Organic Chemistry on Solid Supports**

Jörg S. Früchtel and Günther Jung*

Dedicated to Professor Ivar Ugi on the occasion of his 65th birthday

Until recently, repetitive solid-phase synthesis procedures were used predominantly for the preparation of oligomers such as peptides, oligosaccharides, peptoids, oligocarbamates, peptide vinylogues, oligomers of pyrrolin-4-one, peptide phosphates, and peptide nucleic acids. However, the oligomers thus produced have a limited range of possible backbone structures due to the restricted number of building blocks and synthetic techniques available. Biologically active compounds of this type are generally not suitable as therapeutic agents but can serve as lead structures for optimization. "Combinatorial organic synthesis" has been developed with the aim of obtaining low molecular weight compounds by pathways other than those of oligomer synthesis. This concept was first described in 1971 by Ugi.[56f, g, 59c] Combinatorial synthesis offers new strategies for preparing diverse molecules, which can then be screened to provide lead structures. Combinatorial chemistry is compatible with both solution-phase and solid-phase synthesis. Moreover, this approach is conducive to automation, as proven by recent successes in the synthesis of peptide libraries. These developments have led to a renaissance in solid-phase organic synthesis (SPOS), which has been in use since the 1970s. Fully automated combinatorial chemistry relies not only on the testing and optimization of known chemical reactions on solid supports, but also on the development of highly efficient techniques for simultaneous multiple syntheses. Almost all of the standard reactions in organic chemistry can be carried out using suitable supports, anchors, and protecting groups with all the advantages of solid-phase synthesis, which until now have been exploited only sporadically by synthetic organic chemists. Among the reported organic reactions developed on solid supports are Diels–Alder reactions, 1,3-dipolar cycloadditions, Wittig and Wittig–Horner reactions, Michael additions, oxidations, reductions, and Pd-catalyzed C–C bond formation. In this article we present a comprehensive review of the previously published solid-phase syntheses of nonpeptidic organic compounds.

Keywords: combinatorial chemistry · compound libraries · oligomer synthesis · solid-phase synthesis

1. Introduction

More than three decades ago, Merrifield[1] introduced the concept of solid-phase peptide synthesis. Since then, automated solid-phase syntheses of polypeptides,[2, 3] oligonucleotides,[4] and oligosaccharides[5] have been carried out with increasing regularity. The introduction of synthesis robots for the simultaneous multiple synthesis of peptides[3b, 6] was the logical continuation, and more recently the systematic synthesis of peptide libraries was developed.[7]

Compared with classical synthesis in solution, the solid-phase synthesis of modified peptides, for example lipopeptides such as tripalmitoyl-(*S*)-glycerylcysteine peptides,[8] glycopeptides,[9] and cyclosporin,[10] is simpler and can also be carried out more rapidly. Even for less complicated peptides, several weeks are often required for the classical multistep synthesis in solution including isolation and purification. Synthesis of biopolymers on solid supports has simplified these procedures considerably by obviating the need for elaborate separation steps; however, its prerequisite is a quantitative yield in every step.

[*] Prof. Dr. G. Jung, Dipl.-Chem. J. S. Früchtel
Institut für Organische Chemie der Universität
Auf der Morgenstelle 18, D-72076 Tübingen (Germany)
Fax: Int. code +(7071)296925
e-mail: Jung@AKJung3.orgchemie.chemie.uni-tuebingen.de

[**] The following abbreviations are used in this article: 9-BBN: 9-borabicyclo[3.3.1]nonane; Ac_2O: acetic anhydride; Bn: benzyl; Bpoc: biphenylpropyloxycarbonyl; Bu: butyl; CPG: controlled-pore glass; dba: dibenzylidene acetone; DBU: diazobicyclo[5.4.0]undec-7-ene; DCC: dicyclohexylcarbodiimide; DEAD: diethyl azodicarboxylate; DIAD: diisopropyl azodicarboxylate; DIBAL-H: diisobutylaluminium hydride; DIC: diisopropylcarbodiimide; dipamp: 1,2-ethanediylbis[(2-methoxyphenyl)phenylphosphane]; DIPEA: diisopropylethylamine; DMAP: dimethylaminopyridine; Dmt: dimethoxytrityl; DVB: divinylbenzene, EDC: *N*-ethyl-*N'*-(3-dimethylaminopropyl)carbodiimide; HATU: azabenzotriazol-1-yl-*N*,*N*,*N'*,*N'*-tetramethyluronium hexafluorophosphate; HBTU: *O*-benzotriazol-1-yl-*N*,*N*,*N'*,*N'* tetramethyluronium hexafluorophosphate; HMPB: 4-(4-hydroxymethyl 3-methoxy)-phenoxybutyric acid; HOBT: hydroxybenzotriazole; LDA: lithium diisopropylamide; MBHA: methylbenzhydryl; MCPBA: *m*-chloroperbenzoic acid; nbd: norbornadiene, NMP: *N*-methylpyrrolidinone; NPEOC: *p*-nitrophenylethoxycarbonyl; PEG: polyethylene glycol; Pfp: pentafluorophenyl; ph-capp: 1-phenylcarbamoyl-4-diphenylphosphino-2-diphenylphosphinomethylpyrrolidine; phth: phthaloyl; PNA: peptide nucleic acid; PPTS: pyridinium (toluene-4-sulfonate); PS: polystyrene; PTH: phenylthiohydantoin; $Py \cdot SO_3$: pyridine–SO_3 complex; SCAL: safety catch amide linker; TFA: trifluoroacetic acid; TG: TentaGel; TMAD: *N*,*N*,*N'*,*N'*-tetramethylazocarboxamide; TMSCl: trimethylsilyl chloride; TOF: time-of-flight; Tol, tol: tolyl; Trt: trityl.

Among the simple peptide derivatives, several peptide alcohols show interesting biological activity,[11] and some of them have already undergone clinical trials (e.g. DAGO,[12] Sandostatine[13]). The peptide aldehydes, which are obtained from alcohols, may be protease inhibitors.[14] Such peptide alcohols and N-protected amino acid alcohols have been synthesized only in solution so far.[15] However, the methods proposed by Swistok et al.[16] and Neugebauer et al.[17] may also be applied to the solid-phase synthesis of C-terminal peptide alcohols. It has been demonstrated with increasing frequency that complicated peptidomimetics and biologically active peptides can also be prepared on solid supports.

Until recently, the solid-phase synthesis of nonpeptidic compounds, generally nonpolymeric substances, received less attention. However, the synthesis of DIVERSOMER™ libraries by Hobbs DeWitt et al.[18] and other examples of combinatorial organic synthesis[56] (cf. Section 2.3) has led to a renaissance in organic synthesis on solid supports. Reactions on polymer supports will be especially significant in future for the fast, simultaneous, and multiple synthesis of many new compounds required in the search for lead structures and their optimization for preparation of novel pharmaceuticals.

In this article we make a distinction between Solid-Phase Peptide Synthesis (SPPS) and other types of Solid-Phase Organic Synthesis (SPOS). We will primarily emphasize the methods used to carry out classical organic synthesis on solid supports, which bear little resemblance to peptide, oligonucleotide, and polysaccharide chemistry. In choosing the reactions discussed, we gave special consideration to their applicability for the multiple synthesis of "chemical libraries" and oligomer libraries. We also wish to point out that reactions on polymeric supports are not limited to the coupling and protecting group cleavage reactions in biopolymer synthesis, but have also been applied for some time to other organic reactions.

The solid support based reactions described in this article are of fundamental significance to combinatorial chemistry, the approach in which the pharmaceutical industry is currently investing for the efficient development of new lead structures. Combinatorial chemistry will be dominated by solid-phase synthesis, since reactions on polymer supports are more amenable to multiple and automated syntheses. A review on the combinatorial organic synthesis of small molecules will soon appear in this journal.[161]

2. Organic Synthesis on Solid Supports and Analysis

2.1. Advantages of Solid-Phase Synthesis for Procedures and Product Workup

In discussions of syntheses on polymer supports one must differentiate between polymer-bound reagents and polymeric protecting groups. Reactions with polymer-bound reagents are one-step reactions in which the dissolved substrate is allowed to react with chemical reagents, mostly catalysts or enzymes, that are bound to solid supports (Scheme 1). Many support-bound reagents have been developed[19] for conducting a variety of chemical reactions on supports. Solid supports have been used, for example, for immobilizing triarylphosphanes,[20] hydrogenation catalysts, oxidizing and reducing agents, and chiral auxiliaries and catalysts.[21] A number of these polymer-bound reagents are commercially available; they simplify the performance of reactions and especially the workup of reaction mixtures. Until now, most organic chemists have apparently not recognized the advantages of the support-bound reagents and the opportunities offered by solid-phase synthesis.

This review article will not focus on reactions with immobilized reagents, but rather on reactions in which the polymeric support functions as a protecting group for one functional group of the substrate while another site on the substrate is derivatized. These syntheses always consist of several consecutive reaction steps on the solid support, including anchoring of the substrate and cleavage of the reaction product (Scheme 2).

Günther Jung was born in Tübingen (Germany) in 1937 and received his doctorate from the University of Tübingen in 1967. In 1971 he was granted permission to teach organic chemistry and biochemistry. From 1967 to 1968 he was an assistant professor at the University of Houston in Texas (USA). He received the Max Bergmann Medal in 1989 and the Leonidas Zervas Award of the European Peptide Society in 1991. His research interests include the 3D structure elucidation, biological activity, and biosynthesis of peptide antibiotics and siderophores, structure–activity relationships of neuropeptide Y, models for transmembrane channels, multiple peptide synthesis, peptide libraries, B-, T-helper, and T-killer cell epitope mapping, development of synthetic vaccines, and elucidation of sequence motifs of peptides bound to the major histocompatibility complex (MHC). Combinatorial peptide synthesis is one of his main areas of research.

G. Jung

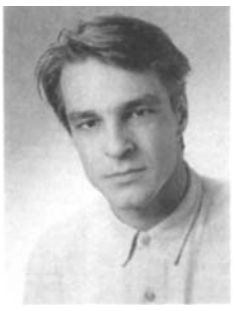

J. S. Früchtel

Jörg S. Früchtel was born in Reutlingen (Germany) in 1967 and studied chemistry at the University of Tübingen from 1987 to 1994. During his studies for the diploma, he started to work in solid-phase combinatory chemistry. He investigated the multiple synthesis of peptoids as analogues of peptide ligands and their binding to MHC class I proteins. In his dissertation, which he started in mid-1994, he has been concentrating on the optimization and development of methods for the combinatorial solid-phase synthesis of small molecules and biopolymer analogues.

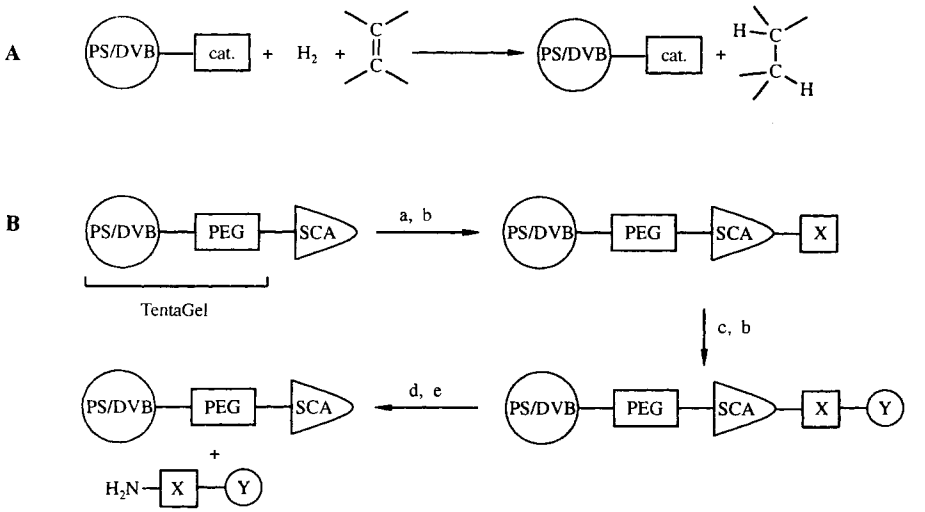

Scheme 1. Schematic representation of A) a one-step reaction with a polymer-supported *reagent*, a covalently bound hydrogenation catalyst [19–21]. B) Schematic representation of a reaction with a polymer-supported *substrate* bound by a support–linker–anchor combination. PS/DVB copolymer (Table 1); PEG: polyethylene glycol as the hydrophilic linker between the anchor and support; SCA: Safety Catch Amide (Table 3) anchor for the covalent and reversible binding of the substrate. a) Coupling of compound **X** to the support; b) removal of excess reagents; c) derivatization of X with Y; d) reduction of the anchor; e) cleavage of the final product.

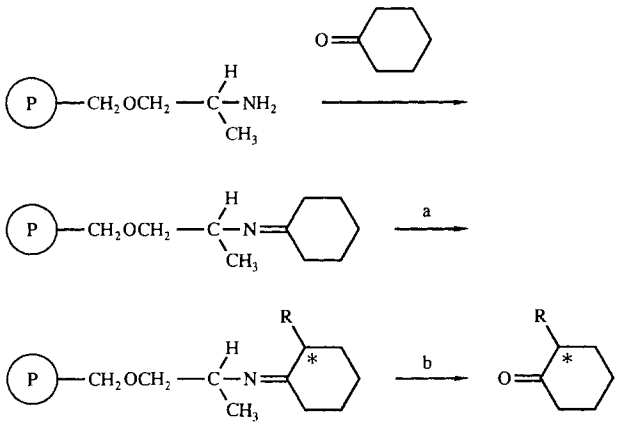

Scheme 2. Example of a multistep synthesis on a solid support (P): Synthesis of chiral 2-alkylcyclohexanone by an enamine reaction according to Stork [21]. a) 1. LDA, 2. RI; b) H^+.

Over three decades, this method has been investigated extensively and optimized for peptide chemistry, especially for carboxyl, amino, thiol, and hydroxyl groups.[22, 23] The following advantages can be expected from this type of solid-phase synthesis.

1) Considerably simplified reaction procedures: Time-consuming purification and isolation steps are eliminated by the covalent binding of the substrate and product to the support. Solutions of reagents in excess are used and the support-bound product is filtered off and washed.
2) Thermodynamic and kinetic influence on the course of the reaction: Higher yields can be obtained by using a large excess of reagents. However, the conditions must also be chosen carefully so that no undesired side reactions such as multisubstitutions take place.
3) Possibility of regenerating the support: The polymeric support can be regenerated and reused for new syntheses if appropriate cleavage conditions and suitable anchor groups are chosen. For industrial syntheses of small molecules involving a few reaction steps, in particular, the support should be chosen such that after cleavage of the product it can be regenerated in a few steps and used again. The price of the support is not an important factor in the multistep synthesis of expensive products. Regenerable supports include chloromethylated PS/DVB resin (Merrifield resin), chlorotrityl-PS/DVB resins, and hydroxymethylated PS/DVB resins (two-step regeneration).
4) Principle of high dilution: Undesired side reactions such as cross-linking and multiple couplings can be suppressed by using supports with low loading (<0.8 mmol g^{-1}) which serve to isolate the reactive sites (see Dieckmann cyclization, Section 3.6).
5) Influencing the stability (thermodynamic, kinetic) of polymer-bound reagents, for example, by making use of the template effect in asymmetric synthesis.
6) Automation: Automated synthesis is a basic requirement for the multiple parallel synthesis of individual products and compound libraries by combinatorial chemistry.

2.2. Supports and Linkers

The correct choice of supports and the bound anchor groups (Scheme 1) is of utmost importance for the success of organic synthesis on solid supports. At present, the choice of available linkers still limits the reaction sequences possible on supports, since these are mostly optimized for biopolymer synthesis.

For reactions in solution extreme conditions are often required for satisfactory results. Synthesis at higher temperatures, the use of reactive substrates, and reactions under inert gas are the rule here and not the exception. When solid-phase syntheses are planned, these factors must be taken into account in the choice of the support and suitable linkers.

So far, no special supports and only a few anchors have been developed for solid-phase organic synthesis. However, the supports developed for peptide chemistry can also be used for numerous organic syntheses (Table 1). The planned reaction sequence ultimately determines what kind of support can be used.

Therefore, the choice of anchors is one of the most decisive factors for the success of a series of reaction steps. Similar to the requirements for peptide chemistry, the anchor and any other necessary protecting groups must be stable to all of the reagents used in the synthesis (orthogonality principle). But it should be possible to remove these groups under mild conditions without damaging the final products.

The anchors developed for peptide chemistry are generally stable to either bases or weak acids, but for the most part they are suitable only for the immobilization of carboxylic acids.[3c]

Table 1. Selected supports (solid phases) used in organic synthesis.

Solid support	Remarks	Ref.
PS/DVB copolymer (1–5% cross-linking)	good swelling properties; swells up to five times its dry volume; at low levels of cross-linking (1%) only limited thermal stability (105–130 °C, dependent on solvent)	[24, 25]
hexamethylenediamine-polyacryl resins and related polymers	polar resins; good swelling properties in H_2O and DMF; do not swell in CH_2Cl_2	[26, 27]
poly[*N*-{2-(4-hydroxyphenyl)ethyl}]acrylamide (Core Q)	SPPS with high loading	[28]
poly(*N*-acryloylpyrrolidine) resins, PAP- and SPARE-polyamide resins	SPPS with high loading; swell in H_2O, DMF, and CH_2Cl_2	[29]
polyethylene functionalized with acrylic acid	synthesis on pins	[30]
kieselgur/polyamide (Pepsyn K)	pressure stable; used in continuous-flow SPPS; low swelling properties due to inorganic support; shaking results in marked wear of the organic polymer	[31]
polyHipe, PS/polydimethylacrylamide copolymer	continuous-flow SPPS; loading capacity up to 5 mmol g^{-1}; high cross-linking of the PS chains	[32] [33]
CPG	pressure and heat stable; stable toward aggressive reagents; low loading	
PS macrobeads	diameter ≦1 mm; loading 50 nmol per bead; available with three different anchors	[34]
TentaGel, PEG-PS/DVB copolymers	polar; swell in H_2O, MeOH, MeCN, DMF, and CH_2Cl_2; pressure stable; suitable for bioassays on resin	[35]

Table 2. Base-stable anchors groups for linking the substrate to the solid phase.

Anchor	Name; reagent for cleavage (acidolysis); application, comments	Ref.
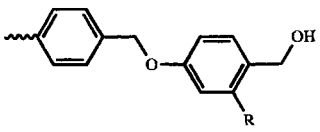	Wang anchor (R = H); 95% TFA; immobilization of carboxylic acids SASRIN anchor (R = OMe); 1% TFA; immobilization of carboxylic acids	[38, 39]
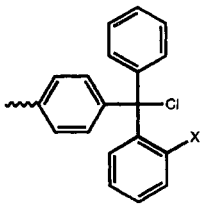	trityl chloride anchor (X = H); weak acids (HOAc); immobilization of nucleophiles 2-chlorotrityl chloride anchor (X = Cl); very weak acids, $HOAc/CH_2Cl_2$(1/4); immobilization of nucleophiles	[36]
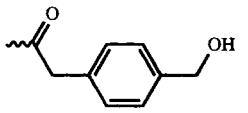	PAM anchor; HF, TFMSA; immobilization of carboxylic acids, 100 times more stable than chloromethylated Merrifield resin	[40]
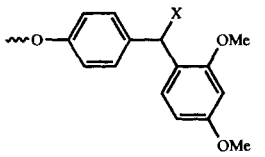	Rink acid (X = OH); $HOAc/CH_2Cl_2$; immobilization of carboxylic acids Rink amide (X = NH-Fmoc); TFA/CH_2Cl_2; immobilization of carboxylic acids by amide formation	[41]
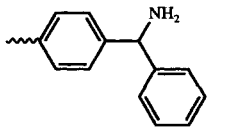	BHA anchor; TFMSA; immobilization of carboxylic acids by amide formation	[42]
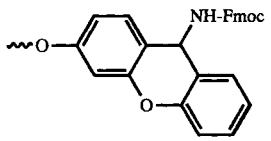	Sieber amide; TFA/CH_2Cl_2 (1/99); immobilization of carboxylic acids by amide formation	[43]

One exception is the chlorotrityl-PS/DVB resin[36] (Table 2), which is a suitable support in theory for all nucleophilic substrates (Section 3.1). Unfortunately, the trityl anchoring bond can be cleaved by very weak acids such as acetic acid.

The Safety Catch Amide Linker (SCAL; Table 3) is very stable to acids and bases in its oxidized form, but after reduction with $(EtO)_2P(S)SH$ it can be cleaved with trifluoroacetic acid (TFA). However, the SCAL group can be used to attach only carboxylic acids to the support, and carboxamides are generated upon cleavage. Additional safety catch linkers have already been investigated and reported.[37] A selection of tested, commercially available (only a few) anchors are listed in Tables 2 and 3. For the reversible attachment of special functional groups, known anchors often have to be derivatized and optimized, or when necessary, completely new anchors must be developed. Some of the modified standard anchors with examples of their applications are presented in this article.

In addition to the previously mentioned, versatile trityl and 2-chlorotrityl anchors, other anchor groups have been developed for coupling compounds having other functional groups. Ellman et al.[54] introduced an anchor group for immobilizing alcohols. The sodium salt of this anchor, (6-hydroxymethyl)-3,4-dihydro-2*H*-pyran, is covalently bound to chloromethylated Merrifield resin by a nucleophilic substitution reaction (Scheme 3). The alcohol is coupled to the support by electrophilic addition in the presence of pyridinium toluene-4-sulfonate (PPTS) in dichloromethane (16 h at 80 °C). The resulting tetrahydropyranyl ether, a common protecting group for alcohols, is stable to base but can be cleaved by transetherification or treatment with 95% trifluoroacetic acid.

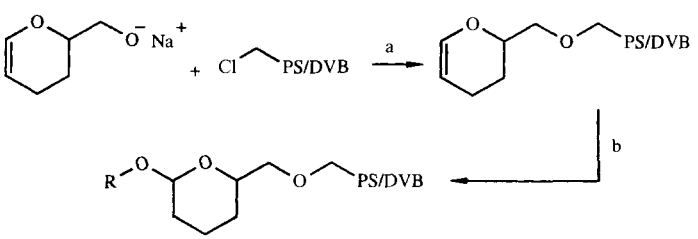

Scheme 3. Preparation of an anchor used for immobilizing alcohols [54]. The reaction of an alcohol with the anchor generates a tetrahydropyranyl ether; this common alcohol protecting group is base-stable but can be cleaved by acidolysis. a) Dimethylacetamide, room temperature, 16 h; b) 2 equiv PPTS, 5 equiv ROH, 80 °C, 16 h.

Sucholeiki[55] coupled benzyl halides to a photolabile α-sulfanyl-substituted phenyl ketone anchor (Scheme 4). In this approach the 2-methoxy-5-[2-{(2-nitrophenyl)dithio}-1-oxopropyl]phenylacetic acid anchor (NpSSMpact) is protected as a disulfide and coupled to an amino-functionalized resin. The disulfide bond is cleaved by reduction, and then various (substituted) benzyl halides can be coupled to the free thiol group. The

Table 3. Acid-stable anchor groups for linking substrate and support.

Anchor	Cleavage conditions (reagents), mechanism; application; comments	Ref.
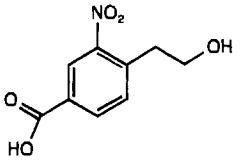	DBU/piperidine, β-elimination; suitable for peptide, oligonucleotide, and oligosaccharide syntheses on aminomethylated solid supports, immobilization of carboxylic acids	[44]
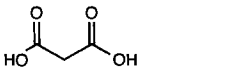	NaOH, saponification; immobilization of alcohols, amines (irreversible) on hydroxymethylated PS/DVB resins	[45]
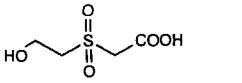	NaOH, β-elimination; immobilization of carboxylic acids on hydroxymethylated PS/DVB resins	[46]
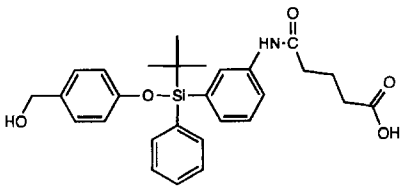	Bu_4NF; immobilization of carboxylic acids on H_2NCH_2-PS/DVB resins; cumbersome synthesis of the linker	[47]
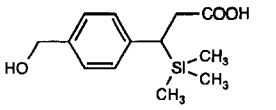	Bu_4NF; as in ref. [47]; immobilization of carboxylic acids on aminomethylated PS/DVB resins	[48]
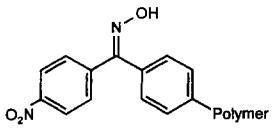	Hydrazine hydrate, hydrazinolysis; stable in 25% TFA; immobilization of carboxylic acids	[49]
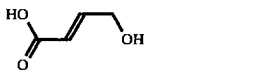	Pd^0/H_2, catalytic hydrogenation; immobilization of carboxylic acids; HYCRAM supports [c]	[50]
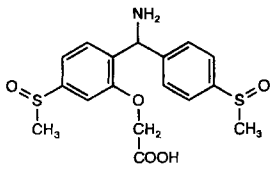	$(EtO)_2P(S)SH$/TFA, reductive acidolysis; in oxidized form stable toward acids and bases SCAL; immobilization of carboxylic acids	[51]
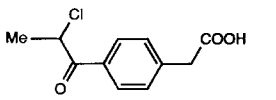	photolysis ($h\nu$ = 350 nm, room temperature, 72 h); stable in 50% TFA, labile in hydrazine hydrate; immobilization of carboxylic acids	[52]
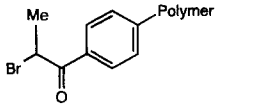	photolysis ($h\nu$ = 350 nm); labile in piperidine/DMF [a], more stable in piperidine/CH_2Cl_2 [b]; immobilization of carboxylic acids	
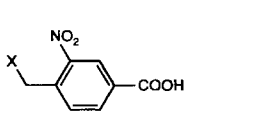	photolysis ($h\nu$ = 350 nm, under inert gas; X = Hal, OH, NH_2); immobilization of carboxylic acids	[53]

[a] Up to 3% loss of peptide per Fmoc cleavage. [b] Up to 1% loss per Fmoc cleavage. [c] HYCRAM = hydroxycrotonylaminomethyl.

photochemical cleavage generates disulfides when unsubstituted benzyl halides are used and toluene derivatives when *p*-arylbenzyl halides are employed.

2.3. Multiple, Parallel Syntheses on Solid Supports

Until a few years ago, new organic compounds were mostly synthesized individually and then tested for their possible biological activity. More recently, the procedures in searching for new lead structures have become tremendously more efficient. Progress in the fields of biotechnology, molecular biology, robotics, and automation have led to the development of new screening assays that can be used to test a series of substances for receptor binding and biological activity in a remarkably short time. As a consequence, the stockpile of new compounds in the pharmaceutical industry requiring testing has been rapidly depleted, and standard methods of synthesis are not efficient enough to supply the demand for new compounds.

In addition to the previously mentioned methods for the automated synthesis of peptides, oligosaccharides, and oligonucleotides, a new method has been developed for the rapid, automated synthesis of a series of oligomeric and nonoligomeric compounds—combinatorial chemistry.[56, 59] Chemists in this area no longer work with three-neck flasks, stirrers, reflux condensers, dropping funnels, and heating mantles. Instead they use the new type of multiple reactors for the parallel and potentially automated simultaneous synthesis of a series of compounds. Reactions on solid supports are especially suitable for this type of synthesis, since the desired products remain bound to the support and can be separated from the excess reagents by filtration (Section 2.1). The starting materials (building blocks) should be versatile, easy to derivatize, and readily accessible. For example, if retrosynthesis leads to a preparative route to a desired product, then multiple procedures can be used to prepare a large series of structurally similar compounds. Generally two strategies are available for this purpose:

1. The multiple parallel synthesis of *individual compounds*. In this case, only one compound is prepared per reaction vessel (arrays). This method is especially suitable for rapidly optimizing previously identified lead structures.
2. The multiple parallel synthesis of *compound libraries*. Here, many different compounds having a common backbone are synthesized simultaneously in each reaction vessel.

Compound libraries can be prepared with relative ease by "divide, couple, and recombine" techniques[75, 76] (Scheme 5). Portions of the anchor–resin combination are allowed to react separately with the first components (A^1–A^3). After the reaction the resins are thoroughly mixed and then redivided into portions of the same size in order to ensure a random distribution of the components. By subsequent reaction with the building blocks B^1–B^3 one obtains, in this example, nine different compounds after only two reaction steps. Depending on the number of individual building blocks and synthesis steps, thousands of different compounds can be synthesized in each reaction vessel, which can be subjected to screening either as polymer-bound products or as polymer-free libraries.

In the development of methods for combinatorial chemistry, reactions known from solution chemistry must be tested for their suitability for solid-phase synthesis of nonpeptidic and nonoligomeric compounds. In the last decade, in addition to the classical condensation used in peptide synthesis, a representa-

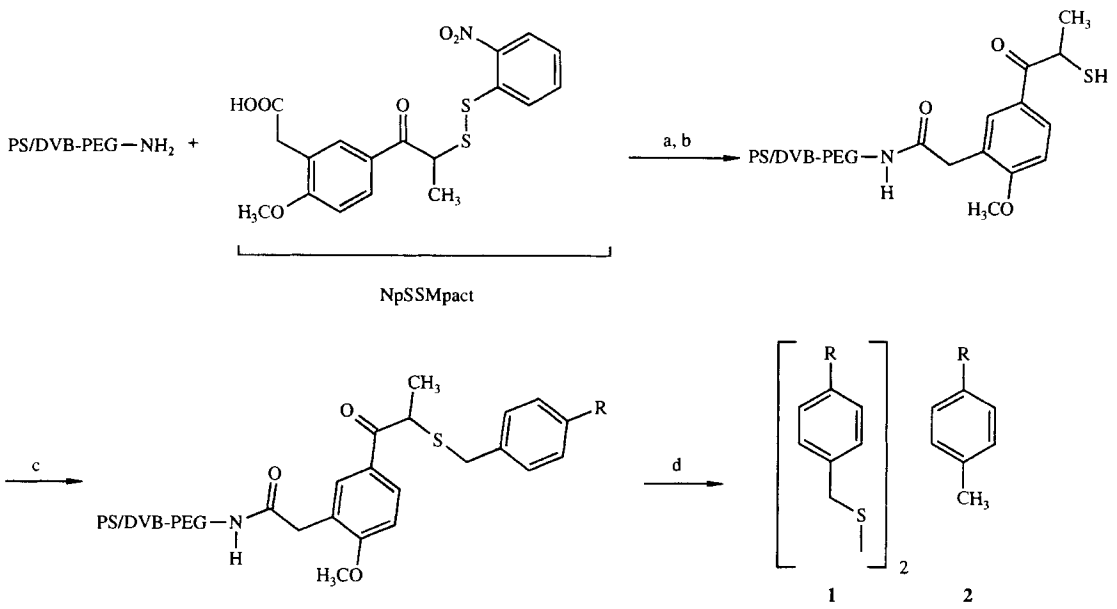

Scheme 4. Preparation of a photochemically cleavable linker for thiols [55]. Toluene derivatives or disulfides are obtained, depending on the reaction conditions. a) DIC, CH_2Cl_2; b) β-sulfanylethanol, DIPEA, DMF; c) a benzyl bromide, DIEA, DMF; d) acetonitrile, $h\nu$ = 350 nm, N_2, 1–5 h. **1** (R = H), **2** (R = aryl).

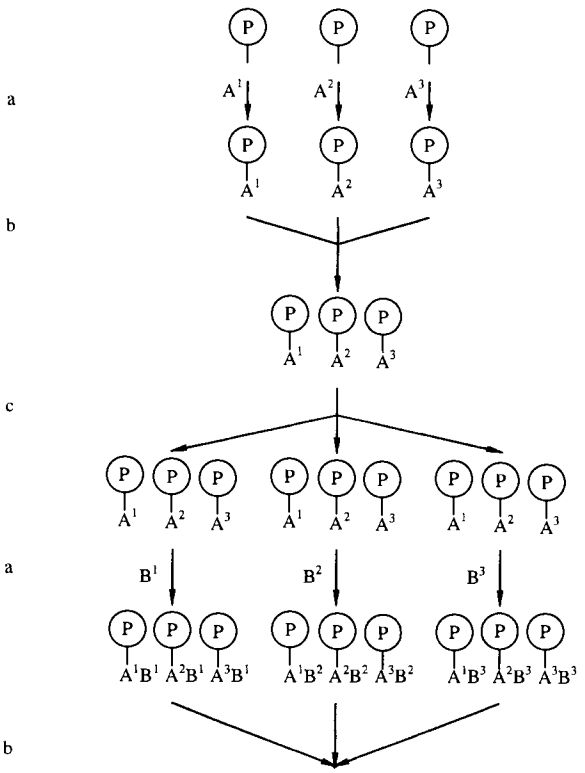

Scheme 5. Preparation of nine different products on a polymeric support Ⓟ by combinatorial chemistry and the the "divide–couple–recombine" method [75,76]. a) Coupling, b) mixing, c) dividing.

tive series of reaction types (Table 4) have been investigated for their applicability to solid-phase organic synthesis (SPOS).

However, the published solid-phase reactions and anchor–resin combinations do not suffice for the preparation of a truly broad spectrum of compounds. The primary goal of solid-phase organic synthesis must be to extend the range of currently available reactions, regardless of whether these reactions are suitable

Table 4. Examples of reactions that can be carried out on solid supports.

Reaction type	Examples of reactions on the support	Ref.
[2+2]cycloadditions	trapping of butadiene	[103]
[2+3]cycloadditions	synthesis of isoxazolines, furans, modified peptoids	[104,108,147]
acetal formation	immobilization of diols, aldehydes, and ketones	[72,82–85]
aldol condensation	derivatization of aldehydes, synthesis of propanediols	[82–85,136]
benzoin condensation	derivatization of aldehydes	[83,84]
cyclocondensations	benzodiazepines, hydantoins, thiazolidines, β-turn mimetics, porphyrins, phthalocyanines	[115–117,119, 123,125,128,129]
Dieckmann cyclization	cyclization of diesters	[124]
Diels–Alder reaction	derivatization of acrylic acid	[104]
electrophilic addition	addition of alcohols to alkenes	[54]
Grignard reaction	derivatization of aldehydes	[83–85]
Heck reaction	synthesis of disubstituted alkenes	[131]
Henry reaction	synthesis of nitrile oxides in situ (see [2+3]cycloaddition)	[108]
catalytic hydrogenation	synthesis of pheromones and peptides (hydrogenation of alkenes)	[70,71,137]
Michael reaction	synthesis of sulfanyl ketones, bicyclo[2.2.2]octanes	[73,142]
Mitsunobu reaction	synthesis of aryl ethers, peptidyl phosphonates, and thioethers	[78–81]
nucleophilic aromatic substitutions	synthesis of quinolones	[118]
oxidation	synthesis of aldehydes and ketones	[69–71,73,123]
Pausen–Khand cycloaddition	cyclization of norbornadiene with pentynol	[106]
photochemical cyclization	synthesis of helicenes	[127]
reactions with organometallic compounds	derivatization of aldehydes and acyl chlorides	[69–71,72d,89, 90,94]
reduction with complex hydrides and Sn compounds	reduction of carbonyl, carboxylic acids, esters, and nitro groups	[54,70,71,72d, 83,84,89,90,141]
Soai reaction	reduction of carboxyl groups	[81]
Stille reaction	synthesis of biphenyl derivatives	[122,132]
Stork reaction	synthesis of substituted cyclohexanones	[21]
reductive amination	synthesis of quinolones	[118]
Suzuki reaction	synthesis of phenylacetic acid derivatives	[134]
Wittig, Wittig–Horner reaction	reactions of aldehydes; pheromones, sulfanyl ketones	[70–73,83,84]

for the synthesis of single compounds or compound libraries. With this in mind, we will discuss the known solid-phase reactions here without differentiating between "combinatorial" and "noncombinatorial" solid-phase chemistry.

The reproducible, in other words automated, synthesis of compound libraries consisting of oligomers (e.g. peptides, oligonucleotides, and biopolymer analogues) or small molecules (e.g. benzodiazepines) is one challenge; the identification and structural elucidation of biologically active compounds from "combinatorial compound libraries" is another.

As a result of the new developments in the synthesis of nonpeptide libraries, heavy demands are put on their analysis. Besides the problem of monitoring the solid-phase synthesis mentioned in Section 2.4, common chromatographic methods such as HPLC and TLC are not suitable for the analysis of the liberated, complex substance libraries. The ^{13}C NMR spectrum of a mixture of hundreds or more similar compounds cannot be interpreted completely and, like an IR spectrum, it is only suitable for the analysis of functional groups. In this case, the typical parameters that determine the quality of a synthesis such as purity, yield, exact structure, and stereospecificity can no longer be determined.

Electrospray mass spectrometry (ES-MS), a method recently introduced for the investigation of peptide libraries,[57] furnishes useful information on the identity and purity of a compound library. The coupling of MS with HPLC,[57] or GC and MS-MS[58] allows the analysis of these mixtures; however, even more complex coupled techniques cannot be used to unequivocally characterize more complex mixtures, especially libraries of low molecular weight compounds.

A series of proposals have been made for the identification of active substances in a library, and a few of them will be illustrated here. A complete presentation and discussion of these methods will be found in an article appearing soon in this journal.[161]

A series of reporter systems have been proposed (tags, code molecules)[59] for the identification of compounds after they have been determined to be active lead structures. The aim in this approach is to label individually the components of a library in a parallel synthesis, thus making the identification easier. Kerr et al.[60] and Nicolaiv et al.[61] have used a peptide code for encoding their synthesized compounds. The coding principle is illustrated here with the compound library prepared by Nicolaiev et al. (Scheme 6). A nonpeptide compound library was prepared by acylation of the support with halocarboxylic acids, followed by nucleophilic substitution and subsequent condensation with cyclic carboxylic acids. A standard protocol was used to synthesize the dipeptide Fmoc-Trp-Lys(Boc) on a TentaGel support modified with the SCAL anchor. After removal of the Fmoc group with piperidine, the compound library was assembled on the free amino group of Trp by using the split–couple–recombine technique.[75, 76] In a parallel synthesis, the ε-amino group of the lysine residue was deprotected with TFA and the code sequence was assembled on this site, such that each building block is encoded by an amino acid. The free library can be obtained by reduction of the anchor followed by cleavage with TFA. If an active substance is found by screening, the structure of the compound can be established by sequencing the peptide code.

However, since this method is very time-consuming and requires elaborate instrumentation, it does not seem to be very useful. Further problems could appear by the coding structure itself, since an orthogonal protection strategy is required and the code peptides can participate in the receptor recognition. Finally, the coding can also cause side reactions and lead to false interpretations of the test results.

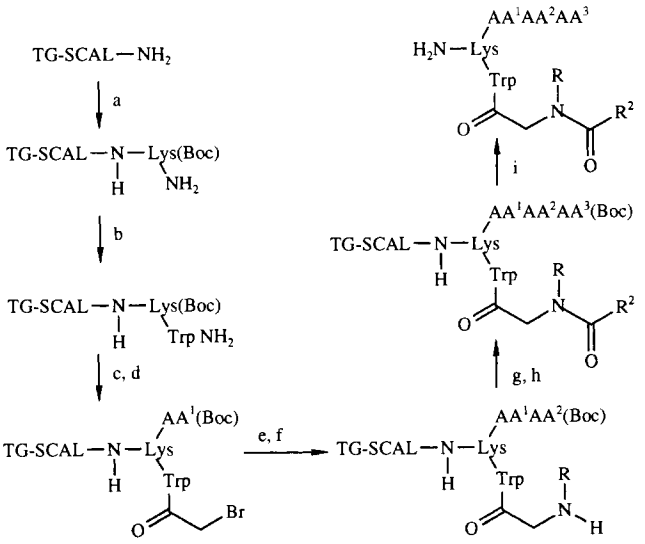

Scheme 6. Example of the synthesis of a peptide-encoded compound library according to Nicolaev et al. [61]. a) 1. Boc-Lys(Fmoc)-OH, DIC/HOBT, 2. piperidine/DMF (1/1); b) 1. Fmoc-Trp-OH, DIC/HOBT, 2. piperidine/DMF (1/1); c) 1. dividing, 2. bromoacetic acid, DIC; d) 1. TFA, 2. encoding with Boc-protected amino acids (Boc-AA^1), DIC, 3. mixing; e) 1. TFA, 2. dividing, 3. Boc-AA^2, DIC/HOBT; f) 1. RNH_2, 2. mixing; g) 1. dividing, 2. coupling of carboxylic acids, DIC/DMF; h) TFA, Boc-AA^3, DIC/HOBT; i) 1. mixing, 2. reductive acidolysis (TFA).

Ohlmeyer et al.[62] encoded their compounds with a chlorophenol binary code that was bound to the resin by a photolabile anchor. In each synthesis step a maximum of 1% of the available anchor positions on each polymer bead were used for the encoding. The remaining binding sites served to link the compound being synthesized. In this way, individual beads, and consequently the compounds synthesized on these beads, are provided with a sort of individual bar code. The code molecules of polymer beads identified by screening were cleaved photolytically from the resin and analyzed by gas chromatography. Due to the extreme sensitivity of this detection method, even the smallest amount of these aryl halide labels can be detected. A variation of this coding was proposed by Baldwin et al.,[140] in which the tag molecules are linked covalently to the resin by carbene insertion. After the synthesis of the compound library the tags are removed by oxidation with ceric ammonium nitrate then silylated, and the code sequence is analyzed by electron capture gas chromatography (EC-GC).

Another completely different method was proposed by Brenner and Lerner.[63] They used a binary code composed of oligonucleotide sequences (DNA-tag) and "read" the code with one of the most sensitive known analytical tools, the polymerase chain reaction (PCR). The DNA-tag of the isolated, active molecule can be amplified with PCR and the code can be decoded by DNA sequencing. Very small amounts of the code molecule can be amplified, identified, and decoded by this approach. However, due to the inherent chemical lability of oligonucleotides, applications of this method are severely limited.

2.4. Analysis and Monitoring of Reactions on Solid Supports

Every step in a multistep synthesis on a solid support yields a resin-bound intermediate whose characterization poses a serious problem. Quantifying the loading (= yield) and determining the structures of the polymer-bound product and possible by-products, which are fairly straightforward in solution-phase syntheses, are very difficult. However, the analysis of resin-bound peptides and peptidomimetics has already reached a high standard even for multiple syntheses. Quantitative determination of coupling yields is possible, for example, by rapid, quantitative UV analysis of the cleavage product formed from the amino acid protecting group Fmoc, by direct sequencing on the support (for individual peptides), and by ES-MS and Edman degradation (for peptides bound to single beads).

By contrast, very few methods have been described for the analysis of compounds on the support during solid-phase organic synthesis, although this is essential information for optimizing successive synthetic steps in combinatorial chemistry. In addition to the standard procedure—1. derivatization, 2. cleavage, 3. purification, and 4. analysis (MS, IR, and/or NMR)—several analytical methods are available for characterizing the polymer-bound compounds and give information on the type and completeness of reactions:

- FT-IR and FT-Raman spectroscopy
- Solid-state and gel-phase ^{13}C NMR spectroscopy[64] as well as ^{1}H and ^{13}C correlation NMR spectroscopy
- High-resolution ^{1}H MAS and MAS-CH correlation in the gel phase[65]
- Matrix-assisted laser desorption ionization time-of-flight (MALDI-TOF) mass spectrometry[66]
- Elemental analysis
- Titration of reactive groups ($-NH_2$, -COOH, ArOH, -SH)
- Gravimetric analysis
- Photometry ($-NH_2$ monitored by photometric Fmoc determination)

Due to the interference of the polymer backbone and low loadings commonly used, conventional IR and NMR spectra are difficult to interpret and are often ambiguous. FT-IR measurements performed under defined conditions furnish qualitative as well as quantitative data. In difference measurements on the free and the loaded support under identical conditions absorption bands can be detected, especially in the fingerprint region, which otherwise are seen only as poorly identifiable shoulders. For example, the absorption band of the H-C-Cl stretching vibration (1250 cm^{-1}) can be used to determine the yield of the coupling of carboxylic acids to a chloromethylated PS-DVB support. By calibrating measurements[72d, 124] on several loaded resins, a calibration curve can be constructed (log(absorption) vs chlorine content) and the completeness of the reaction can be verified.

The developments in the area of solid-state and gel-phase NMR in the last years has led to further suitable methods for monitoring reactions on supports. Gel-phase NMR spectroscopy[64] is a mixture of standard solution-phase and solid-state NMR spectroscopy. For this purpose, a solid sample, for instance PS-DVB resin, is transferred to an ordinary NMR tube and allowed to swell in a suitable solvent (CD_2Cl_2, $CDCl_3$). After the sample is degassed, it can be measured under the conditions typically used for dissolved samples.

The ^{13}C NMR spectra are dominated by the strong resonance signals of the polymeric support, and the weak signals of the polymer-bound substrate are often difficult to see. Due to strong line broadening, one-dimensional ^{1}H NMR spectra cannot be interpreted. High-resolution ^{1}H NMR spectra can be obtained by a combination of MAS (Magic Angle Spinning),[65] a technique normally used in solid-state NMR spectroscopy, and the previously described gel-phase method. As a result line broadening is suppressed effectively, and even with short measuring times the signal-to-noise ratio is improved considerably. However, the proton coupling patterns can be resolved only for support–linker combinations like PS/PEG.

Enger, Langley, and Bradley[66] monitored chemical reactions by matrix-assisted laser desorption ionization time-of-flight mass spectrometry (MALDI-TOF-MS). In this example, a series of peptides were synthesized on the commercially available acid-labile Rink amide PS/DVB support. After every reaction step, 1–100 polymer beads were removed and placed directly in the sample holder. The synthesized compounds were then cleaved from the polymer by addition of suitable cleaving reagents. The polymer beads and liberated compounds were then embedded in a matrix (e. g. 2,5-dihydroxybenzoic acid) and analyzed by MALDI-TOF-MS. This analytical method was initially applied to compounds attached to the extremely acid-labile Rink amide anchor (Table 2) but has been repeated subsequently with compounds on other acid-labile anchors such as MBHA, trityl, *p*-alkoxybenyl (Wang resin), aminotrityl, and hydroxytrityl.[66b] In addition, the photolabile anchors, which can be cleaved by laser light, have been employed.

Other methods also enable quantitative analysis of polymer-bound compounds. Elemental analysis of resins, in particular, is fraught with difficulties. In general, the inaccuracy and deviation of the results obtained is associated with the low loading of the substrates on the support. Information on the real availability of reactive or functional groups on the resin is also very difficult to obtain by such an analysis. The reproducibility of C, H, N, and halogen determinations is too poor to quantitate small variations. Several independent investigations on $BrCH_2(O)CO$-trityl PS/DVB resins[67] gave values between 0.9–1.8 mmole of Br per gram of resin, with a possible maximum loading of 1.47 mmol g^{-1}. Furthermore, it could be shown that because of frequently occurring side reactions (e.g. cross-linking and multiple coupling of the substrate), the results obtained deviated severely from the actual yields of the cleaved products.[72d]

In spite of the great progress made so far, the analysis of support-bound compounds and compound libraries is not satisfactory. Further attempts must be made to optimize the known methods and to introduce new techniques for the direct monitoring of reactions, for example using electrochemical sensors.

3. Examples of Solid-Phase Syntheses of Small Molecules

A frequent problem in preparative chemistry is the selective protection of one of two identical functional groups in a compound. Typically a mixture of di-, mono-, and unprotected

products is obtained, which must be separated by elaborate procedures. In syntheses in solution this problem is often circumvented noneconomically by using an excess of the difunctional starting material. Consequently, the mono-protected derivative is formed predominantly, but it must be separated from the excess of unreacted starting material.

This problem of product isolation does not occur when polymer-bound protecting groups are used, since only one of the functional groups in the substrate is protected by immobilization on the support. Thus, further reactions can be carried out selectively on the unprotected group, and the excess reagents are removed by washing the resin. This reaction is an example of the "fishhook" principle.[68] In particular, the group of Leznoff[69] has worked intensively on the selective blocking of one of many functional groups and the subsequent problems incurred.

3.1. Immobilization and Reactions with Hydroxy Compounds

In extensive studies insect sex attractants were synthesized using polymer-bound symmetrical diols.[70, 71] For this purpose, a series of synthetic procedures were developed, some of which are presented here. A polystyrene (PS) resin heavily cross-linked with 2% divinylbenzene (DVB) served as the support and was functionalized with the acid-labile trityl anchor group. The diols were immobilized on the support by reacting the functionalized resin with a solution of an appropriate alcohol in pyridine (Scheme 7).

Starting with this functionalized resin,[69–71] the solid-phase synthesis of pheromones was achieved by several different procedures. Treatment of the immobilized diol with methanesulfonyl chloride yielded a polymer-bound sulfonate, which was then allowed to react with suitable alkynyllithium compounds to yield a protected alkynol. The compound with R = H can be substituted by deprotonation with butyllithium and subsequent reaction with alkyl halides. However, in contrast to the analogous reaction in solution, a large excess of BuLi must be used for deprotonation on a solid support. Subsequent hydrogenation of the triple bond with H_2/Pd–$CaCO_3$ produces a mixture of *cis* and *trans* alkenes; the stereoselective reduction to *cis* alkenes is possible by using 9-borabicyclo[3.3.1]nonane (9-BBN) or disiamylborane. The resulting alkene is then cleaved and the resin regenerated by hydrolysis with either HCl or acetic acid; the final product can then be esterified by treatment with acetic anhydride in solution.

Further variations of the pheromone synthesis have also been investigated using Wittig and "reverse Wittig" reactions.[69–71] Because of the acid-lability of the trityl anchor, basic to neutral conditions are required for the oxidation of the polymer-bound alcohol to the corresponding aldehyde. In addition, precipitation of the oxidizing agent on the resin, either before or during the reaction, must be prevented. Oxidation can be achieved with $CrCl_2O_2$/pyridine/*tert*-butyl alcohol in dichloromethane (Scheme 8 left). The subsequent reaction with an alkyl triphenylphosphonium halide followed by Wittig reaction yields the *cis* alkene with high stereoselectivity (68–91.5%, as determined by HPLC).

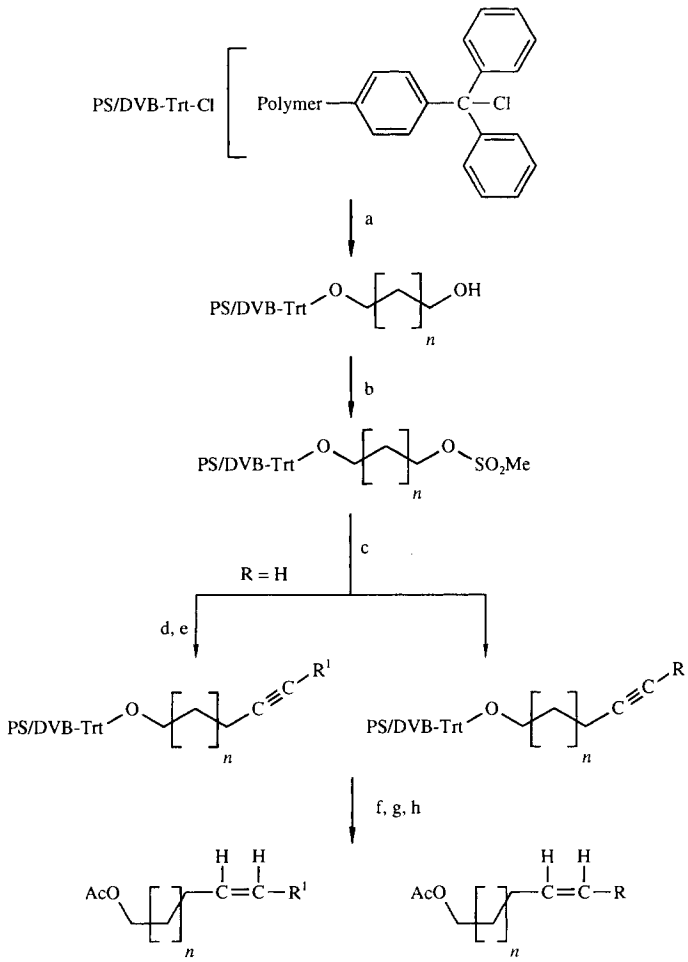

Scheme 7. Synthesis of several insect sex attractants linked by trityl anchors to polymer supports can be carried out by the alkyne method as well as by the two-step alkyne method [69–71]. a) Pyridine; b) $MeSO_2Cl$; c) RC≡CLi (R = H, alkyl, aryl), inert gas; d) BuLi; e) R^1Br; f) reduction (e.g. with 9-BBN); g) HCl or acetic acid; h) Ac_2O.

In the reverse Wittig reaction on solid polymers (Scheme 8, right) the phosphonium salt is prepared on the resin starting from polymer-bound alkyl halides or mesylated alcohols. This reaction requires very drastic conditions, since triphenylphosphane does not react with alkyl halides or with mesylated alcohols at room temperature. Preparation of the polymer-bound Wittig reagent is possible only when the resin is heated with molten phosphane at 100 °C for 24 h.

It is not possible to link the less reactive aromatic diols to the trityl resin. If, instead of the trityl anchor, one uses benzoic acid derivatives such as benzoyl chloride[71c] as the anchor, the aromatic diols can be immobilized readily by esterification. However, owing to the base-lability of this aryl ester bond, only reactions in neutral to acidic media are possible. Thus, for example, monomethyl ethers of resorcinol, hydroquinone, and 7-hydroxy-2-naphthol can be obtained by reaction with diazomethane; their monoalkyl ethers are prepared by reaction with potassium *tert*-butoxide and alkyl halides. The yields after cleavage, and based on the maximal loading of the support, ranged from 22 to 74%. These variations were attributed to incomplete alkylation or cleavage reactions. The possibility that both hydroxyl groups are bound simultaneously to the resin has

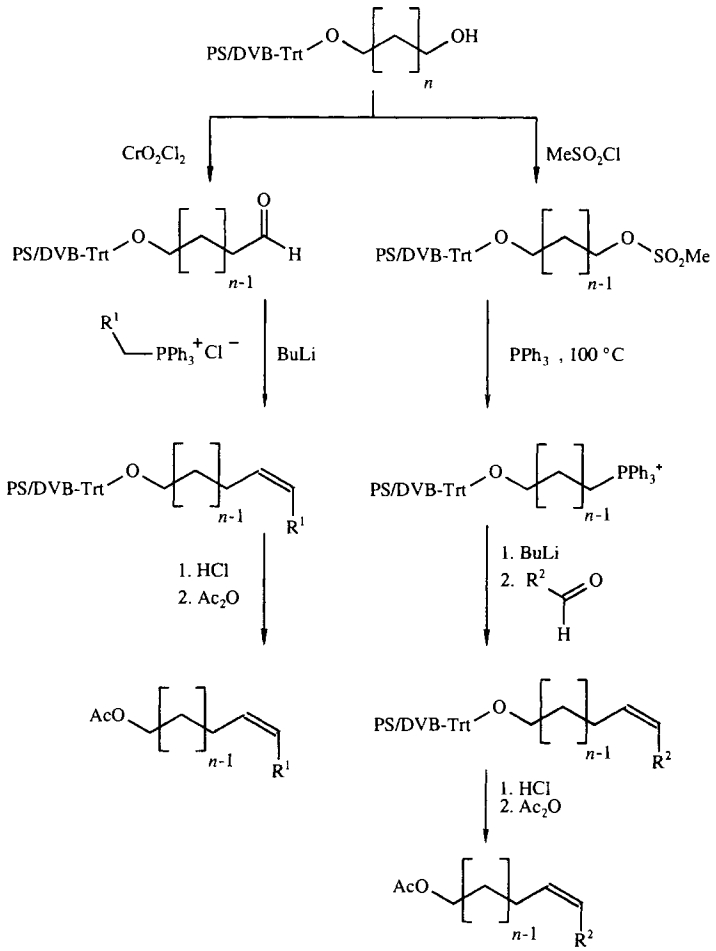

Scheme 8. Preparation of pheromones by Wittig (left) and reverse-Wittig reactions [71, 72] (right) on trityl resin. Because of the sluggish reaction of the mesitylated diol, the resin must be heated with triphenylphosphane at 100 °C. Immobilized halides can also be used as well. R^1, R^2 = alkyl.

also been discussed. But this reaction is not very probable: the best monofunctionalization results have been achieved with hydroquinone, which because of its *para* substitution would be the most suitable diol for cross-linking coupling. Generally, when the experimental results are evaluated, the possibility of a cross-linking reaction involving bifunctional molecules cannot be ruled out.

In addition to the trityl anchor for immobilizing *cis* diols on polymers, Fréchet et al. [72] have investigated the interesting support–anchor combination polystyrene/boric acid. This anchor has several very promising properties: it has moderate to high loading (2–3 mmol g^{-1}), the coupling of the diol as a boronate proceeds simply and with high yield, only *cis* diols are bound, and the resin can be reused without loss of reactivity after the reaction product is cleaved. This anchor has been used for the selective blocking of *cis* hydroxyl groups of carbohydrates. This method has been employed to synthesize desoxysugars on solid supports which otherwise could not have been prepared.

Based on the previous work of Leznoff et al.,[69–71] a recent article has appeared describing a combinatorial method for the simultaneous synthesis of several different β-sulfanyl ketones.[73] In this approach 1,4-butanediol immobilized on a trityl resin is oxidized[74] and subjected to a Wittig–Horner reaction and a Michael addition of an aromatic thiol to afford the resin-bound sulfanyl ketone (Scheme 9), which is cleaved from the resin by acidolysis with formic acid. A series of nine different ketones could be obtained by the divide, couple, and recombine strategy[75, 76] and reactions with three different ylides and three different thiols.

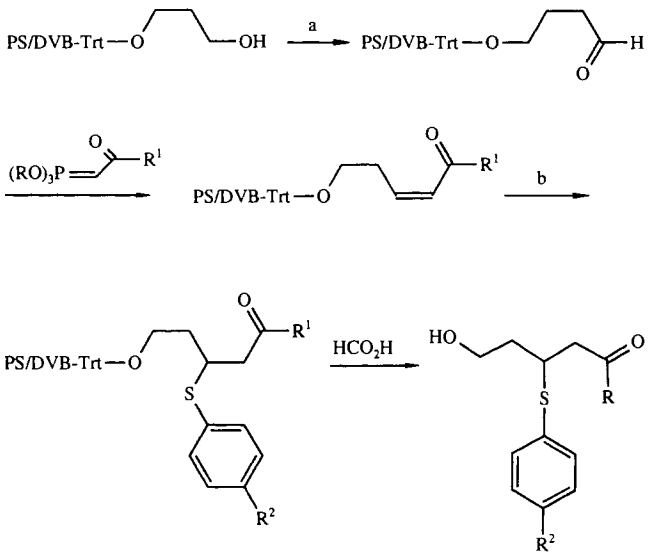

Scheme 9. Synthesis of nine different sulfanyl ketones by a combination of Wittig–Horner reaction and Michael addition [73]. a) Py·SO_3, DMSO, Et_3N, room temperature, 2 h; b) thiophenols, NaOMe (cat.), THF, room temperature, 2 d. R = alkyl, aryl; R^1 = Me, Bu, Ph; R^2 = H, Me, Cl.

3.1.1. Derivatization of Hydroxy Compounds by the Mitsunobu Reaction

The Mitsunobu reaction[77] is an efficient and commonly used organic reaction for the synthesis of esters and aromatic ethers with inversion of configuration. For this reason Richter and Gadek[78] chose this reaction to immobilize *N*-Boc-L-tyrosine methyl ester via its phenolic hydroxyl group on hydroxymethyl-PS/DVB resin. Their aim was to synthesize tail-to-head coupled cyclopeptides. *N*-methylmorpholine was used as the solvent and base for deprotonation of tyrosine, and diethyl azodicarboxylate (DEAD)/triphenylphosphane served as the Mitsunobu reagent. A maximum loading of 0.9 mmole per gram of resin (theoretical maximum loading 1.08 mmol g^{-1}) was obtained.

A modified Mitsunobu reaction was used by Campbell and Bermak[79] to prepare peptide phosphonates from peptides (Scheme 10). As transition state mimetics, peptide phosphonates show inhibitory activity against peptidases, esterases, and metalloproteases. The synthetic method described is compatible with the Fmoc strategy of solid-phase peptide synthesis and enables the unrestricted incorporation of phosphonic acid groups into peptides. An α-*O*-Fmoc-hydroxycarboxylic acid is coupled to the peptide with HOBT/HBTU, and the Fmoc group is then removed with piperidine/*N*-methylpyrrolidinone (NMP). The modified peptide is converted into the peptide phosphonate by reaction with an ethyl α-[*N*-(4-nitrophenylethoxycarbonyl)amino]alkylphosphonate under Mitsunobu

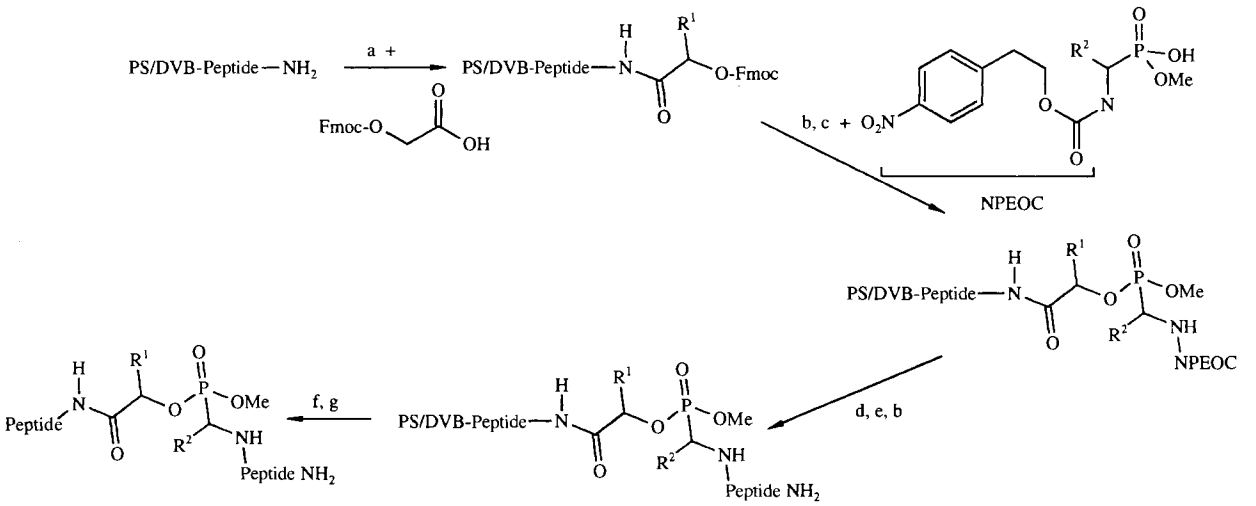

Scheme 10. Preparation of peptide phosphonates by a modified Mitsunobu reaction [79]. a) HBTU, HOBT, DIPEA, NMP; b) piperidine/NMP (3/7); c) $P(4\text{-}ClC_6H_4)_3$, DIAD, DIPEA, THF; d) DBU/NMP (5/95); e) Fmoc-protected amino acids, HBTU, HOBT, DIPEA, NMP; f) thiophenol/triethylamine/dioxane (1/2/2); g) trapping reagent, TFA. R^1 = H, Me, Bn, *i*Bu; R^2 = H, Me, Bn, *i*Pr, *i*Bu.

conditions (DEAD, tri(4-chlorophenyl)phosphane, NMP). After cleavage of the 4-nitrophenylethoxycarbonyl (NPEOC) protecting group under basic conditions (DBU/NMP), the peptide synthesis can be continued. This variant of the Mitsunobu reaction afforded couplings yields of >90% with the alkylphosphonic acids tested.

A classical application of the Mitsunobu reaction for the synthesis of phenol ethers was conducted recently by Rano and Chapman[80] with immobilized substrates (Scheme 11). Two model compounds were used to study the coupling of phenols to polymer-bound alcohols, and of alcohols to the resin-bound phenols. The optimal coupling reagents were found to be *N*,*N*′,*N*″,*N*‴-tetramethylazodicarboxamide and tributylphosphane in THF/CH_2Cl_2. A fivefold excess of the coupling reagents and ten equivalents of the phenol (based on the maximum loading of the TentaGel support) were used, and after a reaction time of about 15 min the phenol ethers were obtained in yields of 72–99% with purities of 89–97% as judged by HPLC. Similarly, the reaction of alcohols with the polymer-bound phenols proceeded smoothly. The coupling reagents and the alcohol were used in fivefold excess. Reactions over 45–60 min resulted in yields of phenol ethers of 68–94% with purities of 81–97%.

The first steps for the synthesis of new oligomers, oligosulfones and oligosulfoxides, have been described by Moran et al.[81] The starting materials for these compounds were polymer-bound thioethers, which were prepared in five steps. To follow the reaction course more accurately, the chromophore 2-(4-carboxybenzyloxy)ethanol was coupled to the Rink amide resin and the terminal hydroxyl group was thioacetylated with thioacetic acid under Mitsunobu conditions (PPh_3, DIAD, THF at 0 °C). Reduction of the thioacetate with $NaBH_4$ generated the free thiol. The thiol was alkylated with (*S*)-2-bromopropionic acid and the carboxyl group was subsequently reduced to the alcohol by using a slightly modified Soai reaction.[82] Further synthesis steps could then be carried out on the free hydroxyl group to obtain polymer-bound thioethers, which were oxidized to oligosulfones and oligosulfonates.

3.2. Immobilization and Derivatization of Aldehydes and Ketones

Immobilization of aldehydes and ketones on polymeric supports is possible by acetalization using resins functionalized with 1,2- or 1,3-diols. The 1,3-dioxolanes and 1,3-dioxanes thus

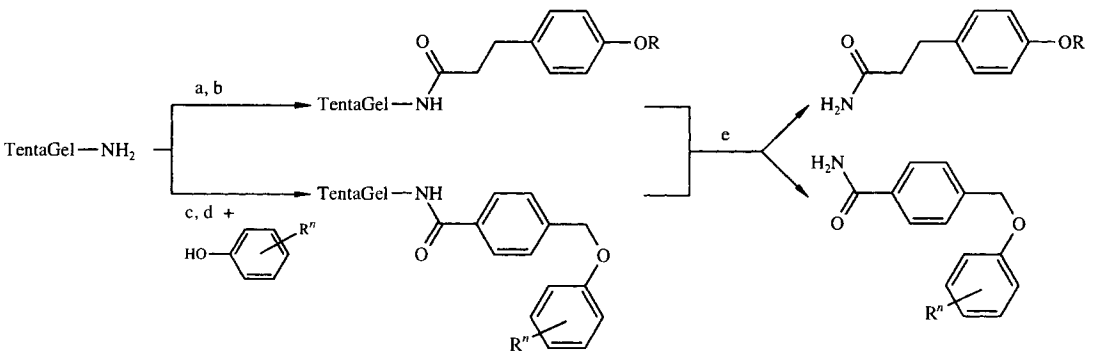

Scheme 11. The classical Mitsunobu reaction for the synthesis of aryl ethers on a polymeric support [80]. a) 3-(4-Hydroxyphenyl)propionic acid, EDC, DMF, 2 h; b) ROH, TMAD, Bu_3P; c) 4-hydroxymethylbenzoic acid, EDC, DMF, 2 h; d) phenol derivatives, TMAD, Bu_3P; e) TFA/H_2O (9/1). R = alkyl, aryl; R″ = H, Ph, OMe, OPh, CN, Br, CHO, CO_2Me.

formed are base-stable but can be cleaved by strong acids. Several of these functionalized polymers have already been prepared by Leznoff et al.[83] (Scheme 12). To prevent cross-linking of the resin, the reaction must be carried out with a large excess of the dicarbonyl compound; the acetal formation is catalyzed by *m*-benzenedisulfonic acid.

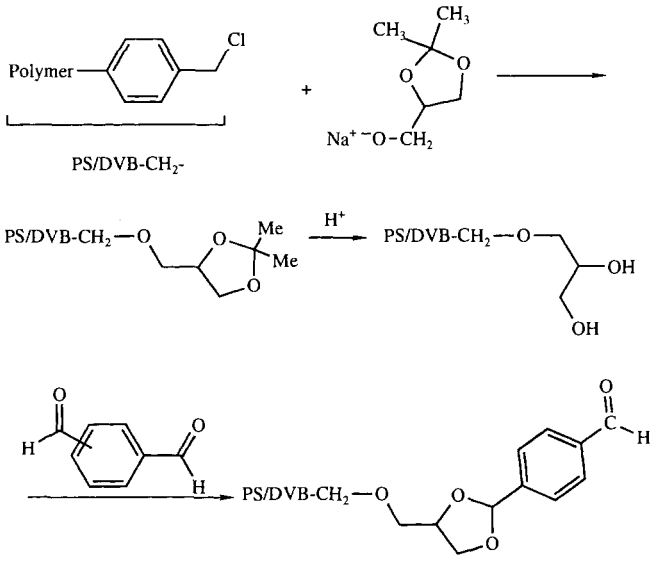

Scheme 12. Preparation of a modified chloromethyl-PS/DVB support for immobilizing aldehydes and ketones [83, 84]. Alternatively, diols can be linked to an aldehyde- or ketone-modified support.

Leznoff et al.[83, 84] developed six methods for derivatizing polymer-bound dialdehydes (Scheme 13). Analogous reactions can be carried out with acetalated ketones. As an example, Grignard reactions on these solid supports yield substituted olefins.[84]

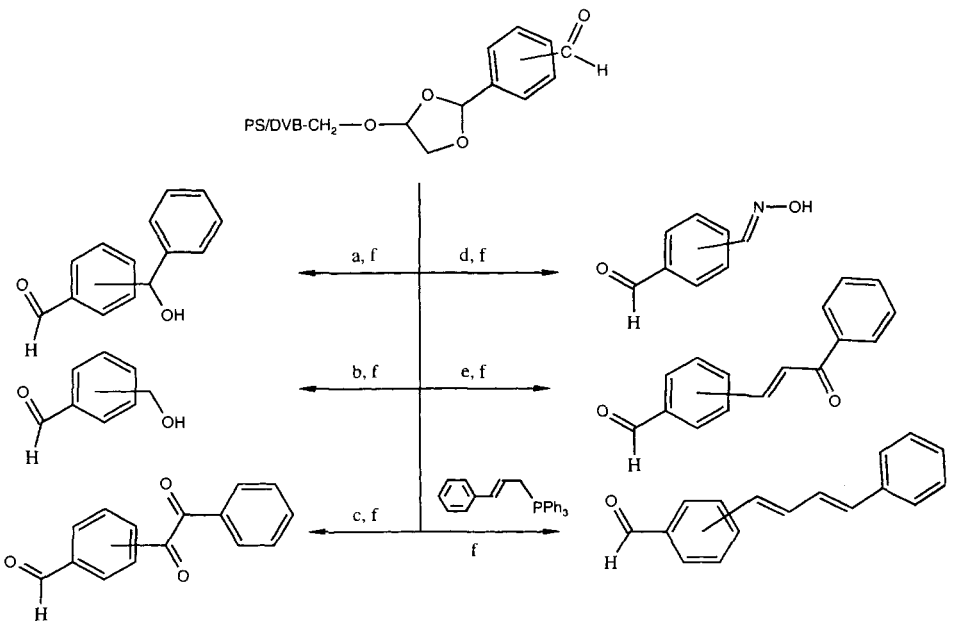

Scheme 13. Several organic reactions carried out by using immobilized aromatic aldehydes, for example preparation of oximes, Grignard reaction, selective reduction of carbonyl groups, benzoin condensation, aldol condensation, and Wittig reaction [83, 84]. a) PhMgBr; b) $Na[AlH_2(OCH_2OCH_3)_2]$; c) PhCHO, NaCN; d) NH_2OH; e) acetophenone; f) acidolysis.

Ren et al.[85] synthesized a 1,3-diol-functionalized polystyrene resin by aldol condensation and disproportionation (mixed Cannizzaro reaction) of a butyrylated PS/DVB copolymer with paraformaldehyde in the presence of NaOH. Aldehydes (terephthalaldehyde is particularly well suited) have been immobilized on this resin and treated with hydroxylamine, NaOH, and Grignard and Wittig reagents. The resulting products, *p*-formylbenzaldoxime, *p*-formylbenzyl formate, mono-*p*-formylstilbene, and mono-*p*-formyldiphenyl formate, were obtained in high yields.

3.3. Immobilization and Derivatization of Dicarboxylic Acids and Their Derivatives

Monoester monoamides are typically prepared by the reaction of monoester carboxylic acid chlorides with ammonia.[86, 87] However, synthesis of these acid chlorides generally proceeds with yields of less than 50%.[88] Only in the reactions using anhydrides are yields of up to 70% achieved. Higher yields of monoester monoamides have been obtained by solid-phase synthesis.[89, 90] As long as strongly acidic conditions are not required, both hydroxymethylated PS/DVB resins and *p*-alkoxy resins[91] (Wang resins) can be functionalized with the corresponding dicarboxylic acid chlorides (Schemes 14, 15; Table 5). Subsequently, the polymer-bound monoester monoamides are further derivatized by reaction with amines (Table 5). Based on the resin loading of 0.3–0.56 mmol g^{-1}, yields of 65–98% have been obtained. The resin–substrate bond is cleaved by alkaline saponification using potassium carbonate.

Ketones can be prepared by treating polymer-bound acyl chlorides with phenylcadmium chloride[92] (Scheme 15). The selective reduction of acyl chlorides to primary alcohols is achieved with $NaBH_4$ without cleavage of the ester group;[93] reaction with alkylmanganese iodides[94] converts acyl chlorides into tertiary alcohols. Some of these alcohols may serve as precursors of 4,4-diphenyl-γ-butyrolactones, which have known biological activity against pathogenic viruses.[95]

Similar reactions have been conducted with a specially derivatized sulfonylethanol-PS/DVB resin.[72d] This anchor combination has ester bonds with different reactivities, one of which can be cleaved by β-elimination. The remaining ethenesulfonyl moiety can be regenerated without loss of reactivity and utilized in further syntheses.

Camps et al.[96] and Patschorkin and Kraus[97] succeeded in finding reaction conditions that allow monoalkylation and monoacylation of polymer-bound carboxylic acids. Side reactions that are often observed in solution synthesis, for example the Claisen condensation, were suppressed completely by using low loading (<0.2 mmol g^{-1}).

Table 5. Starting materials for the solid-phase synthesis of monoamides.

Dicarboxylic acid dichloride	Amine
isophthaloyl dichloride	*tert*-butylamine
terephthaloyl dichloride	*tert*-butylamine
succinyl dichloride [a]	aniline, benzylamine, methylamine, ammonia
glutaryl dichloride	aniline, benzylamine, methylamine, ammonia
adipoyl dichloride	aniline, benzylamine, methylamine, ammonia
sebacoyl dichloride	aniline, benzylamine, methylamine, ammonia

[a] The anhydride can also be used.

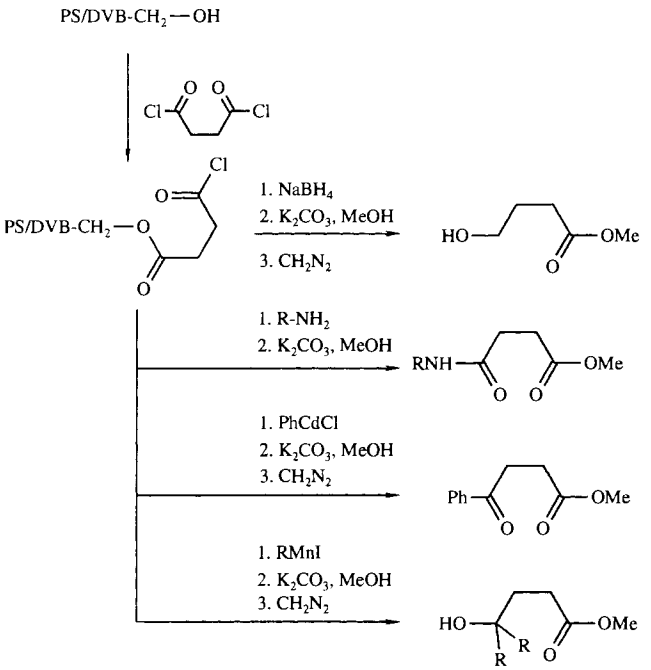

Scheme 14. Linking and derivatization of dicarboxylic acids dichlorides to hydroxymethylated PS/DVB supports [86, 87]. R = Ph, Bu.

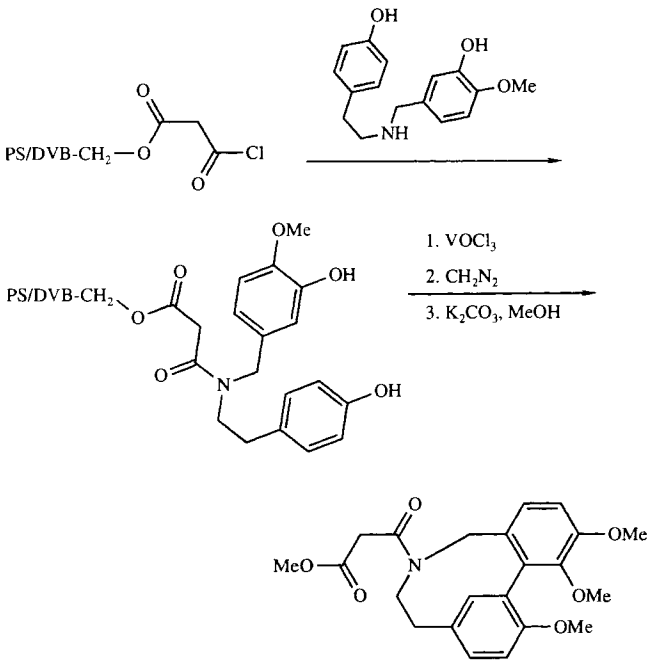

Scheme 15. Oxidative synthesis of a biphenyl derivative on a polymer support [69].

3.4. Ring-Closing Reactions

In this section we will not discuss methods for the cyclization of polymer-bound peptides and proteins,[98] but rather we will focus on adaptations of ring-closing reactions that have been used successfully in solution-phase synthesis.

Due to their high regio- and stereoselectivity, pericyclic reactions are often employed in the synthesis of compounds with defined structures.[100] For this reason several groups are engaged with the investigation of solid-phase cyclization reactions. Blazka and Harwood,[101] for instance, prepared a resin-bound Diels–Alder product by reacting a polymer-bound maleimide with a cyclopentadiene. Nieuwstad and co-workers[102] employed a series of polymer-bound dienes for desulfurizing fume gases by cycloaddition with sulfur dioxide (Scheme 16). However, in both cases the synthesized products were not cleaved from the polymer.

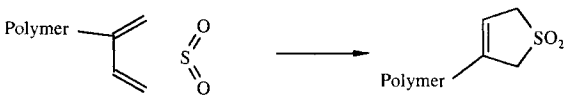

Scheme 16. Gas desulfurization through trapping of SO_2 by immobilized butadienes [102].

Resin-bound dienes and dienophiles have also been used to trap reactive intermediates[103] (Scheme 17). Trapping reactions with reactive polymers could also be interesting for combinatorial chemistry in solution, for example, to facilitate workup and automation.

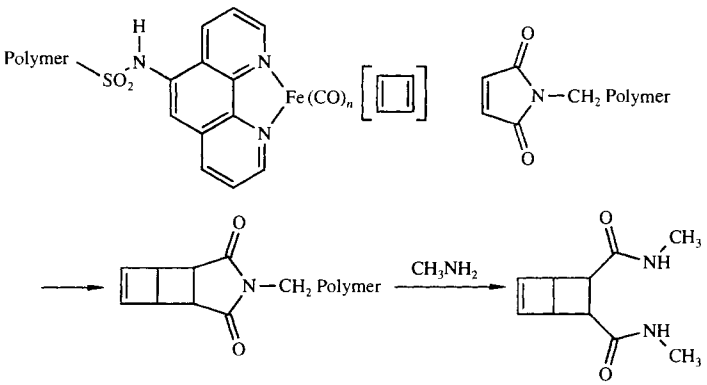

Scheme 17. Two different resins were combined to generate an interesting "trap" for reactive intermediates [103]. The trapping reagent maleimide was immobilized on a support (PS/DVB (2%) copolymer). A butadiene precursor was prepared on the second resin, a chlorosulfonated support, by reaction with 5-amino-*o*-phenanthroline and tricarbonyl(cyclobutadienyl)iron. A suspension of these resins was oxidized with metals or pyridin-1-oxide, the resins were separated, and the product, bicyclo[2.2.0]hexenediamide, was obtained.

The research group led by Leznoff[104] investigated the reaction of substituted 1,3-butadienes with polymer-bound dienophiles, in particular immobilized acrylic acid. In the reaction with electron-deficient dienophiles in solution a mixture of 3,4- and 3,5-disubstituted cyclohexanes results, in which the 3,4-disubstituted isomer is the major product.[105] The aim of these investigations was to shift the reaction in favor of the

3,5-disubstituted product by taking advantage of the increased steric bulk of the resin-bound dienophile. Acrylic chloride was anchored to a hydroxymethylated PS/DVB resin as described in Section 3.3 and was then allowed to react with a hot solution of (*E*)-1-phenyl-1,3-butadiene in xylene (Scheme 18). The Diels–Alder product was removed from the polymer with base.

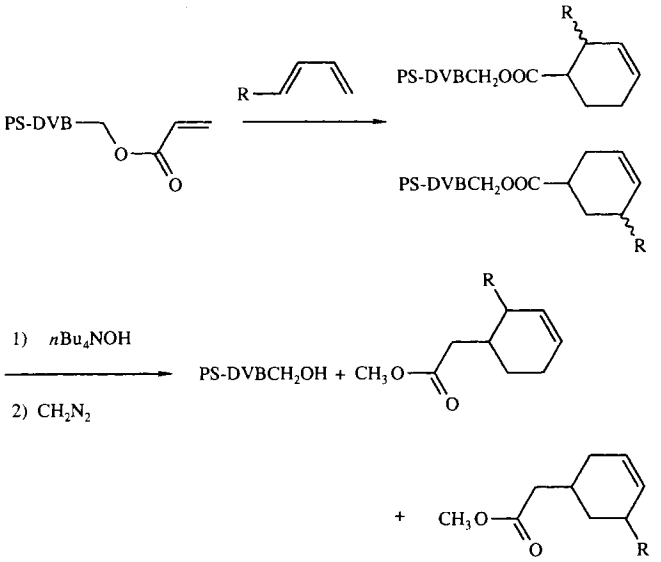

Scheme 18. Diels–Alder reaction of a butadiene (e.g. R = Ph) with polymer-bound acrylic acid [104] and cleavage of the cycloaddition product.

In other studies the regio- and stereoselectivity of 1,3-dipolar cycloadditions of nitrile oxides to polymer-bound alkynes was examined[104] (Scheme 19, see also Section 4.1). The reactions of support-bound propionic and phenylpropionic acids with benzonitrile oxide followed by alkaline cleavage and esterification with diazomethane yielded exclusively methyl 3-phenylisoxazole-5-carboxylate and methyl 3,5-diphenylisoxazole-4-carboxylate, respectively.

Although Leznoff et al.[104] could not demonstrate conclusively that regioselectivity is influenced by the substrate–support linkage in general, these experiments showed that pericyclic reactions can be carried out successfully on polymer supports. The stereoselectivity may not be affected or at best only minimally, but the yields and purity are considerably improved.

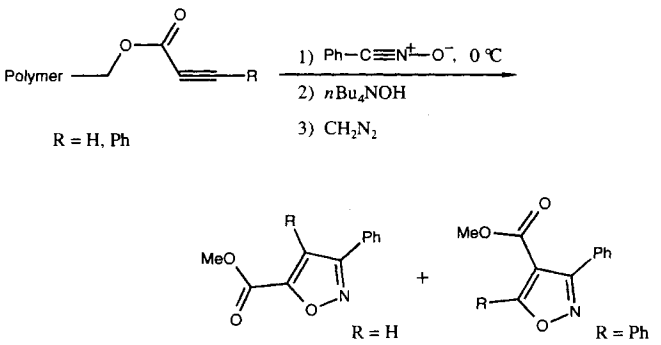

Scheme 19. 1,3-dipolar cycloaddition of nitrile oxides to resin-bound alkynyl carboxylic acids [104].

The findings of Leznoff et al. from the 1980s[104] have served as impetus for more recent studies. Schore and Najdi[106] treated immobilized 4-pentyn-1-ol with excess norbornadiene in a Pauson–Khand cycloaddition[107] and, after hydrolysis, obtained the monocyclic product **3** in 69% yield (26% by solution synthesis; Scheme 20); the bicyclic adduct **6** (20% yield, only traces are found in solution synthesis) could also be isolated when norbornadiene was used in equimolar amounts. An analogously performed reaction with 1-methyl-5-norbornen-2-one furnished a 3:7 mixture of isomers **4** and **5** (total yield 99%; 10% by solution synthesis) (Scheme 21). The formation of **6** can be explained by assuming a cross-linking reaction involving norbornadiene. This has been confirmed in further experiments using 2% cross-linked PS/DVB. It is assumed that the cross-linking reaction is suppressed since the reactive groups of a more highly cross-linked polymer are more isolated. Indeed, formation of **6** could be suppressed under analogous reaction conditions with 2% cross-linked PS/DVB.[106b]

In 1992 Beebe, Schore, and Kurth[108] described the solid-phase synthesis of 2,5-disubstituted tetrahydrofurans by a "tandem" 1,3-dipolar cycloaddition of a support-bound nitrile oxide with 1,5-hexadiene (Scheme 22). Nitrile oxides were produced by reacting nitromethane with polymer-bound aldehydes in a Henry reaction. After protection of the hydroxyl group as a trimethylsilyl ester and dehydrogenation, a cyclization yielded

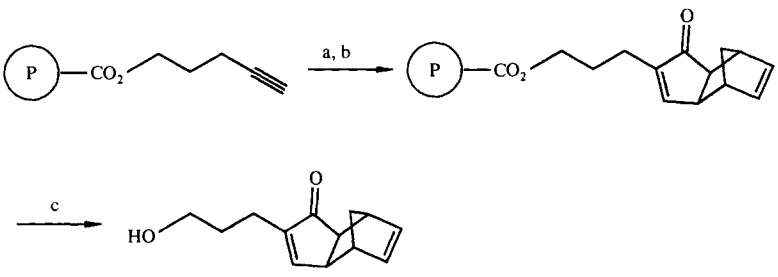

Scheme 20. Dicobalt octacarbonyl mediated Pauson–Khand cycloaddition [106, 107]. a) [Co$_2$(CO)$_8$]; b) norbornadiene, 80–100 °C; c) nBu$_4$NCl, KOH, H$_2$O, 80 °C, 4 h. Ⓟ = polymer.

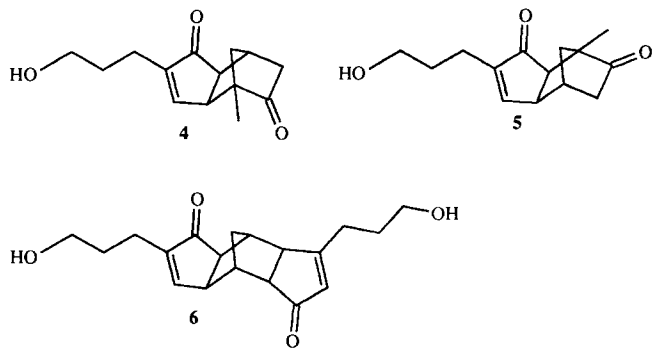

Scheme 21. Compounds prepared by Pauson–Khand cycloaddition [106, 107].

a resin-bound isoxazoline. The subsequent electrophilic cyclization by addition of iodine monochloride (ICl) afforded 2,5-disubstituted dihydrofurans. The *cis* to *trans* ratio was 1:2.1 (1:1.92 in the solution synthesis) with a total yield of 17% based on a maximum loading of 0.65 mmol g^{-1} (18% yield in solution).

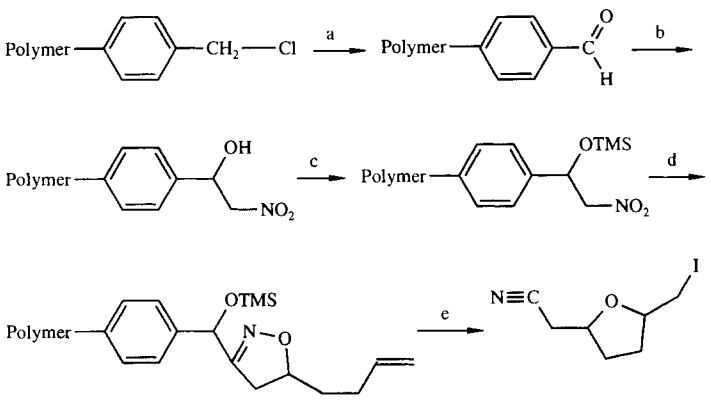

Scheme 22. Tandem 1,3-dipolar cycloaddition for the preparation of substituted tetrahydrofurans [108]. a) DMSO, $NaHCO_3$, 155 °C, 6 h; b) CH_3NO_2, Et_3N, THF, EtOH, 14 h; c) TMSCl, Et_3N; d) PhNCO, Et_2O, PhH, 80 °C, 1,5-dienes; e) ICl, CH_2Cl_2, −78 °C, 1.5 h.

[3 + 2]Cycloaddition reactions have also been carried out to derivatize alkene- and alkyne-substituted peptoids[147] (Section 4.1).

3.5. Synthesis of Heterocyclic Compounds: Benzodiazepines, Hydantoins, and Thiazolidines

The benzodiazepine skeleton is a constituent of many bioavailable therapeutic agents. The CCK receptor A and B antagonists,[109] opiate receptor ligands[110] (e.g. valium), fibrinogen receptor antagonists (GP-IIbIIIa inhibitors),[111, 112] reverse transcriptase inhibitors,[113] and HIV-TAT-RNA antagonists[114] all have benzodiazepine frameworks.

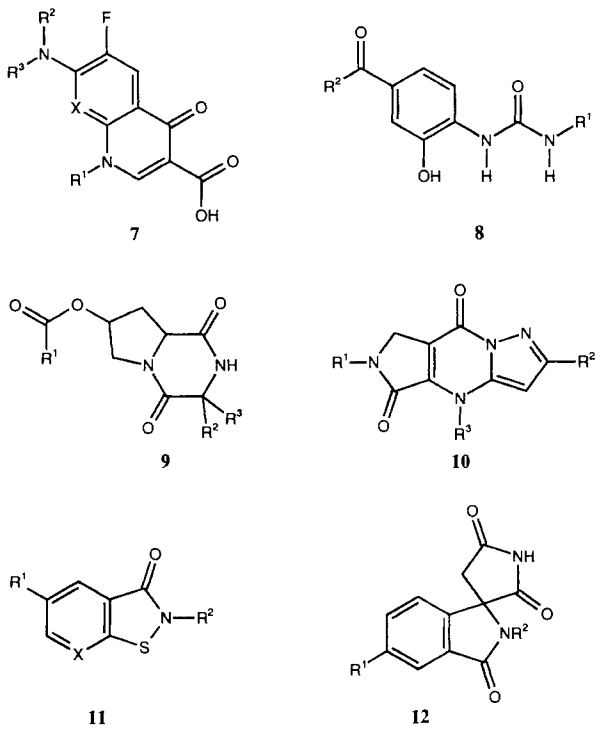

Scheme 24. Other heterocyclic compounds in addition to benzodiazepines and hydantoins prepared by Hobbs DeWitt et al. [117] on solid supports. Quinolones **7** (X = N, CH), (acylphenyl)ureas **8**, dioxopiperazines **9**, pyrimidindiones **10**, benzothiazolones **11** (X = N, CH), spirosuccinimides **12**. R^1, R^2, R^3 = alkyl, aryl.

Following the solid-phase synthesis of benzodiazepines reported by Camps, Castells, and Pi in 1974,[115] Hobbs DeWitt et al.[116] developed a method for the synthesis of benzodiazepines and hydantoins based on the Fmoc strategy (Scheme 23). The synthesis of Camps et al. begins with the coupling of Boc-protected amino acids to hydroxy-functionalized PS/DVB resin using carbonyldiimidazole (CDI) as a coupling reagent (Scheme 23). Benzodiazepines are obtained directly by cleavage of the Boc group, followed by the reaction with acetophenone.

A further development of this reaction led to the simultaneous multiple synthesis of benzodiazepines and hydantoins starting with the resin-bound Boc- or Fmoc-protected amino acids. Hobbs DeWitt et al.[116] synthesized sets of 40 benzodiazepines and hydantoins by reacting five differently loaded resins with eight different benzophenones and isocyanates, respectively. In addition, in a patent published in early 1994 Hobbs-DeWitt et al.[117] described the simultaneous multiple synthesis of a series of heterocyclic compounds starting with commercially available standard resins (hydroxy- or chloromethylated PS/DVB) (Scheme 24).

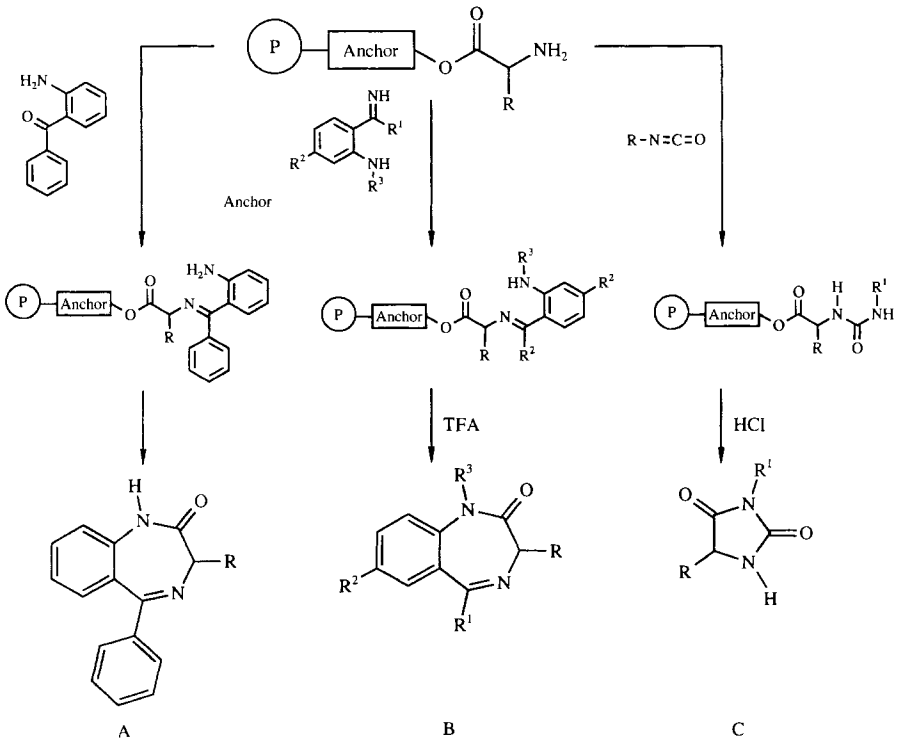

Scheme 23. Solid-phase synthesis of benzodiazepines and hydantoins. Benzodiazepine synthesis according to Camps, Castells, and Pi [115] (A); synthesis of benzodiazepines and hydantoins according to Hobbs DeWitt et al. [116] (B and C, respectively). Ⓟ = polymer; R = amino acid side chains; R^1, R^2, R^3 = alkyl, aryl.

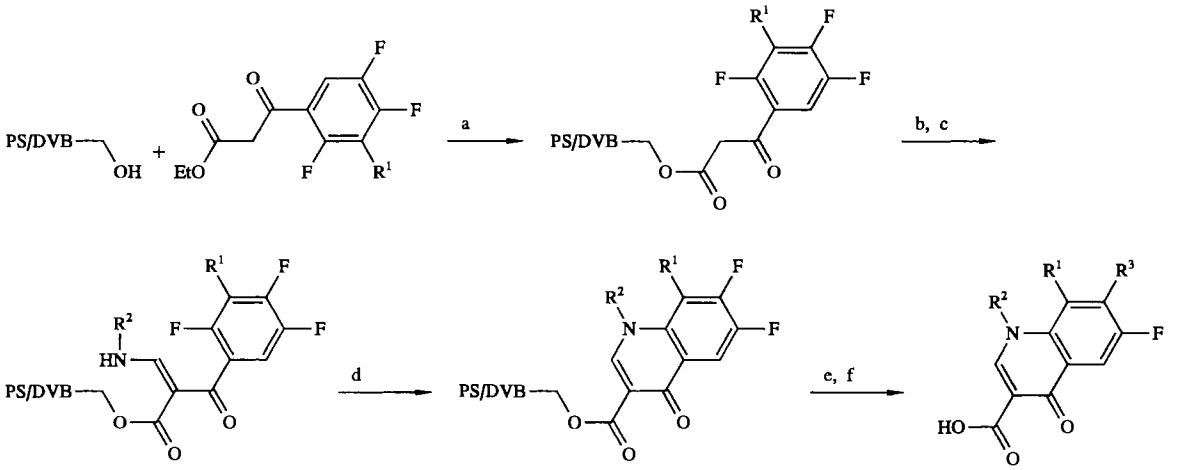

Scheme 25. Solid-phase synthesis of quinolones [188]. a) Toluene, DMAP, 110 °C, 16 h; b) $(CH_3O)_2CHN(CH_3)_2$, THF, 25 °C, 18 h; c) H_2NR^2, 25 °C, 72 h; d) tetramethylguanidine, CH_2Cl_2, 65 °C, 18 h; e) H_2NR^3, NMP, 110 °C, 4 h; f) TFA/CH_2Cl_2 (2/3), 25 °C, 1 h. R^1, R^2, R^3 = alkyl, aryl.

Recently MacDonald and Ramage,[118] in cooperation with Hobbs DeWitt and Hogan, described a procedure for the multiple parallel synthesis of quinolones (Scheme 25). In this approach ethyl 3-(3-alkyl-2,4,5-trifluorophenyl)-3-oxopropionate was coupled to commercially available Wang resin (Table 2) by transesterification and then treated with a series of amines to obtain enamines, which were cyclized by nucleophilic aromatic substitution. The quinolone skeleton was subsequently modified by a further nucleophilic aromatic substitution. The final product was cleaved from the anchor by trifluoroacetic acid/CH_2Cl_2.

Ellman et al.[119] described a slightly different procedure for synthesizing benzodiazepines (Scheme 26). The benzodiazepines were synthesized on a resin by using three different building blocks. An aminobenzophenone derivative (carboxylic acid or alcohol) was attached to the polymer through an acid-labile anchor and subsequently reacted with a Fmoc-protected amino acid fluoride. After deprotection, the diazepine ring was formed by addition of 5% acetic acid. After deprotonation and alkylation with one of a series of alkyl halides, the benzodiazepine product was cleaved from the resin by treatment with acids.

In further investigations, in addition to the solid-phase synthesis of benzophenone derivatives[120] (Scheme 27) a set of 192 benzodiazepines was synthesized simultaneously and their biological activity determined. Thus, microscale syntheses were carried out on derivatized polypropylene pins[121] loaded with two different benzophenones. A block of 96 of these pins was immersed in successive microtiter plates filled with N-protected amino acid fluorides or alkyl halides (a specific compound in each cavity) and subjected to standard reaction conditions.

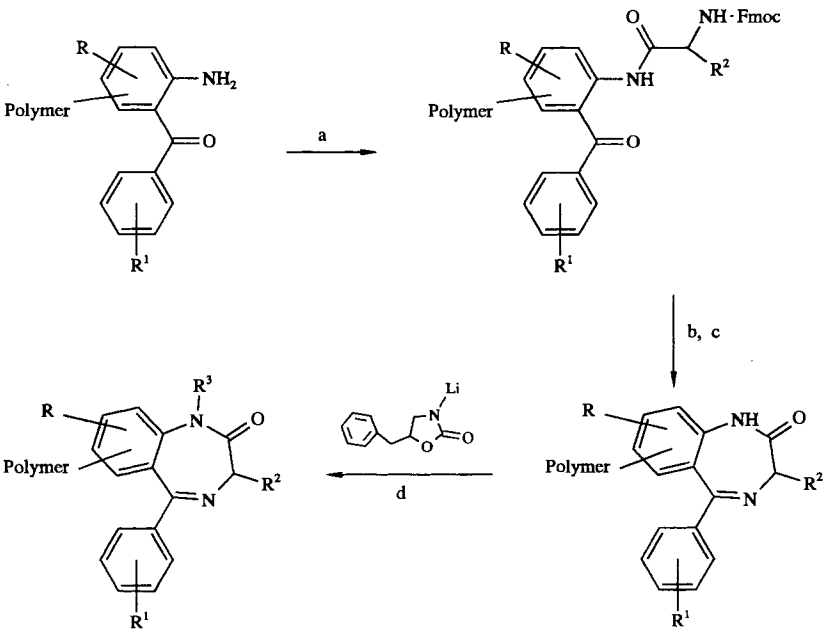

Scheme 26. Benzodiazepine synthesis according to Ellman et al. [119, 120]. a) Fmoc-protected amino acid fluorides; b) piperidine/DMF (1/1); c) HOAc/DMF (5/95); d) alkyl iodides R^3I, DMF. R = Cl, OH; R^1 = OH; R^2 = Me, *i*Pr, 3-indoyl-CH_2; R^3 = H, Et, Bn.

Recently Plunkett and Ellman[122] developed a further method for preparation of benzodiazepines by the Stille reaction (see also Section 3.7) of polymer-bound N-Bpoc protected (2-aminoaryl)stannates with aromatic or aliphatic acyl halides. After removal of the Bpoc protecting group, the free amine was acylated and cyclized to give the benzodiazepine with 5% acetic acid.

Patek et al.[123] published a method for the simple solid-phase synthesis of thiazolidines by cyclocondensation of bound β-sulfanylalkylamine with ketones or aldehydes (Scheme 28). The β-sulfanylalkylamine moieties were introduced in the form of Fmoc-Cys(Trt)-OH, and the Fmoc and Trt groups were removed consecutively. Subsequent reactions with aldehydes or ketones generated the polymer-bound thiazolidine skeleton, which was acylated at the nitrogen atom by a condensation reaction with carboxylic acids in DMF. To enhance the acid-lability of the five-membered ring, the anchor was oxidized

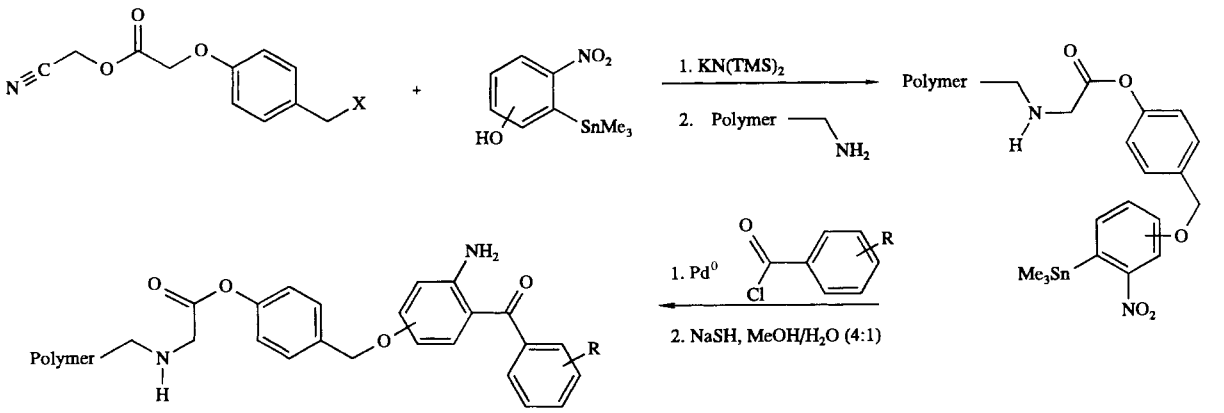

Scheme 27. Synthesis of polymer-bound benzophenones [119, 120]. R = alkyl, aryl; X = halogen.

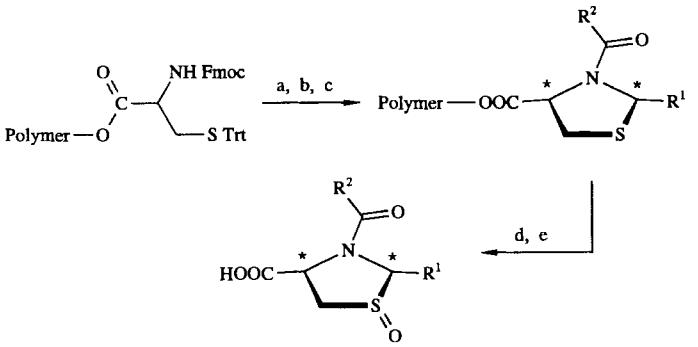

Scheme 28. Preparation of chiral thiazolidines [123]. a) piperidine/DMF (1/4), $TFA/CH_2Cl_2/i$BuSiH$_3$; b) R^1CHO, AcOH; c) R^2COOH, DIC, CH_2Cl_2; d) MCPBA, CH_2Cl_2; e) 0.5% NaOH. R^1 = *t*Bu, *i*Pr, *p*-$NO_2C_6H_4$, thiophenyl; R^2 = alkyl, aryl.

with 3-chloroperbenzoic acid (MCPBA) before cleavage from the support to give the sulfoxide.

The thiazolidine synthesis was further investigated by employing a series of compounds containing carbonyl and carboxyl groups; the yields and ratios of diastereomeric products were determined and compared with the results of the analogous solution reactions. When low yields are obtained, the diastereoselectivity of the solid-phase reaction is on average higher than that of the solution synthesis. The yields ranged from <10 to 90% (in solution 66 to 92%) with d.r. values (d.r. $= 100 \times [(1R,4R)/\{(2R,4R) + (2S,4R)\}]$) of 65 to >97% (in solution 29 to >97%).

3.6. Further Ring Closures on Solid Supports

The intramolecular ester condensation (Dieckmann condensation) of asymmetrically substituted esters generally leads to a mixture of isomers. In the solid-phase procedure developed by Crowley and Rapoport,[124a] this ring-closing reaction is regioselective. An asymmetrically disubstituted diester was synthesized by deprotonation of pimelic acid monomethyl ester and reaction with chloromethylated polystyrene; the product was finally cyclized by addition of a base. By using the monoester labeled with ^{14}C at C1, it could be demonstrated that the condensation proceeds in both possible directions (Scheme 29). Hence, one product is removed from the resin by autocleavage, whereas the other remains immobilized on the resin. This product can be obtained by treatment with base.

By using the three building blocks, α-amino acids, bromocarboxylic acids, and aminoalkylthiols, Virgilio and Ellman[125] (Scheme 30) synthesized simultaneously a series of nine- and ten-membered ring systems that supposedly imitate the β-turn of proteins. Polypropylene pins or PEG/PS graft copolymers were used for the synthesis of β-turn mimetics possessing (*R*) configuration in the $i+1$ position and (*S*) configuration in the $i+2$ position. What makes the reaction interesting is that based on only commercially available building blocks a compound library containing more than 2000 components can be synthesized simultaneously.[126] The multiple-step synthesis (Scheme 30) began with the coupling of a bromocarboxylic acid to the support and displacement of bromine by aminoalkylthiol, protected as a disulfide. The secondary amine formed was condensed with an Fmoc-protected amino acid and, after removal of the Fmoc group, was acylated again with a further bromocarboxylic acid. The disulfide bond was cleaved with tributylphosphane and, finally, a ring-closing nucleophilic cyclization was effected by addition of *N*,*N*′,*N*″,*N*‴-tetramethylguanidine.

Solid-phase synthesis is not limited to the preparation of small-ring systems; syntheses of helicenes,[127] porphyrins,[128] and phthalocyanines[129] have also been reported. The first synthesis of unsymmetrically substituted tetraarylporphyrins on a PS/DVB support was reported in 1977. For this purpose, hy-

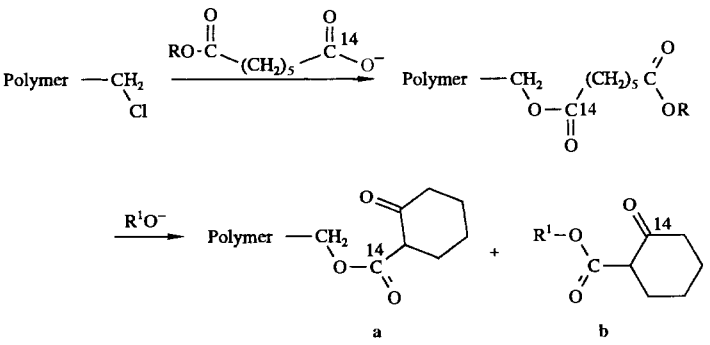

Scheme 29. Dieckmann cyclization of a polymer-bound substrate. The cyclohexanone product **a** remains immobilized on the resin during the reaction, whereas product **b** is liberated by self-cleavage. The polymer-bound product can be cleaved by saponification [124]. R = Et; R^1 = alkyl. 14 = ^{14}C-radiolabeled carbon atom.

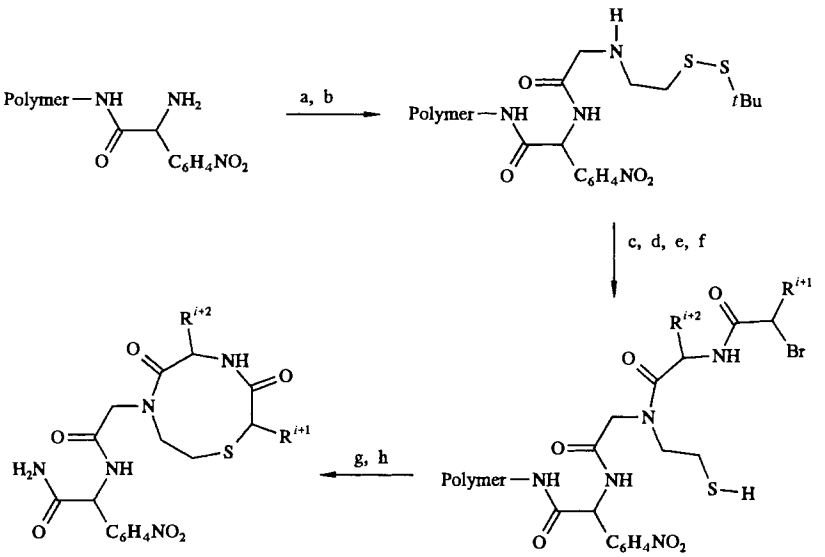

Scheme 30. Preparation of nonpeptidic β-turn mimetics on polymer supports [125]. a) Bromoacetic acid, DIC; b) 2-aminoethyl-*tert*-butylsulfide (or aminopropylthio-*tert*-butyldisulfide); c) Fmoc-protected amino acids, HATU; d) piperidine/DMF (1/1); e) symmetrical α-bromocarboxylic anhydride; f) PBu_3, H_2O; g) tetramethylguanidine; h) TFA/water/Me_2S (18/1/1). R^{i+1} = alkyl, aryl, protected amino acid side chains; R^{i+2} = alkyl, aryl.

droxybenzaldehydes were bound to a resin by means of an acid-labile linker and allowed to react with *p*-methylbenzaldehyde, pyrrole, and propionic acid at high temperature for one hour. In addition to a soluble mixture of several porphyrins, which were removed by extraction, a polymer-bound unsymmetrically substituted porphyrin was also obtained in 4 to 5% yield . The product was obtained in pure form by alkaline saponification. Recently, unsymmetrically substituted phthalocyanines were also synthesized by a similar procedure.[129]

3.7. Palladium-Catalyzed C–C Bond Formation

In recent years numerous articles have described the extension of reactions for C–C bond formation, which are frequently carried out in solution syntheses, to reactions on polymeric supports. A common feature of these solid-phase reactions is the use of soluble palladium compounds as catalysts. Based on the results of the elegant experiments described in this section, further successful applications in this area of combinatorial chemistry can be expected.

The Heck reaction[130] can be used for simple synthesis of disubstituted alkenes and alkynes. The reactions of aryl iodides with alkenes (alkynes) and of styrene with aryl halides in the presence of Pd^{II} acetate produce the correspondingly substituted alkenes (alkynes) with high purity and yields. Yu, Deshpande, and Vyas[131] immobilized the model compounds 4-vinyl- and 4-iodobenzoic acid on Wang resin and reacted them with a series of substrates under Heck conditions (Scheme 31; Table 6). With a few exceptions, such as ethyl propionate which did not react under the chosen conditions, alkenes and alkynes were obtained in high yields.

In related work immobilized 4-iodobenzoic acid was used to investigate the Stille reaction .[132] Reaction of iodobenzoic acid with vinyl- and arylstannanes in the presence of palladium and $As(Ph)_3$ generated substituted arenes and biphenyl derivatives, respectively, in yields of 85 to 92% based on the loading of iodobenzoic acid on the resin (Scheme 32).

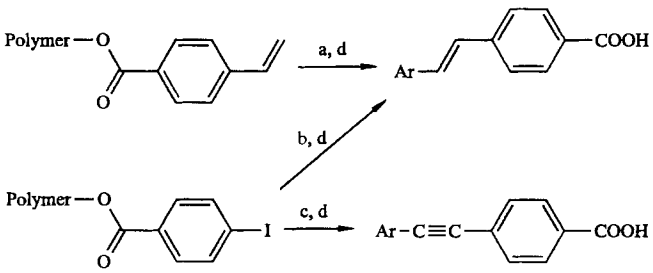

Scheme 31. Palladium-catalyzed Heck reaction [130, 131] for the preparation of substituted arenes. a) Aryl halides, $Pd(OAc)_2$; b) arenes or olefins, Pd; c) aryl-substituted alkynes, $Pd(OAc)_2$; d) TFA/CH_2Cl_2 (9/1).

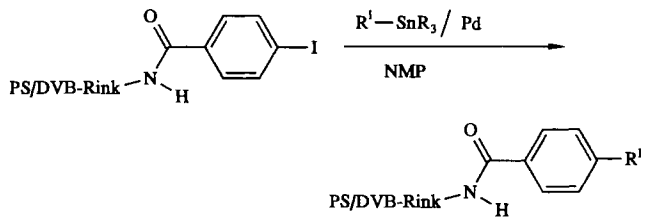

Scheme 32. Stille coupling reaction of a polymer-supported substrate [132]. Substituted arenes are obtained by the reaction of organotin compounds in the presence of Pd^0. The products are cleaved from the resin by TFA. R^1 = vinyl, aryl; R = Me.

Table 6. Starting material and reagents used in Heck reactions on solid phases (Scheme 31) [131].

Polymer [b]	Reagent	Catalyst	T[°C]	t[h]	Yield [%][a]
1	iodobenzene	$[Pd(OAc)_2]$, nBu_4NCl	90	16	81
1	2-bromonaphthalene	$[Pd_2(dba)_3]$, P(2-tol)$_3$	100	20	64
1	2-bromothiophene	$[Pd_2(dba)_3]$, P(2-tol)$_3$	100	20	76
1	3-bromopyridine	$[Pd_2(dba)_3]$, P(2-tol)$_3$	100	20	87
2	methyl 4-vinylbenzoate	$[Pd(OAc)_2]$, nBu_4NCl	90	16	90
2	phenylacetylene	$[Pd_2(dba)_3]$, P(2-tol)$_3$	100	20	90
2	ethyl acrylate	$[Pd(OAc)_2]$, nBu_4NCl	90	16	91

[a] Based on the loading of the support with the substrate. [b] Wang resin with immobilized 4-vinyl- (1) or 4-iodobenzoic acid (2).

Backes and Ellman[134] synthesized a series of phenylacetic acid derivatives on supports by enolate alkylation and subsequent Suzuki reaction[133] (Scheme 33; Table 7). The rarely used Safety-Catch linker[37c] was used since it is stable under the chosen reaction conditions. The active ester pentafluorophenyl 4-bromophenylacetate was immobilized on the support in the presence of dimethylaminopyridine. Deprotonation with LDA gave a trianion, which was then alkylated with alkyl halides (Table 7). For the palladium-catalyzed Suzuki reaction, a series of either arylboronic acids or alkylboranes produced by in situ hydroboration of alkenes served as coupling partners. After methylation of

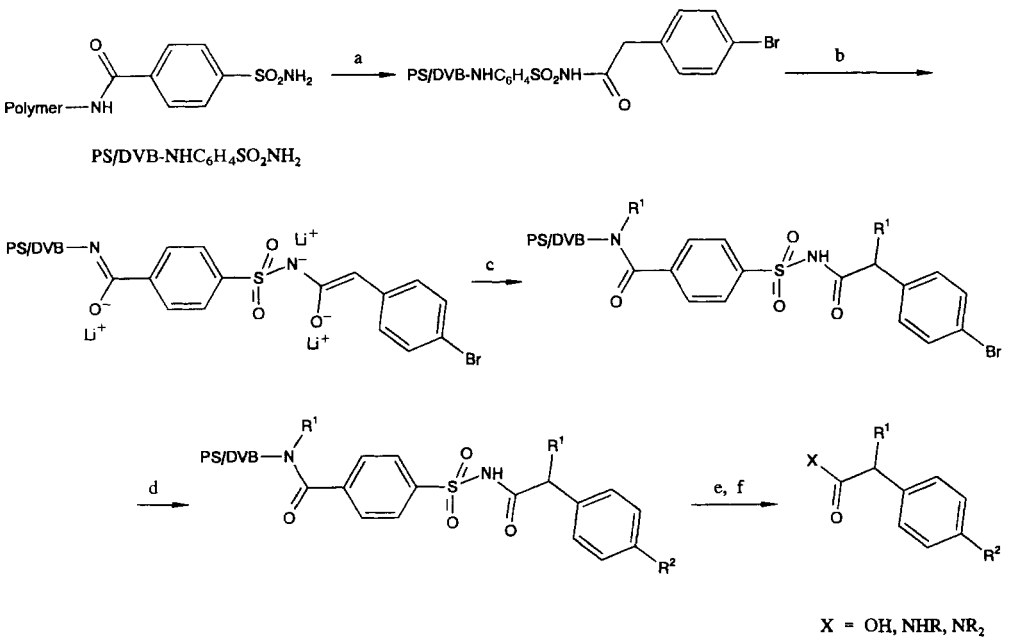

Scheme 33. Solid-phase synthesis of substituted phenylacetic acid derivatives by an enolate alkylation followed by a Suzuki reaction [133, 134]. Backes and Ellman used this procedure to prepare ibufenac (R^1 = H, R^2 = Me_2CHCH_2, X = OH), ibuprofen (R^1 = Me, R^2 = Me_2CHCH_2, X = OH), and felbinac (R^1 = H, R^2 = Ph, X = OH) (see Table 7). a) *p*-$BrC_6H_4CH_2CO_2C_6F_5$, DMAP; b) LDA, THF, 0 °C; c) alkyl halides, 0 °C; d) alkylated 9-BBN or an aryl boronic acid, $[Pd(PPh_3)_3]$, Na_2CO_3, THF, 65 °C; e) diazomethane; f) hydroxide or amine. For R^1, R^2 see Table 7.

Table 7. Starting materials and yields for the solid-phase synthesis of phenylacetic acid derivatives (Scheme 33) [134].

R^1	R^2	Nucleophile	Yield [%]
H	Me_2CHCH_2	H_2O	100[a]
Me	Me_2CHCH_2	H_2O	96[b]
Me	Me_2CHCH_2	$BnNH_2$	96
Bn	Me_2CHCH_2	$BnNH_2$	98
Et	Me_2CHCH_2	$BnNH_2$	92
*i*Pr	Me_2CHCH_2	$BnNH_2$	91
Me	Me_2CHCH_2	piperidine	96
Me	Me_2CHCH_2	aniline	0
H	Ph	H_2O	93[c]
Me	Ph	$BnNH_2$	95
Me	4-$F_3CC_6H_4$	$BnNH_2$	87
Me	4-$MeOC_6H_4$	$BnNH_2$	88
Me	2,4-$Cl_2C_6H_3$	$BnNH_2$	88

[a] Ibufenac. [b] Ibuprofen. [c] Felbinac.

the sulfonamide nitrogen atom of the safety-catch anchor, the reaction products were cleaved by treatment with hydroxide or an amine nucleophile.

The methods presented for C–C bond formation are of particular significance for preparation of molecular diversity, since they allow the synthesis of novel skeletons.

3.8. Further Reactions on Polymeric Supports

A generally applicable method for the synthesis of ureas was described by Hutchins and Chapman[135] (see also Section 4.4). The ureas were produced by treating polymer-bound *p*-nitrophenylcarbamates with primary and secondary amines. The carbamates were obtained in turn from the reaction of immobilized amines with *p*-nitrophenyl chloroformate. Thus, for example, Fmoc-protected glutamic acid was anchored to the polymer through its γ-carboxyl group while the α-carboxyl group was protected as an allyl ester. After removal of the Fmoc group, the free amino group was reacted with *p*-nitrophenyl chloroformate and several amines to obtain the corresponding ureas (Scheme 34). With the exception of *p*-nitroaniline, which did not react, all the amines employed yielded relatively pure products (90–98%, estimated by HPLC). It is also probable that this method can be adapted for the preparation of oligoureas (see Section 4.4).

Kurth et al.[136] described the three-step solid-phase synthesis of a series of 1,3-propanediols (Scheme 35). The synthesis began with the coupling of carboxylic acids (acetic acid, 2-methoxyacetic acid, and 3-phenylpropionic acid) to chloromethylated Merrifield resin. After deprotonation with LDA/THF, they were allowed to undergo an aldol condensation reaction with a series of aromatic carbonyl compounds. In the last step, the

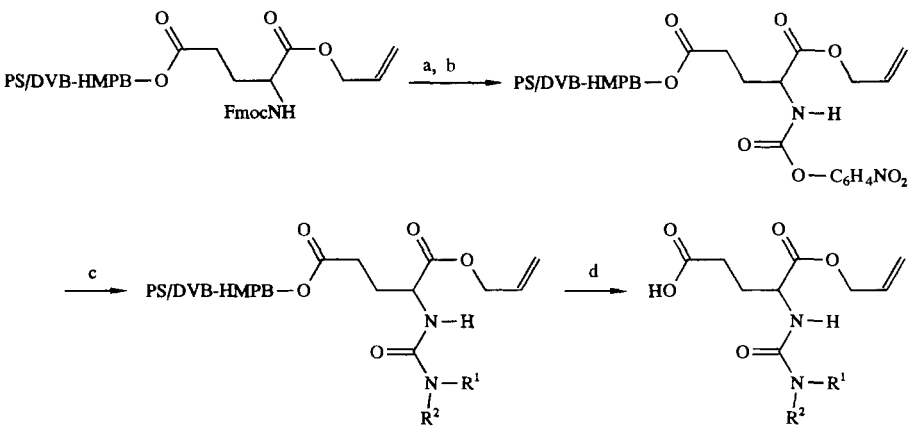

Scheme 34. Preparation of polymer-bound ureas [135]. a) piperidine/DMF (1/4); b) $ClCO_2C_6H_4$-*p*-NO_2, DIPEA, THF/CH_2Cl_2, 0.5 h; c) R^1R^2NH, DMF, 15 min; d) TFA/CH_2Cl_2 (2/98), 10 min. R^1, R^2 = alkyl, aryl.

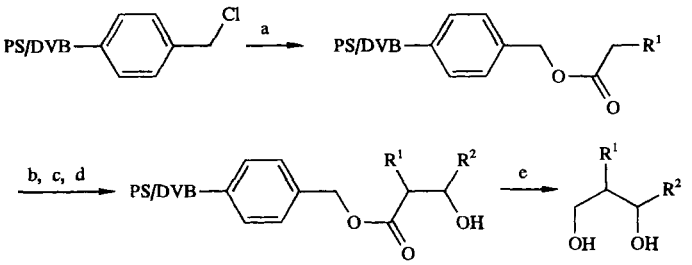

Scheme 35. Solid-phase synthesis of 1,3-propanediols [136]. a) R^1COO_2Na, Bu_4NBr (cat.), THF, Δ; b) LDA, THF; c) $ZnCl_2$, THF; d) aldehyde R^2CHO (or ketone); e) DIBAL-H, toluene. R^1, R^2 = aryl.

immobilized β-hydroxy esters were cleaved reductively (DIBAL-H/toluene, 0 °C) and converted into 1,3-diols. A set of 27 diols was prepared from three carboxylic acids and nine carbonyl compounds.

As already mentioned in Section 2.1, polymers have been used routinely to immobilize palladium hydrogenation catalysts.[19-21] Soluble palladium complexes have also been employed to cleave protecting groups and anchor linkages. Recently, the use of palladium catalysts for the asymmetric catalytic hydrogenation of polymer-bound substrates (alkenes) was also described.[137] For a catalytic reduction step in the synthesis of a tripeptide, various hydrogenation catalysts and reaction conditions were investigated. The tripeptide, which was synthesized in solution and then coupled to Wang resin, contained an α,β-didehydroamino acid, which was then reduced enantioselectively. The best results were achieved with the in situ prepared catalysts [Rh(dipamp)(nbd)]BF_4[138] and [Rh(ph-capp)(nbd)]BF_4[139] in toluene/2-propanol (100% yield; in dioxane a yield of only 46% was obtained). Moreover, the diastereomeric ratios (*R,S*):(*S,S*) were strongly affected by the catalyst and reaction conditions. For [Rh(dipamp)(nbd)]BF_4 diastereomeric ratios of 30.9:69.1 in dioxane and 6.2:93.8 in toluene/2-propanol were obtained; for [Rh(ph-capp)(nbd)]BF_4 these values were 43.6:69.1 and 94.9:5.1, respectively, under analogous conditions.

The most recent results in this area were presented in 1995 at numerous conferences and symposia on combinatorial chemistry and/or organic chemistry. A few reactions, especially those with interesting future prospects, should be mentioned here. Chabal et al.[140] described acylpiperidine and benzopyran libraries as well as the preparation of sulfonamides. Pavia[141] presented the synthesis of dibenzamide phenols by immobilization of 3-nitro-4-aminophenol on resin, followed by a selective reduction of the nitro group with tin(II) chloride and acylation of the new amino group. A tandem Michael addition[142] of phenolates to polymer-bound acrylic acid has also been used to prepare substituted bicyclo[2.2.2.]octanes on Wang resin (Scheme 36). These products were removed from the support either by TFA/CH_2Cl_2 or by reduction with DIBAL-H.

4. Synthesis of Oligomers

In the search for lead structures for therapeutic agents the systematic screening of peptide libraries[3b, 7] is being applied routinely and successfully. When biologically active peptides are

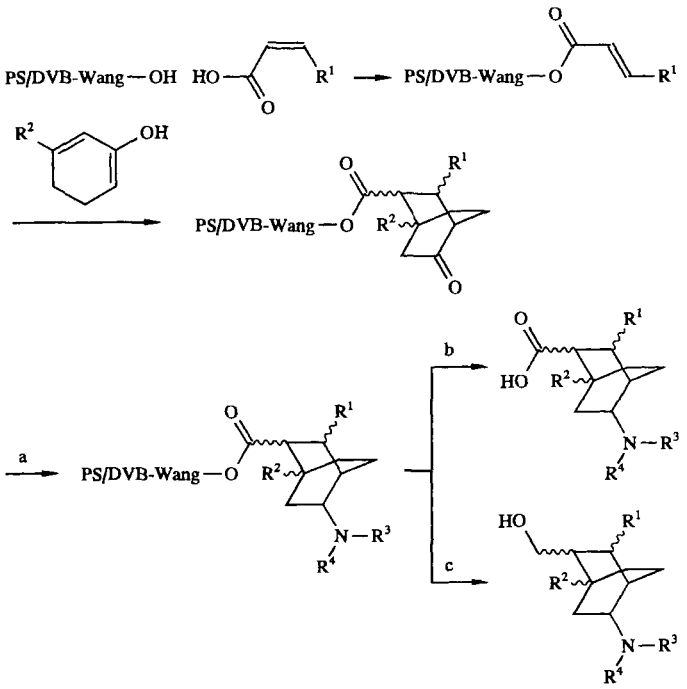

Scheme 36. Solid-phase synthesis of bicyclo[2.2.2]octanes [142]. a) R^3R^4NH, $NaBH(OAc)_3$, ultrasound; b) TFA/CH_2Cl_2; c) DIBAL-H. R^1–R^4 = alkyl, aryl.

found, related low molecular weight peptidomimetics are painstakingly developed that can be applied orally as drugs.[143]

In Section 3.5 two methods were described that help to shorten this search. Thus, the compounds in benzodiazepine and hydantoin libraries are much more closely related to the final biologically active agents than a peptide is. An active compound found in such a library may be converted into more effective derivatives by a few additional steps. In addition to the peptide libraries, oligomer libraries from different building blocks also furnish interesting additional possibilities for the discovery of new biologically active compounds and/or lead structures. In contrast to biopolymers, these oligomer libraries are more stable toward enzymes and often have far higher bioavailability.

4.1. Peptoids

Peptoids, which possess N-substituted glycines (NSGs) as the smallest building blocks, are the compounds most closely related to peptides (Scheme 37). Simon et al.[144] reported a synthesis of peptoids, in which NSG building blocks, presynthesized in solution, are coupled according to a standard protocol with Fmoc protecting groups. Zuckermann[145] and co-workers synthesized NSGs directly on a polymeric support by the coupling of bromoacetic acid with diisopropylcarbodiimide and subsequent reaction of the bromoacyl group with an amine.

Since a tremendous range of amines are commercially available, peptoids with "unnatural" side chains can be used as well as those with natural side chains for the synthesis of a huge number of peptoid libraries. In principle, 10^{18} different hexa-

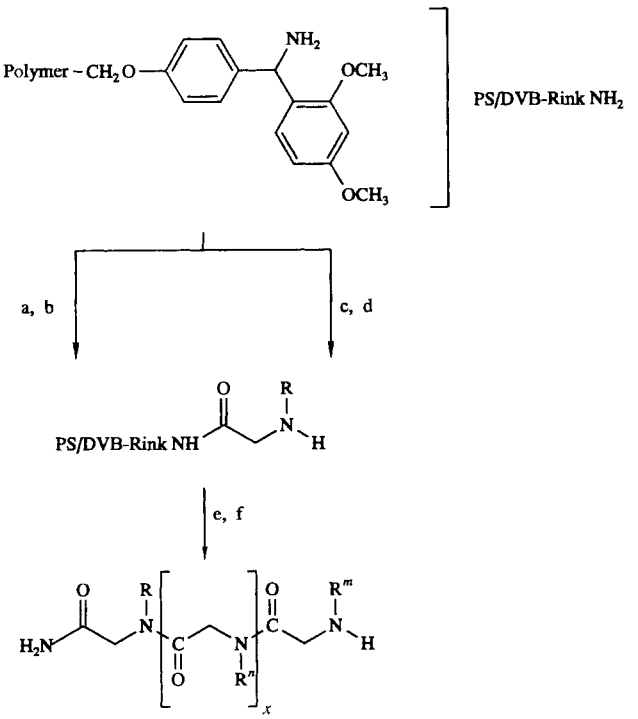

Scheme 37. Synthesis of peptoids on Rink resins. In the monomer method (a,b) of Simon et al. [144] the required monomers are prepared separately by solution procedures: a) *N*-Fmoc-*N*-alkylamino acids, DIC; b) piperidine/DMF (1/1). The submonomer method (c,d) of Zuckermann et al. [145] can be used to prepare immobilized N-substituted glycines from bromoacetic acid and amines: c) bromoacetic acid, DIC/DMF, 2 × 30 min; d) RNH_2, DMSO, 2 h; e) repetitive coupling; f) TFA/CH_2Cl_2. R, R‴, R″ = alkyl, aryl.

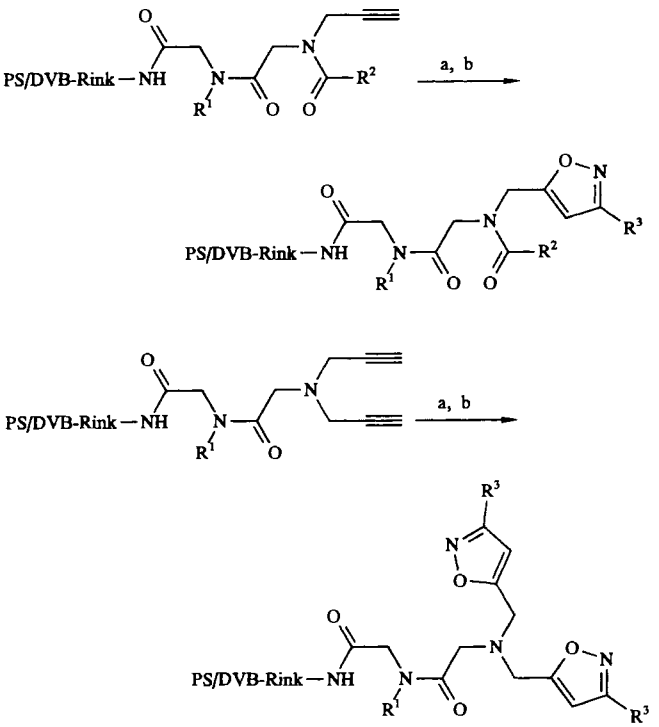

Scheme 38. Subsequent modification of *N*-alkenyl- and *N*-alkynylglycines by [3 + 2]cycloaddition of nitrile oxides prepared in situ [147]. a) Phenylisocyanate, nitroalkyl or nitroaryl compounds, triethylamine, toluene, 100 °C; b) TFA/CH_2Cl_2 (1/4). R^1 = alkyl; R^2 = alkyl, pyridyl, halogen; R^3 = Me, Bu, $HOCH_2$, Ph.

mers can be prepared from 1000 amines. Thus by screening a tetrapeptoid library (4500 individual compounds) with side chains chosen according to required diversity criteria, an α-1-adrenergic receptor antagonist was found in a short time.[146]

The possible variations are not restricted only to the choice of amines (side chains), since new classes of polymers can also be developed by varying the employed halocarboxylic acids. For example, α-alkyl- and ω-bromocarboxylic acids can be used to obtain N- and C_α-disubstituted peptoids or products with chain-extended backbones. Pei and Moos[147] synthesized isoxazoline- and isoxazole-substituted peptoids by reacting nitrile oxides[104, 108] (Section 3.4) with *N*-alkenyl- and *N*-alkynylglycines, respectively (Scheme 38). In these solid-phase syntheses, nitrile oxides were prepared in situ from nitro compounds, isocyanates, and triethylamine, or by oxidation of oximes with sodium hypochlorite in the presence of Et_3N. Nitrile oxides are usually very unstable and yield a series of side products by [3 + 2]cycloaddition. Here, however, the by-products were formed in the solution phase and could be removed by washing the support. Aside from two cases in this series,[147] isoxazoline and isoxazole derivatives were obtained with more than 80% purity (as measured by HPLC).

We carried out the automated synthesis of octa- and nonapeptoids on a preparative scale in our laboratories. Using ligand–receptor assays, we could show, for example, the interesting binding of peptide/peptoid hybrids to the MHC classI proteins[67] of the MHC haplotype K^b in competition with the CTL epitope SIINFEKL.[148] The identity and purity of the peptoids were established by electrospray-MS, HPLC, and for the first time by automated sequencing.[149] The sequencing was optimized for routine procedures and the products of the Edman degradation reaction could be identified. For this purpose, the monomeric NSG was synthesized on chlorotrityl-PS/DVB and converted into the corresponding phenylthiohydantoins (PTH-NSGs). The PTH-NSGs were isolated, purified, and characterized by MS and UV spectroscopy. Afterwards, an HPLC standard was constructed from PTH-NSGs; by coelution the degradation products of sequencing of peptoids and peptide–peptoid hybrids could be identified.

4.2. Oligocarbamates

The solid-phase synthesis of oligocarbamates offers another new source of potentially active oligomers for the search for lead structures. In contrast to the backbone in peptides, the oligocarbamate backbone consists of chiral *ethylene* units connected by relatively rigid carbamate units. As in peptides, the C_α atom can be substituted with different functional groups. Whereas in the first solid-phase synthesis of oligocarbamate by Cho et al.[148, 150] the C_β atom was left unsubstituted, further backbone modifications can be achieved by β-substitutions or by alkylation of the carbamoyl nitrogen atom. Compared to peptides, oligocarbamates are more hydrophobic and more stable toward proteases such as trypsin and pepsin.

Polymer-bound oligocarbamates are obtained by repetitive couplings of commercially available N-protected aminocarbonates (or aminocarbonates prepared by the reduction of protected pentafluorophenylamino acids), to an amino-functionalized resin (Scheme 39). Cleavage from the resin is carried out accord-

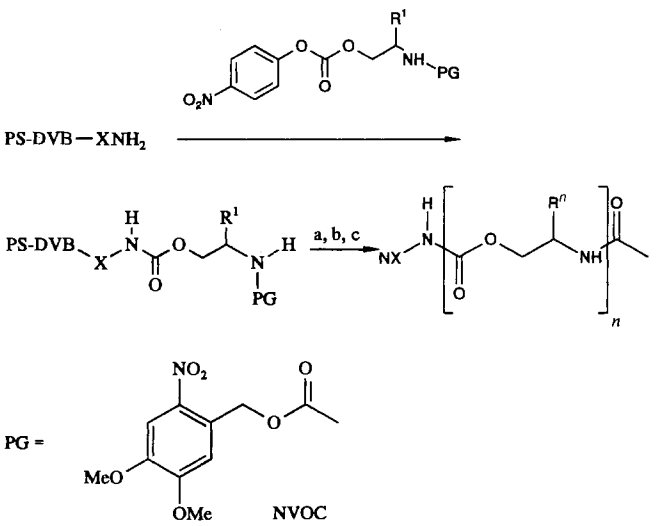

Scheme 39. Solid-phase synthesis of oligocarbamates [150]. a) Deprotection: *hν* = 350 nm (NVOC), piperidine/DMF (1/1) (Fmoc); b) repetitive monomer coupling; c) TFA/CH_2Cl_2. X = spacer or anchor; R^1, R^n = alkyl, aryl, protected amino acid side chain.

ing to routine procedures from peptide chemistry. To demonstrate that these methods can be used to synthesize oligocarbamate libraries, a set of 256 oligocarbamates was prepared using a photolabile amino protecting group (nitroveratroyloxycarbonyl, NVOC) in a photochemical parallel synthesis.[151] The screening of this surface-bound library with an anti-oligocarbamate antibody, obtained by immunization (antigen $AcX^cK^cF^cL^c$), showed the selective binding of antibody to this and to related sequences. The sequence segment F^cL^c was found to be the minimal epitope.

With commercially available amino acid alcohols and the Fmoc strategy, C_α-substituted free oligocarbamates were synthesized in our group on a preparative scale by employing fully automated and considerably simplified procedures.[152]

4.3. Peptide Nucleic Acids

Hybrid oligomers with the properties of both oligonucleotides and peptides were first described in 1991 and designated as peptide nucleic acids (PNAs).[153] Designed as DNA mimetics, these PNA compounds can be varied easily by convenient procedures. It could be shown that the complete DNA backbone can be replaced by a polyamide (pseudo-peptide) structure without impairing the base-specific hybridization. Thus, it is hoped that these compounds can find applications in antisense DNA therapy and in diagnostics.

For the synthesis of PNAs, the nucleobases (only thymine and cytosine were used in initial studies) were first N-substituted using bromoacetic acid and converted into pentafluorophenyl esters (Pfp), which were then reacted with *N*-(*N*-Boc-aminoethyl)glycine (Scheme 40). After a second esterification with PfpOH, the monomers were coupled in situ by DCC according to a standard protocol.

The PNA–DNA binding characteristics were established by determining the melting points of two complementary PNA–DNA strands (dA_{10}, PNA-T_{10}) and the structure by NMR spectroscopic analysis.[153e] The homosequence dA_{10} forms a triple helix with PNA-T_{10} having a melting point of 73 °C.

Replacement of the phosphodiester group in DNA with a diisopropylsilyl analogue led to a DNA-compatible DNA backbone modification. Solid-phase synthesis of this class of compounds has been investigated thoroughly by Saha et al.[154] (Scheme 41). The oligonucleotide analogues were obtained by repetitive coupling of 3′-*O*-diisopropylsilyl deoxyriboucleotide to the already loaded controlled core glass (CPG) support. In addition to "all-silyl" analogues, diisopropylsilyl phosphonate hybrids (60–80% yields based on maximum loading) have also been synthesized and their binding to complementary DNA strands was investigated. By determining the melting temperature of the duplex strands, which depend on the chain length and degree of substitution, values have been obtained ranging from 2 to 5 °C lower than those of the native DNA duplex.

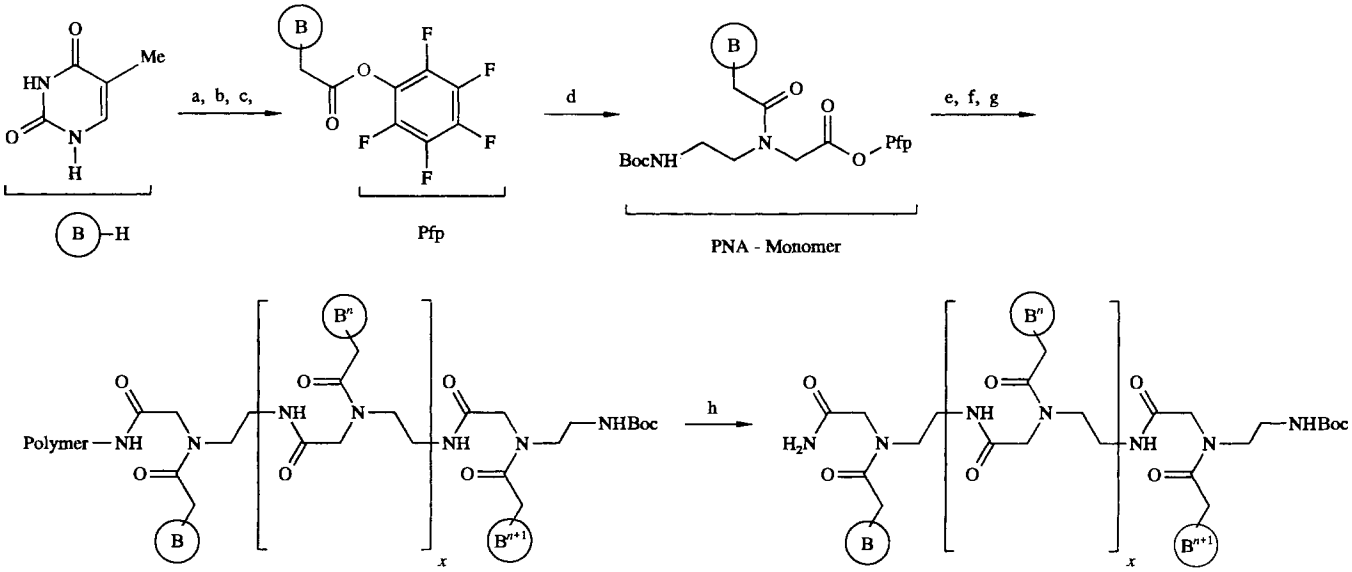

Scheme 40. Synthesis of peptide nucleic acids (PNAs) [153]. a) $BrCH_2CO_2Me$, K_2CO_3; b) NaOH/H_2O, 100 °C; c) PfpOH, DCC, DMF; d) 1. H_2N-Orn(Boc)-OH; 2. PfpOH, DCC, DMF; e) coupling to the amide resin, DMF/CH_2Cl_2; f) TFA; g) repetitive monomer coupling; h) HF. Ⓑ-H = thymine; B^n, B^{n+1} = nucleobases.

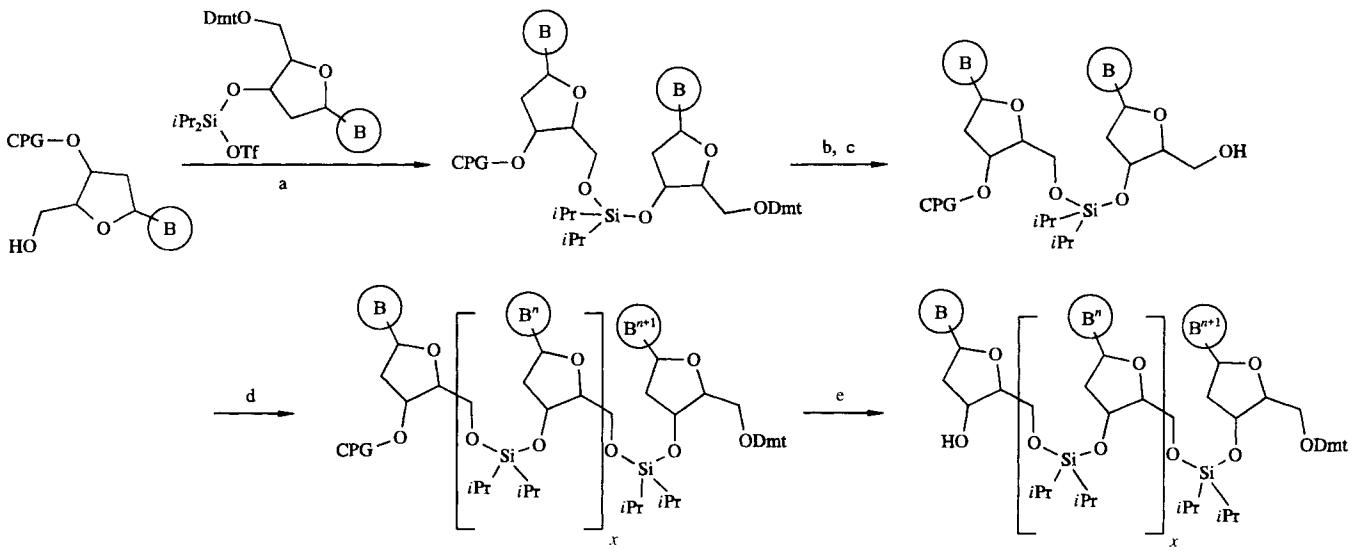

Scheme 41. Synthesis of the Si-bridged oligonucleotide analogues [154]. a) Imidazole; b) Ac_2O, *N*-methylimidazole; c) 3% trichloroacetic acid; d) repetitive monomer coupling; e) cleavage from the support. Ⓑ = nucleobase.

4.4. Oligoureas

Enzyme inhibitors[155] often contain a urea functional group as an important structural element. Recently Burgess et al.[156] reported the possibility of preparing oligoureas by solid-phase synthesis (Scheme 42). The starting point for their synthesis is

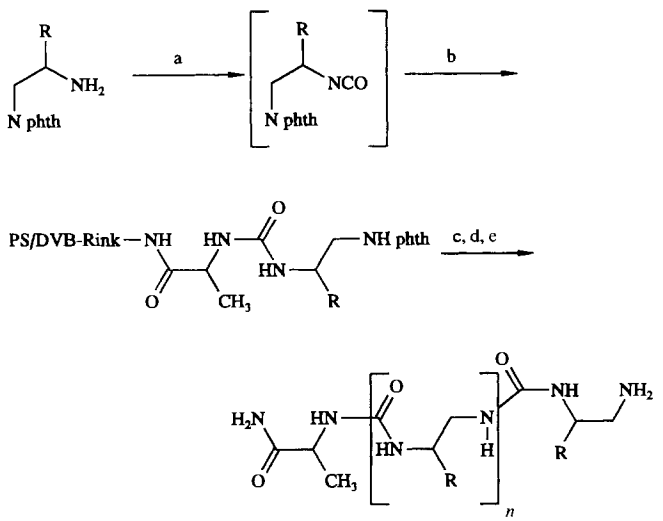

Scheme 42. Solid-phase synthesis of oligoureas [156]. a) 0.33 equiv $(Cl_3CO)_2CO$, Et_3N, CH_2Cl_2; b) PS/DVB-Rink-Ala-NH_2, CH_2Cl_2; c) 60% hydrazine hydrate, DMF, 15 h, 25 °C; d) repeated monomer coupling and protecting group removal; e) cleavage from the resin with TFA. R = H, Me, Ph.

the preparation of a phthaloyl-protected diamine. This monomer was prepared in solution from a Boc-protected amino acid, which was reduced and reacted with phthalimide under the conditions of the Mitsunobu reaction. This diamine was treated with triphosgene (bis(trichloromethyl)carbonate) to give a reactive isocyanate, which can be reacted with amino- or amino acid functionalized polymer supports. After hydrazinolysis (cleavage of the phthaloyl protecting group), the free amino group can be used for repetitive reaction steps. This solid-phase method was used to prepare oligoureas on a preparative scale. The overall yield of a tetrameric test substance was 46%, corresponding to an average coupling yield of 86%. This synthetic route is suitable for preparing not only oligoureas but also peptidomimetics, owing to the use of the hydrazine-labile phthaloyl protecting group.

5. Outlook

In solid-phase synthesis a high excess of reagents can be used without the associated problems of solution-phase organic chemistry. In addition to the possibility of obtaining higher yields, solid-phase organic synthesis has the advantage of facilitating complete automation of all the reaction steps as well as analytical monitoring. The required instrumentation for the automated synthesis of biopolymers has been nearly perfected in recent years. Excess reagents and all soluble by-products can be removed by washing the resin. The examples mentioned in this article demonstrate that almost all organic reactions can be conducted with solid-phase procedures. However, intensive optimization and special adaptation will be required to achieve methods as efficient as those currently in use in biopolymer synthesis.

The methods required for combinatorial chemistry cannot be developed with the equipment available to organic chemists today; instead new PC-controlled robots and reactors are necessary for the simultaneous and parallel syntheses of great numbers of compounds on the 100-mg scale. Therefore, future chemistry research laboratories may in part resemble the present-day assay laboratories for biological screening. Three-neck flasks, reflux condensers, filters, and distillation apparatus will be replaced by minireactors containing a large number of reaction vessels and sensors with fully automated devices for adding and removing reagents. Present investigations focus on new techniques for rapid heating with microwaves as well as on simultaneous and efficient workup procedures for the products of multiple synthesis.

Even though many small companies have been founded with the goal of synthesizing extensive compound libraries for pharmaceutical screening, it is essential that the "combinatorial chemist" systematically optimizes reactions for the simultaneous preparation of single compounds, since as always the problems of realizing extensive compound libraries lie in the experimental details.

In the case of biopolymer libraries and their analogues, as well as the low molecular weight products of combinatorial chemistry, interest will be focused on the free compounds and the strategies without encoding procedures. Practical implementation of label and tagging concepts in libraries already contaminated with by-products cannot be realized easily. In any case, with these libraries the desired and theoretically possible simplification in the discovery of biologically active products is not possible. Concepts relying on directly linking labels to the ligands under investigation have especially little prospect for general application.

Great successes in biological basic research as well as in medical diagnostics and therapy have become possible due to progress made in the multiple solid-phase synthesis of peptides and DNA. Therefore, it can be assumed with certainty that future developments in solid-phase organic chemistry will be revolutionary not only for chemical laboratories but also for the related sciences. The pharmaceutical industry is intensively involved in developing these new techniques. But the universities must also be prepared to train and familiarize students with these new tools.

What exactly are the limits of solid-phase organic chemistry, and in which direction might combinatorial chemistry develop in the coming years? Currently the expectations are very high for what can be achieved by combinatorial chemistry; however, the future will show which of these are reasonable. In addition, the results of future screening programs should demonstrate the feasibility of using combinatorial chemistry, for example, in the search for novel lead compounds. Presently the automation of peptide and nucleic acid synthesis is possible; however, the technical aspects of combinatorial chemistry are still comparatively primitive and fully functioning automatic synthesizers are not commercially available. The future of automation offers two alternatives: either known chemistry must be adapted to suit present technology or the currently available synthesizers and other machines must be radically redesigned to suit new chemistries. Either way, a great deal of developmental work is still needed.

Combinatorial chemists are best advised not to invest great effort in areas where nature excels. It is pointless to synthesize proteins containing more than 100 amino acids when biotechnology can provide cleaner products faster and more economically. Nature is better than combinatorial chemistry for constructing and derivatizing complicated natural products. Several strategies combining the strengths of both approaches have been discussed and described with the terms "combinatorial biosynthesis"[157] and "biological diversity".

An expansion of the pool of natural products is possible if, for example, microorganisms are led to produce new variants of a siderophore[158] or an antibiotic through feeding with unnatural building blocks. These modest possibilities of "directed fermentation" lag far behind the enormous diversity, which, for example, is achievable by polyketide biosynthesis. Using different combinations of polyketide biosynthesis genes, unimaginable numbers of combinations can be achieved[159] for the production of new molecules.

Finally, it should be mentioned that the genetic manipulation of precursor structural genes can lead to the production of a vast array of variants and analogues of ribosomally synthesized polycyclic peptide antibiotics. Thus, several novel enzymes have been found which can effect, for example, dehydration, cyclization, epimerization, and oxidative decarboxylation in the post-translational modification of lantibiotics precursor proteins.[160] In contrast to phage libraries, biosynthesis systems of lantibiotics have been used to prepare numerous conformationally restricted soluble active peptides.

We sincerely thank all of our colleagues who helped and supported us during preparation of this review article: Prof. Austel (Thomae), Dr. C. Tsaklakidis and Dr. R. Heck (Boehringer Mannheim), Dr. R. Jack, Dr. K.-H. Wiesmüller, Priv.-Doz. J. W. Metzger, Dr. J. Jauch, A. Fischer, H. Eickhoff, M. Winter, T. Redemann, W. Haap, and S. Kapitza.

Received: May 11, 1995
Revised version: October 16, 1995 [A 114IE]
German version: *Angew. Chem.* **1996**, *108*, 19–46

[1] R. R. Merrifield, *J. Am. Chem. Soc.* **1963**, *85*, 2149.
[2] a) R. B. Merrifield, *Angew. Chem.* **1985**, *97*, 801; *Angew. Chem. Int. Ed. Engl.* **1985**, *24*, 799.
[3] Reviews: a) M. R. Pavia, T. K. Sawyer, W. H. Moos, *Bioorg. Med. Chem. Lett.* **1993**, *3*, 387; b) G. Jung, A. G. Beck-Sickinger, *Angew. Chem.* **1992**. *104*, 375; *Angew. Chem. Int. Ed. Engl.* **1992**, *31*, 367; c) G. B. Fields, R. L. Noble, *Int. J. Pept. Protein Res.* **1990**, *35*, 161.
[4] Reviews: a) S. L. Beaucage, R. P. Iyer, *Tetrahedron* **1992**, *48*, 2223; b) P. W. Davis, D. Hudson, M. Lyttle, N. D. Sinaha, N. Usman, M. Weiss, P. Wright in *Innovation and Perspectives in Solid Phase Synthestis* (Ed.: R. Epton), Intercept, Andover, **1992**, p. 63; c) F. X. Montserra, A. Grandas, R. Eritja, E. Pendroso, *Tetrahedron* **1994**, *50*, 2617.
[5] a) R. Verduyn, P. A. M. van der Klein, M. Douwes, G. A. van der Marl, J. H. van Boom, *Recl. Trav. Chim. Pays Bas* **1993**, *112*, 464; b) S. J. Danishefsky, K. F. McClure, J. T. Randolph, R. B. Ruggeri, *Science*, **1993**, *260*, 1307; c) S. P. Douglas, D. M. Whitfield, J. J. Kerpinsky, *J. Am. Chem. Soc.* **1991**, *113*, 5095; d) M. Schuster, P. Wang, J. C. Paulson, C.-H. Wong, *ibid.* **1994**, *116*, 1135.
[6] a) R. N. Zuckermann, J. M. Kerr, M. A. Siani, S. Banville, *Int. J. Pept. Protein Res.* **1992**, *40*, 497; b) G. Schnorrenberg, K.-H. Wiesmüller, A. G. Beck-Sickinger, H. Drechsel, G. Jung in *Peptides 1990, Proc. 21st Eur. Pept. Symp.* (Eds.: E. Giralt, D. Andreu), ESCOM, Leiden, **1991**, p. 202.
[7] a) R. A. Houghten, C. Pinilla, S. E. Blondelle, J. R. Appel, C. T. Dooley, J. H. Cuervo, *Nature* **1991**, *354*, 84; b) J. M. Ostresh, G. M. Husar, S. E. Blondelle, B. Dörner, P. A. Weber, R. A. Houghten, *Proc. Natl. Acad. Sci. USA* **1994**, *91*, 11138; d) M. Stankova, S. Wade, K. S. Lam, M. Lebl, *Pept. Res.* **1994**, *7* (6), 292; e) M. A. Gallop, R. W. Barrett, W. J. Dower, S. P. A. Fodor, E. M. Gordon, *J. Med. Chem.* **1994**, *37*, 1233.
[8] L. DeOgny, B. C. Pramanik, L. L. Arndt, J. D. Jones, J. Rush, C. A. Slaughter, J. D. Randolf, M. V. Norgrad, *Pept. Res.* **1994**, *2*, 91.
[9] H. Paulsen, T. Bielfeldt, S. Peters, M. Meldal, K. Bock, *Liebigs Ann. Chem.* **1994**, 369.
[10] Y. M. Angell, T. L. Thomas, G. R. Flentke, D. H. Rich, *J. Am. Chem. Soc* **1995**, *117*, 7279.
[11] J. Pless, W. Bauer, F. Cardinaux, A. Closse, D. Hauser, R. Huguenin, D. Roemer, H.-H. Buescher, R. C. Hill, *Helv. Chim. Acta* **1979**, *62*, 398.
[12] D. Roemer, H.-H. Buescher, R. C. Hill, J. Pless, W. Bauer, F. Cardinaux, A. Closse, D. Hauser, R. Huguenin, *Nature* **1977**, *268*, 547.
[13] D. Roemer, J. Pless, *Life Sci.* **1979**, *24*, 621.
[14] M. Nishikata, H. Yokosawa, S.-I. Ishii, *Chem. Pharm. Bull.* **1986**, *34*, 2931.
[15] G. Kokotos, V. Constantinou-Kokotou in *Peptides 1990, Proc. 21st Eur. Pept. Symp.* (Eds.: E. Giralt, D. Andreu), ESCOM, Leiden, **1991**, p. 23.
[16] J. Swistok, J. W. Tilley, W. Danho, R. Wagner, K. Mulkerins in *Peptides, Chemistry, Structure and Biology* (Eds.: J. E. Rivier, G. R. Marshall), ESCOM, Leiden, **1990**, p. 1017.
[17] W. Neugebauer, M. R. Lefèbvre, R. Lapris, E. Escher in *Peptides, Chemistry, Structure and Biology* (Eds.: J. E. Rivier, G. R. Marshall), ESCOM, Leiden, **1990**, p. 1020.
[18] S. Hobbs DeWitt, J. S. Kiely, C. J. Stankovic, M. C. Schroeder, D. M. Reynolds Cody, M. R. Pavia, *Proc. Natl. Acad. Sci. USA* **1993**, *90*, 6909.
[19] Reviews: a) D. E. Bergbreiter in *Functional Polymers* (Eds.: D. E. Bergbreiter, C. R. Martin) Plenum, New York, **1989**, p. 143; b) P. Hodge in *Synthesis and Separations Using Functional Polymers* (Eds.: D. C. Sherrington, P. Hodge), Wiley, Chichester, **1988**, p. 43; c) A. Akelah, *Reakt. Polym. Ion Exch. Sorbents* **1988**, *8*, 273; d) A. Akelah, *Synthesis* **1981**, 413; e) G. A.

Crosby, *Aldrichimica Acta* **1976**, 15; f) C. G. Overberger, K. N. Sannes, *Angew. Chem.* **1974**, *86*, 139; *Angew. Chem. Int. Ed. Engl.* **1974**, *13*, 99.
[20] Reviews: A. Akelah, G. Abdel, M. Fathy, *Phosphorus Sulfur Relat. Elem.* **1987**, *30*, 91.
[21] a) Reviews: P. Hodge in ref. [21c], p. 273; b) P. M. Worster, C. R. McArthur, C. C. Leznoff, *Angew. Chem.* **1979**, *91*, 255; *Angew. Chem. Int. Ed. Engl.* **1979**, *18*, 221; c) *Innovations and Perspectives in Solid Phase Synthesis* (Ed.: R. Epton), SPCC, Birmingham, **1990**.
[22] a) J. M. J. Fréchet, K. E. Haque, *Macromolecules*, **1975**, *8*, 130; b) C. R. Harrsison, P. Hodge, *J. Chem. Soc. Chem. Commun.* **1974**, 1009; c) N. M. Weinshenker, C. N. Shen, *Tetrahedron Lett.* **1972**, 3281; d) F. Camps, J. Castells, J. Font, F. Vela, *Tetrahedron Lett.* **1971**, 1715.
[23] a) A. Patchornik, M. A. Kraus, *Pure Appl. Chem.* **1975**, *43*, 503; references to more recent literature can be found in ref. [6b].
[24] B. Gutte, R. B. Merrifield, *J. Biol. Chem.* **1971**, *246*, 1922.
[25] A. Guyot in *Synthesis and Separations Using Functional Polymers* (Eds.: D. C. Sherrington, P. Hodge) Wiley, Chichester, **1988**, p. 1.
[26] E. Atherton, R. C. Sheppard in *Peptides 1974, Proc. 13th Eur. Pept. Symp.* (Ed.: Y. Wolman), Halsted Press, New York, **1975**, p. 123.
[27] a) E. Atherton, D. L. J. Clive, R. C. Sheppard, *J. Am. Chem. Soc.* **1975**, *97*, 6584; b) E. Atherton, M. Caviezel, H. Over, R. C. Sheppard, *J. Chem. Soc. Chem. Commun.* **1977**, 819.
[28] a) E. Ashardy, E. Atherton, M. J. Gait, K. Lee, R. C. Sheppard, *J. Chem. Soc. Chem. Commun.* **1979**, 423; b) E. Atherton, D. Jarvis, G. P. Priestley, R. C. Sheppard, B. J. Williams in *Peptides: Structure and Function* (Eds.: E. Gross, J. Meienhofer), Pierce, Rockford, **1979**, p. 361.
[29] a) J. C. Alfred, J.-L. Aubagnac, M. Calmes, J. Daunis, B. Elamarani, R. Jacquir, G. Nkusi, *Tetrahedron* **1988**, *44*, 4407; b) G. L. Stahl, R. Walter, C. W. Smith, *J. Am. Chem. Soc.* **1979**, *101*, 5383; c) B. Calas, J. Parello, *Am. Biotechnol. Lab.* **1985**, 1985.
[30] H. M. Geysen, R. H. Meloen, S. J. Barteling, *Proc. Natl. Acad. Sci. USA* **1984**, *81*, 3998.
[31] A. Dryland, R. C. Sheppard, *J. Chem. Soc. Perkin Trans. 1* **1986**, 125.
[32] P. W. Small, R. C. Sheppard, *J. Chem. Soc. Chem. Commun.* **1989**, 1589.
[33] a) F. Albericio, M. Pons, E. Pendroso, E. Giralt, *J. Org. Chem.* **1989**, *54*, 360; b) K. Büttner, H. Zahn, W. H. Fischer in *Peptides: Chemistry and Biology* (Ed.: G. R. Marschall), ESCOM, Leiden, **1988**, p. 210.
[34] W. Rapp, K.-H. Wiesmüller, B. Fleckenstein, V. Gnau, G. Jung in *Peptides 1994, Proc. 23rd Eur. Pept. Symp.* (Ed.: H. L. S. Maja), ESCOM, Leiden, **1995**, p. 87.
[35] a) E. Bayer, *Angew. Chem.* **1991**,*103*, 117; *Angew. Chem. Int. Ed. Engl.* **1991**, *30*, 113; b) E. Bayer, W. Rapp, *Chem. Pept. Prot.* **1986**, *3*, 3; c) E. Bayer, *Int. J. Pept. Prot. Res.* **1985**, *25*, 178.
[36] a) K. Barlos, D. Gatos, S. Kapolos, G. Paphotiu, W. Schafer, Y. Wenqing, *Tetrahedron Lett.* **1989**, *30*, 3947; b) J. M. J. Fréchet, K. E. Haque, *Tetrahedron Lett.* **1975**, 3055; c) F. Cramer, H. Köster, *Angew. Chem.* **1966**, *78*, 180; *Angew. Chem. Int. Ed. Engl.* **1966**, *5*, 473.
[37] a) D. L. Marshall, I. E. Liener, *J. Org. Chem.* **1970**, *35*, 867; b) T. Wieland, J. Lewalter, C. Birr, *Justus Liebigs Ann. Chem.* **1970**, *740*, 31; c) G. W. Kenner, J. R. McDermott, R. C. Sheppard, *J. Chem. Soc. Dalton Trans.* **1971**, *12*, 636; d) Y. Kiso, T. Fukui, S. Tanaka, T. Kimura, K. Akaji, *Tetrahedron Lett.* **1994**, *35*, 3571; e) R. Sola, P. Saguer, M.-L. David, R. Pascal, *J. Chem. Soc. Chem. Commun.* **1993**, 1786.
[38] R. B. Wang, *J. Am. Chem. Soc.* **1972**, *95*, 1328.
[39] M. Mergler, R. Tanner, J. Gosteli, P. Grogg, *Tetrahedron Lett.* **1988**, *29*, 4005.
[40] A. R. Mitchell, B. W. Erickson, M. N. Raybtsev, R. S. Hodge, R. B. Merrifield, *J. Am. Chem. Soc.* **1976**, *98*, 7357.
[41] H. Rink, *Tetrahedron Lett.* **1987**, *28*, 3787.
[42] a) J. Tam, R. D. DiMarchi, R. B. Merrifield, *Tetrahedron Lett.* **1981**, *22*, 2851; b) A. Hiro, S. Itsuno, I. Hattori, K. Yamaguchi, S. Nakahama, N. Yamazaki, *J. Chem. Soc. Chem. Commun.* **1983**, 25.
[43] P. Sieber, *Tetrahedron Lett.* **1987**, *28*, 2107.
[44] a) F. Albericio, E. Giralt, R. Eritja, *Tetrahedron Lett.* **1991**, *32*, 1515; b) F. Albericio, J. Robles, D. Fernandez-Forner, Y. Palom, C. Celma, E. Pedroso, E. Giralt, R. Eritja in *Peptides 1990, Proc. 21st Eur. Pept. Symp.* (Eds.: E. Giralt, D. Andreu), ESCOM, Leiden, **1991**, p. 134.
[45] J. W. Apsimon, D. M. Dixit, *Synth. Commun.* **1982**, *12*, 113.
[46] S. B. Katti, P. K. Misra, W. Haq, K. B. Mathur, *J. Chem. Soc. Chem. Commun.* **1992**, 843.
[47] D. G. Mullen, G. Barany, *J. Org. Chem.* **1988**, *53*, 5240.
[48] R. Ramage, C. A. Barron, S. Bielecki, D. W. Thomas, *Tetrahedron Lett.* **1987**, *28*, 4105.
[49] W. F. DeGrado, E. T. Kaiser, *J. Org. Chem.* **1980**, *45*, 1295.
[50] a) H. Kunz, B. Dombo, W. Kosch in *Peptides 1988, Proc. 20th Eur. Pept. Symp.* (Eds.: G. Jung, E. Bayer), de Gruyter, Berlin, **1989**, p. 154; b) G. Becker, H. Nguyen-Trong, C. Birr, B. Dombo, H. Kunz, *ibid.*, p. 157.
[51] M. Patek, M. Lebl, *Tetrahedron Lett.* **1991**, *32*, 3891.
[52] a) F.-S. Tjoeng, G. A. Heavner, *J. Org. Chem.* **1983**, *48*, 355; b) S.-S. Wang, *J. Org. Chem.* **1976**, *41*, 3258.
[53] a) G. Barany, N. A. Sole, R. J. Van Abel, F. Albericio in *Innovations and Perspectives in Solid Phase Synthesis* (Ed.: R. Epton), Intercept, Andover, **1992**, p. 29; b) F. Albericio, P. Lloyd-Willams, M. Gairi, G. Jou, C. Celma, N. Kneib-Cordonier, A. Grandas, R. Erityja, E. Pendroso, J. Van Rietschoten, G. Barany, E. Giralt, *ibid.*, p. 39; c) G. Barany, F. Albericio in *Peptides 1990, Proc. 21st Eur. Pept. Symp.* (Eds.: E. Giralt, D. Andreu), ESCOM, Leiden, **1991**, 139; d) R. P. Hammer, F. Albericio, E. Giralt, G. Barany, *Int. J. Pept. Protein Res.* **1991**, *37*, 402; e) D. H. Rich, S. K. Gurwara, *J. Am. Chem. Soc.* **1975**, *97*, 1575.
[54] L. A. Thompson, J. A. Ellman, *Tetrahedron Lett.* **1994**, *35*, 9333.
[55] I. Sucholeiki, *Tetrahedron Lett.* **1994**, *35*, 7307.
[56] Reviews: a) E. M. Gordon, R. W. Barrett, W. J. Dower, P. A. Fodor, M. A. Gallop, *J. Med. Chem.* **1994**, *37*, 1385; b) R. M. J. Liskamp, *Angew. Chem.* **1994**, *106*, 661; *Angew. Chem. Int. Ed. Engl.* **1994**, *33*, 633; c) T. Carell, E. A. Wintner, A. Bashir-Hashemi, J. Rebek, Jr., *Angew. Chem.* **1994**, *106*, 2159; *Angew. Chem. Int. Ed. Engl.* **1994**, *33*, 2059; d) N. K. Terrett, M. Gardner, D. W. Gordon, R. J. Kobylecki, J. Steel, *Tetrahedron* **1995**, *51*, 8135; e) D. J. Ecker, S. T. Crooke, *Biotechnology* **1995**, *13*, 351; f) I. Ugi in *Isonitrile Chemistry* (Ed.: I. Ugi), Academic Press, New York, **1971**, p. 1; g) I. Ugi, lecture at the symposium *Mehrkomponenten-Reaktionen*, Garching, **1995**.
[57] a) J. W. Metzger, K.-H. Wiesmüller, V. Gnau, J. Brünjes, G. Jung, *Angew. Chem.* **1993**, *105*, 901; *Angew. Chem. Int. Ed. Engl.* **1993**, *32*, 894; b) C. L. Brummel, I. N. W. Lee, Y. Zhou, S. J. Benkovic, N. Winograd, *Science* **1994**, *263*, 399.
[58] a) J. W. Metzger, C. Kempter, K.-H. Wiesmüller, G. Jung, *Anal. Biochem.* **1994**, *219*, 261; b) J. W. Metzger, S. Stevanovic, J. Brünjes, K.-H. Wiesmüller, G. Jung, *Methods (San Diego)* **1994**, *6*, 425.
[59] Reviews: a) P. Eckes, *Angew. Chem.* **1994**, *106*, 1649; *Angew. Chem. Int. Ed. Engl.* **1994**, *33*, 1573; b) K. D. Janda, *Proc. Natl. Acad. Sci. USA*, **1994**, *91*, 10779; I. Ugi, A. Bömling, B. Gruber, M. Heilgenbrunner, C. Heiss, W. Hörl in *Software-Entwicklungen in der Chemie, Vol. 9* (Ed.: R. Moll), Gesellschaft Deutscher Chemiker, Frankfurt, **1955**, p. 113.
[60] J. M. Kerr, S. C. Banville, R. N. Zuckermann, *J. Am. Chem. Soc.* **1993**, *115*, 2529.
[61] V. Nikolaiev, A. Stierandova, V. Krchnak, B. Seligmann, K. S. Lam, S. E. Salomon, M. Lebl, *Pept. Res.* **1993**, *3*, 161.
[62] M. H. J. Ohlmeyer, R. N. Swanson, L. W. Dillard, J. C. Reader, G. Asouline, R. Kobayashi, M. Wigler, W. C. Still, *Proc. Natl. Acad. Sci. USA* **1993**, *90*, 10922.
[63] S. Brenner, R. A. Lerner, *Proc. Natl. Acad. Sci. USA* **1992**, *89*, 5181.
[64] a) W. Schoknecht, K. Albert, G. Jung, E. Bayer, *Liebigs Ann. Chem.* **1982**, 1514; b) E. Giralt, J. Rizo, E. Pedroso, *Tetrahedron* **1984**, *40*, 4141; c) E. Giralt, F. Albericio, F. Bardella, R. Eritja, M. Feliz, E. Pedroso, M. Pons, J. Rizo in *Innovations and Perspectives in Solid Phase Synthesis* (Ed.: R. Epton), SPCC, Birmingham, **1990**, p. 111; d) G. C. Look, C. P. Holmes, J. P. Chinn, M. A. Gallop, *J. Org. Chem.* **1994**, *59*, 7588.
[65] a) W. L. Fitch, G. Detre, C. P. Holmes, J. N. Shoolery, P. A. Kiefer, *J. Org. Chem.* **1994**, *59*, 7955; b) R. C. Anderson, M. A. Jarema, M. J. Shapiro, J. P. Stokes, M. Ziliox, *ibid.* **1995**, *60*, 2650, R. C. Anderson, J. P. Stokes, M. Shapiro, *Tetrahedron Lett.* **1995**, *36*, 5311.
[66] a) B. J. Egner, J. L. Langley, M. Bradley, *J. Org. Chem.* **1995**, *60*, 2652; b) M. Bradley, lecture at the *Combinatorial Synthesis Symposium*, Exeter, **1995**.
[67] J. S. Früchtel, K.-H. Wiesmüller, G. Jung, unpublished results.
[68] I. T. Harrison, S. Harrison, *J. Am. Chem. Soc.* **1967**, *89*, 5723.
[69] C. C. Leznoff, *Acc. Chem. Res.* **1978**, *11*, 327.
[70] a) T. M. Fyles, C. C. Leznoff, *J. Chem. Soc. Chem. Commun.* **1976**, 251; b) J. M. J. Fréchet, L. J. Nuyens, *Can. J. Chem.* **1976**, 54, 926; c) J. Y. Wong, C. C. Leznoff, *ibid.* **1973**, *51*, 2452; d) *ibid.* **1972**, *50*, 2892.
[71] a) C. C. Leznoff, T. M. Fyles, *Can. J. Chem.* **1977**, *55*, 1143; b) T. M. Fyles, C. C. Leznoff, *ibid.* **1977**, *55*, 4135; c) C. C. Leznoff, D. M. Dixit, *ibid.* **1977**, *55*, 3351.
[72] a) E. Seymour, J. M. J. Fréchet, *Tetrahedron Lett.* **1976**, 3669; b) *ibid.* **1976**, 1149; c) J. M. J. Fréchet, L. J. Nuyens, E. Seymour, *J. Am. Chem. Soc.* **1979**, *101*, 432; d) J. M. J. Fréchet, *Tetrahedron*, **1981**, 663.
[73] C. Chen, L. A. Ahlberg Randall, R. B. Miller, A. Daniel Jones, M. K. Kurth, *J. Am. Chem. Soc.* **1994**, *116*, 2661.
[74] J. R. Prikh, W. von E. Doering, *J. Am. Chem. Soc.* **1967**, *89*, 5505.
[75] K. S. Lam, S. E. Salmon, E. M. Hersh, V. J. Hruby, W. M. Kazmeiersky, R. J. Knapp, *Nature* **1991**, *354*, 82.
[76] A. Furka, F. Sebestyen, M. Asgedom, G. Dibo, *Int. J. Pept. Protein Res.* **1991**, *37*, 487.
[77] a) O. Mitsunobu, *Synthesis* **1981**, 1; b) D. L. Huges, *Org. React. (NY)* **1992**, *42*, 335.
[78] a) L. S. Richter, T. R. Gadek, *Tetrahedron Lett.* **1994**, *35*, 4705; b) V. Krchnák, D. Cabel, A. Weichsel, Z. Flegelová, *Lett. Pept. Sci.* **1995**, *1*, 277.
[79] D. A. Campbell, J. C. Bermak, *J. Am. Chem. Soc.* **1994**, *116*, 6039.
[80] T. A. Rano, K. T. Chapman, *Tetrahedron Lett.* **1995**, *36*, 3789; siehe auch V. Krchnák, J. Vágner, Z. Flegelová, G. Barany, M. Lebl, *Abstr. Pap. 14th Am. Pept. Symp.* (Columbus, OH) **1995**.
[81] E. J. Moran, T. E. Wilson, C. Y. Cho, S. G. Cherry, P. G. Schultz, *Biopolymers* **1995**, *37*, 213.
[82] a) K. Soai, H. Oyamada, M. Takase, *Bull. Chem. Soc. Jpn.* **1984**, *57*, 2327; b) G. Kokotos, *Synthesis* **1990**, 299.

[83] a) C. C. Leznoff, W. Sywanyk, *J. Org. Chem.* **1977**, *42*, 3203; b) C. C. Leznoff, S. Greenberg, *Can. J. Chem.* **1976**, *54*, 3842; c) C. C. Leznoff, J. Y. Wong, *ibid.* **1973**, *51*, 3756.
[84] Z.-H. Xu, C. R. McArthur, C. C. Leznoff, *Can. J. Chem.* **1983**, *61*, 1405.
[85] Q. S. Ren, W. Q. Wen, P. L. Ho, *React. Polym.* **1989**, *11*, 237.
[86] A. Wohl, *Chem. Ber.* **1910**, *43*, 4374.
[87] D. H. Johnson, *J. Chem. Soc.* **1958**, 1624.
[88] a) G. T. Morgan, E. Walton, *J. Chem. Soc.* **1936**, *902*; b) M. D. Soffer, N. S. Strauss, M. D. Trail, K. W. Sherk, *J. Am. Chem. Soc.* **1947**, *69*, 1684.
[89] C. C. Leznoff, J. M. Goldwasser, *Tetrahedron Lett.* **1977**, 1875.
[90] J. M. Goldwassser, C. C. Leznoff, *Can. J. Chem.* **1978**, *56*, 1562.
[91] S. S. Wang, *J. Am. Chem. Soc.* **1973**, *95*, 1928.
[92] K. M. Patel, H. J. Pownall, J. D. Morrisett, J. T. Sparrow, *Tetrahedron Lett.* **1976**, 4015.
[93] S. W. Chaiken, W. G. Brown, *J. Am. Chem. Soc.* **1949**, *71*, 122.
[94] C. C. Leznoff, V. Yedidia, *Can. J. Chem.* **1980**, *58*, 287.
[95] T. Veda, S. Kato, S. Toyoshima, J. Takada (Dainippon Pharm. Co), JP-B 5873(61), **1957** [*Chem. Abstr.* **1963**, *59*, 2726b].
[96] F. Camps, J. Castells, M. J. Ferrando, J. Font, *Tetrahedron Lett.* **1971**, 1715.
[97] A. Patchorkin, M. A. Kraus, *J. Am. Chem. Soc.* **1970**, *92*, 7587.
[98] a) E. Hoffmann, A. G. Beck-Sickinger, G. Jung, *Liebigs Ann. Chem.* **1991**, 585; b) J. S. McMurray, *Tetrahedron Lett.* **1991**, *32*, 7679; c) S. Plaue, *Int. J. Pept. Protein Res.* **1990**, *35*, 510; d) G. Ösapay, L. Quartara, G. Fabbi, *J. Am. Chem. Soc.* **1990**, *112*, 6046; e) A. M. Felix, C.-T. Wang, E. P. Heimer, A. Fournier, *Int. J. Pept. Protein Res.* **1988**, *31*, 231.
[99] Review: R. G. Pearson, *J. Chem. Educ.* **1981**, *81*, 753.
[100] J. March, *Advanced Organic Chemistry*, 4. Aufl., Wiley, New York, **1992**, p. 846, 875, 1112, 1123.
[101] S. J. Blazka, H. J. Harwood, *Polym. Prep. (Am. Chem. Soc. Div. Polym. Chem.)* **1975**, *16*, 633.
[102] T. J. Nieuwstad, A. P. G. Kienboom, A. J. Breijer, J. van der Linden, H. van Bekkum, *Recl. Trav. Chim. Pays Bas* **1976**, *95*, 225.
[103] a) J. Rebek, Jr., F. Gavina, *J. Am. Chem. Soc.* **1974**, *96*, 7112; b) F. Gavina, P. Gil, B. Palazon, *Tetrahedron Lett.* **1979**, 1333.
[104] V. Yedida, C. C. Leznoff, *Can. J. Chem.* **1980**, **58**, 1144.
[105] a) K. N. Houk, *J. Am. Chem. Soc.* **1973**, 95, 4092; b) K. N. Houk, *Acc. Chem. Res.* **1975**, *8*, 361; c) L. E. Overman, G. F. Taylor, K. N. Houk, L. N. Domelsmith, *J. Am. Chem. Soc.* **1978**, *100*, 3182.
[106] a) N. E. Schore, S. D. Najdi, *J. Am. Chem. Soc.* **1990**, *112*, 441; b) M. J. Kurth, lecture at the *Combinatorial Synthesis Symposium*, Exeter, **1995**.
[107] Review: P. L. Pauson, *Tetrahedron* **1985**, *41*, 5855.
[108] a) X. Beebe, N. E. Schore, M. J. Kurth, *J. Am. Chem. Soc.* **1992**, *114*, 10061.
[109] M. G. Bock, R. M. DiPrado, B. E. Evans, K. E. Rittle, W. L. Whitter, D. F. Veber, P.-S. Anderson, R. M. Freidinger, *J. Med. Chem.* **1989**, *32*, 13.
[110] D. Roemer, H. H. Buescher, R. C. Hill, R. Maurer, T. J. Petcher, H. Zeugner, W. Benson, E. Finner, W. Milkowski, P. W. Thies, *Nature* **1982**, *298*, 759.
[111] E. Kornecki, Y. H. Ehrlich, R. H. Lenox, *Science* **1991**, *254*, 1799.
[112] W. E. Bondinell, J. F. Callahan, W. F. Huffman, W. F. Sherman, M. I. Richman, T. W. Ku, K. A. Newlander (Smithkline Beecham), *International Patent Application* **1991**, WO 93/00095 [*Chem. Abstr.* **1993**, *119*, 493416e].
[113] R. Pauwels, K. Andries, J. Desmyter, D. Schols, M. J. Kukla, H. J. Breslin, A. Raeymaeckers, J. Van Gelder, R. Woestenborghs, J. Heykants, K. Schellekens, M. A. C. Janssen, E. De Clercq, P. A. J. Jannsen, *Nature* **1990**, *343*, 470.
[114] M.-C. Hsu, A. D. Schutt, M. Holly, L. W. Slice, M. J. Sherman, D. D. Richman, M. J. Potash, D. J. Volsky, *Science* **1991**, *254*, 1799.
[115] F. Camps, J. Castells, J. Pi, *An. Quim.* **1974**, *70*, 848.
[116] S. HobbsDeWitt, J. S. Kiely, C. J. Stankovic, M. C. Schroeder, D. M. Reynolds Cody, M. R. Pavia, *Proc. Natl. Acad. Sci. USA* **1993**, *90*, 6909.
[117] D. M. Reynolds Cody, S. HobbsDeWitt, J. C. Hodges, B. D. Roth, M. C. Schroeder, C. J. Stankovic, W. H. Moos, M. R. Pavia, J. S. Kiely (Warner-Lambart Company), WO 9408711 [*Chem. Abstr.* **1995**, *122*, 106536].
[118] A. MacDonald, R. Ramage, S. HobbsDeWitt, E. Hogan, Poster, lecture at the *Combinatorial Synthesis Symposium*, Exeter, **1995**.
[119] a) B. A. Bunin, M. J. Plunkett, J. A. Ellman, *Proc. Natl. Acad. Sci. USA* **1994**, *91*, 4708; b) B. A. Bunin, J. A. Ellman, *J. Am. Chem. Soc.* **1992**, *114*, 10997.
[120] a) L. Weber, *Nachr. Chem. Tech. Lab.* **1994**, *42*, 698; b) E. M. Gordon, R. W. Barrett, W. J. Dower, S. P. A. Fodor, M. A. Gallop, *J. Med. Chem.* **1994**, *37*, 1385; c) J. A. Ellman, lecture at the conference *Exploiting Molecular Diversity for Drug Discovery*, San Diego, CA, **1994**.
[121] H. M. Geysen, S. J. Rodda, T. J. Mason, G. Tribbick, P. G. Schoofs, *J. Immunol. Methods* **1987**, *102*, 259.
[122] M. J. Plunkett, J. A. Ellman, *J. Am. Chem. Soc.* **1995**, *117*, 3306.
[123] M. Patek, B. Drake, M. Lebl, *Tetrahedron Lett.* **1995**, *36*, 2227.
[124] a) J. I. Crowley, H. Rapoport, *J. Am. Chem. Soc.* **1970**, 92, 6363; *J. Org. Chem.* **1980**, *45*, 3215; b) in solution: Y. Yamada, T. Ishii, M. Kimura, K. Hosaka, *Tetrahedron Lett.* **1981**, *22*, 1353.
[125] A. A. Virgilio, J. A. Ellman, *J. Am. Chem. Soc.* **1994**, *116*, 11580.
[126] A. A. Virgilio, J. A. Ellman, lecture at the conference *Exploiting Molecular Diversity, Small Molecule Libraries for Drug Discovery*, La Jolla, CA, **1995**.
[127] J.-M. Vanest, M. Gorsane, V. Libert, J. Pecher, R. H. Martin, *Chimia* **1975**, *29*, 345.
[128] a) C. C. Leznoff, P. I. Svirskaya, *Angew. Chem.* **1978**, *90*, 1001; *Angew. Chem. Int. Ed. Engl.* **1978**, *17*, 647; b) R. K. Pandey, T. P. Forsyth, K. R. Gerzevske, J. J. Lin, K. M. Smith, *Tetrahedron Lett.* **1992** *33*, 5315.
[129] C. C. Leznoff, P. I. Svirskaya, B. Khouw, R. L. Cerny, P. Seymour, A. B. P. Lever, *J. Org. Chem.* **1991**, *56*, 82.
[130] R. F. Heck, *Org. React.* **1982**, *27*, 345.
[131] K.-L. Yu, M. S. Deshpande, D. M. Vyas, *Tetrahedron Lett.* **1994**, *48*, 8919.
[132] M. S. Desphande, *Tetrahedron Lett.* **1994**, *31*, 5613.
[133] A. Suzuki, *Pure Appl. Chem.* **1985**, *57*, 1749.
[134] B. J. Backes, J. A. Ellman, *J. Am. Chem. Soc.* **1994**, *116*, 11171.
[135] S. M. Hutchins, K. T. Chapman, *Tetrahedron Lett.* **1994**, *34*, 4055.
[136] M. J. Kurth, L. A. Ahlberg Randall, C. Chen, C. Melander, R. B. Miller, *J. Org. Chem.* **1994**, *59*, 5862.
[137] I. Ojima, C.-Y. Tsai, Z. Zhang, *Tetrahedron Lett.* **1994**, *35*, 5785.
[138] B. D. Vineyard, W. S. Knwoles, M. J. Sabacky, G. L. Bachmann, D. J. Weinkauff, *J. Am. Chem. Soc.* **1977**, *99*, 5946.
[139] I. Ojima, N. Yoda, *Tetrahedron Lett.* **1980**, *21*, 1051.
[140] a) J. C. Chabala, J. J. Baldwin, J. J. Burbaum, D. Chelsky, L. W. Dillard, I. Henderson, G. Li, M. H. J. Ohlmeyer, T. L. Randle, J. C. Reader, L. Rokosz, N. H. Sigal, *Perspect. Drug Discovery Des.* **1994**, *2*, 305; b) J. C. Chabala, lecture at the conference *Exploiting Molecular Diversity, Small Molecule Libraries for Drug Discovery*, La Jolla, CA, **1995**; c) J. J. Baldwin, J. J. Burbaum, I. Henderson, M. H. J. Ohlmeyer, *J. Am. Chem. Soc.* **1995**, *117*, 5588.
[141] M. R. Pavia, lecture at the conference *Exploiting Molecular Diversity, Small Molecule Libraries for Drug Discovery*, La Jolla, CA, **1995**.
[142] S. V. Ley, D. M. Wynett, W.-J. Koot, poster presented at the *Combinatorial Synthesis Symposium*, Exeter, **1995**.
[143] Reviews: a) R. A. Wiley, D. H. Rich, *Med. Res. Rev.* **1993**, 327; b) G. R. Marshall, *Tetrahedron* **1993**, *49*, 3547; c) W. C. Ripka, D. V. de Lucca, A. C. Bach, R. S. Pottdorf, J. Blaney, *Tetrahedron* **1993**, *49*, 3593; d) M. Chorev, M. Goodman, *Acc. Chem. Res.* **1993**, *26*, 266.
[144] R. J. Simon, R. S. Kania, R. N. Zuckermann, V. D. Huebner, D. A. Jewell, S. Banvill, S. Ng, C. Wang, S. Rosenberg, C. K. Marlowe, D. C. Epellmeyer, R. Tan, A. D. Fankel, D. V. Santi, F. E. Cohen, P. A. Bartlett, *Proc. Natl. Acad. Sci. USA* **1992**, *89*, 9367.
[145] R. N. Zuckermann, J. M. Kerr, S. B. H. Kent, W. H. Moos, *J. Am. Chem. Soc.* **1992**, *114*, 10646.
[146] R. N. Zuckermann, E. J. Martin, D. C. Spellmeyer, G. B. Stauber, K. R. Shoemaker, J. M. Kerr, G. M. Figliozzi, D. A. Goff, M. A. Siani, R. J. Simon, S. C. Banville, E. G. Brown, L. Wang, L. S. Richter, W. H. Moos, *J. Med. Chem.* **1994**, *37*, 2678.
[147] Y. Pei, W. H. Moos, *Tetrahedron Lett.* **1994**, *32*, 5825.
[148] K.-H. Wiesmüller, B. Teufel, R. Brock, J. S. Früchtel, R. Warrass, G. Jung, P. Walden in *Peptides, Chemistry, Structure and Biology* (Eds.: P. T. P. Kaumaya, R. S. Hodges), Mayflower Scientific, Kingswinford (UK), in press.
[149] D. Stoll, J. S. Früchtel, K.-H. Wiesmüller, G. Jung, *Abstr. Pap. 2. Deutsches Peptidkolloquium*, Tübingen, **1995**.
[150] C. Y. Cho, E. J. Moran, S. R. Cherry, J. C. Stephans, S. P. A. Fodor, C. L. Adams, A. Sundaram, J. W. Jacobs, P. G. Schultz, *Science* **1993**, *261*, 1303.
[151] S. P. A. Fodor, *Science* **1991**, *251*, 767.
[152] R. Warrass, K.-H. Wiesmüller, G. Jung, unpublished results.
[153] a) P. E. Nielsen, M. Egholm, R. H. Berg, O. Buchardt, *Science* **1991**, *254*, 1497; b) M. Egholm, O. Buchardt, L. Christensen, C. Behrens, S. M. Freier, D. A. Driver, R. H. Berg, S. K. Kim, B. Norden, P. E. Nielsen, *Nature* **1993**, *365*, 566; c) M. Egholm, O. Buchardt, P. E. Nielsen, R. H. Berg, *J. Am. Chem. Soc.* **1992**, *114*, 1895; d) M. Egholm, O. Buchardt, P. E. Nielsen, R. H. Berg, *Peptides 1992, Proc. 22nd Eur. Pept. Symp.* (Eds.: C. H. Schneider, A. N. Eberle), ESCOM, Leiden, **1993**, p. 152; e) S. C. Brown, S. A. Thomson, J. M. Veal, D. G. Davis, *Science* **1994**, *265*, 777.
[154] A. K. Saha, M. Sarsaro, C. Waychunas, D. Delecki, R. Kutny, P. Cavanaugh, A. Yawman, D. A. Upson, L. I. Kruse, *J. Org. Chem.* **1993**, *58*, 7827.
[155] P. Y. S. Lam, P. K. Jadahav, C. J. Eyermann, C. N. Hodge, Y. Ru, L. T. Bacheler, J. L. Meek, M. J. Otto, M. M. Rayner, Y. N. Wong, C.-H. Chang, P. C. Weber, D. A. Jackson, T. R. Sharpe, S. Erickson-Viitanen, *Science* **1994**, *263*, 380.
[156] K. Burgess, D. S. Linthicum, H. Shin, *Angew. Chem.* **1995**, *107*, 975; *Angew. Chem. Int. Ed. Engl.* **1995**, *34*, 907.
[157] a) H. Decker, S. Haag, G. Udvarnoki, J. Rohr, *Angew. Chem.* **1995**, *107*, 1214; *Angew. Chem. Int. Ed. Engl.* **1995**, *34*, 1107; b) R. A. Houghten, *Methods (San Diego)* **1994**, *6*, 354.
[158] H. Drechsel, M. Tschierske, A. Thieken, G. Jung, H. Zähner, G. Winkelmann, *J. Ind. Microbiol.* **1995**, *14*, 105.
[159] a) C. R. Hutchinson, H. Decker, K. Maddari, S. L. Otten, L. Tang, *Antonie van Leeuwenhoek*, **1994**, *64*, 165; b) H. Fu, S. Ebert-Khosla, D. A. H. Hopwood, C. Khosla, *J. Am. Chem. Soc.* **1994**, *116*, 4166.
[160] a) G. Jung, *Angew. Chem.* **1991**, *103*, 1067; *Angew. Chem. Int. Ed. Engl.* **1991**, *30*, 1051; b) G. Jung, H.-G. Sahl, *Nisin and Novel Lantibiotics*, ESCOM, Leiden, **1991**; c) M. Skaugen, J. Nissen-Meyer, G. Jung, S. Stevanovic, S. Kletten, C. I. Mortvedt Abildgaard, I. Nes, *J. Biol. Chem.* **1994**, *269*, 27183. d) T. Kupke, C. Kempter, G. Jung, F. Götz, *J. Biol. Chem.* **1995**, *270*, 11282; e) N. Zimmermann, J. W. Metzger, G. Jung, *Eur. J. Biochem.* **1995**, *228*, 786.
[161] F. Balkenhohl et al., *Angew. Chem.* **1996**, *108*, in press; *Angew. Chem. Int. Ed. Engl.* **1996**, *35*, in press.

Copper—A "Modern" Bioelement

Wolfgang Kaim* and Jochen Rall

Copper is a bioessential element in biology with truly unique chemical characteristics in its two relevant oxidation states +I and +II. Significant progress has been made in recent years in the elucidation of the frequently surprising biochemistry of this trace element. Those advances were especially furthered through mutual stimulation involving results from biochemistry, molecular biology, and medicine on one hand and the synthesis as well as the structural and spectroscopic characterization of low molecular weight model complexes on the other. The most notable features of protein-bound active copper are its almost exclusive function in the metabolism of O_2 or N/O compounds (NO_2^-, N_2O) and its frequent association with oxidizing organic and inorganic radicals such as tyrosyl, semiquinones, superoxide, or nitrosyl. This unique biological role of copper can be rationalized given its chemical and assumed evolutionary background.

Keywords: bioinorganic chemistry · copper proteins · enzymes · oxygen metabolism · radicals

1. Introduction

Although the bioessential character of copper has been established since about 1925,[1] its biological relevance and prevalence was fully recognized only during the last two decades when the bioinorganic chemistry of this trace element developed rapidly.[2, 3] This remarkable progress was made possible, inter alia, through a growing body of information from trace element analysis,[4] protein crystallography,[5] spectroscopy,[6] and molecular biology.[7, 8] In addition, the popularity of "bioinorganic chemistry" as a new, rapidly burgeoning subfield of inorganic chemistry has stimulated a highly successful interaction between the chemistry of model complexes and metalloprotein biochemistry.[3]

A particularly outstanding example for the usefulness of this interaction is the reinterpretation (end-on → side-on[9]) for the mode of coordination for O_2 in the oxygen-transporting copper protein hemocyanin (Hc) from the hemolymph, the "blood" of certain molluscs and arthropods.[10] This reevaluation came about only *after* a corresponding model complex had been found and structurally identified (Fig. 1).[12] Conversely, the preliminary evidence[13] for an intermediate containing NO coordinated to Cu^I centers in nitrite reductase enzymes of denitrifying bacteria[14, 15] prompted the synthesis of the first such low molecular weight complex to be structurally and electronically characterized (Fig. 2).[16]

This article provides a selective review of the bioinorganic chemistry of copper, emphasizing chemically *and* biologically relevant results from very recent research. The admittedly subjective selection includes generally interesting topics as well as representative special examples of the productive interaction between biological, medical-pharmaceutical, and chemical research. Among the chemical aspects underscored are the unique properties of the copper(I) ion and the peculiar association of the evolutionary rather "modern" bioelement copper (see Section 3) with dioxygen and its metabolites as well as with organic radicals.

2. Structural Preferences and Reactivity of the Copper Oxidation States: A Survey

According to its position as the lightest homologue of group 11 in the periodic table, copper is a very special element: The elements of the neighboring group 12 form only divalent monoions with d^{10} configuration (the oxidation state III has not been unequivocally established for mercury[18a, b]), and the elements of neighboring group 10 also prefer the divalent state, here with d^8 configuration. The coordination chemistry of the heavier homologues of copper, namely silver and gold, is characterized by a preference for even-numbered d electron configurations, very low coordination numbers, "soft" ligand donor centers, and by often unphysiologically high redox potentials. The bioavailability of these two elements is extremely small because of their low abundance in the earth's crust and in sea water.

Copper is distinguished by redox potentials for the transitions Cu^{II}/Cu^I and Cu^I/Cu^0 that can lie close together. A com-

[*] Prof. Dr. W. Kaim, Dipl.-Chem. J. Rall
Institut für Anorganische Chemie der Universität
Pfaffenwaldring 55, D-70550 Stuttgart (Germany)
Fax: Int. code +(711)685-4241
e-mail: kaim@anorg55.chemie.uni-stuttgart.de

 © VCH Verlagsgesellschaft mbH, D-69451 Weinheim, 1996 0570-0833/96/35-0043 $ 10.00+.25/0

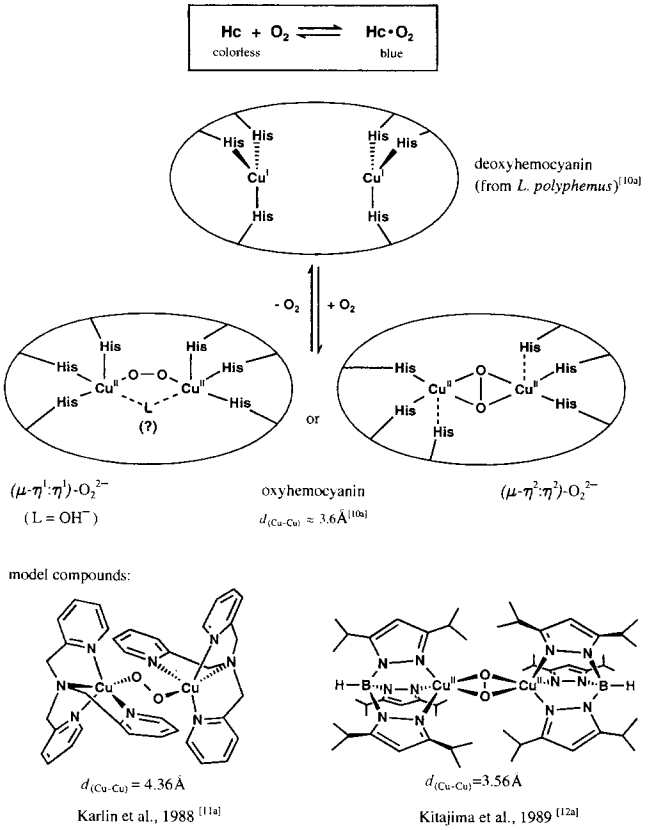

Fig. 1. Hemocyanin (Hc), a class of complex dioxygen transport proteins of arthropods (for example, crustaceans, spiders) or molluscs (for example, squid), contains two cooperatively interacting copper centers per subunit. These change between the colorless deoxy state [Cu^{I}–Cu^{I}] and the blue oxy form [Cu^{II}-O_2^{2-}-Cu^{II}] with antiferromagnetically coupled d^9 metal centers [9,10]. For some time, a μ-η^1:η^1 end-on bridging arrangement was assumed for reversibly coordinated O_2^{2-} ions in the deoxy form, an arrangement supported by model complexes [11]. Only in 1989 was a first synthetic dinuclear complex characterized by Kitajima et al. with sterically demanding tris(3,5-dialkylpyrazolyl)borate ligands and doubly (μ-η^2:η^2) side-on coordinated peroxide [12]. Spectroscopic studies [9] as well as crystal structure analyses [10] have meanwhile established the rather unusual μ-η^2:η^2 alternative coordination mode for oxyhemocyanin.

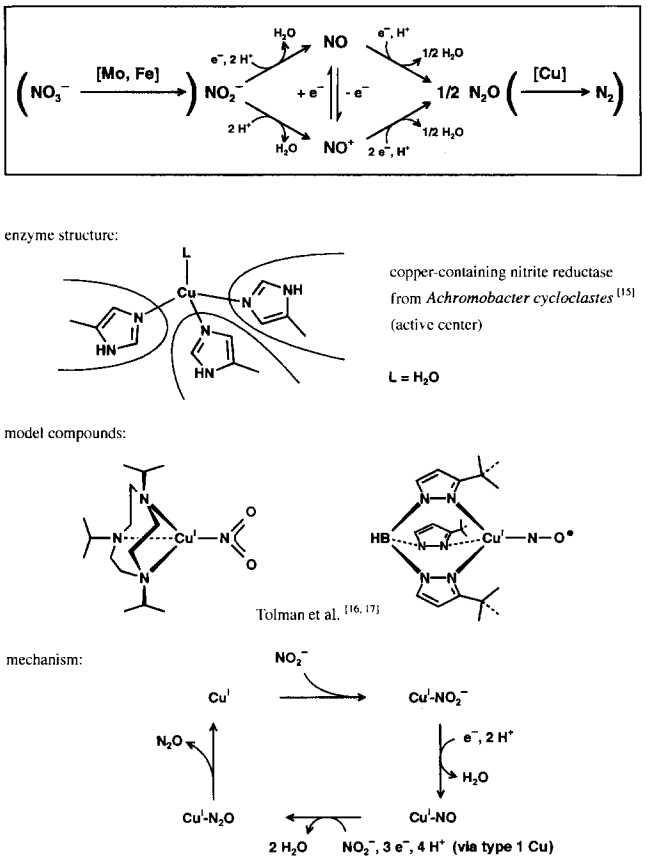

Fig. 2. Mechanistic studies on the transformation of the nitrite ion into dinitrogenoxide through nitrite reductase enzymes of denitrifying organisms in 1989 suggested the existence of a Cu^{I}–nitrosyl intermediate [13a]. This hypothesis [13] prompted the synthesis and structural characterization of several nitrite [17] as well as the first stable mononuclear and dinuclear nitrosylcopper(I) compounds, thus closing a gap in the otherwise well-established chemistry of metal nitrosyl complexes [16]. The catalytically active centers of copper-dependent nitrite reductase were identified as nearly tetrahedral ions even in the Cu^{II} form; they are each coordinated by three histidine ligands from three different protein subunits [15].

W. Kaim J. Rall

Wolfgang Kaim was born in 1951 and studied chemistry at the Universities in Frankfurt am Main and Konstanz. After he had obtained his doctorate under the supervision of Hans Bock in the field of main group organoelement radical chemistry in 1978, he spent the following year working with F. A. Cotton at Texas A & M University on metal–metal multiple bonds. In 1982 he submitted his Habilitation Thesis on the "Coordination Chemistry of Reduced N-Heterocycles" and was awarded a Winnacker Scholarship. In 1987 he moved to the University of Stuttgart as Full Professor of Inorganic Chemistry. Together with B. Schwederski he is the author of a textbook on "Bioinorganic Chemistry" (Literature Award 1993 of the Fonds der Chemischen Industrie). The leitmotiv of his work, as documented in more than 250 publications, is the activation of one or more electrons in novel "complex" compounds: organic and organometallic radical species, mono- and oligonuclear transition metal complexes, and charge-transfer excited states.

Jochen Rall was born in 1966 and studied chemistry at the University of Stuttgart and at the University of Cincinnati. In 1990 he completed his M. Sc. with E. Deutsch, and in 1993 obtained his Diplom in Stuttgart. His graduate studies since 1993 in the research group of W. Kaim have centered around biorelevant paramagnetic copper complexes.

parison of the Cu^{II}/Cu^{I} redox potentials of copper proteins with those of other biologically relevant couples, in particular the Fe^{III}/Fe^{II} redox pairs in functionally analogous,[3a, 19] iron proteins, reveals mostly higher potentials for the copper systems.

Cu^0 refers to metallic copper, which is now produced worldwide to a significant extent by a "geo-biotechnological process", that is, by microbial leaching[20] (Fig. 3). In contrast, neutral

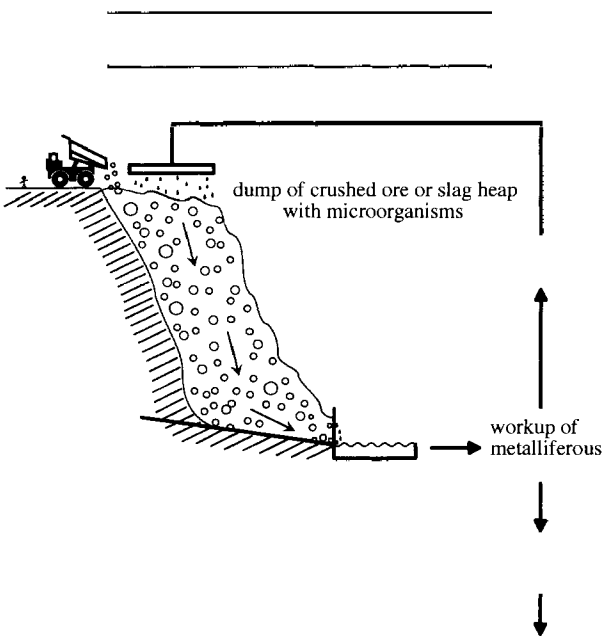

Fig. 3. The microbial leaching Cu^0 recovery process. More than one fourth of the annual world copper production is now estimated to come from microbial leaching (bacterial leaching, biomining), one of the most substantial biotechnological processes in terms of production volume and value ($>10^9$ US$) [20]. The acid-tolerant microorganism *Thiobacillus ferrooxidans* slowly dissolves insoluble sulfidic ores by oxidizing sulfide to sulfate and simultaneously assimilating CO_2. An environmentally friendlier and less expensive metal production is thus possible, not only of copper but also of included metals such as gold [20a].

complexes such as $[Cu(phen)_2]$, which are often referred to as Cu^0 compounds,[21] have recently been identified as Cu^I complexes with one radical anion ligand[22] by using the 1,10-phenanthroline derivative **1** with R = phenyl. The nitrosyl copper complexes mentioned above (Fig. 2) have similarly been characterized as Cu^I–NO· systems by EPR spectroscopy; that is, contributions from formulations like Cu^0–NO^+ or Cu^{II}–NO^- play a subordinate role in the description of these compounds.[16b]

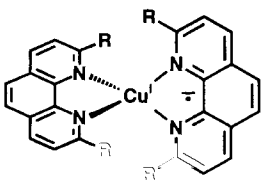

1

As a result of high redox potentials and a propensity for one-electron transfer reactions, organocopper compounds are quite reactive[23] and not biologically relevant—in contrast to organometallic compounds of nickel (methyl-F430 complex[24a])

this unique coordination chemistry of copper are the almost "noble" character of the metal, the intermediate stability and reactivity of the d^{10} configuration in Cu^I,[25] and the comparatively small radius of the Cu^{2+} ion, which contributes to the high energy of hydration and thus to the stability of $Cu^{2+}(aq)$ over $Cu^+(aq)$. The character of the metal–ligand interaction in Cu^{II} complexes is frequently but not always ionic (see Section 7) and favors the stabilization of this state through pronounced Jahn–Teller distortion. Different extents of axial elongation of the octahedron can thus produce square-bipyramidal, square-pyramidal, or square-planar coordination geometries. Deviations from these energy minimum structures, which are necessary for rapid oxidation state changes Cu^{II}/Cu^{I} (and thus for efficient electron transfer), may require specific, strained conformations ("entatic state concept"[26a, b]) through elaborate ligand architecture, either in proteins (type 1 copper centers in "blue" copper proteins, see Section 7[26]) or in low molecular weight model compounds containing specially designed ligands.[27]

Contrary to an earlier[28] suggestion that was propagated in textbooks[18c] (see Section 9.3.2), the Cu^{III} state is *not* a biologically relevant oxidation state; the redox potentials for the transition Cu^{III}/Cu^{II} are generally very high. Instead, there may be one-electron oxidation of cofactors or protein components that can cooperate with the copper(II) centers.[29, 30] Authentic, stable Cu^{III} compounds exist only with very strong donor ligands such as O^{2-}, F^-, or R_2N^-,[31] the d^8 configuration favoring square-planar or square-pyramidal arrangements. In this context the layered structures of high-temperature superconductors, which invariably contain Cu^{III}/Cu^{II} mixed-valent centers,[32] have to be mentioned.

The prototypical Jahn–Teller ion Cu^{2+} is characterized not only by marked axial distortion in its complexes (the most typical result is a square-pyramidal coordination), but also by a strong preference for ligands with nitrogen donor centers. This pertains to complex stabilities (equilibrium aspect) and to the often inert N–Cu^{II} bonds that render a special fixation in biological systems, for example through tetrapyrrole macrocycles, unnecessary. Copper(II) centers form weaker, more labile bonds with normal oxygen donor ligands (that do not undergo back-bonding) or with neutral sulfur and phosphorus donor centers.

Chemically and spectroscopically interesting[6, 33] as well as biologically relevant[26] is the combination of copper(II) ions with potentially reducing thiolate ligands, such as the cysteinate anion. In that case, the usual electron transfer (ET) reaction to Cu^I and diorganodisulfide-forming thiyl radicals can be avoided through appropriate coordination arrangements (Scheme 1).[33a] However, exceptionally intense ligand-to-metal charge transfer (LMCT) absorptions are then observed in the visible spectral region ("blue" copper proteins, see Section 7), which indicate that charge transfer does occur, albeit in the LMCT excited state.[6]

The coordination number and geometry of copper(I) is rather flexible, not least because it has a d^{10} configuration and therefore exhibits no ligand field effects. The usually cited values for the preferred coordination number range from two to four with an optimum between three and four.[34] The metalla-supramolecular chemistry[35, 36] continues to make extensive

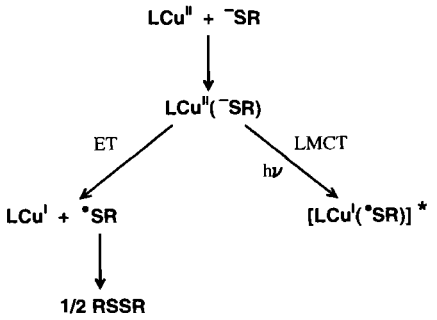

Scheme 1. Two possible reactions for thiolatocopper(II) complexes.

use of the tendency of copper(I) to bind organic ligands[37–42] quite strongly yet in a structurally flexible way, taking advantage of the low charge (that is, little polarization) and the high bond stability, in particular towards ligands with nitrogen donor centers (Fig. 4). The latter feature distinguishes Cu^{+} from other monovalent metal ions such as the alkali metal ions or Tl^{+}; Ag^{I} and Au^{I} display an intricate redox behavior and

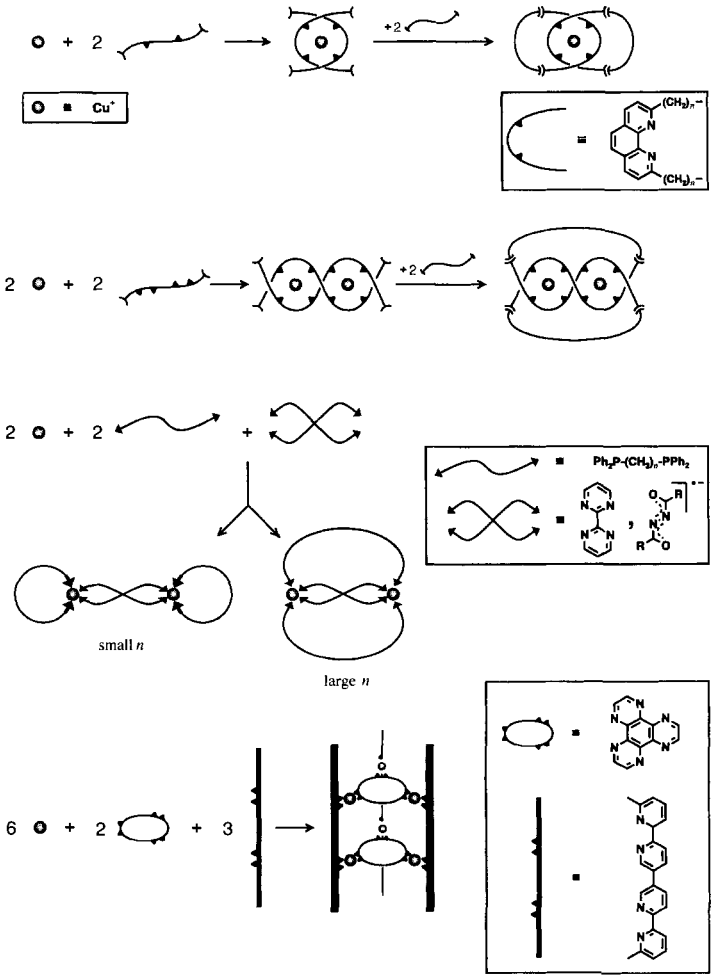

Fig. 4. The suitability of Cu^{+} ions as template for self-assembly processes in supramolecular chemistry is now documented by numerous examples of topologically interesting arrangements in coordination compounds. From top to bottom: catenates [37], molecular knots [38], inverse cryptates [39], molecular tubes [40]. Further examples not included in this figure are (double) helices [41], molecular grids [42a], rotaxanes [42a], or hinged triple-decker sandwiches [34c,d,39b].

show less d_{π} back-donation than Cu^{I} to unsaturated ligands.[25,43]

In agreement with its position next to Ag^{I} (with preferred coordination number 2) and Zn^{II} (with preferred coordination number 4), Cu^{I} favors a coordination number 3 with trigonal-planar geometry.[34] However, this particular arrangement is often associated with coordinative unsaturation,[34b] which, indeed, is frequently complemented in Cu^{I} compounds through formation of weak axial interactions (Scheme 2, top). Some low molecular weight complexes and the type 1 copper centers in the reduced *and* oxidized state of blue copper proteins illustrate this particular situation[6,26,44] (see Section 7).

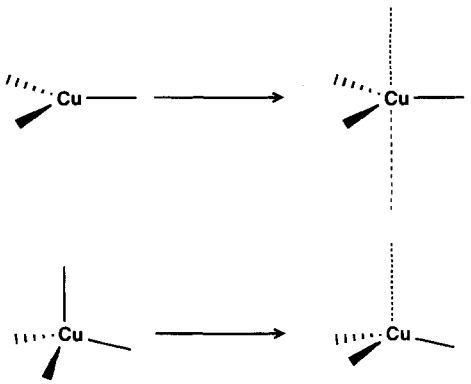

Scheme 2. Extension of the coordination number of three- and fourfold coordinated Cu^{I} centers.

On the other hand, small perturbations of tetracoordinate Cu^{I} may suffice to weaken the bond to one of the four donor atoms, resulting in a change of coordination geometry from approximately tetrahedral to trigonal pyramidal (Scheme 2, see also Scheme 5).[34c,d,39] The ambivalence between coordination number 3 and 4 of Cu^{I} compounds is most evident from the observation that apparently equivalent copper centers of the same molecule may show threefold as well as fourfold coordination (**2**).[45]

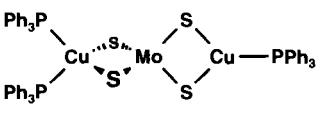

2

The oxidation state I can be stabilized in copper compounds by using "soft" coordinating atoms as in R_3P,[46a–c] R_2S,[46d] or RS^{-} ligands;[47] unsaturated nitrogen donor ligands are also well tolerated.

An outstanding feature of the copper(I) state is its ability to bind and reductively activate molecular oxygen ($^{3}O_2$) despite the closed 3d shell of Cu^{I}. Only three kinds of O_2-activating sites are known in biology; in addition to Cu^{I} centers these include high-spin iron(II) center with four unpaired 3d electrons and the formally antiaromatic 1,5-dihydroflavin system.[48] The affinity of copper(I) for the triplet molecule $^{3}O_2$[49] presumably relies on contributions from unoccupied 4s or 4p orbitals[6c] and thus possible 3d/4s or 3d/4p orbital mixing. Additional activation may result from metal–ligand or metal–metal interactions.[50]

The comparatively open and variable coordination sphere of both the Cu^{I} and Cu^{II} states and their readily accessible redox

transition in the positive potential region render copper a widely used metal in non-organometallic redox catalysis, including organic synthesis and industrial processes;[12c, 51] the majority of the biological functions of this trace element also involves oxidase or oxygenase activity (Fig. 5).

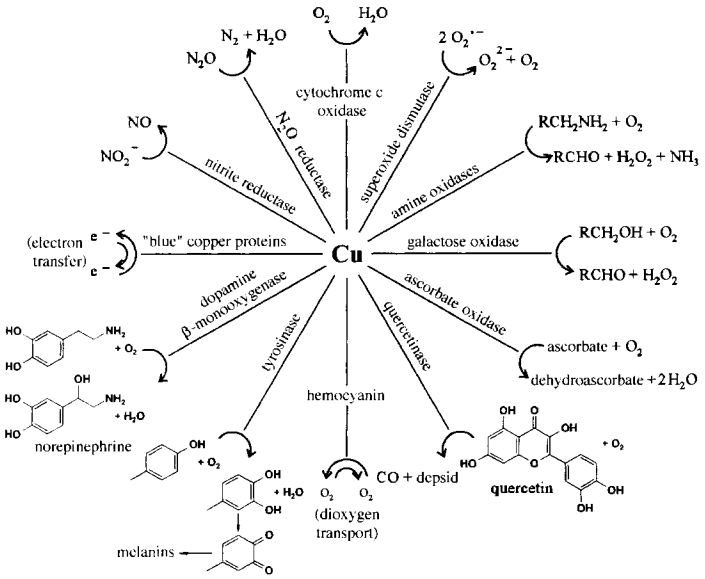

Fig. 5. The essential metabolic functions of copper-containing proteins (mostly enzymes) are summarized in the "biocopper dial". The close association of this bioelement with dioxygen and its secondary products is obvious. Not included are transport, regulatory, and storage proteins for copper.

3. Copper—a "Modern" Bioelement?

In many regards, copper can be designated as a modern bioelement. First of all, the essential trace element character of copper has been known for quite some time, yet the detailed structural background for many of its biological functions has long eluded determination. On a molecular level, such information has become available only in the last decade, allowing for the correction or specification of numerous (textbook) hypotheses. These include the binding of dioxygen in the O_2-transporting system hemocyanin[10] (Fig. 1), the role of copper-containing enzymes in the nitrogen cycle (denitrification)[13-15, 52] (Fig. 2), the precise copper content of the essential respiratory enzyme cytochrome c oxidase[4] (see Fig. 7), the nature of the quinonoid cofactor of copper-containing amine oxidases[53] (see Fig. 9), the oxidation states of the metal in galactose oxidase[29, 30] (see Fig. 10), and the trinuclear arrangement of the catalytic center in "blue oxidases"[5] (see Fig. 8).

However, as R. J. P. Williams has pointed out,[3c, 54] copper can also be regarded as a newcomer among the bioelements[19] under the aspect of the evolution of the biosphere and—as a consequence—of the atmosphere. Due to the high potential necessary for oxidation to the (+ II) state, copper was bioavailable only to a very small extent[55a, b] prior to the biogenic (photosynthetic) generation of an oxidizing environment; in the typical mineral form of halides or chalcogenides, Cu^I compounds are insoluble at pH 7. Only the massive production of oxidation equivalents (and, finally, O_2) by photosynthetic organisms about 3×10^9 years ago[55c] enabled significant oxidation of Cu^I to soluble Cu^{II}, with two important consequences:

- Through oxidation from Fe^{II} to Fe^{III}, the functionally competing iron became *less* bioavailable (iron as limiting trace element in today's seawater[56]), and required bioenergetically costly strategies like complexation and/or intermediate reduction to Fe^{II}.
- Secondly, the presence of an oxidizing atmosphere created the need for a catalytically redox-active metal with potentials between 0.0 and 0.8 V; the $Cu^{II/I}$ redox pair is thus almost ideally suited for catalysis of the typically inhibited reactions of O_2, as evident from many organic-synthetic and industrial reactions.[12c, 51]

It comes as no surprise, therefore, that copper enzymes participate particularly in reactions involving dioxygen (transport, utilization by oxidases and oxygenases) as well as in the degradation of unwanted side products of the O_2 metabolism such as $O_2^{\bullet-}$ radicals (Fig. 5). Similarly, copper enzymes are active within the nitrogen cycle by catalyzing transformations of certain N/O compounds such as NO_2^-, NO', or N_2O, which unavoidably occur in an O_2-containing atmosphere; iron-containing systems also participate in these reactions.[13b, 14, 52] The coexistence of copper compounds and O_2 is also related to the frequent association of copper with biogenic or synthetic radicals, as has been established in many cases;[16b, 29, 30, 39a, 46, 57-59] unusual cooperativities in enzymatic reactions (Figs. 9 and 10)[29, 30, 57] may result from this kind of association.

For an efficient catalysis of more complex redox processes, the accumulation and storage of several single electrons and their controlled release as "multielectron package" at a catalytic center[60] often require the coupling of two or more redox centers. Examples from the field of biological copper chemistry are the heterodimeric center Cu_B–heme a_3 of the terminal respiratory enzyme cytochrome c oxidase, which reduces O_2 to H_2O (see Section 9.3.3),[61, 62] or the trimeric cluster arrangement in "blue oxidases" like ascorbate oxidase or laccase (see Section 9.3.1).[4, 63] ("Blue oxidases" contain a "blue" type 1 copper center with electron transfer function in addition to the catalytic metal cluster.) "Non-blue oxidases" use a different strategy, namely the functional coupling of a single metal center (Cu^I or Cu^{II}) with an organic redox system such as a quinone (amine oxidases, see Figure 9),[57, 64] a modified tyrosyl radical (galactose oxidase, see Fig. 10),[29, 30] or possibly pterins (phenylalanine hydroxylase from *Chromobacterium violaceum*).[65] Such strategies of coupling *one* redox metal center with a redox active ligand are known from the heme system ($Fe^{II}/Fe^{III}/Fe^{IV}$ + porphinato ligand) and are postulated for the cofactor complex in pterin-containing molybdenum or tungsten enzymes.[3a, b, 66]

The rather "modern" status of biological copper (in evolutionary terms) relative to iron, cobalt, or nickel[3c, 54] may be related to the well-known toxicity of the metal for "lower" organisms such as algae or some bacteria[67] and with its predominant location in the extracellular space[54b] (exception: Cu,Zn superoxide dismutase). Another such indication may be seen in the late and only gradual stabilization of the copper metabolism in newborn infants, which can give rise to corresponding dysfunctions.[67a]

4. Medical and Toxicological Aspects

Although copper is definitely an essential element for many life processes in higher organisms (after iron, copper is the second most abundant "genuine" transition metal in the human organism[3a, b]), it is also a toxic (heavy) metal with low legal concentration limits, for example, for drinking water or sewage sludge.[3a, b, 67] The tolerance of an adult human being for, for instance, copper sulfate is surprisingly high,[67a] yet the "therapeutical width" between the concentrations causing deficiency symptoms and those responsible for poisoning is rather small and also quite variable, especially during growth periods or for lower organisms. Infants are particularly vulnerable, and the accumulation of copper in trace concentrations from cooking utensils or acidic (pH < 6) drinking water led through copper-containing pipes can cause "Indian" or "German Childhood Cirrhosis".[67a]

Best known among the environmentally caused disorders of copper metabolism is the molybdenum/copper antagonism in highly food-specific ruminants.[68] It appears to result from a complexation of Cu^{I} by $MoO_nS_{4-n}^{2-}$ as formed under reducing conditions in the stomach of ruminants; "molybdenosis" thus implicates a secondary copper deficiency. Not only are thiomolybdates readily soluble in water, they are also excellent chelating agents for metal centers in low oxidation states such as copper(I)[69] (**2**). The small therapeutic width of copper also leads to copper deficiency symptoms if other competing (Fe, Zn) or antagonistic (S, Se) elements are present.

In view of the increasingly realistic expectations for a therapy aimed at the biological cause of genetic disorders, two hereditary diseases concerning the copper metabolism, Wilson's disease and Menke's syndrome, have attracted special attention.[67] Both diseases occur with a probability of about 1 case per 100 000 births. Wilson's disease involves a pathological accumulation of copper in the liver and brain, and is lethal if left untreated.[67a, c, d] Consequently, the therapy of this disorder consists of the administration of copper-specific chelating agents, in particular D-penicillamine (**3**) or—in case of the not uncommon intolerance to **3**—of triethylenetetramine (**4**) or derivatives.[67a, c] Zinc compounds can stimulate an increased formation of the heavy metal storage protein, metallothionein (see Section 6), and thus also counteract the copper enrichment effects of Wilson's disease.

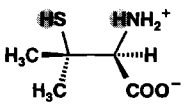

D-penicillamine

(HS : replaceable by Cu^{2+})

3

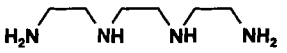

triethylenetetramine

4

D-Penicillamine is also indicated in the treatment of scleroderma, which involves the overproduction of collagen and an embrittlement of the skin. This disorder demonstrates the importance of copper for the controlled synthesis of connective tissue (see Section 9.3.2), as in Menke's syndrome.

In contrast to Wilson's disease, Menke's syndrome is caused by a hereditary dysfunction of the intracellular copper transport and thus insufficient copper storage.[7] If the disorder is not treated very early by continuously supplementing the essential element, for example as "copper histidine" (assumed structure (**5**)), a rapid and eventually lethal degradation occurs in the central nervous system.[70] A characteristic symptom of this disease is the occurrence of "kinky" hair, illustrating again the necessity for copper-containing proteins in the biosynthesis of structural proteins (see Section 9.3.2). Recently, the gene responsible for the disease was identified and isolated; it is situated on the X chromosome.[7] The produced membrane protein is a typical transport ATPase with several copper binding motifs (Cys-X-X-Cys) as they are similarly known from heavy metal regulation and storage proteins of the metallothionein type[71, 72] (Fig. 6).

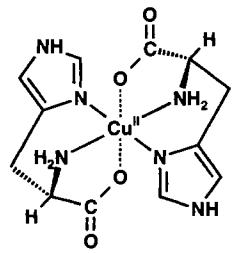

5

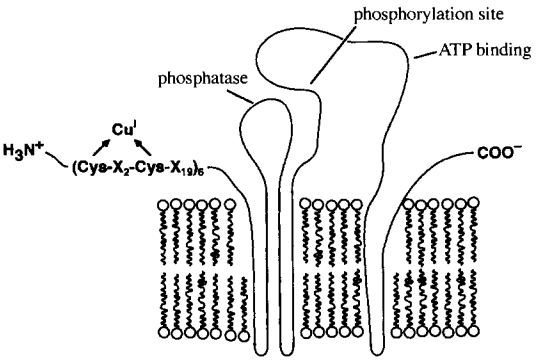

Fig. 6. Based on studies with cloned genetic material, the inadequate intracellular copper transport by an ATPase membrane protein with a cysteine-rich section [7] was found to be responsible for Menke's "kinky hair" syndrome of infants, a lethal disease if untreated. The cysteine-rich sequences are reminiscent of metal-binding sites in regulatory proteins such as CUP2 [78] and in metallothionein (MT) storage proteins as found in yeast cells. Unlike the better known mammalian metallothioneins, the yeast MT proteins are characterized by a special affinity for copper [71]. The genetic defect responsible for Menke's syndrome was localized on the X chromosome [7]. If the disease is recognized early, the subcutaneous administration of Cu^{II}/histidine preparations may contribute to a satisfactory development [70].

Genetic defects causing changes in the amino acid sequence of the antioxidant enzyme Cu,Zn superoxide dismutase (SOD) (see Section 9.4 and Fig. 11) are responsible for the familial form of amyotrophic lateral sclerosis (ALS).[8] ALS is a progressive, irreversibly neurodegenerative disease of the motoric system, which became widely known as the cause of paralysis of prominent persons such as the physicist Stephen Hawking.[8c] In the United States ALS is also known as "Lou Gehrig's disease", named after one of the most famous baseball players, the "iron horse" (first baseman of the New York Yankees), who died of this disease in 1941 at the age of 38.

In 1993 two research teams[8a, b] were able to show that the likely causes for familial ALS are defects in copper-containing SOD, which affect the protein structure and thus diminish the required optimal functioning of this detoxification enzyme (see Section 9.4).

Established symptoms of chronic copper deficiency include arterial weakness and enlargement of the heart; according to

recent research results these symptoms are caused by a decreased synthesis of catecholamine neurotransmitters.[73, 74] The biosynthesis of L-epinephrine (adrenaline), for example, requires a pterin-dependent phenylalanine hydroxylase (with Fe or Cu as metal component)[65] as well as the copper-dependent enzymes dopamine β-monooxygenase[65d, 75] and tyrosinase[76] (Scheme 3). Reduced production of neurotransmitters leads to a diminished formation of "heat shock" proteins (HSPs), which serve in the management of cellular stress.[74]

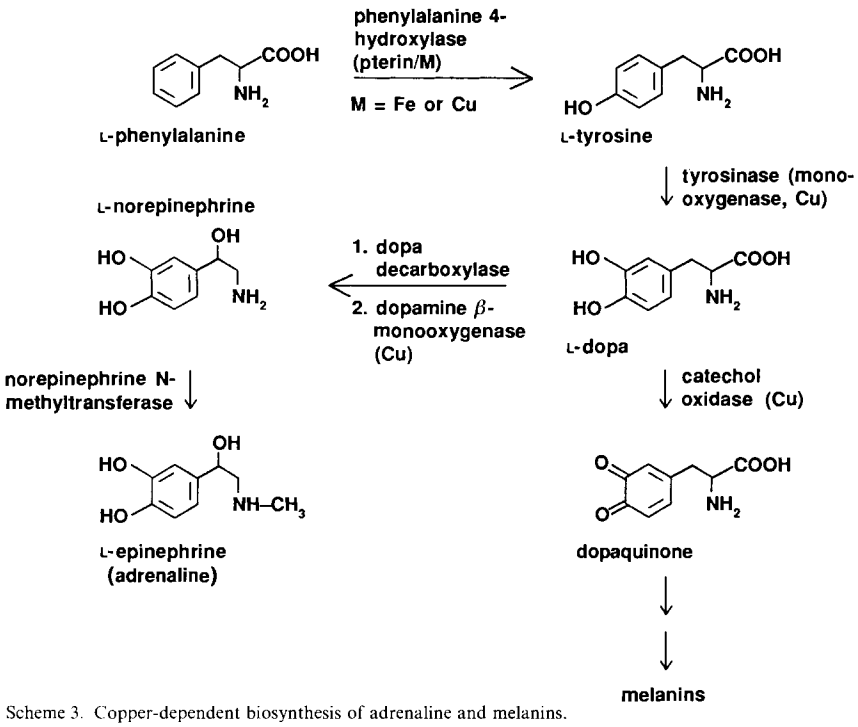

Scheme 3. Copper-dependent biosynthesis of adrenaline and melanins.

5. Old and New Types: The Classification of Biological Copper Centers

The standard division of biologically active copper centers from proteins into "type 1, type 2, and type 3 copper"[3, 6a, b] was initially necessary to correlate function with analytical features (optical absorption, EPR, magnetism). By now, these correlations are largely understood and refined because of increasingly available structural details. On the other hand, several additional biological copper centers have been found that do not fit the conventional scheme. Table 1 summarizes the characteristics of these new centers as well as those of the classical types.

The biological repertoire of copper centers is possibly not exhausted with the representative structures listed in Table 1; future structure determinations may well lead to corrections or to the discovery of further alternatives. Remarkable from the aspect of coordination chemistry is the occurrence of all forms of aggregation, starting from mononuclear species (type 1, and, in part, type 2) through homodinuclear (type 3 or Cu_A), heterodinuclear (Cu_B/Fe in cytochrome c oxidase, Cu/Zn in Cu,Zn superoxide dismutase) and trinuclear centers (for example in ascorbate oxidase), to apparently cysteinate-bridged clusters (6–8 Cu centers[71, 80]) in copper-containing metallothioneins of yeast.

Table 1. Important properties of copper centers in various biomolecules.

	Type 1	Type 2	Type 3	Type (2+3) trimer	Cu_A	MT-Cu
aggregation state	mononuclear (even in oligocopper proteins)	mononuclear	dinuclear	trinuclear	dinuclear	mononuclear to multinuclear (clusters)
specificity, biological function	electron transfer	catalysis and redox reactivity	O_2 activation for transport and oxygenation	O_2 activation for oxidase function	electron transfer	regulation, storage, and transport form
occurrence (examples)	"blue" copper proteins, e.g. plastocyanin, azurin; laccase	amine oxidases, galactose oxidase superoxide dismutase, cytochrome c oxidase (Cu_B)	hemocyanin, tyrosinase	ascorbate oxidase, laccase	N_2O reductase, cytochrome c oxidase	CUP2, metallothionein (MT), Cu transport ATPase (Fig. 6)
structural characteristics						
typical coordination number	3 (trigonal-planar), +1	4 or 5 (square-planar or -pyramidal)	Cu^I: 3 (trigonal-planar)	Cu^I: 3 (trigonal) Cu^{II}: 4	4	3 (trigonal-planar)
coordinated atoms	S^-(Cys$^-$), 2 N (His), +S(Met)	3 N(His), □	2 × 3 N(His); Cu^{II}:μ-η^2:η^2-O_2^{2-}	N(His), partly (O)OH^-	2 S^-(Cys$^-$), 2 N (His), S(Met) or O (peptide)	3 S^-(Cys$^-$)
spectroscopic characteristics of the oxidized or oxygenated form						
EPR	small $^{63}Cu/^{65}Cu$ hyperfine splitting ($A_\parallel$), low g factor ($g_\parallel$)	"normal" Cu^{II} EPR parameters	no signal (strong antiparallel spin–spin coupling)	"normal" Cu^{II} EPR parameters	very small Cu hyperfine splitting due to two equivalent Cu, low g factor	no oxidized form
light absorption	intense absorption in the visible, LMCT (Cys$^-$ → Cu^{2+})	no intense absorption, only "forbidden" ligand field transitions	intense absorptions; LMCT (O_2^{2-} → Cu^{2+})	intense absorptions; LMCT (O_2^{2-} → Cu^{2+})	absorption in the near infrared region (MMCT)	

□: free coordination site, special ligands (organic radicals), or adjacent metal centers (Zn, Fe).

6. Regulation, Transport, and Storage of Copper in Biological Molecules

After resorption in the gastro-intestinal system (requirement about 2 mg per day)[67a] copper is bound by serum albumin, which contains M^{2+}-binding histidine residues.[77] Cysteine-rich metallothionein proteins,[71] which are responsible for homeostasis, transfer copper to ceruloplasmin, a large plasma protein[5a] that has six copper-binding sites and that can also function as ferroxidase by catalyzing the Fe^{III}/Fe^{II} transition.

The control of the copper metabolism requires a highly complex regulatory system, probably similar to that of the more thoroughly studied bioelement iron. A regulatory protein CUP2 (also termed ACE1)[78] is known, which contains several well-conserved cysteine residues. After uptake of several Cu^+ ions, specific DNA-binding of this regulatory protein causes the expression of copper-storing metallothionein. For the particularly good copper-binding metallothionein from the yeast *Saccharomyces cerevisiae*, clusters of six or eight copper(I) centers bridged by cysteinate residues are assumed.[71] Data from X-ray absorption studies (crystallographic data are not yet available) are in accord with a trigonal configuration at the copper(I) centers.[71] Just like numerous mononuclear and oligonuclear copper(I) complexes,[34c, d, 79] the Cu^I-metallothioneins of yeast can exhibit intense luminescence.[71, 80]

7. Type 1 Centers in Blue Copper Proteins: The Cu^I/Cu^{II} Structure Problem and the Quest for Electron Transfer Pathways

The unsymmetrical, but not accidental coordination arrangement (Scheme 4) at type 1 copper centers in blue copper proteins such as plastocyanin or azurin is well conserved according to protein crystallographic data[5a, 44, 81] and has played an important role for the understanding of the structural basis of protein and enzyme reactivity.[26]

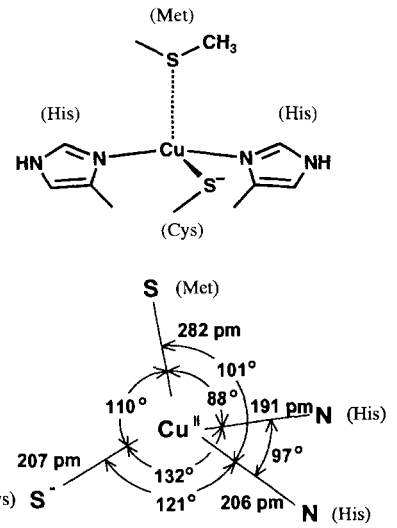

Scheme 4. Coordination of type 1 copper centers in blue copper proteins. Top: general arrangement. Bottom: structural details for plastocyanin [81a].

Especially for the Cu^{II} state, the large structural deviation from the energetically favored square-planar or square-pyramidal geometries has prompted the suggestion that the strain is "external", but enforced by the surrounding polypeptide. This strain implicates a higher potential energy at the start of the reaction, which in turn facilitates the approach to the transition state—in this case, of the Cu^{II}/Cu^I electron transfer reaction (see Scheme 6). The concepts of a "rack" mechanism (the protein as structure-enforcing framework[26c]) or of the "entatic state"[26a, b] of active proteins, in particular of enzymes, have been derived and refined to a substantial extent from attempts to understand the geometry of type 1 copper centers in blue copper proteins.

Detailed structural,[44, 81] kinetic,[82] and spectroscopic[6] studies of *both* copper oxidation states in blue copper proteins have shown that the two sulfur ligands, the π-electron-rich thiolate base of the cysteine anion and the thioether residue of methionine (a weak π-acceptor), contribute to the rapid, vectorial electron transfer at a relatively high potential. The typical coordination of type 1 copper centers is almost optimal for Cu^I, that is, an approximately trigonal-planar coordination by one cysteinate and two histidine residues with an additional long axial bond to methionine (Scheme 4), or glutamine in the case of stellacyanin.[81g] Similarly, weakly perturbed complexes of Cu^I with two N and two P donor ligands (Scheme 5) have a tendency towards trigonal-pyramidal coordination with one long bond to one of the (larger) donor atoms from the third period of the Periodic Table.[34c, d, 39b]

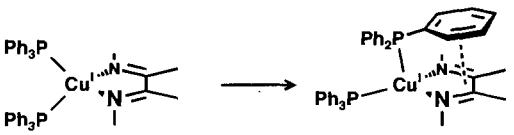

Scheme 5.

Not only does the protein enforce a structural distortion of higher energy; the π-acceptor ligand methionine also destabilizes the copper(II) state with the result that the Cu^{II}/Cu^I redox potentials of type 1 copper centers are rather more positive than those of complexes without such acceptor ligands. Because of this special, unsymmetrical geometry, the higher energy 3d orbitals are no longer degenerate; no reorganization energy (and time) is thus necessary to bring about Jahn–Teller distortion when Cu^I is oxidized to Cu^{II} (Scheme 6).[6c]

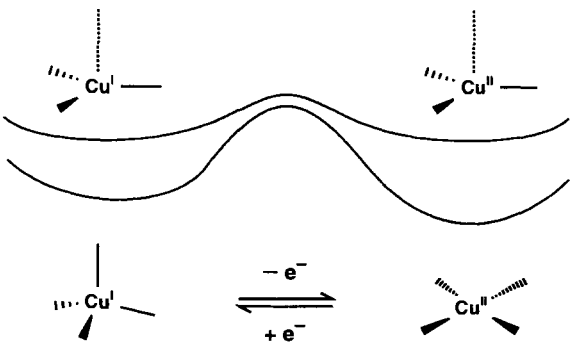

Scheme 6.

A strong π-interaction (Scheme 7) exists in the copper(II) state between the electron-deficient metal ion and the cysteinate anion. The short Cu–S bond has significantly covalent character, as shown by EPR spectroscopy (metal-to-ligand spin delocalization);[6, 83] the typical intense color of these blue copper proteins primarily results from ligand-to-metal charge transfer (LMCT) transitions (Scheme 1).[6]

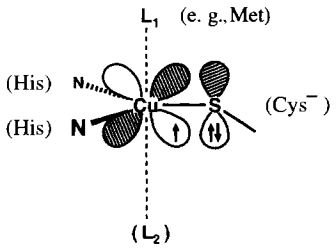

Scheme 7.

The covalency of the copper(II)–cysteinate bond was also confirmed by ENDOR measurements (ENDOR: *e*lectron *n*uclear *d*ouble *r*esonance[84]), which reveal that the unpaired electron density is distributed over the cysteinate sulfur atom and the neighboring β-methylene group to a considerable extent.[83] More sophisticated details of the coordination, such as the less pyramidalized copper (Scheme 4) in azurin, can now be correlated[81c, 82a] with different redox potentials and EPR properties (rhombic or axial *g* anisotropy, respectively). Specifically tailored ligands such as the tris(alkylpyrazolyl)borates (Figs. 1,2), which have become prominent in attempts to model biological copper sites, can be used to mimic the spectroscopic properties of type 1 copper centers while suppressing undesired side reactions such as disulfide formation (Scheme 1).[33]

Since the properties of isolated blue copper proteins are now well understood, the interest has shifted to their interaction with physiological reaction partners. Plastocyanin,[81a, b] for example, transfers electrons from cytochrome f in the photosynthetic membrane to photooxidized chlorophyll P700 of the photosystem I in green plants, whereas amicyanin[81d] is responsible for the specific transfer of electrons from the oxidoreductase enzyme methylamine dehydrogenase (MADH), a quinoprotein,[85] to cytochrome c. Although the actual dynamic situation may be quite complex, crystal structures of ternary protein complexes such as MADH/amicyanin/cytochrome c_{551i}[86] illustrate the crucial role of copper-containing electron transfer proteins (Scheme 8).

According to their function (see Scheme 8), simple blue copper proteins such as plastocyanin contain two preferred electron transfer routes,[82] a short pathway to the electron donor through a rather hydrophobic region and a longer pathway to the acceptor, ending at a polar group. With programs[87] for the calculation of matrix elements of the electronic coupling through π systems, lone pairs, or the σ framework, preferred electron pathways may be assessed and verified through site-directed mutagenesis experiments.[88]

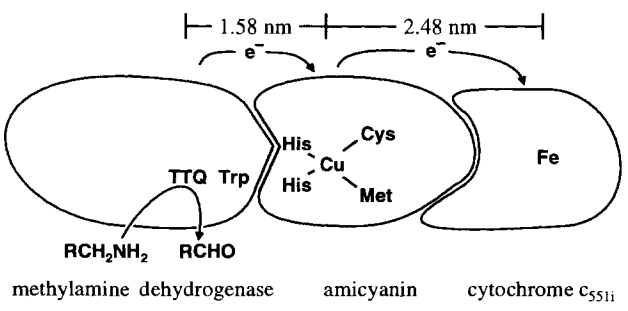

Scheme 8. Amicyanin mediates the electron transfer from methylamine dehydrogenase to cyctochrome c_{551i} (TTQ = tryptophan tryptophylquinone) [85,86].

8. The Dinuclear Cu_A Centers in Cytochrome c Oxidase and N_2O Reductase: Biological Copper in the Oxidation State +1.5

Cytochrome c oxidase ("COX"), the *Atmungsferment* (respiratory enzyme) of Otto Warburg, serves as the terminal "complex IV" of the respiratory chain, yet its metal content has remained poorly defined[4, 61b, 89a] for a long time, despite its obvious importance as final acceptor and converting site for O_2 in mitochondria (Fig. 7).[62, 63] The two heme iron centers in heme *a* and heme a_3 were identified quite early (see Section 9.3.3), and two copper "centers", Cu_A and Cu_B, were differentiated by EPR spectroscopy.[90, 91] However, the Cu_A "center" active in electron transfer could not be classified under the conventional type 1–type 3 copper scheme (Table 1), and even after initial spectroscopic characterization and identification of two invariant cysteine and histidine residues as presumably primary ligands, the dinuclear nature of this center had long been overlooked.[91]

The difficulties in determining the proper metal content partly originated from the complexity of this enzyme, which, in the mammalian form, consists of 13 very different subunits (M_r 204 kDa)[4, 61, 133] and which is embedded in the mitochondrial membrane, thus complicating the collection and purification of the complete protein complex. The Cu_A center is located in subunit II (26 kDa), whereas the heme groups and Cu_B are components of subunit I (60 kDa). Careful trace elemental analyses prompted Buse and coworkers in 1987[4] to postulate a copper-content for COX of *three* copper atoms per enzyme and not—as had long been assumed and widely disseminated[91b–d]—only two. In the meantime, biological copper centers of the Cu_A type had also been detected[14c, 52] in N_2O reductase (Fig. 7) of *Pseudomonas stutzeri*, an enzyme participating in the denitrification process. While the unusual EPR characteristics of the oxidized Cu_A centers had previously been attributed to the coordination of two cysteinate ligands at *one* Cu^{II} center (Cu_A as "super type 1 copper"),[91] Kroneck and coworkers were able to show in 1990 that actually *one* unpaired electron interacts with *two* spectroscopically equivalent metal centers.[92] Natural copper consists of the isotopes ^{63}Cu (69.2% natural abundance, nuclear spin $I = 3/2$, nuclear *g* factor $g_N = 1.484$) and ^{65}Cu (30.8%, $I = 3/2$, $g_N = 1.588$), which leads to a characteristically split[59b] septet in the $A_{\parallel}$ region. These results were confirmed by EPR measurements at different microwave frequencies,[93] and several other groups have since verified the existence of a dinuclear Cu_A center.[94, 133]

There had been two hypotheses about the detailed structure of Cu_A (Fig. 7)[95a, b, d] before the structures of two COX forms were reported in August 1995 (see Chapter 9.3.3).[133] The suggestion by Blackburn et al. was based on reinterpreted[95b, c] EXAFS measurements[95d] and implied for the first time a metal–metal bond in a biomolecule.[95b] The still rather embryonic modeling[89] of both structural proposals does not strictly

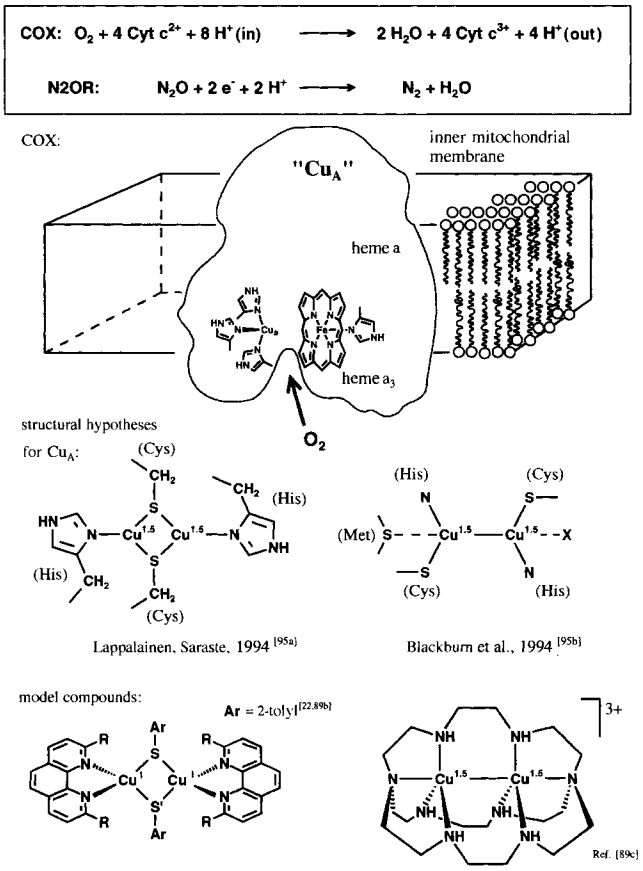

Fig. 7. The terminal respiratory enzyme cytochrome c oxidase [4,62] (COX) and the denitrification enzyme N_2O reductase (N2OR, which contains several copper centers) [52] both exhibit unusual noncatalytic "Cu_A" centers. These centers have an electron transfer function, and the oxidized state is characterized spectroscopically by a long-wavelength absorption at about 800 nm and by an unusual EPR spectrum, distinguished by diminished g anisotropy and small copper hyperfine splitting [91a]. Two histidine residues and two cysteinate anions were established as ligands for Cu_A [91]; however, only very detailed EPR studies at different microwave frequencies [93] revealed the interaction of *one* unpaired electron with *two* spectroscopically equivalent nuclei $^{63}Cu/^{65}Cu$ according to the natural isotopic abundance [59b]. This result, corresponding to a spin-delocalized mixed-valent formulation ($Cu^{1.5+}/Cu^{1.5+}$), confirmed the revised [4a] analytical value of *three* instead of two Cu centers for cytochrome c oxidase (Cu_A dimer and Cu_B/heme a_3 catalytic center). N_2O reductase, a protein dimer, contains eight copper ions, four in two dinuclear Cu_A centers [52]. A distance of about 2.5 Å for the mixed-valent Cu_A dimer was determined by EXAFS spectroscopy in a water-soluble domain of COX of *Bacillus subtilis*, assigned to a Cu–Cu distance, and interpreted as a first metal–metal bond in a biomolecule [95b]. Other structural hypotheses [95a,d] rather invoked two metal-bridging Cys^- ligands. Preliminary low-molecular weight model complexes are available for both structural concepts [89]; crystal structures reported in August 1995 for two COX forms confirmed the thiolate-bridged alternative (see Section 9.3.3) [133].

support this implication, particularly as it is not prudent to deduce the existence of a "bond" in the customary sense from short metal–metal and especially copper–copper distances of 2.3–2.6 Å.[50a, 89a, 96]

The existence of an obviously spin-delocalized mixed-valent (+ II/ + I) dinuclear unit in Cu_A centers[92, 93] suggests strong electronic coupling, either directly across the short distance of about 2.6 Å or through effectively bridging ligands such as cysteinate (thiolate) anions,[89] which are known to mediate "superexchange". As early as 1962, Beinert et al. discussed the possibility of different copper valencies in COX.[90] In comparison with other mixed-valent dimers or higher aggregates in biology,[97] the delocalization according to a $(Cu^{1.5+})_2$ formulation is quite remarkable: Mn^{IV}/Mn^{III} centers in water oxidase and other enzymes[98] as well as Fe^{III}/Fe^{II} systems bridged by oxygen ligands[99] and corresponding reduced [2Fe–2S] centers are spin-localized. Delocalization is only observed in higher iron–sulfur clusters.[100]

9. Copper Proteins and Dioxygen Species O_2^{n-}

9.1. O_2 Transport by Hemocyanin and Variable Coordination in the Cu_k^{II}/O^{n-} System

At the start of this article we drew attention to the reinterpretation[9] of the O_2 binding mode in the oxygen transport protein hemocyanin (Hc),[10] inspired by studies of low molecular weight models[12] (Fig. 1). Hc proteins occur in molluscs and arthropods and maintain an efficient supply of oxygen even in larger animals such as lobster or giant squid. Due to the advantage of allosteric behavior for cooperative O_2 binding, the hemocyanins are oligomeric proteins, like the hemoglobins.[10]

The Hc proteins allow efficient *and* reversible dissociation of the doubly *side-on* coordinated dioxygen molecule in spite of its fourfold contact with the copper centers and the two-electron transfer upon binding. Reim and Krebs[101] have recently published the structure of a tetranuclear complex with μ_4-$(\eta^1)_4$-peroxide surrounded by *four* Cu^{II} centers in which the dioxygen form is irreversibly bound. Iron-containing oxygen transport proteins, on the other hand, display invariably singly end-on coordinated O_2^{n-} ions in their oxy forms.[3, 99] In addition to oligonuclear copper(II) compounds with (μ-η^1:η^1)-,[11] (μ-η^2:η^2)- (Fig. 1),[10, 12] and (μ_4-$(\eta^1)_4$)-peroxide[101], the Cu_k^{II}/O_2^{n-} system ($k = 1-4$) encompasses compounds with end-on (η^1)[58a] and side-on (η^2) coordinated superoxide[58b] as well as bridging $O_2^{\cdot-}$ radical ions;[58c] end-on (η^1) coordinated are hydroperoxide anions in the oxygenated form of ascorbate oxidase (see Section 9.3.1)[5b] and the cumylperoxo ligand ($PhMe_2COO^-$) in a model complex with tris(3,5-dialkylpyrazolyl)borate as additional ligand.[102]

9.2. Copper-containing Monooxygenases in the Metabolism of Natural Products

Dinuclear type 3 copper centers do not only occur in the O_2-transport protein hemocyanin but also in polyphenol oxidases of the tyrosinase type.[76] These enzymes catalyze the *ortho*-hydroxylation of phenols such as tyrosine (monooxygenase reactivity) as well as the further oxidation of the resulting catechols to *ortho*-quinones (catechol oxidase function). Such copper enzymes participate in the biosynthesis of the very many polyphenolic natural products, in particular of catecholamine neurotransmitters (see Scheme 3),[73] in the metabolism of insect cuticula,[103a] in the enzymatic browning of fruit,[103b] and in other melanin-forming processes (Scheme 3).[104]

Mechanistic hypotheses for the function of tyrosinase imply the metal coordination of the phenolic oxygen and an ensuing attack of oxygen at the *ortho* carbon atom.[6, 105] However, there are also copper-dependent enzymes with copper centers other than type 3 that are capable of monooxygenating *aliphatic* C–H bonds. These include a particulate form of methane

monooxygenase that is assumed to contain a copper trimer,[106] as well as dopamine β-monooxygenase,[73] which is essential during neurotransmitter biosynthesis (Scheme 3) and which contains two different copper centers.[65d, 75] One of these centers has an electron transfer role (ascorbate as the physiological electron donor), whereas the other, the catalytic center, has not yet been conclusively defined.[75] As for the iron-containing methane monooxygenase[107] that was crystallized in the absence of copper, the copper-dependent forms are also assumed to generate radicals of the organic substrate as intermediates;[106] a similar assumption holds for dopamine-β-monooxygenase (abstraction of a benzylic hydrogen atom[75, 108]). In this context it is important to realize that recent model complexes with μ-η^2:η^2-coordinated dioxygen can activate C–H bonds (monooxygenation) in alkyl substituents.[109] Based on EPR measurements and in accord with studies on ascorbate oxidase (see Section 9.3.1), a $Cu^{II}OOH$ species may be envisaged as reactive intermediate prior to O–O bond cleavage.

9.3. Strategies for Multielectron Catalysis in Copper-Containing Oxidases

9.3.1. Cu_3 Clusters in "Blue" Oxidases (Ascorbate Oxidase, Laccase)

"Blue" oxidases like the structurally well-established ascorbate oxidase[5b] provide substrate-specific oxidation equivalents by four-electron reduction of O_2 to 2 H_2O. To meet the stringent requirements for multielectron catalysis,[60] these often dimeric enzymes contain four copper atoms per subunit, one center being a separate type 1 copper ion for electron transfer purposes, which is also responsible for the typical blue color of these enzymes. Early spectroscopic studies led to the description of the remaining three metal ions as one type 2 and one (dimeric) type 3 copper center, before more refined spectroscopic investigations[6d] as well as the crystal structure analysis by Messerschmidt et al.[5b] rendered this differentiation based on an artificial classification scheme obsolete (Fig. 8): The arrangement is trinuclear with partially hydroxo-bridged metal centers and metal–metal distances between 3.4 and 5.1 Å, depending on the coordination and on the oxidation state. Structure determinations of the oxidized form, the reduced state, the hydroperoxide-containing oxygenated form, and of a bis(azido) derivative have provided the crystallographic basis for a detailed reaction mechanism.[5b]

Starting from the completely oxidized, but not oxygenated form, a successive, controlled electron flow takes place from the substrate to the catalytic trimer through the type 1 copper center. The latter is separated from the cluster by more than 13 Å and is coordinatively saturated. After complete reduction, the enzyme reacts with oxygen to form a hydroperoxo adduct with oxidation of both "type 3" metal centers, one of which serves as coordination site for HOO^-. (Stable alkylperoxocopper(II) complexes have been isolated with tris(3,5-dialkylpyrazolyl)-borate ligands.[102]) Close to the transition state of the reaction, an additional intramolecular electron transfer from the remaining two Cu^I centers leads to O–O bond cleavage and to the release of two water molecules.[5b]

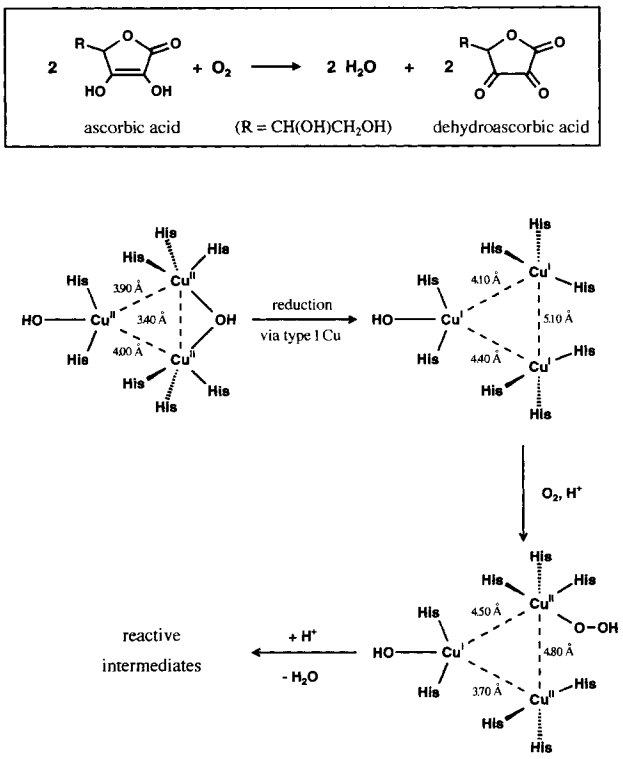

Fig. 8. "Blue" four-electron oxidase enzymes such as ascorbate oxidase contain four copper ions per subunit, one of which is a type 1 copper center for electron transfer. According to protein crystallography, the remaining three copper ions do not strictly behave as one type 2 and one type 3 center (dimer), but rather act as a new trinuclear catalytic site [5b]. Dioxygen is coordinated end-on as hydroperoxide [5b] by one copper center of the trimer, and a controlled electron flow is effected through the type 1 copper ion from the substrate.

9.3.2. Interactions between Copper and "Built-In" Radical Cofactors in "Non-blue" Oxidases

In contrast to the blue oxidases, the non-blue oxidases utilize only the two-electron process $O_2 \rightarrow H_2O_2$ to generate oxidation equivalents for substrate oxidation. These enzymes also contain only one type 2 copper center per subunit, which for the purpose of multielectron catalysis is structurally and functionally linked to the redox system of organic cofactors, which are part of the protein framework. Since the two-electron reaction involves one copper center with a Cu^{II}-to-Cu^I oxidation state change, the cofactors also have to undergo a one-electron transition at relatively high potential—similar to that of the Cu^{II}/Cu^I pair—which should result in the temporary formation of radicals. The necessary requirements for the redox potential, the available coordination sites and catalytic centers, and the stability of radical intermediates are met by the tyrosine-derived "topaquinone/topasemiquinone/topahydroquinone" redox system (see Fig. 9)[53, 57, 64] in the case of copper-dependent amine oxidases, whereas a tyrosyl radical/tyrosine redox pair plays this role in galactose oxidase. There, the tyrosyl radical state is additionally stabilized through a covalent linkage with a cysteinate "substituent" in *ortho* (ε) position (see Fig. 10) and through π–π interaction with a tryptophan side chain.[29]

The foremost role of the metal center is to bind and activate O_2,[29, 30, 57] whereas the organic cofactors participate in substrate conversion. This functional division is particularly evi-

dent in copper-dependent amine oxidases, which, inter alia, serve in the formation and maturation of connective tissue (Scheme 8; see Fig. 9 for Cu-independent forms[85]): The metal participates in a "valence-tautomer" equilibrium Cu^{II}-$Q^{2-} \leftrightarrow Cu^{I}$-$Q^{\bullet -}$ [46, 57] (Q = quinone component), which allows for the controlled binding of O_2 to the copper(I) center. Copper(II) catecholate as well as copper(I) semiquinone and comparable radical complexes can be prepared as stable species (Scheme 9) and are readily identified and differentiated by EPR measurements.[46, 57] The position of the valence-tautomer equilibrium can be influenced by variation of the quinone component Q, by assumed steric and solvent effects,[110] and through the ancillary ligands at the metal:[46] nitrogen donor ligands L favor the Cu^{II}/catecholate form, whereas thioether donor ligands L favor the Cu^{I}/semiquinone state, as do triorganophosphanes, olefins, or carbon monoxide.[46a, d]

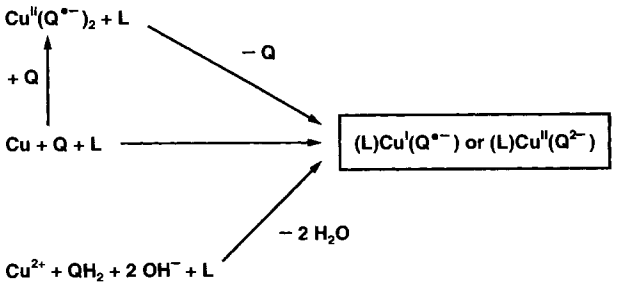

Scheme 9.

Like several other quinoprotein cofactors,[85] the six-membered ring of topaquinone (Q) shows a potentially *ortho*- and *para*-quinonoid structure,[111] protected by substitution in the γ-position. In the oxidized (quinone) state a carbonyl group serves to bind the primary amine substrate, which is eventually converted into the aldehyde product in the course of the reaction; topaquinone is thus reduced to aromatic topahydroquinone (the "catecholate" state) (Fig. 9).[112]

Galactose oxidase is excreted as an extracellular enzyme by some parasitic fungi. It catalyzes the oxidation of primary alcohols to the corresponding aldehydes in a regioselective, but not substrate-specific manner. The biological role of the enzyme is not completely understood; one possible function is the degradation of rotting wood by oxidation of oligosaccharide intermediates, which are preferred substrates of the enzyme. Perhaps, however, the coupled formation of hydrogen peroxide is just as important.[30] H_2O_2 is required for the degradation of lignin by special peroxidases (ligninases) or for chemical defense against bacteria. The most thoroughly studied galactose oxidase was isolated from a strain, previously classified as *Cladobotryum dendroides* (before 1986: *Dactylium dendroides*), but more recently identified as a member of the genus *Fusarium*.[113]

For some time it remained obscure how this enzyme with only one copper center can catalyze a two-electron reaction. The reaction mechanism was explained by a Cu^{III}/Cu^{I} redox pair,[28]

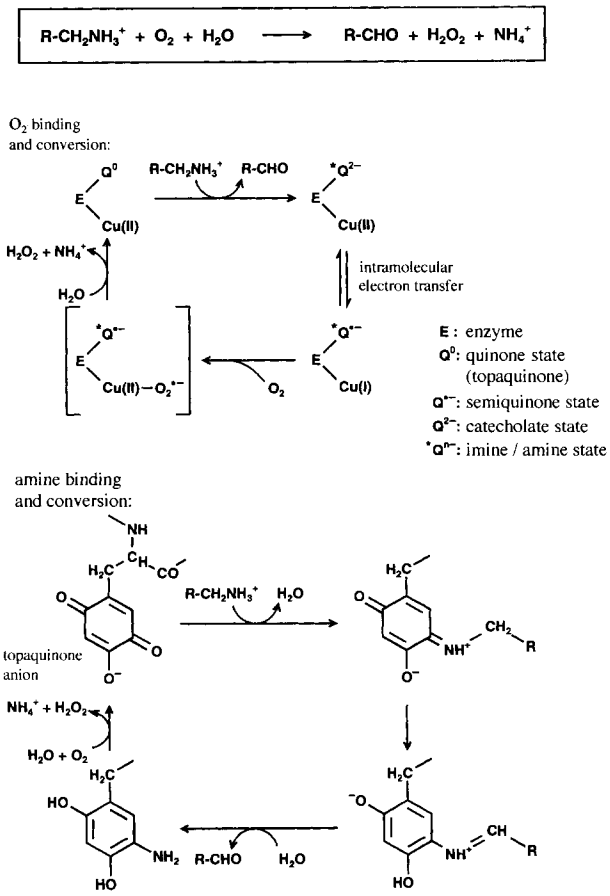

Fig. 9. Copper-containing quinoproteins are involved in amine oxidation, for instance, in the formation of connective tissue (lysyl oxidase) [85]. The coupling of the Cu^{II}/Cu^{I} redox function with that of a modified quinone (Q) firstly guarantees the activation of O_2 by Cu^{I} centers, following an EPR-detectable Cu^{II}-$Q^{2-} \rightarrow Cu^{I}$-$Q^{\bullet -}$ [57] valence tautomerization and secondly allows for the reaction of a free quinone carbonyl function with the primary amine. For some time, pyrroloquinolinequinone (PQQ) had been assumed to be the (dissociable) quinonoid cofactor [85b]; however, Klinman et al. [57] identified covalently anchored topaquinone (TQ) as that redox-active organic entity. TQ is a posttranslationally modified tyrosine which can alternatively form *ortho*- or *para*-quinonoid structures [111].

which seemed to be plausible at first since an external cofactor could not be found. However, detailed spectroscopic and magnetic studies later indicated the presence of a protein-bound, "built-in" organic radical cofactor. The crystal structure of the enzyme finally confirmed this conclusion (Fig. 10):[29] A tyrosine residue positioned in an equatorial coordination site of a square pyramidal arrangement is covalently linked *ortho* (ε) to the sulfur atom of a cysteinate side chain as donor substituent. This arrangement facilitates the oxidation to the tyrosyl radical by lowering the redox potential and allowing for spin delocalization.[114a] Further stabilization of the radical is apparently provided by a tryptophan residue, the indole part of which is situated in a position above the cysteinate-substituted tyrosine—well suited for π–π interactions. In view of this complexity of the metal-containing active center, there are currently few relevant studies with model complexes.[114b] Because they are specific for primary amines or alcohols, two quite important and widespread classes of organic substances, both the amine oxidases and galactose oxidase have become interesting enzymes for biosensor applications.[114c, d]

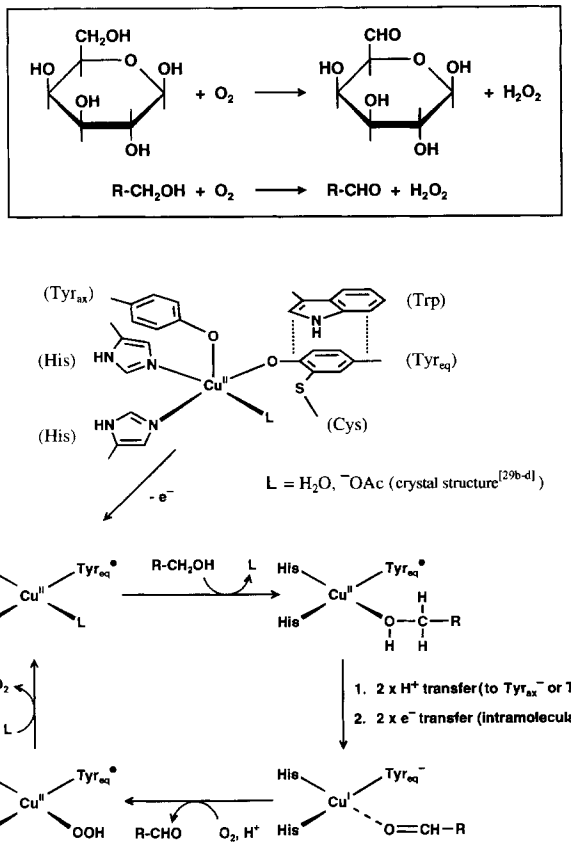

Fig. 10. The catalysis of the depicted two-electron process by galactose oxidase from parasitic fungi was originally attributed to a Cu^{III}/Cu^{I} transition [18c,28], since there is only *one* copper center available. However, the crystal structure of the enzyme showed that a type 2 Cu^{II}/Cu^{I} system is structurally as well as electronically coupled to an equatorially coordinated tyrosinate/tyrosyl radical redox pair. This very special tyrosyl group is further characterized by an unusual covalent linkage to a cysteine sulfur center in *ortho* (ε) position and by $\pi-\pi$ interactions with the indole ring system of a tryptophan residue: a highly sophisticated "built-in" cofactor.[29]

9.3.3. The Catalytic Cu/Fe Center of Cytochrome c Oxidase (COX)

While the dinuclear Cu_A center in subunit II (see Section 8) and the low-spin heme *a* in subunit I of COX have both electron transfer functions,[62d] the actual four-electron reduction of O_2[62] occurs at a heterodinuclear center Cu_B/heme a_3. The metals are separated by about 4–5 Å,[95d, 133] which suggests that the triplet dioxygen molecule possibly binds to the Cu^{I} as well as to the high-spin Fe^{II} center of heme a_3. Apparently, both biologically occurring O_2-activating metal ions (see Section 2) cooperate here to catalyze this mechanistically demanding[60] multielectron reduction. Hydroperoxocopper(II)[5b] and oxoferryl(IV) species[115] were postulated as intermediate species (Scheme 10).[62]

Whereas the Cu_B ion can be regarded as a type 2 copper center based on its ligation and spectroscopy (Fig.7), the special heme a_3 is characterized by a partially unsaturated farnesyl substituent[62a, 116] at the porphyrin ring. The tendency of copper(I) and iron in low oxidation states to form olefinic (Cu) or π-allylic (Fe) complexes led to suggestions aimed at an intermediate coordination of this porphyrin substituent with the heterodinuclear metal center.[116] The reduction of O_2 in this "complex IV" of the respiratory chain is closely linked to the translocation of

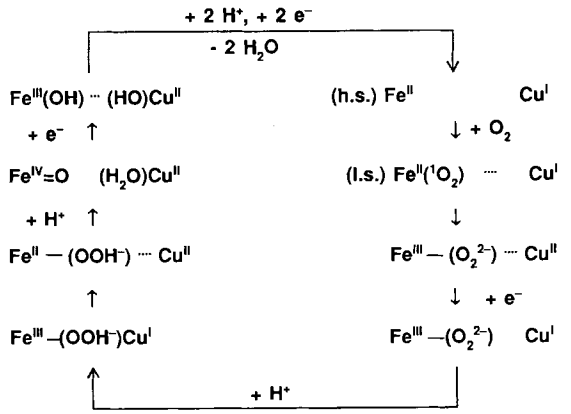

Scheme 10. Catalytic cycle for O_2 reduction by cytochrome c oxidase. h.s. = high spin; l.s. = low spin.

protons through the mitochondrial membrane[62, 133] to eventually form ATP as the energy storage product of this oxidative phosphorylation.

An increasing number of attempts to model the heterodinuclear Cu_B/heme a_3 center of COX structurally as well as functionally has been published since 1994.[117] In addition to the molecular design of the correct Cu–Fe distance and the proper oxidation and spin states, attention has been directed at the reactivity of O_2 activation[117f] and inhibition by bridging cyanide, μ-CN^-.[117c, e] Since cyanide is a diatomic anion that can bridge low-valent transition metal ions at a distance of 4.5–5.5 Å, it is an efficient inhibitor of O_2 coordination at the Cu_B/heme a_3 site and thus of cell respiration (toxicity of cyanide).[118]

Two research teams have recently reported the successful structural characterization of cytochrome c oxidase forms at 2.8 Å resolution. One of the enzymes is the mammalian form derived from bovine heart mitochondria (complete enyzme, "the largest membrane protein yet crystallized and analyzed at atomic resolution"),[133a] and the other is the form of soil bacterium *Parococcus denitrificans* (four subunits, complexed with an antibody fragment).[133b] These studies have revealed the following details concerning the copper centers: The Cu_A site outside the membrane region on the cytosolic side is dinuclear with the two copper ions bridged by two cysteinate residues (cf. the hypothesis on the left of Fig. 7). The copper–copper distance in the planar CuSCu'S' arrangement is 2.7 Å[133a] or 2.6 Å.[133b] Each metal center is coordinated to one histidine residue, while one is additionally connected to a methionine sulfur center and the other to a carbonyl oxygen atom of a peptide link to complete the tetracoordination (distorted tetrahedron). The Cu_B and Fe_{a3} ions are 4.5[133a] or 5.2 Å[133b] apart in the (oxidized) resting state. Cu_B is coordinated to three imidazole rings (ImH) from histidine side chains, one of which seems to be mobile (reported for bacterial COX[133b]) and to participate in the redox-coupled proton translocation. The research team from Frankfurt[133b] proposed a sequence $Cu^{2+}/Im^- \rightarrow Cu^+/ImH \rightarrow O_2/Cu^+ + HImH^+$ for the first stages that connect proton shuttling with dioxygen binding and conversion (cf. the reaction cycle of superoxide dismutase in Fig. 11). In the bovine heart COX the farnesyl side chain engages in hydrogen-bonding interactions that seem to contribute to the structural stabilization of Cu_B.[133a]

9.4. Cu,Zn Superoxide Dismutase (Cu,Zn-SOD)

Cu,Zn superoxide dismutase (SOD)[119, 120] is a widespread enzyme with a function that may go beyond that defined in its name. In addition to its well-established ability for detoxifying $O_2^{\bullet-}/HO_2^{\bullet}$ radicals through catalyzed disproportionation, the enzyme could also have a metal storage and transport function because of its abundance in eukaryotic tissue. The disproportionation ("dismutation") of the metastable superoxide (properly: hyperoxide ion) to give dioxygen and enzymatically further metabolized peroxide can be catalyzed by many redox-active transition metal ions[120] if they can function according to Equations (a) and (b).

$$M^{n+} + O_2^{\bullet-} \longrightarrow M^{(n-1)+} + O_2 \quad (a)$$

$$M^{(n-1)+} + O_2^{\bullet-} + 2H^+ \longrightarrow M^{n+} + H_2O_2 \quad (b)$$

It is therefore not surprising that there are superoxide dismutase enzymes with M = Cu, Fe, or Mn, the latter occurring especially in mitochondria[121, 122] and the former in erythrocytes.[119, 120] In view of the lability of the substrate and the substantial driving force of the reaction, the requirements for SOD enzyme functioning do not appear that compelling at first glance; however, the very rapid diffusion of $O_2^{\bullet-}$ radical ions to the active site has to be guaranteed, and the enzyme must exhibit long-term stability towards O_2, $O_2^{\bullet-}$ ions, H_2O_2, and the surrounding proteins.[126] The first condition is met by the "conduction" of the pseudohalide-type $O_2^{\bullet-}$ anion or its conjugated acid, $HO_2^{\bullet}$, along a funnel-shaped channel bordered by cationic and hydrogen-bond-forming amino acid residues to the active site. This site consists of a type 2 copper center coordinated to three imidazole groups from histidines and one imidazolate anion of a deprotonated and Zn^{2+}-bound histidine.[119, 123] A few years ago the exchange of anionic glutamate in the channel by neutral glutamine was accomplished by site-directed mutagenesis. Under certain conditions, this exchange gave rise to a further increase of the rate of diffusion and, thus, of the overall reaction rate: the optimization of an apparently "perfect" enzyme (Fig. 11).[124]

The second requirement for the high stability of this enzyme is certainly fulfilled, as illustrated most vividly by the largely intact activity of Cu,Zn-SOD from 3000-year-old mummified tissue.[125] In addition to the long-term stability of this enzyme, its structural integrity, and a high tolerance of the aggressive substrate and product molecules, the essential copper ion has to be tightly bound in Cu,Zn-SOD so that it cannot be extracted as Cu^{II} by other proteins such as serum albumin.[126] Presumably, the unusual arrangement with an additional dicationic metal (Zn^{2+}) and the biologically unique bridging imidazolate ion of a histidine side chain also enhance the stability; this stability but not the function of the enzyme seems to be impaired when the zinc ion is selectively removed.

The essential role of Cu,Zn-SOD is not only emphasized by its pharmacological use in the treatment of inflammatory diseases, in the prophylaxis of radiation damage, or by its increasingly recognized importance during the process of ageing.[128] As was pointed out in Section 4, even rather minute mutations can have grave consequences.[8] Although superoxide is produced in a controlled manner in phagocytic cells by the "respiratory burst" and then used for defense purposes in the immune system,[129] its uncontrolled occurrence during the transport of O_2 by erythrocytes,[120] in mitochondrial respiration,[122] or during the activity of molybdenum-containing xanthine oxidase is clearly undesirable.[8c]

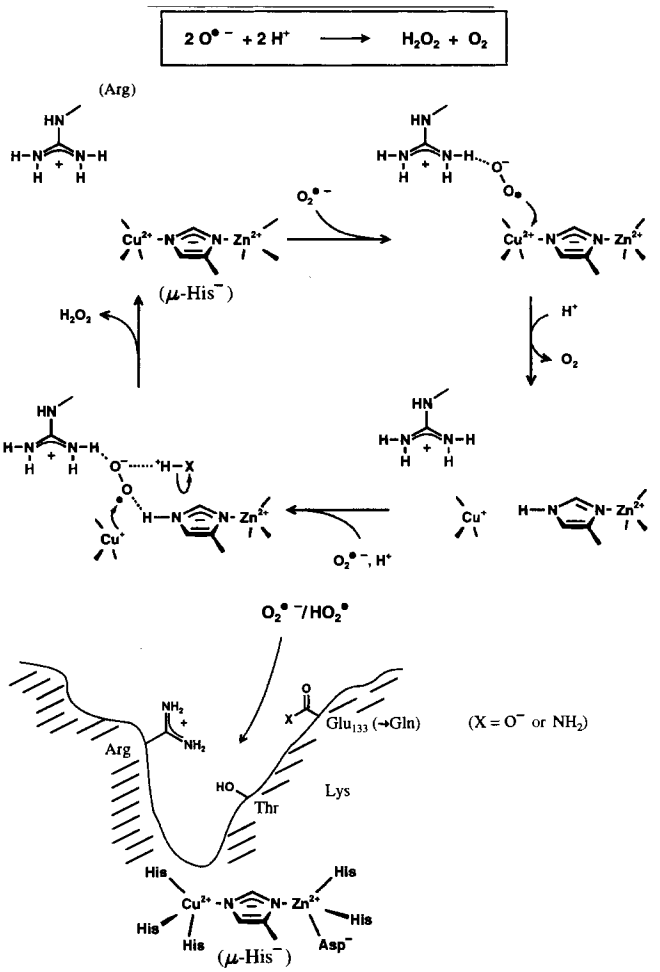

Fig. 11. The superoxide dismutase (SOD) from mammalian erythrocytes is a homodimeric enzyme that contains one zinc and one copper center per subunit. The two metal ions are connected in a biologically unique manner by the functionally essential imidazolate bridging ligand of a histidine side chain [119]. Copper is the redox active metal that reduces metastable superoxide to peroxide when in the Cu^{I} form and oxidizes it to O_2 when in the Cu^{II} state. While the enzyme itself must not be attacked by the aggressive dioxygen species, it has to convert the reactive $O_2^{\bullet-}/HO_2^{\bullet}$ radicals very efficiently, that is, in a diffusion-controlled manner. For proper functioning, rapid electron and proton transfer processes at the actual reaction site are thus crucial as is the supported diffusion of $O_2^{\bullet-}/HO_2^{\bullet}$ ions to the active center; the latter could be accelerated even further by the site-directed mutation $Glu^- \rightarrow Gln$ in the channel leading to the bimetallic site. On the other hand, defect variants of Cu,Zn-SOD are held to be responsible for to the familial form of amyotrophic lateral sclerosis (ALS), an irreversible neurodegenerative disease of the motoric system [8].

Cytotoxic radicals may also contribute to the development of insulin-dependent diabetes mellitus (type I diabetes). There is much evidence[130] that active oxygen species such as superoxide, hydroxyl radical, or peroxynitrite play an important role in the destruction of the insulin-producing β-cells of the pancreas. Experiments on mice with increased production of Cu,Zn superoxide dismutase showed that the the β-cells have a distinctly higher tolerance to induction of diabetes through oxidative stress.[130]

10. Copper in the Nitrogen Cycle

The production of oxidation equivalents and, as a result, of O_2 through photosynthetic organisms has not only led to an increased bioavailability of copper but also to the necessity for a biological metabolism of the nitrogen/oxygen compounds formed.[3a-c] In addition to iron and molybdenum (which became bioavailable[3c, 68b] as the $Mo^{VI}O_4^{2-}$ ion), copper-containing enzymes are also important in biological denitrification.[13b, 14, 15, 52]

Details about N_2O reductase (N2OR, see Fig. 7) from *Pseudomonas stutzeri*, which contains catalytically active "Cu_Z" dinuclear centers[14c, 52] as well as the dinuclear Cu_A centers introduced in Section 8 are known. A multicopper-containing form of microbial nitrite reductase has also been mentioned earlier in this article[14, 52] (Fig. 2); its catalytic metal centers (besides type 1 copper) show an unusual Cu^{II} coordination geometry (nearly tetrahedral) in the crystallographically determined resting state ("pseudo type 2" copper, Fig. 2).[15] Many new results from model complexes with tris(alkylpyrazolyl)borate ligands[16, 17] indicate that the catalytically relevant and spectroscopically remarkable[16b] Cu^{I}–nitrosyl radical complexes as well as the Cu^{II}–nitrite precursor complexes are important intermediates in the reaction. However, the pathway from the nitrosyl state to dinitrogen monoxide is not yet well understood (Fig. 2).[13]

11. Summary and Outlook

Although copper became bioavailable in significant amounts only as Cu^{II}, that is, after sufficient photosynthetic production of oxidation equivalents about 2–3 billion years ago, all biological functions involve copper in the monovalent form, either alone or in form of the Cu^{II}/Cu^{I} redox pair. In contrast to other stable metal monocations, the Cu^{I} state is characterized by high, but not unphysiological, *one-electron* oxidation potentials and by a preference for low coordination numbers (3–4) with a variable coordination geometry, uninfluenced by ligand field effects. Further remarkable properties include the ability to bind olefins and to activate O_2 in its triplet ground state; within biology, this latter, essential activity is only shared by the high-spin iron(II) state and by the formally antiaromatic 1,5-dihydroflavins.

The one-electron redox reactivity in the Cu^{II}/Cu^{I} system with potentials between 0.0 and +1.0 V renders copper centers compatible with weakly oxidizing organic and inorganic radicals in corresponding redox systems; redox pairs identified as such partners of copper centers include quinones/semiquinones, tyrosyl/tyrosine, $O_2/O_2^{\bullet-}/O_2^{2-}$ and $NO^{+}/NO^{\bullet}$.

In the light of the rapid parallel development of medical, microbiological, biochemical, and inorganic-chemical research in the area of copper coordination compounds during the last decade, more surprising discoveries can be anticipated, and new methodologies such as site-directed mutagenesis may be developed to enable targeted design of copper-containing proteins. There are still many intriguing questions open, such as the coordination environment in copper-dependent monooxygenases and the possible role of Cu^{I} sites in the receptor protein of the plant hormone ethylene.[131] Speculative yet fascinating remain the attempts to understand the temporal and functional development of this unique element in the evolution of life.[3c, 19, 54b, 132]

Our own research on the chemistry of copper has been funded by programs of the Deutsche Forschungsgemeinschaft (DFG) and by the Fonds der Chemischen Industrie, which we gratefully acknowledge. We also thank those co-workers directly involved, in particular Dr. Stephan Kohlmann, Dr. Conny Vogler, Dr. Michael Moscherosch, Dipl.-Chem. Eberhard Waldhör, Dipl.-Chem. Andreas Stange, Dipl.-Chem. Christoph Titze, and Dipl.-Chem. Manuela Schwach. We sincerely acknowledge the help of Mrs. Dipl.-Chem. Angela Winkelmann in preparing this manuscript.

Received: May 23, 1995 [A115IE]
German version: *Angew. Chem.* **1995**, *107*, 47–64
Translated by Dr. B. Schwederski, Stuttgart (Germany)

[1] M. C. Linder, C. A. Goode, *Biochemistry of Copper*, Plenum, New York, **1991**.

[2] *Bioinorganic Chemistry of Copper* (Eds.: K. D. Karlin, Z. Tyeklar), Chapman & Hall, New York, **1993**.

[3] a) W. Kaim, B. Schwederski, *Bioanorganische Chemie*, 2nd ed., Teubner, Stuttgart, **1995**; b) *Bioinorganic Chemistry: Inorganic Elements in the Chemistry of Life*, Wiley, Chichester, **1994**; c) J. J. R. Fraústo da Silva, R. J. P. Williams, *The Biological Chemistry of the Elements*, Clarendon, Oxford, **1991**; d) J. A. Cowan, *Inorganic Biochemistry*, VCH, New York, **1993**; e) S. J. Lippard, J. M. Berg, *Principles of Bioinorganic Chemistry*, University Science Books, Mill Valley, **1994**.

[4] a) G. C. M. Steffens, R. Bielwald, G. Buse, *Eur. J. Biochem.* **1987**, *164*, 295; b) G. C. M. Steffens, T. Soulimane, G. Wolff, G. Buse, *ibid.* **1993**, *213*, 1149.

[5] a) R. Huber, *Angew. Chem.* **1989**, *101*, 849; *Angew. Chem. Int. Ed. Engl.* **1989**, *28*, 848; b) A. Messerschmidt, H. Luecke, R. Huber, *J. Mol. Biol.* **1993**, *230*, 997.

[6] a) E. I. Solomon, M. J. Baldwin, M. D. Lowery, *Chem. Rev.* **1992**, *92*, 521; b) E. I. Solomon, M. D. Lowery, *Science* **1993**, *259*, 1575; c) J. A. Guckert, M. D. Lowery, E. I. Solomon, *J. Am. Chem. Soc.* **1995**, *117*, 2817; d) D. J. Spira-Solomon, M. D. Allendorf, E. I. Solomon, *ibid.* **1986**, *108*, 5318.

[7] a) C. Vulpe, B. Levinson, S. Whitney, S. Packman, J. Gitschier, *Nat. Genet.* **1993**, *3*, 7; b) K. Davies, *Nature (London)* **1993**, *361*, 98.

[8] a) D. R. Rosen, T. Siddique, D. Patterson, D. A. Figlewicz, P. Sapp, A. Hentati, D. Donaldson, J. Goto, J. P. O'Regan, H.-X. Deng, Z. Rahmani, A. Krizus, D. McKenna-Yasek, A. Cayabyab, S. M. Gaston, R. Berger, R. E. Tanzi, J. J. Halperin, B. Herzfeldt, R. Van den Bergh, W.-Y. Hung, T. Bird, G. Deng, D. W. Mulder, C. Smyth, N. G. laing, E. Soriano, M. A. Pericak-Vance, J. Haines, G. A. Rouleau, J. S. Gusella, H. R. Horvitz, R. H. Brown, Jr., *Nature (London)* **1993**, *362*, 59; b) H.-X. Deng, A. Hentati, J. A. Tainer, Z. Iqbal, A. Cayabyab, W.-Y. Hung, E. D. Getzoff, P. Hu, B. Herzfeldt, R. P. Roos, C. Warner, G. Deng, E. Soriano, C. Smyth, H. E. Parge, A. Ahmed, A. D. Roses, R. A. Hallewell, M. A. Pericak-Vance, T. Siddique, *Science* **1993**, *261*, 1047; c) J. O. McNamara, I. Fridovich, *Nature (London)* **1993**, *362*, 20; d) J. Marx, *ibid.* **1993**, *261*, 986; e) M. E. Gurney, H. Pu, A. Y. Chiu, M. C. Dal Canto, C. Y. Polchow, D. D. Alexander, J. Caliendo, A. Hentati, Y. W. Kwon, H.-X. Deng, W. Chen, P. Zhai, R. L. Sufit, T. Siddique, *Science* **1994**, *264*, 1772; f) J. A. Graden, L. M. Ellerby, J. A. Roe, J. S. Valentine, *J. Am. Chem. Soc.* **1994**, *116*, 9743; g) L. P. Rowland, *Proc. Natl. Acad. Sci. USA*, **1995**, *92*, 1251.

[9] a) P. K. Ross, E. I. Solomon, *J. Am. Chem. Soc.* **1990**, *112*, 5871; b) M. J. Baldwin, D. E. Root, J. E. Pate, K. Fujisawa, N. Kitajima, E. I. Solomon, *J. Am. Chem. Soc.* **1992**, *114*, 10421; c) F. Tuczek, E. I. Solomon, *ibid.* **1994**, *116*, 6916; d) E. I. Solomon, F. Tuczek, D. E. Root, C. A. Brown, *Chem. Rev.* **1994**, *94*, 827.

[10] a) K. A. Magnus, H. Ton-That, J. E. Carpenter, *Chem. Rev.* **1994**, *94*, 727; b) J. Ling, L. P. Nestor, R. S. Czernuszewicz, T. G. Spiro, R. Fraczkiewicz, K. D. Sharma, T. M. Loehr, J. Sanders-Loehr, *J. Am. Chem. Soc.* **1994**, *116*, 7682.

[11] a) R. R. Jacobson, Z. Tyeklar, A. Farooq, K. D. Karlin, S. Liu, J. Zubieta, *J. Am. Chem. Soc.* **1988**, *110*, 3690; b) Z. Tyeklar, R. R. Jacobson, N. Wei, N. N. Murthy, J. Zubieta, K. D. Karlin, *ibid.* **1993**, *115*, 2677.

[12] a) N. Kitajima, K. Fujisawa, Y. Moro-oka, K. Toriumi, *J. Am. Chem. Soc.* **1989**, *111*, 8975; b) J. Kitajima, K. Fujisawa, C. Fujimoto, Y. Moro-oka, S. Hashimoto, T. Kitagawa, K. Toriumi, K. Tatsumi, A. Nakamura, *ibid.* **1992**, *114*, 1277; c) N. Kitajima, Y. Moro-oka, *Chem. Rev.* **1994**, *94*, 737; d) see also the analogous S_2 complex: K. Fujisawa, Y. Moro-oka, N. Kitajima, *J. Chem. Soc. Chem. Commun.* **1994**, 623.

[13] a) C. L. Hulse, B. A. Averill, J. M. Tiedje, *J. Am. Chem. Soc.* **1989**, *111*, 2322; b) B. A. Averill, *Angew. Chem.* **1994**, *106*, 2145; *Angew. Chem. Int. Ed. Engl.* **1994**, *33*, 2057; c) C. E. Ruggiero, S. M. Carrier, W. B. Tolman, *ibid.* **1994**, *106*, 917 and **1994**, *33*, 895.

[14] a) P. M. H. Kroneck, J. Beuerle, W. Schumacher in *Metal Ions in Biological Systems, Vol. 28* (Eds.: H. Sigel, A. Sigel), Dekker, New York, **1992**, p. 455; b) T. Brittain, R. Blackmore, C. Greenwood, A. J. Thomson, *Eur. J. Biochem.* **1992**, *209*, 793; c) W. G. Zumft, *Arch. Microbiol.* **1993**, *160*, 253.

[15] a) J. W. Godden, S. Turley, D. C. Teller, E. T. Adman, M. Y. Liu, W. J. Payne, J. LeGall, *Science* **1991**, *253*, 438; b) B. D. Howes, Z. H. L. Abraham, D. J. Lowe, T. Brüser, R. R. Eady, B. E. Smith, *Biochemistry* **1994**, *33*, 3171.

[16] a) S. M. Carrier, C. E. Ruggiero, W. B. Tolman, *J. Am. Chem. Soc.* **1992**, *114*, 4407; b) C. E. Ruggiero, S. M. Carrier, W. E. Antholine, J. W. Whittaker, C. J. Cramer, W. B. Tolman, *ibid.* **1993**, *115*, 11285; c) W. B. Tolman, S. M. Carrier, C. E. Ruggiero, W. E. Antholine, J. W. Whittaker in Ref. [2], p. 406; d) P. P. Paul, Z. Tyeklar, A. Farooq, K. D. Karlin, S. Liu, J. Zubieta, *J. Am. Chem. Soc.* **1990**, *112*, 2430.

[17] a) J. A. Halfen, W. B. Tolman, *J. Am. Chem. Soc.* **1994**, *116*, 5475; b) J. A. Halfen, S. Mahapatra, M. M. Olmstead, W. B. Tolman, *ibid.* **1994**, *116*, 2173.

[18] a) R. L. Deming, A. L. Allred, A. R. Dahl, A. W. Herlinger, M. O Kestner, *J. Am. Chem. Soc.* **1976**, *98*, 4132; b) F. A. Cotton, G. Wilkinson, *Advanced Inorganic Chemistry*, 5th ed., Wiley, New York, **1988**, p. 615; c) *ibid.* p. 774.

[19] E.-I. Ochiai, *J. Chem. Educ.* **1986**, 63, 942.

[20] a) A. S. Moffat, *Science* **1994**, *264*, 778; b) M. N. Hughes, R. K. Poole, *Metals and Micro-organisms*, Chapman & Hall, London, **1989**; c) K. Bosecker, *Metall* **1980**, *34*, 36.

[21] M. A. Masood, P. S. Zacharias, *J. Chem. Soc. Dalton Trans.* **1991**, 111.

[22] A. F. Stange, E. Waldhör, M. Moscherosch, W. Kaim, *Z. Naturforsch. B* **1995**, *50*, 115.

[23] a) J. G. Noltes, G. van Koten in *Comprehensive Organometallic Chemistry, Vol. 2* (Eds.: G. Wilkinson, F. G. A. Stone, E. Abel), Pergamon, Oxford, **1982**, p. 709; b) *Organocopper Reagents*, (Ed.: R. J. K. Taylor), Oxford University Press, Oxford, **1994**.

[24] a) A. Berkessel, *Bioorg. Chem.* **1991**, *19*, 101; b) P. J. Toscano, L. G. Marzilli, *Prog. Inorg. Chem.* **1984**, *31*, 105.

[25] W. Kaim, T. Stahl, C. Vogler, S. Kohlmann in *Unkonventionelle Wechselwirkungen in der Chemie metallischer Elemente* (Ed.: B. Krebs), VCH, Weinheim, **1992**, p. 81.

[26] a) In the concept of the entatic (strained) state the high-energy arrangement of the ligands created by a special protein conformation at the active metal center facilitates the course to the transition state of the reaction concerned: B. L. Vallee, R. J. P. Williams, *Proc. Natl. Acad. Sci. USA* **1968**, *59*, 498; b) R. J. P. Williams, *J. Mol. Catal.* (Review Issue) **1986**, 1; c) B. G. Malmström, *Eur. J. Biochem.* **1994**, *223*, 711.

[27] S. Knapp, T. P. Keenan, X. Zhang, R. Fikar, J. A. Potenza, H. J. Schugar, *J. Am. Chem. Soc.* **1990**, *112*, 3452.

[28] G. A. Hamilton, P. K. Adolf, J. De Jersey, G. C. DuBois, G. R. Dyrkacz, R. D. Libby, *J. Am. Chem. Soc.* **1978**, *100*, 1899.

[29] a) N. Ito, S. E. V. Phillips, C. Stevens, Z. B. Ogel, M. J. McPherson, J. N. Keen, K. D. S. Yadav, P. F. Knowles, *Faraday Discuss. Chem. Soc.* **1993**, *93*, 75; b) *Nature (London)* **1991**, *350*, 87; c) P. F. Knowles, N. Ito in *Perspectives on Bioinorganic Chemistry, Vol. 2* (Eds.: R. W. Hay, J. R. Dilworth, K. B. Nolan), Jai Press, London, **1993**, p. 207; d) N. Ito, S. E. V. Phillips, K. D. S. Yadav, P. F. Knowles, *J. Mol. Biol.* **1994**, *238*, 794.

[30] J. W. Whittaker in *Metal Ions in Biological Systems, Vol. 30* (Eds.: H. Sigel, A. Sigel), Dekker, New York, **1994**, p. 315.

[31] a) M. R. McDonald, W. M. Scheper, H. D. Lee, D. W. Margerum, *Inorg. Chem.* **1995**, *34*, 229; b) see also M. Kaupp, H. G. von Schnering, *Angew. Chem.* **1995**, *107*, 1076; *Angew. Chem. Int. Ed. Engl.* **1995**, *34*, 986, and J. P. Snyder, *ibid.* **1995**, *107*, 1076 and **1995**, *34*, 987.

[32] a) K. Prassides, A. Lappas, *Chem. Br.* **1994**, *30*, 730; b) A. W. Sleight, *Acc. Chem. Res.* **1995**, *28*, 103; c) mixed valency according to a formulation $[Cu^{1+\delta}(DCNQI^{-(1+\delta)/2})_2]$ is found for anisotropically conducting crystals and films with partially reduced N,N′-dicyano-*p*-quinodiimine ligands (DCNQI): R. Burkert, H. W. Helberg, J. U. von Schütz, *Synth. Met.* **1993**, *55–57*, 2519.

[33] a) N. Kitajima, *Adv. Inorg. Chem.* **1993**, *39*, 1; b) N. Kitajima, K. Fujisawa, M. Tanaka, Y. Moro-oka, *J. Am. Chem. Soc.* **1992**, *114*, 9232; c) P. K. Bharadwaj, J. A. Potenza, H. J. Schugar, *ibid.* **1986**, *108*, 1351; d) C. R. Andrew, H. Yeom, J. S. Valentine, B. G. Karlsson, N. Bonander, G. van Pouderoyen, G. W. Canters, T. M. Loehr, J. Sanders-Loehr, *ibid.* **1994**, *116*, 11489.

[34] a) H. tom Dieck, L. Stamp, *Z. Naturforsch. B* **1990**, *45*, 1369; b) M. J. Begley, P. Hubberstey, C. E. Russell, P. H. Walton, *J. Chem. Soc. Dalton Trans.* **1994**, 2483; c) C. Vogler, W. Kaim, H.-D. Hausen, *Z. Naturforsch. B* **1993**, *48*, 1470 and references therein; d) C. Vogler, H.-D. Hausen, W. Kaim, S. Kohlmann, H. E. A. Kramer, J. Rieker, *Angew. Chem.* **1989**, *101*, 1734; *Angew. Chem. Int. Ed. Engl.* **1989**, *28*, 1659.

[35] E. C. Constable, *Chem. Ind. (London)* **1994**, 56.

[36] J.-M. Lehn, *Angew. Chem.* **1990**, *102*, 1347; *Angew. Chem. Int. Ed. Engl.* **1990**, *29*, 1304.

[37] a) M. Cesario, C. O. Dietrich-Buchecker, J. Guilhem, C. Pascard, J.-P. Sauvage, *J. Chem. Soc. Chem. Commun.* **1985**, 244; b) C. O. Dietrich-Buchecker, B. Frommberger, I. Lüer, J.-P. Sauvage, F. Vögtle, *Angew. Chem.* **1993**, *105*, 1526; *Angew. Chem. Int. Ed. Engl.* **1993**, *32*, 1434.

[38] a) C. O. Dietrich-Buchecker, J. P. Sauvage, A. DeCian, J. Fischer, *J. Chem Soc. Chem. Commun.* **1994**, 2231; b) see also the knotted structure of copper-containing ascorbate oxidase: C. Liang, K. Mislow, *J. Am. Chem. Soc.* **1994**, *116*, 11189; *ibid.* **1995**, *117*, 4201.

[39] a) M. Moscherosch, J. S. Field, W. Kaim, S. Kohlmann, M. Krejcik, *J. Chem. Soc. Dalton Trans.* **1993**, 211; b) M. Schwach, H.-D. Hausen, W. Kaim, *Chem. Eur. J.*, in press; c) see also S. Kitagawa, M. Kondo, S. Kawata, S. Wada, M. Maekawa, M. Munakata, *Inorg. Chem.* **1995**, *34*, 1455.

[40] P. Baxter, J.-M. Lehn, A. DeCian, J. Fischer, *Angew. Chem.* **1993**, *105*, 92; *Angew. Chem. Int. Ed. Engl.* **1993**, *32*, 69.

[41] a) B. Schoentjes, J.-M. Lehn, *Helv. Chim. Acta* **1995**, *78*, 1; b) E. C. Constable, A. J. Edwards, M. J. Hannon, P. R. Raithby, *J. Chem. Soc. Chem. Commun.* **1994**, 1991.

[42] a) P. N. W. Baxter, J.-M. Lehn, J. Fischer, M.-T. Youinou, *Angew. Chem.* **1994**, *106*, 2432; *Angew. Chem. Int. Ed. Engl.* **1994**, *33*, 2284; b) H. Sleiman, P. Baxter, J.-M. Lehn, K. Rissanen, *J. Chem. Soc. Chem. Commun.* **1995**, 715.

[43] a) W. Kaim, S. Kohlmann, J. Jordanov, D. Fenske, *Z. Anorg. Allg. Chem.* **1991**, *598/599*, 217; b) C. Vogler, W. Kaim, *Z. Naturforsch. B* **1992**, *47*, 1057.

[44] W. E. B. Shepard, B. F. Anderson, D. A. Lewandoski, G. E. Norris, D. N. Baker, *J. Am. Chem. Soc.* **1990**, *112*, 7817.

[45] a) A. Müller, H. Bögge, U. Schimanski, *Inorg. Chim. Acta* **1980**, *45*, L249; b) E. Lastra, M. P. Gamasa, J. Gimeno, M. Lanfranchi, A. Tiripicchio, *J. Chem. Soc. Dalton Trans.* **1989**, 1499; c) J. Kampf, R. Kumar, J. P. Oliver, *Inorg. Chem.* **1992**, *31*, 3626; d) B. J. Wuensch, *Z. Kristallogr.* **1964**, *119*, 437; e) J. K. Burdett, O. Eisenstein, *Inorg. Chem.* **1992**, *31*, 1758.

[46] a) G. Speier, S. Tisza, Z. Tyeklar, C. W. Lange, C. G. Pierpont, *Inorg. Chem.* **1994**, *33*, 2041; b) G. A. Razuvaev, V. K. Cherkasov, G. A. Abakumov, *J. Organomet. Chem.* **1978**, *160*, 361; c) R. M. Buchanan, C. Wilson-Blumenberg, C. Trapp, S. K. Larsen, D. L. Greene, C. G. Pierpont, *Inorg. Chem.* **1986**, *25*, 3070; d) J. Rall, W. Kaim, *J. Chem. Soc. Faraday Trans.* **1994**, *90*, 2905.

[47] a) P. J. Blower, J. R. Dilworth, *Coord. Chem. Rev.* **1987**, *76*, 121; b) I. J. Pickering, G. N. George, C. T. Dameron, B. Kury, D. R. Winge, I. G. Dance, *J. Am. Chem. Soc.* **1993**, *115*, 9498.

[48] V. Massey, *J. Biol. Chem.* **1994**, *269*, 22459.

[49] K. D. Karlin, Y. Gultneh, *Prog. Inorg. Chem.* **1987**, *35*, 219.

[50] a) K. M. Merz, R. Hoffmann, *Inorg. Chem.* **1988**, *27*, 2120; b) M. Hakansson, S. Jagner, E. Clot, O. Eisenstein, *ibid.* **1992**, *31*, 5389.

[51] E. Spodine, J. Manzur, *Coord. Chem. Rev.* **1992**, *119*, 171.

[52] a) H. Jin, H. Thomann, C. L. Coyle, W. G. Zumft, *J. Am. Chem. Soc.* **1989**, *111*, 4262; b) W. G. Zumft, *Nova Acta Leopold.* **1994**, *70 (No. 288)*, 237; c) W. G. Zumft, A. Dreusch, S. Löchelt, H. Cuypers, B. Friedrich, B. Schneider, *Eur. J. Biochem.* **1992**, *208*, 31; d) D. M. Dooley, M. A. McGuirl, A. C. Rosenzweig, J. A. Landin, R. A. Scott, W. G. Zumft, F. Devlin, P. J. Stephens, *Inorg. Chem.* **1991**, *30*, 3006.

[53] S. M. Janes, S. Mu, D. Wemmer, A. J. Smith, S. Kaur, D. Maltby, A. L. Burlingame, J. P. Klinman, *Science* **1990**, *248*, 981.

[54] a) R. J. P. Williams, *Chem. Scr.* **1986**, *26*, 515; b) R. J. P. Williams in *The Chemistry of Copper and Zinc Triads* (Eds.: A. J. Welsh, S. K. Chapman), Royal Society of Chemistry, Cambridge, **1993**, p. 1.

[55] a) E. I. Ochiai, *Origins Life* **1978**, *9*, 81; b) M. G. Schwendinger, R. Tauler, S. Saetia, K. R. Liedl, R. T. Kroemer, B. M. Rode, *Inorg. Chim. Acta* **1995**, *228*, 207; c) C. J. Allègre, S. H. Schneider, *Sci. Am.* **1994**, *271* (4), 44.

[56] a) Z. S. Kolber, R. T. Barber, K. H. Coale, S. E. Fitzwater, R. M. Greene, K. S. Johnson, S. Lindley, P. G. Falkowski, *Nature (London)* **1994**, *371*, 145; b) see also J. H. Martin, K. H. Coale, S. E. Fitzwater, R. M. Greene, K. S. Johnson, S. Lindley, P. G. Falkowski, *Nature (London)* **1994**, *371*, 145; b) vgl. auch J. H. Martin, K. H. Coale, K. S. Johnson, S. E. Fitzwater, R. M. Gordon, S. J. Tanner, C. N. Hunter, V. A. Elrod, J. L. Nowicki, T. L. Coley, R. T. Barber, S. Lindley, A. J. Watson, K. Van Scoy, C. S. Law, M. I. Liddicoat, R. Ling, T. Stanton, J. Stockel, C. Collins, A. Anderson, R. Bidigare, M. Ondrusek, M. Latasa, F. J. Millero, K. Lee, W. Yao, J. Z. Zhang, G. Friederich, C. Sakamoto, F. Chavez, K. Buck, Z. Kolber, R. Greene, P. Falkowski, S. W. Chisholm, F. Hoge, R. Swift, J. Yungel, S. Turner, P. Nightingale, A. Hatton, P. Liss, N. W. Tindale, *ibid.* **1994**, *371*, 123.

[57] a) D. M. Dooley, M. A. McGuirl, D. E. Brown, P. N. Turowski, W. S. McIntire, P. F. Knowles, *Nature (London)* **1991**, *349*, 262; b) see also D. M. Dooley, W. S. McIntire, M. A. McGuirl, C. E. Cote, J. L. Bates, *J. Am. Chem. Soc.* **1990**, *112*, 2782.

[58] a) M. Harata, K. Jitsukawa, H. Masuda, H. Einaga, *J. Am. Chem. Soc.* **1994**, *116*, 10817; b) K. Fujisawa, M. Tanaka, Y. Moro-oka, N. Kitajima, *ibid.* **1994**, *116*, 12079; c) M. Mahroof-Tahir, K. D. Karlin, *ibid.* **1992**, *114*, 7599.

[59] a) W. Kaim, S. Kohlmann, *Inorg. Chem.* **1987**, *26*, 1469; b) W. Kaim, M. Moscherosch, *J. Chem. Soc. Faraday Trans.* **1991**, *87*, 3185; c) W. Kaim, M. Moscherosch, S. Kohlmann, J. S. Field, D. Fenske in *The Chemistry of the Copper and Zinc Triads* (Eds.: A. J. Welch, S. K. Chapman), Royal Society of Chemistry, Cambridge, **1993**, p. 248.

[60] H. Tributsch, *J. Electroanal. Chem.* **1992**, *331*, 783.

[61] a) G. Buse, *Naturwiss. Rundschau* **1986**, *39*, 518; b) H. Beinert, *Chem. Scr.* **1988**, *28A*, 35.

[62] a) G. T. Babcock, M. Wikström, *Nature (London)* **1992**, *356*, 301; b) M. W. Calhoun, J. W. Thomas, R. B. Gennis, *Trends Biochem. Sci.* **1994**, *19*, 325; c) C. Varotsis, Y. Zhang, E. H. Appelman, G. T. Babcock, *Proc. Natl. Acad. Sci. USA* **1993**, *90*, 237; d) B. C. Hill, *J. Biol. Soc.* **1994**, *269*, 2419.

[63] a) O. Farver, M. Goldberg, I. Pecht, *Eur. J. Biochem.* **1980**, *104*, 71; b) J.-M. Latour, *Bull. Soc. Chim. Fr.* **1988**, 508.

[64] a) P. F. Knowles, D. M. Dooley in *Metal Ions in Biological Systems, Vol. 30* (Eds.: H. Sigel, A. Sigel), Dekker, New York, **1994**, p. 361; b) K. Warncke, G. T. Babcock, D. M. Dooley, M. A. McGuirl, J. McCracken, *J. Am. Chem. Soc.* **1994**, *116*, 4028.

[65] a) J. McCracken, S. Pember, S. J. Benkovic, J. J. Villafranca, R. J. Miller, J. Peisach, *J. Am. Chem. Soc.* **1988**, *110*, 1069; b) S. Pember, K. A. Johnson, J. J. Villafranca, S. J. Benkovic, *Biochemistry* **1989**, *28*, 2124; c) N. J. Blackburn, R. W. Strange, R. T. Carr, S. J. Benkovic, *ibid.* **1992**, *31*, 5298; d) N. J. Blackburn in *Bioinorganic Chemistry of Copper* (Eds.: K. D. Karlin, Z. Tyeklar), Chapmann & Hall, New York, **1993**, p. 164.

[66] M. K. Chan, S. Mukund, A. Kletzin, M. W. W. Adams, D. C. Rees, *Science* **1995**, *267*, 1463.

[67] a) S. G. Schäfer, B. Elsenhans, W. Forth, K. Schümann in *Lehrbuch der Toxikologie* (Eds.: H. Marquardt, S. G. Schäfer), BI-Wissenschaftlicher Verlag, Mannheim, **1994**, p. 504, or N. W. Solomons, *J. Am. Coll. Nutr.*, **1985**, *4*, 83; b) N. L. Brown, B. T. O. Lee, S. Silver in *Metal Ions in Biological Systems, Vol. 30* (Eds.: H. Sigel, A. Sigel), Dekker, New York, **1994**, p. 405; c) *Genetic Response to Metals* (Ed.: B. Sarkar), Dekker, New York, **1995**; d) R. P. Csintalan, N. M. Senozan, *J. Chem. Educ.* **1991**, *68*, 365.

[68] a) C. F. Mills, *Chem. Br.* **1979**, *15*, 512; b) R. J. P. Williams in *Molybdenum: An Outline of its Chemistry and Uses* (Eds.: E. R. Braithwaite, J. Haber), Elsevier, Amsterdam, **1994**, p. 419.

[69] A. Müller, E. Diemann, R. Jostes, H. Bögge, *Angew. Chem.* **1981**, *93*, 957; *Angew. Chem. Int. Ed. Engl.* **1981**, *20*, 934.

[70] a) B. Sarkar, K. Lingertat-Walsh, J. T. R. Clarke, *J. Pediatr.* **1993**, *123*, 828; b) see also S. Borman, *Chem. Eng. News* **1993**, *71*, December 13, 23.

[71] a) G. N. George, J. Byrd, D. R. Winge, *J. Biol. Chem.* **1988**, *263*, 8199; b) Y.-J. Li, U. Weser, *Inorg. Chem.* **1992**, *31*, 5526.

[72] *Metallothioneins: Synthesis, Structure, and Properties of Metallothioneins, Phytochelatins, and Metal-Thiolate Complexes*, (Eds.: M. J. Stillman, F. C. Shaw, K. R. Suzuki), VCH, New York, **1992**.

[73] "Catecholamines, Parts I and II": U. Trendelenburg, N. Weiner, *Handb. Exp. Pharmocol.*, **1989**, *90*.

[74] J. M. Matz, M. J. Blake, J. T. Saari, A. M. Bode, *FASEB J.* **1994**, *8*, 97.

[75] a) B. J. Reedy, N. J. Blackburn, *J. Am. Chem. Soc.* **1994**, *116*, 1924; b) G. Tian, J. A. Berry, J. P. Klinmann, *Biochemistry* **1994**, *33*, 226.

[76] a) K. Lerch, *Life Chem. Rep.* **1987**, *5*, 221; b) see also T. N. Sorell, *Tetrahedron* **1989**, *45*, 3.

[77] X. Min, D. C. Carter, *Nature (London)* **1992**, *358*, 209.

[78] K. H. Nakagawa, C. Inouye, B. Hedman, M. Karin, T. D. Tullius, K. O. Hodgson, *J. Am. Chem. Soc.* **1991**, *113*, 3621.

[79] a) O. Horvath, *Coord. Chem. Rev.* **1994**, *135/136*, 303; b) C. Kutal, *ibid.* **1990**, *99*, 213.

[80] a) A. R. Green, A. Presta, Z. Gasyna, M. J. Stillman, *Inorg. Chem.* **1994**, *33*, 4159; b) A. R. Green, M. J. Stillman, *Inorg. Chim. Acta* **1994**, *226*, 275.

[81] a) J. M. Guss, H. D. Bartunik, H. C. Freeman, *Acta Crystallogr. Sect. B* **1992**, *48*, 790; b) M. R. Redinbo, D. Cascio, M. K. Choukair, D. Rice, S. Merchant, T. O. Yeates, *Biochemistry* **1993**, *32*, 10560; c) T. Inoue, Y. Kai, S. Harada, N. Kasai, Y. Ohshiro, S. Suzuki, T. Kohzuma, J. Tobari, *Acta Crystallogr. Sect. D* **1994**, *50*, 317; d) A. Romero, H. Nar, R. Huber, A. Messerschmidt, A. P. Kalverda, G. W. Canters, R. Durley, F. S. Mathews, *J. Mol. Biol.* **1994**, *236*, 1196; e) E. T. Adman, S. Turley, R. Bramson, K. Petratos, D. Banner, D. Tsernoglou, T. Beppu, H. Watanabe, *J. Biol. Chem.* **1989**, *264*, 87; f) K. Petratos, Z. Dauter, K. S. Wilson, *Acta Crystallogr. Sect. B* **1988**, *44*, 628; g) B. A. Fields, J. M. Guss, H. C. Freeman, *J. Mol. Biol.* **1991**, *222*, 1053; see also H. Thomann, M. Bernardo, M. J. Baldwin, M. D. Lowery, E. I. Solomon, *J. Am. Chem. Soc.* **1991**, *113*, 5911.

[82] a) A. G. Sykes, *Adv. Inorg. Chem.* **1991**, *36*, 377; b) O. Farver, I. Pecht, *FASEB J.* **1991**, *5*, 2554; c) H. E. M. Christensen, L. S. Conrad, K. V. Mikkelsen, M. K. Nielsen, J. Ulstrup, *Inorg. Chem.* **1990**, *29*, 2808.

[83] M. M. Werst, C. E. Davoust, B. M. Hoffman, *J. Am. Chem. Soc.* **1991**, *113*, 1533.

[84] a) H. Kurreck, B. Kirste, W. Lubitz, *Electron Nuclear Double Resonance Spectroscopy of Radicals in Solution*, VCH, Weinheim, **1988**; b) B. M. Hoffman, *Acc. Chem. Res.* **1991**, *24*, 164.

[85] a) W. S. McIntire, *FASEB J.* **1994**, *8*, 513; b) J. A. Duine, *Eur. J. Biochem.* **1991**, *200*, 271.

[86] L. Chen, R. C. E. Durley, F. S. Mathews, V. L. Davidson, *Science* **1994**, *264*, 86.

[87] G. M. Ullmann, N. M. Kostic, *J. Am. Chem. Soc.* **1995**, *117*, 4766 and references therein.

[88] a) A. J. Di Bilio, T. K. Chang, B. G. Malmström, H. B. Gray, B. G. Karlsson, M. Nordling, T. Pascher, L. G. Lundberg, *Inorg. Chim. Acta* **1992**, *198–200*, 145; b) B. C. Dave, J. P. Germanas, R. S. Czernuszewicz, *J. Am. Chem. Soc.* **1993**, *115*, 12175.

[89] a) H. Bertagnolli, W. Kaim, *Angew. Chem.* **1995**, *107*, 847; *Angew. Chem. Int. Ed. Engl.* **1995**, *34*, 771; b) R. K. Chadha, R. Kumar, D. G. Tuck, *Can. J. Chem.* **1987**, *65*, 1336; c) M. E. Barr, P. H. Smith, W. E. Antholine, B. Spencer, *J. Chem. Soc., Chem. Commun.* **1993**, 1649; d) J. A. Farrar, V. McKee, A. H. R. Al-Obaidi, J. J. McGarvey, J. Nelson, A. J. Thomson, *Inorg. Chem.* **1995**, *34*, 1302.

[90] a) H. Beinert, D. E. Griffiths, D. C. Wharton, R. H. Sands, *J. Biol. Chem.* **1962**, *237*, 2337; b) see also C. Sigwart, P. Hemmerich, J. T. Spence, *Inorg. Chem.* **1968**, *12*, 2545.

[91] a) T. H. Stevens, C. T. Martin, H. Wang, G. W. Brudvig, C. P. Scholes, S. I. Chan, *J. Biol. Chem.* **1982**, *257*, 12106; b) R. J. Gurbiel, Y.-C. Fann, K. K. Surerus, M. M. Werst, S. M. Musser, P. E. Doan, S. I. Chan, J. A. Fee, B. M. Hoffman, *J. Am. Chem. Soc.* **1993**, *115*, 10888; c) D. Voet, J. G. Voet, *Biochemistry*, 2nd ed., Wiley, New York, **1995**, p. 580, 581; d) A. L. Lehninger, D. L. Nelson, M. M. Cox, *Principles of Biochemistry*, 2nd ed., Worth, New York, **1993**, p. 554; e) L. Stryer, *Biochemistry*, 4th ed., Freeman, New York, **1995**, p. 539, 540.

[92] P. M. H. Kroneck, W. E. Antholine, D. H. W. Kastrau, G. Buse, G. C. M. Steffens, W. G. Zumft, *FEBS Lett.* **1990**, *268*, 274.

[93] W. E. Antholine, D. H. W. Kastrau, G. C. M. Steffens, G. Buse, W. G. Zumft, P. M. H. Kroneck, *Eur. J. Biochem.* **1992**, *209*, 875.

[94] a) M. Kelly, P. Lappalainen, G. Talbo, T. Haltia, J. van der Oost, M. Saraste, *J. Biol. Chem.* **1993**, *268*, 16781; b) B. G. Malmström, R. Aasa, *FEBS Lett.* **1993**, *325*, 49; c) L. P. Pan, Z. Li, R. Larsen, S. I. Chan, *J. Biol. Chem.* **1991**, *266*, 1367; d) C. van Wachenfeldt, S. De Vries, J. van der Oost, *FEBS Lett.* **1994**, *340*, 109.

[95] a) P. Lappalainen, M. Saraste, *Biochim. Biophys. Acta* **1994**, *1187*, 222; b) N. J. Blackburn, M. E. Barr, W. H. Woodruff, J. van der Oost, S. De Vries, *Biochemistry* **1994**, *33*, 10401; c) G. N. George, S. P. Cramer, T. G. Frey, R. C. Prince, *Biochim. Biophys. Acta* **1993**, *1142*, 240; d) see also very recent EXAFS results for the Cu_A dimer and the Cu_B–Fe_{a_3} complex in intact active cytochrome c oxidase from bovine heart mitochondria: G. Henkel, A. Müller, S. Weissgräber, G. Buse, T. Soulimane, G. C. M. Steffens, H.-F. Nolting, *Angew. Chem.* **1995**, *107*, 1615; *Angew. Chem. Int. Ed. Engl.* **1995**, *34*, 1488.

[96] a) J. Strähle in *Unkonventionelle Wechselwirkungen in der Chemie metallischer Elemente* (Ed.: B. Krebs), VCH, Weinheim 1992, p. 357; b) S. W. Lee, W. C. Trogler, *Inorg. Chem.* **1990**, *29*, 1659.

[97] W. Kaim, W. Bruns, J. Poppe, V. Kasack, *J. Mol. Struct.* **1993**, *292*, 221.

[98] K. Wieghardt, *Angew. Chem.* **1989**, *101*, 1179; *Angew. Chem. Int. Ed. Engl.* **1989**, *28*, 1153.

[99] S. J. Lippard, *Angew. Chem.* **1988**, *100*, 353; *Angew. Chem. Int. Ed. Engl.* **1988**, *27*, 344.

[100] a) L. Noodleman, J. G. Norman, H. H. Osborne, A. Aizman, D. A. Case, *J. Am. Chem. Soc.* **1985**, *107*, 3418; b) R. Cammack, *Adv. Inorg. Chem.* **1992**, *38*, 299.

[101] J. Reim, B. Krebs, *Angew. Chem.* **1994**, *106*, 2040; *Angew. Chem. Int. Ed. Engl.* **1994**, *33*, 1961.

[102] N. Kitajima, T. Katayama, K. Fujisawa, Y. Iwata, Y. Moro-oka, *J. Am. Chem. Soc.* **1993**, *115*, 7872.

[103] a) M. G. Peter, *Chem. Unserer Zeit* **1993**, *27*, 189; b) J. R. L. Walker, P. H. Ferrar, *Chem. Ind. (London)* **1995**, 836.

[104] a) M. G. Peter, *Angew. Chem.* **1989**, *101*, 572; *Angew. Chem. Int. Ed. Engl.* **1989**, *28*, 555; b) V. J. Hearing, K. Tsukamoto, *FASEB J.* **1991**, *5*, 2902.

[105] a) M. S. Nasir, B. I. Cohen, K. D. Karlin, *J. Am. Chem. Soc.* **1992**, *114*, 2482; b) L. M. Sayre, D. V. Nadkarni, *ibid.* **1994**, *116*, 3157; c) Z. Tyeklar, K. D. Karlin in Ref. [2], p. 277.

[106] H.-H. T. Nguyen, A. K. Shiemke, S. J. Jacobs, B. J. Hales, M. E. Lidstrom, S. I. Chan, *J. Biol. Chem.* **1994**, *269*, 14995.

[107] A. C. Rosenzweig, S. J. Lippard, *Acc. Chem. Res.* **1994**, *27*, 229.

[108] K. Wimalasena, K. R. Alliston, *J. Am. Chem. Soc.* **1995**, *117*, 1220.

[109] a) S. Itoh, T. Kondo, M. Komatsu, Y. Ohshiro, C. Li, N. Kanehisa, Y. Kai, S. Fukuzumi, *J. Am. Chem. Soc.* **1995**, *117*, 4714; b) S. Mahapatra, J. A. Halfen, E. C. Wilkinson, L. Que, Jr., W. B. Tolman, *ibid.* **1994**, *116*, 9785.

[110] G. A. Abakumov, V. A. Garnov, V. I. Nevodchikov, V. K. Cherkasov, *Dokl. Akad. Nauk SSSR* **1989**, *304*, 107.

[111] E. Waldhör, B. Schwederski, W. Kaim, *J. Chem. Soc. Perkin Trans. 2* **1993**, 2109.

[112] a) C. Hartmann, J. P. Klinman, *Biochemistry* **1991**, *30*, 4605; b) C. Hartmann, P. Brzovic, J. P. Klinman, *ibid.* **1993**, *32*, 2234.

[113] Z. B. Ögel, D. Brayford, M. J. McPherson, *Mycol. Res.* **1994**, *98*, 474.

[114] a) G. T. Babcock, M. K. El-Deeb, P. O. Sandusky, M. M. Whittaker, J. W. Whittaker, *J. Am. Chem. Soc.* **1992**, *114*, 3727; b) H. Adams, N. A. Bailey, D. E. Fenton, Q. He, M. Ohba, H. Okawa, *Inorg. Chim. Acta* **1994**, *215*, 1; c) M. Shaolin, *J. Electroanal. Chem.* **1994**, *370*, 135; d) E. Katz, D. D. Schlereth, H.-L. Schmidt, *ibid.* **1994**, *367*, 59.

[115] S. Han, Y. Ching, D. L. Rousseau, *Nature (London)* **1990**, *348*, 89.

[116] a) W. Woodruff, O. Einarsdottir, R. B. Dyer, K. A. Bagley, G. Palmer, S. J. Atherton, R. A. Goldbeck, T. D. Dawes, D. S. Kliger, *Proc. Natl. Acad. Sci. USA* **1991**, *88*, 2588; b) C. A. James, W. Woodruff, *Inorg. Chim. Acta* **1995**, *229*, 9.
[117] a) S. C. Lee, R. H. Holm, *J. Am. Chem. Soc.* **1993**, *115*, 11789; b) A. Nanthakumar, S. Fox, N. N. Murthy, K. D. Karlin, N. Ravi, B. H. Huynh, R. D. Orosz, E. P. Day, K. S. Hagen, N. J. Blackburn, *ibid.* **1993**, *115*, 8513; c) S. C. Lee, M. J. Scott, K. Kauffmann, E. Münck, R. H. Holm, *ibid.* **1994**, *116*, 401; d) K. D. Karlin, A. Nanthakumar, S. Fox, N. N. Murthy, N. Ravi, B. H. Huynh, R. D. Orosz, E. P. Day, *ibid.* **1994**, *116*, 4753; e) M. J. Scott, S. C. Lee, R. H. Holm, *Inorg. Chem.* **1994**, *33*, 4651; f) J. P. Collman, P. C. Herrmann, B. Boitrel, X. Zhang, T. A. Eberspacher, L. Fu, J. Wang, D. L. Rosseau, E. R. Williams, *J. Am. Chem. Soc.* **1994**, *116*, 9783; g) M. J. Scott, R. H. Holm, *ibid.* **1994**, *116*, 11357; h) M. J. Scott, H. H. Zhang, S. C. Lee, B. Hedman, K. O. Hodgson, R. H. Holm, *ibid.* **1995**, *117*, 568; i) A. Nanthakumar, M. S. Nasir, K. D. Karlin, N. Ravi, B. H. Huynh, *ibid.* **1992**, *114*, 6564.
[118] D. A. Labianca, *J. Chem. Educ.* **1979**, *56*, 788.
[119] J. A. Tainer, E. D. Getzoff, J. S. Richardson, D. C. Richardson, *Nature (London)* **1983**, *306*, 284.
[120] a) A. Gärtner, U. Weser, *Top. Curr. Chem.* **1986**, *132*, 1; b) A. E. G. Cass in *Metalloproteins, Part 1* (Ed.: P. Harrison), VCH, Weinheim, **1985**, p. 121; c) I. Fridovich, *J. Biol. Chem.* **1989**, *264*, 7761.
[121] W. C. Stallings, K. A. Pattridge, R. K. Strong, M. L. Ludwig, *J. Biol. Chem.* **1985**, *260*, 16424.
[122] G. E. O. Borgstahl, H. E. Parge, M. J. Hickey, W. F. Beyer, Jr., R. A. Hallewell, J. A. Tainer, *Cell* **1992**, *71*, 107.
[123] I. Bertini, L. Banci, M. Piccioli, C. Luchinat, *Coord. Chem. Rev.* **1990**, *100*, 67.
[124] E. D. Getzoff, D. E. Cabelli, C. L. Fisher, H. E. Parge, M. S. Viezzoli, L. Banci, R. A. Hallewell, *Nature (London)* **1992**, *358*, 347.
[125] U. Weser, *Forschung - Mitteilungen der DFG* **1994**(4), 11.
[126] J.-L. Pierre, P. Chautemps, S. Refaif, C. Beguin, A. E. Marzouki, G. Serratrice, E. Saint-Aman, P. Rey, *J. Am. Chem. Soc.* **1995**, *117*, 1965.
[127] J. R. J. Sorenson, *Chem. Br.* **1989**, *25*, 169.
[128] W. C. Orr, R. S. Sohal, *Science* **1994**, *263*, 1128.
[129] A. W. Segal, A. Abo, *Trends Biochem. Sci.* **1993**, *18*, 43.
[130] H. M. Kubisch, J. Wang, R. Luche, E. Carlson, T. M. Bray, C. J. Epstein, J. P. Phillips, *Proc. Natl. Acad. Sci. USA* **1994**, *91*, 9956.
[131] E. W. Ainscough, A. M. Brodie, A. L. Wallace, *J. Chem. Educ.* **1992**, *69*, 315.
[132] E. Frieden in *Met. Ions Biol. Syst.* **1981**, *13*, 1.
[133] a) T. Tsukihara, H. Aoyama, E. Yamashita, T. Tomizaki, H. Yamaguchi, K. Shinzawa-Itoh, R. Nakashima, R. Yaono, S. Yoshikawa, *Science* **1995**, *269*, 1069; b) S. Iwata, C. Ostermeier, B. Ludwig, H. Michel, *Nature* **1995**, *376*, 660.

Miller, R.J.D. (ed.)

Surface Electron Transfer Processes

1995. XII, 368 pages
with 137 figures and 3 tables.
Hardcover. DM 128.00.
ISBN 1-56081-036-X
(VCH, New York)

This book gives an extensive theoretical treatment of its theme. The emphasis is on electronic coupling of molecular potentials to conducting band states. The essential role of surface electron transfer in catalysis, electrochemistry, photo imaging, and virtually all charge transfer solid state devices make this process one of the most important single chemical events.

Sandifer, J. R.

Ion-Transfer Kinetics

1995. X, 142 pages with
38 figures and 16 tables.
Hardcover. DM 165.00.
ISBN 1-56081-508-6
(VCH, New York)

In six concise, well-referenced chapters, this book covers the essentials of ion-transfer principles and applications, including computer simulation techniques for ion-transfer kinetics models.

It is addressed to chemists in academia and industry, to physical chemists and to chemical engineers.

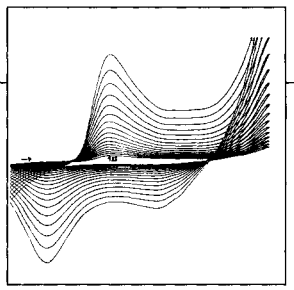

ELECTRO CHEMISTRY

To order please contact your bookseller or:

VCH, P.O. Box 10 11 61,
D-69451 Weinheim,
Telefax (0) 62 01 - 60 61 84

VCH, Hardstrasse 10, P.O. Box,
CH-4020 Basel

VCH, 8 Wellington Court,
Cambridge CB1 1HZ, UK

VCH, 303 N.W. 12th Avenue,
Deerfield Beach, FL 33442-1788, USA
toll-free: 1-800-367-8249
or fax: 1-800-367-8247

VCH, Eikow Building,
10-9 Hongo 1-chome, Bunkyo-ku,
Tokyo 113, Japan

VCH

"New" Reagents for the "Old" Pinacol Coupling Reaction

Thomas Wirth*

An old-timer in the history of chemistry, the pinacol coupling, was first described over 130 years ago in a publication on the synthesis of pinacols.[1a] Today this reaction is still a versatile tool for chemists. This "longevity" can be explained by the continuous development of improved reagents and by the intrisic elegance of the method for the preparation of 1,2-diols (pinacols) by the reductive coupling of carbonyl compounds.[1] Starting with two carbonyl functionalities, a C–C bond is formed and two new adjacent stereocenters created. 1,2-Diols are versatile intermediates in synthesis; for example, they can be used for the preparation of ketones by the pinacol rearrangement or alkenes by the McMurry reaction (Scheme 1).

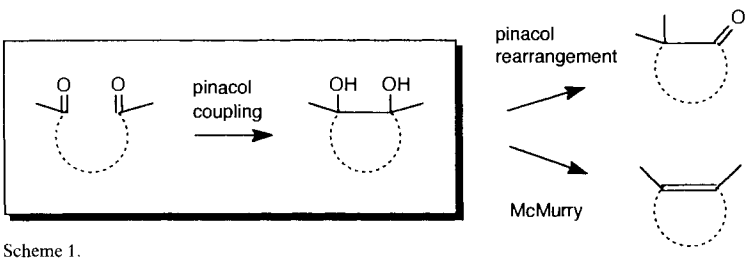

Scheme 1.

Whether the reductive coupling of carbonyl compounds leads to 1,2-diols or to the deoxygenated or rearranged products is dependent on the oxygen affinity of the reducing agent employed. The McMurry reaction uses low-valent titanium compounds, which under certain reaction conditions can transform the 1,2-diol intermediates into alkenes by rapid deoxygenation (Scheme 1). When this reaction was performed on the surface of reduced titanium dioxide, the intermediate 1,2-diols could be isolated.[2]

Reducing agents suitable for the synthesis of pinacols must allow the reaction to be stopped at the 1,2-diol stage. One of the first practical reductants for pinacol coupling reactions was the Mg/MgI_2 system reported by Gomberg and Bachmann.[3] More recently these reducing agents have been extended by a magnesium–graphite system, which is competitive with other currently available reductants.[4] Different low-valent titanium compounds have proved to have similar efficiency for pinacol coupling reactions.[5] They have been used for intramolecular couplings as well as for the formation of unsymmetrical pinacols, and have demonstrated their potential in several key steps of natural product syntheses.[6]

Typical mechanisms for pinacol couplings are shown in Scheme 2. In the first reduction step a ketyl radical is formed, which can dimerize (path A) or add to a second carbonyl group (path B) forming a C–C bond. In path B a second one-electron reduction must then follow. For pinacol coupling reactions mediated by transition metals the insertion of a carbonyl group into the metal–carbon bond of initially formed metal oxiranes has been proposed (path C).

Pinacol coupling reactions can lead to either the *syn*- or *anti*-diols. The stereochemical course of the reaction depends on the reducing agents and, of course, on the structure of the carbonyl compounds. Recent studies employing reagents that form the C–C bond according pathways B and C have met with success.

Previously, tin–ketyl radicals have been added to alkenes only in an intramolecular fashion.[7] In recent publications, however, pinacols and amino alcohols have been prepared by cyclization of dicarbonyl compounds[8] or keto-oximes[9] with tributyltin hydride. Cyclization of 1,5-ketoaldehydes **1** and 1,5-dialdehydes with tributyltin hydride yields *cis*-diols **2** with excellent stereoselectivities, whereas the keto-oxime **4** with four ben-

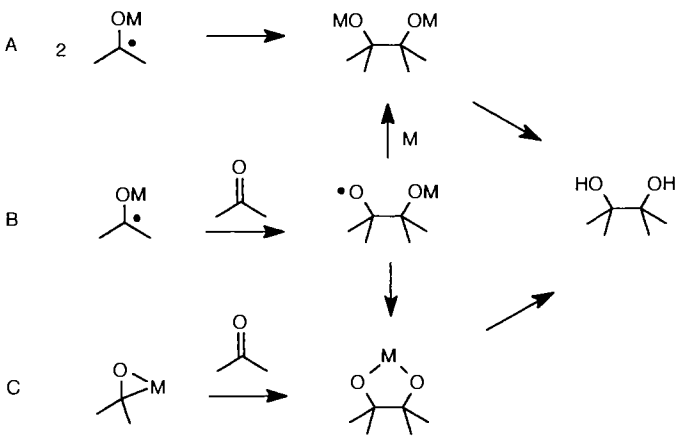

Scheme 2.

[*] Dr. T. Wirth
Institut für Organische Chemie der Universität
St.-Johanns-Ring 19, CH-4056 Basel (Switzerland)
Fax: Int. code + (61)322-6017
e-mail: wirth@ubaclu.unibas.ch

 © *VCH Verlagsgesellschaft mbH, D-69451 Weinheim, 1996* *0570-0833/96/3501-0061 $ 10.00+.25/0*

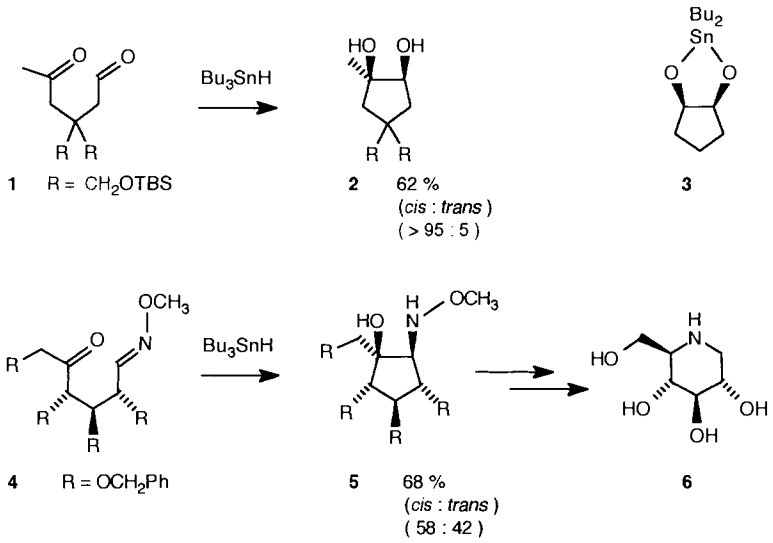

1 2 3 4 5 6

zyloxy substituents affords a 58:42 (*cis*:*trans*) mixture. The *trans* product was transformed in two more steps into the potent glycosidase inhibitor 1-deoxynojirimycin (**6**).[9b] The reversibility of both the addition of the tributyltin radical to the carbonyl group and the intramolecular radical C–C bond formation is believed to be responsible for the high selectivity in the formation of **2**. In the cyclization of 1,5-pentanedial the unhydrolyzed coupling product **3** could be isolated, therefore providing evidence for a new mechanistic variant of the pinacol reaction, in which only 1.2 equivalents of the reducing agent are necessary.

1,6-Dicarbonyl compounds can also be converted into the corresponding pinacols. Tributyltin hydride can again be used as an efficient reducing agent, this time for the stereoselective synthesis of **7**.[8] Other well-established pinacol-forming reagents such as low-valent titanium compounds[1b,c] and samarium diiodide[10] can cyclize 1,*n*-dicarbonyl compounds with comparable stereoselectivities to give 1,2-diols. X-ray crystal structures of a samarium ketyl complex and a samarium pinacolate are further evidence of the reversibility of the coupling reaction under appropriate conditions.[11] Samarium diiodide was used as pinacol coupling reagent for the synthesis of the optically active inositol derivative **8**.[10b]

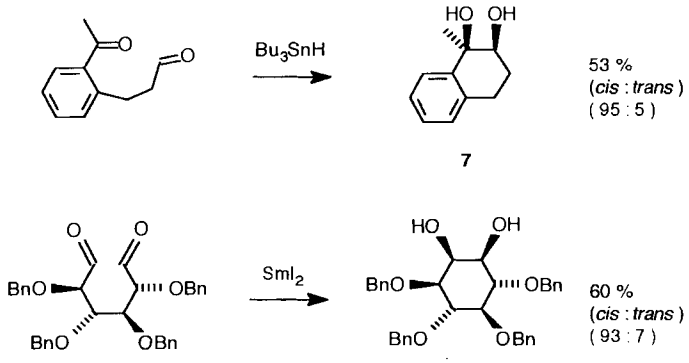

7 8

Low-valent compounds of other early transition metals were shown to be effective reagents for the pinacol coupling. Zirconium, niobium, and ytterbium reagents form metal oxiranes with carbonyl compounds; however, the mechanism of the reaction with vanadium compounds is not clear at present. The mechanism of the pinacol coupling via metal oxiranes is supported by X-ray structure analysis of an intermediate.[12] Vanadium and niobium compounds seem to be particularly attractive reagents for intermolecular pinacol coupling reactions.

The vanadium complex $[V_2Cl_3(thf)_6]_2[Zn_2Cl_6]$ is suitable for the intramolecular coupling of functionalized aldehydes bearing further coordination sites, for example amino aldehydes.[13] The formation of a bidentate or tridentate metal–aldehyde complex is proposed to be the origin of the *threo* selectivity observed in this reaction. The coupling products **9** are interesting target structures because they are potential inhibitors of HIV proteases. They can even be synthesized on a kilogram-scale with good yields.[13b] The niobium reagent $[NbCl_3(dme)]$ can be used to couple imines with carbonyl compounds giving amino alcohols such as **10**, although generally

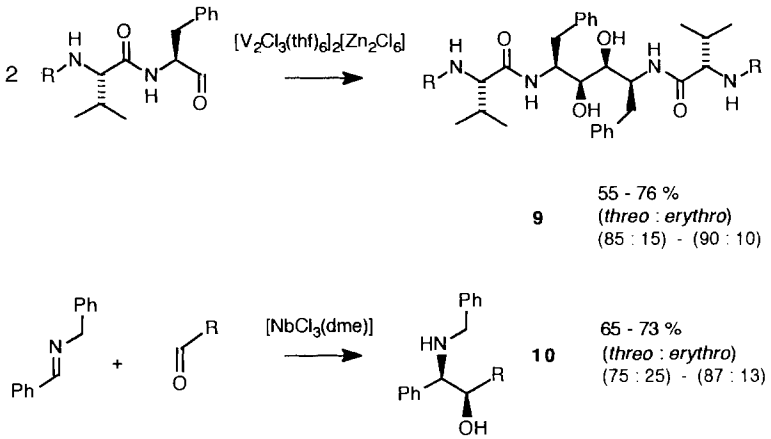

9 10

lower stereoselectivity is observed.[14] In analogy to reactions with other early transition metals, the mechanism is believed to proceed via a niobaziridine, which adds to the carbonyl functionality.

The relative and absolute stereochemistry in pinacol coupling reactions, for instance in the natural product syntheses mentioned earlier,[6] is always controlled by the stereocenters of the substrates. Very little work has concentrated on the control of the absolute stereochemistry in pinacol coupling reactions.[1b] Because of the potential of the reagents presented here, the development of chiral coupling reagents will no doubt be reported in the near future.

German version: *Angew. Chem.* **1996**, *108*, 65–67

Keywords: amino alcohols · diols · pinacols

[1] a) R. Fittig, *Justus Liebigs Ann. Chem.* **1859**, *110*, 23–45; b) review: G. M. Robertson in *Comprehensive Organic Synthesis, Vol. 3* (Eds.: B. M. Trost, I. Fleming, G. Pattenden), Pergamon, Oxford, **1991**, p. 563; c) A. Fürstner, *Angew. Chem.* **1993**, *105*, 171–197; *Angew. Chem. Int. Ed. Engl.* **1993**, *32*, 164–189.

[2] K. G. Pierce, M. A. Barteau, *J. Org. Chem.* **1995**, *60*, 2405–2410.

[3] M. Gomberg, W. E. Bachmann, *J. Am. Chem. Soc.* **1927**, *49*, 236–257.

 © VCH Verlagsgesellschaft mbH, D-69451 Weinheim, 1996 0570-0833/96/3501-0062 $ 10.00+.25/0

[4] A. Fürstner, R. Csuk, C. Rohrer, H. Weidmann, *J. Chem. Soc. Perkin Trans. 1* **1988**, 1729–1734.
[5] J. E. McMurry, *Chem. Rev.* **1989**, *89*, 1513–1524.
[6] a) E. J. Corey, R. L. Danheiser, S. Chandrasekaran, P. Siret, G. E. Keck, J. Gras, *J. Am. Chem. Soc.* **1978**, *100*, 8031–8034; b) C. S. Swindell, W. Fan, P. G. Klimko, *Tetrahedron Lett.* **1994**, *35*, 4959–4962; c) K. C. Nicolaou, Z. Yang, J. J. Liu, H. Ueno, P. G. Nantermet, R. K. Guy, C. F. Claiborne, J. Renaud, E. A. Couladouros, K. Paulvannan, E. J. Sorensen, *Nature* **1994**, *367*, 630–634.
[7] B. Giese, B. Kopping, T. Göbel, J. Dickhaut, G. Thoma, K. J. Kulicke, F. Trach in *Organic Reactions, Vol. 48* (Ed.: L. A. Paquette), Wiley, New York, **1996**, p. 301.
[8] D. S. Hays, G. C. Fu, *J. Am. Chem. Soc.* **1995**, *117*, 7283–7284.
[9] a) T. Naito, K. Tajiri, T. Harimoto, I. Ninomiya, T. Kiguchi, *Tetrahedron Lett.* **1994**, *35*, 2205–2206; b) T. Kiguchi, K. Tajiri, I. Ninomiya, T. Naito, H. Hiramatsu, *ibid.* **1995**, *36*, 253–256.
[10] a) J. L. Chiara, W. Cabri, S. Hanessian, *Tetrahedron Lett.* **1991**, *32*, 1125–1128; b) J. P. Guidot, T. Le Gall, C. Mioskowski, *ibid.* **1994**, *35*, 6671–6672.
[11] Z. Hou, T. Miyano, H. Yamazaki, Y. Wakazuki, *J. Am. Chem. Soc.* **1995**, *117*, 4421–4422.
[12] Z. Hou, H. Yamazaki, Y. Fujiwara, H. Taniguchi, *Organometallics* **1992**, *11*, 2711–2714.
[13] a) A. W. Konradi, S. J. Kemp, S. F. Pedersen, *J. Am. Chem. Soc.* **1994**, *116*, 1316–1323; b) B. Kammermeier, G. Beck, D. Jacobi, H. Jendralla, *Angew. Chem.* **1994**, *106*, 719–721; *Angew. Chem. Int. Ed. Engl.* **1994**, *33*, 685–687.
[14] E. J. Roskamp, S. F. Pedersen, *J. Am. Chem. Soc.* **1987**, *109*, 6551–6553.

Selective Catalytic Reactions at the External Surface of Zeolite Crystals

Stefan Ernst*

Zeolites are crystalline microporous aluminosilicates consisting of SiO_4 and AlO_4 tetrahedra as the primary building units. One salient feature of the crystalline structure of zeolites is the occurrence of strictly regular cavities and pores with sizes of the same order of magnitude as molecular dimensions (0.3–1.5 nm). Zeolites have found widespread applications as catalysts in the petroleum refining industry, in petrochemical processes, and for the manufacture of organic intermediates. Furthermore, they are used as selective adsorbents in separation and purification processes and as phosphate substituents in detergents.[1, 2] Many of the catalytic applications of zeolites are based on the principle of shape-selective catalysis. Shape selectivity effects in microporous solids may occur if the pore width of the solid and the dimensions of the reactant molecules, product molecules, and transition states, which take part in the catalytic reaction, are similar.[3] Consequently in the nomenclature adopted by Csicsery,[4] distinctions are made between *reactant shape selectivity*, *product shape selectivity*, and *restricted transition state shape selectivity* (Fig. 1). Reactant shape selectivity occurs when from at least two reactants only one is "slim" enough to enter the pores of the zeolite where most of the catalytically active (acid) sites are located. Hence, only the less bulky molecule is catalytically converted, whereas the bulky reactants are not. Product shape selectivity may be regarded as the reverse of reactant shape selectivity: all reactants are small enough to enter the zeolite pores, but of the potential products only one species is small enough to leave the pore system. Restricted transition state shape selectivity finally takes place if one of at least two parallel or consecutive reactions is suppressed because it requires a bulky transition state. Thus, this reaction cannot occur if there is insufficient space within the pore system.

There are numerous examples for the three classical types of shape-selective catalysis in zeolites. In some cases, however, experimentally observed selectivities could not be explained based on this early classification. Hence, a number of new concepts

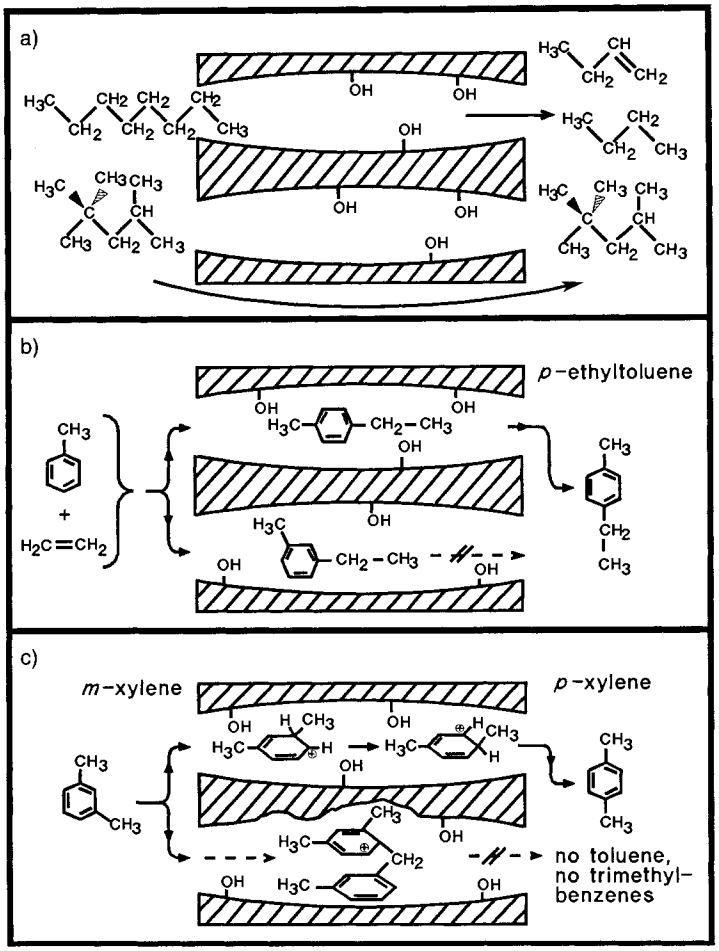

Fig. 1. Examples for the three classical types of shape-selective catalysis in zeolites. a) Reactant shape selectivity: from a mixture consisting of *n*-octane and 2,2,4-trimethylpentane, only the "slim" isomer is able to diffuse to the active sites inside the zeolite pores where it is catalytically cracked. b) Product shape selectivity: the reactants are small enough to enter the zeolite pores, but of the potential products (*o*-, *m*-, and *p*-ethyltoluene), only the "slim" *para* isomer is small enough to leave the pore system. c) Restricted transition state shape selectivity: disproportionation of *m*-xylene into toluene and trimethylbenzenes is suppressed because the required formation of the relatively bulky bimolecular transition state is inhibited due to steric constraints.

[*] Dr.-Ing. S. Ernst
Institut für Technische Chemie I der Universität
D-70550 Stuttgart (Germany)
Fax: Int. code + (711) 685-4065

have been developed which have found varying degrees of acceptance. Examples include the "cage- or window effect",[5] and "molecular traffic control".[6] Also, several attempts have been made to assign shape-selective properties even to the external surface of zeolite crystals[7, 8] (see for example the "nest effect"). However, sophisticated catalytic experiments[10] revealed that the selectivities described earlier, in particular in references [7, 8], can be alternatively explained in a straightforward manner by classical shape-selectivity concepts.

In light of this, recent work by Martens et al.,[11] describing the selective isomerization of long-chain *n*-alkanes over zeolite ZSM-22, is particularly interesting. The pore system of zeolite ZSM-22 consists of linear, non-interconnected channels with crystallographic diameters of about 0.45 nm × 0.55 nm. If this zeolite is modified into its Brønsted acid (H^+) form and loaded by ion exchange with a small amount of a noble metal (for example 0.5 wt.% of platinum), a bifunctional catalyst (i.e., acidic and with hydrogenation/dehydrogenation activity) is obtained which is capable of converting unbranched alkanes into their branched isomers. In their experiments, Martens et al., used *n*-heptadecane (n-$C_{17}H_{36}$) as the model *n*-alkane. At low conversions, monobranched isomers with one methyl group are formed exclusively, namely 2-, 3-, 4-, 5-, and 6-methylhexadecane. Among them, 2-methylhexadecane, that is the isomer with the methyl branching near the end of the hydrocarbon chain, strongly predominates. Isomers with longer side chains (for example ethylpentadecanes or propyltetradecanes) are virtually absent, presumably due to the limited space in the relatively narrow pores of zeolite ZSM-22. The preponderance of methyl branching in the 2-position over this zeolite is in sharp contrast to what is typically observed with zeolites of larger pore widths (for example, zeolite Y): In such a large pore zeolite catalyst, methyl isomers having the branching at or near the center of the long chain are preferentially formed over those with terminal branching (which would be also expected on the basis of the reaction mechanism via protonated cyclopropanes[12]). Furthermore, isomers with ethyl or propyl branchings are also formed over large pore zeolites, even at low conversions. The pronounced selectivity of zeolite ZSM-22 for the formation of the terminal methyl-branched isomer (2-methylhexadecane) has been ascribed in a previous publication to a pore mouth catalysis mechanism, by which isoalkanes with the longest possible linear chain are favored.[13] In this picture, the catalytic reaction does indeed occur inside the pores of the zeolite, however, due to the slow diffusion of the reactant molecules, near the mouths of the pores. The recent work from the same research group takes this one step further.[11] It is postulated that 2-methylhexadecane, which is preferentially formed in the first branching step, arranges on the surface of the zeolite crystals in such a manner that the methyl group is pinned in one pore mouth while the rest of the molecule is stretched across an external [001] crystal face. The second branching is then introduced in a position were a neighboring pore mouth and its active site can be reached. In agreement with this hypothesis, of the 219 theoretically possible dibranched isoheptadecanes essentially only five are formed over zeolite ZSM-22, namely 2,7-, 2,8-, 2,9-, 2,10-, and 2,11-dimethylpentadecane. The distance between the two methyl branchings in these five compounds correlates well with the distance between two adjacent pore entrances in the [001] plane of the zeolite ZSM-22 surface. Supplementary experiments with selected additional reactant molecules (1-nonylcyclopentane; icosane (n-$C_{20}H_{42}$)) seem to support the concept advanced by Martens et al. The authors therefore concluded that, at least for the examples reported in their study, shape-selective catalysis at the external surface of zeolite crystals may occur during which the geometric arrangement of the pore mouths acts as a template for the positions of the methyl branchings. This model may be also helpful for a refined interpretation of previously reported results from the isomerization of long-chain *n*-alkanes over zeolite ZSM-22 and the structurally closely related zeolite ZSM-23.[14]

Although there is already important experimental evidence supporting the new concept advanced by Martens et al., there are still several questions that remain to be answered. For instance: Can the concept be transferred to other reactants and other zeolite structures? Which role do the active sites at the external surface of the zeolite crystals play? What is the influence of the crystal size (and, hence, the proportion of the external as compared to the total surface area) on activity and selectivity of the zeolite? The answers to these (and probably other) questions will determine the future acceptance of the proposed model by the scientific community.

German version: *Angew. Chem.* **1996**, *108*, 67–68

Keywords: catalysis · isomerizations · shape selectivity · zeolites

[1] L. Puppe, *Chem. Unserer Zeit* **1986**, *20*, 117; W. Hölderich, M. Hesse, F. Näumann, *Angew. Chem.* **1988**, *100*, 232; *Angew. Chem. Int. Ed. Engl.* **1988**, *27*, 226; J. M. Thomas, *ibid.* **1994**, *106*, 963 and **1994**, *33*, 913.
[2] N. Y. Chen, W. E. Garwood, F. G. Dwyer, *Shape Selective Catalysis in Industrial Applications*, Dekker, New York, **1989**.
[3] J. Weitkamp, H. Dauns, S. Ernst, E. Gallei, *Chem. Ing. Tech.* **1986**, *58*, 623.
[4] S. M. Csicsery, *ACS Monogr.* **1976**, *171*, 680.
[5] R. L. Gorring, *J. Catal.* **1973**, *31*, 13.
[6] E. G. Derouane, Z. Gabelica, *J. Catal.* **1980**, *65*, 486.
[7] D. Fraenkel, M. Cherniavsky, M. Levy, *Proc. Int. Congr. Catal. 8th, Vol. 4*, Verlag Chemie, Weinheim, **1984**, p. 545.
[8] D. Fraenkel, M. Cherniavsky, B. Ittah, M. Levy, *J. Catal.* **1986**, *101*, 273.
[9] E. G. Derouane, *J. Catal.* **1986**, *100*, 541.
[10] M. Neuber, J. Weitkamp in *Zeolites for the Nineties: Recent Research Reports, 8th International Zeolite Conference* (Eds.: J. C. Jansen, L. Moscou, M. F. M. Post), Amsterdam, **1989**, p. 425.
[11] J. A. Martens, W. Souverijns, W. Verrelst, R. Parton, G. F. Froment, P. A. Jacobs, *Angew. Chem.* **1995**, *107*, 2726; *Angew. Chem. Int. Ed. Engl.* **1995**, *34*, 2528.
[12] J. Weitkamp, *Ind. Eng. Chem. Prod. Res. Dev.* **1982**, *21*, 550.
[13] J. A. Martens, R. Parton, L. Uytterhoeven, P. A. Jacobs, G. F. Froment, *Appl. Catal.* **1991**, *76*, 95.
[14] S. Ernst, G. T. Kokotailo, R. Kumar, J. Weitkamp, *Proc. Int. Congr. Catal. 9th, Vol. 1*, The Chemical Institute of Canada, Ottawa, **1988**, p. 388.

 © VCH Verlagsgesellschaft mbH, D-69451 Weinheim, 1996 0570-0833/96/3501-0064 $ 10.00+.25/0

Tetrasupersilyldiindium(*In–In*) and Tetrasupersilyldithallium(*Tl–Tl*): $(t\mathrm{Bu_3Si})_2\mathrm{M}-\mathrm{M}(\mathrm{Si}t\mathrm{Bu_3})_2$ (M = In, Tl)**

Nils Wiberg,* Kerstin Amelunxen, Heinrich Nöth, Martin Schmidt, and Holger Schwenk

Dedicated to Professor Heinz Peter Fritz

Donor-free, uncharged molecular compounds $(RM)_n$ and $(R_2M)_2$ with clusters formed from the boron homologues M = Al, Ga, In, Tl have—unlike such compounds with boron clusters[1]—only been known for about ten years. In fact, the compounds of the boron homologues have a tendency to disproportionate ($6\,RM \rightarrow 3\,R_2M + 3\,M \rightarrow 2\,R_3M + 4\,M$); however, this process can be stopped at the $(RM)_n$ stage (very bulky groups) or at the $(R_2M)_2$ stage (medium-sized bulky groups) by employing bulky substituents R such as C_5Me_5 (Cp*), $C_5(CH_2Ph)_5$ (Cp**), $CH(SiMe_3)_2$ (Disyl), $C(SiMe_3)_3$ (Trisyl), 2,4,6-$i\mathrm{Pr_3C_6H_2}$ (Trip), 2,4,6-$(CF_3)_3C_6H_2$ (R^F), $Si(SiMe_3)_3$ (Hypersilyl), and $Si t\mathrm{Bu_3}$ (Supersilyl). Known examples of R_4M_2 and $(RM)_n$ compounds with normal covalent M–M bonds are $[(Me_3Si)_2CH]_4M_2$ (M = Al, Ga, In),[1] (2,4,6-$i\mathrm{Pr_3C_6H_2}$)$_4M_2$ (M = Al, Ga),[2] $[2,4,6\text{-}(CF_3)_3C_6H_2]_4M_2$ (M = Ga, In),[1] or $[(Me_3Si)_3Si]_4Tl_2$,[3] and $(RAl)_4$ (R = $Si t\mathrm{Bu_3}$, Cp*),[4] $(RGa)_4$ (R = $C(SiMe_3)_3$,[1] $Si(SiMe_3)_3$[5]) or $[(Me_3Si)_3CIn]_4$,[6] respectively. Only very weak M–M interactions are present in the compounds $(Cp^*In)_6$[7] and $(Cp^{**}M)_2$ (M = In, Tl).[8]

It should be possible to stabilize compounds of the type $(RM)_n$ by using, as we have done previously, the readily accessible and chemically comparably inert supersilyl group.[4a] The ability of this group to potentially stabilize such compounds arises from its very high steric demand[9] and its prominent tendency to donate electrons to its bonding partners[1, 4c] with this donation having a cluster stabilizing effect. Indeed, the reaction of aluminum monochloride in toluene/diethyl ether[10] with supersilylsodium $t\mathrm{Bu_3SiNa}$ in dibutyl ether at −78 °C gave, among others, the deep violet tetraalatetrahedrane $(t\mathrm{Bu_3SiAl})_4$ **1** [Eq. (a)], which as expected was metastable (sublimation at 180 °C under high vacuum; Al–Al: calcd. 2.64 Å, Al–Al dissociation energy per edge of the tetrahedron: calcd. ca. 100 kJ mol^{-1}; for comparison $(Cp^*Al)_4$: thermolysis at 70 °C; Al–Al: found 2.77 Å; Al–Al dissociation energy per edge of the tetrahedron: calcd. 25 kJ mol^{-1}).[4, 11]

$$4\,\mathrm{AlCl} + 4\,t\mathrm{Bu_3SiNa} \xrightarrow[-4\,\mathrm{NaCl}]{\text{(toluene, } Et_2O, Bu_2O)} t\mathrm{Bu_3Si}-\mathrm{Al}\langle(\mathrm{Al}-\mathrm{Si}t\mathrm{Bu_3})_3 \quad \text{(a)}$$

1

To our surprise the reactions of indium bromide and thallium bromide with supersilyl sodium $t\mathrm{Bu_3SiNa}$ in tetrahydrofuran at −78 °C did not lead to the tetrahedranes $(t\mathrm{Bu_3SiM})_4$ (M = In, Tl)[6] but gave the diindium compound **2** and indium and the dithallium compound **3** and thallium, respectively, [Eq. (b)]. In addition, $t\mathrm{Bu_3SiH}$, $t\mathrm{Bu_3SiBr}$, and $(t\mathrm{Bu_3Si})_2$ were formed in these reactions.

$$4\,\mathrm{MBr} + 4\,t\mathrm{Bu_3SiNa} \xrightarrow[-4\,\mathrm{NaBr}]{\text{(THF)}} (t\mathrm{Bu_3Si})_2\mathrm{M}-\mathrm{M}(\mathrm{Si}t\mathrm{Bu_3})_2 + 2\,\mathrm{M} \quad \text{(b)}$$

2 (M = In); **3** (M = Tl)

That **2** and **3**, respectively, are formed in these reactions is probably a result of how the reaction was carried out, since the tetraindatetrahedrane $[(Me_3Si)_3CIn]_4$ is accessible from corresponding starting materials.[6] Possibly, **2** and **3** are formed on the surface of the MBr crystals, which are insoluble in THF. The formation of $(t\mathrm{Bu_3Si})_2$ in high yields indicates the existence of intermediary $t\mathrm{Bu_3Si}^{\cdot}$ radicals.

Compound **2** is obtained as deep violet and compound **3** as black-green crystals, which decompose at about 125 and about 52 °C, respectively. The thermolysis of **2** in [D$_8$]toluene at 40 °C occurs slowly ($t_{1/2} \approx 8$ d), that of compound **3** very quickly; $t\mathrm{Bu_3SiD}$ and $(t\mathrm{Bu_3Si})_2$ are formed in these reactions, together with other $t\mathrm{Bu_3Si}$-containing compounds and elemental thallium, respectively.[12] Compound **2** is attacked only very slowly by methanol at room temperature.[12]

The structures of compounds **2** and **3**, which crystallize isomorphically, were determined by X-ray diffraction (Fig. 1).[13] However, due to the decomposition of compound **3** in the X-ray beam, only its Tl and Si positions could be determined with sufficient precision; thus, in this case the crystal structure analysis should only be considered as evidence for the constitution of the compound. The central structural element of both compounds is the M–M grouping. The M atoms are each coordinated in a trigonal planar fashion by two Si atoms and one M atom; the $MMSi_2$ planes are orthogonal (Si-In-In-Si angle between 89.5 and 90.5°, Fig. 1). The high steric demand of the supersilyl groups leads to the very long M–M distances of 2.921 Å (**2**; for comparison $[(Me_3Si)_2CH]_4In_2$: 2.828 Å[1]) and 2.966 Å (**3**; for comparison $[(Me_3Si)_3Si]_4Tl_2$: 2.914 Å[3]). The angles between the MMR_2 planes are significantly smaller in R_4M_2 compounds with less bulky substituents R, (e.g. $[(Me_3Si)_2CH]_4M_2$:[1] 8° (M = Al), 5.0° (M = Ga), 6.7° (M = In); (2,4,6-$i\mathrm{Pr_3C_6H_2}$)$_4Ga_2$: 43.8°;[2] with regard to the conformation of R_4M_2 see ref.[1]). The Si-M-Si and M-M-Si angles in both compounds are about 130 and 115°, respectively. The C-Si-C angle (av 109.7°) of the supersilyl group $t\mathrm{Bu_3Si}$ in **2** is at the lower end of the normal range of 110–112° (extreme C-Si-C angles are exhibited by the very sterically bulky $(t\mathrm{Bu_3Si})_2$ (107.3°[9a]) and by the less bulky $t\mathrm{Bu_3SiH}$ (113.7°[14])).

[*] Prof. Dr. N. Wiberg, Dipl.-Chem. K. Amelunxen, Prof. Dr. H. Nöth, Dr. M. Schmidt, Dipl.-Chem. H. Schwenk
Institut für Anorganische Chemie der Universität
Meiserstrasse 1, D-80333 München (Germany)
Fax: Int. code +(89)5902-451

[**] Sterically Overloaded Silicon Compounds, Part 8, Silicon Compounds Part 99. This work was supported by the Deutsche Forschungsgemeinschaft. Part 7: N. Wiberg in Progress in Organosilicon Chemistry (Eds.: B. Marciniec, J. Chojnewski), Gordon and Breach Science Publishers, Amsterdam, **1995**, pp. 19–39. Part 6: Ref.[9b]. Part 98: N. Wiberg, M. Link, *Chem. Ber.* **1995**, *128*, 1241.

 © VCH Verlagsgesellschaft mbH, D-69451 Weinheim, 1996 0570-0833/96/3501-0065 $ 10.00+.25/0

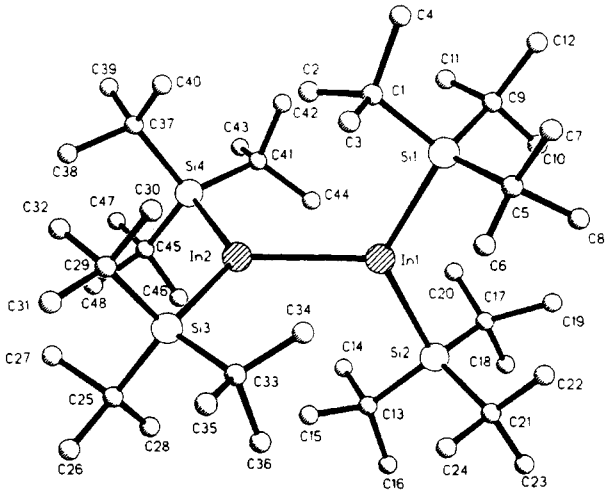

Fig. 1. Crystal structure of **2**. The H atoms were omitted for clarity. Important bond lengths [Å] and angles [°]: In1–In2 2.9217(11), In1–Si1 2.778(4), In1–Si2 2.779(4), In2–Si3 2.778(4), In2–Si4 2.778(4), Si1–C1 1.95(2), Si1–C5 1.94(2), Si1–C9 1.95(2) [mean value of Si–C distances 1.95], C1–C2 1.50(3), C1–C3 1.48(3), C1–C4 1.59(3); Si1-In1-Si2 129.43(11), Si3-In2-Si4 129.25(12), In2-In1-Si1 115.27(9), In2-In1-Si2 115.30(9), In1-In2-Si3 115.15(9), In1-In2-Si4 115.60(9), In1-Si1-C1 108.0(5), In1-Si1-C5 109.7(6), In1-Si1-C9 110.1(6), C1-Si1-C5 110.8(8), C1-Si1-C9 109.0(7), C5-Si1-C9 109.2(9) [mean value of the C-Si-C angles 109.7°]. Crystal structure of **3** (Tl instead of In in Fig. 1). The compound is isomorphic to **2**. Only the Tl and the Si positions can be given with sufficient precision: bond lengths [Å] and angles [°]: Tl1–Tl2 2.966(2), Tl1–Si1 2.801(11), Tl1–Si2 2.765(12), Tl2–Si3 2.800(12), Tl2–Si4 2.790(11) [the Tl–Si bond lengths are of the same length within the limits of error]; Si1-Tl1-Si2 130.3(4), Si3-Tl2-Si4 130.1(3), Tl2-Tl1-Si1 114.4(2), Tl2-Tl1-Si2 115.2(3), Tl1-Tl2-Si3 114.7(2), Tl1-Tl2-Si4 115.2(3) [the bond angles are the same within the limits of error].

Experimental Procedure

2: tBu$_3$SiNa (2.91 mmol) in THF (10 mL) was added dropwise to a suspension of InBr (0.566 g, 2.91 mmol) in THF (15 mL) at −78 °C. The deep brown reaction solution was stirred for 12 h at −78 °C and then allowed to slowly warm to room temperature. According to the ^{1}H NMR spectrum of the crude mixture, compound **2** (33%), tBu$_3$SiH (5%), tBu$_3$SiBr (4%), and (tBu$_3$Si)$_2$ (58%, yields based on the amount of tBu$_3$SiNa employed) were formed. All the volatile compounds were removed in the oil pump vacuum, the residue was taken up in pentane (20 mL) and the dark precipitate (In) was filtered off from the dark violet solution. Compound **2** (0.483 g, 0.47 mmol, 16.2%) precipiated from the latter solution at −23 °C within one week in the form of deep violet crystals. These dissolved very well in nonpolar solvents such as benzene and alkanes, but not very well in polar solvents such as THF and acetone. Heating the crystalline compound **2** obtained from pentane led to the evolution of a gas (pentane?) at 105 °C and subsequent decomposition at 125 °C which was accompanied by an irreversible change in color first to orange and then to black under concomitant formation of (tBu$_3$Si)$_2$. ^{1}H NMR (C_6D_6, TMS, internal): δ = 1.35 (s; 12 tBu); ^{13}C{^{1}H} NMR (C_6D_6, TMS, internal): δ = 26.82 (12 CMe_3), 34.00 (12 CMe_3); ^{29}Si NMR (C_6D_6, INEPT, TMS, external): δ = 76.83 (4 SitBu$_3$); MS: m/z: 513 [$(M/2)^+$]; C,H analysis ($C_{48}H_{108}In_2Si_4$, 1027.4): calcd. C 56.12, H 10.60; found 55.75, H 10.53.

3: tBu$_3$SiNa (2.88 mmol) in THF (10 mL) was added dropwise to a suspension of TlBr (0.826 g, 2.88 mmol) in THF (15 mL) at −78 °C. The resulting solution changed color first to red, then green, and finally brown. The reaction mixture was stirred for 12 h at −78 °C and then slowly allowed to warm to room temperature. According to the ^{1}H NMR spectrum of the crude mixture, compound **3** (27%), tBu$_3$SiH (12%), tBu$_3$SiBr (4%), and (tBu$_3$Si)$_2$ (57%, yields based on the amount of tBu$_3$SiNa employed) were formed [15]. All the volatile compounds were removed in the oil pump vacuum, the residue was taken up in Et$_2$O (20 mL), and the dark precipitate (Tl) was filtered off from the deep green solution. Compound **3** (0.314 g, 0.26 mmol, 9.0%) precipiated from the latter solution at −23 °C within one week in the form of black-green crystals. Compound **3** exhibited a similar solubility to **2**. It decomposed above 52 °C with a change in color to black and concomitant formation of silyl compounds such as (tBu$_3$Si)$_2$. ^{1}H NMR (C_6D_6, TMS, internal): δ = 1.32 (d; ^4J(H,Tl) = 6.7 Hz; 12 tBu); ^{13}C{^{1}H} NMR (C_6D_6, TMS, internal): δ = 28.57 (d, ^2J(C,Tl) = 155.8 Hz; 12 CMe_3), 33.12 (d, ^3J(C,Tl) = 49.9 Hz; 12 CMe_3); ^{29}Si NMR (C_6D_6, INEPT, TMS, external): δ = 100.2 (d, $^1J(^{29}Si,^{205}Tl)$ = 1451, $^1J(^{29}Si,^{203}Tl)$ = 1436 Hz; 4 SitBu$_3$); MS: m/z: 601/603 [$(M/2)^+$; with ^{203}Tl and ^{205}Tl, respectively]; C,H analysis ($C_{48}H_{108}Tl_2Si_4$, 1206.4): calcd. C 47.79, H 9.02; found 53.54, H 10.08.

Received: August 9, 1995 [Z 8296 IE]
German version: *Angew. Chem.* **1996**, *108*, 110–112

Keywords: indium compounds · silicon compounds tetrahedranes · thallium compounds

[1] W. Uhl, *Angew. Chem.* **1993**, *105*, 1449; *Angew. Chem. Int. Ed. Engl.* **1993**, *32*, 1386, and references therein.
[2] X. He, R. A. Bartlett, M. M. Olmstead, K. Ruhlandt-Senge, B. E. Sturgeon, P. P. Power, *Angew. Chem.* **1993**, *105*, 761; *Angew. Chem. Int. Ed. Engl.* **1993**, *32*, 717.
[3] S. Henkel, K. W. Klinkhammer, W. Schwarz, *Angew. Chem.* **1994**, *106*, 721; *Angew. Chem. Int. Ed. Engl.* **1994**, *33*, 681.
[4] a) N. Wiberg in *Frontiers of Organosilicon Chemistry* (Eds.: A. R. Bassindale, P. P. Gaspar), The Royal Society of Chemistry, Cambridge, **1991**, pp. 263–270; b) C. Dohmeier, C. Robl, M. Tacke, H. Schnöckel, *Angew. Chem.* **1991**, *103*, 594; *Angew. Chem. Int. Ed. Engl.* **1991**, *30*, 564; c) with regard to the ab initio calculations see N. Schneider, R. Ahlrichs, H. Horn, A. Schäfer, *ibid.* **1992**, *104*, 327 or **1992**, *31*, 353.
[5] G. Linti, *Inorg. Chem.*, in press.
[6] R. D. Schluter, A. H. Cowley, D. A. Atwood, R. A. Jones, J. L. Atwood, *J. Coord. Chem.* **1993**, *30*, 25; W. Uhl, R. Graupner, M. Layh, U. Schütz, *J. Organomet. Chem.* **1995**, *493*, C1.
[7] O. T. Beachley, Jr., R. Blom, M. R. Churchill, K. Faegrie, J. C. Fettinger, J. C. Pazik, L. Victoriano, *Organometallics* **1989**, *8*, 346.
[8] a) H. Schumann, C. Janiak, J. Pickardt, U. Börner, *Angew. Chem.* **1987**, *99*, 788; *Angew. Chem. Int. Ed. Engl.* **1987**, *26*, 789; H. Schumann, C. Janiak, F. Görlitz, J. Loebel, A. Dietrich, *J. Organomet. Chem.* **1989**, *363*, 243; b) with regard to the ab initio calculations see C. Janiak, R. Hoffmann, *J. Am. Chem. Soc.* **1990**, *112*, 5924.
[9] a) N. Wiberg, H. Schuster, A. Simon, K. Peters, *Angew. Chem.* **1986**, *98*, 100; *Angew. Chem. Int. Ed. Engl.* **1986**, *25*, 79; b) N. Wiberg, C. M. M. Finger, K. Polborn, *ibid.* **1993**, *105*, 1140 and **1993**, *32*, 1054.
[10] M. Tacke, H. Schnöckel, *Inorg. Chem.* **1989**, *28*, 2895.
[11] Additional information to ref.[4a] (established together with H. Schnöckel, T. Passler, C. Dohmeier): On warming a solution of AlCl (4.70 mmol) in toluene/Et$_2$O [10] (20 mL) and tBu$_3$SiNa (4.75 mmol) in Bu$_2$O (25 mL) from −78 °C, the solution became dark red at about 0 °C. According to the ^{1}H NMR spectrum of the crude mixture, tBu$_3$SiH (60%), (tBu$_3$Si)$_2$ (27%), and **1** (13%) are formed together with intermediary traces of a radical (as revealed by the ESR spectrum which shows a line-rich signal indicating a species containing three Al atoms). Compound **1** could so far not be isolated by crystallization from the reaction solution; however, by sublimation of the reaction mixture at 180 °C under high vacuum, **1** was obtained as a deep violet, X-ray amorphous, pentane-soluble, oxygen- and moisture-sensitive solid. ^{1}H NMR (C_6D_6, TMS, internal): δ = 1.35 (br., 12 tBu); ^{29}Si NMR (C_6D_6, TMS, external): δ = 15.34 (br., 4 SitBu$_3$); ^{27}Al NMR (C_6D_6, Al(NO$_3$)$_3$, external in D$_2$O): δ = 64.48 (line width = 148 Hz); MS: m/z: 904 [M^+].
[12] N. Wiberg, K. Amelunxen, unpublished results. Additional properties of **2** and **3**: Compound **2** reacted with AgF$_2$ in heptane at room temperature to give among others (tBu$_3$Si)$_2$InF ($C_{24}H_{54}FInSi_2$ (532.7); ^{1}H NMR (C_6D_6, TMS, internal): δ = 1.27 (s, 6 tBu); ^{29}Si NMR (C_6D_6, INEPT, TMS, internal): δ = 50.27 (d, ^2J(Si,F) = 6.5 Hz; 2 SitBu$_3$); MS: m/z: 532 [M^+]). Its thermolysis in C_6D_6 at 40 °C yields tBu$_3$SiF, (tBu$_3$Si)$_2$, and In. The reaction of **3** with AgF$_2$ in Et$_2$O at room temperature led, possibly via (tBu$_3$Si)$_2$TlF, to tBu$_3$SiF, (tBu$_3$Si)$_2$, and Tl. The reaction of **2** with Na in C_6D_6 at 40 °C led after 3 d to tBu$_3$SiNa, (tBu$_3$Si)$_2$, tBu$_3$SiD, tBu$_3$SiC$_6$D$_5$, and In, whereas the reaction of **3** with Na in C_6D_6 at 40 °C led after 1 d to tBu$_3$SiNa, tBu$_3$SiD as well as to two additional tBu$_3$Si-containing compounds and Tl. Compound **3** shows a line-rich ESR signal in C_6D_6 at room temperature (dissociation in intermediary (tBu$_3$Si)$_2$Tl$^{\cdot}$ radicals?). Compounds **2** and **3** are intensely colored (deep violet and black green; in comparison [(Me$_3$Si)$_2$CH]$_4$In$_2$ and [2,4,6-(CF$_3$)$_3$C$_6$H$_2$]$_4$In$_2$: orange [1]; [(Me$_3$Si)$_3$Si]$_4$Tl$_2$: dark red [3]), which might be attributed to the presence of radicals such as (tBu$_3$Si)$_2$Tl$^{\cdot}$.
[13] Crystallographic data of **2**: $(C_{48}H_{108}In_2Si_4 \cdot C_5H_{12}$, M_r = 1027.34): a = 20.471(3), b = 15.553(3), c = 41.746(6) Å, β = 99.84(1)°, V = 13095(4) Å^3, monoclinic, space group $C2/c$, Z = 8, ρ_{calcd} = 1.042 g cm^{-3}, μ = 8.01 cm^{-1}, $F(000)$ = 4400. Crystal dimensions = 0.6 × 0.6 × 0.5 mm^3. The single crystal was mounted in perfluoroether oil and all measurements were performed at 183 K. Data collection: ω scans, 2θ = 3–50° in $-24 < h < 3$; $0 < k < 18$; $-47 < l < 48$. 11816 measured reflections, 10938 symmetry independent, 6720 with $F > 4\sigma(F)$, max/min transmission: 0.645/0.569. Structure solution and refinement: heavy atom method, full matrix refinement against F^2, 604 parameters refined, 105 restraints, R_1 = 0.086, $wR2$ = 0.229, GOF = 1.129; largest residual electron density = 1.889 e Å^{-3}. The non-hydrogen atoms were refined with anisotropic temperature parameters, the H atoms were included into the refinement in calculated positions with a riding model. The temperature factors indicated that the *tert*-butyl groups were rotationally disordered. For eight of these 36 methyl groups this disorder was taken into consideration by refinement of the sites into two positions. The relatively large residual electron density, which was not located near the In or Si atoms, indicated the presence of a possible additional disordered solvent molecule in the unit cell. Crystallographic data of **3** ($C_{48}H_{108}Tl_2Si_4$, M_r = 1206.4): a = 20.309(6),

$b = 15.387(4)$, $c = 41.57(2)$ Å, $\beta = 99.44(3)^\circ$, $V = 12814.5$ Å^3, monoclinic, space group $C2/c$, $Z = 8$, $\rho_{calcd} = 1.251$ g cm^{-3}, $\mu = 51.2$ cm^{-1}, $F(000) = 4912$. Crystal mounted in perflouroether oil; measurements at 213 K. Data collection: ω scans, $2\theta = 3-46^\circ$ in $h, k, \pm l$. 7738 measured reflections, 7354 of which were independent and 4339 with $F > 4\sigma(F)$. Structure solution and refinement: heavy atom method, Tl and Si atoms anisotropically refined, C atoms isotropically. The structure solution converged without inclusion of H atoms and possible solvent molecules at $R_1 = 0.135$, $wR2 = 0.417$, GOF = 1.097. The crystal decomposed considerably during the measurement; the measurement was stopped when the intensity of two standard reflections became smaller than 50%, which is why the C atoms were not refined anisotropically. Further details of the crystal structure investigation may be obtained from the Fachinformationszentrum Karlsruhe, D-76344 Eggenstein-Leopoldshafen (Germany) on quoting the depository number CSD-404429.

[14] S. H. Down, L. S. Wartell, *J. Molec. Struct.* **1980**, *67*, 249.

[15] The solution contains an additional tBu$_3$Si-containing thallium compound in traces [^{29}Si NMR (C_6D_6, INEPT, TMS, external): $\delta = 99.79$ (d, $^1J(^{29}Si,^{205}Tl) = 1652$, $^1J(^{29}Si,^{203}Tl) = 1636$ Hz)]. This compound was formed from the reaction of CpTl with tBu$_3$SiNa in THF (red reaction solution) in higher yields.

Synthesis and Structure of Seven-Coordinate Bismuth(v) Complexes with Benzenoid and Non-Benzenoid Arene Ligands: Tri(aryl)tropolonatobismuth(v) Complexes**

Uwe Dittes, Bernhard Klaus Keppler,* and Bernhard Nuber

To obtain stable bismuth(v) compounds, starting materials are required that behave as strongly electronegative bonding partners or, at least, show rather large group electronegativities, as is true for substituted phenyl groups and similar aromatic systems.[1] By far the best known example of an arylbismuth(v) compound is pentaphenylbismuth which was prepared by G. Wittig and K. Clauss, and later crystallographically characterized in 1987.[2, 3] Many of the bismuth(v) compounds prepared to date are five-coordinate; the synthesis of the hexaphenylbismutate complex ion provided a six-coordinate bismuth(v) ion.[4, 5] Tri(organo)bismuth sulfonates and tri(aryl)bismuth dicarboxylates are compounds for which a five- and seven-coordinate bismuth(v) ion, respectively, are discussed.[6–9] Little information is available regarding the biological activity of bismuth(v) compounds, since most of these complexes are too unstable for biological and medicinal studies. We now report the synthesis of tri(aryl)tropolonatobismuth(v) complexes that are suitable for such investigations.

Tropolone and its derivatives are well-studied non-benzenoid aromatic systems.[10] Following removal of the proton of the hydroxy group, metals can bind to the two oxygen atoms, resulting in the formation of chelates (Scheme 1). Tropolonatobismuth(III) complexes are stable compounds that have been shown to exhibit biological activity, for example, against *Helicobacter pylori* bacteria, which are responsible for gastritis and other gastrointestinal diseases.[11] The heretofore unknown tropolonatobismuth(v) complexes might have similar properties and for this reason we decided to pursue their synthesis and characterization.

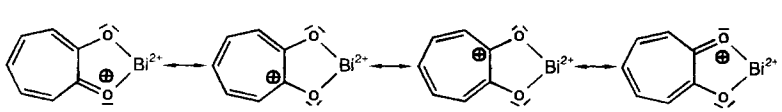

Scheme 1. Mesomeric structures of the tropolone ligands in the tropolonato complexes.

Treatment of diacetetotri(aryl)bismuth(v) compounds with tropolone derivatives results in the cleavage of the two acetate groups and their exchange for two tropolone rings. Diacetatotri(phenyl)bismuth(v) **4** can be prepared readily in ether from triphenylbismuth and acetic acid in the presence of *tert*-butylhydroperoxide.[12] We employed this method to synthesize diacetatotri(*p*-tolyl)bismuth(v) **1** in good yield. The reaction of **1** with tropolone **2** in methanol (heating under reflux for 30 min, yield 69%) led to water- and air-stable yellow crystals of di(*O,O*-tropolonato)tri(*p*-tolyl)bismuth(v) **3**, suitable for a crystal structure analysis (Fig. 1).[13] Complex **3** has a distorted pentagonal-bipyramidal structure; the base of the pyramid comprises a tolyl group (C17) and two tropolone rings (twist angle 11.7°). The remaining two tolyl groups occupy axial positions; the angle between them (C32-Bi1-C20) is 158.8°. The interaction between the oxygen atoms of the tropolone rings and the bismuth atom leads to Bi–O bonds of different lengths; two are shorter (Bi–O1 2.316, Bi–O3 2.310 Å) and two are longer (Bi–O2 2.497, Bi–O4 2.455 Å). Opposite bonds are of approximately similar length. The measured Bi-O-C angles lie in the range 119.5–121.5°, a finding consistent with sp^2-hybridization of the oxygen atoms. For the short Bi–O bond lengths we expected elongation of the corresponding C–O bonds, since the electron pull exerted by the bismuth atom and transmitted through the oxygen atom should weaken the C–O bond. This prediction was indeed confirmed for the O3–C8 bond (1.286 Å) and the O4–C14 bond (1.263 Å); however, the short Bi–O1

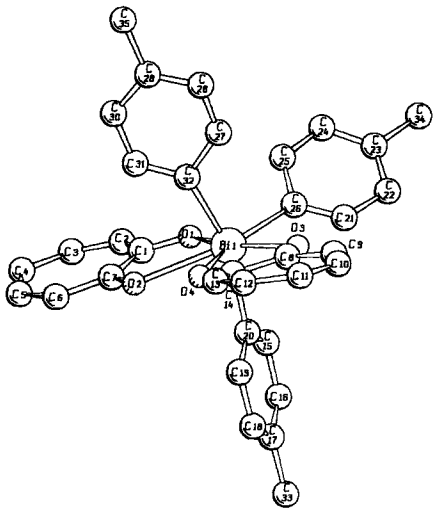

Fig. 1. Molecular structure of **3** in the crystal. Selected distances [Å] and angles [°]: Bi(1)-O(1) 2.317(16), Bi(1)-O(2) 2.498(15), Bi(1)-O(3) 2.310(16), Bi(1)-O(4) 2.456(14), Bi(1)-C(20) 2.215(23), Bi(1)-C(26) 2.156(24), Bi(1)-C(32) 2.119(28), O(1)-C(1) 1.266(31), O(2)-C(7) 1.316(33), O(3)-C(8) 1.286(26), O(4)-C(14) 1.263(31); O(1)-Bi(1)-O(2) 67.6(6), O(1)-Bi(1)-O(3) 156.7(5), O(2)-Bi(1)-O(3) 134.7(5), O(1)-Bi(1)-O(4) 137.4(5), O(2)-Bi(1)-O(4) 70.0(5), O(3)-Bi(1)-O(4) 65.7(5), C(20)-Bi(1)-C(26) 101.7(9), C(1)-Bi(1)-C(32) 93.5(8), O(2)-Bi(1)-C(32) 82.4(7), O(3)-Bi(1)-C(32) 96.0(8), O(4)-Bi(1)-C(32) 76.9(8), C(20)-Bi(1)-C(32) 158.8(9), C(26)-Bi(1)-C(32) 99.4(9), Bi(1)-O(1)-C(1) 121.5(14), Bi(1)-O(2)-C(7) 112.6(13), Bi(1)-O(3)-C(8) 120.7(14), Bi(1)-O(4)-C(14) 119.5(13).

[*] Doz. Dr. Dr. B. K. Keppler, Dipl.-Chem. U. Dittes, Dr. B. Nuber
Anorganisch-chemisches Institut der Universität
Im Neuenheimer Feld 270, D-69120 Heidelberg (Germany)
Fax: Int. code +(6221)564955

[**] This work was supported by the Fonds der Chemischen Industrie and the Deutsche Forschungsgemeinschaft.

bond (2.316 Å) is accompanied by a short C1–O1 bond (1.266 Å), and the long Bi–O2 bond (2.497 Å) is accompanied by a long C7–O2 bond (1.315 Å). The Bi–C distances in **3** range from 2.119–2.215 Å, differing at most by 4.5% from each other; the observed bond lengths are within the range of values previously reported for covalent Bi–C bonds. This finding provides conclusive evidence that the central bismuth atom is seven-coordinate.

We obtained a second seven-coordinate bismuth(v) complex in 73.8% yield in an analogous way by treating diacetatotri(phenyl)bismuth(v) **4** with 5-nitrotropolone **5**.[14] Di(*O*,*O*-5-nitrotropolonato)tri(phenyl)bismuth(v) **6** is likewise air-stable and exhibits a similarly distorted, albeit more symmetric, pentagonal-bipyramidal structure as **3** (Fig. 2).[15] One phenyl ring

Fig. 2. Molecular structure of **6** in the crystal. Selected distances [Å] and angles [°]: Bi(1)-O(1) 2.594(14), Bi(1)-O(2) 2.315(15), Bi(1)-C(13) 2.141(18), Bi(1)-C(17) 2.391(39), Bi(1)-O(1A) 2.594(14), Bi(1)-O(2A) 2.315(15), Bi(1)-C(13A) 2.141(18), O(1)-C(1) 1.243(27), O(2)-C(7) 1.282(30); O(1)-Bi(1)-O(2) 64.7(5), O(1)-Bi(1)-O(1A) 72.3(6), O(2)-Bi(1)-O(1A) 137.1(5), O(1)-Bi(1)-O(2A) 137.1(5), O(2)-Bi(1)-O(2A) 158.2(7), O(1A)-Bi(1)-O(2A) 64.7(5), C(13)-Bi(1)-C(13A) 154.8(7), C(17)-Bi(1)-C(13A) 102.6(3), O(1A)-Bi(1)-C(13A) 76.5(7), O(2A)-Bi(1)-C(13A) 87.9(10), Bi(1)-O(1)-C(1) 114.6(13), Bi(1)-O(2)-C(7) 126.2(13), O(1)-Bi(1)-C(13) 76.5(7), O(2)-Bi(1)-C(13) 87.9(10), O(1)-Bi(1)-C(17) 143.8(3), O(2)-Bi(1)-C(17) 79.1(4).

(C17) and the tropolone rings, which are twisted relative to each other by only 2°, collectively form the base of the pentagonal pyramid. The two remaining phenyl groups occupy axial positions; the measured axial Bi–C distances are the same length (Bi–C13(A) 2.141 Å) and the angle between the phenyl groups is 154.8°. The bonding between the tropolone oxygen atoms and the bismuth atom corresponds to that previously discussed for **3**: the tropolone oxygen atoms are also sp^2-hybridized (Bi-O-C angles 114.6, 126.3°). A long C–O distance (C7(A)–O2(A) 1.281 Å) follows a short Bi–O distance (Bi–O2(A) 2.315 Å), and a short C–O distance (C1(A)–O1(A) 1.243 Å) follows a long Bi–O distance (Bi–O1(A) 2.593 Å). The Bi–C17 (2.390 Å) bond is markedly longer than the other two axial Bi–C bonds (2.141 Å) making it one of the longest Bi–C bonds reported to date. The NMR spectra of complexes **3** and **6** in $CDCl_3$ not only show a significant shift of the tropolone ring protons to lower field, but also loss of the partial C=O double bond character.[16] The latter was also apparent in the shift of the C=O stretching frequencies in the IR spectrum to lower wavenumbers. This finding can be rationalized in terms of ligand deshielding by the electron-pulling nature of the coordinated bismuth(v) cation.

Stability studies show that the new complexes **3** and **6** do not undergo decomposition in aqueous medium, which is attributed to the steric shielding of the bismuth(v) cation. Thus, compounds **3** and **6** are suitable for studying the biological properties of these classes of complexes.

Received: July 12, 1995 [Z81961E]
German version: *Angew. Chem.* **1996**, *108*, 90–92

Keywords: bismuth compounds · complexes with oxygen ligands · tropolone derivatives

[1] P. R. Wells, *Progr. Phys. Org. Chem.* **1968**, *6*, 111.
[2] G. Wittig, K. Clauß, *Justus Liebigs Ann. Chem.* **1952**, *578*, 136.
[3] A. Schmuck, J. Buschmann, J. Fuchs, K. Seppelt, *Angew. Chem.* **1987**, *99*, 1206; *Angew. Chem. Int. Ed. Engl.* **1987**, *26*, 1180.
[4] D. Hellwinkel, G. Kilthau, *Justus Liebigs Ann. Chem.* **1967**, *705*, 66.
[5] D. Hellwinkel, M. Bach, *Justus Liebigs Ann. Chem.* **1968**, *720*, 198.
[6] R. Rüther, F. Huber, H. Preut, *Z. Anorg. Allg. Chem.* **1986**, *539*, 110–126.
[7] G. Ferguson, B. Kaitner, C. Glidewell, S. Smith, *J. Organomet. Chem.* **1991**, *419*, 283–291.
[8] M. Domagala, H. Preut, F. Huber, *Acta Crystallogr. Sect. C* **1988**, *44*, 830–832.
[9] H. Suzuki, T. Ikegami, Y. Matano, N. Azuma, *J. Chem. Soc. Perkin Trans. 1* **1993**, 2411–2415.
[10] H. C. Stevens, J. K. Rinehart, J. M. Lavanish, G. M. Trenta, *J. Org. Chem.* **1971**, *36*, 2780–2784.
[11] R. Diemer, B. K. Keppler, U. Dittes, B. Nuber, V. Seifried, W. Opferkuch, *Chem. Ber.* **1995**, *128*, 335–342.
[12] V. A. Dodonov, A. V. Gushchin, T. G. Brilkina, *J. Gen. Chem. USSR (Engl. Transl.)* **1985**, *55*, 63–68.
[13] a) Crystal data for **3**: crystal dimensions [mm]: 0.15 × 0.35 × 0.40, triclinic space group *P*1 (No. 2), $a = 10.464(7)$, $b = 10.676(8)$, $c = 13.970(1)$ Å, $\alpha = 76.29(6)$, $\beta = 82.58(6)$, $\gamma = 77.48(6)°$, $V = 1475.1$ Å^3, $Z = 2$, $\rho_{calcd} = 1.63$ g cm^{-3}, $F(000) = 712$; 5164 reflections with $3 < 2\theta < 50.0°$, reflections with $I > 2.0\sigma(I)$ not determined. Structure solution and refinement for 3061 independent reflections with $I > 2.5\sigma(I)$ and 362 parameters, no absorption correction possible due to irregular reflection profiles. $R = 0.087$; $R(w) = 0.071$. Residual electron density max. 2.00, min. −2.85 e Å^{-3}. SynTex-R3-diffractometer, $Mo_{K\alpha}$ radiation ($\mu = 5.99$ mm^{-1}); graphite monochromator. Structure solution and refinement was carried out on a Microvax II by using SHELXTL PLUS Release 1.11/V and the Patterson-Fourier method. Hydrogen atoms were included in calculated positions (HFIX). b) Further details of the crystal structure investigations may be obtained from the Fachinformationszentrum Karlsruhe, D-76344 Eggenstein-Leopoldshafen (Germany), on quoting the depository number CSD-59130.
[14] J. W. Cook, A. R. Gibb, R. A. Raphael, A. R. Somerville, *J. Chem. Soc.* **1951**, 503.
[15] a) Crystal data for **6**: crystal dimensions [mm]: 0.27 × 0.34 × 0.34, tetragonal space group $P4_32_12$ (No. 96), $a = 14.837(6)$, $c = 14.189(9)$ Å, $V = 3123.5$ Å^3, $Z = 4$, $\rho_{calcd} = 1.64$ g cm^{-3}, $F(000) = 1504$: 3493 reflections with $3 < 2\theta < 52.5°$, 1143 reflections with $I > 2.0\sigma(I)$. Structure solution and refinement for 957 independent reflections with $I > 2.5\sigma(I)$ and 104 parameters, empirical absorption correction , 4 reflections, $6.8 < 2\theta < 20.3°$. $R = 0.058$; $R(w) = 0.044$. Residual electron density max. 1.26, min. −1.70 e Å^{-3}. AED-II-diffractometer, $Mo_{K\alpha}$ radiation ($\mu = 5.68$ mm^{-1}); graphite monochromator. Structure solution and refinement was carried out on a Microvax II by using SHELXTL PLUS Release 1.11/V and the Patterson-Fourier method. Hydrogen atoms were included in calculated positions (HFIX) [13b].
[16] Spectroscopic data for **3**: ^{1}H NMR ($CDCl_3$, 25 °C, 200 MHz): $\delta = 2.27$ (s, 9H, CH_3-Ph), 6.76 (m, 2H, *p*-Tr.), 7.19 (d, 6H, *m*-Ph), 7.22 (m, 4H, *o*-Tr.), 7.24 (m, 4H, *m*-Tr.), 7.81 (d, 6H, *o*-Ph); ^{13}C NMR ($CDCl_3$, 25 °C, 50 MHz): $\delta = 177.0$, 167.7, 138.8, 137.1, 133.2, 130.7, 125.7, 124.3, 21.2; IR (KBr): $\tilde{\nu} = 1592$ cm^{-1} (C=O), correct C,H analysis. Spectroscopic data for **6**: ^{1}H NMR ($CDCl_3$, 25 °C, 200 MHz): $\delta = 7.16$ (dd, 4H, *o*-5-NTr.), 7.36 (m, 3H, *p*-Ph), 7.50 (dd, 6H, *m*-Ph), 7.92 (dd, 6H, *o*-Ph), 8.41 (dd, 4H, *m*-5-NTr.); ^{13}C NMR ($CDCl_3$, 25 °C, 50 MHz): $\delta = 178.6$, 168.8, 143.6, 133.3, 132.6, 131.0, 130.2, 122.2; IR (KBr): $\tilde{\nu} = 1593$ cm^{-1} (C=O), correct C,H,N analysis.

 © VCH Verlagsgesellschaft mbH, D-69451 Weinheim, 1996 0570-0833/96/3501-0068 $ 10.00+.25/0

Convenient New Synthesis of [7]Circulene**

Koji Yamamoto,* Hiroyuki Sonobe,
Hiroshi Matsubara, Masaaki Sato,
Susumu Okamoto, and Kazuo Kitaura*

Recent advances in carbon cluster chemistry (fullerenes) have renewed the interest in nonplanar polycyclic aromatic compounds with a circular arrangement of benzene rings, known as circulenes.[1] We previously reported the preparation of [7]circulene **11**[2] (pleiadannulene)[3] whose twisted, saddle-shaped structure resulting from a circular arrangement of seven benzene rings can be considered as a subunit of the inner surface of helix-shaped nanotubes.[4] We report here a convenient new synthesis of **11** via the 2,15-ethano-bridged hexahelicene intermediate **9**, and the electrochemical properties of **11**.

The Wittig condensation of 2,7-naphthalenedicarboxaldehyde **1**[5] with triphenyl-*para*-xylylphosphonium bromide in sodium methoxide/DMF gave a mixture of stereoisomers **2**.

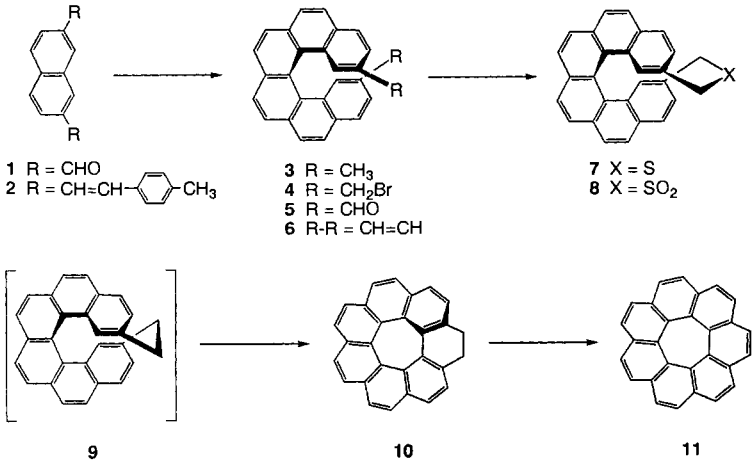

This mixture was dissolved in benzene and irradiated with a high-pressure mercury lamp[6] for 2 h to give 2,15-dimethylhexahelicene **3** (m.p. 212–214 °C, 59% yield from **1**).[7] Bromination of **3** with *N*-bromosuccinimide afforded the dibromide **4** (m.p. 196–198 °C, 40%),[8] which was oxidized with *O*-natrio-2-*aci*-nitropropane in ethanol/benzene to give the dialdehyde **5** (m.p. 202–204 °C, 72%).[9]

Although, reductive coupling of **5** to give the bridged hexahelicene **6** by using low-valent titanium[10] was unsuccessful, invariably giving a polymer as the product, intramolecular cyclization of **4** with sodium sulfide nonahydrate in refluxing benzene/ethanol afforded the hexahelicene sulfide **7** (m.p. 252–254 °C, 48% yield)[11] whose oxidation with hydrogen peroxide gave the sulfone **8** (m.p. >300 °C) in quantitative yield. Flash vacuum pyrolysis (550 °C, 0.01 Torr) of **8** gives the dihydro[7]circulene **10** directly which, as expected from the examination of its molecular model, has a chiral, saddle-shaped structure (yellow prisms, m.p. 225–227 °C, 24% yield)[12] and was isolated by chromatography on silica gel.

The mechanism for this striking transformation presumably involves the initial formation of the ethano-bridged hexahelicene **9** by pyrolysis, followed by dehydrogenation at both ends of the hexahelicene.[13] MM3 calculations[14] predict a strain energy about 32.2 kcal mol^{-1} for **10**, which should make it more than 12 kcal mol^{-1} more stable than **9** (44.3 kcal mol^{-1}). The 500 MHz ^{1}H NMR spectrum of **10** in $CDCl_3$ shows a single peak for the two enantiotopic methylene groups at room temperature ($\delta = 2.70$), but sets of peaks for the aliphatic hydrogens centered at $\delta = 2.98$ and 3.75 at -50 °C ($\Delta\nu = 149.5$ Hz) characteristic of an AA'BB' pattern. The coalescence temperature for those two signals was found to be -10 °C, from which we calculate the barrier for ring inversion in **10** to be $\Delta G^{\ddagger} = 12.2$ kcal mol^{-1} at this temperature.

Finally, dehydrogenation of **10** with 5% Pd/C in 1-methylnaphthalene at 280 °C for 3 h led to [7]circulene **11** (m.p. 295–296 °C, 85% yield) with a twisted saddle-shaped geometry.[2]

The electrochemical properties of **11** were examined by cyclic voltammetry. The voltammograms exhibited one irreversible oxidation peak and two reduction waves, the first of which was reversible, the second irreversible, as in the case of coronene itself (Table 1). A comparison of the oxidation and redox potentials of **11** with those of coronene[15] indicate that it is easier to remove or add electrons to **11**. This observation reveals that structures such as **12** and **13** make a large contribution to the electronic structure of the radical cation and anion, respectively, of the non-alternated benzenoid hydrocarbon **11**.[16]

For a better understanding of the radical ions of [7]circulene, ab initio MO calculations were performed with the GAUSSIAN 92 program.[17] The calculated HOMO energy of [7]circulene is -7.1 eV at the 3-21G SCF level, whereas that of coronene is -7.3 eV.[18] Thus the calculations predict that the ionization potential is smaller for [7]circulene than for coronene, which is consistent with the observed redox potentials. The geometry optimizations of the radical cation and anion of **11** were carried out at the STO-3G UHF level. The doublet spin state was assumed for both ions. Both of the calculated geometries are saddle-shaped with C_2 symmetry, and are remarkably similar. They are also very similar to the structure of the neutral molecule.

Table 1. Results of cyclic voltammetric studies [a].

Compound	E_{ox} [b, d]	E_{red1} [c, e]	E_{red2} [c, f]
coronene	+0.90	−2.05	−2.47
11	+0.73	−1.94	−2.29

[a] Tetrabutylammonium perchlorate (0.2 mol dm^{-3}) as a supporting electrolyte, scan rate 0.3 Vs^{-1}, at 25 °C. [b] Potential in Volts vs. Ag/Ag$^+$ with a glassy carbon working electrode in dichloromethane. [c] Potential in Volts vs. SCE with a hanging mercury drop working electrode in DMF. [d] Irreversible oxidation. [e] Reduction peak potential of a quasi-reversible redox reaction. [f] Irreversible reduction.

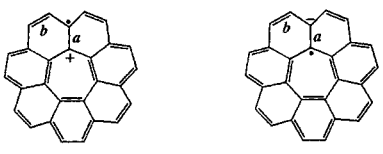

[*] Prof. Dr. K. Yamamoto, Prof. Dr. K. Kitaura, H. Sonobe, Dr. H. Matsubara, Dr. M. Sato
Department of Chemistry, Faculty of Integrated Arts and Sciences
University of Osaka Prefecture, Sakai, Osaka 593 (Japan)
Fax: Int. code +(722) 55-2981
S. Okamoto
Department of Chemistry, Minatogawa College
Yotsutsuji, Sanda, Hyogo 669-13 (Japan)

[**] This work was supported by a Grant-in-Aid for Scientific Research on Priority Areas "Carbon Cluster" (No. 05233105) from the Ministry of Education, Science and Culture, Japan.

 © VCH Verlagsgesellschaft mbH, D-69451 Weinheim, 1996 0570-0833/96/3501-0069 $ 10.00+.25/0

The major differences are that the out-of-plane distortion is a little greater and that the bonds *a* and *b* are about 0.05 Å longer in the radical ions. This suggests some contribution of the localized Kekuléan forms **12** and **13** or of other unidentified localized forms to the resonance hybrids of cation and anion. Details of the calculations will be reported elsewhere.

We are currently investigating the potentially fascinating chemistry of **11** including the energy barrier for the inversion of the twisted saddle structure in mono-substituted derivatives and the synthesis of metal complexes.

Received: April 10, 1995
Revised version: October 18, 1995 [Z 7878 IE]
German version: *Angew. Chem.* **1996**, *108*, 69–70

Keywords: arenes · circulenes · polycycles

[1] J. H. Dopper, H. Wynberg, *J. Org. Chem.* **1975**, *40*, 1957–1966.
[2] K. Yamamoto, T. Harada, Y. Okamoto, H. Chikamatsu, M. Nakazaki, Y. Kai, T. Takano, M. Tanaka, S. Harada, N. Kasai, *J. Am. Chem. Soc.* **1988**, *110*, 3578–3584; K. Yamamoto, Y. Saitoh, D. Iwaki, T. Ooka, *Angew. Chem.* **1991**, *103*, 1202–1203; *Angew. Chem. Int. Ed. Engl.* **1991**, *30*, 1173–1174; K. Yamamoto, *Pure Appl. Chem.* **1993**, *65*, 157–163.
[3] J. S. Siegel, T. J. Seiders, *Chem. Br.* **1995**, 313–316.
[4] S. Iijima, P. M. Ajayan, T. Ichihashi, *Phys. Rev. Lett.* **1992**, *69*, 3100–3104; V. Ivanov, J. B. Nagy, P. Lambin, A. Lucas, X. B. Zhang, X. F. Zhang, D. Bernaerts, G. van Tendeloo, S. Amelinckx, J. van Landuyt, *Chem. Phys. Lett.* **1994**, *223*, 329–335.
[5] Compound **1** was prepared by lithiation of 2,7-dibromonaphthalene followed by formylation with DMF.
[6] Halos, ET-500, Eikosha Co., Osaka (Japan).
[7] J. H. Borkent, W. H. Laarhoven, *Tetrahedron* **1978**, *34*, 2565–2567.
[8] Satisfactory analytical and spectroscopic data have been obtained for all new compounds.
[9] K. Yamamoto, T. Ikeda, T. Kitsuki, Y. Okamoto, H. Chikamatsu, M. Nakazaki, *J. Chem. Soc. Perkin Trans. 1* **1990**, 271–276.
[10] J. E. McMurry, K. L. Kess, *J. Org. Chem.* **1977**, *42*, 2655–2656; A. L. Baumstark, C. J. Closkey, K. E. Witt, *ibid.* **1978**, *43*, 3609–3611.
[11] **7**: MS (EI, 75 eV): *m/z* 386 (M^+); ^{1}H NMR (270 MHz, $CDCl_3$, 25 °C, TMS): δ = 2.55 (d, J = 12.82 Hz, 2H, CH_2), 3.74 (d, J = 12.82 Hz, 2H, CH_2), 7.40 (s, 2H, ArH), 7.93–8.13 (m, 12H, ArH).
[12] **10**: MS: *m/z*: 352 (M^+); ^{1}H NMR (500 MHz, $CDCl_3$, 25 °C, TMS): δ = 2.70 (s, 4H, CH_2), 7.50 (d, J = 7.63 Hz, 2H, ArH), 7.59 (d, J = 8.55 Hz, 2H, ArH), 7.62 (d, J = 7.63 Hz, 2H, ArH), 7.68 (d, J = 8.24 Hz, 2H, ArH), 7.69 (d, J = 8.55 Hz, 2H, ArH), 7.80 (d, J = 8.24 Hz, 2H, ArH); UV/Vis (cyclohexane): $\lambda_{max}(\varepsilon)$ = 251 (46080), 273 (30590), 383 sh (28430), 296 sh (21180), 312 (20400), 333 (9800) nm.
[13] J. H. Dopper, D. Oudman, H. Wynberg, *J. Org. Chem.* **1975**, *40*, 3398–3401.
[14] N. L. Allinger, Y. H. Yuh, J.-H. Lii, *J. Am. Chem. Soc.* **1989**, *111*, 8551–8566; J. C. Tai, L. Yang, N. L. Allinger, *ibid.* **1993**, *115*, 11906–11917.
[15] B. S. Jensen, V. D. Parker, *J. Am. Chem. Soc.* **1975**, *97*, 5211–5217.
[16] J. Janata, J. Gendell, C.-Y. Ling, W. Barth, L. Backer, H. B. Mark, R. D. Lawton, *J. Am. Chem. Soc.* **1967**, *89*, 3056–3058.
[17] M. J. Frisch, G. W. Trucks, M. Head-Gordon, P. M. W. Gill, M. W. Wong, J. B. Foresman, B. G. Johnson, H. B. Schlegel, M. A. Robb, E. S. Replogle, R. Gomperts, J. L. Andres, K. Raghavachari, J. S. Binkley, C. Gonzalez, R. L. Martin, D. J. Fox, D. J. DeFrees, D. J. Baker, J. J. Stewart, J. A. Pople, GAUSSIAN 92, Gaussian Inc., Pittsburgh, PA, USA, **1992**.
[18] The STO-3G SCF optimized geometries were used. The geometries were taken from M. Shen, I. S. Ignatyev, Y. Xie, H. F. Schaefer III, *J. Phys. Chem.* **1993**, *97*, 3212–3216 for [7]circulene and from J. M. Schulman, R. C. Peck, R. L. Disch, *J. Am. Chem. Soc.* **1989**, *111*, 5675–5680 for coronene.

2-Nucleos-5′-*O*-yl-4*H*-1,3,2-benzodioxaphosphinin-2-oxides—A New Concept for Lipophilic, Potential Prodrugs of Biologically Active Nucleoside Monophosphates**

Chris Meier*

Nucleoside analogues such as 3′-azido-2′,3′-dideoxythymidine (AZT), 2′,3′-dideoxy-2′,3′-didehydrothymidine (d4T), 2′,3′-dideoxyinosine (ddI), and 2′,3′-dideoxycytidine (ddC) are used in antiviral chemotherapy against AIDS.[1] One of the major problems in the use of this type of compounds is the intracellular bioavailability of their 5′-phosphorylated derivatives. One concept to overcome this limitation is the intracellular delivery of the 5′-monophosphates from prodrugs ("kinase-bypass").[2] In view of the high antiviral activity of nucleoside analogues, the development of nucleotide prodrugs is a challenging goal.[3]

As part of our ongoing program[4] to develop new prodrug systems, the synthesis of the title compounds **3a–e** and **4a–e** of the nucleoside analogues 2′,3′-dideoxythymidine (ddT) **1** and d4T **2**, respectively, bearing different donor and acceptor substituents on the benzene ring is reported. Furthermore the partition coefficients of **3** and **4** in 1-octanol/phosphate buffer and their hydrolysis behavior in phosphate buffer (pH 7.5) at 37 °C will be discussed.[4a, 5]

The approach reported here differs from other prodrug concepts in that it leads to nucleotides after a *coupled* cleavage of the phenyl- and the benzylester bond in the phosphotriesters **3** and **4**, respectively. The difference in hydrolytic stability of phenyl-[6] and benzylphosphotriesters[7, 8] has already been reported: whereas *acceptor*-substituted phenylphosphotriesters are rapidly hydrolyzed under alkaline conditions, a fast hydrolysis of benzylphosphotriesters was only observed in the case of their *donor*-substituted derivatives.[9] Regardless of the type of phosphotriester, the resulting phosphodiesters are very stable against nonenzymatic hydrolysis.[10] The herein reported prodrug concept of the title compounds **3** and **4** uses precisely this difference in stability of the phenyl and the benzyl phosphate esters for the design of a three-parted prodrug for the selective liberation of phosphorylated nucleosides. The hydrolysis should proceed as follows: in the initial step the phenolic phosphate ester bond is cleaved selectively, since the resulting negative charge can be delocalized over the phenolic oxygen atom in the aromatic ring. The acceptor substituent in the *ortho* position prevents the cleavage of the benzylester bond. As a consequence of this cleavage, together with the "umpolung" of the substituent in the *ortho* position to the methylene group, the second step, the cleavage of the 2-hydroxybenzyl group is induced. The presence of the electron-donating substituent allows cleavage of the benzylic phosphate ester bond, releasing the nucleotides **7** or **8** and the 2-hydroxybenzyl alcohols **9**[3d, 9] (tandem-reaction; Scheme 1).

Furthermore, according to this concept it should be possible to control the initial activation step by varying the substituents in the *para* position to the phenolic phosphate ester bond. For this reason, different *para*-substituted salicyl alcohols **9a, b, d, e** were used as precursors in the synthesis of **3** and **4**. In addition, the different substitution in the *para* position allows one to

[*] Dr. C. Meier
Institut für Organische Chemie der Universität
Marie-Curie-Strasse 11, D-60439 Frankfurt am Main (Germany)
Fax: Int. code + (69)7982-9148

[**] This work was supported by the Deutsche Forschungsgemeinschaft, the Adolf-Messer-Stiftung, and the Fonds der Chemischen Industrie. I thank Prof. Dr. J. W. Engels for his generous support and encouragement.

 © VCH Verlagsgesellschaft mbH, D-69451 Weinheim, 1996 0570-0833/96/3501-0070 $ 10.00+.25/0

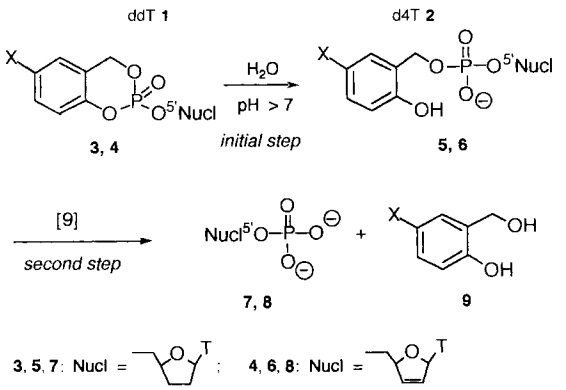

Scheme 1. Hydrolytic degradation of the title compounds **3** and **4** following the tandem mechanism. X = donor or acceptor substituent (see Table 1).

study which of the two steps is rate-determining for the liberation of the nucleotide. Prior to hydrolysis, the phosphotriesters **3** and **4** serve as lipophilic, neutral prodrugs.

The 2-chloro-4*H*-1,3,2-benzodioxaphosphinines **11**, used as starting materials for the synthesis of the cyclic phosphotriesters **3** and **4**,[11] were isolated by distillation under an argon atmosphere in 60–80% yield. The target compounds **3a–e** and **4a–e** were obtained in a one-pot reaction by reacting the nucleoside analogues **1** or **2** with 1.5 equivalents of the chlorophosphinines **11a–e** at 0 °C in the presence of distilled diisopropylethylamine (DIPEA) to give the phosphites **12a–e**, **13a–e** and subsequent in situ oxidation with *tert*-butylhydroperoxide (Scheme 2).

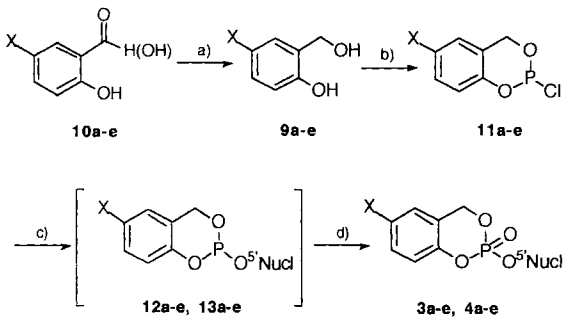

Scheme 2. Synthesis of the title compounds **3a–e** and **4a–e** (X see Table 1, Nucl see Scheme 1). a) $NaBH_4$ ($LiAlH_4$); b) PCl_3, pyridine, Et_2O, −10 °C, 2 h; c) ddT **1** (gives **3** via **12**) or d4T **2** (gives **4** via **13**), DIPEA, CH_3CN, 0 °C, 20 min; d) *t*BuOOH, CH_3CN, 20 °C, 30 min.

After purification (70–85% yield) the phosphotriesters **3** and **4** were obtained as 1:1.2 diastereomeric mixtures with respect to the configuration at the phosphorus atom (Table 1). The diastereomers were not separable in all cases by common chromatographic procedures, but could be distinguished by ^1H, ^{13}C, and ^{31}P NMR spectroscopy. Furthermore **3** and **4** were characterized by circular dichroism (CD),[12] UV spectroscopy, and electrospray mass spectrometry (negative mode).

As a qualitative estimation of the lipophilic properties of the described compounds their partition coefficients (log(PC) values) in 1-octanol/phosphate buffer (pH 6.5) were determined[13] (Table 1). All compounds **3** and **4** showed positive log(PC) values and partition coefficients a factor of 8.1 to 50.5 higher than those of the parent nucleosides ddT **1** and d4T **2**, respectively (Table 1). Consequently, the passive diffusion through a membrane should be easier for these compounds than for the free nucleoside.

Table 1. Partition coefficients and half-lives of the title compounds **3** and **4** and their dependence on the substituents X. Compound **3** is hydrolyzed to **7** and **9**, and compound **4** is hydrolyzed to **8** and **9**. σ_p = Hammett parameters.

Compd.	X	σ_p	^{31}P NMR [δ] "fast"/"slow"	log (PC) [a]	$t_{1/2}$ [b] [h]
3a	OCH_3	−0.28	−8.12/−8.19	0.57	9.33
3b	CH_3	−0.14	−8.27/−8.33	0.97	7.00
3c	H	0.0	−8.34/−8.39	0.54	4.40
3d	Cl	0.24	−8.81/−8.91	1.05	1.56
3e	NO_2	1.27	−9.35/−9.53	0.26	0.20
ddT **1**	–	–	–	−0.64 [14]	–
4a	OCH_3	−0.28	−7.89/−7.96	0.35	9.20
4b	CH_3	−0.14	−8.04/−8.11	0.65	6.86
4c	H	0.0	−8.12/−8.14	0.28	4.50
4d	Cl	0.24	−8.59/−8.66	0.89	1.66
4e	NO_2	1.27	−9.10/−9.34	0.08	0.18
d4T **2**	–	–	–	−0.82 [14]	–

[a] In 1-octanol/phosphate buffer (pH 6.5). [b] In 30 mM phosphate buffer (pH 7.5) at 37 °C.

As a model for the physiological milieu, hydrolysis studies of the new phosphotriesters **3** and **4** were carried out in 30 mM phosphate buffer (pH 7.5) at 37 °C.[14] In all studied cases, **3** and **4** were degraded following pseudo-first order kinetics. The nucleoside monophosphates of ddT **7** or d4T **8** as well as the salicyl alcohols **9** were detected by HPLC analysis as the exclusive products of the hydrolysis. Furthermore, the identification of **7** and **8** was accomplished directly from the hydrolysis mixture by electrospray mass spectrometry. In an additional hydrolysis experiment, the degradation of triester **3d** in borate buffer (30 mM, pH 9) was studied by ^{31}P NMR spectroscopy. Only one signal, which showed the characteristic chemical shift of nucleoside monophosphates and a triplet fine splitting, was observed in the ^{31}P NMR spectrum. Besides the selective hydrolysis to the nucleoside monophosphate, the expected effect of the substitution of the aromatic ring on the $t_{1/2}$ values as well as on the rate-determining step was observed. In the case of the donor-substituted derivatives of **3** and **4**, only their decrease and the increase of the nucleoside monophosphates **7** and **8** could be followed by HPLC. In contrast, the intermediate phosphodiesters **5d**, **5e** and **6d**, **6e**, respectively, were also detected for the acceptor-substituted derivatives **3d**, **3e** and **4d**, **4e**. Consequently, in the latter cases the second step (**5**, **6** → **7**, **8**) is rate-determining (Scheme 1). These results are consistent with the postulated pathway for the hydrolysis shown in Scheme 1.[15] In all studies, no difference was detected between the ddT or the d4T derivatives (Table 1). As a result, the donor-substituted compounds of **3** and **4** should act as suitable prodrugs because their hydrolytic stability ($t_{1/2}$ value) seems to be sufficiently high (Table 1).

In summary, it has been possible for the first time to deliver phosphate monoesters of type **7**, **8** selectively and in a controllable manner from a phosphotriester hydrolytically at physiological pH according to the newly developed tandem-reaction. Thus, an enzymatically catalyzed activation is not a prerequisite for the liberation of nucleotides. We are currently investigating the hydrolysis of **3** and **4** in a RPMI-culture medium containing 10% fetal calf serum, as well as the antiviral activity of our compounds against HIV-1 and HIV-2.

Experimental Procedure

To a solution of dried nucleoside **1** or **2** (0.64 mmol) in acetonitrile (10 mL), diisopropylethylamine (DIPEA) (1.27 mmol) was added at 0 °C. Then the cyclic chlorophosphinines **11** (2.0 equiv., 1.28 mmol in 1 mL acetonitrile) were slowly added. The generated phosphites **12** and **13**, respectively, were oxidized in situ with *tert*-butylhydroperoxide (200 μL) after 20 min. After evaporation of the solvent, the residue was purified by chromatography on a Chromatotron (solvent gradient of

 © VCH Verlagsgesellschaft mbH, D-69451 Weinheim, 1996 0570-0833/96/3501-0071 $ 10.00+.25/0

ethyl acetate and methanol: 40–30% methanol). Further purification was achieved by semipreparative HPLC (70–85% yield). After lyophilization the triesters **3** and **4** were isolated as colorless solids.

Received: June 30, 1995
Revised version: September 29, 1995 [Z 8150 IE]
German version: *Angew. Chem.* **1996**, *108*, 77–79

Keywords: AIDS · chemotherapy · phosphotriesters · prodrugs · thymidine derivatives

[1] *Chem. Eng. News* **1994**, *72*(4), 22.
[2] R. J. Jones, N. Bischofberger, *Antiviral Res.* **1995**, *27*, 1–17.
[3] Several nucleoside phosphotriesters have been studied previously which should liberate nucleoside monophosphates by nonenzymatic [3a] or enzymatic [3b–d] hydrolysis: a) U. Nillroth, L. Vrang, G. Ahlsen, Y. Besidsky, J. Chattopadhyaya, I. Ugi, U. H. Danielson, *Antiviral Chem. Chemother.* **1995**, *6*, 50–64 and references therein; b) D. Farquhar, R. Chen, S. Khan, *J. Med. Chem.* **1995**, *38*, 488–495; c) C. Perigaud, A.-M. Aubertin, S. Benzaria, H. Pelicano, G. Gosselin, A. Kirn, J. L. Imbach, *Biochem. Pharmacol.* **1994**, *48*, 11–14; d) W. Thomson, D. Nicholls, W. J. Irwin, J. S. Al-Mushadani, S. Freeman, A. Karpas, J. Petrik, N. Mahmood, A. J. Hay, *J. Chem. Soc. Perkin Trans. 1* **1993**, 1239–1245; see also ref. [2].
[4] a) C. Meier, *Angew. Chem.* **1993**, *105*, 1854–1856; *Angew. Chem. Int. Ed. Engl.* **1993**, *32*, 1704–1706; b) C. Meier, L. Habel, W. H. G. Laux, J. Balzarini, E. De Clercq, *Nucleosides Nucleotides* **1995**, *14*, 759–762; c) C. Meier, R. Mauritz, *ibid.* **1995**, *14*, 803–804.
[5] Prodrugs for ddT **1**: S. I. Shimizu, J. Balzarini, E. De Clercq, R. T. Walker, *Nucleosides Nucleotides* **1992**, *11*, 583–594; ref. [4a]. Prodrugs for d4T **2**: C. McGuigan, H. M. Sheeka, N. Mahmood, A. Hay, *Bioorg. Med. Chem. Lett.* **1993**, *3*, 1203–1206; C. Sergheraert, C. Pierlot, A. Tartar, Y. Henin, M. Lemaitre, *J. Med. Chem.* **1993**, *36*, 826–830.
[6] S. N. Farrow, A. S. Jones, A. Kumar, R. T. Walker, J. Balzarini, E. De Clercq, *J. Med. Chem.* **1990**, *33*, 1400–1406.
[7] J. W. Engels, E.-J. Schläger, *J. Med. Chem.* **1982**, *20*, 907–911.
[8] C. Meier, L. Habel, J. Balzarini, E. De Clercq, *Liebigs Ann. Chem.* **1995**, in press; L. Habel, Diploma thesis, Universität Frankfurt, **1994**.
[9] Two different mechanisms of benzylester hydrolysis are discussed: 1) a spontaneous heterolytic bond breakage leading to a benzyl cation and a phosphate ester; 2) a nucleophilic attack of water at the benzylic methylene group: a) J. W. Engels, *Z. Naturforsch. B* **1977**, *32*, 807–809; b) A. G. Mitchell, D. Nicholls, W. J. Irwin, S. Freeman, *J. Chem. Soc. Perkin Trans. 2* **1992**, 1145–1150.
[10] C. Meier, unpublished results.
[11] A. Wissner, M. L. Carroll, *J. Med. Chem.* **1992**, *35*, 1650–1662.
[12] The ^{31}P NMR shifts of the diastereomers correlate with their CD properties as well as with their eluting properties during chromatography: the "fast"-eluting diastereomer (semipreparative reversed-phase silica gel HPLC-column) showed an upfield shift in the ^{31}P NMR spectrum and a positive Cotton-effect at 225 nm in the CD spectrum as compared to the "slow"-eluting diastereomer.
[13] J. Balzarini, J. M. Cools, E. De Clercq, *Biochem. Biophys. Res. Commun.* **1989**, *158*, 413–422.
[14] The hydrolysis studies were carried out as described before, see ref. [4a].
[15] It should be mentioned that at pH < 7 no or only a very slow hydrolysis of **3** or **4** was observed, whereas at pH > 7 a pH-dependent hydrolysis occurred.

Chiral Recognition of α-Amino Acid Derivatives with a Homooxacalix[3]arene: Construction of a Pseudo-C_2-Symmetrical Compound from a C_3-Symmetrical Macrocycle

Koji Araki, Kousuke Inada, and Seiji Shinkai*

The NH_3^+ moiety of primary alkylammonium ions (RNH_3^+) possesses C_3 symmetry, and therefore complementary hosts might best possess C_3 symmetry as well. In chiral molecules with two complexing faces, the importance of having the two faces related by C_2 symmetry has been emphasized.[1] A chiral guest molecule interacts identically with the homotopic faces of this type of chiral host. Therefore, for the enantioselective recognition of primary alkylammonium ions, it is desirable for a chiral host molecule to possess a C_2 axis perpendicular to a local C_3 symmetry element. Satisfying these requirements is quite difficult. [18]Crown-6 is one of the few compounds that has these two local symmetry elements—at least when it binds K^+ or RNH_3^+ ions in the solid state. In fact, several chiral [18]crown-6 derivatives are known to bind racemic substrates containing NH_3^+ centers with high enantioselectivity.[2] Here we describe how such a host molecule for chiral recognition can be prepared from a homooxacalix[3]arene.

As the starting material we chose 7,15,23-tri-*tert*-butyl-25,26,27-trihydroxy-2,3,10,11,18,19-hexahomo-3,11,19-trioxacalix[3]arene (**1**H_3),[3] which possesses C_3 symmetry[4] and shows high affinity for primary alkylammonium ions.[5] When two hydroxyl groups in **1**H_3 are converted into ethers (R′) with bulky alkyl groups, which can suppress rotation of the phenylene group, and the third hydroxyl group is transformed into an ether (R) having a small alkyl group, the product, *anti*-**1**RR'_2, is optically active. It behaves like a C_2-symmetrical macrocycle as a result of the free rotation of the phenylene group having the less bulky ether group (Scheme 1). A guest

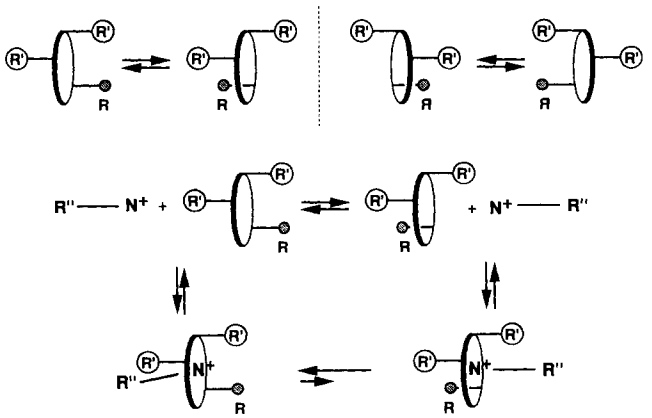

Scheme 1. Schematic representation of the binding of an RNH_3^+ ion (R″–N^+) to a pseudo-C_2-symmetric host.

molecule meets the "same chiral face" of *anti*-**1**RR'_2 regardless of the direction from which it approaches. For this reason we consider *anti*-**1**RR'_2 to have "pseudo-C_2-symmetry".

It is known that rotation of the phenylene groups in **1**H_3 can be suppressed when the substituent on the O atom is bulkier than an *n*-propyl group.[5a] In this study we used *n*-butyl groups (R′ = Bu) to fix the conformation. The reaction of **1**H_3 and *n*-butyl iodide in the presence of NaH gave *anti*-**1**HBu_2 in 48% yield (Scheme 2). Although the unmodified OH group can still pass through the ring, this calix[3]arene is already optically active. As the smaller R group, which can also pass through the annulus, we chose the methyl group. The OH group in *anti*-**1**HBu_2 was methylated with methyl iodide and NaH to give *anti*-**1**$MeBu_2$ in 70% yield. The IR spectrum and elemental analysis data were in satisfactory agreement with expected values. X-ray crystallographic analysis of *anti*-**1**$MeBu_2$ shows that one of the OBu groups is directed upward and the second downward, and that the OMe group points downward (Fig. 1).[6, 7] However, the ^1H NMR spectra of *anti*-**1**$MeBu_2$ are characteristic of a C_2-symmetrical structure: two singlets are observed for the *t*Bu protons with a 1:2 integral intensity ratio, and these signals did not split into doublets even at −85 °C. The results

[*] Prof. S. Shinkai, K. Araki, K. Inada
Department of Chemical Science and Technology
Faculty of Engineering, Kyushu University, Fukuoka 812 (Japan)

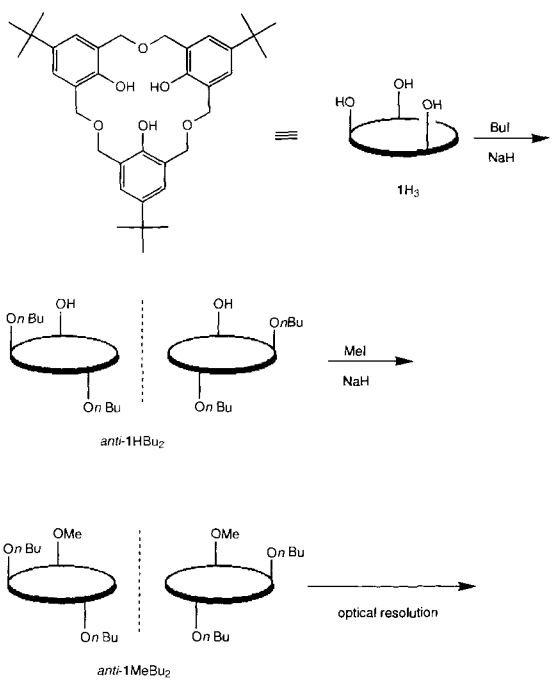

Scheme 2. Synthesis of the pseudo-C_2-symmetrical macrocycle *anti*-$1MeBu_2$ starting from the C_3-symmetrical compound $1H_3$.

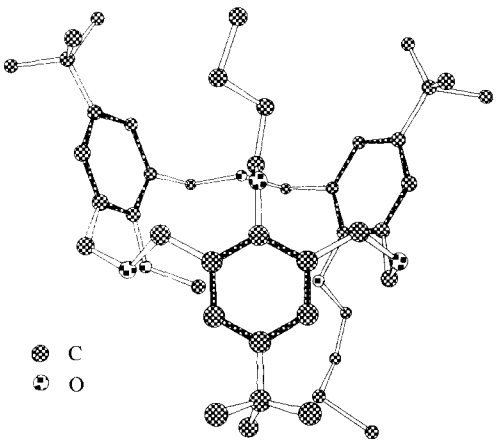

Fig. 1. X-ray crystal structure of *anti*-$1MeBu_2$; only one of the two molecules in the unit cell is shown.

can be explained by two possibilities: either the OMe group lies in the plane of the homooxacalix[3]arene resulting in C_2 symmetry, or in solution the OMe group rotates rapidly on the NMR time scale to give pseudo-C_2-symmetry. However, judging from CPK molecular models and MM3 computations, the first possibility is not likely.[8]

We measured ^1H NMR spectra of *anti*-$1MeBu_2$ in the presence of L-phenylalanine ethyl ester hydrochloride (25 °C, $CDCl_3/CD_3CN$ (3/1), 250 MHz). Most of the signals split into pairs, indicating that *anti*-$1MeBu_2$ is a pair of enantiomers. This compound can bind primary alkylammonium ions through hydrogen-bonding interactions with three oxygen atoms. Judging from the chemical shift changes of $1MeBu_2$, at least two phenolic oxygens and possibly an oxygen atom from à CH_2OCH_2 group may be involved. CPK molecular models indicate that it is sterically impossible for the oxygen atoms from three CH_2OCH_2 groups to form hydrogen bonds with RNH_3^+ ions.

To obtain further insight into the complex structure we measured NOE spectra of the complex of $1MeBu_2$ and neopentylammonium picrate. When the resonance frequency of the *tert*-butyl protons in the neopentyl group was irradiated, the difference NOE signal for the ArH protons in the OMe-substituted phenylene unit was larger than that for those in the OBu-substituted phenylene unit (Fig. 2). This result clearly shows that the alkyl group of this guest is located in the cavity formed by an OMe-substituted and one OBu-substituted phenylene ring.

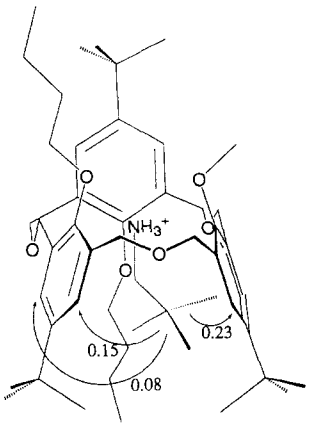

Fig. 2. NOE signal intensities of the ArH protons on irradiation of the resonance frequency of the *t*Bu protons in the *anti*-$1MeBu_2$/neopentylammonium complex (5.0×10^{-3} mol dm^{-3}, 25 °C, $CDCl_3/CD_3CN$ (3/1)).

anti-$1MeBu_2$ was optically resolved by HPLC method (Chiralpak OP(+), *n*-hexane/2-propanol (1/1)). The first fraction ((−)-*anti*-$1MeBu_2$) and the second fraction ((+)-*anti*-$1MeBu_2$) gave symmetrical CD spectra with $\lambda_{max} = 232$ nm and $\theta_{max} = \pm 20200$ deg cm^2 dmol^{-1} (Fig. 3).

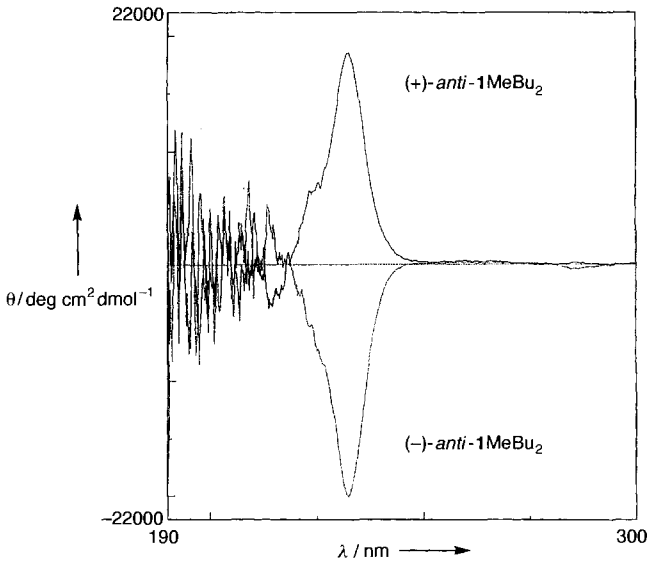

Fig. 3. CD spectra of (−)- and (+)-*anti*-$1MeBu_2$ (1.0×10^{-3} mol dm^{-3}, 25 °C, *n*-hexane).

The association constants (K_{ass}) for α-amino acid ethyl ester picrates and 1-arylethylammonium picrates were determined at 25 °C in chloroform/THF (99/1) by monitoring the change in the absorption spectrum ([picrate] = 1.00×10^{-5} mol dm^{-3}, [*anti*-$1MeBu_2$] = $(0.2-14)\times10^{-5}$ mol dm^{-3}, λ_{max}(picrates) = 345 nm, λ_{max}(complexes) = 380 nm; Table 1).[9] Plots of the absorption A_{380} versus [*anti*-$1MeBu_2$] give an inflection point at [*anti*-$1MeBu_2$]/[picrate] = 1.0, indicating that the complexes have a 1:1 stoichiometry. The association constants for the L-configurated isomers are greater with (−)-*anti*-$1MeBu_2$ than with (+)-*anti*-$1MeBu_2$. The largest chiral discrimination (74% *ee*) was observed for the picrate salt of L-phenylalanine ethyl ester.

 © VCH Verlagsgesellschaft mbH, D-69451 Weinheim, 1996 0570-0833/96/3501-0073 $ 10.00+.25/0

Table 1. Association constants K_{ass} [$dm^3 mol^{-1}$] for the complexes of *anti*-1MeBu$_2$ and picrate salts of α-amino acid ethyl esters and 1-arylethylamines (25 °C, chloroform/THF (99/1)).

Picrate salt	(−)-*anti*-1MeBu$_2$	(+)-*anti*-1MeBu$_2$	K_{ass} (large)/K_{ass} (small)
L-alanine ethyl ester picrate	4500	3200	1.4
L-phenylalanine ethyl ester picrate	1200	180	6.7
(*R*)-1-phenylethylamine picrate	2200	3000	1.4
(*R*)-1-naphthylethylamine picrate	2000	2400	1.2

The foregoing results prove that the molecular design concept proposed in this paper, a pseudo-C_2-symmetrical compound based on a C_3-symmetrical skeleton, is very effective for chiral recognition of optically active primary alkylammonium ions. We believe that the chiral discrimination ability of *anti*-1RR$'_2$ can be further enhanced by elaborating the bulkiness and polarity of the substituents R and R'.

Received: June 16, 1995
Revised version: October 16, 1995 [Z 8110 IE]
German version: *Angew. Chem.* **1996**, *108*, 92–94

Keywords: calixarenes · chiral recognition · host–guest chemistry · macrocycles

[1] a) T. Mizutani, T. Ema, T. Tomita, Y. Kuroda, H. Ogoshi, *J. Am. Chem. Soc.* **1994**, *116*, 4240; b) E. N. Jacobsen, W. Zhang, A. R. Muci, J. R. Ecker, L. Deng, *ibid.* **1991**, *113*, 7063; c) A. Miyashita, A. Yasuda, H. Takaya, K. Toriumi, T. Ito, T. Souchi, R. Noyori, *ibid.* **1980**, *102*, 7932; d) T. Katsuki, K. B. Sharpless, *ibid.* **1980**, *102*, 5974; e) T. J. van Bergen, R. M. Kellogg, *ibid.* **1977**, *99*, 3882.

[2] a) J.-M. Lehn, *Angew. Chem.* **1988**, *100*, 91; *Angew. Chem. Int. Ed. Engl.* **1988**, *27*, 89, and references cited therein; b) D. J. Cram, *ibid.* **1988**, *100*, 1041 and *ibid.* **1988**, *27*, 1009, and references cited therein.

[3] a) Y. Mukoyama, T. Tanno, *Org. Coat. Plast. Chem.* **1979**, *40*, 894; b) B. Dhawan, C. D. Gutsche, *J. Org. Chem.* **1983**, *48*, 1536; c) P. Zerr, M. Mussrabi, J. Vicens, *Tetrahedron Lett.* **1991**, *32*, 1879.

[4] Strictly speaking, 1H$_3$ may not be C_3-symmetrical since the direction of OH groups (above, below the annulus) and the conformation of the ArCH$_2$OCH$_2$Ar groups may be in constant flux. However, the complementarity of 1H$_3$ with C_3-symmetrical RNH$_3^+$ ions described here indicates that this molecule can be considered to be C_3-symmetrical.

[5] a) K. Araki, K. Inada, H. Otsuka, S. Shinkai, *Tetrahedron* **1993**, *49*, 9465; b) K. Araki, N. Hashimato, H. Otsuka, S. Shinkai, *J. Org. Chem.* **1993**, *58*, 5958.

[6] Further details of the crystal structure investigation may be obtained from the Director of the Cambridge Crystallographic Data Centre, 12 Union Road, GB-Cambridge CB21EZ (UK), on quoting the full journal citation.

[7] "Upward" and "downward" have been defined by Gutsche et al. (S. Kanamathareddy, C. D. Gutsche *J. Am. Chem. Soc.* **1993**, *115*, 6572).

[8] This structure is difficult to construct with CPK molecular models, because the bulky OMe group must be included in the cavity of the homooxacalix[3]arene. MM3(92) calculations also predict that the most stable conformations of 1MeBu$_2$ are cone and partial-cone, whereas the structure in which the MeO group is lies in the plane of the ring is much less stable (by at least 1.5 kcal).

[9] The K_{ass} values were evaluated by the Benesi–Hildebrand method: H. Benesi, J. H. Hildebrand, *J. Am. Chem. Soc.* **1949**, *71*, 2703.

A Convergent, Enantioselective Total Synthesis of Hapalosin: A Drug with Multidrug-Resistance Reversing Activity**

Arun K. Ghosh,* Wenming Liu, Yibo Xu, and Zhidong Chen

Hapalosin (**1**), a novel cyclodepsipeptide isolated recently[1] from the blue-green alga *Hapalosiphon welwitschii*, has shown important multidrug-resistance reversing activity.[2] The term multidrug-resistance (MDR), is defined as the ability of tumor cells exposed to one drug to develop cross resistance to seemingly unrelated drugs. This phenomenon is apparently caused by an overexpression of P-glycoprotein, a 170–200 kDa transmembrane protein that acts as an ATP-dependent drug efflux pump.[3] As a consequence, chemotherapy very often becomes ineffective. Thus, the agents that are capable of reversing this P-glycoprotein-induced MDR effect, may have therapeutic potential for patients undergoing cancer chemotherapy. Preliminary biological studies indicated that hapalosin inhibits the P-glycoprotein efflux pump.[1] Also, hapalosin has already been shown to have better MDR-reversing activity than verapamil which is currently under active investigation to test the MDR-reversing hypothesis in the clinic.[4] The structure of hapalosin was assigned by Moore et al.[1] through spectroscopic and degradation studies. Besides important MDR-reversing activity, one of the intriguing features of hapalosin is that the molecule exists as a mixture of two conformers, as shown by ^{1}H and ^{13}C NMR spectroscopy. Perhaps, only one of these conformers is responsible for the potent MDR-reversing activity. In order to study the structure–function relationships as well as to gain information regarding the bioactive conformation, we sought a flexible, enantioselective synthesis of hapalosin. We describe here a convergent and stereocontrolled first total synthesis of hapalosin.

The synthesis of (3*R*,4*S*-4-(*N*-benzyloxycarbonyl-*N*-methylamino)-3-methoxymethoxy-5-phenylpentanoic acid **5** was carried out stereoselectively starting from Weinreb amide **2** (Fig. 1).[5] Treatment of **2** with allylmagnesium bromide (2.2 equiv) in THF at −20 °C afforded the corresponding ketone, which was subsequently reduced with sodium borohydride in propanol at 0 °C to provide the alcohol **3** as a mixture (5:1) of diastereomers in 73% yield.[6] The isomers were separated by chromatography (silica gel, 15% ethyl acetate/hexane). Protection of the major isomer **3** as a methoxymethyl (MOM) ether followed by *N*-methylation with sodium hydride (2 equiv) and methyl iodide (3 equiv) in a mixture of THF/DMF (10:1) at 23 °C afforded the protected amino alcohol **4** in 68% yield after silica gel chromatography.[7] The cleavage of the double bond in **4** with ruthenium trichloride and excess of sodium periodate in a mixture of acetonitrile, carbon tetrachloride, and water at 23 °C for 12 h provided the acid **5** in 84% yield.[8]

The protected β-hydroxy acid **7** was conveniently prepared by an asymmetric aldol reaction utilizing an (1*S*,2*R*)-aminoindan-2-ol derived chiral auxiliary.[9] Thus, reaction of *n*-octanaldehyde and the corresponding chiral propionimide using di-*n*-butylboryl trifluoromethanesulfonate and triethylamine at −78 °C furnished the aldol product **6** in 90% yield after silica

[*] Prof. A. K. Ghosh, W. Liu, Y. Xu, Z. Chen
Department of Chemistry, University of Illinois at Chicago
845 West Taylor Street, Chicago, IL 60607 (USA)
Fax: Int. code +(312) 996-0431

[**] We thank Prof. Robert Moriarty for helpful discussions. Financial support of this project was provided by the University of Illinois at Chicago and Merck Research Laboratories.

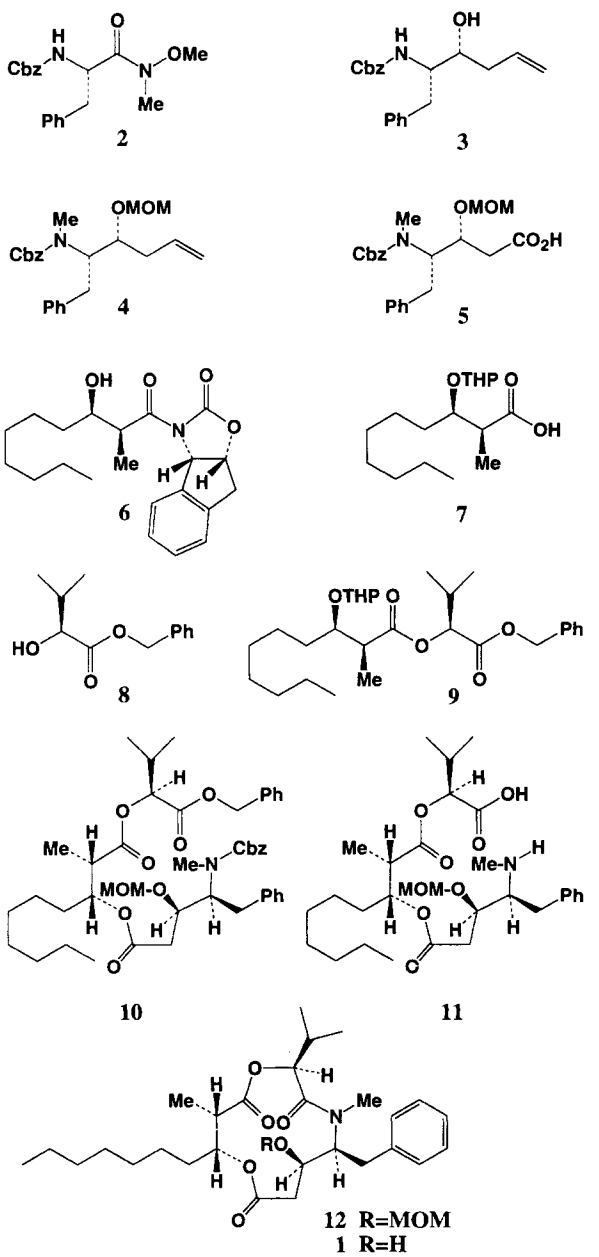

Fig. 1. The compounds employed and synthesized in this work.

gel chromatography.[10, 11] The hydroxyl group was protected as the tetrahydropyranyl ether by treatment with dihydropyran (2 equiv) and a catalytic amount of pyridinium *p*-toluenesulfonate in CH_2Cl_2 at 23 °C for 6 h. The removal of chiral auxiliary was effected with lithium hydroperoxide under standard reaction conditions[12] to provide the acid **7** in 84% yield. Alcohol **8** was prepared by diazotization[13] of L-valine and subsequent esterification with benzyl alcohol in the presence of dicyclohexylcarbodiimide (DCC) (2 equiv) and dimethylaminopyridine (DMAP) (2 equiv) in CH_2Cl_2.[14] The acid **7** was esterified by reaction with 2,4,6-trichlorobenzoyl chloride (1.0 equiv), triethylamine (1.2 equiv), and alcohol **8** (1.2 equiv) to afford the diester **9** in 91% yield.[15] The removal of the THP protecting group of **9** with *p*-toluenesulfonic acid in methanol followed by esterification of the resulting alcohol with acid **5** using an analogous procedure to that described above furnished the tri-ester derivative **10** in 76% yield.[16] Catalytic hydrogenation of **10** over Pearlman's catalyst in ethyl acetate under a hydrogen filled balloon for 5 h provided the requisite precursor **11** for macrocyclization.[17] The amino acid **11** was subjected to macrocyclization conditions without further purification. Thus, the desired cyclization was effected by slow addition of a solution of **11** in DMF with a syringe pump to a mixture of 1-ethyl-3-(3-dimethylaminopropyl)carbodiimide (EDC) (1.5 equiv) and HOBt (1.5 equiv) in the presence of triethylamine (3 equiv) in DMF (0.01 molar solution) at 60 °C to furnish the macrolactam **12** ($[\alpha]_D^{23} = -80.8$, $c = 0.7$, CH_2Cl_2; 30–37% yield after silica gel chromatography). Attempts to improve the yield of the cyclization step by using a variety of reagents and reaction conditions have so far been unsuccessful. Interestingly, the ^1H NMR (400 MHz) spectrum of macrolactam **12** ($CDCl_3$) revealed the presence of a 2:1 mixture of conformers at 23 °C. Removal of the MOM protecting group[18] of **12** by exposure to tetra-*n*-butylammonium bromide (5 equiv) and trimethylsilyl chloride (5 equiv) in CH_2Cl_2 at 23 °C for 24 h furnished the synthetic (−)-hapalosin **1** ($[\alpha]_D^{23} = -40.9$, $c = 0.11$, CH_2Cl_2; ref. [1], $[\alpha]_D^{23} = -49.2$, $c = 0.35$, CH_2Cl_2) as a mixture (2:1) of conformers at 23 °C. Spectral data (IR and 400 MHz ^1H NMR) for the major conformer is identical to that reported for the natural product.[1] The R_f value (0.3 in $MeOH/H_2O$ 9/1) is also identical to the reported value. Thus, the synthesis of hapalosin has provided confirmation of the absolute configurational assignments. To gain insight into the bioactive conformation of hapalosin, we are currently studying the design and synthesis of conformationally restricted structural variants of hapalosin.

Received: July 10, 1995 [Z 8186 IE]
German version: *Angew. Chem.* **1996**, *108*, 73–75

Keywords: chemotherapy · hapalosin · natural products · total syntheses

[1] K. Stratmann, D. L. Burgoyne, R. E. Moore, G. M. L. Patterson, C. D. Smith, *J. Org. Chem.* **1994**, *59*, 7219.
[2] J. A. Endicott, V. Ling, *Annu. Rev. Biochem.* **1989**, *58*, 137.
[3] a) I. Pastan, M. M. Gottesman, *Annu. Rev. Med.* **1991**, *42*, 277; b) N. Kartner, J. R. Riordan, V. Ling, *Science* **1983**, *221*, 1285.
[4] R. F. Ozols, R. E. Cunnion, R. W. Klecker, T. C. Hamilton, Y. Ostchega, J. E. Parrillo, R. C. Young, *J. Clin. Oncl.* **1987**, *5*, 641.
[5] S. Nahm, S. M. Weinreb, *Tetrahedron Lett.* **1981**, *32*, 3815.
[6] The stereochemistry of the major isomers was assigned based upon comparison of the corresponding BOC derivative of **3** with the sample derived from opening the known epoxide [7] 3(*S*)-azido-1,2(*R*)-epoxy-4-phenylbutane with vinylmagnesium bromide (2 equiv) and cuprous cyanide (catalytic) at −20 °C to 0 °C followed by hydrogenation of the azide with 10% Pd-C in ethyl acetate in the presence of BOC_2O (overall isolated yield 20–22%). The resulting 4(*R*)-hydroxy-5(*S*)-*tert*-butyloxycarbonylaminophenylhexane is identical with the hydrogenated BOC derivative of **3**.
[7] A. K. Ghosh, W. J. Thompson, M. K. Holloway, S. P. McKee, T. T. Duong, H. Y. Lee, P. M. Munson, A. M. Smith, J. M. Wai, P. L. Darke, J. A. Zugay, E. A. Emini, W. A. Schleif, J. R. Huff, P. S. Anderson, *J. Med. Chem.* **1993**, *36*, 2300.
[8] P. J. Carlsen, T. Katsuki, V. Martin, K. B. Sharpless, *J. Org. Chem.* **1981**, *46*, 3936.
[9] Available from Sepracor Inc., Marlborough, MA 01752 (USA). For convenient synthesis and resolution see a) A. K. Ghosh, S. P. McKee, W. M. Sanders, *Tetrahedron Lett.* **1991**, *32*, 711; b) W. J. Thompson, P. M. D. Fitzgerald, M. K. Holloway, E. A. Emini, P. L. Darke, B. M. McKeever, W. A. Schleif, J. C. Quintero, J. A. Zugay, T. J. Tucker, J. E. Schwering, C. F. Homnick, J. Nunberg, J. P. Springer, J. R. Huff, *J. Med. Chem.* **1992**, *35*, 1685.
[10] A. K. Ghosh, T. T. Duong, S. P. McKee, *J. Chem. Soc. Chem. Commun.* **1992**, 1673. For other asymmetric aldol reactions with suitable chiral auxiliaries, see ref. [11].
[11] a) D. A. Evans, *Asymmetric Synth.* **1984**, *3*, 1; b) C. H. Heathcock, *ibid.* **1984**, *3*, 111; c) W. Oppolzer, J. Blagg, I. Rodriguez, E. Walther, *J. Am. Chem. Soc.* **1990**, *112*, 2767; c) H. Roder, G. Helmchen, E.-M. Peters, K. Peters, H. G. von Schnering, *Angew. Chem.* **1984**, *96*, 895; *Angew. Chem. Int. Ed. Engl.* **1984**, *23*, 898; d) G. Gardillo, M. Orena, M. Romero, S. Sandri, *Tetrahedron* **1989**, *45*, 1501; e) W. Sankhavasi, M. Yamamoto, S. Kohmoto, K. Yamada, *Bull. Chem. Soc. Jpn.* **1991**, *64*, 1425; f) S. E. Drewes, D. S. Malissar, G. P. Roos, *Chem. Ber.* **1991**, *124*, 2913, and references therein.

 © VCH Verlagsgesellschaft mbH, D-69451 Weinheim, 1996 0570-0833/96/3501-0075 $ 10.00+.25/0

[12] D. A. Evans, T. C. Britton, J. A. Ellman, *Tetrahedron Lett.* **1987**, *28*, 6141.
[13] K. Mori, *Tetrahedron* **1976**, *32*, 1101.
[14] B. Neises, W. Steglich, *Angew. Chem.* **1978**, *90*, 556; *Angew. Chem. Int. Ed. Engl.* **1978**, *17*, 522.
[15] J. Inanaga, K. Hirata, H. Saeki, T. Katsuki, M. Yamaguchi, *Bull. Chem. Soc. Jpn.* **1979**, *52*, 1989.
[16] All new compounds were fully characterized by spectroscopic and analytical methods.
[17] An analytical sample of compound **11** was obtained after chromatography over silica gel (10% MeOH/$CHCl_3$): $[\alpha]_D^{23} = -5.1$ ($c = 0.93$, $CHCl_3$); ^{1}H NMR (400 MHz): $\delta = 0.88$ (t, 3H, $J = 6.9$ Hz, CH_3), 0.98 (d, 3H, $J = 7.0$ Hz, CH_3), 1.02 (d, 3H, $J = 7.1$ Hz, CH_3), 1.18 (d, 3H, $J = 7.0$ Hz, CH_3), 1.17–1.31 (m, 10H, $(CH_2)_5$), 1.51 (m, 1H, CH_2), 1.72 (m, 1H, CH_2), 2.29 (m, 1H, $CH(CH_3)_2$), 2.47 (dd, 1H, $J = 4.0$, 16.2 Hz, CH_2-C=O), 2.66 (s, 3H, N-CH_3), 2.71–2.82 (m, 2H, CH_2-C=O, MeC*H*C=O), 3.00 (dd, 1H, $J = 5.2$, 14.2 Hz, CH_2Ph), 3.18 (dd, 1H, $J = 8.8$, 14.2 Hz, CH_2Ph), 3.35 (s, 3H, CH_3O), 3.55 (br, s, 1H, C*H*-NHMe), 3.66 (br, 1H, N*H*Me), 4.43 (m, 1H, C*H*-OMOM), 4.73 (ABq, 2H, $J = 6.4$, 9.5 Hz, O-CH_2-OMe), 4.79 (d, 1H, $J = 4.1$ Hz, O-C*H*-$CHMe_2$), 5.34 (dt, 1H, $J = 3.1$, 7.6 Hz, C*H*-O-CO-CH_2), 7.20–7.38 (m, 5H, Ph); ^{13}C NMR (100 MHz): $\delta = 9.81$ (CH_3), 14.04 (CH_3), 17.29 (CH_3), 19.28 (CH_3), 22.58 (CH_2), 25.65 (CH_2), 29.11 (CH_2), 29.31 (CH_2), 29.74 (*C*HMe$_2$), 30.42 (CH_2), 30.98 (CH_2), 31.73 (CH_2Ph), 39.22 (CH_2), 40.43 (*C*HMeCO), 41.04 (N*C*H$_3$), 56.20 (O*C*H$_3$), 68.46 (*C*HNMe), 75.27 (*C*HOMOM), 77.17 (O*C*HCHMe$_2$), 78.66 (CH_2*C*HOC=O), 96.50 (O*C*H$_2$OMe), 126.82 (CH), 128.77 (CH), 128.72 (CH), 129.18 (CH), 129.37 (CH), 137.2 (*C*=CH), 169.7 (C=O), 170.0 (C=O), 173.5 (C=O); IR (neat): $\tilde{\nu} = 3660$, 3621, 3020, 2975, 1730, 1716, 1527 cm^{-1}; MS (70 eV): *m/z*: 551 (M^+).
[18] S. Hanessian, D. Delorme, Y. Dufresne, *Tetrahedron Lett.* **1984**, *25*, 2515.

Proton-Induced Switching of Electron Transfer Pathways in Dendrimer-Type Tetranuclear $RuOs_3$ Complexes**

Masa-aki Haga,* Md. Meser Ali, and Ryuichi Arakawa

Supramolecular complexes as precursors for molecular devices have attracted much attention in recent years.[1] Molecular switching by an external stimulus is one of the fundamental functions of supramolecular complexes. Protonation can act as an external trigger in complexes containing basic sites. Recently, protonation has been shown to induce the switching of fluorescence,[2] redox properties,[3] and electron transfer reactions.[3a,4] The chemical principle underlying the switching of redox potential, for example the reversible protonation of an uncoordinated nitrogen site in 2-(2-pyridyl)benzimidazole Ru complexes, has been developed.[3a,c] We have extended this chemistry to dendrimer-type tetranuclear complexes. Two oxidation patterns shown have been reported in ligand-bridged dendrimer tetranuclear complexes (Scheme 1).[5] Pattern A consists of simultaneous oxidation of three peripheral Os^{II} atoms at almost the same potentials prior to one-electron oxidation of the central Ru^{II} atom. Pattern B is the reverse. The two redox patterns can be interchanged by protonation/deprotonation of basic sites.

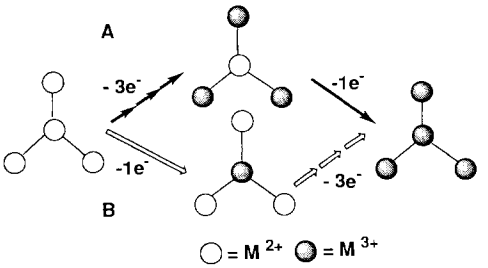

Scheme 1. Two redox patterns in dendrimer-type ligand-bridged tetranuclear metal complexes.

Complex **1** is composed of a central Ru^{II} atom surrounded by three pyridine and three benzimidazole ligands, which are complexed to three $Os^{II}(bpy)_2$ units (Scheme 2). The coordination of Ru and Os by ligands containing extra Brönsted basic sites makes the redox potentials of the metal sensitive to ligand protonation/deprotonation reactions.

$[\{Os(bpy)_2(bbbpyH_2)\}_3Ru](ClO_4)_8$ **1**-$(ClO_4)_8$
bpy = 2,2′-bipyridine
$bbbpyH_2$ = 2,2′-bis(benzimidazol-2-yl)-4,4′-bipyridine

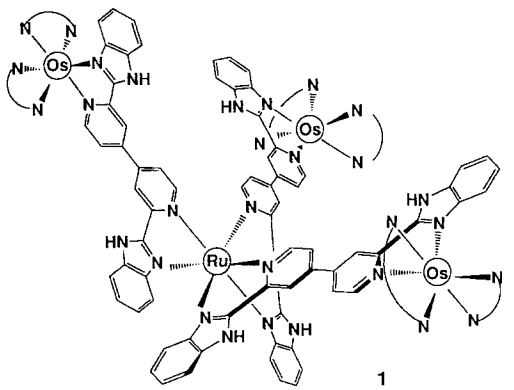

Scheme 2. Schematic representation of **1**.

Complex **1**-$(ClO_4)_8$ was synthesized by the reaction of $RuCl_3 \cdot 3H_2O$ with $[Os(bpy)_2(bbbpyH_2)](ClO_4)_2$ using the "complexes-as-ligands" strategy. Complex **2**-$(ClO_4)_2$, the perchlorate salt of the fully deprotonated product, was obtained by reaction of **1**-$(ClO_4)_8$ with an equimolar amount of sodium methoxide.

$[\{Os(bpy)_2(bbbpy)\}_3Ru](ClO_4)_2$ **2**-$(ClO_4)_2$

The cyclic voltammogram of the perchlorate salt of **1** in CH_3CN with 0.15 mM $HClO_4$ (Fig. 1, top) shows two oxidation waves centered at + 0.38 and + 0.71 V (versus ferrocenium/ferrocene (Fc^+/Fc)), which are assigned to three-electron $Os^{II/III}$-based and one-electron $Ru^{II/III}$-based oxidations, respectively. In the cyclic voltammogram of the fully deprotonated complex **2** (Fig. 1, bottom) the order of the two waves is reversed, and they are shifted to − 0.34 V and + 0.06 V. Thus, deprotonation has switched the site of the first oxidation from the peripheral Os

[*] Prof. M. Haga, Md. Meser Ali
Department of Chemistry, Faculty of Education, Mie University
1515 Kamihama, Tsu, Mie 514 (Japan)
Fax: Int. code + (592) 31-4657
e-mail: haga@libelle.edu.mie-u.ac.jp
Prof. R. Arakawa
Department of Applied Chemistry, Faculty of Engineering
Osaka University, Toyonaka, 560 (Japan)

[**] This work was supported by the Ministry of Education through a Grant-in-Aid for Scientific Research (No.06804036), and by the Iketani Science and Technology Foundation, and the Sumitomo Foundation. M. M. A. also thanks the Japanese Ministry of Education for a Monbusho scholarship. We thank Prof. T. Ohno and Dr. K. Nozaki at Osaka University for measuring the near-IR spectra.

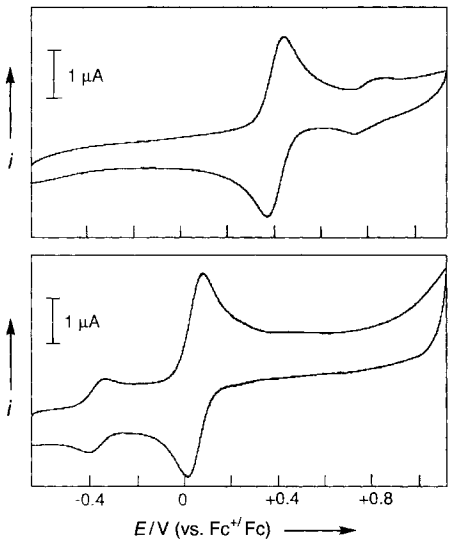

Fig. 1. Cyclic voltammograms of **1**-$(ClO_4)_8$ (top) and **2**-$(ClO_4)_2$ (bottom) in CH_3CN (0.1 M NBu_4BF_4; with added 0.15 mM $HClO_4$ for **1**-$(ClO_4)_8$) recorded with a Pt working electrode at a scan rate of 0.1 Vs^{-1}.

centers to central Ru site. This change is accompanied by negative potential shifts.

Plots of the oxidation potential $E_{1/2}$ versus pH (Pourbaix diagrams, Fig. 2) give lines with slopes of 60 and 120 $mVpH^{-1}$ for the Os- and Ru-based oxidations, respectively, which cross around pH 5.

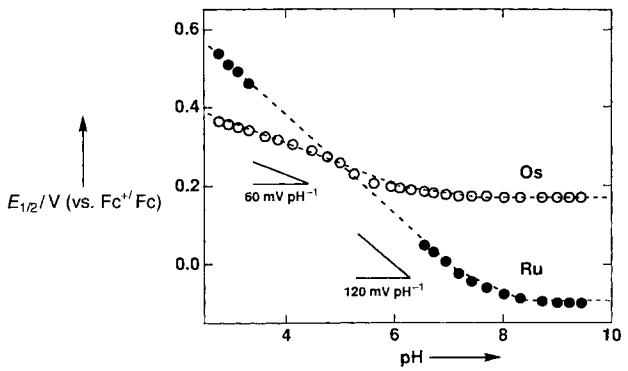

Fig. 2. Plots of the oxidation potential versus pH (Pourbaix diagrams) for **1**-$(ClO_4)_8$ in CH_3CN/Britton-Robinson buffer (1/1) at 25 °C. In this diagram the pH value refers to the apparent pH, which is a direct reading of a pH meter in CH_3CN/Britton-Robinson buffer (1/1).

The one-electron oxidized form of the deprotonated complex $\mathbf{2}^+$ ($Ru^{III}Os^{II}_3$) was generated quantitatively by bulk electrolysis at -0.2 V. The rotating disk voltammogram of this one-electron oxidation product in CH_3CN is shown in Figure 3. The cathodic current at negative potentials is due to the one-electron $Ru^{III} \rightarrow Ru^{II}$ reduction at $E_{1/2} = -0.34$ V. The anodic current is due to the three-electron oxidation $Os^{II} \rightarrow Os^{III}$ of the peripheral sites at $E_{1/2} = +0.06$ V (Fig. 3a).

Following acidification of this solution, positive potential shifts and reversed order of the $3e^-$ and $1e^-$ processes were observed. A significant observation in this case is that a small part of the cathodic current, which is superimposed on the anodic current, remained for the three-electron Os-based process at $E_{1/2} = +0.38$ V. This observation indicates that the electron

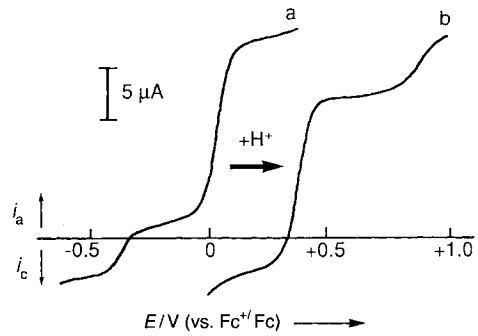

Fig. 3. Rotating disk voltammograms of the deprotonated complex $\mathbf{2}^+$ after one-electron oxidation in CH_3CN (0.1 M NBu_4BF_4) before (a) and after (b) addition of $HClO_4$ (1 mM). The voltammograms were recorded with a glassy-carbon electrode at a rotation rate of 1000 rpm and sweep rate of 0.02 Vs^{-1}.

transfer from the peripheral Os^{II} sites to the central Ru^{III} moiety occurs upon protonation. Addition of base (NBu_4OH) to the acidic solution restores the original voltammogram. Therefore, the process is reversible. To confirm the electrochemical detection of the proton-induced electron transfer reaction, the near-IR spectrum of the complex after one-electron oxidation was recorded. After one-electron oxidation the deprotonated complex does not show absorption in the near-IR region, but protonation induces a drastic change: new bands at 1050, 1900, and 2300 nm appear (Fig. 4). The latter two can be assigned to $d\pi-$

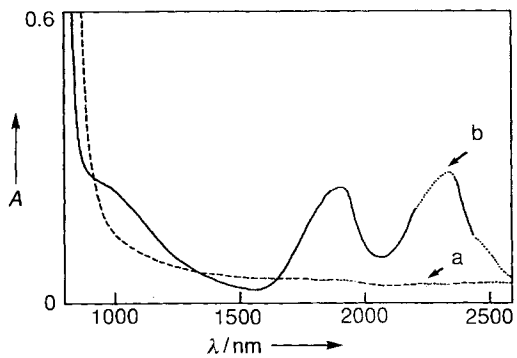

Fig. 4. Near-IR spectra of the deprotonated complex $\mathbf{2}^+$ after one-electron oxidation ($d = 1$ cm, $c = 0.7$ mM) in CH_3CN (0.1 M NBu_4BF_4) before (a) and after (b) addition of $HClO_4$ (1 mM). A = absorption in arbitrary units.

$d\pi$ transitions within the Os^{III} part of the complex.[6] The band at 1050 nm may be assigned to the Ru^{II} to Os^{III} intervalence charge transfer band. Thus, the Os→Ru electron transfer reaction [Eq. (a)] can be induced by protonation of the ligand Brönsted basic sites.

$$[\{Os^{II}(bpy)_2(bbbpy)\}_3Ru^{III}]^{3+} + 6H^+ \longrightarrow [\{Os^{III}(bpy)_2(bbbpyH_2)\}\{Os^{II}(bpy)_2(bbbpyH_2)\}_2Ru^{II}]^{9+} \quad (a)$$

A similar proton-induced electron transfer reaction has been reported for related dinuclear RuOs complexes.[4a,b]

Experimental Procedure

1-$(ClO_4)_8$: A suspension of $RuCl_3 \cdot 3H_2O$ (0.026 g, 0.1 mmol) in 20 mL of glycerol was stirred at 100 °C under nitrogen for 1.5 h. During this period, the color of the suspension changed to green. Then $[Os(bpy)_2(bbbpyH_2)](ClO_4)_2 \cdot 2H_2O$ (0.34 g, 0.3 mmol) was added, and the solution temperature was maintained at 120 °C for 24 h. The violet solution was cooled to room temperature, and 50 mL of H_2O was added to the solution. A saturated solution of $NaClO_4$ was added until complete

 © VCH Verlagsgesellschaft mbH, D-69451 Weinheim, 1996 0570-0833/96/3501-0077 $ 10.00+.25/0

precipitation occurred. The precipitate was collected by filtration and dissolved in a minimum amount of CH_3CN. This solution was loaded onto an SP-Sephadex C-25 column and eluted with CH_3CN/buffer (1/1) by raising the pH of the solution. The desired tetranuclear complex was eluted by adjusting the solution pH to 7.5 with 0.05 M NaCl. The eluate was collected and concentrated by evaporation to half its volume. The complex was precipitated from the resulting solution by addition of $NaClO_4$. The precipitate was collected by filtration and dried under vacuum. Yield: 0.18 g (50%). UV/Vis(CH_3CN): λ_{max} (ε) = 708 (18800), 535 (78800), 345 (118000), 291 nm (221000). Electrospray MS [7]: m/z 1089 $[M-3X^-]^{3+}$, 1055.4 $[M-4X^-+H^+]^{3+}$, 1022.7 $[M-5X^-+2H^+]^{3+}$, 988.4 $[M-6X^-+3H^+]^{3+}$, 955.2 $[M-7X^-+4H^+]^{3+}$, 794.6 $[M-4X^-]^{4+}$, 768.5 $[M-5X^-+H^+]^{4+}$, 743.3 $[M-6X^-+2H^+]^{4+}$, 718.1 $[M-7X^-+3H^+]^{4+}$, 693.8 $[M-8X^-+4H^+]^{4+}$, 595.7 $[M-6X^-+H^+]^{5+}$, 575.4 $[M-7X^-+2H^+]^{5+}$, 555 $[M-8X^-+3H^+]^{5+}$, 496.5 $[M-6X^-]^{6+}$, 480 $[M-7X^-+H^+]^{6+}$, 462.9 $[M-8X^-+2H^+]^{6+}$, where $M = C_{132}H_{96}N_{30}O_{32}Cl_8RuOs_3$, $X^- = ClO_4^-$. Satisfactory C, H, N analysis was obtained for the salt with the formula $C_{132}H_{96}N_{30}O_{32}Cl_8RuOs_3 \cdot H_2O$.

2-$(ClO_4)_2$: A solution of **1**-$(ClO_4)_8$ (0.16 g, 0.045 mmol) in methanol (25 mL) was added to a solution of sodium methoxide formed by the addition of sodium metal (0.006 g, 0.26 mmol) to methanol (3 mL). The mixture was stirred for 10 min with heating and then cooled. The black solution was concentrated to half of its volume and kept in a refrigerator. Analytically pure black microcrystalline solid was obtained. Yield: 0.09 g (69%). UV/Vis (CH_3CN): λ_{max} (ε) = 596 (54000), 513 (55700), 465sh, 347 (108000), 294 nm (203000). Electrospray MS [7]: m/z 922.1 $[M-2X^-+H^+]^{3+}$, 718.1 $[M-X^-+3H^+]^{4+}$, 693.8 $[M-2X^-+2H^+]^{4+}$, 574.6 $[M-X^-+4H^+]^{5+}$, 554.6 $[M-2X^-+3H^+]^{5+}$, 462.7 $[M-2X^-+4H^+]^{6+}$, where $M = C_{132}H_{90}N_{30}O_8Cl_2RuOs_3$ and $X^- = ClO_4^-$. Satisfactory C, H, N analysis was obtained for the salt with the formula $C_{132}H_{90}N_{30}O_8Cl_2RuOs_3 \cdot 33H_2O$.

Received: June 21, 1995 [Z 8120 IE]
German version: *Angew. Chem.* **1996**, *108*, 85–87

Keywords: dendritic complexes · electrochemistry · electron transfer · osmium compounds · ruthenium compounds

[1] a) V. Balzani, L. Moggi, F. Scandola in *Supramolecular Photochemistry* (Ed.: V. Balzani), Reidel, Dordrecht, **1987**, p. 1; b) V. Balzani, F. Scandola, *Supramolecular Photochemistry*, Ellis Horwood, Chichester, **1991**; c) S. Woitellier, J. P. Launay, C. W. Spangler, *Inorg. Chem.* **1989**, *28*, 758; d) J. P. Launay in *Molecular Electronic Devices II* (Ed.: F. L. Carter), Dekker, New York, **1987**, p. 39; e) J. J. Hopfield, J. N. Onuchic, D. N. Beratan, *Science* **1988**, *241*, 817; f) Y. Kim, C. M. Lieber, *Inorg. Chem.* **1989**, *28*, 3990; g) G. J. Kavarnos, *Fundamentals of Photoinduced Electron Transfer*, VCH, New York, **1993**, p. 185.

[2] a) A. W. Czarnik, *Acc. Chem. Res.* **1994**, *27*, 302; b) G. De Santis, M. Di Casa, L. Fabbrizzi, M. Licchelli, C. Mangano, P. Pallavicini, A. Perotti, A. Poggi, D. Sacchi, A. Taglietti in *Transition Metals in Supramolecular Chemistry* (Eds.: L. Fabbrizzi, A. Poggi), Kluwer, Dordrecht, **1994**, p. 133; c) R. A. Bissell, A. P. de Silva, H. Q. N. Gunaratne, P. L. M. Lynch, G. E. M. Maguire, C. P. McCoy, K. R. A. S. Sandanayake, *Top. Curr. Chem.* **1993**, *168*, 223; d) A. L. Moore, T. A. Moore, *J. Am. Chem. Soc.* **1995**, *117*, 1657.

[3] a) M. Haga, T. Ano, K. Kano, S. Yamabe, *Inorg. Chem.* **1991**, *30*, 3843–3849; b) M. Haga, T. Ano, T. Ishizaki, K. Kano, K. Nozaki, T. Ohno, *J. Chem. Soc. Dalton. Trans.* **1994**, 263; c) M. Haga, Md. M. Ali, H. Maegawa, K. Nozaki, A. Yoshimura, T. Ohno, *Coord. Chem. Rev.* **1994**, *132*, 99.

[4] a) G. A. Neyhart, T. J. Meyer, *Inorg. Chem.* **1986**, *25*, 4808; b) W. J. Vining, N. A. Surridge, T. J. Meyer, *J. Phys. Chem.* **1986**, *90*, 2281; c) K. Nozaki, T. Ohno, M. Haga, *ibid.* **1992**, *96*, 10880; d) V. Marvaud, J. P. Launay, *Inorg. Chem.* **1993**, *32*, 1376; e) H. Krenziern, H. Taube, *ibid.* **1982**, *21*, 4001; f) H. Segawa, N. Nakayama, T. Shimidzu, *J. Chem. Soc. Chem. Commun.* **1992**, 785; g) V. Goulle, A. Harriman, J.-M. Lehn, *J. Chem. Soc. Chem. Commun.* **1993**, 1034.

[5] a) G. Denti, S. Campagna, L. Sabatino, S. Serroni, M. Ciano, V. Balzani, *Inorg. Chem.* **1990**, *29*, 4750; b) G. Denti, S. Campagna, S. Serroni, M. Ciano, V. Balzani, *J. Am. Chem. Soc.* **1992**, *114*, 2944; c) S. Serroni, A. Juris, S. Campagna, M. Venturi, G. Denti, V. Balzani, *ibid.* **1994**, *116*, 9086.

[6] a) J. Sen, H. Taube, *Acta Chem. Scand. Ser. A* **1979**, *33*, 125; b) J. D. Buhr, J. R. Winkler, H. Taube, *Inorg. Chem.* **1980**, *19*, 2416; c) M. Haga, T. Matsumura-Inoue, S. Yamabe, *ibid.* **1987**, *26*, 4148.

[7] The electrospray ionization mass spectra of both **1**-$(ClO_4)_8$ and **2**-$(ClO_4)_2$ in CH_3CN can be explained by the general formulas $[M-nX^-+mH]^{(n-m)+}$ for **1**-$(ClO_4)_8$ and $[M-nX^-+mH]^{(n+m)+}$ for **2**-$(ClO_4)_2$, where n and m are the numbers of perchlorate anions and protons, respectively. This spectra indicates that protonation/deprotonation reactions occur during the ionization [8].

[8] a) R. Arakawa, T. Matsuo, H. Ito, I. Katakuse, K. Nozaki, T. Ohno, M. Haga, *Org. Mass. Spectrom.* **1994**, *29*, 289–294; b) R. Arakawa, T. Matsuo, K. Nozaki, T. Ohno, M. Haga, *Inorg. Chem.* **1995**, *34*, 2464.

$[N(CH_3)_4][Mn(N_3)_3]$: A Compound with a Distorted Perovskite Structure through Azido Ligands**

Franz A. Mautner, Roberto Cortés, Luis Lezama, and Teófilo Rojo*

In the last few years the azide ion has been shown to be a very versatile ligand in bridging different transition metals. By using its two possible bridging modes, end-to-end (EE) and end-on (EO), dinuclear,[1–3] tetranuclear,[4] one-dimensional (1D),[2b, 5] and two-dimensional (2D) polymeric complexes[6] have been characterized for the azido ligand. The EE bridges give rise to antiferromagnetic interactions,[5a–c] the EO bridges lead to ferromagnetic coupling[1, 3] even for the manganese(II) ion with $S = 5/2$,[7] and in a 1D compound containing both types of bridging, alternating ferro- and antiferromagnetic interactions are observed.[5d]

Three-dimensional (3D) compounds are of interest in the field of molecular magnets because on the one hand they should help researchers gain a better understanding of the correlation between magnetism and structure, and on the other hand 3D antiferro- or ferromagnets are attractive for possible technical applications. Only a few molecular magnets based on 3D systems are known; however, by employing the versatile coordination ability of the azido ligand it should be possible to tailor systems of this kind.

With this aim in mind we developed a synthesis strategy in which the six vacant coordination sites around the metal ion could be filled by azido ligands. To obtain the desired conformation of a 3D system, the tetramethylammonium ion was selected as positive counterion because of its small size. By using this method, we isolated a 3D Mn^{II} compound of the empirical formula $[N(CH_3)_4][Mn(N_3)_3]$. To our knowledge, this is the first three-dimensional azide compound.

The crystal structure (Fig. 1)[8] of the room temperature phase may be described as a distorted Perovskite structure, that is, the Mn^{II} ion is shifted from the origin of the unit cell by about 0.25 along the b axis. The azido groups act as end-to-end bridging ligands between the manganese centers, thereby forming the three-dimensional network. Each manganese ion shows a slightly distorted octahedral coordination sphere. The $[N(CH_3)_4]^+$ ions are located in the cavities of the manganese(II)-azido sublattice (Fig. 1). The EE azido ligands asymmetrically bridge the metal centers: the Mn-N-N and N-N-Mn′ angles are about 165° and 135°, respectively, the Mn···Mn distance about 6.4 Å. The compound undergoes a reversible phase transformation at approximately 303 K. The pseudo-cubic high-temperature (HT) phase at 310 K has a cell length of 6.446(4) Å, and each unit cell contains one formula unit. The crystal structure of this HT phase is currently under investigation.

[*] Prof. T. Rojo, Dr. L. Lezama
Departamento de Química Inorgánica, Universidad del País Vasco
Aptdo. 644, E-48080 Bilbao (Spain)
Fax: Int. code +(4)4648500
e-mail: QIPROAPT@lg.ehu.es
Dr. R. Cortés
Departamento de Química Inorgánica, Facultad de Farmacia (U. P. V.)
Aptdo. 450, E-01080 Vitoria-Gasteiz (Spain)
Dr. F. A. Mautner
Institut für Physikalische und Theoretische Chemie
Technische Universität Graz, A-8010 Graz (Austria)

[**] This work has been supported by the Spanish DGICYT (Project PB90-0549) and the University of the Basque Country (UPV 130.310-EB017/92). F. A. M. thanks Prof. C. Kratky (Universität Graz, Austria) for the use of experimental equipment.

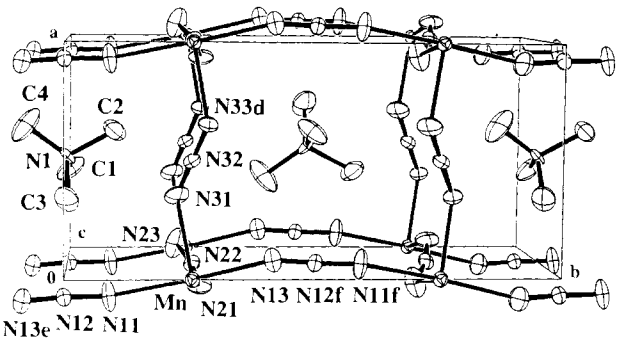

Fig. 1. Crystal structure of $[N(CH_3)_4][Mn(N_3)_3]$. H atoms are omitted for clarity. Selected distances [Å] and bond angles [°] (standard deviations in parentheses): Mn(1)–N(11) 2.21(1), Mn(1)–N(13), 2.22(2), Mn(1)–N(21) 2.20(1), Mn(1)–N(31) 2.24(1), Mn(1)–N(33) 2.21(1), Mn(1)–N(23b) 2.26(1); N(11)-Mn(1)-N(13) 175.4(9), N(11)-Mn(1)-N(21) 85.6(6), N(11)-Mn(1)-N(31) 90.8(7), N(11)-Mn(1)-N(33) 89.5(6), N(11)-Mn(1)-N(23b) 90.4(6), N(13)-Mn(1)-N(21) 90.3(7), Mn(1)-N(11)-N(12) 162(1). N(11)-N(12)-N(13e) 176(1), Mn(1)-N(13)-N(12e) 163(1), Mn(1)-N(21)-N(22) 144(1), N(21)-N(22)-N(23) 164(2), N(22)-N(23)-Mn(1c) 132(1), Mn(1)-N(31)-N(32) 134(1), N(31)-N(32)-N(33d) 177(3), Mn(1)-N(33)-N(32a) 131(1); symmetry code: a) $x-1, y, z$; b) $x, y, z-1$; c) $x, y, z+1$; d) $x+1, y, z$; e) $-x, y-1/2, -z$; f) $-x, y+1/2, -z$.

EPR measurements on this compound at low (cooling with liquid nitrogen) and high temperatures were carried out on powdered samples with a Bruker ESP 300 spectrometer. They show an isotropic signal for the manganese(II) ion, $g = 2.00$. This signal is very sharp and intense and does not change significantly on varying the temperature, which indicates that the octahedral environment of the Mn^{II} ion does not alter to a great extent.

Variable-temperature magnetic susceptibility measurements were performed on a powdered sample in the range 350 to 2 K with a SQUID Quantum Design MPMS-2 magnetometer. Global antiferromagnetic behavior is evident from the magnetic measurements as is shown in Figures 2 and 3. The χ_m value increases as the temperature decreases (Fig. 2), reaching a sharp

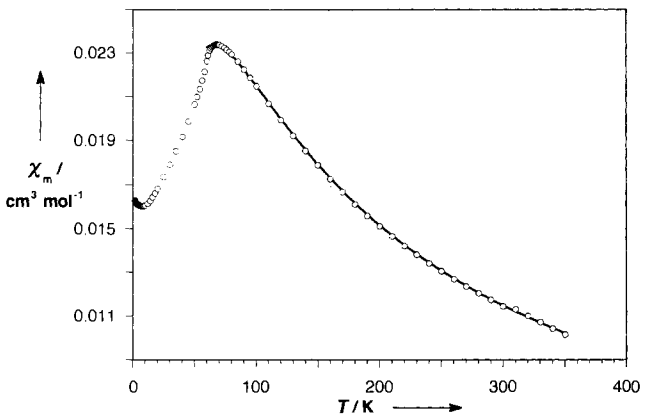

Fig. 2. Plot of χ_m (○) of $[N(CH_3)_4][Mn(N_3)_3]$ versus T. Solid line: best-fit susceptibility curve for an $S = 5/2$ simple cubic Heisenberg antiferromagnetic system derived from the HTS model developed by Rushbrook and Wood [9].

maximum at about 70 K, and then decreases on cooling down to 2 K. The extrapolated value of the susceptibility at 0 K is found to be approximately two-thirds of the value of the susceptiblity maximum. The latter, together with the existence of a sharp maximum on the curve, indicates that three-dimensional antiferromagnetic behavior can be inferred from the susceptibility measurements. Indeed, investigations on single crystals, AC susceptibility measurements, and neutron diffraction would be suitable methods to unambiguously confirm 3D ordering. The $\chi_m T$ value at room temperature is 3.5 $cm^3 K mol^{-1}$ (Fig. 3),

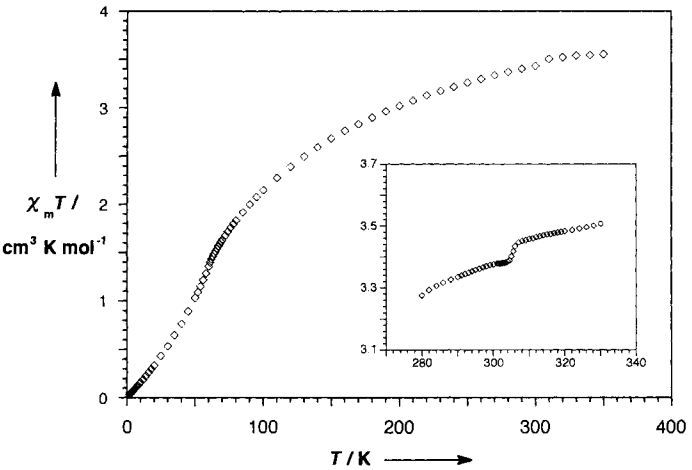

Fig. 3. Thermal variation of $\chi_m T$ (○). Inset: phase transition.

smaller than the value expected for an uncoupled Mn^{II} ion. This value decreases with decreasing temperature tending to zero. The reversible phase transition (305 K) was also evident from these measurements (inset in the $\chi_m T$ vs. T plot). This could be indicative of changes in the Mn-azido-Mn angles in the high-temperature phase, which would lead to a variation in the strength of J and consequently to a modification of the magnetic behavior.

The magnetic behavior of this compound must be explained by assuming a regular three-dimensional network as indicated by the crystal structure. The expression of the magnetic susceptibility for a simple cubic Heisenberg antiferromagnetic system was derived from the high-temperature series expansion (HTS) model developed by Rushbrook and Wood.[9] By taking the exchange Hamiltonian $\mathcal{H} = -2J \sum_{i \neq j} S_i S_j$ into consideration, the expression given in Equation (a) was obtained for the sus-

$$\chi = \frac{35Ng^2\beta^2}{12kT}(1 + C_1x + C_2x^2 + C_3x^3 + C_4x^4 + C_5x^5 + C_6x^6) \qquad \text{(a)}$$

$x = Jk^{-1}T^{-1}$; $C_1 = 35$, $C_2 = 221.67$, $C_3 = 608.22$, $C_4 = 26049.66$, $C_5 = 210986$, $C_6 = 8014980$

ceptibility. Equation (a) is only valid around the maximum (paramagnetic region). The solid line in Figure 2 shows the best least-squares fit of the susceptibility data for $[N(CH_3)_4][Mn(N_3)_3]$ by using Equation (a). The parameters obtained are $Jk^{-1} = -2.5$ K and $g = 2.01$, in good agreement with the results from the EPR measurements.

Experimental Procedure

Manganese nitrate tetrahydrate (2.1 g, 8.4 mmol) was dissolved in a hot aqueous solution of tetramethylammonium azide (45 mL, 48 mmol, $T = 340$ K), saturated with hydrazoic azide. The clear solution was allowed to cool, and colorless, transparent, prismatic crystals were obtained. Elemental analysis: calc. (found): Mn 21.5 (21.4), N 54.9 (54.8), C 18.8 (18.9) H 4.7 (4.7)%.

Received: June 30, 1995 [Z 8154 IE]
German version: *Angew. Chem.* **1996**, *108*, 96–98

Keywords: azides · magnetic properties · manganese compounds · perovskites · solid-state structures

 © VCH Verlagsgesellschaft mbH, D-69451 Weinheim, 1996 0570-0833/96/3501-0079 $ 10.00+.25/0

[1] a) J. Commarmond, P. Plumeré, J. M. Lehn, Y. Agnus, R. Louis, R. Weiss, O. Kahn, I. Morgenstern-Badarau, *J. Am. Chem. Soc.* **1982**, *104*, 6330–6340; b) P. Chaudhuri, M. Guttmann, D. Ventur, K. Weighardt, B. Nuber, J. Weiss, *J. Chem. Soc. Chem. Commun.* **1985**, 1618–1620; c) T. Rojo, L. Lezama, R. Cortés, J. L. Mesa, M. I. Arriortua, G. Villeneuve, *J. Magn. Magn. Mater.* **1990**, *83*, 519-521; d) R. Cortés, J. I. R. Larramendi, L. Lezama, T. Rojo, M. K. Urtiaga, M. I. Arriortua, *J. Chem. Soc. Dalton Trans.* **1992**, 2723–2728; e) R. Cortés, M. K. Urtiaga, L. Lezama, J. I. R. de Larramendi, M. I. Arriortua, T. Rojo, *ibid.* **1993**, 3685–3694 and references therein.

[2] a) R. Vicente, A, Escuer, J. Ribas, M. S. El Fallah, X. Solans, M. Font-Bardía, *Inorg. Chem.* **1993**, *32*, 1920–1924; b) J. Ribas, M. Monfort, C. Diaz, C. Bastos, X. Solans, *ibid.* **1994**, *33*, 484–489.

[3] J. Ribas, M. Monfort, C. Diaz, C. Bastos, X. Solans, *Inorg. Chem.* **1993**, *32*, 3557–3561.

[4] J. Ribas, M. Monfort, R. Costa, X. Solans, *Inorg. Chem.* **1993**, *32*, 695–699.

[5] a) C. G. Pierpont, D. N. Hendrickson, D. M. Duggan, F. Wagner, E. K. Barefield, *Inorg. Chem.* **1975**, *14*, 604–610; b) A. Escuer, R. Vicente, J. Ribas, M. S. El Fallah, X. Solans, M. Font-Bardía, *ibid.* **1993**, *32*, 3727–3732; c) R. Cortés, M. K. Urtiaga, L. Lezama, J. L. Pizarro, A. Goñi, M. I. Arriortua, T. Rojo, *ibid.* **1994**, *33*, 4009–4015; d) R. Cortés, L. Lezama, J. L. Pizarro, M. I. Arriortua, X. Solans, T. Rojo, *Angew. Chem.* **1994**, *106*, 2520–2521; *Angew. Chem. Int. Ed. Engl.* **1994**, *33*, 2488–2489.

[6] a) J. Ribas, M. Monfort, X. Solans, M. Drillon, *Inorg. Chem.* **1994**, *33*, 742–745; b) M. A. S. Goher, F. A. Mautner, *Croat. Chem. Acta* **1990**, *63*, 559–564.

[7] R. Cortés, J. L. Pizarro, L. Lezama, M. I. Arriortua, T. Rojo, *Inorg. Chem.* **1994**, *33*, 2697-2700.

[8] X-ray structure analysis: STOE four-circle diffractometer. Unit cell parameters were determined from automatic centering of 32 reflections $11 < 2\theta < 23°$) and refined by least squares method. Intensities were collected with graphite-monochromatized $Mo_{K\alpha}$ (0.71069 Å) radiation using the ω-scan technique ($\Delta\omega = 1.00$). Lorentz polarization and extinction corrections were made. Data collection, solution and refinement: ω/scan. The structure was solved by standard Patterson methods with the SHELXS-86 program. For structure refinement the twin routine of SHELXL-93 program was used (twin matrix: 1 0 0, 0 −1 0, 0 0 −1). Constraints were applied to the positions of all hydrogen atoms, and the H atoms were assigned a common isotropic temperature factor. $C_4H_{12}N_{10}Mn$ ($M = 255.14$), monoclinic, $P2_1$, $a = 6.264(3)$, $b = 13.150(6)$, $c = 6.375(3)$ Å, $b = 90.00(6)$, $V = 525.1(4)$ Å^3, $Z = 2$, $\rho_{calcd} = 1.614$ g cm^{-3}, $\mu = 12.5$ cm^{-1}, $F(000) = 262$, 1373 reflections were measured in the range $5 < 2\theta < 65$, 891 of which were assumed as observed by applying the condition $I > 4\sigma(I)$, 142 parameters, $R1(F_o) = 0.0296$, $wR2(F_o^2) = 0.0694$ and $S = 1.106$. Mean shift/esd = 0.055. Max. and min. peaks in final difference synthesis were 0.22 and −0.41 e Å^{-3}. Further details of the crystal structure investigation may be obtained from the Director of the Cambridge Crystallographic Data Centre, 12 Union Road, GB-Cambridge CB21EZ (UK), on quoting the full journal citation.

[9] G. S. Rushbrook, P. J. Wood, *Mol. Phys.* **1958**, *1*, 257–283.

Formation of a Zirconocene–Betaine System by Electrophilic Substitution with $B(C_6F_5)_3$ at a Cyclopentadienyl Ligand**

Johannes Ruwwe, Gerhard Erker*, and Roland Fröhlich

Cyclopentadienyl complexes of the late transition elements often readily undergo electrophilic aromatic substitution reactions at the η^5-cyclopentadienyl rings. The corresponding substitution reactions of ferrocene are well-known general examples.[1] Analogous reactions of the bent metallocene complexes of titanium, zirconium, and hafnium are to our knowledge not known. For this reason bent metallocenes with Group 4 metals containing substituted or functionalized Cp ligands are typically synthesized by other routes utilizing suitably functionalized Cp ligand precursors.[2] The development of new methods for synthesizing Cp-functionalized derivatives starting from simple metallocenes would be of great importance because of the general catalytic potential of Group 4 metallocene complexes.[3] We have now found an example of a reaction of a zirconocene complex that can be regarded as a functionalization of a Cp ligand by an electrophilic aromatic substitution reaction similar to that often observed with the ferrocene system. The products, novel metallocene–betaine complexes, may be of interest in the development of new catalysts.[4]

We treated 1,1-bis(cyclopentadienyl)-2,3,4,5-tetramethylzirconacyclopentadiene (**1**) with tris(pentafluorophenyl)borane in toluene solution at ambient temperature. Product **3** formed cleanly and was isolated as a pale yellow solid in 78% yield. Single crystals of **3** suitable for X-ray crystal structure determination were obtained from ether.

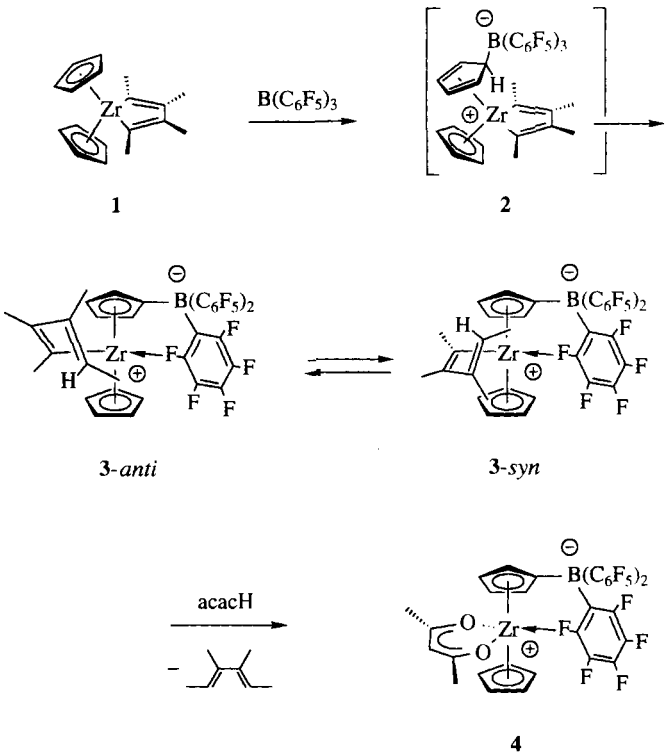

The crystal structure analysis reveals that a zirconium–carbon σ bond is cleaved during the reaction of **1** with $B(C_6F_5)_3$ (Fig. 1). Complex **3** contains a σ-bound trimethylpentadienyl ligand at zirconium. The C1–C2 double bond is oriented coplanar with the Zr–C σ bond in the σ ligand plane of the bent metallocene (dihedral angle Zr-C1-C2-C3 −8.6(5)°). The adjacent C3–C4 double bond is rotated about the C2–C3 σ bond such that the diene conjugation is almost completely lost (dihedral angles C1-C2-C3-C4 −66.9(5)°, C6-C2-C3-C7 −61.0(5)°). Despite this, there is a marginal coordinative interaction between the C3–C4 double bond and the electrophilic zirconium center in **3** (distances C3–Zr 2.932(4) Å, C4–Zr 3.040(4) Å).[5] Complex **3** contains a normal η^5-bound Cp ligand [η^5-C_5H_5] at zirconium and as the most characteristic feature a tris(pentafluorophenyl)borane-substituted cyclopentadienyl unit [η^5-$C_5H_4B(C_6F_5)_3$].[6, 7] Thus, complex **3** formally exhibits a betaine structure with positive partial charge on zirco-

[*] Prof. Dr. G. Erker, Dipl.-Chem. J. Ruwwe, Dr. R. Fröhlich
Organisch-chemisches Institut der Universität
Corrensstrasse 40, D-48149 Münster (Germany)
Fax: Int. code +(251)83-9772
e-mail: erker@uni-muenster.de

[**] This work was supported by the Fonds der Chemischen Industrie, the Alfried-Krupp-von-Bohlen-und-Halbach-Stiftung, and the Ministerium für Wissenschaft und Forschung des Landes Nordrhein-Westfalen.

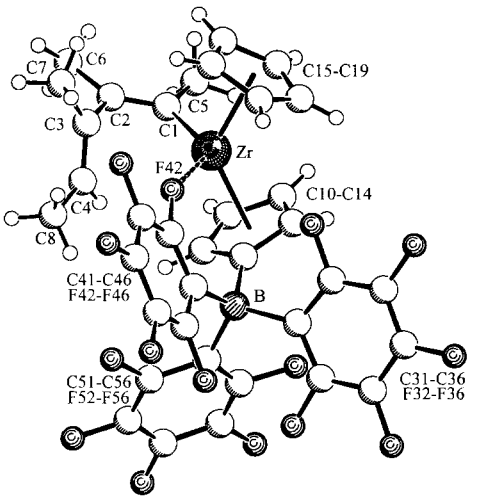

Fig. 1. Molecular structure of **3**-*syn* in the crystal; selected bond lengths [Å] and angles [°]: Zr-C1 2.252(4), C1-C2 1.329(6), C2-C3 1.498(6), C3-C4 1.340(6), C4-C8 1.494(6), C10-B 1.648(5), C10-C11 1.415(5), C10-C14 1.440(5), C11-C12 1.411(5), C12-C13 1.398(6), C13-C14 1.410(6), B-C31 1.653(5), B-C41 1.661(6), B-C51 1.637(5), Zr-F42 2.322(2), C42-F42 1.388(4), C43-F43 1.340(5), C46-F46 1.372(6); C42-F42-Zr 150.6(2), F42-Zr-C1 130.41(12), C2-C1-Zr 110.2(3), C5-C1-Zr 127.7(3), C2-C1-C5 121.5(4), C1-C2-C3 118.0(4), C2-C3-C4 117.9(4), C3-C4-C8 125.8(4).

nium and negative partial charge on boron. But the resulting electron deficiency at zirconium is very efficiently compensated in **3**: an *ortho*-fluorine substituent of one of the C_6F_5 groups

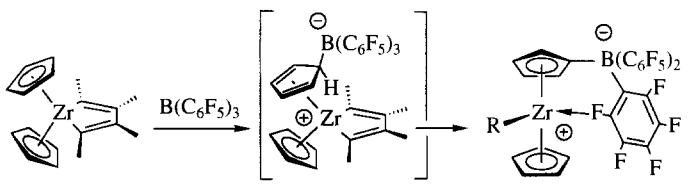

1 **2** **3**

R = -C(CH$_3$)=C(CH$_3$)-C(CH$_3$)=CH(CH$_3$)

occupies the free coordination site. In this way the pseudo-tetrahedral coordination environment at zirconium is retained: the D1-Zr-D2 angle (D1 and D2 denote the centroids of the Cp ring systems) is 130.4°, and the "divalent" fluorine atom F42 is oriented coplanar with the C1–Zr σ bond in the σ ligand plane of the bent metallocene [C1-Zr-F42 130.4(1)°].

Complex **3** is chiral in the crystal, and its chirality is retained in solution. This follows from the characteristic features of its NMR spectra. The η^5-$C_5H_4B(C_6F_5)_3$ ligand gives rise to four ^{1}H NMR signals at δ = 6.34, 5.69, 5.55, 4.82 (^{13}C NMR signals for the Cp ligand at δ = 125.0, 124.8, 119.3, 115.5, 114.3). Therefore, one must assume that the coordination of the fluorine atom to the zirconium center is retained under the conditions of the NMR measurement. Complex **3** exhibits dynamic NMR behavior when the temperature is lowered. At 213 K in [D_8]toluene the expected ^{19}F NMR signal of the bridging fluorine substituent is found at δ = −185. When the temperature is lowered to 188 K, this signal splits into two resonances of almost equal intensity at δ = −184 and −186. In the ^{1}H and ^{13}C NMR spectra there is also evidence for the presence of two almost equally populated diastereomeric complexes [^{1}H NMR in CD_2Cl_2 at 200 K: δ = 6.21/6.00 (s, Cp), 1.28/1.27 (d, each $^3J_{HH}$ = 5.6 Hz, =CHC*H*$_3$); ^{13}C NMR in CD_2Cl_2 at 200 K: pairs of signals for C1 at δ = 182.2/180.0, the η^5-C_5H_5 ligand at δ = 112.7/112.0, and the methyl groups at δ = 22.1/21.1, 15.8/15.5, 13.8/13.7, and 13.2/12.9]. Apparently the characteristic nonplanar conformation of the σ-dienyl ligand is retained in solution. We assume that these diastereomers are the complexes **3**-*syn* and **3**-*anti*, which may rapidly interconvert in solution at room temperature by rotation around the C2–C3 σ bond. The isomers can be observed when this rotation is "frozen" on the NMR time scale at low temperature [$\Delta G^{\neq}$ (267 K) = 12.7 ± 0.5 kcal mol^{-1}]. The majority of the crystals formed from the equilibrating isomers contain the diastereomer **3**-*syn*, in which the C3–C4 double bond and the η^5-$C_5H_4B(C_6F_5)_3$ ligand are *syn* oriented (see Fig. 1).

In the course of the reaction of **1** with $B(C_6F_5)_3$ to yield **3** a hydrogen atom was transferred to an α-carbon center of the metallacyclic five-membered ring system to form the trimethyl-substituted σ-bound pentadienyl ligand [^{1}H/^{13}C NMR at room temperature: δ = 5.36 (q, 1H, ^3J = 6.0 Hz, =C*H*CH$_3$)/ δ = 105.9 ($^1J_{CH}$ = 168 Hz, =*C*HCH$_3$)]. We assume that this hydrogen atom was abstracted from a Cp ring during the course of the reaction.[7] Typically $B(C_6F_5)_3$ abstracts σ-alkyl groups or hydride from organometallic substrates with formation of ionic products.[8] These reactions are apparently so unfavorable with **1** that the usually less favorable addition of the electrophilic reagent to a Cp ring takes place. The addition may lead to the (η^4-cyclopentadienyl)metal complex **2** containing an *exo*-positioned $B(C_6F_5)_3$ substituent and an *endo*-oriented hydrogen atom at C5. The subsequent acid–base reaction to give **3** is probably facilitated by the close spacial proximity of the proton and the Zr–C(sp^2) bond in the intermediate **2**.

Compound **3** is readily available by this route, and it may potentially serve as starting material in studies of the metallocene–betaine chemistry of Group 4 metal complexes containing an internal borate anion covalently bound to a Cp ligand. We have conducted exploratory experiments in this direction. Compound **3** reacts cleanly with acetylacetone at room temperature in toluene solution by protolytic liberation of 3,4-dimethylhexa-2,4-diene and formation of the (acetylacetonato)zirconium–betaine complex **4**. Product **4** exhibits an unsymmetrical acac coordination mode (Fig. 2). This is confirmed in solution by the low-temperature (203 K) ^{1}H NMR spectrum, which shows a pair of methyl resonances of the acac ligand at δ = 2.06 and 1.73 (acac-CH signal at δ = 5.73, η^5-C_5H_5 resonance at δ = 6.16). Complex **4** is apparently chiral due to *o*-fluorine coordination, and

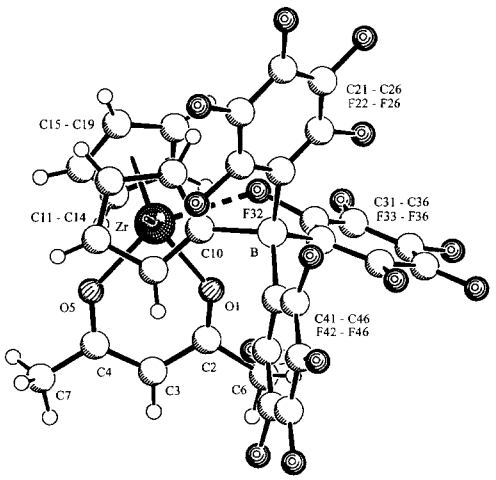

Fig 2. Molecular structure of **4** in the crystal.

four methine resonances of the η^5-$C_5H_4B(C_6F_5)_3$ ligand are evident in the ^1H NMR spectrum at low temperature (δ = 6.65, 6.54, 5.93, and 5.79). At room temperature rapid enantiomerization takes place on the NMR time scale, which results in a much simpler ^1H NMR spectrum after coalescence of the corresponding pairs of resonances. The unsymmetrical coordination of acac and the *o*-fluorine coordination is also confirmed by the structure of **4** in the crystal (Fig. 2). Because of the rather high *R*-value (0.12) details of this structure will not be discussed.

Experimental Procedure

Reaction of **1** with tris(pentafluorophenyl)borane: Compound **1** [9] (640 mg, 1.94 mmol) was dissolved in 50 mL of toluene. Then a solution of $B(C_6F_5)_3$ (980 mg, 1.94 mmol) in 35 mL of toluene was added and the reaction mixture was stirred for 8 h at ambient temperature. The solvent was removed in vacuo. The residue was washed with pentane (2 × 25 mL) and then dired in vacuo to give 1.12 g (78%) of complex **3** as a pale yellow solid. M.p. 101 °C (decomp, DSC); Elemental analysis: $C_{36}H_{22}F_{15}BZr$ (841.6) calcd C 51.35, H 2.64; found C 50.72, H 2.97; ^1H NMR ([D$_6$]benzene, 200 MHz, 300 K): δ = 6.34, 5.69, 5.55, 4.82 (m, each 1H, C_5H_4[B]), 5.51 (s, 5H, Cp), 5.36 (q, ^3J = 6.0 Hz, 1H, $=CHCH_3$), 1.39, 1.31, 1.25 (s, each 3H, CH_3), 0.99 (d, ^3J = 6.0 Hz, 3H, $=CHCH_3$); ^{13}C NMR ([D$_6$]benzene, 50 MHz, 300 K): δ = 182.0 (Zr–C=), 148.9, 139.5 137.7 ($^1J_{CF}$ = 242, 264, 266 Hz, $B(C_6F_5)_3$), 136.7, 125.0, 124.8, 119.3, 115.5, 114.3, 112.7 (Cp), 105.9 ($=CHCH_3$), 22.7, 21.6, 15.8, 15.2 (CH_3); ^{11}B NMR ([D$_6$]benzene): δ = − 16.5; ^{19}F NMR ([D$_6$]benzene, 300 K): δ = − 131.0 to −142.0 (br. m, 6F, *o*-C_6F_5), −153.2 (m, 3F, *p*-C_6F_5), −163.2 (m, 6F, *m*-C_6F_5). X-ray crystal structure analysis of **3** (single crystals from ether): formula $C_{36}H_{22}BF_{15}Zr$, M = 841.57, crystal size 1.4 × 0.5 × 0.2 mm, a = 10.878(1), b = 17.529(1), c = 17.494(1) Å, β = 96.91°, V = 3311.5(4) Å^3, ρ_{calcd} = 1.688 g cm^{-3}, μ = 4.44 cm^{-1}, empirical absorption correction, Z = 4, monoclinic, space group $P2_1/n$ (No. 14), Enraf-Nonius Mach III diffractometer, λ = 0.71073 Å, T = 223 K, 7067 measured reflections (+ h, − k, ± l), $[(\sin\theta)/\lambda]_{max}$ = 0.59 Å^{-1}, 6707 independent and 4745 observed reflections [$I > 2\sigma(I)$], 482 refined parameters, R = 0.044, wR^2 = 0.145, programs used: SHELXS-86, SHELXL-93, SCHAKAL-92. Further details of the X-ray crystal structure analyses may be obtained from the Fachinformationszentrum Karlsruhe, D-76344 Eggenstein-Leopoldshafen (Germany), on quoting the depository number CSD-404021.

Reaction of **3** with acetylacetone: Compound **3** (380 mg, 0.45 mmol) was dissolved in 25 mL of toluene. A solution containing 100 mg (1.00 mmol) of acetylacetone in 5 mL of toluene was added and the mixture was stirred for 1 h at room temperature. The solvent was removed in vacuo and the residue washed with pentane (3 × 20 mL) and then dried in vacuo to give 306 mg (81%) of **4** as a white solid. M.p. 152 °C (decomp, DSC). ^1H NMR ([D$_6$]benzene, 200 MHz, 300 K): δ = 6.05, 5.69 (m, each 2H, C_5H_4[B]), 5.54 (s, 5H, Cp), 4.88 (s, 1H, acac), 1.27 (s, 6H, acac); ^1H NMR (CD_2Cl_2, 200 MHz, 300 K): δ = 6.30 (br. s, 4H, C_5H_4[B]), 6.24 (s, 5H, Cp), 5.82 (s, 1H, acac), 1.96 (s, 6H, acac); ^{13}C NMR ([D$_8$]toluene, 50 MHz, 300 K): δ = 193.2 (acac, *C*), 149.0 ($^1J_{CF}$ = 252 Hz) and 138.0 ($^1J_{CF}$ = 227 Hz, *o*- and *m*-C_6F_5; *p*- and *ipso*-C_6F_5M signals not located), 121.3, 119.3, 117.5 (C_5H_4[B]), 115.5 (Cp), 104.1 (acac, CH), 25.6 (acac, CH_3); ^{11}B NMR ([D$_6$]benzene): δ = −15.8; ^{19}F NMR ([D$_6$]benzene): δ = −138.5, −153.6, −161.8 (*o*, *p*, *m*-C_6F_5). X-ray structure analysis of **4**: formula $C_{33}H_{16}O_2F_{15}BZr$, M = 831.49, crystal size 0.5 × 0.2 × 0.05 mm, a = 13.207(2), b = 14.918(4), c = 15.891(2) Å, V = 3130.9(10) Å^3, ρ_{calcd} = 1.764 g cm^{-3}, μ = 4.73 cm^{-1}, Z = 4, orthorhombic, space group $P2_12_12_1$ (No. 19), Enraf-Nonius Mach III diffractometer, λ = 0.71073 Å, T = 173 K, 3107 measured reflections (+ h, ± k, ± l), $[(\sin\theta)/\lambda]_{max}$ = 0.62 Å^{-1}, 3096 independent and 1815 observed reflections [$I > 2\sigma(I)$], 469 refined parameters, R = 0.121, wR^2 = 0.351.

Received: July 7, 1995
Revised version: October 6, 1995 [Z 8177 IE]
German version: *Angew. Chem.* **1996**, *108*, 108–110

Keywords: betaines · boron compounds · sandwich complexes · substitutions · zirconium compounds

[1] R. B. Woodward, M. Rosenblum, M. C. Whiting, *J. Am. Chem. Soc.* **1952**, *74*, 3458; review: W. E. Watts in *Comprehensive Organometallic Chemistry*, (Eds.: G. Wilkinson, F. G. A. Stone, E. W. Abel), Pergamon, New York, **1982**, *Vol. 8*, Chapter 59, p. 1013.

[2] a) W. P. Hart, D. W. Macomber, M. D. Rausch, *J. Am. Chem. Soc.* **1980**, *102*, 1196; W. P. Hart, D. Shihua, M. D. Rausch, *J. Organomet. Chem.* **1985**, *282*, 111; M. D. Rausch, J. F. Lewison, W. P. Hart, *ibid.* **1988**, *358*, 161; S. S. Jones, M. D. Rausch, T. E. Bitterwolf, *ibid.* **1990**, *396*, 279; M. Ogasa, D. T. Mallin, D. W. Macomber, M. D. Rausch, R. D. Rogers, A. N. Rollins, *ibid.* **1991**, *405*, 41; S. S. Jones, M. D. Rausch, T. E. Bitterwolf, *ibid.* **1993**, *450*, 27; b) K. P. Stahl, G. Boche, W. Massa, *ibid.* **1984**, *277*, 113; C. P. Casey, F. Nief, *Organometallics* **1985**, *4*, 1218; D. Morcos, W. Tikkanen, *J. Organomet. Chem.* **1989**, *371*, 15; W. A. Schenk, C. Labude, *Chem. Ber.* **1989**, *122*, 1489; M. Ogasa, M. D. Rausch, R. D. Rogers, *J. Organomet. Chem.* **1991**, *403*, 279; c) P. Burger, H. H. Brintzinger, *ibid.* **1991**, *407*, 207; W. A. Herrmann, M. J. A. Morawietz, T. Priermeier, *Angew. Chem.* **1994**, *106*, 2025; *Angew. Chem. Int. Ed. Engl.* **1994**, *20*, 2040; G. Erker, S. Wilker, C. Krüger, R. Goddard, *J. Am. Chem. Soc.* **1992**, *104*, 10983; G. Erker, S. Wilker, C. Krüger, M. Nolte, *Organometallics* **1993**, *12*, 2140, and references therein.

[3] H. H. Brintzinger, D. Fischer, R. Mülhaupt, B. Rieger, R. Waymouth, *Angew. Chem.* **1995**, *107*, 1255; *Angew. Chem. Int. Ed. Engl.* **1995**, *34*, 1143.

[4] For other examples of stable metallocene betaines and related systems see: G. G. Hlatky, H. Turner, R. R. Eckman, *J. Am. Chem. Soc.* **1989**, *111*, 2728; M. Bochmann, G. Karger, A. J. Jaggar, *J. Chem. Soc. Chem. Commun.* **1990**, 1038; A. D. Horton, J. H. G. Frijns, *Angew. Chem.* **1991**, *103*, 1181; *Angew. Chem. Int. Ed. Engl.* **1991**, *30*, 1152; D. M. Amorose, R. A. Lee, J. L. Petersen, *Organometallics* **1991**, *10*, 2191; X. Yang, C. L. Stern, T. J. Marks, *J. Am. Chem. Soc.* **1991**, *113*, 3623; *Angew. Chem.* **1992**, *104*, 1406; *Angew. Chem. Int. Ed. Engl.* **1992**, *31*, 1375; C. Sishta, R. M. Hathorn, T. J. Marks, *J. Am. Chem. Soc.* **1992**, *114*, 1112; G. G. Hlatky, R. R. Eckman, H. W. Turner, *Organometallics* **1992**, *11*, 1413; C. J. Schaverien, *ibid.* **1992**, *11*, 3476; M. Bochmann, *Angew. Chem.* **1992**, *104*, 1206; *Angew. Chem. Int. Ed. Engl.* **1992**, *31*, 1181; C. Pellecchia, A. Immirzi, A. Grassi, A. Zambelli, *Organometallics* **1993**, *12*, 4473; C. Pellecchia, A. Grassi, A. Immirzi, *J. Am. Chem. Soc.* **1993**, *115*, 1160; J. J. Eisch, S. I. Pombrik, G.-X. Zheng, *Organometallics* **1993**, *12*, 3856; D. J. Gillis, M. J. Tudoret, M. C. Baird, *J. Am. Chem. Soc.* **1993**, *115*, 2543; K. Mashima, S. Fujikawa, A. Nakamura, *ibid.* **1993**, *115*, 10990; A. R. Siedle, R. A. Newmark, W. M. Lamanna, J. C. Huffman, *Organometallics* **1993**, *12*, 1491; F. Calderazzo, G. Pampaloni, L. Rocchi, U. Englert, *ibid.* **1994**, *13*, 2592; J. L. Kiplinger, T. G. Richmond, C. E. Osterberg, *Chem. Rev.* **1994**, *94*, 373; B. Temme, G. Erker, J. Karl, H. Luftmann, R. Fröhlich, S. Kotila, *Angew. Chem.* **1995**, *107*, 1867; *Angew. Chem. Int. Ed. Engl.* **1995**, *34*, 1755. See also: G. Erker, R. Noe, C. Krüger, S. Werner, *Organometallics* **1992**, *11*, 4174; G. Erker, R. Noe, D. Wingbermühle, J. L. Petersen, *Angew. Chem.* **1993**, *105*, 1216; *Angew. Chem. Int. Ed. Engl.* **1993**, *32*, 1213; G. Erker, R. Noe, D. Wingbermühle, *Chem. Ber.* **1994**, *127*, 805; F. Barsan, M. C. Baird, *J. Chem. Soc. Chem. Commun.* **1995**, 1065.

[5] In the $[Cp_2Zr\text{-}O\text{-}CMe_2CH_2CH_2CH{=}CH_2]^+$ system an internal C=C bond is coordinated to the zirconocene cation. The corresponding zireonium–carbon distances in the crystal structure amount to 2.89(2) Å (Zr–C4) and 2.68(2) Å (Zr–C5): Z. Wu, R. F. Jordan, J. L. Petersen, *J. Am. Chem. Soc.* **1995**, *117*, 5867.

[6] Only a few boron-substituted metallocenes having other central metal atoms are known: B. Lockman, T. Onak, *J. Org. Chem.* **1973**, *38*, 2552; W. Ruf, M. Füller, W. Siebert, *J. Organomet. Chem.* **1974**, *64*, C45; J. M. Burlitch, J. H. Burk, M. E. Leonowicz, R. E. Hughes, *Inorg. Chem.* **1979**, *18*, 1702; B. Wrackmeyer, U. Dörfler, M. Herberhold, *Z. Naturforsch. B* **1993**, *48*, 121; C. Dusemund, K. R. A. S. Sandanayake, S. Shinkai, *J. Chem. Soc. Chem. Commun.* **1995**, 333; A. Appel, H. Nöth, M. Schmidt, *Chem. Ber.* **1995**, *128*, 621; M. Bochmann, S. J. Lancaster, O. B. Robinson, *J. Chem. Soc. Chem. Commun.* **1995**, 2081, and references therein. See also: H. Grundke, P. I. Paetzold, *Chem. Ber.* **1971**, *104*, 1136.

[7] A related reaction was recently observed upon treatment of the metallocene base Cp_2WH_2 with $RBCl_2$ Lewis acids. In this case the metal center itself serves as the base, and the substitution product $(RCl_2B\text{-}C_5H_4)CpWH_3$ is formed: H. Braunschweig, T. Wagner, *Chem. Ber.* **1994**, *127*, 1613. Cf. R. Gleiter, W. Wittwer, *Chem. Ber.* **1994**, *127*, 1797.

[8] A. S. Guram, R. F. Jordan, *J. Org. Chem.* **1993**, *58*, 5595; K. Ishihara, N. Hananki, H. Yamamoto, *Synlett* **1993**, 577, **1994**, 963; X. Yang, C. L. Stern, T. J. Marks, *J. Am. Chem. Soc.* **1994**, *116*, 10015; R. Quyoum, Q. Wang, M.-J. Tudoret, M. C. Baird, *ibid.* **1994**, *116*, 6435; R. Gómez, M. L. H. Green, J. L. Haggitt, *J. Chem. Soc. Chem. Commun.* **1994**, 2607; T. Nagata, T. Toshihiro, T. Yamada, K. Imagawa, T. Mukaiyama, *Bull. Chem. Soc. Jpn.* **1994**, *67*, 2614. B. Temme, G. Erker, *J. Organomet. Chem* **1995**, *488*, 177; D. Röttger, S. Schmuck, G. Erker, *ibid.* in press.

[9] E. Negishi, F. E. Cederbaum, T. Takahashi, *Tetrahedron Lett.* **1986**, *27*, 2829; D. R. Swanson, E. Negishi, *Organometallics* **1991**, *10*, 825.

Heterocumulenes: Reaction of C_3O_2 with Ketenylidenetriphenylphosphorane; Synthesis and Structure of a Spirobis(cyclobutanedione)**

Luciano Pandolfo,* Giacomo Facchin,*
Roberta Bertani, Paolo Ganis,* and Giovanni Valle

Acylketenes (α-oxoketenes) are subject to increasing interest and are used extensively as synthetic building blocks for a large number of interesting compounds.[1] Recently we reported[2] that the simplest stable bis(ketene), carbon suboxide (**1**),[3] reacts with stabilized phosphonium and arsonium ylides[4] bearing a hydrogen atom on the ylidic carbon atom. Depending on the ylide, bis(ylidic) malonil derivatives or zwitterionic pyrone derivatives are formed, but Wittig-type reactions were never observed.

Ketenylidenetriphenylphosphorane **2**[5] is a readily accessible molecule containing both an ylidic and a ketenic function. In contrast to ketenes, **2** displays no tendency to dimerize, and when it is protonated the resulting phosphonium ion shows typical ketene behavior.[6] Thus protonated **2** can undergo [2 + 2]cycloaddition with **2** to form, after reaction with base, the bis(ylidic) cyclobutanedione **3**.[7] Compound **3** reacts with carbonyl compounds yielding the cyclobutane-1,3-dione derivatives **4** by a Wittig-type process.[6, 7] Moreover, cyclobutanedionic derivatives **5** have been obtained through [2 + 2]cycloaddition of **2** with ketenes.[8] Bestmann et al. reported the syntheses and determined the structures of the cyclobutanetrione **6**, obtained by oxidation of **3**, and of the bicyclic bis(ylidic) derivative **7**.[9]

We report the synthesis of the bis(ylidic) spirocyclobutanedione **8** by the double [2 + 2]cycloaddition reaction of two molecules of **2** with one molecule of **1** [Eq. (a)]. The $^{31}P\{^1H\}$ NMR

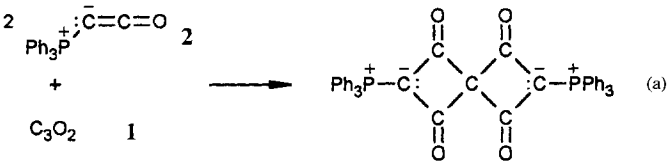

(a)

8

spectrum of **8** shows one singlet at $\delta = -2.91$, which is in the typical range for acyl ylides having a cyclobutane structure.[8-10] The $^{13}C\{^1H\}$ NMR spectrum, in addition to resonances due to the phenyl groups, shows signals at $\delta = 122.59$ and 185.11 attributable to C–P and C=O groups, respectively. A complex signal is also observed at $\delta = 83.10$, which agrees with the values reported for the central carbon atom of related spirocyclobutenones ($\delta = 79.7-84.8$).[11]

In the mass spectrum of **8** under electron impact ionization conditions no molecular ion was detected; however, the protonated molecule was easily generated by fast atom bombardment and detected at *m/z* 673. Accurate mass measurements with PEG 500 as a standard gave a value of 673.1657 (±0.005), in agreement with the proposed structure ($C_{43}H_{31}O_4P_2$, calcd 673.1688). The fragmentation pattern in the mass spectrum will be described elsewhere.

Single crystals of **8** suitable for X-ray structure analysis[12] were obtained by slow evaporation of a CH_2Cl_2 solution. The independent structural unit consists of two molecules of **8** (A and B). They differ mainly in the orientation of the phenyl groups with respect to the molecular backbone. The structures of these two nonequivalent molecules are shown in Figure 1.

Although the molecules of **8** are in principle C_2-symmetric, owing to crystallographic demands they display a total absence of symmetry. Thus, in **8** the molecular structures of four independent cyclobutanedione moieties can be compared.

The lengths of the ylidic P–C bonds, with an average value of 1.737(5) Å, are indicative of substantial double bond character and in agreement with values given in several similar cases.[13a, c, 14] The C=O bonds, with the exception of C(1)B′–O(1)B′ (1.194(9) Å), have an average length of 1.215(7) Å, which is virtually identical with the value reported in the literature (1.217(5) Å) for a C=O bond having partial triple bond character due to dipole formation ($C^{\delta+}=O^{\delta-}$).[13] For comparison, the length of a "normal" C=O bond is 1.230(5) Å.[13c, d, 14] The distances between the P-substituted C atoms and the adjacent O-substituted C atoms are in the range of 1.433(7)–1.464(7) Å. These values correspond with the lengths of C–C bonds in conjugated systems such as C=C–C=C or C=C–C≡C, which are reported to be in the range of 1.43–1.48 Å.[15]

[*] Dr. L. Pandolfo
Dipartimento di Chimica Inorganica, Metallorganica e Analitica
Università di Padova
Via Marzolo 1, I-35131 Padova (Italy)
Fax: Int. code +(49)8275161
e-mail: pandolfo@chim02.chin.unipd.it

Dr. G. Facchin, Dr. R. Bertani
Centro di Studio per la Chimica e Tecnologia dei Composti
Metallorganici degli Elementi di Transizione del CNR
Istituto di Chimica Industriale
Università di Padova, Via Marzolo 9, I-35131 Padova (Italy)
Fax: Int. code +(49)8275525

Prof. P. Ganis
Dipartimento di Chimica, Università di Napoli
Via Mezzocannone 4, I-80134 Napoli (Italy)

Dr. G. Valle
Centro di Studio sui Biopolimeri, Padova (Italy)

[**] This work was supported by the Ministero dell' Università e della Ricerca Scientifica e Tecnologica (MURST) and by the Consiglio Nazionale delle Ricerche (CNR).

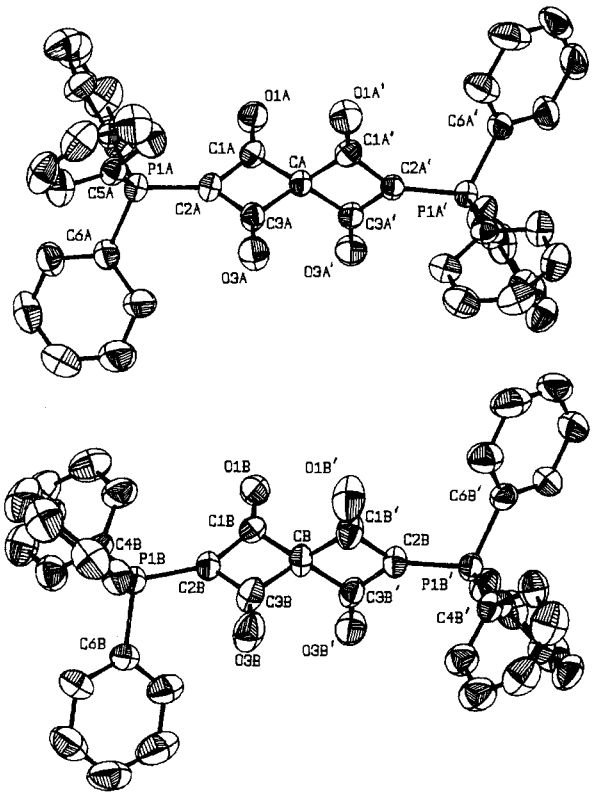

Fig. 1. Molecular structures of the two independent molecules A and B in a crystal of **8**; the two molecules have similar structural parameters and the pseudo-C_2 symmetry. Selected bond lengths [Å] for molecule A (top): P(1)A-C(2)A 1.736(5), P(1)A'-C(2)A' 1.735(5), C(1)A-O(1)A 1.211(6), C(3)A-O(3)A 1.219(6), C(1)A'-O(1)A' 1.204(7), C(3)A'-O(3)A' 1.215(7), C(1)A-C(2)A 1.455(6), C(2)A-C(3)A 1.433(7), C(1)A'-C(2)A' 1.457(7), C(2)A'-C(3)A' 1.462(7), CA-C(1)A 1.533(7), CA-C(3)A 1.549(6), CA-C(1)A' 1.558(6), CA-C(3)A' 1.554(7); for molecule B (bottom): P(1)B-C(2)B 1.741(5), P(1)B'-C(2)B' 1.737(5), C(1)B-O(1)B 1.221(6), C(3)B-O(3)B 1.217(7), C(1)B'-O(1)B' 1.194(9), C(3)B'-O(3)B' 1.217(7), C(1)B-C(2)B 1.444(6), C(2)B-C(3)B 1.447(8), C(1)B'-C(2)B' 1.458(8), C(2)B'-C(3)B' 1.464(7), CB-C(1)B 1.540(7), CB-C(3)B 1.541(8), CB-C(1)B' 1.541(7), CB-C(3)B' 1.558(8).

This structural data is consistent with formal resonance structures in which both mesomeric and inductive effects are supposed to operate (Scheme 1). In **8** the limiting resonance form **a** seems to dominate; form **c**, suggested for compound **6**,[9] cannot explain our data alone, since in this case the C=O bonds would be somewhat longer than those in "normal" keto groups. The other molecular parameters of molecules A and B, including bond and torsion angles, are quite similar to those of analogous compounds;[9, 11] they do not depend upon electronic factors but are chiefly controlled by intramolecular steric requirements and/or crystal field forces.

The ylidic character of **8** is in agreement with the results obtained in the reaction with acetaldehyde [Eq. (b)]. When a

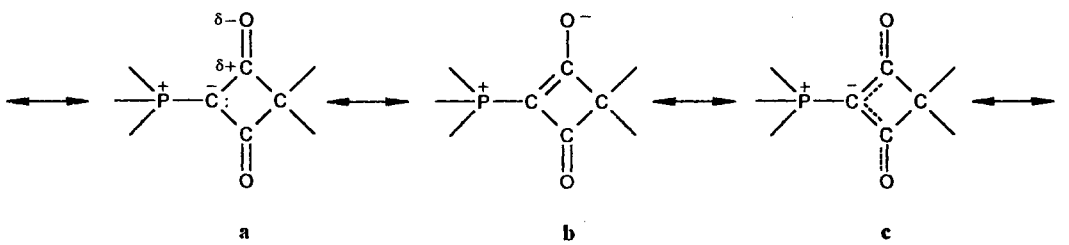

Scheme 1.

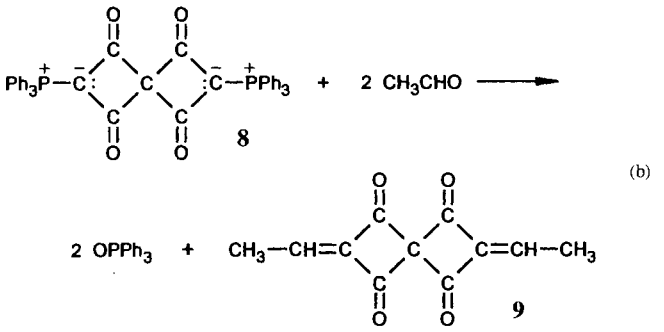

(b)

suspension of **8** in CH_3NO_2 is heated at 60 °C in a sealed vial with two equivalents of CH_3CHO, the solid dissolves rapidly. The $^{31}P\{^1H\}$ NMR spectrum ($CDCl_3$) of the sticky orange compound obtained by evaporation of the solvent shows a unique signal at $\delta = 27.84$ due to $OPPh_3$. The ^1H NMR spectrum of this compound presents two relevant signals at $\delta = 4.40$ (q, $^3J(HH) = 6.1$ Hz) and 1.19 (d, $^3J(HH) = 6.1$ Hz) in a 1:3 ratio, which are attributed to the =CH and CH_3 protons, respectively. In the IR spectrum of the new orange substance the band at 1622 cm^{-1} characteristic of **8** is gone and new intense absorptions at 1678 and 1553 cm^{-1} are evident. These data indicate that **8** undergoes a Wittig reaction to afford compound **9**. At present, the reactivity of compound **8** toward organic and organometallic reagents is under investigation.

Experimental Procedure

8 : A solution of **1** in toluene (0.044 M, 15 mL, 0.66 mmol) was added at room temperature to a stirred solution of **2** (0.395 g, 1.31 mmol) in 25 mL of toluene. A yellow solid immediately precipitated, which was filtered, washed with acetone, and dried under vacuum to give **8** as creamy white crystals. Yield: 0.380 g (86%). M.p. 245–250 °C (decomp); correct C, H analysis. IR (Nujol): 1622 cm^{-1} (ν_{CO}); ^1H NMR (200 MHz, CD_2Cl_2, 25 °C): $\delta = 7.73$–7.55 (m, C_6H_5); $^{13}C\{^1H\}$ NMR (100 MHz, CD_2Cl_2, 25 °C): $\delta = 185.11$ (dd, $^2J(CP) = 5.3$ Hz, $^4J(CP) = 2.6$ Hz, C=O), 122.59 (d, $^1J(CP) = 91.6$ Hz, C=P), 83.10 (m, central C); $^{31}P\{^1H\}$ NMR (80 MHz, $CDCl_3$, 25 °C): $\delta = -2.91$ (s); FAB MS in glycerol: *m/z* (%): 673 (3) $[M + H]^+$, 672 (2) $[M]^+$; FAB MS in *m*-nitrobenzyl alcohol: 673 (30) $[M + H]^+$, 644 (4) $[M - CO]^+$.

Received: July 18, 1995 [Z 8219IE]
German version: *Angew. Chem.* **1996**, *108*, 75–77

Keywords: carbon suboxide · heterocumulenes · ketenylidene phosphoranes · spirocyclobutanes · strained rings

[1] a) T. T. Tidwell, *Ketenes*, Wiley, New York, **1995**; b) M. A. McAllister, T. T. Tidwell, *J. Am. Chem. Soc.* **1994**, *116*, 7233; c) A. D. Allen, M. A. McAllister, T. T. Tidwell, *Tetrahedron Lett.* **1993**, *34*, 1095; d) C. O. Kappe, G. Farber, C. Wentrup, G. Kollenz, *J. Org. Chem.* **1992**, *57*, 7078; e) *Tetrahedron Lett.* **1992**, *33*, 4553; f) H. J. Bestmann, G. Schmid, D. Sandmeier, C. Geismann, *ibid.* **1980**, *21*, 2401.

[2] a) L. Pandolfo, G. Facchin, R. Bertani, P. Ganis, G. Valle, *Angew. Chem.* **1994**, *106*, 586; *Angew. Chem. Int. Ed. Engl.* **1994**, *33*, 576; b) R. Seraglia, P. Traldi, R. Bertani, G. Facchin, L. Pandolfo, *Org. Mass Spectrom.* **1994**, *26*, 619; c) L. Pandolfo, G. Facchin, R. Bertani, L. Zanotto, P. Ganis, G. Valle, R. Seraglia, *Inorg. Chim. Acta* **1995**, *237*, 27.

[3] a) O. Diels, B. Wolf, *Ber. Deut. Chem. Ges.* **1906**, *39*, 689; b) T. Kappe, E. Ziegler, *Angew. Chem.* **1974**, *86*, 529; *Angew. Chem. Int. Ed. Engl.* **1974**, *13*, 491; c) G. Paiaro, L. Pandolfo, *Comments Inorg. Chem.* **1991**, *12*, 213.

[4] A. W. Johnson, *Ylides and Imines of Phosphorus*, Wiley, New York, **1993**, and references therein.

[5] a) C. N. Mattews, G. H. Birum, *Tetrahedron Lett.* **1966**, *46*, 5707; b) H. J. Bestman, D. Sandmeier, *Angew. Chem.* **1975**, *87*, 630; *Angew. Chem. Int. Ed. Engl.* **1975**, *14*, 634; c) *Chem. Ber.* **1980**, *113*, 277.
[6] H. J. Bestmann, *Angew. Chem.* **1977**, *89*, 361; *Angew. Chem. Int. Ed. Engl.* **1977**, *16*, 349.
[7] H. J. Bestmann, G. Schmid, D. Sandmeier, L. Kisielowski, *Angew. Chem.* **1977**, *89*, 275; *Angew. Chem. Int. Ed. Engl.* **1977**, *16*, 268.
[8] G. H. Birum, C. N. Mattews, *J. Am. Chem. Soc.* **1968**, *90*, 3842.
[9] H. J. Bestmann, T. G. Fürst, A. Schier, *Angew. Chem.* **1993**, *105*, 1783; *Angew. Chem. Int. Ed. Engl.* **1993**, *32*, 1746.
[10] H. J. Bestmann, B. Siegel, G. Schmid, *Chem. Lett.* **1986**, *9*, 1529.
[11] S. Polanc, M. C. Labille, Z. Janousek, R. Merényi, M. Vermander, H. G. Viehe, B. Tinant, J. Piret-Meunier, J. P. Declercq, *New. J. Chem.* **1991**, *15*, 79.
[12] Crystal structure analysis of **8**: $C_{43}H_{30}O_4P_2$: $M = 672.65$; crystal dimensions: $0.2 \times 0.2 \times 0.1$ mm; Philips PW 1100 computer-controlled four-circle diffractometer; graphite monochromator, $Mo_{K\alpha}$ radiation, $\lambda = 0.71073$ Å, 298 K; θ-2θ scan method; the lattice constants were determined from 25 reflections: $a = 14.988(4)$, $b = 18.946(6)$, $c = 12.905(3)$ Å, $\alpha = 102.2(1)$, $\beta = 90.4(1)$, $\gamma = 75.4(1)°$; $V = 3461.97$ Å^3, space group $P\bar{1}$, $Z = 2$, $\rho_{calcd} = 1.290$ g cm^{-3}, F(000) = 1400. $\mu(Mo_{K\alpha}) = 1.28$ cm^{-1}; *hkl* range $-17 < h < 17$, $-22 < k < 22$, $0 < l < 12$; of 11 397 independent reflections 6102 were considered "observed" [$F_0 \geq 3(F_0)$]; solution and refinement by standard Patterson methods and subsequent Fourier recycling (SHELX-76); all non-hydrogen atoms were refined with anisotropic displacement parameters; all hydrogen atoms were located and refined isotropically; R (R_w) = 0.050 (0.060 with $w = 1/[\sigma^2(F_0) + 3 \times 10^{-3} F_0^2]$), 241 parameters, maximum residual electron density 0.39 e Å^{-3}. Further details of the crystal structure investigation may be obtained from the Director of the Cambridge Crystallographic Data Centre, 12 Union Road, GB-Cambridge CB21EZ (UK), on quoting the full journal citation.
[13] a) D. R. Davies, J. J. Blum, *Acta Crystallogr.* **1955**, 133, and references therein; b) E. G. Cox, M. W. Dangill, G. A. Jeffrey, *J. Chem. Soc.* **1952**, 4854; c) *Interatomic Distances Supplement*, Chemical Society Special Publ., No. 18, London, **1965**; d) *Handbook of Chemistry and Physics*, 74th ed., **1993**.
[14] *International Tables for X-Ray Crystallography*, Riedel, Boston, MA, **1983**.
[15] a) F. H. Allen, O. Kennard, D. G. Watson, L. Bremmer, A. G. Orpen, R. Taylor, *J. Chem. Soc. Perkin Trans.* **1987**, *2*, S1; b) M. D. Harmony, V. W. Laurie, R. L. Kuczowski, R. H. Schwendeman, D. A. Ramsay, F. J. Lovas, W. J. Lafferty, A. G. Maki, *J. Phys. Chem. Ref. Data*, **1979**, *8*, 619.

The Organometallic Chemistry of Zirconium on an Oxo Surface Provided by *p-tert*-Butylcalix[4]arene**

Luca Giannini, Euro Solari, Antonio Zanotti-Gerosa, Carlo Floriani,* Angiola Chiesi-Villa, and Corrado Rizzoli

The chemistry of calix[*n*]arenes and transition metal complexes[1] is a very young and rather unexplored area.[2–6] Previous applications of calix[*n*]arenes did not extend much beyond their use as a conventional polyoxo coordination environment and, in a few cases, for the *endo* coordination of substrates in their cavity.[3–6]

Calix[*n*]arenes have never been exploited as polyoxo matrices for reactive organometallic functionalities. Their use as ancillary ligands in organometallic chemistry is an interesting application due to their unique structural properties. In this context, some target functionalities that are versatile in organic synthesis were chosen and fixed on a *p-tert*-butylcalix[4]arene tetraoxo matrix to give $[ZrR_2]$,[7] $[ZrR]^+$,[8] and [Zr(diene)] complexes.[9] The starting material, the functionalizable $[ZrCl_2]$ complex **2**, was prepared in two steps from dimethoxy-*p-tert*-butylcalix[4]arene[10] dianion (Scheme 1). Even very small amounts of

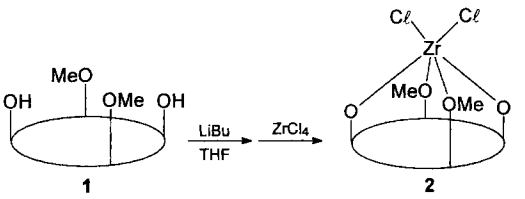

Scheme 1.

impurities in **1** and **2** are particularly troublesome for the further functionalization. Scheme 2 shows how **2** was converted into a number of complexes in which organometallic functionalities are bonded to a polyoxo matrix. This scheme outlines a general entry to the organometallic chemistry of zirconium on a *p-tert*-butylcalix[4]arene support. The present report concerns only the synthesis and the characterization of the compounds; reactivity studies will be conducted later.

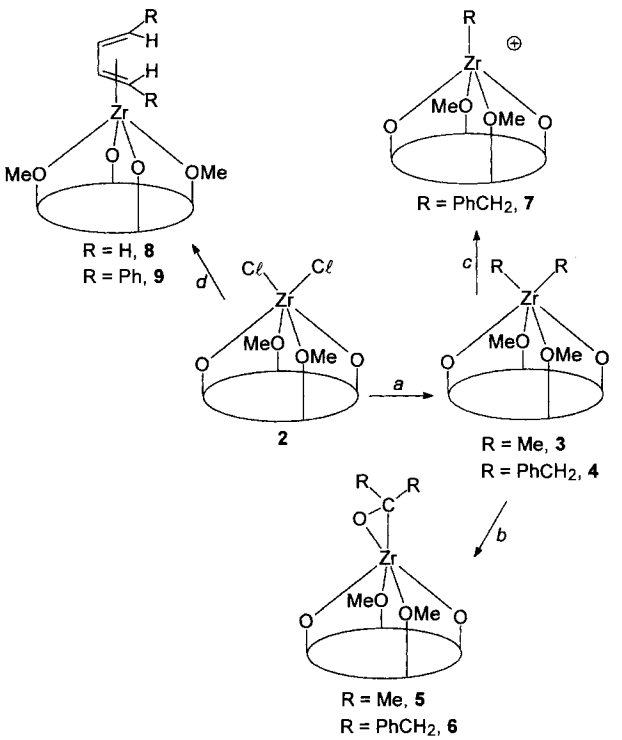

Scheme 2. a) MeLi, toluene, −30 °C; $PhCH_2MgCl$, toluene, −35 °C. b) CO, benzene, 8 °C. c) $[Cp_2Fe]BPh_4$, toluene, −35 °C. d) $[Mg(C_4H_6)(thf)_2]$, toluene, −25 °C; $[Mg(C_{16}H_{14})(thf)_3]$, toluene, −30 °C.

When reaction *a* was carried out with a 1:1 molar ratio of **2** and alkylating agent, a mixture of **2**, **3**, and the monoalkylated analogue were obtained in an approximate 1:1:2 ratio (determined by ^{1}H NMR spectroscopy). Furthermore, the same 1:1:2 mixture was obtained when equimolar solutions of **2** and **3** were mixed. Thus, under the conditions mentioned above, the monoalkylated form cannot be obtained in pure form. Both dialkyl derivatives **3** and **4** show high thermal stability (65 °C for 14 h), while only **4** was found to be photolabile in

[*] Prof. Dr. C. Floriani, Dr. E. Solari, Dr. A. Zanotti-Gerosa, L. Giannini
Institut de Chimie Minérale et Analytique
Université de Lausanne, BCH 3307, CH-1015 Lausanne (Switzerland)
Fax: Int. code +(21)692-3905
Prof. Dr. A. Chiesi-Villa, Dr. C. Rizzoli
Dipartimento di Chimica, Università di Parma (Italy)

[**] This work was supported by the Fonds National Suisse de la Recherche Scientifique (grant no. 20-40268.94) and by Ciba-Geigy SA (Basel, Switzerland). We thank Dr. Marc Weydert for preliminary work on the synthesis of **2**.

C_6D_6. Their reaction with carbon monoxide (reaction *b*) resulted in the migratory insertion of both alkyl ligands affording the corresponding η^2-ketone derivatives.[11] Compounds **5** and **6**, although thermally stable (65 °C for 14 h), are both photolabile and rather reactive. The oxidative cleavage of the Zr–C bond in **4** using the ferrocenyl cation (reaction c)[12] led to the cationic species **7**; the relevance of analogous complexes with ancillary ligands other than *p-tert*-butylcalix[4]arenes is well known.[8]

All the compounds in Scheme 2 were characterized by X-ray structure analyses, except **7**, whose analytical and NMR data are consistent with the formulation given. Compounds **2**–**4** and **7** have C_{2v} symmetry and their ^{1}H NMR spectra show one pair of doublets for the bridging methylene groups and a singlet for the MeO groups. Compounds **5**, **6**, and **9** have C_s symmetry; their ^{1}H NMR spectra show two pairs of doublets for the methylene protons and two singlets for the MeO groups. The diene complex **8** also has C_s symmetry, as evidenced by its ^{1}H NMR spectrum at temperatures below −10 °C (in [D_8]toluene), which is similar to those of the other low-symmetry compounds. However, at temperatures above 40 °C complex **8** exhibits a ^{1}H NMR spectrum similar to those of the previously mentioned C_{2v}-symmetrical compounds. A dynamic process (probably the rotation of the butadiene ligand) increases the apparent symmetry of the compound in solution.

In the X-ray crystal structures of **3**[13] (Fig. 1) and **9**[14] (Fig. 2) with σ- and π-bonded carbon fragments, respectively,

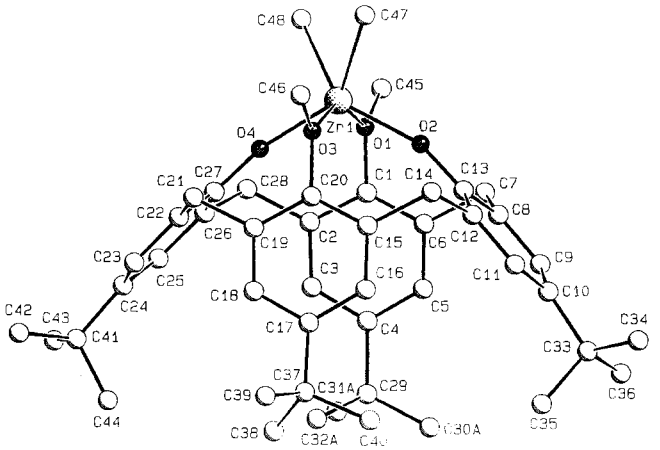

Fig. 1. Crystal structure of complex **3** (SCHAKAL representation). Selected distances [Å]: Zr1-O1 2.401(3), Zr1-O2 1.974(3), Zr1-O3 2.410(4), Zr1-O4 1.964(3), Zr1-C47 2.275(5), Zr1-C48 2.294(7). Selected bond angles [°]: C47-Zr1-C48 77.7(3), O3-Zr1-C47 75.6(2), O3-Zr1-O4 76.8(1), O2-Zr1-O4 120.8(1), O2-Zr1-O3 87.7(1), O1-Zr1-C48 74.6(2), O1-Zr1-O4 88.3(1), O1-Zr1-O3 150.9(1), O1-Zr1-O2 78.6(1), Zr1-O2-C13 161.4(3), Zr1-O4-C27 167.3(3). Disorder affecting the C30–C32 methyl groups has been omitted for clarity.

the structure of the *p-tert*-butylcalix[4]arene moiety is elliptical in cross-section, as dictated by a hexacoordinate metal center.[4] The Zr1–O2 and Zr1–O4 distances, and the related Zr1-O2-C13 and Zr1-O4-C27 angles (see legends of Figs. 1 and 2) support a very strong metal–oxygen π bond.[3–6] The Zr–O1 and Zr–O3 distances are not only much longer than Zr–O2 and Zr–O4, but they also differ significantly for the two complexes. The steric constraints, specifically the methyl···methoxy repulsion, may be the reason why the Zr–O1 distance in **3** is longer than that in **9**, the C47-Zr-C48 angle is very small [77.7(2)°], and C47···C48 distance is rather short [2.865(10) Å]. In complex **9** the plane of the butadiene carbon atoms is nearly parallel to the O_4 plane (dihedral angle −7.2(8)°). The η^4 bonding mode of the butadiene fragment is

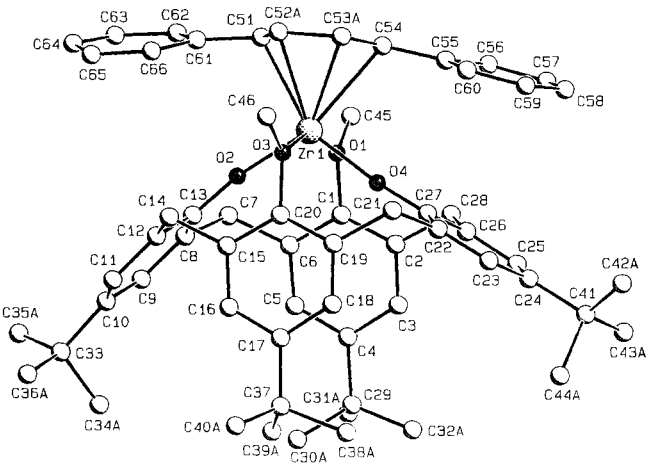

Fig. 2. Crystal structure of complex **9** (SCHAKAL representation). Selected distances [Å]: Zr1-O1 2.304(9), Zr1-O2 1.949(7), Zr1-O3 2.345(9), Zr1-O4 1.950(7), Zr1-C51 2.427(13), Zr1-C52A 2.46(2), Zr1-C53A 2.49(2), Zr1-C54 2.513(12). Selected bond angles [°]: C53A-Zr1-C54 31.4(5), C52A-Zr1-C53A 34.1(6), C51-Zr1-C52A 30.5(6), O3-Zr1-O4 82.5(3), O2-Zr1-O4 112.0(3), O2-Zr1-O3 83.8(3), O1-Zr1-O4 82.2(3), O1-Zr1-O3 155.2(3), O1-Zr1-O2 84.0(3), Zr1-O2-C13 171.0(7), Zr1-O4-C27 174.2(7). Disorder affecting the C52A and C53A carbon atoms and the methyl carbons of all *t*-butyl groups groups is not reflected in this representation.

supported by the Zr–C distances, which fall within a very small range. The lengths of the C–C bonds within the butadiene ligand, for which we have averaged the A and B positions and have considered a large standard deviation, follow the sequence C=C–C=C. Thus, the bonding mode of the diphenylbutadiene in **9** can be described as π^2,η^4. The structural and spectroscopic characteristics of the Zr–diene fragment should be compared to those in the [Cp_2Zr][9] and [(tmtaa)Zr] derivatives (tmtaa = dibenzotetramethyltetraaza[14]annulene dianion];[15] compound **9** is more closely related to the tmtaa complexes. In particular, we can say both for **8** and **9** (although the structure of **8** is approximate) that the *cis* form is the only butadiene conformer detected in the solid state; we did not observe any *cis–trans* isomerization upon heating of **8** or **9**. The ^{1}H NMR signals for **8** and **9** were assigned by a computer simulation.

The splitting patterns for the signals of the butadiene protons in the ^{1}H NMR spectrum for **8** are temperature independent though the chemical shifts are slightly temperature dependent. The data mentioned above emphasize the difference between the butadiene complexes **8** and **9** (π^2,η^4) and the cyclopentene complexes (σ^2,π) in the [Cp_2Zr] series.[9] A variety of bonding modes for zirconium–butadiene compounds ranging from π,η^4 to σ^2,π,η^4 can be found in complexes having subunits other than Cp_2Zr.[15]

Experimental Procedure

2: A solution of BuLi (94 mL, 1.65 M in hexane, 155.1 mmol) was added dropwise to a solution of **1** (51.55 g, 76.25 mmol) in THF (300 mL) to give a golden solution, which was added dropwise to a stirred suspension of [$ZrCl_4(thf)_2$] (29.26 g, 77.58 mmol) in THF (300 mL). The resulting pale yellow solution was stirred at room temperature for 2 h, the volatiles were removed in vacuo, and the residue was extracted overnight with benzene (400 mL). The solvent was evaporated and the residue was extracted again over 2 d with a mixture of hexane (600 mL) and benzene (70 mL) to remove residual LiCl. The resulting suspension was allowed to stand at room temperature for 18 h. A white, microcrystalline powder consisting of **2** with 1.5 molecules of cocrystallized benzene was collected and dried in vacuo (51.2 g, 70%). The X-ray analysis was performed on crystals containing two C_6H_6 molecules of crystallization. Anal. calcd for $C_{55}H_{67}Cl_2O_4Zr$: C 69.23, H 7.08; found: C 69.11, H 7.13; ^{1}H NMR (CD_2Cl_2, 25 °C): δ = 7.37 (s, 9H, benzene), 7.15 (s, 4H, Ar H), 7.11 (s, 4H, Ar H), 4.53 (s, 6H, MeO), 4.33 (d, J = 13.1 Hz, 4H, *endo*-CH_2), 3.43 (d, J = 13.1 Hz, 4H, *exo*-CH_2), 1.29 (s, 18H, *t*Bu), 1.16 (s, 18H, *t*Bu); ^{1}H NMR (C_6D_6, 25 °C): δ = 7.19 (s, 4H, Ar H), 6.77 (s, 4H, Ar H), 4.42 (d, J = 13.0 Hz, 4H,

endo-CH_2), 3.92 (s, 6H, MeO), 3.15 (d, J = 13.0 Hz, 4H, *exo*-CH_2), 1.43 (s, 18H, *t*Bu), 0.65 (s, 18H, *t*Bu).

3: A solution of MeLi (7.7 mL, 1.71 M in Et_2O, 13.17 mmol) was added dropwise to a solution of **2** (6.38 g, 6.69 mmol) in toluene (200 mL) at −30 °C. The mixture was stirred and allowed to warm to room temperature, volatiles were removed in vacuo, and benzene (150 mL) was added. The mixture was heated to reflux, filtered while hot, and concentrated by evaporation in vacuo to a volume of ca. 30 mL. Hexane (200 mL) was added to the resulting white creamy suspension and the mixture was heated to reflux to give a colorless solution. This solution was kept at 9 °C for 3 d to yield colorless crystals of **3**·benzene, which were collected and dried in vacuo (3.66 g, 63%). Anal. calcd for $C_{54}H_{70}O_4Zr$: C 74.18, H 8.07; found: C 74.38, H 8.18. ^{1}H NMR (CD_2Cl_2, 25 °C): δ = 7.36 (s, 6H, benzene), 7.09 (s, 4H, Ar H), 6.95 (s, 4H, Ar H), 4.41 (d, J = 12.5 Hz, 4H, *endo*-CH_2), 4.22 (s, 6H, MeO), 3.31 (d, J = 12.5 Hz, 4H, *exo*-CH_2), 1.25 (s, 18H, *t*Bu), 1.06 (s, 18H, *t*Bu), 0.60 (s, 6H, Me-Zr); ^{1}H NMR (C_6D_6, 25 °C): δ = 7.23 (s, 4H, Ar H), 6.79 (s, 4H, Ar H), 4.46 (d, J = 12.5 Hz, 4H, *endo*-CH_2), 3.69 (s, 6H, MeO), 3.18 (d, J = 12.5 Hz, 4H, *exo*-CH_2), 1.46 (s, 18H, *t*Bu), 1.24 (s, 6H, Me-Zr), 0.77 (s, 18H, *t*Bu). Crystals suitable for X-ray analysis were obtained by preparing a saturated solution of **3** in pentane at room temperature and storing it at 8 °C. (The solution was obtained by using pentane instead of benzene in the workup; the workup with benzene/hexane gave better yields). The product is stable to prolonged heating (65 °C, 14 h) in C_6D_6 and CD_2Cl_2, as judged by its ^{1}H NMR spectrum; it is not photosensitive in C_6D_6. The exchange reaction between $[(CalMe_2)Zr(Me)_2]$ and $[(CalMe_2)Zr(Cl)_2]$ is fast: when equimolar amounts of the two compounds were dissolved in CD_2Cl_2, an equilibrium mixture of the two reagents and a new product were obtained in an approximate 1:1:2 ratio, as judged by the ^{1}H NMR spectrum. Data for the new species: δ = 7.13 (s, 4H, Ar H), 7.04 (s, 4H, Ar H), 4.43 (d, J = 12.5 Hz, 4H, *endo*-CH_2), 4.36 (s, 6H, MeO), 3.37 (d, J = 12.5 Hz, 4H, *exo*-CH_2), 1.27 (s, 18H, *t*Bu), 1.13 (s, 18H, *t*Bu), 0.82 (s, 3H, Me-Zr). Some peaks overlap with those of the two starting compounds.

9: Complex **2** (8.26 g, 8.66 mmol) and $[Mg(C_{16}H_{14})(thf)_3]$ (3.9 g, 8.73 mmol) were suspended in toluene (250 mL) at −30 °C. The mixture, which became deep red in seconds, was stirred and allowed to warm to room temperature. Dioxane (5 mL) was added and the mixture was stirred for 1 h. Volatiles were then removed in vacuo (heating to 50 °C). The residue was extracted overnight with a mixture of hexane (230 mL) and benzene (30 mL). The red suspension was kept at −25 °C for 24 h to give **9** with 1.5 molecules of cocrystallized benzene as a deep red microcrystalline solid, which was collected and dried in vacuo (5.79 g, 61.4%). Anal. calcd for $C_{71}H_{81}O_4Zr$: C 78.26, H 7.49; found: C 78.31, H 7.73. ^{1}H NMR (C_6D_6, 25 °C): δ = 7.36–6.63 (m, 27H, Ar H, benzene), 6.07 (m, 2H, H(5,6)), 4.48 (s, 3H, MeO), 4.31 (d, J = 12.5 Hz, 2H, *endo*-CH_2), 4.00 (m, 2H, H(1,2)), 3.92 (d, 2H, *endo*-CH_2) overlapping with 3.89 (s, 3H, MeO), 3.30 (d, J = 12.5 Hz, 2H, *exo*-CH_2), 2.94 (d, J = 12.5 Hz, 2H, *exo*-CH_2), 1.37 (s, 18H, *t*Bu), 0.70 (s, 9H, *t*Bu), 0.64 (s, 9H, *t*Bu); ^{1}H NMR (CD_2Cl_2, 25 °C): δ = 7.37–6.50 (m, 27H, Ar H, benzene), 6.09 (m, 2H, H(5,6)), 4.97 (s, 3H, MeO), 4.72 (s, 3H, MeO), 4.29 (d, J = 12.5 Hz, 2H, *endo*-CH_2), 3.80 (m, 2H, H(1,2)), overlapping with 3.72 (d, 2H, *endo*-CH_2), 3.32 (d, J = 12.5 Hz, 2H, *exo*-CH_2), 2.86 (d, J = 12.5 Hz, 2H, *exo*-CH_2), 1.20 (s, 18H, *t*Bu), 1.06 (s, 9H, *t*Bu), 1.00 (s, 9H, *t*Bu). Crystals suitable for X-ray analysis were obtained at room temperature from a supersaturated solution of **9** in hexane/benzene (10/1). The product can be refluxed in benzene for hours without appreciable decomposition, as judged by its NMR spectrum, and it is photosensitive (benzene solutions become colorless when exposed to sunlight and the calixarene species formed is the same as that formed in photolysis of **9**). Complex **9** is stable to CO (1 bar) in benzene.

Received: July 21, 1995 [Z 8234 IE]
German version: *Angew. Chem.* **1996**, *108*, 79–82

Keywords: calixarenes · complexes with carbon ligands · complexes with oxygen ligands · zirconium compounds

[1] a) C. D. Gutsche, *Calixarenes, Vol. 1*, The Royal Society of Chemistry, Cambridge, **1989**. b) Preparations of standard calix[4,6,8]arenes: C. D. Gutsche, M. Iqbal, *Org. Synth.* **1989**, *68*, 234–237; C. D. Gutsche, B. Dhawan, M. Leonis, D. Stewart, *ibid.* **1989**, *68*, 238–242; J. H. Munch, C. D. Gutsche, *ibid.* **1989**, *68*, 243–246.

[2] a) S. G. Bott, A. W. Coleman, J. L. Atwood, *J. Chem. Soc. Chem. Commun.* **1986**, 610–611; b) M. M. Olmstead, G. Sigel, H. Hope, X. Xu, P. P. Power, *J. Am. Chem. Soc.* **1985**, *107*, 8087–8091; c) G. E. Hofmeister, F. E. Kahn, S. F. Pedersen, *ibid.* **1989**, *111*, 2318–2319; d) G. E. Hofmeister, E. Alvarado, J. A. Leary, D. I. Yoon, S. F. Pedersen, *ibid.* **1990**, *112*, 8843–8851; e) B. M. Furphy, J. M. Harrowfield, D. L. Kepert, B. W. Skelton, A. H. White, F. R. Wilner, *Inorg. Chem.* **1987**, *26*, 4231–4236.

[3] F. Corazza, C. Floriani, A. Chiesi-Villa, C. Guastini, *J. Chem. Soc. Chem. Commun.* **1990**, 640–641.

[4] F. Corazza, C. Floriani, A. Chiesi-Villa, C. Guastini, *J. Chem. Soc. Chem. Commun.* **1990**, 1083–1084.

[5] F. Corazza, C. Floriani, A. Chiesi-Villa, C. Rizzoli, *Inorg. Chem.* **1991**, *30*, 4465–4468.

[6] J. A. Acho, L. H. Doerrer, S. J. Lippard, *Inorg. Chem.* **1995**, *34*, 2542–2556.

[7] a) D. J. Cardin, M. F. Lappert, C. L. Raston, *Chemistry of Organozirconium and Hafnium Compounds*, Wiley, New York, **1986**; b) S. L. Buchwald, R. B. Nielsen, *Chem. Rev.* **1988**, *88*, 1047–1058; c) M. T. Reetz in *Organometallics in Synthesis* (Ed.: M. Schlosser), Wiley, New York, **1994**, Chapter 3; d) E.-I. Negishi in *Comprehensive Organic Synthesis Vol. 5* (Eds.: B. M. Trost, I. Fleming, L. A. Paquette), Pergamon, Oxford, **1991**, p. 1163; e) E.-I. Negishi, T. Takahashi, *Acc. Chem. Res.* **1994**, *27*, 124–130, and references therein; f) N. E. Schore, In *Comprehensive Organic Synthesis Vol. 5* (Eds: B. M. Trost, I. Fleming, L. A. Paquette), Pergamon, Oxford, **1991**, p. 1037; g) G. Erker, R. Pfaff, C. Krüger, S. Werner, *Organometallics* **1993**, *12*, 3559–3568; h) G. Erker, R. Noe, C. Krüger, S. Werner, *Organometallics* **1992**, *11*, 4174–4177; i) G. Erker, R. Pfaff, *Organometallics* **1993**, *12*, 1921–1926.

[8] R. F. Jordan, *Adv. Organomet. Chem.* **1991**, *32*, 325–387; R. B. Grossman, W. M. Davis, S. L. Buchwald, *J. Am. Chem. Soc.* **1991**, *113*, 2321–2322; A. S. Guram, D. C. Swenson, R. F. Jordan, *ibid.* **1992**, *114*, 8991–8996; A. S. Guram, Z. Guo, R. F. Jordan, *ibid.* **1993**, *115*, 4902–4903; A. S. Guram, R. F. Jordan, *J. Org. Chem.* **1993**, *58*, 5595–5597; T. J Marks, *Acc. Chem. Res.* **1992**, *25*, 57–65; G. W. Coates, R. M. Waymouth, *J. Am. Chem. Soc.* **1993**, *115*, 91–98; G. Erker, M. Aulbach, M. Knickmeier, D. Wingbermühle, C. Krüger, M. Nolte, S. Werner, *ibid.* **1993**, *115*, 4590–4601; G. Guerra, L. Cavallo, G. Moscardi, M. Vacatello, P. Corradini, *ibid.* **1994**, *116*, 2988–2995; X. Yang, C. L. Stern, T. J. Marks, *ibid.* **1994**, *116*, 10015–10031.

[9] G. Erker, C. Krüger, G. Müller, *Adv. Organomet. Chem.* **1985**, *24*, 1–39, and references therein; H. Yasuda, K. Tatsumi, A. Nakamura, *Acc. Chem. Res.* **1985**, *18*, 120–126, and references therein; H. Yasuda, Y. Kajihara, K. Mashima, K. Nagasuna, K. Lee, A. Nakamura, *Organometallics* **1982**, *1*, 388–396; G. Erker, U. Dorf, R. Benn, R.-D. Reinhardt, *J. Am. Chem. Soc.* **1984**, *106*, 7649–7650; G. Erker, K. Engel, U. Korek, P. Czisch, H. Berke, P. Caubère, R. Vanderesse, *Organometallics* **1985**, *4*, 1531–1536; G. Erker, T. Mühlenbernd, R. Benn, A. Rufinska, *ibid.* **1986**, *5*, 402–404; G. Erker, R. Lecht, J. L. Petersen, H. Bönnemann, *ibid.* **1987**, *6*, 1962–1967; M. Akita, K. Matsuoka, K. Asami, H. Yasuda, A. Nakamura, *J. Organomet. Chem.* **1987**, *327*, 193–209; H. B. Bürgi, K. C. Dubler-Steude, *J. Am. Chem. Soc.* **1988**, *110*, 4953–4957; G. Erker, R. Aul, *Organometallics* **1988**, *7*, 2070–2072; G. Erker, F. Sosna, R. Zwettler, C. Krüger, *ibid.* **1989**, *8*, 450–454; H. Yasuda, T. Okamoto, Y. Matsuoka, A. Nakamura, Y. Kai, N. Kanehisa, N. Kasai, *ibid.* **1989**, *8*, 1139–1152; G. Erker, S. Friedrich, N. Ralf, *Chem. Ber.* **1990**, *123*, 821–827; G. Erker, M. Babil, *ibid.* **1990**, *123*, 1327–1329; R. Beckhaus, D. Wilbrandt, S. Flatau, H. Böhmer, *J. Organomet. Chem.* **1992**, *423*, 211–222.

[10] A. Casnati, A. Arduini, E. Ghidini, A. Pochini, R. Ungaro, *Tetrahedron* **1991**, *47*, 2221–2228, and references therein.

[11] L. D. Durfee, I. P. Rothwell, *Chem. Rev.*, **1988**, *88*, 1059–1079. The review contains references also to the related Zr-alkoxo-based organometallic chemistry.

[12] R. F. Jordan, R. E. LaPointe, P. K. Bradley, N. Baenziger, *Organometallics* **1989**, *8*, 2892–2903.

[13] a) Crystal structure analysis of **3**: $C_{48}H_{69}O_4Zr$, M = 801.25, monoclinic, space group $P2_1/c$, a = 16.299(2), b = 13.757(4), c = 20.250(2) Å, β = 93.35(1)°, V = 4533(2) Å^3, Z = 4, ρ_{calcd} = 1.174 g cm^{-3}, F(000) = 1716, $Cu_{K\alpha}$ radiation (λ = 1.54178 Å), $\mu(Mo_{K\alpha})$ = 22.83 cm^{-1}; crystal dimensions 0.15 × 0.26 × 0.43 mm. The structure was solved by the heavy-atom method and refined anisotropically for all non-hydrogen atoms. One of the four *t*-butyl groups was disordered. The hydrogen atoms (except for those of the disordered group) were located from a difference map and introduced as fixed contributors in the last stage of refinement (U_{iso} = 0.10 Å^2). For 5580 unique observed reflections [$I > 2\sigma(I)$] collected at room temperature on a Rigaku AFC6S diffractometer ($5° < 2\theta < 140°$) and corrected for absorption the final R value was 0.052 ($wR2$ = 0.132). b) Further details of the crystal structure investigation may be obtained from the Director of the Cambridge Crystallographic Data Centre, 12 Union Road, GB-Cambridge CB2 1EZ (UK), on quoting the full journal citation.

[14] Crystal structure analysis of **9**: $C_{62}H_{70}O_4Zr \cdot 5C_6H_6$, M = 1087.56, triclinic, space group $P\bar{1}$, a = 14.684(2), b = 17.992(2), c = 13.033(2) Å, α = 109.64(1), β = 103.51(1), γ = 86.55(1)°, V = 3152.6(7) Å^3, Z = 2, ρ_{calcd} = 1.146 g cm^{-3}, F(000) = 1154, $Cu_{K\alpha}$ radiation (λ = 1.54178 Å), $\mu(Mo_{K\alpha})$ = 17.73 cm^{-1}; crystal dimensions 0.15 × 0.26 × 0.43 mm. A statistical distribution around the C51···C54 line in the diphenylbutadiene ligand was evident from a ΔF map calculated after the anisotropic refinement. The two orientations (A and B) of the butadiene framework share the C51 and C54 terminal carbon atoms and form a dihedral angle of 19.9(1.9)°, such that only C52 and C53 appear to be disordered. Refinement of the relative occupancies resulted in a value of 0.69(2) for C52A, C53A and 0.31(2) for C52B, C53B. The four *t*-butyl groups are severely disordered. All the hydrogen atoms except those of the *t*-butyl groups were located in a difference map (including those attached to C52A and C53A) and used in the structure factor calculations (U_{iso} = 0.10 Å^2). For 4273 unique observed reflections [$I > 2\sigma(I)$] collected at room temperature on a Rigaku AFC6S diffractometer ($6° < 2\theta < 140°$) and corrected for absorption the final R value was 0.080 ($wR2$ = 0.194). All calculations were performed by using SHELX76 for the early stages of solution and SHELXL92 for refinements on an Encore 91 computer. See ref. [13b].

[15] L. Giannini, E. Solari, C. Floriani, A. Chiesi-Villa, C. Rizzoli, *Angew. Chem.* **1994**, *106*, 2279–2281; *Angew. Chem., Int. Ed. Engl.* **1994**, *33*, 2204–2206, and references therein.

Synthesis of Fucopeptides as Sialyl Lewis^x Mimetics**

Shih-Hsiung Wu, Makoto Shimazaki, Chun-Cheng Lin, Lei Qiao, Wilna J. Moree, Gabriele Weitz-Schmidt, Chi-Huey Wong*

The Ca^{2+}-dependent interaction between E-selectin of endothelial cells and sialyl Lewis^x (SLe^x) of neutrophils is a critical carbohydrate–protein recognition event that occurs shortly after tissue injury and leads to acute and chronic inflammations.[1] E-selectin is also inducibly expressed in response to inflammatory factors such as tumor necrosis factor (TNF), interleukin-1b (IL-1b), leukotriene B_4, neurotoxins, and endotoxins, while SLe^x is presented by glycoproteins and/or glycolipids on the neutrophil surface. Thus, blocking the SLe^x/E-selectin

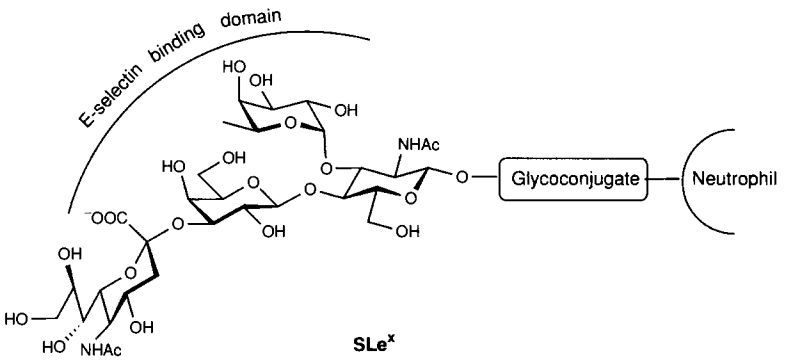

SLe^x

interaction has been considered to be an effective way to treat neutrophil-mediated inflammatory diseases.[2] Although SLe^x has been considered as an antiinflammatory agent, this tetrasaccharide can only be used in acute cases, as it is unstable in the blood and orally inactive. In addition, it is generally difficult to synthesize oligosaccharides on a large scale. It is therefore of great interest to develop oligosaccharide mimetics that are more stable and active, possess better bioavailability, and are easier to make.

The conformation of SLe^x in solution[3] and the three-dimensional structure of the human E-selectin[4] have been determined. The key structural features of SLe^x required for recognition by E-selectin have also been determined.[5] The L-fucose, D-galactose (Gal), and sialic acid moieties of SLe^x are the major components that interact with E-selectin, and the *N*-acetylglucosamine unit acts merely as a linker connecting L-fucose and sialyl galactose. Six functional groups of the SLe^x molecule—the 2-, 3-, and 4-hydroxyl groups of L-fucose, the 4- and 6-hydroxyl groups of Gal, and the carboxylate group of sialic acid—are essential for E-selectin recognition. Compounds containing these functional groups, which mimic the active conformation of SLe^x in space, have been designed and synthesized,[6] and two of them exhibit activities similar to that of SLe^x in the E-selectin binding assay.[6d] Although the C-linked fucopeptide[6d] is highly active, the fucose and the galactose equivalents may not be in the same positions in space as those in SLe^x. We report here the design and synthesis of a simple fucopeptide as a SLe^x mimetic, which has the same activity as SLe^x in the E-selectin binding assay, and compare the binding activity of this mimetic to that of related compounds.

The fucopeptide **1a** contains an L-fucose residue, two hydroxyl groups from (2*S*,3*R*)-2-amino-3,4-dihydroxybutyric acid corresponding to the 4- and 6-hydroxyl groups of the Gal residue, and a carboxylate group from the glutarate residue to mimic the negatively charged group in the sialic acid residue. When L-threonine is used to replace *N*-acetylglucosamine, the configuration of the glycosidic linkages is expected to be retained. Molecular modeling indeed indicates that the six key functional groups in compound **1a** have the same arrangement in space as the analogous groups of the active SLe^x. Compounds **2** and **3** were designed in a similar way except that the dihydroxy amino acid is replaced with another amino acid in order to address its role in recognition.

The synthesis of **1a** is shown in Scheme 1. L-Fucose was first converted into tribenzylfucosyl phosphite by the established method[7] and successfully coupled to Boc-L-Thr-OEt with trifluoromethanesulfonic acid (TfOH) or trimethylsilyl trifluoromethanesulfonate (TMSOTf) as catalyst to give the Boc-(αFuc3,4,5Bn_3)-L-ThrOEt (**4**) in 80% yield. The Boc group was removed from **4** without cleavage of the fucosidic bond by treatment with 30% TFA in CH_2Cl_2 (25 °C, 30 min). The resulting amine was coupled with (2*S*,3*R*)-*N*-Boc-2-amino-4-benzyloxy-3-hydroxy butyric acid[8] to provide **5**. Removal of the Boc protecting group, followed by coupling with monobenzyl glutarate, provided

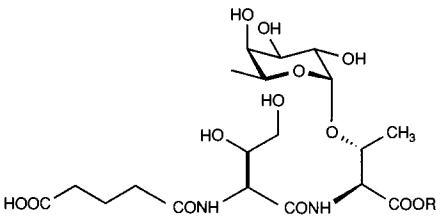

1a, R = Et
1b, R = H

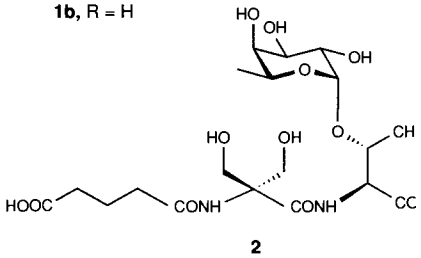

2

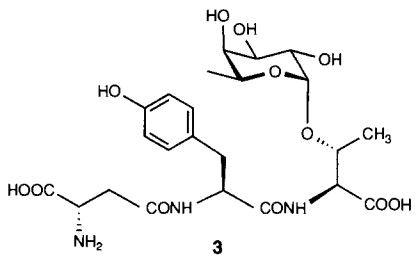

3

[*] Prof. Dr. C.-H. Wong, Dr. M. Shimazaki, Dipl.-Chem. C.-C. Lin, Dr. L. Qiao, Dr. W. J. Moree
Department of Chemistry, The Scripps Research Institute
10666 North Torrey Pines Road, La Jolla, CA 92037 (USA)
Fax: Int. code +(619)554-6731
Prof. Dr. S.-H. Wu
Institute of Biological Chemistry, Academia Sinica, Taipei (Taiwan)
Dr. G. Weitz-Schmidt
Sandoz Pharmaceuticals Ltd., Preclinical Research, Basel (Switzerland)

[**] Financial support of this work was provided by the National Science Foundation (USA), Sandoz Pharmaceuticals Ltd. (Switzerland), the National Science Council of Taiwan (grant to S.-H. W.), and NATO (fellowship to W. J. M.).

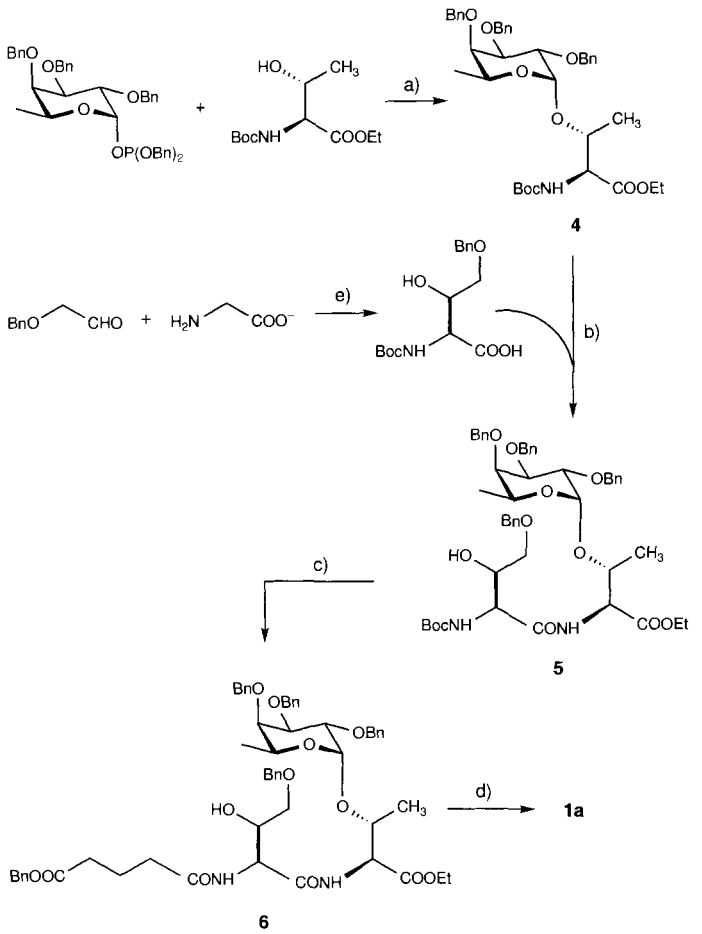

Scheme 1. a) TfOH, CH_2Cl_2, −15 °C, 1 h, 84%; b) 1. 30% TFA in CH_2Cl_2, 25 °C, 30 min; 2. 1.5 equiv HOBt, 1.5 equiv EDCI, CH_2Cl_2, 0 °C, 30 h, 60%; c) 1. 30% TFA in CH_2Cl_2, 25 °C, 30 min; 2. monobenzyl glutarate, 1.5 equiv HOBt, 1.5 equiv EDCI, CH_2Cl_2, 25 °C, 20 h, 70%; d) H_2 (1 atm), 20% $Pd(OH)_2/C$, MeOH, 24 h, 50%; e) 1. threonine aldolase, 86%; 2. $BocN_3$, 90%. Bn = $PhCH_2$; Boc = *tert*-butoxycarbonyl; Tf = CF_3SO_2; TFA = trifluoroacetic acid; HOBt = hydroxybenzotriazole; EDCI = *N*-ethyl-*N'*-(3-dimethylaminopropyl)carbodiimide.

compound **6**. The benzyl groups of **6** were cleaved by hydrogenation over 20% $Pd(OH)_2/C$ in MeOH, and the crude product was purified by Biogel P-2 chromatography to give **1a** (54%). Compound **1a** and other key intermediates were characterized by ^1H NMR spectroscopy and high-resolution mass spectrometry (Table 1). Compounds **2** and **3** were synthesized from the key intermediate **4** by the same methods (Table 1).

An analysis of these compounds as inhibitors of E-selectin gave the following IC_{50} values: **1a**, 0.5 mM; **2**, 1.0 mM; **3**, 1.3 mM.[9] Conversion of **1a** to **1b** decreases the activity (IC_{50} = 1.0 mM). Since compound **1a** has the same biological activity as SLe^x (0.50 mM), all the functional groups required for E-selectin binding in SLe^x must exist in **1a**. Compounds **1b** and **2** are slightly less active than SLe^x, probably due to the presence of the free carboxyl group in the Thr moiety. Compound **3** is, however, surprisingly active, as the OH group of Tyr in **3** does not correspond spatially to the essential OH groups of the Gal residue in SLe^x. Whether the hydrophobic nature of the aromatic group or the additional amino group contributes to binding is unclear. Replacement of the dihydroxy amino acid with L-Thr, L-Ser, Phe, Ala, or Gly, however, results in a nearly complete loss of activity (IC_{50} > 10 mM).

This study thus confirms the minimum structural elements required for E-selectin recognition and provides a new direction for the development of SLe^x mimetics. Compared to the synthesis of SLe^x, the preparation of **1a** is very straightforward and can be scaled up easily. Work is in progress to couple an Arg-Gly-Asp (RGD) containing peptide to the carboxylate group of the Thr residue of **1b** to obtain a potential inhibitor of P- and L-selectins.[10]

Table 1. NMR spectroscopic and mass spectrometric data for **1**–**6**.

1 (amorphous): ^1H NMR (400 MHz, D_2O): δ = 4.98 (d, J = 3.2 Hz, 1H), 4.61 (d, J = 2.2 Hz, 1H), 4.56 (d, J = 7.2 Hz, 1H), 4.46–4.44 (dd, J = 2.2, 6.4 Hz, 1H), 4.28–4.13 (m, 3H), 4.02–3.98 (m, 1H), 3.86–3.59 (m, 5H), 2.42–2.22 (m, 4H), 1.90–1.79 (m, 2H), 1.30–1.18 (m, 9H); electrospray negative-ion mass (−80 V): *m/z*: 523 $[(M-H)^-]$; calcd for $C_{21}H_{36}N_2O_{13}$: 524].

2 (amorphous): ^1H NMR (400 MHz, D_2O): δ = 4.96 (d, J = 3.2 Hz, 1H), 4.68–4.37 (m, 3H), 4.07–3.63 (m, 7H), 2.43–2.37 (m, 4H), 1.85–1.75 (m, 2H), 1.23–1.13 (m, 6H); electrospray negative-ion mass (−80 V): *m/z*: 495 $[(M-H)^-]$; calcd for $C_{19}H_{32}N_2O_{13}$: 496].

3 (amorphous): ^1H NMR (500 MHz, D_2O): δ = 7.02 (d, J = 8.4 Hz, 1H), 6.69 (d, J = 8.3 Hz, 1H), 4.81 (d, J = 4.0 Hz, 1H), 4.57 (dd, J = 4.8, 9.0 Hz, 1H), 4.29–4.07 (m, 3H), 3.85 (q, J = 6.5 Hz, 1H), 3.74–3.55 (m, 3H), 3.05–2.99 (m, 1H), 2.81–2.72 (m, 2H), 2.58–2.50 (m, 1H), 1.01 (d, J = 6.5 Hz, 3H), 0.97 (d, J = 6.0 Hz, 3H); electrospray negative-ion MS (−80 V): *m/z*: 542 $[(M-H)^-]$; calcd for $C_{23}H_{33}N_3O_{12}$: 543].

4: ^1H NMR (400 MHz, $CDCl_3$, TMS): δ = 7.25–7.40 (m, 15H; 3 × Ph), 5.34 (d, J = 9.6 Hz, 1H; NH), 4.92 (d, J = 11.6 Hz, 1H; PhCH), 4.84 (d, J = 3.8 Hz, 1H; Fuc 1-H), 4.79 (d, J = 11.4 Hz, 1H; PhCH), 4.76 (d, J = 11.5 Hz, 1H; PhCH), 4.67 (d, J = 11.7 Hz, 1H; PhCH), 4.62 (d, J = 11.9 Hz, 1H, PhCH), 4.60 (d, J = 11.6 Hz, 1H; PhCH), 4.32–4.28 (m, 2H; Thrα- and β-H), 4.18 (dd, J = 7.2, 10.8 Hz, 1H; Fuc 2-H), 4.10–3.99 (m, 1H; Fuc 5-H), 3.80 (dd, J = 2.8, 10.1 Hz, 1H; Fuc 3-H), 3.69 (q, J = 7.0 Hz, 2H; CH_3CH_2O), 3.60 (d, J = 2.4 Hz, 1H; Fuc 4-H), 1.48 (s, 9H; *t*Bu), 1.24 (t, J = 7.2 Hz, 3H; CH_3CH_2O) 1.21 (d, J = 6.5 Hz, 3H; Thr Me), 1.06 (d, J = 6.4 Hz, 3H; Fuc 6-H); HR-MS for $(C_{38}H_{49}NO_9+Cs)^+$ $[M+Cs^+]$: calcd 796.2462, found 796.2485.

5: ^1H NMR (400 MHz, $CDCl_3$, TMS):δ = 7.21–7.50 (m, 20H; 4 × Ph), 5.38 (d, J = 9.4 Hz, 1H; NH), 4.95–4.57 (m, 9H; 4 × $PhCH_2$), 4.35–3.99 (m, 5H; Thrα- and β-H, $CH(OH)CH_2OBn$, Fuc 2- and 5-H), 3.80–3.60 (m, 7H; CH_3CH_2O, $NHCH(CH(OH)CH_2OBn)$, Fuc 3- and 4-H), 1.48 (s, 9H; *t*Bu), 1.24 (t, J = 7.2 Hz, 3H; CH_3CH_2O), 1.21 (d, J = 6.5 Hz, 3H; Thr Me), 1.06 (d, J = 6.4 Hz, 3H; Fuc 6-H); HR-MS for $(C_{49}H_{62}N_2O_{12}+Cs)^+$ $[M+Cs^+]$: calcd 1003.3357, found 1003.3315.

6: ^1H NMR (400 MHz, $CDCl_3$, TMS): δ = 7.28–7.64 (m, 25H; 5 × Ph), 5.09 (s, 2H; $COOCH_2Ph$), 4.97–4.54 (m, 9H; 4 × $PhCH_2$, Fuc 1-H), 4.27–4.15 (m, 3H; Thr α- and β-H, $CH(OH)CH_2OBn$), 4.05–3.98 (m, 2H; Fuc 2- and 5-H), 3.80 (dd, J = 2.8, 10.2 Hz, 1H; Fuc 3-H), 3.67–3.52 (m, 6H; $NHCH(CH(OH)CH_2OBn)$, CH_3CH_2O, Fuc 4-H), 2.47–2.33 (m, 4H; $OCH_2CH_2CH_2O$), 2.01–1.91 (m, 2H; $OCH_2CH_2CH_2O$), 1.24 (t, J = 7.2 Hz, 3H; CH_3CH_2O), 1.21 (d, J = 6.5 Hz, 3H; Thr Me), 1.07 (d, J = 6.5 Hz, 3H; Fuc 6-H); HR-MS for $(C_{56}H_{66}N_2O_{13}+Cs)^+$ $[M+Cs^+]$: calcd 1107.3614, found 1107.3667.

Received: July 21, 1995 [Z8235IE]
German version: *Angew. Chem.* **1996**, *108*, 106–108

Keywords: glycopeptides · selectins · sialyl Lewis^x

[1] a) M. L. Phillips, E. Nudelman, F. C. A. Gaeta, M. Perez, A. K. Singhal, S. Hakomori, J. C. Paulson, *Science* **1990**, *250*, 1130; b) J. B. Lowe, L. M. Stoolman, R. P. Nair, R. D. Larsen, T. L. Berhend, R. M. Marks, *Cell* **1990**, *63*, 475; c) T. Feizi, *Trends Biochem. Sci.* **1991**, *16*, 84; d) M. Tiemeyer, S. J. Swiedler, M. Ishihara, M. Moreland, H. Schweingruber, P. Hirtzer, B. K. Brandley, *Proc. Natl. Acad. Sci. USA* **1991**, *88*, 1138; e) J. H. Musser, *Annu. Rep. Med. Chem.* **1992**, *27*, 301; f) L. A. Lasky, *Science* **1992**, *258*, 964; g) T. A. Springer, L. A. Lasky, *Nature* **1991**, *349*, 196.

[2] M. Buerke, A. S. Weyrich, Z. Zheng, F. C. A. Gaeta, M. J. Forrest, A. M. Lefer, *J. Clin. Invest.* **1994**, 1140.

[3] a) Y. C. Lin, C. W. Hummel, D.-H. Huang, Y. Ichikawa, K. C. Nicolaou, C.-H. Wong, *J. Am. Chem. Soc.* **1992**, *114*, 5452; b) Y. Ichikawa, Y. C. Lin, D. P. Dumas, G. J. Shen, E. Garcia-Junceda, M. A. Williams, R. Bayer, C. Ketcham, L. E. Walker, J. C. Paulson, C.-H. Wong, *ibid.* **1992**, *114*, 9283; c) G. E. Ball, R. A. O'Neill, J. E. Schultz, J. B. Lowe, B. W. Weston, J. O. Nagy, E. G. Brown, C. J. Hobbs, M. D. Bednarski, *ibid.* **1992**, *114*, 5449.

[4] B. J. Graves, R. L. Crowther, C. Chandran, J. M. Rumberger, S. Li, K. S. Huang, D. H. Presky, P. C. Familletti, B. A. Wolitzky, D. K. Burns, *Nature* **1994**, *367*, 532.

[5] a) B. K. Brandley, M. Kiso, S. Abbas, P. Nikrad, O. Srivastava, C. Foxall, Y. Oda, A. Hasegawa, *Glycobiology* **1993**, *3*, 633; b) S. A. DeFrees, F. C. A. Gaeta, Y. C. Lin, Y. Ichikawa, C.-H. Wong, *J. Am. Chem. Soc.* **1993**, *115*, 7549;

c) J. Y. Ramphal, Z.-L. Zheng, C. Perez, L. E. Walker, S. A. DeFrees, F. C. A. Gaeta, *J. Med. Chem.* **1994**, *37*, 3459; d) D. Tyrrell, P. James, B. N. Narasinga Rao, C. Foxall, S. Abbas, F. Dasgupta, M. Nashed, A. Hasegawa, M. Kiso, D. Asa, J. Kidd, B. K. Brandley *Proc. Natl. Acad. Sci. USA* **1991**, *88*, 10372; e) R. M. Nelson, S. Dolish, A. Aruffo, O. Cecconi, M. P. Bevilacqua, *J. Clin. Invest.* **1993**, *91*, 1157; f) A. Giannis, *Angew. Chem.* **1994**, *106*, 188; *Angew. Chem. Int. Ed. Engl.* **1994**, *33*, 178.

[6] a) N. M. Allanson, A. D. Davidson, F. M. Martin, *Tetrahedron Lett.* **1993**, *34*, 3945; b) J. A. Ragan, K. Cooper, *Bioorg. Med. Chem. Lett.* **1994**, *4*, 2563; c) S. Hanessian, H. Prabhanjan, *Synlett* **1994**, 868; d) T. Uchiyama, V. P. Vassilev, T. Kajimoto, W. Wong, H. Huang, C.-C. Lin, C.-H. Wong, *J. Am. Chem. Soc.* **1995**, *117*, 5395; e) H. Huang, C.-H. Wong, *J. Org. Chem.* **1995**, *60*, 3100; f) J. C. Prodger, M. J. Bamford, P. M. Gore, D. S. Holmes, V. Saez, P. Ward, *Tetrahedron Lett.* **1995**, *36*, 2339; g) B. N. Narasinga Rao, M. B. Anderson, J. H. Musser, J. H. Gilbert, M. E. Schaefer, C. Foxall, B. K. Brandley, *J. Biol. Chem.* **1994**, *269*, 19663.

[7] a) T. Muller, G. Hummel, R. R. Schmidt, *Liebigs Ann. Chem.* **1994**, 325; b) H. Kondo, S. Aoki, Y. Ichikawa, R. L. Halcomb, H. Ritzen, C.-H. Wong, *J. Org. Chem.* **1994**, *59*, 864.

[8] The unusual amino acid was prepared from glycine and *O*-benzylglycolaldehyde by L-threonine aldolase catalyzed reaction: V. P. Vassilev, T. Uchiyama, T. Kajimoto, C.-H. Wong, *Tetrahedron Lett.* **1995**, *36*, 4081. α-Hydroxymethyl serine was prepared according to the procedure described previously: T. T. Otani, M. Winitz, *Arch. Biochem. Biophys.* **1960**, *90*, 254.

[9] The inhibition analysis is based on a cell-free competitive assay. Details will be published separately.

[10] A SLe^x-RGD conjugate has been shown to be a potent inhibitor of P-selectin: U. Sprengard, G. Kretzschmar, E. Bartnik, C. Hüls, H. Kunz, *Angew. Chem.* **1995**, *107*, 1104; *Angew. Chem. Int. Ed. Engl.* **1995**, *34*, 990.

β,β-Dimethylcyclolanthionines, New Constrained Dipeptide Mimetics: Synthesis, Crystal Structures, and Conformational Studies**

Hui Shao, Chang-Woo Lee, Qin Zhu, Peter Gantzel, and Murray Goodman*

Dedicated to Professor Ivar Ugi on the occasion of his 65th birthday

In the past decade extensive efforts have been focused on the design of novel peptidomimetics for biomedical applications.[1] Recently, lanthionine,[2] a monosulfide cystine analog, has been examined by us as a new peptidomimetic (Scheme 1). The results of the chemical, biological, and physiological investigations indicate that lanthionine is an effective building block with conformational constraint and metabolic stability.[3] In this communication, we describe the design and synthesis of new constrained dipeptide mimetics based on β,β-dimethylcyclolanthionine.

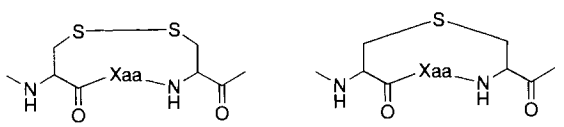

peptide chain with disulfide bridge lanthionine-modified peptide chain

Scheme 1. Representative disulfide and lanthionine structures in peptide chains. Xaa = amino acid residue.

The disulfide bridges between cysteine (Cys) residues in a peptide chain are most important covalent cross-linkages in proteins and peptide hormones[3, 4] (Scheme 1). In particular, the cysteinyl-cysteinyl motif (abbreviated as Cys-Cys), in which the two adjacent cysteine residues are connected by both amide and disulfide bridges, is a unique sequence in some naturally occurring peptides and proteins including malformin A, the γ-subunit of transducin, the nicotinic acetylcholine receptor (AChR), and mercuric reductase.[5, 6] It has been reported that the amide bond in Cys-Cys exists predominantly in the *cis* conformation and in solution it interconverts with the *trans* amide structure; in the solid state only the *cis* amide conformation is found.[5, 7] Furthermore, when Cys-Cys is changed to its penicillamine (Pen, β,β-dimethylcysteine) analog, Cys-Pen, a *trans* amide bond exists both in solution and in the solid state.[8] Our previous studies on cyclolanthionine showed that a *cis* amide bond in the seven-membered ring structure is the only conformation observed both in solution and in the solid state.[3g]

Two stereoisomers of β,β-dimethylcyclolanthionine, **1** and **2**, were prepared stereoselectively by regioselective ring-opening of *N*-Cbz-(*R*)-serine-β-lactone with the methyl esters of *N*-Boc-(*R*)- and -(*S*)-penicillamine, respectively (Scheme 2).[3a] Cyclizations were carried out on an oxime resin to provide the β,β-dimethylcyclolanthionine analogs **1** and **2** in high yields. The structures of these compounds have been analyzed by X-ray crystallography (Fig. 1).[9] Although the two isomers differ in the configuration of one chiral center, the ring structures adopt very similar conformations in the solid state with *cis* amide bonds rather than *trans* amides (Table 1). The only difference between the two diastereomers is the orientation of the carboxymethyl groups relative to the ring structures. The (1*S*,2*R*) configuration of isomer **1** orients the C- and N-terminal groups perpendicular to each other. On the other hand, the (1*S*,2*S*) isomer **2** has an extended conformation. Both conformations

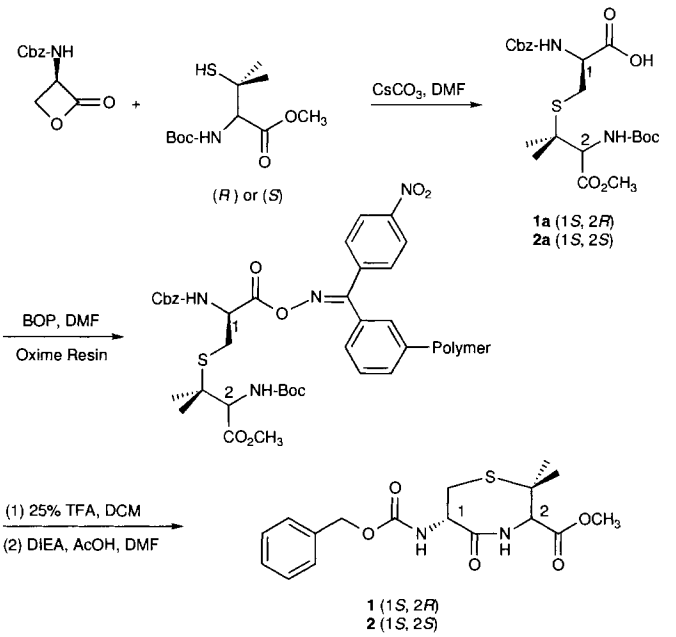

Scheme 2. Synthesis of β,β-dimethylcyclolanthionine analogs **1** and **2**. Bcz = benzyloxycarbonyl, Boc = *tert*-butoxycarbonyl, BOP = benzotriazol-1-yloxy-tris(dimethylamino)phosphonium hexafluorophosphate, DMF = dimethylformamide, TFA = trifluoroacetic acid, DCM = dichloromethane, DIEA = ethyldiisopropylamine.

[*] Prof. M. Goodman, H. Shao, C.-W. Lee, Q. Zhu, P. Gantzel
Department of Chemistry and Biochemistry
University of California, San Diego
La Jolla, CA 92093-0343 (USA)
Fax: Int. code +(619)534-0202

[**] We thank Drs. George Ösapay (UC-Riverside), Yunfei Zhu (Bioresearch Inc.), and Joseph Taulane for helpful discussions. We also thank Dr. Richard Kondrat (UC-Riverside) for mass spectroscopic analyses. This work was supported by the NIH (grant DK-15410).

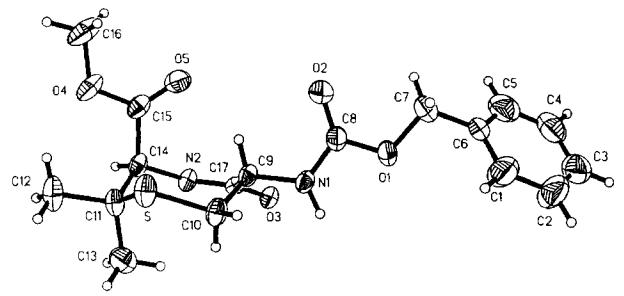

1 (1*S*, 2*R*)

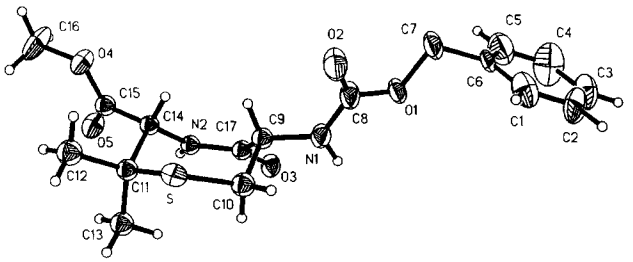

2 (1*S*, 2*S*)

Fig. 1. X-ray crystal structures of **1** and **2** (ORTEP view); thermal ellipsoids at 50% probability.

Table 1. Comparison of the conformations of β,β-dimethylcyclolanthionines **1** and **2** in the solid state and in solution.

Torsion angle [a]	Cmpd **1**		Cmpd **2**	
	Crystal	Solution	Crystal	Solution
Ψ^1	−177	91	−169	−165
ω^1	1	1	5	−1
ϕ^2	69	−151	157	163
χ^{11}	156	−155	154	151
χ^{12}	69	83	61	66
χ^{22}	−68	−38	−54	−61
χ^{21}	80	−47	84	78

[a] See Scheme 3 for a definition of the angles.

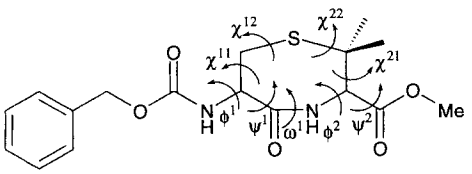

Scheme 3. Definition of the torsion angles in Table 1.

are identical to those we observed for the corresponding unsubstituted cyclolanthionine analogs.[3g]

The conformational preferences of the two isomers in solution were determined by NMR measurements in [D_6]DMSO and by subsequent computer simulations. Both isomers are characterized by *cis* amide bonds between the first and the second residue as indicated by NOE data. The most preferred ring conformations for both isomers in solution were compared with the solid-state conformations (Table 1). For isomer **2** the two conformations are similar. However, for isomer **1** the preferred conformation in solution differs dramatically from that in solid state (Fig. 2). In the X-ray crystal structure the N-terminal group is in the equatorial position of a boat conformation, while the C-terminal group prefers the axial position. In solution the ring structure of **1** exists in a unique folded boat conformation,

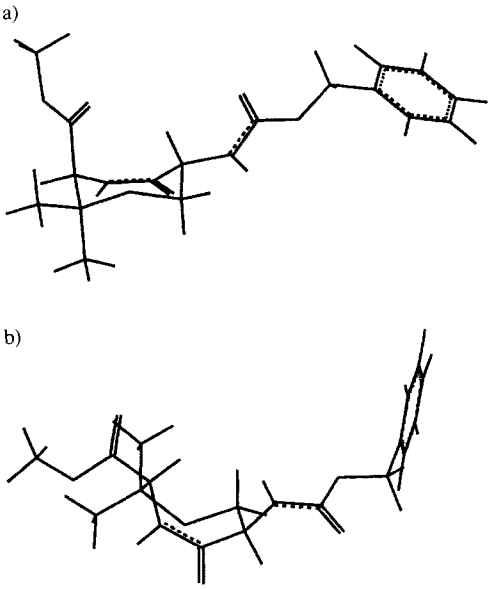

Fig. 2. Comparison of the conformations **1** in the solid state (a) and in solution (b).

which makes the orientations of the N-terminal and C-terminal groups different from the arrays in solid states. Comparison of the two conformations shows that the solid-state conformation is about 2.6 kcal mol^{-1} higher in energy than the conformation in solution. Since the conformations of β,β-dimethylated cyclolanthionines in the crystal structures are similar to the conformations of their corresponding unsubstituted analogs both in the solid state and in solution, the comparison indicates that β,β-dimethylation alters only the conformational preference in solution. In the solid state intermolecular interactions play an important role in stabilizing certain conformations as a result of molecular packing effects. The favorable conformations for molecular packing, of course, are not found in solution. This case illustrates the effect of solvent and crystal packing forces on preferred conformations of peptide-based structures.

We have described the synthesis and structural features of two new dipeptide mimetics, the diastereomeric β,β-dimethylcyclolanthionines **1** and **2**. An interesting feature is the discovery of two different conformations in the solid state and in solution. Our synthetic methods can also lead to (1*R*,2*S*) and (1*R*,2*R*) diastereomers of **1** and **2** if we start with appropriate amino acids. The stereoisomers of β,β-dimethylcyclolanthionine have distinctive structural features that depend on the chirality at each asymmetric center, which make them attractive building blocks or templates for the design of peptidomimetic drugs.

Experiment Procedure

Synthesis of compounds **1** and **2**: Compounds **1a** and **2a** were prepared by methods developed in our group [3]. The synthesis of compounds **1** and **2** were carried out on a Kaiser oxime resin [3] (5 g), which was suspended in CH_2Cl_2 (60 mL) for 1 h. After removal of the solvent the resin-containing vessel was charged with **1a** or **2a** (485 mg, 1 mmol), BOP (664 mg, 1.5 mmol) and anhydrous DMF (20 mL, dried over molecular sieves). Diisopropylethylamine (517 mg, 0.70 mL) was added, and the mixture was shaken for 24 h on a wrist action shaker (model 75, Burrell Corp.). The cyclization and isolation were carried out using procedures described for peptide cyclization on an oxime resin [3]. The crude product was purified by silica gel chromatography with ethyl acetate/hexane (1/1, v/v). The crystals were grown in ethyl acetate solution at room temperature.

1: Colorless solid; m.p. 142 °C; $[\alpha]_D^{20} = -4.4$ ($c = 0.16$, $CHCl_3$); ^{1}H NMR (500 MHz, [D_6]DMSO): $\delta = 1.336$ (3H, s), 1.38 (3H, s), 2.53 (1H, m), 2.82 (1H, m),

3.72 (3H, s), 4.08 (1H, d, J = 7.7 Hz), 4.61 (1H, m), 5.02 (2H, s), 7.31 (1H, m), 7.35 (5H, m), 7.80 (1H, d, J = 7.8 Hz); FAB-MS: m/z: 367 (MH^+); HRMS: m/z calcd for $C_{17}H_{23}O_5N_2S$: 367.1328; found: 367.1348; Anal. calcd for $C_{17}H_{22}O_5N_2S$: C 55.72, H 6.05, N 7.64; found: C 55.64, H 6.16, N 7.51.

2: Colorless solid; m.p. 140 °C; $[\alpha]_D^{20} = -30.9$ (c = 0.57, $CHCl_3$); ^{1}H NMR (500 MHz, [D$_6$]DMSO): δ = 1.36 (3H, s), 1.38 (3H, s), 2.54 (1H, m), 2.82 (1H, m), 3.71 (3H, s), 4.09 (1H, d, J = 7.8 Hz), 4.61 (1H, m), 5.02 (2H, s), 7.31 (1H, m), 7.35 (5H, m), 7.80 (1H, d, J = 6.8 Hz); FAB-MS: m/z: 367 (MH^+); HRMS: m/z calcd for $C_{17}H_{23}O_5N_2S$: 367.1328; found: 367.1333; Anal. calcd for $C_{17}H_{22}O_5N_2S$: C 55.72, H 6.05, N 7.64; found: C 55.70, H 6.20, N 7.53.

NMR Spectroscopy: The ^{1}H NMR spectra were recorded with a Bruker AMX 500 spectrometer at 300 K. Samples were prepared in [D$_6$]DMSO at concentrations of 30–40 mM. The resonance of [D$_5$]DMSO (δ = 2.49) was used as an internal standard. The one-dimensional spectra were collected with 32 K data points and with spectral widths of ±3000 or ±2000 Hz. The two-dimensional DQF COSY experiments were acquired with 2 K data points in the t_2 domain and with 256 data points in the t_1 domain. The ROESY experiments were carried out with a mixing time of 150 ms and a spin lock field of 2.5 KHz, and with 2 K data points in the t_2 domain and 256 data points in the t_1 domain. Zero-fillings were applied in the t_1 domain. Multiplication with phase-shifted sine function was employed in all spectra.

Computer Simulations: All calculations were carried out on an Iris 40-25 and a Challenge L computer. The distance geometry program DGEOM was used to generate structures compatible with NOE constraints. Energy minimizations were carried out with the DISCOVER force field program. Distance-dependent dielectric constants were used for all calculations. Structures generated from DGEOM were minimized by the steepest descent algorithm for 100 steps followed by the VAO9A algorithm until all the derivatives were smaller than 0.001 kcal mol^{-1} Å^{-1}.

Received: July 24, 1995 [Z 8242 IE]
German version: *Angew. Chem.* **1996**, *108*, 88–90

Keywords: lanthionines · peptidomimetics

[1] For recent examples, see: a) M. Goodman, S. Ro, *Burger's Medicinal Chemistry and Drug Discovery, Vol. 1* (Ed.: M. E. Wolff), Wiley, New York, **1995**, pp. 803–861; b) H. Shao, Q. Zhu, M. Goodman, *J. Org. Chem.* **1995**, *60*, 790–791; c) R. Hirschmann, K. C. Nicolaou, S. Pietranico, J. Salvino, E. M. Leahy, P. A. Sprengeler, G. Furst, A. B. Smith, C. D. Strader, M. A. Cascieri, M. R. Candelore, C. Donaldson, W. Vale, L. Maechler, *J. Am. Chem. Soc.* **1992**, *114*, 9217–9218; d) A. B. Smith, M. C. Guzman, P. A. Sprengeler, T. P. Keenan, R. C. Holcomb, J. L. Wood, P. J. Carroll, R. Hirschmann, *ibid.* **1994**, *116*, 9947–9962; e) F. Cornille, U. Slomczynska, M. L. Smythe, D. D. Beusen, K. D. Moeller, G. R. Marshall, *ibid.* **1995**, *117*, 909–917; f) A. Giannis, T. Kolter, *Angew. Chem.* **1993**, *105*, 1303–1326; *Angew. Chem. Int. Ed. Engl.* **1993**, *32*, 1244–1267; g) J. Gante, *ibid.* **1994**, *106*, 1780 and **1994**, *33*, 1699–1720; h) V. J. Hruby, A. Gehring, *Med. Res. Rev.* **1989**, *9*, 343–401.

[2] a) *Nisin and Novel Lantibiotics* (Eds.: G. Jung, H. G. Sahl), Escom, Leiden, **1988**; b) R. Zhang, G. H. Snyder, *J. Biol. Chem.* **1989**, *264*, 18472–18479, and references therein; c) S. Chatterjee, D. K. Chatterjee, S. J. Lad, M. S. Phansalkar, R. H. Rupp, B. N. Ganguli, *J. Antibiot.* **1992**, *45*, 832–838; d) S. Chatterjee, D. K. Chatterjee, R. H. Jani, J. Blumbach, B. N. Ganguli, *ibid.* **1992**, *45*, 839–845.

[3] a) H. Shao, S. H.-H. Wang, C.-W. Lee, G. Ösapay, M. Goodman, *J. Org. Chem.* **1995**, *60*, 2956–2957; b) G. Ösapay, M. Goodman, *J. Chem. Soc. Chem. Commun.* **1993**, 1599–1600; c) A. Polinsky, M. G. Cooney, A. Toy-Palmer, G. Ösapay, M. Goodman, *J. Med. Chem.* **1992**, *35*, 4185–4194; d) G. Ösapay, H. Shao, M. Goodman, J. W. Taylor, *Pept. Chem. Biol. Proc. Am. Pept. Symp. 13th* **1994**, 101–103; e) C.-W. Lee, Q. Zhu, H. Shao, S. H.-H. Wang, G. Ösapay, M. Goodman, *Pept. Proc. Eur. Pept. Symp. 23rd* **1994**, 627–628; f) S. H.-H. Wang, *Pept. Chem. Biol. Proc. Am. Pept. Symp. 14th* **1995**, in press; g) G. Ösapay, Q. Zhu, H. Shao, R. H. Chadha, M. Goodman, *Int. J. Pept. Protein Res.* **1995**, *46*, 290–301.

[4] a) E. E. Sugg, D. Tourwe, W. Kazmierski, V. J. Hruby, G. Van Binst, *Int. J. Pept. Protein Res.* **1988**, *31*, 192–200; b) S. Horvat, B. Gragas, N. Raog, V. Simeon, *ibid.* **1989**, *34*, 346–351.

[5] a) D. K. Sukumaran, M. Prorok, D. S. Lawrence, *J. Am. Chem. Soc.* **1991**, *113*, 706–707; b) M. Bodanszky, G. L. Stahl, *Proc. Natl. Acad. Sci. USA* **1974**, *71*, 2791–2794; c) Y. A. Ovchinnikov, V. M. Lipkin, T. M. Shuvaeva, A. P. Bogachuk, V. V. Shemyakin, *FEBS Lett.* **1985**, *179*, 107; d) P. N. Kao, A. Karlin, *J. Biol. Chem.* **1986**, *261*, 8085–8088; e) S. M. Miller, M. J. Moore, V. Massey, C. Williams, M. D. Distefano, D. P. Ballou, C. T. Walsh, *Biochemistry* **1989**, *28*, 1194–1205.

[6] R. Chandrasekaran, R. Balasubramanian, *Biochim. Biophys. Acta* **1969**, *188*, 1–9.

[7] a) S. Capasso, C. Mattia, L. Mazzarella, *Acta Crystallogr. Sect. B* **1977**, *33*, 2080–2083; b) Y. Hata, Y. Matsuura, N. Tanaka, T. Ashida, M. Kakudo, *ibid.* **1977**, *33*, 3561–3564; c) A. Horne, M. North, J. A. Parkinson, I. H. Sadler, *Tetrahedron* **1993**, *49*, 5891–5904.

[8] R. L. Baxter, S. S. B. Glover, E. M. Gordon, R. O. Gould, M. C. McKie, A. I. Scott, M. D. Walkinshaw, *J. Chem. Soc. Perkin Trans. 1* **1988**, 365–371.

[9] **1**: $C_{17}H_{22}N_2O_5S$, crystals from ethyl acetate; monoclinic, space group $P2_1$, a = 12.041(6), b = 7.467(4), c = 22.20(1) Å, β = 118.59(4)°, Z = 2; ρ_{calcd} = 1.273 g cm^{-3}; μ_{Mo} = 0.197 mm^{-1}; 2162 observed reflections ($I \geq 4.0\,\sigma(I)$); $2\theta_{max.}$ = 55.0°; R = 0.0428; R_w = 0.0608; max. residual electron density 0.37 eÅ^{-3}; C*H* in calculated positions. **2**: $C_{17}H_{22}N_2O_5S$, crystals from ethyl acetate; monoclinic, space group $P2_1$, a = 6.228(3), b = 10.067(5), c = 14.548(6) Å, β = 90.89(3)°, Z = 2; ρ_{calcd} = 1.334 g cm^{-3}; μ_{Mo} = 0.207 mm^{-1}; 2112 observed reflections ($I \geq 4.0\,\sigma(I)$); $2\theta_{max.}$ = 55.0°; R = 0.0505; R_w = 0.0704; max. residual electron density 0.34 eÅ^{-3}; C*H* in calculated positions. Program used: Siemens SHELXTL PLUS (PC Version). Further details of the crystal structure investigations may be obtained from the Director of the Cambridge Crystallographic Data Centre, 12 Union Road, GB-Cambridge CB21EZ (UK), on quoting the full journal citation.

A Sequential Electron-Transfer Relay in Diporphyrin–Porphyrin–Pyromellitimide Triads Analogous to That in the Photosynthetic Reaction Center**

Atsuhiro Osuka,* Satoshi Nakajima, Tadashi Okada,* Seiji Taniguchi, Koichi Nozaki, Takeshi Ohno, Iwao Yamazaki, Yoshinobu Nishimura, and Noboru Mataga*

The reaction center (RC) of photosynthetic bacteria contains a number of cofactors that mediate a series of fast electron transfers, yielding an oxidized electron donor and a reduced electron acceptor on the opposite sides of a membrane. The key steps in this process are the initial charge separation (CS) between tetrapyrrolic pigments and the subsequent charge-shift reaction (CSH) to a quinone acceptor to generate a stable, long-lived, charge-separated state.[1] Numerous model compounds have been prepared to understand the factors controlling electron transfer (ET) reactions in these highly complex systems.[2, 3] In the past decade the advantages of multiple electron transfers have been amply demonstrated.[4, 5] Nevertheless, modeling the sequential electron transfer relay of the reaction center remains very difficult, particularly with regard to the ET reaction scheme outlined above.[6]

Recently, we described the intramolecular charge separation in triads **13** and **14**, which comprise a zinc diporphyrin (Dp), a zinc monoporphyrin (Mp), and a pyromellitimide (Im).[7] Upon photoexcitation in THF at 532 nm, these triads give Dp$^+$-Mp-Im$^-$ ion pairs with lifetimes of 0.25 μs (**13**) and 2.4 μs (**14**) in relatively low quantum yield by the pathway Dp-^{1}Mp*-Im → Dp-Mp$^+$-Im$^-$ → Dp$^+$-Mp-Im$^-$. The low quantum yields are due mainly to efficient intramolecular singlet–singlet energy

[*] Prof. A. Osuka, Dr. S. Nakajima
Department of Chemistry, Faculty of Science
Kyoto University, Kyoto 606 (Japan)
Fax: Int. code +(75)751-2085
Prof. T. Okada, S. Taniguchi
Department of Chemistry, Faculty of Engineering Science
Osaka University, Toyonaka 560 (Japan)
Dr. K. Nozaki, Prof. T. Ohno
Department of Chemistry, Faculty of Science
Osaka University, Toyonaka 560 (Japan)
Prof. I. Yamazaki, Dr. Y. Nishimura
Department of Chemical Process Engineering, Faculty of Engineering
Hokkaido University, Sapporo 060 (Japan)
Prof. N. Mataga
Institute for Laser Technology, Utsubo-Honmachi
Nishiku, Osaka 550 (Japan)

[**] This work was supported by Grants-in-Aid (No. 07228232 to A. O. and No. 2948 to S. N.) from the Ministry of Education, Science, and Culture of Japan and by the Japanese Securities Scholarship Foundation. S. N. thanks the JSPS Foundation for a postdoctoral fellowship.

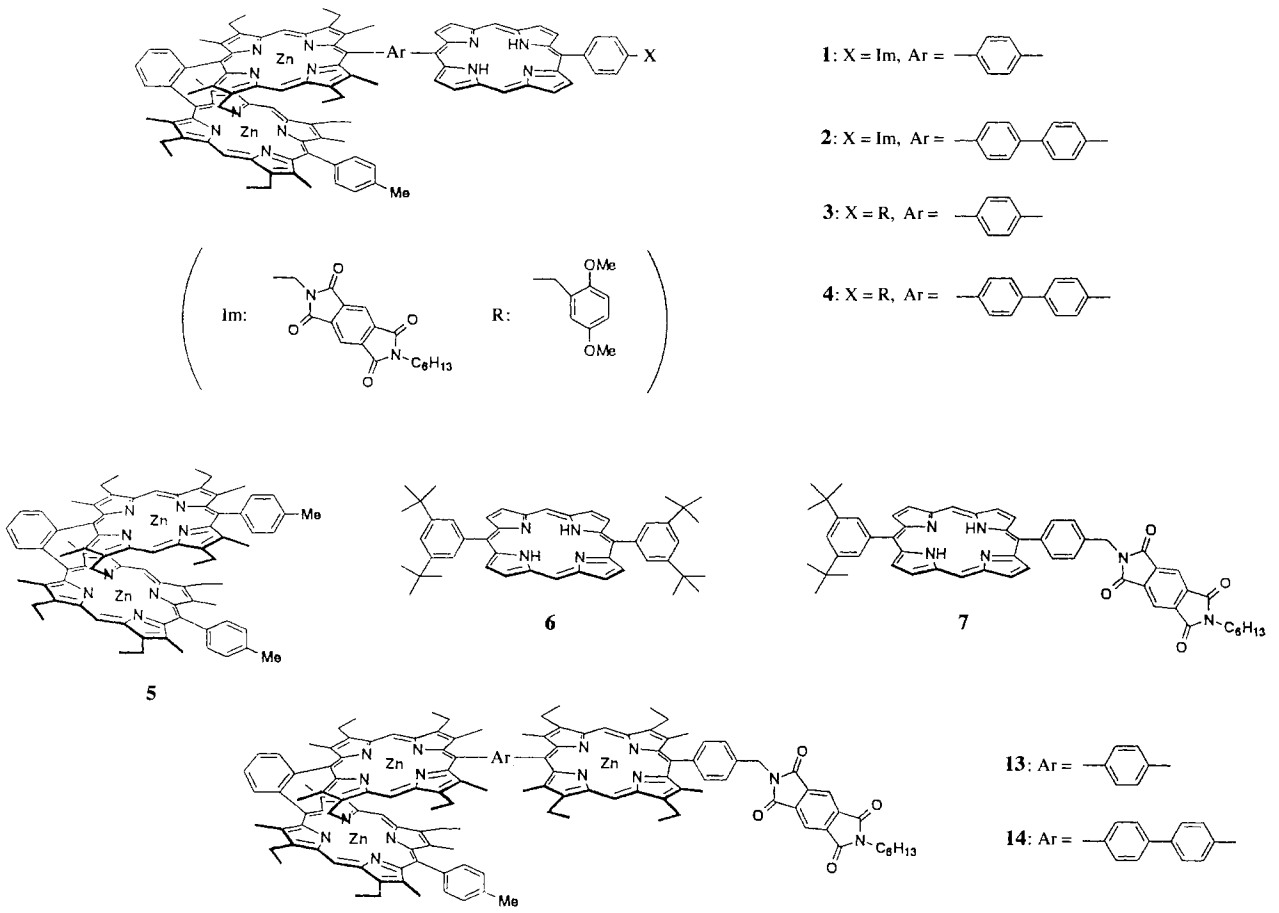

transfer from ^{1}Mp* (2.13 eV) to Dp (1.97 eV); the ^{1}Dp*-Mp-Im thus formed does not undergo electron transfer (ET) reactions.

We report here on the synthesis of triads **1** and **2**, which consist of a zinc diporphyrin, an uncomplexed porphyrin, and pyromellitimide (Dp-Hp-Im). These triads serve as functional models for the photosynthetic RC, since they display an efficient ET relay, ^{1}Dp*-Hp-Im → Dp$^+$-Hp$^-$-Im → Dp$^+$-Hp-Im$^-$, which is quite similar to the primary ET events in the RC. The triads **1** and **2** are designed such that 1) the energy gradient ^{1}Dp*-Hp-Im or Dp-^{1}Hp*-Im > Dp$^+$-Hp$^-$-Im > Dp$^+$-Hp-Im$^-$ allows the occurrence of the ET relay, and 2) the respective oxidized or reduced chromophores exhibit characteristic absorption bands, making the analysis of ET dynamics very easy.[7] The former condition is satisfied by **1**, as shown in Figure 1. Here the energies of the charge-separated pair states were estimated with corrected solvation energies, which were calculated by the Born equation using the one-electron oxidation and reduction potentials.[8]

The synthetic route to **1** is shown in Scheme 1. The acid-catalyzed condensation of formyl-substituted diporphyrins **8**[7] and pyromellitimide-substituted benzaldehyde **9**[9] with dipyrrolylmethane **10**[10] under the previously reported conditions[11] gave triporphyrin **11** in 30% yield (based on **8**). Selective zinc-metalation was performed by careful treatment of **11** with exactly two equivalents of $Zn(OAc)_2$, giving **1** in 60% yield. The eight β-alkyl substituents seem to enhance the basicity of the porphyrin ligand by their electron-donating property, which leads to an enhanced affinity toward zinc(II) ions. The ^{1}H NMR spectrum of **11** shows a broad signal at $\delta \approx 6$ due to the four inner NH protons of the diporphyrin and a signal at $\delta \approx -3$ attributed to the two inner NH protons of the monoporphyrin. The former signal is diagnostic of 1,2-phenylene-bridged diporphyrins. In contrast, the spectrum of **1** exhibits only peaks due to the two inner NH protons at $\delta \approx -3$. Another triad, compound **2**, which bears a 4,4'-biphenylene spacer between Dp and Hp, was prepared from **12**[7] in essentially the same manner as **1** was synthesized from **8**. Pyromellitimide-free molecules **3** and **4** as well as compounds **5**–**7** were also prepared as references.

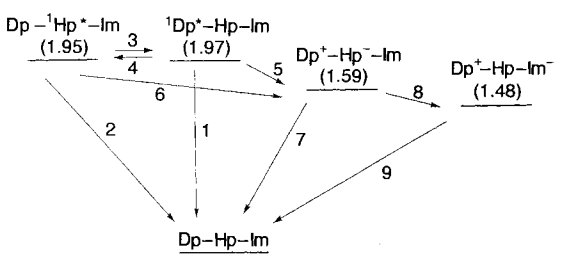

Fig. 1. Reaction scheme and energy diagram for **1** in THF. Numbers in parentheses indicates the approximate energies in eV [8].

The UV/Vis absorption spectra of **1**–**4** are nearly identical to the sum of the spectra of the chromophores **5** and **6**, indicating that electronic interaction is weak in the ground states of **1**–**4**. To understand the dynamics of the photoexcited states of the triads it is appropriate to first consider some simpler reference molecules. The fluorescence intensity of **7** is identical to that of **6** in a wide range of solvents (e.g. benzene, THF, and DMF), indicating that there is no CS in the ^{1}Hp*-Im subunit. This has been confirmed by measurements of the fluorescence lifetime and transient absorption spectra as well.

In contrast, a strong fluorescence quenching in the Dp-Hp subunit has been observed for **1**–**4** in THF. Since the excitation energies to ^{1}Dp* (1.97 eV) and ^{1}Hp* (1.95 eV) are nearly the same, it is very difficult to selectively excite one chromophore.

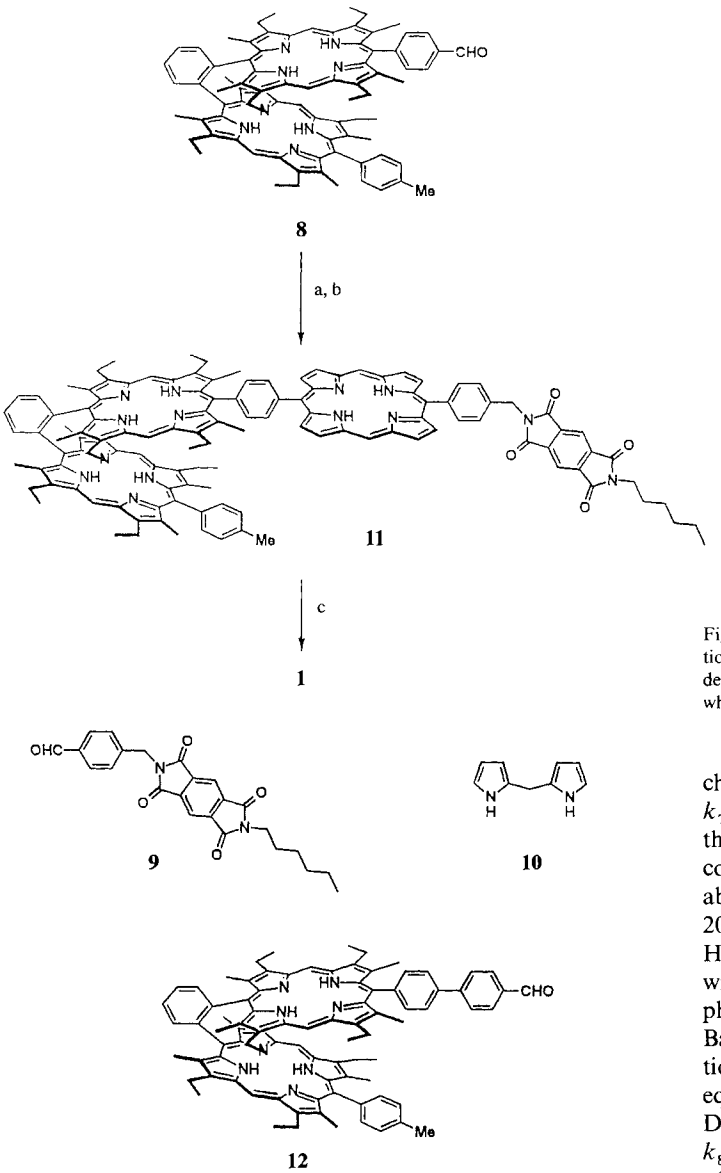

Scheme 1. Synthesis of **1**. a) **9**, **10**, TFA, CH_2Cl_2, ca. 20 °C, 10 h; b) DDQ, ca. 20 °C, 10 h, 30%, c) $Zn(OAc)_2$ (2 equiv), $CHCl_3$/MeOH, ca. 20 °C, 20 min, 60%.

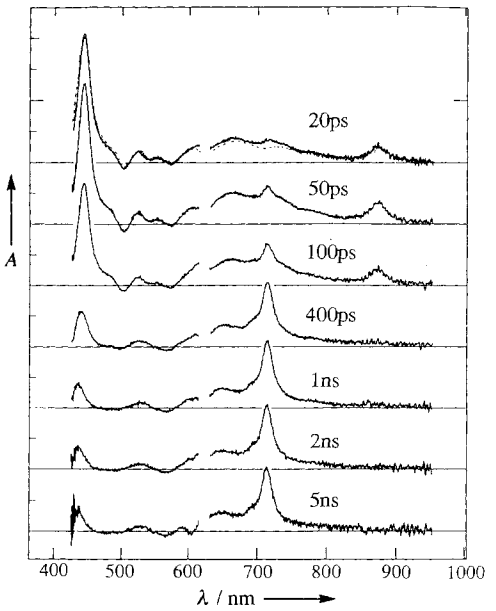

Fig. 2. Transient absorption spectra on the picosecond range of a 1×10^{-4} M solution of **1** in THF with 8 ps, 818 nm pulses. The dotted line in the spectrum at 20 ps delay time is for **3**. The details of the measuring system have been described elsewhere [13]. A = absorbance in 0.2 units per division.

We measured the transient absorption spectra by exciting at 618 nm; at this wavelength the incident light is absorbed by Dp and Hp in a ratio of 3:1. The transient absorption spectrum of **3** in THF recorded after a delay time of 20 ps (the dotted line in Fig. 2, top) shows immediate build-up of the absorption bands at 670 and 870 nm, which are characteristic of Dp^+ and Hp^-, respectively.[12] Figure 2 also displays the transient absorption spectra of the triad **1** recorded after delay times of 20 ps to 5 ns. The spectrum measured with a 20 ps delay time is nearly the same as that of **3** with a 20 ps delay time except for a weak absorption at 715 nm due to Im^-. These two spectra clearly indicate that Dp^+-Hp^--Im and Dp^+-Hp^- form from **1** and **3**, respectively, in high yield within 20 ps. Therefore, the rates of the formation of Dp^+-Hp^--Im and Dp^+-Hp^- are larger than 5×10^{10} s^{-1}n and the CS reactions (steps 5 and 6 in Fig. 1) are almost quantitative for the both models; when the lifetimes of $^1Dp^*$ (900 ps) and $^1Hp^*$ (12 ns) are also considered, estimated values of $k_1 = 1.1 \times 10^9$ s^{-1} and $k_2 = 8.3 \times 10^7$ s^{-1} result. Analysis of the time profile of the 870 nm absorption reveals that the Dp^+-Hp^- state of **3** decays to the ground state by charge recombination with a time constant of 1.2 ns (step 7, $k_7 = 8.3 \times 10^8$ s^{-1}). In the case of the Dp^+-Hp^--Im state of **1**, the decay of the Hp^- absorption is much faster with a time constant of 200 ps. Concomitantly the increase in the 715 nm absorption due to Im^-[7] has exactly the same time constant of 200 ps. These data clearly show that the CSH reaction of Dp^+-Hp^--Im to give Dp^+-Hp-Im^- (step 8, Fig. 1) is in competition with CR to the ground state. Therefore, the behavior of **1** after photoirradiation can be summarized as shown in Figure 1. Based on this scheme, the rate constant of the charge-shift reaction (k_8) was determined to be 4.1×10^9 s^{-1} by the following equation: $k_8 = 1/\tau_2 - 1/\tau_1$, where τ_1 and τ_2 are the lifetimes of Dp^+-Hp^- and Dp^+-Hp^--Im, respectively. It is now evident that k_8 is roughly five times larger than k_7. Therefore, the formation of Dp^+-Hp-Im^- from Dp^+-Hp^--Im is favored, and the overall quantum yield is greater than 0.8. Finally, the lifetime of the secondary ion pair Dp^+-Hp-Im^- was determined to be 280 ns.

Examination of the transient absorption spectra of 4,4′-biphenyldiyl-bridged models **2** and **4** reveal essentially the same type of ET relay. The initial ion pair Dp^+-Hp^--Im, which is formed with a time constant of 120 ps, undergoes a productive CSH reaction to provide Dp^+-Hp-Im^- with $k_8 = 4.6 \times 10^9$ s^{-1}; the CSH reaction is in competition with CR to the ground state with $k_7 = 4.0 \times 10^8$ s^{-1}. The quantum yield for the formation of Dp^+-Hp-Im^- therefore is still as high as 0.79; however, Dp^+-Hp-Im^- has a much longer lifetime (2.1 μs), reflecting the larger separation between the two charges. Comparison of k_8 values in **1** and **2** might be interesting, since it should reflect the electric-field effect exerted by Dp^+ upon the CSH reaction, which should be very significant in nonpolar media. The small differences in the k_{CSH} values (k_8) observed here indicate substantial dielectric shielding in THF. According to the Born equation, the difference in the free energies of the CSH reaction between **1** and **2** is only 0.02 eV.

In the more polar solvent DMF the excitation of **3** leads to the formation of Dp^+-Hp^- within 10 ps, which decays rapidly to the ground state by CR with $k_7 = 1.8 \times 10^{10}$ s^{-1}. The increase of k_7 in polar DMF is notable. Since the very poor solubility of

 © VCH Verlagsgesellschaft mbH, D-69451 Weinheim, 1996 0570-0833/96/3501-0094 $ 10.00+.25/0

1 in DMF hampered the measurement of its transient spectra, we examined the dynamics of the photoexcited states of **2** and **4** in DMF. The energy levels of the ion pairs were calculated to be 1.41 eV for Dp^+-Hp^--Im and 1.19 eV for Dp^+-Hp-Im^-. Analysis of the transient absorption spectra of **2** and **4** reveals the formation of Dp^+-Hp^--Im within 30 ps, and the values of k_7 and k_8 were determined to be 1.0×10^{10} and $1.1 \times 10^9\ s^{-1}$, respectively. Here again the increase of k_7 is large in DMF, while k_8 is slightly smaller. As a consequence, the overall quantum yield decreases to roughly 0.1. The polar environment is of course favorable in lowering the energy level of the charge-separated states for the ET process. But it often accelerates the energy-wasteful CR reaction, which is accompanied by a concomitant decrease of the overall quantum yield of the charge separation, as observed in our system. This kinetic aspect may be quite common and should be taken into account in the future design of more elaborate photosynthetic model systems.

In summary, a sequential ET relay resembling that in the RC and ultimately leading to the formation of long-lived charge separated states has been realized in the Dp-Hp-Im triads **1** and **2**, which have a molecular composition quite similar to that of the RC. The polarity of solvent is crucial in determining the overall CS quantum yield. The polarity of the solvent is crucial for the overall CS quantum yield.

Received: June 26, 1995 [Z 8133 IE]
German version: *Angew. Chem.* **1996**, *108*, 98–101

Keywords: electron transfer · photosynthesis · porphyrinoids

[1] D. Holten, C. Kirmaier, *Photosynth. Res.* **1987**, *13*, 225.
[2] M. R. Wasielewski, *Chem. Rev.* **1992**, *92*, 435.
[3] H. Kurreck, M. Huber, *Angew. Chem.* **1995**, *107*, 929; *Angew. Chem. Int. Ed. Engl.* **1995**, *34*, 849.
[4] D. Gust, T. A. Moore, A. L. Moore, *Acc. Chem. Res.* **1993**, *26*, 198; K. Maruyama, A. Osuka, N. Mataga, *Pure Appl. Chem.* **1994**, *66*, 867.
[5] S. Nishitani, N. Kurata, Y. Sakata, S. Misumi, A. Karen, T. Okada, N. Mataga, *J. Am. Chem. Soc.* **1983**, *105*, 7771; J. Rodriguez, C. Kirmaier, M. R. Johnson, R. A. Friesner, D. Holten, J. L. Sessler, *ibid.* **1991**, *113*, 1652; A. M. Brun, A. Harriman, V. Heitz, J. P. Sauvage, *ibid.* **1991**, *113*, 8657; D. Heiler, G. McLendon, P. Rogalskyj, *ibid.* **1987**, *109*, 604; J. L. Sessler, V. L. Capuano, A. Harriman, *ibid.* **1993**, *115*, 4618; J. Zaleski, W. Wu, C. K. Chang, G. E. Leroi, R. I. Cukier, D. G. Nocera, *Chem. Phys.* **1993**, *176*, 483; F. Pöllinger, H. Heitele, M. E. Michel-Beyerle, C. Anders, M. Futscher, H. A. Staab, *Chem. Phys. Lett.* **1992**, *198*, 645; J. M. Lawson, M. N. Paddon-Row, *J. Chem. Soc. Chem. Commun.* **1993**, 1641; S. I. van Dijk, P. G. Wiering, R. van Staveren, H. J. van Ramesdonk, A. M. Brouwer, J. W. Verhoeven, *Chem. Phys. Lett.* **1993**, *214*, 502.
[6] Recently, an efficient, single-step ET in chlorin-porphyrin-quinone triads was reported: M. R. Wasielewski, G. L. Gaines III, G. P. Wiederrecht, W. A. Svec, M. P. Niemcyzk, *J. Am. Chem. Soc.* **1993**, *115*, 10442.
[7] A. Osuka, S. Nakajima, K. Maruyama, N. Mataga, T. Asahi, I. Yamazaki, Y. Nishimura, T. Ohno, K. Nozaki, *J. Am. Chem. Soc.* **1993**, *115*, 4577; D. Gosztola, H. Yamada, M. R. Wasielewski, *ibid.* **1995**, *117*, 2041.
[8] A. Weller, *Z. Phys. Chem. (Wiesbaden)* **1982**, *93*, 5983. $E(IP) = E_{ox} - E_{red} + \Delta G_s, \Delta G_s = (e^2/2)(1/r_D - 1/r_A)(1/4\pi\varepsilon_0\varepsilon - 1/4\pi\varepsilon_0\varepsilon_r) - e^2/4\pi\varepsilon_0\varepsilon R_{DA}$, where E_{ox} and E_{red} are the oxidation and reduction potentials of the donor and acceptor, respectively, measured in DMF, r_D and r_A are the effective radii of the donor cation and the acceptor anion, and ε_r is the dielectric constant of DMF and ε that of C_6H_6 or THF. The one-electron oxidation potentials of Dp and Hp in DMF are −0.05 and 0.61 V (vs. ferrocene/ferrocenium), respectively, and the one-electron reduction potentials of Hp and Im are −1.61 and −1.24 V, respectively. The radii of Dp^+, Hp^+, Hp^-, and Im^- were assumed to be 5, 5, 5, and 3.5 Å, respectively, and the separations (R_{DA}) between charges were assumed to be 17.9, 29.8, and 13.5 Å for Dp^+-Hp^-, Dp^+-Hp-Im^-, and Hp^+-Im^-, respectively. For ion pairs from **2**, R_{DA} values of 17.9 Å for Dp^+-Hp^- and 29.8 Å for Dp^+-Hp-Im^- give the energies of 1.62 and 1.49 eV, respectively.
[9] T. Nagata, *Bull. Chem. Soc. Jpn.* **1991**, *64*, 3005.
[10] T. Chong, P. S. Clezy, A. J. Liepa, A. W. Nichol, *Aust. J. Chem.* **1969**, *22*, 229.
[11] S. G. DiMagno, V. S.-Y. Lin, M. J. Therien, *J. Org. Chem.* **1993**, *58*, 5983.
[12] J. Fajer, D. C. Borg, A. Forman, D. Dolphin, R. H. Felton, *J. Am. Chem. Soc.* **1970**, *92*, 3451; P. Neta, A. Scherz, H. Levanon, *ibid.* **1989**, *101*, 3624.
[13] Y. Hirata, N. Mataga, *J. Phys. Chem.* **1991**, *95*, 1640.

Cycloadditions of Ruthenium Alkylidyne Complexes with Carbonyl or Thiocarbonyl Compounds**

Robin B. Bedford, Anthony F. Hill,*
Andrew J. P. White, and David J. Williams

Whilst the cycloaddition of carbon–carbon and metal–carbon multiple bonds is central to alkene and alkyne metathesis processes,[1] the addition of heteroallenes and heteroalkenes to alkylidyne complexes has been less intensely studied[2] despite the added intrigue of multiple bond polarity. Reactions of alkylidyne complexes of Group 6 metals with carbon disulfide have been discussed recently by Mayr and Lee,[3] and the processes observed typically involve C–C bond formation. We have been previously concerned with the cycloaddition of SO_2 and iminooxosulfuranes to Group 8 alkylidyne complexes[4] and have suggested that the products derive from M–S and C–O bond formation (Scheme 1).[5] Herein we report the reactions of

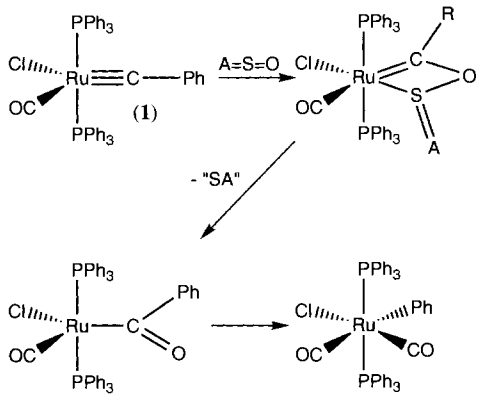

Scheme 1. Addition of sulfur dioxide and iminooxo-λ^4-sulfuranes to a ruthenium benzylidyne complex. A = O, NC_6H_4-4-Me.

a ruthenium benzylidyne complex with CO_2, MeNCS, and CS_2, in which the orientation of addition is opposite to that observed in the analogous reactions with the Group 6 alkylidyne complexes.

Treating a solution of $[Ru(\equiv CPh)Cl(CO)(PPh_3)_2]$ (**1**)[6] with carbon disulfide leads to clean formation of a carbonyl-free complex, spectroscopic data (Table 1) for which are consistent with the formulation $[Ru(\eta^2\text{-}SCPh)Cl(CS)(PPh_3)_2]$ (**2a**) (Scheme 2). The corresponding carbonyl analogue **2b** could be prepared by the route outlined in Scheme 2, and spectroscopic data for the two analogues compare well in all respects but those associated with the thiocarbonyl/carbonyl ligand. This route to **2b** has precedent in the preparation of the complexes $[Os(\eta^2\text{-}SCC_6H_4\text{-}4\text{-}Me)Cl(CO)(PPh_3)_2]$ and $[Ru(\eta^2\text{-}SCSiMe_2OEt)Cl(CO)(PPh_3)_2]$.[7]

[*] Dr. A. F. Hill, Dr. R. B. Bedford
Department of Chemistry
Imperial College of Science, Technology and Medicine
South Kensington, London SW7 2AY (GB)
Fax: Int. code +(171)594-5804
e-mail: a.hill@ic.ac.uk
Dr. A. J. P. White, Dr. D. J. Williams
Chemical Crystallography Laboratory
Department of Chemistry
Imperial College of Science, Technology and Medicine
South Kensington, London SW7 2AY (GB)

[**] This research was supported by the Engineering and Physical Sciences Research Council and the Royal Society.

 © VCH Verlagsgesellschaft mbH, D-69451 Weinheim, 1996 0570-0833/96/3501-0095 $ 10.00+.25/0

Table 1. Selected spectroscopic data of the complexes **2a** and **2b** [a].

	2a	**2b**
IR (Nujol, cm^{-1})		
$\tilde{\nu}$(CA)	1257vs	1928vs, 1906vs [b]
ruthenathiirene	1283s, 1187m, 978w, 829s	1287s, 1187m, 978w, 820s
NMR ($CDCl_3$, 25 °C)		
$^{31}P\{^1H\}$	27.7	30.0
$^{13}C\{^1H\}$		
δRuCS [J (PC)/Hz]	305.9 [t, 15.1]	208.9 [t, 15.1]
δRuSCPh [J (PC)/Hz]	310.6 [t, 8.9]	311.5 [t, 8.1]
FAB-MS (nba-matrix)		
m/z (intensity (%))		
[assignment]	826(2) $[M]^+$	810(1) $[M]^+$
	791(5) $[M - Cl]^+$	782(15) $[M - CO]^+$
	705(2) $[M - SCPh]^+$	775(19) $[M - Cl]^+$
	564(5) $[M - L]^+$	520(8) $[M - CO - L]^+$
	529(11) $[M - Cl - L]^+$	485(4) $[M - CO - Cl - L]^+$

[a] L = PPh_3, nba = nitrobenzyl alcohol. [b] Solid-state splitting: $\tilde{\nu}$(CO) in CH_2Cl_2: 1920 cm^{-1}.

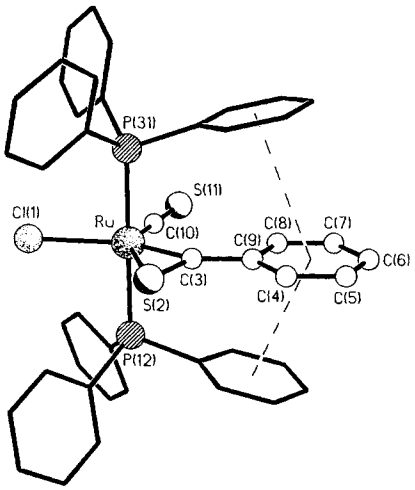

Fig. 1. The structure of **2a** in the crystal, showing the π-π stacking of the phosphane phenyl and thiobenzoyl rings.

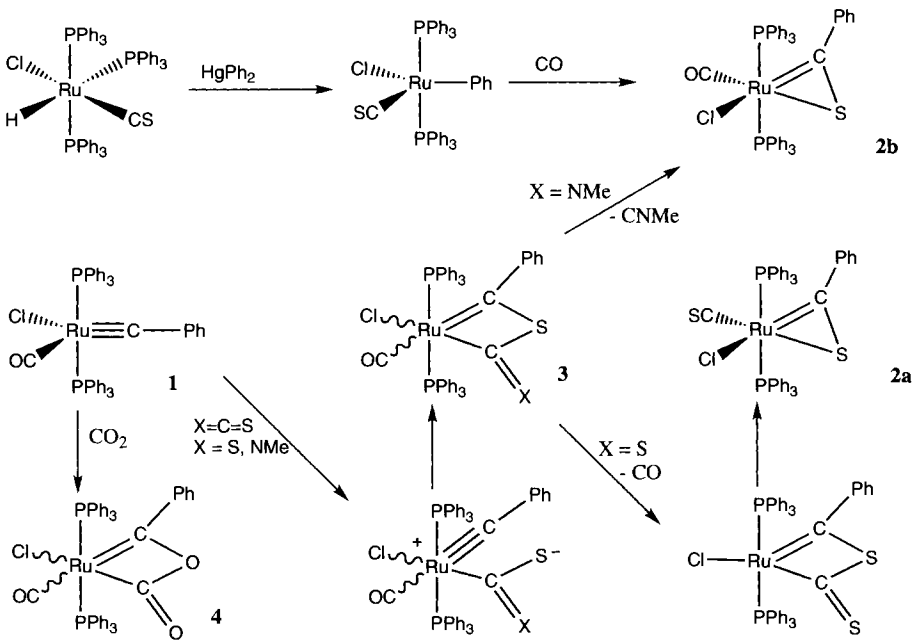

Scheme 2. Preparation of ruthenium(II) thiobenzoyl complexes.

The formulation of $[Ru(\eta^2\text{-SCPh})Cl(CS)(PPh_3)_2]$ (**2a**) was also confirmed by X-ray crystallography.[8] Although the structure is definitive (Fig. 1), detailed analysis of the relative molecular dimensions is precluded by positional disorder (35:65) of the thiocarbonyl and thiobenzoyl ligands about an axis approximately colinear with the Ru–Cl(1) bond such that there is almost perfect overlap between the Ru–S(2) linkage and the thiocarbonyl grouping. Considering the thiobenzoyl group as one ligand, the geometry at the ruthenium center is a distorted trigonal bipyramid; the S(2)-Ru-Cl(1) and C(10)-Ru-Cl(1) angles are noticeably contracted to about 109.0(2) and 104.4(9)°, respectively, and the P(31)-Ru-P(12) angle is 177.6(1)°. Interestingly, the carbon atoms of the thiobenzyl phenyl ring lie in the plane formed from the atoms Cl(1), S(2), C(3), and C(10). This orientation is consistent with conjugation between the aromatic ring and the C–S group of the thiobenzoyl ligand, which enhances the donor role of the ligand. The orientation is further stabilized by face-to-face π-π stacking relationships between the thiobenzoyl phenyl ring and one each of the phosphane phenyl groups (Fig. 1). The associated ring-centroid to ring-centroid distances are about 3.60 and 3.72 Å. This mode of ring stacking is also present for the alternatively disordered structural arrangement.

We favor the following mechanism for the formation of **2a**: Electrophilic attack at the ruthenium center by the carbon atom of CS_2 and subsequent ring closure provide the metallacyclic ruthenium(II) carbene complex **3**. Loss of CO from **3** is then presumably followed by C–S bond cleavage to generate the thiocarbonyl and thiobenzoyl ligands of the product.[9] The facile formation of **2a** raises the question of cycloaddition reactions with other heterocumulenes. We note that the reaction of **1** with MeN=C=S provides low yields of **2b**, whilst **1** reacts with carbon dioxide to give the stable oxoruthenacyclobutenone **4**. This latter metallacycle is noteworthy for two reasons. First, it supports the intermediacy of the related sulfur-based analogue **3** in the formation of **2a**, and second, the orientation of CO_2 in the cycloaddition is opposite to that found in $Et_4N[Et_2N{-}C{\equiv}W(CO)_2(\mu\text{-}PPh_2)_2Mo(CO)_4]$, the product of the carboxylation of $Et_4N[WOC(O)C(NEt_2)(CO)_2(\mu\text{-}PPh_2)_2Mo(CO)_4]$.[2d] We therefore suggest that for low-valent (formally d^8) Group 8 alkylidyne complexes, it is the metal center which is attacked by electrophiles rather than the alkylidyne carbon atom. Indeed, to date all reports of electrophilic attack at such complexes[4, 6] may actually be reinterpreted as proceeding in this way, even when the electrophile ultimately resides on the alkylidyne carbon atom.

Whilst much previous work has focussed on the addition of multiple bonds to alkylidyne complexes of metals of Groups 5–7, clearly the reactivity profile of later transition metal alkylidyne complexes is, as illustrated here, distinct from those of earlier metals and merits further study.

 © VCH Verlagsgesellschaft mbH, D-69451 Weinheim, 1996 0570-0833/96/3501-0096 $ 10.00+.25/0

Experimental Procedure

2a: A solution of **1** (0.100 g, 1.30 mmol) in dichloromethane (10 mL) was treated with carbon disulfide (0.5 mL, excess) and stirred for 2 h and then freed of volatiles. The residue was chromatographed (silica gel, dichloromethane eluant, 25 °C) to provide **2a**. Yield 0.061 g (61 %).

2b: A solution of $[RuHCl(CS)(PPh_3)_3]$ [10] (0.50 g, 0.50 mmol) and $[HgPh_2]$ (0.20 g, 0.56 mmol) in toluene (45 mL) was heated under reflux for 30 min, cooled, and filtered through Kieselguhr. Addition of ethanol to the filtrate and concentration under reduced pressure provided $[Ru(Ph)Cl(CS)(PPh_3)_2]$. Yield 0.31 g (80%). Carbon monoxide was passed through a solution of $[Ru(Ph)Cl(CS)(PPh_3)_2]$ (0.20 g, 0.27 mmol) in dichloromethane (20 mL) for 5 min and then freed of volatiles. The residue was chromatographed (silica gel, dichloromethane eluant, 25 °C) to provide **2b**. Yield 0.14 g (67%).

Received: August 17, 1995 [Z8319IE]
German version: *Angew. Chem.* **1996**, *108*, 94–96

Keywords: cycloadditions · metathesis · ruthenium compounds · sulfur compounds

[1] K. J. Ivin, *Olefin Metathesis*, Academic Press, New York, **1986**.

[2] Cycloadditions of heteroallenes and heteroalkenes to Group 6 alkylidyne complexes include a) carbodiimides, isocyanates, and isothiocyanates: R. Goller, U. Schubert, K. Weiss, *J. Organomet. Chem.* **1993**, *459*, 229; K. Weiss, R. Goller, M. Denzner, G. Lossel, J. Kodel, *NATO ASI Ser. Ser. C* **1992**, *392*, 55; K. Weiss, U. Schubert, R. R. Schrock, *Organometallics* **1986**, *5*, 397; b) azides: C. M. Stegmair, W. Ullrich, W. Schutt, P. Kiprof, F. R. Kreissl, *Chem. Ber.* **1992**, *125*, 1571; C. M. Stegmair, W. Schutt, W. Ullrich, P. Kiprof, J. Ostermeier, F. R. Kreissl, *J. Organomet. Chem.* **1993**, *447*, 251; W. Schutt, E. Herdtweck, F. R. Kreissl, *ibid.* **1993**, *456*, C15; J. Ostermeier, C. Ogric, W. Hiller, F. R. Kreissl, *ibid.* **1994**, *472*, C8; c) phosphaalkynes: A. F. Hill, J. A. K. Howard, T. P. Spaniol, F. G. A. Stone, J. Szameitat, *Angew. Chem.* **1989**, *101*, 213; *Angew. Chem. Int. Ed. Engl.* **1989**, *28*, 210; d) CO_2: E. O. Fischer, A. C. Fillipou, H. G. Alt, U. Thewalt, *ibid.* **1985**, *97*, 215 and **1985**, *24*, 203.

[3] A. Mayr, T. Y. Lee, *Angew. Chem.* **1993**, *105*, 1835; *Angew. Chem. Int. Ed. Engl.* **1993**, *32*, 1726; *J. Am. Chem. Soc.* **1994**, *116*, 10300.

[4] For recent reviews of the chemistry of alkylidyne and thiocarbonyl complexes of Group 8 metals see A. F. Hill, in *Comprehensive Organometallic Chemistry II, Vol 7* (Eds.: E. W. Abel, F. G. A. Stone, G. Wilkinson), Pergamon, Oxford, **1995**.

[5] A. F. Hill, *J. Mol. Cat.* **1991**, *65*, 85.

[6] W. R. Roper, *NATO ASI Ser. Ser. C* **1993**, *392*, 155; W. R. Roper, *J. Organomet. Chem.* **1986**, *300*, 167; M. A. Gallop, W. R. Roper, *Adv. Organomet. Chem.* **1986**, *25*, 121.

[7] G. R. Clark, T. J. Collins, K. Marsden, W. R. Roper, *J. Organomet. Chem.* **1978**, *157*, C23; G. R. Clark, T. J. Collins, K. Marsden, W. R. Roper, *ibid.* **1983**, *259*, 215; C. E. F. Rickard, W. R. Roper, D. M. Salter, L. J. Wright, *Organometallics* **1992**, *11*, 3931.

[8] Crystal data for **2a**·$2CH_2Cl_2$: monoclinic, space group $P2_1$; $a = 11.811(2)$, $b = 16.481(4)$, $c = 12.519(2)$ Å, $\beta = 101.16(1)°$, $V = 2391(1)$ Å^3, $Z = 2$, $\rho_{calcd} = 1.384$ g cm^{-3} $\mu(Mo_{K\alpha}) = 7.92$ cm^{-1}, 4311 independent reflections measured, 3243 observed reflections [$|F_o| > 4\sigma(|F_o|)$, $2\theta \leq 50°$]. Siemens P4/PC diffractometer, $Mo_{K\alpha}$ radiation (graphite monochromator, ω scans). The structure was solved by the heavy atom method and all the major occupancy non-hydrogen atoms of the complex and the major occupancy chlorine atoms of the solvent molecules were refined anisotropically using full-matrix least-squares to give $R_1 = 0.066$ and $wR_2 = 0.159$. Computations were carried out by using the SHELXTL (PC) 5.0 program system. Further details of the crystal structure investigation may be obtained from the Director of the Cambridge Crystallographic Data Centre, 12 Union Road, GB-Cambridge CB2 1EZ (UK), on quoting the full journal citation.

[9] The geometry at the ruthenium center in **2a** established crystallographically represents the thermodynamic product with the ($\sigma + \pi$) dative thione sulfur coordinated *trans* to the superlatively π-acidic thiocarbonyl ligand, although an isomer with *cis*-coordinated thione and thiocarbonyl ligands is presumably an intermediate.

[10] P. J. Brothers, W. R. Roper *J. Organomet. Chem.* **1983**, *258*, 73.

The Heaviest Alkali Metallocene: Structure of an Anionic Cesocene Triple-Decker**

Sjoerd Harder* and Marc Heinrich Prosenc

We recently reported the synthesis and structure of the simplest metallocene sandwich complex, the lithocene anion, which was obtained by reacting two equivalents of CpLi with PPh_4Cl in THF [Eq. (a)].[1] The approximate D_{5d} staggered lithocene sandwich is remarkably similar to the isovalent, diagonally related, alkaline earth analogue Cp_2Mg.[2] At the same time Paquette et al. published the structure of a substituted lithocene anion in which the noncoordinating cation is a bis([12]crown-4) solvated Li cation [Eq. (b)].[3] Since this new class of anionic alkali metallocenes is particularly interesting from a theoretical point of view, we have now focused our attention on the heavier alkali metal analogues.

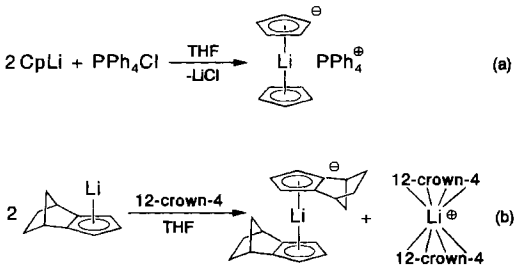

Treatment of cyclopentadienylcesium, prepared from cyclopentadiene and cesium metal, with 0.5 equivalents of PPh_4Cl in THF[4] resulted in the immediate formation of a red solution and rapid precipitation of very small orange-red needles. Recrystallization from warm pyridine yielded larger good quality single crystals of the same color and needlelike habitus which were suitable for X-ray diffraction.

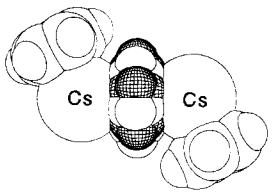

Fig. 1. A space-filling model of the strongly bent $[Cp_3Cs_2]^-$ triple-decker. The bridging Cp ring is positioned on a crystallographic center of inversion and therefore disordered over two positions (50% occupation).

X-ray structure analysis reveals the product formula $[Cp_3Cs_2]^-$·$[PPh_4]^+$.[5] The $[Cp_3Cs_2]^-$ ion (Fig. 1) is a strongly bent triple-decker ($Cp_{centroid}$-Cs-$Cp'_{centroid}$ 115.6(2)°), which closely resembles a recent structure of the first triple-decker structure of a main group metal, the $[Cp_3Tl_2]^-$ ion, in which the $Cp_{centroid}$-Tl-$Cp'_{centroid}$ angle is 134.2°.[6] The bridging Cp ring is positioned on a crystallographic center of inversion and is consequently disordered in a 50/50 ratio. The centers of both disordered Cp rings are only 0.01(1) Å removed from the crystallographic center of inversion and this results in a perfect ring of electron density between the Cs cations. The Cs–C bond lengths for the terminal Cp ligands lie in the range 3.313(6)–3.385(5) Å (av 3.350(5) Å; Cs–$Cp_{centroid}$ = 3.134(5) Å) and

[*] Dr. S. Harder, Dipl.-Chem. M. H. Prosenc
Universität Konstanz
Postfach 5560 - M738, D-78434 Konstanz (Germany)
Fax: Int. code +(7531)883137

[**] The European community is acknowledged for a fellowship (S. H.). Prof. Dr. H.-H. Brintzinger and Prof. Dr. G. Müller are kindly acknowledged for helpful discussions and for providing laboratory facilities. We thank Prof. Dr. L. Brandsma and Chemetall (Reuterweg 14, D-60271 Frankfurt am Main, Germany) for a generous gift of Cs metal and their interest in the current work.

 © VCH Verlagsgesellschaft mbH, D-69451 Weinheim, 1996 0570-0833/96/3501-0097 $ 10.00+.25/0

compare well with the two sets of Cs–C bonds observed for the disordered bridging Cp rings which range from 3.30(2) Å to 3.36(2) Å (av 3.33(2) Å; $Cs-Cp_{centroid} = 3.10(2)$ Å) and from 3.31(2) Å to 3.38(2) Å (av 3.35(2) Å; $Cs-Cp_{centroid} = 3.13(2)$ Å). This narrow range of Cs–C bond lengths leads to a near perfect η^5-Cp–Cs bonding geometry (the largest deviation from the average Cs–C bond length is only 1.2%). The Cp–Cs bonds are extremely long and probably the longest Cp–metal bonds encountered (apart from Cp–metal distances in the hypothetical francocene). The Cp–Cs bonds in the $[Cp_3Cs_2]^-$ ion should be considered as highly ionic; that is, these very long electrostatic $Cp^- - Cs^+$ bonds are weak.[7] It is therefore even more remarkable that these loosely bound Cp ligands show such a perfect η^5-bonding mode. Also remarkable is the similarity in the Cp–Cs bond lengths for terminal and bridging Cp rings. Apparently, the Cs cations in the triple-decker are too far apart ($Cs \cdots Cs' = 6.236(3)$ Å) for a significant repulsive $Cs^+ \cdots Cs^+$ interaction and thus have little influence on the inner Cp–Cs distances.

The huge coordination sphere of the Cs^+ ion cannot be filled by only contacts to two Cp ligands and is therefore supplemented by additional intermolecular interactions. A space-filling packing model of the structure shows alternating layers of $[Cp_3Cs_2]^-$ and $[Ph_4P]^+$ ions (Fig. 2a). The shortest interaction

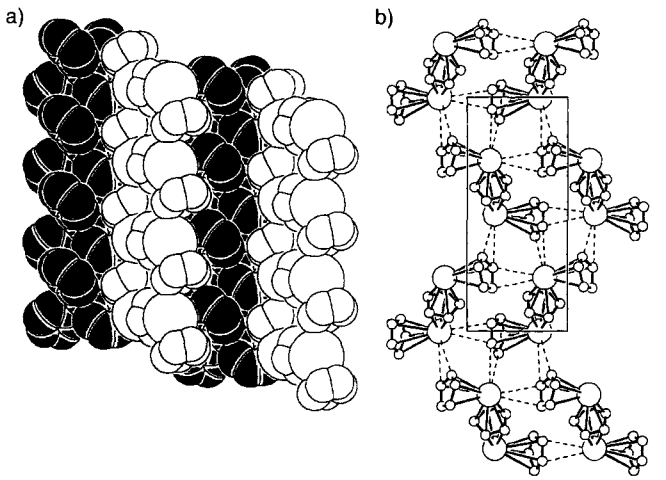

Fig. 2. a) Packing of the alternating layers of $[Cp_3Cs_2]^-$ ions (white) and $[PPh_4]^+$ ions (black) viewed along the *c* axis. b) The layer of $[Cp_3Cs_2]^-$ ions viewed along the *a* axis. The intermolecular Cs···C contacts are denoted by dashed lines.

between the layers corresponds to a (phenyl)C···Cs contact of 3.760(5) Å. More important are the short intermolecular $Cp^- \cdots Cs^+$ contacts within the layers of $[Cp_3Cs_2]^-$ ions. These layers form two-dimensional coordination polymers in which the intermolecular Cp···Cs contacts range from 3.699(5) to 3.810(5) Å (depicted in Fig. 2b by dotted lines). The complete coordination sphere of the Cs cation is shown in Figure 3. One of the Cp rings is bonded "side-on" to the Cs cation and shows close C-H···metal interactions similar to those found between the linear strands in the polymeric chain structure of $(Me_3SiCpK)_\infty$.[8] The other Cp ring is orientated "face-on" and shows π-$Cp^- \cdots Cs^+$ interactions. The intermolecular Cs···Cp contacts are only 10% longer than the intramolecular bonds and should therefore be considered as significant bonding interactions.

The crystal structure of the lithocene anion closely resembles that of the isovalent, diagonally related, magnesocene. Is there

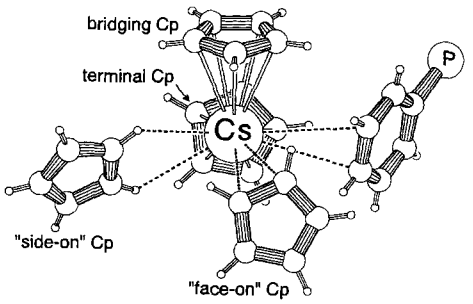

Fig. 3. Complete coordination sphere of the Cs cation (partial structure). Short intermolecular contacts are denoted by dashed lines; (phenyl)C···Cs distances are 3.760(5) and 3.881(5) Å; ("face-on" Cp)C···Cs distances are 3.699(5) and 3.719(5) Å; ("side-on" Cp)C···Cs distances are 3.754(5) and 3.810(5) Å (short H···Cs distances are 3.139 and 3.263 Å).

also structural conformity between the heavy anionic alkali metallocenes and alkaline earth metallocenes? The heavier alkaline earth metallocenes are typified by their bent structures which violate VSEPR rules and simple electrostatic bonding models.[9] It is believed that packing effects do not play a significant role in the solid-state structures of Cp^*_2Ca and Cp^*_2Ba ($Cp^* = C_5Me_5$) and, in particular, are not responsible for the bending at the metal atom (Cp-Ca-Cp 146.3° and Cp-Ba-Cp 131.0°).[10] This argument is supported by the results of the structural analyses of these metallocenes in the gas phase which likewise indicate bent structures.[11] Arguments advanced as explanations for the bending (attractive van der Waals forces between the Cp rings, induced polarization of the metal center by the ligands, and involvement of d orbitals) could to a certain extent similarly be applied to the heavier anionic alkali metallocenes.

Indeed, qualitative high level ab initio calculations show that bent structures play a role in the coordination chemistry of the Cs cation: the minimum energy structure of $Cs^+(H_2O)_2$ is bent with a O-Cs-O angle of 113.3° (cf. the angle of 109.6° in $Ba^{2+}(H_2O)_2$).[12] However, the extremely small linearization energy of only 0.26 kcal mol^{-1} indicates that the potential surface is very shallow (the linearization energy for $Ba^{2+}(H_2O)_2$ is 1.03 kcal mol^{-1}). The energy involved with the intermolecular contacts in the solid-state structure of $[Cp_3Cs_2]^-[PPh_4]^+$, is expected to be much larger. The bent structure as a typical energy minimum for sandwich or triple-decker cesocene complexes is therefore not confirmed by our experimental data. The use of bulky substituted Cp ligands could probably yield anionic cesocene sandwich complexes in which intermolecular $Cp^- \cdots Cs^+$ interactions are neglible. The elucidation of the structures of such compounds will reveal more about their similarity with the bent structures of the heavier alkaline earth metallocenes.

We had expected to isolate a $[Cp_2Cs]^-$ sandwich compound from the $Cp^-/CpCs$ solution, but instead obtained an anionic triple-decker complex. This suggests that the remaining mother liquor might contain species of interesting composition such as $[Cp_3Cs]^{2-}$ or $[Cp_2CsCpCsCp_2]^{3-}$. We anticipate that the $[Cp_2Cs]^-$ sandwich complex and these di- and trianions will be obtained in future research by variation of the reaction conditions.

Received: July 25, 1995 [Z8256IE]
German version: *Angew. Chem.* **1996**, *108*, 101–103

Keywords: cesium compounds · sandwich complexes · structure elucidation

[1] a) S. Harder, M. H. Prosenc, *Angew. Chem.* **1994**, *106*, 1830; *Angew. Chem. Int. Ed. Engl.* **1994**, *33*, 1744; see also a highlight b) D. Stalke, *ibid.* **1994**, *106*, 2256 and **1994**, *33*, 2168.
[2] W. Bünder, E. Weiss, *J. Organomet. Chem.* **1975**, *92*, 1.
[3] F. Zaegel, J. C. Gallucci, P. Meunier, B. Gautheron, M. R. Sivik, L. A. Paquette, *J. Am. Chem. Soc.* **1994**, *116*, 6466.
[4] The syntheses were carried out under argon with use of Schlenk techniques and predried solvents. Cyclopentadiene (ca. 5 mL, ca. 75 mmol) was added dropwise to metallic cesium (5.90 g, 42.1 mmol) in THF (90 mL). The blue color of the solvated electrons disappeared and the solution was slowly warmed to reflux temperature. After complete addition, the yellow solution was heated to reflux for 30 minutes. The solvent was removed under reduced pressure and the crystalline needles were dried under high vacuum for 4 h at 80 °C. This yielded CpCs as a white powder. ^{1}H NMR (250 MHz, [D$_5$]pyridine, 25 °C, TMS): δ = 5.47 (s, Cp); ^{13}C NMR: δ = 106.9 (Cp). A suspension of PPh_4Cl (0.38 g, 1.01 mmol) in THF (6 mL) was added to a solution of CpCs (0.40 g, 2.0 mmol) in THF (10 mL). This immediately resulted in the formation a red reaction mixture from which small orange-red needles rapidly crystallized. The crystals were only slightly soluble in pyridine at room temperature. ^{1}H NMR (250 MHz, [D$_5$]pyridine, 25 °C, TMS): δ = 6.25 (s, Cp); 7.56–7.67 (m, PPh_4^+), 7.78–7.82 (m, PPh_4^+). The $C_5H_5^-/PPh_4^+$ ratio cannot be accurately determined due to partial decomposition of $C_5H_5^-$ (probably partial H/D exchange with pyridine). Recrystallization of the needles from warm pyridine gave larger single crystals (0.29 g; 54% calculated on CpCs) with an identical NMR spectrum which are suitable for X-ray diffraction. Elemental analyses on crystals: found C 58.89, H 4.50%; calcd C 58.52, H 4.41%.
[5] Crystal structure data for $[Cp_3Cs_2]^-[Ph_4P]^+$: monoclinic, a = 29.513(15), b = 6.898(4), c = 18.166(8) Å, β = 116.94(4)°, V = 3297(3) Å^3, space group $C2/c$, formula $\{(C_{15}H_{15}Cs_2)\cdot(C_{24}H_{20}P)\}$, M = 800.5, Z = 4, ρ_{calcd} = 1.613 g cm^{-3}, $\mu(Mo_{K\alpha})$ = 2.267 mm^{-1}; 5342 reflections were measured on a Siemens R3m/V diffractometer ($Mo_{K\alpha}$, graphite monochromator, T = −35 °C), 3237 unique reflections after merging (R_{int} = 0.018), 2541 observed reflections with $F > 4.0\ \sigma(F)$. Solution by Patterson methods with the SHELXTL program, refinement by minimization of $\Sigma w(|F_o| - |F_c|)^2$ to $R(F)$ = 0.032, $wR(F)$ = 0.032 (221 parameters; $w = 1/(\sigma^2(F) + 0.0001(F)^2)$. Non-hydrogens, except those from the disordered Cp rings, were refined anisotropically; hydrogens on $[Cp_3Cs_2]^-$ were calculated and those on $[PPh_4]^+$ were found. Geometry calculations and plots were made with the EUCLID package [13]. Further details of the crystal structure investigation may be obatined from the Fachinformationzentrum Karlsruhe, D-76344 Eggenstein-Leopoldshafen (Germany), on quoting the depositary number CSD-59137.
[6] D. R. Armstrong, A. J. Edwards, D. Moncrieff, M. A. Paver, P. R. Raithby, M.-A. Rennie, C. A. Russell, D. S. Wright, *J. Chem. Soc. Chem. Commun.* **1995**, 927.
[7] C. Lambert, P. von R. Schleyer, *Organometallics* **1993**, *12*, 853.
[8] P. Jutzi, W. Leffers, B. Hampel, S. Pohl, W. Saak, *Angew. Chem.* **1987**, *99*, 563; *Angew. Chem. Int. Ed. Engl.* **1987**, *26*, 583.
[9] Reviews: a) P. Jutzi, *J. Organomet. Chem.* **1990**, *400*, 1; b) T. P. Hanusa, *Chem. Rev.* **1993**, *93*, 1023; c) D. J. Burkey, T. P. Hanusa, *Comments Inorg. Chem.* **1995**, *17*, 41; d) T. V. Timofeeva, J.-H. Lii, N. L. Allinger, *J. Am. Chem. Soc.* **1995**, *117*, 7452.
[10] R. A. Williams, T. P Hanusa, J. C. Huffman, *Organometallics* **1990**, *9*, 1128.
[11] a) R. A. Anderson, J. M. Boncella, C. J. Burns, R. Blom, A. Haaland, H. V. Volden, *J. Organomet. Chem.* **1986**, *312*, C49. b) R. A. Anderson, R. Blom, C. J. Burns, H. V. Volden, *J. Chem. Soc. Chem. Commun.* **1987**, 768.
[12] M. Kaupp, P. von R. Schleyer, M. Dolg, H. Stoll, *J. Am. Chem. Soc.* **1992**, *114*, 8202.
[13] A. L. Spek, The EUCLID package, *Computational Crystallography*, (Ed.: D. Sayre) Clarendon Press, Oxford, **1982**.

On Ligand Design for Catalytic Outer Sphere Reactions: A Simple Asymmetric Synthesis of Vinylglycinol**

Barry M. Trost* and Richard C. Bunt

The importance of enantiomerically pure vinylglycinol as a building block has stimulated much synthetic effort.[1] Not only is it an obvious precursor of vinylglycine; many biologically important targets may be derived from it, such as the tuberculostatic (+)-ethambutol,[2] the antimetabolite antibiotic acivicin,[3a, b] the antibiotic phosphinotricin,[3c] the selective enzyme-activated inhibitor of GABA-T vigabatrin,[4] an inhibitor of calmodulin-activated brain phosphodiesterase pseudodistomin B,[5] adenosine deamimase inhibitor pentostatin,[6] metal-chelating polyamino acid aspergillomarasamine A,[7] and the antibiotic subunit galatinic acid.[8] The most effective syntheses of vinylglycine to date begin with amino acids, only one enantiomer of which is generally available inexpensively.[1] Therefore, a simple asymmetric synthesis that would provide access to both enantiomers is most desirable.

The ready availability of one of the potential starting materials, 3,4-epoxy-1-butene (butadiene monoepoxide, **1**) from the selective, catalytic oxidation of butadiene with dioxygen,[9] makes it quite attractive. However, two hurdles not yet addressed in our asymmetric allylic alkylation program must be overcome to convert racemic epoxide **1** to vinylglycinol: 1) the control of the regioselectivity of alkylation to give the 1,2-adduct, and 2) the design of a racemization step (Scheme 1, **2** to

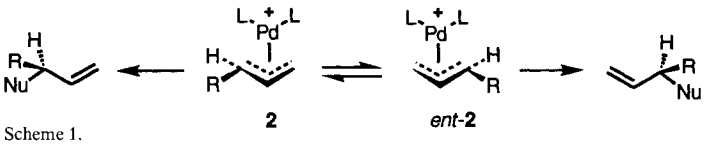

Scheme 1.

ent-**2**) that occurs faster than alkylation so that one of the two complexes (which are diastereomeric when L is chiral) reacts faster than the other.[10] Because most nucleophiles, including amines, add to give 1,4-adducts with **1**,[11] the simplest solution to the regioselectivity problem is to tether the nitrogen nucleophile to the oxygen atom.[12] However, preliminary results with the bisisocyanate of chiral 1-buten-3,4-diol and (*S*,*S*)-**3** gave the

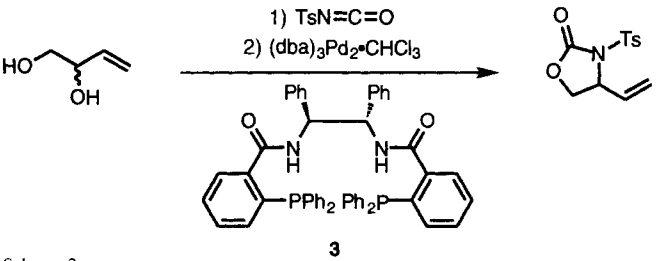

3

Scheme 2.

[*] Prof. B. M. Trost, R. C. Bunt
Department of Chemistry, Stanford University
Stanford, CA 94305-5080 (USA)
Fax: Int. code +(415)725-0259

[**] We thank the National Science Foundation and General Medical Sciences Institute of the National Institutes of Health for their generous support of our programs. R.C.B. was an NSF predoctoral fellow. Johnson Matthey Alfa Aesar provided a generous loan of palladium salts, and Stephen A. Godleski of Kodak a generous sample of 3,4-epoxy-1-butene. Mass spectra were provided by the Mass Spectrometry Facility, University of California-San Francisco, supported by the NIH Division of Research Resources.

 © VCH Verlagsgesellschaft mbH, D-69451 Weinheim, 1996 0570-0833/96/3501-0099 $ 10.00+.25/0

vinyloxazolidin-2-one with only 2% *ee* (Scheme 2), which suggested that racemization did not compete with cyclization.[13] We therefore turned to a bimolecular process in the hope that slowing the attack of nucleophile would enable racemization to compete effectively.

We postulated that increasing the acidity of the N–H of the pronucleophile should increase 1,2-adduct formation because of hydrogen bonding to the oxygen leaving group.[14] Indeed, with triphenylphosphane as the ligand in THF, phthalimide reacted with epoxide **1** to give an approximately 9:1 ratio of the 1,2 or proximal adduct (**4**) to the 1,4 or distal (**5**) adduct but in yields of only 30–40% (Scheme 3). With our standard chiral ligand

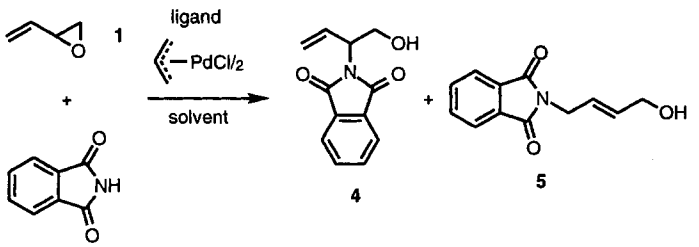

Scheme 3.

6[15] in THF, two quite gratifying observations were made. First, the yield of isolated **4**[16] increased significantly to 87%. Second, the ratio of *S*-**4**:*R*-**4** was 88:12 in THF. Switching the solvent to dichloromethane, which increased the enantioselectivity in other alkylations,[17] led to a slight decline to 83:17 (83% yield of isolated product **4**).

As further attempts to improve the enantiomeric ratio (er) by varying the reaction conditions failed, we turned our attention to the modification of our chiral ligand. We chose to rigidify bonds *a* and *b* (see **6**) by introducing a *peri* interaction as in the naphthalene-derived ligands **7**[16] (bond *a*) and **8**[16] (bond *b*).

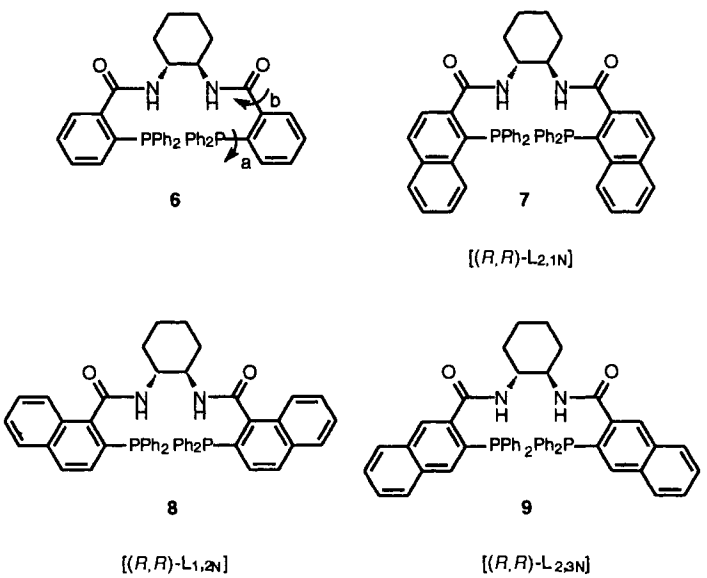

Restricting rotation about bonds *a* or *b* should affect how the chiral scaffold (the diaminocyclohexane unit) communicates its chirality to the conformationally chiral space created by the diphenylphosphino unit. This transference of chirality is critical, because the asymmetric bond-forming process occurs outside the direct coordination sphere of the metal. We hoped that a more rigid ligand would possess a better defined "chiral pocket" and thus give higher levels of asymmetric induction. For completeness, we also synthesized ligand **9**,[16] which, lacking such restraints, was expected to behave like ligand **6**. All three diphenylphosphinonaphthoic acids are readily available from the corresponding hydroxynaphthoic acids by cross-coupling reactions.[18]

To compare these new ligands, we explored the alkylation of 3-acetoxycyclopentene (Scheme 4), since we had a great deal of

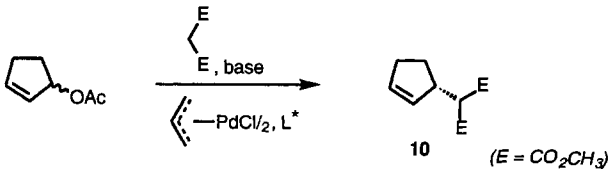

Scheme 4.

experience with this substrate.[17] Each ligand was tested with sodium hydride and cesium carbonate as the base in both THF and dichloromethane under a range of conditions known to influence enantiomeric excesses. Table 1 summarizes these results, and several points are worth noting. First, (R,R)-$L_{2,3N}$ (**9**) and (R,R)-**6** did behave similarly and give very high er's with cesium carbonate as the base in dichloromethane (entries 4 and 8). Second, restricting the diphenylphosphino unit as in (R,R)-$L_{2,1N}$ (**7**) effectively destroyed the chiral recognition (entries 9–12). Third, restricting the carboxylate group as in (R,R)-$L_{1,2N}$ (**8**) maintained a reasonable level of chiral recognition, although somewhat less than for (R,R)-**6** or (R,R)-$L_{2,3N}$ (**9**). In contrast to (R,R)-**6** or (R,R)-$L_{2,3N}$ (**9**), with (R,R)-$L_{1,2N}$ (**8**) the sodium salt of malonate ester gave a higher er than the cesium salt (entries 14 and 16). This reversal of behavior suggests that

Table 1. Comparison of ligands for the alkylation of dimethyl malonate with 3-acetoxycyclopentene. For spectroscopic data, see Table 2.

No.	Ligand	Base	Solvent	Yield [a]	er (*S*:*R*) **10**
1	(R,R)-**6**	NaH	THF	73	67:33 [b]
2	(R,R)-**6**	NaH	CH_2Cl_2	91	74:26 [c]
3	(R,R)-**6**	Cs_2CO_3	THF	89	83:17 [b]
4	(R,R)-**6**	Cs_2CO_3	CH_2Cl_2	82	99:1 [c]
5	(R,R)-$L_{2,3N}$ **9** [d]	NaH	THF	65	63:37 [b]
6	(R,R)-$L_{2,3N}$ **9** [d]	NaH	CH_2Cl_2	85	64:36 [c]
7	(R,R)-$L_{2,3N}$ **9** [d]	Cs_2CO_3	THF	47	76:24 [c]
8	(R,R)-$L_{2,3N}$ **9** [d]	Cs_2CO_3	CH_2Cl_2	91	98:2 [c]
9	(R,R)-$L_{2,1N}$ **7** [e]	NaH	THF	63	53:47 [b]
10	(R,R)-$L_{2,1N}$ **7** [e]	NaH	CH_2Cl_2	88	58:42 [b]
11	(R,R)-$L_{2,1N}$ **7** [e]	Cs_2CO_3	THF	79	53:47 [b]
12	(R,R)-$L_{2,1N}$ **7** [e]	Cs_2CO_3	CH_2Cl_2	87	62:38 [c]
13	(R,R)-$L_{1,2N}$ **8** [f]	NaH	THF	99	84:16 [b]
14	(R,R)-$L_{1,2N}$ **8** [f]	NaH	CH_2Cl_2	96	94:6 [c]
15	(R,R)-$L_{1,2N}$ **8** [f]	Cs_2CO_3	THF	76	70:30 [b]
16	(R,R)-$L_{1,2N}$ **8** [f]	Cs_2CO_3	CH_2Cl_2	90	90:10 [c]

[a] Yield of isolated product. [b] The er was determined by optical rotation for which $[\alpha]_D^{25} = -85.2°$ was established for the enantiomerically pure compound. [c] The er was determined by NMR shift studies with the chiral compound [Eu((+)-hfc)$_3$] in C_6D_6. The er reported is the average of the integration ratios determined for the enantiotopic methyl ester peaks with 0.2 to 0.5 equiv of the shift reagent added in increments of 0.1 equiv. [d] The symbolism denotes the absolute stereochemistry with the ligand having a 2-carboxy-3-phosphino-substituted naphthalene linker. [e] The linker possesses a 2-carboxy-1-phosphino-substituted naphthalene. [f] The linker possesses a 1-carboxy-2-phosphino-substituted naphthalene.

 © VCH Verlagsgesellschaft mbH, D-69451 Weinheim, 1996 0570-0833/96/3501-0100 $ 10.00+.25/0

Table 2. Spectroscopic data of *S*-**4** and **7**–**9**.

(*S*)-**4**: M.p 61–62 °C, $[\alpha]_D^{25} = -71.1$ ($c = 3.06$, CH_2Cl_2). IR (neat): $\tilde{\nu}$ = 3450, 1767, 1704, 1644, 1614, 1469, 1386 cm^{-1}. ^1H NMR (300 MHz, $CDCl_3$): δ = 7.8 (m, 2H), 7.7 (m, 2H), 6.1 (ddd, J = 17.3, 10.2, 6.9 Hz, 1H), 5.3 (m, 2H), 4.9 (m, 1H), 4.2–4.1 (m, 1H), 4.0–3.9 (m, 1H), 2.9 (bs, 1H). ^{13}C NMR (75 MHz, $CDCl_3$): δ = 168.4, 133.9, 132.0, 131.4, 123.0, 118.6, 61.7, 55.5. Anal. calcd for $C_{12}H_{11}NO_3$: C 66.35, H 5.11, N 6.45; found: C 66.60, H 5.33, N 6.65.

(R,R)-$L_{2,1N}$ (**7**): $[\alpha]_D^{25} = -81.9$ ($c = 0.4$, CH_2Cl_2). IR (C_6D_6): $\tilde{\nu}$ = 3398, 3304, 1659, 1585, 1515, 1503, 1481, 1434 cm^{-1}. ^1H NMR (300 MHz, $CDCl_3$): δ = 8.14 (d, J = 8.7 Hz, 2H), 7.78 (dd, J = 8.4, 3.4 Hz, 2H), 7.64 (m, 4H), 7.45 (m, 6H), 7.37 (d, J = 8.4 Hz, 2H), 7.02 (t, J = 8.0 Hz, 2H), 6.89 (m, 14H), 6.73 (d, J = 7.1 Hz, 2H), 4.02 (m, 2H), 2.09 (m, 2H), 1.36 (m, 4H), 1.03 (m, 2H). ^{13}C NMR (75 MHz, C_6D_6): δ = 171.2 (d, J = 6.7 Hz), 148.4 (d, J = 41.5 Hz), 138.1 (d, J = 16.4 Hz), 137.2 (d, J = 15.5 Hz), 135.3, 135.2, 132.7 (d, J = 21.8 Hz), 132.5 (d, J = 21.8 Hz), 132.4, 131.0 (d, J = 26.3 Hz), 130.1 (b), 129.8, 129.00 (d, J = 10.5 Hz), 128.99, 128.2, 126.7 (d, J = 11.8 Hz), 125.3 (d, J = 10.6 Hz), 54.5, 32.1, 25.1. HRMS: calcd for $C_{52}H_{44}N_2O_2P_2$: 790.2878; found: 790.2872.

(R,R)-$L_{1,2N}$ (**8**): M.p. 148–150 °C; $[\alpha]_D^{25} = +13.9$ ($c = 1.19$, CH_2Cl_2). IR ($CDCl_3$): $\tilde{\nu}$ = 3412, 1648, 1602, 1510, 1435, 1313 cm^{-1}. ^1H NMR (300 MHz, $CDCl_3$): δ = 7.8 (d, J = 8.2 Hz, 2H), 7.7 (d, J = 9.1 Hz, 2H), 7.6 (d, J = 8.9 Hz, 2H), 7.4–7.2 (m, 22H), 7.0 (m, 4H), 6.6 (d, J = 5.5 Hz, 2H), 3.8 (m, 2H), 2.3 (m, 2H), 1.7 (m, 2H), 1.3–1.2 (m, 4H). ^{13}C NMR (75 MHz, $CDCl_3$): δ = 169.2 (d, J = 4.2 Hz), 142.0 (d, J = 34.2 Hz), 136.9 (d, J = 11.3 Hz), 136.8 (d, J = 11.3 Hz), 133.5 (d, J = 19.6 Hz), 133.4 (d, J = 19.3 Hz), 133.3, 131.3 (d, J = 18.1 Hz), 129.9 (d, J = 7.9 Hz), 129.4, 129.2, 128.7, 128.7, 128.6, 128.5, 128.4 (d, J = 6.7 Hz), 127.7, 127.2, 126.9, 125.6, 54.7, 31.5, 24.4. Anal. calcd for $C_{52}H_{44}N_2O_2P_2$: C 78.97, H 5.61, N 3.54, P 7.83; found: C 78.76, H 5.86, N 3.38, P 7.67.

(R,R)-$L_{2,3N}$ (**9**): M.p. 154–158 °C, $[\alpha]_D^{25} = -53.9$ ($c = 2.14$, CH_2Cl_2). IR ($CDCl_3$): $\tilde{\nu}$ = 3426, 1651, 1626, 1519, 1435, 1324 cm^{-1}. ^1H NMR (300 MHz, $CDCl_3$): δ = 8.1 (d, J = 3.8 Hz, 2H), 7.6 (m, 2H), 7.5 (m, 2H), 7.4 (m, 4H), 7.3–7.2 (m, 22H), 6.6 (d, J = 7.1 Hz, 2H), 3.9 (m, 2H), 1.9 (m, 2H), 1.7–1.6 (m, 2H), 1.25 (m, 2H), 1.1 (m, 2H). ^{13}C NMR (75 MHz, $CDCl_3$): δ = 169.5, 137.7, 134.9, 134.0 (d, J = 18.8 Hz), 133.7 (d, J = 9.8 Hz), 133.5 (d, J = 11.7 Hz), 132.4, 128.7, 128.5 (d, J = 6.9 Hz), 128.4 (d, J = 6.5 Hz), 128.3, 127.8, 127.5 (d, J = 4.8 Hz), 127.4, 127.1, 54.0, 32.0, 24.7. Anal. calcd for $C_{52}H_{44}N_2O_2P_2$: C 78.97, H 5.61, N 3.54, P 7.83; found: C 78.77, H 5.80, N 3.40, P 7.57.

we may have altered the conformational properties of the chiral pocket as intended.

To further probe the usefulness of (R,R)-$L_{1,2N}$ (**8**), we explored the reaction of the acyclic substrate **11** with dimethyl malonate (Scheme 5) for which the maximum er previously

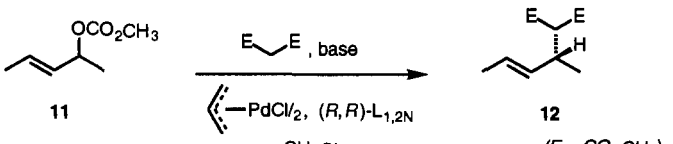

Scheme 5.

recorded was 85:15.[19] With our newly developed ligand, the er of **12** produced was 70:30 for the sodium salt but 93:7 for the cesium salt, the highest yet recorded.

The most dramatic result of this new ligand occurred for the type of chiral recognition required in the case of epoxide **1** (Scheme 2). Adding neat epoxide **1** to a mixture of phthalimide (110 mol%), sodium carbonate (5 mol%), π-allylpalladium chloride dimer (2.5 mol%), and (R,R)-$L_{1,2N}$ (**8**) (7.5 mol%) in dichloromethane (all at ambient temperature) gave a 99% yield of **4** and **5** in a ratio greater than 75:1. The er was assayed by conversion to the *O*-methylmandelate ester **13**[20] followed by HPLC analysis and found to be 99:1 (Scheme 6). Further confirmation of the er, as well as establishment of the absolute configuration, was accomplished by removal of the phthalic acid moiety[21] and formation of the known CBZ derivative **14**[7] (Scheme 6). The observed optical rotation of **14** $[\alpha]_D^{25} = -32.2°$ ($c = 1.47$, $CHCl_3$) is in excellent agreement with the literature value of $[\alpha]_D^{25} = -32.1°$ ($c = 3.1$, $CHCl_3$) for the compound having the *S* absolute configuration. In contrast to **6**, in which a slightly higher er was obtained in THF than dichloromethane, the er in THF with (R,R)-$L_{1,2N}$ (**8**) was only 84:16.

The new ligand **8** permits high enantiodiscrimination between equilibrating diastereomeric complexes. Combined with the unorthodox control of regioselectivity, vinylglycinol of high enantiomeric purity and in either enantiomeric series is available quite simply from racemic 3,4-epoxy-1-butene. Since the conversion of vinylglycinol to vinylglycine is known,[3b] this route provides a synthesis of the latter as well. In this type of asymmetric induction, which requires a kinetic bias for the reaction of one diastereomeric π-allyl palladium complex of a rapidly interconverting pair (cf. Scheme 1), rigidifying the carboxylate group has a dramatic effect in enhancing the selectivity. This same ligand effectively discriminates the enantiotopic termini of the 1,3-dimethylallyl system (cf. Scheme 5). The nature of the chiral cavity of (R,R)-$L_{1,2N}$ (**8**) seems quite distinct from the other ligands **6**, **7**, and **9**. For example, **6** always shows an enhanced er on going from the sodium salt to the cesium salt of malonate as the nucleophile, but (R,R)-$L_{1,2N}$ (**8**) is incongruous, showing the opposite trend with a cyclic substrate and the same trend with an acyclic one. With the larger, cyclic substrate, this tighter pocket less selectively accommodates the larger cesium counterion. However, with the narrower, acyclic substrate (**11**), the larger cesium counterion again shows a higher er than sodium. The differences between achiral and chiral ligands are not limited to asymmetric induction. Quite notably, upon switching from triphenylphosphane to (R,R)-$L_{1,2N}$ (**8**), the regioselectivity increased from about 9:1 to greater than 75:1, and the yield almost tripled (**1** → **4**). Thus, the systematic rigidification of the bonds involved in transmitting the chiral information through the ligand–metal complex resulted in a new chiral ligand, which shows many desirable properties for applications in synthesis.

Received: August 3, 1995 [Z 8277 IE]
German version: *Angew. Chem.* **1996**, *108*, 70–73

Keywords: allylic alkylations · asymmetric induction · catalysis deracemization · palladium compounds

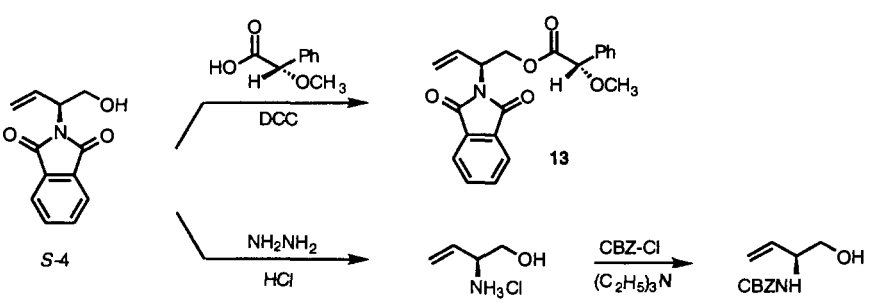

Scheme 6.

[1] For vinylglycinol, see A. McKillop, R. J. K. Taylor, R. J. Watson, N. Lewis, *Synthesis*, **1994**, 31; T. Moriwake, S. Hamano, S. Saito, S. Torii, *Chem. Lett.* **1987**, 2085; Y. Ohfune, N. Kurokawa, *Tetrahedron Lett.* **1984**, *25*, 1071. For vinylglycine, see T. Itaya, S. Shimizu, S. Nakagawa, M. Morisue, *Chem. Pharm. Bull.* **1994**, *42*, 1927; M. Carrasio, R. J. Jones, S. Kamel, H. Rapoport, T. Truong, *Org. Synth.* **1991**, *70*, 29; D. H. R. Barton, D. Crich, Y. Hervé, P. Potier, J. Thierry, *Tetrahedron* **1985**, *41*, 4347; S. Hanessian, S. P. Sahoo, *Tetrahedron Lett.* **1984**, *25*, 1425; A. Afzali-Ardakani, H. Rapoport, *J. Org. Chem.* **1980**, *45*, 4817.

[2] R. G. Wilkinson, R. G. Shepherd, J. P. Thomas, C. Baughn, *J. Am. Chem. Soc.* **1961**, *83*, 2212; C. S. Lee, L. Z. Benet in *Anal. Profiles Drug Subst.* **1978**, *7*, 231–249.

[3] a) D. G. Martin, D. J. Duchamp, C. G. Chidester, *Tetrahedron Lett.* **1973**, 2549; b) D. M. Vygas, Y. Chiang, T. W. Doyle, *J. Org. Chem.* **1984**, *49*, 2037; c) G. M. Ramos Tombo, D. Bellus, *Angew. Chem.* **1991**, *103*, 1219; *Angew. Chem. Int. Ed. Engl.* **1991**, *30*, 1193.

[4] A recent leading reference: Z.-Y. Wei, E. E. Knaus, *Tetrahedron* **1994**, *50*, 5569.

[5] T. Naito, M. Ikai, M. Shirakawa, K. Fiyimoto, I. Ninomiya, T. Kiguchi, *J. Chem. Soc. Perkin 1* **1994**, 773.

[6] T. V. Truong, H. Rapoport, *J. Org. Chem.* **1993**, *58*, 6090.

[7] Y. Ohfune, N. Kurokawa, *Tetrahedron Lett.* **1984**, *25*, 1071.

[8] Y. Ohfune, N. Kurokawa, *Tetrahedron Lett.* **1984**, *25*, 1587.

[9] J. R. Monnier, P. J. Muehlbauer, US-A 5081096, **1992** [*Chem. Abstr.* **1992**, *116*, 114395b]; US-A 5138077, **1992** [*Chem. Abstr.* **1992**, *117*, 212303k].

[10] For a 1,3-diphenylallyl system, see G. J. Dawson, J. M. J. Williams, S. J. Coote, *Tetrahedron Lett.* **1995**, *36*, 461; P. R. Auburn, P. B. MacKenzie, B. Bosnich, *J. Am. Chem. Soc.* **1985**, *107*, 2033; P. B. MacKenzie, J. Whelan, B. Bosnich, *ibid.* **1985**, *107*, 2046.

[11] B. M. Trost, G. A. Molander, *J. Am. Chem. Soc.* **1981**, *103*, 5969; B. M. Trost, J. Cossy, *ibid.* **1982**, *104*, 6881; S. A. Godleski, Y. Hung, PCT Int. Appl. WO 93/25516, **1993** [*Chem. Abstr.* **1994**, *120*, 298062c].

[12] With a chiral ferrocenyl complex, vinyloxazolidin-2-ones having er's up to 86:14 have been obtained: T. Hayashi, A. Yamamoto, Y. Ito, *Tetrahedron Lett.* **1988**, *29*, 99. Chiral derivatives derived from 3,4-epoxy-1-butene: N. W. Boaz, R. L. Zimmerman, *Tetrahedron: Asymmetry* **1994**, *5*, 153; N. W. Boaz, *ibid.* **1995**, *6*, 15.

[13] J. Trauger, unpublished work in these laboratories. Cf. B. M. Trost, D. L. Van Vranken, *J. Am. Chem. Soc.* **1993**, *115*, 444.

[14] Cf. B. M. Trost, P. D. Greenspan, H. Geissler, J. H. Kim, N. Greeves, *Angew. Chem.* **1994**, *106*, 2296; *Angew. Chem. Int. Ed. Engl.* **1994**, *33*, 2182; B. M. Trost, N. Ito, P. D. Greenspan, *Tetrahedron Lett.* **1993**, *34*, 1421 and references therein.

[15] B. M. Trost, D. L. Van Vranken, C. Bingel, *J. Am. Chem. Soc.* **1992**, *114*, 9327.

[16] This compound has been satisfactorily characterized spectroscopically, and its elemental composition was established by combustion analysis and high resolution mass spectrometry.

[17] B. M. Trost, R. C. Bunt, *J. Am. Chem. Soc.* **1994**, *116*, 4089.

[18] Adapted from the cross-coupling with aryl halides: S. E. Tunney, J. K. Stille, *J. Org. Chem.* **1987**, *52*, 748.

[19] P. von Matt, A. Pfaltz, *Angew. Chem.* **1993**, *105*, 614; *Angew. Chem. Int. Ed. Engl.* **1993**, *32*, 566.

[20] B. M. Trost, J. L. Belletire, S. Godleski, P. G. McDougal, J. M. Balkovec, J. J. Baldwin, M. E. Christy, G. S. Ponticello, S. L. Varga, J. P. Springer, *J. Org. Chem.* **1986**, *51*, 2370.

[21] H. R. Ing, R. H. F. Manske, *J. Chem. Soc.* **1926**, 2348.

O-Protonation at a Neutral Ditungsten Carbonyl Dimer to Give a Stable Hydroxycarbyne Complex**

M. Angeles Alvarez, Claudette Bois, M. Esther García, Victor Riera, and Miguel A. Ruiz*

Metal–metal bonds in organometallic compounds behave as nucleophilic centers and, accordingly, they can be often protonated to afford hydrido-bridged complexes.[1] Protonation can also occur at the coordinated ligands, and in this way a wide variety of products can be obtained.[2] The latter, however, is a very rare reaction for coordinated carbon monoxide. The few examples reported so far all involve protonation of bridging CO ligands in anionic carbonyl clusters such as $[M_3H(CO)_{10}]^-$ (M = Fe, Ru, Os),[3] $[Fe_4H(CO)_{13}]^-$,[4] and $[Co_3(CO)_{10}]^-$.[5] The resulting hydroxycarbyne clusters are without exception thermally unstable and could be only characterized at low temperatures. In this paper we report on the unexpected O-protonation of **1**[6] (dppm = $Ph_2PCH_2PPh_2$; Cp = η^5-C_5H_5), which gives the cationic and unsaturated hydroxycarbyne complex **4**.

$[W_2(CO)_4(\mu\text{-dppm})Cp_2]$ **1**

To our knowledge, this is the first example of protonation of a carbonyl ligand in a complex lacking bridging CO ligands,[7] and also in a neutral species. In addition, **4** is stable at room temperature, both in solution and in the solid state, thus allowing the study of its reactivity. The chemical behavior of hydroxycarbyne species is of interest in the context of carbon monoxide reduction.[8]

The reaction of **1** with $HBF_4 \cdot OEt_2$ is strongly dependent on the solvent. Thus, when the reaction is carried out in toluene, a mixture of the known hydrido complexes[9] **2** and **3** is obtained.

$[W_2(\mu\text{-H})(CO)_4(\mu\text{-dppm})Cp_2]BF_4$ **2**-BF_4

$[W_2(\mu\text{-H})(CO)_2(\mu\text{-dppm})Cp_2]BF_4$ **3**-BF_4

$[W_2(\mu\text{-COH})(CO)_2(\mu\text{-dppm})Cp_2]BF_4$ **4**-BF_4

By contrast, the protonation of **1** in CH_2Cl_2 gives the hydroxycarbyne complex **4** almost quantitatively. The salt **4**-BF_4 is stable at room temperature both in the solid state and dissolved in CH_2Cl_2; however, when **4**-BF_4 is dissolved in THF or acetone, a mixture of the hydrido complexes **2** and **3** is instantaneously formed. This strongly suggests that the formation of **2** and **3** in toluene is likely to proceed through **4**, which then rapidly undergoes a proton rearrangement, probably assisted by the solvent. The reactions discussed here are summarized in Scheme 1.

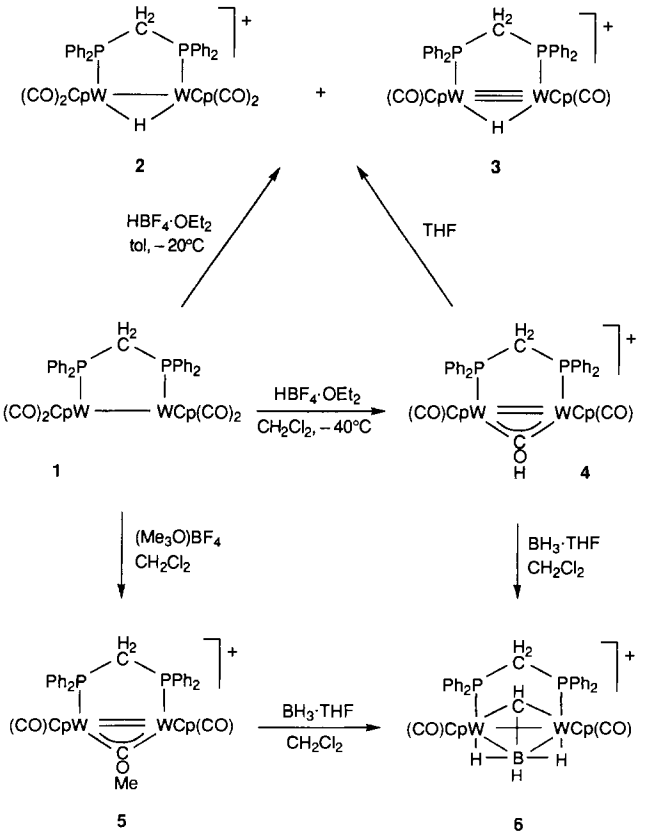

Scheme 1. Tol = toluene; counterion = BF_4^-.

[*] Dr. M. A. Ruiz, Dr. M. A. Alvarez, Dr. M. E. García, Prof. Dr. V. Riera
Departamento de Química Orgánica e Inorgánica - IUQUEM
Universidad de Oviedo, E-33071 Oviedo (Spain)
Fax: Int. code +(8)5103446
Dr. C. Bois
Université P. et M. Curie, Paris (France)

[**] We thank the DGICYT (Spain) for financial suppport and the FICYT (Asturias) for a grant to M. A. A.

The carbonyl ligands in **1** are also susceptible to alkylation. Thus, **1** reacts with $(Me_3O)BF_4$ to give the methoxycarbyne complex **5**, which is isostructural with **4**. The crystal structure of **5**-BF_4 (Fig. 1)[10a] confirms the presence of a rather symmetrical

$[W_2(\mu\text{-COMe})(CO)_2(\mu\text{-dppm})Cp_2]BF_4$ **5**-BF_4

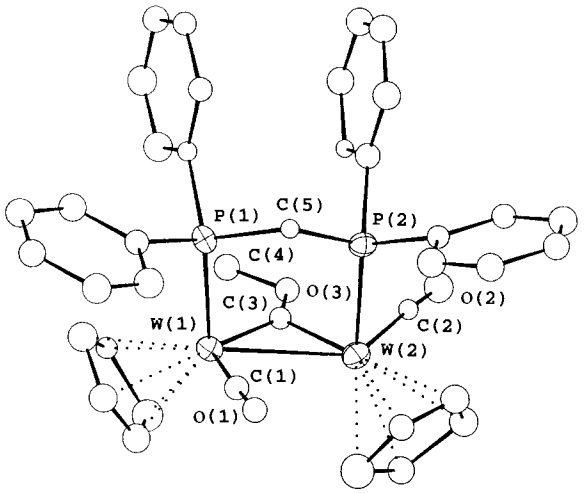

Fig. 1. Molecular structure of **5** in the crystal [10a] (thermal ellipsoids for 30% probability, hydrogen atoms omitted). Selected interatomic distances [Å] and angles [°]: W(1)–W(2) 2.781(3), W(1)–C(1) 1.82(6), W(2)–C(2) 2.02(5), W(1)–C(3) 1.95(5), W(2)–C(3) 1.99(5), C(3)–O(3) 1.42(5), O(3)–C(4) 1.42(6), W(1)–P(1) 2.47(1), W(2)–P(2) 2.45(2); C(1)-W(1)-C(3) 119.8(23), C(2)-W(2)-C(3) 75.2(20), W(1)-W(2)-P(2) 90.6(4), W(2)-W(1)-P(1) 94.7(3), C(1)-W(1)-P(1) 82.3(18), C(2)-W(2)-P(2) 90.7(14), C(3)-O(3)-C(4) 120.3(39).

methoxycarbyne ligand bridging the metal atoms in the cation. The conformation of this ligand is similar to that of other edge-bridging alkoxycarbyne ligands.[11] According to the 18-electron rule, a metal–metal double bond should be formulated for the cations **4** and **5**. In agreement with this, the intermetallic separation in **5** (2.781(3) Å) is about 0.25 Å shorter than those found for related electron-precise species.[9]

In spite of their electronic unsaturation, cations **4** and **5** exhibit some interesting nucleophilic properties. Thus, they are able to react with $BH_3 \cdot THF$ to yield the methylidyne–borane complex **6**. The crystal structure of **6**-BF_4 (Fig. 2)[10b] reveals

$[W_2(\mu\text{-CHBH}_3)(CO)_2(\mu\text{-dppm})Cp_2]BF_4$ **6**-BF_4

that the $CHBH_3$ ligand (H atoms not located) bridges symmetrically a singly bonded ditungsten center (W–W = 3.074(1) Å). The above, together with the NMR data, clearly indicates that one H atom bridges each of the W–B edges, thus formally making the $[CHBH_3]^-$ ligand a 6e-donor group. Only two other complexes containing this type of ligand are known: $[W_2\{\mu\text{-CRBH}_2(CH_2R)\}(CO)_4Cp_2]^+$; R = Me, C_6H_4Me).[12] In the latter, however, it was suggested that the H atoms bridge a B–W edge and a BW_2 face.

In summary, the transformations **1** → **4** → **6** imply a carbonyl to methylidyne reduction, which proceeds via an hydroxycarbyne intermediate and uses BH_3 as reductant. This is in contrast to the more usual carbonyl reduction via formyl intermediates, thought to be an operative pathway in the Fischer–Tropsch synthesis.[13] Further studies on the activity of the hydroxycarbyne complex **4** in C–H and C–C bond formation reactions are now in progress in our laboratory.

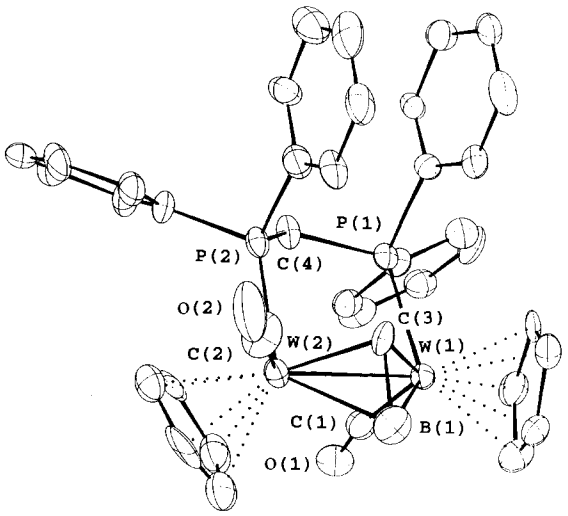

Fig. 2. Molecular structure of **6** in the crystal [10b] (thermal ellipsoids for 30% probability, hydrogen atoms omitted). Selected interatomic distances [Å] and angles [°]: W(1)–W(2) 3.074(1), W(1)–C(1) 1.92(2), W(2)–C(2) 1.95(3), W(1)–C(3) 2.14(2), W(2)–C(3) 2.09(2), W(1)–B(1) 2.40(3), W(2)–B(1) 2.40(3), W(1)–P(1) 2.494(5), W(2)–P(2) 2.465(6), B(1)–C(3) 1.60(4); W(1)-B(1)-W(2) 79.6(8), W(1)-C(3)-W(2) 93.2(9), P(1)-W(1)-B(1) 130.6(8), P(2)-W(2)-B(1) 124.5(8).

Experimental Procedure

4: $HBF_4 \cdot OEt_2$ (12 μL, 0.1 mmol) was added to a solution of **1** (100 mg, 0.1 mmol) in CH_2Cl_2 (30 mL) at −40 °C, and the mixture was stirred for 45 min. The solvent was then removed under vacuum, and the residue washed with toluene and petroleum ether to afford 94 mg (89%) of **4** as a brown powder. Selected spectroscopic data: IR (CH_2Cl_2): $\tilde{\nu}$(CO) [cm^{-1}] = 1943 vs, 1853 s. ^1H NMR (200.13 MHz, CD_2Cl_2, 198 K): δ = 12.97 (br, 1H; COH), 5.36 (s, br, 10H; Cp); $^{31}P\{^1H\}$ NMR (121.50 MHz): δ = 23.9, 13.2 (2 × d, J(P,P) = 48 Hz). $^{13}C\{^1H\}$ NMR (50.32 MHz): δ = 357.8 (s, J(C,W) = 121 Hz; COH), 96.4, 92.6 (2 × s; Cp).

5: $[Me_3O]BF_4$ (10 mg, 0.07 mmol) was added to a solution of **1** (50 mg, 0.05 mmol) in CH_2Cl_2 (15 mL) at room temperature, and the mixture was stirred for 2.5 h. The solution was then filtered, the solvent removed under vacuum, and the residue washed with toluene to give compound **5** as a brown powder (36 mg, 65%). Selected spectroscopic data: IR(Me_2CO): $\tilde{\nu}$(CO) [cm^{-1}] = 1946 vs, 1842 s. ^1H NMR (300.13 MHz, $[D_6]Me_2CO$, 188 K): δ = 5.68 (s, br, 5H; Cp), 5.61 (s, br, 6H; Cp, CH_2), 4.87 (s, 3H; Me), 4.85 (br, 1H; CH_2); $^{31}P\{^1H\}$ NMR (121.50 MHz): δ = 19.3, 13.4 (2 × d, J(P,P) = 48 Hz). $^{13}C\{^1H\}$ NMR (100.61 MHz): δ = 368.5 (s; COMe).

6: $BH_3 \cdot THF$ (2 mL of a 1 M solution in THF, 2 mmol) was added to a solution of **5** (100 mg, 0.1 mmol) in CH_2Cl_2 (15 mL) at −20 °C. The solution was stirred for 1 h and allowed to reach room temperature slowly. Solvent was then removed under vacuum, and the residue washed with toluene/petroleum ether 1/1, extracted with CH_2Cl_2, and filtered. Removal of solvent from the filtrate under vacuum yielded compound **6** as a yellow-orange powder (78 mg, 79%). Selected spectroscopic data: IR (CH_2Cl_2): $\tilde{\nu}$(CO) [cm^{-1}] = 1963 vs, 1841 s. ^1H NMR (400.13 MHz, CD_2Cl_2, 291 K): δ = 7.82 (br, 1H; $HCBH_3$), −1.56 (br, 1H; BH), −12.58 (br, 1H; BHW), −12.95 (br, 1H; BHW). ^{13}C NMR (100.61 MHz): δ = 111.1 (d, br, J(C,H) = 178 Hz; $HCBH_3$).

Received: August 8, 1995 [Z 8293 IE]
German version: *Angew. Chem.* **1996**, *108*, 112–114

Keywords: carbyne complexes · complexes with carbonyl ligands · complexes with phosphorus ligands · tungsten compounds

[1] R. H. Crabtree, *Organometallic Chemistry of the Transition Metals*, 2nd ed., Wiley, New York, **1994**, p. 335.
[2] *Reactions of Coordinated Ligands* (Ed. P. S. Braterman), Plenum, New York, **1986**.
[3] a) H. A. Hodali, D. F. Shriver, C. A. Ammlung, *J. Am. Chem. Soc.* **1978**, *100*, 5239; b) D. C. Pribich, E. Rosenberg, *Organometallics* **1988**, *7*, 1741; c) L. R. Nevinger, J. B. Keister, J. Maher, *ibid.* **1990**, *9*, 1900.
[4] K. H. Whitmire, D. F. Shriver, *J. Am. Chem. Soc.* **1981**, *103*, 6754.
[5] a) G. Fachinetti, *J. Chem. Soc., Chem. Commun.* **1979** 397; b) H.-N. Adams, G. Fachinetti, J. Strähle, *Angew. Chem.* **1981**, *93*, 94; *Angew. Chem. Int. Ed. Engl.* **1981**, *20*, 125.

 © VCH Verlagsgesellschaft mbH, D-69451 Weinheim, 1996 0570-0833/96/3501-0103 $ 10.00+.25/0

[6] M. A. Alvarez, M. E. García, V. Riera, M. A. Ruiz, C. Bois, Y. Jeannin, *J. Am. Chem. Soc.* **1993**, *115*, 3786.
[7] The spectroscopic data for **1** indicates that it is isostructural to its molybdenum analogue, the crystal structure of which shows terminal carbonyl ligands. K. A. Azam, A. J. Deeming, M. S. B. Felix, P. A. Bates, M. B. Hursthouse, *Polyhedron* **1988**, *7*, 1793.
[8] K. M. Nicholas, *Organometallics* **1982**, *1*, 1713.
[9] M. A. Alvarez, M. E. García, V. Riera, M. A. Ruiz, C. Bois, Y. Jeannin, *Angew. Chem.* **1993**, *105*, 1232; *Angew. Chem., Int. Ed. Engl.* **1993**, *32*, 1156.
[10] a) Crystal structure determination of **5**·acetone: crystals from acetone/toluene, monoclinic, space group $P2_1$; $a = 16.387(8)$, $b = 11.489(9)$, $c = 10.806(5)$ Å, $\beta = 91.34(3)°$, $Z = 2$, $\rho_{calcd} = 1.84\ g\,cm^{-3}$. 3734 independent reflections, of which 1262 with $I_o > 3\sigma I_o$ were used for calculations, $R = 0.057$, $R_w = 0.067$; b) crystal structure determination of **6**: crystals from CH_2Cl_2/Et_2O, monoclinic, space group $P2_1/c$, $a = 18.164(6)$, $b = 11.355(6)$, $c = 17.859(2)$ Å, $\beta = 97.51(1)°$, $Z = 4$, $\rho_{calcd} = 1.91\ g\,cm^{-3}$. 6299 independent reflections, of which 3139 with $I_o > 3\sigma I_o$ were used for calculations, $R = 0.051$, $R_w = 0.058$. Further details of the crystal structure investigations may be obtained from the Director of the Cambridge Crystallographic Centre, 12 Union Road, GB-Cambridge CB2 1EZ (UK), on quoting the full journal citation.
[11] a) R. H. Fong, C.-H. Lin, H. Idmoumaz, W. H. Hersh, *Organometallics* **1993**, *12*, 503; b) K. A. Johnson, W. L. Gladfelter, *ibid.* **1990**, *9*, 2101; c) A. A. Aitchison, L. Farrugia, *ibid.* **1987**, *6*, 819.
[12] D. Barrat, S. J. Davies, G. P. Elliot, J. A. K. Howard, D. B. Lewis, F. G. A. Stone, *J. Organomet. Chem.* **1988**, *355*, 231.
[13] a) R. L. Miller, R. Toreki, R. E. LaPointe, P. T. Wolczanski, G. D. van Duyne, D. C. Roe, *J. Am. Chem. Soc.* **1993**, *115*, 5570 and references therein; b) W. A. Herrmann, *Angew. Chem.* **1982**, *94*, 118; *Angew. Chem. Int. Ed. Engl.* **1982**, *21*, 117.

A New Multifunctional Heterobimetallic Asymmetric Catalyst for Michael Additions and Tandem Michael–Aldol Reactions**

Takayoshi Arai, Hiroaki Sasai, Kei-ichi Aoe, Kimio Okamura, Tadamasa Date, and Masakatsu Shibasaki*

Although numerous asymmetric catalysts (chemzymes) have been developed utilizing nearly all the elements in the periodic table, the abilities of chemzymes have, in general, proven inferior to those of enzymes, probably because chemzymes have only one function with which to control asymmetric reactions. It is possible that multifunctional heterobimetallic asymmetric catalysts could compensate for the shortcomings of chemzymes by providing positive cooperation between different metals. Recently, for catalytic asymmetric carbon–carbon bond-forming reactions we introduced a new class of heterobimetallic complexes that consist of a rare earth metal center, an alkali metal center (Li, Na, K), and 2,2′dihydroxy-1,1′-binaphthyl (BINOL).[1, 2] For example, the LaLi–BINOL complex is quite effective in catalyzing asymmetric nitroaldol reactions, and LaNa–BINOL is a very efficient catalyst for asymmetric Michael reactions. Mechanistic studies on LaNa–BINOL-catalyzed Michael reactions have revealed that though this complex acts as a base catalyst (ONa), it simultaneously shows Lewis acid character (La), which makes highly enantioselective reactions possible even at room temperature.[2] This result suggested that extension of the "heterobimetallic concept" to metal centers other than rare earths could lead to heterobimetallic asymmetric catalysts with novel properties. In this paper we report the new heterobimetallic asymmetric catalyst **I** consisting of aluminum, lithium, and BINOL, which makes possible for the first time catalytic asymmetric tandem Michael–aldol reactions.

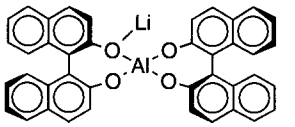

I

We began with the development of an amphoteric asymmetric catalyst made with aluminum and an alkali metal.[3] Initially, in an attempt to prepare the AlLi–BINOL complex **I**, diisobutylaluminum hydride (1.0 M solution in THF) was treated with two equivalents of (*R*)-BINOL in THF at 0 °C for half an hour, and the resulting solution was further treated with one equivalent of BuLi (1.73 M solution in hexane) at 0 °C for half an hour. We were pleased that this new asymmetric catalyst (10 mol%[4]) was also effective in the Michael reaction of cyclohexenone (**6**) with dibenzyl malonate (**4**), giving **7** in 98% *ee*[5] and 46% yield at room temperature. In addition, we observed that the same catalyst **I** was prepared more efficiently from $LiAlH_4$ and two equivalents of (*R*)-BINOL (THF, 0 °C, 1 h). This catalyst (10 mol%[4]) provided high yields of **7** in 99% *ee*, as well as excellent yields of the various Michael adducts **3**, **5**, **9**, and **11** in enantiomeric excesses ranging from 91% to 98% (Table 1).[2]

Table 1. Catalytic asymmetric Michael additions promoted by Al–M–(*R*)-BINOL complexes (10 mol%).

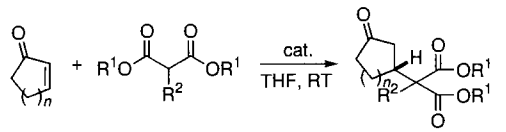

1; $n = 1$
6; $n = 2$

2; R^1 = Et, R^2 = Me
4; R^1 = Bn, R^2 = H
8; R^1 = Me, R^2 = H
10; R^1 = Et, R^2 = H

3; $n = 1$, R^1 = Et, R^2 = Me
5; $n = 1$, R^1 = Bn, R^2 = H
7; $n = 2$, R^1 = Bn, R^2 = H
9; $n = 2$, R^1 = Me, R^2 = H
11; $n = 2$, R^1 = Et, R^2 = H

No.	Enone	Donor	Product	M	*t* [h]	Yield [%]	*ee* [%]
1	**1**	**2**	**3**	Li	72	84	91
2	**1**	**4**	**5**	Li	60	93	91
3	**6**	**4**	**7**	Li	72	88	99
4	**6**	**4**	**7**	Na	72	50	98
5	**6**	**4**	**7**	K	72	43	87
6	**6**	**4**	**7**	Ba	6	100	84
7	**6**	**8**	**9**	Li	72	90	93
8	**6**	**10**	**11**	Li	72	87	95

These are the highest enantiomeric excesses of all known catalytic asymmetric Michael reactions.[2, 6] Although LaLi–BINOL and LaNa–BINOL complement each other in their ability to catalyze asymmetric nitroaldol and Michael reactions,[1, 2] Al–M–(*R*)-BINOL complexes (M = Li, Na, K, and Ba)[7] are commonly useful for the catalytic asymmetric Michael reaction (entries 3–6).

With these excellent results in hand, we set out to determine the structure of **I** unequivocally. Although an X-ray quality crystal[8] of **I** was obtained, it was prone to decomposition during X-ray diffraction studies. However, the complex **II** generated from **I** and cyclohexenone (**6**) in THF provided a crystal that was stable to X-ray crystal analysis.[9] The structure is shown in

[*] Prof. Dr. M. Shibasaki, Dr. H. Sasai, T. Arai
Faculty of Pharmaceutical Sciences, University of Tokyo
Hongo, Bunkyo-ku, Tokyo 113 (Japan)
Fax: Int. code +(3)5684-5206
K. Aoe, K. Okamura, T. Date
Analytical Chemistry Research Laboratory, Tanabe Seiyaku Co., Ltd., Osaka (Japan)

[**] This study was financially supported by a Grant-in-Aid for Scientific Research on Priority Areas from the Japanese Ministry of Education, Science, and Culture.

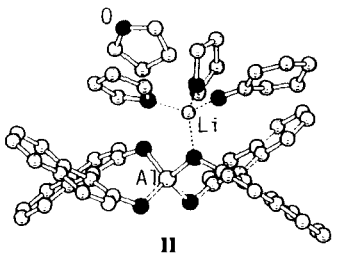

II

Fig. 1. Crystal structure of $C_{40}H_{24}O_4AlLi/C_6H_8O/(C_4H_8O)_3$ (**II**).

Figure 1.[10] The complex has tetrahedral geometry around the aluminum center with average Al–O distances of 1.75 Å. The long Li–O(1) distance of 1.96 Å is indicative of the ionic character of the interaction between Li^+ and $[Al(binol)_2]^-$.[11] The structure of the AlLi–BINOL complex is thus assumed to be **I** or a corresponding dimeric structure.

The small electronegativity value of lithium (1.0) relative to that of aluminum (1.5) suggests that a lithium enolate should be generated from a malonate derivative. However, the role of aluminum in this reaction is not well understood. To study the interaction between the enone and the aluminum atom, an ^{27}Al NMR study was performed.[12] One broad signal was observed for the AlLi–(*R*)-BINOL complex **I** at $\delta = 75$ (S_0). Upon addition of three equivalents of cyclohexenone (**6**) to the complex, two additional signals were obtained at $\delta = 40$ (S_1) and 23 (S_2). The S_2 signal became more intense and was a major peak under conditions of the Michael reaction. This is strong evidence for an octahedral arrangement of six magnetically equivalent ligands around the aluminum cation in THF solution, since all other shifts are upfield relative to S_0.[13] These NMR studies clearly indicate that the carbonyl groups of the enones are coordinated to the aluminum. Consequently, this AlLi–(*R*)-BINOL complex **I** probably also acts as a heterobimetallic multifunctional asymmetric catalyst,[2] making possible efficient Michael reactions even at room temperature.

This aspect of the mechanism suggested that the reaction of a lithium enolate derived from a malonate derivative with an enone would lead to an aluminum enolate intermediate. Further studies were carried out to obtain direct evidence for an aluminum enolate in an effort to learn how to enhance the aluminum enolate's influence on the chemical fate of the Michael adducts. On the basis of the electronegativity of aluminum, the protonation of the aluminum enolate should be slower than that of the corresponding lithium, sodium, or lanthanoid enolates. Could such an Al-enolate then be trapped by an electrophile such as an aldehyde? As was anticipated, the reaction of cyclopentenone (**1**), diethyl methylmalonate (**2**), and 3-phenylpropanal (**12**) in the presence of 10 mol% of the AlLi–(*R*)-BINOL complex gave the three-component coupling product **13** as a single isomer in 91% *ee* (64% yield; Table 2). Quite interestingly, the use of LaLi–BINOL, LaNa–BINOL, or a lithium-free La–BINOL complex[6] gave very unsatisfactory results in the three-component coupling reaction. This is probably because the lanthanum enolate is more reactive toward the acidic proton.[14] Moreover, the use of benzaldehyde (**14**) instead of **12** gave the three-component coupling product **15** in 82% yield. Although **15** was a mixture of diastereomers, its oxidation gave the corresponding diketone derivative **16** as a single isomer in 89% *ee*. This is the first example of a catalytic asymmetric tandem Michael–aldol reaction.

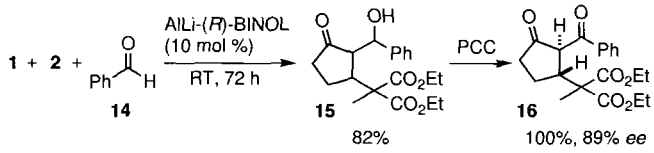

14 **15** 82% **16** 100%, 89% *ee*

We therefore describe the reaction pathway in these three-component coupling reactions as follows (Scheme 1). The reaction of diethyl methylmalonate (**2**) with the AlLi–(*R*)-BINOL complex gives the corresponding lithium enolate (**III**). Enolate **III** then reacts with cyclopentenone (**1**), which is pre-coordinated to the aluminum, to give the aluminum enolate **IV** enantioselectively. Further reaction of enolate **IV** with aldehyde would lead to an alkoxide (**V**). Although it is unclear whether the

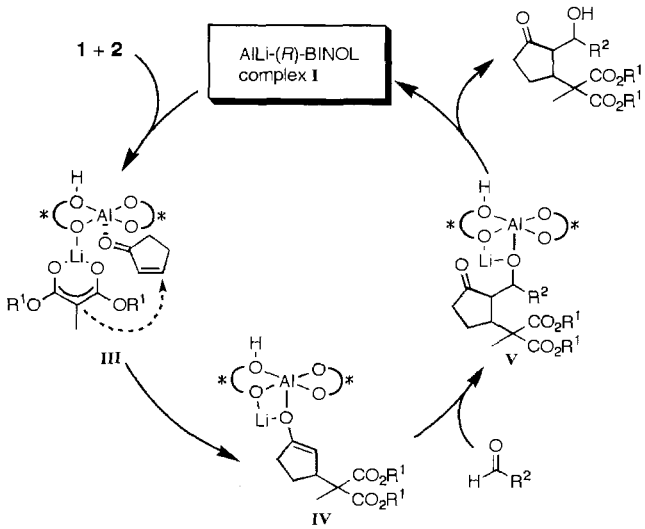

Scheme 1. Possible mechanism for the catalytic asymmetric tandem Michael–aldol reaction promoted by the AlLi–(*R*)-BINOL complex (**I**).

Table 2. Tandem Michael–aldol reactions.

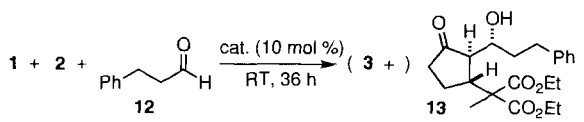

12 **13**

Catalyst	**3**		**13**	
	Yield [%]	*ee* [%]	Yield [%]	*ee* [%]
AlLi-(*R*)-BINOL	7	90	64	91
LaLi-(*R*)-BINOL	46	3	30	– [a]
LaNa-(*R*)-BINOL	73	86	trace	–
La-(*R*)-BINOL [b]	57	83	trace	–

[a] Nonseparable mixture. [b] See Ref. [6].

aluminum or lithium alkoxide is generated, the resulting alkoxide then abstracts a hydrogen atom from an acidic OH group to give the three-component coupling product and regenerate the AlLi–(*R*)-BINOL complex, thereby completing the catalytic cycle.

In conclusion, we have succeeded in developing highly efficient Al–M–(*R*)-BINOL (M = Li, Na, K, or Ba) catalysts for asymmetric Michael reactions. Mechanistic studies on AlLi–(*R*)-BINOL complex revealed that this complex also acts as a multifunctional heterobimetallic asymmetric catalyst. Furthermore, three-component coupling reactions were achieved by trapping the aluminum enolate intermediate with an aldehyde for the first time. These results will provide a very useful method for the catalytic asymmetric synthesis of complex molecules.

 © *VCH Verlagsgesellschaft mbH, D-69451 Weinheim, 1996* *0570-0833/96/3501-0105 $ 10.00+.25/0*

Experimental Procedure

I: To a solution of $LiAlH_4$ (94.9 mg, 2.5 mmol) in THF (5.0 mL) was added a solution of (*R*)-BINOL (20 mL, 5.0 mmol, 0.25 M in THF) at 0 °C. After 30 min stirring at 0 °C, this solution of **I** (0.1 M in THF) was directly used for Michael reactions.

7: To a stirred solution of the catalyst **I** (0.05 mmol) in THF (0.5 mL) was successively added cyclohexenone (**6**) (48 μL, 0.5 mmol) and dibenzyl malonate (**4**) (125 μL, 0.5 mmol) at 0 °C. After 72 h stirring at room temperature, the reaction mixture was treated with 1 N HCl (2.0 mL) and extracted with EtOAc (3 × 10 mL). The combined organic extracts were washed with brine, dried ($NaSO_4$), and concentrated to give an oily residue. Purification by flash chromatography (SiO_2, 25% acetone/hexane) gave the Michael adduct **7** (172.0 mg, 88% yield) in 99% *ee*. The spectral and analytical data of **7** were in agreement with those of Ref. [2].

13: To a solution of cyclopentenone (**1**) (84 μL, 1.0 mmol), methyl diethylmalonate (**2**) (138 μL, 1.0 mmol) and 3-phenylpropanal (**12**) (158 μL, 1.2 mmol) in THF (1.0 mL) was added a solution of the AlLi-(*R*)-BINOL complex **I** (1.0 mL, 0.1 M in THF, 0.1 mmol) at 0 °C. After 36 h stirring at room temperature, the reaction was quenched with 1 N HCl at 0 °C and worked up as described for **7**. The oily residue was purified by flash chromatography (SiO_2, acetone:hexane 1:9) to give **13** (250 mg, 0.64 mmol, 64% yield). The optical purity of **13** was determined by HPLC analysis on a chiral phase (DAICEL CHIRALPAK AD, *i*PrOH:hexane 1:9). $[\alpha]_D^{24} = +18.3$ ($c = 0.66$ in chloroform) (91% ee); ^1H NMR (270 MHz, $CDCl_3$): $\delta = 7.40-7.13$ (m, 5 H), 4.13 (q, $J \approx 7.0$ Hz, 2 H), 4.11 (q, $J = 7.0$ Hz, 1 H), 4.06 (q, $J = 7.0$ Hz, 1 H), 3.75 (dt, $J = 3.8$, 9.6 Hz, 1 H), 2.97 (dt, $J = 6.3$, 8.0 Hz, 1 H), 2.89-2.76 (m, 1 H), 2.70-2.57 (m, 2 H), 2.35 (dd, $J = 3.8$, 6.3 Hz, 1 H), 2.24 (t, $J = 8.4$ Hz, 2 H), 2.19-2.01 (m, 2 H), 1.87-1.68 (m, 2 H), 1.40 (s, 3 H), 1.22 (t, $J = 7.0$ Hz, 3 H), 1.19 (t, $J = 7.0$ Hz, 3 H); ^{13}C NMR ($CDCl_3$): $\delta \approx 218.9$, 171.8, 171.6, 141.8, 128.4, 125.9, 72.0, 61.6, 56.9, 55.9, 43.3, 38.5, 36.1, 32.5, 22.9, 18.6, 14.0, 13.9; IR (neat): $\tilde{\nu} = 3518$, 3085, 1728, 1253 cm^{-1}; MS: *m/z* (%) 391 [M^+], 373 [$M^+ - H_2O$], 175 (100); anal. calcd for $C_{22}H_{30}O_6$: C, 67.67; H, 7.74; found: C, 67.41; H, 7.70.

16: To a solution of cyclopentenone (**1**) (84 μL, 1.0 mmol), methyl diethylmalonate (**2**) (138 μL, 1.0 mmol) and benzaldehyde (**14**) (122 μL, 1.2 mmol) in THF (1.0 mL) was added a solution of the AlLi-(*R*)-BINOL complex (1.0 mL, 0.1 M in THF, 0.1 mmol) at 0 °C. After 72 h stirring at room temperature, the reaction was quenched with 1 N HCl at 0 °C and worked up as described for **7**. The crude product was purified by flash chromatography (SiO_2, acetone:hexane 1:9) to give the diastereomixture of **15** (297 mg, 82%). To a solution of **15** (100 mg, 0.277 mmol) was added molecular sieves (4Å, 200 mg) and pyridinium chlorochromate (PCC, 65 mg, 0.3 mmol) at 0 °C. After 1h of stirring at room temperature, the reaction mixture was diluted by Et_2O (20 mL). The insoluble materials were filtered off through a Celite pad. The filtrate was evaporated to dryness in vacuo. The residue was purified by silica gel chromatography (SiO_2, acetone:hexane 1:9) to give **16** (100 mg, 100% yield). The optical purity of **16** was determined by HPLC analysis on a chiral phase (DAICEL CHIRALCEL OJ, *i*PrOH:hexane 1:4). $[\alpha]_D^{24} = -22.0$ ($c = 1.02$ in chloroform) (89% ee); ^1H NMR (270 MHz, $CDCl_3$): $\delta = 8.00-8.05$ (m, 2 H), 7.62-7.55 (m, 1 H), 7.52-7.45 (m, 2 H), 4.77 (d, $J = 8.6$ Hz, 1 H), 4.13 (q, $J = 7.3$ Hz, 2 H), 4.03 (dq, $J = 7.3$, 10.9 Hz, 1 H), 3.87 (dq, $J = 7.3$, 10.9 Hz, 1 H), 3.68-3.55 (m, 1 H), 2.48-2.26 (m, 3 H), 2.03-1.03 (m, 1 H), 1.49 (s, 3 H), 1.21 (t, $J = 7.3$ Hz, 3 H), 1.04 (t, $J = 7.3$ Hz, 3 H); ^{13}C NMR ($CDCl_3$): $\delta = 211.0$, 195.1, 171.1, 136.5, 133.3, 129.4, 128.5, 61.4, 59.4, 55.6, 44.4, 38.9, 22.7, 19.7, 13.9, 13.6; IR (neat): $\tilde{\nu} = 3463$, 1728, 1677, 1260 cm^{-1}; MS: *m/z* (%) 361 [$M^+ + 1$]), 360 [M^+], 105 (100); anal. calcd for $C_{20}H_{24}O_6$: C, 66.65; H, 6.71; found: C, 66.38; H, 6.76.

Received: August 18, 1995 [Z 83241E]
German version: *Angew. Chem.* **1996**, *108*, 103-105

Keywords: aldol reactions · aluminum compounds · cascade reactions · catalysis · Michael additions

[1] a) H. Sasai, T. Suzuki, S. Arai, T. Arai, M. Shibasaki, *J. Am. Chem. Soc.* **1992**, *114*, 4418; b) H. Sasai, T. Suzuki, N. Itoh, M. Shibasaki, *Tetrahedron Lett.* **1993**, *34*, 851; c) H. Sasai, N. Itoh, T. Suzuki, M. Shibasaki, *ibid.* **1993**, *34*, 855; d) H. Sasai, T. Suzuki, N. Itoh, S. Arai, M. Shibasaki, *ibid.* **1993**, *34*, 2657; e) H. Sasai, W.-S. Kim, T. Suzuki, M. Shibasaki, M. Mitsuda, J. Hasegawa, T. Ohashi, *ibid.* **1994**, *35*, 6123; f) H. Sasai, T. Suzuki, N. Itoh, K. Tanaka, T. Date, K. Okamura, M. Shibasaki, *J. Am. Chem. Soc.* **1993**, *115*, 10372; g) H. Sasai, T. Tokunaga, S. Watanabe, T. Suzuki, N. Itoh, M. Shibasaki, *J. Org. Chem.* **1995**, *60*, 7388; h) H. Sasai, S. Arai, Y. Tahara, M. Shibasaki, *ibid.* **1995**, *60*, 6656.

[2] H. Sasai, T. Arai, Y. Satow, K. N. Houk, M. Shibasaki, *J. Am. Chem. Soc.* **1995**, *117*, 6194, and references therein.

[3] For the previously known asymmetric Al-BINOL reagents and the related compounds, see: a) R. Noyori, *Tetrahedron.* **1994**, *50*, 4259, and references therein; b) K. Maruoka, H. Yamamoto in *Catalytic Asymmetric Synthesis* (Ed.: I. Ojima), VCH, New York, **1993**, p. 413, and references therein.

[4] Calculated on the assumption of quantitative formation of the catalyst.

[5] For information on the absolute configurations and enantiomeric excesses of all Michael adducts, see Refs. [2, 6].

[6] H. Sasai, T. Arai, M. Shibasaki, *J. Am. Chem. Soc.* **1994**, *116*, 1571, and references therein.

[7] Prepared from diisobutylaluminum hydride, two equivalents of (*R*)-BINOL, and one equivalent of NaO*t*Bu, $KN(TMS)_2$, and/or $Ba(OtBu)_2$.

[8] The crystalline **I** (10 mol%) efficiently promoted the Michael reaction of **6** with **4** to give **7** (81% *ee*, 75% yield).

[9] The crystalline **II** (10 mol%) efficiently promoted Michael reaction of **6** with **4** to give **7** (89% ee, 67% yield).

[10] Crystal structure data for **II** ($C_{40}H_{24}O_4AlLi/C_6H_8O/(C_4H_8O)_3$): $T = 223$ K; space group *P*1, $a = 9.510(1)$, $b = 11.063(1)$, $c = 13.052(3)$ Å; $\alpha = 96.42(1)$, $\beta = 95.71(1)$, $\gamma = 64.97(1)°$, $Z = 1$. The structure was solved by direct methods and refined to $R(F) = 0.0520$, $Rw(F) = 0.0490$; further details of the crystal structure investigation are available on request from the Director of the Cambridge Crystallographic Data Centre, 12 Union Road, GB-Cambridge CB2 1EZ (UK) on quoting the full journal citation.

[11] C. Lambert, P. von R. Schleyer, *Angew. Chem.* **1994**, *106*, 1187; *Angew. Chem. Int. Ed. Engl.* **1994**, *33*, 1129.

[12] The chemical shift of the α-proton of **1** in the ^1H and ^{13}C NMR spectra does not change on mixing **1** and the AlLi-BINOL complex.

[13] a) D. Canet, J. J. Delpuech, M. R. Khaddar, P. R. Rubini, *J. Mag. Res.* **1973**, *9*, 329; b) J. J. Delpuech, M. R. Khaddar, A. A. Peguy, P. R. Rubini, *J. Chem. Soc. Chem. Commun.* **1974**, 154; c) *J. Am. Chem. Soc.* **1975**, *97*, 3373.

[14] The mixture *rac*-**3** does not react with **12** in the presence of 10 mol% of the AlLi-(*R*)-BINOL complex.

Enzymatic Synthesis of Peptides and *Ras* Lipopeptides Employing Choline Ester as a Solubilizing, Protecting, and Activating Group**

Michael Schelhaas, Simone Glomsda, Marion Hänsler, Hans-Dieter Jakubke,* and Herbert Waldmann*

For the synthesis of peptides and sensitive complex peptide conjugates, enzymatic transformations offer advantageous alternatives to classical chemical methods.[1, 2] Thus, for instance, biocatalyzed deblocking reactions[1] have proven their efficiency in the construction of glyco-[3] and lipopeptides,[4] and protease-mediated peptide synthesis in ice[5] can be used to couple amino acids and peptides without racemization.

However, enzymatic reactions often are hampered or even prevented by the low solubility of the protected peptides in aqueous reaction media, resulting in limited accessibility of the substrates to the biocatalysts. This difficulty can be overcome by employing solubilizing blocking groups.[6] Their removal, however, often requires reaction conditions that cannot be tolerated in the construction of sensitive peptide conjugates. We now report that choline esters are advantageous solubility-enhancing protecting groups for the synthesis of peptides and lipopeptides under extremely mild conditions.

Peptide choline esters (peptide-Cho) **1** (Scheme 1) can be constructed by treating the corresponding 2-bromoethyl esters with trimethylamine.[7] Alternatively, they are accessible by condensation of amino acid choline ester hydrobromides with C-terminally deblocked peptides (vide infra; Scheme 2).

[*] Prof. Dr. H. Waldmann, Dipl.-Chem. M. Schelhaas, Dipl.-Chem. S. Glomsda
Institut für Organische Chemie der Universität
Richard-Willstätter-Allee 2, D-76128 Karlsruhe (Germany)
Fax: Int. code +(721)608-4825
Prof. Dr. H.-D. Jakubke, Dr. M. Hänsler
Institut für Biochemie der Universität
Talstrasse 33, D-04103 Leipzig (Germany)
Fax: Int. code +(341)295-939

[**] This work was supported by the Deutsche Forschungsgemeinschaft, the Bundesministerium für Forschung und Technologie, and the Fonds der Chemischen Industrie. We are grateful to Degussa AG for the donation of chemicals. We thank Mrs. R. Schauf and Mrs. H. Späth for assistance with the experiments.

The high solubility of these amorphous hygroscopic solids in water, water/dioxane, and water/methanol mixtures is advantageous for the selective removal of the C-terminal protecting group by means of the enzymes butyrylcholine esterase (EC 3.1.1.8) from horse serum or acetylcholine esterase (EC 3.1.1.7) from electric eel. Butyrylcholine esterase accepts a variety of dipeptides as substrates and removes the C-terminal choline ester in high yield under very mild conditions (pH 6.5, room temperature) and with complete selectivity (Scheme 1, Table 1). In the majority of the cases the protected dipeptide

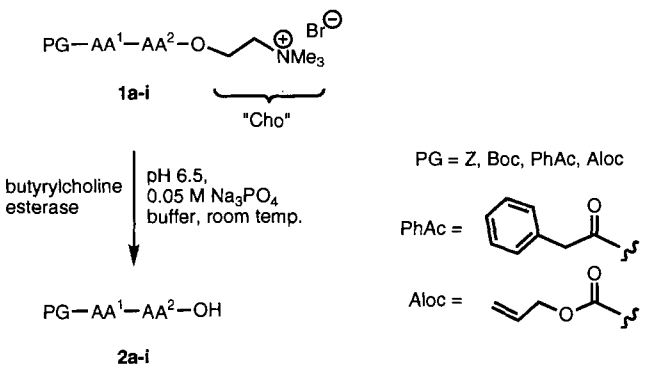

Scheme 1. Enzymatic removal of the choline ester (Cho) from peptides by butyrylcholine esterase. AA = amino acid, PG = protecting group.

Table 1. Results of the enzymatic removal of the choline ester protecting group from the dipeptide choline esters **1** by means of butyryl- and acetylcholine esterase.

No.	**2**	PG	AA^1	AA^2	Vol% CH_3OH	Enzyme [a]	Yield [%] [b]
1	**a**	Boc	Phe	Phe	–	BE	65
2	**a**	Boc	Phe	Phe	–	AE	46
3	**b**	Boc	Ala	Phe	–	BE	50
4	**b**	Boc	Ala	Phe	–	AE	44
5	**c**	Boc	Ile	Ala	–	BE	76
6	**c**	Boc	Ile	Ala	–	AE	60
7	**d**	Boc	Gly	Thr	–	BE	66
8	**e**	Z	Gly	Ala	10	BE	89
9	**f**	Z	Ser	Phe	10	BE	90
10	**g**	PhAc	Phe	Phe	–	BE	70
11	**h**	PhAc	Ile	Phe	–	BE	91
12	**i**	Aloc	Leu	Pro	–	BE	95

[a] BE = butyrylcholine esterase from horse serum; AE = acetylcholine esterase from electric eel. [b] Yields refer to pure deprotected dipeptide **2**. All dipeptide carboxylic acids **2** were characterized by means of their 200 MHz ^1H NMR spectra (in $CDCl_3$) and their FAB mass spectra. The analytical purity of the carboxylic acids **2** was confirmed by HPLC.

esters **1** are freely soluble in the aqueous buffer, and a solubilizing cosolvent is not needed (Table 1). In the enzymatic removal of the N-terminal phenylacetamido (PhAc) group[8] and the C-terminal heptyl (Hep) esters, in particular, the combination of two sterically demanding hydrophobic amino acids posed serious problems due to the low solubility of the respective peptide derivatives in the aqueous media. However, butyrylcholine esterase accepts these combinations, too, and deprotects substrates **1a**, **b**, **g**, **h**, and **1i** in high yield. Since the acetylcholine esterase catalyzed deprotection of peptide choline esters under these mild conditions is slow (Table 1, nos. 2, 4, and 6), butyrylcholine esterase is preferred.

The conditions for the enzymatic deprotection of the choline esters are so mild that this method can be employed to synthesize sensitive S-palmitoylated and S-farnesylated cysteinyl lipopeptides, which, for instance, represent the characteristic partial structures of the *Ras* lipoproteins.

The *Ras* proteins are a class of membrane-bound lipoproteins found in organisms as diverse as mammals, flies, worms, and yeast, and serve as central molecular switches.[10] They translate the signals given by growth factors through a well-balanced series of noncovalent protein/protein interactions into a cascade of highly specific protein phosphorylations terminating in the activation of transcription factors, which then may influence the transcription of the genetic code. Cell growth and proliferation are regulated by this pathway, and if it is disturbed or interrupted, uncontrolled proliferation and finally cancer may occur. Thus, in roughly 40% of all human cancers a point mutation in the *ras* oncogenes coding for the *Ras* proteins is found, a figure that increases to 85% for some of the major malignancies like lung, colon, and pancreas cancer.[11] The human H- and N-*Ras* proteins terminate in an S-farnesylated cysteine methyl ester, and towards the N-terminus one or more S-palmitoylated cysteines are found[12] (see for instance the C-terminal lipohexapeptide of the human N-*Ras* protein **9** (Scheme 2)). The

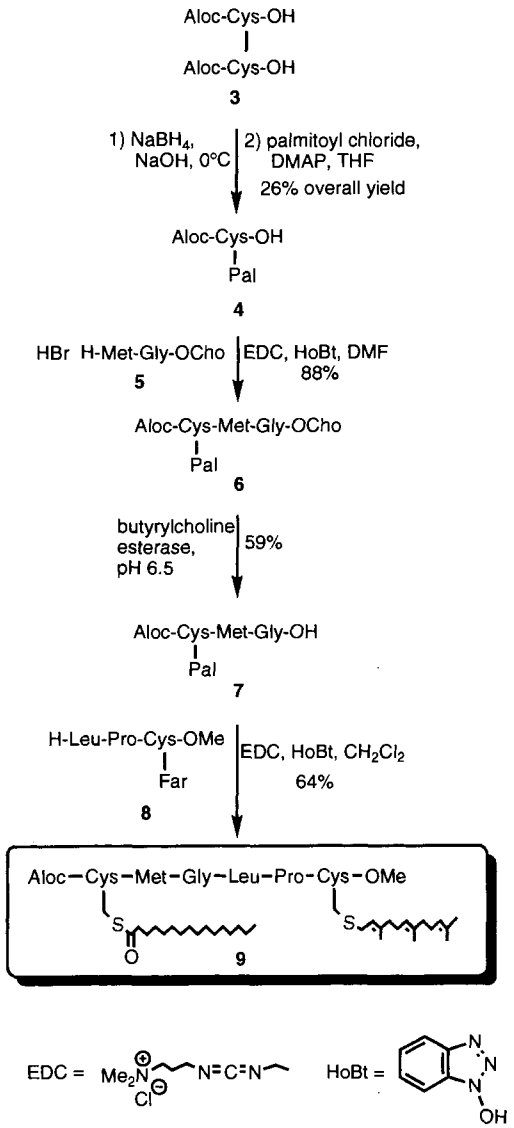

Scheme 2. Enzymatic synthesis of the S-palmitoylated and S-farnesylated *Ras* lipopeptide **9**.

synthesis of characteristic *Ras* peptides is severely complicated by the acid sensitivity of the farnesyl residue and the pronounced base lability of the palmitic acid thioester (vide infra) and excludes the use of acid- or base-labile blocking functions.[4] For this purpose protecting groups have to be employed that can be removed selectively under extremely mild, preferably neutral conditions.

In a retrosynthetic sense the *Ras* peptide **9** was divided into the masked S-palmitoylated tripeptide **7** and the N-terminally deprotected S-farnesylated tripeptide ester **8** to ensure that the final coupling would proceed efficiently (Scheme 2). For the synthesis of **7**, bis[allyloxycarbonyl(Aloc)]-protected cystine **3** was reduced to Aloc-cysteine, which was immediately acylated with palmitoyl chloride to give the correctly functionalized cysteine derivative **4**. Compound **4** was then condensed in high yield with the dipeptide choline ester **5**, which was readily obtained from the corresponding Boc-protected dipeptide choline ester by treatment with HBr/AcOH. The selective removal of the choline ester group from the fully protected tripeptide **6** in the presence of the base-labile thio ester posed a serious challenge. Preliminary experiments revealed that palmitic acid is cleaved from **6** in aqueous solution by nonenzymatic hydrolysis already at pH 6.5, in other words under virtually neutral conditions, without saponification of the choline ester. However, when **6** was treated with the enzyme butyrylcholine esterase at pH 6.5, the chemoselectivity of the hydrolysis was completely reversed, and the C-terminally deprotected lipotripeptide **7** was obtained in 59% yield. We would like to stress that under these extremely mild reaction conditions absolutely no β-elimination of the S-acyl group is observed, a disturbing side reaction that occurs readily for acylated serine and cysteine derivatives at weakly basic pH.[13] The synthesis of the completely functionalized lipopeptide **9**[14] was finally completed by carbodiimide-mediated condensation of the S-palmitoylated peptide carboxylic acid **7** with the S-farnesylated N-terminally deblocked peptide ester **8**[4] (Scheme 2).

Besides the choline esterases, proteases like chymotrypsin, papain, trypsin, subtilopeptidase A, nagarse, and proteinase K also cleave N-protected amino acid and peptide choline esters under mild conditions. For instance, in the chymotrypsin-catalyzed hydrolysis of Z-Phe-OCho **10** the specificity constant[15] has a value of 1.2×10^6 mM^{-1}s^{-1}, which is significantly higher than the values determined for comparable water-soluble *N*-maleinamido amino acid and peptide benzyl and *p*-nitrobenzyl esters. This difference is caused in part by the P'_1 specificity of chymotrypsin for positively charged residues, as we determined previously,[16] and also by the coulombic effect of the positive charge, which leads to enhanced reactivity of the choline ester bond.[17] Due to these excellent substrate properties, we tested choline esters as acyl donors in kinetically controlled peptide syntheses.

In these reactions, too, the excellent solubility of the protected amino acid choline esters in aqueous solvents is a great advantage. Thus, in the presence of chymotrypsin the Z-protected phenylalanine choline ester **10** is coupled in only 30 min with the amino acid amides **11** and **12**, and also with the amino acid benzyl esters **15** and **16**, to give the fully protected peptides **13**, **14**, **17**, and **18**, respectively, in high yield (Scheme 3). The undesired competing hydrolysis of the choline ester can be suppressed simply by adding a precooled solution (0 °C) of the acyl donor slowly to an ice-cold solution (pH 7.8) of the acyl acceptor and the biocatalyst.

The application of the amino acid choline esters for enzymatic peptide synthesis is not restricted to reactions with chymotrypsin as the biocatalyst. For instance, the dipeptide **13** also

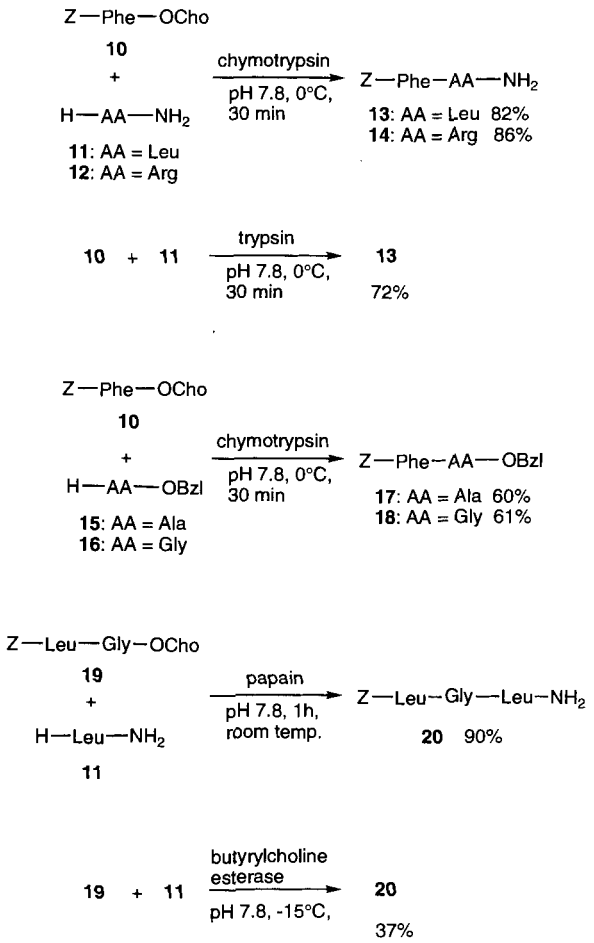

Scheme 3. Enzymatic peptide synthesis employing amino acid and peptide choline esters as acyl donors.

is obtained in high yield by employing trypsin (Scheme 3). In addition, the N-protected peptide choline ester **19** and leucine amide **11** are condensed by papain to give the tripeptide **20** in 90% yield (Scheme 3). Particularly surprising is the finding that butyrylcholine esterase is also able to transfer the acyl moiety from amino acid choline esters to N-nucleophiles; in other words, it catalyzes not only the hydrolysis of choline esters but also the formation of peptide bonds. However, in initial experiments with this biocatalyst tripeptide **20** was obtained from **19** and **11** in 37% yield only at −15 °C in a frozen aqueous system[5] but not at room temperature.

Experimental Procedure

General procedure for the enzymatic cleavage of choline esters by means of butyrylcholine esterase: A solution of 1 mmol of the choline ester and 1000 u of butyrylcholine esterase in 50 mL of 0.05 M Na_3PO_4 buffer (pH 6.5; when necessary 5–10 vol% of methanol was added as cosolvent) was shaken at 37 °C. After the conversion was complete (24–36 h; reaction monitored by thin-layer chromatography with *n*-hexane/ethyl acetate/methanol), the pH was adjusted to 2–3 with 1 N HCl. Depending on the substrate the solution was extracted four to eight times with 40 mL of dichloromethane. The combined organic layers were dried over $MgSO_4$, the solvent was removed in vacuo, and the residue was purified by chromatography on silica gel eluting with *n*-hexane/ethyl acetate/methanol.

7: Colorless oil; $R_f = 0.25$ (*n*-hexane/ethyl acetate/methanol 60/30/5 [v/v/v]); $[\alpha]_D^{22} = -59$ ($c = 0.5$ in CH_3OH); ^{1}H NMR (400 MHz, $CDCl_3$, 25 °C, TMS): $\delta = 0.88$ (t, $J = 7$ Hz, 3H, ω-CH_3 Pal), 1.25 (m, 24H, CH_2 Pal), 1.60–1.68 (m, 2H, β-CH_2 Pal), 1.95–2.09 (m, 2H, β-CH_2 Met), 2.10 (s, 3H, CH_3 Met), 2.53–2.57 (m, 4H, α-CH_2 Pal, γ-CH_2 Met), 3.15–3.27 (m, 2H, β-CH_2 Cys), 3.83–3.93 (m, 1H, CH_{2a} Gly), 4.10–4.20 (m, 1H, CH_{2b} Gly), 4.39–4.78 (m, 4H, α-CH Met, α-CH Cys, OCH_2 Aloc), 5.18–5.38 (m, 3H, CH_2=CH Aloc); FAB-MS (2-NBA/TFA 5/1): *m/z* (%): 654 (63) [M + Na]$^+$.

 © VCH Verlagsgesellschaft mbH, D-69451 Weinheim, 1996 0570-0833/96/3501-0108 $ 10.00+.25/0

General procedure for chymotrypsin-catalyzed peptide synthesis employing N-protected amino acid choline esters: A precooled (0 °C) solution of 1 mmol of the choline ester in 10 mL of water was added with stirring at 0 °C within 3 min to a solution of 2 mmol of the amino acid ester or the amino acid amide and 7.5 mg of chymotrypsin in 7.5 mL of water (pH 7.8), and the reaction mixture was stirred for 30 min. The precipitate was removed by filtration, washed three times with water, dried in vacuo, and recrystallized from methanol/water.

13: M.p. 189–193 °C; FAB-MS (2-NBA): *m/z*: 654 $[M+H]^+$; the purity of **13** was confirmed by HPLC (eluent: CH_3CN/H_2O 2/3 [v/v] and 0.1 vol% trifluoroacetic acid).

Received: August 17, 1995
Revised version: October 19, 1995 [Z 8334/8335 IE]
German version: *Angew. Chem.* **1996**, *108*, 82–85

Keywords: choline esterase · enzymatic catalysis · peptides · *Ras* proteins

[1] Review on enzymatic protecting group techniques: H. Waldmann, D. Sebastian, *Chem. Rev.* **1994**, *94*, 911.
[2] Review on enzymatic peptide syntheses: V. Schellenberger, H.-D. Jakubke, *Angew. Chem.* **1991**, *103*, 1440; *Angew. Chem. Int. Ed. Engl.* **1991**, *30*, 1437.
[3] P. Braun, H. Waldmann, H. Kunz, *Bioorg. Med. Chem.* **1993**, *1*, 197.
[4] E. Nägele, H. Waldmann, *Angew. Chem.* **1995**, *107*, 2425; *Angew. Chem. Int. Ed. Engl.* **1995**, *34*, 2259.
[5] a) M. Schuster, A. Aaviksaar, H.-D. Jakubke, *Tetrahedron* **1990**, *46*, 8093; b) M. Schuster, G. Ullmann, U. Ullmann, H.-D. Jakubke, *Tetrahedron Lett.* **1993**, *34*, 5701.
[6] a) For an enzymatic peptide synthesis employing solubilizing protecting groups see: A. Fischer, A. Schwarz, C. Wandrey, A. S. Bommarius, G. Knaup, K. Drauz, *Biomed. Biochim. Acta* **1991**, *50*, 169; b) for enzymatically removable, solubility-enhancing, C-terminal protecting groups see: H. Kunz, D. Kowalczyk, P. Braun, G. Braum, *Angew. Chem.* **1994**, *106*, 353; *Angew. Chem. Int. Ed. Engl.* **1994**, *33*, 336; G. Braum, P. Braun, D. Kowalczyk, H. Kunz, *Tetrahedron Lett.* **1993**, *34*, 3111.
[7] H. Kunz, M. Buchholz, *Chem. Ber.* **1979**, *112*, 2145.
[8] H. Waldmann, *Liebigs Ann. Chem.* **1988**, 1175.
[9] P. Braun, H. Waldmann, W. Vogt, H. Kunz, *Liebigs Ann. Chem.* **1991**, 165.
[10] Reviews: a) S. E. Egan, R. A. Weinberg, *Nature* **1993**, *365*, 781; b) M. S. Boguski, F. McCormick, *Nature* **1993**, *366*, 643; c) J. L. Bos, *Mutation Res.* **1988**, *195*, 255.
[11] Review: A. Levitsky, *Eur. J. Biochem.* **1994**, *226*, 1.
[12] W. A. Maltese, *FASEB J.* **1990**, *4*, 3319, and references therein.
[13] K. Wakabayashi, W. Pigman, *Carbohydr. Res.* **1974**, *35*, 3.
[14] **9**: Colorless oil; $R_f = 0.75$ (*n*-hexane/ethyl acetate/methanol 50/50/10 [v/v/v]); $[\alpha]_D^{22} = -34$ ($c = 0.7$ in $CHCl_3$); ^1H NMR (400 MHz, $CDCl_3$, 25 °C, TMS): $\delta = 0.88$ (t, $J = 7$ Hz, 3H, ω-CH_3 Pal), 0.94 (d, $J = 7$ Hz, 3H, ω-CH_{3a} Leu), 0.98 (d, $J = 7$ Hz, 3H, ω-CH_{3b} Leu), 1.25 (m, 24H, CH_2 Pal), 1.55–1.75 (m, 14H, β-CH_2 Pal, 4CH_3 Far), 1.95–2.2 (m, 19H, β-CH_2 Met, β-CH_2 Leu, 4CH_2 Far, 2CH_2 Pro, S-CH_3 Met), 2.35 (m, 1H, γ-CH Leu), 2.55 (m, 4H, α-CH_2 Pal, γ-CH_2 Met), 2.65–2.68 (m, 2H, β-CH_2 Cys-S-Far), 2.90–3.30 (m, 4H, β-CH_2 Cys-S-Pal, α-CH_2 Far), 3.60–3.80 (m, 6H, CO_2CH_3, CH_2 Pro, CH_{2a} Gly), 4.24–4.28 (m, 1H, CH_{2b} Gly), 4.50–4.78 (m, 7H, α-CH Met, 2α-CH Cys, α-CH Leu, α-CH Pro, OCH_2 Aloc), 5.10–5.34 (m, 5H, 3CH Far, CH_2=CH Aloc), 5.86–5.93 (m, 1H, CH_2=C*H* Aloc), 6.05 (d, br, NH urethane), 7.05 (d, br, 1H, NH), 7.25 (d, br, 1H, NH), 7.4 (br, 1H, NH), 7.58 (d, br, 1H, NH); FAB-MS (2-NBA/TFA 5/1): *m/z* (%): 1163 (4) $[M+H]^+$, 1185 (20) $[M+Na]^+$.
[15] V. Schellenberger, U. Schellenberger, H.-D. Jakubke, *Coll. Czech. Chem. Commun.* **1988**, *53*, 2884.
[16] V. Schellenberger, H.-D. Jakubke, *Biochim. Biophys. Acta* **1986**, *869*, 54.
[17] P. Sikk, A. Aaviksaar, *Org. React.* **1977**, *14*, 61.

Troubleshooting... with VCH books!

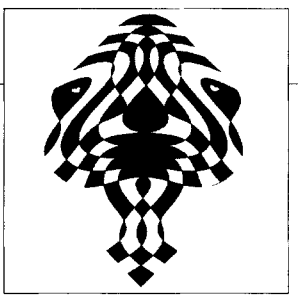

Neuhoff, V.
Scientists in Conference The Congress Organizer's Handbook
1987. X, 223 pages.
Hardcover. DM 68.00
ISBN 3-527-26579-1

Do you have to organize a conference? Well, sometimes, this can't be avoided. But you don't want to get crushed by the wheels of paperwork? And you want to stay in your budget? Then this handy little book is your survival kit!

Schoenfeld, R.
The Chemist's English Third, revised edition with Say It in English, Please!
1990. XII, 195 pages with 9 figures.
Hardcover. DM 48.00
ISBN 3-527-28003-0

"Recommended without qualification; and a suitable gift for friends."
Chemical and Engineering News

"The book might well serve as a prescribed text for PhD students."
Nature

Ebel, H.F. /Bliefert, C. / Russey, W.
The Art of Scientific Writing
From Student Reports to Professional Publications in Chemistry and Related Fields
1990. XIX, 493 pages with 27 figures and 16 tables.
Softcover. DM 48.00
ISBN 3-527-26677-1

First of all, here we have a highly readable text on scientific communication - with all its ramifications from writing the most effective text to getting it published. Never before has so much information on scientific writing been assembled in a single book.

To order please contact your bookseller or:
VCH, P.O. Box 10 11 61,
D-69451 Weinheim,
Telefax (0) 62 01 - 60 61 84
VCH, Hardstrasse 10, P.O. Box,
CH-4020 Basel
VCH, 8 Wellington Court,
Cambridge CB1 1HZ, UK
VCH, 303 N.W. 12th Avenue,
Deerfield Beach, FL 33442-1788,
USA
toll-free: 1-800-367-8249 or
fax: 1-800-367-8247
VCH, Eikow Building,
10-9 Hongo 1-chome, Bunkyo-ku,
Tokyo 113

VCH

 © VCH Verlagsgesellschaft mbH, D-69451 Weinheim, 1996 0570-0833/96/3501-0109 $ 10.00+.25/0

At Last! A Positive Perspective For Chemistry

Designing the Molecular World. Chemistry at the Frontier. By *P. Ball.* Princeton University Press, Princeton, 1994. 376 pp., hardcover $ 29.95.—ISBN 0-691-00058-1

It was high time that this book be written. Chemical research and its applications nowadays receive almost exclusively adverse criticism from the public, and even chemists themselves often take the view that research has exhausted its potential and little new knowledge of importance can be expected. This book is like a clean fresh breeze, and puts the image of chemistry back into proper perspective. In it Philip Ball gives a comprehensive survey of the most recent chemical research. Many of the concepts explained here were unheard of in 1960. All the major research topics that have occupied the universities in recent times are mentioned: the use of flash photolysis and laser techniques to elucidate reaction mechanisms and molecular structures, quasicrystals, interpenetrating networks, the chemistry of life processes and of the self-organization of molecules, crown ethers, cage structures, amphiphilic systems, and so on. No book quite like this has ever appeared before!

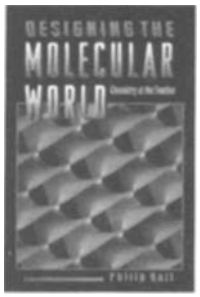

The blurb on the dust-jacket claims that the book is also suitable for readers without a scientific education. This strikes me as somewhat over-optimistic, as Ball rushes with seven-league boots through Rutherford's model of the atom and continues to the frontiers of current research. No lay-person is likely to be able to follow him. On the other hand, the book should be compulsory reading for scientists and for everyone with a basic scientific education. But there is no need to fear such a "duty"; right from the first few pages the book is a pleasure to read. The author's lively and gripping style, in which he does not shrink from phrases containing the word "I", and the clearly constructed sentences serve to clarify even the most complicated relationships in a way that is easy to understand. (Incidentally, a German translation of the book, which one hopes will soon appear, will also need to match this high standard.) The text is illustrated by excellent diagrams and photographs, and together with their accurate and detailed legends these are essentially self-contained units which can be understood independently of the text. Evidently the experience of a skilled scientific editor has helped here. It is certainly to be hoped that the success of this first book by Philip Ball will encourage him to write more. Most importantly of all, the book should be used by every chemistry teacher, from university professor to high school, to help convey to students something of the book's enthusiasm for modern research. I especially liked the chapter "Caught in the Act, Watching Atoms Dance"; it vividly makes the point that all the ideas concerning transition states that were constructed by earlier generations of chemists as a way of understanding reaction mechanisms were not just mental aids, but they actually exist in nature and one can see and almost take hold of them. A significant development that should be noted by epistemologists!

Anyone who has had difficulty up to now in understanding fractals and chaos theory will find this book very helpful, and after reading it will wonder why the subject was made to seem so formidable. Of course the book had to include a chapter on the chemistry of the atmosphere and pollution from human activities. On this subject the book reminds us that long before politicians became concerned about these matters there were already scientists who recognized the problems, studied their causes, and even proposed solutions.

Ball makes an effort in the book to relate chemistry to developments in information technology, microelectronics, consumer electronics, video recorders, color television, news transmission, and the electronics industry. One would perhaps have liked these connections to be explained in more detail, thereby bringing the book even closer to everyday life. Nevertheless, they are adequately sketched here, so that at the end of the book one is convinced that "Not everything is chemistry, but without chemistry nothing can exist."

Rudolf Fahnenstich
Möbris (Germany)

This section contains book reviews and a list of new books received by the editor. Book reviews are written by invitation from the editor. Suggestions for books to be reviewed and for book reviewers are welcome. Publishers should send brochures or (better) books to Dr. Illenora Beckmann, Redaktion Angewandte Chemie, Postfach 101161, D-69451 Weinheim, Federal Republic of Germany. The editor reserves the right of selecting which books will be reviewed. Uninvited books not chosen for review will not be returned.

The book **Inorganic Experiments** (Edited by *J. D. Woollins.* VCH Verlagsgesellschaft, Weinheim, 1994. 286 pp.; hardcover DM 148.00.—ISBN 3-527-29235-7) reviewed by Dr. Johannes Beck, Giessen in the *Angewandte Chemie International Edition in English* (**1995**, *34*, 2565) is now also available as a softcover from VCH Verlagsgesellschaft, Weinheim (DM 58.00/$ 39.95.—ISBN 3-527-29253-5).

 © *VCH Verlagsgesellschaft mbH, D-69451 Weinheim, 1996* *0570-0833/96/3501-0111 $ 10.00+.25/0*

Aluminum(I) and Gallium(I) Compounds: Syntheses, Structures, and Reactions

Carsten Dohmeier, Dagmar Loos, and Hansgeorg Schnöckel*

In memory of Wilhelm Klemm

By the end of the last century there were already the first indications of the possible existence of Al^I halides. However, it was only through the pioneering works of W. Klemm, who would have celebrated his 100th birthday on January 6, 1996, that detailed spectroscopic investigations became possible. Since the end of the 1970s the reactivity of AlX and GaX species in solid noble gases has been confirmed by numerous examples. In recent years formally monovalent Al and Ga species have been successfully synthesized on a preparative scale. In addition to the first halides, organometallic compounds with metal–metal bonds have been isolated and investigated with regard to their chemical properties. The fundamental importance of such species has been documented in this journal among others in the form of two highlight articles in which experimental and theoretical aspects have been examined with examples, and parallels and differences with respect to boron chemistry have been illustrated. This review is intended to give an account of the chronological development of this research area over the last few years, but an attempt is also made to categorize the experimental results achieved not only with respect to structure, thermodynamics, and reactivity, but also with the aid of quantum chemical calculations and by comparative considerations.

Keywords: aluminum compounds · gallium compounds · matrix isolation · subvalent compounds

1. Introduction

A review article from W. Uhl appeared in this journal in 1993,[1] in which mainly organometallic compounds of the formally divalent elements Al and Ga with metal–metal bonds were discussed. Herein, we report on compounds of the formally monovalent elements.[2] Subvalent hydrides,[3] the chalcogenides,[4] and the wide area of intermetallic compounds[4, 5] are omitted to the most part. The main focus is directed towards halogen compounds and organometallic species.

Why are Al^I and Ga^I compounds currently the focus of so much attention? Compared with the fascinating variety of the borane structures or the vast field of the subhalides of indium and thallium, our knowledge of subvalent Al and Ga compounds appears rather scanty. Al^I and Ga^I compounds were only known as high-temperature molecules and considered to be somewhat exotic—something which only spectroscopists would occupy themselves with. For the preparative chemist, this field seemed to be a taboo and hardly fruitful. It was only after this prejudice was eliminated by individual, yet spectacular examples[2, 6] (discussed in the following) that the unanticipated possibilities of this class of compounds became visible.

That Al^I and Ga^I compounds should take up a special place in the third main group is not at all evident at first, because compounds of the monovalent elements have been long known now for both the heavier and lighter homologues of this group. There are, for example, a large number of polyhedral molecular compounds of the type B_nX_n with X = Cl, Br, I.[7] The great variety feigns a general availability, however, because most of these compounds have only been prepared on a mg scale. In contrast, the ionically built-up halides of the heavier homologues In and Tl are readily accessible and known to every freshman in chemistry. When considered from this point of view, it is perhaps astonishing that Al^I and Ga^I compounds that are stable at room temperature were unknown until recently.[8] In the following we aim to show that this can be attributed to the lack of stability on the one hand, for example with regards to disproportionation, and on the other hand to the absence of suitable synthetic methods. The preparative chemistry of analogous compounds with elements from the neighboring groups such as dimeric and even monomeric silylenes has only been achieved in the last few years. Examples are $[SiCp^*_2]$[10] and disilenes with Si=Si bonds.[11]

Based on certain thermodynamic considerations, the energetic situation will first be illustrated taking the monochlorides of the third main group of elements as an example.

[*] Prof. Dr. H. Schnöckel, Dr. C. Dohmeier
Institut für Anorganische Chemie der Universität
Engesserstrasse Geb.-Nr. 30.45, D-76128 Karlsruhe (Germany)
Fax: Int. code +(721)608-4854
Dr. D. Loos
University of Oxford, Inorganic Chemistry Laboratory
South Parks Road, Oxford, OX1 3QR (UK)

 © VCH Verlagsgesellschaft mbH, D-69451 Weinheim, 1996 0570-0833/96/3502-0129 $ 10.00+.25/0

2. Monohalides of the Third Main Group Elements

2.1. Thermodynamic Considerations

In contrast to solid TlCl, gaseous TlCl is unstable with regard to disproportionation to give metal and solid trichloride ($\Delta_R H = -109\ kJ\,mol^{-1}$). As the stabilization of TlCl in the form of an ionic crystal with Tl-Cl-Tl bridges is clearly more favorable with respect to Tl(s) and $TlCl_3$(s) by $299\ kJ\,mol^{-1}$, gaseous TlCl does not disproportionate on cooling (Scheme 1). Only TlCl(g) is suitable for comparative stability considerations, because for the lighter homologues the only data available as yet is on the gaseous monochlorides. Similar relationships are found for molecular InCl, but the energy gain on disproportionation is considerably larger ($267\ kJ\,mol^{-1}$). The instability of the monovalent compounds thus increases, as expected for the lighter homologues. Solid InCl is still slightly favored with respect to the disproportionation products, however ($66\ kJ\,mol^{-1}$). An ionic stabilization of this type has not yet been observed in the case of the monochlorides of the elements Ga, Al, and B, but it is conceivable only for GaCl. For the gaseous monochlorides of Al and B, the disproportionation is so exothermic that the formation of $2M + MCl_3$ from 3 MCl probably represents the energetic minimum in both these systems (Scheme 2).

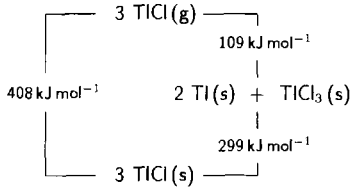

Scheme 1. Energy diagram for the disproportionation of TlCl.

In the case of gaseous BCl, metastable polyhedron compounds with B—B bonds can be isolated in place of an ionic stabilization product, for example molecular B_4Cl_4 with a tetrahedral B_4 framework and terminal chlorine atoms. The energetic relationships between B_4Cl_4(g), BCl(g), and B(s) $+ BCl_3$(g) are illustrated in Scheme 3. They result from a combination of

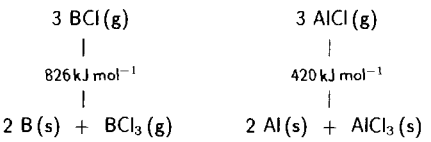

Scheme 2. Energy diagrams for the disproportionations of BCl and AlCl.

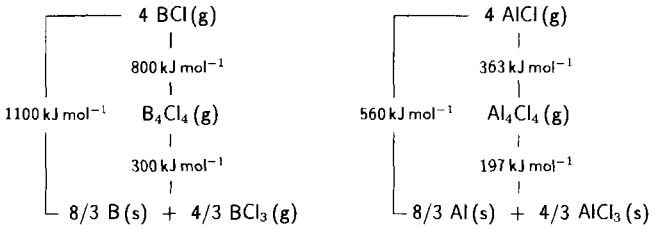

Scheme 3. Energy diagrams for the disproportionations of BCl and AlCl through oligomers.

experimentally determined thermodynamic data [12] and the results of quantum chemical calculations.[13]

Similar oligomers are to be expected in the Al/Cl system as well (Scheme 3), as shown by quantum chemical calculations.[14] For example, Al_4Cl_4 with a tetrahedral structure analogous to that of B_4Cl_4 is energetically favored with respect to a compound with a heterocubane structure. The isolation of this species thus represents a challenge for the preparative chemist. Albeit this synthetic goal has not yet been fully achieved, considerable partial successes have been secured, which will be discussed in Sections 2.3 and 3.[15]

2.2. Spectroscopic Studies on Structure and Reactivity

Spectroscopic studies on low molecular weight species are most appropriate for the systematic analysis of a new class of compounds with regards to structure, thermodynamics, and reactivity. It is advisable to complement these with quantum

Hansgeorg Schnöckel, born in Marienburg, Westpreußen, studied chemistry at the Universität Münster, where he did his doctorate in 1970 under the direction of H. J. Becher. His dissertation was concerned with the spectroscopic investigation of molecules containing boron. Following this, matrix investigations of reactive high-temperature molecules led to his Habilitation in 1981. In 1987 he was named Professor at the Universität Münster and moved to take up a Professorship at the Institut für Anorganische Chemie der Universität München in 1989. He has been Professor für Analytische Chemie at the Universität Karlsruhe since 1993. His research interests are concentrated on spectroscopic and quantum chemical investigations of reactive molecules. Based on works such as these, preparative chemistry involving high-temperature molecules such as aluminum monohalides has become increasingly more important over the last few years.

Carsten Dohmeier, born 1963 in Osnabrück, studied chemistry at the Universität Münster. He did his doctorate in 1994 under the direction of H. Schnöckel at the Ludwig-Maximilians-Universität München. Since then he has worked at the Universität Karlsruhe in the field of low-valent aluminum compounds.

Dagmar Loos, born in München in 1964, studied chemistry at the Ludwig-Maximilians-Universität München where she did her doctorate in 1994 under the direction of H. Schnöckel. Since 1994 she has worked as a post doctoral researcher in the group of A. J. Downs at the University of Oxford investigating low-valent gallium compounds.

chemical calculations. We will not dedicate a separate section to the latter topic, but rather present the results of the theoretical calculations together with the results of the experimental investigations for the individual compounds.

The geometries of the monomeric monohalides, which are only thermodynamically stable as high-temperature molecules in the singlet ground state, have been known for some time.[16] They were identified by analysis of the fine structure of electronic spectra. However, it is not possible to draw conclusions as to the reactivity of the monohalides from these gas phase investigations. Even the simplest of reactions, dimerization, cannot be studied under these conditions, because, due to the low dimerization energy, the proportion of dimeric species at higher temperatures is very small: The ratio of the concentration of dimers to monomers for AlF is only about 10^{-11}:1 at 1473 K (dimerization energy $-55\ kJ\,mol^{-1}$). The thermodynamic data required for an estimation of this type are derived from quantum chemical calculations.[17] A four-membered ring with D_{2h} symmetry was calculated as the equilibrium structure for Al_2F_2 (Scheme 4).

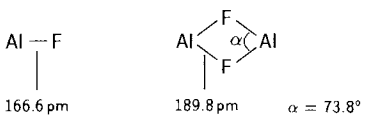

(exp.: 165.4 pm [16])

Scheme 4. Geometric parameters of AlF and Al_2F_2.

The Al—F bonds in Al_2F_2 are significantly weaker than those in monomeric AlF. This is also the reason for the low dimerization energy of AlF. As Al^+ has a relatively large ionic radius due to the doubly occupied 3s AO, d(Al—F) is larger than in AlF_3 for example (163 pm).[18] The geometry of Al_2F_2 is affected by the F—F repulsion. This results from the increase in the dimerization energy when using a larger F basis, which better describes the diffuse charge cloud of F^-. The small F-Al-F angle shows, however, that the Al—Al repulsion dominates. This seems plausible, because the HOMOs in both AlF and Al_2F_2 have Al-3s character.[19] The MOs formed from the F(2p) AOs lie between -0.6 and -0.74 Hartree. We have here, in contrast to the alkali metal halides, the unusual case of an ionogenic compound, in which the MOs localized predominantly on the anion lie energetically lower than those localized on the cation. This is typical for valence unsaturated Al compounds and reflects their strong reduction potential. As the orbital energy ε is a measure of the spatial expansion of an AO ($r^{-1} \sim \sqrt{|\varepsilon|}$),[20] Al^+ with the electronic configuration [Ne] $3s^2$ has an unusually large cation radius which exceeds that of the F^- ion. Even after these considerations, the relatively large Al—F distances and the small F-Al-F angles for AlF and Al_2F_2 are understandable.

Matrix isolation spectroscopy provides an experimental route to oligomeric AlF species. The monomeric high-temperature molecules are first deposited together with a large excess of noble gas onto a cold surface (ca. 15 K).[21] In this way the disproportionation [Eq. (1)], which occurs in the gas phase on cooling due to shifts in the equilibrium, can be avoided.

$$3\ AlF(g) \rightleftharpoons 2\ Al(s) + AlF_3(g) \qquad (1)$$
$$\Delta_R H = -614\ kJ\,mol^{-1}$$

When the monomers are trapped from the gas phase, different amounts of dimeric AlF are formed depending on the reaction conditions (temperature of the cold surface, dilution by the noble gas). Certain statements may be made as to the structure of Al_2F_2 based on its vibrational spectrum: The two IR-active stretching vibrations indicate a four-membered ring structure, and the Al—F force constants calculated from the spectra show that the Al—F bond in Al_2F_2 ($1.2\ N\,cm^{-1}$) is considerably weaker than that in monomeric AlF ($3.92\ N\,cm^{-1}$). These experimental data have been subsequently confirmed by quantum chemical calculations which show that the bond length is elongated from 166.6 pm (AlF) to 189.8 pm (Al_2F_2). The two IR-active stretching vibrations for selected dimeric monohalides with planar ring structures (D_{2h}) found from matrix studies are listed in Table 1. Unfortunately there are no analogous Raman measurements as yet, so there are no complete experimental data on structure or on the force constants matrix.

Table 1. Calculated and experimentally determined frequencies of the IR-active stretching vibrations of some planar [M(μ-X)$_2$M] compounds as well as their calculated geometric parameters and dimerization energy ΔE (2MX → M_2X_2) [25].

	Al_2F_2	Al_2Cl_2	Al_2Br_2	Ga_2F_2	Ga_2Cl_2	Ga_2Br_2
d(M-X) [pm]	188.8	247.9	268.0	200.1	256.2	275.3
∢ (XMX) [°]	73.9	81.8	84.7	73.1	82.8	86.0
ΔE [kJ mol^{-1}]	−91	−30	−33	−118	−57	−52
ν(MX) [cm^{-1}]: exp. (calcd.)	403 [a]	252	-	320	208.5	-
b_{3u} 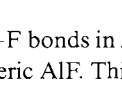	(437)	(270)	(212)	(347)	(210)	(151)
ν(MX) [cm^{-1}]: exp. (calcd.)	430 [a]	270	-	358	220.8 [b]	-
b_{2u} 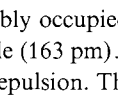	(486)	(272)	(217)	(395)	(221)	(159)

[a] See ref. [17, 26]. [b] See ref. [27].

As these results show, the matrix technique is the method of choice for studying the reactivity of monomeric species—the simplest reaction is the dimerization—and for measuring the vibrational transitions of the reaction products. Trimers, or even larger AlX or GaX oligomers have not yet been identified by the matrix technique, because their concentrations under comparable conditions[22] should be significantly lower than those of the dimers.[23] As in more recent times more sensitive measurement techniques have become available, the detection of additional oligomers should be possible in the near future. Studies of this type are particularly promising, because the vibrational spectra that are expected can be calculated very reliably with quantum chemical methods, and the assignment of the vibrational bands observed can thus be confirmed.[24]

In addition to the dimerization reactions, the reactivity with respect to other species such as atomic oxygen, hydrogen chloride, and molecular hydrogen can also be investigated with the aid of the matrix technique. Oxygen atoms produced from O_2 by microwave discharge react with the monohalide molecules in the matrix to give linear triatomic halide oxides. It was in these compounds that element–oxygen double bonds for Al and Ga were first detected [Eqs. (2a)–(2c); Scheme 5].[28]

$$AlF + O^* \longrightarrow O=AlF \quad [29] \qquad (2a)$$

$$AlCl + O^* \longrightarrow O=AlCl \quad [29] \qquad (2b)$$

$$GaF + O^* \longrightarrow O=GaF \quad [30] \qquad (2c)$$

Scheme 5. Synthesis of molecular halide oxides of Al and Ga in solid noble gases.

AlCl and GaCl react in solid noble gases with hydrogen chloride or molecular hydrogen to form AlH and GaH bonds, respectively [Eqs. (3a)–(3c); Scheme 6].

$$AlCl + HCl \xrightarrow{h\nu} AlCl_2H \quad [31] \qquad (3a)$$

$$GaCl + HCl \xrightarrow{h\nu} GaCl_2H \quad [32] \qquad (3b)$$

$$GaCl + H_2 \xrightarrow{h\nu} GaClH_2 \quad [33] \qquad (3c)$$

Scheme 6. Synthesis of molecular halide hydrides of Al and Ga in solid noble gases.

The study of simple (and subvalent) AlH and GaH compounds takes on a special importance,[3] since here the bonding relationships can be examined particularly reliably by both quantum chemical and spectroscopic methods.[34] With the matrix technique it has been possible to obtain AlH and GaH compounds, starting from monovalent compounds and without the need for bulky substituents, in which the metal atom is only tricoordinate. As regards, for example, the GaH bonds, it remains to be mentioned that they become stronger with increasing chlorine substitution: $GaH_3 < GaClH_2 < GaCl_2H$.[33] For other results concerning the hydride compounds of the trivalent elements the reader is referred to the original works and the review articles cited.[3]

In 1972 indications were that the high-temperature molecule AlCl was unsuitable for synthetic purposes.[35] In the following years the reactivity of such species was confirmed for the first time by matrix experiments, and in recent times it has proved possible to produce Al and Ga monohalides on a preparative scale and use these for syntheses. These results are discussed in the following section.

2.3. Syntheses of Subvalent Al and Ga Halides

For Tl and In the values of the redox potentials M^+/M and M^{3+}/M^+ alone show that only Tl^+ is stable with regards to disproportionation in aqueous solution.[36] It is thus very simple to prepare thallium monohalides by oxidation of the metal with aqueous HX solution. In contrast, the monohalides of the lighter homologues are oxidized under these conditions producing H_2.[37] Recent studies show, however, that InX compounds represent an exception. It has already been mentioned in Section 2.1 that solid InCl is thermodynamically stable with regards to disproportionation. It seems plausible, therefore, that In monohalides may also be isolated from aqueous media under suitable conditions thanks to their low solubilities.[38] The yields obtained are admittedly very low, however. For the synthesis of InX more favorable stoichiometric amounts of suitable starting materials (e.g. indium and InX_3) were heated to 300–400 °C in sealed ampoules.[39]

Al and Ga monohalides that are thermodynamically stable at room temperature are not known.[8] To access metastable AlX and GaX compounds, the gaseous MX species that are thermodynamically stable at high temperatures have to be made first. There are a variety of methods available for their preparation and some examples are shown in Equations (4a)–(4c) (Scheme 7).

$$M + HX \xrightarrow{\Delta} MX + 1/2\,H_2 \qquad (4a)$$

$$2M + X_2 \xrightarrow{\Delta} 2MX \qquad (4b)$$

$$2M + MX_3 \xrightarrow{\Delta} 3MX \qquad (4c)$$

Scheme 7. Possible synthetic routes to MX species (M = Al, Ga; X = halogen).

To largely suppress the formation of the trihalide which is preferred at low temperatures, temperatures of 800–1000 °C are necessary.[40] The gaseous MX species thus formed have to be subsequently quenched at low temperatures in order to prevent the disproportionation which occurs on slow cooling.

The preparation of MX(g) (M = Al, Ga) by the reaction of HX(g) with liquid Al or Ga has already proved itself in the matrix experiments mentioned in Section 2.2. This method also has the advantage that the MX gas stream can be easily added in the correct doses by controlling the amount of HX fed in. Thus, this method of preparation was also used in the synthesis. The apparatus used (Fig. 1) is, in principle, comparable to the experimental construction that was used by Timms for the

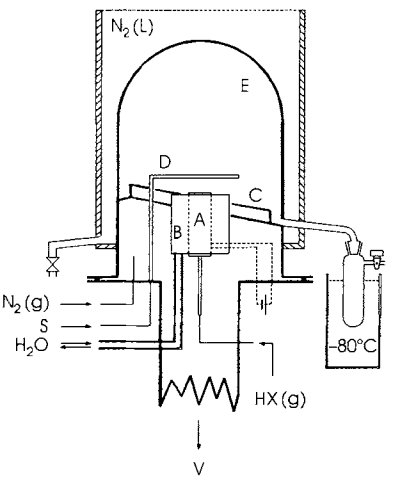

Fig. 1. Schematic representation of the apparatus used for the preparative syntheses. A: Graphite cell, B: Cooling plate, C: Run-off rim, D: Solvent inlet, E: Stainless steel vessel, S: Solvent, V: To vacuum pump.

preparation of other high-temperature molecules (e.g. BF).[35,41] Similar apparatus has been in use for some time now for metal vapor syntheses.[42] The reaction between metal and hydrogen halide (HCl, HBr, or HI) takes place in a graphite cell, located in a stainless steel vessel that can hold about 30 L and is evacuated to approximately 5×10^{-5} mbar. Under these conditions a gaseous equilibrium mixture is formed which—depending on M, HX, and the particular reaction conditions—is made up of between 90% and 100% MX and H_2. The gaseous monohalides continually streaming out of the graphite cell are condensed together with solvent on the inner surface of the stainless steel vessel which is cooled to 77 K. The hydrogen is removed continuously by a high-performance pump system. Approximately 45 mmol MX can be prepared in this way over a period of about two hours. The coolant is subsequently removed and

the melting condensate then collected in a Schlenk vessel located under the run-off rim. The solution thus obtained can be studied by using conventional techniques. To prevent disproportionation of the MX species on melting the condensate, solvents have to be selected that are capable of stabilizing these metastable compounds.[43] The choice of solvents that may be used in this process is limited, especially since protic solvents and halogenated hydrocarbons must be ruled out because of their high reactivity with respect to MX bonds. The possibilities are further limited by the demands placed on the solvent with regards to their physical properties; they must be readily volatile and have good solvating properties at temperatures as low as possible.

Initial attempts at stabilizing AlCl were carried out using pentane. The dark red condensate obtained at 77 K spontaneously turns black on warming above approximately 170 K due to the formation of aluminum as a result of disproportionation ($3\,AlCl \rightarrow 2\,Al + AlCl_3$). Subvalent Al species could not be identified in the solution obtained. Experiments in which pentane was replaced by toluene or other aromatic solvents were similarly unsuccessful.[44] On the other hand, the use of THF appeared promising initially. After melting the condensate, a deep red solution was obtained at $-78\,^{\circ}C$ that reacted violently with water under H_2 evolution. The initial euphoria was quickly followed by sobriety, however, because the THF solutions discolored over a period of several hours or on warming slowly to room temperature. It was shown spectroscopically that this behavior was attributed to ether cleavage reactions,[45, 46] which are also known to occur with boron halides.[47] These undesired reactions can easily be avoided by using a less reactive ether such as diethyl ether for example. Admittedly, it also became apparent that toluene had to be added to the latter to fully dissolve the condensed species on warming. The likewise deep red solution thus obtained can be stored without change for several weeks at about $-50\,^{\circ}C$. The analysis of the elemental ratio of Al to Cl and the amount of hydrogen produced on hydrolysis of the solution ($Al^+ + 2H^+ \rightarrow Al^{3+} + H_2$) seems to support the existence of solvated "AlCl".[44]

Recent studies confirm that "AlBr",[48] "AlI",[49] and "GaX" (X = Cl, Br, I)[50, 51] can be stabilized analogously. As expected, the MX compounds become more stable with respect to disproportionation with increasing atomic numbers of M and X. As exemplified by "AlBr", it was established that the solvent combination toluene/diethyl ether can be replaced by other nucleophilic solvents;[52] the thermal stability increasing with increasing Lewis basicity of the solvent. The addition of an aromatic component further increases the thermal stability.[53] The addition of an arene was as yet only of absolute necessity in combination with diethyl ether, a relatively weak and only slightly polar Lewis base.

Which structures can be expected for the solvated "AlX" species? The influence of the solvent on the stability of the solutions would indicate structures with coordinated solvent molecules. These structures are supported by the ^1H NMR spectra in which the resonances of the particular donors in question are detected greatly shifted in comparison to the noncoordinated solvents. The structures shown in Scheme 8 represent some proposed structures for coordination compounds of the type $[M_nX_n(Do)_m]$ (Do = donor) that are possibly formed; these are based on analogy considerations and quantum chemical calculations. Cyclic or chain structures, for example, show analogies to those of polysilanes, because donor-stabilized Al and Ga monohalides [MX·Do] are isoelectronic with SiR_2 units (Scheme 8, **B**, **C**, **E**).

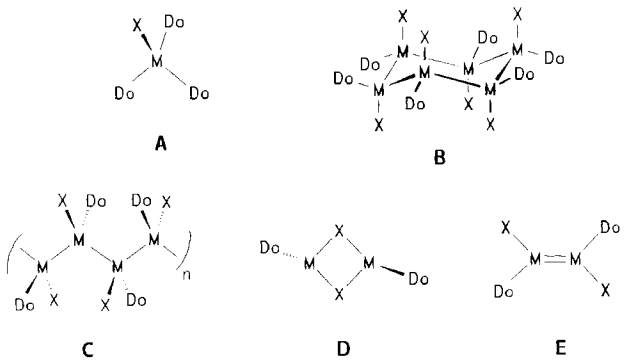

Scheme 8. Proposed structures for donor-stabilized "MX" (M = Al, Ga; X = halogen; Do = donor).

Direct proof of species of these types was not available for a long time. After numerous experiments searching for suitable donors, the stabilization of "AlBr" was finally achieved in a triethylamine/toluene mixture. The adduct of NEt_3 with AlBr can be isolated from the resulting solution in relatively good yield (ca. 50%). The light yellow solid first disproportionates at 95 °C to give metallic aluminum and $AlBr_3 \cdot NEt_3$. The results of the X-ray structure analysis show that the adduct exists as tetrameric $[Al_4Br_4(NEt_3)_4]$ (**1**) and contains a square four-membered Al ring (Fig. 2). The bromine atoms and the donor molecules are arranged in an alternating fashion above and below the ring so that a molecular structure analogous to that of cyclobutane results.[54] Analogously, the isostructural iodine compound $[Al_4I_4(NEt_3)_4]$ **2** was recently isolated from the "AlI"/triethylamine system.[55]

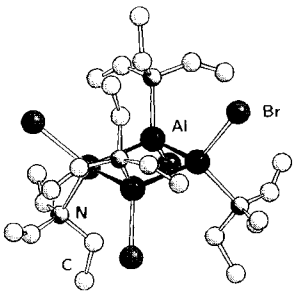

Fig. 2. Molecular structure of $[Al_4Br_4(NEt_3)_4]$ **1** in the solid state (H atoms not shown).

As **1** and **2** were the first Al monohalides whose structures were determined by diffraction methods, only results from quantum chemical calculations are available for evaluation of the observed bond lengths. The structure calculated for the model compound $[Al_4Br_4(NH_3)_4]$ **3** (SCF level)[54] does not differ significantly from that of **1**. For instance, the Al–Al distance calculated for **3** is the same as that experimentally determined for **1** (264 pm). The iodide **2** also has an insignificantly longer metal–metal distance of 265.2 pm. As expected, the Al–halogen distance (d(Al–I) = 264 pm; d(Al–Br) = 242 pm) is longer in both cases than in the gaseous monomeric AlX molecules: d(Al–I) = 254 pm; d(Al–Br) = 230 pm.[16] The long Al–N bonds (**1**: 209.5 pm; **2**: 208.2 pm) also infer Al^I species, because in the trimethylamine adduct of $AlCl_3$, for example, the Al–N distance of 196 pm is considerably shorter.[56]

In addition to the importance of **1** and **2** for structural systematics, these compounds may find numerous uses, particularly as defined starting materials in the synthesis of other Al^I species.

Structures of other donor-stabilized monohalides of Group 13 elements are not known as yet. [InX·0.5tmeda] (tmeda = *N*,*N*,*N'*,*N'*-tetramethylethane-1,2-diamine) has been isolated, but has not yet been characterized by X-ray methods.[57] To our knowledge there are no boron compounds of the type $[B_nX_n(Do)_m]$.

If anisole is used for stabilizing AlX in place of triethylamine, an aluminum monohalide cannot be isolated. Attempts to grow single crystals are made difficult by disproportionation and ether cleavage reactions. These consecutive reactions also occur in "AlX" solutions with other "methylethers".[48, 55] Under suitable conditions, the anisole adduct of $AlBr_2$, **4**, can be isolated in small yields as the least soluble component from a solution of "AlBr" in anisole.[58] $[Al_2Br_4(MeOPh)_2]$ (**4**) is the first Al^{II} halide stable at room temperature.[59] It is presumably formed at low temperatures from "AlBr" and $AlBr_3$, which is produced as a side product in the high-temperature synthesis.[60, 61] Donor-stabilized $AlBr_2$ occurs as a dimer with an Al–Al bond. The coordination spheres of the Al atoms are each completed by one anisole molecule acting as a donor (Fig. 3). An analogous dialane can be characterized in the AlI_2/PEt_3 system.[62]

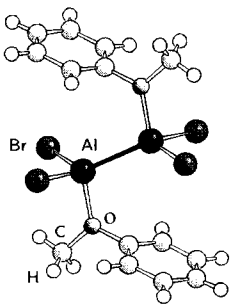

Fig. 3. Molecular structure of $[Al_2Br_4(MeOPh)_2]$ **4** in the solid state.

The Al–Al bond in **4** (d(Al–Al) = 253 pm) is about 11 pm shorter than that in **1**. This considerable difference is probably due to electronic effects rather than steric effects. For instance, a comparison of the Al–Br distances in Al_2Br_6,[18] $[Al_2Br_4(MeOPh)_2]$, and $[Al_4Br_4(NEt_3)_4]$ reveals a continuous increase in the bond lengths (222 (terminal), 230, and 242 pm, respectively). It appears reasonable to attribute both this trend and the different Al–Al distances in **1** and **4** to the increase in the radii in the series Al^{III}, Al^{II}, Al^{I}. The values of the formal oxidation state are reflected in the charge of the Al atoms as calculated by Ahlrichs and Heinzmann:[63] in the model compound $[Al_4Br_4(NH_3)_4]$ **1**, $Q_{Al} = +0.32$, in **4**, $Q_{Al} = +0.62$ (SCF level).[64]

With the exception of Tl, similar ethane-analoguous compounds of the type $[X_2(Do)E–E(Do)X_2]$ with element–element bonds are known for all Group 13 elements.[65] In contrast, under similar conditions, thallium preferentially adopts the mixed-valent ionic form $M^I[M^{III}X_4]$. In the absence of donors, this structure type is also energetically favored for InX_2 and GaX_2 species.[66]

The adduct **4** reacts in solution at room temperature to form Al metal and the anisole adduct of $AlBr_3$. The Al^{II} compound is thus considerably more labile with respect to disproportionation than the homologous $[X_2(Do)M–M(Do)X_2]$ compounds of Ga and In.[67] This stability series of the M^{II} compounds changes when the possibility of disproportionation is blocked, or at least made considerably more difficult, by the use of sterically demanding ligands. For instance, when the alkyl compounds of the formally divalent metals extensively discussed by Uhl ($[R_2M–MR_2]$ with R = $CH(SiMe_3)_2$) are compared with one another,[68] the thermal stability decreases in the same direction in which the M–C and M–M bond energies decrease (Al > Ga > In). The Al compound does not decompose before 217 °C, whereas in the case of the In counterpart, metal deposition occurs at 100 °C.

With sufficiently bulky ligands, it is even possible to force the formation of a Tl–Tl bond. The first example is $[\{(Me_3Si)_3Si\}_2Tl–Tl\{Si(SiMe_3)_3\}_2]$. The Tl^{II} compound is formed together with Tl as a disproportionation product from $[Tl^I(NMe_2)]$ and $Rb[Si(SiMe_3)_3]$.[69] In similar attempts with sterically less demanding σ-bonded substituents, Tl and an organo-Tl^{III} compound are formed as a rule as a result of disproportionation.

If the molecular structures of the donor-stabilized dihalides are compared with those of the organometallic compounds of the type $[R_2M–MR_2]$,[68, 70] it is remarkable that the M–M bonds (see Table 2) in the halogen compounds of Al and Ga are

Table 2. M–M distances [pm] for selected dimetallic compounds. R = aryl, X = halogen, Do = donor.

M	$[R_2M–MR_2]$	Ref.	$[R_2M–MR_2]^{\bullet-}$	Ref.	$[X_2(Do)M–M(Do)X_2]$	Ref.
Al	265–266	[68, 70]	247–253	[71]	253–256	[58, 62]
Ga	248–254	[68, 70]	234	[71]	239–242	[65, 72]

about 5% shorter in spite of the higher coordination number. Even in the reduction of certain $[R_2Al–AlR_2]$ or $[R_2Ga–GaR_2]$ species to their radical anions $[R_2M–MR_2]^{\bullet-}$, the bond is only shortened by between 5–7%, although in this case the metal–metal σ bond is strengthened by a single electron π bond.[71] The reduced coulombic repulsion between the positively charged metal cores as a result of π bonding contributions between the halogen atom and the metal atom and also the coordinated donor can be cited as reasons for the small distance between the metal atoms in the $[X_2(Do)M–M(Do)X_2]$ compounds. Furthermore, in any comparison of the metal–metal bonds steric aspects have to be considered, because repulsive interactions between bulky ligands can also lead to an elongation of M–M bonds.

Just how sensitive the metal–metal distance in bimetallic compounds is to geometric or electronic changes is demonstrated by the recently described digallane **5**, which is stabilized

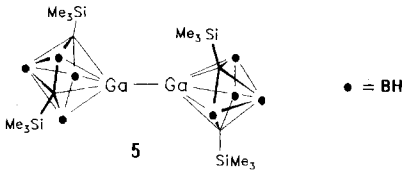

5

by divalent 2,4-bis(trimethylsilyl)-2,4-dicarba-*nido*-hexaborate-(2 −) ligands:[73] The very short Ga–Ga distance of only 234 pm corresponds to that of the radical anion $[R_2Ga–GaR_2]^{\bullet-}$ (R = 2,4,6-$iPr_3C_6H_2$) (Table 2).

To reliably evaluate the effect of electronic and geometric factors, quantum chemical calculations ought to be made as a matter of principle, at least for simple model compounds. Calculations for the parent compound $H_2Al–AlH_2$ give an Al–Al

distance of about 262 pm.[74] Steric effects thus have hardly any influence on the bonding parameters of the compounds of the type $[R_2Al-AlR_2]$ listed in Table 2.

The synthesis of "AlX" solutions already described can be applied to "GaX" systems without any problem. The analytical data of the "GaX" solutions agree with the oxidation state one for gallium, and the thermal stability of the similarly dark red solutions is greater than that of the corresponding AlX system.[50, 51] For this reason, in contrast to the "AlBr" system, no formation of a divalent $[Ga_2X_4(Do)_2]$ side product is observed. As in the case of the "AlX" solutions, the isolation of defined GaX species is difficult, since conventional separation methods such as distillation or chromatographic techniques are not practicable. The experimental possibilities of fractional crystallization are also limited by the thermolability of the species and their high reactivity with respect to many solvents. In the GaCl/diethyl ether system it is possible to isolate $[Ga_5Cl_7(OEt_2)_5]$ ($\equiv [\{(Et_2O)_2ClGa\}Ga\{GaCl_2(Et_2O)\}_3]$) **6** at about $-30\,^{\circ}C$ in a reproducible manner and in acceptable yields (ca. 30 % with respect to Ga). The structure of **6** is shown in Figure 4. The central Ga atom is surrounded by a further four Ga atoms in a distorted tetrahedral fashion. Three of these metal atoms are each bonded to two chlorine atoms and one diethyl ether molecule, whereas the fourth metal atom is surrounded by just one chlorine atom and two donor molecules. The gallium atoms thus display three different formal oxidation states: 0, 1 and 2;[75] the average oxidation state is 1.4.

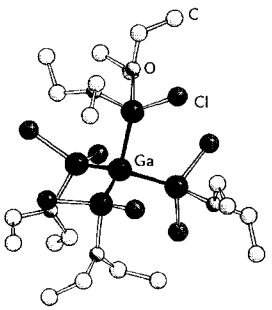

Fig. 4. Molecular structure of $[Ga_5Cl_7(OEt_2)_5]$ **6** in the solid state (H atoms not shown, d(Ga–Ga) = 242–245 pm).

The formation of **6** is possibly a result of the disproportionation of "GaCl", which slowly sets in at $-30\,^{\circ}C$ ($Ga^{I} \rightarrow Ga^{0} + Ga^{III}$ as well as $Ga^{I} \rightarrow Ga^{0} + Ga^{II}$), which under the existing conditions stops at the stage of the poorly soluble metastable intermediate $[Ga_5Cl_7(OEt_2)_5]$.

If $[Ga_2Cl_4(Do)_2]$ is considered as an ethane-analogue, **6** can be interpreted as being the neopentane counterpart in gallium chemistry. On the basis of this kind of analogy consideration, a large number of additional donor-stabilized gallium halides with metal–metal contacts can be envisaged. Their isolation will probably not be trivial, however, because based on the low decomposition temperature of **6** (0 °C), low thermal stabilities are also to be expected for these species.

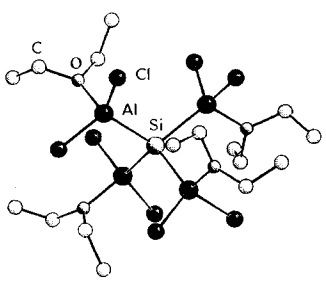

Fig. 5. Molecular structure of $[Si\{AlCl_2(OEt_2)\}_4]$ **7** in the solid state (H atoms not shown).

An Al compound corresponding to **6** is not known. The donor-stabilized ternary chloride $[Si\{AlCl_2(OEt_2)\}_4]$ **7** (Fig. 5) is closely related structurally to the hypothetical $[Al_5Cl_7(OEt_2)_5]$. It is formed rather unexpectedly from "AlCl" and $[SiCp^*_2]$.[76] The central Group 13 atom is replaced in **7** by an Si atom, which is surrounded by four $(AlCl_2 \cdot OEt_2)$ groups (isolobal with CH_3) in a distorted tetrahedral fashion. The Al–Si bond length is 243 pm. Compared with **6**, which disproportionates at about 0 °C, **7** is remarkably stable: it can be heated to 300 °C without decomposition.

X-ray structure analysis is an imperative tool in the unequivocal structural characterization of the compounds described in this section. Admittedly, this method only allows those compounds to be examined that can be obtained in the form of single crystal—and these single crystals do not necessarily represent the structures that are present in solution. Metal nucleus NMR spectroscopy is available as a complementary analytical method. The ^{27}Al NMR resonances of the solvated compounds **1** and **4** appear at about $\delta = 100-130$; thus, they lie in the region which is also typical for species with four-coordinate, trivalent aluminum.[77]

Examination of the solutions of "AlCl", "AlBr", and "AlI" in toluene/diethyl ether by ^{27}Al NMR spectroscopy reveals two signals at room temperature in each case: one very broad signal ($\omega_{1/2}$ ca. 3–4 kHz),[78] which lies at about $\delta = 100-130$, virtually regardless of the halogen, and one signal at higher field strength (AlCl: $\delta = +30$, AlBr: $\delta = +50$, AlI: $\delta = +80$), the intensity of which decreases when the sample is left to stand for prolonged periods at 25 °C. The first signal lies in the region mentioned above and has thus been assigned to donor-stabilized four-coordinate Al species. The assignment of the second signal is not yet possible. It is notable that, in contrast to AlX_3 compounds, the resonance field strength drops with increasing atomic number of the halogen. A possible explanation for this finding is provided by the shifts of non-donor-stabilized AlX (X = F, Cl) species as calculated by quantum chemical methods.[79] In this case too, the smaller chemical shift is determined for the lighter halide.[80] In addition to the donor-stabilized oligomeric AlX compounds, AlX species with different structures also seem to be present in the "AlX" solutions, particularly at low temperatures.

In spite of the diagnostic importance of ^{27}Al NMR spectroscopy, its value in structural elucidation is limited in this case. On the one hand the large full widths at half maximum of the signals prevents a differentiation between different species, on the other hand structural characteristics cannot yet be derived by using the fingerprint method, since only very few comparative data of subvalent compounds are available. This limitation applies to an even greater extent to $^{69/71}Ga$ NMR spectroscopy. The signal widths here are, as a rule, even larger, so that reliable statements regarding structures have only been possible in the case of a few compounds (see Section 3).

As already mentioned in Section 2.2, due to improvements in the technical possibilities, Raman spectroscopy coupled with quantum chemical calculations could prove to be a promising addition to structural analysis techniques in the future, in particular with regards to species in solution.

In addition to the preparation and structural characterization of further more or less donor-stabilized AlX and GaX oligomers, in future the investigation of the properties of these compounds will be of particular interest. Moreover, these species could well provide access to unusual solid-state compounds, which due to their metastable nature are not accessible by high-

temperature methods. Preliminary orientating investigations regarding this topic are currently being carried out in our group. An alternative route to donor-free Al^I and Ga^I halides could be provided by the decomposition of thermally labile MH_2X species ($MH_2X \rightarrow H_2 + MX$).[3b]

2.4. Syntheses with Al and Ga Monohalides

The temperature dependence of the equilibrium $3\,AlCl(g) \rightleftharpoons 2\,Al(s) + AlCl_3(g)$ can be used for the preparation of high purity aluminum or for the formation of thin Al layers by the CVD method.[81] Moreover, the monohalides are of importance for synthetic purposes, because they can be used as synthetic building blocks for new compounds of the trivalent elements.

Reactions that take place in solid noble gases were introduced in Section 2.2; however, monohalides can also be used for preparative syntheses. For this purpose a gas mixture made up of the AlX species prepared at high temperatures, the reaction partner, and an inert solvent are condensed onto a surface cooled with liquid nitrogen. This is subsequently heated slowly. The course of the reaction and the apparatus used correspond to the procedure described in Section 2.3; in this case the stabilizing donor is replaced by the reaction partner. In this way, a dimeric 1,4-dialumina-2,5-cyclohexadiene **8** results from AlCl and 2-butyne [Eq. (5)].[82]

$$4\ AlCl + 4\ Me{-}C{\equiv}C{-}Me \longrightarrow [ClAl\{\mu\text{-}(Me{-}C{=}C{-}Me)\}_2AlCl]_2 \quad (5)$$

8

The most interesting structural characteristic of **8** is the 2e3c bonds between the Al atoms and the C=C bonds (Fig. 6).[83] This unusual dimerization is preferred to the oligomerization

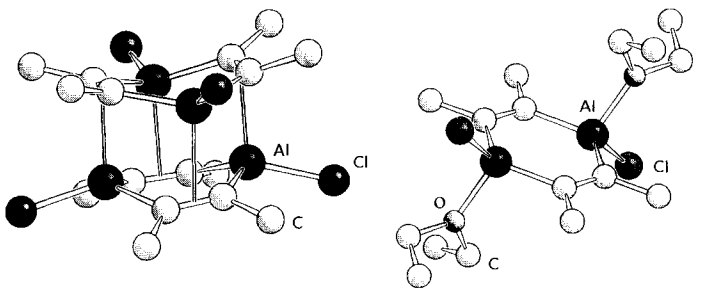

Fig. 6. Molecular structures of the 1,4-dialumina-2,5-cyclohexadienes **8** (left) and **9** (right) (H atoms not shown).

through bridging Cl atoms. The Al–C distances in the Al–olefin units are admittedly relatively long (ca. 235 pm), but all in all the four interactions lead to a remarkable stability of the dimer. The energy gained through each Al–olefin interaction is calculated to be about 25–40 kJ mol^{-1}.[83] As these quantum chemical investigations show, this value also contains small contributions from Al–Al interactions between the tetrahedrally arranged Al atoms. The high stability of the dimer is documented by the vaporization which occurs at about 140 °C without monomerization, and also by the occurrence of the molecular ion $[\mathbf{8}]^+$ in the EI mass spectrum.

If instead of butyne, hexyne is condensed with AlCl, the analogous ethyl-substituted compound is obtained. The structure of this corresponds essentially with that of **8**.[84] In addition to the particular structural characteristics of the dimer, its decomposition in solution to give hexamethylbenzene and hexaethylbenzene is worthy of mention.[45, 85] The mechanism of this decomposition is the subject of current investigation.

The Al–olefin bonds in **8** can be cleaved by ether, leading to the donor-stabilized dialuminahexadiene **9** (Fig. 6),[45, 85] in which the C=C bond is only slightly shorter: d(C=C) = 136.7 pm (**8**), 135 pm (**9**).[85, 86]

If instead of an alkyne, 2,3-dimethyl-1,3-butadiene is used as the organic component, in addition to polymeric products, the cyclic oligomer **10** is obtained [Eq. (6)], the structure of which is

$$6\ AlCl + 6\ H_2C{=}CMe{-}CMe{=}CH_2 \longrightarrow [Al_6\{\mu\text{-}Cl\}_6\{\mu\text{-}(H_2C{-}CMe{=}CMe{-}CH_2)\}_6] \quad (6)$$

10

shown in Figure 7.[87] The neighboring Al atoms of the central twelve-membered Al_6Cl_6 ring are bridged by butenediyl units, so that the coordination number four results for all Al atoms.

The reaction of AlF with bipyridine (bipy) was carried out under very similar conditions. Among others, a product was formed which could be detected by ESR spectroscopy and for which the formula $[FAl^{2+}(bipy^-)_2]_n$ was proposed.[88]

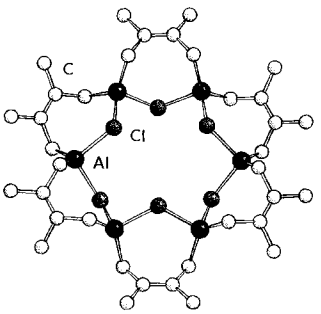

Fig. 7. Molecular structure of **10** in the crystal (H atoms not shown).

Corresponding reactions with GaX are not known to us. Although, GaI is assumed to be formed as an intermediate in the reaction of liquid Ga with I_2 in the presence of an alkyl iodide RI. The reaction is induced by ultrasound and leads to the formation of GaI_2R. In the absence of the alkyl iodide, a pale green product is formed that contains gallium and iodine in the ratio 1:1.[89]

In addition to the reactions introduced here in which Al^I and Ga^I species are oxidized to compounds of the trivalent elements, examples are also known in which the oxidation state I is retained. These metathesis reactions are treated in the following sections.

3. Organometallic Aluminum(I) and Gallium(I) Compounds

In the main, the synthesis of organometallic Al^I and Ga^I compounds has been achieved to date by two methods: a) by substitution of the halogen atoms of dissolved Al^I and Ga^I halides, and b) by reduction of a suitable Al^{III} or Ga^{III} precursor.[90] The former method has an advantage in that it can be carried out under very mild conditions, but also has a disadvantage in that

the preparation of the starting materials is coupled with considerable demands on the apparatus (see Section 2.3). The reductive method involves less demands on the apparatus, but higher temperatures are often required. Thus, this route is not frequently used to prepare temperature sensitive target compounds. In some cases readily accessible gallium dihalides (Ga_2X_4) can also be used in the preparation of Ga^I compounds; however, one equivalent of a Ga^{III} species is also formed. Corresponding reactions of donor-stabilized aluminum dihalides have not yet been investigated. Which of the methods of preparation is the most reasonable for a particular case has to be decided according to the target compound in question and the apparatus available.

3.1. Cyclopentadienyl Compounds of Monovalent Aluminum

Arenes with 6π electrons such as substituted cyclopentadienide anions are, as sterically demanding electron donors, very well suited for stabilizing metals in low oxidation states. For example, several years ago [$SiCp^*_2$] (Cp* = pentamethylcyclopentadienyl) became the first monomeric Si^{II} compound to be obtained which was stable at room temperature.[10] In the third main group of elements corresponding compounds of monovalent In and Tl are also known: [InCp] and [TlCp] were first prepared back in the 1950s.[91] Both of these compounds and their derivatives have been extensively studied and structurally characterized. The corresponding compounds of the lighter homologues were unknown until recently. In 1991 the first example of an Al^I compound stable under normal conditions,[92] namely $[Al_4Cp^*_4]$ (**11**),[93] was prepared from dissolved "AlCl" and $[MgCp^*_2]$ [Eq. (7)]. The compound **11** can be isolat-

$$4\ AlCl + 4\ [MgCp^*_2] \xrightarrow{\text{toluene/Et}_2O} [Al_4Cp^*_4] + 2\ [MgClCp^*(OEt_2)]_2 \quad (7)$$

11

ed in very high yields (85–90 %) in the form of yellow octahedral crystals. It sublimes at 140 °C and decomposes slowly as a solid at about 150 °C. Rather untypically for an Al compound, **11** crystallizes from the solvent mixture toluene/diethyl ether without additional donor molecules. The result of the X-ray crystal structure analysis is shown in Figure 8.

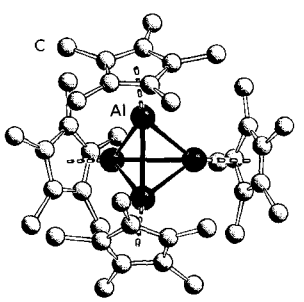

Fig. 8. Molecular structure of solid $[Al_4Cp^*_4]$ **11** (H atoms are not shown).

The most noticeable structural feature of the tetrameric compound is the central Al_4 tetrahedron, a structural element which finds its equivalent in boron chemistry, for example in B_4Cl_4 and B_4tBu_4. Apart from $K_2[Al_{12}iBu_{12}]$, which will be discussed in Section 3.3 in more detail, **11** is thus the only other polyhedral Al compound to date which has been characterized by diffraction methods.

The structure of **11** is not completely unexpected, because the solid structures of the corresponding In and Tl compounds indicate that in the case of the lighter elements of the third main group, decreasing ionic bonding contributions between the ligand and the metal, and stronger metal–metal interactions are to be expected. [TlCp*] thus forms a polymeric zigzag chain structure in the crystal, (Scheme 9) in which Tl atoms and Cp* rings alternate.[95]

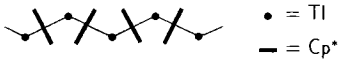

Scheme 9. Schematic representation of the chain structure in solid [TlCp*].

The long and equidistant Tl–C distances (296 pm) to both the η^5-bonded Cp* rings suggest ionic bonding contributions. In contrast to this, the transition to a metal cluster structure is indicated in solid [InCp*], in which hexameric units are present containing an In_6 octahedron.[96] However, the In–In distances of about 395 pm herein are significantly longer than the shortest interatomic distances in In metal (325 pm) or in the diindane $[R_2In–InR_2]$ (R = $CH(SiMe_3)_2$) (282.8 pm)[68] and indicate very weak In–In interactions. In the nonpolar solvent cyclohexane the In_6 cluster dissociates fully into monomeric InCp* units.[96]

The Al–Al distance (276.9 pm) determined for **11** indicates immediately that the interactions between the Al atoms of the AlCp* units in **11** are stronger than those in Al metal, in which the distance is about 9 pm longer. Compared with the calculated bond lengths for other compounds with tetrahedral Al_4X_4 units (X = H, F, Cl; Table 3), however, the Al–Al distances are still relatively long.

Table 3. Calculated equilibrium distances d [pm] and tetramerization energies ΔE [kJ mol^{-1}] of selected Al_4X_4 compounds.

X	d(Al–Al)		ΔE		Ref.
	SCF	MP2	SCF	MP2	
H	261.7	258.3	−373	−569	[97, 98]
$SiiBu_3$	263.8	–	−430	−600 [a]	[99]
SiH_3	261.6	–	−397	−604	[99]
Cl	263.6	259.8	−185	−379	[97, 98]
F	264.0	260.5	−151	−322	[97, 98]
Cp	278.7	268.0	+27	−243	[97, 98]

[a] Estimated from the results found for X = SiH_3.

The ab initio calculation (MP2) for the model compound $[Al_4Cp_4]$ is quite consistent in delivering the rather small tetramerization energy of about −243 kJ mol^{-1}. In contrast, the tetramerization energy of −569 kJ mol^{-1} for a hypothetical Al_4H_4 molecule is very large.

What are the reasons for the relatively weak intermolecular interactions of the AlCp units? In a qualitative MO scheme[97, 99] (Fig. 9) it is possible to see how the framework orbitals of an Al_4X_4 molecule (T_d symmetry) are formed from the frontier orbitals of the monomeric species.[19] The orbitals of the lone pair of electrons (HOMOs) from four AlX molecules split on forming an Al_4X_4 molecule to give a strongly bonding a_1 orbital and three destabilized t_2 orbitals. The latter are further stabilized by interactions with the MOs formed from the p_π

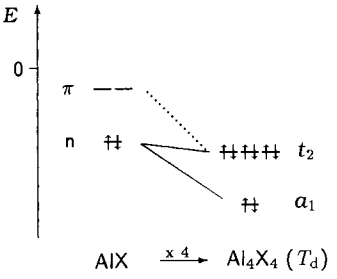

Fig. 9. Section of the qualitative MO diagram for the formation of the framework orbitals of an Al_4X_4 tetrahedron from the frontier orbitals of four AlX molecules [19,97,99].

orbitals of the AlX monomers, so that a bonding interaction results. The strength of the framework bonds in the tetrahedron depends decisively on the stabilization by the $t_2 - \pi$ interaction and thus on the energetic separation between the HOMO and LUMO (i.e. the more similar the energies of the frontier orbitals of the monomer, the more strongly the occupied t_2 orbital is stabilized).

The energies of the frontier orbitals of an AlX molecule are mainly influenced by two factors:[79] a) by the electronegativity of the ligand (high electronegativity on the part of X (e.g. X = F, Cl) leads to a higher positive charge density on the Al atom and thus to a decrease in the HOMO energy) and b) by the size of a possible delocalization of the electrons of filled ligand orbitals into the unoccupied p_π orbitals on the Al atom, which lead to a higher LUMO energy. In the case of [AlCp] the latter effect in particular leads to a large HOMO–LUMO separation and thus to a small tetramerization energy.

As similar bonding relationships are to be expected for [AlCp*], the question is posed as to whether **11** is tetrameric in solution or monomeric like [InCp*] and [TlCp*]. It was not possible to reliably determine the molar mass using cryoscopic methods to clarify this situation because of the poor solubility of **11**. The degree of association of dissolved **11** was finally determined by ^{27}Al NMR spectroscopy.[79] Figure 10 shows a

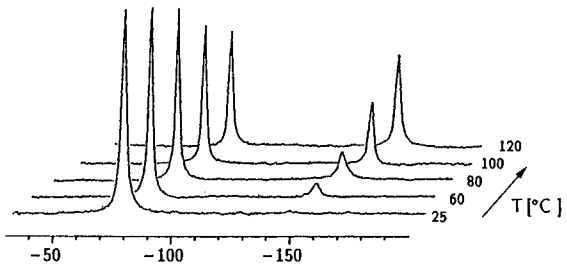

Fig. 10. ^{27}Al NMR spectra of $[Al_4Cp^*_4]$ in solution (C_7D_8).

series of ^{27}Al NMR spectra that were taken at various temperatures. Only one signal was detected at room temperature at $\delta = -80$ ($\omega_{1/2} = 140$ Hz). On raising the temperature a second resonance signal appears at $\delta = -150$ ($\omega_{1/2} = 180 \rightarrow 100$ Hz), the intensity of which increased with increasing temperature at the expense of the original signal. On subsequent cooling the original intensity ratios are restored. This process is thus in agreement with the equilibrium reaction given in Equation 8.

$$[Al_4Cp^*_4] \rightleftharpoons 4\,[AlCp^*] \qquad (8)$$

The assignment of the signals was made possible by calculating the signal positions using the GIAO method.[100] The theoretical shifts determined for the tetramer and monomer ($\delta = -85$ and -143, respectively) are in excellent agreement with the experimentally determined values. The tetramerization energy for [AlCp*] determined from the intensity ratios of the NMR signals is $-150(\pm 20)$ kJ mol^{-1}. As expected, this value is smaller than that calculated for [AlCp] (see Table 3), because repulsive interactions between the sterically more demanding Cp* ligands should additionally lower the tetramerization energy. The extremely effective shielding of the Al nuclei in **11** is mainly attributed to the influence of the Cp* ligands. First, the ring current induced in the π-electron system by the measurement takes effect and weakens the external magnetic field. Second, the η^5-Cp complexes of Al^{I} have large HOMO–LUMO separations due to the high degrees of π bonding between the ligand and aluminum, which then lead to high resonance field strengths due to the inverse proportionality of the chemical shift to the electronic excitation energy.[101, 102] As the extent of π bonding is lessened by the tetramerization in favor of the framework bonds, it is immediately apparent that a higher resonance field strength was found for the monomer than for the tetramer.

In view of the dissociation of **11** which was already detected in solution, it was to be expected that [AlCp*] does not exist in the tetrameric form in the gas phase. In spite of the low volatility and the limited thermal stability of the compound, it was possible to determine the structure of **11** in the gas phase by electron diffraction.[103] In analogy with the Cp* compounds of the heavier homologues, [AlCp*] exists in the gas phase in the monomeric [Al(η^5-Cp)] form with C_{5v} symmetry. The Al–C distance is 239 pm and is thus significantly longer than that in solid $[Al_4Cp^*_4]$ (233 pm). These values, having been determined by different methods of analysis, at different temperatures, and in different states of aggregation, are strictly speaking not comparable. The trend is unambiguous, however; the Al–C distance in the tetramer is shorter than in the monomer. The same change in distance also results from the ab initio (MP2) calculations for tetrameric and monomeric [AlCp] (d(Al–C) = 234.8 pm $[Al_4Cp_4]$; 236.3 pm [AlCp]).[98] An analysis of the molecular orbitals involved shows that these changes are due to a greater s character of the Al–C bond in the tetramer, or due to the dominant p character in the monomer.[79]

A second synthetic route to **11** was reported recently, according to which the compound is accessible by the reductive dehalogenation of $[AlCl_2Cp^*]_2$ [Eq. (9)].[104] This procedure places

$$2\,Al_2Cl_6 \xrightarrow[-4\,ClSiMe_3]{+4\,Cp^*SiMe_3} 2\,[AlCl_2Cp^*]_2 \xrightarrow[110°C]{+8K/-8KCl} [Al_4Cp^*_4]\ \mathbf{11} \qquad (9)$$

only minor demands on the apparatus required, but necessitates more synthetic steps than the first method of preparation. Because of the high thermal strain in the last reaction step the yield remains under 20 % and the target product is contaminated with small amounts of side products.[105] The reductive synthetic route is therefore hardly suitable for thermally less stable Al^{I} compounds.

What influence does the exchange of the methyl groups on the C_5 ring of **11** by other substituents have on the stability and on

the geometrical structure parameters of the cyclopentadienyl Al[I] compounds? Analogous to the preparation of [AlCp*], a yellow compound can be prepared from AlCl and [$MgCp_2$]—presumably oligomeric [AlCp] [Eq. (10)]. At about −60 °C the ex-

$$4\ AlCl + 4\ [MgCp_2] \xrightarrow{\text{toluene/}Et_2O} [Al_4Cp_4] + 2\ [MgClCp(OEt_2)]_2 \quad (10)$$

12

tremely thermolabile compound disproportionates within a few seconds and turns black due to the deposition of metallic aluminum.[79] It has not yet been possible to obtain single crystals of the "oligomer" and thus elucidate its structure by diffraction methods. It can be deduced from the ^{27}Al NMR spectrum obtained at −80 °C, however, that dissolved [AlCp]—like [AlCp*]—exists in the tetrameric form at this temperature.[79] The position of the ^{27}Al NMR signal measured ($\delta = -111$) agrees very well with the quantum chemical resonance calculated ($\delta = -105$) for tetrahedral [Al_4Cp_4] **12**. The full width at half maximum of the signal ($\omega_{1/2} = 1250$ Hz) is almost identical with that determined for the signal of [$Al_4Cp^*_4$] at this temperature. The stronger shielding of the Al nuclei in **12** in comparison to those in **11** is plausible, because the expected higher ionic bonding character between Al and the Cp ligand in the Cp compound leads to a larger HOMO–LUMO separation.

In an alternative synthetic strategy, attempts were made to synthesize **12** from **11**. With this aim in mind, Cp* ligands were to be substituted in a metal exchange reaction with [$MgCp_2$] [Eq. (11)]. As the rate of reaction was too slow even at 20 °C, the

$$[AlCp^*] + [MgCp_2] \longrightarrow [AlCp] + [MgCp^*Cp] \quad (11)$$

thermolabile **12** could not be prepared by this method. Nevertheless, a new yellow product was formed in the reaction mixture which was shown to be [$Al_4(\eta^5\text{-}Cp^*)_3(\eta^5\text{-}Cp)$] **13**,[94] by NMR spectroscopic analysis; thus one AlCp* unit of [$Al_4Cp^*_4$] was replaced by an AlCp fragment. The ^{27}Al NMR spectrum shows two signals in the ratio 3:1. The ^{27}Al NMR resonances for the AlCp* and AlCp partial structures are shifted slightly downfield compared with those for **11** and **12** ($\delta = -77$ and -108, respectively; $\omega_{1/2}$ 300 Hz in both cases).[106]

These experiments show that the substitution of the Cp* ring on [AlCp*] is possible in principle. For this reason [$Al_4Cp^*_4$] was treated analogously with pentabenzylcyclopentadienyllithium and tris(trimethylsilyl)cyclopentadienyllithium. The substitutions take place only slowly at room temperature, but they do go to completion and without disproportionation worthy of mention; however, reaction products [$Al\{C_5(CH_2Ph)_5\}$] (**14**) and [$Al\{C_5H_2(SiMe_3)_3\}$] (**15**) have not yet been isolated in crystalline form. According to the ^{27}Al NMR spectra, both compounds exist in the monomeric form in solution (δ(**14**) $= -155$ (1500 Hz); δ(**15**) $= -165$ (450 Hz)).[94] The isolation of these and other species is the subject of current investigations.

3.2. π Complexes of Monovalent Gallium

The π complexes of Ga^+ have been known for quite some time. Solutions of the mixed-valent gallium dihalides $Ga^+[GaCl_4]^-$ in aromatic solvents contain Ga[I] arene complexes,[107] which can be identified by Ga NMR spectroscopic techniques. The structural element of the 6π-electron arene coordinated η^6 to Ga^+ is also retained in the solid.[9] It is surprising, therefore, that Cp complexes of monovalent Ga were unknown until recently, although the gallium dihalides have long been available as starting materials, in which Ga occurs—at least partially—in the "correct" oxidation state.

The synthesis and identification of [GaCp] (**16**) was first achieved about 35 years after the characterization of [InCp]; its synthesis involves the treatment of dissolved "GaCl" with [$MgCp_2$] or [LiCp] under salt elimination [Eq. (12)]. Mass spec-

$$GaCl + [MCp] \xrightarrow{\text{toluene/}Et_2O} [GaCp] + MCl \quad (12)$$

(M = Li, CpMg) **16**

trometric and NMR techniques reveal that **16** exists in the monomeric form both in the gas phase and in solution. Ab initio calculations (MP2) on the structure and the ^{71}Ga NMR resonance were especially helpful in this respect.[108] According to these—and in analogy to [InCp] and [TlCp]—a C_{5v} symmetric structure with an η^5-coordinated Cp ring represents the minimum of the energy hypersurface for [GaCp] in the gas phase. The ^{71}Ga NMR shift calculated for this molecule is $\delta = -696$. The strong shielding of the metal nucleus seems reasonable in light of the behavior discussed for the Al compounds. In very good agreement with the calculated value, a signal is detected experimentally at $\delta = -714$ ($\omega_{1/2} = 250$ Hz), which indicates that the [Ga(η^5-Cp)] structure can be inferred in solution too.

The unexpectedly high volatility of **16** is quite remarkable. When dissolved in toluene/Et_2O, [GaCp] can be identified by mass spectroscopy in the gas phase using a feed cooled to −78 °C. There are problems associated with this property in trying to isolate pure [GaCp]. It is very easy to separate the product together with the solvent from the other reaction products,[109] but the preparation of solvent-free **16** has not yet been successful. The isolation is made additionally more difficult in that **16** is only stable in dilute form at room temperature and already starts to disproportionate at −70 °C at concentrations greater than 0.2 mol L^{-1}.[51] Small amounts of solid colorless [GaCp] can be precipitated by lowering the solubility through the addition of pentane. Compound **16** is more thermally stable and considerably less volatile as a solid than in solution. An exact determination of the decomposition temperature and the vapor pressure could not yet be carried out due to the problem of isolation.

In analogy with **16**, a series of further ring-substituted cyclopentadienyl compounds of Ga[I] have been prepared.[110] Ga_2Cl_4 can be used as an alternative to "GaCl", but in this case additional products of trivalent Ga are formed that make it more difficult to separate the target compounds. All in all, the isolation of the substituted compounds is considerably easier than that of the parent compound **16** thanks to greater thermal

stability and lower volatility. [GaCp*] (**17**) for example, can be isolated free from solvent by fractional distillation.[110] The ^{71}Ga NMR resonance of **17** appears at $\delta = -653$ ($\omega_{1/2} = 700$ Hz), and compared with that of **16**, it is only slightly shifted downfield. This tends to indicate that **17** also exists in the monomeric [Ga(η^5-Cp)] form in solution. Neither increases nor decreases in the temperature lead to changes in the ^{71}Ga NMR resonances of **16** or **17**, which indicates that neither compound is involved in association equilibria. An oligomerization involving the lone pair of electrons on gallium would thus appear to be less favorable than in the case of the analogous Al compounds, which seems reasonable in view of the larger inert pair effect expected for gallium.

The structure of [GaCp*] in the gas phase was determined by electron diffraction experiments (Fig. 11).[111] [GaCp*] has a pentagonal pyramidal structure with an η^5-coordinated C_5 ring. The Ga–C distance of 240.5 pm, is somewhat shorter than that calculated for **16** (242.0 pm). It is interesting to compare the gaseous molecules [AlCp*] and **17**. The Ga–C distance in **17** is about 0.7% (1.7 pm) longer than the Al–C bond in monomeric [AlCp*]. If the bond lengths of the gaseous compounds GaH, GaCl, and GaF are compared with those of the corresponding Al compounds,[16] it can be seen that here too, the Ga–X bonds are longer. Whereas this difference for the relatively nonpolar hydrides approximately corresponds with that of the Cp* compounds (0.6%), in the case of the polar halides the difference is considerably larger (Cl: 3.3%; F: 7.3%). The nonpolar character of the compounds **11** and **17** already deduced from their physical properties is thus also reflected in their bond lengths.

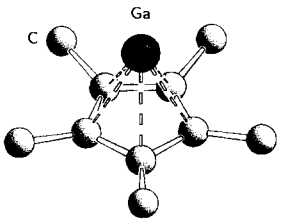

Fig. 11. Molecular structure of [GaCp*] **17** in the gas phase (H atoms not shown).

In addition to [GaCp] and [GaCp*], it was also possible to prepare [Ga(C_5H_4tBu)], [Ga{C_5(CH_2Ph)$_5$}], and [Ga{C_5H_2-($SiMe_3$)$_3$}].[110] According to the spectroscopic data, all of these compounds have, like [GaCp*], a half-sandwich structure and exist in the monomeric form in aromatic solvents. The question as to how the GaCp derivatives are constructed in the solid remains unclear. Do they—like the Al compounds—prefer polyhedral structures, or—like the heavier homologues—polymeric structures with weaker intermolecular interactions? The properties of the dissolved species (e.g. solubility, NMR shifts) would seem to indicate the latter.

3.3. Alkyl and Silyl Compounds of Al^I and Ga^I

As already suggested (see Table 3), alkyl and silyl compounds of Al and Ga should tend to oligomerize to a considerably greater extent than the Cp complexes in which the monomeric units are stabilized by π bonds between the ligand and the metal atom. Prerequisites for the synthesis of AlR and GaR compounds with R = alkyl and silyl are that the ligands R are bulky and kinetically stabilizing and as such prevent the thermodynamically preferred disproportionation from taking place.

Compounds of this type have long been known in boron chemistry.[112] B_4tBu$_4$ recently became the first example of just such an electron-deficient compound to be characterized by X-ray structure analysis.[113] In the meantime, similar species for Al, Ga, and In are also known: the first concrete spectroscopic indications came in 1991. Like [$Al_4Cp^*_4$] (**11**), [Al_4(SitBu$_3$)$_4$] (**18**) can be synthesized by metathesis, in this case by reacting "AlCl" with NaSitBu$_3$ in dibutyl ether.[114] The thermally very stable compound **18** can be separated from the other reaction products by sublimation at 180 °C [115] and characterized as tetrameric [Al(SitBu$_3$)] by mass spectrometry. Unfortunately it has not yet been possible to obtain a solid suitable for X-ray structure analysis. However, quantum chemical calculations (SCF) confirm the tetrahedral structure of **18** (Fig. 12).[99] Compound **18** is characterized by a relatively high tetramerization energy which is a result of the small HOMO–LUMO separation both in the monomeric and in the tetrameric species. Its value corresponds approximately with that of Al_4H_4 and [Al_4(SiH_3)$_4$] and is considerably larger than that of the Cp compounds **11** and [AlCp] (**12**) (see Table 3). In a comparison of **18** with **11** and **12**, this is noticeable not only in the significantly shorter Al–Al bond (263.8 pm in **18**, compared with 276.9 pm in **11** and 278.7 pm (SCF) in **12**), but also in the color: the Cp compounds are yellow, whereas the smaller frontier orbital separation in **18** leads to a blue-violet color. The Al–Al bond in **18** is only insignificantly longer than those calculated in the same manner for Al_4H_4 and [Al_4(SiH_3)$_4$], and it is assumed, therefore, that there are no steric strains of great significance due to interactions between the ligands.

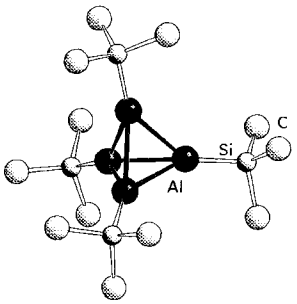

Fig. 12. Calculated structure for [Al_4(SitBu$_3$)$_4$] **18** (Me groups not shown).

A further Al^I compound is accessible by the reduction of di(neopentyl)aluminum chloride with K [Eq. (13)].[116] The results of the molecular mass determination indicates that the compound is the tetrameric [Al_4{$CH_2C(CH_3)_3$}$_4$] **19**. The sluggishness of **19** in entering into reactions leads to the assumption that it has a tetrahedral structure, because in this case the reactive Al_4 core is well shielded by a hydrocarbon shell.

$$2\ AlCl[CH_2C(CH_3)_3]_2 + 8\ K \xrightarrow{-2KCl} 1/4\ [Al_4\{CH_2C(CH_3)_3\}_4] + Al[CH_2C(CH_3)_3]_3 \quad (13)$$

19

As yet there have been no reports of an Al_4R_4 compound with alkyl or silyl ligands that has been characterized by diffraction methods. In contrast, the preparation and characterization of compounds of this type in gallium chemistry has been more successful. Red [Ga_4{$C(SiMe_3)_3$}$_4$] (**20**) was synthesized from the dioxane adduct of Ga_2Br_4 and Li[$C(SiMe_3)_3$] and was the first example found belonging to this class of compounds [Eq. (14)].[117]

$$[Ga_2Br_4(O_2C_4H_8)_2] + 3\ Li[C(SiMe_3)_3] \xrightarrow{-3\,LiBr}$$
$$1/4\ [Ga_4\{C(SiMe_3)_3\}_4] + \text{"}GaBr[C(SiMe_3)_3]_2\text{"} \quad (14)$$
$$\mathbf{20}$$

The structure of this surprisingly stable compound (decomposition > 255 °C) comprises a central tetragallatetrahedrane framework. It corresponds to the structure of **18** shown in Figure 12 when the Al atoms are replaced by Ga atoms and the *t*Bu$_3$Si ligands are replaced by (Me$_3$Si)$_3$C (trisyl) groups. The most interesting structural parameter is almost certainly the Ga–Ga distance of 268.8 pm, which is about 15 pm longer than that in the digallane [R$_2$Ga–GaR$_2$] (R = CH(SiMe$_3$)$_2$).[68] The long Ga–Ga distances are probably due to the repulsive interactions between the bulky trisyl ligands. The relatively facile dissociation of the tetrahedron also tends to indicate that the bonds between the Ga atoms are to be classified as weak. Cryoscopic studies in benzene show an increasing degree of dissociation with increasing dilution. At a concentration of 0.0014 mol L^{-1}, **20** is fully dissociated into monomeric units. In the gas phase too, only monomeric [GaC(SiMe$_3$)$_3$] is observed. The molecular structure of this gallanediyl was determined by electron diffraction experiments.[118]

The dark violet compound [Ga$_4${Si(SiMe$_3$)$_3$}$_4$] **21**, a compound related to **20**, can be prepared from [Ga$_2$Cl$_4$(O$_2$C$_4$H$_8$)$_2$] and Li[Si(SiMe$_3$)$_3$]·3THF.[119] The X-ray structure analysis of **21** shows that the exchange of the tertiary C atoms by Si atoms has a drastic effect on the size of the central Ga$_4$ tetrahedron. The Ga–Si bonds are longer than the Ga–C bonds and lead to considerably longer distances between the ligands, thus allowing the Ga atoms to approach each other to within 259.1 pm. This distance is only slightly longer than the Ga–Ga bond lengths calculated by quantum chemical methods (MP2) for simple tetragallatetrahedranes Ga$_4$X$_4$ (X = H (253 pm), Cl (257 pm), F (259 pm)).[98] Compound **21** should thus be relatively free of steric strain.

Although the tendency to form homonuclear bonds decreases with increasing atomic number in the Group 13 elements, the In compound analogous to **20**, [In$_4${C(SiMe$_3$)$_3$}$_4$] (**22**), also has a tetrahedrane structure in the solid state. The difference to the analogous Ga compound is that the tetrameric structure is retained even in solution. This observation is reasonable, since lower steric strain is to be expected between the substituents of **22** due to the larger M$_4$ tetrahedron. The red-violet compound **22** can be synthesized starting from In$_2$Br$_4$·2tmeda [2, 120] or from InCl on treatment with Li[C(SiMe$_3$)$_3$].[121] The average In–In bond length is 300 pm.[120] This is thus considerably shorter than that in the octahedral "cluster" [In$_6$Cp$^*_6$] (395 pm).[96] A more sensible value for making a comparison is the bond length in the diindane [R$_2$In–InR$_2$] (R = CH(SiMe$_3$)$_2$),[68] which is approximately 20 pm (about 7%) shorter than that in the tetrahedral compound **22**.

If the dimetallic compounds [R$_2$Ga–GaR$_2$] and [R$_2$Al–AlR$_2$] are compared in an analogous manner with the "strain free" tetrahedranes **18** and **21**, the metal–metal bonds in the M$_4$ frameworks are only 2.5% longer for gallium, and in the case of aluminum even about 2.5% shorter, than in the corresponding dimetallic compounds. This finding further reflects the lower tendency of the MR monomers of the heavier elements to tetramerize.

The compounds described in this section up till now give the impression that tetrameric M$_n$R$_n$ compounds are formed preferentially. This collection of tetrahedral oligomers may be due in the first instance to the fact that to date mainly those compounds with very bulky ligands have been studied. The tetrahedron, that is the smallest polyhedron, provides the greatest possible amount of space for the ligands and thus permits the metal atoms to approach one another most closely. In the case of smaller substituents, whose lesser spatial demands would permit the formation of larger polyhedra, it would be expected that the kinetic stabilization would become too small, and that the disproportionation of the compound would come to the fore.

In addition to these steric constraints, the electronic influences should also be of importance for the formation of a particular oligomer. According to Wade's rules,[122] *closo*-polyhedra attain their greatest stability when they have $n + 1$ electron pairs for the framework (n = number of corners on the polyhedron), that is when they are dianions. A large number of compounds are known from boron chemistry and from other fields of chemistry of the main group elements which adhere to this rule. To our knowledge, however, doubly reduced tetrameric M$_4$R$_4$ species of the Group 13 elements are not known. This finding can be explained by use of the MO diagram for tetrahedral MR compounds (Fig. 9). This shows that the four electron pairs from the HOMOs of the monomers already lead to a closed shell occupancy in the tetramer ($a_1 + t_2$).[99] The singly reduced radical anions [B$_4$*t*Bu$_4$]$^{\bullet -}$,[123] [Ga$_4${C(SiMe$_3$)$_3$}$_4$]$^{\bullet -}$,[124] and [In$_4${C(SiMe$_3$)$_3$}$_4$]$^{\bullet -}$ [124] can be identified, but little is known about their structures, for which Jahn–Teller distortion is expected. In the case of [B$_4$*t*Bu$_4$]$^{\bullet -}$, ESR spectroscopic studies lead to the conclusion that this has a butterfly structure.[123] In conclusion, small ligands and reductive reaction conditions that are as mild as possible should be advantageous for the synthesis of large polyhedra.

Polyhedral structural elements have long been known in the field of intermetallic phases—including for the heavy Group 13 elements. At this point only one example of this rather extensive and fascinating field will be mentioned. In Na$_x$Mg$_{5-x}$Ga$_9$ a three-dimensional Ga network is found which contains a Ga$_{12}$ icosahedron; this network is the result of partial reduction of Ga.[125] These structural elements can be treated using Wade's rules in the same way as for dianions of a *closo*-polyhedron, such as [B$_{12}$H$_{12}$]$^{2-}$, when performing an electron count. The role of the ligands is assumed by other atoms of the Ga network. The Ga–Ga distance in the slightly distorted Ga$_{12}^{2-}$ units lies between 269 and 273 pm.

Confirmation of an Al$_{12}$ icosahedron in a molecular compound was a long time in coming. Admittedly, back in 1976 a highly reduced polymeric Al compound was identified in the distillation residue in the reaction of diisobutylaluminum chloride with potassium,[126] but the elucidation of the course of the reaction and the characterization of the products was first achieved in 1991.[127] Dark red K$_2$[Al$_{12}$*i*Bu$_{12}$] (**23**) is made in small but reproducible yields [Eq. (15)]. The X-ray structure

$$AliBu_2Cl + K \xrightarrow[25°C]{hexane}$$
$$K_2[Al_{12}iBu_{12}] + K[AliBu_2Cl_2] + K[AliBuCl_3] \quad (15)$$
$$\mathbf{23}$$

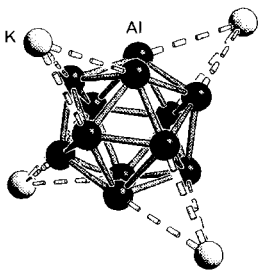

Fig. 13. Depiction of the Al_{12} unit and the surrounding K atoms in $K_2[Al_{12}iBu_{12}]$ **23** (*i*Bu groups not shown).

analysis of **23** confirms the presence of an almost undistorted icosahedral Al_{12} unit (Fig. 13). The Al–Al distance of 268.5 pm is somewhat longer than that in the neutral tetrameric Al_4R_4 (R = H, $SiMe_3$, $SitBu_3$, see Table 3). Compound **23** is rather unstable in solution, but in the solid state it first decomposes above about 150 °C. The redox behavior of the Al_{12} cluster is interesting. As in the case of similar boron compounds, cyclovoltammetric studies show a reversible single-electron oxidation and an irreversible second oxidation step.[2]

The second anionic Al cluster known to date is also formed under reductive conditions. A dark red compound of high thermal stability is formed from AlCl and Li*t*Bu; presumably Al_ntBu_n [Eq. (16)]. If the substance is reduced at 4 °C with Na/K alloy, a compound containing the radical anion $[Al_6tBu_6]^{\bullet -}$ **24** is formed, which has been identified by ESR spectroscopy, but unfortunately not yet been isolated.[128]

$$AlCl + LitBu \xrightarrow{-LiCl} Al_ntBu_n \xrightarrow{Na/K} \underset{\mathbf{24}}{[Al_6tBu_6]^{\bullet -}} \qquad (16)$$

According to SCF calculations, a distorted octahedral structure (D_{3d} symmetry, squashed along the three-fold axis) is expected for the radical anion, with six magnetically equivalent Al atoms (Fig. 14).[129] The singly occupied MO is localized to about 99% on the Al cluster, so that a coupling of the unpaired electron with the Al nuclei can occur, but a coupling with the alkyl groups should not be possible. The hyperfine structure of the ESR spectra obtained from solutions (31 lines) and the small hyperfine coupling constant ($a(^{27}Al) = 8.2$ G) are in agreement with the structure suggested by quantum chemical calculations. According to this, the Al–Al distances are 261.7 and 275.2 pm for the energetically most favorable conformation. Compared with six monomeric Al*t*Bu molecules, the neutral hexamer is already about 540 kJ mol^{-1} more stable on the SCF level.[130] The reduction to the monoanion stabilizes the entity by a further 140 kJ mol^{-1}. Electrochemical studies on this system, for example, the reduction to the dianion, have not yet been carried out.

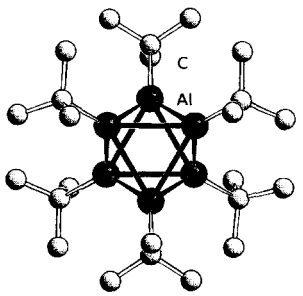

Fig. 14. Calculated structure of the radical anion $[Al_6tBu_6]^{\bullet -}$ **24** (H atoms not shown).

In conclusion, it remains to be mentioned that a mixture of different oligomers of neopentylgallium(I) are accessible by the reduction of di(neopentyl)gallium chloride. The average degree of association of these lies between 8.9 and 10.5.[131]

4. Chemical Properties of $[Al_4Cp^*_4]$

As already mentioned in Section 3, $[Al_4Cp^*_4]$ (**11**) differs from most of the compounds described therein with regard to its tendency to readily dissociate into monomers. This behavior should have an effect on the chemical properties of the compound, because it is to be expected that monomeric alanediyls, like the analogous boranediyls (borylenes),[132] are very reactive. However, the reactivity of [AlCp*] should be lowered by the good donor properties of the Cp* ligands. The previously studied reactions of **11** in solution confirm that indeed a "tamed", but as a result in most cases a very selective alanediyl is present. Compound **11** thus reacts quantitatively with 2,3-dimethyl-1,3-butadiene in toluene at 50 °C [Eq. (17)].[133]

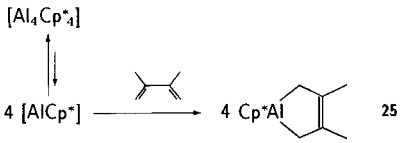

25 (17)

In the solid state **11** is even relatively inert with respect to air, since the aluminum atoms in the tetrameric unit are well shielded by the ligands. Compound **11** is even stable for prolonged periods in water and other polar solvents in which it does not dissolve. In water the surfaces of the crystals are first attacked after about 20 minutes. On the other hand, when in solution, **11** is readily oxidized by air. If a saturated solution of **11** in benzene is brought into contact with air the compound decomposes completely after just 20 minutes.

Rather unexpectedly, solutions of **11** are thermally stable. A solution of **11** in toluene disproportionates fully only after about 20 days at 100 °C, forming Al metal, a considerable amount of pentamethylcyclopentadiene (Cp*H), and an Al^{III} compound.[134] According to the results of spectroscopic studies this is not $AlCp^*_3$, but rather a product arising from this by the elimination of Cp*H.[135]

4.1. Reactions with Lewis Acids

[AlCp*] could function as a base which forms adducts with Lewis acids such as aluminum trihalides or boron trihalides. This type of behavior is known for [InCp], which reacts for example with BF_3 to give the donor–acceptor complex $[CpIn \rightarrow BF_3]$.[136] Furthermore, an insertion into element–halogen bonds is feasible by which, for example, species such as the type represented by **26** could arise.

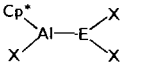

26 (E = B, Al)

In the presence of $AlCl_3$, solutions of **11** in toluene start to disproportionate slowly at 25 °C. If the reaction solution is left at room temperature, Al metal and the aluminum sesquichloride $[Al_2Cl_3Cp^*_3]$ are obtained as the main products. The course of this reaction could be the result of an insertion of [AlCp*] into an Al–Cl bond, by which thermolabile Al subhalides of the type represented by **26** are formed. Their disproportionation would subsequently lead to the products observed.

However, intermediate products of this reaction have not yet been identified.

If this reaction is carried out at higher temperatures, a colorless compound is formed that is extremely sensitive with respect to hydrolysis [Eq. (18)]. The results of the X-ray structure analysis show the compound to be $[AlCp^*_2][AlCl_3Cp^*]$; an ionic isomer of $[Al_2Cl_3Cp^*_3]$.[137]

$$3\,[AlCp^*] + AlCl_3 \xrightarrow[-2\,Al]{\text{toluene/25°C}} [Al_2Cl_3Cp^*_3] \xrightarrow{\Delta} [AlCp^*_2][AlCl_3Cp^*] \quad (18)$$

The $[Al(\eta^5\text{-}Cp^*)_2]^+$ ion **27** of this compound (Fig. 15) is the first ferrocene analogue of a Group 13 element. Since $[BCp^*_2]^+$[138] and $[BeCp_2]$[139] each have just one η^5-coordinated Cp* or Cp ligand, **27** is possibly the smallest metallocene of any main group element.[140] The Al–C bond length is 215.5 pm. Decamethylmagnesocene is isoelectronic with **27**, but due to the smaller positive charge on the central atom it has considerably longer metal–C distances (234.8 pm).[141] The same is also valid for the bis(η^5-dicarbollide)aluminum anion $[Al(\eta^5\text{-}C_2B_9H_{11})_2]^-$ (d(Al–C) = 224–230 pm),[142] which is closely related to **27** from a structural point of view; however, the bonding situation is not exactly comparable with that in **27** (see below). The extremely high ^{27}Al NMR resonance field strength of the cation **27** at $\delta = -114.5$ is quite remarkable and completely untypical for diamagnetic Al^{III} compounds. The calculated ^{27}Al NMR shift (GIAO) for $[Al(\eta^5\text{-}Cp^*)_2]^+$ in D_{5d} symmetry is $\delta = -119.8$ and thus confirms that this structure is also retained in solution.[137] The strong shielding of the Al nuclei, as is the case in the π complexes of Ga^I and Al^I, is mainly attributed to the effect of the ring current. Interestingly, a considerably smaller resonance field strength ($\delta = +54$) is calculated for the Al atom in the bis(η^5-dicarbollide)aluminum anion, which is also surrounded in a sandwich fashion.[143] According to this finding, diamagnetic ring current effects have virtually no effect, that is the bonding differs from that in **27** although according to the usual bonding considerations Cp and dicarbollide ligands should behave similarly.[144, 145]

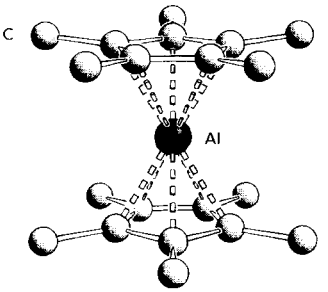

Fig. 15. Structure of the $[Al(\eta^5\text{-}Cp^*)_2]^+$ ion **27** in the crystal (H atoms not shown).

The possibility of insertion of [AlCp*] into element–halogen bonds mentioned at the beginning of this section was reason enough for us to also treat **11** with boron trihalides. In contrast to the reaction of **11** with $AlCl_3$, no Al deposition is observed. In the reactions that we studied no uniform products were obtained, as was the case in reactions of the carbene homologue $[SiCp^*_2]$ with boron trihalides for example.[146] Even at −78 °C, the reaction with BCl_3 in toluene rapidly led to a complicated mixture of products. According to the findings of NMR spectroscopic studies, the carbon framework of the Cp* ligand is also attacked.[147]

Boron tribromide reacts somewhat more selectively. In this case the reaction in toluene first gets underway at higher temperatures and leads to presumably three main products. About 30% of the aluminum used is found in the form of the ionic compound $[BBrCp^*][AlBr_4]$ (**28**), which was identified by its characteristic NMR spectra and by crystal structure analysis. The cation of this compound was already prepared by Jutzi et al. in 1977 in the form of $[BBrCp^*][BBr_4]$ and characterized by NMR spectroscopy in solution as a *nido*-carborane having a pentagonal pyramidal structure.[148] The X-ray structure analysis recently carried out on **28** confirms that this structure type also exists in the solid (Fig. 16). The CH_3 substituents of the Cp* ring are slightly bent towards the boron atom—in agreement with a theoretical prediction.[149, 150] Since both Al and B have the oxidation state III in this compound, but at the same time no aluminum is formed by disproportionation, **28** can be considered as indirect evidence for the (intermediate) occurrence of subvalent boron species. The direct characterization of these intermediates or their consecutive products has still to be made.

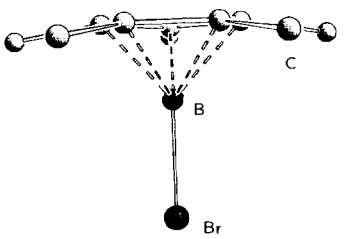

Fig. 16. Structure of the $[BBrCp^*]^+$ ion of **28** in the crystal (H atoms not shown).

The reduction of a suitable B^{III} precursor to make [BCp*] is particularly appealing, and according to the results shown here should also be feasible. This is the last missing member in the series of MCp* compounds (M = B, Al, ... Tl).

[AlCp*] first reacts with the weaker Lewis acid SiF_2Ph_2 at higher temperatures (ca. 110 °C) [Eq. (19)]. It is apparent that in

$$4\,[AlCp^*] + 2\,SiF_2Ph_2 \xrightarrow[3\,d]{\text{toluene/110°C}} [\{Si(AlCp^*F)_2Ph_2\}_2] \quad (19)$$

29

order to cleave the strong Si–F bonds a considerably high activation energy is required. In spite of this $[\{Si(AlCp^*F)_2Ph_2\}_2]$ (**29**) is formed in good yields (88 %) (Fig. 17).[151] Compound **29** can be considered as a dimer of an insertion product of [AlCp*] into the Si–F bonds of SiF_2Ph_2. The Cp* ligands are aprroximately η^2-coordinated. The Al–Si bond length (245.1 pm) corresponds well with the value found for $[Si\{AlCl_2(OEt_2)\}_4]$ (**7**) (see Section 2.3).

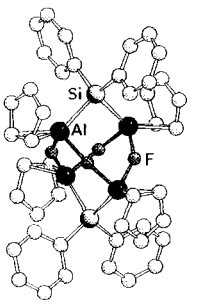

Fig. 17. Structure of $[\{Si(AlCp^*F)_2Ph_2\}_2]$ **29** in the crystal (H atoms not shown).

4.2. Reactions with Elements of the Fifth and Sixth Main Groups

Compound **11** can be oxidized with the elements P, Se, and Te to give interesting products in very good yields. If **11** is treated with white phosphorus in toluene at 25 °C, the unusual cage com-

pound $[(Cp^*Al)_6P_4]$ **30** [Eq. (20); Fig. 18] is obtained in just one synthetic step.[153] Six Al and four P atoms form an Al_6P_4 cage

$$6\ [AlCp^*] + P_4 \xrightarrow[25°C]{\text{toluene}} [(Cp^*Al)_6P_4]\quad \mathbf{30} \qquad (20)$$

with alternating occupancies. This cage can be described as consisting of two face-sharing heterocubanes, the opposite corners of which are missing (Scheme 10). The unexpected bonding in this compound is particularly remarkable. For the formation of two-electron–two-center bonds for the fourteen Al–P contacts in the framework, 28 electrons would be necessary. As can be shown by quantum chemical methods, however, one lone pair of electrons can be attributed to each P atom. As these lone pairs are not delocalized over the cage, only 24 electrons are available for the framework bonds (two from each AlCp* fragment and three from each P atom). Thus, **30** must be regarded as an electron-deficient compound in which 14 bonds are formed by 12 occupied MOs.

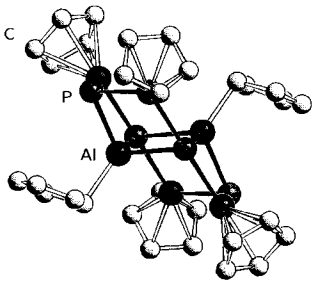

Fig. 18. Molecular structure of $[(Cp^*Al)_6P_4]$ **30** in the solid state (Me groups not shown).

The insertion of one AlCp* unit into each of the six P–P bonds of the P_4 tetrahedron is a feasible mechanism for the formation of **30**. Initially a heteroadamantane (**31**) would be formed, built up from Al and P, which would then rearrange to give the isomer **30**. Quantum chemical studies on the model compound $[(CpAl)_6P_4]$ confirm that isomer **30** is about 30–80 kJ mol^{-1} more stable than isomer **31**. The stabilization is attributed to additional Al–P contacts as well as to significant Al–Al bonding contributions. The structure determined for **30** (Fig. 18) represents a new structural variation of M_6E_4 compounds, in which an additional possibility of stabilization exists due to an electron deficiency.

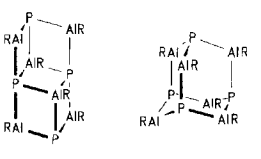

Scheme 10. Schematic representation of the cage compounds **30** and **31**; R = Cp*.

The structures of compounds with other element combinations from the Groups 13 (M) and 15 (E) of the Periodic Table would therefore also be very interesting. A M_3E_2 compound results from the reaction of [AlCp*] with $[Sb_4tBu_4]$ under elimination of the *t*Bu groups. Unfortunately the structure of the product could not be clarified unequivocally. The structure shown in Scheme 11 has been proposed, although it has not been possible to make an exact statement on the Al–Sb and Al–Al interactions as yet.[151] An analogous M_3E_2 framework exists in the compound $[(iPr_2NB)_3P_2]$.[152]

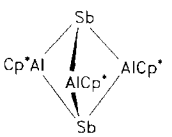

Scheme 11. Propose d structure for $[(Cp^*Al)_3Sb_2]$.

Heterocubanes are formed in high yields by the oxidation of [AlCp*] with Se and Te, in which both the Al atoms and the chalcogen atoms are able to realize their preferred oxidation states and coordination numbers [Eq. (21); Fig. 19].[104]

$$4\ [AlCp^*] + 4\ E \xrightarrow[25°C]{\text{toluene}} [(Cp^*Al)_4E_4] \qquad (21)$$
$$(E = Se\ (\mathbf{32}),\ Te\ (\mathbf{33}))$$

The Cp* ligands on both compounds are η^5-coordinated to the Al atoms; the Al–C bond lengths (as is also the case for the η^5-coordinated Cp* rings in **30**) are about 4–6 pm shorter than those in tetrameric [AlCp*]. The Ga compound analogous to **33** is accessible by silyl halide elimination from $[GaCl_2Cp^*]$ and $Te(SiMe_3)_2$.[154] Unlike in **33**, the Cp* ligands of the Ga–Te heterocubane are η^1-coordinated to the Ga atoms. This finding may be attributed to the lower Lewis acidity of the Ga atoms, and it clearly shows quite impressively the ability of the Cp* ligand to adjust itself to the electronic needs of the particular metal in question.

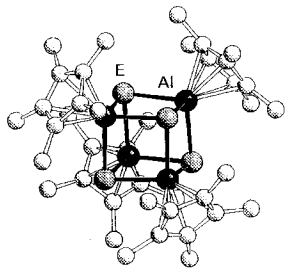

Fig. 19. Molecular structure of the isostructural compounds **32** and **33** (H atoms not shown).

4.3. Reactions with Azides

Because of the isolobal relationship between atoms of the sixth main group and nitrenes (NR), it is not surprising that RAlE (E = chalcogen) and RAlNR′ oligomers have very similar structures. Analogous to the chalcogen compounds described in the previous section, the iminoalanes $(RAlNR')_n$ usually form three-dimensional cross-linked oligomers in which the Al and N atoms are arranged in an alternating fashion and are four-coordinate.[155] Only with very sterically demanding groups does it become possible to stabilize oligomers with $n<4$ and three-coordinate Al centers.[156] The oxidation of [AlCp*] with bulky azides ought, therefore, to be a promising synthetic route for this type of compound.

In the reaction of [AlCp*] with mesitylazide, however, the dimeric aminoalane $[Cp^*Al\{\mu\text{-}NH(C_6H_2\text{-}4,6\text{-}Me_2\text{-}2\text{-}CH_2)\}]_2$ **34** [Eq. (22)] is formed under N_2 elimination instead of an

$$2\ [AlCp^*] + MesN_3 \xrightarrow[-N_2]{\text{toluene / 40°C}} \mathbf{34} \qquad (22)$$

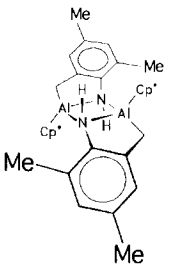

iminoalane.[157] As in an analogous B-N system,[158] the Al atoms here extend their sphere of coordination by the activation of one of the C–H bonds on the mesityl ligand.

If trimethylsilylazide is used instead of mesitylazide, the dimeric iminoalane **35** is obtained in 34% yield, as a result of the unexpected migration of silyl and Cp* groups [Eq. (23)].[157]

$$4\,[AlCp^*] + 4\,Me_3SiN_3 \xrightarrow[-4\,N_2]{\text{toluene / 70°C}} \mathbf{35} \qquad (23)$$

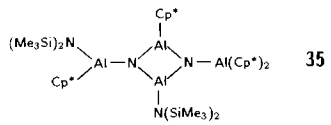

In spite of the fact that all of the Al centers are three-coordinate, the Cp* rings are only bound η^1 or η^2 (Fig. 20). The N atoms thus appear to be able to compete with the Cp* ligands as π donors for the Al atoms. Quantum chemical studies that might shed some light on this interesting bonding situation have sill to be carried out. The very short Al–Al distance in the central four-membered Al_2N_2 ring is also remarkable (ca. 242 pm). A similarly short Al–Al distance has also been calculated for the four-membered Al_2O_2 ring in dimeric OAlF (238.2 pm).[29] A bonding interaction should not be interpreted in either case, however, as the bonding parameters ought to be largely dominated by ionic interactions.

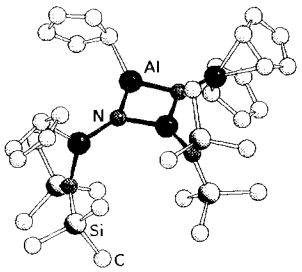

Fig. 20. Molecular structure of **35** in the crystal (Me groups of the Cp* rings and H atoms not shown).

4.4. Reaction with [NiCp$_2$]

Compounds with direct bonds between aluminum and a transition metal have been little studied as yet, although they could play a considerable role in many important catalytic processes.[159] The reaction of [AlCp*] with [NiCp$_2$] provides a simple route to this type of compound. [(NiCp)$_2$(AlCp*)$_2$] (**36**) is formed in good yields (72%) in accordance with Equation (24).[161] It has the butterfly structure shown in Figure 21, in

$$3\,[AlCp^*] + 2\,[NiCp_2] \xrightarrow{\text{toluene, 50°C}} [(NiCp)_2(AlCp^*)_2] + \text{"}[AlCp_2Cp^*]\text{"} \qquad (24)$$

36

which two AlCp* ligands bridge a CpNi–NiCp unit. Ni compounds of this type are also known with numerous other ligands such as CO (isolobal with [AlCp*]).[162] Compound **36** contains the first Ni–Al bond length determined in a molecular compound; the average length is about 228 pm.[160] It is somewhat shorter than the Co–Al distance (233 pm) in the recently reported [{CoCp*(η^2-C_2H_4)}$_2${AlEt}$_2$], which has a planar four-membered Co_2Al_2 ring in which the Al atoms are also three-coordinate.[164] The formation of **36** could be initiated by the intial attack of the alanediyl on the Lewis acidic Ni atom. This type of mechanism is supported, for example, by the reaction of germylenes and stannylenes with [NiCp$_2$], for which insertion products of the carbene analogues into the Cp–Ni bond have been characterized.[165]

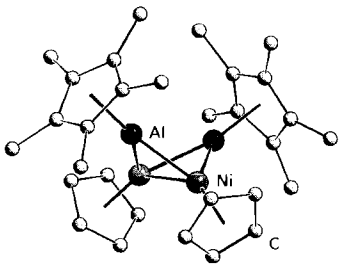

Fig. 21. Molecular structure of [(NiCp)$_2$(AlCp*)$_2$] **36** in the solid state (H atoms not shown).

4.5. Summary

The reactions of [AlCp*] described here show quite clearly that a rather simple route to novel products is frequently possible using this compound; these products are often very interesting from a theoretical standpoint with regards to the bonding aspects.

^{27}Al NMR spectroscopy is a very valuable tool for the characterization of the structures of cyclopentadienylaluminum compounds. Previous studies show that relatively clean signals occur, the resonance field strengths of which permit conclusions to be drawn as to the bonding mode of the Cp ligands. η^1-Cp complexes, for example, have shifts which correspond to those of comparable alkylaluminum compounds, whereas the ^{27}Al NMR resonance frequencies of π-Cp-aluminum compounds are shifted to considerably higher field strengths by anisotropic effects.[166] The well-known relationship between the coordination number and chemical shift in ^{27}Al NMR spectroscopy[77] still appears to be valid, however, although the entire shift region of the π-Cp-Al complexes is found at higher field strengths. The number of the compounds studied to date is still too small to be able to reliably attribute limited frequency regions to certain Al coordinations. Since [AlCp*] may well find wider use as a synthetic building block, extensive data might soon become available.

5. Outlook

Beginning with the matrix isolation technique, the consistent pursuit of an elaborate synthetic method with regards to the demands placed on the apparatus, preparative cryochemistry with reactive high-temperature molecules such as AlCl has led to the development of a new area of main group organometallic chemistry which opens a wide variety of possibilities for theoretical, synthetic, and applied chemistry. It is now expected that other, experimentally less elaborate, routes will increasingly be found for the synthesis of such compounds. In this way the rapid development of this field of research, which has already been manifest in the last few years, will continue to accelerate so that numerous surprising results can be anticipated in the near future.

A particularly interesting aspect is provided by the studies on novel cluster species, on molecular compounds with multiple bonds, and on the preparation of solid materials with metal–metal interactions. The question as to how far the singularly structural and bonding theoretical peculiarities from boron

chemistry, for example in the case of the boranes and carboranes, can be applied to the heavier homologues aluminum and gallium is particularly appealing.[167]

We would like to thank all of the colleagues in our research group for their contributions to this article. In addition we would like to thank Prof. R. Ahlrichs, Dr. J. Gauss, Dr. U. Schneider, F. Kurth, and Dr. R. Köppe for valuable discussions and theoretical studies. Prof. W. Uhl and Dr. G. Linti provided us with as yet unpublished results, for which we are extremely grateful. We thank the Fonds der Chemischen Industrie and the Deutsche Forschungsgemeinschaft for their financial support, the latter in particular for awarding a post-doctoral grant (D. L.).

Received: May 31, 1995 [A 117 IE]
German version: *Angew. Chem.* **1996**, *108*, 141–161

[1] W. Uhl, *Angew. Chem.* **1993**, *105*, 1449; *Angew. Chem. Int. Ed. Engl.* **1993**, *32*, 1386.
[2] Historically important works on Al^{I} Halides: H. Schäfer, *Chemische Transportreaktionen*, Verlag Chemie, Weinheim, **1962**; L. Troost, P. Hautefeuille, *C. R. Hebd. Seances Acad. Sci.* **1885**, *100*, 1220; W. Klemm, E. Voss, K. Geiersberger, *Z. Anorg. Allg. Chem.* **1948**, *256*, 15, 24.
[3] a) A. J. Downs, C. R. Pulham, *Chem. Soc. Rev.* **1994**, 175; b) *Adv. Inorg. Chem.* **1994**, *41*, 171.
[4] See for examples: M. J. Taylor, P. J. Brothers in *Chemistry of Aluminum, Gallium, Indium and Thallium* (Eds.: A. J. Downs), Chapman & Hall, London, **1993**.
[5] See for example: R. Nesper, *Angew. Chem.* **1991**, *103*, 805; *Angew. Chem. Int. Ed. Engl.* **1991**, *30*, 789 and ref. [4].
[6] P. Paetzold, *Angew. Chem.* **1991**, *103*, 559; *Angew. Chem. Int. Ed. Engl.* **1991**, *30*, 544; J. J. Schneider, *ibid.* **1994**, *106*, 1914 and **1994**, *33*, 1830.
[7] See for example: J. A. Morrison, *Chem. Rev.* **1991**, *91*, 35.
[8] The mixed-valence gallium dihalides ($Ga^{+}[GaX_4]^{-}$) (for example G. Garton, H. M. Powell, *J. Inorg. Nucl. Chem.* **1957**, *4*, 84 and ref. [9]) are not considered here.
[9] H. Schmidbaur, *Angew. Chem.* **1985**, *97*, 893; *Angew. Chem. Int. Ed. Engl.* **1985**, *24*, 893; H. Schmidbaur, U. Thewalt, T. Zafiropoulos, *Organometallics* **1983**, *2*, 1550, and references therein.
[10] P. Jutzi, D. Kanne, C. Krüger, *Angew. Chem.* **1986**, *98*, 163; *Angew. Chem. Int. Ed. Engl.* **1986**, *25*, 164; P. Jutzi, U. Holtmann, D. Kanne, C. Krüger, R. Blom, R. Gleiter, I. Hyla-Kryspin, *Chem. Ber.* **1989**, *122*, 1629.
[11] T. Tsumuraya, S. A. Batcheller, S. Masamune, *Angew. Chem.* **1991**, *103*, 916; *Angew. Chem. Int. Ed. Engl.* **1991**, *30*, 902, and references therein.
[12] M. W. Chase, Jr., C. A. Davies, J. R. Downey, Jr., D. J. Frurip, R. A. McDonal, A. N. Syverend, *JANNAF-Thermodynamical Tables, 3rd ed.*, American Chemical Society, American Institute of Physics, US National Bureau of Standards, Midland, MI, **1985**.
[13] R. Ahlrichs, P. Scharf, C. Erhardt, *J. Chem. Phys.* **1985**, *82*, 890; D. J. Swanton, R. Ahlrichs, *Theor. Chim. Acta* **1989**, *75*, 163.
[14] R. Ahlrichs, M. Ehrig, H. Horn, *Chem. Phys. Lett.* **1991**, *183*, 227.
[15] The listed energetic relationships in the third main group are no exception. They are valid for all homologous main group element compounds for example, also for the difluorides of the elements of the fourth main group. Admittedly, PbF_2 is unstable with regard to disproportionation in the gas phase, but this reaction path is not taken as the formation of a PbF_2 ionic crystal is even more favorable. This stabilization possibility does not exist for the lightest homologue. Covalent metastable CF_2 oligomers and polymers are formed instead, some of which demonstrate considerable thermal stability (e.g. Teflon).
[16] K. P. Huber, G. Herzberg, *Molecular Structure IV, Constants of Diatomic Molecules*, Van Nostrand, Reinhold, New York, **1979**.
[17] R. Ahlrichs, L. Zhengyan, H. Schnöckel, *Z. Allg. Anorg. Chem.* **1984**, *519*, 155.
[18] P. A. Akishin, N. G. Rambidi, E. Z. Zasorim, *Kristallografiya* **1959**, *4*, 186; *Sov. Phys. Crystallogr. Engl. Transl.* **1959**, *4*, 167.
[19] Orbital energies [Hartree]: [AlF]: $7\sigma(3s)$: -0.337, $2\pi(2pF)$: -0.611, $6\sigma(2p\sigma F)$: -0.665; $[Al_2F_2]$: $5b_{1u}(3s_{ab})$: -0.299, $7a_g(3s_b)$: -0.335, $4b_{3u}(2p(F))$: -0.633, $6a_g(2p(F))$: -0.749 (1 Hartree = 2625.5 kJ mol^{-1}) [17].
[20] R. Ahlrichs, M. Hoffmann-Ostendorf, T. Hoffmann-Ostendorf, *J. Chem. Phys.* **1978**, *68*, 1402; T. Hoffmann-Ostendorf, M. Hoffmann-Ostendorf, R. Ahlrichs, *Phys. Rev. A* **1978**, *18*, 328.
[21] H. Schnöckel, S. Schunk, *Chem. Unserer Zeit* **1987**, *21*, 73.
[22] In principle, a higher monomer concentration ought to favor the formation of larger oligomers as well. However, a poorer "matrix isolation" is also coupled with this which leads to a broadening of bands and thus under certain circumstances the weak absorptions cannot be detected.
[23] In the matrix investigation of SiO (isoelectronic with AlF), considerable proportions of the trimeric ring are observed under certain conditions (J. S. Anderson, J. S. Ogden, *J. Chem. Phys.* **1969**, *51*, 4189; J. W. Hastie, R. H. Hauge, J. L. Margrave, *Inorg. Chim. Acta* **1969**, *3*, 601). Exclusively trimeric products are obtained in the deposition of PN, which is also isoelectronic with AlF. This experimental finding is in agreement with quantum chemical calculations, according to which the dimerization of PN is endothermic with 19 kJ mol^{-1}, but the trimerization is exothermic with 334 kJ mol^{-1} [3 PN → $(PN)_3$] (R. Ahlrichs, M. Bär, H. S. Plitt, H. Schnöckel, *Chem. Phys. Lett.* **1989**, *161*, 179).
[24] The structures of mass-selected Si_5, Si_6, and Si_9 clusters were investigated with Raman spectroscopy: E. C. Honea, A. Ogura, C. A. Murray, Krishnan Raghararachari, W. O. Sprenger, M. F. Jarrold, W. L. Brown, *Nature* **1993**, *366*, 42.
[25] Geometry optimization as D_{2h} and frequency calculations were performed on SCF level using TURBOMOLE (R. Ahlrichs, M. Bär, M. Häser, H. Horn, C. Kölmel. *Chem. Phys. Lett.* **1989**, *162*, 165) and SVP basis sets (A. Schäfer, H. Horn, R. Ahlrichs, *J. Chem. Phys.* **1992**, *97*, 2571); exponents of the polarization functions for Al, Ga, F, Cl, Br: 0.3, 0.207, 1.4, 0.65, 0.389, respectively. The dimerization energies (ΔE) were calculated according to the single-point-MP2 correction of the SCF geometries (F. A. Kurth, H. Schnöckel, unpublished results).
[26] H. Schnöckel, Habilitation, Universität Münster, **1981**.
[27] R. Köppe, Dissertation, Universität München, **1992**.
[28] The double bond systems of the linear species O=Si=O and O=Ge=O were also identified with the aid of matrix methods before intensive investigations into multiple bonding systems with heavy main group elements began in the 1980s: H. Schnöckel, *Angew. Chem.* **1978**, *90*, 638; *Angew. Chem. Int. Ed. Engl.* **1978**, *17*, 616; A. Bos, J. S. Ogden, *J. Phys. Chem.* **1973**, *77*, 1513; A. Bos, J. S. Ogden, L. Orgee, *ibid.* **1974**, *78*, 1763.
[29] H. Schnöckel, *J. Mol. Struct.* **1978**, *50*, 267. Earlier results on O=AlF (A. Snelson, *High Temp. Sci.*, **1973**, *5*, 77) proved to be wrong; the bands discussed there have to be attributed to matrix-isolated SiF_4, which resulted from the reaction of AlF_3 with the crucible material.
[30] H. Schnöckel, H. J. Göcke, *J. Mol. Struct.* **1978**, *50*, 281.
[31] H. Schnöckel, *J. Mol. Struct.* **1978**, *50*, 275.
[32] R. Köppe, M. Tacke, H. Schnöckel, *Z. Anorg. Allg. Chem.* **1991**, *605*, 35.
[33] R. Köppe, H. Schnöckel, *J. Chem. Soc. Dalton Trans.* **1992**, 3393.
[34] AlH_3 and GaH_3 were recently prepared from metal atoms and H_2 under matrix conditions and characterized; F. A. Kurth, R. A. Eberlein, H. Schnöckel, A. J. Downs, C. R. Pulham, *J. Chem. Soc. Chem. Commun.* **1993**, 1302; C. V. Chertihin, L. Andrews, *J. Phys. Chem.* **1993**, *97*, 10295; P. Pullumbi, Y. Bouteiller, L. Manceron, C. Mijoule, *Chem. Phys.* **1994**, *185*, 25.
[35] P. L. Timms, *Adv. Inorg. Chem. Radiochem.* **1972**, *14*, 142.
[36] Redox potentials [V]: Tl^{+}/Tl: -0.34; Tl^{3+}/Tl^{+}: $+1.25$; In^{+}/In: -0.22; In^{3+}/In^{+}: -0.44.
[37] In addition, no species with M–X bonds (X = Cl, Br) are expected for the lighter homologues in aqueous solution, because the formation of M–O bonds by hydrolysis reactions is energetically favored.
[38] R. Dronskowski, *Inorg. Chem.* **1994**, *33*, 5960, 6201.
[39] See for example K. Wade, A. J. Banister in *Comprehensive Inorganic Chemistry, Vol. 1* (Eds.: A. F. Trotman-Dickenson), Pergamon, Oxford, **1973**, p. 1080.
[40] For all reactions the ratio MX(g) to MX_3(g) is determined by the thermodynamics of the equilibrium $2M(l) + MX_3(g) \rightleftharpoons 3MX(g)$; the influence of entropy increasingly favors the formation of the gaseous monohalides with increasing temperature.
[41] See for example: P. L. Timms, *J. Am. Chem. Soc.* **1967**, *89*, 1629; *ibid.* **1968**, *90*, 4585.
[42] U. Zenneck, *Angew. Chem.* **1990**, *102*, 171; *Angew. Chem. Int. Ed. Engl.* **1990**, *29*, 138.
[43] Preliminary investigations show that the monohalides can also be incorporated into a stabilizing host lattice for example made from simultaneously condensed alkali halide. Novel solid materials are obtained in this way, in which the disproportionation of MX can be followed spectroscopically (H. Schnöckel, unpublished results).
[44] M. Tacke, H. Schnöckel, *Inorg. Chem.* **1989**, *28*, 2895.
[45] M. Tacke, Dissertation, Universität Münster, **1990**.
[46] L. Plaggenborg, Diplomarbeit, Universität Münster, **1989**.
[47] „Borverbindungen": *Gmelin, Handbuch der Anorganischen Chemie* (Supplement to 8th ed.), *Vol. 53*, Springer, Berlin, **1978**.
[48] M. Mocker, Dissertation, Universität München, **1994**.
[49] A. Ecker, Diplomarbeit, Universität Karlsruhe, **1994**.
[50] M. Tacke, H. Kreienkamp, L. Plaggenborg, H. Schnöckel, *Z. Anorg. Allg. Chem.* **1991**, *604*, 35; C. Doriat, H. Schnöckel, unpublished results.
[51] D. Loos, Dissertation, Universität München, **1994**.

[52] Until now, dipropyl ether, *tert*-butylmethyl ether, 1,4-dioxane, anisole, dimethoxyethane, diethyleneglycoldimethyl ether, and triethylamine have been investigated [48].

[53] The role of the arene in the stabilization has not yet been determined. In connection with this, one is reminded of the arene complexes of Ga^+ which are formed on dissolving Ga_2X_4 in aromatic solvents [9]. It is also worth mentioning the complex of "quasi atomic" magnesium with THF and anthracene (Mg atoms can—like AlCl molecules—be regarded as carbenoid species); L. M. Engelhardt, S. Harvey, C. L. Raston, A. H. White, *J. Organomet. Chem.* **1988**, *341*, 39; H. Bönnemann, B. Bogdanović, R. Brinkmann, D.-W. He, B. Spliethoff, *Angew. Chem.* **1983**, *95*, 749; *Angew. Chem. Int. Ed. Engl.* **1983**, *22*, 728.

[54] M. Mocker, C. Robl, H. Schnöckel, *Angew. Chem.* **1994**, *106*, 1860; *Angew. Chem. Int. Ed. Engl.* **1994**, *33*, 1754.

[55] A. Ecker, H. Schnöckel, unpublished results.

[56] D. F. Grant, R. C. G. Killean, J. L. Lawrence, *Acta Crystallogr. B* **1969**, *25*, 377.

[57] C. Peppe, D. G. Tuck, L. Victoriano, *J. Chem. Soc. Dalton Trans.* **1982**, 2165.

[58] M. Mocker, C. Robl, H. Schnöckel, *Angew. Chem.* **1994**, *106*, 946; *Angew. Chem. Int. Ed. Engl.* **1994**, *33*, 862.

[59] The results from an earlier work (G. A. Olah, O. Farooq, S. Morteza, F. Farnia, M. R. Bruce, F. L. Clouet, P. R. Morton, G. K. Surya Prakash, R. C. Stevens, R. Bau, K. Lammertsma, S. Suzer, L. Andrews, *J. Am. Chem. Soc.* **1988**, *110*, 3231) concerning the synthesis of donor-free $AlCl_2$ and $AlBr_2$ at higher temperatures would appear doubtful on the basis of thermodynamic considerations [58].

[60] No $AlCl_3$-etherate can be identified by ^{27}Al NMR spectroscopic methods in an "AlCl" solution even at $-80\,^{\circ}C$. It has to be assumed, therefore, that the $AlCl_3$ formed in the synthesis reacts with "AlCl" at an even lower temperature.

[61] It should be possible to prepare compound **4**, which is only formed as a side product in the synthesis of donor-stabilized "AlBr", in a deliberate manner by slightly altering the reaction conditions. If reaction (4a) is carried out at lower temperatures, in addition to AlBr, more $AlBr_3$ is also formed (see Section 1). At about 600 °C and otherwise unchanged conditions, an equilibrium mixture is obtained that contains roughly equal amounts of AlBr and $AlBr_3$. After the cocondensation of this mixture with a suitable donor, it should be possible to prepare the dihalide in higher yields according to the equation $[M_nX_n(Do)_m] + n\,MX_3 \cdot Do \rightarrow n\,M_2X_4 \cdot 2\,Do$.

[62] The Al–Al distance in $[Al_2I_4(PEt_3)_2]$ is 256 pm, A. Ecker, H. Schnöckel, unpublished results.

[63] E. R. Davidson, *J. Chem. Phys.* **1967**, *46*, 3320; K. R. Roby, *Mol. Phys.* **1974**, *27*, 81; R. Heinzmann, R. Ahlrichs, *Theor. Chim. Acta* **1976**, *42*, 33; C. Erhardt, R. Ahlrichs, *ibid.* **1985**, *68*, 231.

[64] H. Schnöckel, G. Stösser, unpublished results.

[65] For example $B_2Cl_4 \cdot 2\,NMe_3$: N. N. Greenwood in *Comprehensive Inorganic Chemistry, Vol. 1* (Ed.: A. F. Trotman-Dickenson), Pergamon, Oxford, **1973**, p. 928; $Ga_2Cl_4 \cdot 2$ dioxane: J. C. Beamish, R. W. H. Small, I. J. Worrall, *Inorg. Chem.* **1979**, *18*, 220; $In_2Br_3I \cdot 2\,TMEDA$: M. A. Khan, C. Peppe, D. G. Tuck, *Can. J. Chem.* **1984**, *62*, 601.

[66] See for example: M. J. Taylor, P. J. Brothers in ref. [4], p. 198; D. G. Tuck in ref. [4], p. 468.

[67] According to the information currently available, similar stability relationships are also found in solvated donor-stabilized monohalides. This finding would agree with a mechanism proposed for the disproportionation of InX compounds, in which both monovalent and divalent species occur. The disproportionation mechanisms for $M_2X_4 \cdot 2\,Do$ and $[M_nX_n(Do)_m]$ would thus be directly connected with one another: $[M_nX_n(Do)_m] \rightarrow M^0 + MX_3 \cdot Do$ and $[M_nX_n(Do)_m] + n\,MX_3 \cdot Do \rightleftarrows n\,M_2X_4 \cdot 2\,Do$ (see D. G. Tuck, *Polyhedron*, **1990**, *9*, 377 and ref. [57]).

[68] $[R_2M-MR_2]$ (R = $CH(SiMe_3)_2$): M = Al: W. Uhl, *Z. Naturforsch. B* **1988**, *43*, 1113; M = Ga: W. Uhl, M. Layh, T. Hildenbrand, *J. Organomet. Chem.* **1989**, *364*, 289; M = In: W. Uhl, M. Layh, W. Hiller, *ibid.* **1989**, *368*, 139.

[69] S. Henkel, K. W. Klinkhammer, W. Schwarz, *Angew. Chem.* **1994**, *106*, 721; *Angew. Chem. Int. Ed. Engl.* **1994**, *33*, 681.

[70] $[R_2M-MR_2]$: a) R = 2,4,6-$iPr_3C_6H_2$, M = Al: R. J. Wehmschulte, K. Ruhlandt-Senge, M. M. Olmstead, H. Hope, B. E. Sturgeon, P. P. Power, *Inorg. Chem.* **1993**, *32*, 2983; M = Ga: X. He, R. A. Bartlett, M. M. Olmstead, K. Ruhlandt-Senge, B. E. Sturgeon, P. P. Power, *Angew. Chem.* **1993**, *105*, 761; *Angew. Chem. Int. Ed. Engl.* **1993**, *32*, 717; b) R = 2,4,6-$(CF_3)_3C_6H_2$, M = Ga: R. D. Schluter, A. H. Cowley, D. A. Atwood, R. A. Jones, M. R. Bond, C. J. Carrano, *J. Am. Chem. Soc.* **1993**, *115*, 2070; c) R = tetramethylpiperidyl, M = Ga: G. Linti, R. Frey, M. Schmidt, *Z. Naturforsch. B* **1994**, *49*, 958.

[71] $[R_2M-MR_2]^{+-}$: R = $CH(SiMe_3)_2$, M = Al: W. Uhl, A. Vester, W. Kaim, J. Poppe, *J. Organomet. Chem.* **1993**, *454*, 9; C. Pluta, K.-R. Pörschke, C. Krüger, K. Hildenbrand, *Angew. Chem.* **1993**, *105*, 451; *Angew. Chem. Int. Ed. Engl.* **1993**, *32*, 388; R = 2,4,6-$iPr_3C_6H_2$, M = Al, Ga: ref. [70a].

[72] R. W. H. Small, I. J. Worrall, *Acta Crystallogr. Sect. B* **1982**, *38*, 250; *ibid.* **1982**, *38*, 86; J. C. Beamish, A. Boardman, R. W. H. Small, I. J. Worrall, *Polyhedron* **1985**, *4*, 983.

[73] A. K. Saxena, H. Zhang, J. A. Maguire, N. S. Hosmane, A. H. Cowley, *Angew. Chem.* **1995**, *107*, 378; *Angew. Chem. Int. Ed. Engl.* **1995**, *34*, 332.

[74] The energies of the two isomers of Al_2H_4 with a nonbridging Al–Al bond ($H_2Al-AlH_2$ in D_{2d} and D_{2h} symmetry, respectively) represent local minima of the potential hypersurface, but the saltlike isomer $Al^+[AlH_4]^-$ is about 45 $kJ\,mol^{-1}$ more stable (K. Lammertsma, O. F. Güner, R. M. Drewes, A. E. Reed, P. von R. Schleyer, *Inorg. Chem.* **1989**, *28*, 313).

[75] D. Loos, H. Schnöckel, D. Fenske, *Angew. Chem.* **1993**, *105*, 1124; *Angew. Chem. Int. Ed. Engl.* **1993**, *32*, 1059.

[76] C. Dohmeier, H. Krautscheid, R. Köppe, P. Jutzi, H. Schnöckel, unpublished results. In this reaction $[AlCl_2Cp^* \cdot Et_2O]$ is also formed, as well as further Al–Si compounds which are currently under investigation.

[77] See for example R. Benn, A. Rufińska, *Angew. Chem.* **1986**, *98*, 851; *Angew. Chem. Int. Ed. Engl.* **1986**, *25*, 861, and references therein.

[78] The large signal width is possibly due to overlap of several individual signals.

[79] J. Gauss, U. Schneider, R. Ahlrichs, C. Dohmeier, H. Schnöckel, *J. Am. Chem. Soc.* **1993**, *115*, 2402.

[80] The reason for this finding can be easily explained by using an isolated AlX molecule as an example: more electronegative ligands increase, as in the case of AlX_3 species, the effective nuclear charge on the metal atom. This means for AlX molecules that the highest occupied molecular orbital (HOMO) with the lone pair of electrons is lowered energetically. Since the LUMO remains practically unaffected, the electronic excitation energy becomes larger, and the paramagnetic proportion of the chemical shift is thus reduced. The smallest resonance field strength in the series of the AlX species was therefore calculated for AlF [79]. The quantum chemical investigations show that this influence can also be expected in oligomeric AlX species, albeit to a slightly weaker extent.

[81] See for example: T. T. Kodas, M. J. Hampden-Smith, *The Chemistry of Metall CVD*, VCH, Weinheim, **1994**, p. 91; J.-O. Carlsson, U. Jansson, *Progr. Solid State Chem.* **1993**, *22*, 237.

[82] H. Schnöckel, M. Leimkühler, R. Lotz, R. Mattes, *Angew. Chem.* **1986**, *98*, 929; *Angew. Chem. Int. Ed. Engl.* **1986**, *25*, 921.

[83] R. Ahlrichs, M. Häser, H. Schnöckel, M. Tacke, *Chem. Phys. Lett.* **1989**, *154*, 104.

[84] In addition to the compound analogous to **8**, a structural isomer is formed in which an Al_4C_8 ring is present, which in turn is cross-linked by additional Al–olefin bonds to give a cagelike Al–C framework, C. Üffing, A. Ecker, H. Schnöckel, unpublished results.

[85] C. Üffing, Diplomarbeit, Universität Karlsruhe, **1994**.

[86] C. Üffing, E. Möllhausen, H. Schnöckel, unpublished results.

[87] C. Dohmeier, R. Mattes, H. Schnöckel, *J. Chem. Soc. Chem. Commun.* **1990**, 358.

[88] The AlF is not prepared from Al metal and HF, which is not easy to handle experimentally at higher temperatures, but rather by heating a pellet made from AlF_3 and excess Al (W. N. Rowlands, A. D. Willson, P. L. Timms, B. Mile, J. H. Bernard Chenier, J. A. Howard, H. A. Holy, *Inorg. Chim. Acta* **1991**, *189*, 189). Since this reaction takes place spontaneously (solid/liquid), according to our own matrix investigations gaseous AlF_3 is also formed.

[89] M. L. H. Green, P. Mountford, G. J. Smout, S. R. Speel, *Polyhedron* **1990**, *9*, 2763; S. R. Speel, Dissertation, Oxford, **1992**.

[90] MR_2X species (M = Al, Ga) proved to be suitable here. A divalent intermediate is presumably formed in the reduction, the disproportionation of which leads to M^{III} compounds in addition to the desired M^I product.

[91] E. O. Fischer, H. P. Hofmann, *Angew. Chem.* **1957**, *69*, 639; H. Meister, *ibid.* **1957**, *69*, 533.

[92] C. Dohmeier, C. Robl, M. Tacke, H. Schnöckel, *Angew. Chem.* **1991**, *103*, 594; *Angew. Chem. Int. Ed. Engl.* **1991**, *30*, 564.

[93] Spectroscopic and physical data for $[Al_4Cp^*_4]$: ^1H NMR $\delta = 1.89$, ^{13}C NMR: $\delta = 11.4$, 114.1; FT-Raman of the solid (rel. int.): $\tilde{\nu} = 2982(3)$, 2910(10), 2859(4), 2721(2), 1486(2), 1431(5), 1384(3), 1179(1), 1029(1), 601(3), 559(2), 377(br.,4), 125(5) cm^{-1} the "breathing" vibration of the Al_4 tetrahedron is observed at 377 cm^{-1}, and is thus in agreement with a weak framework bond [92]; FT-IR (KBr) (rel. int.): $\tilde{\nu}$ 2972(3), 2909(6), 2957(5), 2722(1), 1639(1), 1492(2), 1430(6), 1374(7), 1038(1), 800(2), 793(1), 595(2), 585(2), 350(10) cm^{-1}; MS (CI), isobutane): *m/z* (%): 513 (17) $[M - Cp^*]^+$, 325 (61) $[M/2 + H]^+$, 324 (100) $[M/2]^+$, 189 (77) $[M/2 - Cp^*]$, 163 (77) $[M/4 + H]^+$; MS (EI): *m/z* (%): 162 (100) $[M/4]^+$; sublimation: 140 °C, decomposition above about 150 °C [94].

[94] C. Dohmeier, Dissertation, Universität München, **1994**.

[95] H. Werner, H. Otto, H. J. Kraus, *J. Organomet. Chem.* **1986**, *315*, C57.

[96] O. T. Beachley, Jr., M. R. Churchill, J. C. Fettinger, J. C. Pazik, L. Victoriano, *J. Am. Chem. Soc.* **1986**, *108*, 4666; O. T. Beachley, B. Blom, M. R. Churchill, K. Faegri, Jr., J. C. Fettinger, J. C. Pazik, L. Victoriano, *Organometallics* **1989**, *8*, 346.

[97] R. Ahlrichs, M. Ehrig, H. Horn, *Chem. Phys. Lett.* **1991**, *183*, 227.

[98] U. Schneider, Dissertation, Universität Karlsruhe, **1993**.

[99] U. Schneider, R. Ahlrichs, H. Horn, A. Schäfer, *Angew. Chem.* **1992**, *104*, 327; *Angew. Chem. Int. Ed. Engl.* **1992**, *31*, 353.

[100] R. Ditchfield, *Mol. Phys.* **1974**, *27*, 789; K. Wolinski, J. F. Hinton, P. Pulay, *J. Am. Chem. Soc.* **1990**, *112*, 8251; M. Häser, R. Ahlrichs, H. P. Baron, P. Weis, H. Horn, *Theor. Chim. Acta* **1992**, *83*, 455; J. Gauss, *Chem. Phys. Lett.* **1992**, *191*, 614.

[101] The paramagnetic shielding term σ_{para} is generally the decisive factor in determining the position of the chemical shift of a metal nucleus, whereas the diamagnetic proportion varies little. As σ_{para} is inversely proportional to the electronic excitation energy, the energetic separation of HOMO and LUMO represents a crude but visual measure for the chemical shift: see ref. [102] and references therein, for example J. A. Pople, *Mol. Phys.* **1964**, *7*, 301; C. J. Jameson, H. S. Gutowsky, *J. Chem. Phys.* **1964**, *40*, 1714).

[102] This effect is also observed in the η^5-Cp complexes of other low-valent main group elements (e.g. Si^{II} or Sn^{II}) (B. Wrackmeyer in *Unkonventionelle Wechselwirkungen in der Chemie metallischer Elemente (DFG Forschungsbericht)* (Ed.: B. Krebs), VCH, Weinheim, **1992**, p. 111). The effect is less pronounced in the case of normally valent compounds such as [LiCp], $[MgCp_2]$, and $[Al(Cp^*)_2]^+$.

[103] A. Haaland, K.-G. Martinsen, S. A. Shlykov, H. V. Volden, C. Dohmeier, H. Schnöckel, *Organometallics* **1995**, *14*, 3116.

[104] S. Schulz, H. W. Roesky, H. J. Koch, G. M. Sheldrick, D. Stalke, A. Kuhn, *Angew. Chem.* **1993**, *105*, 1828; *Angew. Chem. Int. Ed. Engl.* **1993**, *32*, 1729.

[105] The recently determined differences [104] as regards the physical and chemical properties of the products obtained by the various routes are attributed to this impurity. If the compound prepared by the reduction with K is freed from impurities by crystal selection, the properties are identical with those of the product prepared by metathesis. As was unequivocally shown in a recent investigation (S. Schulz, H. W. Roesky, C. Dohmeier, H. Schnöckel, unpublished results), the ^{27}Al NMR spectroscopic results and the behavior on hydrolysis are particularly affected by the foreign substance.

[106] It is remarkable that although **13** is formed relatively quickly, it then reacts under disproportionation only very slowly with $[MgCp_2]$, even when this is added in excess. It is apparent that **13** has a lower tendency toward dissociation into monomers than does **11**; thus only a few AlCp* monomers are available for the reaction with $[MgCp_2]$. Both the observed downfield shift of the ^{27}Al NMR resonances, which as mentioned above is to be expected for a stronger framework bond in the tetramer, and the finding that neither monomeric [AlCp] nor monomeric [AlCp*] can be identified in solutions of **13** even at higher temperatures, are in agreement with this hypothesis.

[107] A review article concerning this class of compounds can be found in ref. [9].

[108] D. Loos, H. Schnöckel, J. Gauss, U. Schneider, *Angew. Chem.* **1992**, *104*, 1376; *Angew. Chem. Int. Ed. Engl.* **1992**, *31*, 1362.

[109] This circumstance possibly prevented an earlier confirmation of the compound [GaCp], since it condensed with the solvent in the cold trap intended for the latter.

[110] D. Loos, H. Schnöckel, *J. Organomet. Chem.* **1993**, *463*, 37.

[111] A. Haaland, K.-G. Martinsen, H. V. Volden, D. Loos, H. Schnöckel, *Acta Chem. Scand.* **1994**, *48*, 172.

[112] See for example $[B_4tBu_4]$: T. Davan, J. A. Morrison, *J. Chem. Soc. Chem. Commun.* **1981**, 250; $[B_9tBu_9]$: S. L. Emery, J. A. Morrison, *J. Am. Chem. Soc.* **1982**, *104*, 6790.

[113] T. Mennekes, P. Paetzold, R. Boese, D. Bläser, *Angew. Chem.* **1991**, *103*, 199; *Angew. Chem. Int. Ed. Engl.* **1991**, *30*, 173.

[114] N. Wiberg in *Frontiers in Organosilicon Chemistry* (Eds.: A. B. Bassindale, P. P. Gaspar), The Royal Society of Chemistry, Cambridge, **1991**, p. 263.

[115] The paramagnetic $[Al_3(SitBu_3)_3]^-$ anion can thus be identified by ESR spectroscopic studies; a slightly distorted three-membered ring structure can be derived from the complex hyperfine structure of the ESR spectrum (T. Passler, Dissertation, Universität München, **1994**; ref. [94]; C. Dohmeier, H. Schnöckel, N. Wiberg, unpublished results).

[116] E. P. Schram, N. Sudha, *Inorg. Chim. Acta* **1991**, *183*, 213.

[117] W. Uhl, W. Hiller, M. Layh, W. Schwarz, *Angew. Chem.* **1992**, *104*, 1378; *Angew. Chem. Int. Ed. Engl.* **1992**, *31*, 1364.

[118] A. Haaland, K.-G. Martinsen, W. Uhl, unpublished results.

[119] G. Linti, *Inorg. Chem.*, submitted.

[120] W. Uhl, R. Graupner, M. Layh, U. Schütz, *J. Organomet. Chem.* **1995**, *493*, C1.

[121] R. D. Schluter, A. H. Cowley, D. A. Atwood, R. A. Jones, J. L. Atwood, *J. Coord. Chem.* **1993**, *30*, 25.

[122] K. Wade, *J. Chem. Soc. Chem. Commun.* **1971**, 792; *Adv. Inorg. Chem. Radiochem.* **1976**, *18*, 1; R. E. Williams, *ibid.* **1976**, *18*, 67.

[123] H. Klusik, A. Berndt, *J. Organomet. Chem.* **1982**, *234*, C17.

[124] W. Uhl et al., unpublished results.

[125] R. Nesper, *Angew. Chem.* **1989**, *101*, 99; *Angew. Chem. Int. Ed. Engl.* **1989**, *28*, 58.

[126] H. Hoberg, S. Krause, *Angew. Chem.* **1976**, *88*, 760; *Angew. Chem. Int. Ed. Engl.* **1976**, *15*, 694.

[127] W. Hiller, K.-W. Klinkhammer, W. Uhl, J. Wagner, *Angew. Chem.* **1991**, *103*, 182; *Angew. Chem. Int. Ed. Engl.* **1991**, *30*, 179.

[128] C. Dohmeier, M. Mocker, H. Schnöckel, A. Lötz, U. Schneider, R. Ahlrichs, *Angew. Chem.* **1993**, *105*, 1491; *Angew. Chem. Int. Ed. Engl.* **1993**, *32*, 1428.

[129] An ideal octahedral symmetry is only expected for dianions according to Wade's rules [122]. In contrast, Jahn–Teller distortion is expected for both the neutral system and the monoanion [128].

[130] An additional stabilization of about 300 kJ mol^{-1} is expected according to calculations on the model compound $[Al_6Me_6]$ on the MP2 level [128].

[131] O. T. Beachley, Jr., J. C. Pazik, M. J. Noble, *Organometallics* **1994**, *13*, 2885.

[132] Boranediyls are assumed to occur as short-lived intermediates in the dehalogenation of $B(NR_2)X_2$ for example; however, a different reaction route was confirmed for the reaction of this compound with alkynes, (R. Schlögl, B. Wrackmeyer, *Polyhedron* **1985**, *4*, 885; A. Meller, W. Maringgele, G. Elter, D. Bromm, M. Noltemeyer, G. M. Sheldrick, *Chem. Ber.* **1987**, *120*, 1437; W. Maringgele, A. Heine, M. Noltemeyer, A. Meller, *J. Organomet. Chem.* **1994**, *468*, 25, and references therein).

[133] C. Dohmeier, H. Schnöckel, unpublished results. Spectroscopic data for **25**: ^1H NMR: $\delta = 1.92$ (t, 6H), 1.75 (s, 15H), 0.34 (q, 4H), ^{13}C NMR: $\delta = 9.73$ (CH_3), 13.3 (br., CH_2), 21.98 (CH_3), 113.51 (C_5), 131.51 (C=C); ^{27}Al NMR: $\delta = +55$ ($\omega_{1/2} = 1650$ Hz); FT-Raman (solid) (rel. int.): $\tilde{\nu} = 2913$ (10.0), 2864 (8.9), 2753 (1.0), 1631 (1.5), 1448 (1.5), 1428 (2.3), 1388 (2.0), 1370 (0.8), 1136 (0.5), 1075 (0.5), 695 (1.0), 664 (1.0), 591 (2.5), 558 (1.0), 479 (0.5), 381 (1.3), 295 (1.2), 193 (1), 162 (1.6), 129 (2.0) cm^{-1}; FT-IR (KBr) (rel. int.): $\tilde{\nu} = 3067$ (1), 2963 (8), 2915 (10), 2859 (9), 1642 (2), 1446 (6), 1378 (4), 1261 (3), 1184 (2), 1137 (6), 1088 (6), 1073 (7), 1022 (5), 888 (8), 799 (9), 736 (9), 694 (10), 668 (10), 614 (7), 475 (5, br.) cm^{-1}; MS (EI, 25 °C): *m/z* (%): 244(7) $[M]^+$, 162(18) $[M - C_6H_{10}]^+$, 136(100) $[C_{10}H_{16}]^+$; m.p.: 82 °C.

[134] $[Al(\eta^5\text{-}Cp^*)_2]^+$ is formed as an intermediate in the thermal decomposition of **11**.

[135] This behavior is similar to the thermolysis of $[ScCp^*_2R]$ in which RH is eliminated and dimeric $[ScCp^*(C_5Me_4CH_2)]$ is formed; $(C_5Me_4CH_2)$ ligands function as η^5-η^1 bridging ligands (M. E. Thompson, J. E. Bercaw, *Pure Appl. Chem.* **1984**, *56*, 1; S. Hajela, W. P. Schaefer, J. E. Bercaw, *Acta Crystallogr. Sect. C* **1992**, *48*, 1771).

[136] J. G. Contreras, D. G. Tuck, *Inorg. Chem.* **1973**, *12*, 2596.

[137] C. Dohmeier, H. Schnöckel, C. Robl, U. Schneider, R. Ahlrichs, *Angew. Chem.* **1993**, *105*, 1714; *Angew. Chem. Int. Ed. Engl.* **1993**, *32*, 1655.

[138] P. Jutzi, A. Seufert, *J. Organomet. Chem.* **1978**, *161*, C5.

[139] A. Almenningen, A. Haaland, J. Lusztyk, *J. Organomet. Chem.* **1979**, *170*, 271; K. W. Nugent, J. K. Beattie, T. W. Hambley, M. R. Snow, *Aust. J. Chem.* **1984**, *37*, 1602.

[140] The Li–C bond in the $[LiCp_2]^-$ ion is about 15 pm longer than the Al–C bond in **27**; S. Harder, M. H. Prosenc, *Angew. Chem.* **1994**, *106*, 1830; *Angew. Chem. Int. Ed. Engl.* **1994**, *33*, 1744.

[141] R. A. Andersen, J. M. Boncella, C. J. Burns, R. Blom, A. Haaland, H. V. Volden, *J. Organomet. Chem.* **1986**, *312*, C49; R. A. Andersen, R. Blom, J. M. Boncella, C. J. Burns, H. V. Volden, *Acta Chem. Scand. A* **1987**, *41*, 24.

[142] M. A. Vol.man, C. B. Knobler, M. F. Hawthorne, *Inorg. Chem.* **1988**, *27*, 2399; D. M. Schubert, M. .A. Vol.man, W. S. Rees, Jr., C. B. Knobler, P. Lu, W. Nam, M. F. Hawthorne, *Organometallics* **1990**, *9*, 2046.

[143] U. Schneider, R. Ahlrichs, *Chem. Phys. Lett.* **1994**, *226*, 491.

[144] See also: P. Jutzi, Pure Appl. Chem. **1990**, *62*, 1035; D. A. Brown, M. O. Fanning, N. J. Fitzpatrick, *Inorg. Chem.* **1978**, *17*, 1620.

[145] A comparison of the ^{27}Al NMR resonances of **27** and monomeric [AlCp*] shows once again quite clearly that in interpreting the ^{27}Al NMR resonances of Al^I compounds not only the ligand effect, but also other influences such as the electronic excitation energy for example, have to be taken into consideration. The shielding of the Al nucleus in [AlCp*] is considerably more effective than is the case in **27**, yet here the Al atoms are surrounded by two Cp* ligands.

[146] P. Jutzi in *Frontiers in Organosilicon Chemistry* (Eds.: A. B. Bassindale, P. P. Gaspar), The Royal Society of Chemistry, Cambridge, **1991**, p. 313.

[147] C. Dohmeier, H. Schnöckel, unpublished results.

[148] P. Jutzi, A. Seufert, *Angew. Chem.* **1977**, *89*, 339; *Angew. Chem. Int. Ed. Engl.* **1977**, *16*, 330; P. Jutzi, A. Seufert, W. Buchner, *Chem. Ber.* **1979**, *112*, 2488.

[149] C. Dohmeier, R. Köppe, C. Robl, H. Schnöckel, *J. Organomet. Chem.* **1995**, *487*, 127.

[150] E. D. Jemmis, P. von R. Schleyer, *J. Am. Chem. Soc.* **1982**, *104*, 4781.

[151] S. Schulz, T. Schoop, H. W. Roesky, L. Häming, A. Steiner, R. Herbst-Irmer, *Angew. Chem.* **1995**, *107*, 1015; *Angew. Chem. Int. Ed. Engl.* **1995**, *34*, 919.

[152] G. L. Wood, E. N. Duesler, C. K. Narula, R. T. Paine, H. Nöth, *J. Chem. Soc. Chem. Commun.* **1987**, 496.

[153] C. Dohmeier, H. Schnöckel, C. Robl, U. Schneider, R. Ahlrichs, *Angew. Chem.* **1994**, *106*, 225; *Angew. Chem. Int. Ed. Engl.* **1994**, *33*, 199.

[154] S. Schulz, M. Andruh, T. Papae, T. Heinze, H. W. Roesky, L. Häming, A. Kuhn, R. Herbst-Irmer *Organometallics* **1994**, *13*, 4004. This method is also successful for example in the synthesis of In-chalcogen-heterocubanes: K. Merzweiler, F. Rudolf, L. Brands, *Z. Naturforsch. B.* **1991**, *47*, 470. In contrast, $[\{(Me_3Si)_3CIn\}_4Se_4]$ can be prepared like **33** by reaction of a monovalent starting product with Se [120].

[155] See for example M. Cesari, S. Cucinella in *The Chemistry of Inorganic Homo- and Heterocycles, Vol. 1* (Eds.: I. Haiduc, D. B. Sowerby), Academic Press, London, **1987**, p. 167.

[156] K. W. Waggoner, H. Hope, P. P. Power, *Angew. Chem.* **1988**, *100*, 1765; *Angew. Chem. Int. Ed. Engl.* **1988**, *27*, 1699.
[157] S. Schulz, L. Häming, R. Herbst-Irmer, H. W. Roesky, G. M. Sheldrick, *Angew. Chem.* **1994**, *106*, 1052; *Angew. Chem. Int. Ed. Engl.* **1994**, *33*, 969.
[158] P. Paetzold, A. Richter, T. Thijssen, S. Würtenberg, *Chem. Ber.* **1979**, *112*, 3811.
[159] Direct Ni Al interactions are discussed for example in the Ni-catalyzed polymerization of ethylene by $AlEt_3$: J. J. Eisch, S. R. Sexsmith, K. C. Fichter, *J. Organomet. Chem.* **1990**, *382*, 273; G. Wilke, *Angew. Chem.* **1988**, *100*, 189; *Angew. Chem. Int. Ed. Engl.* **1988**, *27*, 185; K. R. Pörschke, W. Kleimann, Y.-T. Tsay, C. Krüger, G. Wilke, *Chem. Ber.* **1990**, *123*, 1267.
[160] The spectroscopically determined distance in the high-temperature molecule AlNi is 232.1 pm [163].
[161] C. Dohmeier, H. Krautscheid, H. Schnöckel, *Angew. Chem.* **1994**, *106*, 2570; *Angew. Chem. Int. Ed. Engl.* **1994**, *33*, 2482.
[162] E. O. Fischer, C. Palm, *Chem. Ber.* **1958**, *91*, 1725; L. R. Byers, L. F. Dahl, *Inorg. Chem.* **1980**, *19*, 680.
[163] J. M. Brehm, C. A. Arrington, M. D. Morse, *J. Chem. Phys.* **1993**, *99*, 6409.
[164] $[\{CoCp^*(\eta^2\text{-}C_2H_4)\}_2\{AlEt\}_2]$ is formed from $[CoCp^*(\eta^2\text{-}C_2H_4)_2]$ and $AlHEt_2$ in approximately 2% yield together with an additional Co-Al cluster: J. J. Schneider, C. Krüger, M. Nolte, I. Abraham, T. S. Ertel, H. Bertagnolli *Angew. Chem.* **1994**, *106*, 2537; *Angew. Chem. Int. Ed. Engl.* **1994**, *33*, 2435. Considerably longer metal–metal bonds can be found between the Fe atom and the four-coordinate Al atom in $[Cp(CO)_2Fe{-}Al\{(CH_2)_3NMe_2\}iBu]$ (d(Fe–Al) = 245.6 pm): R. A. Fischer, T. Priermeier *Organometallics* **1994**, *13*, 4306.
[165] M. Veith, L. Stahl, *Angew. Chem.* **1993**, *105*, 123; *Angew. Chem. Int. Ed. Engl.* **1993**, *32*, 106.
[166] This can be clearly seen by comparing the following examples: $[Al(\pi\text{-}Cp)_x(\sigma\text{-}Cp)_y]$ ($x + y = 3$): $\delta(^{27}Al) = +88$ and $AliPr_3$ $\delta(^{27}Al) = +256$, as well as $[Al(\sigma\text{-}Cp)_3(thf)]$ $\delta(^{27}Al) \approx +130$ and $[AliPr_3(thf)]\delta(^{27}Al) = +182$ (R. Benn, E. Janssen, H. Lehmkuhl, A. Rufińska *J. Organomet. Chem.* **1987**, *333*, 155).
[167] After submission of this manuscript further important works connected with this topic have appeared. Some of these are listed here: a digallane with a very short Ga–Ga bond: D. S. Brown, A. Decken, A. H. Cowley, *J. Am. Chem. Soc.* **1995**, *117*, 5421. $[Ga_3R_3]^{2-}$: X.-W. Li, W. T. Pennington, G. H. Robinson, *J. Am. Chem. Soc.* **1995**, *117*, 7578; $[R_2Ga{-}GaR_2]^{-\bullet}$: W. Uhl, U. Schütz, W. Kaim, E. Waldhör, *J. Organomet. Chem.* **1995**, *501*, 79.

Electronegativity and Molecular Properties

D. Bergmann and Juergen Hinze

The paradigm that the properties of the atoms determine the properties of the molecules that they form is systematically presented. To this end, three types of atomic properties are differentiated: a) those that can be determined directly by spectroscopy, b) those based on theoretical concepts, and c) those that can be assigned to the atoms interacting in molecules. On the basis of the electronegativity values of the atoms, which can be determined from spectroscopic data together with the assumption that the electronegativities are equalized in bonds, partial charges of the atoms in molecules are determined. These partial charges are correlated with ESCA data and proton affinities. In addition, simple expressions are given for the reliable estimation of bond lengths, bond energies, and force constants.

Keywords: electronegativity · molecular properties · theoretical chemistry

1. Introduction

The paradigm that the properties of the constituent atoms determine the characteristics of the molecules formed is exceptionally useful in chemistry. It can be founded solidly within quantum mechanics, within the framework of valence-bond (VB) theory for molecular structure.[1, 2] In the VB approach, the molecular wave function is written as a product of the state functions of the constituent atoms. In this description the atomic characteristics, which determine the molecular properties, are readily identified. This makes models based on the VB approximation intuitively appealing, as exemplified by the wide acceptance of Pauling's "Nature of the Chemical Bond"[3, 4] and by the extreme usefulness of Lewis structures and the VSEPR rules[5, 6] based on these structures. Unfortunately, the VB approach becomes unwieldy if the tight binding approximation cannot be maintained, and with its nonorthogonal atomic state functions and localized orbitals, it does not lend itself readily to detailed calculations of molecular wave functions.[7] Therefore theorists generally favor the molecular-orbital (MO) method, where the molecular wave function is composed of orthonormal delocalized orbitals and bears a direct relation to the electronic spectra of the molecules.

On the basis of the MO approach enormous progress has been made in the ab initio characterization of molecular properties,[8–10] and due to rapid computer evolution, which makes increasing computational power more readily available, valuable new programs (for example, GAUSSIAN,[11] GAMESS,[12] or MOLPRO[13]) have been provided to the practical chemist to further his research through the detailed quantum mechanical characterization of the molecules under investigation. Ab initio computations for larger molecules are indeed feasible; however, at present unless undue computational effort is invested, reliable results are possible only for small molecules. Thus, useful, empirical, interpretive models are still needed to further our understanding of chemistry. Within the MO picture many such models have been devised,[14] for example, Hückel theory, the Walsh rules,[15] and the frontier orbital picture of reactivity[16] leading to the Woodward–Hoffmann rules.[17, 18] However, the atomic characteristics that determine the molecular properties are difficult to uncover within MO theory with its delocalized molecular orbitals. Here the VB approach complements the picture, because it provides additional insight and the potential for enormous data reduction when well-defined atomic properties are used to derive the characteristics of the molecules formed. A predictive understanding of molecular properties such as structure, binding energies, charge distribution, electrophilicity, reactivity, and many more can be obtained on the basis of the atomic properties.

Atomic properties that are useful in this context are the atomic state term values and ionization potentials with the corresponding atomic configurations, orbitals and orbital energies, electronegativity and hardness, as well as covalent and van der Waals radii. To be sure, of these only the energies of the atomic term values and the ionization potentials can be measured directly, by spectroscopy, for the free atoms. The association of these with electronic configurations and orbitals requires the independent particle approximation, that is, the theory of atomic structure.[19, 20] Moreover, the electron configurations of the free atoms in their ground states are not those of the atoms in a molecule. For an atom in a molecule the valence-state configuration is required, which depends on the molecular environment of the atom and is thus not strictly an atomic property. Fortunately the valence states of an atom can be determined

[*] Prof. J. Hinze, PhD, Dr. D. Bergmann
Fakultät für Chemie der Universität
Postfach 10 01 31, D-33615 Bielefeld (Germany)
Fax: Int. code +(521) 106-6146

 © VCH Verlagsgesellschaft mbH, D-69451 Weinheim, 1996 0570-0833/96/3502-0150 $ 10.00+.25/0

readily in many cases and are related directly to the spectroscopic term values of the free atom.[21-23] The situation is different for the covalent radii of the atoms. They cannot be determined for the atoms directly; here recourse to a large amount of molecular structure data is necessary. Thus covalent radii of atoms should be considered as an atomic property derived from molecules for data reduction, which facilitates the prediction and understanding of molecular structure.

From this discussion it becomes clear that in the effort to derive molecular information from atomic properties in order to achieve data reduction and an understanding of chemistry, three types of atomic properties should be differentiated:

1. Primary atomic properties can be determined experimentally for the free atoms. These are the ionization potentials, electron affinities, and the spectroscopic term values of the free atoms.
2. Secondary atomic properties require, in addition to the experimentally determined quantities for the free atoms, theoretical concepts generally based on approximations within the quantum mechanical description of the electronic structure of atoms. These are the atomic shell structure, the orbitals, the valence shell, hybridization, the valence state, and the energy required to excite the isolated atom to the valence state (promotion energy).
3. Tertiary atomic properties can not be determined for the free atoms, but are assignable to the atoms in their interaction in gases, solids and molecules. These are van der Waals, ionic, and covalent radii, and the energy of the covalent bond, which require for their determination the analysis of a large database of properties of molecules or of the solid state.

Obviously, primary and, since theoretical concepts will generally be required, secondary atomic properties are to be preferred over tertiary properties, when molecular characteristics are to be derived qualitatively and semiquantitatively from the properties of the constituent atoms.

In the light of these considerations, the concept of electronegativity will be reviewed, with no attempt to be exhaustive. We will rather focus primarily on the concept of orbital electronegativity, which has its origin in Mulliken's original definition of absolute electronegativities.[24] On this aspect we will also present new results to demonstrate how this concept, based on primary and secondary atomic properties, can yield useful and practical correlations and predictions of molecular properties like charge distribution, bond length, and bond energies. To be sure, the secondary properties implied in these considerations, like valence states, atomic orbitals, and localized two-electron bonding valence structures (akin to Lewis structures), entail approximate theoretical models most closely related to the tight binding approximation of VB theory.[1, 2]

2. Electronegativity Scales

2.1. Pauling's Definition

The concept of electronegativity was recognized as a useful ordering principle in chemistry more than 150 years ago.[25] With the definition given by Pauling[3, 4] of electronegativity as "the power of an atom in a molecule to attract electrons to itself" and the electronegativity scale of the elements derived by him from thermochemical data, the concept of electronegativity has become one of the most widely used ordering principles in chemistry. The atomic configuration energy, related to electronegativity,[26] has been considered a necessary supplement to the two-dimensional arrangement of the Periodic Table, providing a third dimension, namely energy,[27] superimposed upon the ordering of the elements according to increasing nuclear charge Z (electron number), in such a way that the columns (groups) correspond to equal valence shell configurations with increasing shell quantum numbers. The apparent dependence of many physical and chemical properties of atoms and molecules on electronegativity has led to many correlations,[28, 29] and thus various different electronegativity scales have been suggested.[30] Thus, the concept of electronegativity has become increasingly ambiguous, to the point that its value has been criticized,[31, 32] because the electronegativity of an atom or of a functional group is neither directly measurable nor has it been uniquely defined.

Jürgen A. M. Hinze, born in Berlin in 1937, studied chemistry at the Technical University of Stuttgart from 1957–1960. From there he went to the University of Cincinnati, Ohio, where he wrote his thesis on electronegativity under the guidance of Professor H. H. Jaffé, in 1962. From 1962–1964 he was postdoctoral fellow with Professor K. S. Pitzer at Rice University in Houston, Texas. Till the beginning of 1966 he worked with T. Förster as assistant at the Institut für Physikalische Chemie der Technische Universität Stuttgart, after which he transferred to the University of Chicago to the Laboratory of Molecular Structure and Spectroscopy, chaired at that time by R. S. Mulliken and C. C. J. Roothaan. In 1967 he became professor at the department of chemistry of the University of Chicago, where he stayed till 1975. During this period he spent half a year's sabbatical at the Max-Planck-Institut für Astrophysik in München in 1973. In 1975 he was appointed professor at the Department of Theoretical Chemistry of the University of Bielefeld. His scientific activities in theoretical chemistry range from the exact quantum mechanical treatment of the three-body problem and electron/atom collision processes to the qualitative theoretical description of chemical phenomena. This is documented in a great number of scientific publications and six books that he has edited.

Pauling proposed originally the thermochemical scale, based on the relation (1).[33, 34] He had observed that the dissociation

$$D_{AB} = \left(\frac{D_{AA}+D_{BB}}{2}\right)+\Delta_{AB} = \left(\frac{D_{AA}+D_{BB}}{2}\right)+23(\chi_A-\chi_B)^2 \quad (1)$$

energy of the heteronuclear bond, D_{AB} between the atoms A and B could be expressed as the arithmetic mean of the corresponding homonuclear bond energies D_{AA} and D_{BB} plus the extra ionic resonance energy Δ_{AB} and that the extra ionic resonance energy was proportional to the square of the difference of two atomic quantities, which he associated with the electronegativity χ_A and χ_B of the atoms A and B. Originally Pauling used the units eV for the dissociation energies and a proportionality constant of 1.[34] Later, when Pauling used kcal mol^{-1} for the dissociation energies in Equation (1), he chose the proportionality constant 23,[3, 4] in order to convert the extra ionic resonance energy $(\chi_A - \chi_B)^2$, thought to be in units of eV, into kcal mol^{-1}. Today the value of the proportionality constant should be 100 with bond energies in kJ mol^{-1}.

By using a large set of thermochemical data with Equation (1), which relates bond dissociation energies and electronegativity, a relative electronegativity scale could be derived. The scale was made absolute by choosing the electronegativity of hydrogen χ_H to be 2.1, the value from Mulliken's publication.[24] Pauling's electronegativity values for the elements were readily accepted by the chemistry community, because a vast amount of chemical information could be correlated and rationalized in terms of electronegativities. The electronegativity values increased from left to right in the periodic table and generally decreased a little from top to bottom within a group. The values obtained by Pauling, in particular for the first row elements ($\chi_{Li} = 1.0$, $\chi_{Be} = 1.5$, $\chi_B = 2.0$, $\chi_C = 2.5$, $\chi_N = 3.0$, $\chi_O = 3.5$, and $\chi_F = 4.0$), were so appealingly simple that Pauling's original scale and "Pauling units" remained the reference for electronegativity, even though the dimension and units seem unnatural. With a dimensionless proportionality constant in Equation (1), the dimension of Pauling electronegativity is square root of energy and "Pauling units" would be $\sqrt{\text{eV}}$. As there is no reason why the proportionality constant must be dimensionless, other units could equally well be justified. It should also be mentioned that Pauling later suggested the use of the geometric rather than the arithmetic mean in Equation (1),[35] in order to overcome the problem of negative extra ionic resonance energies for the alkali hydrides. However, this suggestion has not been used in the extensive determination of electronegativities on the thermochemical scale.

2.2. Mulliken's Definition

Only few years after Pauling's original introduction of the electronegativity concept, Mulliken[24] proposed an absolute scale, in which the electronegativity of an atom was given as the arithmetic mean of the ionization potential IP and the electron affinity EA of an atom, quantities which can be determined experimentally and unambiguously for any atom [Eq. (2)].

$$\chi = \frac{(IP+EA)}{2} \quad (2)$$

Mulliken's definition of electronegativity is based on the consideration of the bond between the atoms (species) A and B in the frame of VB theory as a resonance hybrid of covalent and ionic structures (Scheme 1). The energy required to go from the covalent structure A–B to the ionic structure A^+B^- is the difference between IP_A and EA_B plus the covalent binding energy minus the ionic Coulomb attraction between oppositely charged particles. Similarly, the energy required to go from A–B to A^-B^+ is $IP_B - EA_A$. If the electronegativities of A and B are equal, the two ionic structures A^+B^- and A^-B^+ should have equal weights [Eqs. (3) and (4)].

$$A^+B^- \leftrightarrow A\text{–}B \leftrightarrow A^-B^+$$

Scheme 1. Resonance hybrids as basis for Mulliken's definition of electronegativity.

$$IP_A - EA_B = IP_B - EA_A \quad (3)$$

$$IP_A + EA_A = IP_B + EA_B \quad (4)$$

On the other hand if A were more electronegative than B, the structure A^-B^+ would dominate over the structure A^+B^- [Eqs. (5) and (6)]. Clearly, the ionization potentials and electron

$$IP_A - EA_B > IP_B - EA_A \quad (5)$$

$$IP_A + EA_A > IP_B + EA_B \quad (6)$$

affinities required in Equation (2) are not those of the ground states of atoms, but those of the valence state, that is, those of the orbitals used for bond formation. This was recognized already by Mulliken when he originally proposed his absolute electronegativity scale. This fact, however, has advantages and disadvantages. The disadvantage is that these ionization potentials and electron affinities cannot be measured directly; they can, nevertheless, be derived from the corresponding, experimentally accessible ground-state values and the atomic spectroscopic term values[21–23] within the frame of Slater's theory of atomic structure.[19, 20] Thus electronegativity becomes a derived atomic property, which depends on the valence state of the atom. As this is not a stationary state of the atom, it is not experimentally accessible, but depends on the bonding of the atom in a molecule. This, however, is also the advantage of Mulliken's definition of electronegativity: it permits different electronegativity values for the same atom, depending on the valence state the atom assumes in a molecule. The need for such a dependence was recognized early in the example of carbon, which was known to have a higher electronegativity in the ethynyl group (sp hybridization) than in the methyl group (sp^3 hybridization).[37]

Unfortunately, Mulliken's definition of electronegativity, which is well founded in the quantum theory of the electronic structure of molecules, did not receive the early wide acceptance in chemistry it deserves. This is in part because the experimental determination of electron affinities became reliable only recently.[38] Also the calculation of the required valence-state promotion energies from atomic term values has become possible only after the latter had been determined more completely.[39]

2.3. Comparison Between the Methods To Determine Electronegativity

In their excellent review on the concept of electronegativity, Pritchard and Skinner[40] critically evaluate different suggestions made for the determination of electronegativity values for atoms, most of them based on empirical correlations between atomic and molecular properties and Pauling electronegativity values. Pritchard and Skinner favor Mulliken's scale, as it is based on directly observable spectroscopic data of the atoms. They also succeeded in computing Mulliken electronegativity values for most of the atoms, in some cases even for different valence states, from ionization potentials, electron affinities, and atomic term values as they were known then.

It seems worthwhile here to recall some of the early suggestions made for the determination of electronegativities from molecular properties, as these could be useful when, vice versa, molecular properties are to be determined from known atomic electronegativities.

Malone[41] suggested using "bond" dipole moments μ_{AB} and relating them to the electronegativity difference for the bond A–B by the equation $\mu_{AB} = |\chi_A - \chi_B|$. This correlation, even though it seems obvious, was found not to be very good, and the relation was not used extensively to determine electronegativity values. That such a simple correlation between electronegativity and dipole moment cannot hold is well understood today. There is no reason why first the "ionicity" of a bond should be simply proportional to the electronegativity difference; second, the bond dipole moment should be determined only by the partial charges and not also by the bond distance; and third, the electric moments of lone pairs should be negligible when determining the dipole moment of a molecule from bond moments.

Another early empirical relation was found by Gordy[42,43] between electronegativity and force constants [Eq. (7)], where

$$k_{AB} = \left[1.67N\left(\frac{\chi_A\chi_B}{r_{AB}}\right)^{0.75} + 0.3\right] 10^{-3} \qquad (7)$$

k_{AB} is the stretching force constant of the bond between A and B in dyn Å^{-1} and N is the bond order. As we will see later, a relation like this is useful in determining bond distances and estimating force constants from electronegativities.

The electronegativity of the atoms played an increasingly important role in the qualitative arguments about chemical bonding, since a large amount of chemical information about molecule formation could be systemized and understood with the concept. The need to have reliable electronegativity values available for all of the atoms of the periodic system therefore became urgent. Unfortunately the lack of thermochemical data prevented an extensive use of Pauling's original relation to obtain a complete list of atomic electronegativity values, even though extensive efforts were made by Haissinsky[44,45] and Huggins.[46] A similar situation prevailed with Mulliken's absolute electronegativity values. In particular the electron affinity values of the atoms were not known then, and the definition and calculation of valence states and their promotion energies provided difficulties.

These difficulties in obtaining electronegativity values for the atoms appeared to be resolved by the suggestion of Allred and Rochow[47] that the electronegativity of an atom can be calculated from the empirical relation (8). Here Z_{eff} is the effective

$$\chi = 0.359\,\frac{Z_{eff}}{r^2} + 0.744 \qquad (8)$$

charge of the nucleus screened by the electrons of the atom as estimated by Slater's rules,[48] and r is the covalent radius of the atom as tabulated by Pauling.[49] With this relation electronegativity is given by the radial force an electron would experience one covalent radius from the nucleus of the atom (the "covalent boundary").

The numerical coefficients were determined by fitting the force formula [Eq. (8)] to the then known Pauling electronegativity values. The most significant difference is that in the Allred and Rochow scale the electronegativity value for Ge is larger than that for Si. Allred and Rochow pointed out[50] that this reversal is consistent with chemical evidence and was noted earlier by Sanderson,[51] who attributed it to the d-shell contraction. As the values of Z_{eff}, and apparently also the values for the covalent radii of the atoms, were readily available, it was easy to use Equation (8) and determine the electronegativity values for most of the atoms without the difficulties that afflicted such a determination with Pauling's or Mulliken's definition. Thus, the electronegativity values of Allred and Rochow were readily accepted, to the extent that these values are listed in most explicit periodic charts, where in general also the covalent radii of the atoms are given. That the covalent radius of an atom depends on the valence state of the atom is frequently recognized, but not reflected in the electronegativity values given, even though Allred and Rochow had emphasized it in their original article.

The various atomic and molecular properties that can be correlated with electronegativity have led to many different suggestions[26,28,29,52–71] for the definition and determination of electronegativity values. This has generated some confusion, and we will not discuss these different suggestions here in detail, even though some new insight can be gained from these suggestions if they are derived using an extensive data base and if they have a solid theoretical foundation. It should be mentioned here that in a number of theoretical investigations, using MO as well as VB approaches, connections have been derived between the electronegativity values determined using Mulliken's suggestion [Eq. (2)] and the extra ionic energy as defined in Equation (1).[28,36,72–74]

3. Electronegativity as Electrical Potential

A seemingly rigorous derivation of atomic and molecular electronegativity has been presented on the basis of the density functional theory.[75] Electronegativity is identified as the chemical potential and defined as the partial derivative of the total energy of a system with respect to the total number of electrons, that is, the trace of the charge density. This definition, restricted to the ground state, yields Equation (9) and, therefore, the same

$$\chi = -\left(\frac{\partial E}{\partial N}\right) \qquad (9)$$

electronegativity everywhere for the entire system, atom, or molecule. This electronegativity equalization throughout a

molecule does not seem to be useful and runs counter to chemical intuition and the observation of electro- or nucleophilic centers in a molecule. This global equalization of the electronegativity results because the partial derivative of the energy with respect to the total charge of the system is used; it would even obtain for a system composed of noninteracting subsystems. If the partial derivative were taken with respect to a change of the charge at a particular volume element or locus in the molecule, a space-dependent electronegativity would result for molecules, yielding the electro- and nucleophilic centers required for chemistry. This spatial dependence, desired in chemistry, is recovered through the definition of the Fukui function $f(r)$[76, 77] [Eq. (10)], where $\rho(r)$ is the electron density of the molecule

$$f(r) = \frac{\partial \rho(r)}{\partial N} \tag{10}$$

considered. The Fukui function indicates those regions in a molecule where the charge density changes during a reaction. As numerical approximation for the partial derivatives in Equation (10), the forward difference is used for a nucleophilic attack, while for an electrophilic attack the backward difference is employed. For radical reactions the central difference is recommended. This function is akin to the use of HOMOs (highest occupied MOs) and LUMOs (lowest unoccupied MOs) in the frontier orbital theory of reactivity,[16–18] with the advantage that, because the definition is in terms of the physically real charge density, no recourse to the concept of orbitals is needed. However, as a result the effect of orbital phase relations on reactivity is lost.

The definitions for atoms and molecules, of electronegativity according to Equation (9), and of hardness[78] according to Equation (11), in conjunction with the introduction of the

$$\eta = \frac{1}{2}\left(\frac{\partial^2 E}{\partial N^2}\right) \tag{11}$$

Fukui function [Eq. (10)] within the framework of density functional theory, have the appeal of rigor, as there seems to be no need for the concept of orbitals. However, for the practical use of these definitions, a knowledge of the atomic and molecular electron density functions is required. As this is difficult to obtain experimentally, if at all, recourse to detailed wave function or density functional calculations of these systems becomes necessary. Equations (9) and (11) can be approximated using finite differences instead of differentials, ionization energies, and electron affinities. These aspects have been reviewed recently.[30]

The density functional definition of electronegativity [Eq. (9)] is akin to the earlier definition of atomic electronegativity by Iczkowski and Margrave[79] and to the localized orbital-electronegativity concept introduced by Hinze et al.[80] We will focus here on the latter, since the combination of the localized orbital picture, in the frame of the tight binding approximation of valence-bond theory,[1, 2] with the idea of electronegativity as an electrical potential proves to be rather fruitful, as we hope to show in the following sections. With this definition, the original absolute electronegativity scale introduced by Mulliken[24] is retained and put on a solid theoretical foundation (see appendix A of Ref. [81]). In addition, by using the orbital concept the flexibility required to yield electro- and nucleophilic centers within a molecule is obtained immediately. Furthermore, the extension to a localized "hardness"[78] through the second derivative of the energy with respect to the charge localized in an orbital is retained.

The orbital electronegativity of an atomic orbital, say orbital i, is defined as (12),[80] where n_i is the occupation and q_i the charge in orbital i.

$$\chi_i = -\left(\frac{\partial E}{\partial n_i}\right) = \left(\frac{\partial E}{\partial q_i}\right) \tag{12}$$

This definition makes the electronegativity concept for atoms more complex, yielding more than one electronegativity value for a given atom. Nevertheless, this complexity is desirable if, for instance, the electron shell structure of atoms is to be reflected in the electronegativity values (for example, for a given atom $E(N)$ shows clear discontinuities at $N = 2$, $N = 4$, $N = 10$ etc.) leading to difficulties with the use of Equation (9).

More important for chemistry is the possibility of different electronegativity values for an atom, dependent on its valence state, or, which is more flexible, dependent on the s, p, or d character of the bond-forming hybrid orbital of the atom. Such a valence-state dependence of the electronegativity has been requested on chemical grounds,[37] and the need was recognized already by Mulliken[24] in his original definition of the "absolute" electronegativity scale. Thus, although the electronegativity concept is complicated by orbital electronegativities, the latter definition reflects more realistically the versatility, depending on the different chemical surroundings, of an atom in a molecule. This is particularly apparent in the case of carbon, which has a tetrahedral environment with sp^3 hybrid orbitals in saturated compounds, whereas the environment is trigonal (sp^2 hybrid orbital) or digonal (sp hybrid orbital) in unsaturated compounds. Here large differences in the electronegativity are expected. For most other atoms the variability and therefore the complexity is not so pronounced. Significant differences are also to be expected for the chalcogens, which may be di-, tetra-, or hexavalent and for the elements in the fifth main group, which may be tri- or pentavalent. In addition, as will be shown below, the concept of orbital electronegativities provides a consistent extension to group electronegativities and to the determination of partial charges in molecules.

To use the definition of orbital electronegativity [Eq. (12)] it is necessary to display the energy $E(q_i)$ of an atom as a continuous function of the charge q_i in the i-th spatial valence orbital. It is reasonable to use a quadratic polynomial [Eq. (13)] on empirical as well as theoretical grounds. The orbital electronegativity is then given by Equation (14), and depends on the charge (occupation) of the orbital considered. However, electronegativity should represent the potential for attracting electrons before bond formation, thus the values for empty, singly, or doubly occupied orbitals (that is, for $q_i = 0$, -1, or -2) will be of special significance.

$$E(q_i) = a + bq_i + cq_i^2 \tag{13}$$

$$\chi_i(q_i) = b + 2cq_i \tag{14}$$

Defining the valence-state ionization energy IP_i and electron affinity EA_i for the i-th orbital according to Equa-

tions (15) and (16) yields, on using Equation (13) with the

$$IP_i = E(q_i=0) - E(q_i=-1) \quad (15)$$

$$EA_i = E(q_i=-1) - E(q_i=-2) \quad (16)$$

orbital index i dropped, the relations (17) and (18) for the coefficients b and c.

$$b = \frac{(3IP-EA)}{2} \quad (17)$$

$$c = \frac{(IP-EA)}{2} \quad (18)$$

Substituting these values into Equation (14) results in the electronegativity for a singly occupied orbital, corresponding to the standard electronegativity (19) in accord with the original

$$\chi(-1) = \frac{(IP+EA)}{2} \quad (19)$$

definition of Mulliken.[24] In addition the electronegativity values for empty and doubly occupied orbitals are obtained according to Equations (20) and (21), respectively, which enables

$$\chi(0) = \frac{(3IP-EA)}{2} \quad (20)$$

$$\chi(-2) = \frac{(3EA-IP)}{2} \quad (21)$$

the orbital-electronegativity concept to be used for dative bonds, too. As the orbital occupation can be no smaller than 0 and no larger than 2, $\chi(0)$ is the potential of an empty orbital to attract electrons, while $\chi(-2)$ is the potential to withhold electrons, and only $\chi(-1)$ has both meanings.

The orbital electronegativities obtained in this way have the dimension of an electrical potential, and with the ionization energy and electron affinity in eV, the units for χ will be volts. To convert the results to "Pauling units", more familiar to chemists, the empirical relation (22) may be used, where χ_P is the

$$\chi_P = 0.303\chi_M \quad (22)$$

electronegativity in "Pauling units", while χ_M (Mulliken) is the orbital electronegativity in volts. The proportionality constant in (22) has been obtained by a least squares fit of the computed orbital electronegativities to the generally accepted values of Allred and Rochow.[47] The fit is excellent, and a possible constant term in the fit was found to be statistically insignificant. If ground-state ionization energies and electron affinities are used to determine the χ_M values, such a fit is much less satisfactory, and some inconsistencies arise.[26]

Within the framework of the concepts developed above, a "hardness" parameter η_i akin to the hardness introduced by Pearson[78] may be defined for an orbital according to Equation (23). It has the dimension of energy per square of charge or

$$\eta_i = \frac{1}{2}\frac{\partial^2 E(q_i)}{\partial q_i^2} = \frac{1}{2}\frac{\partial \chi_i(q_i)}{\partial q_i} = c_i \quad (23)$$

potential per charge, which is the same as reciprocal capacitance; if the energy (as used here) is in eV, the units for the hardness will be Ve^{-1}. The concept of "hardness" has been reviewed recently.[82]

In Scheme 2 the standard electronegativity values in "Pauling units" and hardness parameters in Ve^{-1} for the elements are

H χ = 2.17 η = 6.42							He χ = 2.93 η = 14.92
Li χ = 0.91 η = 2.39	Be χ = 1.45 η = 3.77	B χ = 1.88 η = 5.06	C χ = 2.45 η = 6.35	N χ = 2.93 η = 7.29	O χ = 3.61 η = 8.26	F χ = 4.14 η = 9.19	Ne χ = 3.09 η = 11.36
Na χ = 0.86 η = 2.29	Mg χ = 1.21 η = 3.05	Al χ = 1.62 η = 3.53	Si χ = 2.12 η = 4.40	P χ = 2.46 η = 5.32	S χ = 2.64 η = 5.34	Cl χ = 3.05 η = 5.87	Ar χ = 2.71 η = 6.80
K χ = 0.73 η = 1.92	Ca χ = 1.02 η = 2.38	Ga χ = 1.77 η = 3.92	Ge χ = 2.14 η = 4.49	As χ = 2.25 η = 4.91	Se χ = 2.46 η = 4.72	Br χ = 2.83 η = 5.30	Kr χ = 2.36 η = 6.19
Rb χ = 0.71 η = 1.85	Sr χ = 0.96 η = 2.20	In χ = 1.63 η = 3.68	Sn χ = 2.12 η = 3.33	Sb χ = 2.15 η = 4.88	Te χ = 2.29 η = 3.94	I χ = 2.57 η = 4.73	Xe χ = 1.99 η = 5.60
Cs χ = 0.8	Ba χ = 0.9	Tl χ = 2.0	Pb χ = 2.3	Bi χ = 2.0	Po χ = 2.1	At χ = 2.2	Rn χ = 1.8 η = 4.8
Fr χ = 0.7	Ra χ = 0.9						

Sc χ = 1.4	Ti χ = 1.5	V χ = 1.6	Cr χ = 1.7	Mn χ = 1.6	Fe χ = 1.8	Co χ = 1.9	Ni χ = 1.9	Cu χ = 1.4 η = 3.2	Zn χ = 1.5 η = 3.4
Y χ = 1.2	Zr χ = 1.3	Nb χ = 1.5	Mo χ = 2.2	Tc χ = 2.3	Ru χ = 2.3	Rh χ = 2.3	Pd χ = 2.2	Ag χ = 1.4 η = 3.1	Cd χ = 1.4 η = 3.4
La χ = 1.1	Hf χ = 1.3	Ta χ = 1.4	W χ = 2.3	Re χ = 2.2	Os χ = 2.2	Ir χ = 2.2	Pt χ = 2.3	Au χ = 2.5	Hg χ = 2.0

Schema 2. Electronegativity values and hardness parameters for the elements.

presented. These values have been obtained from Equations (19) and (23). The necessary valence-state ionization energies and electron affinities were obtained earlier[83, 84] by combining the corresponding ground-state values with the valence-state promotion energies computed from the atomic term values. Somewhat more detailed information, with the atomic electronegativity parameters required for the determination of the charge distribution in molecules, is presented in Table 1. All the parameters presented here have been reevaluated in the light of the most recent spectroscopic data (more detailed information is given in Refs. [81, 83, 84]); they thus supersede similar data of earlier compilations of Mulliken electronegativity values.[40, 85–88]

The values presented are derived directly from spectroscopic data of atoms and the definition of the atomic valence states that are reasonable on chemical grounds. For the elements of the main groups 1 through 4, the hybrid orbitals s, di (= sp), tr (= sp^2), and te (= sp^3) have been used for the standard values reported. In the case of carbon the orbital electronegativity of the π orbital ($\chi_\pi = 1.73$) is of interest, as well as the values $\chi_{di} = 3.17$ and $\chi_{tr} = 2.69$ obtained for the sp and sp^2 hybrid orbitals, respectively. This demonstrates that the electronegativity of carbon can be quite different, depending on the type of bonding. The situation is not as extreme for most other elements.

The standard electronegativity values reported for the elements of the main groups 5 through 7 have been computed with 15%, 10%, and 5% s character for the bonding orbitals, respectively. For the computation of these values, the parameters b and c were interpolated with a quadratic least squares fit for the experimental data. Although on chemical grounds it is expected that the s character in the bonding orbitals decreases on going to the heavier elements in these groups, the effect on the corre-

Table 1. Atomic electronegativity parameters. The parameters b^0, b^1 (in V), and c (in Ve^{-1}) are defined in Equation (34). In the last two columns the Mulliken and Pauling electronegativity values, χ_M and χ_P, are given.

Atom [a]	IP	EA	b^0	b^1	$c = \eta$	χ_M	χ_P
H(s)	13.599	0.755	20.021	0.000	6.422	7.18	2.17
He [b]	54.402	24.578	69.314	0.000	14.912	9.67	2.93
Li(s)	5.392	0.620	7.778	0.000	2.386	3.01	0.91
Be(di)	8.552	1.018	12.319	6.307	3.767	4.79	1.45
B(tr)	11.250	1.130	16.310	8.823	5.060	6.19	1.88
C(te)	14.423	1.719	20.775	10.741	6.352	8.07	2.45
C(tr)	15.447	2.315	22.013	10.677	6.566	8.88	2.69
C(di)	17.277	3.677	24.077	10.596	6.800	10.48	3.17
C(π)	11.036	0.400	16.354	11.026	5.318	5.72	1.73
N(15% s)	16.974	2.390	24.266	12.900	7.292	9.68	2.93
O(10% s)	20.166	3.644	28.427	14.792	8.261	11.91	3.61
F(5% s)	22.853	4.469	32.045	0.000	9.192	13.66	4.14
Ne [b]	44.274	21.558	55.632	0.000	11.358	10.20	3.09
Na(s)	5.144	0.560	7.436	0.000	2.292	2.85	0.86
Mg(di)	7.029	0.929	10.079	5.070	3.050	3.98	1.21
Al(tr)	8.860	1.806	12.387	6.118	3.527	5.33	1.62
Si(te)	11.384	2.580	15.786	7.225	4.402	6.98	2.12
P(15% s)	13.431	2.785	18.754	8.816	5.323	8.11	2.46
S(10% s)	14.049	3.377	19.385	10.524	5.336	8.71	2.64
Cl(5% s)	15.921	4.183	21.790	0.000	5.869	10.05	3.05
Ar [b]	29.357	15.755	36.158	0.000	6.801	8.95	2.71
K(s)	4.341	0.501	6.261	0.000	1.920	2.42	0.73
Ca(di)	5.747	0.997	8.122	4.108	2.375	3.37	1.02
Cu(s)	7.726	1.226	10.976	0.000	3.250	4.48	1.36
Zn(di)	8.254	1.407	11.678	5.781	3.424	4.83	1.46
Ga(tr)	9.762	1.926	13.680	6.474	3.918	5.84	1.77
Ge(te)	11.544	2.564	16.034	7.397	4.490	7.05	2.14
As(15% s)	12.350	2.534	17.258	9.572	4.908	7.44	2.25
Se(10% s)	12.831	3.401	17.546	9.833	4.715	8.12	2.46
Br(5% s)	14.653	4.057	19.951	0.000	5.298	9.36	2.83
Kr [b]	26.376	13.996	32.566	0.000	6.190	7.81	2.36
Rb(s)	4.176	0.484	6.022	0.000	1.846	2.33	0.71
Sr(di)	5.369	0.979	7.564	3.837	2.195	3.17	0.96
Ag(s)	7.576	1.303	10.713	0.000	3.137	4.44	1.35
Cd(di)	7.790	1.091	11.140	5.645	3.350	4.44	1.35
In(tr)	9.073	1.707	12.756	6.017	3.683	5.39	1.63
Sn(te)	10.346	3.680	13.679	5.986	3.333	7.01	2.12
Sb(15% s)	11.983	2.217	16.866	7.628	4.883	7.10	2.15
Te(10% s)	11.483	3.607	15.421	8.712	3.938	7.54	2.29
I(15%)	13.197	3.741	17.925	0.000	4.728	8.47	2.57
Xe [b]	23.320	12.128	28.916	0.000	5.596	6.53	1.99

[a] In each case the type of hybrid orbital is given in parentheses. s = s orbital, di = sp, tr = sp^2, te = sp^3, π = p orbital available for π bonding. [b] For the inert gases, the electronegativity values given are those for doubly occupied orbitals.

sponding electronegativity values would be minimal. This changes when these elements are not three-, two-, or one-connected, respectively, as was assumed for the standard values reported in Scheme 1. For example, if one would use sp^3d(pe) hybrid orbitals, the electronegativity for pentavalent phosphorus becomes $\chi_{pe} = 3.07$, significantly higher than the standard value. A similar situation obtains for tetra- or hexavalent sulfur; for pentagonal (pe) or octahedral (oh) hybrid orbitals, respectively, the electronegativity values obtained are $\chi_{pe} = 3.22$ and $\chi_{oh} = 3.19$. However, it is not clear at all whether the expansion of the valence shell in these atoms can be attributed to d orbital participation, or whether it is due to three-center bonds. This point will not be considered further here. Thus, by using the standard values for electronegativity as reported above, extended by a few extra values for common valence states, most relevant chemical structures can be accounted for, and it will be necessary only in rare cases to use the more extensive list of possible valence states reported earlier for completeness—for example, more than 40 valence states for sulfur.[81]

The electronegativity values reported in "Pauling units" are converted from the original results obtained in V with the empirical relation (22). They should be adequate for most qualitative considerations. The values given with three significant figures have an uncertainty of ± 0.04 (95% confidence level and interval) due to the conversion from V to "Pauling units" and due to the uncertainty of the s, p, or d character of the bonding orbitals. The latter uncertainty, as well as the lack of atomic spectroscopic data, is even larger for the transition metals and for the last rows of the periodic table; the values for these elements are therefore given with only two significant figures with an implied uncertainty of ± 0.1. Many of these values could not be obtained from spectroscopic data of atoms. For these elements the hardness parameter η is not specified, and the electronegativity values given are those of Allred.[89] The electronegativities for the lanthanides and actinides, not given explicitly, can be obtained only approximately from atomic data. For these elements electronegativity values of 1 or 1.1 are recommended, increasing slightly from left to right in the corresponding row.

The electronegativity values reported in Scheme 2 and Table 1 for the inert gases are the values for doubly occupied orbitals $\chi(-2)$ [see Eq. (21)]. Except for helium, where the s orbital is used, p orbitals are considered.

4. Charge Distribution in Molecules

If it were limited to the determination of the atomic electronegativity values presented in Table 1, the concept of orbital electronegativity would offer little new insight. The electronegativity values determined directly from spectroscopic data differ insignificantly from conventional values, as evidenced by the good correlation between the orbital-electronegativity scale in V, and the conventional Pauling scale obtained in a much less direct way. The few extra values obtained, corresponding to some common valence states of carbon, phosphorus, or sulfur etc., would not justify a new electronegativity concept. The new concept, however, leads to insights into the process of bond formation and the concomitant charge transfer, resulting in the possibility of determining the charge distribution in a molecule without extensive quantum mechanical calculations, and finally to a better understanding of molecular properties, derived from the electronegativity values of the atoms.

The definition of orbital electronegativity as an electric potential [Eq. (12)] provides an immediate rationalization of the electronegativity equalization between two orbitals forming a two electron bond, as suggested by Sanderson.[54, 90, 91] If orbital i on atom A forms a bond with orbital j on atom B, a transfer of charge Δq will occur from the less electronegative orbital to the more electronegative one, until the two electronegativities have become equal, as described in Equation (24). Here q^0 is the

$$\chi_{iA}(q^0_{iA}+\Delta q) = \chi_{jB}(q^0_{jB}-\Delta q) \qquad (24)$$

reference charge in the orbitals before bond formation, and Δq is the charge transferred from the bonding orbital j_B to the orbital i_A. This charge transfer corresponds to an energy lowering in the bond until the two electronegativities are equal,

provided no other energetic effects are connected with this charge transfer process. Such energetic effects have been investigated and discussed extensively. Fortunately, the main two effects—an additional energy lowering due to the coulomb attraction of the partially negative and positive centers A and B formed, and an energy increase due to the weakening of the covalent bond—tend to cancel in the case of bonds formed between singly occupied orbitals. The situation is expected to be different in the case of dative bonds, where both effects are energy lowering.

Using the full electronegativity equalization in a bond as working hypothesis immediately yields the charge transferred from orbital j to orbital i by combining Equations (14) and (24) to give (25).[80, 92]

$$\Delta q = \frac{\chi_j(q_j^0)-\chi_i(q_i^0)}{2(c_j+c_i)} \tag{25}$$

The net energy change due to such a charge transfer is obtained as (26).[28, 92]

$$\Delta E = -\frac{[\chi_j(q_j^0)-\chi_i(q_i^0)]^2}{4(c_j+c_i)} \tag{26}$$

The resulting reduction in energy due to the charge transfer is reminiscent of the extra ionic resonance energy [Eq. (1)] used by Pauling originally in establishing his relative electronegativity scale.[33] Some more recent investigations of the concept of electronegativity equalization,[93] as well as some earlier MO derivations of this concept,[28] seem to indicate that Equations (25) and (26) should also contain the coulomb attraction of the induced partial charges. As these terms would be distance-dependent, their inclusion would require molecular structure information in addition to the simple connectivity for the determination of the partial charges. We therefore proceed here with the simple model that neglects these terms. To what extent the inclusion of these terms will improve the correlations of electronegativity and partial charges with molecular properties remains a topic for future research.

The ideas developed above are adequate for the calculation of the charge transfer in a single two-electron bond. To deal with molecules in general, where the same atom may have several different ligands, an extension of these concepts is required. Consider an atom that uses m orbitals to form m localized two-electron bonds. Due to the orbital-electronegativity equalization, it will have the charge Δq_k transferred into each of the bond forming orbitals, that is, for $k = 1$ through m. The net total charge of the atom is expressed by Equation (27). The orbital

$$Q = \sum_{k=1}^{m} \Delta q_k \tag{27}$$

electronegativities of this atom will presumably depend on the charge transferred in all the other orbitals of the atom. The electronegativity χ_i of a particular orbital i will be a function of $q_i = q_i^0 + \Delta q_i$ [Equation (14)], but it will depend also on the residual charge r_i [Eq. (28)] from all the other bonds of the atom

$$r_i = \sum_{k \neq i} \Delta q_k = Q - \Delta q_i \tag{28}$$

considered. Thus Equation (14) needs to be generalized to (29),

$$\chi_i(r_i,q_i) = b_i(r_i)+2c_i(r_i)q_i \tag{29}$$

in which the parameters b and c depend on the residual charge r_i. Fortunately, the residual charge will be small in general ($|r| < 1$) and the parameter $c = (\mathrm{IP} - \mathrm{EA})/2$, which depends only weakly on the residual charge, can be treated as a constant, while for the parameter b, a linear approximation is adequate [Eq. (30)]. The relation (31) gives b^0 according to (32) and b^1 according to (33). The parameters b^1 can be evaluated from

$$b(r) = b^0 + b^1 r \tag{30}$$

$$b = (3IP - EA)/2 = IP + c \tag{31}$$

$$b^0 = IP^0 + c \tag{32}$$

$$b^1 = \frac{\partial IP}{\partial r} \tag{33}$$

atomic spectroscopic data from for various valence orbitals, just like the parameters b_0 and c. Slightly different b^1 values would be obtained, depending on the orbitals from which the residual charge results. As this dependence would unduly complicate the concept, and since this dependence is weak, b^1 values have been suitably averaged for the main group elements.[83, 84] With these values, the orbital electronegativity can be evaluated from the charge q in the orbital and the residual charge r due to charge transfer in other orbitals of the same atom. This orbital electronegativity [Eq. (34)] for an orbital i can now be used to calcu-

$$\chi_i(r_i,q_i) = b_i^0 + b_i^1 r_i + 2c_{iq_i} \tag{34}$$

late the charge shift Δq_i, using the concept of electronegativity equalization, when orbital i forms a localized two-electron bond with an orbital j of another atom. Since, in this case, $\Delta q_i = -\Delta q_j$, an equation of the form of (35) is obtained for each bond within a molecule. For a molecule with N bonds, N equations of type (35) result, one for each bond. Substituting Equation (34) into Equation (35) and replacing the r_i values by the Δq's [Equations (27) and (28)] yields for a molecule with N

$$\chi_i(r_i,q_i^0+\Delta q_i) = \chi_j(r_j,q_j^0-\Delta q_i) \tag{35}$$

bonds N linear equations (for details see Ref. [18]), which may be solved readily for the N unknowns (the charge shifts Δq in the bonds). This provides an easy method of determining the partial charges Q given by Equation (27) in a molecule, from just the orbital-electronegativity data, the coefficients b and c for the atomic valence orbitals (given in Table 1 and more detailed in Refs. [81, 83, 84]), and the Lewis structure of the molecule. No data on the geometrical structure of the molecule is required, and the determination of the charge distribution is much easier than an analogous quantum chemical calculation; just a set of linear equations containing as many equations as number of bonds needs to be solved. Even small computers (PCs) can handle the solution for large molecules. Not only the charge distribution, which should correlate with a number of experimentally accessible data and which is essential for more detailed molecular mechanics calculations, can be obtained in this way. It is just as easy to determine orbital electronegativities for free radicals or for doubly occupied or empty orbitals. To obtain these values, it is necessary to use Equation (34) together with the r_i value computed in a charge distribution calculation for the group.

It is also possible to determine the orbital hardness parameters [Eq. (9)] for molecular groups. However, here it will not be sufficient to use the c_i value of the corresponding atomic orbital directly, since in the group the residual charge r_i of the orbital considered will have a significant effect on the hardness. To this end it is necessary to use a finite difference approximation to obtain the partial derivative of the corresponding orbital electronegativity in the group. The hardness parameter is thus obtained as Equation (36). Thus two charge distribution calcula-

$$\eta_i = \frac{1}{2}\frac{\partial \chi_i\,(r_i,q_i)}{\partial q_i} \approx \frac{1}{4}\frac{\chi_i\,(r_i^+,\ q_i^0+\Delta q_i)-\chi_i\,(r_i^-,\ q_i^0-\Delta q_i)}{\Delta q_i} \qquad (36)$$

tions are necessary for the group, one with the orbital charge $q_i^0 + \Delta q_i$ to determine r_i^+ and another with $q_i^0 - \Delta q_i$ to determine r_i^-. We have found $\Delta q = 0.1$ to be adequate for the determination of the hardness of a free orbital of a molecular group.

Two problems with the charge distribution calculations should be mentioned. 1) When double or triple bonds are considered, σ and π bonds must be treated together as a localized four or six electron bond with the suitably averaged corresponding b and c parameters, otherwise σ donation and concomitant π back donation become unreasonably amplified. 2) When for the molecules under consideration two or more energetically equal or nearly equal Lewis resonance structures can be drawn, a charge distribution calculation should be performed for each of the resonance structures, and the results suitably averaged. This enables conjugation to be included in a localized orbital description; however, it introduces the ambiguity of the relative weights of these structures in the case of energetically nonequal resonance structures. We have found that for different, reasonably chosen weights, the results are not significantly different.

The theoretical development of the concept of orbital-electronegativity and of electronegativity equalization in a bond can be closed at this point. There are a number of other suggestions in the literature for the determination of partial charges in a molecule through partial[94] or complete[91, 95–100] electronegativity equalization in a molecule. The extent to which these empirical concepts, based on the paradigm that atomic properties (here spectroscopic data to which these of atoms) determine the properties of the molecules formed from these atoms, are useful remains to be demonstrated. To this end it is necessary to find reliable correlations of the computed orbital electronegativities and charge distributions with other results, preferably with molecular properties that can be determined experimentally.

5. Prediction of Molecular Properties

In this section we report some of our results using the concepts and atomic data presented in Sections 3 and 4. Obviously, the correlations we have found between the computed results and experimental data can be used in turn to predict as yet unknown data. Our main interest has been to obtain molecular structure data to use in the parameterization of molecular mechanics models,[101–108] with the aim of reducing the number of seemingly independent parameters in these models. We are sure that a number of additional useful correlations can and will be found in the future.

5.1. Charge Distribution in Molecules

Solving Equation (35) for electronegativity equalization in localized bonds for all the bonds in a molecule, in conjunction with Equations (27), (28), and (34), yields partial atomic charges for all the atoms in the molecule. The procedure is simple, and only primary and secondary atomic data are required together with the Lewis structure of the molecule. In addition, group electronegativity and hardness parameters can be obtained for molecular fragments. Unfortunately, the values for the partial charges in a molecule cannot be determined directly by experiment in order to validate these empirical concepts. The distribution of partial charges in a molecule is related to the uniquely defined charge distribution function $\rho(\boldsymbol{r})$, the first-order reduced electron-density function that is given for an n-electron system by Equation (37) in terms of the elec-

$$\rho(\boldsymbol{r}) = n\int d\sigma_1\, d\tau_2 \ldots d\tau_n\, |\,\Psi(\tau_1 \ldots \tau_n)\,|^2 \qquad (37)$$

tronic wave function of the specific state of the system. Here the integration is over the spin coordinate σ_1 of one electron and the space-spin coordinates τ_i of all the other electrons. To obtain the density function in this way, a full quantum-mechanical electron-structure calculation or a density-functional calculation for the molecule is required. In principle, the charge-distribution function of a molecule could also be determined experimentally with X-ray or electron scattering; however, the resolution obtained today with these methods is not yet satisfactory. Moments of the charge distribution (dipole or quadrupole moments of molecules) are more readily accessible.

But even if the full charge distribution function $\rho(\boldsymbol{r})$ is known, there seems to be no unique way yet to partition the charge distribution into its atomic contributions and thus obtain partial charges, so useful in the interpretation of molecular properties. The problem lies in the difficulty of assigning regions of space to the constituent atoms in a molecule. Several suggestions have been made for such a partition.[109–120] Most, with the exception of that made by Bader[121, 122] (its physical significance has not been established yet), are not unique. All these procedures require initially a full quantum mechanical characterization of the molecule, after which a charge distribution analysis seems to be of limited additional value.

Because of these difficulties, a comparison of the partial charges obtained simply and empirically (using atomic properties and the concepts outlined above) with results from ab initio calculations provides only limited validation of the empirical concepts used. Though a correlation between the partial charges obtained by us and by the more strictly "ab initio" methods is, in general, satisfactory,[81] the absolute values are frequently quite different. It seems more useful to compare molecular properties that can be determined directly by experiment, and which are expected to be related to partial charges, with the data obtained simply from the atomic properties. If the concepts can then be validated, they can be considered to be a useful operational definition of the partial charges in a molecule. In addition, relations are obtained that permit the prediction of observable molecular properties from atomic data.

5.2. ESCA Chemical Shifts

The observed ESCA chemical shifts ΔE relative to some reference compound are, according to the potential model, expected to correlate with partial atomic charges Q according to Equation (38),[124] where R_{AB} is the distance between nucleus A, the

$$\Delta E = c_1 Q_A + c_2 \sum_{B \neq A} \frac{Q_B}{R_{AB}} + c_3 \quad (38)$$

K-shell energy of which is observed, and the other nuclei in the molecule. The coefficients c are global adjustable parameters, and the value of c_3 is determined by the reference used.

We have used Equation (38) to fit 37 observed chemical shifts relative to methane for the carbon atoms of a number of molecules to partial charges computed as outlined above. In the data presented in Table 2, the carbon atoms giving rise to the reported K-shell shift are underlined. In the case of hexafluoro-

Table 2. ESCA C_{1s} shifts in eV, relative to CH_4.

Molecule	Exp.	Calcd	Molecule	Exp	Calcd
$\underline{C}H_4$	0.000	0.190	$\underline{C}_2H_6$	−0.200	0.519
$\underline{C}_2H_4$	−0.100	−0.196	$\underline{C}H_3F$	2.800	2.127
$\underline{C}H_2F_2$	5.600	4.492	$\underline{C}HF_3$	8.280	7.257
$\underline{C}F_4$	11.000	10.503	$\underline{C}H_3CH_2F$	0.200	0.571
$\underline{C}H_3CH_2F$	2.400	2.516	$\underline{C}H_3CF_3$	1.100	0.639
$CH_3\underline{C}F_3$	7.600	7.574	$\underline{C}H_3OH$	1.600	1.988
$CH_3\underline{O}CH_3$	1.400	1.927	$H_2\underline{C}O$	3.300	2.690
$\underline{C}H_3CHO$	0.600	−0.547	$CH_3\underline{C}HO$	3.200	3.383
$\underline{C}H_3COCH_3$	0.500	0.570	$CH_3\underline{C}OCH_3$	3.100	4.344
$\underline{C}H_3CHF_2$	0.660	0.627	$CH_3\underline{C}HF_2$	5.090	4.897
$\underline{C}F_3CF_3$	8.890	8.502	$\underline{C}H_2CHF$	0.140	0.298
$CH_2\underline{C}HF$	2.520	1.935	$\underline{C}H_2CF_2$	0.370	0.829
$CH_2\underline{C}F_2$	5.140	4.699	$\underline{C}HFCF_2$	2.910	3.448
$CHF\underline{C}F_2$	5.290	5.505	$\underline{C}F_2CF_2$	5.580	6.419
cyclo-C_4F_6(te) [a]	6.320	6.627	*cyclo*-C_4F_6(tr) [a]	3.920	4.177
cyclo-C_4F_8	6.290	6.439	$\underline{C}F_3CHCH_2$	7.760	7.991
$CF_3\underline{C}HCH_2$	1.070	0.549	$\underline{C}F_3CHCH_2$	0.600	0.445
$\underline{C}F_3CFCF_2$	8.640	8.634	$CF_3\underline{C}FCF_2$	3.720	4.507
$CF_3CF\underline{C}F_2$	6.020	6.235			

[a] See text.

cyclobutene the four connected carbon is signified by the symbol te and the three-connected one by tr. The resulting fit with a correlation coefficient of $r = 0.984$ and a standard deviation of $s = 0.56$ eV, is quite satisfactory (Fig. 1). The parameters obtained are $c_1 = 20.4$ V, $c_2 = -5.6$ VÅ, and $c_3 = 1.77$ eV. These, together with the partial charges computed simply from atomic data, can thus be used in Equation (38) to predict quite reliably carbon chemical shifts relative to methane. Similar results from fewer data have been obtained earlier by Gasteiger and Marsili,[94] who also used partial electronegativity equalization in the bonds to compute the partial charges.

5.3. Proton Affinities

The proton affinity PA of a species M in the gas phase is defined as the enthalpy of the reaction (39), which is difficult to measure directly for most systems. However, relative proton

$$MH^+ \rightleftharpoons M + H^+ \quad (39)$$

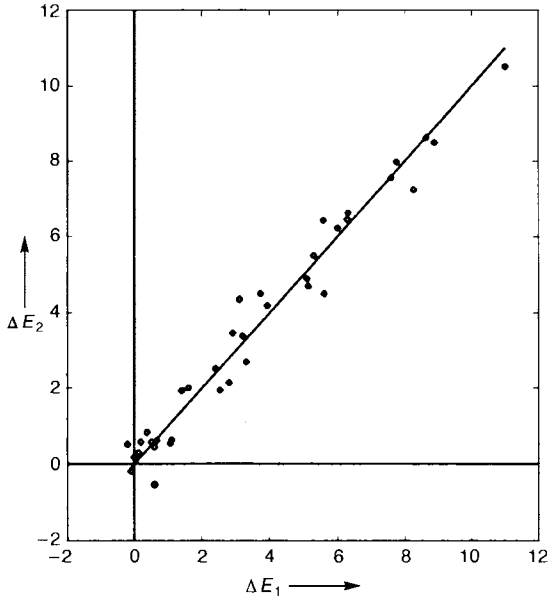

Fig. 1. Correlation of the experimentally determined ESCA C_{1s} shifts (ΔE_1) in eV with computed values (ΔE_2).

affinities are more readily accessible, and based on some absolute measurements Lias et al.[124] have compiled "absolute" values for more than 700 compounds. As the enthalpy of the reaction (39) represents the energy of association between a proton and a Lewis base—in the case of amines the nonbonding electron pair on nitrogen—we expect a correlation with the computed orbital electronegativities $\chi(-2)$ [Eq. (40)] of the corre-

$$PA = a + b\chi(-2) \quad (40)$$

sponding doubly occupied lone pair orbitals. We have fitted this equation to the experimental proton affinities (PA) of those species that have as basic center a lone electron pair on nitrogen and the computed orbital electronegativities of this doubly occupied lone pair ($\chi(-2)$). The simple correlation found from the data reported in Table 3 is reasonably good (correlation coefficient of $r = 0.93$ and a standard deviation $s = 27$ kJ mol^{-1}). The parameters for the nitrogen-containing bases are $a = 966$ kJ mol^{-1} and $b = -59$ kJ mol^{-1} V^{-1}. An earlier attempt at a correlation with the partial charges on nitrogen was not as good,[84] which indicates the important effect of the hybrid character of the lone pair orbital on nitrogen on its basicity. Clearly the parameters a and b would be different for the basicity on atomic centers other than nitrogen.

5.4. Bond Distances

Fundamental to the understanding of the behavior of molecules is their structure, for which internuclear distances and in particular bond lengths are of prime importance. Several suggestions have been made for predicting such bond lengths from atomic data. In one of the earliest, simplest proposals, Pauling and Huggins[126] suggested that the bond length d_{AB} can be computed as the sum of the corresponding covalent radii r_A and r_B [Eq. (41)]. Since the covalent radius of an atom is defined by

$$d_{AB} = r_A + r_B \quad (41)$$

Table 3. Proton affinities [kJ mol^{-1}] and orbital electronegativities [V] of nitrogen bases.

Molecule	PA	$\chi(-2)$	Molecule	PA	$\chi(-2)$
CH_3NH_2	896	0.674	$C_2H_5NH_2$	908	0.668
n-$C_3H_7NH_2$	912	0.673	n-$C_4H_9NH_2$	914	0.675
n-$C_5H_{11}NH_2$	916	0.677	n-$C_6H_{13}NH_2$	916	0.677
n-$C_7H_{15}NH_2$	916	0.677	n-$C_8H_{17}NH_2$	922	0.677
i-$C_3H_7NH_2$	915	0.663	$(CH_3)(C_2H_5)NH$	932	0.573
$(CH_3)_3N$	942	0.503	$(CH_3)_2(C_2H_5)N$	952	0.503
$(C_2H_5)_2NH$	945	0.570	$tert$-$C_4H_9NH_2$	924	0.659
s-$C_4H_9NH_2$	922	0.667	i-$C_4H_9NH_2$	915	0.676
$(CH_3)(C_2H_5)_2N$	962	0.502	$(CH_3)_2(i$-$C_3H_7)N$	961	0.512
$(C_2H_5)(i$-$C_3H_7)NH$	951	0.568	$tert$-$C_5H_{11}NH_2$	930	0.663
neo-$C_5H_{11}NH_2$	917.5	0.679	$(CH_3)_3SiN(CH_3)_2$	946	0.416
$cyclo$-$C_6H_{11}NH_2$	925.5	0.681	$(C_2H_5)_3N$	972	0.501
$(CH_3)_2(tert$-$C_4H_9)N$	971	0.502	$(i$-$C_3H_7)_2NH$	963	0.566
$(n$-$C_3H_7)_2NH$	952	0.578	$(CH_3)_3SiCH_2N(CH_3)_2$	968	0.483
$(C_2H_5)_2(n$-$C_3H_7)N$	971	0.505	$(CH_3)_2(neo$-$C_5H_{11})N$	962	0.512
$(i$-$C_3H_7)_2(C_2H_5)N$	984	0.500	$(tert$-$C_4H_9)_2NH$	976	0.563
$(s$-$C_4H_9)_2NH$	970	0.573	$(i$-$C_4H_9)_2NH$	956	0.584
$(n$-$C_4H_9)_2NH$	956	0.583	$CH_2FCH_2NH_2$	888	0.833
$(CHF_2)CH_2NH_2$	868	1.011	$CF_3CH_2NH_2$	847	1.204
$NC\text{-}CH_2NH_2$	826	1.281	$CH_3N{=}NCH_3$	866	1.431
$(CH_3)_2N\text{-}NH_2$	920	1.094	$F(CH_2)_3NH_2$	911	0.736
$CF_3(CH_2)_2NH_2$	881	0.879	$HC{\equiv}CCH_2NH_2$	882	1.017
$NC(CH_2)_2NH_2$	866	0.905	$NCCH_2NH(CH_3)$	862	1.089
$H_2C{=}C(CH_3)NH_2$	947	0.901	$H_2C{=}CHCH_2NH_2$	903	0.768
$H_3CC(H){=}N(C_2H_5)$	932	0.905	$CF_3CH_2NHCH_3$	878	1.026
$CH_2(CN)_2$	735	4.055	H_2NNH_2	856	1.279
NH_3	835.5	0.819	i-C_3H_7CN	813	3.370
CH_3CN	788	3.415	$ClCH_2CN$	751	3.413
BrCN	746	3.480	CCl_3CN	735.5	3.714
ClCN	735	4.158	HCN	717	4.065
CF_3CN	695	4.948			

means of this tertiary atomic property, the corresponding values can be determined by fitting Eq. (41) to many molecular bond lengths. An improvement in the predicted bond lengths was obtained through the suggestion by Shomaker and Stevenson[127] [Eq. (42)] of including the bond contraction (due to the

$$d_{AB} = r_A + r_B - \beta \mid \chi_A - \chi_B \mid \tag{42}$$

ionic contribution in heteronuclear bonds) as the difference of the electronegativity of the bonded atoms, multiplied by one extra global parameter β. This suggestion has been explored in detail by Polansky and Derflinger.[128] They suggest different values for the parameter β, depending on the type of bond. More recently Sanderson[54] stipulated using radii that are adjusted for the partial charges on the respective atoms in Equation (40). He proposed that the atomic radii be expressed as a function of atomic charges by a truncated Taylor expansion [Eq. (43)]. Sanderson has obtained remarkably good results

$$r = r^0 + b\,Q = r^0 + \left(\frac{\partial r}{\partial Q}\right)_{Q=0} Q \tag{43}$$

with this approach; however, in addition to the covalent radii, it requires the derivatives (that is, the parameters b) as tertiary parameters for each atom. To avoid this doubling of the tertiary atomic parameters we introduce the notion that the parameters b, the partial derivative of the atomic radius with respect to the atomic charge, should be proportional to the softness, the inverse of the atomic hardness parameter. This yields Equation (44), in which c_0 and c_1 are two global parameters that are

$$\left(\frac{\partial r}{\partial Q}\right)_{Q=0} = c_0 + c_1 \frac{1}{\eta} \tag{44}$$

the same for all atoms. In addition, we found it important to use different radii for different hybrid orbitals on the atoms; thus for the orbital radii to be used in Equation (41), we obtain Equation (45) in which the index A_i signifies the hybrid orbital i

$$r_{A_i} = r^0_{A_i} + \left(c_0 + \frac{c_1}{\eta_{A_i}}\right) Q_A \tag{45}$$

on atom A. Using these radii in Equation (41), together with an additional term that accounts for the influence of the Coulomb attraction or repulsion of the partial charges on the bond length, yields the model (46) for bond lengths. The relevant radii and

$$d_{AB} = r^0_A + r^0_B + c_0\,(Q_A + Q_B) + c_1\left(\frac{Q_A}{\eta_A} + \frac{Q_B}{\eta_B}\right) + c_2\,\frac{Q_A Q_B}{(\eta_a + \eta_B)\,d_{AB}} \tag{46}$$

hardness parameters are those for the bond-forming orbitals. The last term, which accounts for the Coulomb interaction effect, introduces another global parameter c_2, as well as a nonlinearity. Fortunately, as this term, in general, is small though significant, it is sufficient to use merely the sum of the two covalent radii, as given by Equation (45), for d_{AB} in the denominator.

Equation (46) was fitted to bond-length data of 543 bonds[83] to determine the parameters, namely, the 51 covalent radii and the three parameters c_0, c_1, and c_2. The data was taken only from structures determined by spectroscopy in the gas phase,[129–132] because X-ray structures would include also packing effects, which are not part of this model. The bond lengths of the homonuclear diatomic molecules H_2 and F_2 and of the alkali metals were eliminated from the regression, as they deviate significantly from the sum of the covalent radii, probably due to a larger Coulomb repulsion of the atomic cores or lone pairs not included in Equation (46). The regression (Fig. 2) is excellent, with a correlation coefficient of $r = 0.997$, a standard error of $\sigma = 0.028$ Å, and a relative standard error of 1.3%.

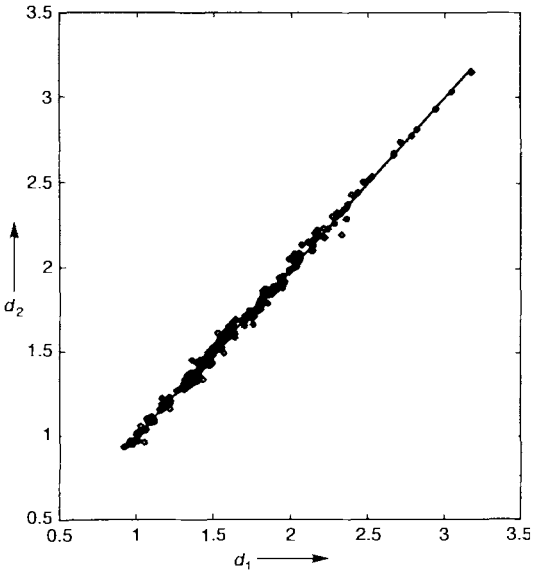

Fig. 2. Correlation between bond lengths in Å determined by experiment (d_1) and those computed with Equation (46) (d_2).

The calculated covalent radii of the orbitals and the three c parameters are compiled in Table 4. Note the different covalent radii for the same atom, depending on the hybrid used in bond formation, as well as on double or triple bonds formed. The data of this table, together with the orbital hardness and the partial charges, can be used in Equation (46) to predict bond length with an error of less than 2%. If just the sum of the covalent radii of the appropriate orbitals were employed, the error would be about 5%.

Table 4. Covalent radii of the atomic orbitals in Å and the global parameters c_0, c_1, and c_2 of Equation (46).

Atom	Type of hybrid orbital	r_{A_i} [Å]	Atom	Type of hybrid orbital	r_{A_i} [Å]	Atom	Type of hybrid orbital	r_{A_i} Å
B^-	te	0.880	B	tr	0.831	B	di	0.831
B	di π	0.619	C	te	0.763	C	r	0.747
C	tr π	0.664	C	di	0.710	C	di π	0.617
C	di π π	0.603	N	te	0.695	N^+	te	0.767
N	tr	0.686	N	tr π	0.601	N	di π	0.562
O	te	0.686	O	tr π	0.552	F	te	0.726
F	p	0.569	Na	p	1.793	Si	te	1.106
Si	p	1.002	P	te	1.018	P^+	te	1.022
P	te π	0.905	P	p	1.097	P	pe	1.006
S	oh	1.029	S	te	1.016	S	te π	0.883
S	p	1.023	S	p π	0.944	Cl	te	0.974
Cl	p	0.988	K	p	2.198	Ge	te	1.192
Ge	p π	1.082	As	p	1.220	Se	p	1.157
Se	p π	1.074	Br	te	1.084	Br	p	1.135
Rb	p	2.374	Sn	te	1.379	Sn	p π	1.278
Sb	p	1.394	Te	p π	1.275	I	te	1.284
I	p	1.338						

c_0 [Å e^{-1}] 0.075 c_1 [V Å e^{-2}] −0.844 c_2 [V Å^2 e^{-3}] 14.558

5.5. Force Constants for Stretching Vibrations

The last, nonlinear term in Equation (46) for the bond lengths has its origin in the VB analysis presented by Polansky and Derflinger.[128] Their analysis led to the suggestion that the sum of the covalent radii should be corrected by a term dependent on the force constant. The bond length is then approximated by Equation (47) in which f_{AB} is the force constant for the stretching vibration. We obtained the last term in Equation (46) by identifying $-\lambda^2 e^2$ with the product of the partial charges $Q_A Q_B$, and by relating the force constants to the orbital hardness parameters as in Equation (48), where c is again a global parameter.

$$d_{AB} = r_A^0 + r_B^0 - \frac{\lambda^2 e^2}{f_{AB} d_{AB}^2} \quad (47)$$

$$f_{AB} = c\frac{\eta_A + \eta_B}{d_{AB}} \quad (48)$$

The correlation between experimental force constants for 65 bonds[128] and those determined with Equation (48) from the orbital hardness parameters of the appropriate atomic orbitals is displayed in Figure 3. The correlation coefficient of $r = 0.98$ is resonably good. The global parameter in Equation (48) is determined to be $c = 0.5$ mdyn e V^{-1} if the force constants are given in mdyn Å^{-1}. In view of the difficulties and uncertainties in the experimental determination of force constants for stretching vibrations the relation (48) can be used effectively in the interpretation of IR spectra, as well as a basis in molecular mechanics force fields.[83]

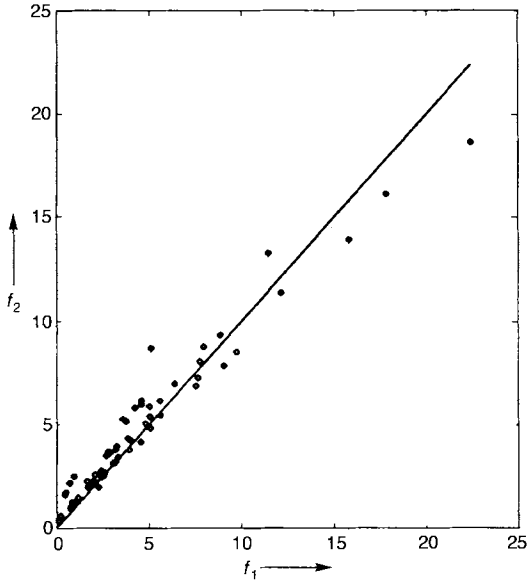

Fig. 3. Correlation between the measured (f_1) and calculated force constants (f_2) in mdyn Å^{-1} for the bond A–B.

5.6. Bond Dissociation Energies

A relation between bond dissociation energies and electronegativity is to be expected on the basis of Pauling's original definition of electronegativity involving the extra ionic resonance energy.[33] As the orbital electronegativity values can be determined directly from spectroscopic data of atoms, it seems natural to use these values for the prediction of bond dissociation energies. Thus, using relation (26) for the extra ionic resonance energy, we have obtained a good fit for the relation (49),

$$D_{AB} = \tfrac{1}{2}(D_{AA} + D_{BB}) + c_3\frac{(\chi_A - \chi_B)^2}{4(\eta_A + \eta_B)} + c_4\frac{Q_A Q_B}{d_{AB}} \quad (49)$$

which is in close accord with Pauling's original suggestion except for the last term, which accounts for the contribution of the Coulomb attraction or repulsion to the bond energy. In the various models tested,[83] this term was found to be essential, particularly in those cases where the bond is between two identical groups, for example the N–N bond or the O–O bond in molecules like N_2H_4 or H_2O_2. In those cases the extra ionic resonance energy would be zero, whereas the Coulomb term can be quite large.

The correlation between the experimentally determined[133] bond dissociation energies and those obtained with Equation (49) is displayd in Figure 4. The correlation (coefficient $r = 0.987$) is quite good. The standard error $\sigma = 5$ kcal mol^{-1} is satisfactory for such a simple relation. The covalent bond dissociation energies determined in this fit, which are tertiary atomic data, are presented in Table 5, together with the values for the global parameters c_3 and c_4. The covalent bond dissociation

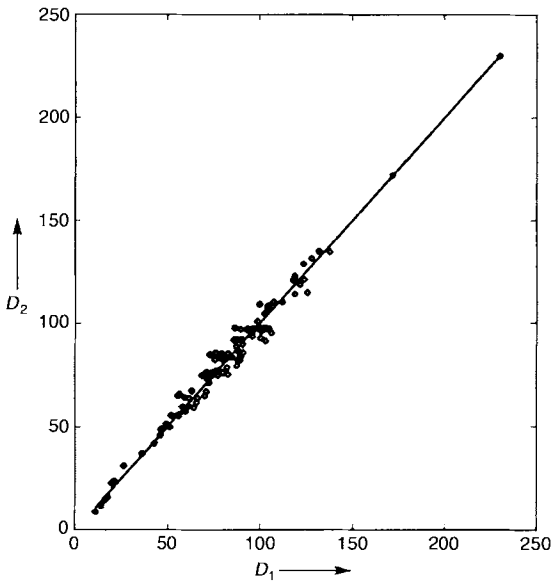

Fig. 4. Correlation between the experimental (D_1) and calculated bond dissociation energies (D_2) in kcal mol^{-1} for the bond A–B.

Table 5. Bond dissociation energies for homonuclear bonds in kcal mol^{-1} and the parameters c_3 and c_4 [Eq. (49)].

Atom	Type of hybrid orbital	D_{AA}	Atom	Type of hybrid orbital	D_{AA}	Atom	Type of hybrid orbital	D_{AA}
H	s	107.5	Li	s	33.0	C	te	85.6
C	tr	(103.)	C	tr π	174.9	C	di	139.2
C	di $\pi\,\pi$	235.8	N	te	778.2	O	p	46.9
F	p	49.7	Na	s	16.2	Si	te	75.9
P	p	57.3	S	p	63.2	Cl	p	62.2
K	s	10.6	Ge	te	62.4	Br	p	44.6
Rb	s	7.1	Sn	te	45.7	Sb	te	23.2
I	p	37.1						
$c_3\left(\frac{\text{kcal}}{\text{mol}\cdot\text{eV}}\right)$		18.51	$c_4\left(\frac{\text{kcal}\cdot\text{A}}{\text{mol}\cdot\text{e}^2}\right)$		−451.4			

energies given are again specific for the type of atomic hybrid orbital used in bond formation. The uncertainty in the values presented is about 4 kcal mol^{-1}, except for C(tr) where the statistical fit yielded $D_{AA} = 75.455$, which is unreasonably low. The reason for this discrepancy can be traced to the fact that the data set available contained only four C–H bonds of this type and three were aldehydes for which a rather low C–H bond energy is given. It is important to realize that, in general, the correction terms accounting for the ionic contributions to the bonds and containing the partial charges in Equation (49) for the dissociation energies and in Equation (46) for the bond length are small, unless the bonding is rather ionic. It is therefore frequently adequate to estimate these corrections for the partial charges on chemical grounds, alleviating the need for their detailed calculation.

6. Conclusion

We have reviewed the concept of orbital electronegativity and hardness, so widely used in the qualitative description of chemistry, and shown how the electronegativity and hardness values for most atoms of interest can be obtained from primary atomic data (spectroscopic data of atoms) provided the concept of atomic orbitals and valence states is used. On the assumption of electronegativity equalization in a bond, it has been possible to determine partial charges on the atoms in a molecule. Reasonable correlations have been obtained between these partial charges and molecular properties such as ESCA data and proton affinities. We anticipate that more such correlations that will be useful for the prediction of molecular properties can be found.

With the additional introduction of tertiary atomic properties such as covalent radii and bond energies, simple models were obtained which are remarkably reliable for the prediction of bond distances, force constants, and bond dissociation energies. In these models the atomic electronegativity and hardness parameters are used in conjunction with the partial charges computed from these values. It is surprising and encouraging how well the experimental data are represented by these simple, zeroth-order models, even though lone pair repulsions and van der Waals and Coulomb interactions of next nearest neighbors are not yet included. This can be done in calculations of molecular mechanics type in which the force field parameters can be derived by and large from the concepts based on the atomic properties presented in this review. Such an effort promises to yield a reliable force field, even though it contains many fewer parameters than the force fields in use today, and what is equally important, most of these parameters are based on atomic properties that can be ascertained experimentally for the free atoms. Thus it appears that to a large extent the molecular properties are determined by the properties of the constituent atoms—the relations have merely to be found. It can be hoped that extensive studies along these lines in the future, with much larger data bases, will yield not only more such relations, but also refinement of the models presented, without complicating them unduly.

The authors are grateful for the financial support of this work from the Fonds der chemischen Industrie.

Received: April 24, 1995 [A 40 IE]
German version: *Angew. Chem.* **1996**, *108*, 162–176

[1] R. McWeeny, *Coulsons Valence*, Oxford University Press, Oxford, **1979**.
[2] R. McWeeny, *Coulsons Chemische Bindung*, 2nd ed., Hirzel, Stuttgart, **1984**.
[3] L. Pauling, *The Nature of the Chemical Bond*, Cornell University Press, Ithaca, NY, **1939**.
[4] L. Pauling, *Die Natur der Chemischen Bindung*, Verlag Chemie, Weinheim, **1973**.
[5] R. J. Gillespie, *Molecular Geometry*, Van Nostrand, London, **1972**.
[6] R. J. Gillespie, *Molekülgeometrie*, Verlag Chemie, Weinheim, **1975**.
[7] J. Gerratt, D. L. Cooper, M. Raimondi in *Valence Bond Theory and Chemical Structure* (Eds.: D. J. Klein, N. Trinajsti), Elsevier, Amsterdam, **1990**, p. 287.
[8] H.-J. Werner, *Adv. Chem. Phys.* **1987**, *69*, 1.
[9] R. Shepard, *Adv. Chem. Phys.* **1987**, *69*, 63.
[10] B. O. Roos, *Adv. Chem. Phys.* **1987**, *69*, 399.
[11] J. A. Pople et al., *GAUSSIAN Series of Programs*, Gaussian Inc., Pittsburgh, PA, **1990**.
[12] W. M. Schmidt et al., *GAMES Users Guide*, Iowa State University, Ames, IA, **1990**.
[13] H.-J. Werner, P. J. Knowles, *Users Manual for MOLPRO*, University of Sussex, Falmer, Brighton, UK, **1991**.
[14] T. A. Albright, J. K. Burdett, M.-H. Whangbo, *Orbital Interactions in Chemistry*, Wiley, New York, **1985**.
[15] A. D. Walsh, *Prog. Stereochem.* **1954**, *1*, 1.
[16] K. Fukui, *Theory of Orientation and Stereoselection*, Springer, Berlin, **1975**; *Angew. Chem.* **1982**, *94*, 852; *Angew. Chem. Int. Ed. Engl.* **1982**, *21*, 801.

[17] R. B. Woodward, R. Hoffmann, *The Conservation of Orbital Symmetry*, Verlag Chemie, Weinheim, **1970**; *Angew. Chem.* **1982**, *94*, 725; *Angew. Chem. Int. Ed. Engl.* **1982**, *21*, 711.
[18] R. B. Woodward, R. Hoffmann, *Die Erhaltung der Orbitalsymmetrie*, Verlag Chemie, Weinheim, **1972**.
[19] J. Slater, *Phys. Rev.* **1929**, *34*, 1293.
[20] E. U. Condon, G. H. Shortley, *The Theory of Atomic Spectra*, Cambridge University Press, Cambridge, **1953**.
[21] J. H. V. Vleck, *J. Chem. Phys.* **1934**, *2*, 20.
[22] W. Moffitt, *Rep. Prog. Phys.* **1954**, *17*, 173.
[23] A. L. Companion, F. O. Ellison, *J. Chem. Phys.* **1958**, *28*, 1.
[24] R. S. Mulliken, *J. Chem. Phys.* **1934**, *2*, 782.
[25] J. J. Berzelius, *Lehrbuch der Chemie, Band 1*, Arnoldsche Buchhandlung, Dresden, **1835**, p. 163 (translated by F. Wöhler).
[26] L. C. Allen, *J. Am. Chem. Soc.* **1989**, *111*, 9003.
[27] L. C. Allen, *J. Am. Chem. Soc.* **1992**, *114*, 1510.
[28] J. Hinze, *Fortschr. Chem. Forsch.* **1968**, *93*, 448.
[29] J. E. Huheey, *Inorganic Chemistry*, Harper & Row, New York, **1978**.
[30] "Electronegativity": *Struct. Bonding (Berlin)*, **1987**, *66*.
[31] V. P. Spiridonov, V. M. Tatevskii, *Zh. Fiz. Khim.* **1963**, 37, 994, 1236, 1583, 1973, 2174.
[32] V. M. Tatevskii, V. P. Spiridonov, *Zh. Khim.* **1964**, *39*, 1284.
[33] L. Pauling, D. M. Yost, *Proc. Natl. Acad. Sci. USA* **1932**, *18*, 414.
[34] L. Pauling, *J. Am. Chem. Soc.* **1932**, *54*, 3570.
[35] L. Pauling, J. Sherman, *J. Am. Chem. Soc.* **1937**, *59*, 1450.
[36] W. Moffitt, *Proc. R. Soc. London A* **1950**, *202*, 548.
[37] A. D. Walsh, *Discuss. Faraday Soc.* **1947**, *2*, 18.
[38] H. Hotop, W. C. Lineberger, *J. Phys. Chem. Ref. Data* **1975**, *4*, 539.
[39] C. E. Moore, *Atomic Energy Levels*, National Bureau of Standards, Washington, DC, **1959**, Vol. I–III and later editions.
[40] H. O. Pritchard, H. A. Skinner, *Chem. Rev.* **1955**, *55*, 745.
[41] J. G. Malone, *J. Chem. Phys.* **1933**, *1*, 197.
[42] W. Gordy, *Phys. Rev.* **1946**, *69*, 130.
[43] W. Gordy, *J. Chem. Phys.* **1946**, *14*, 305.
[44] M. Haissinsky, *J. Phys.* (Paris) **1946**, 7, 7.
[45] M. Haissinsky, *J. Chim. Phys.* **1949**, *46*, 298.
[46] M. L. Huggins, *J. Am. Chem. Soc.* **1953**, *75*, 4123.
[47] A. L. Allred, E. G. Rochow, *J. Inorg. Nucl. Chem.* **1958**, *5*, 264.
[48] J. C. Slater, *Phys. Rev.* **1930**, *36*, 57.
[49] L. Pauling, *J. Am. Chem. Soc.* **1947**, *69*, 542.
[50] A. L. Allred, E. G. Rochow, *J. Inorg. Nucl. Chem.* **1958**, *5*, 269.
[51] R. T. Sanderson, *J. Am. Chem. Soc.* **1952**, *74*, 4792.
[52] R. T. Sanderson, *J. Chem. Educ.* **1952**, *29*, 539.
[53] R. T. Sanderson, *J. Chem. Educ.* **1954**, *31*, 2, 238.
[54] R. T. Sanderson, *Chemical Bonds and Bond Energy*, Academic Press, New York, **1976**.
[55] W. Gordy, *Phys. Rev.* **1946**, *69*, 604.
[56] R. T. Sanderson, *J. Am. Chem. Soc.* **1952**, *74*, 272.
[57] W. Gordy, J. O. Thomas, *J. Chem. Phys.* **1956**, *24*, 439.
[58] S. J. Li, *Acta Chim. Sin. (Engl. Ed.)* **1957**, *23*, 234.
[59] X.-H. Gao, *Acta Chim. Sin. (Engl. Ed.)* **1961**, *27*, 190.
[60] J. C. Phillips, *Covalent Bonding in Crystals, Molecules and Polymers*, University of Chicago Press, Chicago, IL, **1969**.
[61] S. John, A. N. Bloch, *Phys. Rev. Lett.* **1974**, *33*, 1095.
[62] G. Simon, M. E. Zandler, E. R. Talaty, *J. Am. Chem. Soc.* **1976**, *98*, 7869.
[63] P. R. Wells, *Prog. Phys. Org. Chem.* **1968**, *6*, 111.
[64] C. Mande, P. Deshmukh, *J. Phys. B* **1977**, *10*, 2293.
[65] N. Inamoto, S. Masuda, *Tetrahedron Lett.* **1977**, 3287.
[66] N. Inamoto, S. Masuda, K. Tori, Y. Yoshimura, *Tetrahedron Lett.* **1978**, 4547.
[67] R. J. Boyd, G. E. Markus, *J. Chem. Phys.* **1981**, *75*, 3585.
[68] Y. H. Zhang, *Inorg. Chem.* **1982**, *21*, 3886.
[69] S. M. William, W. F. Reynolds, R. W. Taft, R. D. Topsom, *J. Org. Chem.* **1984**, *49*, 959.
[70] H. C. Yuan, *Acta Chim. Sin. (Engl. Ed.)* **1964**, *30*, 341.
[71] Y.-R. Luo, S. W. Benson, *Acc. Chem. Res.* **1962**, *25*, 375.
[72] R. S. Mulliken, *J. Chim. Phys.* **1949**, *46*, 497.
[73] J. Hinze, *Phys. Chem.* **1970**, *5*, 173.
[74] W. Kutzelnigg, *Einführung in die Theoretische Chemie, Band 2*, Verlag Chemie, Weinheim, **1978**, p. 118.
[75] R. G. Parr, R. A. Donelly, M. Levy, W. E. Palke, *J. Chem. Phys.* **1978**, *68*, 3801.
[76] R. G. Parr, W. Yang, *J. Am. Chem. Soc.* **1984**, *106*, 4049.
[77] C. Lee, W. Yang, R. G. Parr, *J. Mol. Struct. THEOCHEM* **1988**, *163*, 305.
[78] R. G. Parr, R. G. Pearson, *J. Am. Chem. Soc.* **1983**, *105*, 7512.
[79] R. P. Iczkowski, J. L. Margrave, *J. Am. Chem. Soc.* **1961**, *83*, 3547.
[80] J. Hinze, M. A. Whitehead, H. H. Jaffé, *J. Am. Chem. Soc.* **1963**, *85*, 148.
[81] D. Bergmann, J. Hinze, *Struct. Bonding (Berlin)* **1987**, *66*, 145.
[82] "Chemical Hardness": *Struct. Bonding (Berlin)* **1993**, *80*.
[83] D. Bergmann, Dissertation, Universität Bielefeld, **1992**.
[84] D. Bergmann, Diplomarbeit, Universität Bielefeld, **1985**.
[85] J. Hinze, H. H. Jaffé, *J. Am. Chem. Soc.* **1962**, *84*, 540.
[86] J. Hinze, H. H. Jaffé, *Can. J. Chem.* **1963**, *41*, 1315.
[87] S. G. Bratsch, *J. Chem. Educ.* **1988**, *65*, 34.
[88] R. G. Pearson, *Inorg. Chem.* **1988**, *27*, 734.
[89] A. L. Allred, *J. Inorg. Nucl. Chem.* **1961**, *17*, 215.
[90] R. T. Sanderson, *Science* **1951**, *114*, 670.
[91] R. T. Sanderson, *Polar Covalence*, Academic Press, New York, **1983**.
[92] J. Hinze, Dissertation, University of Cincinnati, OH, **1962**.
[93] J. Cioslowski, S. T. Mixon, *J. Am. Chem. Soc.* **1993**, *115*, 1084.
[94] J. Gasteiger, M. Marsili, *Tetrahedron* **1980**, *36*, 3219.
[95] R. T. Sanderson, *Chemical Bonds and Bond Energy*, Academic Press, New York, **1987**.
[96] R. F. Nalewajski, *J. Am. Chem. Soc.* **1984**, *106*, 944.
[97] W. J. Mortier, S. K. Ghosh, S. Shankar, *J. Am. Chem. Soc.* **1986**, *108*, 4315.
[98] W. J. Mortier, *Struct. Bonding (Berlin)* **1987**, *66*, 145.
[99] T. K. Ghanty, S. K. Ghosh, *J. Phys. Chem.* **1991**, *95*, 6512.
[100] T. K. Ghanty, S. K. Ghosh, *J. Mol. Struct. THEOCHEM* **1992**, *276*, 83.
[101] C. Altona, D. H. Faber, *Fortschr. Chem. Forsch.* **1974**, *45*, 1.
[102] "The Consistent Force Field: A Documentation": S. R. Niketic, K. Rasmussen, *Lect. Notes Chem.* **1977**, *3*.
[103] "Bonding Forces": O. Ermer, *Struct. Bonding (Berlin)* **1976**, *27*, 163.
[104] "Molecular Mechanics": U. Burkert, N. L. Allinger, *ACS Monogr.* **1982**, *177*.
[105] N. L. Allinger, *Adv. Phys. Org. Chem.* **1976**, *13*, 1.
[106] "Potential Energy Functions in Conformational Analysis": K. Rasmussen, *Lect. Notes Chem.* **1985**, *37*.
[107] E. M. Engler, J. D. Andose, P. von R. Schleyer, *J. Am. Chem. Soc.* **1973**, *95*, 8005.
[108] N. L. Allinger, Y. H. Yuh, J.-H. Lii, *J. Am. Chem. Soc.* **1989**, *111*, 8551.
[109] R. S. Mulliken, *J. Chem. Phys.* **1955**, *23*, 1833.
[110] R. E. Christoffersen, K. A. Baker, *Chem. Phys. Lett.* **1971**, *8*, 4.
[111] K. Jug, *Theor. Chim. Acta* **1971**, *23*, 183.
[112] K. R. Roby, *Mol. Phys.* **1974**, *27*, 81.
[113] R. Heinzmann, R. Ahlrichs, *Theor. Chim. Acta* **1976**, *42*, 33.
[114] M. Yanez, R. F. Pople, *Acta Crystallogr. Sect. A* **1976**, *34*, 641.
[115] F. L. Hirsfeld, *Theor. Chim. Acta* **1977**, *44*, 129.
[116] P. Politzer, R. R. Harris, *J. Am. Chem. Soc.* **1970**, *92*, 6451.
[117] D. L. Grier, J. A. Streitwieser, *J. Am. Chem. Soc.* **1982**, *104*, 3556.
[118] R. Daudel, *C. R. Hebd. Seance Acad. Sci.* **1953**, *237*, 601.
[119] S. Srebrenik, R. Paunz, H. Weinstein, *Chem. Phys. Lett.* **1975**, *32*, 420.
[120] R. G. A. R. Maclagan, *Chem. Phys. Lett.* **1971**, *8*, 114.
[121] R. F. W. Bader, P. M. Beddall, *J. Chem. Phys.* **1972**, *56*, 3320.
[122] "Atoms in Molecules, A Quantum Theory": R. F. W. Bader, *Int. Ser. Monogr. Chem.* **1990**, *22*; *Angew. Chem.* **1994**, *106*, 647; *Angew. Chem. Int. Ed. Engl.* **1994**, *33*, 620.
[123] J. Meister, W. H. E. Schwarz, *J. Phys. Chem.* **1994**, *98*, 8245.
[124] U. Gelius, *Phys. Scr.* **1974**, *9*, 133.
[125] S. G. Lias, J. F. Liebman, R. D. Levin, *J. Phys. Chem. Ref. Data* **1984**, *13*, 695.
[126] L. Pauling, M. L. Huggins, *Z. Kristallogr. Kristallgeom. Kristallphys. Kristallchem.* **1934**, *87*, 205.
[127] V. Shomaker, D. P. Stevenson, *J. Am. Chem. Soc.* **1941**, *63*, 37.
[128] O. E. Polansky, G. Derflinger, *Theor. Chim. Acta* **1963**, *1*, 308.
[129] Landoldt-Boernstein, *Structure Data of Free Polyatomic Molecules, Vol. II/7, New Ser.*, Springer, Berlin, **1976**.
[130] Landoldt-Boernstein, *Structure Data of Free Polyatomic Molecules, Vol. II/15, New Ser.*, Springer, Berlin, **1987**.
[131] F. J. Lovas, E. Tiemann, *J. Phys. Chem. Ref. Data* **1974**, *3*, 609.
[132] G. Herzberg, *Molecular Spectra and Molecular Structure I. Diatomic Molecules*, Van Nostrand, Princeton, NJ, **1950**.
[133] E. R. C. Weast, *Handbook of Chemistry and Physics*, 68th ed., CRC, Boca Raton, FL, **1988**.

New, Efficient Routes to Cyclic Enediynes

Burkhard König*

The special fascination of strained cyclic enediynes lies in their intrinsic tendency to undergo thermal cyclization. This aspect has been stimulating the research on enediynes since its beginnings more than 20 years ago,[1] and it is this reactivity of the enediyne structure that brings about the pharmacological effectiveness of natural products like dynemicin A.[2]

The synthesis of an enediyne parent system calls for mild conditions with, at the same time, a strong driving force for the ring closure reaction. Various approaches have been taken to generate strained cyclic enediynes. Scheme 1 summarizes the major ones: Most often, an acetylide carbonyl addition is used as the ring closure reaction (Scheme 1, routes a and b).[3] Danishefsky et al., however, efficiently obtained highly substituted, 10-membered enediyne cycles by two-fold palladium-catalyzed coupling of iodoacetylene with *cis*-1,2-bis(trimethylstannyl-ethylene) (route c).[4] Substitution reactions can yield 10-membered enediyne cycles as well, though only after the ring strain has been reduced (route d).[5] In contrast to ring closure, Nicolaou et al. employed a ring contraction of cyclic sulfones to synthesize strained cyclic enediynes (route e).[6]

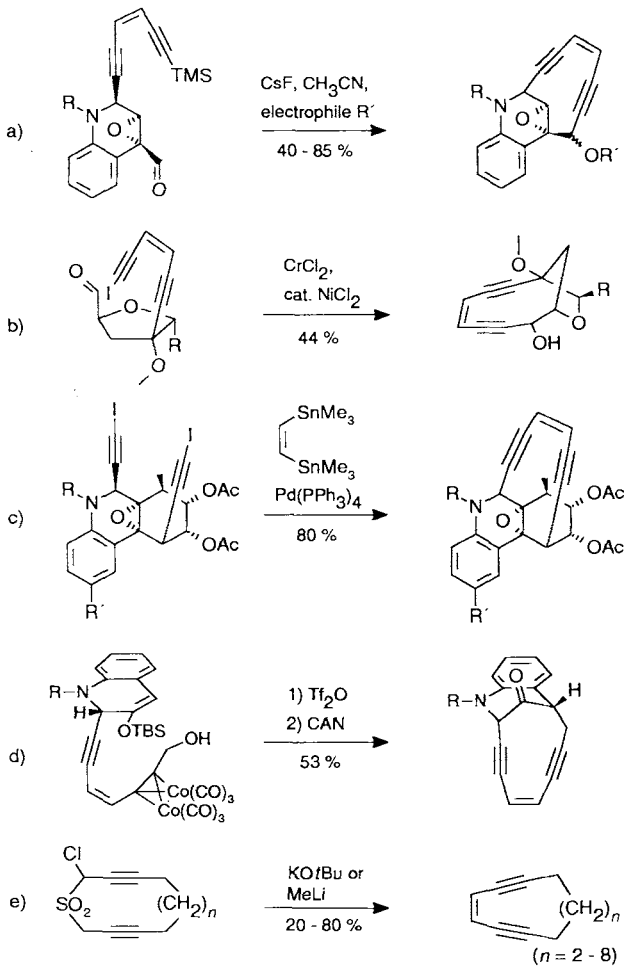

Scheme 1. CAN = cerium ammonium nitrate

Jones, Huber, and Mathews now could demonstrate that strained cyclic enediynes are accessible via carbenoid intermediates, too.[7] Their method is based on a sequence of tandem carbenoid coupling and elimination of two propynylic bromide units, a strategy published last year by the same group:[8] Here the synthesis of the acyclic enediyne bis(trimethylsilyl)hexadiyne (**3**) was achieved by reaction of trimethylsilylpropynylic bromide (**1**) with lithium hexamethyldisilazide (LiHMDS) in THF/HMPT (HMPT = hexamethylphosphoric triamide) at $-85\,^{\circ}C$. A *cis*–*trans* selectivity of about 2:1 was attained with good yields. Probably, a propynylic carbene is formed, which can insert intermolecularly into the C–H bond of another propynylic bromide. The E2 elimination of HBr from the intermediate bromide **2** then leads to the product. As this method proved to be broadly applicable for substituted propynylic substrates, Jones et al. even had it patented.[9] Recently still more highly substituted acyclic enediynes like **4** and **5** were obtained with this approach.[10]

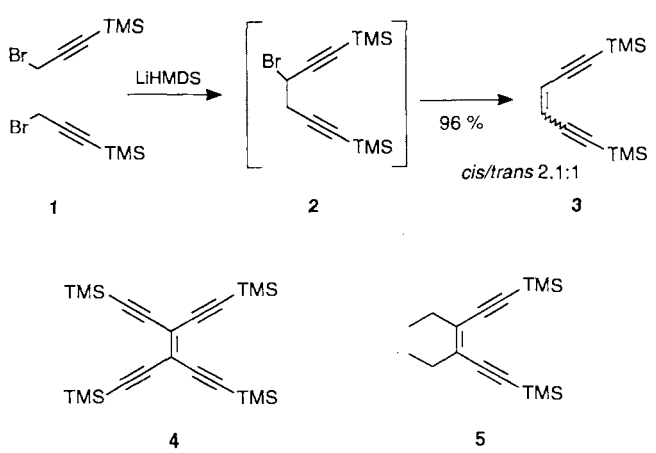

[*] Dr. B. König
Institut für Organische Chemie der Technischen Universität
Hagenring 30, D-38106 Braunschweig (Germany)
Fax: Int. code +(531)391-5388
e-mail: koenig@sgi3.org-chem.nat.tu-bs.de

 © VCH Verlagsgesellschaft mbH, D-69451 Weinheim, 1996 0570-0833/96/3502-0165 $ 10.00+.25/0

The intramolecular variant of this synthesis renders cyclic enediynes. Ten-membered functionalized enediyne cycles (**7**) were generated in yields of up to 95% using slightly altered reaction conditions. Since the starting materials are easily accessible, a synthesis of enediynes in multigram scale can be achieved. Thus, it should be possible to use these functionalized enediyne components to build libraries of enediyne diversomers by the approach of Nicolaou and others.[11] As Jones et al. stated, enediyne steroid conjugates like **8** have been synthesized already.[10]

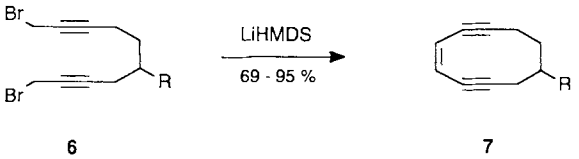

6 **7**

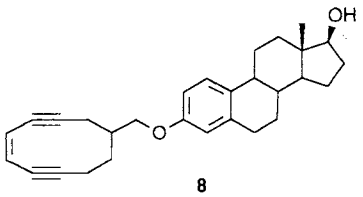

8

Starting from the propynylic bromide **9**, Hopf, Werner, et al. successfully synthesized an only 8-membered cyclic aryl-1,2-diyne (**10**).[12] The remarkably stable molecule was obtained by cyclization with $Bu_3SnSiMe_3/CsF$[13] in 60% yield.

9 **10**

With the mechanistically interesting new approaches described here, the spectrum of methods for the synthesis of strained cyclic enediynes could be enlarged markedly. It is to be expected that the search for simple pharmacologically active enediyne derivatives will benefit accordingly.

German version: *Angew. Chem.* **1996**, *108*, 177–178

Keywords: carbenes · cyclizations · enediynes · macrocycles

[1] a) R. R. Jones, R. G. Bergman, *J. Am. Chem. Soc.* **1972**, *94*, 660–661; b) R. G. Bergman, *Acc. Chem. Res.* **1973**, *6*, 25–31.

[2] Recent reviews on the synthesis and properties of enediyne prodrugs: a) M. E. Maier, *Synlett* **1995**, 13–26; b) K. C. Nicolaou, W.-M. Dai *Angew. Chem.* **1991**, *103*, 1453–1481; *Angew. Chem. Int. Ed. Engl.* **1991**, *30*, 1387–1415. Enediynes as building blocks for new carbon allotropes: c) F. Diederich, *Nature* **1994**, *369*, 199–207. Previous enediyne highlight: d) R. Gleiter, D. Katz, *Angew. Chem.* **1993**, *105*, 884–887; *Angew. Chem. Int. Ed. Engl.* **1993**, *32*, 842–845.

[3] a) P. A. Wender, S. Beckham, D. L. Mohler, *Tetrahedron Lett.* **1995**, *36*, 209–212; b) T. Brandstetter, M. E. Maier, *Tetrahedron* **1994**, *50*, 1435–1448.

[4] M. D. Shair, T. Yoon, S. J. Danishefsky, *J. Org. Chem.* **1994**, *59*, 3755–3757.

[5] P. Magnus, *Tetrahedron* **1994**, *50*, 1397–1418.

[6] K. C. Nicolaou, G. Zuccarello, Y. Ogawa, E. J. Schweiger, T. Kumazawa, *J. Am. Chem. Soc.* **1988**, *110*, 4866–4868.

[7] G. B. Jones, R. S. Huber, J. E. Mathews, *J. Chem. Soc. Chem. Commun.* **1995**, 1791–1792.

[8] a) G. B. Jones, R. S. Huber, *Tetrahedron Lett.* **1994**, *35*, 2655–2658; b) the synthesis of **3** from **1** was reproduced in our laboratory without difficulties. However, the yield and the stereoselectivity were slightly lower than reported.

[9] *A New Route to Enediynes*, G. B. Jones, R. S. Huber, US-A 5436361. **1995**.

[10] G. B. Jones, Clemson University, Clemson, SC (USA), personal communication.

[11] a) K. C. Nicolaou, A. L. Smith, E. W. Yue, *Proc. Natl. Acad. Sci. USA* **1993**, *90*, 5881–5892; b) K. Toshima, K. Otha, A. Ohahsi, T. Nakamura, M. Nakata, S. Matsumura, *J. Chem. Soc. Chem. Commun.* **1993**, 1525–1527, c) M. Tokuda, K. Fujiwara, T. Gomibuchi, M. Hirama, M. Uesugi, Y. Sugiura, *Tetrahedron Lett.* **1993**, *34*, 669–672, d) M. F. Semmelhack, J. J. Gallagher, W. Ding, G. Krishnamurthy, R. Babine, G. A. Ellestad, *J. Org. Chem.* **1994**, *59*, 4357–4359, e) D. L. Boger, J. Zhou, *ibid.* **1993**, *58*, 3018–3024.

[12] a) H. Hopf, C. Werner, P. Bubenitschek, P. G. Jones, *Angew. Chem.* **1995**, *107*, 2592–2594; *Angew. Chem. Int. Ed. Engl.* **1995**, *34*, 2367–2368; for the first synthesis of a cyclooctaenediyne, stabilized as the alkynecarbonylcobalt complex, see: b) G. G. Melikyan, M. A. Khan, K. M. Nicholas, *Organometallics* **1995**, *14*, 2170–2172.

[13] H. Sato, N. Isono, K. Okamura, T. Date, M. Mori, *Tetrahedron Lett.* **1994**, *35*, 2035–2038.

 © VCH Verlagsgesellschaft mbH, D-69451 Weinheim, 1996 0570-0833/96/3502-0166 $ 10.00+.25/0

Vitamin B_{12}: The Haze Clears**

Bernhard Kräutler* and Christoph Kratky*

Dedicated to Professor Albert Eschenmoser on the occasion of his 70th birthday

First isolated nearly 50 years ago, the corrinoid cobalt complex vitamin B_{12} (Scheme 1) continues to be an extraordinarily fascinating compound to chemists, biologists, and physicians. Particularly striking among the several hundred proteins whose

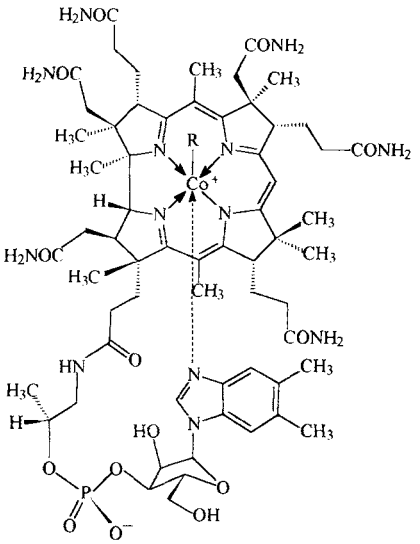

Scheme 1. Structural formulas of vitamin B_{12} derivatives. R = CN: vitamin B_{12}; R = CH_3: methylcob(III)alamin; R = 5'-deoxy-5'-adenosyl: coenzyme B_{12}; R = e^-: cob(II)alamin.

three-dimensional structures were elucidated to atomic resolution last year was the X-ray structure analysis of the B_{12}-binding domain of the (cobalamin-dependent) methionine synthase (a methyl transferase) of *Escherichia coli*.[1, 2] It provided insight into the structure of a B_{12}-binding protein for the first time and revealed quite an unexpected facet of B_{12} chemistry: In this particular protein, a histidine imidazole provided by the peptide chain substitutes the nucleotide function of B_{12}, which coordinates in axial position in solution (see Fig. 3). The dramatic constitutional difference between isolated B_{12} and protein-bound B_{12} casts new light upon the importance of the typical and unique benzimidazole function of the nucleotide-containing B_{12} derivatives. Besides the corrin ligand, it is indeed the nucleotide function that gives the B_{12} derivatives their outstanding position among the porphinoid cofactors.[3]

The pseudo-nucleotide function attached covalently at the periphery of the "complete" corrinoids like that of vitamin B_{12} and other cobalamins always coordinates intramolecularly and in a structurally regular pattern. The intramolecularly coordinating and bulky nucleotide function has recently been shown to cause an increased upward folding of the corrin ligand,[4, 5] a finding of particular interest with regard to the still enigmatic enzymatic activation of coenzyme B_{12} (see, for example, Ref. [6]). Nowadays, a distinct acceleration of the homolysis of the organometallic bond of the protein-bound coenzyme B_{12} is generally considered a crucial prerequisite for the B_{12}-catalyzed enzymatic radical reactions (reviewed in, for example, Refs. [6,7], Fig. 1).

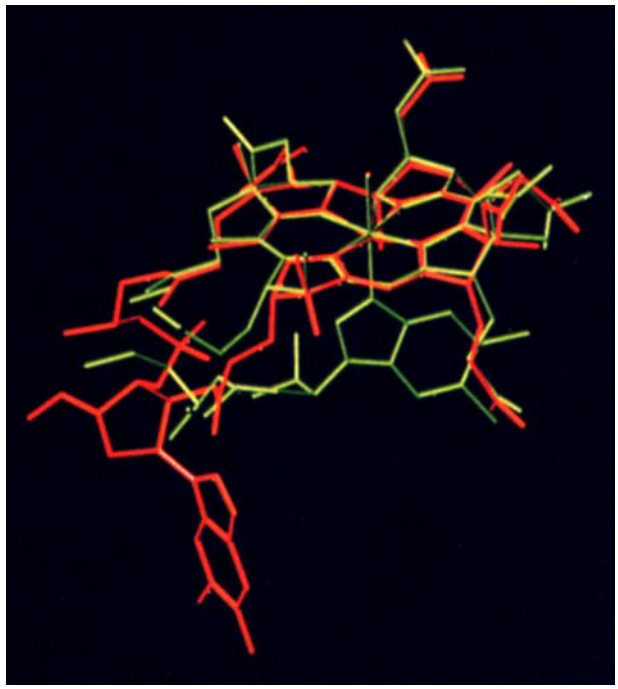

Fig. 1. Superposition of the structures of methylcob(III)alamin in the single crystal ("base-on", green) and in the B_{12}-binding domain of the methionine synthase of *Escherichia coli* ("base-off", red).

On account of the X-ray analysis of the structure of the cobalamin-binding domain of the methionine synthase of *Escherichia coli*[1, 2] published by Drennan, Huang, Drummond, Matthews, and Ludwig, all previous views on the biological role of the intramolecularly binding benzimidazole functions in "complete" vitamin B_{12} derivatives had suddenly to be reconsidered: The investigated 27 kDA segment of the 136 kDa methionine synthase is not able to catalyze the methyl transfer by itself, but

[*] Prof. Dr. B. Kräutler
Institut für Organische Chemie der Universität
Innrain 52a, A-6020 Innsbruck (Austria)
Fax: Int. code +(512)507-2892
e-mail: Bernhard.Kraeutler@uibk.ac.at
Prof. Dr. C. Kratky
Institut für Physikalische Chemie der Universität
Heinrichstrasse 28, A-8010 Graz (Austria)
Fax: Int. code +(316)32-2248
e-mail: kratky@bkfug.kfunigraz.ac.at

[**] The research of both authors in the B_{12} field was supported by the Austrian Fonds zur Förderung der wissenschaftlichen Forschung, Project no. 9334, 10816 (B. K.), 8371, and 9542 (C. K.), and by the Jubiläumsfonds der Österreichischen Nationalbank, Project No. 4991 (C. K.).

 © VCH Verlagsgesellschaft mbH, D-69451 Weinheim, 1996 0570-0833/96/3502-0167 $ 10.00+.25/0

it does bind methylcob(III)alamin. This organometallic corrinoid cofactor is not bound in its "base-on" constitution known from investigations in solution and in single crystals.[8] Instead, and with the help of an external (protein-based) imidazole function as an axial ligand, methylcob(III)alamin is bound in a previously unknown "base-off" form (Fig. 1). In the methionine synthase the imidazole substitute mimics the electronic properties of the coordinating nucleotide function so well that this particular constitutional change was not recognized in earlier ESR and UV/Vis spectra of the holoenzyme.[9]

The methionine synthase of *Escherichia coli* catalyzes the formation of tetrahydrofolate and methionine from N^5-methyltetrahydrofolate and homocysteine. It therefore catalyzes the transfer of a methyl group, which (formally!) occurs by transfer of a methyl cation. This methyl group transfer most probably takes place as a sequence of two nucleophilic substitution steps (Fig. 2), since an overall stereochemical retention (corresponding to a twofold stereochemical inversion) has been established in investigations with isotopically labeled N^5-(HDT)methyltetrahydrofolate (see, for example, Ref. [9]).

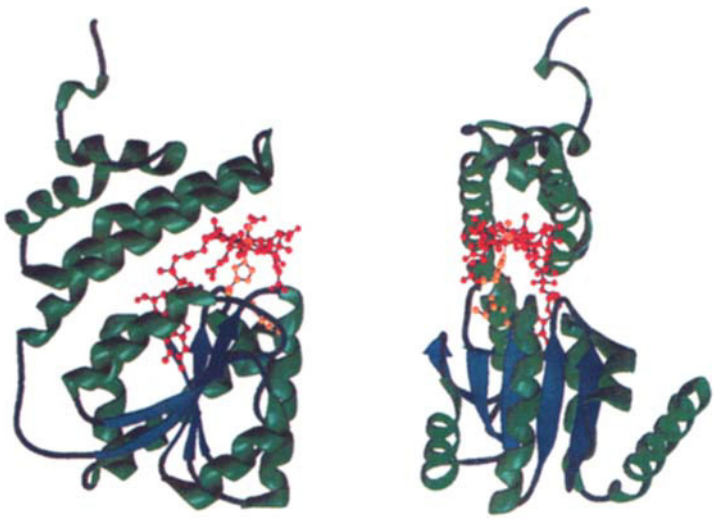

Fig. 3. The cobalamin-binding domain of the methionine synthase of *Escherichia coli* according to Drennan et al. [1, 2]: Ribbons diagrams of the protein part highlighting the amino acid triade His-759, Asp-757, and Ser-810, and the methyl-Co^{III} center (yellow) of the bound methylcob(III)alamin in the "base-off" form (red).

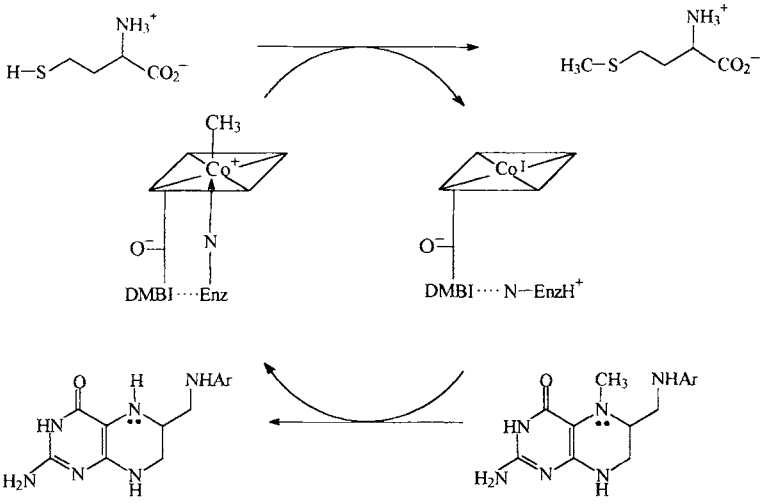

Fig. 2. Schematic representation of the cobalamin-dependent biosynthesis of methionine in *Escherichia coli*: methyl group transfer from N^5-methyl-tetrahydrofolate to homocysteine via enzyme-bound methylcobalamin and cob(I)alamin (DMBI = 5,6-dimethylbenzimidazole).

In the catalytic cycle, the protein-bound corrinoid occurs either as the (now) structurally known, enzyme-bound methylcob(III)alamin or as the oxidation-susceptible and highly nucleophilic cob(I)alamin. Although there is yet little known about the structure of the latter (even in solution), there is evidence that the metal center of cob(I)alamin does not carry any axial ligands. As a consequence, the transition between cob(I)alamin and methylcob(III)alamin (with a hexacoordinate Co^{III} center) implies considerable reorientation at the site of the axial ligand, which allows the enzyme environment to influence the reactivity of the cobalt corrin.[10]

The peptide moiety of the cobalamin-binding fragment of the methionine synthase is essentially composed of two domains (Fig. 3): a "helix bundle" consisting of four antiparallel helices covering the methylated "upper side" of the protein-bound corrinoid, and an α/β-domain, consisting of six α-helices and β-sheets, whose tertiary structure resembles the so-called "Rossmann fold" of nucleotide-binding proteins.[1, 2] The nucleotide function of the protein-bound cobalamin is anchored in a pocket of the α/β-domain. This domain also provides the cobalt-coordinating histidine (His-759), the functional substitute for the nucleotide. His-759 is linked by a hydrogen bond *syn* to an adjacent aspartate (Asp-757) which, in turn, is linked to a serine (Ser-810) by an *anti* hydrogen bond (Fig. 4)

The methionine synthase of *Escherichia coli* contains the new catalytically active tetrade composed of cobalt corrin, histidine, aspartate, and serine (cf. Figs. 3 and 4).[1, 2] Its catalytic activity is mainly due to the reactivity of the cobalt corrin. However, the contribution of the three H-bonded amino acids to the catalysis of the methyl group transfer is not insignificant, considering the important role the axial imidazole ligand plays in methylation equilibria with methyl corrinoids:[11] The stabilization the enzyme experiences in the methylated state (or in the Co^{II} state) on account of the cobalt coordination of His-759 counteracts the tendency to demethylate or reduce to the Co^{I} state.[10] According to electrochemical investigations on intact methionine synthase, the Co^{II}/Co^{I} reduction of the enzyme-bound corrinoid occurs at a potential that is more than 100 mV less negative (relative to the corresponding redox step in aqueous solution) and involves the net uptake of a proton. This indicates a destabilization of the Co^{II} state of the methyl transferase with respect to its Co^{I} state and relative to the redox pair cob(II)alamin/cob(I)alamin in solution. Build-up of strain accompanying the axial histidine coordination might result in loss of the imidazole ligand during demethylation (or reduction) to cob(I)alamin and might be one plausible explanation for the susceptibility to reduction of the protein-bound Co^{II} corrinoid. The actual evidence (deviation from the geometrically ideal bonding of histidine to cobalt and of the two bridging protons to Asp-757) is, however, not conclusive on account of the low nominal resolution of the structure analysis of the B_{12}-binding domain of the methionine synthase.

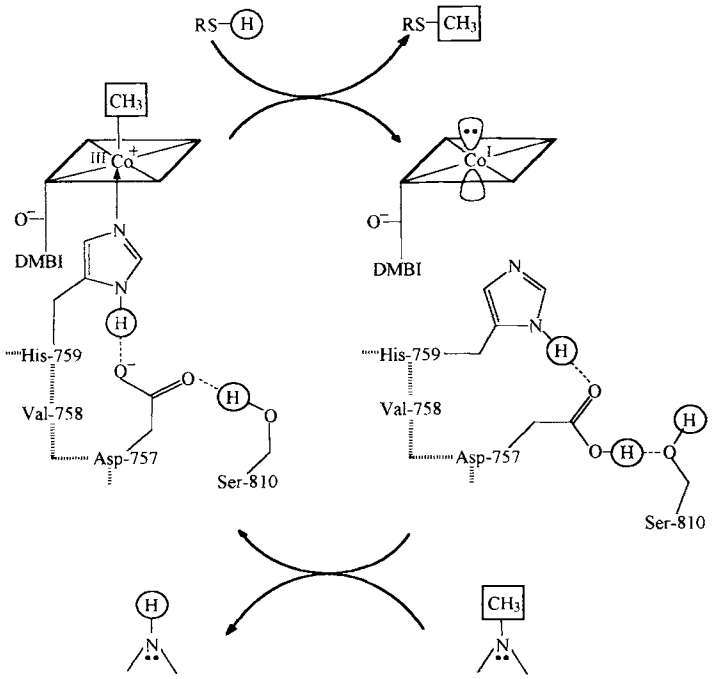

Fig. 4. The catalytically active tetrade of the methionine synthase, enzyme substrates, and products of the methyl transfer steps in a schematic representation, emphasizing potentially relevant stereoelectronic preferences for the formation of hydrogen bonds.

As suggested by Drennan et al., the enzyme-catalyzed methylation of homocysteine to methionine, which implies the demethylation of the protein-bound cofactor from methylcob(III)alamin to cob(I)alamin, involves uptake of a proton by the enzyme.[1, 2] In reverse, the enzyme-catalyzed demethylation of N^5-methyl-tetrahydrofolate to tetrahydrofolate occurs with net release of a proton from the enzyme, whose cofactor is methylated from cob(I)alamin to methylcob(III)alamin during this step. According to Drennan et al. these (hypothetical) protonation and deprotonation steps of the enzyme take place through the amino acid triade His-759, Asp-757, and Ser-810, which stretches from the cobalt center of the protein-bound cofactor to the surface of the B_{12}-domain.

No doubt, the assumed effect of the amino acid triade His-759, Asp-757, Ser-810 on the methyl transfer[12] has to do with the critical axial coordination of the protein-based imidazole ligand (of His-759), and with the structural reorganization occurring during its (de)coordination. However, the ability of His-759 to coordinate depends decisively on the state of protonation:[13] If the protonation of the His-759/Asp^--757 pair leads to $HisH^+$-759/Asp^--757, it completely eliminates the ability of His-759 to coordinate. The nucleophilicity of the imidazole ligand is also reduced when the protonation leads to neutral residues at His-759/Asp-757, as suggested by Drennan et al.[1, 2] Besides, the protonation of the His-759/Asp^--757 pair may lead to a substantial reorientation of the amino acids involved and may therefore indirectly influence the ability of His-759 to coordinate at the cobalt corrin. Indeed, the stereoelectronic preference for the protonation of aspartate at its more basic *syn* lone pair cannot be taken into account unless a change of conformation is postulated, if two hydrogen bonds are to be maintained to His-759 and to Ser-810 (cf. Fig. 4). The role of the H-bonded amino acid triade of the methionine synthase of *Escherichia coli* is therefore potentially that of a "switch" controlled by the degree of protonation and regulating, electronically and conformationally, the "base-on" or "base-off" states of coordination at the cobalt center.

The methionine synthase contains, in the α/β domain, two central amino acids (His-759 and Asp-757) among several other "conserved" amino acids and shows sequence homologies with B_{12}-binding proteins, even with some that use coenzyme B_{12} (adenosylcob(III)alamin) instead of methylcob(III)alamin as cofactor.[14, 15] The expectation that the cofactor of coenzyme B_{12}-binding enzymes might also be bound in a "base-off" form has actually been confirmed for the coenzyme B_{12}-dependent methylmalonyl-CoA-mutase of *Propionibacterium shermanii*.[16, 17] The publication by Phil Evans's group[17] of an X-ray analysis of this enzyme is anticipated in the near future.

The first evidence for cobalt coordination of histidine at a protein-bound "complete" corrinoid was supplied by ESR-spectroscopic data of Stupperich et al.[18] for preparations of the acetogenic bacterium *Sporomusa ovata*, which, however, produces a *p*-cresolylcobamide whose pseudo-nucleotide function is not able to coordinate at cobalt. A *p*-cresolylcobamide-binding protein from *Sporomusa ovata* could be crystallized, and an X-ray structure analysis is presently under way.[19]

Coenzyme B_{12} and the less complex methylcob(III)alamin were the first and only well-documented organometallic coenzymes to be discovered. Their biological functions are closely connected with their organometallic bond. The control and catalysis by the protein of the homolytic cleavage and formation of this bond are relevant for coenzyme B_{12},[20] whereas activation of the corresponding heterolytic reactions are important for methylcob(III)alamin. According to the present state of knowledge, the enzymatic acceleration of the homolysis of the organometallic bond of coenzyme B_{12} can be traced to mechanical steric factors,[6, 7] and the enzyme-catalyzed heterolysis of methylcob(III)alamin to electronic factors.[10]

In spite of the knowledge on the structure of the cobalt complex vitamin B_{12}, the biological function of the corrinoids remained an enigma until the organometallic bond of coenzyme B_{12} was discovered. Similarly, only the X-ray structure analysis of the methionine synthase led to a fundamental broadening of the views on the B_{12} derivatives. Earlier information on the structure of nucleotide-containing B_{12} derivatives obviously concerns molecular transport and storage forms of these unique cofactors, which possess a remarkable potential for self-constitution and have thermodynamically propitious structural properties.[3] Particularly striking among the latter is the structure of the unique nucleotide "loop" which, interestingly enough, plays no functional role in the methionine synthase of *Escherichia coli*. In this particular enzyme the cobalamin cofactor occurs as a special "dinucleotide", which contains, besides a catalytically active moiety of the molecule, a second nucleotide portion that is relevant for the bonding to the apoenzyme. This portion is characterized by an α-configurated pseudo-nucleotide base, but in a B_{12}-specific way. The results presented above cast new light on the question of the biological functions of the intramolecular coordinating benzimidazole function.

German version: *Angew. Chem.* **1996**, *108*, 179–182

 © VCH Verlagsgesellschaft mbH, D-69451 Weinheim, 1996 0570-0833/96/3502-0169 $ 10.00+.25/0

Keywords: biochemistry · cobalt corrin · methyl group transfer vitamin B_{12}

[1] C. L. Drennan, S. Huang, J. T. Drummond, R. G. Matthews, M. L. Ludwig, *Science* **1994**, *266*, 1669–1674.
[2] C. L. Drennan, R. G. Matthews, M. L. Ludwig, *Curr. Op. in Struct. Biol.* **1994**, *4*, 919–929.
[3] A. Eschenmoser, *Angew. Chem.* **1988**, *100*, 5–40; *Angew. Chem. Int. Ed. Engl.* **1988**, *27*, 5–40.
[4] C. Kratky, G. Färber, K. Gruber, K. Wilson, Z. Dauter, H.-F. Nolting, R. Konrat, B. Kräutler, *J. Am. Chem. Soc.* **1995**, *117*, 4654–4670.
[5] B. Kräutler, R. Konrat, E. Stupperich, G. Färber, K. Gruber, C. Kratky, *Inorg. Chem.* **1994**, *33*, 4128–4139.
[6] J. Halpern, *Science* **1985**, *227*, 869–875.
[7] For example, B. T. Golding, D. N. R. Rao, in *Enzyme Mechanisms* (Eds.: M. I. Page, A. Williams), Royal Society of Chemistry, London, **1987**, p. 404.
[8] M. Rossi, J. P. Glusker, L. Randaccio, M. F. Summers, P. J. Toscano, L. G. Marzilli, *J. Am. Chem. Soc.* **1985**, *107*, 1729.
[9] R. G. Matthews, R. V. Banerjee, S. W. Ragsdale, *BioFactors* **1990**, *2*, 147–152.
[10] B. Kräutler, *Proceedings of the Royal Swedish Academy of Sciences Nobel Symposia 1991* (Eds.: C.-I. Brändén, G. Schneider), Oxford University Press, **1994**, pp. 83–92.
[11] B. Kräutler, *Helv. Chim. Acta* **1987**, *70*, 1268–1278.
[12] The "catalytic triade" of the "charge relay" systems of the serine protease chymotrypsin is similarly constructed (but in a different sequence!) with Asp-102, His-57, and Ser-195 (see D. M. Blow, T. A. Steitz, *Ann. Rev. Biochem.* **1970**, *39*, 86).
[13] Evidence that the coordinating His-759 is present as an imidazolate in the methylated Co^{III} form of the methionine synthase of *Escherichia coli* is lacking.
[14] E. N. G. Marsh, D. E. Holloway, *FEBS* **1992**, *310*, 167–170.
[15] In contrast, the B_{12} transport proteins from several sources do not show sequence homologies to the methionine synthase of *Escherichia coli*.
[16] R. Padmakumar, S. Taoka, R. Padmakumar, R. Banerjee, *J. Am. Chem. Soc.* **1995**, *117*, 7033–7034.
[17] F. Mancia, A. Nakagawa, N. H. Keep, P. Leadlay, P. R. Evans, in *Abstr. Pap. 4th Europ. Workshop Crystallog. Biol. Macromol.*, Como, **1995**.
[18] E. Stupperich, H. J. Eisinger, S. P. J. Albracht, *Eur. J. Biochem.* **1990**, *193*, 105–109.
[19] U. G. Wagner, E. Stupperich, P. Aulkemeyer, C. Kratky, *J. Mol. Biol.* **1994**, *236*, 388–989.
[20] J. Retey, *Angew. Chem.* **1990**, *102*, 373–379; *Angew. Chem. Int. Ed. Engl.* **1990**, *29*, 355.

Troubleshooting... with VCH books!

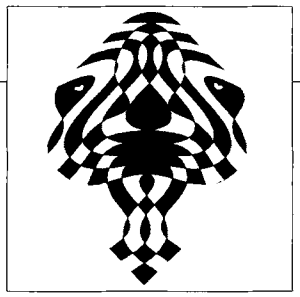

Neuhoff, V.
Scientists in Conference The Congress Organizer's Handbook
1987. X, 223 pages.
Hardcover. DM 68.00
ISBN 3-527-26579-1

Do you have to organize a conference? Well, sometimes, this can't be avoided. But you don't want to get crushed by the wheels of paperwork? And you want to stay in your budget? Then this handy little book is your survival kit!

Schoenfeld, R.
The Chemist's English Third, revised edition with Say It in English, Please!
1990. XII, 195 pages with 9 figures.
Hardcover. DM 48.00
ISBN 3-527-28003-0

"Recommended without qualification; and a suitable gift for friends."
Chemical and Engineering News

"The book might well serve as a prescribed text for PhD students."
Nature

Ebel, H.F. /Bliefert, C. / Russey, W.
The Art of Scientific Writing
From Student Reports to Professional Publications in Chemistry and Related Fields
1990. XIX, 493 pages with 27 figures and 16 tables.
Softcover. DM 48.00
ISBN 3-527-26677-1

First of all, here we have a highly readable text on scientific communication - with all its ramifications from writing the most effective text to getting it published. Never before has so much information on scientific writing been assembled in a single book.

To order please contact your bookseller or:
VCH, P.O. Box 10 11 61,
D-69451 Weinheim,
Telefax (0) 62 01 - 60 61 84
VCH, Hardstrasse 10, P.O. Box,
CH-4020 Basel
VCH, 8 Wellington Court,
Cambridge CB1 1HZ, UK
VCH, 303 N.W. 12th Avenue,
Deerfield Beach, FL 33442-1788,
USA
toll-free: 1-800-367-8249 or
fax: 1-800-367-8247
VCH, Eikow Building,
10-9 Hongo 1-chome, Bunkyo-ku,
Tokyo 113

VCH

$[(AsOH)_3(MoO_3)_3(AsMo_9O_{33})]^{7-}$ and $[(AsOH)_6(MoO_3)_2(O_2Mo\text{-}O\text{-}MoO_2)_2\text{-}(AsMo_9O_{33})_2]^{10-}$: Coupling of Highly Negatively Charged Building Blocks**

Achim Müller,* Erich Krickemeyer, Stephan Dillinger, Jochen Meyer, Hartmut Bögge, and Anja Stammler

Dedicated to Professor C. N. R. Rao on the occasion of his 60th birthday

The design of syntheses in the field of inorganic and supramolecular inorganic chemistry combined with the control of the fundamental reaction pathways would enable the targeted synthesis of complex mesoscopic structures—even with predetermined material properties—on the basis of economical reactions. The realization of this still utopian dream demands the elucidation of formerly largely unknown reaction mechanisms that are fundamental for the formation of large molecular species (for example metal clusters) within conservative self-organization processes and that, for example in the field of polyoxometalate chemistry, have provided an enormous structural diversity, which yields a variety of properties.[1–3] A fundamentally promising route appears to be the strategy of generating large, highly negatively charged (and therefore soluble) intermediates as transferable units in the reaction solution,[4] which can be trapped and stabilized or (!) coupled to each other by progressive condensation reactions by electrophilic protecting groups (for example, As^{3+} [4a] or *fac*-$\{MoO_3\}$ "anti-Lipscomb" units[4b, 5]). We have now succeeded in isolating the mixed-valent, diamagnetic cluster anions **1a** and **2a**, which are the first molybdoarsenates(III) with facial trioxomolybdenum units.

$[(AsOH)_3(MoO_3)_3(AsMo_9O_{33})]^{7-}$ **1a**

$[(AsOH)_6(MoO_3)_2(O_2Mo\text{-}O\text{-}MoO_2)_2(AsMo_9O_{33})_2]^{10-}$ **2a**

The dark blue, mixed-valent salts **1** and **2** were characterized by elemental analysis (including manganometric titration of Mo^V), thermogravimetric analysis (to determine the content of water of crystallization), spectroscopic methods (ESR, IR, UV/Vis, and NIR spectroscopy), and single crystal X-ray structure analysis.[6] The cluster anion **1a** consists of a highly negatively charged $\{AsMo_9O_{33}\}^{13-}$ Keggin fragment (Fig. 1) that is capped by a six-membered ring comprising three electrophilic $\{AsOH\}^{2+}$ and three facial $\{MoO_3\}^0$ units. These units are arranged alternately and linked together as well as to the Mo atoms of the nucleophilic, lacunary $\{AsMo_9O_{33}\}^{13-}$ unit through μ_3-O atoms. The indicated protonation of the terminal oxygen atoms bound in **1a** (and **2a**; see below) to the As^{III} centers is unequivocal from their bond valence sums,[7] the conditions of the synthesis (acidic reaction milieu), and the approximately equally long As-OH and As-μ-O bonds (Figs. 1 and 2).

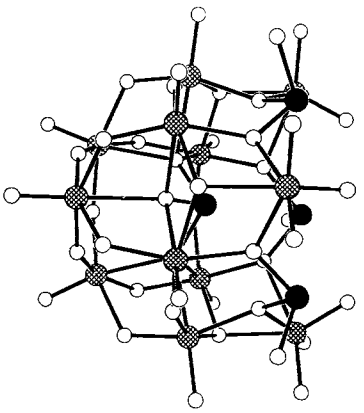

Fig. 1. Structure of the anion **1a** in crystals of **1** (Mo cross-hatched, As black, O white). Selected distances [pm]: Mo···Mo (edge-sharing) 333.7–343.5, Mo···Mo (corner-sharing) 365.6–367.0, Mo–O_{term} ($\{MoO_3\}^0$ units) 173.1–176.0, Mo–O_{term} ($\{AsMo_9O_{33}\}^{13-}$ unit) 167.1–170.3, As-OH 177.4, As-(μ_3-O)($\{AsOH\}^{2+}$ centers) 178.2–179.3, As–(μ_4-O) (central AsO_3 pyramid) 179.4.

Compound **1a** forms in aqueous solution at a pH value of about 4.5. However, if the same reaction is performed at a pH value of 3.0, the highly nucleophilic $\{AsMo_9O_{33}\}^{13-}$ groups react as their stable (trapped) product **1a** to give the "dimeric" cluster ion **2a** (see Fig. 2 and the reaction scheme in Fig. 3).

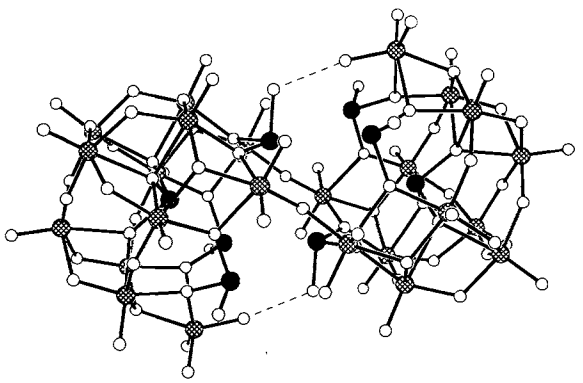

Fig. 2. Structure of the anion **2a** in crystals of **2** (Mo cross-hatched, As black, O white). The two *intramolecular* As^{III}-OH···O=$Mo^{VI}O_2$ hydrogen bonds are depicted as broken lines. Selected distances [pm]: Mo···Mo (edge-sharing) 329.6–347.0, Mo···Mo (corner-sharing) 364.4–368.1, Mo–O_{term} ($\{MoO_3\}^0$ units) 171.0–176.0, Mo–O_{term} ($O_2Mo\text{-}O\text{-}MoO_2$ bridges) 168.5–170.7, Mo–O_{term} ($\{AsMo_9O_{33}\}^{13-}$ unit) 167.4–170.1, As-OH 176.2–179.1, As-(μ_3-O)($\{AsOH\}^{2+}$ centers) 177.2–179.8, As–(μ_4-O) (central AsO_3 pyramid) 178.1–180.0.

According to this scheme, a condensation of four $\{Mo^{VI}O_3\}$ units takes place after protonation, and H_2O is evolved from **1a** on the formation of two $O_2Mo\text{-}O\text{-}MoO_2$ bridges. The two six-membered rings of **2a** therefore have only two facial $\{Mo^{VI}O_3\}$ groups. If at the same pH value a larger amount of As_2O_3 is added to the reaction solution, a further reaction of the remain-

$K_7[(AsOH)_3(MoO_3)_3(AsMo_9O_{33})]\cdot 15H_2O$ **1**

$K_{10}[(AsOH)_6(MoO_3)_2(O_2Mo\text{-}O\text{-}MoO_2)_2(AsMo_9O_{33})_2]\cdot 12H_2O$ **2**

[*] Prof. Dr. A. Müller, E. Krickemeyer, Dr. S. Dillinger, Dipl.-Chem. J. Meyer, Dr. H. Bögge, A. Stammler
Fakultät für Chemie der Universität
Lehrstuhl für Anorganische Chemie I
Postfach 100131, D-33501 Bielefeld (Germany)
Fax: Int. code +(521)106-6003
e-mail: amueller@cheops.chemie.uni-bielefeld.de

[**] We thank Prof. Dr. M. T. Pope and Dr. U. Kortz (both of the Department of Chemistry, Georgetown University, Washington, D. C., USA) for valuable suggestions.

ing trioxomolybdenum units of **2a** in the presence of trimethylammonium ions yields the cluster anion **3a** (cf. the reaction scheme in Fig. 3).[8] Cluster anion **3a** displays four links be-

$[(AsOH)_4(AsO)_2(HOAs\text{-}O\text{-}MoO_2)_2(O_2Mo\text{-}O\text{-}MoO_2)_2(AsMo_9O_{33})_2]^{8-}$ **3a**

tween the two $\{(AsOH)_3(MoO_3)_3(AsMo_9O_{33})\}^{7-}$ units, namely the Mo-O-Mo bridges familiar from **2a** and another two O_2Mo^{VI}-O-$As(OH)_{term}$-O-As bridges (Fig. 3).

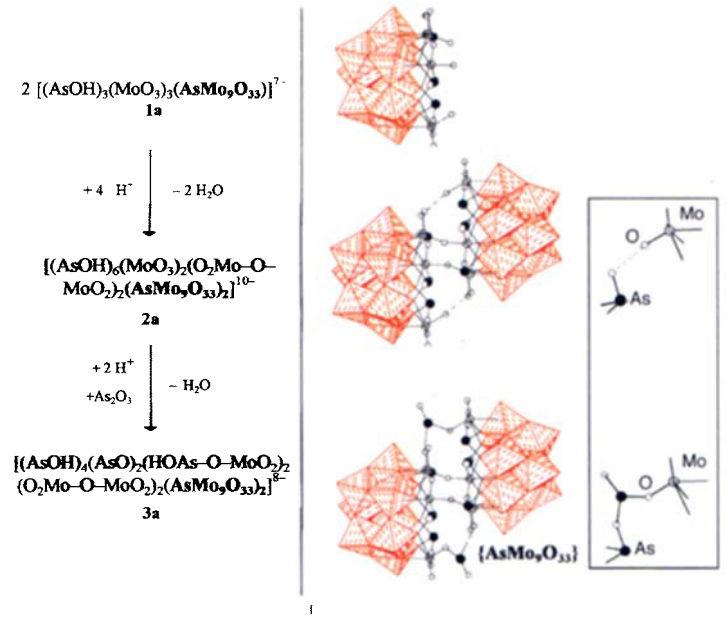

Fig. 3. Reaction scheme depicting the preparation of anions **1a**–**3a** and the linking of the fragments with emphasis on the identical $\{AsMo_9O_{33}\}^{13-}$ unit in each through polyhedral representation.

An important feature is the lone electron pair at the As^{III} center of $\{AsMo_9O_{33}\}^{13-}$ group in compounds **1**–**3** that prevents the adoption of a spherical structure, which can be formed on oxidation of this As^{III} center to an As^{V} center with concomitant rearrangement of the whole cluster framework and would lead to anions of the α-Keggin type with a central AsO_4^{3-} tetrahedron (cf. Ref. [8]).

The facial MoO_3 groups of the cluster anions **1a** and **2a** (that is, at exactly those positions at which further coupling and condensation reactions are possible after protonation) are stabilized by one hydrogen bond each between one of their terminal oxygen atoms and the OH function of the opposite $\{AsOH\}^{2+}$ unit (As^{III}-OH···O=$Mo^{VI}O_2$ distances of 264 pm for **1** and 257 pm for **2**). Whereas in cluster anion **2a** only two *intramolecular* As^{III}-OH···O=$Mo^{VI}O_2$ hydrogen bonds are present, in accordance with its low number of facial trioxomolybdenum units (cf. Fig. 2), every cluster anion in the crystal structure of **1** forms two *intermolecular* As^{III}-OH···O=$Mo^{VI}O_2$ hydrogen bonds to each of its three adjacent ions and therefore the maximal number (six) of such hydrogen bonds. The individual "monomeric" $[(AsOH)_3(MoO_3)_3(AsMo_9O_{33})]^{7-}$ units form a slightly distorted hexagonal closest packing in the crystal lattice and are arranged in such a way that the opening of a cluster anion, whose structure resembles a half-cleaved sphere with a central $As^{III}O_3$ group, points in the direction of the crystallographic *c* axis, while the corresponding openings of its three neighboring cluster anion spheres face in the opposite direction. This type of arrangement of the cluster anions **1a** in the crystal lattice gives rise to a two-dimensional double-layer structure.[9]

According to the results of titrimetric studies and bond valence sum considerations, the $\{AsMo_9O_{33}\}^{13-}$ groups of the cluster compounds **1**, **2**, and **3** have the same electron population (formally four Mo^{V} and five Mo^{VI} centers of type III according to Robin–Day): the number of electrons in 4d states per $\{AsMo_9O_{33}\}^{13-}$ fragment of the anions **1a**, **2a**, and **3a**[8] is always four, and the electrons are delocalized at room temperature[7] over all nine Mo centers of the $O{=}MoO_5$ octahedra that make up the $\{AsMo_9O_{33}\}^{13-}$ unit.

As conclusion the following is important: For otherwise identical reaction conditions, the selection of the reaction routes leading to **1** and **2** is determined exclusively by the different pH values of the reaction solution (**1**: 4.5; **2**: 3.0). One can therefore speak of a new synthesis principle in polyoxometalate chemistry, because ephemeral, highly reactive and otherwise inaccessible reduced, highly negatively charged clusters can be trapped by electrophilic protecting groups like $\{MoO_3\}$ and stabilized.[4b] The protecting groups can themselves cause further coupling of fundamental inorganic units under changed reaction conditions in the context of simple condensation reactions (after protonation at the oxygen atoms with high electron density). The assembly of these preorganized, transferable fundamental inorganic units that exist in aqueous solution to form higher nuclear molybdoarsenates like **2a**, which can be considered successful with respect to the deliberately selected reaction conditions (adjustment of the desired pH value) can be extended to other fields of polyoxometalate chemistry.[4] The interesting question arises whether the disorder (partial linking of units) is the trigger for the crystallization at the nucleation phase of **1**.

Experimental Procedure

1: $K_2MoO_4 \cdot 5H_2O$ (11.2 g, 34.1 mmol; Johnson Matthey), As_2O_3 (6.0 g, 30.3 mmol), and KSCN (20.0 g, 205.8 mmol) were dissolved in H_2O (400 mL) at 95 °C with stirring in a 500 mL Erlenmeyer flask (pH value of the clear solution about 6.2–6.5). After cooling to 85 °C, adjustment of the pH value to about 5.3 with 10% H_2SO_4, and subsequent addition of $N_2H_6SO_4$ (3.2 g, 24.6 mmol), the mixture was stirred for 4 min at this temperature. The pH value of the now deep blue solution was adjusted to about 4.5 with 10% H_2SO_4 (or 10% KOH depending on the resulting pH value) solution, and the reaction mixture rapidly cooled to 25 °C in a water bath. As_2O_3 that again precipitated was filtered off. Slowly, dark blue hexagonal crystals of **1** precipitate from the filtrate in a closed 500 mL round-bottomed flask at 5–7 °C. The As_2O_3 that also precipitates was suspended in the mother liquor by shaking and decanted from the crystals. This purification step was repeated with the filtered mother liquor until all the As_2O_3 had been removed. Yield: 5.8 g (77.7% based on $K_2MoO_4 \cdot 5H_2O$). Some characteristic IR bands (KBr disk; preparation under argon): $\tilde{\nu}$ [cm^{-1}] = 950(vs), 900(m) (Mo–O_{term}), 855(s), 840(s), 750(m), 625(s), 570(s), 540(sh) (As–(OH), As-O-Mo, Mo-O-Mo); UV/Vis (solid-state reflection spectrum with cellulose as white standard): λ [nm] = 315, 650, 790; NIR (KBr pellet, in transmission mode): λ [nm] = 1000, 1500.

2: As for **1** with one decisive difference: the pH value was adjusted to about 3.0 with 10% H_2SO_4 after the reduction with $N_2H_6SO_4$. Yield: 6.6 g (88% based on $K_2MoO_4 \cdot 5H_2O$). Some characteristic IR bands (KBr, preparation under argon): $\tilde{\nu}$ [cm^{-1}] = 950(vs), 910(w) (Mo–O_{term}), 845(m), 750(m), 740(sh), 700(w), 640(m), 560(s–m), 530(sh) (As–(OH), As-O-Mo, Mo-O-Mo); UV/Vis (solid-state reflection spectrum with cellulose as white standard): λ [nm] = 315, 620, 785; NIR (KBr pellet, in transmission mode): λ [nm] = 980, 1540.

Received: July 24, 1995 [Z 8243 IE]
German version: *Angew. Chem.* **1996**, *108*, 183–185

Keywords: arsenic compounds · clusters · molybdenum compounds · polyoxometalates

[1] M. T. Pope, A. Müller, *Angew. Chem.* **1991**, *103*, 56; *Angew. Chem. Int. Ed. Engl.* **1991**, *30*, 34.
[2] M. T. Pope, A. Müller, *Polyoxometalates: From Platonic Solids to Anti-Retroviral Activity*, Kluwer, Dordrecht **1994**.
[3] M. T. Pope, *Heteropoly and Isopoly Oxometalates*, Springer, Berlin, **1983**.
[4] a) A. Müller, E. Krickemeyer, S. Dillinger, H. Bögge, W. Plass, A. Proust, L. Dloczik, C. Menke, J. Meyer, R. Rohlfing, *Z. Anorg. Allg. Chem.* **1994**, *620*, 599; b) M. I. Khan, A. Müller, S. Dillinger, H. Bögge, Q. Chen, J. Zubieta, *Angew. Chem.* **1993**, *105*, 1811; *Angew. Chem. Int. Ed. Engl.* **1993**, *32*, 1780.

 © VCH Verlagsgesellschaft mbH, D-69451 Weinheim, 1996 0570-0833/96/3502-0172 $ 10.00+.25/0

[5] An important working hypothesis of polyoxometalate chemistry is that, in general, metal atoms bearing three or more terminal oxygen atoms in MO_6 octahedra do not occur. For this "Lipscomb rule" see W. N. Lipscomb, *Inorg. Chem.* **1965**, *4*, 132.

[6] Crystal data of **1**: space group $P\bar{3}$, $a = 1432.8(2)$, $c = 1829.8(3)$ pm, $V = 3253(1) \times 10^6$ pm^3, $Z = 2$, $\rho_{calcd} = 2.78$ g cm^{-3}, $T = 188$ K, $R = 0.083$ for 4533 independent reflections ($F > 4.0\sigma(F)$). Crystal data of **2**: space group $P\bar{1}$, $a = 1282.0(4)$, $b = 1380.3(4)$, $c = 1531.5(5)$ pm, $\alpha = 83.46(2)$, $\beta = 77.37(2)$, $\gamma = 68.92(2)$°, $V = 2466(1) \times 10^6$ pm^3, $Z = 1$, $\rho_{calcd} = 3.32$ g cm^{-3}, $T = 294$ K, $R = 0.067$ for 6614 independent reflections ($F > 4.0\sigma(F)$). Further details of the crystal structure investigation may be obtained from the Fachinformationszentrum Karlsruhe, D-76344 Eggenstein-Leopoldshafen (Germany) on quoting the depository number CSD-59227. The cluster anion **2a** was also obtained as ammonium salt $(NH_4)_8[H_2(AsOH)_6(MoO_3)_2(O_2Mo\text{-}O\text{-}MoO_2)_2(AsMo_9O_{33})_2] \cdot 12H_2O$ (**4**).

[7] Calculated bond valence sums (according to I. D. Brown in *Structure and Bondings in Crystals, Vol. II* (Eds.: M. O'Keeffe, A. Navrotsky), Academic Press, New York, **1981**): **1a**: As 3.0, Mo ($\{AsMo_9O_{33}\}$ unit) 5.5, Mo ($\{MoO_3\}^0$ groups) 5.8, O (As-O-H) 1.0; **2a**: As 3.0, Mo ($\{AsMo_9O_{33}\}$ unit) 5.6, Mo ($\{MoO_3\}^0$ groups) 5.9, Mo ($\{O_2Mo\text{-}O\text{-}MoO_2\}$ groups) 5.85, O (As-O-H) 1.0.

[8] A. Müller, E. Krickemeyer, M. Penk, V. Wittneben, J. Döring, *Angew. Chem.* **1990**, *102*, 85; *Angew. Chem. Int. Ed. Engl.* **1990**, *29*, 88.

[9] A precise examination of the structure of an individual crystal of **1** reveals the following disorder: One obtains a maximum of electron density "refinable" as 1/10 As between the oxygen atoms of the opposite $\{AsOH\}^{2+}$ and $\{MoO_3\}^0$ groups within a double layer. This can be interpreted as follows: in the statistical average, about every tenth of the $As^{III}\text{-}OH \cdots O{=}Mo^{VI}O_2$ hydrogen bonds is replaced by a covalent $As^{III}OAs(OH)_{term}\text{-}O\text{-}Mo^{VI}O_2$ bridge. These correspond to the $As^{III}OAs(OH)_{term}\text{-}O\text{-}Mo^{VI}O_2$ bridges in **3**; merely the relative position of the $\{(AsOH)_3(MoO_3)_3(AsMo_9O_{33})\}^{7-}$ units linked thereby is different. The oxygen atom of the terminal $(OH)_{term}$ group bound to this additional arsenic atom was also localized (found disorder: with water of crystallization and potassium ions). The mentioned disorder is more or less pronounced in different crystals of **1**, or not present at all. (We have performed X-ray crystal structure analyses on several single crystals of **1**.)

Synthesis of Chiral 1,1′-Iminodicarboxylic Acid Derivatives from α-Amino Acids, Aldehydes, Isocyanides, and Alcohols by the Diastereoselective Five-Center–Four-Component Reaction

Anton Demharter, Werner Hörl, Eberhardt Herdtweck, and Ivar Ugi*

Dedicated to Professor Paul von Ragué Schleyer

Chemical compounds are usually synthesized in several reaction steps. The intermediates must be separated and purified before they are used as starting materials in the next reaction. The total yield of such an iterative synthesis decreases sharply with the number of steps. Many compounds can also be prepared much faster and with higher yields by one-pot multicomponent reactions (MCR).[1] The scope of the four-component reaction (U-4CR)[2] was only recognized in 1958, shortly after isocyanides had become easily accessible.

A very effective variation of the U-4CR is the five-center–four-component reaction (U-5C-4CR). It combines very high yields (usually more than 95%) and excellent stereoselectivity (de ≈ 80%) with simple preparative procedures.

α-amino acids serve as bifunctional starting materials in the U-5C-4CR instead of the amine and acid components in the familiar U-4CR. They react with equimolar amounts of aldehyde and isocyanide as well as with the alcohol that also serves as a solvent. After one to two days the product, a 1,1′-iminodicarboxylic acid derivative, is obtained in almost quantitative yield.

1,1′-Iminodicarboxylic acids and their derivatives constitute an interesting and thoroughly investigated group of natural substances. They can be isolated from several types of poisonous mushrooms.[3] Opines,[4] such as octopine and nepaline, which have been isolated from crown gall tumors, also belong to this class of compounds. 1,1′-Iminodicarboxylic acid derivatives are also pharmaceutically active as ACE inhibitors.[5] The preparative simplicity and the high yield of the U-5C-4CR make it an ideal approach to this interesting group of compounds.

The postulated reaction mechanism[6] of the U-5C-4CR is given in Scheme 1. First, the amino function of the α-amino acid

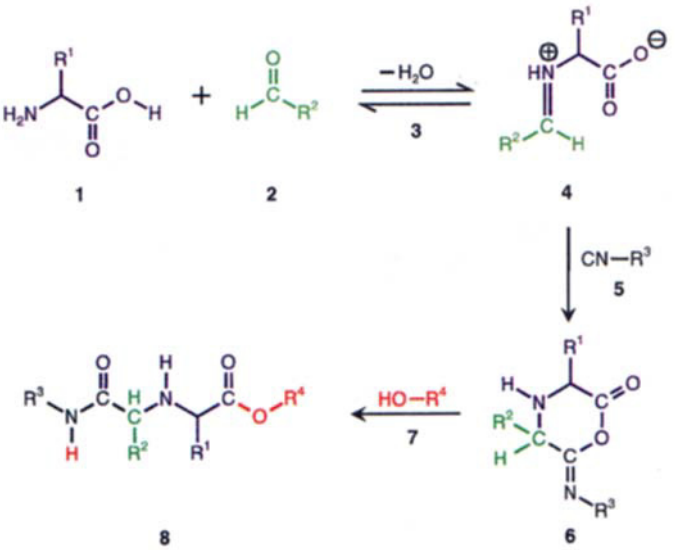

Scheme 1. Postulated reaction mechanism for the U-5C-4CR.

1 condenses with the aldehyde compound **2**, losing water (**3**) to form the imine **4**. After α-addition of the isocyanide **5**, an O-acylamide (**6**) is formed. By the nucleophilic attack of the fourth component (alcohol **7**, the fifth reacting center) at the carboxylic carbon atom and the subsequent rearrangement the U-5C-4CR product, the 1,1′-iminodicarboxylic acid derivative **8** is formed. This is achieved by the esterification of the acid function of the α-amino acid with the alcohol. As in the U-4CR, a secondary amide is formed by the isocyanide. A new stereocenter is created at the initially quaternary carbon atom of the aldehyde. Its prefered absolute configuration is induced by the chiral amino acid employed.

Out of the large number of compounds that have already been synthesized by the U-5C-4CR, three representative examples (for physical data see Table 1) are given in Scheme 2. In accordance with the postulated mechanism, the X-ray structural analysis[7] of **9** (Fig. 1) shows that the new stereocenter has the same absolute configuration (*S*) as the amino acid employed. The assignment of the absolute configuration at the new stereocenter C7 can be unambiguously determined with the help of the second stereocenter C3, which is not affected by the reaction. In the crystal two crystallographically distinct molecules A and B are associated into dimers through weak hydrogen bonds ($N2_A\text{–}H2_A \cdots O2_B$: 297 pm and 174°; $N2_B\text{–}H2_B \cdots O2_A$: 305 pm and 170°). The geometry of the two molecules A and B is marginally different.[7]

[*] Prof. Dr. I. Ugi, Dr. A. Demharter, Dipl.-Chem. W. Hörl
Lehrstuhl für Organische Chemie und Biochemie der Technischen Universität München
Lichtenbergstrasse 4, D-85747 Garching (Germany)
Fax: Int. code +(89)3209-3290
Dr. E. Herdtweck
Lehrstuhl I für Anorganische Chemie der Technischen Universität München

 © VCH Verlagsgesellschaft mbH, D-69451 Weinheim, 1996 0570-0833/96/3502-0173 $ 10.00+.25/0

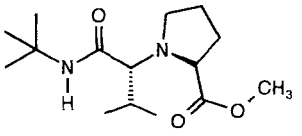

yield: 98%

88% *de*

9

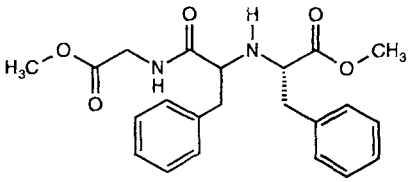

yield: 99%

84% *de*

10

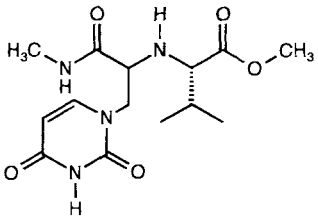

yield: 98%

86% *de*

11

Scheme 2. Selected examples of the U-5C-4CR.

Table 1. Selected physical data of the compounds **9**, **10**, and **11**.

9: ^{1}H NMR (360 MHz, $CDCl_3$): $\delta = 0.88$ (d, 3H, $J = 6.7$ Hz, CH_3CH), 1.02 (d, 3H, $J = 6.7$ Hz, CH_3CH), 1.36 (s, 9H, $(CH_3)_3C$), 1.80 (m, 2H, $CH_2CH_2CH_2$), 1.95, 2.05 (m, je 1H, $CHCH_2CH_2$), 2.05 (m, 1H, $CH(CH_3)_2$), 2.72 (d, 1H, $J = 7.7$ Hz, $CHCH(CH_3)_2$), 3.05, 2.95 (m, each 1H, NCH_2CH_2), 3.55 (dd, 1H, $J = 5.2$, $J' = 8.5$ Hz, $CHCH_2CH_2$), 3.71 (s, 3H, OCH_3), 5.98 (s, 1H, CONH); ^{13}C NMR (90.6 MHz, $CDCl_3$): $\delta = 18.9$ ($CH(CH_3)_2$), 20.3 ($CH(CH_3)_2$), 23.3 ($CHCH_2CH_2$), 28.8 ($(CH_3)_3C$), 28.8 ($CH(CH_3)_2$), 29.7 ($CHCH_2CH_2$), 48.6 (NCH_2CH_2), 51.1 ($(CH_3)_3C$), 51.7 (OCH_3), 62.1 ($CHCH_2CH_2$), 71.7 ($CHCH(CH_3)_2$), 170.5 (CONH), 175.2 (COO); GC-MS (EI, 70 eV): *m/z* (%): 284 (7) [M^+], 184 (100); correct elemental analysis

10: ^{1}H NMR (360 MHz, $CDCl_3$): $\delta = 2.73$ (m, 2H, $CHCH_2$), 2.70 (m, 1H, $CHCH_2$), 3.07 (dd, 1H, $^3J = 4.0$, $^2J = 13.8$ Hz, $CHCH_2$), 3.45 (m, 2H, $CHCO$), 3.65 (s, 3H, CH_3), 3.59 (s, 3H, CH_3), 3.70 (s, 1H, $CHNHCH$), 4.03, 3.92 (dd, each 1H, $^2J = 5.7$, $^3J = 18.0$ Hz, $NHCH_2$), 6.81 (m, 1H, arom.), 6.98 (m, 1H, arom.), 7.1–7.3 (m, 8H, arom.), 7.93 (t, 1H, $J = 5.7$ Hz, $NHCH_2$); ^{13}C NMR (90.6 MHz, $CDCl_3$): $\delta = 38.2$ ($CHCH_2$), 38.9 ($CHCH_2$), 40.9 ($NHCH_2$), 52.0 (CH_3), 52.1 (CH_3), 61.8 ($CHCO$), 62.6 ($CHCO$), 126.7, 126.9, 128.3, 129.0, 129.3, 129.7 (arom.), 170.3 (CONH), 173.7 (CH_2CO), 174.2 ($CHCOO$); GC-MS (CI): *m/z* (%): 399 (100); correct elemental analysis

11: ^{1}H NMR (360 MHz, $CDCl_3$): $\delta = 0.88$ (d, 3H, $J = 6.8$ Hz, $CH(CH_3)_2$), 0.89 (d, 3H, $J = 6.8$ Hz, $CHCH_3)_2$), 1.96 (m, 1H, $J = 6.8$ Hz, $CH(CH_3)_2$), 2.80 (d, 3H, $J = 4.5$ Hz, $NHCH_3$), 3.04 (d, 1H, $J = 5.5$ Hz, $NHCHCH$), 3.41 (t, 1H, $J = 4.8$ Hz, $CHCH_2$), 3.69 (s, 3H, OCH_3), 4.11 (dd, 2H, $J = 4.8$, $J' = 4.4$ Hz, CH_2), 5.67 (d, 1H, $J = 7.7$ Hz, $NCHCHCO$), 7.42 (d, 1H, $J = 7.7$ Hz, $NCHCHCO$), 7.58 (q, 1H, $J = 4.9$ Hz, $CONHCH_3$), 10.4 (br., 1H, CONHCO); ^{13}C NMR (90.6 MHz, $CDCl_3$): $\delta = 18.0$ ($CH(CH_3)_2$), 19.0 ($CH(CH_3)_2$), 26.1 ($NHCH_3$), 31.4 ($CHCH_2$), 51.2 (CH_2), 51.7 (OCH_3), 61.3 ($CHCH_2$), 67.2 ($NHCHCH$), 101.5 ($NCHCHCO$), 146.3 ($NCHCHCO$), 151.8, 164.2 ($CONHCO$), 172.0 (COO), 174.9 (CONH); GC-MS (EI, 70 eV): *m/z* (%): 326 (3) [M^+], 268 (100), 267 (17), 208 (56), 201 (55); correct elemental analysis

Further investigations[8] have shown that the diastereomeric excess can be controlled by temperature and metal catalysts. Apart from alcohols, other classes of compounds such as amines and thiols can react as nucleophiles in U-5C-4CR. Like other

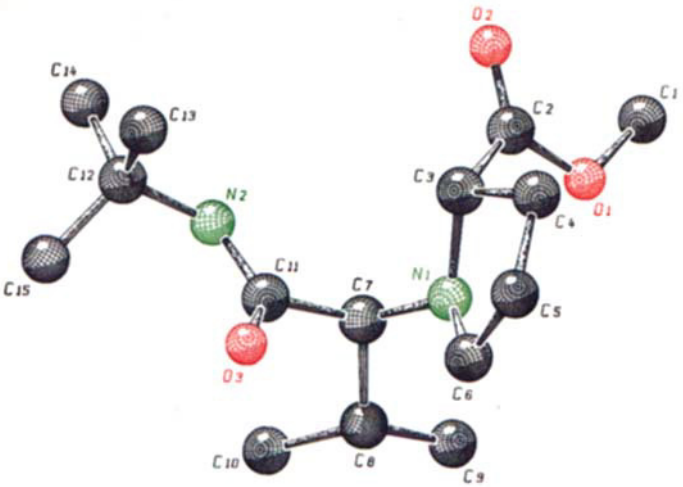

Fig. 1. Crystallographic structure of **9** (SCHAKAL). Selected bond lengths [pm] and angles [°] for molecule A [B]: N1–C3 147.0(2) [145.6(2)], C2–C3 149.0(3) [154.1(2)], C4–C3 157.8(3) [153.1(3)], N1–C7 144.6(2) [145.0(2)], C7–C8 155.0(2) [154.2(2)], C7–C11 153.5(2) [153.2(2)]; N1-C3-C2 114.4(2) [112.1(2)], N1-C3-C4 102.8(2) [103.4(2)], C2-C3-C4 110.0(2) [109.8(2)], N1-C7-C8 111.6(1) [111.6(1)], N1-C7-C11 112.5(1) [111.5(2)], C8-C7-C11 112.2(1) [111.1(1)].

multicomponent reactions, the U-5C-4CR is extremely suitable for generating combinatorial chemical libraries.[9] These findings confirm the authors' opinion that multicomponent reactions in general, and especially the U-4CR, will play a prominent part in research, development, and applications.

Experimental Procedure

The α-amino acid (10 mmol) in methanol (100 mL) was cooled to −30 °C. Then aldehyde and isocyanide (each 10 mmol dissolved in 5 mL methanol) were added. After 3 h the mixture was allowed to warm to room temperature. When the reaction was complete (clear solution, between three hours and two days), the solvent was removed in vacuo. The crude product was virtually free of by-products and often needed no further purification. Small amounts of starting materials could be removed by washing a solution in ether with water. The mixtures of diastereomers were viscous oils or sticky solids. The diastereomers were separated by flash chromatography.

Received: January 25, 1995
Revised version: May 17, 1995 [Z 7659 IE]
German version: *Angew. Chem.* **1996**, *108*, 185–187

Keywords: iminodicarboxylic acids · isocyanides · multicomponent reactions · one-pot reactions

[1] I. Ugi, A. Dömling, W. Hörl, *Endeavour* **1994**, *18*, 115; *GIT Fachz. Lab.* **1994**, *38*, 430.

[2] G. Gokel, G. Lüdke, I. Ugi in *Isonitrile Chemistry* (Ed.: I. Ugi), Academic Press, New York, **1971**, p. 145; I. Ugi, U. Fetzer, C. Steinbrückner, *Angew. Chem.* **1959**, *71*, 386; I. Ugi, S. Lohberger, R. Karl in *Comprehensive Organic Chemistry, Vol. 2* (Eds.: B. M. Trost, I. Fleming, C. H. Heathcock), Pergamon, Oxford, **1991**, pp. 1083–1109.

[3] S. Fushiya, S. Yamada, M. Matsuda, S. Nozoe, *Tetrahedron Lett.* **1994**, *35*, 8201–8204.

[4] J. Tempe, *Chem. Biochem. Amino Acids Pept. Proteins* **1993**, *7*, 134; P. Guyon, M.-D. Chilton, A. Petit, J. Tempe, *Proc. Natl. Acad. Sci. USA* **1980**, *77*, 2693; J. L. Firmin, G. R. Fenwick, *Nature* **1978**, *276*, 842; W. S. Chilton, E. Hood, K. L. Rinehart, M.-D. Chilton, *Phytochemistry* **1985**, *24*, 2945.

[5] C. J. Blankley, J. S. Kaltenbronn, D. E. DeJohn, A. Werner, L. R. Bennett, G. Bobowski, U. Krolls, D. R. Johnson, W. M. Pearlman, M. L. Hoefle, A. D. Essenburg, D. M. Cohen, H. R. Kaplan, *J. Med. Chem.* **1987**, *30*, 992; M. Vincent, G. Rémond, B. Portevin, B. Serkiz, M. Laubie, *Tetrahedron Lett.* **1982**, *23*, 1677; A. Patchett, E. Harris, E. W. Tristram, M. J. Wyvratt, M. T. Wu, D. Taub, E. R. Peterson, T. J. Ikeler, J. ten Broeke, L. G. Payne, D. L. Ondeyka, E. D. Thorsett, W. J. Greenlee, N. S. Lohr, R. D. Hoffsommer, H. Joshua, W. V. Ruyle, J. W. Rothrock, S. D. Aster, A. L. Maycock, F. M. Robinson, R. Hirschmann, C. S. Sweet, E. H. Ulm, D. M. Gross, T. C. Vassil, C. A. Stone, *Nature* **1980**, *288*, 280; R. Bicknell, B. Holmquist, F. S. Lee, M. T. Martin, J. F. Riordan, *Biochemistry* **1987**, *26*, 7291; J. Krapcho, C. Türk, D. W. Cushman, J. R. Powell, J. M. DeForrest, E. R. Spitzmiller, D. S. Karanewsky, M. Duggan, G. Rovnyak, J. Schwartz, S. Natarajan, J. D. Godfrey, D. E. Royono, R. Neubeck, K. S. Atwal, E. W. Petrillo, *J. Med. Chem.* **1988**, *31*, 1148; K. Hayashi, K. Nunami, J. Kato, N. Yoneda, M. Kubo, T. Ochiai, R. Ishida, *ibid.* **1989**, *32*, 289.

 © VCH Verlagsgesellschaft mbH, D-69451 Weinheim, 1996 0570-0833/96/3502-0174 $ 10.00+.25/0

[6] A. Demharter, Dissertation, Technische Universität München, **1992**.
[7] X-ray structural analysis of **9**: $C_{15}H_{28}N_2O_3$, $M_r = 284.4$; monoclinic, $P2_1$ (No. 4); $a = 984.4(1)$, $b = 1000.9(1)$, $c = 1836.1(1)$ pm, $\beta = 104.57(1)$, (25 reflections at high diffraction angles, $2\theta_{min/max} = 79.8/95.7$); $V = 1751 \cdot 10^6$ pm^3; $Z = 4$; $\rho_{calcd} = 1.079$ g cm^{-3}; $F(000) = 624$; CAD4, $Cu_{K\alpha}$ radiation, $\lambda = 154.184$ pm; $\mu = 5.7$ cm^{-1}; $\theta/2\theta$ scan, $1.0 < \theta < 70.0$; $t_{max} = 90$ s. 4621 intensities were collected at $T = (293 \pm 1)$ K. After the LP-correction and the correction for a slight decomposition (106.5 h, −7.7%), 3945 independent reflections remained after averaging. The structure was determined by direct methods. All heavy atoms with anisotropic reflections were refined. The positions of the hydrogen atoms were calculated for ideal geometry and were included in the structure factor calculation. The calculations converge at $R = 0.063$ and $R_w = 0.062$ for all reflections ($I > 0.0$) and 361 variables. A subsequent differential Fourier synthesis showed no anomalies ($e_{min/max} = +0.25/-0.24$ e Å^{-3}). The absolute configuration at C7 was derived from the known configuration at C3. Further details of the crystal structure determination are available on request from the Director of the Cambridge Crystallographic Centre, 12 Union Road, GB-Cambridge CB2 1EZ, on quoting the full journal citation.
[8] W. Hörl, I. Ugi, still unpublished.
[9] I. Ugi, A. Dömling, B. Gruber, M. Heilingbrunner, C. Heiß, W. Hörl, in *Software-Entwicklung in der Chemie 9* (Ed.: R. Moll), Gesellschaft Deutscher Chemiker, Frankfurt, **1995**; I. Ugi, *Proc. Estonian Acad. Sci. Chem.* **1995**, *44*, 237.

Structure and Dynamics of Methanol in a Zeolite**

Ernst Nusterer, Peter E. Blöchl* and Karlheinz Schwarz*

The petrochemical industry relies heavily on zeolite catalysts for petroleum refinement and production of fine chemicals. About 80% of the gasoline currently produced has been in contact with zeolites in the refinement process. Furthermore, zeolites are used during the industrial production of gasoline from methanol, a process by which, for example, about 30% of New Zealand's gas supply is produced. Zeolites are a class of aluminum silicates with large cavities (cages) linked by pores. Only small molecules with certain structural properties can pass through these pores. Acid sites distributed over the large internal surface activate chemical bonds and thus are responsible for zeolites' catalytic function. The acid sites in zeolites typically are AlOH groups that replace SiO fragments in the crystal lattice. The interaction of molecules such as methanol with acid sites is little understood, although it is the key to the catalytic function of most zeolites.

The most direct experimental clues to the mechanisms on a microscopic level come from IR spectroscopy.[1, 2] The interpretation of the IR spectra measured for methanol in a zeolite[2-4] is, however, still a subject of hot debate. Proposals range from absorption of methanol through a weak hydrogen bond with an acid site to fully protonated methanol in the zeolite. The most direct way to correlate measured IR spectra with atomic structures is to compare the experimental results with the results of quantum mechanical simulations. So far, however, the latter are in clear disagreement with the experimental spectra.[5-8] One of the major deficiencies of previous quantum chemical calculations has been the limitation to fairly small fragments of the zeolite crystal.

For this reason we have undertaken dynamic ab initio electronic structure simulations to elucidate the structures and vibrational spectra of methanol trapped in sodalite (Fig. 1). We considered the entire periodic zeolite crystal as it interacts at finite temperature with an adsorbed methanol molecule. Thus we determined the adsorption structures and calculated vibrational spectra, which reproduce the measured IR spectra.

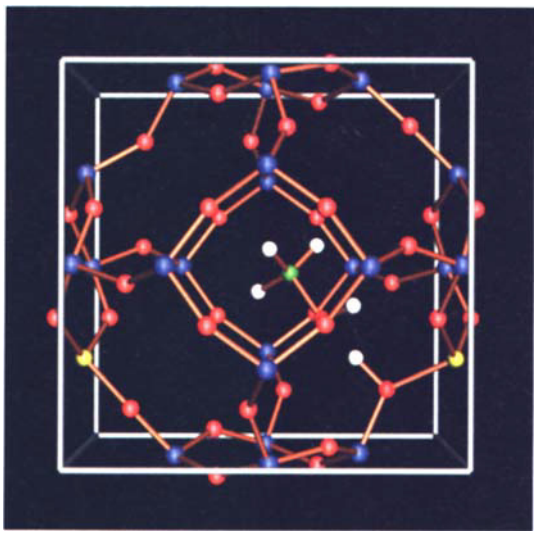

Fig. 1. One unit cell of the silica-rich sodalite (Si = blue, O = red, Al = yellow, H = white) used for the present study is included in the silver box. To complete the sodalite cage, periodic representations of the atoms located near the border of the unit cell are also shown.

Our calculations are based on the density functional theory,[9] including gradient corrections for exchange and correlation,[10, 11] on the ab initio molecular dynamics approach of Car and Parrinello,[12] and on the projector augmented-wave (PAW) method.[13, 14] The accuracy of this approach is comparable to that of correlated quantum mechanical MP2 calculations, but it also takes dynamic effects and finite temperatures into account.

First we examined an isolated acid site (periodically repeated in every other sodalite cage, Fig. 1) in a silicon-rich sodalite[15] as it interacts with methanol. This aluminum-poor zeolite has a silicon-to-aluminum ratio of 11:1. The internal surface is covered with one methanol molecule per acid site. Later we will describe how the resulting picture changes for aluminum-rich zeolites.

For this aluminum-poor sodalite we performed a molecular dyamics simulation for 11 ps at 400 K. The methanol molecule assumes a series of configurations, which we optimized separately to obtain the ground-state structures. Two structure types, **A** and **B** in Figure 2, were observed. In both structures one very strong hydrogen bond exists between the methanol oxygen atom O_m and the proton H_a of the acid site. This hydro-

[*] Prof. Dr. K. Schwarz, E. Nusterer
Technische Universität Wien
Getreidemarkt 9/158
A-1060 Wien (Austria)
Fax: Int. code +(1)586-8937
e-mail: kschwarz@email.tuwien.ac.at
Dr. P. E. Blöchl
IBM Research Division, Zurich Research Laboratory
CH-8803 Rüschlikon (Switzerland)
Fax: Int. code + (1) 724-0809
e-mail: blo@zurich.ibm.com.

[**] We thank the IBM T. J. Watson Research Center for providing access to its SP parallel computers. We are particularly grateful to Dr. G. Eder-Mirth and Dr. A. Kogelbauer for interesting discussions, and thank G. Eder-Mirth for sharing unpublished results. This work was supported by grants from the Swiss Federal Office for Education and Science and the Austrian Science Foundation FWF (grants P9213 and 10842).

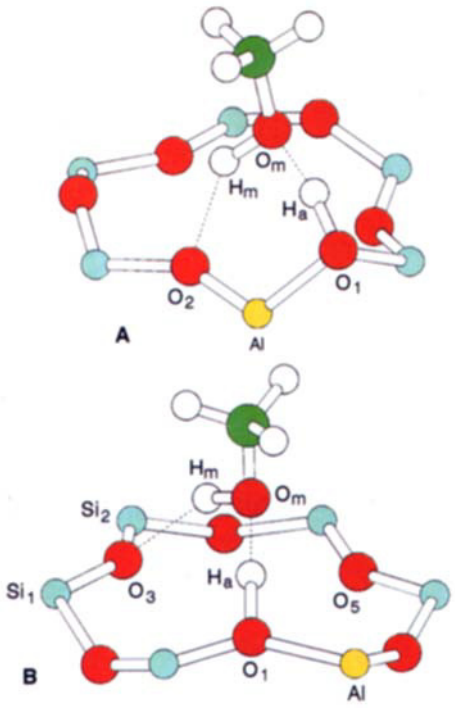

Fig. 2. Schematic drawing of structures **A** (top) and **B** (bottom) showing the adsorption of methanol in sodalite. Only a fragment of sodalite is shown: a ring containing one aluminum and five silicon atoms as well as the corresponding oxygen bridges. The dashed lines indicate hydrogen bonds. For further explanations see text.

gen bond with an O–O distance of 2.4 Å is substantially shorter than a typical hydrogen bond in water (O–O distance = 2.9 Å). It remained intact during our entire simulation. A second hydrogen bond with an O–O distance of 2.7 Å in **A** and 2.9 Å in **B**, similar to the hydrogen bond in water, is formed between the methanol hydrogen atom H_m and various framework oxygen atoms leading to the structures **A** and **B**. At finite temperatures this hydrogen bond breaks and forms again with different framework oxygen atoms. Structure type **B**, of which two virtually identical versions exist, is proposed here for the first time. In previous calculations the zeolite fragments were too small to include this structure, in which the weaker hydrogen bond forms with a framework oxygen atom that is—though located close to the acid site—several bonds away from the acid site. We find that structure **B** is slightly ($\approx 10\ kJ\,mol^{-1}$) more stable than structure **A**.

The crucial test of our structural models is whether our simulation also reproduces the measured IR spectra. The difference vibrational spectra (with and without methanol adsorbed on various zeolites) exhibit four broad characteristic peaks at about 3500, 2900, 2400, and 1700 cm^{-1}.[4] Our simulated spectra are obtained from a histogram of the instantaneous hydrogen stretching vibrations. This instantaneous frequency is obtained directly as $\omega = \pi/\tau$ from the period τ between two consecutive zeros of the hydrogen bond stretching velocity. We have chosen this approach to account for anharmonicities of the system, which result in relatively short lifetimes of the vibrational modes. It should be kept in mind that this procedure works well only for hydrogen stretching vibrations having frequencies clearly separated from those of other modes. This approach predicts the O–H stretching frequency of the isolated acid site (3570 cm^{-1}), in good agreement with experiment (3620 cm^{-1}), while the O–H stretching frequency of isolated methanol is underestimated by 3%.

Our simulated vibrational spectra of methanol in sodalite are shown in Figure 3. Our assignment presented below is consistent with experimental evidence.

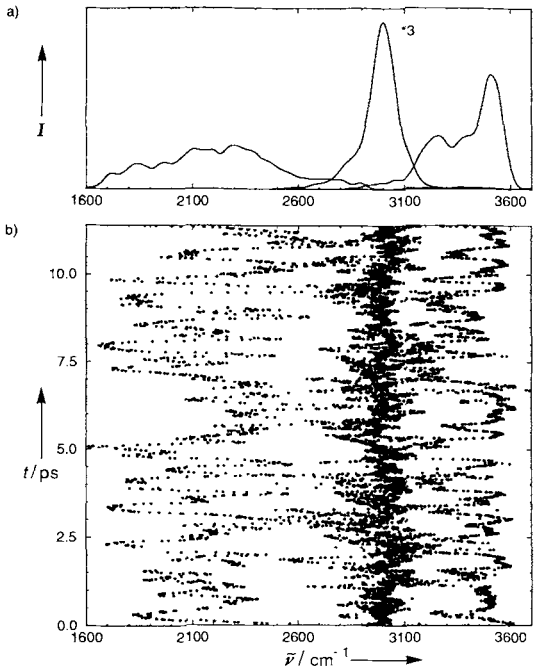

Fig. 3 a) Density of vibrational states I obtained by monitoring the proton stretching frequencies $\tilde{\nu}$ and b) their time evolution $\tilde{\nu}(t)$ during the simulation. In the upper panel the peak at 3500 cm^{-1} corresponds to the O–H stretch of the methanol proton H_m; the band at 3000 cm^{-1} is due to the C–H stretching vibrations of the methyl group; and the lowest band between 2600 cm^{-1} and 1600 cm^{-1} is caused by the O–H stretching vibrations of the acid-site proton H_a.

1) We assign the simulated peak at 3500 cm^{-1} to the methanol O–H stretching vibration (O_m–H_m) at 3300–3600 cm^{-1} in contrast to other assignments involving acid site protons.[4] This peak has also been observed in alkali forms of zeolites,[1] which lack acid sites. There only "normal" hydrogen bonds between the methanol hydrogen and framework oxygens are possible, which are similar to our "weak" hydrogen bond. Hence, our findings conclusively exclude any major contribution from the acid-site proton to this peak.

2) The C–H stretching vibrations are located in the simulated spectrum at 2800–3100 cm^{-1} and are broadened to a width of 200–300 cm^{-1} by weak interactions with the zeolite framework. As shown by recent experiments of Eder-Mirth, they disappear when the methyl group is deuterated. Hence these modes must be C–H vibrations, which are shifted towards lower frequencies when deuterated.

3) The O–H stretching vibration predicted for the acid-site hydrogen forms a very broad band from 1600 to 2600 cm^{-1} and corresponds to the measured broad peaks at about 2400 cm^{-1} and 1690 cm^{-1}. The latter peaks are not found in the alkali forms of the zeolites,[1] in accordance with our interpretation that these modes originate from vibrations of the acid-site proton interacting with the adsorbed methanol. A band for a combination mode of the zeolite lattice near 2000 cm^{-1} decreases upon adsorption and thus may suppress the center of the simulated broad peak and lead to a pseudo double peak in the experimental difference spectra.

In our simulations we observed a correlation between the O–H stretching frequency and the length of the hydrogen bond,

 © VCH Verlagsgesellschaft mbH, D-69451 Weinheim, 1996 0570-0833/96/3502-0176 $ 10.00+.25/0

which allows structural information to be deduced from a measured vibrational spectrum. Strong hydrogen bonds with short O–O distances correlate with long, weakened O–H covalent bonds and low hydrogen stretching vibrations. If the O–O distance is increased, the length of the covalent bond approaches its unperturbed value approximately exponentially; the O–H stretching vibration increases almost linearly as the length of the covalent bond decreases. Aluminum-rich zeolites differ from their aluminum-poor counterparts both in their IR spectra and in their reactivity.[4, 16] In particular, the highest peak at 3500 cm^{-1} seems to vanish as the Si:Al ratio approaches its lower limit of 1:1. Therefore we investigated the interaction of methanol with two acid sites simultaneously. We find that the hydrogen bond between the methanol proton H_m and an oxygen adjacent to another aluminum atom is shortened by about 5% and is therefore stronger than the hydrogen bond formed with an isolated acid site. Preliminary molecular dynamics simulations of 1 ps reveal a downward shift of the H_m–O vibration (located at 3500 cm^{-1} for the methanol hydroxyl group adsorbed on an isolated acid site) of roughly 400 cm^{-1}, which could explain the disappearance of the former absorption band. However, it should be noted that aluminum-rich zeolites exhibit a substantially richer variety of structures for acid-site centers and adsorption complexes than aluminum-poor zeolites, a fact that has not yet been explored exhaustively.

We studied sodalite to unravel processes that should also be relevant for the more complex zeolites actually used in technologically relevant processes. Therefore we should discuss to what extent our results apply to zeolites other than sodalite. We expect that the essential features of structure **A** are rather independent of the zeolite, as the tetrahedral angle on the Si and Al atoms is largely conserved. Structure **B**, however, depends strongly on the local structure. Since it depends on the proximity of distant oxygen atoms, this structure can only occur in sufficiently small or highly deformed larger rings. Rings consisting of four atoms with tetrahedral coordination cannot be bridged, because the acid-site protons point outward. Since the structures **A** and **B** have similar vibrational patterns, we expect only quantitative changes in the IR spectra for zeolites that cannot form structure **B**. The largest deviations in the IR spectra will occur in the lower part (see Fig. 3), because this part is most sensitive to the strength of bond of the acid-site proton.

Our computer experiments predicted adsorption structures of methanol in zeolites which, for the first time, are consistent with the available experimental data. This information forms the basis for the understanding of a large class of zeolite-catalyzed reactions. We have applied a theoretical approach to zeolite chemistry, which allows us to study with a high level of accuracy dynamic behavior of molecules in zeolites at finite temperatures without the limitation of small zeolite fragments. Real-time simulations of chemical reactions in zeolites are currently in progress.

Received: May 11, 1995
Revised version: August 11, 1995 [Z 7977 IE]
German version: *Angew. Chem.* **1996**, *108*, 187–189

Keywords: ab initio calculations · hydrogen bonds · methanol · molecular dynamics · zeolites

[1] G. Mirth, J. A. Lercher, M. W. Anderson, J. Klinowski, *J. Chem. Soc. Faraday Trans.* **1990**, *86*, 3039–3044.
[2] A. Ison, R. J. Gorte, *J. Catal.* **1984**, *89*, 150–158.
[3] A. G. Pelmenschikov, R. A. van Santen, J. H. M. C. Wolput, J. Jänchen, *Stud. Surf. Sci Catal.* **1994**, *84*, 2179–2186.
[4] G. Mirth, A. Kogelbauer, J. A. Lercher, *Proc. 9th Int. Zeolite Conf. Montreal, Canada, 1992, Vol. II* (Eds.: R. von Ballmoos, J. B. Higgins, M. M. J. Treacy), Butterworth-Heinemann, Boston, **1993**, pp. 251–258.
[5] J. Sauer, H. Horn, M. Häser, R. Ahlrichs *Chem. Phys. Lett.* **1990**, *173*, 26–32.
[6] J. Sauer, *Stud. Surf. Sci. Catal.* **1994**, *84*, 2039–2057.
[7] S. Bates, J. Dwyer, *J. Mol. Struct.* (THEOCHEM) **1994**, *306*, 57–65.
[8] R. A. van Santen, *Stud. Surf. Sci. Catal.* **1994**, *85*, 273–294.
[9] W. Kohn, L. J. Sham, *Phys. Rev.* **1965**, *140*, A1133–A1138.
[10] J. P. Perdew, *Phys. Rev. B* **1986**, *33*, 8822–8824.
[11] A. D. Becke, *J. Chem. Phys.* **1992**, *96*, 2155–2160.
[12] R. Car, M. Parrinello, *Phys. Rev. Lett.* **1985**, *55*, 2471–2474.
[13] P. E. Blöchl, *Phys. Rev. B* **1994**, *50*, 17953–17979.
[14] A representative application in which the PAW method was used to calculate the vibrational modes of ferrocene can be found in: P. Margl, K. Schwarz, P. E. Blöchl, *J. Chem. Phys.* **1994**, *100*, 8194–8203.
[15] D. M. Bibby, M. P. Dale, *Nature* **1985**, *317*, 157–158.
[16] A. Kogelbauer, A. A. Nikolopoulos, J. G. Goodwin, Jr., G. Marcelin, *J. Catal.* **1995**, *152*, 122–123.

Single-Chain Polyprenyl Phosphates Form "Primitive" Membranes

Gianluca Pozzi, Véronique Birault, Birgit Werner, Olivier Dannenmuller, Yoichi Nakatani, Guy Ourisson,* and Susumu Terakawa*

Terpenoid components are ubiquitous and very varied in biological membranes (archeal lipids, hopanoids, carotenoids, sterols, dolichols, ubiquinones, etc.). We showed that the structures of various molecular fossils (sedimentary biomarkers), considered along with known biosynthetic mechanisms, permit the deduction of the structures of their precusors, which often appear to be still undiscovered membrane terpenoid lipids. We have thus been led to the conclusion that the universal role of this class of natural products in all living organisms has been in membrane formation or reinforcement.[1]

We also showed that all these demonstrated or postulated membrane terpenoids can be arranged in a hypothetical evolutionary sequence and proposed that the most primitive members of such a group of substances involved in one common biological function should be sought among those accessible by the simplest possible "azymatic" reactions, that is, reactions not requiring enzymes.[2] This led us to postulate that the most primitive membrane constituents may have been some acyclic polyprenoid phosphates, whose chains are an adequate length

[*] Prof. G. Ourisson
Centre de Neurochimie CNRS
Laboratoire de Chimie Organique des Substances Naturelles
Université Louis Pasteur, 5 rue Blaise Pascal, F-67084 Strasbourg (France)
Fax: Int. code +88-60-7620
Dr. G. Pozzi
Centro C. N. R. Sintesi e Stereochimica Speciali Sistemi Organici, Milano (Italy)
V. Birault, O. Dannenmuller, Prof. Y. Nakatani
Université Louis Pasteur, Strasbourg
Dr. B. Werner
Organisch-chemisches Institut der Technischen Universität München (Germany)
Prof. S. Terakawa
Hamamatsu University School of Medicine, Photon Medical Research Center, Hamamatsu (Japan)

[**] Prebiomimetic Chemistry, Part 3 (Part 1: Ref. [3]; Part 2: M. Keller, D. Hafenbradl, K. O. Stetter, G. Teller, Y. Nakatani, G. Ourisson, *Angew. Chem.*, **1995**, *107*, 2015–2017; *Angew. Chem. Int. Ed. Engl.*, **1995**, *34*, 1898–1900). This work was supported by the Centre National de la Recherche Scientifique and the Université Louis Pasteur as part of the ULP/Research Development Corporation of Japan "Supermolecules" Programme. G. P. thanks CNRS and the Académie des Sciences (Marion-Merrell-Dow/ULP Fellowship), B. W. the CNRS and the Alexander-von-Humboldt Stiftung (Lynen Fellowship), and V. B. Rhône-Poulenc-Rorer for post-doctoral fellowships.

to achieve the amphipathic ratio required for spontaneous vesicle formation: these phosphates could have been formed by essentially one synthetic reaction, of the general type (a).

$$C^+ + C{=}C \longrightarrow C{-}C{-}C^+ \qquad (a)$$

We had synthesized a series of dipolyprenyl phosphates and had shown that their salts indeed formed vesicles (revealed by electron microscopy and encapsulation of dyes); this was the case for sodium digeranylphosphate (**1**) and its higher isoprenologs with two C_{15} or C_{20} chains.[3] On water, the same dipolyprenyl phosphates give monolayers, which, like those of di-*n*-acylphospholipids, become denser on the addition of cholesterol or of hopanoids.[4] It has also been shown that addition of diphytanyl phosphate (mixture of (*R*,*S*) diastereomers) improves the barrier properties of vesicles of dipalmitoylphosphatidylcholine.[5]

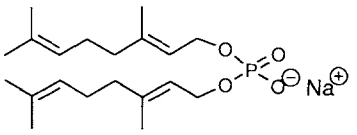

1

We wondered whether, like some fatty acids[6] and many other single-chain amphiphiles,[7] monopolyprenyl phosphates and/or pyrophosphates would not also be able to self-assemble into bilayer structures, in particular closed vesicles. These phosphates and the corresponding pyrophosphates have been described as intermediates in the biosynthesis of polyterpenoids,[8] but their phase behavior has not been studied, except for the brief mention that (uncharacterized) "micelles" might be formed in slightly acidic water dispersions of ammonium salts of monofarnesyl phosphate.[9] It has also been shown that phytanyltrimethylammonium phytanylphosphate (**7**) did form stable vesicles, albeit of a particular type in which cationic and anionic head-groups are located on identical lipophilic chains.[10] If the sodium salts of monopolyprenyl phosphates were to form vesicles, this would not only enable us to go one step backwards towards simpler, potentially more primitive membranes than the dipolyprenyl phosphates, but it would also be an experimental confirmation of part of the hypotheses presented by Wächtershäuser, in the completely different framework of his theory of a "pyrite-pulled" chemoautotrophic origin of life, for the formation of polyterpenoid membranes.[11] That these phosphates could indeed have interesting phase properties was suggested by the well-known uses of long-chain alkyl phosphates as industrial surfactants, though they have mostly been described as forming micelles, not closed vesicles.[12]

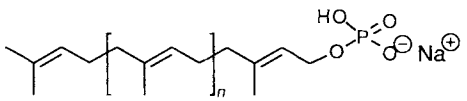

2 : $n = 0$
3 : $n = 1$
4 : $n = 2$

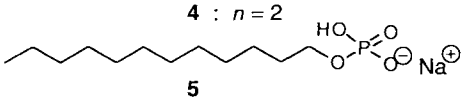

5

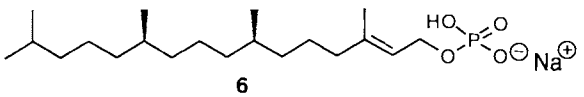

6

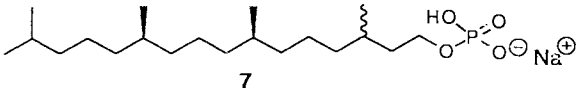

7

For the preparation of the phosphates derived from the unsaturated polyprenyl chains, one can, of course, not use hydrogenolysis of diphenyl phosphates, as had been described for the first clean preparation of long-chain *n*-alkyl phosphates.[13] We have now synthesized a series of monopolyprenyl phosphates—those of geraniol (**2**), farnesol (**3**), geranylgeraniol (**4**), dodecanol (**5**, for comparison), phytol (**6**), and (3*R*,3*S*)-phytanol (**7**)—as their sodium or ammonium salts, by the Cramer phosphorylation procedure adapted by Danilov et al.,[14] and isolated the products from the reaction mixture as the cyclohexylammonium salts, as reported by Julia et al.[15] For the pyrophosphates of geraniol (**8**), farnesol (**9**), geranylgeraniol (**10**), phytol (**11**), and phytanol (**12**), we used the fast synthetic

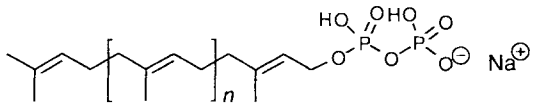

8 : $n = 0$
9 : $n = 1$
10 : $n = 2$

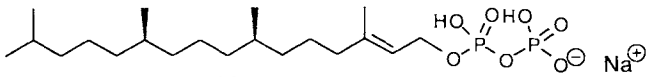

11

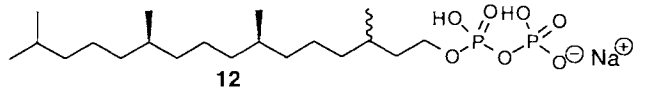

12

method of Keller and Thompson.[16] These pyrophosphates could again be used to obtain the phosphates by controlled hydrolysis. After cation exchange to obtain the sodium or ammonium salts, the products, visualized as single spots on TLC, were characterized by their potentiometric curves (pK_{a_1} 3.2–3.3, pK_{a_2} 6.6–6.7 for the phosphates; for the pyrophosphates, hydrolysis occurred during titration, and the pK_a's observed corresponded to the phosphate) and their ^1H and ^{31}P NMR spectra. Suspensions in water were examined by electron microscopy (cryomicroscopy), and their formation from the solid phosphates in the presence of a series of buffers was followed by two types of optical microscopy: by differential interference contrast microscopy, or by confocal microscopy, both of which can only reveal "giant" vesicles.

Table 1 summarizes the results obtained. Compounds **2** and **8**, with only the C_{10} chain of geraniol, were apparently completely

Table 1. Obtention of closed vesicles (see Experimental Procedure) [a].

Substance	Electron microscopy	Optical microscopy	pH or pH range
2	n.t.	– (soluble in water)	
3	+	– (vesicles too small)	
4	+	+	2–8
5	n.t.	+	3–10
6	n.t.	+	3–9
7	n.t.	+	2.5–12.5
8	n.t.	– (soluble in water)	
9	n.t.	+	1.5
10	n.t.	+	2
11	n.t.	+	2–10
12	n.t.	+	2.5

[a] n.t.: not tested; +: vesicle formation; –: no vesicle formation (empty field); pH tested, or range of pH buffers leading to vesicle formation.

 © VCH Verlagsgesellschaft mbH, D-69451 Weinheim, 1996 0570-0833/96/3502-0178 $ 10.00+.25/0

soluble in water across the whole pH range. No giant vesicle of farnesyl phosphate could be seen by optical microscopy, though electron microscopy did show the presence of small vesicles. All the other phosphates and pyrophosphates formed giant vesicles (diameter larger than 10 μm, Fig. 1) on simple contact of the

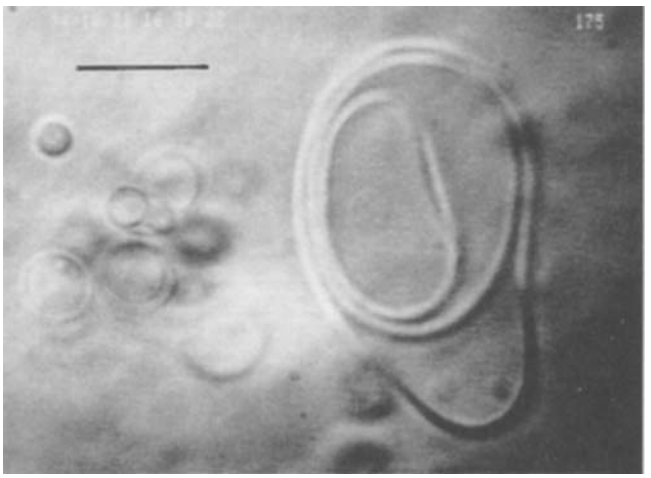

Fig. 1. Copy of a video frame of the differential interference contrast image of a multivesicular structure of sodium geranylgeranylphosphate in a buffer at pH 4.1 and 23 °C. The bar represents 5 μm.

solid with an appropriate buffer. They were observed to bud from the solid by a variety of processes: formation of warts, growing until they detached as closed vesicles from the surface of the solid, or formation of tubules, the distal end of which progressively grew into an intumescence, then into a bubble, and finally into a free vesicle. The best conditions for observation of the giant vesicles were at about pH 4 in an acetate or phthalate buffer. Hydrolysis of the pyrophosphates, however, appeared to occur within a few minutes. We must also note that our setups do not allow us to vary the temperature, which was in all cases about 23 °C. This appears to be above the transition temperature of these polyprenylphosphates anyway; it should be remembered that branchings on the lipophilic chains appear to lower the phase transition temperature enough to make it impossible to measure, if one generalizes from the case of archeal lipids.[17]

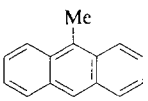

13

We also added 5% of the fluorescent hydrocarbon 9-methylanthracene (**13**, Nile Red) to the vesicle preparation and used the laser equipment of the confocal microscope to observe the fluorescence of the vesicle preparation after excitation at $\lambda = 485$ and 551 nm in the *xz* and *xy* planes (Fig. 2). This demonstrated that at least some of the vesicles were quasi-spherical, and formed by one lipophilic layer (emitting in the green in the first case and in the red in the second); furthermore it established directly that lipophilic molecules are selectively extracted into the vesicle bilayer, as expected, a fact of some importance in the discussion of the establishment of increasing complexity in self-organized systems.[2]

It is obvious that **2**–**4** (or **8**–**10**) are much more plausible primitive membrane constituents than the *n*-alkyl amphiphiles or the meteoritic mixtures of aromatic acids previously postulated for that role.[18] We are presently studying the properties of these novel vesicles (in particular to elucidate the importance of

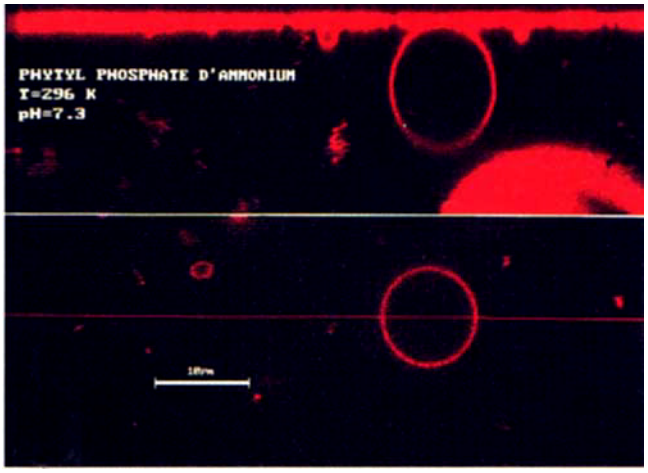

Fig. 2. Confocal fluorescence images of a vesicle of ammonium phytylphosphate containing 5% Nile Red (**13**) grown from the solid, in a buffer at pH 7.3 and 23 °C. Wavelength of excitation light: 551 nm. The same vesicle is seen in two orthogonal sections, the *xy* and *xz* planes. The bar represents 10 μm.

the chain-branchings and unsaturation, which are not yet clear at all), as well as their formation under the prebiomimetic conditions suggested earlier.[2, 11]

Experimental Procedure

Differential interference contrast microscopy: Inverted microscope (Axiovert 135, 63x/1.40 Plan Achromat Oil DIC objective, × 2.5 insertion lens, Carl Zeiss), charge-coupled device (CCD) camera (C2400-75i, Hamamatsu Photonics), image processor (Argus-20, Hamamatsu Photonics), S-VHS video recorder (SVO-9500MDP, Sony), video monitor (PVM-1443, Sony), and video printer VP-1500, Seikosha).

Confocal microscopy: Inverted confocal microscope (LSM Invert 410, Plan Apo X63 objective, Carl Zeiss), laser sources Ar (488 nm, bandpass 515–565 filter) and He/Ne (543 nm, Longpass 595 filter), image processor (Matrox 4MW), PC 486-488PX microcomputer, color monitor (FT 3420 ETKL, Mitsubishi), printer (VP-1800 EPM, Sony), and digital image recorder (Focus).

Observations: A typical procedure was as follows: the phosphate (3 mg) was dissolved in 300 mL of a 2:1 mixture of chloroform and methanol. An aliquot (1.5 mL) of the solution was dropped on a coverglass (0.17 mm thick). After 10 min of drying, the lamellar solid remaining on the slide was brought into focus and 4.5 mL of a buffer (for example an acetate buffer, pH 4.1) at 25 °C was added. Vesicles were observed to grow from the edges of the solid. Besides multilamellar structures shown in the figure, unilamellar vesicles and tubules were also observed. The membranes appear to be thick because of the diffraction-limited resolution of the optical system.

Received: January 26, 1995
Revised version: August 2, 1995 [Z 7663 IE]
German version: *Angew. Chem.* **1996**, *108*, 190–192

Keywords: membranes · microscopy · polyprenyl phosphates · prebiotic chemistry · vesicles

[1] G. Ourisson, *Pure Appl. Chem.* **1990**, *62*, 1401–1404.
[2] G. Ourisson, M. Rohmer, K. Poralla, *Ann. Rev. Microbiol.* **1987**, *41*, 301–333; G. Ourisson, Y. Nakatani, *Chem. Biol.* **1994**, *1*, 11–23; G. Ourisson in *Early Life on Earth. Nobel Symp. Nr 84* (Ed.: S. Bengtson), Columbia University Press, New York, **1994**, pp. 259–269.
[3] N. Plobeck, S. Eifler, A. Brisson, Y. Nakatani, G. Ourisson, *Tetrahedron Lett.* **1992**, *33*, 5249–5252.
[4] A. Kamino, K. Ariga, T. Kunitake, V. Birault, G. Pozzi, Y. Nakatani, G. Ourisson, *Coll. Surf. A*, **1995**, *103*, 183–194.
[5] N. Nishikawa, H. Mori, M. Ono, *Chem. Lett.* **1994**, 767–770.
[6] J. M. Gebicki, M. Hicks, *Nature* **1973**, *243*, 232–233; W. R. Hargreaves, D. W. Deamer, *Biochemistry* **1978**, *17*, 3759–3768; D. P. Cistola, J. A. Hamilton, D. Jackson, D. M. Small, *ibid.* **1988**, *27*, 1881–1888.
[7] T. Kunitake, *Angew. Chem.* **1992**, *104*, 692–710; *Angew. Chem. Int. Ed. Engl.* **1992**, *31*, 709–726.
[8] S. L. Spurgeon, J. W. Porter, *Biosynth. Isoprenoid Compd.* **1981**, *1*, 1–46.
[9] E. F. Brody, C. D. Gutsche, *Tetrahedron* **1977**, *33*, 723–729.

 © VCH Verlagsgesellschaft mbH, D-69451 Weinheim, 1996 0570-0833/96/3502-0179 $ 10.00+.25/0

[10] K. Yamauchi, Y. Yoshida, T. Moriya, K. Togawa, M. Kinoshita, *Biochim. Biophys. Acta* **1994**, *1193*, 41–47.
[11] G. Wächtershäuser, *Microbiol. Rev.* **1988**, *52*, 452–484.
[12] A. A. Ruzza, M. R. K. Walter, F. Nome, D. Zanette, *J. Phys. Chem.* **1992**, *96*, 1463–1467, and references therein; J. H. Fendler, *Membrane Mimetic Chemistry*, Wiley, New York, **1982**; T. Tahara, I. Satake, R. Matuura, *Bull. Chem. Soc. Jpn.* **1969**, *42*, 1201–1205.
[13] D. A. Brown, T. Malkin, G. K. Maliphant, *J. Chem. Soc.* **1955**, 1584, 1588.
[14] L. L. Danilov, T. N. Druzhinina, N. A. Kalinchuk, V. N. Maltsev, V. N. Shibaev, *Chem. Phys. Lipids* **1989**, *51*, 191–203.
[15] M. Julia, H. Mestdagh, C. Rolando, *Tetrahedron* **1986**, *42*, 3841–3849.
[16] R. K. Keller, R. Thompson, *J. Chromatogr.* **1993**, *645*, 161–167.
[17] D. Blöcher, R. Gutermann, B. Henkel, K. Ring, *Biochim. Biophys. Acta* **1984**, *778*, 74–80; D. Blöcher, L. Six, R. Gutermann, B. Henkel, K. Ring, *ibid.* **1985**, *818*, 333–334.
[18] D. W. Deamer, E. Harang Mahon, G. Bosco in *Early Life on Earth, Nobel Symp. Nr 84*, (Ed.: S. Bengtson), Columbia University Press, New York **1994**, pp. 107–123.

Shape-Selective Catalysis with Microporous Amorphous Mixed Oxides**

Wilhelm F. Maier,* Johan A. Martens, Stephan Klein, Jens Heilmann, Rudy Parton, Karen Vercruysse, and Pierre A. Jacobs

The increasing demand on new chemical processes has led to a growing need for more selective catalysts. Selectivity based on the hindered diffusion of larger molecules in micropores, so-called shape selectivity, is the key to the success of zeolites;[1] however, fundamental limitations restrict the general applicability of these highly porous crystalline solids. The stable isomorphic substitution of elements other than alumina in the silica matrix of catalytically active zeolite structures is limited to a few elements and small contents. The pore size and pore architecture are not variable and can only be selected from the many known structures. Thus, there is a demand for alternative materials with shape-selective catalytic properties.

We have shown recently that amorphous microporous silica, titania, zirconia, and alumina with a narrow pore size distribution can be synthesized in the absence of organic templating agents by a specific sol–gel process.[2] These microporous materials form only under acid-catalyzed sol–gel conditions. Rheological studies show a simultaneous increase in the elasticity and viscosity under these sol–gel conditions, indicative of a linear chain growth in the polycondensation process.[3] We are convinced that the release of organic products during the slow and careful drying on these glasses is responsible for the pore size and porosity of the final products. We have now succeeded with this sol–gel process in synthesizing homogeneous microporous amorphous mixed metal oxides with narrow pore size distribution and high porosity.[4] These materials will be denoted in the following as amorphous microporous mixed oxides AMM-M_xSi, in which Si stands for silica as a base oxide and x for the atom% of the additional oxide M.

The porosity of the calcined materials was characterized by nitrogen and argon adsorption/desorption isotherms. All glasses show type I isotherms,[5] characteristic of purely microporous materials (Fig. 1). Table 1 shows the BET surface and pore diameter of the materials. The micropore distribution, determined by using the Horvath–Kawazoe method,[6] is monomodal and very narrow, comparable with the pore size distribution of zeolites. The effective pore diameters are between 0.65 and 0.77 nm, which is the range also found for large-pore 12-ring zeolites. The amorphous state of the AMM materials was identified by temperature-dependent X-ray diffraction, high-resolution transmission electron microscopy (TEM), and electron diffraction. X-ray analysis of selected areas of various sizes (from 1 μm to 2 nm) revealed that the materials have a homogeneous mixed oxide composition and that domain formation is absent. Figure 2 shows a representative micrograph of the AMM-$Ti_{17}Si$ glass. IR studies of the AMM-Ti_xSi materials by diffuse reflectance exhibit the Si-O-Ti band at 960 cm^{-1}, which is indicative of isomorphic Ti substitution in the TS zeolites. The observation of this band is only meaningful, when the presence of surface SiOH vibrations in the investigated spectral region has been excluded by in situ temperature treatment of the mixed oxides.

Transmission IR spectra of adsorbed pyridine show similar intensities for the V- and Ti-containing glasses at 1540 cm^{-1}, indicative of Brønsted acidity. With increasing Ti or V content the absorption signals associated with Lewis and Brønsted acidity increase. A similar correlation between acidity and titanium content was observed in other amorphous titanium silicates,

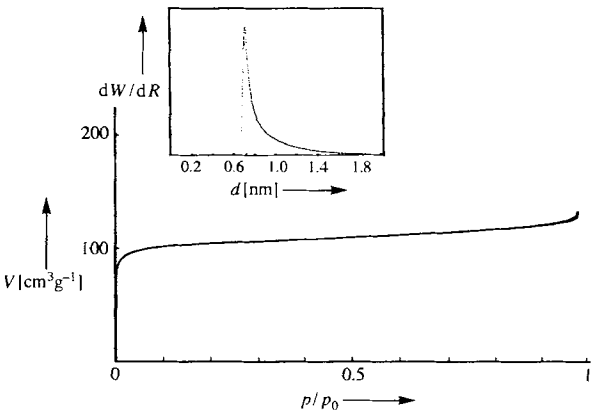

Fig. 1. N_2 adsorption isotherm at 77 K of AMMTi_3Si. V = adsorbed volume; insert: pore size distribution, d = effective pore diameter.

Table 1. BET surface and pore diameter of the AMM glasses. The pore diameters have been calculated by the HK method [a].

Mixed metal oxide	BET surface [$m^2 g^{-1}$]	Pore diameter [nm]
AMM-Ti_3Si	523	0.73
AMM-$Ti_{17}Si$	395	0.76
AMM-$V_{10}Si$	480	0.62

[a] The standard parameters of the Omnisorb-software have been used for the pore size calculation. In our tests these parameters reproduced the trend and pore sizes of H-ZSM5 and HY zeolites correctly.

[*] Prof. Dr. W. F. Maier, Dipl.-Chem. S. Klein, Dr. J. Heilmann
Max-Planck-Institut für Kohlenforschung
Kaiser-Wilhelm Platz 1, D-45470 Mülheim an der Ruhr (Germany)
Fax: Int. code +(2 08) 3 06-29 87
e-mail: maier@dsa.mpi-muelheim.mpg.de
Prof. Dr. J. A. Martens, Dr. R. Parton, Dr. K. Vercruysse,
Prof. Dr. P. A. Jacobs
Centrum voor Oppervlaktechemie en Katalyse
KU Leuven, B-3001 Heverlee (Belgium)

[**] S. K. acknowledges the German Fonds der Chemischen Industrie for a fellowship. R. P. and J. A. M. acknowledge the Flemish National Science Foundation for a fellowship and a research position, respectively. Parts of the work were sponsored by the Belgian Federal Government within the frame of an IUAP program and by the German Fonds der Chemischen Industrie.

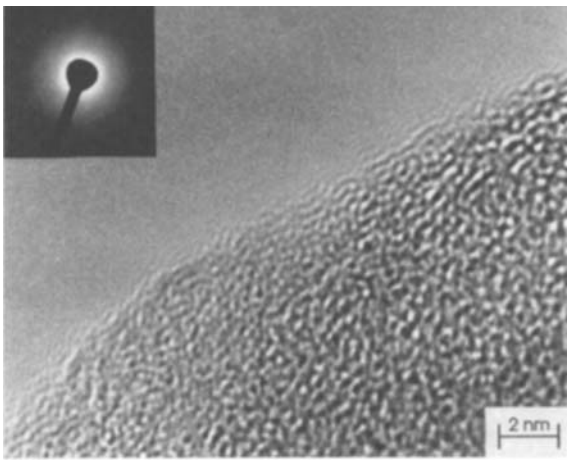

Fig. 2. Representative high-resolution TEM image of AMM-$Ti_{17}Si$ (electron optical magnification 1.5×10^6); the insert shows the electron diffraction at an amplification of 2×10^5 and a camera length of 0.2 m.

and attributed to Ti atoms in octahedral environments linked to silica tetrahedra, the hydroxyl ligands of which have Brønsted acidic properties.[7]

Crystalline mircoporous titanium silicates catalyze the epoxidation of olefins.[8, 9] Amorphous mesoporous Ti-containing aerogels also show good epoxidation properties, however, only with organic hydroperoxides as oxidation agent.[10] The AMM-Ti_xSi materials are comparable epoxidation catalysts with *tert*-butylhydroperoxide (TBHP) as oxidizing agent. In contrast to crystalline TS-1, the AMM-Ti_xSi materials show no epoxidation activity with H_2O_2 as the oxidizing agent. With linear and cyclic olefins, the rate of epoxidation with the AMM-Ti_3Si catalyst decreases rapidly with increasing number of carbon atoms (Fig. 3). This behavior is unexpected, as the reactivity of terminal alkenes is barely affected by chain length. A similar decrease of the rate of epoxidation with increasing number of carbon atoms in the epoxidation of alkenes with TS-1 was ascribed to molecular shape selectivity.[11] On TS-1, however, the epoxidation of hex-1-ene is much quicker than that of cyclohexene,

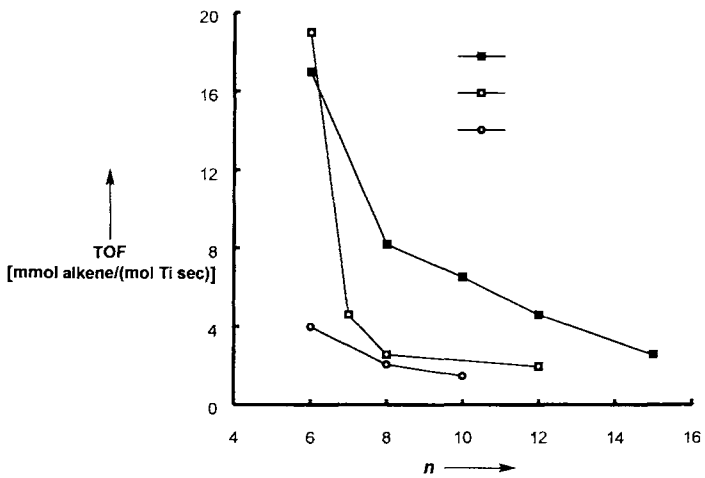

Fig. 3. Relative rate of epoxidation (TOF = turnover frequency) of 1-alkenes and cycloalkenes with AMM-Ti_3Si. Reaction conditions: batch reactor 353 K, 15.8 mmol alkene, 3 mmol TBHP (3 M in isooctane), 50 mg catalyst. The data on Ti-β (at 333 K) are taken from reference [11a]. n = number of carbon atoms of the alkene. ■ = 1-alkene (AMM-Ti_3Si), □ = cycloalkene (AMM-Ti_3Si), ○ = 1-alkene (Ti-β).

whereas on AMM-Ti_3Si the two alkenes are converted at comparable rates, confirming the presence of larger pores in the AMM catalyst. Compared to the zeolite Ti-β, the Ti atoms in the AMM catalyst are also much more efficiently used.[11a] The yield of peroxide relative to TBHP is nearly quantitative. These data indicate that with the preparation of a purely microporous Ti-Si glass with narrow pore size distribution a new, shape-selective epoxidation catalyst with pores in the range of the large-pore 12-ring zeolites with high epoxidation activity has been developed.

Since significant shape selectivity has only been observed with crystalline zeolites, this indication of shape selectivity with a purely amorphous material seems of special importance. The presence of Brønsted acidic centers in AMM-Ti_xSi and AMM-V_x-Si materials allows, besides the mentioned redox catalysis, the investigation of acid-catalyzed reactions. The hydrocracking of decane is of special value for the characterization of the pore architecture of crystalline zeolites. This established test reaction[12] allows a precise assignment of pore structure on the basis of product distribution by comparison with the data bank of known zeolites. The hydrocracking of decane was carried out under standardized reaction conditions, after the AMM materials had been impregnated with 0.5 wt% Pt. Table 2 summarizes the obtained indices of the AMM materials together with the data from the zeolites H-Y and ZSM-5. The position of the AMM materials relative to known zeolites with regard to the ethyloctane criterion is shown in Figure 4.[13]

Table 2. Characterization of the microporous materials by the hydrocracking test of decane [a].

Microporous material	CI*	EC8	PC7	3EC8/4EC8	DBiC10	iC5	DI
USY	1.5	12.5	1.9	0.6	–	50	–
AMM-Ti_3Si	1.5	10.3	0.9	0.7	30	30.5	–
AMM-$Ti_{17}Si$	1.7	11.8	1.1	0.7	–	–	15
AMM-$V_{10}Si$	3.4	3.8	0.9	1.0	17.3	13.3	12
ZSM5	6.6	0	0	–	–	11	–

[a] CI* = content of 2-methylnonane/5-methylnonane at 5% conversion; EC8 = content of ethyloctanes/methylnonanes; PC7 = content of 4-propylheptane in monobranched isomers at 75% conversion; 3-EC8/4-EC8 = content of 3-ethyloctane/4-ethyloctane; DBiC10 = content of dibranched isodecanes at maximal isomerization; iC5 = mol isopentane per 100 mol cracked decane; DI = molar yields of (C3–C7) + (C4–C6) (expressed as mol per 100 mol cracked) at 35% cracking.

The refined constraint index (CI*)[12a] of AMM-Ti_3Si (CI* = 1.5) and of AMM-$Ti_{17}Si$ (CI* = 1.7) positions the pore size of the materials in the range of large-pore 12-ring zeolites ($1 < CI^* < 2.2$). In such large-pore zeolites the extent of the rather bulky ethyl isomers correlates with pore size (Fig. 4). This confirms the assignment of the AMM-Ti materials in the family of large-pore zeolites based on the pore diameter of 0.73 nm from the adsorption isotherm. The decane test further identifies the AMM-Ti_xSi materials as tubular pore systems lacking additional larger cavities and pore intersections, as derived from the high dimensionality index (DI) values ($DI > 5$).[12d] The slightly larger pore size of AMM-Ti_3Si compared to AMM-$Ti_{17}Si$ is confirmed by both the argon adsorption (Table 1) and the decane test (Fig. 4).

The V-containing AMM-$V_{10}Si$ with a CI* of 3.4 is positioned in the zeolite-free range between the medium-pore 10-ring and the large-pore 12-ring zeolites. The high DI of 12 identifies the material as a system of unconnected tubular pores without inner cages like the Ti-containing AMM. The results of the argon

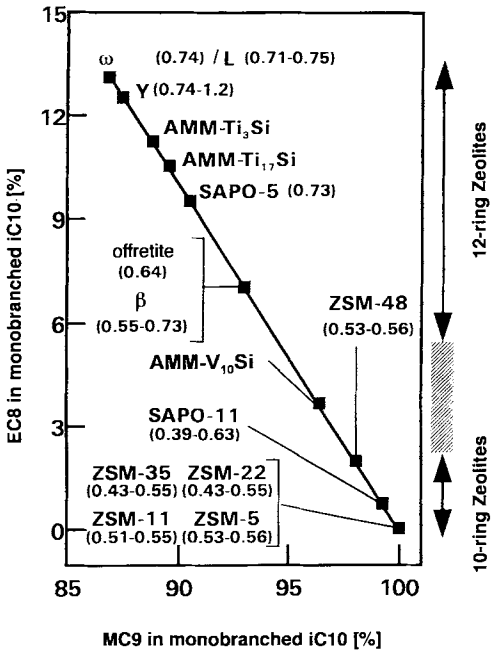

Fig. 4. Comparison of the amorphous AMM glasses with known zeolites, based on the ethyl octane criterion from the decane test [13]. Minimum and maximum diameters of pore cross sections given in brackets. The zeolite data were taken from reference [12]. EC8 = ethyloctanes, MC9 = methylnonanes, iC10 = isodecane.

adsorption (Table 1) and the decane test (Fig. 4) revealed that the pores of the AMM-V_{10}Si are slightly smaller than those of the AMM-Ti_xSi. HR-TEM studies of the materials after the decane test show that the amorphous nature of the AMM materials is stable at high temperatures. However, a slight reduction of the overall surface by about 20% was found with the catalysts used (heated to 550 °C). The temperature-dependent X-ray diffraction exhibits no detectable crystallinity up to 800 °C. The stability of the AMM materials was confirmed by thermogravimetric analysis (TGA) and differential scanning calorimetry (DSC), which showed no change in the range of 200 to 600 °C, while in the range below 200 °C the expected weight loss due to drying was observed.

These results show that microporous amorphous glasses have shape-selective properties in redox and hydrocracking catalysis, a property up to now only observed with crystalline zeolites. There are no known zeolites with the pore architecture and pore sizes of the AMM glasses, thus, these glasses supplement the known zeolites. These studies also confirm that the shape-selective catalytic properties of microporous materials like zeolites are not associated with the crystallinity but with the narrow pore size distribution and small pore size of these materials. The preparation of purely microporous glasses with shape-selective catalytic properties opens the door for the synthesis of new shape-selective catalysts. Compared to traditional zeolite synthesis, the sol–gel route avoids the use of organic templating agents that have to be eliminated through calcination and does not require hydrothermal synthesis conditions. In contrast to zeolites, the chemical composition and pore size of these materials is not limited. The sol–gel process also opens new possibilities for the manufacture of inorganic permselective catalytic membranes and monolithic materials. Thus with the preparation of microporous amorphous mixed oxides it may be possible to overcome many of the limitations of traditional zeolite chemistry.

Received: August 3, 1995 [Z 8275IE]
German version: *Angew. Chem.* **1996**, *108*, 222–224

Keywords: catalysis · sol–gel process · titanium compounds vanadium compounds · zeolites

[1] *Zeolites and Related Materials: State of the Art 1994*, (Eds.: J. Weitkamp, H. G. Karge, H. Pfeifer, W. Hölderich), Elsevier, Amsterdam, **1994**; W. Hölderich, M. Hesse, F. Näumann, *Angew. Chem.* **1988**, *100*, 232; *Angew. Chem. Int. Ed. Engl.* **1988**, *27*, 226.
[2] W. F. Maier, I.-C. Tilgner, M. Wiedorn, H.-C. Ko, *Adv. Mater.* **1993**, *5*, 726.
[3] I.-C. Tilgner, P. Fischer, F. M. Bohnen, H. Rehage, W. F. Maier, *Micropor. Mater.* **1995**, *5*, 77.
[4] The materials were prepared by acid-catalyzed copolycondensation of tetraethoxysilane (TEOS) with tetraisopropoxytitanium TiPOT ((46.3 − *x*) mmol TEOS + *x* mmol TiPOT (or $[VO(acac)_2]$)) in EtOH (100 mmol), dropwise addition of 8 N HCl (2 mL). Hydrolysis, condensation, and gelation were carried out at room temperature. After drying for three days at room temperature, the gels were heated to 338 K at a heating rate of 0.1 K min^{-1}, kept for 5 h at this temperature and then heated at the same heating rate to a final temperature of 523 K and kept there for additional 5 h. The material is allowed to cool to room temperature at a cooling rate of 1 K min^{-1}. The amorphous microporous vanadium-containing SiO_2 was obtained by the same procedure by the use of *x* mmol $[VO(acac)_2]$.
[5] S. Lowell, J. E. Shields, *Powder Surface Area and Porosity*, 3rd ed., Chapman & Hall, London, **1991**.
[6] G. Horvath, K. Kawazoe, *J. Chem. Eng. Jpn* **1983**, *16*, 470.
[7] Z. Liu, R. J. Davis, *J. Phys. Chem.* **1994**, *98*, 1253.
[8] B. Notari, *Stud. Surf. Sci. Catal.* **1988**, *37*, 413.
[9] J. S. Reddy, R. Kumar, P. Ratnasamy, *Appl. Catal.* **1990**, *58*, L1.
[10] D. C. M. Dutoit, M. Schneider, A. Baiker, *J. Catal.* **1995**, *153*, 165.
[11] a) A. Corma, P. Esteve, A. Martinez, S. Valencia, *J. Catal.* **1995**, *152*, 18; b) M. G. Clerici, P. Ingallina, *ibid.* **1993**, *140*, 71.
[12] a) P. A. Jacobs, J. A. Martens, *Pure Appl. Chem.* **1986**, *58*, 1329; b) J. A. Martens, M. Tielen, P. A. Jacobs, J. Weitkamp, *Zeolites* **1984**, *4*, 98; c) J. A. Martens, P. A. Jacobs, *Zeolites* **1986**, *6*, 334; d) M. M. Olken, J. Garcès, *Proc. 9th. IZC*, Montreal **1992**, *Vol. II* (Eds.: R. von Ballmoos, J. B. Higgins, M. M. J. Treacy), Butterworth-Heinemann, Boston **1993**; e) J. A. Martens, P. A. Jacobs, S. Cartlidge, *Zeolites* **1989**, *9*, 423.
[13] Content of ethyloctanes plotted against methylnonanes in the monobranched isomerization products at 5% isomerization yield in the hydrocrack test of decane. The AMM-Ti_xSi materials are compared to 10-ring and 12-ring zeolites. Reaction conditions: continuous-flow, fixed-bed reactor with a total pressure of 0.45 MPa, a decane and water partial pressure of 1.2 kPa; a space time of decane of 1.7 kg s $mmol^{-1}$; a temperature range of 473 to 673 K. AMM-Ti_xSi samples were loaded with 0.1 wt% Pt metal by impregnation with an aqueous $[Pt(NH_3)_4Cl_2]$ solution, calcination in oxygen, and reduction in hydrogen at 673 K.

Asymmetric Dihydroxylation Enables Rapid Construction of Chiral Dendrimers Based on 1,2-Diols**

Han-Ting Chang, Chien-Tien Chen, Teruyuki Kondo, Gary Siuzdak, and K. Barry Sharpless*

Research in dendrimers is a rapidly expanding area at the interface between conventional organic chemistry and polymer science.[1] These macromolecules consist of a polyfunctional central core covalently linked to layers of repeating units bearing functionalized branches, leading to structures with a discrete number of generations and functional end groups. The main quest in dendrimer research has been to find reliable strategies for their efficient construction, especially regarding control of homogeneity, branching patterns, interior cavity size, topology,

[*] Prof. K. B. Sharpless, H.-T. Chang, Dr. C.-T. Chen, Dr. T. Kondo, Dr. G. Suizdak
Department of Chemistry, The Scripps Research Institute
10666 N. Torrey Pines Road, La Jolla, CA 92037 (USA)
Fax: Int. code +(619) 784-7562
e-mail: sharples@scripps.edu

[**] K.B.S thanks the U.S. National Institutes of Health (GM 28384) and the W. M. Keck Foundation for financial support. We are grateful to Dr. Pui Tong Ho for many helpful discussions.

and surface functionality. More recently, following success in the aforementioned areas, the emphasis has shifted toward the elaboration of components with specific functions in both the peripheral and interior domains of the dendrimer.[2] Nevertheless, relatively few studies have focused on chiral dendrimers. Most of those cases involve the use and derivatization of chiral pool materials such as nucleotides, amino acids, and tartaric acid as building blocks or as terminal groups for the construction of biopolymers[3] and abiotic cascade molecules.[4, 5] The Seebach group has done the pioneering work in the synthesis of chiral starburst dendrimers.[6]

Interest in applications of the asymmetric dihydroxylation process attracted us to this field. The primary goal was to introduce chiral cavities into these materials, creating the potential for asymmetric catalysis, chiral recognition, and resolution. Since two stereogenic centers can be created in the asymmetric dihydroxylation (AD) of prochiral olefins,[7] we sought to utilize these readily available 1,2-diols as branch units for the construction of chiral dendrimers, in which the hydroxyl groups provide the covalent linkage points. Here we describe our initial results on the assembly of chiral polyether dendrimers by a "double exponential dendrimer growth" approach.[8]

On the basis of several considerations, three functionalized acetonides **1a–c** with various R substituents in the acetonide and the chloromethyl group in different positions on the aromatic ring were chosen as chiral monomer units. First, these chiral isopropylidene ketals can be readily prepared in enantiomerically pure form by the AD of appropriate 3- or 4-chloromethylphenyl alkenes. Second, the acetonide protecting group can be removed under mildly acidic conditions and also greatly simplifies spectroscopic analysis. Third, the aromatic spacer reduces steric congestion, enabling propagation to higher generations, and also bears the functionality for anchoring to the central core. Of special importance in this latter role is the benzylic activation facilitating the Williamson ether couplings.

To efficiently employ the alternative double exponential approach, judicious selection of a focal protective group compatible with both stages of propagation was essential. We chose the *p*-methoxyphenyl (PMP) ether group due to its stability under both basic (etherification) and acidic (hydrolysis) reaction conditions. The PMP ether functionality was installed at the focal site of **1a–c** by reaction with 4-hydroxyanisole in the presence of K_2CO_3 and a catalytic amount of Bu_4NI under reflux in 2-butanone;[9] quantitative yields were obtained in all cases. The masked diol functionality of the resulting PMP ether was released by exposure to 3 N hydrochloric acid in acetonitrile at ambient temperature.[10] The corresponding 1,2-diols **2a–c**, each prepared in greater than 95% yield, were then subjected to double etherification with the individual benzylic chlorides **1a–c**. Instead of the commonly employed Williamson etherification conditions (NaH/THF or DMF), we took advantage of a KOH/toluene-based benzylation technique for the propagation step. Virtually quantitative formation of the bis(acetonides) **3a–c** can be accomplished by simply refluxing the requisite diol and benzylic chloride in toluene in the presence of KOH pellets with concomitant azeotropic removal of water.[11, 12]

The double exponential dendrimer growth process[13] pioneered by Moore and co-workers[8] comprises the repetitive use of a three-reaction sequence for a doubly protected subunit: 1) selective deprotection of the peripheral groups (acetonides), 2) selective unmasking and functionalization of the focal group (PMP), and 3) coupling of these two components. Hydrolysis of the common intermediates **3a–c** under conditions similar to those described previously provided tetraols **4a–c** in yields

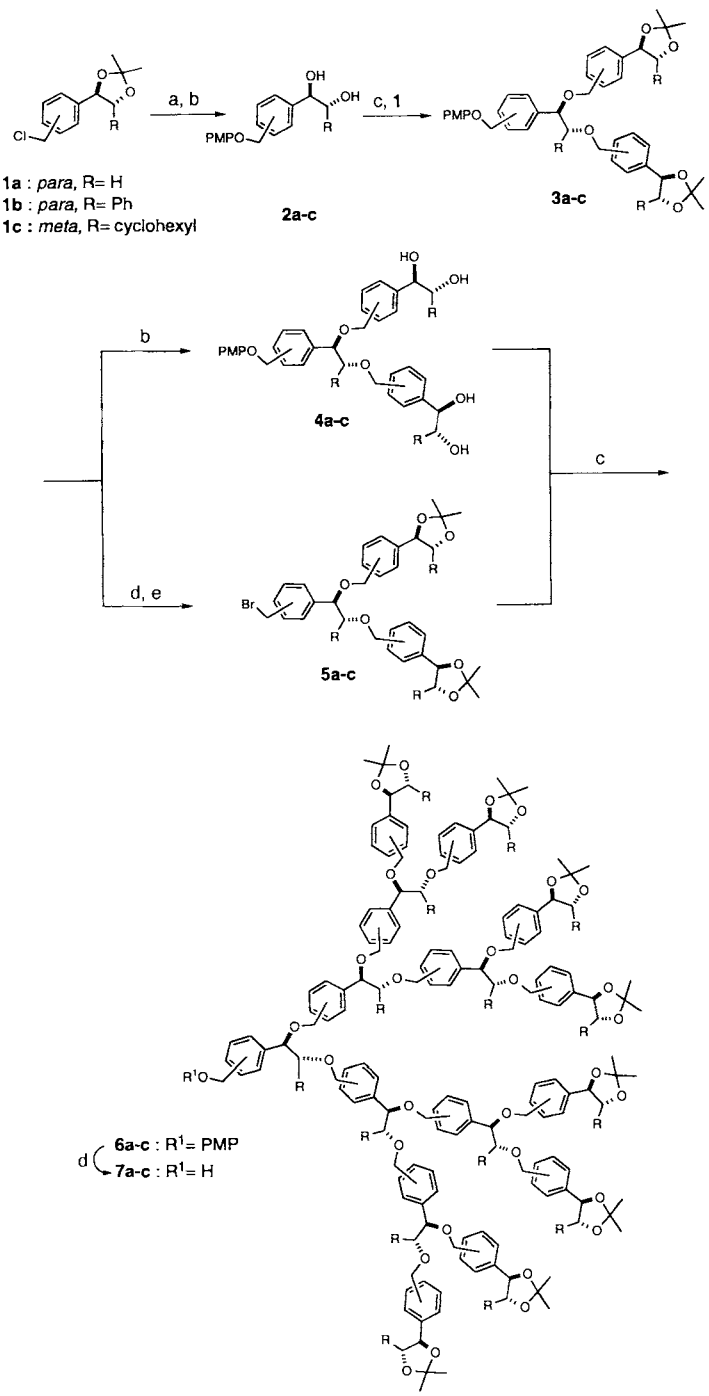

Scheme 1. a) $CH_3OC_6H_4OH$, K_2CO_3, Bu_4NI (5%), 2-butanone, reflux; b) 3 N HCl/CH_3CN (1/10 or 1/3 v/v), room temperature; c) KOH pellets (1.3–3 equiv), toluene, Dean–Stark; d) CAN (2.2–3 equiv), CH_3CN or C_2H_5CN/H_2O (2/1 v/v), −10 °C or 0 °C; e) PPh_3 (1.1 equiv), NBS (1.1–1.8 equiv), CH_2Cl_2, 0 °C.

ranging from 70% (R = cyclohexyl) to 97% (R = H, Ph). The PMP group in **3b** (R = Ph) was cleaved oxidatively by cerium ammonium nitrate (CAN) in CH_3CN/H_2O at 0 °C providing the corresponding benzylic alcohol in 93% yield.[14] However, for ether **4a** removal of the PMP group (95% yield) must be carried out at −10 °C to prevent concomitant hydrolysis of the peripheral acetonides, which are more sensitive in this less substituted series. To overcome the problem associated with the low solubility of **3c** (R = cyclohexyl) in the solvent system employed, propionitrile was ultimately found to be the best substi-

 © VCH Verlagsgesellschaft mbH, D-69451 Weinheim, 1996 0570-0833/96/3502-0183 $ 10.00+.25/0

tute for CH_3CN (yield increased from 78 to 92%). Conversion of the resulting benzylic alcohols to the bromides **5a–c** (88–93%) proceeded smoothly upon treatment with PPh_3 and *N*-bromosuccinimide in CH_2Cl_2 at 0 °C.[15] In the final stage, the second-generation tetraols **4a–c** were propagated to the fourth-generation monodendrons **6a–c** by the KOH/toluene-mediated coupling with the respective benzylic bromides **5a–c**. These exhaustive, fourfold etherifications provided **6a–c**, which have eight end groups, in good yields ranging from 88 to 93%. Electrospray and/or FAB mass spectral analyses of these monodendrons exhibited no signs of products with defects that would arise from incomplete branches, thus demonstrating the overall efficiency of this approach.

After the final coupling the PMP group was removed by our modified oxidative cleavage conditions without overoxidation of the resulting alcohol.[16] The fourth-generation benzylic alcohols **7a–c** were thus obtained in yields of 84 to 89%. A variety of chiral dendrimers can be constructed by anchoring these chiral dendritic components onto a polyfunctional molecular core. As a model for the synthesis of C_3-symmetric dendrimers, 1,3,5-benzenetricarbonyl trichloride was coupled directly with benzylic alcohols **7a** (R = H) and **7b** (R = Ph) in the presence of 4-dimethylaminopyridine in benzene (Scheme 2). The fourth-generation dendrimer **8a** with 45 monomer units, 45 stereogenic centers, and a molecular weight of 7929 Da was synthesized in 75% yield (101 mg) at ambient temperature. In contrast, for the couplings with **7b**, which has more steric congestion, heating to reflux was required. The corresponding fourth-generation dendrimer **8b** possessing 45 monomer units, 90 stereogenic centers, and a molecular weight of 11 354 Da was obtained in 67% yield (130 mg). Important features allowing us to confirm unambiguously the structural integrity and identity of this type of dendrimer are the characteristic ^1H NMR shifts of the aromatic hydrogens in the core unit and the benzylic hydrogens at the focal point. For example, in **8b** these two signals appear as sharp singlets at $\delta = 8.9$ and 5.3, respectively, in a ratio of 1 to 2 (Fig. 1a). Further confirmation of structure and purity was obtained by size exclusion chromatography (Fig. 1b) and MALDI-TOF mass spectroscopy (Fig. 1c).

We have developed an efficient approach to chiral polyether dendrimers. The examples described here are C_3-symmetric dendrimers consisting of 45 chiral monomers and bearing 24 acetonide groups in the periphery. Nature uses α-amino acids as the fundamental repeat units for protein synthesis; this asymmetric dihydroxylation methodology for dendrimers may offer an abiotic counterpart, holding promise for the construction of chiral macromolecules of either antipode and with a vast array of spacer functionality, directionality (branching patterns), and surface chemistry by simple permutations of the 1,2-diol monomer units. In current research we are exploring the properties of this class of dendrimers in chiral recognition[17] and for the preparation of C_3-symmetric dendritic phosphanes as potential ligands for transition metal catalyzed asymmetric transformations.

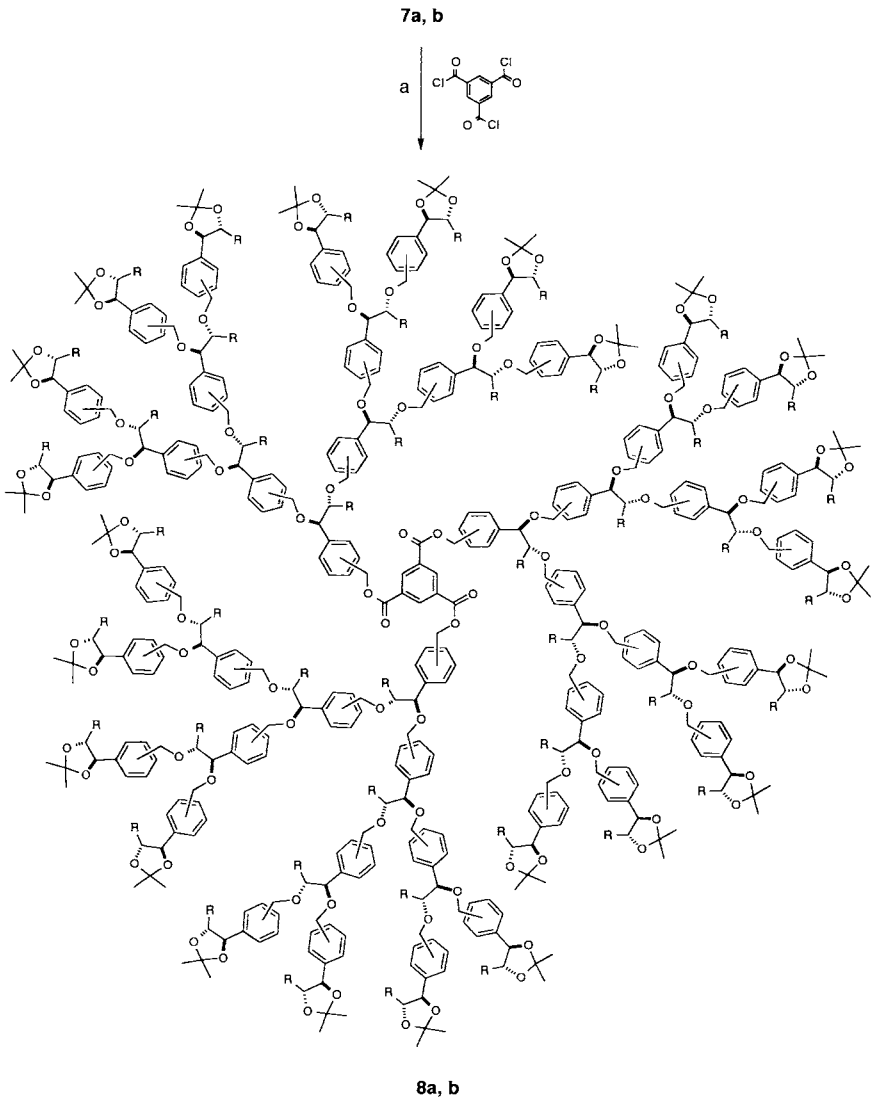

Scheme 2. a) DMAP (3 equiv), PhH, room temperature or reflux.

Experimental Procedure

6a: A single-necked flask fitted with a Dean–Stark apparatus and a magnetic stir bar was charged under a nitrogen atmosphere with tetraol **4a** (746 mg, 1.3 mmol), benzyl bromide **5a** (3.8 g, 6.25 mmol), and 60 mL of toluene. This stirred solution was heated to reflux for 0.5 h, followed by addition of three pellets of KOH (these contain 15 wt.% H_2O, ca. 410 mg, 6.5 mmol). The reaction was monitored by thin-layer chromatography until intermediates were no longer observed; if the reaction seemed too slow in reaching completion, more KOH was added, and the reaction mixture was refluxed an additional hour (approximately 12 h total). After solvent removal in vacuo, the residue was dissolved in 25 mL of CH_2Cl_2, filtered through Celite, and purified by flash chromatography (3.10 g, 88% yield; $R_f = 0.13$, 2/3 EtOAc/hexane).

8b: A two-necked flask fitted with a Dean–Stark trap (filled with molecular sieves) and a condenser was charged with **7b** (211 mg, 0.057 mmol), DMAP (19 mg, 0.15 mmol), and 20 mL of benzene. The resulting solution was stirred and refluxed for 2 h, then cooled to room temperature. 1,3,5-Benzenetricarbonyl trichloride (4.52 mg, 0.017 mmol) was added and the solution refluxed an additional 4 h. Following removal of the solvent in vacuo, flash chromatography gave 130 mg of **8b** (67% yield; $R_f = 0.63$, 2/3 EtOAc/hexane). (An additional 33 mg (25% yield) of a product ($R_f = 0.13$, 2/3 EtOAc/hexane) resulting from incomplete esterification, the diester carboxylic acid, was recovered—presumably a consequence of trace amounts of water.) ^1H NMR (400 MHz, $CDCl_3$): $\delta = 8.90$ (s, 3H, $C_6H_3(CO_2CH_2Ar)_3$), 7.27–7.05 (m, 405H, $45 \times C_6H_4 + 45 \times C_6H_5$), 5.32 (s, 6H, $C_6H_3(CO_2CH_2Ar)_3$), 4.70 (s, 48H, methine protons of

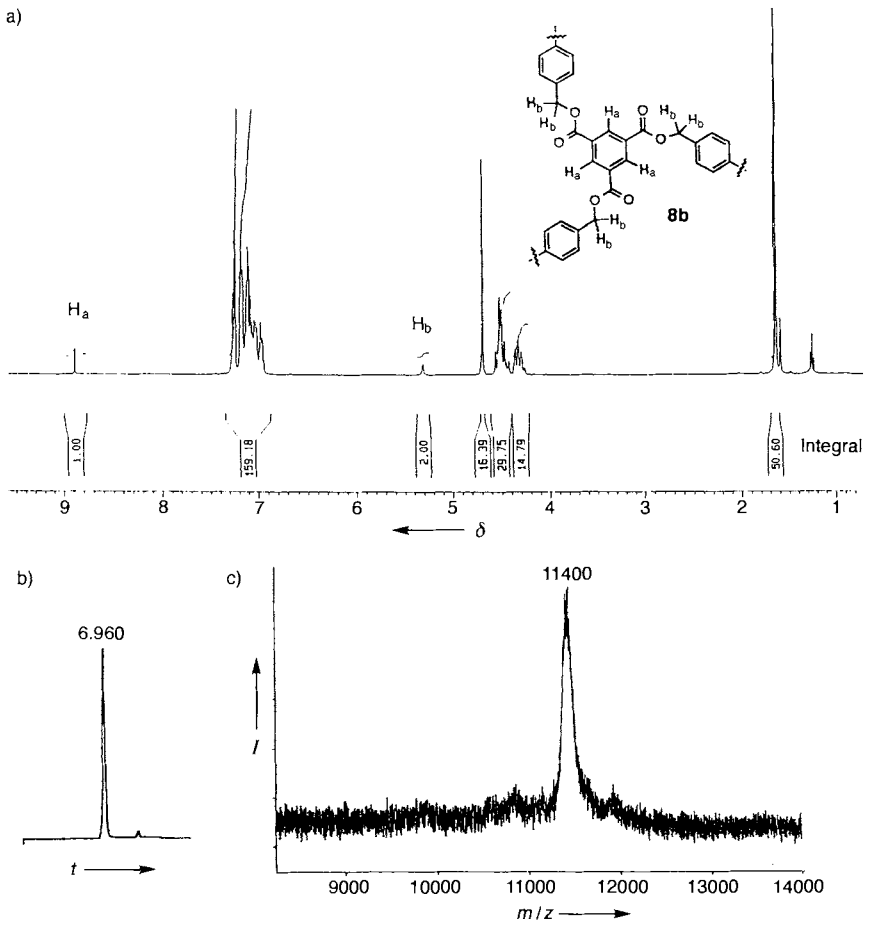

Fig. 1. Characterization of dendrimer **8b**. a) ^{1}H NMR spectrum (400 MHz, $CDCl_3$); b) size exclusion chromatogram (Waters Styragel HR 3, 7.8 × 300 mm, 1 mL min^{-1}, THF); c) MALDI-TOF mass spectrum, resolution ±0.1%.

the peripheral shell), 4.57–4.27 (m, 126H, 42 methine protons of the inner layers + 42 × OCH_2Ar), 1.65 (s, 72H, $C(CH_3)_2$), 1.64 (s, 72H, $C(CH_3)_2$); ^{13}C NMR (100 MHz, $CDCl_3$): δ = 164.80 (CO), aromatic quaternary carbons: 138.61, 138.50, 138.44, 138.26, 137.87, 137.80, 137.70, 137.56, 137.49, 136.75, 135.71, 131.25 (core); aromatic methine carbons: 134.54 (core), 128.36, 128.18, 127.87, 127.78, 127.53, 126.98, 126.64, 126.59, 109.25 ($C(CH_3)_2$), 85.32, 85.25, 85.03, 84.98, 84.82, 84.65, 70.76, 70.60, 67.19 (CO_2CH_2Ar), 27.18 ($C(CH_3)_2$), 27.16 ($C(CH_3)_2$); IR (KBr): $\tilde{\nu}$ = 3062, 2983, 1729 (CO), 1454, 1371, 1236, 1167, 897, 700 cm^{-1}; MS (MALDI-TOF) calcd for $C_{756}H_{732}O_{96}$ + K: 11393; found: 11400 ± 0.1%. Anal. calcd for $C_{756}H_{732}O_{96}$: C 79.97, H 6.5; found: C 79.79, H 6.65.

8a: A procedure analogous to that for the synthesis of **8b** was used except the reaction was performed at room temperature (140 mg of **7a** gave 101 mg of **8a**, 75% yield; R_f = 0.4 on aluminum oxide (IB-F), 1/1 EtOAc/hexane). ^{1}H NMR (400 MHz, $CDCl_3$): δ = 8.92 (s, 3H, $C_6H_3(CO_2CH_2Ar)_3$), 7.46–7.25 (m, 180H, 45 × C_6H_4), 5.39 (s, 6H, $C_6H_3(CO_2CH_2Ar)_3$), 5.06–5.02 (m, 24H, methine protons of the peripheral shell), 4.72–4.33 (m, 105H, 21 methine protons of the inner layers + 42 × OCH_2Ar of all layers), 4.28–4.25 (m, 24H, one methylene proton of the peripheral shell), 3.80–3.51 (m, 42H, both protons from 21 methylene units of the inner layers), 3.68–3.64 (m, 24H, 24 one methylene proton of the peripheral shell), 1.53 (s, 72H, $C(CH_3)_2$), 1.47 (s, 72H, $C(CH_3)_2$); ^{13}C NMR (100 MHz, $CDCl_3$): δ = 164.82 (CO), aromatic quaternary carbons: 139.80, 138.59, 138.50, 138.30, 138.27, 138.21, 138.18, 131.23 (core); aromatic methine carbons: 135.10 (core), 128.73, 127.84, 127.82, 127.75, 127.69, 127.39, 127.10, 126.18, 109.66 ($C(CH_3)_2$), 80.87, 80.37, 77.66, 75.18, 74.83, 73.29, 73.20, 72.97, 71.62, 71.56, 70.76, 70.55, 70.30, 67.23 (CO_2CH_2Ar), 26.60 ($C(CH_3)_2$), 25.95 ($C(CH_3)_2$); IR (KBr): $\tilde{\nu}$ = 2985, 1729 (CO), 1371, 1221, 1064, 820, 732 cm^{-1}; MS (MALDI-TOF) calcd for $C_{486}H_{552}O_{96}$ + Na: 7953; found: 7949 ± 0.1%.

Received: July 3, 1995 [Z 8163 IE]
German version: *Angew. Chem.* **1995**, *107*, 202–206

Keywords: asymmetric syntheses · chirality · dendrimers · dihydroxylations · diols · polyethers

[1] a) D. A. Tomalia, A. M. Naylor, W. A. Goddard III, *Angew. Chem.* **1990**, *102*, 119; *Angew. Chem. Int. Ed. Engl.* **1990**, *29*, 138; b) D. A. Tomalia, *Aldrichim. Acta* **1993**, *26*, 91; c) G. R. Newkome, C. N. Moorefield, G. R. Baker, *ibid.* **1992**, *25*, 31; d) H.-B. Mekelburger, W. Jaworek, F. Vögtle, *Angew. Chem.* **1992**, *104*, 1609; *Angew. Chem. Int. Ed. Engl.* **1992**, *31*, 1571; e) J. Issberner, R. Moors, F. Vögtle, *ibid.* **1994**, *106*, 2507 and **1994**, *33*, 2413; f) "Genealogically Directed Synthesis: Starburst Cascade Dendrimers and Hyperbranched Structures", *Top. Curr. Chem.* **1993**, *165*, 193; g) D. A. Tomalia, *Adv. Mater.* **1994**, *6*, 1710; h) G. R. Newkome, *Advances in Dendritic Macromolecules*, JAI, Greenwich, CT, **1993**.

[2] a) J. M. J. Fréchet, *Science* **1994**, *263*, 1710; b) R. F. Service, *ibid.* **1995**, *267*, 458.

[3] a) R. G. Denkewalter, J. F. Kolc, W. J. Lukasavage, US-A 4410688, **1983** [*Chem. Abstr.* **1984**, *100*, 103907p]; b) S. M. Aharoni, C. R. Crosby III, E. K. Walsh, *Macromolecules* **1982**, *15*, 1093; c) S. M. Aharoni, N. S. Murthym, *Polym. Commun.* **1983**, *24*, 132; d) H. E. Hudson, M. J. Damha, *J. Am. Chem. Soc.* **1993**, *115*, 2119; e) J. Shao, J. P. Tam, *ibid.* **1995**, *117*, 3893; f) J. C. Spetzler, J. P. Tam, *Int. J. Pept. Protein Res.* **1995**, *45*, 78.

[4] a) H. Brunner, S. Altmann, *Chem. Ber.* **1994**, *127*, 2285; b) L. J. Twyman, A. E. Beezer, J. C. Mitchell, *Tetrahedron Lett.* **1994**, *35*, 4423; c) H.-F. Chow, L. F. Fok, C. C. Mak, *ibid.* **1994**, *35*, 3547; d) H.-F. Chow, C. C. Mak, *J. Chem. Soc. Perkin Trans. 1* **1994**, *16*, 2223.

[5] a) G. R. Newkome, X. Lin, C. D. Weis, *Tetrahedron: Asymmetry* **1991**, *2*, 957; b) S. Bauer, H. Fischer, H. Ringsdorf, *Angew. Chem.* **1993**, *105*, 1658; *Angew. Chem. Int. Ed. Engl.* **1993**, *32*, 1589; c) R. Roy, D. Zanini, S. J. Meunier, A. Romanowska, *J. Chem. Soc. Chem. Commun.* **1993**, 1869; d) J. F. G. A. Jansen, E. M. M. de Brabander-van den Berg, E. W. Meijer, *Science* **1994**, *266*, 1226.

[6] a) D. Seebach, J.-M. Lapierre, G. Greiveldinger, K. Skobridis, *Helv. Chim. Acta* **1994**, *77*, 1673; b) D. Seebach, J.-M. Lapierre, K. Skobridis, G. Greiveldinger, *Angew. Chem.* **1994**, *106*, 457; *Angew. Chem. Int. Ed. Engl.* **1994**, *33*, 440. A dendrimer having core with achiral branches was synthesized as a 1:1 mixture of enantiomers; c) J. A. Kremers, E. W. Meijer, *J. Org. Chem.* **1994**, *59*, 4262.

[7] H. C. Kolb, M. S. VanNieuwenhuize, K. B. Sharpless, *Chem. Rev.* **1994**, *94*, 2483.

[8] A similar *achiral* approach has been reported recently and was named "double exponential dendrimer growth", by the authors: T. Kawaguchi, K. L. Walker, C. L. Wilkins, J. S. Moore, *J. Am. Chem. Soc.* **1995**, *117*, 2159.

[9] C. F. H. Allen, J. W. Gates, Jr., *Org. Synth.* **1955**, *3*, 140.

[10] G. A. Crispino, P. T. Ho, K. B. Sharpless, *Science* **1993**, *259*, 64.

[11] This unusual process harkens back to the old days of sugar chemistry in Germany [12]. However, its use here requires comment since the best modern conditions for ether formation (NaH, DMF, cat. R_4NI) fail in these systems due to formation of insoluble alkoxides. Furthermore, for the perbenzylation of smaller, less oxygenated polyols (e.g. pentaerythritol and methyl glycosides) the present Zemplén conditions [12a] are much poorer (i.e. deliver a lot of the expected $ArCH_2OCH_2Ar$ by-product) than the NaH/DMF conditions (H.-T. Chang, K. B. Sharpless, unpublished results). We believe that the large polyether polyols in this study cover the surface of the solid KOH and serve as solid/liquid phase-transfer catalysts, such that the $ArCH_2X$ species is denied access to hydroxide ion. Whatever the explanation, the Zemplén etherification procedure is uniquely effective for construction of these polyether dendrimers.

[12] a) G. Zemplén, Z. Csürös, S. Angyal, *Chem. Ber.* **1937**, *70*, 1848; b) C. M. McCloskey, *Adv. Carbohydr. Chem.* **1957**, *12*, 137; c) H. G. Fletcher, *Methods Carbohydr. Chem.* **1963**, *2*, 166; d) R. M. Hann, W. T. Haskins, C. S. Hudson, *J. Am. Chem. Soc.* **1942**, *64*, 986.

[13] For a double convergent growth approach see: K. L. Wooley, C. J. Hawker, J. M. J. Fréchet, *J. Am. Chem. Soc.* **1991**, *113*, 4252.

[14] a) D. R. Kronenthal, C. Y. Han, M. K. Taylor, *J. Org. Chem.* **1982**, *47*, 2765; b) P. Jacob III, P. S. Callery, A. T. Shulgin, N. Castagnoli, Jr., *ibid.* **1976**, *41*, 3627.

[15] Bromination of the benzylic alcohols **6a–c** was less satisfactory using the Fréchet protocol (PPh_3/CBr_4) [15a] for dendritic polyether synthesis, owing to competitive deprotection of the acetonide functionality [15c]. a) C. J. Hawker, J. M. J. Fréchet, *J. Am. Chem. Soc.* **1990**, *112*, 7638; b) K. C. Nicolaou, C. A. Veale, S. E. Webber, H. Katerinopoulos, *ibid.* **1985**, *107*, 7515; c) H. Hayashi, K. Nakanishi, C. Brandon, J. Marmur, *ibid.* **1973**, *95*, 8749.

 © *VCH Verlagsgesellschaft mbH, D-69451 Weinheim, 1996* *0570-0833/96/3502-0185 $ 10.00+.25 0*

[16] Oxidation of benzylic alcohols to aldehydes by CAN has been reported: W. S. Trahanovsky, L. B. Young, *J. Chem. Soc.* **1965**, 5777.

[17] Since this type of dendrimer has unsymmetrical branch cells leading to surfaces with higher fractal dimensions [1a, 3a, 17a–c], it could possibly provide a chiral environment. a) B. B. Mandelbrot, *Fractals: Form, Chance and Dimensions*, Freeman, New York, **1977**; *The Fractal Geometry of Nature*, Freeman, New York, **1982**; b) B. H. Kaye: *A Random Walk Through Fractal Dimensions*, VCH, Weinheim, New York, **1989**; c) A. B. Blumen, H. Schnörer, *Angew. Chem.* **1990**, *102*, 158; *Angew. Chem. Int. Ed. Engl.* **1990**, *29*, 113. One preliminary investigation of these dendrimers' properties examined the relationship of the optical rotation with generation numbers on the styrene-based dendrons and of dendrimer **8a**. We found that the molar optical rotation is approximately proportional to the number of repeat units. Hence, the molar optical rotation of the PMP/acetonide-protected dendrons per repeat unit is as follows: 1st generation, $-143°$ (molar rotation, $-143°$; 1 unit; $[\alpha]_D^{25}$ $-45.6°$ ($c = 3.0$ in $CHCl_3$)); 2nd generation, $-165°$ (molar rotation, $-495°$; 3 units; $[\alpha]_D^{25}$ $-75.6°$ ($c = 1.0$ in $CHCl_3$)); 3rd generation, $-156°$ (molar rotation, $-1095°$; 7 units; $[\alpha]_D^{25}$ $-82.0°$ ($c = 13.6$ in $CHCl_3$)); 4th generation, $-189°$ (molar rotation, $-2836°$; 15 units; $[\alpha]_D^{25}$ $-105.2°$ ($c = 4.25$ in $CHCl_3$)) and dendrimer **8a**, $-163°$ (molar rotation, $-7345°$; 45 units; $[\alpha]_D^{25}$ $-92.7°$ ($c = 0.8$ in $CHCl_3$)).

A Novel Lithocenophane Derivative of a Trisgermole Dianion: [Li(thf)(tmeda)][2,3,4,5-Et_4-*Ge*,*Ge*-{Li(2,3,4,5-$Et_4C_4Ge)_2$}C_4Ge]**

Jang-Hwan Hong, Youlin Pan, and Philip Boudjouk*

Only two lithocenes, $[Cp_2Li]^-$ and $[(isodicyclopentadiene)_2Li]^-$, have been reported to date.[1] Studies on lithium cyclopentadienide ions show that they are in a monomer–dimer equilibrium.[2] Group 14 "heterole" anions are of particular interest because they are potentially aromatic[3, 4] and offer the promise of a rich and varied chemistry similar to their carbon congeners. In the case of silole anions, the ^{29}Si and ^{13}C NMR chemical shifts led to the conclusion that the degree of aromaticity was significant in these species.[5, 6] Recent high-level calculations support this conclusion.[7] The novel transition metal complexes $[(\eta^5\text{-}C_5Me_5)Ru\{\eta^5\text{-}C_4Me_4SiSi(SiMe_3)_3\}]$ and $[(\eta^5\text{-}C_5Me_5)Ru\{\eta^5\text{-}C_4Me_4GeSi(SiMe_3)_3\}]$, in which the heterole rings appear highly delocalized, have been prepared and characterized.[8, 9] Germole anions, on the other hand, once considered resonance stabilized based on pK_a data,[10] do not have NMR characteristics consistent with extensive delocalization.[11] In contrast, a NMR study of the unique 2,3,4,5-tetraphenylgermole dianion $[Ph_4C_4Ge]^{2-}$ provided evidence that this species exhibits significant π delocalization.[12]

To our knowledge, there are no examples of lithocene-type complexes of Group 14 heteroles. Herein, we report the synthesis and characterization of a novel trisgermole complex of lithium (**3**). X-ray analysis of a single crystal reveals that this species

[Li(thf)(tmeda)][2,3,4,5-Et_4*Ge*,*Ge*-{Li(2,3,4,5-$Et_4C_4Ge)_2$}C_4Ge] **3**

has a sandwich structure in the solid state. NMR studies indicate that the dianion is in dynamic equilibrium in solution but that the sandwich structure is maintained.

[*] Prof. Dr. P. Boudjouk, Adj. Prof. Dr. J.-H. Hong, Dr. Y. Pan
Center for Main Group Chemistry
Department of Chemistry, North Dakota State University
Fargo, ND 58105 (USA)
Fax: Int. code +(701) 231-7947 or 8831

[**] This work was supported by the Air Force Office of Scientific Research through Grants No. 91-0197 and 49620-929-J0431 and the National Science Foundation through Grant No. OSR 9452892.

Sonication of 1,1-dichloro-2,3,4,5-tetraethylgermole (**1**) with excess Li in THF in the presence of tetramethylethylenediamine (TMEDA) gives a red solution (**3**) which, upon addition of MeI, leads to the trigermole **2** in high yield [Eq. (a)]. The intermediate

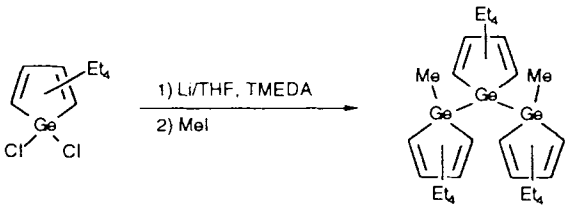

(a)

1 **2**

salt **3** was isolated as crystals and analyzed by X-ray diffraction. The essential structural features of **3** (Fig. 1)[13] are: 1) two differently π-complexed rings, one with only π bonding to the Li center, the other with π bonding to the Li center plus a σ Ge–Li bond; 2) apparent η^5 and η^4 bonding to the Li(1) center; 3) two terminal rings, the germanium atoms in which tilt away from the

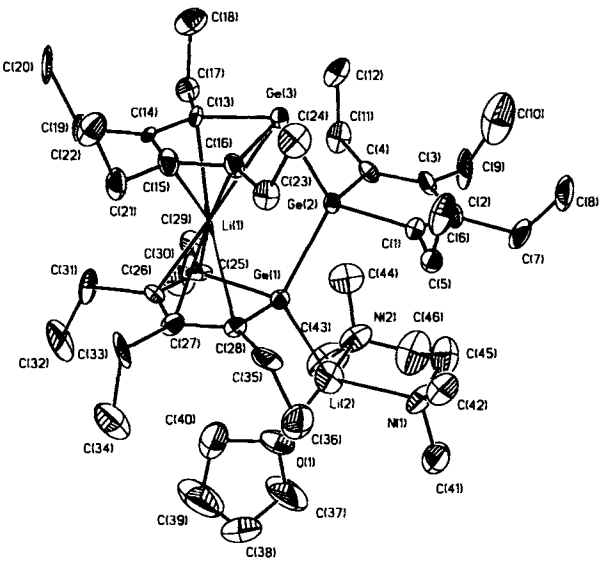

Fig. 1. Structure of **3** in the solid state. Selected bond lengths [Å] and angles [°]: Ge(1)-Ge(2) 2.527(2), Ge(2)-Ge(3) 2.508(2), Ge(1)-C(25) 2.002(16), Ge(1)-C(28) 2.009(13), C(25)-C(26) 1.358(26), C(26)-C(27) 1.476(24), C(27)-C(28) 1.369(23), Ge(2)-C(1) 1.980(16), Ge(2)-C(4) 1.982(14), C(1)-C(2) 1.354(23), C(2)-C(3) 1.533(23), C(3)-C(4) 1.357(22), Ge(3)-C(13) 2.019(14), Ge(3)-C(16) 1.976(16), C(13)-C(14) 1.363(22), C(14)-C(15) 1.507(23), C(15)-C(16) 1.371(22), Ge(1)-Li(1) 2.759(24), Ge(1)-Li(2) 2.716(31), Ge(3)-Li(1) 2.700(28), C(13)-Li(1) 2.179(32), C(14)-Li(1) 2.262(29), C(15)-Li(1) 2.288(28), C(16)-Li(1) 2.304(28), C(25)-Li(1) 2.382(28), C(26)-Li(1) 2.394(31), C(27)-Li(1) 2.406(34), C(28)-Li(1) 2.411(32), C(25)-Ge(1)-C(28) 84.1(7), C(1)-Ge(2)-C(4) 88.9(7), C(13)-Ge(3)-C(16) 84.4(6), Ge(1)-Ge(2)-Ge(3) 123.1(1), Ge(2)-Ge(1)-Li(2) 124.1(8).

π complexed lithium (the angle between the two least-squares planes Ge(1), C(25), C(26), C(27), C(28) and Ge(3), C(13), C(14), C(15), C(16) is 10.7°); and, 4) ring to Li bond lengths close to those in lithocenes.[1] Other noteworthy structural features are that the Ge–Ge bonds are longer than typical Ge–Ge bonds (2.41–2.46 Å) in trigermanes,[14] but shorter than typical Ge–Ge bonds (2.53–2.59 Å) in cyclotrigermanes.[15] The Ge(2)–Li(1) distance of 2.794 Å indicates the absence of a significant bonding interaction between Ge(2) and Li(1).[16]

The structure of **3** consists of three rings, the middle ring (C_4Ge(2)) of which bridges the other two rings by Ge–Ge

bonds. This middle ring is a typical germole.[17] The germanium atoms of the two terminal rings are slightly out of the ring's plane. For example, the deviations from the least-squares planes are 0.072 Å for $C_4Ge(1)$, and 0.082 Å for $C_4Ge(3)$. Li(1) is positioned close to the center of the two planes defined by $C_4Ge(1)$ and $C_4Ge(3)$, similar to the situation in lithocene or ferrocenophane derivatives.[18] Li(2) is tetrahedrally coordinated by the two nitrogen atoms of the TMEDA molecule, the oxygen atom of the THF molecule and Ge(1). The Ge(1)–Ge(2) bond (2.527(2) Å) is longer than the Ge(2)–Ge(3) bond (2.508(2) Å).

Delocalization in the $C_4Ge(1)$ and $C_4Ge(3)$ rings is not as complete as in lithocene derivatives[1] and $[(\eta^5\text{-}C_5Me_5)Ru\{\eta^5\text{-}C_4Me_4GeSi(SiMe_3)_3\}]$.[9] (See the values of $C_\beta C_\beta$–$C_\alpha C_\beta$ and the bond lengths in Table 1.) These intra-ring bond lengths notwithstanding, the Li(1)–$C_4Ge(3)_{centroid}$ distance of 1.918 Å compares favorably to the Li–$C_{5centroid}$ distance of 1.987–2.008 Å in the lithocene anion.[1] In contrast, the Li(1)–$C_4Ge(1)_{centroid}$ distance of 2.046 Å is a little out of that range, which is attributed to the significant bonding interaction[16] between Ge(1) and Li(2) (Table 1). Thus, Li(1) is η^5 coordinated to the $C_4Ge(3)$ ring but Ge(1) is sp^3 hybridized, and Li(1) is η^4 coordinated to the $C_4Ge(1)$ ring.

Table 1. Structural data for **3** and a related ruthenium compounds.

	Ge(1)	Ge(2)	Ge(3)	Ru*
C_β–C_β [Å]	1.476(24)	1.533(23)	1.507(23)	1.425(11)
(C_α–C_β) [Å] [a]	1.364	1.356	1.367	1.425
$C_\beta C_\beta$–$C_\alpha C_\beta$	0.112	0.177	0.140	0.00
(Ge–C_α) [Å] [a]	2.006	1.981	1.998	1.900
C_α–Ge–C_α [°]	84.1(7)	88.9(7)	84.4(6)	89.1(1)

[a] Average length. Cp* = pentamethylcyclopentadienyl. Ru* = $[(Cp^*)Ru\{\eta^5\text{-}C_4Me_4GeSi(SiMe_3)_3\}]$.

The NMR spectra of **3** indicate that the sandwich structure is preserved in solution even at room temperature; one Li cation is in a highly anisotropic environment as in lithocene, while the other Li cation is in an environment similar to that in common organolithium compounds. The two terminal rings can be distinguished by low-temperature ^1H NMR spectroscopy (Table 2). At 25 °C, two broad peaks are observed in the ^7Li NMR spectrum which, upon cooling to −50 °C, form two sharp resonances at $\delta = -4.98$ and $\delta = -0.93$ (Table 2). The former is consistent with π bonding in cyclopentadienyllithium derivatives ($\delta = -8.2$ to -12.5),[19] while the latter is typical of coordinated lithium ions.[20] In the ^1H NMR spectrum only two sets of two ethyl peaks in the ratio of 1:2 are observed, consistent with C_2 symmetry, over the temperature range +50 to +10 °C. Upon cooling from +50 to −50 °C, the two broad quartets of methylene absorptions become four well-defined quartets, indicating the coordination of the second lithium ion to a germanium atom (Table 2).

Table 2. ^1H and ^7Li NMR shifts of **3** at various temperatures.

T [°C]	^1H NMR (CH_2 groups) [δ]						^7Li NMR [δ] [a]	
	Ge(1,3)		Ge(2)	Ge(2)	Ge(1,3)			
50	2.88 (br.q)		2.73 (q)	2.35 (q)	2.28 (br.q)		−2.7 (br.s)	
15	2.88 (br.s)		2.71 (q)	2.32 (q)	2.28 (br.s)		−1.2 (br.s)	−4.6 (br.s)
10	2.87 (v br.s)		2.71 (q)	2.32 (q)	2.27 (v br.s)			
5	2.95 (br.s)	2.79 (br.s)	2.71 (q)	2.32 (q)	2.30 (br.s)	2.24 (br.s)		
−10	3.03 (br.s)	2.72 (br.s)	2.70 (br.q)	2.31 (br.q)	2.40 (br.s)	2.14 (br.s)	−0.93 (br.s)	−4.85 (br.s)
−30	3.05 (br.s)	2.71 (br.s)	2.71 (br.s)	2.32 (br.s)	2.41 (br.s)	2.13 (br.s)	−0.93 (br.s)	−4.98 (br.s)
−40	3.05 (br.q) [b]	2.73 (br.q)	2.69 (br.q)	2.31 (br.q)	2.40 (br.q) [b]	2.08 (br.q) [b]	−0.93 (br.s)	−4.98 (br.s)
−48	3.06 (q) [b]	2.73 (q)	2.70 (q)	2.30 (q)	2.40 (q) [b]	2.08 (q) [b]	−0.93 (ss)	−4.98 (ss)

[a] ^7Li NMR (155 MHz, $[D_8]$THF, external LiBr (1 M/THF)). [b] AB system.

These observations can be explained by a simple process in which the σ-bound lithium ion becomes solvated and is reattached to the ring, as shown in Figure 2. The NMR spectroscopic data do not rule out a more complex bimolecular process in which lithium atoms are passed between rings without the intermediacy of a solvated lithium ion.

^{13}C NMR data for **3** at 25 °C (Tables 3 and 4) show that the chemical shifts assigned to the $C_4Ge(2)$ ring are typical of a conventional neutral germole. The signals of the α and β carbon atoms in the $C_4Ge(1)$ and $C_4Ge(3)$ rings, however, appear much further downfield than those in other neutral germoles, including the $C_4Ge(2)$ ring in **3**. These downfield shifts are in contrast to the upfield shifts in shifts in silole anions which possess signif-

Table 3. ^{13}C NMR chemical shifts in **1**, **2**, and **3**.

	1 [a] Ge	**2** [a] Ge(1,3)		**2** [a] Ge(2)		**3** [b] Ge(1,3)		**3** [b] Ge(2)	
C_α	132.12	142.98		144.60		156.00		142.18	
C_β	149.62	149.38		148.96		171.72		146.35	
T	563.58	584.72		587.12		655.44		577.06	
	α-Et β-Et	α-Et	β-Et	α-Et	β-Et	α-Et	β-Et	α-Et	β-Et
CH_2	20.93 21.72	21.01	24.02	21.30	24.20	22.50	28.23	21.94	26.28
CH_3	14.21 14.58	15.06	15.91	14.95	16.88	16.71	21.94	16.90	18.24

[a] 68 MHz in $CDCl_3$, 25 °C, external TMS as standard. [b] 100 MHz in $[D_8]$THF, 25 °C, δ(solvent) = 25.30; T: The total chemical shifts of the C_α and C_β atoms.

Table 4. ^{13}C NMR chemical shift differences for **1**, **2**, and **3**.

	3 − **2** Ge(1,3)	Ge(2)	**3** − **1** Ge(1,3)	Ge(2)
ΔC_α	13.02	−2.42	23.88	10.06
ΔC_β	22.34	−2.61	21.90	−3.27

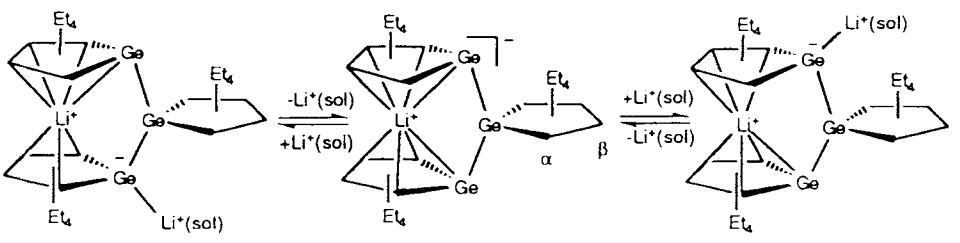

Fig. 2. Postulated mechanism for the solvation/coordination of a lithium ion in **3** (sol = solvated).

 © VCH Verlagsgesellschaft mbH, D-69451 Weinheim, 1996 0570-0833/96/3502-0187 $ 10.00+.25/0

icant π delocalization,[5-7] instead, they are similar to the downfield shifts for the ring carbon atoms in 1-lithio-2,3,4,5-tetramethyl-1-1-phenylgermacyclopentadienide [$\Delta\delta(C\alpha) = 10.5$ ppm and $\Delta\delta(C\beta) = 2.6$ ppm], in which the negative charge is localized on the germanium atom.[11] We attribute the downfield shifts of the signals in **3** to a field effect induced by the incompletely delocalized negative charges on Ge(1) and Ge(3).

Experimental Procedure

All reactions and manipulations were performed under an inert nitrogen or argon atmosphere and anhydrous conditions. NMR spectra were recorded on JEOL GSX270 and GSX400 spectrometers. GC-MS and solid sample MS data were obtained on a Hewlett-Packard 5988A GC-MS system equipped with a methyl silicon capillary column. Elemental analyses were performed by Desert Analytics, Tucson, Arizona. All ^{13}C NMR data are given in Table 2 [21].

1: A mixture of Mg (4.86 g, 200 mmol) and $HgCl_2$ (5.43 g, 20 mmol) in THF (70 mL) was stirred for 40 min. To this was added a solution of $[Cp_2ZrCl_2]$ (14.62 g, 50 mmol) and 3-hexyne (11.34 mL, 8.20 g, 100 mmol) in THF (200 mL) with stirring at room temperature [22]. The mixture was stirred overnight to give a dark red solution which was decanted into a 500 mL flask and cooled to −78 °C. To this was added $GeCl_4$ (5.70 mL, 10.72 g, 50 mmol) with stirring. The mixture was warmed to room temperature and stirred overnight to produce a clear, light orange solution [23]. After solvent was removed under reduced pressure, the residue was extracted with pentane. Removal of solvents under reduced pressure gave **1** as a colorless liquid. Yield: 9.84 g (64%, 99% pure by GC), b.p. 87–89° C/0.1 mm Hg, correct elemental analysis for $C_{12}H_{20}Ge_2Cl_2$; ^1H NMR (270 MHz, $CDCl_3$, ext. TMS), $\delta = 1.04$ (q, $^3J(H,H) = 7.3$ Hz, 6H; Me), 1.23 (q, $^3J(H,H) = 7.3$ Hz, 6H; Me), 2.33 (t, $^3J(H,H) = 7.3$ Hz, 4H; CH_2), 2.45 (t, $^3J(H,H) = 7.3$ Hz, 4H; CH_2); MS (70 eV): *m/z* (%): 312 (1.2) [$M^+ + 4$], 311 (0.7) [$M^+ + 3$], 310 (4.2) [$M^+ + 2$], 309 (1.4) [$M^+ + 1$], 308 (7) [M^+, 7], 306 (5.40) [$M^+ - 2$], 304 (2.4) [$M^+ - 4$], 164 (32) [$C_4Et_4^+$], 149 (100) [$C_4Et_4^+ - 15$], 135 (86), 107 (79), 91 (43).

2: Crystals of **3** (1.0 g) were dissolved in THF (30 mL) and slowly added to an excess of methyl iodide at 0 °C. Additional stirring at room temperature for 4 h produced a colorless solution and a white solid. Removal of all volatiles, extraction with hexane, followed by column chromatography gave a colorless oil which solidified slowly at room temperature. The yield of **2** was quantitative as determined by GC and ^1H NMR. Correct elemental analysis for $C_{38}H_{66}Ge_3$; ^1H NMR (270 MHz, $CDCl_3$, ext. TMS), $\delta = 0.64$ (s, 6H; $GeCH_3$), 0.87–1.03 (overlapped t, 36H; CH_3), 2.15–2.48 (brd m, 24H; CH_2).

3: Sonication of **1** (6.30 g, 20.5 mmol) in an ultrasonic cleaning bath [24] with excess Li (0.68 g, 97.14 mmol) in THF (70 mL) and TMEDA (6.5 mL, 5.01 g, 43 mmol) for 10 h gave a red-orange solution. After the unconverted lithium was filtered, all volatiles were removed under vacuum. The residue was extracted with hexane. The resulting solution produced orange-red crystals of **3**. ^1H NMR (270 MHz, [D$_8$]THF, 25 °C, solvent: $\delta = 1.73$), $\delta = 0.94$ (t, $^3J(H,H) = 7.3$ Hz, 12H; CH_3 of Ge(1,3)), 1.07 (t, $^3J(H,H) = 7.3$ Hz, 6H; CH_3 of Ge(2)), 1.12 (t, $^3J(H,H) = 7.3$ Hz, 12H; CH_3 of Ge(1,3)), 1.24 (t, $^3J(H,H) = 7.3$ Hz, 6H; CH_3 of Ge(2)), 2.29 (brd s, 8H; CH_2 of G(1,3)), 2.34 (q, $^3J(H,H) = 7.3$ Hz, 4H; CH_2 of Ge(2)), 2.72 (q, $^3J(H,H) = 7.3$ Hz, 4H; CH_2 of Ge(2)), 2.88 (brd s, 8H; CH_2 of Ge(1,3)). All peak assignments are based on proton homo decoupling, INEPT ^{13}C, and ^{13}C-^1H correlation 2D experiments.

Received: August 7, 1995 [Z 8289 IE]
German version: *Angew. Chem.* **1996**, *108*, 213–216

Keywords: aromaticity · germanium compounds · germoles · heterocycles · lithocenes

[1] S. Harder, M.H. Prosenc, *Angew. Chem.* **1994**, *106*, 1830; *Angew. Chem. Int. Ed. Engl.* **1994**, *33*, 1744; F. Zaegel, J. C. Galluci, P. Meunier, B. Gautheron, M. R. Sivik, L. A. Paquette, *J. Am. Chem. Soc.* **1994**, *116*, 6466; for the crystal structure of lithium-7b*H*-indeno[1,2,3-*jk*]fluorenide see: D. Bladauski, W. Broser, H.-J. Hecht, D. Rewicki, H. Dietrich, *Chem. Ber.* **1979**, *112*, 1380.

[2] For NMR studies of cyclopentadienyllithium see: L. A. Paquette, M. R. Sivik, W. Bauer, P. von R. Schleyer, *Organometallics* **1994**, *13*, 4919; W. Bauer, M. R. Sivik, D. Fridrich, P. von R. Schleyer, L. A. Paquette, *ibid.* **1992**, *11*, 4178; W. Bauer, G. A. O'Doherty, P. von R. Schleyer, L. A. Paquette, *J. Am. Chem. Soc.* **1991**, *113*, 7093; L. A. Paquette, W. Bauer, M. R. Sivik, M. Bühl, M. Feigel, P. von R. Schleyer, *ibid.* **1990**, *112*, 8776.

[3] H. Grüntzmacher, *Angew. Chem.* **1995**, *107*, 323; *Angew. Chem. Int. Ed. Engl.* **1995**, *34*, 295; J. Dubac, A. Laporterie, G. Manuel, *Chem. Rev.* **1990**, *90*, 215; E. Colomer, R. J. P. Corriu, M. Lheureux, *ibid.* **1990**, *90*, 265.

[4] P. von R. Schleyer, P. K. Freeman, H. Jiao, B. Goldfuss, *Angew. Chem.* **1995**, *107*, 332; *Angew. Chem. Int. Ed. Engl.* **1995**, *34*, 337 and references therein.

[5] J.-H. Hong, P. Boudjouk, *J. Am. Chem. Soc.* **1993**, *115*, 5883.

[6] J.-H. Hong, P. Boudjouk, S. Castellino, *Organometallics* **1994**, *13*, 3387.

[7] B. Goldfuss, P. von R. Schleyer, *Organometallics* **1995**, *14*, 1555.

[8] W. P. Freeman, T. D. Tilley, A. L. Rheingold, *J. Am. Chem. Soc.* **1994**, *116*, 8428.

[9] W. P. Freeman, T. D. Tilley, A. L. Rheingold, R. L. Ostrander, *Angew. Chem.* **1993**, *105*, 1841; *Angew. Chem. Int. Ed. Engl.* **1993**, *32*, 1744.

[10] M. D. Curtis, *J. Am. Chem. Soc.* **1967**, *89*, 4241; *ibid.* **1969**, *91*, 6011.

[11] P. Dufour, J. Dubac, M. Dartiguenave, Y. Dartiguenave, *Organometallics* **1990**, *9*, 3001.

[12] J.-H. Hong, P. Boudjouk, *Bull. Soc. Chim. Fr.* **1995**, *132*, 495.

[13] X-ray structure analysis of **3**: $C_{50}H_{94}Ge_3Li_2N_2O_2$, $M = 986.9$, monoclinic, $P2_1/c$, $a = 10.846(2)$, $b = 21.013(4)$, $c = 23.881(4)$ Å, $\beta = 100.57(2)°$, $V = 5351(2)$ Å^3, $Z = 4$, $\rho_{calcd} = 1.225$ g cm^{-3}, $Mo_{K\alpha}$, $\lambda = 0.71073$ Å, $T = 223$ K; 6981 independent reflections were collected, of which 3263 reflections with F_0 greater than $4.0\sigma(F_0)$ were used for refinement. $R(F) = 0.066$, $R_w(F) = 0.076$, GOP = 6.34. X-ray-quality crystals of **2** were grown by slowly cooling a concentrated hexane solution of **2** at −25 °C. Data were collected at 223 K on a Siemens R 3m/V diffractometer at $2\theta = 3.5$ to 45.0° using graphite monochromated $Mo_{K\alpha}$ radiation. All calculations were performed with Siemens SHELXTL PLUS (VMS) programs. The structure was solved by Patterson and refined by the full matrix least-square procedure. Further details of the crystal structure investigation may be obtained from the Director of the Cambridge Crystallographic Data Centre, 12 Union Road, GB-Cambridge CB2 1EZ (UK), on quoting the full journal citation.

[14] S. Roller, D. Simon, M. Draeger, *J. Organomet. Chem.* **1986**, *301*, 27; M. Draeger, D. Simon, *ibid.* **1986**, *306*, 183; K. Haeerle, M. Draeger, *ibid.* **1986**, *312*, 155.

[15] T. Tsumuraya, S. A. Batcheller, S. Masamune, *Angew. Chem.* **1991**, *103*, 916; *Angew. Chem. Int. Ed. Engl.* **1991**, *30*, 902 and references are therein.

[16] The van der Waals radii of Ge is not available, but the Li–Ge distance in the monogermanides lies between 2.70 and 2.88 Å in the normal pressure phase and between 2.64 and 3.24 Å in the high-pressure phase. J. Evers, G. Oehlinger, G. Sextl, H.-O. Becker, *Angew. Chem.* **1987**, *327*, 260; *Angew. Chem. Int. Ed. Engl.* **1987**, *26*, 76.

[17] The bond lengths and angles in $Ph_4C_4Ge(CCPh)_2$ are 1.927 Å (Ge–C_α), 1.353 Å (C=C), 1.510 Å (C–C), and 91.4° (C_α-Ge-C_α) in S. V. Lindeman, V. E. Shklover, Yu. T. Struchkov, N. A. Vasneva, A. M. Sladkov, *Cryst. Struct. Commun.* **1981**, *10*, 827.

[18] For the structure of (1,1′-ferrocenediyl)diphenylgermane and (1,1′-ferrocenediyl)phenylphosphane, see: H. Stoeckli-Evans, A. G. Osborne, R. H. Whiteley, *J. Organomet. Chem.* **1980**, *194*, 91. For the structure of (1,1′-ferrocenediyl)diphenylsilane, see: H. Stoeckli-Evans, A. G. Osborne, R. H. Whiteley, *Helv. Chim. Acta* **1976**, *7*, 2403.

[19] P. Jutzi, W. Letters, S. Pohl, W. Saak, *Chem. Ber.* **1989**, *122*, 1449.

[20] R. Cox, H. Terry, *J. Magn. Reson.* **1974**, *14*, 317.

[21] Detailed ^1H, ^{13}C, and ^7Li NMR data are available upon request from the authors.

[22] The synthetic procedures of $[Cp_2Zr(EtCCEt)_2]$ were modified from a published procedure: A. J. Ashe, III, J. W. Kampf, S. M. Al-Taweel, *J. Am. Chem. Soc.* **1992**, *114*, 372.

[23] P. J. Fagan, W. A. Nugent, *J. Am. Chem. Soc.* **1988**, *110*, 2310.

[24] P. Boudjouk in *Current Trends in Sonochemistry*, *Organometallic Processes Promoted by Ultrasound* (Ed.: G. J. Price), The Royal Society of Chemistry, Cambridge, **1992**, p. 110–122.

Patterns of Multiple Additions to Fullerene C_{70}: Isolation and Structural Characterization of $[C_{70}\{Pt(PPh_3)_2\}_4]$**

Alan L. Balch,* Leijun Hao, and Marilyn M. Olmstead

Fullerenes provide the chemist with a rich framework for the assembly of large molecules with remarkably complex and frequently aesthetically pleasing structures.[1-4] Since the fullerenes contain a multiplicity of similar carbon–carbon bonds that appear to be only weakly interconnected electronically, the pat-

[*] Prof. Dr. A. L. Balch, Dr. L. Hao, Dr. M. M. Olmstead
Department of Chemistry
University of California, Davis
Davis, CA 95616 (USA)
Fax: Int. code +(916) 752-8995
e-mail: albalch@ucdavis.edu

[**] This work was supported by the U.S. National Science Foundation (Grant CHE 9321257). We thank Johnson Matthey, Inc. for a loan of platinum salts.

terns of reactivity, which frequently involve multiple addition reactions, require experimental exploration. Single and multiple additions to C_{60} have been studied in detail, and some factors leading to regiospecific multiple additions have been identified.[5] However, comparable information relevant to the patterns of additions to the higher fullerenes such as C_{70} is limited. Here we report on the results of addition reactions of $Pt(PPh_3)_2$ units to C_{70} which involves the successive formation of adducts **1**–**4** with the eventual addition of four platinum atoms in a plane about the fullerene.

$[C_{70}\{Pt(PPh_3)_2\}]$ **1** $[C_{70}\{Pt(PPh_3)_2\}_2]$ **2**

$[C_{70}\{Pt(PPh_3)_2\}_3]$ **3** $[C_{70}\{Pt(PPh_3)_2\}_4]$ **4**

The structure of C_{70}, which is shown in Figure 1, contains five types of carbon atoms in layers, a–e, and eight types of carbon–carbon bonds. Additions to C_{70} are governed by considerations of both π-bond order and the fullerene curvature. Of the four C–C bonds at 6-6 ring junctions, those at the C_c–C_c and C_a–C_b bonds have the highest π-bond orders, 1.74 and 1.66, respectively.[6] The curvature of C_{70} is greatest at the poles so that the C_a–C_b bonds are the most pyramidalized.[7–9] Formation of organometallic complexes of C_{70} by addition of one or two molecules of Vaska's complex $[Ir(CO)Cl(PR_3)_2]$ has been shown to involve addition to the C_a–C_b bonds, the most pyramidalized bonds in this fullerene.[7, 8] In this case the only double addition product that crystallizes has isomeric structure **B**.[8] Osmylation of C_{70} produces two isomeric monoaddition products that involve addition to the C_a–C_b and C_c–C_c bonds.[9] Diels–Alder adducts of C_{70} have been obtained in which addition has occurred at three of the possible 6-6 ring junctions to produce adducts involving the C_a–C_b, C_c–C_c, and C_d–C_e bonds.[10, 11] Three biscyclopropanation adducts of C_{70} have been observed to form; the isomeric form **B** is predominant (relative ratio of isomers: **A**, 0.19; **B** 0.68; **C**, 0.13).[12]

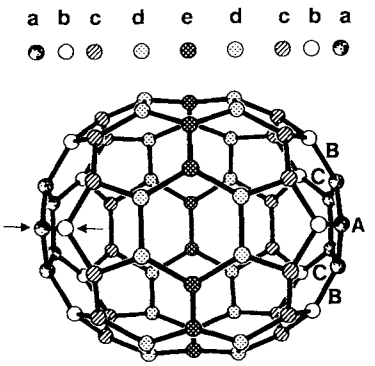

Fig. 1. Structure of C_{70} emphasizing the layers of five types (C_a–C_e) of carbon atoms. For double addition to C_{70}, in which the first addition occurs at the bond denoted by the arrows, three isomeric products are possible. Addition at bonds A, B, and C produce isomers **A**, **B**, and **C**, respectively.

Addition of four molar equivalents of $[Pt(C_2H_4)(PPh_3)_2]$ to a solution of C_{70} in benzene produces a deep brown solution from which **4** can be obtained by evaporation. The complex can be recrystallized from benzene by the slow diffusion of diethyl ether/methanol. The results of a single-crystal X-ray diffraction study of **4** · 6.5 benzene · 0.5 methanol are shown in Figure 2.[13] The adduct **4** has no crystallographically imposed symmetry, but the $C_{70}Pt_4P_8$ unit does have effective C_{2v} symmetry with the twofold axis passing through the centers of the C36–C37 and C31–C32 bonds. The four platinum atoms reside in a single plane (maximum deviation: ±0.051 Å for Pt3 and Pt4). Two of the platinum atoms, Pt1 and Pt2, are coordinated to C_a–C_b bonds and thus are in sites that are analogous to those utilized in the binding of Vaska's compound to C_{70}. However,

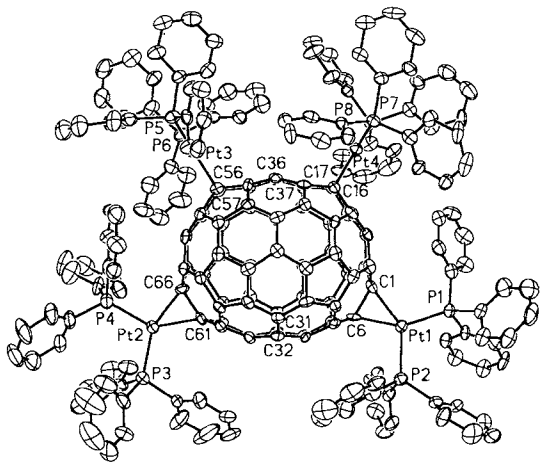

Fig. 2. A perspective drawing of the structure of **4** (50% thermal contours for all non-hydrogen atoms). Selected bond lengths [Å]: Pt(1)-C(1) 2.122(12), Pt(1)-C(6) 2.092(12), Pt(2)-C(61) 2.146(11), Pt(2)-C(66) 2.092(12), Pt(3)-C(56) 2.140(11), Pt(3)-C(57) 2.112(12), Pt(4)-C(16) 2.086(11), Pt(4)-C(17) 2.136(11), Pt(1)-P(1) 2.280(3), Pt(1)-P(2) 2.295(3), Pt(2)-P(3) 2.280(3), Pt(2)-P(4) 2.282(3), Pt(3)-P(5) 2.267(3), Pt(3)-P(6) 2.297(3), Pt(4)-P(7) 2.286(3), Pt(4)-P(8) 2.258(3), C(1)-C(6) 1.51(2), C(16)-C(17) 1.48(2), C(56)-C(57) 1.495(14), C(61)-C(66) 1.51(2).

the other two platinum atoms, Pt3 and Pt4, are attached to C_c–C_c bonds. This compound represents the first case in which direct attachment of a metal center to a C_c–C_c bond in C_{70} has been observed and is currently the highest adduct of C_{70} to be fully characterized. As Figure 3 shows, this arrangement of platinum bearing addends results in effective coverage of the two

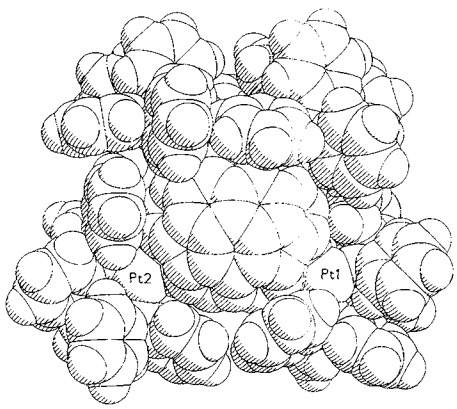

Fig. 3. Van der Waals surfaces of **4**.

poles of the fullerene by phenyl groups of the phosphane ligands. As seen previously for $[C_{70}Ir(CO)Cl(PPh_3)_2]$ and $[C_{70}\{Ir(CO)Cl(PPhMe_2)_2\}_2]$,[7, 8] two of the phenyl groups addends attached to the C_a–C_b bonds make face-to-face π–π contact with the fullerene, but there is no contact of this sort by the ligands attached to the C_c–C_c bonds. In contrast to the situation at the poles, the central portion of the C_{70} moiety, especially the C_e–C_e bonds, is exposed and accessible for chemical reaction. Consequently steric factors, symmetry considerations, and solubility play major roles in determining the pattern of addition seen in the formation of **4**.[14] Notice that the placement of the platinum complexes on the specific C_c–C_c bonds, C16–C17 and C56–C57, places these as far as possible from the platinum complexes at the C_a–C_b bonds, C1–C6 and C61–C66. The resulting arrangement of four groups about

 © VCH Verlagsgesellschaft mbH, D-69451 Weinheim, 1996 0570-0833/96/3502-0189 $ 10.00+.25/0

the C_{70} core has the highest possible symmetry for such a tetraaddition product.

It is important to note that information obtained about the favored geometry of bisaddition products cannot be used to predict the pattern of higher addition products of C_{70} at least in the case of relatively labile addenda. From the structural study of $[C_{70}\{Ir(CO)Cl(PPhMe_2)_2\}_2]$[8] and work on the biscyclopropanation of C_{70},[12] it may be concluded that isomer **B** is the favored geometry for double addition. However, the arrangement of $Pt(PPh_3)_2$ groups at the C_a-C_b bonds of **4** does not correspond to isomer **B** of a double addition product. Rather it corresponds to isomer **A**, the statistically least favored isomer.

Attempts to add more than four $Pt(PPh_3)_2$ groups to C_{70} by increasing the $[Pt(C_2H_4)(PPh_3)_2]/C_{70}$ ratio have not been successful, but it has been possible to observe the formation of the lower adducts **1**–**3**. When C_{70} is treated with $[Pt(C_2H_4)(PPh_3)_2]$ in benzene in ratios of 1:1, 1:2, and 1:3, brown solids are obtained upon evaporation of the solvent. Analysis by ^{31}P NMR spectroscopy shows that each sample contains a spectroscopically discrete species. The 1:1 adduct **1** has been briefly described and identified as having the platinum bound to a C_a-C_b bond.[15] Our ^{31}P NMR data ($\delta = 28.0$ [d, 1P, $^1J(Pt,P) = 4038$ Hz, $^2J(P,P) = 24$ Hz], 25.3 [d, 1P, $^1J(Pt,P) = 3866$ Hz, $^2J(P,P) = 24$ Hz] in C_6D_6) are consistent with this interpretation. Additionally we have X-ray crystallographic data that shows that the related complex $[C_{70}Pd(PPh_3)_2]$ has the palladium center coordinated to a C_a-C_b bond.[16] The ^{31}P NMR data obtained for **2** ($\delta = 28.5$ [d, 2P, $^1J(Pt,P) = 4032$ Hz, $^2J(P,P) = 29$ Hz], 26.3 [d, 2P, $^1J(Pt,P) = 3868$ Hz, $^2J(P,P) = 29$ Hz] in C_6D_6) are similar to those for **1** and are consistent with addition to the C_a-C_b bonds at opposite poles of C_{70}. Three isomers of **2**, **A** with C_{2v} symmetry and **B** and **C** with C_2 symmetry,[8] are possible and further structural characterization will have to await a crystalline sample suitable for X-ray diffraction. For **3**, the ^{31}P NMR data ($\delta = 30.0$ [s, 2P, $^1J(Pt,P) = 4000$ Hz], 29.6 [d, 1P, $^1J(Pt,P) = 3932$ Hz, $^2J(P,P) = 41$ Hz], 28.9 [d, 1P, $^1J(Pt,P) = 4002$ Hz, $^2J(P,P) = 34$ Hz], 27.8 [d, 1P, $^1J(Pt,P) = 3876$ Hz, $^2J(P,P) = 41$ Hz], 27.0 [d, 1P, $^1J(Pt,P) = 3889$ Hz, $^2J(P,P) = 34$ Hz] in C_6D_6) suggest that two of the $Pt(PPh_3)_2$ groups (those with $\delta = 28.9$ and 27.0) are bound to C_a-C_b bonds, while the third ($\delta = 30.0$) is attached to a C_c-C_c bond. These spectroscopic data combined with the X-ray crystallographic structure for **4** indicate that binding of the platinum centers preferentially occurs at the C_a-C_b bonds and only after the two poles are blocked with addends, does binding to the less pyramidalized C_c-C_c bonds occur. As a result of steric considerations and the low reactivity of the exposed C_e-C_e bonds, addition of $Pt(PPh_3)_2$ groups to C_{70} stops after the formation of the tetraadduct **4**. In contrast, up to six $Pt(PR_3)_2$ groups have been added to the smaller fullerene C_{60}.[2, 3]

Experimental Procedure

All reactions were carried out under a N_2 atmosphere using Schlenk techniques. The solvents were dried and freshly distilled. $[Pt(C_2H_4)(PPh_3)_2]$ was prepared by a literature method [17].

4: Solid $[Pt(C_2H_4)(PPh_3)_2]$ (57 mg, 0.076 mmol) was added to a solution of C_{70} (16 mg, 0.019 mmol) in benzene (20 mL). The red-brown solution of C_{70} darkened immediately. The mixture was stirred for 20 min. The solvent was then removed under vacuum to give the product as a dark brown solid in 85% yield. Well-shaped black crystals of **4** · 6.5 benzene · 0.5 methanol that were suitable for X-ray diffraction were obtained by diffusion of diethyl ether/methanol (10/1, v/v) into a solution of **4** in benzene. IR (KBr pellet): $\tilde{\nu} = 1478$ (m), 1433 (s), 1094 (s), 742 (s), 692 (vs), 674 (m), 534 (m), 517 (s), 507 (s) cm^{-1}. $^{31}P\{^1H\}$ NMR (in C_6D_6): $\delta = 29.9$ [s, 4P, $^1J(Pt,P) = 4000$ Hz], 28.7 [d, 2P, $^1J(Pt,P) = 3923$ Hz, $^2J(P,P) = 41$ Hz], 27.9 [d, 2P, $^1J(Pt,P) = 3901$ Hz, $^2J(P,P) = 41$ Hz].

Samples of the other addition products **1**–**3** were obtained similarly as dark brown solids. These were examined by ^{31}P NMR spectroscopy but so far have not produced crystals suitable for single crystal X-ray diffraction.

Received: August 7, 1995
Revised version: October 4, 1995 [Z 8290 IE]
German version: *Angew. Chem.* **1996**, *108*, 211–213

Keywords: fullerenes · platinum compounds

[1] a) R. Taylor, D. M. R. Walton, *Nature* **1993**, *363*, 685; b) A. Hirsch, *Angew. Chem.* **1993**, *105*, 1189; *Angew. Chem. Int. Ed. Engl.* **1993**, *32*, 1138; c) A. Hirsch, *The Chemistry of the Fullerenes*, Thieme, Stuttgart, **1994**.
[2] P. J. Fagan, J. C. Calabrese, B. Malone, *Acc. Chem. Res.* **1992**, *25*, 134.
[3] P. J. Fagan, J. C. Calabrese, B. Malone, *J. Am. Chem. Soc.* **1991**, *113*, 9408.
[4] A. L. Balch in *The Chemistry of Fullerenes* (Ed.: R. Taylor), World Scientific Publishing Co., in press.
[5] A. Hirsch, I. Lamparth, T. Grösser, H. R. Karfunkel, *J. Am. Chem. Soc.* **1994**, *116*, 9385; A. Hirsch, I. Lamparth, H. R. Karfunkel, *Angew. Chem.* **1994**, *106*, 453; *Angew. Chem. Int. Ed. Engl.* **1994**, *33*, 437; I. Lamparth, C. Maichle-Mössmer, A. Hirsch, *Angew. Chem.* **1995**, *107*, 1755; *Angew. Chem. Int. Ed. Engl.* **1995**, *34*, 1607.
[6] J. Baker, P. W. Fowler, P. Lazzeretti, M. Malagoli, R. Zanai, *Chem. Phys. Lett.* **1991**, *184*, 182.
[7] A. L. Balch, V. J. Catalano, J. W. Lee, M. M. Olmstead, S. R. Parkin, *J. Am. Chem. Soc.* **1991**, *113*, 8953.
[8] A. L. Balch, J. W. Lee, M. M. Olmstead, *Angew. Chem.* **1992**, *104*, 1400; *Angew. Chem. Int. Ed. Engl.* **1992**, *31*, 1356.
[9] J. M. Hawkins, A. Meyer, M. A. Solow, *J. Am. Chem. Soc.* **1993**, *115*, 7499.
[10] A. Herrmann, F. Diederich, C. Thilgen, H.-U. ter Meer, W. H. Müller, *Helv. Chim. Acta* **1994**, *77*, 1689.
[11] P. Seiler, A. Herrmann, F. Diederich, *Helv. Chim. Acta* **1995**, *78*, 344.
[12] C. Bingel, H. Schiffer, *Liebigs Ann.* **1995**, 1551.
[13] Crystal data for **4** · $6.5C_6H_6$ · $0.5CH_3OH$: black parallelepipeds of $C_{253.50}H_{161}O_{0.50}P_8Pt_4$ that were obtained by diffusion of diethyl ether into a benzene solution of the compound under dioxygen-free conditions form in the triclinic space group $P\bar{1}$ with $a = 14.948(3)$, $b = 21.280(4)$, $c = 29.334(4)$ Å, $\alpha = 91.521(14)$, $\beta = 90.27(2)$, $\gamma = 105.39(2)°$ at 130(2) K with $Z = 2$ with the use of graphite monochromated $Mo_{K\alpha}$ ($\lambda = 0.71073$ Å) radiation. Refinement of 31664 reflections with 2272 parameters and 18 restraints yielded $wR2 = 0.2158$ (based on F^2) and a conventional $R_1 = 0.074$ (based on F) for 21833 reflections with $I > 2\sigma(I)$. Further details of the crystal structure investigation are available on request from the Director of the Cambridge Crystallographic Data Centre, 12 Union Road, GB-Cambridge CB2 1EZ, on quoting the full journal citation.
[14] A. L. Balch, J. W. Lee, B. C. Noll, M. M. Olmstead, *Inorg. Chem.* **1994**, *33*, 5238.
[15] M. Iyoda, Y. Ogawa, H. Matsuyama, H. Ueno, K. Kikuchi, I. Ikemoto, Y. Achiba, *Fullerene Sci. Tech.* **1995**, *3*, 1.
[16] A. L. Balch, L. Hao, M. M. Olmstead, unpublished results.
[17] R. A. Head, *Inorg. Synth.* **1990**, *28*, 132.

Acyclic Stereocontrol in Radical Reactions: ρ-Selectivity with Oxazolidinone Auxiliaries**

Mukund P. Sibi* and Jianguo Ji

Stereocontrol in reactions of acyclic radicals is a subject of considerable interest.[1] ρ-Diastereoselective radical reactions mediated by chiral auxiliaries[2] have been investigated by the research groups of Curran,[3] Porter,[4] Giese,[5] Garner,[6] and others.[7] However, the use of oxazolidinone auxiliaries[8] in radical reactions has been hampered because the reactive rotomer is not available in the absence of Lewis acid additives.

[*] Prof. M. P. Sibi, Dr. J. Ji
Department of Chemistry, North Dakota State University
Fargo, ND 58105-5516 (USA)
e-mail: sibi@plains.nodak.edu
Fax: Int. code + (701) 231-8831

[**] This work was supported in part by the NSF (OSR-9108770). We thank Prof. Craig Jasperse for helpful discussions.

Until recently, the application of Lewis acids in radical reactions has been rather sparse.[9] We surmised that a proper combination of a chelating Lewis acid and the R substituent in the chiral auxiliary would allow for highly diastereoselective radical reactions if the radical were to react from a single rotamer. Of the several possible rotamers (**1**–**4**), type **1** is attainable when a Lewis acid chelates the two carbonyls, and steric interaction orients R^1 *syn* to the carbonyl group.[10] The rotamer population having been thus controlled, radical addition to the substrate should occur from the least hindered face opposite to the 4-substituent of the oxazolidinone. This communication describes outstanding levels of *p*-diastereoselectivity in Lewis acid mediated radical allylation with a simple, readily available, and easily removable oxazolidinone chiral auxiliary. Additionally, the first examples of the successful use of $Sc(OTf)_3$ in radical reactions are described.

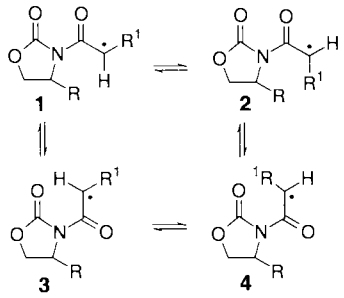

The reaction we chose to test the *p*-diastereoselectivity when oxazolidinone auxiliaries are used was the transfer of an allyl group with allyl stannane [Eq. (a)].[11] The starting material **5**

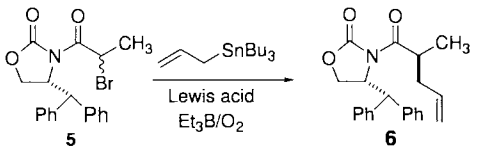

(a)

was prepared by standard acylation of our new oxazolidinone, derived from diphenylalaninol,[12] with racemic α-bromopropionic acid. The reaction of **5** with allyltributylstannane and triethylborane/oxygen[13] as the radical initiator produced **6** as a 1:1.8 diastereomeric mixture in 93% chemical yield (Table 1, entry 1). The absolute configuration of the newly formed stereocenter for the major diastereomer was established as (*R*).

Table 1. The results of allylations according to Equation (a) [a].

Entry	Lewis Acid	Reaction Conditions	% Yield[b]	Ratio (*RS*:*RR*) [c]
1	None	−78 °C, CH_2Cl_2, 3 h	93	1:1.8
2	$BF_3 \cdot OEt_2$	−78 °C, CH_2Cl_2, 2.5 h	85	1:1.4
3	Et_2AlCl	−78 °C, CH_2Cl_2, 3 h	44	1.8:1
4	$ZnCl_2$	−78 °C, CH_2Cl_2, 2 h	95	6:1
5	$Zn(OTf)_2$	−78 °C, CH_2Cl_2/THF (1:1), 2 h	86	7.6:1
6	MgI_2	−78 °C, CH_2Cl_2, 2 h	57(39)	≥100:1
7	$MgBr_2$	−78 °C, CH_2Cl_2, 2 h	94	≥100:1
8	$MgBr_2$	25 °C, CH_2Cl_2, 2 h	94	30:1
9	$Yb(OTf)_3$ [d]	−78 °C, CH_2Cl_2/THF (1:1), 2 h	64(14)	5:1
10	$Yb(OTf)_3$ [d]	−78 °C, THF, 2 h	86(5)	5:1
11	$Yb(OTf)_3$ [d]	−78 °C, Et_2O, 2 h	91	16:1
12	$Yb(OTf)_3$ [d]	−78 °C, Et_2O, H_2O (10 eq.), 2 h	77(3)	9:1
13	$Sm(OTf)_3$ [d]	−78 °C, Et_2O, 2 h	90	7:1
14	$Sc(OTf)_3$ [d]	−78 °C, Et_2O, 2 h	94	≥100:1

[a] 2 equiv of Lewis acid was used in all reactions unless otherwise noted. [b] Yield of isolated product; yield of the reduction product in parentheses. [c] Diastereomer ratios were determined by ^1H NMR spectroscopy (400 MHz). [d] 1 equiv of the Lewis acid was used.

The next series of experiments involved the screening of several mono- and multidentate Lewis acid additives of varying strength. Several entries in Table 1 are noteworthy. Outstanding levels of diastereoselectivity and high chemical yields were obtained with several Lewis acids (entries 6–8 and 14). The scandium and magnesium Lewis acids gave the highest selectivity.[14] *These experiments provide the first examples of the use of scandium triflate in radical reactions.* Lewis acids capable of chelation gave higher selectivities than those which give only single point coordination (compare entries 6–8 and 14 with 2). Increasing the temperature from −78 °C to room temperature led to a reduction in diastereoselectivity (compare entries 7 and 8). The absolute stereochemistry of **6** obtained with Lewis acid additives was (*S*), opposite to that obtained in the absence of a Lewis acid.[15] The sense of stereoinduction in Lewis acid mediated radical allylation was the same as that of enolate allylation, and these two reactions provide comparable diastereoselectivity.[16]

We have also examined the effect of the oxazolidinone ring's 4-substituent on diastereoselectivity in the allylation reaction [Eq. (b), Table 2]. Some trends are discernible from the data.

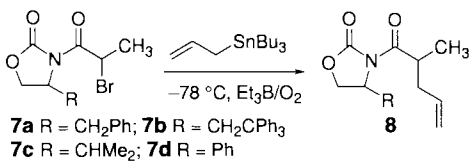

(b)

7a R = CH_2Ph; **7b** R = CH_2CPh_3
7c R = $CHMe_2$; **7d** R = Ph

Table 2. Effect of the chiral auxiliary's substituent on the diastereoselectivity of reaction (b).

Entry	Auxiliary[b]	Reaction Conditions	% Yield	Ratio [b]
1	**5** (*R*)	$MgBr_2$ (2 equiv), −78 °C, CH_2Cl_2, 2 h	94	≥100:1 (1:1.8) (*S*)
2	**5** (*R*)	$Sc(OTf)_3$ (1 equiv), −78 °C, Et_2O, 2 h	94	≥100:1 (1:1.8) (*S*)
3	**7a** (*R*)	$MgBr_2$ (2 equiv), −78 °C, CH_2Cl_2, 2 h	84	17:1 (1:1) (*S*)
4	**7a** (*R*)	$Sc(OTf)_3$ (1 equiv), −78 °C, Et_2O, 2 h	91	58:1 (1:1) (*S*)
5	**7b** (*R*)	$MgBr_2$ (2 equiv), −78 °C, CH_2Cl_2, 2 h	94	≥100:1 (1:1) (*S*)
6	**7b** (*R*)	$Sc(OTf)_3$ (1 equiv), −78 °C, Et_2O, 2 h	88	≥100:1 (1:1) (*S*)
7	**7c** (*S*)	$MgBr_2$ (2 equiv), −78 °C, CH_2Cl_2, 2 h	85	2.8:1 (1:1)[c]
8	**7d** (*S*)	$MgBr_2$ (2 equiv), −78 °C, CH_2Cl_2, 2 h	92	3:1 (1.5:1)[c]

[a] The absolute configuration of the auxiliary is indicated in parentheses. [b] The ratio for reactions without Lewis acid additive and the absolute configuration of the newly formed stereocenter are given in parentheses. Diastereomer ratios were determined by ^1H NMR spectroscopy (400 MHz). [c] The absolute configuration of the products was not determined.

Oxazolidinones with aromatic substituents (**5**, **7a**, **7b**, entries 1–6) gave higher diastereoselectivities than those with the isopropyl substituent (**7c**, entry 7). Of all the oxazolidinones examined in this study, the auxiliary derived from diphenylalaninol and the tritylmethyl-substituted auxiliary gave highest selectivity. It is interesting to note that allylation with the valinol auxiliary (**7c**) under radical conditions gave **8c** with lower diastereoselectivity than enolate allylation.[17] Substrate **7d** with an auxiliary derived from phenylglycine gave poor selectivity.

We present here a working hypothesis for the stereoselectivities observed for the Lewis acid mediated allylations with different auxiliaries [Eq. (a) and (b)]. For reactions with **5**, coordination with a bidentate Lewis acid leads to the chelated intermediate **9** with an s-(*Z*) orientation of the C–CH_3 group.

Addition of the allyltin occurs from the face opposite to the large diphenylmethyl substituent, leading to **6** with the observed (*S*) stereochemistry. The low selectivity observed for **7c** with an isopropyl substituent (see **10**) relative to that for **5** and **7a** with

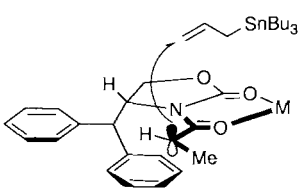

9

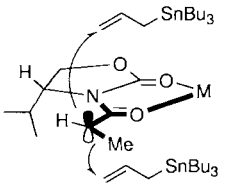

10

diphenylmethyl and benzyl substituents suggests that other factors in conjunction with steric effects may be responsible for the high selectivities observed with these auxiliaries.[18]

In conclusion we have shown that the versatile oxazolidinone auxiliaries can be used in conjunction with Lewis acids to provide outstanding levels of ρ-selectivities. The first use of scandium triflate in radical reactions was also illustrated. The extension of these studies to more complex systems and reactions with other radical acceptors is underway.

Experimental Procedure

Allylation of **5**: To a flask containing **5** (194 mg, 0.5 mmol), $MgBr_2 \cdot Et_2O$ (258 mg, 1.0 mmol), and CH_2Cl_2 (5 mL) under N_2 was added allyl tributylstannane (333 mg, 1 mmol) at $-78\,^{\circ}C$. Triethylborane (1 M in hexane, 1.0 mL, 1 mmol) and finally oxygen (5 mL, over 2 min) were added by syringe. The reaction mixture was stirred at $-78\,^{\circ}C$ for 2 h. After the reaction was complete, the mixture was diluted with CH_2Cl_2 (20 mL), washed with brine (3 × 3 mL), and the organic layer dried over $MgSO_4$. The product was purified by chromatography on silica gel (eluent: hexane/ethyl acetate 9/1). Yield 164 mg (94%).

6: M.p. 98–100 °C; $R_f = 0.6$ (80/20 hexane/ethyl acetate); ^1H NMR (400 MHz, $CDCl_3$): δ = 7.08–7.33 (m, 10H), 5.6 (m, 1H), 5.29 (m, 1H), 5.01 (m, 2H), 4.66 (d, J = 6.6 Hz, 1H), 4.35 (d, J = 5.1 Hz, 2H), 3.62 (m, 1H), 2.28 (m, 1H), 1.89 (m, 1H), 1.05 (d, J = 6.6 Hz, 3H); ^{13}C NMR (65 MHz, $CDCl_3$): δ = 176.1, 153.0, 139.5, 138.1, 135.5, 129.2, 128.9, 128.6, 128.4, 128.3, 127.8, 127.0, 117.0, 64.9, 56.5, 51.2, 37.3, 16.0; $[\alpha]_D^{26} = -111.93$ (c = 0.352, CH_2Cl_2); C,H,N analysis: calcd for $C_{22}H_{23}NO_3$: C 75.62, H 6.63, N 4.01; found: C 75.34, H 6.82, N 4.24.

Received: August 18, 1995 [Z 8321 IE]
German version: *Angew. Chem.* **1996**, *108*, 198–200

Keywords: asymmetric syntheses · chiral auxiliaries · oxazolidinones · radical reactions

[1] a) B. Giese, *Radicals in Organic Synthesis. Formation of Carbon–Carbon Bonds*, Pergamon, Oxford, **1986**; b) N. A. Porter, B. Giese, D. P. Curran, *Acc. Chem. Res.* **1991**, *24*, 296; c) W. Smadja, *Synlett* **1994**, 1, and references therein.

[2] For a definition of this terminology, see Ref. [1b].

[3] a) D. P. Curran, A. C. Abraham, H. Liu, *J. Org. Chem.* **1991**, *56*, 4335; b) D. P. Curran, W. Shen, J. Zhang, T. A. Heffner, *J. Am. Chem. Soc.* **1990**, *112*, 6738.

[4] a) N. A. Porter, E. Swann, J. Nally, A. T. McPhail, *J. Am. Chem. Soc.* **1990**, *112*, 6740; b) N. A. Porter, J. D. Bruhnke, W.-X. Wu, I. J. Rosenstein, R. A. Breyer, *ibid.* **1991**, *113*, 7788.

[5] a) B. Giese, M. Zehnder, M. Roth, H.-G. Zeitz, *J. Am. Chem. Soc.* **1990**, *112*, 6741; b) A. Veit, R. Lenz, M. E. Seiler, M. Neuberger, M. Zehnder, B. Giese, *Helv. Chim. Acta* **1993**, *76*, 441; c) B. Giese, U. Hoffmann, M. Roth, A. Veit, C. Wyss, M. Zehnder, H. Zipse, *Tetrahedron Lett.* **1993**, *34*, 2445.

[6] P. P. Garner, P. B. Cox, S. J. Klippenstein, *J. Am. Chem. Soc.* **1995**, *117*, 4163.

[7] a) P. Renaud, M. Ribezzo, *J. Am. Chem. Soc.* **1991**, *113*, 7803; b) D. Crich, J. W. Davies, *Tetrahedron Lett.* **1987**, *28*, 4205; c) D. P. G. Hamon, R. A. Massy-Westropp, P. Razzino, *Tetrahedron* **1993**, *49*, 6419; d) M.-Y. Chen, J.-M. Fang, Y.-M. Tsai, R.-L. Yeh, *J. Chem. Soc. Chem. Commun.* **1991**, 1603; e) E. Baciocchi, E. Muraglia, C. Villani, *Synlett* **1994**, 821.

[8] a) Use of an oxazolidinone auxiliary for ρ-addition giving insignificant diastereoselectivity has been reported by Crich and Davies: Ref. [7b]. b) A Lewis acid mediated allylation of an oxazolidinone substituted α-bromoglycinate showed moderate to good levels of diastereoselectivity: Y. Yamamoto, S. Onuki, M. Yumoto, N. Asao, *J. Am. Chem. Soc.* **1994**, *116*, 421. (c) For another use of an oxazolidinone auxiliary in a radical reaction, see D. Badone et. al. *Angew. Chem. Int. Ed. Engl.*, **1995**, *35*, No. 3.

[9] The sparse use of Lewis acid in radical reactions can be attributed to the general incompatibility of these reagents with typical conditions for radical generation. For selected recent examples on the use of Lewis acids in radical reactions see a) P. Renaud, M. Gerster, *J. Am. Chem. Soc.* **1995**, *117*, 6607; b) M. Nishida, E. Ueyama, H. Hayashi, Y. Ohtake, Y. Yamaura, E. Yanaginuma, O. Yonemitsu, A. Nishida, N. Kawahara, *ibid.* **1994**, *116*, 6455; c) M. Nishida, H. Hayashi, Y. Yamaura, E. Yanaginuma, O. Yonemitsu, A. Nishida, N. Kawahara, *Tetrahedron Lett.* **1995**, *36*, 269; d) D. P. Curran, L. H. Kuo, *J. Org. Chem.* **1994**, *59*, 3259; e) P. Renaud, N. Moufid, L. H. Kuo, D. P. Curran, *ibid.* **1994**, *59*, 3547; f) H. Urabe, K. Yamashita, K. Suzuki, K. Kobayashi, F. Sato, *ibid.* **1995**, *60*, 3576; g) T. Toru, Y. Watanabe, M. Tsusaka, Y. Ueno, *J. Am. Chem. Soc.* **1993**, *115*, 10464; h) M. Murakata, H. Tsutsui, O. Hoshino, *J. Chem. Soc. Chem. Commun.* **1995**, 481; i) Y. Guindon, J.-F. Lavallée, M. Llinas-Brunet, G. Horner, J. Rancourt, *J. Am. Chem. Soc.* **1991**, *113*, 9701; j) M. P. Sibi, C. P. Jasperse, J. Ji, *ibid.* **1995**, *117*, 10779.

[10] For a discussion on the preference of the bulky substituent to orient itself *syn* to the C–O double bond see Ref. [1b], and references therein.

[11] G. E. Keck, E. J. Enholm, J. B. Yates, M. R. Wiley, *Tetrahedron* **1985**, *41*, 4079.

[12] a) On the preparation of the auxiliary see M. P. Sibi, P. K. Deshpande, A. J. La Loggia, J. W. Christensen, *Tetrahedron Lett.*, **1995**, *36*, 8961. b) For the use of the oxazolidinone auxiliary in aldol, alkylation, and Diels–Alder reactions see M. P. Sibi, P. K. Deshpande, J. Ji, *ibid.*, **1995**, *36*, 8965.

[13] No allylation product was formed without radical initiation with triethylborane/oxygen.

[14] A control experiment in the presence of Galvinoxyl, a radical scavenger, led to complete recovery of the starting material.

[15] On hydrolysis with $LiOH/H_2O_2$ **6** gave (*S*)-2-methyl-4-butenoic acid ($[\alpha]_D^{25} = 10.52$ (c = 1.150, $CHCl_3$); published value: 10.5 ($CHCl_3$); R. G. Riley, R. M. Silverstein, *Tetrahedron* **1974**, *30*, 1171)).

[16] Enolate allylation of 4-(diphenylmethyl)-3-(1-oxopropyl)-2-oxazolidinone gave **6** in 63% yield with >99% *de* [12b].

[17] Enolate allylation of 4-(methylethyl)-3-(1-oxopropyl)-2-oxazolidinone gave a 98:2 mixture of the allylated products: D. A. Evans, M. D. Ennis, D. J. Mathre, *J. Am. Chem. Soc.* **1982**, *104*, 1737.

[18] The higher selectivity with aryl-containing auxiliaries indicates that some π-stacking may be operative with these systems. Experiments are underway to understand these results.

A Sustainable Catalyst for the Partial Oxidation of Methane to Syngas: $Ni/Ca_{1-x}Sr_xTiO_3$, Prepared In Situ from Perovskite Precursors

Takashi Hayakawa,* Hideaki Harihara, Arnfinn G. Andersen, Andrew P. E. York, Kunio Suzuki, Hiroyuki Yasuda, and Katsuomi Takehira*

The catalytic partial oxidation of methane to syngas has been intensively studied.[1–4] This process has advantages over the conventional steam reforming of methane to make syngas, since this process is highly endothermic and produces syngas with a H_2/CO ratio ≥ 3. The partial oxidation of CH_4, expected to afford syngas with a H_2/CO ratio of about 2, makes methanol synthesis an ideal follow-up process. Precious metals such as

[*] Dr. T. Hayakawa, Dr. K. Takehira, H. Harihara, Dr. A. P. E. York, Dr. K. Suzuki
Department of Surface Chemistry
National Institute of Materials and Chemical Research, AIST, 1-1 Higashi, Tsukuba, Ibaraki 305 (Japan)
Fax: Int. code +(298)54-4709
e-mail: takehira@nimc.go.jp
Dr. H. Yasuda
Institute of Research and Innovation, Takada 1201, Kashiwa, Chiba 277 (Japan)
Dr. A. G. Andersen
Nycomed Imaging AS, P. O. Box 4220, Torshov, N-0401 Oslo (Norway)

Ru, Rh, Pd, Ir, and Pt, supported on alumina,[1] or platinum and rhodium surfaces in a metal-coated ceramic monolith[3] were suitable as catalysts for this oxidation. Interestingly, some transition metal oxides combined with alkaline earth or rare earth oxides were found to be catalytically active at low temperatures (300 °C);[4] however, hot spots have been observed in the catalyst bed where the actual temperature was up to 370 K higher than the temperature measured by a thermocouple.[5] Ni/Al_2O_3, a typical catalyst for the steam reforming process, was tested with regard to its suitability for the partial oxidation of CH_4 at temperatures above 700 °C.[2] This process was thought to involve the initial oxidation of some of the CH_4 to H_2O and CO_2, followed by the reforming reactions of CH_4 with H_2O and CO_2.

In the production of syngas from CH_4, coke formation over the catalyst frequently takes place, resulting in catalyst deactivation. However, coke formation has been largely ignored,[2-5] except by Claridge et al.,[6] who observed that the relative rate of coke formation follows the order Ni > Pd > Rh > Ir.[6] We recently reported on the activity of a (Ca,Sr)(Ti,Ni) oxide in the oxidation of CH_4 to syngas; the Ni catalyst was prepared by in situ reduction of perovskite-like precursors.[7] The $Ca_{1-x}Sr_xTiO_3$ perovskite probably has an important role as the carrier of the Ni catalyst. We report herein the details of the activity of the (Ca,Sr)(Ti,Ni) oxide catalyst and its sustainability against coke formation in the partial oxidation of CH_4 to syngas.

To confirm that the perovskite carrier influences the efficiency of the catalyst, the Ni catalysts were prepared by three methods, that is, the citrate method ($Ni/Ca_{0.8}Sr_{0.2}TiO_3$ (cit)), the impregnation method ($Ni/Ca_{0.8}Sr_{0.2}TiO_3$ (imp)), and the mixing method ($Ca_{0.8}Sr_{0.2}Ti_{1.0}Ni_{0.2}O$). The results of the CH_4 oxidation over these catalysts are shown in Figure 1. The most

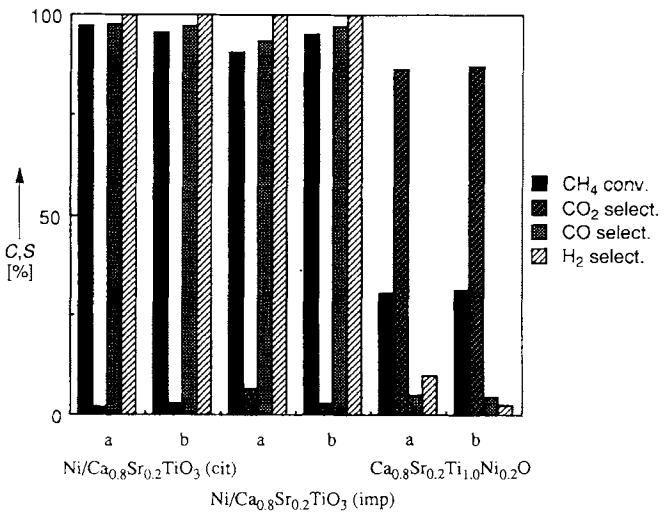

Fig. 1. CH_4 oxidation over the Ni catalyst. a: Directly after increase to 800 °C; b: After reduction with CH_4 (1.0 L h^{-1}) for 2 h. C = conversion, S = selectivity.

active catalyst was $Ni/Ca_{0.8}Sr_{0.2}TiO_3$ (cit), followed by $Ni/Ca_{0.8}Sr_{0.2}TiO_3$ (imp). After reduction with CH_4 (1.0 L h^{-1}) for 2 h, the activity of the $Ni/Ca_{0.8}Sr_{0.2}TiO_3$ (imp) catalyst increased to almost the same value as the $Ni/Ca_{0.8}Sr_{0.2}TiO_3$ (cit) catalyst. $Ca_{0.8}Sr_{0.2}Ti_{1.0}Ni_{0.2}O$ showed a very low activity for syngas production and gave small amounts of C_2 compounds as the by-products. In all reactions, the total amount of carbon in the effluent gas, ΣC, was almost constant.

X-ray diffraction (XRD) measurements revealed that both $Ni/Ca_{0.8}Sr_{0.2}TiO_3$ (cit) and $Ni/Ca_{0.8}Sr_{0.2}TiO_3$ (imp) are composed of orthorhombic $Ca_{0.8}Sr_{0.2}TiO_3$ perovskite and NiO. NiO was reduced to Ni metal after the testing. $Ca_{0.8}Sr_{0.2}Ti_{1.0}Ni_{0.2}O$ contains CaO, TiO_2 (rutile), and NiO together with small amounts of $CaTiO_3$. In this case, after the catalytic testing, NiO was only partly reduced to Ni metal, which helps to explain the marked contrast to the results obtained with $Ni/Ca_{0.8}Sr_{0.2}TiO_3$ (cit) and $Ni/Ca_{0.8}Sr_{0.2}TiO_3$ (imp), where NiO was almost completely reduced to Ni metal.

The particle sizes of Ni metal in the catalysts after the catalytic testing, determined from X-ray line broadening measurements based on the most intense reflection, that is the (111) reflection for Ni, were as follows: citrate, 20 nm; impregnation, 33 nm, and mixing, 40 nm. X-ray photoelectron spectra (Ni 2d) of the catalysts revealed peaks at 852.7 eV (Ni^0) and around 855.5 eV (Ni^{2+} and Ni^{3+}); the former peak was clearly enhanced after the studies on the catalytic activity, showing that NiO had reduced to Ni metal during the CH_4 oxidation. The composition of the catalyst after the tests on the catalytic activity was calculated from the X-ray photoelectron spectra[8] (Fig. 2). The amount of Ni present was obtained by summing

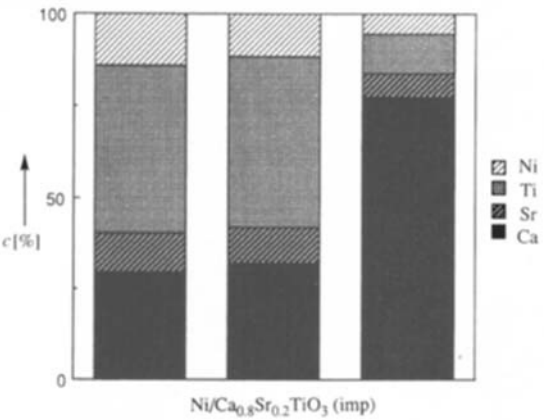

Fig. 2. Composition of the surface of the Ni catalyst. c = relative concentration.

the amounts of Ni^0, Ni^{2+} and Ni^{3+}. Similar metal distributions were observed for $Ni/Ca_{0.8}Sr_{0.2}TiO_3$ (cit) and $Ni/Ca_{0.8}Sr_{0.2}TiO_3$ (imp), except that a higher Ni content was obtained for the former catalyst, contrary to our expectations. In $Ca_{0.8}Sr_{0.2}Ti_{1.0}Ni_{0.2}O$ the Ca content increased, whereas the Ti and Ni contents decreased.

Scanning electron microscopic images of $Ni/Ca_{0.8}Sr_{0.2}TiO_3$ (cit) showed that the particle size of 10 μm prior to testing the catalytic activity decreased to 1 μm after the testing, suggesting that the catalyst particles were pulverized during the CH_4 oxidation. This may be due to the reduction of NiO to Ni metal: NiO was separated from the perovskite structure and may be located at the grain boundaries in the catalyst particles prior to the testing. The catalyst particles may be pulverized to fine particles as the "binder" NiO is no longer present after the testing. Thus nickel probably appears on the catalyst surface. On the other hand, the $Ca_{0.8}Sr_{0.2}Ti_{1.0}Ni_{0.2}O$ catalyst showed particles of tight agglomerates, which may be formed by sintering of small metal oxide particles; these agglomerates were not decomposed during the reaction. Only the surface morphology changed after the catalytic testing. These observations, and the low nickel concentration on the surface of $Ca_{0.8}Sr_{0.2}Ti_{1.0}Ni_{0.2}O$ (Fig. 2)

 © VCH Verlagsgesellschaft mbH, D-69451 Weinheim, 1996 0570-0833/96/3502-0193 $ 10.00+.25/0

were consistent with the partial reduction of NiO to Ni metal observed in the XRD analyses of the catalysts. In $Ca_{0.8}Sr_{0.2}Ti_{1.0}Ni_{0.2}O$, the NiO in the catalyst bulk cannot be easily reduced and does not appear on the catalyst surface. Only NiO species on the surface of the catalyst particles were reduced to Ni metal. Interestingly, among the methods of preparation tested, the citrate method gave both the most active catalyst and that with the highest Ni content.

To test the lifetime of the catalysts, $Ni/Ca_{0.8}Sr_{0.2}TiO_3$ (cit) and $Ni/Ca_{0.8}Sr_{0.2}TiO_3$ (imp) were used for the CH_4 oxidation for 150 h at 800 °C. The activity of both these catalysts remained constant; the $Ni/Ca_{0.8}Sr_{0.2}TiO_3$ (cit) catalyst gave higher selectivities to syngas than $Ni/Ca_{0.8}Sr_{0.2}TiO_3$ (imp) (Fig. 3).

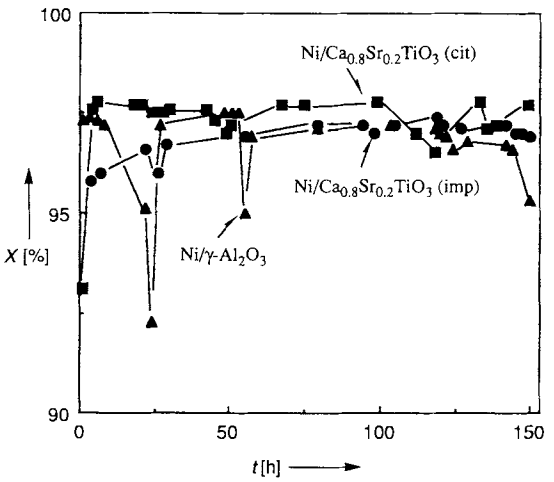

Fig. 3. CH_4 oxidation over the Ni catalysts. Dependence of the CO selectivity X on the reaction time t. Conditions: CH_4 1 Lh^{-1} (41.6 $mmol\,h^{-1}$); air: 2.4 Lh^{-1} (O_2: 21.0 $mmol\,h^{-1}$; N_2: 78.9 $mmol\,h^{-1}$); catalyst: 0.3 g; reaction temperature 800 °C.

$Ni/\gamma\text{-}Al_2O_3$ was used for comparison. Its activity varied, and both the selectivity and the conversion oscillated periodically (with a considerable time interval between the oscillations). At each oscillation the selectivity for syngas decreased, while the complete oxidation to CO_2 was accelerated. This is also evident from Figure 4, in which a sudden decrease in the value of ΣC is

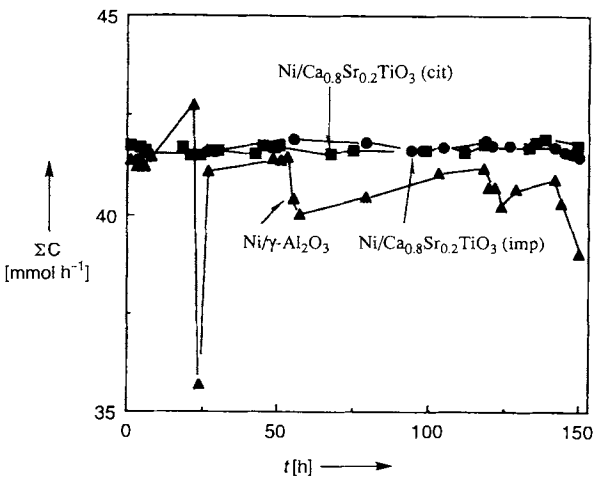

Fig. 4. CH_4 oxidation over the Ni catalysts. Dependence of the total carbon content ΣC in the effluent gas on the reaction time t. Conditions: CH_4 1 Lh^{-1} (41.6 $mmol\,h^{-1}$); air: 2.4 Lh^{-1} (O_2: 21.0 $mmol\,h^{-1}$; N_2: 78.9 $mmol\,h^{-1}$); catalyst: 0.3 g; amount of Ni: 11.5 wt% on $\gamma\text{-}Al_2O_3$ or 8.1 wt% on $Ca_{0.8}Sr_{0.2}TiO_3$ ($Ni/Ca_{0.8}Sr_{0.2}TiO_3$ (imp) and $Ni/Ca_{0.8}Sr_{0.2}TiO_3$ (cit)); reaction temperature 800 °C.

observed at each oscillation point, while both $Ni/Ca_{0.8}Sr_{0.2}TiO_3$ (cit) and $Ni/Ca_{0.8}Sr_{0.2}TiO_3$ (imp) showed constant ΣC values in the effluent gas, close to the theoretical value of 42 $mmol\,h^{-1}$. This oscillation may be caused by the progressive build-up of a carbon layer over the catalyst, finally resulting in a blockage in the reactor. Since CH_4 and air were controlled by separate mass flow controllers with an entrance pressure of 1 and 3 $kg\,cm^{-2}$, respectively, the back pressure resulting from the reactor blockage would lead to a preferential decrease in the CH_4 flow rate. A decrease in the CH_4 partial pressure in the reactor would result in a more favorable composition of the reaction mixture for the formation of CO_2 and, more importantly, to the combustion of some of the deposited carbon to CO_2 and the recovery of the original steady state conditions. Furthermore, since the partial oxidation of CH_4 to syngas over the $Ni/\gamma\text{-}Al_2O_3$ catalyst proceeds by the complete oxidation followed by the reforming reactions, and the catalyst bed consists of two zones (the first zone comprises NiO under the oxygen-rich atmosphere, while the second comprises Ni metal under the reducing atmosphere[2]), the oscillation can probably also be related to a balance between the zones in the catalyst and thus to a balance between the complete oxidation and the reforming equilibria. After 150 h, the reactor was cooled to room temperature in N_2 gas flow. The catalyst was then treated in air (1.5 Lh^{-1}) by increasing the temperature at 2.5 $K\,min^{-1}$ to measure the amount of coke formed over the catalyst during the CH_4 oxidation. The coke over the catalyst was oxidized to CO_2; the rate of its formation was plotted against temperature as shown in Figure 5. CO_2 formation was evident above 250 °C; the main peaks

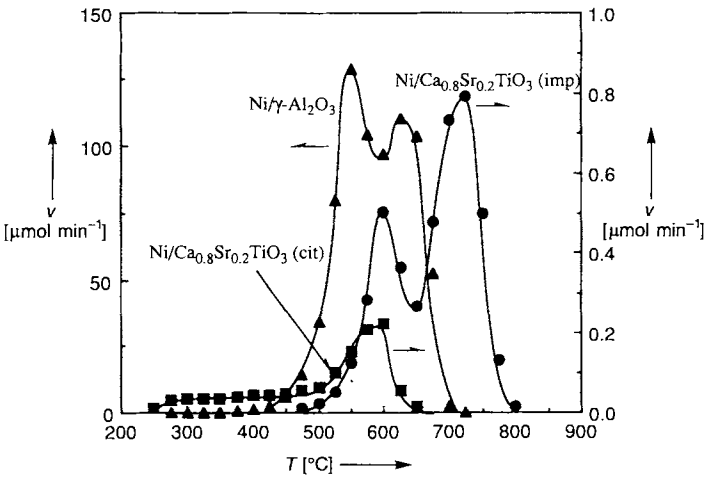

Fig. 5. Carbon deposition over the Ni catalysts. Dependence of the rate of formation of CO_2 (v) on the temperature T. After the reactions for 150 h, the catalysts were treated in air (1.5 Lh^{-1}) by increasing the temperature at 2.5 $K\,min^{-1}$. The arrows indicate which scale for the rate of formation of CO_2 is applicable to a particular catalyst.

were observed between 500–800 °C. Integration of the rate gave the total amount of CO_2, from which the amount of coke formed over the catalyst was calculated. The following values were obtained: 29.3 wt% on $Ni/\gamma\text{-}Al_2O_3$, 0.17 wt% on $Ni/Ca_{0.8}Sr_{0.2}TiO_3$ (imp), and 0.05 wt% on $Ni/Ca_{0.8}Sr_{0.2}TiO_3$ (cit).

Transmission electron microscopic studies of the surface of $Ni/\gamma\text{-}Al_2O_3$ after the reaction for 150 h showed that in the coke formation, the typical tubular carbon filaments (whisker carbon) formed with a small nickel particle at the end.[9] On the other hand, no coke formation was observed on the surface of $Ni/Ca_{0.8}Sr_{0.2}TiO_3$ (cit); the size of the nickel particles increased

 © VCH Verlagsgesellschaft mbH, D-69451 Weinheim, 1996 0570-0833/96/3502-0194 $ 10.00+.25/0

after the reaction. Prior to the reaction, NiO particles were evenly dispersed on $Ni/Ca_{0.8}Sr_{0.2}TiO_3$ (cit) and their average sizes were below 5 nm, while after the reaction they had grown to about 50 nm diameter.

Ni catalysts supported on $(Ca,Sr)TiO_3$ oxidize CH_4 to syngas. The most active of these catalysts is $Ni/Ca_{0.8}Sr_{0.2}TiO_3$ (cit) prepared by the citrate method from the perovskite precursor. Coke formation over $Ni/Ca_{0.8}Sr_{0.2}TiO_3$ (cit) was negligible, even after reaction for 150 h. Thus, nickel, which is abundant and cheap, can now be used in place of the expensive platinum group metals as a component of catalysts for the production of syngas.

Experimental Procedure

The catalysts were prepared by the citrate, impregnation, and mixing methods. In the citrate process [10], nickel nitrate, alkaline earth carbonates, and tetraisopropoxidotitanium were treated and heated with citric acid and ethylene glycol to make a sol. This was subsequently decomposed in two steps by heating to 200 °C for 5 h and then to 500 °C for 5 h, and finally calcined at 850 °C in air for 10 h. In the impregnation process, nickel nitrate, citric acid, and ethylene glycol were added to an aqueous suspension of the perovskite $Ca_{0.8}Sr_{0.2}TiO_3$, which had previously been prepared by the citrate method. The suspension was evaporated and calcined at 850 °C in air for 5 h. In the mixing method, a mixture of metal oxides was ground and calcined at 850 °C in air for 5 h. The Ni metal content was fixed at 8.1 wt% in all three catalysts. The Ni/γ-Al_2O_3 catalyst, used for comparison, was prepared by the impregnation method with γ-Al_2O_3 (Sumitomo Chemical Co., NK-124). The Ni metal content was 11.5 wt%.

The structure of the catalysts was studied by powder X-ray diffractometry (MAC Science MXP-18 diffractometer with $Cu_{K\alpha}$ radiation) and X-ray photoelectron spectroscopy (PHI-5000 spectrometer employing $Al_{K\alpha}$ radiation and an electron flood gun). The surface areas of the catalysts ($1\ m^2 g^{-1}$) used were almost identical, as measured by the N_2-BET method with a Micromeritics model 2200.

All the catalysts were tested at 800 °C in a mixture of air ($2.4\ L h^{-1}$) and CH_4 ($1.0\ L h^{-1}$) using a quartz reactor. 300 mg of catalyst was dispersed in 2 mL of quartz wool to avoid sintering and clogging of the reactor. Product gases were sampled immediately after the reactor and injected into a gas chromatograph for analysis. The selectivities for C_2 compounds, CO_2, CO, and H_2 were calculated based on the numbers of carbon and hydrogen atoms in CH_4.

Received: August 16, 1995 [Z83131E]
German version: *Angew. Chem.* **1996**, *108*, 231–234

Keywords: catalysis · methane oxidation · nickel compounds · perovskite · synthesis gas

[1] A. T. Ashcroft, A. K. Cheetham, J. S. Foord, M. L. H. Green, C. P. Grey, A. J. Murrell, P. D. F. Vernon, *Nature* **1990**, *344*, 319–321.
[2] D. Dissanayake, M. P. Rosynek, K. C. C. Kharas, J. H. Lunsford, *J. Catal.* **1991**, *132*, 117–127.
[3] D. A. Hickman, L. D. Schmidt, *Science* **1993**, *259*, 343–346.
[4] V. R. Choudhary, A. M. Rajput, B. Prabhakar, *J. Catal.* **1993**, *139*, 326–328.
[5] D. Dissanayake, M. P. Rosynek, J. H. Lunsford, *J. Phys. Chem.* **1993**, *97*, 3644–3646.
[6] J. B. Claridge, M. L. H. Green, S. C. Tsang, A. P. E. York, A. T. Ashcroft, P. D. Battle, *Catal. Lett.* **1993**, *22*, 299–305.
[7] T. Hayakawa, A. G. Andersen, M. Shimizu, K. Suzuki, K. Takehira, *Catal. Lett.* **1993**, *22*, 307–317; K. Takehira, T. Hayakawa, H. Harihara, A. G. Andersen, K. Suzuki, M. Shimizu, *Catal. Today* **1995**, *24*, 237–242.
[8] D. R. Penn, *J. Electron Spectrosc. Relat. Phenom.* **1976**, *9*, 29–40.
[9] J. R. Rostrup-Nielsen, in *Catalysis, Science and Technology Vol. 5* (Eds.: J. R. Anderson, M. Boudart), Springer, Berlin, **1984**, pp. 1–117.
[10] M. S. G. Baythoun, F. R. Sale, *J. Mater. Sci.* **1982**, *17*, 2757–2769.

Resolving the Puzzling Eclipsed Conformation of the Methyl Group in a Tricyclic Orthoamide Trihydrate**

Ito Chao* and Jye-Chan Chen

It is well known that a staggered conformation around a $C_{sp^3}-CH_3$ bond is preferred over an eclipsed one. Nevertheless, the striking crystal structure of the trihydrate of tricyclic orthoamide **1** ($\mathbf{1}\cdot 3H_2O$) was pointed out by Seiler et al.[1] as the first example of a nearly eclipsed arrangement for a $C_{sp^3}-CH_3$ bond (N-C-C-H dihedral angle is 8°). In this unusual crystal structure, each C–H bond of the methyl group seemed to be engaged in C–H···O hydrogen bonding[2] with a H_2O molecule surrounding the orthoamide molecule, according to the intermolecular C–H···O distance (2.67 Å) and angle (170°). Because a staggered $C_{sp^3}-CH_3$ conformation was found in the crystal structure of *anhydrous* **1**, Seiler et al. carried out ab initio calculations on $CH_3-C(NH_2)_3$, $CH_4\cdots OH_2$, and $CH_4\cdots OH_2\cdots NH_3$[3] as models to study the magnitude of the torsional barrier for the rotation of the methyl group (ΔE_{rot}) in **1** and the strength of C–H···O interactions in the $\mathbf{1}\cdot 3H_2O$ crystal. Their results were in line with the assumption that the eclipsed conformation in $\mathbf{1}\cdot 3H_2O$ originated from C–H···O H-bonding (about 2 kcal mol^{-1} for each C–H···O interaction), which is higher for the three hydrogen bonds than the estimated ΔE_{rot} of $C_{sp^3}-CH_3$ (about 5.5 kcal mol^{-1} at the RHF/6-31G* level).[1a] An important implication of their finding was that the conformation of aliphatic moieties of molecules next to clusters of H_2O molecules may be different from that in non-aqueous environments.

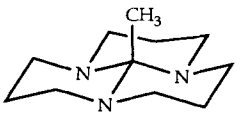

1

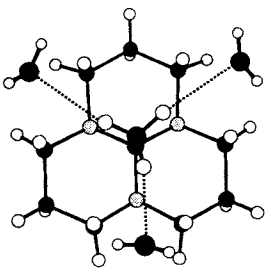

$\mathbf{1}\cdot 3H_2O$

However, the conclusion by Seiler et al. based on theoretical results was later questioned by Novoa et al.[4] They pointed out that a large part of the C–H···O stabilization energy reported by Seiler et al. came from basis set superposition errors (BSSEs). The BSSE-corrected $CH_4\cdots OH_2$ binding energy was calculated to be 0.59 kcal mol^{-1} based on MP2 calculations with a near Hartree–Fock (HF) limit basis set.[5] To reexamine the problem, Novoa et al. calculated ΔE_{rot} for the model compounds $CH_3-C(NH_2)_3$ and $CH_3-C[N(CH_3)_2]_3$ with a larger basis set, 6-31 + + G**. Furthermore, to model C–H···O interactions

[*] Dr. I. Chao, J.-C. Chen
Institute of Chemistry
Academia Sinica
Nankang, Taipei 115 (Taiwan)
Fax: Int. code +(2)783-1237
e-mail: ichao@chem.sinica.edu.tw

[**] This work was financially supported by the National Science Council, Republic of China (Taiwan). The granting of computer time from the National Center for High-performance Computing and the Computing Center of Academia Sinica, Taiwan is gratefully acknowledged.

in $1\cdot 3H_2O$, they carried out MP2/6-31 + + G** calculations on $CH_4\cdots OH_2$, $CH_4\cdots(OH_2)_2$, $CH_4\cdots(OH_2)_3$, and $CH_4\cdots OH_2\cdots NH_3$, AM1 calculations on **1** and $1\cdot 3H_2O$, and atom–atom potential calculations on crystalline $1\cdot 3H_2O$. The ab initio HF/6-31 + + G** calculations for $CH_3-C(NH_2)_3$ and $CH_3-C[N(CH_3)_2]_3$ still supported a ΔE_{rot} value of about 5.5 kcal mol^{-1} for **1**. However, the total stabilization energy provided by the three C–H···O contacts was estimated to be about 2.5 kcal mol^{-1} by the ab initio method and less than 3 kcal mol^{-1} by all methods used. Therefore, Novoa et al. did not agree that the C–H···O H-bonds resulted in the eclipsed arrangement of the methyl group in the $1\cdot 3H_2O$ crystal and suggested that the observed structure of $1\cdot 3H_2O$ may be a local energy minimum.[4]

Since computing resources are limited, it is often imperative to use small model systems to solve chemical problems in the real world. However, it is not trivial to assess the validity of models. It has been shown that the H-accepting ability of a H-bond acceptor can be estimated by the most negative value (V_{min}) of its molecular electrostatic potential (MEP).[6] Likewise, the H-donating ability of a H-bond donor can be estimated by the most positive value (V_{max}) on a MEP surface defined by the 0.002 e bohr^{-3} contour of the electron density (ρ) of the molecule.[7] Therefore, we calculated the MEP at the RHF/6-31G* level to assess dependence of the H-bond forming ability on the size of model systems.[8a] Figure 1a and b show that the V_{min} of H_2O (−62.1 kcal mol^{-1}) is smaller than that of $H_2O\cdots NH_3$ (−78.6 kcal mol^{-1}). This is in agreement with the finding that polarization of H_2O by NH_3 increases the strength of C–H···O H-bonding.[1a, 4] In fact, in the $1\cdot 3H_2O$ crystal each H_2O molecule is not only H-bonded to an N atom and a C–H bond of **1**, but also to two nearby H_2O molecules. Overall, six water molecules form a chairlike cluster, which is sandwiched by two molecules of **1** with their N sides facing the H_2O cluster. The V_{min} value shown in Figure 1c reveals that adding two more H_2O molecules to the $H_2O\cdots NH_3$ model reduces the C–H···O H-bonding ability of H_2O. However, if all heteroatoms in the H-bonded cluster are accounted for in the model (Fig. 1d), the V_{min} value is more negative than that of the $H_2O\cdots NH_3$ model.[9] Because many-body effects in the solid state are expected to enhance electronic polarization of heterobonds, H_2O in $1\cdot 3H_2O$ crystal should be a better H-bond acceptor than isolated H_2O or $H_2O\cdots NH_3$. On the other hand,

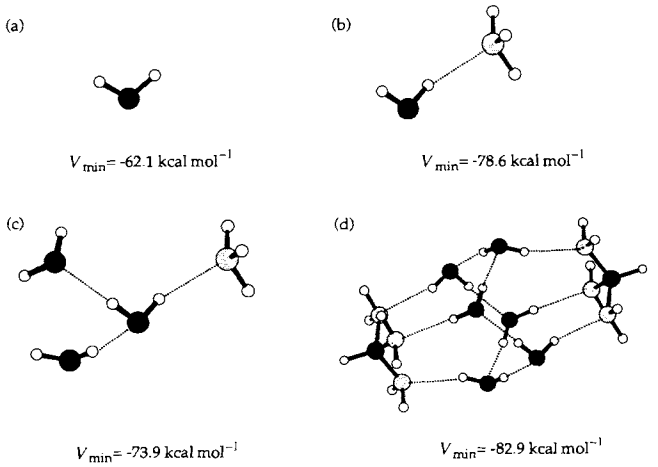

Fig. 1. V_{min} of a) an isolated H_2O molecule, b) H_2O H-bonded to NH_3, c) H_2O H-bonded to one NH_3 and two H_2O, and d) H_2O in the presence of the complete network of O–H···O and O–H···N bonds. All geometries are taken directly from X-ray coordinates.

V_{max} values of CH_4 and **1** are 11.7 and 12.5 kcal mol^{-1}, respectively. If the V_{max} of a good H-donor CHF_3 (V_{max} = 42.3 kcal mol^{-1}) is taken as reference, the H-donating ability of **1** is slightly larger than CH_4.[10] Based on above analyses, we believe models studied by Novoa et al. provide the lower limit of the strength of C–H···O bonds in the $1\cdot 3H_2O$ crystal.[11]

We evaluated ΔE_{rot} of **1** by carrying out ab initio HF and density functional theory (DFT) calculations on the molecule itself, rather than on a simplified model.[8] Since ΔE_{rot} values for ethane calculated at HF/6-31G* and HF/6-31 + + G**[4] levels (both afforded 2.98 kcal mol^{-1}) agreed well with experiment (2.88 kcal mol^{-1}),[12] the same theory levels were used to calculate **1**. The calculated ΔE_{rot} barriers were 1.96 and 2.00 kcal mol^{-1} at 6-31G* and 6-31 + + G** levels, respectively. These energy barriers are more than 3 kcal mol^{-1} lower than that of model compounds calculated at the same theory level. More importantly, these low energy barriers make it possible for C–H···O interactions to induce the nearly eclipsed conformation in $1\cdot 3H_2O$. Results from DFT calculations also support the above conclusion. The ΔE_{rot} of **1** is 1.56 kcal mol^{-1} at the BLYP/6-31G* level and 1.04 kcal mol^{-1} at the BLYP/6-31 + + G**//BLYP/6-31G* level.[13]

One may wonder what the reason is for this significant difference between the ΔE_{rot} of **1** and that of $CH_3-C(NH_2)_3$. On examining the RHF/6-31 + + G** optimized geometry of **1** we found that the distances between H_a and H_b in **1** are smaller than the sum of the van der Waal radius of the H atom (2.4 Å) in both the eclipsed and the staggered forms (Fig. 2), whereas this type of short contact is absent in $CH_3-C(NH_2)_3$. The crowdedness around the methyl group generated by the axial H atom of **1** explains why the values of the $H_a\cdots N$ distances and H-C_1-C_2 angles of **1** are larger than those of the corresponding conformations of $CH_3-C(NH_2)_3$ (Fig. 2). However, it was not apparent why the eclipsed **1** and $CH_3-C(NH_2)_3$ have similar C_1-C_2 bond lengths, whereas the staggered **1** has a longer C_1-C_2 bond than $CH_3-C(NH_2)_3$. We sought insights by looking into molecular orbitals (MOs) of **1** and $CH_3-C(NH_2)_3$. We found that the orbital energies of two thirds of the occupied MOs of staggered **1** are reduced upon rotation to the eclipsed conformation. Although the energies of most MOs decrease by a small amount upon rotation, some of them decrease by a significant amount. For example, rotating **1** from the staggered conformation to the eclipsed, the orbital energy of degenerate orbitals 47 and 48 decreases by 2.58 kcal mol^{-1} (Fig. 3). For $CH_3-C(NH_2)_3$ the orbital energies of most occupied orbitals of the staggered form increase upon rotation to the eclipsed conformation. For orbitals whose energies decrease upon rotation, the magnitudes of the energy decrease are less significant than in **1** (the largest energy decrease is 1.04 kcal mol^{-1}). In other words, the absence of the axial H atom in $CH_3-C(NH_2)_3$ makes it a poor model for estimating ΔE_{rot} of **1**. Similarly, fully optimized

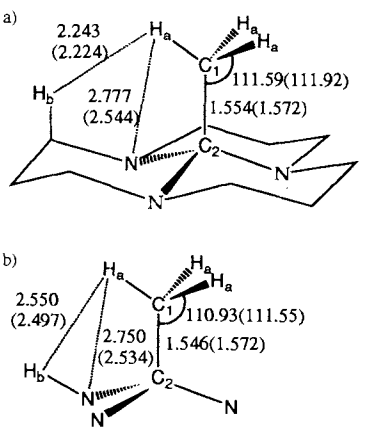

Fig. 2. Selected bond lengths [Å] and bond angle [°] of RHF/6-31 + + G** optimized **1** (a) and CH_3-$C(NH_2)_3$ (b). Numbers in parentheses are for the eclipsed conformer. The rest are for the staggered conformer.

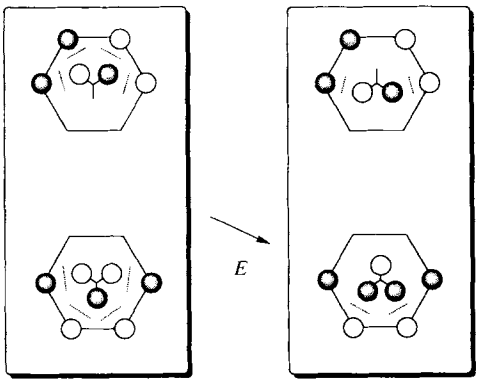

Fig. 3. Simplified representation of (47th and 48th) degenerate orbitals of the staggered and the eclipsed **1**. Only positions of axial and methyl H are shown. Nodal planes between H in close contact are shown by dashed lines. The orbital energy of the eclipsed conformer is lower than that of the staggered conformer by 2.58 kcal mol^{-1}, because it has fewer nodal planes.

CH_3-$C[N(CH_3)_2]_3$[4] is not a good model of **1** either. This is because the H atom of the $-N(CH_3)_2$ groups will not occupy the corresponding axial positions in **1**, in order to avoid strong repulsion between neighboring H atoms (Fig. 4). Finally, it should be noted that MM3[14] molecular mechanical calculations, without any MO concept in the underlying principles, afford 3.98 and 4.38 kcal mol^{-1} for the ΔE_{rot} of **1** and CH_3-$C(NH_2)_3$, respectively.

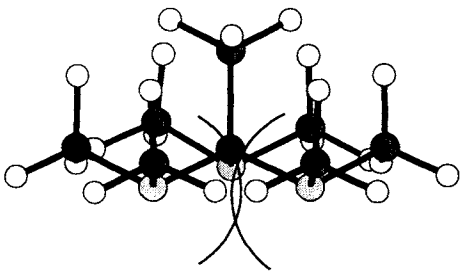

Fig. 4. Unfavorable contacts between H of CH_3-$C[N(CH_3)_2]_3$.

In summary, we found that 1) the strength of the three C-H···O H-bonds in **1**·3H_2O estimated by Novoa et al. (2.5 kcal mol^{-1}) is the lower limit of these interactions and 2) ΔE_{rot} of **1** is equal to or less than 2 kcal mol^{-1} because of the existence of proximal axial H atoms. Therefore, our results lead to the conclusion that the unique crystal structure of **1**·3H_2O is a result of the C-H···O interactions that overcome the low rotational barrier of **1**. Furthermore, these results demonstrate the danger of relying on small model systems for solving delicate problems of large molecules.

Received: August 7, 1995 [Z 8292 IE]
German version: *Angew. Chem.* **1996**, *108*, 200-202

Keywords: hydrogen bonds · molecular electrostatic potential · semiempirical calculations

[1] a) P. Seiler, G. R. Weisman, E. D. Glendening, F. Weinhold, V. B. Johnson, J. D. Dunitz, *Angew. Chem.* **1987**, *99*, 1216; *Angew. Chem. Int. Ed. Engl.* **1987**, *26*, 1175; b) P. Seiler, J. D. Dunitz, *Helv. Chim. Acta* **1989**, *72*, 1125.

[2] R. D. Green, *Hydrogen Bonding by C-H Groups*, Wiley, New York, **1974**. G. R. Desiraju, *Acc. Chem. Res.* **1991**, *24*, 290 and references therein. J. Bernstein, M. C. Etter, L. Leiserowitz in *Structural Correlation, Vol.2* (Eds.: H.-B. Bürgi, J. D. Dunitz), VCH, Weinheim, **1994**, pp 431-507.

[3] In the crystal structure of **1**·3H_2O, each H_2O molecule engaged in C-H···O hydrogen bonding also forms a hydrogen bond with the N atom of a nearby **1**.

[4] J. J. Novoa, P. Constans, M.-H. Whangbo, *Angew. Chem.* **1993**, *105*, 640; *Angew. Chem. Int. Ed. Engl.* **1993**, *32*, 588.

[5] J. J. Novoa, B. Tarron, M.-H. Whangbo, J. M. Williams, *J. Chem. Phys.* **1991**, *95*, 5179.

[6] J. S. Murray, S. Raganathan, P. Politzer, *J. Org. Chem.* **1991**, *56*, 3734.

[7] J. S. Murray, P. Politzer, *J. Org. Chem.* **1991**, *56*, 6715.

[8] a) All MEP calculations and HF optimizations used the Gaussian 92 program: M. J. Frisch, G. W. Trucks, M. Head-Gordon, P. M. W. Gill, M. W. Wong, J. B. Foresman, B. G. Johnson, H. B. Schlegel, M. A. Robb, E. S. Replogle, R. Gomperts, J. L. Andres, K. Raghavachari, J. S. Binkley, C. Gonzales, R. L. Martin, D. J. Fox, D. J. Defrees, J. Baker, J. J. P. Stewart, J. A. Pople, Gaussian, Inc., Pittsburgh, PA, **1992**. For CH_4, CHF_3, and **1**, V_{max} were values at ρ = 0.002 e bohr^{-3} along the C-H bond vector. b) All DFT calculations used the Gaussian 94 program: M. J. Frisch, G. W. Trucks, H. B. Schlegel, P. M. W. Gill, B. G. Johnson, M. A. Robb, J. R. Cheeseman, T. A. Keith, G. A. Petersson, J. A. Montgomery, K. Raghavachari, M. A. Al-Laham, V. G. Zakrzewski, J. V. Ortiz, J. B. Foresman, J. Cioslowski, B. B. Stefanov, A. Nanayakkara, M. Challacombe, C. Y. Peng, P. Y. Ayala, W. Chen, M. W. Wong, J. L. Andres, E. S. Replogle, R. Gomperts, R. L. Martin, D. J. Fox, J. S. Binkley, D. J. Defrees, J. Baker, J. P. Stewart, M. Head-Gordon, C. Gonzalez, J. A. Pople, Gaussian, Inc., Pittsburgh PA, **1995**.

[9] Since a C-H···O H-bond is significantly weaker than O···H···O and O-H···N bonds, we did not include any C-H···O bond in any model shown in Figure 1.

[10] At the RHF/6-31G* level, the BSSE-uncorrected C-H···O binding energies of CH_4···H_2O and CHF_3···H_2O are −0.56 (Ref. [5]) and −4.05 kcal mol^{-1}, respectively.

[11] When using MEP as a measure of H-bond donor/acceptor ability, we overlooked the dispersion energy contribution to nonbonded interactions. However, due to the attractive nature of dispersion energy and because more dispersion forces are present in the crystal than in the models, our conclusion that model systems provide the lower limit of the strength of C-H···O interactions remains unchanged.

[12] E. Hirota, Y. Endo, S. Saito, J. L. Duncan, *J. Mol. Spectrosc.* **1981**, *89*, 285.

[13] a) The abbreviation BLYP implies that the Becke functional (A. D. Becke, *Phys. Rev. A* **1988**, *38*, 3098) is used for the exchange energy and the Lee, Yang, and Parr functional (C. Lee, W. Yang, R. G. Parr, *Phys. Rev. B* **1988**, *37*, 785) for correlation energy. b) The C_{sp^3}-CH_3 torsional barrier calculated for ethane is 2.75 kcal mol^{-1} at the BLYP/6-31G* level and 2.65 kcal mol^{-1} at the BLYP/6-31 + + G** level; for CH_3-$C(NH_2)_3$ it is 5.07 kcal mol^{-1} at the BLYP/6-31G* level and 4.62 kcal mol^{-1} at the BLYP/6-31 + + G** level.

[14] MM3(92): N. L. Allinger, University of Georgia, Athens, GA.

Synthesis of the Nonamannan Residue of a Glycoprotein with High Mannose Content**

Peter Grice, Steven V. Ley,* Jörg Pietruszka, and Henning W. M. Priepke

AIDS (Acquired Immunodeficiency Syndrome) is a vicious retroviral disease characterized by immunosupression associated with opportunistic infections, secondary neoplasms, and neurological manifestations. Despite an extensive international research effort, the viral infection caused by the human immunodeficiency virus (HIV) remains incurable. In the United States it is presently the fourth leading cause of mortality for men between the age of 15 and 54.[1]

The heavily glycosylated surface glycoprotein gp120 plays a critical role for HIV infection of cells. Gp120 is responsible not only for the attachment and penetration of target cells, but also for the antiviral immune response. There is evidence that the

[*] Prof. Dr. S. V. Ley, Dr. P. Grice, Dr. J. Pietruszka, Dr. H. W. M. Priepke
University of Cambridge, Department of Chemistry
Lensfield Road, GB-Cambridge CB21EW (UK)
Telefax: Int. code + (1223) 336-442

[**] Cyclohexane-1,2-diacetals in Synthesis. Part 4. This work was supported by the BP Research Endowment (to S. V. L.), the Zeneca Strategic Research Fund, the Deutsche Forschungsgemeinschaft (postdoctoral fellowship to J. P.), and Schering Agrochemicals Ltd, now AgrEvo, (Schering Fellowship in Bioorganic Chemistry to H. W. M. P). Parts 1-3: Ref. [7a-c]

glycans of the viral envelope are possible targets for immunotherapy and/or vaccine development.[2] No less than 29 N-linked oligosaccharides have been identified, the main fraction being of the high mannose type, for example **1**,[3] a ubiquitous undecasaccharide.[4] In view of the remarkable activity of antibodies directed against the mannose residues of HIV-1 glycoprotein gp120 in vitro,[5] the mannan moiety of this glycoprotein is a very attractive synthetic target.[6] In this paper we describe the preparation of the model nonasaccharide **2** with our CDA methodology (CDA = cyclohexane-1,2-diacetal) for oligosaccharide assembly.[7]

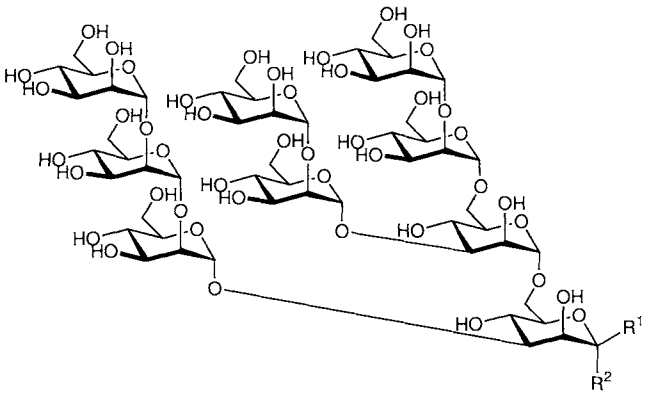

1, R^1 = 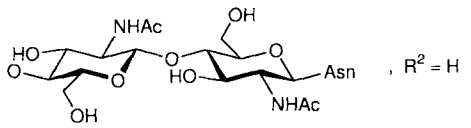 , R^2 = H

2, R^1 = H, R^2 = OMe

Recently we reported that the reactivity of glycosyl donors can be tuned by the selective introduction of different protecting and leaving groups, thus enabling highly efficient oligosaccharide synthesis.[7] Four levels of reactivity are provided by these methods. This led us to propose a synthetic plan for **2** including the five building blocks **A**–**E** (Scheme 1).[8] We anticipated that the final step for assembling the nonasaccharide would be the coupling between an ethylthio pentasaccharide donor and a tetrasaccharide acceptor unit. The preparation of the two segments should be straightforward, since the CDA group decreases the reactivity of glycosyl donors relative to the per-O-benzylated compounds (reactivity **A** > **B**).[7] In addition, phenylseleno glycosides are more reactive than the ethylthio analogues (reactivity **B** > **C**,**E**), whereas the O-glycoside **D** is virtually unreactive in the presence of iodonium sources.[9]

Unfortunately it was not possible to selectively benzylate the 6-position of CDA-protected mannose donors, which would have led directly to **3a** (**B**) and **4a** (**C**).[8] Instead we began with the TPS-protected (TPS = 6-*O*-*tert*-butyldiphenylsilyl) analogues **3b** and **4b** and performed appropriate deprotections and reprotections at later stages. First we synthesized the "common" disaccharide **6** from **5** (**A**) and **3b** in 55% yield (Scheme 2), by a fast reaction (reaction time less than ten minutes) that is selective towards activation with *N*-iodosuccinimide/triflic acid (NIS/TfOH). Subsequent protecting group manipulation (desilylation/benzylation) furnished **7** in 84% yield. Two equivalents of **7** then reacted selectively with **8a** (**E**) to form the pentasaccharide **9** (80%). The benzoyl group in the 2-position of **8a** is essential not only for high α-selectivity in the following coupling reaction, but also for the successful formation of **9**, since the 2-O-benzyl compound **8b** reacted with NIS faster than disaccharide **7**.

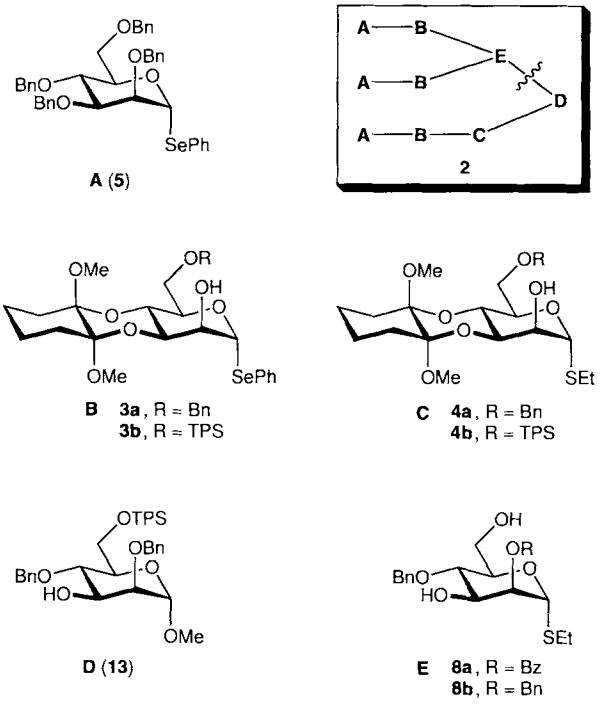

Scheme 1. Building blocks **A**–**E** for the synthesis of **2** (schematic representation at the top right).

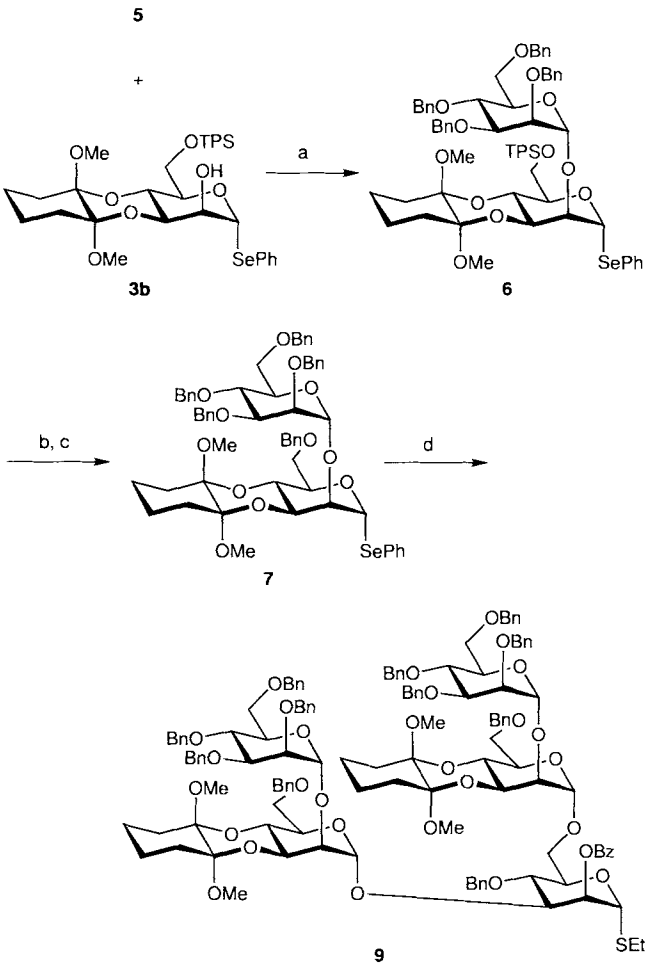

Scheme 2. a) NIS/TfOH(cat.), dichloroethane/Et_2O (1/1), 4 Å molecular sieves, 55%; b) TBAF/AcOH (3%), THF; c) NaH, BnBr (Bn = $PhCH_2$), DMF, 84% over two steps. d) **8a** (0.4 equiv), NIS/TfOH(cat.), dichloroethane/Et_2O (1:1), 4 Å molecular sieves, 80%.

 © VCH Verlagsgesellschaft mbH, D-69451 Weinheim, 1996 0570-0833/96/3502-0198 $ 10.00+.25/0

Next we focused on the synthesis of the trisaccharide **10** for further elaboration to the tetrasaccharide **11** (Scheme 3). For the formation of disaccharide **6** the difference in glycosyl reactivity originated from the choice of protecting groups. For the formation of trisaccharide **10**, however, the difference in glycosyl reactivity could be exclusively controlled by changing from the phenylselenoglycoside **3b** to the ethylthioglycoside **4b** without changing the protecting groups. The desired trisaccharide **10** was thus formed in an excellent yield (80%); after protecting group manipulation **12** was obtained in 70% yield over two steps. Finally, tetrasaccharide **11** was formed by activation of **12** in the presence of acceptor **13** with NIS/TfOH and desilylation with tetrabutylammonium fluoride (TBAF)/acetic acid (66% over two steps, Scheme 3).

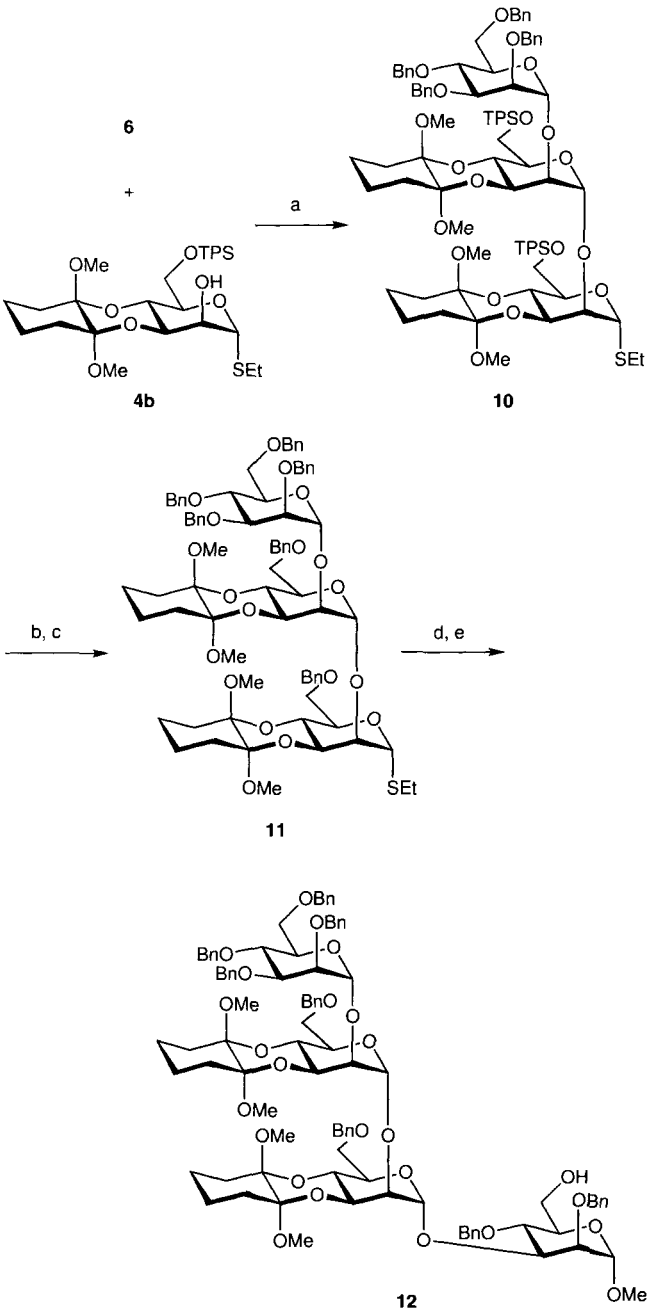

Scheme 3. a) NIS/TfOH(cat.), dichloroethane/Et_2O (1/1), 4 Å molecular sieves, 80%; b) TBAF/AcOH (3%), THF; c) NaH, BnBr, DMF, 70% over two steps; d) **12** (1.1 equiv), NIS/TfOH(cat.), dichloroethane/Et_2O (1/1), 4 Å molecular sieves; e) TBAF/AcOH (3%) in THF, 66% over two steps.

The final glycosidation step—activation of **9** in the presence of **11**—provided the desired nonasaccharide **14** (Scheme 4). However, the low 30% yield of this reaction was disappointing. More successful preliminary results with other tetrasaccharide

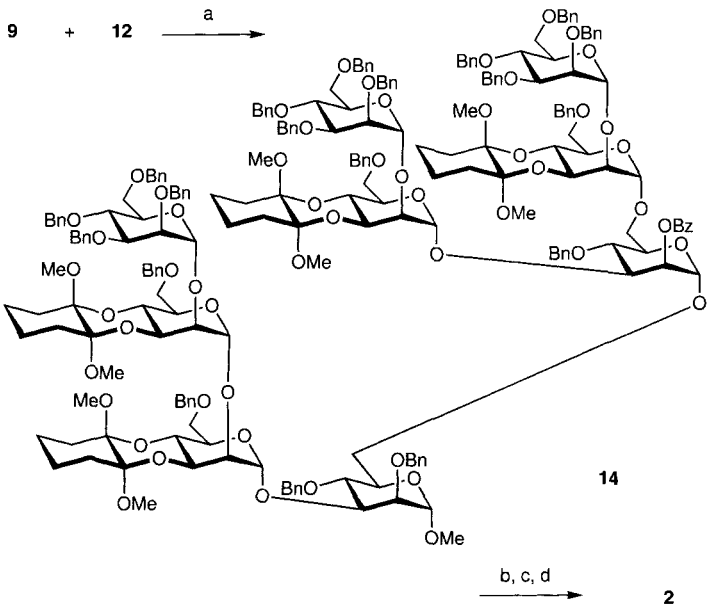

Scheme 4. a) NIS/TfOH(cat.), dichloroethane/Et_2O (1/1), 4 Å molecular sieves, 30%; b) CF_3CO_2H/H_2O (20/1), 5 min, (43%); c) $NaOCH_3$ in MeOH, Amberlite IR 120, (55%); d) $Pd(OH)_2$ on activated charcoal, MeOH, quantitative.

acceptors indicate that this may be due to a steric mismatch of the two partners, a phenomenon which has been previously noted.[10] Deprotection of **14** to yield the target molecule **2** was straightforward. The global cleavage of the CDA groups was achieved with trifluoroacetic acid/water (20/1) in an acceptable 43% yield (81% per CDA unit). Debenzoylation mediated by sodium methoxide in methanol at 55 °C (no reaction at room temperature) followed by removal of the benzyl groups by catalytic hydrogenation occurred smoothly to afford **2**.[11]

In summary, we have achieved a short synthesis of the mannan residue of a high mannose type oligosaccharide present on the viral coat of HIV-1. We efficiently assembled the protected nonasaccharide **14** from monosaccharide building blocks using only one promotor system (NIS/TfOH) to activate the different glycosyl donors and only minor protecting group manipulation. Furthermore, this synthesis demonstrates that the strategy of tuning the reactivity of glycosides is a powerful tool for the concise and rapid preparation of complex oligosaccharides. The synthesis of a nonasaccharide with a β-O-linker (instead of the α-O-methyl group) that would permit binding of the glycan to a protein (hence providing us with a tool for further biological/medical testing) is currently under investigation.

Received: July 24, 1995 [Z 8250 IE]
German version: *Angew. Chem.* **1996**, *108*, 206–208

Keywords: AIDS · mannose · oligosaccharide · protecting groups

[1] R. S. Cotran, V. Kumar, S. L. Robbins, *Robbins Pathologic Basis of Disease*, Saunders, Philadelphia, London, **1994**, Chap. 6, and references therein.

[2] J.-E. S. Hansen, H. Clausen, C. Nielsen, L. S. Teglbjærg, L. L. Hansen, C. M. Nielsen, E. Dabelsteen, L. Mathiesen, S.-i. Hakomori, J. O. Nielsen, *J. Virol.* **1990**, *64*, 2833–2840; J.-E. S. Hansen, C. Nielsen, M. Arendrup, S. Olofsson, L. Mathiesen, J. O. Nielsen, H. Clausen, *ibid.* **1991**, *65*, 6461–6467; J.-E. S. Hansen, C. M. Nielsen, C. Nielsen, P. Heedegaard, L. R. Mathiesen, J. O.

Nielsen, *AIDS* **1989**, *3*, 635–641; A. Kobata, *Alfred Benzon Symp.* **1994**, *36*, 246–256; J.-E. S. Hansen, H. Clausen, T. Sørensen, T. White, H. H. Wandall, *ibid.* **1994**, *36*, 297–310; J.-E. S. Hansen, B. Hofmann, T. Sørensen, H. Clausen, *ibid.* **1994**, *36*, 414–427, and references therein.

[3] T. Mizuochi, M. W. Spellman, M. Larkin, J. Solomon, L. J. Basa, T. Feizi, *Biochem. J.* **1988**, *254*, 599–603.

[4] H. Lis, N. Sharon, *J. Biol. Chem.* **1978**, *253*, 3468; E. Li, S. Kornfeld, *ibid.* **1979**, *254*, 1600; L. Dorland, H. van Halbeek, J. F. G. Vliegenthart, H. Lis, N. Sharon, *ibid.* **1981**, *256*, 7708.

[5] W. E. G. Müller, H. C. Schröder, P. Reuter, A. Maidhof, G. Uhlenbruck, I. Winkler, *AIDS* **1990**, *4*, 159–162.

[6] Synthesis of major segments of high mannose glycoproteins: H. Paulsen, *Angew. Chem.* **1990**, *102*, 851–867; *Angew. Chem. Int. Ed. Engl.* **1990**, *29*, 823, and references therein; J. R. Merritt, E. Naisang, B. Fraser-Reid, *J. Org. Chem.* **1994**, *59*, 4443–4449.

[7] a) S. V. Ley, H. W. M. Priepke, S. L. Warriner, *Angew. Chem.* **1994**, *106*, 2410–2412; *Angew. Chem. Int. Ed. Engl.* **1994**, *33*, 2290–2292; b) S. V. Ley, H. W. M. Priepke, *ibid.* **1994**, *106*, 2412–2414 and **1994**, *33*, 2292–2294; c) P. Grice, S. V. Ley, J. Pietruszka, H. W. M. Priepke, E. P. E. Walther, *Synlett* **1995**, 781–784; d) T. Ziegler, *Angew. Chem.* **1994**, *106*, 2362–2365; *Angew. Chem. Int. Ed. Engl.* **1994**, *33*, 2272–2275.

[8] Preparation of building blocks with full experimental details will be reported in due course.

[9] S. Mehta, B. M. Pinto, *J. Org. Chem.* **1993**, *58*, 3269–3276; H. M. Zuurmond, P. H. van der Meer, P. A. M. van der Klein, G. A. van der Marel, J. H. van Boom, *J. Carbohydr. Chem.* **1993**, *12*, 1091–1103; G. H. Veeneman, J. H. van Boom, *Tetrahedron Lett.* **1990**, *31*, 275–278; G. H. Veeneman, S. H. van Leeuwen, J. H. van Boom, *ibid.* **1990**, *31*, 1331–1334.

[10] Y.-M. Zhang, A. Brodzky, P. Sinaÿ, G. Saint-Marcoux, B. Perly, *Tetrahedron: Asymmetry* **1995**, *6*, 1195–1216.

[11] **2**: ^{1}H NMR (500 MHz, D_2O, 297.3 K): δ = 5.29 (s, 1H, 1-H_a), 5.22 (s, 1H, 1-H_b), 5.19 (s, 1H, 1-H_c), 5.04 (s, 1H, 1-H_d), 4.93 (s, 3H, 1-H_e, 1-H_f, 1-H_g), 4.76 (s, 1H, 1-H_h), 4.61 (s, 1H, 1-H_i), 3.40-4.07 (m, 54H), 3.29 (s, 3H, OCH_3); ^{13}C NMR (100 MHz, D_2O): δ = 102.2, 102.2 (2×), 100.9, 100.6 (2×), 100.5, 99.4, 98.0 (anomeric C), 54.74 (OCH_3); MALDI-TOF-MS: *m/z*: 1513 ([*M* + Na]$^+$). MALDI = matrix-supported laser desorption/ionization, TOF = time of flight.

Chiral Phosphanyldihydrooxazoles in Asymmetric Catalysis: Enantioselective Heck Reactions**

Olivier Loiseleur, Peter Meier, and Andreas Pfaltz*

The development of enantioselective variants of the Heck reaction has added a new dimension to this important method for C–C bond formation.[1, 2] Excellent enantioselectivities have been achieved and several remarkable applications in the synthesis of complex natural products have been reported. So far, the most effective ligand for these reactions has been BINAP.[1–3] However, the application range of Pd(BINAP) catalysts seems limited to certain classes of substrates and their activity is often low. In addition, these catalysts promote C=C bond migration which sometimes leads to useful products but unfortunately often results in mixtures of isomers. Therefore, it is necessary to search for other ligands and catalysts to enhance the scope of enantioselective Heck reactions.

In the course of our work on phosphanyldihydrooxazoles **1**,[4–6] which have proven to be effective ligands for enantioselective Pd-[4a, 5] and W-catalyzed[6] allylic substitution, we have

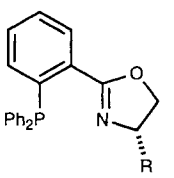

1a R = CH_3
1b R = $CH(CH_3)_2$
1c R = $C(CH_3)_3$
1d R = C_6H_5
1e R = $CH_2(C_6H_5)$
1f R = $CH_2CH(CH_3)_2$
1g R = $CH_2C(CH_3)_3$

tested these ligands in intermolecular Heck reactions of cyclic olefins. The reaction between 2,3-dihydrofuran and 1-cyclohexenyl triflate, previously reported by Ozawa, Hayashi et al.,[2b] was chosen to screen different ligands and catalyst precursors and to optimize the reaction conditions (Table 1). The best enantioselectivity and also the highest catalyst activity was observed with the *tert*-butyldihydrooxazole derivative **1c**. With 3 mol% of catalyst, prepared in situ from [Pd(dba)$_2$][7] and 1.5–2 equivalents of ligand **1c**, the 2,5-dihydrofuran derivative **2** was formed in high yield and with excellent enantioselectivity [Eq. (a), Table 1]. The corresponding 2,3-dihydrofuran derivative was not detected, in contrast to the Pd(BINAP)-catalyzed reaction[2b] which yields the thermodynamically more stable 2,3-dihydro isomer as the main product with 58% yield and 87% *ee*. With Pd(BINAP) catalysts, 1,8-bis(dimethylamino)-naphthalene (proton sponge) has to be used as base for optimum results, whereas in our case simpler bases such as triethylamine or *N*,*N*-diisopropylethylamine are equally effective. Catalysts derived from analogous ligands with less bulky substituents at the stereogenic center are significantly less reactive and the resulting *ee* values are slightly lower [% conversion/% *ee*: 97/98 for **1c**, 24/90 for **1e**, 18/95 for **1f**; proton sponge, 50 °C, other conditions, see Equation (a)].

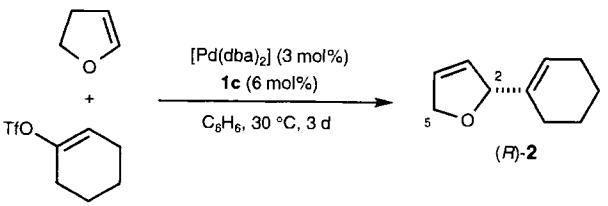

Table 1. Enantioselective Heck reaction of 2,3-dihydrofuran to give (*R*)-**2** [Eq. (a)].

Base	*ee* [%]	Yield [%] [a]
1,8-bis(dimethylamino)naphthalene	98	95
2,2,6,6-tetramethylpiperidine	99	95
triethylamine	>99	78
N,*N*-diisopropylamine	>99	92
N,*N*-diisopropylethylamine	99	98 [b]
sodium carbonate	98	34
sodium acetate	98	50

[a] Determined by GC with *n*-tridecane as internal standard. [b] Yield of purified product: 92%.

Similar results were obtained with phenyl and 1-cyclopentenyl triflate (Scheme 1). Arylation of 4,7-dihydro-1,3-dioxepin, which leads to a masked hydroxyaldehyde, also proceeds with good enantioselectivity and satisfactory yield. The corresponding Pd(BINAP)-catalyzed process[2d] was reported to give 72% *ee* and 84% yield.

The reaction was found to be highly sensitive to traces of chloride ions and chloroform. No reaction was observed in the presence of Et_4NCl or with [(**1c**)$PdCl_2$]/BuLi as catalyst precur-

[*] Prof. Dr. A. Pfaltz,[+] Dipl.-Chem. O. Loiseleur, P. Meier
Institut für Organische Chemie der Universität
St.-Johanns-Ring 19, CH-4056 Basel (Switzerland)

[+] New address: Max-Planck-Institut für Kohlenforschung
Kaiser-Wilhelm-Platz 1, D-45470 Mülheim an der Ruhr (Germany)
Fax: Int. code +(208)306-2992

[**] Financial support of this work by the Swiss National Science Foundation and Hoffmann-La Roche AG, Basel, is gratefully acknowledged.

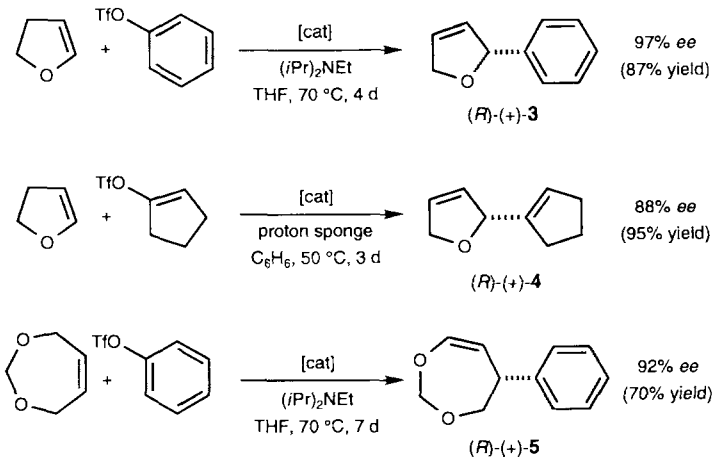

Scheme 1. [cat] = [Pd(dba)$_2$] (3 mol%), **1c** (6 mol%).

sor. [$Pd_2(dba)_3 \cdot CHCl_3$] as catalyst precursor gave lower conversion than [$Pd_2(dba)_3 \cdot dba$], and large fluctuations in yields and enantiomeric excesses were observed.[8]

The low tendency of (phosphanyldihydrooxazole)palladium catalysts to promote C=C bond migration allows the use of substrates such as cyclopentene, which are converted to mixtures of isomers with Pd(BINAP) catalysts (Scheme 2). The product distributions are strongly dependent on the solvent and the base. However, under optimized conditions, the desired chiral 3-substituted cyclopentene derivatives **6** and **9** are formed in good yield and with high preference over the corresponding achiral isomers **7** and **10**. Other isomers are formed only in trace amounts under these conditions, in contrast to the corresponding Pd(BINAP)-catalyzed reactions which give complex mixtures of isomers and low *ee* values due to extensive double bond migration in the five-membered ring.

A mechanistic interpretation of the observed selectivities will have to wait until more is known about the structure, relative stability, and reactivity of the intermediates in the catalytic cycle.[1] Unless we can distinguish between two possible pathways, one involving *cis* the other *trans* coordination of the olefin and the P atom, no meaningful mechanism of enantioselection can be proposed.

The remarkable selectivities obtained with phosphanyldihydrooxazoles point to a considerable potential of P,N ligands of this type for enantioselective Heck reactions. Because of the low extent of C=C bond migration, the product distribution can differ substantially from analogous Pd(BINAP)-catalyzed reactions. Phosphanyldihydrooxazoles are attractive ligands because they are readily synthesized from simple precursors[4, 5] and because their modular structure allows extensive and independent variation of the backbone, the dihydrooxazole ring, and the phosphane group. Thus it should be possible to improve the catalysts described here still further by optimizing the steric and electronic properties of the ligand.

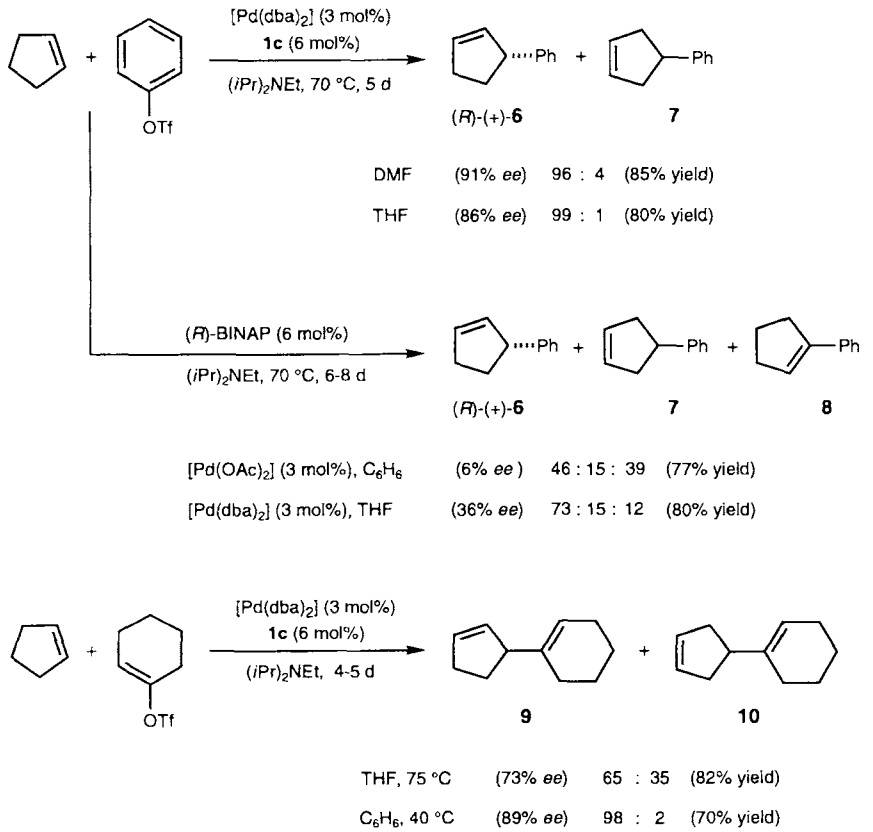

Scheme 2. Heck reactions with cyclopentene. Comparison of ligand **1c** with BINAP.

Experimental Procedure

[$Pd_2(dba)_3 \cdot dba$] (77.5 mg, 0.135 mmol) and (−)-(*S*)-**1c** (104.6 mg, 0.270 mmol) were placed under Ar in an ampoule equipped with a magnetic stirring bar and a Young valve and treated with a solution of 1-cyclohexenyl triflate (1.048 g, 4.55 mmol) and *n*-tridecane (424 mg, 2.30 mmol) as internal GC standard in Ar-saturated benzene (10 mL), followed by 2,3-dihydrofuran (1.35 mL, 17.9 mmol), *N,N*-diisopropylethylamine (1.57 mL, 9.17 mmol), and Ar-saturated benzene (40 mL). The ampoule was sealed under argon and the mixture stirred at 24 °C (red solution, precipitation of *N,N*-diisopropylethylammonium triflate) until the reaction was complete according to GC analysis (65 h; MN Permabond OV 1701; 50 m, 90–210 °C, 0.7 °C min^{-1}, 120 kPa: t_R = 21.7 min (*n*-tridecane), 22.3 min (**2**)). The reaction mixture was diluted with pentane (ca. 150 mL) and the resulting red suspension was filtered through a 2 cm layer of silica gel (∅ = 7 cm). Further elution with Et_2O and concentration gave a red oil which was purified by flash chromatography (silica gel, 4 × 25 cm; *n*-pentane/CH_2Cl_2 1:1) followed by Kugelrohr distillation (125 °C, 12 kPa) to afford (*R*)-(+)-**2** (629 mg, 92%) as a colorless oil [9]. $[\alpha]_D$ = + 201 (*c* = 1.06, $CHCl_3$, 24 °C, 99% *ee* by GC). GC (Chiraldex γ-CD-TFA; 30 m, 80–140 °C, 0.3 °C min^{-1}, 60 kPa): 29.3 min (*S*), 30.4 min (*R*).

Received: September 18, [Z 8409 IE]
German version: *Angew. Chem.* **1996**, *108*, 218–220

Keywords: asymmetric catalysis · dihydrooxazoles · Heck reactions · palladium catalysts · P,N ligands

[1] Reviews: a) H. G. Schmalz, *Nachr. Chem. Tech. Lab.* **1994**, *42*, 270; b) R. C. Larock, *Adv. Met. Org. Chem.* **1994**, *3*, 97; c) A. de Meijere, F. E. Meyer, *Angew. Chem.* **1994**, *106*, 2473; *Angew. Chem. Int. Ed. Engl.* **1994**, *33*, 2379; d) W. Cabri, I. Candiani, *Acc. Chem. Res.* **1995**, *28*, 2.

[2] See for example a) Y. Sato, M. Sodeoka, M. Shibasaki, *J. Org. Chem.* **1989**, *54*, 4738; K. Kondo, M. Sodeoka, M. Mori, M. Shibasaki, *Synthesis.* **1993**, 920; K. Kondo, M. Sodeoka, M. Shibasaki, *J. Org. Chem.* **1995**, *60*, 4322; b) F. Ozawa, A. Kubo, T. Hayashi, *J. Am. Chem Soc.* **1991**, *113*, 1417; F. Ozawa, Y. Kobatake, T. Hayashi, *Tetrahedron Lett.* **1993**, *34*, 2505; F. Ozawa, A. Kubo, Y. Matsumoto, T. Hayashi, E. Nishioka, K. Yanagi, K. Moriguchi, *Organometallics* **1993**, *12*, 4188; c) A. Ashimori, T. Matsuura, L. E. Overman, D. J. Poon, *J. Org. Chem.* **1993**, *58*, 6949; L. E. Overman, *Pure Appl. Chem.* **1994**, *66*, 1423; d) Y. Koga, M. Sodeoka, M. Shibasaki, *Tetrahedron Lett.* **1994**, *35*, 1227; e) L. F. Tietze, R. Schimpf, *Angew. Chem.* **1994**, *106*, 1138; *Angew. Chem. int. Ed. Engl.* **1994**, *33*, 1089.

[3] BINAP = 2,2'-bis(diphenylphosphano)-1,1'-binaphthyl: R. Noyori, H. Takaya, *Acc. Chem. Res.* **1990**, *23*, 345.
[4] a) P. von Matt, A. Pfaltz, *Angew. Chem.* **1993**, *105*, 614; *Angew. Chem. Int. Ed. Engl.* **1993**, *32*, 566; P. von Matt, O. Loiseleur, G. Koch, A. Pfaltz, C. Lefeber, T. Feucht, G. Helmchen, *Tetrahedron: Asymmetry* **1994**, *5*, 573; b) G. Koch, G. C. Lloyd-Jones, O. Loiseleur, A. Pfaltz, R. Prétôt, S. Schaffner, P. Schnider, P. von Matt, *Recl. Trav. Chim. Pays-Bas* **1995**, *114*, 206.
[5] See also: a) J. Sprinz, M. Kiefer, G. Helmchen, M. Reggelin, G. Huttner, O. Walter, L. Zsolnai, *Tetrahedron Lett.* **1994**, *35*, 1523; P. Sennhenn, B. Gabler, G. Helmchen, *ibid.* **1994**, *35*, 8595; b) G. J. Dawson, C. G. Frost, J. M. J. Williams, S. J. Coote, *ibid.* **1993**, *34*, 3149; G. J. Dawson, J. M. J. Williams, *ibid.* **1995**, *36*, 461; I. C. Baldwin, J. M. J. Williams, R. P. Beckett, *Tetrahedron: Asymmetry* **1995**, *6*, 679.
[6] G. C. Lloyd-Jones, A. Pfaltz, *Angew. Chem.* **1995**, *107*, 534; *Angew. Chem. Int. Ed. Engl.* **1995**, *34*, 462.
[7] $[Pd_2(dba)_3 \cdot dba]$: Y. Takahashi, T. Ito, S. Sakai, Y. Ishii, *J. Chem. Soc. Chem. Commun.* **1970**, 1065; T. Ukai, H. Kawazura, Y. Ishii, J. J. Bonnet, J. A. Ibers, *J. Organomet. Chem.* **1974**, *65*, 253.
[8] For the effect of halide ions in Heck reactions, see for example ref. [1d]. Facile oxidative addition of chloroform to [(diphosphane)(dba)Pd^0] complexes has been reported: W. A. Herrmann, W. R. Thiel, C. Brossmer, K. Öfele, T. Priermeier, W. Scherer, *J. Organomet. Chem.* **1993**, *461*, 51.
[9] Configurational assignments: **2** and (*R*)-(−)-2-(1-cyclohexenyl)2,3-dihydrofuran [2b] were converted to (*R*)-(+)-2-(1-cyclohexenyl)tetrahydrofuran. (*R*)-(+)-**3**: ref. [2b]. (*R*)-(+)-**4**: CD comparison with (*R*)-(+)-**2**. (*R*)-(+)-**5**: ref. [2d]. (*R*)-(+)-**6**: H. B. Hopps, *Diss. Abstr.* **1962**, *23*, 439.

Molecular Recognition of Carboxylate Ions Based on the Metal–Ligand Interaction and Signaled through Fluorescence Quenching**

Giancarlo De Santis, Luigi Fabbrizzi,* Maurizio Licchelli, Antonio Poggi, and Angelo Taglietti

Molecular recognition of a given substrate can be signaled in a number of ways: the change in the the potential of an electrode, the shift of an NMR signal, an abrupt color change. However, the most spectacular and easily detectable signaling effect is probably a change in fluorescence. Fluorescent sensing procedures have been developed over the last decade for several metal ions.[1] Usually the recognition of the metal center is communicated to the outside through the quenching (for transition metal ions)[2] or the revival (for alkali and alkaline earth metal cations)[3] of the fluorescence of a light-emitting unit linked to the receptor. In any case, the variation of the fluorescence emission is related to an intramolecular electron transfer process, which directly involves the metal center. On the other hand, fluorescence sensing of anions is a much less developed field, which may be due to the low energy of the receptor–substrate interactions (hydrogen bonding, electrostatic effects). A successful case is the binding of hydrogen phosphate to a polyammonium unit, to which an anthracene subunit is appended as a fluorescent group.[4]

We considered that the metal–ligand interaction, which can be significantly stronger than hydrogen bonding and other van der Waals interactions, could be conveniently used for anion recognition. In this connection, we first appended a 9-anthracenyl group to a peripheral nitrogen atom of tris(2-aminoethyl)amine (tren). The resulting anthrylamine **1** was reacted with Zn^{II} to give the corresponding complex. In the two-component system $[Zn^{II}(\mathbf{1})]^{2+}$, the four-coordinate metal center has a

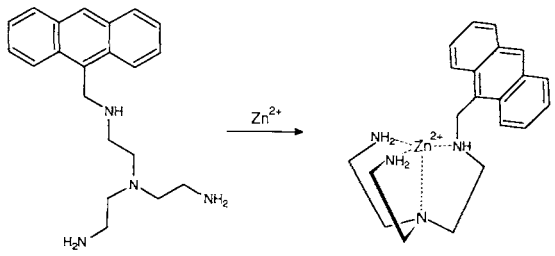

1 $[Zn^{II}(\mathbf{1})]^{2+}$

vacant site for coordination of a solvent molecule or for an anion to give a trigonal-bipyramidal arrangement. The proximate luminescent unit is in a favorable position to signal the occurrence of the anion recognition. In methanolic solutions $[Zn^{II}(\mathbf{1})]^{2+}$ shows a strong affinity towards anions bearing a carboxylate group. In particular, a stable 1:1 adduct is formed with the benzoate ion, as shown by spectrophotometric titrations. However, parallel titration experiments carried out in the spectrofluorimetric cuvette indicate that anion binding does not interfere with the photophysical activity of the proximate anthracene group, whose emission spectrum was not altered even after the addition of several equivalents of the anion. Thus, in this case the anthracene subunit is only a "silent witness" of the anion binding to the Zn^{II} center.

However, when a solution of $[Zn^{II}(\mathbf{1})]^{2+}$ was titrated with the 4-*N*,*N*-dimethylaminobenzoate ion (X^-), the fluorescence intensity progressively decreased until complete quenching (Fig. 1). The plot of fluorescence intensity (I_F) versus equiva-

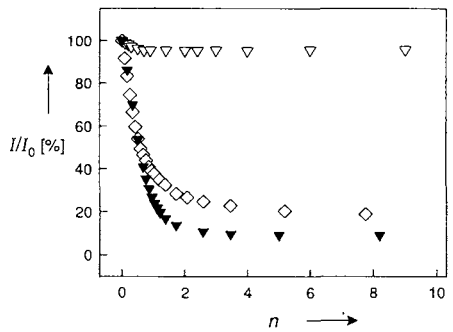

Fig. 1. Spectrofluorimetric titrations of the $[Zn^{II}(\mathbf{1})]^{2+}$ receptor in methanolic solution (10^{-4} M) with standard methanolic solutions of *N*,*N*-dimethylaminobenzoate (▾), acetate (▿); *N*,*N*-dimethylaminobenzoate + acetate (○); n = equivalents of anion/equivalents of complex.

lents of anion added indicates that the 1:1 adduct $[Zn^{II}(\mathbf{1})X]^+$ is formed, and least-squares treatment of the curve gave a $\lg K$ value of 5.45 ± 0.03 for the equilibrium $[Zn^{II}(\mathbf{1})]^{2+} + X^- \rightleftharpoons [Zn^{II}(\mathbf{1})X]^+$.[5] It is suggested that fluorescence quenching is due to an intramolecular electron transfer (ET) process within the $[Zn^{II}(\mathbf{1})X]^+$ adduct, in particular from the Zn^{II}-bound dimethylaminobenzoate subunit D to the photo-excited anthracene unit *An. The electron donor tendencies of *N*,*N*-dimethylaniline

[*] Prof. Dr. L. Fabbrizzi, Dr. G. De Santis, Dr. M. Licchelli, Prof. Dr. A. Poggi, Dr. A. Taglietti
Dipartimento di Chimica Generale, Università di Pavia
Via Taramelli 12, I-27100 Pavia (Italy)
Fax: Int. code + (382) 528544

[**] This work was supported by the Italian National Council of Research (CNR: Progetto Strategico: Tecnologie Chimiche Innovative) and by the European Union (HCM program: Network Contract no. ERBCHRXCT940492).

and its derivatives are well recognized.[6] Moreover, the D → *An ET process is thermodynamically feasible, as indicated by the distinctly negative value of $\Delta G^{\circ}_{ET} = E_{0-0} - \Delta G_{D^+/D} + \Delta G_{An/An^-} = (-3.1 + 0.3 + 2.4)\,eV = -0.4\,eV$. The ET nature of *An quenching has been confirmed by spectrofluorimetric studies at 77 K. It is known that immobilization of the solvent molecules in a frozen matrix prevents charge separation and strongly disfavors the ET process, thus restoring fluorescence.[7] Indeed, when an ethanolic solution containing $[Zn^{II}(\mathbf{1})]^{2+}$ and an excess of 4-*N*,*N*-dimethylaminobenzoate, which does not emit at room temperature, was frozen at 77 K, fluorescence of the anthracene subunit was restored, demonstrating the ET nature of the quenching at room temperature.

To verify the selectivity of the $[Zn^{II}(\mathbf{1})]^{2+}$ receptor, spectrofluorimetric titration experiments were carried out with the following inorganic anions: NO_3^-, NCS^-, and Cl^-. The anthracene emission was not altered or showed an intensity decrease of less than than 5% (Cl^-). Competitive titration experiments were also conducted. A 5×10^{-5} M solution of $[Zn^{II}(\mathbf{1})]^{2+}$ in methanol was titrated with a solution containing equimolecular amounts of 4-*N*,*N*-dimethylaminobenzoate and the particular anion. The I_F titration curves obtained with NO_3^- and NCS^- were identical to that with 4-*N*,*N*-dimethylaminobenzoate alone, indicating no competition for the binding to the metal center. However, in the presence of Cl^-, I_F was not fully quenched, but decreased to about 80% of the value observed in the titration with 4-*N*,*N*-dimethylaminobenzoate alone. This indicates that the chloride ions compete successfully with the X^- ions, binding about 20% of the available $[Zn^{II}(\mathbf{1})]^{2+}$ complex cations. The acetate ion behaved in a similar way. The acetate alone does not exert any quenching effect on the anthracene unit of the $[Zn^{II}(\mathbf{1})]^{2+}$ receptor; however, in a competitive titration experiment (CH_3COO^-, X^-), fluorescence quenching was not complete, but corresponded to about 85% of that observed in the titration with 4-*N*,*N*-dimethylaminobenzoate alone (see Fig. 1). This would imply a ratio of the equilibrium constants for the adduct formation $K_{benzoate}/K_{acetate} \approx 6$. The distinctly higher value of the binding constant observed for the 4-*N*,*N*-dimethylaminobenzoate anion may suggest that a $\pi-\pi$ interaction between the Zn^{II}-bound benzoate group and the anthracene subunit provides an additional contribution to the solution stability of the $[Zn^{II}(\mathbf{1})X]^+$ adduct.

In this context, it should be noted that the occurrence of the intramolecular ET process in the $[Zn^{II}(\mathbf{1})X]^+$ supramolecular system requires that the fluorophore and the acceptor are close enough for the appropriate orbitals to overlap. Stacking of benzoate and anthracene fragments may favor electron transfer and induce the nonradiative deactivation of the *An state. A pictorial representation of the intramolecular ET process is sketched in Figure 2. A similar stereochemical arrangement has been proposed for the 1:1 adduct between the benzoate anion and a Zn^{II}-cyclen complex with an acridine pendant.[8] Noticeably, interaction of the thymine anion with the Zn^{II} center of the same complex induced a distinct decrease of the intensity of acridine fluorescence emission.[9]

In any case, fluorescence quenching of the excited anthracene unit of the $[Zn^{II}(\mathbf{1})]^{2+}$ receptor should not be limited to 4-*N*,*N*-dimethylaminobenzoate, but should be feasible for any benzoate anion bearing either a donor or an acceptor group, provided that the thermodynamic requirements for the transfer of an electron to or from the photo-excited fluorophore are fulfilled. In fact, titration of $[Zn^{II}(\mathbf{1})]^{2+}$ with 4-nitrobenzoate ion in methanolic solution induced the decrease and quenching of the fluorescence, according to a profile analogous to that displayed in Figure 1. Nitrobenzene and its derivatives are

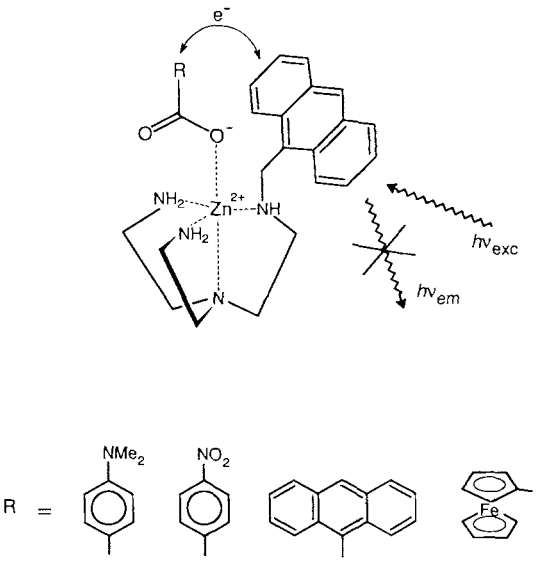

Fig. 2. Representation of the electron transfer mechanism responsible for the fluorescence quenching of the excited anthracene unit *An, which signals the binding of a carboxylate anion by the Zn^{II} center.

classical acceptors. Thus, fluorescence quenching has to be ascribed to an intramolecular ET process from *An to the metal-bound 4-nitrobenzoate ion A. The negative value of $\Delta G^{\circ}_{ET}[= E_{0-0} + \Delta G_{A/A^-} - \Delta G_{An^+/An} = (-3.1 + 1.3 + 0.8)\,eV = -1.0\,eV]$ accounts for its thermodynamic feasibility. Quite interestingly, decrease and almost complete quenching of the fluorescence was observed also when $[Zn^{II}(\mathbf{1})]^{2+}$ was titrated with 9-anthracenoate ion, which itself is fluorescent. Fluorescence quenching should arise from the "disproportionation" process involving an electron transfer between the two anthracene subunits of the supramolecular adduct: $*An + An \rightleftharpoons An^- + An^+$. Both the anthracenoate-to-anthracene and anthracene-to-anthracenoate electron transfer processes exhibit a slightly negative ΔG°_{ET} value (−0.2 eV). In any case, the observed revival of the fluorescence emission in an ethanolic solution frozen at 77 K demonstrates also for the present system that electron transfer is responsible for the quenching of the photo-excited aromatic subunit.

The $[Zn^{II}(\mathbf{1})]^{2+}$ system is able to signal the binding of carboxylate ions other than benzoates, provided that they have definite donor or acceptor properties in a photophysical sense. For instance, fluorescence quenching is observed also on titration of $[Zn^{II}(\mathbf{1})]^{2+}$ with 1-ferrocenecarboxylate (Fcc^-). Ferrocene (Fc) and its derivatives are quite strong donors, and the $Fcc^- \rightarrow *An$ electron transfer is thermodynamically favored: $\Delta G^{\circ}_{ET} = E_{0-0} + \Delta G_{An/An^-} - \Delta G_{Fcc^+/Fcc^-} = (-3.1 + 2.4 + 0.3)\,eV = -0.4\,eV$. In this case, too, the electron transfer nature of the quenching process was confirmed by the fluorescence revival observed at 77 K.

The Zn^{II} ion was deliberately chosen as a Lewis acid for carboxylate binding owing in part to its photophysical innocuosness. Transition metal ions bind to the tren framework to form even more stable adducts with inorganic and organic anions, but tend to complicate the photophysical response. This is the case with the $[Cu^{II}(\mathbf{1})]^{2+}$ system, which, even in absence of any coordinating anion, displays a much less intense emission spectrum (about 15% of that observed for $[Zn^{II}(\mathbf{1})]^{2+}$). This partial fluorescence quenching has to be ascribed to a direct interaction between the Cu^{II} center and the *An fragment. We note that freezing an ethanolic solution of $[Cu^{II}(\mathbf{1})]^{2+}$ at 77 K did not induce any

fluorescence revival. This may suggest that quenching takes place through an *An-to-Cu^{II} energy transfer process, although the occurrence of a very fast electron transfer process cannot be excluded in principle. The Cu^{II} ion (d^9) is well inclined to undergo an energy transfer process, as it has a half-filled d level of low energy ($x^2 - y^2$), which is available for a double electron exchange process (Dexter mechanism).[10] In any case, titration of $[Cu^{II}(\mathbf{1})]^{2+}$ with 4-nitrobenzoate or 4-*N*,*N*-dimethylaminobenzoate caused complete quenching of the residual fluorescence emission.

This work has demonstrated that metal–ligand interactions can be conveniently used for anion binding and recognition. The coordination environment provided by the tren ligand leaves one binding site of the metal center free for the approach of anions of various sizes and shapes: the selectivity is essentially determined by the energy of the metal–anion coordinative interaction. Then, the appended fluorescent unit signals the occurrence of the recognition. A further element of selectivity is introduced by the signal transduction mechanism: only the interactions with anions displaying distinctive electron donor or electron acceptor tendencies will be signaled and sensed. The Zn^{II}-containing system described is well suited for carboxylate anions. Following a similar approach, more sophisticated systems can be designed for the recognition and sensing of anions of various types and complexities.

Experimental Procedure

1: Anthracene-9-carbaldehyde (2.0 mmol) was allowed to react with an excess of tren (6.0 mmol) in 30 mL of a 1:1 EtOH/MeCN mixture at room temperature for 36 h. The solvent and most of the excess tren were distilled off at reduced pressure. The remaining oil was dissolved in 30 mL of EtOH and the resulting solution was treated with 0.7 g of $NaBH_4$, in small portions, then heated at 50 °C for 4 h. On concentration at reduced pressure, a sticky solid was obtained, to which 25 mL of water was added. The suspension that formed was extracted with three 25 mL portions of CH_2Cl_2. The organic layer was dried over $MgSO_4$ and the solvent removed on a rotary evaporator to give **1** as a bright orange oil. Yield 75%. MS (ESI): *m/z* (%) 337 (100) ($M^+ + H$). The corresponding Zn^{II} complex was obtained as the salt $[Zn^{II}(\mathbf{1})](ClO_4)_2$ in the form of a pale yellow solid, through reaction of equimolar amounts of **1** and $Zn(ClO_4)_2 \cdot 6H_2O$ in ethanol. The salt gave a satisfactory C,H,N analysis.

Emission spectra were recorded on a Perkin-Elmer LS-50 luminescence spectrometer and were not corrected for instrument response. Emission spectra at 77 K were measured in dry ethanol by using quartz sample tubes and the same luminescence spectrometer equipped with a low-temperature luminescence accessory (Perkin-Elmer). Pertinent electrode potentials (of the A/A^- and D^+/D redox couples) for the relevant acceptor and donor units (4-nitrobenzoate, 4-*N*,*N*-dimethylaminobenzoate, 9-anthracenecarboxylate, and 1-ferrocenecarboxylate as sodium salts) were determined through differential pulse voltammetry experiments (vs. the Fc^+/Fc internal reference couple, MeCN, 0.1 M Bu_4NClO_4). A platinum microsphere was used as the working electrode. The calculated ΔG°_{ET} values refer to the MeCN medium, as $\Delta G^\circ_{Ox/Red}$ values ($= -FE^\circ_{Ox/Red}$) were obtained in MeCN solutions. Corresponding δG°_{ET} values in MeOH solution should be even more negative, and the ET process more favorable, due to the higher solvent polarity.

Received: July 26, 1995
Revised version: September 25, 1995 [Z8259IE]
German version: *Angew. Chem.* **1996**, *108*, 224–227

Keywords: anion recognition · anthracene derivatives · fluorescent sensors · supramolecular chemistry · zinc compounds

[1] *Fluorescent Chemosensors for Ion and Molecule Recognition* (Ed.: A. W. Czarnik) (*ACS Symp. Ser.* **1993**, *538*).
[2] L. Fabbrizzi, M. Licchelli, P. Pallavicini, A. Perotti, D. Sacchi, *Angew. Chem.* **1994**, *106*, 2051–2053; *Angew. Chem. Int. Ed. Engl.* **1994**, *33*, 1975–1977.
[3] R. A. Bissell, A. P. de Silva, H. Q. N. Gunaratne, P. L. M. Lynch, G. E. M. Maguire, C. P. McCoy, K. R. A. S. Sandanayake, *Top. Curr. Chem.* **1993**, *168*, 223–264.
[4] M. E. Huston, E. U. Akkaya, A. W Czarnik, *J. Am. Chem. Soc.* **1989**, *111*, 8735–8737.
[5] The HYPERQUAD program was used: A. Sabatini, A. Vacca, P. Gans, *Coord. Chem. Rev.* **1992**, *120*, 389–405.
[6] G. J. Kavarnos, *Fundamentals of Photoinduced Electron Transfer*, VCH, New York, **1993**, p. 40.
[7] M. R. Wasielewski, G. L. Gaines III, M. P. O'Neil, M. P. Niemczyk, W. A. Svec in *Supramolecular Chemistry* (Eds.: V. Balzani, L. De Cola), Kluwer, Dordrecht, **1992**, p. 202.
[8] E. Kimura, T. Ikeda, M. Shionoya, M. Shiro, *Angew. Chem.* **1995**, *107*, 711–713; *Angew. Chem. Int. Ed. Engl.* **1995**, *34*, 663–664.
[9] M. Shionoya, T. Koike, E. Kimura, M. Shiro, *J. Am. Chem. Soc.* **1994**, *116*, 3848–3859.
[10] V. Balzani, F. Scandola, *Supramolecular Photochemistry*, Ellis Horwood, London, **1991**, p. 71.

$[S(NtBu)_3]^{2-}$—A Cap-Shaped Dianion, Isoelectronic with the Sulfite Ion and Oxidizable to a Stable Radical Anion**

Roland Fleischer, Stefanie Freitag, Frank Pauer, and Dietmar Stalke*

Dedicated to Professor Herbert W. Roesky on the occasion of his 60th birthday

Recently we have been interested in the synthesis of new ligands with main group elements in low oxidation states as central atoms. These tripodal ligands, as a result of the lone pair on the central atom, have potentially Lewis base character; metal atoms are coordinated by nitrogen atoms in the substituents on the ligands and not by the central atom. Tripodal ligands of this kind include, in particular, compounds with structural units such as $E(NR)_3^-$ (E = Ge, Sn, Pb),[1] as well as polypyrazolylgermanates and -stannates;[2] trislithium tris(trimethylsilylamino)silanes $[(LiNSiMe_3)_3SiR]_2$, R = Me, *t*Bu, Ph;[3] R = H[4] and $[\{(thf)LiNSiMe_2tBu\}_3SiPh]$ [5] are described as trianionic tripodal ligands.

Our aim was to extend this range of mono- and trianionic ligands by synthesizing a dianionic ligand system, to make homoleptic complexes of low-coordinate bivalent metals accessible. Here we report on the tris(*tert*-butyl)triazasulfite ligand, which is formally derived from the dianionic SO_3^{2-} ion in that the three oxygen atoms were substituted by isoelectronic *t*BuN groups. Together with bivalent metals this ligand could lead to interesting organometallic precursors for II/VI semiconducting materials.

In analogy to the addition of organo alkali metal compounds to sulfurdiimines, which leads to aminoiminosulfinates,[6] we have added alkali metal amides to sulfurdiimides. Although equimolar amounts of the starting materials were used, the equimolar addition of lithium *tert*-butylamide to di(*tert*-butyl)sulfurdiimide did not occur, but two equivalents of the sulfurdiimide react with four equivalents of lithium *tert*-butylamide to give the dimeric bislithium tris(*tert*-butyl)triazasulfite **1** [Eq. (a)].

$$2\,S(NtBu)_2 + 4\,LiNHtBu \xrightarrow{\text{toluene}} \underset{\mathbf{2}}{[Li_2(NtBu)_3S]_2} + 2\,H_2NtBu \qquad (a)$$

[*] Priv.-Doz. Dr. D. Stalke,[+] R. Fleischer,[+] Dr. S. Freitag, Dr. F. Pauer
Institut für Anorganische Chemie der Universität
Tammannstrasse 4, D-37077 Göttingen (Germany)
Fax: Int. code +(551)392582
[+] New address:
Institut für Anorganische Chemie der Universität
Am Hubland, D-97074 Würzburg (Germany)

[**] This work was supported by the Deutsche Forschungsgemeinschaft and the Fonds der Chemischen Industrie. We thank Dr. D. Marsh, Max-Planck-Institut für Biophysikalische Chemie, Göttingen, for recording the ESR spectra.

The crystal structure analysis[7] shows a dimer, comprising two cap-shaped dianions, the concave sides of which face each other. Between these caps, there are four lithium atoms each coordinated by three nitrogen atoms (Fig. 1). The lengths of the three crystallographically independent S–N bonds (av 165.0 pm) do not differ significantly. Thus, the negative charge is completely delocalized over the whole ligand. The average N-S-N angle of 102.1° reveals that the central sulfur(IV) atom has trigonal-pyramidal coordination.

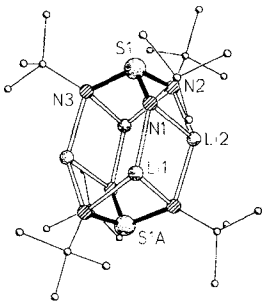

Fig. 1. Structure of **1** in the crystal. Selected bond lengths [pm] and angles [°]: S1–N1 164.8(2), S1–N2 165.8(1), S1–N3 164.4(1), av Li–N 200.6(4); N1-S1-N2 100.08(7) N1-S1-N3 105.34(7) N2-S1-N3 100.85(7) av S1-N-C 116.3(1).

To date there are only two structurally characterized derivatives of triazasulfite compounds. In the solid state both are solvent-separated ion pairs with N-bonded sulfonyl groups. In $S(NR)_3^{2-}$, with R = $S(O)C_6H_4Me$, the S–N distance is 164.3 pm and the N-S-N angle is 101.7°;[8] in the derivative with R = $S(O)C_6H_5$, these values are 162 pm and 103.2°, respectively.[9]

Pure **1** is a white pyrophoric solid. Both as a solid and in solution, **1** turns dark blue if it is handled in an inert gas atmosphere (Ar 5.0) without an additional oxygen absorber. On the other hand, by using an oxygen absorber, both can be handled for a short time with Schlenk techniques. This phenomenon suggests that a radical is formed in the reaction with oxygen. Indeed, a dark blue solution of oxidized **1** in hexane shows an ESR signal even at room temperature. The hyperfine splitting of the signal to give a septet (intensity ratio 1:3:6:7:6:3:1) with a coupling constant of a = 8 G confirms that the unpaired electron interacts with three equivalent ^{14}N atoms (I = 1/2) (Fig. 2). An additional septet (intensity ratio 1:2:3:4:3:2:1) with a coupling constant of a = 0.8 G can be resolved, which might indicate further interaction of the unpaired electron with two equivalent ^{7}Li atoms (I = 3/2).

The radical anion is not only generated by exposure to oxygen but also by reaction with elemental iodine. The final product of the oxidation with iodine is the triiminosulfur(VI) compound $S(NtBu)_3$.[10] Dark blue crystals can be grown from the blue solution. The structure analysis of these crystals provides almost identical structural parameters to those of **1**. The only noticeable difference between the parameters of the blue compound and those of the white one is that for the blue compound the amplitude of the anisotropic displacement parameters of the lithium atoms is marginally higher. This may indicate that not all metal atom positions are occupied in the crystal. The blue crystals probably comprise two compounds—a radical monoanion coordinated by one lithium atom, and a dianion coordinated by two lithium atoms—that together form a dimer. The unoccupied lithium atom position is thus disordered over the two crystallographically independent positions. The ESR spectrum of the blue solid shows no hyperfine splitting.

$[\{Li_2(tBuN)_3S\}_2(thf)]$ **2** is obtained, if the triazasulfite is synthesized in THF. Like in **1**, the concave sides of the cap-shaped dianions face each other. However, in contrast to **1**, only three lithium atoms are located between the staggered *t*BuN groups. The fourth, Li4 (Fig. 3), is only coordinated to two nitrogen atoms (N2 and N3) of the dianion **A** and to a single thf molecule. While the nitrogen atoms N2–N6 are coordinated to two lithium atoms each, N1 is exclusively coordinated to Li1.

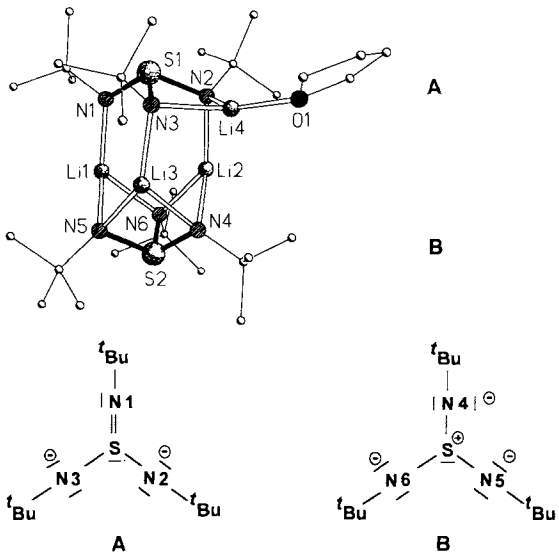

Fig. 3. The structure of **2** in the crystal (top) and the related mesomeric forms (bottom). **A**: S1–N1 160.7(2), S1–N2 168.0(2), S1–N3 168.1(2) pm; N1-S1-N2 108.0(1), N1-S1-N3 108.5(1), N2-S1-N3 93.0(1)°. **B**: S2–N4 163.2(3), S2–N5 164.2(3), S2–N6 164.1(3) pm; N4-S2-N5 100.5(2), N4-S2-N6 100.4(2), N5-S2-N6 98.8(2)

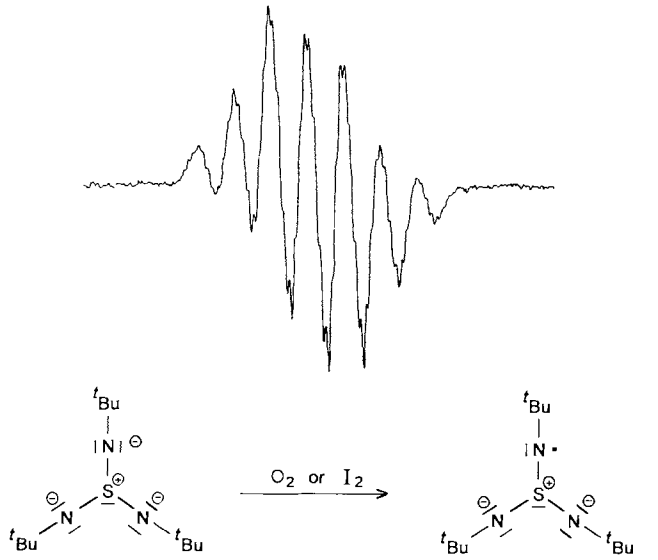

Fig. 2. Oxidation of **1** in hexane at 20 °C. The unpaired electron is delocalized over the three nitrogen atoms.

The significantly different coordination of the metals in **2** compared to **1** gives rise to completely different structural parameters in the two dianionic caps. Cap **A** is described more adequately by a mesomeric form in which one of the three nitrogen atoms (N1) is double-bonded to the central sulfur atom. In cap **B**, all three S–N bonds are approximately the same length. The S1–N1 bond (160.7 pm) is more than 7 pm shorter than the two remaining S–N bonds. Hence this bond can be assigned more double bond character.

The central sulfur atom in the triiminosulfur(VI) compound is coordinated in a trigonal-planar arrangement by three double-bonded imino groups.[10] The S=N distances in this compound are, depending on the substiuents, 12–14 pm shorter than those in the triazasulfite molecules, the S=N distances in the solid-state structures of sulfurdiimides $S(NR)_2$ a further 7–8 pm

 © VCH Verlagsgesellschaft mbH, D-69451 Weinheim, 1996 0570-0833/96/3502-0205 $ 10.00+.25 0

shorter.[11] Hence, the distance between S1 and N1 in **2** indicates only partial double bond character. The N-S-N angle opposite this partial double bond is about 15° smaller than the other two N-S-N angles, since a double bond is more sterically demanding than a single bond and the nitrogen atoms N2 and N3 are bridged by Li4. The cap **B** adopts almost ideal local threefold symmetry. The S–N bonds are identical within their estimated standard deviations. The N-S-N angles in **B** are on average more acute than in **A**, because all nitrogen atoms are μ_2 bridged by a lithium atom.

Tris(*tert*-butyl)triazasulfite, which is isoelectronic to the SO_3^{2-} ion, is a promising ligand that can be oxidized to a stable radical monoanion.[15] The structural motif with only three lithium atoms between the two caps also seems to be favored for steric reasons, as demonstrated in the conversion of **1** to **2**: in the presence of a donor molecule, one of the four lithium atoms (Li4, Fig. 3) leaves the sterically crowded inner region between the caps to take up a less congested position on the periphery.

Experimental Procedure

1: *tert*-Butylamine (30 mmol, 0.69 mL) was added dropwise to a solution of *n*-butyllithium (30 mmol, 20 mL of a 1.52 M solution in hexane) at −78 °C and the mixture was subsequently stirred for 30 min at room temperature. Di(*tert*-butyl)sulfurdiimide (2.61 g, 15 mmol) was added dropwise to the resulting suspension of lithium *tert*-butylamine at room temperature. After all volatile components had been removed in vacuum, the solid was dissolved in toluene to give a red solution from which colorless crystals of **1** (2.9 g, 75%) were obtained after one day at 0 °C. The pyrophoric product melted at 260 °C (decomp.); satisfactory elemental analysis. ^{1}H NMR (250 MHz, [D$_8$]toluene, 25 °C): $\delta = 1.31$ (s, 54H, *t*Bu); ^{7}Li NMR (155 MHz, [D$_8$]toluene, 25 °C): $\delta = 2.88$ (s); ^{13}C NMR (400 MHz, [D$_8$]toluene, 25 °C): $\delta = 33.88$ (s; $C(CH_3)_3$), 53.66 (s; $C(CH_3)_3$); MS(EI): *m/z* (%): 518 (11), M^+; 266 (56), $S(NtBu)_3Li_3$; 103 (59), $SNtBu$; 58 (100), SNC.

2: **2** (3.0 g, 68%) was obtained after recrystallization of **1** from THF/hexane (1:1). The product decomposed at temperatures slightly higher than 100 °C; satisfactory elemental analysis. ^{1}H NMR (250 MHz, [D$_8$] toluene, 25 °C): $\delta = 1.39$ (s, 9H, N-*t*Bu); 1.45, 3.56 (8H, thf); ^{7}Li NMR (155 MHz, [D$_8$]toluene, 25 °C): $\delta = 4.75$ (s); ^{13}C NMR (400 MHz, [D$_8$]toluene, 25 °C): $\delta = 25.67$ (s; $O(CH_2)_2(CH_2)_2$), 34.02 (s; $C(CH_3)_3$), 53.61 (s; $C(CH_3)_3$), 68.16 (s; $O(CH_2)_2(CH_2)_2$); MS(EI): *m/z* (%): 518 (4), $M^+ - THF$; 266 (25), $[(tBuN)_3S]Li_3$; 103 (50), $SNtBu$; 58 (100), SNC.

Received: August 18, 1995 [Z 8323 IE]
German version: *Angew. Chem.* **1996**, *108*, 208–211

Keywords: nitrogen compounds · structure elucidation · sulfur compounds · triazasulfite

[1] a) Reviews from: M. Veith *Angew. Chem.* **1987**, *99*, 1; *Angew. Chem. Int. Ed. Engl.* **1987**, *26*, 1; *Chem. Rev.* **1990**, *90*, 3; 3) *Adv. Organomet. Chem.* **1990**, *31*, 269; b) M. Veith, W. Frank, *Angew. Chem.* **1985**, *97*, 213; *Angew. Chem. Int. Ed. Engl.* **1985**, *24*, 223; c) M. Veith, S. Becker, V. Huch, *Angew. Chem.* **1990**, *102*, 186; *Angew. Chem. Int. Ed. Engl.* **1990**, *29*, 216; d) A. J. Edwards, M. A. Paver, P. R. Raithby, C. A. Russell, A. Steiner, D. Stalke, D. S. Wright, *Inorg. Chem.* **1994**, *33*, 2370.

[2] a) A. Steiner, D. Stalke, *J. Chem. Soc. Chem. Commun.* **1993**, 1702; b) A. Steiner, D. Stalke, *Inorg. Chem.* **1995**, *34*, 4846.

[3] a) D. J. Brauer, H. Bürger, G. R. Liewald, J. Wilke, *J. Organomet. Chem.* **1985**, *287*, 305; b) D. J. Brauer, H. Bürger, G. R. Liewald, *ibid.* **1986**, *305*, 119.

[4] P. Kosse, E. Popowski, M. Veith, V. Huch, *Chem. Ber.* **1994**, *127*, 2103.

[5] I. Hemme, U. Klingebiel, S. Freitag, D. Stalke, *Z. Anorg. Allg. Chem.*, in press.

[6] a) O. J. Scherer, R. Schmitt, *J. Organomet. Chem.* **1969**, *16*, P11; b) O. J. Scherer, R. Wies, *Z. Naturforsch. B* **1970**, *25*, 1486; c) J. Kuyper, K. Vrieze, *J. Chem. Soc. Chem. Commun.* **1976**, 64; d) J. Kuyper, P. C. Keijzer, K. Vrieze, *J. Organomet. Chem.* **1976**, *116*, 1; e) F. Pauer, D. Stalke, *ibid.* **1991**, *418*, 127; f) F. Pauer, J. Rocha, D. Stalke, *J. Chem. Soc. Chem. Commun.* **1991**, 1477; g) F. T. Edelmann, F. Knösel, F. Pauer, D. Stalke, W. Bauer, *J. Organomet. Chem.* **1992**, *438*, 1; h) S. Freitag, W. Kolodziejski, F. Pauer, D. Stalke, *J. Chem. Soc. Dalton Trans.* **1993**, 3479.

[7] Crystal data for **1**: $C_{12}H_{27}Li_2N_3S$, $M = 259.31$, monoclinic, space group $P2_1/c$, $a = 1040.4(2)$, $b = 1638.5(4)$, $c = 1009.9(1)$ pm, $\beta = 112.54(1)°$, $V = 1.5901(5)$ nm^3, $Z = 4$, $\rho_{calcd} = 1.083$ Mg m^{-3}, $F(000) = 568$, $\lambda = 71.073$ pm, $T = 153$ K, $\mu(Mo_{K\alpha}) = 0.189$ mm^{-1}. Data were collected on a Stoe-Siemens-AED diffractometer using an oil-coated, rapidly cooled [12] crystal of dimensions $0.7 \times 0.5 \times 0.4$ mm by the $2\theta/\omega$ method ($4° < 2\theta < 42°$). Of a total of 4989 collected reflections, 2085 were independent ($R_{int} = 0.019$) and 2084 were used to refine 172 parameters, maximum and minimum of the final difference Fourier synthesis: 250 and −316 e nm^{-3}, $R1(F > 4\sigma(F)) = 0.033$ and $wR2 = 0.093$ (all data) with $R1 = \Sigma||F_o| - |F_c||/\Sigma|F_o|$ and $wR2 = (\Sigma w(F_o^2 - F_c^2)^2/\Sigma w(F_o^2)^2)^{0.5}$. Crystal data for **2**: $C_{24}H_{54}Li_4N_6S_2 \cdot$thf, $M = 590.72$, triclinic, space group $P\bar{1}$, $a = 971.9(1)$, $b = 1241.1(1)$, $c = 1619.8(2)$ pm, $\alpha = 84.88(1)$, $\beta = 86.13(1)$, $\gamma = 69.61(1)°$, $V = 1.8227(3)$ nm^3, $Z = 2$, $\rho_{calcd} = 1.076$ Mg m^{-3}, $F(000) = 648$, $\lambda = 71.073$ pm, $T = 153$ K, $\mu(Mo_{K\alpha}) = 0.174$ mm^{-1}. Data were collected on a Stoe-Siemens-AED diffractometer using an oil-coated, rapidly cooled [12] crystal of dimensions $0.6 \times 0.3 \times 0.3$ mm by the $2\theta/\omega$ method ($4° < 2\theta < 45°$). Of a total of 4791 collected reflections, 4746 were independent ($R_{int} = 0.100$) and 4742 were used to refine 490 parameters (720 restraints), maximum and minimum of the final difference Fourrier synthesis: 338 and −333 e nm^{-3}. $R1(F > 4\sigma(F)) = 0.052$ and $wR2 = 0.135$ (all data); defined as above. Both structures were solved by direct methods (SHELXS-90) [13] and refined by full-matrix least-squares procedures on F^2 (SHELXL-93) [14]. The hydrogen atom positions were geometrically idealized and refined by using a riding model. Further details on the crystal structure investigation can be obtained from the Director of the Cambridge Crystallographic Data Center, 12 Union Road, GB-Cambridge CB2 1EZ (UK), by quoting the full journal citation.

[8] A. Gieren, P. Narayanan, *Acta Crystallogr. Sect. A* **1975**, *31*, 120.

[9] H. W. Roesky, W. Schmieder, W. Isenberg, W. S. Sheldrick, G. M. Sheldrick, *Chem. Ber.* **1982**, *115*, 2714.

[10] a) O. Glemser, S. Pohl, F.-M. Tesky, R. Mews, *Angew. Chem.* **1977**, *89*, 829; *Angew. Chem. Int. Ed. Engl.* **1977**, *16*, 789; b) S. Pohl, B. Krebs, U. Seyer, G. Henkel, *Chem. Ber.* **1979**, *112*, 1751.

[11] a) D. G. Anderson, H. E. Robertson, D. W. H. Rankin, J. D. Woollins, *J. Chem. Soc. Dalton Trans.* **1989**, 859; b) M. Herberhold, S. Gerstmann, B. Wrackmeyer, H. Borrmann, *J. Chem. Soc. Dalton Trans.* **1994**, 633.

[12] T. Kottke, D. Stalke, *J. Appl. Crystallogr.* **1993**, *26*, 615.

[13] G. M. Sheldrick, *Acta Crystallogr. Sect. A* **1990**, *461*, 467.

[14] G. M. Sheldrick, SHELXL-93, Program for crystal structure refinement, **1993**, Universität Göttingen.

[15] Note in proof (Dec. 20, 1995): Recently the structure of $[Li_2(NtBu)_3Te]_2$ analogous to that of **1** was described (T. Chivers, X. Gao, M. Parvez, *Angew. Chem.* **1995**, *107*, 2756; *Angew. Chem.* **1995**, *34*, 2549). It would be interesting to determine whether this compound can also be oxidized to a stable radical.

Epoxidation of Electron-Deficient Olefins by a Nucleophilic Iron(III) Peroxo Porphyrinato Complex, Peroxo(tetramesitylporphyrinato)ferrate(1 −)**

Marlene F. Sisemore, Judith N. Burstyn, and Joan S. Valentine*

Heme complexes in which a peroxo ligand is bound to an iron center are probable intermediates in reactions of cytochromes P-450 and related enzymes. Peroxo(porphyrinato)iron(III) complexes have been synthesized as models for such intermediates and characterized with respect to their physical and chemical properties.[1, 2] The reactivities of peroxo transition metal complexes have been classified in the past as either electrophilic or nucleophilic on the following basis:[3] electrophilic peroxo complexes react readily with normal (that is, electron-rich) olefins to give epoxides, while some nucleophilic peroxo complexes such as $[Pt(O_2)(PPh_3)_2]$ react with very electron-poor olefins, for example tetracyanoethylene.[4] Likewise, only electrophilic peroxo complexes oxidize the butyl anion to butoxide.[5] The oxo(diperoxo)rhenium(VII) complex $[ReO(O_2)_2(CH_3)(H_2O)]$, however, is

[*] Dr. J. S. Valentine, M. F. Sisemore
Department of Chemistry and Biochemistry
University of California, Los Angeles, CA 90095 (USA)
Fax: Int. code +(310) 206-7197
e-mail: jsv@chem.ucla.edu
Dr. J. N. Burstyn
Department of Chemistry
University of Wisconsin, Madison, WI 53706 (USA)

[**] We thank Dr. Arthur Cho, Dr. Christopher Foote, Dr. Jon Fukuto, and Dr. David Myles for helpful discussions. This work was supported by the National Science Foundation.

an exception in that it epoxidizes both electron-rich and electron-poor substrates.[6] Previous studies of peroxo(porphyrinato)iron(III) complexes demonstrated that they did not display strongly electrophilic reactivities such as direct hydroxylation of hydrocarbons or epoxidation of electron-rich olefins.[7, 8] Such complexes instead have been shown to be nucleophilic; for example, manganese[9] and iron peroxo porphyrinato complexes[10] react with acyl halides, and iron(III) peroxo porphyrinato complexes react with aldehydes[11] and with carbon dioxide.[12] We recently realized that it might be possible to transfer an oxygen atom directly to an olefin from a bound peroxo ligand by a nucleophilic pathway if we used an electron-deficient olefin. We report here that peroxo complexes of iron(III) porphyrins do indeed react cleanly with electron-deficient olefins, such as enones and quinones, to give the corresponding epoxides. To our knowledge, this is the first time that a peroxo(porphyrinato)iron(III) complex has been shown to insert oxygen directly into an olefinic bond.

In order to investigate further the electronic character of peroxo(porphyrinato)iron(III) complexes, we prepared $[Fe(O_2)TPP]^-$[7, 13] in situ by stirring [FeTPPCl] (1.85 mM) with an excess of tetramethylammonium superoxide[14] in THF[13] for six hours, followed by filtration to remove the excess superoxide salt.[15] Two equivalents of superoxide are required to form the peroxo(porphyrinato)iron(III) complex (Scheme 1).[1]

$$[Fe^{III}Cl(TPP)] + TMA^+O_2^- \longrightarrow [Fe^{II}(TPP)] + O_2 + TMA^+Cl^-$$

$$[Fe^{II}(TPP)] + TMA^+O_2^- \longrightarrow TMA^+[Fe^{III}(O_2)(TPP)]^-$$

Scheme 1. Stepwise reaction of $[Fe^{III}Cl(TPP)]$ with superoxide to give $[Fe^{III}(O_2)(TPP)]^-$.

Formation of $[Fe(O_2)TPP]^-$ was confirmed by the characteristic visible spectrum.[1, 2] Following the procedure described by Regen and Whitesides,[5] butyllithium (1.5 M in hexane) was added to $[Fe(O_2)TPP]^-$, and the resulting solution was stirred for between 5 and 60 min. An excess of acetic anhydride was added, and the solution stirred for another hour to trap and convert any butoxide that might be formed into the acetate. The reaction mixture was analyzed by gas chromatography; no butyl acetate was detected. As a control, $[MoO_5(HMPA)]$,[13, 16] which is known to be an electrophilic Mo^{VI} peroxo complex, was subjected to the same treatment; in this case 1.0 equiv of butyl acetate per peroxo ligand was detected. These results confirmed our earlier conclusion,[7] based on its lack of reactivity with electron-rich olefins, that the peroxo(porphyrinato)iron(III) complex is not electrophilic.

Reactions of the tetraphenyl- and tetramesitylporphyrinato peroxo complexes with electron-deficient olefins were carried out in a similar fashion.[15] An aliquot of the peroxo(porphyrinato)iron(III) solution was removed prior to substrate addition, in order to confirm spectrophotometrically the presence of the metalloperoxide complex.[17] Two equivalents of either 2-methyl-1,4-naphthoquinone (menadione), or 2-cyclohexen-1-one was then added to aliquots of the peroxo(porphyrinato)iron(III) solution. The solutions were stirred vigorously, and aliquots of the reaction mixture were removed after between 2 and 15 minutes for analysis.[18] The results of these reactions are summarized in Table 1.

Reaction of $[Fe(O_2)TMP]^-$ with two equivalents of menadione produced menadione epoxide in $(76\pm8)\%$ yield. Reaction with $[Fe(O_2)TPP]^-$ afforded menadione epoxide in $(52\pm10)\%$ yield. The control reactions with KO_2[19] resulted in $(8\pm1)\%$ epoxide formation. Reaction of $[Fe(O_2)TMP]^-$[20] with two equivalents of 2-cyclohexen-1-one resulted in a $(23\pm2)\%$ yield of epoxide. Addition of a large excess of 2-cyclohexen-1-one (80 equiv) did not increase the epoxide yield. The control reaction with KO_2 alone gave less than 3% epoxide by GC-MS.

Table 1. Reactions of peroxo(tetramesitylporphyrinato)ferrate(1−) with electron-deficient olefins.

Substrate	c ([FeCl-(TMP)]) [mM]	Time [min]	c (Epoxide) [mM]	Yield [a]
menadione	0.10	10–15	0.076 ± 0.008	$76\pm8\%$
KO_2 (0.10 mM control)	0.00	10–15	0.008 ± 0.001	$8\pm1\%$
$H_2O_2/KHCO_3$ (0.10 mM control)	0.00	10–15	0.005 ± 0.001	$5\pm1\%$
2-cyclohexen-1-one	3.44	2–4	0.78 ± 0.06	$23\pm8\%$
KO_2 (3.44 mM control)	0.00	2–4	<0.10	<3%

[a] Yields are based on the starting concentration of [FeCl(TMP)] or of the oxidant in control reactions.

Titration of $[Fe(O_2)TMP]^-$ with aliquots (0.25 equiv) of menadione was monitored by visible absorption spectroscopy. The intensity of the Soret band of $[Fe(O_2)TMP]^-$ (at 434 nm) decreased by approximately 25% upon each addition of menadione. The clean isosbestic points obtained at 424 and 543 nm indicates that $[FeTMP]^-$ reacted directly with the olefin to give the product epoxide. The best results were obtained when the successive aliquots were all added within five minutes, which implies that $[Fe(O_2)TMP]^-$ might react slowly with the epoxide product; this conclusion was confirmed in separate experiments by the observation of the disappearance of the EPR signal due to the peroxo complex and of the loss of epoxide detected by HPLC when the two were mixed.

The mechanism that we propose for this reaction (Scheme 2) is analogous to that proposed for the reaction of electron-deficient olefins with basic hydrogen peroxide, HO_2^-:[21, 22]

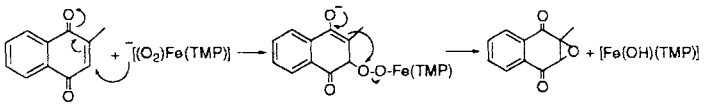

Scheme 2. The epoxidation of menadione (or 2-cyclohexen-1-one) by $[Fe(O_2)TMP]^-$ probably proceeds through a peroxy intermediate, which rearranges to give the epoxide.

$[Fe(O_2)TMP]^-$ attacks menadione (or cyclohexenone) to form a peroxy intermediate, which then rearranges to give menadione epoxide and a porphyrin product whose UV-Vis absorption spectrum resembles that of [Fe(OH)(TMP)].[23] The organic products obtained from reaction with $[Fe(O_2)TMP]^-$ are identical to those resulting from reaction with HO_2^-, which suggests that the mechanisms are analogous. It is conceivable that HO_2^- could dissociate from the peroxoporphyrin complex to epoxidize the olefin. However, since control reactions (Table 1) with HO_2^-, prepared from 0.10 mM $H_2O_2/KHCO_3$, produced only $(5\pm1)\%$ menadione epoxide after 10–15 minutes (Table 1), we conclude that the high yields of epoxide obtained with $[Fe(O_2)TMP]^-$ are due to reactions of the iron(III) complex itself and not to free HO_2^-.

Our results indicate that peroxo(porphyrinato)iron(III) complexes behave as nucleophiles toward electron-deficient olefins, a finding that lends further support to the studies carried out with acyl halides,[9, 10] aldehydes,[11] and carbon dioxide.[12] Similar nucleophilic peroxo heme species are proposed as reac-

 © VCH Verlagsgesellschaft mbH, D-69451 Weinheim, 1996 0570-0833/96/3502-0207 $ 10.00+.25/0

tive intermediates in a series of reactions with cytochrome P-450 aromatase,[24] an enzyme that converts androgens into estrogens (which is implicated in breast cancer), with cytochrome P-450 2B4 (which aromatizes the bicyclic steroid analog, 3-oxodecalin-4-ene-10-carboxaldehyde[25]), and with NO synthase[26] (which converts arginine to citrulline and nitric oxide gas; NO gas is important in neurotransmission, vascular dilation, and macrophage toxicity to name but a few of its biological functions). The nucleophilic chemistry of the peroxo(porphyrinato)iron(III) complex described here may be a good model for such enzymatic intermediates.

Received: July 12, 1995 [Z 8201 IE]
German version: *Angew. Chem.* **1996**, *108*, 195–196

Keywords: enzyme mimetics · epoxidations · peroxo complexes · porphyrinoids

[1] a) E. McCandlish, A. R. Miksztal, M. Nappa, A. Q. Sprenger, J. S. Valentine, J. D. Strong, T. G. Spiro, *J. Am. Chem. Soc.* **1980**, *102*, 4268–4271; b) J. N. Burstyn, J. A. Roe, A. R. Miksztal, B. A. Shaevitz, G. Lang, J. S. Valentine, *ibid.* **1988**, *110*, 1382–1388.
[2] A. R. Miksztal, J. S. Valentine, *Inorg. Chem.* **1984**, *23*, 3548–3552.
[3] R. A. Sheldon, J. K. Kochi, *Metal-Catalyzed Oxidations of Organic Compounds*, Academic Press, **1981**, pp. 81–97.
[4] R. A. Sheldon, J. A. van Doorn, *J. Organomet. Chem.* **1975**, *94*, 115–129.
[5] S. L. Regen, G. M. Whitesides, *J. Organomet. Chem.* **1973**, *59*, 293–297.
[6] a) W. A. Herrmann, R. W. Fischer, D. W. Marz, *Angew. Chem.* **1991**, *103*, 1706–1709; *Angew. Chem. Int. Ed. Engl.* **1991**, *30*, 1638–1641; b) W. A. Herrmann, R. W. Fischer, W. Scherer, M. U. Rauch, *ibid.* **1993**, *105*, 1209–1212 and **1993**, *32*, 1157–1160.
[7] J. N. Burstyn, *Ph.D. Dissertation*, University of California, Los Angeles, **1986**.
[8] J. S. Valentine, J. N. Burstyn, L. D. Margerum, *Mechanisms of Dioxygen Activation in Metal-Containing Monooxygenases: Enzymes and Model Systems*, Plenum, New York, **1988**.
[9] J. T. Groves, Y. Watanabe, T. J. McMurry, *J. Am. Chem. Soc.* **1983**, *105*, 4489–4490.
[10] A. M. Khenkin, A. A. Shteinman, *J. Chem. Soc. Chem. Commun.* **1984**, 1219–1220.
[11] Y. Watanabe, Y. Ishimura, *J. Am. Chem. Soc.* **1989**, *111*, 410–411, 8047–8049.
[12] M. Schappacher, R. Weiss, R. Montiel-Montoya, A. Trautwein, A. Tabard, *J. Am. Chem. Soc.* **1985**, *107*, 3736–3738.
[13] Abbreviations used in the text: THF = tetrahydrofuran, TPP = tetraphenylporphyrin dianion, TMA = tetramethylammonium, TMP = tetramesitylporphyrin dianion = K222 = 1,10-diaza-4,7,13,16,21,24-hexaoxabicyclo[8.8.8]-hexacosane, HMPA = hexamethylphosphoramide.
[14] D. T. Sawyer, T. S. Calderwood, K. Yamaguchi, C. T. Angelis, *Inorg. Chem.* **1983**, *22*, 2577–2583.
[15] All reactions to prepare the peroxoiron(III) complexes were carried out in an inert atmosphere chamber (Vacuum Atmospheres) under helium. Solvents were rigorously dried before use (THF from potassium/benzophenone and acetonitrile from calcium hydride). [FeCl(TMP)] (1–3.44 mM) was treated for 20 min with ground KO_2 (2 equiv) and K222 (2.6 equiv) in acetonitrile that had been passed over neutral alumina (Super I) prior to use. Dilutions were made as needed, prior to substrate addition.
[16] H. Mimoun, *J. Mol. Catal.* **1980**, *7*, 1–29.
[17] UV/Vis spectrum of peroxo(tetramesitylporphyrinato)ferrate(1–): 434, 549sh, 567, 595sh, 612 nm.
[18] Menadione and its epoxide were analyzed by C18 HPLC (Beckmann 114M solvent delivery module, flow 1 mL min^{-1}, acetonitrile/water 65/35, with a 165 variable-wavelength detector set at 265 nm, 421 controller, and Econosphere cartridge) and by GC-MS (HP 5890A capillary column coated with 5% methylphenylsilicone connected to an HP 9570 detector). 2-Cyclohexen-1-one and its epoxide were analyzed by GC-MS using decane as an internal standard. Epoxide yields were determined by comparison against standard curves.
[19] Prior to analysis, 0.10 mM KO_2 was treated with 2 equiv menadione for 10–15 min, or 3.44 mM KO_2 with 2 equiv 2-cyclohexen-1-one for 2–4 min.
[20] $[Fe(O_2)TMP]^-$ was used for the reactivity studies with 2-cyclohexen-1-one because of the higher epoxide yields obtained with menadione.
[21] L. F. Fieser, M. Fieser, *Reagents for Organic Synthesis, Vol. 1*, Wiley, New York, **1967**, p. 466.
[22] D. Felix, C. Wintner, A. Eschenmoser, *Org. Synth. Collective, Vol. 6* **1988**, 679–682.
[23] R.-J. Cheng, L. Latos-Grazynski, A. L. Balch, *Inorg. Chem.* **1982**, *21*, 2412–2418.
[24] a) M. Akhtar, M. R. Calder, D. L. Corina, J. N. Wright, *J. Chem. Soc. Chem. Commun.* **1981**, 129–130; b) P. A. Cole, C. H. Robinson, *J. Am. Chem. Soc.* **1991**, *113*, 8130–8137.
[25] A. D. N. Vaz, K. J. Kessel, M. J. Coon, *Biochemistry* **1994**, *33*, 13651–13661.
[26] M. A. Marletta, *J. Biol. Chem.* **1993**, *268*, 12231–12234.

Synthesis and Structure of the Bis(imido)gold Complex $[Au^{I}_5(NtBu)_2(PPh_3)_4]^+Cl^- \cdot 2C_6H_5CH_3$; a Higher Homologue of the Organotris-(triphenylphosphaneaurio)ammonium Ions**

Robert E. Allan, Michael A. Beswick, Michael A. Paver, Paul R. Raithby, Alexander Steiner, and Dominic S. Wright*

Recently we investigated the syntheses and structures of main group metal imido compounds generated from the reactions of the dimethylamido metal complexes with primary amines (RNH_2) or metalated primary amines (RNHLi).[1] Of particular interest has been the development of Group 15 (Sb and Bi) metal imido anions,[1c,d] which are novel ligands for transition metals. Hence, the transmetalation reaction of $[\{Sb_2(Ncy)_4\}_2Li_4]$ with CuCl gives $[\{Sb_2(Ncy)_4\}_2Cu_4]$ (cy = cyclohexyl), in which a Cu_4 square-planar core is stabilized by $[Sb_2(Ncy)_4]^{2-}$ dianions.[2] Our most recent studies have focused on the applications of $[Sn(NMe_2)_x]$ ($x = 2$ or 4) in the syntheses of anionic Sn^{II} and Sn^{IV} ligands.[1e]

In an attempt to generate in situ a mixed-metal Sn^{IV}/Au^{I} complex containing a $[Sn(NtBu)_4]^{4-}$ tetraanion, [*t*BuNHLi] was treated with $[Sn(NMe_2)_4]$ in the molar ratio 4:1. However, addition of $[AuCl(PPh_3)]$ (4 equiv) to this mixture affords the bis(imido)gold(I) complex **1**, in which imido group transfer

$[Au_5(NtBu)_2(PPh_3)_4]^+Cl^- \cdot 2C_6H_5CH_3$ **1** $\cdot 2C_6H_5CH_3$

has occurred, rather than formation of the mixed-metal aggregate which was sought. Evidently, $[Sn(NMe_2)_4]$ functions simply as a base in this reaction. This became clear when **1** was also formed when [*t*BuNHLi] was treated directly with $[AuCl(PPh_3)]$ (1 equiv), the excess [*t*BuNHLi] now acting as the base. Compound **1** is most conveniently prepared by this latter route (see Experimental Procedure).

The synthetic strategies used to date to generate imidogold(I) cations $[Au_3(\mu_3\text{-}NR)(PPh_3)_3]^+$ have involved reactions of RNH_2 or RNCO with $[(AuPPh_3)_3O]^+BF_4^-$ and resulted in the formation of the organotris(triaurio)ammonium salts and H_2O or CO_2, respectively.[3] Although the exact mechanism of formation of **1** is uncertain, we assume that the cation of **1** finally results from the interaction of $[Au_2(\mu\text{-}N\text{-}tBu)(PPh_3)_2]$, formed during the reaction, with $[AuCl(PPh_3)]$ (Scheme 1).

The low-temperature X-ray structure of **1**[4] shows that it is an ion-separated species consisting of a bis(imido)-Au_5 cation and a Cl^- anion (Fig. 1). Additionally, two lattice-bound

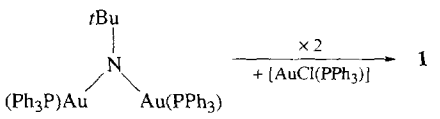

Scheme 1.

[*] Dr. D. S. Wright, R. E. Allan, Dr. M. A. Beswick, M. A. Paver, Dr. P. R. Raithby, Dr. A. Steiner
University Chemical Laboratory
Lensfield Road, GB-Cambridge, CB2 1EW (UK)
Fax: Int. code +(1223) 33 63 62
e-mail: DSW1000@Cam.ac.uk

[**] We gratefully acknowledge the Engineering and Physcial Sciences Research Council (R. E. A., M. A. B., M. A. P., P. R. R.), the Royal Society (D. S. W., P. R. R.), the Nuffield Foundation (D. S. W.), the Associated Octel Co. Ltd., Ellesmere Port, UK (M. A. P., D. S. W.), and the European Community (Fellowship for A. S.). We also thank Johnson Matthey for generous loans of $[HAuCl_4 \cdot nH_2O]$.

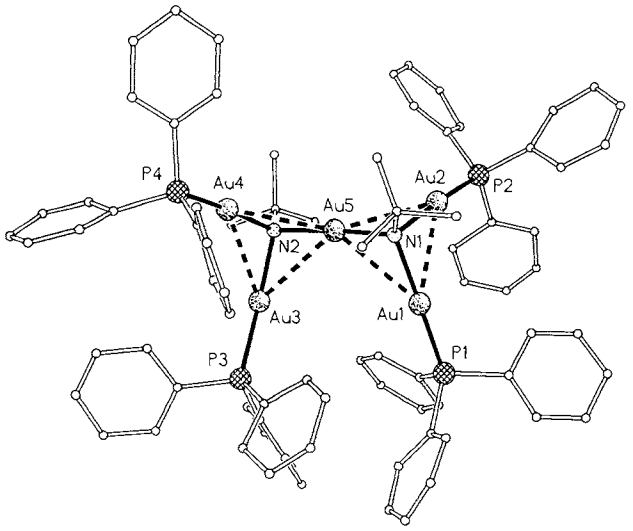

Fig. 1. Molecular structure of **1** in the crystal. Hydrogen atoms and the lattice-bound toluene molecules have been omitted for clarity. Selected bond lengths [Å] and angles [°]: Au1–N1 2.03(4), Au2–N1 2.11(3), Au5–N1 2.00(3), Au5–N2 2.07(3), Au3–N2 2.05(4), Au4–N2 2.09(3), Au1···Au2 2.945(3), Au5···Au1 3.110(2), Au5···Au2 3.005(2), Au5···Au3 3.016(2), Au5···Au4 3.033(2); N1-Au5-N2 176(2), av N-Au-P 173.6, av Au-N-Au 94.0.

toluene molecules are present for each formula unit of **1**. The two triangular Au_3 moieties of the "bowtie-shaped" core of the cation are interlocked by the central Au5 atom; the planes of these Au_3 units are inclined at an angle of about 43° to each other. The Au···Au distances between the central Au5 atom and the four terminal, phosphane-complexed Au centers (av 3.04 Å) are considerably longer than those formed between the terminal metal atoms of the "bowtie" (av 2.94 Å). These Au···Au distances correspond to those found in the few structurally characterized imidogold(I) complexes (in the $[Au_3(\mu_3\text{-}NR)(PPh_3)_3]^+$ ions: 2.93–3.30 Å).[3] The two Au_3 rings are capped by μ_3-N*t*Bu ligands at opposite faces of the Au_5 core, resulting in an overall transoid conformation for the cation. The cation of **1** can be regarded as a "naked" Au^I center which has been complexed by two neutral $[Au_2(\mu_2\text{-}NtBu)(PPh_3)_2]$ units. Interestingly, both the terminal Au atoms (av P-Au-N 174°) and the central Au (N-Au-N 176°) atom all have essentially linear ligand coordination geometries.

Although there has been considerable fundamental interest in the nature and influence of the "aurophilic" interaction spurred by the recent structural characterizations of the $[(PPh_3)_4Au_4(\mu_4\text{-}N)]^+$[5] and $[(PPh_3)_5Au_5(\mu_5\text{-}N)]^{2+}$[6] nitridogold(I) cations, all the imido complexes that have been structurally elucidated are cations of the type $[Au_3(\mu_3\text{-}NR)(PPh_3)_3]^+$.[3] The Au_5 cation of **1** is composed of similar $Au_3(\mu_3\text{-}N)$ units and can be regarded as the next homologue of a potential series of cations, constructed from interlocked Au_3 units, of the general formula $[Au_{(3+2n)}(\mu_3\text{-}NR)_{(1+n)}(PR'_3)_{(3+n)}]^+$. As such, **1** is the largest imidogold(I) complex to be structurally characterized so far. Several mixed-metal cluster compounds have been structurally characterized in which "bowtie-shaped" Au_5 units akin to that in the cation of **1** are capped by another transition metal center[7] (e.g. in the cation $[Rh(C\text{-}NC_8H_9)_3(AuPPh_3)_5]^{2+}$).[7b] The cation of **1** is a potential precursor for the formation of analogous mixed-metal species. We are currently investigating the reactions of transition metal anions with **1** with a view to synthesizing bimetallic complexes in a targeted way.

Experimental Procedure

1: *n*BuLi (0.31 mL, 1.6 M in hexanes, 0.5 mmol) was added to a solution of $[tBuNH_2]$ (0.5 mL, 0.5 mmol) in toluene (5 mL). After the mixture had been heated to reflux for 5 min, a pale yellow solution was formed. This was subsequently cooled to −78 °C, $[AuCl(PPh_3)]$ (0.25 g, 0.5 mmol) was added, and the mixture stirred for 30 min at −78 °C. The reaction mixture was allowed to warm to room temperature; most of the solid that had formed dissolved. The solution was filtered through Celite. Reduction of the volume of the filtrate under vacuum (ca. 2 mL) gave a white solid, which redissolved when the solution was warmed gently; hexagonal, colorless crystals grew at room temperature (24 h). Although two lattice-bound toluene molecules are present per molecular unit of **1** in the crystal, placing **1** under vacuum (ca. 15 min, 10^{-1} Torr) leads to unsolvated, amorphous samples in which all the lattice solvent is apparently removed. The following analytical and spectroscopic investigations were carried out on the dry amorphous material: yield 0.18 g (80%); decomposition to give a black solid at about 145 °C; elemental analyses for $(C_{80}H_{78}Au_5ClN_2P_4)_n$, found: C 42.1, H 3.5, N 1.2, P 5.4; calcd: C 43.4, H 3.5, N 1.3, P 5.6; IR (Nujol), $\tilde{\nu}$ [cm^{-1}] = ca. 3040 (aryl C-H stretching vibration), 1435 (P-Ph stretching vibration), 743, 691 (aryl bending vibration); ^1H NMR (250 MHz, +25 °C, $CDCl_3$), δ = 7.50–7.15 (10H, br., m, C_6H_5-), 1.34 (3H, s, *t*Bu); ^{31}P NMR (101.25 MHz, +25 °C, $CDCl_3$), δ = −113.2 (s, PPh_3); ^{13}C NMR (100.61 MHz, +25 °C, $CDCl_3$), 134.1–128.9 (PPh_3), 42.8 (*t*Bu).

Received: August 28, 1995 [Z83491E]
German version: *Angew. Chem.* **1996**, *108*, 220–221

Keywords: aurophilicity · complexes with nitrogen ligands · gold compounds · imides

[1] a) A. J. Edwards, N. E. Leadbeater, M. A. Paver, P. R. Raithby, C. A. Russell, D. S. Wright, *J. Chem. Soc. Dalton Trans.* **1994**, 1479; b) A. J. Edwards, M. A. Paver, P. R. Raithby, M.-A. Rennie, C. A. Russell, D. S. Wright, *ibid.* **1994**, 2963; c) A. J. Edwards, M. A. Paver, M.-A. Rennie, P. R. Raithby, C. A. Russell, D. S. Wright, *Angew. Chem.* **1994**, *106*, 1334; *Angew. Chem. Int. Ed. Engl.* **1994**, *33*, 1277; d) R. A. Alton, D. Barr, A. J. Edwards, M. A. Paver, P. R. Raithby, M.-A. Rennie, C. A. Russell, D. S. Wright, *J. Chem. Soc. Chem. Commun.* **1994**, 1481; e) R. E. Allan, M. A. Beswick, A. J. Edwards, M. A. Paver, P. R. Raithby, M.-A. Rennie, D. S. Wright, *J. Chem. Soc. Dalton Trans.*, in press.

[2] D. Barr, A. J. Edwards, M. A. Paver, S. Pullen, P. R. Raithby, M.-A. Rennie, C. A. Russell, D. S. Wright, *Angew. Chem.* **1994**, *106*, 1960; *Angew. Chem. Int. Ed. Engl.* **1994**, *33*, 1875.

[3] a) V. Ramamoorthy, P. R. Sharp, *Inorg. Chem.* **1990**, *29*, 3336; b) A. Grohmann, J. Riede, H. Schmidbaur, *J. Chem. Soc. Dalton Trans.* **1991**, 783; c) H. Schmidbaur, A. Kolb, P. Bissinger, *Inorg. Chem.* **1992**, *31*, 4370; d) A. Kolb, P. Bessinger, H. Schmidbaur, *Z. Anorg. Allg. Chem.* **1993**, *619*, 1580.

[4] Crystal data for **1**: $C_{94}H_{94}Au_5ClN_2P_4$, M_r = 2395.87, space group, monoclinic, $P2_1/c$, a = 19.892(8), b = 11.052(3), c = 39.16(2) Å, β = 90.35(5)°, V = 8609(6) Å^3, Z = 4, λ = 0.71073 Å, ρ_{calcd} = 1.849 M gm^{-3}, $\mu(Mo_{K\alpha})$ = 8.642 mm^{-1}. Data were collected on a Siemens-Stoe AED diffractometer using an oil-coated [8] crystal of dimensions 0.15 × 0.13 × 0.12 mm by the θ/ω method ($8.0 \le 2\theta \le 45.0°$). Of a total of 12347 reflections collected, 11135 were independent. A semiempirical absorption correction was applied (max. and min. transmission, 0.536 and 0.188, respectively). The structure was solved by direct methods [9] and refined by full-matrix least-squares on F^2 [10] to final values of $R1$ ($F > 4\sigma F$) = 0.092 and $wR2$ = 0.320 (all data) [$R1 = \Sigma||F_o| - |F_c||/\Sigma|F_o|$, $wR2 = \{[\Sigma w(F_o^2 - F_c^2)^2]/\Sigma wF_o^4\}^{0.5}$, $w = 1/[\sigma^2(F_o^2) + (xP)^2 + yP]$, $P = (F_o^2 + 2F_c^2/3)$. Largest features in the final difference map, 2.093 and −1.841 e Å^{-3}. The crystal used in the experiment was irregularly shaped and gave a weak diffraction pattern even at 153 K. When restraints were applied to the light atoms, a chemically sensible structure was obtained with an R value of less than 0.10. However, as pointed out by one of the referees, this refinement procedure leads to large estimated standard deviations. Further details of the crystal structure investigation can be obtained from the Director of the Cambridge Crystallographic Data Centre, 12 Union Road, GB-Cambridge CB2 1EZ (UK), on quoting the full citation.

[5] Y. L. Slovokhotova, Y. T. Struchkov, *J. Organomet. Chem.* **1984**, *277*, 143; E. Zeller, H. Beruda, A. Kolb, H. Schmidbaur, *Nature* **1991**, *352*, 141.

[6] A. Grohmann, J. Riede, H. Schmidbaur, *Nature* **1990**, *345*, 140.

[7] a) P. D. Boyle, B. J. Johnson, A. Buehler, L. Pignolet, *Inorg. Chem.* **1986**, *25*, 5; b) S. G. Bott, H. Fleischer, M. Leach, D. M. P. Mingos, H. Powell, D. J. Watkins, M. J. Watson, *J. Chem. Soc. Dalton Trans.* **1991**, 2569; c) T. G. M. M. Kappen, A. C. M. van den Broek, P. P. J. Schlebos, J. J. Bour, W. P. Bosman, J. M. M. Smit, P. T. Beurskens, J. J. Steggerda, *Inorg. Chem.* **1992**, *31*, 4075.

[8] D. Stalke and T. Kottke, *J. Appl. Crystallogr.* **1993**, *26*, 615.

[9] G. M. Sheldrick, *SHELXS 86*, Göttingen, **1986**.

[10] G. M. Sheldrick, *SHELXL 93*, Göttingen, **1993**.

Synthesis of the First Titana[3]radialene and Its Ring Enlargement to a Titanacyclopentene**

Adalbert Maercker* and Andreas Groos

Dedicated to Professor Harald Günther on the occasion of his 60th birthday

The ready availability of 3,4-dilithio-2,5-dimethyl-2,4-hexadiene (**1**)[1] and its conversion into heteroradialenes[2] with boron,[3] silicon,[4] tin,[5] and phosphorus[6] as heteroatoms challenged us to investigate the existence of transition metal derivatives.

Indeed, the reaction of **1** with titanocene dichloride (**2**) led to the expected titana[3]radialene **3**, which underwent a fast rearrangement with ring enlargement to give titanacyclopentene **4**.

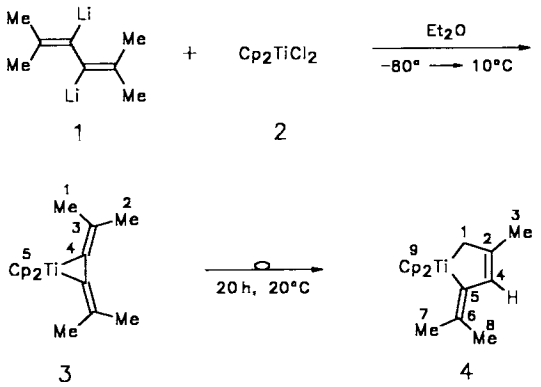

Intermediate **3** could not be isolated. The structures of both titanium compounds **3** and **4** were determined unequivocally by their NMR spectra, and data for derivatives of **4**, compounds **12** and **13**, lent further support (Table 1). Even just the ^{13}C chemical shifts of the carbon atoms C-3 ($\delta = 121.24$) and C-4 ($\delta = 191.63$) indicate that the proposed structure of the initial product is **3** and not, for example, **5** or **6**. Compound **7**, the zirconium analogue of **6** obtained from the reaction of **1** and zirconocene dichloride,[7] shows totally different ^{13}C chemical shifts ([D_6]benzene: $\delta = 60.57$ (C-2), 103.97 (C-3)). The number of methyl signals in the ^1H and ^{13}C NMR spectra also indicate that **5** and **6** are not the initial products; like **7** these compounds should give rise to only one methyl signal, whereas

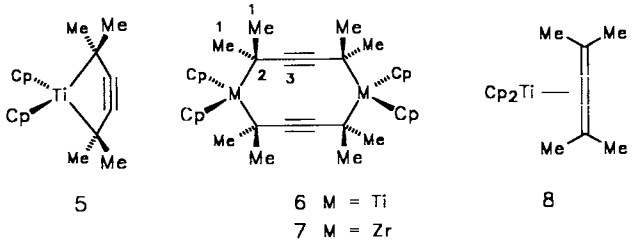

the initial product **3** gives rise to two methyl signals (cf. also: butadiyne–zirconocene complexes of Rosenthal et al.[8] and Erker et al.,[9] which have two more electrons, and also the butadiyne–titanocene complexes of Rosenthal et al.[10]).

Furthermore, the number of NMR signals excludes an unsymmetrical structure. Due to the integration of the ^1H NMR signals one can also exclude a butatriene-bridged dimer structure. The question whether **3** is a titanium(IV) or titanium(II) compound is only a formal one. The actual structure must be between that of **3** and **8**.[11] It has been proposed, however, that the mesomeric resonance structure **8** is only a minor contributor, since the ^1H NMR chemical shift of the cyclopentadienyl signal of titanium(II) compounds should be shifted upfield by up to 2 ppm;[12] here this signal is observed at low field (([D_8]THF): $\delta = 6.38$).

When **1** is allowed to react with **2** in the presence of 2-butyne, the titanacyclopentadiene **11**[13] is formed, possibly via **9** and certainly via the titanacyclopropene intermediate **10**[14], together with **3** and **4**. A reaction of titana[3]radialene **3** with 2-butyne did not occur.

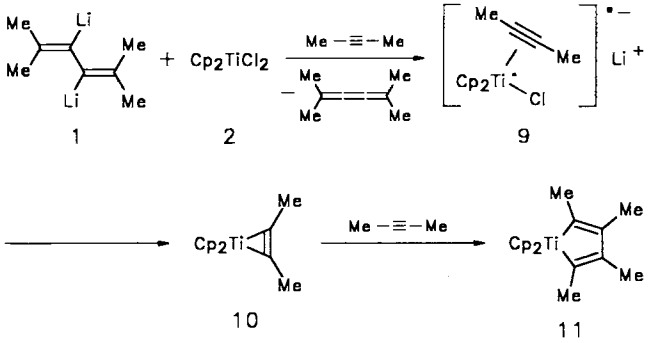

In contrast, the titanacyclopentene **4** reacts slowly with 2-butyne and titanacyclopentene **12** is formed by insertion (Table 1). With 1-hexyne a fast and strictly regioselective reaction leads to **13**, in which the butyl group of hexyne is directly adjacent to the titanium center (Table 1). This can be explained by assuming

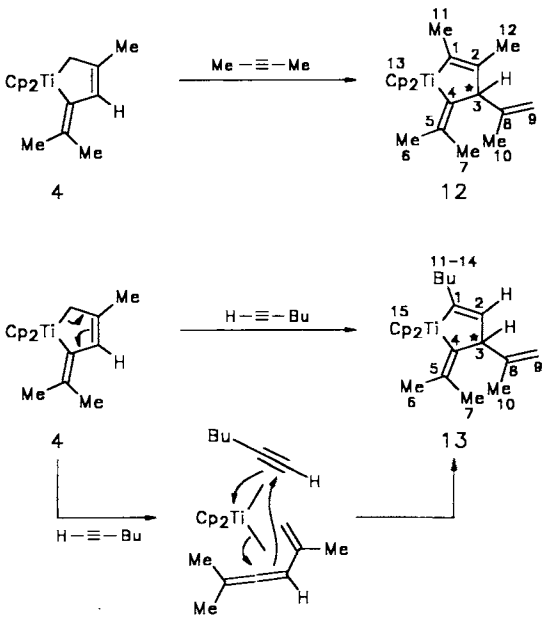

[*] Prof. Dr. A. Maercker, Dr. A. Groos
Institut für Organische Chemie der Universität
Adolf-Reichwein-Strasse, D-57068 Siegen (Germany)
Fax: Int. code +(271)740-2330

[**] Polylithiumorganic Compounds, Part 22. This work was supported by the Volkswagen-Stiftung and the Fonds der Chemischen Industrie. We thank Prof. Dr. H. Kisch, Erlangen, and the referees for valuable suggestions. Part 21: A. Maercker, J. Fischenich, *Tetrahedron* **1995**, *51*, 10209–10218.

Table 1. Important spectroscopic data of compounds **3**, **4**, **12**, and **13**.

3: ^{1}H NMR [a] (400 MHz, [D$_8$]THF): δ = 0.46 (6H-1), 1.52 (6H-2), 6.38 (10H-5); ^{13}C NMR (100 MHz, [D$_8$]THF): δ = 25.51 (C-1), 26.63 (C-2), 115.08 (C-5), 121.24 (C-3), 191.63 (C-4)

4: ^{1}H NMR [a, b] (400 MHz, [D$_8$]THF): δ = 0.96 (3H-7), 1.44 (3H-3), 1.48 (3H-8), 1.65 (2H-1), 5.48 (1H-4), 6.12 (10H-9); ^{13}C NMR (100 MHz, [D$_8$]THF): δ = 20.78 (C-3), 25.57 (C-7), 28.99 (C-8), 56.86 (t, ^1J = 128.7 Hz, C-1), 113.56 (C-9), 124.37 (C-4), 127.40 (C-2), 137.34 (C-6), 182.58 (C-5); MS: M^+ peak not detectable

12: ^{1}H NMR [c] (200 MHz, [D$_8$]THF): δ = 0.62 (d, ^5J = 1.6 Hz, 3H-6), 1.03 (dq, ^4J = 1.8, ^5J = 0.8 Hz, 3H-12), 1.09 (dq, ^5J = 0.9, 0.8 Hz, 3H-11), 1.32 (d, ^5J = 1.1 Hz, 3H-7), 1.71 (dd, ^4J = 1.4, 0.7 Hz, 3H-10), 3.34 (br.s, 1H-3), 4.56 (dm, ^2J = 2.9, ^4J = 0.7 Hz, 1H-9), 4.66 (dq, ^2J = 2.9, ^4J = 1.4 Hz, 1H-9), 6.23 (s, 5H-13), 6.32 (s, 5H-13); ^{13}C NMR (50 MHz, [D$_8$]THF): δ = 15.77 (C-11), 19.89 (C-10), 20.46 (C-12), 23.13 (C-7), 24.87 (C-6), 65.32 (C-3), 112.82 (C-9), 115.07 (C-13), 115.44 (C-13), 125.55 (C-2), 128.94 (C-5), 149.44 (C-8), 188.57 (C-4), 190.29 (C-1); HR-MS: *m/z* (calcd) 340.16705, *m/z* (found) 340.16735

13: ^{1}H NMR [a, c] (200 MHz, [D$_8$]THF): δ = 0.75 (3H-6), 0.87 (3H-14), 0.8–1.5 (6H-11–H-13), 1.26 (3H-7), 1.70 (3H-10), 3.23 (1H-3), 4.58 (1H-9), 4.67 (1H-9), 4.84 (1H-2), 6.22 (5H-15), 6.28 (5H-15); ^{13}C NMR (50 MHz, [D$_8$]THF): δ = 14.55 (C-14), 20.86 (C-10), 22.60 (C-7), 23.82 (C-13), 24.69 (C-6), 32.18 (C-12), 38.90 (C-11), 55.51 (C-3), 109.29 (C-9), 114.79 (C-15), 115.07 (C-15), 118.69 (C-2), 129.27 (C-5), 151.31 (C-8), 186.53 (C-4), 201.05 (C-1)

[a] Only broad singlets were observed due to the presence of paramagnetic impurities. Thus coupling constants could not be determined. [b] Assignment by inverse C,H shift correlation. [c] Assignment by C,H shift correlation.

that when complex **4** coordinates the alkyne initially, the bulky butyl group avoids the triene ligand. A direct insertion of the alkyne into **4** by formation of a titanacycloheptadiene was not observed. Compounds **4**, **12**, and **13** show some unique structural features similar to those of compounds described by Doxsee et al.[15]

Since *no* intermediates were detected during the rearrangement **3** → **4**, the mechanism can only be speculative. The reaction may follow the path shown in Scheme 1. When the rearrangement was monitored by NMR spectroscopy no further hydrocarbons or titanium compounds could be found.

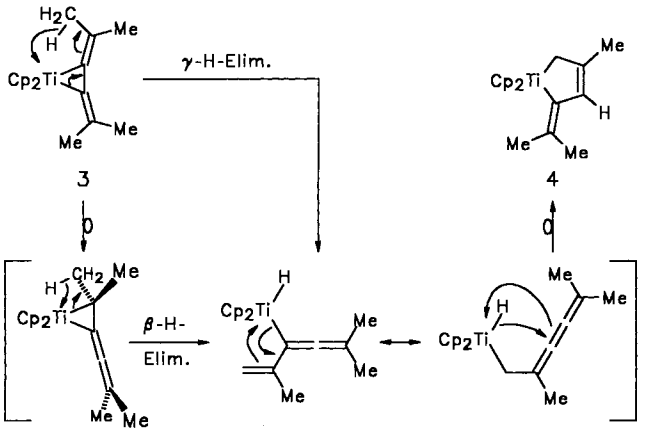

Scheme 1.

The five-membered ring compound **4** reacts with oxygen, with selenium, and with $CDCl_3$ giving 2,5-dimethyl-1,3,4-hexatriene (**14**), which was identified by comparison of the NMR and MS data with reported values.[16] No deuterium from $CDCl_3$ was incorporated into **14**. The titanacyclopentene **4** can be stored at ambient temperature in [D$_8$]THF under argon for some days without noticeable decomposition.

The reaction of 3,4-dilithio-2,5-dimethyl-2,4-hexadiene (**1**) with zirconocene dichloride (instead of titanocene dichloride

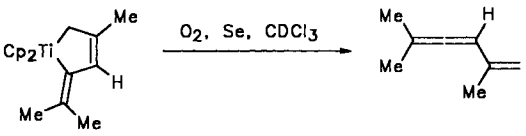

(**2**)) led to other types of products. Neither a zircona[3]radialene nor a compound like **4** could be detected. The ten-membered ring compound **7** was obtained in addition to other compounds.[7]

Experimental Procedure

3 and **4**: To a stirred solution of **1** in diethyl ether (30 mL of a 1 M solution, 30 mmol) diluted with 280 mL of diethyl ether was added **2** (7.47 g, 30 mmol; Merck) in one portion at −80 °C. The mixture was allowed to warm up to 10 °C within 1 h and then filtered through a G3 glass sinter frit under argon. The solvent was removed in vacuo and 100 mL of pentane was added to the residue. The mixture was stirred for 30 min and filtered again through a G3 glass sinter frit under argon. The solvent was removed in vacuo. The crude product (6.7 g) consisted of **3** (50%) together with **4** (^{1}H NMR). Pentane (100 mL) was added to the crude product and after sedimentation of some solid, the solution was transferred into another Schlenk flask. Then the solution was concentrated to a volume of 20 mL, and after one week at −25 °C solid **4** formed (2.5 g, 29%). After the mother liquor was removed by pipette, the solid was dried under high vacuum.

14: Black selenium (0.8 g, 10 mmol; Merck) was added to a solution of **4** (1.4 g, 5 mmol) in 30 mL of pentane at room temperature, and the mixture was stirred for 48 h. The mixture was filtered through a G3 glass sinter frit under argon and the solvent removed in vacuo. The residue contained **4** and **14** in a molar ratio of 2:1 (^{1}H NMR). When oxygen was introduced into a benzene solution of **4**, or **4** was added to $CDCl_3$, **14** formed as main product.

12: At ambient temperature 2-butyne (1.6 g, 30 mmol) was added in two portions with an interval of 1 h to a stirred solution of **4** (7.3 g, 25.5 mmol) in 150 mL of pentane. The mixture was stirred for another 5 h then filtered through a G3 glass sinter frit under argon. The solvent was removed in vacuo and 40 mL pentane was added to the residue (7.8 g; **12** and **4** ca. 1:1.3). After one week at −25 °C pure **12** (1.92 g, 22%) had precipitated. The mother liquor was removed by pipette and **12** was dried at high vacuum. **13** was synthesized in the same way.

Received: June 14, 1995
Revised version: October 30, 1995 [Z80971E]
German version: *Angew. Chem.* **1996**, *108*, 216–218

Keywords: heteroradialenes · lithium compounds · rearrangements · titanium compounds · zirconium compounds

[1] A. Maercker, R. Dujardin, *Angew. Chem.* **1985**, *97*, 612–613; *Angew. Chem. Int. Ed. Engl.* **1985**, *24*, 571–572; A. Maercker, R. Dujardin, F. Brauers, *Organomet. Synth.* **1988**, *4*, 362–365.

[2] Review: A. Maercker, *Methoden der Organischen Chemie (Houben-Weyl) 4th ed. 1952 –*, Vol. E19d, **1993**, pp. 448–556.

[3] A. Maercker, W. Brieden, T. Schmidt, H. D. Lutz, *Angew. Chem.* **1989**, *101*, 477–479; *Angew. Chem. Int. Ed. Engl.* **1989**, *28*, 477–479.

[4] A. Maercker, F. Brauers, W. Brieden, B. Engelen, *J. Organomet. Chem.* **1989**, *377*, C45–C51; A. Maercker, W. Brieden, F. Kastner, A. Mannschreck, *Chem. Ber.* **1991**, *124*, 2033–2036.

[5] A. Maercker, F. Brauers, W. Brieden, M. Jung, H. D. Lutz, *Angew. Chem.* **1988**, *100*, 413–414; *Angew. Chem. Int. Ed. Engl.* **1988**, *27*, 404–405.

[6] A. Maercker, W. Brieden, *Chem. Ber.* **1991**, *124*, 933–938; W. Brieden, T. Kellersohn, *Chem. Ber.* **1993**, *126*, 845–847.

[7] A. Groos, *Neue Darstellungsmethoden von Chalkogen- und Metallocen-Verbindungen mit 3,4-Dilithio-2,5-dimethyl-2,4-hexadien unter besonderer Berücksichtigung heterocyclischer Verbindungen*, Shaker, Aachen, **1995**, p. 82.

[8] U. Rosenthal, A. Ohff, W. Baumann, R. Kempe, A. Tillack, V. V. Burlakov, *Angew. Chem.* **1994**, *106*, 1678–1680; *Angew. Chem. Int. Ed. Engl.* **1994**, *33*, 1605–1607.

[9] B. Temme, G. Erker, R. Fröhlich, M. Grehl, *Angew. Chem.* **1994**, *106*, 1570–1572; *Angew. Chem. Int. Ed. Engl.* **1994**, *33*, 1480–1482.

[10] U. Rosenthal, A. Ohff, A. Tillack, W. Baumann, H. Görls, *J. Organomet. Chem.* **1994**, *468*, C4–C8.

[11] Cf.: P. C. Wailes, R. S. P. Coutts, H. Weigold, *Organometallic Chemistry of Titanium, Zirkonium and Hafnium*, Academic Press, New York, **1974**; G. Erker, F. Rosenfeldt, *J. Organomet. Chem.* **1982**, *224*, 29–42; G. Erker, K. Engel, C. Krüger, A.-P. Chiang, *Chem. Ber.* **1982**, *115*, 3311–3323; G. Erker,

K. Engel, C. Krüger, G. Müller, *Organometallics* **1984**, *3*, 128–133; M. Albrecht, G. Erker, C. Krüger, *Synlett* **1993**, 441–448; C. McDade, J. E. Bercaw, *J. Organomet. Chem.* **1985**, *279*, 281–315; S. A. Cohen, J. E. Bercaw, *Organometallics* **1985**, *4*, 1006–1014; S. L. Buchwald, B. T. Watson, J. C. Huffman, *J. Am. Chem. Soc.* **1987**, *109*, 2544–2546; S. L. Buchwald, R. B. Nielsen, *Chem. Rev.* **1988**, *88*, 1047–1058.

[12] G. Avar, W. Rüsseler, H. Kisch, *Z. Naturforsch. B* **1987**, *42*, 1441–1446.

[13] CAS No. 96363-96-1; cf.: H. G. Alt, H. E. Engelhardt, M. D. Rausch, L. B. Kool, *J. Am. Chem. Soc.* **1985**, *107*, 3717–3718; H. G. Alt, H. E. Engelhardt, M. D. Rausch, L. B. Kool, *J. Organomet. Chem.* **1987**, *329*, 61–67.

[14] CAS No. 130320-35-3; cf.: H. G. Alt, G. S. Herrmann, *J. Organomet. Chem.* **1990**, *390*, 159–169.

[15] K. M. Doxsee, J. J. J. Juliette, K. Zientara, G. Nieckarz, *J. Am. Chem. Soc.* **1994**, *116*, 2147–2148.

[16] CAS No. 10412-57-4; cf.: A. C. Day, M. C. Whiting, *J. Chem. Soc. (B)* **1967**, 991–1003; L. Skattebøl, *Tetrahedron* **1967**, *23*, 1107–1117.

Model Compounds for the Homogeneous Hydrodesulfurization of Benzothiophene: Insertion of Manganese into the S–C(aryl) Bond**

Conor A. Dullaghan, Shouheng Sun, Gene B. Carpenter, Brandon Weldon, and Dwight A. Sweigart*

The great importance of heterogeneous hydrodesulfurization (HDS)[1] has spawned numerous studies with homogeneous model systems.[2] Of particular interest has been the activation of derivatives of thiophene (T), benzothiophene (BT), and dibenzothiophene (DBT). While all three of these sulfur-containing molecules are relevant to HDS, the latter two are especially so because they are more difficult to desulfurize and thus are much more abundant in fossil fuels. The key step in HDS is cleavage of the S–C bonds, and a reasonable way for this to occur is by initial coordination to a metal followed by insertion into the S–C bond. In particular, precoordination of the metal to the sulfur atom of the thiophene unit is thought to be crucial to S–C bond cleavage.[3–5] In the case of BT (**1**), several examples of the insertion of metal fragments ML_n into the S–C(vinyl) bond to give **2** (M = Fe, Ru, Rh, Ir, Pt[3b, 5, 6]) have been reported; however, there have been no reports of S–C(aryl) bond cleavage to give **3**. The X-ray structure[4] of [(BT)Re(CO)$_2$Cp*] (Cp* = C_5Me_5), in which the rhenium

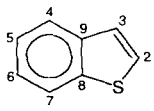

1

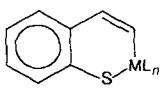

2

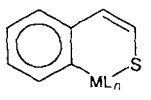

3

atom is η^1-bonded to the sulfur atom, suggests that η^1-S coordination selectively weakens the S–C(vinyl) bond but not the S–C(aryl) bond, thus providing an explanation[6e] for why **2**, and not **3**, is formed. Herein we demonstrate that the insertion of a metal atom into the S–C(aryl) bond of BT to give complexes of type **3** can, in fact, be readily accomplished.

[*] Prof. D. A. Sweigart, C. A. Dullaghan, S. Sun, Prof. G. B. Carpenter, B. Weldon
Department of Chemistry, Brown University
Providence, RI 02912 (USA)
Fax: Int. code +(401)863-2594

[**] This work was supported by a grant from the National Science Foundation (CHE-9400800). The X-ray equipment was purchased with assistance from the NSF (Grant CHE-8206423) and the National Institutes of Health (Grant RR-06462).

$[(\eta^6\text{-polyarene})Mn(CO)_3]^+$ ions, in which the polyarene is a naphthalene-type ligand, are converted by one equivalent of reducing agent to *syn*-facial bimetallic $[(\eta^4,\eta^6\text{-polyarene})Mn_2(CO)_5]$ complexes containing a Mn–Mn bond.[7] In analogy to this, it was anticipated that reduction of the readily available[8] $[(\eta^6\text{-BT})Mn(CO)_3]^+$ ion **4** would yield a bimetallic η^4,η^5-BT complex. However, reduction of **4** with cobaltocene under an atmosphere of CO produced a high yield of the bimetallic complex **5a**, which contains a $Mn(CO)_4$ moiety inserted into the S–C(aryl) bond of BT. When the reduction of **4** was carried out under N_2 and in the presence of one equivalent of $P(OR)_3$, the analogous bimetallic products **5b** and **5c**

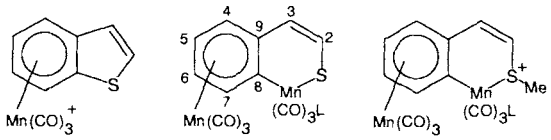

4 **5a-c** **6a,b**

a: L = CO, **b**: L = $P(OMe)_3$
c: L = $P(OEt)_3$

were obtained, in which $Mn(CO)_3P(OR)_3$ is inserted into the S–C(aryl) bond. Complexes **5b** and **5c** could also be synthesized in comparable yield directly from **5a** by the thermal displacement of a CO ligand with one equivalent of $P(OR)_3$. Both synthetic methods produced **5b** (as well as **5c**) as a mixture of two isomers in a ratio of ten or more to one. The red-purple isomers, which were easily separated by chromatographic techniques, give *very* similar but perceptibly different IR and NMR spectra, indicating that the $P(OR)_3$ ligand is bonded to the same manganese atom in the two isomers (see Experimental Procedure).

Complexes **5a–c** are stable under N_2 in the solid state and suffer no detectable decomposition over 24 h in CH_2Cl_2 or CH_3CN. They are reversibly oxidized at a platinum electrode in CH_2Cl_2/Bu_4NPF_6 at potentials only moderately more positive than the ferrocenium/ferrocene couple.[9] The results of X-ray structural analysis of **5a** and **5c** are given in Figures 1 and 2, respectively.[10] The neutral molecules are, in effect, zwitterions in which the $Mn(CO)_3$ unit bears a formal +1 charge, while the inserted manganese atom formally carries a −1 charge. The Mn–S bond length in **5a** is 2.369(2) Å, a value similar to that reported for $[(C_6H_6)Mn(CO)_2SPh]$ (2.35 Å).[11] The most significant structural feature of **5a**, however, is the nonplanarity of the metallacyclic ring (Fig. 1 bottom). Mn2 and C3 are essentially coplanar with the highly planar C4–C9 carbocyclic ring. However, C2 and S1 are 0.53 Å and 1.05 Å, respectively, above this plane. Complex **5c** also has a highly nonplanar metallacyclic ring and is structurally very similar to **5a** except that an "axial" CO is replaced by $P(OEt)_3$ to give a *facial* ligand arrangement about Mn2 (Fig. 2).[12] The position of the sulfur atom in **5a** and **5c** is particularly interesting as it is seemingly rather exposed and may therefore be susceptible to electrophilic extraction; the formal negative charge on the adjacent manganese atom would serve to enhance such behavior.

The nucleophilicity of the sulfur atom in **5a** (and **5b**) was tested by treating a solution of the complex in CH_2Cl_2 with methyl triflate. The initially red-purple solution turned yellow within minutes and the product was isolated in high yield as a triflate salt by the addition of diethyl ether. Examination of the spectra indicated that methylation occurred cleanly at the sulfur to afford **6a,b**.[13] Thus, the IR spectra of **5a,b** and **6a,b** in the

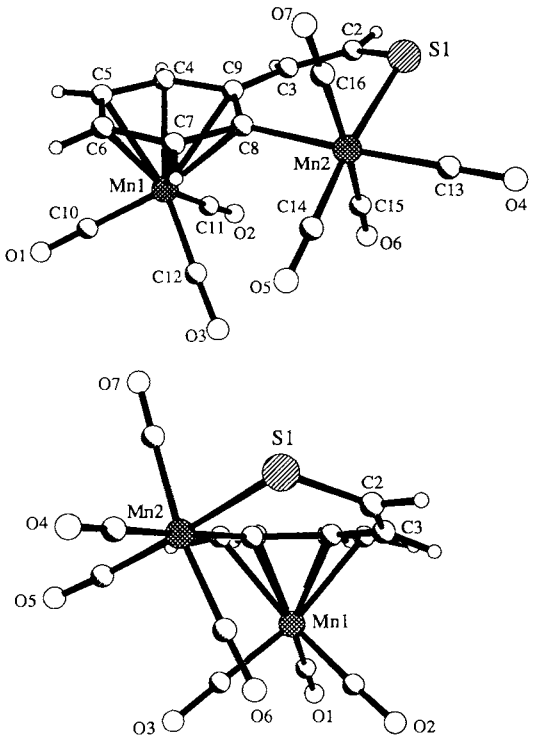

Fig. 1. Crystal structure of **5a**. Top: View showing the atom numbering scheme. Bottom: A side-on view parallel to the carbocyclic ring. Selected bond lengths [Å]: S1–C2 1.720(7), C2–C3 1.324(9), C3–C9 1.455(9), Mn1–C4 2.179(6), Mn1–C5 2.172(6), Mn1–C6 2.175(6), Mn1–C7 2.184(6), Mn1–C8 2.312(5), Mn1–C9 2.301(5), Mn2–S1 2.369(2), Mn2–C8 2.091(6), Mn2–C13 1.835(8), Mn2–C14 1.804(7), Mn2–C15 1.863(7), Mn2–C16 1.868(7).

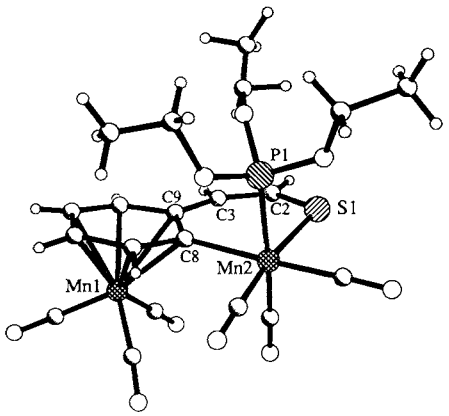

Fig. 2. Crystal structure of **5c**. Selected bond lengths [Å]: S1–C2 1.69(2), C2–C3 1.34(2), C3–C9 1.43(2), Mn2–S1 2.344(5), Mn2–C8 2.10(1), Mn2–P1 2.268(6).

ν_{CO} region are very similar except for the expected shift of the peaks of the latter to higher wavenumbers. The NMR chemical shifts of the hydrogen atoms of the SMe group in **6a,b** are similar to those reported for methyl thioethers coordinated to manganese carbonyl units,[11, 14] and are inconsistent with the presence of a Mn–Me linkage. Furthermore, the reaction of **5a,b** in CH_2Cl_2 with methyl triflate to give **6a,b** occurred in comparable yield whether the reaction was performed under CO or under N_2. This shows that Mn–S (or Mn–C) bond cleavage does not accompany methylation, since such cleavage would generate a free coordination site at which CO would bind. The sulfur center in **6a,b** is chiral and the methyl group can be in an *exo* or *endo* orientation. ^{1}H NMR spectroscopic studies showed that on the timescale of the reaction, **6a** was formed as a single diastereomer. However, **6b** was formed as a diastereomeric mixture in a ratio of about 2:1. Over a period of hours in solution, or days in the solid state, the diastereomeric mixture of **6b** transformed cleanly into a single diastereomer.[15]

In conclusion, the S–C(aryl) bond in benzothiophene can be activated by reduction of the $[(\eta^6\text{-BT})Mn(CO)_3]^+$ ion, leading to the bimetallic complexes **5a–c**. That the S–C(aryl) bond can be readily cleaved means that this mode of activation should be considered in HDS reactions. The mechanism of formation of **5a–c** is currently under investigation with an emphasis on the probable influence of the first manganese on the insertion of the second metal. Possibly, S–C(aryl) bond cleavage requires initial η^6-coordination of a metal to the carbocyclic ring, suggesting that this type of precoordination should not be discounted[4, 16] in heterogeneous HDS reactions. Indeed, one pathway for the catalytic desulfurization of BT may involve simultaneous coordination of the carbocyclic and the thiophene rings prior to insertion into a S–C bond. The sulfur atom in the nonplanar metallacyclic ring in **5a–c** is nucleophilic and, accordingly, can be methylated to give **6**. The reaction of **5a–c** with other electrophilic reagents, as well as dihydrogen, is under investigation.

In analogy with the behavior of the $[(\eta^6\text{-BT})Mn(CO)_3]^+$ ion, the $[(\eta^5\text{-thiophene})Mn(CO)_3]^+$ ion **7** also undergoes insertion of manganese into a S–C bond when reduced with cobaltocene. The bimetallic product **8** has the metallacyclic ring π-bonded (η^5) through C2-C3-C4-C5-S to a $[Mn(CO)_3]$ moiety (Fig. 3).[17] As a consequence of this π bonding, and in sharp contrast to the situation with **5a**, the C_4S segment of the metallacyclic ring is highly planar (mean deviation = 0.030 Å) and the sulfur atom in **8** is not nucleophilic towards HBF_4 or MeOTf.[18] Reduction of the $[(\eta^5\text{-}2,5\text{-}Me_2T)Mn(CO)_3]^+$ ion was found to afford a bimetallic complex completely analogous to **8**. A thorough study of manganese insertion into these thiophene complexes is underway.

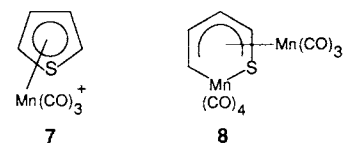

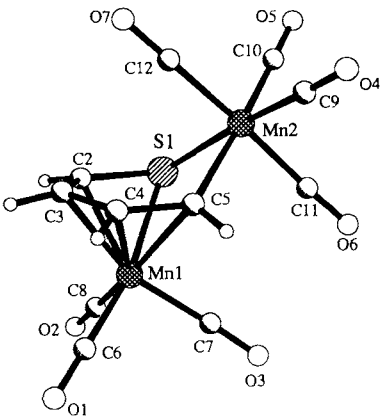

Fig. 3. Crystal structure of **8**. Selected bond lengths [Å]: S1–C2 1.718(6), C2–C3 1.370(7), C3–C4, 1.442(8), C4–C5 1.362(7), Mn1–S1 2.379(2), Mn1–C2 2.117(5), Mn1–C3 2.149(5), Mn1–C4 2.174(5), Mn1–C5 2.403(4), Mn2–S1 2.346(2), Mn2–C5 2.109(5), Mn2–C9 1.806(6), Mn2–C10 1.821(6), Mn2–C11 1.855(6), Mn2–C12 1.846(6).

Experimental Procedure

5a: Cobaltocene (0.31 mmol) and **4**-BF_4 (0.30 mmol) were combined in CH_2Cl_2 (5 mL), and the mixture was stirred under CO at room temperature for 20 min and then passed through deactivated neutral alumina (10% water) with CH_2Cl_2 as eluant. After the solvent had been removed under vacuum, the resulting red-purple solid was washed with pentane and dried. Yield 80%; IR (CH_2Cl_2): ν_{CO}

 © VCH Verlagsgesellschaft mbH, D-69451 Weinheim, 1996 0570-0833/96/3502-0213 $ 10.00+.25/0

$[cm^{-1}]$ = 2074(m), 2049(s), 1995(s), 1980(s), 1932(m); IR (hexanes): ν_{CO} $[cm^{-1}]$ = 2076(m), 2050(s), 2000(s), 1995(s), 1979(s), 1939(m); ^1H NMR (CD_2Cl_2): δ = 7.55 (d, J = 9.6 Hz, H2), 6.85 (d, J = 5.5 Hz, H7), 6.18 (d, J = 9.4 Hz, H3), 6.04 (t, J = 5.6 Hz, H6), 5.49–5.41 (m, H4,5); anal. calcd: C 40.91, H 1.36; found: C 41.00, H 1.36. Crystals suitable for X-ray studies were grown by slow evaporation of a pentane solution at −20 °C.

5b: To a mixture of cobaltocene (0.61 mmol) and $P(OMe)_3$ (48 μL, 0.41 mmol) in CH_2Cl_2 (10 mL) under N_2 was added **4**-BF_4 (0.41 mmol), and the solution was stirred for 20 min. After concentration and filtration through a short deactivated neutral alumina column, purification was completed by TLC on silica gel with Et_2O/hexanes (1/1). The first band contained traces of a red-purple minor isomer, which separated cleanly from the red-purple major isomer. Complex **5c** was prepared similarly. **5b**: yield of major isomer 85%; IR (hexanes): ν_{CO} $[cm^{-1}]$ = 2052(vs), 2012(s), 1996(s), 1975(s), 1950(s), 1914(m); ^1H NMR ($CDCl_3$): δ = 7.63 (d, J = 9.7 Hz, H2), 7.05 (d, J = 6.6 Hz, H7), 6.09 (d, J = 9.7 Hz, H3), 5.88 (t, J = 6.0 Hz, H6), 5.20–5.35 (m, H4,5), 3.57 (d, J = 10.3 Hz, OMe); yield of minor isomer <5%; IR (hexanes): ν_{CO} $[cm^{-1}]$ = 2052(vs), 2025(m), 1995(s), 1975(s), 1946(s), 1917(m); ^1H NMR ($CDCl_3$): δ = 3.74 (d, J = 11 Hz, OMe), otherwise identical to major isomer. **5c**: yield of major isomer 76%; IR (hexanes): ν_{CO} $[cm^{-1}]$ = 2052(vs), 2010(s), 1996(s), 1975(s), 1946(s), 1912(m); ^1H NMR (CD_3COCD_3): δ = 7.44 (d, J = 9.6 Hz, H2), 7.12 (d, J = 6.4 Hz, H7), 6.43 (t, J = 6.0 Hz, H6), 6.17 (d, J = 9.7 Hz, H3), 5.76 (t, J = 6.1 Hz, H5), 5.68 (d, J = 6.8 Hz, H4), 3.91 (q, J = 7.0 Hz, OCH_2), 1.16 (t, J = 7.0 Hz, Me); anal. calcd: C 41.53, H 3.67; found: C 41.73, H 3.69. Complex **5b** was also synthesized in about the same yield by the following alternative procedure: **5a** (0.10 mmol) and $P(OMe)_3$ (0.20 mmol) were mixed in CH_2Cl_2 (3 mL) under N_2. After the mixture had been stirred for 1 h, the solvent was removed and the residue chromatographed on neutral alumina. Impurities, as well as the minor isomer, were eluted with Et_2O/hexanes (1/1) and the major isomer was eluted with Et_2O/hexanes (4/1). Complex **5c** was also made by this method except that the elution solvents were Et_2O/hexanes (1/5 and 1/3, respectively). Small single crystals of **5c** were grown by slow evaporation of a pentane solution at −20 °C.

6a: Methyl triflate (0.30 mmol) was added to complex **5a** (0.10 mmol) in CH_2Cl_2 (5 mL) under CO or N_2, and the solution stirred for 30 min during which time the color changed from red-purple to yellow. After concentration to 2 mL, Et_2O was added to precipitate the product as fine yellow microcrystals. Yield 81%; IR (CH_2Cl_2): ν_{CO} $[cm^{-1}]$ = 2097(m), 2066(vs), 2020(vs), 1979(m); ^1H NMR (CD_3COCD_3): δ = 7.18 (d, J = 9.9 Hz, H2), 7.10 (d, J = 6.4 Hz, H7), 7.03 (d, J = 9.9 Hz, H3), 6.81 (t, J = 6.3 Hz, H6), 6.61 (d, J = 6.6 Hz, H4), 6.51 (t, J = 6.1 Hz, H5), 2.98 (s, Me).

6b: Methyl triflate (0.30 mmol) was added to **5b** (0.10 mmol) in CH_2Cl_2 (10 mL) under CO or N_2. After the mixture had been stirred for 30 min, the solution was concentrated and transferred to a dry acidic alumina column, washed with CH_2Cl_2 and eluted with acetone. Yield 79%; IR (CH_2Cl_2): ν_{CO} $[cm^{-1}]$ = 2067(s), 2030(s), 2010(s), 1963(ms), 1940(ms); ^1H NMR (CD_3COCD_3): δ = 7.08–7.04 (m, H2,7), 6.88 (d, J = 10.1 Hz, H3), 6.73 (t, J = 6.3 Hz, H6), 6.48 (d, J = 6.4 Hz, H4), 6.37 (t, J = 6.3 Hz, H5), 3.74 (d, J = 10.5 Hz, OMe), 2.84 (s, Me).

8: Cobaltocene (0.24 mmol) and **7**-BF_4 (0.22 mmol) [19] were combined in CH_2Cl_2 (8 mL) under an atmosphere of CO. After the reaction mixture had been stirred for 20 min, it was concentrated and eluted through a column of deactivated neutral alumina with CH_2Cl_2 to yield the product as a microcrystalline orange solid. Yield 71%; IR (hexanes): ν_{CO} $[cm^{-1}]$ = 2081(m), 2039(s), 1999(sh,s), 1994(s), 1979(m/s), 1962(s); ^1H NMR ($CDCl_3$): δ = 6.94 (t, J = 6 Hz, 1H), 6.09 (d, J = 6 Hz, 1H), 6.04 (dd, J = 10.5, 5.5 Hz, 1H), 5.09 (d, J = 10 Hz, 1H). Large crystals of **8** were easily grown from pentane solutions at −20 °C.

Received: September 13, 1995
Revised version: October 9, 1995 [Z 8398 IE]
German version: *Angew. Chem.* **1996**, *108*, 234–237

Keywords: complexes with sulfur ligands · desulfurization · manganese compounds · metallacycles

[1] a) B. C. Gates, J. R. Katzer, G. C. A. Schuit, *Chemistry of Catalytic Processes*, McGraw-Hill, New York, **1979**, Chapter 5; b) R. Prins, V. H. J de Beer, G. A. Somorjai, *Catal. Rev.-Sci. Eng.* **1989**, *31*, 1; c) R. J. Angelici in *Encyclopedia of Inorganic Chemistry, Vol. 3* (Ed.: R. B. King), Wiley, New York, **1994**, p. 1433; d) J. Benson, G. L. Schrader, R. J. Angelici, *J. Mol. Catal.* **1995**, *96*, 283.

[2] a) R. J. Angelici, *Acc. Chem. Res.* **1988**, *21*, 387; b) R. A. Sánchez-Delgado, *J. Mol. Catal.* **1994**, *86*, 287; c) T. B. Rauchfuss, *Prog. Inorg. Chem.* **1991**, *39*, 260.

[3] a) L. Dong, S. B. Duckett, K. F. Ohman, W. D. Jones, *J. Am. Chem. Soc.* **1992**, *114*, 151; b) W. D. Jones, L. Dong, *ibid.* **1991**, *113*, 559.

[4] M.-G. Choi, R. J. Angelici, *Organometallics* **1992**, *11*, 3328.

[5] C. Bianchini, V. Herrera, M. V. Jiménez, A. Meli, R. Sánchez-Delgado, F. Vizza, *J. Am. Chem. Soc.* **1995**, *117*, 8567.

[6] a) A. E. Ogilvy, M. Draganjac, T. B. Rauchfuss, S. R. Wilson, *Organometallics* **1988**, *7*, 1171; b) H. E. Selnau, J. S. Merola, *ibid.* **1993**, *12*, 1583; c) A. J. Arce, Y. DeSanctis, A. Karam, A. J. Deeming, *Angew. Chem.* **1994**, *106*, 1459; *Angew. Chem. Int. Ed. Engl.* **1994**, *33*, 1381; d) C. Bianchini, A. Meli, M. Peruzzini, F. Vizza, S. Moneti, V. Herrera, R. A. Sánchez-Delgado, *J. Am. Chem. Soc.* **1994**, *116*, 4370; e) J. J. Garcia, B. E. Mann, H. Adams, N. A. Bailey, P. M. Maitlis, *ibid.*, **1995**, *117*, 2179.

[7] S. Sun, C. A. Dullaghan, G. B. Carpenter, A. L. Rieger, P. H. Rieger, D. A. Sweigart, *Angew. Chem.* **1995**, *107*, 2735; *Angew. Chem. Int. Ed. Engl.* **1995**, *34*, 2540.

[8] S. Sun, L. K. Yeung, D. A. Sweigart, T.-Y. Lee, S. S. Lee, Y. K. Chung, S. R. Switzer, R. D. Pike, *Organometallics* **1995**, *14*, 2613.

[9] $E_{1/2}$ is +0.35 for **5a** and +0.04 V for **5c** (relative to the Fc^+/Fc couple).

[10] a) The crystal structures of **5a** and **5c** were determined with a Siemens P4 diffractometer. Data was collected at 25 °C with $Mo_{K\alpha}$ radiation, and refinements based on F^2 were carried out with the SHELXL 93 package. For **5a**: triclinic, space group $P\bar{1}$, a = 7.469(2), b = 8.4800(10), c = 13.444(2) Å, α = 78.190(10), β = 86.840(10), γ = 72.63(2)°, V = 795.5(3) Å^3, Z = 2, ρ_{calcd} = 1.838 g cm^{-3}, μ = 1.754 mm^{-1}, θ range 2.57–25.00°, 226 variables refined with 2762 independent reflections ($I > 2\sigma(I)$) to R = 0.0668, $wR2$ = 0.1669, and GOF = 1.040. X-ray data for **5c** were of rather low quality due to the small size of the crystal. Because of this only about 1500 reflections were collected with $I > 2\sigma(I)$ and only the S, P, and Mn atoms were refined anisotropically. In spite of the resultant large standard deviations, the data were sufficient to unambigously define the structure. The unit cell contains two independent molecules of **5c**, which differ insignificantly. Crystal data for **5c**: monoclinic, space group $P2_1/c$, a = 15.346(3), b = 10.877(2), c = 30.688(5) Å, β = 103.101(14)°, V = 4988.9(14) Å^3, Z = 8, ρ_{calcd} = 1.540 g cm^{-3}, μ = 1.206 mm^{-1}, θ range 1.99–22.50°, 306 variables refined with 1480 independent reflections ($I > 2\sigma(I)$) to R = 0.0744, $wR2$ = 0.1607, and GOF = 0.773. b) Further details of the crystal structure investigations are available on request from the Director of the Cambridge Crystallographic Data Centre, University Chemical Laboratory, Lensfield Road, GB-Cambridge CB2 1EW (UK), on quoting the full journal citation.

[11] M. Schindehutte, P. H. van Rooyen, S. Lotz, *Organometallics* **1990**, *9*, 293.

[12] IR and NMR spectra of the *same* crystal that was used for the X-ray study verified that the major isomer of **5c** is *facial*; it is likely that the minor isomer has a *meridional* ligand arrangement about Mn2.

[13] Methylation of the sulfur atom in metallacyclic complexes of type **2** is known: C. Bianchini, P. Frediani, V. Herrera, M. V. Jiménez, A. Meli, L. Rincón, R. Sánchez-Delgado, F. Vizza, *J. Am. Chem. Soc.* **1995**, *117*, 4333 and references therein.

[14] R. L. Bennett, M. I. Bruce, I. Matsuda, R. J. Roedens, R. G. Little, J. T. Veal, *J. Organomet. Chem.* **1974**, *67*, C72.

[15] This timeframe for inversion at a chiral sulfur center is typical: M. Mikolajczyk, J. Drabowicz, *Topics Stereochem.* **1982**, *13*, 333.

[16] S. C. Huckett, R. J. Angelici, *Organometallics* **1988**, *7*, 1491.

[17] The crystal structure of **8** was determined under the same conditions as used for **5a** and **5c**, with the following results: triclinic, space group $P\bar{1}$, a = 7.209(2), b = 8.540(2), c = 12.142(4), α = 69.58(2), β = 79.97(3), γ = 85.75(2)°, V = 689.7(4) Å^3, Z = 2, ρ_{calcd} = 1.878 g cm^{-3}, μ = 2.009 mm^{-1}, θ range 1.81–24.99°, 190 variables refined with 2401 independent reflections ($I > 2\sigma(I)$) to R = 0.0501, $wR2$ = 0.1276, and GOF = 0.968. See ref. [10b]

[18] A number of bimetallic complexes involving insertion into a thiophene ring are known (although none have a structure analogous to **8**): see a) A. E. Ogilvy, M. Draganjac, T. B. Rauchfuss, S. R. Wilson, *Organometallics* **1988**, *7*, 1171; b) S. Luo, A. E. Ogilvy, T. B. Rauchfuss, A. L. Rheingold, S. R. Wilson, *ibid.* **1991**, *10*, 1002; c) W. D. Jones, R. M. Chin, *ibid.* **1992**, *11*, 2698; d) J. Chen, L. M. Daniels, R. J. Angelici, *J. Am. Chem. Soc.* **1991**, *113*, 2544; e) J. Chen, V. G. Young, R. J. Angelici, *ibid.* **1995**, *117*, 6362; f) K. M. K. Dailey, T. B. Rauchfuss, A. L. Rheingold, G. P. A. Yap, *ibid.* **1995**, *117*, 6396; g) A. Bacchi, C. Bianchini, V. Herrera, M. V. Jiménez, C. Mealli, A. Meli, S. Moneti, M. Peruzzini, R. A. Sánchez-Delgado, F. Vizza, *J. Chem. Soc. Chem. Commun.* **1995**, 921.

[19] D. A. Lesch, J. W. Richardson, R. A. Jacobson, R. J. Angelici, *J. Am. Chem. Soc.* **1984**, *106*, 2901.

Poly(A·A·U) Triple Helix Formation Promoted by Porphyrin Assembly**

Rosaria Lauceri, Tiziana Campagna, Annalinda Contino, and Roberto Purrello*

Porphyrins are aromatic molecules whose properties (planarity, large molar absorption coefficients, tunable absorption and emission properties) make them ideal building blocks in supramolecular complexes that are models for molecular devices that store electronic[1] or solar energy.[2].

Porphyrins having polar groups in the *meso* position are water-soluble. Some of them (like *trans*-bis(N-methylpyridinium-4-yl)diphenylporphine (*t*-H_2Pagg), Scheme 1) have a pronounced tendency to self-stack in aqueous solution even at micromolar concentrations and low ionic strengths ($I = 0.02$ M), both in the absence and in the presence of charged matrices (DNA, poly-L/D-glutamate).[3,4] Furthermore, the interaction of cationic porphyrins with DNA or RNA could be relevant for medical and biological applications.[5]

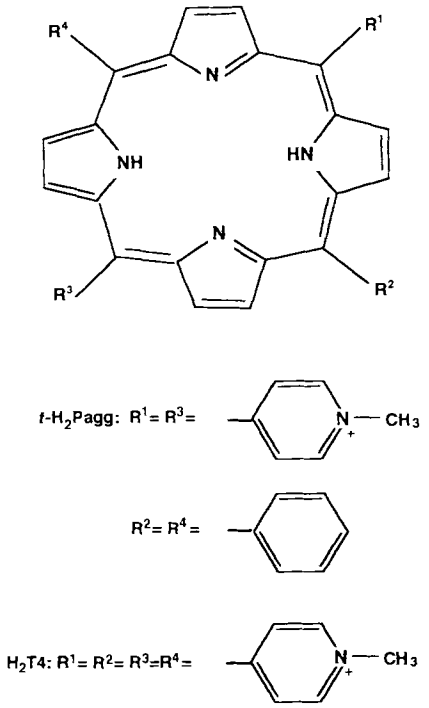

Scheme 1. Counterion Cl^-.

Recently tetrakis(*N*-methylpyridinium-4-yl)porphine (H_2T4, Scheme 1), which does not have any tendency to self-associate, was also found to form extended aggregates on single-stranded (*ss*) poly(A) but not on *ss* poly(dA),[4] poly(C), poly(G), and poly(U).[6] These findings demonstrate that aggregation of porphyrins on matrices of opposite charge is not necessarily correlated to their tendency to self-aggregate but also involves molecular recognition processes. Aggregation of porphyrins on chiral matrices can be detected easily by means of circular dichroism (CD) measurements; it leads to an induced CD band in the Soret region having a characteristic shape (conservative) and unusually large intensity ($|\Delta\varepsilon| > 100\ M^{-1}cm^{-1}$).[7]

The specificity of the interaction of H_2T4 with *ss* poly(A) encouraged us to study the poly(A)–poly(U) system in the presence of this free-base porphyrin. Poly(A) and poly(U) can form three types of complexes: the double-stranded (*ds*) helix poly(A·U) and the three-stranded helices poly(U·A·U)[8] and poly(A·A·U).[9] The latter helix forms in the presence of 0.15 M NaCl and 5 mM $MgCl_2$ after one week of incubation at 4 °C.[9] Fresco and co-workers have also shown that the complex forms only when the degree of polymerization (dp) of poly(A) is between 28 and 150, whereas the length of poly(U) does not affect the triple helix formation.[9]

Because of coulombic repulsions between the negative arrays of phosphate groups, most triple helices form at high salt concentrations or in the presence of divalent cations in millimolar concentrations. Here we report evidence that the presence of cationic porphyrins in micromolar concentrations "induces" the formation of the poly(A·A·U) triple helix also under unfavorable conditions, for example with poly(A) strands having an average dp higher than 400 base residues. We anticipate that the "catalytic" action of porphyrins occurs through specific molecular recognition processes on the "external" poly(A) strand. Figure 1 shows the absorbance mixing curves monitored at

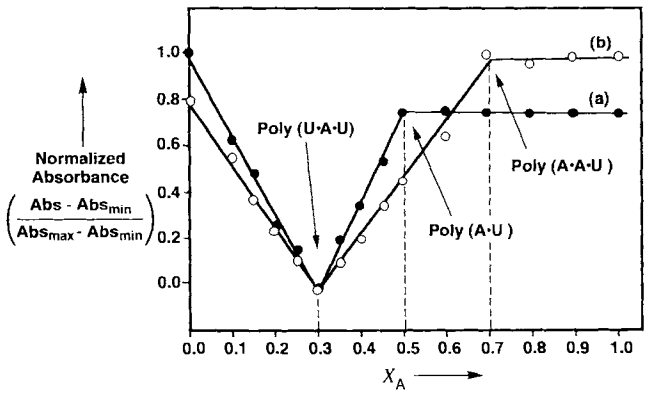

Fig. 1. Absorbance mixing curves of poly(A)–poly(U) mixtures (total concentration = 100 μM) in the absence (a) and in the presence (b) of H_2T4 (4 μM). Poly(A) dp > 400. $I = 0.1$ M (NaCl). X_A = mole fraction of adenine residues.

280 nm[10] for poly(A)–poly(U) mixtures incubated for one hour at room temperature in the absence and in the presence of H_2T4 at $I = 0.1$ M (NaCl).[11] As expected, when no porphyrin is added (Fig. 1a) the curve shows two clear endpoints at $X_A = 0.3$ and $X_A = 0.5$, corresponding to the three-stranded helix poly(U·A·U) and the double helix poly(A·U), respectively.[8,9] In the presence of porphyrin (Fig. 1b) the endpoint at $X_A = 0.5$ is absent,[12] but an additional endpoint at $X_A \approx 0.7$ is present. This corresponds to a helix with A_2U stoichiometry and shows that H_2T4 is an effective "catalyst" for the formation of a poly(A·A·U) triple helix.

CD spectra of the poly(A)–poly(U) mixtures containing H_2T4 were recorded soon after the absorption spectra. The intensity of bands in the Soret region are plotted in Figure 2 as

[*] Prof. Dr. R. Purrello, Dr. A. Contino
Dipartimento di Scienze Chimiche, Università di Catania
Viale Andrea Doria 8, I-95125 Catania (Italy)
Fax: Int. code +(95)580138
Dr. R. Lauceri
Istituto per lo Studio delle Sostanze Naturali di Interesse Alimentare e Chimico-Farmaceutico del CNR, Catania (Italy)
T. Campagna
Consorzio Catania Ricerche, Catania (Italy)

[**] This work was supported in part by the Consiglio Nazionale delle Ricerche (CNR), the Ministero dell'Università e della Ricerca Scientifica e Tecnologica (MURST), and the EEC (HCM project CHRXC 920014). We thank Prof. R. F. Pasternack and Prof. E. Rizzarelli for helpful discussions.

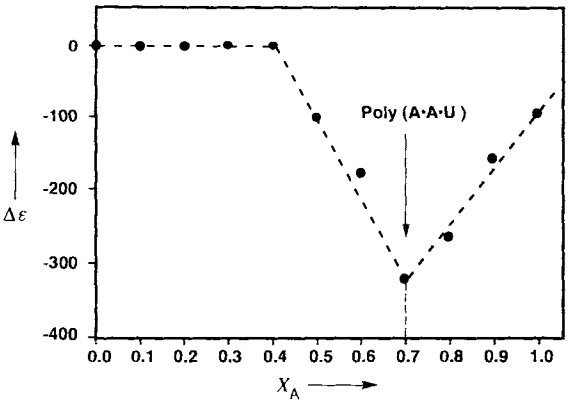

Fig. 2. Plot of the intensity of the CD bands ($\Delta\varepsilon$ [$M^{-1}cm^{-1}$)] at 450 nm of poly(A)–poly(U) mixtures in the presence of H_2T4 vs. mole fraction of adenine residues.

a function of the mole fraction of adenine residues (X_A). For $X_A < 0.5$[12] the CD spectra do not show any induced features, implying that porphyrins are essentially monodispersed on the surface of the polynucleotide (as indicated by hypochromism and the frequency shift of the Soret band observed in the absorption experiments). In contrast, for $X_A \geq 0.5$ the intensity of the induced CD bands increases with the mole fraction of A, reaches a maximum ($\Delta\varepsilon = -320\ M^{-1}cm^{-1}$) at $X_A = 0.7$, and then decreases. The unusually large intensity and the nonconservative shape of the CD signals indicate that for $X_A \geq 0.5$ porphyrins are assembled on polynucleotides. Thus, UV and CD data show that 1) under our experimental conditions the poly(A·A·U) helix forms only in the presence of H_2T4, and 2) CD intensities maximize at $X_A = 0.7$, suggesting that specific aggregation of H_2T4 is a key step in the formation of the triple helix.

To further investigate this last point we conducted the same experiments with copper(II) and zinc(II) derivatives of H_2T4. CuT4 (which also aggregates on *ss* poly(A)[4] and not on poly(U)[6]) behaves in the same way as the free-base porphyrin, showing clear endpoints at $X_A = 0.7$ in the absorption and CD titrations. In contrast, absorption titration curves obtained in the presence of ZnT4 are identical to those obtained when no porphyrin is added and show only the endpoints at $X_A = 0.3$ and $X_A = 0.5$. Moreover, the CD spectra measured in the presence of ZnT4 do not show any features in the Soret region over the entire mole fraction range. We would like to recall that ZnT4 aggregation is severely limited by the presence of a water molecule axially coordinated to the Zn^{II} center.[4] These results underline that aggregation is crucial for the whole assembly process.

The following experimental findings obtained for *t*-H_2Pagg show that, to "catalyze" poly(A·A·U) formation, porphyrin aggregation must be specific on *ss* poly(A). *t*-H_2Pagg has a very strong tendency to aggregate on DNA and RNA polymers[3a, b, 4b] and therefore lacks specificity. We noted, in fact, aggregation on both *ss* poly(U) and poly(A).[6] However, absorbance and CD titrations performed on poly(A)–poly(U) mixtures in the presence of *t*-H_2Pagg do not show clear endpoints. Most likely, indiscriminate aggregation on all the constituents of the mixtures hinders not only the formation of the triple-stranded helix but also the formation of poly(A·U) and poly(U·A·U) helices, confirming that the interactions of porphyrins on single strands can strongly affect the formation of double and triple helices.[4a] The results obtained with ZnT4 and *t*-H_2Pagg indicate that 1) the formation of the poly(A·A·U) triple helix is fostered only by porphyrins that recognize (through aggregation) *ss* poly(A), and 2) the recognition process involves the "external" poly(A) because we noted aggregation only for solutions having $X_A \geq 0.5$.

A possible explanation for this behavior is that aggregation of cationic porphyrins occurs on a single strand of poly(A); this leads to a partial "neutralization" of the phosphate negative charges thus facilitating the approach of the third strand to an already formed poly(A·U) double helix. We also hypothesize that porphyrins aggregate in a "face-on" fashion (i.e. with the porphyrin plane parallel to the helix axis) because this arrangement may allow a more efficent "contact" (neutralization) between porphyrins and phosphate groups. Studies on the dependence of the system on ionic strength and concentration are currently in progress.

Experimental Procedure

Poly(U) and poly(A) were obtained both from Sigma and Pharmacia. The average dp for poly(A) was certified to be higher than 400 bases. Tetrakis(*N*-methylpyridinium-4-yl)porphine and *trans*-bis(*N*-methylpyridinium-4-yl)diphenylporphine were purchased from Mid-Century. The porphyrin were metalated as described in the literature [13]. Circular dichroism spectra were recorded on a JASCO J-600 spectrometer. Absorption spectra were measured on an HP-8462A spectrometer. Porphyrin-containing solutions were always kept in the dark. Doubly distilled water was used throughout.

Received: July 27, 1995 [Z8263IE]
German version: *Angew. Chem.* **1996**, *108*, 227–229

Keywords: aggregates · molecular recognition · nucleotides · porphyrinoids · supramolecular chemistry

[1] a) H. L. Anderson, *Inorg. Chem.* **1994**, *33*, 972–981; b) C. M. Drain, J.-M. Lehn, *J. Chem. Soc. Chem. Commun.* **1994**, 2313–2314; c) D. W. Bruce, M. A. Wali, Q. M. Wang, *J. Chem. Soc. Chem. Com.* **1994**, 2089–2090.

[2] a) J.-H. Fuhrhop, C. Demoulin, C. Boettcher, J. Konig, U. Siggel, *J. Am. Chem. Soc.* **1992**, *114*, 4159–4165; b) J. Seth, V. Palaniappan, T. E. Johnson, S. Sreedharan, J. S. Lindsey, D. F. Bocian, *ibid.* **1994**, *116*, 10578–10592; c) J. Sessler, B. Wang, A. Harryman, *ibid.* **1995**, *117*, 704–714.

[3] a) E. J. Gibbs, I. Tinoco, Jr., M. F. Maestre, P. A. Ellinas, R. F. Pasternack, *Biochem. Biophys. Res. Commun.* **1988**, *157*, 350–358; b) R. F. Pasternack, C. Bustamante, P. J. Collings, A. Giannetto, E. J. Gibbs, *J. Am. Chem. Soc.* **1993**, *115*, 5393–5399; c) R. F. Pasternack, A. Giannetto, P. Pagano, E. J. Gibbs, *ibid.* **1991**, *113*, 7799–7800; d) N. E. Mukundam, G. Petho, D. W. Dixon, M. S. Kim, L. G. Marzilli, *Inorg. Chem.* **1994**, *33*, 4676–4687.

[4] a) C. Bustamante, S. Gurrieri, R. F. Pasternack, R. Purrello, E. Rizzarelli, *Biopolymers* **1994**, *34*, 1099–1104; b) R. F. Pasternack, S. Gurrieri, R. Lauceri, R. Purrello, *Inorg. Chim. Acta*, in press.

[5] L. G. Marzilli, *New J. Chem.* **1990**, *14*, 409–420.

[6] R. Purrello, E. Bellacchio, R. Lauceri, unpublished.

[7] Porphyrins are D_{4h}-symmetric and therefore they show an "induced" CD spectrum in the Soret region only when they interact with chiral molecules [3] or when they form chiral superstructures [2b]. The interaction of porphyrins with polynucleotides leads to modest negative CD signals when intercalation occurs. In contrast, external binding is associated with at most low positive bands [3].

[8] a) W. Saenger, *Principles of Nucleic Acid Structure*, Springer, New York, **1988**; b) C. R. Cantor, P. R. Schimmel, *Biophysical Chemistry*, Freeman, New York, **1980**.

[9] S. L. Broitman, D. D. Im, J. R. Fresco, *Proc. Natl. Acad. Sci. USA*, **1987**, *84*, 5120–5124.

[10] Absorbance mixing curves are plots of absorbances vs. the fractional composition of the mixtures at constant total concentration [8b]. In analogy to Fresco et al. [9], we monitored the absorbances at 280 nm.

[11] Mixtures with porphyrin were prepared adding H_2T4 as the last component shortly after the polynucleotides.

[12] We hypothesize that the endpoint at $X_A = 0.5$ is obscured by the disproportionation reaction (a), which disfavors formation of the double helix. Our

$$2\,\text{poly(A·U)} + n\,H_2T4 \rightleftharpoons \text{poly(U·A·A)}\cdot n\,H_2T4 + \text{poly(U)} \quad \text{(a)}$$

hypothesis is confirmed by the CD data which show that 1) H_2T4 does not aggregate up to $X_A = 0.5$ (which means that H_2T4 does not aggregate on *ds* poly(A·U), because it is not conceivable that poly(A·U) is not present at $X_A = 0.4$), and 2) H_2T4 is suddenly extensively aggregated ($\Delta\varepsilon = 120\ M^{-1}cm^{-1}$) at $X_A = 0.5$, where triple helix formation begins.

[13] O. Hermann, S. Husain Mehdi, A. Corsini, *Can. J. Chem.* **1978**, *56*, 1084–1087.

A General and Efficient Method for the Monohydroxylation of Alkanes**

Gregorio Asensio,* Rossella Mello, María Elena González-Núñez, Gloria Castellano, and Julia Corral

The selective functionalization of alkanes is an important challenge in synthetic organic chemistry. In this context, several methodologies have been developed to oxidize hydrocarbons.[1] The cyclic peroxide methyl(trifluoromethyl)dioxirane (**1**) has been revealed as a selective and very efficient oxidant for alkanes under very mild conditions.[2] Dioxirane **1** discriminates tertiary C–H bonds in the presence of methylene and methyl groups to give tertiary alcohols with a remarkably high selectivity. However, methylene groups are oxidized to ketones, since the secondary alcohol produced in the first oxygen transfer step reacts with **1** faster than the starting alkane.[1–3] Analogously, in the few examples reported of oxidation of methyl groups,[4] carboxylic acids are the reaction products.

During our studies on the factors influencing the selectivity of the O-atom insertion into C–H bonds by dioxiranes, we found that acylated primary and secondary alcohols are protected against oxidation by **1**. This result prompted us to study the control of the oxidation of methyl and methylene groups at the alcohol stage. Now we report that unactivated primary and secondary C–H bonds are selectively monohydroxylated by **1** with excellent yields when reactions are carried out in the presence of a tenfold excess of trifluoroacetic anhydride [Eq. (a)].

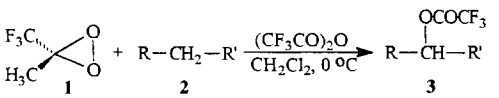

(a)

R= alkyl, aryl
R'= H, alkyl, aryl

The reaction products were the trifluoroacetates **3** in all cases. Overoxidation to carboxylic acids or ketones was not observed in any case under our reaction conditions. The yields of monohydroxylation products decreased with the use of a threefold excess of trifluoroacetic anhydride; the resulting trifluoroacetic acid esters were stable under the reaction conditions. The results are shown in Table 1.

The formation of the trifluoroacetic acid esters **3** is easily understood if we consider that the alcohols formed initially by oxidation of a C–H bond undergo acylation by trifluoroacetic anhydride, present in excess, faster than any further oxidation by **1**. The oxygen transfer is nearly quantitative in all cases to give only monohydroxylated products; moreover, no product resulting from the radical chain decomposition of **1** is detected.[5] A model of concerted electrophilic O-atom insertion[6] into C–H bonds best accommodates the above observations. Our results parallel those reported in the oxidation of methylene groups to ketones by **1**; the presence of trifluoroacetic anhydride in the medium has obviously no any significant influence on the course of the oxygen transfer process.

[*] Prof. Dr. G. Asensio, Dr. R. Mello, Prof. Dr. M. E. González-Núñez, G. Castellano, J. Corral
Departamento de Química Orgánica, Facultad de Farmacia
Universidad de Valencia
Avda. Vicente Andrés Estellés s.n., E-46100 Burjassot, Valencia (Spain)
Fax: Int. code +(6)386-4939

[**] This work was supported by the Spanish Dirección General de Investigación Científica y Técnica (PB93-0681). We thank the S. C. S. I. E. Universidad de Valencia for the use of NMR and GC-MS facilities.

Table 1. Reaction of alkanes **2** with **1** in the presence of trifluoroacetic anhydride [a].

Substrate	Reaction time	Product(s) (Yield [%]) [b]
2a	60 h	**3a** (>99)
2b	40 min	(±)-**3b** (58) (±)-**3b'** (42)
2c	10 min	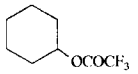 **3c** (>99)
2d	2 min	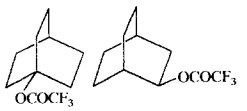 **3d** (50) (±)-**3d'** (50)
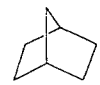 **2e**	40 min	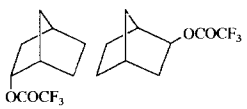 (±)-**3e** (5) (±)-**3e'** (95)
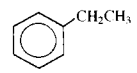 **2f**	20 min	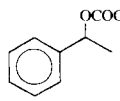 (±)-**3f** (75)[c]
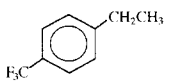 **2g**	1 h	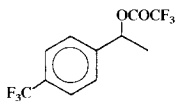 (±)-**3g** (>99)[d]

[a] Substrate concentration (in CH_2Cl_2) about 0.1 M in all cases; initial molar ratio of **2**/**1** = 1/1.2. The substrate conversion was quantitative except where otherwise indicated (see [c, d]). [b] Determined by GC analysis; all values are within 1% error limits. [c] Substrate conversion 12%. [d] Substrate conversion 75%.

2,2,3,3-Tetramethylbutane (**2a**) was selected for the study of the oxidation of methyl groups (Table 1). The stoichiometric reaction takes 60 hours to afford monoester **3a**, which reveals the low reactivity of primary C–H bonds. *n*-Hexane (**2b**) reacts in 40 min to give a mixture of secondary esters **3b**, and **3b'** in a nearly statistical ratio. Cyclohexane (**2c**) reacts much faster (in only 10 min) to afford cyclohexyltrifluoroacetate (**3c**) as the only product.

Bicyclo[2.2.2]octane (**3d**) is monohydroxylated in the tertiary and secondary positions in a 1:1 ratio in accord with the known preference of **1** to react with tertiary C–H bonds. Norbornane (**2e**)[2, 7] is hydroxylated at C2 with high *exo*-selectivity (*exo*/*endo* ratio 95/5). Benzylic positions are also monohydroxylated by this process. In this case, an important side reaction, the oxidation of the activated aromatic ring, causes lower yields (for instance, of monoester **3f**). If the aromatic ring carries an electron-withdrawing trifluoromethyl group as in **2g**, this side reaction does not take place, but the rate of O-atom insertion into the benzylic C–H bond decreases (see **2f** and **2g** in Table 1).

In conclusion, the methodology reported for oxidation with **1** enables highly selective monohydroxylation of alkanes.

Experimental Procedure

General procedure: A 1.2-fold excess of **1** (0.37 M) in ketone-free [5] CH_2Cl_2 was added to a solution of alkane **2** (0.5–1.0 mmol, 0.13–0.15 M) in CH_2Cl_2 containing a tenfold excess of trifluoroacetic anhydride at 0 °C. The progress of the reactions

 © VCH Verlagsgesellschaft mbH, D-69451 Weinheim, 1996 0570-0833/96/3502-0217 $ 10.00+.25/0

was monitored by iodometric titration [8] until the iodometric titer was constant. Then the solutions were treated with solid sodium carbonate at 0 °C for 1 h with stirring and subsequently filtered; the volatile products were removed under vacuum at 0 °C to yield the trifluoroacetate esters **3**. Yields were determined by GC analysis of the crude reaction mixture (internal standard p-$ClC_6H_4CO_2CH_3$) after neutralization. All the products were isolated and identified by comparison (^1H and ^{13}C NMR, and GC-MS) with authentic samples.

Received: July 4, 1995
Revised version: October 30, 1995 [Z8170IE]
German version: *Angew. Chem.* **1996**, *108*, 196–198

Keywords: alkanes · dioxiranes · hydroxylations · oxidations

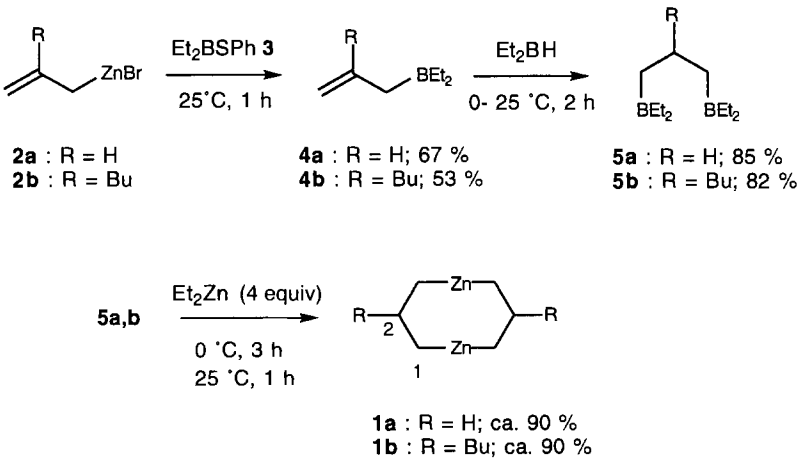

Scheme 1.

[1] a) O. Reiser, *Angew. Chem.* **1994**, *106*, 73; *Angew. Chem. Int. Ed. Engl.* **1994**, *33*, 69; b) D. H. R. Barton, D. Doller, *Acc. Chem. Res.* **1992**, *25*, 504; c) B. Meunier, *Chem. Rev.* **1992**, *92*, 1411; d) J. F. Larrow, E. N. Jacobsen, *J. Am. Chem. Soc.* **1994**, *116*, 12129; e) K. Nomura, S. Uemura, *J. Chem. Soc. Chem. Commun.* **1994**, 129; f) A. Tenaglia, E. Terranova, B. Waegell, *Tetrahedron Lett.* **1989**, *30*, 5271; g) P. H. J. Carlsen, *Synth. Commun.* **1987**, *17*, 19; h) D. D. Desmarteu, A. Donadelli, V. Montanari, V. A. Petrov, G. Resnati, *J. Am. Chem. Soc.* **1993**, *115*, 4897; i) M. D. Kaufman, P. A. Grieco, D. W. Bougie, *ibid.* **1993**, *115*, 11648; j) A. de Meijere, F. Wolf, *Methoden Org. Chem. (Houben-Weyl) 4th ed. 1952–*, E13, **1988**, pp. 971–990, and references therein; k) G. A. Olah, G. K. S. Prakash, J. Sommer, *Superacids*, Wiley, New York, **1985**, and references therein.
[2] R. Mello, M. Fiorentino, C. Fusco, R. Curci, *J. Am. Chem. Soc.* **1989**, *111*, 6749.
[3] R. Mello, L. Cassidei, M. Fiorentino, C. Fusco, W. Hümmer, V. Jäger, R. Curci, *J. Am. Chem. Soc.* **1991**, *113*, 2205.
[4] a) D. Kuck, A. Schuster, C. Fusco, M. Fiorentino, R. Curci, *J. Am. Chem. Soc.* **1994**, *116*, 2375; b) G. D. Maynard, L. A. Paquette, *J. Org. Chem.* **1991**, *56*, 5480.
[5] W. Adam, M. E. González-Núñez, R. Mello, R. Curci, *J. Am. Chem. Soc.* **1991**, *113*, 7654.
[6] R. D. Bach, M.-D. Su, *J. Am. Chem. Soc.* **1994**, *116*, 10103.
[7] a) D. H. Giamalva, D. F. Church, W. A. Pryor, *J. Org. Chem.* **1988**, *53*, 3429; b) *J. Am. Chem. Soc.* **1986**, *108*, 7679.
[8] W. Adam, G. Asensio, R. Curci, M. E. González-Núñez, R. Mello, *J. Am. Chem. Soc.* **1992**, *114*, 8345.

Preparation of 1,3-Dizinc Compounds by a Boron–Zinc Exchange**

Holger Eick and Paul Knochel*

1,3-Dimetallic reagents are interesting building blocks that have proved to be especially useful for the preparation of metallacyclic transition metal complexes.[1] However, applications of these dimetallic reagents in organic synthesis have been hampered by their difficult preparation. Thus, treatment of 1,3-dibromopropane with metals such as Li, Mg, and Zn affords cyclopropanes as major products, but 1,3-dimetallic compounds can only be obtained in modest yields.[2] Alternatively, the transmetalation of 1,3-dimercury compounds[1, 2] constitutes a satisfactory approach to 1,3-dimagnesio-[1, 2] and 1,3-dilithiopropanes;[1] however, the high toxicity of mercury compounds precludes broad synthetic applications of this chemistry. Recently we developed an efficient synthesis of polyfunctional dialkylzinc compounds by a boron–zinc exchange reaction.[3] Herein, we report an application of this reaction to the preparation of 1,3-dizinc compounds **1a,b** (Scheme 1).

[*] Prof. Dr. P. Knochel, Dipl.-Chem. H. Eick
Fachbereich Chemie der Universität
Hans-Meerwein-Strasse, D-35032 Marburg (Germany)
Fax: Int. code +(6421) 28 21 89

[**] This work was supported by the Fonds der Chemischen Industrie and the Deutsche Forschungsgemeinschaft (SFB 260). We thank BASF, Witco, Schering, Callery, Bayer, Sipsy, and Chemetall for the generous gift of chemicals.

Thus, treatment of the allylic zinc bromides **2a,b**[4] with diethylthiophenylborane **3**[5] affords the corresponding allylic diethylboranes **4a,b**. These air-sensitive organoboranes can be isolated in pure form by distillation under reduced pressure (53–67% yield). The hydroboration of **4a,b** with diethylborane/methyl sulfide complex[3, 6] (25 °C, ca. 2 h) affords the 1,3-bis(diethylboryl)propanes **5a,b** in 82–85% yield as clear oils. Treatment of **5a,b** with diethylzinc (4 equiv, neat, 0 °C, 0.5 h) leads as expected to a fast boron–zinc exchange. After removal of the excess diethylzinc by application of vacuum, the crude 1,3-dizinc species **1a,b** are obtained as sole products (ca. 90% yield) as shown by ^1H and ^{13}C NMR analysis.[7] NMR experiments and a comparison with the pioneering work by F. Bickelhaupt et al. on the structures of 1,4-, 1,5- and 1,6-dizinc compounds[8] led us to propose an eight-membered cyclic structure for **1a,b** rather than an open-chain polymeric structure $[(ZnCH_2CH_2CH_2)_n]$. The ^{13}C NMR spectrum of the 2-butyl-substituted 1,3-dizinc derivative **1b**[7] shows two sharp signals each for C(1), C(2), and the CH_2 group attached to C(2), suggesting the formation of a 1:1 *cis*/*trans* mixture for **1b**. The reaction of an equimolar mixture of **5a** and **5b** with diethylzinc gives a mixture of products. The ^{13}C NMR signals are broader and of unequal intensity for C(1), C(2), and the CH_2 group attached to C(2), which can be explained by the additional formation of the 1,5-dizincacyclooctane **6**.[9]

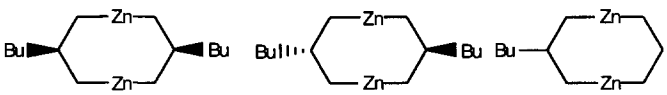

cis-**1b** *trans*-**1b** **6**

The dimetallic reagents **1a,b** do not react directly with electrophiles;[10] however, in the presence of copper(I) salts like $CuCN \cdot 2LiCl$,[11] allylic halides and propargyl bromide are converted at −60 °C to the bisallyl products **7a,b** and **8a,b**, and the bisallene **9**, respectively, in excellent yields (84–89%) (Scheme 2). With less reactive electrophiles, higher temperatures are required. The intermediate 1,3-dicopper reagents are significantly less stable than the 1,3-dizinc precursors, and some decomposition of these compounds occurs under the reaction conditions required for performing an acylation (−10 °C, 10 h) or an addition to ethyl propiolate (−15 °C, 3 h), leading to lower yields (ca. 40%) of the respective products **10a,b** and **11**.

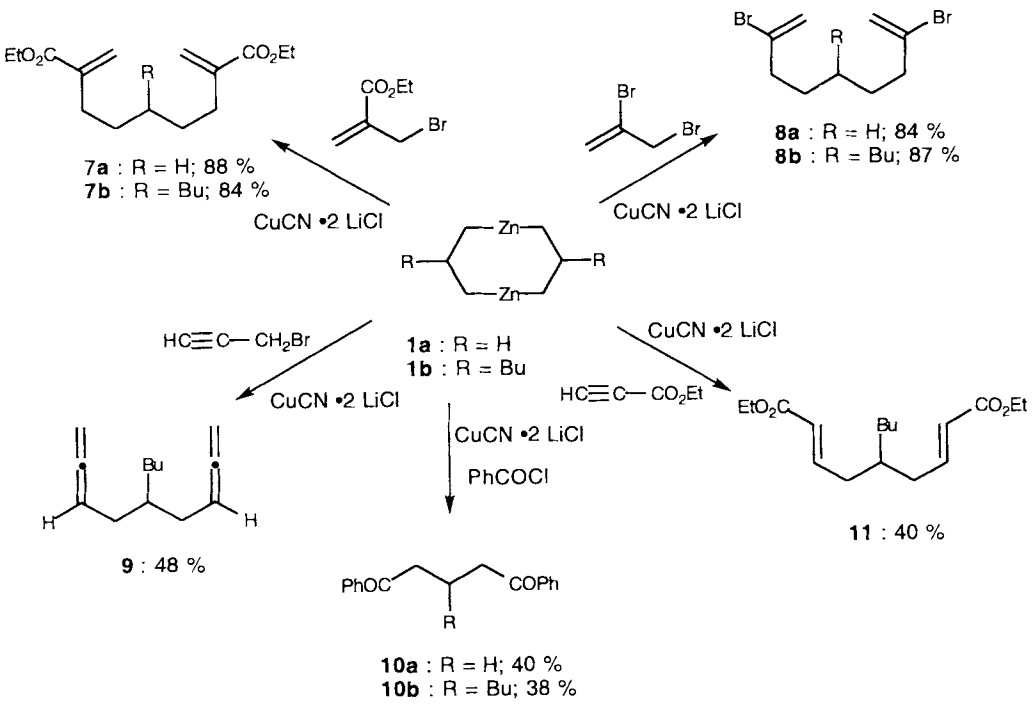

Scheme 2.

An allylated, reduction side product (1-phenyl-3-buten-1-yl benzoate) is formed during the reaction of **1a** with benzoyl chloride. Similarly, Bickelhaupt has observed that 1,3-dimagnesium compounds can play the role of a hydride donor. This reaction pathway is observed when **1b** is treated with tosyl cyanide.[12] In this case, the unsaturated cyanide **12** is obtained as sole product in 82% yield (Scheme 3). Finally, the reaction of

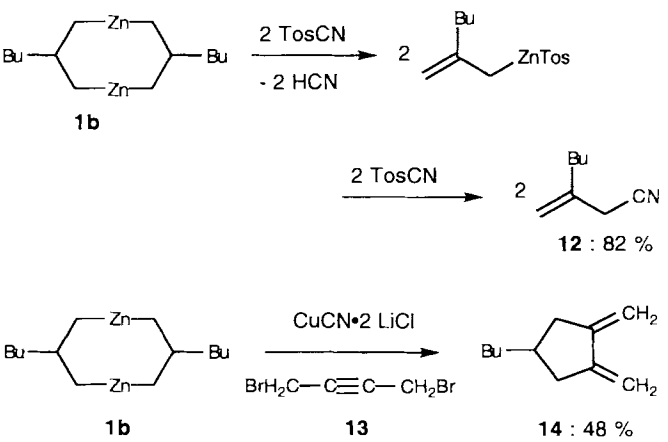

Scheme 3.

1b with a bis-electrophile like 1,4-dibromo-2-butyne (**13**)[13] allows a short one-step synthesis of the 1,2-bis(exomethylene)-cyclopentane **14** in 48% yield (Scheme 3).

In summary, we have developed a new simple synthesis of 1,3-dizinc derivatives using the boron–zinc exchange reaction and have shown that these reagents can be allylated and allenylated in excellent yield. Furthermore, we have reported a new cyclization reaction. Further investigations into the synthesis, structure, and reactivity of 1,3-dizinc compounds are currently underway in our laboratories.

Experimental Procedure

Diethyl(2-butylallyl)borane **4b**: A solution of 2-butylallyl bromide (16.29 g, 92 mmol) in THF (90 mL) was added dropwise to pieces of zinc foil (6.9 g, 92 mmol) in THF (2 mL) in such a way that the temperature of the solution did not rise above 10 °C [4]. The reaction was complete after stirring 2 h at 25 °C and gave the corresponding zinc reagent **2b** (ca. 70% yield according to GC analysis of an iodolyzed reaction mixture aliquot). Diethylthiophenylborane **3** [3] (11.40 g, 64 mmol) was added. The crude reaction mixture was purified by distillation (b. p. 31 °C/0.2 mmHg) to give **4b** (8.15 g, 49 mmol, 53% yield) as a colorless liquid.

1,3-Bis(diethylboryl)-2-butylpropane **5b**: The allylic borane **4b** (2.15 g, 12.9 mmol) prepared as described above was treated with diethylborane methyl sulfide complex [3] (1.17 g, 12.9 mmol) for 2 h at 25 °C. The unconverted diethylborane and methyl sulfide was distilled off to leave crude **5b** (2.49 g, 10.6 mmol, 82% yield) which was used directly in the next step.

5-Butyl-1,2,7,8-nonatetraene **9**: A 50 mL two-necked flask equipped with an argon inlet and a rubber septum was charged with **5b** (1.2 g, 5 mmol) and diethylzinc (2.0 mL, 20 mmol) at 0 °C. After 0.5 h at 0 °C the excess diethylzinc and resulting triethylborane were removed under vacuum (0 °C, 3 h, then 25 °C, 1 h at 0.1 mmHg) to give the crude 3,7-dibutyl-1,5-dizincacyclooctane **1b** as a gray oil. Satisfactory ^{1}H and ^{13}C NMR spectra were obtained. The zinc compound **1b** is stable for at least 1 day at 0 °C in the dark (no appreciable change of the NMR spectra was detected). The crude **1b** was diluted with THF (8 mL), cooled to −60 °C, and CuCN·2LiCl [10] (10 mmol) in THF (12 mL) was added by syringe. Subsequently, propargyl bromide (2.60 g, 17.5 mmol) was added, and the reaction mixture was slowly allowed to warm up to 25 °C and stirred for 0.5 h. After the usual workup [10], the crude oil obtained after evaporation of the solvents was purified by flash chromatography (hexane) to give **9** (760 mg, 4.35 mmol; 89% yield) as a yellow oil.

Received: September 7, 1995 [Z83751E]
German version: *Angew. Chem.* **1996**, *108*, 229–231

Keywords: boron compounds · 1,5-dizincacyclooctane · zinc compounds

[1] a) F. Bickelhaupt, *Angew. Chem.* **1987**, *99*, 1020–1035; *Angew. Chem. Int. Ed. Engl.* **1987**, *26*, 990–1005; b) *J. Organomet. Chem.* **1994**, *475*, 1–14; c) J. W. F. L. Seetz, G. Schat, O. S. Akkerman, F. Bickelhaupt, *Angew. Chem.* **1983**, *95*, 242–243; *Angew. Chem. Int. Ed. Engl.* **1983**, *22*, 248–249; d) *J. Am. Chem. Soc.* **1983**, *105*, 3336–3337; e) J. Levisalles, H. Rudler, D. Villemin, *J. Organomet. Chem.* **1980**, *193*, 69–82.

[2] L. C. Costa, G. M. Whitesides, *J. Am. Chem. Soc.* **1977**, *99*, 2390–2391.

[3] a) F. Langer, J. R. Waas, P. Knochel, *Tetrahedron Lett.* **1993**, *34*, 5261–5264; b) F. Langer, A. Devasagayaraj, P.-Y. Chavant, P. Knochel, *Synlett* **1994**, 410–412; c) L. Schwink, P. Knochel, *Tetrahedron Lett.* **1994**, *35*, 9007–9010; d) A. Devasagayaraj, L. Schwink, P. Knochel, *J. Org. Chem.* **1995**, *60*, 3311–3317.

[4] Allylic zinc bromides are readily prepared by the direct insertion of zinc from pieces of zinc foil to the corresponding allylic bromides (THF, 5–10 °C, 2–3 h, 90–95% yield): M. Gaudemar, *Bull. Soc. Chim. France* **1962**, 974–987.

[5] a) A. Pelter, K. Rowe, D. N. Sharrocks, K. Smith, C. Subrahmanyam, *J. Chem. Soc. Dalton* **1976**, 2087–2090; b) F. Langer, Diplomarbeit, Universität Marburg, **1993**.

[6] R. Köster, G. Griasnow, W. Larbig, P. Binger, *Liebigs Ann. Chem.* **1964**, *672*, 1–34.

[7] ^{1}H and ^{13}C NMR data of **1a,b**; **1a**: ^{1}H NMR (300 MHz, [D$_8$]THF): δ = 0.22 (m, 8H), 1.82 (m, 4H); ^{13}C NMR (75 MHz, [D$_8$]THF): δ = 22.4 (C(1)), 27.7 (C(2)). **1b**: ^{1}H NMR (500 MHz, [D$_8$]THF): δ = 0.30–0.55 (m, 8H), 0.80–0.95 (m, 6H), 1.10–1.35 (m, 12H), 2.10–2.20 (m, 2H); ^{13}C NMR (125 MHz, [D$_8$]THF), 15.0 (CH$_3$), 24.5 (CH$_2$), 30.0, 30.3 (C(1)), 32.0 (CH$_2$), 38.5, 38.9 (C(2)), 48.3, 49.1 (CH$_2$ attached at C(2)).

 © VCH Verlagsgesellschaft mbH, D-69451 Weinheim, 1996 0570-0833/96/3502-0219 $ 10.00+.25/0

[8] F. J. M. Freijee, J. W. F. L. Seetz, O. S. Akkerman, F. Bickelhaupt, *J. Organomet. Chem.* **1982**, *224*, 217–221.
[9] Numerous attempts to determine the degree of aggregation of compounds **1** by using differential-vapor osmometry in anology to the experiments of Bickelhaupt et al. led to the expected association value of 2, but with a low reproducibility of our results and a large standard deviation.
[10] For a recent review on the reactions of organozinc derivatives: P. Knochel, R. Singer, *Chem. Rev.* **1993**, *93*, 2117–2188.
[11] P. Knochel, M. C. P. Yeh, S. C. Berk, J. Talbert, *J. Org. Chem.* **1988**, *53*, 2390–2392.
[12] I. Klement, K. Lennick, C. E. Tucker, P. Knochel, *Tetrahedron Lett.* **1993**, *34*, 4623–4626.
[13] a) L. Zhu, R. D. Rieke, *Tetrahedron Lett.* **1991**, *32*, 2865–2866; b) H. Ochiai, Y. Tamaru, K. Tsubaki, Z. Yoshida, *J. Org. Chem.* **1987**, *52*, 4418–4420.

New Catalysts and Conditions for a C–H Insertion Reaction Identified by High Throughput Catalyst Screening**

Kevin Burgess,* Hee-Jong Lim, Alexander M. Porte, and Gary A. Sulikowski

Diazo compounds with suitably oriented substituents can undergo intramolecular cyclizations by metal-promoted reactions that presumably involve insertion of metallocarbenes into C–H bonds.[1, 2] Most of the known reactions of this type involve rhodium complexes,[3] typically bearing optically pure ligands from amino acids,[4] but two of us recently reported that optically active copper catalysts seemed to be superior for the reaction shown in Scheme 1.[5] In the best case, the product **3** was isolated in 64% yield as a 2.3:1.0 mixture of diastereomers. The object of the current study was to use high throughput catalyst screening to improve these results.

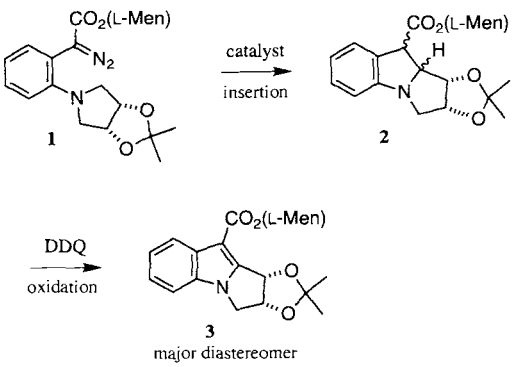

Scheme 1. L-Men = L-menthyl.

[*] Prof. K. Burgess, H.-J. Lim, A. M. Porte, Prof. G. A. Sulikowski
Department of Chemistry, Texas A & M University
College Station, TX 77843-3255 (USA)
Fax: Int. code +(409)845-8839
e-mail: burgess@chemvx.tamu.edu

[**] We thank the Petroleum Research Foundation and the Robert A. Welch Foundation for financial support. K. B. thanks the National Institutes of Health for an NIH Research Career Development Award, and the Alfred P. Sloan Foundation for a Fellowship. G. A. S. thanks the American Cancer Society for a Junior Faculty Research Award, and American Cyanamid for a Cyanamid Faculty Award.

Our strategy was based on examining 96 potential systems for the transformation of diazo compound **1** into **2**, using a microtitre plate format. Solvents and reagents were mixed in the plate, which was then gently agitated under an inert atmosphere for 18 h at ambient temperature. The plate was then brought into the air, and the product was oxidized by adding 2,3-dichloro-5,6-dicyano-1,4-benzoquinone (DDQ) into each well. Each reaction mixture was then filtered through a silica gel plug, an internal standard (naphthalene) was added to each, and their compositions were analyzed by using an HPLC equipped with an autosampler. In this way, 96 sets of approximate yield and stereoselectivity data could be obtained in less than a week. Finally, the most promising leads would be reinvestigated in the standard way, that is sequentially.

Table 1 shows the ligand/metal/solvent combinations that were used and the data that was obtained from the high throughput screen. In summary, three different bis(oxazolidine) ligands,[6–8] a salen-type ligand,[9] and sparteine were used in combination with seven different metal salts (although not for each ligand), and four different solvents. Copper(1+) and rhodium(1+) ions were combined with the following, less well investigated, metal candidates: silver(1+), scandium(3+), gold(1+), lanthanum(3+), and ytterbium(3+) ions. Silver(1+) and scandium(3+) ions were used in more wells than the other metals of the latter category.

The original study had demonstrated that the influence of the menthyl group on the diastereomeric ratio was negligible: all the stereoselectivity could be attributed to the catalyst.[5] Inclusion of the menthyl group gives diastereomers of product **3** which can be separated by using analytical HPLC on a silica column.[5] Convenient analyses are a prerequisite for high throughput screening, hence the menthyl ester **1** was chosen for this work, in preference to esters of any achiral alcohols.

There are two main reasons for uncertainties in the screening process. First, small quantities are involved in the reactions performed in microtitre plates (ca. 10 mg of **1**, 0.6–1.4 mg of ligand, and 0.63–1.5 mg of metal salt) hence there can be significant weighing errors. Second, the agitation process may also effect the results obtained from this type of screen. Consequently, the procedure can only be considered to render leads for further investigations. To further explore the most encouraging results from the screening process, several of the reactions from the plate therefore were repeated on a larger scale (10 mol% of catalyst, throughout) with stirring, under more carefully controlled conditions. Under those conditions the following systems gave relatively poor yields of product as judged by HPLC: sparteine (ligand **7**) with $(CuOTf)_2 \cdot C_6H_6$ (THF, 25 °C, 12 h), with $Sc(OTf)_3$ (THF, 25 °C, 12 h), with $[Rh(nbd)]BPh_4$ (MePh, 10 °C, 24 h); and ligand **8**[9] with $(CuOTf)_2 \cdot C_6H_6$ (MePh, 10 °C, 24 h). Moreover, the diastereomeric ratio of product **3** formed in all these reactions was no greater than 1.3:1. Discrepancies between the latter data and that from the screen can be attributed mainly to the factors outlined above. Two sets of conditions, however, did give very interesting results. Ligand **5**[10] with $(CuOTf)_2 \cdot C_6H_6$ (THF, 10 °C, 12 h), and with $AgSbF_6$ (THF, 25 °C, 24 h), gave diastereomeric ratios for product **3** of 3.9:1 and 3.5:1, respectively. HPLC traces and isolated yields for the copper- and silver-based processes indicated that the product yield was better in the latter case (61% and 75%, respectively).

The results of the screening process suggest that ligand **5** was superior to many others, as inferred in the original study.[5] However, THF seems to be a better solvent than chloroform (the solvent originally reported), and when the reaction was repeated at a slightly reduced temperature using

Table 1. Diastereomeric ratios and yields [%] for the 96 different systems that were screened for efficacy in the reaction shown in Scheme 1.

Ligand [a]	Metal salt [b]	Diastereomic ratio (yield [%]) [c]			
		THF	MeCN	$CHCl_3$	MePh
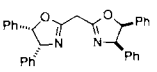 4	$AgSbF_6$	1.5:1 (45)	1.1:1 (54)	2.3:1 (6.7)	1.9:1 (25)
	$Sc(OTf)_3$	– [d]	–	–	1.6:1 (36)
	$[Rh(nbd)]BPh_4$	1:1.6 (43)	1:1.5 (15)	1:1.9 (9.8)	1:1.2 (23)
	$(CuOTf) \cdot C_6H_6$	3.4:1 (44)	1:1.0 (21)	1.9:1 (41)	1.7:1 (47)
	$La(Otf)_3$	1.5:1 (12)	1.1:1 (0.26)	1:1.2 (27)	1:1.3 (19)
	$Yb(OTf)_3$	1.3:1 (0.71)	–	–	1:1.4 (0.40)
	$AuCl(SMe_2)$	1:1.0 (20)	1.2:1 (9.3)	1:1.2 (18)	1:1.2 (15)
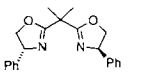 5	$AgSbF_6$	2.7:1 (44)	1.2:1 (36)	1:1.1 (1.9)	1.1:1 (32)
	$Sc(OTf)_3$	1.1:1 (9.9)	–	1:1.2 (3.2)	1.6:1 (45)
	$[Rh(nbd)]BPh_4$	1:1.1 (14)	1.1:1 (6.6)	1:1.5 (25)	1:2.1 (36)
	$(CuOTf) \cdot C_6H_6$	4.4:1 (47)	1.3:1 (18)	4.0:1 (13)	2.9:1 (44)
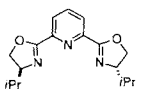 6	$AgSbF_6$	2.0:1 (10)	1.4:1 (8.0)	1:1.4 (7.9)	1:1.4 (36)
	$Sc(OTf)_3$	–	–	–	1:1.5 (43)
	$[Rh(nbd)]BPh_4$	1.2:1 (11)	1:1.1 (6.9)	1:1.4 (19)	1:2.3 (17)
	$(CuOtf) \cdot C_6H_6$	2.0:1 (7.0)	2.0:1 (5.0)	1.2:1 (19)	1:1.3 (21)
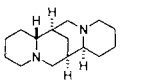 7	$AgSbF_6$	1.7:1 (0.47)	1.7:1 (8.1)	1:1.2 (39)	1:1.4 (37)
	$Sc(OTf)_3$	3.4:1 (0.91)	1.3:1 (0.08)	1:1.3 (2.3)	1:1.1 (34)
	$[Rh(nbd)]BPh_4$	1:1.4 (30)	1:1.0 (7.2)	1:1.7 (33)	1:2.4 (29)
	$(CuOTf) \cdot C_6H_6$	5.9:1 (23)	2.1:1 (5.1)	1.2:1 (24)	1.3:1 (44)
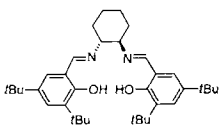 8	$AgSbF_6$	1.8:1 (15)	1.3:1 (3.4)	1.2:1 (0.45)	1.4:1 (14)
	$Sc(OTf)_3$	1:1.5 (0.15)	1.7:1 (0.08)	1.3:1 (0.09)	–
	$[Rh(nbd)]BPh_4$	1.5:1 (9.6)	1.1:1 (6.3)	1:1.8 (12)	1:2.3 (15)
	$(CuOTf) \cdot C_6H_6$	3.2:1 (4.1)	1.7:1 (0.31)	1.3:1 (4.0)	1.3:1 (1.5)
	$AuCl(SMe_2)$	1:1.0 (5.8)	1:1.1 (1.8)	1:1.3 (22)	1:1.4 (14)

[a] Substrate **1**:ligand:salt ratio is 1:0.1:0.1 throughout. [b] Tf = trifluoromethanesulfonyl, nbd = norbornadiene. [c] After DDQ oxidation, accessed by HPLC. Throughout, the first value quoted in the ratios refers to the isomer shown in the reaction shown in Scheme 1 [11]. [d] Where no data is quoted, insufficient product was obtained for analysis.

$(CuOTf)_2 \cdot C_6H_6$, the diastereomeric ratio was improved from the value of 2.3:1 (CH_2Cl_2, 25 °C) as reported in the original work, to 3.9:1 (THF, 10 °C). With respect to yield, the combination of ligand **5** with $AgSbF_6$ was better than the copper-based system, and the stereoselectivity for this catalyst was almost as good as for the best copper system identified. Use of silver complexes in C–H insertion reactions is at least extremely rare, and perhaps unprecedented.

Stereoselective processes of the type depicted in Scheme 1 are difficult to control since there are two possible pathways to each of the diastereomeric products. Scheme 2 shows the four different processes by which the two diastereomers of **3** may form. Any catalyst that is intended to favor production of one of these

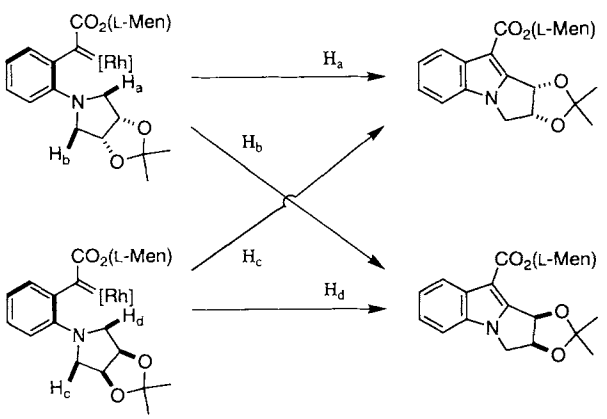

Scheme 2. The origin of both diastereomers in the reaction shown in Scheme 1.

isomers has to selectively reduce a specific combination of two of the four activation energies involved. Consequently, it may be difficult to obtain high diastereoselectivities in this transformation.

We have shown how 96 different catalyst systems were screened for their potential to mediate a challenging asymmetric C–H insertion reaction. The best stereoselectivity was observed with a copper catalyst, but comparable diastereoselectivities and superior yields were obtained with a silver-based catalyst. Use of silver complexes in these reactions may be unique.

In general, high throughput catalyst screening can have several advantages over the usual approach wherein experimentalists perform only a limited number of test reactions simultaneously. First, the plate format is much more efficient when many catalysts are to be screened. Second, parallel screening encourages the researcher to try a wide variety of systems, some of which would otherwise have been regarded as too unusual to warrant testing in a sequential fashion. In this respect, the concept of high throughput screening encourages creativity. Moreover, given a model reaction, high throughput catalyst screening with incremental changes could be very useful for optimization situations commonly encountered in industrial process development.

There are obvious parallels with this research and the concept of "combinatorial catalysis" wherein extremely large numbers of catalysts (many more than 96) might be generated by combining reagents, and screened in parallel. Experimentally, that idea is likely to be extremely difficult to put into practice. We strongly advocate a "one catalyst per well" strategy until a truly combinatorial method is devised for screening varied catalysts for a range of different reaction types.

Experimental Procedure

Screening in microtitre plates: All operations preceding the DDQ oxidation were performed in a glove box. Weighed amounts of metal salts (10 mol%) and then ligands (10 mol%) were introduced into the wells of a microtitre plate. A solvent (100 μL), then 100 μL of a 10 mg/100 μL solution of substrate **1** in the same solvent, were added by using a micropipetter. The plate was gently agitated for 18 h at 25 °C. The plate was brought out into the air, and DDQ (20 mg) was added as a solid to each well. The plate was agitated for 1 h at 25 °C. The solvents were allowed to evaporate. The contents of each well were passed through a short column of silica eluted with 1.5 mL of 2:3 EtOAc/hexanes, then 50 μL of a 1 mg mL^{-1} solution of naphthalene (internal standard) in 2:3 EtOAc/hexanes was microsyringed into each reaction mixture. Finally, an autosampler was used to input each sample into an HPLC (10 × 250 mm Dynamax, 60 Å pore size, silica gel column; isocratic 3 mL min^{-1} solvent flow of 9:1 hexanes/EtOAc; UV detection at 290 nm).

3: The following procedure is illustrative of the larger scale reactions. Silver hexafluoroantimonate (1.4 mg, 0.0057 mmol) and ligand **5** (1.9 mg, 0.0057 mmol) were weighed into a reaction flask in a glove box. THF (1 mL) was added to generate the catalyst system. A solution of substrate **1** (25 mg, 0.057 mmol) in THF (0.5 mL) was then added to the catalyst and stirred at 25 °C for 24 h. Solid DDQ (0.086 mmol) was added to the mixture, and it was then stirred for 1 h. An aliquot of the reaction mixture was taken for HPLC analysis. Solvent was removed form the reaction mixture and the product redissolved in ether (10 mL). Subsequent washes with $NaHCO_3$ (3 × 5 mL) and brine (5 mL) and drying of the organic layer over $MgSO_4$ followed by flash chromatography produced **3**.

Received: October 6, 1995 [Z8452IE]
German version: *Angew. Chem.* **1996**, *108*, 192–194

Keywords: carbene complexes · catalysis · combinatorial chemistry · insertions

[1] H. Brunner, *Angew. Chem.* **1992**, *104*, 1208–1210; *Angew. Chem. Int. Ed. Engl.* **1992**, *31* 1183–1185.
[2] T. Ye, M. A. McKervey, *Chem. Rev.* **1994**, *94*, 1091–1160.
[3] M. P. Doyle, *Chem. Rev.* **1986**, *86*, 919–939.
[4] M. P. Doyle, A. B. Dyatkin, G. H. P. Roos, F. Canas, D. A. Pierson, A. van Basten, *J. Am. Chem. Soc.* **1994**, *116*, 4507–4508.
[5] H.-J. Lim, G. A. Sulikowski, *J. Org. Chem.* **1995**, *60*, 2326-2327.
[6] R. E. Lowenthal, A. Abiko, S. Masamune, *Tetrahedron Lett.* **1990**, *31*, 6005-6008.
[7] H. Fritschi, U. Leutenegger, K. Siegmann, A. Pfaltz, W. Keller, C. Kratky, *Helv. Chim. Acta* **1988**, *71*, 1541–1552.
[8] A. Pfaltz, *Acc. Chem. Res.* **1993**, *26*, 339–345.
[9] E. N. Jacobsen, W. Zhang, A. R. Muci, J. R. Ecker, L. Deng, *J. Am. Chem. Soc.* **1991**, *113*, 7063–7064.
[10] D. A. Evans, K. A. Woerpel, M. M. Hinman, M. M. Faul, *J. Am. Chem. Soc.* **1991**, *113*, 726–728.
[11] P. V. Roey, G. D. Smith, T. M. Balasubramanian, G. R. Marshall, *Acta Crystallogr. Sect. B* **1981**, *37*, 1785–1788.

Correction of "1,1-Di-, 1,2,3-Tri- and 1,1,4,4-Tetra-*tert*-butyl-1,3-butadiene"

Henning Hopf,* Ralf Hänel, Peter G. Jones, and Peter Bubenitschek

We recently reported the preparation and crystal structure of 1,1,4,4-tetra-***tert*-butyl-1,3-butadiene** (**1** in this note, compound **8** of the original publication[1]). The structure displayed unusual aspects such as a very wide C1-C2-C2′ angle [142.2(2)°] and equal bond lengths in the butadiene chain (C1–C2 134.6(2), C2–C2′ 135.3(4) pm). For this reason a referee requested us to check the structure carefully for possible errors. However, we could find no obvious signs of serious basic errors: low temperature measurements had led to a conventional *R*-value of 0.061; there were no regions of significant residual electron density (max. 267 e nm^{-3}) and no unusually large displacement parameters (e.g., U_{eq} 456 pm^2 for C2; see footnote [4] in Ref. [1]).

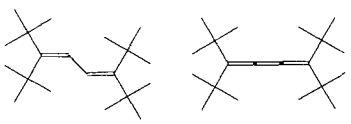

1 **2**

Since the appearance of our article, many colleagues have again asked us whether the structure analysis is reliable. In retrospect the equal bond lengths did indeed appear suspicious to us, although the wide angles could conceivably have been the result of steric effects. We therefore decided to repeat the structure with a new sample of **1**.[2]

The new structure (Fig. 1) displays the expected alternating bond lengths in the butadiene chain [C1–C2 134.9(2), C2–C2′ 145.8(3) pm], and the angle C1-C2-C2′ is at 131.1(2)° not as markedly widened. It is therefore clear that the original structure determination was incorrect. The probable cause is the contamination of the first crystal (which unfortunately was not preserved and thus could not be subjected to spectroscopic checks) by a significant amount of the cumulene **2** (compound **9** in the original), which was formed as a by-product in all preparations of **1**. The new crystal was taken from a sample that had been scrupulously checked for purity. In addition, no traces of impurity could be detected in the measured crystal by NMR spectroscopy and gas chromatography.

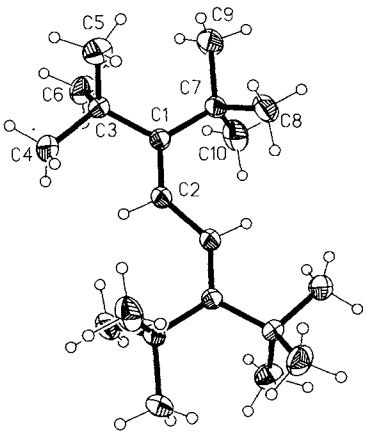

Fig. 1. The revised structure of **1** in the crystal. Ellipsoids correspond to 50% probability levels. Hydrogen radii are arbitrary. Only the asymmetric unit is numbered.

This case shows that unsuspected disorder phenomena can lead to totally incorrect results even when a structure determination appears satisfactory.

Received: December 18, 1995

[*] Prof. Dr. H. Hopf, Dipl.-Chem. R. Hänel, Dipl.-Chem. P. Bubenitschek
Institut für Organische Chemie der Technischen Universität
Hagenring 30, D-38106 Braunschweig (Germany)
Fax: Int. code +(531)391-5388
Prof. Dr. P. G. Jones
Institut für Anorganische und Analytische Chemie der Technischen Universität Braunschweig

[**] We thank Ina Dix for the new data collection.

[1] H. Hopf, R. Hänel, P. G. Jones und P. Bubenitschek, *Angew. Chem.* **1994**, *106*, 1444–1445; Angew. Chem. Int. Ed. Engl. **1994**, *33*, 1369–1370.
[2] Crystal data for **1**: $C_{20}H_{38}$, triclinic, $P\bar{1}$, $a = 608.93(12)$, $b = 825.4(2)$, $c = 1022.4(2)$ pm, $\alpha = 76.496(12)$, $\beta = 85.998(14)$, $\gamma = 70.587(14)°$, $T = -100$ °C, $Z = 1$. The cell constants are significantly different from those in Ref. [1]. Refinement on F^2 [3] led to $wR_2 = 0.149$, $R_1 = 0.053$, $\Delta\rho_{max.}$ 196 e nm^{-3}, $S = 0.94$ for 2129 reflections and 97 parameters. The displacement parameters, particularly those of C2 ($U_{eq} = 261$ pm^2), were appreciably smaller than in Ref. [1]. Further details can be obtained from the Fachinformationszentrum Karlsruhe, D-76344 Eggenstein-Leopoldshafen (Germany), quoting the deposition number CSD-400686.
[3] SHELXL-93, A Program for Refining Crystal Structures: G. M. Sheldrick, Universität Göttingen, **1993**.

Once Exotic, Now Essential

Transition Metal Chemistry. By *M. Gerloch* and *E. C. Constable*. VCH Verlagsgesellschaft, Weinheim/VCH Publishers, New York, 1994. 211 pp., hardcover DM 128.00/XI $ 75.00; paperback DM 58.00/$ 35.00.—ISBN 3-527-29218-7/1-56081-885-9

Brief, concise, and yet fundamental introductions to scientific fields are welcomed not only in education, but also in research, because it has become increasingly interdisciplinary. Although abundant in the periodic system, the transition metals have frequently been regarded as rather "exotic" elements; however, increasing knowledge of their chemistry has turned out to be very useful for furthering progress in the areas of organic chemistry (synthetic methodology, supramolecular compounds), chemical technology (catalysis), biochemistry ("bioinorganic" chemistry) as well as physical chemistry and physics (optical and magnetic properties).

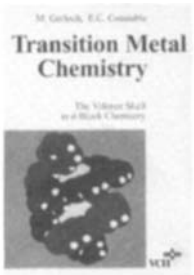

The book by *Gerloch* and *Constable* contains a well readable and succinct description of the structural and electronic properties of transition metal complexes, the theoretical–mathematical treatment being kept to a minimum. As the authors admit, the actual "chemistry" (e.g. reactivity) receives less consideration in comparison to spectroscopic and structural aspects, and for the training of chemists the book will have to be supplemented accordingly. The text is, however, well suited for interested researchers from other areas.

The problem of starting with highly symmetrical compounds as primary, "simple" examples without completely losing the relation to the more complex everyday systems has been adequately solved by the authors. Unfortunately, compounds of the 4d and 5d transition metals are mentioned only sporadically. Yet these compounds have received more attention in recent research than the lighter (3d) transition metals which are predominantly featured in this book.

After an elementary introduction (including the notorious 3d/4s problem) the following 55 pages contain a well-presented description of crystal field theory and the correlation of optical spectra with d-electron configurations. After what is probably the best chapter, "Spin and Magnetism", ligand field theory and the concept of back-bonding are introduced by using the molecular orbital approach. Correlations between structure and d^n configuration as rationalized by perturbation theory are described in a further chapter in which square-planar d^8 systems and the Jahn–Teller effect receive comprehensive treatment.

The next chapter concerns thermodynamic properties such as complex stabilities (including a nonkinetic representation of the chelate effect) and the classical manifestations of crystal field stabilization energy. The penultimate chapter introduces less stringent but unavoidable concepts like the 18-electron rule, the "hard/soft" concept, and the stability of oxidation states, followed by a rather short section on the reactivity of simple complexes. The last, brief chapter is dedicated to the lanthanoid elements.

When a directly accessible albeit comprehensive description is attempted within a limited space, it is inevitable that many questions remain open and alternative examples come to mind. The charge transfer phenomenon, for example, is described on page 114 in such an abstract way that the nonexpert cannot understand why Mn^{VII} compounds are colored. On page 168 it could have been easily explained *why* Co^{II} tends to form tetrahedral complexes. The lanthanoid element chapter could have profited if ground and excited states of NMR shift reagents had been used as examples and, more generally, practical aspects are hardly covered. Neither the repeatedly emphasized use of the model by *Kepert* to explain structural preferences nor the strict classification of low, intermediate, and high oxidation states with different functions of the d electrons and binding characteristics seem to be compelling to this reviewer.

Factual errors and misprints in the text are rare ("Frank–Condon", p. 32; "coordninates", p. 69) but unfortunately the first citation of one of the author's (M. G.) articles in the preface is incorrect (p. 117 instead of p. "199"). Other errors concern the Laporte rule (transitions between orbitals or states of different parity are *allowed* and not "forbidden", p. 64), and $Ru(bpy)_3^{3+}$ is certainly not a "labile" complex (p. 190).

Two aspects of the book warrant more severe critism: Several figures are of low quality, e.g. absorption spectra and functions drawn by shaky hand on pages 22, 143, or 199. Secondly, the few references are of little help: In addition to citing their own previous books and articles (which, for a considerable part, serve as components of this book), the authors have restricted themselves largely to the classical literature from their own impressionable years; about half of the "further reading" material is more than 25 years old!

Despite these two irritating aspects, the book is excellently suited as an introduction to the realm of transition metal complexes. Its strong point is the step-by-step approach in the interpretation of spectra, magnetism, and structure which does not overburden the reader with mathematical equations and formalisms. Considering the price of this text, students as well as interested researchers from neighboring fields will be able to use it for increasing their knowledge in an enjoyable way.

Wolfgang Kaim
University of Stuttgart (Germany)

This section contains book reviews and a list of new books received by the editor. Book reviews are written by invitation from the editor. Suggestions for books to be reviewed and for book reviewers are welcome. Publishers should send brochures or (better) books to Dr. Illenora Beckmann, Redaktion Angewandte Chemie, Postfach 101161, D-69451 Weinheim, Federal Republic of Germany. The editor reserves the right of selecting which books will be reviewed. Uninvited books not chosen for review will not be returned.

 © *VCH Verlagsgesellschaft mbH, D-69451 Weinheim, 1996* *0570-0833/96/3502-0223 $ 10.00+.25/0*

Stereocontrol in Organic Synthesis Using the Diphenylphosphoryl Group

Jonathan Clayden* and Stuart Warren

In 1959, Horner showed that metalated alkyldiphenylphosphane oxides react with aldehydes or ketones to give alkenes. With this reaction, the diphenylphosphoryl (Ph_2PO) group made its entrance into synthetic organic chemistry. In the thirty-six years since that date, extensive research has shown that this olefination, the Horner–Wittig reaction, has unique properties that make it much more than simply the phosphane oxide cousin of the more famous phosphorus-based olefinations—the Wittig reaction (based on phosphonium salts) and the Wadsworth–Emmons reaction (based on phosphonate esters). Early work on the Horner–Wittig reaction concentrated on the reactivity of phosphane oxides and the regioselectivity of their reactions, but more recently the power of the Ph_2PO group to control the stereochemistry of alkenes, and to produce "on demand" either stereoisomer in high stereochemical purity, has emerged. From the study of these stereocontrolled Horner–Wittig reactions arose the realization that the Ph_2PO group is useful not only for the control of the two-dimensional stereochemistry of alkenes, but also of three-dimensional stereochemistry in general.

After a brief introduction to phosphane oxide chemistry, this review will examine the Horner–Wittig reaction, in both its original and "stereocontrolled" varieties. From there, we will move on to an account of the stereoselective construction of molecules containing the Ph_2PO group, concentrating on the stereochemical directing effects of the Ph_2PO group and on the role of its unique combination of attributes—steric bulk, electronegativity, and Lewis basicity—in controlling these reactions. Finally, we will present what is intended as a practical guide to this chemistry, covering the type of functionalized alkenes that have been made with the help of the Ph_2PO group and giving guidelines that we hope will help the organic chemist to make the most of the chemistry the Ph_2PO group has to offer.

Keywords: alkenes · asymmetric syntheses · Horner–Wittig reactions · phosphane oxides · synthetic methods

1. Introduction

Horner's first olefinations with phosphane oxides[1–3] were carried out by metalating benzyldiphenylphosphane oxides **1** (R^1 = Ar) with a potassium base (KO*t*Bu) and then adding an aldehyde or a ketone to give an alkene in one step (Scheme 1).

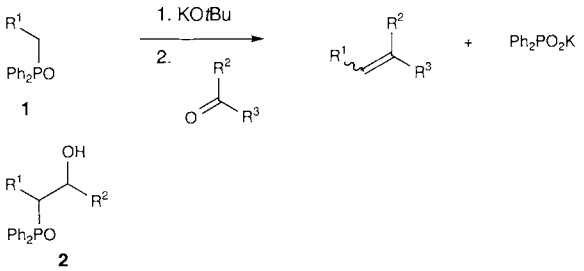

Scheme 1. Horner's olefination with phosphane oxides.

[*] Dr. J. Clayden
Department of Chemistry, University of Manchester
Oxford Road, GB-Manchester M13 9PL (UK)
Fax: Int. code +(161)275-4598
e-mail: j.p.clayden@man.ac.uk
Dr. S. Warren
University Chemical Laboratory
Lensfield Road, GB-Cambridge CB2 1EW (UK)

With lithium bases, however, the reaction did not give the alkene, but stopped at an intermediate adduct **2**.[1–4] These β-hydroxy phosphane oxide intermediates are generally quite stable even at 20 °C, and it is their existence as normal, isolable, and usually crystalline compounds that underlies the degree of control the chemist can exert over the Horner–Wittig reaction when compared with its Wittig[5–7] and Wadsworth–Emmons[7, 8] analogues. As we shall see, our ability to reach right into the center of the Horner–Wittig reaction, adjusting stereochemistry and conditions to favor the required stereoisomer, compares with the fine adjustments a mechanic might make to the engine of a car. In contrast, stereochemical control in the Wittig or Wadsworth–Emmons reactions seems more like pressing buttons on the dashboard or choosing what is to be put in the fuel tank.

We will refer only rarely to the Horner–Wittig *reaction*, but rather more often to its two synthetically separable mechanistic components, the Horner–Wittig *addition* of a lithiated alkyldiphenylphosphane oxide to an aldehyde, and the Horner–Wittig *elimination*, the concerted extrusion of diphenylphosphinic acid from a β-hydroxy phosphane oxide (Scheme 2). Many Horner–Wittig eliminations we will discuss will not be from β-hydroxy phosphane oxides made directly by Horner–Wittig additions. Any reaction sequence leading to an alcohol

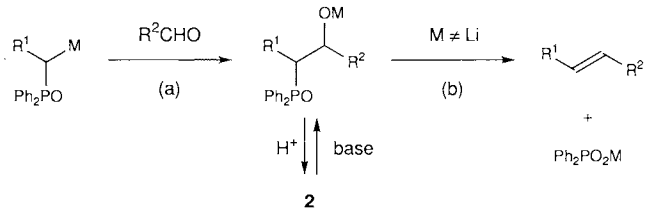

Scheme 2. The Horner–Wittig reaction; a) Horner–Wittig addition, b) Horner–Wittig elimination.

bearing a β-Ph_2PO group can be used to make a Horner–Wittig intermediate, and it is on the stereochemical control inherent in these reactions, often directed by the unique properties of the Ph_2PO group, that we will concentrate.

The usefulness of the Ph_2PO group in synthesis derives not just from the stereoselectivity of the reactions of phosphane oxides. Compounds containing the Ph_2PO group are very often crystalline. This property is important for the synthetic application of stereoselective reactions because it allows the separation and purification of stereoisomers by crystallization.[9] Because of the electronegativity of the Ph_2PO group, its stereochemical disposition relative to other polar groups in a molecule dominates the overall polarity of the molecule. This aids greatly the separation of diastereomers by flash chromatography.[9]

The anion-stabilizing ability of the Ph_2PO group makes compounds containing it easy to build. Complicated structures can be built up rapidly by metalation and alkylation, hydroxyalkylation, or acylation of simple alkyldiphenylphosphane oxides. The most common methods for making the starting materials for such a sequence are shown in Equations (a)–(e) in Scheme 3: a) nucleophilic displacement with triphenylphosphane followed by hydrolysis of the phosphonium salt,[9] b) nucleophilic displacement with lithium diphenylphosphanide followed by oxidation of the phosphane,[10–12] c) the Arbuzov reaction,[13, 14] d) phosphorylation of an organometallic compound by Ph_2POCl, and e) (for allylic phosphane oxides) the Arbuzov rearrangement.[15] They have also been made by addition of a phosphorus nucleophile to aldehydes[16] and by Wittig reaction of cyclic phosphonium salts.[17–22] Clearly these methods can also be used at a later stage in a synthesis to introduce the Ph_2PO group to a well-developed carbon skeleton.[11, 23, 24]

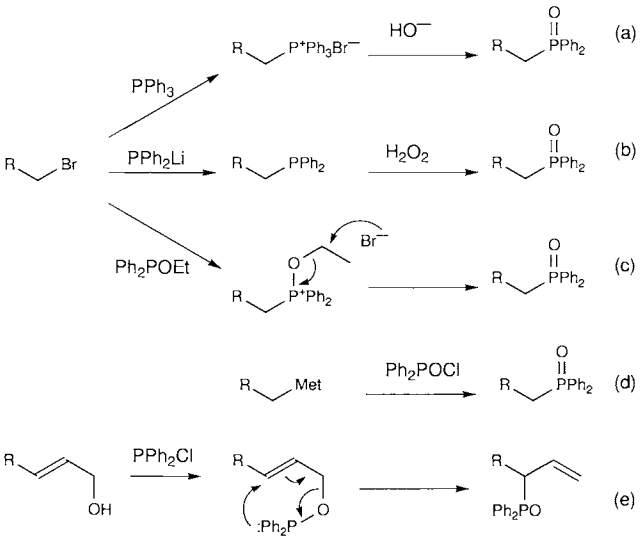

Scheme 3. Methods for making simple phosphane oxides.

Structure **3** illustrates the way we will refer to the chiral centers and substituents in an elaborated phosphane oxide. The two chains on the carbon atom bearing the Ph_2PO group are distinguished by the presence of the hydroxyl group that will ultimately undergo Horner–Wittig elimination, and the Greek letters denote the positions relative to the phosphorus atom.

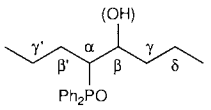

3

2. Two-Dimensional Stereocontrol with the Ph_2PO Group: The Horner–Wittig Reaction

The chemistry of the diphenylphosphoryl group is well suited for syntheses of molecules containing C=C bonds. Early work in this area concentrated on the connective and regioselective aspects of such syntheses, but more recently the power of the Ph_2PO group to control the two-dimensional stereochemistry of alkenes, and to produce either stereoisomer in high geometrical purity, has emerged. The stereochemical control offered by the Ph_2PO group is in fact only a special case of the three-dimensional stereocontrol we will examine in detail Section 3.

Jonathan Clayden was born in 1968 in Kampala, Uganda, and brought up in Bradwell-on-sea on the east coast of Essex (UK). In 1989 he gained a degree in chemistry from the University of Cambridge. He remained in Cambridge to carry out research on phosphane oxides under the direction of Dr. Stuart Warren, leading to a Ph.D. in 1992. He then moved to Paris, spending 18 months in the laboratories of Prof. Marc Julia at the École Normale Supérieure, where he worked on transition metal catalyzed reactions of sulfones. In 1994 he was appointed as a Lecturer in the Department of Chemistry of the University of Manchester. His research interests include stereoselectivity in organic reactions and organo-main group chemistry. He lives in Manchester with his wife and son.

2.1 The One-Step Horner–Wittig Reaction

Metalated alkyldiphenylphosphane oxides **1** bearing certain functional groups in the α position (R^1 = benzyl,[4, 25] allyl,[10, 12, 26–31] CN,[32] isoxazole,[33] NR_2,[14] OR,[34, 35] SR[36]), can undergo a "one-step" Horner–Wittig reaction with aldehydes or ketones like that shown in Scheme 1. Horner–Wittig elimination follows directly after Horner–Wittig addition without isolation of an intermediate. These reactions have been widely used by Lythgoe et al.[10, 26, 37] and others[29–31] in syntheses of vitamin D and its analogues. The penultimate step of the synthesis of milbemycin β_3 by Smith et al.[38] is an important recent example (Scheme 4).

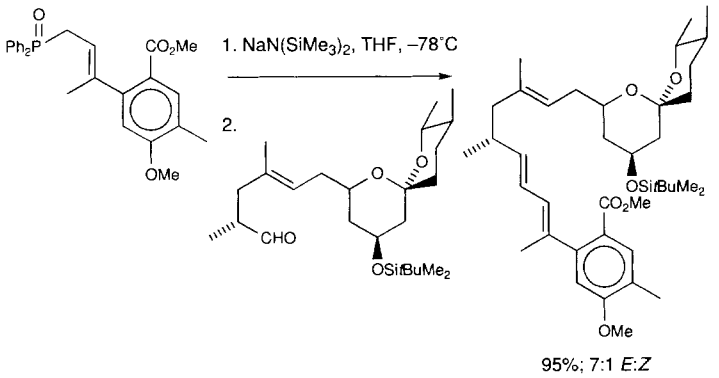

Scheme 4. Part of the synthesis of milbemycin β_3 by Smith et al.

One-step Horner–Wittig reactions are usually (*E*)-selective, like the corresponding Wadsworth–Emmons reactions (Scheme 5).[7] The metalated Horner–Wittig adduct decomposes easily in these one-step reactions because R^1 provides conjugation or stabilization of the negative charge and lowers the activation energy for the elimination. The (*E*) stereoselectivity is almost certainly a result of the reversibility of the addition to a carbonyl group of an alkyldiphenylphosphane oxide bearing an additional anion-stabilizing group. This reversibility allows interconversion of the two diastereomers of the adducts, and faster elimination from the *syn* adduct means that the (*E*) isomer of the product alkene is formed selectively (Scheme 5). Vedejs[5] has challenged an analogous explanation for the (*E*) selectivity of Wittig olefinations of stabilized phosphonium ylides, as he doubts the existence of the intermediate betaines. In the Horner–Wittig reaction the "betaines" are formed—they can

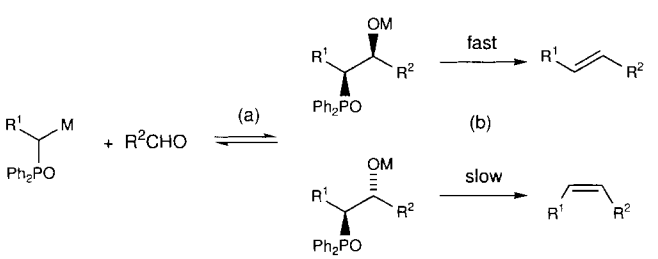

Scheme 5. The (*E*)-selective one-step Horner–Wittig reaction; a) reversible when R^1 is anion-stabilizing, b) reaction rates increase when R^1 is anion-stabilizing or conjugating. In this and all subsequent schemes only relative configurations will be shown (except in Sections 3.3.2, 3.3.3, and 4.5).

be isolated—so there is no reason to rule out this explanation. Indeed, treatment of the Horner–Wittig adduct *anti*-**6** with NaH/DMF gave a mixture of starting phosphane oxide **4** and alkene (*E*)-**5**, proving that equilibration can occur during the elimination: stereospecific elimination directly from *anti*-**6** would give (*Z*)-**5**.[33]

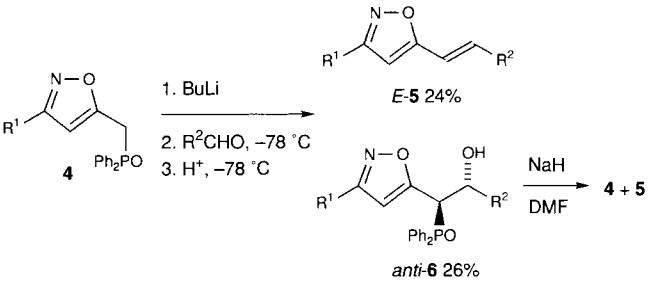

Many of these one-step reactions have direct analogues in the Wittig and Wadsworth–Emmons series, and do not specifically make use of some of the properties more particular to the Ph_2PO group. In many of the cases in which the one-step Horner–Wittig reaction has been used in a synthetic route, the phosphane oxide variant was chosen simply because it performed better than the alternatives.[35, 37, 39] An advantage that the Horner–Wittig reaction shares with the Wadsworth–Emmons is the water-solubility of the elimination by-product, a diphenylphosphinate salt. A common practical problem with the Wittig reaction is the removal of its elimination by-product, triphenylphosphane oxide, from the desired alkenes. With the Horner–Wittig reaction a simple aqueous wash suffices.

2.2. The Two-Step Horner–Wittig Reaction

For the reactions described in Section 2.1 and summarized in Scheme 5, both Horner–Wittig addition of the lithiated phosphane oxide to the aldehyde and the reverse reaction are fast, as is the sterically preferred Horner–Wittig elimination of lithium diphenylphosphinate from the *syn* adduct to give an (*E*) alkene. For simple, "unstabilized" lithiated phosphane oxides, however, this is not the case. Neither the reverse reaction nor the elimination takes place when R^1 = alkyl or H, and aqueous quenching of a Horner–Wittig reaction mixture at 0 or at 20 °C gives not an alkene but a stable, often crystalline, β-hydroxy phosphane oxide.[9] Even the Horner–Wittig adducts from stabilized lithium derivatives of phosphane oxides **1** (R^1 = benzyl,[9, 25] allyl,[40–42] isoxazole,[33] NR_2,[39, 43] OR,[44, 45] SR[46]) can be isolated before elimination if conditions are adjusted carefully (e.g. adducts **2** of benzyldiphenylphosphane oxide **1** (R^1 = Ph) must be quenched below −50 °C).[25] Crucial to this control is the use of a lithium base: the lithium counterion binds strongly to the oxyanion formed in the reaction and prevents it from attacking the electrophilic Ph_2PO group. This unique attribute of the phosphane oxides, which distinguishes them from their phosphonium and phosphonate analogues, permits the synthesis of alkenes of very high stereochemical purity. The diastereomers of the Horner–Wittig adduct **2** (typically formed

in a ratio of 85:15 *anti*:*syn*) are usually easily separated by flash chromatography or by crystallization.[9] Treatment of each pure diastereomer with a sodium or potassium base in a dipolar aprotic solvent (usually NaH in dimethylformamide (DMF), or KOH in dimethyl sulfoxide (DMSO)),[47] which generates a much more nucleophilic oxyanion, then leads stereospecifically[47] to a single stereoisomer by *syn* elimination of sodium or potassium diphenylphosphinate.[9, 20, 48, 49] We call this stepwise sequence (Horner–Wittig addition, purification of the intermediate, and Horner–Wittig elimination) the "stereocontrolled Horner–Wittig Reaction"[9] (Scheme 6).

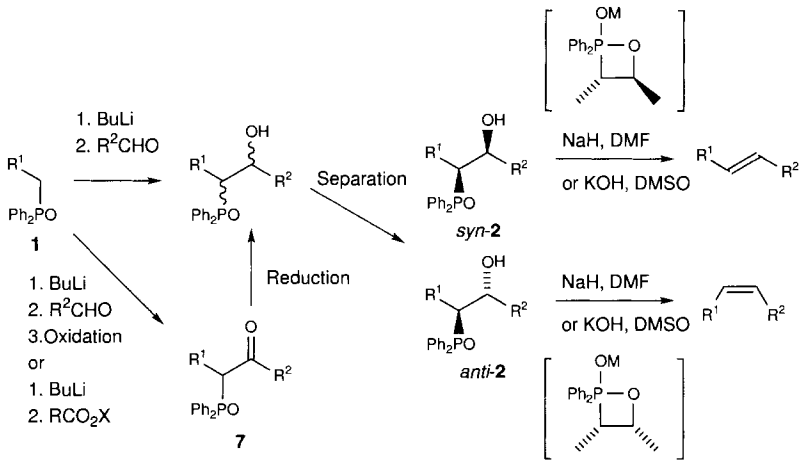

Scheme 6. The stereocontrolled Horner–Wittig reaction.

Because of the *anti* selectivity of the Horner–Wittig addition (the diastereomers *anti*-**2** can usually be isolated in pure form in 60–80% yield) this route is usually suitable only for the synthesis of (*Z*) alkenes. The practical synthesis of (*E*) alkenes by the Horner–Wittig elimination requires a high-yielding route to the *syn* diastereomer *syn*-**2**.[50] The usual approach[9, 13, 51] makes use of a β-oxo phosphane oxide **7**, easily prepared by acylation of an alkyldiphenylphosphane oxide or by oxidation of the mixture of diastereomers of the adduct **2** obtained from a Horner–Wittig addition. Reduction of the ketone **7** with $NaBH_4$ followed by purification generally returns the *syn* diastereomer of the adduct **2** in a yield of 80–95%.[9, 51]

The Horner–Wittig elimination from either *syn* or *anti* β-hydroxy phosphane oxides **2** is usually carried out with NaH/DMF or KOH/DMSO. During the reaction with NaH/DMF a thick, feathery precipitate of sodium diphenylphosphinate is usually formed. Recent results suggest that KOH/DMSO is marginally preferable in some cases, as it can reduce the formation of by-products (e.g. from fragmentation reactions[52]) and increase the stereospecificity of the elimination.[42]

The relative stereochemistry of the Horner–Wittig adducts **2**, and hence the *syn* specificity of the elimination, has been confirmed by X-ray crystallography. Clear differences in the NMR spectra of the *syn* and *anti* diastereomers of **2** allow reliable stereochemical assignments to be made by inspection of the NMR spectra of other compounds.[47] The elimination is, in general, 100% stereospecific, giving pure (*Z*) alkenes from pure *anti* β-hydroxy phosphane oxides, and pure (*E*) alkenes from pure *syn* β-hydroxy phosphane oxides. This stereospecificity is compromised only if R^1 of **2** is a conjugating or anion-stabilizing group, in which case the increased rate of Horner–Wittig reverse reaction of *anti*-**2** may allow "stereochemical leakage" to produce some of the more rapidly eliminating *syn* diastereomer, and hence the (*E*) alkene.[9, 25]

3. Three-Dimensional Stereocontrol with the Ph_2PO Group

We have already seen that β-hydroxy phosphane oxides are stable, often crystalline, compounds. This fact, along with the stereospecificity of the Horner–Wittig elimination, means that any stereoselective route to a β-hydroxy phosphane oxide can lead to a pure stereochemically defined alkene. With this in mind, a wide variety of reactions have been examined in which the Ph_2PO group directs the stereoselective construction of an adjacent hydroxyl-carrying center, often over several steps of a synthesis. This work led to the idea that the Ph_2PO group is useful not just for the control of the stereochemistry of double bonds, but also in the stereoselective construction of chiral centers in general. Section 3 will expand this idea, and demonstrate that the stereochemical influence of the Ph_2PO group in a molecule can reach far beyond just an adjacent hydroxyl-carrying carbon atom, and that Ph_2PO chemistry can therefore form the basis for the stereoselective synthesis of molecules in which three-dimensional as well as two-dimensional stereocontrol is required.

The stereochemical control exerted by the Ph_2PO group can be rationalized in terms of its three important attributes: its size, its electronegativity, and its ability to participate in hydrogen bonds and Lewis acid/base complexes.

3.1. Addition Reactions of Lithiated Alkyldiphenylphosphane Oxides

The anion-stabilizing ability of the Ph_2PO group permits easy α metalations, and the reaction of an α-lithiated alkyldiphenylphosphane oxide with a carbonyl electrophile is often stereoselective, making it a valuable method for the construction of molecules containing the Ph_2PO group.

3.1.1. The Structure of Lithiated Alkyldiphenylphosphane Oxides

To explain the reactions of lithiated phosphane oxides, we need to consider their structure. Ab initio calculations suggest that, in THF solution, lithiated alkyldiphenylphosphane oxides contain four-membered P-C-Li-O rings as the monomeric unit, complexed with one or two THF molecules: structure **8** is proposed for the lithiated methyldiphenylphosphane oxide.[53]

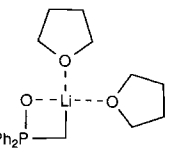

8

Recent work[54a] has shown that lithiated phosphane oxides are not configurationally stable about a stereogenic carbon atom bearing phosphorus and lithium.

For example, when enantiomerically pure (>95% *ee*) phosphane oxide **9** was treated with BuLi or lithium diisopropylamide (LDA) at −78 °C and quenched with a variety of electrophiles under Grignard or Barbier conditions, the products **10** were all racemic. Vedejs and Garcia-Rivas[55] have reported that benzylic phosphane oxides **11** can be lithiated and then quenched with chiral proton sources to return the starting phosphane oxides with very high enantiomeric excesses.

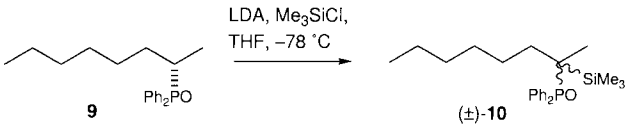

9 (±)-**10**

11

3.1.2. Additions to Aldehydes and Ketones: The Horner–Wittig Addition

As we mentioned in Section 2.2, the Horner–Wittig addition usually produces preferentially the *anti* diastereomer of the product alcohol. Table 1 lists the stereoselectivities obtained in some representative Horner–Wittig additions of phosphane oxides **12** to aldehydes and ketones. If we take the selectivity shown in entries 1–5 (about 85:15) as the standard, we can say that the *anti* selectivity is 1) fairly independent of R^2, but reduced slightly if R^2 is very large (entry 6) or very small (entries 7, 8), 2) reduced significantly if R^1 is large (entries 9–12), 3) reduced significantly if R^1 carries a functional group capable of complexing lithium (entries 13–18), and, in a special case of this situation, 4) inverted, giving excellent *syn* selectivity, if the complexing group contains a lithiated nitrogen atom (entry 19).

Secondary phosphane oxides **12** ($R^3 \neq H$) react with low stereoselectivity (entry 20); similarly, additions to ketones ($R^4 \neq H$) are unselective (entry 21) unless there is a very large size difference between the two groups R^2 and R^4 (entry 22).

The model we now favor for the transition state of the Horner–Wittig reaction helps understand these observations. Ab initio calculations on the reactive complex formed between uncomplexed $LiCH_2P(O)H_2$ and H_2CO, coupled with the understanding we have gained from structural studies on lithiated alkyldiphenylphosphane oxides, suggest that the reaction passes through a butterfly-shaped transition state structure **14**.[53] Both R^1 and R^2 occupy the less sterically demanding *exo* positions, hence the *anti* selectivity. Increasing the bulk of R^1 increases the steric interaction between R^1 and R^2, and between R^1 and the *exo* phenyl ring. R^1 then tends to flip to the pseudoequatorial *endo* position, leading to the observed drop in *anti* selectivity with branched R^1 substituents. For R^2 the pseudoequatorial *exo* position and the pseudoaxial *endo* position

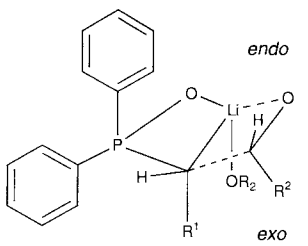

14 R_2O = THF

Table 1. Horner–Wittig additions.

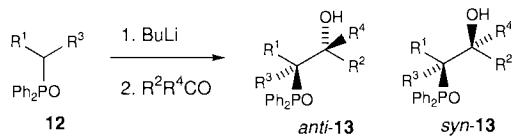

12

Entry	R^1	R^2	R^3	R^4	Yield[%]	*anti*:*syn*	Ref.
1	Me	Ph	H	H	88	88:12	[9]
2	Et	Ph	H	H	86	85:15	[9]
3	Bu	Ph	H	H	84	84:16	[9]
4	*i*Bu	Ph	H	H	81	80:20	[9]
5	Ph	Ph	H	H	88	83:17	[9]
6	Me	C_6H_{11} [a]	H	H	86	79:21	[9]
7	Me	Me	H	H	93	75:25	[9]
8	Ph	Me	H	H	97	72:28	[9]
9	*i*Pr	*n*Pr	H	H	84	57:43	[82]
10	*i*Pr	Ph	H	H	79	67:33	[82]
11	C_6H_{11} [a]	*n*Pr	H	H	100	53:47	[82]
12	C_6H_{11} [a]	Ph	H	H	80	80:20	[82]
13	OMe	*n*-C_6H_{13}	H	H	79	50:50	[44]
14	$(CH_2)_2OSiMe_2tBu$	Et	H	H	–	50:50	[75]
15	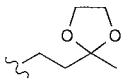	Pr	H	H	67	69:31	[117]
16	$(CH_2)_2OLi$	Ph	H	H	–	75:25	[62, 75]
17	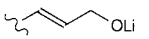	Et	H	H	59	60:40	[42]
18	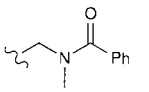	Me	H	H	68	55:45	[60]
19	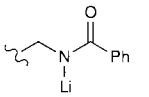	Ph	H	H	80	5:95	[60]
20	$(CH_2)_2Ph$	Me	Me	H	81	47:53	[63]
21	CH_2Ph	Et	H	Me	79	53:47	[63]
22	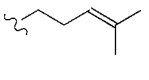	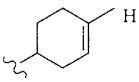	H	Me	57	98:7	[63]

[a] Cyclohexyl.

(which suffers from strong 1,3-diaxial interactions with the *endo* phenyl ring) are much more clearly differentiated, and, in almost every case, R^2 will prefer the *exo* face. Only very small R^2 groups can occupy the *endo* position, lowering the *anti* selectivity. Very large R^2 groups may lower *anti* selectivity by forcing R^1 to take the *endo* position. The low selectivity with unsymmetrical ketones and secondary alkyldiphenylphosphane oxides results because at least one alkyl group must be *endo*. The decrease in selectivity in the presence of coordinating functional groups is harder to explain quantitatively: clearly coordination of these groups to the lithium atom in the reacting complex changes the structure of the complex and therefore necessarily the stereochemical outcome of the reaction.

With a few notable exceptions, preexisting chiral centers in either the phosphane oxide or the aldehyde exert little chiral induction over the formation of the new C–C bond and the two new chiral centers. For example, additions of lithiated **15**,[42] **16**,[56, 57] **17**,[58] and **18**[57] to aldehydes generally give all four

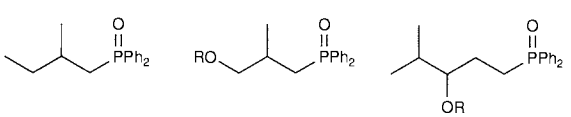

15 **16** **17**

possible diastereomers in more or less equal quantities. On the other hand, **18** gives only one diastereomer of the products **19** and **20** on lithiation and addition to cyclohexanone and Me_3SiCl, respectively.[58, 59] A β-LiO group induces weak *anti*

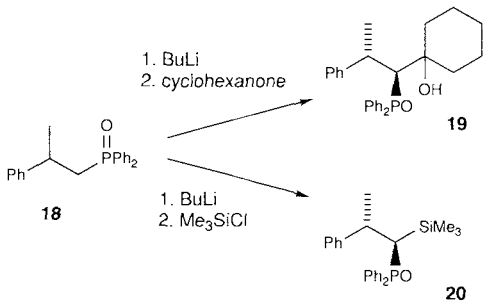

selectivity across the existing C–C bond and reduces the *anti* selectivity in the formation of the new C–C bond to about 70:30. As an example, lithiated **21** reacts with acrolein, and lithiated **23** with propionaldehyde, to give products **22** with about the same diastereomeric distribution.[42] A β-amido group has a similar effect;[60] addition of lithiated **24** to acrolein gives predominantly the *anti* diastereomers of **25**.[52] Control of this chiral center in the β' position is achieved more reliably by acyl transfer (Section 3.1.4) or by alkylation of Ph_2PO-lactones (Section 3.3.5).

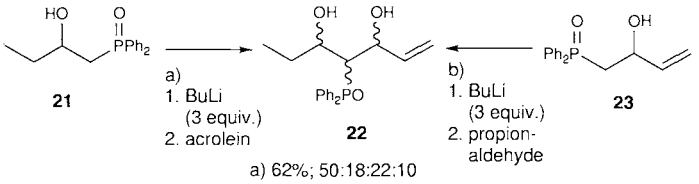

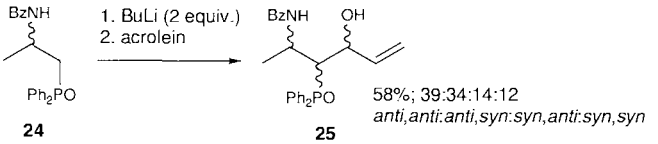

Ketones bearing chiral auxiliaries have been used to prepare optically active functionalized phosphane oxides.[54b] For example, lithiation of methyldiphenylphosphane oxide with MeLi/LiBr in toluene and addition to the chiral ketones **26** (R = Me, Ph) gave the adducts **27** as an 85:15 mixture of diastereomers. Separation and hydrolysis yielded **28** with >97% *ee*. An alternative procedure with THF as the solvent gave a 35:65 mixture of diastereomers; here the sense of the induction is reversed by disruption of the chelation presumed responsible for the selectivity in toluene.

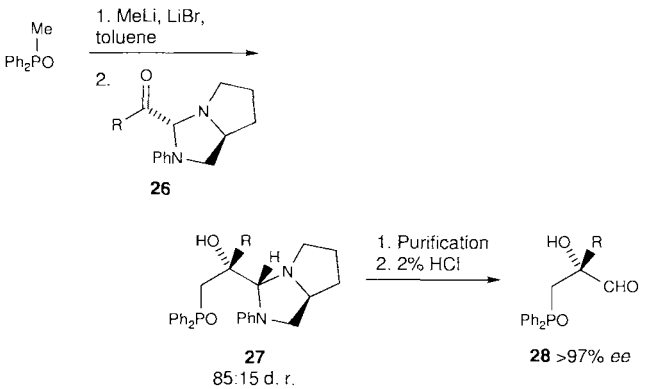

3.1.3. Acylation with Esters, Lactones, Acyl Chlorides, and Acid Anhydrides

The β-oxo phosphane oxides **7**, which are formed by acylation of an alkyldiphenylphosphane oxide, are important starting materials for the stereoselective additions and reductions described in Section 3.2. The cleanest acylations are achieved by reacting the lithiated phosphane oxide with an acid anhydride, an ester,[61] or a lactone,[40, 58, 62, 63] or by reacting a copper derivative with an acid chloride.[64] As only one chiral center is formed in these reactions, the question of stereocontrol does not usually arise. Interestingly, however, phosphane oxide **18** can be acylated stereoselectively with ethyl benzoate;[58] the major diastereomer of the product **29** is dependent on the temperature

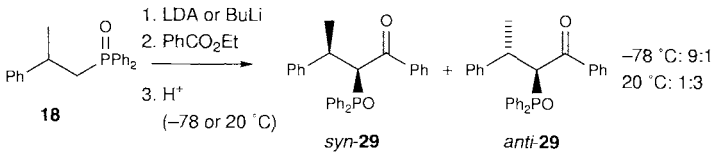

at which the reaction is quenched.[58, 65] Low-temperature quenching returns the kinetic product, while, at higher temperatures the thermodynamic product is produced.

3.1.4. Intramolecular Acylation: The Acyl Transfer Reaction

Phosphane oxides can also be acylated intramolecularly. For example, treatment of the ester **30** with LDA gives the hydroxy ketone **31** in high yield.[66, 67] The reaction has been used as a

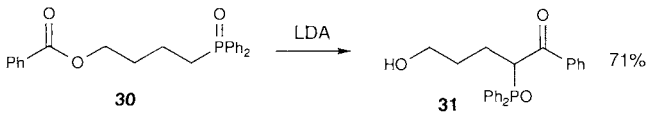

method for ring expansion,[68] but its stereoselective aspects are more important. In contrast to its intermolecular counterpart, intramolecular acylation is stereoselective for a range of substrates,[9, 58, 67, 69] allowing control of up to three chiral centers in one step. The cyclic transition state of the reaction means that preexisting chiral centers within the molecule have a powerful influence over the stereochemistry at the new carbon–carbon bond α to Ph_2PO, and the construction of chiral centers quite distant from the Ph_2PO group can be controlled.

Compounds **32**[66, 67] and **34**,[58] with chiral centers γ and β to phosphorus, respectively, undergo stereoselective 1,4 O→C acyl transfers to give only one diastereomer at the newly formed C–C bond (**33a**). In both cases the products exist partly as a mixture of the anomers of hemiacetals **33b** and **35**, respectively. In the analogous acyl transfer reaction of **36** internal trapping of the reaction's tetrahedral intermediate as **37** showed that it ex-

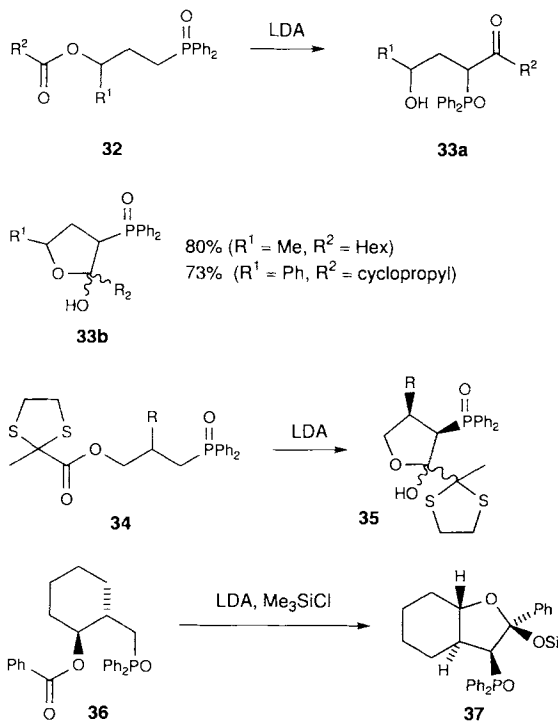

32 **33a** **33b** **34** **35** **36** **37**

ists as only one diastereomer, even at the anomeric center.[70] Thermodynamic equilibration to the mixture of hemiacetals (such as **33b** and **35**) must occur only later.

1,5 O → C Acyl transfer is also stereoselective for **38**, which has chiral centers γ and δ to phosphorus, but not for esters of **40**, with only a γ chiral center.[58] Conveniently, the acyl transfer product could be trapped as the oxo ester **39** by acylation with

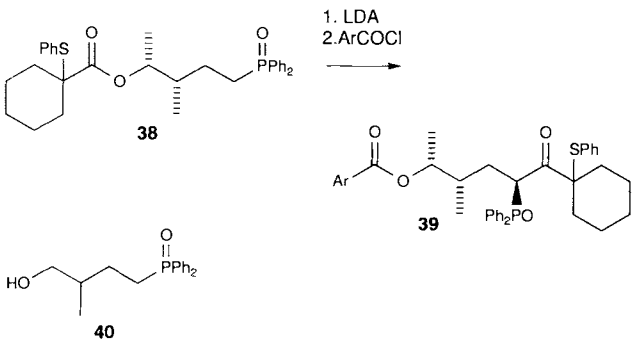

38 **39** **40**

2,4-dinitrobenzoyl chloride. Other attempts to avoid hemiacetal formation by protection of the hydroxyl group have not always been so successful.[71]

Acyl transfers are best with unenolizable esters and are low-yielding with α,β-unsaturated esters.[58, 72]

3.1.5. *Additions to Epoxides*

Lithiated alkyldiphenylphosphane oxides can be added to epoxides to give γ-hydroxy phosphane oxides in good yield. Thus, lithiated methyldiphenylphosphane oxide gives the adduct **41** in a reaction in which the stereochemistry is merely a consequence of the necessary inversion at the electrophilic center.[67] A new chiral center α to Ph_2PO may nonetheless also be introduced with excellent selectivity. While lithiated ethyldiphenylphosphane oxide gives a 50:50 mixture of the two diastereomers of **42**, reaction of lithiated ethyl- and propyldiphenylphosphane oxide with styrene oxide yields the diastereomers of **43** in ratios of 91:9 and >96:4, respectively.[67] High stereoselectivity is also obtained when ethyldiphenylphosphane oxide reacts with cyclic epoxides to give **44** and **45**.[73, 74]

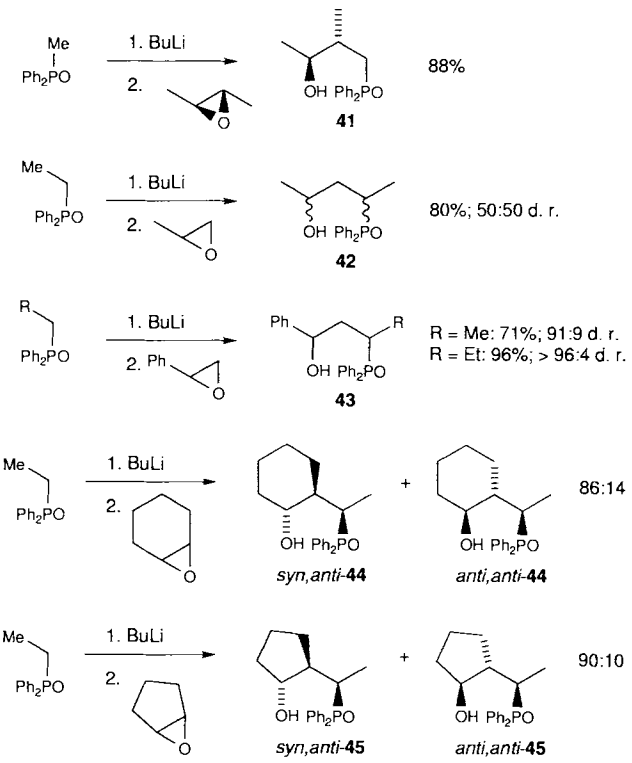

41 **42** **43** *syn,anti*-**44** *anti,anti*-**44** *syn,anti*-**45** *anti,anti*-**45**

3.2. Ph_2PO-Directed Addition to a Carbonyl Group

Section 3.1 concentrated on the stereocontrolled formation of carbon–carbon bonds where the Ph_2PO group was initially not at a chiral center. The new carbon–carbon bond was formed by using the anion-stabilizing ability of the Ph_2PO group, and the stereoselectivity derived from the size of the Ph_2PO group and from its ability to coordinate to a lithium atom through its oxygen atom. The next two sections will turn to the formation of new chiral centers directed by a preexisting chiral center bearing a Ph_2PO group. Section 3.2 will deal with stereocontrolled nucleophilic additions to carbonyl groups and Section 3.3 with stereocontrolled electrophilic additions to alkenes.

3.2.1. *Reduction of β-Oxo Phosphane Oxides*

As we saw in Section 2.2, the reduction of β-oxo phosphane oxides **46** (R^3 = H) by sodium borohydride is usually stereoselective, favoring formation of the *syn* isomer. Table 2 gives an outline of the dependence of this selectivity on the substitution pattern of the ketone. This selectivity is often higher, and less

dependent on the size or type of the substituents, than the complementary *anti* selectivity obtained in the Horner–Wittig addition. With unfunctionalized alkyl or aryl substituents at R^1 and R^2 the *syn* selectivity is usually of the order of 85:15 to 90:10 (entries 1–5), but the selectivity is reduced slightly if R^1 is very large (entries 6–9), particularly if R^2 is also small. The selectivity is also reduced if R^1 or R^2 contains a Lewis-basic functional group (other than hydroxyl) anywhere along the chain (entries 10–17). If R^1 contains a hydroxyl (or carboxyl) group, the *syn* selectivity is usually reduced (entries 18, 19), and the effect *increases* when the hydroxyl group is further from the Ph_2PO group (entries 20–23). For certain R^1 the selectivity may even be enhanced if the hydroxyl or carboxyl group is close (γ) to Ph_2PO (entries 18, 19). If R^2 contains a hydroxyl group, the *syn* selectivity is also reduced (entries 24–26). For ketones **46** derived from secondary phosphane oxides ($R^3 \neq H$), the selectivity is also lower (entry 28), though a γ-hydroxyl group can improve it significantly (entry 29).

Higher selectivities (practically 100%) are obtained by hydrogenation over PtO_2 or with some bulky hydrides, though the conversion is low.[9] Most other reducing agents tried (e.g. $Zn(BH_4)_2$, $LiBHEt_3$, $LiAlH_4$, and B_2H_6)[9, 69, 75] give products in lower yields or with lower selectivities.

Table 2. Borohydride reductions.

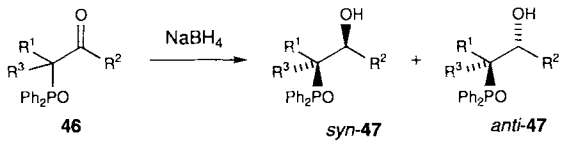

46 *syn*-**47** *anti*-**47**

Entry	R^1	R^2	R^3	Yield[%]	*syn*-**47**:*anti*-**47**	Ref.
1	Me	Ph	H	89	89:11	[51]
2	Me	C_6H_{11}[a]	H	87	91:9	[51]
3	Et	Ph	H	88	89:11	[51]
4	Bu	Ph	H	81	89:11	[51]
5	*i*Bu	Ph	H	77	89:11	[51]
6	*i*Pr	*n*Pr	H	71	54:46	[82]
7	*i*Pr	Ph	H	75	83:17	[51, 81]
8	C_6H_{11}[a]	*n*Pr	H	74	62:38	[82]
9	C_6H_{11}[a]	Ph	H	71	76:24	[81, 82]
10	$(CH_2)_2OSitBuPh_2$	Me	H	–	62:38	[75]
11	$(CH_2)_4OSitBuPh_2$	Me	H	–	48:52	[75]
12	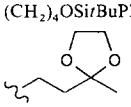	Me	H	91	78:32	[117]
13	Me	$(CH_2)_2OSitBuPh_2$	H	–	67:33	[75]
14	Me	$(CH_2)_4OSitBuPh_2$	H	–	71:29	[75]
15	Me	$(CH_2)_{10}OSitBuPh_2$	H	–	64:36	[75]
16	Me	$(CH_2)_4CO_2Me$	H	–	58:42	[119, 139]
17	Me	$(CH_2)_4CO_2H$	H	–	66:34	[119, 139]
18	$(CH_2)_2OH$	Ph	H	–	92:8	[66, 67]
19	CH_2CO_2H	*i*Pr	H	–	94:6	[95]
20	$(CH_2)_2OH$	Me	H	–	75:25	[66, 67]
21	$(CH_2)_3OH$	Me	H	–	64:36	[75]
22	$(CH_2)_4OH$	Me	H	–	63:37	[75]
23	$(CH_2)_{10}OH$	Me	H	–	37:63	[75]
24	Me	$(CH_2)_2OH$	H	–	65:35	[75]
25	Me	$(CH_2)_3OH$	H	–	74:26	[75]
26	Me	$(CH_2)_5OH$	H	–	74:26	[75]
27	Me	$(CH_2)_{14}OH$	H	–	52:48	[75]
28	$(CH_2)_2Ph$	Me	Me	98	67:33	[63]
29	$(CH_2)_2OH$	Ph	Me	–	80:20	[62, 67]

[a] Cyclohexyl.

The *syn* selectivity of the borohydride reduction is easily explained by a Felkin–Anh[76, 77] transition state structure **48**,[51] in which the large, electronegative Ph_2PO group occupies a position perpendicular to the carbonyl group; the larger of the two remaining groups, R^1, adopts the position furthest from R^2. Larger R^2 groups increase this preference, though larger R^1 groups have little effect unless, like *i*Pr, they rival Ph_2PO in angular bulk. Complexing functional groups can clearly modify the selectivity by favoring small changes in the structure of the transition state, but these effects (like those in the Horner–Wittig addition) are difficult to quantify.[62]

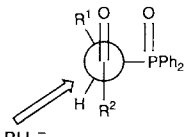

48

3.2.2. *Luche Reduction of β-Oxo Phosphane Oxides*

The presence of $CeCl_3$[78–80] can have dramatic and unexpected effects on the stereoselectivity of these reductions. Table 3 outlines the selectivities obtained in $NaBH_4/CeCl_3$ reductions of β-oxo phosphane oxides **7** and compares them with the selectivities for $NaBH_4$ reductions of the same compounds. In most cases, except those in which a further coordinating hydroxyl group in the molecule complicates the situation, the addition of $CeCl_3$ shifts the stereoselectivity towards the *anti* diastereomer of the product. When R^1 is a simple, unbranched alkyl group, this effect is weak, and the selectivity of the reaction is either weakly *syn* or just reversed to weakly *anti* (entries 1–3). However, when R^1 is β'-branched, the stereoselectivity swings dramatically towards the *anti* diastereomer. These compounds are reduced by $NaBH_4/CeCl_3$ to give *anti* β-hydroxy phosphane oxides *anti*-**2**, often with no trace of the *syn* isomers (entries 4–14).

The shift in selectivity toward the *anti* product, which is enhanced greatly by β'-branched substituents, can be rationalized by assuming that the cerium ions can be chelated by the carbonyl group and the Ph_2PO group, distorting the transition state structure for the reduction from **48** towards **49**.[81, 82] If R^1 is large and β'-branched (in which case structure **49** will be more favorable than **48**, as interactions between R^1 and both R^2 and the complexed carbonyl oxygen atom are minimized), the left-hand side of the carbonyl group in **49** is more shielded than the right, so the predominant isomer of the product will be *anti*. Otherwise, with small R^1, chelation simply serves to lift the blocking Ph_2PO group partly out of the way of the incoming nucleophile, lessening the group's *syn* directing effect. For *anti*-selective $NaBH_4/CeCl_3$ reduction of compounds with unbranched R^1, we have to turn to a modified analogue of the Ph_2PO function, the dibenzophosphole group,[83] but discussion of this is beyond the scope of this review.

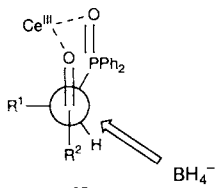

49

As an exception to these principles, compounds with a free γ'-hydroxyl group, which are reduced in the presence of cerium chloride with excellent *syn* selectivity, whether they are β'-branched or not, in complete reversal of the effect described above (Table 3, entries 15–17). The free γ'-hydroxyl group is

Table 3. Luche reductions of β-oxo phosphane oxides **7**.

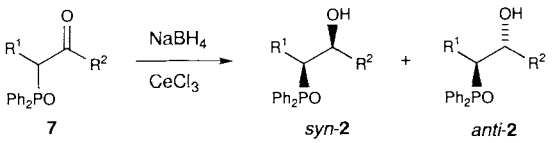

7 *syn*-**2** *anti*-**2**

Entry	R^1	R^2	$NaBH_4$ Yield[%]	$NaBH_4/CeCl_3$ Yield[%]	$NaBH_4$ *syn*-**2**:*anti*-**2**	$NaBH_4$ $CeCl_3$ *syn*-**2**:*anti*-**2**	Ref.
1	Me	Ph	-	-	89:11	70:30	[51,81]
2	Et	Ph	-	-	89:11	77:33	[51,81]
3	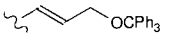	Et	97	95	53:47	50:50	[42]
4	*i*Pr	Me	71	83	65:35	23:77	[82]
5	*i*Pr	Et	84	100	61:39	7:93	[82]
6	*i*Pr	*n*Pr	71	77	54:46	11:89	[82]
7	*i*Pr	Ph	75	96	83:17	5:95	[51,81]
8	*i*Pr	4-$MeOC_6H_4$	82	100	72:28	3:97	[82]
9	*i*Pr	2-furyl	75	96	83:17	<2:98	[82]
10	C_6H_{11}[a]	*n*Pr	74	84	62:38	<4:96	[82]
11	C_6H_{11}[a]	Ph	71	100	76:24	5:95	[81,82]
12	*i*Pr		-	-	-	<5:95	[81]
13			-	-	-	<5:95	[81]
14	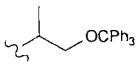		-	-	-	<5:95	[81]
15	$(CH_2)_2OH$	Me	-	-	67:33	>95:5	[75]
16	$(CH_2)_2OH$	$(CH_2)_2CO_2Me$	64	77	69:31	>95:5	[69,81]
17	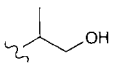		-	-		100:0	[58]
18	$(CH_2)_3OH$	Me	-	-	64:36	55:45	[75]
19	$(CH_2)_4OH$	Me	-	-	63:37	56:44	[75]
20	$(CH_2)_{10}OH$	Me	-	-	37:63	72:28	[75]
21	Me	$(CH_2)_2OH$	-	-	65:35	41:59	[75]
22	Me	$(CH_2)_5OH$	-	-	74:26	48:52	[75]
23	$(CH_2)_2OSitBuPh_2$	Me	-	-	62:38	73:27	[75]
24	Me	$(CH_2)_2OSitBuPh_2$	-	-	67:33	50:50	[75]

[a] Cyclohexyl.

essential for this stereochemical reversal: compounds with more distant OH groups (entries 18–20), with OH groups in R^2 (entries 21, 22), or with OH groups protected as ethers (entries 23, 24) are reduced with weakened *syn* selectivity, like the compounds in entries 1–3. Again, chelation effects appear to be responsible. By chelating the γ-OH group, cerium ion can now pull R^1 away from its blocking position on the left-hand side of the carbonyl group in **49** and allow attack *anti* to Ph_2PO, as shown in **50**, giving a product with a *syn* hydroxyl group.[81]

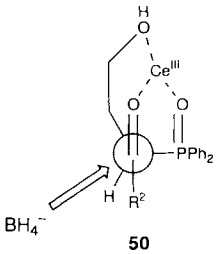

50

3.2.3. *Pinacol Cross-Coupling of α-Ph_2PO Aldehydes*

Vanadium(II)-promoted coupling of the two aldehydes **51** and R^3CHO gives diols **52** in excellent yields (Table 4).[84] When $R^1 \neq R^2$ the stereochemistry of the third chiral center, α to Ph_2PO, is remarkably well controlled, even for pairs of usually

Table 4. Pinacol coupling of **51** [84].

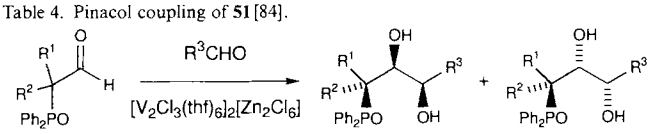

51 *syn*-**52** *anti*-**52**

Entry	R^1	R^2	R^3	Yield[%]	*syn*-**52**:*anti*-**52**
1	Me	Me	*i*Pr	84	-
2	Et	Me	$PhCH_2CH_2$	82	93:7
3	Bn	Me	$PhCH_2CH_2$	89	98:2
4	*i*Pr	Me	*i*Bu	94	>99:1
5	*i*Pr	Et	Pr	81	88:12

only weakly contrasting groups such as Et and Me (entry 2) or Et and *i*Pr (entry 5). As with the $CeCl_3$-catalyzed reductions, a chelated transition state structure **53** explains the sense of the chiral induction, in which R^3CHO approaches from the same side as the smaller of the two substituents R^1 and R^2.

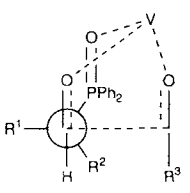

53

3.2.4. A Vinylogous Cram Rule—Reduction of γ-Ph_2PO Enones

The stereodirecting effect of the Ph_2PO is not limited only to nearby chiral centers. An impressive demonstration of the size of the sphere of influence of the Ph_2PO group in a molecule is provided by the remarkably stereoselective reductions of the enones **54** to give *syn* δ-hydroxy phosphine oxides **55**.[85] The

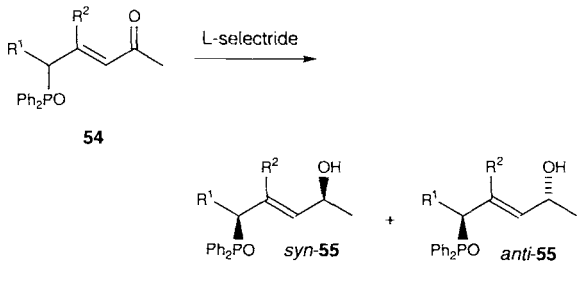

55a (R^1 = *n*-C_5H_{11}; R^2 = Me): >85:15 *syn*:*anti*
55b (R^1 = *n*-C_5H_{11}; R^2 = H): 72:28 *syn*:*anti*
55c (R^1 = *i*Pr; R^2 = H): 87:13 *syn*:*anti*

bulky reducing agent L-selectride performs better than $NaBH_4$ in this reaction, in which the bulk of the Ph_2PO group directs not only the stereoselectivity but also the regioselectivity of the reduction by crowding the enone. This inductive effect, exerted over the full length of a *trans* double bond, follows the "vinylogous Cram rule" discussed and sought by Fleming et al.[86] The reaction is even more remarkable in the light of evidence from IR studies that both the s-*cis* and s-*trans* conformations of enones **54** (R^2 = Me) are populated.[87]

In Section 3.2 we have seen that the Ph_2PO group is capable of directing highly stereoselective nucleophilic attack at a carbonyl group. Important characteristics of the Ph_2PO group are 1) its size, strikingly demonstrated by the reductions in Section 3.2.4; 2) its electronegativity, which helps fix the reactive conformation in the Felkin-style additions described in Section 3.2.1; and 3) its ability to coordinate to metal cations, which controls the reductions in Section 3.2.2 and the couplings in Section 3.2.3. The $NaBH_4/CeCl_3$ reductions of bulky ketones in Section 3.2.2 show how, in some cases, these attributes of the Ph_2PO group can have opposing effects, and by choosing which we want to be important, we can determine the stereochemical outcome of a reaction.

In Section 3.3 we will go on to consider stereocontrolled reactions of carbon–carbon double bonds directed by the Ph_2PO group, and we will see that the same themes will emerge. In Section 3.3.1 another nice example of the complementarity of the Ph_2PO group's steric and coordinating effects will be presented.

3.3. Ph_2PO-Directed Additions to C–C Double Bonds

The reactions of alkenes with an allylic chiral center have been well studied and form the basis of some of the most effective methods for the stereocontrolled introduction of new chiral centers into a molecule. When the allylic chiral center carries a Ph_2PO group, some remarkable examples of allylic stereocontrol can be observed.

In Sections 3.3.1 to 3.3.4 we will discuss the stereochemistry of electrophilic additions to allylic phosphane oxides. We will rationalize these reactions in terms of the transition state conformations for electrophilic attack on chiral alkenes proposed by Houk et al.[88] and recently clarified by Fleming et al.[89, 90] The lowest energy conformation for reactions of allylic phosphane oxide **56** will be considered to be **56a**, in which H (the

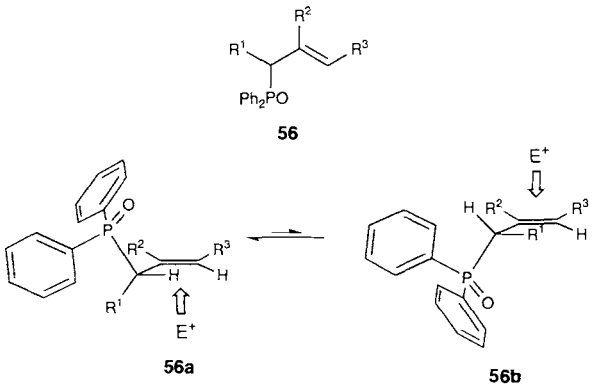

smallest group) more or less eclipses the double bond. We will see that the major diastereomeric product in each reaction can usually be explained by a reaction of this conformation; the electrophile E^+ approaches the double bond *anti* to the bulky Ph_2PO group. However, if R^1 is small (e.g. R^1 = Me) the next lowest energy reactive conformation **56b** may also become important. This conformation is strongly disfavored only when a large R^1 group generates too much 1,3-allylic strain with the *cis* vinylic hydrogen atom of the double bond. Electrophilic attack on the less hindered face of the double bond in this conformation reverses the stereochemical result of the reaction. We will see that the transition state structure **56b** also becomes significant if the electrophile is bulky and interacts strongly with R^1 in **56a**. As with the examples discussed in Section 3.2, we will also see that this fundamental selectivity pattern can be altered significantly by coordination effects involving the phosphoryl oxygen atom.

3.3.1. Epoxidation with Peracids

Epoxidation of allylic phosphane oxides **56** with *m*-chloroperbenzoic acid (*m*CPBA) is *anti* selective (Table 5); the major diastereomer of the product **57** is formed via transition state

Table 5. Epoxidation of **56**.

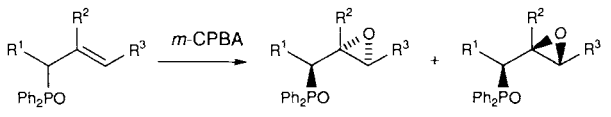

Entry	R^1	R^2	R^3	*anti*-**57**:*syn*-**57**	Ref.
1	Me	H	Me	66:34	[92]
2	Pr	H	Me	85:15	[92]
3	*i*Pr	H	CH_2OSi*t*$BuMe_2$	86:14	[92, 127]

56a, and a selectivity of about 6:1 is obtained when $R^1 > Me$ (entries 2, 3). When $R^1 = Me$ the reaction is less *anti* selective (entry 1), probably because the alternative conformation **56b** is then low enough in energy to lead to a significant amount of *syn* product. Magnesium monoperoxyphthalate (MMPP) also epoxidizes allylic phosphane oxides with *anti* selectivity.[91]

If the allylic phosphane oxide also contains a δ-hydroxyl group, some interesting and unusual effects arise (Table 6).[92] Hydroxyl groups are strong directors of peracid epoxidations,

Table 6. Epoxidation of *syn*-**55** and *anti*-**55** with *m*CPBA [92].

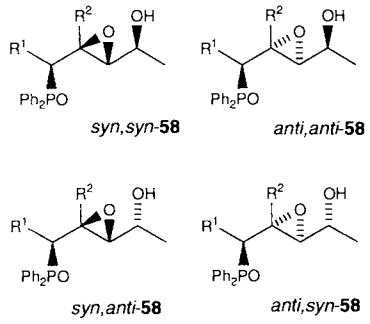

Entry	Starting cmpd.	R^1	R^2	Epoxidation of *syn*-**55**: *syn,syn*-**58**:*anti,anti*-**58**	Epoxidation of *anti*-**55**: *anti,syn*-**58**:*syn,anti*-**58**
1	**55a**	n-C_5H_{11}	Me	93:7	100:0
2	**55b**	n-C_5H_{11}	H	73:27	56:44
3	**55c**	*i*Pr	H	81:29	53:47

encouraging a *syn* attack on the double bond by hydrogen bonding to the epoxidizing agent.[93] As expected, therefore, *syn*-**55a** and *anti*-**55a** are both epoxidized *syn* to the hydroxyl group with high stereoselectivity (entry 1). Any effect arising from the chiral center α to phosphorus is completely dominated by the chiral center carrying the hydroxyl group in the δ position, because the methyl group (R^2 = Me) *cis* to this hydroxyl group firmly fixes the reactive conformation **59** at this center.

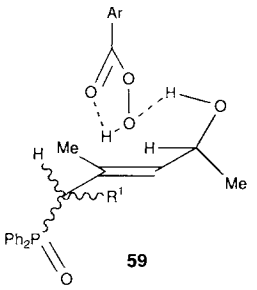

The epoxidations of *syn*- and *anti*-**55b** and *syn*- and *anti*-**55c** show that removal of this methyl group allows both chiral centers to play a role in directing the epoxidation. For these compounds matched and mismatched diastereomers exist in which the effects of the two chiral centers are engaged in cooperation and in competition, respectively (entries 2, 3). Unexpectedly, the matched diastereomer is that in which epoxidation occurs *syn* to the OH group and *syn* to the Ph_2PO group, and not *anti* to the Ph_2PO group as would be expected from the results with simpler allylic phosphane oxides (Table 5).

This effect persists even when the hydroxyl group is not attached to a chiral center, but disappears if it is protected. Thus, **60** is epoxidized with 73:27 *syn* selectivity, while **61** is epoxidized with 86:14 *anti* selectivity [Eqs. (f), (g)]. Reducing the size of the group R^1 of **62** reduces this *syn* selectivity, and with R^1 = Me the *anti* epoxide product dominates (Table 7).[92]

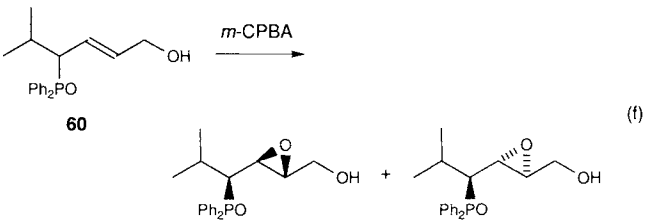

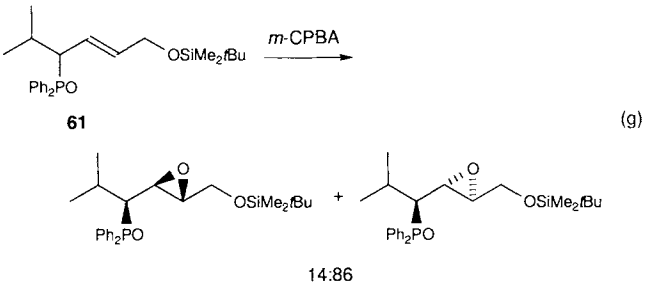

Table 7. Epoxidation of **62** with *m*CPBA [92].

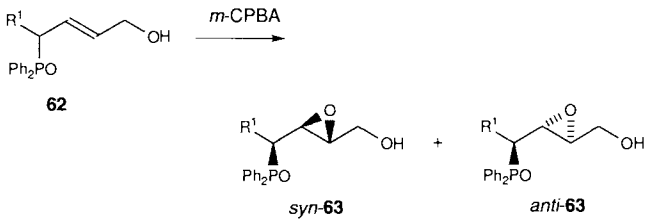

Entry	R^1	*syn*-**63**:*anti*-**63**
1	*i*Pr	73:27
2	C_6H_{11} [a]	69:31
3	n-C_5H_{11}	54:46
4	Et	53:47
5	Me	29:71

[a] Cyclohexyl.

The *syn* selectivity in the presence of an allylic hydroxyl group probably arises from a hydrogen bond between the Ph_2PO group and the acidic hydrogen atom of the peracid, favoring the reactive conformation **64**.[92] This is another example of the opposition of the Ph_2PO group's coordinating ability to its steric effects. Why the free hydroxyl group should encourage formation of this cyclic structure is not clear, though a similar effect has been noted by Johnson and Kishi in the epoxidation of benzyl ethers.[94] In any case, the stereoselectivity of the epoxidation of **60**, though remarkable, is low enough for us to deduce that a significant amount of reaction still takes place without hydrogen bonding to the Ph_2PO group, on the *anti* face of the double bond. For compounds **62** with smaller R^1 groups, population of the eclipsed conformation **56b** increases the amount of *anti* epoxide produced.

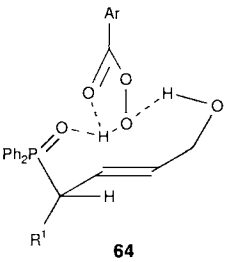

The Ph_2PO group can also have an influence over the epoxidation of a more distant double bond. For example, while the

allylic alcohol *anti*-**65** is epoxidized very cleanly to give an *anti* product [Eq. (h)], its diastereomer *syn*-**65** is epoxidized with only 75:25 selectivity in favor of the *anti* diastereomer [Eq. (i)].[57] A kind of match/mismatch effect involving the two

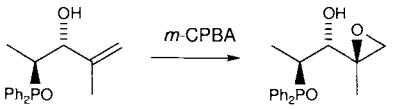

anti-**65** 92% (h)

syn-**65** 75:25 *syn,syn*:*syn,anti* (i)

chiral centers is evidently in operation, though in fact the selectivities of both diastereomers are remarkable considering that allylic alcohols with this substitution pattern are usually epoxidized with almost no selectivity.[93] The lactones **66**, with their hydroxyl groups protected and conformational mobility restricted, are epoxidized with *syn* selectivity (85:15 to 90:10) [Eq. (j)].[95]

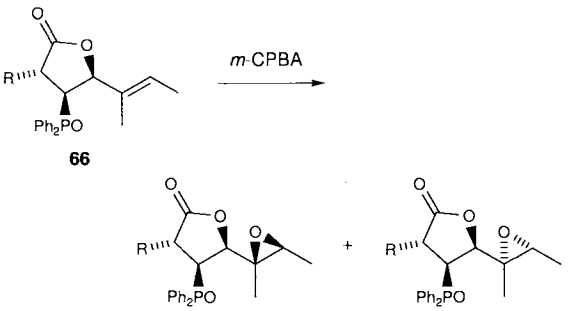

66 (j)

85:15 - 90:10

3.3.2. *Asymmetric Epoxidation*

Sharpless's asymmetric epoxidation[96–99] is an important way of functionalizing an alkene enantioselectively. Allylic phosphane oxides can be epoxidized with this method if they are also allylic alcohols: epoxidation of **67** under the standard stoichiometric conditions of Sharpless's asymmetric epoxidation (*t*BuOOH, $Ti(OiPr)_4$, L- or D-diethyl tartrate)[96] gives **68** in high yield and enantiomeric excess.[100] Under these conditions similar compounds are kinetically resolved if they have a chiral center α to the hydroxyl group. Kinetic resolution of **69** gives only one (*anti*) epoxide **70** with high *ee* at 50% completion; the allylic alcohol starting material **69** is also returned in high enantiomeric excess.[100] Interestingly, and contrary to precedent,[97] these kinetic resolutions are significantly affected by a second chiral center carrying a Ph_2PO group located *trans* to the allylic hydroxyl group. As with the peracid epoxidations described in Section 3.3.1, **55c** demonstrates cooperation and competition between the two chiral centers of its diastereomers. In this case the matched diastereomer *syn*-**55c** is epoxidized (this time with

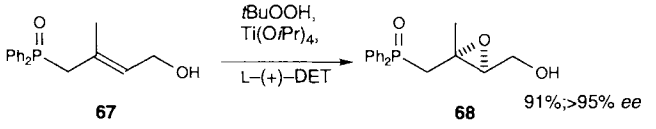

67 **68** 91%;>95% *ee*

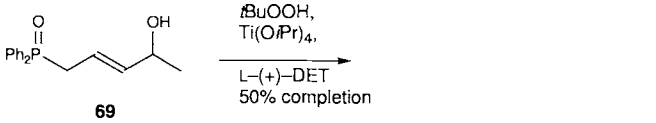

69

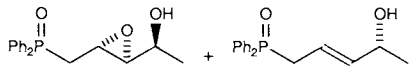

70 >95% *ee* (*R*)-**69** 95% *ee*

L-(+)-diisopropyl tartrate) *anti* to both the OH and Ph_2PO groups, and at 52% completion the kinetic resolution yields starting material *syn*-**55c** and a single epoxide product *anti,anti*-**58** with excellent enantiomeric excesses. Epoxidation of the mismatched diastereomer *anti*-**55c** results in poor conversion, low selectivies, and the appearance of ketones as by-products.

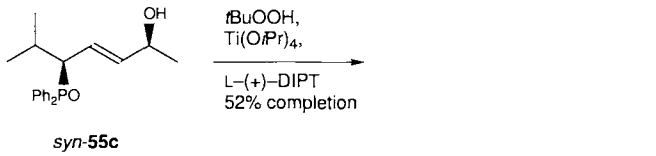

syn-**55c**

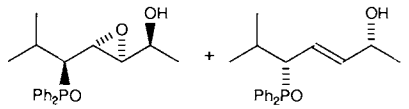

anti,anti-**58** >99% *ee** *syn*-**55c** 89% *ee*

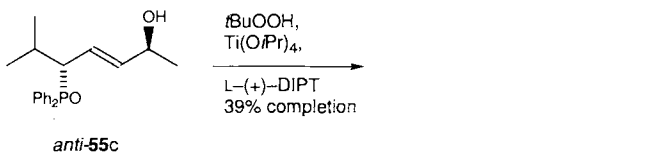

anti-**55c**

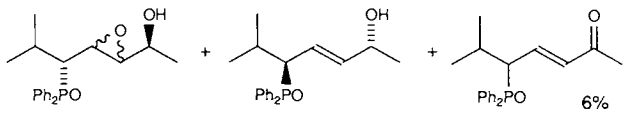

anti,syn-**58**: *syn,anti*-**58** 76:24 *anti*-**55c** 37% *ee*

A single chiral center α to phosphorus is sufficient to drive a kinetic resolution as long as one of the other two groups at this chiral center is also large (Table 8).[100] When $R^1 = iPr$ or cyclohexyl, **62** can be kinetically resolved with efficiency, giving high selectivity for the *anti* epoxide *anti*-**63**, and returning enantiomerically enriched starting material (entries 1, 2). However, with small R^1 groups the kinetic resolutions are not so efficient.

Again, the transition states **56a** and **56b** can be used to explain these selectivities. In this case the added complication of the enantiomerically pure epoxidizing agent means that epoxidation is possible only on the bottom face of the double bond, as

Table 8. Kinetic resolution of **62** [100].

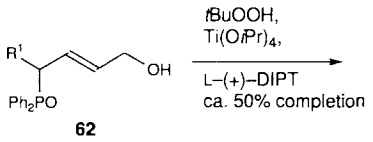

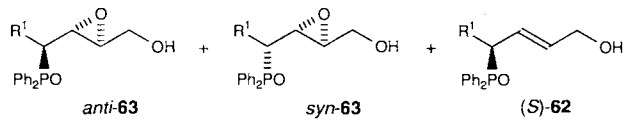

Entry	R^1	*anti*-**63**:*syn*-**63**	*ee*(*anti*-**63**)[%]	*ee*(**62**, recovered)[%]
1	*i*Pr	90:10	75	63
2	C_6H_{11}[a]	93:7	86	65
3	n-C_5H_{11}	68:32	[b]	36
4	Et	71:29	82	31
5	Me	54:46	[b]	10

[a] Cyclohexyl. [b] Not determined.

shown in **71a–d**. For the conformation and configuration shown in **71a**, this means approach of the bulky titanium–tartrate–peroxide reagent alongside R^1, while for the configuration shown in **71c**, the catalyst must approach alongside the much larger Ph_2PO group. When conformations **71b** and **71d** are unpopulated (i.e.

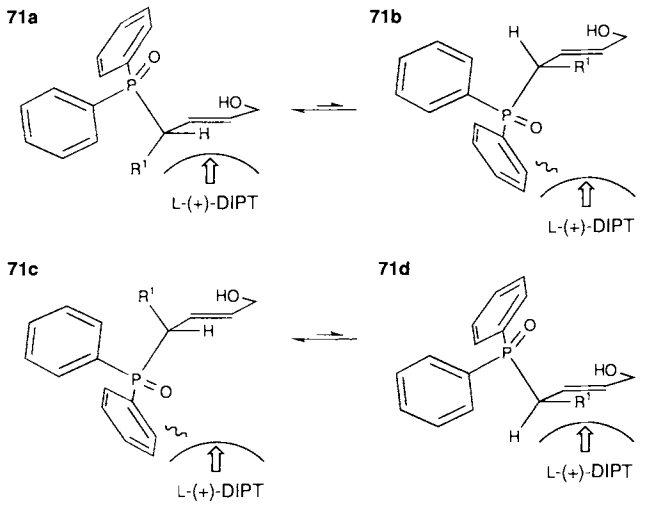

when R^1 is large), the outcome of this interplay of effects is that the epoxidation of the enantiomer of **62** in **71a** is much faster than epoxidation of the enantiomer of **62** in **71c**, and an efficient kinetic resolution results. By this model the faster reacting enantiomer of **62** gives the observed *anti* epoxide *anti*-**63**.

If R^1 is smaller than *i*Pr or cyclohexyl, the conformation of **62** depicted in **71b** and **71d** can be populated to some extent. The relative rates of epoxidation of the two enantiomers of **62** in these conformations are reversed: for the configuration in **71b**, the titanium–tartrate–peroxide reagent must approach alongside the bulky Ph_2PO group, while for the configuration in **71d** it is hindered only by a hydrogen atom. So, the more **71b** and **71d** are populated, the less efficient is the kinetic resolution. This also fits our observed trend in the decrease in efficiency for resolution of **62** with R^1 groups in the series *sec*-alkyl > *n*-alkyl > Me (Table 8).

3.3.3. *Dihydroxylation with Osmium Reagents*

Hydroxylations of allylic phosphane oxides with osmium reagents are *anti* selective: The reaction of **72** with OsO_4 and morpholine *N*-oxide gives mainly the *anti,syn* diastereomer of the diol **73**.[91] Recent results have shown that this *anti* selectivity is dependent on the solvent and reagent used for the reaction: with $OsCl_3/[K_3Fe(CN)_6]$, **73** was formed with only 60:40 selectivity.[101]

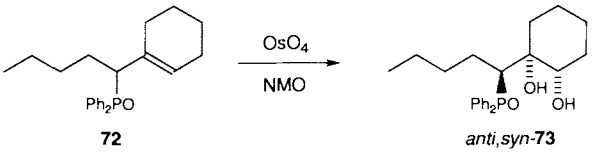

Asymmetric dihydroxylation (AD) of achiral phosphane oxides **74** with commercially available AD-mixes[102] produced optically active diols **75**; the enantiomeric excess of the product is highest with the largest, most hydrophobic groups R^1 and R^2 (Table 9).[103]

Table 9. Asymmetric dihydroxylation of **74** [103].

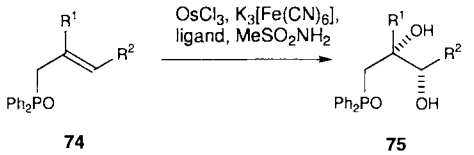

Entry	R^1	R^2	Yield(**75**)[%]	*ee*(**75**)[%]
1	$-(CH_2)_4-$		73	18
2	H	Me	84	10
3	H	*n*Bu	61	49
4	H	Ph	66	74
5	Me	H	75	55
6	Ph	H	74	86

3.3.4. *[3 + 2]Cycloadditions with Nitrile Oxides*

Allyldiphenylphosphane oxide **76** reacts with nitrile oxides RCNO with aliphatic R groups under ultrasound sonication to give excellent yields of the isoxazolines **77**.[15, 104] The reaction

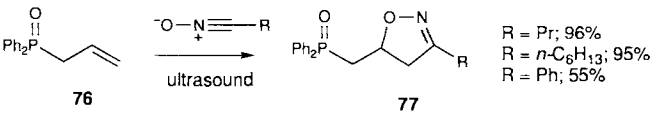

proceeds with 100% regioselectivity; a C–O bond is formed with the carbon atom β to Ph_2PO. Phosphane oxides **78** with a chiral center α to the Ph_2PO group give predominantly the *syn* diastereomer of the isoxazoline products **79** (Table 10),[15, 105] in contrast with the *anti* selectivity of the epoxidation reactions of similar compounds (Section 3.3.1). The stereoselectivity is relatively insensitive to the substitution pattern of either the nitrile oxide or the phosphane oxide component. However, increasing the size of R^1 marginally reduces the selectivity (entries 1–3), and very big R^1 groups stop the reaction (entry 4).

Table 10. Cycloadditions of nitrile oxides R^2CNO and **78**.

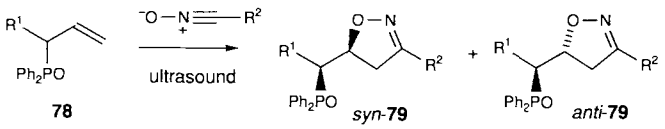

Entry	R^1	R^2	*syn*-**79**:*anti*-**79**	Ref.
1	Me	n-$C_{11}H_{23}$	80:20	[15, 104]
2	Et	n-$C_{11}H_{23}$	78:22	[15, 104]
3	Pr	n-$C_{11}H_{23}$	72:28	[15, 104]
4	*i*Pr	n-$C_{11}H_{23}$	– [a]	[15, 104]
5	OMe	Ph	76:24	[105]
6	OEt	Ph	80:20	[105]

[a] No product formed.

The *syn* stereochemistry of the products is consistent with the results of Houk et al.[106] for nitrile oxide cycloadditions. It can be explained along the lines of transition states **56a** and **56b** if we consider the nitrile oxide to be a very large electrophile, which can therefore interact strongly with the allylic substituent R^1 in the transition states **80a** and **80b**. This interaction raises the energy of conformation **80a**, and favors reaction via **80b**, in which R^1 eclipses the double bond, but only a hydrogen atom is directed at the nitrile oxide. When R^1 is very large, reaction in neither conformation is possible.

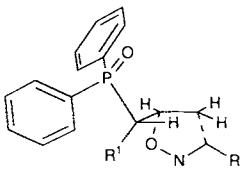

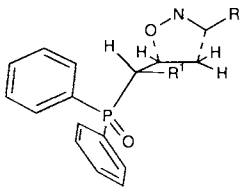

For allylic ethers the stereoselectivities of nitrile oxide cycloadditions are usually greater because of the electronic "inside alkoxy effect"—the double bond is most nucleophilic when the interaction between π and the σ^* orbitals of the C–O bond is least.[107] The absence of this effect in the reaction of **78** with R = OMe or OEt (entries 5, 6) is perhaps due to the presence of two electronegative groups at the chiral center.

Cycloadditions of allylic phosphane oxides to nitrones can also be carried out, but they are fairly unstereoselective.[108]

3.3.5. Alkylation of Ph_2PO-Substituted Lactones

The power of the Ph_2PO group to direct stereoselective reactions is amplified when conformations are restricted by the presence of a ring. Alkylation of the enolates of lactones **81**, which were prepared by treatment with lithium hexamethyldisilazide (LiHMDS) in the presence of *N*,*N*′-dimethyl-*N*,*N*′-propylene urea (DMPU), gave single diastereomers of the products **82** (according to NMR spectra), with attack of the electrophile on the enolate occurring *anti* to the Ph_2PO group.[95]

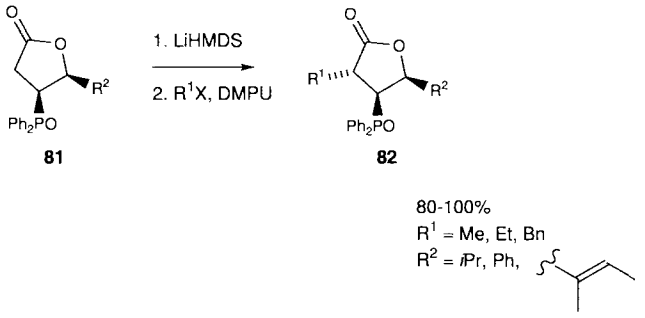

3.3.6. Stereospecific Allylic Rearrangements

We have already seen, in the epoxidations of **65**, how a chiral center bearing a hydroxyl group can be used to "relay" chiral information further along a carbon chain. Another way of propagating chiral centers distant from the Ph_2PO group, yet with a defined stereochemistry relative to it, is to perform stereospecific allylic rearrangements of single diastereomers of unsaturated β-hydroxy phosphane oxides **83** (R^3 = H) to give the unsaturated δ-hydroxy phosphane oxides **84** (R^3 = H). Several methods, each demonstrating a different degree of stereocontrol, have been used to rearrange these compounds, usually via their esters (Table 11).

Table 11. Rearrangement of **83** to **84**.

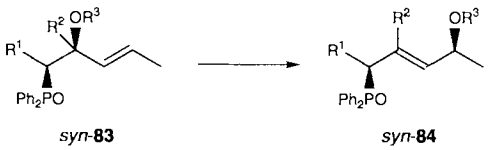

a: R^1 = n-C_5H_{11}; R^2 = Me
b: R^1 = n-C_5H_{11}; R^2 = H
c: R^1 = *i*Pr; R^2 = H

Entry	Starting cmpd.	R^3	Method [b]	Product	R^3	*syn*-**84**:*anti*-**84**	Ref.
1	*syn*-**83a**	H	A	**84a**	Ac	44:56	[85]
2	*anti*-**83a**	H	A	**84a**	Ac	33:67	[85]
3	*syn*-**83b**	H	A	**84b**	Ac	65:35	[85]
4	*anti*-**83b**	H	A	**84b**	Ac	35:65	[85]
5	*syn*-**83b**	[a]	B	**84b**	[a]	90:10	[85]
6	*anti*-**83b**	[a]	B	**84b**	[a]	7:93	[85]
7	*anti*-**83b**	Ac	C	**84c**	Ac	0:100	[111, 112]

[a] *p*-Nitrobenzoyl. [b] Methods: A: Ac_2O, AcOH, TsOH (cat.), 0 °C, 5 min.; B: PhCN, 190 °C, 1 h; C: $[PdCl_2(MeCN)_2]$ (5 mol%), 20 °C, 2 h.

The acid-catalyzed rearrangements of **83** to give **84** (R^3 = Ac) probably via the acetates **83** (R^3 = Ac) are partially stereoselective (both diastereomers of the starting material form predominantly the *anti* diastereomer of the product) and partially stereospecific (the amount of *syn* product formed from *syn* starting material is greater than the amount of *syn* product formed from *anti* starting material) (entries 1, 2). This rearrangement passes through a cationic intermediate

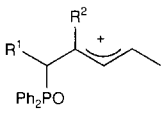

85

85.[85] The cationic intermediate generated from compounds **83b,c** lacks one of the stabilizing methyl substituents and must therefore remain more tightly bound as an ion pair. A greater amount of suprafacial migration of the acetate group then takes place, and the reaction is more stereospecific (entries 3, 4).

The thermal rearrangement of the *p*-nitrobenzoates of **83** is even more stereospecific, since in the absence of acid the transition state is an ion pair (entries 5, 6). However, the best method makes use of Overman's Pd^{II}-catalyzed allylic ester transposition (entry 7).[109, 110] This method is also higher yielding and tolerates a wider range of substitution patterns than the acid-catalyzed or thermal rearrangements.[42, 111, 112] Some spectacular double transpositions have also been carried out by this method: starting from **86**, a 1,7-chiral relationship is controlled in the product **87**.[42]

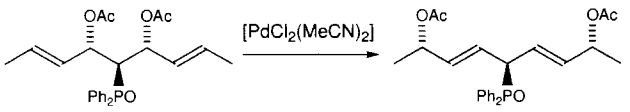

86 **87**

The role of the Ph_2PO group in these reactions is twofold. Firstly, it makes possible the easy synthesis and separation of the diastereomerically pure starting materials for the rearrangements. Secondly, it acts as a driving force for the rearrangements, probably for steric reasons. For example, while the rearrangement of **83a** may be driven by the increase in substitution of the double bond, the rearrangements of **83b**, **83c**, and **90** must be driven by steric repulsion between the Ph_2PO group and the migrating acetate group, since both the starting material and the product are alkenes with equal numbers of substituents on their double bonds.

4. Stereochemically Controlled Organic Synthesis Using the Ph_2PO Group

The first three sections of this article have considered the reactions of compounds containing the Ph_2PO group, placing particular emphasis on stereoselective aspects. In this last section we shall examine these reactions in the context of a practical guide to making molecules, in particular alkenes, using Ph_2PO chemistry. We will highlight those compounds for which this chemistry is exceptionally appropriate.

The simplest alkenes containing no other functional groups will be considered first. Ph_2PO chemistry lends itself particularly well to the synthesis of certain types of alkenes, but we will show that careful consideration of the possible reaction sequences can enhance the chances of making any given alkene in good yield and stereochemical purity. Alkenes containing functional groups can be made by the same routes as those used for unfunctionalized alkenes. However, these functional groups often lower the stereoselectivity and stereospecificity of the classic Horner–Wittig reaction. Better results can be obtained by making these functional groups active participants in the construction of the molecules—in other words by making full use of the stereoselective reactions described in Section 3. This is particularly true for alkenes carrying two or more chiral centers or those that are required in optically active form.

4.1. Simple Alkenes

Except in the case of (*E*) alkenes bearing stabilizing substituents (e.g. polyenes, styrenes, vinyl sulfides, ethers; see Section 4.2), the two-step Horner–Wittig reaction (Section 2.2) is well-suited to making simple (*E*) or (*Z*) alkenes. As we have already discussed, the stereospecificity of the Horner–Wittig elimination usually means that the problem of producing pure (*E*) or (*Z*) alkenes is reduced to the much easier task of purifying *syn* or *anti* β-hydroxy phosphane oxides, and the best yields will be obtained if we can make the required diastereomer with high stereoselectivity. In addition, for a specific alkene there are usually two β-hydroxy phosphane oxide precursors, in which R^1 and R^2 are exchanged (Scheme 7). We need to consider firstly

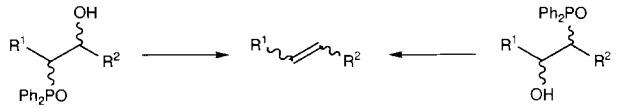

Scheme 7. Two routes to one alkene.

which route to each candidate β-hydroxy phosphane oxide would give the best yield, and then, on the basis of these yields, which of the two candidates we will use to make our alkene, bearing in mind that certain anion-stabilizing groups at R^1 lower the stereospecificity of elimination to give (*Z*) alkenes.[9] Sometimes, further considerations will also be important: for example, if pure samples of both the (*E*) and the (*Z*) isomer of an alkene are required, high yields for each isomer may be sacrificed for the convenience of using the same starting materials for each route. In this case, a particularly *un*selective Horner–Wittig addition might be chosen and the products would be separated to obtain both isomers.

4.1.1. *Disubstituted (E) Alkenes*

The only reliable route to simple *syn* β-hydroxy phosphane oxides is reduction of a β-oxo phosphane oxide **7** with sodium borohydride. The selectivity for this reduction is usually of the order of 90:10 *syn*:*anti* unless R^1 is large [Eq. (k)]. Thus, the

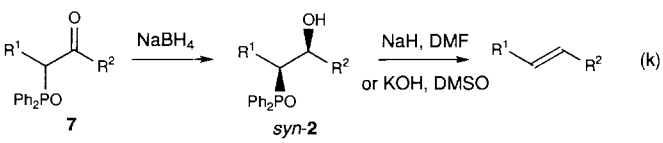

7 *syn*-**2** (k)

best yields will be obtained when R^1 is the smaller substituent. The reduction of **88**, in which R^1 = isoprenyl, led to pure (*E*)-**89** in high yield (Scheme 8).[9]

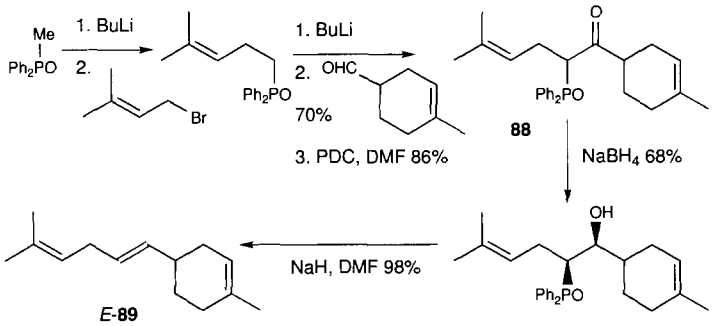

Scheme 8. Synthesis of the disubstituted alkene (*E*)-**89**; PDC = pyridinium dichromate.

Bridges and Whitham used the stereospecific opening of *cis* epoxides by phosphorus nucleophiles as a route to *syn* β-hydroxy phosphane oxides. This method can be used to invert the stereochemistry of alkenes and is particularly suited to the control of double-bond stereochemistry in medium rings (Scheme 9).[113]

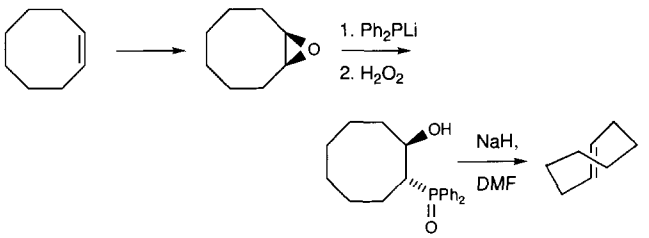

Scheme 9. Inversion of double-bond stereochemistry by Bridges and Whitham.

4.1.2. Disubstituted (*Z*) Alkenes

anti β-Hydroxy phosphane oxides *anti*-**2** can be made selectively by two routes: a) Horner–Wittig addition of a lithiated β-hydroxy phosphane oxide to an aldehyde, or b) Luche reduction ($NaBH_4/CeCl_3$) of β-oxo phosphane oxides **7** having a β′-branched R^1 group (Scheme 10). While Horner–Wittig addition is generally more useful since it tolerates most substituents R^1 and R^2, in those cases where the *anti*-selective Luche reduction is successful, it is spectacularly so, giving almost quantitative yields of the *anti* isomer.[82] We can therefore deduce two strategies: if one of the alkene substituents is α-branched (e.g. isopropyl or cyclohexyl), this should be specified as R^1 and route 2 used; otherwise, the smaller of the two substituents should be designated R^1 and a Horner–Wittig addition applied (as for the $NaBH_4$ reduction, the stereoselectivity is lowered by when R^1 is large).[9]

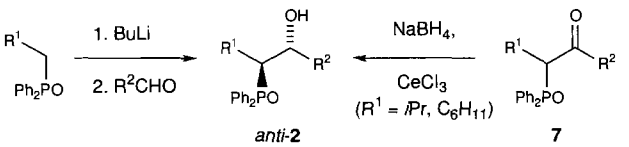

Scheme 10. Two routes to *anti* β-hydroxy phosphane oxides.

Van den Nieuwendijk and van der Gen needed the (*Z*) alkene (*Z*)-**92** for a synthesis of an unusual unsaturated fatty acid.[114] Addition of lithiated heptyldiphenylphosphane oxide **90** to 5-hydroxypentanal, followed by purification of the major diastereomer, gave the *anti* β-hydroxy phosphane oxide **91**, which underwent stereospecific elimination to give (*Z*)-**92**.

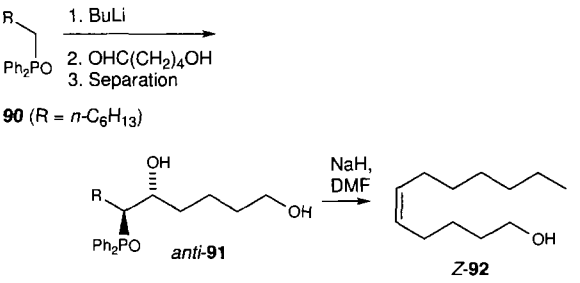

4.1.3. Trisubstituted Alkenes

Both (*E*) and (*Z*) trisubstituted alkenes can be made by the two-step Horner–Wittig route.[63] Two combinations of starting materials are possible: a lithiated primary alkyldiphenylphosphane oxide and a ketone, or a lithiated secondary alkyldiphenylphosphane oxide and an aldehyde (Scheme 11). In general, as neither addition proceeds with good stereoselectivity, overall yields tend to be low. In the elimination step, the additional complication of Horner–Wittig reversal can arise, but syntheses starting from secondary phosphane oxides are less prone to this problem. Nonetheless, elimination of the pure *anti* β-hydroxy phosphane oxide **95** isolated from the mixture of adducts of phosphane oxide **93** and ketone **94** gave the perfumery compound (*Z*)-α-bisabolene **96**. Interestingly, the second, unfunctionalized chiral center of **95** (γ-C) does not affect chromatographic separation of the mixture into a *syn* pair and an *anti* pair. Denmark and Amburgey have recently described the stereoselective contruction of trisubstituted double bonds using phosphoramidates.[115]

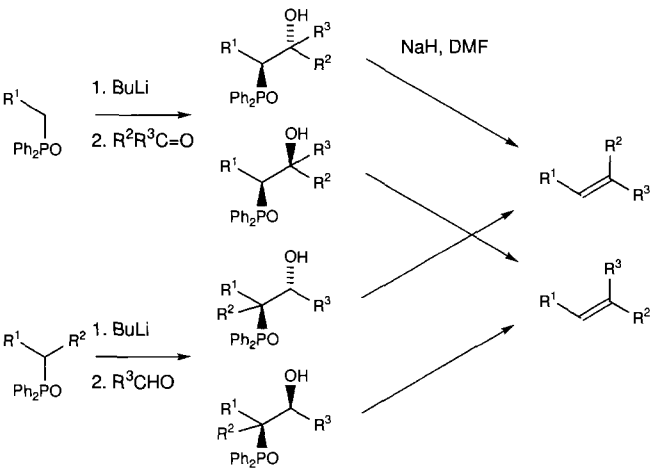

Scheme 11. Routes to trisubstituted alkenes.

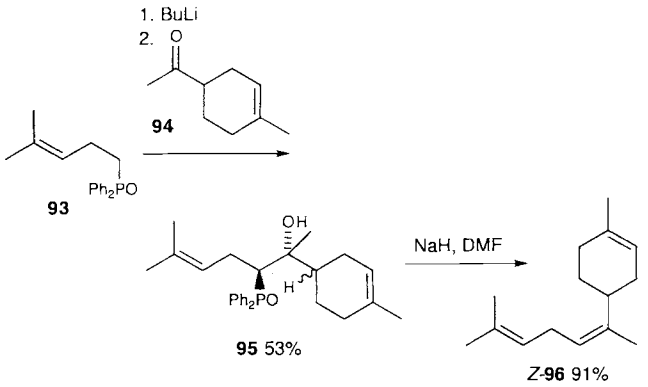

4.2. Functional Groups at Vinylic Positions

If the target alkene carries an anion-stabilizing or a conjugated aryl or alkenyl substituent, two further effects need to be taken into consideration in planning a synthesis. Firstly, the reversal of the Horner–Wittig addition step is accelerated by anion-stabilizing groups at R^1, leading to "stereochemical leakage" during the Horner–Wittig elimination and contamination of the alkene with its stereoisomer. In some cases, for example in the synthesis of alkenyl isoxazoles,[33] this reversal makes the two-step Horner–Wittig reaction almost unusable, as the driving force of the elimination is required for the Horner–Wittig addition to reach completion. Secondly, conjugating groups at R^1 or R^2 stabilize an incipient double bond and accelerate the Horner–Wittig elimination, making one-step reactions particularly successful. Deciding on the best strategy means comparing the relative importance of these two factors. If a pure (*E*) or (*Z*) alkene is required, and the two stereoisomers are separable only with difficulty, it would be important to avoid Horner–Wittig reversal; a two-step Horner–Wittig reaction would be more appropriate with R^2 as a conjugating group. If some contamination with a stereoisomer is not important, R^1 could be the conjugating group and the simplicity of a one-step Horner–Wittig reaction exploited.

4.2.1. Stilbenes

Owing to the equilibration of Horner–Wittig adducts made from benzyldiphenylphosphane oxides, it is very difficult to make (*Z*)-stilbenes by the Horner–Wittig reaction.[25] (*E*)-Stilbenes have, however, been made by using one-step Horner–Wittig reactions.[1–3] For example, lithiation of phosphane oxide **97** and addition to aldehyde **98** gave (*E*)-stilbene **99**.[16]

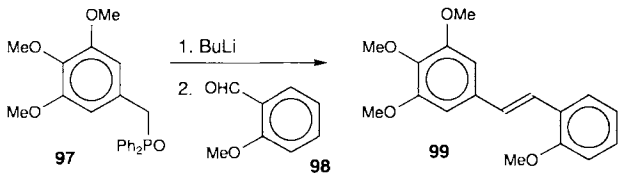

4.2.2. Styrenes

Because of the danger of nonstereospecific eliminations of β-hydroxy phosphane oxides having R^1 = Ar, (*Z*)-styrenes must be made by two-step Horner–Wittig reactions with R^2 = Ar.[9, 25] Thus, both isomers of isosafrole **100** could be made from the same starting materials by a two-step Horner–Wittig sequence.[9] For (*E*)-styrenes, R^1 can be Ar, and Kallmerten and Wittman[13] obtained only the (*E*) product (*E*)-**102** from the *syn* β-hydroxy phosphane oxide **101** in their synthesis of the oudemansins (Scheme 12b).

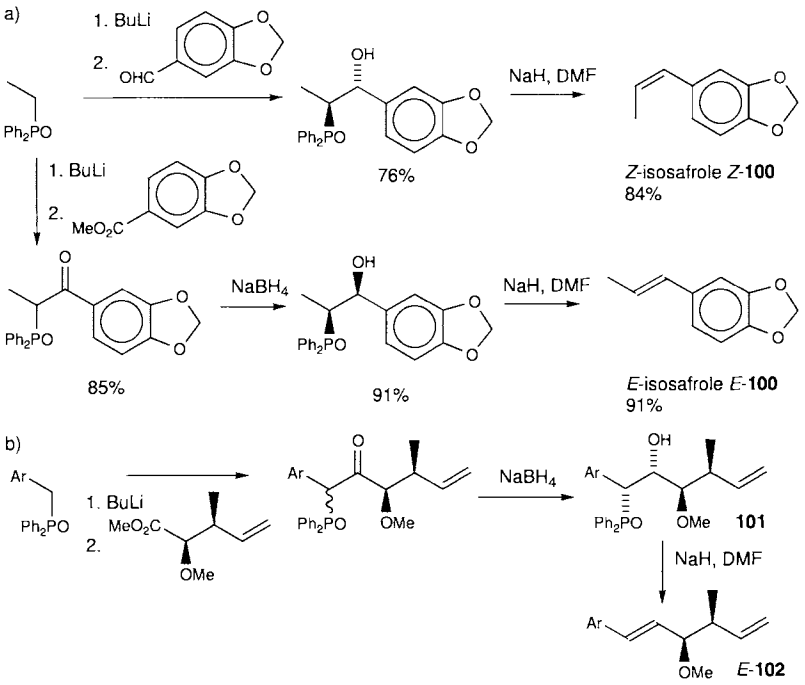

Scheme 12. Synthesis of (*Z*)- and (*E*)-isosafrole (a) and of the oudemansin precursor (*E*)-**102** (b).

4.2.3. Polyenes

4.2.3.1. One-Step Horner–Wittig Reactions

As discussed in Section 2.1, all-(*E*) polyenes are easily made by reacting the lithium, sodium, or potassium derivative of an allylic phosphane oxide with an aldehyde or ketone, and conditions of time and temperature can be used that allow the elimination to go to completion. Several examples exist, especially in vitamin D chemistry,[10, 26, 29–31, 37] but also in other fields,[12, 27, 28] of connective polyene syntheses in which allylic phosphane oxides perform better than their phosphonate or phosphonium salt analogues. Nearly all of these syntheses feature a one-step Horner–Wittig reaction. This variant is quite appropriate, since Horner–Wittig reversal, in conjunction with fast elimination, serves to increase the proportion of (*E*) product.

Polyenes containing a (*Z*) double bond can be made by a one-step Horner–Wittig reaction, by starting with a (*Z*) allylic phosphane oxide. Unlike allylic phosphonium salts, allylic phosphane oxides react stereospecifically, retaining their stereochemistry.[7] One example is the synthesis of (*E*,*Z*) diene **104** from the (*Z*) allylic phosphane oxide **103** described by Dolle and Nicolaou.[28]

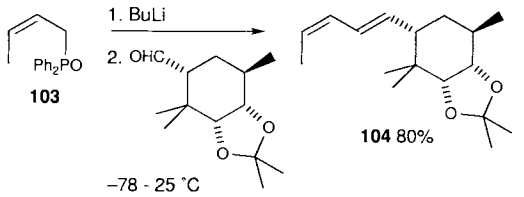

4.2.3.2. Two-Step Horner–Wittig Reactions

The stereoselectivities obtained in Horner–Wittig additions of allylic phosphane oxides to aldehydes or in reductions of ketones **7** (R^1 = allyl) are often poor.[42] Nonetheless, the two diastereomers are often separable, and elimination of the individual diastereomers can lead to pure (*E*,*E*) and (*E*,*Z*) dienes, albeit in low overall yield. The dienes (*Z*)- and (*E*)-**106** were made by this sort of two-step route.[41]

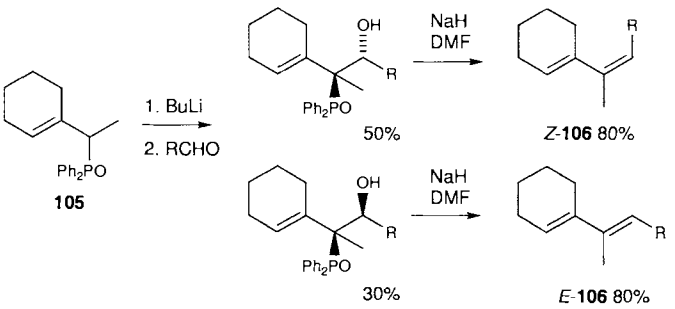

Stereochemically pure dienols are interesting because of their potential use in intramolecular Diels–Alder reactions. Addition of **67** to cyclohexanone, followed by Horner–Wittig elimination, gave dienol **107** [Eq. (l)].[40] Some attempted stereocontrolled syntheses of dienols have been frustrated by difficulty in separating the two diastereomers of the β-hydroxy phosphane oxides **109**.[40, 42] Diastereomeric mixtures of the diols, diacetates, and bis(trimethylsilyl) ethers of **109a** were inseparable, and separation of the diols **109b** was achieved only by converting them into the diacetates **110**.[42] Hydrolysis, protection, and elimination completed a synthesis of the protected (*E*,*E*) and (*E*,*Z*) dienols **111**, intermediates in the synthesis of some insect pheromones (Scheme 13). In this case KOH/DMSO was found to be more effective than NaH/DMF in promoting the stereospecific elimination leading to (*E*,*Z*)-**111**.

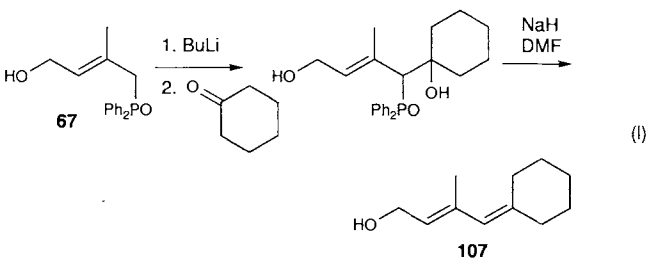

The allylic and hydroxyallylic phosphane oxide starting materials for these two examples of two-step Horner–Wittig routes to dienes were all made by rearrangement: the allylic phosphane oxides **105** by acid-catalyzed dehydration,[41] and the hydroxyallylic phosphane oxides **108** by acid-catalyzed,[40, 85] or, more generally, palladium-catalyzed[111] rearrangement of allylic acetate **112** to **113**. In the synthesis of **110** (Scheme 14) the addition and rearrangement steps may be successfully reversed by using the phosphane oxide version of Corey's SCOOPY reaction.[42]

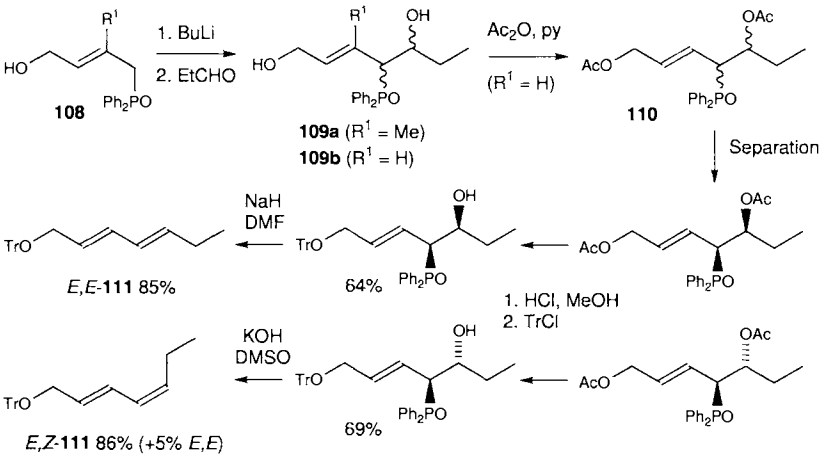

Scheme 13. Synthesis of the dienes (*E*,*E*)- and (*E*,*Z*)-**111**; Py = pyridine, Tr = Ph_3C.

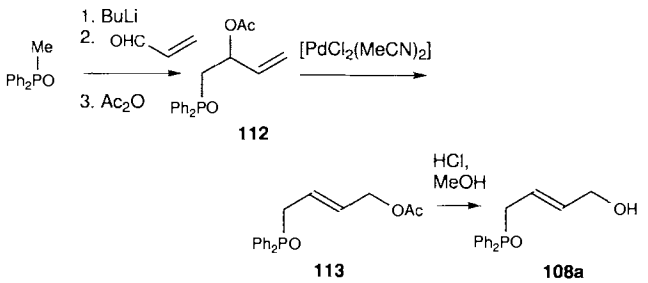

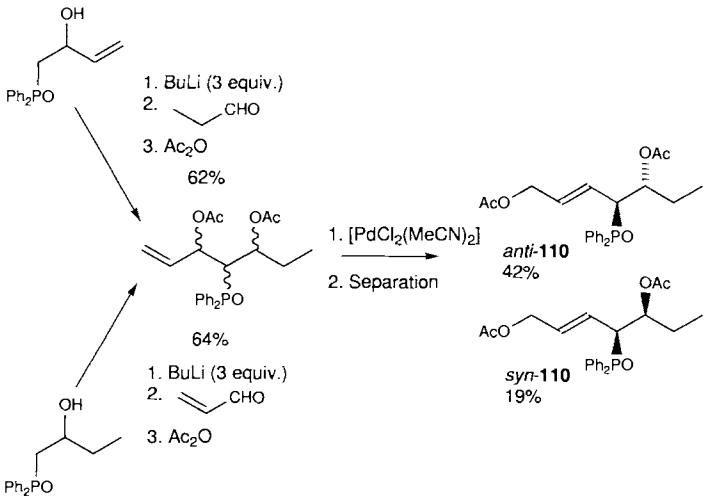

Scheme 14. Synthesis of the allylic phosphane oxides *anti*- and *syn*-**110** by a modified SCOOPY reaction [42].

4.2.4. Alkenyl Isoxazoles

(*E*) Alkenyl isoxazoles **115** and **5** are interesting as leukotriene analogues. They have been made in a one-step Horner–Wittig reaction from phosphane oxides **114** and **4**, which are easily synthesized by cycloaddition chemistry.[33] Two-step Horner–Wittig reactions of these phosphane oxides were unsuccessful due to Horner–Wittig reversal of the intermediate β-hydroxy

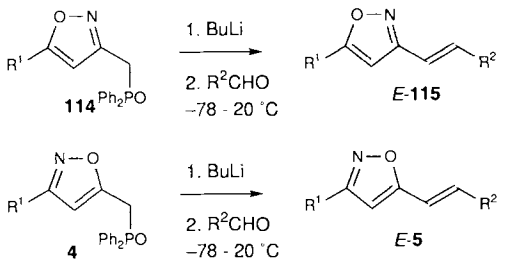

phosphane oxides (Section 2.1). The alternative addition of ethyldiphenylphosphane oxide to aldehydes **116** was unselective as well, and elimination of the pure *anti* isomer **117** gave mixtures of (*E*) and (*Z*) alkenes **118** (Scheme 15). Reduction of the corresponding ketone gave *syn*-**117**, which could be converted stereospecifically into (*E*) alkenes (*E*)-**118**, but none of these approaches was as good as the one-step route.

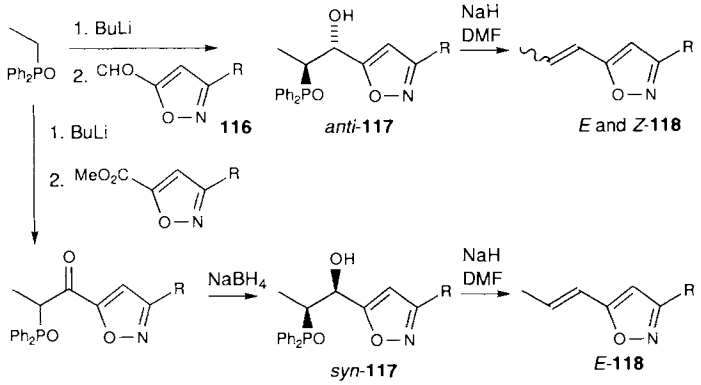

Scheme 15. Synthesis of the alkenyl isoxazoles (*E*)- and (*Z*)-**118**.

4.2.5. *Heteroatoms in Vinylic Positions*

Horner–Wittig routes to alkenes carrying heteroatoms in vinylic positions are successful, providing R^1 is the functional group containing the hetereoatom. Vinyl sulfides, ethers, and amines have all been made by stereocontrolled two-step Horner–Wittig routes, but in the case of the sulfides, completion of the elimination is rapid and special precautions must be taken to isolate the intermediates.

4.2.5.1. *Vinyl Sulfides*

Lithiation of **119** and addition to an aldehyde gives a diastereomeric mixture of β-hydroxy phosphane oxide adducts **120**, which can be isolated as the alcohols **121** by quenching with acid at low temperature.[46] If the reaction mixture is instead warmed to room temperature, Horner–Wittig elimination takes place and a mixture of stereoisomers of the vinyl sulfide **122** is isolated.[36, 116] This one-step olefination is moderately (*E*) selective, and the selectivity is determined by the ratio of diastereomers formed in the addition step. Pure (*E*) and (*Z*) vinyl sulfides **124** have been prepared by elimination of single diastereomers of **123**, which are obtained from α-phenylthiopropyldiphenylphosphane oxide.[46]

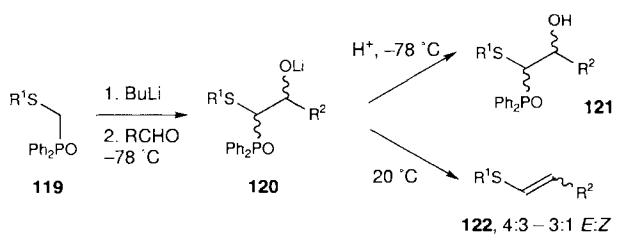

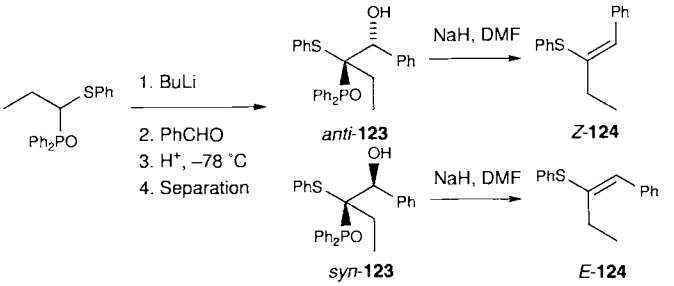

4.2.5.2. *Enol Ethers*

When alkoxyalkyldiphenylphosphane oxides are lithiated with LDA, they add successfully to aldehydes and ketones.[44] The C–C bond forming additions are unselective, but separation of the diastereomers and elimination allows stereospecific synthesis of (*E*) and (*Z*) enol ethers such as (*E*)- and (*Z*)-**125** (Scheme 16). Ketene acetals **126** have been made by a similar route [Eq. (m)].[45] In this case, there is no question of stereo-

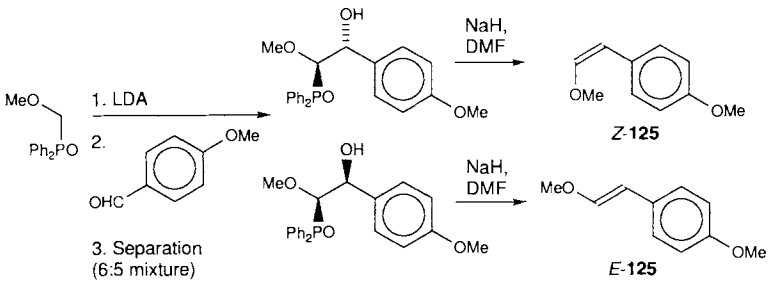

Scheme 16. Synthesis of enol ethers (*Z*)- and (*E*)-**125**.

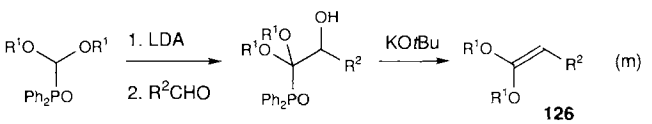

chemistry, and the olefination can be carried out as a one-step reaction if the addition reaction mixture is warmed. Bosch used a one-step Horner–Wittig addition to make enol ether **127** [Eq. (n)].[35] This elimination is presumably encouraged by conjugation.

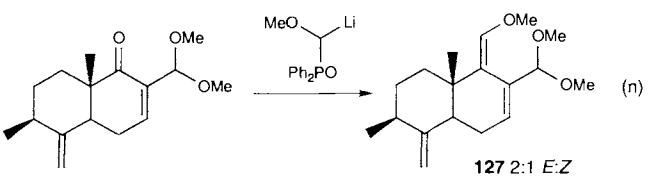

Enol ethers bearing amino groups have been made using nitrile oxide cycloadditions (Section 4.3.4).[105]

4.2.5.3. Enamines

Van der Gen et al. have shown that although addition of lithiated amino phosphane oxides **128** to aldehydes gives a mixture of diastereomers **129**, which can be isolated, elimination of these mixtures with potassium bases leads exclusively to the (*E*) enamines **130**.[14, 39] They ascribe this to an isomerization of the enamine during the workup.

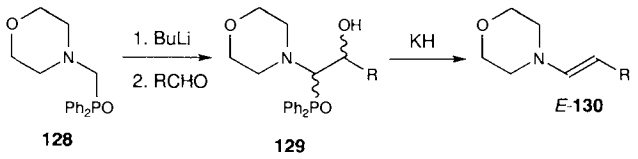

4.3. Functional Groups in Homoallylic and More Remote Positions

4.3.1. Unsaturated Ketones

4.3.1.1. γ,δ-Unsaturated Ketones

γ,δ-Unsaturated ketones can be made by the two-step Horner–Wittig reaction.[117] The carbonyl group is included in the alkyl phosphane oxide as an acetal **131**. In contrast with protected β-Ph_2PO ketones (see Section 4.3.1.2), these protected γ-Ph_2PO ketones undergo Horner–Wittig additions to aldehydes with good *anti* selectivity. Purification of the *anti* diastereomer *anti*-**132** and elimination with NaH/DMF gives the protected ketone (*Z*)-**133**.

(*E*)-γ,δ-Unsaturated ketones are made by stereoselective reduction of the ketones **134** with $NaBH_4$. Purification of the major *syn* isomer and elimination gives ketone (*E*)-**133**.

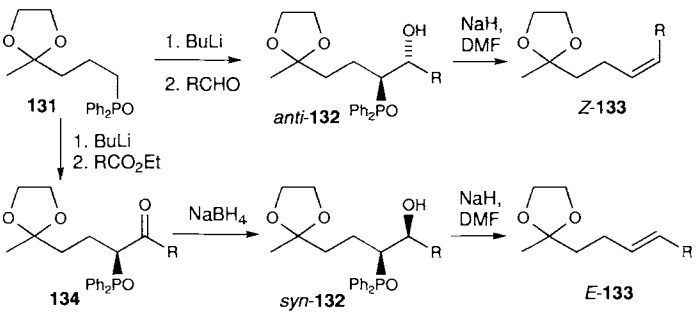

4.3.1.2. β,γ-Unsaturated Ketones

Horner–Wittig reactions of protected β-Ph_2PO ketones **135** can be used to make β,γ-unsaturated ketones **137**[118] in much the same way that γ-Ph_2PO ketones give γ,δ-unsaturated ketones. However, the stereoselectivity of the addition is poor, and the diastereomers of the intermediate hydroxy phosphane oxides **136** are hard to separate. In only one case (R = *n*Pr) was it possible to isolate the pure intermediate *anti*-**138**: as expected, elimination gave the (*Z*) alkene (*Z*)-**139**. Nonetheless, elimination of mixtures of diastereomers of **136** produced by the Horner–Wittig reaction gives good yields of mixtures of alkenes; the protecting acetal group can then be removed without shifting the double bond into conjugation. Protected β-Ph_2PO ketones therefore perform well as homenolate equivalents, provided single stereochemical isomers of the product alkenes are not required.

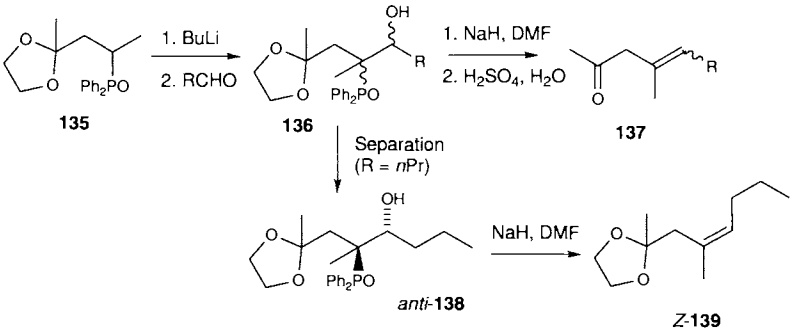

4.3.2. Unsaturated Carboxylic Acids

Horner–Wittig eliminations leading to carboxylic acids **141** are best carried out directly with the lactones **140**.[119] The lactones are hydrolyzed with an excess KOH in aqueous THF, and the solvents removed by freeze-drying to give a solid mixture of KOH and the potassium salt of the hydroxy carboxylic acid. The Horner–Wittig elimination takes place stereospecifically when the dried salt is dissolved in DMSO.

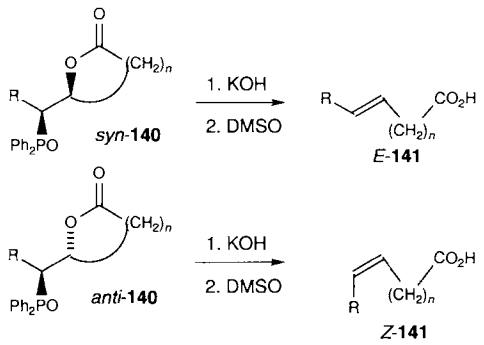

The problem of making single stereoisomers of unsaturated carboxylic acids is therefore reduced to making and separating the two diastereomeric lactones **140**. This has been achieved by two complementary routes: the first is more successful for (*E*) carboxylic acids, and the second for (*Z*), though each is applicable to both.

4.3.2.1. Route Recommended for (E) Unsaturated Carboxylic Acids

Diphenylphosphoryl carboxylic acids, even as polyanions, do not undergo Horner–Wittig addition reactions.[119] Reduction of the oxo carboxylic acids or oxo esters **142** with $NaBH_4$ is successful but only marginally stereoselective, and the diastereomeric products **143**, are difficult to separate. However, the lactones **140** are crystalline and easily separable. After lactonization of the mixture of esters **143** *syn*- and *anti*-**140** can be separated, and hence the (*E*) and (*Z*) unsaturated acids **141** prepared.

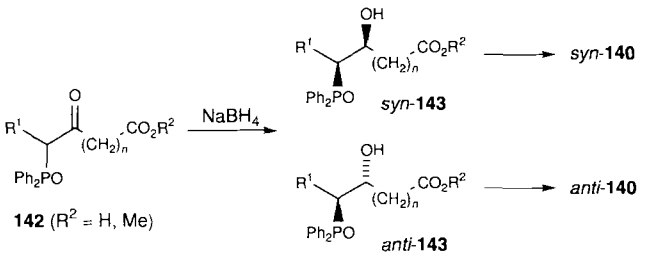

4.3.2.2. Route Recommended for (Z) Unsaturated Carboxylic Acids

An alternative approach uses the cyclic alcohols **144** (Scheme 17).[73] These compounds can be made with high stereoselectivity by addition of lithiated alkyldiphenylphosphane oxides to epoxides (Section 3.1.5). Oxidation of **144** gives pure *anti*-**145**, which is converted into the lactone *anti*-**146** by Baeyer–Villiger oxidation. Subsequent hydrolysis and elimination according to the procedure described above gives the pure (*Z*) carboxylic acid (*Z*)-**141**.

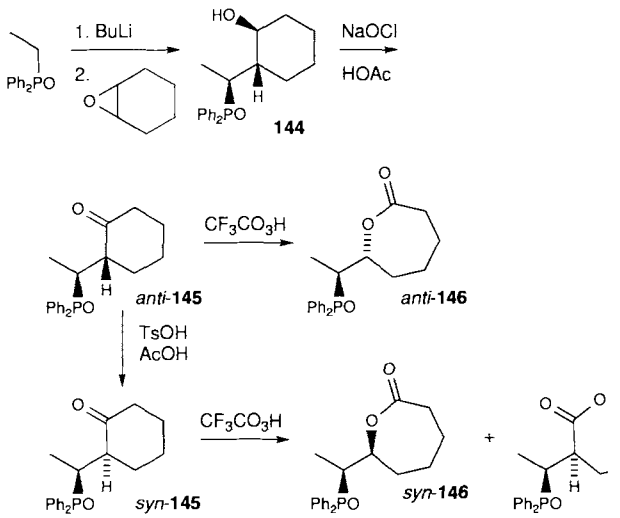

Scheme 17. Synthesis of a precursor for a (*Z*) unsaturated carboxylic acid; Ts = $H_3CC_6H_4SO_2$.

The *syn* ketone *syn*-**145** is made by epimerization of the ketone *anti*-**145**. Exposure to TsOH/AcOH for one week converts *anti*-**145** into 10:1 mixture of *syn*-**145** and *anti*-**145**, from which pure *syn*-**145** can be isolated in 81% yield. In this case, however, the Baeyer–Villiger reaction is not regiospecific, giving two inseparable lactones *syn*-**146** and **147**, and lowering the overall yield. After hydrolysis and elimination of the mixture, the (*E*) carboxylic acid can be separated from the by-products, as only one of the hydroxy carboxylic acids can undergo Horner–Wittig elimination.

4.3.3. Unsaturated Alcohols

4.3.3.1. (Z) Unsaturated Alcohols

Although Horner–Wittig additions of alkyldiphenylphosphane oxides carrying hydroxy or silyloxy groups are usually rather unselective, giving the product as 50:50 to 70:30 mixtures of diastereomers in favor of the *anti* adduct, separation of the product alcohols and elimination can lead to pure (*E*) or (*Z*) unsaturated alcohols. The (*Z*) homoallylic alcohol (*Z*)-**149** was made from phosphane oxide **148** and benzaldehyde by this strategy [Eq. (o)].[75] Van den Nieuwendijk and van der Gen made the (*Z*) unsaturated alcohol (*Z*)-**92** by the alternative route, addition of a phosphane oxide to a hydroxy aldehyde.[114]

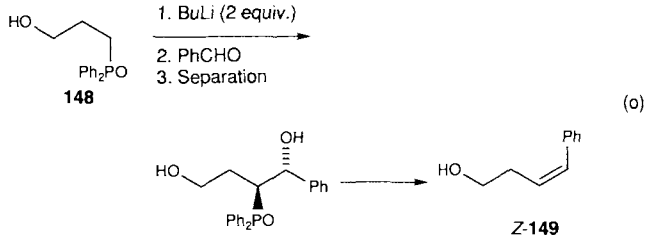

4.3.3.2. (E) Unsaturated Alcohols

(*E*) Unsaturated alcohols can be made by *syn*-selective reduction of the oxo alcohols **150** or **151**. Oxo alcohols **150** are available by addition of lithiated phosphane oxides to lactones and are best reduced with $NaBH_4$.[63, 75] This route was used to make (*E*)-dec-5-en-1-ol (*E*)-**152**, a pheromone of the peach twig borer moth (Scheme 18).[63] Oxo alcohols **151** are available by

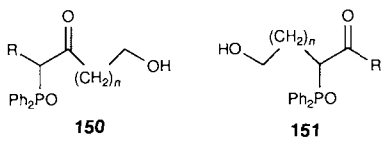

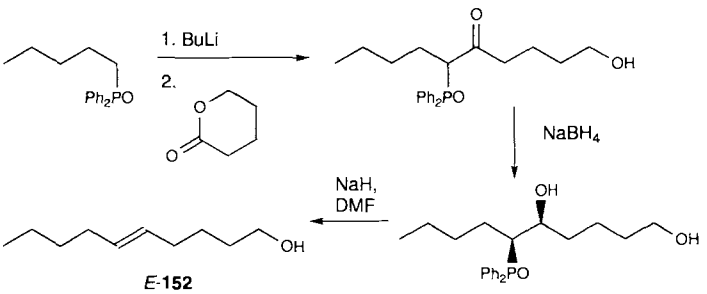

Scheme 18. Synthesis of the pheromone (*E*)-**152** from the peach tree borer moth.

intramolecular acyl transfer and can be *syn*-selectively reduced either with $NaBH_4$[67] (e.g. **153**) or, for **154** (≡**151**, $n = 1$), with $NaBH_4/CeCl_3$ (Luche conditions) (Scheme 19).[75] (*E*) Homoallylic alcohols are among the very best target compounds that can be prepared by phosphane oxide chemistry because Luche reduction of their precursor ketones is extremely (>95:5) *syn* selective.

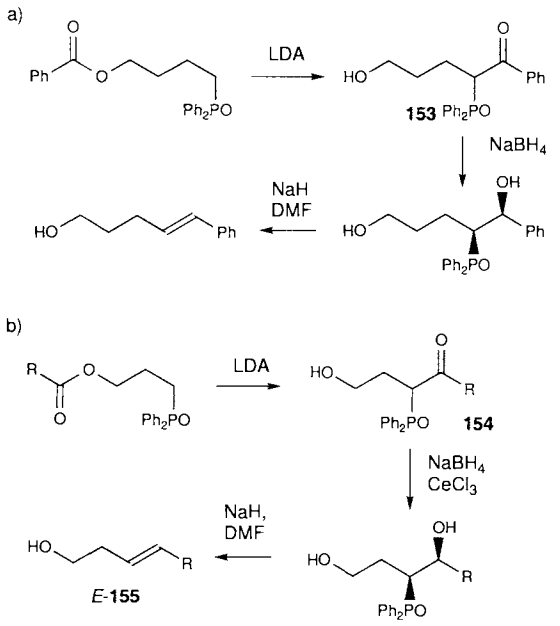

Scheme 19. Synthesis of the (*E*) unsaturated alcohols (*E*)-5-phenylpent-4-enol-1 (a) and (*E*)-**155** (b).

The starting materials for a synthesis of an (*E*) homoallylic alcohol by this route are the alcohols **156**, which are available either by addition of a lithiated phosphane oxide to an epoxide[67] or by hydroboration[58] of an allylic phosphane oxide [Eq. (p)]. When the starting alcohol contains a chiral center, the

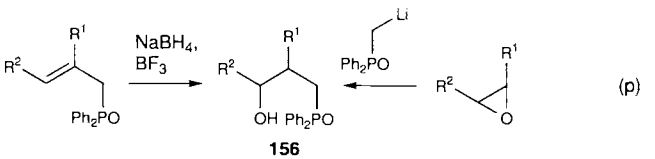

(p)

acyl transfer can be stereoselective, allowing the synthesis of homoallylic alcohols with chiral substituents such as **158** (Scheme 20).[58] Although simple Horner–Wittig additions have been used to make chiral alkenes (e.g. **96**), there is always the danger that a third chiral center could complicate the clean separation of diastereomers. The method describes here avoids this problem, since construction of all three chiral centers of **157** is controlled, though stereochemical information is lost in the elimination step.

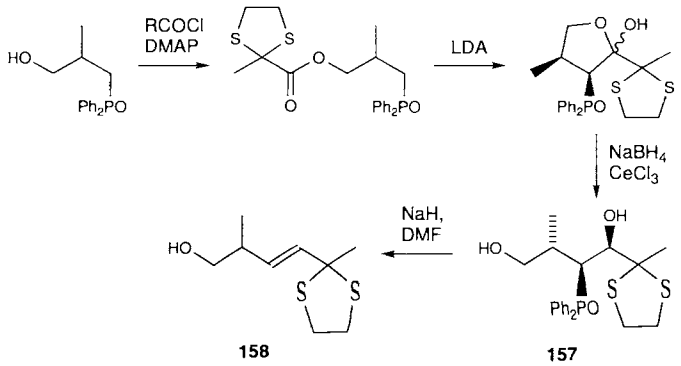

Scheme 20. Synthesis of the homoallylic alcohol **158**; DMAP = 4-dimethylaminopyridine.

Interestingly, treatment of the oxo alcohols **154** with base can lead to phosphoryl migration and formation of cyclopropyl ketones **159** or γ-hydroxy ketones **160** (Scheme 21).[58, 67]

Certain branched (*E*) homoallylic alcohols can also be synthesized by opening epoxy phosphane oxides with carbon nucleophiles (Section 4.5).

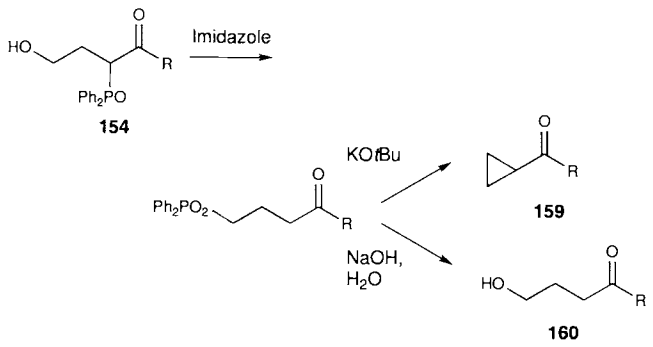

Scheme 21. Base-catalyzed migration of the Ph_3PO group of **154** leading to **159** and **160**.

4.3.4. Homoallylic Amines

Cycloaddition of a nitrile oxide to an allylic phosphane oxide **78** is an effective way of stereoselectively introducing the hydroxyl and amino functional groups needed to make a homoallylic amine by Horner–Wittig elimination.[15] As discussed in Section 3.3.4, this reaction is regio- and stereoselective, giving mainly the *syn* isomer *syn*-**79**. The diastereomers of the cyclo-

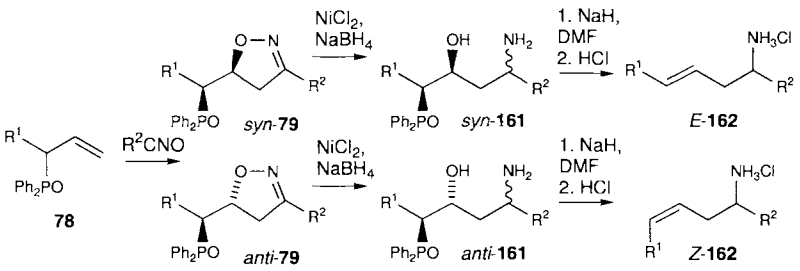

adduct are easily separated by chromatography. Reduction of the isoxazoline to reveal the alcohol needed for Horner–Wittig elimination is achieved with nickel boride. This reaction is moderately stereoselective too, though the diastereomers of the amino alcohols **161** are very difficult to separate. This is unimportant from a practical point of view, since, in the final step, both of these diastereomers give the same homoallylic amine (*E*) or (*Z*)-**162**. The *syn* and *anti* diastereomers of the cycloadducts **79** can be carried through to elimination separately, giving stereospecifically the (*E*) and (*Z*) homoallylic amines **162**, respectively. The amines are most easily isolated as their hydrochloride salts.

4.4. Functional Groups in Allylic Positions

4.4.1. α,β-Unsaturated Ketones

α,β-Unsaturated ketones **164** are very easily made by the Wadsworth–Emmons reaction of β-oxo phosphonates **163** (Scheme 22).[120, 121] However, the Horner–Wittig equivalent

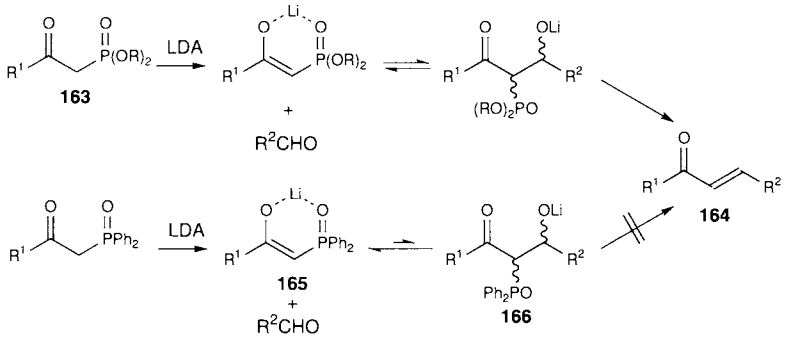

Scheme 22. Synthesis of the α,β-unsaturated ketones **164**.

of this reaction fails.[122] Presumably the Wadsworth–Emmons reaction is driven to completion by spontaneous elimination of phosphate. In the Horner–Wittig reaction the equilibrium between the lithiated α-Ph_2PO ketone **165**[61] and the adducts **166** clearly lies on the side of the starting materials, and as elimination of phosphonate has to be a separate step, only starting materials can be recovered.

Azaenolates formed from imines **167** do, however, combine with aldehydes to give enones **164** [Eq. (q)].[123, 124] The lithiated Ph_2PO-imines were heated with the aldehydes to complete the elimination.

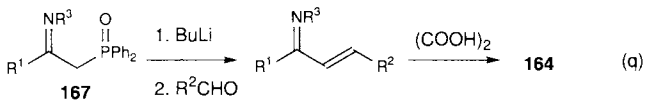

(q)

4.4.2. Allylic Amines and Amides

Lithiated alkyldiphenylphosphane oxides **168** with functional groups X in the β position are prone to fragmentation to give vinyl phosphane oxides **169** [Eq. (r)], and are therefore usually

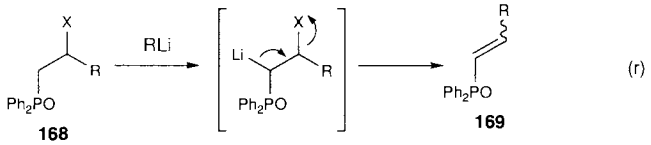

(r)

poor choices as starting materials for Horner–Wittig additions. It is for this reason that the more uncoventional routes to the β-hydroxy phosphane oxides, which are needed to make the allylic functionalized compounds discussed towards the end of this review, have been developed. However, when the β-substituent X is a poor leaving group, such as R_2N, RCONLi, or OLi, the lithiated compounds are stable, and Horner–Wittig additions are possible.

As usual for functionalized phosphane oxides capable of chelating Li^+, the stereoselectivity in the Horner–Wittig addition of the amines **170** is low, but the isomers of the product **171** could be separated and gave the (*E*) and (*Z*) allylic amines stereospecifically (Scheme 23).[60] (*E*) and (*Z*) amides **174** could be made by the same route, starting with bis-lithiation of phosphane oxides **172**. Separation of the two diastereomers **173** formed in the addition to acetaldehyde followed by elimination gave the (*E*) and (*Z*) amides **174** stereospecifically. Interestingly, only two diastereomers of **173** arise from this reaction, just as in the reaction of the **172** with symmetrical ketones. Both have the same (*anti*) relative stereochemistry at the third chiral center, though this is irrelevant to the stereochemistry of the allylic amides **174**.

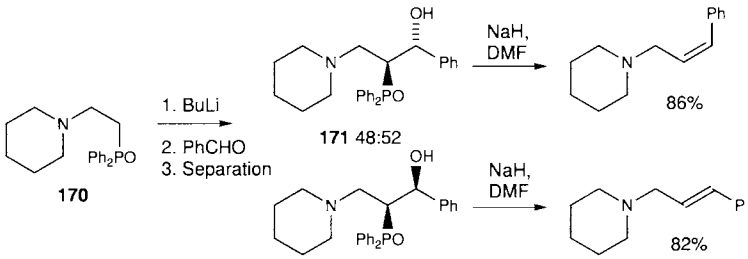

Scheme 23. Synthesis of allylic amines.

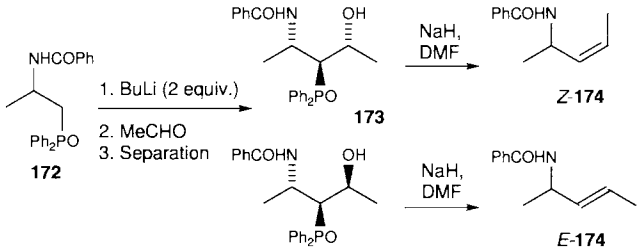

In additions of the amide **175** (doubly lithiated) to aldehydes high stereoselectivity was observed for the formation of the two new chiral centers. Moreover, the major isomer (formed almost exclusively in the reaction of **175** with benzaldehyde) was remarkably the *syn* diastereomer *syn*-**176**. Horner–Wittig elimination gave (*E*) allylic amide (*E*)-**177** in excellent overall yield

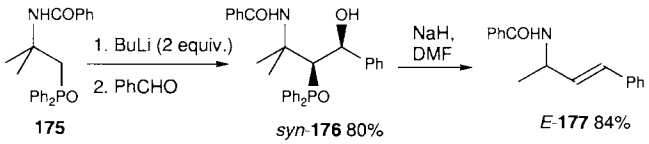

from **175**. Such unexpected results mean that although the Horner–Wittig route may not be the first choice in the synthesis of an allylic amide, in certain cases it may significantly outperform its competitors.

4.4.3. Allylic Alcohols

anti-Selective osmylation of allylic phosphane oxides gives *anti,syn* diols, which undergo Horner–Wittig elimination to give (*Z*) alkenes. The otherwise difficult to make exocyclic (*Z*) alkene **178** was made in this manner [Eq. (s)].[91]

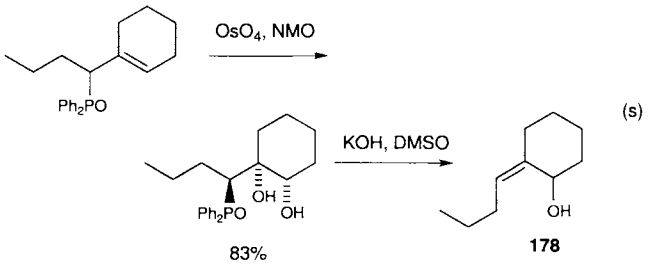

An altogether different route makes use of a reduction step rather than a Horner–Wittig elimination to remove the Ph_2PO group used to construct the carbon skeleton of the alkene. Treatment of the alcohols **180**, prepared by Horner–Wittig addition of lithiated allylic phosphane oxides **179** to aldehydes, with $LiAlH_4$ gives (*E*) allylic alcohols **182**.[125] It is presumed that the hydroxyl group delivers the reducing agent to the allylic phosphane oxide (**181**). The (*E*) stereochemistry in this case is the result of stereoselective migration of a double bond rather than a stereospecific elimination.

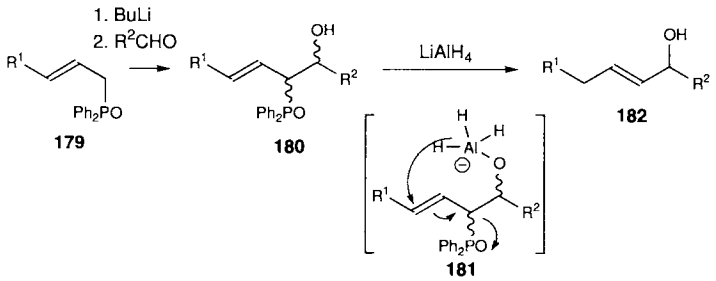

(*E*) allylic alcohols with trisubstituted double bonds can be made from the major diastereoisomer formed with excellent stereoselectivity in the vanadium(II)-promoted mixed pinacol reactions of aldehydes such as **183** and 3-phenylpropanal.[84] Crystallization of the diol **184** removes traces of the unwanted diastereomer, and elimination with NaH/THF gives excellent yields of the allylic alcohols **185**.

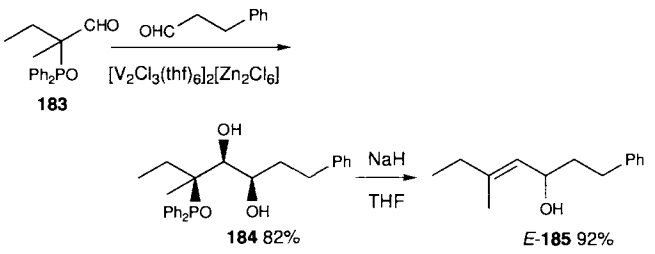

(*E*) and (*Z*) allylic alcohols bearing substituents in homoallylic position have been made from Ph_2PO epoxy alcohols (Section 4.5).

4.4.4. *Allylic Sulfides*

The epoxide **187** of an allylic phosphane oxide **186** is an excellent starting point for synthesizing a whole variety of compounds **189** functionalized in the allylic position. As discussed in Section 3.3, epoxidations can be *syn* or *anti* selective, and even

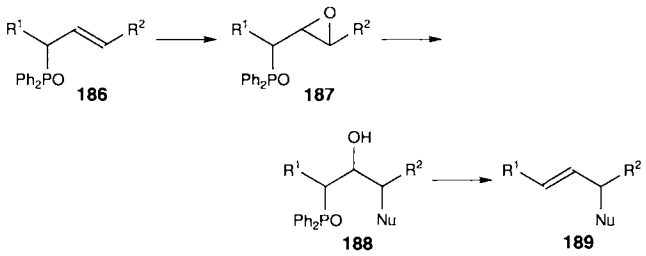

enantioselective, and through epoxide opening a range of functional groups can be introduced yielding products **188**. For example, the allylic sulfides **191** were made by epoxidation of the allylic phosphane oxide **190**, regioselective nucleophilic ring opening with a thiolate, and Horner–Wittig elimination (Scheme 24).[91, 126] Similar reactions form the basis of most of the chemistry discussed in the remainder of this review.

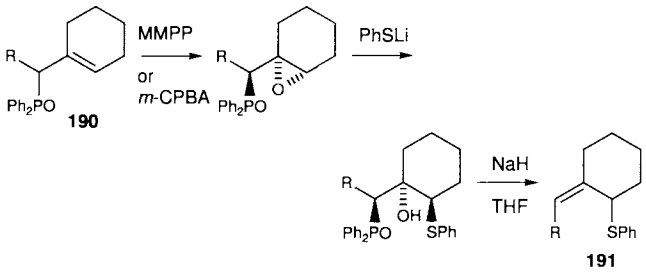

Scheme 24. Synthesis of the allylic sulfides **191**; MMPP = magnesium monoperoxyphthalate.

4.5. Functional Groups in Both Allylic and Homoallylic Positions

The compounds discussed in this section are the products of reactions of epoxy alcohols **193** and **197**. In Sections 3.3.1 and 3.3.2 we described how these compounds can be made from **192** and **196**, respectively, by diastereo- and enantioselective epoxidation reactions. A regioselective (and stereospecific) ring-opening reaction and Horner–Wittig elimination of the resulting alcohols **194** and **196** completes the stereocontrolled synthesis of alkenes **195** and **199**, which have functional groups

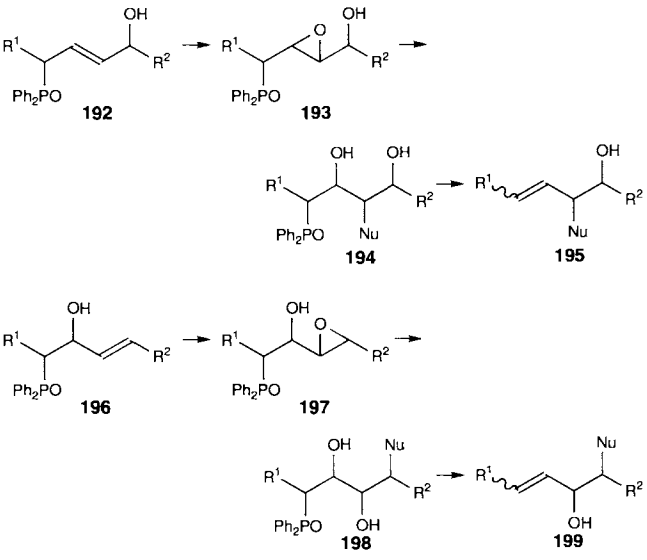

in allylic and homoallylic positions, respectively. By modifying reagents or route, either enantiomer of any diastereomer of the epoxy alcohol **193** can be made, and each enantiomer will stereospecifically produce an enantiomerically pure diastereomer of a substituted alkene **195**. The main problem encountered in using this strategy is the regioselectivity of the epoxide-opening step, and ways of synthesizing the required regioisomer selectively for are discussed for each of the classes of target compound.

4.5.1. Unsaturated Hydroxy Sulfides

Epoxy alcohols **201** and **205**, which result from the cooperative epoxidation of the respective allylic alcohols **200** and **204** (Section 3.3.1), react with thiolate nucleophiles stereospecifically at their less hindered terminal carbon atoms to give sulfides **202** and **206**, respectively.[57] Horner–Wittig elimination of these sulfides gave the (*Z*) allylic alcohols **203** and **207**. Only the

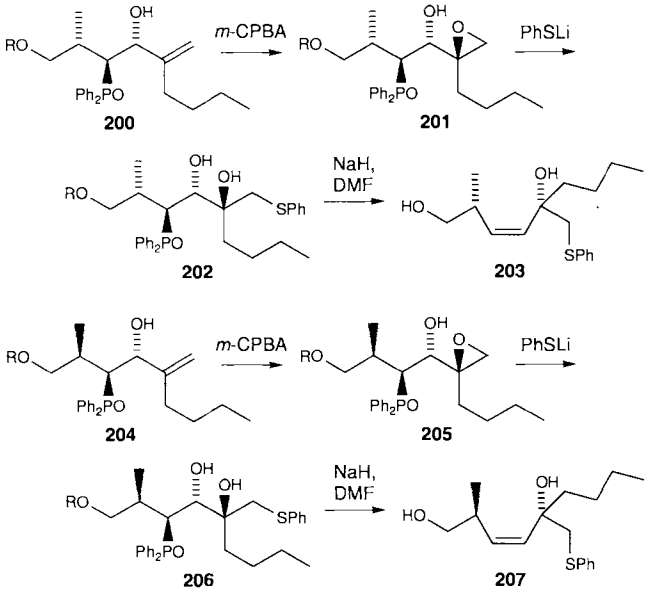

(*Z*) alkenes can be made in this way because only *anti* β-hydroxy phosphane oxides can be epoxidized stereoselectively. The stereoselectivity of the epoxidation is in fact important only because a fourth chiral center is present in the molecule. The 1,4-chiral relationship in these alkenes will be discussed further in Section 4.6.

Epoxy alcohols **193**, which are formally the Payne-rearranged analogues of epoxy alcohols **197**, are valuable as intermediates because they can be made enantioselectively by Sharpless asymmetric epoxidation and kinetic resolution.[100] By making use of the complementarity between the stereoselectivity of the kinetic resolution and of the *syn*-selective peracid epoxidation[92] it is in fact possible to make both diastereomers of the epoxides in each enantiomeric sequence from the same starting materials by choice of route.[127–129] For example, optically active *anti* epoxide *anti*-**208** is the main product of kinetic resolution of **60**. Treatment of the enantiomerically enriched remaining starting material with *m*CPBA gives optically active *syn* epoxide *syn*-**208**. Either enantiomer of each diastereomer of **208** is available

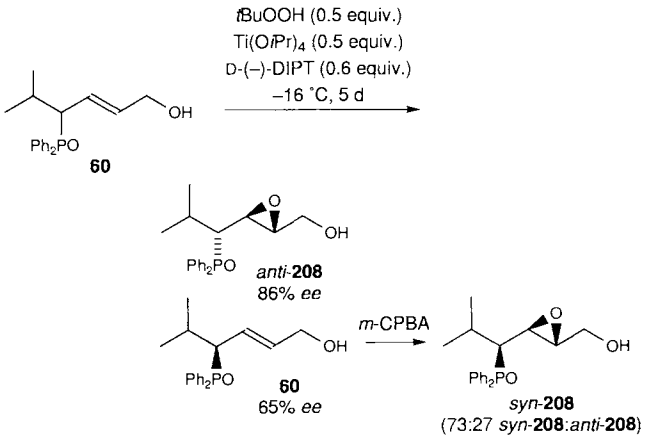

simply by using the appropriate enantiomer of tartrate ester in the kinetic resolution. Application of these epoxides in synthesis does, however, pose some problems, firstly because of the lack of regioselectivity in the reactions of 1,2-disubstituted epoxides, and secondly because they are prone to undergo base-catalyzed elimination reactions to give vinylic phosphine oxides **209** [Eq. (t)].

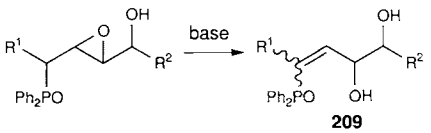

(t)

The asymmetric synthesis of the sulfides **214** from enantiomerically enriched epoxides **210** (Scheme 25) aimed to avoid the regioselectivity problem by using a Payne rearrangement to produce a terminal epoxide **213**, which would undergo regiose-

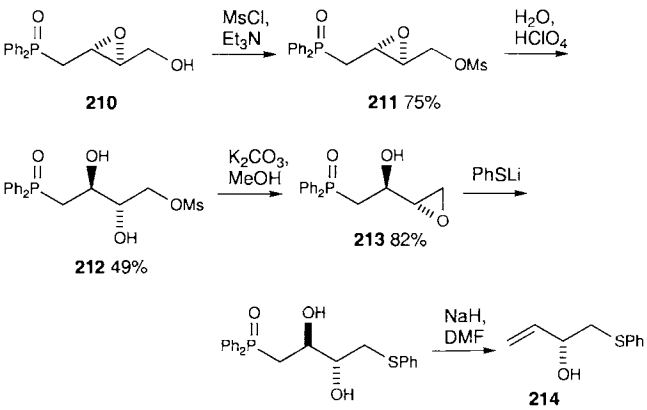

Scheme 25. Synthesis of the unsaturated hydroxysulfide **214**.

lective ring opening. The Payne rearrangement could not be carried out under basic conditions because of the problem of base-catalyzed elimination, so Sharpless's stepwise controlled Payne route[130] was used. Epoxide opening and Horner–Wittig elimination gave the allylic alcohol **214**. Unfortunately, regiocontrol still posed a problem because the nonregioselective addition of water to epoxide **211** resulted in reduced enantiomeric excess in the product diol **212**.[128]

Lack of regioselectivity in the attack of thiolate nucleophiles on epoxy alcohols **215** and **219** was overcome by first oxidizing them to ketones **216** and **220** (Scheme 26).[128, 131] Nucleophilic

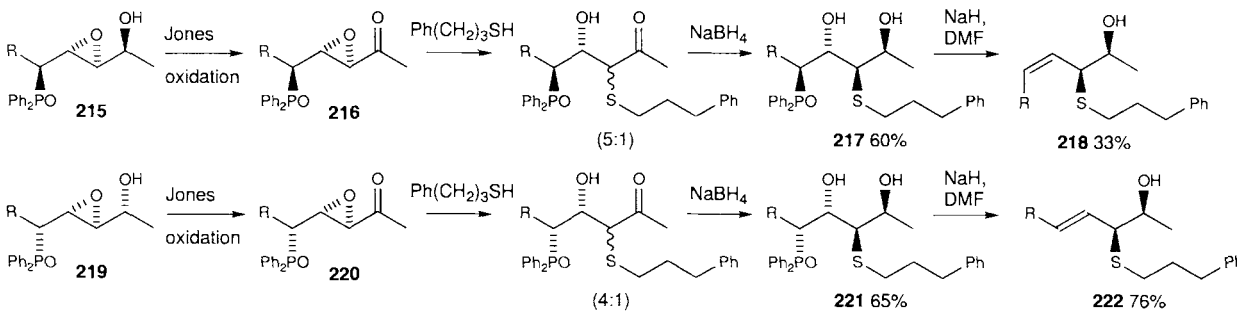

Scheme 26. Synthesis of the unsaturated hydroxysulfide **214**.

addition was then regioselective, though not completely stereospecific, and small quantities of epimerized sulfides were produced. Horner–Wittig eliminations of these compounds proved impossible because of a competing fragmentation. However, reduction to the alcohols **217** and **221** was stereoselective; the reaction was directed by the arylthio substituent and gave the diastereomer predicted by a Felkin–Anh transition state. Horner–Wittig elimination gave stereospecifically the (*E*) and (*Z*) allylic sulfides **218** and **222**.

The regioselectivity of the ring opening of the optically active epoxides **208** by thiolate nucleophiles was controlled by using a Lewis acidic reagent, trimethylaluminum.[128] The aluminum thiolate gave only one regioisomer of the products **223** and **225**, while lithium thiolates led to mixtures of regioisomers in low yield. Horner–Wittig eliminations gave the optically active allylic sulfides (*E*)- and (*Z*)-**224**. The low yield of (*Z*)-**224** illustrates a general problem with the synthesis of alkenes bearing groups that can stabilize anions (e.g. thio or acyl substituents). Often these groups encourage fragmentation rather than Horner–Wittig elimination. This problem is especially noticeable with slower eliminations leading to (*Z*) alkenes.

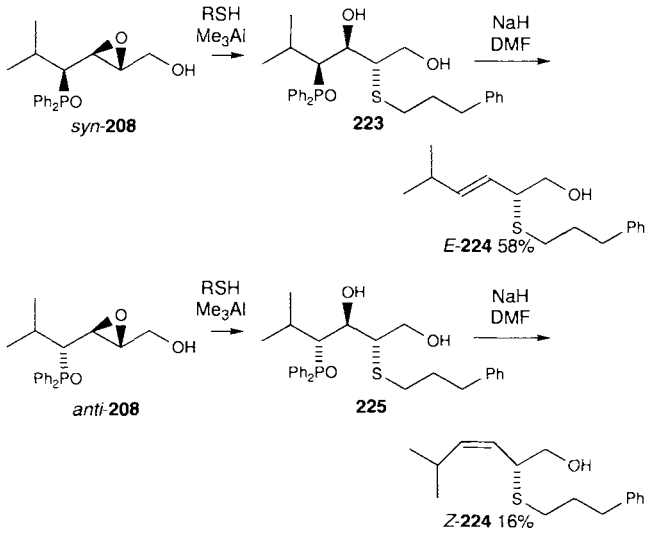

Lewis acid promoted regioselective epoxide opening was also used to introduce nitrogen and carbon nucleophiles. The reaction was surprisingly substrate dependent: *syn*-**208** was much more reactive than *anti*-**208**.[128] Horner–Wittig elimination of **226** gave the optically active (*E*) homoallylic alcohol (*E*)-**227**.

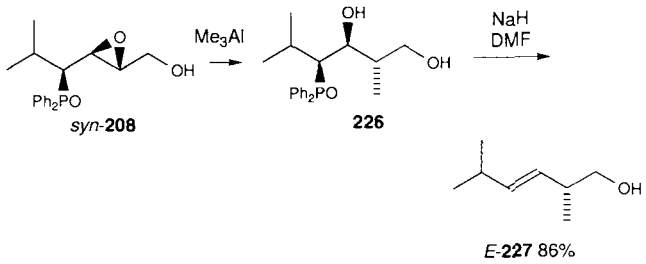

4.5.2. *Unsaturated Amino Acids*

After the epoxy alcohols **228** were oxidized to the acids **229**, regioselective ring opening succeeded with benzylamine.[127, 128] The product of this reaction is a protected amino acid, and Horner–Wittig elimination of **230** and **232** led to the interesting unsaturated protected amino acids (*E*)- and (*Z*)-**231**. Choice of synthetic route and of chiral catalyst allowed access to either enantiomer of either (*E*)/(*Z*) isomer.[127]

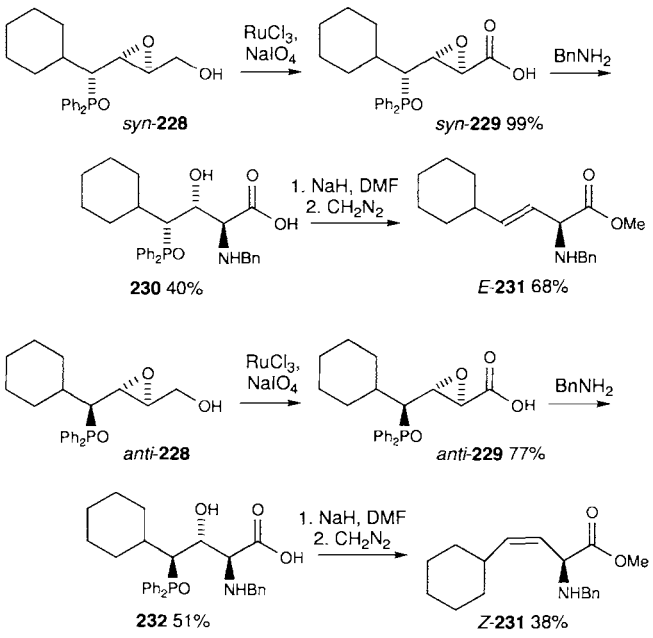

4.5.3. *Alkenyl Oxazolidinones*

A third strategy for ensuring regioselective ring opening was used to make single enantiomers and (*E*)/(*Z*) isomers of the

alkenyl oxazolidinones **234**.[129, 132] The nucleophile (a masked benzylamine equivalent) was tethered to the hydroxyl group of *syn*-**208** with formation of urethane **233**. Deprotonation with KOH in DMSO promoted attack of the nitrogen nucleophile on

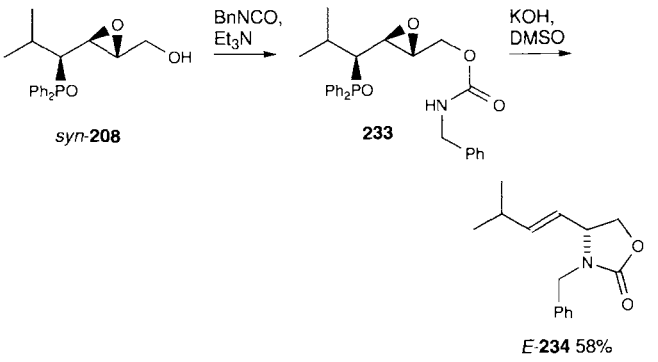

the nearer end of the epoxide to give a potassium oxyanion, which collapsed immediately in a Horner–Wittig elimination to give the alkenyl oxazolidinones **234**. Both enantiomers of both (*E*)/(*Z*) isomers could be made available in this way, and derivatives with further chiral centers could be prepared by starting with epoxides **235** and **236** (Scheme 27).

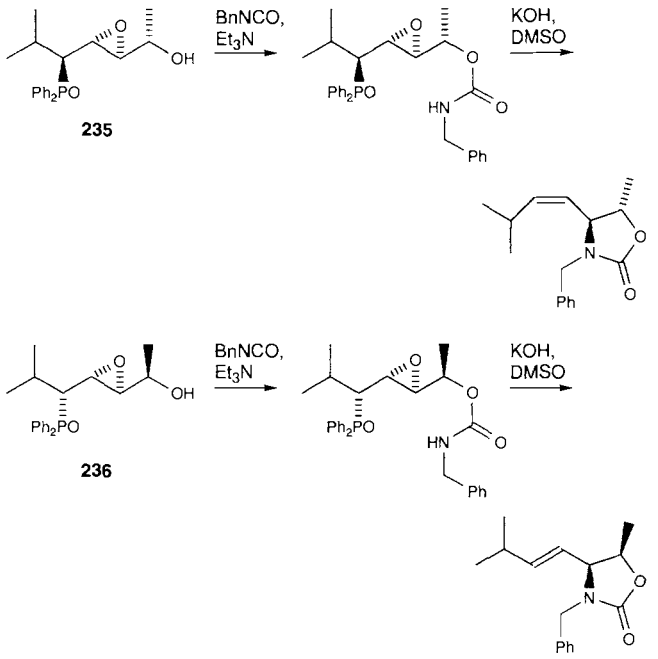

Scheme 27. Synthesis of alkenyloxazolidinones from epoxides **235** and **236**.

4.6. Remote Stereocontrol

Alkenes with chiral centers in the 1- and 4-positions have been synthesized by a number of strategies, most usually involving stereospecific allylic rearrangement of chiral centers from a 1,2- to a 1,4 relationship.[133–136] 1,4-Chiral relationships across (*Z*) double bonds are harder to control. Ph_2PO chemistry can be used to set up a sequence of four chiral centers, from which the middle two are converted by stereospecific elimination into a double bond of either stereochemistry. The diastereomeric pair of racemic (*Z*) alkenes **203** and **207** was made in this way (Section 4.4.4). Similar conversions may be used to control 1,4,5-related chiral centers across an (*E*) double bond. Stereoselective alkylation (Section 3.3.5) and stereoselective epoxidation (Section 3.3.1) gave epoxide **237**. Epoxide opening, reduction, and Horner–Wittig elimination gave a single diastereomer of the alkene **238** (Scheme 28).[95]

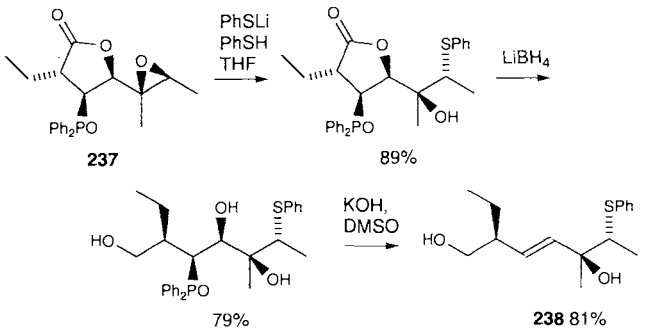

Scheme 28. Stereocontrolled synthesis of alkene **238**.

More recent work has extended this strategy to both (*E*) and (*Z*) alkenes in the homochiral series. Addition of lithiated **239** to acrolein gave a more or less random mixture of all four diastereomers of **240** (Scheme 29). Allylic rearrangement[111] converted these four into two diastereomers of **241**, which could be separated by HPLC after hydrolysis to give the alcohols *syn*- and *anti*-**242**. By using a combination of kinetic resolution[100] and peracid epoxidation,[92] all four diastereomers of the epoxides **243** were made, and each was elaborated with the tethered nucleophile employed to make alkenyl oxazolidinones. One-step ring opening of the epoxide and Horner–Wittig elimination then gave, stereospecifically, the four isomers **244**, one from each diastereomer of epoxide (Scheme 29).[129, 132] Although the other enantiomeric series was not made, it is clearly available just by using the other enantiomer of tartrate ester in the Sharpless kinetic resolution step.

5. Modifications and Improvements to the Ph_2PO Group

We have considered a large number of the reactions of compounds containing the Ph_2PO group, in which starting materials, reagents, and conditions were changed to achieve the level and sense of stereocontrol required. One thing we have not considered altering is the Ph_2PO group itself. Variations on the Ph_2PO group have nonetheless been used to great effect. It has been shown, for example, that Horner–Wittig additions of alkyl bis(*ortho*-anisyl)phosphane oxides **245** are significantly more stereoselective than Horner–Wittig additions of their Ph_2PO counterparts [Eq. (u)].[137] The result of altering the steric bulk of the Ph_2PO group by linking the two phenyl rings together as in a dibenzophosphole system has also been investigated: while

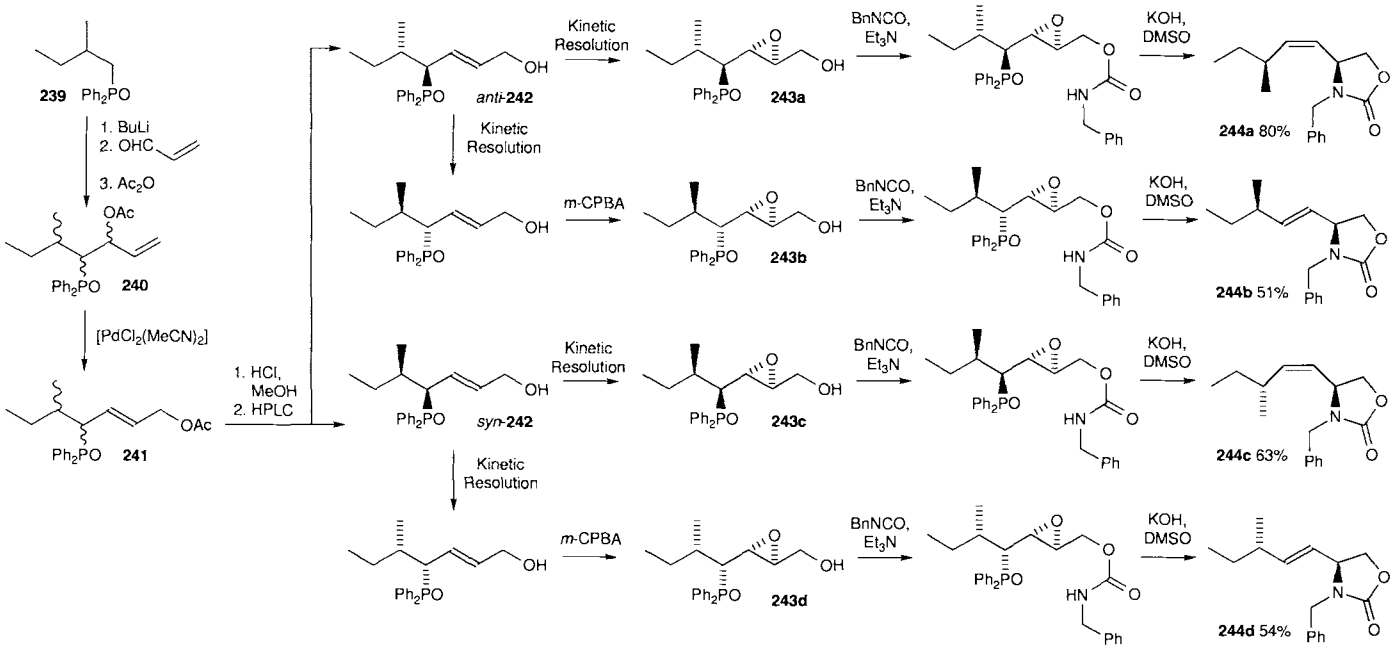

Scheme 29. Stereocontrolled synthesis of all four diastereomers of alkenyl oxazolidinone **244**.

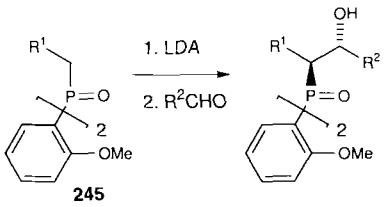

(u)

$NaBH_4$ reductions of α-dibenzophospholyl ketones such as **246** are *syn* selective, Luche reductions are invariably *anti* selective, in contrast with the strong substituent dependence of analogous reductions of Ph_2PO compounds. This result was applied to the synthesis of both (*E*)- and (*Z*)-isosafrole [(*E*)- and *Z*-**100**].

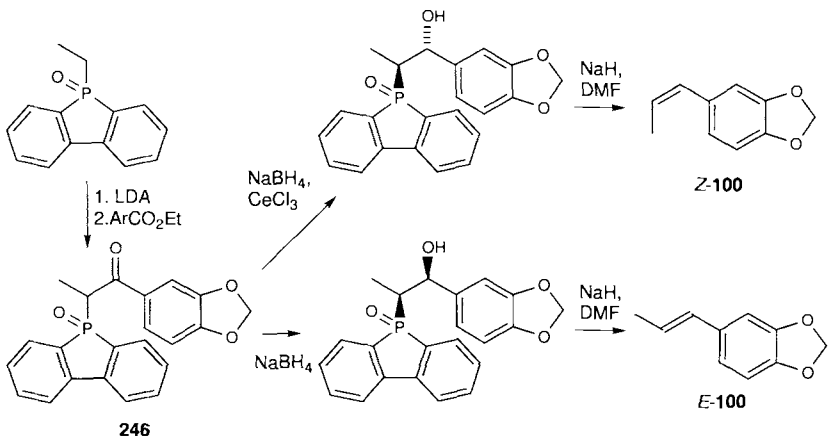

Scheme 30. Synthesis of (*Z*)- and (*E*)-**100** with a dibenzophosphole.

Asymmetric induction using chiral versions of the Ph_2PO group are currently under investigation: the anisylphenylphosphane oxide **247**[91] and the dihydrodibenzophosphepin oxide **248**[138] are being used to make individual (*E*) and (*Z*) isomers of homochiral compounds. Work is continuing in this area with the aim of developing new syntheses of enantiomerically pure alkenes with a recyclable phosphine oxide based chiral auxiliary.[138]

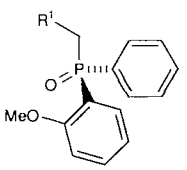

247

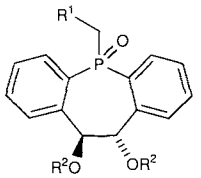

248

6. Summary

Chemists usually consider two chiral centers with a controlled three-dimensional relationship to be of greater "synthetic value" than a double bond with controlled stereochemistry in two dimensions: many synthetic strategies rely on the stereospecific transformation of a double bond into chiral centers with a three-dimensional chiral relationship. Transformations like the Horner–Wittig elimination that move in the other direction, sacrificing two controlled chiral centers for a double bond, therefore seem wasteful. This is particularly the case when the stereochemical information contained in a second controlled chiral relationship to a third chiral center is completely lost, as, for example, in the synthesis of racemic allylic alcohols by osmylation (Section 4.4.3). When that third chiral center is retained (as in the enantiomerically pure amino acids in Sec-

tion 4.5.2), or when two chiral centers and their controlled relationship are retained (e.g. **218** and **222**), such strategies seem more profitable. But in fact single (*E*)/(*Z*) isomers of alkenes are in general harder to make and purify than single diastereomers of chiral compounds, especially by connective methods. It is here that lies the greatest strength of the Horner–Wittig reaction, since it simplifies the production of stereochemically pure alkenes to the production of stereochemically pure diastereomers. Our aim in this review has been to demonstrate that the Ph_2PO group facilitates all three stages of this process: the stereoselective synthesis of these single diastereomers, their purification, and their stereospecific elimination to give pure alkenes.

Received: April 19, 1995 [A112IE]
German version: *Angew. Chem.* **1996**, *108*, 261–291

[1] L. Horner, H. Hoffmann, H. G. Wippel, G. Klahre, *Chem. Ber.* **1959**, *92*, 2499.
[2] L. Horner, H. Hoffmann, W. Klink, H. Ertel, V. G. Toscano, *Chem. Ber.* **1962**, *95*, 581.
[3] L. Horner, *Pure Appl. Chem.* **1964**, *9*, 225.
[4] L. Horner, W. Klink, *Tetrahedron Lett.* **1964**, 2467.
[5] E. Vedejs, *Top. Stereochem.* **1994**, *21*, 1.
[6] M. Schlosser, *Top. Stereochem.* **1970**, *5*, 1.
[7] B. E. Maryanoff, A. B. Reitz, *Chem. Rev.* **1989**, *89*, 863.
[8] W. S. Wadsworth, *Org. React.* **1977**, *25*, 73.
[9] A. D. Buss, S. Warren, *J. Chem. Soc. Perkin Trans. 1* **1985**, 2307.
[10] B. Lythgoe, T. A. Moran, M. E. N. Nambudiry, S. Ruston, *J. Chem. Soc. Perkin Trans. 1* **1976**, 2386.
[11] G. H. Posner, T. D. Nelson, *J. Org. Chem.* **1991**, *56*, 4339.
[12] E. Vedejs, J. B. Campbell, R. C. Gadwood, J. D. Rodgers, K. L. Spear, Y. Watanabe, *J. Org. Chem.* **1982**, *47*, 1534.
[13] J. Kallmerten, M. D. Wittman, *Tetrahedron Lett.* **1986**, *27*, 2443.
[14] B. H. Bakker, D. S. Tjin A-Lim, A. van der Gen, *Tetrahedron Lett.* **1984**, *25*, 4259.
[15] S. K. Armstrong, E. W. Collington, J. G. Knight, A. Naylor, S. Warren, *J. Chem. Soc. Perkin Trans. 1* **1993**, 1433.
[16] K. M. Brown, N. J. Lawrence, J. Liddle, F. Muhammad, D. A. Jackson, *Tetrahedron Lett.* **1994**, *35*, 6733.
[17] T. Fujimoto, Y. Hotei, H. Takeuchi, S. Tanaka, K. Ohta, I. Yamamoto, *J. Org. Chem.* **1991**, *56*, 4799.
[18] T. Fujimoto, Y. Uchiyama, Y. Kodama, K. Ohta, I. Yamamoto, *J. Org. Chem.* **1993**, *58*, 7322.
[19] I. Yamamoto, T. Fujimoto, K. Ohta, K. Matsuzaki, *J. Chem. Soc. Perkin Trans. 1* **1987**, 1537.
[20] I. Yamamoto, S. Tanaka, T. Fujimoto, K. Ohta, *J. Org. Chem.* **1989**, *54*, 747.
[21] D. Lednicer, *J. Org. Chem.* **1970**, *35*, 2307.
[22] D. Lednicer, *J. Org. Chem.* **1971**, *36*, 3473.
[23] P. F. Newton, G. H. Whitham, *J. Chem. Soc. Perkin Trans. 1* **1979**, 3067.
[24] S. L. Schreiber, T. Sammakia, D. E. Uehling, *J. Org. Chem.* **1989**, *56*, 15.
[25] A. D. Buss, S. Warren, J. S. Leake, G. H. Whitham, *J. Chem. Soc. Perkin Trans. 1* **1983**, 2215.
[26] B. Lythgoe, T. A. Moran, M. E. N. Nambudiry, J. Tideswell, P. W. Wright, *J. Chem. Soc. Perkin Trans. 1* **1978**, 590.
[27] J. M. Clough, G. Pattenden, *Tetrahedron Lett.* **1978**, 4159.
[28] R. E. Dolle, K. C. Nicolaou, *J. Chem. Soc. Chem. Commun.* **1985**, 1016.
[29] W. G. Dauben, R. R. Ollmann, A. S. Funhoff, S. S. Leung, A. W. Norman, J. E. Bishop, *Tetrahedron Lett.* **1991**, *32*, 4643.
[30] W. G. Dauben, L. J. Greenfield, *J. Org. Chem.* **1992**, *57*, 1597.
[31] K. L. Perlman, H. F. de Luca, *Tetrahedron Lett.* **1992**, *33*, 2937.
[32] A. Loupy, K. Sogadji, J. Seyden-Penne, *Synthesis* **1977**, 126.
[33] E. W. Collington, J. G. Knight, C. J. Wallis, S. Warren, *Tetrahedron Lett.* **1989**, *30*, 877.
[34] M. Schlosser, H. B. Thuong, *Chimia* **1976**, *30*, 197.
[35] M. P. Bosch, F. Camps, J. Coll, A. Guerrero, T. Tatsuoka, J. Meinwald, *J. Org. Chem.* **1986**, *51*, 773.
[36] J. I. Grayson, S. Warren, *J. Chem. Soc. Perkin Trans. 1* **1977**, 2263.
[37] B. Lythgoe, *Chem. Soc. Rev.* **1980**, 449.
[38] S. R. Schow, J. D. Bloom, A. S. Thompson, K. N. Winzenburg, A. B. Smith, *J. Am. Chem. Soc.* **1986**, *108*, 2662.
[39] N. L. J. M. Broekhof, F. L. Jonkers, A. van der Gan, *Tetrahedron Lett.* **1979**, 2433.
[40] P. S. Brown, N. Greeves, A. B. McElroy, S. Warren, *J. Chem. Soc. Perkin Trans. 1* **1991**, 1485.
[41] A. H. Davidson, S. Warren, *J. Chem. Soc. Perkin Trans. 1* **1976**, 639.
[42] J. Clayden, S. Warren, *J. Chem. Soc. Perkin Trans. 1* **1994**, 1529–1539.
[43] N. L. J. M. Broekhof, F. L. Jonkers, A. van der Gen, *Tetrahedron Lett.* **1980**, *21*, 2671.
[44] C. Earnshaw, C. J. Wallis, S. Warren, *J. Chem. Soc. Perkin Trans. 1* **1979**, 3099.
[45] T. A. M. van Schaik, A. V. Henzen, A. van der Gen, *Tetrahedron Lett.* **1983**, *24*, 1303.
[46] C. Earnshaw, J. I. Grayson, S. Warren, *J. Chem. Soc. Perkin Trans. 1* **1979**, 1506.
[47] A. D. Buss, W. B. Cruse, O. Kennard, S. Warren, *J. Chem. Soc. Perkin Trans. 1* **1984**, 243. The assignment of the protons in Table 4 of this paper is incorrect: H^A and H^B have (clearly) been reversed.
[48] T. K. Jones, S. G. Mills, R. A. Reamer, D. Askin, R. Desmond, R. P. Volante, I. Shinkai, *J. Am. Chem. Soc.* **1989**, *111*, 1157.
[49] J. M. Muchowski, M. C. Venuti, *J. Org. Chem.* **1981**, *46*, 459.
[50] N. J. Lawrence, F. Muhammad, *J. Chem. Soc. Chem. Commun.* **1993**, 1187.
[51] A. D. Buss, R. Mason, S. Warren, *Tetrahedron Lett.* **1983**, *24*, 5293.
[52] J. Clayden, S. Warren, unpublished results.
[53] D. G. Barr, M. G. Davidson, G. Hutton, R. Snaith, S. Warren, D. R. Armstrong, unpublished results.
[54] a) P. O'Brien, S. Warren, *Tetrahedron Lett.* **1995**, *36*, 8473; b) *ibid.* **1995**, *36*, 2681.
[55] E. Vedejs, J. A. Garcia-Rivas, *J. Org. Chem.* **1994**, *59*, 6517.
[56] M. J. Doyle, D. Hall, P. R. Raithby, N. Skelton, S. Warren, *J. Chem. Soc. Perkin Trans. 1* **1993**, 517.
[57] D. Hall, A.-F. Sévin, S. Warren, *Tetrahedron Lett.* **1991**, *32*, 7123.
[58] P. M. Ayrey, S. Warren, *Tetrahedron Lett.* **1989**, *30*, 4581.
[59] C. Guéguen, P. O'Brien, M. Russell, S. Warren, unpublished results.
[60] D. Cavalla, W. B. Cruse, S. Warren, *J. Chem. Soc. Perkin Trans. 1* **1987**, 1883.
[61] R. S. Torr, S. Warren, *J. Chem. Soc. Pakistan* **1979**, *1*, 15.
[62] A. D. Buss, N. Greeves, D. Levin, P. Wallace, S. Warren, *Tetrahedron Lett.* **1984**, *25*, 357.
[63] A. D. Buss, N. Greeves, R. Mason, S. Warren, *J. Chem. Soc. Perkin Trans. 1* **1987**, 2569.
[64] F. Mathey, P. Savignac, *Tetrahedron* **1978**, *34*, 649.
[65] C. Guéguen, P. O'Brien, S. Warren, unpublished results.
[66] P. Wallace, S. Warren, *Tetrahedron Lett.* **1985**, *26*, 5713.
[67] P. Wallace, S. Warren, *J. Chem. Soc. Perkin Trans. 1* **1988**, 2971.
[68] P. Wallace, S. Warren, *J. Chem. Soc. Perkin Trans. 1* **1992**, 3169.
[69] N. Greeves, S. Warren, *Tetrahedron Lett.* **1986**, *27*, 259.
[70] N. Feeder, G. Hutton, S. Warren, *Tetrahedron Lett.* **1994**, *35*, 5911.
[71] A.-F. Sévin, G. Hutton, S. Warren, unpublished results.
[72] A.-F. Sévin, S. Warren, unpublished results.
[73] D. Levin, S. Warren, *J. Chem. Soc. Perkin Trans. 1* **1992**, 2155.
[74] D. Levin, S. Warren, *Tetrahedron Lett.* **1986**, *27*, 2265.
[75] P. M. Ayrey, M. A. Bolton, A. D. Buss, N. Greeves, D. Levin, P. Wallace, S. Warren, *J. Chem. Soc. Perkin Trans. 1* **1992**, 3407.
[76] M. Chérest, H. Felkin, N. Prudent, *Tetrahedron Lett.* **1968**, 2199.
[77] N. T. Anh, *Top. Curr. Chem.* **1980**, *88*, 145.
[78] J.-L. Luche, *J. Am. Chem. Soc.* **1978**, *100*, 2226.
[79] J.-L. Luche, L. R. Hahn, P. Crabbe, *J. Chem. Soc. Chem. Commun.* **1978**, 601.
[80] A. L. Gemal, J.-L. Luche, *J. Am. Chem. Soc.* **1981**, *103*, 5454.
[81] J. Elliott, D. Hall, S. Warren, *Tetrahedron Lett.* **1989**, *30*, 601.
[82] G. Hutton, T. Jolliff, H. Mitchell, S. Warren, *Tetrahedron Lett.* **1995**, *36*, 7905.
[83] J. Elliott, S. Warren, *Tetrahedron Lett.* **1986**, *27*, 645.
[84] J. Park, S. F. Pederson, *J. Org. Chem.* **1990**, *55*, 5924.
[85] J. Clayden, E. W. Collington, J. Elliott, S. J. Martin, A. B. McElroy, S. Warren, D. Waterson, *J. Chem. Soc. Perkin Trans. 1* **1993**, 1849.
[86] I. Fleming, H. Kühne, K. Takaki, *J. Chem. Soc. Perkin Trans. 1* **1986**, 725.
[87] J. Clayden, A. B. McElroy, S. Warren, unpublished results.
[88] K. N. Houk, N. G. Rondan, Y.-D. Wu, J. T. Metz, M. N. Paddon-Row, *Tetrahedron* **1984**, *40*, 2257.
[89] I. Fleming, *J. Chem. Soc. Perkin Trans. 1* **1992**, 3363.
[90] I. Fleming, J. J. Lewis, *J. Chem. Soc. Perkin Trans. 1* **1992**, 3257.
[91] N. J. S. Harmat, S. Warren, *Tetrahedron Lett.* **1990**, *31*, 2743.
[92] J. Clayden, E. W. Collington, E. Egert, A. B. McElroy, S. Warren, *J. Chem. Soc. Perkin Trans. 1* **1994**, 2801.
[93] B. E. Rossiter, T. R. Verhoeven, K. B. Sharpless, *Tetrahedron Lett.* **1979**, 4733.
[94] M. R. Johnson, Y. Kishi, *Tetrahedron Lett.* **1979**, 4347.
[95] H. J. Mitchell, S. Warren, submitted to *Tetrahedron Lett.*
[96] T. Katsuki, K. B. Sharpless, *J. Am. Chem. Soc.* **1980**, *102*, 5974.
[97] M. G. Finn, K. B. Sharpless, in *Asymmetric Synthesis, Vol. 5* (Ed.: J. D. Morrison), Academic, New York, **1985**, p. 247.
[98] B. E. Rossiter, in *Asymmetric Synthesis, Vol. 8* (Ed.: J. D. Morrison), Academic Press, New York, **1985**, p. 194.
[99] R. A. Johnson, K. B. Sharpless, in *Comprehensive Organic Synthesis, Vol. 7* (Eds.: B. M. Trost, I. Fleming), Pergamon, Oxford, **1990**, p. 389.
[100] J. Clayden, S. Warren, *J. Chem. Soc. Perkin Trans. 1* **1994**, 2811.
[101] J. Eames, H. J. Mitchell, A. Nelson, P. O'Brien, S. Warren, P. Wyatt, *Tetrahedron Lett.* **1995**, *36*, 1719.

[102] K. B. Sharpless, W. Amberg, Y. L. Bennani, G. A. Crispino, J. Hartung, K.-S. Jeong, H. L. Kwong, K. Morikawa, Z.-M. Wang, D. Xu, X.-L. Zhang, *J. Org. Chem.* **1992**, *57*, 2768.
[103] A. Nelson, P. O'Brien, S. Warren, *Tetrahedron Lett.* **1995**, *36*, 2685.
[104] S. K. Armstrong, S. Warren, E. W. Collington, A. Naylor, *Tetrahedron Lett.* **1991**, *32*, 4171.
[105] S. K. Armstrong, E. W. Collington, S. Warren, *J. Chem. Soc. Perkin Trans. 1* **1994**, 515.
[106] K. N. Houk, H.-Y. Duh, Y.-D. Wu, S. R. Moses, *J. Am. Chem. Soc.* **1986**, *108*, 2754.
[107] K. N. Houk, S. R. Moses, Y.-D. Wu, N. G. Rondan, V. Jäger, R. Schohe, F. R. Fronczek, *J. Am. Chem. Soc.* **1984**, *106*, 3880.
[108] S. K. Armstrong, E. W. Collington, J. Stonehouse, S. Warren, *J. Chem. Soc. Perkin Trans. 1* **1994**, 2825.
[109] L. E. Overman, F. M. Knoll, *Tetrahedron Lett.* **1979**, 321.
[110] L. E. Overman, *Angew. Chem.* **1984**, *96*, 565; *Angew. Chem. Int. Ed. Engl.* **1984**, *23*, 579.
[111] J. Clayden, S. Warren, *J. Chem. Soc. Perkin Trans. 1* **1993**, 2913.
[112] J. Clayden, E. W. Collington, S. Warren, *Tetrahedron Lett.* **1992**, *33*, 7039.
[113] A. J. Bridges, G. H. Whitham, *J. Chem. Soc. Chem. Commun.* **1974**, 142.
[114] A. M. C. H. van den Nieuwendijk, A. van der Gen, *Phosphorus, Sulfur, Silicon Relat. Elem.* **1993**, *77*, 168.
[115] S. E. Denmark, J. Amburgey, *J. Am. Chem. Soc.* **1993**, *115*, 10386.
[116] J. I. Grayson, S. Warren, A. T. Zaslona, *J. Chem. Soc. Perkin Trans. 1* **1987**, 967.
[117] C. A. Cornish, S. Warren, *J. Chem. Soc. Perkin Trans. 1* **1985**, 2585.
[118] C. Earnshaw, R. S. Torr, S. Warren, *J. Chem. Soc. Perkin Trans. 1* **1983**, 2893.
[119] D. Levin, S. Warren, *J. Chem. Soc. Perkin Trans. 1* **1988**, 1799.
[120] W. S. Wadsworth, W. D. Emmons, *J. Am. Chem. Soc.* **1961**, *83*, 1733.
[121] J. Boutagy, R. Thomas, *Chem. Rev.* **1974**, *74*, 87.
[122] R. S. Torr, S. Warren, *J. Chem. Soc. Perkin Trans. 1* **1983**, 1173.
[123] N. A. Portnoy, C. J. Morrow, M. S. Chattha, J. C. Williams, A. M. Aguiar, *Tetrahedron Lett.* **1971**, 1397, 1401.
[124] N. A. Portnoy, K. S. Yong, A. M. Aguiar, *Tetrahedron Lett.* **1971**, 2559.
[125] R. R. Arndt, S. Warren, *Tetrahedron Lett.* **1978**, 4089.
[126] R. S. Torr, S. Warren, *J. Chem. Soc. Perkin Trans. 1* **1983**, 1169.
[127] J. Clayden, E. W. Collington, S. Warren, *Tetrahedron Lett.* **1993**, *34*, 1327.
[128] J. Clayden, A. B. McElroy, S. Warren, *J. Chem. Soc. Perkin Trans. 1* **1995**, 1913.
[129] J. Clayden, S. Warren, unpublished.
[130] C. H. Behrens, S. Y. Ko, K. B. Sharpless, F. J. Walker, *J. Org. Chem.* **1985**, *50*, 5687.
[131] A. B. McElroy, S. Warren, *Tetrahedron Lett.* **1985**, *26*, 5709.
[132] J. Clayden, E. W. Collington, R. B. Lamont, S. Warren, *Tetrahedron Lett.* **1993**, *34*, 2203.
[133] T. Ibuka, K. Nakai, H. Habashita, Y. Hotta, N. Fujii, N. Mimura, Y. Miwa, T. Taga, Y. Yamamoto, *Angew. Chem.* **1994**, *106*, 693; *Angew. Chem. Int. Ed. Engl.* **1994**, *33*, 652.
[134] P. J. Murphy, G. Procter, *Tetrahedron Lett.* **1990**, *31*, 1059.
[135] V. K. Aggarwal, I. Coldham, S. McIntyre, S. Warren, *J. Chem. Soc. Perkin Trans. 1* **1991**, 451.
[136] R. C. Hartley, S. Warren, I. C. Richards, *J. Chem. Soc. Perkin Trans. 1* **1994**, 507.
[137] T. Kauffmann, P. Schwartze, *Chem. Ber.* **1986**, *119*, 2150.
[138] S. Warren, P. J. Wyatt, submitted to *Tetrahedron Lett.*
[139] D. Levin, S. Warren, *Tetrahedron Lett.* **1985**, *26*, 505.

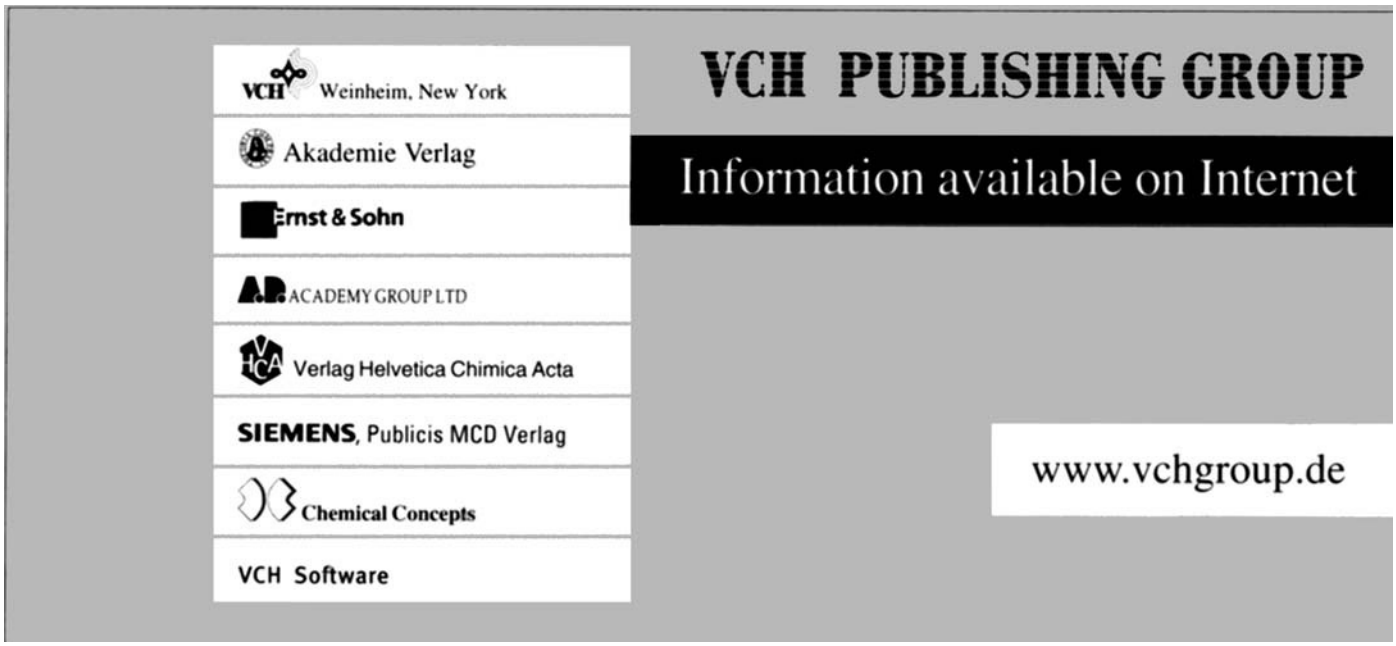

Metallophosphaalkenes—from Exotics to Versatile Building Blocks in Preparative Chemistry

Lothar Weber

The chemistry of low-valent organophosphorus compounds such as phosphaalkenes and phosphaalkynes has undergone rapid development in the last two decades. This development also includes the coordination chemistry of these species, which can act as versatile ligands in metal complexes. Metallophosphaalkenes are compounds in which one or more of the organic substituents on the P=C unit is replaced by a transition metal complex fragment. Metallophosphaalkenes have emerged from an existence as laboratory curiosities to become a link between main group and organometallic complex chemistry. The great richness of their chemistry not only mirrors the specific properties of the individual building block, but also shows novel and individual traits. Particular examples are cycloadditions of these electron-rich heteroalkenes with electron-deficient alkenes, alkynes, azo, and diazo compounds. These often lead to novel types of reaction and compounds. Metallophosphaalkenes are also important as intermediates in all metal-assisted cyclooligomerizations of phosphaalkynes.

Keywords: metallophosphaalkenes · phosphaalkenes · transition metal compounds

1. Introduction

The rapid development in the chemistry of low-valent phosphorus compounds during the last twenty years includes their coordination chemistry.[1, 2] There are now five types of complexes known containing phosphaalkene ligands (**A**–**E**) (Scheme 1).[2] The structural integrity of the phosphaalkene ligand is largely retained in complexes **A**–**E**. In metallophosphaalkenes, on the other hand, one or more of the substituents R on the phosphaalkene is replaced by a transition metal complex fragment; thus five basically different types of compound (I–V) can be differentiated (Scheme 2). Like phosphaalkenes with purely organo substituents, the phosphorus atom as well as the P=C-π bond in compounds of type I–V are capable of acting as donors and are therefore, in principle, in the position to interact further as ligands with other metal centers. Moreover, since metallophosphaalkenes are polyfunctional molecules, they are valuable starting materials for a wide range of chemical transformations with both organic and inorganic partners.

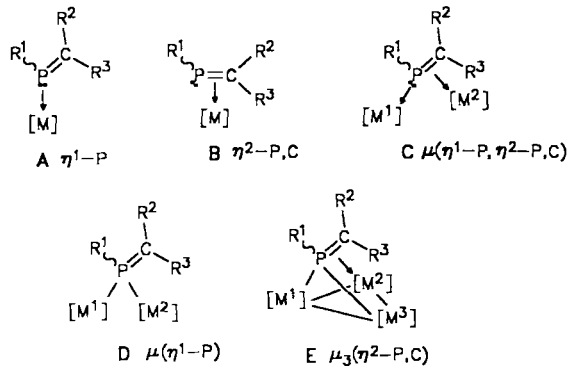

Scheme 1. Basic types of phosphaalkene transition metal complexes.

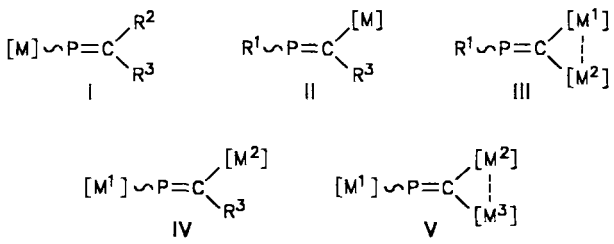

Scheme 2. Basic types of metal-functionalized phosphaalkenes (metallophosphaalkenes).

This review provides an overview of metal-functionalized P=C systems with particular emphasis placed on the preparative and structural aspects of this chemistry.

[*] Prof. Dr. L. Weber
Fakultät für Chemie der Universität
Universitätsstrasse 25, D-33615 Bielefeld (Germany)
Fax: Int. code +(521)106-6146

2. Synthetic Methods

2.1. *P*-Metallophosphaalkenes (Type I)

P-Metallophosphaalkenes [M]–P=R^2R^3 are now available by several synthetic routes; however, three general principles, a–c, are discernable (Scheme 3). In syntheses following route (a), the P=C bond is constructed from starting materials with [M]–P bonds such as metallophosphanes, in route (b), a M–P bond is formed between a P-functionalized phosphaalkene and a metal complex, and in route (c), phosphaalkynes are reduced within the coordination sphere of transition metal complexes.

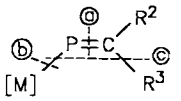

Scheme 3. Routes to metallophosphaalkenes of type I.

2.1.1. Syntheses by Route a

The first *P*-metallophosphaalkenes were obtained from the reaction of metallodisilylphosphane **1** with acid chlorides **2** (Scheme 4).[3] The reaction sequence of condensation and silyl migration resembles the synthesis of phosphaalkenes from acid chlorides and organodisilylphosphanes,[4] in which, in contrast to transient **3**, the primarily formed acyl(silyl)phosphanes were detectable by ^{31}P NMR spectroscopy.

The principle of the synthesis outlined in Scheme 4 cannot be subjected to unlimited generalization (Scheme 5). Thus, the reaction of pentamethylcyclopentadienyl (Cp*) derivatives [Cp*$(CO)_2$M–P$(SiMe_3)_2$] of iron (**5**)[5] and ruthenium (**6**)[6] with mesitoyl chloride (**2a**) leads cleanly to the metallophosphaalkenes **8a** and **9a**, respectively, whilst treatment with benzoyl chloride (**2b**) leads to mixtures of **8b** and **9b**, respectively, together with the dibenzoylphosphido complexes **11b** and **12b**, respectively. With pivaloyl chloride (**2c**) only the diacylphosphido complexes **11c** and **12c**, respectively, are formed. These limitations are even more valid for the osmium complex **7**, which, even with **2a**, produces mixtures of the osmiophosphaalkene **10a** and the dimesitoylphosphido complex **13a**.[7]

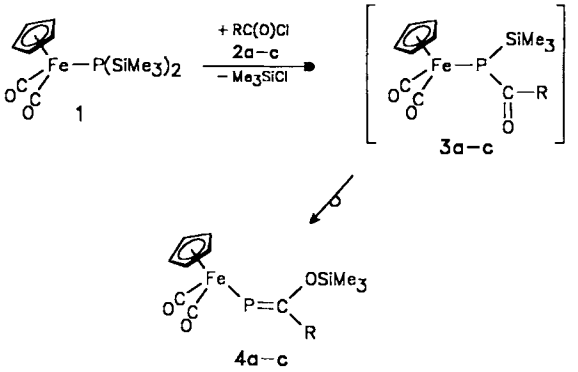

Scheme 4. Syntheses of the metallophosphaalkenes **4**. R = mesityl (Mes) (**a**), Ph (**b**), *t*Bu (**c**).

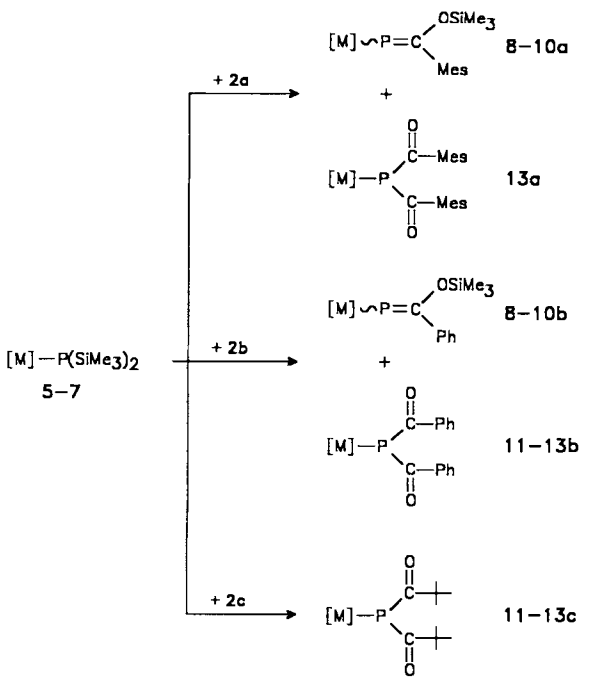

Scheme 5. Reaction of [Cp*$(CO)_2$M–P$(SiMe_3)_2$] with acid chlorides. M = Fe: **5**, **8**, **11**; Ru: **6**, **9**, **12**; Os: **7**, **10**, **13**; R = Mes (**a**), Ph (**b**), *t*Bu (**c**).

Another successful synthesis of ferriophosphaalkenes (such as **8**) following route (a) is based on the lithiation of the acyl(metallo)phosphanes **14a–c** and the subsequent treatment of the enolates **15a–c** with chlorotrimethylsilane. Compound **8c** is also accessible by this route (Scheme 6).

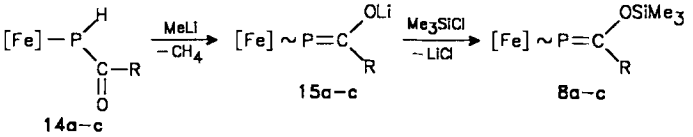

Scheme 6. Ferriophosphaalkenes from acylferriophosphanes. [Fe] = Cp*$(CO)_2$Fe; R = Mes (**a**), Ph (**b**), *t*Bu (**c**).

Lothar Weber was born in 1944 in Langenöls in Schlesien. He studied at the Universität Marburg and received his doctorate there under the supervision of Professor Günter Schmid in 1973. Thereafter, he carried out post-doctoral studies with Professor Barry M. Trost at the University of Wisconsin in Madison, USA. On his return to Marburg, he began the experimental work towards his Habilitation, which was completed in 1982 at the Universität Essen. His work centered on the coordination chemical aspects of sulfur ylides. In 1985, he became a C2 Professor, before he received the call to the Fakultät für Chemie der Universität Bielefeld. His research interests also include the chemistry of compounds with low-coordinate elements of the fifth main group, the synthesis of small homo- and heterocycles with heavy elements as well as metal complex catalyzed reactions of multiply bonded systems.

2.1.2. *Syntheses by Route b*

A particularly efficient method for the synthesis of the metallophosphaalkenes **16**–**27** utilizes the reaction of halogeno(methylene)phosphanes $XP{=}C(R)(SiMe_3)$ with carbonylmetalate ions. The products, with the exceptions of **16** and **20**, are obtained as stable solids in good yield (Scheme 7).[8–10]

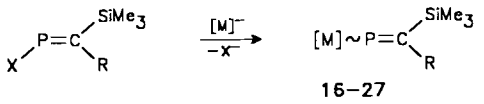

16–27

	[M]	R		[M]	R
16	$[Cp(CO)_3Mo]$	Me_3Si	**22**	$[Cp(CO)_3Mo]$	Ph
17	$[Cp^*(CO)_3Mo]$	Me_3Si	**23**	$[Cp^*(CO)_3Mo]$	Ph
18	$[Cp(CO)_3W]$	Me_3Si	**24**	$[Cp(CO)_3W]$	Ph
19	$[Cp^*(CO)_3W]$	Me_3Si	**25**	$[Cp^*(CO)_3W]$	Ph
20	$[Cp(CO)_2Fe]$	Me_3Si	**26**	$[Cp(CO)_2Fe]$	Ph
21	$[Cp^*(CO)_2Fe]$	Me_3Si	**27**	$[Cp^*(CO)_2Fe]$	Ph

Scheme 7. Metallophosphaalkenes from carbonylmetalates and halogenophosphaalkenes. X = Cl, Br.

The thermal stability of these metallophosphaalkenes decreases with increasing electron density on the metal ($Mo(d^4) < Fe(d^6)$) as well as with decreasing steric demand of the π ligand ($C_3H_5 < Cp < Cp^*$). Thus, the thermolabile complexes **20** and $[(\eta^3\text{-}C_3H_5)(CO)_2FeP{=}C(SiMe_3)_2]$ readily undergo further reaction to **28** and **29**, respectively (Scheme 8).[11]

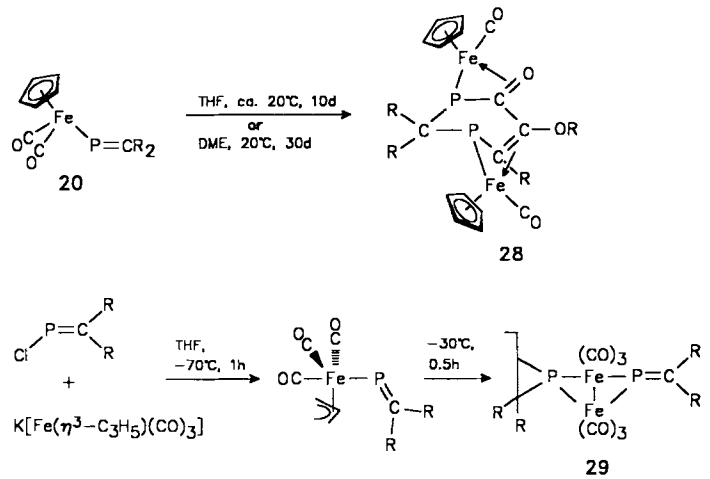

Scheme 8. Subsequent reactions of unstable metallophosphaalkenes **20** and $[(\eta^3\text{-}C_3H_5)(CO)_3Fe{-}P{=}CR_2]$. R = Me_3Si. DME = 1,2-dimethoxyethane. THF = tetrahydrofuran.

There have been some reports on the oxidative addition of P-halogenophosphaalkenes to low-valent nickel and platinum centers (Scheme 9). Whilst the platinum complex **30**, a cream-colored solid, is stable, the nickel compounds **31a** and **31b** rapidly decompose in solution.[12]

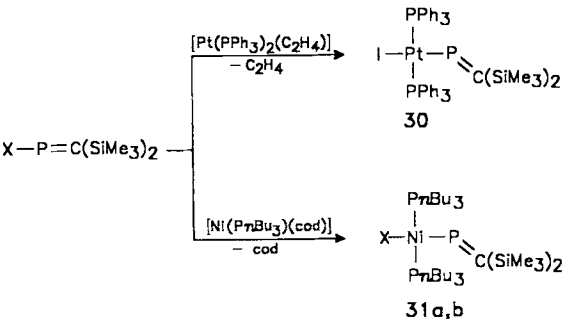

Scheme 9. *P*-Nickelio- and *P*-platiniophosphaalkenes by oxidative addition. X = Cl (**a**), I (**b**), cod = 1,5-cyclooctadiene.

Oxidative addition takes place in competition with η^1 and η^2 coordination of the halogenophosphaalkenes and is particularly favored for the reactive P–I bond (184 kJ mol^{-1}). In contrast, the phosphaalkene $F{-}P{=}C(SiMe_3)_2$ has a strong P–F bond (490 kJ mol^{-1}) and has only been observed so far as a η^1 and η^2 ligand for example in *trans*-$[Rh(PPh_3)_2(Cl)\{\eta^1\text{-}P(F){=}C(SiMe_3)_2\}]$ or $[Ni(PnBu_3)_2\{\eta^2\text{-}P(F){=}C(SiMe_3)_2\}]$.[13] The nature of the transition metal complex fragment clearly influences the reaction behavior of the corresponding chlorophosphaalkene [dissociation energy (P–Cl) = 319 kJ mol^{-1}]. Here, along with **31a**, η^1 complexes are known such as *trans*-$[RhCl(PPh_3)_2\{\eta^1\text{-}P(Cl){=}C(SiMe_3)_2\}]$[13] and η^2 complexes such as $[Pt(PPh_3)_2\{\eta^2\text{-}P(Cl){=}C(SiMe_3)_2\}]$.[12]

As an alternative to the methods described in Scheme 7, the pentamethylcyclopentadienyl metal derivatives **17** and **19** can be obtained from $Cp^*P{=}C(SiMe_3)_2$ and the kinetically labile complexes $[M(MeCN)_3(CO)_3]$ (M = Mo, W). Here, the metal complex fragment is inserted into the labile P–C(Cp*) bond (1.931(4) Å[14]) (Scheme 10).

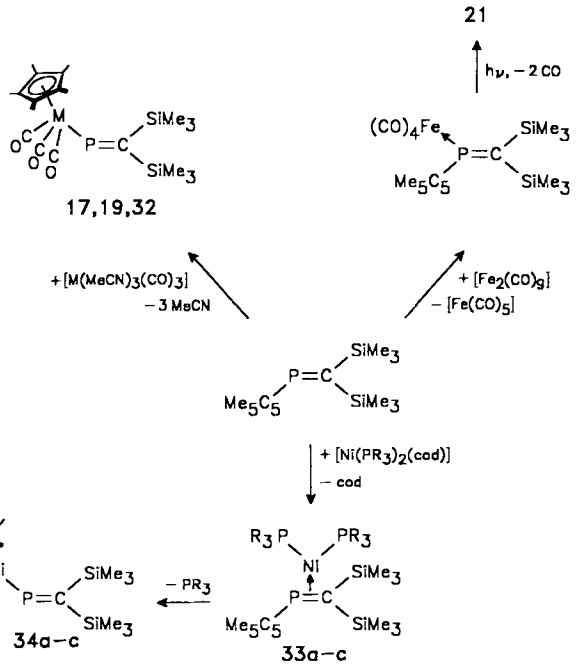

Scheme 10. Oxidative additions with $Cp^*P{=}C(SiMe_3)_2$. M = Mo (**17**), W (**19**), Cr (**32**); R = Ph (**a**), Et (**b**), *n*Bu (**c**).

Complexes **17** and **19** are synthesized photochemically; however, the analogous chromiophosphaalkene **32** is produced by thermolysis. Formation of **21** from $Cp^*P{=}C(SiMe_3)_2$ and $[Fe_2(CO)_9]$ proceeds by the photolysis of the isolable complex $[\{\eta^1\text{-}Cp^*P{=}C(SiMe_3)_2\}Fe(CO)_4]$. The synthesis approach for **17**, **19**, and **21** based on $Cp^*P{=}C(SiMe_3)_2$ does not show any advantages over the method given in Scheme 7 (which generates greater yields), because the organophosphorus starting material has to be prepared from $Cl{-}P{=}C(SiMe_3)_2$ beforehand. No alternatives, however, exist for the synthesis of the chromium complex **32** and the nickeliophosphaalkenes **34a–c**.[10]

The particularly electron-rich metallophosphaalkenes **35** and **36** are obtained by condensation of the bromo complexes $[MCp^*(CO)_2Br]$ (M = Fe, Ru) with $Me_3Si{-}P{=}C(NMe_2)_2$ (Scheme 11).[15]

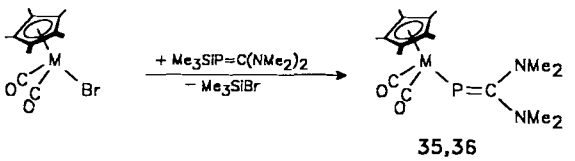

Scheme 11. Metallophosphaalkenes from $Me_3SiP{=}C(NMe_2)_2$ by condensation. M = Fe (**35**), Ru (**36**).

2.1.3. *Syntheses by Route c*

Phosphaalkynes oligomerize within the coordination sphere of transition metals to furnish a wide range of new compounds[1f, 2] some of which display the structural characteristics of *P*-metallophosphaalkenes. Thus, cyclotrimerization of *t*BuC≡P or 1-AdC≡P on the $[CpRu]^+$ fragment of **37** yields complexes **38a** and **38b**, respectively, in which all the acetonitrile ligands have been displaced by the phosphaalkyne. The fluorine atom in the products originates from the hexafluorophosphate ion (Scheme 12).[16]

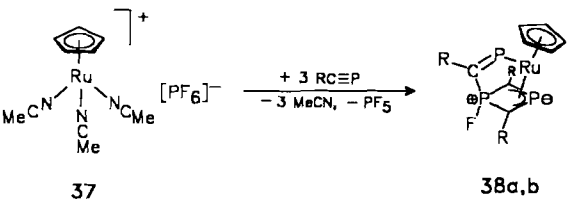

Scheme 12. Synthesis of a *P*-rutheniophosphaalkene by cyclotrimerization of phosphaalkynes; R = *t*Bu (**a**), 1-adamantyl (1-Ad) (**b**).

Treatment of $[Rh(C_2H_4)_2Cl]_2$ with trimethylphosphane and *tert*-butylphosphaacetylene in the molar ratio of 1:4:4 produces a 1:2 mixture of the 1,4-diphospha-2-rhodacyclopentadiene **39** and the 1,3-diphosphacyclobutadiene derivative **40**. Reaction of **40** with indenyllithium cleanly yields the sandwich complex **41** (Scheme 13).[17] Rhodiophosphaalkene **39** is a model complex for an important intermediate product in metal-induced cyclooligomerizations of phosphaalkynes. On cobalt, rhodium,[1f] and iron[18] centers this usually leads to η^4-ligated 1,3-diphosphacyclobutadienes. On the other hand, cyclodimerization of *t*BuC≡P on $[Cp_2Zr]$ and $[Cp_2Hf]$ fragments yields complexes with 1,3-diphosphabicyclo[1.1.0]butanediyl ligands.[19] A highly efficient cyclotetramerization of the phosphaalkyne occurs on

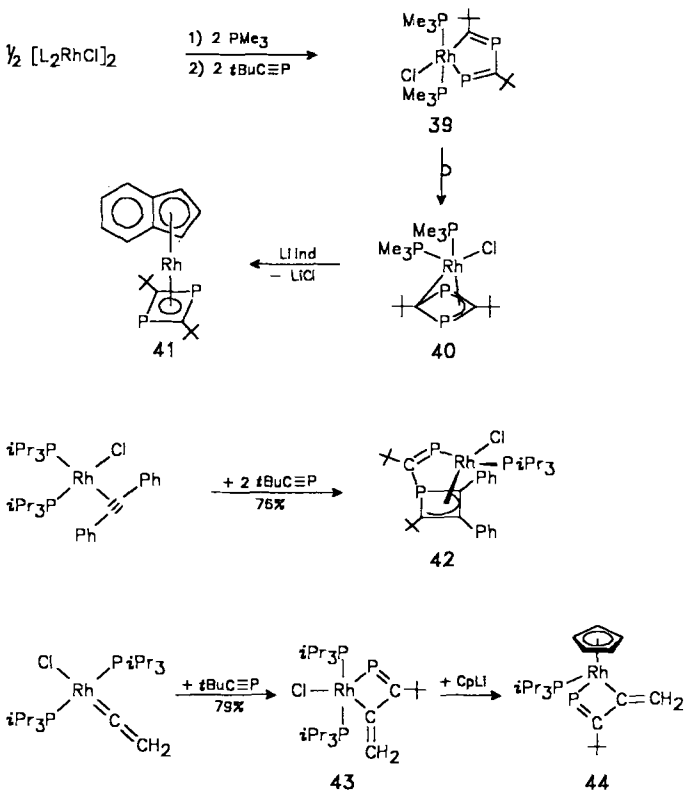

Scheme 13. Synthesis of cyclic rhodiophosphaalkenes. Ind = indenyl.

the (η^8-cyclooctatetraene)zirconium fragment to give a (η^4-1,3,5,7-tetraphosphabarralene)zirconium complex, and here reactive metallophosphaalkynes are also postulated as intermediates.[20]

The tolanrhodium complex $[Rh(PiPr_3)_2(Cl)(\eta^2\text{-}PhC{\equiv}CPh]$ reacts with two equivalents of *t*BuC≡P, undergoing a cyclodimerization to yield **42**. One molecule of phosphaalkyne adds to the alkyne to generate a η^3-phosphacyclobutenyl ligand. The second molecule of phosphaalkyne bridges the P atom of the four-membered ring to the metal center, thus producing a rhodiophosphaalkene (Scheme 13).[21]

The cyclo-cooligomerization of alkynes with phosphaalkynes is sensitively dependent on the nature of the other ligands on the metal center. Thus, in the reaction of $[RhCp(PiPr_3)(\eta^2\text{-}PhC{\equiv}CPh)]$ with *t*BuC≡P only one molecule of the phosphaalkyne is incorporated to give the η^4-phosphacyclobutadiene-rhodium complex $[CpRh(\eta^4\text{-}\overline{PC(Ph)C(Ph)C}\,t\text{Bu})]$.[21]

Another type of [2+2]cycloaddition occurs between the vinylidene complex $[(PiPr_3)_2(Cl)Rh{=}C{=}CH_2]$ and *t*BuC≡P. Here, the cyclic rhodiophosphaalkene **43** is produced, which subsequently reacts smoothly with cyclopentadienyllithium to yield **44** (Scheme 13).[21]

2.2. *C*-Metallophosphaalkenes (Type II)

2.2.1. *From Lithiosilylphosphanes and Carbonylmetal Cations*

The syntheses of the first *C*-metallophosphaalkenes **46a–c** were contrived by the addition of lithiosilylphosphanes to the carbonylrhenium cation $[Cp^*Re(CO)_2(NO)]^+$ in ether at

-80 °C (Scheme 14). The initially formed complexes **45a–c** can be detected by ^{31}P NMR spectroscopy, they rearrange above -40 °C to the products **46a–c**. Analogously, the extremely sensitive compound [Cp(CO)(NO)Re–C(OSiMe$_3$)=P*t*Bu] is obtained from the reaction of [CpRe(CO)$_2$(NO)]BF$_4$ with LiP(*t*Bu)(SiMe$_3$).[22]

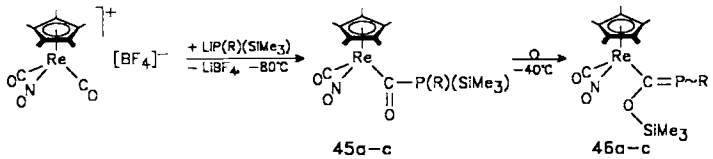

Scheme 14. Synthesis of *C*-rheniophosphaalkenes. R = Me$_3$Si (**a**), *t*Bu (**b**), Ph (**c**).

This type of synthesis, however, has only a limited range of application. Thus, treatment of the manganese complex cation [Cp*Mn(CO)$_2$(NO)]$^+$ with LiP(SiMe$_3$)$_2$ produces the complex [Cp*(CO)$_2$Mn–P(SiMe$_3$)$_2$] instead of a *C*-manganiophosphaalkene.[23]

The tendency of formation and stability of *C*-metallophosphaalkenes are also sensitively influenced by the spatial requirements of the other ligands in the complex and by the substituents on the P atom. This is particularly valid for the corresponding iron and ruthenium compounds. The cation [CpFe(CO)$_3$]$^+$ is attacked at the cyclopentadienyl ligand by LiP(R)(SiMe$_3$) (R = SiMe$_3$, *t*Bu) at -78 °C in ether. The *exo*-phosphinocyclopentadiene complexes **47** thus formed rearrange at room temperature to the metallophosphanes [Cp(CO)$_2$Fe–P(R)(SiMe$_3$)] (Scheme 15).[24]

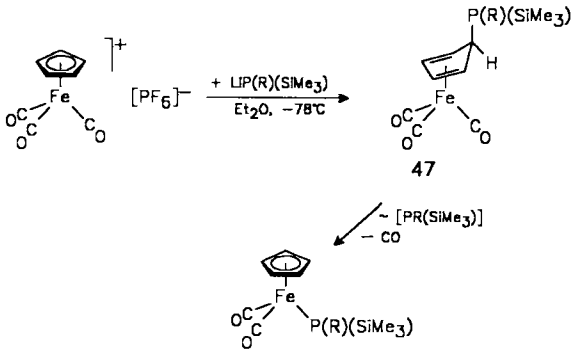

Scheme 15. Reaction of [FeCp(CO)$_3$]$^+$ with lithiosilylphosphanes. R = Me$_3$Si (**a**), *t*Bu (**b**).

If the analogous pentamethylcyclopentadienyl cation [Cp*(CO)$_3$Fe]$^+$ is used, the attack by the phosphide on the ring ligand does not occur, however, the desired *C*-metallophosphaalkene **49** is only produced in the case of the bulky supermesityl group (Mes* = 2,4,6-*t*Bu$_3$C$_6$H$_2$) on the P atom (Scheme 16).[25] For R = SiMe$_3$ and *t*Bu the 1,3-silyl migration does not occur, and the phosphinocarbonyl complexes **48a** and **48b**, respectively, are isolated as the final products (Scheme 16).[26] Similar results are obtained in the chemistry of the ruthenium derivative [Cp*Ru(CO)$_3$]$^+$.[25, 27]

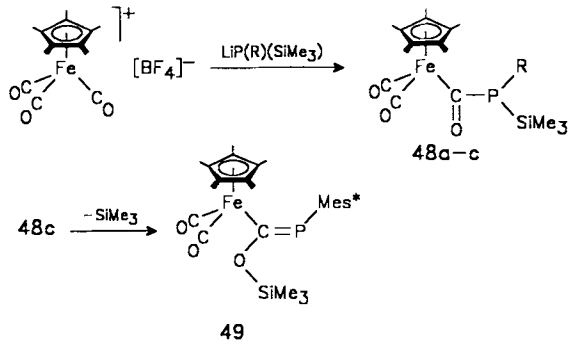

Scheme 16. Synthesis of (phosphino)carbonyl complexes **48a–c** and a *C*-ferriophosphaalkene **49**. R = Me$_3$Si (**a**), *t*Bu (**b**), Mes* (**c**).

2.2.2. *From C-Functionalized Phosphaalkenes*

Two research groups have succeeded in synthesizing *C*-metallophosphaalkenes from phosphaalkenes that have halogen functions on the methylene carbon atom.[28, 30] The *trans*-configured compounds **50a** and **51** result from the oxidative addition of equimolar amounts of Cl$_2$C=PMes* and [M(PEt$_3$)$_4$] in benzene or hexane at 20 °C (Scheme 17). Similarly, the bromoplatinum derivative **50b** is obtained from [Pt(PEt$_3$)$_4$] and Br$_2$C=PMes*. The analogous bromopalladium compound could not be isolated due to decomposition to *trans*-[Pd(PEt$_3$)$_2$Br$_2$] and Mes*C≡P.[28a, c]

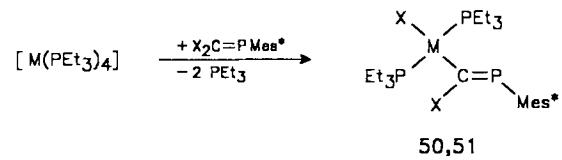

Scheme 17. Synthesis of *C*-palladio- and *C*-platiniophosphaalkenes; M = Pt, X = Cl (**50a**), X = Br (**50b**); M = Pd, X = Cl (**51**).

The *cis* isomer corresponding to **50a** is formed from Cl$_2$C=PMes* and [Pt(PEt$_3$)$_4$] in hexane at -50 °C and can be isolated as analytically pure crystals at this temperature. However, in solution *cis*-[(Et$_3$P)$_2$(Cl)Pt{C(Cl)=PMes*}] rearranges in the presence of PEt$_3$ and above -30 °C to the *trans* isomer.[28c] An alternative synthesis of **50a** utilizes a ligand exchange reaction between *trans*-[Pt(PEt$_3$)$_2$Cl$_2$] and LiC(Cl)=PMes*.[28c]

The principle of synthesis outlined in Scheme 17 is also subject to narrow limits: 1. To date there are only a few *C*-halogenomethylenephosphanes known, and these carry, with the exception of the 2,2,6,6-tetramethylpiperidino and bis(trimethylsilyl)amino substituents, the supermesityl group on phosphorus. 2. The stability of the products discussed here is as follows: Pt > Pd; Cl > Br; PEt$_3$ > PPh$_3$.

In agreement with this, the reaction of [Pt(η^2-C$_2$H$_4$)(PPh$_3$)$_2$][28c] or [Pd(PPh$_3$)$_4$][29] with Cl$_2$C=PMes* does not lead to stable *C*-metallophosphaalkenes, but only to the phosphaalkyne Mes*C≡P and to *cis*-[Pt(PPh$_3$)$_2$Cl$_2$] and *trans*-[Pd(PPh$_3$)$_2$Cl$_2$], respectively.

The organolithium compound (*Z*)-Mes*P=CHLi reacts with one equivalent of HgCl$_2$ to give the mercuriophosphaalkene

(*Z*)-**52**, whilst treatment with only 0.5 equiv of $HgCl_2$ generates the bis(phosphaalkenyl)mercury derivative (*Z*/*Z*)-**53** (Scheme 18).[30] If, instead of the single isomer of the lithium compound, the mixture (*E*/*Z*)-Mes*P=CHLi is used, as is produced from the lithiation of the phosphaalkene mixture (*E*/*Z*)-Mes*P=CHI (80:20), the mercury compound is also obtained as a mixture of (*E*/*E*)-**53** and (*Z*/*Z*)-**53**. The isomers can be separated by crystallization.[30]

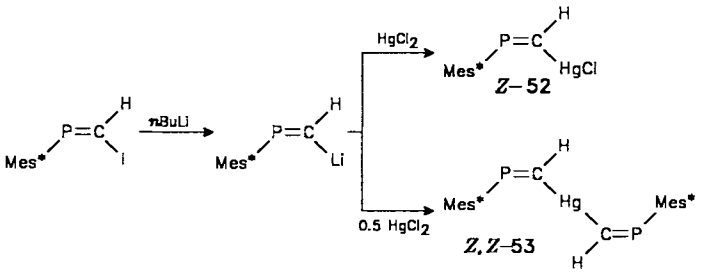

Scheme 18. Synthesis of *C*-mercuriophosphaalkenes **52** and **53**.

2.2.3. *From Phosphaalkynes or η^2-Phosphaalkyne Complexes*

Cyclo-codimerizations of *t*BuC≡P with alkenes and alkynes within the coordination sphere of titanocenes and zirconocenes lead to metallaheterocycles with structural features of *C*-metallophosphaalkenes. If, for example, a solution of **54** in *n*-heptane is heated with the phosphaalkyne for several hours at 80 °C, the zirconiophosphaalkene **55** is obtained as a red powder and a η^2-dehydrobenzene complex is postulated as an intermediate (Scheme 19). A titanium derivative analogous to **55** has also been reported.[31]

The *C*-metallophosphaalkenes **57a–d** are readily accessible from the phosphaalkyne complex **56** by reaction with the alkynes HC≡CH, MeC≡CMe, PhC≡CPh, and PhC≡CH, respectively, if the released phosphane is removed from the equilibrium by adduct formation with triethylborane (Scheme 19). However, codimerization fails with silylated alkynes such as $HC{\equiv}CSiMe_3$, $PhC{\equiv}CSiMe_3$, $Me_3SiC{\equiv}CSiMe_3$ as well as with dimethyl acetylenedicarboxylate. In the absence of trapping agents the coordinatively unsaturated complex **58**, formed from **56** by abstraction of phosphane, trimerizes to **59**.[32] The cyclic *C*-metallophosphaalkenes **55** and **57** are the first stable representatives of a class of compounds which are most probably intermediates playing an important role in all metal-induced cyclo-cooligomerizations, but which have, to date, evaded detection. This is true not only for the formation of (η^4-phosphacyclobutadiene)cobalt[33] and -rhodium[21] complexes but also for the synthesis of (1,3-diphosphinine)iron compounds.[18] A highly reactive nickeliophosphaalkene has been proposed as an intermediate in the synthesis of a tetraphosphatricyclooctadiene.[34]

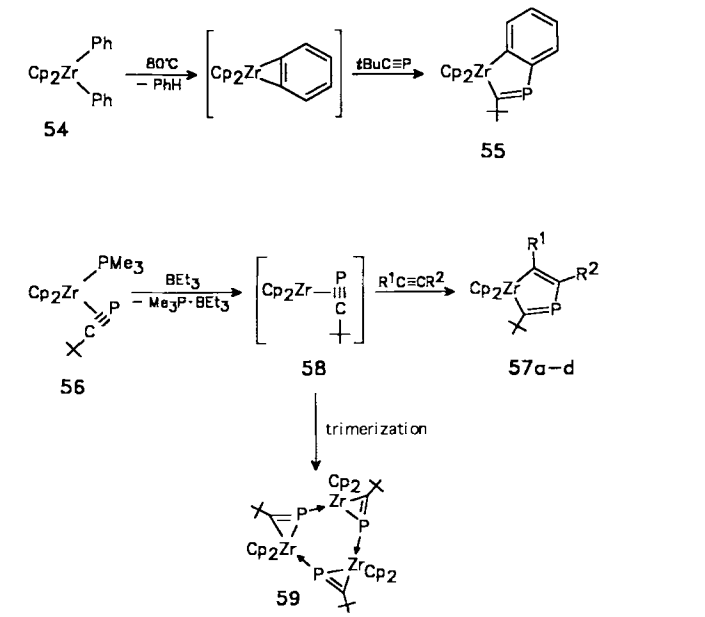

Scheme 19. *C*-Zirconiophosphaalkenes from alkyne, phosphaalkyne, and zirconocene building blocks. $R^1 = R^2 = H$ (**a**), Me (**b**), Ph (**c**); $R^1 = H$, $R^2 = Ph$ (**d**).

The 1-phospha-3-zirconia[3.1.0]bicyclohex-1-enes **60a–e** can be synthesized from **58** and cyclopropene derivatives. If **58**, generated in situ, is treated with acetone, benzophenone, benzaldehyde, or isobutyraldehyde, metallaheterocycles **61** are obtained. Treatment of 1,1-dimethylallene or triphenylketeneimine with **58** produces complexes **62** and **63**, respectively (Scheme 20).[32] The titanium derivatives analogous to **60a–c** and **61c,d** have also been prepared.[32]

The insertion of a methylene group into the metal–phosphorus bond can be achieved when **56** or the trimer **59** is treated with the ylides $Ph_3P{=}CH_2$ or $Me_3P{=}CH_2$ as well as with the adduct $Ph_3P{=}CH_2 \cdot BEt_3$ (Scheme 21).[32]

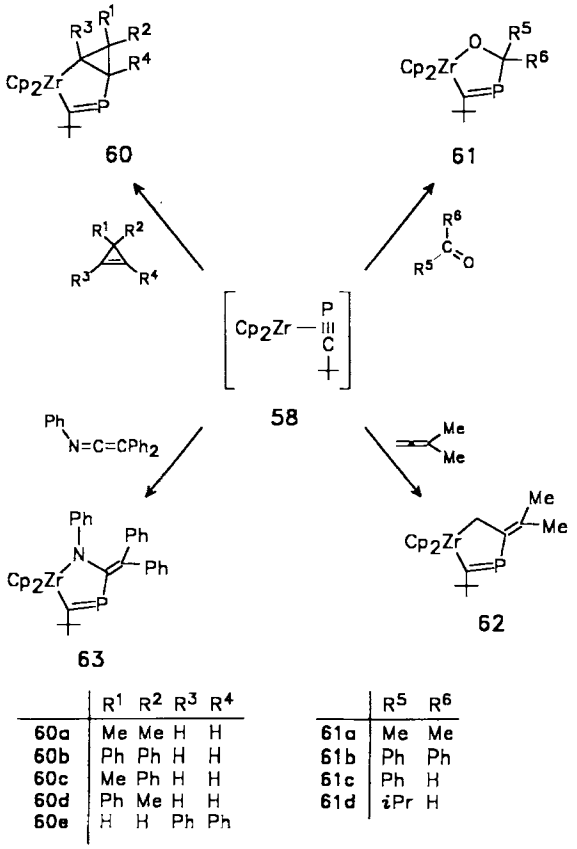

	R^1	R^2	R^3	R^4
60a	Me	Me	H	H
60b	Ph	Ph	H	H
60c	Me	Ph	H	H
60d	Ph	Me	H	H
60e	H	H	Ph	Ph

	R^5	R^6
61a	Me	Me
61b	Ph	Ph
61c	Ph	H
61d	*i*Pr	H

Scheme 20. Synthesis of cyclic *C*-zirconiophosphaalkenes.

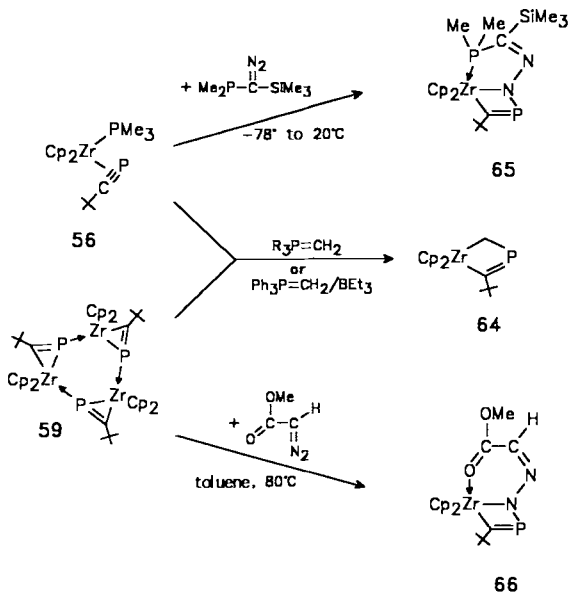

Scheme 21. Reaction of (η^2-phosphaalkyne)zirconocene complexes with ylides and diazo compounds. R = Me, Ph.

The reaction of **56** or **59** with diazo compounds does not lead to the expected loss of N_2 and insertion of the carbene fragment into the Zr–P bond. Instead, a cycloaddition reaction yields the 2-aza-1-phospha-3-zirconiacyclobut-4-enes **65** and **66**, respectively, which, like **64**, have the structural motif of a *C*-metallophosphaalkene in the heterocycle (Scheme 21).[32]

2.3. *C,C*-Dimetallophosphaalkenes (Type III)

For compounds of this type, which can also be regarded as μ-isophosphaalkyne or phosphoisonitrile complexes, there are two methods of synthesis available so far. These complexes deserve particular attention, as the ligated isophosphaalkynes C≡P(aryl) are unknown as the free species, and all attempts to synthesize them up to now afforded only the already well known phosphaalkyne isomers (aryl)C≡P. The first complexes of this type, **68** (Scheme 22), are obtained by the oxidative addition of

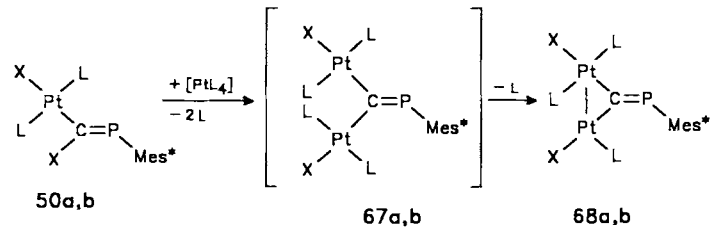

Scheme 22. Synthesis of *C,C*-diplatiniophosphaalkenes. X = Cl (**a**), Br (**b**); L = PEt_3.

one equivalent of $[Pt(PEt_3)_4]$ to the *C*-metallophosphaalkenes **50**; the dinuclear complexes **67** are assumed to be the primary products.[28a–d]

Experiments to produce heterodimetallic complexes of type **68** with Pt and Pd proceed by a different route:[28d] The complexes **70** and **71** are the only organometallic products detectable following the reaction of **50** with $[Pd(PEt_3)_4]$ for 24 h; however, the metallophosphaalkynes **70** could not be isolated. Their subsequent treatment with $[Pt(PEt_3)_4]$ leads to **72** with the novel $\mu(\eta^1:\eta^2)$-phosphaethynyl ligand (Scheme 23).[28d]

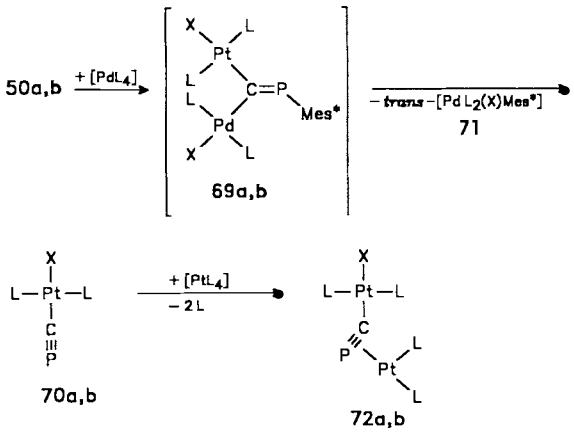

Scheme 23. Synthesis of $\mu(\eta^1:\eta^2)$-phosphaethynyl complexes. X = Cl (**a**), Br (**b**); L = PEt_3.

An alternative method for the synthesis of *C,C*-dimetallophosphaalkenes employs base-induced condensation of aryl(silyl)phosphanes **74a–d** with the μ-carbynediiron complex **73** (Scheme 24).[35,36] Compounds **75a–c** are obtained by column chromatography as dark red, air-stable, crystalline substances, whereas **75d** has not yet been isolated undecomposed. On the basis of findings to date, the condensation described above is limited to bulky aryl(silyl)phosphanes.

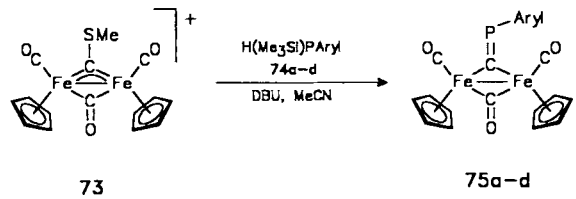

Scheme 24. Synthesis of *C,C*-diferriophosphaalkenes. Aryl = Mes (**a**), 2,4,6-$iPr_3C_6H_2$ (**b**), Mes* (**c**), 2,4,6-$(CF_3)_3C_6H_2$ (**d**); DBU = diazabicycloundecene.

2.4. *C,P*-Dimetallophosphaalkenes (Type IV)

The only compound with this type of structure known so far, **77**, is obtained by the addition of *t*BuC≡P to the Pt–Pt fragment of the diplatinum complex **76** (Scheme 25).[37]

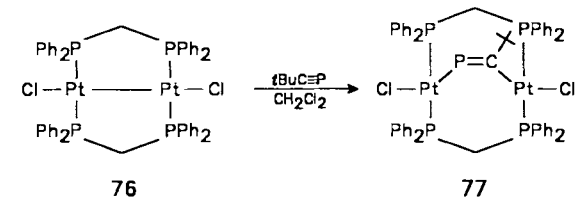

Scheme 25. Synthesis of a *C,P*-diplatiniophosphaalkene.

3. Structures and Bonding Properties

3.1. Molecular Structures of Metallophosphaalkenes

The most noticeable structural change that a classical phosphalkene undergoes on exchanging an organic substituent on the phosphorus atom for a transition metal complex fragment is the opening of the valence angle on the phosphorus atom. The angle M-P-C varies from 113.8(2)° in the [CpFe] complex **4c** (see Scheme 4)[3] to 126.2(3)° in the [Cp*Fe] complex **21**[9] (Fig. 1). In the parent compound $HP{=}CH_2$ the calculated value for the angle H-P-C is 97.4°,[38, 39] whilst in phosphaalkenes with organic substituents the value for this angle usually varies between 100–114° depending on the spatial requirements of the substituents.[40] The unusually large valence angle N-P-C in $Mes^*(Me_3Si)N{-}P{=}C(SiMe_3)_2$ (121.38(6)°) undoubtedly results from steric repulsion within the molecule.[41] The opening of the angle in metallophosphaalkenes is due not only to steric but also to electronic effects which arise from the low electronegativity of the metal substituent. In the parent compound, the orbital of the lone pair on the phosphorus has mainly 3s character. This changes in the metallophosphaalkenes: the p character of the lone pair increases. This causes an opening of the angle on phosphorus and a decrease in the ionization energy of the n orbital. In metallophosphaalkenes, this orbital then becomes energetically the HOMO, whilst the π orbital becomes HOMO − 1. All in all, the energy difference HOMO–LUMO (the latter is a π*-orbital) is smaller than that in $HP{=}CH_2$.[38, 39]

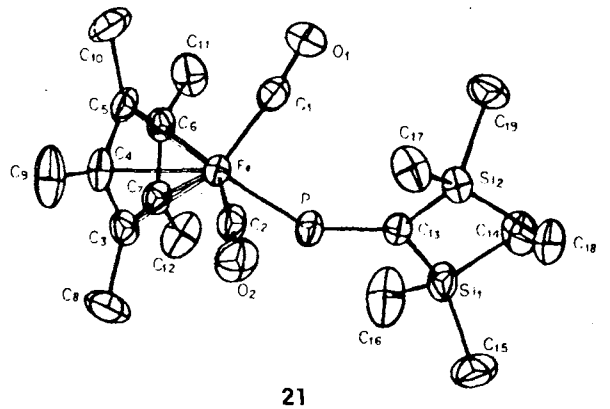

21

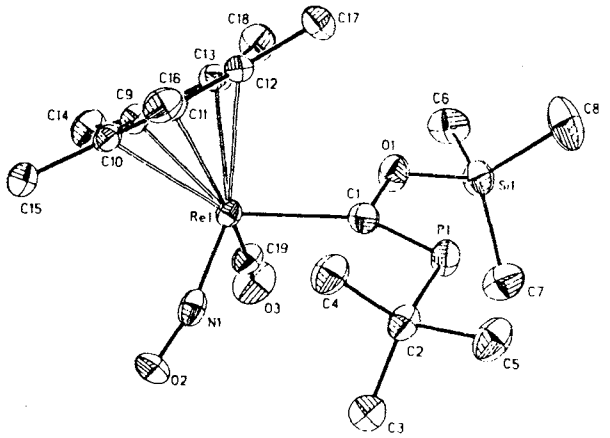

46b

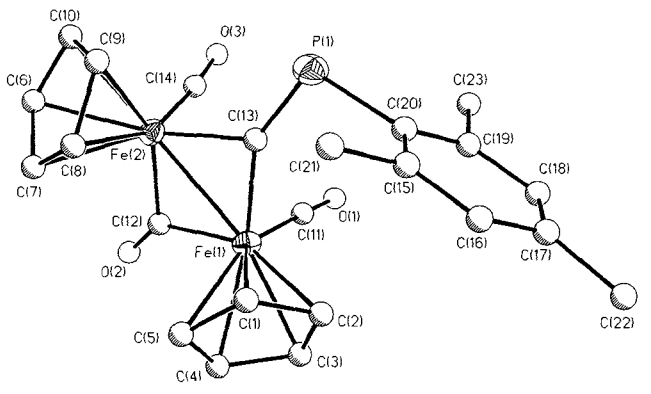

75a

Fig. 1. Crystal structures of the metallophosphaalkenes **21**, **46b**, and **75a**. Selected bond lengths [Å] and angles [°]: **21**: P-C13 1.680(9), Fe-P 2.256(2); Fe-P-C13 126.2(3); **46b**: P1-C1 1.704(4), Re1-C1 2.138(4), C1-O1 1.399(5); C1-P1-C2 112.3(2); **75a**: P1-C13 1.683(12), C13-Fe1 1.903(16), C13-Fe2 1.927(16); C13-P1-C20 104.5(7).

In the *C*-rheniophosphaalkene **46b**[22] and in the *C*,*C*-diferriophosphaalkene **75a**,[35] C-P-C bond angles of 112.3(2)° and 104.5(7)°, respectively, have been measured (Fig. 1).

The molybdeniophosphaalkene **16** (see Scheme 7) has the shortest P=C distance observed to date for a *P*-metallophosphaalkene (1.665(3) Å;[8] calc.: 1.673 Å[38]). π-Conjugation with the lone pairs on oxygen or nitrogen atoms of heterosubstituents generally leads to a small elongation of the P=C bond (e.g. 1.701(4) Å in *t*Bu(OSiMe$_3$)C=P complex **4c**[3] or 1.709 Å in the $(NMe_2)_2C{=}P$ complex **35**[15]). The same is true of the P=C bond lengths in **46b** (1.704(4) Å) and **75a** (1.683(17) Å). The metal–phosphorus distances in *P*-metallophosphaalkenes are in agreement with single bonds with negligible π-bond contributions.

3.2. NMR Spectra

The characteristic ^{31}P and ^{13}C NMR shifts for selected compounds are summarized in Table 1.

The ^{31}P NMR chemical shifts of phosphaalkenes vary in the wide range between $\delta = -62.0$ for $(Me_2N)C{=}PH$[42] to $\delta = 740.5$ in the nickel complex **34b**.[9, 10] The ^{31}P NMR data of compounds containing low-coordinate phosphorus published up to 1987 are summarized in a review.[43] Inspite of the large problems associated with the theoretical collation and interpretation of these large differences in shift, which generally occur for compounds containing two-coordinate phosphorus, some trends can be discerned for metallophosphaalkenes.

In metallophosphaalkenes strong downfield shifts of the ^{31}P resonances relative to the signals of the analogous, purely organo-substituted compounds are typical, this points to a small HOMO–LUMO gap. The effect can be correlated to the σ-donor effect of the complex fragment which is dependent not only on the donor strength of the 3d metal (Cr in **32** ($\delta = 605.4$) < Fe in **21** ($\delta = 641.5$) < Ni in **34b** ($\delta = 740.5$)), but also on the ring ligand. Thus, the exchange of a Cp for a Cp* ligand causes a deshielding of $\Delta\delta(^{31}P)$ of 42.9 to 60.3.

Table 1. ^{13}C and ^{31}P NMR data of selected *P*-metallophosphaalkenes and phosphaalkenes[a]

Compound		$\delta(^{31}P)$	$\delta(^{13}C)$	$^1J(P,C)$/ Hz	Ref.
(*Z*)-*t*Bu–P=C(OSiMe$_3$)(*t*Bu)		176.0	213.0	76.5	[44]
(*Z*)-[Cp(CO)$_2$Fe–P=C(OSiMe$_3$)(*t*Bu)]	**4c**	215.2	213.5	95.7	[3]
(*Z*)-[Cp*(CO)$_2$Fe–P=C(OSiMe$_3$)(*t*Bu)]	**8c**	258.1	211.2	87.7	[5]
(*Z*)-*t*Bu–P=C(OSiMe$_3$)(Ph)		188.0	199.6	59.0	[45]
(*Z*)-[Cp(CO)$_2$Fe–P=C(OSiMe$_3$)(Ph)]	**4b**	237.7	202.1	78.2	[3]
(*Z*)-[Cp*(CO)$_2$Fe–P=C(OSiMe$_3$)(Ph)]	**8b**	287.1	199.7	72.6	[5]
(*Z*)-[Cp*(CO)$_2$Ru–P=C(OSiMe$_3$)(Ph)]	**9b**	264.1	196.7	72.6	[6]
(*Z*)-[Cp*(CO)$_2$Os–P=C(OSiMe$_3$)(Ph)]	**10b**	225.7			[7]
(*Z*)-[Cp(CO)$_2$Fe–P=C(OSiMe$_3$)(Mes)]	**4a**	208.2	198.6	71.8	[3]
(*Z*)-[Cp*(CO)$_2$Fe–P=C(OSiMe$_3$)(Mes)]	**8a**	251.9	196.1	65.4	[5]
(*E*)-[Cp*(CO)$_2$Ru–P=C(OSiMe$_3$)(Mes)]	(*E*)-**9a**	254.8			[6]
(*Z*)-[Cp*(CO)$_2$Ru–P=C(OSiMe$_3$)(Mes)]	(*Z*)-**9a**	230.0	192.6	64.3	[6]
(*Z*)-[Cp*(CO)$_2$Os–P=C(OSiMe$_3$)(Mes)]	(*Z*)-**10a**	193.7	189.8	58.8	[7]
*t*Bu–P=C(SiMe$_3$)$_2$		438.7	194.4	94.3	[46]
[Cp(CO)$_2$Fe–P=C(SiMe$_3$)$_2$]	**20**	593.2	211.2	110.9	[10]
[Cp*(CO)$_2$Fe–P=C(SiMe$_3$)$_2$]	**21**	641.5	208.9	106.1	[10]
[Cp(CO)$_3$Mo–P=C(SiMe$_3$)$_2$]	**16**	528.5	213.6	109.5	[10]
[Cp(CO)$_3$W–P=C(SiMe$_3$)$_2$]	**18**	505.2	210.1	106.4	[10]
[Cp*(CO)$_3$Cr–P=C(SiMe$_3$)$_2$]	**32**	605.4	222.2	107.6	[10]
[Cp*(CO)$_3$Mo–P=C(SiMe$_3$)$_2$]	**17**	588.8	218.0	106.9	[10]
[Cp*(CO)$_3$W–P=C(SiMe$_3$)$_2$]	**19**	564.3	210.6	105.0	[10]
[Cp*(PEt$_3$)Ni–P=C(SiMe$_3$)$_2$]	**34b**	740.5	202.6	94.7	[10]
trans-[(Bu$_3$P)$_2$(Cl)Ni–P=C(SiMe$_3$)$_2$]	**31a**	633.4			[12]
trans-[(Bu$_3$P)$_2$(I)Ni–P=C(SiMe$_3$)$_2$]	**31b**	645.4			[12]
trans-[(Ph$_3$P)$_2$(I)Pt–P=C(SiMe$_3$)$_2$]	**30**	585.0			[12]
Mes–P=C(NMe$_2$)$_2$		8.05	197.8	72.5	[47]
[Cp*(CO)$_2$Fe–P=C(NMe$_2$)$_2$]	**35**	135.5	202.4	97.0	[15]
[Cp*(CO)$_2$Ru–P=C(NMe$_2$)$_2$]	**36**	121.2	201.4	92.6	[15]

[a] In C_6D_6; 85% H_3PO_4 as external standard for the ^{31}P NMR signals.

In contrast, the exchange of iron in **8b** for the heavier homologues Ru and Os causes upfield shifts ($\Delta\delta(^{31}P) = -23.0$ and -38.4, respectively). Similar results are observed in the CpMo and CpW complexes **16** and **18** ($\Delta\delta^{31}P = -23.2$) as well as in the Cp*Cr, Cp*Mo, and Cp*W complexes **32**, **17**, and **19** ($\Delta\delta^{31}P = -16.6$ and -24.5, respectively). As in nonmetalated phosphaalkenes, substituents on the heteroatom lead to an increased shielding of the phosphorus nucleus by conjugation of a lone pair with the P=C bond.

Up to now there are only a few examples known of (*E*/*Z*) isomerism of *P*-metallophosphaalkenes. In these compounds the more strongly sterically hindered (*E*) isomers absorb at somewhat lower field than the (*Z*) isomers (e.g. δ((*E*)-(**9a**)) $-\delta$((*Z*)-(**9a**)) = 24.8[6]).

Downfield shifts of the ^{31}P NMR signal are also observed for *C*-metallophosphaalkenes of type [RP=C[M](OSiMe$_3$)] when a *tert*-butyl group on the methylene carbon atom is exchanged for a carbonylcyclopentadienyl metal complex fragment. This is attributed essentially to changes in the paramagnetic shift contribution. Thus, the singlet in (*E*)-[Cp*(CO)(NO)Re–C(OSiMe$_3$)=PPh] ((*E*)-**46b**)[22] observed at δ = 194.4 is shifted downfield relative to that in (*E*)-PhP=C(OSiMe$_3$)(*t*Bu) (δ = 135.0[44]) by $\Delta\delta$ = 59.4. For the pair of compounds (*E*)-[Cp*(CO)(NO)ReC(OSiMe$_3$)=PSiMe$_3$] ((*E*)-**46a**) (δ = 214.4[22]) and (*E*)-Me$_3$SiP=C(OSiMe$_3$)(*t*Bu)[48] the corresponding downfield shift is $\Delta\delta$ = 99.4. The *P*-aryl-*C*,*C*-dimetallophosphaalkenes **68a**[28] and **75c**[35] give singlets at $\delta(^{31}P)$ = 151.3 and 258.0, respectively.

The ^{13}C NMR spectra of phosphaalkenes show characteristic doublets for methylene carbon atoms at δ = 170–210; the *P*-metallophosphaalkenes are found in the upper region of the range. As the electron density on the metal atom increases, the ^{13}C NMR chemical shift decreases. This also applies when the substitution pattern on the phosphaalkenyl fragment remains the same within a triad ((d^4): Cr > Mo > W; (d^6): Fe > Ru > Os) as well as for 3d metals with increasing atomic number (Cr(d^4) > Fe(d^6) > Ni(d^8)).

In *C*-metallophosphaalkenes **46**[22] and **49**,[25] the ^{13}C NMR resonances lie at noticeably lower field (δ = 210.0–252.5 (d), $^1J_{C,P}$ = 80.7–113.5 Hz). The corresponding signals in the ^{13}C NMR spectra of the *C*,*C*-dimetallophosphaalkenes **75a–c** are doublets at even lower field (δ = 338.8–345.8 (d), $^1J_{P,C}$ = 92–97 Hz)[35] and therefore within the range of signals observed for carbenium ions.[49]

4. Reactivity

Metallophosphaalkenes of types I–IV are polyfunctional molecules with various reactive centers that can undergo chemical transformations. The reactivity of *P*-metallophosphaalkenes (type I) has been the most extensively investigated to date. These species react readily with electrophiles, and several types of reaction and products are often observed. The initial step is frequently a Lewis acid–base interaction, in which the phosphaalkene plays the part of the Lewis base through the lone pair of electrons on phosphorus. Therefore, it seems reasonable to organize this section according to the nature of the reaction partner. The subdivision of the metallophosphaalkenes, types I–IV, remains unchanged.

4.1. Reactivity of the *P*-Metallophosphaalkenes (Type I)

4.1.1. Protic Reagents

The tungstiophosphaalkene **18** is protonated at the P atom by trifluoromethanesulfonic acid in CH_2Cl_2 at $-78\,^\circ C$ to afford the cationic η^1-phosphaalkene complex **78** (Scheme 26).[8]

Equimolar amounts of **21** and 1,1,1,3,3,3-hexafluoropropane-2,2-diol dihydrate (hexafluoroacetone trihydrate) react in benzene to give the ferriophosphane oxide **79**, which can be isolated as pale yellow crystals in 30% yield.[50] The hydration is catalyzed by the fluoroorganic compound, a weak protic acid (pK_a = 6.58).[51]

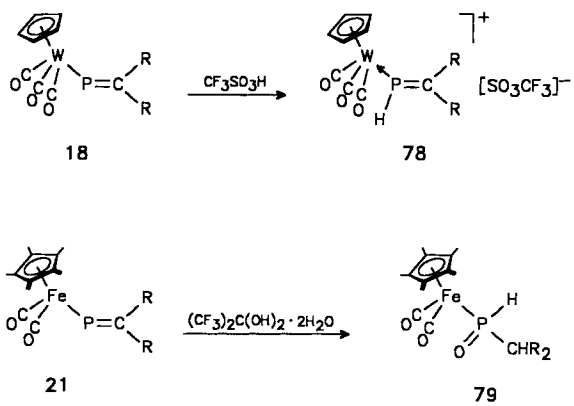

Scheme 26. Reaction of metallophosphaalkenes **18** and **21** with protic reagents. R = Me$_3$Si.

4.1.2. *Chalcogens*

Reactions of **18** and **24** with sulfur and selenium follow an unexpected course. Instead of the anticipated oxidation to products of type **80**, the chalcogen is inserted into the phosphorus–metal bond to produce complexes **81** and **83**, respectively (Scheme 27). Double sulfurization of **24** gives the $1,2\lambda^5$-thiaphosphirane **82** with preservation of the P–W bond. Compounds **80a** and **80b**, respectively, are postulated as intermediates.[10]

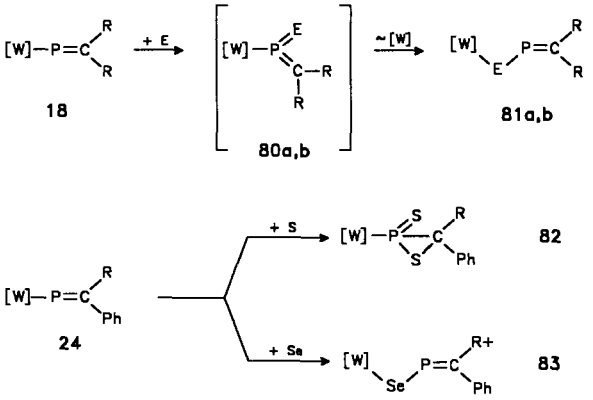

Scheme 27. Chalcogenation of tungstiophosphaalkenes; [W] = $Cp(CO)_3W$; E = S (**a**), Se (**b**); R = Me_3Si.

4.1.3. C_1 *Building Blocks*

4.1.3.1. *Alkylating Agents*

The cationic η^1-[bis(trimethylsilyl)methylene]methylphosphane complex **84** can be prepared by the alkylation of **18** with methyl trifluoromethanesulfonate (Scheme 28).[10]

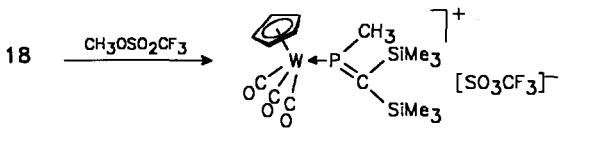

Scheme 28. Methylation of $[Cp(CO)_3W–P=C(SiMe_3)_2]$ **18**.

4.1.3.2. *Diazoalkanes*

Diphosphenes react smoothly with diazoalkanes with the loss of N_2 to produce diphosphiranes.[1h] As yet there are no reports of a similar phosphirane synthesis from phosphaalkenes and diazo compounds. The first 1,2,3-diazaphospholes with metal functions on nitrogen (**86a,b**), are obtained unexpectedly from the treatment of **35** with equimolar amounts of diazoacetates (Scheme 29).[52] The reaction proceeds by a 1,3-dipolar cycloaddition, in which the P atom of **35** is negatively polarized.[52] 1,3-Dipolar cycloadditions between acyldiazoalkanes and phosphaalkenes such as $Me_3SiP=C(R)(OSiMe_3)$ or $ClP=C(R)(SiMe_3)$, which contain positively polarized phosphorus centers, usually lead to 1,2,4-diazaphospholes.[53] Intermediates such as **85** were not detectable.

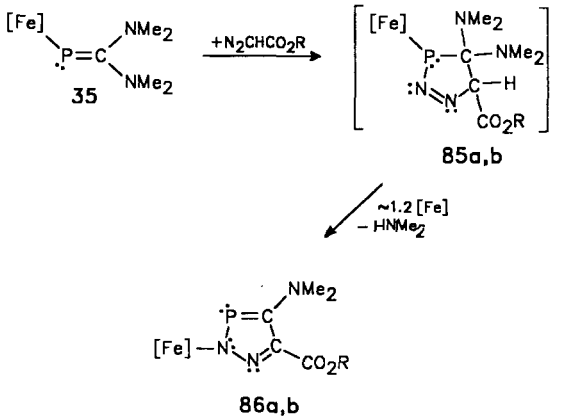

Scheme 29. [3+2]Cycloaddition between **35** and diazoacetates. [Fe] = $Cp^*(CO)_2Fe$, R = Et (**a**), *t*Bu (**b**).

Evidently, after cycloaddition of the starting materials to produce **85**, there is a subsequent rapid elimination of dimethylamine and a 1,2-metal migration (Scheme 29). Compound **35** and trimethylsilyldiazomethane do not react with one another.

4.1.3.3. *Sulfur Ylides*

Sulfur ylides are known to be excellent alkylidene transfer reagents that readily convert diphosphenes to diphosphiranes.[1h] The reaction of **21** with $Me_2S(O)=CH_2$ or $Me(Me_2N)S(O)=CH_2$, however, does not lead to the expected *P*-metallophosphirane, but to the "butterfly" complex **87** (Scheme 30).[54]

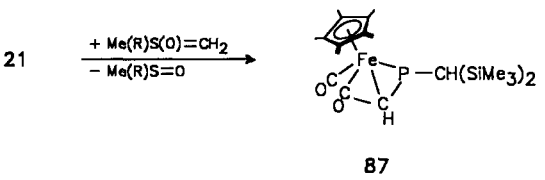

Scheme 30. Reaction of **21** with sulfur ylides. R = Me, Me_2N.

4.1.3.4. *Isocyanides*

The red, crystalline 2-imino-*P*-metallophosphiranes **88a–c** result from a formal [2+1]cycloaddition of aryl isocyanides to **21** (Scheme 31).[55] A striking feature in the molecular structure of **88a** (Fig. 2) is the P(1)–C(14) bond which is markedly elongated relative to the P(1)–C(13) bond. The endocyclic angle on the phosphorus atom [45.3(3)°] is strongly compressed com-

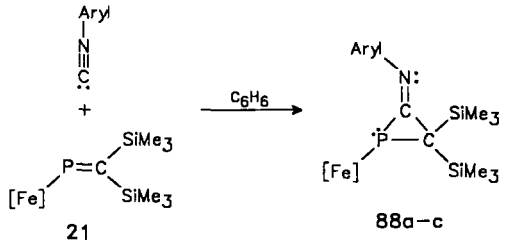

Scheme 31. Reaction of **21** with aryl isocyanides. Aryl = Ph (**a**), *o*-MeC_6H_4 (**b**), 2,6-$Me_2C_6H_3$ (**c**); [Fe] = $Cp^*(CO)_2Fe$.

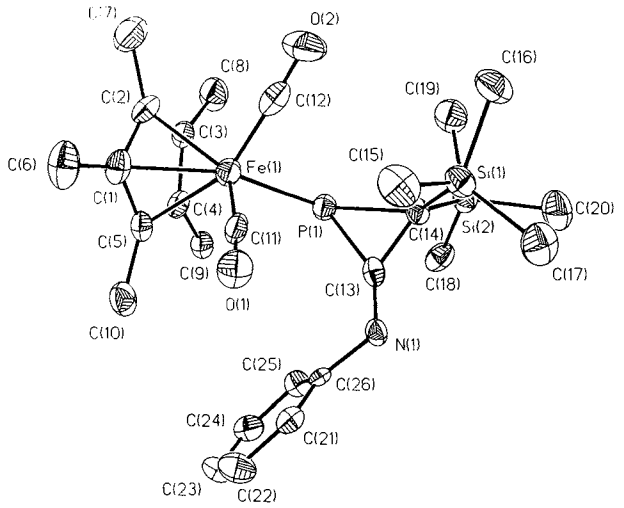

Fig. 2. Crystal Structure of **88a**. Selected bond lengths [Å] and angles [°]: Fe1-P1 2.279(2), P1-C13 1.799(7), P1-C14 1.990(7), C13-C14 1.469(8), N1-C13 1.273(7); C13-P1-C14 45.3(3), P1-C14-C13 60.9(3), P1-C13-C14 74.3(4).

pared to that on the ring carbon atoms C(13) [74.3(4)°] and C(14) [60.5(3)°].[55]

In contrast, the ferriophosphaalkene **35** is not attacked by isocyanides on the P—C double bond under similar conditions, but reacts with CO substitution to afford [Cp*(CO)(RNC)-Fe—P=C(NMe$_2$)] (R = *t*Bu, *c*C$_6$H$_{11}$, 2,6-Me$_2$C$_6$H$_3$).[56a]

4.1.4. C_2 Building Blocks

4.1.4.1. Alkenes

Since α,β-unsaturated carboxylic acid esters and nitriles are electrophilic, they are suitable partners for reaction with electron-rich metallophosphaalkenes. As a result of a two-step [2 + 2]cycloaddition, *P*-metallophosphetanes of type **89** are, a priori, the expected products (Scheme 32). However, treatment of **35** with fumarodinitrile and dimethyl fumarate lead instead to the *P*-metallo-1,2-dihydrophosphetes **90**; the initial products **89a,b** were not detectable by spectroscopy.[15] The reaction of ferriophosphaalkene **21** with fumarodinitrile proceeds completely differently and leads to the insertion product **91**. X-ray structure analysis of the deep violet phosphido complex **91** reveals that the two cyano groups occupy *cis* positions at the C=C bond (Scheme 32).[56b]

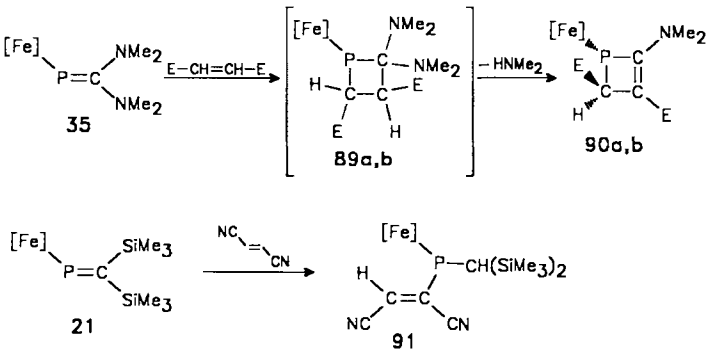

Scheme 32. Reactivity of ferriophosphaalkenes towards electron-deficient alkenes. [Fe] = Cp*(CO)$_2$Fe; E = CO$_2$Me (**a**), CN (**b**).

4.1.4.2. Alkynes

The reactivity of metallophosphaalkenes towards carbonyl-activated alkynes is determined largely by the substituents on the reaction partners concerned, as well as by the solvent and by the stoichiometry of the starting materials. There have been no cases of the isolation of *P*-metallo-1,2-dihydrophosphetes, which should result from a formal [2 + 2]cycloaddition. Thus, the reaction of *C*-silylated metallophosphaalkenes **21** or **27** with one equivalent of dimethyl acetylenedicarboxylate **92a** produced the [3 + 2]cycloadducts **93** and **94**, respectively (Scheme 33). In this case, the role of the 1,3-dipole is played by the OC-Fe-P fragment which is polarized negatively on the P atom and positively on the carbonyl carbon atom.[57]

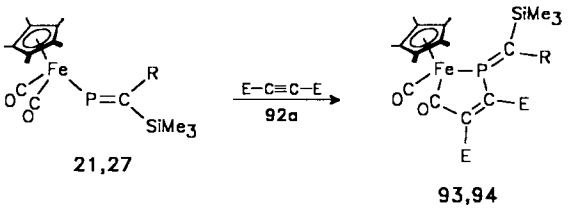

Scheme 33. Reaction of the ferriophosphaalkenes **21** and **27** with dimethyl acetylenedicarboxylate; E = CO$_2$Me; R = Ph: **27**, **94**; R = Me$_3$Si: **21**, **93**.

The metallaheterocycle **95a**, which is analogous to **93** and **94**, however, is only a minor product of the reaction between **35** and **92a**. The main product is the 1-metallo-1-phospha-1,3-butadiene **97a**, which is isolated as a stable, red-brown solid (Scheme 34).[58] The synthesis of **97a** from **35** and the alkyne is plausible if it is assumed that the initial reaction step is a non-concerted [2 + 2]cycloaddition to give 1,2-dihydrophosphete **96a**. The four-membered ring evades spectroscopic detection by spontaneous [2 + 2]cycloreversion to **97a** (Scheme 34).[58] This result is unusual because, as a rule, heterobutadienes with phosphorus fragments can only be isolated if the P=C bond is kinet-

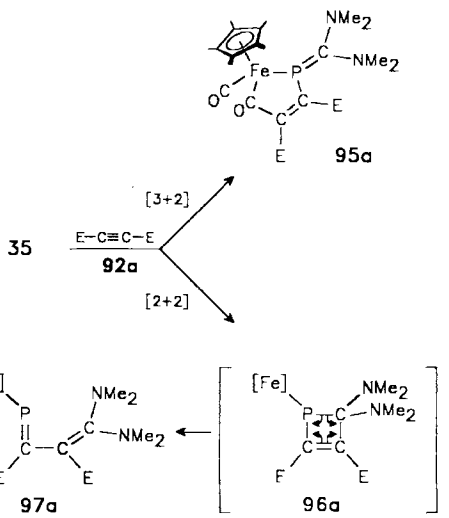

Scheme 34. Reaction of **35** with dimethyl acetylenedicarboxylate. [Fe] = Cp*(CO)$_2$Fe; E = CO$_2$Me.

ically stabilized by bulky substituents.[1a, 59] If there is insufficient steric shielding, the 1-phosphabutadienes spontaneously cyclize to 1,2-dihydrophosphetes. Mathey et al. postulate an equilibrium between 1,2-dihydrophosphetes and 1-phosphabutadienes (Scheme 35). At high temperatures this equilibrium shifts towards the heterodiene, which can be detected by trapping reactions.[60]

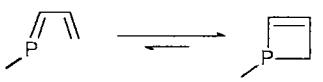

Scheme 35. Equilibrium between 1-phosphabutadienes and 1,2-dihydrophosphetes.

In the synthesis of **97a**, however, the reverse reaction from a ring to an acyclic compound was accomplished for the first time, without the resulting heterodiene having particularly bulky substituents.

According to the X-ray structure analysis of **97a** (Fig. 3), the molecule has a cisoid conformation with a localized P=C bond. The C4–C5 and C4–C8 distances are similar and provide evidence for the pronounced delocalization of the C=C bond in the diene moiety of the molecule.

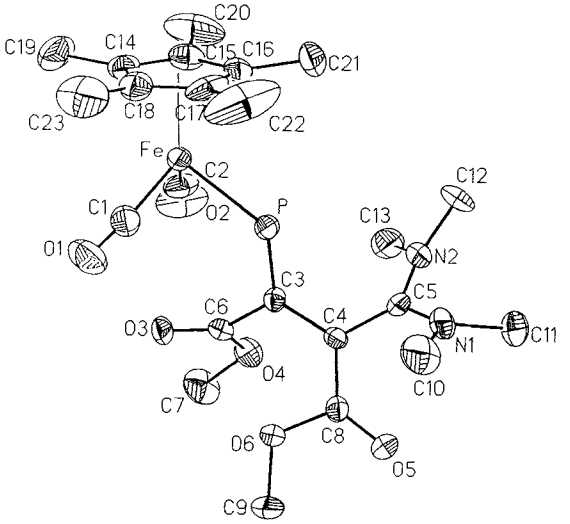

Fig. 3. Crystal Structure of **97a**. Selected bond lengths [Å] and angles [ ]: Fe-P 2.259(2), P-C3 1.688(7), C3-C4 1.451(9), C4-C5 1.427(10), C3-C6 1.513(11), C4-C8 1.428(10); Fe-P-C3 119.3(3).

The ferriophosphaalkenes **21** and **27** are not attacked by methyl 2-butynoate (**92b**); however, if equimolar amounts of **35** and **92b** are allowed to react in *n*-pentane, the 1-phosphabutadiene **97b** precipitates as a red-brown solid (42% yield) (Scheme 36). Approximately equal amounts of **95b** and the 2-methylene-1,2-dihydrophosphete **98** can be detected in the mother liquor. In ether or benzene, **97b** cyclizes rapidly to **98** with release of dimethylamine. In keeping with this, treatment of **35** with the alkyne **92b** in ether leads directly to orange microcrystalline **98** as the main product (41% yield).[58]

On the other hand, alkyl propiolates $HC{\equiv}CCO_2R$ behave completely differently towards ferriophosphaalkenes. Compound **21** adds two equivalents of the alkyne in pentane to form the bicyclic, red, crystalline *P*-metallo-ylide **99** (Scheme 37); no intermediates were detected by ^{31}P NMR spectroscopy.[61] For-

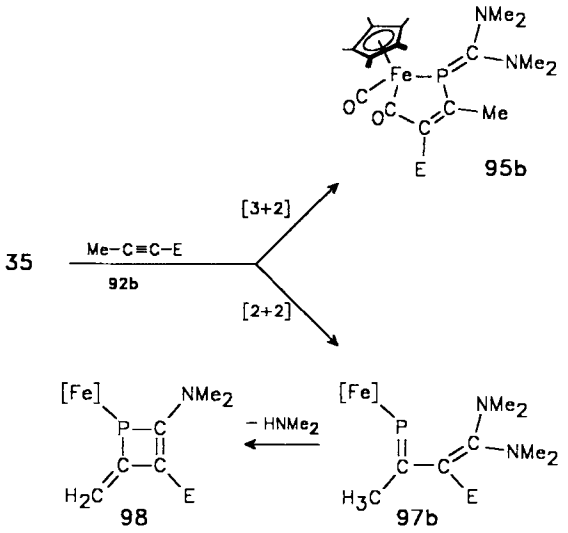

Scheme 36. Reaction of **35** with methyl 2-butynoate. E = CO_2Me. [Fe] = $Cp^*Fe(CO)_2$.

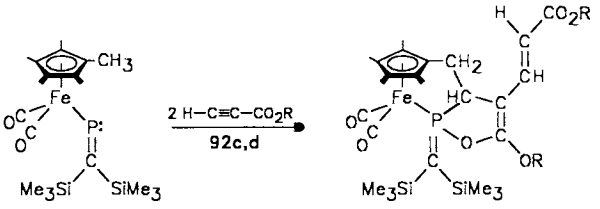

Scheme 37. Reaction of **21** with propiolates. R = Me (**92c**), Et (**92d**).

mation of the product is evidently preceded by the addition of two equivalents of the ester onto the P atom of **21** and a proton transfer from the ring methyl group to the end of the diene chain.[61]

Equimolar amounts of **35** and methyl propriolate (**92c**) react in *n*-pentane to a furnish a mixture of the metallaheterocycle **95c** and the 1-phosphabutadiene **97c** (Scheme 38). The reaction between the ferriophosphaalkene and three molar equivalents of alkyne is more straightforward, here the bicyclic compound **100**

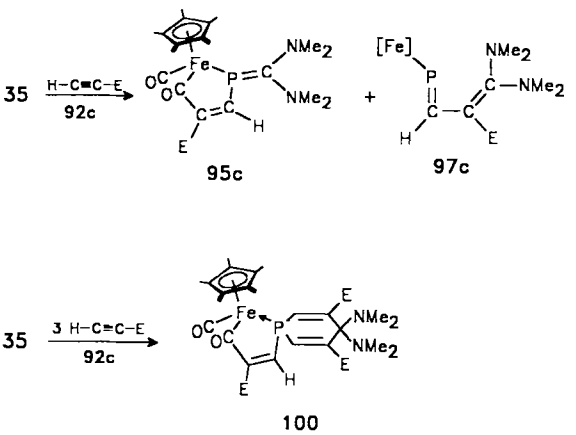

Scheme 38. Reactions of **35** with methyl propiolate. E = CO_2Me; [Fe] = $Cp^*(CO)_2Fe$.

is obtained as the sole product in good yield. It is conceivable that **97c** forms a reactive [4+2]cycloadduct with the second equivalent of **92c** and is then rapidly converted to the final product by the third equivalent of alkyne.[61]

4.1.5. *Azo Compounds*

Azodicarboxylates E–N=N–E induce the intramolecular condensation of a ring-methyl group with the P=C function in the metallophosphaalkene **35** to afford complexes **101a–c** in 48–54% yield (Scheme 39). This reaction is important because this was the first such condensation involving the η^5-C_5Me_5 ligand. An essential advantage of this ring ligand in its complexes, along with its donating ability and bulk, is its pronounced reluctance to chemical transformations.[62]

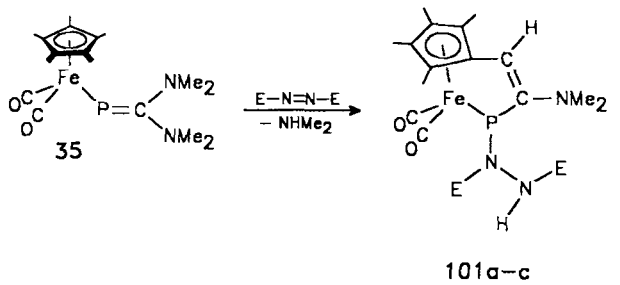

Scheme 39. Treatment of **35** with azodicarboxylates. E = CO_2Et (**a**), CO_2tBu (**b**), CO_2CH_2Ph (**c**).

The X-ray structure analysis of **101b** (Fig. 4) reveals that the η^5-ring ligand is additionally bonded to the metal atom by a

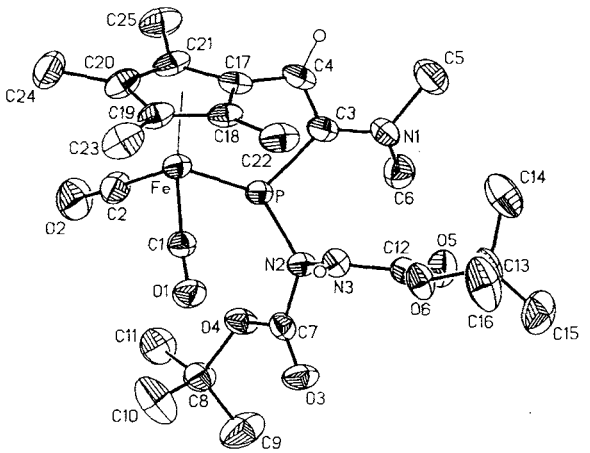

Fig. 4. Crystal Structure of **101b**. Selected bond lengths [Å] and angles [ ]: Fe-P 2.307(2), P-C3 1.843(5), P-N2 1.781(5), C3-C4 1.338(9); Fe-P-C3 102.1(2), P-C3-C4 113.3(4), P-C3-N1 121.4(5), N1-C3-C4 124.7(5).

C=C–P chain. The C3–C4 distance of 1.338(9) Å corresponds to a double bond. The trigonal pyramidally surrounded phosphorus atom also bears a hydrazido substituent (N2–N3 1.399(6) Å).[62]

4.2. Reactivity of the Metallophosphaalkenes of Type II and III

4.2.1. *Rearrangement of Phosphametallabicyclohexenes*

If the phosphazirconiabicyclic compounds **60a–c** are heated in toluene to 60 °C, they undergo ring opening to generate unstable vinylcarbene complexes. Subsequent "dimerization" of the carbene–metal fragment with the phosphaalkyne ligand produces four-membered rings of the type in compound **102**, which also show structural properties of C-metallophosphaalkenes (Scheme 40). The corresponding titanium derivatives are also accessible.[32]

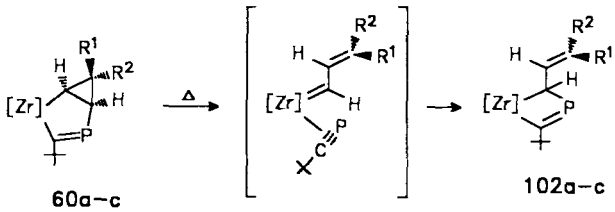

Scheme 40. Thermal rearrangement of the bicyclic compounds **60a–c**. [Zr] = Cp_2Zr; **a**: $R^1 = R^2$ = Me (89%), **b**: $R^1 = R^2$ = Ph (97%), **c**: R^1 = Me, R^2 = Ph (64%).

4.2.2. *Thermolysis of the Phosphazirconiacyclopentadiene 57a*

On warming a yellow solution of **57a** in toluene to 60 °C, it changes color to deep red over a period of 72 h with formation of the 1,4-diphosphinine complex **103** (92% yield) (Scheme 41).[32] The same product arises almost quantitatively from an equimolar mixture of **57a**, **56**, and BEt_3 on warming from −78 °C to 20 °C.[32]

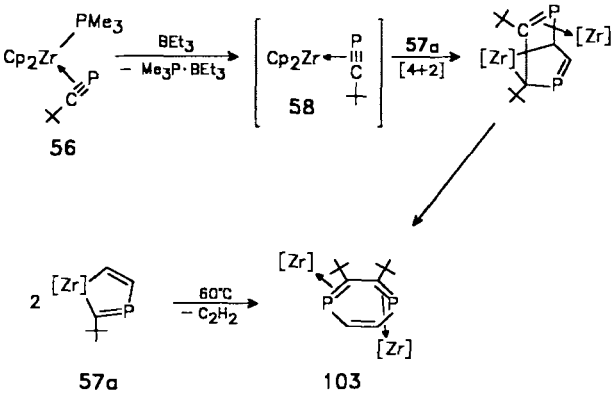

Scheme 41. Synthesis of a (1,4-diphosphinine)dizirconium complex. [Zr] = Cp_2Zr.

4.2.3. *Thermolysis of C-Platiniophosphaalkenes*

The metallophosphaalkenes **50a,b** rearrange at 20 °C in dichloromethane within 24 h to the bicyclic compounds **104a,b** which can be isolated without decomposition from the polar solvent (Scheme 42). In *n*-hexane, however, the products rapidly decompose to Mes*C≡P and *trans*-$[Pt(PEt_3)_2X_2]$.[28c]

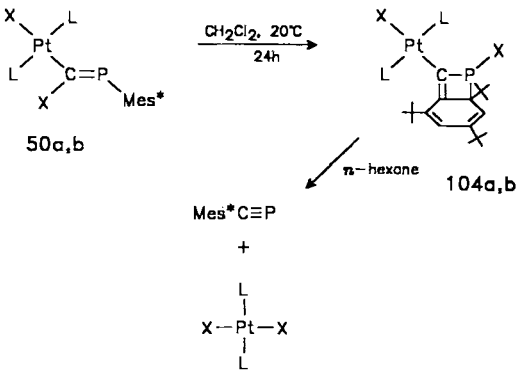

Scheme 42. Intramolecular cyclization of *C*-platiniophosphaalkenes **50a,b**. L = PEt_3; X = Cl (**a**), Br (**b**).

5. Coordination Chemistry of Metallophosphaalkenes

5.1. *P*-Metallophosphaalkenes as Ligands

Akin to their organo-substituted prototypes, the metallophosphaalkenes $L_nMP{=}CR^2R^3$ (type I) can also act as ligands in transition metal complexes. In principle, the coordination modes **G**–**K** are conceivable. (Scheme 43).

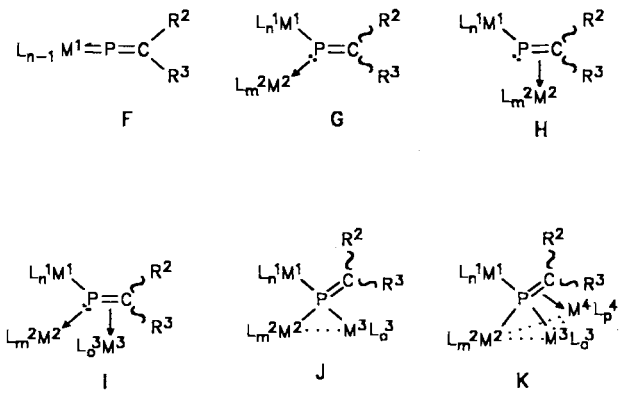

Scheme 43. Coordination modes of metallophosphaalkenes in transition metal complexes.

The metallophosphaalkenes of the four other structural types (II–V) should show comparable ligand properties. In contrast to the coordination behavior of conventional phosphaalkenes, it is possible for the lone pair of electrons on the phosphorus atom in *P*-metallophosphaalkenes to displace a loosely bound two-electron donor (2e donor) intramolecularly from the metal, so that the organophosphorus fragment becomes a 3e ligand. Similar behavior is known from phosphido and phosphenium ligands PR_2,[63] and, of course, from NO ligands. In the case discussed here, phosphavinylidene complexes **F** are formed.

5.1.1. Phosphavinylidene Complexes (Type F)

This type of complex is known with molybdenum, tungsten and nickel; the first, the complex **105a**, was obtained from the reaction of $K[Mo(CO)_3Cp]$ with $ClP{=}C(SiMe_3)_2$ in THF (Scheme 44).[64]

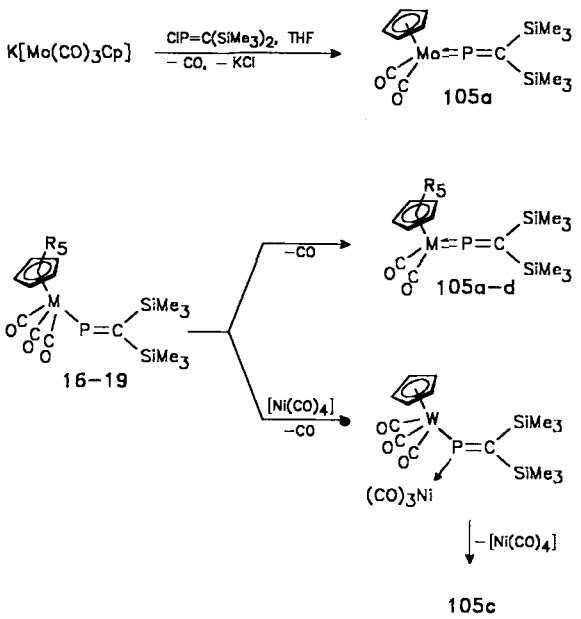

Scheme 44. Syntheses of phosphavinylidene complexes of molybdenum and tungsten. **a**: M = Mo, R = H; **b**: Mo, Me; **c**: W, H; **d**: W, Me.

The metallophosphaalkenes **16**–**19** undergo thermal decarbonylation in solution to give the phosphavinylidene complexes **105a**–**d** (Scheme 44). The reaction conditions required for the cleavage of the CO ligand depend on the stability of the metal–CO bond as well as on the substituents on the phosphaalkenyl fragment. Accordingly, cleavage of CO from the molybdeniophosphaalkenes **16** and **17** in nonpolar solvents commences at room temperature, whilst the formation of the tungsten derivatives **105c,d** requires several hours reflux in benzene. For the ferriophosphaalkene **21** as well as for the phenyl-substituted metallophosphaalkenes **22**–**27**, elimination of CO to form phosphavinylidene complexes is not observed under thermal nor under photochemical conditions.[10]

Abstraction of CO can also be carried out chemically. Thus, the adduct obtained from **18** and nickel tetracarbonyl at low temperatures rapidly decomposes in solution at 20 °C to afford **105c** and $[Ni(CO)_4]$ (Scheme 44).[10]

An interesting route to the (phosphavinylidene)nickel cation **107** is based on the treatment of $[Ni(PPh_3)_2(cod)]$ with triphenyl(phosphaalkenyl)phosphonium ion **106** (Scheme 45). No intermediates were detected by spectroscopy.[65]

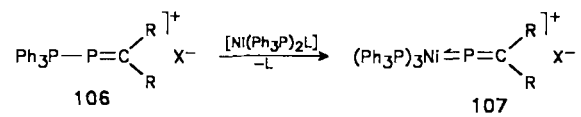

Scheme 45. Synthesis of a (phosphavinylidene)nickel complex. L = 1,5-cyclooctadiene, R = Me_3Si, X = $AlCl_4$.

5.1.2. Metallophosphaalkenes as η^1 Ligands (Type G)

Transition metal complexes with η^1-metallophosphaalkene ligands of type **G** are formally divided into those without metal–metal interactions (e.g. **108** and **109**) and those with **M**–**M** bonding (e.g. **110** and **112**). The former usually arise from

the treatment of metallophosphaalkenes, for example **24**, with transition metal complexes containing labile ligands (Scheme 46).[110]

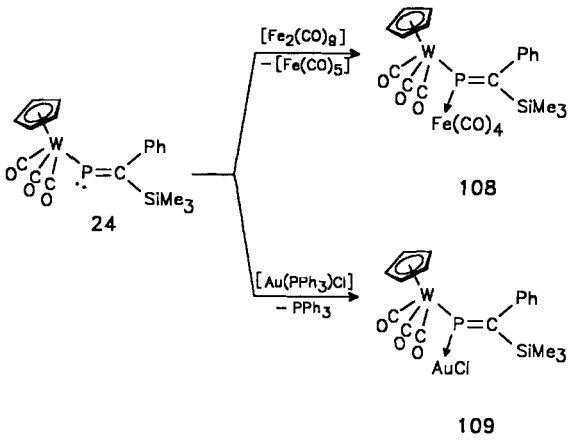

Scheme 46. *P*-Metallophosphaalkenes as η^1-ligands without M–M bonds.

The preparation of the dinuclear complex **110** with an Fe–Fe bond was carried out by the reaction of $ClP{=}C(SiMe_3)_2$ with excess $[Na_2Fe(CO)_4]\cdot 1.5$ dioxane in the presence of diazabicycloundecene (Scheme 47).[66]

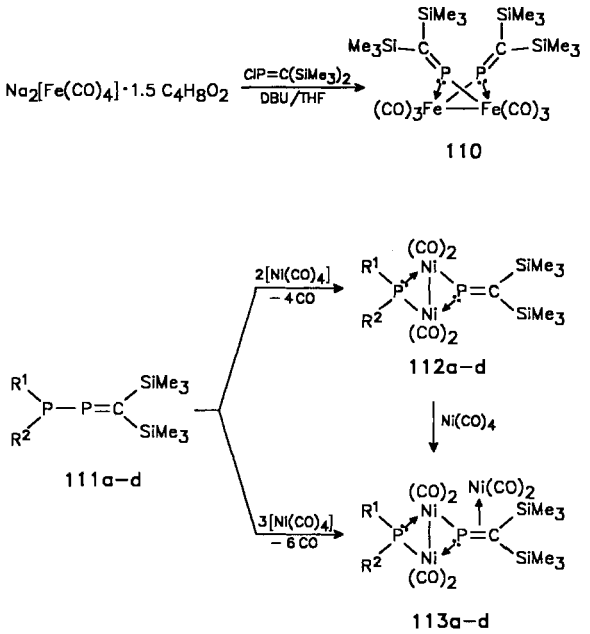

Scheme 47. *P*-Metallophosphaalkenes as η^1-ligands with M–M bonds. **a**: $R^1 = R^2 = c\text{-}C_6H_{11}$; **b**: *t*Bu; **c**: Me_3Si; **d**: $R^1 = t$Bu, $R^2 = Me_3Si$.

Dinuclear carbonylnickel complexes **112a–d** with μ-phosphaalkenyl and μ-phosphido ligands result from the treatment of 1,2-diphosphapropenes **111a–d** with two molar equivalents of $[Ni(CO)_4]$ (Scheme 47). If a larger excess of nickel carbonyl is added, the trinuclear species **113a–d** are formed in which the P=C bond also acts as a π donor. Compounds **112a–d** also react directly with $[Ni(CO)_4]$ to give **113a–d**.[67] Derivatives of type **112** are also known with iron and molybdenum centers.[67]

5.1.3. *P*-Metallophosphaalkenes as η^2 Ligands (Type H)

Compounds containing a metallophosphaalkene with this mode of coordination usually arise from peripheral reactions of phosphaalkynes with transition metal complexes. For example, the reaction of $[Cp^*_2(CO)_2Rh_2]$ or $[Cp^*_2(CO)_2CoRh]$ with *t*BuC≡P readily affords the complexes **114** (Scheme 48).[68, 69] Complex **115a** is formed as a side-product and can be regarded as a metallodiphosphadiene which is additionally π-bound through both C=P functions to a Cp*Rh fragment. The reaction of $[Cp^*_2(CO)_2Rh_2]$ with AdC≡P proceeds similarly.

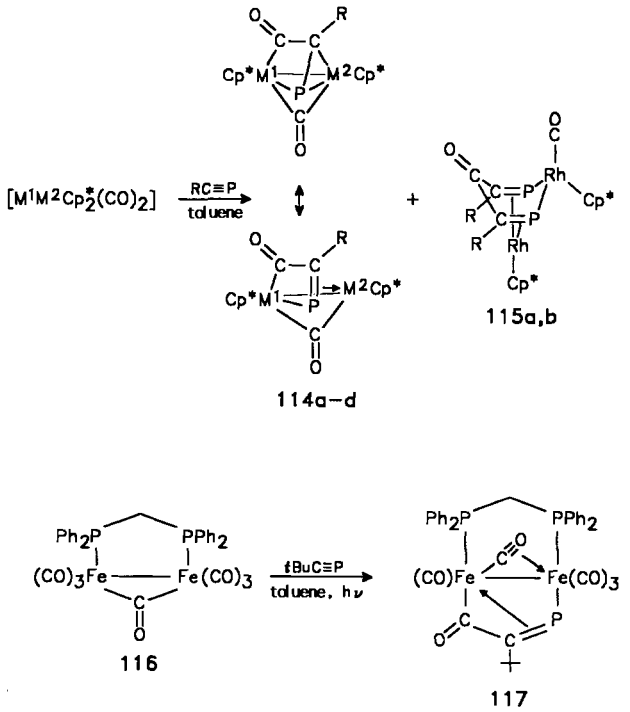

Scheme 48. Metallophosphaalkenes as η^2 ligands; **a**: $M^1 = M^2 = Rh$, R = *t*Bu; **b**: $M^1 = M^2 = Rh$, R = 1-adamantyl; **c**: $M^1 = Rh$, $M^2 = Co$, R = *t*Bu; **d**: $M^1 = Co$, $M^2 = Rh$, R = *t*Bu.

A mode of coordination similar to that present in **114** is encountered in the dinuclear iron complex **117**, which is produced by the photolysis of **116** in the presence of *t*BuC≡P (Scheme 48).[70]

5.1.4. Metallophosphaalkenes as η^1:η^2 Ligands (Type I)

It appeared reasonable to extend the principle of synthesis for *C,C*-dimetallophosphaalkenes, outlined in Scheme 24, to the preparation of *C,C,P*-trimetallophosphaalkenes $[[M^1]{-}P{=}C{-}([M^2])[M^3]]$ (type V, Scheme 2). Condensation of the cation **73** with metallodisilylphosphanes **5** or **6** gave, instead of the expected threefold functionalized phosphaalkenes, the trinuclear complexes **118a** and **118b**, respectively, in which the η^1:η^2-metallophosphaalkene ligand bridges the $[Fe_2Cp_2(CO)(\mu\text{-}CO)]$ skeleton (Scheme 49). Compound **118a** can also be obtained from the reaction of $[FeCp^*(CO)_2(PH_2)]$ and **73** under analogous conditions.[71]

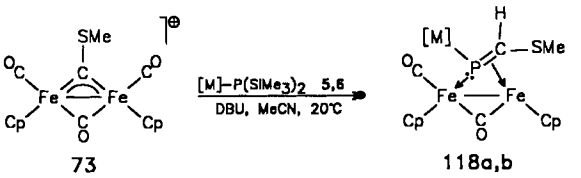

Scheme 49. Synthesis of complexes with η^1:η^2-metallophosphaalkene ligands; **a**: [M] = Cp*(CO)$_2$Fe; **b**: [M] = Cp*(CO)$_2$Ru.

5.2. Miscellaneous

Metallophosphaalkenes of type II and IV (Scheme 2) can also function as ligands in transition metal complexes. For example, the η^1 complexes **119** containing a *C*-metallophosphaalkene ligand are obtained from the action of thermolabile carbonylmetal complexes such as [Cr(cyclooctene)(CO)$_5$][72] or [Fe$_2$(CO)$_9$][73] on compound **87** (Scheme 50). However, if **87** or **119b** is treated with excess [Fe$_2$(CO)$_9$], the trinuclear complex **120** is isolated, which has a formal μ_3-1-oxa-4-phosphabutadiene ligand.[73]

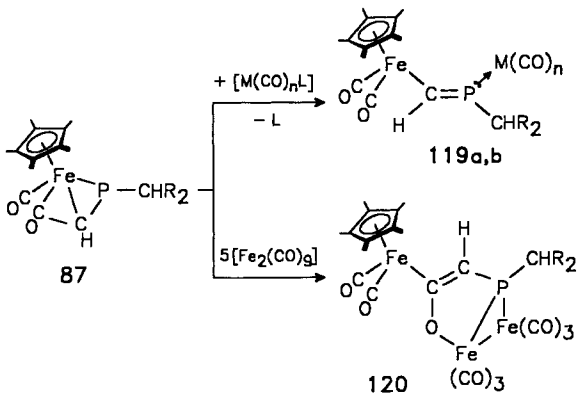

Scheme 50. Reaction of **87** with carbonylmetal complexes. R = Me$_3$Si; **a**: L = cyclooctene, M(CO)$_n$ = Cr(CO)$_5$; **b**: L = Fe(CO)$_5$, M(CO)$_n$ = Fe(CO)$_4$.

The coordination mode which the dimetallophosphaalkene **75a** displays towards transition metal fragments is controlled by the nature of the complex building unit. The reaction with equimolar amounts of [Cr{(*Z*)-cyclooctene}(CO)$_5$] or [Fe$_2$(CO)$_9$] leads to the black-brown microcrystalline compounds **121** and **122**, respectively (Scheme 51). In complex **123**, obtained from the treatment of **75a** with [Pt(PPh$_3$)$_2$(η^2-C$_2$H$_4$)], the dimetallophosphaalkene can be described as a η^3-1-phospha-3-ferraallyl ligand bound to a [Pt(PPh$_3$)] fragment.

The X-ray crystal structure analysis of **123** (Fig. 5) reveals that the molecular framework of **75a** has remained largely intact. The trigonal-planar surrounded donor site C(12) (sum of angles = 359.2°) symmetrically bridges the iron atoms. The P=C bond is elongated to 1.737(10) Å on account of π coordination to the Pt atom. In order to saturate its coordination, the platinum atom also bonds to Fe(1) and C(13). Alternatively, the framework can be regarded as an *arachno* cluster of atoms Pt(1), P(2), C(12), Fe(1), and C(13).[36]

The complex anions **125a–d**, which arise from the reaction of carbonylhydridometalates **124a–d** with equimolar amounts of *t*BuC≡P (Scheme 52), contain a μ_3-η^2-phosphaalkyne ligand,

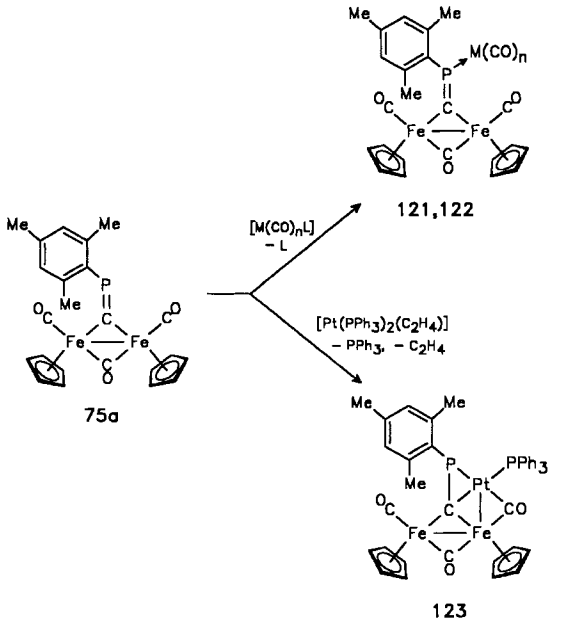

Scheme 51. The *C*,*C*-Diferriophosphaalkene **75a** as a ligand in Cr, Fe, and Pt complexes. **121**: M(CO)$_n$ = Cr(CO)$_5$, L = cyclooctene; **122**: M(CO)$_n$ = Fe(CO)$_4$, L = Fe(CO)$_5$.

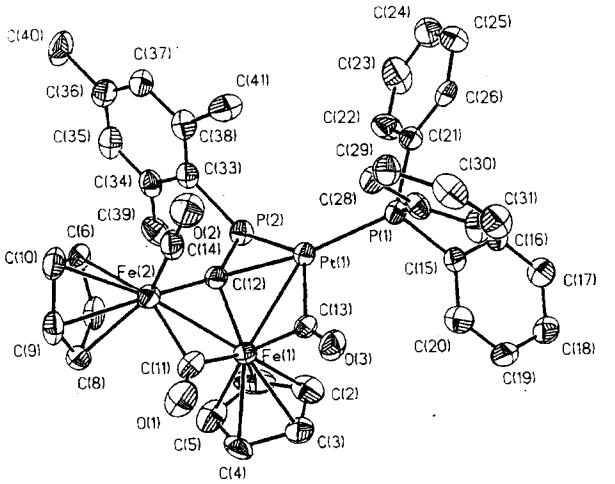

Fig. 5. Crystal Structure of **123**. Selected bond lengths [Å] and angles [°]: Pt1-Fe1 2.577(2), Pt1-P1 2.240(2), Pt1-P2 2.471(2), Pt1-C12 2.162(9), Pt1-C13 1.997(2), Fe1-C13 1.951(9), P2-C12 1.737(10), Fe1-Fe2 2.518(4); Fe1-C12-P2 130.6(5), Fe2-C12-P2 146.5(5), Fe1-C12-Fe2 82.1(4).

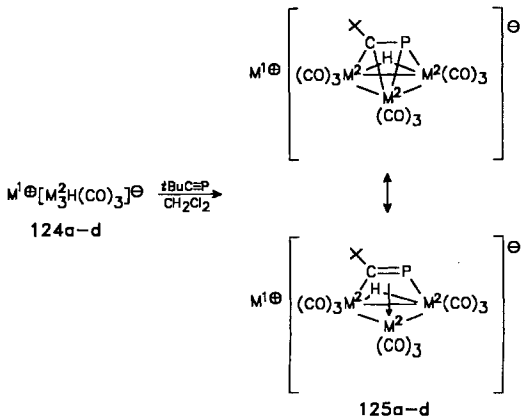

Scheme 52. Complex anions with a *C*,*P*-dimetallophosphaalkene as a η^2-ligand. **a**: M^1 = PPh$_4$, M^2 = Fe; **b**: M^1 = (Ph$_3$P)$_2$N, M^2 = Ru; **c**: M^1 = Na, M^2 = Ru; **d**: M^1 = NEt$_4$, M^2 = Ru.

which unsymmetrically spans the metal triangle. Alternatively, these anions may also be regarded as *C,P*-dimetallophosphaalkenes in which the C=P bond maintains a π interaction with a third metal atom.[74]

6. Chemical Properties of Phosphavinylidene Complexes

In agreement with the polarization $P^{\delta+}-C^{\delta-}$ of the P=C bond in the molybdenumphosphavinylidene complex **105a**, protic substances, HX, add regioselectively to the double bond to form the phosphenium complexes **126** (Scheme 53).[44b] The

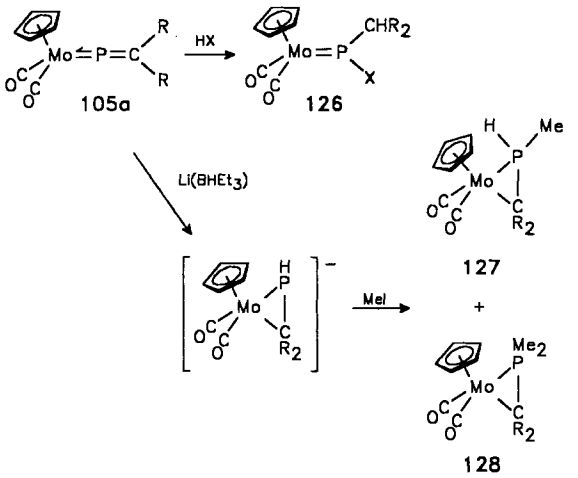

Scheme 53. Reactions of **105a** with proton and hydride donors. R = Me_3Si; X = EtO, Me_2N, C_6F_5S.

behavior of **105a** towards the hydride donor $Li(BHEt_3)$ is explained similarly. If a solution of the phosphavinylidene complex is treated with one equivalent of $Li(HBEt_3)$ and subsequently with excess methyl iodide, heterocycles with three-membered rings, **127** and **128**, are produced. Here, hydride attack on the phosphorus atom of **105a** plays the key role.[75]

Equimolar amounts of the phosphavinylidene complexes **105a** or **105c** and the sulfur ylide $Me_2S(O)=CH_2$ in ether react to form the phosphenium complexes **129** (Scheme 54), which

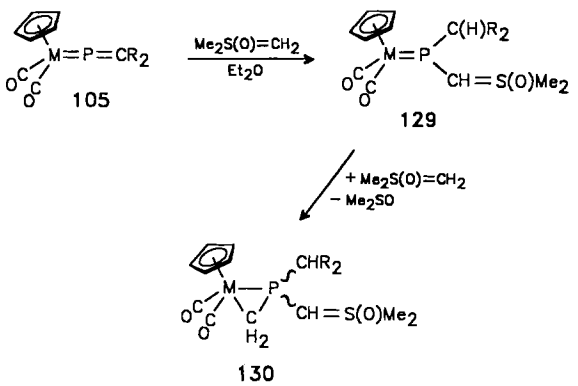

Scheme 54. Reaction of phosphavinylidene complexes of molybdenum and tungsten with $Me_2S(O)=CH_2$. M = Mo, W.

are isolated as brick red solids in yields of about 70%. Evidently, the addition of the carbanionic ylide center onto the P atom is accompanied by a rapid transylidation. A second ylide molecule subsequently "cyclopropanizes" the M=P bond to yield the metallaheterocycle **130**.[76]

7. Summary and Future Prospects

This review demonstrates that the chemistry of metal-functionalized phosphaalkenes has developed rapidly in recent years. In the beginning the interest focused on the synthesis and structural elucidation of such complexes. Ever increasingly it has shifted towards the reactivity of these compounds which are to be found in the border regions of organophosphorus, organometallic, and complex chemistry.

The combination of electrophilic and nucleophilic centers on the P=C unit as well as on the organometallic fragment makes metallophosphaalkenes versatile reaction partners, and we have only just begun to explore the great richness of their chemistry.

The possibilities for the synthesis of metallophosphaalkenes with their structural variations are by no means exhausted. Novel reactive compounds, such as the recently discovered phosphane-stabilized methylenediylphosphenium salts ($(Ph_3P-P=CR_2)X$) continually lead to novel metallophosphaalkenes. Even phosphaalkynes, which are in the meantime so well-known, serve further as a valuable source for the synthesis of metallophosphaalkenes. Metallophosphaalkenes play a key role as intermediates in the metal-mediated oligomerization of phosphaalkynes to phosphorus–carbon heterocycles and cages. The understanding of the chemical properties of metallophosphaalkenes not only casts light onto such oligomerization processes, but also should be an aid in the planning of efficient syntheses.

In future, along with purely preparative considerations, physico-chemical investigations will make an important contribution to this field, in particular, electrochemical, kinetic, and mechanistic studies, as well as theoretical calculations. Application-orientated aspects such as polymerization and copolymerization of suitably substituted derivatives are also waiting to be discovered.

I would like to thank all my coworkers who have contributed with great commitment to the development of this field. Their names can be found in the literature citations. I owe many thanks to Professors E. Niecke (Bonn) and W. W. Schoeller (Bielefeld) for helpful discussions. I thank Mrs M. Schimmel for writing up the manuscript. Much of the cited work was supported by the Deutsche Forschungsgemeinschaft, the Fonds der Chemischen Industrie, and the companies BASF AG, Ludwigshafen, and DEGUSSA AG, Hanau.

Received: February 23, 1995
Revised version: May 26, 1995 [A 1061E]
German version: *Angew. Chem.* **1996**, *108*, 292–310
Translated by G. Scheibelein, Offenburg (Germany)

[1] Reviews: P=C: a) R. Appel in *Multiple Bonds and Low Coordination in Phosphorus Chemistry* (Eds.: M. Regitz, O. J. Scherer), Thieme, Stuttgart, **1990**, pp. 157–219; b) R. Appel, F. Knoll, *Adv. Inorg. Chem.* **1989**, *33*, 259–361; c) L. N. Markovskii, V. D. Romanenko, *Tetrahedron* **1989**, *45*, 6019–6090; d) R. Appel, F. Knoll, I. Ruppert, *Angew. Chem.* **1981**, *93*, 771–784; *Angew. Chem. Int. Ed. Engl.* **1981**, *20*, 731. P≡C: e) M. Regitz, *Chem. Rev.* **1990**, *90*, 191–213;

f) M. Regitz, P. Binger, *Angew. Chem.* **1988**, *100*, 1541–1565; *Angew. Chem. Int. Ed. Engl.* **1988**, *27*, 1484. P=N: g) E. Niecke, D. Gudat, *ibid.* **1991**, *103*, 251–270 and **1991**, *30*, 217. P=P, P=As, As=As: h) L. Weber, *Chem. Rev.* **1992**, *92*, 1839–1906.

[2] J. F. Nixon, *Chem. Rev.* **1988**, *88*, 1327–1362.

[3] L. Weber, K. Reizig, M. Frebel, R. Boese, M. Polk, *J. Organomet. Chem.* **1986**, *306*, 105–114.

[4] Review: G. Becker, W. Becker, O. Mundt, *Phosphorus Sulfur* **1983**, *14*, 267–283.

[5] L. Weber, K. Reizig, M. Frebel, *Chem. Ber.* **1986**, *119*, 1857–1867.

[6] L. Weber, D. Bungardt, K. Reizig, R. Boese, *Z. Naturforsch. B* **1986**, *41*, 1096–1106.

[7] L. Weber, D. Bungardt, *J. Organomet. Chem.* **1986**, *311*, 269–280.

[8] D. Gudat, E. Niecke, W. Malisch, U. Hofmockel, S. Quashie, A. H. Cowley, A. M. Arif, B. Krebs, M. Dartmann, *J. Chem. Soc. Chem. Commun.* **1985**, 1687–1689.

[9] D. Gudat, E. Niecke, A. M. Arif, A. H. Cowley, S. Quashie, *Organometallics* **1986**, *5*, 593–595.

[10] E. Niecke, H.-J. Metternich, M. Nieger, D. Gudat, P. Wenderoth, W. Malisch, C. Hahner, W. Reich, *Chem. Ber.* **1993**, *126*, 1299–1309.

[11] H.-J. Metternich, E. Niecke, J. F. Nixon, *J. Chem. Soc. Chem. Commun.* **1992**, 232–233.

[12] D. Gudat, M. F. Meidine, J. F. Nixon, E. Niecke, *J. Chem. Soc. Chem. Commun.* **1989**, 1206–1208.

[13] P. B. Hitchcock, M. F. Meidine, J. F. Nixon, H. Wang, D. Gudat, E. Niecke, *J. Organomet. Chem.* **1989**, *368*, C29–C32.

[14] D. Gudat, E. Niecke, B. Krebs, M. Dartmann, *Chimia* **1985**, *39*, 277–279.

[15] L. Weber, O. Kaminski, H.-G. Stammler, B. Neumann, V. D. Romanenko, *Z. Naturforsch. B* **1993**, *48*, 1784–1794.

[16] P. B. Hitchcock, C. Jones, J. F. Nixon, *Angew. Chem.* **1994**, *106*, 478–480; *Angew. Chem. Int. Ed. Engl.* **1994**, *33*, 463.

[17] P. Binger, B. Biedenbach, R. Mynott, C. Krüger, P. Betz, M. Regitz, *Angew. Chem.* **1988**, *100*, 1219–1221; *Angew. Chem. Int. Ed. Engl.* **1988**, *27*, 1158.

[18] a) U. Zenneck, *Angew. Chem.* **1990**, *102*, 171–182; *Angew. Chem. Int. Ed. Engl.* **1990**, *29*, 138; b) D. Böhm, F. Knoch, S. Kummer, U. Schmidt, U. Zenneck, *ibid.* **1995**, *107*, 251–253 and **1995**, *34*, 198–201.

[19] P. Binger, B. Biedenbach, C. Krüger, M. Regitz, *Angew. Chem.* **1987**, *99*, 798–799; *Angew. Chem. Int. Ed. Engl.* **1987**, *26*, 764–765.

[20] P. Binger, G. Glaser, B. Gabor, R. Mynott, *Angew. Chem.* **1995**, *107*, 114–116; *Angew. Chem. Int. Ed. Engl.* **1995**, *34*, 81–83.

[21] P. Binger, J. Haas, A. T. Herrmann, F. Langhauser, C. Krüger, *Angew. Chem.* **1991**, *103*, 316–318; *Angew. Chem. Int. Ed. Engl.* **1991**, *30*, 310.

[22] L. Weber, K. Reizig, R. Boese, M. Polk, *Organometallics* **1986**, *5*, 1098–1103.

[23] L. Weber, G. Meine, *Chem. Ber.* **1987**, *120*, 457–459.

[24] L. Weber, K. Reizig, *Z. Naturforsch. B* **1984**, *39*, 1350–1354.

[25] L. Weber, K. Reizig, G. Meine, *Z. Naturforsch. B* **1985**, *40*, 1698–1702.

[26] L. Weber, K. Reizig, R. Boese, *Chem. Ber.* **1985**, *118*, 1193–1203.

[27] L. Weber, K. Reizig, R. Boese, *Organometallics* **1985**, *4*, 2097–2101.

[28] a) H. Jun, V. G. Young, Jr., R. J. Angelici, *J. Am. Chem. Soc.* **1991**, *113*, 9379–9380; b) H. Jun, R. J. Angelici, *Organometallics* **1993**, *12*, 4265–4266; c) H. Jun, V. G. Young, Jr., R. J. Angelici, *ibid.* **1994**, *13*, 2444–2453; d) H. Jun, R. J. Angelici, *ibid.* **1994**, *13*, 2454–2460.

[29] V. D. Romanenko, M. Sanchez, T. V. Sarina, M. R. Mazieres, R. Wolf, *Tetrahedron Lett.* **1992**, *21*, 2981–2982.

[30] S. J. Goede, H. P. van Schaik, F. Bickelhaupt, H. Kooijman, A. L. Spek, *Organometallics* **1992**, *11*, 3844–3848.

[31] a) P. Binger, B. Biedenbach, R. Mynott, M. Regitz, *Chem. Ber.* **1988**, *121*, 1455–1456; b) P. Binger, S. Barth, B. Biedenbach, J. Haas, A. T. Herrmann, R. Milczarek, R. Schneider, *Phosphorus, Sulfur, Silicon Relat. Elem.* **1993**, *77*, 1–4; c) B. Biedenbach, Dissertation, Universität Kaiserslautern, **1990**.

[32] A. T. Herrmann, Dissertation, Universität Kaiserslautern, **1990**.

[33] P. Binger, R. Milczarek, R. Mynott, M. Regitz, *J. Organomet. Chem.* **1987**, *323*, C35.

[34] B. Geissler, S. Barth, U. Bergsträsser, M. Slany, J. Durkin, P. B. Hitchcock, M. Hofmann, P. Binger, J. F. Nixon, P. von R. Schleyer, M. Regitz, *Angew. Chem.* **1995**, *107*, 485–488; *Angew. Chem. Int. Ed. Engl.* **1995**, *34*, 484–487.

[35] L. Weber, I. Schumann, T. Schmidt, H.-G. Stammler, B. Neumann, *Z. Anorg. Allg. Chem.* **1993**, *619*, 1759–1764.

[36] L. Weber, I. Schumann, H.-G. Stammler, B. Neumann, *Chem. Ber.* **1994**, *127*, 1349.

[37] S. I. Al-Resayes, J. F. Nixon, *Inorg. Chim. Acta* **1993**, *212*, 265–269.

[38] Review: W. W. Schoeller in *Multiple Bonds and Low Coordination in Phosphorus Chemistry* (Eds.: M. Regitz, O. J. Scherer), Thieme, Stuttgart, **1990**, pp. 5–32.

[39] W. W. Schoeller, J. Strutwolf, U. Tubbesing, C. Begemann, *J. Phys. Chem.* **1995**, *99*, 2329–2334.

[40] a) R. Appel, V. Barth, F. Knoch, *Chem. Ber.* **1983**, *116*, 938–950; b) R. Appel, U. Kündgen, F. Knoch, *ibid.* **1985**, *118*, 1352–1370.

[41] A. N. Chernega, A. V. Ruban, V. D. Romanenko, L. N. Markovskii, A. A. Korkin, N. Y. Struchkov, *Heteroat. Chem.* **1991**, *2*, 229–241.

[42] V. D. Romanenko, T. V. Sarina, N. V. Kolotilo, L. N. Markovskii, *Zh. Obshch. Khim.* **1985**, *55*, 1188–1190; *J. Gen. Chem. USSR* **1985**, *55*, 1060–1061.

[43] Review: K. Karaghiosoff in *Multiple Bonds and Low Coordination in Phosphorus Chemistry* (Eds.: M. Regitz, O. J. Scherer), Thieme, Stuttgart, **1990**, pp. 463–471, and references therein.

[44] G. Becker, *Z. Anorg. Allg. Chem.* **1976**, *423*, 242–254.

[45] a) G. Becker, W. Becker, G. Uhl, *Z. Anorg. Allg. Chem.* **1994**, *518*, 21–35; b) W. Uhl, Dissertation, Universität Karlsruhe, **1980**.

[46] K. Issleib, H. Schmidt, C. Wirkner, *Z. Anorg. Allg. Chem.* **1981**, *437*, 85–90.

[47] L. Weber, A. Kakoschke, unpublished results.

[48] G. Becker, *Z. Anorg. Allg. Chem.* **1977**, *430*, 66–76.

[49] H.-O. Kalinowski, S. Berger, S. Braun, *^{13}C-NMR-Spektroskopie*, Thieme, Stuttgart, **1984**, p. 371.

[50] L. Weber, S. Buchwald, A. Rühlicke, H.-G. Stammler, B. Neumann, *Z. Anorg. Allg. Chem.* **1993**, *619*, 934–942.

[51] W. J. Middleton, R. V. Lindsay, Jr., *J. Am. Chem. Soc.* **1964**, *86*, 4948–4952.

[52] L. Weber, O. Kaminski, H.-G. Stammler, B. Neumann, *Organometallics* **1995**, *14*, 581–583.

[53] A. Schmidpeter, K. Karaghiosoff in *Multiple Bonds and Low Coordination in Phosphorus Chemistry* (Eds.: M. Regitz, O. J. Scherer), Thieme, Stuttgart, **1990**, pp. 258–286, and references therein.

[54] L. Weber, E. Lücke, R. Boese, *Chem. Ber.* **1990**, *123*, 23–28.

[55] L. Weber, A. Rühlicke, H.-G. Stammler, B. Neumann, *Organometallics* **1993**, *12*, 4653–4656.

[56] a) L. Weber, O. Kaminski, unpublished results; b) L. Weber, A. Rühlicke, B. Quasdorff, R. Boese, unpublished results.

[57] L. Weber, A. Rühlicke, *J. Organomet. Chem.* **1994**, *470*, C1–C3.

[58] L. Weber, O. Kaminski, H.-G. Stammler, B. Neumann, R. Boese, *Z. Naturforsch. B* **1994**, *49*, 1693–1706.

[59] a) R. H. Neilson, B. A. Boyd, D. A. Dubois, R. Hani, G. M. Scheide, J. T. Shore, U. G. Wettermark, *Phosphorus Sulfur Relat. Elem.* **1987**, *30*, 463–466; b) B. A. Boyd, R. J. Thoma, R. H. Neilson, *Tetrahedron Lett.* **1987**, *28*, 6121–6124; c) B. A. Boyd, R. J. Thoma, W. H. Watson, R. H. Neilson, *Organometallics* **1988**, *7*, 572–574.

[60] a) F. Mathey, C. Charrier, N. Maigrot, A. Marinetti, C. Ricard, N. H. Tran Huy, *Comments Inorg. Chem.* **1992**, *13*, 61–90; b) N. H. Tran Huy, F. Mathey, *Tetrahedron Lett.* **1988**, *29*, 3077–3078; c) F. A. Ajulu, S. S. Al-Juaid, D. Carmichael, P. B. Hitchcock, M. F. Meidine, J. F. Nixon, F. Mathey, N. H. Tran Huy, *J. Organomet. Chem.* **1991**, *406*, C20–C24.

[61] L. Weber, O. Kaminski, A. Rühlicke, B. Quasdorff, H.-G. Stammler, B. Neumann, *Organometallics*, in press.

[62] L. Weber, O. Kaminski, R. Boese, D. Bläser, *Organometallics* **1995**, *14*, 820–824.

[63] Review: M. Sanchez, M.-R. Mazières, L. Lamandé, R. Wolf in *Multiple Bonds and Low Coordination in Phosphorus Chemistry* (Eds.: M. Regitz, O. J. Scherer), Thieme, Stuttgart, **1990**, pp. 129–148.

[64] a) A. H. Cowley, N. C. Norman, S. Quashie, *J. Am. Chem. Soc.* **1984**, *106*, 5007–5008; b) A. M. Arif, A. H. Cowley, C. M. Nunn, S. Quashie, N. C. Norman, A. G. Orpen, *Organometallics* **1989**, *8*, 1878–1884.

[65] G. David, E. Niecke, M. Nieger, J. Radseck, W. W. Schoeller, *J. Am. Chem. Soc.* **1994**, *116*, 2191–2192.

[66] A. M. Arif, A. H. Cowley, S. Quashie, *J. Chem. Soc. Chem. Commun.* **1985**, 428–429.

[67] G. Bruder, Dissertation, Universität Bonn, **1989**.

[68] P. B. Hitchcock, M. J. Maah, J. F. Nixon, *Heteroat. Chem.* **1991**, *2*, 243–252.

[69] G. Becker, W. A. Herrmann, W. Kalcher, G. Kriechbaum, C. Pahl, C. T. Wagner, M. L. Ziegler, *Angew. Chem.* **1983**, *95*, 417; *Angew. Chem. Int. Ed. Engl.* **1983**, *22*, 413; *Angew. Chem. Suppl.* **1983**, 501–526.

[70] a) P. B. Hitchcock, T. J. Madden, J. F. Nixon, *J. Chem. Soc. Chem. Commun.* **1989**, 1660–1661; b) *J. Organomet. Chem.* **1993**, *463*, 155–162.

[71] L. Weber, I. Schumann, H.-G. Stammler, B. Neumann, *Organometallics* **1995**, *14*, 1626–1631.

[72] L. Weber, E. Lücke, A. Müller, H. Bögge, *Z. Anorg. Allg. Chem.* **1990**, *583*, 91–101.

[73] L. Weber, U. Nolte, H.-G. Stammler, B. Neumann, *Chem. Ber.* **1991**, *124*, 989–996.

[74] M. F. Meidine, J. F. Nixon, R. Mathieu, *J. Organomet. Chem.* **1986**, *314*, 307–310.

[75] C. J. Carrano, A. H. Cowley, C. M. Nunn, M. Pakulski, S. Quashie, *J. Chem. Soc. Chem. Commun.* **1988**, 170–171.

[76] L. Weber, T. Matzke, R. Boese, *Chem. Ber.* **1990**, *123*, 739–745

Pericyclic Reactions in Biological Systems—Does Nature Know About the Diels–Alder Reaction?

Sabine Laschat*

Pericyclic reactions, that is one-step processes that proceed through cyclic transition states under control of orbital symmetry, represent an import tool for the synthetic organic chemist. A large number of pericyclic key steps also occurs in biological systems.[1] The classical example, which led Woodward and Hoffmann to establish the rules of conservation of orbital symmetry, is the formation of vitamin D_3 from 7-dehydrocholesterol by a photochemically induced, conrotatory cycloreversion of the steroid B-ring, followed by a thermally allowed [1,7]sigmatropic H-shift. Claisen rearrangements are also found in natural systems. The [3,3]sigmatropic Claisen rearrangement of chorismic acid (**1**) to prephenic acid (**2**), which is catalyzed by the enzyme chorismate mutase, can be considered as the key step in the biosynthesis of aromatic compounds, that is the so-called shikimic acid pathway. The chairlike transition state geometry **3** was confirmed by double isotope labeling experiments.[2]

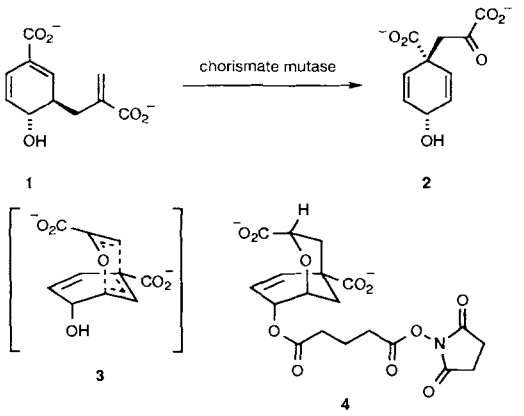

1 **2** **3** **4**

However, in the laboratory this particular reaction can be accelerated not only by enzymes but also by catalytic antibodies.[3] For the generation of such antibodies haptens such as **4** were used, that is, molecules whose structure is very similar to the transition state of the particular reaction and which at the same time are tightly bound by the antibody.

However, pericyclic reactions in natural systems do not necessarily require the participation of an enzyme. Several reactions proceed spontaneously, for example the above-mentioned 1,7-H shift in the biosynthesis of vitamin D_3. Recently Boland et al. reported that the ectocarpenes **6** and related substances, which were isolated from the brown algae *Ectocarpus siliculosus*, are not the sexual pheromones of the algae but that these cycloheptadienes **6** are formed from the actual pheromones, namely the thermolabile *cis*-divinylcyclopropanes **5**, by a spontaneous Cope rearrangement.[4] Thus, the Cope rearrangement of **6** resembles a deactivation pathway of the pheromones **5**.

5 R = H, Et, $CH=CH_2$ **6**

Diels–Alder reactions have been postulated as key steps in a number of biosynthetic conversions. The biosynthesis of the endiandric acids **13** and **14** is discussed below as an example for

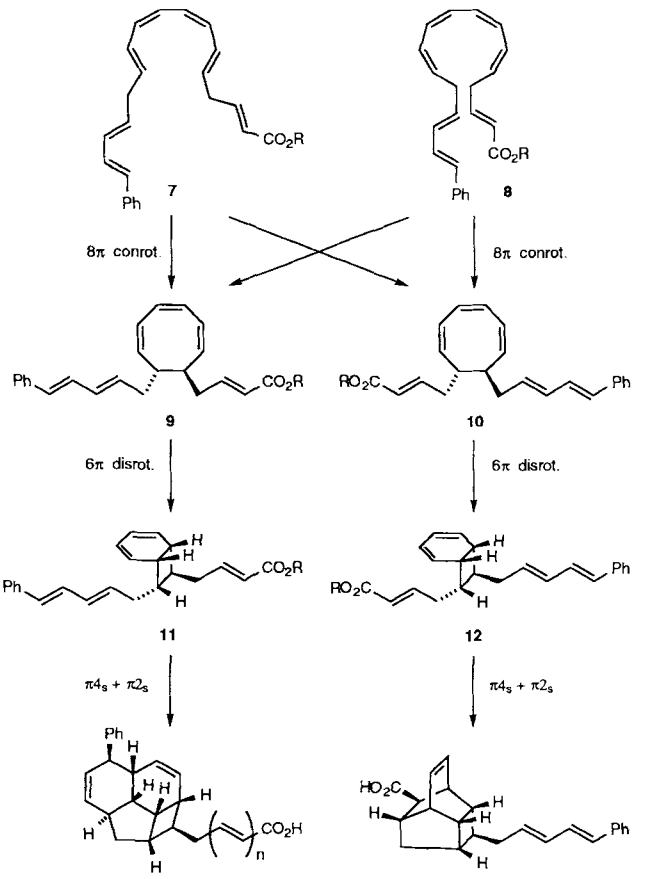

7 **8** **9** **10** **11** **12**

13a n = 0 endiandric acid A
13b n = 1 endiandric acid B
14 endiandric acid C

[*] Dr. S. Laschat
Organisch-chemisches Institut der Universität
Corrensstrasse 40, D-48149 Münster (Germany)
Fax: Int. code +(251)83-8772

 © VCH Verlagsgesellschaft mbH, D-69451 Weinheim, 1996 0570-0833/96/3503-0289 $ 10.00+.25/0

a spontaneous [4 + 2]cycloaddition. This class of compounds which is produced by the Australian plant *Endiandra introsa (Lauraceae)* is remarkable, because different constitutional isomers were formed simultaneously and in all cases racemic mixtures were synthesized by the plant. It was first postulated by Black et al.[5] and later confirmed by biomimetic total syntheses by Nicolaou et al.[6] that the endiandric acids A, B, and C (**13a**, **13b**, and **14**, respectively) are formed by a cascade of electrocyclic reactions. The cascade is initiated by a conrotatory 8π-electron ring closure of the polyene carboxylic acids **7** and **8** to the isomeric cyclooctatrienes **9** and **10**, respectively, which subsequently undergo a disrotatory 6π-electron cyclization to **11** and **12**, respectively. Termination of the cascade by an intramolecular Diels–Alder reaction yields either the tetracyclic endiandric acids **13a**,**b** or the bridged derivative **14**.

Besides those spontaneous processes a variety of [4 + 2]-cycloadditions exists for which it still remains unclear whether they are Diels–Alder reactions and if so, whether they proceed spontaneously or only in the presence of an enzyme.[7] In this respect the stereospecific synthesis of the sesterpenoid heliocide H_2 (**15**), an insecticide isolated from cotton wool, from hemigossypolon (**16**) and myrcene (**17**)[8, 9] should be mentioned. Other examples of biomolecules that are probably formed by Diels–Alder reactions include the chalcone kuwanon J (**19**) from the mulberry tree *Morus alba L.*, the mycotoxins chaetoglobosin A (**21**)[11] and brevianamide A (**23**),[12]

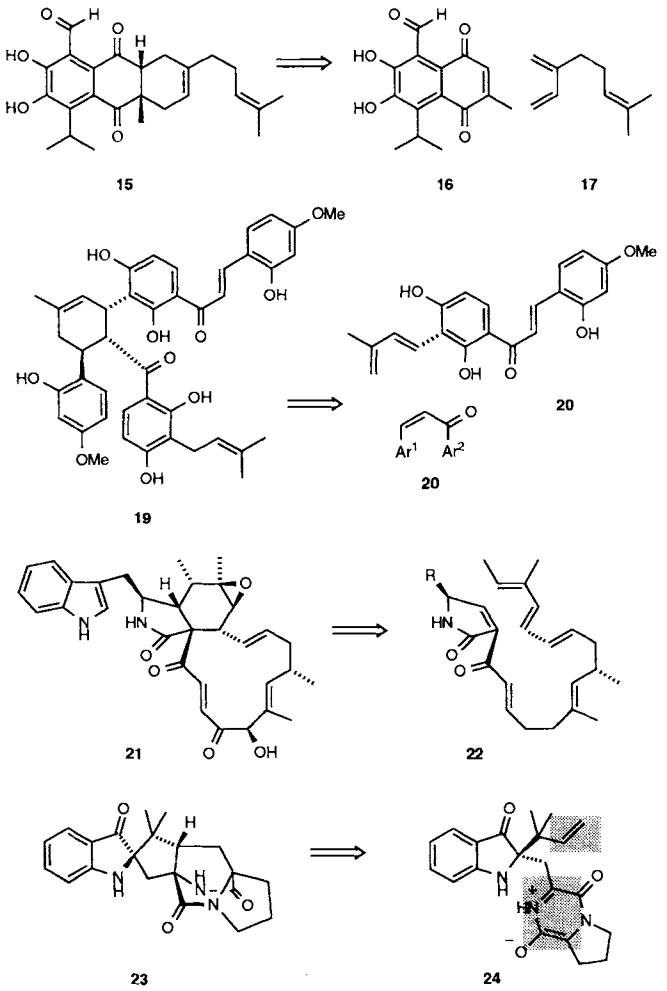

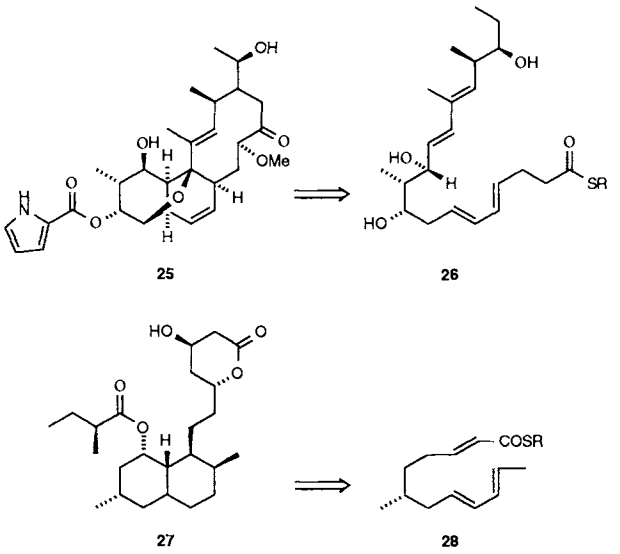

the polyketide nargenicin (**25**),[13] and mevinolin (**27**), a metabolite of the fungus *Aspergillus terreus* MF4845, which is used as a drug for reducing the blood cholesterol level.[14] However, until now there is no case known where the corresponding enzyme system, that is the Diels–Alder-ase, could be detected. Even in the biosynthesis of the iboga and aspidosperma alkaloids the final proof for a Diels–Alder reaction is still missing.[15] In 1970 Scott et al. were able to elucidate nearly the whole biosynthetic pathway by feeding experiments with plant seedlings.[16] According to Scott et al. isovincoside (**29**) is converted to stemmadenine (**30**) in several steps. Heterolytic ring opening and concomitant dehydration leads to the postulated intermediate dehydrosecodine **31**. Starting from the acrylic ester **31** two [4 + 2]cycloadditions are possible. If the 2-dehydropyridine system of **31** reacts as a dienophile, the aspidosperma alkaloid tabersonine (**32**) is formed, whereas participation of the 2-dihydropyridine moiety as a diene leads to the iboga alkaloid

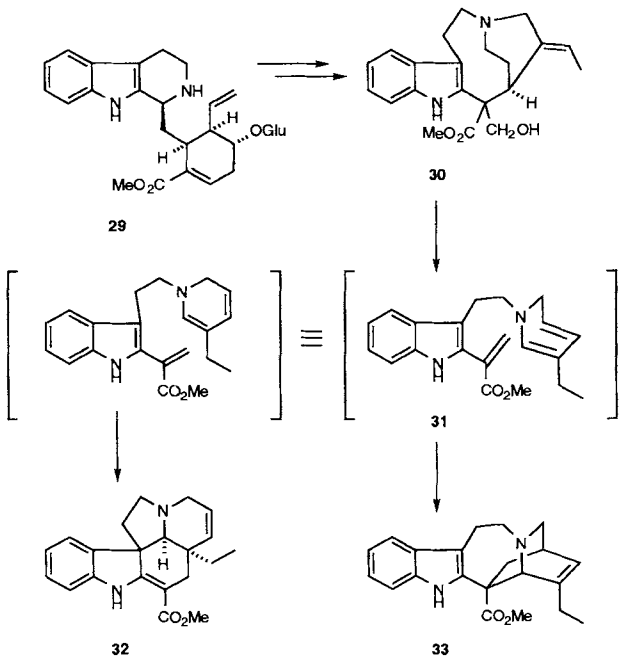

 © VCH Verlagsgesellschaft mbH, D-69451 Weinheim, 1996 0570-0833/96/3503-0290 $ 10.00+.25/0

catharanthine (**33**). The reversibility of the reactions led the authors to assume stepwise Michael additions.

In view of the difficulties in detecting and isolating Diels–Alder-ases, one might assume that there are no enzyme-catalyzed [4 + 2]cycloadditions involved in natural systems. However, this assumption seems to be incorrect. Recently Oikawa, Ishihara et al. published experimental evidence that the solanapyrones **36** and **37**, two phytotoxins produced by the

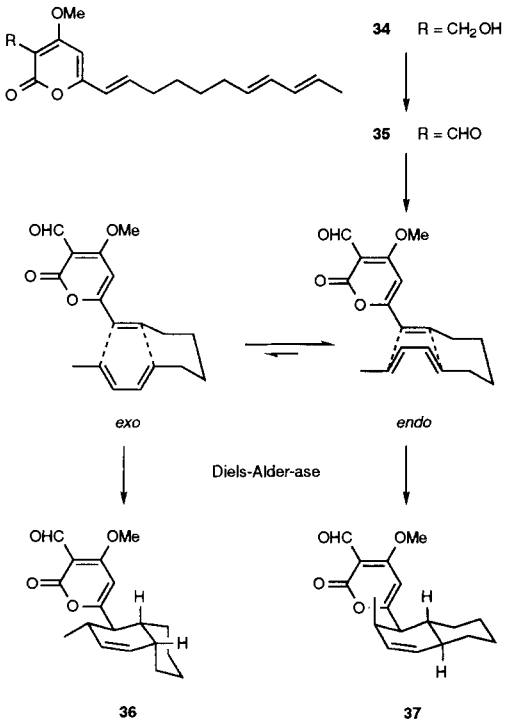

pathogenic fungus *Alternaria solani*, are probably formed by enzyme-catalyzed [4 + 2]cycloadditions.[17] Treatment of prosolanapyrone III (**35**) with a cell-free extract of *A. solani* at 30 °C for 10 min yielded a mixture of **36** and **37** (25% conversion) with an *exo*/*endo* ratio of 53:47. In the absence of the cell-free extract under the same conditions the aldehyde **35** undergoes an uncatalyzed Diels–Alder reaction to **36** and **37** (15% conversion) with an *exo*/*endo* ratio of 3:97.[18] Treatment of **35** with the denatured cell-free extract yielded likewise an *exo*/*endo* ratio of 3:97 (10% conversion). Thus, the enzyme-related conversion is about 15% and the *exo*/*endo* ratio 87:13 (>92% *ee* for **36**). The high *exo* selectivity is remarkable, because it cannot be achieved by chemical methods. It should be emphasized, however, that in the above-mentioned investigations no isolated enzymes were used but a cell-free extract. Thus the postulated Diels–Alder mechanism needs to be further confirmed by characterization of the enzyme or enzyme complex. The biosynthesis of the solanapyrones **36** and **37** shows an additional feature worthy of mention. Whereas the alcohol prosolanapyrone II (**34**) does not form any cycloaddition products in aqueous medium without any catalyst, the presence of the cell-free extract induces the production of 19% of the solanapyrones **36** and **37** (*exo*/*endo* 85:15) and 6% of the aldehyde **35**. Apparently, the Diels–Alder-ase is accompanied by a dehydrogenase which catalyzes the oxidation of **34** to **35**. Further studies with isolated enzymes are required to investigate whether these are separated enzymes or coupled in an enzyme complex. However, in light of these results further biosynthetic pathways for which Diels-Alder reactions will be found and the isolation of the corresponding enzymes are eagerly awaited in the near future.

German version: *Angew. Chem.* **1996**, *108*, 313–315

Keywords: biochemistry · enzymatic catalysis · Diels–Alder reactions · pericyclic reactions

[1] U. Pindur, G. H. Schneider *Chem. Soc. Rev.* **1994**, *94*, 409–415.
[2] Despite various mechanistic investigations, it is still a matter of debate whether the enzymatic Claisen rearrangement proceeds through a concerted mechanism. See: Y. Asano, J. J. Lee, T. L. Shieh, F. Spreafico, C. Kowal, H. G. Floss, *J. Am. Chem. Soc.* **1985**, *107*, 4314–4320; J. J. Delany, R. E. Padykula, G. A. Berchtold, *J. Am. Chem. Soc.* **1992**, *114*, 1394–1397 and references therein.
[3] Reviews: P. G. Schultz, R. A. Lerner, *Acc. Chem. Res.* **1993**, *26*, 391–395; J. D. Stewart, L. J. Loitta, S. J. Benkovic, *ibid.* **1993**, *26*, 396–404; D. Burton, *ibid.* **1993**, 404–411; P. G. Schultz, *Angew. Chem.* **1989**, *101*, 1336–1348; *Angew. Chem. Int. Ed. Engl.* **1989**, *28*, 1283–1295; R. A. Lerner, S. J. Benkovic, P. G. Schultz, *Science* **1991**, *252*, 659–667.
[4] W. Boland, G. Pohnert, I. Maier *Angew. Chem.* **1995**, *117*, 1717–1719; *Angew. Chem. Int. Ed. Engl.* **1995**, *34*, 1602–1604.
[5] W. M. Bandaranayake, J. E. Banfield, D. S. C. Black, *J. Chem. Soc. Chem. Commun.* **1980**, 902–903.
[6] K. C. Nicolaou, N. A. Petasis, R. E. Zipkin, J. Uenishi *J. Am. Chem. Soc.* **1982**, *104*, 5555–5564.
[7] To avoid the problem of product inhibition in antibody-catalyzed Diels–Alder reactions resulting from the close structural similarity between the transition state (or hapten respectively) and the product, the cycloaddition must be either followed by a cheleotropic reaction or the hapten must be bulkier than the corresponding transition state. See: D. Hilvert, K. W. Hill, K. D. Nared, M. T. M. Auditor, *J. Am. Chem. Soc.* **1989**, *111*, 9261–9262; A. C. Braisted, P. G. Schultz, *ibid.* **1990**, *112*, 7430–7431.
[8] R. D. Stipanovic, A. A. Bell, D. H. O'Brien, M. J. Lukefahr, *Tetrahedron Lett.* **1977**, *18*, 567–570.
[9] In addition an enzymatic prenylation of the sesquiterpene hydroquinone to the corresponding sesterpene **15** might be a possible alternative to the Diels–Alder mechanism.
[10] Y. Hano, A. Ayukawa, T. Nomura, *Naturwissenschaften* **1992**, *79*, 180–182.
[11] H. Oikawa, Y. Murakami, A. Ichihara, *J. Chem. Soc. Perkin Trans. 1* **1992**, 2955–2959.
[12] J. F. Sanz-Cervera, T. Glinka, R. M. Williams, *J. Am. Chem. Soc.* **1993**, *115*, 347–348.
[13] D. E. Cane, W. Tan, W. R. Ott, *J. Am. Chem. Soc.* **1993**, *115*, 527–535.
[14] Y. Yoshizawa, D. J. Witter, Y. Liu, J. C. Vederas, *J. Am. Chem. Soc.* **1994**, *116*, 2693–2694.
[15] W. A. Carrol, P. A. Grieco, *J. Am. Chem. Soc.* **1993**, *115*, 1164–1165. W. G. Bornmann, M. E. Kuehne, *J. Org. Chem.* **1992**, *57*, 1752–1760.
[16] A. I. Scott, *Acc. Chem. Res.* **1970**, *3*, 151–157; E. Wenkert, *J. Am. Chem. Soc.* **1962**, *84*, 98–102.
[17] H. Oikawa, K. Katayama, Y. Suzuki, A. Ichihara, *J. Chem. Soc. Chem. Commun.* **1995**, 1321–1322.
[18] This ratio is comparable to the *endo* ratio of other Diels–Alder reactions in aqueous media.

 © *VCH Verlagsgesellschaft mbH, D-69451 Weinheim, 1996* *0570-0833/96/3503-0291 $ 10.00+.25/0*

Boron-Substituted Heterocycles as π-Donors in Organometallic Chemistry—A Sandwich Complex with 1-*H*-Boratabenzene and Lithium

H. Nöth* and Martin Schmidt

Since the discovery of ferrocene, aromatic π-donor ligands have become an indispensible part of organometallic chemistry. In particular, complexes with cyclopentadienyl ions and benzene, as well as with the derivatives of these ligands, revolutionized the coordination chemistry of the transition metals.

Far less thoroughly studied is the chemistry of the heterocyclic, isoelectronic analogs of these compounds. If, for example, a CH fragment in a cyclopentadienyl ion **A** is replaced by an isoelectronic and isolobal BH^- group, the result is the borole(2−) anion (Scheme 1). Just like Cp^-, it is a 6-π electron

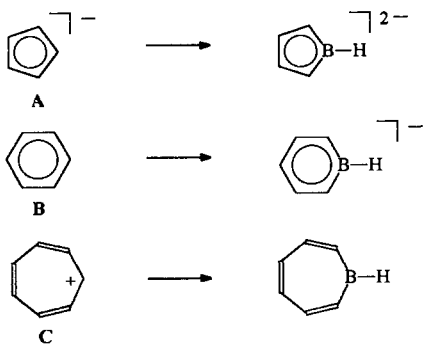

Scheme 1. The replacement of CH units by BH^- groups.

donor. Analogously, replacement of a CH fragment in benzene **B** by a BH^- group affords the boratabenzenes. An expansion of this substitution pattern leads to the formulation of the electroneutral borepine,[1] derived from the tropylium ion **C**, as an aromatic π-donor. Of course, this replacement need not be restricted to only one CH fragment, but can be extended in all cases.[2]

Metal complexes prepared with boron-substituted heterocycles containing a hydrogen substituent at the boron atom are in the minority. The most common examples contain amino or phenyl substituents in this positon. The examples **D**–**F** represent an arbitrary selection of the different sized heteroring systems.[3–5] As in the metal complexes of the congeners **A**–**C**, the aromatic character of the boron-substituted ligands is detected, inter alia, by the experimentally confirmed planarity of the rings.

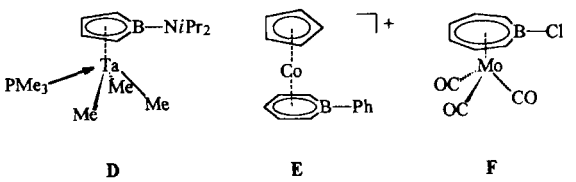

D **E** **F**

[*] Prof. Dr. H. Nöth, Dr. M. Schmidt
Institut für Anorganische Chemie der Universität
Meiserstrasse 1, D-80333 München (Germany)
Fax: Int. code +(89)5902451

The replacement of a CH fragment by an isoelectronic BR^- group is accompanied by an increase in the electron density in the π-electron system of the ligands. Such electron-rich species should thus be particularly suitable for coordination to electron-poor metal centers of the transition metal elements, as well as to alkali or alkali earth metals. In contrast to cyclopentadienyl compounds of the alkali and alkali earth metals, several representatives of which have been characterized and structurally analyzed,[6,7] only a few complexes of these metals with benzene are known. Infrared spectroscopic studies by L. Andrews et al. on $Li(C_6H_6)$ and $Li(C_6H_6)_2$ in an argon matrix showed that the sandwich structure typical of the transition metal complexes with aromatic ligands is also adopted with alkali metals and, in particular, with lithium (Scheme 2).[8]

Scheme 2. The structures of $Li(C_6H_6)$ and $Li(C_6H_6)_2$ as determined by IR spectroscopy.

Fu et al. have now succeeded in synthesizing the boratabenzene compound $Li_2[H_5C_5BH]_2 \cdot 4THF$ (**1**), which besides $Fe[H_5C_5BH]_2$ prepared by Ashe et al.[9] is the second derivative of a boratabenzene containing a hydrogen substituent at the boron atom and the only example that has been characterized by X-ray crystallography.[10] The synthesis of **1** is based on a prescription by Paetzold et al. for the corresponding pyridine derivative.[11] Fu et al.'s route proceeded via the accessible PMe_3 adduct of borabenzene (**2**) according to Equation (a).

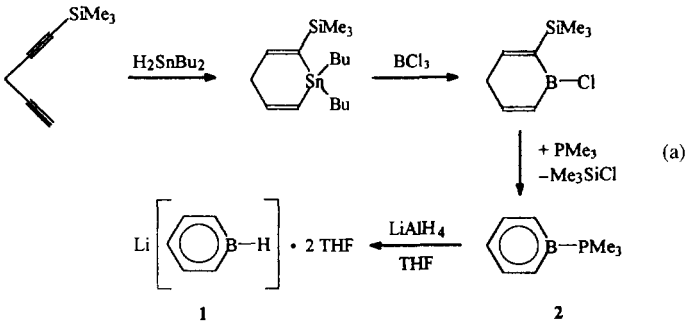

As the X-ray analysis indicates, **1** is a dimer incorporating four THF molecules (Fig. 1). Two boratabenzene ions coordinate to the lithium ion in a sandwich structure. The lithium ion lies on a crystallographic inversion center: the boron atoms of the ligands are therefore as far apart as possible. The second lithium ion, which compensates for the negative charge of the sandwich anion, is separated from the sandwich anion by four THF donor solvent molecules.

The lithium ion in the anion of **1** does not lie in the center above or below these two ring planes. The two boratabenzene anions are shifted relative to each other in such a way that the lithium ion is closest to the carbon atom *para* to the boron

 © VCH Verlagsgesellschaft mbH, D-69451 Weinheim, 1996 0570-0833/96/3503-0292 $ 10.00+.25/0

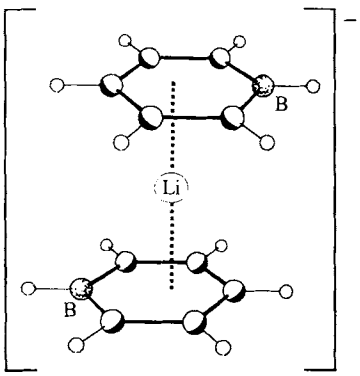

Fig. 1. Crystal structure of the anion in **1**.

atoms. This distance is 2.413(3) Å, whereas the B–Li distance is 2.474(4) Å. The B–Li distance is shorter than that in $[Li\{Me_2NC_2H_4NMe_2\}][H_5C_5B(NMe_2)]$, studied by Herberich et al.[12] In this compound the π-symmetric orbital at the boron atom interacts strongly with the lone electron pair of the N atom. This compound can therefore be better described as a η^5-cyclohexadienyl complex.

In **1** the distance between the lithium ion and the ring planes is comparable with those found in other lithocene derivatives; for example in $[Cp_2Li]^-PPh_4^+$ it is 1.98 Å.[13]

Fu et al. were recently also able to structurally analyze the PMe_3 adduct of borabenzene (**2**, Fig. 2).[14] As in the previously characterized pyridine adduct,[11] the boron-containing heterocycle is planar. Just as in the anionic boratabenzene and dictated by the different covalent radii of boron and carbon, the ring geometries cannot be described by a regular hexagon. The differences between corresponding bond parameters of **1** and **2** are, however, only slight.

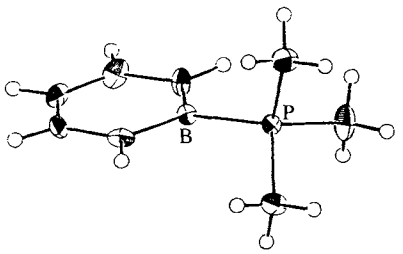

Fig. 2. Crystal structure of **2**.

With the synthesis of **1** Fu et al. advanced both the organometallic chemistry of the alkali metals and organoboron chemistry. This important contribution can give new impetus to both these fields of inorganic chemistry. Compound **1** will also be a challenge to theoreticians to study the coordination behavior of boron-substituted heterocycles theoretically.[15] Perhaps one day the stabilization of solvent-free borabenzene by coordination to metal centers, which has still not been accomplished, will also be achieved.

German version: *Angew. Chem.* **1996**, *108*, 311–312

Keywords: boron compounds · sandwich complexes

[1] A. J. Ashe III, J. W. Kampf, Y. Nakadaira, J. M. Pace, *Angew. Chem.* **1992**, *104*, 1267–1269; *Angew. Chem. Int. Ed. Engl.* **1992**, *31*, 1255–1258.
[2] In the diborol–metal complexes studied by the group of W. Siebert, the ligands of type 1,3-$B_2C_3R_5^-$ are only 4-π donors because of the single negative charge. See also W. Siebert, *Angew. Chem.* **1985**, *97*, 924–939; *Angew. Chem. Int. Ed. Engl.* **1985**, *24*, 943–958.
[3] G. C. Bazan, G. Rodriguez, *Polyhedron* **1995**, *14*, 93–102.
[4] G. E. Herberich, H. Ohst, *Adv. Organomet. Chem.* **1986**, *25*, 199–236; G. E. Herberich, B. Schmidt, U. Englert, *Organometallics* **1995**, *14*, 471–480.
[5] A. J. Ashe III, J. W. Kampf, W. Klein, R. Rousseau, *Angew. Chem.* **1993**, *105*, 1112–1113; *Angew. Chem. Int. Ed. Engl.* **1993**, *32*, 1065–1066.
[6] P. Jutzi, *J. Organomet. Chem.* **1990**, *400*, 1–17; *Adv. Organomet. Chem.* **1986**, *26*, 217–295.
[7] L. A. Paquette, W. Bauer, M. R. Sivik, M. Feigel, P. von R. Schleyer, *J. Am. Chem. Soc.* **1990**, *112*, 8776–8789.
[8] L. Manzeron, L. Andrews, *J. Am. Chem. Soc.* **1988**, *110*, 3840–3846.
[9] A. J. Ashe III, W. Butler, H. F. Sandford, *J. Am. Chem. Soc.* **1979**, *101*, 7066–7067.
[10] D. A. Hoic, W. M. Davis, G. C. Fu, *J. Am. Chem. Soc.* **1995**, *117*, 8480–8481.
[11] R. Boese, N. Finke, J. Henkelmann, G. Maier, P. Paetzold, H. P. Reisenauer, G. Schmidt, *Chem. Ber.* **1985**, *118*, 1644–1654.
[12] G. E. Herberich, B. Schmidt, U. Englert, T. Wagner, *Organometallics* **1993**, *12*, 2891–2893.
[13] S. Harder, M. H. Prosenc, *Angew. Chem.* **1994**, *106*, 1830–1832; *Angew. Chem. Int. Ed. Engl.* **1994**, *33*, 1744–1746.
[14] D. A. Hoic, J. R. Wolf, W. M. Davis, G. C. Fu, *Organometallics*, in print.
[15] J. Ciosłowski, P. J. Hay, *J. Am. Chem. Soc.* **1990**, *112*, 1707–1710.

 © VCH Verlagsgesellschaft mbH, D-69451 Weinheim, 1996 0570-0833/96/3503-0293 $ 10.00+.25/0

Synthesis and Structure of the First Cyclopentadienyl(halogeno)metal(VI) Complex of the Chromium Triad $[(\eta^5\text{-}C_5Me_5)WF_5]$**

Katrin Köhler, Axel Herzog, Alexander Steiner, and Herbert W. Roesky*

Dedicated to Professor Marianne Baudler on the occasion of her 75th birthday

The development of transition metal complexes with one cyclopentadienyl ligand and halogeno ligands is of great interest, since these compounds can be used as readily accessible precursors in the synthesis of numerous organometallic compounds containing metals in both low and high oxidation states.[1] Since the discovery of the pentamethylcyclopentadienyl-substituted metal chlorides $[Cp^*MoCl_4]$[2] and $[Cp^*WCl_4]$[3] ($Cp^* = \eta^5\text{-}C_5Me_5$), many monocyclopentadienyl compounds of molybdenum and tungsten have been prepared in which the metal atoms are present in the formal oxidation states +III and +V. The synthesis of compounds containing molybdenum in the rarely observed +IV oxidation state was only achieved very recently.[4–6]

We report herein on the synthesis of the first fluorinated pentamethylcyclopentadienyltungsten complexes $[Cp^*WF_4]$ **1**, $[(\eta^5\text{-}C_5Me_4Et)WF_4]$ **2**, $[Cp^*WF_4(thf)]$ **3**, and $[Cp^*WF_5]$ **4**, as well as on the crystal structure of the tungsten(VI) fluoride.

Within the context of our investigations on cyclopentadienyl(fluoro) transition metal complexes, we have shown that by using trimethyltin fluoride[7] as a metathetically acting fluorinating reagent it is possible to prepare organometallic fluorides of Group 4 of the type $[Cp^*MF_3]$ (M = Ti, Zr, Hf) as well as main group element fluorides such as PF_3 and SOF_2.[8] Herein we report that these fluorinating reagents can be used to synthesize completely new cyclopentadienyl fluorides of Group 6.

The reaction of the tetrachloro complexes $[(\eta^5\text{-}C_5Me_4R)WCl_4]$ (R = Me,Et) with trimethyltin fluoride in the molar ratio 1:4 leads to the fluorides $[Cp^*WF_4]$ **1** and $[(\eta^5\text{-}C_5Me_4Et)WF_4]$ **2** [Eq. (a)]. The trimethyltin chloride formed during the reaction can be easily separated from the products by sublimation in vacuum and can be subsequently converted back into Me_3SnF by reaction with aqueous KF solution. Both compounds **1** and **2** are obtained from the reaction as beige solids with melting points above 300 °C.

1 R = Me
2 R = Et

The bands at 300–400 cm^{-1} characteristic for tungsten–chlorine vibrations are absent in the IR spectra of **1** and **2**. Instead, very strong absorption bands (576 cm^{-1} **1** and 572 cm^{-1} **2**) appear that may be assigned to tungsten–fluorine vibrations. The ESR signal of the solid **1**, detected at room temperature, has a *g* value of 1.82.[9] A comparable ESR signal was found for the analogous chlorine compound $[Cp^*WCl_4]_2$.[3] The color of complex **1**, atypical for a paramagnetic compound, indicates the presence of at least a dimer, which results in an intermolecular coupling of the unpaired electrons. The very low intensity peak in the EI mass spectrum (correct isotopic distribution) of **1** for $[M_2]^+$ minus four fluorine atoms may serve as an indication of this dimer formation. Further characterization by elemental analysis confirms the presence of both compounds.

Complexes **1** and **2** are insoluble in *n*-hexane and toluene, but can be recrystallized from THF as violet solids. The one obtained from **1** was characterized by mass spectrometry and elemental analysis as its THF adduct $[Cp^*WF_4(thf)]$ **3**. It may be assumed that **3** exists as a monomeric d^1 complex, and that its color originates through the uncoupled spin of the electron. The ESR spectrum of solid **3**, recorded at room temperature, exhibits a *g* value of 1.82.[9] In comparison, the complex $[Cp^*WCl_4(PMe_3)]$ shows, like the Lewis base free chloride, a *g* factor of about 1.9.[3]

To investigate the sensitivity of the complex to hydrolysis, a solution of **1** in THF was exposed to air. The deep violet solution changed to orange over a period of twelve hours. Slow evaporation of the solvent yielded orange crystals that were identified as the tungsten(VI) complex $[Cp^*WF_5]$ **4** by a single-crystal X-ray analysis (Fig. 1).[10]

Compound **4** crystallizes in the orthorhombic space group $Pna2_1$. The tungsten atom in the monomeric complex resides in

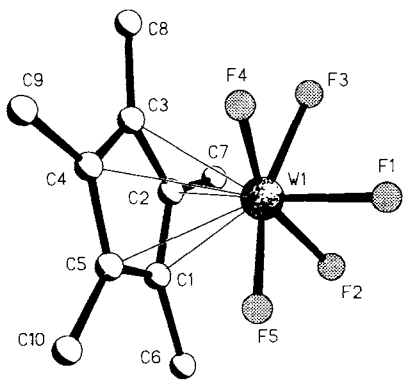

Fig. 1. Crystal structure of **4**. Selected bond lengths [pm] and angles [°]: W(1)-F(1) 192.5(1), W(1)-F(2) 187(2), W(1)-F(3) 190(2), W(1)-F(4) 187(2), W(1)-F(5) 191(2), F(2)-W(1)-F(5) 90.7(1); F(2)-W(1)-F(1) 83.2(8), F(3)-W(1)-F(1) 87.1(7), F(4)-W(1)-F(3) 86.1(1), F(2)-W(1)-F(4) 156.6(9), F(3)-W(1)-F(5) 158.8(9), F(2)-W(1)-F(3) 86.0(9), F(4)-W(1)-F(5) 88.8(1), F(4)-W(1)-F(1) 74.4(8), F(5)-W(1)-F(1) 71.6(9).

[*] Prof. Dr. H. W. Roesky, Dr. K. Köhler, Dr. A. Herzog, Dr. A. Steiner
Institut für Anorganische Chemie der Universität
Tammannstrasse 4, D-37077 Göttingen (Germany)
Fax: Int. code +(551)39-3373

[**] This work was supported by the Deutsche Forschungsgemeinschaft, the Volkswagen-Stiftung, and the Bundesministerium für Bildung und Forschung. We thank Dr. D. Marsh, MPI für Biophysikalische Chemie, Göttingen, for recording the ESR spectra.

a square-bipyramidal (distorted octahedral) environment, surrounded by a pentamethylcyclopentadienyl ligand and five fluorine atoms; the center of the Cp ligand is considered as one apex of the pyramid. The square basal plane around the metal center is formed by the four fluorine atoms F2, F3, F4, and F5. The angles between these atoms are on average 87.9°, that is, the deviation from the sum of angles (360°) in the square is only 8.4°. The bond angles between opposite fluorine atoms (F2-W1-F4 = 156.6° and F3-W1-F5 = 158.5°) show that the tungsten atom does not lie in the plane of the square base of the pyramid, but is somewhat projected out of this plane. In the ideal octahedron, the basal plane would be oriented perpendicular to the fifth fluorine atom F1. The average angle, however, is 75.6°, indicating a distortion of the octahedron. The average tungsten–fluorine distance is 189.5 pm and is thus in good agreement with the bond lengths in the compound $[F_4W\{NS(O)Me_2\}_2]$[11] (mean value of the W–F bonds is 190.5 pm).

After crystallization of **4** from THF, it was not possible to redissolve the compound in that solvent. However, **4** is readily soluble in acetone, and thus the NMR spectra were recorded in deuterated acetone or an acetone/acetonitrile mixture. The ^{19}F NMR spectrum of **4** confirms the existence of nonequivalent fluorine atoms. In contrast to $[Cp^*WMe_5]$, for which a rapid exchange of the methyl groups is observed at room temperature,[13] compound **4** at room temperature reveals a signal for the four equatorial fluorine atoms as a doublet at $\delta = 102.20$, and a corresponding signal for the axial fluorine atom as a quintet at $\delta = 90.80$. Thus, both signals lie in the range of chemical shifts expected for fluorine atoms terminally bonded to transition metals.[8] In the ^1H NMR spectrum of **4**, the signal for the protons of the pentamethylcyclopentadienyl ligand appears at $\delta = 2.99$. The occurrence of the signal as a doublet of quintets may be explained by the existence of H–F through-space coupling. The downfield shift of the signal is unusual compared to the proton resonance signals of other Cp*-substituted complexes. A corresponding deshielding of the hydrogen atoms can be ascribed to the strong electron-withdrawing effects of the WF_5 unit.

After filtration of the orange crystals and concentration of the THF solution, a yellow solid is obtained as the major product. The latter is characterized as the cyclopentadienyl-substituted oxofluoride $[Cp^*WO_2F]$ **5**. The singlet that appears at $\delta = -153.9$ in the ^{19}F NMR spectrum of **5** indicates the presence of a bridging fluorine atom. In addition to the molecular peak of **5**, even heavier fragments that are indicative of a polynuclear complex are also found in the mass spectrum of the compound. The IR spectrum of the compound shows in addition to a strong absorption band at 578 cm^{-1}, which can be ascribed to the tungsten–fluorine vibration, other absorptions in the region from 933 to 875 cm^{-1} that confirm the presence of W–O groups.

The disproportionation reaction that **1** undergoes upon contact with air may be understood as the first step in the hydrolysis of the tungsten(v) fluoride **1**. A simultaneously formed species in a low oxidation state could not be detected, since it is presumably immediately converted to the corresponding oxotungsten(VI) compound **5** in the presence of oxygen in the air. Compound **4** can be handled in air for only a limited time; it hydrolyzes further to **5**. This "hydrolysis start", which initially appeared not usual, has also been observed by us in other systems, for example, in the onset of hydrolysis of imidotungsten(v) complexes.[12]

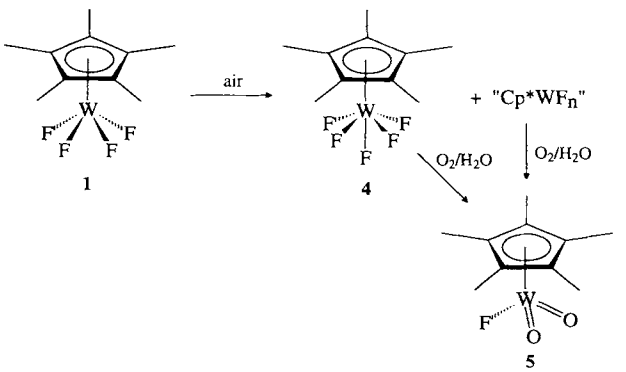

Experimental Procedure

1 (Method a): $[Cp^*WCl_4]$ (5.35 g, 11.6 mmol) and freshly sublimed Me_3SnF (8.45 g, 46.4 mmol) were combined as solids. After addition of toluene (60 mL), the initially orange-colored suspension was stirred for five days at room temperature. During this time, the color changed to dark yellow. After the solid was filtered off, toluene and the Me_3SnCl resulting from the reaction were removed in vacuum. The solid was washed with *n*-hexane (3 × 30 mL). After removal of the *n*-hexane, the residue was dried in vacuum. Compound **1** (3.94 g, 86%) was obtained as a beige powder with a melting point above 300 °C.

1 (Method b): $[Cp^*WCl_4]$ (5.35 g, 11.6 mmol) and freshly sublimed Me_3SnF (8.45 g, 46.4 mmol) were combined as solids. After addition of dichloromethane (60 mL), the suspension was stirred for 8 h at room temperature. The solvent and the Me_3SnCl resulting from the reaction were removed in vacuum. The residue was washed with toluene (30 mL) and *n*-hexane (30 mL) and the remaining solid was dried in vacuum. Compound **1** (4.10 g) was obtained in 89.5% yield. IR (CsI): $\tilde{\nu}$ = 1261, 1192, 1078, 1021, 802, 650, 576 (W–F), 477 cm^{-1}. MS (70 eV): *m/z* (%): 702 (3) $[(M_2)^+ - 4F]$, 395 (18) $[M^+]$, 135 (100) $[C_5Me_5]$. Elemental analysis [16] of $C_{10}H_{15}WF_4$: calc. C 30.4, H 3.8, F 19.3; found C 31.1, H 3.9, F 19.6.

2: The preparation was carried out analogously to that of **1** (method a or b). $[(\eta^5\text{-}C_5Me_4Et)WCl_4]$ (3.20 g, 7.8 mmol) and Me_3SnF (5.73 g, 31.2 mmol) afforded **2** as a beige solid with a melting point above 300 °C in 80% (2.55 g) and 88% (2.82 g) yield, respectively. IR (CsI): $\tilde{\nu}$ = 1261, 1191, 1095, 1050, 1029, 801, 722, 572 (W–F) cm^{-1}. MS (70 eV): *m/z* (%): 409 (38) $[M^+]$, 149 (100) $[C_5Me_4Et]$. Elemental analysis [16] of $C_{11}H_{17}WF_4$: calc. C 32.3, H 4.2, F 18.6; found C 31.1, H 4.3, F 19.0.

3: **1** (2.0 g, 5.1 mmol) was dissolved in warm THF (40 mL). After the solution was allowed to cool to room temperature, it was concentrated, and **3** crystallized as violet crystals, which were filtered off and dried in vacuum. Yield 93% (2.2 g). M.p. 205 °C. IR (CsI): $\tilde{\nu}$ = 2610, 1074, 1026, 875, 573, 540 cm^{-1}. MS (70 eV): *m/z* (%): 395 (18) $[M^+]$, 357 (100) $[M^+ - 2F]$. Elemental analysis of $C_{14}H_{23}WF_4O$: calc. C 36.0, H 5.0, F 16.3; found C 35.3, H 5.0, F 16.1.

4: **1** (0.50 g, 1.2 mmol) was dissolved in THF (50 mL). The violet solution was exposed to air for 12 h during which time the solution turned orange. The clear orange solution was concentrated in vacuum to about 30 mL. At −20 °C, compound **4** (0.04 g, 15%) was obtained as an orange crystalline solid with a melting point of 212 °C. IR (CsI): $\tilde{\nu}$ = 1262, 1169, 1155, 1079, 966, 802, 655, 641, 584 (W–F), 544 cm^{-1}. MS (70 eV): *m/z* (%): 414 (2) $[M^+]$, 395 (100) $[M^+ - F]$. ^1H NMR ([D$_6$]acetone/CD_3CN, 250 MHz, TMS): δ = 2.99 (d quint, $J(H,F_{equatorial})$ = 1.1 Hz, $J(H,F_{axial})$ = 0.7 Hz, 15H; C_5Me_5). ^{19}F NMR ([D$_6$]acetone, 250 MHz, $CFCl_3$): δ = 102.20 (d quart, $^2J(F,F)$ = 140 Hz, $J(W,F)$ = 10 Hz, $J(H,F)$ = 4.5 Hz, 4F; $F_{equatorial}$), 90.80 (quint, $^2J(F,F)$ = 140 Hz, $J(W,F)$ = 62 Hz, 1F; F_{axial}). Elemental analysis of $C_{10}H_{15}WF_5$: calc. C 29.0, H 3.6, F 22.9; found C 28.9, H 3.7, F 22.7.

5: After the THF solution had been decanted from the orange crystals of **4**, the solution was further concentrated in vacuum. This led to the precipitation of **5** in the form of a pale yellow solid, which was separated by filtration and dried in vacuum. Compound **5** (0.15 g, 62%) was obtained as a pale yellow powder with a melting point of 168 °C. IR (CsI): $\tilde{\nu}$ = 1262, 1169, 1032, 933 (W=O), 875, 761, 578 (W–F), 481, 448, 423, 370, 312 cm^{-1}. MS (70 eV): *m/z* (%): 370 (100) $[M^+]$. ^1H NMR ($CDCl_3$, 250 MHz, TMS): δ = 2.16 (s 15H; C_5Me_5). ^{19}F NMR ($CDCl_3$, 250 MHz, $CFCl_3$): δ = −153.9 (s, 1F). Elemental analysis [16] of $C_{10}H_{15}WFO_2$: calc. C 32.4, H 4.0, F 5.1; found C 31.2, H 3.9, F 5.4.

Received: March 24, 1995
Revised version: November 8, 1995 [Z 7830 IE]
German version: *Angew. Chem.* **1996**, *108*, 331–333

Keywords: complexes with carbon ligands · complexes with halogeno ligands · fluorine compounds · structure elucidation

[1] R. Poli, *Chem. Rev.* **1991**, *91*, 509.
[2] R. C. Murray, L. Blum, A. H. Liu, R. R. Schrock, *Organometallics* **1985**, *4*, 953.
[3] A. H. Liu, R. C. Murray, J. C. Dewan, B. D. Santarsiero, R. R. Schrock, *J. Am. Chem. Soc.* **1987**, *109*, 4282.
[4] J. C. Gordon, V. Lee, R. Poli, *Inorg. Chem.* **1993**, *32*, 4460.
[5] F. Abugideiri, G. A. Brewer, J. U. Desai, J. C. Gordon, R. Poli, *Inorg. Chem.* **1994**, *33*, 3745.
[6] J. U. Desai, J. C. Gordon, H.-B. Kraatz, B. E. Owens-Waltermire, R. Poli, A. L. Rheingold, *Angew. Chem.* **1993**, *105*, 1506; *Angew. Chem. Int. Ed. Engl.* **1993**, *32*, 1486.
[7] E. Krause, *Ber. Dtsch. Chem. Ges.* **1918**, *51*, 1447.
[8] A. Herzog, F.-Q. Liu, H. W. Roesky, A. Demsar, K. Keller, M. Noltemeyer, F. Pauer, *Organometallics* **1994**, *13*, 1251; H. W. Roesky, A. Herzog, F.-A. Liu, *J. Fluorine Chem.* **1995**, *71*, 161; H. W. Roesky, A. Herzog, K. Keller, *Z. Naturforsch. B.* **1994**, *49*, 981.
[9] The ESR spectra were recorded on a Varian Century (Line Series 9 GHz) X-Band spectrometer at a working frequency of 9.108 GHz.
[10] $C_{10}H_{15}F_5W$, $M = 414.08$, orthorhombic, space group $Pna2_1$, $a = 1154.1(3)$, $b = 761.2(2)$, $c = 1341.3(3)$ pm, $V = 1.1783(5)$ nm^3, $Z = 4$, $\rho = 2.334$ Mg m^{-3}, $\mu = 9.838$ mm^{-1}, 4042 measured, 1535 independent reflections, 1533 used for the refinement, $2\theta_{max} = 45°$, $R1 = \Sigma|F_o - F_c|/\Sigma F_o = 0.075$ ($F > 2\sigma F$) and $wR2 = [\Sigma w(F_o^2 - F_c^2)^2/\Sigma wF_o^4]^{1/2} = 0.193$ (all data) from $w^{-1} = \delta^2(F_o^2) + (g1P)^2 + g2P$ with $P = (F_o^2 + 2F_c^2)/3$ and $g1 = 0.103$, $g2 = 33.87$, max. residual electron density: 1.8×10^3 e nm^{-3}. The data for the structure were collected on a Stoe-Siemens diffractometer. The intensities were measured with graphite-monochromated $Mo_{K\alpha}$ radiation ($\lambda = 71.073$ pm) at 293(2) K. Semi-empirical absorption corrections were carried out on all data. The structure was solved by direct methods (SHELXS-90) [13]. All non-hydrogen atoms were refined anisotropically against (F^2) [14]. The refinement of the Flack x parameter [$x = 0.45(6)$] revealed a racemic twinning of the crystal structure of **4** [15]. Further details of the crystal structure investigation can be obtained from the Director of the Cambridge Crystallographic Data Centre, 12 Union Road, GB-Cambridge CB2 1EZ, on quoting the complete journal citation.
[11] H. W. Roesky, M. Scholz, F. Edelmann, M. Noltemeyer, G. M. Sheldrick, *Chem. Ber.* **1987**, *120*, 1881.
[12] K. Köhler, H. W. Roesky, A. Herzog, H. Gornitzka, A. Steiner, I. Usón, *Inorg. Chem.*, in press.
[13] G. M. Sheldrick, *Acta Crystallogr. Sect. A* **1990**, *46*, 467.
[14] G. M. Sheldrick, SHELXL-93, program for crystal structure refinement, **1993**, Universität Göttingen.
[15] H. D. Flack, *Acta Crystallogr. Sect. A* **1983**, *39*, 876.
[16] Satisfactory carbon values were not obtained because of incomplete combustion (tungsten carbide formation).

A Freely Hinged Macrotricycle with a Molecular Cavity**

Ziyan Wu and Jeffrey S. Moore*

We describe here the synthesis and characterization of the carbon-rich macrotricycle **1**, whose strands form the perimeter of a $36 \times 12 \times 12$ Å molecular cavity (Fig. 1a, b). The topology of **1** is analogous to that of the prototypical three-dimensional network of three-connected silicon atoms in the intermetallic compound α-$ThSi_2$ (Fig. 1c).[1] One of the simplest cyclic fragments of this network is an 18-membered tricycle in which four parallel central edges are joined in pairs to the four, three-connected bridgeheads. Closure of the tricycle is accomplished with a three-vertex chain that links the bridgehead pairs at each end. All edges of this quadruple-bridged tricycle are joined at angles of 120° (i.e. each vertex has trigonal-planar coordination). In other words, the 18-membered tricycle **1** is to α-$ThSi_2$, what adamantane is to diamond (Fig. 1c, d).

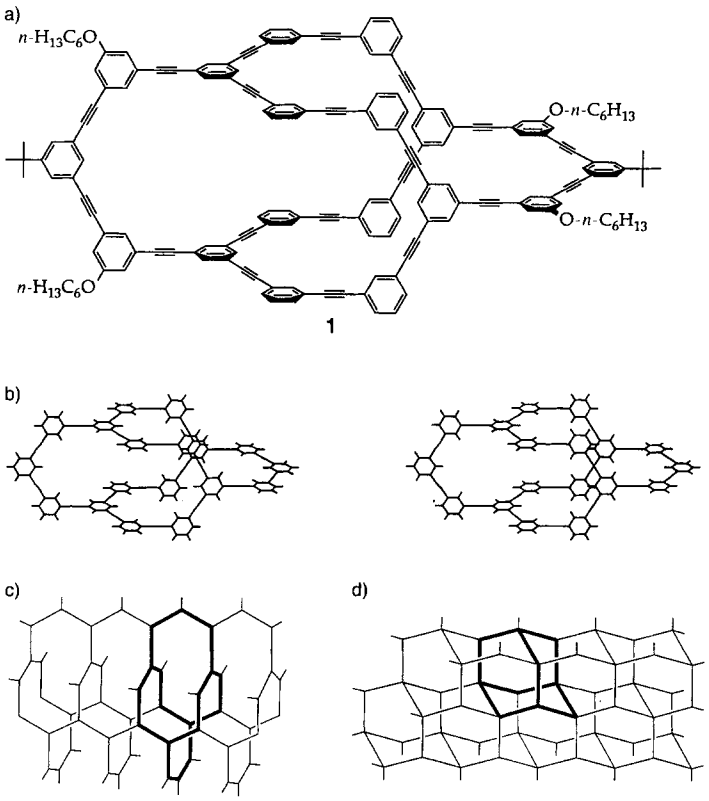

Fig. 1. a) The structural formula of macrotricycle **1**, b) stereoview of the carbon skeleton of **1** (computer-generated model; the pendant groups are removed for clarity), c) the silicon framework of α-$ThSi_2$, and d) the carbon framework of diamond. The bold lines in (c) and (d) denote the simplest cage motifs in these networks.

Many structural motifs based on the silicon network of α-$ThSi_2$ have received considerable attention of late. In 1983 Hoffmann et al. described a hypothetical carbon allotrope with the α-$ThSi_2$ topology as an alternative packing to graphite for trigonal-planar sp^2 carbon atoms.[2] Later, Diederich and Rubin postulated other carbon networks having the α-$ThSi_2$ connectivity.[3, 4] In 1993 a theoretical paper by Baughman and Galvão[5] showed how such a topology could give rise to materials with unusual mechanical (i.e. negative Poisson's ratio or auxetic[6] behavior) and thermal properties, provided that the network was expanded so as to retain a significant fraction of internal volume (the "uncrowded" hinged network phase). These hinged networks have the peculiar feature that the entire lattice can undergo reorganization by a nearly barrierless type of twisting motion around a set of parallel bonds that extends throughout the lattice.

Interestingly, supramolecular approaches to compounds of the expanded α-$ThSi_2$ structure type have recently been attempted. Single-crystal X-ray structures have shown that silver(I) salts complexed to certain tritopic, planar ligands give metal coordination networks possessing the α-$ThSi_2$ connectivity.[7, 8] Although these networks have the proper topology, they are heav-

[*] Prof. J. S. Moore
Roger Adams Laboratory, Box 55
Departments of Chemistry and Materials Science & Engineering
and The Beckman Institute for Advanced Science and Technology
University of Illinois
Urbana, IL 61801 (USA)
Fax: Int. code +(217) 244-8068
e-mail: moore@aries.scs.uiuc.edu
Dr. Z. Wu
Department of Chemistry, University of Michigan
Ann Arbor, MI 48109-1055 (USA)

[**] This work was supported by the National Science Foundation (CHE-94-23121) and the NSF Young Investigator Program (Grant CHE-94-96105). Additional support from the 3M Company and the Camille Dreyfus Teacher-Scholar Awards Program is gratefully acknowledged.

ily interpenetrated[9] leaving behind no open space along a direction that would permit large-scale mechanical deformation. One approach to prevent the formation of interpenetrated networks in these supramolecular constructions might involve the use of cyclic building blocks.[10] Because of their covalent connectivity, such building blocks would be incapable of forming catenated networks during crystallization. Properly functionalized derivatives of macrotricycle **1** should be geometrically predisposed to organize into expanded α-$ThSi_2$ supramolecular networks.

Each of the 18 vertices of **1** is constructed from a 1,3-diconnected or a 1,3,5-triconnected aromatic ring. All of the arene units are linked by linear ethynyl bridges. As a result of these "expanded" vertices and edges, the framework of **1** possesses a large internal void (Fig. 1b). Molecular mechanics calculations[11] on **1** confirm that a compliant, hinge-like rotation about the $C_{sp}-C_{sp^2}$ single bonds is possible for lateral deformations. In contrast, the structure is relatively stiff along its longitudinal axis, both in compression and under tension. The hingelike lateral conformational change occurs as the result of a concerted torsional rotation around the eight parallel edges in **1**. This rotational motion is restricted only when the macrocycle has collapsed upon itself, leading to a nearly planar, folded structure. This motion is purely torsional, occurring without any significant change in bond lengths. The simulated mechanical response of this finite fragment is thus similar to that of the infinite lattice structures described by Baughman and Galvão.[5]

The synthesis of **1** involved back-to-back cyclization steps using preassembled branched sequences. We have previously described an efficient method for synthesizing branched phenylacetylene sequences[12, 13] and showed how these could be double-cyclized to three-dimensional macrobicycles.[14] The sequences were designed carefully and their connection planned to uniquely obtain the topology of macrotricycle **1**. Scheme 1 illustrates this point by showing three synthetic routes leading to two isomeric macrotricycles from a pair of branched sequences. Here A and B refer to functional groups capable of forming a new covalent bond, while A_p and B_p are corresponding protected versions of these groups. For all three routes shown in Scheme 1 the first cyclization step entails a tandem bimolecular coupling of two branched segments and subsequent intramolecular cyclization. The second step involves double-cyclization of the resulting branched sequence. The three routes differ with regard to the substitution pattern on the branched sequences. Only one of these routes leads unambiguously to the desired connectivity. Specifically, the desired macrotricycle is the only isomer obtained by combining one sequence that is symmetrically substituted across its branch junctures with another sequence that is unsymmetrically substituted across its branch junctures.

The preparation of the required sequences **2** and **3** followed from repetitive methods previously developed in our laboratory.[12-14] The first cyclization step [Eq. (a)] was most crucial since it involved tandem bimolecular coupling and unimolecular cyclization. Besides uncontrolled oligomerization, the desired

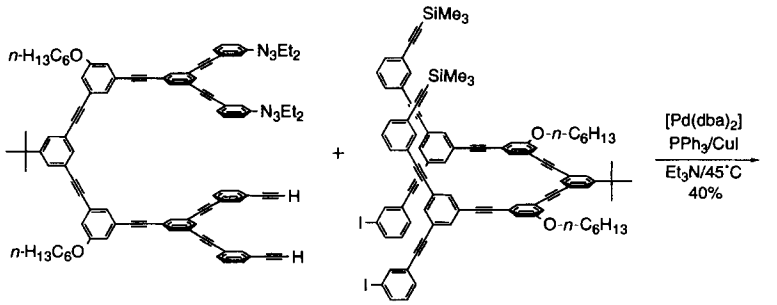

2 **3**

(a)

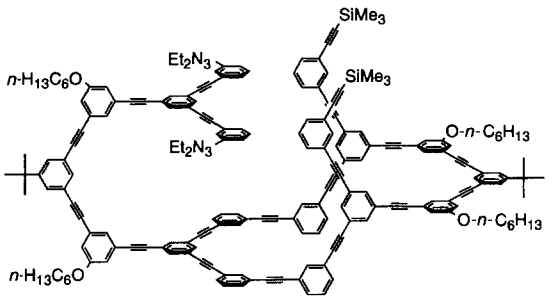

4

cross-coupling reactions also had to compete against oxidative dimerization, which is an important side reaction common to this chemistry producing diacetylene by-products. This side reaction is probably catalyzed by adventitious molecular oxygen. Extensive experimentation established that a catalyst to sequence molar ratio of 1:2 and a sequence concentration of 0.002 M (in dry triethylamine) gave the best yield of compound **4** [Eq. (a)]. Strict exclusion of oxygen and reaction at low temperature for extended times was optimal. Interestingly, the best mode of addition was to mix both sequences together at the start, rather than slowly add as solution of one sequence to a solution of the other. Product **4** was isolated by silica gel chromatography in 40% yield. Following removal of the triazene and trimethylsilyl groups, the resulting sequence was subjected to double cyclization [Eq. (b)] to afford macrotricycle **1** in 50% yield as a white powder.

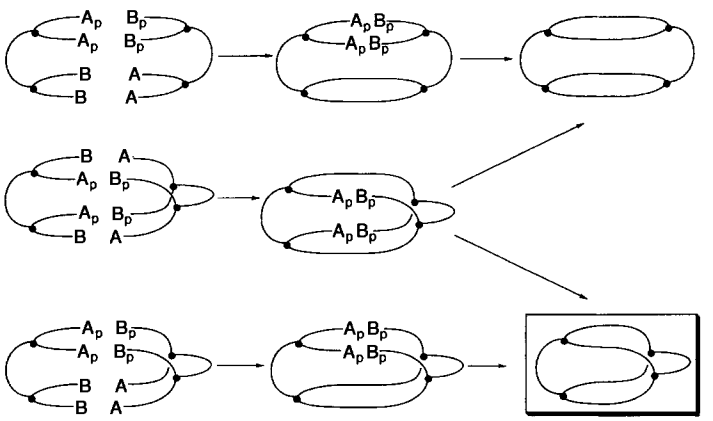

Scheme 1. Three cyclization strategies leading to macrocycles of different topologies.

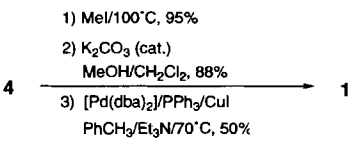

4 → **1** (b)

 © VCH Verlagsgesellschaft mbH, D-69451 Weinheim, 1996 0570-0833/96/3503-0298 $ 10.00+.25/0 Angew. Chem. Int. Ed. Engl. 1996, 35, No. 3

Table 1. Assignments of the ^{1}H NMR signals of **1** in the aromatic region [a].

Aromatic ring	Spin system	Relative intensity	δ
1	A_2X	1	7.54, 7.48
2	ABX	2	7.34, 7.05, 7.02
3	A_2B	2	7.66 [b]
4	ABMX	4	7.52, 7.43, 7.36, 7.27

[a] 500 MHz, $CDBr_3$, 100 °C. [b] The chemical shifts of this ABC spin system are apparently equivalent.

Macrotricycle **1** has low solubility in common organic solvents, which hampered its characterization. The ^{1}H NMR spectrum of **1** ($CDBr_3$, 100 °C) was assigned from a two-dimensional ^{1}H,^{1}H-COSY experiment at 500 MHz (Table 1). The COSY spectrum (Fig. 2) shows the expected four aromatic spin systems A_2X, ABX, A_2B, and ABMX present in the intensity ratio 1:2:2:4. In addition, only one singlet resonance is observed for the *tert*-butyl groups, consistent with the D_{2d} symmetry of **1**. Size exclusion chromatography (SEC) showed only one narrow, symmetrical peak confirming the purity of macrotricycle **1**. The SEC retention time of **1** is slightly longer than that of the branched precursor **4**, as expected owing to its more compact size. The elemental composition of **1** was verified by silver chemical ionization, laser desorption FT mass spectrometry[15] (MS calcd for $C_{180}H_{132}O_4Ag$ 2465.9244, found 2465.9420).[16]

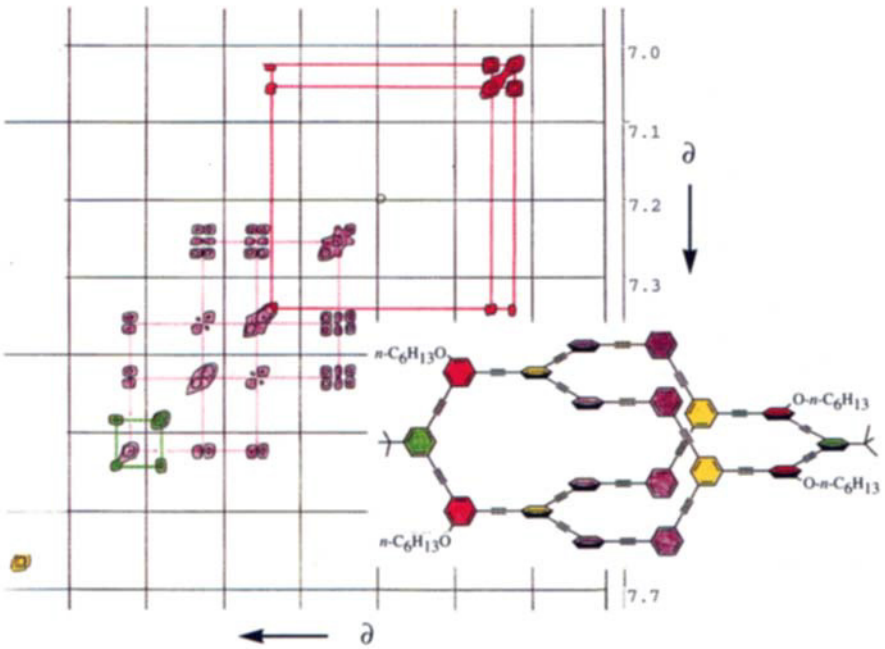

Fig. 2. Aromatic region of ^{1}H,^{1}H-COSY NMR spectrum of macrotricycle **1** (500 MHz, $CDBr_3$) at 100 °C. Color coding has been used to indicate the four unique spin systems.

In summary, a freely hinged macrocycle with a molecular cavity was prepared whose carbon-based skeleton represents a finite fragment of the α-ThSi_2 network. Properly functionalized derivatives of macrotricycle **1** might be useful as nanomechanical building blocks for constructing the noninterpenetrated, open networks required for the rational design of molecular-based auxetic materials.

Experimental Procedure

4: A single-neck flask with a side arm was charged with **3** (94.8 mg, 0.06 mmol), **2** (82.9 mg, 0.06 mmol), bis(dibenzylideneacetone)palladium(0) (31.4 mg, 0.03 mmol), triphenylphosphane (78.8 mg, 0.16 mmol), copper(I) iodide (5.2 mg, 0.015 mmol), and dry triethylamine (100 mL). The flask was stoppered, evacuated, and flushed with nitrogen three times, and the mixture was stirred at 45 °C for 24 h. The disappearance of the starting sequences was monitored by TLC. After the reaction was complete, the mixture was diluted with dichloromethane, washed three times with water and brine, dried over anhydrous magnesium sulfate, and filtered. The crude mixture was separated by column chromatography eluting with hexane/dichloromethane (1/1) to give the major product **4** as a clear, colorless glasslike material (70.1 mg, 40%): $R_f = 0.5$ (dichloromethane/hexane 1/1); ^{1}H NMR (360 MHz, C_6D_6): $\delta = 8.15$ (m, 2H), 7.95 (d, $J = 6.4$ Hz, 4H), 7.90 (d, $J = 8.7$ Hz, 2H), 7.80 (m, 3H), 7.76 (m, 1H), 7.71 (m, 5H), 7.67 (m, 3H), 7.65 (m, 2H), 7.64–7.60 (m, 10H), 7.41–7.29 (m, 14H), 7.22 (t, $J = 1.6$ Hz, 2H), 6.90 (td, $J = 7.7$, 1.6 Hz, 4H), 6.81 (t, $J = 7.7$ Hz, 2H), 3.55 (m, 8H), 3.35 (br s, 8H), 1.56 (m, 8H), 1.26–1.17 (m, 24H), 1.14 (s, 9H), 1.12 (s, 9H), 1.08–0.86 (m, 24H), 0.25 (s, 18H); ^{13}C NMR (125 MHz, $CDCl_3$): $\delta = 158.84$, 158.82, 151.64, 151.61, 151.14, 135.07, 134.95, 134.60, 134.22, 134.03, 133.98, 133.94, 132.12, 131.90, 131.82, 131.52, 131.39, 128.99, 128.95, 128.81, 128.57, 128.37, 128.18, 127.54, 127.22, 124.37, 124.33, 124.19, 124.03, 123.88, 123.83, 123.62, 123.54, 123.40, 123.35, 123.12, 123.05, 122.92, 121.29, 118.08, 117.89, 117.75, 117.28, 103.97, 95.13, 90.98, 89.98, 89.81, 89.79, 89.72, 89.60, 89.47, 89.45, 89.38, 89.19, 88.61, 88.57, 88.41, 88.39, 88.25, 88.19, 87.99, 87.94, 87.30, 68.29, 48.0 (br), 42.0 (br), 34.72, 31.54, 31.09, 29.10, 25.66, 22.61, 14.04, 12.0 (br), −0.11.

1: Procedures for transforming the triazene to the corresponding aryl iodide and the trimethylsilyl-protected alkyne to the corresponding terminal alkyne are similar to those previously described [12]. The double cyclization procedure is as follows: A septum-stoppered flask with a side arm charged with bis(dibenzylideneacetone)palladium(0) (37 mg, 0.031 mmol), copper(I) iodide (6.1 mg, 0.016 mmol), and triphenylphosphane (92.7 mg, 0.173 mmol) was evacuated and flushed with nitrogen. Dry triethylamine (10 mL) and toluene (20 mL) were added and the solution was stirred at 65 °C. The deprotected sequence (56 mg, 0.021 mmol) was dissolved in dry triethylamine (10 mL) and toluene (10 mL) and added to the flask by a syringe pump at a rate of 1.67 mL h^{-1}. White solid started to precipitate after the first half hour. At the end of the addition the mixture was heated at 70 °C for another 10 h and then the reaction mixture was cooled to room temperature. The solid was filtered and dissolved in large amount of chloroform. The solution was washed with 1 N aqueous HCl, water, and brine, and then dried over magnesium sulfate. After the solvent was removed, the residue was reprecipitated with chloroform and ether to afford a white powder (24.3 mg, 50% yield). Mass spectrometrie and ^{1}H NMR data for 1 are given in the text and Table 1.

Received: August 22, 1995 [Z 8332 IE]
German version: *Angew. Chem.* **1996**, *108*, 320–322

Keywords: carbon compounds · macrocycles · polycycles

[1] A. F. Wells, *Structural Inorganic Chemistry*, Oxford University Press, New York, **1993**, pp. 110–116.
[2] R. Hoffmann, T. Hughbanks, M. Kertész, P. H. Bird, *J. Am. Chem. Soc.* **1983**, *105*, 4831–4832.
[3] F. Diederich, Y. Rubin, *Angew. Chem.* **1992**, *104*, 1123–1146; *Angew. Chem. Int. Ed. Engl.* **1992**, *31*, 1101–1123.
[4] F. Diederich, *Nature* **1994**, *369*, 199–207.
[5] R. H. Baughman, D. S. Galvão, *Nature* **1993**, *365*, 735–737.
[6] I. E. Evans, M. A. Nkansah, I. J. Hutchinson, S. C. Rogers, *Nature* **1991**, *353*, 124.
[7] G. B. Gardner, D. Venkataraman, J. S. Moore, S. Lee, *Nature* **1995**, *374*, 792–795.
[8] L. Carlucci, G. Ciani, D. M. Proserpio, A. Sironi, *J. Am. Chem. Soc.* **1995**, *117*, 4562–4569.
[9] O. Ermer, L. Lindenberg, *Helv. Chim. Acta* **1991**, *74*, 825–877.
[10] D. Venkataraman, S. Lee, J. Zhang, J. S. Moore, *Nature* **1994**, *371*, 591–593.
[11] DISCOVER, Biosym Technologies Inc., 10065 Barnes Canyon Road, San Diego, CA (USA).
[12] J. Zhang, D. J. Pesak, J. J. Ludwick, J. S. Moore, *J. Am. Chem. Soc.* **1994**, *116*, 4227–4239.
[13] J. K. Young, J. C. Nelson, J. S. Moore, *J. Am. Chem. Soc.* **1994**, *116*, 10841–10842.
[14] Z. Wu, S. Lee, J. Moore, *J. Am. Chem. Soc.* **1992**, *114*, 8730–8732.
[15] M. S. Kahr, C. L. Wilkins, *J. Am. Soc. Mass Spectrom.* **1993**, *4*, 453–460.
[16] We are grateful to Dr. Michael S. Kahr and Prof. Charles L. Wilkins, University of California, Riverside, for collecting this data.

 © VCH Verlagsgesellschaft mbH, D-69451 Weinheim, 1996 0570-0833/96/3503-0299 $ 10.00+.25/0

Tris(chalcogenato)carbenium Ions $[C(XR)_3]^+$ (X = O, S, Se, Te): An Experimental and Quantum-Chemical Comparison**

Dietmar Ohlmann, Christina M. Marchand, Hansjörg Grützmacher,* Grace Shiahuy Chen, David Farmer, Rainer Glaser,* Antonio Currao, Reinhard Nesper, and Hans Pritzkow

Dedicated to Professor H. W. Roesky on the occasion of his 60th birthday

We have performed a systematic study of tris(chalcogenato)carbenium ions $[(RX)_3C]^+$ (X = S, Se, Te) to obtain a better understanding as to how donor atoms of the higher periods influence carbenium ion stability. Extensive experimental[1] and theoretical[2] studies have shown that carbenium ions $[H_{3-n}CY_n]^+$ can be stabilized by substituents Y (Y = NR_2, PR_2, OR, SR, and halogen) that contain electronegative heteroatoms with lone pairs that may engage in π donation as well as by substituents Y (Y = Li, Na, BeH) with electropositive elements which act as σ donors. In general, the stabilization energies (SE) can be quantified by the reaction energies of the hydride-transfer reactions [Eq. (a)] and the respective values for the cations $[H_{3-n}C(XH)_n]^+$ (X = O, S, Se, Te; $n = 1, 2, 3$) are listed in Table 1.

$$[H_{3-n}CY_n]^+ + n\,CH_4 \longrightarrow CH_3^+ + n\,H_3CY \qquad (a)$$

The oxocarbenium ion $[H_2C(OH)]^+$ (SE ≈ 64 kcal mol^{-1}; see also[1d, 2e-g]) has almost the same stabilization energy as the $[H_2C(XH)]^+$ ions (SE ≈ 64–68 kcal mol^{-1}; see also[1d, 2e-g]). The stabilization energies increase as the number of XH groups in the ions $[H_{3-n}C(XH)_n]^+$ increase. This increase is about the same for the thio-, seleno-, and telluro-substituted ions (average values: ΔSE(1 → 2) = 22.3 kcal mol^{-1}; ΔSE(1 → 3) = 33.3 kcal mol^{-1}; where ΔSE(1 → 2) = $SE[HC(XH)_2]^+ - SE[H_2C(XH)]^+$ and ΔSE(1 → 3) = $SE[C(XH)_3]^+ - SE[H_2C(XH)]^+$). The SE values increase particularly for the ions $[HC(OH)_2]^+$ and $[C(OH)_3]^+$ (ΔSE(1 → 2) = 40.7 kcal mol^{-1} and ΔSE(1 → 3) = 71.5 kcal mol^{-1}), and these ions are significantly more stabilized (by about 18 and 38 kcal mol^{-1}, respectively) than the homologous S, Se, and Te ions. These results are surprising in light of the decrease of the electronegativity χ_{spec}[3] in the order O ≫ S > Se > Te and of the concomitant increases of the σ- as well as of the π-donating ability of the heteroatom X.[2a,c] On the other hand, the χ_{spec} values of S, Se, and Te are relatively similar and we report herein experimental results that suggest that the bonding situations in the ions $[C(XR)_3]^+$ (X = S, Se, Te) also are comparable to each other, while they are clearly distinct from those in the $[C(OR)_3]^+$ ions.

Table 1. Stabilization energies (SE) [a] at the QCISD(T, full)/LANL1DZ + P′//MP2(full)/LANL1DZ + P′ level.

Molecule [b]	Element X: O	S	Se	Te
$[C(XH)_3]^+$	135.31	100.37	96.55	100.79
$[HC(XH)_2]^+$	104.56	89.00	86.01	89.61
$[H_2CXH]^+$ [c]	63.83	65.65	64.40	67.72

[a] SE calculated as the reaction energy ΔE_{HTR} of the hydride transfer reaction: $[H_{3-n}C(XH)_n]^+ + n CH_4 \rightarrow [H_3C]^+ + n H_3C(XH)$. [b] Trisubstituted cations in C_{3h} symmetry; di- and monosubstituted cations in C_s symmetry. All energies in kcal mol^{-1}. [c] In good agreement with results obtained at comparable levels and reported in ref. [2g].

Since the usual synthetic routes for the preparation of $[C(XR)_3]^+$ cations with X = O, S by protonation or alkylation of $(RX)_2C{=}X$ cannot be extended to the selenium and tellurium compounds, we have devised a new synthesis for these cations (Scheme 1). The copper complexes **1b, c** can be prepared in situ by addition of 2,2′-bipyridine to the copper chalcogenolates [Cu(XR)] (X = S,[4] Se;[5] R = 2,4,6-iPr$_3$C$_6$H$_2$) and **1d** can be obtained by reaction of $[\{(bpy)CuBr\}]_2$[6] with $[(thf)_2LiTeR]$.[7] The complexes **1b–d** react with CBr_4 (**2**) in CH_3CN (**1b, c**) or toluene (**1d**) to form the desired carbenium ions **3b–d** with dibromocuprate counterions. Exchange of the $CuBr_2^-$ ion by the PF_6^- ion yields the salts **6b–d** as yellow (**6b**), orange (**6c**), and pink (**6d**) solids, respectively. The corresponding oxocarbenium ion $[C(OR)_3]^+$ with R = 2,4,6-iPr$_3$C$_6$H$_2$ has not yet been prepared, but many such ions with other R groups were prepared by alkylation of carbonates and are well characterized. The salts **3b–d** and **6b–d** are remarkably soluble in apolar solvents such as benzene and Et_2O and can be handled in air.

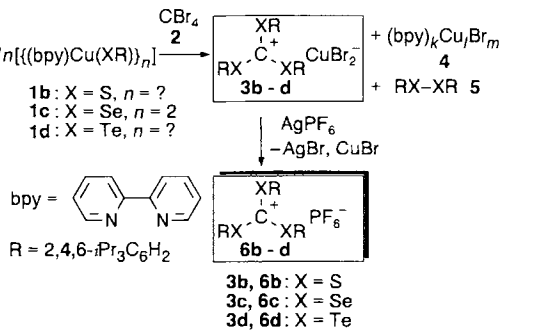

Scheme 1. Synthesis of **3b–3d** and **6b–6d**.

The result of a single-crystal X-ray structure determination of **6d** is shown in Figure 1.[8] Selected average distances and angles of **6d** are listed in Table 2 together with the respective data for the cations of **3b, c**.[9] The central carbon atom in all of the cations of **3b, c** and **6d** is coordinated in a trigonal-planar fashion (sum of angles at the carbon center = 360°) and the X-C-X angles vary only marginally (119.0°–121.3°). The C-X-C angles decrease in the series S > Se > Te as expected (**3b**: 102.5°; **6c**: 97.8, **6d**: 93.6°). Remarkably, the X–C bond to the central carbon atom C1 is shortened by about the same percentage (3.4–4.3%) in all cations. For the calculation of these percentages, we employed the $X-C_{aryl}$ bonds as internal standard for the $X-C(sp^2)$ bond length. This indicates that the S–C, Se–C,

[*] Prof. Dr. H. Grützmacher, D. Ohlmann, C. M. Marchand, A. Currao, Prof. Dr. R. Nesper
Eidgenössische Technische Hochschule Zürich
Laboratorium für Anorganische Chemie
Universitätstrasse 6, CH-8092 Zürich (Switzerland)
Fax: Int. code +(1) 632-1090
e-mail: gruetz@elwood.ethz.ch
Prof. Dr. R. Glaser, G. S. Chen, D. Farmer
Department of Chemistry, University of Missouri-Columbia
Columbia, MO 65211 (USA)
Fax: Int. code +(314)882-2754
e-mail: chemrg@showme.missouri.edu
Dr. H. Pritzkow
Anorganisch-chemisches Institut der Universität
Im Neuenheimer Feld 270, D-69120 Heidelberg (Germany)

[**] This research was supported in part by NATO (CRG 940399), the Fonds der Chemischen Industrie, and the Deutsche Forschungsgemeinschaft. We thank Prof. Dr. P. von R. Schleyer for making a preprint (ref. [2g]) available to us.

Table 2. Selected bond lengths [Å] and angles [°] for the cations of **3b,c**, **6d**, and **7a–d**. The Δ values specify the percentage shortening of the C1–X bond relative to the C_{aryl}–X bond. The calculated values (in italics) for **7a–d** were obtained at the MP2(full)/LANL1DZ+P′ level. The redox potentials for **6b–d** were measured in CH_3CN/nBu_4NPF_6 with a Pt electrode using a Ag electrode with ferrocene as standard. A reversible redox wave (ΔE = 0.85 mV) was observed in the cyclic voltammogram for **6b** at T = 298 K and for **6c,d** at T = 238 K.

Cmpd.	X	d(C1–X)	$d(C_{aryl}$–X)	∢(C–X–C(H))	Δ [%]	$\delta(^{13}C)$	δ(X)	λ_{max} ε [nm] [eL mol^{-1} cm^{-1}]	E_p^{red} [V]	E_{HOMO} [eV]	E_{LUMO} [eV]	ΔE [eV]
6a	O		-	-		166.3[b]	-	< 190[c]	-			
7a	*O*	*1.289*		*102.5*	5.9[a]					-21.99	-2.10	19.89
3b/**6b**	S	1.706	1.767	102.5	3.4	239.5		309/31065	-0.68			
7b	*S*	*1.710*		*97.8*	-			-		-16.13	-4.72	11.41
3c/**6c**	Se	1.839	1.933	97.8	4.9	253.7	^{77}Se: 770	388/16835	-0.65			
7c	*Se*	*1.855*		*95.8*		-	-	-		-14.77	-4.69	10.08
6d	Te	2.049	2.142	93.6	4.3	230.6	^{125}Te: 1279	500/22940	-0.67			
7d	*Te*	*2.050*	-	*94.6*		-	-	-		-13.15	-4.70	8.45

[a] The calculated percent shortening Δ is based on a C_{aryl}–O distance of 1.370 Å[10]. [b] Ref. [11a]. [c] Refers to $[C(OMe)_3][BF_4]$[11b].

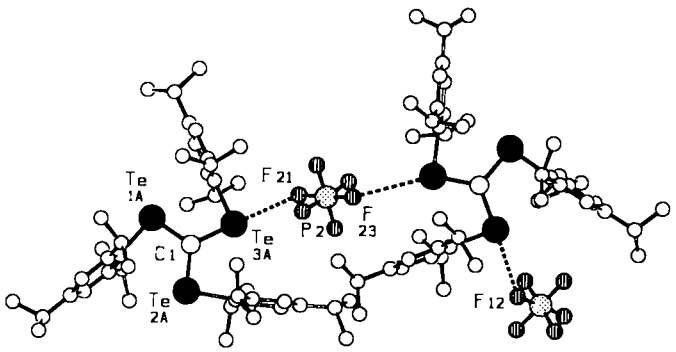

Fig. 1. SCHAKAL drawings of the two $[C(TeR)_3][PF_6]$ complexes (R = 2,4,6-iPr$_3$C$_6$H$_2$) in the asymmetric unit of **6d** which are connected through one shorter (3.061(15) Å) and one longer Te–F (3.637(15) Å) contact. Selected averaged distances and angles are given in Table 2.

and Te–C bonds are electronically rather similar in these cations. This expectation can be corroborated by experimental results: a) The chemical shifts of the central carbon atom C1 (Table 2) fall in the same range for all cations; b) cyclic voltammetry in acetonitrile/nBu$_4$NPF$_6$ electrolytes showed nearly identical peak potentials at about −0.66 V for the reductions of the cations. These observations suggest that the LUMO energies—which depend on the (p-p)π interactions between the donor atom X and the acceptor atom C1—deviate from each other only marginally in all cations of **6b–d**. On the other hand, the lowest energy absorptions in the UV/Vis spectra of the salts **6b–d** exhibit a bathochromic shift of 79 nm when S is replaced by Se and a further shift of 112 nm when Se is replaced by Te (Table 2). Evidently, an increasing destabilization of the HOMO is associated with varying the X atom in the series S, Se, and Te. In contrast, the ^{13}C NMR signal of protonated carbonic acid $[C(OH)_3]^+$ (**6a**) occurs at significantly higher field (Table 2), and no absorptions with wavelengths above 190 nm are observed in the UV/Vis spectra of tris(alkoxy)carbenium ions.[11b] In these compounds the HOMO–LUMO gap thus is significantly larger.

The experimental observations are consistent with calculations of the cations $[C(XH)_3]^+$ **7a–d** at the MP2(full)/LANL1DZ+P′ level[12] (Table 2) which establish strict C_{3h} symmetry for all of the trigonal-planar monocations and demonstrate excellent agreement between theoretical and experimental bond lengths and angles (average deviations are < 0.01 Å and < 3°, respectively). Information about the bonding situations and, for example, the size of the atoms in the molecules can be obtained from a topological electron density analysis (TEDA). TEDA is based on properties of the gradient vector field of the electron density distributions in Cartesian space and, in Figure 2, the gradient vector fields are exemplified for **7a** and **7b**.

The corresponding plots for the Se- and Te-containing cations greatly resemble the plot for **7b**. It becomes immediately apparent that the "bond critical points" (BCPs) for the C–X bonds (X = S, Se, Te) are closer to the X atoms than to the C atoms, which is in sharp contrast to the C–O bond in **7a**. The electron densities at the locations of the bond critical points (ρ_b) decrease in the series O > S > Se > Te. These TEDA results clearly demonstrate the umpolung of the C–X bond on going from the second to the third period and allow for an interpretation of the SE values (Table 1). As was previously described by Bernardi et al.,[2c] the stabilization of the RO-substituted carbenium ions can largely be attributed to the high polarity of the $C^{\delta+}$–$O^{\delta-}$

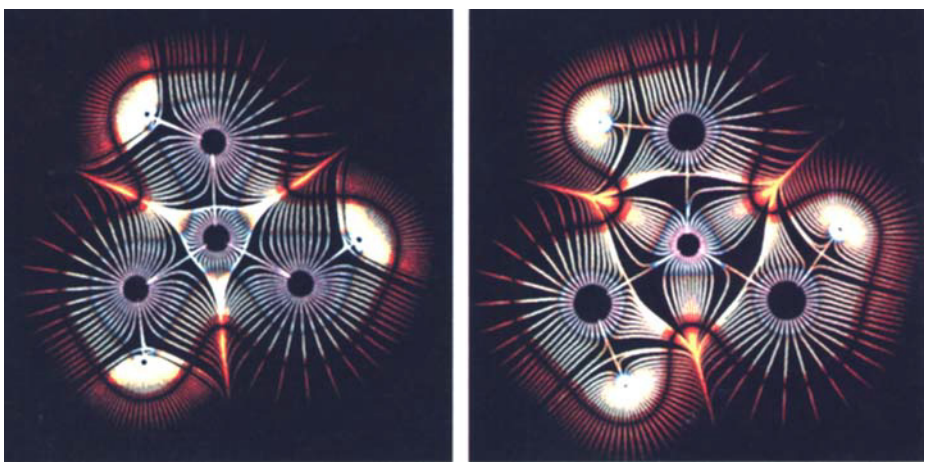

Fig. 2. Graphical representations of the gradient vector fields of the electron density distributions in the ions $[C(OH)_3]^+$ (**7a**, left) and $[C(SH)_3]^+$ (**7b**, right). The color coding reflects the magnitude of the electron density (pink 3–0.7, blue 0.35–0.3, yellow 0.2–0.1, red 0.05–0.01 e a_0^{-3}). The bond paths and the cross sections of the zero-flux surfaces also are shown and the bond critical points occur at their intersections.

bonding in the cations $[H_{3-n}C(OR)_n]^+$. This bond polarity results in spite of significant X→C π-bonding contributions, which, however, do not suffice to compensate the stronger C→X electron density shifts in the σ system. Consequently, instead of the expected charge *dispersal* an increased charge *separation* occurs. This interpretation also is consistent with the particularly large increase of the stabilities of the oxocarbenium ions (X = O) with increasing n in $[H_{3-n}C(XR)_n]^+$ ions because the Coloumb term contributes significantly to the binding energy in this case and increases the stability compared to the neutral compound $HC(XH)_3$. In contrast, the homologous cations $[R_{3-n}C(XR)_n]^+$ are stabilized by σ- and π-dative X→C bonding. Again an increasing electron density shift to the C atom is observed in the series S < Se < Te which goes beyond formal charge dispersal and results in $X^{\delta+}-C^{\delta-}$ bond polarizations that contribute to the stability of the cations. The nearly equal SE values of the $[H_2C(XH)]^+$ cations are fortuitous and result from different mechanisms of charge stabilization, which becomes clear only when the SE values associated with multiple substitution are considered.

Experimental Procedure

6b, c: Cu(XR) (3.35 mmol) (1.00 g **1b** or 1.16 g **1c**) was dissolved in acetonitrile (50 mL) and treated with freshly sublimed 2,2'-bipyridine (3.35 mmol, 523 mg). The deep red solution was cooled to 0 °C and a solution of CBr_4 (372 mg, 1.12 mmol) in acetonitrile (5 mL) was added by syringe over the course of 1 min. The solution was stirred overnight at room temperature. The resulting precipitate was separated by using a filtering crucible (fritted glass disk D4), and the acetonitrile was removed under vacuum. The dark, oily residue was stirred with warm hexane (3 × 10 mL) and after this treatment the yellow crude product **3b, c** was obtained after drying under high vacuum. The crude product was treated with $AgPF_6 \cdot 2CH_3CN$ (for **3b** (211 mg, 0.63 mmol), for **3c** (270 mg, 0.81 mmol)) in THF (20 mL) in the dark. After the mixture had been stirred for 1 h, the THF was removed under high vacuum, the residue was taken up in CH_2Cl_2 (20 mL), and the solution was filtered through silica. CH_2Cl_2 was removed under high vacuum and the remaining solid was washed with hexane and dried. **6b**: Yield 542 mg (56%) (m.p. 211 °C); ^1H NMR ($CDCl_3$): $\delta = 1.19$ (d, 18H, $J(H,H) = 6.8$ Hz, *o*-CH_3), 1.27 (d, 18H, $J(H,H) = 6.8$ Hz, *p*-CH_3), 1.42 (d, 18H, $J(H,H) = 6.8$ Hz, *o*-CH_3), 3.03 (m, 9H, $J(H,H) = 6.8$ Hz, *o*- and *p*-CH), 7.27 (s, 6H$_{aryl}$); ^{13}C NMR ($CDCl_3$): $\delta = 23.29$ and 23.57 (*o*-CH_3), 25.04 (*p*-CH_3), 32.97 (*o*-CH), 34.44 (*p*-CH), 117.22 (*p*-C_{aryl}), 124.50 (H-C_{aryl}), 152.73 (*o*-C_{aryl}), 156.52 (*ipso*-C_{aryl}), 239.51 ($C_{central}$); ^{31}P NMR ($CDCl_3$): $\delta = -144.5$ (m, $J(P,F) = 711$ Hz); ^{19}F NMR ($CDCl_3$): $\delta = -74.4$ (d, $J(F,P) = 711$ Hz); UV (Et_2O) λ_{max} (ε): 214 (60810), 256 (59310), 309 (31065), 375 nm (5665) strong offset shoulder. **6c**: Yield 809 mg (72%) (> 185 °C decomp.); ^1H NMR ($CDCl_3$): $\delta = 1.19$ (d, 18H, $J(H,H) = 6.8$ Hz, *o*-CH_3), 1.28 (d, 18H, $J(H,H) = 6.8$ Hz, *p*-CH_3), 1.39 (d, 18H, $J(H,H) = 6.8$ Hz, *o*-CH_3), 2.98 (m, 3H, $J(H,H) = 6.8$ Hz, *p*-CH), 2.99 (m, 6H, $J(H,H) = 6.8$ Hz, *o*-CH), 7.29 (s, 6H$_{aryl}$); ^{13}C NMR ($CDCl_3$): $\delta = 22.73$ and 22.83 (*o*-CH_3), 24.01 (*p*-CH_3), 33.43 (*p*-CH), 34.16 (*o*-CH), 123.25 (*p*-C_{aryl}), 123.66 (H-C_{aryl}), 151.26 (*o*-C_{aryl}), 155.03 (*ipso*-C_{aryl}), 253.71 [$C_{central}$, $^1J(^{77}Se, ^{13}C) = 210.5$ Hz]; ^{77}Se NMR ($CDCl_3$): $\delta = -769.5$; ^{31}P NMR ($CDCl_3$): $\delta = -144.4$ (m, $J(P,F) = 712$ Hz); ^{19}F NMR ($CDCl_3$): $\delta = -74.0$ (d, $J(F,P) = 712$ Hz); UV (Et_2O) λ_{max} (ε): 208 (63265), 254 (40490), 343 (9565) shoulder, 388 nm (16835).

6d: $[(thf)_2LiTeR]$ (1.61 g, 3.35 mmol) and $[(bipy)CuBr]_2$ (1.00 g, 1.67 mmol) were mixed and THF (50 mL) was added at −80 °C. The mixture was allowed to warm to −30 °C and stirred until a clear deep red solution was obtained. At 0 °C, half of the THF was removed under high vacuum and replaced by toluene. The solution was further reduced to about 15 mL and toluene (25 mL) was added subsequently. This solution was stored overnight at −70 °C. Precipitated LiBr was separated by filtration (fritted filter D4). The red-brown solution was brought to 0 °C and a solution of CBr_4 (372 mg, 1.12 mmol) in toluene (5 mL) was added by syringe over the course of 1 min. The solution was stirred overnight at room temperature, the resulting solid was separated by filtration (fritted filter D4) and toluene was removed in a high vacuum. The residue was stirred with warm hexane (3 × 10 mL). After drying in high vacuum, crude **3d** was obtained as a pink solid. As with **6b,c**, **6d** was prepared with $AgPF_6 \cdot 2CH_3CN$ (128 mg, 0.38 mmol). **6d**: Yield 437 mg (34%) (m.p. 152 °C); ^1H NMR (C_6D_6): $\delta = 1.16$ (d, 18H, $J(H,H) = 6.8$ Hz, *o*-CH_3), 1.26 (d, 18H, $J(H,H) = 6.8$ Hz, *p*-CH_3), 1.39 (d, 18H, $J(H,H) = 6.8$ Hz, *o*-CH_3), 2.89 (m, 3H, $J(H,H) = 6.8$ Hz, *p*-CH), 3.11 (m, 6H, $J(H,H) = 6.8$ Hz, *o*-CH), 7.37 (s, 6H$_{aryl}$); ^{13}C NMR (C_6D_6): $\delta = 23.92$ (*p*-CH_3), 24.92 and 25.05 (*o*-CH_3), 34.70 (*p*-CH), 40.08 (*o*-CH), 124.61 (H-C_{aryl}), 129.83 (*p*-C_{aryl}), 154.60 (*o*-C_{aryl}), 155.58 (*ipso*-C_{aryl}), 230.39 [$C_{central}$, $^1J(^{125}Te, ^{13}C) = 535$ Hz]; ^{125}Te NMR (C_6D_6): $\delta = 1278.8$; ^{31}P NMR (C_6D_6): $\delta = -145.0$ (m, $J(P,F) = 714$ Hz); ^{19}F NMR (C_6D_6): $\delta = -75.0$ (d, $J(F,P) = 714$ Hz); UV (Et_2O) λ_{max} (ε): 210 (65415), 275 (34565), 361 (2705), 500 nm (22940).

Received: September 15, 1995
Revised version: November 16, 1995 [Z 8405 IE]
German version: *Angew. Chem.* **1996**, *108*, 317 - 320

Keywords: ab initio calculations · carbenium ions · chalcogen compounds

[1] Reviews: a) *Carbonium Ions, Vol. I - V* (Eds.: G. A. Olah, P. von R. Schleyer), Wiley, New York, **1976**; b) M. Hanack, *Methoden Org. Chem. (Houben-Weyl)*, **1990**, Vol. 19c, p. 285ff., c) J. Hocker, F. Jonas, *ibid.* **1983**, Vol. E4, p. 677ff.; d) P. von R. Schleyer, *Pure Appl. Chem.* **1987**, *59*, 1647; e) T. Okuyama, *Rev. Heteroatom Chemistry, Vol. 1* (Ed.: S. Oae), **1988**, p. 46; f) L. Hevesi in *The Chemistry of Organic Selenium and Tellurium Compounds, Vol. 1* (Eds.: S. Patai, Z. Rappoport), Wiley, **1986**, p. 307ff. Experimental structural data of $[R^1C(XR)_2]^+$ ions (X = N, O, S, Se) see for example: g) M. Sundaralingam, A. K. Chwang in *Carbonium Ions, Vol. V* (Eds.: G. A. Olah, P. von R. Schleyer), Wiley, New York, **1976**, p. 2427; h) L. Hevesi, S. Desauvage, B. Georges, G. Evrard, P. Blanpain, A. Michel, S. Harkema, G. J. van Hummel, *J. Am. Chem. Soc.* **1984**, *106*, 3784; i) L. O. Atovmyan, V. I. Ponomarev, *Zh. Strukt. Khim.* **1975**, *16*, 920; j) H. Vancik, E. Sunko, *J. Am. Chem. Soc.* **1990**, *112*, 7418, citations 4 and 7; k) for X = PR, see: U. Heim, H. Pritzkow, H. Schönberg, H. Grützmacher, *J. Chem. Soc. Chem. Commun.* **1993**, 673; l) for X = Cl see: T. Laube, E. Bannwart, S. Hollenstein, *J. Am. Chem. Soc.* **1993**, *115*, 1731, m) for X = I see: R. Weiss, M. Rechinger, F. Hampel, *Angew. Chem.* **1994**, *106*, 901; *Angew. Chem. Int. Ed. Engl.* **1994**, *33*, 893.

[2] a) F. Bernardi, A. Mangini, N. D. Epiotis, J. R. Larson, S. Shaik, *J. Am. Chem. Soc.* **1977**, *99*, 7465; b) Y. Apeloig, P. von R. Schleyer, J. A. Pople, *ibid.* **1977**, *99*, 1291; c) F. Bernardi, A. Bottoni, A. Venturini, *ibid.* **1986**, *108*, 5395; d) A. M. Aissani, J. C. Baum, R. F. Langler, J. L. Ginsburg, *Can. J. Chem.* **1986**, *64*, 532; e) Y. Apeloig, M. Karni, *J. Chem. Soc. Perkin Trans. 2* **1988**, 625; f) J. C. White, R. J. Cave, E. R. Davidson, *J. Am. Chem. Soc.* **1988**, *110*, 6308; g) J. Kapp, C. Schade, A. M. El-Nahas, P. von R. Schleyer, unpublished results, h) P. G. Jasien, W. J. Stevens, *J. Chem. Phys.* **1985**, *83*, 2984. i) For a theoretical analysis of Y conjugate systems with NR_2 and O as π donors, see: A. Gobbi, G. Frenking, *J. Am. Chem. Soc.* **1993**, *115*, 2362, and references therein.

[3] We refer to the spectroscopic electronegativities determined by Allen: $\chi_{spec}(O) = 3.610$; $\chi_{spec}(S) = 2.589$; $\chi_{spec}(Se) = 2.424$; $\chi_{spec}(Te) = 2.158$; L. C. Allen, *J. Am. Chem. Soc.* **1989**, *111*, 9003.

[4] I. Schröter-Schmid, J. Strähle, *Z. Naturforsch. B* **1990**, *45*, 1537, and references therein.

[5] D. Ohlmann, H. Pritzkow, H. Grützmacher, M. Anthamatten, R. Glaser, *J. Chem. Soc. Chem. Commun.* **1995**, 1011.

[6] B. W. Skelton, A. F. Waters, A. H. White, *Aust. J. Chem.* **1991**, *44*, 1207.

[7] W.-W. du Mont, H. U. Meyer, S. Kubiniok, S. Pohl, W. Saak, *Chem. Ber.* **1992**, *125*, 761.

[8] Structure analysis of **6d**: $C_{46}H_{69}F_6Te_3P$, 1149.82 g mol^{-1}. Data acquisition: diffractometer STOE IPDS, $\lambda(Mo_{K\alpha}) = 0.71073$ Å; crystal dimensions about 0.30 × 0.30 × 0.2 mm; dark red, Lp corrections applied, no absorptions corrections applied, temperature − 200 K. Crystal data: triclinic, space group $P\bar{1}$ (No. 2), $a = 16.969(6)$, $b = 18.200(6)$, $c = 18.788(7)$ Å, $\alpha = 86.47(3)$, $\beta = 75.84(3)$, $\gamma = 72.93(3)°$; $V = 5377(3)$ Å^3, $\rho_{calcd} = 1.420$ g cm^{-3}, $Z = 4$, (two complexes in asymmetric unit), $\mu(Mo_{K\alpha}) = 1.69$ mm^{-1}, $2\theta_{max} = 48.3°$; 29422 reflections measured, 15896 independent reflections ($R_{int} = 0.0485$), 12988 independent reflections with $|F^2| > 2\sigma|F_2|$; 1009 parameters; *wR* (for $|F^2| > 2\sigma|F^2|$) = 0.2355, *wR* (for all reflections) = 0.2529, *R* (for $|F^2| > 2\sigma|F^2|$) = 0.0874, *wR* (for all reflections) = 0.1047, residual electron density (electrons Å^{-3}) min. = −1.04, max = 2.72; structure solved by heavy atom method (SHELX-86, G. M. Sheldrick, *Acta Crystallogr. Sect. A*, **1990**, *46*, 467), structure refinement by full matrix least-square refinement of $|F^2|$ (SHELXL-93, G. M. Sheldrick, Göttingen, **1993**), all non-hydrogen atoms were refined by using anisotropic thermal parameters, all H atoms were placed in calculated positions using fixed thermal parameters ($U_{iso} = 0.08$ Å^2). Further details of the crystal structure investigation may be obtained from the Fachinformationszentrum Karlsruhe, D-76344 Eggenstein-Leopoldshafen, on quoting the depository number CSD-59188.

[9] The salts **3b–d** were characterized by single-crystal X-ray diffraction as well. The parameters obtained for **3d** deviate only marginally from those found for **6d**. D. Ohlmann, H. Pritzkow, H. Grützmacher, unpublished results.

[10] F. H. Allen, O. Kennard, D.G. Watson, L. Brammer, A. G. Orpen, R. Taylor, *J. Chem. Soc. Perkin Trans. 2*, **1987**, S1.

[11] a) G. A. Olah, A. M. White, *J. Am. Chem. Soc.* **1968**, *90*, 1884; b) B. G. Ramsey, R. W. Taft, *ibid.* **1966**, *88*, 3058.

[12] a) W. J. Hehre, L. Random, P. von R. Schleyer, J. A. Pople, *Ab initio Molecular Orbital Theory*, Wiley, New York, **1986**; b) *Gaussian92/DFT*, Revision G.2: M. J. Frisch, G. W. Trucks, H. B. Schlegel, P. M. Gill, B. G. Johnson, M. W. Wong, J. B. Foresman, M. A. Robb, M. Head-Gordon, E. S. Replogle, R. Gomperts, J. L. Andres, K. Raghavachari, J. S. Binkley, C. Gonzalez, R. L.

Martin, D. J. Fox, D. J. Defrees, J. Baker, J. J. P. Stewart, J. A. Pople, Gaussian Inc., Pittsburgh, PA, **1993**; c) R. Bader, *Atoms in Molecules. A Quantum Theory*, Oxford University Press, New York, **1990**; d) "CCGVF-Color Coded Gradient Vector Fields", R. Glaser, D. Farmer, University of Missouri, Columbia, **1995**, unpublished results; e) LANL1DZ + P' refers to the LANL1DZ basis sets (P. J. Hay, W. R. Wadt, *J. Chem. Phys.* **1985**, *82*, 270 and 284) augmented by single sets of six Cartesian d-type polarization functions with the exponents 0.8 (C and O) and 0.65 (S) recommended for use with Pople's 6-31G* basis set and with exponents 0.338 (Se) and 0.237 (Te) suggested by Huzinaga, et al. (S. Huzinaga, J. Andzelm, M. Klobukowski, E. Radzio-Andzelm, Y. Sakai, H. Tatewaki, *Gaussian Basis Sets for Molecular Calculations*, Elsevier, New York, **1984**.) f) The gradient vector field analyses employed all-electron RHF wavefunctions and were based on the structures optimized at the all-electron RHF level. The all-electron basis sets were the 6-31G* basis set for H, C, O, and S atoms and the basis sets (43321/4321/311*) and (433321/43321/4211*) for Se and Te, respectively, as suggested by Huzinaga, et al.

Conformational Differences of O- and C-Glycosides in the Protein-Bound State: Different Conformations of C-Lactose and Its O-Analogue are Recognized by Ricin B, a Galactose-Binding Protein**

Juan-Félix Espinosa, F. Javier Cañada, Juan Luis Asensio, Hansjörg Dietrich, Manuel Martín-Lomas, Richard R. Schmidt, and Jesús Jiménez-Barbero*

Dedicated to Prof. Dr. Manuel Bernabé on the occasion of his 60th birthday

The interest in the chemistry of C-disaccharides as structural analogues of O-glycosides continues to grow[1] since these carbon-bridged compounds are thought to affect the activity of glycosidases as competitive inhibitors of the natural compounds. Therefore, it is extremely important that both compounds, the natural substrate and its C-glycoside analogue, are recognized by the enzyme in a similar way. The conformation of free C-glycosides has usually been assumed to be the same as that of the corresponding O-analogues.[2] However, we have recently demonstrated that, at least for O- and C-lactoses, this is not the case.[3]

To the best of our knowledge, it is not yet known whether both compounds are recognized by a carbohydrate-binding protein in the same conformation. Apart from the presence of the key interacting groups in the nonnatural substrate, this would be an essential requirement for an important inhibitory activity. On this basis, we report now on the use of 2D transferred NOE (TR-NOESY) and transferred ROE (TR-ROESY) experiments[4] to study the complexation of C-lactose (**1**) by a galactose-binding protein, ricin B.[5] In addition, we compare the obtained results with those reported for the complexation of regular lactose analogues.[6] Taking advantage of the large size of lectins, TR-NOE (TR-ROE) experiments have recently been used to determine the 3D structure of protein-bound carbohydrates[7] by focusing on the easily detected NMR signals of the free ligand.

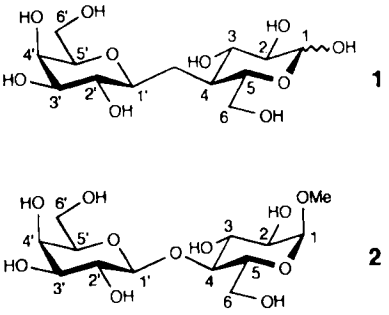

Fig. 1. Views of C-lactose (**1**) and methyl α-lactoside (**2**) showing the atomic numbering.

Figure 1 shows compound **1** and its O-analogue, methyl α-lactoside (**2**), along with their atomic numbering. The glycosidic dihedral angles are defined as Φ (H1'-C1'-O1'(C_x)-C4) and Ψ (C1'-O1'(C_x)-C4-H4). We have recently reported on the conformational study of **1** and **2** using NMR spectroscopy and only the basic features will be presented here.[3, 8] Both compounds adopt the *exo*-anomeric conformation around the glycosidic bonds but the conformation around the aglyconic bonds are rather different. For **2**, about 90% of the population is located in the central low-energy region (minimum A, Φ/Ψ 54/18), while roughly 10% of population presents similar Φ values but has Ψ values around 180° (minimum B, Φ/Ψ 36/180). These two different dispositions around the aglyconic bond are referred to as *syn* and *anti*, respectively.[9a] However, for **1** approximately 55% of the population adopts the *anti* conformation, while about 40% presents the *syn* orientation. The experimental data also indicate that minimum C (Φ/Ψ 180/0) is also populated (ca. 5%). Therefore, C-lactose exhibits much higher flexibility than its O-analogue. Table 1 summarizes the exclusive NOEs[9b] that characterize each region for **1**.

Table 1. Normalized NOESY and TR-NOESY intensities [%] for **1** at 30 °C in D_2O at (Varian, 500 MHz). The mixing times for the NOESY and TR-NOESY experiments were 700 and 300 ms, respectively.

Proton pair	NOE [%] Free	Bound
H^{pro-R}/H3	5.7	0.0
H^{pro-S}/H5	3.0	0.0
H^{pro-S}/H6 [a]	2.7	0.0
H1'/H4	2.1	−1.2
H1'/H3	5.9	−3.1
H^{pro-R}/H6 [a]	5.1	−5.4

[a] These NOEs were obtained by adding the contributions of both H6 protons.

The conformational changes that occur when methyl α-lactoside is bound to ricin B have been studied using TR-NOESY and TR-ROESY experiments.[6a] In summary, the bound conformation deviates slightly from the *exo*-anomeric conformation towards smaller Φ angles, while the orientation around the aglyconic bond is exclusively *syn*. The relevant interproton distances (H1'–H4 ca. 2.2–2.3 Å) are in agreement with those reported previously for the binding of methyl β-lactoside to ricin.[6b]

For C-lactose in the presence of ricin B the observed NOEs are negative, an indication of binding. The NOESY spectra of **1** (Fig. 2) recorded in the absence and in the presence of the lectin show important differences. First, the presence of both H1'/H3 and H^{pro-R}/H6 cross peaks, which define the population around minimum B, indicates that the *anti* conformation is indeed recognized by the protein, in contrast with the results

[*] Dr. J. Jiménez-Barbero, J.-F. Espinosa, Dr. F. J. Cañada, Dr. J.-L. Asensio, Dr. H. Dietrich, Prof. Dr. M. Martín-Lomas
Grupo de Carbohidratos, Instituto Química Orgánica, C. S. I. C.
Juan de la Cierva 3, E-28006 Madrid (Spain)
Fax: Int. code + (1)5644853
e-mail: IQOJJ01@pinar1.csic.es
Prof. Dr. R. R. Schmidt
Fakultät für Chemie der Universität Konstanz (Germany)

[**] Financial support by the Dirección General de Investigación Científica y Técnica (DGICYT, PB93-0127) is gratefully acknowledged. J.-F. E. thanks the Ministerio de Educación y Ciencia (MEC) for a FPU fellowship.

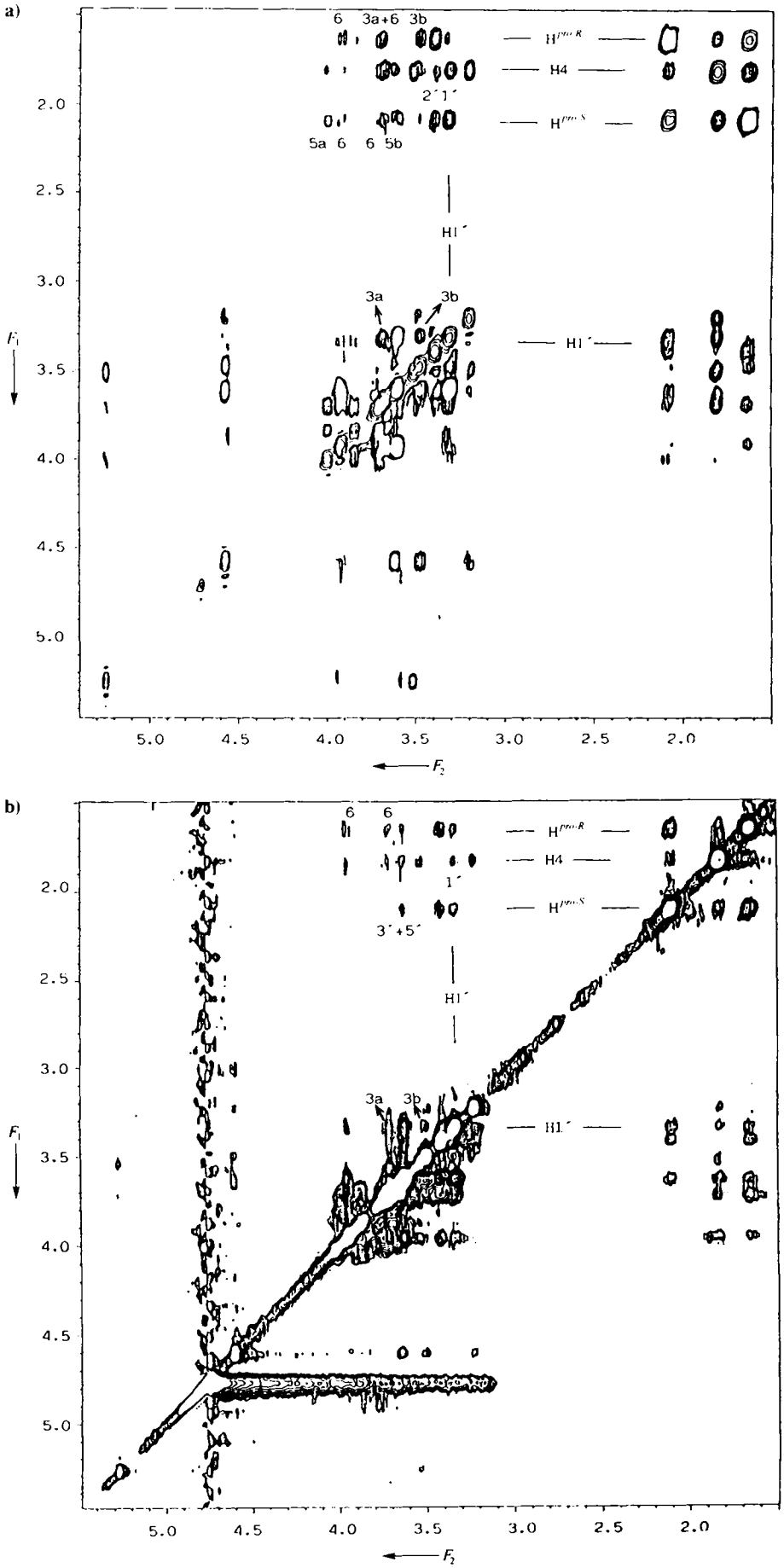

obtained for methyl α-lactoside (**2**).[6] Moreover, a total of four NOEs, which were observed for free **1**, are not detected in the complex (Table 1, Fig. 3). The H4/H2′ NOE (an exclusive NOE of the region around minimum C) is not present, indicating that this conformation is not bound. In addition, three exclusive NOEs for the *syn* conformation (H^{pro-R}/H3, H^{pro-S}/H5, and H^{pro-S}/H6) are also absent in the TR-NOESY spectrum (Fig. 2) and, thus, the *syn* conformation is not recognized by the lectin. The presence of the H1′/H4 cross peak seems to be a contradiction. However, a careful study of the spectrum shows that, for the complex, the NOE between H1′ and H^{pro-S} NOE (ca. −3%) is much more intense than that between H1′ and H4 (ca. −1%), while, for free **1**, these cross peaks have the same intensity. Since spin diffusion is extremely efficient for a molecular complex of this size,[10] it may be that this H1′/H4 NOE is mediated by an indirect effect in the complex. Indeed, the presence of the two methylene protons in **1** provides important diffusion pathways, and therefore an indirect H1′/H4 cross peak via H^{pro-S} may be expected. To confirm this hypothesis and to differentiate spin diffusion effects from direct NOE enhancements, TR-ROESY experiments are essential,[6a, 10] since under spin-locking conditions direct and three-spin effects are of opposite sign. The major disadvantage of TR-ROESY is that cross relaxation of the free ligand cannot be neglected and must be measured in a separate experiment. The experimental data show that the H1′/H3 ROE is roughly three times more intense in the spectrum recorded in the presence of protein than in the spectra for free **1** at the same mixing time. In contrast, the H1′/H4 NOE has the same magnitude in both cases, hence demonstrating that the corresponding TR-NOESY cross peak detected in the complex between **1** and the lectin is mediated by an indirect effect. The presence of the H1′/H4

Fig. 2. 2D NOESY ^{1}H NMR spectra (Varian, 500 MHz, 30 °C, D_2O) of **1** in the absence (a) and in the presence (b) of protein. Samples of ricin B were concentrated after repeated cycles of exchange with deuterated sodium phosphate and transferred to the NMR tube; the final pH was 6.5, the concentration 0.12 mM, and the molar ratio of C-lactose/ricin B 20:1. Mixing times of 700 and 300 ms were used for free and bound **1**, respectively. TR-NOESY experiments were also carried out with mixing times of 120, 400, and 500 ms.

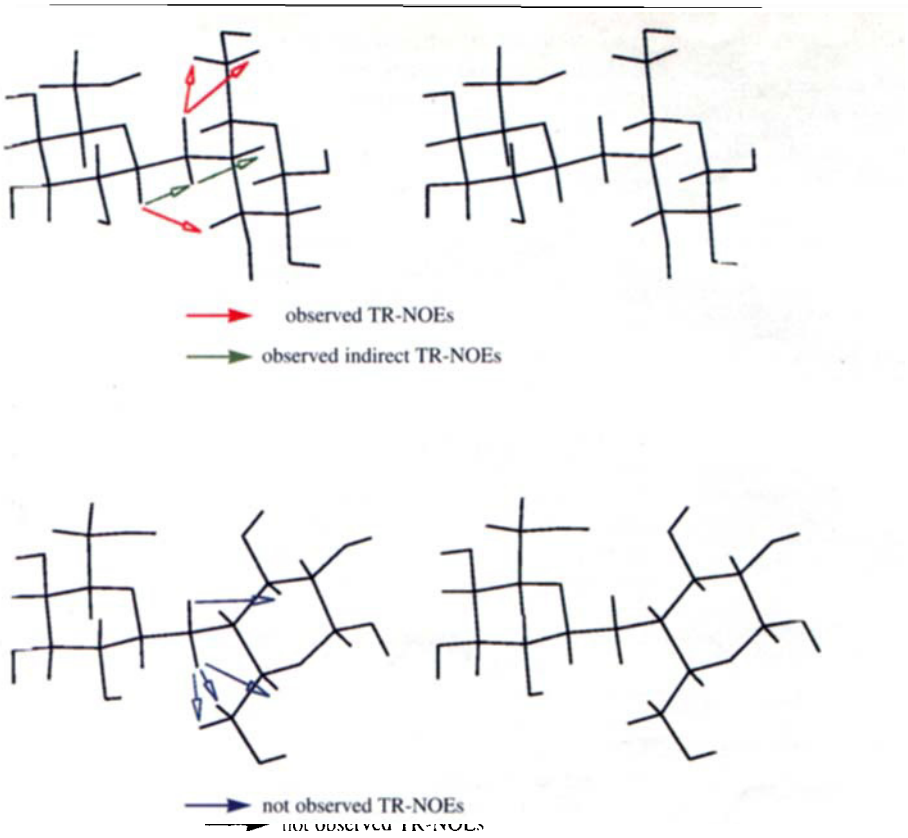

Fig. 3. Stereoscopic views of the *syn* (minimum A, Φ, Ψ 54/18) and *anti* (minimum B, Φ Ψ 36/180) conformations of **1** with the exclusive NOEs in each case.

cross peak in the TR-ROESY experiment is evidently due to the excess of free ligand. Differences between TR-NOESY and TR-ROESY spectra are also found for H1′/H4′, H^{pro-S}/H3′ + H5′, and H^{pro-R}/H3′ + H5′ cross peaks, which disappear in the TR-ROESY spectrum.[11] Our results confirm recent reports that indicate that spin diffusion plays a significant role in transferred NOE experiments.[10] A quantitative analysis of the TR-NOE data obtained for C-lactose/ricin B was attempted by simulation of the TR-NOESY spectrum according to the full relaxation matrix method.[12] However, it was not possible to completely reproduce the experimental data by using a rigid model of the ligand within the binding site.[13] This fact confirms that C-lactose is mobile even in the binding site and that several conformers within the *anti* valley defined by minimum B are still possible.

More importantly, the experimental results indicate (Fig. 2) unequivocally and unexpectedly that ricin B selects differentconformers of **1** (*anti*), and its O-analogue, **2** (*syn*) (Fig. 4).

Crystallographic and binding studies of the ricin B/lactose complex[5c] have shown that the lectin contains two noncooperative β-galactose binding sites.[5d] To estimate the relative binding affinities of **1** and **2**, competitive TR-NOESY experiments were performed with different **1**:**2** ratios. It was observed that the increase in the amount of **2** added to the NMR tube induced a decrease in the negative NOE cross peak intensities of **1**. When a 1:1 ratio was reached, the NOEs of **1** became positive, whereas strong negative NOEs were clearly observed for **2**. These results lead to two conclusions: a) both ligands compete for the same binding sites of the lectin, and b) the affinity constant of **1** is smaller than that of its O-analogue **2**.

The study of the crystal structure of the complex of ricin B with lactose does not give any unambiguous explanation for the change in conformation on going from **1** to **2**. The lack of recognition of the *anti* conformation of **2** by the lectin could be explained by a steric interaction between the hydroxymethyl group of the glucose moiety and the protein.[6a] Although merely speculative, the higher flexibility and the larger distances between the pyranoid rings might allow the recognition of the *anti* conformation of C-lactose. Nevertheless, no obvious reason has been found for the exclusive binding of this conformation to the protein.

In conclusion, we have shown for the first time that not only the 3D structure of a C-glycoside may be different from that of its corresponding O-glycoside in the free state, but also that a carbohydrate-binding protein may select different conformations of these types of compounds. Although the case presented here cannot be generalized, care should be taken in the design of competitive inhibitors of glycosidases based on C-glycosides, since these compounds may have different preferred conformations than their natural substrates.

Received: August 3, 1995
Revised version: October 20, 1995 [Z82781E]
German version: *Angew. Chem.* **1996**, *108*, 323–326

Keywords: C-glycosides · carbohydrates · lectins · molecular recognition · NMR spectroscopy

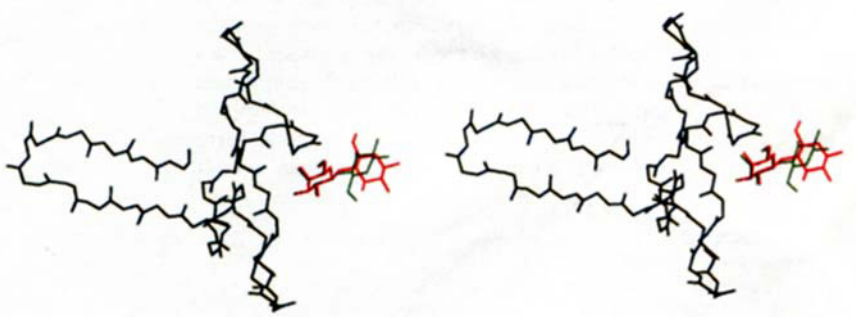

Fig. 4. Stereoscopic view of compounds **1** (red) and **2** (green) docked into the 1α subdomain of ricin B as constructed from the crystallographic coordinates [5c]. Both ligands were docked in the selected conformation into the protein to fit the hydrogen bond pattern observed in the crystal for the galactose moiety. Extensive minimization of each complex with the CVFF program was performed as described [6a]. This figure should be regarded as just a model of the conformation of the ligands within the binding site of ricin B, since protein–carbohydrate contacts have not been detected experimentally.

 © VCH Verlagsgesellschaft mbH, D-69451 Weinheim, 1996 0570-0833/96/3503-0305 $ 10.00+ .25/0

[1] a) H. Dietrich, R. R. Schmidt, *Liebigs Ann. Chem.* **1994**, 975–981, and references therein; b) A. Wei, A. Haudrechy, C. Audin, J. Hyuk-Sang, N. Haudrechy-Bretel, Y. Kishi, *J. Org. Chem.* **1995**, *60*, 2160–2169, and references therein.

[2] a) Y. Wang, P. G. Goekjian, D. V. Ryckman, W. H. Miller, S. A. Babirad, Y. Kishi, *J. Org. Chem.* **1992**, *57*, 482–489; b) C.-H. Wong, R. L. Halcomb, Y. Ichikawa, T. Kajimoto, *Angew. Chem.* **1995**, *107*, 569–593; *Angew. Chem. Int. Ed. Engl.* **1995**, *34*, 521–546.

[3] J.-F. Espinosa, M. Martin-Pastor, J. L. Asensio, H. Dietrich, M. Martin-Lomas, R. R. Schmidt, J. Jiménez-Barbero, *Tetrahedron Lett.* **1995**, *36*, 6329–6332.

[4] a) G. M. Clore, A. M. Gronenborn, *J. Magn. Reson.* **1982**, *48*, 402–417; b) A. P. Campbell, B. D. Sykes, *Annu. Rev. Biophys. Biomol. Struct.* **1993**, *22*, 99–122.

[5] a) Ricin B was purchased from Sigma. b) S. Olsnes, A. Pihl, *The Molecular Actions of Toxines and Viruses*, Elsevier Biomedical Press, New York, **1982**, pp. 52–105; c) E. Rutenber, J. D. Robertus, *Proteins* **1991**, *10*, 260–269; d) D. Solis, P. Fernandez, T. D. Mauriño, J. Jiménez-Barbero, M. Martin-Lomas, *Eur. J. Biochem.* **1993**, *214*, 677–683.

[6] a) J. L. Asensio, F. J. Cañada, J. Jiménez-Barbero, *Eur. J. Biochem.* **1995**, *233*, 618–630; b) V. L. Bevilacqua, D. S. Thomson, J. H. Prestegard, *Biochemistry* **1990**, *29*, 5529–5537.

[7] a) T. Weimar, T. Peters, *Angew. Chem.* **1994**, *106*, 79–82; *Angew. Chem. Int. Ed. Engl.* **1994**, *33*, 88–91; b) D. R. Bundle, N. M. Young, *Curr. Opin. Struct. Biol.* **1992**, *2*, 655–660.

[8] J. L. Asensio, J. Jiménez-Barbero, *Biopolymers* **1995**, *35*, 55–73.

[9] a) J. Dabrowski, T. Kozár, H. Grosskurth, N. E. Nifant'ev, *J. Am. Chem. Soc.* **1995**, *117*, 5534–5539; b) L. Poppe, C. W. von der Lieth, J. Dabrowski, *ibid.* **1990**, *112*, 7762–7771.

[10] S. R. Arepalli, C. P. J. Glaudemans, G. D. Daves, P. Kovac, A. Bax, *J. Magn. Reson.* **1995**, *106*, 195–198.

[11] They are probably due to indirect effects mediated by H3'/H5' in the first case and by H1' in the last two cases.

[12] R. E. London, M. E. Perlman, D. G. Davis, *J. Magn. Reson.* **1992**, *97*, 79–98.

[13] The correlation times for the bound state and the exchange rate constants that fit all the intragalactose NOEs did not reproduce all the intra- and interglycosidic NOEs involving the glucose unit. In contrast, for **2**/ricin B all the experimental TR-NOEs could be fitted by a simple set of parameters [6a].

Catenane Chameleons: Environment-Sensitive Translational Isomerism in Amphiphilic Benzylic Amide [2]Catenanes**

David A. Leigh,* Karen Moody, John P. Smart, Karen J. Watson, and Alexandra M. Z. Slawin

The organization of two or more amphiphilic molecules into oligomeric and polymeric ensembles such as micelles, reverse micelles, and lipid bilayers[1, 2] is a spectacular example of molecular self-assembly which gives rise to supramolecular structures with properties exploited by both nature (for example cell membranes[3]) and mankind (for example detergents,[4] drug delivery systems[5, 6]). Here we report the synthesis, structure, and properties of a new class of constitutionally simple, but topologically complex, compounds containing amphiphilic units connected by noncovalent, mechanical linkages to form catenanes.[7–14] These remarkable *unimolecular* species exhibit in solution conformational and dynamic properties reminiscent of the micellar and reverse micellar behavior of classical, *multimolecular* amphiphilic systems. In particular, in polar solvents the amphiphilic units of the catenanes arrange themselves such that the polar groups are at the surface of the supramolecular structure where they can form hydrogen bonds with solvent molecules and the lipophilic chains are on the inside where their interaction with the solvent is minimized. In nonpolar media the situation is reversed, that is the catenanes undergo a chameleon-like translational isomerism, adopting a supramolecular conformation to suit the character of the local environment. The X-ray crystal structure of one of the catenanes is consistent with the preferred conformation in nonpolar solvents: one macrocycle (the "host"[15]) of each catenane adopts a conformation that has convergent hydrogen bonding sites; the other (the "guest") one with divergent hydrogen bonding sites. Extraordinary double bifurcated hydrogen bonding occurs between host and guest in the solid state and, together with polarphobic forces, determines the supramolecular conformations adopted by the amphiphilic catenanes in solution.

We recently described[16, 17] the synthesis of a series of octaamide benzylic amide catenanes that exhibit a range of dynamic behavior, dependent upon both steric and electronic factors,[17] and solvent-controlled rates of macrocyclic ring rotation mediated by the strength of the intermacrocyclic ring hydrogen bonding. The solid-state structure[16] of one catenane revealed six intramolecular, interring hydrogen bonds per catenane and an extensive network of π-stacks composed of four aromatic rings that together were proposed to provide the driving force for the formation of the topologically complex product. We have now investigated the effect on the benzylic amide catenane self-assembly process of removing some of the amide groups and aromatic rings in the catenane precursors.

Initial base-promoted reactions of the diol **1** and sebacoyl chloride (Scheme 1) in various polar solvents (e.g. THF, MeCN, pyridine, DMF; **1** is insoluble in halogenated and less polar solvents) led to the (1 + 1) and (2 + 2) macrocycles **2** and **3**, respectively, in combined yields of up to 80%, but no catenanes could be detected. Since directional hydrogen bonds are weak in these solvents, we sought methods that would allow the use of **1** in less polar media so as to maximize the strength of

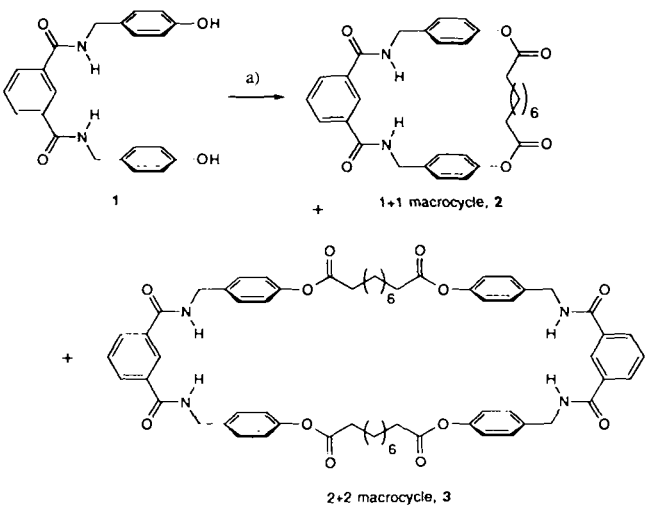

Scheme 1. The condensation of the diol **1** with sebacoyl chloride and triethylamine in polar solvents. a) $ClOC(CH_2)_8COCl$, Et_3N, polar solvents (e.g. THF, MeCN, pyridine, DMF).

[*] Dr. D. A. Leigh, K. Moody, Dr. J. P. Smart, Dr. K. J. Watson
Department of Chemistry
University of Manchester Institute of Science and Technology
Sackville Street, Manchester M60 1QD (UK)
Fax: Int. code +(161)200-4539
A. M. Z. Slawin
Department of Chemistry
Loughborough University of Technology (UK)

[**] Supported in part by EPSRC Innovative Polymer Synthesis Initiative Grant No. GR/J/88579.

the hydrogen bonding interactions necessary for benzylic amide catenane assembly.

Stannylation with di- and trialkyltin compounds has been exploited, particularly in carbohydrate chemistry, to modify the reactivity of hydroxyl groups and to solubilize polyols in nonpolar solvents.[18] Although the attempted preparation of the bis(dibutylstannylene ether) derivative of **1** led to an insoluble gum, the analogous bis(tributylstannylene ether) derivative **4** could be prepared quantitatively in toluene by removal of water (Dean–Stark apparatus) and proved highly soluble in common halogenated solvents. In contrast to the results obtained by using the underivatized diol, **4** reacts with sebacoyl chloride in the presence of triethylamine[19] in anhydrous chloroform under high dilution conditions to give the (1 + 1 + 1 + 1) [2]catenane **5** in 18% yield, together with **2** (19%) and **3** (14%, Scheme 2). The different macrocycles were distinguished unambiguously by mass spectrometry and the (1 + 1 + 1 + 1) catenane **5** was discernible from the isomeric (2 + 2) macrocycle **3** by FAB-MS fragmentation patterns, ^{1}H NMR spectroscopy, and X-ray crystallography (see below).

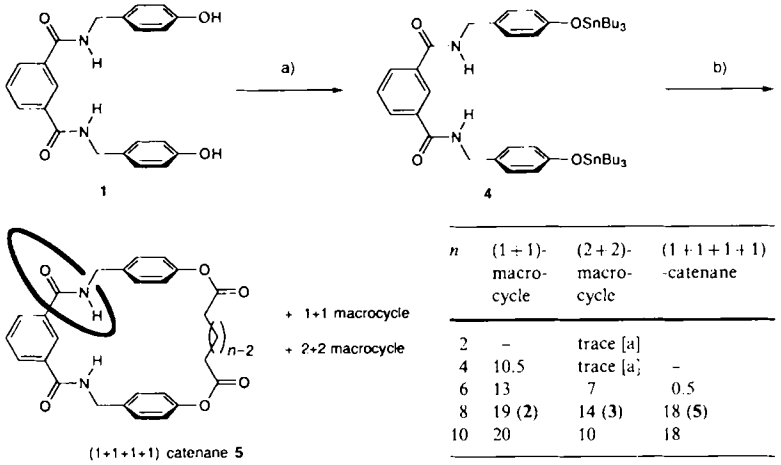

n	(1+1)-macrocycle	(2+2)-macrocycle	(1+1+1+1)-catenane
2	–	trace [a]	
4	10.5	trace [a]	–
6	13	7	0.5
8	19 (**2**)	14 (**3**)	18 (**5**)
10	20	10	18

Scheme 2. Preparation of **4** and its condensation with *n*-alkanedicarboxylic acid dichlorides and triethylamine in anhydrous chloroform. a) $(Bu_3Sn)_2O$, toluene, Dean-Stark apparatus; b) $ClOC(CH_2)_nCOCl$, Et_3N, anhydrous $CHCl_3$ [29]. [a] From FAB-MS (MS-MS excludes catenane formation); however, these compounds proved too insoluble to be isolated.

Single crystals of **5** suitable for investigation by X-ray diffraction were obtained from $CHCl_3$/cyclohexane mixtures by vapor diffusion. The crystal structure analysis (Figs. 1a–d) shows that

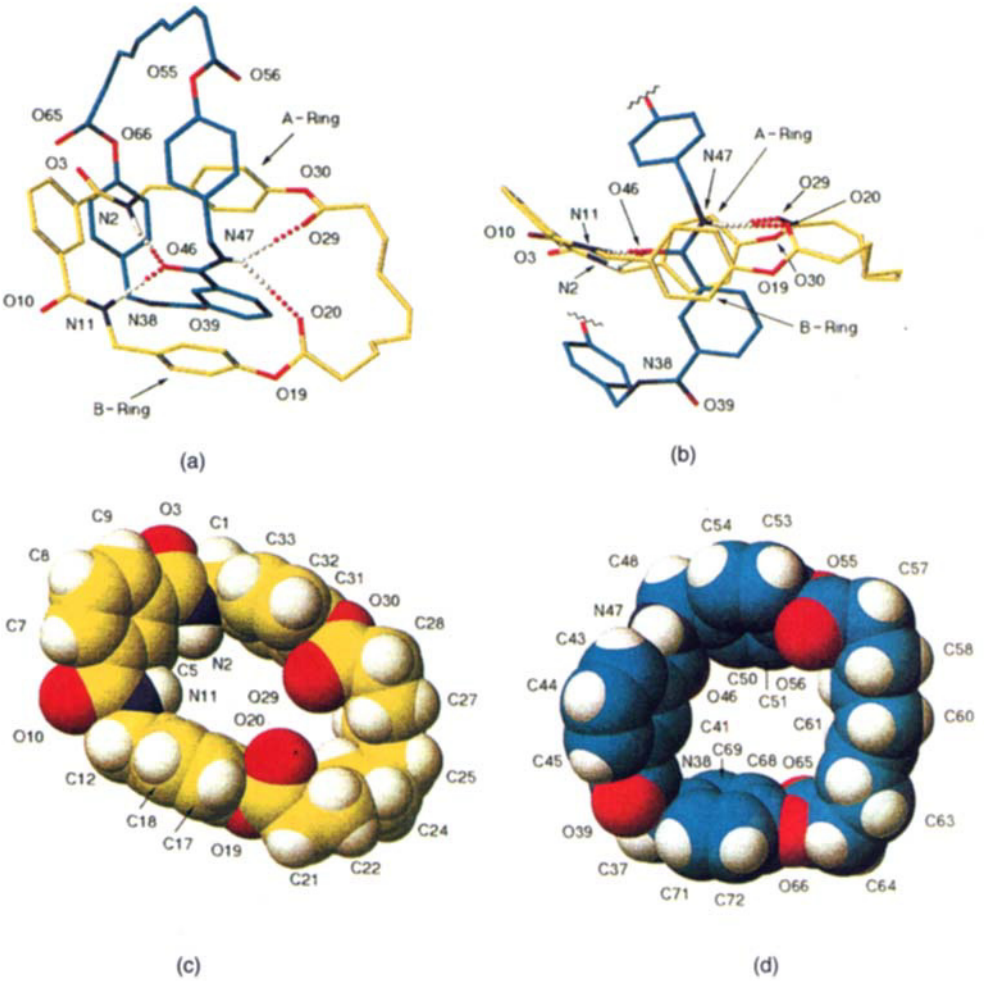

Fig. 1. Solid-state structure of the [2]catenane **5** as determined by X-ray crystallography [26] (for clarity carbon atoms of the "host" macrocyclic ring of the catenane are shown in yellow and those of the guest in blue; oxygen atoms are depicted red, nitrogen atoms purple, and hydrogen atoms white). a) Framework representation of the [2]catenane illustrating the double bifurcated hydrogen bonding. Intramolecular hydrogen bond lengths [Å]: N2···O46 3.232 [2.230 for NH···O]; N11···O46 2.989 [2.610 for NH···O]; O29···N47 3.365 [2.801 for NH···O]; O20···N47 3.483 [3.112 for NH···O]. Intermolecular hydrogen bonding occurs in the packed structure between N38-H and O10 (N···O distance 2.861 Å; 2.569 for NH···O) of adjacent catenanes. b) Framework representation of the [2]catenane illustrating π stacking between two aromatic rings of the host macrocycle and a benzamide unit of the guest. Closest contact distances [Å]: "External" (ring-B, Fig. 1b) host aromatic ring···guest benzamide unit 3.541; "internal" (ring-A, Fig. 1b) host aromatic ring···guest benzamide unit 3.296. c) Space-filling representation of the host macrocycle. Selected bond lengths [Å]: O10–C10 1.228, N11–C10 1.319, N11–C12 1.441, O19–C20 1.343, O20–C20 1.156, O29–C29 1.189, O30–C29 1.327, N2–C1 1.533, N2–C3 1.184, O3–C3 1.332. Selected bond angles [°]: C4-C3-O3 112.11, O3-C3-N2 121.44, C3-N2-C1 117.52, N2-C1-C34 110.53, C31-O30-C29 123, O30-C29-O29 118.81, O29-C29-C28 130.65, C21-C20-O20 131.66, O20-C20-O19 125.64, C20-O19-C16 117.77, C13-C12-N11 112.55, C12-N11-C10 122.20, N11-C10-O10 120.72, O10-C10-C6 120.998. Selected dihedral angles [°]: C5-C4-C3-O3 145.499, C5-C4-C3-N2 −22.600, C4-C3-N2-C1 −170.190, C3-N2-C1-C34 141.808, C36-C31-O30-C29 −112.517, C31-O30-C29-O29 0.557, C15-C16-O19-C20 131.868, C16-O19-C20-C21 −12.378, C5-C6-C10-O10 −155.454, C5-C6-C10-N11 26.886, C10-N11-C12-C13 −167.526. d) Space-filling representation of the guest macrocycle. Selected bond lengths [Å]: O46–C46 1.258, N47–C46 1.324, N47–C48 1.445, O55–C56 1.32, O56–C56 1.498, O65–C65 1.227, O66–C65 1.334, N38–C37 1.472, N38–C39 1.309, O39–C39 1.209. Selected bond angles [°]: C40-C39-O39 122.233, O39-C39-N38 121.540, C39-N38-C37 123.448, N38-C37-C70 113.641, C67-O66-C65 118.481, O66-C65-O65 120.935, O65-C65-C64 125.207, C57-C56-O56 150.622, O56-C56-O55 120.004, C56-O55-C52 119.767, C49-C48-N47 113.861, C48-N47-C46 123.208, N47-C46-O46 122.360, O46-C46-C42 118.356. Selected dihedral angles [°]: C41-C40-C39-O39 13.985, C41-C40-C39-N38 −164.060, C40-C39-N38-C37 −178.542, C39-N38-C37-C70 −88.195, C72-C67-O66-C65 115.517, C67-O66-C65-O65 −2.234, C53-C53-O55-C56 −1.466, C52-O55-C56-C57 0.213, C41-C42-C46-O46 157.344, C41-C42-C46-N47 −22.595, C46-N47-C48-C49 168.699.

 © VCH Verlagsgesellschaft mbH, D-69451 Weinheim, 1996 0570-0833/96/3503-0307 $ 10.00+.25/0

the two chemically identical component macrocycles of the [2]catenane adopt very different conformations in the solid state. One macrocycle (Fig. 1c, carbon atoms shown in yellow) effectively acts as a "host" for the other and binds through four hydrogen bonds in an extraordinary double bifurcated motif to *both* sides of an amide group on the other ("guest") macrocycle (Fig. 1d, carbon atoms shown in blue).

The host macrocycle (Fig. 1c) adopts a flattened chairlike conformation which is almost D_2-symmetric; the cisoid isophthaloyl 1,3-diamide group and the carbonyl groups of the phenolic esters are directed into the cavity to form precisely positioned convergent hydrogen bonding sites. The guest macrocycle (Fig. 1d) has a more open and less regular geometry which allows both the isophthaloyl amides and the phenolic ester groups to adopt their preferred transoid orientations. The O46-C46-N47-H amide group of the guest is accessible by virtue of the open conformation of the macrocycle and acts as the divergent double hydrogen bonding site for the host macrocycle. In addition to the four hydrogen bonding groups, the aromatic A- and B-rings of the host form close noncovalently bonded contacts with the extended π-system of the C42-C46-(-O46)-N47 benzamide group of the guest (closest π-stacking distances 3.541 and 3.296 Å, Fig. 1b). However, in contrast to the amide catenane solid-state structures reported previously,[16, 20, 21] there are no other π-stacking interactions found in the crystal structure of **5**, suggesting that such interactions are, after all, of limited importance in the catenane assembly process.

As seen with both the benzylic amide [2]catenanes[16] and the catenane systems investigated by Hunter and Vögtle,[20, 21] the bifurcated hydrogen bonding to the amide carbonyl group (O46, Fig. 1a and b) does not occur to the lone pairs of the oxygen atom—such an interaction is prevented in these molecules on steric grounds—but rather orthogonal to them. In the absence of the conventional H···lone pair hydrogen bond geometry the thermodynamic driving force for this unusual (but clearly strong since it drives the entire catenane assembly process and has short NH···O bond lengths of 2.23 and 2.61 Å) interaction appears to be either a general, nondirectional electrostatic association between the δ^- oxygen and δ^+ hydrogen atoms, or a specific directional interaction between the two amide hydrogen atoms and the π electrons of the carbonyl group. In contrast, the weaker O···H(N)···O bifurcated hydrogen bonding (2.80 and 3.11 Å) from the ester carbonyl groups (O20 and O29) to the amide (N47) hydrogen atom occurs in a standard fashion to the lone pairs of the sp^2-hybridized oxygen atoms.

A comparison of the ^{1}H NMR spectra (Fig. 2a) of the (1 + 1) macrocycle **2** (the (2 + 2) macrocycle **3** is insoluble in halogenated solvents) and the (1 + 1 + 1 + 1) catenane **5** allows the determination of the "supramolecular conformation" adopted by the [2]catenane in $CDCl_3$ solution.[22] The chemical shifts of the *h*, *i*, *j*, and *k* protons in the sebacoyl chains are virtually identical for **2** and **5**, suggesting that in the catenane the alkyl chains spend little time in close proximity to aromatic rings which would cause shielding or deshielding effects. In contrast, the protons of the benzylic spacer (*e*, *f*, and *g*) show large shielding (up to $\Delta\delta = 0.7$) in the catenane with respect to the analogous protons in the macrocycle. These observations are consistent with the preferred conformation of the catenane in $CDCl_3$ being similar to that determined by X-ray crystallography for the solid state (Fig. 3, conformation **I**). The lipophilic sebacoyl chains are on the surface of the molecule away from the aromatic rings and polar regions, whereas the hydrogen bonding groups are buried in the middle of the supramolecular structure involved in intermacrocycle, intramolecular hydrogen bonding shifting the amide protons (*d*) downfield by $\Delta\delta = -1.5$. The network of hydrogen bonds locks the aromatic rings in close proximity to each

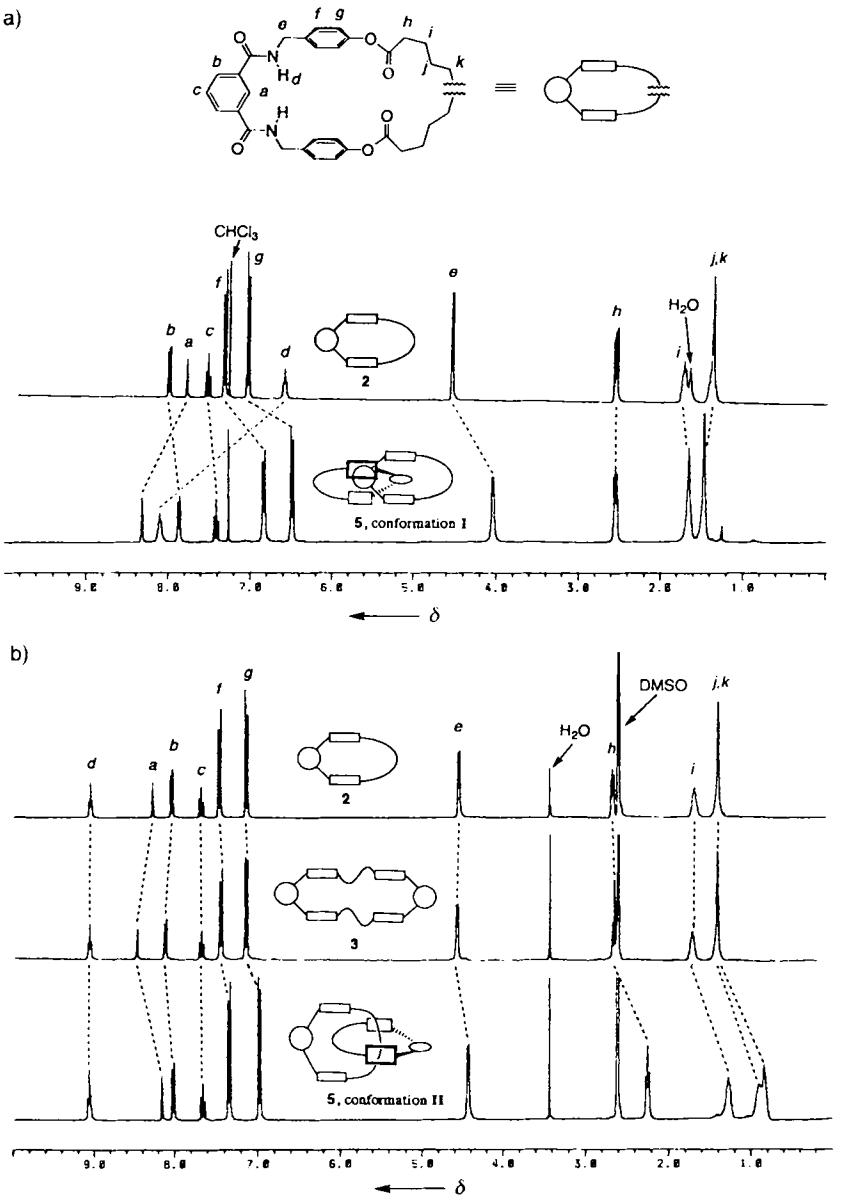

Fig. 2. a) ^{1}H NMR spectra (300 MHz, $CDCl_3$) of **2** and **5**. b) ^{1}H NMR spectra (300 MHz, [D$_6$]DMSO) of **2**, **3**, and **5**.

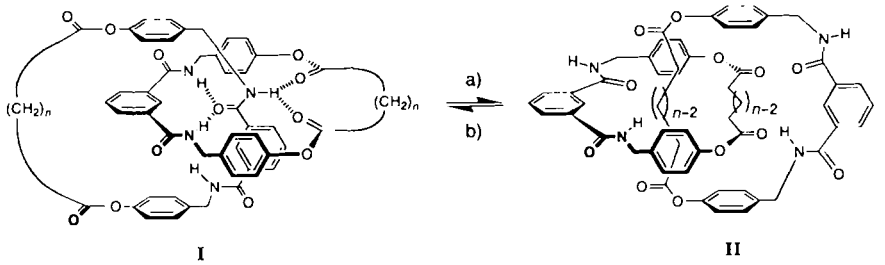

Fig. 3. Translational isomerism of amphiphilic benzylic amide [2]catenanes in nonpolar (conformation **I**) and polar solvents (conformation **II**). The preferred supramolecular conformation in nonpolar solvents is similar to that determined for the solid-state by X-ray crystallography.

other leading to the shielding effects seen in the ^{1}H NMR spectra. Further supporting evidence is found in the relative chemical shift of the isophthaloyl ring protons; the protons *b* and *c* show small shielding shifts, but proton *a* is substantially deshielded ($\Delta\delta = 0.5$) by the cone of the carbonyl group which occurs through the bifurcated hydrogen bonding geometry seen in the X-ray crystal structure (cf. conformation **I**, Fig. 3).

In [D$_6$]DMSO, a hydrogen bond accepting solvent, comparison of the ^{1}H NMR spectra (see Fig. 2b) of the (1 + 1) and (2 + 2) macrocycles and the (1 + 1 + 1 + 1) catenane shows that in this solvent a dramatically different supramolecular conformation is adopted by the catenane. The aromatic protons of the two macrocycles and the catenane occur at similar chemical shifts, indicating that little shielding/deshielding is taking place in the catenane, that is the aromatic rings are spending little time close to one another. However, the protons of the sebacoyl chain of the catenane are heavily shielded with respect to those of the two macrocycles. This is consistent with a structure where the lipophilic chains of the catenane are buried in the center of the catenane (Fig. 3, conformation **II**) and shielded by the aromatic spacer groups that line the cavity, and the hydrogen bonding amide groups are exposed to interact with the polar solvent. The driving force for such a geometry is twofold: the hydrogen bonding of the amide groups with the solvent and the polarphobic benefit of shielding the lipophilic chains from the polar media.[23]

The synthesis of **5** is not unique (see Scheme 2). Variation in the length of the alkyl chain of the dicarboxylic acid dichloride shows that a minimum of six carbon atoms is required to allow catenane formation, in broad agreement with inspection of CPK space-filling models. The yields of (1 + 1) macrocycle and [2]catenane decrease on shortening of the alkyl chain, reflecting the increase in strain and preorganization required for the ring closure reactions. The ^{1}H NMR spectra of each of the [2]catenanes in $CDCl_3$ and [D$_6$]DMSO mirror the trends outlined above for the sebacoyl (C_8) spacer.

The simplicity of the catenane NMR spectra suggest that whichever supramolecular conformation is preferentially adopted the rotation of the macrocyclic rings is rapid on the NMR timescale at room temperature in either type of solvent. Low-temperature ^{1}H NMR studies in $CDCl_3$ give a rate of rotation (circumvolution) of the component macrocyclic rings of the [2]catenane **5** of 8100 s^{-1} at room temperature ($\Delta G^{\ddagger}$ = 11.3 kcal mol^{-1}; T_c = 240, $\Delta\nu$ = 105 Hz, k_c 233 s^{-1}).[24] Although a similar experiment with [D$_6$]DMSO is not possible because of the freezing point of the solvent, in neat [D$_7$]DMF (an alternative hydrogen bond accepting solvent) circumvolution of **5** at room temperature was found to occur at a rate greater than 100000 s^{-1} ($\Delta G^{\ddagger} < 10.2$ kcal mol^{-1}).[25] Initial results suggest that the solvent-mediated rotation frequency is a continuum and that mixing of two or more solvents (e.g. [D$_4$]MeOH and $CDCl_3$) allows regulation of the rate of circumvolution of the macrocyclic rings at a given temperature. Such tunable control over the frequency and mode of translational isomerism is of fundamental importance to the design of nanoscale devices based upon molecular shuttles and switches.

The amphiphilic benzylic amide catenanes described illustrate well how the noncovalent assembly of even the simplest of molecules can result in materials with remarkable and unexpected properties by virtue of their supramolecular architectures. The chameleon-like ability of the catenanes to alter their shape, conformation, and surface properties in accordance with their local environment offers fascinating possibilities in areas where interactions at surfaces or interfaces are important, such as drug delivery systems, surfactants, nanoemulsions, vesicles, interfacial arrays, thin films, and "nanotape". The opportunities for new strategies in organic synthesis will be discussed elsewhere. Finally, the discovery of a double bifurcated binding site for an amide group provides a route to the design of synthetic receptors for amino acids and peptides and serves as a reminder that although hydrogen bonding is considered amongst the best understood of supramolecular forces, the rules regarding its geometrical requirements are, as yet, nowhere near complete.

Experimental Procedure

4: To a stirred suspension of the diol **1** (0.451 g, 1.2 mmol) in toluene (30 mL) was added bis(tributyltin)oxide (0.715 g, 1.2 mmol). The mixture was heated at reflux for 20 h with removal of water by azeotropic distillation (Dean-Stark apparatus). The resulting clear solution was cooled and the toluene removed under reduced pressure. After drying for 2 h in vacuo the product **4** was obtained as a cream gum (1.14 g, 100%) and used immediately.

Preparation of **5**, **2**, and **3**: A solution of sebacoyl chloride (0.32 g, 1.34 mmol) in anhydrous $CHCl_3$ (10 mL) [29] and **4** (1.14 g, 1.2 mmol) in anhydrous $CHCl_3$ (20 mL) [29] were added simultaneously over 2 h, by using motor-driven syringe pumps, to a stirred solution of triethylamine (0.35 mL, 2.53 mmol) in anhydrous $CHCl_3$ (100 mL) [29] at room temperature under argon. After 24 h the reaction mixture was filtered and the combined filtrates washed successively with 0.1 M hydrochloric acid (50 mL), distilled water (3 × 50 mL), 10% aqueous potassium fluoride solution (50 mL), and distilled water (3 × 50 mL). The organic washings were dried over anhydrous $MgSO_4$, filtered, the solvent removed under reduced pressure, and the resulting solid subjected to column chromatography on silica gel (98:2 $CHCl_3$:MeOH as eluent) to give as the first fraction eluted the [2]catenane **5** (0.117 g, 18%); m.p. 309 °C; ^{1}H NMR (300 MHz, $CDCl_3$): δ = 1.45 (bs, 16H, H-j,k), 1.75 (bs, 8H, H-i), 2.58 (t, J = 6 Hz, 8H, H-h), 4.05 (d, J = 6 Hz, 8H, H-e), 6.45 (AA', J = 8 Hz, 8H, H-g), 6.85 (BB', J = 8 Hz, 8H, H-f), 7.4 (t, J = 8 Hz, 2H, H-c), 7.85 (d, J = 8 Hz, 4H, H-b), 8.10 (bt, 4H, H-d), 8.30 (s, 2H, H-a); ^{13}C NMR (75 MHz, $CDCl_3$): δ = 24.47 (C-k), 28.12 (C-j), 29.03 (C-i), 33.86 (C-h), 43.82 (C-e), 120.92, 127.46, 127.62, 130.06, 130.12 (C-a,b,c,f,g), 134.95, 135.59 (quaternary C), 149.48 (*C*-OCO), 166.87 (*C*ONH), 172.74 (O*C*=O); FAB-MS: m/z 1085 [M + H], 565 [M/2 + Na], 543 [M/2 + H]; anal. calcd for $C_{64}H_{88}N_4O_{12}$: C 70.8, H 6.3, N 5.2; found C 70.5, H 6.3, N 4.9. The second fraction eluted was characterized as the (1 + 1) macrocycle **2** (0.124 g, 19%): m.p. 262–263 °C; ^{1}H NMR (300 MHz, $CDCl_3$)[22]: δ = 1.40 (bs, 8H, H-j,k), 1.78 (bs, 4H, H-i), 2.60 (t, J = 6 Hz, 4H, H-h), 4.60 (d, J = 6 Hz, 4H, H-e), 6.50 (bt, 2H, H-d), 7.00 (AA', J = 8 Hz, 4H, H-g), 7.35 (BB', J = 8 Hz, 4H, H-f), 7.55 (t, J = 8 Hz, 1H, H-c), 7.80 (s, 1H, H-a), 8.05 (d, J = 8 Hz, 2H, H-b); ^{13}C NMR (75 MHz, $CDCl_3$): δ = 24.90 (C-k), 28.44 (C-j), 29.25 (C-i), 34.01 (C-h), 43.88 (C-e), 122.01, 123.68, 129.46, 129.52, 130.89 (C-a,b,c,f,g), 134.69, 135.30 (quaternary C), 150.25 (*C*-OCO), 166.59 (*C*ONH), 172.29 (O*C*=O); FAB-MS: m/z 565 [M + Na], 543 [M + H], anal. calcd for $C_{32}H_{34}N_2O_6$: C 70.8, H 6.3, N 5.2; found C 70.5, H 6.0, N 5.1. The third fraction eluted was characterized as the (2 + 2) macrocycle **3** (0.091 g, 14%): m.p. 301–303 °C; ^{1}H NMR (300 MHz, [D$_6$]DMSO): δ = 1.40 (bs, 16H, H-j,k), 1.85 (bs, 8H, H-i), 2.65 (t, J = 6 Hz, 8H, H-h), 4.56 (d, J = 6 Hz, 8H, H-e), 7.17 (AA', J = 8 Hz, 8H, H-g), 7.43 (BB', J = 8 Hz, 8H, H-f), 7.65 (t, J = 8Hz, 2H, H-c), 8.00 (d, J = 8 Hz, 4H, H-b), 8.39 (s, 2H, H-a), 9.06 (bt, 4H, H-d); ^{13}C NMR (75 MHz, [D$_6$]DMSO): δ = 28.304 (C-k), 32.436 (C-j), 32.573 (C-i), 37.691 (C-h), 46.243 (C-e), 125.666, 130.248, 132.468, 132.550, 134.014 (C-a,b,c,f,g), 138.561, 141.085 (quaternary C),

153.325 (*C*-OCO), 169.879 (CONH), 175.955 (OC-O); FAB-MS: *m/z* 1107 [*M* + Na], 1085 [*M* + H]; anal. calcd for $C_{64}H_{68}N_4O_{12}$: C 70.8, H 6.3, N 5.2; found C 70.3, H 5.9, N 5.1.

Received: September 7, 1995 [Z 8373 IE]
German version: *Angew. Chem.* **1996**, *108*, 326–331

Keywords: amphiphiles · catenanes · hydrogen bonds · isomerism · supramolecular chemistry

[1] J. H. Fendler, *Membrane Mimetic Chemistry: Characterizations and Applications of Micelles, Microemulsions, Monolayers, Bilayers, Vesicles, Host Guest Systems, and Polyions*, Wiley, Chichester, **1982**.
[2] V. Degiorgio, M. Corti, *Physics of Amphiphiles - Micelles, Vesicles and Microemulsions*, North-Holland, New York, **1983**.
[3] C. Tanford, *The Hydrophobic Effect: Formation of Micelles and Biological Membranes*, 2nd ed., Wiley, New York, **1980**.
[4] E. H. Lucassen-Reynders, *Anionic Surfactants, Physical Chemistry of Surfactant Action*, (*Surfactant Sci. Ser.* **1981**, 11).
[5] *Liposomes: From Physical Structure to Therapeutic Applications* (Ed.: G. C. Knight), Elsevier, Amsterdam, **1981**.
[6] *Liposome Technology* (Ed.: G. Gregoriadis), CRC, Boca Raton, FL, **1984**.
[7] G. Schill, *Catenanes, Rotaxanes and Knots*, Academic Press, New York, **1971**
[8] J.-F. Nierengarten, C. O. Dietrich-Buchecker, J.-P. Sauvage, *J. Am. Chem. Soc.* **1994**, *116*, 375–376.
[9] D. B. Amabilino, P. R. Ashton, C. L. Brown, E. Córdova, L. A. Godinez, T. T. Goodnow, A. E. Kaifer, S. P. Newton, M. Pietraszkiewicz, D. Philp, F. M. Raymo, A. S. Reder, M. T. Rutland, A. M. Z. Slawin, N. Spencer, J. F. Stoddart, D. J. Williams, *J. Am. Chem. Soc.* **1995**, *117*, 1271–1293.
[10] C. A. Hunter, *J. Am. Chem. Soc.* **1992**, *114*, 5303–5311.
[11] F. Vögtle, S. Meier, R. Hoss *Angew. Chem.* **1992**, *104*, 1628–1631; *Angew. Chem. Int. Ed. Engl.* **1992**, *31*, 1619–1622
[12] M. J. Gunter, M. R. Johnston, *J. Chem. Soc. Chem. Commun.* **1992**, 1163–1165.
[13] M. Momenteau, F. Le Bras, B. Loock, *Tetrahedron Lett.* **1994**, *35*, 3289–3292.
[14] M. Fujita, F. Ibukuro, H. Hagihara, K. Ogura, *Nature (London)* **1994**, *367*, 720–723.
[15] Cram's original definition of a host is a molecule possessing convergent binding sites; guests contain divergent binding sites [E. P. Kyba, R. C. Helgeson, K. Madan, G. W. Gokel, T. L. Tarnowski, S. S. Moore, D. J. Cram, *J. Am. Chem. Soc.* **1977**, *99*, 2564].
[16] A. G. Johnston, D. A. Leigh, R. J. Pritchard, M. D. Deegan, *Angew. Chem.* **1995**, *107*, 1324–1327; *Angew. Chem. Int. Ed. Engl.*, **1995**, *34*, 1209–1212.
[17] A. G. Johnston, D. A. Leigh, L. Nezhat, J. P. Smart, M. D. Deegan, *Angew. Chem.* **1995**, *107*, 1327–1331; *Angew. Chem. Int. Ed. Engl.*, **1995**, *34*, 1212–1216.
[18] S. David, S. Hanessian, *Tetrahedron* **1985**, *41*, 643. For recent examples and experimental procedures from our group, see A. Glen, D. A. Leigh, R. P. Martin, J. P. Smart, A. M. Truscello, *Carbohydr. Res.* **1993**, *248*, 365–369; D. A. Leigh, R. P. Martin, J. P. Smart, A. M. Truscello, *J. Chem. Soc., Chem. Commun.* **1994**, 1373–1374; S. David, *Chemtracts: Org. Chem.* **1993**, *6*, 315–319.
[19] The necessity of the triethylamine is at first sight somewhat surprising and was originally included by mistake; however, the reaction does not proceed in the absence of the amine! The phenolic stannylene derivative **4** is less reactive than the alkoxystannylene derivatives used routinely with acid chlorides in carbohydrate chemistry and therefore the role of the triethylamine may be to activate the stannylene acetal derivative either directly, by nucleophilic attack on tin, or indirectly by liberating the stannophilic chloride ion from the acid chloride.
[20] S. Ottens-Hildebrandt, M. Nieger, K. Rissanen, J. Rouvinen, S. Meier, G. Harder, F. Vögtle, *J. Chem. Soc. Chem. Commun.* **1995**, 777–778.
[21] H. Adams, F. J. Carver, C. A. Hunter, *J. Chem. Soc. Chem. Commun.* **1995**, 809–810.
[22] The ^{1}H NMR spectra of the macrocycle **2** in $CDCl_3$ (but not [D_6]DMSO) is slightly concentration dependent due to self-association ($K_a = 0.1\ M^{-1}$); however, the shifts of all non-amide hydrogen atoms are very small ($\Delta\delta < 0.02$). All the NMR spectra reported here were carried out at 5 mM concentration)
[23] A less dramatic, but equally fascinating, example of solvent-dependent translational isomerism occurs with one of the catenanes described by Stoddart et al., and was attributed to ion solvation effects: P. R. Ashton, M. Blower, D. Philp, N. Spencer, J. F. Stoddart, M. S. Tolley, R. Ballardini, M. Ciano, V. Balzani, M. T. Gandolfi, L. Prodi, C. H. McLean, *New J. Chem.* **1993**, *17*, 689.
[24] I. O. Sutherland, *Ann. Rep. NMR Spectrosc.* **1971**, *4*, 71.
[25] Because of the symmetry of conformation **II**, the rate of rotation in [D_7]DMF was calculated by line broadening of protons passing through the macrocycle cavity rather than by the coalescence method [see J. Sandström, *Dynamic NMR Spectroscopy*, Academic Press, London, **1982**].
[26] Crystal data for **5**: $C_{64}H_{68}O_{12}N_4$, $M = 1085.26$, a clear block crystal, dimensions $0.6 \times 0.6 \times 0.58$ mm, was mounted in epoxy resin on a quartz fiber, monoclinic, space group $P2_1/n$ (no. 14), $a = 14.722(2)$, $b = 20.447(2)$, $c = 20.056(3)$ Å, $\beta = 105.17(1)^\circ$, $V = 5826(1)$ Å^3, $\rho_{calcd} = 1.24$ g cm^{-3}, $Z = 4$; 9358 reflections were measured on a Rigaku AFC7S diffractometer by using the ω-scan technique, of which 8968 were unique ($R_{int} = 0.02$), and 5720 observed ($I > 3\sigma I$, $2\theta_{max} = 120.2^\circ$, $Cu_{K\alpha}$ radiation at $T = 293.2$. The data were corrected for Lorentz and polarization effects and for absorption using DIFABS [27] ($\mu = 6.6$ cm^{-1}, min/max transmission 0.60/1.00). The structure was solved and refined on 286 variables [20.0 reflection/parameter ratio] using the teXsan crystallographic package of Molecular Structure Corporation [28]. The crystal decayed by 19.3% during data collection and a linear correction factor was applied to account for this phenomenon. Some disorder was observed in the middle region of the alkyl chains and at O65 and O66, and these could not always be separated into discrete partial occupancy carbon and oxygen atoms. All six-membered rings were refined as rigid isotropic bodies with a common *B* factor. The nitrogen, oxygen, and all other carbon atoms were refined anisotropically. All hydrogen atoms on carbon atoms were placed in idealized fixed geometries. All hydrogen atoms on nitrogen atoms were located from a ΔF map and allowed to refine. The disorder in the alkyl chains and decay leads to a fairly high agreement factor of $R = 0.197$ and $R_w = 0.210$, refined against $|F|$, with a residual electron density of 0.77 e Å^{-3}. Further details of the crystal structure investigation are available on request from the Director of the Cambridge Crystallographic Data Centre, 12 Union Road, GB-Cambridge CB2 1EZ (UK), on quoting the full journal citation.
[27] N. Walker, N. Stuart, *Acta Crystallogr.* **1983**, *A39*, 158.
[28] TeXsan: Crystal Structure Analysis Package, **1985**, Molecular Structure Corporation, 3200A Research Forest Drive, The Woodlands, TX 77381 (USA).
[29] Stabilized with amylenes not ethanol, see ref. [16].

A Chelating Triscarbene Ligand and Its Hexacarbene Iron Complex**

Ulrich Kernbach, Matthias Ramm, Peter Luger, and Wolf P. Fehlhammer*

Dedicated to Professor Henri Brunner on the occasion of his 60th birthday

Here we report on a triscarbene ligand which has the topology of Trofimenko's tris(pyrazolyl)borate,[1] and thus perfectly meets all requirements for the synthesis of novel chelate-like poly- and percarbene complexes. At the same time we present the first hexacarbene iron complex with this ligand.

The first hexacarbene complexes **1** were synthesized by us in 1985 from simple metal compounds and 2-hydroxyalkyl isocyanides, which proved to be a highly efficient approach to homoleptic carbene complexes.[2] The easy access mainly to tetrakis(oxazolidin-2-ylidene) complexes of the nickel triad[3] and their straightforward handling prompted us to study the reactivity of the coordinated ligand. Here, a particularly attractive goal was the linking together of ligands to form C-porphyrin-type systems and C cages (from hexacarbene moieties), that is, possibly highly stable materials with interesting properties. Unfortu-

[*] Prof. Dr. W. P. Fehlhammer
Deutsches Museum
D-80306 München (Germany)
Fax: Int. code +(89)2179-425
e-mail: KDQ01AF@SUNMAIL.LRZ-MUENCHEN.DE
Dr. U. Kernbach
Institut für Anorganische und Analytische Chemie der Freien Universität
Fabeckstrasse 34-36, D-14195 Berlin (Germany)
Prof. Dr. P. Luger, Dr. M. Ramm
Institut für Kristallographie der Freien Universität
Takustrasse 3, D-14195 Berlin (Germany)

[**] Homoleptic Carbene Complexes, Part 7. This work has been supported by the Deutsche Forschungsgemeinschaft, the Fonds der Chemischen Industrie, and the Bundesministerium für Bildung und Wissenschaft (Graduiertenkolleg "Synthese und Strukturaufklärung niedermolekularer Verbindungen"). Part 6: ref. [6].

nately, all experiments in this direction were unsuccessful which we attributed to the "wrong" conformation found in all structures of the five-membered heterocycles. These were arranged almost perpendicular with respect to the coordination plane of the metal. It is for the same reason, presumably, that even the precursor complex **2** is unable to react in the desired fashion.[4] As regards functionality and reactivity, **2** appeared particularly predisposed to an eightfold(!) ring closure to give **3**. In contrast, both the classical addition of amines (here of diamines) to isocyanide ligands and the deprotonation of bisimidazolium salts in the presence of palladium iodide turn out to be feasible routes at least to the first chelating percarbene complexes **4** and **5**, respectively.[5, 6]

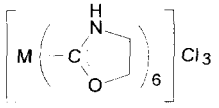

1
(M = Co^{III}, Rh^{III})

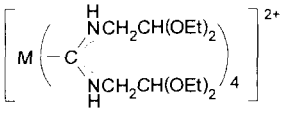

2
(M = Pd^{II}, Pt^{II})

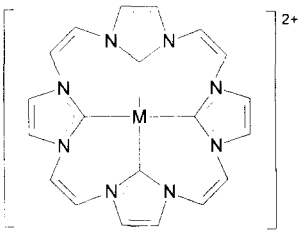

3
(M = Pd^{II}, Pt^{II})

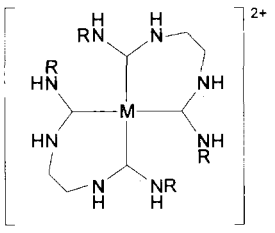

4
(M = Pd^{II}, Pt^{II})

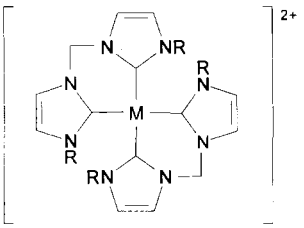

5
(M = Pd^{II}, R = Me, Et)

By an extension of the latter approach, that is by trialkylation of tris(imidazolyl)borate to give **6** followed by deprotonation with *n*BuLi, coordination to Fe^{2+}, and precipitation with tetraphenylborate, we have now obtained the bis(tricarbene)iron complex **7** [Eq. (a)] (see Experimental Procedure). As in the case of complexes **5** no efforts were made to isolate the intermediate free tricarbene.[7]

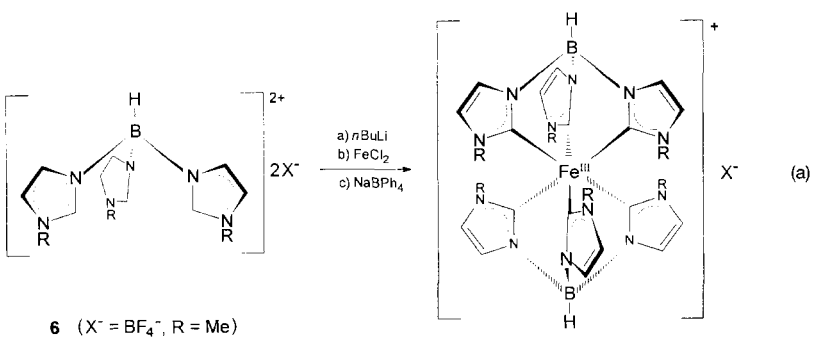

6 (X^- = BF_4^-, R = Me)

7 (X^- = BPh_4^-)

(a)

Surprisingly, the red solid that crystallized from the red solution is a saltlike substance with a complex cation, thus indicating the presence of an iron(III) compound. This is unequivocally confirmed by the magnetic moment which shows the expected value for a low-spin d^5 system.[8] At present it is still unclear when and how the oxidation occurred. After the reaction an iron(III) content of 2.6 wt% was determined in the iron(II) starting material, an amount which, of course, cannot explain the 25% yield of **7**.

Nevertheless, the stability of the organometallic 17-electron species is really astonishing, particularly in view of the reducing character of the reaction mixture. This might be explained, however, by the extraordinary donor abilities of diheteroatom-stabilized carbene ligands which clearly favor higher valent metals for bonding.[2] Closely related findings are, for example, the isolation of the "purely open-chain" hexakis(2-hydroxyethyl isocyanide)iron(II) complex $[Fe^{II}(CNCH_2CH_2OH)_6][BPh_4]_2$[9] and the noncyclization of the 2-hydroxyethyl isocyanide ligands in the product resulting from $H_4[Fe(CN)_6]$ and ethylene oxide, namely $[Fe^{II}(CN)_2(CNCH_2CH_2OH)_4]$[10], that is the nonexistence of a polycarbene iron(II) species.[11] Though as yet, no corresponding iron(III) complex is known either.

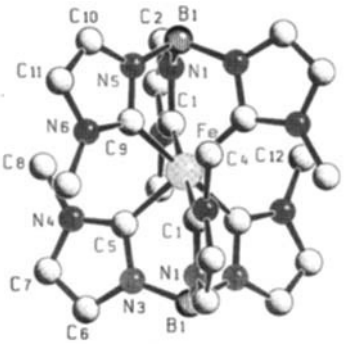

Fig. 1 SCHAKAL drawing of a complex cation of **7** in the crystal. Selected bond lengths [Å] and angles [°]: Fe1–C1 1.987(3), Fe1–C5 1.975(3), Fe1–C9 1.988(4), N1–C1 1.352(3), N1–C2 1.383(4), N1–B1 1.547(4), N2–C1 1.369(3), N2–C3 1.383(4), N2–C4 1.459(4), C2–C3 1.335(4); C5-Fe1-C1 92.22(11), C5-Fe1-C9 87.09(13), C1-Fe1-C9 87.08(14), C1-N1-C2 110.6(2), C1-N1-B1 119.2(3), C2-N1-B1 130.1(3), C1-N2-C3 110.4(2), C1-N2-C4 126.7(3), C3-N2-C4 122.9(3), N1-C1-N2 104.6(2), N1-C1-Fe1 120.4(2), N2-C1-Fe1 135.0(2), C3-C2-N1 107.5(3), C2-C3-N2 106.9(3).

Fig. 2. The highly symmetric (S_6) hexacarbene iron cation of **7** as viewed along the B-Fe-B axis.

The X-ray crystal structure analysis of **7**[12] shows an iron atom which is spherically surrounded by six five-membered heterocycles and is common to six six-membered metallacycles, thereby achieving the same highly symmetric *quasi* cage structure as in numerous bis[hydridotris(pyrazolyl)borato]metal complexes (Figs. 1 and 2).[1] The average Fe–C distance (1.984 Å) as taken from the two crystallographically independent complex cations[13] is greater than the Fe^{III}–N bond lengths of the isomeric bis[hydridotris(3,5-dimethyl-1-pyrazolyl)borato]iron(III) PF_6^- (1.964 Å) and $TCNQ^-$ salts (1.966 Å; TCNQ = 7,7,8,8-tetracyano-*p*-quinodimethane)[14] by a little less than the difference between the atomic radii, $r(N_{sp^2}) - r(C_{sp^2})$,[15] which points to very similar bonding situations without metal–ligand multiple bonds. This was certainly to be expected, since

according to the Fe–C(carbene) bond lengths in **8** (2.007(5) Å) and **9** (1.951(10) Å)[16] even in Fe^0-carbene complexes "in case of CO competition" there is no appreciable back donation to the *N,N'*-carbene ligand.

$[Fe(CO)_4\{\overline{CN(Me)CHCHNMe}\}]$ **8**

$[Fe(CO)_3\{\overline{CN(Me)CHCHNMe}\}(PEt_3)]$ **9**

Finally, a comparison of the bonding parameters within the different five-membered heterocycles of the two types of tripod ligands, tris(pyrazolyl)borate and tris(imidazolin-2-ylidene)-borate, is quite informative. While the bond lengths in the pyrazole rings vary very little (1.37 ± 0.02 Å) in spite of the presence of three different combinations of elements (NN, CN, CC), the carbenoid imidazole, as already reported a number of times, exhibits a tendency to break up into two more or less localized π systems that are characterized by short C(carbene)–N bonds (av 1.358 Å) and a C–C double bond (1.332 Å) loosely tied together by two longer C–N bonds (1.383 Å).[5, 6, 17] This structural phenomenon which frequently is even more pronounced has been described by us as "activation of heterocycles"; in fact, recently we have discovered a chemical consequence thereof—the epoxidation of the isolated C–C double bond of carbenoid 4-aminoimidazoles on their oxidative removal from the metal with $KMnO_4/Fe^{3+}$.[18]

The straightforward synthesis, the great similarity to cyclopentadienyl, and the evident stability of its metal complexes are sufficient to predict a brilliant future for the tridentate *C,C',C''* ligand and its organometallic and coordination chemistry. Judging from the recent extremely positive experiences with the "Arduengo carbenes"[19] we are convinced that its application particularly in homogeneous catalysis, for example in the place of triphosphanes, will open new opportunities.

Experimental Procedure

6: Trimethyloxonium tetrafluoroborate (2.25 g, 15.24 mmol) was added to a suspension of potassium hydridotris(imidazolyl)borate (1.28 g, 5.08 mmol) [20] in dichloromethane (50 mL) at 0 °C. The mixture was then stirred for 24 h at 25 °C after which time the solid was filtered off and washed several times with small amounts of ethanol followed by diethyl ether. After the mixture had been dried in high vacuum, **6** (1.55 g, 71%) was obtained as a colorless hygroscopic powder. ^1H NMR (250 MHz, [D$_6$]DMSO, 25 °C, TMS): δ = 3.80 (s, 3H, Me), 7.55 (s, 1H, CH), 7.75 (s, 1H, CH), 8.80 (s, 1H, CH); ^{13}C NMR (62 MHz, [D$_6$]DMSO): δ = 35.3, 123.1, 124.6, 139.4; IR (KBr): $\tilde{\nu}$ = 3075, 2487, 1570, 1271, 1033 cm^{-1}; MS (FAB (positive ion), Xe, DMSO, 3-nitrobenzyl alcohol): *m/z* (%) = 345 (100) [$M^+ - BF_4^-$], 257 (66) [$M^+ - 2BF_4^- - H^+$]; elemental analysis: calcd. (for $C_{12}H_{19}B_3F_8N_6$): C 33.32, H 4.43, N 19.44; found C 31.20, H 4.65, N 18.01%.

7: A solution of *n*BuLi in hexane (1.60 M, 6.02 mL, 9.63 mmol) was added to a suspension of **6** (1.39 g, 3.21 mmol) in THF (100 mL) at −78 °C under argon. After the reaction mixture had been stirred for 30 min at 0 °C, it was again cooled to −78 °C, and anhydrous $FeCl_2$ (0.20 g, 1.60 mmol; Fluka) was added. The suspension was allowed to warm to room temperature and stirred for another 24 h during which time the color changed from a greenish gray to bright red. The red solid was collected on a D4 frit, washed with small portions of THF and diethyl ether, and dissolved in methanol (20 mL). On addition of a saturated solution (5 mL) of sodium tetraphenylborate in methanol, the bordeaux-red complex salt **7** (0.35 g, 25%) precipitated immediately, which was recrystallized from dichloromethane. M.p. 305–307 °C (decomp.); IR (KBr): $\tilde{\nu}$ = 3122, 3053, 2983, 2945, 2463, 1197, 731, 705 cm^{-1}; MS (FAB (positive ion), Xe, DMSO, 3-nitrobenzyl alcohol): *m/z* (%) = 566 (100) [Fe(C-tripod)$_2^+$], 311 (43) [Fe(C-tripod)$^+$]; elemental analysis: calcd. (for $C_{48}H_{52}B_3FeN_{12}$): C 65.05, H 5.92, N 18.98; found C 63.91, H 5.89, N 18.35%. No further defined compound has been obtained from a work-up of the red filtrate by concentration and column chromatography.

Received: July 10, 1995 [Z 8187 IE]
German version: *Angew. Chem.* **1996**, *108*, 333–335

Keywords: carbene complexes · iron compounds · triscarbene chelate ligands

[1] S. Trofimenko, *Prog. Inorg. Chem.* **1986**, *34*, 115.
[2] U. Plaia, H. Stolzenberg, W. P. Fehlhammer, *J. Am. Chem. Soc.* **1985**, *107*, 2171–2172.
[3] a) K. Bartel, W. P. Fehlhammer, *Angew. Chem.* **1974**, *86*, 588–589; *Angew. Chem. Int. Ed. Engl.* **1974**, *13*, 599–600; b) W. P. Fehlhammer, K. Bartel, U. Plaia, A. Völkl, A. T. Liu, *Chem. Ber.* **1985**, *118*, 2235–2254.
[4] T. Bliss, *PhD Thesis*, Freie Universität Berlin, **1991**.
[5] W. P. Fehlhammer, T. Bliss, W. Sperber, J. Fuchs, *Z. Naturforsch. B* **1994**, *49*, 494–500.
[6] W. P. Fehlhammer, T. Bliss, U. Kernbach, I. Brüdgam, *J. Organomet. Chem.* **1995**, *490*, 149–153.
[7] A stable tricarbene consisting of a benzene ring carrying three (imidazol-2-ylidene-1-yl)methyl functions has recently been described: H. V. R. Dias, W. Jin, *Tetrahedron Lett.* **1994**, *35*, 1365–1366.
[8] Magnetic moment μ(298.3 K) = 2.086 μ_B. We thank Dr. Frank Hintermaier (research group of Prof. W. Beck, Universität München) for the measurements.
[9] U. Plaia, *PhD Thesis*, Freie Universität Berlin, **1986**.
[10] In contrast, most other cyano complexes such as $[Pt(CN)_4]^{2-}$ or $[Au(CN)_2]^-$ give rise to the corresponding oxazolidin-2-ylidene(carbene) species: W. Weigand, U. Nagel, W. Beck, *Z. Naturforsch. B* **1988**, *43*, 328.
[11] The coexistence in **A** of all three forms of 2-hydroxyisocyanide, the cyclic

$[Fe^{II}Cp(\overline{CNC_6H_4\text{-}2\text{-}O})(CNC_6H_4\text{-}2\text{-}OH)(\overline{CN(H)C_6H_4\text{-}2\text{-}O})]$ **A**

carbenoid, the carbanionic, and the "open-chain" form, is a beautiful demonstration of how a ligand sphere seeks to adjust to the electronic situation about a metal: F. E. Hahn, M. Tamm, *J. Chem. Soc. Chem. Commun.* **1995**, 569.
[12] X-ray structure analysis of **7**: $C_{48}H_{52}B_3FeN_{12}$, M = 885.4; a = 19.336(3), b = 21.878(2), c = 10.823(2) Å, β = 90.31(1)°, V = 4578.4(1) Å^3, Z = 4, ρ_{calcd} = 1.284 g cm^{-3}, μ = 3.081 mm^{-1}, monoclinic, space group $P2_1/a$ (No. 14), STOE-AED diffractometer, $Cu_{K\alpha}$ (λ = 1.54178 Å), ω-2θ scan, total number of reflections 9721, 4666 of which were independent and 3386 observed [$F > 4\sigma(F)$], direct methods, refinement with F^2 [21], 789 refined parameters, R = 0.0325, wR_2 = 0.0853 (all data), H atoms refined isotropically, residual electron densities 0.243 (−0.169) e Å^{-3}, SCHAKAL 92 [22]. Further details of the crystal structure investigation may be obtained from the Fachinformationszentrum Karlsruhe, D-76344 Eggenstein-Leopoldshafen (Germany), on quoting the depository number CSD-401749.
[13] In the crystal structure, the Fe atoms occupy special positions on the centers of symmetry at (1/2,0,0) and (1/2,1/2,0). Half a complex cation each on (1/2,0,0) and (1/2,1/2,0) together with the anion residing on a general position form the asymmetric unit. The structural parameters of the two crystallographically independent hexacarbene complex cations differ only marginally.
[14] S. J. Mason, C. M. Hill, V. J. Murphy, D. O'Hare, D. J. Watkin, *J. Organomet. Chem.* **1995**, *485*, 165–171.
[15] Atomic radii: C_{sp^2} = 0.667 Å, N_{sp^2} = 0.62 Å. L. Pauling, *The Nature of the Chemical Bond*, 3rd ed. Cornell University Press, Ithaca, New York, **1960**.
[16] a) G. Huttner, W. Gartzke, *Chem. Ber.* **1972**, *105*, 2714; b) P. B. Hitchcock, M. F. Lappert, S. A. Thomas, A. J. Thorne, A. J. Carty, N. J. Taylor, *J. Organomet. Chem.* **1986**, *315*, 27.
[17] W. P. Fehlhammer, T. Bliss, J. Fuchs, G. Holzmann, *Z. Naturforsch. B* **1992**, *47*, 79.
[18] D. Rieger, S. D. Lotz, U. Kernbach, C. André, J. Bertran-Nadal, W. P. Fehlhammer, *J. Organomet. Chem.* **1995**, *491*, 135.
[19] a) W. A. Herrmann, K. Öfele, M. Elison, F. E. Kühn, P. W. Roesky, *J. Organomet. Chem.* **1994**, *480*, C7; b) W. A. Herrmann, personal communication.
[20] S. A. A. Zaidi, T. A. Kahn, S. R. A. Zaidi, Z. A. Siddiqi, *Polyhedron* **1985**, *7*, 1163.
[21] G. M. Sheldrick, SHELXL 93, A Program for Crystal Structure Determination, Göttingen, **1993**.
[22] E. Keller, SCHAKAL 92, Universität Freiburg, **1993**.

Synthesis, Structure, and Reactivity of a 2,3,4-Triphosphapentadienide**

Vera Thelen, Dietmar Schmidt, Martin Nieger, Edgar Niecke,* and Wolfgang W. Schoeller

Dedicated to Professor Ralf Appel on the occasion of this 75th birthday

Pentadienides **I**, which, as a result of their different configurations (W, U, S form) and modes of coordination (η^1, η^3, η^5 coordination) have proven to be versatile ligands for d- and f-block metals,[1] have recently attracted interest as π ligands for metals of the s-block.[2] In the context of our work on phosphaallylic anions[3] we became interested in the corresponding vinylogous heteroallylic systems (phospha- and polyphosphapentadienides **II**) about which little is known.[4] Their corresponding cyclic analogues (phospha- and polyphosphacyclopentadienides **III**) are known for their manifold coordination chemistry[6] (σ and π coordination) and are of interest as building blocks for P/C cage compounds.[7] Here we report on the synthesis and structural elucidation of the first lithium salt of a 2,3,4-triphosphapentadienide (**IV**) as well as on the consecutive reactions of this species.

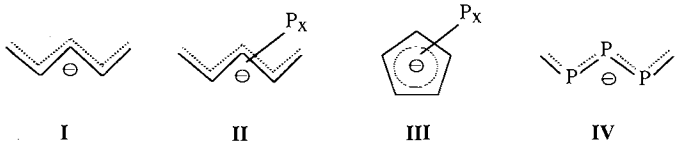

I **II** **III** **IV**

Treatment of the chloromethylenephosphane[8] **1** with two equivalents[9] of lithium bis(trimethylsilyl)phosphanide[10] **2** in DME, led to the lithium salt of the 1,2-diphosphapropenide[11] **3**, which was isolated as a microcrystalline solid. Subsequent reaction of **3** with chloromethylenephosphane **1** proceeded by elimination of trimethylchlorosilane and formation of the lithium salt of the persilylated 2,3,4-triphosphapentadienide **4** · Li(dme)$_3$, suitable crystals of which were obtained for an X-ray structural analysis.[12] The structure determination shows **4** as a discrete anion in the crystal; the shortest contact between the lithium atom, which is coordinated in a distorted octahedral fashion by three dme solvent molecules, and the phosphorus atom P(2) is 620 pm. The anion adopts a W geometry with crystallographic C_s symmetry, as has been established for a variety of pentadienides[1] (Fig. 1). The all-*trans* arrangement of the lone pairs at the phosphorus atoms is energetically most favorable. The atoms of the Si_2C-P-P-P-CSi_2 skeleton are nearly in one plane (average deviation from the best plane: 3.1 pm). Hence, they span a delocalized five-center/six-electron pπ electron system. The large differences in the valence angles at the two-coordinate phosphorus centers are unusual (P(2): 88.3(1)° vs. P(1/3): 113.6(1)°. Associated with this are comparably long P–P distances (213.7(1) pm), which are compensated by a contraction of the P–C bonds (168.7(3) pm).

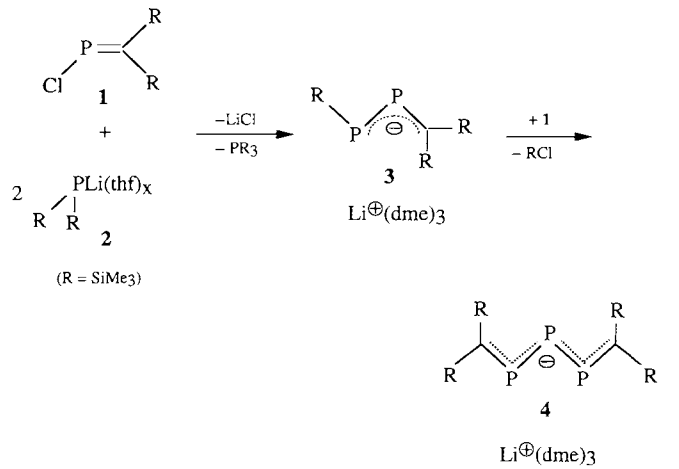

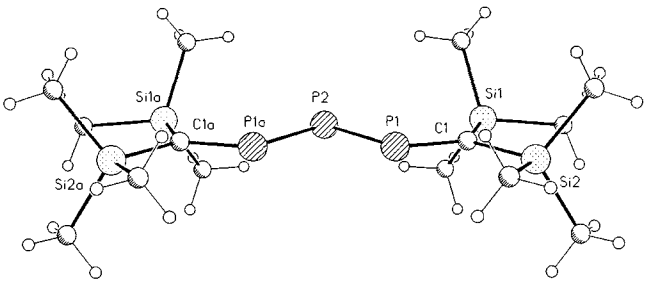

Fig. 1. Structure of the anion **4**. Selected bond lengths [pm] and angles [°]: P1-P2 213.7(1), P1-C1 168.7(3), C1-Si1 185.3(3), C1-Si2 185.8(3); P1-P2-P1a 88.3(1), C1-P1-P2 113.6(1), P1-C1-Si1 126.6(2), P1-C1-Si2 112.6(2), Si1-C1-Si2 120.9(2).

The results of an ab initio calculation[14] on the model system, $[(H_3Si)_2CPPPC(SiH_3)_2]^-$ **V** are in agreement, with respect to the P–C and P–P distances, with those determined experimentally for **4**. On the other hand, the calculated P-P-P angle is wider than the one found in **4** (Fig. 2). According to a vibrational analysis, the structure is highly flexible. On this basis, deviations from the experimentally determined structure can be attributed to steric hindrance. A NBO analysis on the parent system **V**[16] reveals the expected density distribution for the π-space to be most strongly pronounced at the positions 1, 3, and 5. The stabilizing effect of the silyl substituents (Fig. 2) is indicated by the energy of the HOMO (π_3, b_1 in C_{2v}) which is lower than that of the parent system $[H_2CPPPCH_2]^-$.[17]

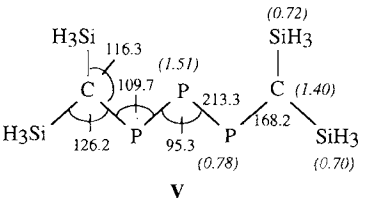

V

Fig. 2. Calculated [6-31 + G*] π-electron density for 1,1,5,5-tetrasilyl-2,3,4-triphosphapentadienide **V**.

The observed multiplet structure of the resonance signals in the ^{31}P NMR spectrum of **4** (δ = 494.1(d), 295.5(t); J(P, P) = 430 Hz) indicates the preference of the W geometry in solution as well. Diagnostic criteria for the constitution of **3** are the significant ^{31}P and ^{13}C NMR data [^{31}P NMR: δ = 86.1, 510.8; ^1J(P, P) = 487 Hz); ^{13}C NMR: δ = 137.6 (dd, ^1J(C, P) = 97.6 Hz, ^2J(C, P) = 4.6 Hz)]. The *cis* position of the P-bound trimethylsilyl group with respect to the lone pair at the central phosphorus atom is evidenced by the large value of ^3J(P, C) = 18.6 Hz.

[*] Prof. Dr. E. Niecke, Dipl.-Chem. V. Thelen, Dr. D. Schmidt, Dr. M. Nieger
Anorganisch-chemisches Institut der Universität
Gerhard-Domagk-Strasse 1, D-53121 Bonn (Germany)
Fax: Int. code + (228)73-5327
Prof. Dr. W. W. Schoeller
Fakultät für Chemie der Universität Bielefeld (Germany)

[**] This work was supported by the Deutsche Forschungsgemeinschaft and the Fonds der Chemischen Industrie.

The lithium salt of the heteropentadienide anion **4** is remarkably stable in DME solution; however, above 100 °C, it rearranges to the corresponding salt of the 1,2,4-triphospholenide **6**, which was characterized by its NMR data [^{31}P NMR: $\delta = -71$ (d), 377 (t), $^2J(P,P) = 15.3$ Hz; ^{13}C NMR: $\delta = 94.1$ (m)]. Decomposition of **4** into the trimethylsilylphosphaalkyne[16] **5** and the 1,2-diphosphaallylanion **3** appeared plausible as a primary step of this "rearrangement". Subsequent [2+3]cycloaddition of **3** and **5**, followed by silyl group migration yields **6**.[18] The formation of **6** from **3** and **5** is comparable to that of the dihydrophospholyl system from 1-phosphaallyl anions and alkynes.[3b] In the presence of air the heterocyclic anion **6** was transformed to the 1,2,4-triphospholide **7**[19] by removal of the two trimethylsilyl groups at the phosphorus atoms. The lithium salt of **7** was isolated as a yellow, crystalline solid. The formation of three two-coordinate phosphorus centers in **7** is evidenced by the low-field shift of all ^{31}P NMR signals [$\delta = 313$ (t), 328 (d), $^2J(P,P) = 31.8$ Hz], a diagnostic tool for polyphospholid ions.[6].

Unexpectedly in the presence of traces of moisture the thermolysis of **4** yields the 1,2,3-triphosphabicyclo[1.1.0]butane **9**, which probably forms from a valence isomerization of the 1,2,3-triphosphabutadiene intermediate **8**. The bicyclic structure of compound **9** follows from the characteristic[20] ^{31}P NMR data of this class of compounds [$\delta = -72.5$ (t), -263.5 (dd), $^1J(P,P) = 179.3$ Hz].

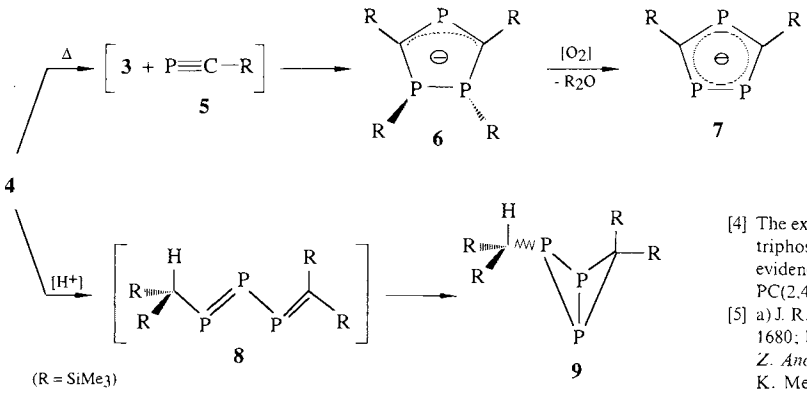

Experimental Procedure

3: A solution of $LiP(SiMe_3)_2 \cdot 1.8$ THF (1.56 g, 5 mmol) in DME (10 mL) was added to a stirred and cooled (−40 °C) solution of $ClP{=}C(SiMe_3)_2$ (0.56 g, 2.5 mmol) in DME (5 mL). After the solution was allowed to warm up to 25 °C the volatiles were removed under vacuum and the residue was taken up in benzene (20 mL). The solution was filtered, the solvent removed, and the residue dried under vacuum. Yield: 76%; m.p. 35–37 °C. $^{31}P\{^1H\}$ NMR (121.5 MHz, DME): $\delta = 86.1$ (d), 510.8 (d, $^1J(P,P) = 487$ Hz). ^{1}H NMR (300 MHz, C_6D_6): $\delta = 0.72$ (s, 9H, $CSiMe_3$-*exo*); 0.76 (s, 9H, $CSiMe_3$-*endo*); 0.95 (s, 9H, $PSiMe_3$). ^{13}C NMR (75.5 MHz, C_6D_6): $\delta = 4.9$ (d, $^3J(C,P) = 13.7$ Hz, $PCSiC_3$-*exo*), 8.7 (d, $^3J(C,P) = 10.3$ Hz, $PCSiC_3$-*endo*), 6.2 (m, $|^2J(C,P) + {}^3J(C,P)| = 18.6$ Hz, $PPSiC_3$). 137.6 (dd, $^1J(C,P) = 97.6$, $^2J(C,P) = 4.6$ Hz, PPC).

4: A solution of **1** (0.62 g, 2.5 mmol) in DME (8 mL) was added dropwise to a solution of **3** (2.5 mmol) in DME (10 mL) at −78 °C. The reaction mixture was allowed to warm up to 20 °C and stirred, the volatiles were removed under vacuum, and the residue was taken up in a small amount of DME. Compound **4** crystallized from the concentrated solution at −25 °C as deep red prismlike crystals. Yield: 58%. Concentration of the mother liquor and crystallization afforded further pure product. $^{31}P\{^1H\}$ NMR (121.5 MHz, DME): $\delta = 494.1$ (d), 295.5 (t, $^1J(P,P) = 430.1$ Hz); ^{1}H NMR (300 MHz, ext. ref., DME): $\delta = 0.4$ (s, 9H, $CSiMe_3$), 0.5 (s, 9H, $CSiMe_3$). ^{13}C NMR (75.5 MHz, ext. ref., DME): $\delta = 2.3$ (d, $^3J(C,P) = 9.9$ Hz, $PCSiC_3$), 3.0 (m), $|^3J(C,P) + {}^4J(C,P)| = 12.5$ Hz, $PPCSiC_3$), 156.8 (m, X part of a ABB'X spin system: $^2J(C,P) = 4.5$ Hz; $|^1J(C,P) + {}^3J(C,P)| = 60.3$ Hz. MS (EI, 70 eV): *m/z* (%): $[M^+ + H]$ 410(3), $[M^+ + H - SiMe_3]$ 377(2.6), $[PPCSiMe_3]^+$ 147 (15), $[SiMe_3]^+$ 73(100).

6: A solution of **4** (2 mmol) in DME was heated to reflux for 2 h at 100 °C, during which the reaction mixture changed color from deep red to violet. The volatiles were removed under vacuum at 25 °C to afford **6** as a red-violet oil. ^{31}P NMR (121.5 MHz, DME): $\delta = -71$ (d); 377 (t) ($^2J(P,P) = 15.3$ Hz). ^{1}H NMR (300 MHz, ext. ref., DME): $\delta = 0.4$ (s), 0.5 (s) ($SiMe_3$). ^{13}C NMR (75.5 MHz, ext. ref., DME): $\delta = 0.1$ (m, $|^2J(C,P) + {}^3J(C,P)| = 15.2$ Hz, $PPCSiC_3$), 5.4 (dd, $^3J_{CP} = 4.6$, 1.5 Hz, $PPCSiC_3$), 94.1 (m, X part of an AMM'X spin system: $^1J(C,P_A) = 70$ Hz, $|^1J(C,P_M) + {}^2J(C,P_{M'})| = 61.8$ Hz). MS (EI, 20 eV): *m/z*: (%): $[M^+ + H]$ 410(4), $[M^+ - 2\,SiMe_3 + H]$ 265(5), $[M^+ - PC(SiMe_3)_2]$ 221(6), $[PPCSiMe_3]^+$ 147(21), $[SiMe_3]^+$ 73(100).

7: A solution of **4** was stirred at room temperature in an open atmosphere under exclusion of moisture for 24 h, during which the solution changed color from red-violet to yellow. The volatiles were removed under vacuum and the residue was washed several times with *n*-pentane. In this way **7** was obtained as a microcrystalline solid. Yield: 72%. $^{31}P\{^1H\}$ NMR (121.5 MHz, DME): $\delta = 313$ (t), 328 (d), ($^2J(P,P) = 31.8$ Hz). ^{13}C NMR (75.5 MHz, C_6D_6): $\delta = 179.1$ (m, X part of an ABB'X spin system: $^1J(C,P_A) = 77.8$ Hz, $|^1J(C,P_B) + {}^2J(C,P_{B'})| = 51.5$ Hz), 5.4 (m, SiC_3). MS (EI, 70 eV): *m/z*: (%): $[M^+ + H]$ 264(2), $[M^+ - PC(SiMe_3)_2]$ 221(2), $[PPCSiMe_3]^+$ 147(52), $[SiMe_3]^+$ 73(100).

9: A solution of **2** in DME, containing traces of moisture, was heated for 2 h at 100 °C, during which time the solution changed color from deep red to pale yellow. After removing the solvent under vacuum **9** remained as a yellow oil. ^{31}P NMR (121.5 MHz, C_6D_6): $\delta = -72.5$ (t), -263.5 (dd); $^1J(P,P) = 179.3$ Hz; $^2J(P,H) = 9$ Hz. MS (EI, 70 eV): *m/z* (%): $[M^+]$ 410(21), $[M^+ - P_2]$ 348(28), $[M^+ - PC(SiMe_3)_2]$ 221 (33), $[PPCSiMe_3]^+$ 147(52), $[SiMe_3]^+$ 73(100).

Received: September 18, 1995 [Z 8407 IE]
German version: *Angew. Chem.* **1996**, *108*, 354–356

Keywords: heterocycles · pentadienides · phosphorus compounds · triphosphapentadienides

[1] Review: P. Powell, *Adv. Organomet. Chem.* **1986**, *26*, 125–164.
[2] T. P. Hanusa, J. S. Overby, *Angew. Chem.* **1994**, *106*, 2300–2303; *Angew. Chem. Int. Ed. Engl.* **1994**, *33*, 2191–2193. See also: D. Stalke, *ibid.* **1994**, *106*, 2256–2259; **1994**, *33*, 2220–2222.
[3] a) E. Niecke, M. Nieger, P. Wenderoth, *J. Am. Chem. Soc.* **1993**, *115*, 6989–6990; b) *Angew. Chem.* **1994**, *106*, 362–363; *Angew. Chem. Int. Ed. Engl.* **1994**, *33*, 353–354; c) *ibid.* **1994**, *106*, 2045–2046 and **1994**, *33*, 1945–1947; d) K. Paasch, M. Nieger, P. Wenderoth, E. Niecke, unpublished results.
[4] The existence of a free 1-phosphapentadienide [5a]; 1,3-diphospha- and 1,3,5-triphosphapentadienide [5b] had been based on ^{31}P NMR spectroscopic evidence only. A stable 1,2,4-triphosphapentadienide, $[Me_3Si\text{-}PPC(Mes)\text{-}PC(2,4,6\text{-}Me_3C_6H_2SiMe_3]^-$, is known [5c].
[5] a) J. R. Bleeke, A. M. Rohde, K. D. Robinson, *Organometallics* **1995**, *14*, 1674–1680; b) R. Appel, P. Fölling, B. Josten, W. Schuhn, H. V. Wenzel, F. Knoch, *Z. Anorg. Allg. Chem.* **1988**, *556*, 7–22; c) G. Becker, G. Ditten, K. Hübler, K. Merz, M. Niemeyer, N. Seidler, M. Westermann, "The Function of the Trimethylsilyl Substituent in the Synthesis of Low-valent Phosphorus and Arsenic Containing Compounds" in *Organosilicon Chemistry II* (Eds.: N. Auner, J. Weis), VCH, Weinheim, **1996**, pp. 161–186.
[6] F. Mathey, *Coord. Chem. Rev.* **1994**, *137*, 1–552, and references therein; N. Maigrot, N. Avarvari, C. Charrier, F. Mathey, *Angew. Chem.* **1995**, *107*, 623–624; *Angew. Chem. Int. Ed. Engl.* **1995**, *34*, 590–592.
[7] a) R. Bartsch, P. B. Hitchcock, J. F. Nixon, *J. Chem. Soc. Chem. Commun.* **1989**, 1046–1048; b) *J. Organomet. Chem.* **1989**, *373*, C31.
[8] R. Appel, A. Westerhaus, *Tetrahedron Lett.* **1981**, *22*, 2159–2160.
[9] Treatment of **1** and **2** in the molar ratio 1:1 led to the fully silylated 1,2-diphosphapropene, $(Me_3Si)_2P{-}P{=}C(SiMe_3)_2$ [ruby-red crystals, yield: 85%, m.p. 26–28 °C. $\delta(^{31}P) = 434$, -134.5, $J(P,P) = 237$ Hz)].
[10] G. Fritz, J. Z. Härer, *Z. Anorg. Allg. Chem.* **1981**, *481*, 185–200.
[11] A 1,2-diphosphapropenide, $[Me_3Si\text{-}PPC(Ph)SiMe_3]^-$, was first obtained in the reaction of **1** and ethyl benzoate [5c].
[12] X-ray structure analysis of **4** · Li(dme)$_3$: $[C_{14}H_{36}P_3Si_4]$ $[Li(dme)_3]^+$: red crystals, crystal dimensions $0.28 \times 0.40 \times 0.45$ mm: $M = 687.0$; orthorhombic, space group *Pnma* (No. 62), $a = 15.411(1)$, $b = 20.003(2)$, $c = 12.249(3)$ Å, $V = 4342(1)$ Å^3, $Z = 4$, $\mu(Cu_{K\alpha}) = 2.55$ mm^{-1}; $T = 208$ K, $F(000) = 1496$. 4288 reflections up to $\theta_{max.} = 140°$ were collected on an Enraf-Nonius CAD4 diffractometer with $Cu_{K\alpha}$ radiation, of these 4208 were independent and used for the calculations. The structure was solved by direct methods and refined on F^2 anisotropic; the H atoms were refined with a riding model (program SHELXL-93 [12]). The final quality factor $wR^2(F^2)$ was 0.188, with a conventional $R(F) = 0.064$ for 231 parameters. An absorption correction based on Ψ scans and an extinction correction were carried out. Two DME molecules are disordered. Further details of the crystal structure investigations may be obtained from the Fachinformationszentrum Karlsruhe, D-76344 Eggenstein-Leopoldshafen (Germany), on quoting the depository number CSD-404621.

[13] G. M. Sheldrick, SHELXL-93, University of Göttingen, **1993**.
[14] All calculations were carried out with the Gaussian 92/DTF program (Revision G3) [15].
[15] M. J. Frisch, G. W. Trucks, H. B. Schlegel, P. M. W. Gill, B. G. Johnson, M. W. Wong, J. B. Foresman, M. A. Robb, M. Head-Gordon, E. S. Replogle, R. Gomperts, J. L. Andres, K. Raghavachari, J. S. Binkley, C. Gonzalez, R. L. Martin, D. J. Fox, D. J. Defrees, J. Baker, J. J. P. Stewart, J. A. Pople, Gaussian Inc., Pittsburgh, PA, USA, **1993**.
[16] A. F. Reed, L. A. Curtiss, F. Weinhold, *Chem. Rev.* **1988**, *88*, 899. 6-31+G* basis set with diffuse functions: T. Clark, J. Chandrasekhar, G. W. Spitznagel, P. von R. Schleyer, *J. Comput. Chem.* **1983**, *4*, 294; M. J. Frisch, J. A. Pople, J. S. Binkley, *J. Chem. Phys.* **1984**, *80*, 3265.
[17] The frontier orbitals [RHF/6-31+G(d,p)] of $[H_2CPPPCH_2]^-$ and $[(H_3Si)_2CPPPC(SiH_3)_2]$ are: HOMO (π_3, b_1 in C_{2v}) −2.5 [−3.5] eV; HOMO-1 (n_3(P), a_1 in C_{2v}) −4.1 [−4.9] eV. NBO analysis of $[H_2CPPPCH_2]^-$ (π space): C (1.31), P (0.88), P (1.68 eV).
[18] a) R. Appel, A. Westerhaus, *Tetrahedron Lett.* **1981**, *22*, 2159–2160; b) G. David, E. Niecke, M. Nieger, J. Radseck, *J. Am. Chem. Soc.* **1994**, *116*, 2191–2192.
[19] A lithium 1,2,4-triphospholenide, $[Me_3SiP\text{-}P(SiMe_3)C(Ph)C(Ph)P]^-$, has been obtained by cyclization of a 1,2,4-triphosphapentadienide [5c].
[20] a) R. Appel, B. Niemann, M. Nieger, *Angew. Chem.* **1988**, *100*, 957; *Angew. Chem. Int. Ed. Engl.* **1988**, *27*, 957; b) E. Niecke, O. Altmeyer, M. Nieger, *J. Chem. Soc. Chem. Commun.* **1988**, 945–946.

Reactivity of Tungstenocene with B–B and B–H Bonds versus C–H Bonds**

John F. Hartwig* and Xiaoming He

The oxidative addition of B–H and B–B bonds of borane reagents to transition metals is a crucial step in the mechanism of metal-catalyzed borane additions to carbon–carbon multiple bonds.[1–8] An understanding of the factors controlling these addition reactions will help to determine which metal centers would be effective catalysts for such catalytic hydroboration and diboration reactions. Preferences for additions of C–H bonds rather than C–C bonds are well established and can serve as a benchmark for evaluating additions of main group hydride and element–element bonds.[9] In homogeneous systems, oxidative addition of C–H bonds is preferred over addition of unstrained C–C bonds, except in highly unusual cases.[10]

We report herein that tungstenocene, $[Cp_2W]$, which is known to readily add C–H bonds of arenes,[11] exclusively forms $[Cp_2W(Bcat')_2]$ (Cat' = 4-*t*Bu$C_6H_3O_2$) (**1**) by addition of the B–B bond of Cat'BBCat' in the presence of arene solvent when generated either thermally or photochemically, whereas catecholborane is eliminated from $[Cp_2W(H)(Bcat)]$ (**2**) under photochemical conditions to form $[Cp_2WH(Ph)]$ (**3**) in benzene as solvent. An X-ray structure of the bisboryl complex **1** showed a nondistorted structure with ligand orientations indicative of π bonding.

[*] Prof. J. F. Hartwig, Dr. X. He
Department of Chemistry, Yale University,
P. O. Box 208107, New Haven, CT 06520-8107
Fax: Int. code +(203)432-6144

[**] We are grateful for support from the National Science Foundation (CHE and NYI Award program) the donors of the Petroleum Research Fund, administered by the American Chemical Society, the Dreyfus Foundation for a New Faculty Award, DuPont for a Young Faculty Award, Union Carbide for an Innovative Recognition Award, and Yale University for a Junior Faculty Fellowship.

The reactivity of $[Cp_2W]$ with regard to borane additions and eliminations is shown in Scheme 1. Irradiation of $[Cp_2WH_2]$ (**4**) with a medium-pressure mercury arc lamp is known to generate the highly reactive intermediate $[Cp_2W]$ that reacts further to

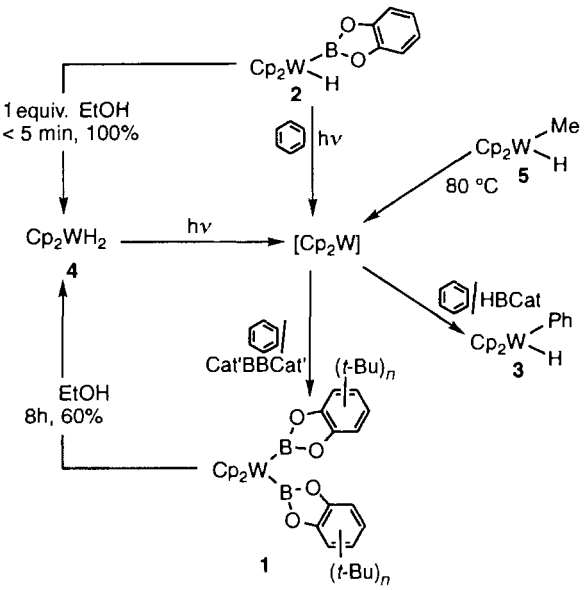

Scheme 1. Formation and reactivity of $[Cp_2W]$ and tungstenocene–boron compounds.

give the phenyl hydride **3** when benzene is used as solvent.[11] However, irradiation of **4** for 6.5 h in a benzene solution containing just one equivalent of Cat'BBCat' gave the B–B bond oxidative addition product $[Cp_2W(BCat')_2]$ (**1**) in 82% yield by ^{1}H NMR spectroscopy.[12] No phenyl hydride product **3** was formed in this reaction. Product **1** was isolated in 55% yield by concentration of the reaction solution and layering with pentane. The bisboryl compound displayed a ^{11}B NMR spectrum with a signal at $\delta = 59.3$, which is close to but slightly downfield from the $\delta = 57.2$ chemical shift of $[Cp_2WH(BCat)]$ (**2**).[13] Our data indicates that the phenyl hydride **3** is not formed as a kinetic product that would subsequently undergo photochemical conversion to diboron compound **1**, since isolated samples of **3** were stable in the presence of Cat'BBCat' under reaction conditions identical to those employed for the conversion of the **4** to **1**.

An X-ray diffraction study of **1** (Fig. 1) was conducted on a sample obtained from benzene/pentane solvent mixture. Compound **1** crystallized in the space group $P2/n$ and showed well-separated monomeric units with no intermolecular contacts.[14] The unit cell contains one benzene molecule per tungsten complex. The two boryl ligands are oriented in a fashion that allows for π bonding between the basic metal center and each electrophilic boron atom. This orientation is also observed in the boryl compound **2**.[13] Moreover, the metal–boron distances of **1** are similar to that reported for **2**, which appeared to be shortened by π bonding. Finally, the B1-W-B2 angle of 78.0(4)° in **1** is identical to the H-W-B angle in **2** and the calculated ideal angle for d^2 Cp_2ML_2 compounds.[15] A similar B-M-B angle is also found in pseudo square planar and octahedral bis boryl compounds in which the idealized angle would be 90°.[4, 16] In the case of **1**, however, the small B-W-B angle reflects the ideal angle of the metallocene system and does not contain any distortion relative to the geometry of other metallocene compounds that could be attributed to B–B interactions.

 © VCH Verlagsgesellschaft mbH, D-69451 Weinheim, 1996 0570-0833/96/3503-0315 $ 10.00+.25/0

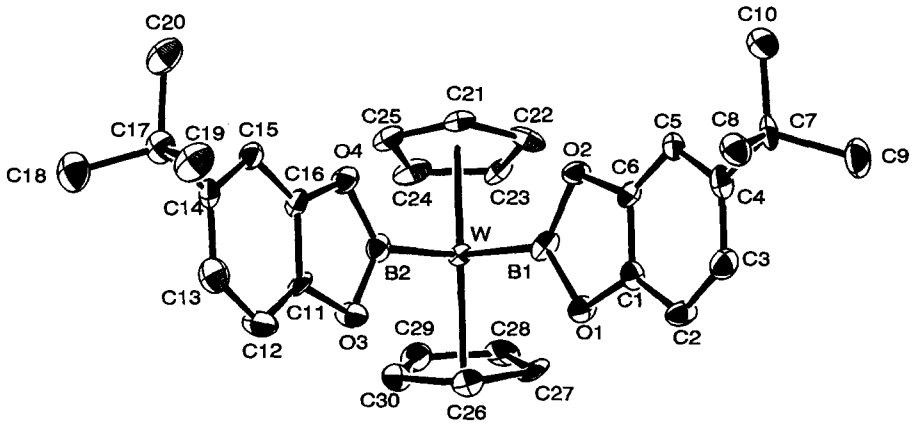

Fig. 1. ORTEP drawing of **1**. Selected bond lengths [Å] and angles [°]: W–B1 2.19(19; W–B2 2.23(1), W-Cp1 1.96, W–Cp2 1.97; B1-W-B2 78.0(4), Cp1-W-Cp2 142.

The selectivity for B–B over C–H bond addition is independent of whether tungstenocene is generated photochemically or thermally. Gentle thermolysis of $[Cp_2W(H)(Me)]$ (**5**) is known to generate $[Cp_2W]$.[17, 18] If a solution of **5** in benzene is heated for 4 h at 80 °C in the presence of 1–2 equivalents of Cat'BBCat', **1** is formed in 70% yield. No phenyl hydride **3** was observed during the course of the reaction; **3** is stable in benzene at 80 °C in the presence of Cat'BBCat'. Therefore, **3** is, again, not even a reaction intermediate in the synthesis of **1**.

The clean oxidative addition chemistry of diboron compounds led us to probe the potential oxidative addition chemistry of catecholborane by $[Cp_2W]$. Irradiation of a solution of dihydride **4** for 6 h in benzene containing HBCat (6 equiv) led to the solvent C–H activation product **3**, rather than the borane addition product **2**. At short reaction times (30 and 60 min), however, we did observe small amounts of the B–H activation product **2** (10–20% relative to **3**). The formation of this product in benzene indicates that catecholborane addition is kinetically preferred over benzene addition. However, at longer reaction times the small amounts of **2** were converted to the phenyl hydride **3**.

Thus, it appeared that isolated **2** should undergo photochemically induced reductive elimination to generate $[Cp_2W]$. Indeed, irradiation of pure **2** in benzene for only 10 min gave **3** in 90% yield. If the reaction was carried out in [D$_6$]benzene, the ^{1}H NMR spectra of final reaction mixtures showed the absence of a hydride resonance, and the ^{11}B NMR spectra showed the presence of a doublet resonance for catecholborane. This suggests that clean reductive elimination of borane to form $[Cp_2W]$ takes place, rather than a photochemically induced C–H activation reaction by intact **2** or a radical generated from it.

Attempts to induce thermal reductive elimination of catecholborane were unsuccessful. Compound **2** was stable for several days at 120 °C. Attempts to induce thermal oxidative addition of catecholborane to $[Cp_2W]$ by warming compound **5** in the presence of catecholborane led to several reaction products, including MeBCat, which was presumably formed from exchange reactions with $[Cp_2W(H)(Me)]$ (**5**), similar to those observed previously in other systems.[19–21]

These studies led to the following series of photochemical stabilities: $[Cp_2W(BCat')_2] > [Cp_2W(Ph)(H)] > [Cp_2W(BCat)(H)]$. These selectivities by $[Cp_2W]$ for B–B over C–H bond activation are precedented by the oxidative addition of diboron compounds with systems that do not undergo intermolecular C–H activation.[3, 4, 16] However, the overall selectivity for C–H over B–H activation with Cp_2W contrasts the selectivities of systems that add the B–H bond of catecholborane but do not add the C–H bond of hydrocarbons.[6–8] Furthermore, the resulting selectivity for B–B over B–H activation is exactly the opposite of the general preference for C–H over C–C bond activation.

We have shown previously with an electron-rich, third row system, albeit an iridium system, that the metal–boron bond is stronger thermodynamically than the corresponding metal–hydrogen bond.[22] The stability of the tungsten bisboryl compound may be derived from a similar high bond dissociation energy of the metal–boron linkage. A kinetic effect that enhances selectivity for the boranes may result from the favorable match-up of the electron-rich d^4 $[Cp_2W]$ with the electrophilic diboron reagent.

Experimental Procedure

1: A solution of $[Cp_2WH_2]$ (42.0 mg, 0.133 mmol) was dissolved in either benzene or toluene (4 mL) and the solution was added to a vial containing (tBu-C$_6$H$_3$O$_2$B)$_2$ (1.0 equiv, 49.5 mg). The solution was divided into four NMR sample tubes, which were irradiated. ^{11}B NMR spectra that were taken periodically showed complete reaction after 3.5 h. The samples were then transferred to the drybox, the solutions were combined, and the volume was reduced to 0.5 mL. This toluene or benzene solution was then layered with pentane to afford yellow crystals of **1**. Samples obtained from a toluene/pentane mixture revealed the presence of one solvent of crystallization by ^{1}H NMR spectroscopy in C_6D_6 and gave satisfactory microanalysis. Crystals suitable for X-ray diffraction analysis were obtained from a benzene/pentane solvent mixture. Yield 52 mg (57%). ^{1}H NMR (300 MHz, [D$_6$]benzene, 25 °C, TMS): δ = 7.13 (d, ^4J(H·H) = 2.0 Hz, 1H, C-H), 6.93 (d, ^3J(H·H) = 8.2 Hz, 1H), 6.73 (dd, ^3J(H,H) = 8.2 Hz, ^4J(H·H) = 2.0 Hz, 1H), 4.70 (s, 10H, Cp), 1.16 (s, 9H, tBu); ^{11}B NMR (96.38 MHz, [D$_6$]benzene, 25 °C, BF_3-OEt$_2$): δ = 59.3; ^{13}C{^{1}H} NMR (75.48 MHz, [D$_6$]benzene, 25 °C, TMS): δ = 151.19, 149.14, 143.69, 117.2, 109.5, 108.27, 81.59, 34.42, 31.86. Anal. Calcd for $C_{30}H_{34}WB_2O_4 \cdot C_7H_7$: C 58.85, H 5.47. Found: C 58.59, H 5.56.

Received: September 8, 1995 [Z8377IE]
German version: *Angew. Chem.* **1996**, *108*, 352–354

Keywords: B–B activation · B–H activation · boron compounds · C–H activation · tungsten compounds

[1] For a review see: K. Burgess, M. J. Ohlmeyer, *Chem. Rev.* **1991**, *91*, 1179.
[2] T. Ishiyama, N. Matsuda, N. Miyaura, A. Suzuki, *J. Am. Chem. Soc.* **1993**, *115*, 11018-11019.
[3] P. Nguyen, G. Lesley, N. J. Taylor, T. B. Marder, N. L. Pickett, W. Clegg, M. R. J. Elsegood, N. C. Norman, *Inorg. Chem.* **1994**, *33*, 4623.
[4] C. N. Iverson, M. R. Smith, *J. Am. Chem. Soc.* **1995**, *117*, 4403.
[5] R. T. Baker, P. Nguyen, T. B. Marder, S. A. Westcott, *Angew. Chem.* **1995**, *107*, 1451; *Angew. Chem. Int. Ed. Engl.* **1995**, *34*, 1336.
[6] H. Kono, K. Ito, Y. Nagai, *Chem. Lett.* **1975**, 1095.
[7] K. Burgess, W. A. van der Donk, S. A. Westcott, T. B. Marder, R. T. Baker, G. C. Calabrese, *J. Am. Chem. Soc.* **1992**, *114*, 9350.
[8] S. A. Westcott, N. J. Taylor, T. B. Marder, R. T. Baker, N. J. Jones, J. C. Calabrese, *J. Chem. Soc. Chem. Commun.* **1991**, 304.
[9]R. H. Crabtree, *Chem. Rev.* **1985**, *85*, 245.
[10] S.-Y. Liou, M. Gozin, D. Milstein, *J. Am. Chem. Soc.* **1995**, *117*, 9774, and references therein.
[11] M. L. H. Green, D. O'Hare, *Pure Appl. Chem.* **1985**, *57*, 1897.
[12] The *tert*-butyl-substituted reagent was employed, rather than the parent catB-Bcat for solublility reasons.
[13] J. F. Hartwig, S. R. De Gala, *J. Am. Chem. Soc.* **1994**, *116*, 3661.
[14] Crystal parameters: $P2/n$, a = 14.829(4), b = 7.976(2), c = 27.282(5) Å, β = 98.76(2)°, V = 3189(2) Å^3, Z = 4, ρ_{calcd} = 0.03, $2\theta_{max}$ = 52.6°, Mo$_{K\alpha}$ (λ = 0.71069 Å), ω-2θ, 1.0–16.5° min^{-1} (in ω), (0.53 + 1.10 tanθ)°, −119 °C, 7198 reflections with 6929 unique. The data were corrected for Lorentz and polarization factors. An empirical absorption correction based on azumuthal

scans was applied, which resulted in transmission factors ranging from 0.77 to 1.00. The structure was solved by Patterson methods. The SHELXS program was used. No. observations ($I > 3.00\sigma(I)$) = 4288 and number of variables = 388. H atoms were included in calculated positions, with one methyl hydrogen located on each methyl group. $R = 0.041$, $R_w = 0.50$, refined against $|F|$. Further details of the crystal structure investigation may be obtained from the Director of the Cambridge Crystallographic Data Centre, 12 Union Road, GB-Cambridge CB2 1EZ (UK), on quoting the full journal citation.

[15] J. W. Lauher, R. Hoffmann, *J. Am. Chem. Soc.* **1976**, *98*, 1729.

[16] $Fe(CO)_5$ oxidatively adds cat'BBcat'to form $[Fe(CO)_4(Bcat')_2]$: X. He, J. F. Hartwig, *Organometallics* in press.

[17] M. L. H. Green, *Pure Appl. Chem.* **1978**, *50*, 27.

[18] R. M. Bullock, C. E. L. Headford, K. M. Hennessy, S. E. Kegley, J. R. Norton, *J. Am. Chem. Soc.* **1989**, *111*, 3897.

[19] J. F. Hartwig, S. Bhandari, P. R. Rablen, *J. Am. Chem. Soc.* **1994**, *116*, 1839.

[20] S. A. Westcott, H. P. Blom, T. B. Marder, R. T. Baker, J. C. Calabrese, *Inorg. Chem.* **1993**, *32*, 2175.

[21] J. A. Marsella, K. G. Caulton, *J. Am. Chem. Soc.* **1982**, *104*, 2361.

[22] P. R. Rablen, J. F. Hartwig, S. P. Nolan, *J. Am. Chem. Soc.* **1994**, *116*, 4121.

Specific Protein Docking to Chelator Lipid Monolayers Monitored by FT-IR Spectroscopy at the Air–Water Interface

Lutz Schmitt, Tom M. Bohanon, Steffen Denzinger, Helmut Ringsdorf, and Robert Tampé*

The concept of fusion proteins is widespread in molecular biology for the identification, one-step purification, and characterization of gene products. Among the most prominent examples are histidine-tagged fusion proteins, which can be isolated by immobilized metal ion affinity chromatography.[1, 2] To combine this strategy with the fundamental properties of lipid interfaces such as self-organization, supramolecular assembly, and the interplay of fluidity and rigidity, we have synthesized a novel class of chelator lipids bearing a nitrilotriacetic acid (NTA) head group.[3, 4] Thin films of these lipids are highly sensitive towards nickel ions,[3] forming complexes and thereby generate binding sites for the histidine tag.[5, 6] We describe here how the specific docking of a histidine-tagged protein to a chelator lipid monolayer at the air–water interface was monitored directly by external reflection Fourier transform infrared spectroscopy (FT-IR) at the air–water interface. Evidence for complex formation and specific and reversible binding was obtained.

External reflection FT-IR at the air–water interface can be used to study the physical properties of lipid monolayers,[7] for example configurations of the lipid acyl chain.[8, 9] This technique requires no extrinsic probes like fluorescent dyes, which could perturb the properties of the system under investigation. Until now, the adsorption or even specific binding of proteins to lipid monolayers at the air–water interface was not studied directly. We combined a film balance setup with an FT-IR spectrometer that collected spectra in the external reflection mode (Fig. 1 bottom). The specific binding of imidazole and histidine-tagged biomolecules to these chelator lipids was revealed by film balance techniques, fluorescence spectroscopy, and reflection interference contrast microscopy.[3–6] Complex formation and specific binding of histidine-tagged fusion proteins to the novel chelator lipids used in the IR experiments are illustrated in Figure 1 top.

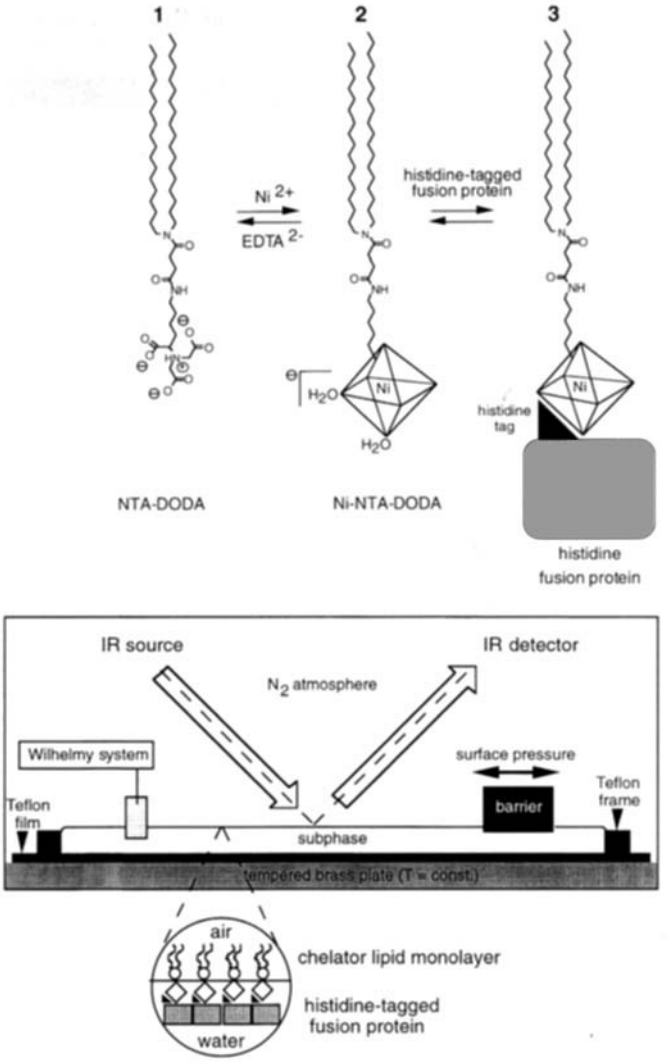

Fig. 1. Top: Compounds used in the experiments: nonloaded (NTA-DODA **1**) and nickel-loaded chelator lipids (Ni-NTA-DODA **2**), and a nickel-loaded chelator lipid with an immobilized histidine-tagged protein (protein/Ni-NTA-DODA **3**). The chelator lipid N^{α},N^{α}-bis(carboxymethyl)-N^{ε}-[(dioctadecylamino)succinyl]-L-lysine (NTA-DODA) was synthesized and used in unloaded and loaded forms as described in ref. [3]. For the IR experiments, 30 nmol of Ni-NTA-DODA or NTA-DODA was spread onto subphase buffer (10 mM HEPES, 140 mM NaCl, pH 8.0). As a model compound for histidine-tagged fusion proteins, a heat shock factor from tomato (HSF24) was used [15], which kindly provided by Oliver Boscheinen and Dr. Klaus-Dieter Scharf (University Frankfurt, Germany). HSF24 was expressed in *E. coli* as fusion protein containing a C-terminal sequence of six histidines [17]. The functionality of this protein is demonstrated by DNA gel retardation assays [15, 17]. Bottom: Experimental setup for external reflection FT-IR spectroscopy at the air–water interface; details are given in ref. [21]. All spectra were recorded with a resolution of 8 cm^{-1} by Fourier transformation of 5000 scans, and analyzed using the software provided by Nicolet. Automatic baseline and automatic smooth corrections were applied for all the spectra.

For reasons of sensitivity and simplicity, pure lipid layers were used for the measurements. First, we were interested in whether we could detect any differences between a nonloaded and a metal-loaded chelator lipid layer. To directly compare the symmetric and asymmetric stretching vibrations of the methylene groups near 2850 and 2920 cm^{-1}, respectively, of a nonloaded (NTA-DODA) and nickel-loaded chelator lipid monolayer (Ni-NTA-DODA), the spectra were recorded at the

[*] Dr. R. Tampé
Max-Planck-Institut für Biochemie
Am Klopferspitz 18a, D-82152 Martinsried (Germany)
Fax: Int. code +(89)8578-2641
e-mail: tampe@vms.biochem.mpg.de
Dipl.-Chem. L. Schmitt, Dr. R. Tampé
Lehrstuhl für Biophysik E22, Technische Universität München (Germany)
Dr. T. M. Bohanon, Dipl.-Chem. S. Denzinger, Prof. Dr. H. Ringsdorf
Institut für Organische Chemie der Universität Mainz (Germany)

same area per molecule. The spectrum of the NTA-DODA monolayer was recorded at 20 mN m^{-1} and that of the Ni-NTA-DODA monolayer at 15 mN m^{-1} in the coexistence region of the liquid expanded (LE) and liquid condensed (LC) phase (Fig. 2a). While changes in the homogenous LC or LE phase are negligible over a large range, changes in the coexistence region drastically influence the IR bands for the CH_2 stretching modes, as was previously determined for similar lipid systems.[8] As expected, complex formation at the lipid head group decreases the repulsive forces between the negatively charged lipid head groups and thereby lowers the pressure for a given area per molecule. For both lipid systems (Fig. 2b,c) the positions of these IR bands were identical (2847 cm^{-1}/2916 cm^{-1}). Complexation of the NTA head group does not affect the conformational order of the alkyl chains within the experimental error.

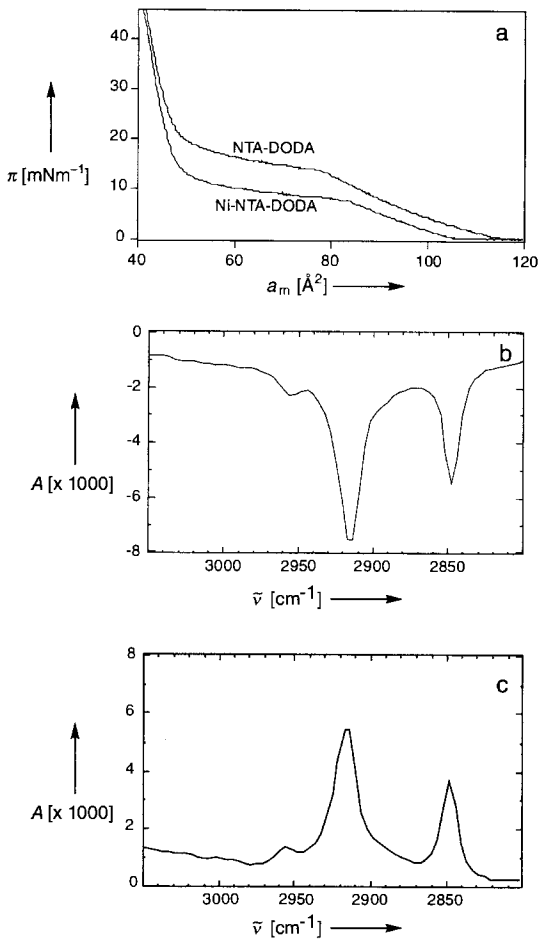

Fig. 2. a) Area–pressure diagram for a nonloaded NTA-DODA monolayer and a loaded Ni-NTA-DODA monolayer. The molar ratio Ni^{2+}:NTA-DODA was 1:1. Compressions were performed at 22 °C (1.8 Å^2 molecule^{-1} min^{-1}) as described in ref. [3]. FT-IR spectra of the NTA-DODA (b) and Ni-NTA-DODA monolayer (c) in the range 3050–2800 cm^{-1}. Spectra were recorded in the coexistence regions at 20 mN m^{-1} (22 °C) for the NTA-DODA system and 15 mN m^{-1} (22 °C) for the Ni-NTA-DODA system. a_m = area per molecule, A = absorption.

IR spectra recorded in the transmission mode are dominated by the attenuation constant (k) of the complex refractive index ($\hat{n} = n + ik$) and are fairly insensitive towards the real part of the refractive index (n). In reflection mode IR spectra the real part (n) of the complex refractive index dominates.[10, 11] In addition, incoming light is reflected at several interfaces with different Fresnel reflection coefficients. The most significant difference between the spectra of an nonloaded NTA lipid (Fig. 2b) and a loaded Ni-NTA lipid monolayer (Fig. 2c) is the inversion of the absorption signal, which can be explained only by the presence of a nickel layer complexed by the lipid interface. In contrast to the expected negative absorption sign of the NTA lipid monolayer,[12, 13] the positive absorption signals of the Ni-NTA lipid monolayer suggests a comparison with lipid monolayers at air–metal interfaces. But the assignment of a macroscopic value, the refractive index $\hat{n}$, to a monoatomic layer of complexed nickel ions is not justified in our case, and one must use caution when comparing peak areas from external reflection IR spectra. Nevertheless, it is interesting to note that the peak areas of the CH_2 stretching bands are nearly identical. Because the peak areas of the IR bands for the alkyl stretching vibration of the Ni-NTA lipid monolayer did not change over 12 h, dissociation of the complexed nickel ions just after spreading or within this time period can be excluded. In accord with the minute concentration of nickel ions, which was calculated to be 200 nM for our subphase volume of a loaded Ni-NTA (1:1) complex, the formation constant for the lipid head group complex seems to be high (10^{-12} M in solution[14]). This concept offers in principle a new perspective for the design of biofunctionalized interfaces by specific docking of histidine-tagged biomolecules to these chelator lipids.

To investigate the specific functionalization of a chelator lipid interface by histidine-tagged fusion proteins, the heat shock factor HSF24 containing a C-terminal histidine tag[15] was injected into the subphase of a Ni-NTA-DODA monolayer at 15 mN m^{-1} to yield a final concentration of 0.5 nM. After 1 h additional IR signals of the immobilized protein were detected. To circumvent any steric interference during protein binding, the monolayer was expanded to 4 mN m^{-1} for 12 h. After recompression to 15 mN m^{-1}, IR spectra were recorded. A new signal was observed at 3014 cm^{-1} (Fig. 3b), not seen in the spectrum of a Ni-NTA-DODA monolayer (Fig. 3a), which corresponds to intramolecular hydrogen bonds of the NH groups or an overtone of the amide II absorption;[16] another new band around 2200 cm^{-1} (Fig. 4a) was also recorded. Because of the overlap with the CO_2 signal, the latter band was taken into account only in qualitative analysis.

To evaluate the amount of unspecific versus specific immobilization, the experiment was repeated with a nonloaded NTA-DODA monolayer (Fig. 3c) under identical conditions (final pressure 15 mN m^{-1}). In this case, only weak protein bands at 3014 cm^{-1} and around 2200 cm^{-1} were found. In these protein binding experiments the positions of the CH_2 stretching modes are identical, indicating that the immobilized protein does not drastically affect the conformational order of the lipid chains. Interestingly, the peak areas of these bands are nearly identical in the presence and absence of immobilized protein. Assuming that the transition dipole moments of the protein bound to both layers are identical, we can estimate the amount of nonspecifically bound protein to be 20%. This unspecific binding is in agreement with the results of film balance and epifluorescence microscopy studies.[17] In these experiments HSF24 was only functionally immobilized if it was bound through the histidine tag and chelator lipid. HSF24 nonspecifically bound to lipid monolayers was not functional in DNA binding. In an additional control experiment the heat shock factor without the histidine tag did not specifically interact with a nickel-loaded chelator lipid layer.

Biotinylated lipids are very useful for immobilizing biotinylated proteins through an additional (strept)avidin layer as docking station.[18, 19] But the orientation of the attached mole-

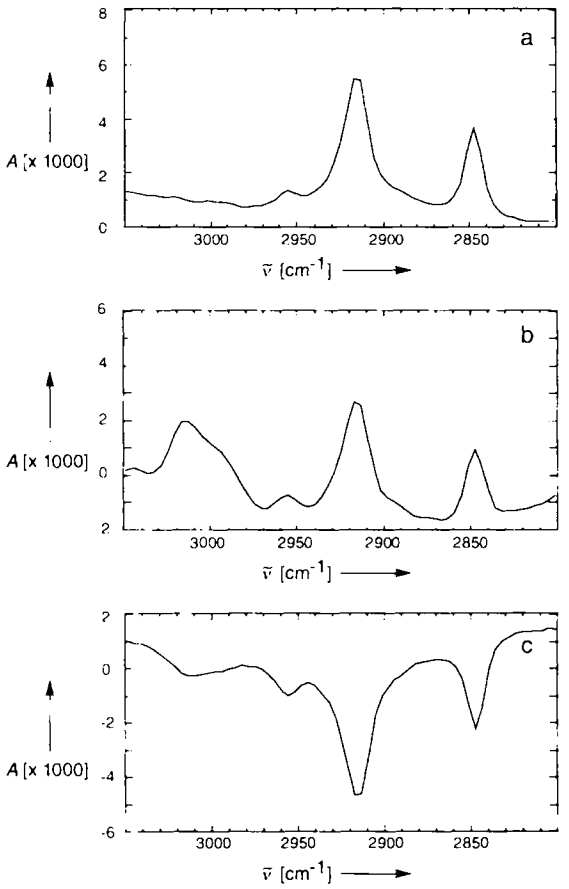

Fig. 3. FT-IR spectra of the Ni-NTA-DODA monolayer in the absence (a) and presence of the HSF24 (b) as well as the NTA-DODA monolayer (c) in the presence of HSF24 in the range 3050–2800 cm^{-1}. The experimental conditions are described in the legend of Fig. 2. For protein binding experiments, 80 pmol of HSF24 was injected into the subphase at 15 mN m^{-1} (22 °C), yielding a final concentration of 0.5 nM (lipid:protein = 380:1 mol mol^{-1}). After 1 h the monolayer was expanded to 4 mN m^{-1} and after 12 h recompressed to 15 mN m^{-1} (22 °C).

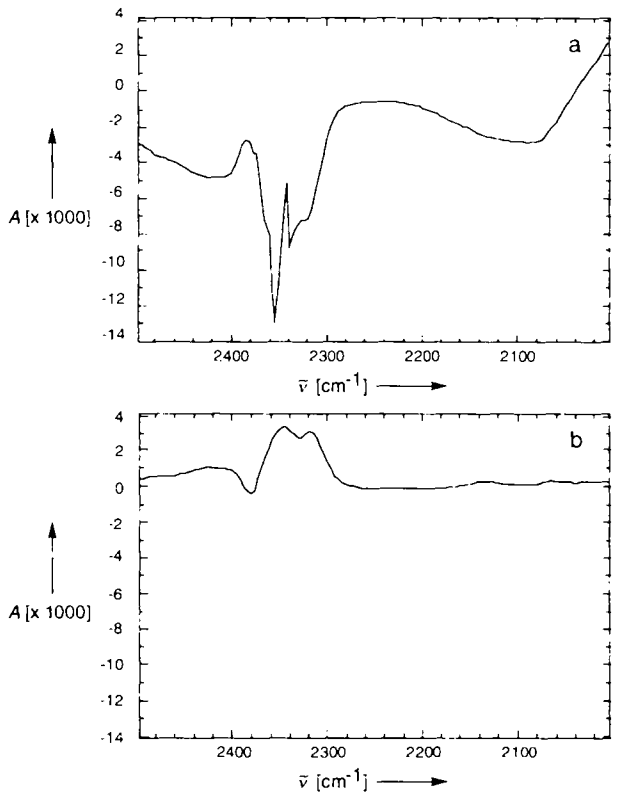

Fig. 4. a) FT IR spectra of the Ni-NTA-DODA monolayer in the presence of the HSF24 as described in the legend of Fig. 3b in the range 2500–2000 cm^{-1}. b) FT IR spectra of the Ni-NTA-DODA monolayer 30 min after the injection of EDTA yielding a final concentration 0.8 mM.

cules is limited by the regioselectivity and stoichiometry of chemical biotinylation. In contrast, the concept of NTA lipids makes use of a vast variety of proteins carrying the affinity tag at well-defined positions. A further advantage is that the binding is reversible. The dissociation of any immobilized protein can be achieved either by competition with imidazole, by complexing the Ni^{2+} ions with stronger chelating agents such as EDTA, or by lowering the pH.[5, 6] To examine this reversibility, EDTA was injected into an immobilized protein monolayer. Because EDTA has strong absorption peaks at 3015 and 2982 cm^{-1},[20] the detected protein absorption at 3014 cm^{-1} could not be used to follow the disassembly of the protein. But within 30 min after EDTA addition, firstly the absorption signal was again inverted, which implies dissociation of the Ni-NTA complex (data not shown), and secondly the protein peak around 2200 cm^{-1} was not detected (Fig. 4b). Note, in the absence of EDTA the Ni-NTA-DODA monolayer gave invariant spectra over 12 h. The peak positions of the CH_2 stretching modes are identical before and after EDTA addition. Comparison of the peak areas of these modes yields a ratio of 3:1 for the unloaded versus loaded chelator lipid layer. This incomplete complexation of the nickel ions by EDTA is not surprising because the dissociation generates a negatively charged surface, depleting EDTA from its interface. An alternative explanation could be that EDTA itself binds to the Ni-NTA head group. In order to achieve complete unloading, EDTA, imidazole, or low pH should be applied in a continuous-flow experiment.

External reflection FT-IR spectroscopy at the air–water interface was used to demonstrate specific and reversible protein docking at chelator lipid interfaces for the first time. This method also permits studies of lipid–protein and lipid–ligand interactions without labels or probes and is restricted by scan time only. Due to the vast variety of histidine-tagged fusion proteins already available, the concept of chelator lipids should make it possible to organize and orient biomolecules in a well-defined way, generating two-dimensional protein arrays for studying molecular mechanisms of membrane recognition, vesicle targeting, docking and fusion, the immune response in the cell, and adhesion processes.

Received: July 11, 1995 [Z 8192 IE]
German version: *Angew. Chem.* **1996**, *108*, 344–347

Keywords: immobilization · IR spectroscopy · lipids · molecular recognition · proteins

[1] J. Porath, J. Carlsson, I. Olsson, G. Belfrage *Nature* **1975**, *258*, 598–599.
[2] E. Hochuli, W. Bannwarth, H. Döbeli, R. Gentz, D. Stüber, *Bio/Technology* **1988**, *6*, 1321–1325.
[3] L. Schmitt, C. Dietrich, R. Tampé, *J. Am. Chem. Soc.* **1994**, *116*, 8485–8491.
[4] R. Tampé, C. Dietrich, G. Elender, S. Gritsch, L. Schmitt, *Nanofabrication and Biosystems: Integrating Material Science, Engineering and Biology* (Eds.: H. H. Loch, L. Jelinski, H. Craighead), Cambridge University Press, London, **1995**.
[5] C. Dietrich, L. Schmitt, R. Tampé, *Proc. Natl. Acad. Sci. USA* **1995**, *92*, 9014–9018.
[6] S. Gritsch, K. Neumaier, L. Schmitt, R. Tampé, *Biosensors*, **1995**, *10*, 805–812.
[7] R. Mendelsohn, H. H. Mantsch, *Progress in Protein-Lipid Interaction 2*, Elsevier, Amsterdam, **1986**.
[8] M. L. Mitchell, R. A. Dluhly, *J. Am. Chem. Soc.* **1988**, *110*, 712–718.

[9] R. A. MacPhail, H. L. Strauss, R. G. Synder, C. A. Elliger, *J. Phys. Chem.* **1984**, *88*, 334–341.
[10] D. L. Allara, A. Baca, C. A. Pryde, *Macromolecules* **1978**, *11*, 1215–1220.
[11] R. A. Dluhly, K. E. Reilly, R. D. Hunt, M. L. Mitchell, A. J. Mautone, R. Mendelsohn, *Biophys. J.* **1989**, *56*, 1173–1181.
[12] J. D. E. McIntyre, *Adv. Electrochem. Electrochem. Eng.* **1973**, *9*, 61–166.
[13] R. A. Dluhly, D. G. Cornell, *J. Phys. Chem.* **1985**, *89*, 3195–3197.
[14] R. J. Angelici, *Inorganic Biochemistry*, *Vol. 1*, Elsevier, Amsterdam, **1972**.
[15] K.-D. Scharf, S. Rose, W. Zott, F. Schöffl, L. Nover, *EMBO J.* **1990**, *9*, 4495–4501.
[16] L. J. Bellamy, *The Infrared Spectra of Complex Molecules*, *Vol. 1*, Chapman and Hall, London, **1975**.
[17] C. Dietrich, O. Boscheinen, K.-D. Scharf, L. Schmitt, R. Tampé, *Biochemistry* **1995**, in press.
[18] R. Blankenburg, P. Meller, H. Ringsdorf, C. Salesse, *Biochemistry* **1989**, *28*, 8214–8221.
[19] W. Mueller, H. Ringsdorf, E. Rump, G. Wildburg, X. Zhang, L. Angermaier, W. Knoll, M. Liley, J. Spinke, *Science* **1993**, *262*, 1707–1708.
[20] B. Schrader, *Raman-Infrared Atlas of Organic Compounds*, *Vol. 2*, VCH, Weinheim, **1989**, B3-32.
[21] T. M. Bohanon, S. Denzinger, R. Fink, W. Paulus, H. Ringsdorf, M. Weck, *Angew. Chem.* **1995**, *107*, 102–104; *Angew. Chem. Int. Ed. Engl.* **1995**, *34*, 58–60.

The Crystal Structure of Difluoroamine**

Martin Frank Klapdor, Helge Willner,* Wolfgang Poll, and Dietrich Mootz*

Dedicated to Professor Hans Joachim Seifert on the occasion of his 65th birthday

The structure of difluoroamine, HNF_2, has been well studied by vibrational and microwave spectroscopy and ab initio calculations. The results for the geometry and self-association of this small and prominent molecule of inorganic fluorine chemistry have now been independently confirmed and significantly complemented by a crystal structure analysis at low temperature.

Caution! Difluoroamine (m.p. −117, b.p. −23 °C) is potentially explosive (particularly in the solid state) and should be handled only on a mmol scale and with suitable protective measures.[1] We observed no explosion when working with submmol quantities. For the synthesis of HNF_2, N_2F_4 was treated with excess thiophenol.[2] DNF_2 was prepared by treating 0.5 mmol HNF_2 with an excess of D_2O (ca. 50 mmol, 99.9%, Merck, Sharpe and Dohme) at ambient temperature. After one day the reaction mixture was fractionated by "trap to trap" condensation at −80, −120, −196 °C. The trap at −120 °C contained pure DNF_2. In sealed glass tubes at −20 °C, gaseous HNF_2/DNF_2 could be kept without decomposition for years.

On cooling with liquid nitrogen, small amounts of the compound were condensed into thin-walled quartz-glass capillaries and sealed. A single crystal was grown by miniature zone melting with focused heat radiation[3] in situ on a diffractometer. The structure of HNF_2 was determined at −150 °C in the usual way.[4]

The values obtained for the N–F bond lengths and F–N–F bond angle, of 139.6(2) and 139.2(2) pm and 102.4(1)°, respectively, are quite similar to those determined from the microwave spectrum[5] (N–F: 140.0 pm, F–N–F: 102.9°, N–H: 102.6 pm, F–N–H: 99.8°) and ab initio calculations[6] for the free molecule. As common in X-ray analysis, the H atom is less accurately localized (N–H: 86(3) pm, F–N–H: 99(2) and 106(2)°), but clearly in an ordered position (Fig. 1).

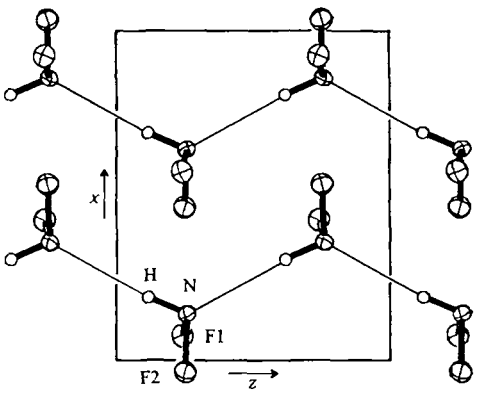

Fig. 1. Crystal structure of difluoroamine. Projection of two chains (see text) at different heights onto the *a,c* plane of the unit cell, with hydrogen bonds as thin lines and with ellipsoids with 25% probability [7].

In the crystal, the molecules are linked by weak hydrogen bonds of the type N–H···N (N···N: 314.9(2) pm, H···N: 230(3) pm, N–H···N: 171(2)°) to form zigzag chains of uniform (parallel) polarity, extending along the crystallographic *c* axis (Fig. 1). The presence of hydrogen bonds N–H···N (as distinguished from N–H···F) in the solid as in the liquid state has already been inferred from IR and Raman spectra.[1] The crystal structure of HNF_2 is hence similar to that previously determined[8] for HOF (hypofluorous acid) with chains (here antiparallel) of hydrogen bonds of the type O–H···O, that is, also not involving the particularly electronegative F atom.

Received: September 11, 1995 [Z 8389 IE]
German version: *Angew. Chem.* **1996**, *108*, 336

Keywords: difluoroamine · fluorine compounds · hydrogen bonds · structure elucidation

[*] Prof. Dr. H. Willner
Institut für Anorganische Chemie der Universität
Callinstrasse 9, D 30167 Hannover (Germany)
Fax: Int. code +(511)762-3006
Prof. Dr. D. Mootz, Dipl. Chem. M. F. Klapdor, Dr. W. Poll
Institut für Anorganische Chemie und Strukturchemie der Universität
Universitätsstrasse 1, D 40225 Düsseldorf (Germany)
Fax: Int. code +(211)81-13085

[**] In part from the Dissertation in progress by M. F. Klapdor. Supported by Fonds der Chemischen Industrie and the Dr. Jost Henkel-Stiftung.

[1] K. O. Christe, R. D. Wilson, *Inorg. Chem.* **1987**, *26*, 920, and references therein.
[2] J. P. Freeman, A. Kennedy, C. B. Colburn, *J. Am. Chem. Soc.* **1960**, *82*, 5304.
[3] D. Brodalla, D. Mootz, R. Boese, W. Osswald, *J. Appl. Crystallogr.* **1985**, *18*, 316.
[4] Crystal system: orthorhombic, space group $Pca2_1$, $Z = 4$; $a = 671.9(4)$, $b = 487.1(3)$, $c = 557.8(4)$ pm; $V = 182.6(2) \times 10^6$ pm^3 at −150 °C. Diffractometer: Siemens/Stoe AED2, $Mo_{K\alpha}$-radiation, graphite monochromator, $2\theta(\max.) = 70°$, ω/θ-Scan, 433 independent reflections with $F_o^2 > -3\sigma_{F^2}$, of which 413 with $F_o > 4\sigma_F$ observed. Direct methods with SHELXS-86 [9], refinement against F^2 with SHELXL-93 [10], 32 varied parameters, $R(F)$ (obs) = 0.038, $R(F)$ (all) = 0.041, $wR(F^2) = 0.136$, residual electron density $-0.33 - 0.31 \times 10^{-6}$ e pm^{-3}. The structure analysis on a single crystal of deuterated material, DNF_2, showed no significant differences. Further details of the crystal structure investigations may be obtained from the Fachinformationszentrum Karlsruhe, D-76344 Eggenstein-Leopoldshafen (Germany), on quoting the depository numbers CSD-404200 (HNF_2) and 404201 (DNF_2).
[5] D. R. Lide, Jr., *J. Chem. Phys.* **1963**, *38*, 456.
[6] H. G. Mack, D. Christen, H. Oberhammer, *J. Mol. Struct.* **1988**, *190*, 215, and references therein.
[7] SHELXTL PLUS, Structure Determination System, Revision 4.21/V, Siemens Analytical X-ray Instruments, Madison, WI, USA, **1990**.
[8] W. Poll, G. Pawelke, D. Mootz, E. H. Appelman, *Angew. Chem.* **1988**, *100*, 425; *Angew. Chem. Int. Ed. Engl.* **1988**, *27*, 392.
[9] G. M. Sheldrick, *Acta Crystallogr. Sect. A* **1990**, *46*, 467.
[10] G. M. Sheldrick, Program for the Refinement of Crystal Structures, Universität Göttingen, **1993**.

Multiple Sialyl Lewis^X N-Glycopeptides: Effective Ligands for E-Selectin**

Ulrich Sprengard, Manfred Schudok, Wolfgang Schmidt, Gerhard Kretzschmar, and Horst Kunz*

Dedicated to Professor A. Eschenmoser on the occasion of his 70th birthday

Selectins, a special group of transmembrane glycoproteins on platelets and endothelial cells, play a key role in the early stages of leukocyte adhesion.[1] The transient binding of selectins to oligosaccharide ligands like sialyl Lewis^X mediates the so-called rolling of leukocytes on the vascular endothelium. This event is the first in a complex cascade of macromolecular interactions involving other adhesion molecules in the extravasation of leukocytes into the tissue. Complex glycoproteins bearing the sialyl Lewis^X epitope and related saccharide moieties have been identified as efficient ligands for the selectins.[2, 3] Mucins with multiple oligosaccharide moieties at very high surface densities have been identified as endogenous selectin ligands.[4] Multivalent interactions between ligand and protein may increase the efficacy of selectin–glycoprotein binding.

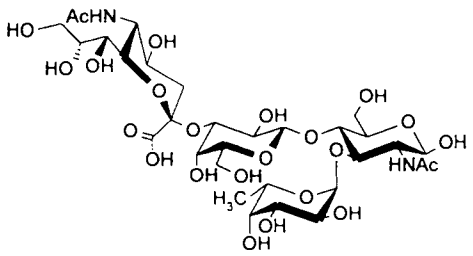

sialyl Lewis^X unit

Simple model compounds have been synthesized, for example diol-bridged bivalent sialyl Lewis^X analogues[5] and trivalent sialyl Lewis^X conjugates[6] derived from a nitromethanetripropionic acid template. Inspired by the endogenous ligands, we designed the trivalent N-glycopeptides **7a** and **7b** based on sialyl Lewis^X. These compounds showed improved inhibitory activity in an E-selectin cell adhesion assay. We prepared the cyclic N-glycopeptides containing three asparagine-linked sialyl Lewis^X tetrasaccharides by a synthetic strategy involving orthogonally stable protective groups for both the peptide and oligosaccharide synthesis. The sequential introduction of glycosylated, presynthesized amino acid building blocks might be an alternative strategy;[7] however, this approach would require the use of a considerable excess of coupling agents and valuable, temporarily protected glycosyl amino acids. In addition, the acid lability of fucose restricts the application of trifluoroacetic acid and other reagents often used in solid-phase synthesis.[8, 9]

The synthesis of trivalent sialyl Lewis^X glycopeptides was achieved by means of a combined strategy utilizing solid-phase peptide synthesis and fragment condensation in solution: a) The cyclic peptides **4a** and **4b** were prepared in high purity as versatile templates in a combined solid-phase and solution synthesis. b) The 4′-lactone of neuraminic acid served as an internal protective group during the synthesis and masked the carboxyl function of the partially blocked sialyl Lewis^X unit **1**.[2,7] c) The threefold condensation of the partially deblocked sialyl Lewis^X unit **1** with the cycloheptapeptides **4a** and **4b** led to the N-glycosidically linked sialyl Lewis^X glycopeptides **5a** and **5b**, respectively. d) The protecting group strategy allowed final deblocking of the glycosylated cyclopeptides by mild catalytic hydrogenolysis of 15 benzyl ether groups.

The linear heptapeptide containing D-alanine for more efficient cyclization was synthesized according to the Fmoc solid-phase strategy on acid-labile Sasrin resin.[10] Detachment of the partially protected heptapeptide **2a** from the resin under mild conditions (1% TFA in CH_2Cl_2) with retention of the orthogonally stable protective groups proceeded in 62% yield.[11] Sub-

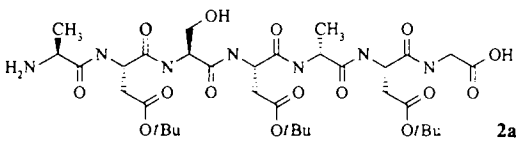

2a

$Ala_{(1)}$-$Asp(OtBu)_{(3)}$-Ser-$Asp(OtBu)_{(2)}$-D-$Ala_{(2)}$-$Asp(OtBu)_{(1)}$-Gly-OH

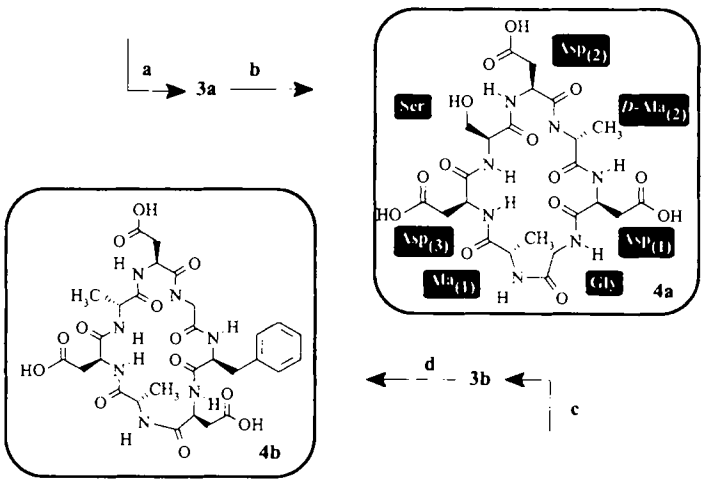

Ala-Asp(OtBu)-D-Ala-Asp(OtBu)-Gly-Phe-Asp(OtBu)-OH

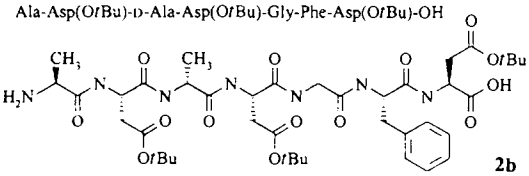

2b

Scheme 1. Synthesis of **4a,b**. The subscripted numbers in parentheses facilitate the assignment of the amino acid positions in the linear and cyclic peptides **2a** and **4a**, respectively. The NH hydrogen atoms were sometimes omitted from the formulae for clarity. These remarks are also valid for Schemes 2 and 3. a) **2a** (1 mmol L^{-1}), HATU/HOAT/DIPEA (3 equiv each), **3a**: 50%; b) TFA (with 5% water), **4a**: 96%; c) **2b** (1 mmol L^{-1}), HATU/HOAT/DIPEA (1 equiv each), after 1 h additional HATU/HOAT/DIPEA (0.8 equiv each), **3b**: 83%; d) TFA (with 5% water), **4b**: 81%.

[*] Prof. Dr. H. Kunz
Institut für Organische Chemie der Universität
J.-J.-Becher-Weg 18–20, D-55099 Mainz (Germany)
Telefax: Int. code +(6131)39 4786
Dipl.-Chem. U. Sprengard
Institut für Organische Chemie der Universität Mainz and
Zentralforschung, Hoechst AG, Frankfurt (Germany)
Dr. M. Schudok
Pharmaforschung, Hoechst AG, Frankfurt (Germany)
Dr. G. Kretzschmar, Dr. W. Schmidt
Zentralforschung, Hoechst AG, Frankfurt (Germany)

[**] The authors thank Dr. Kogler (Pharmaforschung, Hoechst AG) for stimulating discussions and for performing valuable NMR experiments. In this article the following abbreviations are used: Asp = asparagine, COSY = correlated spectroscopy, DIPEA = diisopropylamine, EEDQ = *N*-ethoxycarbonyl-2-ethoxy-1,2-dihydroquinoline, ESI = electrospray ionization, Fmoc = (9*H*-fluoren-9-ylmethoxy)carbonyl, Fuc = fucosyl, Gal = D-galactose, Glc = D-glucose, Gly = glycine, HATU = *O*-(7-azabenzo-triazol-1-yl)-1,1,3,3,-tetramethyluronium hexafluorophosphate, HMBC = H-detected multiple-bond correlation, HMQC = heteronuclear multiple-quantum coherence (NMR), HOAT = 1-hydroxy-7-azabenzotriazole, HOBt = 1-hydroxy-1*H*-benzotriazol, HSQC = heteronuclear single-quantum coherence (NMR), PHDQF = phase-sensitive double quantum filtered, Ser = serine, TBTU = (1*H*-benzotriazol-1-yloxy)bis(dimethylamino)methylium tetrafluoroborate, TCP = chlortrityl-polystyrene (PepChem, Tübingen), TFA = trifluoroacetic acid, TOCSY = total correlation spectroscopy (2D NMR).

sequent cyclization of the linear peptide, deblocked at the N- and C-termini, using HATU/HOAT/DIPEA[12] in dilute solution ($c_{peptide}$ = 0.001 M) afforded **3a** in 50% yield (Scheme 1). Cyclization with EEDQ via mixed anhydrides generated in situ resulted in complex mixtures of products. This may be due to aspartimide formation through the activation of β-carboxyl groups. The *t*-butyl protecting groups of **3a** were removed with TFA (5% water) leading to **4a** in 96% yield.

The acid- or base-catalyzed formation of aspartimides in asparagine-containing peptides and the subsequent transpeptidation are well-known side reactions.[13] This has been observed in particular in the case of Asp-Gly- and Asp-Ser-containing sequences; however, HSQC- and PHDQF-COSY NMR experiments confirmed the sequential integrity of the conformationally restricted cyclopeptide. The analysis of long-range couplings (^2J, ^3J, and ^4J couplings) obtained by proton-detected multiple-bond coherence (HMBC) experiments made structure determination possible even when the proton spin system is interrupted by heteroatoms and nonprotonated carbonyl groups (Table 1).[14]

Table 1. ^{1}H and ^{13}C NMR shifts of **4a**.

	δ						
	Ala^1	Asp^3	Ser	Asp^2	D-Ala^2	Asp^1	Gly
1-C	174.8	173.5	171.1	173.0	174.5	173.6	171.2
2-C	49.9	52.4	56.3	51.7	50.1	51.5	43.0
3-C	16.7	38.5	60.9	38.5	16.7	38.5	
4-C		177.7		177.4		177.6	
α-H	4.34	4.51	4.31	4.60	4.33	4.66	3.92
β_1-H	1.35	2.76	3.88	2.67	1.37	2.70	
β_2-H		2.71	3.84	2.61		2.53	

Fragment condensation of the sialyl Lewis^X unit **1** with cyclopeptide **4a** using HATU/HOAT/DIPEA produced the partially protected sialyl Lewis^X cyclopeptide **5a** in 48% yield (Scheme 2). The 4'-lactone group of the sialic acid was not affected during this step. Cleavage of the benzyl ether groups by hydrogenolysis over Pd/C in methanol/acetic acid/dioxane (5/1/1) gave **6a** in 88% yield. The lactone was opened by mild, alkaline hydrolysis in 96% yield, and the cyclic sialyl Lewis^X glycopeptide **7a** was purified by gel permeation chromatography on Biogel P2. The structure of **7a** was confirmed by electrospray ionization mass spectrometry (ESI-MS) and HSQC-, HMBC-, HSQC-TOCSY and HMQC-COSY NMR experiments. The PHDQF-COSY NMR spectrum (Table 2) showed almost complete coincidence of the signals for each of the three GlcNAc, Fuc, Gal, and NeuNAc residues.[15] This indicates that the trivalent cyclopeptide barely restricts the flexibility of the three sialyl Lewis^X ligands compared to the monomeric tetrasaccharide.

Table 2. ^{1}H and ^{13}C NMR shifts of **7a**.

	δ							
	GlcNAc		Fuc		Gal		NANA	
	H	C	H	C	H	C	H	C
1	5.07	77.73	5.07	98.2	4.50	101.12		173.44
	5.08	77.61						
2	4.0	54.08	3.66	67.17	3.5	68.77		99.19
	3.98							
3	3.88	74.89	3.86	68.77	4.05	75.15	1.76	39.3
							2.72	
4	3.93	72.4	3.75	71.4	3.89	66.85	3.65	67.86
5	3.61	76.53	4.79	66.25	3.54	74.45	3.81	51.22
6	3.89	59.03	1.14	14.82	3.66	61.06	3.62	72.4
7							3.55	67.65
8							3.86	71.4
9							3.60	62.13
							3.83	
CH_3	1.95	21.75					1.99	21.57
	1.96	21.73						
C=O		173.73						174.53
		173.81						

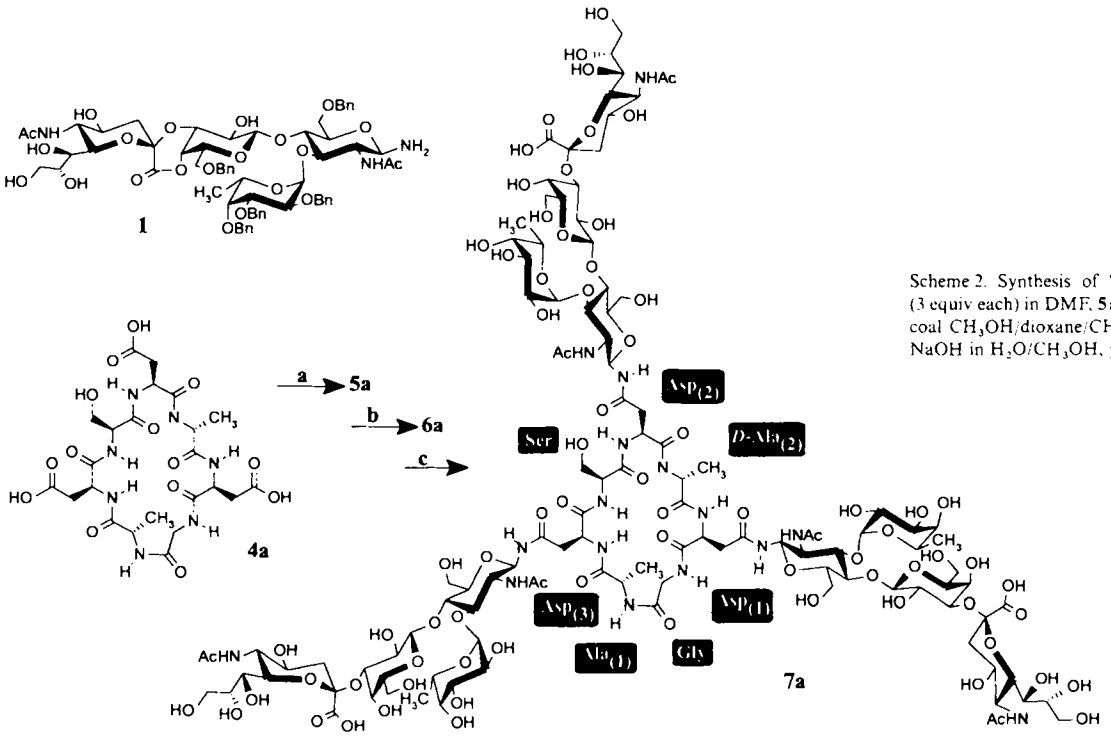

Scheme 2. Synthesis of **7a**. a) HATU/HOAT/DIPEA (3 equiv each) in DMF, **5a**: 48%; b) H_2, Pd active charcoal CH_3OH/dioxane/CH_3COOH (5/1/1), **6a**: 88%; c) NaOH in H_2O/CH_3OH, pH = 10.4, **7a**: 96%.

The partially protected, linear heptapeptide **2b** having a different peptide sequence was synthesized in analogy to **2a** by solid-phase Fmoc methods. Detachment from the extremely acid-labile TCP resin[16] with retention of the *t*-butyl esters could be carried out under substantially milder conditions (acetic acid/methanol/dioxane 5/1/4) than those typically applied in solid-phase synthesis.[17] In principle, these conditions should be compatible with the solid-phase glycopeptide synthesis of fucosylated structures since the loss of acid-labile fucose should not occur.[18] Cyclization of **2b** using HATU/HOAT/DIPEA (**3b**: 83% yield) and cleavage of the *t*-butyl esters with aqueous trifluoroacetic acid furnished **4b** (81% yield). Subsequent fragment condensation using HATU/HOAT/DIPEA gave **5b**, and hydrogenolytic cleavage of the benzyl ether groups and saponification of the lactone afforded the sialyl Lewis^X glycopeptide **7b** in an overall yield of 80%. (Scheme 3).

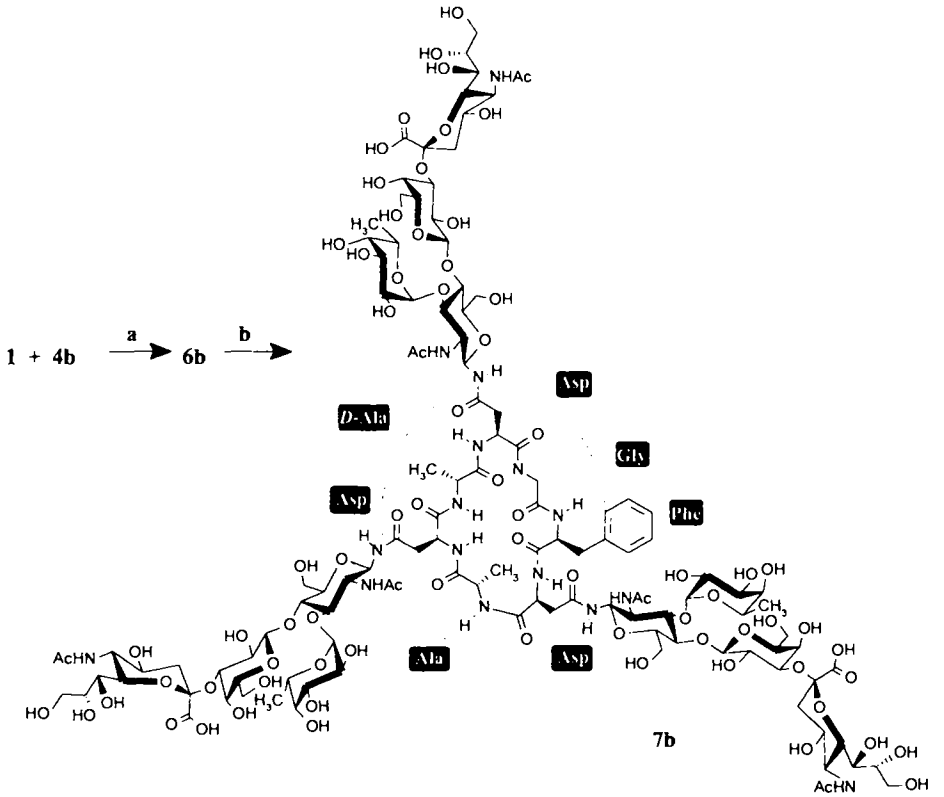

Scheme 3. Synthesis of **7b**. a) HATU, HOAT, DIPEA (1.5 equiv each) in DMF, after 4 h additional HATU/HOAT/DIPEA (0.5 equiv each) then H_2, Pd active charcoal, CH_3OH/dioxane/CH_3COOH (1:1:1), **6b**: 92%; b) NaOH in H_2O/CH_3OH (4:1), pH = 10.6, **7a**: 87%.

An efficient condensation was required for linking the aspartic acid unit in **4b** with the amine in **1** due to the adjacent bulky phenylalanine residue. The conditions used here permitted a complete N-glycoside formation between the sterically hindered aspartic acid and the sialyl Lewis^X amine **1**.

The synthesis of topologically functionalizable cyclopeptide templates involving an orthogonal protective group strategy allowed access to N-glycosides containing various oligosaccharides. In the past, solid-phase or solution glycopeptide synthesis using presynthesized glycosyl amino acids have been applied to reach this goal.[7] Owing to the good solubility of the partially protected tetrasaccharide unit **1**, a broad spectrum of organic solvents (dichloromethane, DMF, methanol) could be used for N-glycoside formation with lipophilic as well as with hydrophilic components. The partially protected sialyl Lewis^X unit has proven useful for multiple formation of N-glycosides on trivalent templates,[6, 27] and the convergent synthetic strategy has opened up a route to multivalent glycopeptide structures with repetitive oligosaccharide units. Until now, related strategies have been applied only for smaller glycopeptides.[19]

In cell adhesion tests measuring the binding of **7b** to recombinant human E-selectin–immunoglobulin fusion proteins (E-selectin–IgG[20]) in competition to tumour cells carrying sialyl Lewis^X ligands (cell line HL_{60}), **7b** proved to be an active synthetic ligand. The trivalent glycopeptide inhibited the adhesion of HL_{60} cells with an IC_{50} of 0.35–0.6 mM, which is two to three times more efficient than monomeric sialyl Lewis^X. In an extension of the concept, multiple conjugation of sialyl Lewis^X with biocompatible, peptide-derived polymers led to multivalent saccharide clusters which proved to be efficient inhibitors of leukocyte adhesion.[21, 22] Besides highly active, monovalent sialyl Lewis^X mimetics,[23–27] multivalent antagonists seem to be valuable antiinflammatory agents for selectin-mediated leukocyte adhesion.

Received: September 15, 1995 [Z84031E]
German version: *Angew. Chem.* **1996**, *108*, 359–362

Keywords: cell adhesion · cyclopeptides · glycopeptides · selectins · sialyl Lewis^X

[1] T. A. Springer, *Cell* **1994**, *76*, 301–314; D. N. Granger, P. Kubes, *J. Leukocyte Biol.* **1995**, *55*, 662–675, and references therein.
[2] T. P. Patel, S. E. Goelz, R. R. Lobb, R. B. Parekh, *Biochemistry* **1994**, *33*, 14815–14824.
[3] M. R. Stroud, K. Handa, K. Ito, M. E. K. Salyan, H. Fang, S. B. Levery, S. Hakomori, B. B. Reinhold, V. N. Reinhold, *Biochem. Biophys. Res. Commun.* **1995**, *209*, 777–787.
[4] P. A. Van der Merwe, A. N. Barclay, *TIBS* **1994**, *19*, 354–358.
[5] S. A. DeFrees, W. Kosch, W. Way, J. C. Paulson, S. Sabesan, R. L. Halcomb, D.-H. Huang, Y. Ichikawa, C.-H. Wong, *J. Am. Chem. Soc.* **1995**, *117*, 66–79.
[6] G. Kretzschmar, U. Sprengard, H. Kunz, E. Bartnik, W. Schmidt, A. Toepfer, B. Horsch, M. Krause, D. Seiffge, *Tetrahedron* **1995**, *51*, 13015–13030.
[7] H. G. Garg, K. von dem Bruch, H. Kunz, *Adv. Carbohydr. Chem. Biochem.* **1994**, *50*, 277–310.
[8] H. Kunz, C. Unverzagt, *Angew. Chem.* **1988**, *100*, 1763–1765; *Angew. Chem. Int. Ed. Engl.* **1988**, *27*, 1697–1699.
[9] The development of the allylic anchor, which can be cleaved under mild conditions, enables the synthesis of sensitive glycopeptides on solid supports: H. Kunz, B. Dombo, *Angew. Chem.* **1988**, *100*, 732; *Angew. Chem. Int. Ed. Engl.* **1988**, *27*, 711; O. Seitz, H. Kunz, *ibid.* **1995**, *107*, 94–97 and **1995**, *34*, 803–805.
[10] M. Mergler, R. Tanner, J. Gosteli, P. Grogg, *Tetrahedron Lett.* **1988**, *29*, 4005–4008.
[11] Solid-phase synthesis on Sasrin resin: a) 20% piperidine in DMF; b) 2 equiv temporarily blocked amino acid, TBTU, HOBT, DIPEA (2 equiv each); c) TFA (1% in CH_2Cl_2), then pyridine, **2a**: 62%.
[12] For reactions with HOAT: L. A. Carpino, *J. Am. Chem. Soc.* **1993**, *115*, 4397–4398; for reactions with EEDQ see: B. Belleau, G. Malek, *J. Am. Chem. Soc.* **1968**, *90*, 1651.
[13] M. Bodanszky, J. Z. Kwei, *Int. J. Pept. Protein Res.* **1978**, *12*, 69; M. Bodanszky, J. C. Tolle, S. S. Deshmane, A. Bodanszky, *ibid.* **1978**, *12*, 57.
[14] M. F. Summers, L. G. Marzilli, A. Bax, *J. Am. Chem. Soc.* **1986**, *108*, 4285.
[15] Characterization of **7a**: $[\alpha]_D^{20} = -41.3$ ($c = 1$ in water); ^{1}H NMR (400 MHz, D_2O): $\delta = 1.33$ (d, 3H, $J_{\beta,\alpha} = 7.3$ Hz, β-Ala^3), 1.36 (d, 3H, $J_{\beta,\alpha} = 7.3$ Hz, β-Ala^2), 2.66 (dd, 1H, $J_{\beta,\alpha} = 7$, $J_{gem} = 16$ Hz, β-Asp^1), 2.75 (dd, 1H, $J_{\beta,\alpha} = 7$, $J_{gem} = 16$ Hz, β-Asp^2), 2.73 (dd, 1H, $J_{\beta,\alpha} = 7$, $J_{gem} = 16$ Hz, β-Asp^3), 2.76 (dd, 1H, $J_{\beta,\alpha} = 7$ Hz, β-Asp^1), 2.85 (dd, 1H, $J_{\beta,\alpha} = 7.2$ Hz, β-Asp^2), 2.94 (dd, 1H,

$J_{\beta,\alpha}$ = 6 Hz, β-Asp³), 3.84 (β-Ser), 4.26 (m, 2H, α-Ala¹, α-Ala²), 4.28 (dd, 1H, α-Ser), 4.52 (1H, α-Asp³), 4.72 (1H, α-Asp²), 4.79 (1H, α-Asp¹); ^{13}C NMR (125.8 MHz, D_2O): δ = 15.57 (β-Ala²), 16.11 (β-Ala¹), 35.53 (β-Asp¹), 35.67 (β-Asp²), 35.99 (β-Asp³), 41.62 (α-Gly), 49.27 (α-Ala²), 49.78 (α-Ala¹), 49.08, 49.19, 50.57 (α-Asp¹, α-Asp², α-Asp³), 55.24 (α-Ser), 59.89 (β-Ser), 170.46, 170.57 (C=O¹ Ser), (C=O² Gly), 171.62, 171.69, 171.79, 171.88, 172.22, 172.34 (C=O¹ Asp¹), (C=O² Asp²), (C=O¹ Asp³), (C=O⁴ Asp¹), (C=O⁴ Asp²), (C=O⁴ Asp³), 174.3 (C=O Ala¹), 174.70 (C=O Ala²); ESI-MS: 1540 $(M^+ + 2Na)^{2+}$, 1034 $(M^+ + 3Na)^{3+}$.

[16] K. Barlos, D. Gatos, J. Kallitsis, G. Papaphotiou, Y. Wenqing, W. Schäfer, *Tetrahedron Lett.* **1989**, *30*, 394.

[17] Solid-phase synthesis on TCP resin: a) 20% piperidine in DMF; b) 3 equiv temporarily blocked amino acid, HBTU/HOBT/DIPEA (3 equiv each); c) $CH_3COOH/CH_3OH/CH_2Cl_2$, **2b**: 36%.

[18] D. Vetter, D. Tumelty, S. K. Singh, M. A. Gallop, *Angew. Chem.* **1995**, *107*, 94–97; *Angew. Chem. Int. Ed. Engl.* **1995**, *34*, 60–63.

[19] K. Gall-Istok, E. Zara Kaczian, L. Kisfaludy, G. Deak, *Acta. Chim. Acad. Sci. Hung.* **1981**, *107*, 221–229; M. Tamura, H. Okai, *Carbohydr. Res.* **1984**, *133*, 207–218; T. Takeda, A. Utsuno, N. Okamoto, Y. Ogihara, *ibid.* **1990**, *207*, 71–79; T. Takeda, K. Kojima, Y. Ogihara, *Chem. Pharm. Bull.* **1991**, *39*, 2699–2701; G. Arsequell, S. Y. C. Wong, G. R. Guile, T. W. Rademacher, R. A. Dwek, *Abstr. Pap. Eur. Pept. Symp. 22nd* (Interlaken, Switzerland) **1992**, A416.

[20] A. Aruffo, W. Kolanus, G. Walz, P. Fredman, B. Seed, *Cell* **1991**, *67*, 35–44; test system in analogy to: B. M. C. Chan, M. J. Elices, E. Murthy, M. E. Hemler, *J. Biol. Chem.* **1992**, *267*, 8366–8370.

[21] W. Stahl, U. Sprengard, M. Ahlers, B. Hörsch, A. Walch, G. Kretzschmar, *Tetrahedron Lett.*, submitted; B. Hörsch et al., unpublished results.

[22] Biophysical investigation of the neutrophile–selectin interaction in hydrodynamic flow systems might improve out understanding of transient binding of clustered carbohydrate ligands and their receptors.

[23] F. Dasgupta, B. N. N. Rao, *Expert Opin. Invest. Drugs* **1995**, *3*, 709–724.

[24] W. Stahl, U. Sprengard, G. Kretzschmar, H. Kunz, *Angew. Chem.* **1994**, *106*, 2186–2188; *Angew. Chem. Int. Ed. Engl.* **1994**, *33*, 2096–2098.

[25] W. Stahl, U. Sprengard, G. Kretzschmar, D. W. Schmidt, H. Kunz, *J. Prakt. Chem.* **1995**, *337*, 441–445.

[26] H. Huang, C.-H. Wong, *J. Org. Chem.* **1995**, *60*, 3100–3106.

[27] U. Sprengard, G. Kretzschmar, E. Bartnik, C. Hüls, H. Kunz, *Angew. Chem.* **1995**, *107*, 1104–1107; *Angew. Chem. Int. Ed. Engl.* **1995**, *34*, 990–993.

Synthesis and Dynamic Behavior of the Heptafluorotrisilacyclohexane Anion: A New Fluxional Silicate with Rapid Intramolecular Exchange of Fluoride Ligand

Dalci Brondani, Francis H. Carré, Robert J. P. Corriu,* Joel J. E. Moreau,* and Michel Wong Chi Man

The search for new silicon-based polymers and materials[1, 2] led to a growing interest in polyfunctional organosilicon precursors. These molecules are important for the preparation of hypervalent silicon species, which exhibit interesting structural properties and also unusual chemical reactivity.[3] Recent work has also revealed some unique properties of polysilylated hypervalent molecules: new structural and dynamic behaviors involving rapid intramolecular exchange of a fluoride ligand between silicon atoms were observed in disilyl- and hexasilylbenzene derivatives.[4, 5]

We recently reported that functional Grignard reagents provide a short route to carbosilane oligomers,[6] which are precursors of ceramic and sol–gel materials.[7] We thought that the cyclosilane **1** [Eq. (a), e.g. R = Me, Et] would be an interesting type of precursor for hypervalent species that, owing to the presence of three functionalized silicon atoms, might demonstrate unusual dynamic behavior. We report here the preparation of a new silicate anion which exhibits a rapid intramolecular ligand exchange in solution and in the solid state.

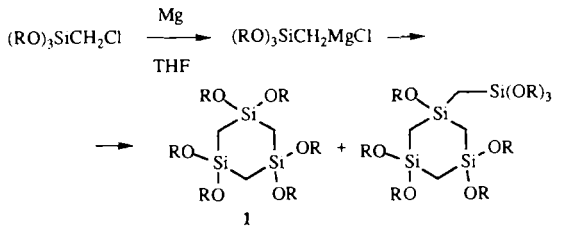

(a)

1

The 1,1,3,3,5,5-hexafluoro-1,3,5-trisilacyclohexane **2** was readily obtained when the hexamethoxy derivative **1** (R = CH_3) was[6b] treated with BF_3 and Et_2O [Eq. (b)].[8a] The reaction

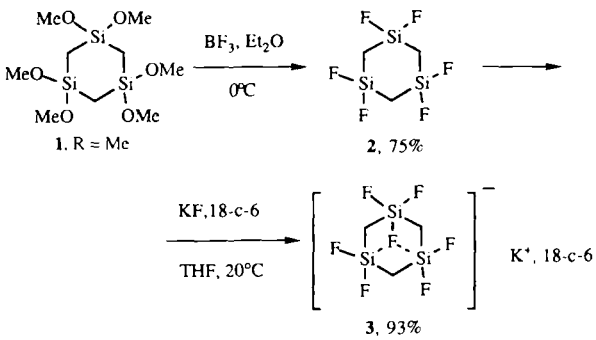

(b)

action of **2** with 1 mol of KF in the presence of [18]crown-6 (18-c-6) led to crystalline derivative **3** in 93% yield. Analysis of compound **3** indicated that it was a heptafluorosilicate derivative; single lines were observed in both the ^{19}F and ^{29}Si NMR spectra.[8b]

Evidence for the fluxional behavior was obtained upon NMR analysis of compound **3**. The observation of a single resonance in the ^{19}F spectrum indicated that rapid intramolecular ligand exchange occurred. Even at low temperature (as low as 183 K), the ^{19}F NMR spectrum of compound **3** in THF contains a single line at δ = −108.8.

More information can be gleaned from the ^{29}Si NMR analysis. At room temperature, the ^{29}Si NMR spectrum consists of a sharp singlet centered at δ = −25.56. This is consistent with a fluoride ligand exchange that is rapid on the NMR time scale; the environment of the three silicon atoms is thus averaged. Moreover, the absence of Si–F coupling suggests rapid intermolecular exchange in solution as well. It is also interesting to note that the ^{29}Si resonance occurs at δ = −25.56, intermediate between the expected chemical shift for a tetracoordinate difluorosilane $(CH_2SiF_2)_3$ (δ = −2.38[8a]) and the chemical shift of a pentacoordinate trifluorosilicate in a related cyclic structure $[CH_2(CH_2)_4SiF_3]$ (δ = −76.9[9]). The value for the ^{29}Si NMR chemical shift observed for **3** indicates that the seventh fluoride ligand is "equally shared" by the three silicon atoms in **3**.

Upon lowering the temperature, the signal broadened, and at 183 K a coupled signal was observed ($J_{Si,F}$ = 85.55 Hz, Fig. 1). The spectrum appeared as an octuplet (1:7:21:35:35:21:7:1), although the intensities of the external

[*] Prof. Dr. R. J. P. Corriu, D. Brondani, F. H. Carré
Précurseurs Organométalliques de Matériaux, CNRS UMR44
Case Courrier 007, Département de Chimie Organique Fine, Université de Montpellier II, Sciences et Techniques du Languedoc
F-34095 Montpellier Cédex 5 (France)
Fax: Int. code +(67)14-3888
Prof. Dr. J. J. E. Moreau, M. Wong Chi Man
Laboratoire de Chimie Organométallique, ENS Chimie Montpellier
8 rue de l'École Normale, 34053 Montpellier, Cedex 01 (France)

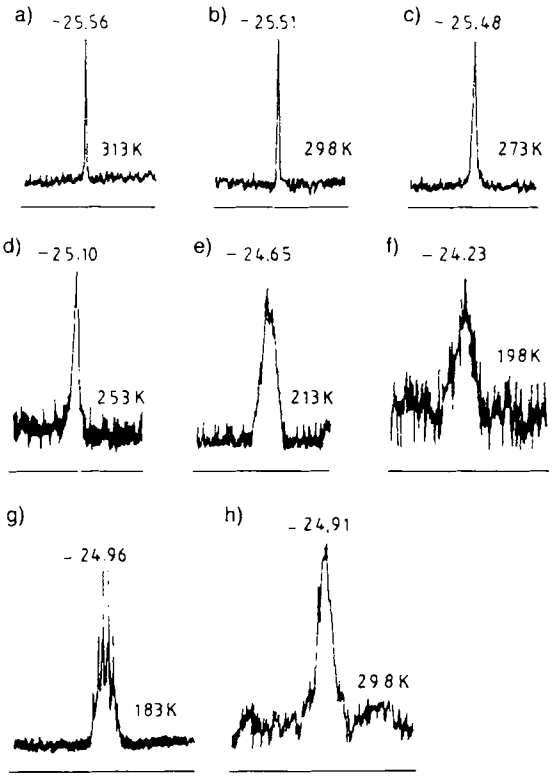

Fig. 1. ^{29}Si NMR spectra of **3** in [D_6]acetone at various temperatures (a–g) and the ^{29}Si CP MAS NMR spectrum of **3** at 298 K (h).

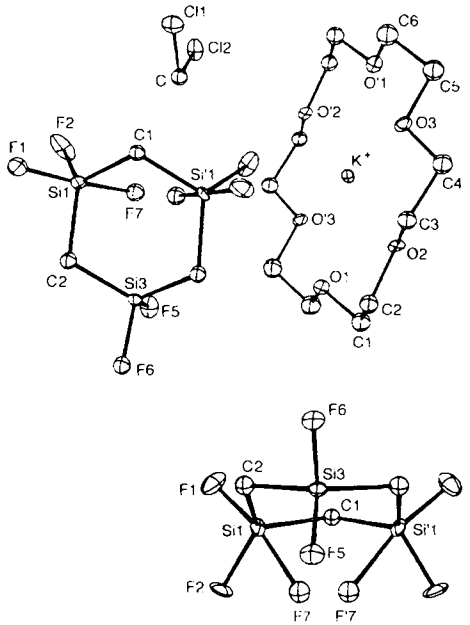

Fig. 2. Top: ORTEP projection of the crystal structure of **3** (hydrogen atoms are omitted for clarity; the ellipsoids and spheres enclose 20% of the electron density). Selected bond lengths [Å] and angles [°]: Si1–F1 1.62(1), Si1–F2 1.57(1), Si3–F5 1.59(2), Si3–F6 1.60(2), Si1–F7 1.86(2), C1-Si1-C2 117.6(9), F1-Si1-F2 95.9(7), F1-Si1-C1 102.7(7), F1-Si1-C2 98.6(7), F1-Si1-F7 169(1), C2-Si3-C2' 116.3(9), F5-Si3-F6 101.2(8); bottom: projection of the trisilacyclohexane anion of **3**. The distance between the two disordered positions F7 and F7' is 1.04(3) Å. An increase in the mean values of the C-Si-C and Si-C-Si angles of as much as 115.5° is observed; this increase results in a flatter trisilacyclohexane ring.

lines is quite low. The multiplicity is confirmed by the relative intensities (1:3:5) observed for the six internal lines (which would be 1:5:10 for a sextuplet). These observations show that even at 183 K a rapid intramolecular exchange occurs and that each silicon atom in **3** is coupled to seven equivalent fluorine atoms.

Interestingly, evidence for a rapid exchange of fluoride within the molecule was obtained even in the solid state. The ^{29}Si CP/MAS NMR spectrum of crystals of **3** revealed a single broad resonance at $\delta = -24.91$ (Fig. 1). The observed chemical shift indicates that even in the solid state, rapid exchange of the fluoride ligand between the three silicon atoms of **3** takes place.

The structure of compound **3** was determined by single-crystal X-ray diffraction analysis.[10] The crystals were unstable. The measurements were therefore made at 178 K by immersing the crystal in a cold stream of dry nitrogen. Two ORTEP diagrams of the heptafluorotrisilacyclohexane anion are shown in Figure 2.

The potassium cation is located at an inversion center of the lattice and is surrounded by six oxygen atoms at a mean distance of 2.79(1) Å and two fluorine atoms. The F2···K^+ distance is 2.68(1) Å. The dominant feature of the crown ether ring is the 1-point geometry in which pairs of atoms correspond to each other through the inversion center.

Figures 1 and 2 depict the hexafluorotrisilacyclohexane moiety in which the two half-occupied positions of the seventh fluorine atom are displaced (F7 and F'7, mirror images). We think that the F7/F'7 disorder induces an additional, corresponding, although smaller, disorder in the F1 and F2 atomic positions. It was not possible to detect such weak displacements. The values for the coordinates reported here for atoms F1 and F2 must be taken as mean values. In other words silicon atom Si1 (or Si1') should have tetrahedral geometry, while atom Si1' (or Si1) should be close to the center of a trigonal bipyramid. The X-ray diffraction methods can lead to only an average view of such disorder. Hence the resulting geometry around Si1 can be compared to either a capped tetrahedron or a distorted trigonal bipyramid in which the fluorines F1 and F7 occupy the axial sites [F1-Si1-F7 is 169(1)°]. In fact, the mean value for the F1-Si-F2, F1-Si1-C1, and F1-Si1-C2 is 99° as opposed to a mean value of only 81° for the angles F7-Si-F2, F7-Si1-C1, and F7-Si1-C2.

A significant difference in bond length is also observed between the axial bonds Si1–F1 [1.62(1) Å and Si1–F7 [1.86(2) Å]. It is noteworthy that, except for the Si1–F7 bond, the Si–F bond lengths are equal within the experimental error; the mean value is 1.60(1) Å. The separation between the two disordered positions F7 and F7' is only 1.04(3) Å in the solid state at 178 K, whereas the distance between F7 and Si3 is as much as 2.75(2) Å. At higher temperatures minor deformations of the six-membered ring are induced. It can be assumed that the fluorine anion moves easily between positions. The trisilacylclohexane moiety is somewhat flattened: the mean value for the bond angles in the ring atoms (both C and Si) is 115.5° (for the cyclohexane ring it is 109.5°). Such a geometry allows the molecule more fluxional character; thus the F7 atom should easily reach its new position on the Si3–F6 bond axis, *opposite* to the F6 atom. Actually, this theoretical position (calculated coordinates: 0.3904, 0.25, and −0.0262) is only 1 Å away from the F7 (or F7') atomic position, which is close to the F7···F7' separation reported above. It is consistent with the observed disorder in the solid state structure of **3** and with the presence of a single resonance in the ^{29}Si CP/MAS NMR spectrum of **3**.

The heptafluorotrisilacyclohexane anion does exhibit a unique dynamic behavior. The structure may be described as a $C_3Si_3F_6$ ring in a chair conformation with a seventh "bridging"

fluoride ion in an averaged position between the three silicon atoms. The presence of bridging fluoride ligand was recently proposed by Tamao et al.[4] and Sakurai et al.[5] to account for rapid exchange processes in ortho(fluorosilyl)benzene derivatives. For silicate **3** the mechanism in Scheme 1 accounts for the

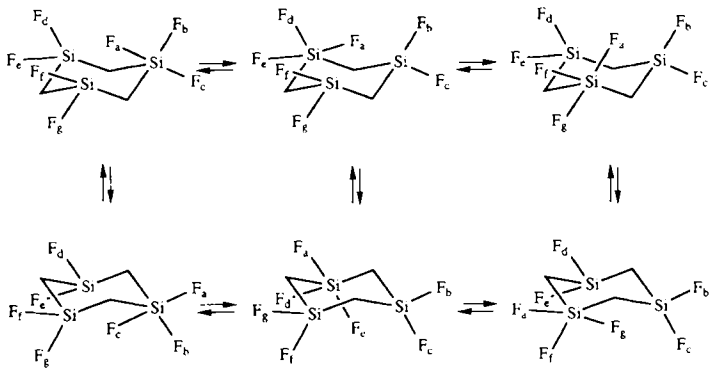

Scheme 1.

facile intramolecular ligand exchange at low temperatures. The mechanism involves a rapid transfer of the fluoride between silicon atoms and a conformational equilibrium of the six-membered ring. As shown in Scheme 1, successive fluoride transfers and chair inversions will shuttle the fluoride ligand from the "bridging" to the equatorial and axial positions. These low-energy processes are probably responsible for the observed dynamic behavior. In particular, the barrier to intramolecular fluoride transfer between silicon atoms is presumably of very low energy.

Received: July 26, 1995 [Z82551E]
German version: *Angew. Chem.* **1996**, *108*, 349–352

Keywords: dynamics · hypervalent compounds · silicon compounds

[1] a) "Inorganic and Organometallic Polymers": M. Zeldin, K. J. Wynne, M. R. Allcock, *ACS Symp. Ser.* **1988**, *360*, and references therein; b) "Inorganic and Organometallic Polymers with special Properties": R. M. Laine, *Nato ASI Ser. Ser. 206*, **1992** and references therein.

[2] a) C. J. Brinker, G. W. Scherer, *Sol-Gel Sciences*, Academic Press, London, **1990**; b) H. K. Schmidt, *Mater. Res. Soc. Symp. Proc.* **1990**, *180*, 9621, and references therein.

[3] a) R. J. P. Corriu, C. Guérin, J. J. E. Moreau, *Top. Stereochem.* **1985**, *15*, 43; b) R. J. P. Corriu, J. C. Young in *Hypervalent Silicon Compounds in the Silicon - Heteroatom Bond* (Eds.: S. Patai, Z. Rappoport), Wiley, New York, **1991**, p. 1, and references therein; c) C. Chuit, R. J. P. Corriu, C. Reye, J. C. Young, *Chem. Rev.* **1993**, *93*, 1371, and references therein.

[4] K. Tamao, T. Hayashi, Y. Ito, M. Shiro, *Organometallics* **1992**, *11*, 2099.

[5] K. Ebata, T. Irada, C. Kabuto, H. Sakurai, *J. Am. Chem. Soc.* **1994**, *116*, 3595.

[6] a) D. J. Brondani, R. J. P. Corriu, E. El Ayoubi, J. J. E. Moreau, M. Wong Chi Man, *J. Organomet. Chem.* **1993**, *451*, C1; b) *Tetrahedron Lett.* **1993**, *34*, 2111.

[7] D. J. Brondani, R. J. P. Corriu, L. Lutsen, J. J. E. Moreau, M. Wong Chi Man, still unpublished.

[8] a) Selected data for **2**: Anal. calcd for $C_3H_6F_6Si_3$: C 14.99, H 2.51; found: C 14.79, H 2.53. NMR ($CDCl_3$, δ) ^{1}H: 0.78 (q, ^3J(H,F) = 2.3 Hz); ^{19}F: 124.7 (s); ^{13}C: 1.1 (tq, ^1J(C,H) = 116, ^3J(C,F) = 12 Hz); ^{29}Si: −2.38 (q, ^2J(Si,F) = 292, ^3J(Si,F) = 11 Hz). b) Selected data for **3**: m.p. 170–173 °C (decomp.); anal. calcd for $C_{15}H_{30}F_5Si_3O_6K$: C 32.01, H 5.37, F 23.63; found: C 32.12, H 5.4, F 23.58. NMR ($CDCl_3$, δ): ^{1}H: 0.01 (6H, s), 3.39 (24H, s); ^{19}F: −108.8; ^{13}C: 4.99 (t), 71.09 (t), ^{29}Si: −25.56(s).

[9] S. E. Johnson, J. S. Payne, R. O. Day, J. M. Holmes, R. R. Holmes, *Inorg. Chem.* **1989**, *28*, 3190.

[10] The single crystal structure of **3** was determined *twice* with crystals from different experiments. Both discrepancy factors R had high values (0.150 and 0.142), probably due to the low quality of the crystals (milky instead of colorless crystals). Results of the analysis of **3**: orthorhombic, space group P_{nma}, a = 18.328(2), b = 18.421(6), c = 8.354(2) Å, V = 2820(1) Å^3, ρ_{calcd} = 1.525 g cm^{-3}, $\mu(Mo_{K\alpha})$ = 5.76 cm^{-1}, Z = 4. 3338 unique reflections up to $(\sin\theta)/\lambda$ = 0.704, 1374 with $F_o > 3.0(F_o)$. Enraf-Nonius CAD4 diffractometer, $Mo_{K\alpha}$ radiation, λ = 0.71069, T = 178 K. Solution by direct methods (MULTAN-80, assuming the $Pna2_1$ space group). $R(Rw)$ = 0.142(0.140), $\omega = 1/(\sigma^2(F_o) + 0.0286F^2)$ for 127 refined parameters; the hydrogen atoms were taken into account in the refinement with isotropic temperature factors, and methyl groups were considered as rigid (SHELX 76). Residual electron density: 2.25 e Å^{-3}, near the potassium peak; further details of the crystal structure investigation may be obtained from the Cambridge Crystallographic Data Centre, University Chemical Laboratory, 12 Union Road, GB-Cambridge CB2 1EZ (UK), on quoting the full journal citation.

A Reversible Transition between an α-Helix and a 3_{10}-Helix in a Fluorescence-Labeled Peptide**

Graham Hungerford, Marta Martinez-Insua, David J. S. Birch, and Barry D. Moore*

A key goal of molecular electronics is to synthesize molecular-based systems that can be rapidly and reversibly switched between two or more states in response to specific stimuli.[1] Ideally the switch should include a sensitive transduction mechanism so that changes occurring at a molecular level can be detected at a macroscopic level.[2, 3] Towards this end we have used oligopeptides to develop molecular switches for which different conformational states can be probed optically by monitoring the extent of intramolecular electron transfer quenching of fluorescence of internal labels.[2] Our eventual aim is to develop generic switching systems that can be tuned to respond to a wide range of stimuli by the inclusion of different functionality in the peptide chain. Here we describe a novel peptide that can be switched between two helical states, an α-helix and a 3_{10}-helix. Evidence for this transition has been obtained from circular dichroism (CD), infrared spectroscopy (IR), and photoinduced electron transfer (PET) fluorescence quenching.

Transitions between peptide secondary structures such as α-helix to random coil and α-helix to β-sheet have been very well studied.[4, 5] In contrast much less attention has been paid to the transition between the two most common types of peptide helix, the α- and 3_{10}-helices, although it has been implicated in the function of enzymes.[6, 7] Figure 1 shows schematically the difference between the two forms. The 3_{10}-helix is more highly pitched and has a different hydrogen bonding pattern. It is most often found in short peptides containing α-aminoisobutyric acid (Aib) residues[8] and at the termini of longer α-helical stretches in proteins.[9] Studies of a number of peptide families have shown that the relative stability of the two conformations can be

[*] Dr B. D. Moore, Dr G. Hungerford, M. Martinez-Insua
Department of Pure and Applied Chemistry
University of Strathclyde
Thomas Graham Building, 295 Cathedral Street, Glasgow, G1 1XL, Scotland (UK)
Fax: Int. code + (141) 552-5664
e-mail: b.d.moore@strath.ac.uk
Prof. D. J. S. Birch
Department of Physics and Applied Physics, University of Strathclyde

[**] We acknowledge funding from the EPSRC and thank Sharon Kelly and Nicholas Price at the BBSRC circular dichroism facility, University of Stirling. The authors also would like to thank Fiona Donald for valuable advice and NovaBiochem/Calbiochem for their generous support.

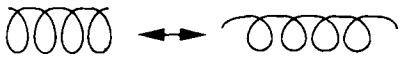

	α-helix	3_{10}-helix
H-bond pattern	$i, i+4$	$i, i+3$
backbone dihedral angles (φ, ψ)	-63, -42	-57, -30
pitch (Å/residue)	1.56	1.94
residues per turn	3.63	3.24

Fig. 1. General properties for an α helix and a 3_{10}-helix [29].

altered by changing the sequence,[10] the length of the peptide,[11, 12] and its environment.[13] Molecular dynamics simulations have shown that there is a well-defined pathway between the two forms[14, 15] and that the transition occurs over 15 picoseconds.[15] It therefore provides an attractive system for the development of a molecular switch.

We synthesized a series of peptides of differing length and sequence in which changes in conformational state can be probed by measuring the rate of PET between specific amino acids.[16] The peptides all include three or more Aib residues to promote helicity[17, 18] and two differently modified glutamic acids (at relative positions i and $i+4$). One glutamic acid is conjugated with a fluorescent methoxynaphthalene electron donor (Don) and the other with a piperidone electron accepting group (Acc) (Fig. 2).

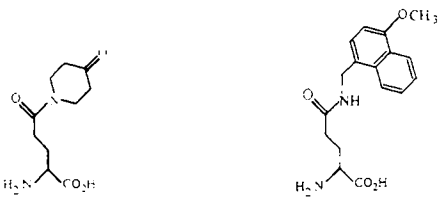

Acc Don

1) Ac-Ala-Aib-Ala-Acc-Leu-Aib-Ala-Don-Ala-Aib-Leu-Ala-NH_2

2) Ac-Ala-Ala-Aib-Ala-Phe-Ala-Acc-Leu-Aib-Ala-Don-Ala-Aib-Leu-Ala-NH_2

Fig. 2. Sequences of peptides **1** and **2** and the structures of Don and Acc [16, 30].

The CD spectra in acetonitrile of the shorter members (twelvemers) of the series including **1** are indicative of an incompletely formed helical structure that is nevertheless stable over the temperature range 0 to 60 °C. Intriguingly PET fluorescence quenching studies on **1** suggested that at low temperature (below 0 °C) two different conformations were present in solution.[16]

To obtain more information peptide **2** was synthesized. This had the same central sequence as **1** but was three amino acids longer in order to promote greater helicity. The CD spectrum of **2** in acetonitrile was measured over the temperature range −40 to 60 °C. At lower temperatures it was highly characteristic of an α-helix,[19–22] with two pronounced minima of similar intensity at 208 nm and 222 nm (Fig. 3a). The intensity of the spectrum at −30 °C shows that almost all the peptide is α-helical.[19] On warming above −20 °C the CD spectrum changed rapidly with a large loss in the relative intensity of the 222 nm minimum (Fig. 3b). This continued up to 20 °C. Further heating to 60 °C left the spectrum largely unchanged (Fig. 3c). This data provides convincing evidence for a sharp thermal transition from an α-helical conformation at lower temperatures to another stable conformation at higher temperatures. This is neither a random coil nor a β-sheet structure as evidenced by the constant inter-

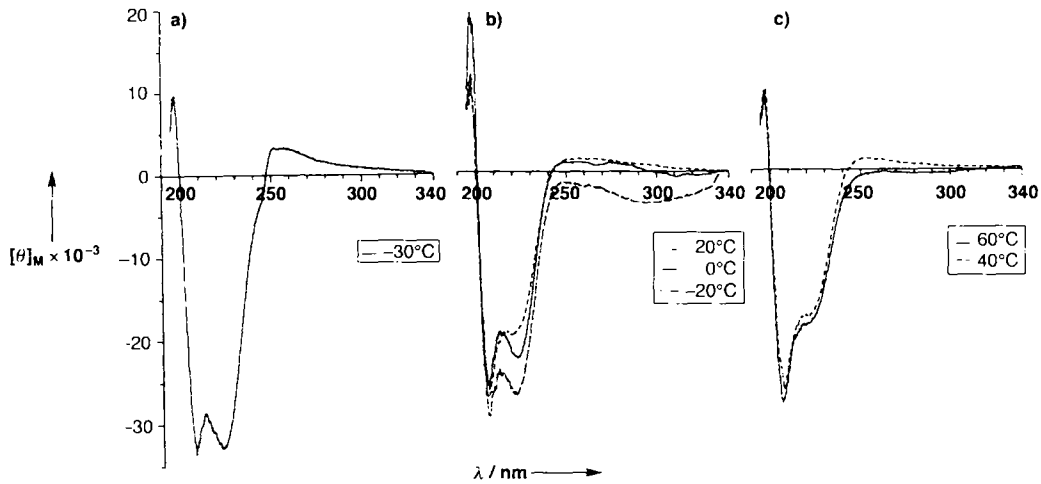

Fig. 3. Circular dichroism spectra of peptide **2** in acetonitrile at −30 °C (a), −20 to 20 °C (b), and 40 and 60 °C (c) [31].

cept of the x axis at 200 nm and the nearly constant intensity of the θ_{208} minimum.[19] Comparisons with other published CD spectra of helical peptides strongly suggest that this conformation is a 3_{10}-helix.[13, 20, 23] These spectra show a minimum at θ_{208} and a shoulder at θ_{222} with an intensity ratio $\theta_{222}:\theta_{208}$ in the range 0.5 to 0.8.[23, 21] This is comparable with the ratio of 0.7 at 20 °C found for peptide **2**.

Further evidence for the formation of a 3_{10}-helix was obtained from the room temperature infrared spectrum of **2** in acetonitrile, which showed a strong amide I band at 1662 cm^{-1}. This lies outside the 1650–1655 cm^{-1} range usually associated with the amide I band for an α-helix,[24] but is within the 1662–1665 cm^{-1} range measured for short $(Aib)_n$ homopeptides, known to form well characterized 3_{10}-helices.[25] It also coincides with the amide I band found for the antibiotic alamethicin in fluid phospholipid membranes and methanol, where it is reported to be a combination of α- and 3_{10}-helices.[24]

Although the CD spectra are consistent with a reversible change in the conformation of the whole peptide, it might be argued that only part of the backbone alters. Both X-ray[26] and NMR[27] measurements of helical peptides have shown stretches of α- and 3_{10}-helices within the same molecule, and α-helical stretches in proteins are often found to terminate with a 3_{10}-turn.[9] We introduced labeled glutamic acid residues within the central segment of the peptide to investigate this possibility further, as the results obtained should reflect changes in this section of the peptide. The fluorescence behavior of the peptide solution was monitored over the same temperature range as that used for

the CD measurements. At all temperatures it was possible to distinguish two species from their different fluorescence lifetimes. The relative amounts of each species varied reversibly with temperature, and the greatest change was observed over the same range as in the CD spectrum. These results show that the peptide exists in two discrete conformations that are in thermal equilibrium. Figure 4 shows the percentage of peptide exhibiting the shorter fluorescence lifetime plotted against temperature, along with the ratio of θ_{222} to θ_{208} for comparison. The latter gives a measure of the interconversion from α- to 3_{10}-helix, and it can be seen that the two data sets are strongly correlated. They both show a sharp transition indicative of a cooperative process. A similar melting range (ΔT) of 44 °C was measured by CD and PET fluorescence quenching, but the melting temperature (T_m) was -8 ± 4 °C by fluorescence and $4 + 10$ °C by circular dichroism. The fluorescence data shows clearly that the conformational changes seen in the CD measurements must also affect the central region of the peptide backbone where the labels are attached. By comparison we can assign the short lifetime component to peptide in the 3_{10} state, which indicates that PET fluorescence quenching is more efficient in this form.

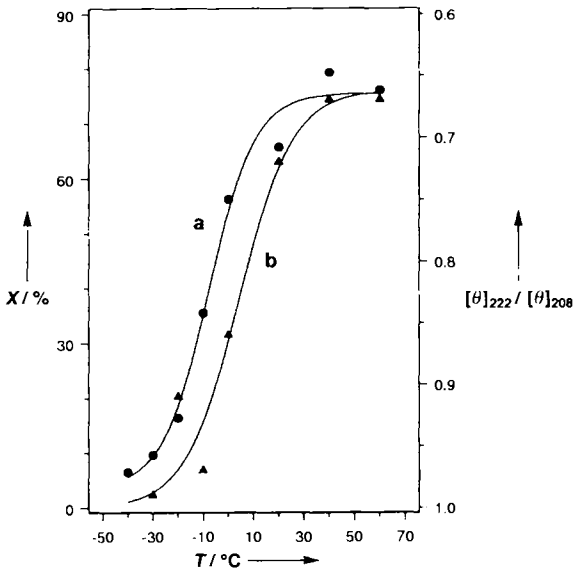

Fig. 4. The percentage X of the short lifetime component [32] (●, curve a) and the ratio of the intensities of the 222 nm and 208 nm CD minima (▲, curve b) against temperature for peptide **2** in acetonitrile.

The observed formation of a stable 3_{10}-helix at higher temperature indicates that there is a favorable entropic term associated with this conformation. Figure 5 shows the average conformations of the peptide in the two helical forms obtained from molecular dynamics simulations. It can be seen that in the 3_{10}-helix the bulky labeled side chains are, on average, further apart. The greater degree of conformational freedom this allows is consistent with a switch to this conformation at higher temperature (see Fig. 5). The lack of any detectable random coil formation in the accessible temperature range could be ascribed to the inclusion of three strongly helix-forming Aib residues and the use of an aprotic solvent, acetonitrile, which promotes strong intramolecular hydrogen bonding. The puzzling question why the fluorescence quenching is more efficient in this form is currently under investigation. Interestingly, de Rege et al. have predicted that distinct secondary structural motifs may modulate donor–acceptor electronic coupling differently.[28]

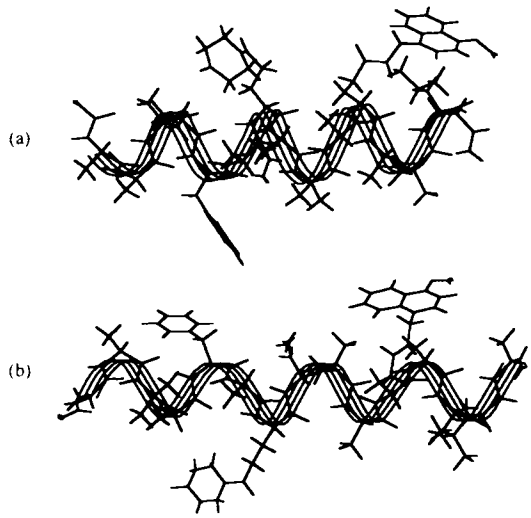

Fig. 5. The average conformation obtained from a 200 ps molecular dynamics simulation on peptide **2** with the peptide constrained in an α-helix (a) and in a 3_{10} helix (b) [33].

These results prove that a well-defined α- to 3_{10}-helical transition is possible in a synthetic peptide. This is the first step towards a molecular switch based on these conformational states. The well-defined transition seen here suggests that it will be possible to synthesize more complex peptides that respond to different stimuli such as the binding of ions or molecules. This will enable the development of the logic functions required for molecular electronics.

Received: August 14, 1995 [Z8303IE]
German version: *Angew. Chem.* **1996**, *108*, 356–359

Keywords: circular dichroism · electron transfer · fluorescence · molecular switches · peptides

[1] J. M. Lehn, *Angew. Chem.* **1990**, *102*, 1347–1362; *Angew. Chem. Int. Ed.* **1990**, *29*, 1304–1319.
[2] A. P. Desilva, C. P. McCoy, *Chem. Ind.* **1994**, *24*, 992–996.
[3] A. P. Desilva, H. Q. N. Gunaratne, C. P. McCoy, *Nature* **1993**, *364*, 42–44.
[4] S. Lee, T. Iwata, H. Oyagi, H. Aoyagi, M. Ohno, K. Anzai, Y. Kirino, G. Sugihara, *Biochim. Biophys. Acta* **1993**, *1151*, 76–82.
[5] A. P. Todd, G. L. Millhauser, *Biochemistry* **1991**, *30*, 5515–5523.
[6] C. A. McPhalen, M. G. Vincent, D. Picot, J. N. Jansonius, A. M. Lesk, C. Chothia, *J. Mol. Biol.* **1992**, *227*, 197–213.
[7] M. Gerstein, C. Chothia, *J. Mol. Biol.* **1991**, *220*, 133–149.
[8] K. Otoda, S. Kimura, Y. Imanishi, *Biochim. Biophys. Acta* **1993**, *1150*, 1–8.
[9] D. Pathak, D. Ollis, *J. Mol. Biol.* **1990**, *214*, 497–525.
[10] G. Basu, D. Anglos, A. Kuki, *Biochemistry* **1993**, *32*, 3067–3076.
[11] W. R. Fiori, S. M. Miick, G. L. Millhauser, *Biochemistry* **1993**, *32*, 11957–11962.
[12] K. Otoda, Y. Kitagawa, S. Kimura, Y. Imanishi, *Biopolymers* **1993**, *33*, 337–1345.
[13] T. Iwata, S. Lee, O. Oishi, H. Aoyagi, M. Ohno, K. Anzai, Y. Kirino, G. Sugihara, *J. Biol. Chem.* **1994**, *269*, 4928–4933.
[14] S. E Huston, G. R. Marshall, *Biopolymers* **1994**, *34*, 75–90.
[15] J. Tirado-Rives, D. S. Maxwell, W. L. Jorgensen, *J. Am. Chem. Soc.* **1993**, *115*, 11590–11593.
[16] F. Donald, G. Hungerford, D. J. S. Birch, B. D. Moore, *J. Chem. Soc. Chem. Commun.* **1995**, 313–314.
[17] C. Toniolo, G. M. Bonora, A. Bavoso, E. Benedetti, B. di Blasio, V. Pavone, C. Pedone, *Biopolymers* **1983**, *22*, 205–215.
[18] I. L. Karle, P. Balaram, *Biochemistry* **1990**, *29*, 6747–6756.
[19] N. Greenfield, G. D. Fasman, *Biochemistry* **1969**, *8*, 4108–4116.
[20] M. C. Manning, R. W. Woody, *Biopolymers* **1991**, *31*, 569–586.
[21] R. W. Woody, *Peptides* (London) **1985**, *7*, 15–114.
[22] W. C. Johnson, *Proteins: Struct., Funct. Genet.* **1990**, *7*, 205–214.
[23] T. S. Sudha, E. K. S. Vijayakumar, P. Balaram, *Int. J. Pept. Protein Res.* **1983**, *22*, 464–468.
[24] P. I. Haris, D. Chapman, *Biopolymers* **1995**, *37*, 251–263.

[25] D. F. Kennedy, M. Crisma, C. Toniolo, D. Chapman, *Biochemistry* **1991**, *30*, 6541–6548.
[26] R. O. Fox, F. M. Richards, *Nature* **1982**, *300*, 325–330.
[27] E. K. Bradley, J. F. Thomason, F. E. Cohen, P. A. Kosen, I. D. Kuntz, *J. Mol. Biol.* **1990**, *215*, 607–622.
[28] P. J. F. de Rege, S. A. Williams, T. J. Therien, *Science* **1995**, *269*, 1409–1413.
[29] C. Toniolo, E. Benedetti, *Trends Biochem. Sci.* **1991**, *16*, 350–353.
[30] The peptides were synthesized with a NovaSyn Crystal solid phase peptide synthesizer on a modified Rink type resin using 9-fluorenylmethoxycarbonyl (FMOC) protecting group strategies and benzotriazol-1-yloxytris(pyrrolidino)phosphonium hexafluorophosphate (PyBOP) coupling protocols. Following cleavage with 10% trifluoroacetic acid in dichloromethane, the crude peptide was purified by reversed-phase high-performance liquid chromatography and characterized with electrospray mass spectrometry.
[31] The spectra were recorded at a concentration of about 10^{-5} M with a Jasco J600 spectropolarimeter (1 cm pathlength cell). $[\theta]_M$ is in units of deg cm^2 dmol^{-1}. The experiment was performed by first heating to 60 °C then cooling to −40 °C. Identical spectra were obtained over several cycles.
[32] The fluorescence data were obtained at a peptide concentration of about 5×10^{-5} M in degassed acetonitrile with a time-resolved single-photon counting fluorometer with a coaxial flashlamp excitation source which gives an instrumental response of about 1.2 ns at full width half maximum. The excitation and emission wavelengths of 300 nm and 360 nm, respectively, were selected by monochromators. At 0 °C the lifetimes recovered were 4.14 and 6.32 ns, whilst the lifetime without fluorescence quenching was 7.59 ns. The curve fitted to both sets of data was a logistic sigmoid of the form $F(T) = y_{min} + [(y_{max} - y_{min})/(1 + \exp(-A(T - T_m)))]$, where A is a constant, T is temperature, and T_m is the melting temperature. The melting range ΔT was obtained by taking the center 80% of the curve between the upper and lower y data values. The uncertainty in the T_m value was taken as two standard errors.
[33] Calculations were performed with the software packages InsightII, Discover, and Analysis from BioSym Technologies on a Silicon Graphics Iris Indigo workstation. The force field used was CVFF, dynamics were run at 293 K in a vacuum, and the peptide was constrained in each helical form by fixing the α carbon atoms.

Stable, Highly Unsaturated Glycerides—Enzymatic Synthesis with a Carotenoic Acid**

Vassilia Partali, Lise Kvittingen, Hans-Richard Sliwka,* and Thorleif Anthonsen

The recent interest in highly unsaturated long-chain glycerides has resulted in the development of several synthetic and concentration methods.[1–4] However, glycerols of polyunsaturated fatty acids such as icosapentaenoic acid (C20:5), docosahexaenoic acid (C22:6), and the conjugated ajenonoic acids (C12:5, C14:5) are at least as unstable as the free fatty acids and can therefore only be handled at low temperature under an inert atmosphere or with stabilizers such as carotenoids.[4–6]

Thus, the synthesis of stable, highly unsaturated glycerides has to be based on stable highly unsaturated fatty acids. This requirement is met by the approximately 25 carotenoic acids that occur in low concentrations in nature.[7] One of these acids, 8′-apo-β-carotenoic acid (C30:9), is a stable, vitamin A active carotenoid, which is commercially available as the ethyl ester (C30-ester) **2** (see Scheme 1).[8,9]

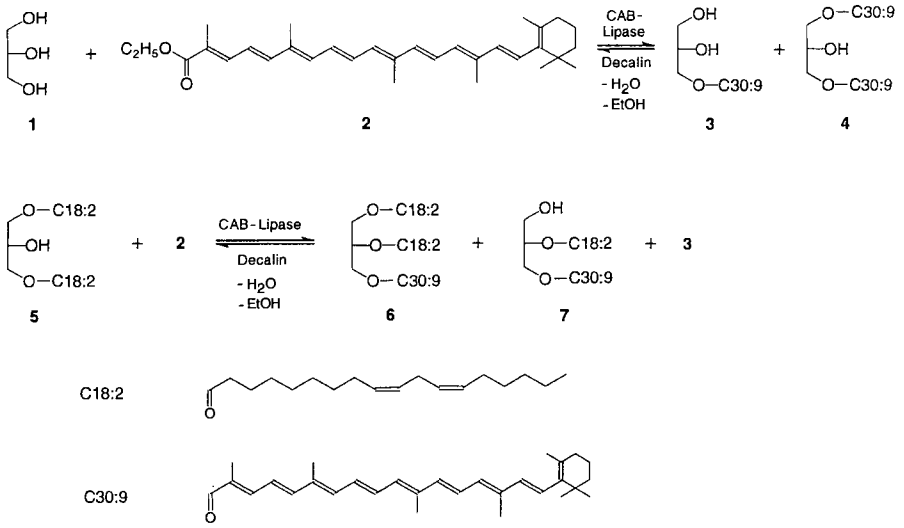

Scheme 1. Enzymatic synthesis of carotenoid glycerides.

Glycerides with a carotenoid as fatty acid have not been encountered in nature, although the carotenoic acid **2** can be considered as a dehydrogenated form of the naturally occurring branched fatty acids.[8,10]

We expect the carotenoid glycerides **3**, **4**, **6**, and **7** to combine the many physiological effects of fatty acids with those of carotenoids.[11–13] The carotenoid glycerides will probably be better absorbed and therefore their pharmacological effects might be higher than those of free carotenoids, which, even when esterified with palmitic acid, are not easily absorbed by man and animals.[14–16] The carotenoid fats **6** and **7** are polyfunctional glyceride derivatives in which the antioxidant carotenoid part can function as an intramolecular stabilizer for the fatty acid acyl groups in the molecule, while, simultaneously, the fatty acid acyl groups promote the absorption of the carotenoid.[17] We report here on the synthesis of the first stable highly unsaturated, conjugated glycerides.

The classical syntheses of glycerides (transesterification, direct synthesis) appeared to be less suitable as a route to these compounds, since the carotenoid ester **2**, like most carotenoids, is decomposed under the reaction conditions (high temperature or presence of acids) required.[18,19] Therefore, the conjugated mono-, di-, and trinonaenoylglycerol derivatives **3**, **4**, **6**, and **7** were synthesized with the help of enzymatic catalysis (Scheme 1), a method, which has not often been applied in carotenoid chemistry.[4,20–22]

Compounds **3** and **4** were obtained by esterification, and fats **6** and **7** by transesterification. Glycerol (**1**) was treated with **2** in decalin at 30–37 °C under reduced pressure in the presence of lipase from *Candida Antartica B* (CAB). This gave the mono- and diglycerides **3** and **4**, respectively, in about equal amounts (total yield 43%). The reaction of the diglyceride **5** with **2** produced the triglyceride **6** and the glycerides **3** and **7** in a ratio of 9:2:1 (total yield 38%). The yield of the enzymatic esterification of glycerol (**1**) with unsaturated fatty acids decreases with the

[*] Dr. H.-R. Sliwka
Norges Teknisk Naturvitenskapelige Universitet
Institutt for Organisk Kjemi-NTH
N-7034 Trondheim (Norway)
Fax: Int. code + (73) 59 54 73
e-mail: hrs@nvg.unit.no
Dr. V. Partali, Dr. L. Kvittingen, Dr. T. Anthonsen
Norges Teknisk Naturvitenskapelige Universitet, Kjemisk Institutt-AVH (Norway)

[**] We thank P. Halling for discussions on enzymatic catalysis and H. Anthonsen, B. Olsrød, A. Melbye, S. Liaaen-Jensen for NMR spectroscopy, mass spectrometry, and technical support.

increasing proximity of the double bond to the carbonyl group.[4] Nevertheless, the yield of carotenoyl glycerols in the esterification and the transesterification reaction between the carbonyl conjugated ester **2** and glycerol (**1**) or glyceride **5** can be considered as satisfactory.

The reaction of diglyceride **5** with ester **2** can give, statistically, nine glyceride products, not including possible positional and stereoisomers. In theory the formation of the products depends on an overall equilibrium constant which itself is a function of the three hydrolytic equilibrium constants for the tri-, di-, and monoglycerides. In fact, the product formation is also dependent on the reactant concentration, the solvent, the position specificity of the lipase, and, eventually acyl migration. By reducing the pressure, the products water and ethanol are continuously removed, which has a favorable effect on the formation of higher glycerides. Despite the complexity of the transesterification reaction, the main product was triglyceride **6**, with smaller amounts of mono- and diglycerides **3** and **7**, respectively.

The carotenoid glycerols were separated from the few by-products, unconverted **2**, and colorless glycerides by chromatographic work-up.

The structure of the new fats was confirmed by UV-Vis, ^{1}H, ^{13}C NMR, and IR spectroscopy, and mass spectrometry. After work-up of the reaction mixture, NMR spectroscopy revealed the presence of only the 1,3-derivative **4**, the triglyceride **6**, and the 1,2-isomer **7**, although acyl migration cannot be excluded.[23]

Mono- and diglycerides of medium- and long-chain fatty acids form stable emulsions in water.[24] Thus, compounds **3**, **4**, and **7** may be suitable for preparing easily absorbable carotenoid dispersions without relying on additional emulsifiers.[25]

Experimental Procedure

Esterification: **1** (83 mg, 0,90 mol), **2** (73 mg, 0.16 mmol), and CAB-lipase (350 mg) were stirred in decahydronaphthalene (10 mL) at 35 °C at reduced pressure (10 Torr) for 4 days.

Transesterification: **5** (7.4 mg, 0.012 mmol), **2** (12 mg, 0.026 mmol), and CAB-lipase (60 mg) were stirred in decahydronaphthalene (2 mL) at 35 °C at reduced pressure (10 Torr) for 8 days. After evaporation of the solvent, the yellow-red carotenoid glyceride products from both reactions were separated by column or preparative TLC chromatography on silica gel with hexane/acetone mixtures as eluents. Colorless glycerides were not analyzed. The esterification reaction gave the products **3** and **4** in the ratio 1:1 in 43% yield. The transesterification reaction afforded the products **3**, **6**, and **7** in 38% yield in a ratio of 9:2:1. The VIS spectra of products **3**, **4**, **6**, and **7** (λ_{max} = 456 nm, CH_2Cl_2) were identical with that of the starting material **2**.

Esterification reaction: Recovered **2**: 22 mg. **3**: Obtained: 15 mg. MS (70 eV) *m/z*: 506 [M^+], 414 [$M^+ - 92$]; IR (KBr): $\tilde{\nu}$ = 3428 (OH), 1700 (conj. C=O) cm^{-1}; ^{1}H NMR (500 MHz, $CDCl_3$, TMS): glyceryl part: (ABMXY system) δ = 3.91, (quin, H-2), (H-2), 3.56 and 3.65, (both dd, 2H-3), 4.20 and 4.23, (both dd, 2H-1); carotenoyl part: δ = 6.0–6.8, (12H), 1.95 (12H, 4 CH_3), 1.73 (3H, 1 CH_3-C5), 0.95 (6H, 2 CH_3-C1), 1.48 (2H, CH_2-C2), 1.55 (2H, CH_2-C3), 2.01 (2H, CH_2-C4).

4: Obtained: 15 mg. MS: *m/z*: 936 [M^+], 844 [$M^+ - 92$]; IR: $\tilde{\nu}$ = 3460 (OH), 1700 (conj. C=O) cm^{-1}; ^{1}H NMR: glyceryl part: (AA'BB'X system) δ = 4.16 (quin, H-2), 4.24 and 4.27 (2H A, and 2H A', respectively (J(A,A') = 11.1, J(A,X) = 5.0 Hz); carotenoyl part: δ = 6.0–6.7 (24H, 2 × 12H),0.96 (12H, 4 × CH_3-C1), 1.65 (6H, 2 × CH_3-C5), 1.90, 1.91, 1.92, 1.94 (24H, 2 × 4 CH_3), 1.40 (4H, 2 × CH_2-C2), 1.55 (4H, 2 × CH_2-C3), 1.96 (4H, 2 × CH_2-C4); ^{13}C NMR: (100 MHz, $CDCl_3$): glyceryl part: δ = 65.86 (C1, C3); carotenoyl part: δ = 168.6 (C=O), 39.66 (C2), 33.13 (C4), 28.98 (2 CH_3-C1), 21.77 (CH_3-C1), 19.27 (C3), 12.8–12.9 (4 CH_3).

Transesterification reaction: Recovered **2**: 4.6 mg. **6**: Obtained: 3.4 mg. MS: *m/z*: 1030 [M^+], 938 [$M^+ - 92$], 599 [$M^+ - 431$]; IR: 1742 (C=O), 1712 (conj. C=O) cm^{-1}; ^{1}H NMR: glyceryl part: (ABMXY system), δ = 5.2 (m, H-2), 4.11 and 4.21,(m, each 1H), 4.27, (m, 2H); carotenoyl part: δ = 6.0–6.8 (12H), 1.90, 1.95, (12H, 4 CH_3), 0.95 (6H, 2 CH_3-C1), 1.73 (3H, CH_3-C5), 1.48 (2H, CH_2-C2), 1.60 (2H, CH_2-C3); linoleoyl part: δ = 5.27 (m, 8H, 2 × 4H *cis*-alkene), 0.88 (t 6H, 2 × CH_3-C18), 1.25 (m, 32H, 2 × 16 CH_2), 2.28 (m, 4H, 2 × CH_2CO), 2.70 (m, 4H, 2 × $=CCH_2C=$), 1.8–2.0, (m, 8H, 4 × $=CCH_2$).

7: Obtained: 0.8 mg. MS: *m/z*: 768 [M^+], 676 [$M^+ - 92$], 337 [$M^+ - 431$]; IR: $\tilde{\nu}$ = 3450 (OH), 1730 (C=O), 1711 (conj. (C=O) cm^{-1}; ^{1}H NMR: glyceryl part: (ABMXY system), δ = 5.09 (m, H-2), 3.69 (m, 2H-3), 4.24 (m, 2H-1); carotenoyl part: δ = 6.0–6.7 (12H), 1.92, 1.98 (12H, 4 CH_3), 1.66 (3H, CH_3-C5), 0.95 (6H, 2 CH_3-C1), 1.55 (2H, CH_2-C3), 1.41 (2H, CH_2-C2); linoleoyl part: δ = 5.27 (m, 4H *cis*-alkene), 0.82 (t, 3H, CH_3-C18), 1.25 (m, 16H, 8 CH_2), 2.28 (m, 2H, CH_2CO), 2.70 (m, 2H, $=CCH_2C=$), 1.8–2.0 (m, 4H, 2 $=CCH_2$).

3: Obtained: 0.4 mg.

Received: May 29, 1995
Revised version: September 28, 1995 [Z80361E]
German version: *Angew. Chem.* **1996**, *108*, 342–344

Keywords: carotenoids · enzymatic catalysis · lipids

[1] E. Solar, J. Røttingen, P. Grimstad, A. Askeland, *US-A* 5336792, **1994**. [*Chem. Abstr.* **1994**, *114*, 162805r].
[2] C. F. Moffat, A. S. McGill, R. Hardy, R. S. Anderson, *J. Am. Oil Chem. Soc.* **1993**, *70*, 133.
[3] Y. Tanaka, J. Hirano, T. Funada, *J. Am. Oil Chem. Soc.* **1994**, *71*, 331.
[4] G. G. Haraldsson, B. Ö. Gudmundsson, Ö. Almarsson, *Tetrahedron* **1995**, *51*, 941.
[5] J. Cason, R. Davies, M. H. Sheehan, *J. Org. Chem.* **1971**, *36*, 2621.
[6] W. T. Wang, D. B. Min, *ACS Symp. Ser.* **1994**, 15.
[7] H. P. Pfander, M. Gerspacher, M. Rychener, R. Schwabe, *Key to Carotenoids*, Birkhäuser, Basel, **1987**.
[8] J. C. Bauernfeind, *J. Agric. Food Chem.* **1972**, *20*, 456.
[9] Produced by BASF AG, Ludwigshafen.
[10] P. Nuhn, M. Gutheil, B. Dobner, *Fette, Seifen, Anstrichm.* **1985**, 135.
[11] J. L. Harwood, A. Cryer, M. I. Gurr, P. Dodds in *The Lipids Handbook* (Eds.: F. D. Gunstone, J. L. Harwood, F. B. Badley), Chapmann and Hall, London **1994**, S. 665.
[12] N. I. Krinsky, *Pure Appl. Chem.* **1994**, *66*, 1003.
[13] T. D. Shultz, B. P. Chew, W. R. Seaman, L. O. Wedecke, *Cancer Lett. (Shannon Irel.)* **1992**, *63*, 125.
[14] J. A. Olsen, *Pure Appl. Chem.* **1994**, *66*, 1011.
[15] P. Jayarajan, V. Reddy, M. Mohanram, *Indian J. Med. Res.* **1980**, *71*, 53.
[16] J. K. Tyczkowski, J. L. Schaeffer, P. B. Hamilton, *Poultr. Sci.* **1989**, *68*, 1246.
[17] O. Hirayama, K. Nakamura, S. Hamada, Y. Kobayasi, *Lipids* **1994**, *29*, 149.
[18] K. Schiedt, S. Liaaen-Jensen in *Carotenoids, Vol. 1A* (Eds.: G. Britton, S. Liaaen-Jensen, H. Pfander), Birkhäuser, Basel, **1995**, S. 81.
[19] F. Gunstone in *The Lipids Handbook* (Eds.: F. D. Gunstone, J. L. Harwood, F. B. Badley), Chapman and Hall, London, **1994**, S. 594.
[20] C. Paden, R. Seiden (Procter & Gamble) *US-A* 5288512, **1994** [*Chem. Abstr.* **1994**, *112*, 54088j].
[21] P. H. Brown, F. D. Carvallo, R. C. Dinwoodie, M. T. Dueber, D. K. Hayashi, R. G. Krishnamurthy, J. J. Myrick, R. S. Silver, C. Thomas (Kraft General Foods) *US-A* 5288619, **1994** [*Chem. Abstr.* **1994**, *115*, 113289h].
[22] V. Partali, H.-R. Sliwka, T. Anthonsen, S. Liaaen-Jensen, *Biocatalysis* **1992**, *6*, 145.
[23] D. R. Kodali, A. Tercyak, D. A. Fahey, D. M. Small, *Chem. Phys. Lipids* **1990**, *52*, 163.
[24] M. Berger, M. Schneider, *Fett. Wiss. Technol.* **1993**, *95*, 169.
[25] L. Schweikert, C. Sambale (BASF AG) *US-A* 5350773 **1994** [*Chem. Abstr.* **1994**, *119*, 138086q].

Synthesis of Tailor-Made Glycoconjugates Showing AT III-Mediated Inhibition of Blood Coagulation Factors Xa and Thrombin**

Pieter Westerduin, Jan E. M. Basten, Marc A. Broekhoven, Vera de Kimpe, Will H. A. Kuijpers, and Constant A. A. van Boeckel*

The sulfated glycosaminoglycan heparin binds with high affinity to the plasma protein antithrombin III (AT III), thereby accelerating its inhibitory activity towards factor Xa and thrombin, two serine proteases involved in blood coagulation.[1, 2] The AT III-binding region in heparin consists of a unique pentasaccharide (PS) domain,[3, 4] the synthetic counterpart of which was found to accelerate the AT III-mediated inhibition of factor Xa but not that of thrombin.[5, 6]

In the course of studies on the preparation of PS analogues[7, 8] the molecular requirements for the specific binding of PS to AT III became transparent and a three-dimensional model of the interaction of PS and AT III could be constructed.[9, 10] In addition, easily accessible, highly potent O-sulfated/O-methylated PS analogues such as **1** have been identified.[11–13]

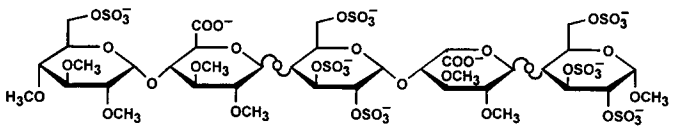

1

The next challenge was to extend the concept of AT III-mediated inhibition of factor Xa by PS towards synthetically feasible derivatives displaying both antifactor Xa and antithrombin activity.

It is now well recognized that for AT III-mediated inhibition of thrombin a heparin fragment comprising at least 18 saccharide units is required,[14] facilitating the binding of AT III and thrombin to the same polysaccharide chain (the so-called "bridge" or "template" mechanism) (Fig. 1).[15] In the formation of the heparin/AT III/thrombin ternary complex the unique PS sequence interacts specifically with AT III, and any sulfated oligosaccharide fragment along the heparin chain interacts in a less specific mode with thrombin.[15, 16] Our recent model of the heparin/AT III/thrombin ternary complex reveals that heparin analogues may be obtained when a thrombin-binding oligosaccharide is tethered to the nonreducing terminus of the AT III-binding pentasaccharide with a spacer about 50 atoms in length (Fig. 1).[17] To this end, glycoconjugate **I** (see Scheme 3) has been synthesized, which comprises the AT III-binding PS **1** (AT III-binding domain, ABD), a linear spacer, and a persulfated maltotrioside moiety (thrombin-binding domain, TBD). For the construction of a pentasaccharide (ABD) containing a functionalized molecular spacer at its nonreducing end, the following key synthetic steps have to be performed (Scheme 1): a) glycosylation of the tetrasaccharide acceptor **3** with 6-*O*-acetyl-4-*O*-(11-azido-3,6,9-trioxaundecane)-2,3-di-*O*-methyl-D-glucopyranosyl trichloroacetimidate (**2**) to give the protected pentasaccharide **4** having a 1-azidotetraethylene glycol moiety[18] and b) linkage of the amino group in compound **5** with the thioacetyl-substituted bifunctional spacer **6**, and subsequent *O*-sulfation.

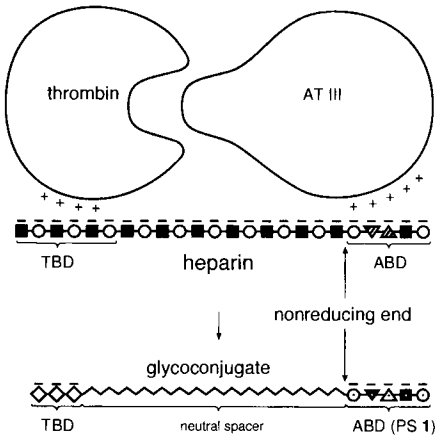

Fig. 1. Schematic representation of the heparin/AT III/thrombin ternary complex, leading to the concept of synthetic heparin analogues such as glycoconjugates **I**–**VI**.

To synthesize donor **2**, methyl 6-*O*-benzyl-2,3-di-*O*-methyl-α-D-glucopyranoside[19] was treated with tetraethylene glycol ditosylate in DMF in the presence of sodium hydride at 40 °C followed by addition of sodium azide to the reaction mixture and elevation of the temperature to 70 °C. Subsequent acetolysis using 1% sulfuric acid in acetic anhydride at −20 °C and treatment with piperidine and trichloroacetonitrile/cesium carbonate afforded the glycosyl donor **2** in 30% overall yield.

Trimethylsilyl trifluoromethanesulfonate (TMSOTf) mediated coupling of **2** with **3** at −20 °C afforded the α-linked pentasaccharide **4** in 65% yield after purification (Scheme 1). Concomitant hydrogenolysis of benzyl esters, benzyl ethers, and the azide group of **4** followed by saponification gave pentasaccharide **5** (75% overall yield), which bears an amino function for attaching the bifunctional spacer **6**. The latter was synthesized by a seven-step procedure starting from tetraethylene glycol: 1) monosilylation (*tert*-butyldimethylsilyl chloride/NaH in DMF), 2) introduction of a methylene carboxylate ester (NaH/*tert*-butylbromoacetate in DMF), 3) desilylation (tetrabutylammonium fluoride), 4) tosylation (tosyl chloride, pyridine, 20 h, room temperature), 5) substitution of tosylate with thioacetate (KSAc/acetone, 18 h, room temperature), 6) cleavage of the *tert*-butyl ester (trifluoroacetic acid in dichloromethane), and 7) activation of the carboxyl group (diisopropylcarbodiimide/*N*-hydroxysuccinimide) to give **6** in 20% overall yield.

Coupling of **5** with **6** afforded, after sulfation with triethylamine/sulfur trioxide complex in DMF at 50 °C, a mixture of **7a** and **7b**. HPLC and mass spectrometry indicated that the amide group in the spacer moiety was partly sulfated (65%) giving derivative **7a**. Nevertheless, this problem could be overcome easily: treatment of the crude mixture with 0.2 N hydrochloric acid at 0 °C for 24 h led to selective desulfation of the amide sulfate group (without any observed cleavage of the $O-SO_3^-$ bond) to give the desired ABD moiety **7b** in quantitative yield.

To equip glycoconjugate **I** with a spacer about 50 atoms in length, the polysulfated maltotrioside (TBD) fragment should bear a spacer about 25 atoms in length. In addition, the latter should carry a thiophilic group to allow coupling with the thiol

[*] Prof. Dr. C. A. A. van Boeckel, Dr. P. Westerduin, J. E. M. Basten, M. A. Broekhoven, V. de Kimpe, Dr. Ir. W. H. A. Kuijpers
Department of Medicinal Chemistry, N. V. Organon
P. O. Box 20, NL-5340 BH Oss (The Netherlands)
Fax: Int. code +(412) 662546

[**] This work was carried out in collaboration with Sanofi Recherche, France. We thank Dr. M. Petitou (Sanofi Recherche, France) for useful discussions, Dr. P. A. van Veelen (N. V. Organon) for the MALDI MS measurements, and T. G. van Dinther and E. van As (N. V. Organon) for determining the in vitro biological activities.

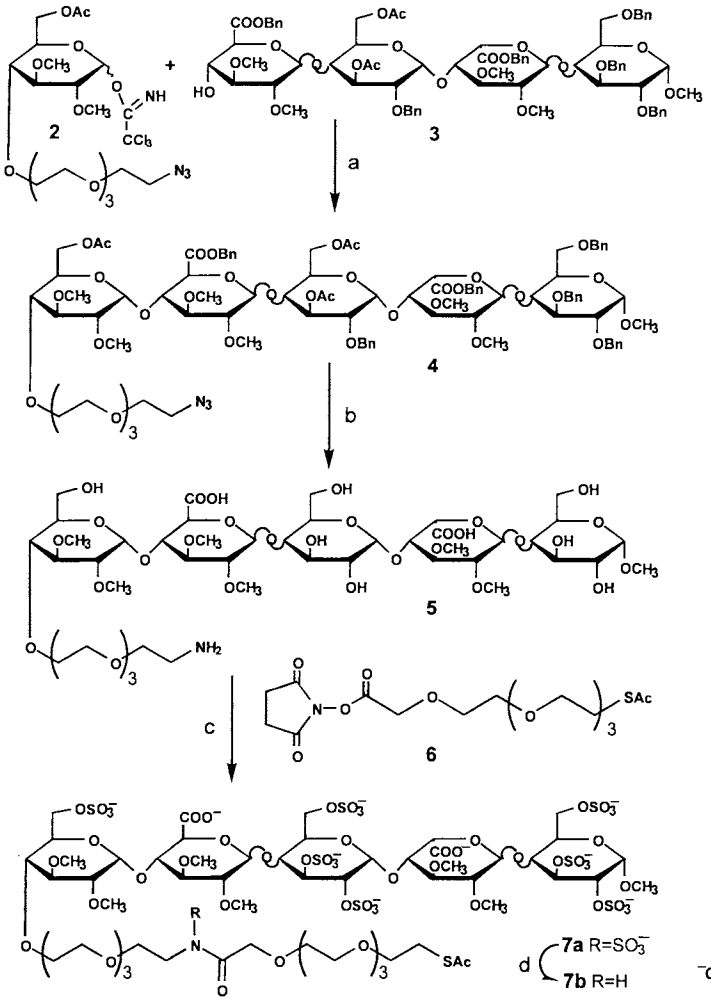

Scheme 1. a) TMSOTf, CH_2Cl_2, 4 Å molecular sieves, 1 h, −20 °C (65%); b) Pd/C, H_2, DMF, H_2O, HOAc, 24 h and 0.3 M NaOH, CH_3OH, H_2O, 1/1, v/v, 4 h (75%); c) H_2O, DMF, *N*-methylmorpholine, 15 min, (80%); $Et_3N{\cdot}SO_3$, DMF, 50 °C, 16 h; d) 0.2 N HCl, 24 h, 0 °C, (100%).

function of deprotected **7b**. Thus, TMSOTf-promoted coupling of peracetylated maltotriose trichloroacetimidate[20] and 1-azido-17-hydroxy-3,6,9,12,15-pentaoxaheptadecane[21] was performed giving 1-azidohexaethylene glycol glycoside **8**. Saponification, subsequent sulfation, and catalytic hydrogenation provided the polysulfated maltotrisaccharide 1-amino-hexaethylene glycol derivative **9** in 55% yield (Scheme 2), which was then condensed with sulfosuccinimidyl (4-iodoacetyl-amino)benzoate (**10**, sulfo-SIAB) to give the TBD moiety **11** in 70% yield after G-15 size exclusion chromatography (Scheme 3). The ABD and TBD units were linked in a one-step procedure. A solution of **7b** (ABD) and **11** (TBD) in 0.1 M sodium hydrogenphosphate buffer (pH 7.5) was treated with 0.05 M hydroxylamine under argon atmosphere to furnish, after G-50 size exclusion chromatography, conjugate **I** in 65% yield and in

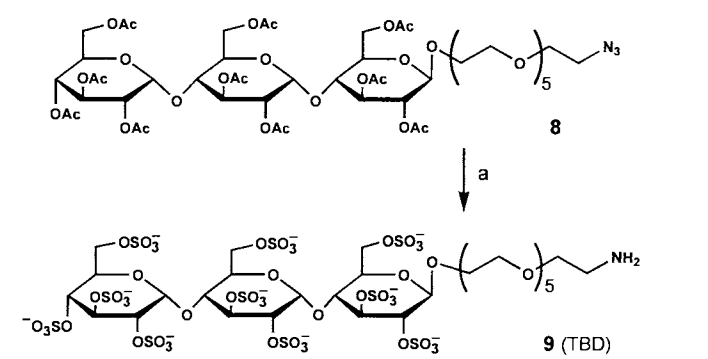

Scheme 2. a) KO*t*Bu, MeOH, 6 h; $Et_3N{\cdot}SO_3$, DMF, 50 °C, 16 h; Pd/C, H_2, H_2O, HOAc, 24 h (55%).

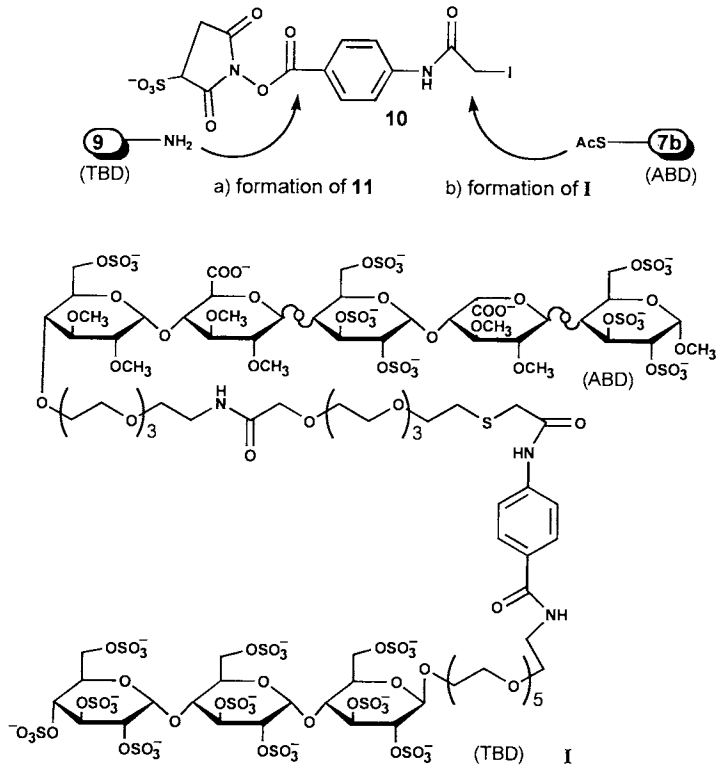

Scheme 3. a) sulfo-SIAB (**10**), DMF/H_2O (70%); b) **7b** and **11**, 0.1 M aqueous Na_2HPO_4 (pH 7.5), 0.05 M $NH_2OH{\cdot}HCl$, 4 h (65%).

excellent purity as revealed by ^1H NMR spectroscopy[22] and reversed UV capillary electrophoresis (**I** $[\alpha]_D^{21}$ 40.1 ($c = 1$ in water)). In addition, the identity of **I** was corroborated unambiguously by matrix-assisted laser desorption ionization (MALDI) mass spectrometry.[23, 24]

The ABD and TBD fragments in glycoconjugate **I** are separated by a 53-atom spacer, and the compound has roughly the same length as a heparin fragment of about 18 saccharide units. Indeed compound **I** displays a substantial antithrombin activity (Table 1), thus demonstrating that the syn-

Table 1. In vitro AT III-mediated anti-Xa and anti-thrombin activities of glycoconjugates **I**–**VI**, PS **1**, and heparin.

Compound	TBD moiety[a]	anti-Xa activity [U mg^{-1}]	anti-thrombin activity [U mg^{-1}]	anti-Xa/ anti-thrombin activity
I	maltotriose (10)	490	64	7.6
II	cellobiose (7)	740	10	74
III	maltopentaose (16)	280	330	0.9
IV	TBD = ABD (7)	770	14	55
V	TBD = ABD (9)	640	36	18
VI	TBD = ABD (11)	280	160	1.75
PS 1		1600	–	∞
heparin	oligosaccharide	160	160	1

[a] The number of sulfate groups in the TBD is in parentheses.

thesis of large, complex heparin-like oligosaccharides can be circumvented elegantly and efficiently by the demonstrated spacer strategy.

We also wished to study the requirements for the binding of TBD to thrombin. For this purpose a disaccharide and a pentasaccharide, cellobiose heptasulfate and maltopentaose hexadecasulfate, were prepared and attached to ABD **7b** in a similar fashion as described for conjugate **I**, furnishing ABD–TBD conjugates **II** ($[\alpha]_D^{21} = 24.8$ ($c = 1$ in water)) and **III** ($[\alpha]_D^{21} = 30.6$ ($c = 0.4$ in water)), respectively.

We were anxious to find out if the ATIII-binding pentasaccharide itself may also act as a thrombin-binding domain. These studies would require a symmetric pentasaccharide conjugate such as compound **IV**, which should be accessible by oxidative coupling of a thiol like **7b** after removal of the acetyl protecting group. Indeed, dimerization of functionalized pentasaccharide **7b** was accomplished in a single step by treatment with hydroxylamine in the presence of oxygen; the symmetric conjugate **IV** was isolated in 90% yield after G-50 size exclusion chromatography (Scheme 4). The identity of **IV** ($[\alpha]_D^{21} = 46.9$ ($c = 1$ in water)) was corroborated unambiguously by ^{1}H NMR spectroscopy and MALDI mass spectrometry.[25] Conjugates **V** ($[\alpha]_D^{21} = 42.9$ ($c = 1$ in water)) and **VI** ($[\alpha]_D^{21} = 31.6$ ($c = 0.82$ in water)) were obtained by procedures analogous to those used in the synthesis of **IV**.

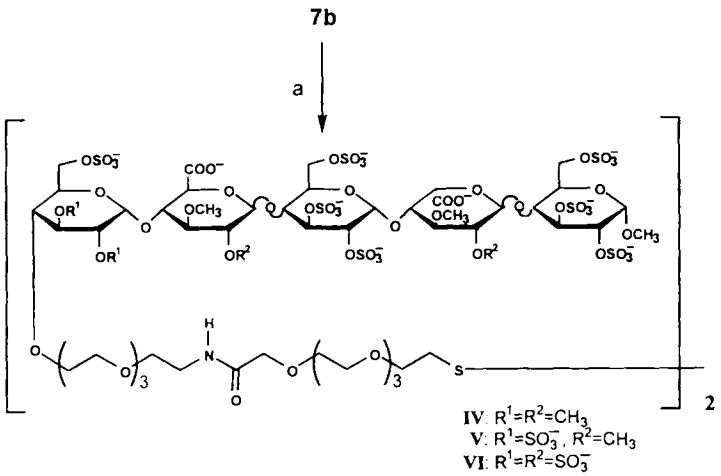

Scheme 4. a) 0.1 M aqueous Na_2HPO_4 (pH 7.5), 0.05 M $NH_2OH \cdot HCl$, O_2 stream, 16 h (90%).

The conjugates **I**–**VI** were tested in vitro for ATIII-mediated antifactor Xa and antithrombin activity, and the results were compared to those with heparin and PS **1** (Table 1). The glycoconjugates **I**–**VI** display good to strong ATIII-mediated antifactor Xa and antithrombin activity, while the activities of glycoconjugates **III** and **VI** even exceed that of heparin. It is clearly shown that the increase in charge of the TBD moiety gives rise to higher antithrombin activity. In this way, a chemical basis is provided for imparting a desired antifactor Xa and antithrombin activity to one synthetic glycoconjugate, leading to tailor-made antithrombotics.

Received: September 4, 1995 [Z 8366 IE]
German version: *Angew. Chem.* **1996**, *108*, 339–342

Keywords: antithrombotics · enzyme inhibitors · heparin

[1] B. Casu, *Adv. Carbohydr. Chem. Biochem.* **1985**, *43*, 51.
[2] *Heparin. Chemical and Biological Properties, Clinical Applications* (Eds.: D. A. Lane, U. Lindahl), Edward Arnold, London, **1989**.
[3] J. Choay, J. C. Lormeau, M. Petitou, P. Sinaÿ, J. Fareed, *Ann. NY Acad. Sci.* **1981**, *370*, 644.
[4] L. Thunberg, G. Backstrom, U. Lindahl, *Carbohydr. Res.* **1982**, *100*, 393.
[5] J. Choay, M. Petitou, J. C. Lormeau, P. Sinaÿ, B. Casu, G. Gatti, *Biochem. Biophys. Research Commun.* **1983**, *116*, 492.
[6] G. M. T. Vogel, D. G. Meuleman, F. G. M. Bourgondien, P. M. J. Hobbelen, *Thromb. Res.* **1989**, *54*, 399.
[7] M. Petitou, C. A. A. van Boeckel in *Progress in the Chemistry of Natural Products, Vol. 60* (Eds.: W. Hertz, G. W. Kirby, C. Tamm), Springer, Berlin, **1992**, p. 143.
[8] C. A. A. van Boeckel, M. Petitou, *Angew. Chem.* **1993**, *105*, 1741; *Angew. Chem. Int. Ed. Engl.* **1993**, *32*, 1671.
[9] P. D. J. Grootenhuis, C. A. A. van Boeckel, *J. Am. Chem. Soc.* **1991**, *113*, 2743.
[10] C. A. A. van Boeckel, P. D. J. Grootenhuis, A. Visser, *Nat. Struct. Biol.* **1994**, *1*, 423.
[11] J. Basten, G. Jaurand, G. Olde-Hanter, P. Duchaussoy, M. Petitou, C. A. A. van Boeckel, *Bioorg. Med. Chem. Lett.* **1992**, *2*, 905.
[12] H. Lucas, J. E. M. Basten, P. Konradsson, C. A. A. van Boeckel, *Angew. Chem.* **1993**, *105*, 462; *Angew. Chem. Int. Ed. Engl.* **1993**, *32*, 434.
[13] P. Westerduin, C. A. A. van Boeckel, J. E. M. Basten, M. A. Broekhoven, H. Lucas, A. Rood, H. van der Heijden, R. G. M. van Amsterdam, T. G. van Dinther, D. G. Meuleman, A. Visser, G. M. T. Vogel, J. B. L. Damm, G. T. Overklift, *Bioorg. Med. Chem.* **1994**, *2*, 1267.
[14] D. L. Lane, J. Denton, A. M. Flynn, L. Thunberg, U. Lindahl, *Biochem. J.* **1984**, *218*, 725.
[15] S. T. Olson, I. Björk, *J. Biol. Chem.* **1991**, *266*, 6353.
[16] S. T. Olson, H. R. Halvarson, I. Björk, *J. Biol. Chem.* **1991**, *266*, 6342.
[17] P. D. J. Grootenhuis, P. Westerduin, D. Meuleman, M. Petitou, C. A. A. van Boeckel, *Nat. Struct. Biol.* **1995**, *2*, 736.
[18] The imidate glycosylation procedure: R. R. Schmidt, *Angew. Chem.* **1986**, *98*, 213; *Angew. Chem. Int. Ed. Engl.* **1986**, *25*, 212.
[19] P. J. Garegg, H. Hultberg, *Carbohydrate Res.* **1981**, *93*, C10.
[20] Prepared in three steps from commercially available maltotriose by standard procedures.
[21] Prepared according to the method described for 1-azido-11-hydroxy-3,6,9-trioxaundecane: C. R. Bertozzi, M. D. Bednarski, *J. Org. Chem.* **1991**, *56*, 4326.
[22] **I**: ^{1}H NMR (Bruker BRX 400 spectrometer, 400 MHz, D_2O, 300 K, δ(HOD) = 4.76): ABD unit 1 (reducing end): δ = 5.19 (d, 1H, $J_{1,2}$ = 4.0 Hz, H-1), 4.20 (m, H-2), 4.69 (m, H-3), 4.01 (m, H-4), 4.08 (m, H-5), 4.4 (m, H-6, H-6'); ABD unit 2: 5.39 (br. s, 1H, H-1), 3.56 (m, H-2), 3.85 (m, H-3), 4.19 (m, H-4), 4.87 (d, 1H, $J_{4,5}$ = 3 Hz, H-5); unit 3: 5.44 (d, 1H, d, $J_{1,2}$ = 4.0 Hz, H-1), 4.62 (t, 1H, $J_{2,3}$ = 9.0 Hz, H-3), 4.06 (m, H-4), 4.25 (m, H-5); ABD unit 4: 4.71 (d, 1H, $J_{1,2}$ = 6.0 Hz, H-1), 3.29 (dd, 1H, $J_{1,3}$ = 6.0 Hz, $J_{2,3}$ = 7.0 Hz, H-2), 3.57 (m, H-4), 3.75 (m, H-5); ABD unit 5 (nonreducing end): 5.49 (d, 1H, $J_{1,2}$ = 3.0 Hz, H-1), 3.35 (dd, 1H, $J_{1,2}$ = 3.0 Hz, $J_{2,3}$ = 7.0 Hz, H-2), 3.57 (m, H-3), 3.48 (t, 1H, J = 7 Hz, H-4), 3.89 (m, H-5); TBD unit 1 (reducing end): 4.99 (d, 1H, $J_{1,2}$ = 5.0 Hz, H-1), 4.54 (t, 1H, J = 5 Hz, H-2), 4.18 (m, H-4), 4.62 (m, H-5); TBD unit 2: 5.57 (d, 1H, $J_{1,2}$ = 4.0 Hz, H-1), 4.69 (m, H-2), 4.95 (dd, 1H, J = 6, 7 Hz, H-3), 4.18 (m, H-4); TBD unit 3: 5.67 (d, 1H, $J_{1,2}$ = 4.0 Hz, H-1), 4.95 (m, H-3), 4.63 (m, H-4); Spacer: 2.63 (AB, 2H, J = 40, 16 Hz, $SCH_2C(O)$), 2.92 (t, 2H, J = 6.0 Hz, CH_2CH_2S).
[23] MALDI mass spectrometry of heparin derived oligosaccharides: P. Juhasz, K. Biemann, *Carbohydr. Res.* **1995**, *270*, 131.
[24] MALDI mass spectrum of mixed conjugate **I** (Vision 2000 spectrometer, $(Arg\text{-}Gly)_{10}$ as basic peptide for formation of ionic complexes, 3-hydroxypicolinic acid as matrix): calcd for ($\mathbf{I} + 2(Arg\text{-}Gly)_{10} + H^+$): 7971; found: 7972 ($M + 2(Arg\text{-}Gly)_{10} + H^+$).
[25] The ^{1}H NMR spectrum of the symmetric conjugate **IV** is virtually identical to the spectrum of its precursor **7b** (and the ABD carbohydrate part of compound **I** [22]), except for the CH_2S triplet: δ(**7b**) = 3.26 (t, CH_2SAc); δ(**IV**) = 2.79 (t, CH_2SSCH_2) (Bruker BRX 400 spectrometer, 400 MHz, D_2O, 300 K, δ(HOD) = 4.76); MALDI mass spectrum of symmetric conjugate **IV** (Vision 2000 spectrometer, $(Arg\text{-}Gly)_{10}$ as basic peptide for formation of ionic complexes, 3-hydroxypicolinic acid as matrix): MH^+ (**IV** + $2(Arg\text{-}Gly)_{10} + H^+$) found 8180, calcd 8181.2.

(15*R*)-16-*m*-Tolyl-17,18,19,20-tetranorisocarbacyclin: A Stable Ligand with High Binding Affinity and Selectivity for a Prostacyclin Receptor in the Central Nervous System**

Masaaki Suzuki,* Koichi Kato, Ryoji Noyori, Yumiko Watanabe, Hajime Takechi, Kiyoshi Matsumura, Bengt Långström, and Yasuyoshi Watanabe

Prostaglandins (PGs) are known to exhibit diverse biological activities controlling a wide range of physiological functions in the circulatory, reproductive respiratory, and digestive systems.[1] In recent years there has been strong interest in elucidating the role of PGs in brain function.[2]

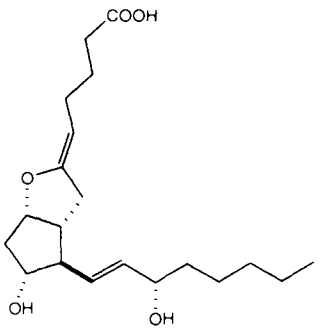

1

Prostacyclin (PGI_2, **1**) is a potent vasodilator and plays an important role in the circulatory system through antithrombotic actions.[3] Several lines of evidence suggest that PGI_2 has neuromodulatory actions as well.[4] Quite recently, a quantitative in vitro autoradiographic mapping of a PGI_2 receptor in the rat brain using [^{3}H]iloprost,[5] a stable specific agonist for a PGI_2 receptor, demonstrated a high density distribution in four regions of the lower brain stem including the medial and commissural subnuclei of the nucleus tractus solitarius (NTS).[6] Precise analysis of the role of PGI_2 in the brain requires the development of a specific molecular probe capable of sharply discriminating its action in the central and peripheral nervous systems. In this context, our interest has been directed towards designing a new ligand selectively responsive to a receptor in the central nervous system. We describe here a tolyl-functionalized isocarbacyclin derivative with high binding affinity and selectivity for a PGI_2 receptor in the thalamus.

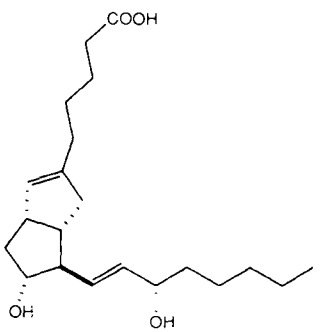

2

The title compound was devised based on the structural modification of the ω side chain of isocarbacyclin (**2**), a chemically stable PGI_2 agonist,[7] starting from the aldehyde intermediate **3**[8] shown in Scheme 1.[9] Incorporation of the tolyl group at the terminus of the the PG ω side chain in **3** was planned in the hope of later conversion into a $^{11}CH_3$-containing hypersensitive ligand usable for positron emission tomography (PET).[11] Thus the starting methyl *m*-tolylacetate **4**[12] was condensed with the anion of dimethyl methylphosphonate, which was generated by action of *n*-butyllithium in THF at −78 °C, to give the β-keto phosphonate **5** as a Horner–Emmons reagent in 48% yield.

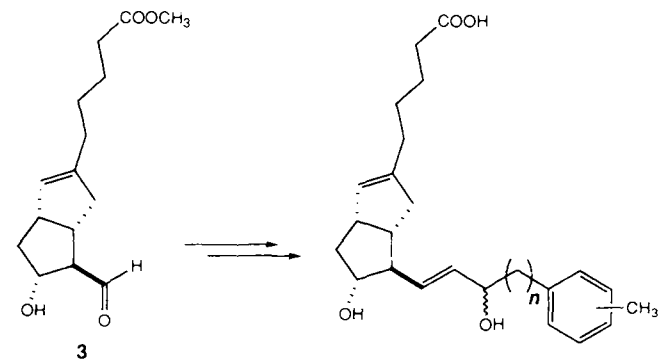

3

Scheme 1. Structural modification of the ω side chain.

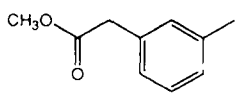

4

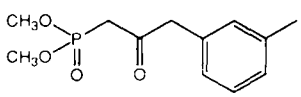

5

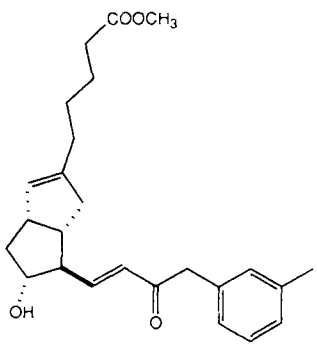

6

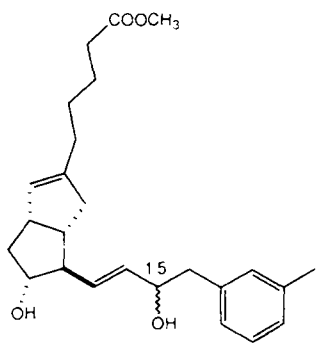

7

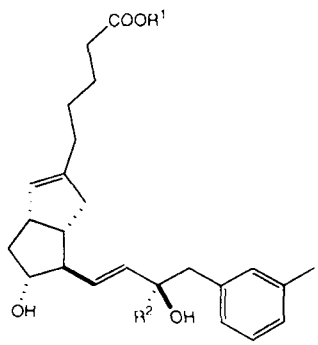

8, $R^1 = CH_3$; $R^2 = H$
10, $R^1 = H$; $R^2 = H$
[^{3}H]-**10**, $R^1 = H$; $R^2 = {}^3H$

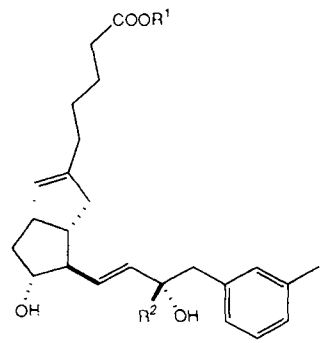

9, $R^1 = CH_3$; $R^2 = H$
11, $R^1 = H$; $R^2 = H$
[^{3}H]-**11**, $R^1 = H$; $R^2 = {}^3H$

[*] Prof. Dr. M. Suzuki
Department of Applied Chemistry, Faculty of Engineering
Gifu University, Gifu 501-11 (Japan)
Fax: Int. code +(58)293-2635
K. Kato, Prof. Dr. R. Noyori
Department of Chemistry, Nagoya University, Nagoya 464-01 (Japan)
Dr. Yumiko Watanabe, Dr. H. Takechi, Dr. K. Matsumura, Dr. Yasuyoshi Watanabe
Subtemtomole Biorecognition Project, Research Development Corporation of Japan and Department of Neuroscience, Osaka Bioscience Institute
Osaka 565 (Japan)
Prof. Dr. B. Långström
Department of Chemistry and PET Centre
Uppsala University, Uppsala (Sweden)

[**] This work was supported in part by a Grant-in-Aid from the Ministry of Education, Science, and Culture of Japan.

Other Horner–Emmons reagents required for the ω side-chain modification were prepared in a similar manner by combining the same phosphonate with the corresponding longer chain ester substrates.[14] The phosphonate **5** was then condensed with the aldehyde **3**[8] in 1,2-dimethoxyethane with sodium hydride as the base to afford the enone **6** in 96% yield, which then reduced with sodium borohydride in the presence of cerium(III) chloride in methanol to give the diol **7** (as a 1:1 mixture of stereoisomers at C-15) in quantitative yield. The stereoisomers were separated by conventional silica gel column chromatography to give the stereochemically pure alcohols **8** and **9** (each in 50% yield) as the less and more polar materials, respectively (TLC on silica gel (ethyl acetate/hexane 1/1) R_f = 0.26 and 0.18, respectively). Finally, alkaline hydrolysis of **8** and **9** led to the corresponding tolylisocarbacyclin derivatives **10** and **11** in quantitative yields.[13] Other tolylisocarbacyclin derivatives subjected to the binding assay were also synthesized by a similar method using the corresponding Horner–Emmons reagents as described above.[14, 15]

The absolute configuration at C-15 of the tolylisocarbacyclin derivatives **10** and **11** was determined unambiguously at the stage of the ester by chemical correlation[8] as outlined in Schemes 2 and 3. Thus selective masking of the double bond in one of the five-membered rings of **9** by transformation to a tricyclic compound followed by esterification of the C-15 hydroxyl group with (*S*)-α-methoxy-α-(trifluoromethyl)phenylacetyl chloride [(*S*)-MTPA chloride] gave the MTPA ester **12** (Scheme 2). Then, oxidative cleavage of the double bond in the ω side chain, reduction of the resulting aldehyde to give the alcohol, and MTPA esterification provided the tolyl group containing, optically active bis(MTPA) ester **13** and the tricyclic residue. The stereodefined ester (2*S*)-**13** was prepared independently from the optically pure glycerol derivative (2*S*)-**14** by Grignard reaction with an aldehyde and Barton's deoxygenation of the resulting alcohol (Scheme 3).[16] The corresponding diastereomeric mixture of (2*R*)- and (2*S*)-**13** was also prepared via the racemic **14**. HPLC analysis of these authentic samples indicated that the retention time of **13** obtained by degradation of the isocarbacyclin derivative **9** was identical with that of (2*S*)-**13**,[17] thus indicating that the C-15 stereocenter of **11** has the *S* configuration, and thereby the *R* configuration can be assigned to **10**.

The binding assay of the isocarbacyclin derivatives was conducted for PGI_2 receptor proteins in frozen tissue sections containing either the thalamus or the NTS as representative of the central or peripheral nervous systems, respectively, using C-15 tritium-labeled isocarbacyclin ([^{3}H]isocarbacyclin) as a radioligand. The 50% inhibitory concentrations of the binding (IC_{50} values) were determined on the basis of the degree of

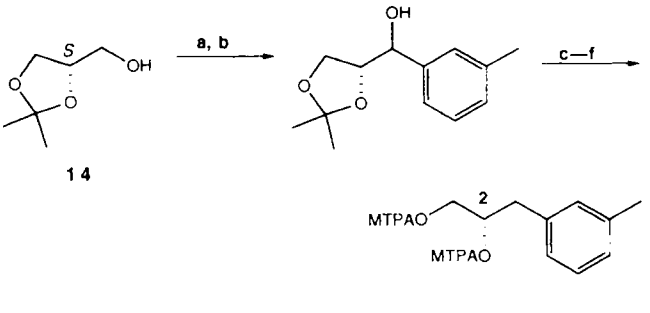

Scheme 3. a) PCC, CH_2Cl_2; b) *m*-$CH_3C_6H_4MgCl$, ether; c) NaH, THF, then CS_2, CH_3I, 98%; d) nBu_3SnH, toluene, reflux, 66%; e) CF_3COOH, THF/H_2O (4:1); f) (*S*)-MTPACl, pyridine.

displacement of 10 nM [^{3}H]isocarbacyclin bound to the receptor by its nonradioactive derivatives. We found that (15*R*)-16-*m*-tolyl-17,18,19,20-tetranorisocarbacyclin [**10**, referred to as (15*R*)-TIC], among other tolylisocarbacyclin derivatives, exhibited the highest binding affinity sufficient for a receptor in the thalamus (IC_{50} = 31 nM) but showed very weak binding with a receptor in the NTS (IC_{50} = 1.2 μM). The (15*S*) isomer **11** [referred to as (15*S*)-TIC] showed slightly lower binding (IC_{50} = 38 nM) in the thalamus than **10** and still maintained considerably strong binding affinity (IC_{50} = 32 nM) in the NTS. Other tolylisocarbacyclin derivatives[15] showed weaker thalamus binding affinity. Isocarbacyclin (**2**), the lead compound for this study, exhibited high binding affinity in the thalamus (IC_{50} = 31 nM) and NTS (IC_{50} = 23 nM). The resulting binding profile of (15*R*)-TIC (**10**), as illustrated by plots A and B in Figure 1,

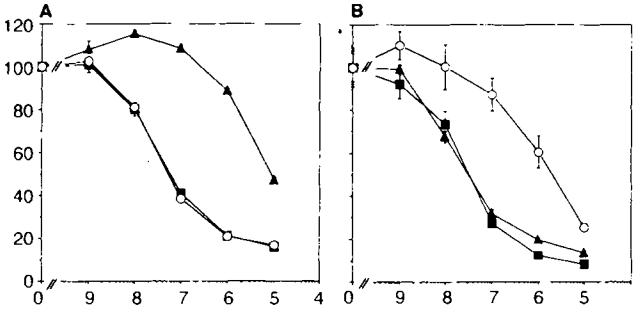

Fig. 1. Displacement of 10 nM [^{3}H]isocarbacyclin binding by nonradioactive (15*R*)-TIC (**10**) (○), isocarbacyclin (**2**) (■), and cicaprost (**15**) (▲) to thalamus (**A**) and the NTS (**B**) of rat brain. The frozen sections of rat brain (10 μm thick) containing thalamus and the NTS of medulla oblongata were incubated with 10 nM [^{3}H]isocarbacyclin in the absence or presence of different concentrations of the above displacers at 4 °C for 120 min. The sections were then washed, air-dried, and exposed to imaging plates (BAS TR2040, Fuji Film Co., Ltd., Tokyo, Japan). After calibration with plastic tritium scales, densitometric analysis of the radioautograms was performed with the image analyzing program NIH image. The quantitated data are expressed as % control of the 10 nM [^{3}H]isocarbacyclin binding without displacer. The plotted data are the means ± standard deviations of four determinations, each determination consisting of 5–8 sections. Some standard deviation bars are too small to be visible. The concentration of the ligands (−log M) is plotted on the x axes.

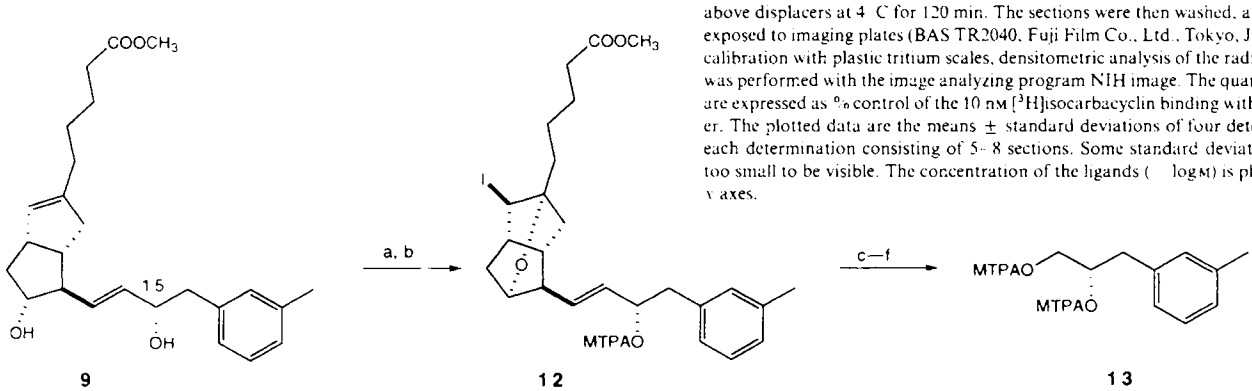

Scheme 2. a) I_2, CH_3OH, H_2O (3:1), 89%; b) (*S*)-MTPACl, pyridine, 92%; c) OsO_4, pyridine; d) $NaIO_4$, THF/ether/H_2O (2:1:1); e) $NaBH_4$, CH_3OH; f) (*S*)-MTPACl, pyridine, 20% overall yield from **12**.

contrasts markedly with that of cicaprost (**15**),[18] a stable PGI_2 agonist belonging to the iloprost family, which shows high binding affinity and selectivity for a PGI_2 receptor in the NTS (IC_{50} – 30 nM). In agreement with these binding experiments, (15*R*)-TIC (**10**) showed a very weak inhibitory effect (IC_{50} > 400 nM)[19] on platelet aggregation, while cicaprost (**15**) and isocarbacyclin (**2**) exhibit potent inhibitory effects (IC_{50} = 3.2 nM[18] and 2.5 nM[19], respectively). Thus we have succeeded in finding a stable PGI_2 analogue based on a structural modification of **2** which acts with high selectivity on the central nervous system.[20] We hope that this ligand will ameliorate the biological problems arising from the instability of PGI_2 and the lack of a stable analogue specific to a PGI_2 receptor expressed in the central nervous system.

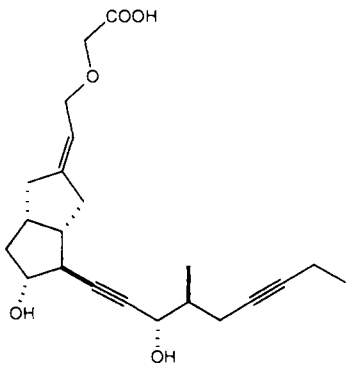

15

The fascinating binding characteristics of (15*R*)-TIC (**10**) and its potential usefulness as an efficient molecular probe for a PGI_2 receptor in the central nervous system prompted us to synthesize the corresponding tritium-labeled derivative. Thus radioisotope labeling was achieved at the stage of the enone **6** by reduction using [^{3}H]$NaBH_4$ (60 Ci mmol^{-1}) in the presence of cerium(III) chloride. The tritium-labeled compound [^{3}H]-**7** was obtained as a 1:1 mixture of epimers with a specific activity of roughly 15 Ci mmol^{-1}.[8, 21] Separation of these epimers with reversed-phase HPLC followed by ester hydrolysis gave [^{3}H]-(15*R*)-TIC ([^{3}H]-**10**) and [^{3}H]-(15*S*)-TIC ([^{3}H]-**11**) in pure forms.

The biological study, including the successful quantitative in vitro autoradiographic mapping of a new PGI_2 receptor subtype in the rat brain using [^{3}H]-(15*R*)-TIC, will be reported separately.[22]

Received: September 13, 1995 [Z 8399 IE]
German version: *Angew. Chem.* **1996**, *108*, 366–369

Keywords: prostacyclin receptors · tolylisocarbacyclin · molecular probes

[1] Reviews: N. A. Nelson, R. C. Kelly, R. A. Johnson, *Chem. Eng. News* **1982**, *60*, 30–44; J. R. Vane, *Angew. Chem.* **1983**, *95*, 782–794; *Angew. Chem. Int. Ed. Engl.* **1983**, *22*, 741–752; B. Samuelsson, *ibid.* **1983**, *95*, 854–864 and **1983**, *22*, 805–815; S. Bergström, *ibid.* **1983**, *95*, 865–873 and **1983**, *22*, 858–866; P. W. Collins, S. W. Djuric, *Chem. Rev.* **1993**, *93*, 1533–1564; see also: *Adv. Prostaglandin, Thromboxane, Leukotriene Res.* **1983–1995**, *11–23*.

[2] Reviews: L. S. Wolfe, F. Coceani, *Ann. Rev. Physiol.* **1979**, *41*, 669–684; L. S. Wolfe, *J. Neurochem.* **1982**, *38*, 1–14; T. Shimizu, L. S. Wolfe, *J. Neurochem.* **1990**, *55*, 1–15; O. Hayaishi, *FASEB J.* **1991**, *5*, 2575–2581.

[3] S. Moncada, R. Gryglewsky, S. Bunting, J. R. Vane, *Nature* **1976**, *263*, 663–665; P. J. Kadowitz, B. M. Chapnick, L. P. Feigen, A. L. Hyman, P. K. Nelson, E. W. Spannhake, *J. Appl. Physiol.* **1978**, *45*, 408–413; see also ref. [1].

[4] Y. Hori, M. Katori, Y. Harada, Y. Uchida, K. Tanaka, *Eur. J. Pharmacol.* **1986**, *132*, 47–52; D. J. Chapple, G. J. Dusting, J. R. Vane, *Br. J. Pharmacol.* **1980**, *68*, 437–447; O. Rimoldi, S. Pierini, M. R. Pagani, M. Pagani, *Cardiovasc. Res.* **1991**, *25*, 793–801; I. H. Zucker, M. J. Panzenbeck, S. Barker, W. Tan, A. Hajdu, *Am. J. Physiol.* **1988**, *254*, 424–430; H. I. Chen, M. W. Chapleau, T. S. McDowell, F. M. Abboud, *Circulation Res.* **1990**, *67*, 1394–1404; S. H. Ferreira, M. Nakamura, M. S. A. Castro, *Prostaglandins* **1978**, *16*, 31–37; G. J. Birrell, D. S. McQueen, A. Iggo, R. A. Coleman, B. D. Grubb, *Neurosci. Lett.* **1991**, *124*, 5–8; M. Devor, D. M. White, E. J. Goetzl, J. D. Levine, *Neuro Report* **1992**, *3*, 21–24; Y. O. Taiwo, J. D. Levine, *Brain Res.* **1990**, *537*, 372–374; T. Inoue, Y. Ito, *Br. J. Pharmacol.* **1985**, *84*, 289–298; M. Nakajima, N. Toda, *Eur. J. Pharmacol.* **1986**, *120*, 309–318; R. M. Gaion, M. Trento, *Br. J. Pharmacol.* **1983**, *80*, 279–286; Y. Makita, *ibid.* **1983**, *78*, 517–527; I. Bishai, F. Coceani, *Biochim. Biophys. Acta* **1981**, *664*, 1–9; T. Ogorochi, S. Narumiya, N. Mizuno, K. Yamashita, H. Miyazaki, O. Hayaishi, *J. Neurochem.* **1984**, *43*, 71–82.

[5] W. Skuballa, H. Vorbüggen, *Angew. Chem.* **1981**, *93*, 1080–1081; *Angew. Chem. Int. Ed. Engl.* **1981**, *20*, 1046–1048; W. Skuballa, H. Vorbrüggen, *Adv. Prostaglandin, Thromboxane, Leukotriene Res.* **1983**, *11*, 299–305.

[6] K. Matsumura, Yu. Watanabe, H. Onoe, Y. Watanabe, *Neuroscience* **1995**, *65*, 493–503.

[7] M. Shibasaki, Y. Torisawa, S. Ikegami, *Tetrahedron Lett.* **1983**, *24*, 3493–3496; Y. Mizushima, R. Igarashi, K. Hoshi, A. K. Sim, M. E. Cleland, H. Hayashi, J. Goto, *Prostaglandins* **1987**, *33*, 161–168.

[8] M. Suzuki, H. Koyano, R. Noyori, H. Hashimoto, M. Negishi, A. Ichikawa, S. Ito, *Tetrahedron* **1992**, *48*, 2635–2658.

[9] In this context, we recently synthesized an azido-functionalized isocarbacyclin derivative, referred to as APNIC[8], from the same aldehyde intermediate **3**. APNIC acts as a specific probe for a PGI_2 receptor in mastocytoma P-815 cells. We succeeded in identifying PGI_2 receptor proteins and determining their molecular weights in these cells and in porcine and human platelets for the first time by photoaffinity labeling with a [^{3}H]APNIC ligand[10].

[10] S. Ito, H. Hashimoto, M. Negishi, M. Suzuki, H. Koyano, R. Noyori, *J. Biol. Chem.* **1992**, *267*, 20326–20330; R. Noyori, M. Suzuki, *Science* **1993**, *259*, 44–45; R. Noyori, H. Koyano, M. Mori, R. Hirata, Y. Shiga, T. Kokura, M. Suzuki, *Pure Appl. Chem.* **1994**, *66*, 1999–2005.

[11] J. R. Barrio, J. C. Mazziotta, M. E. Phelps in *Positron Emission Tomography and Autoradiography* (Eds.: M. E. Phelps, J. C. Mazziotta, H. R. Schelbert), Raven, New York, **1986**, Chapters 10, 11.

[12] A. Dorville, I. M. Tranchepain, D. Vichard, W. Sather, R. Maroun, P. Ascher, B. P. Roques, *J. Med. Chem.* **1992**, *35*, 2551–2562.

[13] **10**: ^{1}H NMR (600 MHz, $CDCl_3$): δ = 1.2–1.7 (m, 7H, 2 CH_2, CH, 2 OH), 1.8–2.1 (m, 4H, 2 CH_2), 2.2–2.5 (m, 8H, CH_3, $CH_2C(O)$, CH_2, CH), 2.78 (dd, *J* = 6.4, 13.4 Hz, 1H, C*H*H), 2.87 (dd, *J* = 7.0, 13.4 Hz, 1H, C*H*H), 2.9–3.0 (br, 1H, allylic CH), 3.63 (dt, *J* = 7.4, 9.6 Hz, 1H, CHO), 4.35 (q, *J* = 6.6 Hz, 1H, CHO), 5.28 (d, *J* = 1.0 Hz, 1H, vinyl in ring), 5.44 (dd, *J* = 8.8, 15.4 Hz, 1H, vinyl in chain), 5.62 (dd, *J* = 6.6, 15.4 Hz, 1H, vinyl in chain), 7.00 (d, *J* = 7.4 Hz, 1H, aromatic), 7.02 (s, 1H, aromatic), 7.05 (d, *J* = 7.4 Hz, 1H, aromatic), 7.20 (t, *J* = 7.4 Hz, 1H, aromatic); ^{13}C NMR (67.5 MHz, $CDCl_3$): δ = 21.5, 24.4, 27.1, 30.5, 33.8, 39.3, 39.5, 44.1, 44.3, 45.7, 58.2, 73.7, 77.3, 126.7, 127.4, 128.4, 128.6, 130.4, 133.0, 134.3, 137.9, 138.2, 141.4, 178.7. **11**: ^{1}H NMR: δ = 1.2–1.7 (m, 7H), 1.8–2.1 (m, 4H), 2.2–2.5 (m, 8H), 2.80 (dd, *J* = 7.3, 13.6 Hz, 1H), 2.84 (dd, *J* = 5.9, 13.6 Hz, 1H), 2.9–3.0 (br, 1H), 3.73 (dt, *J* = 7.3, 9.5 Hz, 1H), 4.34 (q, *J* = 6.6 Hz, 1H), 5.29 (br. s, 1H), 5.47 (dd, *J* = 8.8, 15.4 Hz, 1H), 5.64 (dd, *J* = 6.6, 15.4 Hz, 1H), 7.01 (d, *J* = 7.4 Hz, 1H), 7.02 (s, 1H), 7.04 (d, *J* = 7.4 Hz, 1H), 7.20 (t, *J* = 7.4 Hz, 1H); ^{13}C NMR: δ = 21.5, 24.4, 27.0, 30.4, 33.8, 39.3, 39.4, 43.9, 44.3, 45.6, 58.1, 73.9, 77.3, 126.7, 127.3, 128.3, 128.9, 130.5, 133.4, 134.5, 137.8, 138.0, 141.2, 178.4.

[14] Details of the synthesis are not discussed because of space limitations.

[15] Other tolylisocarbacyclin derivatives synthesized in this study include: 17-*m*-tolyl-18,19,20-trinorisocarbacyclin (1:1 mixture of stereoisomers at C-15); 17-*p*-tolyl-18,19,20-trinorisocarbacyclin (1:1 mixture of stereoisomers at C-15); (15*R*)-18-*m*-tolyl-19,20-dinorisocarbacyclin; (15*S*)-18-*m*-tolyl-19,20-dinorisocarbacyclin; 19-*m*-tolyl-20-norisocarbacyclin (1:1 mixture of stereoisomers at C-15); 19-*p*-tolyl-20-norisocarbacyclin (1:1 mixture of stereoisomers at C-15).

[16] D. H. R. Barton, S. W. McCombie, *J. Chem. Soc. Perkin Trans.* **1975**, 1574–1585.

[17] Retention times for (2*S*)-**13** and (2*R*) **13** were 29.3 and 31.7 min, respectively (Jasco PU-980, CHIRALCEL-OD (Daicel), 0.46 cm × 25 cm, hexane/2-propanol (60:1), flow rate 1 mL min^{-1}).

[18] W. Skuballa, E. Schillinger, C.-S. Stürzebecher, H. Vorbrüggen, *J. Med. Chem.* **1986**, *29*, 313–315.

[19] The biological activity was examined at Teijin Co.

[20] In this context, a subtype of the PGI_2 receptor expressed in the central nervous system has been proposed: H. Takechi, K. Matsumura, Yu. Watanabe, K. Kato, R. Noyori, M. Suzuki, Y. Watanabe, *J. Biol. Chem.* submitted.

[21] The tritium incorporation was carried out at Amersham International plc, UK.

[22] Yu. Watanabe, H. Takechi, K. Matsumura, K. Kato, R. Noyori, M. Suzuki, Y. Watanabe, unpublished.

Supramolecular Catalysis of H/D Exchange in Malonate Ions by Macrocyclic Polyamines: A Model Enzyme with Enolase Activity**

Hicham Fenniri, Jean-Marie Lehn,* and Annie Marquis-Rigault

The enolization of carbonyl compounds such as carboxylic acids and ketones is a crucial event in a wide variety of key reactions in chemical and in biochemical transformations.[1] Examples include enzyme-catalyzed carbon- carbon bond formation,[2] racemization,[3] β-elimination,[4] and isomerization.[5] Model systems have been designed and schemes proposed for elucidating the many steps of this process.[6] Of special interest is the question how a catalytic group of an enzyme whose pK_a is usually less than 8 can efficiently abstract a proton from a substrate with a pK_a greater than 20.[7, 8]

We now report that binding malonate ions to the polyammonium macrocycles **1** and **2** greatly accelerates the H/D exchange at the CH_2 group. This supramolecular catalytic process[9] markedly facilitates enolization and provides information about the mechanistic factors involved.

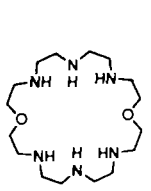

1 [24]ane N_6O_2

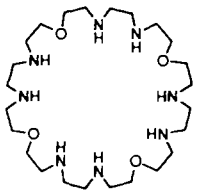

2 [36]ane N_8O_4

Macrocyclic polyamines possess the remarkable property of simultaneously 1) carrying a high positive charge through protonation,[10, 11] 2) presenting unprotonated nucleophilic sites, and 3) serving as a potential proton reservoir in a reaction on a bound substrate. These features come into play in the catalysis of ATP hydrolysis and of phosphorylation reactions by various macrocyclic polyamines, in particular by the [24]ane N_6O_2 macrocycle **1**.[9a, 12] It appeared that they could also provide a pathway for facilitating enolization processes.

Protonated macrocyclic polyamines form stable complexes with polycarboxylate substances.[11, 13] In particular, the protonated compound **1** binds malonate ions,[14] which are geometrically and electrostatically complementary to this receptor.[15] The predominant species around pH $\approx$ 7 is the complex between the tetraprotonated form of **1** and the malonate dianion;[16] it displays a stability constant of 240 M^{-1}.[14] Thus, **1** was a good candidate for investigating the effect of binding on the H/D exchange in malonate ions. The most extensive studies were performed with this more readily available compound **1** and complemented by experiments with macrocycle **2**.

The reaction was followed by ^1H NMR spectroscopy[17] ($D_2O > 98\%$) under different conditions to investigate the effects of pH, ionic strength, and temperature on the enolization process in the presence and absence of macrocycle **1**. It was found to display Michaelis-Menten kinetics with saturation behavior (Fig. 1). The Lineweaver-Burk plot of the same data (Fig. 1, insert) yielded $K_m = 3.8\,10^{-3}$ M and $k_{cat} = 1.75\ 10^{-3}\ s^{-1}$,

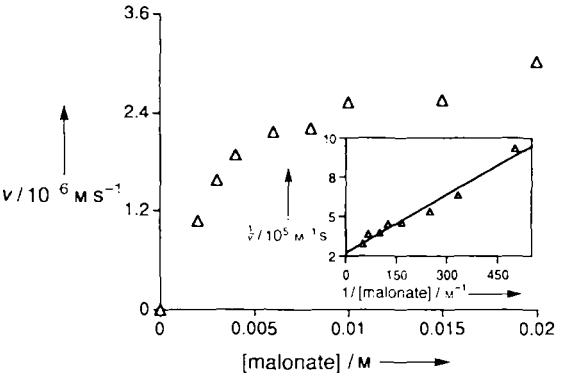

Fig. 1. Michaelis-Menten and Lineweaver-Burk (insert) plots for H/D exchange at the α position in malonate catalyzed by the macrocyclic polyamine **1**; [**1**] = 2 mM, [malonate] = 2, 3, 4, 6, 8, 12, 15, and 20 mM, pD = 7, 25 °C, D_2O; $K_m = 3.8 \times 10^{-3}$ M, $k_{cat} = 1.75 \times 10^{-3}\ s^{-1}$, $v_{max} = 3.5 \times 10^{-6}\ M\,s^{-1}$.

which gave a large rate enhancement ($k_{cat}/k_{uncat} \approx 1.4 \times 10^3$) relative to the uncatalyzed reaction ($k_{uncat} = 1.2 \times 10^{-6}\ s^{-1}$; Table 1).[18] Similar values were obtained from Eadie-Hofstee plots of v versus v/[malonate] (Table 1). In comparison, diethylenetriamine (DET), which is the reactive structural subunit of **1**, gave a rate acceleration of a factor of only about 6 (Table 1). As expected, the H/D exchange at the α position of malonate ions in the absence of **1** is more sensitive to acid catalysis than to base catalysis: the rate is slowest in the pH 7-11 range (Fig. 2).[19]

Table 1. Kinetic data for H/D exchange at the α position in malonate ions in the presence and absence of catalyst (25 °C, pD = 7 in D_2O).

Catalyst	k_{cat} [s^{-1}] [a]	K_m [M] [a]	v_{max} [$M\,s^{-1}$] [a]	k_{cat}/k_{uncat} [a]
-	1.2×10^{-6} [b]	-	-	-
DET	7.2×10^{-6} [c]	-	-	-
1	1.75×10^{-3}	3.8×10^{-3}	3.5×10^{-6}	1.4×10^3
	(1.62×10^{-3})	(4.0×10^{-3})	(3.25×10^{-6})	(1.3×10^3)
2	0.22	7×10^{-2}	2.16×10^{-5}	1.8×10^5
	(0.215)	(6.6×10^{-2})	(2.15×10^{-5})	(2.0×10^5)

[a] Data obtained from Lineweaver-Burk or from Eadie-Hofstee plots (values in parentheses) in a similar fashion for the two catalysts under the conditions given in Fig. 1 for **1** and in Ref. [23] for **2**; the pD was adjusted by addition of small amounts of NaOH or HCl and checked at the end of the reaction (less than $\pm$ 0.1 pD unit variation). [b] k_{uncat} is the slope of the relationship $v = k_{uncat}$ · [malonate] for [malonate] = 2, 5, and 10 mM. [c] k_{obs} obtained for [DET] = 2 mM and [malonate] = 10 mM; under the same conditions **1** gives $k_{obs} = 225 \times 10^{-6}\ s^{-1}$.

In the presence of the macrocycle **1** the rate depends on the protonation state of the polyamine. At low pH (< 2), malonate ions are protonated[16] and hence do not interact with the protonated polyamine; at high pH (> 10) the polyamine is unprotonated and does not bind malonate ions; at neutral pH, malonate is dianionic, and the polyamine is tetraprotonated,[10] allowing the formation of a moderately stable complex.[14] The rate acceleration in this pH domain indicates that the H/D exchange is catalyzed through complex formation, in agreement with the saturation kinetics, which indicates that the reaction proceeds through the formation of a Michaelis-Menten complex.

[*] Prof. Dr. J.-M. Lehn, Dr. A. Marquis-Rigault
Laboratoire de Chimie Supramoléculaire, URA 422 des CNRS
Institut Le Bel, Université Louis Pasteur
4 rue Blaise Pascal, F-67000 Strasbourg (France)
Fax: Int. code +(88)41 10 20
H. Fenniri
The Scripps Research Institute, La Jolla, California (USA)

[**] Communicated in part at the XVIIIth International Symposium on Macrocyclic Chemistry, Enschede, The Netherlands, 1993.

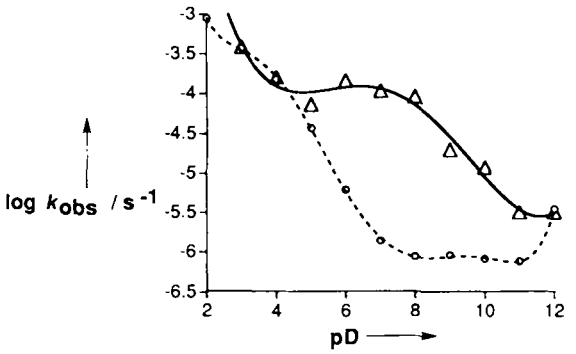

Fig. 2. Dependence of the observed rate constant for H/D exchange at the α position in malonate on pD in the presence (Δ) and absence (○) of the macrocyclic polyamine **1**; [**1**] = 2 mM, [malonate] = 10 mM, [$NaClO_4$] = 100 mM, 25 °C, D_2O.

Ionic strength has a negligible effect on the uncatalyzed reaction, whereas in the presence of a large excess of NaCl (500 equiv) the polyamine can be completely inhibited.[20]

The highest rate acceleration was obtained for the octa ammine [36]ane N_8O_4 **2**[21, 22] for which $k_{cat}/k_{uncat} \approx 1.8 \times 10^5$ (Table 1).[18, 23] This result is seemingly at variance with the apparent structural features of **2**, such as its ring size. It may indicate that the protonated polyamine **2** adopts a special conformation responsible for its high activity. Indeed, the crystal structure of the octahydrobromide of **2**[24] displays a pocket-shaped conformation into which a malonate unit would fit quite well.

The complexation of the dianionic substrate by the polyprotonated receptors could accelerate the rate of H/D exchange by activating the enolization through several combined effects: 1) neutralization of the negative charges resulting in a dicationic complex; 2) electrostatic facilitation of the approach of an electron rich base; 3) introduction of acidic proton transfer sites NH^+ and of weakly basic sites (the central N of each triamine subunit, which might participate in proton abstraction)

Electrophilic catalysis in the case of mandelic acid enolization can induce a decrease of the pK_a of the α-CH site by up to 15 units upon protonation of the carbonyl group,[4a, 8b, 8c] and concerted general acid–base catalysis is capable of providing a low-energy route for α-proton exchange.[4a] In the present case, more or less concerted proton abstraction from the CH_2 group and proton transfer to one of the carboxylates of the malonate dianion would yield a dianionic species $^-O_2CCH{\cdot}C(O^-)OH$; the conservation of the dianionic character of the substrate would ensure that it is bound throughout the whole process; such a (strongly) hydrogen-bonded enolate intermediate could be compatible with the requirements for electrophilic catalysis of α-proton exchange.[4a] Transfer of a second proton would lead to a less well (but perhaps sufficiently) bound intermediate $^-O_2CCH{\cdot}C(OH)_2$. Rapid reprotonation of either species at the α-C atom and back-transfer of the OH proton(s) regenerates the (exchanged) malonate ion. Whatever the exact amount of negative charge generated and the timing of the proton transfer processes, it is clear that stabilization of the intermediate and transition states is provided by strong electrostatic interaction between the anionic substrate and the cationic receptor, with respect to the corresponding intermediates for unbound malonate ions. Structure **3** represents schematically one of the possible arrangements of the substrate and the receptor in the reactive supramolecular species with an external base as proton abstraction agent.

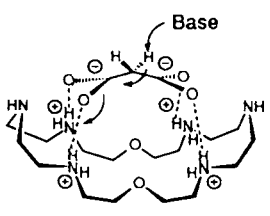

3

The present systems provide models for supramolecular electrophilic catalysis in the activation of α-proton exchange in carboxylic acids. High rate accelerations are achieved by structurally very simple macrocyclic polyamine receptors; they compare favorably with those displayed by catalytic antibodies[25] and by hydrogen-bonded supramolecular species that operate in organic solvents[26] (acceleration factors of about 10^4 and 10^3, respectively). It may be possible to obtain even larger rate increases by exploring further structural variations. Extension to H/D exchange in ketoacids (such as pyruvate)[27] and to aldolization reactions may be considered. Such studies give insight into the factors that control the activation of proton transfer and the catalysis of reactions involving this process.

Received: April 29, 1995
Revised version: October 16, 1995 [Z 7944 IE]
German version: *Angew. Chem.* **1996**, *108*, 337–339

Keywords: enolization · macrocycles · proton transfer · supramolecular chemistry

[1] a) W. P. Jencks, *Catalysis in Chemistry and Enzymology*, McGraw-Hill, New York, **1969**; b) I. A. Rose, *Methods Enzymol.* **1982**, *87*, 84.
[2] a) L. C. Kurz, S. Shah, B. R. Crane, L. J. Donald, H. W. Duckworth, G. R. Drysdale, *Biochemistry* **1992**, *31*, 7899; b) P. Dowd, S. W. Ham, S. J. Geib, *J. Am. Chem. Soc.* **1991**, *113*, 7734; c) J. R. Knowles, *Annu. Rev. Biochem.* **1989**, *58*, 195.
[3] a) V. M. Powers, C. W. Koo, G. L. Kenyon, J. A. Gerlt, J. W. Kozarich, *Biochemistry* **1991**, *30*, 9255; b) W. J. Albery, J. R. Knowles, *ibid.* **1986**, *25*, 2572.
[4] a) J. A. Gerlt, P. G. Gassman, *J. Am. Chem. Soc.* **1992**, *114*, 5928; b) V. E. Anderson in *Enzyme Mechanisms from Isotope Effects* (Ed.: P. F. Cook), CRC Press, Cleveland, **1991**, Chap. 16.
[5] a) P. J. Lodi, J. R. Knowles, *Biochemistry* **1993**, *32*, 4338; b) J. R. Knowles, *Nature* **1991**, *350*, 121; c) L. Xue, P. Talalay, A. S. Mildvan, *Biochemistry* **1990**, *29*, 7491.
[6] a) E. T. Harper, M. L. Bender, *J. Am. Chem. Soc.* **1965**, *87*, 5625; b) R. P. Bell, D. W. Earls, *J. Chem. Soc. Perkin Trans. 2* **1976**, 45; c) R. P. Bell, S. Grainger, *ibid.* **1976**, 1367; d) B. M. Tadayoni, J. Huff, J. Rebek, Jr., *J. Am. Chem. Soc.* **1991**, *113*, 2247; e) F. Cramer, *Chem. Ber.* **1953**, *86*, 1576; f) A. J. Kirby, *Adv. Phys. Org. Chem.* **1980**, *17*, 183; g) J. R. Keefe, A. J. Kresge in *The Chemistry of Enols* (Ed.: H. Rappoport), Wiley, New York, **1990**, Chap. 7; h) A. F. Hegarty, J. Dawling, *J. Chem. Soc. Chem. Commun.* **1991**, 996; i) A. F. Hegarty, W. P. Jencks, *J. Am. Chem. Soc.* **1975**, *97*, 7188; j) W. J. Albery, *J. Chem. Soc. Faraday Trans. 1* **1982**, 1579; k) R. Breslow, A. Graff, *J. Am. Chem. Soc.* **1993**, *115*, 10988; l) J. Wolfe, A. Muehldorf, J. Rebek, Jr., *ibid.* **1991**, *113*, 1453; m) B. Siegel, A. Pinter, R. Breslow, *ibid.* **1977**, *99*, 2309.
[7] J. A. Gerlt, J. W. Kozarich, G. L. Kenyon, P. G. Gassman, *J. Am. Chem. Soc.* **1991**, *113*, 9667.
[8] a) P. Renaud, M. A. Fox, *J. Am. Chem. Soc.* **1988**, *110*, 5705; b) A. J. Kresge, *Pure Appl. Chem.* **1991**, *63*, 213; c) Y. Chiang, A. J. Kresge, *Science* **1991**, *253*, 395; d) B. Zeng, R. M. Pollack, *J. Am. Chem. Soc.* **1991**, *113*, 3838.
[9] a) J.-M. Lehn, *Pure Appl. Chem.* **1979**, *51*, 979; *Ann. N. Y. Acad. Sci.* **1986**, *471*, 41; *Angew. Chem.* **1988**, *100*, 91; *Angew. Chem. Int. Ed. Engl.* **1988**, *27*, 89; b) C. Sirlin, *Bull. Soc. Chim. Fr. 2* **1984**, 5.
[10] B. Dietrich, M. W. Hosseini, J.-M. Lehn, R. B. Sessions, *Helv. Chim. Acta* **1983**, *66*, 1262.
[11] a) A. Bianchi, M. Micheloni, P. Paoletti, *Coord. Chem. Rev.* **1991**, *110*, 17; b) E. Kimura, *Top. Curr. Chem.* **1985**, *128*, 113.
[12] Review: M. W. Hosseini, *Bioorg. Chem. Front.* **1993**, *3*, 67.
[13] a) B. Dietrich, M. W. Hosseini, J.-M. Lehn, R. B. Sessions, *J. Am. Chem. Soc.* **1981**, *103*, 1282; b) M. W. Hosseini, J. M. Lehn, *Helv. Chim. Acta* **1986**, *69*, 587; c) *ibid.* **1988**, *71*, 749.
[14] R. J. Motekaitis, A. E. Martell, *Inorg. Chem.* **1992**, *31*, 5534.
[15] Crystal structure of the hexahydrochloride of **1**: S. Boudon, A. DeCian, J. Fischer, M. W. Hosseini, J. M. Lehn, G. Wipff, *J. Coord. Chem.* **1991**, *23*, 113.
[16] Ionization constants: $pK_a = 2.63$ and 5.27 [14].
[17] The course of the reaction was monitored at 25 ± 3 °C with the integrated CH_2 signal. The exchange of each proton and the isotope effect of the first exchange on the second one were studied [19]. Since we followed the exchange of both protons, the present values constitute a lower limit for the H/D exchange rate. The spectra were recorded 1–5 min after sample mixing. Concentration, pH, and temperature are given in the legend of each figure. The pH was adjusted by adding very small volumes of concentrated aqueous HCl or NaOH.

[18] It was not possible to perform measurements under saturation conditions, because the rates k_{obs} became too fast for determination by the NMR method. The factor of about 100 between the ratios k_{cat}/k_{uncat} produced by **1** and **2** can also be illustrated by the fact that, at the same malonate concentration (10 mM), k_{obs} for **2** is about the same as that for **1** (about 260×10^{-6} s^{-1}) at a 20-fold lower concentration (10^{-4} M for **1** versus 10^{-3} M for **2**, that is, under conditions much further from saturation for **2** than for **1**.
[19] E. W. Hansen, P. Ruoff, *J. Phys. Chem.* **1988**, *92*, 2641.
[20] Cl^--forms stable complexes with protonated polyamines (M. W. Hosseini, J. P. Kintzinger, J. M. Lehn, A. Zahidi, *Helv. Chim. Acta* **1989**, *72*, 1078). Furthermore, Na^+ can compete with H^+ for the interaction with the polyamine [13c].
[21] This macrocycle had been synthesized in the course of other work: A. Marquis-Rigault, J.-M. Lehn, unpublished results; another approach has been reported recently [22].
[22] T. Shimada, M. Kodera, H. Okawa, S. Kida, *J. Chem. Soc. Dalton Trans.* **1992**, 1121.
[23] [**2**] = 10^{-4} M, [malonate] = $2.5 \times 10^{-3} - 10^{-2}$ M. Lineweaver-Burk plot (6 points, $r = 0.996$).
[24] N. Kyritsakas, J. Fischer, H. Fenniri, J.-M. Lehn, unpublished result.
[25] Rate acceleration for proton transfer to an enol ether catalyzed by a catalytic antibody: J. L. Reymond, G. K. Jahangiri, C. Stoudt, R. A. Lerner, *J. Am. Chem. Soc.* **1993**, *115*, 3909.
[26] J. Wolf, A. Castero, J. Rebek, Jr., *Israel J. Chem.* **1992**, *32*, 97.
[27] H. Fenniri, C. Dallaire, J.-M. Lehn, unpublished results.

Effects of Strained Bicyclic Annelation on the Benzene Nucleus: The X-Ray Crystal Structures of a Triphenylene and Two Anthracene Derivatives**

Francesca Cardullo, Daniele Giuffrida, Franz H. Kohnke,* Françisco M. Raymo, J. Fraser Stoddart, and David J. Williams

In the course of our studies on the assembly of molecular doughnuts, cages, and ribbons using repetitive Diels–Alder reactions between molecular building blocks containing endocyclic dienophilic double bonds, and exocyclic butadiene units grafted onto either norbornane or 7-oxanorbornane skeletons, we have synthesized the bisdienophiles **1** and **2** and the trisdienophiles **3**.[1] Here we report[2, 3] on the X-ray structural analyses of *anti*-**1b**, *anti*-**1c**, and *anti*-**3**. The structure of *anti*-**3** shows significant bond length alternation within its benzene unit. This feature is not observed in *anti*-**1b** and *anti*-**1c**.

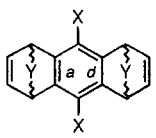

1a: X = H; Y = O
b: X = Me; Y = CH_2
c: X = Br; Y = O

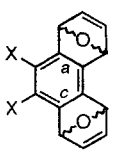

2a: X = H
b: X = Me

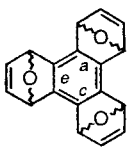

3

Bond length alternation within the benzene nucleus as a result of annelation to small rings was first postulated by Mills and Nixon.[4] Although they based their work on the wrong model of benzene, the idea that annelation to small rings could induce bond length alternation has survived up to the currently accepted model of benzene.[5] Multiple angular [*a*,*c*] and [*a*,*c*,*e*] annelation was expected to be more effective at promoting bond length alternation than linear [*a*,*d*] bisannelation because in the former case the strain imposed by each of the small rings on to the benzene nucleus would act cooperatively. However, with the exception of compound **8**,[6] in which electronic factors play a major role, the latest findings indicate that there is no significant bond length alternation in the planar compounds **4**–**7**.[7] In

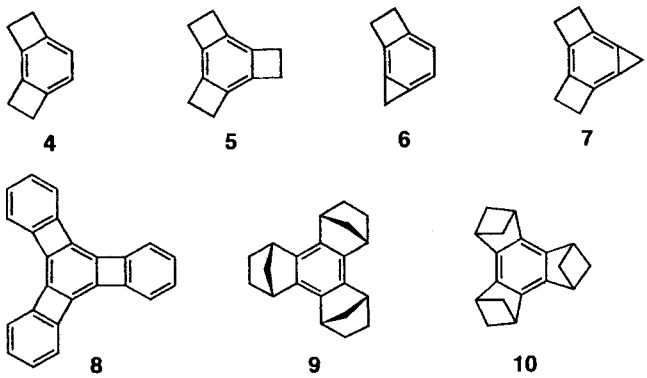

4 **5** **6** **7**

8 **9** **10**

these compounds angular distorsion appears to lead to the formation of bent bonds instead.[7] Yet the crucial role of strained bicyclic annelation in the induction of bond length alternation in the benzene nucleus has recently been fully confirmed by the results of computational and X-ray structural analysis of **9**[8] and **10**[9], and the interpretation of this effect in terms of the Mills–Nixon theory has finally been rejected.[9]

Besides angular strain, bicyclic annelation such as that in **1**–**3** is recognized to introduce anomalous effects by σ through-bond coupling of the attached framework and additional coupling to the σ-linked π bonding orbitals of the ethylenic group.[10]

In the X-ray crystal structure of *anti*-**3**[2] (Fig. 1) the average lengths of the bonds in the benzene ring *endo* and *exo* to the annelated bicyclic systems are 1.425 and 1.353 Å, respectively.

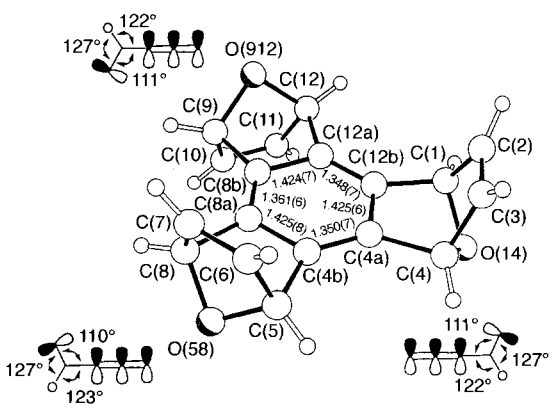

Fig. 1. The X-ray crystal structure of *anti*-**3**. The values of relevant dihedral angles involving the oxygen bridges are indicated beside each associated ring system.

[*] Prof. F. H. Kohnke, F. Cardullo, Dr. D. Giuffrida, F. M. Raymo
Dipartimento di Chimica Organica e Biologica
Università di Messina
Salita Sperone 31, I-98166 Messina (Italy)
Fax: Int. code +(90)393895
Prof. J. F. Stoddart
School of Chemistry, The University of Birmingham
Edgbaston, GB-Birmingham B15 2TT (UK)
Dr. D. J. Williams
Chemical Crystallography Laboratory, Department of Chemistry
Imperial College of Science, Technology and Medicine
South Kensington, GB-London SW7 2AY (UK)

[**] This work was sponsored by the Consiglio Nazionale delle Ricerche (Italy) and the Engineering and Physical Sciences Research Council (UK).

The corresponding values observed for **9** (1.417 and 1.379 Å) and for **10** (1.438 and 1.349 Å) indicate that bond length alternation in *anti*-**3** is intermediate to those in these two hydrocarbons. This is consistent with the increasing angular distortion of the σ bonds between the aromatic and the methine carbon atoms, which subtend with the *endo* bond angles of 106.5, 104, and 102.3° in **9**, *anti*-**3**, and **10**, respectively. In the recently reported structure of **3** calculated at the 6-31G(d) level,[11] the bond lengths are 1.438 Å (*exo*) and 1.340 Å (*endo*); the angles formed by the σ bonds between the arene and the methine carbon atoms and the *endo* annelated bonds are 103.0°.

Accompanying the pronounced bond alternation within the benzene nucleus in *anti*-**3**, there are subtle perturbations in the conformation of the molecule as a whole. The oxymethine carbon atoms all lie slightly out of the plane of the benzene nucleus: the deviations, which are in the range of 0.02–0.05 Å, are consistent with a repulsion between the oxygen lone pairs and the aromatic π system. Thus, C(9) and C(12) lie below the plane of the aromatic ring, while C(1) and C(4), and C(5) and C(8) all lie above this plane (Fig. 1). The dihedral angle between the plane containing the oxygen bridge and the one containing the olefinic double bond is in each case greater than that formed by the plane containing the oxygen bridge and the plane containing the pair of annelated aromatic carbon atoms. Thus, the repulsive interaction of the oxygen lone pairs is more pronounced in the former case than in the latter. A study of the packing of the molecules in the crystal reveals (Fig. 2) an elegant network of weak but cooperative C–H···O hydrogen bonds, involving both olefinic and methine hydrogen atoms. All three oxygen atoms within each molecule are implicated in hydrogen bonding interactions.[12]

The structural evidence obtained previously[13] supports the proposal that when the benzenoid ring is linearly bisannelated with bicyclic units, no significant bond alternation occurs within the aromatic ring. Further direct evidence for the absence of bond alternation is provided by the crystal structures of *anti*-**1b** and *anti*-**1c** (Fig. 3). Both of these structures have molecular C_{2h} and crystallographic C_i symmetry. In *anti*-**1c** the methine carbon atoms lie 0.023 and 0.041 Å out of the aromatic ring plane in a direction opposite to that of the bridging oxygen atoms. In *anti*-**1b** this effect is not observed to any significant extent. In *anti*-**1c** the dihedral angles between the principal planes within the bicyclic residues, that is, those containing the olefinic bond and the oxygen bridge, do not differ significantly from those observed in *anti*-**3**. In *anti*-**1b** the replacement of the oxygen atoms by methylene groups is accompanied by a reduction in the analogous dihedral angle (123.9° in **1b**, cf. 126.2° in **1c**, Fig. 3). An inspection of the packing of the molecules in both these structures does not reveal any notable intermolecular interactions.

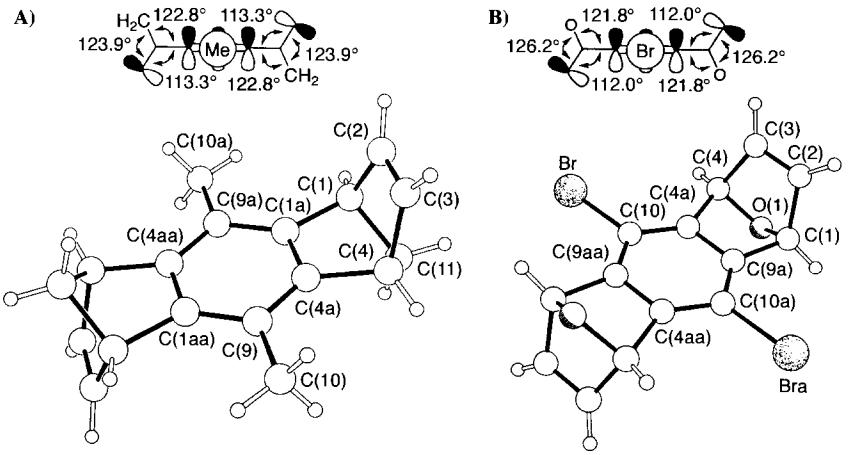

Fig. 3. The X-ray crystal structures of A) *anti*-**1b** and B) *anti*-**1c**. The relevant dihedral angles involving the one-atom bridges are indicated beside each associated ring system.

In contrast with the structures observed for the linear bisdienophiles, the bond length alternations observed for the benzene rings in the crystal structures of the bisdienophiles **2b**[14] confirms that the angular fusion allows the two 2,5-dihydrofuran residues to act upon the aromatic nucleus in a cooperative manner. The relative magnitudes of the effects in **2b** (average lengths of the *endo* and *exo* bonds are 1.422 and 1.367 Å, respectively) and in *anti*-**3** are consistent with this.

The definitive experimental evidence for bond alternation provided by the structure of *anti*-**3** and support for the predicted through-space and through-bond interactions between the aromatic ring and the bicyclic annelated units provides an explanation for the difficulties encountered[1d] in the synthesis of angularly annelated systems.

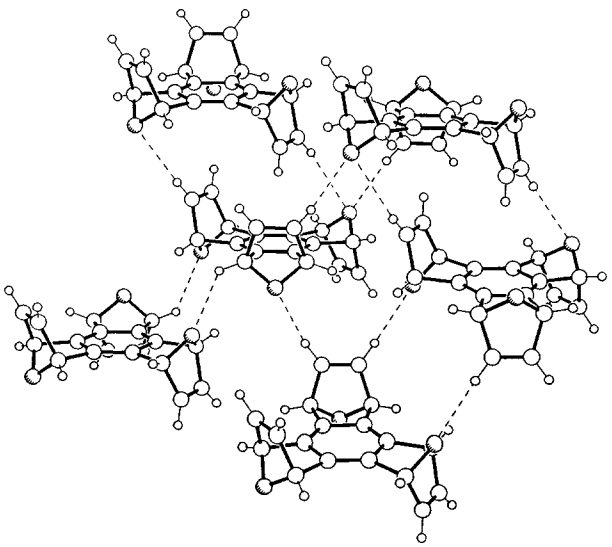

Fig. 2. The packing of *anti*-**3** in the solid state; the elegant network of C–H···O hydrogen bonds is indicated by the dotted lines.

Received: July 17, 1995
Revised version: October 5, 1995 [Z 8211 IE]
German version: *Angew. Chem.* **1996**, *108*, 347–349

Keywords: bond-length alternation · Mills–Nixon effect · polycycles · strained rings · triepoxytriphenylenes

[1] a) P. R. Ashton, G. R. Brown, N. S. Isaacs, D. Giuffrida, F. H. Kohnke, J. P. Mathias, A. M. Z. Slawin, D. R. Smith, J. F. Stoddart, D. J. Williams, *J. Am. Chem. Soc.* **1992**, *144*, 6330–6353; b) P. R. Ashton, U. Girreser, D. Giuffrida, F. H. Kohnke, J. P. Mathias, F. M. Raymo, A. M. Z. Slawin, J. F. Stoddart, D. J. Williams, *ibid.* **1993**, *115*, 5422–5429; c) For **1b** see: H. Hart, C. Lai, G. C. Nowkogu, S. Shamouilian, *Tetrahedron* **1987**, *43*, 5203–5224; d) For **1c** and **3** see also: F. M. Raymo, F. H. Kohnke, F. Cardullo, U. Girreser, J. F. Stoddart, *Tetrahedron*, **1992**, *48*, 6827–6838 and references therein.

[2] Crystal data for *anti*-**3**: monoclinic, $a = 13.718(2)$, $b = 8.661(2)$, $c = 11.178(2)$ Å, $\beta = 102.62(2)°$, $V = 1295.9(4)$ Å^3, space group $P2_1/c$, $Z = 4$, $\mu(Cu_{K\alpha}) = 7.8$ cm^{-1}, $\rho_{calcd} = 1.42$ g cm^{-3}. Siemens P3/PC diffractometer, ω scans, $Cu_{K\alpha}$ radiation (graphite monochromator). The structure was solved by direct methods and the non-hydrogen atoms refined anisotropically to give $R = 0.061$,

$R_w = 0.057$ for 1097 independent observed reflections [$2\theta = 3$–$116°$, $|F_o| > 3\sigma(|F_o|)$]. b) Further details of the crystal structure investigations can be obtained from the Director of the Cambridge Crystallographic Data Centre, 12, Union Road, GB-Cambridge CB2 1EZ (UK), by quoting the full literature citation.

[3] Crystal data for *anti*-**1b**: monoclinic, $a = 8.420(16)$, $b = 7.364(13)$, $c = 10.90(2)$ Å, $\beta = 109.7(2)°$, $V = 637(2)$ Å^3, space group $P2_1/c$, $Z = 2$, $\mu(Cu_{K\alpha}) = 5.1$ cm^{-1}, $\rho_{calcd} = 1.22$ g cm^{-3}. Crystal data for *anti*-**1c**: monoclinic, $a = 4.956(2)$, $b = 15.915(2)$, $c = 7.493(2)$ Å, $\beta = 93.36(2)°$, $V = 590.0(3)$ Å^3, space group $P2_1$, a, $Z = 2$, $\mu(Cu_{K\alpha}) = 86.4$ cm^{-1}, $\rho_{calcd} = 2.07$ g cm^{-3}. Siemens P3 PC diffractometer (for *anti*-**1b**), Nicolet R3m/E diffractometer (for *anti*-**1c**), ω scans, $Cu_{K\alpha}$ radiation (graphite monochromator). The structures were solved by direct methods and the non-hydrogen atoms refined anisotropically, (using absorption corrected data for *anti*-**1c**) to give for *anti*-**1b**, $R = 0.051$, $R_w = 0.051$ for 597 independent observed reflections [$2\theta = 3$–$116°$, $|F_o| > 4\sigma(|F_o|)$], and for *anti*-**1c**, $R = 0.032$, $R_w = 0.041$ for 772 independent observed reflections [$2\theta = 3$–$116°$, $|F_o| > 4\sigma(|F_o|)$]. See ref. [2b].

[4] W. H. Mills, I. G. Nixon, *J. Chem. Soc.* **1930**, 2510–2524.

[5] J. S. Siegel, *Angew. Chem.* **1994**, *106*, 1808; *Angew. Chem. Int. Ed. Engl.* **1994**, *33*, 1721–1723 and references therein.

[6] a) R. Faust, F. D. Glendening, A. Streitwieser, K. P. C. Vollhardt, *J. Am. Chem. Soc.* **1992**, *114*, 8263–8268; b) K. K. Baldridge, J. S. Siegel, *J. Am. Chem. Soc.* **1992**, *114*, 9583–9587.

[7] R. Boese, D. Bläser, W. E. Billups, M. M. Haley, A. H. Maulitz, D. L. Mohler, K. P. C. Vollhardt, *Angew. Chem.* **1994**, *106*, 321; *Angew. Chem. Int. Ed. Engl.* **1994**, *33*, 313–317.

[8] N. L. Frank, K. K. Baldridge, P. Gantzel, J. S. Siegel, *Tetrahedron Lett.* **1995**, *36*, 4389–4392.

[9] a) H.-B. Bürgi, K. K. Baldridge, K. Hardcastle, N. L. Frank, P. Gantzel, J. S. Siegel, J. Ziller, *Angew. Chem.* **1995**, *107*, 1575–1577; *Angew. Chem. Int. Ed. Engl.* **1995**, *34*, 1454–1456 b) N. L. Frank, K. K. Baldridge, J. S. Siegel, *J. Am. Chem. Soc.* **1995**, *117*, 2102–2103.

[10] a) J. S. Craw, N. S. Hush, S. Sternhell, C. W. Tansey, *J. Phys. Chem.* **1992**, *96*, 5753–5759; b) M. N. Paddon-Row, H. K. Patney, J. B. Peel, G. D. Willet, *J. Chem. Soc., Chem. Commun.* **1984**, 564–566; c) M. N. Paddon-Row *Acc. Chem. Res.* **1982**, *15*, 245–251; d) K. N. Houk, N. G. Rondan, M. N. Paddon-Row, C. W. Jefford, P. T. Huy, P. D. Burrow, K. D. Jordan, *J. Am. Chem. Soc.* **1983**, *105*, 5563–5569; e) R. Gleiter, *Angew. Chem.* **1974**, *86*, 770; *Angew. Chem. Int. Ed. Engl.* **1974**, *13*, 696–701; f) R. Hoffmann, *Acc. Chem. Res.* **1971**, *4*, 1–9.

[11] N. L. Frank, J. Siegel, *Advances in Theoretically Interesting Molecules, Vol. 3*, (Ed.: R. P. Thummel), JAI, Greenwich (USA), **1995**, pp. 209–260. We thank Professor J. S. Siegel for supplying us with details on the calculated structure of **3**.

[12] For recent accounts on hydrogen bond networks in the solid state see: a) C. B. Aakeröy, K. R. Seddon, *Chem. Soc. Rev.* **1993**, *22*, 397–407; b) M. C. Etter, *Acc. Chem. Res.* **1990**, *23*, 120–126; c) G. Desirasu, *ibid.* **1991**, *24*, 290–296; d) G. M. Whitesides, E. E. Simanek, J. P. Mathias, C. T. Seto, D. N. Chin, M. Mammen, D. N. Gordon, *ibid.* **1995**, *28*, 37–45. The [H···O] interactions are of two types: stronger ones where the H···O distances are in the range 2.42–2.50 Å, and weaker linkages between centrosymmetrically related pairs of molecules where the H···O distance is 2.61 Å. The C–H···O angles are in the range 132–171°.

[13] a) F. H. Kohnke, J. F. Stoddart, A. M. Z. Slawin, D. J. Williams, *Acta Crystallogr. Sect. C* **1988**, *44*, 738–740; b) *ibid.* **1988**, *44*, 740–742; c) *ibid.* **1988**, *44*, 742–745; d) F. H. Kohnke, J. P. Mathias, J. F. Stoddart, A. M. Z. Slawin, D. J. Williams, *ibid.* **1990**, *46*, 1043–1046; e) F. H. Kohnke, J. P. Mathias, J. F. Stoddart, A. M. Z. Slawin, D. J. Watts, D. J. Williams, *ibid.* **1990**, *46*, 1046–1049; f) *ibid.* **1990**, *46*, 1049–1051.

[14] For *anti*-**2b** see: F. H. Kohnke, J. P. Mathias, J. F. Stoddart, A. M. Z. Slawin, D. J. Williams, *Acta Crystallogr. Sect. C*, **1992**, *48*, 663–665; for *syn*-**2b**, see ref. [13b].

Asymmetric Catalysis in the Complexation of Prochiral Dienes by the Tricarbonyliron Fragment: A Novel Methodology for the Enantioselective Synthesis of Planar Chiral Tricarbonyl(diene)iron Complexes**

Hans-Joachim Knölker* and Holger Hermann

Tricarbonyl(η^4-1,3-diene)iron complexes are important building blocks for organic synthesis.[1] The bulky tricarbonyliron moiety ensures in most cases a complete diastereoselectivity of reactions at these complexes. Applications of tricarbonyl(η^4-1,3-diene)iron complexes to asymmetric synthesis have demonstrated that the metal fragment may also serve as a chiral auxiliary.[2] The methods available for the preparation of enantiopure complexes include the classical separation of racemic complexes through diastereoisomers,[3] the diastereoselective complexation of enantiopure diene ligands,[4] the separation of planar chiral complexes by enzymatic reactions,[5] and the enantioselective complexation of prochiral 1,3-dienes by chiral tricarbonyliron transfer reagents.[6] We recently introduced (η^4-1-aza-1,3-butadiene)tricarbonyliron complexes as highly efficient novel tricarbonyliron transfer reagents.[7–9] The 1-aza-1,3-butadienes serve as catalysts for the complexation of 1,3-dienes with pentacarbonyliron.[7–9]

Based on these findings we investigated the possibility of achieving an asymmetric induction in the complexation of prochiral 1,3-dienes with the tricarbonyliron fragment by using chiral enantiopure 1-aza-1,3-butadienes as catalysts. We describe herein the first asymmetric catalysis of the complexation of a prochiral ligand by a transition metal fragment, in which an optically active, planar chiral transition metal π complex is generated.

The reaction of 1-methoxy-1,3-cyclohexadiene (**1**) with pentacarbonyliron [Eq. (a)], in which the corresponding planar chiral tricarbonyliron complex was generated, was used as a model reaction to optimize the catalytic system with respect to yield and asymmetric induction (Table 1).

Condensation of (*R*)- and (*S*)-1-phenylethylamine with cinnamaldehyde afforded the azadienes (*S*)-**3** and (*R*)-**3** shown in Scheme 1.[10] The fact that stoichiometric complexation of these chiral azadienes by the tricarbonyliron fragment is nonstereoselective is of no consequence for the present investigations, since epimerization of the two diastereoisomers occurs under the reaction conditions.[11] Under standard reaction conditions (2 equiv $Fe(CO)_5$, 0.125 equiv of catalyst, benzene, 80 °C), the catalyst (*S*)-**3** provided complex **2** in 69% yield with 6% *ee* of the *R* enantiomer. Correspondingly, complexation in presence of catalyst (*R*)-**3** gave **2** with 6% *ee* of the *S* enantiomer. The enantiomeric excess in each case was determined by separation of the planar chiral tricarbonyliron complexes **2** on a permethylated β-cyclodextrin column by HPLC.[12]

The axially chiral binaphthyl-substituted azadienes (*S*)-**4** and (*S*)-**5** were prepared by reaction of the enantiopure (*S*)-2-

[*] Prof. Dr. H.-J. Knölker, Dipl.-Chem. H. Hermann
Institut für Organische Chemie der Universität
Richard-Willstätter-Allee, D-76131 Karlsruhe (Germany)
Fax: Int. code +(721)698-529
e-mail: knoe@ochhades.chemie.uni-karlsruhe.de

[**] Transition Metal-Diene Complexes in Organic Synthesis, Part 28. This work was supported by the Deutsche Forschungsgemeinschaft (Gerhard-Hess-Förderpreis) and the Fonds der Chemischen Industrie. We are grateful to Priv. Doz. Dr. P. Metz, Universität Münster, for providing us his optimized procedure for the synthesis of enantiopure 2-amino-2'-methoxy-1,1'-binaphthyl prior to publication. Part 27: H.-J. Knölker, G. Baum, J.-B. Pannek, *Tetrahedron* **1996**, *52*, in press.

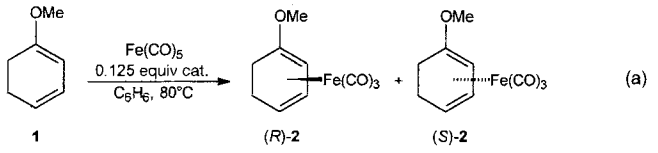

Table 1. Results of the asymmetric catalysis of the complexation of 1-methoxy-1,3-cyclohexadiene (**1**) with pentacarbonyliron.

Catalyst	t [h]	**2**, Yield [%]	*ee* [%] (abs. config.)[a]
(*S*)-**3**	45	69	6 (*R*)
(*R*)-**3**	45	68	6 (*S*)
(*S*)-**4**	42	87	25 (*R*)[b]
(*S*)-**5**	16	20	28 (*R*)
(*R*)-**9**	16	20	6 (*R*)
(*S*,*R*)-**10**[c]	44	20	16 (*S*)
(*S*)-**11**	16	24	20 (*R*)
(*S*,*S*)-**12**	16	6	34 (*R*)
(*S*,*R*)-**12**	16	2	14 (*S*)
(*R*)-**13**	38	29	33 (*R*)
(*R*)-**14**	38	67	33 (*R*)
(*R*)-**15**	16	9	62 (*S*)
(*S*)-**15**	40	11	56 (*R*)

[a] Determined by chiral HPLC on a permethylated β-cyclodextrin column [12]. [b] $[\alpha]_D^{20} = -35.3$, $c = 1.32$ in $CHCl_3$. [c] (*S*,*R*)-**10** is almost insoluble in C_6H_6.

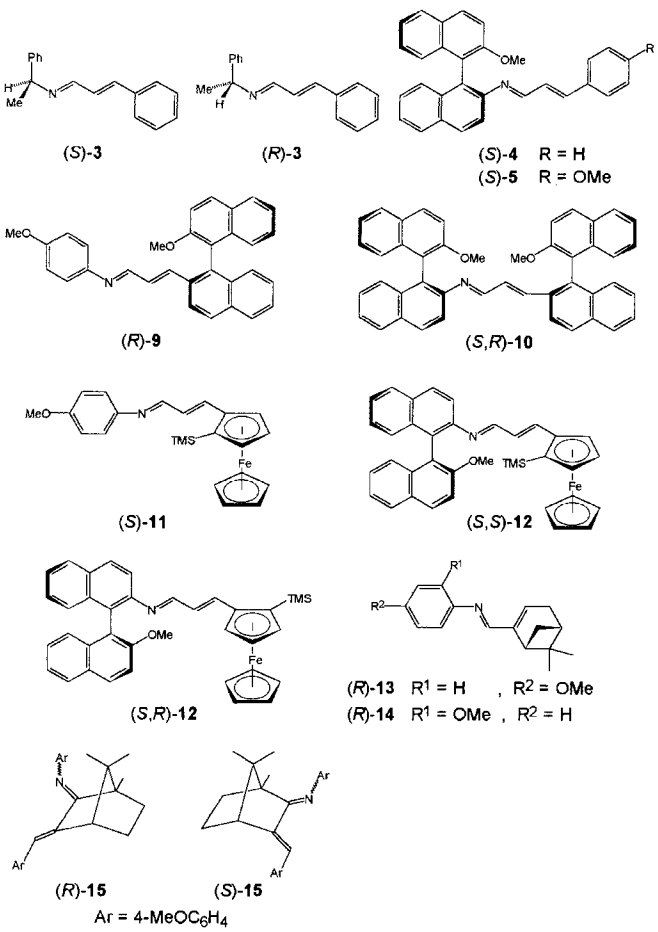

Scheme 1. Formulae of the catalysts employed.

amino-2′-methoxy-1,1′-binaphthyl[13] with cinnamaldehyde and *p*-methoxycinnamaldehyde (yields: 90 and 79%, respectively). Complexation of **1** with pentacarbonyliron in the presence of catalyst (*S*)-**4** afforded after a reaction time of 42 h complex **2** in 87% yield with 25% *ee* of the *R* enantiomer. The determination of the absolute configuration of complex **2** was based on correlation of the value for optical rotation ($[\alpha]_D^{20} = -35.3$, $c = 1.32$ in $CHCl_3$) with data previously published by Birch.[14] By using (*S*)-**5** as catalyst, complex **2** was obtained after 16 h in 20% yield with 28% *ee* of the *R* enantiomer.

In this context, two experimental observations are noteworthy. First, the pure enantiomers of complex **2** are stable under the reaction conditions and no racemization occurs. This has been demonstrated by heating an enantioenriched sample of (*R*)-**2** (18% *ee*) in benzene at reflux for four days without any detectable change of the *ee* value. Second, the asymmetric induction is independent of the concentration of the azadiene catalyst. The use of 0.03 equivalents of (*S*)-**4** in the above reaction afforded complex **2** with the same *ee* value (25% *ee* of the *R* enantiomer). However, as previously reported for the non-chiral catalysts,[7, 8] the best chemical yields were obtained by using 0.125 equivalents of the catalyst. Thus, in the asymmetric catalysis an extension of the reaction time led to higher turnovers and therefore higher yields without causing a decrease in the *ee* value.

We then decided to introduce the axially chiral binaphthyl moiety, which was successfully utilized as chiral auxiliary in the 1-position of 1-aza-1,3-butadiene for the asymmetrically catalyzed complexation, at the 4-position of the 1-aza-1,3-butadiene catalyst. In the mechanism, which we proposed for the 1-aza-1,3-butadiene catalyzed complexation of 1,3-dienes, a [(1-η)-1-aza-1,3-butadiene]tricarbonyliron complex was suggested as the crucial intermediate of the catalytic process.[8] Based on this 16-electron η^1-imine tricarbonyliron complex as the reactive species of the catalytic cycle, the degree of asymmetric induction was expected to be lower by having the chiral auxiliary at C-4, because of the larger distance to the reactive center. The synthesis of the catalyst is depicted in Scheme 2. Reduction of the

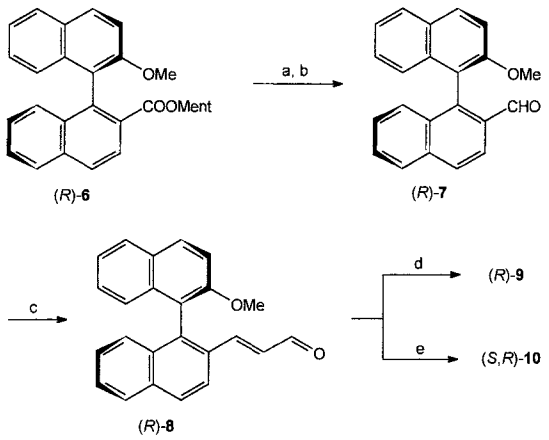

Scheme 2. a) 1.5 equiv $LiAlH_4$, Et_2O, 0 °C, 30 min (95%); b) 1.2 equiv $(COCl)_2$, 2.6 equiv DMSO, 5 equiv Et_3N, CH_2Cl_2, −78 °C, 30 min (86%); c) 1.4 equiv $(EtO)_2P(O)CH{=}CHN(t\text{Bu})Li$, THF, −78 °C → room temperature (RT) (47%); d) 1.0 equiv *p*-anisidine, molecular sieves 4 Å, benzene, RT, 6 h (82%); e) 1.0 equiv (*S*)-2-amino-2′-methoxy-1,1′-binaphthyl, molecular sieves 4 Å, benzene, 80 °C, 24 h (95%). Ment = D-(+)-menthyl.

(+)-menthyl ester (*R*)-**6**[13] followed by Swern oxidation afforded the aldehyde (*R*)-**7**, which was transformed to the α,β-unsaturated aldehyde (*R*)-**8** according to the method of Nagata et al. and Meyers et al.[15] Imine condensation of (*R*)-**8** with *p*-anisidine or (*S*)-2-amino-2′-methoxy-1,1′-binaphthyl provided the catalysts (*R*)-**9** and (*S*,*R*)-**10**, respectively. As expected, the asymmetric induction using (*R*)-**9** as the catalyst for the complexation of **1** was disappointing. However, compound (*S*,*R*)-**10**, which contains chiral binaphthyl units at the 1- and 4-posi-

tion, gave better results (16% *ee* of the *S* enantiomer of **2**). Moreover, with the bis(binaphthyl)-substituted 1-aza-1,3-butadiene **10** we realized that we get *matched* and *mismatched* pairs of the two chiral auxiliaries in the catalysts. By using the enantiopure diastereoisomeric compound (*S,S*)-**10**, prepared from (*S*)-**6** as described for (*S,R*)-**10** in Scheme 2, we obtained only 8% *ee* of the *S* enantiomer. Therefore, it is possible to achieve a double stereodifferentiation in this novel asymmetric catalysis by having two different chiral auxiliaries bound to the catalyst.[16] This finding will be of great value for the future design of novel catalysts, particularly with respect to optimization directed towards high asymmetric inductions in the complexation.

Asymmetric induction on complexation of **1** was expected to be even more efficient by using a catalyst with planar chiral auxiliaries. Based on this assumption we prepared complex (*S*)-**11** by condensation of the corresponding enantiopure (*S*)-ferrocenylpropenal[17] with *p*-anisidine (81% yield). Although the chiral center of compound (*S*)-**11** is at the unfavorable 4-position of the 1-aza-1,3-diene (see above), this catalyst led to an asymmetric induction of the complexation of **1** affording 20% *ee* of the *R* enantiomer of **2**. Combination of planar chirality and axial chirality in the catalyst by reaction of the (*S*)-2-amino-2′-methoxy-1,1′-binaphthyl with the (*S*)- and (*R*)-ferrocenylpropenal,[17] provided us with the enantiopure diastereoisomeric catalysts (*S,S*)-**12** (75% yield) and (*S,R*)-**12** (74% yield), respectively. With these catalysts a further impressive example of double stereodifferentiation in the asymmetric catalysis was observed. Catalysis of the complexation of **1** by (*S,S*)-**12** gave 34% *ee* of the *R* enantiomer of **2**, whereas the complexation catalyzed by (*S,R*)-**12** led to a lower *ee* of the opposite enantiomer (14% *ee* of (*S*)-**2**). As mentioned above, increasing the reaction time of the asymmetrically catalyzed complexation leads to higher yields without a decrease of the *ee* value. At this stage of our investigations we were therefore mainly interested in achieving higher asymmetric inductions by optimizing the catalyst.

In this context, we tested several enantiopure 1-aza-1,3-butadienes derived from the chiral pool. Condensation of (1*R*)-( )-myrtenal with *p*-anisidine led to the catalyst (*R*)-**13** (62% yield) which in the catalyzed complexation of **1** provided (*R*)-**2** in 33% *ee* and 29% yield. Catalysis with (*R*)-**14** (obtained from condensation of (1*R*)-(-)-myrtenal with *o*-anisidine, 62% yield) afforded after the same reaction time (*R*)-**2** of the same optical purity in 67% yield. The beneficial effect of an *ortho*-methoxy substituent in the arylamine moiety of the 1-aza-1,3-butadiene was previously reported by us for the achiral catalysts.[8] The catalysts (*R*)-**15** and (*S*)-**15** were easily prepared from (1*R*)-(+)-camphor and (1*S*)-(−)-camphor, respectively, by aldol condensation with *p*-methoxybenzaldehyde and subsequent imine condensation with *p*-anisidine (43% overall yield). Without having attempted to optimize the yields (see above), our initial results indicated that asymmetric catalysis of the complexation of **1** by (*R*)-**15** and (*S*)-**15** afforded (*S*)-**2** in 62% *ee* and (*R*)-**2** 56% *ee*, respectively. This asymmetric induction was accurately determined by HPLC separation of (*R*)-**2** and (*S*)-**2** on a permethylated β-cyclodextrin-bound chiral stationary phase (Figs. 1 and 2).[12]

Finally, we were also able to achieve an asymmetric catalysis in the complexation of the prochiral diene **16** (Scheme 3). The resulting iron complex **17** is an important building block for diastereoselective iron-mediated spiroannulations.[18] Asymmetric complexation of **16** with pentacarbonyliron in presence of the binaphthyl-substituted catalyst (*S*)-**4** provided complex **17** in 26% yield and, as determined by chiral HPLC,[12] with 19% *ee* of the *R* enantiomer.[19]

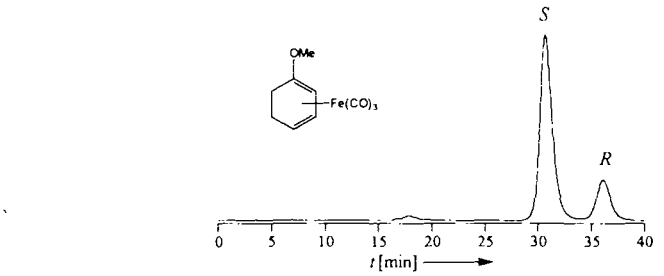

Fig. 1. Chiral HPLC of **2** with 62% *ee* of the (*S*) (+) enantiomer [12]. *t* = retention time.

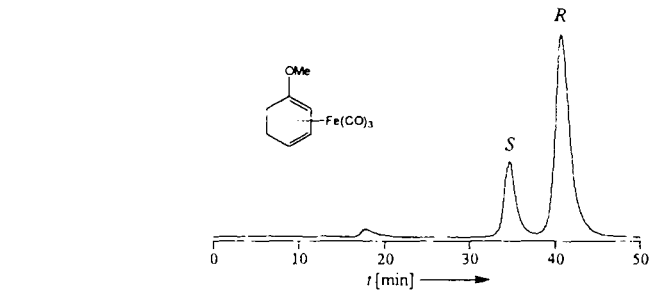

Fig. 2. Chiral HPLC of **2** with 56% *ee* of the (*R*) (−) enantiomer [12]. *t* = retention time.

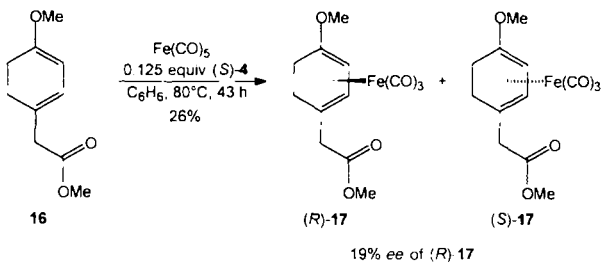

Scheme 3.

In conclusion, we have shown for the first time the feasibility of generating planar chirality by asymmetric catalysis[20] of the complexation of prochiral ligands with transition metal fragments. Therefore, the results described above may have a major impact on the applications of planar chiral transition metal π complexes in synthetic organic chemistry.

Received: November 15, 1995 [Z 8549 IE]
German version: *Angew. Chem.* **1996**, *108*, 363–365

Keywords: asymmetric catalysis · chirality · dienes · iron compounds

[1] A. J. Pearson, *Acc. Chem. Res.* **1980**, *13*, 463; A. J. Pearson in *Comprehensive Organometallic Chemistry*, *Vol. 8*, (Eds.: G. Wilkinson, F. G. A. Stone, E. W. Abel), Pergamon, Oxford, **1982**, Chap. 58; A. J. Pearson, *Metallo-organic Chemistry*, Wiley, Chichester, **1985**, Chap. 7 and 8; R. Grée, *Synthesis* **1989**, 341; H.-J. Knölker in *Organic Synthesis via Organometallics* (Eds.: K. H. Dötz, R. W. Hoffmann), Vieweg, Braunschweig, **1991**, p. 119; H.-J. Knölker, *Synlett* **1992**, 371; A. J. Pearson, *Iron Compounds in Organic Synthesis*, Academic Press, London, **1994**, Chap. 4 and 5; H.-J. Knölker *in Advances in Nitrogen Heterocycles*, *Vol. 1*, (Ed.: C. J. Moody), JAI Press, Greenwich (CT), **1995**, p. 173.

[2] A. J. Pearson, M. W. Zettler, *J. Chem. Soc. Chem. Commun.* **1987**, 1243; M. Laabassi, R. Grée, *Tetrahedron Lett.* **1988**, *29*, 611; A. J. Birch, L. F. Kelly, D. V. Weerasuria, *J. Org. Chem.* **1988**, *53*, 278; P. Pinsard, J.-P. Lellouche, J.-P. Beaucourt, R. Grée, *Tetrahedron Lett.* **1990**, *31*, 1140; M. Franck-Neumann, P.-J. Colson, *Synlett* **1991**, 891.

[3] A. J. Birch, B. M. R. Bandara, *Tetrahedron Lett.* **1980**, *21*, 2981; A. Monpert, J. Martelli, R. Grée, R. Carrié, *ibid.* **1981**, *22*, 1961; M. Franck-Neumann, C. Briswalter, P. Chemla, D. Martina, *Synlett* **1990**, 637; S. Nakanishi, H. Yamamoto, Y. Otsuji, H. Nakazumi, *Tetrahedron: Asymmetry* **1993**, *4*, 1969.
[4] P. W. Howard, G. R. Stephenson, S. C. Taylor, *J. Chem. Soc. Chem. Commun.* **1988**, 1603; *ibid.* **1990**, 1182; A. J. Pearson, K. Chang, D. B. McConville, W. J. Youngs, *Organometallics* **1994**, *13*, 4; H.-G. Schmalz, E. Hessler, J. W. Bats, G. Dürner, *Tetrahedron Lett.* **1994**, *35*, 4543.
[5] N. W. Alcock, D. H. G. Crout, C. M. Henderson, S. E. Thomas, *J. Chem. Soc. Chem. Commun.* **1988**, 746; J. A. S. Howell, M. G. Palin, G. Jaouen, S. Top, H. E. Hafa, J. M. Cense, *Tetrahedron: Asymmetry* **1993**, *4*, 1241; M. Uemura, H. Nishimura, S. Yamada, Y. Hayashi, K. Nakamura, K. Ishihara, A. Ohno, *ibid.* **1994**, *5*, 1673.
[6] A. J. Birch, W. D. Raverty, G. R. Stephenson, *Tetrahedron Lett.* **1980**, *21*, 197; *Organometallics* **1984**, *3*, 1075; T. Jenny, V. Schmid, *Chimia* **1993**, *47*, 296 (abstract 135).
[7] H.-J. Knölker, P. Gonser, *Synlett* **1992**, 517.
[8] H.-J. Knölker, P. Gonser, P. G. Jones, *Synlett* **1994**, 405.
[9] H.-J. Knölker in *Encyclopedia of Reagents for Organic Synthesis Vol 1* (Ed.: L. A. Paquette), Wiley, Chichester, **1995**, p. 333.
[10] T. N. Danks, S. E. Thomas, *J. Chem. Soc. Perkin Trans. 1* **1990**, 761.
[11] H.-J. Knölker, G. Baum, P. Gonser, *Tetrahedron Lett.* **1995**, *36*, 8191.
[12] ET200/8,4 Nucleodex β-PM from Macherey-Nagel; a complete baseline separation of the peaks resulting from a racemic mixture of the two enantiomers can be achieved by using a technique developed in our laboratories by cooling the column to 0 °C and using $MeCN/H_2O$ as the eluent: H.-J. Knölker, P. Gonser, T. Koegler, unpublished results.
[13] T. Hattori, M. Shijo, S. Kumagai, S. Miyano, *Chem. Express* **1991**, *6*, 335; T. Hattori, H. Hotta, T. Suzuki, S. Miyano, *Bull. Chem. Soc. Jpn.* **1993**, *66*, 613; P. Metz, B. Hungerhoff, unpublished results.
[14] A. J. Birch, W. D. Raverty, G. R. Stephenson, *J. Chem. Soc. Chem. Commun.* **1980**, 857; *J. Org. Chem.* **1981**, *46*, 5166.
[15] W. Nagata, Y. Hayase, *Tetrahedron Lett.* **1968**, 4359; A. I. Meyers, K. Tomioka, M. P. Fleming, *J. Org. Chem.* **1978**, *43*, 3788.
[16] For a review on double stereodifferentiation, see: S. Masamune, W. Choy, J. S. Peterson, L. R. Sita, *Angew. Chem.* **1985**, *97*, 1; *Angew. Chem. Int. Ed. Engl.* **1985**, *24*, 1.
[17] The enantiopure (*R*)-2-trimethylsilylferrocenylcarbaldehyde ($[\alpha]_D^{20} = -222$, $c = 0.295$ in EtOH) and (*S*)-2-trimethylsilylferrocenylcarbaldehyde ($[\alpha]_D^{20} = +221$, $c = 0.295$ in EtOH) were prepared by modification of a literature procedure: G. Gokel, P. Hoffmann, H. Kleimann, H. Klusacek, D. Marquarding, I. Ugi, *Tetrahedron Lett.* **1970**, 1771. Elongation using the method of Nagata and Meyers [15] provided (*R*)-3-(2-trimethylsilylferrocenyl) 2-propenal and (*S*)-3-(2-trimethylsilylferrocenyl)-2-propenal: H.-J. Knölker, H. Hermann, P. Gonser, unpublished results.
[18] H.-J. Knölker, R. Boese, K. Hartmann, *Angew. Chem.* **1989**, *101*, 1745; *Angew. Chem. Int. Ed. Engl.* **1989**, *28*, 1678; H.-J. Knölker, R. Boese, K. Hartmann, *Tetrahedron Lett.* **1991**, *32*, 1953; H.-J. Knölker, K. Hartmann, *Synlett* **1991**, 428.
[19] The absolute configuration of the excess enantiomer was assigned based on an X-ray analysis of an enantiopure derivative of (*R*) **17** which was obtained by separation of diastereoisomers: H.-J. Knölker, E. Baum, T. Koegler, unpublished results.
[20] For a compilation of asymmetric catalysis, see: *Catalytic Asymmetric Synthesis* (Ed.: I. Ojima), VCH, Weinheim, **1993**.

Brian Kaye
Chaos & Complexity
Discovering the Surprising Patterns of Science and Technology

1993. XXII, 593 pages with 257 figures, 2 in color
Hardcover. DM 148.-/öS 1154.-/sFr 140.-.
ISBN 3-527-29039-7 (VCH, Weinheim)
Softcover. DM 78.-/öS 608.-/sFr 75.-.
ISBN 3-527-29007-9 (VCH, Weinheim)

The surprising patterns of chaos and complexity are to be found in many areas of nature and science, examples ranging from cabbages to coastlines.

Quite often, those who could benefit most from an understanding of the principles behind chaos and complexity are denied access to the power and wonders of the field by the mathematical and unnecessarily convoluted way the topic is usually presented.

This book makes these sometimes complicated wonders accessible to students and professionals alike. Amusing tales and cartoons are used to explain the concepts and demonstrate the fascinating applications of this powerful technique.

To order please contact your local bookseller or:

VCH, P.O. Box 10 11 61, D-69451 Weinheim, Fax 0 62 01 - 60 61 84

VCH, Hardstrasse 10, P.O. Box, CH-4020 Basel

VCH, 8 Wellington Court, Cambridge CB1 1HZ, UK

VCH, 220 East 23rd Street, New York, NY 10010-4606, USA

VCH, Eikow Building, 10-9 Hongo 1-chome, Bunkyo-Ku, Tokyo 113, Japan

VCH

What's in a Gene?

Dictionary of Gene Technology. By *G. Kahl.* VCH Verlagsgesellschaft, Weinheim, 1994. 550 pp., hardcover DM 184.00.—ISBN 3-527-30005-8

It is an undisputed fact that the importance of gene technology was first recognized in the USA, and it was there that its applications were most vigorously pursued. This circumstance has given rise to a whole vocabulary of English terms that have become firmly established in the everyday language of molecular biology. For many of us in the German-speaking world, the difficulty of finding a German equivalent for an English technical term in gene technology or molecular biology is already a familiar problem. Many of the expressions used to describe processes, phenomena, etc. cannot actually be translated, since it is the privilege of the discoverer to invent a name for his brain-child. In many cases the name is an abbreviation.

The *Dictionary of Gene Technology* acknowledges this development and sets out to define and explain, in English, the increasing flood of technical terms, names, and abbreviations used to describe methods, processes, substances, materials, and biological macromolecules. What sort of terms should be included in such a dictionary, and how much detail can be put into the definitions and explanations? In many cases the decisions are not easy. In this compilation the main emphasis is on keywords that are concerned, in the broadest sense, with nucleic acids and their structures, synthesis, analysis, transfer, modification, and processing. Although the dictionary includes many terms belonging to related fields outside gene technology, the author has not aimed at a complete coverage of these peripheral areas.

The result is an impressive compilation of technical terms with explanations that are mostly brief and easily understandable, occasionally rather more detailed but never long-winded, and nearly always absolutely correct. The author has set out to meet the needs of a wide readership, especially scientists working in the relevant disciplines and their students, but also specialists in neighboring areas of science as well as journalists and politicians. The book has not been written for the lay reader, as it assumes an understanding of the language and jargon commonly used by molecular biologists. However, the great majority of the envisaged readership should find the book useful, especially in view of the fact that their educational backgrounds differ widely. The clear and simple diagrams, the practical examples included for illustration, and the more detailed explanations where these are appropriate, all contribute to the usefulness of the work.

Of course one does not actually read through a dictionary, but even on just randomly leafing through it the many cross-references gently lead one to read further. These cross-references are indicated by small arrows which tend to dominate the appearance of the text, so that in many of the entries their effect is at first sight rather irritating. However, on closer examination one discovers that they are very useful, as they serve to form a network linking the various terms and to place each individual term within a wider context. A dictionary cannot be a substitute for a textbook or practical handbook and is certainly not intended as such. It can explain the principle of a technique, remind one of a formula, show the structure of a molecule, or give the meaning of an abbreviation. It is a reference source which can help to call things to mind or to fill gaps in one's knowledge. This book fulfills those aims very well.

It will certainly not be an easy task to update such a book in printed form so as to keep place with future developments. Even now there are a few important and highly topical techniques, such as "two-hybrid system", "interaction trap", and "knock-out animal", that should have been included. These omissions are all the more surprising in view of the fact that in the preface the author emphasizes that new technological developments are included. Other readers will undoubtedly be able to list other omissions. Also a few of the definitions could have been better expressed or expanded, such as those of "gene expression" and "repressor". The explanations of some of the keywords seem too short or too dull.

A dictionary, by its very nature, informs one about matters that are treated more fully and with more explanation elsewhere. Its advantage lies in its convenience, allowing one to look things up very quickly. It seems to me an almost impossible task for a single author to write a book of this kind that is complete and free of mistakes. On the whole, however, that appears to have been achieved in this case. This is a comprehensive, balanced, and useful work of reference, and it will certainly find an assured place on the office desk and in the laboratory.

Michael Meisterernst
Laboratorium für Molekulare Biologie
und Genzentrum
der Universität München (Germany)

Integrated Chemical Systems. A Chemical Approach to Nanotechnology. (Baker Lecture Series.) By *A. J. Bard.* Wiley, Chichester, 1994. 324 pp., hardcover £ 41.50.—ISBN 0-471-00733-1

This book contains the text of a course of lectures which the author, who is best known to electrochemists and physical chemists, gave during 1987. The reader will recognize in the title two keywords that are of particular interest: "nanotechnology" and "integrated". Although it is now some time since microelectronics gave birth to the microtechnologies, which are already almost part of the everyday scene, the next stage in this field, the nanotechnology referred to in the title, is still in an exciting and very promising state of development. The word "integrated" is also associated with novel and high-

This section contains book reviews and a list of new books received by the editor. Book reviews are written by invitation from the editor. Suggestions for books to be reviewed and for book reviewers are welcome. Publishers should send brochures or (better) books to Dr. Illenora Beckmann, Redaktion Angewandte Chemie, Postfach 101161, D-69451 Weinheim, Federal Republic of Germany. The editor reserves the right of selecting which books will be reviewed. Uninvited books not chosen for review will not be returned.

ly topical advances in technology. Both these concepts are synonymous with very rapid developments, and the delay in producing this book therefore seems unfortunate.

Probably only those few readers who make a pastime of phantasizing about future developments will start off with an idea of what an integrated chemical system might consist of. The rest must wait for several pages before coming to the following definition: "We define these integrated chemical systems (ICSs) as heterogeneous, multiphase systems involving several different components (e.g., semiconductors, polymers, catalysts, membranes) designed and arranged for specific functions or to carry out specific reactions or processes. Often the different components will be organized structurally and will show synergistic effects. Usually it is the interaction of the components of the ICS that determines its properties." Unfortunately many readers will still not have a clear picture of an ICS from this definition. However, some examples follow which should help in making the breakthrough. In the biological field chloroplasts and mitochondria are cited as typical ICSs, while in chemistry a heterogeneous catalyst coupled to a redox system is given as an example, in photography the instant color film is cited, and in chemical analysis various sensor systems are mentioned. In accordance with the author's aim of giving a systematic overview of nanotechnology the following chapters describe methods for constructing and characterizing ICSs, which could perhaps be incorporated into future nanotechnological developments. Many of the methods described will already be familiar to some readers from their acquaintance with microtechnology. Others based on self-organizing structures are common knowledge, while some, such as the use of a scanning electron microscope for fabricating components, are speculative. The methods proposed for characterizing ICSs are mainly drawn from surface and thin film analytical techniques, although some new advances in these will be needed to enable them to be applied to ICSs.

This is followed by chapters on chemically modified electrodes and methods for characterizing these, as well as developments in photoelectrochemistry, both of which are stages on the way to nanostructured systems. The author describes advances towards producing these, which are already well covered in existing review articles. The choice of substrates, reactants, and systems is discussed, with some complicated examples related to the development of sensors and highly selective electrocatalytic films. The description of electrochemical methods used to study such modified electrodes concentrates mainly on potentiodynamic measurements; nonclassical methods are not discussed. This omission is surprising if one assumes that nanostructured surfaces for many of the functions envisaged will need to have a specific well-defined surface topography or other properties that cannot be investigated by electrochemical methods. The following chapter is concerned with semiconductors and their photochemistry; starting with the band model, this gives a thorough and detailed account of current knowledge. This is then related to the development of ICSs by discussing photosemiconducting electrodes with modified surfaces and finely-divided photosemiconductor particles as components for such systems. The final chapter is an appraisal of future prospects and research trends in the areas of microsensors, microreactors, and composite materials. The book is completed by a comprehensive index which provides a useful key to the contents. The numerous figures are mostly successful in illustrating and clarifying even the more complicated discussions. However, many of these are of inferior quality, occasionally making them difficult to understand.

One must now ask who are the readers most likely to benefit from the book. It will be of interest to scientists entering the field of methods for modifying surface properties and for generating surface structures with molecular dimensions. Experienced electrochemists and specialists in microtechnology will gain little new knowledge from the book.

Rudolf Holze
Institut Chemie – Abt. Elektrochemie
der Technischen Universität Chemnitz-Zwickau
Chemnitz (Germany)

A New Dimension to Quantum Chemistry. Analytic Derivative Methods in Ab-Initio Molecular Electronic Structure Theory. By *Y. Yamaguchi, Y. Osamura, J. D. Goddard* and *H. F. Schaefer*. Oxford University Press, Oxford, 1994. 471 pp., hardcover £ 60.00.— ISBN 0-19-507038-3

It is probably no exaggeration when, in the title of this book, the development of analytical derivative methods for ab-initio wave-function calculations is described as a new dimension in quantum chemistry. Following on from the pioneering work of P. Pulay in the late 1960s, the standing of ab-initio methods of calculation has been considerably enhanced through the advantages of analytical gradients, especially their use for reliably determining equilibrium structures and saddle points. In addition, however, the development and appropriate implementation of algorithms for analytical calculations of derivatives of the energy function has now made it possible to calculate harmonic vibration frequencies, anharmonic corrections, IR and Raman intensities, and many other properties. There already exist a number of review articles and collections of papers on this topic, but this book by Schaefer and coauthors is the most detailed and thorough retrospective survey to appear so far. Starting from a concise introduction to the LCAO-MO formalism, the authors derive explicit expressions for the first and second derivatives of various Hartree–Fock (HF) SCF wave-functions and of wave-functions of the configurational interaction (CI), two-configurational SCF, and general multiconfigurational SCF (MCSCF) types. This is followed by chapters describing in detail the methods for solving "coupled perturbed" HF, CI, or MCSCF equations. Next there is a discussion of higher derivatives and of the special case of derivatives involving an electric field. The mathematical part of the book ends with a short chapter on the "Z-vector" method recently developed by Handy and Schaefer for calculating analytical derivatives. In the penultimate chapter the authors describe a number of typical applications of analytical derivatives for obtaining answers to chemical problems. The final (20th) chapter offers an optimistic assessment of likely future developments. This is followed by 28 appendices which summarize the key equations from all the chapters. The book ends with a bibliography listing the relevant original papers, which is commendably up-to-date as it extends up to 1993.

The quality of production is up to the same excellent standard as others in this series from the same publisher. However, after even an initial brief glance through the book one is struck by the large proportion of space devoted to mathematical expressions, which is unusual even for a monograph on a theoretical subject. In fact the work is essentially a collection of formulas relieved only by a small amount of explanatory text. The structure of the chapters is rigid and very formalized. Chapters treating related aspects have an almost identical structure, with only small differences in the wording. As a result the book makes arid and heavy reading. Who are the readers most likely to benefit from

this book? Whether it is suitable for the advanced students envisaged in the preface seems rather doubtful, since the style is too condensed and the amount of mathematics too demanding; also the book makes few concessions to the need to show the subject within a wider context. On the other hand, for the specialist it should certainly be useful as a work of reference. Even here, however, it must be said that the authors have concentrated on discussing their own research, with the result that apart from the Hartree - Fock case the main emphasis is on the derivatives of CI and MCSCF energy functions. It is unfortunate that there is no discussion of the popular methods based on perturbation theory, nor of the increasingly important coupled-cluster methods. In conclusion, therefore, the book can be recommended only for a rather restricted circle of theoretical chemists.

Wolfram Koch
Institut für Organische Chemie
der Technischen Universität Berlin
(Germany)

The Surface Science of Metal Oxides. By *V. E. Henrich* and *P. A. Cox*. Cambridge University Press, Cambridge, 1994. 464 pp., hardcover £ 55.00. –ISBN 0-521-44389-X

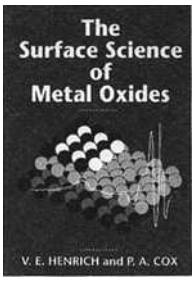

In the interdisciplinary field of "surface science", which encompasses surface physics and surface chemistry, the physical aspects are at present much more developed than the chemical. This is mainly due to progress in the single crystal physics of metal surfaces and in semiconductor studies. So far as the chemistry is concerned, the investigations have been limited to a relatively small number of reactions and to only a few studies of chemical compounds with well-characterized surfaces (which in this book means single crystal surfaces). This situation applies especially to the large class of solid oxides. Despite their great scientific and technological importance, which far outweighs that of pure metal surfaces, little progress has so far been achieved in oxide studies. The reasons for this are clearly explained in a general context in the introduction to this book, and are illustrated more specifically by the many examples described later.

The work is a critical survey of the most important results achieved by research into the surface physics and chemistry of oxide single crystals. Many examples are discussed, including oxides of the main-group elements magnesium, aluminum, zinc, and tin (silicon oxide is excluded, being an oxide of a nonmetal) and of the sub-group elements titanium, vanadium, and iron. Other oxides are also included where it has been possible to find sufficient published work. Regrettably the alkali metal oxides, which would have fitted appropriately into the subject matter of the book, are not mentioned, presumably due to the lack of examples involving single crystals. Thin films of metal oxides with monocrystalline surfaces are also absent, despite the fact that there is currently much research activity in this area.

Nevertheless, these omissions are outweighed by the thoroughness of the treatment of those oxides that are included. After a short introduction to ideal structures, the electronic properties of the main- and sub-group metal oxides are treated in detail and at a high standard, starting with a chapter on the relevant lattice vibrations, which have a considerable influence on the physical properties of the surfaces. This is followed by two long chapters on the surface chemistry of molecular compounds and reactions at their interfaces with other oxides or metals. However, the sections on heterogeneous catalysis and ceramic superconductors included here can only be rated as a fair attempt at their targets rather than a direct hit.

A noteworthy feature of the book is that the chemical and physical aspects are treated with equal competence and rigor. Consequently the reader needs to have an appropriate background of knowledge in both disciplines; this is certainly not an introductory text. One of the characteristics of interdisciplinary research is that the same terms are sometimes used with different meanings, and wherever appropriate that is pointed out and clarified. The different definitions of hybridization on page 104 are a good example of this.

The value of the exhaustive analysis of the relevant literature, in some cases with information-packed tables summarizing the results, can hardly be overstated. This makes the book a useful work of reference for the scientist engaged in research in this field. In this respect it is far more than a monograph and has the status of a standard work.

This high quality is also evident in the examples, which are illustrated by excellent figures; in some of the more important examples, such as the surface chemistry of titanium oxide (Ch. 6.4), these contain so much detail that one would learn little more by reading the original papers. The book's usefulness as a reference source is further enhanced by around 1000 literature citations, a well arranged contents list, and indexes of keywords and compounds.

A less favorable aspect is the inconsistency in the frequency of references in the text; often one has to search for a long time to find the reference corresponding to a particular topic. Also the claim that this book is the first of its kind is not quite correct. Two other works are in fact mentioned in the introduction, but the main text contains no mention of other monographs on the subject, such as that by Nowottny and Dufour.

Altogether, however, this is an extremely useful book which gives a competent and reliable survey of the field. It can be recommended as a standard work on the subject, and everyone working in this area will find it a reliable source of information. The general observations that are offered should provide many useful ideas when designing one's own research projects in the currently burgeoning field of surface science. The style of presentation, the instructive diagrams, and not least the outstandingly good treatment of the literature also make the book a valuable resource for those engaged in research in related disciplines such as solid state physics, oxides chemistry, materials science, and catalysis. Libraries are strongly recommended to buy it as a comprehensive monograph with a long life expectancy.

Robert Schlögl
Fritz-Haber-Institut
der Max-Planck-Gesellschaft
Berlin (Germany)

Control of the Structure and Functions of Biomaterials by Light

Itamar Willner* and Shai Rubin

Vision and other light-triggered biochemical transformations in plants and living organisms represent a sophisticated biological processes in which optical signals are recorded and transduced as (physico)chemical events. Photoswitchable biomaterials are a new class of substances in which optical signals generate discrete "On" and "Off" states of biological functions, resembling logic gates that flip between 0 and 1 states in response to the changes in electric currents in computers. The (photo)chemistry of photochromic materials has been extensively developed in the past four decades. These materials isomerize reversibly upon light absorption, and the discrete photoisomeric states exhibit distinct spectral and chemical features. Integration of photoisomerizable (or photochromic) units into biomaterials allow their secondary functions such as biocatalysis, binding, and electron transfer to be tailored so that they can be switched on or off. This can be accomplished by chemical modification of the biomaterial by photoisomerizable units and by integration of biomaterials in photoisomerizable microenvironments such as monolayers or polymers. The photoswitchable properties of chemically modified biomaterials originate from the light-induced generation or perturbation of the biologically active site, whereas in photoisomerizable matrices they depend upon the regulation of the physical or chemical features of the photoisomerizable assemblies of polymers, monolayers, or membranes. Light-triggered activation of catalytic biomaterials provides a means of amplifying the recorded optical signal by biochemical transformations, and photostimulated biochemical redox switches allow its electrochemical transduction and amplification. The field of photoswitches based on biomaterials has developed extensively in the past few years within the general context of molecular switching devices and micromachinery. The extensive knowledge on the manipulation of biomaterials through genetic engineering and the fabrication of surfaces modified by biologically active materials enables us to prepare biomaterials with improved optical-switching features. Their application in optoelectronic or bioelectronic devices has been transformed from fantasy to reality. The use of photoswitchable biomaterials in information storage and processing devices (biocomputers), sensors, reversible immunosensors, and biological amplifiers of optical signals has already been demonstrated, but still leaves important future challenges.

Keywords: bioelectronics · enzymes · optoelectronics · photoswitchable systems

1. Introduction

Diverse biological processes are triggered by light signals. Photosynthesis[1, 2] and vision[3, 4] are the most fundamental light-controlled biological mechanisms. Other processes, such as photomovement at various biological levels[5] (movement of motile organisms, dynamics of plant tissues), photomorphogenesis[6, 7] (seed germination, induction of flowering, synthesis of chlorophyll), and conversion of light energy into chemical energy[8, 9] (ATP synthesis, proton pumps, and ion-transport) add important light-triggered biological mechanisms. The common feature of all these systems is the participation of a chromophore (photosensor or photoreceptor) that upon light absorption activates a series of chemical transformations in the chromophore surrounding the biomembrane or protein. Such light-activated biochemical cycles represent reversible photobiological optical switches: the bioevent is switched on upon recording of the optical signal and off in the dark. To identify the fundamental characteristics of biological photoswitches, the functions of the extensively studied bacteriorhodopsin system will be mentioned here briefly.

Bacteriorhodopsin is a retinal-containing protein in *Holobacterium halobium* that converts light energy into chemical energy by synthesizing ATP.[10] The 11-*trans*-retinal chromophore of bacteriorhodopsin is embedded in the bacterium membrane, and upon absorption of light it activates the net transport of protons from the inner (cytoplasm) to the outer (extracellular) side of the cell membrane. The generated potential gradient activates a membrane-bound ATPase for ATP synthesis.[11] Scheme 1 summarizes the interactions of the photoreceptor with its surrounding protein that causes the formation of a potential

[*] Professor I. Willner, Dr. S. Rubin
Institute of Chemistry and Farkas Center for Light-Induced Processes
The Hebrew University of Jerusalem
Jerusalem 91904 (Israel)
Fax: Int. code + (2)6527715

 © *VCH Verlagsgesellschaft mbH, D-69451 Weinheim, 1996* *0570-0833/96/3504-0367 $ 15.00+.25/0*

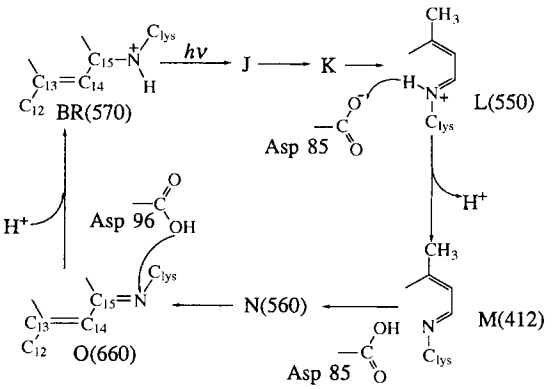

Scheme 1. Interactions of rhodopsin photoisomers with the surrounding membrane, resulting in a proton-pump.

gradient and provides a mode of relaxation for the optical switch. Photoisomerization of the chromophore BR to state L results in deprotonation of the protonated, isomerized Schiff base by a proton transfer to the Asp85 residue. In the subsequent isomerization of state O a proton is translocated from Asp96 to regenerate the initial chromophore and complete the photocycle. The bacteriorhodopsin photocycle illustrates the basic principles of biological photoswitches:

1) The optical signal is recorded by the photosensor site and triggers a structural change in the chromophore.

2) Isomerization of the chromophore is transduced to the surrounding protein. The protein, and thereby an ion-pump, is stimulated.

3) The photosensor–protein assembly provides a relaxation pathway by which the photosensor is recycled for a secondary optical recording event.

The rapid transformation of photobiological switches between different states enables their application as optical memory devices.[12] The photostimulated transitions of bacteriorhodopsin from BR through M back to BR allows repeated "write and erase" cycles.[13] Various optical applications[14] such as holographic pattern recording,[15] dynamic optical filtering,[16] and associative optical memories[17] were developed with bacteriorhodopsin as photosensor. This highlights the broad practical implications of the photochemical control of the functions of biomaterials.

Recent efforts have been directed towards the development of semisynthetic photobiological switches.[18] A photobiological switch is a biological material or a biological environment that is activated to perform its biochemical function upon exposure to light. Two fundamental subclasses of photobiological switches have been developed.

1. Single-cyle photoswitches are a class of biological photoswitches in which the biomaterial is deactivated by attachment of photosensitive chemical protecting groups (Scheme 2). The

Scheme 2. A single-cycle photobiological switch. I = inactive assembly, II = active assembly, S = photosensitive group.

biomaterial is activated by light-stimulated removal of the protective group to restore the biologically active structure.[19, 20] Activation of enzymes,[21–23] photoinduced formation of specific ion-chelators,[24–26] and light-triggered activation of important biological components such as cAMP,[27] cGMP,[28] ATP,[29] and InP_3[30] have been used in this approach. Several review articles summarize the subject of single-cycle photoswitches.[31–33]

2. Multicycle photobiological switches are the results of efforts to transform biomaterials or biological environments into light-activated matrices operating reversibly between a mute bioactive state (switch "Off") and an activated biological function (switch "On") (Fig. 1). Three different methodologies to reversibly photostimulate biomaterials are envisaged:

a) Chemical modification of biomaterials by photoisomerizable units could lead to photoswitchable biological assemblies (Fig. 1a). Synthetic modification of the biomaterial with one photosensor state (state B) could distort the biomaterial or its active site (that is, the protein) and deactivate it. Upon photoisomerization of the photosensor to state A the structural

Itamar Willner was born in 1947. He completed his Ph. D. studies in Chemistry in 1978 at The Hebrew University of Jerusalem. After a postdoctoral stay with M. Calvin at the University of California, Berkeley, he acted as research associate at the Lawrence Berkeley Laboratory until he joined the Institute of Chemistry at the Hebrew University as Senior Lecturer in 1982. In 1986 he accepted a position as Professor there. His research interests encompass light-induced electron transfer processes and artificial photosynthesis, photo- and electroswitchable molecular, macromolecular, and biological assemblies, including their application in optoelectronics and bioelectronics, supramolecular chemistry and photochemistry, and nanoscale chemical and photochemical transformations at monolayer interfaces.

S. Rubin

I. Willner

Shai Rubin finished his B. Sc. studies at The Hebrew University of Jerusalem in 1988 and his Ph. D. studies there in 1994. He is currently a postdoctoral fellow at the Los Alamos National Laboratory, Material Science and Technology Division. His research interests include the photochemical and electrochemical activation of biomaterials, self-assembled monolayers, and the physical characterization of thin-film assemblies.

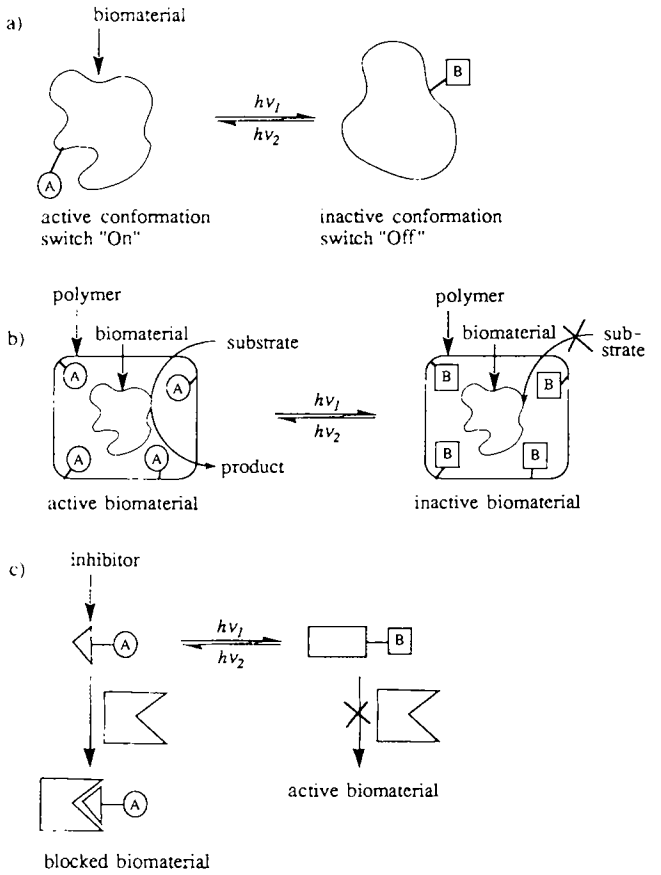

Fig. 1. Methods for tailoring reversible photobiological switches: a) by covalent attachment of photoisomerizable units to the biomaterial; b) by embedding the biomaterial in a photoisomerizable environment; c) by use of a low molecular-weight photoisomerizable inhibitor.

perturbations originally induced on the biomaterial diminish, and the biomaterial restores its active-site structure and is activated to its biochemical function (switch "On"). By reversible photochemical isomerization of the photosensor site, cyclic activation of the biomaterial's functions such as biocatalysis or binding can be switched "On" and "Off".

b) Entrapment of biomaterials in photoisomerizable environments provides a further means to switch "On" and "Off" biochemical functionalities (Fig. 1b). Physicochemical properties of photoisomerizable membrane-mimetic assemblies (for example, polymers, monolayers, and liposomes) are controlled by light.[34-38] The wettability,[39] sol–gel transitions,[40] effective volume viscosity,[41] and permeability[42] of such assemblies are controlled by light. Figure 1b outlines schematically the photostimulation of the biocatalytic functions of an enzyme by a photoisomerizable membrane. In one isomeric state of the environment the membrane is nonpermeable to the substrate, and the membrane-entrapped enzyme is switched off. Upon photoisomerization of the membrane to state B it becomes permeable to the substrate, and the protein can perform its biological function (switch "On").

c) Application of low molecular-weight photoisomerizable compounds that are recognized by biological macromolecules provides a third method to reversibly activate biomaterials (Fig. 1c). Inhibitors or cofactors act as low molecular-weight deactivators or activators of proteins, respectively. Thus, by the application of a photoisomerizable inhibitor the reversible activation of the biomacromolecule is feasible. In one photoisomeric state the inhibitor blocks the protein's active site, and its biological function is switched off. In the complementary photoisomeric state, the low molecular-weight component lacks inhibition properties, and it is released from the active site of the protein.[33,43-49] Similarly, use of a photoisomerizable cofactor that has only one state recognizable by the biomaterial could reversibly switch its biological functions.

The photochemistry of reversibly photoisomerizable compounds has been extensively reviewed in the context of photochromic compounds.[50-53] Various classes of reversibly photoisomerizable substances are available, including isomerization across double bonds (stilbenes, azobenzenes, indigo, and thioindigo derivatives),[54,55] photochemical $(4n+2)\pi$-electron ring closures and openings (fulgides (= dialkylidene butanedioic anhydrides), spiropyrans, spirooxazines),[56,57] photoisomerization of $(4n)\pi$-electron ring systems (oxiranes and aziridines),[58] photoisomerization based on cycloaddition reactions,[59] and photoisomerization by light-induced tautomerism (*N*-salicylidenanilines, anils, *aci*-nitro compounds).[60,61]

These classes of compounds could be coupled to biological substances, membrane mimetic assemblies, and molecular inhibitors (or cofactors) to act as photosensor sites.

Diverse potential applications of photoswitchable biomaterials can be envisaged.[18,62] Fast photobiological switches as interfaces for the recording and readout of optical signals are the basis for optical memory devices and biocomputers.[63,64] Amplification of weak light signals by a photoswitchable catalytic biomacromolecule (enzyme) whose resting state is the mute—"Off"—position represents a further optoelectronic application: absorption of a weak light signal by the photosensor site activates the enzyme, and the chemical transformation driven by the biocatalyst chemically amplifies the light signal by the cyclic formation of the reaction product.[65] Various therapeutic uses and the development of reversible biosensor devices based on photoswitchable biomaterials seem feasible.[33] As many enzymes or their reaction products act as therapeutic agents,[66,67] their reversible light-induced activation and deactivation allows targeting and controlled release of the therapeutic agent by irradiation of the infected organism. The use of photoswitchable biomaterials in the organization of reversible biosensor devices is schematically shown in Figure 2. Numerous biosensors (immunosensors) transduce the binding process between an analyte and the biological sensing receptor into a physical output (color, fluorescence, or electrochemical response).[68-70] However, due to the strong receptor–analyte interactions, many of these biosensors operate as single-cycle (that is, not reusable)

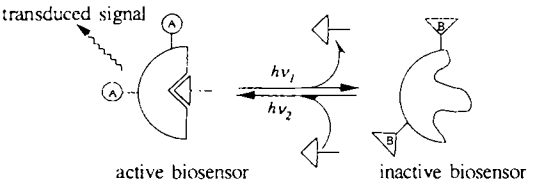

Fig. 2. Scheme illustrating the operation of a reversible biosensor, which utilizes a photoisomerizable biomaterial sensing interface.

analytical devices. Use of a photoisomerizable biomaterial as sensing interface enables the biosensor's active interface to be recycled. The bioreceptor modified by the photosensor in isomeric state A is activated towards the analyte and permits the sensing process. Photoisomerization of the biological interface to state B upon completion of the first sensing cycle yields a biological interface of low affinity for the analyte, which facilitates its release. The analyte is then washed off, and further reisomerization of the biological receptor to state A regenerates the active sensing interface for the subsequent analysis cycle.[33]

The present review summarizes recent advances in the development of photobiological switches based on covalent attachment of photoisomerizable units to biological materials and on immobilization of biomaterials in photoisomerizable environments.

2. Photoregulation of Structures and Functions of Biomaterials and Related Macromolecules by Anchored Photoisomerizable Units

Photochemical isomerization of small molecules attached to macromolecules are known to induce pronounced structural perturbations on the macromolecular matrix; these changes are reflected in the photoswitchable physical properties of the macromolecular assembly.[39, 71–75] Similarly, photoisomerizable units covalently linked to biomaterials provide a means of controlling by light the functions of the biological macromolecules.

2.1. Photochemical Control of the Structure of Polypeptides

Polypeptides are synthetic analogs of proteins, and they organize as random-coil, β-sheet, and α-helix structures, depending on the reaction medium, pH, and temperature.[76] Photochemical control of polypeptide structures by covalently linked photoisomerizable components[77] represents the junction between photostimulated biomaterials and synthetic photoisomerizable polymers.

Poly(L-glutamic acid) was modified with nitrospiropyran units, and the resulting polymer was stabilized in hexafluoropropanol (HFP) in the merocyanine isomeric structure **1b**. The basicity of the phenolate group results in protonation by the solvent, and the protonated merocyanine poly(L-glutamic acid) (**1a**) turns the polymer into a positively charged matrix. Illumination of the stable mixture of **1a** and **1b** with visible light induces isomerization to the spiropyran poly(L-glutamic acid) (**1c**) that undergoes thermal relaxation to the merocyanine isomers **1a** and **1b**. Spiropyran poly(L-glutamic acid) (**1c**) has an α-helix structure that is reflected by typical CD curves with two negative bands at λ = 208 and 222 nm. Thermal back-isomerization of **1c** to **1a** and **1b** decreases the intensity of the CD signal, which implies that the peptide is transformed into an extended coil conformation. The reason for the light-stimulated ordering of **1c** was attributed to the hydrophobic apolar state of the isomer that enables the polymer to form intramolecular H-bonds, thus adopting the α-helix structure.[78, 79] Thermal isomerization to **1a**/**1b** results in electrostatic repulsions between the positively charged photoisomer units tagged to the polypeptide that perturb the α-helix structure and an extended coil conformation results (Scheme 3). These light-stimulated α-helix → random coil changes in polymer **1** are reversible.

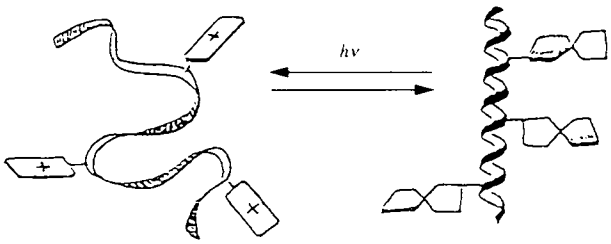

Scheme 3. Schematic representation of photostimulated random-coil/helix transitions of a spiropyran-modified poly(L-glutamic acid) (**1**).

Closely related photoregulation of polypeptide structures was accomplished with azobenzene-modified poly(L-glutamic acid)[80, 81] (**2**) and azobenzene-modified poly(L-lysine)[82] (**3**) in the presence of appropriate surfactants. *Trans*-azobenzene-poly(L-glutamic acid) (**2a**) undergoes reversible photoisomerization. Upon illumination at λ = 370 nm it transforms into *cis*-azobenene-poly(L-glutamic acid) (**2b**), which reisomerizes to **2a** upon illumination at 450 nm. The pK_a values of the free carboxylic acid functionalities of an azobenzene poly(L-glutamic acid) polymer (35 mol% loading) depend on the isomeric structures of the azobenzene units (pK_a 6.8 for **2a** and 6.3 for **2b**). The difference in the pK_a values of the polymer was attributed to the polarity of *cis*-azobenzene units, which enhances the local dielectric constant of neighboring carboxylic acid functionalities. As a result, photoisomerization in an aqueous solution (pH = 6.5) transforms *trans*-isomer **2a** to the *cis*-isomer **2b**.[83] Not only the acidity of adjacent carboxylic acid functionalities but also the structure of the polymer is influenced by the photochemical isomerization. The *trans*-isomer **2a** (which includes a 20 mol% loading of the photoisomerizable units) was found to exist in the presence of dodecylammonium chloride micelles in a

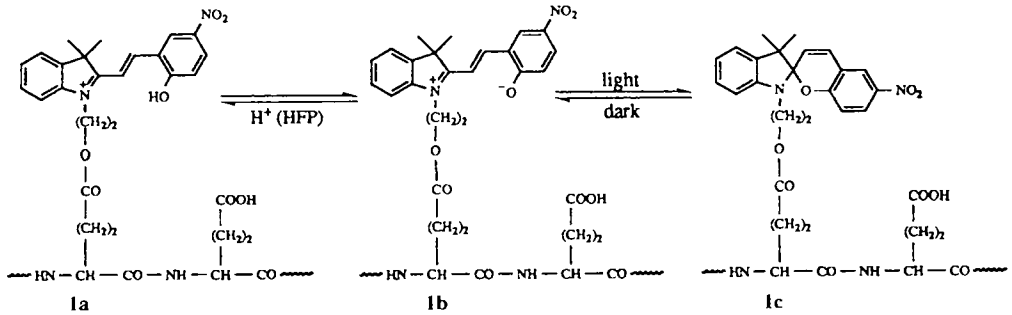

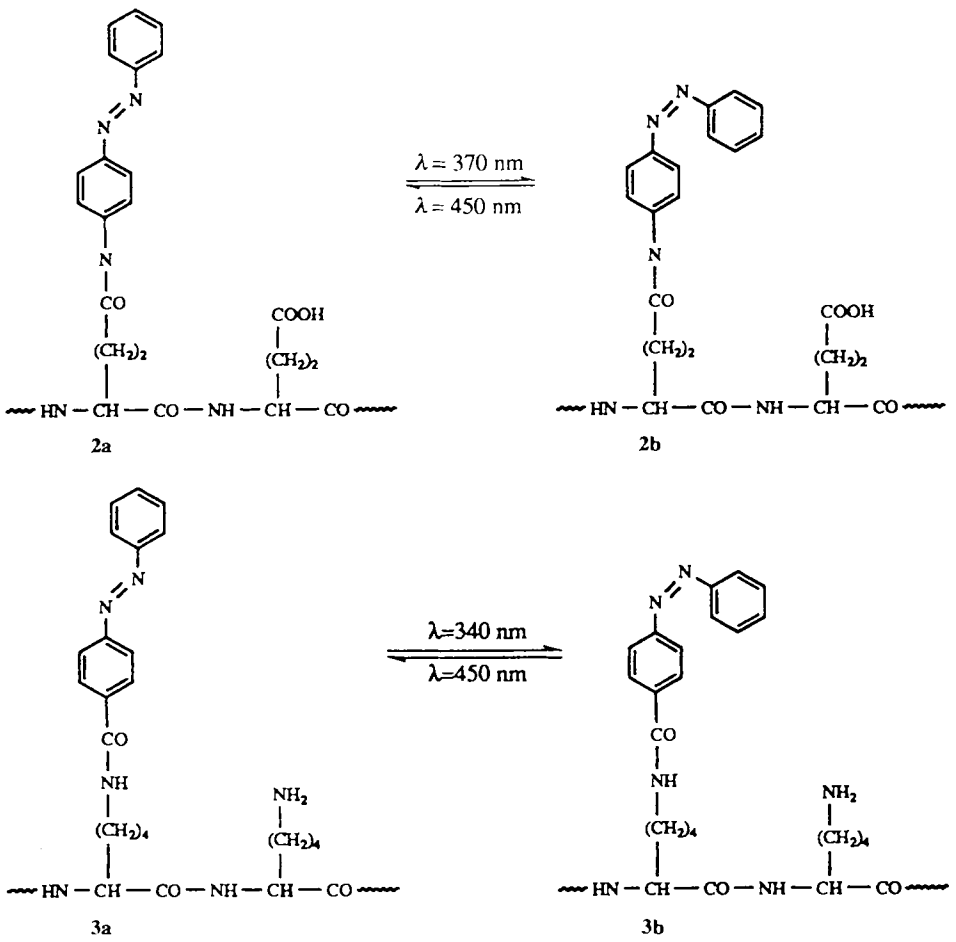

random coil conformation. Photoisomerization to **2b** induces a coil-to-helix transition, which is evident from CD bands at 210 and 228 nm. The existence of the *trans*-isomer **2a** in a disordered coil structure was attributed to the hydrophobic character of the *trans*-azobenzene units: the distortion of the polymer results from the incorporation of the hydrophobic units into the core of micelles. Photoisomerization to **2b** forms the polar *cis*-azobenzene polypeptide units, which leave the micelles, and the stabilized α-helix conformation of the polymer is favored in the aqueous phase.[84] Similar photomodulated structural control of azobenzene poly(L-lysine) (**3**) was observed in a hexafluoropropanol/water/sodium dodecylsulfate system (the polymer contained 43 mol% of azobenzene units). The CD spectrum of the *trans* isomer **3a** was characteristic of a polypeptide in a β-sheet conformation. Upon irradiation at 340 nm and isomerization to **3b** the β-sheet structure was disrupted, and an α-helix polypeptide conformation was promoted (50% α-helix content). Upon further photoisomerization of **3b** to **3a** (illumination at $\lambda = 450$ nm) the β-sheet structure was reconstituted. These photostimulated β-sheet → α-helix transitions were ascribed to the different geometries and polarities of the polymer-anchored azobenzene units. Polypeptide β-sheets are stabilized by hydrophobic interactions of the polymer's side chains. Accordingly, the planar structure of *trans*-azobenzene units and their hydrophobic nature contribute to the stabilization of the β-sheets. Photoisomerization to **3b**, which has polar side-chain chromophoric units, favors the α-helix conformation.[85]

2.2. Photoregulated Binding of Proteins

Intermolecular recognition is a fundamental function of biomaterials. Catalysis within the recognition pair, transport of specific substrates across natural membranes, and storage of materials, specifically small molecular-weight compounds, represent biological processes where recognition and binding play a primary role. Modification of biomaterials with photoisomerizable components provides a general means to control by light the binding affinities of the complementary components. Whereas in one photoisomeric state the biomaterial's binding site is preserved and the formation of the intermolecular complex is facilitated, the second photoisomeric state distorts the biomaterial's recognition site and binding is blocked.

The lectin concanavalin A (Con. A) was modified by photoisomerizable components, and its binding properties towards α-D-mannopyranose and α-D-glucopyranose were regulated by light.[86-89] Con. A is a globular lectin composed of four subunits ($M \approx 26$ kDa). Each subunit includes binding sites for Mn^{2+} and Ca^{2+}, which act cooperatively in the recognition of α-D-mannopyranose (**4**) and α-D-glucopyranose (**5**). Con. A was modified by photoisomerizable

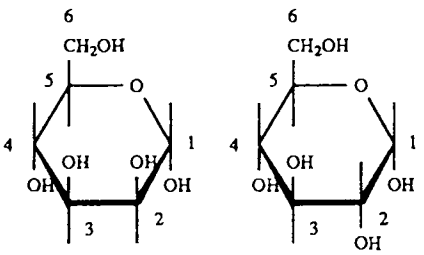

4 **5**

thiophenefulgide[86] and nitrospiropyran[87] components (Scheme 4). The photosensitive proteins undergo reversible photoisomerization: thiophenefulgide-modified Con. A (**6a**) undergoes electrocyclization to **6b** upon irradiation at $\lambda = 300$–400 nm, whereas **6b** is photoisomerized into **6a** upon exposure to visible light ($\lambda > 475$ nm). Spiropyran-modified Con. A (**7a**) undergoes a 6π-electron photochemical ring-opening to the zwitterionic merocyanine-Con. A (**7b**) upon illumination at $\lambda = 300$–400 nm. The latter photoisomer is reversibly electrocyclyzed to **7a** by irradiation with visible light ($\lambda = 475$ nm). Table 1 gives the association constants for the binding between

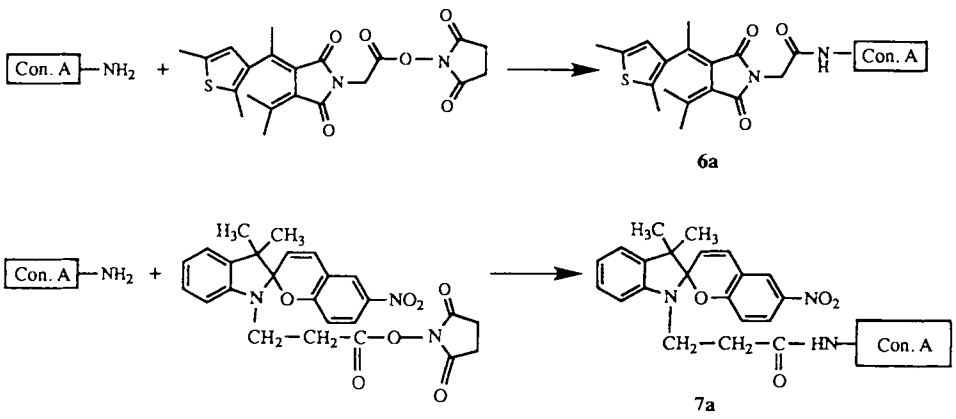

6a

7a

Scheme 4. Chemical modification of concanavalin A with the photoisomerizable thiophenefulgide (top) and spiropyran photoisomerizable units (bottom).

6 or **7** and nitrophenyl-α-D-mannopyranose **8** for several protein loadings. For thiophenefulgide-modified Con. A the isomeric

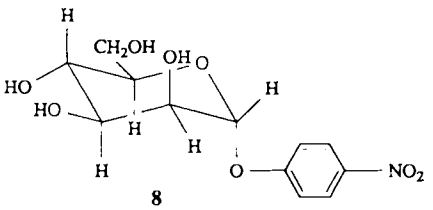

8

state **6b** exhibits higher affinity towards α-D-mannopyranose, while for spiropyran-modified Con. A the photoisomeric state **7a** exhibits enhanced binding properties for the monosaccharide. The difference between the binding properties of the concanavalin A photoisomeric states is very sensitive to the loading degree. While low loadings do not substantially change the binding affinities of the two photoisomeric proteins that recognize the substrate, high loadings result in a significant decrease in the binding properties, presumably due to substantial distortion of the proteins.

Table 1. Association constants K_a for the binding of **8** to the two photochromic states of **6** and **7** as a function of degree of loading by the photochromic substituent.

Degree of loading	K_a [M^{-1}] **6a**	K_a [M^{-1}] **6b**	K_a [M^{-1}] **7a**	K_a [M^{-1}] **7b**
0	22000		24000	
3			23000	23000
6	16400	20000	18000	12000
8			10000	7300
9	7800	12100		
12	6400	6400		

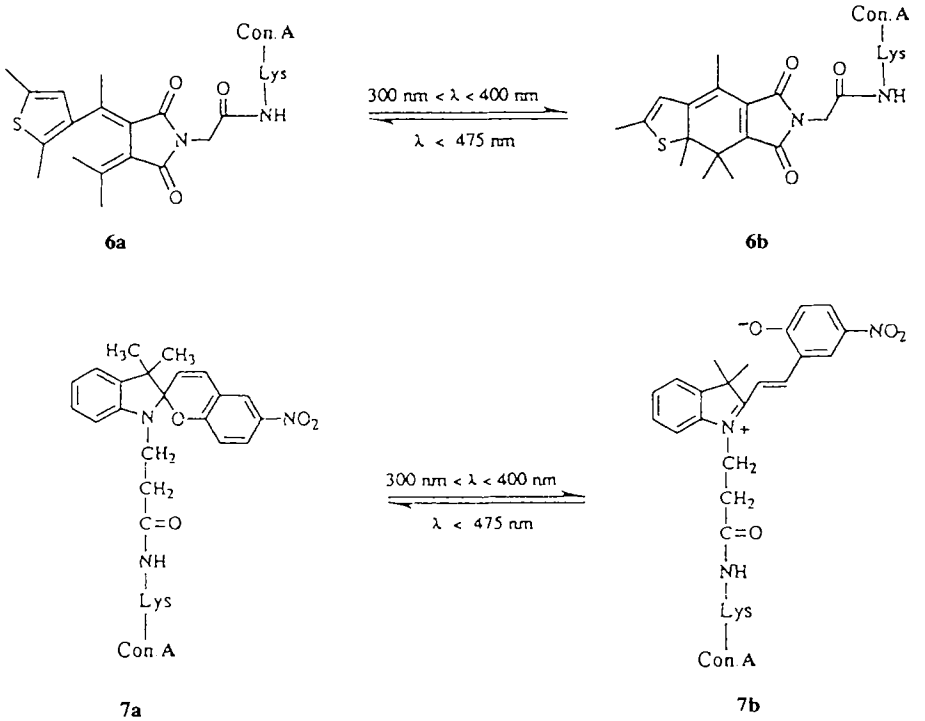

6a **6b**

7a **7b**

The difference in the affinities of **6a** and **6b** for α-D-mannopyranose was utilized for reversible photostimulated association of the host-substrate to the protein (Fig. 3). In this system the concentration of free α-D-mannopyranose in solution is controlled by the photoisomeric state of Con. A. In state **6b** the monosaccharide binds efficiently to the protein, and its free concentration is low. Upon photoisomerization of **6b** to **6a** the binding constant of the substrate to the protein decreases, and the free monosaccharide concentration in the solution increases. This intermolecular complex formation and dissociation is fully reversible upon photoswitching Con. A between states **6b** and **6a**.

The binding process of the monosaccharides to the photoisomerizable Con. A proteins was not only thermodynamically controlled; a kinetic control of the protein–substrate association processes was also revealed.[90] Self-assembled monolayers of the guest monosaccharides

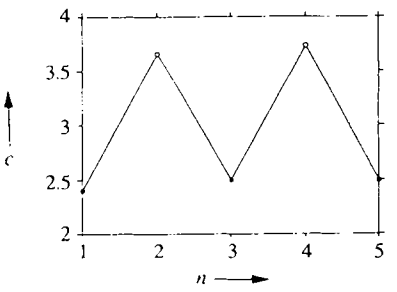

Fig. 3. Reversible photostimulated association and dissociation of **8** and **6**. ●: protein in **6a** state, ○: protein in **6b** state. c = concentration of the complex of **6** and **8** in μM. n = number of cycles.

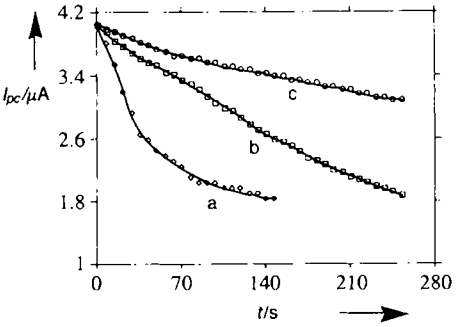

Fig. 5. Decay of current (I_{pc}) of a $[Fe(CN)_6]^{4-}$ redox probe upon interaction of phenyl-α-D-glucopyranose monolayer Au electrode with native Con. A (a), **7a** (b), and **7b** (c). All experiments were performed in a three-electrode cell with Ag/AgCl as reference electrode; electrolyte composition: 1×10^{-3} M $K_4[Fe(CN)_6]$, 1×10^{-3} M KCl in phosphate buffer (0.1 M, pH = 8); concentration of added protein: 0.01 mg mL^{-1}; T: 20 ± 1 °C; scan rate: 200 mV sec^{-1}.

were organized on Au electrodes (Fig. 4). The kinetics of the association of the spiropyran-modified Con. A (**7a**) and merocyanine-derivatized Con. A (**7b**) to the monosaccharide monolayer on the electrode was followed by inspecting the extent of electrode insulation towards a redox probe in solution. Figure 5 depicts the kinetics of insulation by native Con. A, **7a**, and **7b** of an electrode modified by the thiourea-linked phenyl-α-D-glucopyranose monolayer. Native Con. A reveals the highest affinity for the substrate-coated electrode, as reflected by the rapid insulation of this monolayer electrode. The photoisomer **7b** that exhibits a low association constant for α-D-glucopyranose (K_a = 12000 M^{-1}) reveals slow kinetics of interaction with the electrode. In contrast, the photoisomeric protein **7a** (K_a = 18000 M^{-1}) associates faster with the electrode. Table 2 presents the time constants for association of the photoisomers **7a** and **7b** to various monosaccharide monolayer electrodes.

The different association properties of the monosaccharides to photoisomerizable Con. A were attributed to enhanced perturbations by one of the photoisomeric states to the structure of the protein and specifically its binding site. Evidence for the structural distortion of Con. A following the photoisomerization of **7a** to **7b** and the associated dynamics was revealed by time-resolved light-scattering experiments.[91] Photoisomerization of **7a** to **7b** is accompanied by a transient increase in the light-scattered signal by the protein, which implies protein shrinkage upon isomerization. The dynamics of the protein condensation is reflected by the time constants of the intensity of the scattered light. For a protein loaded with six photoisomerizable units the matrix shrank within 60 msec. At a loading of eight units the dynamics of structural perturbation revealed biexponential kinetics, where shrinkage to a metastable protein configuration occurred within 60 msec, and the matrix condensed further on a longer time scale (t = 250 msec).

Table 2. Time constant $\tau_{1/2}$ [sec] [a] for the association of Con A and spiropyran-modified Con A (7) to monosaccharide substrates.

Substrate	$\tau_{1/2}$ (Con. A)	$\tau_{1/2}$ (**7a**)	$\tau_{1/2}$ (**7b**)
phenyl-α-D-mannopyranoside	40	60	160
phenyl-α-D-glucopyranoside	85	220	670
phenyl-β-D-glucopyranoside	100	100	100

[a] $\tau_{1/2}$ is the time required for the cathodic peak current I_{pc} to decay to half of its original value in the cyclic voltammogram of the $[Fe(CN)_6]^{4-}$ redox probe. At this stage the monolayer is half-covered by the protein.

Mutual recognition of antibody and antigen was photostimulated in a photoisomerizable antigen. A monoclonal antibody (Z1H01) for the hapten Glu-(*trans*-azobenzene Ala)-Gly_2 (**9a**)

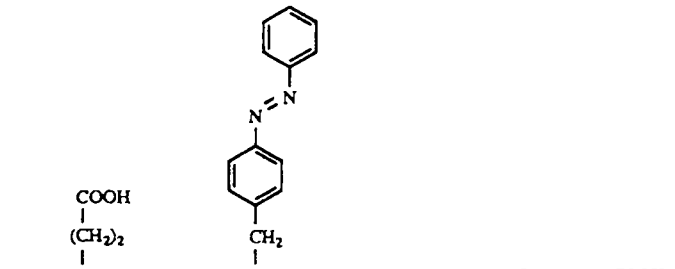

9a

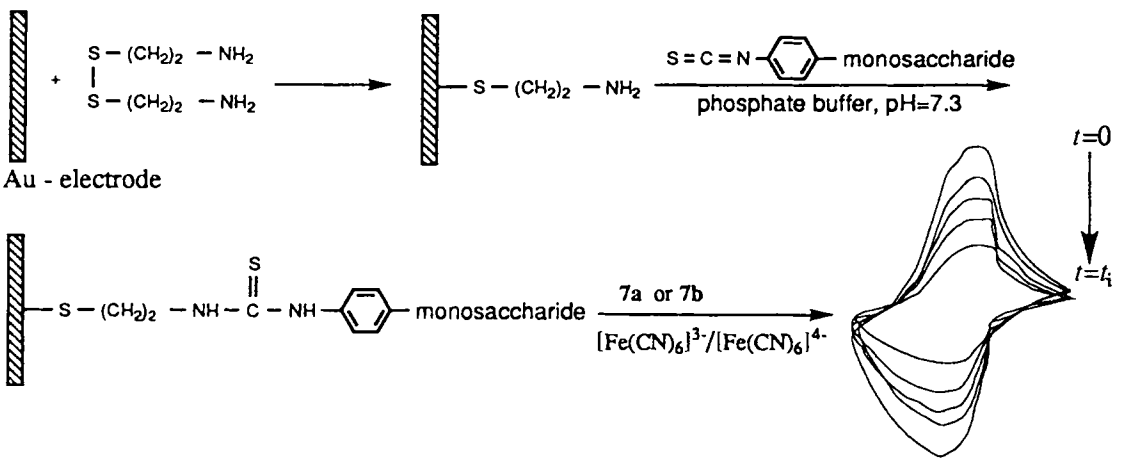

Fig. 4. Construction of monosaccharide monolayers on Au electrodes and cyclic voltammograms of a soluble redox probe at different time intervals as schematic representation of the insulation of the electrodes through association with the photoisomerizable proteins. The monosaccharides used were α-D-manno-, α-D-gluco-, and β-D-glucopyranoside.

was prepared.[92] The *trans*-azobenzene hapten state exhibits high affinity for the antibody. The binding process was followed by quenching of the antibody fluorescence through energy transfer to the associated azobenzene hapten. The value of the derived association constant K_a is $5 \times 10^7\,M^{-1}$. Photoisomerization of **9a** to the *cis*-azobenzene hapten **9b** (λ = 360 nm) resulted in a hapten isomer with poor affinity for the antibody as reflected by inefficient quenching of the antibody fluorescence. Further illumination of the photoisomer **9b** to **9a** by illumination with visible light (λ = 430 nm) restored the active hapten recognized by the antibody. Uptake and release of the hapten to and from the antibody was accomplished reversibly and followed by the fluorescence resulting from the system (Fig. 6). The light-induced association and dissociation of antigen–antibody pairs could provide a general means for the development of reversible immunosensor devices (for a specific example see Section 3.3).

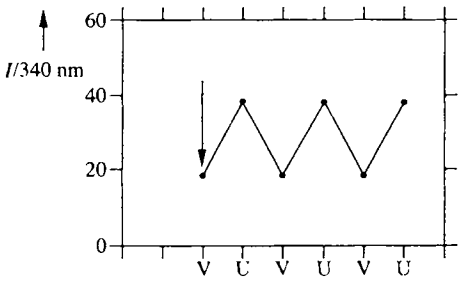

Fig. 6. Reversible photostimulated binding and dissociation of the photoisomerizable hapten **9** to and from the monoclonal antibody Z1HO1. V indicates hapten in the **9a** (*trans*) configuration; U indicates hapten in the **9b** (*cis*) isomeric state. The arrow indicates addition of **9a**; *I* is the intensity of the fluorescence at 340 nm.

The monoclonal antibody against *trans*-azobenzene units was recently applied in the reversible photostimulation of biocatalytic activities. The *trans*-azobenzene-modified NAD^+-cofactor (**10a**) was prepared.[93] This cofactor exhibits photoisomerizable properties, and upon UV irradiation of **10a** (λ = 320 nm) the *cis*-azobenzene-NAD^+-cofactor (**10b**) is formed. Further illumination of **10b** with visible light ($\lambda > 420$ nm) restores **10a**. While **10a** binds to the corresponding antibody, **10b** is not recognized and is released from it. Accordingly, coupling of NAD^+-dependent enzymes with the *trans*-azobenzene-NAD^+-antibody provides a mechanism for controlling the availability of the cofactor for biocatalyzed transformations: association of the cofactor in state **10a** to the antibody eliminates the free cofactor from solution, and the enzyme activity is inhibited; photoisomerization of **10a** to state **10b** dissociates the antibody–antigen complex, and the cofactor is released to solution and activates the enzyme. In Scheme 5 the photostimulated activation and deactivation of NAD^+-mediated biocatalyzed transformations with the photoisomerizable cofactor **10** and the *trans*-azobenzene antibody is described schematically. The two NAD^+/NADH-dependent enzymes are alcohol dehydrogenase and diaphorase. The cofactor in state **10a** is associated to the antibody, and the activities of the two enzymes are blocked. Photoisomerization of **10a** to *cis*-azobenzene-NAD^+ (**10b**) releases the cofactor from the antibody. The free cofactor is then reduced by ethanol in the presence of alcohol dehydrogenase to form *cis*-azobenzene-NADH, which is oxidized by 2,6-dichlorophenol–indophenol (DCIP) in the presence of diaphorase. The biocatalyzed reduction of DCIP by ethanol in the presence of the two enzymes can be blocked by reisomerization of **10b** to **10a** and entrapment of the cofactor in the antibody matrix. This indirect approach to photomodulating enzyme activities by antibodies specific to the photoisomerizable unit that is linked to a cofactor seems to be generally applicable to the design of reversible photoswitchable biomaterials. Attachment of photoisomerizable units to inhibitors, coenzymes, activating proteins, etc., and utilization of the appropriate antibodies could trigger enzyme activities by selective release of the biocatalyst-dependent co-component.

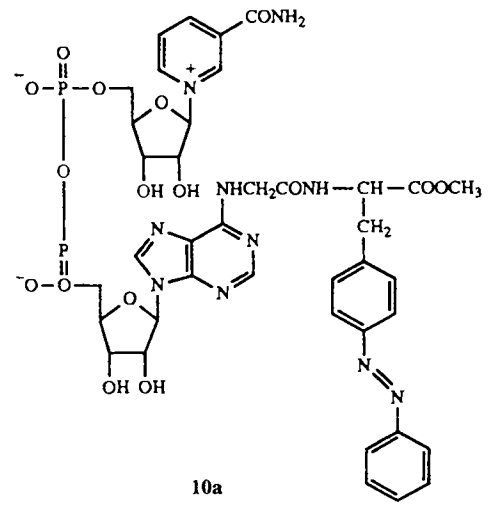

10a

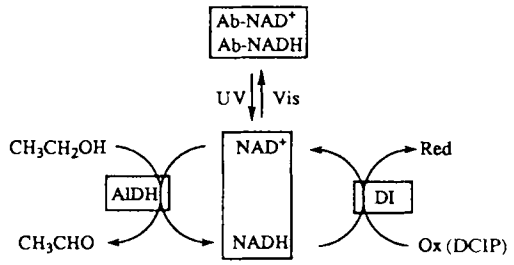

Scheme 5. Reversible photostimulation of alcohol dehydrogenase (AlDH) by the photoisomerizable azobenzene-modified NAD^+ (**10**) in the presence of the monoclonal antibody Z1HO1 (Ab). Diaphorase (DI) is used to regenerate the oxidized cofactor. The Ab complexes at the top of the scheme are inactive.

2.3. Photostimulation of Enzyme Activities

Attachment of photoisomerizable units to enzymes provides a general means of regulating biocatalytic activities (Fig. 7). In one photoisomeric state the tertiary structure of the protein and the conformation of its active site are preserved, and the enzyme is switched "On" with respect to its native activity. Photoisomerization induces distortion of the protein structure that could originate from electrostatic interactions between the isomeric state and the protein, steric distortions, or disruption of hydro-

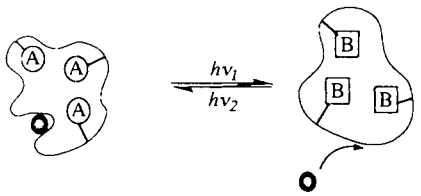

Fig. 7. Schematic representation of the photoswitchable activation and deactivation of an enzyme by covalently linked photoisomerizable components. The binding site is accessible in the undistorted protein (on the left), but not in the distorted protein (on the right).

gen bonds associated with the tertiary enzyme structure. The initial attempts at "On–Off" photostimulation of an enzyme by this method were reported by Montagnoli et al., who modified aldolase at Cys 237 and Cys 287 by attaching different diazonium salts.[94, 95] The resulting diazo-modified aldolases (**11a**) exhibited photoisomerizable properties, but the two states **11a** and **11b** exhibited little differences in their biocatalytic proper-

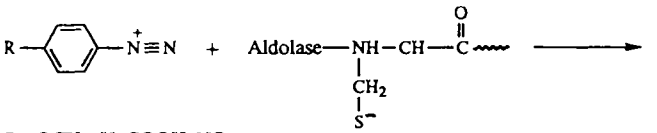

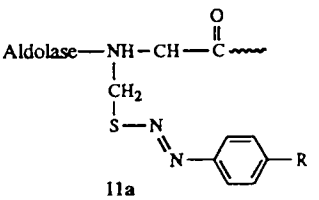

ties. The isomeric states gave different mobilities in gel electrophoresis, which implies that they have different structures, but the protein-embedded active site is not sufficiently distorted to reveal switchable biocatalytic activities.

The approach has been successfully applied to photoregulate the activity of papain.[96] This enzyme was modified by covalent coupling of either *trans*-4-carboxyazobenzene (**12**), *trans*-3-carboxyazobenzene (**13**), or *trans*-2-carboxyazobenzene (**14**) to its

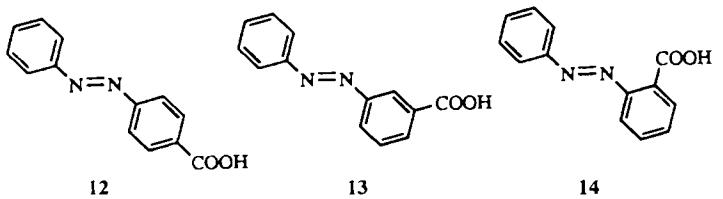

lysine residues. The different azobenzene-modified papains undergo reversible *trans* → *cis* photoisomerization [Eq. (a)]. The activity of the modified enzymes depends on the nature of the azobenzene components. (*Trans*-4-carboxyazobenzene)-papain, (*trans*-3-carboxyazobenzene)-papain, and (*trans*-2-carboxyazobenzene)-papain retain 80%, 36%, and 1%, respectively, of the activity of the native enzyme. The best photostimulated activities were detected with the 4-carboxyazobenzene derivative **15** for a loading corresponding to five photoactive units per enzyme. In this protein assembly, the *trans*-isomer **15a** was

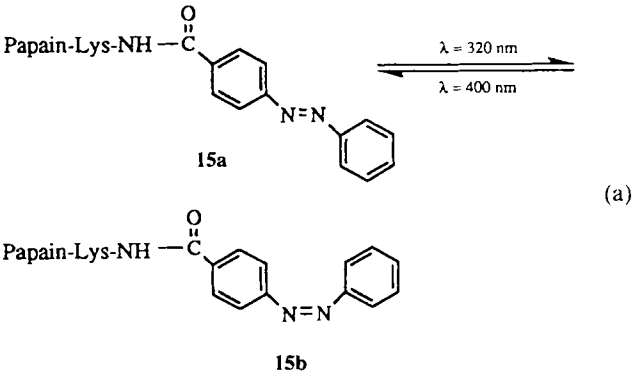

(a)

about 2.75 times more active than the *cis*-isomer **15b** towards the hydrolysis of *N*-benzyl-D,L-arginine-nitroanilide [**16**, Eq. (b)]. Since photoisomerization of **15a** to **15b** yields a photo-

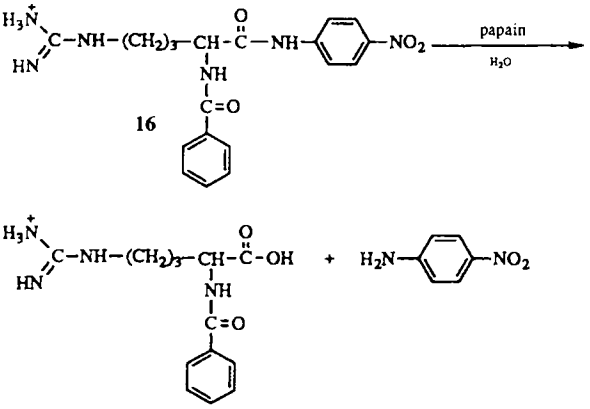

(b)

stationary equilibrium where [**15b**]/[**15a**] = 0.89, even partial transformation into the *cis*-state is sufficient to retard the hydrolytic activity of the enzyme. The different activities of the papain photoisomeric states **15a** and **15b** enabled reversible cyclic photostimulation of the hydrolytic process of Equation (b) (Fig. 8). Kinetic analyses of the biocatalysts in the two

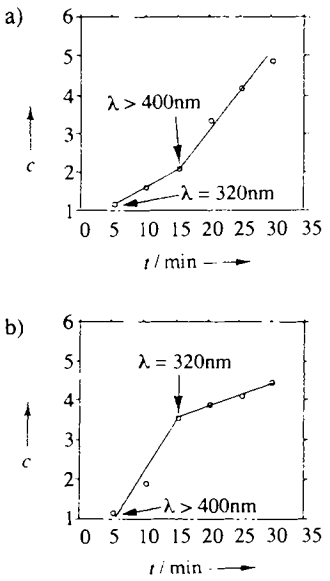

Fig. 8. Photostimulated hydrolysis of **15** by azobenzene-modified papain. a) Hydrolysis is initiated by the *cis*-isomer **15b** and switched on by irradiation (marked by an arrow) that transforms **15b** into the *trans*-derivative **15a**. b) Hydrolysis is initiated with **15a** and switched off by irradiation (marked by an arrow) that transforms **15a** into **15b**. *c* = concentration of product in 10^{-5} M.

photoisomeric states **15a** and **15b** were conducted to elucidate the mechanism of photoswitchable activity of the enzyme. The two photoisomeric states of papain (**15a** and **15b**) exhibit similar V_{max} values ((1.9 ± 0.2) mM min^{-1}) but differ in their K_m values ($K_m = (2.2 \pm 0.2)$ mM for **15a** and (6.5 ± 0.6) mM for **15b**). These results suggested that the binding of the substrate to the enzyme's active site was inhibited in the "Off" state of papain (**15b**) but the catalytic functions of the active center were not influenced by photoisomerization.

Closely related reversible activation of biocatalysts' functions were reported for a series of spiropyran-modified enzymes.[97, 98] Spiropyran units were covalently linked to a series of enzymes [Eq. (c)], and the resulting enzymes exhibited reversible photoisomerization [Eq. (d)]. Table 3 summarizes the

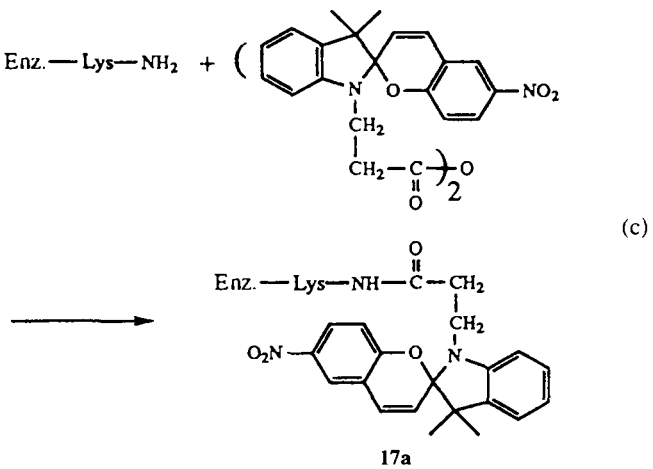

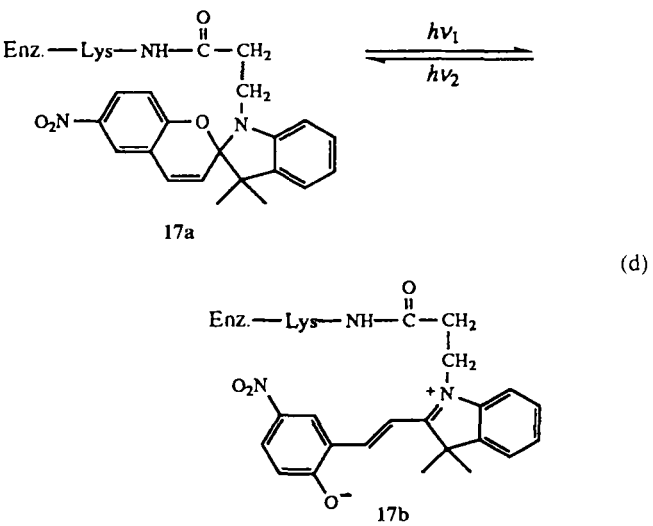

different enzymes used in this study, the substrates used to assay them, and the relative activities of the enzyme's isomeric states **17a** and **17b**. The K_m values of the enzymes' isomeric states are also provided. The highest photoswitchable activation/deactivation is observed for β-amylase, for which the activity in the isomeric state **17b** is only about a tenth of the activity in state **17a**. The substantially higher K_m value of the α-amylase in state **17b** suggests that the binding to the protein's active site is perturbed in this conformation.

Table 3. Activities and affinity parameters of photoisomerizable spiropyran-modified enzymes **17**.

Enzyme	Substrate	17a		17b	
		Activity	K_m [mM]	Activity	K_m [mM]
α-chymotrypsin	*N*-benzoyl-L-tyrosinethylester	1	15	1.5	4.3
β-glucosidase	*p*-nitrophenyl-β-D-glucoside	1	4.0	1.15	3.3
β-amylase	amylose	1	3.4	0.13	60
α-amylase	amylose	1	12	0.64	15

Modification of enzymes by attaching photoisomerizable units led to incomplete photoswitchable activities of the biocatalysts in aqueous media, as the enzymes in the "Off" states exhibited residual biocatalytic properties. It has been suggested that better light-controlled biocatalysts could be obtained by employing the photoisomerizable enzymes in organic solvents,[99] because proteins should then be more sensitive to structural perturbations induced by the photoactive units due to the limited amount of water that participates in the stabilization of the biopolymer's tertiary structure.[100–102] Accordingly, α-chymotrypsin was modified with thiophenefulgide units to introduce reversible photoisomerizable properties [states **18**-E and **18**-C, Eq. (e)]. The two photoisomeric states have similar

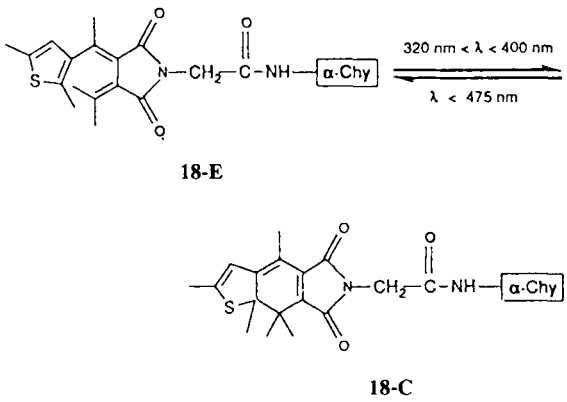

hydrolytic activities in an aqueous solution (assayed by hydrolysis of *N*-acetyl-*N*-phenylalanine ethyl ester or *N*-succinyl-L-phenylalanine-*p*-nitroanilide). However, the photoisomerizable α-chymotrypsin exhibits light-controlled biocatalytic activities in an organic solvent (cyclohexane). Esterification of *N*-acetyl-L-phenylalanine (**19**) by ethanol is slow in the presence of **18**-E, and photoisomerization to **18**-C accelerates the reaction by about a factor of 5 [Fig. 9 and Eq. (f)].

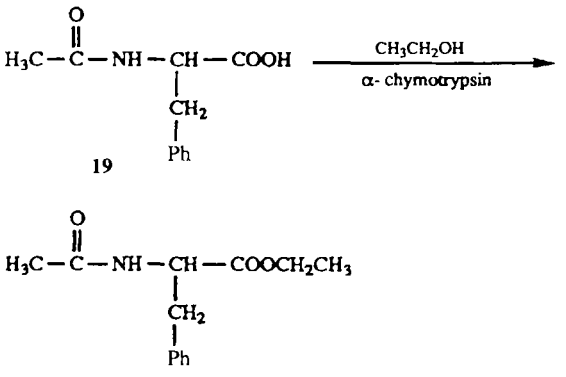

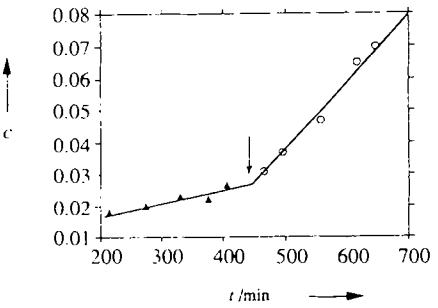

Fig. 9. Photostimulation of the esterification of **19** by ethanol in cyclohexane by using thiophenefulgide-modified α-chymotrypsin (**18**). The biocatalyzed transformation is initiated with **18-E** and switched on by photoisomerization of the biocatalyst to state **18-C** ($320\ nm < \lambda < 400\ nm$, at the time indicated by the arrow). c = concentration of the product in 10^{-3} M.

The control of enzyme activities by photoswitchable, covalently linked, isomerizable groups has involved random chemical substitution of the proteins by photoisomerizable groups, and superior switchable activities were observed at high loadings. It has been suggested that at high loadings maximal steric distortions of the proteins are induced, leading to inhibited catalytic or binding properties of the biomaterial's active sites. A significant advance, however, would include the specific mutation of selected amino acid residues by photoisomerizable units. This would allow direct correlation between computational analyses of the tertiary structure of the isomerizable mutants, and specifically their active sites, and the observable photoswitchable properties.

Preliminary studies based on these concepts have recently been reported by the semisynthesis of a photoisomerizable mutant of phospholipase A_2.[103] This lipolytic enzyme cleaves 2-acyl bonds of phosphoglycerides, and its activity is enhanced towards substrates associated with aggregated interfaces such as micelles or vesicles. It was suggested that the N-terminus of phospholipase A_2, composed of Ala-1, Leu-2, Trp-3, Arg-6, Leu-15, Met-20, Leu-31, and Try-69, adopts an α-helical conformation that generates a recognition site at the interface.[104, 105] This site facilitates the association of the enzyme at lipid–water interfaces and thereby enhances the hydrolysis of substrates at such boundaries.[106] Covalent linkage of a photoisomerizable unit to an amino acid residue associated with the recognition site of the interface enables photostimulation of the enzyme activity. A photoisomerizable phospholipase A_2 mutant was prepared by a semisynthetic approach (Scheme 6).[103] The ε-amidinated enzyme was subjected to three consecutive Edman degradations to degrade the terminal amino acids Ala-1, Leu-2, and Trp-3. The protein was then reconstituted by the stepwise synthesis of the tripeptide Boc-Ala-Leu-(*trans*-azobenzene-Phe) (X_{aa} = *trans*-azobenzene-phenylalanine) followed by its coupling to the 121-mer obtained in the initial cleavage step. The procedure specifically substituted the Trp-3-residue with the photoisomerizable azobenzene-Phe.

The activities of the photoisomerizable phospholipase A_2 mutant were assayed towards hydrolysis of the lipids associated with palmitoyl phosphatidylcholine vesicles. (Radio-labeled lipids or vesicle-encapsulated fluorescence probes were used to monitor lipid hydrolyses). The mutant in the *trans*-azobenzene-phenylalanine conformation does not exhibit any hydrolytic activity towards the lipid hydrolysis. Photoisomerization of the mutant to the *cis*-azobenzene-Phe isomer activates it towards hydrolysis. The mutant in the *cis*-conformation retains about 10% of the native enzyme activity. CD spectra of the mutant phospholipase A_2 revealed that the α-helix content of the *cis*-isomer is substantially higher than in the *trans*-mutant. The enzyme recognition site adopts the α-helical conformation and is the active counterpart for the biocatalytic lipid hydrolysis. This suggests that in the *trans*-form of the mutant the recognition site of the interface is perturbed, and the enzyme activity is blocked. Upon photoisomerization to the *cis*-mutant, the recognition site is reconstituted (as evidenced by the α-helical conformation deduced from the CD spectrum), and the enzyme is switched on towards the hydrolytic process.

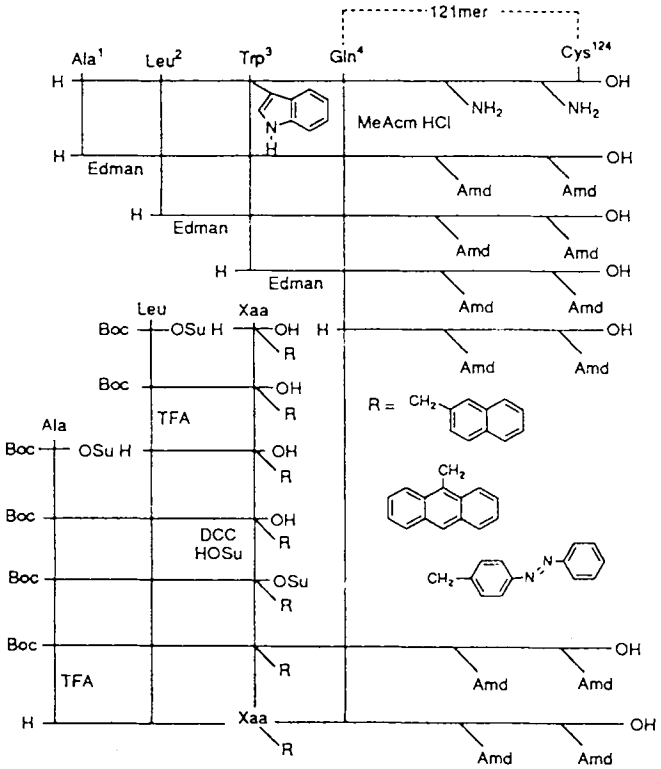

Scheme 6. Semisynthetic method for cleavage of phospholipase A_2 to constitute azobenzene-modified phospholipase A_2. Acm = acetamidate, Amd = ε-amidinated, DCC = dicyclohexylcarbodiimide, HOSu = *N*-hydroxysuccinimide, TFA = trifluoroacetic acid, Xaa = *trans*-azobenzene phenylalanine.

Photoswitchable biomaterials exhibit the fundamental optical recording feature of an optoelectronic active interface. Recorded optical signals are translated into mute or chemically activated functions. Fast read-out of the recorded optical information, preferably by a different physical signal, is essential for applications of photoswitchable biomaterials as active interfaces in optoelectronics. Amperometric transduction of recorded optical signals was recently demonstrated with a photoisomerizable redox enzyme, which acted as the optical recording and transducing matrix.[107] Glucose oxidase (GOD) was modified by nitrospiropyran photoisomerizable units. The modified enzyme is photoisomerizable between the nitrospiropyran-GOD (SP-GOD, **20a**) and the protonated merocyanine-GOD (MRH^+-GOD, **20b**) states and displays light-controlled activities: **20a** is about twice as active as **20b**. The

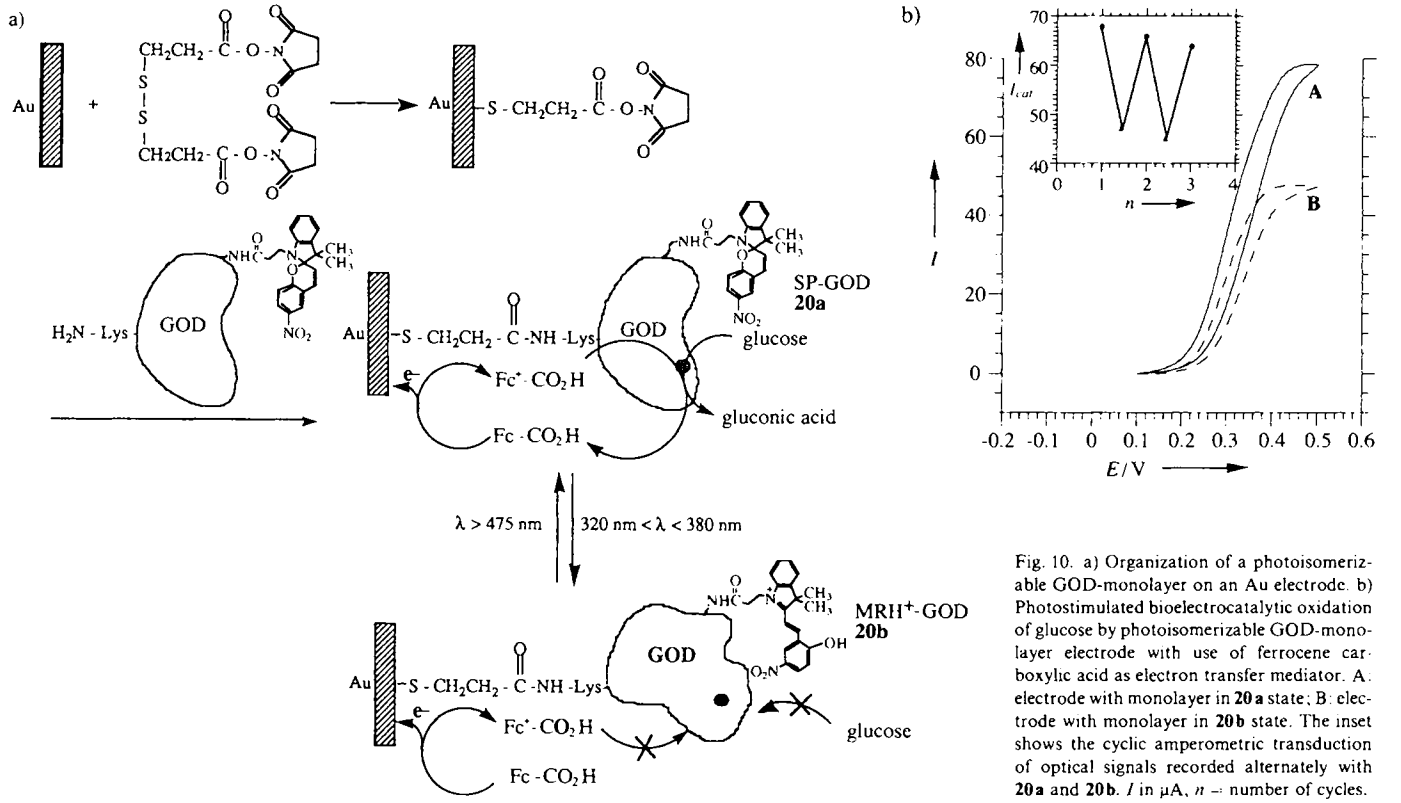

Fig. 10. a) Organization of a photoisomerizable GOD-monolayer on an Au electrode. b) Photostimulated bioelectrocatalytic oxidation of glucose by photoisomerizable GOD-monolayer electrode with use of ferrocene carboxylic acid as electron transfer mediator. A: electrode with monolayer in **20a** state; B: electrode with monolayer in **20b** state. The inset shows the cyclic amperometric transduction of optical signals recorded alternately with **20a** and **20b**. I in μA, n = number of cycles.

photoswitchable amperometric activities of the photoisomerizable GOD were used for the transduction of recorded optical signals. Enzyme **20a** was assembled as a monolayer on an Au electrode (Fig. 10a). The electrode coated with the monolayer in **20a** state exhibits electrobiocatalytic properties: In the presence of ferrocene carboxylic acid as electron transfer mediator, electrocatalyzed oxidation of glucose gives rise to an electrocatalytic anodic current (I_{cat}). Upon photoisomerization of the monolayer to the **20b** state the enzyme is deactivated, and the efficiency of the bioelectrocatalytic oxidation of glucose decreases. This is reflected by a lower amperometric response of the enzyme-electrode. By cyclic photoisomerization of the monolayer between these states, the recorded optical signals are amperometrically transduced (Fig. 10b).

3. Modulation of Biomaterial Functions by Photoisomerizable Environments

The effects of photoisomerizable components on the physical and chemical properties of membrane mimetic assemblies such as micelles, microemulsions, and liposomes are well documented.[108-112] Photochemical control of the organization of liquid crystal phases[113-116] and sol-gel transitions of polymers[117-119] containing appropriate photoisomerizable components exemplifies the regulation by light of the structure and properties of microscopic and macroscopic phases. If biomaterials are incorporated into such photomodulated phases, their functions could be triggered by environmental effects. This is schematically presented in Figure 11, in which the catalytic function (Fig. 11a) or the binding properties (Fig. 11b) of a biomaterial immobilized into a liposome that contains a photoisomerizable component as a part of the membrane boundary are triggered by light. In photoisomeric state B (Fig. 11a) the liposome is nonpermeable towards the substrate, and the enzyme activity is switched off. Upon photoisomerization to state A the liposome becomes permeable towards the substrate, and the catalytic function of the protein is switched on. The permeability of the membrane could be modulated by a phase transition of the hydrophobic boundary or by utilizing the photoisomeric state A as substrate carrier. In Figure 11b the light-stimulated binding of an antibody is illustrated. The environment in isomeric state A does not include any recognition

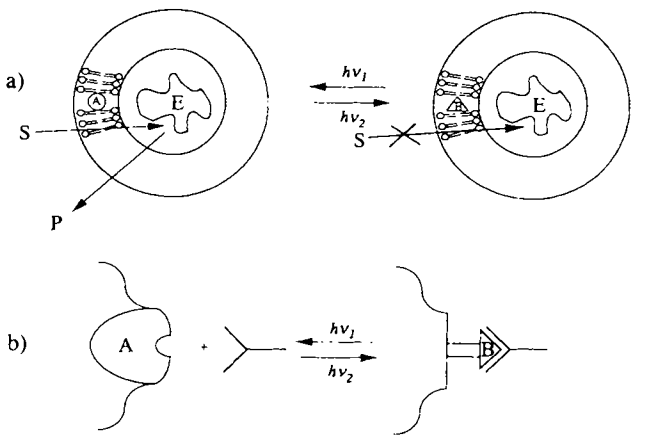

Fig. 11. Principles for photostimulation of a biomaterial's functions by photoisomerizable environments: a) "On-Off" activation of an enzyme by controlling permeability to the substrate (S) of a photoisomerizable liposome. P = product. b) Photoswitchable binding of an antibody to a photoisomerizable antigenic interface.

element towards the antibody. As a result, no binding interactions between the antibody and its surroundings exist. Photoisomerization of the environment to state B generates an antigenic interface, and binding of the antibody is switched on. Upon reversible photoisomerization to state A the antigen interface is perturbed, and the complex between antibody and the surrounding phase dissociates. In the following subsections the light-stimulated activation and deactivation of biomaterials by photoisomerizable environments will be discussed with particular emphasis on the practical implications of such systems.

3.1. Light-Controlled Structure and Permeability of Membrane Mimetic Systems

Monolayers provide two-dimensional arrays that mimic membrane assemblies. Monolayers of poly(L-lysine) with 43% loading of azobenzene groups were prepared.[82] Exposure of the *trans*-azobenzene monolayer compressed to a pressure of 7 $mN\,m^{-1}$ to UV irradiation results in isomerization to the *cis*-azobenzene monolayer and a decrease in the monolayer surface pressure corresponding to $(1.8 \pm 0.2)\,mN\,m^{-1}$. On restoration of the *trans*-azobenzene monolayer by illumination with visible light the monolayer surface pressure increased reversibly. These changes in the monolayer surface pressure were attributed to the different structures of the monolayers: the *trans* isomer exhibits an extended structure of higher surface area, and the *cis* isomer exists in an α-helix monolayer configuration. Similar observations were made with spiropyran-modified poly(methyl methacrylate) (**21a**) monolayers.[120] Upon irradiation of this monolayer with UV light and isomerization of the monolayer to the merocyanine isomer, the monolayer surface pressure increases by $10^{-3}\,N\,m^{-1}$ and $0.3 \times 10^{-3}\,N\,m^{-1}$ at pH = 1.5 and pH = 5.5, respectively. Reversible photoisomerization to the spiropyran monolayer is accompanied by a decrease in the surface pressure to its original value. The pH dependence was attributed to the protonation of the photoisomerized spiropyran polymer. While at pH < 3 it exists as a protonated *o*-hydroxystyrylic cation (**21c**), at pH > 4 the zwitterionic merocyanine isomer (**21b**) is formed. It was also concluded that changes in the surface area are influenced by the location of the chromophores in the monolayer assembly. The charged chromophores of the isomer monolayers **21b** and **21c** are located close to aqueous subphase within the formed monolayer at the air–water interface, while the apolar spiropyran isomer (**21a**) is buried in the hydrophobic monolayer and does not contribute significantly to the surface pressure.

Control of the adhesion and the functions of vesicles was possible by the incorporation of a photoisomerizable polypeptide into the bilayer membrane of the vesicle.[121] Azobenzene-modified poly(γ-methyl-L-glutamate–co(L-glutamic acid)) (**22a**) was incorporated into the bilayer of distearyldimethyl-

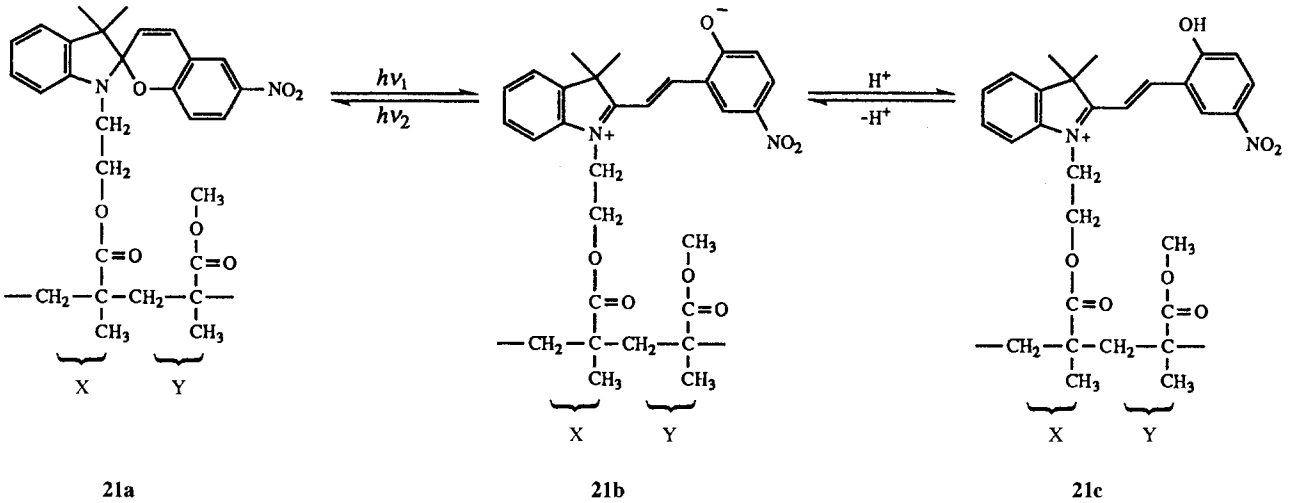

21a **21b** **21c**

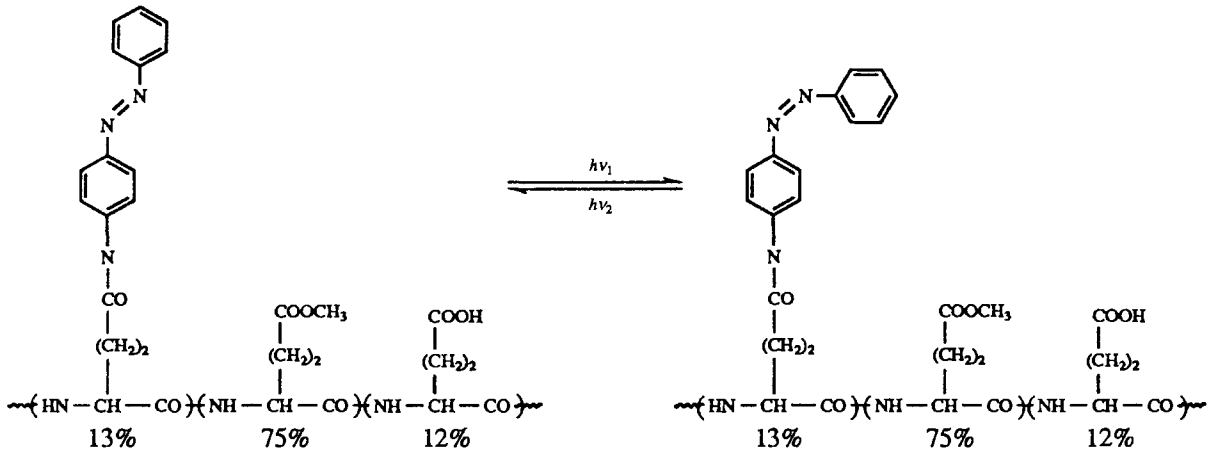

22a **22b**

ammonium chloride vesicles. Upon photoisomerization of **22a** to the *cis* isomer **22b** the polypeptide chain translocated to the exterior hydrophilic subphase of the liposome. Upon photoisomerization of the *cis* isomer back to **22a** with visible light, the polypeptide did not reorganize to its interior boundary position, but retained its translocated position. In a vesicle assembly kept above the gel–liquid phase transition temperature, translocation of the *trans*-azobenene polypeptide **22a** into the interior part of the bilayer did occur, and upon cooling the reconstituted vesicles exhibited properties similar to the original vesicles. The positions and translocation of the polypeptide isomers **22a** and **22b** within the vesicles was characterized by following the polarity effects of the microenvironment on the emission of the fluorescence probe linked to copolymer **22** in the *trans*- and *cis*-configurations. Light-stimulated translocation of the cis-azobenzene-modified polypeptide **22b** has important effects on the vesicle's properties and functions. Adhesion between vesicles containing **22b** at the exterior boundary occurred, presumably through intervesicular interactions of the polypeptide chains. Permeation of ions across the vesicle boundary is controlled by the position of the photoisomerizable polypeptide. The vesicle membrane that includes the interlaced *trans*-polypeptide **22a** is permeable to Na^+, and the permeability to the ion decreases approximately fivefold upon photoisomerization to **22b** and translocation of the polypeptide chain to the exterior boundary of the bilayer. Dissociation of the intervesicular aggregates and restoration of the ion permeability properties of the vesicles was accomplished by photoisomerization of the polypeptide to state **22a** followed by heating the vesicle assembly to the gel–liquid phase transition temperature ($T_c = 40\,^{\circ}C$).

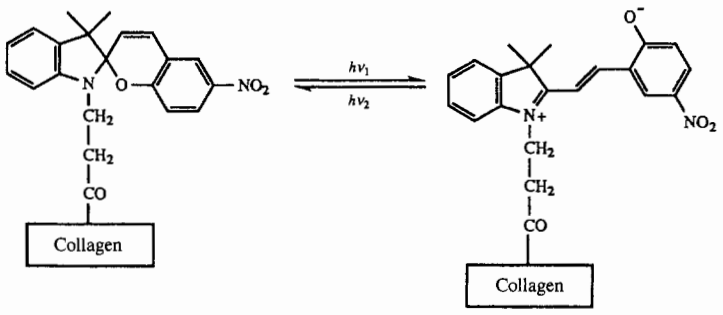

23a **23b**

membrane **23a**. The permeability of the membrane states **23a** and **23b** to the urea substrate is similar and cannot account for the different activities of the biocatalyst. It has been suggested that the enhanced activity of urease in the polymer **23b** originates from the faster release of the reaction product (NH_4^+) from the active complex in the polar isomeric state of the collagen membrane.

Control of the permeation of substrates across photoisomerizable polymers provides a general means to photostimulate polymer-entrapped enzymes (see Fig. 11a). The series of polymers **24**–**26** serve as macromolecular matrices for encapsulation

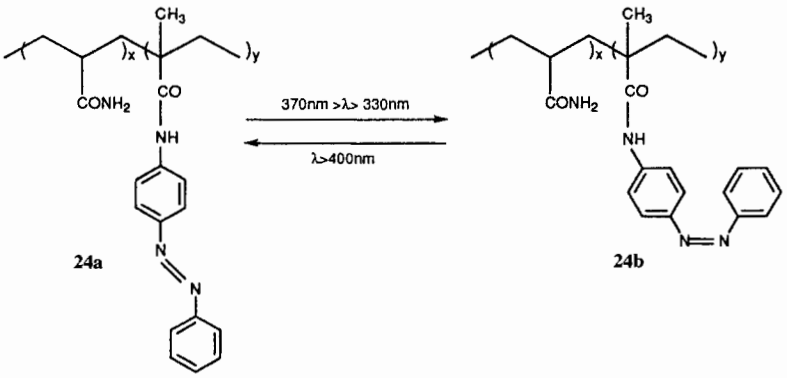

24a **24b**

3.2. Control by Light of Catalytic Functions of Biomaterials by Photoactive Environments

Attempts to affect protein functions by photoisomerizable environments were initiated by Balasurbamanian et al. as early as 1975, who studied the influence of model membrane systems containing photoisomerizable compounds on α-chymotrypsin activity.[122]

These investigations showed that addition of *trans*-4-carboxyazobenzene (**12**) to a microemulsion within a lamellar bilayer structure that contains α-chymotrypsin led to photochemically controllable enzyme activity. The biocatalyst activity was enhanced eightfold in the presence of *cis*-4-carboxyazobenzene. Although the origin of the photostimulation of α-chymotrypsin is not clear, it has been suggested that the photoisomerizable additive affects the lamellar bilayer structure. The photostimulation of α-chymotrypsin was attributed to different interactions of the enzymes with the light-controlled states of the bilayer membrane.

Immobilization of urease in a spiropyran-modified collagen membrane (**23**) led to light-controllable enzyme activity.[123–125] The biocatalyst decomposes urea within the merocyanine collagen membrane **23b** at a rate that is about twice that within the spiropyran

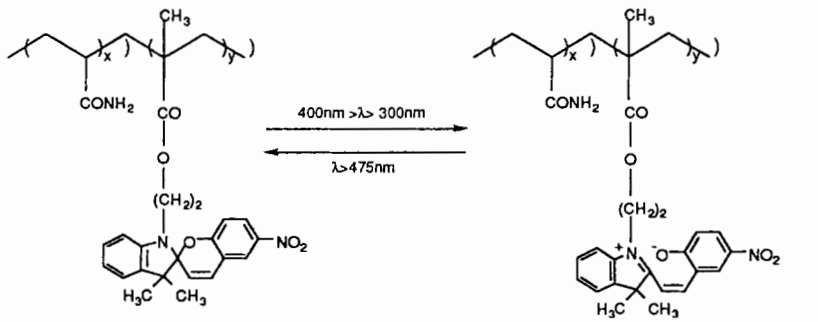

25a **25b**

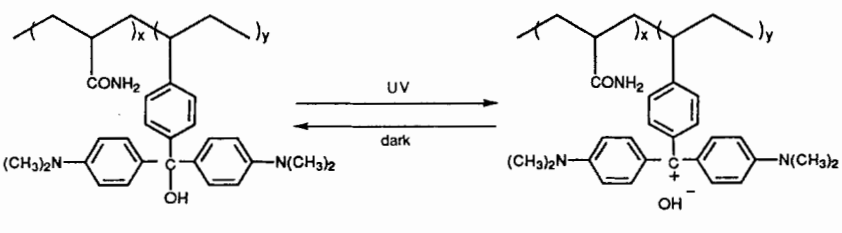

26a **26b**

of α-chymotrypsin and its reversible photoactivation.[126-128] Figure 12 shows the rate of hydrolysis of *N*-(3-carboxypropionyl)-L-phenylalanine-*p*-nitroanilide (**27**) by α-chymotrypsin immobilized in the azobenzene-acrylamide copolymer **24** or in

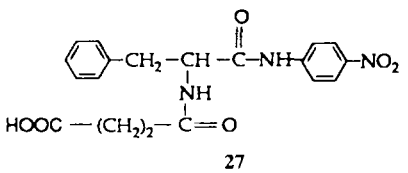

27

the spiropyran-acrylamide copolymer **25**. At a polymer loading of 0.5 mol% azobenzene units, the hydrolytic activity of the immobilized enzyme is entirely blocked in the *trans*-azobenzene copolymer **24a** (Fig. 12A). Photochemical isomerization to the

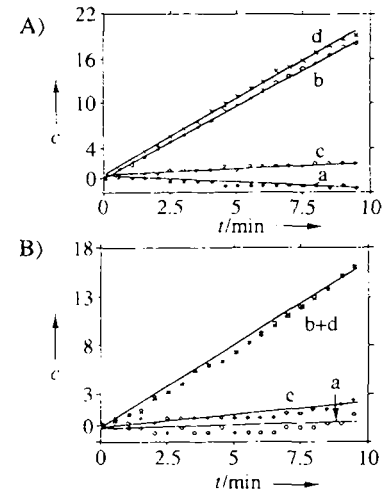

Fig. 12. Reversible photoactivation of α-chymotrypsin towards hydrolysis of **27** by immobilization in photoisomerizable polymers: A) Immobilization in polymer **24**. Curves a and c represent the rates of hydrolysis in **24a** generated by illumination with light of wavelength $\lambda > 400$ nm and curves b and d that in polymer **24b** generated by completing the cycle of illumination with light within the range 330 nm $< \lambda <$ 370 nm. B) Immobilization in polymer **25**. Curves a and c refer to **25a** (illumination at $\lambda > 475$ nm) and curves b and d to **25b** generated by completing a cycle of illumination (300 nm $< \lambda <$ 400 nm). c = concentration of product in 10^{-6} M.

cis-azobenzene copolymer **24** (330 nm $< \lambda <$ 370 nm) switches on the biocatalyst's activity ($V_{max} = 2$ mM min^{-1}). Photoisomerization of **24b** back to **24a** ($\lambda > 400$ nm) switches off the enzyme activity. The biocatalytic transformation is repeatedly switched "On" and "Off" by cyclic isomerization of the polymer between states **24a** and **24b**.

Similar results are observed for the spiropyran-acrylamide copolymer **25** (Fig. 12B). The enzyme activity is almost blocked in the copolymer **25a** that contains 0.12 mol% spiropyran units. In the copolymer state **25b** the activity of α-chymotrypsin is ten times higher ($V = 1.5$ μm min^{-1}). The "On–Off" photostimulated activation of the biocatalyst is fully reversible upon cyclic photoisomerization of the copolymer between states **25a** and **25b**.

Copolymer **26** does not undergo reversible photoisomerization. Upon illumination of **26a** the cationic copolymer state **26b** is formed, which relaxes *thermally* to the copolymer form **26a**. α-Chymotrypsin immobilized in copolymer **26a** loaded by 0.2 mol% of the photoisomerizable units is fully deactivated towards hydrolysis of **27**, whereas it reveals pronounced hydrolytic activity upon photoisomerization (330 nm $< \lambda <$ 370 nm) of the copolymer to state **26b** ($V = 1$ μM min^{-1}). Complementary flow-dialysis experiments, in which the permeability of the two isomeric states of polymers **24**, **25**, and **26** to **27** were examined, revealed that the photostimulated activities of α-chymotrypsin correlate with the permeability of the polymer membranes. That is, polymer states **24a**, **25a**, and **26a** exhibit poor permeability towards the enzyme's substrate, whereas the copolymer membranes in states **24b**, **25b**, and **26b** show effective permeability of the reaction substrates. It was suggested that the high dipole moment of *cis*-azobenzene units linked to copolymer **24b** (3.0 D vs. $\mu = 0$ for *trans*-azobenzene units), and the electrical charges associated with copolymer states **25b** and **26b** yield porous membrane assemblies because of electrical repulsion. Such pores facilitate permeation of the substrate **27** into the polymer and allow its transport to the enzyme's active site.

3.3. Photoswitchable Binding of Biomaterials in Photoisomerizable Environments

Photoisomerizable monolayers associated with surfaces provide organized two-dimensional membrane mimetic microenvironments in which the interactions of biomaterials with the monolayer and the base solid surface are controlled by light. Light-switchable interactions of antibodies with a photoisomerizable, self-assembled monolayers of antigens have been the basis for the development of reversible amperometric immunosensors.[129] Figure 13 shows the organization of a dinitrospiropyran monolayer electrode by self-assembly. The spiropyran monolayer can be reversibly photoisomerized between the monolayer states **28a** and **28b**. In a homogeneous phase, this monolayer exhibits high affinity for the anti-DNP-antibody, while the affinity of the merocyanine isomer **28b** for this antibody is poor. The switchable binding interactions of isomers **28a** and **28b** provide the foundation for an amperometric immunosensor electrode, and specifically a reversible amperometric immunosensor. In an electrochemical cell that includes a redox couple R^+/R (such as $[Fe(CN)_6]^{3-}/[Fe(CN)_6]^{4-}$) the spiropyran monolayer electrode (**28a**) gives an electrochemical response. Challenging the electrode with the DNP antibody resulted in the antibody's binding to the antigen monolayer and in the electrode's insulation towards the redox couple (Fig. 14). The amount of antibody interacting with the monolayer electrode and the extent of insulation of the electrode is dependent on the concentration of the antibody in solution. By appropriate calibration of the electrode's amperometric response as a function of antibody concentration, quantitative amperometric analysis of the antibody was achieved. In contrast to antigen electrodes that are single-cycle devices, the photoisomerizable properties of the antigen monolayer **28a** provide a means of regenerating the active antigen electrode. Photoisomerization of the antigen monolayer to state **28b** resulted in an interface with poor affinity towards the antibody, which could be washed off. The antibody-free monolayer electrode was then reisomerized to state **28a** and reactivated towards a second immuno-amperometric sensing cycle (Fig. 15, top). Figure 15 (bottom) shows the

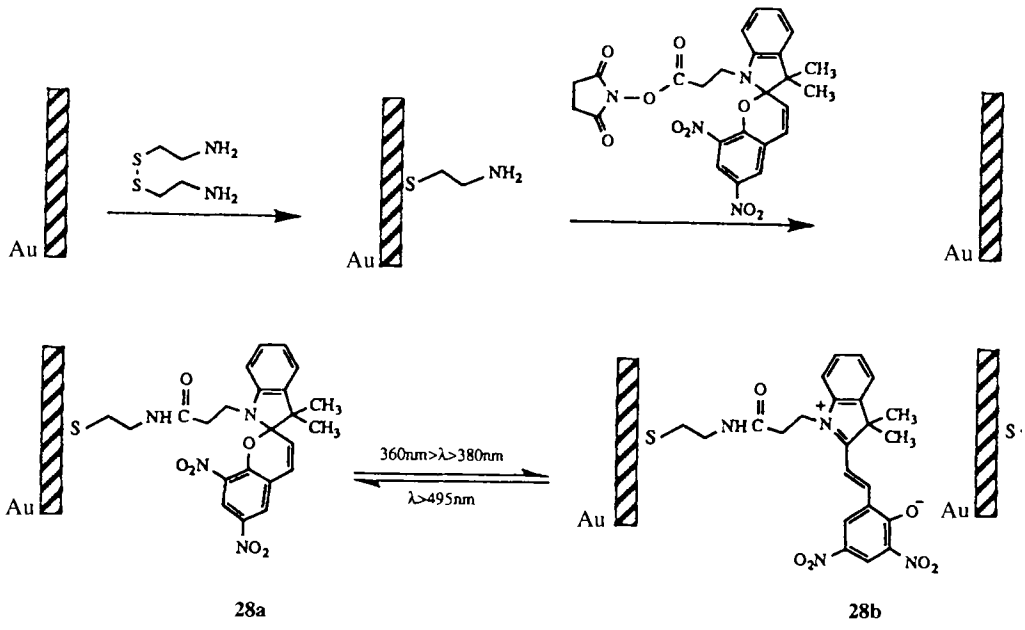

28a 28b

Fig. 13. Organization of a dinitrospiropyran photoisomerizable monolayer on an Au electrode.

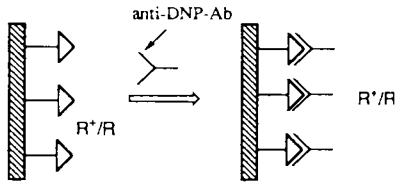

Fig. 14. Principles for the application of an antigen monolayer electrode for amperometric analysis (shown at the bottom) of an antibody (anti-DNP-Ab).

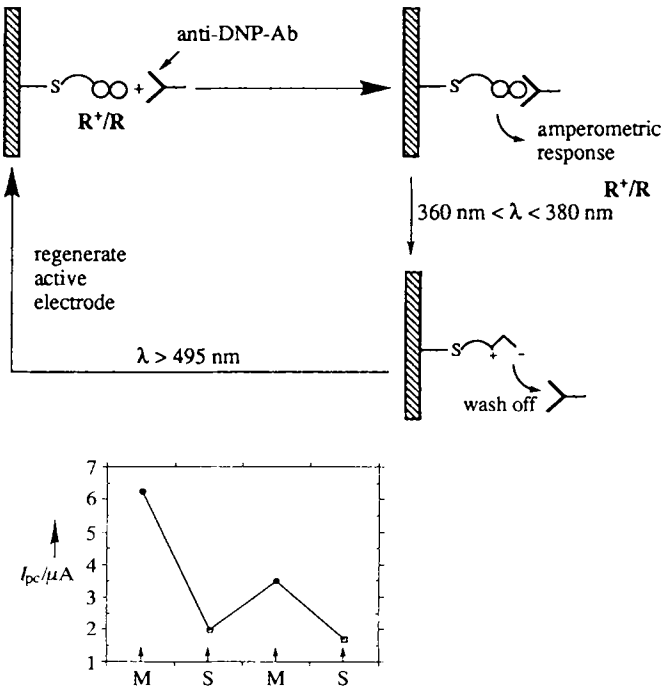

Fig. 15. Top: Principles for the application of the dinitrospiropyran-modified monolayer electrode for reversible amperometric analysis of the antibody anti-DNP-Ab. Bottom: Reversible amperometric response of the monolayer electrode (**28** as monolayer) in the presence of 1.5 mM anti-DNP-Ab. ■ electrode in **28a** state (S, generated by irradiation at $\lambda > 495$ nm); ● electrode in **28b** state (M, generated by irradiation in the range 360 nm $< \lambda <$ 380 nm). Electrodes were washed prior to each measurement.

reversible operation of the dinitrospiropyran/merocyanine monolayer electrode in the amperometric detection of anti-DNP-antibody. Initially, the electrode in state **28b** is challenged with the antibody. Due to poor interaction with the monolayer, the electrode is not insulated and gives rise to a high amperometric response. Photoisomerization to state **28a** yields the active antigen surface that binds the DNP antibody, which insulates the electrode and decreases its amperometric response. Subsequent photoisomerization of the electrode to state **28b** releases the antibody and enhances the electrode's electrochemical response.

The changes in potential at an electrode modified by a photoisomerizable polymer matrix were used to probe antibody–antigen interactions. Carboxyl-substituted polyvinyl chloride was applied as a coating polymer membrane on a glassy-carbon electrode. Into this polymer were incorporated 2,4-dinitrophenyldecylamine and spiro(2*H*-1-benzopyran-2,2'-indoline) (**29a**).[130] The latter component turned the polymer into a photoisomerizable membrane assembly. The electrode potential is sensitive to the photoisomeric state, and upon light-induced isomerization of state **29a** to the merocyanine isomer **29b**, the electrode potential increased by about 120 mV. Figure 16A shows the reversible light-stimulated potential switches of the electrode upon cyclic photoisomerization of **29a** to **29b** and back. Introduction of the anti-dinitrophenyl-BSA antibody to the system consisting of the electrode coated with the polymer membrane in state **29b** (high electrode potential) results in a decrease in the electrode potential (Fig. 16B). At an antibody concentration corresponding to 15 mg ml^{-1} the electrode potential drops by about 100 mV. The decrease in the electrode potential is dependent on the DNP-antibody concentration and hence provides a quantitative measure for the antigen–antibody interactions. The decrease of the electrode potential upon association of the antibody to the antigen membrane-coated elec-

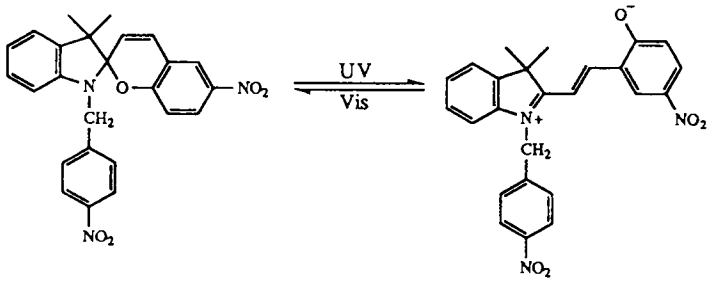

29a 29b

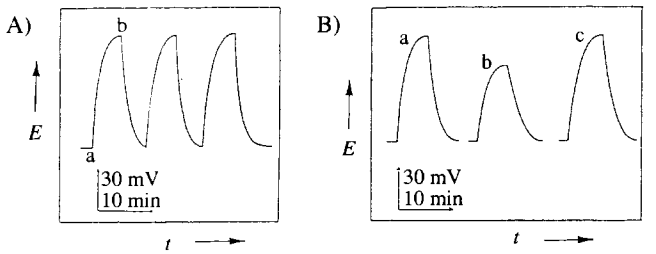

Fig. 16. A) Photostimulated changes in the potential of a poly(vinyl chloride)-modified electrode that contains **29**. Potential values a and b correspond to the electrode in states **28a** and **28b**, respectively. B) Photostimulated potentials of a poly(vinyl chloride)-modified polymer electrode that contains **29**, in the presence and absence of the anti-DNP-antibody. a: Electrode potential in the state **29b** in the absence of DNP-Ab. b: Electrode potential in state **29b** in the presence of the DNP-Ab. c: Electrode potential after the **29b** electrode with bound Ab had been isomerized to state **29a**, the DNP-Ab washed off, and the electrode subsequently reisomerized from state **29a** to state **29b**.

trode was attributed to the perturbation of the electrolyte gradient at the polymer-solution interface as a result of the antibody adsorption. The electrode could be reused by washing off the adsorbed antibody in a pure electrolyte solution.

Light-controlled association of cytochrome c (Cyt. c) to a photoisomerizable monolayer membrane associated with an electrode is of specific relevance to the vision process.[131] A mixed monolayer consisting of pyridine units and nitrospiropyran photoisomerizable components was assembled on an Au electrode surface (Fig. 17). The pyridine units act as promoting site that associates Cyt. c to the monolayer interface. Association of Cyt. c to the monolayer facilitates electrical communication between the redox center of the heme of Cyt. c and the electrode. Photoisomerization of the monolayer results in the protonated nitromerocyanine mixed monolayer. Electrostatic repulsion of the positively charged Cyt. c from the monolayer blocks the electrical communication between Cyt. c and the electrode surface. Recording of cyclic optical signals by the monolayer is transduced into amperometric responses as a result of "On–Off" photostimulated electrical communication between Cyt. c and the electrode (Fig. 18). Amplification of the transduced amperometric signal is observed upon coupling the light-stimulated electrical communication of Cyt. c to an enzymatic

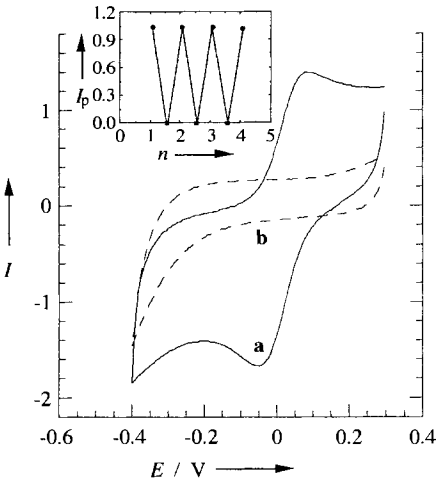

Fig. 18. Photostimulated electrical communication of cytochrome c with the photoisomerizable mixed pyridine monolayer electrode in a) the SP state and b) the MRH^+ state (see Fig. 17). The inset shows the amperometric transduction of the optical signals recorded by the monolayer electrode. I in μA; n = number of cycles.

transformation. In the pyridine–nitrospiropyran monolayer electrode state, electrical communication between Cyt. c and the electrode is maintained. Reduced Cyt. c was coupled to the reduction of cytochrome c oxidase (COX) that biocatalyzed the reduction of molecular oxygen. The enzymatic transformation regenerates the electrical interaction of Cyt. c with the electrode, and the optical signal triggering the electron transfer is amplified. The enzymatic cascade is alternately activated and blocked through photoisomerization of the monolayer and control of the primary electrical interactions of Cyt. c with the electrode

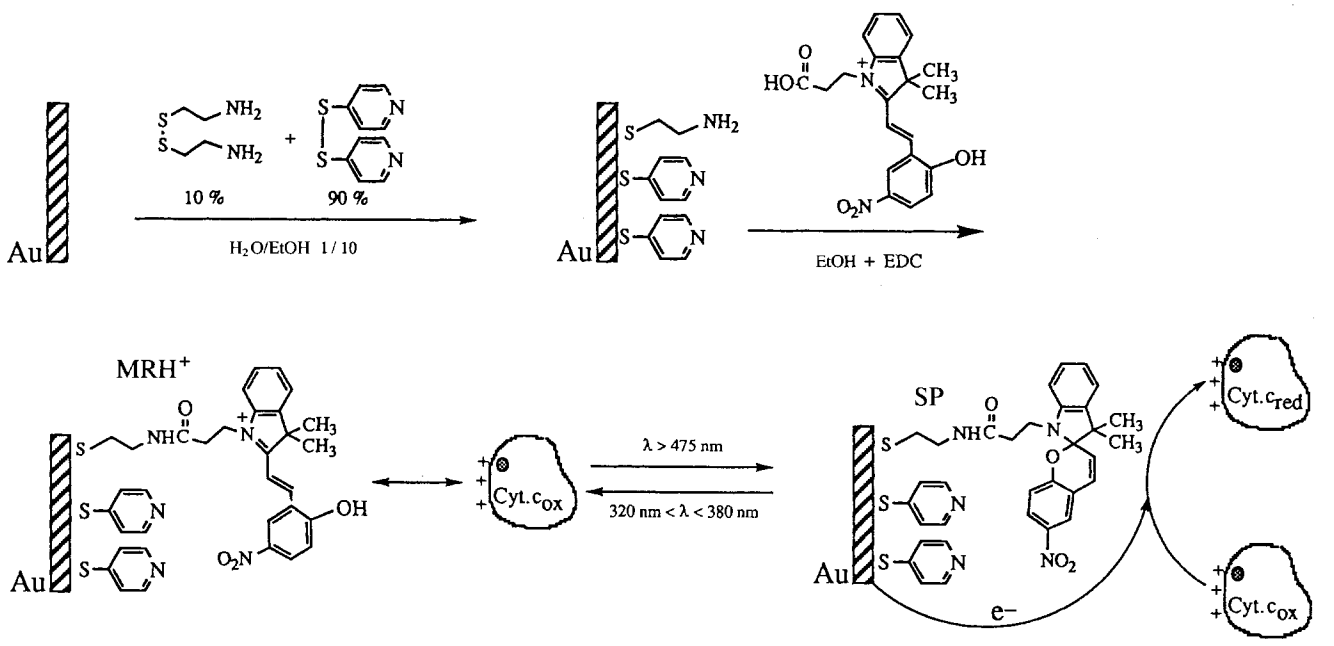

Fig. 17. Organization of a mixed nitrospiropyran/nitromerocyanine–pyridine monolayer on an Au electrode.

(Fig. 19). This system resembles features of the vision process:[132] isomerization of the protein-bound 11-*cis*-retinal transforms the protein into an appropriate conformation that binds the G-protein. The associated G-protein triggers an enzymatic cascade, which ultimately yields c-GMP that activates the neural response. In the example presented above, the mixed monolayer associated with the electrode controls the binding of Cyt. c to the photoisomerizable membrane. Binding of Cyt. c to the monolayer results in electrical communication with the electrode and triggers an enzymatic cascade that reduces oxygen. The optical signal is amplified by the enzymatic cascade and transduced by an electrochemical amperometric output.

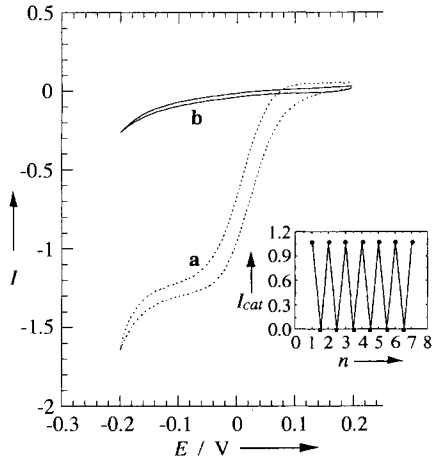

Fig. 19. Photostimulated amplified amperometric transduction of optical signals recorded by the photoisomerizable mixed pyridine monolayer electrode described in Figure 17 with Cyt. c/COX as enzymatic cascade. a) Electrode in the SP state; (b) electrode in the MRH^+ state. The inset shows amperometric transduction of the optical signals recorded by the monolayer. I in μA; n = number of cycles.

4. Summary and Outlook

We have presented an overview on the scientific progress in the development of reversible photobiological switches. Two general methodologies to transform bioactive materials into light-regulated assemblies were discussed. One approach involved the chemical modification of the biomaterial by means of synthetic photoisomerizable components. In this approach the two photoisomeric states of the photoreceptor stimulate "On–Off" activities of the biomaterial. That is, in one photoisomeric state the biomaterial retains its bioactive structure and its biological function switched on, while in the complementary photoisomeric state the biomaterial structure is distorted and consequently switched off towards its bioactivity. The second methodology to photostimulate biomaterials involved its entrapment in a photoisomerizable environment. Control of the physical properties of the photoisomerizable matrix such as membrane permeability, phase viscosity, or local electrical potential, have led to activation and deactivation of the immobilized biomaterial by light. Development of such artificial photobiological switches represents a scientific effort to mimic photoswitchable biological systems in nature, like the process of vision. Photobiological switches can therefore be viewed as the chemist's approach to transforming bioactive materials into "intelligent" new materials whose function responds to external light signals.

Potential applications of photoswitchable biomaterials in the tailoring of targeted light-activated bioactive drugs, the design of reversible biosensors, and the organization of light amplification devices have been discussed. Future goals include the challenge of applying photoswitchable biomaterials as bioelectronic devices. The recording of an optical output by a biochemical transformation is undesirable for practical reasons. Nonetheless, the progress in electrical communication of redox protein with electrodes[133–136] and the novel techniques to organize biomaterials as self-assembled monolayers on electrode surfaces[136–138] imply that optical recording by photoswitchable biomaterials and electrochemical read-out of the information is an attractive path to follow. Indeed, the recently reported amperometric transduction of recorded optical signals by photoisomerizable redox proteins[107] and by photoisomerizable monolayer coupled to redox proteins[131] demonstrated the viability of this approach. It is envisaged that photoswitchable biomaterials will find extensive use in the future for information storage, recording, and transfer. Clearly, photoswitchable biomaterials offer exciting perspectives at the frontiers of chemistry, biology, physics, medicine, and materials science.

The research project on photobiological switches is supported by a grant from the Ministry of Science and Technology, Israel, and the Commission of the European Union.

Received: December 5, 1995
Revised version: July 6, 1995 [A96 IE]
German version: *Angew. Chem.* **1996**, *108*, 419–439

[1] G. Feher, J. P. Allen, M. Okamura, D. C. Rees, *Nature* **1989**, *339*, 111.
[2] S. Kartha, R. Das, J. R. Norris in *Metal Ions in Biological Systems* (Eds.: H. Sigel, A. Sigel), Dekker, New York, **1991**, p. 323.
[3] L. Stryer, *Am. Rev. Neurosci.* **1986**, *9*, 87.
[4] F. Siebert in [51], p. 756.
[5] W. Haupt, *Philos. Trans. R. Soc. London B* **1983**, *303*, 467.
[6] H. Senger, W. Schmidt in *Photomorphogenesis in Plants* (Eds.: R. E. Kendrick, G. H. M. Kronenberg), Nijhoff, Dordrecht, **1986**, p. 137.
[7] H. Smith, *Phytochrome and Photomorphogenesis*, McGraw-Hill, London, **1975**, p. 22.
[8] R. R. Birge, *Biochem. Biophys. Acta* **1991**, *1016*, 293.
[9] T. Merinetti, *Biophys. J.* **1987**, *52*, 115.
[10] W. Stoeckenius, R. A. Bogomolni, *Annu. Rev. Biochem.* **1982**, *52*, 587.
[11] T. Kouyama, K. Kinosita, A. Ikegami, *Adv. Biophys.* **1988**, *24*, 123.
[12] C. Bräuchle, N. Hampp, D. Oesterhelt, *Adv. Mater.* **1991**, *3*, 420.
[13] N. Hampp, C. Bräuchle, D. Oesterhelt, *Biophys. J.* **1990**, *58*, 83.
[14] *Optical Processing and Computing* (Eds.: H. H. Arsenault, T. Szoplik, B. Macukow) Academic Press, New York, **1989**.
[15] N. Hampp, C. Bräuchle in [51], p. 954.
[16] R. Thoma, N. Hampp, C. Bräuchle, D. Oesterhelt, *Opt. Lett.* **1991**, *16*, 651.
[17] A. Yariv, S. K. Kwong, *Opt. Lett.* **1986**, *11*, 186.
[18] F. L. Carter, A. Schultz, D. Duckworth in *Molecular Electronic Devices II* (Ed.: F. L. Carter), Dekker, New York, **1987**, p. 183.
[19] V. N. R. Pillai, *Synthesis* **1990**, 1.
[20] R. W. Binkley, T. W. Flechtner in *Synthetic Organic Photochemistry* (Ed.: W. M. Horspool), Plenum, New York, **1984**, p. 375.
[21] A. D. Turner, S. V. Pizzo, G. Rozakis, N. A. Porter, *J. Am. Chem. Soc.* **1988**, *110*, 244.
[22] N. A. Porter, J. D. Bruhnke, *Photochem. Photobiol.* **1990**, *51*, 37.
[23] P. M. Koenigs, B. C. Faust, N. A. Porter, *J. Am. Chem. Soc.* **1993**, *115*, 9371.
[24] S. R. Adams, J. P. Y. Kao, Y. Tsien, *J. Am. Chem. Soc.* **1989**, *111*, 7957.
[25] G. C. R. Ellis-Davies, J. H. Kaplan, *J. Org. Chem.* **1988**, *53*, 1966.
[26] R. Warmuth, E. Grell, J.-M. Lehn, J. W. Bats, G. Quinkert, *Helv. Chim. Acta* **1991**, *74*, 671.
[27] J. Nargeot, J. M. Nerbonne, J. Engels, H. A. Lester, *Proc. Natl. Acad. Sci. USA* **1983**, *80*, 2395.
[28] J. M. Nerbonne, S. Richard, J. Nargeot, H. A. Lester, *Nature* **1984**, *310*, 74.
[29] J. H. Kaplan, R. J. Hollis, *Nature* **1980**, *288*, 587.

[30] J. W. Walker, A. V. Somlyo, Y. E. Goldman, A. P. Somlyo, D. R. Trentham, *Nature* **1987**, *327*, 249.
[31] A. M. Gurney, H. A. Lester, *Physiol. Rev.* **1987**, *67*, 583.
[32] H. A. Lester, J. M. Nerbonne, *Annu. Rev. Biophys. Bioeng.* **1982**, *11*, 151.
[33] "Biological Applications of Photochemical Switches": I. Willner, B. Willner in: *Bioorganic Photochemistry, Vol. 2* (Eds.: H. Morrison), Wiley, **1993**, p. 1.
[34] H. R. Allcock, C. Kim, *Macromolecules* **1991**, *24*, 2846.
[35] V. A. Krongauz, E. S. Goldburt, *Macromolecules* **1981**, *14*, 1382.
[36] J. Verborgt, G. Smets, *J. Polym. Sci.* **1974**, *12*, 2511.
[37] S. Kato, M. Aizawa, S. Suzuki, *J. Membr. Sci.* **1976**, *1*, 289.
[38] J. Anzai, K. Sakamura, T. Osa, *J. Chem. Soc. Chem. Commun.* **1992**, 888.
[39] K. Ishihara, A. Okazaki, N. Negishi, I. Shinohara, T. Okano, K. Kataoka, Y. Sakurai, *J. Appl. Polym. Sci.* **1982**, *27*, 239.
[40] A. Mamada, T. Tanaka, D. Kungwatchakum, M. Irie, *Macromolecules* **1990**, *23*, 1517.
[41] M. Irie, K. Hayashi, *J. Macromol. Sci. Chem.* **1979**, *A13*, 511.
[42] S. M. Fatahur Rahman, K. Fukurishi, M. Kuwabara, H. Yamanaka, M. Momura, *Bull. Chem. Soc. Jpn.* **1993**, *66*, 1461.
[43] J. Bieth, S. M. Vratsanos, N. H. Wassermann, B. F. Erlanger, *Proc. Natl. Acad. Sci. USA* **1969**, *64*, 1103.
[44] J. Bieth, N. H. Wassermann, S. M. Vratsanos, B. F. Erlanger, *Proc. Natl. Acad. Sci. USA* **1970**, *66*, 850.
[45] K. T. Galley, M. DeSorgo, W. Prins, *Biochem. Biophys. Res. Commun.* **1973**, *50*, 300.
[46] M. A. Wainberg, B. F. Erlanger, *Biochemistry* **1971**, *10*, 3816.
[47] E. Bartels, N. H. Wassermann, B. F. Erlanger, *Proc. Natl. Acad. Sci. USA* **1971**, *68*, 1820.
[48] P. R. Westmark, J. P. Kelly, B. D. Smith, *J. Am. Chem. Soc.* **1993**, *115*, 3416.
[49] B. F. Erlanger, *Annu. Rev. Biochem.* **1976**, *45*, 267.
[50] *Photochromism* (Ed.: G. H. Brown), Wiley, New York, **1971**.
[51] *Photochromism: Molecules and Systems* (Eds.: H. Dürr, H. Bouas-Laurent), Elsevier, Amsterdam, **1990**.
[52] *Organic Photochromism* (Ed.: A. V. Elstov), Plenum, New York, **1990**.
[53] *Applied Photochromic Polymer Systems* (Eds.: C. B. McArdle), Chapman & Hall, New York, **1992**.
[54] J. Saltiel, Y. P. Sun in Ref. [51], p. 64.
[55] D. L. Ross, J. Blanc in Ref. [50], p. 471.
[56] J. Whittall in Ref. [51], p. 467.
[57] R. Guglielmetti in Ref. [51], p. 314.
[58] C. Schulz, H. Dürr in Ref. [51], p. 193.
[59] H. Bouas-Laurent, J.-P. Desvergne in Ref. [51], p. 561.
[60] E. Hadjoudis in Ref. [51], p. 685.
[61] M. Ottolenghi, D. S. McClure, *J. Chem. Phys.* **1967**, *46*, 4613.
[62] K. Schaumburg, J.-M. Lehn, C. Goulle, S. Roth, H. Byrne, S. Hagen, J. Poplawsky, K. Brufeldt, K. Beechgard, T. Bjornholm, P. Fredericksen, M. Jorgensen, K. Lerstrup, P. Sommer-Larsen, O. Goscinsky, J.-L. Calais, L. Erikson in *Nanostructure Based Molecular Materials* (Eds.: W. Göpel, C. Ziegler), VCH, Weinheim, **1992**, p. 153.
[63] D. A. Parthenopoulos, P. M. Rentzepis, *Science* **1989**, *245*, 843.
[64] Z. F. Liu, K. Hashimoto, A. Fujishima, *Nature* **1990**, *347*, 658.
[65] K. Martinek, I. V. Berezin, *Photochem. Photobiol.* **1979**, *29*, 637.
[66] H. Flohe, R. Giertz, R. Beckmann, *Handbook of Information, Vol. 5*, Elsevier, Amsterdam, **1985**.
[67] K. Lechner, *Blutgerinnungsstörungen*, Springer, Berlin, **1982**.
[68] *Biosensors: Fundamentals and Applications* (Eds.: A. P. F. Turner, I. Karube, G. S. Wilson), Oxford University Press, **1989**.
[69] F. Scheller, F. Schubert, *Tech. Instrum. Anal. Chem.* **1992**, *11*.
[70] a) *Biosensors and Chemical Sensors* (Eds.: P. G. Edelman, J. Wang) American Chemical Society, Washington, D. C., **1991**; b) K. Cammann, U. Lemke, A. Roken, J. Sander, H. Wilken, B. Winter, *Angew. Chem.* **1991**, *103*, 519; *Angew. Chem. Int. Ed. Engl.* **1991**, *30*, 516.
[71] M. Irie in *Applied Photochromic Polymer Systems* (Ed.: C. B. McArdle), Chapman & Hall, New York, **1992**, p. 174.
[72] M. Irie, *Adv. Polym. Sci.* **1990**, *94*, 27.
[73] G. Smets, *Adv. Polym. Sci.* **1983**, *50*, 17.
[74] M. Irie, Y. Hirano, S. Hashimoto, K. Hayashi, *Macromolecules* **1981**, *14*, 262.
[75] M. Irie, M. Hosoda, *Makromol. Chem. Rapid Commun.* **1985**, *6*, 533.
[76] L. Stryer, *Biochemistry*, Freeman, New York, **1988**, p. 25.
[77] O. Pieroni, A. Fissi, *J. Photochem. Biol. B* **1992**, *12*, 125.
[78] F. Ciardelli, D. Fabbri, O. Pieroni, A. Fissi, *J. Am. Chem. Soc.* **1989**, *111*, 3470.
[79] O. Pieroni, A. Fissi, A. Viegi, D. Fabbri, F. Ciardelli, *J. Am. Chem. Soc.* **1992**, *114*, 2734.
[80] O. Pieroni, J. L. Houben, A. Fissi, P. Costantino, F. Ciardelli, *J. Am. Chem. Soc.* **1980**, *102*, 5913.
[81] J. L. Houben, A. Fissi, D. Baccida, N. Rosato, O. Pieroni, F. Ciardelli, *Int. J. Biol. Macromol.* **1983**, *5*, 94.
[82] B. R. Malcolm, O. Pieroni, *Biopolymers* **1990**, *29*, 1121.
[83] F. Ciardelli, O. Pieroni, A. Fissi, J. L. Houben, *Biopolymers* **1984**, *23*, 1423.
[84] O. Pieroni, D. Fabbri, A. Fissi, F. Ciardelli, *Makromol. Chem. Rapid Commun.* **1988**, *9*, 637.
[85] A. Fissi, O. Pieroni, F. Ciardelli, *Biopolymers* **1987**, *26*, 1093.
[86] I. Willner, S. Rubin, J. Wönner, F. Effenberger, P. Bäuerle, *J. Am. Chem. Soc.* **1992**, *114*, 3150.
[87] S. Rubin, I. Willner, *Mol. Cryst. Liq. Cryst.* **1994**, *246*, 201.
[88] I. Willner, S. Rubin, *React. Polym.* **1993**, *21*, 177.
[89] E. Zahavy, S. Rubin, I. Willner, *Mol. Cryst. Liq. Cryst.* **1994**, *246*, 195.
[90] I. Willner, S. Rubin, Y. Cohen, *J. Am. Chem. Soc.* **1993**, *115*, 4937.
[91] E. Zahavy, S. Rubin, I. Willner, *J. Chem. Soc. Chem. Commun.* **1993**, 1753.
[92] M. Harada, M. Sisido, J. Hirose, M. Nakanishi, *FEBS Lett.* **1991**, *286*, 6.
[93] T. Hohsaka, K. Kawashima, M. Sisido, *J. Am. Chem. Soc.* **1994**, *116*, 413.
[94] G. Montagnoli, S. Monti, L. Nannicini, R. Felicioli, *Photochem. Photobiol.* **1976**, *23*, 29.
[95] S. Monti, G. Montagnoli, L. Nannicini, *J. Am. Chem. Soc.* **1977**, *99*, 3808.
[96] I. Willner, S. Rubin, A. Riklin, *J. Am. Chem. Soc.* **1991**, *113*, 3321.
[97] M. Aizawa, K. Namba, S. Suzuki, *Arch. Biochem. Biophys.* **1977**, *182*, 305.
[98] K. Namba, S. Suzuki, *Chem. Lett.* **1975**, 947.
[99] I. Willner, M. Lion-Dagan, S. Rubin, J. Wörner, F. Effenberger, P. Bäuerle, *Photochem. Photobiol.* **1994**, *59*, 491.
[100] A. M. Klibanov, *CHEMTECH* **1986**, 354.
[101] C. S. Chen, C. J. Sih, *Angew. Chem.* **1989**, *101*, 711; *Angew. Chem. Int. Ed. Engl.* **1989**, *28*, 695.
[102] J. S. Dordick, *Enzyme Microb. Technol.* **1989**, *11*, 194.
[103] T. Ueda, K. Murayama, T. Yamamoto, S. Kimura, Y. Imanishi, *J. Chem. Soc. Perkin Trans. 1* **1994**, 225.
[104] R. Verger, M. C. E. Mieras, G. H. de Haas, *J. Biol. Chem.* **1973**, *248*, 4023.
[105] W. A. Pieterson, J. C. Vidal, J. J. Volwerk, G. H. de Haas, *Biochemistry* **1974**, *13*, 1455.
[106] M. C. E. van Dam-Mieras, M. C. E. A. J. Slotboom, W. A. Pieterson, G. H. de Haas, *Biochemistry* **1975**, *14*, 5387.
[107] a) M. Lion-Dagan, S. Marx-Tibbon, E. Katz, I. Willner, *Angew. Chem.* **1995**, *107*, 1730; *Angew. Chem. Int. Ed. Engl.* **1995**, *34*, 1604; b) I. Willner, M. Lion-Dagan, S. Marx-Tibbon, E. Katz, *J. Am. Chem. Soc.* **1995**, *117*, 6581.
[108] J. Sunamoto, K. Iwamoto, Y. Mohri, T. Kominato, *J. Am. Chem. Soc.* **1982**, *104*, 5502.
[109] I. Willner, S. Sussan, S. Rubin, *J. Chem. Soc. Chem. Commun.* **1992**, 100.
[110] S. Marx-Tibbon, I. Willner, *J. Chem. Soc. Chem. Commun.* **1994**, 1261.
[111] M. Aoyama, J. Watanabe, S. Inoue, *J. Am. Chem. Soc.* **1990**, *112*, 5542.
[112] J. Anzai, Y. Hasebe, A. Ueno, T. Osa, *Bull. Chem. Soc. Jpn.* **1987**, *60*, 1515.
[113] T. Seki, M. Sakuragi, Y. Kawanishi, Y. Suzuki, T. Tamaki, R. Fukuda, K. Ichimura, *Langmuir* **1993**, *9*, 211.
[114] Y. Kawanishi, T. Tamaki, T. Seki, M. Sakuragi, Y. Suzuki, K. Ichimura, K. Aoki, *Langmuir* **1991**, *7*, 1314.
[115] K. Ichimura, Y. Suzuki, T. Seki, A. Hosoki, K. Aoki, *Langmuir* **1988**, *4*, 1214.
[116] K. Aoki, T. Seki, Y. Suzuki, T. Tamaki, A. Hosoki, K. Ichimura, *Langmuir* **1992**, *8*, 1007.
[117] M. Irie, H. Tanaka, *Macromolecules* **1983**, *16*, 210.
[118] T. Amiya, T. Tanaka, *Macromolecules* **1987**, *20*, 1162.
[119] A. Suzuki, T. Tanaka, *Nature* **1990**, *346*, 345.
[120] R. Vilanove, H. Hevet, H. Gruler, F. Rundale, *Macromolecules* **1983**, *16*, 825.
[121] M. Higuchi, A. Takizawa, T. Kinoshita, Y. Tsujita, *Macromolecules* **1987**, *20*, 2888.
[122] D. Balasubramanian, S. Subramani, C. Kumar, *Nature* **1975**, *254*, 252.
[123] I. Karube, Y. Nakamoto, S. Suzuki, *Biochim. Biophys. Acta* **1976**, *445*, 774.
[124] I. Karube, Y. Nakamoto, K. Namba, S. Suzuki, *Biochim. Biophys. Acta* **1976**, *429*, 975.
[125] Y. Hasebe, J.-I. Anzai, A. Ueno, T. Osa, *J. Phys. Org. Chem.* **1988**, *1*, 309.
[126] I. Willner, S. Rubin, T. Zor, *J. Am. Chem. Soc.* **1991**, *113*, 4013.
[127] I. Willner, S. Rubin, R. Shatzmiller, T. Zor, *J. Am. Chem. Soc.* **1993**, *115*, 8690.
[128] I. Willner, S. Rubin, *React. Polym.* **1993**, *21*, 171.
[129] I. Willner, R. Blonder, A. Dagan, *J. Am. Chem. Soc.* **1994**, *116*, 9365.
[130] J.-I. Anzai, K. Sakamura, Y. Hasebe, T. Osa, *Anal. Chim. Acta* **1993**, *281*, 8543.
[131] M. Lion Dagan, E. Katz, I. Willner, *J. Chem. Soc. Chem. Commun.* **1994**, 2741.
[132] L. Stryer, *Biochemistry*, Freeman, New York, **1988**, p. 1028.
[133] R. Maidan, A. Heller, *Anal. Chem.* **1992**, *64*, 2889.
[134] Y. Degani, A. Heller, *J. Phys. Chem.* **1987**, *91*, 1285.
[135] I. Willner, N. Lapidot, A. Riklin, R. Kasher, E. Zahavy, E. Katz, *J. Am. Chem. Soc.* **1994**, *116*, 1428.
[136] I. Willner, A. Riklin, B. Shoham, D. Rivenzon, E. Katz, *Adv. Mater.* **1993**, *5*, 912.
[137] I. Willner, A. Riklin, *Anal. Chem.* **1994**, *66*, 1535.
[138] I. Willner, E. Katz, A. Riklin, R. Kasher, *J. Am. Chem. Soc.* **1992**, *114*, 10965.

Nonstabilized Alkyl Complexes and Alkyl-Cyano-Ate Complexes of Iron(II) and Cobalt(II) as New Reagents in Organic Synthesis**

Thomas Kauffmann*

Alkyl transition metal reagents are being increasingly used for alkylations in organic synthesis. They have various advantages over alkyllithium and alkylmagnesium reagents including higher selectivity, lower basicity, and as long as the transition metal is not in its highest oxidation state—their willingness to undergo oxidative addition with electrophiles. Alkyl derivatives of Fe^{II} and Co^{II}, which are not stabilized by special ligands but still can be easily handled, are in many cases superior to the well-known alkyl-Cu^{I} and -Mn^{II} reagents and can also undergo unexpected reactions. The introduction of alkyl-cyano-ate complexes of Fe^{II} and Co^{II}, the cyanide ligands of which (in contrast to neutral π-acidic ligands) do not reduce the reactivity, has led to further advances. Reaction mechanisms will be discussed and comparisons will be made with alkylating reagents containing Cu^{I}, Mn^{II}, Ni^{II}, or Ti^{IV} as well as with Pd-catalyzed coupling reactions. Furthermore, it will be shown that super-ate Fe^{II} complexes are almost certainly the reactive species in highly selective catalytic alkylations.

Keywords: alkylations · catalysis · cobalt compounds · iron compounds

1. Introduction

Collman's reagent $Na_2[Fe(CO)_4]$ and its half-sandwich analog $Na[Fe(C_5H_5)(CO)_2]$ react with alkyl halides by oxidative addition to afford alkyl-Fe^{II} compounds (e.g. $[(C_5H_5)(CO)_2FeEt]$, which are stabilized by π-acidic ligands and are useful reagents for C–C bond formations.[2] Prior to the investigations reported herein little was known about alkyl-Fe^{II} reagents that contain no stabilizing ligands or about analogous Co^{II} compounds. After various unsuccessful or questionable attempts had been made by other authors to obtain "homoleptic" alkyl derivatives of Fe^{II} and Co^{II}, Berthold et al.[3] described the isolation of $[Me_4FeLi_2(Et_2O)_2]$ and $[Me_4FeLi_2(dioxane)_{1.25}]$ in 1973, while in 1975 Wilkinson et al.[4] obtained $[Me_4CoLi_2(tmeda)_2]$ (TMEDA = tetramethylethylenediamine). Some years earlier Corey and Posner[5] had synthesized the complexes R_3FeLi (R = Me, *n*Bu) and Me_3CoLi in situ by transmetalation of FeI_2 and CoI_2 and had established that Me_3FeLi undergoes cross-coupling reactions in good yields with (*E*)-1-iodo-1-nonene, (*E*)-β-bromostyrene, and (*E*)-1-bromocyclohexene but does not react with alkyl halides. As far as Me_3CoLi is concerned, they stated that "the predominant course of reaction with most of the halides was via metal–halogen replacement; a predominance of the cross-coupling was only observed with vinyl bromides and iodides." Perhaps mainly because of the incorrect statement[5] that nBu_3FeLi, which in contrast to Me_3FeLi is potentially able to undergo decomposition by β-elimination, is unsuitable for cross-coupling reactions and the fact that Corey and Posner used their reagent Me_3FeLi in an unnecessary fivefold excess, the synthetic potential of the reagents R_3MLi (M = Fe, Co) was apparently considered to be very low in comparison with that of alkyl cuprates.[6] In contrast to the R_3MnLi reagents, also first introduced by Corey and Posner,[7] they remained unused for many years.

In 1983, as part of a broad comparative study of alkyl transition metal reagents, members of the author's research group commenced their studies of alkyl derivatives of Fe^{II} and Co^{II} that are not stabilized by special ligands. The low thermal stabilities of these reagents were not considered to be a disadvantage, since low temperatures are generally required for selective reactions. Since the stability of the divalent state of the middle and late 3d elements has its minimum at Fe^{II} [Mn^{II} (half-filled 3d shell) > Fe^{II} < Co^{II} < Ni^{II})[8]], it seemed likely that alkyl-Fe^{II} reagents would be particularly tolerable of the oxidative addition of electrophiles and thus offer advantages over other similar reagents.

2. Synthesis and Characterization of Fe and Co Reagents

2.1. Reagents with Simple Alkyl Groups

The Fe and Co reagents that we have used were usually obtained in situ by transmetalation of alkyllithium compounds

[*] Prof. Dr. T. Kauffmann
Organisch-chemisches Institut der Universität
Corrensstrasse 40, D-48149 Münster (Germany)
Fax: Int. code +(251)839772

[**] Alkyliron and Alkylcobalt Reagents, Part 11. Part 10: ref. [1].

with $FeCl_2$,[9, 10] $CoCl_2$,[11, 12] $Fe(CN)_2$,[1] or $Co(CN)_2$[1] according to Schemes 1 and 2. In some cases Grignard reagents were also subjected to transmetalations. It was possible to use either pure $[FeCl_2(thf)_{1.5}]$[13] or to prepare $FeCl_2$ in situ by reducing[14] $FeCl_3$ with one equivalent of MeLi at $-78\,^{\circ}C$. Pure $CoCl_2$ is commercially available, while $Fe(CN)_2$ and $Co(CN)_2$ can be obtained preparatively.[1] No methane or ethane is set free in reactions carried out according to Schemes 1 and 2 (in contrast to the reaction of MeLi with $FeCl_3$), so that apparently

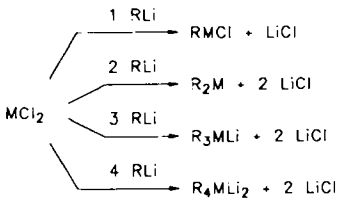

Scheme 1. R = Me, *n*Bu, *n*-octyl, cyclopropyl; M = Fe, Co.

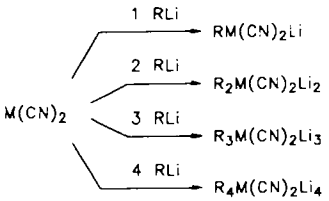

Scheme 2. R = Me, *n*Bu; M = Fe, Co, Ni.

reduction to the M^I or M^0 state is not involved. As far as reactivity and selectivity is concerned there is no difference between the isolated complexes $[Me_4FeLi_2(Et_2O)_2]$[3] and $[Me_4CoLi_2(tmeda)]$[4] referred to above and the $[Me_4ML_{i2}(thf)_n]$ (M = Fe, Co) complexes prepared in situ. Thus, there is no advantage in using the isolated complexes. The formulae in Schemes 1 and 2 are based solely on the stoichiometry of the reactants. Since LiCl is formed in the in situ syntheses carried out according to Scheme 1, this salt may possibly form complexes with the alkyl transition metal compounds. Thus, for example the hetero-ate complexes $Me_2Co(Cl)Li$ or $Me_2Co(Cl)_2Li_2$ might be present rather than simply Me_2Co; this must be taken into account in mechanistic discussions. The hetero-ate complexes "$Me_3M(CN)_2Li_3$" and "$Me_4M(CN)_2Li_4$" (M = Fe, Co), obtained according to Scheme 2, are in fact probably compounds of the type $Me_2M(CN)_2Li_2$ containing one or two equivalents of MeLi[1] (see below). Further hetero-ate complexes of Fe^{II} are dealt with in Section 4.5 and Scheme 26.

The *β-bromostyrene–ketone test*[9-11] can be applied to determine whether the organolithium reagent has been completely used up in transmetalation reactions carried out according to Scheme 1: equimolar amounts of β-bromostyrene and a ketone are added, and gas chromatography is used to check whether only the styrene derivative has been alkylated; see Section 3.1.1. The *aldehyde–ketone test*[14] also gives reliable results (equimolar amounts of an aldehyde and a ketone are added, and gas chromatography is used to determine whether only the aldehyde has undergone alkylation). Neither test can be used if the transmetalations are carried out according to Scheme 2, either because free MeLi is present in the reaction mixture or because the cyano-ate complexes formed are strongly nucleophilic towards ketones. In these cases the transmetalation becomes evident from the resulting change in selectivity (see Section 4.1).[11] Schemes 1 and 2 are a considerable simplification of the reaction processes, since in each case only a single product is stated to result from the transmetalation step. In fact several alkyl- or cyano-ate complexes can be formed in each case and can undergo rapid interconversion. Which species in fact actually reacts can be proposed from the stoichiometry but not determined with certainty, since no relevant studies have been carried out.

As in the case of the alkyl–Mn^{II} compounds,[7] the thermal stability of the alkyl derivatives of Fe^{II} and Co^{II} (Scheme 3)[10, 11] decreases in the series $R_3MLi > RMCl > R_2M$. The hypothetical cyano-ate complexes of Fe^{II} (black

MeFeCl	Me_2Fe	Me_3FeLi	Me_4FeLi_2	nBu_4FeLi_2
0	-10	+25	+40	-20
MeCoCl	**Me_2Co**	**Me_3CoLi**	**Me_4CoLi_2**	**nBu_4CoLi_2**
-30	-40	-15	-10	-70

Scheme 3. Approximate decomposition temperature [°C] of the reagents in THF.

suspension) and Co^{II} (blue suspension) depicted in Scheme 2 do not change color on warming to 0 °C. Since no gases are liberated under these conditions the reagents appear to be stable up to 0 °C. In the case of the *n*-butyl-cyano-ate complexes this indicates an increase in their stability compared to that of nBu_4MLi_2 (M = Fe, Co). Thus cross-coupling reactions can be carried out with $nBu_2Co(CN)_2Li_2$, although not with nBu_4CoLi_2 (see Section 3.3).

The paramagnetism of the solutions obtained according to Scheme 1 prevented NMR measurements. It was also not possible to obtain crystals of the isolated complex $[Me_4FeLi_2(Et_2O)_2]$[1] that were suitable for X-ray crystallographic analysis. It has been shown, however, that the iron atom

Thomas Kauffmann was born in Reutlingen in 1924, studied at the Universität Würzburg, carried out research and taught at Technische Hochschule Darmstadt, and has been a Professor for Organic Chemistry at the Universität Münster since 1965 (Emeritus Professor in 1990). His main research interests have focused on sodium hydrazide as a reagent in organic synthesis, hetarynes, homocoupling by organocopper compounds, 1,3-anionic cycloaddition, preparative application of the areno-analogy principle, organoelement–lithium reagents and organo transition metal reagents for organic syntheses, chele- and anticheleselectivity, and the additive ARCD reductive carbonyl dimerization (reaction).

in $[(1\text{-naphthyl})_4FeLi_2(Et_2O)_2]$ is in an octahedral environment; the two ether ligands occupy equatorial positions (X-ray structure analysis).[15] The cyano-ate complexes of Fe and Co, which were obtained as paramagnetic suspensions, provided no analyzable NMR and IR spectra. The corresponding Ni compounds, which can be obtained from $Ni(CN)_2$ as diamagnetic solutions according to Scheme 2, exhibit IR spectra with a strong vibration at 2047 cm^{-1}, which is attributed to cyano groups bonded to Ni. ^1H and ^{13}C NMR spectra of solutions of "$Me_4Ni(CN)_2Li_4$" reveal the presence of free MeLi as well as of two different types of methyl group bonded to nickel. This, together with the diamagnetism of the solution, indicates the presence of *cis and trans* isomers of the square-planar anion $[Me_2Ni(CN)_2]^{2-}$.[1]

2.2. Reagents with Functionalized Alkyl Groups

The α-transition metalated carboxylates **2**–**5**,[16] *N*,*N*-diethylcarboxamides **7** and **8**,[17o] and cyanides **10**–**12**[18] were synthesized in situ according to Scheme 4. The transmetalation

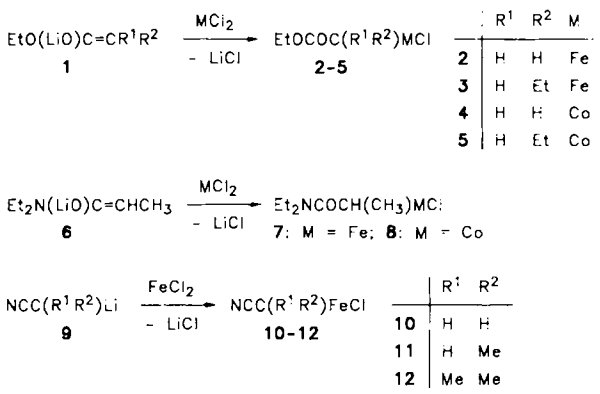

Scheme 4.

of the lithium enolates **1** cannot be checked by using the Gilman test with Michler's ketone,[19] the aldehyde–ketone test,[14] or the β-bromostyrene–ketone test,[10] but is evident from the anticheleselectivity (see Section 4.1.2) of the transmetalation products **2**–**5** and from a shift of the band at about 1650 cm^{-1} to about 1600 cm^{-1} in the IR spectrum. The carbonyl band of the Reformatsky reagent **13**[20] also lies at about 1600 cm^{-1}, thus suggesting the presence of an analogous dimeric structure (**14**) for **2**–**5**. An additional argument for structure **14** is the appearance of a carbonyl band at about 1600 cm^{-1} observed for the Cr^{III} reagent formed by oxidative addition of ethyl α-bromobutanoate to two equivalents of $CrCl_2$.[16] The transmetalation of **6** and **9** according to Scheme 4 is demonstrated by the change in

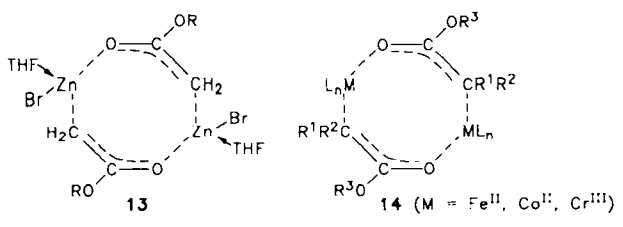

selectivity (see Section 4.1), and in the case of **9** also by the shift of the CN band in the IR spectrum from 2051 to 2190 cm^{-1}. Because of their anticheleselectivity (see Section 4.1.2) it is assumed that the reagents **7**, **8**, and **10**–**12** are aggregated in THF.[17o, 55]

3. Cross-Coupling with Organic Halides and Triflates[*]

3.1. 1-Alkenyl Halides and Triflates

3.1.1. 1-Alkenyl Bromides

Methyl derivatives of Fe^{II} and Co^{II} appear likely to become important reagents for stiochiometric cross-coupling reactions with 1-alkenyl halides. In this respect they are certainly superior to the Gilman reagent Me_2CuLi and the methylmanganates Me_3MnLi and Me_4MnLi_2, since unlike Me_2CuLi they do not need to be used in excess but can be employed in less than stoichiometric amounts, while unlike the methylmanganates they react rapidly at −78 °C. A comparison of the activity of Me_4FeLi_2 in cross-coupling with (*E*)-β-bromostyrene with that of Me_2CuLi and methylmanganates has been reported.[10] Me_4CoLi_2 is as good as Me_4FeLi_2 for the methylation of (*E*)-β-bromostyrene; however, Me_4FeLi_2 is more efficient with respect to functionalized 1-alkenyl bromides (Table 1).[11, 12] The

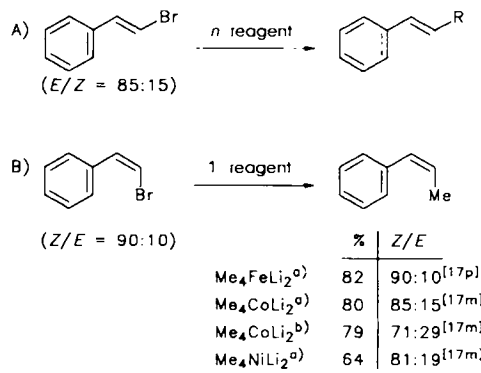

Scheme 5. A) Conditions and results of reactions from Scheme 5A: see Table 1. B) a) THF, 1 h, −78 °C; b) THF, −78 to 20 °C in 18 h.

Table 1. Cross-coupling with (*E*)-β-bromostyrene (*E*:*Z* = 85:15) according to Scheme 5A [17p] (n.d. = not determined).

n Equiv reagent	Product yield [%]	*E*:*Z*	Substrate recovered [%]
1 Me_4FeLi_2 [a]	92	90:10	0
0.5 Me_4FeLi_2 [b]	80	88:12	10
0.5 Me_4CoLi_2 [b]	91 [c]	85:15	<1
0.25 Me_4CoLi_2 [b]	67 [c]	n.d.	10
1 nBu_4FeLi_2 [a]	95	87:13	0
0.5 nBu_4FeLi_2 [a]	83	88:12	0
1 sBu_4FeLi_2 [a]	66	90:10	0
0.5 sBu_4FeLi_2 [a]	57	88:12	0
1 tBu_4FeLi_2 [a]	0	–	n.d.
1 nBu_4CoLi_2 [a]	16	n.d.	n.d.
1 nBu_4MnLi_2 [d]	37	81:19	0
1 nBu_2CuLi [d]	36	89:11	55

[a] THF; −78 °C (0.5 h). [b] THF, −78 to 20 °C in 18 h. [c] These results: ref. [11]. [d] Et_2O, −40 °C (0.5 h).

[*] Triflate = trifluoromethanesulfonate.

cyano-ate complexes $Me_2Fe(CN)_2Li_2$ and $Me_2Co(CN)_2Li_2$ have comparable methylation activity, as shown in 1:1 reactions with α-bromostyrene[11] (yield of α-methylstyrene with $Me_2Fe(CN)_2Li_2$: 89% in ether and 69% in THF; in comparison, yield with 0.5 equivalents of Me_4FeLi_2: 82% in THF).[17p] The iron complexes also give good results in the *n*- and *s*-butylation of (*E*)-β-bromostyrene (Table 1). In the cross-coupling with (*E*,*Z*)-1-bromo-4-phenyl-1,3-butadiene to give (*E*,*Z*)-1-phenyl-1,3-pentadiene both Me_4FeLi_2 and Me_4CoLi_2 give considerably better results than Me_3CuLi_2 and Me_4MnLi_2[17p] (Scheme 6; reaction conditions optimized in each case), while

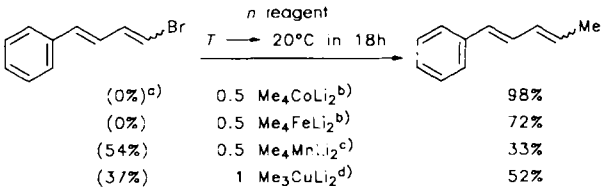

Scheme 6. a) Recovery; b) THF, $T = -78$ °C; c) Et_2O, $T = 0$ °C; d) THF, $T = 0$ °C. See also ref. [17p].

β,β-dibromostyrene reacts with one equivalent of Me_4FeLi_2 (THF, 1 h, −78 °C)[17p] or with Me_2CuLi (Et_2O, 3 h, −80 °C),[21] to give medium yields (43 and 40%, respectively) of β,β-dimethylstyrene (for the probable mechanism see Scheme 22). The *n*-octylation of a 1-alkenyl bromide is shown in Scheme 9. The Fe and Co derivatives of functionalized alkanes obtained according to Scheme 4 are unexpectedly found to be inactive towards 1-alkenyl bromides[17f, 17a] (cf. Section 4.1.4).

Stereoselectivity: As in the case of the cross-couplings with (*E*)-β-bromostyrene (Table 1), those with (*Z*)-β-bromostyrene (Scheme 5B) occur with predominant retention of configuration. One exception is provided by the reaction of Me_4CoLi_2 with (*Z*)-β-bromostyrene in which the reaction mixture was allowed to warm from −78 to 20 °C (Scheme 5). A mechanistic interpretation of the more pronounced reversal of configuration in the reaction of Me_4CoLi_2 with the β-hydroxyalkenyl bromide **15** (Scheme 7) has been reported.[12]

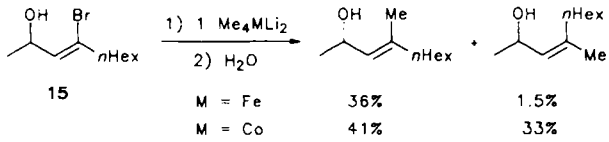

Scheme 7. Different stereoselectivities of Me_4FeLi_2 and Me_4CoLi_2 [12]. Reaction conditions: −78 °C (0.5 h) to 20 °C in 18 h.

Chemoselectivity and Neighboring Group Effects: alkyl-Fe^{II}[9, 10] and methyl-Co^{II} reagents[11] exhibit a high *aldehyde-versus-ketone selectivity* in competition experiments. Since this is also valid for $Me_3Ni(MgBr)$,[17m] this type of selectivity[8, 14] has now been demonstrated for alkyl derivatives of all the 3d metals. At −78 °C the reagents R_4FeLi_2 (R = Me, *n*Bu, *n*-octyl, cyclopropyl) and Me_4CoLi_2 react exclusively or almost exclusively with the bromide when treated with a 1:1 mixture of (*E*)-β-bromostyrene and 4-methyl-2-pentanone, while alkyllithium or alkylmagnesium reagents attack only the ketone. This result enables confirmation of transmetalation reactions carried out according to Scheme 1 with the help of the *β-bromostyrene–ketone test*,[9, 10] although this test cannot be applied to the cyano-ate complexes prepared according to Scheme 2.[1] Me_4CoLi_2, in fact, methylates (*E*)-β-bromostyrene much faster than benzaldehyde in competition experiments: when 0.5 equivalents of the reagent in THF were allowed to react at −78 °C, (*E*)-β-methylstyrene was formed in 97% yield and 1-phenylethanol in only 17% yield.[17m] In alkylation of ketones with transition metal reagents, basic groups α or β to the keto group exert a reaction-promoting neighboring group effect that leads to highly selective alkylations ("*cheleselectivity*").[22] Corresponding effects (for a mechanistic interpretation see reference [23]) of basic groups (OH, OMe, NEt_2, NH-*n*-C_6H_{13}, CN) in the α-, β-, or γ-position to the bromine atoms in 1-alkenyl bromides are observed in intermolecular competition experiments carried out with Me_4FeLi_2 (Scheme 8) and R_4MnLi_2 (R = Me, *n*Bu).[23] Me_4CoLi_2 is much too reactive for highly selective reactions of this type (Scheme 8 bottom), and Me_2CuLi is completely deactivated by the functionalized 1-alkenyl bromides. Thus, the reagents Me_4FeLi_2 and R_4FeLi_2 appear to have an important preparative potential.

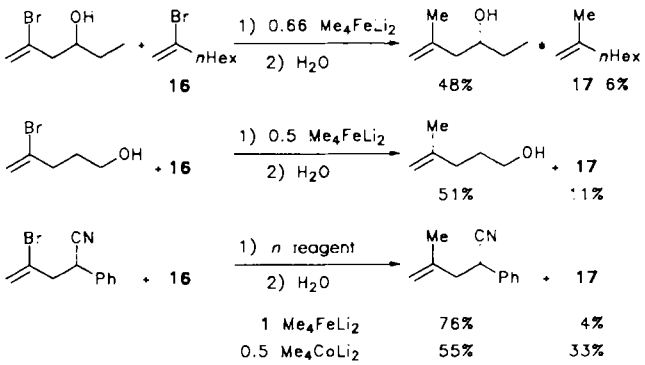

Scheme 8. Cheleselective cross-coupling [23]. Reaction conditions: THF, −78 to 20 °C in 1 h. Details of the substrate recovery see ref. [23].

Regioselectivity: As expected from the results of the competition experiments with two substrates, the compounds **18**, **22**, and **27**, which contain two competing reactive groups, are alkylated in cross-coupling reactions with a high degree of regioselectivity and with retention of configuration (Scheme 9, Table 2).

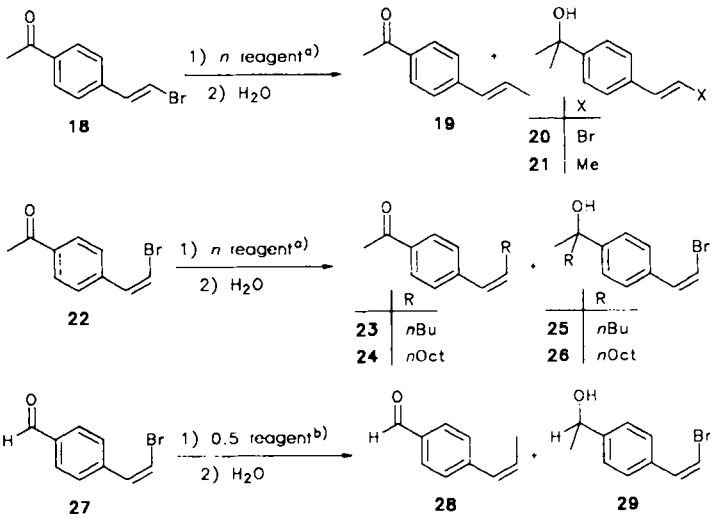

Scheme 9. Regioselective cross-coupling (*n*Oct = *n*-octyl) [17j,m]. Reaction conditions: a) THF, −78 to 20 °C in 18 h; b) THF, −78 °C, 1 h; Yields: Table 2.

Table 2. Regioselective alkylation of **18**, **22**, and **27** according to Scheme 9 [17j,m].

n Equiv reagent	Yield [%]		Recovered [%]
	19	**20**	**18**
1 $Me_3FeMgBr$	87	3	7
1 Me_2Co	85	0	5
0.5 Me_4CoLi_2	96	0	0
1 $Me_3MnMgBr$	25	20 [a]	15
	23/24	**25/26**	**22**
1 nBu_2Fe	57	0	0
1 $nOct_2Fe$	54	0	30
1 $nOct_4FeLi_2$	78	0	0
	28	**29**	**27**
0.5 Me_4CoLi_2	56	0	17

[a] In this case the dimethylation product **21** is formed in 21% yield. In all other cases no dialkylation product is formed.

3.1.2. 1-Alkenyl Chlorides, Fluorides, and Triflates

Several methods for cross-coupling involving 1-alkenyl chlorides have been described; the more effective of these are catalytic in nature (for a review see ref. [24]). The Pd-catalyzed Stille and Suzuki couplings (see Section 3.8) are apparently not possible for 1-alkenyl chlorides and fluorides; in the other catalytic methods the reaction mixture contains free alkyllithium or alkylmagnesium compounds, which can lead to unselective alkylation if the substrate contains an additional electrophilic group apart from the 1-alkenyl chloride functionality. Me_4FeLi_2, Me_4CoLi_2, and Me_3CoLi, which, in contrast to Me_3CuLi_2,[25] are not in equilibrium with MeLi according to the β-bromostyrene–ketone test (see Section 3.1.1), have shown themselves to be suitable reagents for cross-coupling reactions with *1-alkenyl chlorides* (yields 68–99%).[24] In the case of (*Z*)-1-chloro-1-octene, Me_3CoLi couples with complete retention, Me_4CoLi_2 with partial inversion of configuration, and the higher ate-complex Me_5CoLi_3 with complete inversion of configuration.[17k] In competition experiments Me_4FeLi_2 is able to differentiate better between different 1-alkenyl chlorides than Me_3CoLi or Me_4CoLi_2. The variation in the electrophilic character of 1-alkenyl chlorides towards Me_4FeLi_2, Me_4CoLi_2, and Me_3CoLi is shown in Scheme 10.[24] Me_4FeLi_2 methylates

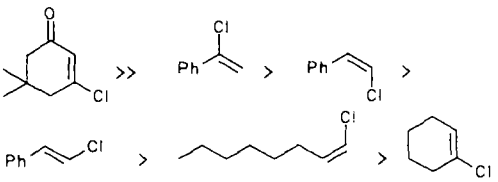

Scheme 10. Variation in electrophilicity of alkenyl chlorides towards Me_4FeLi_2, Me_4CoLi_2, and Me_3CoLi.

(*E*,*Z*)-4-(2-chlorethenyl)benzyl chloride almost exclusively at the chloroethenyl functionality, while with Me_2CuLi virtually only the chloromethyl group is attacked.[24]

While Me_2CuLi is completely inert towards (*Z*)-β-fluorostyrene,[26] cross-coupling between (*E*,*Z*)-β-fluorostyrene and Me_4CoLi_2 or Me_4FeLi_2 occurs in 92 and 59% yield, respectively.[24] 1-Fluoronaphthalene, which because of the high double-bond character of the α,β-bond of the naphthalene system can be considered as an alkenyl fluoride, can be methylated in good yield by Me_4CoLi_2 (see Section 3.3). In an important alkene synthesis ketones are transformed to 1-alkenyl triflates, followed by a cross-coupling with alkyl cuprates.[27] It is thus of interest that Me_4FeLi_2 gives better yields in cross-coupling with 1-alkenyl triflates than the particularly reactive cuprate Me_3CuLi_2 or Me_4CoLi_2 and Me_4MnLi_2 (Scheme 11).[17p]

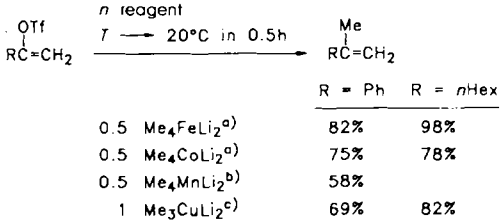

		R = Ph	R = *n*Hex
0.5	Me_4FeLi_2 [a]	82%	98%
0.5	Me_4CoLi_2 [a]	75%	78%
0.5	Me_4MnLi_2 [b]	58%	
1	Me_3CuLi_2 [c]	69%	82%

Scheme 11. 1-Alkenyl triflates as substrates [17p] (*n*Hex = *n*-hexyl). a) THF, $T = -78$ °C; b) Et_2O, $T = 0$ °C, c) THF, $T = 0$ °C.

3.2. Acyl Chlorides

An important application of alkyl transition metal complexes is the transformation of acyl chlorides to ketones without the subsequent reaction to tertiary alcohols. Alkyl–Mn^{II} compounds are regarded as reagents that are particularly suitable for such ketone syntheses.[7] As is shown by the generally high yields obtained in reactions between *monoacyl chlorides* and Me_2Fe, Me_2Co, Me_2Fe, Me_3CoLi, nBu_2Fe, and nBu_3FeLi,[28] these reagents are just as suitable as the Mn reagents. The *bisacyl chlorides* **30** and **31** are converted into the corresponding

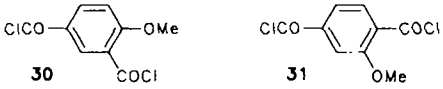

diketones by three equivalents of Me_2Fe in 86 and 65% yields, respectively. The acyl chloride group of **30** and **31** without adjacent substituents is methylated when only 1.25 equivalents of Me_2Fe are used, while Me_2CuLi reacts predominantly with the other acyl chloride group (for Fe-catalyzed synthesis of ketones from acyl chlorides see Section 3.7).

3.3. Aryl Halides

Alkyl cuprates of the type R_2CuLi are not particularly suitable for cross-coupling with aryl halides, since a large excess of the reagent must generally be used and the yield of the cross-coupling product is reduced by halogen/hydrogen exchange reactions (see for example reference [29]). The hypothetical hetero-ate complexes $Me_3Fe(CN)_2Li_3$ and $Me_nCo(CN)_2Li_n$ ($n = 2-4$) are excellent reagents for cross-coupling with *1-halogenonaphthalenes* (Scheme 12).[1] Since they give much higher yields of cross-coupling product and cause much less reduction of the halides to naphthalene they are clearly superior to the homo-ate complexes Me_3FeLi, Me_4FeLi_2, and Me_4CoLi_2. In contrast to the behavior of $Me_4Co(CN)_2Li_4$, the reaction between 1-fluoronaphthalene and Me_3CuLi_2 leads

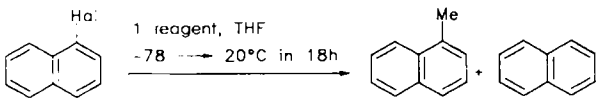

Hal = Br	$Me_3Fe(CN)_2Li_3$	86%	10%
Hal = Br	$Me_2Co(CN)_2Li_2$	89%	5%
Hal = Br	$Me_3Co(CN)_2Li_3$	95%	4%
Hal = Cl	$Me_3Co(CN)_2Li_3$	77%	16%
Hal = F	$Me_4Co(CN)_2Li_4$	67%	1%

Scheme 12. See also ref. [1].

mainly to the cine-substitution product 2-methylnaphthalene.[17k] While nBu$_4$CoLi$_2$ is completely unsuitable for cross-coupling with 1-bromonaphthalene, the reaction proceeds in 28% yield when nBu$_2$Co(CN)$_2$Li$_2$ is used, thus demonstrating the lower tendency of the cyano-ate complex to decompose by β-H-elimination. Up to now *bromobenzene* has only been treated with cobalt cyano-ate complexes: $Me_3Co(CN)_2Li_3$, the most suitable reagent, affords toluene (70%), benzene (14%), and biphenyl (7%) under the conditions in Scheme 12.[1]

3.4. 1-Alkynyl Halides

Although 1-alkynyl halides are more strongly electrophilic towards organometallic reagents than are 1-alkenyl halides, no good method for *alkylating* cross-coupling with these substrates has been reported. [nBuCu·MgBr$_2$] is relatively useful for this purpose, since it reacts with 1-iodo-, 1-bromo-, and 1-chloro-1-heptyne to give the cross-coupling products in 71, 33, and 19%, respectively.[30, 31] Me_4FeLi_2 has shown itself to be a good reagent for methylating cross-coupling reactions with 1-bromo- and 1-chloro-2-phenylethyne and with 1-chloro-3-phenoxypropyne (yields 46,[17p] 70,[17k] and 80%,[17l] respectively), while Me_4CoLi_2, Me_4MnLi_2, Me_2Cu, and Me_3CuLi_2 gave disappointing results.[24] Ether is not a suitable solvent for these reactions, and 1,2-dimethoxyethane is better than THF. $MeCo(CN)_2Li$, the optimum reagent for cross-coupling with 1-bromo-2-phenylethyne, gives the methylation product via **32** in 81% yield; 1,4-diphenyl-1,3-butadiyne (7%) and phenylethyne (3%) are also formed (Scheme 13; for the reaction mechanism see Section 3.6).[1] There was no evidence for the formation of a vinylidene complex by methyl migration in the acetylide complex. Substitution of the Cl atom in 1-chloro-2-phenylethyne by n-butyl, n-octyl, or phenyl groups is carried out more effectively by using the catalytic system [RMgBr + 2.5 mol% $FeCl_3$] (R = nBu, nOct, Ph; yields 75, 63, and 96%, respectively) than by nBu$_4$FeLi$_2$ or R$_4$Fe(MgBr)$_2$ with R = nBu, nOct, Ph; yields 18–28%.[24, 17l] It appears possible that the active catalysts in the catalytic system are super-ate

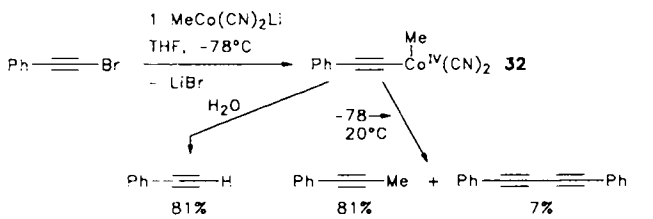

Scheme 13. Products formed from 1-bromo-2-phenylethyne and a rationalization of their formation [1].

complexes of the type [R$_4$Fe(MgBr)$_2$·(RMgBr)$_n$] (see Section 3.7). Competition experiments, in which the reagent was given the choice of two reaction partners (reagent:substrate ratio 1:1:1), gave the following order of the electrophilic behavior towards Me_4FeLi_2: benzoyl chloride > 1-bromo-2-phenylethyne > (*E*)-β-bromostyrene.

3.5. Alkyl Halides

3.5.1. *Monohalides*

Cross-coupling with alkyl halides is well known to be a domain of the organocuprates and organoheterocuprates (e.g. R$_2$Cu(CN)Li$_2$[25]). It was recognized in the study by Corey and Posner mentioned above[5] that Me_3FeLi is not suitable for cross-coupling with 1-iododecane and iodocyclohexane (3 and 1% of methylation product, respectively). Co-workers of the author also obtained very low yields of coupling product in the reactions of 1-bromooctane and 1-bromo-3-phenylpropane in THF with Me_4MLi_2 (M = Fe, Co, −78 °C, in 18 h) or Me_4MnLi_2 (0 to 20 °C, in 18 h). The identification of all the products (for the results of the reaction of Me_4FeLi_2 or Me_4CoLi_2 with 1-bromooctane see Scheme 14 A; similar results

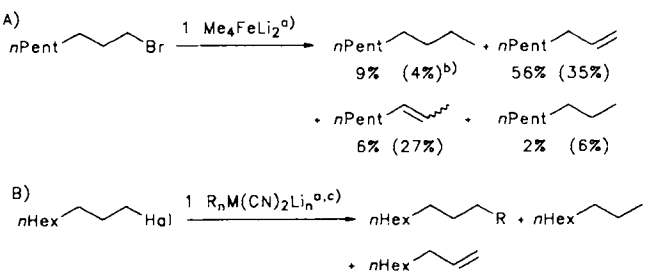

Scheme 14. The reactivity of Me_4FeLi_2 and alkyl-cyano-ate complexes towards alkyl halides [1,17p] (nPent = n-pentyl; nHex = n-Hexyl). a) THF, −78 °C to 20 °C in 18 h; b) yields in parentheses: corresponding reactions with Me_4CoLi_2; c) results for Scheme 14 B: Table 3.

were obtained in reactions with 1-bromo-3-phenylpropane or by using Me_4MnLi_2) showed that the predominant reaction involved dehydrobromination and led to the formation of the terminal alkene and an alkene in which the double bond is shifted by one C atom.[17p] Cyano-ate complexes of Fe^{II} and Ni^{II} are, however, very good reagents for cross-coupling with monohalogenoalkanes[1, 17q] (Scheme 14 B and Table 3). A compari-

Table 3. Cross-coupling of n-nonyl halides with alkyl-cyano-ate complexes in THF (−78 °C to 20 °C in 18 h) in a molar ratio of 1:1 according to Scheme 14B.

Reagent	Hal	Yield [%] Decane	Nonane	1-Nonene	Halide recovered [%]
$Me_2Fe(CN)_2Li_2$	Br	71	21	0	0
$Me_4Fe(CN)_2Li_4$	Br	83	10	0	0
$Me_3Co(CN)_2Li_3$	Br	36	3	51	0
$Me_3Ni(CN)_2Li_3$	Br	84	0	3	0
$Me_4Ni(CN)_2Li_4$	Br	90 (53) [a]	0 (0)	0 (0)	0 (27) [a]
$Me_4Ni(CN)_2Li_4$	Cl	80 (0)	6 (0)	0 (0)	7 (quant.)
$Me_4Ni(CN)_2Li_4$	F	0	0	0	quant.
		tridecane	nonane	1-nonene	
nBu$_4$Ni(CN)$_2$Li$_4$	Br	42	19	0	0

[a] Values in parentheses for yield and recovery: 1 h at −78 °C.

son of the reactivity of $Me_2Fe(CN)_2Li_2$ and Me_4FeLi_2 towards such substrates shows that the cyano ligands alter the course of the reaction (for a mechanistic interpretation see Section 3.6). The use of $Fe(CN)_2$ as a source of iron in the preparation of the reagent thus represents an important advance in the area of iron reagents.

3.5.2. *Geminal Dihalides*

The main reaction that occurs when geminal dihaloalkanes are allowed to react with an excess of Me_2CuLi is the exchange of both halogen atoms by methyl groups.[32] In contrast, Me_4FeLi_2, Me_4CoLi_2, and nBu_4FeLi_2 convert such halides into alkenes.[17k, p] When Me_4FeLi_2, which in this case is a better choice than Me_4CoLi_2, is allowed to react with 1,1-dichlorocyclopentane and 1,1-dichlorocyclohexane, the predominant or sole product is the corresponding methylenecycloalkane (for the probable mechanism see Section 3.6), while in the reaction of nBu_4FeLi_2 with 1,1-dichlorocyclohexane the double bond formed initially is shifted to a large extent into the ring. This and analogous olefinations are shown in Scheme 15.

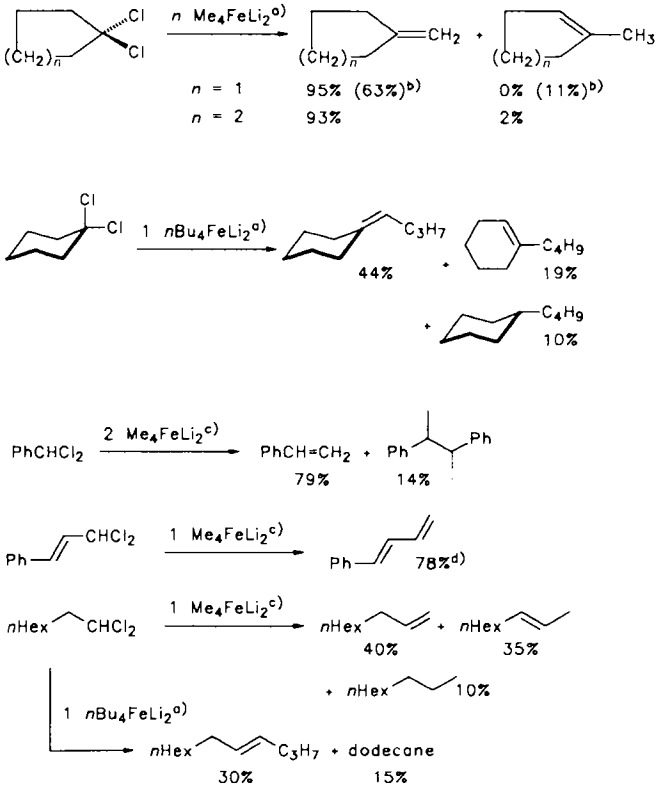

Scheme 15. Olefination of geminal alkyl dichlorides [17k,q]. a) THF, −78 °C (1 h) to 20 °C in 1 h; b) yields in parentheses: corresponding reactions with Me_4CoLi_2; c) Et_2O, −78 °C (1 h); d) THF, −78 °C; d) sole product.

3.5.3. *Allyl Halides, 3-Chloro-1-octyne, and Benzyl Bromide*

"In general, substitution reactions of allylic substrates without (or with) complete allylic rearrangement via organometallics are still unpredictable processes." This statement made in 1980[33] is still valid today (with few exceptions). Substitution reactions involving alkyl–Cu complexes and primary allyl bromides occur in high yield, but often give two regioisomers[6, 33, 34] (for an example see Scheme 16). In contrast, the reactions of Me_4FeLi_2 and Me_4CoLi_2 with 3-chloro- and 3-bromo-1-propene lead exclusively to the unrearranged substitution product **33** (Scheme 16). Me_4FeLi_2 reacts in an analogous manner with 3-chloro-1-octyne to give only 1-methyl-3-pentylallene (58%, THF, −55 °C).[17k]

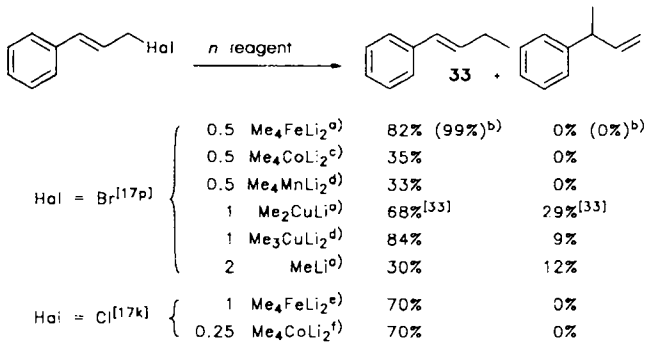

Scheme 16. Regiospecific cross-coupling reactions with allyl halides. a) Et_2O, −78 °C, 1 h; b) 1 molar equivalent of the reagent rather than 0.5; c) THF, −78 °C, 1 h; d) Et_2O, 0 °C, 1 h; e) THF, −40 to 20 °C in 0.5 h; f) THF, −78 to 20 °C in 0.5 h.

The Fe and Co derivatives of *functionalized alkanes* obtained according to Scheme 4, which are inert towards (*E*)-β-bromostyrene and the S_N1-inactive alkyl halide 1-bromocyclohexane, are found to be reactive towards S_N1-active bromides. They react with allyl bromides in good yields to give unrearranged cross-coupling products.[17f, i, n] Cross-coupling also occurs readily with benzyl bromide and 2-methoxybenzyl bromide.[17f, n] The reagent **34**, obtained in a manner analogous to **11**, does not react with vinylic bromine but well with allylic bromine; this enables the regiospecific cross-coupling to give **35**[12, 17i] (Scheme 17).

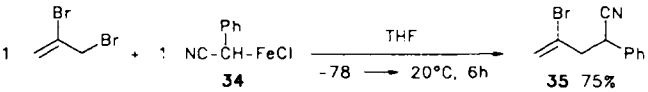

Scheme 17. See also ref. [12].

3.6. Discussion of the Reaction Mechanism of Stoichiometric Cross-Coupling

The reactions of alkyl derivatives of Fe^{II} and Co^{II} with organic substrates often resemble the well-studied reactions of dialkyl cuprates with such substrates. Although the mechanistic rationales devised for dialkyl cuprates are in part controversial, they do provide valuable guidelines for attempts to determine the mechanisms of cross-coupling reactions involving alkyl derivatives of Fe^{II} and Co^{II}. The following features are characteristic of cross-couplings of Me_2CuLi with *alkyl halides*:[35] complete inversion of configuration as in classical S_N2 reactions, second-order kinetics, and the structure–reactivity pattern methyl halide > primary > secondary > tertiary alkyl halide and I > Br > Cl ≫ F. The following mechanisms have been

discussed:[36] 1) normal S_N2 process (methyl "anion" attacks the halide), 2) S_N2 process in which the Cu attacks the alkyl halide (= two-electron transfer process via Cu^{III} species), and 3) one-electron transfer process in which both Cu atoms of the dimeric Me_2CuLi are temporarily oxidized to Cu^{II}. It has been suggested that the second mechanism is not compatible with the highly selective formation of the coupling products R–Me; however, this argument can be countered by the observation that larger alkyl residues are generally more rapidly eliminated than methyl groups because of the release of steric strain. The reaction of Me_2CuLi with 6-iodo-1-heptene leads to the initial generation of a free radical, as can be seen from the formation of a cyclopentane derivative.[37] In contrast, the analogous reaction of Me_3FeLi with 6-bromo-1-hexene[17a] (Scheme 18) is a nonradical process, as is shown by the absence of a cyclization product; the same is true for Me_3MnLi.[17d] The presence of the coupling product **36** indicates that the main product, 1,5-hexadiene, is not formed by the classical E1cB-mechanism[38] (E1 at the carbanion) but by Br/Fe exchange with subsequent β-H-elimination (Scheme 18). The initial reaction step is thus most probably a two-electron oxidative addition.

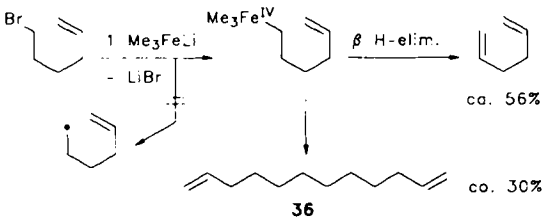

Scheme 18. Study of the mechanism of the reaction between Me_3FeLi and an alkyl bromide [17a]. Reaction conditions: THF, −78 to 20 °C in 18 h.

Halogen/Fe exchange must also be assumed for the second phase of the reaction of 1,1-dichlorocyclopentane (**37**) with Me_4FeLi_2 and Me_4CoLi_2 (see Scheme 15 and Scheme 19) and

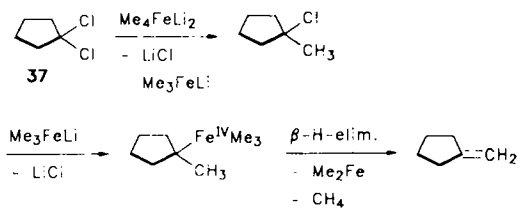

Scheme 19. Mechanistic rationale for the methylenation of a geminal dichloride [17q].

for the initial phase of the reaction of 2-bromopropiophenone (**38**) with Me_3FeLi[17a] (Scheme 20). In the former case this provides a simple explanation for the formation of the olefinic double bond (Scheme 19) and in the latter for the three reaction products (Scheme 20). The 1,4-diketone **39** could also be formed by radical dimerization subsequent to a one-electron transfer process, rather than by homocoupling. While Me_4FeLi_2 reacts with 1-octyl bromide to give 1-octene as the main product (see Scheme 14), the analogous reaction of $Me_2Fe(CN)_2Li_2$ with 1-nonyl bromide gives no olefins but only

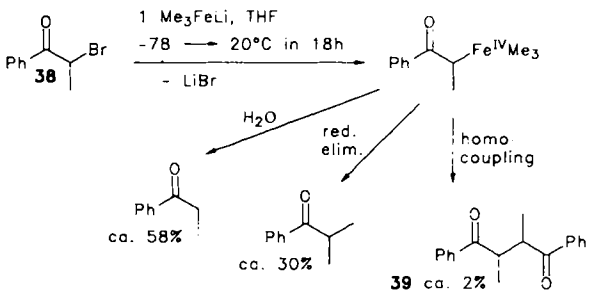

Scheme 20. Mechanistic rationale for the product formation in the reaction of 2-bromopropiophenone with Me_3FeLi [17a].

the coupling product decane in 83% yield[1] (Table 3; Scheme 21). The increase in the length of the carbon chain by one carbon atom in the bromide is hardly likely to play an important role here. Thus the cyano ligands apparently prevent the β-H-elimination that leads to the formation of olefins. It appears likely that because of delocalization of the negative charge, as shown in **40**, the basicity of the Fe atom is reduced to such an extent that it is no longer able to carry out the proton abstraction necessary for β-elimination to occur.

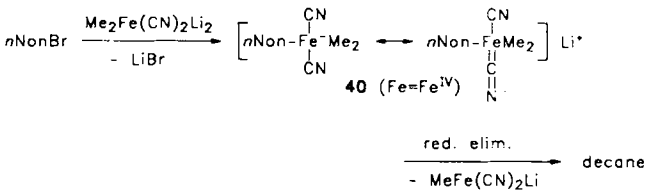

Scheme 21. Control of the course of the reaction by cyanide ligands (*n*Non = *n*-nonyl).

In the reaction of one equivalent of $MeCo(CN)_2Li$ with 1-bromo-2-phenylethyne,[1] the Co^{IV} intermediate **32** (see Scheme 13) and thus a two-electron oxidative addition of the bromide as the initial step, appears almost certain, since there is no other plausible explanation for the formation of the two products (each in 81% yield) when different reaction conditions are used. A one-electron oxidative addition to form 1-methyl-2-phenylethyne (81%) via a Co^{III} intermediate would require two equivalents of the reagent. Homocoupling of **32** (see Scheme 13) gives 1,4-diphenyl-1,3-butadiyne in 7% yield. Little can be said with certainty about the mechanism of the cross-coupling of alkyl derivatives of Fe^{II} and Co^{II} with *1-alkenyl bromides*, which occurs with retention of configuration, and also about the corresponding reactions with Me_2CuLi.[6] A process analogous to that shown in Scheme 13 appears most likely. In the same way the formation of 2,3-dimethyl-1,4-diphenyl-1,3-butadiene (10%) in the reaction referred to in Section 3.1.1 (Scheme 22) of β,β-dibromostyrene with Me_4FeLi_2 to give β,β-dimethylstyrene indicates that an electron-transfer step is involved in the second methylation step; the butadiene derivative is formed either by homocoupling of **41** or by the dimerization of the radical **42** formed in a one-electron transfer process.

The reagents $MeTiCl_3$, $MeNbCl_4$, Me_2NbCl_3, and $MeTi(OiPr)_3$, in which the metals are in their highest possible oxidation states, are not suited for the transformation of *acyl chlorides* into methyl ketones: the three chlorides are inert or

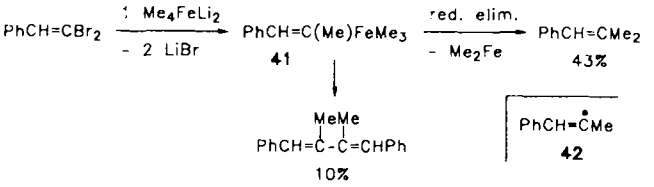

Scheme 22. Mechanistic rationale of product formation in the reaction of β,β-dibromostyrene with Me_4FeLi_2 [17p].

almost inert towards such substrates,[39] while $MeTi(OiPr)_3$ transfers an *O*iPr group instead of its methyl group.[40] In contrast, methyl derivatives of Fe^{II} and Co^{II}, like those of other low-valent transition metals, react readily with acyl chlorides to give cross-coupling products (see Section 3.2). It is thus almost certain that these methyl transfer reactions proceed by oxidative addition followed by reductive elimination; the reaction proposed by Hegedus et al.[41] for the cross-coupling of benzoyl chloride with alkyl-Rh^I complexes (initial formation of an η^1-acyl-M(Cl) complex by oxidative addition of the C-Cl bond) appears most probable. Because of the complete agreement between the observations made for the methylation of acyl chlorides on the one hand and of phenyl isocyanate on the other (with respect to Ti^{IV} reagents, see Section 4.4), there is a slight possibility that cross-coupling reactions of acyl chlorides proceed by *oxidative addition of the CO double bond* (in analogy to Scheme 34) followed by reductive elimination and subsequent β-elimination with renewed formation of the carbonyl function.

3.7. Catalytic Cross-Coupling: Highly Selective Super-Ate Complexes as Catalysts

In the period 1971-1975 Kochi et al.[42] described Fe-catalyzed cross-coupling reactions of *1-alkenyl bromides* with Grignard reagents and catalytic amounts of $FeCl_3$ or Fe^{III} complexes carried out at 25 °C in THF (yields 25 99%) and surmised that labile Fe^I species could well be the active catalytic species. Analogous catalytic cross-coupling reactions of *acyl chlorides at* $-65\,^{\circ}C$ with $FeCl_3$ as the iron source afford ketones in high yields.[43] These ketone syntheses were postulated to involve Fe^{III} catalysts;[44,45] this is extremely unlikely, since $FeCl_3$ is reduced very rapidly to Fe^{II} by MeMgBr or *n*BuMgBr in THF or Et_2O even at $-78\,^{\circ}C$.[28,17l,p]

On the basis of the idea that Me_4FeLi_2 is converted into Me_3FeLi in the reaction with 1-alkenyl bromides and that Me_4FeLi_2 can be regenerated by adding MeLi to Me_3FeLi, the author's group studied Fe-catalyzed cross-couplings of *1-alkenyl bromides* with MeLi or *n*BuLi as well as of *acyl chlorides* with MeMgBr in THF at about $-78\,^{\circ}C$.[28] Use of the systems [RLi +5 mol% $FeCl_3$] or [MeMgBr +2.5 mol% $FeCl_3$] led in each case to high yields of cross-coupling products; in both cases the catalytic species was most probably an Fe^{II} compound.[28,46] Competition reactions with α-bromostyrene/(*E*)-β-bromostyrene showed that the selectivity increases in the series Me_3FeLi, Me_4FeLi_2, and [MeLi +5 mol% $FeCl_3$] (competition constants $K_k = 3.0$, 3.6, 11.1, respectively). In corresponding experiments with benzoyl chloride and 2-methoxybenzoyl chloride the selectivity increased in the analogous series MeFeCl, Me_2Fe, $Me_3Fe(MgBr)$, $Me_4Fe(MgBr)_2$, and [MeMgBr +2.5 mol% $FeCl_3$] ($K_k = 9.9$, 10.7, 10.9, 15.0, and about 110, respectively). These results for the "competition constant method"[47] indicate the presence of "super-ate complexes" [$Me_4FeLi_2 \cdot n$MeLi] and [$Me_4Fe(MgBr)_2 \cdot n$MeMgBr].[28,46] The high selectivity of these catalysts is explained on the basis that their outer sphere, which consists of MeLi or MeMgBr and solvent molecules, hinders the attack of relatively large organic halides at the Fe atom.[28] The catalytic cycle proposed for [$Me_4FeLi_2 \cdot n$MeLi] is shown in Scheme 23.

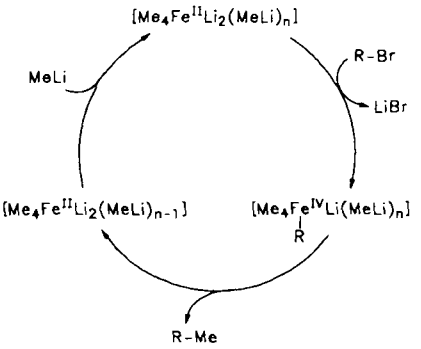

Scheme 23. Postulated catalytic cycle for catalytic cross-coupling of 1-alkenyl bromides with the system [MeLi +5 mol% $FeCl_3$].

The main advantage of catalytic cross-coupling over the stoichiometric procedure is its high chemoselectivity. Its disadvantage is that, because of the presence of MeLi or MeMgBr in the mixtures, catalytic systems cannot be used when the halide contains a functional group that is strongly electrophilic towards MeLi or MeMgBr (e.g. **18**, **22**, **27**). The catalytic rearrangement of terminal epoxides in the presence of [MeLi +2.5 mol% $FeCl_3$] to give methyl ketones (see Section 5.3) is also assumed to involve a super-ate complex as the active catalyst.[46]

3.8. A Comparison with Pd-Catalyzed Cross-Coupling

The cross-coupling reactions discussed in Sections 3.1-3.5 and 3.7 must also be compared with the Pd-catalyzed cross-coupling processes of Stille[48] and Suzuki.[49] The alkylating *Stille coupling*[48] (alkyl-Sn^{IV} compound +Pd catalyst; substrates: allyl, benzyl, aryl, and acyl halides, 1-alkenyl iodides, bromides, and triflates; mild conditions, high stereo- and regioselectivity) has the clear advantage over the *catalytic* cross-couplings described in Section 3.7 that the electrophilic groups >C=O, -COOR, $-CONR_2$, -CN, and even -CHO are tolerated. Nothing is, however, known as to whether these couplings permit a good differentiation between similar substrates, as is the case for the Fe-catalyzed couplings. As far as the comparison with the *stoichiometric* cross-couplings discussed in Sections 3.1-3.5 is concerned, there is the important limitation that in contrast to the couplings with the methylcyanoferrates and alkylcyanonickelates listed in Table 3 (as well as with organocuprates and organocyanocuprates), substrates which bear a hydrogen atom at the sp^3-C atom β to the leaving group (such as RCH_2CH_2Hal, where the intermediate species $RCH_2CH_2Pd(L)_2Hal$ rapidly eliminates alkene) are not suitable

for Stille coupling. (This limitation does not apply to the organotin reagent). In addition the Stille coupling cannot be applied to 1-alkenyl chlorides and fluorides or to aryl chlorides and fluorides. In many cases it will, however, be a useful alternative to the couplings described in Sections 3.1–3.5.

In the case of the alkylating *Suzuki coupling*[49] (β-alkyl-9-borabicyclo[3.3.1]nonane derivative + Pd catalyst + base; substrates aryl and 1-alkenyl halides (Hal = I, Br)), the limitations with respect to the substrate are much more severe; this reaction, which differs mainly from the much more widely studied Stille coupling in that the Pd catalyst is alkylated by a boron compound rather than a tin compound, requires the presence of a strong base; thus, base-sensitive substrates cannot be used. In addition the reaction temperatures are relatively high (generally reflux temperature in THF + H_2O).

4. Reactions with Carbonyl Compounds, Azomethines, and Nitriles

The cyano-ate complexes of Fe, Co, and Ni which have been referred to several times in Section 3 will not be discussed in this section, since relevant studies have not yet been carried out.

4.1. Chemoselective Alkylation of Aldehydes and Ketones

4.1.1. Aldehyde versus Ketone Selectivity

Alkyl derivatives of Cu, Mn, Ti, Cr, and other transition metals have been shown to exhibit a high chemoselectivity in competition reactions with aldehyde/ketone pairs ("aldehyde selectivity"): for a survey see reference [10]. Alkyl derivatives[8a, 9, 11] and functionalized alkyl derivatives[16, 18] of Fe and Co, obtained according to Schemes 1 and 4, are also highly aldehyde-selective. In this respect the *α-cyanoalkyl–Fe complexes* **10–12** are either as good as the corresponding Ti^{IV} complexes or even superior.[18]

4.1.2. Chele- and Anticheleselectivity

Alkyl derivatives of certain transition metals alkylate ketones that contain a basic group in the α-position ("1,2-chelator ketones")[22] or in the β-position ("1,3-chelator ketones")[22] much faster than normal ketones.[22, 50, 51] Me_2Mg methylates α-alkoxy ketones more rapidly than α-siloxy ketones,[52] and Grignard reagents alkylate β-dimethylamino ketones somewhat more rapidly than normal ketones.[50] This "cheleselectivity",[22] which is due to chelate formation in a reaction intermediate, has also been observed for alkyl derivatives of Fe^{II}[9, 17h] and (in a much less pronounced form) for methyl derivatives of Co^{II}[17f, 53d] and Ni[17m]. Alkyl derivatives of Ti^{IV}, Cr^{III}, Mn^{II}, Fe^{II}, and Ag^{I} are probably the best choice for preparative cheleselective alkylation reactions.[22] The preferential alkylation of the β-dimethylamino ketone **43** by Fe and Co reagents in the presence of a normal ketone is shown in Scheme 24.[17h, m, 53d] The *n*-butylation and *n*-octylation of **43** results in almost complete formation of the *S,R/R,S*-diastereoisomer of **44**. This corresponds to an alkylation according to the

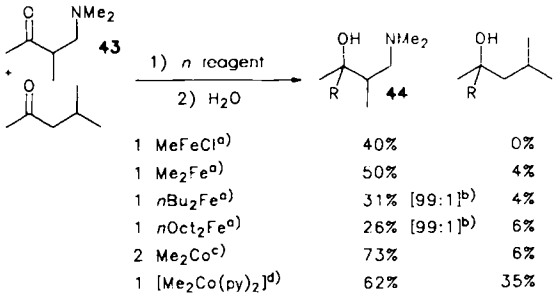

1	MeFeCl[a]	40%	0%
1	Me_2Fe[a]	50%	4%
1	nBu_2Fe[a]	31% [99:1][b]	4%
1	$nOct_2Fe$[a]	26% [99:1][b]	6%
2	Me_2Co[c]	73%	6%
1	$[Me_2Co(py)_2]$[d]	62%	35%

Scheme 24. Cheleselective carbonyl alkylations. a) THF, −78 to 20 °C in 18 h, reagents prepared from RLi [17h]; b) ratio of *S,R/R,S* to *S,S/R,R* diastereoisomers; c) THF, −78 to 20 °C in 18 h, reagent prepared from MeMgBr [53d]; d) Et_2O, −50 to 20 °C in 18 h, reagents prepared from MeLi [53d].

cyclic model proposed by Cram and Kopecky;[54] thus, the formation of an iron chelate intermediate is extremely likely. The decrease in the cheleselectivity in the series Me_2Fe, nBu_2Fe, and $nOct_2Fe$ (as shown in Scheme 24) can easily be explained on the basis of the decreasing tendency to chelation because of the increasing size of the alkyl groups. In contrast to the situation when Ti or Cr reagents are used,[22] the reaction-accelerating effect of a methoxy group in reactions of methyl–Fe reagents only becomes apparent (see Scheme 4 in reference [9]) when the very weakly basic CH_2Cl_2 is used as the solvent and when the Fe reagents (e.g. Me_2Fe) are prepared from MeMgBr rather than from MeLi. This indicates that Mg chelates may be responsible for the cheleselectivity.

Cheleselectivity is also observed when the Fe and Co reagents **2–5**, **7**, **8**, and **10–12** (prepared according to Scheme 4) containing functionalized alkyl groups are allowed to react with *1,2-chelator ketone/ketone competition systems* (for examples see reference [16] and Scheme 25[17o, f]). However, in reactions involving *1,3-chelator ketone/ketone competition systems* the transfer of the functionalized alkyl group occurs in an anticheleselective manner (for examples see references [16,22] and Scheme 25[17o]). The reason for the anticheleselectivity, which in stereochemically relevant cases is always accompanied by low

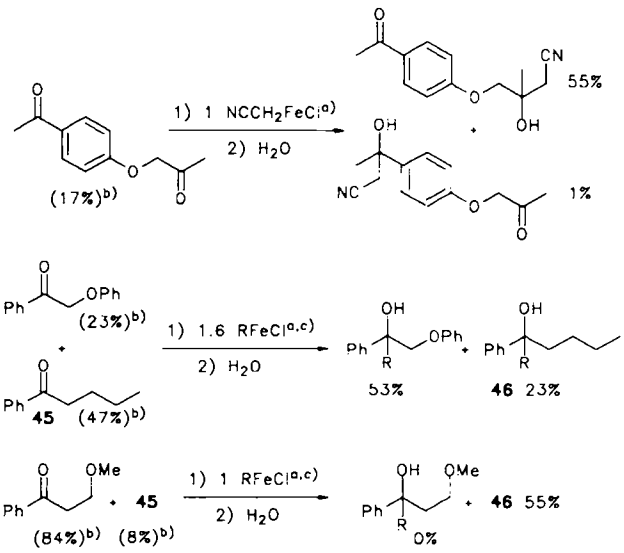

Scheme 25. Chele- and anticheleselectivity of Fe derivatives of functionalized alkanes [17f,o]. a) THF, −78 to 20 °C in 18 h; b) recovery; c) R = $Et_2NCOCH(Me)$.

or even zero diastereoselectivity, is likely to lie in aggregation of the transition-metalated functionalized alkanes[16, 55] (see Section 2.2). The above-mentioned change from chele- to anticheleselectivity, which is also observed for titanated functionalized alkanes,[22] is probably due to the fact that for entropy reasons the formation of a five-membered chelate occurs more readily than that of a six-membered one. Kinetic studies of cheleselective reactions, such as those on alkyl derivatives of Ti^{IV}[51] and Mg^{II}[52], remain to be carried out for the alkyl derivatives of Fe^{II}, Co^{II}, and Ni^{II}.

4.1.3. 99:1 Equatorial-Diastereoselective Addition to Substituted Cyclohexanones

The competition between equatorial and axial attack in nucleophilic additions to substituted cyclohexanones is of both theoretical and synthetic interest. Small nucleophiles such as the hydride ion attack in an axial manner, while organometallic compounds tend towards equatorial attack (for a survey see reference [56]). The degree of selectivity observed is often unsatisfactory. The alkyl–Fe complexes (prepared according to or in analogy to Scheme 1) and Ph_2Fe, as well as the hetero-ate complexes $R_2Fe(acac)_2Li_2$ (R = Me, Ph; Hacac = pentane-1,3-dione) obtained from in situ transmetalation of RLi with Fe $(acac)_2$, were allowed to react with **47** and a second alkylated cyclohexanone by Reetz et al.[56] The results (for examples see Scheme 26) show that the methyl-, *n*-butyl-, and phenyl–Fe

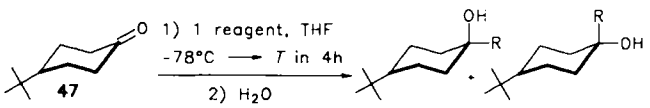

Me_2Fe[a]	99:1 (98%)[b]
Me_3FeLi[a]	98:2 (99%)
$Me_2Fe(acac)_2Li_2$[a,c]	99:1 (85%)
nBu_2Fe[d]	99:1 (60%)
Ph_2Fe[e]	93:7 (64%)
$Ph_2Fe(acac)_2Li_2$[a,c]	97:3 (76%)

Scheme 26. Highly equatorial-selective alkylation and phenylation of a cyclohexanone derivative [56]. a) $T = -22$ °C; b) total yield; c) Hacac = pentane-2,4-dione; d) $T = -15$ °C; e) $T = 0$ °C.

reagents alkylate in an equatorial manner with a diastereoselectivity superior to any achieved previously; thus, the axial alcohols are virtually the sole products. Even the planar phenyl group, which is normally very problematic in such reactions,[57] can be attached to **47** with an equatorial diastereoselectivity of 97:3. For the two hetero-ate complexes, which have been suggested to have the structures **48** and **49**,[56] the methyl derivative is not as good as Me_2Fe, while the phenyl derivative is better than Ph_2Fe. Cholestanone reacts with Me_2Fe to give the axial

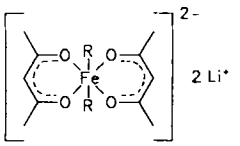

48: R = Me
49: R = Ph

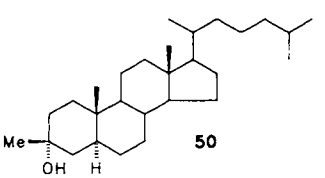

50

alcohol **50** (78%) with a diastereoselectivity of 99:1 (**48**: yield 36%, diastereoselectivity 98:2). A possible explanation of the extreme equatorial selectivity is given in Section 4.4.

4.1.4. Regioselective Addition to Conjugated Enones

Not only organocuprates but also homoleptic alkyl complexes of Mn^{II},[58, 59, 17d] Fe^{II},[60, 17h] Co^{II}[11, 17m] as well as of some later 4d metals[60] react with conjugated enones under 1,4-addition. Nevertheless, organocuprates remain the reagents of choice for 1,4-addition, since in difficult cases (transfer of large residues, open-chain enones) they react in a highly selective manner and give high yields.

In the reactions of the methyl–Fe complexes shown in Table 4 with *2-cyclohexenone* (**51**) (Scheme 27) an increase in the number of methyl groups bonded to the Fe atom correlates with

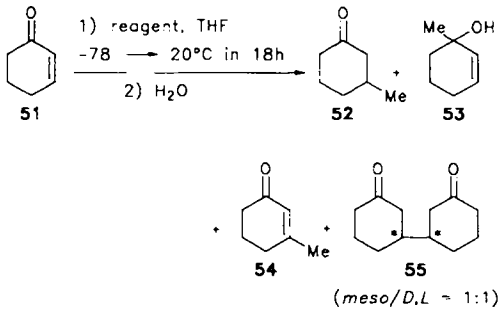

Scheme 27. Reagents and yields: Table 4.

decrease in the yield of the 1,4-addition product **52**, while the opposite is true for methyl–Co and methyl–Mn complexes (Table 4); this indicates the presence of different mechanisms (a possible explanation is given in Section 4.4). The dihydrodimers formed as by-products, *meso*-**55** (m.p. 97 °C and D,L-**55** (m.p. 63–65 °C), are already known,[61] and their structure has been determined by proton NMR spectroscopy.[17h] In contrast to the methyl reagents listed in Table 4 and the hetero-ate complexes nBuFe(OtBu)$_2$Li and nBuFe(SPh)$_2$Li referred to in Section 4.5, the reagents **3** and **5** (Scheme 4), which contain functionalized alkyl groups, react with **51** to give almost exclu-

Table 4. Reactions of Fe [17h,60] and Co reagents [11,17m] and for comparison of Mn reagents [17d] with 2-cyclohexenone (**51**) in a molar ratio of 1:1 according to Scheme 27 (n.d. = not determined).

Reagent [a]	Yield [%]				Recovered [%]
	52	**53**	**54**	**55**	**51**
Me_2Fe	87	3	0	0	3
Me_3FeLi	64	10	0	3 [c]	0
Me_4FeLi_2 [b]	0	35	0	54 [c]	0
$Me_4Co(MgBr)_2$	69	3	0	n.d. [d]	0
Me_3CoLi_4	64	5	6	n.d. [d]	1
Me_3CoLi	44	13	19	n.d. [d]	1
Me_3Co	15	27	17	n.d. [d]	8
Me_3MnLi	60	2	0	19	2
Me_2Mn	57	9	0	4	1
MeMnCl	43	2	0	21	5

[a] Prepared (with the exception of $Me_4Co(MgBr)_2$) from MeLi according to Scheme 1. [b] Almost identical results are obtained by using isolated Me_4FeLi_2. [c] 1:1 mixture of *meso*- and D,L-**55**. [d] Up to four dihydromers $C_{12}H_{18}O_2$ of unknown structure are formed.

sively products derived from 1,2-addition.[17n] Since these aggregated reagents also differ clearly from those obtained according to Scheme 1 in that they do not react with 1-alkenyl bromides, it appears likely that they are not able to undergo oxidative addition of organic substrates because of stabilization of the oxidation states of their metal atoms.

By using *methyl vinyl ketone*[17m,h] as the open-chain substrate, the addition of Me_2Fe, Me_3FeLi, and Me_4CoLi_2 occurs highly selectively in a 1,4-manner (in 1:1 reactions 2-pentanone is formed in 32, 39, and 32% yield, respectively), while Me_4FeLi_2 again gives only the 1,2-addition product (26%). In all cases the dihydrodimers $C_8H_{14}O_2$ are formed in high yields (27–50%).

4.2. Reactions with Esters of Carboxylic Acids and *N,N*-Diethylbenzamide

While the Fe reagents prepared according to Scheme 1 are virtually inert towards esters of carboxylic acids, the methyl–Co reagents listed in Scheme 28 react under mild conditions with ethyl benzoate to give predominantly 2-phenyl-2-propanol,[11,17m] while Me_2CuLi yields only acetophenone.[17c]

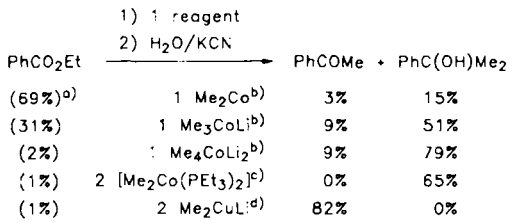

Scheme 28. a) Recovery; b) Et_2O, −78 to 20 °C in 18 h [17m]; c) Et_2O, −78 to 20 °C in 30 min [53b]; d) Et_2O, −50 to 20 °C in 18 h [17c].

In the former case the second methylation step is apparently faster than the first, indicating the intermediate formation of free acetophenone. This is, however, not the case when *N,N*-diethylbenzamide is allowed to react with Me_3CoLi (Scheme 28): acetophenone is almost the sole product obtained when the reaction mixture is treated with an aqueous solution of KCN, suggesting that the initial product is a complex of acetophenone that is stable in nonaqueous media, possibly complex **56**. Me_3CoLi also methylates the ethoxycarbonyl group of ethyl valerate. A 1:1 reaction in Et_2O (−78 to 20 °C in 18 h) affords hexanone (8%) and 2-methyl-2-hexanol (44%).[17m] Me_3CoLi is unable to differentiate between ethyl valerate and *N,N*-diethylbenzamide in 1:1 competition experiments carried out in THF. The reagent is deactivated to such an extent by the two substrates that almost no methyl transfer is observed. However, an analogous experiment with (*E*)-β-bromostyrene and *N,N*-diethylbenzamide leads to the chemospecific formation of (*E*)-β-methylstyrene in 95% yield.[17m]

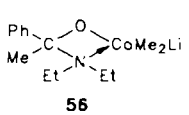

56

4.3. Reactions with Compounds Containing a C–N Multiple Bond

4.3.1. Addition and Substitution Reactions

The reactions described here are of considerable mechanistic interest, since a series of observations indicate that the organic substrates undergo oxidative addition to the reagents (see Section 4.4). It is of interest with regard to synthesis that methyl–Fe and methyl–Co reagents can replace the strongly basic alkyllithium reagents in nucleophilic substitution reactions at heteroarenes; apart from their lower basicity, the former have the further advantage that the addition step is followed by β-H-elimination, which leads to spontaneous rearomatization.

Me_3MnLi reacts with *phenyl isocyanate* in the molar ratio 0.33:1 (THF at −50 to 20 °C) to afford acetanilide in 98% yield.[62] This requires that all three methyl groups are transferred, though this could not be confirmed in attempts[53c] to repeat the work (yield 63%). In contrast to reactions of methyl–Ti^{IV} reagents or $MeNbCl_4$, reactions carried out according to Scheme 29 with the methyl derivatives of Fe, Co, and Ni listed

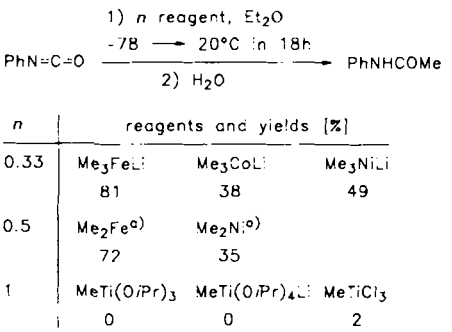

n	reagents and yields [%]		
0.33	Me_3FeLi	Me_3CoLi	Me_3NiLi
	81	38	49
0.5	Me_2Fe[a]	Me_2Ni[a]	
	72	35	
1	$MeTi(OiPr)_3$	$MeTi(OiPr)_4Li$	$MeTiCl_3$
	0	0	2

Scheme 29. See also ref. [53e]. a) These reagents were prepared from MeMgBr in analogy to Scheme 1.

there also gave acetanilide; the best yields are obtained with Me_3FeLi and Me_2Fe.[53e] The mechanism of these methylations is discussed in Section 4.4. 1:1:1 Competition experiments carried out in analogy to Scheme 8 (Et_2O, −78 to 20 °C in 18 h) suggest the following variation of the electrophilic character towards Me_3FeLi:[53e] PhCHO > PhN=C=O > PhCOMe. Me_2CuLi reacts faster with PhN=C=O than with PhCHO.[53e] No studies have yet been carried out to establish whether (as expected) methyl derivatives of Fe^{II} or Co^{II} will methylate carbon dioxide.

In terms of the mechanism, the reaction of Me_3FeLi with *benzalaniline*[17a] (Scheme 30) is remarkable, since the coupling

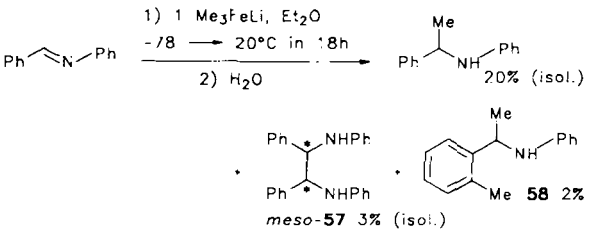

Scheme 30.

product *meso*-**57** indicates the presence of an electron transfer process (see Section 4.4). The assignment of the configuration of *meso*-**57** was determined by ^{1}H NMR spectroscopy: δ(PhC*H*) − 5.01;[63] *meso*-**57** δ = 4.95, D,L-**57** δ = 4.55. The *ortho*-methylation product **58** is discussed in Section 5.1. Under the conditions shown in Scheme 31, the reactions of Me_3FeLi[17a]

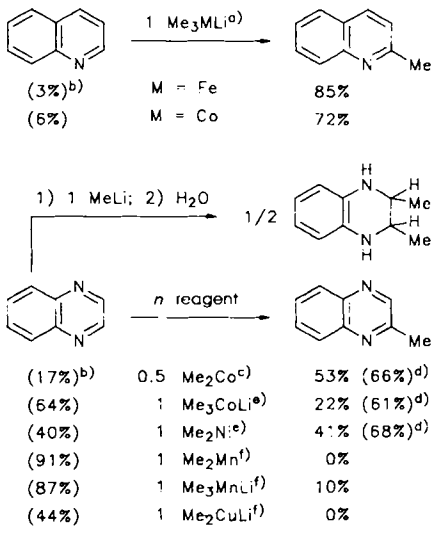

Scheme 31. a) THF, −78 to 20 °C in 18 h [17a,63]; b) recovery; c) Et_2O, −70 °C, 5 days [53d]; d) yields based on unconverted quinoxaline; e) Et_2O, −78 to 20 °C in 18 h [17m]; f) 1 h, −30 °C, 18 h, 20 °C.

or Me_3CoLi[64] with *quinoline* gave 2-methylquinoline in high yield. This product is certainly not formed via MeLi, since neither of the reagents used splits off MeLi in THF (see the β-bromostyrene test in Section 3.1.1); in addition, MeLi would give predominantly 1,2-dihydro-2-methylquinoline under the reaction conditions used which would have to undergo oxidation to form 2-methylquinoline. The products also differ when a transition metal reagent or MeLi is allowed to react with *quinoxaline* (Scheme 31): MeLi does not lead to 2-methylquinoxaline but (in high yield) to 2,3-dimethyl-1,2,3,4-tetrahydroquinoxaline.[17e, 53d] In contrast, the reactions with 0.5 equivalents of Me_3Co[53b, 53d] or Me_2Ni[17m] (Scheme 31) lead to the formation of medium yields of 2-methylquinoxaline as the sole low-molecular weight product, while Me_2Fe[17h] and Me_2Mn[17e] are almost inert towards this heteroarene. The reason for the spontaneous rearomatization that occurs prior to the addition of the transition metal reagents to quinoline and quinoxaline is discussed in Section 4.4.

Nitriles are normally resistant or rather unreactive towards alkyl transition metal reagents. In the case of the well-studied dialkylcuprates this is documented by their position in the "Posner series"[65] RCOCl > RCHO > epoxides > RI > RR'CO > RCO_2R' > RCN. Alkyl-Ti^{IV} derivatives, the second most intensively studied class of alkyl transition metal reagents,[14, 66] are inert towards nitriles, and both $MeHfCl_3$[17b] and Me_3MnLi[17a, d] do not react with benzonitrile. It is thus surprising that the CN group of benzonitrile undergoes quantitative addition with Me_3FeLi under the mild conditions of Scheme 32; subsequent hydrolysis with 2N HCl leads to acetophenone (**59**; 83%) and 2-methylacetophenone (**60**; 17%; due to *ortho*-

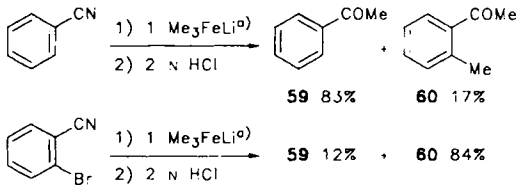

Scheme 32. a) THF, −78 to 20 °C in 18 h.

methylation, see Section 5.1). This attack occurs very rapidly: the yield of acetophenone was 54% after one equivalent of Me_3FeLi was allowed to react for two minutes in THF at −20 °C.[17a] The high reactivity of Me_3FeLi towards the cyano group is confirmed by the reaction with 2-bromobenzonitrile to give **59** and **60**[17a] (Scheme 32). The reactions shown in Scheme 32 could theoretically be caused by MeLi formed by dissociation of Me_3FeLi; apart from the results of the β-bromostyrene-ketone test when carried out with Me_3FeLi (the ketone is not attacked), the formation of the *ortho*-methylation product **60** is also not consistent with such a postulate, since it is not formed when MeLi is allowed to react with benzonitrile.

4.3.2. Stereocontrol of a 1,3-Anionic Cycloaddition by Interactions with Fe Orbitals

The reaction of 1,3-diphenyl-2-azaallyllithium, which can be obtained by lithiation of *N*-benzylidenebenzylamine (**61**) by lithium diisopropylamide (LDA), with acenaphthylene leads to a 1:1 mixture of *endo*-**62** and the thermodynamically more stable *exo*-**62**.[67, 68] If, however, **61** is allowed to react with one molar equivalent of Me_3FeLi (THF, −78 to 20 °C in 18 h) and then treated with acenaphthylene (−78 °C, 18 h) the sole product is *endo*-**62** (55%)[17a] (Scheme 33). The kinetically controlled formation of *endo*-**62** is of more general interest, as it demonstrates that 1,3-anionic cycloadditions[67] are subject to steric control by a transition metal.

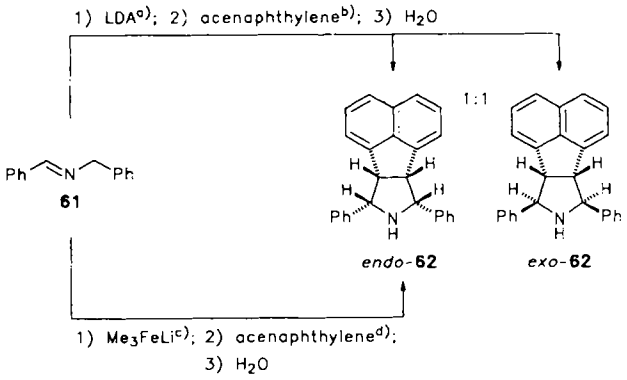

Scheme 33. 1,3-Anionic cycloaddition directed by Fe orbitals. a) THF, −60 to 20 °C; b) 0 °C [67]; c) −78 to 20 °C in 18 h; d) 20 °C [17a].

4.4. Discussion of Reaction Mechanisms

Two classes of methyl reagents containing 3d metals can presently be distinguished: in *category A reagents*, for example $MeTiCl_3$, $MeTi(OiPr)_3$, $MeTi(OiPr)_4Li$, $MeHfCl_3$, $MeV(O)Cl_2$, Me_2NbCl_3, and $MeTaCl_4$, the transition metal is

in its highest possible oxidation state; the reagent is characterized by low basicities, as well as reactivity towards aldehydes, ketones, epoxides, and S_N1-active alkyl halides such as allyl and benzyl halides and α-halogenated carboxylates). In *category B reagents*, for example $MeCrCl_2$, Me_3MnLi, Me_2Fe, Me_4CoLi_2, and Me_2CuLi, the transition metal is not in its highest oxidation state; apart from typical substrates for reactions of category A reagents these can also attack S_N1-inactive alkyl halides, 1-alkenyl, aryl, and 1-alkynyl halides, phenyl isocyanate and azomethines as well as (to some extent) electrophilic heteroarenes, nitriles, esters, amides, and CO_2.[69] In their reactions with alkyl halides the category B reagents make use of their ability to undergo oxidative additions (see Section 3.6). They employ this potential in reactions with substrates containing a CO double or CN multiple bond when other modes of reaction are unfavorable. Comparative studies carried out in the author's research group have demonstrated that the nucleophilicity of methyl derivatives of the following metals towards (*E*)-β-bromostyrene and the heteroarene quinoxaline follows the same order in each case: $Mn^{II} < Co^{II} > Cu^{I}$.

It is not clear whether ketones react with category B reagents by the addition mechanism normally found for carbanions or whether the reagent attacks by an oxidative addition. The surprisingly high equatorial selectivity[56] of the methylation of 4-*tert*-butylcyclohexanone (**47**) by Me_3FeLi discussed in Section 4.1.3 could be due to oxidative addition in which the trimethyliron residue (increased in size due to the presence of coordinated THF molecules) is forced to attack from the equatorial side; thus, after reductive elimination the methyl group is located solely in this position (Scheme 34). However, no trace of a dihydrodimerization product of **47** (of the pinacol type) was found; the presence of such a product would also have indicated an oxidative addition step.

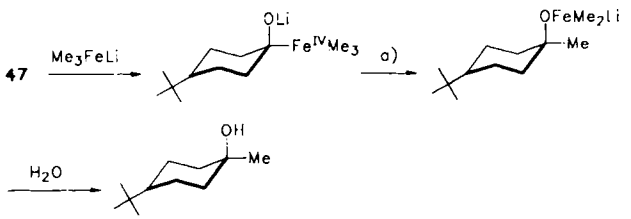

Scheme 34. Possible mechanism for the highly equatorial-selective methylation of 4-*tert*-butylcyclohexanone (**47**) with Me_3FeLi (see also Scheme 26). a) Reductive elimination and complexation of the liberated Me_2Fe to the alkoxide group.

There are several indications that an electron transfer process may be involved in the reactions of category B reagents with CN multiple bonds. When Me_3FeLi is allowed to react with *benzalaniline* (Scheme 30) the formation of a dihydrodimerization product indicates the presence of an oxidative addition step. Assuming that Me_3FeLi reacts as a monomer, the mechanisms A, B, and C shown in Scheme 35 may be involved. The dihydrodimerization product could be formed via the radical **64** or via a species (e.g. **63**) in which the benzylic carbon atom is linked to iron. In the former case D,L-**57** should be formed as well as *meso*-**57** (compare the formation of *meso*-**55** and D,L-**55** in Scheme 27). Since only *meso*-**57** is detected (see Scheme 30), the second possibility (analogous to the homocoupling **65** → *meso*-**66**[70] in Scheme 35) is much more likely.

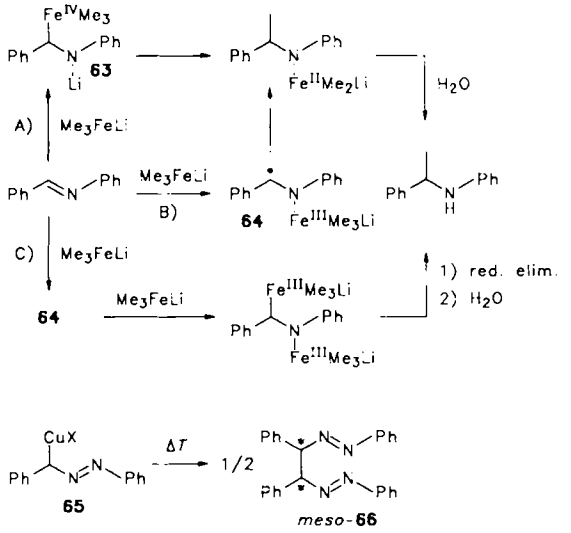

Scheme 35. Possible electron-transfer processes A–C in the methylation of benzalaniline according to Scheme 30 and an interesting stereospecific homocoupling which is of interest in this context [70].

In analogy to the behavior of category A reagents towards acyl chlorides (see Section 3.6) the reagents $MeTiCl_3$, $MeTi(OiPr)_3$, $MeTi(OiPr)_4Li$, $MeTi(OiPr)_4MgBr$, $MeHfCl_3$ and Me_2NbCl_4, which are reactive towards aldehydes and generally also towards ketones, methylate *phenyl isocyanate* only to a very small extent if at all;[53e] the same is true for the behavior of $Me_2V(O)Cl$ towards *methyl isocyanate*[53c] (when the above-mentioned isopropoxytitanium reagents are allowed to react with phenyl isocyanate they instead form PhNHCOO*i*Pr in 40–80% yield[53e]). Phenyl isocyanate is, however, methylated in medium to good yields by $MeCrCl_2$,[53c] Me_3MnLi,[62] $Me_3MnMgBr$,[62] and the derivatives of Fe, Co, and Ni shown in Scheme 29.[53e] Thus, it is likely that these reactions also involve an oxidative addition; in this context it is worth mentioning the two-electron oxidative addition of CO_2 to $(Me_3P)_4Fe$ which leads to the ferraoxirane **67**.[71]

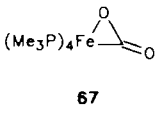

67

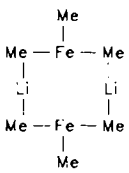

68

In the methylation of the heteroarenes *quinoline* and *quinoxaline* according to Scheme 31, as well as of *nitriles* according to Scheme 32, the surprisingly high nucleophilicity of the reagents towards these substrates provides evidence for the occurrence of an oxidative addition. Analogous mechanisms to those formulated in Scheme 35 for benzalaniline thus appear likely for the addition step. A synchronous *cis*-addition (insertion) of a Me–Fe or Me–Co bond is also possible. Since in each case these reactions lead to a single species in which the transition metal is bound to the N atom, the spontaneous rearomatization that occurs in the case of quinoline and quinoxaline can readily be explained on the basis of a transition metal induced β-H-elimination, as formulated for compound **69** in Scheme 36. As in the case of all the other mechanistically discussed reactions of Me_3FeLi, the possibility must also be taken into account that this reagent, analogous to Me_2CuLi, can perhaps exist and react in the dimeric form **68**.

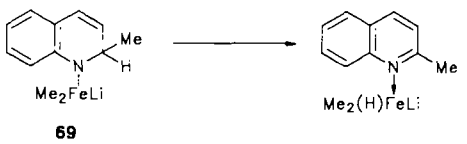

69

Scheme 36.

Two processes have been discussed for the often-studied "1,4-addition" of Me_2CuLi to *2-cyclohexenone* (**51**): an initial one-electron transfer step to give a radical anion and alternatively an attack of the dimeric Me_2CuLi at the enone in analogy to the Michael addition at position C-3.[72] When **51** is methylated by methyl–Fe reagents, the ratio of 1,4- to 1,2-addition product (**52**:**53**) decreases with increasing degree of methylation of the transition metal, while the opposite is true for methylation with Co reagents (Table 4). This clearly suggests that two different mechanisms are involved; these could differ in that (as formulated for Me_4CoLi_2 and Me_3FeLi in Scheme 37) the transition

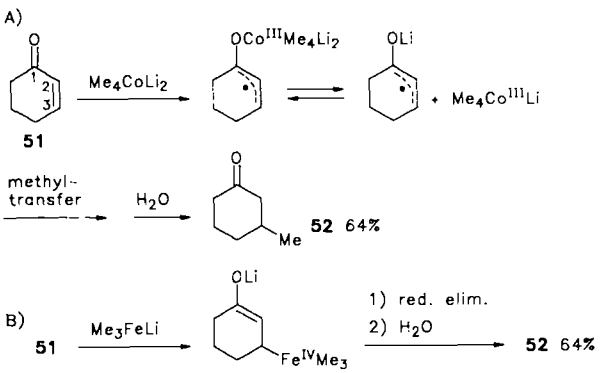

Scheme 37. Possible mechanisms for the methylation reactions **51** → **52** (see also Scheme 27 and Table 4).

metal attacks at either the O atom or at C-3 of **51**. The increase in the ratio **52**:**53** as the degree of methylation at the cobalt atom increases (Table 4) can be explained (assuming a mechanism of type A in Scheme 37) on the basis of increasing steric hindrance to methyl transfer to C-1. The dihydrodimer **55** obtained when Me_3FeLi or, in particular, Me_4FeLi_2 is used (Scheme 27) indicates a one-electron transfer process; compound **55** is probably formed by radical dimerization and not by homocoupling, since a 1:1 mixture of the *meso*- and D,L-forms is obtained.

4.5. The Influence of Stabilizing Neutral Ligands and the Anionic Ligands *t*BuO$^-$ and PhS$^-$ on Reactivity and Selectivity

Is it possible to increase the stability of thermolabile alkyl transition metal reagents by means of complexation with neutral ligands without any excessive loss of reactivity and selectivity? This question was posed in the case of Me_2Co, which decomposes at −40 °C in Et_2O or THF (see Scheme 3). The complexes **70**[71] (isolated, stable up to 20 °C) and **71**–**73** (prepared in situ from the corresponding known dichlorides[73–75] and two equivalents of MeLi) in Table 5 exhibited a considerably lower reactivity than Me_2Co itself in reactions with benzaldehyde and quinoxaline carried out in Et_2O; this corresponds to the observation that the nucleophilicity of Me_2Co in Et_2O is higher than in the more basic solvent THF. A better

Table 5. Comparison of the reactivity of the complexes **70**–**73** with Me_2Co. Reaction conditions: Et_2O, −78 to 20 °C in 18 h.

n Equiv reagent	Substrate	Product	Yield [%]
2 Me_2Co	benzaldehyde	1-phenylethanol [53b]	90
2 [$Me_2Co(PMe_3)_2$] **70**			52
2 [$Me_2Co(PEt_3)_2$] **71**			23
1 Me_2Co	quinoxaline	2-methylquinoxaline [53d]	26 [a]
1 [Me_2Co(dppe)] **72** [b]			2
1 [$Me_2Co(py)_2$] **73**			1

[a] Under optimum conditions 53% (Scheme 31). [b] dppe = 1,2-bis(diphenylphosphino)ethane.

yield than that from Me_2Co was, however, obtained when [$Me_2Co(PEt_3)_2$] (**71**) was allowed to react with ethyl benzoate (see Scheme 28), probably because of the higher thermal stability of **71**. Compounds **71** and [$Me_2Co(py)_2$] (**73**), both of which are stable at −10 °C, were studied with respect to selectivity: compound **71** showed itself to be completely unselective in competition experiments with benzaldehyde/acetophenone and heptanal/3-pentanone,[53b] and the cheleselectivity of **73** is much lower than that of Me_2Co[53d] (see Scheme 24).

The hetero-ate complexes $RFe(OtBu)_2Li$,[53a] $RFe(SPh)_2Li$,[53a] $R_2Fc(OtBu)_2Li_2$,[53f] and $R_2Fe(SPh)_2Li$[53f] (R = Me, *n*Bu) have only been the subject of preliminary studies and will thus only be mentioned in passing: while the methyl complexes were generally much less favorable with respect to both reactivity and selectivity than the methyl-homo-ate complexes prepared according to Scheme 1, the *n*-butyl complexes were found to be superior to the corresponding homo-ate complexes, indicating a greater thermal stability. Two 1:1 reactions with 2-cyclohexenone (**51**) (THF, −78 °C, 1 h, rising to 20 °C in 45 min) are used as examples: *n*BuFe(OtBu)$_2$Li reacted predominantly (3-*n*-butylcyclohexanone (79%), *n*-butylcyclohex-2-enol (15%)) and *n*BuFe(SPh)$_2$Li[53a] solely by 1,4-addition (3-*n*-butylcyclohexanone (71%)). Alkyl–Co^{II} complexes with *t*BuO$^-$ or PhS$^-$ as ligands were less effective than the analogous Fe complexes.

5. Reactions with Other Substrates

5.1. *ortho*-Methylation of Azobenzene and 4-Dimethylaminoazobenzene

A small amount of *ortho*-methylation product is formed in each case when Me_3FeLi is allowed to react with benzalaniline and benzonitrile (see Schemes 30 and 32, respectively). The formation of these compounds, which certainly involves the intermediate formation of a cyclometalation product (cf. ref. [76]), is by no means surprising, since the postulated mechanisms involve an intermediate that can be considered a suitable precur-

sor for *ortho*-methylation. *ortho*-Methylation was the sole reaction observed when Me_3FeLi was allowed to react with *azobenzene* (Scheme 38) or *4-dimethylaminoazobenzene*.[17a, 77] *In the case of the latter substrate the ortho*-methylation of the dimethylamino-substituted (and thus electron-richer) benzene ring occurs to a lesser extent than that of the other benzene ring. An explanation of this result is presented in reference [77]. MeLi, which reacts by an alternative mechanism, *ortho*-methylates 4-dimethylaminobenzene preferentially at the dimethylamino-substituted ring.[77]

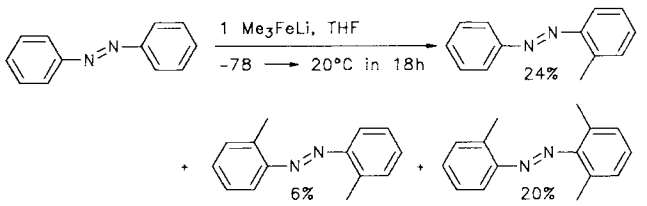

Scheme 38. See also ref. [77].

5.2. Addition to C–C Double and C–C Triple Bonds

(*Z*)-Stilbene and tolane (as examples of substrates with a nonpolarized C–C multiple bond) were allowed to react with one molar equivalent of Me_3FeLi.[17a] The main reaction of *(Z)-stilbene* was its rearrangement to (*E*)-stilbene, making the presence of the radical **74** (and thus a one-electron oxidative addition) very probable. The formation of the by-products **75**–**77** can easily be explained, as shown in Scheme 39. Under the conditions given in Scheme 39, small amounts of several products were obtained from *tolane* (recovered in 65% yield), the most predominant of these were identified by GLC-MS coupling as **75** and **76**. When methyl phenylpropynoate, a substrate with a polarized C–C triple bond, was allowed to react with one equivalent of Me_3FeLi (THF, −78 to 20 °C in 18 h) the main product was methyl (*E,Z*)-2-methylcinnamate (66%) with a *Z*/*E* ratio of 67:33[17a] (for comparison the corresponding reactions with other ate-complexes: with Me_3MnLi *Z*:*E* = 4:96;[17d] with Me_2CuLi according to ref. [78] 100% *Z*-selectivity, but according to ref. [17a] *Z*:*E* = 75:25).

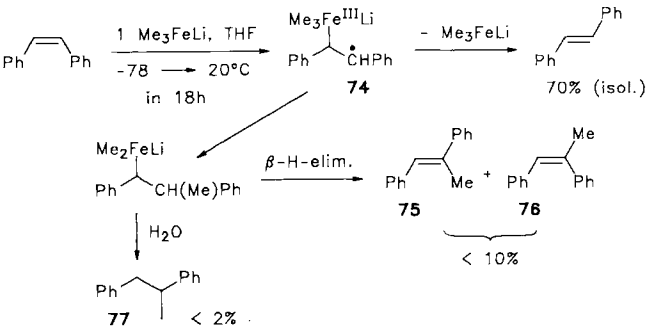

Scheme 39. Products formed from (*Z*)-stilbene and Me_3FeLi and mechanistic rationale for their formation [17a].

5.3. Regiospecific Epoxide Rearrangement

Terminal aliphatic epoxides can undergo rearrangement to aldehydes when treated with Lewis acids.[79] Their rearrangement to give methyl ketones, which has previously been carried out with $Co_2(CO)_8$ or noble metal catalysts (for a survey see ref. [46]), also occurs in high yields when Me_4FeLi_2, Me_3FeLi, or the catalytic systems [RLi +2.5 mol% $FeCl_3$] (R = Me, *n*Bu)[17g, p, 46] are used (for an example see Scheme 40). Alkylating ring opening, the main reaction when alkyl derivatives of Cu^I and Ti^{IV} react with epoxides, is not observed. Me_4CoLi_2 and Me_4NiLi_2 also cause terminal aliphatic epoxides such as **78** to rearrange to methyl ketones, but the yields are lower (ca. 30%) because of the occurrence of side reactions. The following order of the electrophilicity towards Me_4FeLi_2 was determined by means of competition experiments with two substrates carried out in analogy to Scheme 8: 1-alkenyl bromides > ketones > terminal epoxides > alkyl bromides. Thus, this reagent reacts with **79** in a highly selective manner at the epoxide group (78% rearrangement) and with **80** at the vinyl bromide group (90% cross-coupling).[46] The aromatic epoxides styrene oxide and α-methylstyrene oxide are converted by Me_4FeLi_2 into product mixtures.[46] The mechanism formulated in Scheme 40, which involves the ferraoxetane **81**, was postulated for the catalytic rearrangement of 1-decene oxide (**78**) with [MeLi +2.5 mol% $FeCl_3$].[46] The stoichiometric rearrangement with Me_4FeLi_2 or Me_3FeLi probably occurs in an analogous manner.

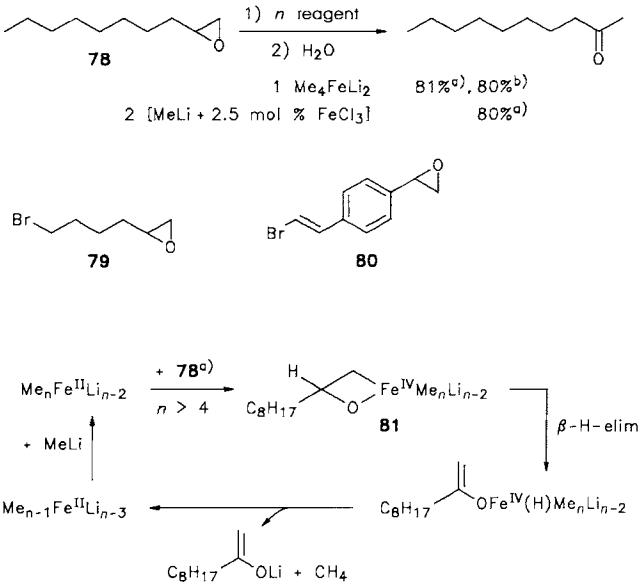

Scheme 40. Rearrangement of terminal epoxides with Fe reagents [46]. a) Et_2O, −78 to 20 °C in 18 h; b) Et_2O, −78 °C 45 min.

6. Summary and Future Prospects

Alkyl derivatives of Cu^I, Mn^{II}, Ti^{IV}, and Ce^{III} have well-established uses in organic synthesis; the nonstabilized alkyl derivatives of Fe^{II} and Co^{II} as well as the alkyl-cyano-ferrates, -cobaltates, and -nickelates whose chemistry is discussed above form

a welcome addition to the arsenal of mild, selective alkylation reagents for organic electrophiles (Table 6 gives a summary of favorable applications). Such compounds are clearly superior to the alkyl–Cu^{I} and alkyl–Mn^{II} reagents (the reactivities of which are comparable) in several respects. These observations, as well as some unexpected reactions (Schemes 31, 32, and 40) point (in comparison with alkyl derivatives of Cu^{I} and Mn^{II}) to an increased willingness to undergo oxidative addition with electrophiles. Depending on the reactivity of the substrates this can apparently be either a *two-electron oxidative addition* (for organic halides that are not S_N1-active; see Scheme 13, 18, and 34) or a *one-electron oxidative addition* (for unsaturated compounds that can stabilize unpaired electrons, see Schemes 37A and 39). It is not surprising that alkyl derivatives of Fe^{II} are particularly willing to tolerate the oxidative addition of electrophiles, since the stability of the divalent oxidation state of the elements Mn, Fe, Co, and Ni is at its lowest for Fe.[8] The cyanide ligands of the cyano-ate complexes of Fe, Co, and Ni prevent β-H-elimination subsequent to the oxidative addition of alkyl halides and thus facilitate cross-couplings with these substrates in high yields. As far as Fe-catalyzed alkylations (in principle long-known) is concerned (see Section 3.7), the extremely high selectivity and the nature of the active species has been recognized.

Table 6. Alkyl complexes of Fe, Co, Ni, Cu, and Mn that can be recommended as reagents for C–C bond formation reactions with the given organic electrophiles (*n*Oct = *n*-octyl)

Substrates	Reaction type	Reagents
1-alkenyl halides		
Hal = Br	cross-coupling	Me_4MLi_2 (M = Fe, Co), nBu_4FeLi_2, $nOct_2Fe$, $Me_2Fe(CN)_2Li_2$
Hal = Br	cheleselective cross-coupling	Me_4FeLi_2, R_4MnLi_2 (R = Me, *n*Bu)
Hal = Cl	cross-coupling	Me_4MLi_2 (M = Fe, Co), Me_3CoLi
Hal = F	cross-coupling	Me_4CoLi_2
1-bromo-4-phenyl-1,4-butadiene	cross-coupling	Me_4CoLi_2
1-alkenyl triflates	cross-coupling	Me_4FeLi_2
acyl chlorides	cross-coupling	alkyl-Mn^{II} reagents, Me_2M (M = Fe, Co), nBu_2Fe, nBu_3FeLi
1-halogenonaphthalenes		
Hal = Br	cross-coupling	$Me_3M(CN)_2Li_3$ (M = Fe, Co)
Hal = Cl	cross-coupling	$Me_3Co(CN)_2Li_3$
Hal = F	cross-coupling	$Me_4Co(CN)_2Li_4$
bromobenzene	cross-coupling	$Me_3Co(CN)_2Li_3$
1-alkynyl halides (Hal = Br,Cl)	cross-coupling	$MeCo(CN)_2Li$, Me_4FeLi_2
alkyl halides (Hal = Br, Cl)	cross-coupling	alkyl-Cu^{I} reagents, $Me_nFe(CN)_2Li_n$ (n = 2–4), $R_4Ni(CN)_2Li_4$ (R = Me, *n*Bu)
gem. dichloroalkanes	methylenation	Me_4FeLi_2
allyl halides (Hal = Br, Cl)	cross-coupling without rearrangement	Me_4MLi_2 (M = Fe, Co) al well as alkyl-Fe- and alkyl-Co-reagents with functional groups in the alkyl groups (see Scheme 4)
4-*tert*-butylcyclohexanone	equatorial-diastereoselective addition	Me_2Fe, Me_3FeLi, nBu_2Fe
conjugated enones	1,4-addition	alkyl-Cu^{I} reagents
PhCOOEt	substitution	Me_2CuLi
	substitution +addition	Me_4CoLi_2

An appropriate continuation of the investigations described above[80] would involve the extension of the chemistry of the cyano-ate complexes of Fe, Co, and Ni, which have so far only been subjected to reaction with organic halides, to include unsaturated organic compounds, the exploration of the potential of alkyl derivatives of these metals as mild alkylating reagents for electrophilic heteroarenes, and the question as to whether super-ate complexes—possibly in combination with chiral anionic ligands—of Mn, Co, and Ni can function as highly selective alkylation catalysts.

I thank those co-workers (their names can be found in the list of references) who were members of the highly effective team that worked with great personal initiative on the research group's last project (either nerved by failures or inspired by successes) and who did not let the gas chromatographs get cold even during the Institute's holiday periods! Those who were involved in the project thank the Deutsche Forschungsgemeinschaft, the Volkswagen-Stiftung, and the Fonds der Chemischen Industrie for financial support.

Received: March 23, 1995 [A 110 IE]
German version: *Angew. Chem.* **1996**, *108*, 401–418
Translated by Prof. T. N. Mitchell, Dortmund, Germany

[1] T. Kauffmann, H. Nienaber, *Synthesis* **1995**, 207–211.
[2] J. P. Collman, *Acc. Chem. Res.* **1975**, *8*, 342–347.
[3] H. J. Spiegl, G. Groh, H. J. Berthold, *Z. Anorg. Allg. Chem.* **1973**, *398*, 225–230.
[4] R. A. Andersen, E. Carmona-Guzman, K. Mertis, E. Sigurdson, G. J. Wilkinson, *J. Organomet. Chem.* **1975**, *99*, C19–C20.
[5] E. J. Corey, G. H. Posner, *Tetrahedron Lett.* **1970**, 315–318.
[6] F. Naso, G. Marchese in *The Chemistry of Functional Groups*, Supplement D (Eds.: S. Patai, Z. Rappoport), Wiley, New York, **1983**, p. 1353–1449.
[7] J. F. Normant, G. Cahiez in *Modern Synthetic Methods* (Ed.: R. Scheffold), Salle und Sauerländer, Frankfurt, **1983**, S. 173–216.
[8] A. F. Hollemann, E. Wiberg, *Lehrbuch der Anorganischen Chemie* (Ed.: N. Wiberg), 91.–100. ed., de Gruyter, Berlin, **1985**, p. 1125.
[9] T. Kauffmann, B. Laarmann, D. Menges, K.-U. Voß, D. Wingbermühle, *Tetrahedron Lett.* **1990**, *31*, 507–510.
[10] T. Kauffmann, B. Laarmann, D. Menges, G. Neiteler, *Chem. Ber.* **1992**, *125*, 163–169.
[11] T. Kauffmann, G. Hopp, B. Laarmann, D. Stegemann, D. Wingbermühle, *Tetrahedron Lett.* **1990**, *31*, 511–514.
[12] T. Kauffmann, D. Stach, *Chem. Ber.* **1992**, *125*, 913–921.
[13] M. Aresta, C. F. Nobile, D. Petruzzelli, *Inorg. Chem.* **1977**, *16*, 1817–1818.
[14] M. Reetz, *Organotitanium Reagents in Organic Synthesis*, Springer, Berlin, **1986**, p. 75.
[15] T. A. Bazhenova, R. M. Lobkovskaya, R. P. Shibaeva, A. K. Shilova, M. Gruselle, G. Leny, E. Deschamps, *J. Organomet. Chem.* **1983**, *244*, 375–382.
[16] T. Kauffmann, T. Möller, H.-W. Wilde, *Chem. Ber.* **1994**, *127*, 2277–2283.
[17] Dissertations, Universität Münster: a) J. Sander, **1986**; b) C. Pahde, **1986**; c) M. Kolb, **1987**; d) S. Raedeker, **1987**; e) J. C. Baune, **1988**; f) H.-J. Kieper, **1990**; g) C. Neiteler, **1991**; h) D. Menges, **1991**; i) D. Stach, **1991**; j) D. Schlosser, **1991**; k) R. Sälker, **1991**; l) K.-U. Voss, **1992**; m) D. Stegemann, **1992**; n) H.-W. Wilde, **1992**; o) E. Bischoff, **1993**; p) G. Neiteler, **1994**; q) H. Nienaber, **1994**.
[18] T. Kauffmann, H. Kieper, H. Pieper, *Chem. Ber.* **1992**, *125*, 899–905.
[19] H. Gilman, F. Schulze, *J. Am. Chem. Soc.* **1925**, *47*, 2002–2005.
[20] M. Gaudemar, M. Martin, *C. R. Acad. Sci. Ser. C* **1968**, *267*, 1053–1056.
[21] J. Klein, R. Levene, *Tetrahedron Lett.* **1974**, *15*, 2935–2938.
[22] Review: T. Kauffmann, *Synthesis* **1995**, 745–755.
[23] T. Kauffmann, H. Nienaber, D. Stach, *Inorg. Chim. Acta* **1994**, *220*, 85–92; T. Kauffmann, D. Stach, *Angew. Chem.* **1991**, *103*, 1683–1685; *Angew. Chem. Int. Ed. Engl.* **1991**, *30*, 1684–1685.
[24] T. Kauffmann, R. Sälker, K.-U. Voss, *Chem. Ber.* **1993**, *126*, 1447–1452.
[25] B. H. Lipshutz, J. A. Kozlowski, C. M. Breneman, *J. Am. Chem. Soc.* **1985**, *107*, 3197–3204; review on "higher order" organocuprates": B. H. Lipshutz, R. S. Wilhelm, J. A. Kozlowski, *Tetrahedron* **1984**, *40*, 5005–5038; B. H. Lipshutz, *Synthesis* **1987**, 325–341; *Synlett* **1990**, 119–128.
[26] C. V. Maffeo, G. Marchese, F. Naso, L. Ronzini, *J. Chem. Soc. Perkin Trans. 1* **1979**, 92–97.
[27] J. E. McMurry, W. J. Scott, *Acc. Chem. Res.* **1988**, *21*, 47–54.
[28] T. Kauffmann, K.-U. Voss, G. Neiteler, *Chem. Ber.* **1993**, *126*, 1453–1459.
[29] E. J. Corey, G. H. Posner, *J. Am. Chem. Soc.* **1967**, *89*, 3911–3912; G. M. Whitesides, W. F. Fischer, Jr., J. J. Filippo, Jr., R. W. Bashe, H. O. House, *ibid.* **1969**, *91*, 4871–4882.

[30] A. Commerçon, J. F. Normant, J. Villieras, *Tetrahedron* **1980**, *36*, 1215–1221.
[31] J. F. Normant in *New Applications of Organometallic Reagents in Organic Synthesis* (Ed.: D. Seyferth), Elsevier, Amsterdam, **1976**, S. 238.
[32] G. H. Posner, D. J. Brunelle, *Tetrahedron Lett.* **1972**, *13*, 293–296.
[33] Y. Yamamoto, S. Yamamoto, H. Yatagai, K. Maruyama, *J. Am. Chem. Soc.* **1980**, *102*, 2318–2325.
[34] K. Maruyama, Y. Yamamoto, *J. Am. Chem. Soc.* **1977**, *99*, 8068–8070.
[35] A. Yamamoto, *Organotransition Metal Chemistry*, Wiley, New York, **1986**, p. 400.
[36] J. P. Collman, L. S. Hegedus, J. R. Norton, R. G. Finke, *Principles and Applications of Organotransition Metal Chemistry*, University Science Books, Mill Valley, CA, USA, **1987**, p. 686.
[37] E. C. Ashby, R. N. DePriest, A. Tuncay, S. Srivastava, *Tetrahedron Lett.* **1982**, *23*, 5251–5254.
[38] J. March, *Advanced Organic Chemistry*, 3. ed., Wiley, New York, **1985**, p. 882–886.
[39] T. Kauffmann, T. Abel, C. Beirich, G. Kieper, C. Pahde, M. Schreer, E. Toliopoulos, R. Wiescholleк, *Tetrahedron Lett.* **1986**, *27*, 5355–5358.
[40] B. Weidmann, D. Seebach, *Angew. Chem.* **1983**, *95*, 12–26; *Angew. Chem. Int. Ed. Engl.* **1983**, *22*, 31–45.
[41] L. S. Hegedus, S. M. Lo, D. E. Bloss, *J. Am. Chem. Soc.* **1973**, *95*, 3040–3042.
[42] S. M. Neumann, J. K. Kochi, *J. Org. Chem.* **1975**, *40*, 599–606; M. Tamura, J. K. Kochi, *J. Am. Chem. Soc.* **1971**, *93*, 1487–1489.
[43] W. C. Percival, R. W. Wagner, N. C. Cook, *J. Am. Chem. Soc.* **1953**, *75*, 3731–3734.
[44] R. T. Morrison, M. Wishman, *J. Am. Chem. Soc.* **1954**, *76*, 1059–1061.
[45] J. Cason, K. W. Kraus, *J. Org. Chem.* **1961**, *26*, 1768–1772.
[46] T. Kauffmann, C. Neiteler, G. Neiteler, *Chem. Ber.* **1994**, *127*, 659–665.
[47] R. Huisgen, J. Sauer, *Angew. Chem.* **1960**, *72*, 91–108.
[48] Review: J. K. Stille, *Angew. Chem.* **1986**, *98*, 504–519; *Angew. Chem. Int. Ed. Engl.* **1986**, *25*, 508–524. This publication also deals with the transfer of groups other than alkyl by Stille coupling.
[49] N. Miyaura, T. Ishiama, H. Sasaki, M. Ishikawa, M. Satoh, A. Suzuki, *J. Am. Chem. Soc.* **1989**, *111*, 314–321. This account also includes literature on the transfer of aryl and 1-alkenyl groups by Suzuki coupling.
[50] T. Kauffmann, T. Möller, H. Rennefeld, S. Welke, R. Wieschollek, *Angew. Chem.* **1985**, *97*, 351–352; *Angew. Chem. Int. Ed. Engl.* **1985**, *24*, 348–349; T. Kauffmann, C. Neiteler, S. Robbe, *Chem. Ber.* **1992**, *125*, 2409–2418.
[51] M. T. Reetz, S. Maus, *Tetrahedron* **1987**, *43*, 101–108; M. T. Reetz, *Acc. Chem. Res.* **1993**, *26*, 462–468.
[52] X. Chen, E. R. Hortelano, E. L. Eliel, S. V. Frye, *J. Am. Chem. Soc.* **1992**, *114*, 1778–1784.
[53] Diploma theses, Universität Münster: a) U. Lügger, **1984**; b) J. C. Baune, **1985**; c) W. Bonrath, **1985**; d) G. Hopp, **1989**; e) H.-W. Wilde, **1989**; f) H. Nienaber, **1990**.
[54] D. J. Cram, K. R. Kopecky, *J. Am. Chem. Soc.* **1959**, *81*, 2748–2755.
[55] T. Kauffmann, H. Kieper, *Chem. Ber.* **1992**, *125*, 907–912.
[56] M. T. Reetz, S. Stancher, *J. Chem. Soc. Chem. Commun.* **1993**, 328–330.
[57] M. T. Reetz, H. Hanig, S. Stancher, *Tetrahedron Lett.* **1992**, *33*, 6963–6966.
[58] T. Kauffmann, M. Bisling, *Tetrahedron Lett.* **1984**, *25*, 293–296.
[59] G. Cahiez, M. Alami, *Tetrahedron Lett.* **1986**, *27*, 569–572.
[60] T. Kauffmann, A. Hülsdünker, D. Menges, H. Nienaber, L. Rethmeier, S. Robbe, D. Scherler, J. Schrickel, D. Wingbermühle, *Tetrahedron Lett.* **1990**, *31*, 1553–1556.
[61] J. Dunouguès, R. Calas, M. Bolourtchian, C. Biran, N. Duffant, B. Barbe, *J. Organomet. Chem.* **1973**, *57*, 55–69.
[62] G. Friour, G. Cahiez, A. Alexakis, J. F. Normant, *Bull. Soc. Chim. France* **1979**, 515–517.
[63] A. Collet, M.-J. Brienne, J. Jacques, *Bull. Soc. Chim. Fr.* **1972**, 336–342.
[64] T. Kauffmann, B. Laarmann, unpublished results, **1988**.
[65] Ref. [36], p. 685.
[66] D. Seebach, B. Weidmann, L. Widler in *Modern Synthetic Methods* (Ed.: R. Schefford), Salle und Sauerländer, Frankfurt, **1983**, p. 217–353.
[67] T. Kauffmann, *Angew. Chem.* **1974**, *86*, 715–727; *Angew. Chem. Int. Ed. Engl.* **1974**, *13*, 627–639.
[68] T. Kauffmann, K. Habersaat, E. Köppelmann, *Chem. Ber.* **1977**, *110*, 638–644.
[69] The alkyl–Ce^{III} reagents (RLi or RMgHal + $CeHal_3$) described by T. Imamoto (*Pure Appl. Chem.* **1990**, *62*, 747–752, and references therein) behave more like Category A reagents (ready addition to enolizable ketones because of their low basicity, as for alkyl–Ti^{IV} compounds; 1,2-addition to conjugated enones) than category B reagents (nBuCeI$_2$ reacts with 4-iodoacetophenone not by cross-coupling but at the keto group to give 4-I-$C_6H_4C(OH)(CH_3)C_4H_9$ in 93% yield; no cross-coupling reactions with other aryl halides or with 1-alkenyl halides are known). However, their ready addition to esters and amides of carboxylic acids as well as to nitriles demonstrates a behavior that is untypical of category A reagents.
[70] T. Kauffmann, *Angew. Chem.* **1974**, *86*, 321–335; *Angew. Chem. Int. Ed. Engl.* **1974**, *13*, 291–306.
[71] H.-F. Klein, H. H. Karsch, *Chem. Ber.* **1976**, *109*, 1453–1464.
[72] J. P. Collman, L. S. Hegedus, *Principles and Applications of Organotransition Metal Chemistry*, University Science Books, Mill Valley, CA, USA, **1980**, p. 552.
[73] K. K. Chow, W. Levason, C. A. McAuliffe, *Transition Metal Complexes of Phosphorus, Arsenic and Antimony Ligands*, McMillan Press, London, **1973**, p. 94.
[74] W. D. Horrocks, Jr., G. R. van Hecke, D. W. Hall, *Inorg. Chem.* **1967**, *6*, 694–699.
[75] F. Reitzenstein, *Justus Liebigs Ann. Chem.* **1894**, *282*, 267–280.
[76] M. I. Bruce, *Angew. Chem.* **1977**, *85*, 75–89; *Angew. Chem. Int. Ed. Engl.* **1977**, *16*, 73.
[77] T. Kauffmann, J. Jordan, J. Sander, *Chem. Ber.* **1992**, *125*, 153–155.
[78] E. J. Corey, J. A. Katzenellenbogen, *J. Am. Chem. Soc.* **1969**, *91*, 1851–1852.
[79] D. Dietrich, *Methoden Org. Chem.* (Houben-Weyl), 4th ed. 1952- Bd. 7/2a, **1978**, p. 932.
[80] Experimental studies ceased in 1993 due to the author's emeritus state.

Radical Reactions as Key Steps in Natural Product Synthesis

Ulrich Koert*

Radical reactions have developed into indispensable methods in organic synthesis[1] and are often used as key steps in the construction of complex natural products. Impressive demonstrations are found in the following examples taken from the current literature: the synthesis of dactomelyne by Lee et al.,[2] that of camptothecin by Curran et al.,[3] and of 7-deoxypancratistatin by Keck et al.,[4] and the approaches towards aspidospermidine by Murphy et al.[5] and pseudopterosin A by Schmalz et al.[6]

The total synthesis of the marine natural product (3*Z*)-dactomelyne (**1**) requires the elaboration of the *cis*-linked pyranopyran skeleton and the stereoselective introduction of halogen atoms on the tetrahydropyran rings. Lee et al.[2] solved this problem by using β-alkoxyacrylates twice as radical acceptors. Radical cyclization of the trichloro compound **2** afforded the bicyclic product **3**. The selective monodehalogenation of the dichloro compound **3** giving **4** was accomplished with a radical reaction as well. Important for the desired stereoselectivity was the use of the silane $(Me_3Si)_3SiH$. Stannanes like nBu$_3$SnH gave the other epimer **5** as the major product. The highlight of the synthesis was the construction of the second tetrahydropyran ring and simultaneous stereoselective introduction of the bromo-substituted stereocenter: the radical reaction of β-alkoxyacrylate **6** with nBu$_3$SnH gave exclusively the desired bicyclic product **7**. The authors propose the chairlike transition state **8** to explain the observed stereoselectivity. The bicyclic product **7** was converted in a few steps into the target compound (3*Z*)-dactomelyne (**1**).

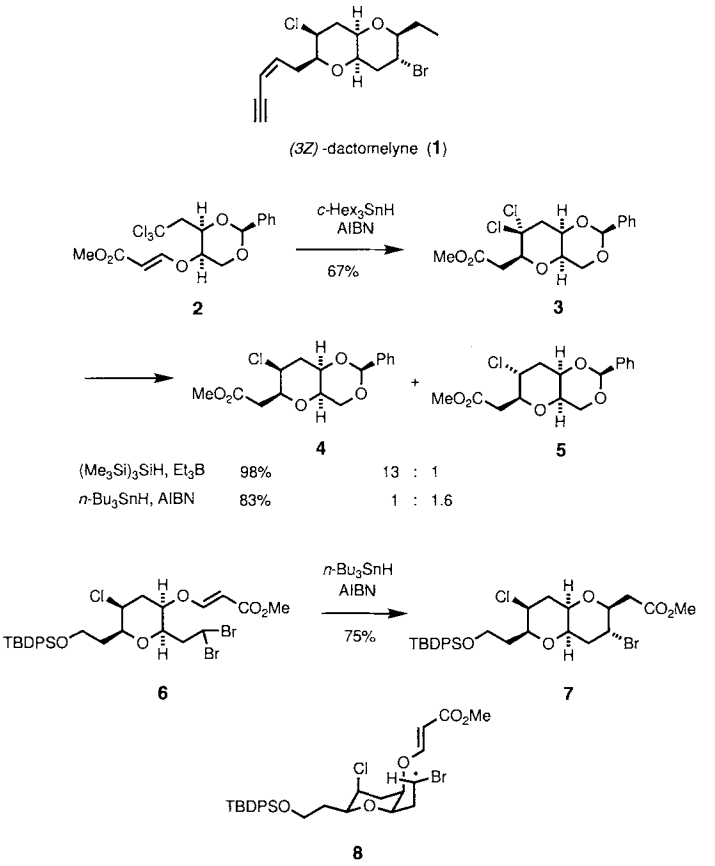

The potent antitumor agents camptothecin (**11**) and its derivatives are currently the targets of extensive synthetic activities.[7] A major contribution to this research area came from the laboratory of D. P. Curran[3] in Pittsburgh with a total synthesis of camptothecin relying on radical chemistry. In the key step of this synthesis the iodoalkyne **9** was allowed to react with phenyl isonitrile to provide the target compound **11**. In this radical cascade reaction, an excellent example of a "sequential reaction",[8] the simultaneous construction of the B- and C-rings of camptothecin was accomplished. The mechanism for radical reaction is best explained by the transformation of the structurally less complex bromoalkyne **12** into the tetracyclic compound **16**. First, a trimethylstannyl radical produced from hexamethyldistannane attacks the C–Br bond of compound **12**.

[*] Dr. U. Koert
Fachbereich Chemie der Universität
Hans-Meerwein-Strasse, D-35032 Marburg (Germany)
Fax: Int. code +(6421)288-917

The resulting pyridone radical **13** reacts intermolecularly with isocyanide **10** to yield the radical intermediate **14**. An intramolecular attack of the radical center in **14** on the alkyne functionality leads to radical **15**. Finally, the A-ring is attacked by the radical center in **15** leading to **16**, which rearomatizes to yield the desired compound **17**.

The alkaloid pancratistatin (**18**) isolated from *Amaryllidaceous* plants displays promising antineoplastic and antiviral activity.[9a] The 7-deoxy compound **19** exhibits both better therapeutic properties and decreased toxicity.[9b] The group of G. E. Keck[4] successfully completed the total synthesis of 7-deoxypancratistatin (**19**) using a radical reaction as a key step. Here, the radical precursor **20** was treated with nBu$_3$SnH to yield the benzyl radical **21**, which reacted further by a 6-*exo* cyclization affording the cyclohexylamine **22**. Important for the excellent stereoselectivity of this step was the conformational control dic-

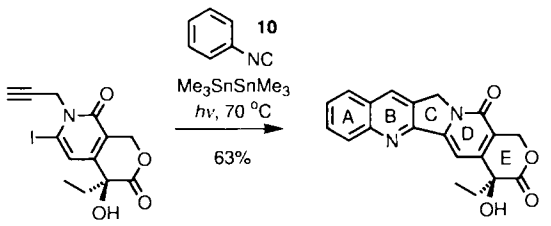

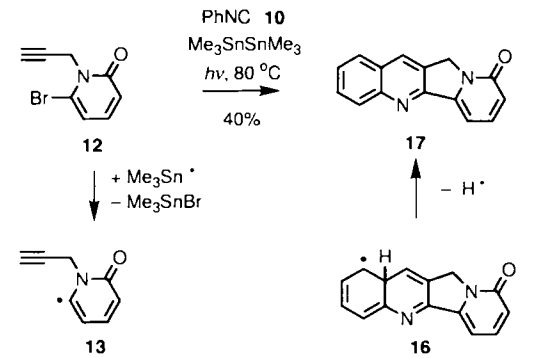

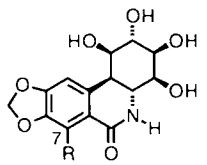

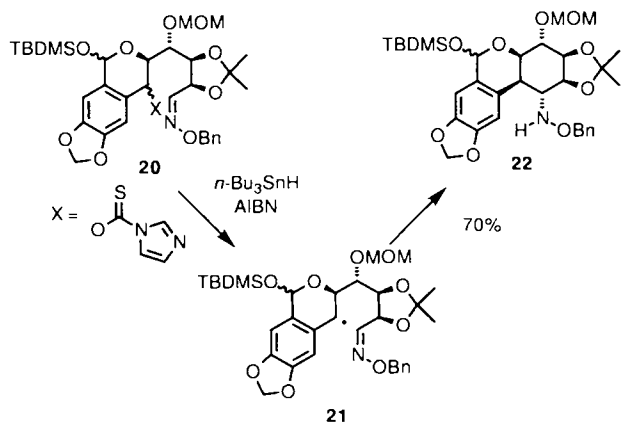

tated by the *tert*-butyldimethylsilyl (TBDMS) protected six-membered lactol ring. Compound **22** was then transformed in few standard steps into the target compound **19**.

J. A. Murphy et al.[5] were able to show the synthetic potential of radical reactions in a short and efficient synthesis of the ABCE ring system of aspidospermidine (**23**). They used a tandem radical cyclization to directly convert the aryl iodide **24** into the tetracycle **25**. The mechanism of this reaction sequence was rationalized as follows: A silyl radical produced from $(Me_3Si)_3SiH$ attacks the aryl iodide bond in **24** forming the aryl radical **26**. Intramolecular attack of the radical center in **26** on the double bond then affords the alkyl radical **27**. Lastly, addition of this alkyl radical to the azide function followed by loss of N_2 gives the observed product **25** via the N-radical intermediate **28**. The high stereoselectivity and the excellent yield of this tandem radical cyclization is noteworthy.

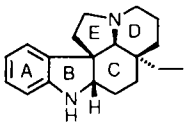

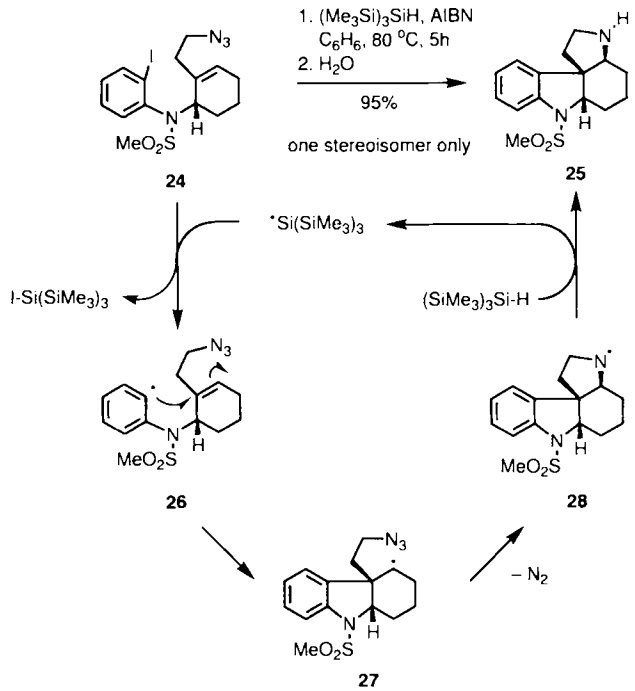

New perspectives are opened by the combination of radical reactions with organometallic chemistry, as was demonstrated recently by the group of H.-G. Schmalz at the TU in Berlin.[6] In the course of synthetic studies towards pseudopterosin A (**29**) and related compounds they succeeded in the SmI_2-induced cyclization of the arenetricarbonylchromium complex **30** to give the tricyclic pseudopterosin scaffold **31**. The authors propose the following mechanism for this reaction: In the first step the ketyl radical **32** is produced, which adds to the arene ring to give **33**. A second transfer of one electron by SmI_2 affords the anionic η^5 complex **34**. Subsequent protonation yields η^4 complex **35**, from which the final product **31** is obtained after elimination of methanol and hydrolytic workup. It should be noted that the pendant trisubstituted double bond does not lead to any side reactions.

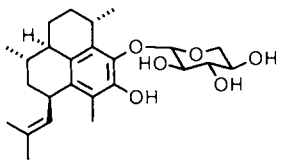

pseudopterosin A (**29**)

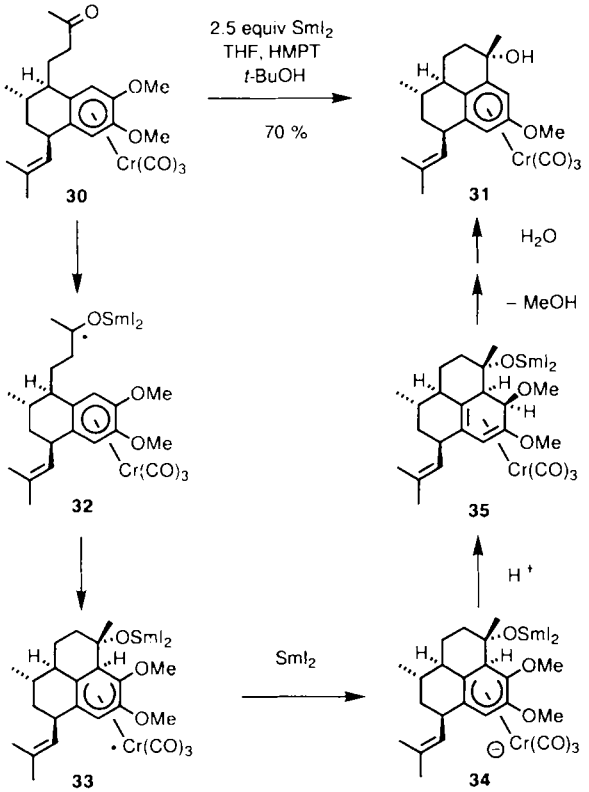

The present selection of natural product syntheses with radical reactions as key steps demonstrates the extraordinary potential applications of modern radical chemistry. However, one limitation is evident: four out of the five reaction sequences presented involved an intramolecular cyclization reaction.[10] Intermolecular radical bond formations with high yields and stereoselectivities are still very rare in the total synthesis of bioactive compounds. One exception is the camptothecin synthesis by Curran et al. However, progress in acyclic stereoselection of radical reactions[11] should soon help to formulate new solutions for these synthetic challenges.

German version: *Angew. Chem.* **1996**, *108*, 441–443

Keywords: natural products · radical reactions · tandem reactions · total syntheses

[1] a) B. Giese, *Radicals in Organic Synthesis: Formation of Carbon-Carbon Bonds*, Pergamon, Oxford, **1986**; b) D. P. Curran in *Comprehensive Organic Synthesis*, *Vol 4*. (Eds.: B. M. Trost, I. Fleming, M. F. Semmelhack), Pergamon, Oxford, **1991**, p. 779.
[2] E. Lee, C. M. Park, J. S. Yun, *J. Am. Chem. Soc.* **1995**, *117*, 8017.
[3] a) D. P. Curran, S.-B. Ko, H. Josien, *Angew. Chem.* **1995**, *107*, 2948; *Angew. Chem. Int. Ed. Engl.* **1995**, *34*, 2683; b) D. P. Curran, H. Liu, *J. Am. Chem. Soc.* **1992**, *114*, 5863.
[4] G. E. Keck, S. F. McHardy, J. A. Murry, *J. Am. Chem. Soc.* **1995**, *117*, 7289.
[5] M. Kizil, J. A. Murphy, *J. Chem. Soc. Chem. Commun.* **1995**, 1409.
[6] a) H.-G. Schmalz, S. Siegel, J. W. Bats, *Angew. Chem.* **1995**, *107*, 2597; *Angew. Chem. Int. Ed. Engl.* **1995**, *34*, 2383; b) I thank Prof. H.-G. Schmalz for personal communication of additional, still unpublished results.
[7] a) D. P. Curran, *J. Chin. Chem. Soc.* **1993**, *40*, 1; b) U. Koert, *Nachr. Chem. Tech. Lab.* **1995**, *43*, 686.
[8] L. F. Tietze, U. Beifuss, *Angew. Chem.* **1993**, *105*, 137; *Angew. Chem. Int. Ed. Engl.* **1993**, *32*, 131.
[9] a) G. R. Pettit, V. Gaddamidi, G. M. Cragg, *J. Nat. Prod.* **1984**, *47*, 1018; b) S. Ghosal, S. Singh, Y. Kumar, R. S. Srivastava, *Phytochemistry* **1989**, *28*, 611.
[10] D. P. Curran, J. Xu, E. Lazzarini, *J. Am. Chem. Soc.* **1995**, *117*, 6603.
[11] a) W. Smadja, *Synlett* **1994**, 1; b) W. Damm, J. Dickhaut, F. Wetterich, B. Giese, *Tetrahedron Lett.* **1993**, *34*, 431; c) N. A. Porter, B. Giese, D. P. Curran, *Acc. Chem. Res.* **1991**, *24*, 296; d) P. Renaud, M. Gerster, *J. Am. Chem. Soc.* **1995**, *117*, 6607.

Enantioselective Catalytic Hydrogenation

Judith Albrecht and Ulrich Nagel*

Enantioselective catalysis is one of the most important tools in asymmetric synthesis.[1, 2] With its assistence biologically active substances can be prepared in enantiomerically pure form—this purity can be a crucial factor with pharmaceutical products. In the field of crop protection the use of enantiomerically pure compounds provides irrefutable advantages for both economic and ecological reasons.[3, 4]

Enantioselective transition metal catalyzed hydrogenation has an important place among the methods of asymmetric synthesis. A large range of substrates can be enantioselectively hydrogenated in this way, which is extremely important for the preparation of natural and also nonnatural amino acids, because it enables the directed synthesis of all possible amino acid derivatives from the many prochiral enamides and ketones. Recently great progress has been made in this field. Very high *ee* values are achieved, and even sterically demanding substrates like β,β-disubstituted enamides are able to be hydrogenated in good optical yield.[5, 6]

Since the beginning of the 90's Burk et al. have been exploring the development of novel electron-rich phosphane ligands that give powerful catalysts for enantioselective hydrogenation on complexation with rhodium.[7] The ligands they use each contain two phospholanes *trans*-substituted in 2,5 position, whose

[*] Prof. Dr. U. Nagel, J. Albrecht
Institut für Anorganische Chemie der Universität
Auf der Morgenstelle 18, D-72076 Tübingen (Germany)
Fax: Int. code +(7071)29-2436
e-mail: ulrich.nagel@uni-tuebingen.de

phosphorus atoms are linked together through different groups as backbone. The carbon atoms adjacent to the phosphorus atoms are chiral and in these catalysts are situated in the immediate vicinity of the rhodium atoms (Scheme 1).

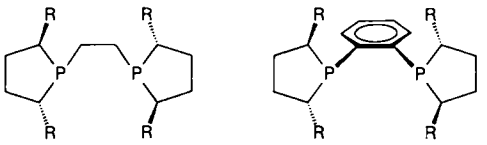

BPE DuPHOS

Scheme 1. The bisphospholane ligands BPE and DuPHOS; R = Me, Et, *n*Pr, *i*Pr (to give Me-, Et-, *n*Pr-, and *i*Pr-BPE or -DuPHOS).

Initially the phospholanes were synthesized by derivatization of homochiral 1,4-diols with mesyl chloride. The dimesylates were then transformed into the 2,5-disubstituted phenylphospholanes with dilithiumphenylphosphide. The phenyl group was cleaved with pure lithium metal, and the resulting lithium phosphide could then be converted into the bridged system with 1,2-dichloroethane, ethyleneglycoldi-*p*-tosylate, or 1,3-dichloropropane. The yields with this synthetic route were moderate and depended strongly on the purity of the lithium metal.[8]

A later optimized synthesis also starts from the 1,4-diols. They are then converted into cyclic sulfates with thionyl chloride on mediation of ruthenium chloride and sodium periodate. The sulfates are transformed with dilithiumbis(phosphido)-ethane into bis(phospholanyl)ethane ligands (BPE) or with dilithium-1,2-bis(phosphido)benzene into a bis(phospholanyl)-benzene (DuPHOS) ligand. Ring closure to form phospholanes is achieved by addition of *n*BuLi[9] (Scheme 2).

The differently substituted BPE and DuPHOS rhodium complexes were applied in the hydrogenation of *N*-acetyl enamines. Of the BPE ligands, the ethyl-substituted derivative gave the highest *ee* values (93% for methyl α-acetylaminocinnamate and 98% for methyl α-acetylaminoacrylate). Higher enantioselectivities were achieved with the DuPHOS ligands. Under optimized conditions some systems afforded *ee* values of over 99%. In particular the sterically demanding *n*Pr-DuPHOS gave *ee* values of 99.8% (enantiomer ratio 1000:1).

In all enantioselective hydrogenations the ability of the substrate to form a chelate ring with the catalyst is extremely important. For this reason the enantioselective reductive amination of ketones is always particularly difficult, because these compounds usually do not have a structure suitable for the required chelation. Burk et al. circumvent this problem by reversible derivatization. The ketones are converted into *N*-acetylhydrazones, whose structures resemble those of enamides.[10] The C–N double bond can then be hydrogenated by *n*Pr-DuPHOS–rhodium with *ee* values almost as high as those for C–C double bonds of enamines. The *N*-acetylhydrazines obtained thus can either be transformed into the free hydrazines by acid hydrolysis or into amines by treatment with samarium diiodide. In this way a large number of ketones can be reductively aminated.[11]

To hydrogenate prochiral ketones to the corresponding chiral alcohols, Noyori et al. have developed ternary catalyst systems from $[RuCl_2(binap)(dmf)_n]$, a chiral diamine, and KOH.[12, 13] By this route methyl(1-naphthyl)ketone can be hydrogenated to 1-(1-naphthyl)ethanol with $[RuCl_2(binap)(dmf)_n]$, 1,2-diphenylethyldiamine, and KOH in the ratio 1:1:2 in 2-propanol (substrate:catalyst = 500:1, 4 bar H_2, 28 °C, 6 h) in greater than 99% yield with 97% *ee*.

Other sources of hydrogen can be used instead of elemental hydrogen gas. In transfer hydrogenations a secondary alcohol has been employed as hydrogen donor. Noyori et al. have also made advances in this field. They use a catalyst system from $[RuCl_2(\eta^6\text{-mesitylene})]_2$, *N*-(*p*-toluenesulfonyl)-1,2-diphenylethylenediamine, and KOH in 2-propanol. At room temperature acetophenone can be reduced in 15 h with this complex prepared in situ (substrate:catalyst = 200:1) to 1-phenylethanol in 95% yield with an optical purity of 97%.[14] Catalyst systems with a β-amino alcohol as auxiliary are faster, as shown by the reduction of acetophenone to 1-phenylethanol under otherwise identical conditions with $[RuCl_2(\eta^6\text{-hexamethylbenzene})]_2$, 2-methylamino-1,2-diphenylethanol, and KOH within as little as 1 h in 94% yield and 92% *ee* (Scheme 3).[15]

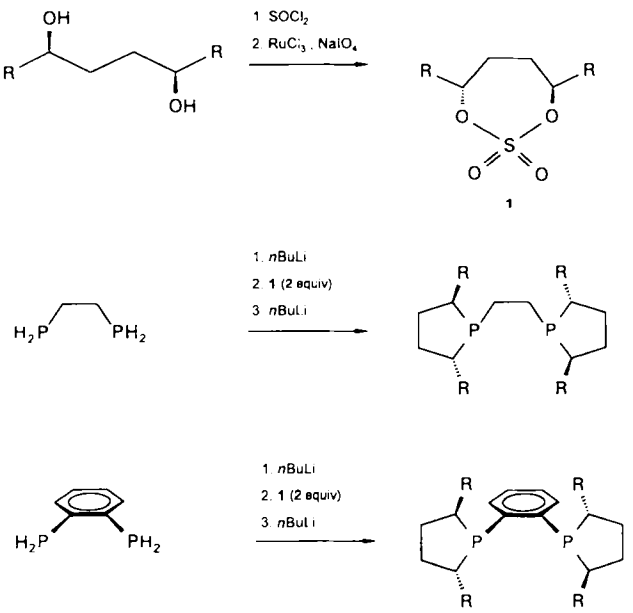

Scheme 2. Synthesis of BPE and DuPHOS ligands.

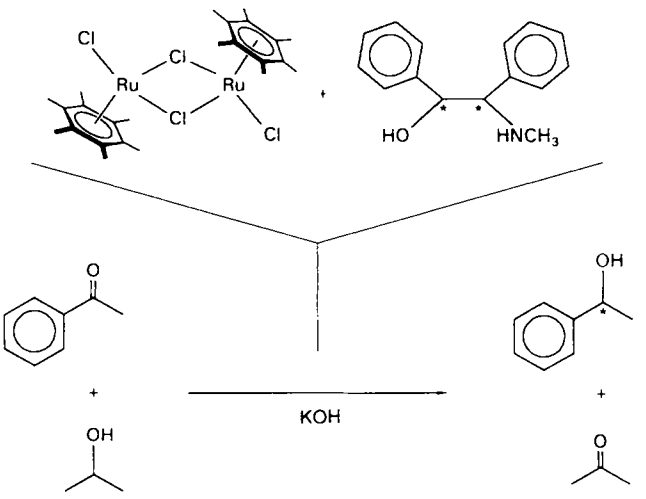

Scheme 3. Transfer hydrogenation of acetophenone.

The *N*-acetylhydrazones used by Burk et al. are ketone derivatives, and their structures therefore correspond to those of the β,β-disubstituted *N*-acetylaminoacrylic acids. This and the finding that both the (*E*)- and the (*Z*)-enamides are hydrogenated with almost the same enantioselectivity by the BPE and DuPHOS complexes prompted them to investigate the ability of the phospholane ligands to enantioselectively hydrogenate β,β-disubstituted *N*-acetylaminoacrylic acids.[5]

Attempts to use the ligands Et-, *n*Pr-, and *i*Pr-DuPHOS, which were most successful for the *N*-acetyl enamines, gave unsatisfactory results: the *ee* values were 74, 45, and 14%, respectively. In supercritical CO_2 as solvent[16] they improved to 90%. The use of supercritical CO_2, however, puts a greater demand on the hydrogenation apparatus than conventional conditions, since it must be able to withstand high pressures. The temperature must also be precisely controlled, because in supercricital systems merely a small temperature difference can lead to enormous effects.

The *trans* chelate ligands developed by Ito et al. are also used for enantioselective hydrogenation of β,β-disubstituted *N*-acetylaminoacrylic acids.[6] These ligands fall into the class of TRAP ligands (Scheme 4, TRAP = 2,2″-bis[1-(dialkylphosphanyl)-ethyl]-1,1″-biferrocene), with which good *ee* values are achieved. Methyl α-*N*-acetylamino-β,β-dimethylacrylate can be hydrogenated with Bu-TRAP at a catalyst:substrate ratio of 1:1000 in 24 h (15 °C, 1 bar H_2) to form the corresponding propane carboxylic acid in 88% *ee*.

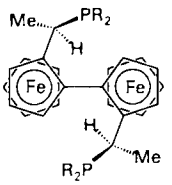

Scheme 4. Ito's TRAP ligand.

Further progress in the hydrogenation of β,β-disubstituted *N*-acetyl enamines was made with the sterically less hindered Me-DuPHOS–rhodium catalyst. In this system an *ee* value of 92% was obtained.[5]

The best enantioselectivities till now have been reached with the Me-BPE ligand. With this ligand a large variety of β,β-disubstituted *N*-acetyl enamines were hydrogenated with very high *ee* values of over 99% in some cases. For a catalyst:substrate ratio of 1:500 under mild conditions (25 °C, 6 bar H_2) β-methyl- and β-ethylphenylalanine derivatives could be prepared from the corresponding β,β-disubstituted *N*-acetylaminoacrylates in 12–24 hours with optical yields of 99.4 and 99%, respectively.

The Pr-DuPHOS ligand is one of the best ligands for the hydrogenation of sterically less congested substrates, whereas for the sterically more demanding β,β-disubstituted compounds the ligand Me-BPE is the better choice. The astoundingly different behavior of derivatives of these catalysts is hard to predict, yet because of the opportunities for variation in the synthesis of the bisphospholanes, the broadest possible tailoring of the ligands to a problem at hand is assured.

An old but graphic picture to explain the enantioselectivities with different ligands is that of the blocked quadrants[17] (Scheme 5). The rigid benzene ring in the backbone of the

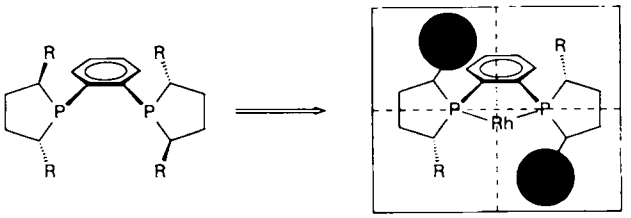

Scheme 5. Blocked quadrants.

DuPHOS ligands blocks two diagonally oriented quadrants at the metal atom through the substituents on the phospholane ring. The bulkier the substituent and the more rigidly it is held in its position, the better the quadrants are blocked. For most of the sterically less hindered substrates like β-monosubstituted acetylaminoacrylic acids the optimum is reached with the *n*Pr-DuPHOS ligand. The ligand in the catalyst may not be so bulky that the binding of the substrate is overly restricted. Thus the *ee* values for hydrogenations with the bulkier *i*Pr-DuPHOS–rhodium catalyst decrease.[9]

In the case of the tetrasubstituted acrylic acids the rigid DuPHOS ligands block both diagonally oriented quadrants so severly that the larger space requirements of these substrates cannot be accommodated. Here the more flexible Me-BPE ligand with its smaller methyl groups performs better.

German version: *Angew. Chem.* **1996**, *108*, 444–446

Keywords: asymmetric syntheses · enamides · hydrogenations · phosphane ligands · supercritical phases

[1] R. Noyori, *Asymmetric Catalysis in Organic Synthesis*, Wiley, New York, **1994**.
[2] *Catalytic Asymmetric Synthesis* (Ed.: I. Ojima), VCH, Weinheim, **1993**.
[3] W. A. Nugent, T. V. RajanBabu, M. J. Burk, *Science* **1993**, *259*, 479–483.
[4] G. M. Ramos Tombo, D. Belluš, *Angew. Chem.* **1991**, *103*, 1219–1241; *Angew. Chem. Int. Ed. Engl.* **1991**, *30*, 1193–1215.
[5] M. J. Burk, M. F. Cross, J. P. Martinez, *J. Am. Chem. Soc.* **1995**, *117*, 9375–9376.
[6] M. Sawamura, R. Kuwano, Y. Ito, *J. Am. Chem. Soc.* **1995**, *117*, 9602–9603.
[7] M. J. Burk, J. E. Feaster, R. L. Harlow, *Organometallics* **1990**, *9*, 2653–2655.
[8] M. J. Burk, J. E. Feaster, R. L. Harlow, *Tetrahedron: Asymmetry* **1991**, *2*, 569–592.
[9] M. J. Burk, J. E. Feaster, W. A. Nugent, R. L. Harlow, *J. Am. Chem. Soc.* **1993**, *115*, 10125–10138.
[10] M. J. Burk, J. E. Feaster, *J. Am. Chem. Soc.* **1992**, *114*, 6266–6267.
[11] M. J. Burk, J. P. Martinez, J. E. Feaster, N. Cosford, *Tetrahedron* **1994**, *50*, 4399–4428.
[12] T. Ohkuma, H. Ooka, S. Hashiguchi, T. Ikariya, R. Noyori, *J. Am. Chem. Soc.* **1995**, *117*, 2675–2676.
[13] T. Ohkuma, H. Ooka, S. Hashiguchi, T. Ikariya, R. Noyori, *J. Am. Chem. Soc.* **1995**, *117*, 10417–10418.
[14] S. Hashiguchi, A. Fujii, J. Takehara, T. Ikariya, R. Noyori, *J. Am. Chem. Soc.* **1995**, *117*, 7562–7563.
[15] J. Takehara, S. Hashiguchi, A. Fujii, S. Inoue, T. Ikariya, R. Noyori, *J. Chem. Soc. Chem. Commun.*, im Druck.
[16] M. J. Burk, S. Feng, M. F. Cross, W. Tumas, *J. Am. Chem. Soc.* **1995**, *117*, 8277–8278.
[17] W. S. Knowles, *Acc. Chem. Res.* **1983**, *16*, 106.

 © VCH Verlagsgesellschaft mbH, D-69451 Weinheim, 1996 0570-0833/96/3504-0409 $ 15.00+.25/0

Synthesis of Highly Substituted Cyclopentane and Tetrahydrofuran Derivatives by Crossed Olefin Metathesis**

Matthias F. Schneider and Siegfried Blechert*

The metathesis of olefins, a reaction which has been known for many years, is the metal-catalyzed exchange of the alkylidene groups of two olefins.[1] This synthetically very interesting reaction has very often been employed in the past in ring-opening metathesis polymerization (ROMP).[2] More recently, many reports have been published about the use of ring-closing metathesis (RCM) for the synthesis of carbo- and heterocycles (Scheme 1).[3] The mechanism of such C–C coupling proceeds by [2+2]-cycloadditions and reversions of metal-alkylidene complexes.[4] With the discovery of novel catalysts[5] capable of tolerating a wider range of functional groups, olefin metathesis is becoming increasingly important.

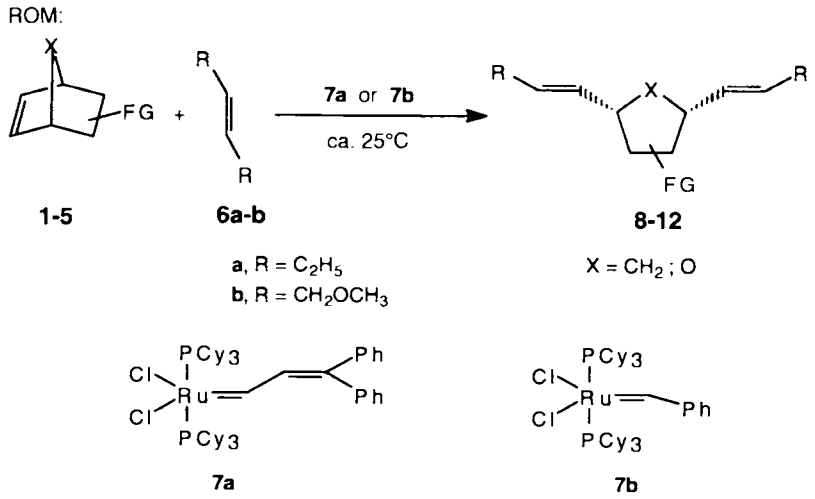

Scheme 2. Crossed olefin metathesis. Top: synthesis of **8**–**12** from **1**–**5** and **6a,b**. FG = functional group. For conditions and results, see Table 1. Bottom: ruthenium catalysts used. Cy = cyclohexyl.

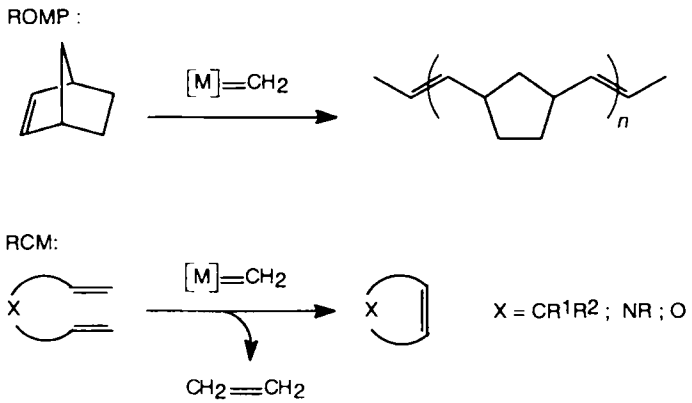

Scheme 1. Ring-opening methathesis polymerization (ROMP) and ring-closing methasis (RCM) with metal complex catalysts. [M] = metal complex fragment.

Mixed olefin metatheses, in which two different olefins are employed in a bimolecular C–C bond forming reaction, appears particularly exciting to us. We wanted to trap the intermediate from a ring-opening with a second alkene. In this way the production of monomers would be possible.

A crossed metathesis was recently described which involved the reaction of cyclobutene derivatives with monosubstituted alkenes.[6] With symmetrical olefins the reaction led exclusively to polymers. We now wish to report the successful crossed ring-opening metatheses (ROM) of functionalized bicycles with symmetrical olefins (Scheme 2).[7]

[*] Prof. Dr. S. Blechert, Dipl.-Chem. M. F. Schneider
Institut für Organische Chemie der Technischen Universität
Strasse des 17. Juni, D-10623 Berlin (Germany)
Fax: Int. +30 31423619
e-mail: sibl@wap0105.chem.tu-berlin.de

[**] This work was funded by the Fonds der Chemischen Industrie.

We utilized the ring strain of norbornene derivatives as the driving force for the ring opening. To avoid polymerization we carried out the reactions in dilute solution (max. 0.1 M) and with a tenfold excess of *trans*-3-hexene (**6a**). The ruthenium complex **7a**[8] was used as catalyst. The course of the reactions was followed by gas chromatography. The results are listed in Table 1.

The yields are high, with the exception of **11**. Because of the relatively high volatility of **8a**, **9**, and **10**, yields were determined by gas chromatography with octadecane as internal standard. The conversion of the crude products into less volatile substances led to similar yields (for example, the conversion of **9** into the diol with $LiAlH_4$ and subsequent workup: 94% over two steps). The lower yield obtained from the ring-opening of the β-lactam **4** is apparently due to the competitive formation of oligomers detectable with ^1H NMR spectroscopy and mass spectrometry. In this case the polymerization cannot be avoided by use of higher dilution. As expected, the double bond in the newly formed olefins does not always have the same conformation. Mixtures of all-*trans* and *cis*-*trans* products are formed. In every case, the major product is the all-*trans* compound. In the case of **11a** a small amount of the all-*cis* olefin was also detected.

After the successful reaction with *trans*-3-hexene (**6a**), we investigated reactions with the diacetate of *cis*-2-butene-1,4-diol. The desired reactions did not take place with this substrate. Consistent with other experiments we have carried out, the catalyst **7a** apparently does not tolerate allylic acetates or carbonates. However, reactions with *trans*-1,4-dimethoxy-2-butene (**6b**) were successful, as shown by examples with **8b** and **12b**.

These ring openings are not restricted solely to norbornene derivatives. The Diels-Alder adduct **5**, readily accessible from furan, can be used in crossed olefin metathesis, yielding products in high yield (see Table 1, **12a,b**).

The reactions described above proceed by cycloadditions and cycloreversions. The conformation of the olefin should therefore influence the course of the reaction. The use of *cis*-3-hexene

Table 1. Results of the ring-opening metatheses of the norbornene and 7-oxanorbornene derivatives **1**–**5** with the trapping reagents **6a**–**c**.

Starting material	Product	Yield [%]	Conditions	*E,E*:*E,Z*-isomer ratio
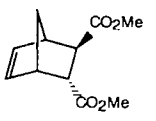 **1**	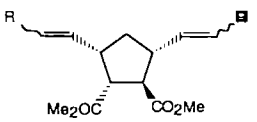 **8a**: R = C_2H_5; **8b**: R = CH_2OCH_3	**8a**: 91 [b]	2 mol% **7a**; 19 h	4.5
		94 [b, c]	2 mol% **7a**; 5 h	3.5
		75 [b, d]	6 mol% **7b**; 13 h	5
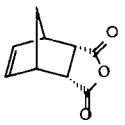 **2**	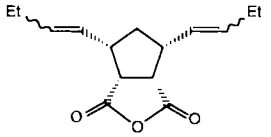 **9**	**8b**: 68 [a]	2 mol% **7a**; 9 h	1.5
		94 [a]	6 mol% **7a**; 4 d	2
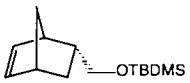 **3**	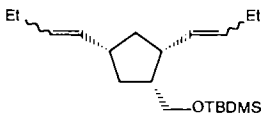 **10**	85 [a]	2 mol% **7a**; 14 h	2
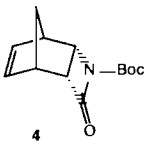 **4**	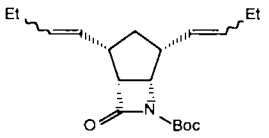 **11**	34 [b]	4 mol% **7a**; 20 h	1.5
		73 [b]	8 mol% **7b**; 3 h	1.5
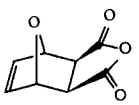 **5**	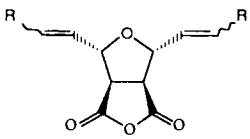 **12a**: R = C_2H_5; **12b**: R = CH_2OCH_3	**12a**: 98 [b]	2 mol% **7a**; 2 h	3.5
		12b: 89 [b, e]	2 mol% **7a**; 15 h	

[a] Benzene. [b] CH_2Cl_2. [c] 10 equiv *cis*-3-hexene **6c**. [d] 1.5 equiv *cis*-3-hexene **6c**. Isomer ratio cannot be determined unequivocally. BOC = *tert*-butoxycarbonyl. TBDMS = *tert*-butyldimethylsilyl.

6c provided confirmation of this supposition. The reaction with **1**, under otherwise identical conditions as those described for **6a**, proceeded significantly more rapidly. After 3 h the conversion of **1** was essentially complete. The maximum yield was achieved after 5 h. In contrast, the required reaction time for **6a** was 19 h. The isomer ratio was essentially unchanged by the use of *cis*-3-hexene **6c**.

By capitalizing on the higher rate of reaction of **6c** and by use of the new ruthenium catalyst **7b**[5] we could also almost totally suppress the competing oligomerization found in the ring opening of the β-lactam **4**. Thus, the yield could be more than doubled to 73%.

The use of a smaller excess of the trapping olefin is desirable for worthwhile preparative use of ring opening metathesis. This was possible with a revised experimental methodology. The catalyst **7b** and only 1.5 equivalents of **6c** were added to CH_2Cl_2. Bicycle **1**, dissolved in CH_2Cl_2, was then slowly added over 4 h. The yield of 75% thus achieved is acceptable.

A mechanism for crossed olefin metathesis appears plausible in which the ring opening proceeds via a carbene complex of the acyclic olefin. A subsequent reaction of the cyclopentyl-substituted carbene complexes with the trapping olefin should lead to product and to renewed formation of the catalytically active carbene complex.

Bicycles **1**–**5** containing diverse substituents, many of which are enantiomerically pure, are easily accessible. The process described should therefore offer attractive possibilities for the preparation of highly substituted five membered rings.

Experimental Procedure

A typical procedure for ring opening metathesis can be illustrated with **8a**: All metatheses are carried out under an atmosphere of argon. Benzene or dichloromethane can be used as solvent. Ruthenium catalyst **7a** (5.2 mg, 5.6 μmol, 2 mol%) are dissolved in CH_2Cl_2 (2 mL). *trans*-3-Hexene **6a** (240 mg, 2.8 mmol) dissolved in CH_2Cl_2 (1 mL), and **1** (60 mg, 0.28 mmol) dissolved in CH_2Cl_2 (3 mL) were then added. The resulting mixture is allowed to stir at room temperature for 19 h. The reaction can be monitorred by gas chromatography. After complete conversion the solvent is removed under reduced pressure.

The crude product is purified by column chromatography (Kieselgel, Et_2O:isopentane = 1:9). Compound **8a** (70 mg, 0.238 mmol, 85%) is obtained as a colorless oil.

Variation of the metathesis with 1.5 equivalents of trapping reagent: ruthenium catalyst **7b** (14 mg, 16.6 μmol, 6 mol%) and **6c** (34 mg, 0.42 mmol) are dissolved in CH_2Cl_2 (6 mL). A solution of 58 mg (0.276 mmol) **1** in 12 mL CH_2Cl_2 is added to this solution over a period of 4 h by syringe pump, and the mixture is stirred for 13 h at room temperature. Yield: 75%.

All new compounds have been unequivocally characterized by spectroscopy. The structural determination was accomplished by two dimensional NMR spectroscopy and by NOE experiments. Spectroscopic data for (*E,E*)-**8a**: ^{1}H NMR (400 MHz, $CDCl_3$): δ = 5.51 (2H, dt, J = 15, 6 Hz), 5.40 (1H, ddt, J = 15, 7.5, 1 Hz), 5.22 (1H, ddt, J = 15, 8.5, 1 Hz), 3.65 (3H, s), 3.61 (3H, s), 3.25 (1H, dd, J = 10, 8.5 Hz), 3.04–2.91 (1H, m), 2.99 (1H, dd, J = 10.5, 8.5 Hz), 2.67 (1H, ddt, J = 10.5, 10.5, 7.5 Hz), 1.99 (4H, dq, J = 7.5, 6 Hz), 1.56–1.40 (1H, m), 0.95 (3H, t, J = 7.5 Hz), 0.92 (3H, t, J = 7.5 Hz); ^{13}C NMR (50.32 MHz, $CDCl_3$): δ = 174.7 (C), 173.4 (C), 133.9 (CH), 133.0 (CH), 129.9 (CH), 128.1 (CH), 52.3 (CH_3), 52.0 (CH), 51.7 (CH_3), 51.3 (CH_3), 47.1 (CH), 44.4 (CH), 39.2 (CH_2), 25.3 (CH_2), 13.7 (CH_3); IR (CCl_4): $\tilde{\nu}$ = 2964, 1736, 1436, 1199, 1169, 969 cm^{-1}. MS: *m/z* (%): 294 (6) [M^+], 262 (63), 234 (90), 205 (43), 192 (44), 175 (100), 153 (22), 145 (20), 133 (18), 119 (21), 109 (19), 91 (27), 79 (26), 67 (20), 55 (41); high-resolution MS: calcd for $C_{17}H_{26}O_4$ [M^+]: 294.1831, found: 294.1831.

Received: November 2, 1995 [Z 8519 IE]
German version: *Angew. Chem.* **1996**, *108*, 479–481

Keywords: catalysis · cyclopentanes · olefin metathesis · tetrahydrofurans

[1] a) R. H. Grubbs, S. H. Pine in *Comprehensive Organic Synthesis, Vol. 5* (Eds.: B. M. Trost, I. Fleming, L. A. Paquette), Pergamon, New York, **1991**, Chap. 9.3; b) R. R. Schrock, *The Strem Chemiker, Vol. XIV*, Strem Chemicals, Newburgport, **1992**, No. 1, p. 1–6.

[2] a) B. M. Novak, R. H. Grubbs, *J. Am. Chem. Soc.* **1988**, *110*, 960; b) R. H. Grubbs, W. Tumas, *Science* **1989**, *243*, 907–915; c) S. T. Nguyen, L. K. Johnson, R. H. Grubbs, *J. Am. Chem. Soc.* **1992**, *114*, 3974; d) D. J. Brunelle, *Ring-Opening Polymerization, Mechanism, Catalysis, Structure, Utility*, Hanser, München, **1993**.

[3] a) H.-G. Schmalz, *Angew. Chem.* **1995**, *107*, 1981–1984; *Angew. Chem. Int. Ed. Engl.* **1995**, *34*, 1833–1836; b) U. Koert, *Nachr. Chem. Tech. Lab.* **195**, *43*, 809.

[4] a) J. L. Hérisson, Y. Chauvin, *Makromol. Chem.* **1970**, *141*, 161; b) J. P. Collman, L. S. Hegedus, J. R. Norton, R. G. Finke, *Principles and Applications of Organotransition Metall Chemistry*, University Science Books, Mill Valley, **1987**, pp. 475–485.

[5] P. Schwab, M. B. France, J. W. Ziller, R. H. Grubbs, *Angew. Chem.* **1995**, *107*, 2179–2181; *Angew. Chem. Int. Ed. Engl.* **1995**, *34*, 2039–2041.

[6] M. L. Randell, J. A. Tallarico, M. L. Snapper, *J. Am. Chem. Soc.* **1995**, *117*, 9610–9611.

[7] M. F. Schneider, S. Blechert, lecture at the workshop of the Sonderforschungsbereichs 260 „Metallorganische Verbindungen", Marburg, **1995**.

[8] G. C. Fu, S. T. Nguyen, R. H. Grubbs, *J. Am. Chem. Soc.* **1993**, *115*, 9856; b) S. T. Nguyen, R. H. Grubbs, *ibid.* **1993**, *115*, 9858.

A Versatile New Preparation of Cyclopropylamines from Acid Dialkylamides**

Vladimir Chaplinski and Armin de Meijere*

Dedicated to Professor Herbert W. Roesky on the occasion of his 60th birthday

Not only has the cyclopropane ring established its role as a particular functional group[1] and as a part of valuable "composite functionalities"[2] in organic synthesis; it has also become indispensable as a skeleton or substituent in a variety of biologically active compounds.[3] Among the most important precursors for such compounds are cyclopropylamine and substituted cyclopropylamines, yet only a few methods exist for their preparation.[4] Our completely different approach to aminocyclopropanes from acid dialkylamides, which appears to have a wide potential, complements existing methodology and substantially broadens the range of easily accessible derivatives.

The facile preparation of cyclopropanols from alkyl carboxylates and ethylmagnesium bromide (EtMgBr) in the presence of titanium tetra(2-propanolate)[5] [Ti(O*i*Pr)$_4$] was the force behind the idea to transform carboxylic acid dialkylamides **1** to cyclopropylamines in an analogous way. Indeed, when *N*,*N*-dimethylacetamide was treated analogously to an ester[5b] with 2.1 equivalents of EtMgBr in the presence of 0.2 equivalents of Ti(O*i*Pr)$_4$, and the reaction mixture worked up appropriately, 1-dimethylamino-1-methylcyclopropane (**3a**) was obtained, but in poor yield ($\leq 30\%$).

The yield was significantly improved when a stoichiometric amount (1 equivalent with respect to **1**) of Ti(O*i*Pr)$_4$ was employed (Scheme 1 and entry 1 in Table 1). The method is equally

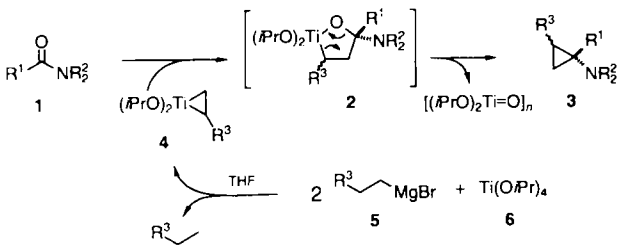

Scheme 1. Synthesis of cyclopropylamines. For conditions and further details see Table 1.

applicable to acid *N*,*N*-dibenzylamides, but at elevated temperature[6] yields 1-alkyl-1-dibenzylaminocyclopropanes **3b–d** (entries 2–4), from which primary cyclopropylamines can be obtained by catalytic hydrogeneration.[7] Higher homologues of alkylmagnesium bromides give 1,2-dialkylsubstituted cyclopropylamines **3e–h** in moderate yields (35–51%, entries 5–8).

This demonstrates that the titanacyclopropane **4**, which is assumed to form by β-hydride elimination from a dialkyloxo-di(propan-2-olato)titanium intermediate initially formed from two equivalents of alkylmagnesium bromide **5** and titanium tetra(2-propanolate) **6**,[5,9] can add across the C=O double bond of an acid amide to give an amino-substituted titanaoxacyclopentane (**2**). Because of the oxophilicity of titanium and the poor leaving characteristics of the dialkylamino group, this intermediate apparently cycloreverts, probably aided by the attack of the donor solvent THF on titanium, to yield the aminocyclopropane **3** and an oligomeric titanium species, which is eventually solvolyzed to TiO_2. This must be the reason why yields of **3** drop drastically when substoichiometric amounts of Ti(O*i*Pr)$_4$ are employed.

It is remarkable that the titanacyclopropane **4** readily attacks the weakly electrophilic carbonyl group of an *N*,*N*-dialkyl-

Table 1. Substituted and unsubstituted *N*,*N*-dialkylaminocyclopropanes **3** [8] from carboxylic acid *N*,*N*-dialkylamides **1**, alkylmagnesium bromides **5**, and titanium(IV) tetra(2-propanolate) **6**.

Entry	Starting Material 1	5	Conditions [a]	Product 3		Yield [%][b]
1			A, 5 h		**3a**	56
2			B, 10 h		**3b**	60
3			B, 24 h		**3c**	63
4			B, 24 h		**3d**	52
5			B, 24 h		**3e**	50[c]
6			B, 24 h		**3f**	51[c]
7			B, 24 h		**3g**	38[c]
8			B, 24 h		**3h**	35[c]
9			C 5 h		**3i**	73
10			C, 10 h	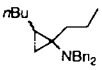	**3j**	74[c]
11			C, 10 h		**3k**	74[c]
12			C, 10 h		**3l**	69[c]
13			D 3 d		**3m**	76[c]
14			E 10 d		**3n**	20
15			B, 24 h		**3o**	63[c]
				cis/*trans* 1:1		
16			B, 24 h		**3p**	52[c]
				cis/*trans* 1:2.3		

[a] A: To 2.5 equiv of RMgBr in THF was added at -78 °C 1 equiv of Ti(O*i*Pr)$_4$ in THF, then 1 equiv of an acid *N*,*N*-dialkylamide **1** in THF. The mixture was warmed to 20 °C and stirred for the given time. B: Same as A, except that the reaction mixture was finally heated under reflux for the given time. C: At $+20$ °C EtMgBr in Et$_2$O (2.5 equiv) was added within 20 s to 1 equiv of *N*,*N*-dialkylformamide and 1.1 equiv of Ti(O*i*Pr)$_4$ in THF. The mixture was warmed to 45 °C and stirred at $+20$ °C for the given time. D: Same as A, except that 6 equiv of RMgBr and 3 equiv of Ti(O*i*Pr)$_4$ were used. E: Same as D, except that the reaction mixture was finally heated under reflux for the given time. [b] Isolated as the hydrochloride, unless otherwise stated. [c] Isolated as the free amine by column chromatography.

[*] Prof. Dr. A. de Meijere, Dipl.-Chem. V. Chaplinski
Institut für Organische Chemie der Universität
Tammannstrasse 2, D-37077 Göttingen (Germany)
Fax: Int. +551 39 94 75
e-mail: ameijer1@gwdg.de

[**] Cyclopropyl Building Blocks for Organic Synthesis. Part 33. This work was supported by the Deutsche Forschungsgemeinschaft, the Fonds der Chemischen Industrie, and by the companies BASF, Bayer, Degussa, and Hüls AG (chemicals). V. C. is indebted to the Gottlieb-Daimler- und Carl-Benz-Stiftung for a graduate fellowship. The authors are grateful to Dr. B. Knieriem for his careful reading of the manuscript. Part 32: S. Bräse, A. de Meijere, *Angew. Chem.* **1995**, *107*, 2741; *Angew. Chem. Int. Ed. Engl.* **1995**, *34*, 2545.

amide.[10] That accepted, however, it is not surprising that *N,N*-dialkylformamides react more rapidly than higher acid amides. The procedure can be drastically simplified for formamides (entries 9–12 in Table 1) and yet gives better yields (69–74%). Although with two bulky isopropyl groups the reaction required heating under reflux for 3 days, the sterically congested cyclopropyldiisopropylamine **3m** was obtained from diisopropylformamide[11] in 76% yield, and even *N,N*-di-*tert*-butylformamide,[12] when treated with a threefold excess of the reagent at elevated temperatures for an extended time, gave cyclopropyldi-*tert*-butylamine (**3n**), the most highly congested tertiary amine known to date,[13] albeit in low yield. A competition experiment disclosed that the cyclopropanation of dibenzylformamide proceeds more rapidly than that of *tert*-butyl acetate. Dialkylformamides can also be cyclopropanated with reagents generated from β-substituted ethylmagnesium bromides and $Ti(OiPr)_4$, but the 2-alkyl-1-dialkylaminocyclopropanes **3o, p** are obtained with no or low diastereoselectivity only (entries 15, 16 in Table 1).

Experimental Procedure

General procedure for the cyclopropanation of acid *N,N*-dialkylamides: To a suspension of the alkylmagnesium bromide (50 mmol, 25% excess) in THF (200 mL, cooled to −78 °C) was added $Ti(OiPr)_4$ (20 mmol in 10 mL of THF) under nitrogen through a steel cannula. After the mixture had been stirred for 2 min, the dialkylamide (20 mmol in 10 mL of THF) was added, and the mixture allowed to warm to 20 °C. It was stirred for an additional 3 h before volatile amines (with boiling points close to that of THF and isopropyl alcohol together with THF were distilled from the reaction mixture, without adding water, under reduced pressure (100 Torr) into a cold trap (−78 °C). Addition of a solution of hydrogen chloride in ether precipitated the hydrochloride of the cyclopropylamine. The crystals were collected and recrystallized from $CHCl_3/Et_2O$.

Amines with higher boiling points (containing one or two benzyl, isopropyl, or cyclopropyl groups in addition to the newly formed cyclopropane ring) were isolated by first adding saturated ammonium chloride solution (150 mL) and water (50 mL), then filtering the solution to remove the any precipitate that may have formed, and extracting it with ether (3 × 50 mL) after the solution had been made basic (pH > 11) with 15% sodium hydroxide solution. The combined ethereal extracts were washed with saturated sodium chloride solution, dried over $MgSO_4$ or K_2CO_3, and concentrated under reduced pressure (amines with C_8–C_{11} were first converted into nonvolatile salts with hydrogen chloride solution). Large amounts were purified by distillation.

Simplified procedure for the transformation of dialkylformamides: To a solution of dialkylformamide (5 mmol) in THF (30 mL) was added $Ti(OiPr)_4$ (5.5 mmol) and then at ambient temperature within 20 s a 2.85 M ethylmagnesium bromide solution in ether (12.5 mmol, 4.4 mL). On warming to 45 °C the mixture turned black, and ethane was evolved. After the mixture had been stirred for an additional 10 h, it was treated with 15 mL of saturated ammonium chloride solution, filtered if necessary to remove precipitated TiO_2, and the filtrate extracted with ether (3 × 20 mL). The combined ethereal extracts were washed with 20 mL of sodium chloride solution, dried over K_2CO_3, and concentrated.

Received: June 30, 1995 [Z 8147 IE]
Publication delayed at authors' request
German version: *Angew. Chem.* **1996**, *108*, 491–492

Keywords: amides · amines · cyclopropanes · titanium compounds

[1] a) *Small Ring Compounds in Organic Synthesis I–IV (Top. Curr. Chem.)* **1986**, *133*; **1987**, *135*, **1988**, *144*, **1990**, *155*; **1996**, *178*; b) H.-U. Reissig in *The Chemistry of the Cyclopropyl Group* (Ed.: Z. Rappoport), Wiley, Chichester, **1987**, p. 375; c) H. N. C. Wong, M.-Y. Hon, C.-W. Tse, Y.-C. Yip, J. Tanko, T. Hudlicky, *Chem. Rev.* **1989**, *89*, 165; d) J. Salaün, *ibid.* **1989**, *89*, 1247.

[2] B. M. Trost in *Strain and its Implications in Organic Chemistry (NATO ASI Ser. Ser. C)* **1989**, *273*.

[3] a) Probably the most abundant cyclopropyl compound in nature is aminocyclopropane carboxylic acid (ACC): H.-W. Liu, C. T. Walsh in *The Chemistry of the Cyclopropyl Group* (Ed.: Z. Rappoport), Wiley, Chichester, **1987**, p. 1010ff.; b) the modern broad-spectrum antibiotic "ciprofloxacin" from Bayer contains a cyclopropyl substituent on a nitrogen: *Pharmakologie und Toxikologie* (Eds.: W. Forth, D. Henschler, W. Rummel, K. Starke), Wissenschaftsverlag, Mannheim, **1993**, p. 655ff.; c) a more recent example is the natural peptide lactone "hormaomycin" containing two (2′-nitrocyclopropyl)alanine moieties: N. Andres, H. Wolf, H. Zähner, E. Rössner, A. Zeeck, W. A. König, V. Sinnwell, *Helv. Chim. Acta* **1989**, *72*, 426.

[4] Cf. a) D. Wendisch, *Houben-Weyl, Methoden der Organischen Chemie, 4th ed., Vol. IV/3* (Ed.: E. Müller), Thieme, Stuttgart, **1971**, b) *The Chemistry of the Cyclopropyl Group* (Ed.: Z. Rappoport), Wiley, Chichester, **1987**; *Houben-Weyl, Methoden der Organischen Chemie, 4th ed., Vol. E 19b* (Ed.: M. Regitz), Thieme, Stuttgart, **1989**.

[5] This fascinating reaction was first reported only a few years ago: a) O. G. Kulinkovich, S. V. Sviridov, D. A. Vasilevskii, T. S. Prityts kaya, *Zh. Org. Khim.* **1989**, *25*, 2245; *J. Org. Chem. USSR (Engl. Transl.)* **1990**, *25*, 2027; b) O. G. Kulinkovich, S. V. Sviridov, D. A. Vasilevskii, *Synthesis* **1991**, 234; c) O. G. Kulinkovich, D. A. Vasilevskii, A. I. Savchenko, S. V. Sviridov, *Zh. Org. Khim.* **1991**, *27*, 1428; *J. Org. Chem. USSR (Engl. Transl.)* **1992**, *27*, 1249; it has been applied by other groups: d) A. de Meijere, S. I. Kozhushkov, T. Späth, N. S. Zefirov, *J. Org. Chem.* **1993**, *58*, 502; and developed into an enantioselective variant: e) E. J. Corey, S. Achyutha Rao, M. C. Noe, *J. Am. Chem. Soc.* **1994**, *116*, 9345.

[6] In contrast to previous reports [5], the titanium reagent formed in this reaction survives heating to 55 °C for extended periods.

[7] Although the cyclopropane ring can undergo hydrogenolytic ring-opening under drastic conditions, it survives the reductive debenzylation of an adjacent dibenzylamino group: a) M. Es-Sayed, C. Gratkowski, N. Krass, A. I. Meyers, A. de Meijere, *Synlett* **1992**, 962; b) M. Es-Sayed, C. Gratkowski, N. Krass, A. I. Meyers, A. de Meijere, *Tetrahedron Lett.* **1993**, *34*, 289.

[8] All new compounds were fully characterized by spectroscopic methods (^1H and ^{13}C NMR, IR) and by mass spectrometry, and their molecular formulas were established by elemental analysis or high-resolution mass spectrometry.

[9] O. G. Kulinkovich, A. I. Savchenko, S. V. Sviridov, D. A. Vasilevski, *Mendeleev Commun.* **1993**, 192.

[10] In general, alkyltitanium reagents are less basic and less reactive than the corresponding magnesium and lithium reagents: M. Reetz in *Organometallics in Synthesis* (Ed.: M. Schlosser), Wiley, Chichester, **1994**, and references therein.

[11] *Houben Weyl, Methoden der Organischen Chemie, 4th ed., Vol. E5/2* (Ed.: J. Falbe), Thieme, Stuttgart, **1985**, p. 1043.

[12] C. A. Audeh, S. E. Fuller, R. J. Hutchinson, J. R. L. Smith, *J. Chem. Res. Synop.* **1979**, 270; *J. Chem. Res. Miniprint* **1979**, 2984.

[13] According to a literature search, the only known tertiary amine with two *tert*-butyl groups on nitrogen has been di-*tert*-butylmethylamine [12].

A Step-Growth Approach to Metal-Capped One-Dimensional Carbon Allotropes: Syntheses of C_{12}, C_{16}, and C_{20} μ-Polyynediyl Complexes**

Tamás Bartik, Berit Bartik, Monika Brady, Roman Dembinski, and J. A. Gladysz*

The three-dimensional and two-dimensional carbon allotropes, diamond and graphite, have been known since antiquity. However, the one dimensional carbon allotrope, which would consist of sp hybridized carbons, remains by comparison only exigously described. Over the last thirty years several syntheses have been claimed.[1, 2] Recently mixtures of lower (C_{16}–C_{28}) and higher (C_{75}–C_{150}) oligomers have been prepared by novel synthetic techniques with various organic endgroups.[3–6] These reports foreshadow many fascinating properties, the precise delineation of which requires samples that are homogeneous in chain length.

We have sought to prepare compounds in which elemental carbon chains span two transition metals. We previously isolated dirhenium μ-polyynediyl complexes of the formula $[\{Re^*\}(C\equiv C)_n\{Re^*\}]$ (n = 2, **C4**; 3, **C6**; 4, **C8**; $\{Re^*\} = (\eta^5\text{-}C_5Me_5)Re(NO)(PPh_3)$) from coupling or cross-coupling reac-

[*] Prof. Dr. J. A. Gladysz, Dr. T. Bartik, Dr. B. Bartik, Dr. M. Brady, Dr. R. Dembinski
Department of Chemistry, University of Utah
Salt Lake City, UT 84112 (USA)
Fax: Int. code +(801) 585-7807
e-mail: gladysz@rhenium.chem.utah.edu

[**] We thank the National Science Foundation for support of this research.

tions of the corresponding [{Re*}(C≡C)$_n$H] species ($n = 1, 2$).[7] In this communication, we detail new step-growth chain extension methodology that leads to analogous complexes with up to twenty-carbon bridges. This strategy appears to carry no upper bound for chain length and should allow access to a complete family of well-defined oligomers.

The racemic butadiynyl complex [{Re*}(C≡CC≡CH)] (**1**; Scheme 1) was treated with *n*BuLi in THF (1.1 equiv, −45 °C) to generate the previously reported C_4Li complex [{Re*}(C≡C–C≡CLi)] (**2**).[8] Then CuI was added (− 20 °C). The sample was warmed and kept at room temperature for a short time. IR and ^{31}P NMR spectra showed broad signals indicating complete conversion to a new complex or mixture of complexes. These were presumed to have the empirical formula [{Re*}(C≡CC≡CCu)] (**3**; Scheme 1).[9]

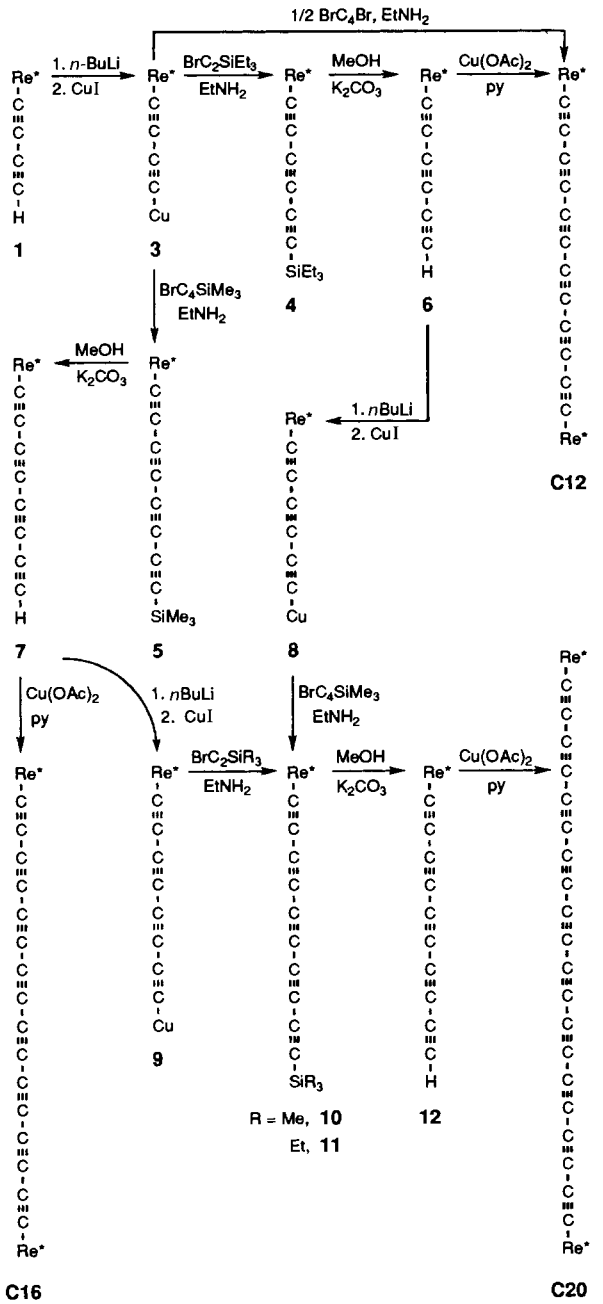

Scheme 1. Syntheses of [{Re*}(C≡C)$_n${Re*}] [n = 6 (**C12**), 8 (**C16**), 10 (**C20**)]; {Re*} = (η^5-C_5Me_5)Re(NO)(PPh_3); py = pyridine.

Under suitable conditions copper-substituted and bromine-substituted alkynes couple to 1,3-diynes.[10] However, to our knowledge such "Cadiot-Chodkiewicz" protocols have not been applied in metal coordination spheres. Thus, solutions of **3** were treated with excess $EtNH_2$ (− 20 °C). Then $BrC{\equiv}CSiEt_3$[11] or $BrC{\equiv}CC{\equiv}CSiMe_3$[12] (1.0–1.1 equiv) were added. Workup gave the analytically pure C_6Si and C_8Si complexes [{Re*}(C≡CC≡CC≡CSiEt$_3$)] (**4**) and [{Re*}-(C≡CC≡CC≡CC≡CSiMe$_3$)] (**5**) in 51–77% yield after crystallization. Complexes **4** and **5** exhibited spectroscopic properties similar to those of lower homologs reported earlier.[7] However, IR spectra showed additional $\nu_{C\equiv C}$ bands.[9b]

Reactions of **4** and **5** with K_2CO_3/CH_3OH gave the corresponding C_6H and C_8H complexes [{Re*}(C≡CC≡CC≡CH)] (**6**) and [{Re*}(C≡CC≡CC≡CC≡CH)] (**7**) in 91–98% yield after workup. These were moderately air-sensitive as solids, and more air-sensitive in solution (**7** > **6**). Subsequent reactions with $Cu(OAc)_2$ (1.0 equiv, 50 °C) in pyridine gave the μ-dodecahexaynediyl and μ-hexadecaoctaynediyl complexes [{Re*}-(C≡C)$_6${Re*}] (**C12**) and [{Re*}(C≡C)$_8${Re*}] (**C16**) in 71–67% yield. Key properties are summarized below.

"Second generation" chain extensions of **6** and **7** were investigated. Reactions with *n*BuLi and CuI similar to those above were presumed to generate the C_6Cu and C_8Cu species [{Re*}(C≡CC≡CC≡CCu)] (**8**) and [{Re*}-(C≡CC≡CC≡CC≡CCu)] (**9**). Treatment of **8** with excess $EtNH_2$ and then with $BrC{\equiv}CC{\equiv}CSiMe_3$, as described for **3** above, gave the analytically pure $C_{10}Si$ complex [{Re*}-(C≡CC≡CC≡CC≡CC≡CSiMe$_3$)] (**10**) in 51% yield. Similar reactions of **8** and $BrC{\equiv}CC{\equiv}CSiEt_3$[13] or **9** and $BrC{\equiv}CSiEt_3$ gave the triethylsilyl analog **11** in 24–26% yields.

Reaction of **11** and K_2CO_3/MeOH gave a $C_{10}H$ complex, [{Re*}(C≡CC≡CC≡CC≡CC≡CH)] (**12**), which was partially characterized. The crude sample was treated with $Cu(OAc)_2$ in pyridine as described above. Workup gave the μ-icosadecaynediyl complex [{Re*}(C≡C)$_{10}${Re*}] (**C20**) in 41% yield. Finally, a more convergent chain extension route was probed. The C_4Cu species **3** was treated with excess $EtNH_2$ and then the *di*bromide $BrC{\equiv}CC{\equiv}CBr$.[14] Workup gave **C12** in 45% yield.

The sp carbon chains in **C12**, **C16**, and **C20** are by far the longest tether between two metals to date.[7, 8, 15, 16] All three compounds are microcrystalline or amorphous powders and show only slight decomposition after one week in air at room temperature. When heated they decompose (above 100 °C) without melting or explosion. Mass spectra exhibit strong molecular ions. Correct microanalyses have been obtained for **C12** and **C16**, but not yet for **C20**. Solubilities are high in CH_2Cl_2 and THF but low in hexane. In solution **C20** is noticeably more labile than **C12** or **C16**.[16]

Some physical properties of **C12**–**C20** should asymptotically approach those of a one-dimensional sp carbon allotrope. For example, ^{13}C NMR spectra show Re*C*≡*C* signals at $\delta = 127$–114. Interestingly, the remaining signals cluster in the narrow range of $\delta = 68$–63 (Fig. 1). Similar trends occur in mixtures of oligomers with organic endgroups, reported by Lagow.[3] Also, the colors of solutions deepen from red (**C12**) to black cherry (**C16**) to brown-black (**C20**). Accordingly, UV/Vis spectra exhibit progressively red-shifted bands of markedly increasing intensities, as illustrated in Figure 2. Some have molar extinction coefficients of well over 100000 $M^{-1}cm^{-1}$. Importantly, PES and MO studies of metal ethynyl and butadiynyl complexes[17] suggest that the HOMOs of **C12**–**C20** likely have appreciable metal d *and* (C≡C)$_n$ π character.

Cyclic voltammograms of **C4**–**C8** show two chemically reversible one-electron oxidations under suitable conditions.[7b]

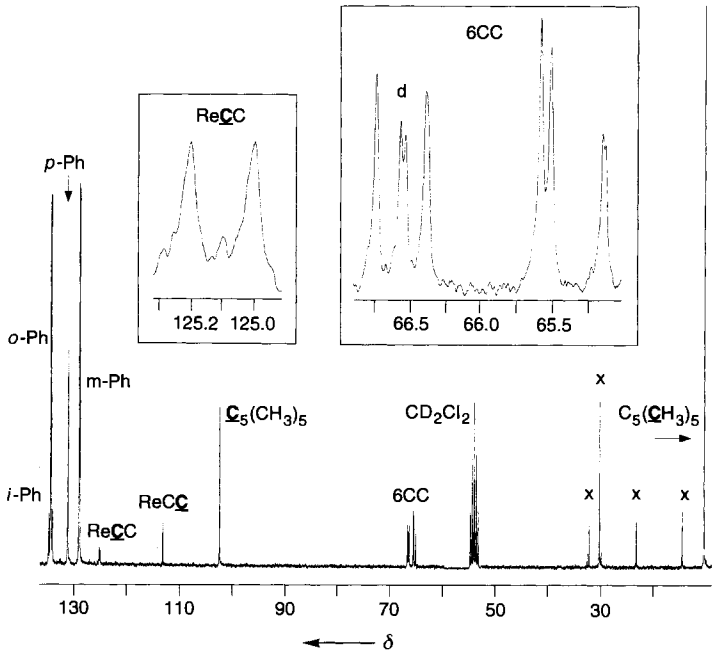

Fig. 1. ^{13}C NMR spectrum of **C16** (75 MHz, CD_2Cl_2, 20 °C) and expanded sp carbon region (insets); x = solvent impurities; d = doublet.

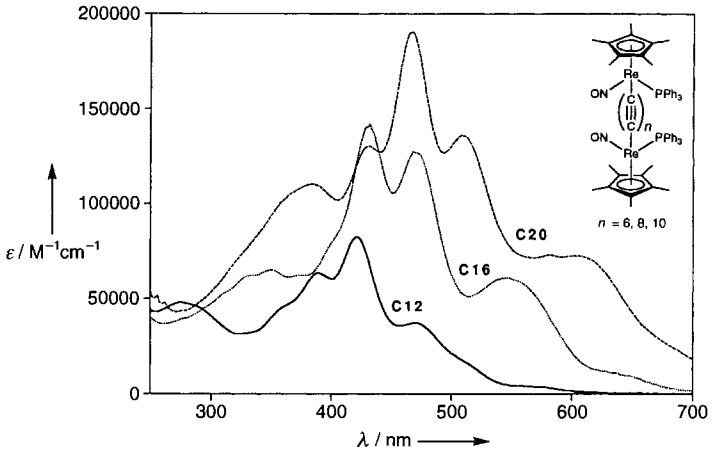

Fig. 2. UV/Vis spectra of **C12**, **C16**, and **C20** (CH_2Cl_2, ambient temperature).

Table 1. Cyclic voltammetry data [a].

Compound	$E_{p,a}$ [V]	$E_{p,c}$ [V]	E^0 [V]	ΔE [mV]	i_a/i_c [b]
C4	0.15	0.06	0.11	90	1
	0.68	0.59	0.64	90	1
C6	0.24	0.17	0.20	70	1
	0.62	0.55	0.58	70	1
C8	0.37	0.30	0.34	70	>1
	0.66	0.59	0.62	70	>1
C12	0.60	0.52	0.56	80	≫1
	0.79	0.69	0.75	100	≫1
C16	0.70	0.64	0.67	60	≫1
	0.79	0.73	0.76	60	≫1
C20	0.80	0.67	0.74	130	⋙1

[a] The first line shows the potential of the first oxidation, and the second line that of the second oxidation. **C20** undergoes only one oxidation (see text). $7-9\times10^{-5}$ M in 0.1 M $Bu_4N^+BF_4^-/CH_2Cl_2$ at ambient temperature, Pt working and counter electrodes, ferrocene standard, potential vs. Ag wire pseudoreference; scan rate 100 mVs^{-1}. p = potential. a = anode. c = cathode. [b] Improved reversibility is generally seen at lower temperatures.

These generate monocations and dications, which have been isolated in the C_4 series. Data acquired under identical conditions with **C12**–**C20** are summarized in Table 1. Some striking trends are evident. For example, as the carbon chain lengthens, the first oxidation potential becomes thermodynamically less favorable (**C4** vs. **C16**, $\Delta E^\circ = 0.56$ V). The second potential varies by a smaller amount (**C4**/**C6** vs. **C16**, $\Delta E^\circ = 0.12/0.18$ V). Consequently, the E° values approach each other, and with **C20** they merge to give a single—presumably two-electron—oxidation. This signifies the chain length at which the two rhenium atoms start to behave independently, at least in a redox sense.

The final step in each synthesis of **C12**–**C20** can be viewed as "convergent". However, especially for **C20**, a number of iterative steps are required. Importantly, many ways can be envisioned to optimize or combine the individual steps, or to employ longer building blocks. In summary, we have shown that it is possible to rationally synthesize metal-capped oligomers of sp carbon atoms that are homogeneous in chain length. Additional properties of the title compounds, and syntheses of analogs, will be reported in the near future.

Received: October 6, 1995 [Z 8453 IE]
German version: *Angew. Chem.* **1996**, *108*, 467–469

Keywords: alkynyl complexes · carbon allotropes · polyynes · rhenium compounds

[1] Representative syntheses: a) V. I. Kasatochkin, A. M. Sladkov, Y. P. Kudryavtsev, N. M. Popov, V. V. Korshak, *Dokl. Chem. Engl. Transl.* **1967**, *177*, 1031–1034; b) K. Akagi, M. Nishiguchi, H. Shirakawa, Y. Furukawa, I. Harada, *Synth. Met.* **1987**, *17*, 557–562.

[2] Reviews and critical analyses: a) V. M. Mel'nichenko, A. M. Sladkov, Yu. N. Nikulin, *Russ. Chem. Rev. Engl. Transl.* **1982**, *51*, 421–438; b) P. P. K. Smith, P. R. Buseck, *Science* **1982**, *216*, 984–986.

[3] R. J. Lagow, J. J. Kampa, H.-C. Wei, S. L. Battle, J. W. Genge, D. A. Laude, C. J. Harper, R. Bau, R. C. Stevens, J. F. Haw, E. Munson, *Science* **1995**, *267*, 362–367.

[4] T. Grösser, A. Hirsch, *Angew. Chem.* **1993**, *105*, 1390–1392; *Angew. Chem. Int. Ed. Engl.* **1993**, *32*, 1340–1342.

[5] Homogeneous *t*-butyl capped species, $Me_3C(C{\equiv}C)_nCMe_3$ (n = 4–8, 10, 12), have been prepared by classical techniques and characterized by UV/Vis spectra and melting points. For summaries of this early work and data on related compounds, see: a) F. Bohlmann, *Angew. Chem.* **1953**, *65*, 385–389; b) A. M. Sladkov, Yu. P. Kudryavtsev, *Russian Chem. Rev. Engl. Transl.* **1963**, *32*, 229–243; c) E. R. H. Jones, H. H. Lee, M. C. Whiting, *J. Chem. Soc.* **1960**, 3483–3489; d) T. R. Johnson, D. R. M. Walton, *Tetrahedron* **1972**, *28*, 5221–5236.

[6] Similar $R_3Si(C{\equiv}C)_nSiR_3$ species have been reported (n = 4–10, 12, 16), but the higher oligomers were generated in solution, characterized by UV/Vis spectra, and not purified further: R. Eastmond, T. R. Johnson, D. R. M. Walton, *Tetrahedron* **1972**, *28*, 4601–4616.

[7] a) Y. Zhou, J. W. Seyler, W. Weng, A. M. Arif, J. A. Gladysz, *J. Am. Chem. Soc.* **1993**, *115*, 8509–8510; b) M. Brady, W. Weng, J. A. Gladysz, *J. Chem. Soc. Chem. Commun.* **1994**, 2655–2656.

[8] a) W. Weng, T. Bartik, J. A. Gladysz, *Angew. Chem.* **1994**, *106*, 2269–2272; *Angew. Chem. Int. Ed. Engl.* **1994**, *33*, 2199–2202; b) W. Weng, T. Bartik, M. Brady, B. Bartik, J. A. Ramsden, A. M. Arif, J. A. Gladysz, *J. Am. Chem. Soc.* **1995**, *117*, 11922–11931.

[9] a) Complete spectroscopic data for new compounds are available upon request from the authors. b) All compounds gave IR $\tilde{\nu}_{NO}$ bands at 1653–1662 (vs), and $\tilde{\nu}_{C\equiv C}$ bands as follows (cm^{-1}, THF): **3** 2010 m br; **4** 2133 m, 2111 m, 1979 vs; **5** 2115 m, 2069 m sh, 2046 vs, 1971 s; **6** 2140 s, 2080 m, 1970 m; **7** 2109 s, 2036 s, 1971 m; **10** 2158 w, 2133 w, 2070 w, 2037 vs, 1955 vs; **11** 2157 vw, 2132 vw, 2069 w, 2035 vs, 1955 vs; **C12** 2115 m, 2056 vs, 1952 s; **C16** 2074 m, 2014 vs, 1941 vs; **C20** 2150 vw, 2116 vw, 1991 m, 1925 vs. c) UV/Vis (λ in nm, CH_2Cl_2 (ε in $M^{-1}cm^{-1}$); see also Fig. 1): **C12** 230 (60500), 280 (47600), 364 sh (47300), 390 (63400), 422 (82700), 470 (37350), 512 sh (16600), 568 (3850); **C16** 232 (62600), 328 (61700), 348 (65300), 402 sh (81500), 430 (142000), 470 (128000), 548 (61200), 644 (9900); **C20** 228 (78000), 384 sh (110000), 430 (131000), 466 (191000), 508 (136000), 582 (73000), 602 (73000).

[10] G. Eglinton, W. McCrae, *Adv. Org. Chem.* **1963**, *4*, 225.

[11] R. Eastmond, D. R. M. Walton, *Tetrahedron* **1972**, *28*, 4591–4599 and references therein.

[12] W. de Graaf, A. Smits, J. Boersma, G. van Koten, W. P. M. Hoekstra, *Tetrahedron* **1988**, *44*, 6699–6704.

[13] B. N. Ghose, D. R. M. Walton, *Synthesis* **1974**, *12*, 890–891.

[14] a) F. Straus, L. Kollek, H. Hauptmann, *Ber. Dtsch. Chem. Ges. B* **1930**, *63*, 1886–1899; b) E. Heilbronner, V. Hornung, J. P. Maier, E. Kloster-Jensen, *J. Am. Chem. Soc.* **1974**, *96*, 4252–4262.
[15] Some lead references: a) H. Lang, *Angew. Chem.* **1994**, *106*, 569; *Angew. Chem. Int. Ed. Engl.* **1994**, *33*, 547–550; b) N. Le Narvor, L. Toupet, C. Lapinte, *J. Am. Chem. Soc.* **1995**, *117*, 7129–7138.
[16] Presumably **C12**–**C20** are 50:50 mixtures of diastereomers, as established for lower homologs **C4**–**C8**. However, in each case only a single set of NMR signals is observed. Other spectroscopic properties, and redox behavior, are also presumed to be identical. We have not yet been able to obtain single crystals, perhaps in part due to the presence of two diastereomers.
[17] D. L. Lichtenberger, S. K. Renshaw, A. Wong, C. D. Tagge, *Organometallics* **1993**, *12*, 3522–3526, and references therein.

Photochemically Induced Metathesis Reactions of Tetradehydrodianthracene: Synthesis and Structure of Bianthraquinodimethanes**

Stefan Kammermeier and Rainer Herges*

Dedicated to Professor Ivar Ugi on the occasion of his 65th birthday

Photochemical [2+2] cycloadditions[1] with subsequent [2+2] cycloreversion in the sense of an overall metathesis reaction often lead to interesting products that are otherwise difficult to prepare.[2] With the example of 5,12:6,11-di[1,2]benzenodibenzo[*a*,*e*]cyclooctene[3] (9,9′,10,10′-tetradehydrodianthracene, ethylene*super*phane;[4] **1**), we demonstrate that this concept of two-step (photochemical and thermal) metathesis can be used to synthesize spherically deformed, polycyclic, aromatic hydrocarbons.

The highly strained, but stable diene **1** contains two bridgehead double bonds 2.42 Å apart,[3] which are *syn*-pyramidalized.[5] The unusual configuration (pyramidalization, through-space interaction) gives rise to a decrease in the $\pi-\pi^*$ gap, which is mainly due to a lowering of the LUMO.[6] Consequently, the reactivity of the double bonds towards electrophilic[7] and (even more pronounced) towards nucleophilic[8] reagents should be enhanced. Therefore **1** should be particularly reactive towards electron-rich alkenes in cycloadditions. As part of our investigations into the reactivity of **1** we performed photochemical [2+2] cycloadditions with a number of alkenes and cycloalkenes. Compound **1** gives three absorption bands in the UV range above 200 nm: 282 ($\varepsilon = 1270$), 270 ($\varepsilon = 2500$), and 233 nm ($\varepsilon = 10\,700$). The longest wavelength band can probably be attributed to the symmetry-forbidden $\pi-\pi^*$ transition and therefore to the excited state that correlates with the [2+2] cycloadducts.

Ethene adds photochemically (benzene, 150 W Hg high-pressure lamp, quartz, room temperature, 90 min) to **1** forming a very strained but isolable cyclobutane derivative **2a** in 32% yield (Scheme 1). Upon heating (toluene, 90 °C, 30 min) a cycloreversion[9] takes place to give the previously unknown, unsubstituted bianthraquinodimethane **3a** (yield 57%).[10, 11] Because of the repulsion between the *peri*-hydrogen atoms the bianthraquinoid systems cannot adopt a planar conformation. In contrast to bianthrone, which avoids this steric hindrance by distorting to a (more stable) *anti*-pyramidalized or a (less stable)

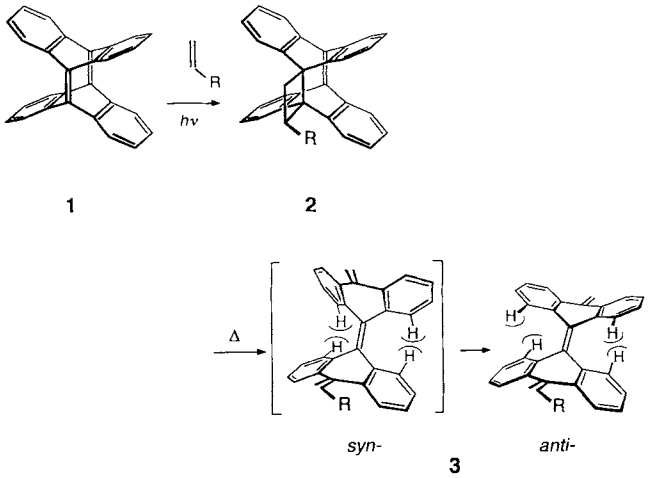

Scheme 1. Metathesis of tetradehydrodianthracene **1** with acyclic alkenes; **a**, R = H; **b**, R = Me. Important data of compounds **2a**, **3a**, and **3b** are given in Table 2.

twist conformation,[12] bianthraquinodimethane **3a** has, according to our calculations[13] at different levels of theory, an *anti*- and a *syn*-pyramidalized form as conformational minima. The twist conformation in this case is not a minimum. As expected, the *anti*-pyramidalized form (C_{2h} symmetry) is more stable than the *syn* isomer (C_{2v} symmetry).[6] At the highest level of theory applied the energy difference is 9.35 kcal mol^{-1} (Table 1). Presumably the *syn*-pyramidalized bianthraquinodimethane **3a**, which is formed upon thermochemical ring opening of **2a**, immediately changes pyramidalization to give the more stable *anti*-conformation (Scheme 1).

Table 1. Absolute electronic energies E_{tot} of both isomeric forms of the unsubstituted bianthraquinodimethane **3a** calculated at different levels of theory.

Level of theory	E_{tot} [Hartree]		ΔE
	anti-Isomer	*syn*-Isomer	[kcal mol^{-1}]
HF/3-21G	−1141.27370	−1141.25725	10.32
HF/6-31G*	−1147.68297	−1147.66766	9.60
Becke3LYP/6-31G*//HF/6-31G*	−1155.21041	−1155.19551	9.35

The product of the photochemical [2+2] cycloaddition with propene (**2b**) is not stable under our reaction conditions (see above). The thermochemical [2+2] cycloreversion giving **3b** (yield 53%) proceeds so fast that the cyclobutane intermediate could not be detected. This agrees with observations that the [2+2] cycloreversion of cyclobutanes is accelerated by alkyl substituents.[9] A rough estimation of the Gibbs activation energies[14] predicts that in our case the methyl group lowers the barrier of activation for the [2+2]cycloreversion by at least 5.5 kcal mol^{-1}. This is substantially more than in the cyclobutane parent system (1.3 kcal mol^{-1}).[9]

With cycloalkenes as reaction partner (toluene:cycloalkene = 5:1, 150 W Hg high-pressure lamp, quartz, room temperature, 120 min) cyclophane-like bridged bianthraquinodimethanes **5a** and **5c**–**e** (Scheme 2) were formed. In this case as well, the cyclobutane intermediates **4** could not be isolated. A by-product in all reactions is bianthryl (probably formed by hydrogen transfer from the cycloalkene to one of the double bonds of **1** and subsequent electrocyclic ring opening[15]). The cyclophane-like bridged bianthraquinodimethanes **5a** and **5c**–**e** are fixed by the alkane chain in the usually less stable *syn*-pyramidalized form. Moreover, the X-ray analysis of **5d** (Fig. 1)[16]

[*] Priv.-Doz. Dr. R. Herges, Dipl.-Chem. S. Kammermeier
Institut für Organische Chemie der Universität Erlangen-Nürnberg
Henkestrasse 42, D-91054 Erlangen (Germany)
Fax: Int. +(9131) 85-9132

[**] This work was supported by the Deutsche Forschungsgemeinschaft and the Fonds der Chemischen Industrie (Scholarship to S.K.).

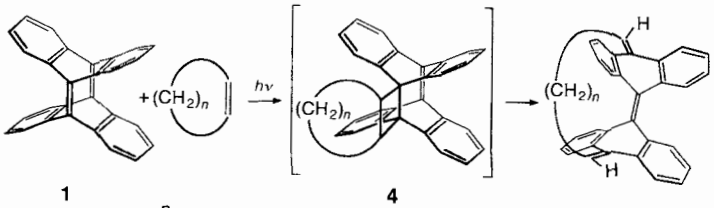

1 4

n		n		
3	cyclopentene	3	**5a**	11 %
4	cyclohexene	4	**5b**	0 %
5	cycloheptene	5	**5c**	29 %
6	cyclooctene	6	**5d**	60 %
8	cyclodecene	8	**5e**	26 %

Scheme 2. Metathesis of tetradehydrodianthracene **1** with cycloalkenes. Important data of the product **5** are given in Table 2.

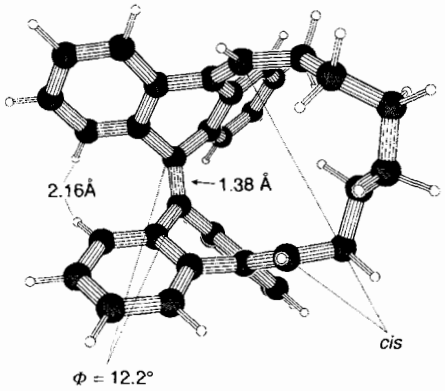

Fig. 1. Crystal structure of **5d**. Φ = pyramidalization angle at the olefinic carbon atoms.

proves that the aliphatic chain is *cis* with respect to both quinoid double bonds (C_s symmetry). The stereochemistry of the cycloalkene (*cis*) is preserved in both steps of the metathesis reaction.

The central pyramidalized double bond of **5d** in the X-ray structure is 1.38 Å long, and the pyramidalization angle is 12.2°. Both anthracenediylidene units are not planar but are bent outwards to resemble a roof. The central six-membered rings thus have a boat conformation. The distance between the *peri*-hydrogen atoms facing each other from the two anthracene units is only 2.16 Å. This is substantially less than the sum of the van der Waals radii. There is, however, no twist in the central double bond to compensate for the repulsive interaction.

Surprisingly, addition of cyclohexene to **1** is not observed. However, norbornene, which contains a conformationally fixed cyclohexene and norbornadiene, undergoes a metathesis reaction in relatively high yields.[17] NOE experiments with the metathesis product show that the addition proceeds in *exo* position.

The multiple addition of **1** to cyclic polyenes should be of interest for the generation of extended polyaromatic systems consisting of several bianthraquinodimethane units. The first step of such a metathesis reaction can be successfully performed by irradiation of **1** in benzene[18] (150 W Hg high-pressure lamp, quartz, room temperature, 4 h). In contrast with **5d**, in the ring-opened product **6** (yield 25%, Table 2), the unsaturated bridging chain has *trans* conformation with respect to both quinoid double bonds. The resulting C_2 symmetry[19] of **6** is verified by a strong NOE effect between the inner *peri*-hydrogen atoms that are spatially very close (in **5d** this distance is only 2.16 Å, see Fig. 1). If **6** had C_s symmetry (*cis* conformation of

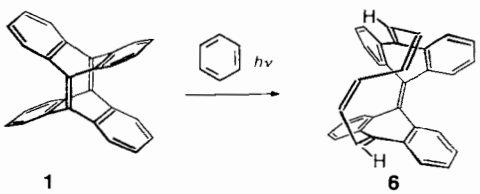

1 6

Table 2. Selected data of compounds **2a**, **3a**, **3b**, **5a**, **5c–e**, and **6**.

2a: ^{1}H NMR (400 MHz, $CDCl_3$): δ = 7.16 (m, 4H; CH), 7.10 (m, 4H; CH), 6.90 (m, 8H; CH), 3.02 (s, 4H; CH_2); ^{13}C NMR (100.6 MHz, $CDCl_3$): δ = 151.07 (2 C, C=C), 145.56 (4 C, C_q), 143.73 (4 C, C_q), 125.46 (4 C, CH), 125.42 (4 C, CH), 124.18 (4 C, CH), 123.23 (4 C, CH), 64.44 (2 C, C_q), 16.88 (2 C, CH_2); UV/Vis (CH_2Cl_2): λ_{max} (ε) = 232 nm (5600); MS (70 eV): *m/z* (%): 380 (100) [M^+]

3a: ^{1}H NMR (400 MHz, $CDCl_3$): δ = 7.66 (m, 4H; CH), 7.21 (m, 4H; CH), 6.95 (m, 8H; CH), 5.83 (s, 4H; CH_2); ^{13}C NMR (100.6 MHz, $CDCl_3$): δ = 143.64 (2 C, C_q), 137.73 (4 C, C_q), 134.94 (4 C, C_q), 131.51 (2 C, C_q), 129.06 (4 C, CH), 126.91 (4 C, CH), 125.71 (4 C, CH), 124.34 (4 C, CH), 108.94 (2 C, CH_2); UV/Vis (CH_2Cl_2): λ_{max} (ε) = 258 (18000), 232 nm (21000); MS (70 eV): *m/z* (%): 380 (100) [M^+]

3b: ^{1}H NMR (400 MHz, $CDCl_3$): δ = 7.67 (m, 2H; CH), 7.53 (m, 2H; CH), 7.21 - 6.87 (m, 12H; CH), 6.38 (q, ^3J(H,H) = 7.3 Hz, 1H; vinyl-CH), 5.82 (s, 2H; CH_2), 2.29 (d, ^3J(H,H) = 7.3 Hz, 3H; CH3); ^{13}C NMR (100.6 MHz, $CDCl_3$): δ = 143.60 (1 C, C_q), 140.77 (1 C, C_q), 137.61 (1 C, C_q), 137.57 (1 C, C_q), 137.32 (1 C, C_q), 136.93 (1 C, C_q), 136.29 (1 C, C_q), 134.87 (1 C, C_q), 134.81 (1 C, C_q), 132.51 (1 C, C_q), 131.53 (1 C, C_q), 130.47 (1 C, C_q), 129.2 (1 C, CH), 129.17 (1 C, CH), 129.02 (1 C, CH), 128.60 (1 C, CH), 127.40 (1 C, CH), 126.83 (3 C, CH), 125.95 (1 C, CH), 125.70 (2 C, CH), 125.30 (1 C, CH), 125.22 (1 C, CH), 124.7 (1 C, CH), 124.29 (1 C, CH), 123.89 (1 C, CH), 122.32 (1 C, vinyl-CH), 108.91 (1 C, CH_2), 15.99 (1 C, CH3); UV/Vis (CH_2Cl_2): λ_{max} (ε) = 255 (11000), 235 nm (18000); MS (70 eV): *m/z* (%): 394 (100) [M^+], 191 (10)

5a: ^{1}H NMR (400 MHz, $CDCl_3$): δ = 7.86 (m, 4H; CH), 7.22 (m, 12H; CH), 5.69 (dd, ^3J(H,H) = 11.2, ^3J(H,H) = 2.9 Hz, 2H; vinyl-CH), 2.45 (m, 4H; CH_2), 1.30 (m, 4H; CH_2), 0.75 (m, 2H; CH_2); ^{13}C NMR (100.6 MHz, $CDCl_3$): δ = 140.20 (2 C, C_q), 140.17 (2 C, C_q), 139.86 (2 C, C_q), 137.57 (2 C, C_q), 136.84 (2 C, C_q), 136.06 (2 C, C_q), 130.19 (2 C, vinyl-CH), 127.18 (2 C, CH), 126.78 (2 C, CH), 126.26 (2 C, CH), 126.14 (2 C, CH), 125.39 (2 C, CH), 125.06 (2 C, CH), 124.64 (2 C, CH), 122.54 (2 C, CH), 30.84 (2 C, CH_2), 29.18 (1 C, CH_2); MS (70 eV): *m/z* (%): 420 (100) [M^+]

5c: ^{1}H NMR (400 MHz, $CDCl_3$): δ = 7.86 (m, 4H; CH), 7.22 (m, 12H; CH), 5.69 (dd, ^3J(H,H) = 12.2, ^3J(H,H) = 3.4 Hz, 2H; vinyl-CH), 2.45 (m, 4H; CH_2), 1.30 (m, 4H; CH_2), 0.75 (m, 2H; CH_2); ^{13}C NMR (100.6 MHz, $CDCl_3$): δ = 140.73 (2 C, C_q), 139.06 (2 C, C_q), 137.66 (2 C, C_q), 136.72 (2 C, C_q), 135.70 (2 C, C_q), 135.15 (2 C, C_q), 130.11 (2 C, CH), 128.83 (2 C, vinyl-CH), 127.70 (2 C, CH), 127.21 (2 C, CH), 127.02 (2 C, CH), 125.42 (2 C, CH), 125.07 (2 C, CH), 123.95 (2 C, CH), 122.58 (2 C, CH), 29.43 (2 C, CH_2), 28.86 (1 C, CH_2), 28.37 (2 C, CH_2); MS(70 eV): *m/z* (%): 448 (100) [M^+]

5d: ^{1}H NMR (400 MHz, $CDCl_3$): δ = 7.84 (m, 4H; CH), 7.14 (m, 12H; CH), 5.74 (dd, ^3J(H,H) = 10.0, ^3J(H,H) = 2.9 Hz, 2H; vinyl-CH), 2.43 (m, 4H; CH_2), 1.40 (m, 4H; CH_2), 1.08 (m, 4H; CH_2); ^{13}C NMR (100.6 MHz, $CDCl_3$): δ = 140.18 (2 C, C_q), 139.03 (2 C, C_q), 136.65 (2 C, C_q), 135.90 (2 C, C_q), 135.76 (2 C, C_q), 135.17 (2 C, C_q), 130.86 (2 C, vinyl-CH), 129.73 (2 C, CH), 127.77 (2 C, CH), 126.86 (2 C, CH), 126.53 (2 C, CH), 125.42 (2 C, CH), 124.94 (2 C, CH), 124.01 (2 C, CH), 122.00 (2 C, CH), 29.99 (2 C, CH_2), 28.46 (2 C, CH_2), 27.80 (2 C, CH_2); UV/Vis (CH_2Cl_2): λ_{max} (ε) = 320 (26000), 240 nm (35000); MS (70 eV): *m/z* (%): 462 (100) [M^+]

5e: ^{1}H NMR (400 MHz, $CDCl_3$): δ = 7.91 (m, 4H; CH), 7.10 (m, 12H; CH), 5.89 (dd, ^3J(H,H) = 10.2, ^3J(H,H) = 3.4 Hz, 2H; vinyl-CH), 2.49 (m, 4H; CH_2), 1.38 (m, 4H; CH_2), 1.21 (m, 4H; CH_2), 0.87 (m, 4H; CH_2); ^{13}C NMR (100.6 MHz, $CDCl_3$): δ = 139.62 (2 C, C_q), 138.72 (2 C, C_q), 136.33 (4 C, C_q), 135.82 (2 C, C_q), 135.51 (2 C, C_q), 129.31 (2 C, CH), 128.88 (2 C, CH), 128.62 (2 C, vinyl-CH), 126.70 (2 C, CH), 126.54 (2 C, CH), 125.83 (2 C, CH), 124.80 (2 C, CH), 124.16 (2 C, CH), 123.45 (2 C, CH), 29.58 (2 C, CH_2), 29.31 (2 C, CH_2), 28.10 (2 C, CH_2), 27.31 (2 C, CH_2); MS (70 eV): *m/z* (%): 490 (100) [M^+]

6: ^{1}H NMR (400 MHz, $CDCl_3$): δ = 7.62 (d, ^3J(H,H) = 6.6 Hz, 2H; CH arom.), 7.57 (d, ^3J(H,H) = 6.8 Hz, 2H; CH arom.), 7.32 (m, 2H; CH arom.), 7.05 (m, 10H; CH arom.), 6.85 (dd, ^3J(H,H) = 8.9, ^3J(H,H) = 9.0 Hz, 2H; CH), 6.18 (d, ^3J(H,H) = 8.9 Hz, 2H; CH), 5.95 (d, ^3J(H,H) = 9.0 Hz, 2H; CH); ^{13}C NMR (100.6 MHz, $CDCl_3$): δ = 140.73 (2 C, C_q), 138.94 (2 C, C_q), 138.87 (2 C, C_q), 138.67 (2 C, C_q), 137.30 (2 C, C_q), 135.23 (2 C, C_q), 131.65 (2 C, CH), 131.31 (2 C, CH), 127.25 (4 C, CH arom.), 126.72 (2 C, CH arom.), 125.85 (2 C, CH), 124.91 (4 C, CH arom.), 124.84 (2 C, CH arom.), 124.09 (2 C, CH arom.), 122.77 (2 C, CH arom.); UV/Vis (isomeric mixture) (CH_2Cl_2): λ_{max} (ε) = 280 (29000), 250 nm (36000); MS (70 eV): *m/z* (%): 430 (100) [M^+], 215 (15)

 © VCH Verlagsgesellschaft mbH, D-69451 Weinheim, 1996 0570-0833/96/3504-0418 $ 15.00+.25/0 Angew. Chem. Int. Ed. Engl. 1996, 35, No. 4

the bridging chain), such a NOE effect could not be observed, because the facing hydrogen atoms would be magnetically equivalent. Presumably the *trans* product is preferred during metathesis on thermodynamic grounds. According to AM1 calculations[20], the *trans* form is about 9 kcal mol^{-1} less strained than the *cis*-bridged isomer.[21] In solution at room temperature the metathesis product **6** is in a rapidly established equilibrium with about 5–10% of an isomer or conformer that can be completely separated by HPLC (Silicagel Grom-sil, Si 100, 5 µ, column 250 × 20, petroleum ether:dichloromethane = 2:1). However, after a few minutes the original equilibrium again is restored. Because of the small amounts and its instability the less concentrated isomer could not be characterized.

In compound **6** the completely conjugated π system with 14 electrons in the perimeter is formally suitable for subsequent cycloadditions. In contrast to normal arenes, the p orbitals are not orthogonal to a common nodal plane but approximately perpendicular to the surface of a cylinder ("beltlike" conjugation). The repeated addition of **1** to **6**, as well as the dimerization or cyclic oligomerization of **1**, are further worthwhile avenues that we are currently pursuing. This could lead to beltlike molecules, which are interesting targets in view of the topical expanding field of research on molecular cavities and graphitic tubes.

Received: April 27, 1995
Revised: November 29, 1995 [Z 7936 IE]
German version: *Angew. Chem.* **1996**, *108*, 470–472

Keywords: aromaticity · bridgehead olefins · cycloadditions metathesis · polycycles

[1] a) W. Carruthers, *Cycloaddition Reactions in Organic Synthesis*, Pergamon, Oxford, **1990**, p. 332–367; b) J. Ninomiya, T. Naito, *Photochemical Synthesis*, Academic Press, New York, **1989**, p. 59–109; c) N. J. Turro, *Modern Molecular Photochemistry*, University Science Books, Mill Valley, CA, **1991**, p. 414–472.

[2] a) G. Mehta, *J. Chem. Educ.* **1982**, *59*, 313–316; b) W. Oppolzer, *Acc. Chem. Res.* **1982**, *15*, 135–141; c) K. B. Wiberg, M. Matturro, R. Adams, *J. Am. Chem. Soc.* **1981**, *103*, 1600–1602; d) P. Camps, M. Font-Bardia, F. Pérez, X. Solans, S. Vásquez, *Angew. Chem.* **1995**, *107*, 1011–1012; *Angew. Chem. Int. Ed. Engl.* **1995**, *34*, 912–914; e) B. A. R. C. Murty, P. Spurr, R. Pinkos, C. Grund, W.-D. Fessner, D. Hunkler, H. Fritz, W. R. Roth, H. Prinzbach, *Chimia* **1987**, *41*, 32–36; f) W.-D. Fessner, B. A. R. C. Murty, H. Prinzbach, *Angew. Chem.* **1987**, *99*, 482–484; *Angew. Chem. Int. Ed. Engl.* **1987**, *26*, 451–452.

[3] R. L. Viavattene, F. D. Greene, L. D. Cheung, R. Majeste, L. M. Trefonas, *J. Am. Chem. Soc.* **1974**, *96*, 4342–4343.

[4] For notation see R. Gleiter, D. Kratz, *Acc. Chem. Res.* **1993**, *26*, 311–318.

[5] a) W. T. Borden, *Chem. Rev.* **1989**, *89*, 1095–1109; b) W. Luef, R. Keese, *Top. Stereochem.* **1991**, *20*, 231–318.

[6] W. V. Volland, E. R. Davidson, W. T. Borden, *J. Am. Chem. Soc.* **1979**, *101*, 533–537.

[7] R. Herges, H. Neumann, *Liebigs Ann.* **1995**, 1283–1289.

[8] R. Herges, H. Neumann, F. Hampel, *Angew. Chem.* **1994**, *106*, 1024–1026; *Angew. Chem. Int. Ed. Engl.* **1994**, *33*, 993–995.

[9] E. Schaumann, R. Ketcham, *Angew. Chem.* **1982**, *94*, 231–253; *Angew. Chem. Int. Ed. Engl.* **1982**, *21*, 225–247.

[10] Derivatives of bianthraquinonedimethane have already been described: a) S. Yamaguchi, T. Hanafusa, T. Tanaka, M. Sawada, K. Kondo, M. Irie, H. Tatemitsu, Y. Sakata, S. Misumi, *Tetrahedron Lett.* **1986**, *27*, 2411–2414; b) A. J. Moore, M. R. Bryce, *J. Chem. Soc. Perkin Trans. 1* **1991**, 157–168.

[11] The anthracene analogous to **3a**, 9,10-anthraquinodimethane, is only stable at low temperatures and high dilution because of its pronounced tendency to self addition: J. H. Golden, *J. Chem. Soc.* **1961**, 3741–3748. The 1,4-dimethyl-substituted system, however, is stable (because of steric hindrance):

[12] a) E. Harnik, G. M. Schmidt, *J. Chem. Soc.* **1954**, 3295–3302; b) R. Korenstein, K. A. Muszkat, S. Sharafy-Ozeni, *J. Am. Chem. Soc.* **1973**, *95*, 6177–6181; c) G. Kortüm, W. Zoller, *Chem. Ber.* **1967**, *100*, 280–292.

[13] a) Gaussian 92: M. J. Frisch, G. W. Trucks, M. Head-Gordon, P. M. W. Gill, M. W. Wong, J. B. Foresman, B. G. Johnson, H. B. Schlegel, M. A. Robb, E. S. Replogle, R. Gomperts, J. L. Andres, K. Raghavachari, J. S. Binkley, C. Gonzalez, R. L. Martin, D. J. Fox, D. J. DeFrees, J. Baker, J. J. P. Stewart, J. A. Pople, Gaussian Inc., Pittsburgh, PA, **1992**; b) *New Methods and Features in Gaussian 92 DFT (adding density functional capabilities to Gaussian 92)*, Gaussian Inc., Pittsburgh, PA, **1993**; c) J. W. Labanowski, J. Andzelm, *Density Functional Methods in Chemistry*, Springer, New York, **1991**; d) R. G. Parr, W. Yang, *Density Functional Theory of Atoms and Molecules*, Oxford University Press, New York, **1989**.

[14] Eyring's equation was used for estimation of the activation parameters. The half-life for **2b** at 85 °C is 200 min (determined by NMR spectroscopy), which corresponds to a free energy of activation of 26.6 kcal mol^{-1}. The half-life for **3b** at 20 °C should be less than 10 min. An upper value for the free energy of activation of 21.1 kcal mol^{-1} can thus be derived.

[15] M. M. Weinshenker, F. D. Greene, *J. Am. Chem. Soc.* **1968**, *90*, 506.

[16] The *R* value of our X-ray structure analysis is only 0.103 because of the thermal flexibility of the alkane chaines. The topology of the structure, however, can be unambiguously derived from the data.

[17] Besides the low ring strain, symmetry grounds are most probably also responsible for the unusually low reactivity of cyclohexene. Presumably the C_2 conformation of the ground state is not favorable for an addition, because the transition state of the cycloaddition should have C_s symmetry according to the Woodward–Hoffmann rules. Thus, during the reaction an energetically unfavorable conformational transition of the cyclohexene ring from C_2 to C_s symmetry must take place. This explanation concurs with the fact that norbornene, which can be viewed as a C_s-fixed cyclohexene, reacts smoothly. All other reactive cycloalkenes have (at least local) C_s symmetry with respect to the π plane of the double bond. A remarkably low reactivity of cyclohexene towards cycloadditions for the series of cycloalkenes was also found by other groups. See, for example, T. Hierstetter, B. Tischler, J. Sauer, *Tetrahedron Lett.* **1992**, *33*, 8019–8022; A. Hassner, H. W. Pinnick, J. M. Ansell, *J. Org. Chem.* **1978**, *43*, 1774–1776; K. Ziegler, H. Froitzheim-Kühlhorn, *Liebigs Ann.* **1954**, *589*, 157.

[18] With copper(I) triflate as catalyst, irradiation times are shorter and the yields are somewhat higher: R. G. Salomon, J. K. Kochi, *Chem. Commun.* **1972**, 559–560; *Tetrahedron Lett.* **1973**, 2529–2532.

[19] The *cis* configuration of the hydrogen atoms at both double bonds in the bridging unit was deduced from the vicinal coupling constant ^3J(H,H) of 8.9 Hz. The coupling constant ^3J(H,H) of 9.0 Hz can be assigned to the coupling of the two quinoid hydrogen atoms and the neighboring vinyl H atoms.

[20] VAMP 5.0: G. Rauhut, J. Chandrasekhar, A. Alex, T. Steinke, T. Clark, Oxford Molecular Limited, **1993**.

[21] In the metathesis products **5a** and **5c–e** the *cis*-annelation is favored on thermodynamic grounds, according to AM1 calculations. Compound **5d**, which was shown to be *cis*-bridged by X-ray analysis, is 6.3 kcal mol^{-1} more stable than the corresponding *trans* isomer.

Structural Characterization of a Tris-Agostic Lanthanoid–H–Si Interaction**

William S. Rees, Jr.,* Oliver Just, Herbert Schumann,* and Roman Weimann

Dedicated to Professor Herbert W. Roesky on the occasion of his 60th birthday

As speed and area efficiency demands in silicon-based electronic circuitry reach near-theoretical limits, attention is turning toward the potential for optical communication, computation, and connection. One approach to overcome the intrinsic direct band gap of silicon is to capitalize on the rich electronic manifold inherent in rare earth elements (Ln).[1] The initial work in

[*] Prof. Dr. W. S. Rees, Jr., Dr. O. Just
Georgia Institute of Technology
School of Chemistry and Biochemistry and School of Materials Science and Engineering and Molecular Design Institute
Atlanta, GA 30332-0400 (USA)
Fax: Int. code +(404)894-1144
e-mail: will.rees@chemistry.gatech.edu
Prof. Dr. H. Schumann, Dr. R. Weimann
Institut für Anorganische und Analytische Chemie
Technische Universität
Strasse des 17. Juni 135, D-10623 Berlin (Germany)
Fax: Int. code +(30)314-22168
e-mail: schn0530@mailszrz.zrz.TU-Berlin.d400.de

[**] This work was supported by the Deutsche Forschungsgemeinschaft and the U. S. Air Force Office of Scientific Research (Small Business Innovation Research contract from the Ballistic Missile Defense Organization to Spire Cooperation subcontract to Georgia Institute of Technology).

this area[2] was followed by results of rare earth element doped lattices grown by chemical vapor deposition (CVD).[3] As one component of research in the area of designed dopant sources for CVD use, previous success had been garnered by employing metal amide compositions for nitrogen doping of ZnSe.[4, 5] Thus, it was of interest to explore the potential of $Ln(NR_2)_3$ compounds as dopants in epitaxial semiconducting layers. Following preliminary fruition in this field,[6] a demand for Ln amide sources with higher vapor pressures emerged.[7] During the search for such materials, a novel interaction of Si–H and erbium was observed for one of these precursors. The present report contains details related to what is, to the best of our knowledge, the initial finding of what is attributed to be a tris-agostic interaction for a lanthanoid element.

The seminal reports of lanthanide tris(amide) compounds[8] relied on the well-known bis(trimethylsilyl) moiety popularized by decades of success in Bradley's group.[9] Subsequent structurally characterized examples include the dysprosium and erbium tris[bis(trimethylsilyl)amide] entries.[10] It was unsurprising that the metal centers in these compounds were observed to be three-coordinate, due to the rather large effective cone angle of $N[Si(CH_3)_3]_2^-$ as a ligand, coupled with its electron-donating properties to the electropositive Ln^{3+} ion. As a consequence of this rarity of coordination number three for lanthanides, it was of interest to probe the boundaries of utilizing less spacially demanding, and concomitantly less electron-donating, substituents on the nitrogen atom.

The first step in such a progression was the preparation of $[Er\{N(t\text{Bu})[Si(CH_3)_3]\}_3]$, pseudoisosteric with $[Er\{N[Si(CH_3)_3]_2\}_3]$, yet electronically perturbing to the Er^{3+} ion. The vapor pressure data for these two compounds were compared ($[Er\{N(t\text{Bu})[Si(CH_3)_3]\}_3]$: vapor pressure $p = 10^{-3}$ Torr/120 °C and $[Er\{N[Si(CH_3)_3]_2\}_3]$: $p = 10^{-4}$ Torr/140 °C) and then attention was turned toward the selective replacement of substituents at the silyl subunit. During the present investigation, independent publications of the structural characterization of five-coordinate yttrium and neodymium[10] compounds $[ML_3L'_2]$, as well as a four-coordinate neodymium[11] derivative occurred (L = amido ligand; L' = neutral coordinated THF). The vapor pressure of $[Er\{N(t\text{Bu})[Si(CH_3)_2(H)]\}_3]$ (**1**), synthesized according to Scheme 1, was observed to be surprisingly high in comparison

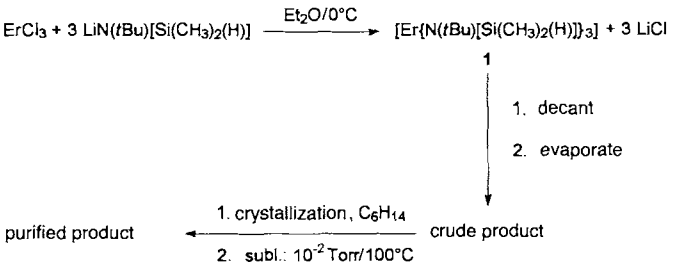

Scheme 1. Synthetic route to **1**.

with other known examples of compounds of this class. Additionally, the melting point was seen to deviate substantially from the values evaluated previously for a range of derivatives.[12] Thus, the search for the origin of these properties compelled a crystallographic characterization of the compound.

The structure[13] of compound **1** is depicted in Figure 1. Remarkably, all the *tert*-butyl groups are present on the same face of the N_3 plane, while there is a uniform rotation of each $Si[(CH_3)_2(H)]$ subunit which places all six methyl groups toward the periphery of the opposing hemisphere of the molecule. This rotation presumably is dictated by the interaction between the three silyl hydrogen atoms and the erbium center, as no indication of structure-influencing intramolecular forces was found in the unit cell. In 1983 Brookhart and Green[16] coined the term agostic to describe interactions of this type. Since then, several examples have been reported[17] for transition metals and C–H as well as N–H units. Very recently $\eta^2(H_2)$[18] and η^2(Si-H) interactions[19] with transition elements have been observed; a rigorous comparison of agostic and η^2 interactions presently is unwarranted, based on available data. To our knowledge, no earlier publications describe potential interactions between lanthanide elements and Si–H units, either originating from inter- or intramolecular coordination.

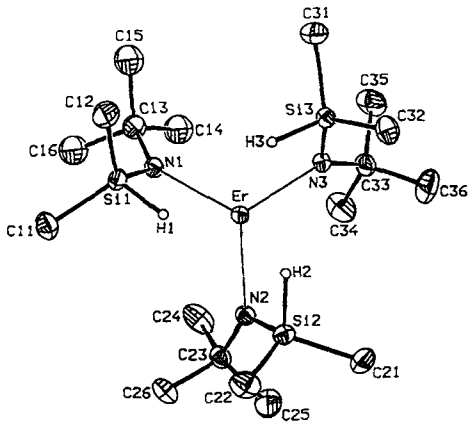

Fig. 1. ZORTEP plot [15] of the structure of **1** in the crystal (thermal ellipsoids are scaled to the 30% probability level). Selected interatomic distances [pm] and angles [°] (standard deviations are given in parentheses): Er–N1 220.6(2), Er–N2 220.6(2), Er–N3 220.6(2), Er–H1 232(3), Er–H2 241(3), Er–H3 237(3), N1–Si1 168.9(3), N1–C13 147.6(4), N2–Si2 169.1(3), N2–C23 146.3(4), N3–Si3 168.6(3), N3–C33 147.5(4), Si1–H1 141.1(3), Si2–H2 146.1(3), Si3–H3 148.1(3); N1-Er-N2 118.97(9), N1-Er-N3 114.60(9), N2-Er-N3 116.85(9), Er-N1-Si1 99.34(11), Si1-N1-C13 126.2(2), Er-N1-C13 133.6(2), Er-N2-Si2 99.85(11), Si2-N2-C23 126.9(2), Er-N2-C23 133.1(2), Er-N3-Si3 99.73(11), Si3-N3-C33 127.1(2), Er-N3-C33 133.1(2).

As can be gleaned from an examination of the interatomic distance and angle data of homoleptic tris(amido)lanthoid derivatives (Table 1), compound **1** has substantially shorter M–N contacts (220 pm). Furthermore, the N-M-N interatomic angles of 116° ± 2° are, in comparison to the corresponding average angle of 111° ± 3° in the four-coordinate entity $[Nd\{N(C_6H_5)[Si(CH_3)_3]\}_3](THF)$, considerably closer to the

Table 1. Interatomic angles [°] and distances [pm] involving M–N interactions for homoleptic lanthanide tris(amide) compounds.

Compound	M–N Distances	MN_2 Angles
$[Er\{N(t\text{Bu})[Si(CH_3)_2(H)]\}_3]$ [a]	Er-N1 220.6(2)	N1-Er-N2 118.97(9)
1	Er-N2 220.6(2)	N1-Er-N3 114.60(9)
	Er-N3 220.6(2)	N2-Er-N3 116.85(9)
$[Nd\{N(C_6H_5)[Si(CH_3)_3]\}_3](THF)$ [11]	Nd-N1 230.8(3)	N1-Nd-N2 107.8(1)
	Nd-N2 229.8(2)	N1-Nd-N3 109.4(1)
	Nd-N3 232.0(3)	N2-Nd-N3 114.0(1)
$[Nd\{N[Si(CH_3)_2(H)]_2\}_3(THF)_2]$ [10]	Nd-N1 235.3(4)	N1-Nd-N2 113.7(2)
	Nd-N2 232.6(5)	N1-Nd-N3 129.9(2)
	Nd-N3 235.1(5)	N2-Nd-N3 129.2(2)
$[Y\{N[Si(CH_3)_2(H)]_2\}_3(THF)_2]$ [10]	Y-N1 227.5(4)	N1-Y-N2 111.1(1)
	Y-N2 222.9(4)	N1-Y-N3 134.8(1)
	Y-N3 227.6(4)	N2-Y-N3 116.9(2)

[a] This work.

 © VCH Verlagsgesellschaft mbH, D-69451 Weinheim, 1996 0570-0833/96/3504-0420 $ 15.00+.25/0

predicted value of 120° for a VSEPR-optimized three-coordinate structure (VSEPR = valence shell electron pair repulsion). This value is approximated for other homoleptic tris(ligand) lanthanide derivatives with sterically demanding ligands.[20] Additionally, the dihedral angles lie around 0° [H(*n*)-Si(*n*)-N(*n*)-Er; $n = 1$: 2.5(13)°; $n = 2$: −4.6(11)°; $n = 3$: −0.1(11)°]; a consequence of the above-mentioned rotation of the dimethylsilyl groups. This further reinforces the concept that the structural motif of compound **1** is dominated by the controlling influence of the tris-agostic Er-H-Si interactions.

The IR data given in Table 2 also support the presence of the Er-H-Si interactions. A comparison of the Si–H vibrational frequencies in free HN(*t*Bu)[Si(CH$_3$)$_2$(H)] and in the complex

Table 2. IR spectroscopic data for compounds with metal–Si–H interactions and representative values for non-interacting systems.

Example	Si–H [cm^{-1}]	Ref.
HN(*t*Bu)[Si(CH$_3$)$_2$(H)]	2111	this work [a]
[Er{N(*t*Bu)[Si(CH$_3$)$_2$(H)]}$_3$] **1**	1858	this work [a]
unperturbed Si–H	2081–1972	[26]
Mo-η^2(Si–H)	1750–1730	[26]

[a] In C_6D_6 solution.

1 reveals the expected shift (253 cm^{-1}) to long wavelength.[21] The well-documented difficulty in obtaining precise NMR data on lanthanide compounds has hampered an examination of the ^2J(Si,H) coupling constant for the silyl-bound hydrogen atoms present in compound **1**. Such a probe of the "unstretched" Si–H character is restricted in the present case.[22] The Si–H interatomic distances (141–148 pm) are, however, within the range of values found for rather rare unstretched complexes, as compared to the typical stretched complexes.[22a] Presumably such an observation is predominately attributable to the influence of a d^0 metal center. In such instances, the possibility of back donation is eliminated, and all indications favor the highly unusual unstretched case. Furthermore, compound **1**, unlike the CH(SiMe$_3$)$_2^-$ unit, cannot be discussed in terms of γ-C-H-Ln versus β-Si-Me-Ln interaction.[23] Examples of Ln-N-Si-Me also have been reported,[24] as well as other γ-agostic or β-methyl interactions;[25] however, the tris-agostic M-H-Si interaction described here appears to be unique.

In conclusion, the tris-agostic Si–H–Er interaction in the solid-state structure of **1** is a possible source of the origin of the observed high vapor pressure and low melting point.

Experimental Procedure

An aliquot of $ErCl_3$ (0.91 g, 3.35 mmol) was suspended in Et_2O (40 mL) and stirred at 0 °C for 1 h. Freshly synthesized LiN(*t*Bu)[Si(CH$_3$)$_2$(H)] (1.38 g, 10.07 mmol) in Et_2O (60 mL) was added dropwise with rapid stirring. The mixture was allowed to warm to ambient temperature and the resultant pink solution was stirred overnight. Subsequently, the clear ether phase was decanted and evaporated. The residue from the ether solution was extracted with hexanes (50 mL). The resultant solution was filtered and its volume reduced in vacuum to 20 mL. Pink crystals of compound **1**, obtained from this solution after three days at −80 °C, were washed three times with cold (−78 °C) hexane and dried at 20 °C and 10^{-2} Torr. Subsequent sublimation at 100 °C and 10^{-2} Torr yielded an air-sensitive, pink powder. Yield = 0.78 g (42%); m.p. 48 °C; ^{13}C NMR (100.569 MHz, C_6D_6, 22 °C, Si(CH$_3$)$_4$ relative to residual C_6D_5H): δ = −227.12 (s, *C*(CH$_3$)$_3$), −127.75 (s, C(*C*H$_3$)$_3$), −8.99 (s, Si(*C*H$_3$)$_2$); ^{29}Si NMR (79.4521 MHz, C_6D_6, 22 °C, external standard: Si(CH$_3$)$_4$): δ = 429 (s, *Si*(CH$_3$)$_2$(H)); MS (EI, 70 eV, 156 °C): *m/z* (%): 559 (6.6) [M^+ + 1], 558 (17.5) [M^+], 543 (20.7) [M^+ − Me], 528 (1.0) [M^+ − 2Me], 501 (2.0) [M^+ − *t*Bu], 499 (2.7) [M^+ − Si(CH$_3$)$_2$(H)], 485 (2.4) [M^+ − N[Si(CH$_3$)$_2$(H)]], 428 (3.5) [M^+ − N[*t*Bu][Si(CH$_3$)$_2$(H)]], 427 (4.7) [M^+ − N[*t*Bu][Si(CH$_3$)$_2$(H)] − (H)], 412 (21.7) [M^+ − N[*t*Bu][Si(CH$_3$)$_2$(H)] − (CH$_3$)(H)], 397 (9.8) [M^+ − N[*t*Bu][Si(CH$_3$)$_2$(H)] − (CH$_3$)$_2$(H)], 369 (12.8) [M^+ − N[*t*Bu][Si(CH$_3$)$_2$(H)] − [Si(CH$_3$)$_2$(H)]], 355 (8.0) [M^+ − N[*t*Bu][Si(CH$_3$)$_2$(H)] − N[Si(CH$_3$)$_2$(H)]], 298 (2.4) [M^+ − N[*t*Bu][Si(CH$_3$)$_2$(H)] − N[*t*Bu][Si(CH$_3$)$_2$(H)]], 130 (6.5) [N[*t*Bu][Si(CH$_3$)$_2$(H)]$^+$], 116 (100) [[*t*Bu][Si(CH$_3$)$_2$(H)]$^+$], 73 (20.3) [N[Si(CH$_3$)$_2$(H)]$^+$], 59 (38.1) [[Si(CH$_3$)$_2$(H)]$^+$].

Received: 16 June, 1995
Revised version: November 20, [Z8100IE]
German version: *Angew. Chem.* **1996**, *108*, 481–483

Keywords: agostic interactions · amido complexes · lanthanide compounds

[1] G. Pomrenke, H. Ennen, W. Haydl, *J. Appl. Phys.* **1986**, *59*, 601–610.
[2] a) J. E. Colon, D. W. Elsaesser, Y. K. Yeo, R. L. Hengehold, G. S. Pomrenke in *Rare Earth Doped Semiconductors, Vol. 301* (Eds.: G. S. Pomrenke, P. B. Klein, D. W. Langer), MRS, Pittsburgh, **1993**, p. 169; b) D. W. Elsaesser, J. E. Colon, Y. K. Yeo, R. L. Hengehold, G. S. Pomrenke, *ibid.* p. 251; c) F. Scholz, J. Weber, K. Pressel, A. Dörnen, *ibid.* p. 3.
[3] a) B. A. Block, B. W. Wessels, *Appl. Phys. Lett.* **1994**, *1*, 25–27; b) X. Z. Wang, B. W. Wessels, *ibid.* **1994**, *5*, 584–586; c) *ibid.* **1994**, *7*, 845–847.
[4] W. S. Rees, Jr., T. J. Anderson, D. M. Green, E. Bretschneider in *Wide Band-Gap Semiconductors, Vol. 242*, (Eds.: T. M. Moustakas, J. I. Pankove, Y. Hamakawa), MRS, Pittsburgh, **1992**, p. 281.
[5] a) W. S. Rees, Jr., D. M. Green, W. Hesse, T. J. Anderson, B. Pathangey in *Chemical Perspectives of Microelectronic Materials, Vol. 282*, (Eds.: C. R. Abernathy et al.), MRS, Pittsburgh, **1992**, p. 63; b) W. S. Rees, Jr., D. M. Green, T. J. Anderson, B. Pathangey, J. Kim, *J. Electron. Mater.* **1992**, *21*, 361–366; c) W. S. Rees, Jr., D. M. Green, W. Hesse, *Polyhedron* **1992**, *11*, 1667-1669.
[6] W. S. Rees, Jr., U. W. Lay, A. C. Greenwald in *Gas-Phase and Surface Chemistry in Electronic Materials Processing, Vol. 334*, (Eds.: T. J. Mountziaris, G. R. Paz-Pujalt, F. T. J. Smith, P. R. Westmoreland), MRS, Pittsburgh, **1994**, p. 207.
[7] A. C. Greenwald, W. S. Rees, Jr., U. W. Lay in *Rare Earth Doped Semiconductors, Vol. 301* (Eds.: G. S. Pomrenke, P. B. Klein, D. W. Langer), MRS, Pittsburgh, **1993**, p. 21.
[8] a) J. S. Ghotra, M. B. Hursthouse, A. J. Welch, *J. Chem. Soc. Chem. Commun.* **1973**, 669-670; b) P. G. Eller, D. C. Bradley, M. B. Hursthouse, D. W. Meek, *Coord. Chem. Rev.* **1977**, *24*, 1–195; c) R. A. Andersen, D. H. Templeton, A. Zalkin, *Inorg. Chem.* **1978**, *17*, 2317–2319.
[9] a) D. C. Bradley, J. S. Ghotra, F. A. Hart, *J. Chem. Soc. Chem. Commun.* **1972**, 349–350; b) *J. Chem. Soc. Dalton Trans.* **1973**, 1021–1023; c) D. C. Bradley, J. S. Ghotra, F. A. Hart, M. B. Hursthouse, P. R. Raithby, *J. Chem. Soc. Dalton Trans.* **1977**, 1166–1172.
[10] W. A. Herrmann, R. Anwander, F. C. Munck, W. Scherer, V. Dufaud, N. W. Huber, G. R. J. Artus, *Z. Naturforsch. B* **1994**, *49*, 1787–1797.
[11] H. Schumann, J. Winterfeld, E. C. E. Rosenthal, H. Hemling, L. Esser, *Z. Anorg. Allg. Chem.* **1995**, *621*, 122–130.
[12] A slight increase in vapor pressure for the purified product **1** versus the crude product **1** was noted. One potential source for the observation of a depression in the vapor pressure in the crude product is the presence of 'ate' complexes. Recently such species have been isolated in this laboratory by reacting $ErCl_3$ with three equivalents of LiN{(*t*Bu)[Si(CH$_3$)$_3$]} and crystallizing the reaction product from Et_2O. Details of crystallographic characterization of the obtained [Li(Et$_2$O)$_3$][Er{N(*t*Bu)[Si(CH$_3$)$_3$]}$_3$Cl] will be reported separately. It is noted that the formation of such 'ate' species appears to be irreversible, that is, once formed, they resist successful removal of LiCl and subsequent conversion to a neutral, homoleptic lanthanide tris[(silyl)(alkyl)amide] species.
[13] X-ray crystal structure analysis data: $C_{16}H_{48}N_3Si_3Er$, M_r = 534.10 g mol^{-1}, monoclinic, space group $P2_1/n$, a = 11.128(2), b = 14.430(3), c = 17.943(3) Å, β = 90.73(2)°, V = 28.810(9) Å^3, Z = 4, ρ_{calcd} = 1.231 g cm^{-3}, crystal size 0.33 × 0.53 × 0.4 mm^3, number of reflections for lattice parameters = 25 (19.5° ≤ 2θ ≤ 26.6°), T = 185 K, μ = 3.041 mm^{-1}, F(000) = 1100. Data collection and correction: Enraf-Nonius CAD-4 diffractometer, $Mo_{K\alpha}$ radiation (λ = 0.71073 Å), graphite monochromator, aperture 2.5 mm, scan time variable, max. 45 s, scan angle (0.93 + 0.35 tanθ)°, scan technique ω-2θ, range 2° < 2θ < 48°, *hkl* boundaries: −12 ≤ *h* ≤ 12, 0 ≤ *k* ≤ 16, 0 ≤ *l* ≤ 20, total number of measured reflections: 4971, unique reflections: 4346 (R = 0.0227), observed reflections with [|F_o| ≥ 4σ|F_o|]: 4340, corrections: Lorentz, polarization, absorption (DIFABS: correction factors: min. 0.917, max. 1.164). Solution and refinement: structure solution by Patterson method, full-matrix least-squares refinement, 236 parameters refined. The methyl groups in the *t*Bu moiety attached to nitrogen N1 were found to be disordered over two sites (C14–C16/C141–C161), each occupying a population parameter of 0.5. The disordered carbon atoms and the agostic hydrogen atoms H1, H2, H3 each were refined with isotropic, whereas all other non-hydrogen atoms were refined with anisotropic, thermal parameters. All hydrogen atoms were calculated in idealized positions (C–H 96 pm, U_{iso} = 0.08 Å^2, final residue value R_1 = $\Sigma(|F_o| - |F_c|)/\Sigma|F_o|$ = 0.0190, R_2 = $[\Sigma_w(|F_o| - |F_c|)^2/\Sigma_w(|F_o|^2)]^{1/2}$ = 0.0417

($w = 1/\sigma^2(F_o)$), Goof = $[\Sigma_w(|F_o| - |F_c|)^2/(n-p)]1/2 = 1.051$, $\Delta\rho$(max./min.) = max. 0.404 e Å^{-3} and min. -0.300 e Å^{-3}. All refinements were performed by using the SHELXL-93 program system [14]. Further details of the crystal structure investigation are available on request from the Fachinformationszentrum Karlsruhe GmbH, D-76344 Eggenstein-Loepoldshafen (Germany) on quoting the dispository number CSD-404714.

[14] G. M. Sheldrick, SHELXL-93, Program for Crystal Structure Determination, University Göttingen, **1993**.

[15] L. Zsolnai, H. Pritzkow, ZORTEP, ORTEP Program for PC, University Heidelberg, **1993**.

[16] M. Brookhart, M. L. H. Green, *J. Organomet. Chem.* **1983**, *250*, 395–408.

[17] *Encyclopedia of Inorganic Chemistry*, *Vol. 1*, (Ed. R. B. King), Wiley, Chichester, England, **1994**, p. 35.

[18] G. J. Kubas, *Acc. Chem. Res.* **1988**, *21*, 120–128.

[19] a) X. L. Luo, G. J. Kubas, J. C. Bryan, C. J. Burns, C. J. Unkefer, *J. Am. Chem. Soc.* **1994**, *116*, 10312–10313; b) E. Spaltenstein, P. Palma, K. A. Kreutzer, C. A. Willoughby, W. M. Davis, S. L. Buchwald, *ibid.* **1994**, *116*, 10308–10309.

[20] H. Schumann, M. Glanz, H. Hemling, F. E. Hahn, *Z. Anorg. Allg. Chem.* **1995**, *621*, 341–345.

[21] J. Weidlein, U. Müller, K. Dehnicke, *Schwingungsfrequenzen I Hauptgruppenelemente*, 1st ed., Thieme, Stuttgart, **1981**, p. 261.

[22] a) R. H. Crabtree, *Angew. Chem.* **1993**, *105*, 828–845; *Angew. Chem. Int. Ed. Engl.* **1993**, *31*, 789–805; b) *Acc. Chem. Res.* **1990**, *23*, 95–101.

[23] a) C. J. Schaverien, G. J. Nesbitt, *J. Chem. Soc. Dalton Trans.* **1992**, 157–167; b) G. Jeske, H. Lauke, H. Mauermann, P. N. Swepston, H. Schumann, T. J. Marks, *J. Am. Chem. Soc.* **1985**, *107*, 8091–8103; c) G. Jeske, L. E. Schock, P. N. Swepston, H. Schumann, T. J. Marks, *ibid.* **1985**, *107*, 8103–8110.

[24] T. D. Tilley, R. A. Andersen, A. Zalkin, *J. Am. Chem. Soc.* **1982**, *104*, 3725–3727.

[25] a) D. M. Barnhart, D. L. Clark, S. K. Grumbine, J. G. Watkin, *Inorg. Chem.* **1995**, *34*, 1695–1699; b) D. L. Clark, M. M. Miller, J. G. Watkin, *ibid.* **1993**, *32*, 772–774; c) D. M. Barnhart, D. L. Clark, J. C. Gordon, J. C. Huffman, J. G. Watkin, B. D. Zwick, *J. Am. Chem. Soc.* **1993**, *115*, 8461–8462; d) K. H. den Haan, J. L. de Boer, J. H. Teuben, A. L. Spek, B. Kojic-Prodic, G. R. Hays, R. Huis, *Organometallics*, **1986**, *5*, 1726–1733; e) W. G. Van Der Sluys, C. J. Burns, A. P. Sattelberger, *ibid.* **1989**, *8*, 855–857.

[26] X. L. Luo, G. J. Kubas, C. J. Burns, J. C. Bryan, C. J. Unkefer in *Book of Abstracts*, 209th ACS National Meeting, Anaheim, **1995**, Division of Inorganic Chemistry, entry 082.

Eight-Coordinate Iron(II) and Iron(III) Ions in Complexes with Distorted Dodecahedral FeN_8 Environments: Synthesis and Structures of Bis(2,11-diaza[3.3](2,6)pyridinophane)iron Complexes**

Welf O. Koch, Adriana Barbieri, Michael Grodzicki, Volker Schünemann, Alfred X. Trautwein, and Hans-Jörg Krüger*

The classical coordination chemistry of iron is dominated by four-, five-, and six-coordinate metal ions, while coordination numbers higher than six are only occasionally encountered in discrete molecules.[1] To our knowledge, only four complexes with eight-coordinate iron ions have been confirmed by X-ray structure determinations: three with an iron(II)[2–4] and one with an iron(III) ion.[5] The formation of these compounds is strongly dependent on the type of ligands used in the synthesis and is confined 1) to bidentate ligands (nitrate,[5] 1,8-naphthyridine = napy[2]) with small chelate bites, which render four-membered chelate rings with the metal ion, 2) to tetradentate ligands (O_4-[12]ane),[3] which form sandwich-like complexes, and 3) to octadentate ligands,[4] in which the backbone of the ligand is specially designed for the encapsulation of the central metal ion by all eight donor atoms. In these studies, only neutral nitrogen or oxygen donor atoms were found to coordinate iron(II) ions, while the coordination of iron(III) ion was restricted to anionic oxygen donors. The ligand donor atoms are generally arranged in the form of a distorted square prism or a distorted dodecahedron.

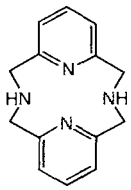

L-N_4H_2

We utilized derivatives of the tetraazamacrocyclic ligand 2,11-diaza[3.3](2,6)pyridinophane L-N_4H_2.[6] In eight-coordinate iron complexes that contain tetraoxocyclododecane[3] or tetraazacyclododecane derivatives[4] as ligands all donor atoms of the macrocyclic ring lie in a plane. This cannot occur in L-N_4H_2-containing complexes because of the ligand's rigidity due to the pyridine rings and its preference to assume a boat–boat conformation upon coordination.[6] With this ligand all four nitrogen donors are arranged in a rhombus which is bent along the shorter diagonal (= $N_{py}-N_{py}$ axis). This arrangement also occurs in dodecahedral coordination geometries; thus, utilization of two molecules of L-N_4H_2 per metal ion was considered to be a promising route to the synthesis of complexes with eight-coordination at the central ion. We report here on the synthesis and structures of iron complexes of the type $[Fe(L\text{-}N_4H_2)_2]^{n+}$.

The reaction of two equivalents of L-N_4H_2 with iron(II) perchlorate in methanol under a nitrogen atmosphere and subsequent metathesis with sodium tetraphenylborate yields a yellow precipitate, which after recrystallization in acetonitrile/ether analyzes correctly for a complex of the composition **1**.

$[Fe(L\text{-}N_4H_2)_2](BPh_4)_2 \cdot Et_2O$ **1**

As a solid and even in solution, **1** is not oxygen-sensitive. Its cyclic voltammogram (Fig. 1) displays an oxidative electron transfer reaction at +385 mV vs. SCE[7] which approaches electrochemical reversibility ($\Delta E_p = 70$ mV and $i_{pc}/i_{pa} \approx 1$ at all scan rates, $i_p/v^{1/2}$ = constant). The electrolysis of a solution of **1** in acetonitrile at an applied potential of +590 mV vs. SCE

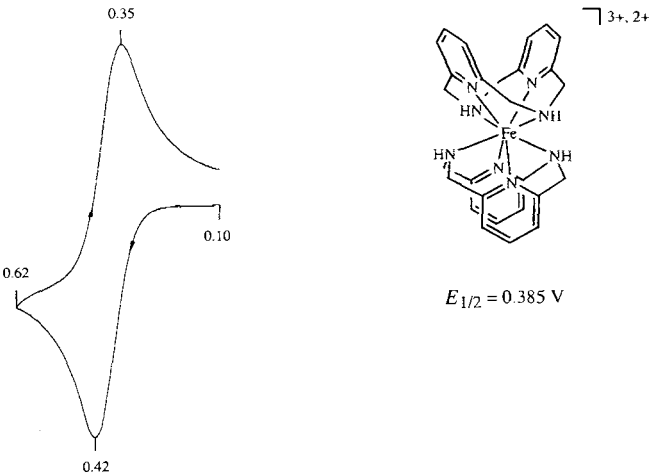

Fig. 1. Cyclic voltammogram (50 mV s^{-1}) of $[Fe(L\text{-}N_4H_2)_2]^{2+}$ at a Pt foil electrode in acetonitrile at 25 °C; peak potentials and half-wave potential vs. SCE are indicated.

[*] Dr. H.-J. Krüger, W. O. Koch
Institut für Anorganische und Angewandte Chemie der Universität Hamburg
Martin-Luther-King-Platz 6, D-20146 Hamburg (Germany)
Fax: Int. code +(40)41232893
A. Barbieri, Dr. habil. M. Grodzicki, Dr. V. Schünemann,
Prof. Dr. A. X. Trautwein
Institut für Physik der Medizinischen Universität Lübeck (Germany)

[**] This work was in part supported by a grant from the Deutsche Forschungsgemeinschaft.

renders a pale yellow solution after a total transfer of 1.00 e^- per molecule of **1**. Re-reduction of the iron(III) species at +190 mV accounts for 96% of recovery of the initial iron(II) complex, indicating that the oxidized species is sufficiently stable to warrant a bulk preparation. However, attempts to synthesize the iron(III) complex directly from iron(III) perchlorate and the free ligand or alternatively by chemical oxidation of complex **1** have failed. The iron(III) complex was eventually obtained by bulk electrolysis of **1** in acetonitrile at +590 mV vs. SCE and isolated as **2**. Magnetic susceptibility measurements at room temperature revealed that complexes **1** and **2** contain high-spin iron.

$[Fe(L\text{-}N_4H_2)_2](ClO_4)_3$ **2**

Complexes **1** and **2** could be obtained as single crystals; their structures were determined by X-ray diffraction[8] (Fig. 2). In both complexes the iron ion is coordinated by all nitrogen

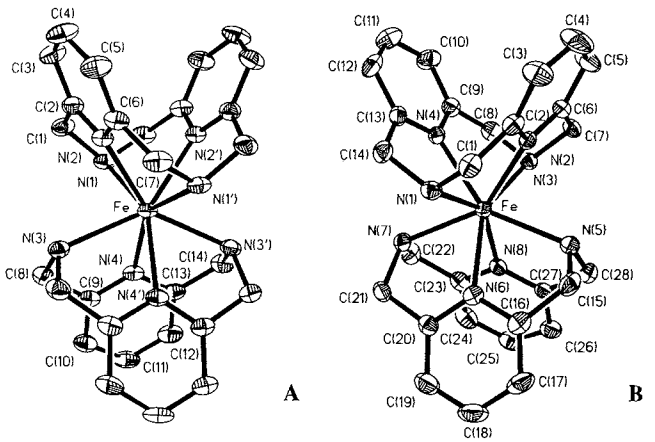

Fig. 2. Crystal structures of the $[Fe(L\text{-}N_4H_2)_2]^{2+}$ (**A**) and $[Fe(L\text{-}N_4H_2)_2]^{3+}$ ions (**B**) showing thermal ellipsoids at 50% probability and the atom numbering schemes. Selected distances [Å] and angles [°]: **A** (the primed and unprimed atoms are related by a twofold rotation axis): Fe–N(1) 2.372(2), Fe–N(2) 2.290(2), Fe–N(3) 2.392(2), Fe–N(4) 2.305(2); N(1)-Fe-N(2) 71.67(6), N(1)-Fe-N(3) 82.46(6), N(1)-Fe-N(4) 78.99(6), N(1)-Fe-N(1') 133.34(8), N(1)-Fe-N(2') 71.23(6), N(1)-Fe-N(3') 116.48(7), N(1)-Fe-N(4') 146.12(6), N(2)-Fe-N(3) 78.86(6), N(2)-Fe-N(4) 140.26(6), N(2)-Fe-N(2') 73.09(9), N(2)-Fe-N(3') 146.23(6), N(2)-Fe-N(4') 121.86(7), N(3)-Fe-N(4) 71.10(7), N(3)-Fe-N(3') 133.20(9), N(3)-Fe-N(4') 71.51(6), N(4)-Fe-N(4') 72.38(9). **B**: Fe–N(1) 2.290(3), Fe–N(2) 2.211(3), Fe–N(3) 2.325(3), Fe–N(4) 2.218(3), Fe–N(5) 2.299(3), Fe–N(6) 2.236(3), Fe–N(7) 2.313(3), Fe–N(8) 2.218(3); N(1)-Fe-N(2) 72.8(1), N(1)-Fe-N(3) 136.9(1), N(1)-Fe-N(4) 74.0(1), N(1)-Fe-N(5) 114.1(1), N(1)-Fe-N(6) 77.3(1), N(1)-Fe-N(7) 82.3(1), N(1)-Fe-N(8) 145.1(1), N(2)-Fe-N(3) 73.2(1), N(2)-Fe-N(4) 74.6(1), N(2)-Fe-N(5) 76.2(1), N(2)-Fe-N(6) 121.3(1), N(2)-Fe-N(7) 146.0(1), N(2)-Fe-N(8) 139.6(1), N(3)-Fe-N(4) 72.1(1), N(3)-Fe-N(5) 82.1(1), N(3)-Fe-N(6) 144.4(1), N(3)-Fe-N(7) 114.21(9), N(3)-Fe-N(8) 76.49(9), N(4)-Fe-N(5) 145.4(1), N(4)-Fe-N(6) 140.5(1), N(4)-Fe-N(7) 76.6(1), N(4)-Fe-N(8) 120.0(1), N(5)-Fe-N(6) 71.9(1), N(5)-Fe-N(7) 136.4(1), N(5)-Fe-N(8) 73.8(1), N(6)-Fe-N(7) 73.2(1), N(6)-Fe-N(8) 73.3(1), N(7)-Fe-N(8) 71.7(1).

donors of the two ligand molecules; thus, the metal ions in both complexes are unambiguously eight-coordinate. The coordination geometries are best described as distorted dodecahedrons. Instead of a torsional angle of 90° between both ligand moieties, as is required in an ideal dodecahedral geometry (D_{2d} symmetry), the angle found is only 70°. Hence, the overall structures of both complexes approach D_2 symmetry.

In complex **1**, the average $Fe-N_{py}$ and $Fe-N_{amine}$ bond lengths are 2.298 ± 0.008 and 2.382 ± 0.010 Å, respectively; which are about 0.1 Å larger than those observed in octahedral high-spin iron(II) complexes with $L\text{-}N_4H_2$ ligands.[6] Upon oxidation, the Fe–N bond lengths decrease to 2.221 ± 0.014 and 2.307 ± 0.018 Å, respectively, which are also considerably longer than those found in six-coordinate high-spin iron(III) complexes.[6] The substantial decrease in Fe–N bond lengths upon oxidation is a clear sign of metal-centered oxidation. The N_{py}-Fe-N_{py} and N_{amine}-Fe-N_{amine} angles, defined by the Fe–N bonds to the same ligand moiety (72.7° and 133.3° for **1** and 73.9° and 136.6° for **2**), hardly change upon oxidation of the iron ion. As in octahedral iron complexes containing this ligand, the metal ion is not placed on the intersecting line of the least-squares planes of those pyridine rings belonging to the same ligand unit. The angles included by these planes are only 46° for **1** and 55° for **2**.

The only Mössbauer study, to our knowledge, carried out on discrete high-spin eight-coordinate iron(II) complexes involved the complex $[Fe(napy)_4]^{2+}$, where $\Delta E_Q = +4.54$ mm s^{-1} constitutes one of the largest quadrupole splittings ever found for an iron(II) compound.[9] The Mössbauer spectra of **1** as a solid and in rapidly frozen acetonitrile solution were recorded at 4.2 K. Both spectra consist of a doublet with an isomer shift $\delta_{IS} = 1.24(1)$ mm s^{-1} (relative to α-Fe at 300 K) and a quadrupole splitting $\Delta E_Q = 3.05(1)$ mm s^{-1}, indicating that in solution the same distorted dodecahedral coordination geometry of the iron ion is present as in the crystalline solid. An additional measurement of **1** as a solid at 150 K in a field of 4 T $\perp \gamma$ documented the asymmetry parameter η and the sign of the electric field gradient: $\eta = 0.1(1)$, ΔE_Q (150 K) $= -3.02(1)$ mm s^{-1}.

Molecular orbital calculations in local spin density approximation by the SCC-Xα method[10] using the experimentally determined atomic positions of the cation in **1** yield $\Delta E_Q = -3.30$ mm s^{-1} and a small asymmetry parameter ($\eta = 0.14$). The direction of the main component V_{zz} of the electric field gradient tensor coincides with the bisectors of the angles N(2)-Fe-N(2') and N(4)-Fe-N(4') (cf. Fig. 2, **A**). Taking this direction as the molecular z axis, the Fe(3d) shell occupation of the high-spin ground state for the iron(II) complex is approximately $(d_{z^2})^2(d_{x^2-y^2})^1(d_{xz})^1(d_{xy})^1(d_{yz})^1$.[11] In conclusion, the results of the Mössbauer investigations show that a large quadrupole splitting ($\Delta E_Q \geq 4$ mm s^{-1}) is not a general property of the eight-coordinate iron(II) ion but reflects the particular electronic structure of a high-spin iron(II) complex. On the one hand, complex **1**, which contains an eight-coordinate iron(II) ion, yields a quadrupole splitting ΔE_Q of about 3 mm s^{-1}, whereas, on the other hand, five-coordinate iron(II) porphyrin complexes with anionic axial ligands, exhibit ΔE_Q values of ≥ 4 mm s^{-1}.[12]

For the first time, eight-coordinate iron ions have been established in a pair of iron complexes with identical ligand environments. These complexes differ only in the oxidation state of the metal ion. Compound **2**[13] is the first eight-coordinate iron(III) complex with a neutral donor atom set. In contrast to $[Fe(napy)_4]^{2+}$ and $[Fe(NO_3)_4]^-$ ions with four-membered chelate rings, only five-membered chelate rings are found in **1** and **2**. The current study has demonstrated that the use of the ligand $L\text{-}N_4H_2$ provides a systematic way to synthesize complexes with eight-coordination at the central ion. An extended investigation with other metal ions, especially with those of the first transition metal row, is currently in progress.

While some of the previously reported eight-coordinate iron complexes change their coordination environment on dissolution,[9b, 14] complexes **1** and **2** are stable and maintain their coordination geometry in solution. They are, therefore, well suited for a detailed investigation of the electronic properties of eight-coordinate iron ions.

Experimental Procedure

1: Under an atmosphere of pure nitrogen a solution of $[Fe(H_2O)_6](ClO_4)_2$ (91 mg, 0.25 mmol) in methanol (15 mL) was added to a solution of L-N_4H_2 (120 mg, 0.5 mmol) in methanol (30 mL). The mixture was heated to reflux and then cooled again to room temperature before it was treated with a solution of sodium tetraphenylborate (171 mg, 0.5 mmol) in methanol (15 mL). The reaction mixture was subsequently heated to reflux for a short time, and the resulting yellow precipitate was collected by filtration under air and washed twice with small amounts of methanol. Recrystallization by ether diffusion into a solution of the complex in acetonitrile afforded **1** (249 mg) as analytically pure, large yellow crystals (80% yield). Anal. calcd. for $C_{80}H_{82}B_2FeN_8O$: C 76.93, H 6.62, N 8.97; found: C 76.90, H 6.77, N 9.08. Magnetic moment $\mu = 4.89\ \mu_B$.

2: Over a period of 7.5 h, **1** (290 mg, 0.23 mmol) was electrolyzed at +590 mV vs. SCE in acetonitrile (60 mL) containing tetrabutylammonium perchlorate (4.1 g) as supporting electrolyte. The electrolysis was carried out at a platinum net electrode with a PAR Model 273A Potentiostat/Galvanostat controlled by the Model 270 Research Electrochemistry Software. After the passage of 96.6% of the theoretical amount of electrons, the resulting pale-yellowish solution which contained already partially precipitated product was stored at −30 °C overnight. The precipitate was isolated by filtration and washed with copious amounts of ethanol and ether. Ether diffusion into a solution of the solid in acetonitrile yielded pale-yellow crystals of the composition $[Fe(L\text{-}N_4H_2)_2](ClO_4)_3 \cdot MeCN$. Since the acetonitrile molecule in the crystal lattice is quite volatile, the solid was kept under vacuo for one day rendering 137 mg of analytically pure product (71% yield). Anal. calcd. for $C_{28}H_{32}Cl_3FeN_8O_{12}$: C 40.29, H 3.86, N 13.42; found: C 40.07; H 3.87; N 13.24. Magnetic moment $\mu = 5.54\ \mu_B$.

Warning: Perchlorate salts are potentially explosive and should be handled with care [15]. Since the solid does explode upon grinding, such procedures, if they are absolutely necessary, should only be carried out with small amounts of complex!

Received: July 10, 1995 [Z 8183 IE]
German version: *Angew. Chem.* **1996**, *108*, 484–486

Keywords: coordination · iron compounds · macrocycles · Mössbauer spectroscopy

[1] a) P. N. Hawker, M. V. Twigg in *Comprehensive Coordination Chemistry, Vol. 4* (Eds.: G. Wilkinson, R. D. Gillard, J. A. McCleverty), Pergamon Press, Oxford, **1987**, chapter 44.1; b) S. M. Nelson, *ibid.* chapter 44.2; c) S. J. Lippard, *Prog. Inorg. Chem.* **1967**, *8*, 114.

[2] napy = 1,8-naphthyridine; a) P. Singh, A. Clearfield, I. Bernal, *J. Coord. Chem.* **1971**, *1*, 29; b) A. Clearfield, P. Singh, I. Bernal, *J. Chem. Soc. Chem. Commun.* **1970**, 389.

[3] O_4-[12]ane = 1,4,7,10-tetraoxocyclododecane; K. Meier, G. Rihs, *Angew. Chem.* **1985**, *97*, 879; *Angew. Chem. Int. Ed. Engl.* **1985**, *24*, 858.

[4] M. Di Vaira, F. Mani, P. Stoppioni, *J. Chem. Soc. Dalton* **1992**, 1127.

[5] T. J. King, N. Logan, A. Morris, S. C. Wallwork, *J. Chem. Soc. Chem. Commun.* **1971**, 554.

[6] a) H.-J. Krüger, *Chem. Ber.* **1995**, *128*, 531; b) W. O. Koch, H.-J. Krüger, *Angew. Chem.* **1995**, *107*, 2928; *Angew. Chem. Int. Ed. Engl.* **1995**, *34*, 2671; c) W. Koch, H.-J. Krüger, unpublished results.

[7] Under these conditions the ferrocene/ferrocenium redox couple has a redox potential at +390 mV vs. the saturated calomel electrode (SCE). ΔE_p = separation of the peak potentials, i_{pa} = anodic peak current, i_{pc} = cathodic peak current, v = scan rate.

[8] Crystallographical data of $[Fe(L\text{-}N_4H_2)_2](BPh_4)_2 \cdot Et_2O$ (**1**): crystal size $0.3 \times 0.5 \times 0.8$ mm, crystal system monoclinic, space group $C2/c$, a = 22.856(4), b = 15.015(4), c = 21.469(5) Å, β = 115.76(3)°, V = 6636(3) Å^3, $Z = 4$, $\rho_{calcd} = 1.25\ g\,cm^{-3}$; $2\theta_{max} = 102.02°$, $\lambda = 1.54178$ Å, scan method ω-2θ, temperature 153 K, 7426 collected reflections; 3564 unique reflections (3428 reflections with $F_0 > 4\sigma(F_0)$), $\mu(Cu_{K\alpha}) = 22.31\ cm^{-1}$, Enraf-Nonius-CAD4-diffractometer; graphite monochromatized $Cu_{K\alpha}$ radiation; structure solution and refinement: direct methods (SHELXS-86) and full-matrix least-squares on F^2 (SHELXL-93); 427 parameters; anisotropic refinement of all non-hydrogen atoms, isotropic refinement of calculated hydrogens; $R = 0.0372$ ($F_0 > 4\sigma(F_0)$); $R_w = 0.0876$, largest diff. peak and hole = 0.225 and −0.479 e Å^{-3}. Crystallographical data of $[Fe(L\text{-}N_4H_2)_2](ClO_4)_3 \cdot MeCN$ (**2**·MeCN): crystal size $0.3 \times 0.3 \times 0.3$ mm, crystal system monoclinic, space group $P2_1/n$, a = 11.833(4), b = 17.110(5), c = 17.924(8) Å, β = 91.17(3)°, V = 3628(2) Å^3, $Z = 4$, $\rho_{calcd} = 1.603\ g\,cm^{-3}$; $2\theta_{max} = 50.1°$, $\lambda = 0.71073$ Å, scan method ω-2θ, temperature 153 K, 8019 collected reflections; 6426 unique reflections (4512 reflections with $F_0 > 4\sigma(F_0)$), $\mu(Mo_{K\alpha}) = 7.12\ cm^{-1}$, Hilger & Watts diffractometer; graphite monochromatized $Mo_{K\alpha}$ radiation; structure solution and refinement: direct methods (SHELXS-86) and full-matrix least-squares on F^2 (SHELXL-93); 529 parameters; anisotropic refinement of all non-hydrogen atoms, isotropic refinement of calculated hydrogens; $R = 0.0422$ ($F_0 > 4\sigma(F_0)$); $R_w = 0.0837$, largest diff. peak and hole = 0.352 and −0.381 e Å^{-3}. Further details of the crystal structure investigations are available on request from the Fachinformationszentrum Karlsruhe, D-76344 Eggenstein-Leopoldshafen (Germany), on quoting the depository numbers CSD-404023 (**1**) and CSD-404024 (**2**·MeCN).

[9] a) E. König, G. Ritter, E. Lindner, I. P. Lorenz, *Chem. Phys. Letts.* **1972**, *13*, 70; b) E. Dittmar, C. J. Alexander, M. L. Good, *J. Coord. Chem.* **1972**, *2*, 69; c) E. Zimmermann, H. Spiering, G. Ritter, *Chem. Phys.* **1974**, *4*, 133.

[10] a) M. Grodzicki, *J. Phys.* **1980**, *B13*, 2683; b) M. Grodzicki, Theorie und Anwendungen der Self-Consistent-Charge-Xα-Methode, Thesis of Habilitation, Hamburg, **1985**; c) R. Bläs, J. Guillin, E. L. Bominaar, M. Grodzicki, V. R. Marathe, A. X. Trautwein, *J. Phys.* **1987**, *B20*, 5627.

[11] In more detail the local spin density calculation renders the occupation numbers $d_\uparrow^{4.99} d_{z^2\downarrow}^{0.97} d_{x^2-y^2\downarrow}^{0.11} d_{xy\downarrow}^{0.15} d_{xz\downarrow}^{0.14} d_{yz\downarrow}^{0.15}$. The d_{z^2} orbital is almost nonbonding for both spin directions, while the occupation numbers of the other four "spin-down" Fe(3d) orbitals reveal some covalent contributions from the Fe–N bonds, resulting in a reduction of the electric field gradient arising from the d_{z^2} orbital alone. These results emphasize that the cation in complex **1** cannot be compared with the $[Fe(napy)_4]^{2+}$ ion, for which a positive quadrupole splitting is found and in which the d_{xy} orbital is the doubly occupied molecular orbital [9c]. Detailed molecular orbital calculations are currently under way to elucidate the differences in electronic structure between the two eight-coordinate iron(II) complexes.

[12] E. L. Bominaar, X.-Q. Ding, A. Gismelseed, E. Bill, H. Winkler, A. X. Trautwein, H. Nasri, J. Fischer, R. Weiss, *Inorg. Chem.* **1992**, *31*, 1845.

[13] Complex **2** exhibits broad and unresolved Mössbauer spectra due to intermediate electronic relaxation in the whole temperature range between 4.2 and 300 K. Mössbauer measurements under strong applied field and their spin-Hamiltonian analysis are in progress.

[14] R. L. Bodner, D. G. Hendricker, *Inorg. Chem.* **1973**, *12*, 33.

[15] a) W. C. Wolsey, *J. Chem. Educ.* **1973**, *50*, A335; b) K. N. Raymond, *Chem. Eng. News* **1983**, *61*, (49), 4.

Transition Metal Stabilized Al^I and Ga^I Complexes; Structure of $[(CO)_5Cr-Ga\{(CH_3)(tmeda)\}]$**

Markus M. Schulte, Eberhardt Herdtweck, Gabriele Raudaschl-Sieber, and Roland A. Fischer*

The chemistry of low-valent Al and Ga compounds, pioneered by Schnöckel et al.[1] and Uhl et al.[2], is currently undergoing rapid development. Recently, high-vacuum co-condensation techniques have been employed to obtain compounds such as E^IX (E = Al, Ga; X = Cl, Br) as metastable solutions that were subsequently used in synthesis.[1] E–E bonds are a typical structural feature of E^IR systems in the solid-state (R = halogen, alkyl, η^5-C_5R_5).[1, 2] We report here on the first transition metal stabilized Al^I and Ga^I complexes that do not contain E–E bonds and on some of the applications of these volatile precursors in MOCVD processes (MOCVD = metal organic chemical vapor deposition) for the deposition of intermetallic thin films.

Equimolar amounts of Cl_2ER (E = Al, Ga; R = Cl, alkyl) and $K_2[Cr(CO)_5]$ react in THF according to Scheme 1 to give the anionic species $K[(CO)_5Cr-E(Cl)(R)]$, which could be isolated after salt metathesis as solvent-free Ph_4P or PPN salts (PPN = $Ph_3P{=}N{=}PPh_3$). If the THF is replaced successively by CH_2Cl_2, the potassium salts eliminate the second equivalent

[*] Dr. habil. R. A. Fischer,[+] Dipl.-Chem. M. M. Schulte, Dr. E. Herdtweck, Dr. G. Raudaschl-Sieber
Anorganisch-chemisches Institut der Technischen Universität München
Lichtenbergstrasse 4, D-85747 Garching (Germany)
Fax: Int. code +(89)3209-3473

[+] New address: Anorganisch-chemisches Institut der Universität
Am Neuenheimer Feld 270, D-69120 Heidelberg (Germany)

[**] Organo-Group 13 Metal Complexes of the d-Block Elements, Part 13. This work was supported by the Fonds der Chemischen Industrie and the Deutsche Forschungsgemeinschaft. We also thank the Anorganisch-chemisches Institut for generous support. Part 12: see ref. [3]. tmeda = *N,N,N',N'*-tetramethylenediamine.

of KCl. In this way, $[(CO)_5Cr-Ga(Cl)(thf)_2]$ was obtained. In contrast, Cl abstraction from the respective Ph_4P or PPN salts was achieved only with $Tl[PF_6]$. Addition of a bidentate Lewis base to solutions of the potassium species in CH_2Cl_2 leads to the formation of compounds **1**–**5** (Scheme 1), which crystallize as

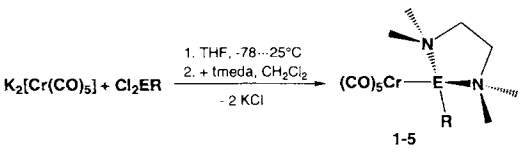

Scheme 1. **1**–**3**: E = Ga; **4**,**5**: E = Al; **1**: R = Me; **2**, **4**: R = Et; **3**, **5**: R = Cl.

colorless to yellow cubes or prisms from concentrated CH_2Cl_2 solutions (yields >90%). The Ga compounds, in particular, are quite air and moisture stable, even for longer periods of time, whereas the related Ga^{III} complexes[3] $[L_nM-GaR_2(Do)]$ (Do = donor ligand) decompose instantaneously. Thus, Raman spectra on the single crystals could be recorded without any special precautions.[4]

Only for In have complexes structurally analogous to **1**–**5** been confirmed by X-ray crystallography ($[(CO)_5Cr-In-Br(thf)]$[5] and $[\{HB(3,5\text{-}Me_2pz)_3\}In-M(CO)_n]$ (M = Fe, $n = 4$; M = W, $n = 5$; 3,5-Me_2pz = 3,5-dimethylpyrazolyl)).[6] The former is polymeric in the solid state (intermolecular In···Br–In contacts). The X-ray structure analysis of **1**[7] (Fig. 1) exemplifies the monomeric structure of the compounds

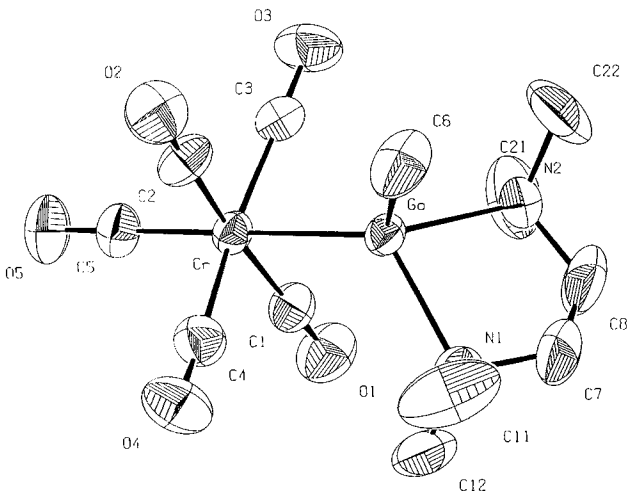

Fig. 1. Structure of **1** in the crystal (ORTEP plot). Hydrogen atoms were omitted for clarity. Selected bond lengths [pm] and angles [°]: Ga–Cr 247.85(11), Ga–N1 217.3(5), Ga–N2 217.4(5), Ga–C6 198.4(6), Cr–C1 186.9(6), Cr–C2 183.9(6), Cr–C3 186.8(6), Cr–C4 186.0(6), Cr–C5 184.7(6); Cr-Ga-N1 120.6(1), Cr-Ga-N2 119.8(2), Cr-Ga-C6 122.5(2), N1-Ga-N2 82.32(19), N1-Ga-C6 101.6(2), N2-Ga-C6 101.6(3), Ga-Cr-C1 89.3(2), Ga-Cr-C2 85.3(2), Ga-Cr-C3 84.7(2), Ga-Cr-C4 85.4(2), Ga-Cr-C5 179.4(2).

reported herein. This is considered to be responsible for their volatility. The Cr–Ga bond (247.8(2) pm) in **1** is unprecedented for molecular compounds.[8] The description of **1**–**5** as Al^I and Ga^I systems is supported by the structural analogy to the In^I systems. Additional evidence is provided by the vibrational spectra. The IR absorptions in the ν(CO) range lie between 1880 and 2030 cm^{-1} and are shifted to significantly *higher* energies than those of the anionic intermediates (1830–1990 cm^{-1}). An analysis of the ν(CO) force constants by using the "CK" approximation[4] confirmed the analogy of **1**–**5** with neutral $L(CO)M^0$ complexes (L = phosphine, arsine). The fragments $[E(R)(tmeda)^0]$ are isolobal to PR_3 and AsR_3 (R = alkyl, Cl) and are regarded as potent σ donors; however, some π-acceptor capabilities are evidently still present (similar to PCl_3). In this sense the bonding in these M–E systems is similar to that in donor-stabilized transition metal silylene complexes.[9] A description of **1**–**5** as complex $M-E^{III}$ contact ion pairs, under the assumption of strongly negatively polarized 18-electron $(CO)_5M^{2-}$ fragments and twofold positively charged $ER(Do)_2^{2+}$ units, appears inappropriate, even when the group electronegativities of the $(CO)_nM$ fragments (which are about 4) are taken into consideration.[10] The exchange of the basic ligand TMEDA by N-base ligands with conjugated π-electron systems (bipyridine, diazabutadiene) gave intense metal–ligand charge-transfer bands in the UV/Vis spectra.[11] In contrast to some E^{III} complexes, it is also remarkable that the metal–metal bonds are preferred over isocarbonyl structures M–C=O–E (E = Al, Ga),[12] and that **1**–**5** are stable to heterolytic bond dissociation in coordinating solvents such as THF and CH_3CN.[3] The ^{27}Al NMR resonances ($\delta = +156$ for **5**) are shifted to higher field compared to those of the Al^{III} complexes $[L_nM-AlR_2(Do)]$ ($\delta = +200 \pm 10$).[12] Qualitatively, this is consistent with the results of ab initio calculations for solvated Al^ICl.[13] Also the mass spectra of complexes **1**–**3**, which volatilize at 110–130 °C and 10^{-3}–10^{-4} Torr without decomposition, show unexpected effects compared to the spectra of the E^{III} complexes. After loss of TMEDA, a series of complex fragments $[(CO)_mMGaR]$ ($m \leq n$) containing an intact M–Ga bond are observed. In contrast, cleavage of the M–Ga bond is preferred for all Ga^{III} complexes $[L_nM-GaR_2(Do)]$. These complexes react cleanly with halogens X_2 by oxidative M–E bond cleavage to give $[(CO)_5M(X)]^-$ and $[(X)(R)E(tmeda)]^+$. Because $[(CO)_5M(X)]^-$ can be described as a Lewis acid base adduct of X^- to the 16-electron fragment $(CO)_5M^0$, the assumption of an oxidation $E^I \rightarrow E^{III}$ is plausible. A selective functionalization of the E–Cl units is possible. Thus, **3** and **5** could be converted smoothly with LiH and $LiBH_4$ into the corresponding hydrides and boranates, respectively.

MOCVD experiments with the Cr–Ga complex **2** were carried out in an isothermal horizontal, hot-wall reactor (10^{-3} Torr, 250 °C).[14] Ex situ analysis (atomic absorption spectroscopy (AAS), scanning electron microscopy–energy-dispersive X-ray analysis (SEM-EDX), and X-ray photoelectron spectroscopy (XPS), Fig. 2) of the resulting metallic, shiny,

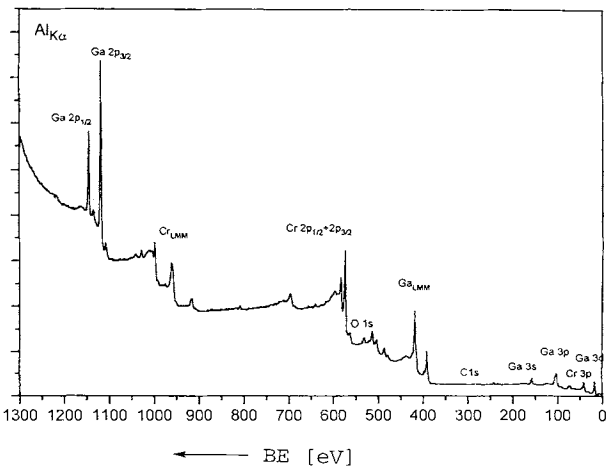

Fig. 2. X-ray photoelectron spectra of a typical CrGa film grown on SiO_2 (BE = bonding energy); quantative XPS analysis (at.% ± 2): Ga 38, Cr 36, O 11, C 15. SEM-EDX of the same sample (at.% ± 0.1): Ga/Cr = 1.06.

 © VCH Verlagsgesellschaft mbH, D-69451 Weinheim, 1996 0570-0833/96/3504-0425 $ 15.00+.25/0

thin films (ca. 1.5 μm thickness; quartz, Si substrates) show the exact metal stoichiometry of 1:1.[15] Thus, compound **2** allows precise control of the stoichiometry even at low substrate temperatures. This result is in accord with previous findings made for the Ga^{III} systems $[L_nM-GaR_2(Do)]$: precursors with GaR_2 units loose GaR_3 (stable against pyrolysis) under mild deposition condtitions to give Ga-deficient films.[16] In this sense the monoalkylated precursors with a $Ga^{I}R$ fragment are far superior to the dialkylated systems with $Ga^{III}R_2$ units. The analysis of the volatile exhaust gases (in situ mass spectrometry, GC/MS and NMR spectroscopy after condensation of the gases) revealed the presence of the unfragmented base ligand. The only hydrocarbon species observed was ethene, which supports a β-H-elimination mechanism.

In conclusion, it is anticipated that the results with the model systems **1**–**5** will have ramifications for the development of improved single-source precursors for the MOCVD of relevant intermetallic phases[17] particularly for III/V semiconductors.

Experimental Procedure

1: A suspension of $K_2[Cr(CO)_5]$ (2 mmol) in THF was added to a solution of Cl_2GaCH_3 (2 mmol) in THF at −78 °C. After the mixture had been stirred for 2 h at 25 °C, TMEDA (1 equiv) was added, and the mixture was stirred for an additional hour. The THF was then exchanged for CH_2Cl_2. After filtration and concentration to 20 mL, **1** crystallized at −30 °C. (yellow cubes, 770 mg, yield 98%). Compounds **2**–**5** were obtained in an analogous manner.

Selected physical data: **1**: Yellow cubes (m.p. 119 °C, subl. 110 °C, 10 − 3 Torr). ^{1}H NMR (399.78 MHz, CD_2Cl_2, 25 °C, TMS): $\delta = -0.01$ (s, 3H, $GaCH_3$), 2.52 (s, 6H, NCH_3), 2.79 (s, 6H, NCH_3), 2.87 (m, 4H, NCH_2, AA'BB'); ^{13}C NMR (100.53 MHz, CD_2Cl_2, 25 °C, TMS): $\delta = 6.3$ (q, ^1J(C,H) = 120 Hz, CH_3), 47.7 (q, ^1J(C,H) = 138 Hz, NCH_3), 48.9 (q, ^1J(C,H) = 139 Hz, NCH_3), 57.8 (t, ^1J(C,H) = 139 Hz, CH_2N), 227.9 (CO), 231.6 (CO). IR (CH_2Cl_2, [cm^{-1}]): ν(CO) = 2013 (vs), 1920 (s), 1884 (vs). CI-MS (isobutene) *m/z* (%): 392 (3) [M^+] (correct isotope pattern), 377 (2) [$M - CH_3^+$], 276 (11) [M − tmeda$^+$], 248 (4) [M − tmeda − CO$^+$], 117 (100) [tmeda + H$^+$]. Correct C, H, N, Cr, and Ga analysis.

5: Yellow prisms. ^{1}H NMR (399.78 MHz, CD_2Cl_2, 25 °C, TMS): $\delta = 2.86$ (s, 6H, NCH_3), 2.91 (s, 6H, NCH_3), 3.09 (m, 4H, NCH_2, AA'BB'). ^{13}C{^{1}H} NMR (100.53 MHz, CD_2Cl_2, 25 °C, TMS): $\delta = 48.3$ (NCH_3), 49.6 (NCH_3), 57.5 (CH_2N), 228 (CO). ^{27}Al{^{1}H} NMR (104.17 MHz, CD_2Cl_2, 25 °C, {[Al(H$_2$O)$_6$]$^{3+}$ external}) $\delta = 156$ ($F_{1/2} = 4680$ Hz). IR (CH_2Cl_2, [cm^{-1}]): ν(CO) = 2015 (s), 1926 (vs), 1876 (vs). Correct C, H, N, Al, and Cr analysis.

Received: August 15, 1995
Revised version: October 16, 1995 [Z8310IE]
German version: *Angew. Chem.* **1996**, *108*, 489–491

Keywords: aluminum compounds · chemical vapor deposition · gallium compounds · CVD precursors

[1] a) C. Dohmeier, C. Robl, M. Tacke, H. Schnöckel, *Angew. Chem.* **1991**, *103*, 594–595; *Angew. Chem. Int. Ed. Engl.* **1991**, *30*, 564–565; b) D. Loos, H. Schnöckel, J. Gauss, U. Schneider, *ibid.* **1992**, *104*, 1376–1378; and **1992**, *31*, 1362–1364; c) M. Mocker, C. Robl, H. Schnöckel, *ibid.* **1994**, *106*, 1860–1861; and **1994**, *33*, 1754–1755; d) D. Loos, H. Schnöckel, *J. Organomet. Chem.* **1993**, *463*, 37–40; e) C. Dohmeier, D. Loos, H. Schnöckel, *Angew. Chem.* **1996**, *108*, 141–161; *Angew. Chem. Int. Ed. Engl.* **1996**, *35*, 129–149.

[2] W. Uhl, W. Hiller, M. Layh, W. Schwarz, *Angew. Chem.* **1992**, *104*, 1378–1380; *Angew. Chem. Int. Ed. Engl.* **1992**, *31*, 1364–1366.

[3] R. A. Fischer, A. Miehr, T. Priermeier, *Chem. Ber.* **1995**, *128*, 831-843.

[4] F. A. Cotton, C. S. Kraihanzel, *J. Am. Chem. Soc.* **1962**, *84*, 4432–4439. The assignement of ν(CO) bands was confirmed by IR/Raman spectroscopic data ("CK" force constant analysis). In addition ν(MGa) [cm^{-1}] data were obtained, for example **1**: ν(CrGa) = 166; ν(MoGa) = 159 for [(CO)$_5$MoGa(Cl)(tmeda)] and ν(WGa) = 156 for [(CO)$_5$WGa(Cl)(tmeda)].

[5] H. Behrens, M. Moll, E. Sixtus, G. Thiele, *Z. Naturforsch. B* **1977**, *32*, 1109–1113.

[6] D. L. Reger, S. S. Mason, A. L. Rheingold, B. S. Haggerty, F. P. Arnold, *Organometallics* **1994**, *13*, 5049–5053.

[7] X-ray single-crystal structure analysis of **1**: $C_{12}H_{19}CrGaN_2O_5$, $M = 393.01$; yellow cubes ($0.15 \times 0.08 \times 0.33$ mm^3); monoclinic, $P2_1/n$ (no. 14), $a = 900.6(1)$, $b = 1611.9(2)$, $c = 1189.7(2)$ pm, $\beta = 95.73(1)°$ (25 reflections at high angle, $2\theta_{min/max} = 40.0°/45.4°$, $V = 1718 \times 10^6$ pm^3, $Z = 4$, $\rho_{calcd} = 1.519$ g cm^{-3}; $F(000) = 800$; $\mu = 22.2$ cm^{-1}; MACH3, oscillating anode, $Mo_{K\alpha}$ radiation, $\lambda = 71.073$ pm. Structure solution by using a combination of direct methods, difference Fourier syntheses, and least-squares refinements (STRUX-V, SIR-92, SHELXS-93, full matrix). $R1 = 0.044$ and $wR2 = 0.134$ for 2740 independent reflections and 185 variables, residual electron density ($e_{min/max} = +0.72/-0.37$ eÅ^{-3}). The TMEDA ligand exhibits a typical thermal libration, which can be explained by a flip-flop mechanism at C7–C8. Further details of the crystal structure investigation may be obtained from the Fachinformationszentrum Karlsruhe, D-76344 Eggenstein-Leopoldshafen, on quoting the depository number CSD-404120.

[8] A systematic search in the CSD database (version 5.09; 4/95) showed no entry. F. H. Allen, O. Kennard, R. Taylor, *Acc. Chem. Res.* **1983**, *16*, 146–153.

[9] a) R. Probst, C. Leis, S. Gamper, E. Herdtweck, C. Zybill, N. Auner, *Angew. Chem.* **1993**, *101*, 1155–1157; *Angew. Chem. Int. Ed. Engl.* **1991**, *30*, 1132–1135; b) R. Corriu, G. Lanneau, C. Priou, *ibid.* **1991**, *103*, 1153–1155; and **1991**, *30*, 1130–1132.

[10] K. D. Sen, M. C. Böhm, P. C. Schmidt, *Struct. Bonding (Berlin)*, **1987**, *66*, 99–123.

[11] Furthermore, the orange or deep violet compounds exhibit an extensive solvatochromic behavior.

[12] R. A. Fischer, T. Priermeier, *Organometallics* **1994**, *13*, 4306–4314 and references therein.

[13] J. Gauss, U. Schneider, R. Ahlrichs, C. Dohmeier, H. Schnöckel, *J. Am. Chem. Soc.* **1993**, *115*, 2402–2408.

[14] For a general procedure and reactor configuration: R. A. Fischer, A. Miehr, M. M. Schulte, *Adv. Mater.* **1995**, *7*, 58–61.

[15] The CrGa films obtained from **2** still contain some impurities of C and O (ca. 10 atom%), which could be explained because of the comparatively porous structure (SEM) of the poly-phased (XRD) material. The X-ray powder diffraction patterns of the untreated and the annealed samples (500 °C, 5h, H_2) reveal that chromium carbide and chromium oxide phases are not important and that Ga_4Cr_3 is the main phase (JCPDS card number 29-447). The films "age" rapidly in air (but also under inert gases); thus without in situ analysis it is difficult ascertain the ultimately achievable quality and purity of the thin films from **2**.

[16] R. A. Fischer, W. Scherer, M. Kleine, *Angew. Chem.* **1993**, *105*, 778–780; *Angew. Chem. Int. Ed. Engl.* **1993**, *32*, 748–750.

[17] R. S. Williams, *Appl. Surf. Sci.* **1992**, *60/61*, 619–624.

Synthesis of a Stable Hexagonally Packed Mesoporous Niobium Oxide Molecular Sieve Through a Novel Ligand-Assisted Templating Mechanism**

David M. Antonelli and Jackie Y. Ying*

Although recent efforts have suggested that it should be possible to synthesize mesoporous materials from transition metal oxides by molecular self-assembly of organic templating agents and inorganic oxides,[1, 2] to date there has been no report of this technique successfully generating such materials which could maintain a stable mesoporous structure upon removal of the organic micelles. Mesoporous materials, such as the aluminosilicate-based MCM-41,[3, 4] have pores with diameters in the 20–100 Å range; in contrast, the pore diameters in zeolites are less than 15 Å. Mesoporous oxides have potential application as solid electrolyte devices, as sorbents, and in catalytic processes where high surface area, fast diffusion, and large pore sizes are necessary for high performance. The synthesis of a stable mesoporous transition metal oxide should provide heterogeneous catalysts suitable for methane oxidation, NO_x decomposition,

[*] Prof. J. Y. Ying, D. M. Antonelli
Department of Chemical Engineering
Massachusetts Institute of Technology
Cambridge, MA 02139 (USA)
Fax: Int. code +(617) 258 8224

[**] This work was supported by the National Science Foundation (CTS-9257223, CTS-9411901, and DMR-9400334). The authors acknowledge Dr. A. Nakahira for his assistance with the transmission electron microscopy and Dr. T. Sun for helpful discussions.

hydrodesulfurization, photocatalytic decomposition of organic halides, and solid acid catalysis. Recently we described the synthesis of Ti-TMS1, the first hexagonally packed mesoporous transition metal oxide, by using a modified sol–gel method in conjunction with phosphate surfactants and titanium alkoxides.[5, 6] One of the important features of this synthesis route was the use of acetylacetone to slow down the condensation of the titanium alkoxide precursor sufficiently to allow the Ti centers to interact with the phosphate head groups on the micellated surfactant molecules. This material, however, underwent partial collapse of the mesostructure during template removal by calcination, yielding surface areas of about 200 $m^2 g^{-1}$.

Herein we describe the synthesis of the niobium oxide molecular sieve (Nb-TMS1), an ultrahigh surface area, hexagonally packed mesoporous transition metal oxide material which is the first such material *completely* stable to surfactant removal. The synthesis of this material was achieved through a novel approach by using the condensation of an organometallic precursor in which the propagating niobium alkoxide moiety is chemically linked through a Nb–N bond to a long-chain amine surfactant molecule. The initial reaction between the amine and $Nb(OEt)_5$ was conducted in the absence of water to ensure that an interaction between the Nb and the surfactant was established prior to condensation. This new approach thus obviates the use of acetylacetone and other chelating agents to control the condensation reaction. Covalent binding of the surfactant to the inorganic phase contrasts to already established routes which employ hydrogen bonding[8] or coulombic forces[1–4] to achieve the desired interaction.

Previous efforts to synthesize hexagonally packed mesoporous oxides have focused on a liquid-crystal templating mechanism involving the adjustment of pH, inorganic precursor, and surfactant head group to achieve an optimal electrostatic charge balance between the organic and inorganic phases during the assembly process.[7] Although claims have been made that such a route should provide a general method for synthesizing mesoporous materials of desired composition by judicious choice of the synthesis parameters, most efforts have led to formation of layered phases. The hexagonally packed mesoporous oxides of tungsten, antimony, lead, and iron derived by such an approach were found to be thermally unstable.[7] High surface areas and well-defined porosities could not be maintained in these systems upon surfactant removal, unlike the case of alumina-[10] or silicate-based systems.[3]

When a solution of niobium(v) ethoxide $Nb(OEt)_5$ (5.0 g) in ethanol (10 mL) was treated with tetradecylamine (0.25–1 equivalents), a new amino(ethoxy)niobium complex was obtained. The reaction of $Nb(OEt)_5$ with donor ligands such as amines is well documented.[9] When this solution was further treated with water (10–20 mL), a rapid reaction ensued, giving a white gelatinous precipitate. If this gel was aged at 100–180 °C for seven days, a white powder (Nb-TMS1) was obtained with a characteristic hexagonal X-ray powder diffraction (XRD) pattern (Fig. 1a) similar to those recorded for MCM-41 with the exception that the (110) and (200) peaks are not well resolved. The transmission electron micrograph (TEM) of Nb-TMS1 shown in Figure 2a also confirms the nature of this material as structurally analogous to MCM-41. While regions of local disorder do exist, the general arrangement of the pores is hexagonal. Prior to our reports[5, 6] and this paper, early transition metal alkoxides have only been used to dope MCM-41, for example 1% Ti in either MCM-41,[8] or its alumina-based analogue.[10]

The surfactant was best removed from Nb-TMS1 by careful treatment with $EtOH/HNO_3$ at 40 °C and pH = 1–2 followed

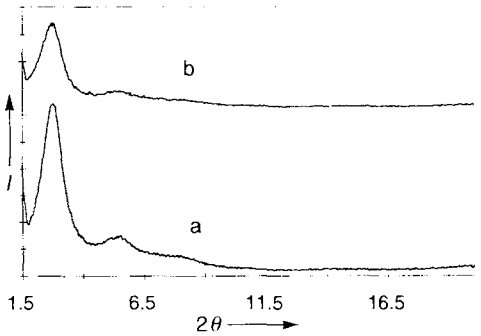

Fig. 1. a) XRD pattern of Nb-TMS1 synthesized with tetradecylamine (I = intensity in arbitrary units, 2θ is measured in degrees). The d spacing for the (100) reflection appears at 34 Å, which is slightly smaller than the value of ≈35 Å observed for as-synthesized MCM-41 made with trimethyltetradecylammonium bromide, possibly reflecting the greater degree of extension of the trimethylammonium head group over the amine head group for the same alkyl chain length. The (110), (200), and (210) reflections appear between 4° and 7° for 2θ as expected; however, the (110) and (200) peaks are not well resolved. This effect was observed previously in samples of MCM-41 and Ti-doped MCM-41, and has been attributed to the small particle size and/or the regions of local disorder where the nanometer-sized tubes are not stacked in a perfectly hexagonal array [8, 10]. b) XRD pattern of the same sample of Nb-TMS1 after $EtOH/HNO_3$ washes, which demonstrates that although the peaks are not as intense, the overall hexagonal structure was maintained after the successful surfactant removal.

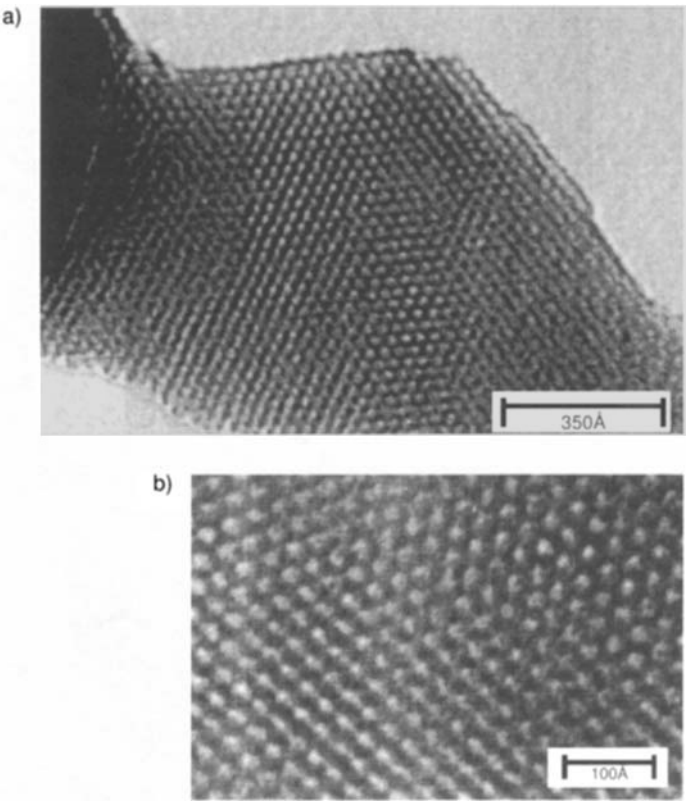

Fig. 2. High-resolution TEM images of the as-prepared Nb-TMS1 synthesized by using tetradecylamine a) prior to and b) after treatment with $EtOH\ HNO_3$. a) The pores are hexagonally packed, with an opening of about 27 Å and wall thickness of about 8 Å. The sum of these numbers agrees well with the value of about 35 Å calculated for the hexagonal repeat distance, a_o ($a_o = 2d_{100}/3^{1/2}$), from XRD. In general, the hexagonally ordered domains are about 100 nm, while samples of MCM-41 may have domain sizes on the micron level. Regions consisting of randomly packed cylindrical pores also exist. b) The pores are hexagonally packed, with an opening of about 25 Å. This pore size is in excellent agreement with the value of 27 Å as measured by N_2 adsorption, although direct comparison between pore sizes obtained from the BJH method (BJH = Barrett–Joyner–Halenda) and those obtained by TEM or XRD are not always valid due to the nature of the method.

 © VCH Verlagsgesellschaft mbH, D-69451 Weinheim, 1996 0570-0833/96/3504-0427 $ 15.00+.25/0

by extensive washing in ethanol. This process led only to a slight reduction of the XRD peak intensity (Fig. 1b). Treatment with HNO_3 at pH values lower than 1 led to reduction of the intensity of the X-ray pattern without loss of the high surface area or narrow pore size distribution. We attribute this to decreased size of the crystal domains. In general, samples made at lower surfactant-to-metal ratios (about 1:2 to 1:3) showed the greatest stability towards acid treatment at lower pH values, as measured by XRD peak intensities. The TEM of surfactant-free Nb-TMS1 (Fig. 2b) confirms that we have synthesized a structural analogue of hexagonally packed mesoporous MCM-41. After acid washing, this material retains only a small amount of surfactant and surface nitrate, as determined by photoacoustic IR spectroscopy. There is also evidence of Nb–OH groups, indicating that this material is partially hydrated. This result is consistent with EDAX studies (EDAX = energy dispersive analysis by X-rays) which show that this material contains slightly less Nb and more O than pure Nb_2O_5. Elemental analysis of these samples further supports the nature of this material as hydrated Nb_2O_5. The BET surface area of a typical sample Nb-TMS1 synthesized from tetradecylamine and washed in the manner described above was 434 $m^2 g^{-1}$. This value agreed well with that for samples of MCM-41 (about 1000 $m^2 g^{-1}$) with similar d spacings, after corrections for the molar weight ratio between $NbO_{2.5}$ and SiO_2 (132.9/61). The N_2 adsorption–desorption isotherms of Nb-TMS1 (Fig. 3a) presented only slight hysteresis. The pore size distribution of this material (Fig. 3b) showed one narrow peak at 27 Å.

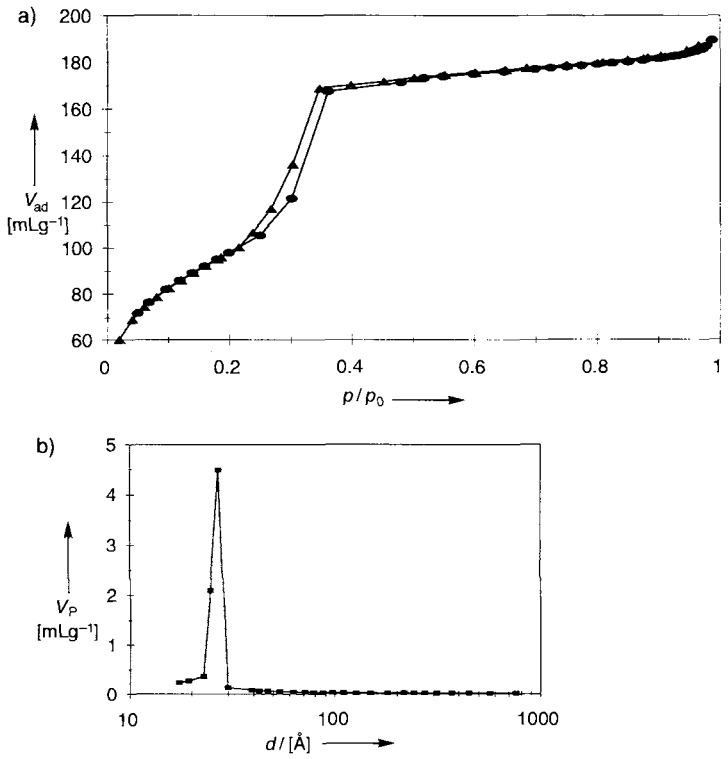

Fig. 3. a) The N_2 adsorption(●) – desorption(▲) isotherms (V_{ad} = volume N_2 adsorbed, p/p_0 = relative pressure of N_2) for heat-treated (400 °C, 2 h) Nb-TMS1 synthesized with tetradecylamine and washed three times with EtOH/HNO_3 at 40 °C. The isotherms display the sharp incline at values of p/p_0 in the range which is typical of other mesoporous materials studied (0.2 to 0.4) [12,13]. b) BJH pore size (d = pore diameter, V_p = pore volume) distribution of the same Nb-TMS1 sample, illustrating the narrow pore opening range, centered at 27 Å. The N_2 adsorption data of this sample prior to heat treatment was nearly identical to that shown apart from the fact that the surface area decreased from 434 to 380 $m^2 g^{-1}$ and the pores decreased in size by about 1 Å after heat treatment.

We have also tried other methods for surfactant removal. Washing the as-synthesized sample with ethanol produced materials with surface areas of about 5 $m^2 g^{-1}$. This is in contrast to recent results[10] which showed that amine surfactants could be removed from samples of silica- and alumina-based mesoporous materials by stirring them in ethanol at room temperature. This finding demonstrates that the amine surfactant was more strongly bonded to the inorganic wall in Nb-TMS1 than in the silica- and alumina-based systems where hydrogen bonding has been invoked to explain the self-assembly process.

The thermal and hydrothermal stability of surfactant-free Nb-TMS1 was studied with N_2 adsorption. This revealed that this material retains mesoporosity, crystallinity, and high surface area to at least 400 °C, a temperature that is well above those previously reported by other researchers for the as-synthesized mesostructured W, Sb, Pb, and Fe oxide materials.[2,7] These results indicate that the Nb-TMS1 synthesized by this novel approach would be very attractive as a high surface area catalytic material with thermal stability and uniform pore sizes. As a transition metal oxide with variable oxidation states, Nb-TMS1 would also offer additional unique catalytic properties not possible in the conventional alumina- or silicate-based MCM-41 systems.

The route to Nb-TMS1 described in Scheme 1 is novel in that the surfactant is covalently bonded to the metal atom in the precursor and possibly throughout the entire aging process. Our new mechanism contrasts to that proposed for the synthesis of MCM-41, where a covalent ligand interaction between the tetraalkylammonium surfactant head group and the Si center is neither present nor possible. In the formation of MCM-41, it has been proposed that the surfactant phase acts as template for the assembly of the inorganic phase either by preformed micelles[11] or electrostatic charge matching between the silicate oligomers and the individual surfactant head groups.[1,2,7] In the synthesis of Nb-TMS1, such a mechanism is not feasible since the surfactant is not soluble in water under the synthesis conditions applied. We propose instead that the Nb–N bond present in the precursor remains intact during at least the initial phase of the synthesis. This is supported by solution and solid-state MAS ^{15}N NMR studies conducted on ^{15}N-labeled samples of the dodecylamine niobium ethoxide precursor in [D_8]toluene and Nb-TMS1 synthesized from ^{15}N dodecylamine. The presence of substantial line broadening (about 450 Hz), attributable to the ^{93}Nb quadrupole (I = 9/2), in both the $^{15}N\{^1H\}$ NMR spectrum of the precursor complex in [D_8]toluene and the $^{15}N\{^1H\}$ MAS NMR spectrum of Nb-TMS1 is strong evidence of a N–Nb bond in both substances. The difference of the chemical shifts of 6.40 ppm between the precursor complex (δ = − 351.13) and free dodecylamine (δ = − 357.53) in [D_8]toluene is virtually identical to the difference of 5.96 ppm between solid Nb-TMS1 (δ = − 361.96) and solid dodecylamine (δ = − 367.92). This suggests that the nitrogen nucleus in Nb-TMS1 has remained bonded to Nb throughout the course of the synthesis process. Furthermore, addition of niobium ethoxide to an alcohol/water solution of dodecylamine led only to formation of amorphous materials. This emphasizes the importance of forming the bond between the metal and the head group prior to exposure to water. Also, while the organic phase in samples of MCM-41 prepared with amine surfactants at neutral pH can be removed by stirring in ethanol for one hour, little if any surfactant is removed from Nb-TMS1 under these conditions. This further supports that Nb–N bonds may well be intact in the as-synthesized material.

The strong interaction between the micelle head groups and the inorganic precursor molecule provided by our ligand-assist-

 © VCH Verlagsgesellschaft mbH, D-69451 Weinheim, 1996 0570-0833/96/3504-0428 $ 15.00+.25/0

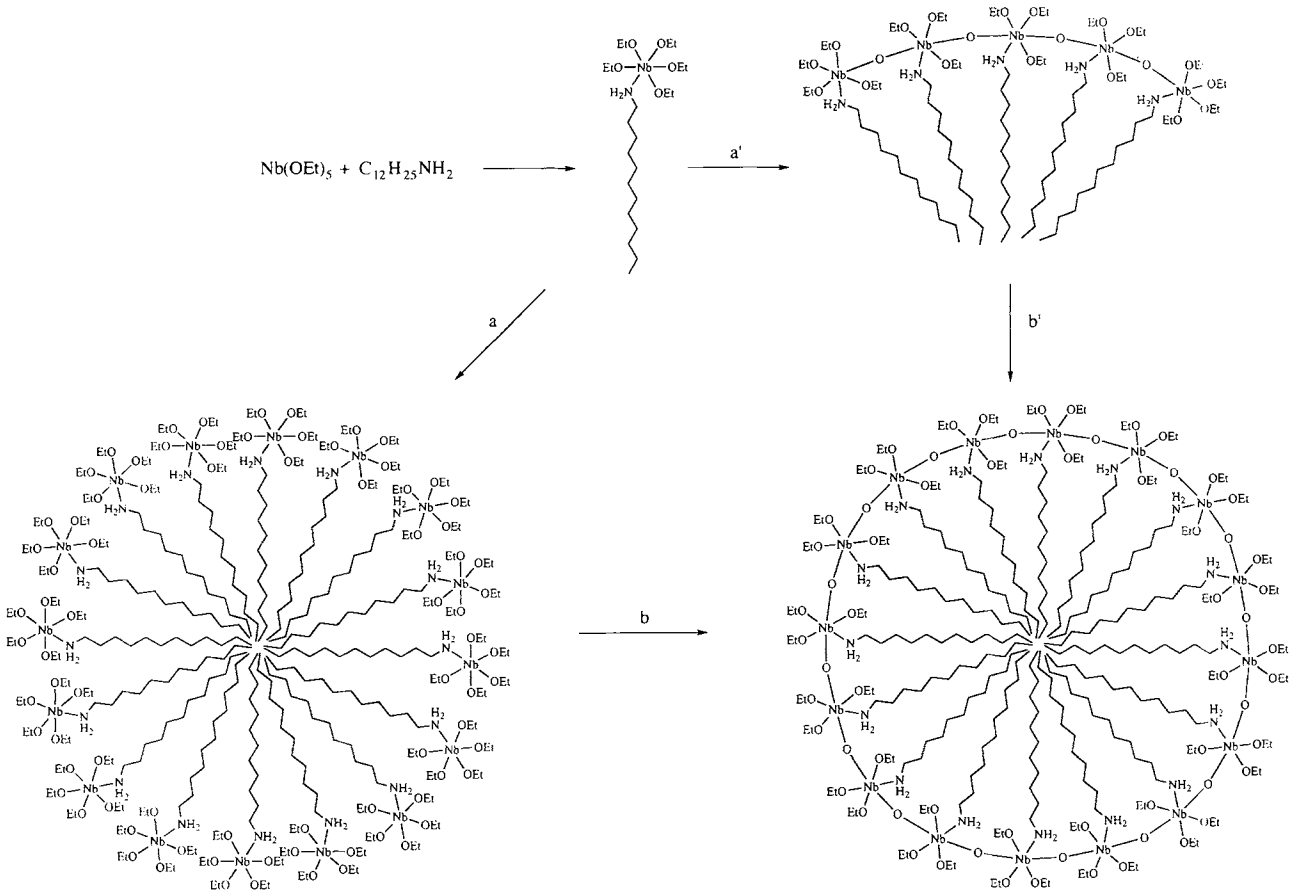

Scheme 1. Schematic representation of two possible synthesis pathways for Nb-TMS1 under a ligand-assisted templating mechanism. In pathway 1, the organometallic precursor self-assembles in ethanol prior to hydrolysis (a). The micellar array thus formed holds the Nb-containing head groups in place during subsequent condensation (b). Although alcohol can disrupt micelle formation, this phenomenon is largely dependent on concentration of the surfactant and the dielectric constant of the medium [14–16]. Due to the high concentrations of the niobium precursor used in the synthesis of Nb-TMS1 and the polar nature of ethanol, micelle formation is possible. Although the niobium head group is not hydrophilic, we think that because of ethoxy exchange with the free ethanol in the solvent, it would prefer to occupy regions of the solution rich in ethanol, while the hydrophobic tail groups would tend to cluster together. Evidence for this is that ethoxo complexes are usually soluble in ethanol, while long-chain hydrocarbons are not. In pathway 2, the self-assembly step (b') occurs only after sufficient propagation of the alkoxide hydrolysis and polycondensation (a'). The self-assembly of polymers containing hydrophobic and hydrophilic regions during chain growth has been noted before. Although the niobium head group is initially hydrophobic, the hydrolytic replacement of ethoxo groups with hydroxo and oxo groups may have given rise to progressively more hydrophilic head group assembly in forming the final mesostructure depicted.

ed templating approach is unique. It has enabled us to synthesize the first mesoporous transition metal oxide, Nb-TMS1, which has excellent thermal stability. We have further applied this methodology to prepare mesoporous oxides of Ti, Zr, Ta, Ce, and Y, and it has great potential to be general to a myriad of related mesoporous materials constructed from transition metal, lanthanide, and actinide oxides. Availability of such materials with well-defined hexagonally packed mesoporous structures of high thermal stability will greatly advance a variety of catalytic and other applications. The ability to intentionally vary the pore size of such material through varying surfactant chain lengths and addition of swelling agents will offer increased selectivity in reactions involving large molecules. The new possibility of generating transition metal oxide based systems with ease of dopant introduction will further provide attractive compositional control for tailoring catalytic materials characteristics.

Experimental Procedure

The X-ray powder diffraction data were recorded on either a Siemens D-5000 θ-θ diffractometer with $Cu_{K\alpha}$ radiation and a scintillation detector at 2.2 kW or a Rigaku RU-300 θ-2θ with a rotating anode using $Cu_{K\alpha}$ radiation at 10 kW. High-resolution transmission electron microscopy (TEM) images and electron diffraction patterns were obtained on a JEOL 2010 transmission electron microscope operated at 200 kV. Samples were prepared by sonication in 2-propanol and suspension on carbon-coated copper grids. N_2 adsorption data were collected on a Micromeritics ASAP 2000 Sorption Analyzer.

In a typical procedure, tetradecylamine (1.68 g, 7.87 mmol) was dissolved in niobium(v) ethoxide (5.0 g, 15.74 mmol). The solution was stirred until homogeneous and ethanol (5 mL) was added. Water (15 mL) was then added and the mixture was stirred, which caused the immediate precipitation of a white solid. This mixture was then left overnight at ambient temperature and further aged at 80 °C, 100 °C, and 180 °C for 1, 1, and 7 days, respectively. The product was collected by suction filtration and washed with three 50 mL portions each of water, ethanol, and ether. After drying in a vacuum oven at 100 °C, the surfactant was removed by treatment with 70% nitric acid at pH 1–2 in ethanol for 1–12 hours at room temperature, followed by stirring in ethanol for 12–24 hours. Materials prepared in this manner have pore sizes of about 27 Å and surface areas of 400 to 600 $m^2 g^{-1}$ with an XRD (100) peak centered at a d value of 31 Å.

Received: September 13, 1995 [Z 8400 IE]
German version: *Angew. Chem.* 1996, *108*, 461–464

Keywords: mesoporous materials · molecular sieves · niobium compounds · template synthesis

[1] Q. Huo, D. I. Margolese, U. Cielsa, P. Feng, T. E. Gier, P. Sieger, R. Leon, P. M. Petroff, F. Schüth, G. Stucky, *Nature* **1994**, *368*, 317–320.
[2] A. Monnier, F. Schüth, Q. Huo, D. Kumar, D. Margolese, R. S. Maxwell, G. D. Stucky, M. Krishnamurty, P. Petroff, A. Firouzi, M. Janicke, B. F. Chmelka, *Science* **1993**, *261*, 1299–1303.
[3] C. T. Kresge, M. E. Leonowicz, W. J. Roth, J. C. Vartulli, J. S. Beck, *Nature* **1992**, *359*, 710–714.

[4] J. S. Beck, J. C. Vartuli, W. J. Roth, M. E. Leonowicz, C. T. Kresge, K. D. Schmitt, C. T.-W. Chu, D. H. Olson, E. W. Shepard, S. B. McCullen, J. B. Higgins, J. L. Schlenker, *J. Am. Chem. Soc.* **1992**, *114*, 10834–10843.
[5] D. M. Antonelli, J. Y. Ying, *Angew. Chem.* **1995**, *107*, 2202–2204; *Angew. Chem. Int. Ed. Engl.* **1995**, *34*, 2014–2017.
[6] J. Y. Ying, D. M. Antonelli, U. S. patent pending.
[7] Q. Huo, D. I. Margolese, U. Ciesla, D. G. Demuth, P. Feng, T. E. Gier, P. Sieger, A. Firouzi, B. F. Chmelka, F. Schüth, G. Stucky, *Chem. Mater.* **1994**, *6*, 1176–1191.
[8] P. T. Tanev, M. Chibwe, T. J. Pinnavaia, *Nature* **1994**, *368*, 321–323.
[9] R. C. Mehrotra, A. K. Rai, P. N. Kapoor, R. Bohra., *Inorg. Chim. Acta* **1976**, *16*, 237–267.
[10] P. T. Tanev, T. J. Pinnavaia, *Science* **1995**, *267*, 865–867.
[11] C.-Y. Chen, S. L. Burkette, H.-X. Li, M. E. Davis, *Microporous Mater.* **1993**, *2*, 27–34.
[12] C.-Y. Chen, H.-X. Li, M. E. Davis, *Microporous Mater.* **1993**, *2*, 17–26.
[13] J. C. Vartuli, K. D. Schmitt, C. T. Kresge, W. J. Roth, M. E. Leonowicz, S. B. McCullen, S. D. Hellring, J. S. Beck, J. L. Schlenker, D. H. Olson, E. W. Sheppard, *Chem. Mater.* **1994**, *6*, 2317–2326.
[14] Y. Moroi, *Micelles, Theoretical and Applied Aspects*, Plenum, New York, **1992**.
[15] C. Gamboa, H. Rios, L. Sepulveda, *J. Phys. Chem.* **1989**, *93*, 5540–5543.
[16] K. Fontell, B. Khan, K. B. Lidstrom, D. Maciejewska, S. Puang-Ngern, *Colloid Polym. Sci.* **1991**, *269*, 727–742.

Chiral Borane–Amine Adducts in Asymmetric Synthesis: Alkylation of Alanine Derivatives

Vincent Ferey, Loïc Toupet, Thierry Le Gall, and Charles Mioskowski*

Current interest in the α-methyl-α-amino acids stems from their use as conformational modifiers in peptides and as components of biologically active peptides.[1] Hence, in recent years, various synthetic approaches to this class of compounds have been developed.[2, 3] Herein we present a method that allows the enantioselective synthesis of α-methyl-α-methylamino esters **4** (see Scheme 2) from methyl (*S*)-*N*-benzyl-*N*-methylalaninate. This approach does not rely on a chiral auxiliary reagent, but is based on the self-regeneration of the stereogenic center.[4] The key reaction, the α-alkylation of an enolate containing a chiral borane–amine moiety,[5–7] proceeds with up to 82% *ee*.

Amino ester **1** (90% *ee*)[8] was prepared from L-alanine methyl ester in two steps: N-benzylation (PhCHO, $NaBH_4$, 80%) and N-methylation (HCHO, HCO_2H, MeOH, 86%) (Scheme 1). Treatment of **1** with BH_3–SMe_2 in THF (Table 1, entry 1) led to a mixture of diastereomeric borane–amino ester adducts **2** and **3**, which were separated by column chromatography. Their structures were established unambigously by a single-crystal X-ray analysis of the less polar diastereomer **2** (Fig. 1).[9] Interestingly, in the solid state, the C2 proton in **2** is antiperiplanar with respect to the bulkier substituent on the nitrogen atom, the benzyl group.

We later noticed that the two diastereomers equilibrate in THF at room temperature, and then we conducted the complexation in other solvents (Table 1). We found that, in hexane, it

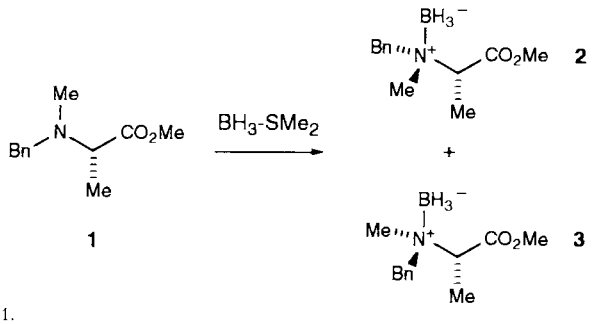

Scheme 1.

Table 1. Formation of borane–amino ester adducts from **1** (Scheme 1).

Entry	Solvent	Equiv borane	*T* [°C]	Time [h]	Ratio **2**/**3**	Yield [%]
1	THF	1.1	0	1	46/54	64 [a]
2	3:1 hexane:CH_2Cl_2	1.05	0	1	53/47	[b]
3	toluene	1.05	0	1	60/40	[b]
4	hexane	0.95	20	6	90/10	62 [c]
5	hexane	0.95	20	24	95/5	78 [d]

[a] Combined yield of diastereomers **2** and **3** after chromatographic separation. [b] Yield not determined. [c] Combined yield of diastereomers **2** and **3** (isolated as a solid). [d] Yield of diastereomer **2** after recrystallization.

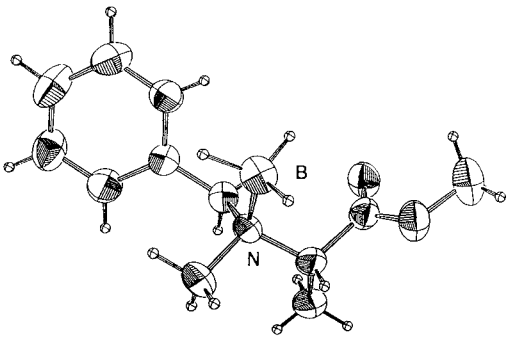

Fig. 1. Crystal structure of the borane–amino ester adduct **2**.

was possible to obtain selectively diastereomer **2**, which crystallized during the reaction, in good yield (Table 1, entry 5). This phenomenon can be described as an asymmetric crystallization-induced disequilibrium,[10] a principle previously applied to the synthesis of enantiomerically pure borane–amine complexes with a chiral boron atom.[11]

The diastereomer **2** was alkylated with various halides (Scheme 2; Table 2, entries 1–5). Potassium hexamethyldisilazide (KHMDS) was employed as base when benzylic or allylic electrophiles were used. Under the same conditions, other non-activated halides did not react with the enolate even at 0 °C. In these cases lithium diisopropylamide (LDA) was used and hexamethylphosphoric triamide (HMPA) (2 equiv) was added prior to the introduction of the electrophile. When the reaction was complete, the reaction mixture was hydrolyzed with a saturated aqueous NH_4Cl solution, which led to compounds **4**. The products were then purified by column chromatography. The yields were generally good; however, compound **4d** was obtained from pentyl iodide in only 50% yield. The enantiomeric excesses were determined by ^1H NMR spectroscopy of **4** or of alcohols **5** (obtained by reduction of **4** with diisobutylaluminum hydride) in presence of [Eu(hfc)$_3$]. The values given are corrected for 90%

[*] Dr. C. Mioskowski, V. Ferey, Dr. T. Le Gall
CEA-Saclay, Service des Molécules Marquées, Bât. 547
Département de Biologie Cellulaire et Moléculaire
F-91191 Gif-sur-Yvette cedex (France)
Fax: Int. code +(1)6908-7991
Dr. L. Toupet
Groupe Matière Condensée et Matériaux
Université de Rennes 1 (France)

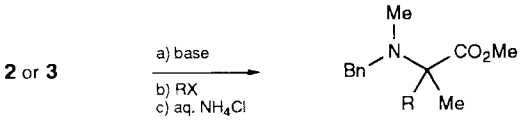

4

Scheme 2.

Table 2. α-Alkylation of **2** and **3** (Scheme 2) [a].

Entry	RX	Base	Substrate	Product	$[\alpha]_D$ (MeOH)	Yield [%]	*ee* [b] [%]
1	$PhCH_2Br$	KHMDS	**2**	**4a**	+35	78	82 [c]
2	(*E*)-$PhCH{=}CHCH_2Br$	KHMDS	**2**	**4b**	+1	72	82 [d]
3	$CH_2{=}CHCH_2Br$	KHMDS	**2**	**4c**	+2	67	74 [d]
4	$CH_3(CH_2)_4I$	LDA	**2**	**4d**	+4.5	50	68 [d]
5	MeO_2CCH_2Br	LDA	**2**	**4e**	−3	82	80 [c]
6	$PhCH_2Br$	KHMDS	**3**	**4a**	−27	66	68 [c]
7	$CH_2{=}CHCH_2Br$	KHMDS	**3**	**4c**	−2	66	40 [d]
8	$CH_3(CH_2)_4I$	LDA	**3**	**4d**	−3.5	50	36 [d]

[a] See Experimental Procedure for details; all products have been fully characterized. [b] Enantiomeric excesses were determined from the ^1H NMR spectrum of **4** or of alcohol **5** in the presence of $[Eu(hfc)_3]$. The values given are corrected for 90% optical purity of the starting material **1**. [c] Enantiomeric excess determined with amino ester **4**. [d] Enantiomeric excess determined with amino alcohol **5**.

optical purity of the starting material **1** used. Thus, the *ee* values observed for the alkylation reactions of **2** range from 68 to 82%.[12] The main enantiomer in **4a** was shown to have *S* absolute configuration by chemical correlation with the known alcohol **6**.[14]

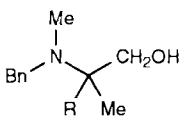

5

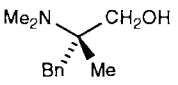

6

Alkylation reactions were also performed with diastereomer **3** (which contained 5% of diastereomer **2**). As expected, the optical rotations of the products of these reactions are of opposite sign to those of the corresponding compounds obtained from **2** (Table 2, entries 6–8). However, the *ee* values of the products were lower than expected in this case, probably because **3** epimerizes partially, at the chiral nitrogen center, under the reaction conditions.[15]

Isolation and separation of the diastereomeric borane–amine intermediates formed in the alkylation reactions could have, in principle, provided a means for improving the enantiomeric excesses of the final products; however, all attempts to isolate the intermediates in the reaction of **2** with benzyl bromide failed. Moreover, no borane–amine adducts were obtained in the reaction of compound **4a** with BH_3–SMe_2. Steric crowding on the nitrogen atom probably prevents formation of a stable adduct.

A Felkin model of the transition state[16] can be used to explain the stereochemical outcome of the reactions. If one assumes that the incoming electrophile RX attacks *anti* to the benzyl group, the larger substituent on nitrogen, two conformations **A** and **B** can be adopted by the enolate derived from diastereomer **2**. Experimental results are in agreement with predominant alkylation through transition state **A**, which should be favored on the basis of steric and electronic effects: BH_3 is larger than the methyl group, and the two negative charges localized on the boron atom and on the carboxylate function are far from each other. This explains the exceptionally high enantiomeric excesses observed here for the alkylation of an acyclic α-amino ester derivative.

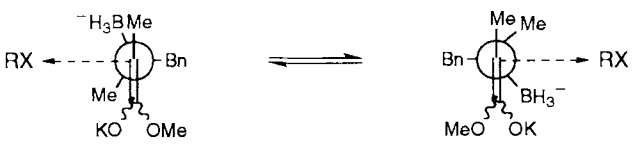

A B

The application of the optically active adducts of chiral amines and borane in synthetic organic chemistry has until now been limited to the enantioselective reduction of ketones and ketone derivatives,[17] to the enantioselective hydroboration of alkenes[18] and, via their corresponding amine–boryl radicals, to the kinetic resolution of carbonyl compounds.[7c] In our new application for borane–amine adducts in asymmetric synthesis a temporarily chiral, quaternary nitrogen atom serves to induce the enantioselective formation of a carbon–carbon bond.

Experimental Procedure

2, 3: To a solution of amino ester **1** (10 g, 48.3 mmol) in THF (150 mL) was added dropwise at 0 °C BH_3–SMe_2 (5.31 mL, 53.1 mmol). The reaction mixture was stirred for 1 h at 0 °C before the solvent was removed by evaporation. The ^1H NMR spectrum of the crude product showed that the ratio of the two diastereomers **2** and **3** was 46:54. Purification by column chromatography (silica gel, hexane/CH_2Cl_2 (3/2)) afforded 2.267 g of borane–amino ester **2**, 2.51 g of a mixture of the two diastereomers, and 2.047 g of borane–amino ester **3** (combined yield of **2** and **3**: 64%).

2: Colorless solid, m.p. 77 °C; $([\alpha]_D^{23} = -68.4$ ($c = 1.9$ in CH_2Cl_2)); ^1H NMR ($CDCl_3$): $\delta = 1.15$–2.20 (m, 3H), 1.58 (d, $J = 7.1$ Hz, 3H), 2.79 (s, 3H), 3.63 (q, $J = 7.1$ Hz, 3H), 3.72 (s, 3H), 4.08 (d, $J = 12.3$ Hz, 1H), 4.22 (d, $J = 12.3$ Hz, 1H), 7.30–7.50 (m, 5H); ^{13}C NMR ($CDCl_3$): $\delta = 13.8$, 44.1, 51.8, 64.1, 65.2, 127.6, 128.7, 131.2, 132.6, 171.6; ^{11}B NMR ($CDCl_3$): $\delta = -10.0$ (br q, $J = 95$ Hz); IR: $\tilde{\nu} = 3009$, 2954, 2416, 1743, 1452, 1433, 1221, 1166, 1114, 866, 748, 700 cm^{-1}; elemental analysis calcd. for $C_{12}H_{20}BNO_2$: C 65.19, H 9.12, B 4.89, N 6.33; found: C 64.93, H 9.11, B 5.05, N 6.28.

3: Colorless solid, m.p. 92–93 °C; $[\alpha]_D^{23} = -63.2$ ($c = 1.9$ in CH_2Cl_2)); ^1H NMR ($CDCl_3$): $\delta = 1.15$–2.15 (br m, 3H), 1.59 (d, $J = 7.1$ Hz, 3H), 2.56 (s, 3H), 3.76 (s, 3H), 3.79 (q, $J = 7.1$ Hz, 3H), 3.99 (d, $J = 12.2$ Hz, 1H), 4.39 (d, $J = 12.2$ Hz, 1H), 7.30–7.55 (m, 5H); ^{13}C NMR ($CDCl_3$): $\delta = 13.1$, 46.1, 51.9, 61.6, 65.8, 127.7, 128.7, 131.2, 132.6, 170.7; ^{11}B NMR ($CDCl_3$): $\delta = -10.5$ (m); IR: $\tilde{\nu} = 2958$, 2379, 1740, 1451, 1397, 1211, 1176, 1087, 858, 743, 699 cm^{-1}; elemental analysis calcd. for $C_{12}H_{20}BNO_2$: C 65.19, H 9.12, B 4.89, N 6.33; found: C 65.08, H 9.21, B 4.85, N 6.31.

Selective preparation of **2**: To a solution of amino ester **1** (300 mg, 1.45 mmol) in hexane (8 mL) was added dropwise at room temperature BH_3–SMe_2 (0.135 mL, 1.375 mmol). After 5 min a white precipitate began to separate. Stirring was continued for 24 h, then the reaction mixture was filtered. The solid was washed with a little hexane, then dried in vacuo. The ^1H NMR spectrum showed that the ratio of the two diastereomers **2** and **3** was 95:5. Recrystallization from hexane/CH_2Cl_2 (3/1) afforded 225 mg of **2** (78%).

Alkylation of **2** using KHMDS: A cooled solution of **2** (50 mg, 0.23 mmol) in toluene (0.5 mL) was added to a solution of KHMDS (0.545 mL of a 0.5 M solution in toluene, 0.27 mmol) in THF (3 mL) at −78 °C. The reaction mixture was stirred for 15 min at −23 °C then cooled to −78 °C; benzyl bromide (0.041 mL, 0.34 mmol) was added by syringe. The reaction mixture was stirred for 2 h at −78 °C then allowed to warm to 0 °C over 2 h. Saturated aqueous NH_4Cl (2 mL) was added, resulting in the formation of a white precipitate, which was dissolved by adding 2 mL of H_2O. The aqueous phase was extracted with CH_2Cl_2 (5 × 10 mL); the combined organic layers were washed with brine, dried over $MgSO_4$, then concentrated to dryness. Purification of the residue by column chromatography (silica gel, hexane/ethyl acetate (98/2)) afforded 52 mg of amino ester **4a** (78%).

Alkylation of **2** using LDA/HMPA: A fresh solution of LDA was prepared by adding 1.3 M *n*-butyllithium in hexane (0.577 mL, 0.75 mmol) to diisopropylamine (0.115 mL, 0.818 mmol) in THF (3 mL) at 0 °C, and stirring at this temperature for 15 min. A cooled solution of **2** (150 mg, 0.68 mmol) in toluene (0.5 mL) was added to the LDA solution cooled at −78 °C. The reaction mixture was stirred for 15 min at −23 °C then cooled to −78 °C. HMPA (0.237 mL, 1.364 mmol) was added rapidly, followed by methyl bromoacetate (0.097 mL, 1.023 mmol), dropwise. The reaction mixture was stirred for 2 h at −78 °C then allowed to warm to 0 °C over 2 h. Saturated aqueous NH_4Cl (2 mL) was added, resulting in the formation of a white precipitate, which was dissolved by adding some H_2O. The aqueous phase was extracted with diethyl ether (5 × 10 mL); the combined organic layers were washed

with brine, dried over $MgSO_4$, then concentrated to dryness. Purification of the residue by column chromatography (silica gel, hexane/ethyl acetate (98/2)) afforded 155 mg of amino diester **4e** (82%).

Received: June 29, 1995
Revised version: November 24, 1995 [Z8145IE]
German version: *Angew. Chem.* **1996**, *108*, 475–477

Keywords: amino acids · asymmetric syntheses · boron compounds · chirality · enolates

[1] H. Heimgartner, *Angew. Chem.* **1990**, *103*, 271; *Angew. Chem. Int. Ed. Engl.* **1991**, *30*, 238, and references therein.

[2] a) R. M. Williams, *Synthesis of Optically Active α-Amino Acids*, Pergamon, Oxford, **1989**, and references therein; b) T. M. Zydowski, E. de Lara, S. G. Spanton, *J. Org. Chem.* **1990**, *55*, 5437; c) M. Ihara, M. Takahashi, N. Taniguchi, K. Yasui, H. Niitsuma, K. Fukumoto, *J. Chem. Soc. Perkin Trans. 1* **1991**, 525; d) G. T. Bourne, D. Crich, J. W. Davies, D. C. Horwell, *ibid.* **1991**, 1693; e) E. C. Roos, M. C. López, M. A. Brook, H. Hiemstra, W. N. Speckamp, B. Kaptein, J. Kamphuis, H. E. Schoemaker, *J. Org. Chem.* **1993**, *58*, 3259; f) M. J. O'Donnell, S. Wu, *Tetrahedron Asymmetry* **1994**, *3*, 591; g) S.-W. Moon, Y. Ohfune, *J. Am. Chem. Soc.* **1994**, *116*, 7405; h) T. Kawabata, T. Wirth, K. Yahiro, H. Suzuki, K. Fuji, *ibid.* **1994**, *116*, 10809; i) C. Cativiela, M. D. Diaz de Villegas, J. A. Gálvez, *Synlett* **1994**, 302; j) D. B. Berkowitz, M. K. Smith, *J. Org. Chem.* **1995**, *60*, 1233.

[3] a) E. Vedejs, S. C. Fields, M. R. Schrimpf, *J. Am. Chem. Soc.* **1993**, *115*, 11612; b) E. Vedejs, R. W. Chapman, S. C. Fields, S. Lin, M. R. Schrimpf, *J. Org. Chem.* **1995**, *60*, 3020; c) E. Vedejs, S. C. Fields, S. Lin, M. R. Schrimpf, *ibid.* **1995**, *60*, 3028.

[4] This concept was introduced by Seebach et al.; see: D. Seebach, R. Imwinkelried, T. Weber, in *Modern Synthetic Methods, Vol. 4* (Ed.: R. Scheffold), Springer, Berlin, **1986**, p. 125, and references therein.

[5] Preparation and use of borane–α-amino esters adducts: a) E. F. Rothgery, L. F. Hohnstedt, *Inorg. Chem.* **1971**, *10*, 181; b) M. F. Grundon, D. G. McCleery, J. W. Wilson, *J. Chem. Soc. Perkin Trans. 1* **1981**, 231; c) V. Ferey, T. Le Gall, C. Mioskowski, *J. Chem. Soc. Chem. Commun.* **1995**, 487.

[6] For examples of alkylation of cyclic α-amino acid derivatives having a boron–nitrogen bond, see: a) N. E. Miller, *Inorg. Chem.* **1974**, *13*, 1459; b) T. Mancilla, S. L. Galvez, *Main Group Met. Chem.* **1992**, *15*, 9; c) ref. [3].

[7] For recent examples of formation of borane adducts of optically active amines, see: a) H. Tlaxhuet, F. Santiesteban, E. García-Báez, R. Contreras, *Tetrahedron Asymmetry* **1994**, *5*, 1579; b) R. Contreras, F. Santiesteban, M. A. Paz-Sandoval, B. Wrackmeyer, *Tetrahedron* **1984**, *40*, 3829; c) H.-S. Dang, V. Diart, B. P. Roberts, *J. Chem. Soc. Perkin Trans. 1* **1994**, 1033.

[8] The optical purity of **1** was determined by ^1H NMR spectroscopy in presence of [Eu(hfc)$_3$].

[9] X-ray crystal data for compound **2**: $BC_{12}H_{20}O_2N$, $M = 221.11$, orthorhombic, $P2_12_12_1$, $a = 6.365(3)$, $b = 7.985(1)$, $c = 25.421(5)$ Å, $V = 1292.0(7)$ Å^3, $Z = 4$, $\rho_{calcd} = 1.137$ Mgm^{-3}, $\lambda(Mo_{K\alpha}) = 0.70926$ Å, $\mu = 0.70$ cm^{-1}, $F(000) = 480$, $T = 294$ K, final $R = 0.032$ for 1092 observations. The crystal ($0.25 \times 0.25 \times 0.45$ mm) was studied on an automatic Enraf-Nonius CAD4 diffractometer with graphite-monochromated $Mo_{K\alpha}$ radiation. The cell parameters were obtained by fitting a set of 25 reflections with high θ values. The data collection ($2\theta_{max} = 50°$, scan $\omega/2\theta = 1$, $\tau_{max} = 60$ s, range HKL: H 0.7, K 0.9, L 0.30, intensity controls without appreciable decay (0.4%) gives 1380 reflections of which 1092 have $I > 3\sigma(I)$. Further details of the crystal structure investigation may be obtained from the Director of the Cambridge Crystallographic Data Centre, 12 Union Road, GB-Cambridge CB21EZ (UK), on quoting the full journal citation.

[10] J. Jacques, A. Collet, S. H. Wilen, *Enantiomers, Racemates, and Resolutions*, Wiley, New York, **1981**, Chapter 6.

[11] B. Gyori, J. Emri, *J. Organomet. Chem.* **1982**, *238*, 159.

[12] A sample of enantiomerically pure **2** ($[\alpha]_D^{23} = -75.2$ ($c = 1.9$ in CH_2Cl_2)) has been prepared from (*S*)-*N*-benzyl-*N*-methylalanine [13] in two steps (MeOH, H_2SO_4; then BH_3–Me_2S, hexane). The alkylation reaction of **2** with benzyl bromide afforded, in 73% yield, compound **4a** ($[\alpha]_D^{24} = +37.1$ ($c = 1.7$ in methanol), 82% *ee*).

[13] P. Quitt, J. Hellerbach, K. Vogler, *Helv. Chim. Acta* **1963**, *46*, 327.

[14] E. J. Corey, R. J. McCaully, H. S. Sachdev, *J. Am. Chem. Soc.* **1970**, *92*, 2476.

[15] This observation was made at the beginning of the complexation experiments leading to the selective preparation of diastereomer **2** from the amino ester **1** in hexane.

[16] M. Chérest, H. Felkin, N. Prudent, *Tetrahedron Lett.* **1968**, 2199. See also: N. T. Anh, *Top. Current Chem.* **1980**, *88*, 145; P. Caramella, N. G. Rondan, M. N. Paddon-Row, K. N. Houk, *J. Am. Chem. Soc.* **1981**, *103*, 2438.

[17] a) J.-C. Fiaud, H.-B. Kagan, *Bull. Soc. Chim. Fr.* **1969**, 2742; b) M. Periasamy, J. V. Bhaskar Kanth, C. Kishan Reddy, *J. Chem. Soc. Perkin Trans. 1* **1995**, 427; c) M. Nishizawa, R. Noyori, in *Comprehensive Organic Synthesis, Vol. 8* (Ed.: B. M. Trost, I. Fleming), Pergamon, Oxford, **1991**, p. 170, and references therein.

[18] C. Narayana, M. Periasamy, *J. Chem. Soc. Chem. Commun.* **1987**, 1857.

Heterobimetallic Hydroxy Complexes: $[Re_3(CO)_9(\mu_2\text{-}OH)_3(\mu_3\text{-}OH)]^-$ as a Novel Tripodal Ligand**

Wolfgang A. Herrmann,* André Egli, Eberhardt Herdtweck, Roger Alberto, and Franz Baumgärtner

Hydroxy and alkoxy complexes of transition metals have recently received renewed interest in terms of applications both in catalysis and—as precursors of metal oxides—in material science.[1–3] Hydroxy groups frequently bridge two or three metals, thus leading to oligomeric structures.[4] A notable example is the cubane-type rhenium cluster **1**, which forms from

$[Re_4(CO)_{12}(\mu_3\text{-}OH)_4]$ **1**

photolysis of the parent rhenium carbonyl complex $[Re_2(CO)_{10}]$ in water.[5] Hardly any chemistry has as yet unfolded for compounds of this type because of their perfectly closed structures. If it were possible, however, to remove a $[Re(CO)_3]^+$ corner from **1**, the resulting new anionic Re_3 cluster should display a rich coordination chemistry provided a) no redox instability is associated with this structure, and b) metal ions of the correct size are introduced as reaction partners.

The tetraethylammonium salts of **2** and **3** are easily accessible from $[N(C_2H_5)_4]_2[ReBr_3(CO)_3]$.[6] Both hydroxyrhenates were isolated from aqueous solution at room temperature after simply adding 1.33 equivalents of alkali hydroxides for **2** and more than 1.5 equivalents for **3** (Scheme 1). Whereas the dinuclear **3** exhibits triply hydroxy-bridged $[Re(CO)_3]^+$ moieties, the trinuclear **2** is an incomplete cubane-type structure missing one rhenium corner. The perfect cubane **1** does not form this way in alkaline aqueous solution.

$[Re_3(CO)_9(\mu_2\text{-}OH)_3(\mu_3\text{-}OH)]^-$ **2**

$[Re_2(CO)_6(\mu_2\text{-}OH)_3]^-$ **3**

The hydroxymetalate **2** acts as a novel tripodal ligand for a wide range of metals. Thus, divalent manganese and copper form the heterobimetallic, electroneutral complexes **4a** and **4b** in near quantitative yields as fully air- and water-stable crystalline compounds.[7]

$[MRe_6(CO)_{18}(\mu_3\text{-}OH)_8]$ **4a** ($M = Mn^{II}$), **4b** ($M = Cu^{II}$)

A single-crystal X-ray diffraction study of the Re_6Mn complex **4a** (Re^I/Mn^{II}) revealed a "double-cubane" type structure, in which the common corner is occupied by the divalent metal ion.[8] The average Mn–O distance of 2.177(7) Å agrees well with common Mn^{II}–O lengths and particularly with the bond lengths in the related homonuclear complex $[Mn_7(CO)_{18}(\mu_3\text{-}OH)_8]$ (av.: 2.169(2) Å).[9] The Re–O distances are slightly longer (2.157(8)–2.212(9) Å, av. 2.182(8) Å) than in the free ligand **2** (2.146(6)–2.174(8) Å),[6] but they are still shorter than in the closed cubane **1** (2.207(8) Å,[10] 2.159(26)–

[*] Prof. Dr. W. A. Herrmann, Dr. A. Egli, Dr. E. Herdtweck
Anorganisch-chemisches Institut der Technischen Universität
Lichtenbergstrasse 4, D-85747 Garching (Germany)
Fax: Int. code +(89) 3209-3473
Dr. R. Alberto
Laboratorium für Radiopharmazie des Paul-Scherrer-Instituts
Villigen (Germany)
Prof. Dr. F. Baumgärtner
Institut für Radiochemie der Technischen Universität München (Germany)

[**] This work was supported by the Alexander von Humboldt Foundation through a research fellowship to A. E.

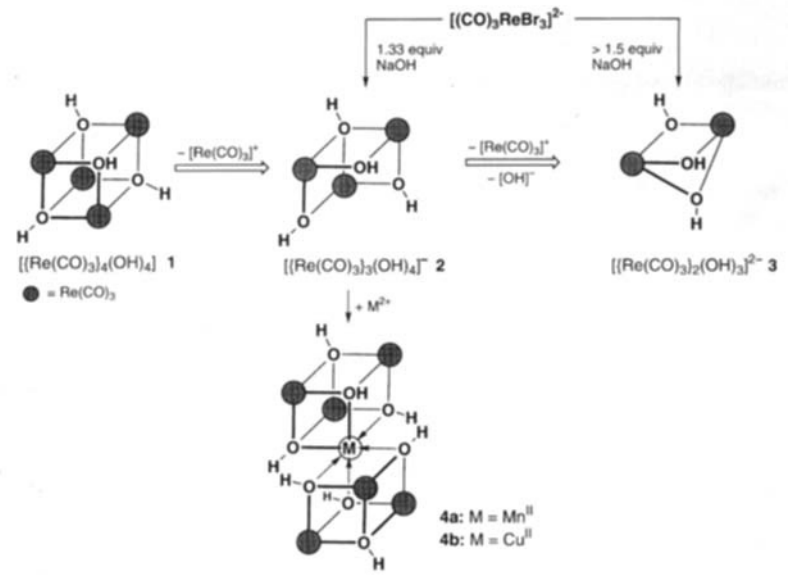

Scheme 1.

2.224(27) Å[11]). The central manganese atom shows an unusual geometry in that it resembles a trigonal prism more than an octahedron (see Fig. 2, left).

A space-filling model reveals the hydrophobic shell resulting from the 18 peripheral carbonyl ligands. However, the intermolecular alignment that depends on hydrogen bonds between the hydroxy ligands and cocrystallized water molecules shows clearly that this shell is upset by the hydroxy groups of the complex. Thus, the twisted core geometry can be rationalized from these peripheral interactions between hydroxy and carbonyl ligands. Those hydroxy groups not engaged in coordination with the manganese center are not captured by water but rather by ether molecules, derived from the preparation of the complex.[7] This results in a layered arrangement in the crystal, assembled from parallel rods of the complex. The space between the layers is occupied by the ethyl groups of ether molecules (Fig. 1, left).

With respect to the Re–O distances (2.151(10)–2.225(9) Å, av. 2.187(10) Å), the copper complex resembles the manganese derivative. However, the coordination sphere of the Cu^{II} center is an octahedron with tetragonal distortion (Fig. 2, left). The bond lengths differ as much as 0.44 Å, ranging from 1.992(9) to 2.428(10) Å.

Like its manganese analogue, the copper complex compound exhibits a layered arrangement in the crystal (Fig. 1, right). However, **4b** crystallizes with only two water molecules per complex (in contrast to six in **4a**), which form hydrogen bonds with the μ_3-OH ligands of one flank of the complex. The μ_3-OH ligands of the other flank form very weak hydrogen bonds to the μ_3-OH ligands of a second and third complex. As in **4a**, the layers are coated with diethyl ether molecules. In contrast to **4a**, the complexes are rotated around the copper ion within the layer plane, which probably facilitates hydrogen bonding. Though the differences in layering of the complexes might arise from different coordination geometries of the heterometals, this suggestion is merely speculative.

The characteristics of **2** as organometallic, tridentate, ligand binding through oxygen bears a certain resemblance to those of silsesquioxanes[12–15] and ligands of the type $[CpCo\{P(O)R'R''\}_3]^-$.[16,17] As opposed to the π-donor properties of the latter, **2** and silsesquioxanes are pure σ-donors, and both form cubane-type structures. However, the hydroxy groups of **2** are not deprotonated upon coordination.

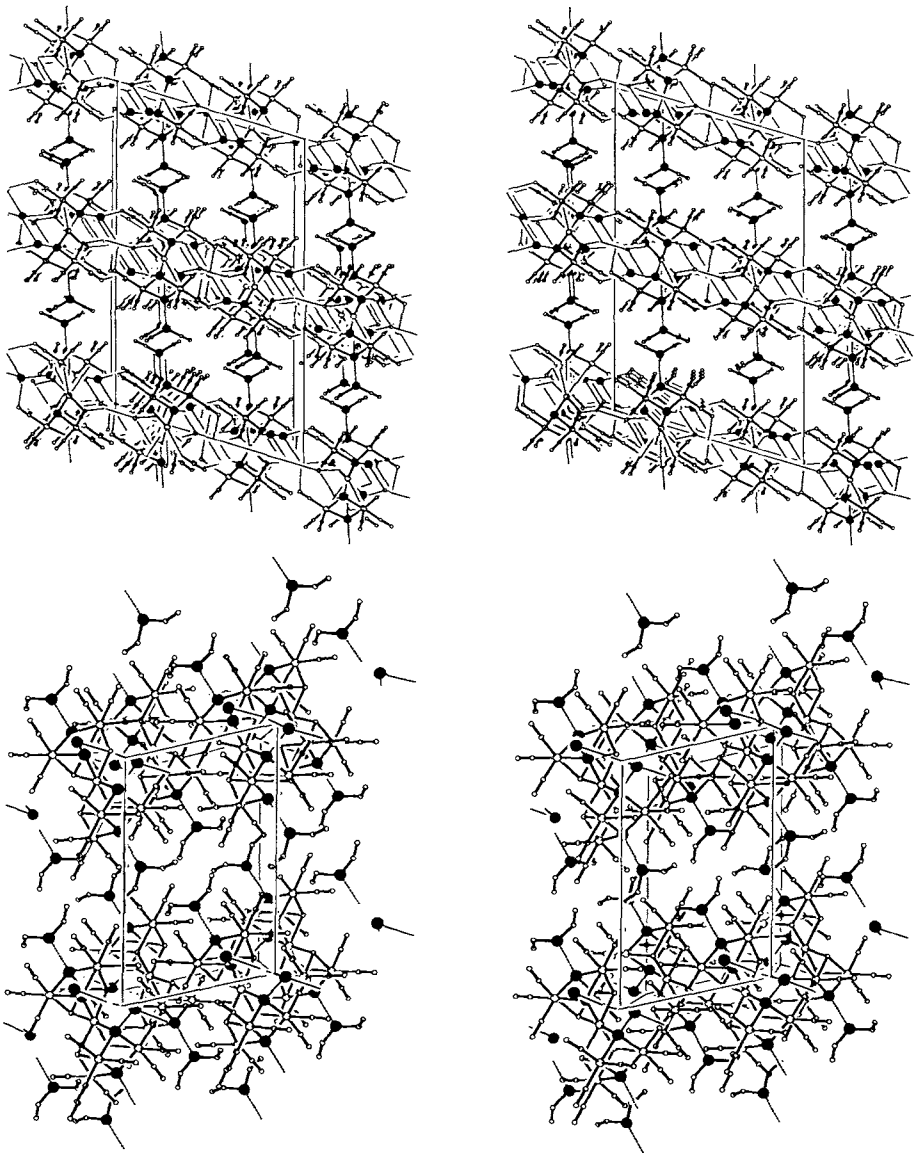

Fig. 1. The layered arrangement of the complex compounds **4a** (left) and **4b** (right) in the crystal (PLUTON drawing). The views are directed between the layers. Dotted lines indicate hydrogen-bridged O···O bonds with 2.59 Å < D–H···A < 2.80 Å.

 © VCH Verlagsgesellschaft mbH, D-69451 Weinheim, 1996 0570-0833/96/3504-0433 $ 15.00+.25/0

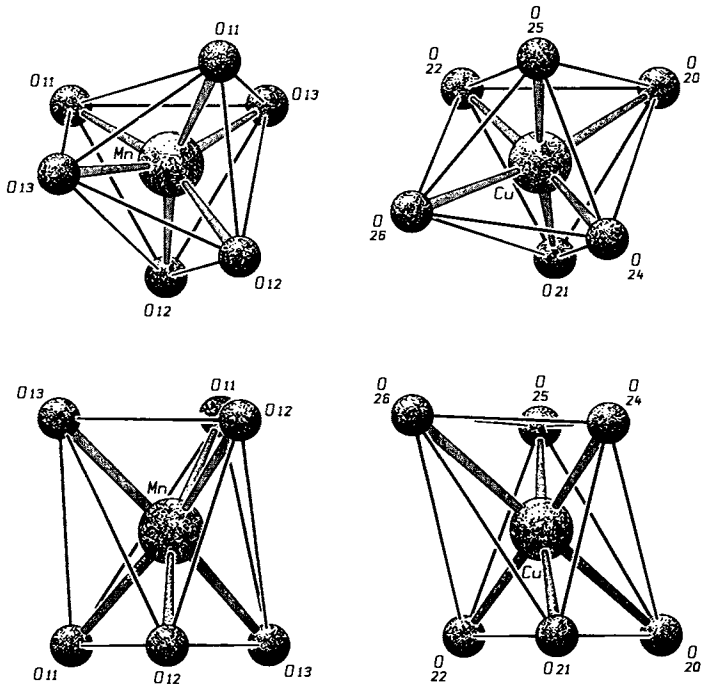

Fig. 2. Comparison of the Mn^{II} and Cu^{II} coordination sphere of **4a** and **4b** (SCHAKAL drawing).

The very different coordination geometries of **4a** and **4b** demonstrate that the new organometallic ligand **2** combines tridentate complexation with a highly flexible core geometry. In addition, the notably different bond lengths and the ability to complex hard as well as soft metal centers illustrate the potential of hydroxymetalates in coordination chemistry.

Received: July 27, 1995 [Z 8265 IE]
German version: *Angew. Chem.* **1996**, *108*, 486–489

Keywords: carbonyl complexes · hydroxyl ligands · rhenium compounds · tripodal ligands

[1] J. W. Gilje, H. W. Roesky, *Chem. Rev.* **1994**, *94*, 895–910.
[2] K. G. Caulton, L. G. Hubert-Pfalzgraf, *Chem. Rev.* **1990**, *90*, 969–995.
[3] W. A. Herrmann, N. W. Huber, O. Runte, *Angew. Chem.* **1995**, *107*, 2371–2390; *Angew. Chem. Int. Ed. Engl.* **1995**, *34*, 2187–2206.
[4] C. F. Baes, R. E. Mesmer, *The Hydrolysis of Cations*, Wiley, New York, **1976**.
[5] M. Herberhold, G. Süss, *Angew.Chem.* **1975**, *87*, 710; *Angew. Chem. Int. Ed. Engl.* **1975**, *14*, 700.
[6] R. Alberto, A. Egli, U. Abram, K. Hegetschweiler, V. Gramlich, P. A. Schubiger, *J. Chem. Soc. Dalton Trans.* **1994**, 2815–2820.
[7] Since the formation of the trinuclear unit takes time, the ligand solution should be prepared several hours before complexation of the second metal M. For this purpose NaOH (1 M solution, 133 μL) is suspended in 2 mL of an aqueous solution of $[N(C_2H_5)_4]_2[ReBr_3(CO)_3]$ (77 mg, 0.1 mmol). The latter compound can be prepared either from $[Re_2(CO)_{10}]$ [6] or perrhenate (R. Alberto, R. Schibli, A. Egli, P. A. Schubiger, W. A. Herrmann, G. Artus, U. Abram, T. A. Kaden, *J. Organomet. Chem.* **1995**, *492*, 217–224). Compounds **4a**, **b** are prepared by the addition of a solution of the appropriate metal salts (0.0166 mmol) in water (0.5 mL) to the ligand solution. The reaction solution is then extracted with diethyl ether (5 mL). After separation of the phases, the ether is removed in vacuo. IR (KBr): **4a**: ν(CO) 2031, 1926, 1898; **4b**: ν(CO) 2024, 1905 cm^{-1}. An excess of the metal salts decreases the yield of 1:2 complexes. Analysis by IR spectroscopy of the residue from the aqueous phase of **4a**, which was evaporated to dryness, displayed a significant shift of the carbonyl stretching bands to lower wavenumbers (2014 (A_1) and 1875 cm^{-1} (E)). The dependence on the stoichiometry suggests formation of 1:1 complexes. The shift in wavenumbers might be caused by anions coordinated to the manganese center.
[8] Crystallographic data for $C_{18}H_8MnO_{26}Re_6 \cdot 6H_2O \cdot 2(C_2H_5)_2O$ (**4a**): $M_r = 2068.7$, monoclinic, $C2/c$ (No. 15), $a = 2980.1(4)$, $b = 1010.8(1)$, $c = 1781.7(2)$ pm, $\beta = 106.74(1)^\circ$, $V = 5139.5(11) \times 10^6$ pm^3; $Z = 4$; $\rho_{calcd} = 2.674$ $g\,cm^{-3}$, $F_{000} = 3772$, $\mu = 144.0$ cm^{-1}. Data were collected on a STOE IPDS diffractometer with graphite monochromator, $\lambda(Mo_{K\alpha}) = 0.71073$ Å. For general details about the data collection see Ref. [19]. During data collection no decay was observed, absorption correction [20], and correction for extinction effects were applied. From 16916 collected data, 1333 were rejected because of negative intensities and 303 because of systematic absences. After merging ($R_{int} = 0.088$) 4349 from 4350 unique data ($I > 0.0\sigma(I)$) were used in the final refinement. The structure was solved with direct methods and refined by full-matrix least-squares calculations, with anisotropic thermal parameters for all non-hydrogen atoms. Hydrogen atoms were calculated in ideal positions except for those located at the solvent water and the ether molecules. Refinement was concluded with $R1 = 0.060$ and $wR2 = 0.115$; SHELXL weights. All software and the sources of the scattering factors are contained in the STRUX-V system [18] using the programs PLATON-92, PLUTON-92, SCHAKAL, SHELXS-86, and SHELXL-93. Crystallographic data for $C_{18}H_8CuO_{26}Re_6 \cdot 2H_2O \cdot 2(C_2H_5)_2O$ (**4b**): $M_r = 2005.3$, triclinic, $P\bar{1}$ (No. 2), $a = 922.1(1)$, $b = 1494.8(2)$, $c = 1724.9(2)$ pm, $\alpha = 89.84(1)^\circ$, $\beta = 88.91(1)$, $\gamma = 76.93(1)^\circ$, $V = 2315.5(5) \times 10^6$ pm^3; $Z = 2$; $\rho_{calcd} = 2.876$ $g\,cm^{-3}$, $F_{000} = 1814$, $\mu = 161.6$ cm^{-1}. Data were collected on a STOE IPDS image plate diffractometer with graphite monochromator, $\lambda(Mo_{K\alpha}) = 0.71073$ Å. For general details concerning the data collection see Ref. [19]. During data collection no decay was observed, absorption correction [20], and correction for extinction effects were applied. From 23199 collected datas 2800 were rejected (negative intensities). After merging ($R_{int} = 0.098$) all 7401 unique data ($I > 0.0\sigma(I)$) were used in the final refinement. The structure was solved with direct methods, and refined by full-matrix least-squares calculations, with anisotropic thermal parameters for all non-hydrogen atoms. Hydrogen atoms were calculated in ideal positions except the hydrogen atoms located at the solvent water molecules. Refinement was concluded with $R1 = 0.081$ and $wR2 = 0.110$, SHELXL weights. All software and the sources of the scattering factors are contained in the STRUX-V [18] system using the programs PLATON-92, PLUTON-92, SCHAKAL, SHELXS-86, and SHELXL-93. Further details of the crystal structure investigation are available on request from the Fachinformationszentrum Karlsruhe, D-76344 Eggenstein-Leopoldshafen 2, on quoting the depository number CSD-404020 for **4a** and 401988 for **4b**.
[9] M. D. Clark, M. J. Zaworotko, *J. Chem. Soc. Chem. Commun.* **1991**, 1607–1608.
[10] B. Nuber, F. Oberdorfer, M. L. Ziegler, *Acta Crystallogr. Sect. B* **1981**, *37*, 2062–2064.
[11] J. Breimair, C. Robl, W. Beck, *J. Organomet. Chem.* **1991**, *411*, 395–404.
[12] F. J. Feher, D. A. Newman, J. F. Walzer, *J. Am. Chem. Soc.* **1989**, *111*, 1741–1748.
[13] F. J. Feher, T. A. Budzichowski, J. W. Ziller, *Inorg. Chem.* **1992**, *31*, 5100–5105.
[14] F. J. Feher, K. Rahimian, T. A. Budzichowski, J. W. Ziller, *Organometallics* **1995**, *14*, 3920–3926.
[15] W. A. Herrmann, R. Anwander, V. Dufaud, W. Scherer, *Angew. Chem.* **1994**, *106*, 1338–1340; *Angew. Chem. Int. Ed. Engl.* **1994**, *33*, 1285–1286.
[16] W. Kläui, *Angew. Chem.* **1990**, *102*, 661–670; *Angew. Chem. Int. Ed. Engl.* **1990**, *29*, 627–637.
[17] R. Colton, A. D'Agostino, J. C. Traeger, W. Kläui, *Inorg. Chim. Acta* **1995**, *233*, 51–57.
[18] W. Scherer, G. Artus, E. Herdtweck, "STRUX-V", A Program System to Handle X-ray Data, Technische Universität München, Germany, **1995**.
[19] W. Schütt, E. Herdtweck, F. Hahn, F. R. Kreißl, *J. Organomet. Chem.* **1993**, 443, C33–C36 and references therein.
[20] IPDS-Operating system; program DECAY Version 2.5. STOE & CIE. GmbH, Darmstadt, **1995**.

Synthesis and Structure of a Bridging Germylidyne Complex: A Stable Germyl Cation**

Lisa K. Figge, Patrick J. Carroll, and Donald H. Berry*

The isolation of three-coordinate silicon cations, R_3Si^+, have been the subject of many recent reports.[1, 2] However, analogous germanium cations have not been described. In a related vein, Ogino, Tobita and co-workers have isolated a cationic diiron complex bridged by a germanium center. This germanium center is substituted with one alkyl group and a Lewis base[3a] and can be viewed as a base-stabilized germyl cation. We now report the synthesis and structure of a germanium-bridged tungsten dimer, which formally contains a base-free dimetalated germyl cation (germylium ion).

Thermolysis of $[Cp_2W(SiMe_3)(GeMe_2OTf)]$ (**1**)[4] in a solution of benzene at 80 °C results in the formation of three new products, trimethylsilyl triflate ($Me_3SiOSO_2CF_3$), $[Cp_2W(SiMe_3)(GeMe_3)]$ (**2**), and the dinuclear compound **3** [Eq. (a)]. Interestingly, the reaction also occurs when the solid is heated at 80 °C in the absence of a solvent.

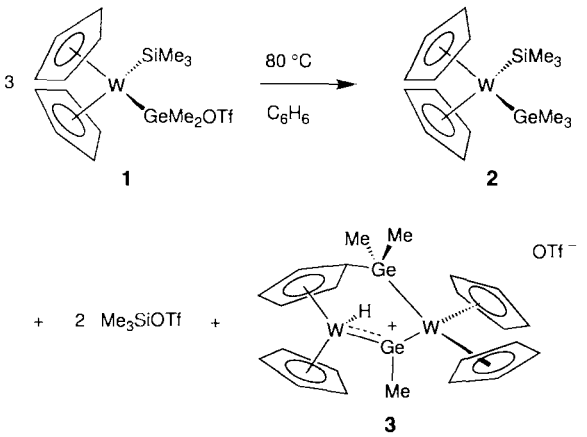

Trimethylsilyl triflate was identified by ^1H and ^{19}F NMR spectroscopy and compared with an authentic sample. The tungsten germyl silyl complex **2** has previously been synthesized independently.[4] The dimeric compound **3** has been isolated in good yield (93% of theoretical) as a bright orange powder, which is moderately soluble in acetonitrile. The ^1H NMR spectrum (in CD_3CN) exhibits three singlets for the intact Cp rings and three broad multiplets for the substituted C_5H_4 ring. The resonance for the remaining C_5H_4 proton is obscured by the Cp signals. Two singlets correspond to the nonequivalent methyl groups of the $C_5H_4GeMe_2$ fragment and a singlet at $\delta = 1.73$ to the methyl group on the germanium bridging the two tungsten centers, more than 1 ppm downfield from the $GeMe_2$ resonance. A singlet corresponding to the tungsten hydride is observed at $\delta = -10.8$ ($^1J_{W,H} = 79.9$ Hz). Significantly, both this hydride chemical shift and tungsten coupling constant are normal for tungstenocene hydrides (cf. **4**,; see below), which indicates that there is no nonclassical Ge···H–W interaction between the three-coordinate germanium atom and the tungsten hydride.

Although the identity of **3** could not be conclusively established by ^1H NMR, the structure of **3** has been unambiguously determined by single-crystal X-ray diffraction methods.[5] The structural analysis reveals a dinuclear compound with one normal Cp_2W unit and second tungsten (W2) with one intact Cp ring and one germanium-substituted Cp ring (Fig. 1). The tungsten hydride observed in the ^1H NMR spectrum was located in the structure at a chemically reasonable position (W–H = 1.53 Å), but did not refine satisfactorily. There is no indication of any interaction between the hydride and the three-coordinate germanium (Ge1···H = 2.80 Å). The germanium on the ring has two methyl groups and is bonded to one of the tungsten metal centers. The second germanium in the structure bridges the two tungsten centers and has only a single methyl substituent. The triflate counterion is totally dissociated; the closest contact to the three-coordinate germanium is 3.707(8) Å.

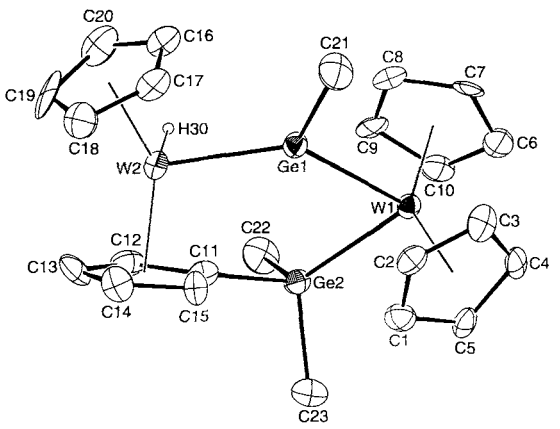

Fig. 1. Crystal structure of **3** (ORTEP drawing showing 30% probability thermal ellipsoids). The hydrogen atoms and the triflate ion have been omitted for clarity. Selected bond lengths [Å] and angles [°]: W1–Ge1 2.583(2), W1–Ge2 2.605(2), W2–Ge1 2.487(2), Ge1–C21 2.001(18); W1-Ge1-C21 108.9(6), W2-Ge1-C21 121.2(6), W1-Ge1-W2 129.9(1).

The geometry about the three-coordinate germanium atom Ge1 is planar (angle sum 360.0°), and it lies only 0.009 Å above the plane defined by the two tungsten centers and the methyl substituent. The tungsten–germanium bond length from W1 to the four-coordinate germanium atom Ge2 is comparable to the W–Ge single bond in $[Cp_2W(SiMe_3)(GeMe_2Cl)]$.[4] In addition, the bond between W1 and Ge1 is also typical of a W–Ge single bond. However, the W2–Ge1 distance is significantly shorter at 2.487(2) Å.

Three possible resonance structures for the bonding about the three-coordinate germanium center are shown in Scheme 1. Structure I depicts the case in which the cationic charge is localized on germanium. In structures II and III, the charge is delo-

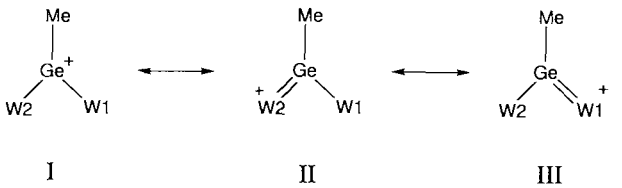

Scheme 1. The three possible resonance structures to describe the bonding about the three-coordinate germanium atom.

[*] Prof. D. H. Berry, L. K. Figge, P. J. Carroll
Department of Chemistry and Laboratory for Research on the Structure of Matter
University of Pennsylvania
Philadelphia, PA 19104-6323 (USA)
Fax: Int. code +(215)573-2112
e-mail: berry@a.chem.upenn.edu

[**] This work was supported by the National Science Foundation.

calized onto the tungsten centers by π-back bonding to the germanium atom. Although delocalization of the charge to both tungsten centers is possible, the presence of one normal and one short W–Ge distance suggests that only W2 is involved in back bonding. The valence orbitals in bent Cp_2M complexes lie in the equatorial plane between the Cp ligands.[7] Therefore, maximum π-bonding is achieved when the acceptor orbital on germanium is also located in the equatorial plane.

Scheme 2 illustrates the relative orientation of each tungsten center to the bridging three-coordinate germanium, as determined in the crystal structure. The two Cp rings on

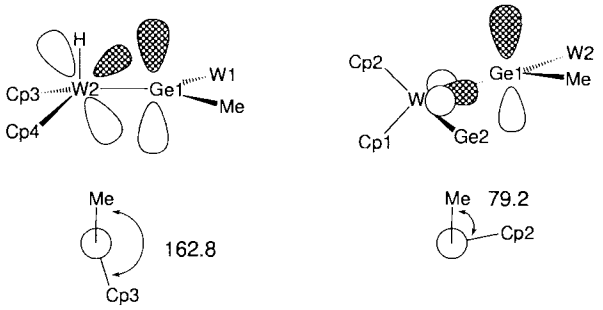

Scheme 2. The relative orientation of each tungsten center to the bridging three-coordinate germanium atom (Ge1).

W2 and the two substituents on Ge1 (W1 and C21) are nearly eclipsed (dihedral angle Cp3-W2-Ge-C21 = 162.8°) This positions the p-orbital on germanium coplanar with a tungsten valence orbital of π-symmetry (with respect to the W–Ge bond), and π-back bonding from the d^2, 18-electron tungsten center should be possible. On the other hand, the rings on W1 are nearly perpendicular to the substituents on Ge1 (dihedral angle Cp2-W1-Ge-C21 = 79.2°); thus only minimal overlap should be possible with the π-symmetry orbital. This is consistent with the normal W1–Ge1 and short W2–Ge1 distances observed in the structure. Once again it should be stressed that although the W2–H30 bond also lies in the plane of the Ge p-orbital, the spectroscopic parameters are typical of an unperturbed tungsten hydride and appear to preclude a bridging or nonclassical interaction with the germanium atom.

Some insight into the formation of **3** has been gained from the following experiments: Treatment of a suspension of **3** in THF with CH_3MgBr yields a soluble dimeric product, tentatively assigned as **4** on the basis of ^1H NMR [Eq. (b)].

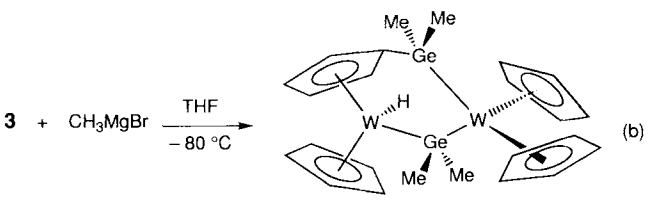

4

Although **4** decomposes in solution over hours and has not been isolated as a pure compound, treatment of **4** with **1** at room temperature leads to the rapid formation of **2** and precipitation of **3** [Eq. (c)].

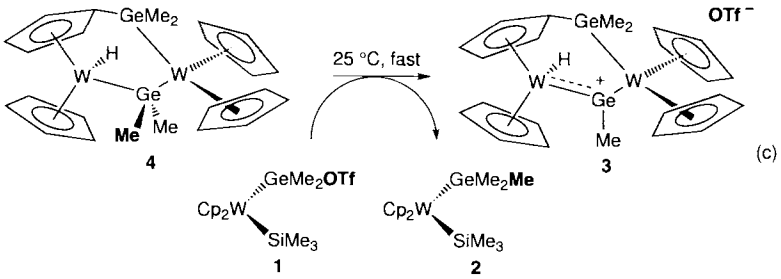

Thus **1** is capable of abstracting a methyl group from the dimetalated $GeMe_2$ unit in **4**, and this seems a probable final step in the formation of **3** from **1**. Our group has recently reported an intermolecular methyl group migration in a related tungsten germyl silyl complex,[4] and, in addition, Tilley and Grumbine have directly observed a comparable intermolecular migration in the reaction of $[Cp^*Ru(PMe_3)_2(SiMe_3)]$ with the stable silylene complex, $[Cp^*Ru(PMe_3)_2(SiPh_2)]^+$.[8]

The process by which **4** is formed from **1** remains obscure, but could involve dimerization and rearrangement of the neutral germylene complex formed by 1,2-elimination of Me_3SiOTf from **1**. Alternatively, the stepwise intermolecular elimination of Me_3SiOTf could also achieve the same end. Activation of Cp ring carbon atoms is a well-documented process often associated with metallocene dimerization.[9]

Compound **3** bears some relation to the cationic base-stabilized bridging germylidyne, and analogous silylidyne complexes, reported by the Ogino group.[3] Tilley and Grumbine have also reported a neutral bridging silylidyne complex, $[(CO)_4Os\{Si(S\text{-}p\text{-}Tol)\}RuCp^*(PMe_3)_2]$, in which a Si(STol) group bridges the two metals.[10] Similarly, **3** can be viewed as a cationic complex with germylidyne bridges.

Other important examples of two- and three-coordinate germanium centers stabilized by transition metals include dimetalated cumulenes of the type M=E=M)[11] (for example, $[Cp'(CO)_2Mn{=}Ge{=}MnCp'(CO)_2]$[11a]) and the "inidene" complexes extensively studied by Huttner et al.[12] The anionic inidene complex $[Cp'(CO)_2Mn{\cdots}Ge(I){\cdots}MnCp'(CO)_2]^-$ is of particular note, as it bears the strongest structural resemblance to **3**. One apparent difference is that the inidenes are generally viewed as having a rather electron-rich main group element (for example Ge^0) which undergoes π-bonding to satisfy the electron count at the metal centers. On the other hand, the three-coordinate germanium atom in the cation of **3** is clearly electron deficient; hence the π-backbonding from the 18-electron tungsten center serves to delocalize the positive charge. This difference has chemical consequences: the methyl germanium center in **3** is electrophilic and reacts with the methyl Grignard compound to yield **4**, whereas the structure of $[Cp'(CO)_2Mn{\cdots}Ge(I){\cdots}MnCp'(CO)_2]^-$ suggests the iodide is best depicted as an anion weakly coordinating to a Ge^0 center.

Experimental Procedure

3: Compound **1** (290 mg, 0.45 mmol) was placed in a glass bomb, which was evacuated and placed in an 80 °C oil bath for 48 hours. The pale yellow powder became bright orange. The volatiles (trimethylsilyl triflate) (0.050 g, 0.22 mmol, 75% of theory) were removed under vacuum, and the orange powder was washed with petroleum ether to remove $[Cp_2W(SiMe_3)(GeMe_3)]$ (0.068 g, 0.134 mmol, 90% yield). Yield of **3**: 136 mg (93%). C,H anal. calcd for $C_{24}H_{29}W_2Ge_2O_3F_3S$: C, 29.80; H, 3.02; found: C, 29.92; H, 2.71. ^1H NMR (200 MHz, CD_3CN, 303 K): δ = 5.88 (m, 1H, C_5H_4Ge), 5.30 (m, 1H, C_5H_4Ge), 5.17 (m, 1H, C_5H_4Ge), 4.91 (s, 5H, Cp), 4.75 (s, 5H, Cp), 4.59 (s, 5H, Cp), 1.73 (s, 3H, GeMe), 0.48 (s, 3H, $GeMe_2$), 0.44 (s, 3H, $GeMe_2$), −10.80 (s, 1H, WH; $^1J(W,H)$ = 79.9 Hz).

4: A THF solution (7 mL) of **3** (30 mg, 0.031 mmol) was cooled to −80 °C and a 3.0 M solution of CH_3MgBr (0.030 mmol) in diethyl ether (10 μL) was added. The reaction was warmed to room temperature and stirred for 10 minutes. The volatiles

 © VCH Verlagsgesellschaft mbH, D-69451 Weinheim, 1996 0570-0833/96/3504-0436 $ 15.00+.25/0

were removed under vacuum to yield a yellow solid. ^{1}H NMR (200 MHz, C_6D_6, 303 K): 4.95 (m, 1H, C_5H_4Ge) 4.14 (s, 5H, Cp), 4.12 (s, 5H, Cp), 3.96 (s, 5H, Cp), 3.21 (m, 1H, C_5H_4Ge), 0.77 (s, 3H, GeMe), 0.75 (s, 3H, GeMe), 0.62 (s, 3H, GeMe), 0.61 (s, 3H, GeMe), −11.32 (s, 1H, WH; ^1J(W,H) = 81.7 Hz). Two additional C_5H_4Ge resonances are believed to be obscured by the other Cp resonances or the large residual THF resonance.

Reaction of **4** with **1**: Immediately following the isolation of **4**, the solid was dissolved in C_6D_6 (0.5 mL) and filtered. This solution was added to an NMR tube containing **1** (16 mg, 0.025 mmol). The tube was sealed under vacuum. Immediately after addition a bright orange precipitate forms. The ^{1}H NMR indicates that only **2** and **1** (in excess) are present in solution.

Received: September 21, 1995
Revised: December 6, 1995 [Z 8414 IE]
German version: *Angew. Chem.* **1996**, *108*, 465–467

Keywords: bridging ligands · germanium compounds · germyl cations · tungsten compounds

[1] a) J. B. Lambert, S. Zhang, S. M. Ciro, *Organometallics* **1994**, *13*, 2430–2443; b) J. B. Lambert, S. Zhang, C. L. Stern, J. C. Huffman, *Science* **1993**, *260*, 1917.

[2] a) Z. Xie, R. Bau, A. Benesi, C. A. Reed, *Organometallics* **1995**, *14*, 3933–3941; b) C. A. Reed, Z. Xie, R. Bau, A. Benesi, *Science* **1993**, *262*, 402.

[3] a) J. Fujita, Y. Kawano, H. Tobita, M. Simoi, H. Ogino, *Chem. Lett.* **1994**, 1353–1356; b) Y. Kawano, H. Tobita, M. Simoi, H. Ogino, *J. Am. Chem. Soc.* **1994**, *116*, 8575–8581.

[4] L. K. Figge, P. J. Carroll, D. H. Berry, *Organometallics* **1996**, *15*, 209–215.

[5] X-ray structure analysis of **3**: $C_{24}H_{29}W_2Ge_2SF_3O_3$ (M_r = 967.43), orange crystals, crystal dimensions 0.05 × 0.03 × 0.04 mm; monoclinic, space group $P2_1/n$ (no. 14), a = 8.8533(2) b = 15.9110(4), c = 18.2630(5) Å, β = 93.666(1)°, V = 2567.35(10) Å^3, Z = 4, $\mu(Mo_{K\alpha})$ = 113.89 cm^{-1}, T = 235 K, $F(000)$ = 1808.00. A total of 18150 reflections were measured over the ranges $4 \le 2\theta \le 50°$, $0 \le h \le 10$, $-18 \le k \le 18$, $-21 \le l \le 21$ on a Rigaku/MSC RAXIS IIc image plate area detector with graphite monochromated $Mo_{K\alpha}$ radiation. The *hkl* data were extracted using the bioTex software package [6a] and subsequent data reduction and solution of the structure was accomplished with the teXsan [6b] package. Cell constants were refined in bioteX using a total of 14366 reflections. Thus eight variables (a, b, c, three orientation angles, and the mosaicity) were refined using 14366 experimental observations. This technique is typical for data sets collected with an area detector, but this large overdetermination results in extremely small esd's for the cell constants. The actual errors are probably somewhat higher due to the uncertainty in $\lambda(Mo_{K\alpha})$. The intensity data were corrected for Lorentz and polarization effects, and an empirical absorption correction was applied [6c]. A total of 4533 reflections were independent, and 3086 reflections with $F^2 > 3\sigma(F^2)$ were used for all calculations. The structure was solved by direct methods and 317 parameters refined based on F, minimizing the quantity $\sum w(|F_o| - |F_c|)^2$ with $w = 1/\sigma^2(F)$. Non-hydrogen atoms were refined anisotropically, and hydrogen atoms were included as constant contributions to the structure factors and were not refined. The hydride on tungsten was located, but could not be refined. Final agreement factors of R_1 = 0.0491, R_2 = 0.0508, and GOF = 1.755 were obtained. Further details of the crystal structure investigation may be obtained from the Director of the Cambridge Crystallographic Data Center, 12 Union Road, GB-Cambridge CB2 1EZ (UK), on quoting the full journal citation.

[6] a) Molecular Structure Corporation, bioteX, **1995**; b) Molecular Structure Corporation, teXsan, **1995**; c) T. Higashi, ABSCOR, Rigaku Corp., **1995**.

[7] J. W. Lauher, R. Hoffmann, *J. Am. Chem. Soc.* **1976**, *98*, 1729.

[8] S. K. Grumbine, T. D. Tilley, *J. Am. Chem. Soc.* **1994**, *116*, 6951.

[9] a) J. Bashkin, M. L. H. Green, M. L. Poveda, K. Prout, *J. Chem. Soc. Dalton Trans.* **1982**, 2485–2494; b) M. Berry, K. Elmitt, M. L. H. Green, *ibid.* **1980**, 29–40; c) D. H. Berry, T. S. Koloski, P. J. Carroll, *Organometallics* **1990**, *9*, 2952–2962.

[10] S. D. Grumbine, T. D. Tilley, *J. Am. Chem. Soc.* **1993**, *115*, 358.

[11] a) W. Gäde, E. Weiss, *J. Organomet. Chem.* **1981**, *213*, 451–460; b) W. A. Herrmann, *Angew. Chem.* **1986**, *98*, 57; *Angew. Chem. Int. Ed. Engl.* **1986**, *25*, 56; c) W. A. Herrmann, H.-J. Kneuper, E. Herdtweck, *ibid.* **1985**, *97*, 1060–1061 and **1985**, *24*, 1062–1063; d) B. Schiemenz, G. Huttner, *ibid.* **1993**, *105*, 1840–1841 and **1993**, *32*, 1772–1774.

[12] B. Schiemenz, G. Huttner, *Chem. Ber.* **1994**, *127*, 2129–2133; F. Ettel, G. Huttner, L. Zsolnai, *Angew. Chem.* **1989**, *101*, 1525–1527; *Angew. Chem. Int. Ed. Engl.* **1989**, *28*, 1496–1498; A. Strube, G. Huttner, L. Zsolnai, *ibid.* **1988**, *100*, 731–732 and **1988**, *27*, 1529–1530.

The First Recombinant Hydroxynitrile Lyase and its Application in the Synthesis of (*S*)-Cyanohydrins**

Siegfried Förster, Jürgen Roos, Franz Effenberger,* Harald Wajant, and Achim Sprauer

Dedicated to Professor Manfred Regitz on the occasion of his 60th birthday

Recently we have reported comprehensively on syntheses and reactions of optically active cyanohydrins.[1] That overview points out that the hydroxynitrile lyase isolated from bitter almond (PaHNL) [EC 4.1.2.10] catalyzes the enantioselective addition of hydrocyanic acid to aldehydes to give (*R*)-cyanohydrins with high optical purities. Because of the very broad substrate range and the easy availability of the enzyme, this procedure is the simplest approach to (*R*)-cyanohydrins.

The conditions for the enzyme-catalyzed preparation of (*S*)-cyanohydrins are, however, essentially different. The application of hydroxynitrile lyase from *Sorghum bicolor* (SbHNL) [EC 4.1.2.11] as catalyst proved so far to be the most successful method for the enantioselective addition of HCN to aldehydes, yielding (*S*)-cyanohydrins.[2, 3] Although this enzyme is now available from Sorghum seedlings in larger amounts for preparative applications, this source is insufficient for technical processes. In addition to the problems of availability, the limited substrate range of SbHNL, which accepts only aromatic and heteroaromatic but not aliphatic aldehydes as substrates, is a severe disadvantage for the application of this enzyme.[2] The (*S*)-hydroxynitrile lyase from *Hevea brasiliensis*, recently applied in the preparation of (*S*)-cyanohydrins, accepts aliphatic aldehydes as substrates but also has the disadvantage of more difficult accessibility.[4]

In view of the disadvantages of both (*S*)-hydroxynitrile lyases used in organic synthesis to date, we were interested in developing an (*S*)-HNL that shows a broad substrate range and can easily be obtained in large amounts by genetic engineering. Investigations with the cloned SbHNL[5] have so far shown that its functional expression requires complex posttranslational processing.[5b] For this reason enzymatically active SbHNL will not be able to be produced genetically in the foreseeable future.

Better results should be obtainable with a hydroxynitrile lyase isolated from *Manihot esculenta* (MeHNL) [EC 4.1.2.37],[6] which is serologically distinct from the other hydroxynitrile lyases.[7] It not only promises more convenient conditions for the functional expression but also more flexibility of substrate range, as first synthetic applications of the natural enzyme have shown.[7] We have now overexpressed the in pQE4 cloned MeHNL-gene (pQE4-MeHNLwt)[7b] in *E. coli* M15[pREP4] cells.[7b]

Activity measurements of lysate of transformed M15[pREP4] cells (M15-MeHNL) show an HNL activity of 0.5 units per milliliter of culture, whereas no activity could be detected in the lysate of untransformed cells.[7b]

[*] Prof. F. Effenberger, Dr. S. Förster, Dipl.-Chem. J. Roos
Institut für Organische Chemie der Universität
Pfaffenwaldring 55, D-70569 Stuttgart (Germany)
Fax: Int. code +(711)6854269
Dr. H. Wajant
Institut für Zellbiologie und Immunologie der Universität Stuttgart (Germany)
Dipl.-Ing.(FH) A. Sprauer
Institut für Technische Biochemie der Universität Stuttgart (Germany)

[**] Enzyme-Catalyzed Reactions, Part 23. This work was supported by the Bundesministerium für Bildung und Forschung and by the Fonds der Chemischen Industrie. Part 22: F. Effenberger, S. Heid, *Tetrahedron Asymmetry* **1995**, *6*, 2945–2952.

The M15-MeHNL cells were disrupted at pH 5.4 and then treated with benzonase. MeHNL was purified by anion exchange chromatography on Q-Sepharose FF. After ultrafiltration the activity of the purified recombinant MeHNL was 900 U mL^{-1}. An 80 L M15-MeHNL culture with 150–200 g wet weight yields approximately 40000 U of recombinant MeHNL. The same quantity of enzyme from plant material would require 100–200 kg of dried cassava leaves. Thus, for the first time an (*S*)-hydroxynitrile lyase has become available in large quantities in a simple way. The biochemical properties of the recombinant MeHNL and MeHNL isolated from *Manihot esculenta* are identical.[7b]

Although the first experiments to determine the catalytic potential of the MeHNL isolated from cassava leaves demonstrated a broad substrate range, the achieved optical yields of the (*S*)-cyanohydrins obtained were unsatisfactory.[7a]

With the recombinant enzyme, available now in sufficient amounts and with 25 times higher specific activity than the natural enzyme, we have investigated the enantioselective addition of hydrocyanic acid to several aldehydes (Scheme 1, Table 1) and ketones (Scheme 2, Table 2). To achieve the highest possible optical purity, diisopropyl ether was chosen as solvent.[1] Although cellulose (Avicel or cellulose P100 PSC) has proved to be very suitable as supporting material for the reactions with PaHNL and SbHNL,[1,8] the reactions with the recombinant MeHNL on cellulose support gave only moderate optical yields.[9] However, by using nitrocellulose as support, which possesses a higher affinity for proteins than cellulose, the enantioselectivity is high in most cases (Tables 1 and 2).

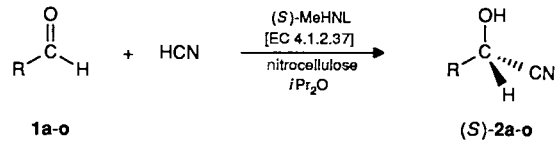

1, 2	R	1, 2	R	1, 2	R
a	Et	i	Ph	m	
b	Bu	j		n	
c	*i*Pr	k		o	
d	Me_3C				
e	CH_2=CH				
f	MeCH=CH				
g	$Me(CH_2)_2CH$=CH				
h	*c*-C_6H_{11}				

Scheme 1. Synthesis of (*S*)-cyanohydrins by MeHNL-catalyzed addition of HCN to aldehydes.

Table 1. (*S*)-cyanohydrins (*S*)-**2** prepared by MeHNL-catalyzed addition of HCN to aldehydes **1** in diisopropyl ether as solvent at 25 °C.

Aldehydes **1** R		Enzyme [U mmol^{-1} **1**]	*t* [h]	(*S*)-Cyanohydrins **2** Yield [%][a]	*ee* [%][b]
a	C_2H_5	34	4.3	86	91
b	*n*-C_4H_9	61	4.0	100	91
c	$(H_3C)_2CH$	32	6.5	91	95
d	$(H_3C)_3C$	39	8.8	80	94
e	H_2C=CH	119	0.5	100	47
		100	1.0 [c]	70	56
f	*E*-H_3CCH=CH	145	1.0	100	92
g	*E*-$H_3C(CH_2)_2CH$=CH	130	3.0	82	97
h	*c*C_6H_{11}	70	5.3	100	92
i	C_6H_5	58	7.0	100	98
j	2-Cl-C_6H_4	107	8.7	100	92
k	4-H_3CO-C_6H_4	130	9.5	82	98
l	3,4-CH_2O_2-C_6H_3	110	10.3	84	86
m	2-thienyl	134	6.0	85	96
n	3-thienyl	149	4.0	98	98
o	3-furyl	141	6.5	98	92

[a] The yields of (*S*)-**2a**–**j** refer to the isolated pure products; those of (*S*)-**2k**–**o** are determined by ^{1}H NMR spectroscopy. [b] Determined by gas chromatography on β-cyclodextrin phases after acetylation with acetic anhydride [1,9]. [c] At 0 °C.

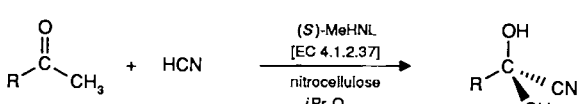

3, 4	a	b	c	d	e	f	g
R	Et	Pr	Bu	C_5H_{11}	Me_2CHCH_2	Me_3C	Ph

Scheme 2. Synthesis of (*S*)-ketone cyanohydrins by MeHNL-catalyzed addition of HCN to methyl ketones.

Table 2. (*S*)-ketone cyanohydrins (*S*)-**4** prepared by MeHNL-catalyzed addition of HCN to methyl ketones **3** in diisopropyl ether as solvent at 25 °C.

Ketones **3** R		Enzyme [U mmol^{-1} **3**]	*t* [h]	(*S*)-Ketone cyanohydrins **4** Yield [%][a]	*ee* [%][b]
a	C_2H_5	53	4.0	91	18
b	*n*-C_3H_7	123	0.5	36	69 [c]
c	*n*-C_4H_9	123	0.5	58	80 [c]
d	*n*-C_5H_{11}	126	2.0	39	92
e	$(H_3C)_2CHCH_2$	107	0.7	69	91
f	$(H_3C)_3C$	107	0.8	81	28
g	C_6H_5	112	7.0	13[d]	78

[a] The yields refer to the isolated pure products. [b] Determined by gas chromatography on β-cyclodextrin phases after acetylation with acetic anhydride or saponification to carboxylic acid and subsequent esterification to methyl ester, or by gas chromatography of diastereomeric (*S*)-MPTA esters (MPTA = α-methoxy-α-trifluoromethylphenyl acetic acid) [1,9]. [c] Comparison with Ref. [11]. [d] Yield determined by ^{1}H NMR spectroscopy.

Table 1 shows that MeHNL exhibits a similar broad substrate range as (*R*)-hydroxynitrile lyase from bitter almond: that is, not only aromatic and heteroaromatic but also aliphatic aldehydes are accepted as substrates. Even the sterically very demanding pivalaldehyde (**1d**) reacts highly enantioselectively.

The enzyme-catalyzed enantioselective addition of HCN to ketones was established for PaHNL,[10a] as well as for hydroxynitrile lyase from *Linum usitatissimum*.[10b] Both enzymes catalyze the formation of (*R*)-ketone cyanohydrins. The synthesis of (*S*)-ketone cyanohydrins catalyzed by an (*S*)-hydroxynitrile lyase has not yet been published. (*S*)-Ketone cyanohydrins have been recently prepared from racemic ketone cyanohydrins by enantioselective transcyanation with (*R*)-hydroxynitrile lyase PaHNL.[11]

In Table 2 our results of the MeHNL catalyzed preparation of (*S*)-ketone cyanohydrins (*S*)-**4** are summarized. As expected, in the reactions of alkyl methyl ketones the optical yields of the products obtained improve with increasing size of the alkyl group.[10a] While branching in the β-position of the alkyl substituent has no disadvantage on the enantioselectivity (**4e**), a bulky substituent in the α-position to the carbonyl group (**4f**) decreases the optical purity. MeHNL accepts even an aromatic ketone such as acetophenone as substrate (Table 2).

Experimental Procedure

Overexpression of MeHNL in *E. coli*: The coding region of the MeHNL gene was amplified from oligo(dT) primed first strand cDNA with PCR (forward primer: GCA GGG CCG GAT CCC ATT TCC AAA ATG GTA ACT GCA CA; rewind primer: GCA GGG CCG GAT CCA CAC AAC GTG GAA CTC TCC CAT ATT;

underlined sequences correspond to position 16–39 and 933–910 of the MeHNL gene published) [6b] and cloned in the correct reading frame in the pQE4 expression vector (Quiagen). The resulting expression plasmid pQE4-MeHNLwt was transformed in *E. coli* M15[pREP4] cells for overexpression (M15-MeHNL).

An overnight culture (2 mL) of a single colony of M15-MeHNL in LB medium containing ampicillin (100 $\mu g mL^{-1}$) and kanamycin (25 $\mu g mL^{-1}$) was used to inoculate an 8 L culture that was then grown for 12 h at 37 °C. This culture was used to inoculate a 100 L fermenter (Bioengineering). The M15-MeHNL cells were grown at 30 C for 1 h and expression of recombinant MeHNL was induced by adding isopropyl-β-D-thiogalactosid (IPTG) to a final concentration of 1 mM. The cells were grown for an additional 3.5 h and concentrated to about 7.5 L by cross-flow concentration (Maxisette system) with a 0.3 μm membrane (0.46 m^2) (Filtron). To remove the remaining LB medium the cells were centrifuged for 10 min at $10000 \times g$. The resulting pellet was resuspended in 2 L sodium acetate buffer (50 mM, pH 5.4), and the cells were disrupted by high-pressure homogenization (500 bar, 3 cycles; Rannie-APV MiniLab). To destroy chromosomal DNA the crude lysate (total amount of MeHNL 40000 U, spec. activity 2.8 $U mg^{-1}$) was digested with benzonase (Merck) (final concentration of 5000 $U L^{-1}$) for 1 h at room temperature. After centrifugation at $130000 \times g$ for 1 h MeHNL was enriched to a spec. activity of 12 $U mg^{-1}$ by anion exchange chromatography. A Q-Sepharose FF 100/1200 column was equilibrated in 20 mM sodium acetate, pH 5.7 (buffer A) and bound proteins were eluted with a 7200 mL linear gradient of 0–1 M NaCl in buffer A at a flow rate of 50 mL min^{-1}. MeHNL eluted after 450 mL salt gradient.

Enzyme-catalyzed preparation of (*S*)-cyanohydrins: The support (50 mg nitrocellulose) was soaked in 3 mL sodium citrate buffer (0.02 M, pH 3.3) for 30 min. After decanting, centrifuging (30 min, $5700 \times g$), and drying under high vacuum (5 h), a concentrated solution of MeHNL (900 $U mL^{-1}$, amounts as in Tables 1 and 2) was added dropwise. After 15 min the enzyme-charged support was centrifuged (at −5 °C, 30 min, $3650 \times g$) and transferred to a flask. Diisopropyl ether (5 mL), substrates **1** or **3** (0.3–0.4 mmol) and HCN (100 µL, 2.6 mmol) were added, and the mixture stirred at room temperature for the time given in Tables 1 and 2. The support was filtered off and washed with diethyl ether. The combined filtrates were dried, and solvent and unchanged starting materials (**1a–g**, **3a–f**) distilled off. Thus pure aldehyde cyanohydrins (*S*)-**2a–j** (Table 1) and ketone cyanohydrins (*S*)-**4a–f** (Table 2) were isolated. To obtain compounds (*S*)-**2k–o** and (*S*)-**4g** in pure form it was necessary to convert them into acetates or trimethyl silyl ethers for the separation from unchanged starting materials. The yields obtained correspond to those determined by ^1H NMR spectroscopy (Tables 1 and 2).

Received: October 11, 1995 [Z 8461 IE]
German version: *Angew. Chem.* **1996**, *108*, 493–494

Keywords: asymmetric syntheses · (*S*)-cyanohydrins · enzymatic catalysis · lyases

[1] F. Effenberger, *Angew. Chem.* **1994**, *106*, 1609–1619; *Angew. Chem. Int. Ed. Engl.* **1994**, *33*, 1555–1564.
[2] F. Effenberger, B. Hörsch, S. Förster, T. Ziegler, *Tetrahedron Lett.* **1990**, *31*, 1249–1252.
[3] a) U. Niedermeyer, M.-R. Kula, *Angew. Chem.* **1990**, *102*, 423–425; *Angew. Chem. Int. Ed. Engl.* **1990**, *29*, 386–387; b) M.-R. Kula, U. Niedermeyer, I. M. Stuertz (Degussa AG), EP-B 350908. **1990**; DE-B 3823866. **1988** [*Chem. Abstr.* **1990**, *113*, 57462h].
[4] a) N. Klempier, H. Griengl, M. Hayn, *Tetrahedron Lett.* **1993**, *34*, 4769–4772; b) N. Klempier, U. Pichler, H. Griengl, *Tetrahedron Asymmetry* **1995**, *6*, 845–848.
[5] a) H. Wajant, H. Böttinger, K.-W. Mundry, *Biotechnol. Appl. Biochem.* **1993**, *18*, 75–82; b) H. Wajant, unpublished results.
[6] a) F. J. P. De C. Carvalho, Dissertation, University of California, Davis, **1981**; b) J. Hughes, F. J. P. De C. Carvalho, M. A. Hughes, *Arch. Biochem. Biophys.* **1994**, *311*, 496–502.
[7] a) H. Wajant, S. Förster, H. Böttinger, F. Effenberger, K. Pfizenmaier, *Plant Sci. (Limerick, Irel.)* **1995**, *108*, 1–11; b) H. Wajant, unpublished results.
[8] F. Effenberger, J. Eichhorn, J. Roos, *Tetrahedron Asymmetry* **1995**, *6*, 271–282.
[9] J. Roos, Diplomarbeit, Universität Stuttgart, **1995**.
[10] a) F. Effenberger, B. Hörsch, F. Weingart, T. Ziegler, S. Kühner, *Tetrahedron Lett.* **1991**, *32*, 2605–2608; b) J. Albrecht, I. Jansen, M.-R. Kula, *Biotechnol. Appl. Biochem.* **1993**, *17*, 191–203.
[11] E. Menéndez, R. Brieva, F. Rebolledo, V. Gotor, *J. Chem. Soc. Chem. Commun.* **1995**, 989–990.

Hexa-*tert*-butyltribenzodecacyclenyl: A Six-Stage Amphoteric Redox System

Takashi Kubo, Kagetoshi Yamamoto, Kazuhiro Nakasuji,* Takeji Takui, and Ichiro Murata

Some organic compounds[1] show amphoteric redox behavior, that is the numerical sum (E^{sum}) of oxidation potential (E^{ox}) and reduction potential (E^{red}), $E^{sum} = E^{ox} + (-E^{red})$, is very small. These compounds are oxidized or reduced easily by an electron transfer. Recently we synthesized the four-stage amphoteric redox hydrocarbons bearing two phenalenyl units, which are crucial for the amphoteric redox behavior. To study the properties of higher amphoteric hydrocarbons, we designed the tribenzodecacyclenyl **1a**, which contains three phenalenyl units. Compound **1a** is expected to behave as a six-stage amphoteric redox compound (Scheme 1)[2] and to readily generate super-charged species such as the trication and trianion. We now

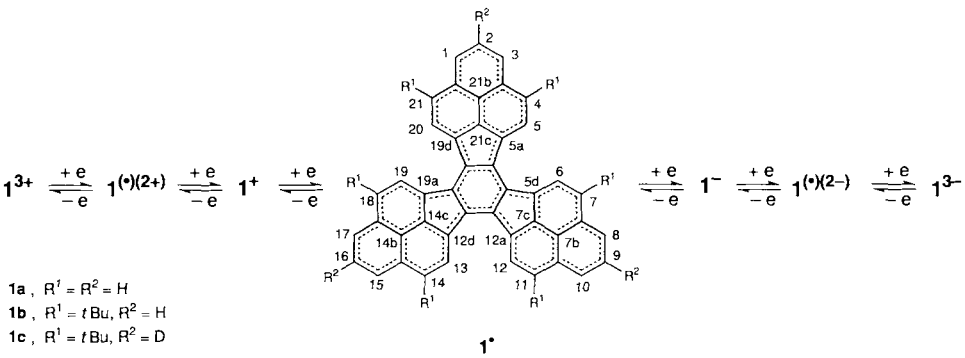

Scheme 1. Six-stage amphoteric redox behavior of **1**•.

report the synthesis of **1b**, the hexa-*tert*-butyl derivative of **1a**, and the properties of **1b**•, $\mathbf{1b}^{3+}$, and $\mathbf{1b}^{3-}$.

The starting material, 2,5,8,11,14,17-hexa-*tert*-butyldecacyclene (**2**),[3] was formed directly by Friedel–Crafts alkylation of decacyclene (Scheme 2).[4] The bromination of **2** furnished an isomeric mixture of the tribromides **3** in 76% yield,[5] which were converted to tris(propionic acid) derivatives **7** by the usual method (only one isomer is shown in Scheme 2). Friedel–Crafts cyclization of **7** gave the triketones **8**, which were reduced and subsequently dehydrated to afford trihydro compounds **10**.[6] The dehydrogenation of **10** with *p*-benzoquinone or *p*-chloranil provided the neutral monoradical species **1b**• as an air-sensitive brown solid (Scheme 2).

The ESR signal of **1b**• was observed, but lack of resolution prevented the determination of the hyperfine coupling (hfc) constants. However, the ESR spectrum of the deuterated compound **1c**• gave hyperfine structure,[7] from which two hfc constants were obtained, 1.43 G (6H), 0.47 G (6H). The hfc

[*] Prof. Dr. K. Nakasuji, T. Kubo, Prof. Dr. K. Yamamoto, Prof. Dr. I. Murata[+]
Department of Chemistry, Faculty of Science
Osaka University
Toyonaka, Osaka 560 (Japan)
Fax: Int. code +(6)850-5395
Prof. Dr. T. Takui
Department of Chemistry, Faculty of Science
Osaka City University
Sumiyoshi-ku, Osaka 558 (Japan)
[+] Current address: Fukui Institute of Technology, Gakuen, Fukui 910 (Japan)
[**] This work was supported by a Grant-in-Aid for Scientific Research on Priority Areas from the Ministry of Education, Science and Culture, Japan. We thank Dr. Kay-Uwe Klabunde for preliminary efforts in this study.

 © VCH Verlagsgesellschaft mbH, D-69451 Weinheim, 1996 0570-0833/96/3504-0439 $ 15.00+.25/0

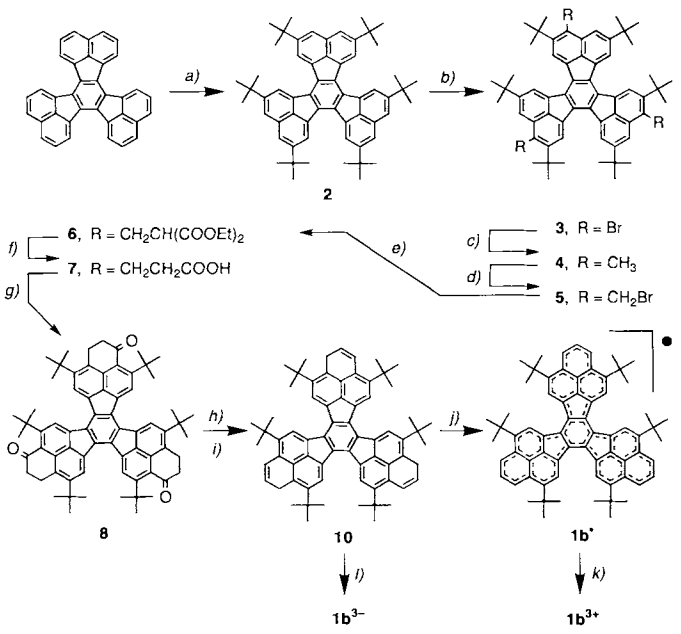

Scheme 2. Synthesis of **1b**•, **1b**$^{3+}$, and **1b**$^{3-}$. Reaction conditions: a) *t*BuCl, $AlCl_3$, CH_2Cl_2, room temperature, 2 h, 74% ; b) Br_2, CH_2Cl_2, 2 h, room temperature, 76%; c) *n*BuLi, CH_3I, THF, −78 °C to room temperature, 81%; d) NBS, benzoyl peroxide, benzene, reflux, 10 min, 96%; e) NaOEt, $CH_2(CO_2Et)_2$, benzene + ethanol, room temperature, 1 d, 36%; f) 1) aqueous KOH, EtOH, 2) 4 N HCl, 3) 100 °C, 95%; g) 1) $(COCl)_2$, 2) $AlCl_3$, CH_2Cl_2, −50 °C, 4 h, 99%; h) $NaBH_4$, CH_2Cl_2 + ethanol, reflux, 1 d, 92%; i) cat. *p*-toluenesulfonic acid, benzene, reflux, 5 min, 90%; j) *p*-benzoquinone or *p*-chloranil, benzene, reflux, 10 min; k) conc. D_2SO_4 or 3 equiv $[(p\text{-}BrC_6H_4)_3N]^+[SbCl_6]^-$; l) K mirror, under vacuum, [D$_8$]THF, −78 °C, 1 week.

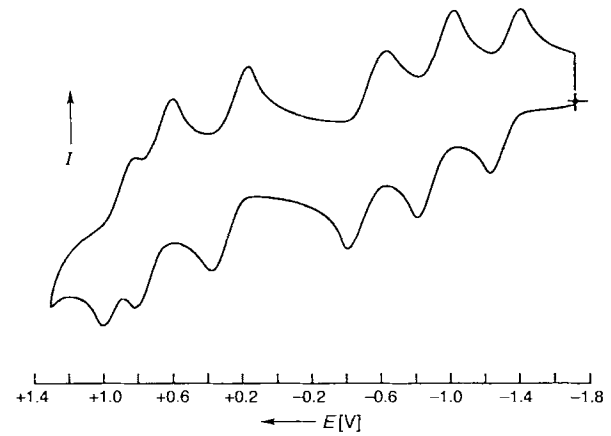

Fig. 1. Cyclic voltammogram of **1b**• measured in dichloromethane with 0.1 M nBu_4NClO_4 as supporting electrolyte at 0 °C; sweep rate 100 mVs^{-1}.

Table 2. Cyclic voltammetric data [V vs. SCE] of **1b**• and some related compounds.

	E_3^{ox}	E_2^{ox}	E_1^{ox}	E_1^{red}	E_2^{red}	E_3^{red}	E_1^{sum} [b]	E_2^{sum} [b]	E_3^{sum} [b]
1b• [a]	+0.87	+0.68	+0.27	−0.51	−0.89	−1.25	0.78	1.57	2.12
PDPL [c]		+1.02	+0.56	−0.43	−1.17		0.99	2.19	
*i*Pr-IDPL [d]		+0.84	+0.62	−0.48	−1.07		1.10	1.91	

[a] Measured against the saturated calomel electrode (SCE) in dichloromethane with 0.1 M nBu_4NClO_4 as supporting electrolyte at 0 °C; sweep rate 100 mVs^{-1}. [b] $E_n^{sum} = E_n^{ox} + (-E_n^{red})$. [c] PDPL = pentaleno[1,2,3-*c*,*d*:4,5,6-*c*′*d*′]diphenalene [1d]. [d] IDPL = *s*-indaceno[1,2,3-*c*,*d*:5,6,7-*c*′*d*′]diphenalene [1f].

constants of the hydrogen atoms H-2, H-9, and H-16 in **1b**• were determined by a computer simulation. Assignments of hfc constants $a_H\mu$ to protons in the position μ were based on a HMO-McLachlan calculation ($\lambda = 1.2$)[8] of the spin density of **1a**•. The hfc constants and the calculated spin densities are listed in Table 1. The linear relationship between the hfc constants

Table 1. Hyperfine coupling constants a_{H_μ} and spin densities ρ_μ for **1b**•, and ^{1}H and ^{13}C NMR chemical shifts (δ) for **1b**$^{3+}$ and **1b**$^{3-}$.

Position μ	**1b**•		**1b**$^{3+}$		**1b**$^{3-}$	
	a_{H_μ} [G][a]	ϱ_μ[b]	$\delta(^1H)$	$\delta(^{13}C)$[c]	$\delta(^1H)$	$\delta(^{13}C)$[c]
1, 3, 8, 10, 15, 17 (α^1)	1.43	0.055	9.68	148.32	7.97	113.40
2, 9, 16 (β^1)	0.37	−0.012	8.31	132.40	7.50	118.63
4, 7, 11, 14, 18, 21 (α^2)				183.45		126.98
5, 6, 12, 13, 19, 20 (β^2)	0.47	−0.009	8.86	125.37	9.49	120.10
5a, 5d, 12a, 12d, 19a, 19d (α^3)				152.57		114.27

[a] ESR measured in toluene at −30 °C. [b] Spin densities (McLachlan method, $\lambda = 1.2$). [c] Other ^{13}C NMR signals of **1b**$^{3+}$ (D_2SO_4 at 60 °C) and **1b**$^{3-}$ ([D$_8$]THF at 25 °C): $\delta = 133.54$ and 130.75 (3a, 7a, 10a, 14a, 17a, 21a), respectively; 145.31 and 119.03 (5b, 5c, 12b, 12c, 19b, 19c), respectively; 125.63 and 129.58 (7b, 14b, 21b), respectively; 136.95 and 127.62 (7c, 14c, 21c), respectively; 41.77 and 37.16 ($C(CH_3)_3$), respectively; 35.20 and 32.55 ($C(CH_3)_3$), respectively.

stants and the theoretical values for the spin densities suggests that the unpaired electron delocalization is not confined to one phenalenyl unit but is operative over the entire C_3 symmetric molecule.

The cyclic voltammogram of **1b**• measured in dichloromethane exhibited six reversible one-electron redox waves (Fig. 1). The electrochemical data of **1b**• and related hydrocarbons bearing two phenalenyl units are summarized in Table 2. The sum of the redox potentials E_1^{sum} of **1b**• is substantially smaller than those reported so far for hydrocarbons. Such a small E_1^{sum} value can be explained in terms of the electronic stability of three redox states of the phenalenyl unit owing to the delocalization of the generated charges or the unpaired electron over the molecules.

The trication **1b**$^{3+}$ was obtained as a dark green solution by dissolving **1b**• in concentrated D_2SO_4 or as dark green needles[9] by treating **1b**• with three equivalents of tris(4-bromophenyl)aminium hexachloroantimonate. The trianion **1b**$^{3-}$ was generated as a red purple solution[10] by the reaction of the trihydro compound **10** with a potassium mirror in a sealed degassed tube at −78 °C for a week. The ^{1}H and ^{13}C NMR chemical shifts of **1b**$^{3+}$ and **1b**$^{3-}$ are given in Table 1. The total ^{13}C chemical shift change ($\Sigma\Delta\delta_C$) of the sp^2 carbon atoms on going from **1b**$^{3+}$ to **1b**$^{3-}$ is 1041.63 (or 173.61 per electron), which supports the idea of the presence of the trication and the trianion, respectively.[11] The shift changes ($\Delta\delta_C$) are large for the C atoms at positions α^1, α^2, and α^3, which correspond to the α positions of the phenalenyl,[12] but small for the C atoms at other positions except for the central benzene ring. This finding suggests that the phenalenyl units contribute largely to the stability of both triply charged species.[13]

The most striking feature is that the signals of the protons at the position β^2 of **1b**$^{3-}$ unexpectedly appear at lower field than the signals of the corresponding protons of **1b**$^{3+}$, in spite of the shielding effect caused by the three negative charges. The ^{13}C chemical shifts of the C atoms at position β^2 reveal that the electron density at the position β^2 is slightly larger in **1b**$^{3-}$ than in **1b**$^{3+}$. These findings clearly suggest the effect of a diamagnetic ring current in **1b**$^{3-}$. Ring currents of **1b**$^{3+}$ and **1b**$^{3-}$ were calculated by London–McWeeny's method.[14] For **1b**$^{3+}$, the phenalenyl unit causes a weakly diamagnetic effect and the

 © VCH Verlagsgesellschaft mbH, D-69451 Weinheim, 1996 0570-0833/96/3504-0440 $ 15.00+.25/0 Angew. Chem. Int. Ed. Engl. 1996, 35, No. 4

trindenyl unit a paramagnetic effect. In contrast, $\mathbf{1b}^{3-}$ exhibits pronounced diamagnetic ring currents along the periphery of the molecule.

Received: September 19, 1995 [Z 8412 IE]
German version: *Angew. Chem.* **1996**, *108*, 456–457

Keywords: hydrocarbons · phenalenes · radicals · redox reactions

[1] a) V. D. Parker, *J. Am. Chem. Soc.* **1976**, *98*, 98; b) K. Deuchert, S. Hünig, *Angew. Chem.* **1978**, *90*, 927; *Angew. Chem. Int. Ed. Engl.* **1978**, *17*, 875; c) K. Nakasuji, K. Yoshida, I. Murata, *J. Am. Chem. Soc.* **1982**, *104*, 1432; d) *ibid.* **1983**, *105*, 5136; e) *Chem. Lett.* **1982**, 969; f) I. Murata, S. Sasaki, K. -U. Klabunde, J. Toyoda, K. Nakasuji, *Angew. Chem.* **1991**, *103*, 198.; *Angew. Chem. Int. Ed. Engl.* **1991**, *30*, 172; g) K. Takahashi, T. Suzuki, *J. Am. Chem. Soc.* **1989**, *111*, 5483.

[2] To our knowledge, only a few examples are known of compounds that exhibit six-stage amphoteric redox behavior. See: J. Heinze, *Angew. Chem.* **1981**, *93*, 186; *Angew. Chem. Int. Ed. Engl.* **1981**, *20*, 202.

[3] The structure of **2** was confirmed unambigously by X-ray analysis. Yellow needles of **2** suitable for X-ray structure analysis were grown by slow evaporation of a solution of **2** in CH_2Cl_2 and *n*-hexane. Details of the structure will be reported in a separate paper.

[4] Decacyclene (Aldrich) was recrystallized from a xylene solution twice.

[5] Two regioisomeric tribromides could not be separated by column chromatography or recrystallization; however, this did not disrupt our synthesis, because they were converted to a single symmetrical product in the final steps, **10** to **1b**$^{\bullet}$, and **10** to $\mathbf{1b}^{3-}$.

[6] Compounds **2**–**10** were fully characterized spectroscopically (^{1}H NMR, MS, IR).

[7] Neutral monoradical species **1b**$^{\bullet}$ and **1c**$^{\bullet}$ were stable in degassed toluene; their ESR signals did not change for a week at room tempetrature.

[8] A. D. McLachlan, *Mol. Phys.* **1960**, *3*, 233.

[9] Elemental analysis: found C 43.06, H 3.60%; calcd for $C_{69}H_{69}(SbCl_6)_3$, C 43.58, H 3.66%; m.p. > 300 °C; UV/Vis (H_2SO_4): $\lambda_{max}(\varepsilon)$ = 775 (sh, 7760), 676 (sh, 26700), 601 (42500), 550 (sh, 37900), 494 (118000), 231 nm (81800).

[10] UV/Vis (THF): $\lambda_{max}(\varepsilon)$ = 543 (56300), 507 (52300), 421 (21000), 361 (37300), 333 (34300), 256 nm (39200).

[11] H. Spiesecke, W. G. Schneider, *Tetrahedron Lett.* **1986**, *27*, 937.

[12] In phenalenyl derivatives the positions 1, 3, 4, 6, 7, and 9 are referred to as α and 2, 5, and 8 as β. The shift changes ($\Delta\delta_C$) are 51.8 at the α position and 4.9 at the β position. I. Sethson, D. Johnels, U. Edlund, A. Sygula, *J. Chem. Soc. Perkin Trans. 2* **1990**, 1339.

[13] For super-charged mono- and polycyclic ions, see: K. Müllen, *Chem. Rev.* **1984**, *84*, 603; M. Rabinovitz, I. Willner, A. Minsky, *Acc. Chem. Res.* **1983**, *16*, 298.

[14] F. London, *J. Phys. Radium.* **1937**, *8*, 397; R. McWeeny, *Mol. Phys.* **1958**, *1*, 311.

An Intramolecular Base-Catalyzed Proton Transfer in 1,3-Bis(4-fluorophenyl)triazene

Ferdinand Männle and Hans-Heinrich Limbach*

Proton transfer processes are elementary steps in many acid- and base-catalyzed organic and biochemical reactions.[1–6] Because of their complexity, simple model compounds are required if the proton motion is to be followed experimentally, for example, by NMR spectroscopy or other fast reaction techniques. Model systems are also important for the theoretical treatment of proton transfers.[7–10] Whereas several model systems for double proton transfer within or between neutral molecules have been devised,[11–13] only a few model systems involving degenerate single proton transfer processes, which are coupled to charge transfer and therefore to solvent reorientation, are currently available. Recently, in the conjugated porphyrin monoanion[14] an intramolecular single proton transfer that is characterized by a high activation barrier was observed. In contrast, the barrier for proton transfer is very low in hydrogen-bonded complexes formed by acetic acid and pyridine at low temperatures in organic solvents.[15] Here we introduce a model system that lies between these two extremes: bis(4-fluorophenyl)[1,3-$^{15}N_2$]triazene (**1**, Fig. 1) dissolved in an aprotic solvent together with a base such as trimethylamine (**2**). The NMR experiments described below show that the intramolecular proton transfer in **1** occurs only in the presence of **2**. Therefore, **2** acts as catalyst carrying the mobile proton of **1** from one nitrogen site to the other, as illustrated in Figure 1a.

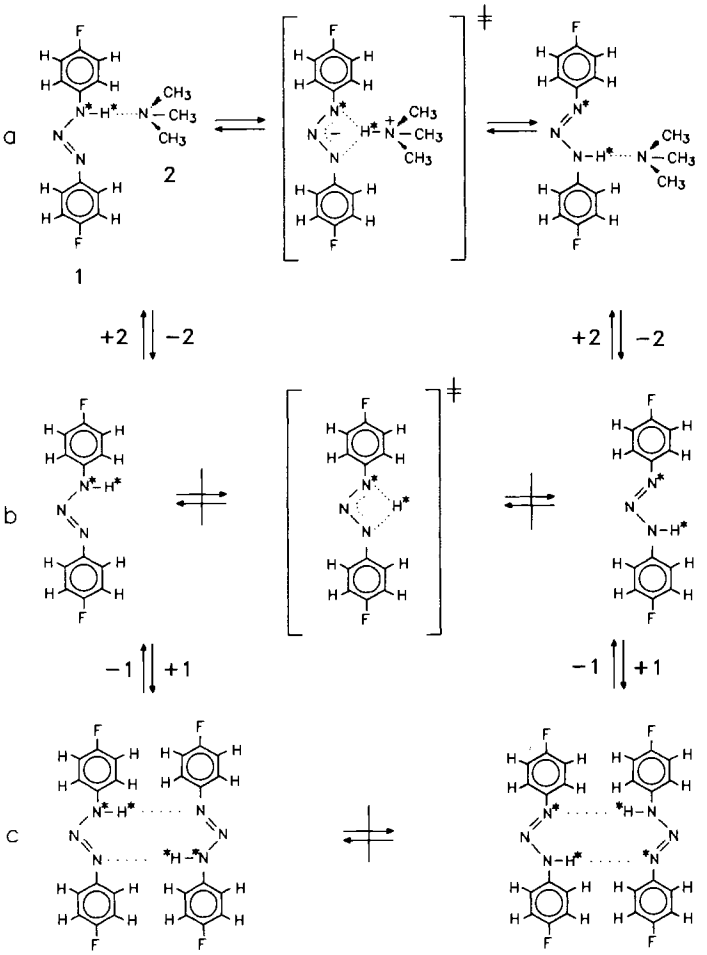

Fig. 1. Proton transfer pathways for 1,3-bis(4-fluorophenyl)[1,3-$^{15}N_2$]triazene (**1**): a) intramolecular proton transfer, catalyzed by trimethylamine; b) hypothetical intramolecular uncatalyzed proton transfer; c) intermolecular double proton transfer in hypothetical cyclic dimers of **1**.

The ^{1}H NMR spectra of sealed samples of **1** in deuterated ethyl methyl ether that are carefully prepared with well-established vacuum techniques to exclude water and other acid or basic impuritites do not show any sign of proton mobility. The partial room-temperature ^{1}H NMR spectrum of such a sample is shown in Figure 2a. The signal of the mobile proton of **1** is split into a doublet by scalar coupling with a single ^{15}N nucleus of **1** ($^1J_{N,H}$ = 93.5 Hz), which indicates that the mobile proton is localized at a single nitrogen site. More precisely, potential

[*] Prof. Dr. H.-H. Limbach, Dipl.-Chem. Dr. F. Männle
Institut für Organische Chemie der Freien Universität
Takustrasse 3, D-14195 Berlin (Germany)
Fax: Int. code +(30)838-5310
e-mail: limbach@chemie.fu-berlin.de

[**] This work was supported by the Deutsche Forschungsgemeinschaft and the Fonds der Chemischen Industrie.

intramolecular proton jumps (Fig. 1b), intermolecular double proton transfer in a hypothetical dimer (Fig. 1c), and intermolecular proton exchange catalyzed by impurities as discussed previously[16–19] are slow on the NMR time scale. This also applies if a small amount of trimethylamine (**2**) is added before recording the spectrum at 137 K (Fig. 2c). Due to enhanced hydrogen bond formation the proton signal shifts to low field. However, if the temperature is increased to 248 K, a triplet can be observed, indicating a scalar coupling to both ^{15}N atoms ($^1J_{N,H}$ = 47 Hz). In the absence of **2** this doublet–triplet transition does not occur. The observation of this triplet verifies that a fast intramolecular proton transfer according to Figure 1a is mediated by **2**. Intermolecular proton exchange would lead to a doublet–singlet transition.[13] Since only one signal was observed for the mobile proton of **1**, the hydrogen-bond exchange between solvated monomeric **1** and its 1:1 complex with **2** is fast on the NMR time scale. The same proton therefore shuttles frequently between the two nitrogen sites of **1**, whereas a different base molecule (**2**) catalyzes each jump.

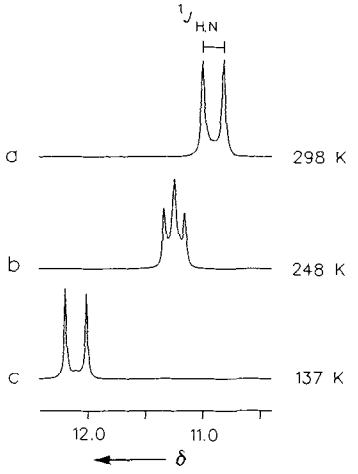

Fig. 2. a) ^1H NMR (500 MHz) signal of the mobile proton of a 0.1 M solution of **1** in [D_8]ethyl methyl ether, at 298 K. b),c) Corresponding signals at 248 and 137 K at the same concentration of **1**, but with 0.02 M trimethylamine (**2**) added.

During the proton carrier process the proton must be temporarily transferred from **1** to **2**—this creates a contact ion pair. The properties of the contact pair ensure that proton transfer to the initial or second nitrogen site of **1** is faster than the dissociation of the contact ion pair that would lead to intermolecular proton exchange. This finding is plausible, because the free energy of dissociation of the contact ion pair is enormous in a solvent with a low dielectric constant as a result of the Coulomb interaction. By contrast, the dissociation energy of the molecular 1:1 complex between **1** and **2** is minimal, leading to the fast hydrogen bond exchange mentioned above.

The uncatalyzed intramolecular proton transfer of **1** is understandably slow, since no intramolecular hydrogen bond is present. Furthermore, **1** does not form cyclic dimers in which a double proton transfer could take place according to Figure 1c, as is the case with the related diarylamidines.[13] This observation can be rationalized, because **1** is planar, and the associated steric repulsion between the aromatic protons within a dimer hinders the approach of the two molecules and the formation of strong hydrogen bonds.

In conclusion, in an aprotic but not necessarily apolar solvent, bases such as trimethylamine are capable of picking up mobile protons at one molecular site and carrying them rapidly to another site. The transfer occurs faster than the dissociation of the intermediate contact ion pair. The system diaryltriazene/trimethylamine therefore is an interesting model for further experimental and theoretical studies of proton carrier processes, which could perhaps contribute to the understanding of the mechanisms of enzyme reactions.

Received: November 17, 1995 [Z 8561 IE]
German version: *Angew. Chem.* **1996**, *108*, 477–479

Keywords: catalysis · NMR spectroscopy · proton transfer

[1] D. F. Cook, *Enzyme Mechanism from Isotope Effects*, CRC, Boca Raton, FL, **1991**.
[2] R. D. Gandour, R. L. Schowen, *Transition States of Biochemical Processes*, Plenum, New York, **1978**.
[3] R. P. Bell, *The Proton in Chemistry*, Chapman and Hall, London, **1973**.
[4] E. F. Caldin, V. Gold, *Proton Transfer Reactions*, Chapman and Hall, London, **1973**.
[5] M. Eigen, L. de Mayer, *Techniques of Organic Chemistry. Investigation of Rates and Mechanisms, Vol. 8, Part 2* (Eds.: E. S. Lewis, A. Weissberger), Wiley, New York, **1961**.
[6] J. G. Belasco, W. J. Albery, J. R. Knowles, *Biochemistry* **1986**, *25*, 2552.
[7] J. R. Reimers, T. X. Lü, M. J. Crossley, N. S. Hush, *J. Am. Chem. Soc.* **1995**, *117*, 2855.
[8] P. M. Kiefer, V. B. P. Leite, R. M. Whitnell, *Chem. Phys.* **1995**, *194*, 33.
[9] A. Staib, D. Borgis, J. T. Hynes, *J. Chem. Phys.* **1995**, *102*, 2487.
[10] a) H. H. Limbach, *Dynamic NMR Spectroscopy in the Presence of Kinetic Hydrogen/Deuterium Isotope Effects, (NMR Basic Princ. Prog.)* **1991**, *23*, pp. 66–167); b) H. H. Limbach, G. Scherer, L. Meschede, F. Aguilar-Parrilla, B. Wehrle, J. Braun, C. Hoelger, H. Benedict, G. Buntkowsky, W. P. Fehlhammer, J. Elguero, J. A. S. Smith, B. Chaudret in *Ultrafast Reaction Dynamics and Solvent Effects*, (Eds: Y. Gauduel, P. J. Rossky), American Institute of Physics, New York, **1994**, p. 225.
[11] M. Schlabach, H. Rumpel, H. H. Limbach, *Angew. Chem.* **1989**, *101*, 84; *Angew. Chem. Int. Ed. Engl.* **1989**, *28*, 76; H. Rumpel, H. H. Limbach, *J. Am. Chem. Soc.* **1989**, *111*, 5429; M. Schlabach, G. Scherer, H. H. Limbach, *ibid.* **1991**, *113*, 3550. F. Aguilar-Parrilla, G. Scherer, H. H. Limbach, M. C. Foces-Foces, F. H. Cano, J. A. S. Smith, C. Toiron, J. Elguero, *ibid.* **1992**, *114*, 9657; M. Schlabach, H. H. Limbach, E. Bunnenberg, A. Shu, B. R. Tolf, C. Djerassi, *ibid.* **1993**, *115*, 4554; C. G. Hoelger, B. Wehrle, H. Benedict, H. H. Limbach, *J. Phys. Chem.* **1994**, *98*, 843; J. Braun, M. Schlabach, B. Wehrle, M. Köcher, E. Vogel, H. H. Limbach, *J. Am. Chem. Soc.* **1994**, *116*, 6593; G. Scherer, H. H. Limbach, *ibid.* **1994**, *116*, 1230; C. G. Hoelger, H. H. Limbach, *J. Phys. Chem.* **1994**, *98*, 11803; G. Scherer, H. H. Limbach, *Croat. Chem. Acta*, **1994**, *67*, 431.
[12] P. Ahlberg, K. Janné, S. Löfås, F. Nettelblad, L. Swahn, *J. Phys. Org. Chem.* **1989**, *2*, 4290.
[13] a) H. H. Limbach, L. Meschede, G. Scherer, *Z. Naturforsch.* **1989**, *44a*, 459; b) L. Meschede, D. Geritzen, H. H. Limbach, *Ber. Bunsenges. Phys. Chem.* **1988**, *92*, 469; c) L. Meschede, H. H. Limbach, *J. Phys. Chem.* **1991**, *95*, 10267.
[14] J. Braun, C. Hasenfratz, R. Schwesinger, H. H. Limbach, *Angew. Chem.* **1994**, *106*, 2302; *Angew. Chem. Int. Ed. Engl.* **1994**, *33*, 2215.
[15] N. S. Golubev, S. Smirnow, V. A. Gindin, G. S. Denisov, H. Benedict, H. H. Limbach, *J. Am. Chem. Soc.* **1994**, *116*, 12055.
[16] D. N. Kravtsov, A. N. Nesmeyanov, L. A. Fedorov, E. I. Fedin, A. S. Peregudov, E. V. Borisov, P. O. Okulevich, S. A. Postovoi, *Dokl. Akad. Nauk. SSSR Ser. Khim.* **1978**, *242*, 347.
[17] A. N. Nesmeyanov, E. V. Borisov, D. N. Kravtsov, A. S. Peregudov, E. I. Fedin, *Izv. Akad. Nauk. SSSR Ser. Khim.* **1981**, *30*, 110.
[18] F. J. Weigert, W. A. Sheppard, *J. Org. Chem.* **1976**, *41*, 4006.
[19] L. Lunazzi, G. J. Panciera, *J. Chem. Soc. Perkin Trans. 2* **1980**, 52.

Regioselective Palladium-Catalyzed Hydrostannylation of Unsymmetrical Oxabicyclic Alkenes**

Mark Lautens* and Wolfgang Klute

Hydrometalation reactions are widely used for the generation of stereochemically defined organometallic compounds. Transition metal catalysts have been shown to accelerate the hydroboration,[1] hydrosilylation,[2] and hydroalumination of alkenes.[3] Significant control of the regio-, stereo-, and enantioselectivity has been achieved.

[*] Prof. M. Lautens, Dr. W. Klute
Department of Chemistry, University of Toronto
Toronto, Ontario M5S1A1 (Canada)
Fax: Int. code +(416)978-6083
e-mail: mlautens@alchemy.chem.utoronto.ca

[**] M. L. thanks NSERC (Canada) for support of this work in the form of an E. W. R Steacie Fellowship. W. K. thanks the Deutsche Forschungsgemeinschaft for a postdoctoral fellowship.

We are interested in demonstrating the utility of oxabicycloheptenes and -octenes as precursors to functionalized and synthetically useful cycloalkenols.[4] We reported that nickel-catalyzed hydroalumination–elimination of bridgehead-substituted substrates such as **1** occurs regioselectively affording the secondary alcohol **2**.[5] Methodology that would selectively lead to the regioisomeric tertiary alcohol **3** would be equally useful. We

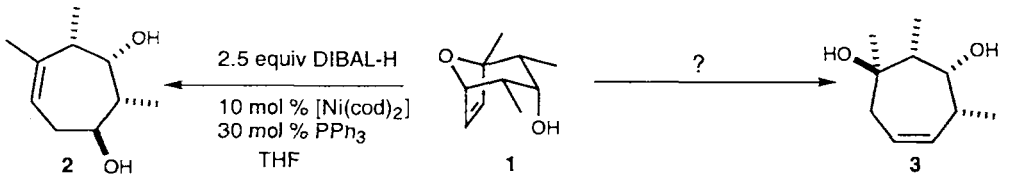

now report a two-step procedure that accomplishes this goal by a regioselective palladium-catalyzed hydrostannylation and organolithium-induced elimination.

Addition of trialkyl- or triaryltin hydride to multiple bonds has typically been achieved under radical conditions.[6] However, there are several recent reports of Pd- and Rh-catalyzed hydrostannylation of enones[6] and triple bonds,[7] and a single example with an allene[8] and a conjugated double bond.[9] To our knowledge simple alkenes have not been examined to date.

Our initial investigations focused on the feasibility of a Pd-catalyzed hydrostannylation of the unsymmetrical oxabicycloheptene **4**. To determine the reactivity of the alkene in the absence of a catalyst, **4** and tributyltin hydride were stirred for 16 h at room temperature. (Scheme 1, step a; Table 1, entry 1).

Table 1. Dependence of the regioselectivity of the Pd-catalyzed hydrostannylation of **6** on the ligand:metal ratio.

Entry	Catalyst	*t* [h]	Yields [%] [a]		
			5a + **5b**	**7a** + **7b**	**7a**/**7b** [b]
1		16	78[c]	95	91.9/8.1
2	, 10 mol % galvinoxyl added[d]	16	76[c]	–	–
3	2.6 mol % $[Pd_2(dba)_3]$,	2	53	89	92.5/7.5
4	2.0 mol % $[Pd_2(dba)_3]$, 9 mol % PPh_3	2	95	85	98.5/1.5
5	2 mol % $[Pd_2(dba)_3]$, 47 mol % PPh_3	16[e]	90	88	99.4/0.6

[a] Yield of isolated product. [b] Determined by capillary gas chromatography on a Chiraldex β-TA column; for an authentic sample of **7b**, see Ref. [5a, 15]. [c] 90/10 mixture by ^{1}H NMR spectroscopy. [d] Galvinoxyl = [2,6-di-*tert*-butyl-4-oxo-2,5-cyclohexadien-1-ylidene)-*p*-tolyloxy, free radical. [e] Addition over 2 h, then stirred for 14 h.

A 90:10 mixture of stannanes **5a** and **5b** was formed; the major isomer arose from addition of the tributyltin moiety to the sterically less encumbered carbon.[10] Addition of galvinoxyl failed to inhibit this reaction, which suggests that a polar pathway might be important (entry 2).[7b, 11]

In the presence of a catalytic amount of $[Pd_2(dba)_3]$ (dba = dibenzylidene acetone), the rate of reaction was much faster, and all the starting material was consumed in less than 2 h (entry 3). Addition of a phosphane ligand improved the chemical yield of the hydrostannylated product and the regioselectivity (entries 4 and 5).[10, 12] Increasing the ligand-to-metal ratio from 2.25:1 (entry 4) to 11.75:1 led to a slight improvement in the ratio of **5a** to **5b**[10] (entry 5), but this increase was insufficient to justify using a such a large amount of the ligand. Most other substrates gave acceptable levels of selectivity with a Ph_3P:Pd ratio of 2.5:1. We observed that tributyltin hydride rapidly decomposes to Bu_6Sn_2 and H_2 in the presence of the Pd catalyst, and so a solution of tributyltin hydride was added slowly by syringe pump over 2 h to a solution of the substrate and catalyst.[7c] Yields in excess of 90% were obtained under the optimized conditions.

The correlation between regioselectivity and ligand-to-metal ratio is best explained by a mechanism of the hydrostannylation that involves a hydropalladation followed by a reductive elimination

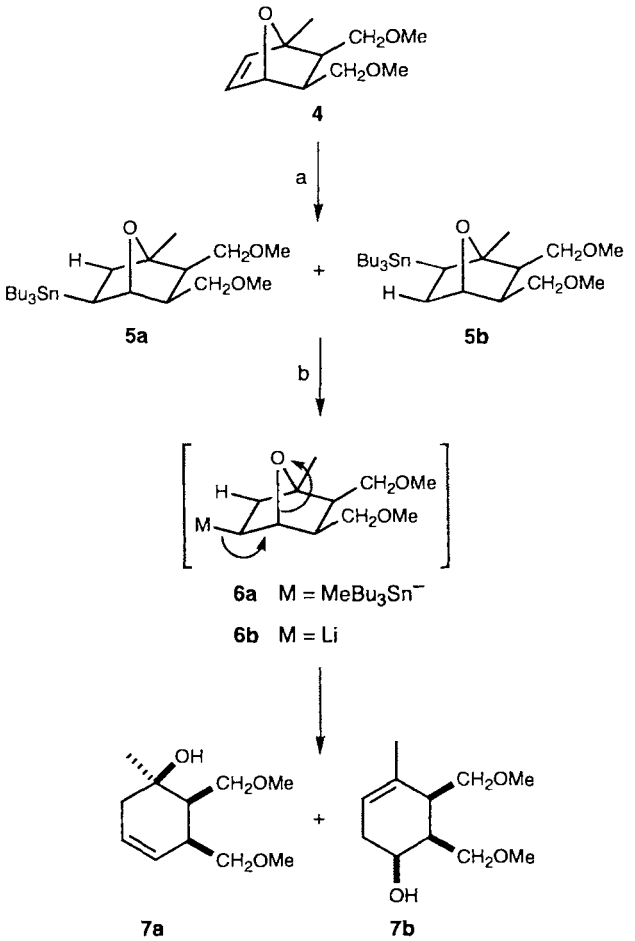

Scheme 1. a) See Table 1; b) 1.5 equiv MeLi, THF, room temperature, 10 min.

with formation of the carbon–tin bond. Higher selectivity would be expected upon increasing the steric bulk of the catalyst.

Transmetalation of simple tetraalkylstannanes with an organolithium typically leads to equilibrium mixtures when the basicities of the organolithium derived from the alkyl stannane and the organolithium reagent used to promote the transmetalation are similar. However, by coupling the transmetalation step to an elimination reaction it was possible to obtain excellent yields of **7a**, **b** upon treatment of **5a**, **b** with methyllithium (Scheme 1, step b).[13–15] The elimination probably proceeds

Table 2. Regioselective hydrostannylation–elimination sequence applied to 8-oxa- and 8-azabicyclo[3.2.1]alkenes.

Entry	Olefin	Major stannane [a]	Yield [%] [b]	Alcohol [c]	Yield [%] [d]	Selectivity [e]
1	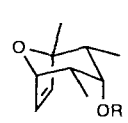 **a**: R = H **b**: R = TBS **c**: R = Me	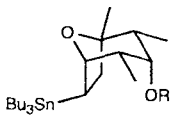	**a**: 80 **b**: 97 **c**: 88	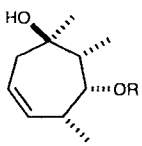	**a**: 84 (A) **b**: 88 (A) **c**: 95 (A)	>97/3 >97/3 97/3 [f]
2	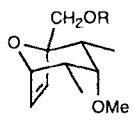 **a**: R = H **b**: R = TBS	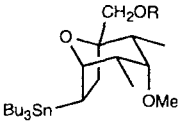	**a**: 62 (76/24) **b**: 98	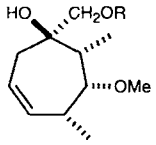	**a**: 85 (B) **b**: 79 (B)	75/25 >97/3
3	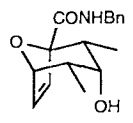	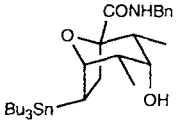	61 [g]	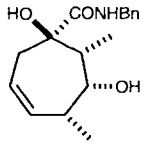	96 (B)	>97/3
4	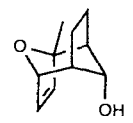	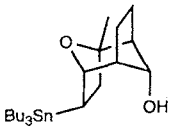	88	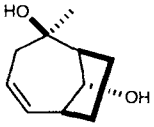	85 (A)	>99/1 [f]
5	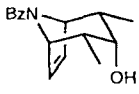	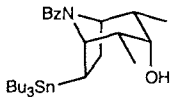	77 [h]	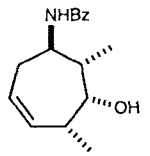	95 (B) [i]	

[a] Conditions: 1.5 equiv Bu_3SnH, 2 mol% $[Pd_2(dba)_3]$, 10 mol% PPh_3, toluene, room temperature (RT), 2 h. [b] Yields of isolated products; in all cases the selectivity was greater or equal to 97/3 (according to ^1H NMR spectroscopy). [c] Conditions: 3–5 equiv *n*BuLi (A) or MeLi (B), THF, RT, 1 h. [d] Yield of isolated products. [e] Based on ^1H NMR spectroscopy; for authentic samples of the other regioisomer see Ref. [5a, 15]. [f] Based on capillary gas chromatography (carbowax HP5 column). [g] 4 mol% $[Pd_2(dba)_3]$, 38 mol% PPh_3, 6 h, THF. [h] THF was used as the solvent. [i] The transmetalation was performed at −78 °C.

directly from the ate complex **6a**, although dissociation to the secondary organolithium species **6b**, which then undergoes elimination, is also possible.

The scope of the hydrostannylation–elimination sequence was demonstrated by carrying out reactions with a variety of bridgehead-substituted oxabicyclo[3.2.1]octenes (Table 2). In all cases the tributyltin moiety was delivered preferentially to the sterically less crowded carbon of the bicyclic system and subsequent elimination gave the tertiary alcohol. The selectivity was typically greater than 95:5 except for the hydrostannylation of the hydroxymethyl-substituted bicycle, where a 75:25 mixture was obtained (entry 2a). However, following protection of the free alcohol as a silyl ether, the selectivity improved dramatically (entry 2b, TBS = *tert*-butyldimethylsilyl). A larger excess of triphenylphosphane and addition of tributyltin hydride over 6 h was required for a substrate bearing an amide at the bridgehead in order to obtain the product in high yield (entry 3). Finally, an N-benzoyl-protected azabicyclooctene efficiently undergoes hydrostannylation and elimination to furnish the amidocycloheptene (entry 5, Bz = benzoyl).

The difference in regioselectivity for the palladium-catalyzed hydrostannylation and nickel-catalyzed hydroalumination is intriguing, and further studies are underway to understand the factors controlling the reaction pathway.[5a, 14] One possibility is that a hydrometalation is occurring in one system, whereas a metallometalation dominates in the other. Experiments designed to differentiate these two pathways are in progress. As a consequence of this difference in regioselectivity, access to the complementary series of ring-opened products has now been achieved.

Experimental Procedure

5a: A solution of tributyltin hydride (200 mg, 0.68 mmol) in dry toluene (1 mL) was slowly added by syringe pump to a solution of **4** (1.3 mg, 0.309 mmol), $Pd_2(dba)_3$ (5.7 mg, 6.2 μmol), and triphenylphosphane (7.6 mg, 29 μmol) in toluene (4 mL). During the addition the color of the solution changed from yellow to brown. The solvent was evaporated, and the residue purified by flash chromatography (EtOAc:hexanes = 1:9) yielding 143.4 mg (0.293 mmol, 95%) of **5a** as a colorless oil. ^1H NMR (400 MHz, $CDCl_3$) δ = 4.26 (s, ^3J(H,Sn) = 68.2 Hz, 1H), 3.39 (m, 1H), 3.20–3.32 (m, 3H), 3.30 (s, 3H), 3.26 (s, 3H), 2.25 (dt, ^3J(H,H) = 9.4, 4.3 Hz, 1H), 2.08 (q, ^3J(H,H) = 7.0 Hz, 1H), 1.90 (dd, ^3J(H,H) = 11.7, 9.5 Hz, 1H), 1.40–1.55 (m, 8H), 1.37 (s, 3H), 1.27 (sex, ^3J(H,H) = 7.3 Hz, 6H), 0.74–0.89 (m, 15H); ^{13}C NMR (100 MHz, $CDCl_3$) δ = 85.6, 81.6, 71.4, 70.5, 58.7, 58.4, 51.2, 47.4, 43.0, 29.2, 27.6, 27.5, 18.0, 13.7, 8.6; HRMS: *m/z* calcd for M^+ 490.2469, found 490.2470.

7a: A solution of **5a** (88.9 mg, 0.182 mmol) in dry THF (2 mL) was treated at room temperature with a solution of methyllithium (0.3 mL, 0.42 mmol) in ether. After 10 min the reaction was quenched with NH_4Cl, extracted four times with ethyl acetate, and the combined organic phases were washed with saturated brine and dried over Na_2SO_4. The solvent was evaporated, and the residue purified by flash chromatography (EtOAc:hexanes = 1:4). Compound **7a** was obtained as colorless crystals (32.6 mg, 0.163 mmol, 89%). M.p. 37–38 °C; ^1H NMR (400 MHz, $CDCl_3$) δ = 5.67 (dq, ^3J(H,H) = 9.9, 3.7 Hz, 1H), 5.47 (dq, ^3J(H,H) = 9.8, 2.2 Hz, 1H), 4.64 (s, 1H), 3.62 (dd, ^3J(H,H) = 9.5, 8.4 Hz, 1H), 3.49 (dd, ^3J(H,H) = 9.9, 7.0 Hz, 1H), 3.37 (s, 1H), 3.36 (s, 1H), 3.35 (s, 3H), 3.33 (s, 3H), 2.65 (ddt, ^3J(H,H) = 11.9, 5.9, 2.9 Hz, 1H), 2.08–2.24 (m, 3H), 1.21 (s, 3H); ^{13}C NMR

(100 MHz, $CDCl_3$) δ = 126.5, 126.1, 72.8, 71.6, 70.2, 59.0, 58.9, 43.7, 39.4, 38.2, 27.5; HRMS: *m/z* calcd for M^+ 200.1412, found 200.1407.

Received: September 22, 1995
Revised version: November 27, 1995 [Z 8420 IE]
German version: *Angew. Chem.* **1996**, *108*, 472–475

Keywords: alcohols · bicyclic alkenes · catalysis · hydrostannylations · regioselectivity

[1] Recent review: K. Burgess, M. J. Ohlmeyer, *Chem. Rev.* **1991**, *91*, 1179.
[2] a) T. Hiyama, T. Kusumoto in *Comprehensive Organic Synthesis, Vol. 8* (Eds.: B. M. Trost, I. Fleming), Pergamon, Oxford, **1991**, p. 763 and references therein; b) T. Hayashi, Y. Uozomi, *Pure Appl. Chem.* **1992**, *64*, 1991.
[3] a) G. Wilke, *Angew. Chem.* **1988**, *100*, 189; *Angew. Chem. Int. Ed. Engl.* **1988**, *27*, 185; b) J. J. Eisch in *Comprehensive Organic Synthesis, Vol. 8* (Eds.: B. M. Trost, I. Fleming), Pergamon Press, Oxford, **1991**, p. 733.
[4] a) M. Lautens, *Synlett* **1993**, 177. b) *Pure Appl. Chem.* **1992**, *64*, 1873 and references therein; c) J. Mann, *Tetrahedron* **1986**, *42*, 464;. d) P. Vogel, D. Fattori, F. Gasparini, C. Le Drian, *Synlett* **1990**, 173.
[5] a) M. Lautens, P. Chiu, S. Ma, T. Rovis, *J. Am. Chem. Soc.* **1995**, *117*, 532. b) Uncatalyzed hydroaluminations of oxabicyclic alkenes: M. Lautens, P. Chiu, J. Colucci, *Angew. Chem.* **1993**, *105*, 267; *Angew. Chem. Int. Ed. Engl.* **1993**, *32*, 281; S. Woo, B. A. Keay, *Tetrahedron Lett.* **1992**, *33*, 2661. c) Hydroboration: H. C. Brown, J. V. N. Vara Prasad, *J. Org. Chem.* **1985**, *50*, 3002. d) Hydrosilylation: Y. Uozomi, T. Hayashi, *Tetrahedron Lett.* **1993**, *34*, 2335.
[6] W. P. Neumann, *Synthesis* **1987**, 665, and references therein.
[7] a) Y. Ichinose, H. Oda, K. Oshima, K. Utimoto, *Bull. Chem. Soc. Jpn.* **1987**, *60*, 3468; b) K. Kikukawa, H. Umekawa, F. Wada, T. Matsuda, *Chem. Lett.* **1988**, 881; c) H. X. Zhang, F. Guibé, G. Balavoine, *J. Org. Chem.* **1990**, *55*, 1857; d) S. Casson, P. Kocienski, *Synthesis* **1993**, 1133.
[8] a) Y. Ichinose, K. Oshima, K. Utimoto, *Bull. Chem. Soc. Jpn.* **1988**, *61*, 2693; b) K. Koerber, J. Gore, J.-M. Vatele, *Tetrahedron Lett.* **1991**, *32*, 1187; c) T. N. Mitchell, U. Schneider, *J. Organomet. Chem.* **1991**, *405*, 195.
[9] H. Miyake, K. Yamamura, *Chem. Lett.* **1992**, 507.
[10] The ratio of the isomeric stannanes was assumed to be equal to the ratio of the alcohols obtained following the transmetalation step.
[11] A. J. Leusink, H. A. Budding, *J. Organomet. Chem.* **1968**, *11*, 533.
[12] The preliminary studies of the Pd-catalyzed hydrostannylation of symmetrical bicycloheptenes and -octenes and the *n*-BuLi-induced ring opening were performed by J. Blackwell.
[13] a) N. Meyer, D. Seebach, *Chem. Ber.* **1980**, *113*, 1290; b) R. H. Newman-Evans, B. K. Carpenter, *Tetrahedron Lett.* **1985**, *26*, 1141.
[14] The choice of the organolithium reagent was crucial for the success of the transmetalation in the [2.2.1] series. *n*-BuLi led to the formation of by-products.
[15] S. Ma, University of Toronto, unpublished results; the regioisomers were prepared according to Ref. [5a].

Pairing Properties of Alanyl Peptide Nucleic Acids Containing an Amino Acid Backbone with Alternating Configuration**

Ulf Diederichsen*

Peptide nucleic acids (PNAs) contain a peptide or polyamide backbone and side chains that are substituted with the nucleobases of DNA or RNA.[1] This class of biomolecules gained importance because of its antisense or antigene potential.[2] In a PNA backbone isomorphous to DNA and RNA, six bonds of the sugar phosphate backbone correlate in terms of their length to two amino acids. Therefore, the repeating unit of a potential antisense PNA is built of an amino acid pair[3] containing a base-substituted and a proteinogenic amino acid.[4] If possible, the pairing complex adopts a conformation with an idealized distance for base pair stacking of about 3.5 Å. This might be achieved by modulating the pitch of a double strand through helicalization.[5] By keeping the distance between base pairs constant, the shortening of the backbone results in an unwinding of the helix until the linear double strand is reached; this is the case when the distances of the base pairs and the backbone between consecutive repeating units is identical. A PNA with a regular peptide strand in β-sheet conformation fulfills the prerequisites for a linear pairing complex except that the consecutive side chains are oriented antiperiplanar (Scheme 1). By using

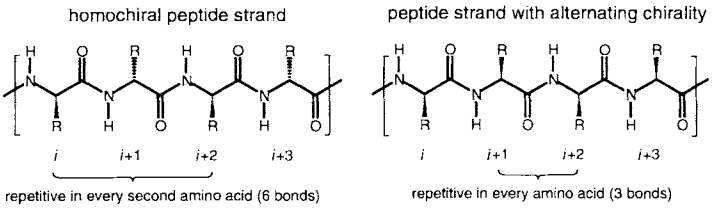

Scheme 1. An antisense PNA isomorphous to DNA needs six backbone bonds for a repetitive unit like in a pair of amino acids. A PNA strand with alternating configuration and β-sheet conformation is repetitive in every side chain.

alternating configurations of the amino acids an orientation of all side chains on the same side of the β-sheet can be achieved,[6] and thus a PNA repetitive in every monomeric unit is obtained. Taking an alanyl PNA with alternating sense of chirality as an example, we now introduce new PNA–PNA pairing complexes based on recognition of the bases adenine and thymine.

The PNA model described in Scheme 2 was regarded as a working hypothesis at the start of our project: A regular alanyl

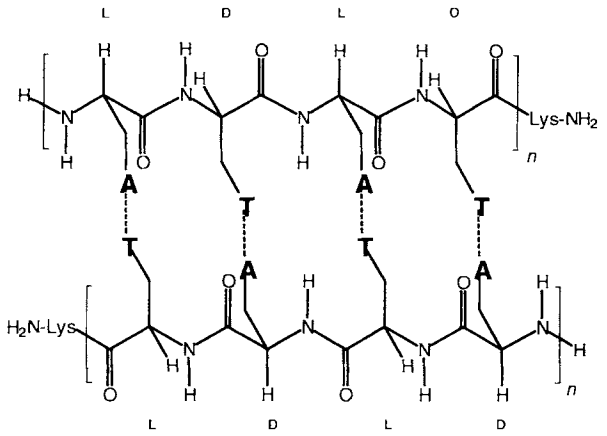

Scheme 2. Model of a linear pairing complex between the enantiomeric alanyl PNA oligomers H-(AlaA-AlaT)$_n$-Lys-NH_2 and H-(AlaA-AlaT)$_n$-Lys-NH_2. AlaA = β(adenine-9-yl)alanine, AlaT = β(thymine-1-yl)alanine, D-configurated amino acids are underlined. There is a specificity of the double strand pairing with antiparallel strand orientation and homochiral base pair connectivity. The C-terminal lysine amide was added for solubility reasons.

peptide strand, whose side chains are β-substituted by the nucleobases adenine and thymine, is repetitive when adopting a β-sheet conformation, and when the amino acid units have alternating configuration. A double strand formed by base pairing is characterized by colinear strands and orthogonal planes of base pairs with a distance of 3.5 Å. Further structural features are lack of charge repulsion, parallel/antiparallel strand orientation, and hetero-/homochiral base pair connectivity. We synthesized

[*] Dr. U. Diederichsen
Institut für Organische Chemie und Biochemie
der Technischen Universität München
Lichtenbergstrasse 4, D-85747 Garching (Germany)
Fax: Int. code +(89) 170 8294

[**] This work was supported by the Fonds der Chemischen Industrie with a Liebig fellowship. I am grateful to Professor H. Kessler for generous support and Professors A. Eschenmoser, A. Vasella, and C. Leumann for the opportunity to measure the UV and CD spectra, and for the characterization of the oligomers by MALDI-TOF-MS.

PNA oligomers to determine their pairing stabilities and to identify double strands based on A–T or A–A, T–T pairing.

The enantiomerically pure amino acids *N*-Boc-thyminylalanine **1** and *N*-Boc-adeninylalanine **2**[7] used for oligomerization were prepared as described by Eschenmoser and Lohse.[8] Nucleophilic ring opening of *N*-Boc-serine-β-lactone **3**[9] with the bases thymine and adenine provided amino acids **1** and **2**, respectively, with an enantiomeric purity of >98% (HPLC of amino acid dimers) (Scheme 3). The PNA oligomers were obtained by solid-phase synthesis on a MBHA-polystyrene (MBHA = 4-methylbenzhydrylamine) resin loaded with L- or D-lysine(Z)-OH (Z = benzyloxycarbonyl) in yields of >98% when HATU (HATU = *O*-(7-azabenzotriazol-1-yl)-1,1,3,3-tetramethyluronium hexafluorophosphate)[10] was used as the coupling reagent. After cleavage from the resin the PNA oligomers were purified by HPLC (RP-C18), isolated in yields of 11–25%, and characterized by ^{1}H NMR spectroscopy and matrix-assisted laser desorption/ionization time-of-flight mass spectrometry (MALDI-TOF-MS).

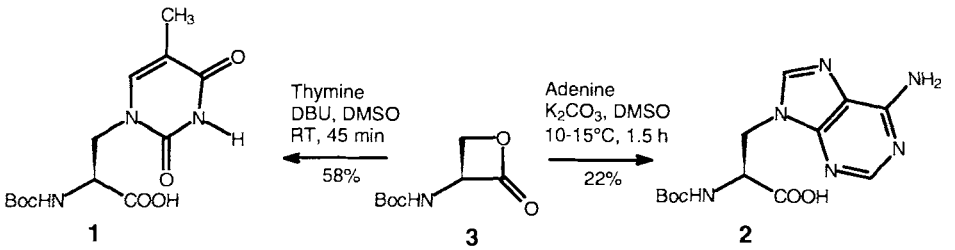

Scheme 3. Synthesis of the base-substituted L-alanyl monomers **1** and **2** by ring opening of L-serinelactone **3** (taken from the thesis of Lohse [8] with kind permission of A. Eschenmoser). RT = room temperature; DBU = 1,8-diazabicyclo[5.4.0]-undec-7-ene; DMSO = dimethyl sulfoxide.

The expected pairing of oligomers in a double strand was investigated by temperature-dependent UV spectroscopy. Cooperative depairing of a double strand, which is based on hydrogen bonds and base stacking, can be recognized as a sigmaoidal increase of the UV absorption A_{rel} with increasing temperature (hyperchromicity), as known from DNA melting curves. All the curves described herein were measured under identical conditions (0.1 M NaCl, 0.01 M Na_2HPO_4/H_3PO_4, pH 7); prior to heating, the samples were kept at 0 °C for 30 minutes until the absorption remained constant. On cooling, the starting absorption was achieved for each of the cooling curves; however, the pairing process occurred only below 5 °C. The melting curve of the oligomer H-(AlaA-AlaT)$_4$-Lys-NH$_2$ (D-configurated amino acids are underlined) has two cooperative transitions at T_m = 14 °C and 25 °C (Fig. 1) indicating that in addition to self-pairing in the double strand there seems to be a second coordination. The equimolar mixture of this oligomer H-(AlaA-AlaT)$_4$-Lys-NH$_2$ with the enantiomeric compound H-(AlaA-AlaT)$_4$-Lys-NH$_2$ yields a temperture-dependent UV spectrum in which the melting temperature is T_m = 31 °C. The pairing of enantiomeric oligomers is more stable than self-pairing of one enantiomer and exhibits almost doubled hyperchromicity (Fig. 1). The nonlinear dependence of the absorption on the temperature below 20 °C, which is indicative of additional associations, has been observed particularly in melting curves of A/T alternating octamers. The CD spectra of the oligomer H-(AlaA-AlaT)$_4$-Lys-NH$_2$ and the enantiomeric oligomer each show the depairing process at about T_m = 14 °C (Fig. 2). This suggests that the pairing complex is highly symmetrical, because the curves measured at 0 °C have a lower Cotton effect, while the intensity increases at 10 and 25 °C. The formation of a pairing complex of A/T alternating octamers at lower temperatures is further supported by a comparison with the CD spectrum of the single-stranded (UV absorption is temperature independent) tetramer H-(AlaA-AlaT)$_2$-Lys-NH$_2$ (Fig. 3). Whereas at 0 °C there is an obvious difference between the curves of octamer and tetramer, at 60 °C, when oligomer H-(AlaA-AlaT)$_2$-Lys-NH$_2$ is destacked and H-(AlaA-AlaT)$_4$-Lys-NH$_2$ is depaired, the CD curves are very similar.

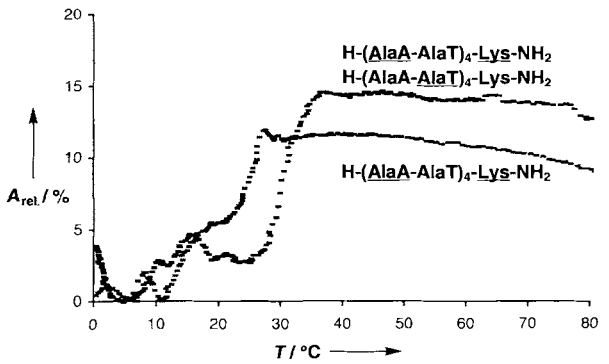

Fig. 1. Melting curves of H-(AlaA-AlaT)$_4$-Lys-NH$_2$ (6 mM) and an equimolar mixture of the enantiomeric oligomers H-(AlaA-AlaT)$_4$-Lys-NH$_2$ and H-(AlaA-AlaT)$_4$-Lys-NH$_2$ (3 mM each, 260 nm, 0.1 M NaCl, 0.01 M Na_2HPO_4/H_3PO_4, pH 7).

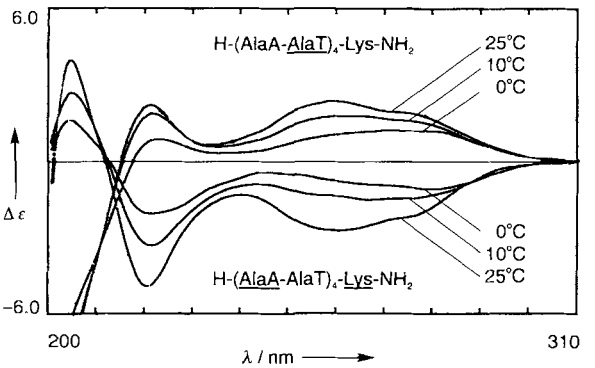

Fig. 2. CD spectrum of the oligomers H-(AlaA-AlaT)$_4$-Lys-NH$_2$ and H-(AlaA-AlaT)$_4$-Lys-NH$_2$ measured independently (6 mM, 0.1 M NaCl, 0.01 M Na_2HPO_4/H_3PO_4, pH 7).

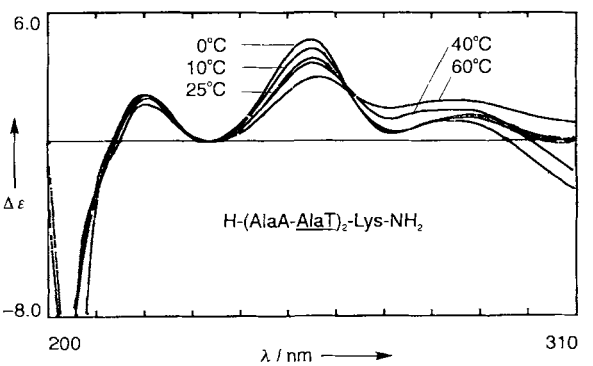

Fig. 3. CD spectrum of H-(AlaA-AlaT)$_2$-Lys-NH$_2$ (12 mM, 0.1 M NaCl, 0.01 M Na_2HPO_4/H_3PO_4, pH 7).

 © VCH Verlagsgesellschaft mbH, D-69451 Weinheim, 1996 0570-0833/96/3504-0446 $ 15.00+.25/0

In principle, pairing of A/T alternating oligomers is possible either by formation of A–T or A–A, T–T base pairs. Simple model studies suggest that an A–T Watson–Crick pairing alanyl PNA forms a complex with antiparallel strand orientation and homochiral base pair connectivity (Scheme 4). Switching one strand to get a parallel pairing complex does not change the geometry but inverts the configuration at C-α (heterochiral base pair connectivity). The A–A, T–T pairing type is formed by parallel (antiparallel) strand orientation and homochiral (heterochiral) base pair connectivity, regardless of the pairing mode. Furthermore, the model shows that the strands of the self-pairing oligomer H-(AlaA-AlaT)$_4$-Lys-NH$_2$ are oriented parallel for both pairing modes, or in contrast, antiparallel in the case of the pairing complex with the two enantiomers. Although the base pairs are orthogonal to the strand the model suggests selectivity of strand orientation. The higher stability observed for the complex of the mixture of enantiomers is consistent with antiparallel strand orientation. With charge separation of the lysine side chains protonated at pH 7 and an additional A–T base pair, antiparallel strand orientation should be the preferred option.

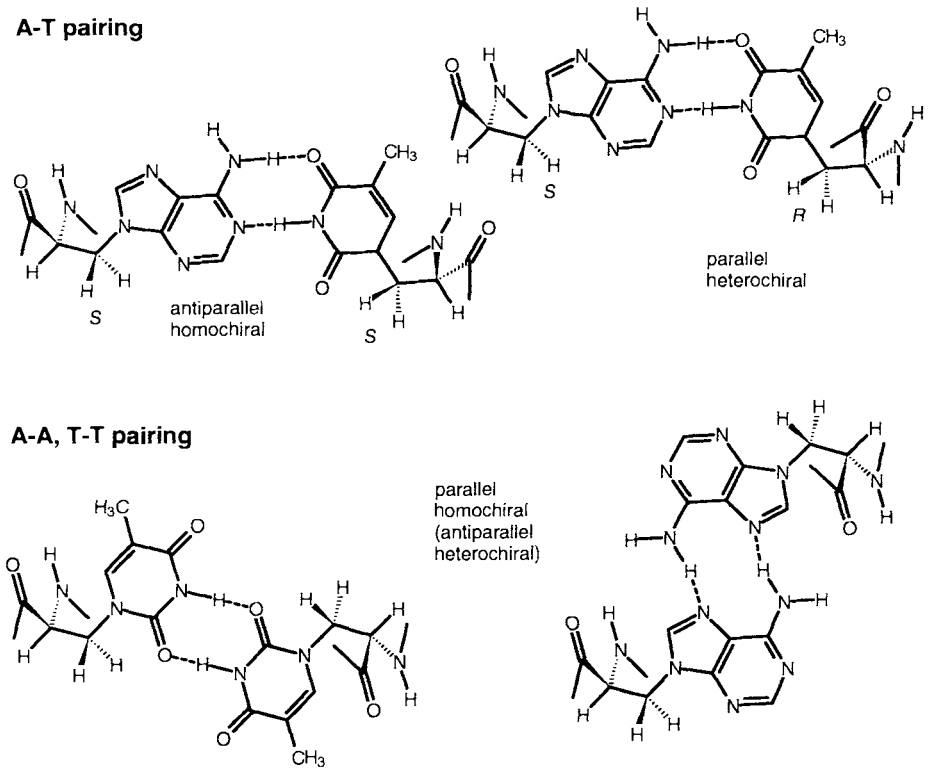

Scheme 4. According to simple model studies, self-pairing in the A–T mode is only possible with parallel strand orientation and the pairing of enantiomeric strands requires antiparallel strand orientation. Formation of double strands with A–A and T–T base pairing is an interesting alternative, because both base pairs described need comparable backbone distances and are C_2-symmetrical.

The oligomers H-(AlaA-AlaA)$_3$-Lys-NH$_2$ and H-(AlaT-AlaT)$_3$-Lys-NH$_2$ have also been synthesized with the intention of forming an A/T pairing complex. H-(AlaT-AlaT)$_3$-Lys-NH$_2$ does not form pairing complexes as indicated by the temperature independence of the UV absorption and the CD curves (not shown). The melting curve of the H-(AlaA-AlaA)$_3$-Lys-NH$_2$ oligomer (Fig. 4), however, indicates two cooperative transitions at melting temperatures of T_m = 9 and 31 °C. Model studies suggest formation of a double strand and further coordination of one or two energetically equivalent adenine hexamers; the latter is possible only by formation of hydrogen bonds with every second adenine. The pairing mode of this adenine self-pairing is currently under investigation. The possibility of correlating an adenine hexamer with a stable complex, which has a nucleobase specificity, has to be interpreted as an indication of a β-sheet conformation of the peptide strand. The repetitive backbone conformation[11] of a 3_{10}-helix has to have 3.0 amino acids per turn. Therefore, a PNA with alternating configuration would only be repetitive in every seventh amino acid. Deorganization of a stable conformation like a peptide helix also is unlikely to be the reason for the melting curves we observed, because in this case there should be no difference between the melting curve of one enantiomeric A–T octamer and the racemic mixture.

The temperature-dependent UV spectrum of an equimolar mixture of oligomers H-(AlaA-AlaA)$_3$-Lys-NH$_2$ and H-(AlaT-AlaT)$_3$-Lys-NH$_2$ (Fig. 5) shows there is no reorganization of the adenine self-pairing double strand on addition of a thymine hexamer. The melting temperature of T_m = 31 °C as well as the hyperchromicity remain unchanged. Therefore, the A–A pairing is more

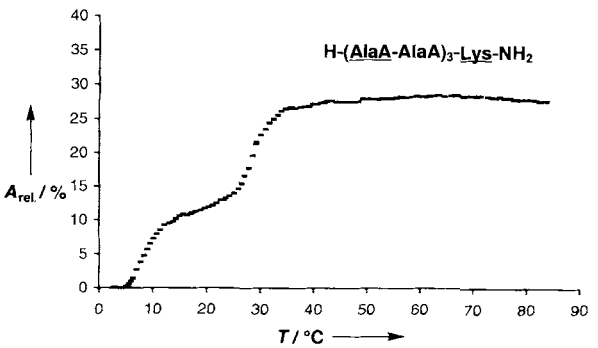

Fig. 4. Melting curve of H-(AlaA-AlaA)$_3$-Lys-NH$_2$ (17 mM, 260 nm, 0.1 M NaCl, 0.01 M Na_2HPO_4/H_3PO_4, pH 7).

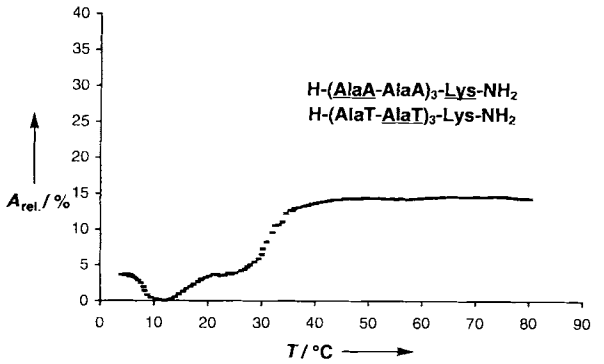

Fig. 5. Melting curve of an equimolar mixture of H-(AlaA-AlaA)$_3$-Lys-NH$_2$ and H-(AlaT-AlaT)$_3$-Lys-NH$_2$ (each 6 mM, 260 nm, 0.1 M NaCl, 0.01 M Na_2HPO_4/H_3PO_4, pH 7).

stable than the A–T mode. The addition of H-(AlaT-AlaT)$_3$-Lys-NH$_2$ only results in a hypochromicity at the lower melting temperature of the self-pairing oligomer H-(AlaA-AlaA)$_3$-Lys-NH$_2$.

The CD spectrum of an equimolar mixture of oligomers H-(AlaA-AlaA)$_3$-Lys-NH$_2$ and H-(AlaT-AlaT)$_3$-Lys-NH$_2$ differs very little from that of the hexamer H-(AlaA-AlaA)$_3$-Lys-NH$_2$ alone (not shown) and can be interpreted as the sum of the single measurements. This again points to the higher stability of the A–A pairing compared with A–T.

Alanyl peptide nucleic acids with alternating configuration of the amino acids form defined pairing complexes, the nature of which is dependent on the kind and sequence of the nucleobases. The rules known for pairing of DNA are not valid for the PNA complexes discussed herein since A–A turned out to be more stable than A–T. Model studies indicate the presence of a linear pairing complex; thus, because of the linearity and the uncharged peptide backbone, the dimer or higher complexes are likely to be more closely packed and formation of unnatural base pairs is possible. Future investigations, for example with 7-carbaadenine which can only form Watson–Crick base pairs, are required to determine the pairing modes. Furthermore, experiments to determine the conformational parameters with multidimensional NMR spectroscopy are planned.

Received: September 22, 1995
Revised version: November 14, 1995 [Z84181E]
German version: *Angew. Chem.* **1996**, *108*, 458–461

Keywords: β-sheet structures · peptide nucleic acids · self-organization

[1] a) P. E. Nielsen, M. Egholm, O. Buchardt, *Bioconjugate Chem.* **1994**, *5*, 3; b) U. Diederichsen, H. W. Schmitt, *Tetrahedron Lett.* **1996**, *37*, 475.
[2] a) P. E. Nielsen, M. Egholm, R. H. Berg, O. Buchardt, *Science* **1991**, *254*, 1497; b) K. L. Dueholm, M. Egholm, C. Behrens, L. Christensen, H. F. Hansen, T. Vulpius, K. H. Petersen, R. H. Berg, P. E. Nielsen, O. Buchardt, *J. Org. Chem.* **1994**, *59*, 5767; c) P. Wittung, P. E. Nielsen, O. Buchardt, M. Egholm, B. Norden, *Nature* **1994**, *368*, 561.
[3] a) H. Moser, A. Fliri, A. Steiger, G. Costello, J. Schreiber, A. Eschenmoser, *Helv. Chim. Acta* **1986**, *69*, 1224; b) M. T. Doel, A. S. Jones, R. T. Walker, *Tetrahedron* **1974**, *30*, 2755.
[4] a) P. Garner, J. U. Yoo, *Tetrahedron Lett.* **1993**, *34*, 1275; b) A. Lenzi, G. Reginato, M. Taddei, E. Trifilieff, *ibid.* **1995**, *36*, 1717.
[5] J. Hunziker, H.-J. Roth, M. Böhringer, A. Giger, U. Diederichsen, M. Göbel, R. Krishnan, B. Jaun, C. Leumann, A. Eschenmoser, *Helv. Chim. Acta* **1993**, *76*, 259.
[6] M. R. Ghadiri, K. Kobayashi, J. R. Granja, R. K. Chadha, D. E. McRee, *Angew. Chem.* **1995**, *107*, 76; *Angew. Chem. Int. Ed. Engl.* **1995**, *34*, 93.
[7] a) M. T. Doel, A. S. Jones, N. Taylor, *Tetrahedron Lett.* **1969**, *27*, 2285; b) J. D. Buttrey, A. S. Jones, R. T. Walker, *Tetrahedron* **1975**, *31*, 73.
[8] a) P. Lohse, Dissertation ETH Zürich **1992**, Nr. 9937; b) P. Lohse, B. Oberhauser, B. Oberhauser-Hofbauer, A. Eschenmoser, *Croatica Chim. Acta* in press.
[9] a) L. D. Arnold, T. H. Kalantar, J. C. Vederas, *J. Am. Chem. Soc.* **1985**, *107*, 7105; b) L. D. Arnold, R. G. May, J. C. Vederas, *ibid.* **1988**, *110*, 2237.
[10] L. A. Carpino, A. El-Faham, C. A. Minor, F. Albericio, *J. Chem. Soc. Chem. Commun.* **1994**, 201.
[11] A. Eschenmoser, M. Dobler, *Helv. Chim. Acta* **1992**, *75*, 218.

A New Ligand Class for the Asymmetric Dihydroxylation of Olefins**

Heinrich Becker and K. Barry Sharpless*

Dedicated to Professor Ivar Ugi on the occasion of his 65th birthday

The catalytic asymmetric dihydroxylation (AD) of olefins using and dihydroquinidine (DHQD) or dihydroquinine (DHQ) derivatives as ligands has become a useful and reliable transformation in organic synthesis.[1] High regio- and stereoselectivity for a broad range of substrates are the most outstanding characteristics of this reaction. To date, over 500 different ligands have been tested in our group and a few superior structural types have been identified (Scheme 1). Ligands based on phthalazine (PHAL) such as (DHQD)$_2$PHAL and (DHQ)$_2$PHAL,[2] along with their recently developed analogs

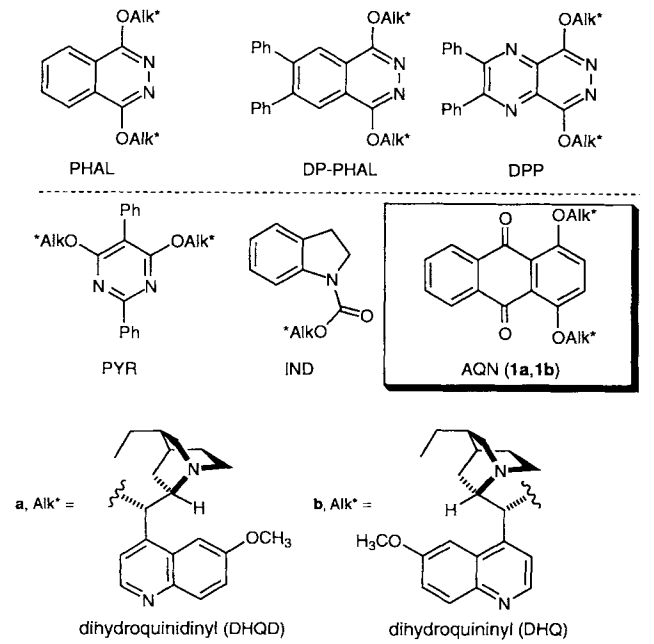

Scheme 1. Ligands used in the asymmetric dihydroxylation.

[*] Prof. K. B. Sharpless, Dr. H. Becker
Department of Chemistry, The Scripps Research Institute
10666 N. Torrey Pines Road, La Jolla, CA 92037 (USA)
Fax: Int. code +(619) 784-7562
e-mail: sharples@scripps.edu

[**] This work was supported by the National Institutes of Health (GM 28384), the W. M. Keck Foundation, and the Fonds der Chemischen Industrie (postdoctoral fellowship for H. B.). We are very grateful to Prof. A. Paul Krapcho for inspiring us to prepare this new ligand class. We thank Paul Richardson for performing the reaction with allyl tosylate (Table 1, entry 5), and Koenraad Vanhessche for permission to include many of his unpublished results in the tables for comparison.

having diphenyl having diphenylphthalazine (DP-PHAL) and diphenylpyrazinopyridazine (DPP) cores,[3] are the most general and lead to high enantioselectivities with most olefins. Ligands based on pyrimidine (PYR) have been found superior for sterically congested olefins (especially terminal olefins).[4] *cis*-1,2-Disubstituted olefins can usually not be dihydroxylated with satisfactory enantioselectivities; however, stereoselectivities in the 70–90% range have been realized for several types of *cis*-1,2-disubstituted olefins.[1a, 5] Despite the recent improvements in ligands for the AD reaction,[3, 5] some important types of olefins, for instance the ubiquitous vinyl compounds, cannot be dihydroxylated reliably with good results.

In this paper we introduce 1,4-bis(dihydroquinidinyl)anthraquinone $(DHQD)_2AQN$ **1a** and 1,4-bis(dihydroquininyl)-anthraquinone $(DHQ)_2AQN$ **1b** (Scheme 1) as a new set of ligands for the AD reaction, which have properties complementary to those of known ligands. The new ligands are easily prepared by nucleophilic substitution of 1,4-difluoroanthraquinone (**3**) with the lithium salt of dihydroquinidine or dihydroquinine in THF at room temperature (Scheme 2). 1,4-Difluoroanthraquinone is obtained by Friedel–Crafts reaction of phthalic anhydride (**2**) and aluminum trichloride in 1,4-difluorobenzene followed by cyclization with polyphosphoric acid (PPA).[6, 7]

The new anthraquinone ligands lead to excellent results in the AD reactions of many allylically substituted terminal olefins. In reactions with the new AQN ligands, most examples of this important class of olefins (Table 1, entries 1–5) can now be dihydroxylated with satisfying enantioselectivities, making a variety of small chiral nonracemic building blocks easily available.[8, 9] Also, reactions of olefins containing multiple halogen atoms (Table 1, entries 6–8; Table 2, entry 16) show significant improvement. The increase in enantioselectivities for terminal olefins with aliphatic substituents (Table 1, entries 10–13) and di- and tri-substituted olefins (Table 2, entries 14–18) is moderate in reactions with the AQN ligands. For sterically congested olefins (Table 1, entries 8 and 13) the pyrimidine-based ligands are still superior. Olefins with aromatic substituents (Table 2, entries 19–24) are usually not dihydroxylated with competitive enantioselectivities in AD reactions with the new ligands; however, the results with indene and allylbenzene (Table 2, entries 23 and 24, respectively) are the best yet for these substrates.

The frequently observed decrease in *ee* values upon changing from DHQD to DHQ ligands is also found for the anthraquinone ligands; in most cases the decrease is moderate. Use of the less expensive quinidine- and quinine-derived ligands instead of their dihydro analogs is possible, but a decrease in *ee* values usually results.[10] The new ligands not only lead to better enantioselectivities, the AD reactions are also faster for certain substrates. For example, 1-decene reacts with OsO_4 about 10% faster in the presence of $(DHQD)_2AQN$ than in the presence of $(DHQD)_2PHAL$.[11]

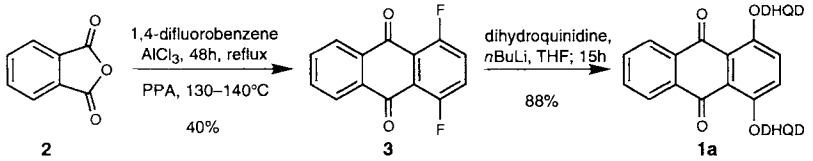

Scheme 2. Synthesis of $(DHQD)_2AQN$ **1a**. $(DHQ)_2AQN$ **1b** can be prepared analogously (see Experimental Procedure).

Table 1. Enantioselectivities for the asymmetric dihydroxylation of terminal olefins using the anthraquinone ligands **1a** and **1b**, and comparisons to the best results obtained previously.

Entry	Olefin	*ee* Values $(DHQD)_2AQN$ **1a**	best ligand known previously	Diol config.
1	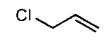	**90%**	63% [$(DHQD)_2PHAL$]	*S*
2	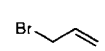	**89%** **85%** [$(DHQ)_2AQN$]	72% [$(DHQD)_2DPP$]	*S* *R*
3	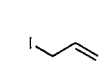	**83%** **82%** [$(DHQ)_2AQN$]	77% [$(DHQD)_2DP$-PHAL]	*S* *R*
4	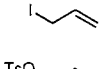	**83%**	40% [$(DHQD)_2PHAL$]	*S*
5	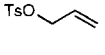	**84%**		*S*
6	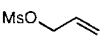	**72%**	63% [$(DHQD)_2PHAL$]	*S*
7	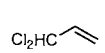	**81%**	64% [$(DHQD)_2PYR$]	*S*
8	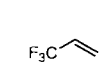	77%	**86%** [$(DHQD)_2PYR$]	*S*
9		**88%**	77% [$(DHQD)_2PHAL$]	*S*
10	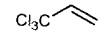	**92%** **87%** [$(DHQ)_2AQN$]	89% [$(DHQD)_2DPP$] 85% [$(DHQ)_2DPP$]	*R* *S*
11	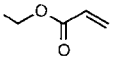	**92%**	87% [$(DHQD)_2PYR$]	*R*
12	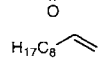	**87%**	**87%** [$(DHQD)_2PYR$]	*R*
13	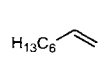	86%	**96%** [$(DHQD)_2PYR$]	*R*

Table 2. Enantioselectivities for the asymmetric dihydroxylation of various olefins with aliphatic and aromatic substituents using the anthraquinone ligands **1a** and **1b**, and comparisons to the best results obtained previously.

Entry	Olefin	*ee* Values $(DHQD)_2AQN$ **1a**	best ligand known previously	Diol config.
14	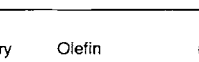	**98%** **96%** [$(DHQ)_2AQN$]	97% [$(DHQD)_2PHAL$] 93% [$(DHQ)_2PHAL$]	*R,R* *S,S*
15	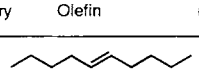	**99%**	**99%** [$(DHQD)_2PHAL$]	*2S,3R*
16	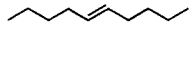	**96%**	94% [$(DHQD)_2PHAL$]	*S,S*
17	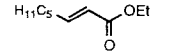	**99%** **96.5%** [$(DHQ)_2AQN$]	**99%** [$(DHQD)_2DP$-PHAL] 95% [$(DHQ)_2PHAL$]	*R* *S*
18	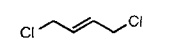	**85%**	81% [$(DHQD)_2DP$-PHAL]	*R*
19	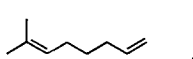	89% 85% [$(DHQ)_2AQN$]	**99%** [$(DHQD)_2DPP$] **97%** [$(DHQ)_2DPP$]	*R* *S*
20	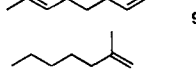	82%	**96%** [$(DHQD)_2DPP$]	*R*
21	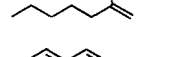	92%	**98%** [$(DHQD)_2DPP$]	*R,R*
22	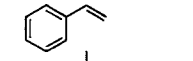	45%	**72%** [DHQD-IND]	*1R,2S*
23	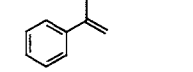	**63%**	53% [$(DHQD)_2DP$-PHAL]	*1R,2S*
24	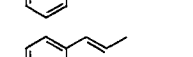	**78%**	44% [$(DHQD)_2PHAL$]	*R*

 © VCH Verlagsgesellschaft mbH, D-69451 Weinheim, 1996 0570-0833/96/3504-0449 $ 15.00+.25/0

In summary, the new anthraquinone-based ligands lead to superior enantioselectivity in the asymmetric dihydroxylation of *almost all* olefins having only aliphatic substituents.[1,2] As these ligands are easy to prepare, their use constitutes an important extension of the AD methodology. The enantioselectivities and rates of reaction for terminal olefins, the most common and most useful class of olefins, show significant improvement. Except in reactions of olefins with aromatic or sterically demanding substituents, the new ligand pair $(DHQD)_2AQN$/$(DHQ)_2AQN$ is now the ligand of choice for the AD reaction.

Experimental Procedure

For general experimental conditions see "Supporting Information" to ref.[3]. Typical procedure for the asymmetric dihydroxylation reactions and workup at 1 mmol scale: $(DHQD)_2AQN$ (8.6 mg, 0.01 mmol, 1 mol%), $K_3Fe(CN)_6$ (990 mg, 3 mmol), K_2CO_3 (420 mg, 3 mmol), and $K_2OsO_2(OH)_4$ (1.4 mg, 0.004 mmol, 0.4 mol%) were dissolved in *tert*-butyl alcohol/water (5 mL of each) at room temperature. For 1,2-disubstituted and trisubstituted olefins $CH_3SO_2NH_2$ (95 mg, 1 mmol) was added. The solution was cooled to 0 °C and the olefin was added. The mixture was stirred at 0 °C, usually for ca. 12 h. In the workup $Na_2S_2O_5$ or Na_2SO_3 (0.8 g) was slowly added and the suspension was warmed to room temperature with vigorous stirring. Ethyl acetate (ca. 20 mL) was added, and the aqueous layer was further extracted with ethyl acetate (2 × 5 mL). If $CH_3SO_2NH_2$ was used the combined organic layers were washed with ca. 20 mL of 2 M aqueous NaOH. The combined organic layers were dried over $MgSO_4$ and then concentrated. The crude product was purified by flash chromatography on silica gel to afford the diol in yields of 65–90%.

Optical rotations of the diols and methods for the determination of enantiomeric excesses: All optical rotations (EtOH, abs.) are given for the products from the reaction of the olefin with $(DHQD)_2AQN$. The *ee* values of the diols or their derivatives were determined by HPLC using Chiracel columns (except for entry 17 in Table 2). Abbreviations used: PMBz = *para*-methoxybenzoyl, IPA = isopropyl alcohol, Bz = benzoyl, NBA = nitrobenzyl alcohol. Entry 1: $[\alpha]_D^{23} = +8.8$ ($c = 1.32$); (bis-PMBz), OD-H, 10% IPA/hexane, 1 mL min^{-1} [retention times: 14.6 min (*S*), 28.0 min (*R*)]; Entry 2: $[\alpha]_D^{23} = +5.9$ ($c = 1.50$); bis-PMBz, OD-H, 10% IPA/hexane, 1 mL min^{-1} [15.3 min (*S*), 30.8 min (*R*)]; Entry 3: $[\alpha]_D^{23} = +5.0$ ($c = 1.10$); diol, OD-H, 5% IPA/hexane, 0.75 mL min^{-1} [22.0 min (*S*), 24.4 min (*R*)]; Entry 4: $[\alpha]_D^{23} = +5.9$ ($c = 1.10$); diol, AD, 10% IPA/hexane, 1 mL min^{-1} [26.8 min (*R*), 29.1 min (*S*)]; Entry 5: $[\alpha]_D^{23} = +14.1$ ($c = 1.30$); bis-PMBz, OD-H, 30% IPA/hexane, 1 mL min^{-1} [38.0 min (*R*), 53.4 min (*S*)]; Entry 6: $[\alpha]_D^{23} = +4.2$ ($c = 1.01$); bis-PMBz, OD-H, 10% IPA/hexane, 1 mL min^{-1} [11.1 min (*S*), 20.7 min (*R*)]; Entry 7: $[\alpha]_D^{23} = -11.7$ ($c = 0.94$); bis-PMBz, OD-H, 10% IPA/hexane, 1 mL min^{-1} [7.4 min (*S*), 16.0 min (*R*)]; Entry 8: $[\alpha]_D^{23} = -23.4$ ($c = 1.02$); bis-PMBz, OD-H, 10% IPA/hexane, 1 mL min^{-1} [9.6 min (*S*), 14.0 min (*R*)]; Entry 9: $[\alpha]_D^{23} = -4.0$ ($c = 1.13$); bis-PMBz, OD-H, 40% IPA/hexane, 0.75 mL min^{-1} [14.8 min (*R*), 45.6 min (*S*)]; Entry 10: $[\alpha]_D^{23} = +14.7$ ($c = 1.04$); bis-PMBz, OD-H, 5% IPA/hexane, 0.75 mL min^{-1} [12.4 min (*R*), 16.6 min (*S*)]; Entry 11: $[\alpha]_D^{23} = +15.8$ ($c = 0.91$); bis-PMBz, OD-H, 5% IPA/hexane, 0.75 mL min^{-1} [13.0 min (*R*), 17.3 min (*S*)]; Entry 12: $[\alpha]_D^{23} = +17.8$ ($c = 0.95$); bis-PMBz, OD-H, 5% IPA/hexane, 0.70 mL min^{-1} [14.4 min (*R*), 20.6 min (*S*)]; Entry 13: $[\alpha]_D^{23} = -4.8$ ($c = 0.96$); bis-Bz, OF, 2.5% IPA/hexane, 0.8 mL min^{-1} [12.9 min (*R*), 17.6 min (*S*)]; Entry 14: $[\alpha]_D^{23} = +38.6$ ($c = 0.96$); bis-PMBz, AD, 5% IPA/hexane, 0.7 mL min^{-1} [18.2 min (*S,S*), 21.7 min (*R,R*)]; Entry 15: $[\alpha]_D^{23} = +12.5$ ($c = 1.01$); bis-PMBz, OD-H, 10% IPA/hexane, 0.5 mL min^{-1} [14.2 min (2*S*,3*R*), 18.4 min (2*R*,3*S*)]; Entry 16: $[\alpha]_D^{23} = -20.1$ ($c = 1.12$); bis-PMBz, AD, 10% IPA/hexane, 1 mL min^{-1} [13.7 min (*S,S*), 16.9 min (*R,R*)]; Entry 17: $[\alpha]_D^{23} = +39.5$ ($c = 1.14$); diol, GLC, CDX-B, 125 °C isotherm [10.0 min (*S*), 10.2 min (*S*)]; Entry 18: $[\alpha]_D^{23} = +2.9$ ($c = 0.99$); mono-Bz, OD-H, 1% IPA/hexane, 1 mL min^{-1} [22.6 min (*R*), 24.3 min (*S*)]; Entry 19: $[\alpha]_D^{23} = -31.9$ ($c = 1.00$); diol, OB-H, 10% IPA/hexane, 0.5 mL min^{-1} [14.3 min (*R*), 18.1 min (*S*)]; Entry 20: $[\alpha]_D^{23} = -4.4$ ($c = 0.96$); bis-Bz, OD-H, 2.5% IPA/hexane, 1 mL min^{-1} [18.4 min (*R*), 22.3 min (*S*)]; Entry 21: $[\alpha]_D^{23} = -1.7$ ($c = 1.05$); diol, AD, 10% IPA/hexane, 0.5 mL min^{-1} [17.4 min (*S,S*), 20.7 min (*R,R*)]; Entry 22: $[\alpha]_D^{23} = -9.9$ ($c = 0.99$); cyclic carbonate, AD, 2.5% IPA/hexane, 1 mL min^{-1} [22.7 min (1*R*,2*S*), 26.0 min (1*S*,2*R*)]; Entry 23: $[\alpha]_D^{23} = +24.1$ ($c = 1.12$); diol, OK, 10% IPA/hexane, 0.8 mL min^{-1} [11.7 min (1*R*,2*S*), 14.4 min (1*S*,2*R*)]; Entry 24: $[\alpha]_D^{23} = +22.9$ ($c = 1.05$); cyclic carbonate, OD-H, 10% IPA/hexane, 1 mL min^{-1} [31.8 min (*R*), 35.4 min (*S*)].

3: A mixture of **2** (5.00 g, 33.8 mmol), $AlCl_3$ (18.0 g, 135 mmol), and 35 mL of 1,4-difluorobenzene was heated at reflux for 48 h. The excess (ca. 25 mL) 1,4-difluorobenzene was removed by distillation and 200 mL of 1 N aq. HCl was added slowly. The mixture was extracted with CH_2Cl_2 (1 × 300 mL, 3 × 100 mL). The combined organic layers were dried by filtration through cotton. The solvent was evaporated and the residue was taken up in 20 mL of $CHCl_3$. Hexane (50 mL) was added and the mixture was cooled to 0 °C, then to −20 °C. The resulting precipate was filtered and dried in vacuo, then 25 mL of polyphosphoric acid was added and the mixture was heated to 130–140 °C for 2 h. The black mixture was poured on to ca. 200 g of ice and then allowed to warm to room temperature with stirring. After neutralization with solid K_2CO_3, the mixture was extracted with CH_2Cl_2 (4 × 100 mL). The combined organic layers were dried by filtration through cotton and concentrated in vacuo. The crude product was filtered through a 5 × 10 cm column of basic alumina (Act. I) eluting with CH_2Cl_2. It was then purified by flash chromatography (4 × 15 cm column of silica gel, hexane/ethyl acetate 2/1, then 1/1) to afford 3.31 g (13.5 mmol, 40%) of **3** as slightly yellow solid. M.p. 220–223 °C; FT-IR (KBr): $\tilde{\nu}$ = 3087 (m), 3051 (w), 1683 (s), 1590 (m), 1472 (m), 1416 (m), 1335 (m), 1258 (s), 1171 (m), 722 (s), 567 (m) cm^{-1}; ^{1}H NMR ($CDCl_3$, 400 MHz): δ = 7.45–7.50 (m, 2H), 7.80 (dd, J = 5.8, 3.3 Hz, 2H), 8.24 (dd, J = 5.8, 3.3 Hz, 2H); ^{13}C NMR ($CDCl_3$, 100 MHz): δ = 121.6, 124.6 (dd, ^2J(C,F) = 20 Hz, ^3J(C,F) = 14 Hz), 127.0, 133.2, 134.3, 156.2 (dd, ^1J(C,F) = 268 Hz, ^4J(C,F) = 4 Hz), 180.6; ^{19}F NMR ($CDCl_3$ [$CFCl_3$], 375 MHz): δ = −180.4 (t, $J \approx 7$ Hz); MS (FAB$^+$/nitrobenzyl alcohol (NBA)/CsI) calculated for $C_{14}H_6F_2O_2$ (MH^+), 245.0414; found, 245.0410.

$(DHQD)_2AQN$ **1a**: A solution of dihydroquinidine [13] (3.35 g, 10.25 mmol, 2.5 equiv) in dry THF was cooled to −50 °C and 6.4 mL (10.25 mmol, 2.5 equiv) of 1.6 M *n*BuLi in hexane was added slowly over 10 min. The solution turned slightly red at the end of the addition. It was stirred for 15 min, warmed to 0 °C, and then **2** (1.00 g, 4.10 mmol) was added as a solid. The reaction mixture was warmed to room temperature, stirred for 18 h, warmed to ca. 40 °C, and stirred for another 2 h. For reactions conducted on a larger scale, the THF was removed in vacuo at this point. Ethyl acetate (200 mL) was added along with sat. aqueous $NaHCO_3$ solution (100 mL). The aqueous phase was extracted with ethyl acetate (2 × 100 mL), and the combined organic layers were dried with $MgSO_4$. After removal of the solvent in vacuo, the raw product was purified by flash chromatography on silica gel (4 × 15 cm, $CHCl_3$ + 5% MeOH + 0.5% NH_4OH) to afford 3.107 g (3.625 mmol, 88%) of $(DHQD)_2AQN$ **1a** as yellow solid. M.p. 152–157 °C; $[\alpha]_D^{23} = -487$ (c = 1.10, $CHCl_3$); UV (MeOH): λ_{max} = 415 nm (ε = 5260), λ_{max} = 335 nm (ε = 11030); FT-IR (KBr): $\tilde{\nu}$ = 2934 (s), 2871 (m), 1669 (s), 1620 (m), 1508 (m), 1463 (m), 1260 (s), 1243 (s), 1030 (m) cm^{-1}; ^{1}H NMR ($CDCl_3$, 400 MHz): δ = 0.84 (t, J = 7.3, 6H), 1.25–1.77 (m, 14H), 2.41 (br s, 2H), 2.40–2.81 (m, 8H), 3.24 (br s, 2H), 3.92 (s, 6H), 5.87 (br s, 2H), 6.65 (s, 2H), 7.36 (dd, J = 9.4, 2.2 Hz, 4H), 7.49 (d, J = 4.2 Hz, 2H), 7.79 (dd, J = 5.7, 3.3 Hz, 2H), 8.02 (d, J = 9.4 Hz, 2H), 8.22 (dd, J = 5.8, 3.3 Hz, 2H), 8.65 (d, J = 4.5 Hz, 2H); ^{13}C NMR ($CDCl_3$, 100 MHz): δ = 12.1, 24.5, 26.5, 27.2, 37.8, 50.2, 51.0, 55.7, 60.3, 81.0 (br), 100.7 (br), 119.1 (br), 120.4, 122.0, 123.4, 126.2, 126.5, 132.0, 133.3, 134.3, 143.0, 144.6, 147.6, 151.2, 158.0, 182.9; MS (FAB$^+$/NBA/CsI) calculated for $C_{54}H_{56}O_6N_4$ (MH^+), 857.4278; found, 857.4242.

$(DHQ)_2AQN$ **1b**: The synthesis is analogous to that of **1a**. Dihydroquinine [13] (3.35 g, 10.25 mmol, 2.5 equiv), 1.6 M *n*BuLi in hexane (6.4 mL, 10.25 mmol, 2.5 equiv), and **3** (1.00 g, 4.10 mmol) afforded 2.967 g (3.462 mmol, 84% yield) of $(DHQ)_2AQN$ **1b** as a yellow solid. M.p. 177–180 °C; $[\alpha]_D^{23} = +579$ (c = 1.18, $CHCl_3$); FT-IR (KBr): $\tilde{\nu}$ = 2954 (m), 2931 (s), 2871 (m), 1669 (s), 1621 (m), 1509 (m), 1461 (m), 1262 (m), 1243 (s), 1005 (m) cm^{-1}; ^{1}H NMR ($CDCl_3$, 400 MHz): δ = 0.80 (t, J = 7.3 Hz, 6H), 1.14–1.44 (m, 8H), 1.59 (br s, 2H), 1.92 (br s, 2H), 2.05 (br s, 2H), 2.35–2.61 (m, 6H), 3.05 (dd, J = 13.4, 10.0 Hz, 2H), 3.23 (br s, 4H), 3.92 (s, 6H), 5.95 (br s, 2H), 6.61 (br s, 2H), 7.32 (br s, 2H), 7.37 (dd, J = 9.2, 2.5 Hz, 2H), 7.43 (d, J = 4.5 Hz, 2H), 7.79 (dd, J = 5.7, 3.3 Hz, 2H), 8.03 (d, J = 9.2 Hz, 2H), 8.28 (dd, J = 5.7, 3.3 Hz, 2H), 8.64 (d, J = 4.5 Hz, 2H); ^{13}C NMR ($CDCl_3$, 100 MHz): δ = 12.1, 20.9, 25.6, 27.7, 27.8, 37.6, 43.5, 55.8, 58.9, 60.0, 80.4 (br), 100.6 (br), 118.7 (br), 120.6, 122.0, 123.4, 126.2, 126.4, 132.1, 133.3, 134.3, 142.8, 144.6, 147.6, 151.0, 158.2, 182.7; MS (FAB$^+$/NBA/CsI) calculated for $C_{54}H_{56}O_6N_4$ (MCs^+), 989.3254; found, 989.3286.

Received: August 28, 1995 [Z8348IE]
German version: *Angew. Chem.* **1996**, *108*, 447–449

Keywords: asymmetric dihydroxylation · catalysis · chiral ligands · cinchona alkaloids · osmium compounds

[1] For reviews on the asymmetric dihydroxylation reaction see: a) H. C. Kolb, M. S. VanNieuwenhze, K. B. Sharpless, *Chem. Rev.* **1994**, *94*, 2483; b) R. A. Johnson, K. B. Sharpless in *Catalytic Asymmetric Synthesis* (Ed.: I. Ojima), VCH, Weinheim, **1993**, pp. 227–272.

[2] a) K. B. Sharpless, W. Amberg, Y. L. Bennani, G. A. Crispino, J. Hartung, K.-S. Jeong, H.-L. Kwong, K. Morikawa, Z.-M. Wang, D. Xu, X.-L. Zhang, *J. Org. Chem.* **1992**, *57*, 2768; b) W. Amberg, Y. L. Bennani, R. K. Chadha, G. A. Crispino, W. D. Davis, J. Hartung, K.-S. Jeong, Y. Ogino, T. Shibata, K. B. Sharpless, *ibid.* **1993**, *58*, 844.

[3] H. Becker, S. B. King, M. Taniguchi, K. P. M. Vanhessche, K. B. Sharpless, *J. Org. Chem.* **1995**, *60*, 3940–3941.

[4] G. A. Crispino, K.-S. Jeong, H. C. Kolb, Z.-M. Wang, D. Xu, K. B. Sharpless, *J. Org. Chem.* **1993**, *58*, 3785–3786.

[5] L. Wang, K. B. Sharpless, *J. Am. Chem. Soc.* **1992**, *114*, 7568–7570.

[6] A. P. Krapcho, Z. Getahun, *Synth. Commun.* **1985**, *15*, 907–910.

[7] Larger quantities of 1,4-difluoroanthraquinone (**3**) are more easily prepared by the chlorination/fluorination procedure with leucoquinizarine described in ref.[6].

[8] The *ee* of the diol of allyl tosylate (Table 1, entry 5) can be increased to 94% by one recrystallization from MeOH.
[9] For a review on nonracemic glycidol and its relatives see: R. M. Hanson *Chem. Rev.* **1991**, *91*, 437–475.
[10] When quinidine- or quinine-derived ligands are used, the operative ligands are the corresponding tetraols.
[11] Reactions with pseudo-first-order rates were conducted in *t*BuOH at 25 °C with concentrations of OsO_4, olefin, and ligand of 0.0002 M, 0.002 M, and 0.002 M, respectively. The rates were determined by monitoring the formation of the osmate ester at $\lambda = 680$ nm using a Cary 4 spectrophotometer. The rates are: $(DHQD)_2PHAL$/1-decene: $0.95 \times 10^{-2}\ s^{-1}$; $(DHQD)_2AQN$/1-decene: $1.10 \times 10^{-2}\ s^{-1}$; $(DHQD)_2PHAL$/styrene: $3.30 \times 10^{-2}\ s^{-1}$; $(DHQD)_2AQN$/styrene: $1.03 \times 10^{-2}\ s^{-1}$.
[12] Recently the DPP ligands have been found to be excellent for the AD reaction of olefins with aromatic substituents. See ref.[3].
[13] Dihydroquinidine and dihydroquinine were obtained from their hydrochloride or hydrobromide salts as described in the "Supplementary Material" to ref.[2a]. The ligands are available from Aldrich.

Catalytic Asymmetric Aminohydroxylation (AA) of Olefins**

Guigen Li, Han-Ting Chang, and K. Barry Sharpless*

Dedicated to the memory of Fèlix Serratosa

The β-hydroxyamino group is frequently found in biologically active molecules. We report here that this important unit can now be synthesized directly from olefins in enantiomerically enriched form. The new osmium-catalyzed asymmetric process is exemplified by the synthesis of the enantiomers of the taxol side chain (**2** and *ent*-**2**) from methyl cinnamate (**1**) (Scheme 1).

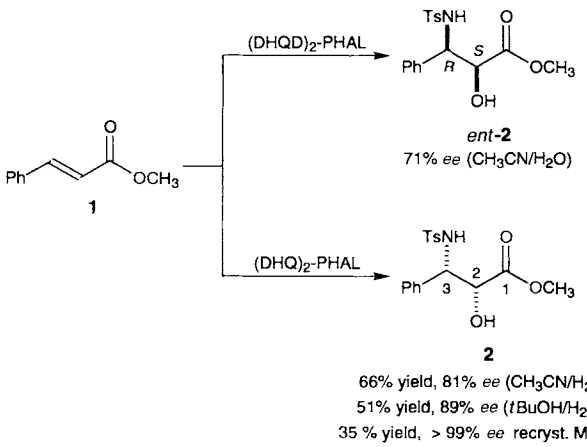

Scheme 1. $K_2OsO_2(OH)_4$, 4%; $(DHQ)_2$-PHAL or $(DHQD)_2$-PHAL, 5%; TsNClNa·3H$_2$O, 3 equiv; CH_3CN/H_2O or *t*BuOH/H_2O, v/v = 1/1; room temperature, 3 h, 0.07 M olefin. See preceding communication for details on the ligands $(DHQ)_2$-PHAL and $(DHQD)_2$-PHAL.

[*] Prof. K. B. Sharpless, Dr. G. Li, H.-T. Chang
Department of Chemistry, The Scripps Research Institute
10666 N. Torrey Pines Road, La Jolla, CA 92037 (USA)
Fax: Int. code +(619)784-7562
e-mail: sharples@scripps.edu

[**] This work was supported by the National Science Foundation (CHE-9296055), the National Institutes of Health (GM 28384), PPG Industries, Sepracor Inc., Merck Research Laboratories, and the W. M. Keck Foundation. We thank Dr. Pui Tong Ho for many helpful discussions. K. B. S. is extremely grateful to Professor Tohru Fukuyama of Rice University for communication of his sulfonamide deprotection discovery[8] and generously suggesting we try it in our earlier osmium-[5] and selenium-catalyzed[9] processes. Taking his advice led us to encounter, serendipitously, these long-sought conditions for achieving catalytic turnover in the AA.

This *catalytic* asymmetric aminohydroxylation (AA) is obviously a close relative of the catalytic asymmetric dihydroxylation (AD).[1] In fact, the *stoichiometric* variant was first reported in 1980 as a footnote in the initial report on the stoichiometric asymmetric dihydroxylation process.[2] However, our studies on both the AD and AA reactions, which were at first only stoichiometric transformations, were pushed aside by rapid developments in the titanium-catalyzed asymmetric epoxidation process (AE), also discovered in 1980.[3] Ever since the development of the *catalytic* AD in 1987,[1a] we have tried to render the AA *catalytic*. Success was very limited[4] until recently when several adjustments in the reaction conditions led to useful catalyst turnover rates. The new process otherwise relies on a simple combination of the phthalazine ligands of the AD reaction and the conditions of the old, but efficient, osmium-catalyzed aminohydroxylation from the 1970s.[5] Other than the asymmetric induction, the most dramatic effect of the cinchona alkaloid ligand is on the regioselectivity. In the original study with methyl cinnamate (**1**),[5a] in which no ligand was used, the C-3 sulfonamide isomer **2** and its C-2 regioisomer were produced in a 2:1 ratio. In the present system this ratio is improved to $\geq 5{:}1$.[6] The reaction of ethyl crotonate (Table 1, entry 2) benefits from this same ligand effect (cf. ref.[5b]). Another positive effect of the ligand is its ability to suppress formation of the diol by-product, which in the absence of the ligand is substantial in this new system.

Table 1 reveals that the process in its present form leads to only modest enantioselectivities (33–81% *ee*). On the other hand, the first report on the catalytic AD reaction did not look much better (20–88% *ee*),[1a] and this new process offers considerably more variables for optimization. Even the present results are useful since hydroxysulfonamides tend to be highly crystalline; enantiomeric purity near 100% can often be reached by recrystallization. This is the case for the derivative of the taxol side chain, **2**, which can be deprotected by treatment with 33% HBr in acetic acid for 10 hours at 75 °C to give the enantiomerically pure α-hydroxy-β-amino acid in 77% yield.[7] While the core functionality of toluenesulfonamide derivative **2** survives these strongly acidic conditions, many compounds would not. Indeed, the notorious problems associated with deprotection of sulfonamides are a serious concern for this AA process. Fortunately, a recent breakthrough from the Fukuyama group[8] promises to make sulfonamide protection for nitrogen extremely popular.[9–11] In any case, the strongly acidic conditions successful for deprotection of the precursor of the taxol side chain indicate that more molecules than previously imagined may tolerate the old "brute-force" approach for hydrolysis of aromatic sulfonamides.

Initial experience has been largely with CH_3CN/H_2O as solvent (procedure 1, Table 1), but *t*BuOH/H_2O is also a good solvent system (procedure 2, Table 2) and both are worth trying with new substrates. For the examples given in Table 2, the products are insoluble in *t*BuOH/H_2O and for *trans*-stilbene, the starting material is also insoluble. In these cases, the reported yields and *ee* values are for the product isolated by direct filtration of the reaction mixture (no workup, not even reduction with sulfite). The products are almost pure by NMR and HPLC analysis. Another virtue of this approach is that the toluenesulfonamide by-product remains in the mother liquor. In procedure 1, the excess $TsNH_2$ can be difficult to remove.

Mechanistic studies on the AA are underway and we have evidence[12] that there is more than one catalytic cycle, which is reminiscent of the AD process when *N*-methylmorpholine *N*-oxide (NMO) is the oxidant.[13] For the present, we eschew further speculation on the mechanism except to note four key

Table 1. Catalytic asymmetric aminohydroxylation in CH_3CN/H_2O (1/1) (see procedure 1 in the Experimental Procedure).

Entry	Substrate	Product [a]		*ee* Values [%] $(DHQ)_2$-PHAL [b]	*ee* Values [%] $(DHQD)_2$-PHAL [c]	Yield [%]	*t* [h]	M.p. [°C] [b]	$[\alpha]_D^{25}$ [b]
1	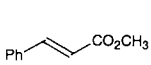 **1**	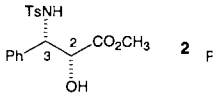 **2**	F	81 (99)	71	64	3	154–155	+19.8 ($c = 0.50$)
2	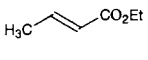	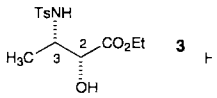 **3**	F	74	60	52	1.5	oil	−20.3 ($c = 1.25$)
3		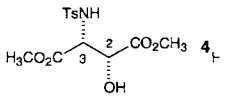 **4**	F	77 (93)	53	65	3	140–141	−7.9 ($c = 0.63$)
4 [d]	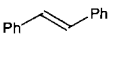	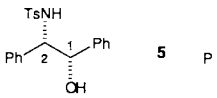 **5**	P	62 (99)	50	52	14	167–168	−15.9 ($c = 0.43$)
		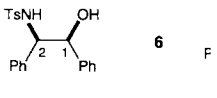 **6**	F						
5		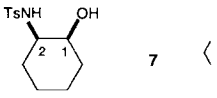 **7**	⟨	33 (99)	48	48	3	227–228	+53.0 ($c = 0.11$)
6				45 (99)	36	64	6	117–119	+1.8 ($c = 0.60$)

[a] All absolute configurations have been determined (see Experimental Procedure). [b] Numbers in parentheses are *ee* values after recrystallization from methanol. (In some cases [7] it is the mother liquor that is enantioenriched when the racemate crystallizes preferentially.) The melting points and optical rotations (in 95% ethanol) are for the samples with the highest *ee* values listed in the $(DHQ)_2$-PHAL column of Table 1. [c] The *ee* values in this column are for the products that are enantiomeric to those in the Product column. [d] CH_3CN/H_2O (4/3) was used as the solvent.

facts. 1) The AA process is obviously an asymmetric version of the catalytic aminohydroxylation process discovered twenty years ago.[5a] 2) The ligand suppresses the formation of the diol by-product. 3) The ligand leads not only to enantioselectivity, but in some cases also accelerates catalytic turnover (ligand-accelerated catalysis, LAC[14]).[15] 4) The ligand influences the regioselectivity, sometimes strongly so. The latter effect is perhaps fortunate for reactions of unsaturated carbonyl compounds such as cinnamate and crotonate (Table 1, entries 1 and 2). The ligand steers the nitrogen center to the β-carbon atom producing a class of amino acids (e.g. **2** and **3**), which are useful in the synthesis of peptidomimics.

Table 2. Catalytic asymmetric aminohydroxylation in *t*BuOH/H_2O (1/1) (see procedure 2 in the Experimental Procedure).

Substrate	Product	*ee* Values [%] $(DHQ)_2$-PHAL	Yield [%]	*t* [h]
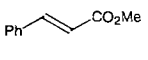	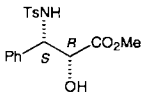 **2**	82 (89 [a])	60 (51 [a])	3
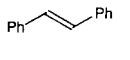	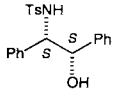 **5**	64 (99 [b])	78 (50 [b])	3
	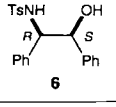 **6**	50	57	2.5

[a] In this case, one-half of the olefin was added at the beginning of the reaction and the rest was added in portions over 45 min starting one hour later. [b] The minor enantiomer was completely removed by two triturations with ethyl acetate leaving a 50% yield of enantiopure (*S*,*S*)-**5**.

Two features of this AA process are surprising: 1) Even strongly electron-deficient olefins such as dimethyl fumarate (Table 1, entry 3) react rapidly and with good *ee* values,[16] whereas in the AD reaction dimethyl fumarate reacts extremely slowly and with less than 40% *ee*. 2) *cis*-Disubstituted olefins appear to be promising substrates, even symmetrical compounds which of course give achiral *meso* diols in the AD. Although the enantioselectivities are low for *cis*-stilbene and cyclohexene (Table 1, entries 5 and 6, respectively), AA reactions of heterocyclic *cis* olefins have exceeded 77% *ee*.[17]

For the *trans*-disubstituted olefins examined here the face selection rule follows that for the AD reaction; that is, with the olefin drawn as in Scheme 1, $(DHQD)_2$-PHAL directs addition to the β-face and $(DHQ)_2$-PHAL directs addition to the α-face. For *trans* olefins it is now the DHQ series that generally gives higher *ee* values (Table 1, entries 1–4), the inverse of the situation for the AD reaction.[1] Another trend, which fits our current speculation on the mechanism,[18] is that with electronically unsymmetrical olefins the nitrogen becomes attached to the carbon

 © VCH Verlagsgesellschaft mbH, D-69451 Weinheim, 1996 0570-0833/96/3504-0452 $ 15.00+.25/0

atom distal to the strongest electron-withdrawing group (Table 1, entries 1 and 2).

In summary, the asymmetric aminohydroxylation (AA) of olefins is now an effective catalytic process. Much work lies ahead to establish the scope and utility of the reaction, but it should already prove useful in research laboratories. The AA shares with the AD three desirable features. The first is simplicity: only catalytic amounts of both osmium and chiral ligand are required; the reactions are performed at close to room temperature with commercially available reagents and are not influenced by water or oxygen; and the products can often be isolated by filtration of the crude reaction mixture. The second feature is the crucial functional group transformations AA and AD provide: under essentially neutral conditions and with great reliability an olefin undergoes *cis*-vicinal addition of two heteroatoms.[19] Last but not least is scope: like the AD, the AA has no requirement for auxiliary functional groups.

Experimental Procedure

General procedure: All reagents and solvents were purchased from commercial sources and used as received unless stated otherwise. Stoichiometries are calculated based on the purities reported by the manufacturer (*trans*-stilbene: 96%; Chloramine-T trihydrate: 98%). $K_2OsO_2(OH)_4$ should be mauve colored rather than brown/black and should be dry for the best yields and *ee* values (the hygroscopic nature of the salt affects the amount of osmium available). All new compounds gave satisfactory spectroscopic analyses (^{1}H NMR and IR spectroscopy, HRMS). Enantiomeric excesses were determined by HPLC using Chiracel columns (Daicel Chemical Industries) and isopropyl alcohol/hexane (v/v) mobile phases; the retention time of the major enantiomer from the $(DHQ)_2$-PHAL reaction is in italics. The vicinal hydroxysulfonamides derived from AA reactions using $(DHQ)_2$-PHAL as the chiral ligand were correlated to compounds of known absolute configuration by HPLC.

Procedure 1: Ethyl (2*R*,3*S*)-*N*-(*p*-toluenesulfonyl)-3-amino-2-hydroxybutanoate (**3**): To a stirred solution of $(DHQ)_2$-PHAL (0.11 g, 0.14 mmol, 5 mol%) in 20 mL of acetonitrile and 20 mL of water, in any convenient-sized glass vessel or vial, were added *trans*-ethyl crotonate (0.32 g, 2.8 mmol), Chloramine-T trihydrate (2.42 g, 8.4 mmol, 3 equiv), and $K_2OsO_2(OH)_4$ (41.6 mg, 0.112 mmol, 4 mol%). As the reaction proceeded to completion over the course of about 90 min at room temperature, the color of the solution changed from yellow to pale green, then deep green, and finally back to yellow (for entry 3 in Table 1, the yellow color remains throughout). After addition of aqueous sodium sulfite (1.0 g in 15 mL H_2O), the phases were separated and the aqueous phase was extracted with ethyl acetate (3 × 15 mL). The combined organic extracts were washed with brine, dried over $MgSO_4$, and concentrated to dryness to give the crude product, which also contains the *p*-toluenesulfonamide by-product produced upon the reduction of the excess Chloramine-T. Flash chromatography (hexane/$CHCl_3$/MeOH (6/4/1)) of this material provided 0.44 g (52% yield, 74% *ee*) of **3** as a clear oil eluting before the *p*-toluenesulfonamide impurity. When the 3 equiv of Chloramine-T was replaced with 1.5 equiv of Chloramine-T and 1.5 equiv of Et_4NOAc, comparable results were obtained and the amount of *p*-toluenesulfonamide by-product formed was reduced. This can greatly simplify product isolation, especially when the product and the toluenesulfonamide have similar chromatographic mobilities. Nonchromatographic methods for removing the $TsNH_2$ will be described elsewhere.

Procedure 2: (1*S*,2*S*)-*N*-(*p*-Toluenesulfonyl)-2-amino-1,2-diphenylethanol (**5**): To a solution of $(DHQ)_2$-PHAL (2.20 g, 2.80 mmol, 5 mol%) in *t*BuOH (100 mL) and water (100 mL) in a 500 mL Erlenmeyer or round-bottomed flask were added in order, *trans*-stilbene (10.5 g, 56.0 mmol), Chloramine-T trihydrate (48.4 g, 0.168 mol, 3.0 equiv), and $K_2OsO_2(OH)_4$ (0.824 g, 2.24 mmol, 4 mol%). The reaction flask was immersed in a room-temperature water bath and the slurry stirred for 2.5 h. Over the course of the reaction, the color changed from brown to deep green and then to yellow as the stilbene slurry became a hydroxysulfonamide slurry. The product was isolated by filtration and the crude solid was washed once with cold (ca. 5 C) *t*BuOH:H_2O (1 1, 15 mL) to yield 16.1 g of **5** (78% yield, 64% *ee*, pure by NMR spectroscopy and HPLC). Trituration of this product twice with ethyl acetate (2 × 15 mL) at room temperature in a sintered glass funnel left crystals of enantiomerically pure **5** (10.3 g, 50% yield, >99% *ee*, m.p. 166–167 °C). See ref. [20] for analogous solid-to-solid AD procedures.

Analysis of enantiomeric excesses: **2**: Chiralcel OG, 30% *i*PrOH/hexane, 1 mL min^{-1}; 21.8 min (2*S*,3*R*), 28.3 min (2*R*,3*S*). **3**: Chiralcel OD-H, 15% *i*PrOH/hexane, 1 mL min^{-1}, 7.5 min (2*S*,3*R*), 13.4 min (2*R*,3*S*). **4**: Chiralcel OG, 30% *i*PrOH/hexane, 1 mL min^{-1}, 16.7 min (2*S*,3*S*), 21.8 min (2*R*,3*R*). **5**: Chiralcel OD-H, 15% *i*PrOH/hexane, 1 mL min^{-1}, 16.2 min (1*S*,2*S*), 26.0 min (1*R*,2*R*). **6**: Chiralcel OD-H, 15% *i*PrOH/hexane, 0.5 mL min^{-1}, 18.5 min (1*S*,2*R*), 22.1 min (1*R*,2*S*). **7**: Chiralcel OG, 15% *i*PrOH/hexane, 0.5 mL min^{-1}, 28.5 min (1*S*,2*R*), 34.4 min (1*R*,2*S*).

Correlation of the absolute configurations: (2*R*,3*S*)-**2**: Authentic (2*R*,3*S*)-**2** was synthesized from *N*-benzoyl-(2*R*,3*S*)-3-phenylisoserine methyl ester (taxol C13 side chain[20]) [6 N HCl, reflux (methyl ester and *N*-benzoyl groups removed); $SOCl_2$, methanol (esterification); TsCl, K_2CO_3, acetone/water (1/1) (*N*-sulfonylation)] [HPLC: vide supra]. (2*R*,3*S*)-**3**: (2*R*,3*S*)-**3** was converted to *N*-tosyl-(2*S*)-alanine methyl ester [6 N HCl (hydrolysis); $RuCl_3/H_5IO_6$ (oxidative cleavage); $SOCl_2$, methanol (esterification)] [HPLC: Chiralcel OD-H, 15% *i*PrOH/hexane, 1 mL min^{-1}, 16.1 min (2*R*), 17.0 min (2*S*)]. (2*R*,3*R*)-**4**: (2*R*,3*R*)-**4** was converted to its *N*-tosyl-(2*R*,3*R*)-2-oxazolidinone derivative, which was also independently synthesized from (1*S*,2*S*)-**5** [carbonyl diimidazole, CH_2Cl_2; $RuCl_3$, H_5IO_6 (oxidative degradation of the phenyl groups)[21]; $SOCl_2$, methanol (esterification)] [HPLC: Chiralcel OD-H, 15% *i*PrOH/hexane, 1 mL min^{-1}, 26.0 min (1*R*,2*R*), 47.2 min (1*S*,2*S*)]. (1*S*,2*S*)-**5**: An authentic sample of (1*S*,2*S*)-**5** was synthesized from (1*R*,2*S*)-**6** [CrO_3, H_2SO_4 (oxidation of alcohol to ketone); DIBAL-H reduction gave a 4:1 mixture of (1*R*,2*S*)-**6** and (1*S*,2*S*)-**5**] [HPLC: vide supra]. (1*S*,2*R*)-**6**: An authentic sample of (1*R*,2*S*)-**6** was synthesized from (1*R*,2*S*)-2-amino-1,2-diphenylethanol [TsCl, K_2CO_3, acetone/water] [HPLC: vide supra]. (1*S*,2*R*)-**7**: *N*,*N*′-Ditosyl-(1*R*,2*R*)-diaminocyclohexane was synthesized from (1*S*,2*R*)-**7** [SO_2Cl_2, Et_3N, EtOAc; NaH (cyclic sulfamidate formation); NaN_3 (opening); H_2, Pd/C (azide reduction); TsCl, K_2CO_3, acetone/water (1/1)] and compared to the compound derived from authentic (1*R*,2*R*)-diaminocyclohexane[22] [HPLC: Chiralcel AS, 20% *i*PrOH/hexane, 1 mL min^{-1}, 23.2 min (1*R*,2*R*), 32.3 min (1*S*,2*S*)].

Received: September 22, 1995 [Z8421IE]
German version: *Angew. Chem.* **1996**, *108*, 449–452

Keywords: β-amino alcohols · asymmetric aminohydroxylation · Chloramine-T · osmium compounds · taxol side chain

[1] a) E. N. Jacobsen, I. Markó, W. S. Mungall, G. Schröder, K. B. Sharpless, *J. Am. Chem. Soc.* **1988**, *110*, 1968; b) H. C. Kolb, M. S. VanNieuwenhze, K. B. Sharpless, *Chem. Rev.* **1994**, *94*, 2483.

[2] See ref. [22] in S. G. Hentges, K. B. Sharpless, *J. Am. Chem. Soc.* **1980**, *102*, 4263. Stoichiometric AA reactions have also been reported recently: a) H. Rubinstein, J. S. Svendsen, *Acta Chem. Scand.* **1994**, *48*, 439; b) C. Y. Park, Ph.D. Thesis, Massachusetts Institute of Technology, Cambridge, MA, USA, **1991**; c) see also ref.[14], p. 1067.

[3] T. Katsuki, K. B. Sharpless, *J. Am. Chem. Soc.* **1980**, *102*, 5974.

[4] The first, albeit inefficient, catalytic asymmetric aminohydroxylations were performed by Christopher J. Burns and Declan G. Gilheany in the Sharpless laboratory at the Massachusetts Institute of Technology in 1987, unpublished results.

[5] a) K. B. Sharpless, A. O. Chong, K. Oshima, *J. Org. Chem.* **1976**, *41*, 177; b) E. Herranz, K. B. Sharpless, *ibid.* **1978**, *43*, 2544; c) E. Herranz, S. A. Biller, K. B. Sharpless, *J. Am. Chem. Soc.* **1978**, *100*, 3596; d) E. Herranz, K. B. Sharpless, *J. Org. Chem.* **1980**, *45*, 2710; e) E. Herranz, K. B. Sharpless, *Org. Synth.* **1981**, *61*, 85; f) E. Herranz, K. B. Sharpless, *ibid.* **1981**, *61*, 93; for palladium-promoted aminohydroxylation (oxyamination) see: J. E. Bäckvall, E. E. Björkman, *J. Org. Chem.* **1980**, *45*, 2893; J. E. Bäckvall, *Tetrahedron Lett.* **1975**, *26*, 2225.

[6] In fact, at an early stage (ca. 5% conversion) of the reaction with methyl cinnamate this ratio is >20:1 and the enantiomeric purity of the major regioisomer (**2**) is about 95% *ee*. Both regio- and enantioselectivity drop continuously as the reaction proceeds. This is tentatively attributed to intrusion of a "second cycle" (see refs.[12,13]).

[7] G. Li, K. B. Sharpless, *Acta Chem. Scand.*, in press. This paper describes a one-third mole scale synthesis of the precursor of the taxol side chain based on the solution-to-solid AA of methyl cinnamate (procedure 2, Table 2, but with only 2.5 mol% ligand and 2.0 mol% osmium catalyst). See also ref. [22].

[8] T. Fukuyama, C.-K. Jow, M. Cheung, *Tetrahedron Lett.* **1995**, *36*, 6373.

[9] M. Bruncko, T.-A. V. Khuong, K. B. Sharpless, *Angew. Chem.* **1996**, *108*, 453; *Angew. Chem. Int. Ed. Engl.* **1996**, 35, 454.

[10] A highlight on this topic is in preparation.

[11] Preliminary results indicate that the chloramines derived from Fukuyama's 2- and 4-nitrosulfonamides are effective in the AA process.

[12] K. B. Sharpless et al., unpublished results.

[13] J. S.-M. Wai, I. Markó, J. S. Svendsen, M. G. Finn, E. N. Jacobsen, K. B. Sharpless, *J. Am. Chem. Soc.* **1989**, *111*, 1123.

[14] D. J. Berrisford, C. Bolm, K. B. Sharpless, *Angew. Chem.*, **1995**, *108*, 1159; *Angew. Chem. Int. Ed. Engl.* **1995**, *34*, 1059.

[15] The ligand, in this case $(DHQ)_2$-PHAL, substantially accelerates the rate of catalysis for the α,β-unsaturated ester substrates (Table 1, entries 1–3). However, for stilbene and the remaining entries in Table 1 the catalysis is faster in the absence of ligand—an example of the more common phenomenon of LDC (ligand-decelerated catalysis)[14]. It is too early to speculate on the origin of these opposite effects of the ligands.

[16] Despite their electron deficiency, reactions of α,β-unsaturated carbonyl compounds are among the fastest to date in the catalytic AA.

[17] A. Houri, K. B. Sharpless, unpublished results.
[18] In the AA the putative organometallic intermediate (see mechanistic section of the AD review [1b]) can be either an oxametallacycle or an azametallacycle. The AA results to date suggest the azametallacycle is preferred, especially for substrates like methyl cinnamate and ethyl crotonate (entries 1 and 2 in Table 1).
[19] a) A remarkably efficient and highly enantioselective catalytic route from *meso* epoxides to *threo* vicinal amino alcohols of high enantiopurity has just been discovered: L. E. Martinez, J. L. Leighton, D. H. Carsten, E. N. Jacobsen, *J. Am. Chem. Soc.* **1995**, *117*, 5897. b) For alternative noncatalytic routes to enantiopure β-amino alcohols, see: R. Polt, M. A. Peterson, L. DeYoung, *J. Org. Chem.* **1992**, *57*, 5469, and references therein.
[20] a) Z.-M. Wang, H. C. Kolb, K. B. Sharpless, *J. Org. Chem.* **1994**, *59*, 5104; b) Z.-M. Wang, K. B. Sharpless, *J. Org. Chem.* **1994**, *59*, 8302.
[21] a) M. T. Nuñez, V. S. Martín, *J. Org. Chem.* **1990**, *55*, 1928; b) P. H. J. Carlsen, T. Katsuki, V. S. Martín, K. B. Sharpless, *J. Org. Chem.* **1981**, *46*, 3936.
[22] E. N. Jacobsen, W. Zhang, A. R. Muci, J. R. Ecker, L. Deng, *J. Am. Chem. Soc.* **1991**, *113*, 7063.

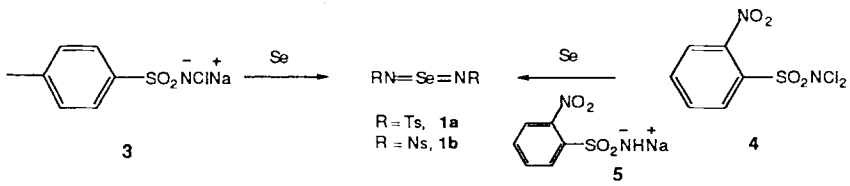

Scheme 2.

Allylic Amination and 1,2-Diamination with a Modified Diimidoselenium Reagent**

Milan Bruncko, Tinh-Alfredo V. Khuong, and K. Barry Sharpless*

Allylic amines and 1,2-diamino-3-alkenes are compounds of great interest[1] predominantly for the synthesis of natural products,[2] medicinal agents,[3] and amino and 1,2-diamino carboxylic acids.[4] Several methods for allylic aminations have been developed,[5] but these require severe reaction conditions or several sequential reactions. Many of the methods employ alkenes that have already been functionalized at the allylic position.[6] The recently published discovery of a simple method for deprotection of nitro-substituted benzenesulfonamides by Fukuyama et al.[7] encouraged us to return to selenium chemistry. We report here on a modification and significant improvement in a method for the allylic amination of olefins utilizing diimidoselenium reagents.[8]

Diimidoselenium compounds **1** have been shown to react in a manner similar to selenium dioxide (Scheme 1).[9] Oxidation of an allylic position in alkenes using SeO_2 proceeds by an ene reaction followed by [2,3]sigmatropic rearrangement, and **1** can effect allylic amination by an analogous pathway. The in situ synthesis of selenium reagent **1a** involves treatment of sodium

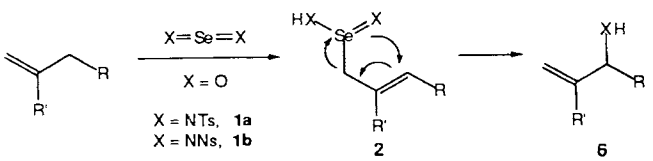

Scheme 1. Ts = *p*-toluenesulfonyl (tosyl), Ns = *o*-nitrobenzenesulfonyl (nosyl).

[*] Prof. K. B. Sharpless, Dr. M. Bruncko, T.-A. V. Khuong
Department of Chemistry, The Scripps Research Institute
10666 N. Torrey Pines, La Jolla, CA 92037 (USA)
Fax: Int. code +(619)784-7562
e-mail: sharples@scripps.edu

[**] This work was supported by the National Institutes of Health (GM 28384), Merck Research Laboratories, and the W. M. Keck Foundation. This research was made possible by the exciting discovery of a superior alkylation/deprotection strategy for amines by Fukuyama et al.[7]. We are deeply indebted to him for encouraging us to try it in our old selenium-mediated allylic aminations.

N-chloro-*p*-toluenesulfonamide (Chloramine-T) (**3**) with elemental selenium in dichloromethane under anhydrous conditions (Scheme 2).[10] Due to the poor solubility of both of these reagents the overall reaction is slow (24–48 h). Subsequent deprotection of the amino function of the allylic amines by removal of the *p*-toluenesulfonyl group requires harsh conditions that are incompatible with many other functionalities. Replacement of the insoluble Chloramine-T (**3**) with a more reactive and entirely soluble dichloramine derivative such as **4** results in a substantial process improvement (Scheme 2). Reagent **4** is very reactive. Therefore we have developed two procedures for allylic amination with **1b**. For reactions on less than a 10 mmol scale all reagents (Se, **4**, **5**) are mixed and dichloromethane is added quickly. For larger scale reactions a solution of **4** in dichloromethane is added to the suspension of selenium and sodium sulfonamide **5**. By these modifications, the whole process can be accomplished in one pot in less than three hours.

The reaction of the selenium reagent **1b** with different alkenes was investigated, and the results are summarized in Table 1. Allylic amination of the simple terminal olefin 1-hexene (Table 1, entry 1), provided the 2-nitrobenzenesulfonyl derivative **6a** in 51% yield. This yield is slightly lower than that ob-

Table 1. Allylic amination of alkenes[a].

Entry	Alkene	Product	Yield [%] [b]
1	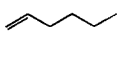	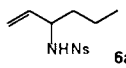 **6a**	51 (54) [c]
2	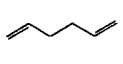	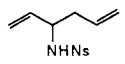 **6b**	21
3		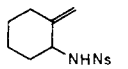 **6c**	64 (74) [c]
4		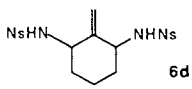 **6d**	39 [d]
5		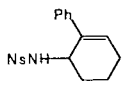 **6e**	59

[a] For reaction conditions see the Experimental Procedure. [b] All yields were determined by isolation of products. [c] Numbers in brackets correspond to yields obtained with the tosyl reagent [8]. [d] 2.1:1 mixture of diastereomers.

tained with the selenium reagent prepared from Chloramine-T. Treatment of two equivalents of methylenecyclohexane (Table 1, entry 3) with one equivalent of **1b** afforded the 2-nosylamido product **6c** in 64% yield. With the opposite proportions, two equivalents of **1b** and one equivalent of the same substrate (Table 1, entry 4), the 2,6-bis(nosylamido) product **6d** was obtained as a 2.1:1 mixture of diastereomers in 39% yield. An acyclic substrate such as 1,5-hexadiene nevertheless afforded the

mono-substituted nosylamido product **6b** (Table 1, entry 2), even when the amount of **1b** was increased to two equivalents. 1-Phenylcyclohexene (Table 1, entry 5) provided 6-nosylamido product **6e** in 59% yield as a single regioisomer. A trace amount (<5%) of a product of an allylic chlorination and subsequent hydrolysis at the 6-position was observed.[11] Allylic chlorination with *N*-chlorosuccinimide and catalytic selenium has been described previously.[12] Attempts to achieve allylic amination of substrates such as 1-phenyl-3,4-dihydronaphthalene and 1,4-cyclohexadiene using the diimidoselenium reagent were unsuccessful.

1,3-Dienes react with **1a** by a Diels–Alder reaction and subsequent [2,3]sigmatropic rearrangement to give *cis*-1,2-diaminoalkenes (Scheme 3).[10] The reaction of cyclopentadiene with **1b** affording **7a** (Table 2, entry 1) proceeds in much higher yield than the analogous reaction with **1a**. The reaction of 1,3-cyclohexadiene (Table 2, entry 2) with **1b** was more complex,

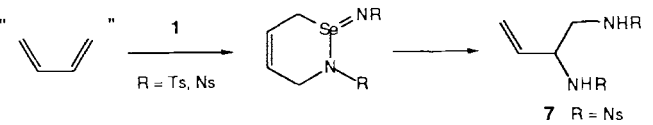

Scheme 3.

providing not only the expected diamino product **7b** (29%) but also a series of selenium-containing by-products and/or by-products formed after allylic amination. The diamination

Table 2. Formation of 1,2-diamino-3-alkenes from 1,3-dienes according to Scheme 3[a].

Entry	Diene	Product	Yield [%] [b]
1		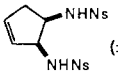 (±)-**7a**	65 (40) [c]
2		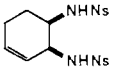 (±)-**7b**	29 (37) [c]
3		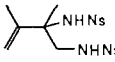 **7c**	46 (68) [c]
4		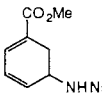 **6g**	7 [d]

[a] For reaction conditions see the Experimental Procedure. [b] All yields were determined by isolation of products. [c] Numbers in brackets correspond to yields obtained with the tosyl reagent[10]. [d] Only the product of allylic amination was isolated.

product **7c** (Table 2, entry 3) was isolated in 46% yield along with the product of allylic monoamination **6f** (17%) in the reaction of **1b** with 2,3-dimethyl-1,3-butadiene. With this diene the tosyl reagent provided only the vicinal diamine product.[10] This difference in reactivity can be explained by the higher electrophilicity of **1b**.

To study the influence of electron-withdrawing groups on the reactivity of **1b**, 1,3-dienes such as methyl 1,3-cyclohexadiene-1-carboxylate, ethyl sorbate, and methyl furoate were examined. However, the allylic amination of methyl 1,3-cyclohexadiene-1-carboxylate with **1b** (Table 2, entry 4) gave the precursor **6g** of (±)-gabaculine[12b, 6b, 13] in very poor yield (7%). The electron-withdrawing substituent apparently renders these 1,3-dienes quite inert under the standard reaction conditions.

To demonstrate the utility of this method, functionalized 1,2-diaminocyclopent-3-enes **9a–c** were synthesized (Scheme 4). The advantage of nitro-substituted benzenesulfonyl residues as protecting groups for amino functions, which were recently introduced by Fukuyama et al.,[7] lies in the ease of deprotection. Dimethyl (**8a**), diallyl (**8b**), and dibenzyl derivatives (**8c**) were prepared in excellent yields by treatment of **7a** with alkyl halides in DMF and in the presence of K_2CO_3. Removal of the nosyl protecting group in **8a–c** proceeded in the presence of thiophenoxide in DMF, via the Meisenheimer complexes, to provide the secondary vicinal diamines **9a–c** in good yields (Scheme 4). Under the same conditions sulfonamide **6e** was also deprotected.

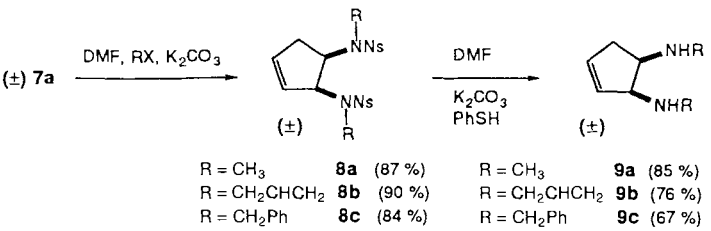

Scheme 4. DMF = dimethylformamide.

A further application of these methods is the preparation of amino acids by the oxidative cleavage of the double bond in the aminated or diaminated products. For example, this was accomplished by oxidation of **7a** with periodic acid and a catalytic amount of $RuCl_3 \cdot 3H_2O$.[14] Dicarboxylic acid **11** was isolated as a white crystalline solid in 64% yield (Scheme 5).

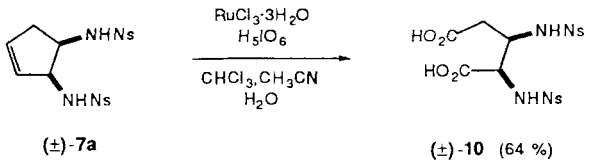

Scheme 5.

In conclusion, we have described a modified and improved procedure for allylic amination of olefins and 1,2-diamination of 1,3-dienes that employs nosyl protecting groups on the intermediate diimidoselenium compound.

Experimental Procedure

Allylic aminations and 1,2-diaminations:

A) General procedure for reactions on scales less than 10 mmol: Dry 2-nitrobenzene-*N*,*N*-dichlorosulfonamide **4** (1.084 g, 4 mmol), sodium 2-nitrobenzenesulfonamide **5**[15] (1.838 g, 8.2 mmol), selenium (0.332 g, 4.2 mmol), and molecular sieves 3Å were placed into a flame-dried flask under nitrogen, and dry dichloromethane (20 mL) was quickly added. The reaction mixture was stirred for 3 h at room temperature. Alkene or diene (8 mmol) was added to the white slurry and the reaction mixture was stirred for another 16–48 h. The reaction mixture was poured into 5% NaOH/ethyl acetate (100 mL/100 mL) and stirred for 20 min. The organic layer was separated, washed with another portion of 5% NaOH (100 mL), and dried over $MgSO_4$. The solvent was removed in vacuo and the brown residue purified by flash column chromatography (silica gel, ethyl acetate/hexane 10–40%).

B) General procedure for reactions on scales over 10 mmol: Dry sodium 2-nitrobenzenesulfonamide **5** (9.19 g, 40 mmol), selenium (1.66 g, 21 mmol) and molecular sieves 3Å were placed into a flame-dried flask under nitrogen, and dry dichloromethane (80 mL) was added. A solution of 2-nitrobenzene-*N*,*N*-dichlorosulfonamide **4** [15] (5.42 g, 20 mmol) in dichloromethane (40 mL) was added dropwise by syringe or cannula. The reaction mixture was stirred for 3 h at room temper-

ature. Alkene or diene (3.3 mL, 2.64 g, 40 mmol) was added to the white slurry and the reaction mixture was stirred for another 16–48 h. The workup was the same as that described above.

6a: 51% yield of the oily product. ^{1}H NMR ($CDCl_3$, 400 MHz): δ = 0.87 (t, ^3J = 7.3 Hz, 3H), 1.30–1.39 (m, 2H), 1.47–1.56 (m, 2H), 3.93 (quint, ^3J = 7.5 Hz, 1H), 4.86 (dt, ^3J = 10.3 Hz, ^4J = 0.9 Hz, 1H), 4.97 (dt, ^3J = 17.1 Hz, ^4J = 1 Hz, 1H), 5.33 (d, ^3J = 8.6 Hz, 1H), 5.51 (ddd, ^3J = 7, 10.3, 17.2 Hz, 1H), 7.67–7.72 (m, 2H), 7.79–7.83 (m, 1H), 8.04–8.07 (m, 1H). ^{13}C NMR ($CDCl_3$, 400 MHz): δ = 13.40, 18.39, 37.48, 57.24, 116.06, 125.05, 130.85, 132.62, 133.37, 134.62, 137.13, 146.71. FT-IR (neat): $\tilde{\nu}$ = 3336, 1537, 1411, 1355, 1167 cm^{-1}. HRMS-FAB: calcd for $C_{12}H_{16}N_2O_4SCs^+$: 416.9885; found: 416.9869.

6b: 21% yield of the oily product. ^{1}H NMR ($CDCl_3$, 400 MHz): δ = 2.29–2.34 (m, 2H), 4.05–4.10 (m, 1H), 4.98 (dt, ^3J = 10.4 Hz, ^4J = 1 Hz, 1H), 5.04 (s, 1H), 5.06 (s, 1H), 5.07–5.11 (m, 1H), 5.41 (d, ^3J = 8.2 Hz, 1H), 5.57–5.68 (m, 2H), 7.69–7.73 (m, 2H), 7.82–7.86 (m, 1H), 8.06–8.11 (m, 1H). ^{13}C NMR ($CDCl_3$, 400 MHz): δ = 39.86, 56.54, 116.48, 119.32, 125.20, 130.87, 132.32, 132.70, 133.39, 134.81, 136.63, 147.69. FT-IR (neat): $\tilde{\nu}$ = 3338, 1538, 1410, 1346, 1168 cm^{-1}. HRMS-FAB: calcd for $C_{12}H_{14}N_2O_4S + H^+$: 283.0753; found: 283.0792.

6c: 64% yield of the oily product. ^{1}H NMR ($CDCl_3$, 400 MHz): δ = 1.30–1.57 (m, 4H), 1.60–1.67 (m, 1H), 1.72–1.83 (m, 1H), 1.87–1.96 (m, 1H), 2.18 (dt, ^3J = 4.8, 14 Hz, 1H), 3.92–3.99 (m, 1H), 4.59 (s, 1H), 4.71 (s, 1H), 5.52 (d, ^3J = 8.6 Hz, 1H), 7.67–7.72 (m, 2H), 7.77–7.80 (m, 1H), 8.03–8.07 (m, 1H). ^{13}C NMR ($CDCl_3$, 400 MHz): δ = 23.69, 26.97, 33.40, 35.10, 56.99, 107.80, 124.97, 130.47, 132.67, 132.71, 133.39, 134.38, 146.83. FT-IR (neat): $\tilde{\nu}$ = 3343, 2932, 1538, 1444, 1356, 1167 cm^{-1}. HRMS-FAB: calcd for $C_{13}H_{16}N_2O_4SNa^+$: 319.0728; found: 319.0737.

6d: 39% yield of a mixture of diastereomers (2.1:1 ratio by NMR). ^{1}H NMR ($CDCl_3$, 400 MHz): δ = 1.56–1.67 (m, 6H), 4.13–4.17 [3.93–3.98] (m, 2H), 4.83 [4.90] (s, 2H), 5.49 [5.55] (d, ^3J = 8 [8.4] Hz, 2H), 7.69–7.73 (m, 4H), 7.83–7.86 (m, 2H), 7.98–8.02 [8.04–8.08] (m, 2H). ^{13}C NMR ($CDCl_3$, 400 MHz): δ = 20.19 [24.36], 33.57 [34.89], 55.34 [56.55], 111.39 [106.45], 125.66 [125.17], 131.03 [130.30], 132.94 [132.99], 133.66 [133.55], 133.89 [134.58], 144.25 [146.90], 147.61 [147.50]. FT-IR (neat): $\tilde{\nu}$ = 3330, 2938, 1537, 1421, 1357, 1165 cm^{-1}. HRMS-FAB: calcd for $C_{19}H_{20}N_4O_8S_2Cs^+$: 628.9777; found: 628.9759.

6e: 59% yield of the oily product. ^{1}H NMR ($CDCl_3$, 400 MHz): δ = 1.69–1.81 (m, 3H), 2.03–2.23 (m, 3H), 4.43 (br s, 1H), 5.44 (d, ^3J = 5 Hz, 1H), 6.04 (dd, ^3J = 2.8, 4.8 Hz, 1H), 6.87–7.02 (m, 5H), 7.60–7.70 (m, 3H), 8.07 (d, ^3J = 7.6 Hz, 1H). ^{13}C NMR ($CDCl_3$, 400 MHz): δ = 16.27, 25.40, 30.75, 50.83, 125.73, 126.18, 126.89, 127.88, 130.58, 131.70, 132.81, 133.04, 134.02, 136.13, 139.36, 146.76. FT-IR (neat): $\tilde{\nu}$ = 3358, 2931, 1539, 1403, 1354, 1168 cm^{-1}. HRMS-FAB: calcd for $C_{18}H_{18}N_2O_4SCs^+$: 491.0042; found: 491.0055.

6g: 7% yield of the oily product. ^{1}H NMR ($CDCl_3$, 400 MHz): δ = 2.50 (ddd, ^3J = 7.9, 18.2 Hz, ^4J = 2.4 Hz, 1H), 2.75 (dd, ^3J = 5.6, 18.2 Hz, 1H), 4.27–4.34 (m, 1H), 5.50 (d, ^3J = 8.9 Hz, 1H), 6.00 (dd, ^3J = 5.1, 9.4 Hz, 1H), 6.20 (dd, ^3J = 5.5, 9.3 Hz, 1H), 7.05 (dd, ^3J = 5.5 Hz, ^4J = 2.4, 1H), 7.75–7.79 (m, 2H), 7.87–7.90 (m, 1H), 8.18–8.21 (m, 1H). ^{13}C NMR ($CDCl_3$, 400 MHz): δ = 28.64, 47.44, 51.89, 125.57, 126.26, 130.38, 130.55, 131.79, 133.03, 133.17, 133.68, 135.10, 147.35, 166.53. FT-IR (neat): $\tilde{\nu}$ = 3285, 1706, 1537, 1436, 1354, 1262, 1166 cm^{-1}. HRMS-FAB: calcd for $C_{14}H_{14}N_2O_6SNa^+$: 361.0470; found: 361.0482.

7a: 65% yield, m.p. 158–159 °C (dichloromethane/pentane). ^{1}H NMR ($CDCl_3$, 400 MHz): δ = 2.23–2.31 (m, 1H), 2.46–2.53 (m, 1H), 4.17 (q, ^3J = 6.6 Hz, 1H), 4.45 (d, ^3J = 6.5 Hz, 1H), 5.44–5.48 (m, 1H), 5.68 (br s, 1H, NH), 5.84–5.86 (m, 1H), 5.98 (br s, 1H, NH), 7.70–7.75 (m, 4H), 7.83–7.86 (m, 2H), 8.05–8.10 (m, 2H). ^{13}C NMR ($CDCl_3$, 400 MHz): δ = 37.43, 54.85, 60.22, 125.58, 128.94, 130.50, 130.67, 132.98, 133.06, 133.73, 133.79, 133.83, 134.14, 147.64, 147.77. FT-IR (KBr): $\tilde{\nu}$ = 3358, 3309, 1535, 1418, 1350, 1160 cm^{-1}. Correct elemental analysis.

7b: 29% yield. ^{1}H NMR ($CDCl_3$, 400 MHz): δ = 1.67–1.73 (m, 2H), 1.98–2.16 (m, 2H), 3.78–3.85 (m, 1H), 4.07–4.13 (m, 1H), 5.21–5.26 (m, 1H), 5.57 (d, ^3J = 9 Hz, 1H, NH), 5.73 (d, ^3J = 8.8 Hz, 1H, NH), 5.76–5.81 (m, 1H), 7.68–7.77 (m, 4H), 7.82–7.86 (m, 2H), 8.03–8.06 (m, 1H), 8.07–8.10 (m, 1H). ^{13}C NMR ($CDCl_3$, 400 MHz): δ = 22.26, 25.53, 52.35, 52.48, 124.43, 125.46, 125.52, 130.32, 130.51, 131.87, 132.98, 133.10, 133.69, 133.88, 134.06, 134.43, 147.61, 147.67. FT-IR (neat): $\tilde{\nu}$ = 3339, 1536, 1413, 1351, 1166 cm^{-1}. HRMS-FAB: calcd for $C_{18}H_{18}N_4O_8S_2Cs^+$: 614.9620; found: 614.9640.

7c: 46% yield of the crystalline product; m.p. 114–117 °C; ^{1}H NMR ($CDCl_3$, 400 MHz): δ = 1.43 (s, 3H), 1.52 (s, 3H), 3.33 (dd, ^3J = 7.2, 12.8 Hz, 1H), 3.50 (dd, ^3J = 6, 12.8 Hz, 1H), 4.93 (d, ^4J = 1.2 Hz, 1H), 5.00 (s, 1H), 5.66–5.71 (m, 2H), 7.66–7.76 (m, 4H), 7.79–7.84 (m, 2H), 7.94–7.99 (m, 1H), 8.08–8.12 (m, 1H). ^{13}C NMR ($CDCl_3$, 400 MHz): δ = 18.71, 22.96, 49.91, 62.20, 114.81, 125.16, 125.45, 130.67, 130.83, 132.66, 132.98, 133.59, 133.63, 133.87, 134.94, 143.49, 147.58, 147.80. FT-IR: $\tilde{\nu}$ = 3334, 1540, 1412, 1354, 1169 cm^{-1}. HRMS-FAB: calcd for $C_{18}H_{20}N_4O_8S_2Cs^+$: 616.9777; found: 616.9757.

6f: Isolated as less polar fraction, 17% yield of the oily product. ^{1}H NMR ($CDCl_3$, 400 MHz): δ = 1.76 (s, 3H), 3.97 (d, ^3J = 5.8 Hz, 1H), 4.98 (s, 1H), 5.00 (s, 1H), 5.13 (s, 1H), 5.15 (s, 1H), 5.53 (bt, 1H), 7.71–7.75 (m, 2H), 7.85–7.89 (m, 1H), 8.10–8.13 (m, 1H). ^{13}C NMR ($CDCl_3$, 400 MHz): δ = 20.77, 46.48, 113.69, 115.62, 125.31, 131.14, 132.75, 133.52, 133.79, 140.23, 141.82, 147.82. FT-IR (neat): $\tilde{\nu}$ = 3349, 2918, 1538, 1359, 1162 cm^{-1}.

Received: September 22, 1995 [Z8422IE]
German version: *Angew. Chem.* **1996**, *108*, 453–455

Keywords: aminations · 1,2-diaminations · Diels–Alder reactions · ene reactions · imidoselenium reagents

[1] Z.-Y. Wei, E. E. Knaus, *Synthesis* **1994**, 1463.
[2] a) P. Jain, H. M. Garraffo, T. F. Spande, H. J. C. Yeh, J. W. Daly, *J. Nat. Prod.* **1995**, *58*, 100; b) M. Reina, A. H. Merioli, R. Cabrere, A. Gonzales-Coloma, *Phytochemistry* **1995**, *38*, 355; c) Y. Genisson, M. Mehmandoust, C. Marazano, B. C. Das, *Heterocycles* **1994**, *39*, 811; d) C. M. Hill, D. P. Caiger, S. A. Pearson, A. J. Smith, L. J. Rogers, *Biochem. Soc. Trans.* **1986**, *14*, 36; e) M. Bergdahl, R. Hett, T. L. Friebe, A. R. Gangloff, J. Iqbal, Y. Wu, P. Helquist, *Tetrahedron Lett.* **1993**, *34*, 7371.
[3] E. T. Michalson, J. Szmuszkovicz, *Prog. Drug. Res.* **1989**, *33*, 135.
[4] M. T. Cox, J. J. Gormley, Ch. F. Hayward, N. N. Petter, *J. Chem. Soc. Chem. Commun.* **1980**, 800.
[5] a) R. S. Srivastava, K. M. Nicholas, *Tetrahedron Lett.* **1994**, *35*, 8739; b) *J. Org. Chem.* **1994**, *59*, 5365; c) P. Magnus, I. Coldham, *J. Am. Chem. Soc.* **1991**, *113*, 672; d) T. J. Katz, S. Shi, *J. Org. Chem.* **1994**, *59*, 8297; e) M. A. Brimble, C. H. Heathcock, *ibid.* **1993**, *58*, 5261; f) G. Kresze, H. Munsterer, *ibid.* **1983**, *48*, 3561; g) G. E. Keck, J. B. Yates, *Tetrahedron Lett.* **1979**, 4627; h) S. Tsushima, Y. Yamada, T. Onami, K. Oshima, M. O. Chaney, N. D. Jones, J. K. Swartzendruber, *Bull. Chem. Soc. Jpn.* **1989**, *62*, 1167; i) J. P. Mahy, G. Bedi, P. Battioni, D. Mansuy, *Tetrahedron Lett.* **1988**, *29*, 1927; j) M. Johannsen, K. A. Joergensen, *J. Org. Chem.* **1995**, *60*, 5979; k) R. B. Cheikh, A. Laurent, P. Mison, A. Nafti, *Synthesis* **1983**, 685; l) P. Magnus, J. Lacour, I. Coldham, B. Mugrage, W. B. Bauta, *Tetrahedron* **1995**, *51*, 11087; m) A. Uzarewicz, J. Scianowski, I. Wyzlic, *Pol. J. Chem.* **1995**, *69*, 1153; n) A. Uzarewicz, I. Wyzlic, J. Scianowski, *ibid.* **1995**, *69*, 681.
[6] a) A. Yamazaki, K. Achiwa, *Tetrahedron Asymmetry* **1995**, *6*, 51; b) B. M. Trost, E. Keinan, *J. Org. Chem.* **1979**, *44*, 3451; c) H. H. Baer, Z. S. Hanna, *Carbohydr. Res.* **1980**, *78*, C11; d) P. von Matt, O. Loiseleur, G. Koch, A. Pfaltz, C. Lefeber, T. Feucht, G. Helmchen, *Tetrahedron Asymmetry* **1994**, *5*, 573; e) J. E. Nystroem, T. Rein, J. E. Baeckvall, *Org. Synth.* **1989**, *67*, 105; f) T. Hayashi, K. Kishi, A. Yamamoto, Y. Ito, *Tetrahedron Lett.* **1990**, *31*, 1743; g) T. Hayashi, A. Yamamoto, Y. Ito, E. Nishioka, H. Miura, K. Yanagi, *J. Am. Chem. Soc.* **1989**, *111*, 6301; h) R. Tamura, L. S. Hegedus, *ibid.* **1982**, *104*, 3727; i) H. H. Baer, Z. S. Hanna, *Carbohydr. Res.* **1981**, *94*, 43; j) Y. Nishibayashi, T. Chiba, K. Ohe, S. Uemura, *J. Chem. Soc. Chem. Commun.* **1995**, 1243; k) R. G. Shea, J. F. Fitzner, J. E. Fankhauser, A. Spaltenstein, P. A. Carpino, R. M. Peevey, D. V. Pratt, B. J. Tenge, P. B. Hopkins, *J. Org. Chem.* **1986**, *51*, 5243; l) M. Mukhopadhay, M. M. Reddy, G. C. Maikap, J. Iqbal, *ibid.* **1995**, *60*, 2670.
[7] T. Fukuyama, C.-K. Jow, M. Cheung, *Tetrahedron Lett.* **1995**, *36*, 6373.
[8] K. B. Sharpless, T. Hori, L. K. Truesdale, C. O. Dietrich, *J. Am. Chem. Soc.* **1976**, *98*, 269.
[9] a) P. C. B. Page, T. J. McCarthy (Oxidation Adjacent to C=C Bonds) in *Comprehensive Organic Synthesis, Vol. 7* (Eds.: B. M. Trost, I. Fleming), Pergamon, Oxford, **1991**, p. 83; b) C. Paulmier (Oxidation Reactions) in *Selenium Reagents and Intermediates in Organic Synthesis* (Ed.: J. E. Baldwin), Pergamon, Oxford, **1986**, p. 353; c) M. A. Umbreit, K. B. Sharpless, *J. Am. Chem. Soc.* **1977**, *99*, 5526; d) K. B. Sharpless, R. F. Lauer, *ibid.* **1972**, *94*, 7154; e) D. Arigoni, A. Vasella, K. B. Sharpless, H. P. Jensen, *ibid.* **1973**, *95*, 7917; f) H. P. Jensen, K. B. Sharpless, *J. Org. Chem.* **1975**, *40*, 264; g) N. Y. Derkach, E. S. Levchenko, *Russ. Chem. Rev.* **1989**, *58*, 507; h) A. Haas, J. Kasprowski, M. Pryka, *Coord. Chem. Rev.* **1994**, *130*, 301.
[10] K. B. Sharpless, S. P. Singer, *J. Org. Chem.* **1976**, *41*, 2504.
[11] F. Bellesia, F. Ghelfi, U. M. Pagnoni, A. Pinetti, *Gazz. Chim. Ital.* **1991**, *121*, 559.
[12] a) T. Hori, K. B. Sharpless, *J. Org. Chem.* **1979**, *44*, 4204; b) T. Hori, K. B. Sharpless, *ibid.* **1979**, *44*, 4208.
[13] a) S. P. Singer, K. B. Sharpless, *J. Org. Chem.* **1978**, *43*, 1448; b) G. Fratér, U. Müller, U. Schopfer, *Tetrahedron Lett.* **1984**, *25*, 281; c) H. Hiemstra, W. J. Klaver, W. N. Speckamp, *ibid.* **1986**, *27*, 1411; d) *Recl. Trav. Chim. Pays-Bas* **1986**, *105*, 299.
[14] a) P. H. J. Carlsen, T. Katsuki, V. S. Martin, K. B. Sharpless, *J. Org. Chem.* **1981**, *46*, 3936; b) M. T. Nunez, V. S. Martin, *ibid.* **1990**, *55*, 1928.
[15] Sodium 2-nitrobenzenesulfonamide (**5**) was prepared from 2-nitrobenzenesulfonamide and NaOH in $MeOH/H_2O$, concentrated and dried under high vacuum.

 © VCH Verlagsgesellschaft mbH, D-69451 Weinheim, 1996 0570-0833/96/3504-0456 $ 15.00+.25/0

The Scent of Success?

Organosulfur Chemistry. Synthetic Aspects. Edited by *P. Page*. Academic Press, London, 1995. 277 pp., hardcover £ 55.00.—ISBN 0-12-543560-6

In almost every area of organic chemistry, from asymmetric synthesis and catalysis, through heterocyclic and dyestuffs chemistry and the synthesis and modification of natural products, to supramolecular and macromolecular chemistry, we find sulfur in a remarkably wide variety of oxidation states, coordination numbers, and bonding situations. Few other elements compare with the ability of sulfur, either in elemental form or as any of its many simple compounds, to become incorporated into organic substrates when activated thermally, chemically, or photolytically. Organosulfur chemistry is particularly well suited as an aid to fulfilling the objectives of the synthetic chemist. On the one hand sulfur compounds in the form of electrophiles, nucleophiles, or free radicals can facilitate reactions in which sulfur acts in an enabling role, while on the other hand there are many organosulfur compounds that have valuable properties in their own right. In accordance with the important role of sulfur in organic chemistry, there exist a great many monographs, specialist journals, and review articles covering the field. The book reviewed here is concerned primarily with synthetic aspects, while also dealing with some bioorganic and pharmaceutical applications of sulfur compounds. It consists of five chapters in which different classes of sulfur compounds are treated by recognized experts.

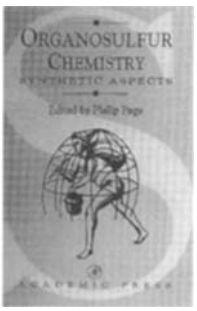

In the first chapter the authors review the use of optically active β-ketosulfoxides and analogous compounds in asymmetric synthesis. A concise survey of methods for synthesizing chiral sulfoxides is followed by descriptions of stereoselective reactions using such chiral auxiliaries. The β-ketosulfoxides are easily prepared and can be used to achieve efficient diastereoselective reductions to give β-hydroxysulfoxides, which are useful precursors for synthesizing carbinols, secondary allyl alcohols, epoxides, and lactones. Their use in total syntheses of insect pheromones, macrolides, polyhydroxylated natural products, and other compounds follows logically from this, and is described with the help of some informative reaction schemes. The next section is concerned with Diels–Alder reactions using sulfinyl compounds, which can act both as dienophiles and as dienes. As well as syntheses of enantiomerically pure sulfinyl acrylates and maleimides, several important [4+2]-cycloaddition reactions are described, some of which are catalyzed by Lewis acids. These reactions, in which the stereoselectivity has been shown to be controlled by the S=O group, yield precursors for synthesizing nucleosides and cancerostatic agents. Some representative cycloaddition reactions in which the regiochemistry is of special importance lead to interesting products such as phenols with well-defined substitution patterns, naphthoquinones and anthraquinones, and homochiral sulfinylquinones. The chapter ends with some examples of reactions of dienes that are activated by sulfinyl groups.

Chapter 2 is concerned with homolytic processes at the sulfur center, and deals in detail with reactions initiated by free radicals, which have probably been known for longer than any others. As well as the trivial case of addition to carbon–carbon multiple bonds, the discussion includes an application of these species that is especially attractive from the standpoint of organic synthesis, namely inter- and intramolecular carbon–carbon bond formation resulting from the β-elimination of thiyl and sulfonyl radicals. The importance of this method is reflected in the great variety of syntheses that are described, including transannular bond formation in cyclic polyenes, rearrangements of cyclopentane derivatives, efficient preparations of the synthetically important alkylstannanes, and Barton's *O*-acylthiohydroxamate method for attachment of side-chains to steroids. Due attention is also given to an application of thiyl radicals which has been known for more than twenty years but has only recently begun to be thoroughly investigated, namely the initiation of the cyclopropylmethyl-3-butenyl rearrangement. Following nature's example of glutathione, it has been shown that thiols can also serve as an efficient source of hydrogen atoms for quenching alkyl radicals. Another application of this reaction is in the reductive substitution of halogen atoms or OH groups, a method which is justifiably treated at some length. The next section deals with extrusion methods, emphasizing the value of sulfur-containing functional groups for mediating such reactions. As well as the cyclophane syntheses that are now well established methods, the discussion also includes modern applications such as Nicolaou's method for oxapolycyclenes. The final part of the chapter makes the point that carbon free radicals too can undergo selective reactions with organosulfur compounds. These include interesting intramolecular thiolactonization reactions and further developments based on the Barton–McCombie reaction.

Chapter 3 contains a survey of synthetic transformations involving thiiranium ions as intermediates. These cationic heterocycles with a three-membered ring, which can also be regarded as carbenium ions stabilized by β-thio groups, can undergo S_N1 or S_N2 ring-opening reactions depending on their substituents. The author gives a very good account of synthetic applications, describing how thiiranium ions formed in situ can react with a variety of nucleophiles. The methods for introducing oxy-, aza-, or carboxysulfenyl groups based on this principle are de-

This section contains book reviews and a list of new books received by the editor. Book reviews are written by invitation from the editor. Suggestions for books to be reviewed and for book reviewers are welcome. Publishers should send brochures or (better) books to Dr. Illenora Beckmann, Redaktion Angewandte Chemie, Postfach 101161, D-69451 Weinheim, Federal Republic of Germany. The editor reserves the right of selecting which books will be reviewed. Uninvited books not chosen for review will not be returned.

scribed with instructive examples; in many cases there is the additional bonus of a high degree of regio- and stereoselectivity. Some useful guidelines for predicting reactivities and cyclization routes, for example in the intramolecular etherification of unsaturated alcohols, are also included here.

Chapter 4, the longest in the book, is concerned with developments in the chemistry of 1,3-dithioacetals. This class of compounds is closely associated with "Umpolung" processes, but these are deliberately avoided in this chapter, as they are already very adequately covered elsewhere. At the beginning of the chapter is a very useful table listing review articles on 1,3-dithioacetals. Applications of these compounds in pharmacology and plant protection are then described. These include various interesting examples that act as mimetics of cyclohexane rings or as "super-*t*-butyl groups", and have applications as calcium channel blockers, leucotriene antagonists, or highly efficient insecticides. The sections on the synthesis of these compounds and their properties as functional groups are especially important from the synthetic chemist's standpoint. Various methods of synthesis are presented in the form of tables, including such details as advice on differentiating between aldehydes and ketones; analogous procedures have been used for regenerating carbonyl functions. The chapter ends with a brief section on applications in asymmetric synthesis, transformations yielding dithiins or geminally-substituted difluoro compounds, and reductions giving methylene groups.

The final chapter is devoted to thioaldehydes, and provides evidence that these are by no means birds of paradise (although thioformaldehyde has been found to occur in interstellar space!), but are useful intermediates for syntheses. Some interesting physicochemical properties of these compounds are also described. Their synthesis, properties, and reactions are treated, classifying them into transient species and stable compounds. In accordance with the chemical nature of these species, the main emphasis is on cycloadditions and their retro-variants and on sigmatropic processes. Their crystal structures and spectroscopic properties are also discussed.

Despite a few errors, especially in the reaction schemes, and some poorly drawn structural formulas, the book contains a valuable review of selected topics in organosulfur chemistry. It can be especially recommended for reading by synthetic chemists and as a source of ideas.

Rainer Beckert
Institut für Organische
und Makromolekulare Chemie
der Universität Jena (Germany)

Introduction to Biocatalysis Using Enzymes and Micro-Organisms. By *S. M. Roberts, N. J. Turner, A. J. Willetts*, and *M. K. Turner*. Cambridge University Press, Cambridge, 1995. 195 pp., hardcover £ 11.95.—ISBN 0-521-43070-4

Twenty or thirty years ago the study of biotransformations of organic substrates was still more a matter of academic interest than of practical significance, but in recent years this field has increased greatly in importance, with regard to applications and future potential. This growing recognition has been accompanied by the appearance of a huge wealth of review articles and books. The authors of this book, who are recognized experts in the field of biotransformations of organic molecules, define their aim as being "to give the non-specialist a comprehensive insight into the science of biotransformations".

The book begins with a historical introduction of about 30 pages, starting from the beginnings of modern biochemistry in the early 19th century, exemplified by the development of the technologies of brewing and fermentation processes. The scientific developments described range from the contributions of Kirchhoff and Pasteur to the work of Reichstein, and the chapter makes interesting and enjoyable reading. Chapter 2 (40 pp.) begins by describing the use of enzymes and discussing the advantages and drawbacks of this method compared with the use of whole cells. Problems of immobilizing enzymes are discussed, as well as optimization strategies. The chapter contains a wealth of useful practical advice, but stops short of being a laboratory handbook. Appendix A, which describes the breeding and cultivation of microorganisms, seems rather out of place here, and the information about sterile procedures seems somewhat trivial.

Chapter 3 (about 20 pp.) is concerned with hydrolysis, which the authors illustrate by describing examples from their own synthetic work. These examples (including syntheses of the nucleoside analogs neplanocin, carbovir, aristeromycin, and others) are certainly highly topical, but does that necessarily make them good examples for teaching purposes? The chapter ends with an explanation of the "*E*-value" introduced by C. Sih. Unfortunately, however, the bibliography does not include a reference to the original publication. Also it would have greatly helped the non-specialist readers, for whom the book is intended, if the authors had included diagrams showing the relationship between (enantiomeric excess)/(conversion rate) and enantiomer ratio.

The descriptions of the basic reactions are completed by Chapter 4 (20 pp.) on redox reactions, with many examples from the authors' own research, and Chapter 5 (also 20 pp.) on methods for forming carbon–carbon, carbon–nitrogen, carbon–oxygen, and carbon–sulfur bonds. Chapter 6 (40 pp.) describes processes for the manufacture of various important fine chemicals, including antibiotics, amino-acids, nucleic acids, peptides, and oligosaccharides, and summarizes the basic principles of genetic engineering. A separate section is devoted to "novel reaction conditions"; however, the curiosity awakened by this misleading title is soon dispelled, as one finds here only some further reactions in non-aqueous media. Hardly any applications in inorganic or organometallic chemistry are mentioned.

Much of the book is intended specifically for newcomers to the field, with the aim of encouraging them to incorporate biotransformations into the planning of their synthetic work. Nevertheless, even specialists will find here and there some useful bits of information, though unfortunately without references to the original publications. Each chapter has an appendix giving references, but only to review articles and books, and even these lists are incomplete. Both the bibliographies and the text contain annoying mistakes, which could easily have been avoided by a little more care on the part of the authors and final checking by the publishers. Already it has come to be regarded as something of an achievement to avoid incorrect spellings of names such as Liebig, which are hardly unfamiliar. The book is a useful addition to the many excellent publications covering the field of biocatalysis. It makes no claim to be comprehensive. Reading it will not make one an expert on the subject, but that was not the authors' intention. With a little more love and care it could have been a very good book; however, despite the fact that it has some shortcomings, I enjoyed reading it.

René Csuk
Institut für Organische Chemie
der Universität Halle-Wittenberg
(Germany)

 © VCH Verlagsgesellschaft mbH, D-69451 Weinheim, 1996 0570-0833/96/3504-0458 $ 15.00+.25/0

Metallomesogens. Synthesis, Properties, and Applications. Edited by **J. L. Serrano.** VCH, Weinheim/New York, **1996.** 498 pp., hardcover, DM 298.00.—ISBN 3-527-29296-9

Active Metals. Preparation, Characterization, Applications. Edited by **A. Fürstner.** VCH, Weinheim/New York, **1996.** 464 pp., hardcover, DM 248.00.—ISBN 3-527-29207-1

Modelling Molecular Structures. By **A. Hinchliffe.** Wiley, Chichester, **1996.** 256 pp, paperback, £ 24.95.—ISBN 0-471-95923-5

Fundamentals of Chemical Kinetics. By **S. R. Logan.** Longman, Harlow, **1996.** 264 pp., paperback, 264 pp., £ 19.99. ISBN 0-582-25185-0

Solving Problems with NMR Spectroscopy. By **Atta-ur-Rahman, M. I. Choudhary.** Academic Press, New York, **1996.** 430 pp., softcover, $ 34.95.—ISBN 0-12-066320-1

Anorganische Chemie. Prinzipien von Struktur und Reaktivität. 2nd edition. By **J. E. Huheey, E. A. Keiter, R. L. Keiter.** De Gruyter, Berlin, **1995.** 1261 pp., hardcover, DM 158.00. ISBN 3-11-013557-4

Umweltbiochemie. By **J. Berndt.** Fischer, Stuttgart, **1995.** 278 pp, paperback, DM 34.80.—ISBN 3-8252-2838-4

Advances in Inorganic Chemistry. Vol. 42. Edited by **A. G. Sykes.** Academic Press, San Diego, **1995.** 408 pp., hardcover, $ 99.00. ISBN 0-12-023642-7

Das Buch des Umweltmanagements. Schitag Ernst & Young, VCH, Weinheim, **1995.** 298 pp., hardcover, DM 98.00. ISBN 3-527-28734-5

Compendium of Terminology and Nomenclature of Properties in Clinical Laboratory Sciences. (Recommendations 1995). By **J. C. Rigg et al.** Blackwell Science, Oxford, **1995.** 290 pp., paperback, £ 18.95.—ISBN 0-86542-612-0

Spektroskopische Methoden in der organischen Chemie. Fifth revised edition. By **M. Hesse, H. Meier, B. Zeeh.** Georg Thieme Verlag, Stuttgart, **1995.** 364 pp., paperback, DM 82.00. ISBN 3-13-576105-3

Inductively Coupled and Microwave Induced Plasma Sources for Mass Spectrometry. By **E. H. Evans et al.** Royal Society of Chemistry, Cambridge, **1995.** 108 pp, hardcover, £ 32.50. ISBN 0-85404-560-0

Palladium Reagents and Catalysts. Innovations in Organic Synthesis. By **J. Tsuji.** Wiley, Chichester, **1995.** 560 pp., hardcover, £ 125.00.—ISBN 0-471-95483-7

Multidimensional Spectroscopy of Polymers: Vibrational, NMR, and Fluorescence Techniques. ACS Symposium Series No. 598. Edited by **M. W. Urban, T. Provder.** American Chemical Society, Washington, **1995.** 616 pp., hardcover, $ 139.95.—ISBN 0-8412-3262-8

Fire and Polymers II: Materials and Tests for Hazard Prevention. ACS Symposium Series No. 599. Edited by **G. L. Nelson.** American Chemical Society, Washington, **1995.** 672 pp., hardcover, $ 129.95.—ISBN 0-8412-3231-8

Explosivstoffe. 8th revised edition. By **J. Köhler, R. Meyer.** VCH, Weinheim, **1995.** 436 pp., DM 165.00.—ISBN 3-527-28641-1

IIC Studies. Studies in Industrial Property and Copyright Law. (Published by the Max Planck Institute for Foreign and Inter-national Patent, Copyright and Competition Law, Munich) Vol. 16. Experimental Use and Patents. By **D. Gilat.** VCH, Weinheim, **1995.** 141 pp., paperback, DM 128.00.—ISBN 3-527-28660-8

Ullmann's Encyclopedia of Industrial Chemistry. Index to Vols. A1 to A25, B1 to B6. Fifth Completely Revised Edition. Edited by **B. Elvers, S. Hawkins, W. Russey, M. Pikart-Müller.** VCH, Weinheim, **1995.** 626 pp., paperback, DM 295.00.—ISBN 3-527-20 149-1

Ullmann's Encyclopedia of Industrial Chemistry. Vol. A26. Surgical Materials to Thiourea. Fifth Completely Revised Edition. Edited by **B. Elvers, S. Hawkins, W. Russey.** VCH, Weinheim, **1995.** 815 pp., hardcover, DM 625.00.—ISBN 3-527-20126-2

Ullmann's Encyclopedia of Industrial Chemistry. Index on CD Rom. VCH, Weinheim, **1995.** DM 248.00.—ISBN 3-527-20153-X

Sicherer Umgang mit Gefahrstoffen. Sachkunde für Naturwissen-schaftler. By **H. F. Bender.** VCH, Weinheim, **1995.** 233 pp., paperback, DM 59.00.—ISBN 3-527-28742-6

Electric Field Applications in Chromatography, Industrial and Chemical Processes. Edited by **T. Tsuda.** VCH, Weinheim, **1995.** 311 pp., hardcover, DM 260.00.—ISBN 3-527-28687-X

Sensors. Vol. 8. (Micro- and Nano-sensor Technology/Trends in Sensor Markets). Volume Editors: **H. Meixner, R. Jones.**

A Comprehensive Survey. Edited by **W. Göpel, J. Hesse, J. N. Zemel.**

VCH, Weinheim, **1995.** 565 pp., hardcover, DM 410.00.—ISBN 3-527-26774-3

Advances in Electrochemical Science and Engineering. Vol. 4. Edited by **H. Gerischer, C. W. Tobias.** VCH Weinheim, **1995.** 430 pp., hardcover, DM 248.00.—ISBN 3-527-29205-5

Quality Assurance in Analytical Chemistry. By **W. Funk, V. Dammann, G. Donnevert.** VCH Weinheim/New York, **1995.** 238 pp., hardcover, DM 125.00.—ISBN 3-527-28668-3

The Neem Tree. Source of Unique Natural Products for Integrated Pest Management, Medicine, Industry and Other Purposes. Edited by **H. Schmutterer.** VCH, Weinheim, **1995.** 696 pp., hardcover, DM 198.00.—ISBN 3-527-30054-6

Organic Synthesis Highlights II. Edited by **H. Waldmann.** VCH, Weinheim/New York, **1995.** 407 pp., hardcover, DM 148.00. ISBN 3-527-29200-4

The Extraordinary Chemistry of Ordinary Things. 2nd Edition. By **C. H. Snyder.** John Wiley, Chichester, **1995.** 656 pp., paperback, £ 28.50.—ISBN 0-471-11157-0

Dynamics of Solutions and Fluid Mixtures by NMR. Edited by **J.-J. Delpuech.** John Wiley, Chichester, **1995.** 587 pp., hardcover, £ 70.00.—ISBN 0-471-95411-X

Introduction to nonlinear science. By **G. Nicolis.** Cambridge University Press, Cambridge, **1995.** 254 pp., paperback, £ 13.95.—ISBN 0-521-46782-9

Monosaccharides. Their Chemistry and Their Roles in Natural Products. By **P. M. Collins, R. J. Ferrier.** John Wiley, Chichester **1995.** 574 pp., paperback, £ 22.50.—ISBN 0-471-95343-1

Biotransformations in Organic Chemistry. A Textbook. By **K. Faber.** Springer-Verlag, Berlin, **1995.** 356 pp., paperback, DM 58.00.—ISBN 3-540-58503-6

Chemometrics. Experimental Design. By **E. Morgan.** John Wiley, Chichester, **1995.** 294 pp., paperback, £ 19.50.—ISBN 0-471-95832-8

Practical Organic Mass Spectrometry. 2nd Edition. A Guide for Chemical and Biochemical Analysis. By **J. R. Chapman.** John Wiley, Chichester, **1995.** 344 pp., paperback, £ 18.95.—ISBN 0-471-95831-X

Das Qualitätssicherungs-Handbuch im Labor. Ein Leitfaden zur Erstellung. By **K. Söhngen.** Springer-Verlag, Berlin, **1995.** 172 pp., hardcover, DM 78.00.—ISBN 3-540-59124-9

Iron-Sulfur Proteins/Perovskites. Structure and Bonding. Vol. 83. Edited by **M. J. Clarke et al.** Springer-Verlag, Berlin, **1995.** 100 pp., hardcover, DM 99.00.—ISBN 3-540-59105-2

Synthesis and Photosynthesis. Advances in Polymer Science. Vol. 123. Edited by **A. Abe et al.** Springer-Verlag, Berlin, **1995.** 255 pp., hardcover, DM 238.00.—ISBN 3-540-58908-2

Aroma Biotechnology. By **R. G. Berger.** Springer-Verlag, Berlin, **1995.** 240 pp., hardcover, DM 186.00.—ISBN 3-540-58606-7

Qualitätive Anorganische Analyse. Ein Begleitbuch für Theorie und Praxis. By **E. Gerdes.** Vieweg, Wiesbaden, **1995.** 295 pp., paperback, DM 32.00.—ISBN 3-528-06667-9

Overlap Determinant Method in the Theory of Pericyclic Reactions. Lecture Notes in Chemistry. Vol. 65. By **R. Ponec.** Springer-Verlag, Berlin, **1995.** 126 pp., paperback, DM 48.00.—ISBN 3-540-59189-3

Biochemische Labormethoden. By **M. Holtzhauer.** Springer-Verlag, Berlin, **1995.** 249 pp., paperback, DM 48.00.—ISBN 3-540-58584-2

Bioelectrochemistry: General Introduction. Edited by **S. R. Caplan, I. R. Miller, G. Milazzo.** Birkhäuser Verlag, Basel, **1995.** 384 pp., hardcover, $ 148.00.—ISBN 3-7643-2687-5

Process Engineering Handbook Series. Solids/Liquids Separation. By **P. N. Cheremisinoff.** Technomic, Basel, **1995.** 400 pp., paperback, SFr. 93.00.—ISBN 1-56676-246-4

Mobile Umweltanalytik. By **G. Schwedt.** Vogel, Würzburg, **1994.** 187 pp., hardcover, DM 49.00.—ISBN 3-8023-1529

Organic Photoreceptors for Imaging Systems. Optical Engineering Series 39. By **P. M. Borsenberger, D. S. Weiss.** Marcel Dekker, New York, **1995.** 472 pp., hardcover, $ 150.00.—ISBN 0-8247-8926-1

Polymers for Lightwave and Integrated Optics. Technology and Applications. Optical Engineering Series 32. Edited by **L. A. Hornak.** Marcel Dekker, New York, **1995.** 768 pp., hardcover, $ 165.00. ISBN 0-8247-8697-1

Thin Films for Optical Systems. Optical Engineering Series 49. Edited by **F. R. Flory.** Marcel Dekker, New York, **1995.** 616 pp., hardcover, $ 165.00.—ISBN 0-8247-9633-0

The Synergy Between Dynamics and Reactivity at Clusters and Surfaces. Edited by **L. J. Farrugia.** Kluwer, Dordrecht, **1995.** 376 pp., hardcover, $ 184.00.—ISBN 0-7923-3522-8

Structure and Dynamics of Atoms and Molecules: Conceptual Trends. Edited by **J. L. Calais, E. S. Kryachko.** Kluwer, Dordrecht, **1995.** 288 pp., hardcover, $ 120.00.—ISBN 0-7923-3388-8

Theoretical Aspects of Homogeneous Catalysis. Applications of Ab Initio Molecular Orbital Theory. Edited by **P. W. N. M. von Leeuwen, K. Morokuma, J. H. van Lenthe.** Kluwer, Dordrecht, **1995.** 216 pp., hardcover, $ 109.00.—ISBN 0-7923-3107-9

Mathematische Einführung in die Thermodynamik der Gemische. By **I. Aavatsmark.** Akademie Verlag, Berlin, **1995.** 171 pp., paperback, DM 48.00.—ISBN 3-05-501662-9

Englisch-Deutsches Wörterbuch der Industriellen Werkstofftechnik. By **C. Goetzel, U. Goetzel.** Carl Hanser, München, **1995.** 754 pp., hardcover, DM 198.00.—ISBN 3-446-17531-8

Diazo Chemistry II. Aliphatic, Inorganic and Organometallic Compounds. By **H. Zollinger.** VCH, Weinheim/New York, **1995.** 522 pp., hardcover, DM 198.00.—ISBN 3-527-29222-5

The Schenck Ene Reaction: Diastereoselective Oxyfunctionalization with Singlet Oxygen in Synthetic Applications**

Michael Prein and Waldemar Adam*

Dedicated to Professor Georg O. Schenck on the occasion of his 80th birthday

Oxyfunctionalized molecules are principal building blocks in organic synthesis. In cellular processes highly efficient enzymes serve as selective catalysts for the formation of such synthetic units, for example the oxygenases oxyfunctionalize substrates by activating molecular oxygen. To date no comparable effective chemical oxidation system has been found. A useful photochemical process is the oxyfunctionalization of allylic substrates by sensitized photooxygenation, for which molecular oxygen and light serve as natural sources. This allylic oxidation of olefins by the ene reaction with singlet oxygen (Schenck reaction) figures as a highly versatile synthetic method. While the regioselectivity of this transformation has been studied for decades, only during the last years has attention focused on stereocontrol. Through these recent efforts it has become possible to control high stereoselectivity in the photooxygenation of organic substrates. This breakthrough has enhanced substantially the utility of singlet oxygen in diastereoselective synthesis.

Keywords: asymmetric syntheses · ene reactions · oxygenations · Schenck reactions · singlet oxygen

1. Sensitized Photooxygenation

1.1. General Aspects

The reaction of organic substrates with molecular oxygen, the most abundant and accessible oxidant, has always been an attractive method for the preparation of oxyfunctionalized target molecules. Since molecular oxygen exists in a triplet ground state ($^3O_2$), the spin conservation rule restricts its transformations to radical-type reactions, which are normally quite unselective.[1] In contrast, in its singlet excited state, O_2 ($^1\Delta_g$) circumvents the problem of spin-forbidden reactions and, consequently, selective novel cycloadditions become possible, which complement in a useful way the activation of dioxygen by metal complexes.[2] Besides the chemical generation of singlet oxygen,[3-5] photosensitization of triplet molecular oxygen by visible light is by far the most common and convenient method for in situ generation of this highly reactive, yet selective oxidant.

In the past there has been considerable dispute about the nature of the species involved in sensitized photooxygenation.[6] This, unfortunately, has at times distracted attention from the synthetic utility of reactions with singlet oxygen, although the experimental setup for photooxygenation is quite straightforward and the workup and product isolation often entails merely evaporation of the solvent. Selective oxidations combined with the practical simplicity render sensitized photooxygenation a most attractive method for the synthetic chemist.

During the last two decades three monographs[7-9] and several review articles[10-14] have appeared on reactions of singlet oxygen in synthesis. The majority of the $^1O_2$ reactions with olefins can be divided into three major groups according to their pathways (Scheme 1): 1) conjugated dienes react preferably

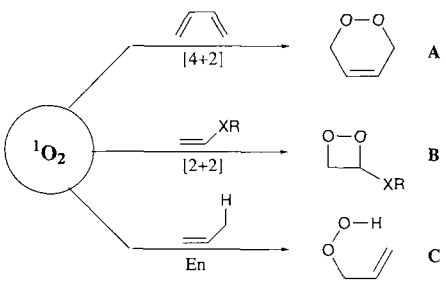

Scheme 1. Reactions of singlet oxygen.

by [4+2] cycloaddition to form endoperoxides (pathway A),[15-17] 2) electron-rich olefins give preferably 1,2-dioxetanes by the [2+2] cycloaddition (pathway B),[9,16,18] and 3) unactivated olefins with allylic hydrogen atoms undergo ene-type reaction to form allylic hydroperoxides (pathway C).[10,19] This review will focus on the stereoselectivity of the latter reaction type, for synthetic applications the most important reaction with singlet oxygen, and provide an updated mechanistic rationalization of the observed experimental results.

[*] Prof. Dr. W. Adam, Dr. M. Prein
Institut für Organische Chemie der Universität
Am Hubland, D-97074 Würzburg (Germany)
Fax: Int. code + (931)888-4756
e-mail: adam@vax.rz.uni-wuerzburg.d400.de

[**] Parts of this review were presented at the meeting of the German Chemical Society (Photochemistry Section) in November 1993.

 © VCH Verlagsgesellschaft mbH, D-69451 Weinheim, 1996 0570-0833/96/3505-0477 $ 15.00+.25/0

1.2. The Schenck Reaction

1.2.1. General Aspects

The ene reaction with singlet oxygen was discovered in 1943 by Schenck,[20] many years after the classical [4+2] cycloaddition,[21] but before the [2+2] cycloaddition, which affords 1,2-dioxetanes.[22] Schenck called this type of hydroperoxidation reaction the "indirect substitutive addition in the allylic position";[23] later it was termed the "Schenck reaction" by Schönberg,[24] although this recognition of its discoverer has not received widespread support.

The allylic hydroperoxides that result from the Schenck reaction have proven to be synthetically useful intermediates (Scheme 2).[9,12,13,25] While reduction leads to allylic alcohols,

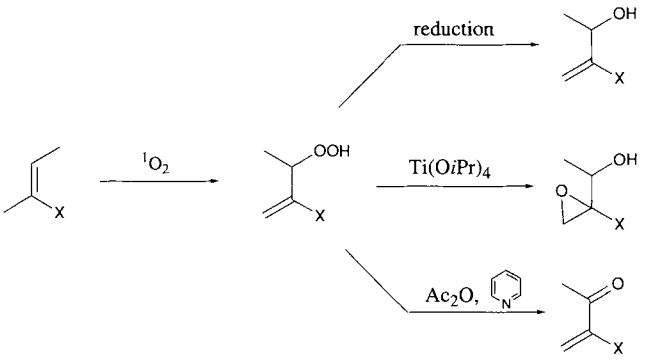

Scheme 2. Synthetic applications of allylic hydroperoxides.

the reaction with Ti^{IV} complexes has been utilized to prepare epoxy alcohols from simple olefins in a one-pot operation.[26,27] Finally, dehydration[28] provides convenient access to synthetically useful enones with silicon ($X = SiR_3$)[29] or tin substituents ($X = SnR_3$)[30] at the α-C atom.

1.2.2. Mechanism

Over the years a diversity of mechanisms has been proposed to account for the complex structure–reactivity relationships of the Schenck reaction (Fig. 1). Depending on the rigor of the

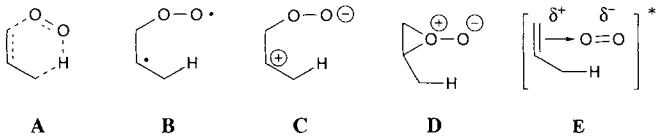

Fig. 1. Possible transition states and intermediates for the Schenck reaction.

theoretical work, arguments in favor of the concerted pathway via the transition state **A**[31] and stepwise mechanisms via the biradical intermediate **B**[32] or the perepoxide-like intermediate **D**[33] have been proposed. This reflects a general problem in scrutinizing reactions of electronically excited molecules such as singlet oxygen by theoretical methods[34] and obliges the mechanistic chemist to rely mainly on experimental data. Although much research has been dedicated to this mechanistic enigma,[7–9,35–42] discussions in this review will be limited to points relevant to understanding the stereoselectivity of the Schenck reaction.

Kinetic data[36,37] clearly favor a stepwise mechanism, while the recognized suprafacial nature[36,39] and the lack of Markovnikov orientation[38] rule out the intermediacy of longer-lived diradical (Fig. 1, **B**) or zwitterionic (Fig. 1, **C**) intermediates. Most experimental data accumulated so far suggest that a bona fide perepoxide **D** or a exciplex **E** of similar geometry occur along the reaction coordinate.[35,36,40,41] The perepoxide intermediate was proposed as early as 1960 by Sharp.[43] The exciplex constitutes an excited state charge transfer complex between singlet oxygen and the substrate, for which on the basis of experimental kinetic data reversible formation has been argued.[41,42]

Waldemar Adam was born in the Ukraine in 1937. He studied chemistry at the University of Illinois in Chicago and the Massachusetts Institute of Technology. In 1961 he received his Ph. D. degree with the thesis "The Diacyl Peroxide–Olefin Reaction" under the direction of Prof. F. D. Greene. In 1962 he carried out postdoctoral research with Prof. R. Criegee at the University of Karlsruhe. In 1961 he was appointed Assistant Professor at the University of Puerto Rico, where he was promoted to Associate Professor in 1965 and Professor in 1970. Since 1980 he has held the Chair of Organic Chemistry at the University of Würzburg. His main research interest is physical organic chemistry with emphasis on high-energy molecules (dioxetanes and dioxiranes), chemi- and bioluminescence, the photobiological oxidation of DNA, laser chemistry, high-spin systems (di- and polyradicals), the application of peroxides and singlet oxygen in organic synthesis, and enzyme- and metal-catalyzed oxyfunctionalization.

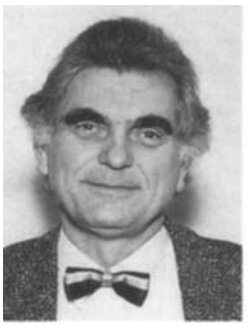
W. Adam

M. Prein

Michael Prein, born in Bad Kissingen (Germany) in 1967, studied chemistry at the University of Würzburg. He received his "Diplom" in 1992 and his doctor's degree in March 1995 with the dissertation "Diastereoselectivity of the [4+2] Cycloaddition of Singlet Oxygen" under the direction of Prof. Adam. At present he is with Prof. Padwa at Emory University, Atlanta, GA (USA), as a NATO postdoctoral fellow. His research interests are cycloadditions and stereochemistry.

1.2.3. Regioselectivity

Since singlet oxygen is a highly reactive oxidant that undergoes reactions with a wide variety of substrates, selectivity in its transformations is mandatory for synthetic utility. A central problem of the Schenck reaction is that of regioselectivity. When a given substrate has several allylic hydrogen atoms, abstraction can take place at all possible sites to lead to complex mixtures of isomeric products. This problem has been studied intensively over the years and several empirical rules have been proposed to allow the a priori determination of the regioselectivity of reactions with a variety of substrates. For example, the "*cis* effect" describes the finding that H abstraction takes place preferably at the more highly substituted side of the double bond (Fig. 2a).[44] The "*gem* effect" applies to *gem*-substituted

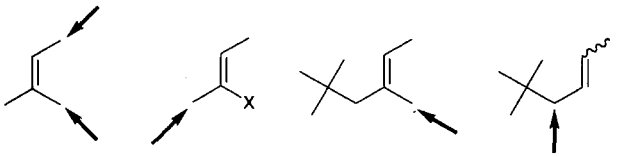

a) *cis* effect b) *gem* effect c) "large group nonbonding effect"

Fig. 2. Regioselectivity of the Schenck reaction.

olefins (X = C(O)R, SO_xR, CN, SiR_3, SnR_3, Ph), for which abstraction at the geminal position predominates (Fig. 2b).[45–48] The "*large group nonbonding effect*",[49] the least general of the regioselectivity rules, describes the preferred site of abstraction for highly substituted olefins (Fig. 2c). Nevertheless, while some progress has been made recently in controlling the regioselectivity of the Schenck reaction, it is important to emphasize that the complexities of the regioselectivity also influence the stereoselectivity of this reaction.

1.2.4. Stereoselectivity

Owing to the inherent lack of stereochemical features in the linear diatomic singlet oxygen molecule, stereoselectivity in the Schenck reaction is directed by the substrate; reactions of this type have been reviewed recently in detail.[50] The presence of two diastereotopic faces in a given chiral substrate allows for two diastereomeric transition states of different energies in the attack of singlet oxygen. In the product-forming step, hydrogen abstraction takes place either at the neighboring alkyl group or directly at the stereogenic center. In the latter case the stereochemistry of the resulting double bond reflects the π-facial selectivity of the initial singlet oxygen attack, provided suprafacial attack applies (Scheme 3). The latter requirement has been examined by Stephenson et al. with the cleverly designed substrate **1**.[39] In the photooxygenation of the optically active olefin **1** the observed products [H]-**2** and [D]-**2** (Scheme 4) differ in the absolute configuration at the newly formed stereogenic center. These stereochemical results clearly demonstrate the suprafacial attack of singlet oxygen, as exhibited in the transition states [D]-$\mathbf{2}^+$ and [H]-$\mathbf{2}^+$. The present case also exhibits another stereochemical feature of the Schenck reaction, namely that for hydrogen abstraction at a prochiral center (Scheme 3, $R^1 = H$) the *E* isomer of the two possible products generally prevails for

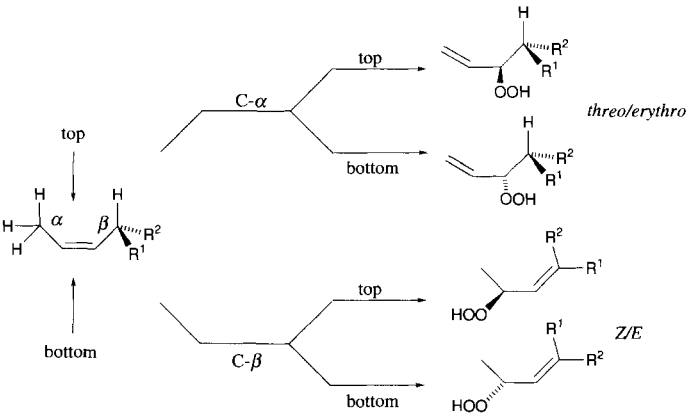

Scheme 3. Stereochemical possibilities for chiral substrates in the Schenck reaction.

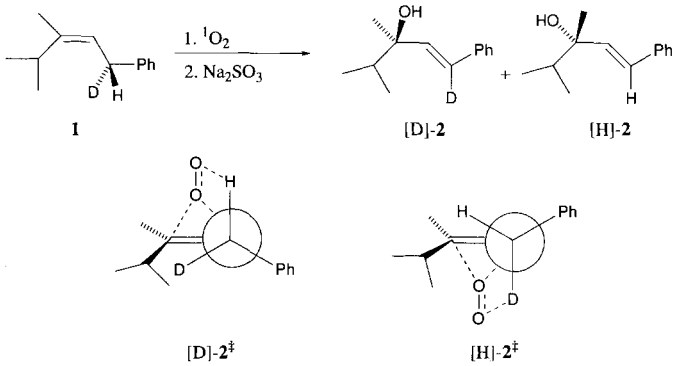

Scheme 4. Suprafacial attack of singlet oxygen in the Schenck reaction.

steric reasons. In the present review we will concentrate on ene reactions with singlet oxygen in which the original stereogenic center is maintained throughout the reaction; in other words, hydrogen abstraction takes place at a neighboring alkyl group with formation of an additional stereogenic center and shift of the double bond (Scheme 3). This pathway predominates in most Schenck reactions. Since the highly functionalized products of this transformation are very useful in synthesis, it is most desirable to find novel methods for their highly diastereoselective preparation.

The factors governing π-facial selectivity can be divided into four distinct types (Fig. 3), which we shall discuss and illustrate in detail. In the case of steric control (Fig. 3a), nonbonding repulsion between substrate and reagent makes one π face of the double bond more accessible to the attacking singlet oxygen than the other. This type of interaction is present in all types of substrates and should show little or no solvent dependence. This stereocontrol is expected to be most important for rigid systems

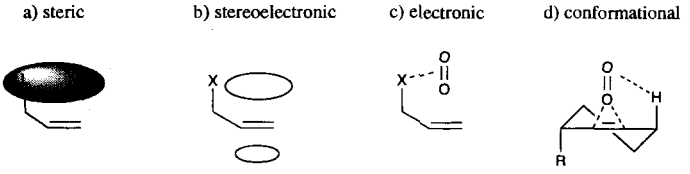

Fig. 3. Factors that determine diastereoselectivity in the Schenck reaction. a) Nonbonding interactions: repulsion, b) electron density: attraction or repulsion; c) direct interaction with substituents: attraction or repulsion; d) availability of abstractable hydrogen atoms.

(cyclic and polycyclic substrates), which cannot adjust their conformations to minimize steric interactions.

Such repulsive interactions between the reaction partners can be modulated by stereoelectronic and electronic factors. Although in this context the distinction between these two factors is not clearcut, we use the term "stereoelectronic control" (Fig. 3b) to describe those cases in which one face of the substrate displays a higher π electron density due to special features of the overall geometry of the substrate molecule, for instance orbital distortion. In contrast, the term "electronic control" (Fig. 3c) describes specific interactions between a substituent of the substrate and the incoming singlet oxygen enophile. This includes attractive hydrogen bonding interactions and electrostatic attractions and repulsions. Thus, ene reactions with singlet oxygen, which are controlled primarily by electronic factors, are expected to be highly sensitive to solvent polarity.[50]

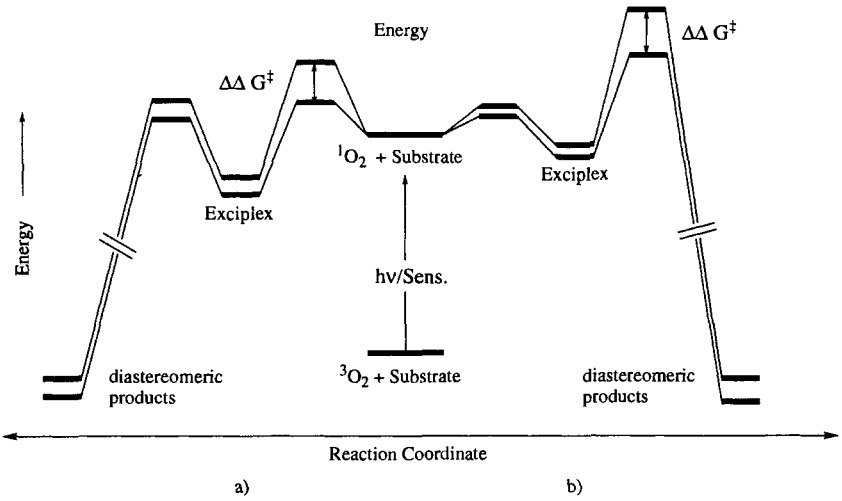

Fig. 4. Energy profiles for the Schenck reaction of chiral substrates. a) Formation of the exciplex determines the diastereoselectivity; b) formation of the exciplex is reversible; the subsequent step leading to the perepoxide or directly to the product determines the diastereoselectivity.

While the three stereocontrolling factors presented so far apply to a wide variety of substrate-directed reactions, the special features of the Schenck reaction make it necessary to include an additional mechanistic criterion, namely conformational features (Fig. 3d). Since the product-forming step involves abstraction of an allylic hydrogen atom, which must not only be present in the substrate molecule but also aligned correctly, conformational control may play a dominant role (Fig. 3d). This is expected to be important especially in cyclic systems, in which allylic hydrogen atoms may be accessible only on one π face of the substrate, and, therefore, express a pronounced influence on the observed stereoselectivity. Since the most suitable geometry for effective hydrogen atom abstraction requires a perpendicular arrangement of the C–H bond with respect to the plane passing through the four atoms attached to the double bond (the plane of the double bond), subtle conformational features may be decisive factors. These stereocontrolling factors alone make understanding the experimental stereoselectivities of the Schenck reaction quite complex. Further complexity, however, derives from the fact that along the reaction coordinate a reversible step has been postulated, which on the basis of kinetic data has been ascribed to exciplex formation between singlet oxygen (electronically excited) and the olefinic substrate.[42]

The postulated energy profile of the Schenck reaction incorporating reversible exciplex formation is featured in Figure 4. Exciplex formation proceeds with a nearly zero activation enthalpy and is thus controlled by the entropy of activation. Therefore, the stereoselectivity of the ene reaction appears to be determined by the difference in activation energies for the subsequent transformation of the reversible, diastereomeric exciplexes (Fig. 4, right). For some substrates this step may proceed directly to the products or proceed via perepoxide intermediates.[35] For the mechanistic rationalization of π-facial selectivity, this distinction is not particulary relevant since perepoxide formation is quite late along the reaction coordinate. Furthermore, even if formation of the perepoxide were reversible, similar geometrical and electronic features for the exciplexes and the corresponding perepoxide intermediates would be expected, which would lead to the same sense of stereoselectivity.

Since the formation of the exciplex is fast and reversible, the situation displayed on the left side of Figure 4 is much less likely, namely the π-facial selectivity in the initial encounter of singlet oxygen and the olefinic substrate to form diastereomeric exciplexes will in most cases not directly determine the final diastereomeric ratio. Nevertheless, one should bear in mind that also the subsequent step from the exciplex to the products, or even through possible perepoxide intermediates, may be quite fast. Consequently, when exciplex formation is not completely reversible, it may also influence π-facial selectivity.[51]

We will analyze the observed diastereoselectivities of the Schenck reaction in terms of the electronic and geometric characteristics (Fig. 3) of the exciplex. However, for ene reactions with high overall reaction rates, ground state properties of the substrate will also have to be taken into consideration, if subtle features are to be understood mechanistically. Since the exciplex and the corresponding perepoxide have apparent structural similarities, rationalizing the selectivity-determining factors may be facilitated by considering the characteristics of the perepoxide.

2. Diastereoselectivity in the Schenck Reaction: Case Studies

The consideration of the general factors that may influence the diastereoselectivity in the Schenck reaction (Section 1) showed that a rather complex situation can be expected when one tries to find a common rationalization of the experimental results for diverse substrates. Fortunately, at least in most cases, the experimental conditions (solvent, sensitizer, light source) have little or no effect on the diastereoselectivities. Moreover, the photooxygenations have been conducted under a variety of experimental conditions; in the older literature, in particular, exact reaction conditions (light source, reaction time) are rarely described. Therefore, in this review we will generally not give

exact reaction conditions for the particular photooxygenations but will refer to the reactant as $^1O_2$, whereby it is understood that the $^1\Delta_g$ electronic state is involved. However, for reactions in which the diastereoselectivity depends strongly on the reaction conditions (especially solvent effects), these will be given and discussed explicitly.

It should be also noted that some of the diastereomeric ratios reported in the literature were determined either after purification of the initial crude product mixture by column chromatography or after reduction of the labile hydroperoxides to the corresponding alcohols, a reaction that generally occurs in nearly quantitative yields and with complete retention of configuration. Therefore, the values reported here may not in all cases reflect the exact diastereoselectivity for the initial attack of singlet oxygen; however, the deviations are expected to be generally quite small.

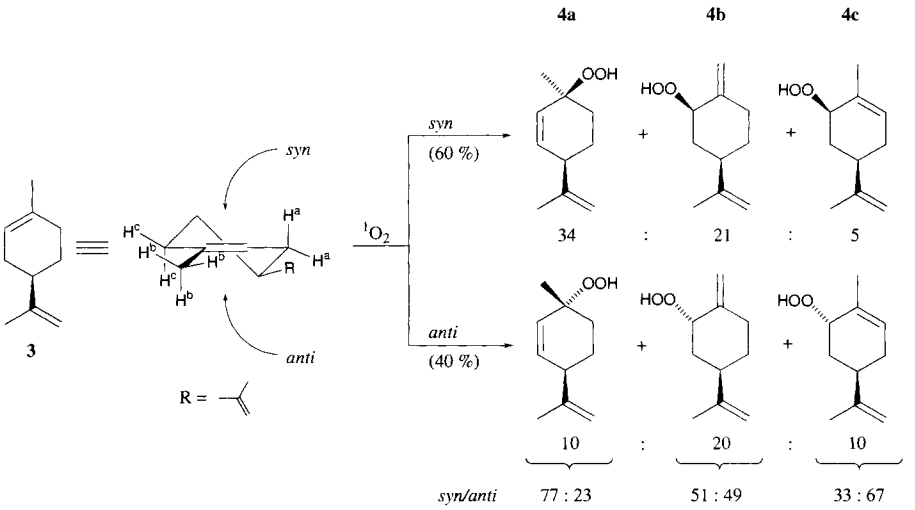

Scheme 5. Schenck reaction of (+)-limonene (**3**).

As mentioned in Section 1.2.4, the ene reaction with singlet oxygen is a substrate-controlled reaction and, therefore, any attempted classification should concentrate on common features of the olefin substrates employed. Whereas the photooxygenation of chiral mono- and polycyclic olefins has been studied ever since the very discovery of the Schenck reaction in 1943, recent results from our group have shown convincingly that high stereocontrol can be achieved in open-chain systems as well. Stereocontrol in reactions of cyclic and polycyclic substrates and that in transformations of acyclic substrates appear to stem from quite different structural features. Whereas through the inherent rigidity of cyclic and polycyclic substrates steric and stereoelectronic effects will principally determine π-facial selectivity, for open-chain olefins electronic interactions take the dominant role in controlling diastereoselectivity. In view of this marked difference between cyclic and acyclic systems, the classification of the olefinic substrates according to this structural feature is convenient on mechanistic grounds.

2.1. Cyclic Olefins

2.1.1. Monocyclic Hydrocarbons

This class of substrates, for which the monoterpenes are good prototypes, was studied by Schenck et al. as far back as 1943. The lack of heteroatom substituents restricts the factors that may influence the diastereoselectivity to steric and conformational effects. One prominent representative is (+)-limonene (**3**), which gives on photooxygenation a mixture of regio- and diastereomeric hydroperoxides **4** in very characteristic ratios (Scheme 5).[52] Historically pertinent, this olefin was used to prove the involvement of singlet oxygen in oxygenation reactions and to rule out radical pathways.[53]

On inspection of the data in Scheme 5, it is evident that there is little overall *syn*/*anti* selectivity (60:40). This is expected since there seems to be no special steric preference for attack from either side of the double bond in the substrate. Nevertheless, if one looks at the regioisomeric hydroperoxides **4a–c** in detail, remarkable differences in the diastereoselectivity become apparent. The observed diastereoselectivity can be explained by the previously discussed preference for abstraction of hydrogen atoms perpendicular to the plane of the double bond (Fig. 3d). Therefore, with the assumption of the preferred ground state conformation displayed in Scheme 5, abstraction of atom H^a should occur preferentially from the *syn* face. Indeed, for the corresponding hydroperoxides **4a** a notable 77:23 *syn*/*anti* preference was found. For abstration of H^c, the opposite applies (67:33 *anti*/*syn* preference for **4c**), while for abstraction at the methyl group, which is conformationally not fixed, abstraction from either face is equally likely. Once the preferences for *syn* and *anti* attack are estimated, the regioselectivity of the abstraction can be examined. An alternative interpretation of the limonene results is to consider the reversible formation of an exciplex intermediate. Stereocontrolled attack of singlet oxygen would be expected to occur from that π face which bears the *better* set of abstractable allylic hydrogen atoms. That this may indeed have a remarkable influence on π-facial selectivity will become evident in Section 2.1.2.

There are numerous other examples for the photooxygenation of monoterpenes without heteroatom substituents,[8–11,54,55] but the general trend shows that low overall *syn*/*anti* selectivities are obtained for substrates in which the double bond is in a six-membered ring. Furthermore, the ground state conformation, specifically the availability of abstractable allylic hydrogen atoms, has a remarkable effect on the diastereoselectivity in many cases.

2.1.2. Bi- and Polycyclic Hydrocarbons

As we have seen, the Schenck reaction of monocyclic olefins shows complex stereoselectivity with little if any overall *syn*/*anti* preference. The photooxygenation of the bicyclic octalene **5** (Scheme 6) shows similar stereoselectivity.[56] Here, too, slight changes in the substitution pattern alter the distribution of both regio- and stereoisomeric products, but the deciding factors are interconnected so subtly that the selectivities are difficult to rationalize mechanistically. The 4a-methyl group seems to block

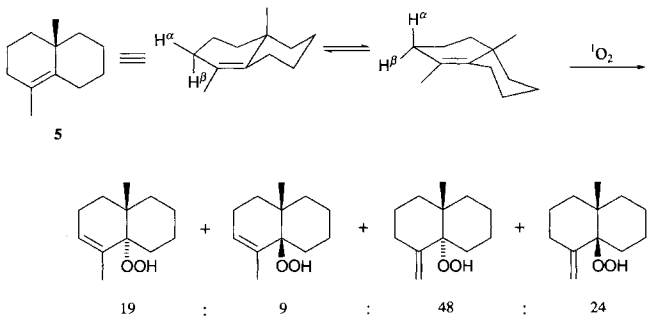

Scheme 6. Schenck reaction of 1,10-dimethyl-1(9)-octalene (**5**).

the β face to some extent, and a slight overall preference (67:33) for the less shielded α face is found. The diastereoselectivity in the photooxygenation of steroids is also governed mainly by steric shielding through angular methyl substituents.[57–59] Furthermore, the rigid conformation of these substrates plays an important role with regard to π-facial selectivity, since hydrogen atoms perpendicular to the plane of the double bond may be accessible from only one π face.

Similar selectivity control is expected for [2.2.1], [3.1.1], and [4.1.0] bicyclic substrates, a class of compounds for which the monoterpenes in the rosette of Scheme 7 are representative and instructive. As expected for these rigid, bicyclic substrates, steric bias induces high π-facial selectivities. The experimental results can in all cases be explained straightforwardly: the favored attack takes place on the sterically less congested π face. While 2-methylnorbornene (**6**)[60] reacts with high *exo* selectivity, as known for other types of electrophilic[65] and nucleophilic[66] additions to norbornene derivatives, two methyl groups at the methylene bridge alter the stereochemical outcome.[67] Thus, quite generally, a dimethylmethylene bridge, as in α-pinene (**8**), Δ^4-carene (**9**), Δ^3-carene (**10**), and *cis*-Δ^2-carene (**11**), is distinctly *anti*-directing, and thus, the hydroperoxides that result from *syn* attack are formed only in traces. In this context it is interesting that *trans*-Δ^2-carene (**12**) is inert to photooxygenation.[62] The reason is that the *syn* face is blocked sterically towards attack of singlet oxygen and the accessible *anti* face bears no abstractable hydrogen atoms. Therefore, physical quenching prevails, and the initially formed *anti* exciplex reverts to the starting material without net reaction. The reaction of α-thujene (**13**) illustrates that the methylene bridge results in complete *anti* selectivity in a [3.1.0] bicyclic substrate.

Paquette and co-workers[68] examined the photooxygenation of a series of cyclopropanated cyclohexenes **14** (Scheme 8). In contrast to the reaction of **13**, for these [4.1.0] bicyclic systems attack occurs diastereoselectively either *syn* or *anti* to the methylene bridge and depends on the overall substitution pattern. Conformational features are important for these particular substrates. Clearly, subtle changes in the substitution pattern of olefin **14** are enough to effect amazingly high levels of either *syn* or *anti* diastereoselectivity.

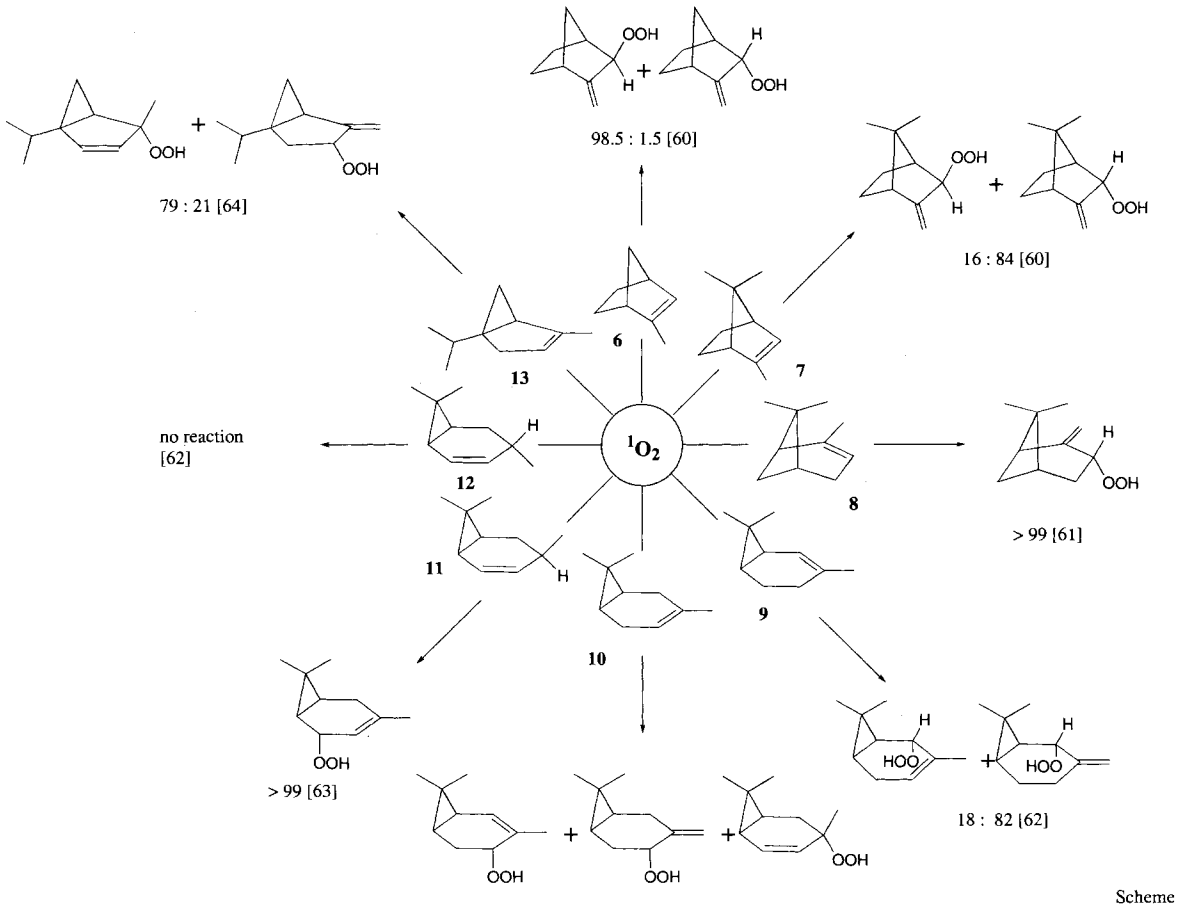

Scheme 7. Schenck reaction of bicyclic hydrocarbons **6**–**13**.

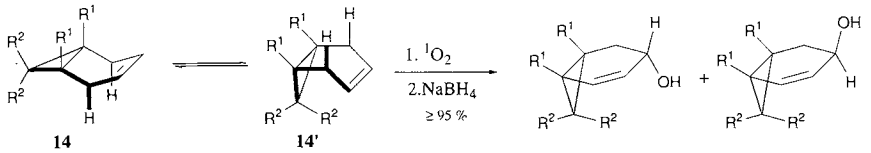

14 **14'**

	R^1	R^2	*syn*		*anti*
14a	H	H	100	:	0
14b	Me	H	0	:	100
14c	H	Me	0	:	100
14d	$-(CH_2)_3-$	H	100	:	0

Scheme 8. Photooxygenation of cyclopropanated cyclohexenes **14**.

The numerous other examples of the Schenck reaction with bi- and polycyclic hydrocarbons,[7–10] mostly natural products, display diastereoselectivities similar to those presented above. Most of these can be explained by simple steric arguments. An increase in the rigidity of the olefinic substrate, for example on going from mono- to bi- and polycyclic systems, leads to a remarkable selectivity enhancement. Conformational adjustment either to minimize steric hindrance with the attacking singlet oxygen or to bring a hydrogen atom into the proper position for abstraction by singlet oxygen on either diastereotopic π face is not usually possible for rigid substrates.

2.1.3. Cyclic Olefins with Heteroatom Substituents

This section will feature cyclic substrates that bear an additional functional group. While for simple hydrocarbons (Sections 2.1.1 and 2.1.2) π-facial selectivity is determined mainly by steric and conformational effects, substitution of the carbon framework with one or more heteroatom-containing functional groups requires that stereoelectronic and electronic features also come into play. Therefore, the rationalization of experimental diastereoselectivities for this type of substrate is less straightforward than for those examined in the previous sections. Nevertheless, the rigidity of cyclic systems will circumvent the difficulties that may complicate simple explanations in the conformationally flexible open-chain derivatives.

One relatively simple, but highly interesting substrate is the substituted 7-isopropylidenenorbornene **15b** (Scheme 9).[69] In this compound the substituents are located too far from the

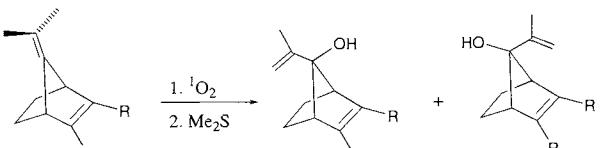

	R	Yield [%]	*syn*		*anti*
15a	H	92	17	:	83
15b	COOMe	90	46	:	54

Scheme 9. Photooxygenation of 7-isopropylidenenorbornenes **15**.

reacting double bond to have any steering influence by direct attraction or repulsion of the incoming singlet oxygen enophile. Nevertheless, substitution by the electron-withdrawing ester groups reduces the diastereoselectivity from 83:17 for the parent system **15a** to 54:46 for derivative **15b**. A very similar situation is encountered in the photooxygenation of substituted 7-isopropylidenebenzonorbornenes **16** (Scheme 10).[69–71] Here, too, reaction of the parent system **16b** shows moderate *anti* selectivity (76:24). Substitution of the benzene ring with electron-donating substituents as in derivative **16a** leads to a slight increase of *anti* preference, whereas electron-withdrawing substituents such as F (**16c**) or Cl (**16d**) even invert the overall selectivity so that now *syn* attack is preferred. In these reactions singlet oxygen shows the same stereochemical behavior as other uncharged electrophiles, for example *m*-chloroperbenzoic acid (*m*CPBA), *N*-methyl-1,2,4-triazolinedione, and *N*-bromosuccinimide (NBS),[70] whereas strong and highly electron-deficient electrophiles such as CH_3CO^+, CCl_2, and *tert*-butyl hypochlorite/H^+ give preferably *syn* attack.

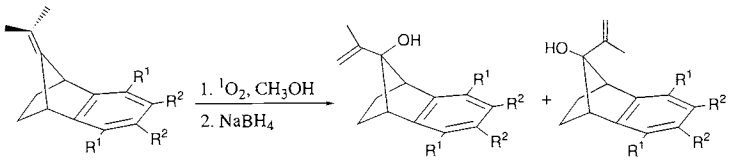

	R^1	R^2	*syn*		*anti*
16a	OMe	H	21	:	79
16b	H	H	24	:	76
16c	F	F	56	:	44
16d	Cl	Cl	59	:	41

Scheme 10. Photooxygenation of 7-isopropylidenebenzonorbornenes **16**.

The attempts to rationalize these results evoked considerable dispute over the years. Okada and Mukai[69] favored orbital distortion at the reacting double bond through σ–π mixing due to the perturbation caused by the C2–C3 double bond. Paquette, Gleiter, et al.[71] stressed the importance of π bond assistance in the transition state through homoconjugative charge delocalization on the side opposite to the incoming electrophile. This is expected to be important for weak, uncharged electrophiles.

This matter was recently reexamined by Houk et al.,[72] who on the basis of RFG/6-31G* calculations concluded that the attack is determined mainly by electrostatic interactions. The overall electron density in substrates **15a** and **16b** is higher on the less reactive *syn* face of the reacting double bond; attack on this face is also slightly preferred for steric reasons. For uncharged electrophiles with lone pair electrons and high electron densities such as singlet oxygen, which are defined by Hehre et al.[73] as "transvestial enophiles", attack from the *syn* face is disfavored due to repulsion of these "negative" enophiles by the high electron density of the double bond. Another way to rationalize this effect is to propose that in the exciplex the attacking singlet oxygen enophile bears a partial negative charge which is unfavorable for attack at the more electron-rich *syn* face.

It is evident from the substrates **15** and **16** that for these rigid systems the lack of conformational flexibility leads to permanently disturbed electron densities on the diastereotopic faces of the reacting double bond and, consequently, to diastereoselec-

tive attack of singlet oxygen. Such stereoelectronic effects must be also considered in cyclic systems that bear a heteroatom substituent in a suitable position for interacting with the incoming singlet oxygen enophile.

Unfortunately, the photooxygenation of only a few examples of this informative class of olefinic substrates has been reported. The simplest cases, namely 2-cyclopentenol (**17**) and 2-cyclohexenol (**18**), were recently examined in our group.[74] In the reaction of **17** high *trans* selectivity (>90:10) was observed (Scheme 11). This is in complete contrast to the epoxidation of

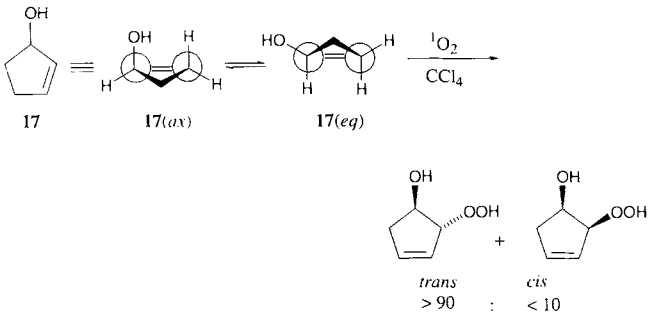

Scheme 11. Photooxygenation of 2-cyclopentenol (**17**).

this particular substrate with *m*CPBA, in which the reagent is directed to the *syn* face through hydrogen bond formation with the free hydroxyl group.[75] The low overall reaction rate in the photooxygenation of these cyclic, chiral allylic alcohols implies substantial reversibility in the exciplex formation. Consequently, it is unlikely that any preference for one of the two possible ground state conformations **17**(*ax*) and **17**(*eq*) dictates the final product ratio. An explanation of the observed π-facial *anti* selectivity is that attack on the *syn* face and abstraction of a hydrogen atom aligned perpendicular to the plane of the double bond from conformation **17**(*ax*) is disfavored due to steric interactions of the incoming singlet oxygen with the axial hydroxyl functionality. However, as we have seen in Section 2.1.1, such simple steric effects are usually not sufficient to induce high selectivities in monocyclic systems and electronic effects must also be invoked. Evidently, the hydroxyl functionality in **17** plays no beneficial role in directing the incoming singlet oxygen to the *syn* face, a result in sharp contrast to what will be encountered in the photooxygenation of acyclic, chiral allylic alcohols (cf. Section 2.2). For the present cyclic substrate only the conformations **17**(*ax*) and **17**(*eq*) are accessible, which bear the heteroatom substituent on the *syn* face. Therefore, stereoelectronic effects come into play in that due to the electron-accepting nature of the oxygen substituent, a high overall electron density accumulates on the *syn* face of the substrate. This would be expected[76] to cause electrostatic repulsion of the "transvestial enophile", as discussed previously for **15** and **16**. This repulsive effect is not counterbalanced by effective attractive interactions of the incoming enophile with the hydroxyl functionality through hydrogen bonding, as in the case of *m*CPBA epoxidation.

A similar outcome is observed for the photooxygenation of 2-cyclohexenol (**18**)[74] (Scheme 12). In this case the products **19b,c**, which arise from regioisomeric hydrogen abstraction,

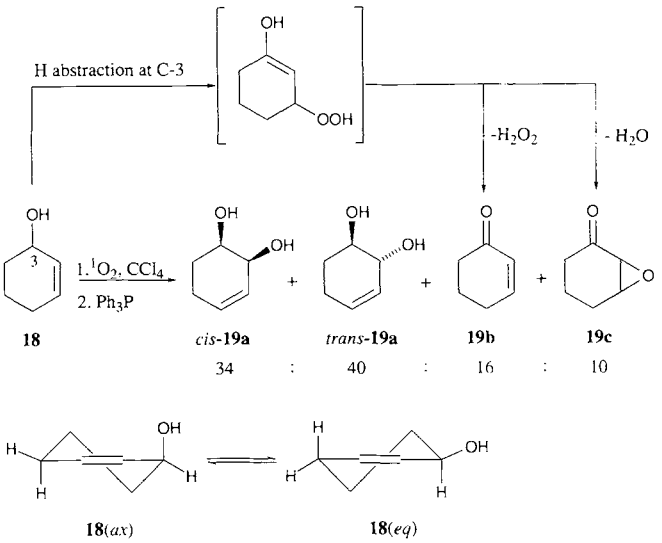

Scheme 12. Schenck reaction of 2-cyclohexenol (**18**).

complicate matters a bit because the stereochemical information is lost. However, these products are formed by *anti* attack since only one allylic hydrogen atom is available at the chiral center. Thus, a moderate overall *anti* selectivity (66:34) is observed. The conformational situation for hydrogen abstraction at the C6 position in cyclohexene **18** is actually opposite to that in the cyclopentene **17**. Because of the perpendicular arrangement of the abstractable hydrogen atom with respect to the plane of the double bond on the *syn* face in conformer **18**(*eq*), the hydroxyl functionality is in a pseudo-equatorial position, where it should not present any steric obstacle towards singlet oxygen attack. This may explain the observed increased *syn* attack in this case.[77]

Preferred *anti* attack of singlet oxygen with respect to the hydroxyl functionality is also observed in reactions of homoallylic alcohols **20a**[78] and **20b**[79] (Scheme 13). Analogous to the

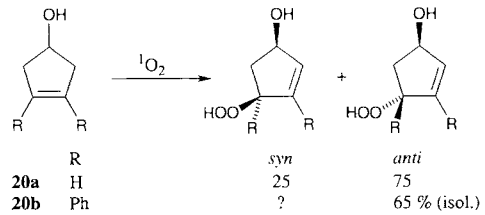

Scheme 13. Schenck reaction of 3-cyclopentenols **20**.

mechanistic rationalization for the allylic alcohols **17** and **18**, repulsion of the singlet oxygen by the enhanced electron density on the *syn* face may be responsible for the observed *anti* diastereoselectivity. The present results seem to indicate a moderate to high *anti*-directing propensity for the hydroxyl functionality in cyclic systems. Similar effects seem to apply for carboxylic acids and their anions, as was recently shown in the photooxygenation of the 1,4-cyclohexadienes **21**[80] (Scheme 14). The complete reversal of π-facial selectivity from preferred *anti* attack with respect to the carboxylate group for R = Me (*syn*:*anti* = 87:13) to strongly favored *syn* attack for R = *i*Pr

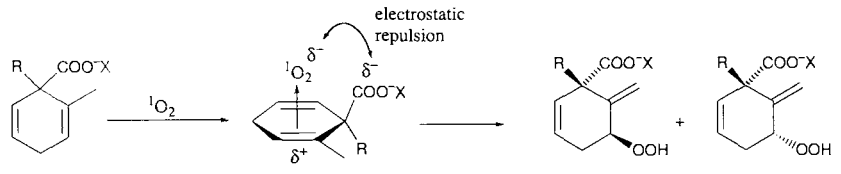

	R	X	*anti*	:	*syn*
21a	Me	H^+	87	:	13
21b	Me	Na^+	92	:	8
21c	Me	PyH^+	> 96	:	< 4
21d	Et	H^+	30	:	70
21e	Et	Na^+	43	:	57
21f	Et	PyH^+	75	:	25
21g	*i*Pr	H^+	< 4	:	> 96

Scheme 14. π-Facial selectivity in the Schenck reaction of 2,5-cyclohexadiene-1-carboxylic acids **21**. Py = pyridine.

(*syn*:*anti* = 4:96) shows that this rigid, almost planar system is quite sensitive to steric effects. Nevertheless, the selectivity in the reaction of derivative **21a**, which opposes steric preference, clearly demonstrates the involvement of stereoelectronic and/or electronic effects in determining the π-facial selectivity. Accordingly, these experimental results have been rationalized[80] in terms of electrostatic repulsion between the carboxylate group and the partially negatively charged singlet oxygen in the exciplex or a perepoxide intermediate (Scheme 14). The trend for increased *anti* selectivity observed for the pyridinium and sodium salts **21b, c, e, f** implies that this electronic effect (electrostatic repulsion) is general.

From the few examples mentioned we can conclude that for cyclic olefins no functional group has yet been found that exercises a *syn*-directing effect on singlet oxygen in the Schenck reaction.[81,82] The reasons for this may be that electron-accepting substituents (inductive effects) that reside on one π face of the substrate molecule render attack of singlet oxygen unfavorable due to long-range electrostatic repulsion. This may occur either through direct interaction between the singlet oxygen enophile and the electron acceptor, as proposed for carboxylic acids, or by an increase in the overall electron density of a particular π face of the olefinic substrate. Although many cyclic olefins have been photooxygenated,[7-11] no systematic studies have been conducted to probe the directing propensity of a variety of common substituents and answer these mechanistic queries. Such studies would provide a better understanding of the diastereoselectivities in reactions of cyclic systems and would allow the synthetic chemist to use the Schenck reaction for applications with predicted stereocontrol.

2.2. Acyclic Systems

The diastereoselective Schenck reaction of acyclic, chiral substrates would be of great benefit to the synthetic chemist for the oxyfunctionalization of olefins. Compared to cyclic systems, which were discussed in the previous section, the enhanced conformational flexibility of open-chain substrates would be expected to reduce the influence of steric and stereoelectronic effects but increase the effect of electronic factors. The ability of a functional group to direct the attack of singlet oxygen preferentially to one π face of the substrate would be decisive for stereocontrol.

Two approaches to the diastereoselective photooxygenation of acyclic substrates have been employed. One option is to introduce a nonracemic, chiral auxiliary to an achiral substrate, which may, after the diastereoselective ene reaction with singlet oxygen, be removed for the preparation of enantiomerically enriched allylic hydroperoxides. Another method for the synthesis of highly oxyfunctionalized, chiral compounds is the diastereoselective photooxygenation of olefins bearing an adjacent stereogenic center. As will be seen, the latter approach has been used for the selective oxyfunctionalization of substrates that bear a variety of functional groups at the stereogenic center.

2.2.1. Chiral Auxiliaries

The use of auxiliaries from the chiral pool has proven successful for a variety of chemical transformations,[83] and consequently, its utility was tested also in ene reactions with singlet oxygen. All attempts reported so far have concentrated on the incorporation of an α,β-unsaturated carboxylic acid unit into a chiral environment; regioselective hydrogen abstraction at the *gem*-substituted position should produce a β-hydroperoxy carboxylic acid.[45] The keystone of this approach is that the conformation of the α,β-unsaturated carboxylic acid has to be fixed by secondary interactions so that singlet oxygen is forced to attack preferentially only on one of the π faces.

One early but unsuccessful attempt is featured in Scheme 15. Photooxygenation of a series of 2-alkenyldihydrooxazoles **22**,

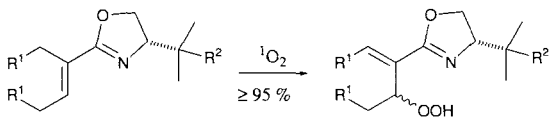

22 **23**

R^1,R^1	R^2	d.r.
H,H	H	50 : 50
H,H	Me	50 : 50
$-CH_2-$	H	50 : 50
$-CH_2-$	Me	50 : 50

Scheme 15. Lack of stereocontrol in the Schenck reaction of chiral oxazolinones **22**.

which can be prepared easily from the corresponding carboxylic acids and optically active amino alcohols, yielded in each case only a 50:50 mixture of the diastereomeric hydroperoxides **23**.[84] Despite its lack of selectivity, this reaction is instructive with regard to the reaction mechanism. For example, to explain the observed geminal regioselectivity, Ensley et al.[85] proposed initial [4+2] cycloaddition of singlet oxygen to the α,β-unsaturated carbonyl moiety as heterodiene partner. The allyldihydrooxazoles **22** should adopt a cisoid conformation for effective [4+2] cycloaddition, attack of singlet oxygen on the *si* face would be severely hindered by the bulky alkyl substituents on

the oxazole ring, and appreciable diastereoselectivity would be expected. However, the enophile $^1O_2$ does not discriminate between the two π faces, indicating that the proposed[85] cisoid conformation is unlikely in the ene reaction.

A very recent and more successful case is documented in Scheme 16. Photooxygenation of the substituted cyclohexyl tiglates **24** gave the corresponding hydroperoxides.[86] While

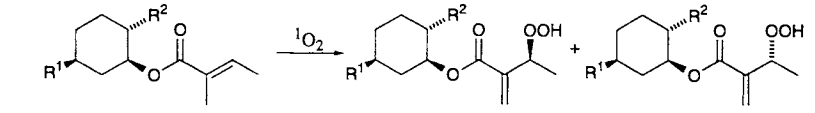

	R^1	R^2	Solvent	T [°C]	d.r.
24a	H	Ph	CCl_4	25	50 : 50
24b	H	Np	CCl_4	25	50 : 50
24c	Me	CMe_2Ph	CCl_4	25	67 : 33
24d	Me	CMe_2Np	CCl_4	25	70 : 30
24e	Me	CMe_2Np	CH_2Cl_2	-60	82 : 18

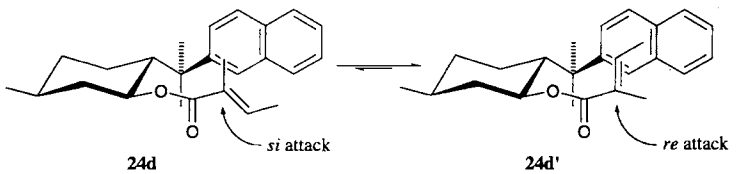

24d **24d'**

Scheme 16. Schenck reaction of chiral enoates **24**. Np = naphthyl.

esters **24a,b** with an aromatic ring attached directly to the cyclohexyl group showed no diastereoselectivity in the ene reaction, the menthol-derived esters **24c,d** displayed moderate π-facial selectivity at room temperature. The diastereoselectivities could be enhanced significantly when the reaction was carried out at −60 °C. These experimental results have been rationalized in terms of different populations of the conformers **24d** and **24d'** (Scheme 16); at lower temperatures the difference is enhanced. The conformer **24d'**, which can be attacked by singlet oxygen only from the *re* face, is lower in energy due to π stacking of the enoate with the aromatic system. The coplanar arrangement and, therefore, maximized π stacking can be optimally achieved for esters **24c,d**, while for the derivatives **24a,b** such a favorable arrangement is not possible due to considerable tilting of the substituents on the cyclohexane.[86]

The lack of an ideal coplanar arrangement of enoate and aromatic ring and, consequently, loss of conformational preference due to π stacking, is presumably also responsible for the lack of π-facial selectivity in the Schenck reaction of 3-naphthylborneol tiglates[86] and for the closely related ester **25a**[87] (Scheme 17). Steric bias alone, as in tiglate **25b**, is also not sufficient to induce good π-facial selectivity. The enoate may

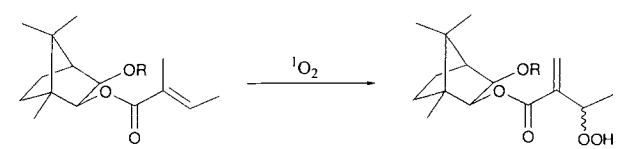

	R	T [°C]	d.r.
25a	CH_2Ph	-50	60 : 40
25b	CH_2tBu	0	56 : 44

Scheme 17. Photooxygenation of chiral enoates **25**.

adopt either a cisoid or a transoid conformation, which both react with singlet oxygen at comparable rates, explaining the observed low π-facial selectivity.

At the present time the use of chiral auxiliaries in the photooxygenation of tiglates has provided only limited success. Since the cisoid and transoid conformations of the enoate show similar reactivity towards singlet oxygen, control of conformer population is essential. The use of π-stacking concepts will require more carefully constructed substrates to guarantee progress along these lines. It should also be noted that in one attempt to induce asymmetry in the Schenck reaction the heterogeneous photooxygenation of 2-methoxy-2-butene was conducted within the dissymmetric cavities of a clathrate, namely *tri-o*-thymotide.[88] The resulting hydroperoxides indeed showed low optical activity; however, the absolute configuration and the enantiomeric excess were unfortunately not determined.

2.2.2. *Olefins Bearing Adjacent Stereogenic Centers*

The alternative approach to achieving high diastereocontrol in the formation of oxyfunctionalized products is by substrate control, in other words by starting with chiral olefins. Numerous such substrates are available for the Schenck reaction, but to apply successfully diastereoselective ene reactions with singlet oxygen in synthesis, the basic features of stereocontrol in such systems must be understood. Mechanistically relevant questions to be examined are: 1) How effective is steric bias in open-chain substrates? 2) Which functional groups at the stereogenic center direct the attack of singlet oxygen in the Schenck reaction? 3) What special structural features should the olefin have for high diastereoselectivities?

During the last five years considerable efforts have been expended on these questions and some general trends on the scope and limitations of this highly attractive synthetic route to stereochemically defined oxyfunctionalized products have become apparent. These make the Schenck reaction even more useful for preparative chemists, especially since the yields of the desired oxyfunctionalized products are generally ≥85%, and in addition excellent regiocontrol is also achieved.

2.2.2.1. Substrates without Heteroatom Functional Groups at the Stereogenic Center

In reactions of chiral olefins bearing only carbon substituents at the stereogenic center the electronic effects should be minimized, and these compounds should thus serve as probes for the effect of steric bias on the stereochemical course of the Schenck reaction in acyclic systems. Photooxygenation of alkene **26** gave a moderate preference for *erythro*-**27** (71:29)[89] (Scheme 18). This result can be rationalized with the Newman projection of alkene **26**. The presence of a methyl group *cis* to the stereogenic center induces considerable 1,3-allylic strain,[90] and in the preferred orientation the hydrogen atom at the stereogenic center is directed inward. Consequently, the singlet oxygen attacks main-

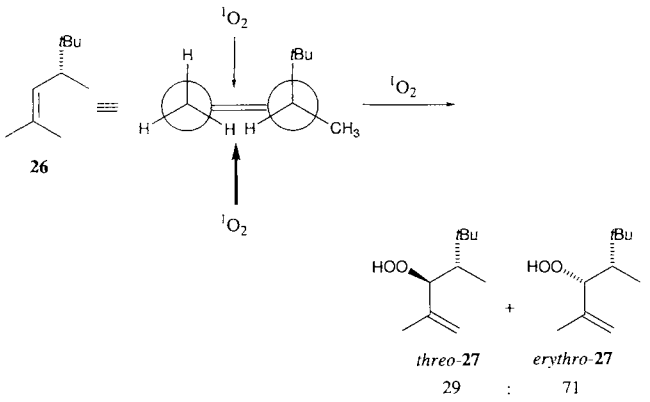

Scheme 18. Stereocontrol in the photooxygenation of chiral olefin **26**.

ly the bottom face, that is, opposite the *tert*-butyl group, to afford preferentially the *erythro* product.

A similar situation is encountered in the photooxygenation of the phenyl-substituted alkenes **28a,b**[91,92] (Scheme 19). Again, the *erythro* hydroperoxide is formed mainly, and the explanation in terms of steric effects is quite similar to that for the

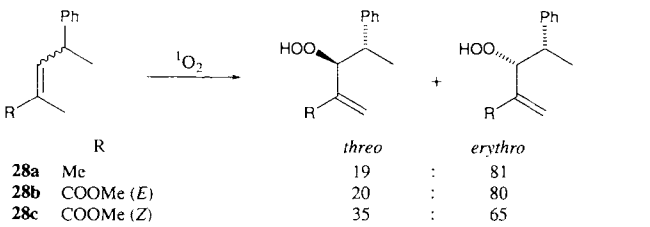

	R	*threo*		*erythro*
28a	Me	19	:	81
28b	COOMe (*E*)	20	:	80
28c	COOMe (*Z*)	35	:	65

Scheme 19. Schenck reaction of chiral olefins **28**.

reaction of the *tert*-butyl-substituted alkene **26**. The slight drop in π-facial selectivity for the *Z*-configurated ester **28** (Scheme 19) arises because the ester group is less effective in inducing 1,3-allylic strain than the spherical methyl group in substrates **26** and **28a,b**. In conclusion, steric bias effects only low to moderate *erythro* selectivities in the Schenck reaction of chiral, open-chain substrates. Next the steering properties of polar heteroatom substituents at the stereogenic center will be scrutinized.

2.2.2.2. *Allylic Alcohols and Derivatives*

Chiral allylic alcohols are readily available substrates for testing the diastereoselectivity of the Schenck reaction and thereby assessing the electronic factors on the steering propensity of the hydroxyl group in open-chain substrates. As we have seen for cyclic allylic alcohols (Section 2.1.3), the hydroxyl group increases the electron density on one π face of the system and through electrostatic interaction repels the attacking singlet oxygen. For acyclic, allylic alcohols such stereoelectronic effects are expected to be much less important since the stereogenic center can adopt a variety of conformations which may place the hydroxyl functionality on either π face. Consequently, long-range, electrostatic repulsion towards the approaching singlet oxygen enophile is expected to be reduced and electronic interactions may come into play during exciplex formation.

In the definitive experiment featured in Scheme 20 a series of *Z*-configurated chiral allylic alcohols **29** were photooxygenated in chlorinated solvents to afford for every derivative in high preference (d.r. ≥93:7) the *threo*-configurated hydroxyhydroperoxides **30**.[93] The size of the aliphatic substituent at the stereogenic center does not influence the diastereoselectivity, which confirms that steric control is not important in the Schenck reaction of these substrates.

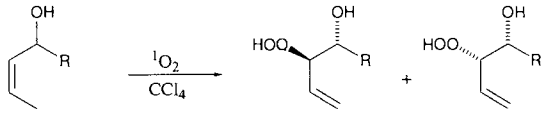

	R	*threo*-**30**		*erythro*-**30**
(*Z*)-**29a**	Me	93	:	7
29b	Et	94	:	6
29c	*i*Pr	94	:	6
29d	*t*Bu	95	:	5

Scheme 20. The directing effect of the hydroxyl group in the photooxygenation of alcohols **29**.

For the mechanistic interpretation of these stereochemical results, it is important to compare them to those for the *E*-configurated allylic alcohol (*E*)-**29a** (Scheme 21).[93] In this second set of experiments essentially no π-facial selectivity was observed, which stresses again the requirement of a substituent in the *cis* position relative to the hydroxyalkyl group to induce 1,3-allylic strain, which is essential for high diastereoselectivity.

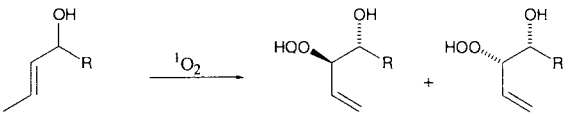

(*E*)-**29a** *threo*-**30a** : *erythro*-**30a** = 54 : 46

Scheme 21. Unselective Schenck reaction due to lack of 1,3-allylic strain in (*E*)-**29a**.

The experiments in Scheme 22 offer insights into the mechanism of the Schenck oxyfunctionalization. As expected, the photooxygenation of allylic alcohol **31a** displays *threo* selectivity in nonpolar solvents; however, in polar and protic solvents a significant drop in diastereoselectivity is observed.[93] This again

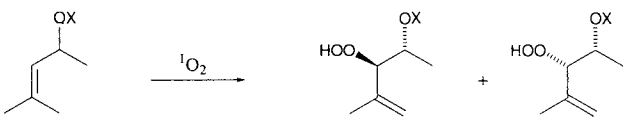

	X	Solvent	Yield [%]	*threo*		*erythro*
31a	H	CCl_4	96	93	:	7
31a	H	$CHCl_3$	96	92	:	8
31a	H	CH_2Cl_2	96	90	:	10
31a	H	CH_3CN	96	76	:	24
31a	H	CH_3OH	96	73	:	27
31b	$SiMe_3$	CCl_4	74	80	:	20
31c	$SiMe_2tBu$	CCl_4	67	83	:	17
31d	Me	CCl_4	80	72	:	28
31e	Ac	CCl_4	82	39	:	61

Scheme 22. Solvent effects and product distribution in the Schenck reaction of chiral allylic alcohol derivatives **31**.

indicates that electronic effects may be responsible for the observed π-facial selectivity in the present system. Thus, protection of the free hydroxyl group by either electron donors (**31b–d**) or by an electron acceptor (**31e**) leads to a substantial drop in the π-facial selectivity compared to that with the parent allylic alcohol **31a**. For the acetate **31e** the *erythro*-configurated hydroperoxide was even the major product.

Based on the stereochemical data from Schemes 20–22, a conclusive mechanistic picture can be drawn for the ene reaction of singlet oxygen with chiral allylic alcohols. The steric factors without electronic interactions are represented in the Newman projections of conformers **31** and **31′** (Fig. 5). To minimize 1,3-allylic strain the smallest substituent at the stereogenic center,

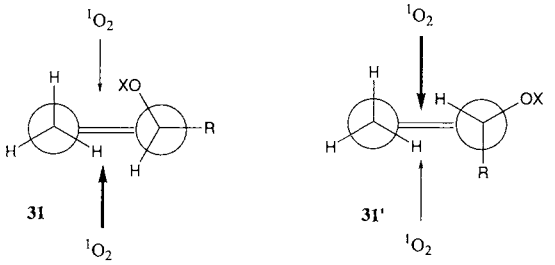

Fig. 5. Steric control in the photooxygenation of chiral allylic alcohol derivatives.

the hydrogen atom, is directed preferentially towards the inside position. When the OX and R substituents at the stereogenic center have roughly the same steric demand, the conformers **31** and **31′** are similar in energy. As a result both π faces of the olefin are exposed towards the attacking singlet oxygen enophile and low diastereoselectivity would be expected. Indeed, the low to moderate π-facial selectivities in the photooxygenation of the alcohol derivatives **31b–e** are all within the range that might be explained in terms of steric factors. Thus, to account for the high diastereoselectivity in the reaction of the free alcohol **31a**, hydrogen bonding is proposed in the exciplex between the hydroxyl group of the allylic alcohol and the partially negatively charged singlet oxygen (Fig. 6). This type of stabilizing electron-

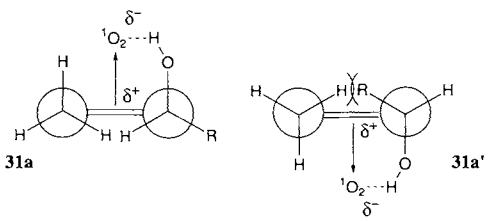

Fig. 6. Stabilization of the *threo* exciplex through hydrogen bonding.

ic interaction in the exciplex is effective only in conformer **31a**, which leads to the *threo*-configurated product; conformer **31a′** does not come into play owing to unfavorable 1,3-allylic strain. A similar rationale applies to the allylic alcohol (*Z*)-**29a** (Scheme 20), but not to its diastereomer (*E*)-**29a**. Since the latter lacks effective 1,3-allylic strain (no *cis* methyl group), the two conformers analogous to structures **31a** and **31a′** are similar in energy. Thus, hydroxyl assistance alone can no longer discriminate between the two π faces and consequently diastereoselectivity is lost. This mechanistic rationalization is further substantiated by the fact that the allylic alcohols show surprisingly high regioselectivity in the Schenck reaction: alcohol **31a** gives products arising from hydrogen abstraction at the stereogenic center in only 4% yield.[93] The Newman projections for the conformers **31a** and **31a′** in Figure 6 clearly reveal that coordination of singlet oxygen to the hydroxyl group precludes hydrogen abstraction at the stereogenic center. Also the observed solvent effect can be explained directly: with increasing polarity of the reaction medium, electronic interactions such as hydrogen bonding will be reduced and, consequently, the preference for the *threo* product diminished. Moreover, the lack of steric effects for the R group in the allylic alcohols **29** (Scheme 20) is evident; for the preferred conformer **31a** (Fig. 6) this substituent is located at the periphery and steric interactions are nominal, in other words, R = Me is large enough to generate sufficient allylic strain.

The high π-facial selectivity in photooxygenations of unprotected allylic alcohols through the directing effect of the hydroxyl group[93] is in accord with the "transvestial nature"[73] of the singlet oxygen enophile. On one hand, singlet oxygen is an electrophilic enophile and responds to high electron densities of the substrate; on the other hand, when it is complexed to the substrate in the form of an exciplex, stabilizing nucleophilic interactions through hydrogen bonding, for example, come into play. This recognition is of general importance[94] and when applied to nonracemic allylic alcohols, the preparation of optically active, highly oxyfunctionalized target molecules can be achieved with high stereocontrol. This was recently demonstrated by application of the novel hydroxyl group assisted Schenck reaction in natural product synthesis.[95]

As we have seen, 1,3-allylic strain plays a decisive role in the hydroxyl group directed ene reaction with singlet oxygen. But how important is 1,2-allylic strain caused by a geminal substituent near the stereogenic center in determining the stereoselectivity of the Schenck reation? To answer this question, the alcohols (*E*)-**32** and (*Z*)-**32** were photooxygenated in nonpolar solvents (Scheme 23).[96] The diastereomer (*E*)-**32**, which does

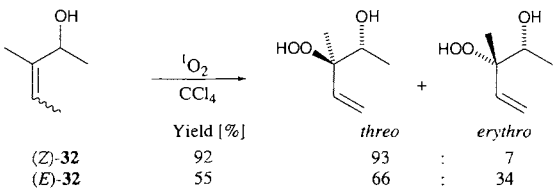

	Yield [%]	*threo*		*erythro*
(*Z*)-**32**	92	93	:	7
(*E*)-**32**	55	66	:	34

Scheme 23. Schenck reaction of chiral allylic alcohols **32**.

not have a methyl group *cis* to the stereocenter, showed only moderate *threo* selectivity (66:34). In contrast, the *Z*-configurated alcohol led to the *threo*-hydroperoxide with high π-facial selectivity (93:7), which is in fact as high as that found in the photooxygenation of (*Z*)-**29a** (Scheme 20) and **31a** (Scheme 22), allylic alcohols without geminal substituents.[93] These results clearly establish that 1,2-allylic strain does not effectively compete with 1,3-allylic strain in differentiating the relative energy of the corresponding diastereomeric exciplexes (Fig. 7). Although significant 1,2-allylic strain is implicated in

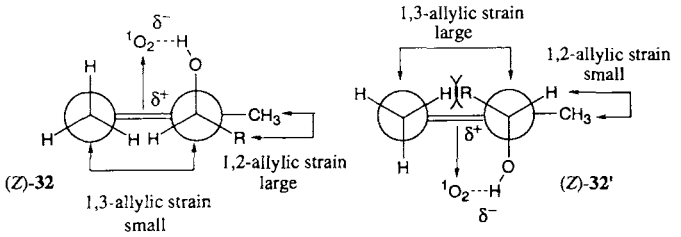

Fig. 7. Competition between 1,2- and 1,3-allylic strain in alcohol (*Z*)-**32**.

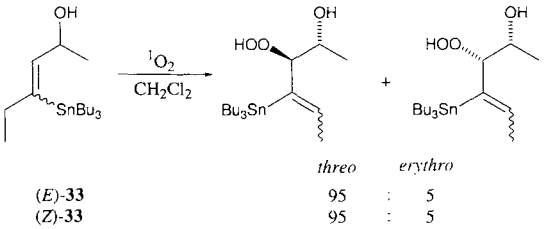

Scheme 24. Schenck reaction of stannyl alcohols **33**.

the conformer (*Z*)-**32**, the *threo* product is formed preferentially, while conformer (*Z*)-**32'** is unimportant. That 1,2-allylic strain by itself is indeed quite ineffective, is emphasized by the photooxygenation of the diastereomer (*E*)-**32**. Here only 1,2-allylic strain may operate and a low π-facial selectivity was found (diastereomer ratio d.r. = 66:34). These results imply that the C-C-C-O dihedral angle α in the exciplex is roughly 90–110° (Fig. 8a), analogous to that in the transition state postulated for the epoxidation by peracids (Fig. 8b).[97] A smaller angle would significantly enhance the importance of 1,2-allylic strain,[50,98] as observed in vanadium-catalyzed oxygen transfer reactions (Fig. 8c).

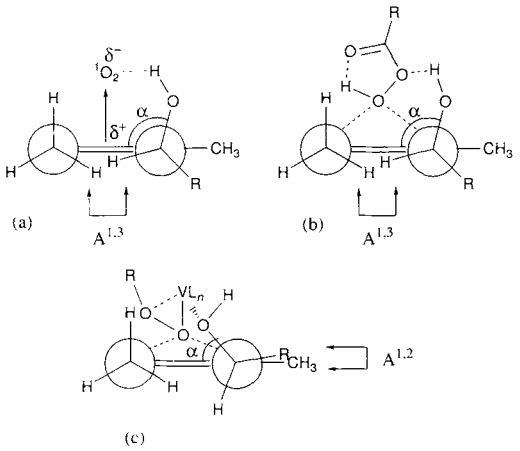

Fig. 8. Transition states in the Schenck reaction (a), the peracid epoxidation (b), and the vanadium(v)-catalyzed epoxidation (c) of chiral allylic alcohols. $A^{1,2}$, $A^{1,3}$: 1,2- and 1,3-allylic strain, respectively.

It may be argued that the π-facial selectivity in the Schenck reaction of (*E*)-**32** is minimal because in this particular substrate a hydrogen atom must be abstracted from a methyl group that is located *trans* to the stereogenic center. In other words, the directing effect of the hydroxyl group may hold only for hydrogen abstraction from an alkyl group located *cis* to the stereocontrolling chiral center. That this assumption does not apply, is shown in the photooxygenation of the stannyl alcohols (*E*)-**33** and (*Z*)-**33** (Scheme 24). In this case for both isomers high *threo* selectivities (95:5) were found.[99] Therefore, also chiral allylic alcohols such as (*Z*)-**33**, for which hydrogen abstraction has to take place from the "wrong" side of the double bond, react with high π-facial selectivity.

This brings up the important question as to the structure of the intermediate stabilized by the hydroxyl group. Two logical alternatives come to mind: the unsymmetrical perepoxide structure (Fig. 9a) and the symmetrical arrangement (Fig. 9b), in which the O–O and C–C bonds are oriented crosswise to each other. In the case of the perepoxide structure, for the hydroxyl group directing effect to be operative in the abstraction at R^1, inversion of the epoxide ring at O1 would be necessary. Such an inversion is unlikely, since the isoelectronic *N*-chloroaziridines,

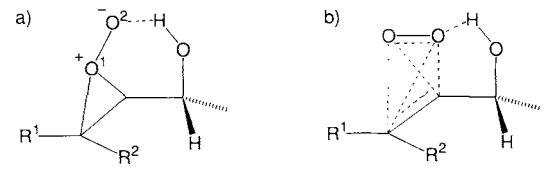

Fig. 9. Hydroxyl group stabilized perepoxide (a) and exciplex (b).

which may be taken as models, are configurationally stable and have been resolved into enantiomers even at room temperature.[100] Therefore, we propose the novel symmetrical structure (Fig. 9b) for the exciplex as a more likely stereocontrolling intermediate. Product formation by allylic hydrogen abstraction may take place either at R^1 or at R^2, depending on the substitution pattern. Whether the product is formed via a bona fide perepoxide intermediate is of no particular consequence for the product distribution because the π-facial selectivity is decided already at the exciplex stage.

For preparative purposes it would be most desirable to be able to use other functional groups to obtain preferentially the *erythro*-configurated product; this would complement the *threo*-selective photooxygenation of chiral allylic alcohols mediated by the hydroxyl group. The Schenck reaction of the allylic acetate **31e** (Scheme 22), which proceeded with modest *erythro* selectivity (61:39), is the only example known so far. The modest *erythro* control that is observed presumably arises from repulsion between the incipient negatively charged singlet oxygen and the negatively charged carbonyl oxygen of the acetate substituent in the exciplex.

To explore this further, a series of allylic esters was photooxygenated to determine which combination of steric and electronic features for the ester functionality would enhance formation of the *erythro* product (Scheme 25). Unfortunately, the results show that this goal is difficult to achieve for allylic esters because both steric and electronic repulsions are too weak to be effective in differentiating the π faces in these substrates.[99]

In summary, the hydroxyl group directed Schenck reaction of open-chain, allylic alcohols provides a mild and highly efficient method for the preparation of *threo*-configurated alkenediols in high yields. The concept can be applied to chiral di-, tri-, and tetrasubstituted olefins; the only prerequisite for high π-facial

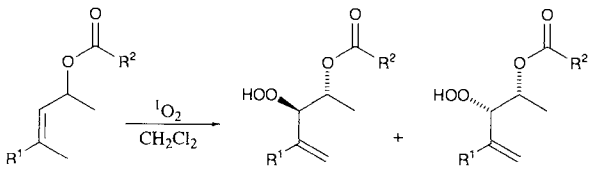

	R^1	R^2	*threo*		*erythro*
31e	Me	Me	70	:	30
34a	H	Me	57	:	43
34b	$SnBu_3$	Me	69	:	31
34c	$SnBu_3$	*t*Bu	62	:	38
34d	$SnBu_3$	OMe	76	:	24
34e	$SnBu_3$	*p*-$C_6H_4NO_2$	67	:	33
34f	$SnBu_3$	CF_3	66	:	34

Scheme 25. Schenck reaction of chiral allylic esters **34**.

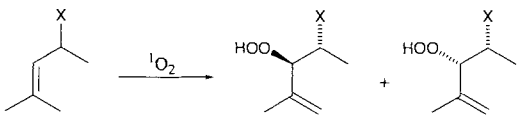

	X	Solvent	Yield [%]	*threo*		*erythro*
35a	NH_2	CCl_4	87	95	:	5
35a	NH_2	$CDCl_3$	90	92	:	8
35a	NH_2	CD_3OD	87	85	:	15
35b	NH_3^+	$CDCl_3$	90	94	:	6
35c	NHAc	CCl_4	93	28	:	72
35d	NHBoc	CCl_4	80	24	:	76
35e	$NBoc_2$	CCl_4	78	5	:	95
35f	NPhth	CCl_4	78	11	:	89
35f	NPhth	$CDCl_3$	92	22	:	78

Scheme 26. Solvent effects and product distribution in the Schenck reaction of chiral allylic amine derivatives **35**. Boc = *tert*-butoxycarbonyl, Phth = phthaloyl.

selectivity is the presence of a *Z*-configurated double bond with a substituent vicinal to the stereogenic center in the allylic alcohol. Mechanistically significant is the fact that the hydrogen atom may also be abstracted from a *trans* alkyl group without loss of diastereoselectivity. This finding speaks for a symmetrical exciplex with crossed bonds as the stereocontrolling initial intermediate rather than the unsymmetrical, end-on perepoxide structure. The observed *threo* selectivity is based on the favored pathway, which features hydrogen bonding of the incoming enophile and for which 1,3-allylic strain is minimal. Unfortunately, no chiral substrates with an oxygen functionality in the allylic position are known to date that undergo the ene reaction with singlet oxygen to give exclusively *erythro* products.

2.2.2.3. *Allylic Amines and Acylated Derivatives*

While the hydroxyl group directed Schenck reaction can be used to prepare *threo*-configurated 1,2-diols after reduction of the hydroperoxy functionality, for preparative purposes, it would be also most desirable to have access to 1,2-amino alcohols of defined stereochemistry through photooxygenation of appropriate allylic amines. For these substrates chemoselectivity is an additional criterion for synthetic utility since a diastereoselective transformation will be useful only when side reactions, for example oxidation at the nitrogen atom[101] or oxidative cleavage of C–N bonds,[102] can be suppressed in favor of the ene reaction.

The results of the photooxygenation are shown in Scheme 26.[89,103] Like the reactions of the allylic alcohols previously discussed (Section 2.2.2.2), the Schenck reaction of the unprotected amine **35a** also shows high *threo* selectivity in nonpolar solvents, which decreases in the polar, protic methanol. Similarly, photooxygenation of the hydrochloride **35b** yielded also the *threo*-configurated β-hydroperoxy amine highly selectively (94:6). This again indicates that hydrogen bonding in the exciplex is the decisive stereochemical directing effect. For the monoacylated amines **35c,d**, which are comparable to the previously mentioned acetate **31e**, only moderate selectivity was achieved with the *erythro* product as the major one. In contrast photooxygenation of the diacylated derivatives **35e,f** produced again the *erythro*-configurated β-hydroperoxyamines diastereoselectively in high yields; this reaction is unquestionably most useful for synthesis. These stereochemical results can again be explained by the formation of the preferred *threo* product from the hydrogen-bonded exciplex **35** (Fig. 10). Thus, in the reaction of the allylic amines, like that of the structurally related allylic alcohols, the *erythro* product does not benefit by the hydrogen bonding stabilization since increased 1,3-allylic strain, as in exciplex **35'**, would be the consequence.

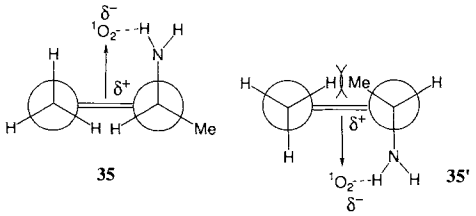

Fig. 10. The directing effect of the amino group in the photooxygenation of chiral allylic amines.

For monoacylated amines **35c,d** this effect no longer applies, possibly because of the increased steric bulk at the nitrogen atom. Synthetically more interesting, however, is the highly diastereoselective formation of the *erythro*-configurated product in the Schenck reaction of the diacylated amines **35e,f**. As mentioned previously (cf. Section 2.2.2.1), steric control alone leads to the *erythro* product, and additional electrostatic repulsion between the carbonyl oxygen atoms and the incoming singlet oxygen enophile further enhances *erythro* control; thus for these substrates steric and electronic effects operate synergistically. This stereochemical steering by electrostatic repulsion will be discussed in more detail in Section 2.2.2.4, but suffice it to say here, the observed solvent effect in the photooxygenation of phthalimide **35f** (Scheme 26) clearly substantiates this mechanistic rationalization.

Compared to the directing effect of the hydroxyl group in the Schenck reaction of allylic alcohols, that of the amino group appears to be of less synthetic applicability, since the readily oxidized amino functionality can interfere in the reactions of substrates with diminished ene reactivity. While allylic amines **35**, which have a trisubstituted double bond, do not suffer from such a drawback and give high yields of the corresponding hydroperoxides, the photooxygenation of allylic amines with a disubstituted double bond is problematic since for these less

reactive substrates the ene reaction cannot compete with other oxidations.[89] Of course, this is only a problem for the unprotected amines; diacylated derivatives are insensitive to such oxidative damage and are converted efficiently into *erythro*-configurated products. Secondary and tertiary amines can also not be employed due to predominant oxidative dealkylation under these reaction conditions.[102] The use of the less nucleophilic hydrochlorides, however, might in these cases be the solution.

Unquestionably, the Schenck reaction of chiral allylic amines and their acyl derivatives provides a highly stereoselective entry to either *threo*- or *erythro*-configurated hydroperoxyamines, which can be readily reduced to the corresponding amino alcohols. This spectacular switch in diastereoselectivity by simple acylation of the amino functionality promises interesting applications in the preparation of oxyfunctionalized allylic amines.[104] For this ene reaction to be of general utility, however, geminal substitution should be explored to assess the effects of 1,2-allylic strain.

2.2.2.4. *Other Functional Groups at the Stereogenic Center*

As we have seen, for allylic alcohols (Section 2.2.2.2) and amines (Section 2.2.2.3) numerous examples reveal the general scope and limitations of the stereochemical steering propensity of hydroxyl and amino functional groups in the Schenck reaction. For compounds with other functional groups at the stereogenic center, however, little if anything is presently known, besides the few recent examples conducted in our research group (Scheme 27).[105] With the exception of the homoallylic alcohol

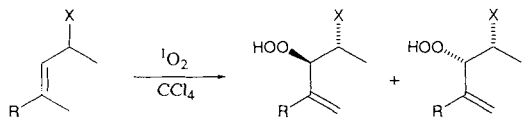

	X	R	Yield [%]	*threo*		*erythro*
36a	Cl	Me	81	< 10	:	> 90
36b	Br	Me	78	< 10	:	> 90
36c	SO_2Ph	Me	87	< 5	:	> 95
36d	OOH	Me	≥ 95	34	:	66
36e	CH_2OH	H	79	55	:	45
36f	COOH	H	88	20	:	80
36f	COOH/Py	H	90	15	:	85
36g	COOEt	H	77	22	:	78

Scheme 27. Directing propensities of various functional groups in the allylic position.

36e, the few substrates examined all display *erythro* diastereoselectivity, irrespective of whether the substituent bears a free OH group, which could serve as a hydrogen bond donor, as in derivatives **36d–f**. Apparently, the geometric requirements for efficient hydrogen bonding are no longer fulfilled for a homoallylic OH group (Fig. 11a). For the allylic halides **36a, b** and the sulfone **36c**, electrostatic repulsion between the substituent and the incoming singlet oxygen in the exciplex (Fig. 11b) appears to be responsible for the high preference of the *erythro*-configurated product. This argumentation has been applied previously to rationalize the stereoselectivities in the reactions of cyclic carboxylic acids (Section 2.1.3) and acyclic diacylated allylic amines (Section 2.2.2.3). Moreover, it seems most reasonable

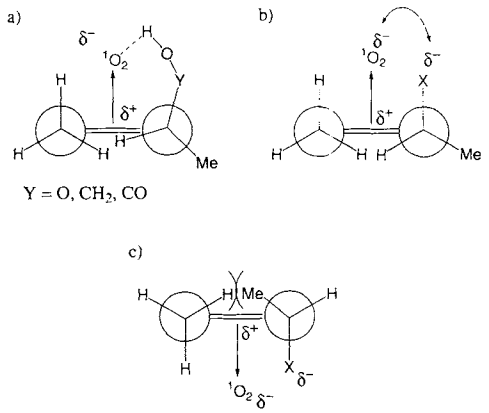

Fig. 11. Stereocontrolling factors in the Schenck reaction of chiral olefins **27**. a) Inefficient hydrogen bonding, b) electrostatic repulsion, c) 1,3-allylic strain.

for compounds with highly electronegative halogen substituents or with the negatively charged oxygen atoms of the electron-attracting sulfonyl group. Furthermore, the slightly enhanced *erythro* selectivity in the Schenck reaction for the pyridinium salt of the carboxylic acid **36f** (d.r. = 15:85) compared to that of the parent acid (d.r. = 20:80) also indicates that such electrostatic effects are operating. Thus, the carboxylate anion is expected to exert a larger repulsion on the incoming singlet oxygen than the carboxylic acid itself.

While for the allylic alcohols and amines hydrogen bonding in the exciplex provides extra stabilization and leads to *threo* control in the Schenck oxyfunctionalization, for the derivatives **36** electrostatic repulsion disfavors approach of singlet oxygen from the π face with the electron acceptor and, therefore, renders formation of the *erythro* product the major pathway. The *erythro* exciplex is not destabilized through such electrostatic repulsion since this would require a structure with significant 1,3-allylic strain (Fig. 11c).

For the sulfoxide **37** an additional stereochemical feature comes into play through the stereogenic sulfur center (Scheme 28).[105] Unfortunately, in the preparation of the sulf-

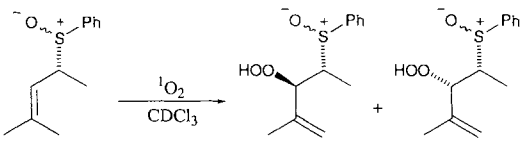

	threo		*erythro*
37a	< 5	:	> 95
37b	15	:	85

Scheme 28. Schenck reaction of chiral allylic sulfoxides **37**.

oxide the two diastereomers **37a, b** were obtained whose relative configurations could not be assigned. While the Schenck reaction of the diastereomer **37a** gave essentially exclusively the *erythro* product (d.r. ≥ 95:5), the π-facial selectivity was significantly lower for sulfoxide **37b**. These results clearly demonstrate that the stereogenic center at the sulfur atom exercises some stereocontrol in this ene reaction.[106] Since the steric demand of the allylic substituents in the diastereomeric sulfoxides **37a** and **37b** must be very similar, electronic reasons are presumably

responsible for the observed difference in the stereocontrol. In agreement with the previous rationalization that the *erythro* exciplex is destabilized by electrostatic repulsion, diastereomer **37a** can easily adopt a conformation in which such a repulsion can operate efficiently, while for sulfoxide **37b** this appears to be more difficult. Since we do not have any information at the present time on the relative stereochemistry of the starting sulfoxides **37**, the stereochemically controlling conformations are not known.

In summary, halogen-, sulfinyl-, and sulfonyl-substituted stereogenic centers exhibit a pronounced propensity for *erythro* control in the Schenck reaction. Furthermore, homoallylic protic groups (e.g. CH_2OH, OOH, COOH) are much less effective than allylic ones (OH, NH_2, NH_3^+) in dictating *threo* stereocontrol through hydrogen bonding in the exciplex.

For the future, it should be of interest to test the directing propensities of other functional groups at the stereogenic center, for example chiral amine oxides, nitriles, azides, imines, aldehydes, ketones, phosphonates, and phosphine oxides. It should be instructive to design chiral substrates having both *threo*- and *erythro*-directing functionalities at the same stereogenic center to assess synergistic effects by electrostatic repulsion of singlet oxygen on one π face reinforced by attractions through hydrogen bonding on the other. This concept, which has already been applied successfully in the photooxygenation of chiral silyl cyanohydrins **38** (d.r. $\geq 99:1$ in Scheme 29),[107] should be tested for chiral β,γ-unsaturated amino and hydroxyl acids.

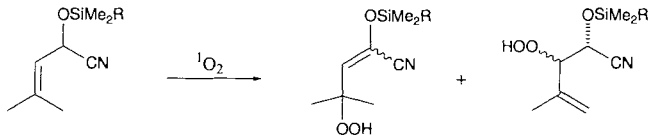

	R	33 :	67
		d.r.	d.r.
38a	Me	96 : 4	96 : 4
38b	*t*Bu	≥ 99 : 1	≥ 99 : 1

Scheme 29. Schenck reaction of chiral silyl cyanohydrins **38**.

We have seen that the ene reaction with singlet oxygen can proceed with amazingly high levels of stereocontrol in open-chain systems. Electronic effects seem to determine the sense and extent of diastereoselectivity. While hydrogen bonding benefits the *threo* products in the photooxygenation of chiral allylic alcohols and amines, electrostatic repulsion in the *threo* exciplex seems to be responsible for the preferred formation of *erythro* products for other functional groups at the stereogenic center. All these directing effects critically depend on the presence of a substituent *cis* to the stereogenic center. Only the effective differentiation in the energies of the different conformers in the exciplex through 1,3-allylic strain can efficiently guide the attack of singlet oxygen preferentially on one of the diastereotopic faces and, thus, give the product with high π-facial selectivity.

3. Summary

The large number of stereoselective photooxygenations that were compiled in the present review clearly demonstrate that the Schenck reaction constitutes a versatile and efficient oxyfunctionalization in organic chemistry. As we have seen, over the years many different methods have been developed to control stereoselectivity efficiently. Several special factors are involved in the stereocontrol of ene reactions with singlet oxygen, and it is impossible to explains the results obtained from the diverse substrates in terms of a single mechanistic picture. This is expected in view of the fact that stereoselectivity in reactions with singlet oxygen is substrate-controlled since this symmetrical reagent lacks stereochemical information. Nevertheless, at this point we will try to evaluate some of the more important features in order to compile a guide for the preparative chemist in the application of the stereoselective Schenck reaction in synthesis. In Table 1 the more important substrate classes that were covered in Section 2 are summarized with respect to type, sense, extent, and scope of stereocontrol in the Schenck reaction. The selective formation of either diastereomer by simple modification of the electronic properties of the functional group at the chiral center would be most useful, as described for different allylic amines in Section 2.2.2.3.

Table 1. Substrate-dependent π-facial selectivity in the Schenck reaction.

Substrate class	Stereocontrol			Scope
	Type[a]	Extent	Sense[b]	
monocyclic olefins	steric conformational	low	*anti*	general
bi- and polycyclic olefins	steric conformational	moderate to high	*anti*	limited
functionalized cyclic olefins	steric stereoelectronic	low to high	*anti*	limited
acyclic allylic alcohols	electronic	high	*threo*	general[c]
acyclic allylic ethers and esters	steric	low	*threo*/*erythro*	general
acyclic allylic amines	electronic	high	*threo*	general[c, d]
diacylated acyclic allylic amines	steric electronic	high	*erythro*	?
acyclic allylic halides, sulfoxides, and sulfones	electronic	high	*erythro*	?

[a] Major selectivity-determining effects as defined in Section 1. [b] For cyclic substrates *syn*/*anti*, for acyclic ones *threo*/*erythro*. [c] A *cis* substituent adjacent to the stereogenic center must be present. [d] Limitations due to side reactions for unreactive amines.

Inspection of the compilation in Table 1 shows that effective stereocontrol has not yet been achieved for cyclic systems. Polycyclic systems in particular will in many cases give very high levels of diastereoselectivity, but only if the substrate itself already bears very special structural features. This applies to many natural products such monoterpenes and steroids, but for synthetic utility it would be much more important if simple monocyclic model substrates would react with high and predictable stereocontrol. However, especially for this class of substrates the stereoselectivity is poor. Thus, incorporating into a synthetic sequence a potentially stereoselective Schenck reaction for a cyclic substrate is problematic. For monocyclic systems, which are easily prepared, low levels of π-facial selectivity are to be expected, while the more difficult to prepare polycyclic substrates still bear the risk of an unselective ene reaction. Too many effects are involved in the Schenck reaction of cyclic substrates to reduce the experimental data to some simple rules.

Nonbonding repulsion, that is, steric control, will in all cases make its contribution, but due the small size of singlet oxygen molecule and its symmetrical structure high levels of stereocontrol cannot be expected. Conformational effects will in many cases also play a major role. Since singlet oxygen is an electronically excited compound, its reactions will always proceed exothermically. This means that early transition states are involved and that even conformational preferences in the substrate may be evident in the final product ratio. This may be effective in some cases, but an a priori evaluation is extremely difficult.

Furthermore, for the Schenck reaction of cyclic systems, no effective methods are known to date for taming singlet oxygen sufficiently by attractive interactions to overcome the steric bias of the substituent and favor *syn* attack. However, repulsion of singlet oxygen by functional groups may be a useful approach in the future for controlling *anti* attack in the preparation of ene products. For synthetic utility it will be important whether highly selective *anti* attack can be achieved for simple cyclic allylic alcohols or carboxylic acids.

Surprisingly, the situation looks much more promising for acyclic systems. The Schenck reaction of acyclic allylic alcohols and amines constitutes a very general and efficient method for the diastereoselective preparation of highly oxyfunctionalized, *threo*-configurated target molecules. The only prerequisite for the substrate structure is the presence of a substituent located *cis* with respect to the chiral center, which allows for efficient differentiation in the energies of the different conformers through 1,3-allylic strain. Furthermore, simple diacylation of the free allylic amine can be used to prepare efficiently the *erythro* product. Also other hetero substituents, for example sulfinyl, sulfonyl, and halogen groups, seem to have remarkable *erythro*-directing propensity, but for these substrates it is still necessary to define the scope and limitations.

What was unfavorable for cyclic substrates, namely the relatively low sensitivity of singlet oxygen to steric effects and the critical dependence on certain conformational arrangements, may be most beneficial in open-chain systems. In these highly flexible substrates, electronic effects such as hydrogen bonding and electrostatic repulsion come into play and override any possible steric effects. Furthermore, for abstraction at an acyclic alkyl site, the optimal arrangement of the hydrogen atom perpendicular to the plane of the double bond can usually be readily achieved, so that conformational effects will also not be decisive. The high sensitivity to solvent effects clearly demonstrates that the operating electronic effects in the photooxygenation are only very weak. Since the list of suitable, nonpolar solvents includes very common ones such as carbon tetrachloride, chloroform, and aromatic hydrocarbons, this should be no major drawback for synthetic applications. The substrate-directed Schenck reaction of olefins with an adjacent, heteroatom-substituted chiral center is a very versatile and mild method for the predicted stereoselective oxyfunctionalization of acyclic substrates. The effects encountered seem to be rather general and, therefore, application in a synthetic sequence should be profitable.

We have shown that singlet oxygen, although it is a highly reactive oxidant, can be utilized in a highly stereoselective manner in the Schenck reaction for the preparation of a variety of valuable oxyfunctionalized target molecules. The operative mechanistic features are highly diverse and complex, nevertheless, most interesting. While quite special mechanistic rationalizations apply for the individual substrates, consideration of all the case studies reported here leads also to a better understanding of the behavior of singlet oxygen in general. Since single oxygen is electronically excited, the oxyfunctionalization reaction starts out on a high-energy potential enery surface with expected shallow wells. The electronically excited system will tend to dissipate the excess energy by either physical quenching or chemical formation of a product. It is this feature of singlet oxygen that makes it difficult to predict and rationalize the chemo-, regio-, and stereoselectivity of photooxygenations. Nevertheless, we have shown that this highly reactive oxidant can be guided to perform selective oxyfunctionalizations for practical applications. Unquestionably, the electronically excited singlet oxygen enophile continues to present an intellectual challenge for both experimental and theoretical chemists!

Our work in this area was generously supported by the Deutsche Forschungemeinschaft (Schwerpunktprogramm "Peroxidchemie: Mechanistische und präparative Aspekte des Sauerstofftransfers") and the Fonds der Chemischen Industrie (doctoral fellowship for M. P.).

Received: February 10, 1995
Revised version: May 5, 1995 [A 1041E]
German version: *Angew. Chem.* **1996**, *108*, 519–538

[1] M. Hudlicky, *Oxidation in Organic Chemistry*, American Chemical Society, Washington, DC, **1990**, p. 1.
[2] *Oxygen Complexes and Oxygen Activation by Transition Metals* (Eds.: A. E. Martell, D. T. Sawyer), Plenum, New York, **1987**; D. H. R. Barton, D. Doller, *Pure Appl. Chem.* **1991**, *63*, 1567–1576; T. Funabiki, H. Ishida, S. Yoshida, *Chem. Lett.* **1991**, 1819–1822.
[3] R. W. Murray, M. L. Kaplan, *J. Am. Chem. Soc.* **1969**, *91*, 5358–5364.
[4] H. H. Wasserman, J. R. Scheffer, *J. Am. Chem. Soc.* **1967**, *89*, 3075–3076.
[5] J. M. Aubry, B. Cazin, F. Duprat, *J. Org. Chem.* **1989**, *54*, 726–728.
[6] T. Vidóczy, *J. Photochem. Photobiol. B* **1992**, *14*, 139–142.
[7] *Singlet Molecular Oxygen* (Ed.: A. P. Schaap), Dowden, Hutchinson Ross, Stroudsburg, PA, **1976**.
[8] *Singlet Oxygen* (Eds.: H. H. Wasserman, R. W. Murray), Academic Press, New York, **1979**.
[9] *Singlet Oxygen* (Ed.: A. A. Frimer), CRC, Boca Raton, FL, **1985**.
[10] K. Gollnick, *Adv. Photochem.* **1968**, *6*, 1–123.
[11] R. W. Denny, A. Nickon, *Org. React. (NY)* **1973**, *20*, 133–336.
[12] F. Ohloff, *Pure Appl. Chem.* **1975**, *43*, 481–502.
[13] H. H. Wasserman, J. L. Ives, *Tetrahedron* **1981**, *37*, 1825–1852.
[14] A. A. Gorman, M. A. J. Rodgers, *Chem. Soc. Rev.* **1981**, *10*, 205–231.
[15] E. L. Clennan, *Adv. Oxygenated Processes* **1988**, *1*, 85–122.
[16] E. L. Clennan, *Tetrahedron* **1991**, *47*, 1343–1382.
[17] E. L. Clennan, C. S. Foote in *Organic Peroxides* (Ed.: W. Ando), Wiley, Chichester, **1992**, p. 255.
[18] E. L. Clennan, K. Nagraba, *J. Am. Chem. Soc.* **1988**, *110*, 4312–4318.
[19] "Allylic Oxidation with Singlet Molecular Oxygen": W. Adam, A. Griesbeck, *Methoden Org. Chem. (Houben-Weyl) 4th ed. 1952–*, E 22, in press.
[20] G. O. Schenck, DE-B 933925, **1943**.
[21] K. Gollnick, G. O. Schenck in *1,4-Cycloaddition Reactions* (Ed.: J. Hamer), Academic Press, New York, **1967**, Chapter 10.
[22] W. Adam, M. Heil, T. Mosandl, C. R. Saha-Möller in *Organic Peroxides* (Ed.: W. Ando), Wiley, Chichester, **1992**, p. 221.
[23] G. O. Schenck, *Naturwissenschaften* **1948**, *35*, 28–29.
[24] A. Schönberg, *Preparative Organic Photochemistry*, Springer, Berlin, **1958**.
[25] N. A. Porter in *Organic Peroxides* (Ed.: W. Ando), Wiley, Chichester, **1992**, p. 157.
[26] W. Adam, M. Braun, A. Griesbeck, V. Lucchini, E. Staab, B. Will, *J. Am. Chem. Soc.* **1989**, *111*, 203–212.
[27] W. Adam, M. J. Richter, *Acc. Chem. Res.* **1994**, *27*, 57–62.
[28] E. D. Mihelich, D. J. Eickhoff, *J. Org. Chem.* **1983**, *48*, 4135–4137.
[29] W. Adam, M. J. Richter, *Synthesis* **1994**, 176–180.
[30] W. Adam, P. Klug, *Synthesis* **1994**, 557–559.

[31] K. Yamaguchi, S. Yabushita, T. Fueno, K. N. Houk, *J. Am. Chem. Soc.* **1981**, *103*, 5043–5046; A. G. Davies, C. H. Schiesser, *Tetrahedron* **1991**, *47*, 1707–1726.

[32] L. B. Harding, W. A. Goddard III, *J. Am. Chem. Soc.* **1980**, *102*, 439–449.

[33] S. Inagaki, H. Fujimoto, K. Fukui, *J. Am. Chem. Soc.* **1975**, *97*, 7480–7484; M. J. S. Dewar, W. Thiel, *ibid.* **1977**, *99*, 2339–2340; M. Hotokna, B. Roos, P. Siegbahn, *ibid.* **1983**, *105*, 5263–5269.

[34] M. A. McCarrick, Y. D. Wu, K. N. Houk, *J. Org. Chem.* **1993**, *58*, 3330–3343.

[35] A. A. Frimer, *Chem. Rev.* **1979**, *79*, 359–387.

[36] J. R. Hurst, S. L. Wilson, G. B. Schuster, *Tetrahedron* **1985**, *41*, 2191–2197.

[37] M. Orfanopoulos, I. Smonou, C. S. Foote, *J. Am. Chem. Soc.* **1990**, *112*, 3607–3614.

[38] L. M. Stephenson, D. E. McClure, P. K. Sysak, *J. Am. Chem. Soc.* **1973**, *95*, 7888–7889.

[39] M. Orfanopoulos, L. M. Stephenson, *J. Am. Chem. Soc.* **1980**, *102*, 1417–1418.

[40] K. Gollnick, H. Hartmann, H. Paur in *Oxygen and Oxyradicals in Chemistry and Biology* (Eds.: M. A. J. Rodgers, E. L. Powers), Academic Press, New York, **1981**, pp. 379–395.

[41] A. A. Gorman, I. R. Gould, I. Hamblett, *J. Am. Chem. Soc.* **1982**, *104*, 7098–7104.

[42] A. A. Gorman, I. Hamblett, C. Lambert, B. Spencer, M. C. Standen, *J. Am. Chem. Soc.* **1988**, *110*, 8053–8059.

[43] D. B. Sharp, *Abstr. Pap. 138th Nat. Meet. Am. Chem. Soc.*, New York, **1960**, p. 79.

[44] M. Orfanopoulos, M. J. Grdina, L. M. Stephenson, *J. Am. Chem. Soc.* **1979**, *101*, 275–276; L. M. Stephenson, M. J. Grdina, M. Orfanopoulos, *Acc. Chem. Res.* **1980**, *13*, 419–425; V. Rautenstrauch, W. Thommen, K. H. Schulte-Elte, *Helv. Chim. Acta* **1986**, *69*, 1638–1643; M. Orfanopoulos, M. Stratakis, Y. Elemes, F. Jensen, *J. Am. Chem. Soc.* **1991**, *113*, 3180–3181; M. Stratakis, M. Orfanopoulos, *Tetrahedron Lett.* **1995**, *36*, 4291–4294.

[45] Aldehydes and ketones: H. E. Ensley, R. V. C. Carr, R. S. Martin, T. E. Pierce, *J. Am. Chem. Soc.* **1980**, *102*, 2836–2838; B.-M. Kwon, R. C. Kanner, C. S. Foote, *Tetrahedron Lett.* **1989**, *30*, 903–906; H. E. Ensley, *Adv. Oxygenated Processes* **1990**, *2*, 181–202.

[46] Carboxylic acids and their derivatives: W. Adam, A. Griesbeck, *Angew. Chem.* **1985**, *97*, 1071–1072; *Angew. Chem. Int. Ed. Engl.* **1985** *24*, 417; M. Orfanopoulos, C. S. Foote, *Tetrahedron Lett.* **1985**, *26*, 5991–5994; W. Adam, A. Griesbeck, *Synthesis* **1986**, 1050–1052; T. Akasaka, K. Takeuchi, W. Ando, *Heterocycles* **1989**, *28*, 445–451; M. Orfanopoulos, M. Stratakis, *Tetrahedron Lett.* **1991**, *32*, 7321–7324.

[47] Sulfoxides: T. Akasaka, Y. Misawa, M. Goto, W. Ando, *Tetrahedron* **1989**, *45*, 6657–6666.

[48] Vinylsilanes and -stannanes: W. E. Fristad, T. R. Bailey, L. A. Paquette, R. Gleiter, M. C. Böhm, *J. Am. Chem. Soc.* **1979**, *101*, 4420–4423; W. E. Fristad, T. R. Bailey, L. A. Paquette, *J. Org. Chem.* **1980**, *45*, 3028–3037; W. Adam, M. J. Richter, *ibid.* **1994**, *59*, 3335–3340; W. Adam, P. Klug, *ibid.* **1993**, *58*, 3416–3420; *ibid.* **1994**, *59*, 2695–2699.

[49] M. Orfanopoulos, M. Stratakis, Y. Elemes, *Tetrahedron Lett.* **1989**, *30*, 4875–4878; *J. Am. Chem. Soc.* **1990**, *112*, 6417–6419; M. Stratakis, M. Orfanopoulos, *Synth. Commun.* **1993**, *23*, 425–430.

[50] A. H. Hoveyda, D. A. Evans, G. C. Fu, *Chem. Rev.* **1993**, *93*, 1307–1370.

[51] Ene reactions of carbonyl enophiles: Z. Song, P. Beak, *J. Am. Chem. Soc.* **1990**, *112*, 8126–8134.

[52] G. O. Schenck, *Angew. Chem.* **1952**, *64*, 12–28; G. O. Schenck, K. Gollnick, G. Buchwald, S. Schroeter, G. Ohloff, *Justus Liebigs Ann. Chem.* **1964**, *674*, 93–117.

[53] K. Gollnick, G. Schade, *Tetrahedron Lett.* **1973**, 857-860; C. S. Foote, S. Wexler, W. Ando, *ibid.* **1965**, 4111–4118.

[54] K. Gollnick, F. Frenken, G. Schade, G. Dörhöfer, *Ann. NY Acad. Sci.* **1970**, *171*, 89.

[55] K. H. Schulte-Elte, M. Gadola, B. L. Müller, *Helv. Chim. Acta* **1971**, *54*, 1870–1880.

[56] J. A. Marshall, A. R. Hochstetler, *J. Org. Chem.* **1966**, *31*, 1020–1025.

[57] G. O. Schenck, O.-A. Neumüller, W. Eisfeld, *Justus Liebigs Ann. Chem.* **1958**, *618*, 202–210; A. Nickon, W. L. Mendelson, *J. Am. Chem. Soc.* **1965**, *87*, 3921–3928; A. Nickon, N. Schwartz, J. B. DiGiorgio, D. A. Widdowson, *J. Org. Chem.* **1965**, *30*, 1711–1717.

[58] A. Nickon, J. B. DiGiorgio, P. J. L. Daniels, *J. Org. Chem.* **1973**, *38*, 533–539.

[59] H. E. Ensley, R. V. C. Carr, *Tetrahedron Lett.* **1977**, 513–516.

[60] C. W. Jefford, A. F. Boschung, *Helv. Chim. Acta* **1974**, *57*, 2242–2257.

[61] G. O. Schenck, H. Eggert, W. Denk, *Justus Liebigs Ann. Chem.* **1953**, *584*, 177–198.

[62] K. Gollnick, G. Schade, *Tetrahedron Lett.* **1966**, 2335–2341.

[63] K. Gollnick, S. Schroeter, G. Ohloff, G. Schade, G. O. Schenck, *Justus Liebigs Ann. Chem.* **1965**, *687*, 14–25.

[64] E. Klein, W. Rojahn, *Chem. Ber.* **1965**, *98*, 3045–3049.

[65] H. C. Brown, J. H. Kawakami, K. T. Liu, *J. Am. Chem. Soc.* **1973**, *95*, 2209–2216; C. W. Jefford, C. G. Rimbault, *ibid.* **1978**, *100*, 6516–6517.

[66] H. C. Brown, J. Muzzio, *J. Am. Chem. Soc.* **1966**, *88*, 2811–2822.

[67] C. W. Jefford, C. G. Rimbault, *J. Am. Chem. Soc.* **1978**, *100*, 6437–6445; C. W. Jefford, C. G. Rimbault, *J. Org. Chem.* **1978**, *43*, 1908–1912.

[68] L. A. Paquette, C. C. Liao, D. C. Liotta, W. E. Fristad, *J. Am. Chem. Soc.* **1976**, *98*, 6412–6413.

[69] K. Okada, T. Mukai, *J. Am. Chem. Soc.* **1978**, *100*, 6509–6512.

[70] L. A. Paquette, L. W. Hertel, R. Gleiter, M. Böhm, *J. Am. Chem. Soc.* **1978**, *100*, 6512–6513; L. W. Hertel, L. A. Paquette, *ibid.* **1979**, *101*, 7622–7623.

[71] L. A. Paquette, L. W. Hertel, R. Gleiter, M. C. Böhm, M. A. Beno, G. C. Christoph, *J. Am. Chem. Soc.* **1981**, *103*, 7106–7121.

[72] Y.-D. Wu, Y. Li, J. Na, K. N. Houk, *J. Org. Chem.* **1993**, *58*, 4625–4628.

[73] A. R. Chamberlin, R. L. Mulholland, Jr., S. D. Kahn, W. J. Hehre, *J. Am. Chem. Soc.* **1987**, *109*, 672–677.

[74] W. Adam, H. G. Brünker, unpublished results.

[75] H. B. Henbest, *Proc. Chem. Soc.* **1963**, 159–165.

[76] For a discussion on cyclopentadienols see: S. D. Kahn, W. J. Hehre, *J. Am. Chem. Soc.* **1987**, *109*, 663–666.

[77] For other cyclohexenol derivatives: F. W. A. M. Miesen, J. L. J. van Dongen, E. W. Meijer, *Rec. Trav. Chim. Pays Bas* **1994**, *113*, 307–317.

[78] W. Adam, B. Nestler, unpublished results.

[79] G. Rio, M. Charifi, *Bull. Soc. Chim. Fr.* **1970**, 3598–3600; G. Rio, D. Bricout, *ibid.* **1971**, 3557–3560.

[80] T. Linker, L. Fröhlich, *Angew. Chem.* **1994**, *106*, 2064–2066; *Angew. Chem. Int. Ed. Engl.* **1994**, *33*, 1971–1972; *J. Am. Chem. Soc.* **1995**, *117*, 2694–2697.

[81] G. O. Schenck, K. Gollnick, O. A. Neumüller, *Justus Liebigs Ann. Chem.* **1957**, *603*, 46–59; A. Nickon, W. L. Mendelson, *J. Am. Chem. Soc.* **1961**, *83*, 1498–1508; *ibid.* **1965**, *87*, 3921–3928.

[82] J. G. Luis, L. S. Andrés, W. Q. Fletcher, *Tetrahedron Lett.* **1994**, *35*, 179–182.

[83] Atta-ur-Rahman, Z. Shah, *Stereoselective Synthesis in Organic Chemistry*, Springer, New York, **1993**.

[84] W. Adam, H.-G. Brünker, B. Nestler, *Tetrahedron Lett.* **1991**, *32*, 1957–1960.

[85] H. E. Ensley, R. V. C. Carr, R. S. Martin, T. E. Pierce, *J. Am. Chem. Soc.* **1980**, *102*, 2836–2838; H. E. Ensley, *Adv. Oxygenated Processes* **1990**, *2*, 181–201.

[86] P. H. Dussault, K. R. Woller, M. C. Hillier, *Tetrahedron* **1994**, *50*, 8929–8940; see also G. B. Jones, B. J. Chapman, *Synthesis* **1995**, 475–497.

[87] B. Nestler, Dissertation, Universität Würzburg, **1993**.

[88] R. Gerdil, G. Barchietto, C. W. Jefford, *J. Am. Chem. Soc.* **1984**, *106*, 8004–8005.

[89] H.-G. Brünker, W. Adam, *J. Am. Chem. Soc.* **1995**, *117*, 3976–3982.

[90] R. W. Hoffmann, *Chem. Rev.* **1989**, *89*, 1841–1860.

[91] H. Kropf, R. Reichwaldt, *J. Chem. Res.* **1987**, 412–413.

[92] W. Adam, B. Nestler, *Liebigs Ann. Chem.* **1990**, 1051–1053.

[93] W. Adam, B. Nestler, *J. Am. Chem. Soc.* **1992**, *114*, 6549–6550; **1993**, *115*, 5041–5049.

[94] For an early example of hydroxyl group directed stereocontrol see: K. H. Schulte-Elte, B. L. Müller, G. Ohloff, *Helv. Chim. Acta* **1971**, *54*, 1899–1910.

[95] W. Adam, P. Klug, *Synthesis* **1994**, 567–572.

[96] W. Adam, B. Nestler, *Tetrahedron Lett.* **1993**, *34*, 611–614.

[97] B. E. Rossiter, T. R. Verhoeven, K. B. Sharpless, *Tetrahedron Lett.* **1979**, 4733–4736; K. B. Sharpless, T. R. Verhoeven, *Aldrichim. Acta* **1979**, *12*, 63–74; M. G. Finn, K. B. Sharpless, *Asymmetric Synth.* **1985**, *5*, 247–368.

[98] A. S. Narula, *Tetrahedron Lett.* **1982**, *23*, 5579–5582.

[99] W. Adam, O. Gevert, P. Klug, *Tetrahedron Lett.* **1994**, *35*, 1681–1684.

[100] S. J. Brois, *J. Am. Chem. Soc.* **1968**, *90*, 506–508; *Trans. NY Acad. Sci.* **1969**, *31*, 931–951.

[101] R. S. Davidson, K. R. Trethewey, *J. Chem. Soc. Chem. Commun.* **1975**, 674–675; R. S. Davidson, K. R. Trethewey, *J. Chem. Soc. Perkin Trans 2* **1977**, 173–178.

[102] M. H. Fisch, J. C. Gramain, J. A. Olesen, *J. Chem. Soc. Chem. Commun.* **1970**, 13–14; *J. Chem. Soc. Chem. Commun.* **1971**, 663; J. H. E. Lindner, H. J. Kuhn, K. Gollnick, *Tetrahedron Lett.* **1972**, 1705–1706.

[103] W. Adam, H.-G. Brünker, *J. Am. Chem. Soc.* **1993**, *115*, 3008–3009.

[104] For a recent application in natural product synthesis see: W. Adam, H.-G. Brünker, *Synthesis* **1995**, 1066–1067.

[105] W. Adam, H.-G. Brünker, S. Kumar, *J. Am. Chem. Soc.*, in press.

[106] Other examples: E. L. Clennan, X. Chen, *J. Am. Chem. Soc.* **1989**, *111*, 5787–5792; T. Akasaka, Y. Misawa, M. Goto, W. Ando, *Tetrahedron* **1989**, *45*, 6657–6666.

[107] W. Adam, L. H. Catalani, A. G. Griesbeck, *J. Org. Chem.* **1986**, *51*, 5494–5496.

Electron Domains and the VSEPR Model of Molecular Geometry

Ronald J. Gillespie* and Edward A. Robinson

The valence shell electron pair repulsion (VSEPR) model—also known as the Gillespie–Nyholm rules—has for many years provided a useful basis for understanding and rationalizing molecular geometry, and because of its simplicity it has gained widespread acceptance as a pedagogical tool. In its original formulation the model was based on the concept that the valence shell electron pairs behave as if they repel each other and thus keep as far apart as possible. But in recent years more emphasis has been placed on the space occupied by a valence shell electron pair, called the domain of the electron pair, and on the relative sizes and shapes of these domains. This reformulated version of the model is simpler to apply, and it shows more clearly that the Pauli principle provides the physical basis of the model. Moreover, Bader and his co-workers' analysis of the electron density distribution of many covalent molecules have shown that the local concentrations of electron density (charge concentrations) in the valence shells of the atoms in a molecule have the same relative locations and sizes as have been assumed for the electron pair domains in the VSEPR model, thus providing further support for the model. This increased understanding of the model has inspired efforts to examine the electron density distribution in molecules that have long been regarded as exceptions to the VSEPR model to try to understand these exceptions better. This work has shown that it is often important to consider not only the relative locations and sizes, but also the shapes, of both bonding and lone pair domains in accounting for the details of molecular geometry. It has also been shown that a basic assumption of the VSEPR model, namely that the core of an atom underlying its valence shell is spherical and has no influence on the geometry of a molecule, is normally valid for the nonmetals but often not valid for the metals, including the transition metals. The cores of polarizable metal atoms may be nonspherical because they include nonbonding electrons or because they are distorted by the ligands, and these nonspherical cores may have an important influence on the geometry of a molecule.

Keywords: electron density distribution · electron pair domains · molecular geometry · VSEPR model

1. Introduction

The valence shell electron pair repulsion (VSEPR) model has for many years provided a useful basis for understanding and rationalizing molecular geometry, and its simplicity has led to its widespread acceptance as a pedagogical tool.[1–3] Nevertheless it has often been regarded as a purely empirical theory having no real physical basis, or as a classical electrostatic theory. It is the purpose of this review to show that 1) the model continues to provide a simple explanation of the structures of many new molecules that have been prepared in recent years, including many detailed features of their structures that often cannot be easily accounted for in any other way; 2) the formulation of the model in terms of electron domains is simpler to understand and to apply than the original version of the model; 3) the Pauli principle is the physical basis of the electron pair domain concept and therefore of the VSEPR model; 4) the domain version of the VSEPR model provides a complement to the conventional orbital models that is useful in introductory chemistry for discussing not only the topic of molecular geometry but also the concept of the chemical bond itself; 5) the domain version of the model is supported by the analysis of the total electron density of a molecule in terms of both electron density deformation maps and the Laplacian of the electron density; 6) the analysis of the Laplacian of the electron density leads to a better understanding of the structures of metal–nonmetal type molecules, including those of the transition metals and shows how the VSEPR model can be modified so that it applies to such molecules.

[*] Prof. R. J. Gillespie
Department of Chemistry, McMaster University
1280 Main Street West
Hamilton, Ontario, L8S 4M1 (Canada)
Fax: Int. code + (905) 522-2509
e-mail: gillespi@mcmail.cis.mcmaster.ca
Prof. E. A. Robinson
Department of Chemistry, University of Toronto (Canada)

2. The Pauli Principle and Electron Pair Domains

2.1. The Pauli Principle

The Pauli principle provides the physical basis for the VSEPR model. In its most general form it states the following: *The total wave function for a system must be antisymmetric to the exchange*

 © VCH Verlagsgesellschaft mbH, D-69451 Weinheim, 1996 0570-0833/96/3505-0495 $ 15.00+.25/0

of any two electrons.[4] A direct conclusion is that two electrons of the same spin have a zero probability of being at the same point in space and a maximum probability of being as far apart as possible, in other words, electrons with the same spin tend to keep apart in space.[5] The Pauli principle places no restrictions on electrons of opposite spin, however, which may indeed be close together or even at the same location.

The importance of the Pauli principle in determining molecular geometry can be clearly seen if we consider the valence shell of eight electrons (the octet) that is commonly found for many atoms in their molecules. In such a valence shell there are four electrons of α spin and four of β spin. As a consequence of the Pauli principle there is a high probability that the four electrons of α spin will have a mutually tetrahedral arrangement, as will the four β electrons (Fig. 1a, b, d, e).[5] From the point of view of the Pauli principle the two tetrahedral sets of electrons are not correlated. However, electrostatic repulsion not only reinforces the tendency of each set of electrons to adopt a tetrahedral arrangement but also tends to keep the two tetrahedra apart. In a free atom such as the neon atom no external force restrains the free movement of the two tetrahedral sets of electrons, which results in an overall spherical total electron density. In contrast, in a molecule the positive cores of one or more ligand atoms attract the valence shell electrons of the central atom. In accordance with the Pauli principle a ligand core may attract two electrons of opposite spin into the same region to form a bond. If A is the central atom with tetrahedral arrangements of both α electrons and β electrons in its valence shell, the formation of two A–H (or two A–X bonds where X is a singly bonded ligand) brings the α spin tetrahedron into approximate coincidence with the β spin tetrahedron, thus forming four electron pairs—two bonding pairs and two nonbonding (lone) pairs (Fig. 1c, f). Each pair of electrons is approximately localized in a part of the valence shell of A—one pair in each of two bonding regions and one pair in each of two nonbonding regions.

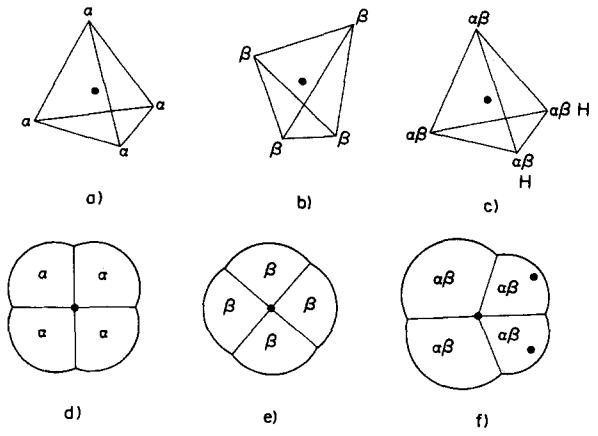

Fig. 1. Most probable arrangement of four valence shell electrons with spin α (a) and spin β (b), and of eight valence shell electrons in an AH_2 molecule (c). Two dimensional representations of the domains of four valence shell electrons with spin α (d) and spin β (e), and of eight valence shell electrons (f) in an AH_2 molecule.

2.2. Electron Pair Domains

We call the region of space in the valence shell in which an electron pair is most probably to be found an electron pair domain. Daudel[6] has previously called such a region of space a loge. Thus a valence shell containing four electron pairs may

R. J. Gillespie

E. A. Robinson

Prof. Ronald J. Gillespie graduated from University College London, obtaining his Ph.D. degree in 1949 and DSc. in 1957. He was a Lecturer at University College London from 1948 to 1958 when he moved to McMaster University as Associate Professor, becoming Professor in 1960 and Emeritus Professor in 1989. After his Ph.D. research on aromatic nitration in sulphuric acid with Sir Christopher Ingold, he did extensive work on the chemistry of superacid media such as H_2SO_4, HSO_3F, and HF including the preparation of noble gas fluorocations and a large number of novel polyatomic cations of the nonmetals. He has received many awards for his work, including election to the Fellowship of the Royal Society of London in 1977 and the American Chemical Society awards for Creative Work in Fluorine Chemistry and for Distinguished Service to Inorganic Chemistry. He has had a long standing interest in Chemical Education and in the use of simple models in the teaching of chemistry. He first proposed the widely used VSEPR model with Ronald S. Nyholm in 1957.

Born in London, England, in 1933, E. A. (Peter) Robinson obtained his Ph.D. under Ronald J. Gillespie in 1958 at the University College, London. Then he moved to McMaster University and worked as an original member of the Gillespie research group in Canada. From 1961 to 1994 he was at the University of Toronto, where he is now Professor Emeritus. In 1965 he became a founding member of the University of Toronto's Erindale Campus in Mississauga. As the first Associate Dean, the second Dean, and the third Principal, he played a major role in the organization and construction of the newest Toronto campus, which is now equally recognized for the quality of its teaching and research. Ongoing research interests include the understanding of both lengths in terms of the Lewis octet rule and expanded octets, and hydrogen bonding involving C–H bonds. He was awarded a D.Sc. by the University of London in 1969.

be thought of as being divided into four tetrahedrally arranged regions or domains in each of which the probability of finding an electron pair is high. We will see later that it is important to consider the shapes of domains but as a rough first approximation we may consider that a domain has a spherical shape, as first proposed by Bent in his tangent-sphere model.[7] Four spheres pack as closely as possible around a point (the core of the atom) by adopting a tetrahedral arrangement, which demonstrates in a simple way that four equivalent domains are expected to have a tetrahedral arrangement (Fig. 2). Similarly

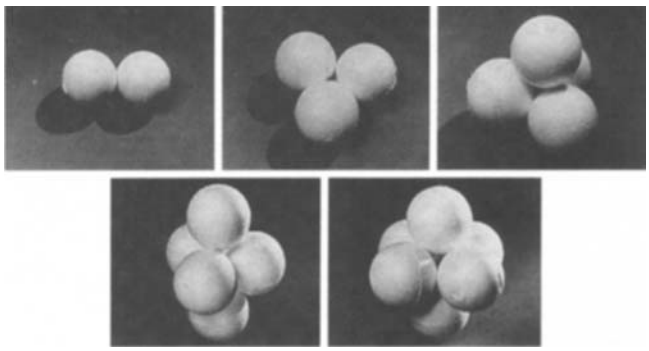

Fig. 2. Arrangements of two to six spherical domains surrounding the core.

two spheres representing two electron pair domains adopt a linear arrangement, three spheres a triangular arrangement, five spheres a trigonal-bipyramidal arrangement, and six spheres an octahedral arrangement (Fig. 2). In the arrangements of two, three, four, and six electron pairs all the domains are equivalent. However, it is not possible to have an arrangement of five equivalent domains, except by arranging them in a plane. But this arrangement does not keep the domains as far apart as possible. In the trigonal-bipyramidal arrangement there is a set of three equivalent (equatorial) domains and a set of two equivalent (axial) domains (Fig. 2). As a result AX_5, molecules with five identical ligands do not have five equal AX bonds, but have two longer axial bonds and three shorter equatorial bonds.

The basic assumption of the VSEPR model in its original form was that a given number of valence shell electron pairs, considered as points, adopt that arrangement that keeps them as far apart as possible (the points-on-a-sphere model). This formulation of the model has sometimes led to the misunderstanding that it is just electrostatic repulsion that keeps electron pairs apart. But the formulation of the model in terms of electron pair domains makes it clear that the formation of electron pairs that keep as far apart as possible is a consequence of the Pauli exclusion principle, electron–nucleus attraction, and electron–electron repulsion.

2.3. Single Bond and Lone Pair Domains

In the valence shell of an atom that obeys the octet rule there are four electron pair domains. When these domains are equivalent, as in an AX_4 molecule where X is a singly bonded ligand, the four equivalent single bond domains are arranged tetrahedrally, and the molecule has a tetrahedral geometry. In an AX_3E molecule, where E is a lone pair, there are three single bond domains giving a triangular-pyramidal molecule with an approximately tetrahedral bond angle. In an AX_2E_2 molecule two single bond domains and two lone pair domains give a molecule with an angular geometry and a bond angle of approximately 109° (Fig. 3).

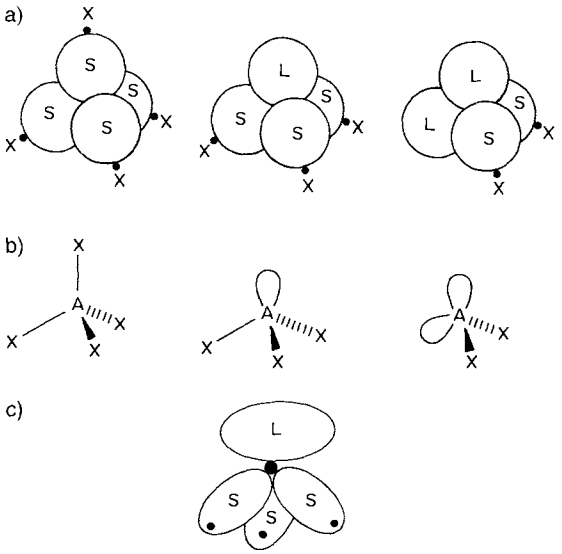

Fig. 3. AX_4, AX_3E, and AX_2E_2 molecules. a) Domain models; S is a single bond domain and L a lone pair domain. b) Conventional bond line structures. c) Approximate relative shapes and sizes of the domains in an AX_3E molecule.

Deviations in bond angles from the ideal angles corresponding to the various most probable electron pair arrangements can be accounted for by recognizing that bonding and nonbonding domains are not equivalent, and in particular, by assuming that they have different shapes and sizes. A nonbonding valence shell electron pair is attracted by just one positive core and so its domain tends to surround the core and thus take up as much space as possible in the valence shell. However, a single bond domain is restricted in size and has a different shape because the two electrons are attracted by two positive cores. Thus in any valence shell a nonbonding domain is larger and is closer to the core than a bonding domain (Fig. 3c). The larger size of a lone pair domain accounts for the observation that in very many molecules in which an atom has one or more lone pairs the angles between the bonds are smaller than the ideal values. For example, they are smaller than 109.5° for AX_3E and AX_2E_2 molecules (Tables 1 and 2) and smaller than 90° for an AX_5E molecule (Table 3). Although electron pair domains are not as localized as shown in Figures 2 and 3 it is very convenient, as we shall see, to think of them as nonoverlapping. So the representations of the domains in Figures 2 and 3 can be regarded as approximately denoting those regions where there is a relatively high probability of finding an electron pair.

In its original form[8] the VSEPR model postulated that the strength of the repulsions between electron pairs decreases in the order lone-pair–lone-pair > lone-pair–bond-pair > bond-pair–bond-pair. This assumption leads to the same conclusions about bond angles as the domain model, although the conclu-

Table 1. Bond angles α [°] in trigonal-pyramidal AX_3E molecules and ions.

Molecule	α	Ref.	Molecule	α	Ref.
NH_3	107.3	[44]	PI_3	102	[58]
PH_3	93.8	[45]	AsI_3	100.2	[59]
AsH_3	91.8	[46]	SbI_3	99.1	[60]
SbH_3	91.7	[46]	$(CH_3)_3N$	110.9	[61]
NF_3	102.2	[47]	$(CH_3)_3P$	98.6	[61]
PF_3	97.8	[48]	$(CH_3)_3As$	96.0	[62]
AsF_3	96.1	[49, 50]	$(CH_3)_3Sb$	94.2	[61]
SbF_3	87.3	[51]	$(CH_3)_3Bi$	96.7	[63]
NCl_3	107.1	[52]	$(CF_3)_3N$	110.9	[64]
PCl_3	100.3	[53]	$(CF_3)_3P$	97.2	[65]
$AsCl_3$	98.6	[50]	$(CF_3)_3As$	100.0	[66]
$SbCl_3$	97.2	[54]	$(CF_3)_3Sb$	100.0	[66]
$BiCl_3$	100	[55]	SF_3^+	97.5	[67]
PBr_3	101.1	[56]	SeF_3^+	94.5	[68]
$AsBr_3$	99.8	[57]	TeF_3^+	90(2)	[69]
$SbBr_3$	98.2	[54]	SCl_3^+	103.3	[70]
$BiBr_3$	100(4)	[55]			

Table 2. Bond angles α [°] in angular AX_2E_2 molecules and ions.

Molecule	α	Ref.	Molecule	α	Ref.
OH_2	104.5	[71]	ClF_2^+	96	[87, 88]
SH_2	92.1	[72]	BrF_2^+	92	[88]
SeH_2	90.6	[73]	ICl_2^+	93	[89]
TeH_2	90.3	[74]	HOF	97.2	[90]
OF_2	103.1	[75]	HOCl	102.5	[91]
SF_2	98.2	[76]	HOBr	110	[92]
SeF_2	94	[77]	CF_3OF	104.8	[93]
OCl_2	111.2	[78]	CH_3OH	108.6	[94]
SCl_2	102.8	[79]	CH_3SH	96.5	[95]
$SeCl_2$	99.6	[80]	CH_3SeH	95.5	[96]
$TeCl_2$	97.0	[81]	CF_3SH	111.2	[97]
$O(CH_3)_2$	111.7	[82]	CH_3SCl	99.4	[98]
$S(CH_3)_2$	99.1	[83]	CF_3SF	97.1	[85]
$Se(CH_3)_2$	96.3	[84]	CF_3SCl	98.9	[85]
$S(CF_3)_2$	97.3	[85]	ClO_2^-	108.6	[99]
$Se(CF_3)_2$	95.6	[86]	NH_2^-	99.4	[2]
			NF_2^-	96.7	[2]

Table 3. Bond angles α(ax–eq) [°] and bond lengths d [pm] in AX_5E molecules and ions.

Compound	d_{ax}	d_{eq}	α	Ref.
$XeF_5^+ SbF_6^-$	179.3(9)	184.5(8)	–	[100]
$XeF_5^+ (AgF_4^-)$	182.6(9)	185.2(19)	77.7(3)	[101]
$XeF_5^+ (PtF_6^-)$	181.0	184.3	79	[102]
ClF_5	157(1)	167(2)	86(2)	[103]
BrF_5	168.9(8)	177.4(3)	84.8(1)	[104]
IF_5	184.4(25)	186.9(5)	81.9(1)	[104]
$TeF_5^- Na^+$	186.2(4)	195.2(4)	87.8	[105]
$SbF_5^{2-} (NH_4^+)_2$	191.6(4)	207.5(2)	88.0	[106]
$SbCl_5^{2-} (NH_4^+)_2$	236	258–269	85	[107]

sions are not always reached so simply. Because electrons of the same spin have a low probability of being close together, electron pair domains resist overlap. It is in this sense that domains may be said to repel each other, and so larger domains appear to repel other domains more strongly than smaller domains.

The importance of considering the relative sizes and shapes of electron pair domains was pointed out by Gillespie many years ago,[1] although the term electron domain was not introduced at that time. However, even though it has several advantages over the electron-pair repulsion formulation, the domain concept has not often been used in the discussion of molecular shapes in terms of the VSEPR model. These advantages are particularly evident for AX_4E, AX_3E_2 and AX_2E_3 molecules. It is simple to understand, for example, why a lone pair always occupies an equatorial position in these types of molecules. An equatorial position is less crowded than an axial position because it has two neighboring axial positions at 90° and two equatorial positions further away at 120°, whereas an axial position has three neighboring equatorial positions at 90°. Because they are larger than bond pair domains, lone pair domains always occupy the less crowded equatorial positions of these molecules, so that AX_4E molecules such as SF_4 always have a disphenoidal shape, AX_3E_2 molecules such as ClF_3 always have a T-shape, and AX_2E_3 molecules such as XeF_2 always have a linear shape (Fig. 4). Another advantage of the domain model is that it allows us to understand how a lone pair domain may exert direc-

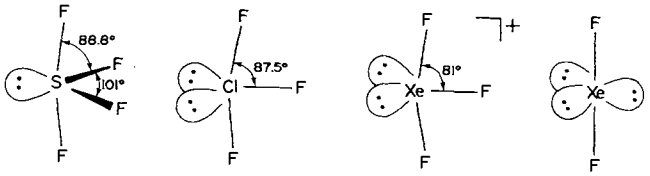

Fig. 4. Examples of AX_4E, AX_3E_2, and AX_2E_3 molecules in which lone pairs always occupy equatorial positions.

tional repulsive effects. The angles between the domains in the equatorial plane of AX_4E, AX_3E_2, and AX_2E_3 molecules are larger than the angles between the axial and equatorial domains. Accordingly a lone pair domain in an equatorial position spreads out more in the equatorial direction than in the axial direction giving it a noncylindrically symmetrical shape, and distorting a larger equatorial bond angle more than a smaller axial–equatorial bond angle. Thus in SF_4, for example, the more easily distorted $F_{eq}SF_{eq}$ angle is reduced by 19° from the ideal value of 120°, while the $F_{ax}SF_{eq}$ angles are reduced by only 1.2° from the ideal angle of 90°. Other similar data are given in Table 4. A recent analysis of the electron density of the SF_4 molecule through its Laplacian[9] (discussed in Section 3.2) has confirmed the unsymmetrical shape of its lone pair domain.

We can similarly understand the shape of the planar XeF_5^- ion, the unique example of an AX_5E_2 molecule (Fig. 5).[10] Although the best arrangement of seven equivalent domains cannot be predicted with certainty,[2] it is reasonable to suppose that the geometry of XeF_5^- would be based on that of the closely related IF_7 and TeF_7^- molecules, which have a pentagonal-bipyramidal geometry.[11, 12] In the pentagonal-bipyramidal arrangement of seven domains in a valence shell more space is available in the axial positions, which make angles of 90° with the neighboring equatorial positions, than in an equatorial position, which makes two angles of 72° and two of 90° with neighboring positions. Hence, large lone pair domains are always expected to occupy the axial positions in a pentagonal bipyramidal arrangement of seven domains leading to the observed pentagonal-planar shape of the XeF_5^- ion.

Table 4. Bond angles α [°] and bond lengths d [pm] in disphenoidal AX_4E and T-shaped AX_3E_2 molecules and ions.

Molecule	d_{ax}	d_{eq}	α		Ref.
AX_4E					
PF_4^-	174	160	$F_{ax}PF_{ax}$	168.3	[108]
			$F_{eq}PF_{eq}$	99.9	
SF_4	164.6(3)	154.5(3)	$F_{ax}SF_{ax}$	173.1(5)	[109]
			$F_{eq}SF_{eq}$	101.6(5)	
$FS\text{-}SF_3$	167.3(7)	156.9(8)	$F_{ax}SF_{ax}$	167.0	[110]
			$F_{eq}SS_{eq}$	104.9(14)	
CH_3SF_3	168.9(1)	157.5(5)	$F_{ax}SF_{ax}$	174.6(8)	[111]
			$F_{eq}SC_{eq}$	102.9(8)	
CF_3SF_3	167.9(4)	159.6(11)	$F_{ax}SF_{ax}$	165.2(25)	[111]
			$F_{eq}SC_{eq}$	100.7(16)	
$(CF_3)_2SF_2$	168.1(3)	188.8(4)	$F_{ax}SF_{ax}$	173.9(8)	[112]
			$C_{eq}SC_{eq}$	97.3(8)	
$(CH_3)_2N\text{-}SF_3$	167.0(7)	156.3(9)	$F_{ax}SF_{ax}$	174.0(12)	[113]
			$F_{eq}SN_{eq}$	104.6(10)	
$[(CH_3)_2N]_2SF_2$	177.0(2)	164.8(2)	$F_{ax}SF_{ax}$	174.7(1)	[114]
			$F_{eq}SN_{eq}$	102.3(1)	
$Ph_2S[OC(CF_3)_2Ph]_2$	188.9(4)	180.7(7)	$O_{ax}SO_{ax}$	175.1(2)	[115]
			$C_{eq}SC_{eq}$	104.4(3)	
$(ClC_6H_4)_2SCl_2$	226–232	178	$Cl_{ax}SCl_{ax}$	174.5(11)	[116]
			$C_{eq}SC_{eq}$	91.4(3)	
SeF_4	177.1(4)	168.2(4)	$F_{ax}SeF_{ax}$	169.2(7)	[117]
			$F_{eq}SeF_{eq}$	100.6(7)	
$(CF_3)_2SeF_2$	182.7	202.2	$F_{ax}SeF_{ax}$	157.8	[118]
			$C_{eq}SeC_{eq}$	118.7	
$(C_6H_5)_2SeCl_2$	230(5)	–	$Cl_{ax}SeCl_{ax}$	180(5)	[119]
			$C_{eq}SeC_{eq}$	118	
$(CH_3C_6H_4)_2SeCl_2$	238	–	$Cl_{ax}SeCl_{ax}$	177.5	[120]
			$C_{eq}SeC_{eq}$	106.5	
$(C_6H_5)_2SeBr_2$	252(1)	191(3)	$Br_{ax}SeBr_{ax}$	180(3)	[121]
			$C_{eq}SeC_{eq}$	110(10)	
$(CH_3C_6H_4)_2SeBr_2$	255	–	$Br_{ax}SeBr_{ax}$	177	[120]
			$C_{eq}SeC_{eq}$	108	
$(C_6H_5)_2TeF_2$	200.6	211.5(3)	$F_{ax}TeF_{ax}$	175.3(1)	[122]
			$C_{eq}TeC_{eq}$	96.9(1)	
$(CH_3)_2TeCl_2$	251	210	$Cl_{ax}TeCl_{ax}$	172.3(3)	[123]
			$C_{eq}TeC_{eq}$	98.2(11)	
$(2\text{-}C_3H_6Cl)_2TeCl_2$	250	215	$Cl_{ax}TeCl_{ax}$	169	[124]
			$C_{eq}TeC_{eq}$	98	
$(C_6H_5)_2TeCl_2$	250.6	210.7	$Cl_{ax}TeCl_{ax}$	175.5(1)	[125]
			$C_{eq}TeC_{eq}$	99.0(3)	
$(C_6H_5)_2TeBr_2$	268.2(3)	218(3)	$Br_{ax}TeBr_{ax}$	177.9(2)	[126]
			$C_{eq}TeC_{eq}$	95.4	
$(CH_3)_2TeI_2$	285–299	210–216	$I_{ax}TeI_{ax}$	177–180	[127]
			$C_{eq}TeC_{eq}$	91–97	
$(C_6H_5)_2TeI_2$	292.8(1)	213.3(13)	$I_{ax}TeI_{ax}$	175.5(5)	[128]
			$C_{eq}TeC_{eq}$	95.3(5)	
BrF_4^+ ($Sb_2F_{11}^-$)	186	177	$F_{ax}IF_{ax}$	173.5	[129]
			$F_{eq}IF_{eq}$	92.4	
IF_4^+	184	177	$F_{ax}IF_{ax}$	160	[130]
			$F_{eq}IF_{eq}$	92	
$ClOF_3$	171.3(3)	160.3(4)	$F_{ax}ClF_{ax}$	170.5	[131]
		140.5(3) [a]	$F_{eq}ClO_{eq}$	108.9	
$IO_2F_2^-$	200	193	$F_{ax}XeF_{ax}$	180	[132]
			$O_{eq}IO_{eq}$	100	
XeO_2F_2	189.9(3)	171.4(4)	$F_{ax}XeF_{ax}$	183.2(2)	[133]
			$O_{eq}XeO_{eq}$	105.7(3)	
AX_3E_2					
ClF_3	169.8(5)	159.8(5)	$F_{ax}ClF_{ax}$	175(4)	[134]
BrF_3	181.0	172.1	$F_{ax}BrF_{ax}$	172.4	[135]
$C_6H_5ICl_2$	245	200	$Cl_{ax}ICl_{ax}$	172	[136]
XeF_3^+ (SbF_6^-)	190.5(15)	183.5(10)	$F_{ax}XeF_{ax}$	160.9(5)	[137]
$[Br_2Se\text{-}CN]^-$	258	174	$Br_{ax}SeBr_{ax}$	179.2	[138]

[a] Cl=O bond length.

2.4. Single Electron Domains

In some free radicals the unpaired electron is located mainly on a single atom. A single electron can be considered to occupy a single electron domain that is expected to be smaller than an electron pair domain, so it affects the geometry of a molecule

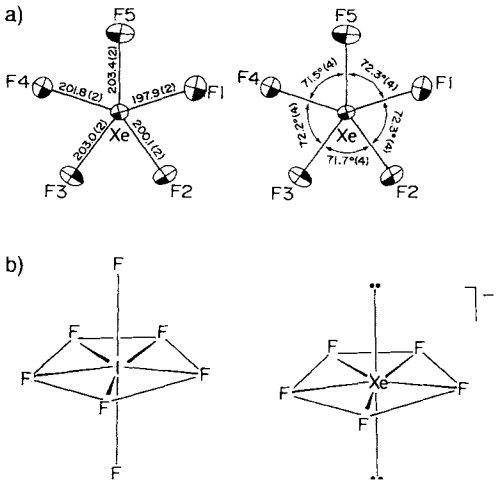

Fig. 5. a) Structure of the XeF_5^- ion (bond lengths in pm). b) Comparison of the structure of IF_7 (an AX_7 molecule) and XeF_5^- (an AX_5E_2 molecule).

less than a lone pair as exemplified by the three molecules NO_2^+, NO_2, and NO_2^-, which have bond angles of 180°, 134°, 115° respectively (Fig. 6a). The difference in size between an electron pair domain and a single electron domain is also seen clearly in the calculated structure of the SF_4^- radical, which has C_{4v} symmetry. This structure is consistent with a trans arrangement of the lone pair and the single electron and with the bending of the SF bonds, away from the lone pair towards the single electron (Fig. 6b).[113] SF_4^- may be said to have an AX_4Ee geometry, where e represents a single electron domain.

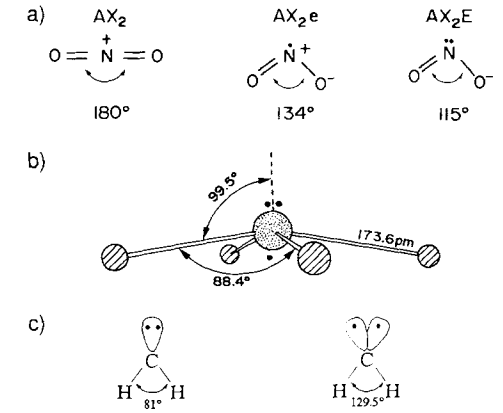

Fig. 6. Single electron domains. a) The bond angle decreases in the series NO_2^+, NO_2, NO_2^-. b) The SF_4^- radical has a C_{4v} structure consistent with the smaller domain for a single nonbonding electron and a larger domain for the nonbonding lone pair. c) Bond angles in the singlet (left) and triplet (right) states of CH_2.

The different stereochemical influence of single electron domains and those of lone pairs is further exemplified by the singlet and triplet states of carbene (Fig. 6c). In the singlet state CH_2 may be described as an AX_2E molecule and, as expected, has a bonding angle small than 120°. The triplet state, which may be described as an AX_2E_2 molecule, has a bond angle larger than the tetrahedral angle, showing the smaller stereochemical effect of the single electron domains.[113b]

2.5. Single Bond Domains and Electronegativity

The space occupied by a single bond domain in the valence shell of A depends on the relative electronegativities of the central atom A and the ligand X. The larger the electronegativity of X and the smaller the electronegativity of A, the less space the A–X bond domain occupies in the valence shell of the central atom A and the smaller the angle between the A–X bond and other neighboring bonds, as can be seen in many of the examples in Tables 1–4. If we consider a lone pair as a bond pair that is bonding a ligand of zero electronegativity we can again see why a lone pair has a domain that is larger than that of any bond pair.

The bond angles of the hydrides of the elements of groups V (that is, Group 15) and VI (that is, Group 16), however, appear to be exceptions to the rule that the X-A-X bond angle decreases with increasing electronegativity of X. The bond angles in PH_3 and H_2S, for example are smaller than in PF_3 and SF_2, although hydrogen is less electronegative than fluorine (Tables 1 and 2). However, hydrogen is a unique element in several ways. One important difference between hydrogen and any other ligand is that the electron pair of an A–H bond has to play the role of both a bonding pair and a nonbonding pair in that it also shields the proton on the opposite side to the bond, in other words the domain of this pair of electrons is not confined to the bonding region but extends into the nonbonding region of the hydrogen atom. Hence the electron density in an A–H bond is smaller than in other single bonds. It follows that A–H bonds can be squeezed together by lone pairs on A much more easily than any A–X bonds, thereby giving a smaller bond angle.

The existence of SF_6, SeF_6, and BrF_6^+, but not of ClF_7 and BrF_7, suggests that the elements of periods 3 and 4 can accommodate up to, but no more than, six electron pair domains with an octahedral arrangement in their valence shells.[14] A few molecules such as $SeCl_6^{2-}$ that appear to be exceptions to this rule are discussed later (Section 3). Hence it is reasonable to suppose that the repulsions between bonding domains in the valence shells of these elements only become significant as the angle between them approaches 90°---the bond angle in an octahedral arrangement of six domains. Hence the bond angles in PH_3, AsH_3, H_2S, and H_2Se approach this limiting value of 90°. However, for all other ligands, repulsions between the bond pair domains become significantly large before the bond angle is close to 90°.

It has long been recognized that more electronegative ligands have a preference for the axial sites and less electronegative ligands a preference for the equatorial sites of a trigonal-bipyramidal structure, as in the examples in Figure 7. The electron pair domains in the axial positions are more crowded than those in the equatorial positions, so the smaller domains bonding the more electronegative ligands favor the axial sites, while the larger domains bonding the less electronegative ligands favor the equatorial sites. In contrast in a pentagonal-bipyramidal AX_7 structure, the axial sites are less crowded and the equatorial sites are more crowded, and the less electronegative ligands favor the axial sites (Fig. 8).

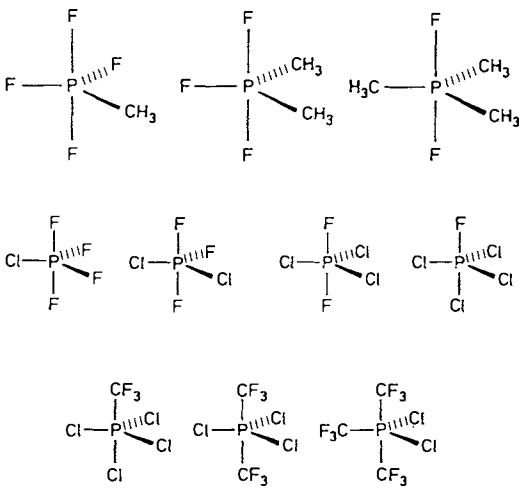

Fig. 7. Examples of PX_5 molecules in which the less electronegative ligands always occupy the equatorial positions.

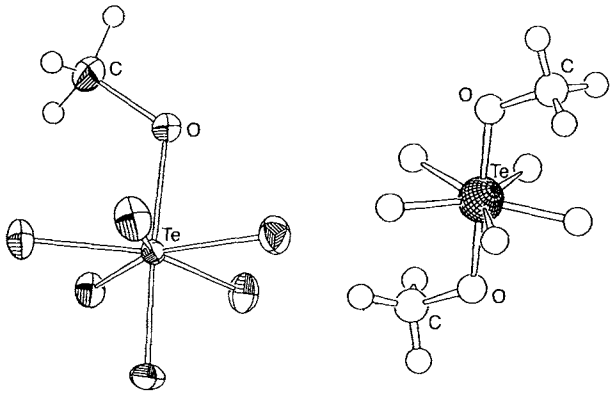

Fig. 8. Structures of the pentagonal-bipyramidal molecules $TeF_6(OMe)$ (left) and $TeF_5(OMe)_2$ (right) in which the less electronegative OMe group preferentially occupies an axial position.

2.6. Multiple Bond Domains

A double bond is formed by the sharing of two electron pair domains between two atoms and a triple bond by the sharing of three electron pair domains between two atoms (Fig. 9a, b). These representations of multiple bonds correspond to the classical bent bond descriptions (Fig. 9c, d), which account for the planar shape of the ethene molecule and the linear shape of the ethyne molecule, and for the decreased CC bond lengths in these molecules.[15] However, we would not expect the HCH bond angle in ethene to retain the ideal tetrahedral angle. The two bonding pairs are attracted toward the same two positive carbon cores and are therefore squeezed together, which allows the repulsion between the CH bond domains to open the HCH bond angle to 117.4° in ethene. In C_2F_4 the FCF bond angle of 112.4° is still smaller and is closer to the tetrahedral angle (Table 5).

Alternatively, and often more conveniently, the two single bond electron pair domains forming a double bond may be considered to be overlapped to such an extent that they form

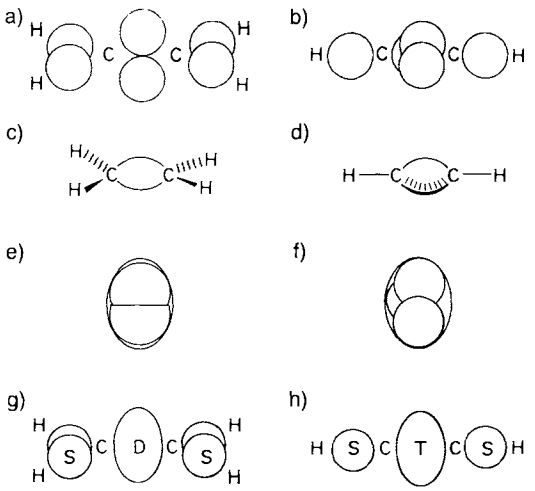

Fig. 9. Representations of the structures of ethene and ethyne. a), b) Electron pair domain models. c), d) Bent bond structural diagrams. e) Prolate ellipsoidal double bond domain formed from two electron pair domains. f) Oblate ellipsoidal triple bond domain formed from three electron pair domains. g) Domain model of ethene showing the AX_3 triangular arrangement of two single bond domains S and a prolate ellipsoidal double-bond domain D at both carbon atoms. h) Domain model of ethyne showing the linear AX_2 arrangement of a single-bond domain S and an oblate ellipsoidal triple-bond domain T at both carbon atoms.

one double bond domain containing four electrons in which the two separate pairs cannot be distinguished (Fig. 9e). The total electron density distribution has an elliptical cross section with a maximum on the CC axis. Figure 9g shows the arrangement of the single and double bond domains giving a planar ethene molecule. Similarly the three single electron pair domains forming a triple bond may be considered to be overlapped to form one six electron triple bond domain (Fig. 9f). Figure 9h shows the arrangement of single and triple bond domains giving a linear ethyne molecule.

The bent bond picture of a double or a triple bond is sometimes criticized, because it appears to suggest that there is an absence of electron density along the bond axis. However, this is an incorrect interpretation of the bent bond model, because bond lines give no indication of the size of the corresponding electron pair domain; in particular they do not show that there is considerable overlap of the bent bond domains to give a double or triple bond domain that has an electron density along the CC axis that is greater than along any other line between the two nuclei. The bent bond model is also sometimes criticized on the grounds that the photoelectron spectrum of ethene shows two ionization energies associated with the double bond, whereas the bent bond model implies that all four of the bond electrons are equivalent. The photoelectron spectrum does not, however, tell us anything about the ground state of ethene but only that, when one electron is removed from the double bond, two states of the ion may be obtained, which can be described as $\sigma^2\pi^1$ and as $\sigma^1\pi^2$. Clearly it is convenient when discussing such spectra to represent the ground state as $\sigma^2\pi^2$, but it is not essential to do so, because a bent bond description, for example one based on sp^3 hybrid orbitals, is essentially equivalent.[15] The bent bond description is, however, not convenient for the ionized state because the unpaired electron is more delocalized than this description permits.

Table 5. Examples of bond lengths d [pm] and single bond–double bond angles in $X_2C=CY_2$ and $X_2C=Z$ molecules.

Molecule	Bond	d	Bond angles				Ref.
			X-C-X	Y-C-Y	X-C-C	Y-C-C	
$H_2C=CH_2$	C–H	108.7(1)	117.4	117.4	121.3	121.3	[139]
	C=C	133.9(1)					
$F_2C=CH_2$	C–F	131.5(3)	110.6	119.3	124.7	120.3	[140]
	C–H	109.1(10)					
	C=C	134.0(6)					
$F_2C=CF_2$	C–F	131.9(1)	112.4	112.4	123.8	123.8	[141]
	C=C	131.1(3)					
$F_2C=CCl_2$	C–F	131.5(15)	112.1	119.0	124.0	120.5	[142]
	C–Cl	170.6(8)					
	C=C	134.5(25)					
$Cl_2C=CCl_2$	C–Cl	171.9(3)	115.6	115.6	122.2	122.2	[143]
	C=C	135.5(3)					
$Br_2C=CBr_2$	C–Br	188.2(3)	115.2	115.2	122.4	122.4	[144]
	C=C	136.3(9)					
$I_2C=CI_2$	C–I	210.6(5)	114.2	114.2	122.9	122.9	[143]
	C=C	136.3(15)					
$(CH_3)_2C=C(CH_3)_2$	C–C	151.1(2)	113.2	113.2	123.4	123.4	[145]
	C=C	135.1(3)					
$(CH_3)_2C=CH_2$	C–C	150.7(1)	115.6	117.4	122.2	121.3	[146]
	C–H	109.5(20)					
	C=C	134.2(1)					
			X-C-X		X-C-Y		
$H_2C=O$	C–H	–	116.5		121.8		[147]
	C=O	120.8(3)					
$F_2C=O$	C–F	131.6(1)	107.7		126.2		[148]
	C=O	117.2(1)					
$Cl_2C=O$	C–Cl	173.8(2)	111.8		124.1		[149]
	C=O	117.6(3)					
$Br_2C=O$	C–Br	192.3(5)	112.3		123.8		[150]
	C=O	117.8(9)					
$(CH_3)_2C=O$	C–C	151.7(2)	116.7		121.7		[151]
	C=O	121.1(2)					
$(CF_3)_2C=O$	C–C	154.9(8)	121.4		119.3		[152]
	C=O	124.6(14)					
$(CF_3)_2C=NH$	C–C	155.1(7)	121.6		119.2		[152]
	C=N	129.6(29)					
$H_2C=S$	C–H	109.2(2)	116.9		121.6		[153]
	C=S	161.1(2)					
$F_2C=S$	C–F	131.6(2)	107.1		126.5		[154]
	C=S	158.9(2)					
$Cl_2C=S$	C–Cl	172.9(3)	111.2		124.4		[155]
	C=S	160.1(3)					
$Br_2C=S$	C–Br	189.4(9)	111.6		124.2		[156]
	C=S	159.7(5)					

Only the most electronegative atoms attract electrons strongly enough to pull two or three electron pairs into the bonding region against their mutual repulsion so that in the vast majority of multiple bonds at least one of the atoms is C, N, or O. Only a few examples of molecules containing double bonds between third and subsequent period elements exist, because their smaller electronegativity than that of period 2 elements allows the repulsion between the four electrons to produce a larger, more diffuse and hence more reactive domain that is very readily attacked by electrophilic reagents. The only stable examples of such molecules have large bulky groups protecting the double bond from attack, as for example in tetramesityldisilene $(Mes)_2Si=Si(Mes)_2$.

The general shapes of molecules containing multiple bonds can be readily predicted simply on the basis of the number of single, double, triple, and lone-pair domains in the valence shell of any given atom by using the basic rule that the domains share out the space in the valence shell of an atom so as to keep as far apart as possible. So three domains (single, double, triple, or lone-pair) always have a trigonal planar arrangement, four do-

mains a tetrahedral arrangement, five domains a trigonal-bipyramidal arrangement, and six domains an octahedral arrangement. Examples of shapes of molecules containing multiple bonds are given in Figure 10.

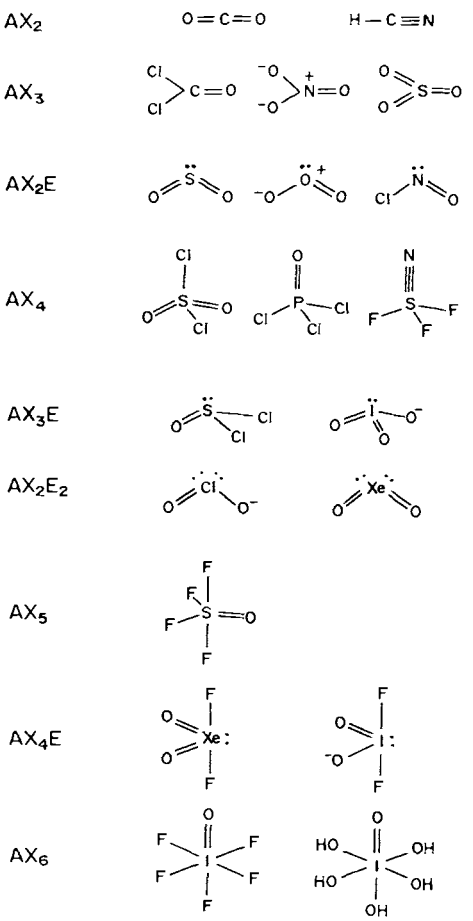

Fig. 10. Shapes of molecules containing multiple bonds.

Qualitative predictions about the relative magnitudes of bond angles in molecules containing multiple bonds can be made on the basis of the relative sizes of the single, double, and triple bond domains. It is clear that a double bond domain must be larger than a single bond domain, and a triple bond domain larger still. For example, in ethene the H-C-C angles that involve the double bond domain are larger (121.3°) than the H-C-H bond angle (117.4°); in SO_2Cl_2 the angle between the two S–O double bonds (123.5°) is much larger than that between the two S–Cl single bonds (100.3°). Other examples are given in Tables 5 and 6.

The larger size of a multiple bond domain compared to a single bond domain also explains the observation that a doubly bonded ligand Y, like a lone pair, always occupies an equatorial site in trigonal-bipyramidal and related molecules, as can be seen from the examples given in Figure 11. Similarly in the case of the pentagonal-bipyramidal seven-coordinated molecule IOF_6^- the doubly bonded oxygen atom occupies a less crowded axial site (Fig. 12).[112] Unlike the IF_7 molecule that is nonrigid and fluxional[111,112] IOF_6^- has a rigid structure, which can be attributed to the resistance of the I–O double bond domain against moving into a more crowded position.[112]

Table 6. Examples of bond lengths d [pm] and bond angles [°] in $X_2S(=Y)_2$ molecules.

Molecule	Bond	d	Bond angles X-S-X	Bond angles Y-S-Y	Ref.
F_2SO_2	S–F	153.0(3)	96.1(2)	124.0(2)	[157]
	S=O	140.5(3)			
Cl_2SO_2	S–Cl	201.2(4)	100.3(2)	123.5(2)	[158]
	S=O	141.8(3)			
$(HO)_2SO_2$	S–OH	157.4(10)	101.3(10)	123.3(10)	[159]
	S=O	142.2(10)			
$(CH_3)_2SO_2$	S–C	177.1(4)	102.6(9)	119.7(11)	[160]
	S=O	143.5(3)			
$(CH_2{=}CH)_2SO_2$	S–C	176.9(4)	–	119.5(12)	[161]
	S=O	143.8(3)			
$[(CH_3)_2N]_2SO_2$	S–N	162.3(5)	112.6(4)	119.7(4)	[162]
	S=O	144.5(5)			
$(CH_3)_2S(NH)_2$	S–C	179.3(2)	101.2(14)	135.0(12)	[163]
	S=N	153.5(2)			

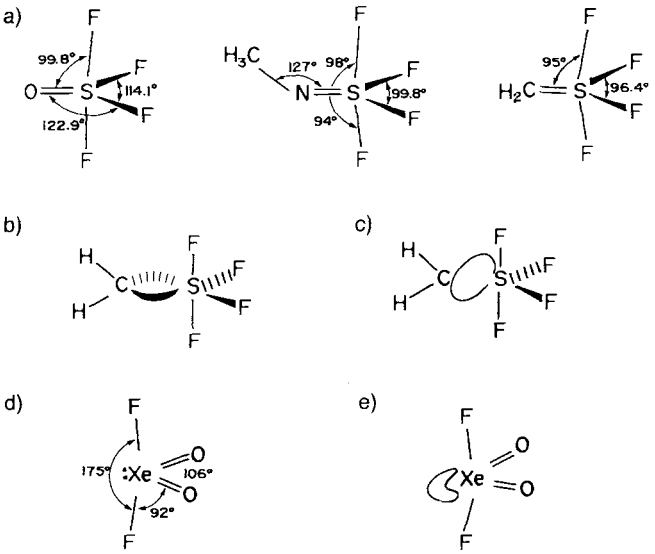

Fig. 11. a) Shapes of some $AX_4=Y$ molecules in which the doubly bonded ligand Y always occupies a less crowded equatorial position. b) Bent bond model of $H_2C=SF_4$ showing that the CH_2 group lies in the axial plane of the SF_4 group. c) Model showing the ellipsoidal double bond domain with its long axis in the equatorial plane of the SF_4 group. d) Structure of XeO_2F_2. e) Illustration of the XeO_2F_2 molecule showing the approximate shape of the xenon lone pair domain.

In interpreting details of molecular geometry it is often important to take into account not only the size of a multiple bond domain but also its shape, which depends on the directions of the other bonds formed by the two bonded atoms. In the common case of a carbon atom forming one double and two single bonds, the double bond domain has a prolate ellipsoidal shape; its long axis is constrained to lie perpendicular to the CX_2 plane to minimize its interaction with the single bond domains. In the ethene molecule the two CH_2 groups are thereby constrained to lie in the same plane, and so the molecule overall is planar (Fig. 9g).

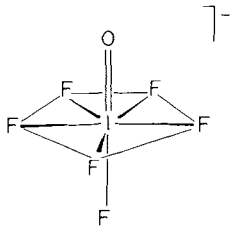

Fig. 12. The double bond domain occupies a less crowded axial position in an $AX_6=Y$ pentagonal bipyramidal molecule such as IOF_6^-.

Another example of the importance of taking into account the shape of a multiple bond domain is seen in the molecules OSF_4 and H_2CSF_4. Here the large size of the SO and SC double bond domains compared to the SF single bond domains causes all the F-S-F angles to be smaller than the ideal angles of 120° and 90° (Fig. 11a). The SC double bond domain is forced by the CH_2 group to have a prolate ellipsoidal shape with its long axis perpendicular to the CH_2 plane (Fig. 11c). To minimize its interaction with the axial SF bond domains, the double bond domain lies in the equatorial plane (with the CH_2 group perpendicular to this plane) so that it decreases the F_{eq}-S-F_{eq} angle from 120° to 96.4°, while it only decreases the F_{ax}-S-F_{ax} angle from 180° to 170°.[16a] Here the bent bond model of the double bond is particularly appropriate (Fig. 11b), as all the angles approach the ideal angle of 90° for an octahedral arrangement of six domains. In contrast the OS double bond domain is not constrained to have an ellipsoidal shape, by any bonds on the oxygen atom so it has an almost cylindrically symmetrical shape. Therefore the SO double bond domain in SOF_4 affects the F_{eq}-S-F_{eq} angle, which is decreased to 114.7°, much less than does the CS double bond in H_2CSF_4, while it has a larger effect on the F_{ax}-S-F_{ax} angle, which is reduced to 160.4°.[9] These conclusions about the shapes of the SO and SC double bonds domains have been confirmed in a study of the Laplacian of the electron density of these molecules (Section 3.2). The shape of the SC double bond domain is also shown to be elliptical in an electron density deformation map of the related molecule $(CF_3)(CH_3)(C{=}SF_4$.[16b]

It is interesting to note that the F-Xe-F angle in the AX_2Y_2E molecule XeO_2F_2 is less than 180° (174.7°) rather than greater than 180° as is normally the case for AX_4E molecules such as SF_4 (Fig. 9f). Because of the large size of the xenon core the lone pair domain is expected to be much more spread out in the equatorial plane than in the axial plane; indeed, while it exerts a strong repulsion on the Xe=O bonds it exerts a weaker repulsion on the Xe–F bond domains than do the Xe=O bond domains. Consequently, the Xe–F bonds bend towards the lone pair and away from the Xe=O bonds.

2.7. Linear Molecules

In linear (cylindrically symmetrical) molecules such as HF and CO_2 there is no requirement that the domains of electrons of opposite spin are brought into coincidence. This was recognized many years ago by Linnett when he formulated the double quartet model.[5] For example, in the HF molecule two electrons of opposite spin are attracted into the bonding region, but the two tetrahedra of electrons of opposite spin are still free to rotate around the bond axis so that the remaining electrons do not form pairs but keep apart due to electrostatic repulsion (see Fig. 13a, b). Similarly in the CO_2 molecule the tetrahedra of electrons of opposite spin are not brought into coincidence and so do not form close pairs (Fig. 13c, d). Rather there are four noncoincident single electron domains forming a cylindrically symmetric double bond (Fig. 13e). Thus the CO_2 molecule can be described as a linear AX_2 molecule in which there is a linear arrangement of two cylindrically symmetric double bond domains. As the electron–electron repulsion in this kind of double bond domain should be less than in an elliptical double bond domain in which the electrons are more closely paired, it is not surprising that the C=O bond in CO_2 (116 pm) is shorter than the standard C=O bond distance (118 pm).

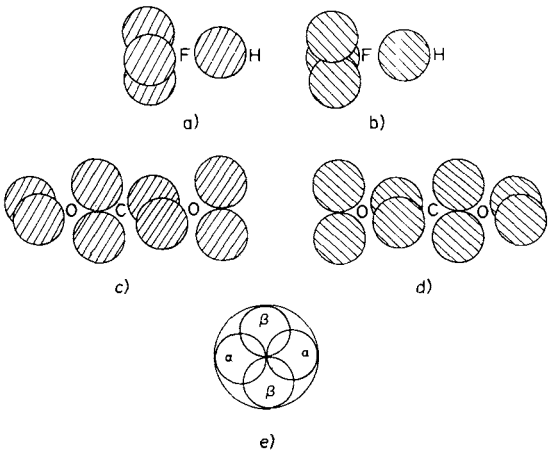

Fig. 13. Domain version of the Linnett double quartet model for the HF and CO_2 molecules: Domains of the α electrons (a) and the β electrons (b) of HF. Domains of the α electrons (c) and the β electrons (d) in CO_2. e) Cross-section of the C–O double bond showing the two α electron domains and the two β electron domains which lead to overall cylindrical symmetry.

3. The Analysis of Electron Density Distributions

The domain model is a very approximate description of the electron density distribution in a molecule and yet a useful tool for the understanding of molecular geometry. But an increasing amount of accurate information about the total electron density in molecules is now forthcoming from X-ray crystallographic studies and from ab initio calculations, and increasing attention is being paid to the analysis of these electron density distributions in an attempt to extract from them the concepts of bonding and nonbonding electron pairs or domains and to improve our understanding of molecular geometry. However, because the electron density changes accompanying bond formation are relatively very small, very accurate low-temperature X-ray crystallographic studies or high-level ab initio calculations are needed to obtain sufficiently accurate electron density distributions to justify a detailed analysis.

At first sight the total electron density distribution provides little information of interest to the chemist, because there is apparently no evidence of the localized pairs of electrons that chemists associate with bonds and lone pairs, as we see, for example, in the illustration of the total electron density of the water molecule in Figure 14. The electron density distribution of a molecule is dominated by the very large electron density close to each nucleus while the electron density in the interatomic regions in which changes in the electron density distribution due to bond formation occur are relatively very small and correspondingly difficult to detect. Bader et al.[17] has shown that the total electron density of a molecule can be partitioned into atomic densities by a rigorous quantum mechanical method and that between any two bonded atoms there is a line, called the bond path, along which the electron density is greater than

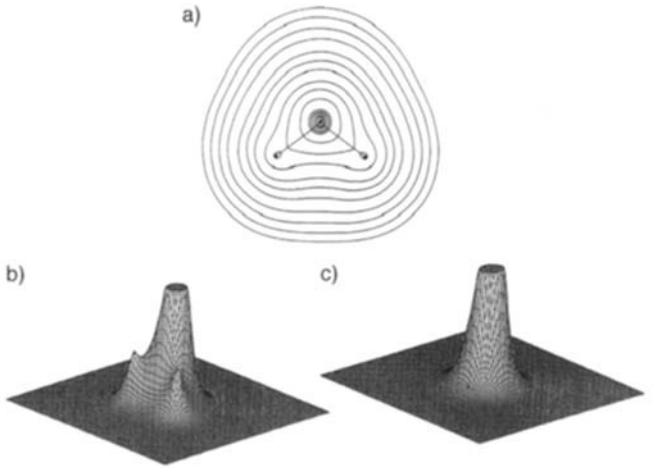

Fig. 14. Electron density distribution in the water molecule. a) Contour map in the plane in which all atoms lie. b) Relief map of the electron density in the plane depicted in (a). c) Relief map of the electron density in the plane through the oxygen atom, perpendicular to the plane depicted in (a) and bisecting the HOH angle.

along any other line between the two nuclei. The bond path appears as a ridge connecting two bonded nuclei in a relief map of the electron density in a plane containing all atoms of the molecule (Fig. 14b). However, there is no indication of bonding or nonbonding electron pairs in these plots of the electron density. There have been several approaches to the problem of analyzing the electron density distribution to provide support for the concept of localized bonding and nonbonding electron pairs. We next consider two of these: the calculation of electron density deformation maps and the analysis of the total electron density in terms of its Laplacian.

3.1. Electron Density Deformation Maps

Electron density deformation maps are obtained by subtracting from the experimental or calculated total electron density of a molecule the density of a promolecule constructed from spherical atoms with the same geometrical arrangement as the actual molecule. In principle such a deformation map should show the changes in electron density that occur on bond formation, and in many cases such maps do show concentrations of electron density in bonding regions and in lone pair regions that correspond to the bond pair and lone pair domains of the VSEPR model. Thus these studies provide some support for the model. An early electron density deformation map is that obtained for the AX_4E molecule $(CH_3)_2TeCl_2$ (Fig. 15a), which clearly shows electron density corresponding to the lone pair.[18] A recent example shows the noncylindrically symmetrical (ellipsoidal) shape of the C=S bond in the molecule $(CF_3)(CH_3)C{=}SF_4$ (Fig. 15b).[16b] However, such deformation maps do not always show the presence of the expected bonding or lone pair densities and there are serious difficulties associated with the construction of an appropriate promolecule.[19] Increasing attention is therefore being paid to other methods for the analysis of the electron density distribution, such as the topological analysis of its Laplacian.

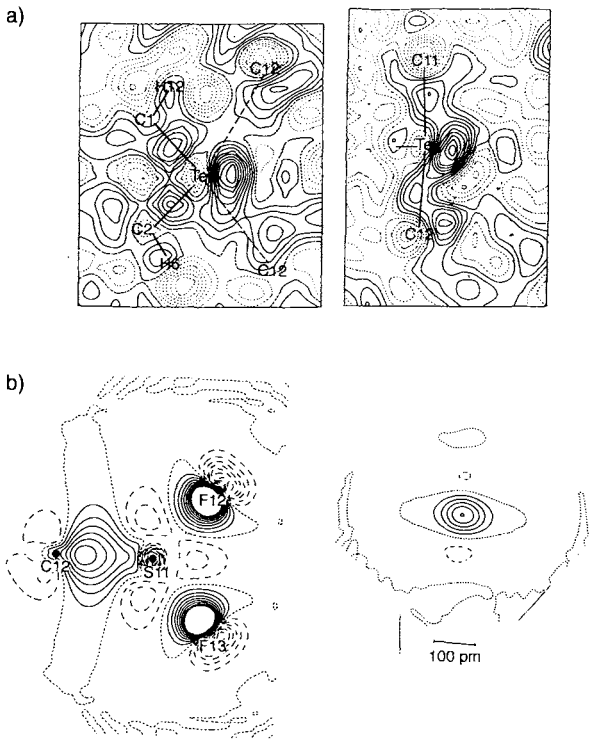

Fig. 15. a) Electron density deformation maps of $Te(CH_3)_2Cl_2$ in the equatorial plane (left) and the axial plane bisecting the angle between the CH_3 ligands (right) showing the deformation density associated with the lone pair. b) Deformation maps of the $(CF_3)(CH_3)C{=}SF_4$ molecule in the FSF equatorial plane (left) and in a plane bisecting the C=S bond showing the anisotropy of the bond corresponding to an ellipsoidal shaped double bond domain.

3.2. The Topological Analysis of the Electron Density and its Laplacian

Bader et al.[17] have shown that the total electron density of a molecule can be usefully analyzed by studying the Laplacian $\nabla^2\rho$ of the electron density ρ, which is given in Equation (a).

$$\nabla^2\rho = \partial^2\rho/\partial x^2 + \partial^2\rho/\partial y^2 + \partial^2\rho/\partial z^2 \quad \text{(a)}$$

This function has the property of magnifying very small variations in the electron density and revealing small local electron density concentrations (charge concentrations) that are not apparent in the total electron density distribution (see appendix). For example, in a free atom there is a continuous decrease in the total density with increasing distance from the nucleus, and there are no maxima and minima in the total electron density corresponding to the successive electron shells. But these shells are revealed clearly in the Laplacian as a local concentration of electron density in the form of a spherical shell surrounded by a spherical region of density depletion (Fig. 16). Although the electron shells in a free atom are also apparent in the radial distribution function, the radial distribution function has no meaning in a molecule. However, the Laplacian of a molecule still reveals the electron shells as regions of concentration and depletion of electron density but distorted by bond formation. In a large number of covalent molecules the valence shell charge concentration exhibits maxima corresponding to each of the bonds and each of the lone pairs expected from the conventional Lewis diagram for the molecule as shown in Figures 17–19 for

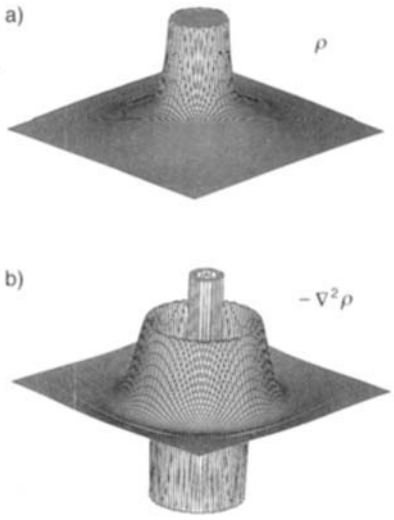

Fig. 16. a) Relief map of the electron density (ρ) in a plane through the nucleus of the argon atom. b) Relief map of the negative Laplacian ($-\nabla^2\rho$) of the electron density in the same plane.

the H_2O, ClF_3 and SF_4 molecules.[17a] Moreover, these local charge concentrations have the same locations and the same relative sizes as the electron pair domains of the VSEPR model.

In the valence shell of the oxygen atom in the water molecule there are charge concentrations in an approximately tetrahedral arrangement that correspond to two bonding and two nonbonding (lone pair) domains of the VSEPR model. Similarly the valence shell of the chlorine atom in ClF_3 contains three bond-

In the valence shell of the oxygen atom in the water molecule there are charge concentrations in an approximately tetrahedral arrangement that correspond to two bonding and two nonbonding (lone pair) domains of the VSEPR model. Similarly the valence shell of the chlorine atom in ClF_3 contains three bonding and two nonbonding charge concentrations in a trigonal-bipyramidal arrangement. And in the valence shell of sulfur in SF_4 the four bonding and one lone pair charge concentration

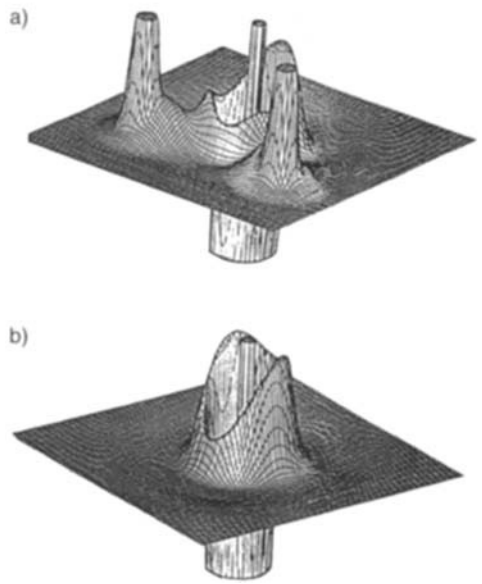

Fig. 17. Relief map of $-\nabla^2\rho$ for the mirror planes σ_v (a) and σ_v' (b) of the H_2O molecule. Two of the maxima in the valence shell charge concentration of O in a) are bonding charge concentrations. The third apparent maximum in a) is the saddle between the two maxima observed in b) that are nonbonding (lone pair) charge concentrations.

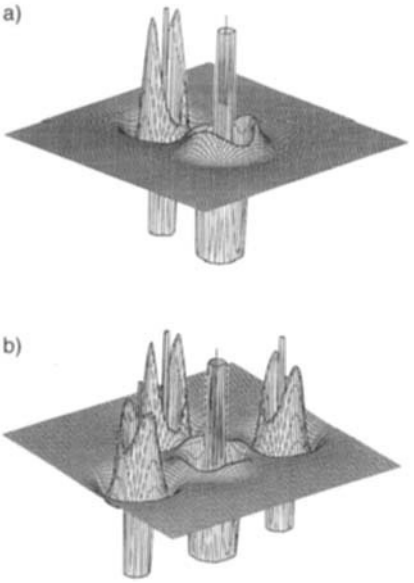

Fig. 18. Relief map of $-\nabla^2\rho$ for the mirror planes σ_v' (a) and σ_v (b) of the ClF_3 molecule. In a) the three maxima in the valence shell of Cl correspond to two nonbonding charge concentrations and a nonbonding (lone pair) charge concentration. In b) three bonding charge concentrations can be seen. The fourth apparent maximum represents the saddle between the two nonbonding maxima in a).

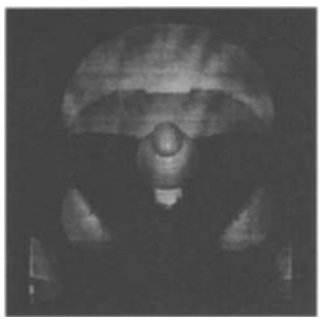

Fig. 19. Isosurface of the Laplacian distribution of the sulfur atom in SF_4, showing a large charge concentration for the lone pair two small charge concentrations for the bonding equatorial electrons, and two still smaller charge concentrations for the axial bonding electrons surrounding a spherical core. Parts of the valence shell charge concentrations of the equatorial fluorine atoms are seen in the lower corners.

are in a trigonal bipyramidal arrangement. Moreover, the Laplacian provides confirmation (Fig. 20) of the increasingly

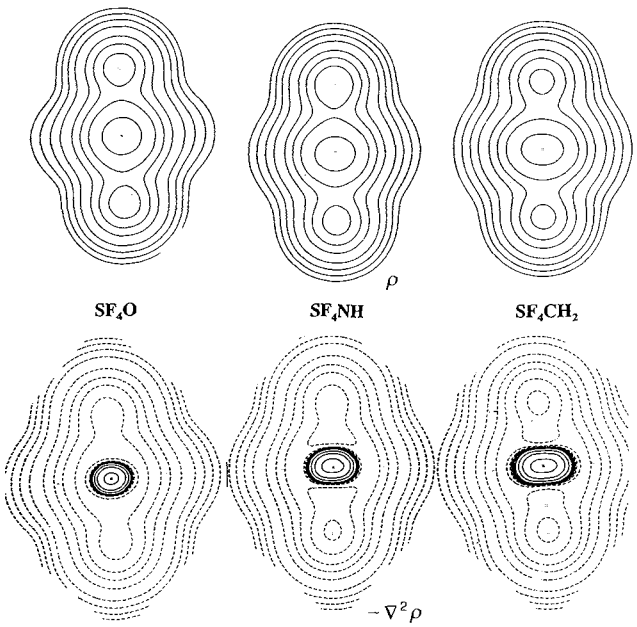

Fig. 20. Contour plot of the electron density ρ (top) and of $-\nabla^2\rho$ (bottom) in a plane through the maximum of $-\nabla^2\rho$ for the double bond in $O=SF_4$, $HN=SF_4$, and $H_2C=SF_4$ showing the increasing ellipticity of the double bond.

elliptical shape of the double bond domain in the series $O=SF_4$, $HN=SF_4$, and $H_2C=SF_4$ that we discussed in Sections 2.2 and 2.5.[9]

The Laplacian therefore provides evidence that the domain version of the VSEPR model has a real physical basis. Although electrons are not as localized into pairs as the domain model depicts them, local concentrations of electron density nevertheless correspond to and have the same properties of relative size and shape as, both bonding and nonbonding electron pair domains.

4. Exceptions to the VSEPR Model

As we have seen in the preceding sections the VSEPR model accounts very successfully for the general shapes of the molecules of the main group nonmetals and also in a qualitative way for deviations of the bond angles from the "ideal" values. However, certain exceptions to the predictions of the model have been recognized, particularly among metal–nonmetal molecules. The rest of this review is concerned with these exceptions, real or apparent. Because the model is so successful in many cases, it is worthwhile examining the exceptions in an attempt to discover why the model breaks down in some cases. In this way we can hope to improve our understanding of bonding and to see if the VSEPR model can be appropriately modified to cover the apparent exceptions. First we discuss exceptions among the main group elements.

4.1. AX_5 Molecules

Although the trigonal bipyramid with longer axial than equatorial bonds is the preferred structure, the energy of the square pyramid is only slightly higher, as is shown, for example, by the fact that it is the transition state in the Berry pseudorotation of a trigonal-bipyramidal molecule. PX_5 and AsX_5 molecules all have the expected trigonal-bipyramidal structures with longer axial than equatorial bonds, as do most SbX_5 molecules. Examples are $SbCl_5$, $Sb(CH_3)_5$,[20a] and also $Bi(CH_3)_5$.[20b] In contrast, $Sb(C_6H_5)_5$[21a] and $Bi(C_6H_5)_5$[21b] in the solid state have structures that can best be described as square pyramids, although they both are somewhat distorted towards trigonal-bipyramidal geometry. However, the closely related molecules $Sb(p\text{-}CH_3C_6H_4)_5$ and $Bi(o\text{-}FC_6H_4)_5$ are trigonal-bipyramidal in the solid state, although the latter exists as an equilibrium mixture of both trigonal-bipyramidal and square-pyramidal molecules in solution.[22] It is clear that the energy difference between the trigonal-bipyramidal and square-pyramidal structures is very small; moreover, it is to be expected that the difference in energy between the two structures will decrease with the decreasing interaction between the bonding domains as the size of the central atom increases, so it is not surprising that it is essentially zero for $Bi(o\text{-}FC_6H_4)_5$. It seems clear therefore that because of the very small energy difference between the trigonal-bipyramidal and square-pyramidal structures of AX_5 molecules, solid-state effects cause the square pyramid to be the preferred structure in a few molecules of antimony and bismuth.

4.2. Stereochemically Inactive Lone Pairs

As we have mentioned, $SeCl_6^{2-}$ and the other AX_6E molecules listed in Table 7 are exceptions to the duodecet rule: they appear to have seven electron pairs in the valence shell of the central atom whereas six is the maximum number normally observed.

Table 7. Bond lengths in some AX_6E ions with octahedral geometry.

Ion	Bond length [pm] obs.	calcd [a]	difference [%] [b]	Ref.
$SnCl_6^{4-}$	283	239	18.4	[164]
$SnBr_6^{4-}$	308	254	21.3	[165]
$PbCl_6^{4-}$	289	252	14.7	[165]
$PbBr_6^{4-}$	313	267	17.2	[166]
PbI_6^{4-}	322	286	12.6	[167]
$SbCl_6^{3-}$	265	242	9.5	[168]
$SbBr_6^{3-}$	279	257	8.6	[169]
$BiCl_6^{3-}$	266	248	7.3	[170]
$BiBr_6^{3-}$	285	263	8.4	[171]
BiI_6^{3-}	307	282	8.9	[172]
$SeCl_6^{2-}$	240	216	11.1	[173]
$SeBr_6^{2-}$	258	231	11.7	[174]
$TeCl_6^{2-}$	254	234	8.5	[175]
$TeBr_6^{2-}$	269	249	8.0	[176]
TeI_6^{2-}	293	268	9.3	[177]
BrF_6^-	185	168 [c]	10.1	[25]

[a] Sum of covalent radii r_{cov}. [b] Observed/calculated ratio. [c] $r_{cov}^{Br} + r_{cov}^{F} = (114 + 54) = 168$ pm, where the covalent radius of fluorine has the value of 54 pm as we suggested recently [178].

They are also exceptional in another sense: they appear to have regular octahedral structures, so the lone pair is said to be stereochemically inactive or to be an "inert pair".[23] However, the experimental evidence on the structures of these molecules is not always clear: For solid state structures disorder in the crystal may lead to an average octahedral structure and in solution the spectroscopic evidence for an octahedral structure is not always unambiguous.[24] In solution some of the molecules may appear to be octahedral because they have fluxional non-octahedral structures. However, it seems certain that some of these molecules have octahedral structures. Apparently in these cases either the valence shell electron pairs and/or the ligands would be too crowded if the valence shell contained seven electron pair domains. So the lone pair is forced inside the six bond domains to occupy a spherical domain surrounding the core. This explanation is given some support by the observation that the bonds in these molecules are unusually long (Table 7).

That crowding of the electron pairs in the valence shell of the central atom is important in determining the octahedral structures of some AX_6E molecules is supported by the observations that, although the BrF_6^- ion has an octahedral structure,[25] both IF_6^-[26] and XeF_6[27] with larger cores and therefore less crowding of the electron pair domains have monocapped octahedral structures with the lone pair in the capping position. But if the crowding of the electron pairs in the valence shell of xenon is increased as in the XeF_8^{2-} ion,[28] which is an AX_8E molecule, the lone pair again becomes "inert", because this ion has the square antiprismatic structure expected for an AX_8 molecule, just like IF_8^-. That the Xe–F distances are longer than the I–F distances in IF_8^- again suggests that the lone pair occupies an inner spherical domain.

4.3. "Ionic" Molecules

Molecules of the type OX_2E_2 are expected to be angular with bond angles smaller than the tetrahedral angle. Although this is the case in H_2O and F_2O, for example (Table 2), in other molecules of this type such as $(SiH_3)_2O$ and $(GeH_3)_2O$ the bond angles are 144° and 126°, respectively, and in Li_2O and Na_2O the bond angles are 180°. The VSEPR model rests on the assumption that the ligands X in an AX_n molecule attract the electrons of the central atom A sufficiently strongly to form relatively well localized pairs. This is the case when X has an electronegativity that is comparable to, or greater than, the electronegativity of A, for example when the ligands are F, =O, or OH, and so such molecules always have the VSEPR-predicted geometry. However, when the ligands are less electronegative than the central atom, the electrons on A are not well localized into pairs. In an extreme case such as Na_2O, there is little localization of the electrons in the oxygen valence shell; consequently the molecule can be described as consisting of a slightly distorted oxide ion and two sodium ions. In such a case ligand–ligand repulsions dominate to give a linear molecule. Many ligands are less electronegative than oxygen, and in such cases we expect the bonds to have considerable ionic character and the oxygen electrons to be only poorly localized giving bond angles larger than the tetrahedral angle. For example, the charges on oxygen and silicon in $(SiH_3)_2O$ have been found from ab initio calculations[28a] to be −1.7 and +3.1, respectively, the molecule has considerable ionic character consistent with the large bond angle. The analogous $(CH_3)_2O$ molecule has a bond angle of 112°, which is slightly larger than 109°, consistent with the smaller electronegativity difference between oxygen and carbon than between oxygen and silicon and the smaller ionic character of the C–O bonds. In general, the VSEPR rules only apply when the ligands have an electronegativity that is comparable to that of the central atom with the result that the bonds are predominately covalent.

5. Metal–Nonmetal Molecules

The largest number of apparent exceptions to the VSEPR model are found among molecules of the metals, including the transition metals. For this reason and because the bonds in many metal–nonmetal molecules are predominantly ionic, it is widely believed that the model does not apply to these molecules, although it was shown over twenty years ago that, if distortion of the core of the metal atom to a nonspherical shape is taken into account, many of these exceptions can be accounted for.[1] Recent studies of the Laplacian of the core electron density in several metal–nonmetal molecules have given support to this view and provided important information on the nature of the core distortion. We review this recent work in this section.

5.1. The Alkaline Earth Dihalides and Related Molecules

It was suggested some time ago[29] that polarization of the metal atom core in the alkaline earth dihalide molecules by the halide ligands could account for the angular shape of some of the alkaline earth dihalides in the gas phase, although a simple electrostatic model for an ionic molecule and the VSEPR model for a covalent molecule would both predict a linear geometry. For CaF_2 it was later proposed[1,2] that, if the molecule is considered to be predominately ionic, the interaction of the negatively charged fluorine ligands with the polarizable Ca^{2+} core would cause the eight electrons of the outer shell of the core to become partially localized to form four tetrahedrally oriented pairs, hence giving the core a nonspherical shape. According to this model the negatively charged ligands tend to adopt the arrangement that places them opposite two of the faces of this tetrahedron, so as to minimize their interaction with these four partially localized electron pairs (Fig. 21c). Thus, if the core is sufficiently polarized an MX_2 molecule will have an angular rather than a linear geometry (Fig. 21a, b). According to this model the bond angle would be expected to decrease from 180° with increasing polarizability of the metal, that is from Be to Ba, and with increasing polarizing power of the ligand from I to F, as is observed (Table 8).

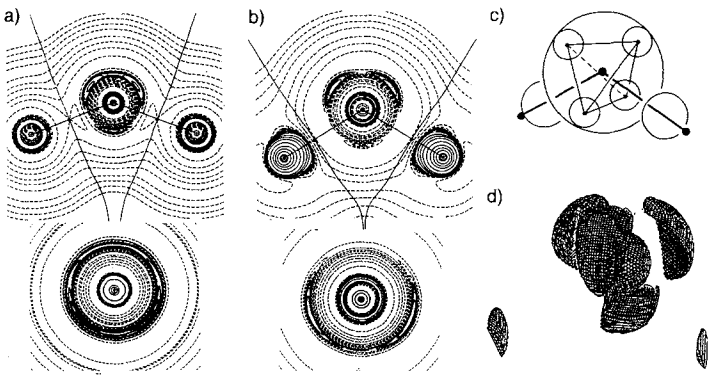

Fig. 21. Structures of the alkaline earth dihalides a) Contour maps of $-\nabla^2\rho$ for SrF_2 in the plane of the molecule (top) and perpendicular to this plane and bisecting the F-Sr-F angle (bottom). b) Contour maps of $\nabla^2\rho$ for BaH_2 in the plane of the molecule (top) and perpendicular to this plane and bisecting the H-Ba-H angle (bottom). c) Model originally proposed to explain the angular shape of the CaF_2 molecule showing four tetrahedrally arranged partially localized electron pairs. d) Three-dimensional plot of an isosurface of $-\nabla^2\rho$ for BaH_2 showing the four charge concentrations in the outer shell of the core surrounding the spherical inner core.

Table 8. Bond angles [°] of halides of Group II in the gaseous phase [2].

MX_2	X = F	Cl	Br	I
BeX_2	180	180	180	180
MgX_2	180	180	180	180
CaX_2	133–155	180	173–180	180
SrX_2	108–135	120–143	133–180	161 180
BaX_2	100–117	100–127	95–135	102–105

Ab initio calculations have likewise shown that the dihalides and the dihydrides of Ca, Sr, and Ba should have an angular shape,[30a,b] and the total electron densities obtained from these calculations have been analyzed in terms of their Laplacians. Although the Laplacian of the calculated electron density of each of the fluorides and hydrides of Ca, Sr, and Ba, and of $Ca(CH_3)_2$, does not display a valence shell charge concentration, presumably because of the ionic nature of the molecules, in

each case it does show that the outer shell of the core is nonspherical with four approximately tetrahedrally arranged charge concentrations (Fig. 21).[30b] Two of these core charge concentrations (CCs) are on the opposite side of the core from the ligands. These CCs arise from the repulsion of the core electrons by the ligands, while the other two charge concentrations arise from the operation of the Pauli principle. Thus the model proposed earlier is fully confirmed by the Laplacian of the electron density. The formation of four charge concentrations in the outer shell of the core of the metal in these molecules is analogous to the formation of four charge concentrations in the valence shell of the oxygen atom in the water molecule. In the water molecule it is the *attraction* of the hydrogen nuclei for electrons combined with the Pauli principle that determines the formation of two bonding charge concentrations and two nonbonding charge concentrations. In contrast in the BaF_2 molecule, for example, it is the *repulsion* of the core electrons by the fluoride ion ligands that causes the formation of four charge concentrations in the outer shell of the core; the fluoride ions adopt positions opposite the "holes" between the charge concentrations thus giving an angular molecule.

It is reasonable to suppose that the bent structure of bis(pentamethylcyclopentadienyl)calcium[31] is similarly due to distortion of the calcium core by the ligands.

5.2. Compounds of d^0 Transition Metals

It has usually been assumed that the VSEPR model does not apply to compounds with transition metals and most recent discussions of the shapes of such molecules have been based on the molecular orbital (MO) model. Nevertheless, the VSEPR model does apply to many molecules containing transition metals, although the number of exceptions is rather large. The application of the VSEPR model to transition metal atoms is, at first sight, straightforward as the lack of nonbonding electrons in the valence shell of the metal yields no other predicted shapes than the AX_2, AX_3, ... AX_n shapes. As a consequence, the predicted shapes are completely independent of the ionic character of the bonds; the packing of negative ions around a central positive ion and the packing of electron pair domains in the valence shell of the central atom give the same shapes. However, even some d^0 metal molecules have nonVSEPR shapes. We will now see that these shapes may be accounted for by the distortion of the core by the ligands (as we have seen for the group 2 halides and hydrides) and that this core distortion has been confirmed in some cases by studies of the Laplacian of electron density of the core of the metal atom.

5.2.1. MX_3 Molecules

The calculated structures of ScH_3, TiH_3^+ and $Ti(CH_3)_3^+$ are pyramidal[32, 33] rather than planar. This pyramidal structure is consistent with the formation of a tetrahedral arrangement of charge concentrations as in BaH_2. The pyramidal geometry of these molecules then results from the ligands' occupying positions opposite the "holes" between these CCs (Fig. 22). This conclusion awaits conformation by the study of the Laplacian of the electron density.

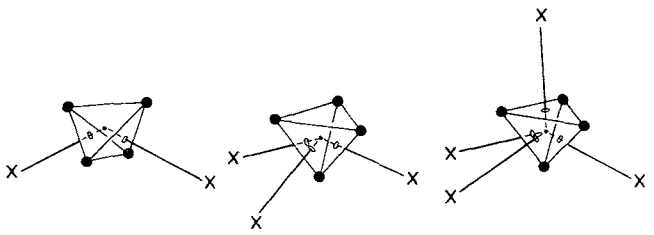

Fig. 22. Diagrammatic representation of the effect of four tetrahedral core charge concentrations on the structures of MX_2, MX_3, and MX_4 molecules (M is a polarizable metal atom) giving angular, pyramidal, and tetrahedral molecules respectively.

5.2.2. MX_4, MX_3Y, MX_2Y_2, and MX_3Z Molecules

Four ligands are expected to produce four core CCs. If the ligands have a tetrahedral arrangement they will be opposite the holes between these CCs, and so no distortion of the VSEPR-predicted tetrahedral geometry is expected (Fig. 22). All MX_4 molecules with a central d^0 transition metal atom have been found to have the regular tetrahedral structure, including the tetrahalides of Ti, Zr, and Hf, all the MO_4^n ions, and the tetraoxides RuO_4 and OsO_4. The tetrahedral structure of TiH_4 has been shown by calculation to be a local minimum, and it is also very probably a global minimum.[34] All MX_3Y, MX_2Y_2,

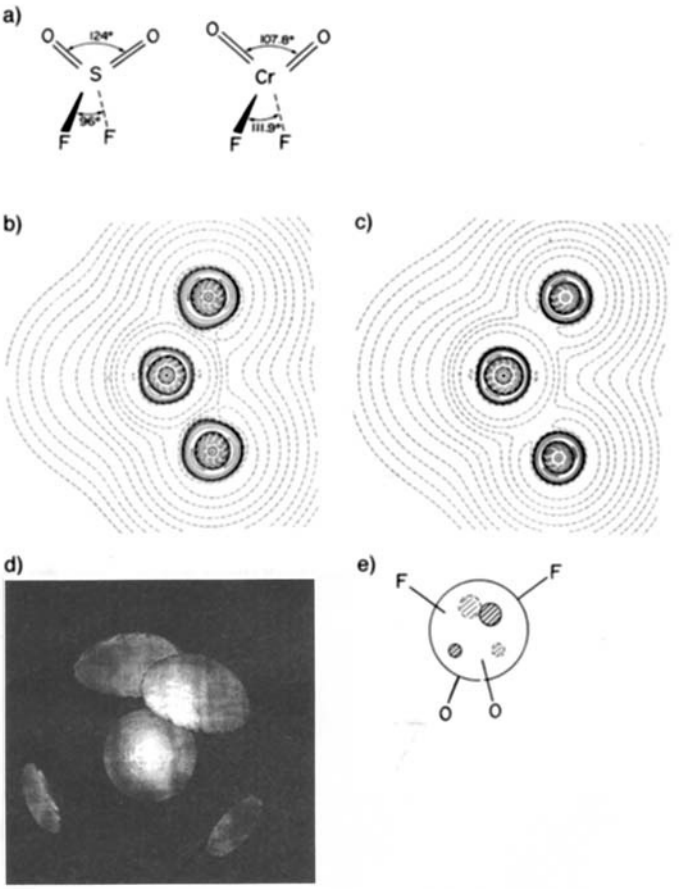

Fig. 23. a) Structural parameters of the SO_2F_2 and CrO_2F_2 molecules. b)–e) Details for CrO_2F_2: Contour map of $-\nabla^2\rho$ in the OCrO plane (b) and the FCrF plane (c). Three-dimensional plot of an isosurface of $-\nabla^2\rho$ for the core of the Cr atom (d) showing four charge concentrations, two larger concentrations opposite the O atoms and two smaller concentrations opposite the F atoms, surrounding a spherical inner core. Diagrammatic representation of CrO_2F_2 molecule (e) showing the ligands and the core charge concentrations.

and MX_3Z molecules such as VOF_3, $VOCl_3$, $MoNF_3$, CrO_2F_2, CrO_2Cl_2, and WNF_3 also have a tetrahedral geometry, although the bond angles are distorted in an unexpected way from the ideal tetrahedral angle.[2] For example, in CrO_2F_2 and CrO_2Cl_2 the O=Cr=O angles are smaller than the tetrahedral angle, whereas in an analogous molecule with a central main group element such as SO_2F_2 this angle is, as expected, larger than the tetrahedral angle (Fig. 23a). The Laplacian of the electron density[35] shows no valence shell charge concentration but charge concentrations in the outer shell of the core opposite each ligand; those opposite the oxygen ligands are larger than those opposite the halogen ligands (Fig. 23b–d). Interaction of the double bond domains with these larger charge concentrations reduces the O=Cr=O bond angle allowing the F-Cr-F angle to increase (Fig. 23e). Similarly in $VOCl_3$ the O-V-Cl bond angles are smaller than tetrahedral, whereas in $POCl_3$ the O-P-Cl angles are larger than tetrahedral as expected because of the large size of the P–O double bond domain. In this case also, a large charge concentration is found in the outer shell of the core opposite the oxygen atom, which tends to open up the Cl-V-Cl angles and thereby reduce the O-V-Cl angles (Fig. 24).[36] A similar situation is observed in the calculated structures of $MoNF_3$ and WNF_3, where the N-Mo-F (104.5°) and N-W-F (105.8°) angles are smaller than the tetrahedral angle, and large CCs are observed opposite the triply bonded nitrogen atom.[37]

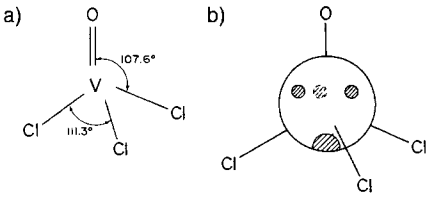

Fig. 24. a) Structural parameters and b) location of the core charge concentrations relative to the ligands in the $VOCl_3$ molecule.

5.2.3. MX_5 and MX_4Y Molecules

The known pentahalides of V, Nb, and Ta all have the geometry predicted by the VSEPR model: trigonal-bipyramidal with longer axial than equatorial bonds. However, $Ta(CH_3)_5$ has square-pyramidal geometry,[20a] and the calculated structures of $Ta(CH_3)_5$ and the hypothetical molecules VH_5, $V(CH_3)_5$, and TaH_5 are also square-pyramidal.[38]

The Laplacian of the electron density has been studied for VF_5, VH_5, and $V(CH_3)_5$. In each case there is no valence shell charge concentration but there are five ligand opposed charge concentrations in the outer shell of the core (Fig. 25).[35] In the trigonal-bipyramidal VF_5 model the equatorial fluorine ligands are opposite holes in the core but the axial fluorine ligands are opposite charge concentrations, whereas in the square-pyramidal VH_5 and $V(CH_3)_5$ molecules all the ligands are opposite holes in the core. The interaction of the ligands with the core charge concentrations would be expected to increase the energy of the trigonal-bipyramidal structure relative to that of the square pyramid. So if the interaction of the ligands with the core is sufficiently great, the square pyramidal structure will be stabilized with respect to the trigonal bipyramid. Thus the more

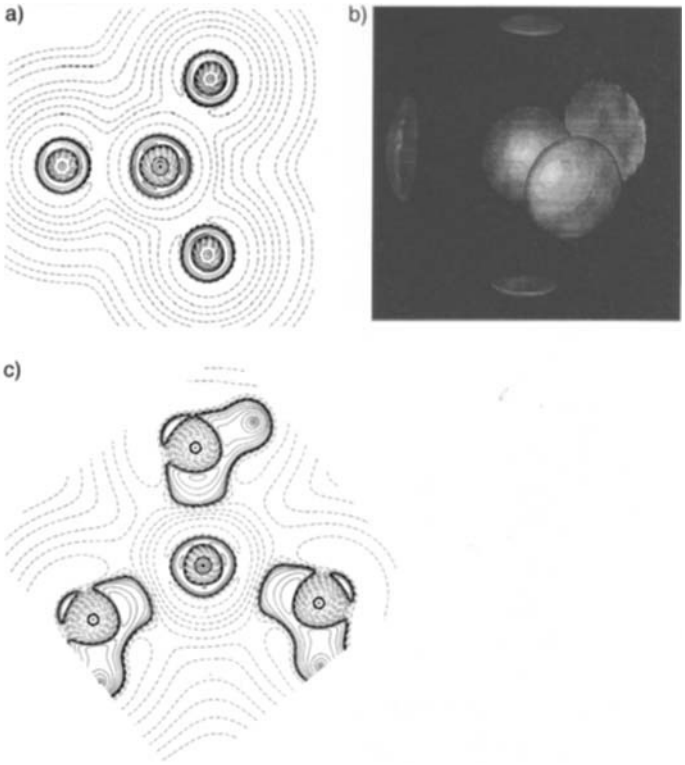

Fig. 25. a) Contour map of $-\nabla^2\rho$ in the equatorial plane of the trigonal-bipyramidal VF_5 molecule. b) Isosurface of $-\nabla^2\rho$ for the core of the vanadium atom in VF_5, showing five ligand opposed charge concentrations surrounding the inner spherical core. c) Contour map of $-\nabla^2\rho$ for the plane through the C_4 axis of the square planar $V(CH_3)_5$ molecule containing two basal and the axial CH_3 groups.

covalently bound ligands such as -H and $-CH_3$ stabilize the square pyramid structure as in VH_5, TaH_5, and $Ta(CH_3)_5$, whereas the less covalently bound halide ligands, such as the halogens, do not perturb the core sufficiently to make this the preferred structure, and the VSEPR-predicted trigonal-bipyramidal structure is retained in molecules such as VF_5.

All the known $(d^0\text{-}M)X_4Y$ molecules such as $CrOF_4$, $MoOF_4$, and $WSCl_4$ have square-pyramidal structures[2] rather than the expected trigonal-bipyramidal structure of the analogous SOF_4 molecule. The Laplacian of the electron density of $CrOF_4$ and $MoOF_4$[35] shows that, as in VF_5, there is no valence shell charge concentration but in each case the core has five CCs in a square-pyramidal arrangement. The CC produced by the doubly bonded oxygen is larger than those produced by the singly bonded F ligands (Fig. 26a–c). This large charge concentration produced by oxygen is responsible for stabilizing the square pyramidal structure with respect to the trigonal bipyramidal structure (Fig. 26). The structures of these square-pyramidal MX_4Y molecules of transition metals bear a noteworthy similarity to the square pyramidal AX_5E molecules of the main group elements, such as BrF_5, in which the nonbonding electron pair E occupies a position in the base of the square pyramid completing an octahedral arrangement of six valence shell domains. The large charge concentration opposite the oxygen in $MoOF_4$ and $CrOF_4$ behaves like a lone pair in that it distorts the trigonal bipyramid to a square pyramid. But as we might expect, the distortion is less than that caused by the lone pair in an AX_5E molecule; the X_b-A-X_a angles in the square-pyramidal

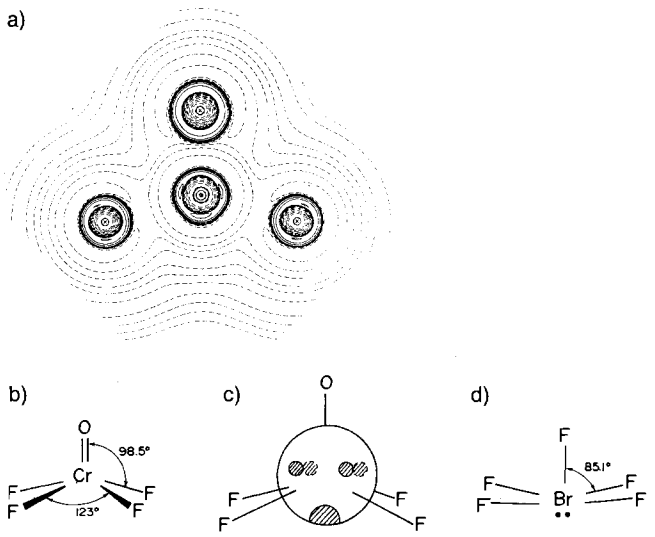

Fig. 26. a) Contour map of $-\nabla^2\rho$ in a vertical plane containing two basal atoms of the square-pyramidal $CrOF_4$ molecule. b) Structural parameters and c) arrangement of the Cr core charge concentrations relative to the ligands in $CrOF_4$. d) Shape of the BrF_5 molecule.

molecules of transition metals are greater than 90° whereas in the AX_5E molecules they are smaller than 90° (Fig. 26d).

In all cases that have been studied so far a doubly bonded ligand such as oxygen distorts the core more than a singly bonded ligand such as fluorine or chlorine. Moreover, it appears from the Laplacian of the calculated electron densities of nitrido complexes such as $MoNF_3$ and $MoNF_4^-$ that the triply bonded nitrogen atom perturbs the metal atom core even more strongly than a doubly bonded oxygen atom.[37] So $MoNF_4^-$ has a square pyramidal structure like $MoOF_4$.

5.2.4. MX_6 Molecules

Two structures have been found for MX_6 molecules of d^0 transition metals—the VSEPR-predicted octahedron for CrF_6, MoF_6, WF_6, WCl_6, WBr_6, TiF_6^{2-}, $ZrCl_6^{2-}$, $W(NMe_2)_6$, and $W(OMe)_6$[38] and the trigonal prism for WMe_6,[39] and $ZrMe_6^{2-}$.[40] The Laplacian of the electron density of the metal atom core in CrF_6 has six LOCCs in an octahedral arrangement, so each ligand is opposite a charge concentration (Fig. 27).[35] The Laplacian of the electron density has not been calculated for either WMe_6 or $ZrMe_6^{2-}$, but it has been calculated for an assumed trigonal prismatic structure for $CrMe_6$ (Fig. 27b, c).[35] Five LOCCs were found in a trigonal bipyramidal arrangement with each ligand opposite one of the six faces of the trigonal bipyramid—that is, opposite holes in the charge density of the core. Apparently, interaction between the fluorine ligands and the core is not strong enough to modify the VSEPR-predicted octahedral structure of CrF_6, but for $CrMe_6$ the stronger interaction of the methyl ligand distorts the Cr core more strongly and causes the change to the trigonal prism in which the interaction between the ligands and the LOCCs is minimized.[35]

On the basis of an accumulating number of examples it seems reasonable to conclude that the cores of metal atoms are distorted by the ligands acting in conjunction with the Pauli principle to form a number of charge concentrations. These charge concentrations have an arrangement that minimizes their mutual

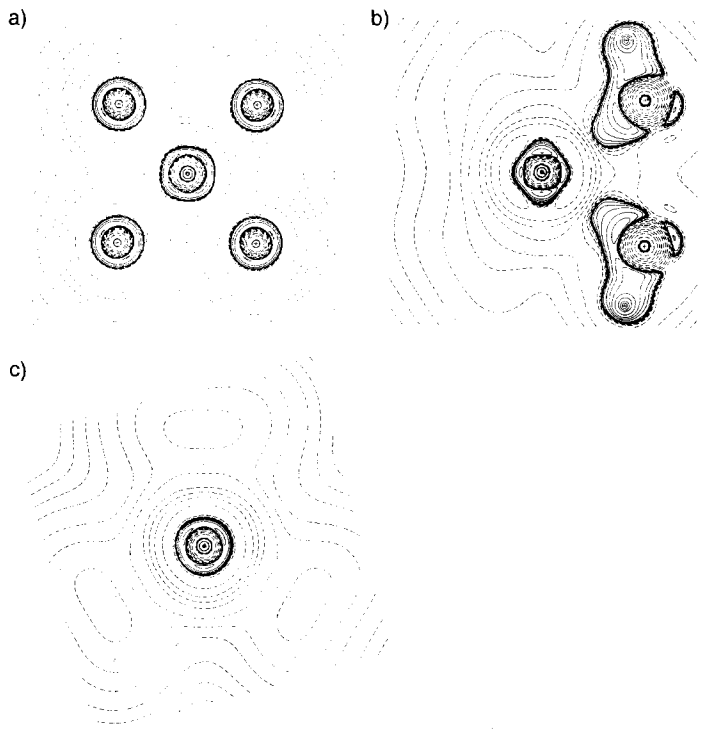

Fig. 27. Contour map of $-\nabla^2\rho$ in an equatorial plane of the octahedral CrF_6 molecule. b) Contour map of $-\nabla^2\rho$ in a vertical plane containing a C_2 axis of the trigonal-prismatic $Cr(CH_3)_6$ molecule. c) Contour map of $-\nabla^2\rho$ for the horizontal symmetry plane of $Cr(CH_3)_6$.

interaction: four CCs have a tetrahedral arrangement, five a trigonal-bipyramidal or square-pyramidal arrangement, and six an octahedral arrangement. Ligands that interact sufficiently strongly with the core of the metal atom (in particular $-H$, $-CH_3$, and $=O$ in the case of transition metals, and F, H, and CH_3 in the case of the more polarizable group 2 metals) adopt a geometry that in some cases differs from the VSEPR-predicted geometry, in which they occupy sites opposite the "holes" in the core between the CCs and which therefore minimizes their interaction with these CCs while it does not greatly increase the ligand–ligand interactions. The geometry of molecules containing ligands that interact only weakly with the core, for example F in the case of the transition metals, is dominated by the interactions between the bonding electron pairs or the ligands, so they have the expected VSEPR geometry. Moreover, it appears that the more strongly covalently bonded ligands induce a larger distortion of the core electrons. For example, in the series ScH_6^{3-}, TiH_6^{2-}, VH_6^-, CrH_6, MnH_6^+, ab initio calculations[33] have shown that for the more ionic molecules ScH_6^{3-} and TiH_6^{2-} the octahedral structure has a lower energy than the trigonal prismatic structure, whereas the trigonal prism has the lower energy for the more covalent VH_6^-, CrH_6, and MnH_6^+ molecules. Further studies are needed before these hypotheses can be fully confirmed.

5.3. Compounds with d^1–d^{10} Transition Metals

It seems clear that the shapes of molecules containing non-transition metal and d^0 transition metal centers are distorted from the VSEPR-predicted shapes by the interaction between

the ligands and a distorted (nonspherical) core of the metal's electrons. So it is reasonable to assume that the shapes of compounds with d^1-d^{10} transition metal centers will also be determined by the shape of the metal atom's core. Indeed, if it is assumed, as a rough first approximation, that an incompletely filled d shell (d^1-d^9) has either a prolate or oblate ellipsoidal shape, the geometry of many such molecules can be accounted for.[2] For example, a prolate ellipsoidal core can result in a square-planar AX_4 molecule, a square-pyramidal AX_5 molecule, and a square-bipyramidal molecule (D_{4h}).

A preliminary study of the Laplacian of the electron density of molecules with transition metal centers with incomplete d shells has been reported by MacDougall and Hall.[41] As yet there have been too few similar studies to enable any general conclusions to be drawn about the influence of the core on the shapes of these molecules. Laing[42] has drawn attention to the striking fact that molecules with transition metal centers that obey Sidgwick's effective atomic number rule[43] (in which, therefore, the metal atom has a total of 18 bonding and nonbonding electrons in its outer shell) always have the predicted VSEPR geometry. No simple and general explanation of Sidgwick's rule has yet been proposed, but it seems reasonable to suppose that further studies of the electron density distribution of the core of the metal atom will eventually lead to a much better understanding of how the shape of the core modifies the VSEPR-predicted geometry for all molecules containing transition metals. And it seems reasonable to hope that a modified VSEPR model can be developed that will prove as useful for transition metal molecules as the original model has been for nonmetal molecules.

6. Conclusions and Pedagogical Considerations

The VSEPR model, particularly when formulated in terms of electron pair domains, continues to be the most useful and most easily used model for the qualitative prediction of molecular shape. It enables us to understand in a qualitative way many features of the structures of molecules that are not readily accounted for in other ways, and it continues to form the basis for the discussion and understanding of the structures of many new molecules. Its physical basis rests on the Pauli principle, and it is independent of any orbital model. It thus provides a useful alternative to the familiar valence bond and molecular orbital methods that can also give us useful new insights into molecular geometry.

Elementary treatments of bonding and molecular geometry are almost always based on hydrogen-like atomic orbitals. It is commonly stated at this level that "an orbital may be thought of as a region of space where there is a high probability of finding an electron". An orbital is often pictured as a charge cloud of varying density. The shapes of s, p, and sometimes d orbitals are then described—usually in a very approximate manner—but are not derived, explained, or otherwise accounted for. A bond in this model is considered to be a "merging or overlapping of the orbitals of the bonded atoms to create a charge cloud that spreads over and between the nuclei and binds them together." Because atomic orbitals are not suitable as a basis for this type of description of many molecules including those of carbon, the concept of hybrid orbitals is introduced, and the hybrid orbitals are chosen to match the observed geometry. Again the mathematical operation of forming hybrid orbitals cannot be explained at the introductory level, and the conventional diagrams of these hybrid orbitals give the incorrect impression that hybridization of a set of atomic orbitals to give a set of hybrid orbitals is a physical phenomenon that results in a change in the total electron density of the atom. Not only does this conventional introductory treatment give no explanation of molecular geometry, it introduces incorrect, or at least very misleading, ideas. In contrast the domain version of the VSEPR model provides a straightforward and readily understandable picture of the chemical bond, while at the same time leading directly to an explanation of molecular geometry without giving incorrect or misleading descriptions of quantum mechanical concepts that cannot be adequately dealt with at the introductory level.

Good quantitative predictions of molecular shape can be made by ab initio molecular orbital calculations for many molecules, but because of the complexity of the large set of basis functions (modified atomic orbitals) used in these calculations they provide little understanding of the factors that determine molecular shape. However, from these calculations, as well as from very careful, low-temperature X-ray crystallographic studies we can obtain a rather accurate map of the electron density distribution in a molecule; from its analysis we may hope to obtain a better understanding of bonding. It is particularly important to derive more electron density distributions from low-temperature X-ray crystallographic studies to confirm the results of ab initio calculations. It is also important to note that the electron density distribution of a molecule is an observable property of the molecule that is independent of the particular experimental or theoretical method used to determine it, provided that it is determined with sufficient accuracy. It is therefore incorrect to claim, as has sometimes been done, that the analysis of an electron density distribution obtained by ab initio calculations using the molecular orbital method cannot yield any more information than is provided by a molecular orbital description of the molecule.

The analysis of the electron density distribution in terms of its Laplacian has been particularly fruitful. The Laplacian of the electron density of molecules containing the main group nonmetals shows that the local concentrations of electron density correspond rather closely in location, size, and shape to the electron pair domains of the VSEPR model, thus giving substantial support to the model, which can be regarded as giving a very crude but nevertheless useful picture of the valence shell electron density distribution in a molecule. Moreover, the study of the Laplacian of the electron density provides considerable insight into the reasons why certain molecules appear to be exceptions to the VSEPR model. In particular it has been shown that it is important to take into account not only the relative sizes of lone pairs and multiple bonds but also their shapes. A basic assumption of the VSEPR model, namely that the core of an atom is spherical and therefore has no effect on the arrangement of the surrounding ligands appears to be true for the compounds of nonmetals, but recent studies of the Laplacian of the cores of metal atoms in their molecules show that they often have nonspherical cores, which do affect the geometry of the

molecule. Even though we cannot yet predict the shapes of molecules with transition metal centers with certainty in all cases, it is clear that the nonspherical shape of the core is an important factor that must be taken into account. Further studies of the shapes of the cores of molecules containing transition metals are needed to give us a better understanding of their geometries and to enable us to extend the VSEPR model to such molecules.

R. J. G. thanks Trevellyan College, University of Durham (UK) for the award of a fellowship in 1994, which enabled him to write the first draft of this article, and Professor K. Wade for fruitful discussions and useful comments.

Appendix: The Laplacian of the Electron Density

The Laplacian of a function $[\nabla^2 f(x,y,z)]$ is the second derivative of this function of x, y, and z. To understand, in an approximate way, how the Laplacian of the electron density distribution of a molecule ($\nabla^2\rho$) reveals features that are not readily apparent in the total electron density, we consider the derivatives of a one-dimensional function such as that shown in Figure 28. This function might represent the radial behavior of the

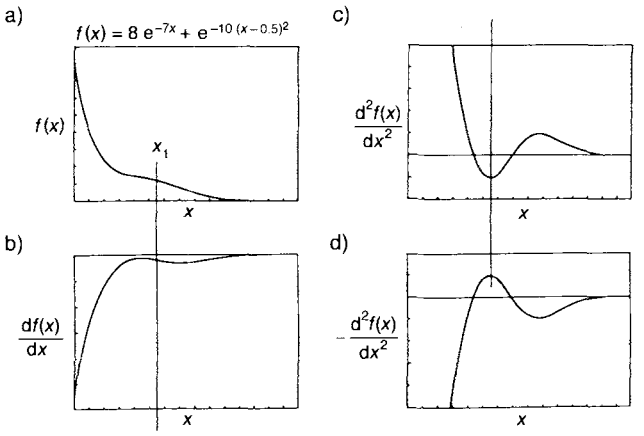

Fig. 28. a) The function $f(x) = 8e^{-7x} + e^{-10(x-0.5)^2}$, b) its first derivative $f'(x)$, c) its second derivative $f''(x)$, and d) the negative of the second derivative $-f''(x)$.

electron density of an atom although in real cases the shoulder at x_1, where $f(x)$ is greater than the average of $f(x + dx)$ and $f(x - dx)$, would not be so apparent. The first derivative $df(x)/dx$ (Fig. 28b) is negative for all values of x, showing the absence of any maximum in $f(x)$, but it has a point of inflection at x_1. At this point the second derivative (Fig. 28c) has a pronounced minimum and therefore $-d^2f(x)/dx^2$ (Fig. 28d) has a maximum. So the shoulder at x_1 at which $f(x) > [f(x + dx) + f(x - dx)]/2$ is made much more apparent in $-d^2f(x)$. If this function represents the radial behavior of the electron density, we could say that the electron density is locally concentrated in the radial direction. Similarly a maximum in $-\nabla^2\rho$ indicates a local concentration in the three-dimensional electron density distribution. Maxwell (*Treatise on Electricity and Magnetism, Vol. 1*, p. 31, Dover reprint, New York, **1954**) coined the phrase *locally concentrated* to signify that the value of a function of r (in this case $\rho(r)$) at a particular r is larger than the average value of ρ on the surface of an infinitesimal sphere centered at r. Thus in the regions in which $-\nabla^2\rho$ is positive (or $\nabla^2\rho$ negative) the electron density is locally concentrated. Analogously, regions where $-\nabla^2\rho$ has negative values correspond to regions of local depletion of electron density. A more detailed discussion of the Laplacian of the electron density is given in Ref. [17].

Received: July 15, 1994
Revised: June 12, 1995 [A 75 IE]
German version: *Angew. Chem.* **1996**, *108*, 539–560

[1] R. J. Gillespie, *Molecular Geometry*, Van Nostrand Reinhold, London, **1972**.
[2] R. J. Gillespie, I. Hargittai, *The VSEPR Model of Molecular Geometry*, Prentice-Hall, New Jersey, **1991**.
[3] R. J. Gillespie, *Chem. Soc. Rev.* **1991**, *21*, 59.
[4] P. W. Atkins, *Quanta*, 2nd ed., Oxford University Press, Oxford, **1991**, p. 268; *Quanten*, VCH, Weinheim, **1993**, p. 239.
[5] J. W. Linnett, *The Electronic Structure of Molecules*, Wiley, New York, **1964**.
[6] R. Daudel, *The Fundamentals of Theoretical Chemistry*, Pergamon, Oxford, **1968**.
[7] H. A. Bent, *J. Chem. Educ.* **1963**, *40*, 446, 523; *ibid.* **1965**, *42*, 302, 348; *ibid.* **1967**, *44*, 5126.
[8] R. J. Gillespie, R. S. Nyholm, *Q. Rev. Chem. Soc.* **1957**, 339.
[9] R. J. Gillespie, I. Bytheway, R. S. DeWitte, R. F. W. Bader, *Inorg. Chem.* **1994**, *33*, 2115.
[10] K. O. Christe, E. C. Curtis, D. A. Dixon, H. P. Mercier, J. C. P. Saunders, J. G. Schrobilgen, *J. Am. Chem. Soc.* **1991**, *113*, 3351.
[11] W. J. Adams, H. B. Thompson, L. S. Bartell, *J. Chem. Phys.* **1970**, *53*, 4050.
[12] K. O. Christe, D. A. Dixon, A.-R. Mahjoub, H. P. A. Mercier, J. C. P. Saunders, K. Seppelt, G. J. Schrobilgen, W. W. Wilson, *J. Am. Chem. Soc.* **1993**, *115*, 2696.
[13] a) K. O. Christe, D. A. Dixon, I. B. Goldberg, C. J. Schak, B. W. Walther, J. T. Wang, F. Williams, *J. Am. Chem. Soc.* **1993**, *115*, 1129; b) P. J. MacDougall, R. F. W. Bader, *Can. J. Chem.* **1986**, *64*, 1496.
[14] E. A. Robinson, *J. Mol. Struct. (Theochem)* **1989**, *186*, 9.
[15] L. Pauling, *The Nature of the Chemical Bond*, 3rd ed., Cornell University Press, **1960**, p. 137; E. A. Robinson, R. J. Gillespie, *J. Chem. Educ.* **1980**, *57*, 324; R. J. Gillespie, *ibid.* **1992**, *69*, 116; R. P. Messmer, *THEOCHEM* **1988**, *46*, 187; R. P. Messmer, P. H. Schultz, *J. Am. Chem. Soc.* **1993**, *115*, 10925.
[16] a) A. Simon, E. M. Peters, D. Lentz, K. Seppelt, *Z. Anorg. Allg. Chem.* **1980**, *468*, 7; b) J. Buschmann, T. Koriatsanszky, R. Kuschel, P. Luger, K. Seppelt, *J. Am. Chem. Soc.* **1991**, *113*, 233.
[17] a) R. F. W. Bader, *Atoms in Molecules; A Quantum Theory*, Oxford University Press, Oxford, **1990**; b) R. F. W. Bader, P. L. A. Popelier, T. A. Keith, *Angew. Chem.* **1994**, *106*, 647; *Angew. Chem. Int. Ed. Engl.* **1994**, *33*, 620.
[18] R. F. Ziolo, J. M. Troup, *J. Am. Chem. Soc.* **1983**, *105*, 229.
[19] P. Coppens, D. Feil in *The Application of Charge Density Research to Chemistry and Drug Design* (Eds.: G. A. Jeffrey, J. F. Pinella), Plenum, New York, **1991**, p. 7–23, and other articles in this volume.
[20] a) A. Haaland, A. Hammel, K. Rypdal, H. P. Verne, H. V. Volden, C. Pulham, J. Brunvoll, J. Weidlein, M. Greune, *Angew. Chem.* **1992**, *104*, 1534; *Angew. Chem. Int. Ed. Engl.* **1992**, *31*, 1464; b) S. Wallenhauer, K. Seppelt, *ibid.* **1994**, *106*, 1044 and **1994**, *33*, 976.
[21] a) A. Schmuck, J. Buschmann, J. Fuchs, K. Seppelt, *Angew. Chem.* **1987**, *99*, 1206; *Angew. Chem. Int. Ed. Engl.* **1987**, *26*, 1180; b) A. L. Beauchamp, F. J. Bennett, F. A. Cotton, *J. Am. Chem. Soc.* **1968**, *90*, 6675.
[22] A. Schmuk, P. Pyykkö, K. Seppelt, *Angew. Chem.* **1990**, *102*, 211; *Angew. Chem. Int. Ed. Engl.* **1990**, *29*, 213.
[23] P. Pyykkö, J. P. Descaux, *Acc. Chem. Res.* **1979**, *12*, 276; P. Pyykkö, *Chem. Rev.* **1988**, *88*, 563.
[24] For an extensive review of the literature, see P. A. Wheeler, P. N. V. Pavan Kumer, *J. Am. Chem. Soc.* **1992**, *114*, 4776.
[25] A.-R. Mahjoub, A. Hoser, J. Fuchs, K. Seppelt, *Angew. Chem.* **1989**, *101*, 1528; *Angew. Chem. Int. Ed. Engl.* **1989**, *28*, 1526.
[26] A.-R. Mahjoub, K. Seppelt, *Angew. Chem.* **1991**, *103*, 309; *Angew. Chem. Int. Ed. Engl.* **1991**, *30*, 323.
[27] R. M. Gavin, L. S. Bartell, *J. Chem. Phys.* **1968**, *48*, 2460, 2466.
[28] a) S. W. Peterson, J. H. Holloway, J. M. Williams, *Science* **1971**, *173*, 128; b) R. J. Gillespie, S. Johnson, T.-H. Tang, not yet published.
[29] E. S. Rittner, *J. Chem. Phys.* **1951**, *19*, 1030.
[30] a) M. Kaupp, P. von R. Schleyer, H. Stoll, H. Preuss, *J. Chem. Phys.* **1991**, *94*, 1360; M. Kaupp, P. von R. Schleyer, *J. Am. Chem. Soc.* **1992**, *114*, 491; *ibid.* **1993**, *115*, 1120; b) I. Bytheway, R. J. Gillespie, T.-H. Tang, R. F. W. Bader, *Inorg. Chem.* **1995**, *34*, 2407.
[31] R. A. Andersen, J. M. Boncella, C. J. Burns, R. Blom, A. Haarland, H. V. Volden, *J. Organomet. Chem.* **1986**, *312*, C49.
[32] C. A. Jolly, D. S. Marynick, *Inorg. Chem.* **1989**, *28*, 2893.
[33] D. G. Musaev, O. P. Charkin, *Koord. Khim.* **1989**, *15*, 161.

[34] J. R. Thomas, G. E. Quelch, E. T. Seidl, H. F. Schaeffer III, *J. Chem. Phys.* **1992**, *96*, 6857.
[35] R. J. Gillespie, I. Bytheway, R. S. deWitte, T.-H. Tang, R. F. W. Bader, *Inorg. Chem.*, in press.
[36] P. J. MacDougall, M. B. Hall, R. F. W. Bader, J. R. Cheeseman, *Can. J. Chem.* **1989**, *67*, 1842.
[37] A. Neuhaus, A. Veldkamp, G. Frenking, *Inorg. Chem.* **1994**, *33*, 5278.
[38] S. K. Kang, H. Tang, T. A. Albright, *J. Am. Chem. Soc.* **1993**, *115*, 1971; E. G. Hope, W. Levanson, J. S. Ogden, *Inorg. Chem.* **1991**, *30*, 4873.
[39] A. Haaland, A. Hammel, K. Rypdal, H. V. Volden, *J. Am. Chem. Soc.* **1990**, *112*, 4547.
[40] P. M. Morse, G. S. Girolani, *J. Am. Chem. Soc.* **1989**, *111*, 4114.
[41] P. J. MacDougall, M. B. Hall, *Trans. Am. Crystallogr. Assoc.* **1990**, *26*, 105.
[42] "Coordination Chemistry: A Century of Progress": M. Laing, *ACS Symp. Ser.* **1994**, *565*, 193.
[43] N. V. Sidgwick, R. W. Bailey, *Proc. R. Soc. (London)* **1934**, *144*, 521.
[44] P. Helminger, F. C. De Lucia, F. W. Gordy, *J. Mol. Spectrosc.* **1971**, *39*, 94.
[45] L. S. Bartell, L. C. Hirst, *J. Chem. Phys.* **1959**, *31*, 449.
[46] G. S. Blevins, A. W. Jache, W. Gordy, *Phys. Rev.* **1955**, *97*, 684.
[47] M. Otake, C. Matsumura, T. Morino, *J. Mol. Spectrosc.* **1968**, *28*, 316.
[48] Y. Morimo, K. Kuchitsu, T. Moritani, *Inorg. Chem.* **1969**, *8*, 867.
[49] F. B. Clippard, L. S. Bartell, *Inorg. Chem.* **1970**, *9*, 805.
[50] S. Konaka, M. Kimura, *Bull. Chem. Soc. Jpn.* **1970**, *43*, 1693.
[51] A. J. Edwards, *J. Chem. Soc. A* **1970**, 2751.
[52] H. B. Bürgi, D. Stedman, L. S. Bartell, *J. Mol. Struct.* **1971**, *10*, 31.
[53] M. Isaki, K. Hedberg, *J. Chem. Phys.* **1962**, *36*, 589.
[54] S. Konaka, M. Kimura, *Bull. Chem. Soc. Jpn.* **1973**, *46*, 404, 413.
[55] H. A. Skinner, L. E. Sutton, *Trans. Faraday Soc.* **1940**, *36*, 681.
[56] K. Kuchitsu, T. Shibata, A. Yokozeki, C. Matsumura, *Inorg. Chem.* **1971**, *10*, 2584.
[57] S. Samdal, D. M. Barnhart, K. Hedberg, *J. Mol. Struct.* **1976**, *35*, 67; A. G. Robiette, ibid. **1976**, *35*, 81.
[58] E. T. Lance, J. M. Haschke, D. R. Pencor, *Inorg. Chem.* **1976**, *15*, 780, 848.
[59] Y. Morino, T. Ukaji, T. Ito, *Bull. Chem. Soc. Jpn.* **1966**, *39*, 71.
[60] A. Almenningen, T. Bjorvatten, *Acta Chem. Scand.* **1963**, *17*, 2573.
[61] B. Beagley, A. R. Medwid, *J. Mol. Struct.* **1977**, *38*, 229.
[62] E. J. Jacob, S. Samdal, *J. Am. Chem. Soc.* **1977**, *99*, 5656.
[63] B. Beagley, K. T. McAloon, *J. Mol. Struct.* **1973**, *17*, 429.
[64] H. Burger, H. Niepel, G. Pawelke, *J. Mol. Struct.* **1979**, *54*, 159.
[65] C. J. Marsden, L. S. Bartell, *Inorg. Chem.* **1976**, *15*, 2713.
[66] H. J. M. Bowen, *Trans. Faraday Soc.* **1954**, *50*, 463.
[67] Y. Yang, L. D. Calvert, S. K. Brownstein, *Acta Crystallogr. Sect. B* **1980**, *36*, 1523.
[68] D. J. Gibler, C. J. Adams, M. Fischer, A. Zalkin, N. Bartlett, *Inorg. Chem.* **1972**, *11*, 2325.
[69] A. J. Edwards, P. Taylor, *J. Chem. Soc. Dalton Trans.* **1973**, 2150.
[70] B. M. Christian, M. J. Collins, R. J. Gillespie, J. F. Sawyer, *Inorg. Chem.* **1986**, *25*, 777.
[71] R. L. Cook, F. C. De Lucia, P. Helminger, *J. Mol. Spectrosc.* **1974**, *53*, 62.
[72] T. H. Edwards, N. K. Moncur, L. E. Snyder, *J. Chem. Phys.* **1967**, *46*, 2139.
[73] R. A. Hill, T. H. Edwards, *J. Chem. Phys.* **1965**, *42*, 1391.
[74] N. K. Moncur, P. D. Willson, T. H. Edwards, *J. Mol. Spectrosc.* **1974**, *52*, 181, 380.
[75] Y. Morino, S. Saito, *J. Mol. Spectrosc.* **1966**, *19*, 435; W. H. Kirchhoff, *ibid.* **1972**, *41*, 333.
[76] W. H. Kirchhoff, D. R. Johnson, F. X. Powell, *J. Mol. Spectrosc.* **1973**, *48*, 157.
[77] D. M. De Leeuw, R. Mooyman, C. A. DeLange, *J. Chem. Phys.* **1979**, *38*, 21.
[78] B. Beagley, A. H. Clark, T. G. Hewitt, *J. Chem. Soc. A* **1968**, 658.
[79] Y. Morino, Y. Murata, T. Ito, J. Nakamura, *J. Phys. Soc. Jpn.* **1962**, *17*, Suppl. BII, 37.
[80] L. Fernholt, A. Haaland, R. Seip, R. Kniep, L. Korte, *Z. Naturforsch. B* **1983**, *38*, 1072.
[81] L. Fernholt, A. Haaland, H. V. Volden, R. Kniep, *J. Mol. Struct.* **1985**, *128*, 29.
[82] K. Kimura, M. Kubo, *J. Chem. Phys.* **1959**, *30*, 151.
[83] T. Ijima, S. Tsuchiya, M. Kimura, *Bull. Chem. Soc. Jpn.* **1977**, *50*, 2564.
[84] G. K. Pandey, H. Dreizler, *Z. Naturforsch. A* **1977**, *32*, 482.
[85] H. Oberhammer, W. Gombler, H. Willner, *J. Mol. Struct.* **1981**, *70*, 273.
[86] C. J. Marsden, G. M. Sheldrick, *J. Mol. Struct.* **1971**, *10*, 405.
[87] A. J. Edwards, K. O. Christe, *J. Chem. Soc. Dalton Trans.* **1976**, 175.
[88] R. Bougon, W. U. Cicha, M. Lance, L. Meublat, M. Nierlich, *Inorg. Chem.* **1991**, *30*, 102.
[89] T. Birchall, R. D. Myers, *Inorg. Chem.* **1981**, *20*, 2207.
[90] H. Kim, E. F. Pearson, E. H. Appelman, *J. Chem. Phys.* **1972**, *56*, 1.
[91] A. M. Mirri, F. Scappini, G. Cazzoli, *J. Mol. Spectrosc.* **1971**, *38*, 218.
[92] I. Schwager, A. Arkell, *J. Am. Chem. Soc.* **1967**, *89*, 6006.
[93] F. P. Diodati, L. S. Bartell, *J. Mol. Struct.* **1971**, *8*, 395; J. F. Olsen, *J. Fluorine Chem.* **1977**, *9*, 471.
[94] M. C. L. Gerry, R. M. Lees, G. Winnewisser, M. Winnewisser, *J. Mol. Spectrosc.* **1976**, *61*, 231.
[95] T. Kojima, *J. Phys. Soc. Jpn.* **1960**, *15*, 1284.
[96] C. H. Thomas, *J. Chem. Phys.* **1973**, *59*, 70.
[97] A. Guarnieri, L. Charpentier, B. Kuck, *Z. Naturforsch. A* **1973**, *28*, 1721; C. J. Marsden, *J. Mol. Struct.* **1974**, *21*, 168.
[98] N. V. Alekseev, F. K. Velichko, *Zh. Strukt. Khim.* **1967**, *8*, 8.
[99] C. Tarimci, R. D. Rosenstein, E. Schlempp, *Acta Crystallogr. Sect. B* **1976**, *32*, 610.
[100] M. Gerries, D. D. Gibson, D. F. Morell, A. Zalkin, N. Bartlett, *Inorg. Chem.* **1973**, *12*, 1717.
[101] K. Lutar, A. Jesih, I. Leban, B. Zemva, N. Bartlett, *Inorg. Chem.* **1989**, *28*, 3467.
[102] N. Bartlett, F. Einstein, D. F. Stewart, J. Trotter, *J. Chem. Soc. A* **1967**, 1190.
[103] A. B. Altman, I. N. Myakshin, V. F. Sukhoverkhov, G. V. Romanov, V. P. Spiridonov, *Dokl. Akd. Nauk. SSSR* **1978**, *241*, 360.
[104] A. G. Robiette, R. H. Bradley, P. N. Prier, *Chem. Commun.* **1971**, 1567.
[105] S. H. Martin, R. R. Ryan, L. B. Asprey, *Inorg. Chem.* **1970**, *9*, 2100.
[106] R. R. Ryan, D. T. Cromer, *Inorg. Chem.* **1972**, *11*, 2322.
[107] M. Webster, S. Keats, *J. Chem. Soc. A* **1971**, 942.
[108] K. O. Christe, D. A. Dixon, H. P. A. Mercier, J. P. Sanders, G. J. Schrobilgen, W. W. Wilson, *J. Am. Chem. Soc.* **1994**, *116*, 2850.
[109] W. M. Tolles, W. D. Gwinn, *J. Chem. Phys.* **1962**, *36*, 1119; K. Kimura, S. H. Bauer, *ibid.* **1963**, *39*, 3172.
[110] M. V. Carlowitz, H. Oberhammer, H. Willner, J. E. Boggs, *J. Mol. Struct.* **1983**, *100*, 161.
[111] A. J. Downs, G. S. McGrady, E. A. Barnfield, D. W. H. Rankin, H. E. Robertson, J. E. Boggs, K. D. Dobbs, *Inorg. Chem.* **1989**, *28*, 3292.
[112] H. Oberhammer, R. C. Kumar, G. D. Knerr, J. M. Shreeve, *Inorg. Chem.* **1981**, *20*, 3871.
[113] A. H. Cowley, *J. Am. Chem. Soc.* **1979**, *101*, 5620.
[114] W. Heilemann, R. Mews, H. Oberhammer, *J. Fluorine Chem.* **1987**, *39*, 261.
[115] N. C. Baenzinger, R. E. Buckle, R. J. Maner, T. D. Simpson, *J. Am. Chem. Soc.* **1972**, *94*, 5010.
[116] N. C. Baenzinger, R. E. Buckle, R. J. Maner, T. D. Simpson, *J. Am. Chem. Soc.* **1969**, *91*, 5749.
[117] I. C. Bowater, R. D. Brown, F. R. Burden, *J. Mol. Spectrosc.* **1968**, *28*, 454.
[118] P. L. Baxter, A. J. Downs, A. M. Forster, M. J. Goode, D. W. H. Rankin, H. E. Robertson, *J. Chem. Soc. Dalton. Trans.* **1985**, 941.
[119] J. D. McCullough, G. Hamburger, *J. Am. Chem. Soc.* **1942**, *64*, 508.
[120] J. D. McCullough, R. E. Marsh, *Acta Crystallogr.* **1950**, *3*, 41.
[121] J. D. McCullough, G. Hamburger, *J. Am. Chem. Soc.* **1941**, *63*, 803.
[122] F. J. Berry, A. J. Edwards, *J. Chem. Soc. Dalton Trans.* **1980**, 2306.
[123] G. D. Christofferson, R. A. Sparks, J. D. McCullough, *Acta Crystallogr.* **1958**, *11*, 782.
[124] D. Kobelt, E. F. Paulus, *J. Organomet. Chem.* **1971**, *27*, C63.
[125] N. W. Alcock, W. D. Harrison, *J. Chem. Soc. Dalton Trans.* **1982**, 251.
[126] G. D. Christofferson, J. D. McCullough, *Acta Crystallogr.* **1958**, *11*, 249.
[127] L. Y. Y. Chan, F. W. B. Einstein, *J. Chem. Soc. Dalton Trans.* **1972**, 316.
[128] N. W. Alcock, W. D. Harrison, *J. Chem. Soc. Dalton Trans.* **1984**, 869.
[129] M. D. Lind, K. O. Christe, *Inorg. Chem.* **1972**, *11*, 608.
[130] A. J. Edwards, P. Taylor, *J. Chem. Soc. Chem. Commun.* **1975**, 2174.
[131] H. Oberhammer, K. O. Christe, *Inorg. Chem.* **1982**, *21*, 273.
[132] L. Helmholtz, M. T. Rogers, *J. Am. Chem. Soc.* **1940**, *62*, 1537.
[133] S. W. Peterson, R. Willett, J. L. Huston, *J. Chem. Phys.* **1973**, *59*, 453.
[134] D. F. Smith, *J. Chem. Phys.* **1953**, *21*, 609.
[135] D. W. Magnusson, *J. Chem. Phys.* **1957**, *27*, 223.
[136] E. M. Archer, T. G. D. van Schalkwyk, *Acta Crystallogr.* **1953**, *6*, 88.
[137] P. Boldrini, R. J. Gillespie, P. R. Ireland, G. J. Schrobilgen, *Inorg. Chem.* **1974**, *13*, 1690.
[138] U. Geiser, H. H. Wang, J. A. Schlueter, J. M. Williams, J. L. Smart, A. C. Cooper, S. K. Kumar, M. Caleca, J. D. Dudek, K. D. Carlson, J. Ren, M.-H. Whangbo, J. E. Schriber, W. R. Bayless, *Inorg. Chem.* **1994**, *33*, 5101.
[139] E. Hirota, Y. Endo, S. Saito, K. Yoshida, I. Yamaguchi, K. Macheda, *J. Mol. Spectrosc.* **1981**, *89*, 223.
[140] F. C. Mijlhoff, G. H. Renes, K. Kohata, K. Oyanagi, K. Kuchitsu, *J. Mol. Struct.* **1977**, *39*, 241.
[141] J. L. Carlos, R. R. Karl, S. H. Bauer, *J. Chem. Soc. Faraday Trans. 2* **1974**, *70*, 177.
[142] A. H. Lowrey, P. D'Antonio, C. George, *J. Chem. Phys.* **1976**, *64*, 2884.
[143] T. G. Strand, *Acta Chem. Scand.* **1967**, *21*, 2111.
[144] T. G. Strand, *Acta Chem. Scand.* **1967**, *21*, 1033.
[145] J. L. Carlos, S. H. Bauer, *J. Chem. Soc. Faraday Trans. 2* **1974**, *70*, 171.
[146] T. Fukuyama, M. Sugié, I. Tokue, K. Kuchitsu, *Acta Crystallogr. Sect. A* **1972**, *28*, S18.
[147] C. Kato, S. Konaka, T. Iijima, M. Kimura, *Bull. Chem. Soc. Jpn.* **1969**, *42*, 2148.
[148] J. H. Carpenter, *J. Mol. Spectrosc.* **1974**, *50*, 182; M. Nakata, K. Kohata, T. Fukuyama, K. Kuchitsu, C. J. Wilkins, *J. Mol. Struct.* **1980**, *68*, 271.
[149] M. Nakata, T. Fukuyama, K. Kuchitsu, H. Takeo, C. Matsumura, *J. Mol. Spectrosc.* **1980**, *83*, 118; M. Nakata, K. Kohata, T. Fukuyama, K. Kuchitsu, *ibid.* **1980**, *83*, 105.

[150] M. Nakata, T. Fukuyama, C. J. Wilkins, K. Kuchitsu, *J. Mol. Struct.* **1981**, *71*, 195.
[151] C. Kati, S. Konaka, T. Iijima, *Bull. Chem. Soc. Jpn.* **1969**, *42*, 2148.
[152] R. L. Hilderbrandt, A. L. Andreassen, S. H. Bauer, *J. Phys. Chem.* **1970**, *74*, 1586.
[153] D. R. Johnson, F. X. Powell, W. H. Kirchhoff, *J. Mol. Spectrosc.* **1971**, *39*, 136.
[154] H. W. Careless, H. W. Croto, B. M. Landsberg, *Chem. Phys.* **1973**, *1*, 371; D. Christen, H. Oberhammer, W. Zeil, A. Haas, A. Darmadi, *J. Mol. Struct.* **1980**, *66*, 203.
[155] J. H. Carpenter, D. F. Rimmer, G. Smith, D. H. Whiffen, *J. Chem. Soc. Faraday Trans. 2* **1975**, *71*, 1752.
[156] D. Christen, *J. Mol. Struct.* **1980**, *66*, 211.
[157] D. R. Lide, D. E. Mann, R. M. Fristrom, *J. Chem. Phys.* **1957**, *26*, 734.
[158] M. Hargittai, I. Hargittai, *J. Mol. Struct.* **1981**, *73*, 253.
[159] R. L. Kuczkowski, R. D. Suenram, F. J. Lovas, *J. Am. Chem. Soc.* **1981**, *103*, 2561.
[160] M. Hargittai, I. Hargittai, *J. Mol. Struct.* **1974**, *20*, 283.
[161] I. Hargittai, B. Rozsondai, B. Nagel, P. Bulcke, G. Robinet, J.-F. Labarre, *J. Chem. Soc. Dalton Trans.* **1978**, 861.
[162] T. Jordan, H. W. Smith, L. L. Lohr, W. N. Lipscomb, *J. Am. Chem. Soc.* **1963**, *85*, 846.
[163] H. Oberhammer, W. Zeil, *Z. Naturforsch. A* **1969**, *24*, 1612.
[164] T. Kimura, T. Sakurai, *J. Solid State Chem.* **1980**, *34*, 369.
[165] R. H. Andrews, S. J. Clark, J. D. Donaldson, J. C. Dewan, J. Silver, *J. Chem. Soc. Dalton Trans.* **1983**, 767.
[166] H. P. Beck, W. Milius, *Z. Anorg. Allg. Chem.* **1988**, *562*, 102.
[167] B. R. Vincent, K. N. Robertson, T. S. Cameron, O. Knop, *Can. J. Chem.* **1987**, *87*, 1042.
[168] K. Prassides, P. Day, A. K. Cheetham, *J. Am. Chem. Soc.* **1983**, *105*, 3366; *Inorg. Chem.* **1985**, *24*, 545.
[169] S. L. Lawton, R. A. Jacobson, *Inorg. Chem.* **1986**, *25*, 743.
[170] A. du Bois, W. Abriel, *Z. Naturforsch. B* **1988**, *43*, 1003; *Z. Kristallogr.* **1988**, *182*, 36.
[171] W. G. McPherson, E. A. Meyers, *J. Phys. Chem.* **1968**, *72*, 3117; F. Lazarini, *Acta Crystallogr. Sect. C* **1985**, *41*, 1617; *Acta Crystallogr. Sect. B* **1980**, *36*, 2748.
[172] R. A. Wheeler, P. N. V. Pavan Kumar, *J. Am. Chem. Soc.* **1992**, *114*, 4776.
[173] W. Abriel, *Acta Crystallogr. Sect. C* **1986**, *42*, 1113.
[174] W. Abriel, *Z. Naturforsch. B* **1987**, *42*, 415.
[175] A. du Bois, W. Abriel, *Z. Naturforsch. B* **1990**, *45*, 573.
[176] S. C. Abrahams, J. Ihringer, P. Marsh, *Z. Kristallogr.* **1989**, *186*, 1; W. Abriel, A. du Bois, *Acta Crystallogr. Sect. C* **1989**, *45*, 2002.
[177] W. Abriel, A. du Bois, *Z. Naturforsch. B* **1989**, *44*, 1187.
[178] R. J. Gillespie, E. A. Robinson, *Inorg. Chem.* **1992**, *31*, 1960.

Time is money...

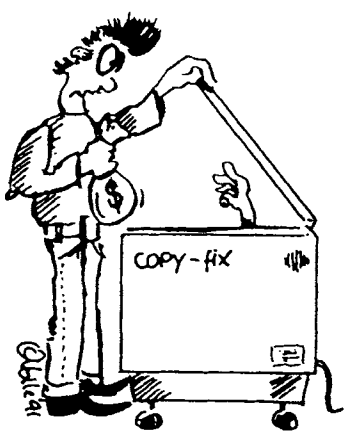

Save both by starting a personal subscription to *Angewandte Chemie* (now with *Chemistry - A European Journal*). At 9¢ per page you can't go wrong. With your own private copy you can read the "hot" articles before they cool, and waste less time in front of the copier.

Order now!
An order form can be found on the last page of this issue.

Voids in Variable Chemical Surroundings: Mesoporous Metal Oxides

Peter Behrens*

The design of the structure of materials is a current challenge in solid-state chemistry. However, binary metal oxides, for example, typically possess only one or a few thermodynamically stable modifications, providing only a limited range for design. If, however, the formation of solid oxides is carried out at low temperatures and thus under kinetic control, it is possible to prepare metastable modifications and to influence the reaction process. Following these guidelines, several groups have recently reported on the preparation of mesoporous metal oxides, that is metal oxide structures that are penetrated by regular arrangements of holes of the same size. Among these metal oxides are alumina,[1-3] titania,[4] niobia,[5] and zirconia.[6]

The preparative methods used are based on classical syntheses of zeolite-type solids and rely on the fact that small organic molecules (templates in the sense of structure directors) are occluded by crystallizing inorganic frameworks during hydrothermal synthesis and that these molecules thus influence the structure of these frameworks.[7] The tetrahedral network is composed typically of silicates, aluminosilicates, or aluminophosphates; correspondingly, the microporous solids are designated as porosils, porolites (zeolites belong to this class), or "AlPOs". The size and shape of the organic molecules that are added to the synthesis mixture influence the arrangement of the TO_4 building units (T = tetrahedrally surrounded atom; Si, Al, etc.) such that the resulting tetrahedral network forms voids for the occlusion of the molecules. The framework structure of these typical host–guest compounds[8] can be determined to a certain degree by the choice of the molecule ("structure-directed solid-state synthesis"). The maximum size of the pores is restricted to cage and channel diameters of about 15 Å, but due to the crystalline structure of these substances their pore-size distribution is very narrow. Thus, in addition to the important industrial applications of microporous materials, the idea of controlling the structure of inorganic solids by organic molecules is appealing to the preparative solid-state chemist. Classical synthetic methods for solid compounds, such as reaction of solids at high temperatures, offer hardly any possibilities to direct the reaction. There is a good chance that the structure-directing effect of organic molecules may some day make it possible to "design" solid-state syntheses.[9]

[*] Prof. Dr. P. Behrens
Institut für Anorganische Chemie der Universität
Meiserstrasse 1, D-80333 München (Germany)
Telefax: Int. code +(89)590-578
e-mail: pbe@anorg.chemie.uni-muenchen.de

A substantial extension of this approach to the synthesis of porous materials was achieved by chemists from Mobil Oil at the beginning of the nineties.[10, 11] Instead of using single molecules as templates, they employed supramolecular long-range ordered aggregates of surfactant molecules which form in aqueous solutions. Use of these lyotropic phases led to mesostructured materials (silicates, aluminosilicates, alumophosphates) with different structure types (Fig. 1). After calcination these mesostructured materials leave ordered arrangements of pores; the diameter of these pores can be tuned between 20 and 100 Å by varying the length of the hydrophobic part of the surfactant. These materials, designated as M41S, are not crystalline, and so their pore-size distributions are not as narrow as those of the microporous substances. Nevertheless, these substances may legitimately be called the "big brothers" of zeolite-type materials. They are currently being tested in several applications which are analogous to those of zeolites and which appear appropriate to be extended to larger molecules.

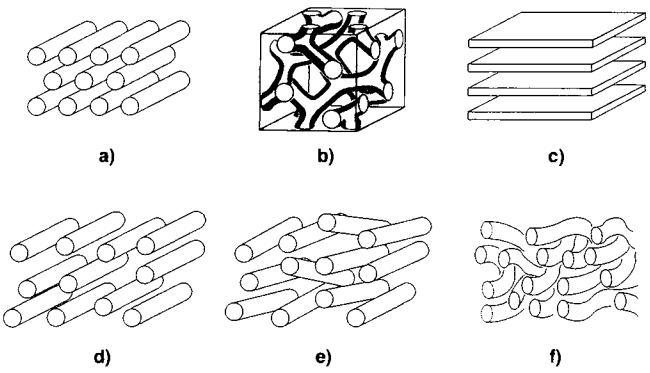

Fig. 1. Structures of mesostructured phases. The top row shows structures with long-range order: a) hexagonal phase, b) cubic $Ia\bar{3}d$ phase, c) lamellar phase. The bottom row shows possible disordered structures, as they may occur in some of the mesoporous metal oxides: d) disordered arrangement of parallel cylindrical pores, e) disordered packing of cylindrical pores (according to ref. [24]), f) worm-shaped pores.

One of these applications is shape-selective catalysis. In the realm of microporous solids, the research in this area during the last ten years has focused on the production of specific reactivities by framework substitutions. The most well-known example is possibly titanium silicalite-1 (TS-1).[12] Substitution of only one percent of the Si atoms in the SiO_2 framework of silicalite-1 creates a highly reactive and shape-selective catalyst for oxidations with hydrogen peroxide. Other substitutions (Ga, Fe, Co)

 © VCH Verlagsgesellschaft mbH, D-69451 Weinheim, 1996 0570-0833/96/3505-0515 $ 15.00+.25/0

of Al or Si in the framework of silicates or aluminophosphates allow the controlled tuning of the acidic catalytic activity of these solid acids. In the last two years, it was shown that such framework substitutions are also possible in M41S materials.[13]

The chemical variability of structure direction with lyotropic phases, however, extends far beyond the incorporation of small amounts of metals in typical framework builders such as silicate, aluminosilicate, and aluminophosphate. Mesostructured phases can be prepared with oxides of a wide variety of metals (Fe, W, Pb, Sb, Mn, Ga) and with salts such as zinc phosphate, as was first shown by the groups of Stucky and Schüth.[14]

For the construction of such mesostructures it is important to adapt the headgroup chemistry of the surfactants to that of the inorganic component. In aqueous solution, the latter forms—in a certain pH range—oligomeric cations or anions that are able to undergo further condensation. Silicate mesopores were originally synthesized in basic solutions in which the silicate species occur as oligoanions. Thus, cationic surfactants S^+ were used for the structuring of negatively charged inorganic species I^-. Such organic–inorganic mesostructures are designated as S^+I^- mesostructures (Fig. 2a). Examples of S^-I^- mesostructures are cationic lead oxide species structured by anionic surfactants such as alkylsulfonates (Fig. 2b). Surprisingly, also

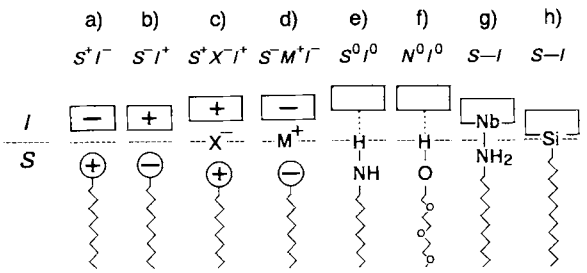

Fig. 2. Interactions at the interface between organic phase (S, N) and inorganic phase (I): a) to d) ionic interactions, e) and f) hydrogen bonding, g) and h) covalent bonds.

organic–inorganic combinations with identically charged partners are possible, but then the formation of the mesostructure is mediated by counter-charged ions which must be present in stoichiometric amounts: $S^+X^-I^+$ mesostructures (Fig. 2c, for example with S^+ = tetraalkylammonium ion, X^- = bromide, and I^+ = cationic silica species which form in strongly acidic solutions) or $S^-M^+I^-$ mesostructures (Fig. 2d, for example with S^- = alkylcarboxylate, $M^+ = Na^+$, and I^- = zincate ions).[14b]

However, most oxides only gave organic–inorganic composites possessing a lamellar structure (Fig. 1c) when the synthesis was based on the compensation of the ionic charges at the S/I interface. These mesostructures collapse upon removal of the organic component and yield dense (in most cases amorphous) metal oxides. They are thus not appropiate for the preparation of mesoporous phases. Iron, tungsten, lead, and antimony oxides also formed hexagonal mesostructured phases (Fig. 1a), and antimony oxide in addition gave cubic ones (Fig. 1b). However, these phases also did not exhibit porosity after calcination: The ordered mesostructure collapsed.[14] The reason for this is probably that the degree of condensation of the oligomeric ions, which form the walls, is lower than in silicates; the redox instability of the metal cations may also play a role. Milder routes for template removal were also tested: For silicate mesophases it was shown that surfactant cations can be extracted from S^+I^- combinations by solvents that contained cations for exchange; treatment of $S^+X^-I^+$ combinations based on silica with ethanol liberates the S^+X^- ion pairs. However, in the case of mesostructured metal oxides based on charge compensation at the S/I interface, this route does not seem to work.

Initial progress with regard to a milder route to template removal from mesostructured metal oxides was achieved by Pinnavaia and co-workers.[1, 2] Interestingly, mesostructures can also be formed without the participation of charges: S^0I^0 combinations were introduced by the formation of hexagonal silica materials that were prepared by using neutral amine surfactants S^0 (Fig. 2e).[11] Also nonionic polyethylene oxide surfactants N^0 can act as structure directors in a N^0I^0 combination (Fig. 2f).[2] In the case of these neutral templating routes the interaction at the S/I interface probably occurs through hydrogen bonds.[15] Thus, the forces at the interface are weak compared to electrostatic coupling. This allows extraction of the neutral template molecules by washing with ethanol.

It was also possible to prepare mesoporous aluminum oxides by S^0I^0 and N^0I^0 combinations.[1, 2] The use of neutral structure directors opens the possibility of forming hexagonal phases (ionic coupling at the interface produces only lamellar surfactant/alumina composites), and template removal can be performed under mild conditions by extraction with ethanol. Aluminum oxide mesostructures that were prepared by using surfactants based on polyethylene oxide/polypropylene oxide copolymers can even be calcined at 773 K to give mesoporous materials.[2, 3] The specific surface areas of these samples range from 420 to 535 $m^2 g^{-1}$ (Table 1).

Table 1. Specific surface areas of mesoporous metal oxides.

Material	Approximate composition [b]	Specific surface area [a] $[m^2 g^{-1}]$	$[10^3 m^2 mol^{-1}]$	Ref.
M41S	SiO_2	>1000	>60	[10]
MSU-1	$AlO_{1.5}$	535	27.3	[3]
Ti-TMS1	TiO_2	<200	<16	[4]
Nb-TMS1	$NbO_{2.5}$	434	100.8	[5]
zirconia	ZrO_2	280	34.5	[6]
zirconium oxo phosphate	ZrO_2	390	48	[6]

[a] In the original publications, the specific surface areas are always related to mass and are given in $m^2 g^{-1}$. To be able to make a better comparison of the surface areas of mesoporous materials of different composition, here also the areas related to one mol of metal atoms are provided, together with the typical value for mesoporous silicates. [b] This composition was used for the transformation of mass-related to molar-specific surface area.

In the syntheses by Pinnavaia et al., alkoxides such as tetraethylorthosilicate or aluminum tri-*sec*-butoxide were used for the construction of the inorganic walls. Metal alkoxides may generally be considered as the precursors of choice for the generation of metal oxide walls in aqueous solutions that are structured by surfactants. However, attempts to prepare mesostructured titania from titanium propoxide and surfactants with different headgroups (phosphate, carboxylate, sulfate) failed and only yielded the dense anatase modification.[4] Evidently, the condensation reaction was too fast so that the species formed by the hydrolysis of the titanium alkoxide could not be

 © VCH Verlagsgesellschaft mbH, D-69451 Weinheim, 1996 0570-0833/96/3505-0516 $ 15.00+.25/0

directed into mesostructural arrangements by the surfactant molecules. By clever use of the coordination chemistry at the metal center Antonelli and Ying[4] were able to correct this negative result: If titanium (acetylacetonate)triisopropoxide is used as the metal alkoxide, the hydrolysis rate is slowed down so that a common hexagonal mesostructure of the surfactant and the inorganic species can form, although only surfactants with phosphate headgroups can be used successfully. The composite produced by using this modified sol–gel process was the first transition metal oxide that could be calcined with a partial conservation of the mesostructure: The calcination yields Ti-TMS-1, a mesoporous material with a narrow pore-width distribution but with a specific surface area of only about 200 $m^2 g^{-1}$. This is quite a small value, even when the difference in relative molecular masses between TiO_2 and SiO_2 is taken into account (Table 1). The phosphate headgroups at least in part remain in the mesoporous material.[4]

By taking advantage of the possibilities of varying the coordination chemistry at the metal center of an alkoxide, Antonelli and Ying[5] recently succeeded in preparing a stable transition metal oxide mesostructure from which the template could easily be removed. The authors first allowed niobium(v) ethoxide to react with a long-chain alkylamine in the absence of water to form an amino(tetraethoxy)niobium complex. In this way they obtained a covalent connection between the organic and the inorganic component. This type of interface interaction may perhaps best be represented by a bonding dash as in "*S–I*" (Fig. 2g). After this composite surfactant had been given sufficient time to form ordered hexagonal structures, water was added to hydrolyze the Nb–O–C bonds. The condensation reaction started immediately and was reinforced by hydrothermal treatment. Template removal was most easily achieved by washing the sample with a HNO_3/EtOH solution at 40 °C. In this way Nb-TMS1, a mesoporous, hydrated niobium oxide, was obtained that exhibited a specific surface area of 434 $m^2 g^{-1}$ (see Table 1). This ligand-assisted template synthesis should also be applicable to the metal oxides of Ti, Zr, Ta, Ce, and Y.[5] We are currently investigating similar structuring processes in silicate systems, in which the headgroup of the surfactant is simultaneously a building unit of the inorganic material (Fig. 2h). For this purpose we use trialkoxyalkylsilanes. Their Si–O–C bonds are hydrolyzed during the synthesis, thus generating an anionic surfactant. In a reaction with tetraethoxysilane a self-organization process occurs that—until now—however, has mainly led to lamellar phases.[16]

In this issue of *Angewandte Chemie* the synthesis of mesoporous zirconium oxide derivatives is reported by Schüth and co-workers.[6] The hydrolysis of zirconium propoxide in a strongly acidic solution of the common S^+ surfactant alkyltrimethylammonium yields hexagonally structured zirconium oxide, when the solution also contains $(NH_4)_2SO_4$. Calcination at 773 K leaves a zirconium oxide that contains only a small amount of sulfur and that has a specific surface area of 280 $m^2 g^{-1}$ (see Table 1). When zirconium sulfate hydrate is used instead of the propoxide and ammonium sulfate, a hexagonal mesostructure is also formed, but this one collapses on calcination. Only treatment with a phosphoric acid solution provides sufficient stability. Possibly, the phosphate ions increase the degree of interlinking in the walls which probably possess only a small degree of condensation. The calcination gives mesoporous materials with a narrow pore-width distribution and specific surface areas of up to 390 $m^2 g^{-1}$ (see Table 1). These materials still contain a considerable amount of phosphorus and should be designated as zirconium oxo phosphate. In the products of their surfactant-based syntheses of zirconium oxides, M. J. Hudson et al. find similar values for the specific surface area, but no ordered pore system.[17]

For all mesoporous metal oxides described here, sorption measurements and a peak appearing at small angles in their X-ray diffraction diagram indicate that the pore size in one sample is rather uniform. In most cases, however, there are no additional X-ray diffraction reflections, whereas well-ordered hexagonal silica materials exhibit three or four of these. This finding indicates that the pores in the metal oxides do not possess a long-range order as perfect as that in the silica materials. Transmission electron microscopic images substantiate this idea (Fig. 4 in ref. [4], Fig. 2 in ref. [5]). The available data can best be explained by structural models containing disorder like those shown in Figure 1d and 1e. In the case of mesoporous aluminum oxide, electron microscopy (for example Fig. 2 in ref. [3]) indicates a drastically changed pore shape. Evidently, the pores are not straight cylinders, but appear with a curved wormlike shape, although of uniform diameter (Fig. 1f).

The application of mesoporous metal oxides in heterogeneous catalysis is evident. Alumina has been known as a catalyst support for a long time. The availability of this support with high surface area and regular pore distribution should in many cases lead to substantial advantages. Larger molecules may possibly be transformed with shape-selectivity like that zeolites demonstrate for small molecules. Transition metal oxides introduce their redox activity as an additional component and could possibly be used directly as redox catalysts. These materials could also be of interest as sorbents because sorption processes depend on the chemical composition of the walls.

Apart from these classical applications mesoporous metal oxides are interesting for other reasons. As the structuring of the mesoporous metal oxides occurs on a length scale where quantum confinement of the electronic states can be expected, these oxides should also possess altered electronic structures. For example, investigations on mesoporous rhenium(VI) oxide would be of interest. As a bulk solid this a metallic conductor; thus a size-induced metal–semiconductor transition should occur as a function of the pore diameter, because the quantum restrictions decrease the overlap of bands. The length of an organic alkyl group would thus ultimately determine the electronic properties of an inorganic solid. In mesoporous materials of semiconducting metal oxides ("expanded semiconductors"),[18] the band gap should widen with increasing pore diameter. Such mesoporous semiconductors with their large internal surface might find applications as highly sensitive sensors if their electronic surface states react to the substances to be detected.

The examples given above for the structure-directed synthesis of mesoporous metal oxides show how strongly the success of these labile kinetically controlled formation processes of inorganic solids depends on minor, delicately tuned manipulations of the synthesis systems. Use of the fine-tuned interplay of the coordination chemistry of metal alkoxide precursors and the additional interlinking of weakly condensed wall material by

 © VCH Verlagsgesellschaft mbH, D-69451 Weinheim, 1996 0570-0833/96/3505-0517 $ 15.00+.25 0

phosphate ions (which plays a role in the synthesis of Ti-TMS-1 and zirconium oxo phosphate) are particularly worthy of mention in this context. Finally, it should not be forgotten that also in the area of structuring inorganic solids, nature is the true master. In biomineralization processes of highly and lowly developed living creatures, supramolecular aggregates of organic substances also serve as structure directors for the construction of inorganic solids; products are created that are optimized for their respective tasks, but which often also are aesthetically pleasing.[19] Recent work in the area of "biomimetic solid-state synthesis" by the groups of Mann[20] and Ozin may point the way ahead.[21] Walsh and Mann prepared hollow spheres of $CaCO_3$-aragonite that possess a striking resemblance to the skeletons of marine algae (Fig. 3 in ref. [20]). In these solid-state syntheses, a microemulsion of didodecyl(dimethyl)ammonium bromide, tetradecane, and water (in which calcium hydrogencarbonate was dissolved) acted as structure director, again a supramolecular structure built from simple organic substances.[20] Oliver, Coombs, and Ozin prepared hollow aluminophosphate spheres by combining phosphoric acid, primary alkylamines, and pseudoboehmite in tetraethyleneglycol.[21b] However, this group also calls the attention to the fact, that these "skeletons from the beaker" have been standing in the archives cupboards of science for quite some time:[22] As far back as 1872 the Dutch scientist Pieter Harting published his investigations "*On the Artificial Production of Some of the Principal Organic Calcareous Formations*", which he had started in 1840, stressing the importance of the controlling action of organic substances.[23]

German version: *Angew. Chem.* 1996, *108*, 561–564

Keywords: catalysis · mesoporosity · metal oxides · surfactants

[1] P. T. Tanev, T. J. Pinnavaia, *Science* **1995**, *267*, 865–867.
[2] S. A. Bagshaw, S. A. Prouzet, T. J. Pinnavaia, *Science* **1995**, *269*, 1242–1244.
[3] S. A. Bagshaw, T. J. Pinnavaia, *Angew. Chem.* **1996**, *108*, in press.
[4] D. M. Antonelli, J. Y. Ying, *Angew. Chem.* **1995**, *107*, 2202–2206; *Angew. Chem. Int. Ed. Engl.* **1995**, *34*, 2014–2017.
[5] D. M. Antonelli, J. Y. Ying, *Angew. Chem.* **1996**, *108*, 461–464; *Angew. Chem. Int. Ed. Engl.*, **1996**, *35*, 426–430.
[6] U. Ciesla, S. Schacht, G. D. Stucky, K. K. Unger, F. Schüth, *Angew. Chem.* **1996**, *108*, 597–600; *Angew. Chem. Int. Ed. Engl.*, **1996**, *35*, 541–543.
[7] M. E. Davis, R. F. Lobo, *Chem. Mater.* **1992**, *4*, 756.
[8] A. Müller, H. Reuter, S. Dillinger, *Angew. Chem.* **1995**, *107*, 2505–2539; *Angew. Chem. Int. Ed. Engl.* **1995**, *34*, 2311–2361.
[9] M. E. Davis, *CHEMTECH* **1994**, 22.
[10] C. T. Kresge, M. E. Leonowicz, W. J. Roth, J. C. Vartuli, J. S. Beck, *Nature* **1992**, *359*, 710–712; J. S. Beck, J. C. Vartuli, W. J. Roth, M. E. Leonowicz, C. T. Kresge, K. D. Schmitt, C. T. W. Chu, D. H. Olson, E. W. Sheppard, S. B. McCullen, J. B. Higgins, J. L. Schlenker, *J. Am. Chem. Soc.* **1992**, *114*, 10834–10843.
[11] P. Behrens, *Adv. Mater.* **1993**, *5*, 127–131; P. Behrens, G. D. Stucky, *Angew. Chem.* **1993**, *105*, 729–732; *Angew. Chem. Int. Ed. Engl.* **1993**, *32*, 696–699.
[12] G. Perego, G. Bellussi, C. Gorno, M. Taramasso, *Stud. Surf. Sci. Catal.* **1986**, *28*, 129; B. Notari, *ibid.* **1988**, *37*, 413.
[13] P. T. Tanev, M. Chibwe, T. J. Pinnavaia, *Nature* **1994**, *368*, 321–323; A. Corma, M. T. Navarro, J. Perez-Pariente, *J. Chem. Soc. Chem. Commun.* **1994**, 147–148; D. Zhao, D. Goldfarb, *ibid.* **1995**, 875–876; Z. Y. Yuan, S. Q. Liu, T. H. Chen, J. Z. Wang, H. X. Li, *ibid.* **1995**, 973–974; A. Sayari, C. Danumah, I. L. Moudrakovski, *Chem. Mater.* **1995**, *7*, 813–815; S. Gontier, A. Tuel, *Zeolites*, **1995**, *15*, 601–610; *Microporous Mater.* **1995**, *5*, 161–171.
[14] a) Q. Huo, D. I. Margolese, U. Ciesla, P. Feng, T. E. Gier, P. Sieger, R. Leon, P. M. Petroff, F. Schüth, G. D. Stucky, *Nature* **1994**, *368*, 317–321; b) Q. Huo, D. I. Margolese, U. Ciesla, D. G. Demuth, P. Feng, T. E. Gier, P. Sieger, A. Firouzi, B. F. Chmelka, F. Schüth, G. D. Stucky, *Chem. Mater.* **1994**, *6*, 1176–1191; c) U. Ciesla, D. Demuth, R. Leon, P. Petroff, G. D. Stucky, K. Unger, F. Schüth, *J. Chem. Soc. Chem. Commun.* **1994**, 1387–1388.
[15] Recently an interesting variation of the neutral templating route was described (G. S. Attard, J. C. Glyde, C. G. Göltner, *Nature* **1995**, *378*, 366–368). These authors used commercially available nonionic surfactants such as octaethyleneglycolhexadecyl ether in concentrations that were so high that the aqueous solution of the surfactant formed a uniform and continuous liquid crystalline phase. By adding silicate solution it was possible to obtain monolithic surfactant/silicon dioxide mesostructures, quite in contrast to the usual synthesis which yields only fine powders. However, the monoliths suffered from cracks upon heating. If their temperature stability can be raised and when mesoporous monoliths become available, this would significantly broaden the applicability of this class of materials.
[16] P. Behrens, A. M. Schneider, unpublished results; this research is funded by the Deutsche Forschungsgemeinschaft in the framework of the Schwerpunktprogramm "Spezifische Phänomene in der Si-Chemie" (Be 1664/5-1).
[17] J. A. Knowles, M. J. Hudson, *J. Chem. Soc. Chem. Commun.* **1995**, 2083.
[18] G. A. Ozin, *Adv. Chem. Ser.* **1995**, *245*, 334.
[19] L. Addadi, S. Weiner, *Angew. Chem.* **1992**, *105*, 159–176; *Angew. Chem. Int. Ed. Engl.* **1992**, *31*, 153–169; *Biomineralization, Chemical and Biochemical Perspectives* (Eds.: S. Mann, J. Webb, R. J. P. Williams, VCH, Weinheim, **1989**.
[20] D. Walsh, S. Mann, *Nature* **1995**, *377*, 320–323.
[21] a) S. Oliver, A. Kuperman, N. Coombs, A. Lough, G. A. Ozin, *Nature* **1995**, *378*, 47; b) S. Oliver, N. Coombs, G. A. Ozin, *Adv. Mater.* **1995**, *7*, 931–935; c) G. A. Ozin, S. Oliver, *ibid.*, **1995**, *7*, 943–947.
[22] S. Oliver, G. A. Ozin, L. A. Ozin, *Adv. Mater.* **1995**, *7*, 948–951.
[23] P. Harting, *Quart. J. Microsc. Sci.* **1872**, *12*, 118–123.
[24] C.-Y. Chen, S.-Q. Xiao, M. E. Davis, *Microporous Mater.* **1995**, *4*, 1–20.

The "Magic" Diarylhydroxymethyl Group

Manfred Braun*

Anyone following the rapid development of asymmetric synthesis during the last decade has certainly noticed the increasing use of the diarylhydroxymethyl group as a structural unit in covalently bound auxiliaries, in ligands, and in catalysts. Although it is not a stereogenic unit, it plays a crucial role in various stereoselective reactions or at least leads to an enhancement of selectivity. After numerous applications the function of the "magic" diarylhydroxymethyl group is now under intense examination.

When acetal-protected (*R*,*R*)-diethyl tartrate was treated with aryl Grignard reagents by Seebach's group in 1983, the first α,α,α′,α′-tetraaryl-1,3-dioxolane-4,5-dimethanols were obtained. The original "TADDOL" **1** ($R^1 = R^2 = CH_3$; Ar = Ph) was followed by a number of analogous compounds with different aryl groups (Ar) and acetal moieties (R^1, R^2).[1] Simultaneously, more and more applications were developed, leading to enantiomerically pure targets: metal complexes **2** with TADDOL ligands, used in stoichiometric or catalytic amounts, make possible enantioselective aldol additions, formation of cyanohydrins, inter- and intramolecular Diels–Alder reactions, [2 + 2]cycloadditions, ene reactions, hydrophosphonylations, iodolactonizations, and transesterifications.[2]

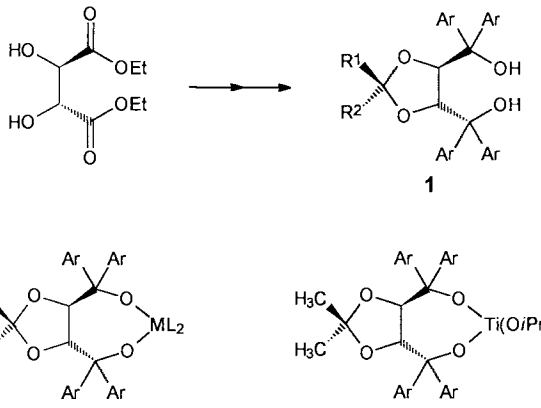

The large number of TADDOL-catalyzed enantioselective additions of polar alkyl-, aryl-, and allylmetal compounds to aldehydes and nitro olefins is exemplified by the reaction of diethylzinc with heptanal. The titanates **3** usually generated from TADDOLs and titanium tetraisopropoxide control the addition of diethylzinc by ligand-accelerated catalysis. An increase in selectivity is achieved not only by using the β-naphthyl derivative **3b** instead of the titanium complex **3a** but, surprisingly, also in the presence of excess achiral titanium tetraisopropoxide (relative to the amount of catalyst) and catalytic amounts of either of the chiral titanates **3a** and **3b** (Scheme 1). Evidently the titanium tetraisopropoxide takes over the alkoxide formed during the addition of diethylzinc, thus regenerating the active catalyst **3**. Titanates like **4** can also catalyze the addition of diethylzinc, albeit with poorer enantioselectivity. Therefore ligand exchange (**4** → **3**) has to take place in order to suppress this competitive reaction.[3a]

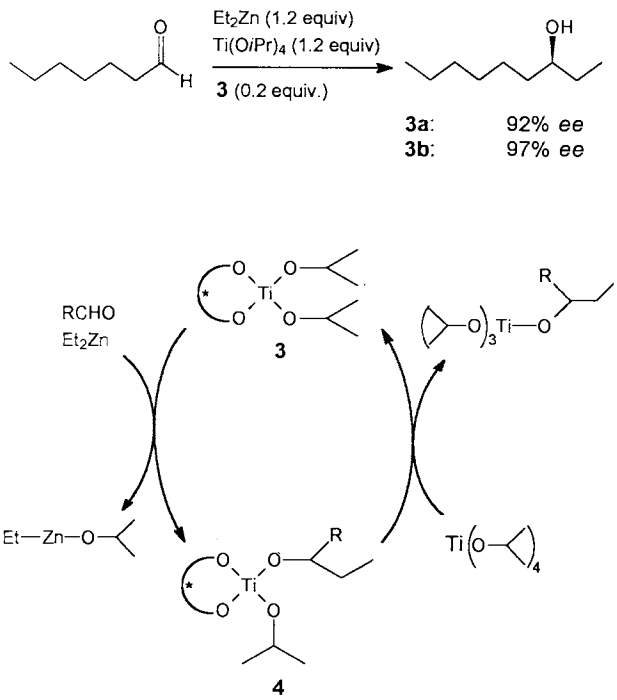

Scheme 1. Reaction of diethylzinc with heptanal in the presence of **3**, and mechanism of the TADDOL-catalyzed addition of diethylzine to aldehydes.

Extensive studies of the titanate-catalyzed addition of diethylzinc employing various TADDOL ligands and TADDOL analogues, for the most part characterized by X-ray crystal structure analysis, have shown a uniform topicity for the nucleophilic attack on aldehydes. All titanium–TADDOL complexes derived from (*R*,*R*)-tartaric acid effect preferential addition to the *Si* face of the aldehyde. This is apparently due to the pseudoaxial arrangement of one of the two geminal diaryl groups, which is clearly observed in crystal structure analyses of TADDOLs as well as their titanium complexes. According to a model suggested by Seebach, an isopropoxide ligand is displaced and the titanium atom coordinates, and thereby activates, the carbonyl oxygen of the aldehyde. In the transition state models represented in **5** and **6** the metal atom is in the foreground (the dioxolane ring in (*R*,*R*) configuration has been omitted for clarity). Consequently, the transfer of the nucleophile should take place from the side of the titanates **5** and **6** directed

[*] Prof. Dr. M. Braun
Institut für Organische und Makromolekulare Chemie der Universität
Universitätsstrasse 1, D-40225 Düsseldorf (Germany)
Fax: Int. code +(211)81-13085
e-mail: braunm@clio.rz.duesseldorf.de

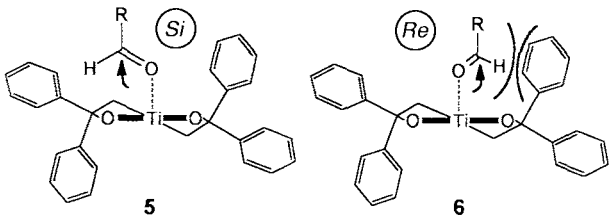

5 6

toward the observer. The diarylmethoxide moiety is responsible for the preference of transition state model **5** (attack from the *Si* face) over the diastereomorphous alternative **6** (*Re*-face attack); the steric interaction between the aldehyde hydrogen and the pseudo-axial aryl unit offers a plausible explanation. Accordingly, the titanate of tetrabenzyl TADDOL (**1**, $R^1 = R^2 = CH_3$; CH_2Ph instead of Ar), in which the aryl groups are no longer conformationally fixed, leads to only marginal enantioselectivity (8% *ee* for the addition of diethylzinc to benzaldehyde). The pseudo-equatorial aryl groups are essential to the ligand-accelerated catalysis of TADDOL titanates as well as those in pseudo-axial positions, as they permit fast exchange of an isopropoxide ligand for the aldehyde. In their absence the addition of diethylzinc is not only slower, but also less stereoselective.[3b]

TADDOLs form clathrates with a wide variety of organic compounds such as tetrachloromethane, alcohols, carbonyl compounds, and amines. These clathrates can be used for resolutions of racemates as well as in enantioselective solid-state reactions.[4a] The TADDOL unit can also serve as a template in the anionic homopolymerization of methacrylates. The isotactic polymer obtained after liberation of the template is chiral and shows optical activity if the two chain ends are not identical and if the degree of polymerization is not too high.[4b]

(*R*)- and (*S*)-triphenylglycols **7** are available through addition of phenylmagnesium bromide to the corresponding enantiomer of methyl mandelate [Eq. (a)]. The monoacetates of triphenylglycol, (*R*)-and (*S*)-HYTRA **8a** (HYTRA = 2-hydroxy-1,2,2-triphenylethyl acetate), which were developed shortly after and independently of TADDOLs, can be utilized for the stereoselective addition of an acetate enolate to aldehydes.[5] As shown in the example of the reaction with isobutyraldehyde [Eq. (b)], this

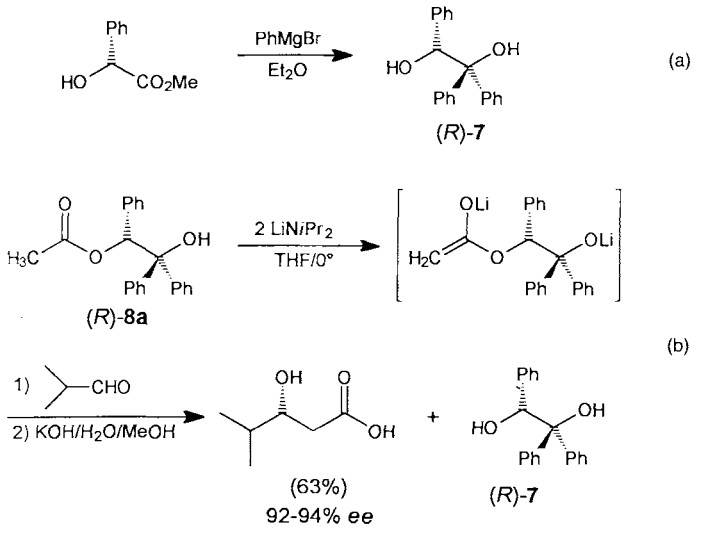

offers a practical solution to the problem of the acetate aldol reaction.[6]

Although the X-ray structure analysis of the HYTRA enolate has not been carried out (yet), research on its derivatives and analogues has shown the (deprotonated) hydroxydiphenylmethyl group again to be responsible for the stereoselectivity of the aldol reaction. The propionate **8b** derived from triphenylglycol **7** permits *anti*- and diastereofacially selective aldol additions.[7a] Ester–imine condensations show a surprising stereodivergence, probably due to the different configurations of the enolate (*E* or *Z*). Whereas the lithium enolates of the O-protected esters **8b** and **8c** lead to *cis*-β-lactams **9**, the condensation of the doubly deprotonated propionate **8d** with imines yields the *trans* diastereomers **10** with high enantiomeric excess.[7b]

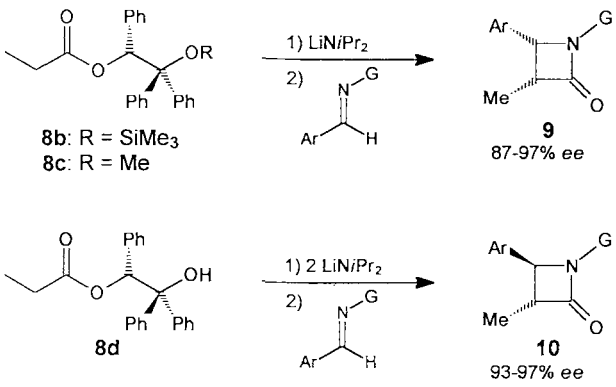

G = Ph, 4-MeOC$_6$H$_4$; Ar = Ph, 2-furyl

The diphenylmethyl unit is also found in the cyclic sulfites **12** used by Kagan and Rebiere to synthesize enantiomerically pure sulfoxides. In this case lactic acid is used as a chiral auxiliary. The diphenylpropanediol **11** derived from (*S*)-ethyl lactate reacts diastereoselectively (*90:10*) with thionyl chloride, resulting in the cyclic sulfite **12**, which can be recrystallized to give the diastereomerically pure substance (Scheme 2). Subsequent substitution at the heterocycle **12** through alkyllithium or Grignard reagents leads to complete inversion at the sulfur atom. However, in principle the formation of two regioisomers is possible, depending on whether the secondary or the tertiary alkoxide serves as the leaving group. Fortunately the regiochemistry of the ring opening reaction is controlled largely by the size of the nucleophile. If R^1 is small, the reaction should proceed via the trigonal-bipyramidal transition state **13** with the two geminal phenyl groups in equatorial position (assuming an S_N2-type reaction without pseudorotation). As a result the secondary alkoxide is the leaving group and the sulfinate **15** is the main product. Bulky nucleophiles with large R^1 groups push the geminal diphenyl group into the axial position to minimize steric interactions. This puts the sterically demanding groups in the trigonal-bipyramidal **14** in the *anti* position, and the tertiary alkoxide is now the leaving group; consequently sulfinate **16** is formed as the main product. In both cases the predominantly produced isomer **15** or **16** can be obtained in pure form by recrystallization. The subsequent second substitution yields the enantiomerically pure sulfoxides **17** and **18**, both with complete inversion at the sulfur atom. This method has the advantage of

 © VCH Verlagsgesellschaft mbH, D-69451 Weinheim, 1996 0570-0833/96/3505-0520 $ 15.00+.25/0

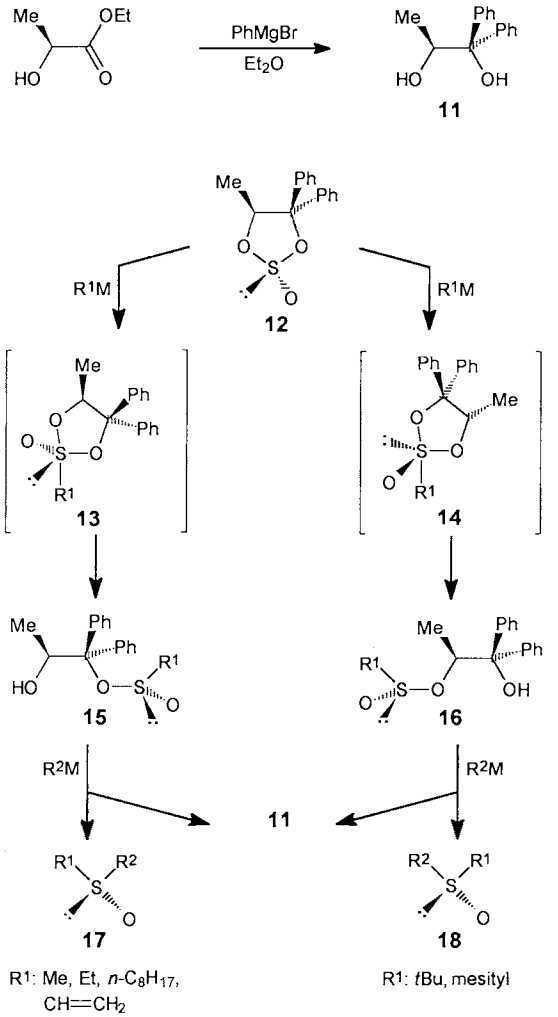

Scheme 2. Synthesis of the chiral auxiliary **11** from (*S*)-ethyl lactate, and conversion of the cyclic sulfite **12** into the enantiomerically pure sulfoxides **17** and **18**.

making sulfoxides with predictable absolute configuration accessible.[8]

The enantioselective reduction of prochiral ketones has long been researched intensively in the context of asymmetric synthesis, leading to numerous publications on chirally modified aluminum and boron hydrides.[9] Itsuno and co-workers were the first to report on the use of the geminally diphenyl-substituted amino alcohol **19** for the enantioselective control of the reduction of ketones by boranes.[10] In one example of this, initially stoichiometric, procedure (*R*)-1-phenylethanol is obtained in 94% *ee* by reduction of acetophenone. In work starting in 1987 Corey's group not only identified the structure of Itsuno's reagent **20**, but also worked out a catalytic variant.[11] Eventually the derivatives of open-chain α-amino acids were replaced by the oxazaborolidine **21**, the (*S*) enantiomer of which is easily available from L-proline. The high cost of D-proline made an alternative approach to the (*R*) reagent **21** desirable. This was accomplished by starting from pyroglutamic acid and resolving an intermediate.[11b] In typical procedures, ketones such as chloroacetophenone react with $BH_3 \cdot SMe_2$, $BH_3 \cdot THF$ or catechol borane in the presence of 1–10 mol% of oxazaborolidine **21** [Eq. (c)].[11c] As a rule, selectivities of more than 90% *ee*

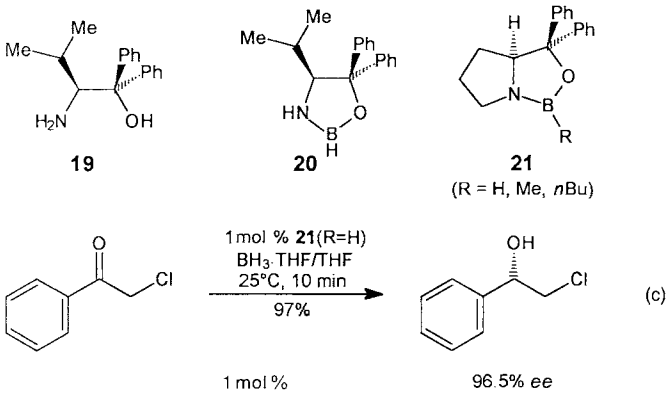

can be achieved. Various analogous ligands, for example **22** and **23**, were described, some of them capable of catalyzing other enantioselective reactions besides the borane reduction.[12] Oxazaborolidines **21** derived from diphenylprolinol[13] have so far found the widest range of applications. The B-methyl derivative (R = Me), a colorless solid, is stable at room temperature and can be handled in air. The borane adduct **24** is available in large quantities through reaction of the oxazaborolidine **21** (R = Me) with $BH_3 \cdot SMe_2$.[14]

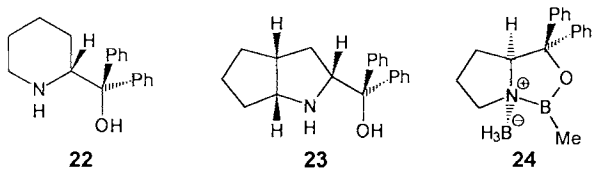

The following mechanism seems plausible to explain the catalytic activity of the oxazaborolidines (Scheme 3). In the first step the reagents **21** and borane·THF form adduct **24** in an equilibrium reaction. The Lewis-acidic boron atom of the heterocycle coordinates the carbonyl oxygen of the ketone (structure **25**). In

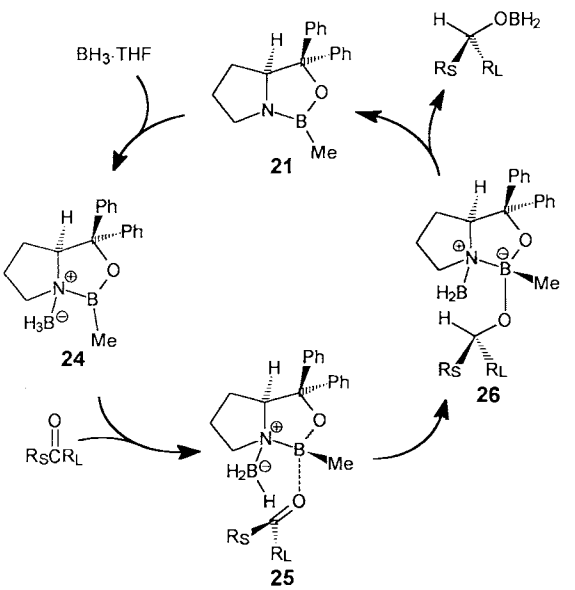

Scheme 3. Proposed mechanism for the reduction of ketones with $BH_3 \cdot THF$ and a catalytic amount of oxazaborolidine **21**.

the subsequent six-membered transition state a hydride is transferred to the ketone (R_S = small, R_L = large substituent), leading predominantly to diastereomer **26**. Finally detachment of the alkoxide takes place, thus regenerating the catalyst.[11a]

The energies of the diastereomeric chair and boat transition states for the reduction of acetophenone with a variety of oxazaborolidine–BH_3 complexes were obtained through MNDO calculations. In the lowest energy chair conformation **27** shown for the parent compound **21** the ketone phenyl group assumes the favored *anti* position (in relation to R) and lies parallel to the axial phenyl group of the geminal diphenylmethoxide unit with a ring distance of at least 5.5 Å. In the diastereomeric transition state **28**, which is 3.5 kcal mol^{-1} higher in energy, the acetophenone methyl substituent is 1.5 Å closer to the axial phenyl group.[15] Again the pseudo-axially orientated aryl group of the diphenylmethoxide unit seems to be essential for high selectivity: the calculated *ee* value of 98% is matched by an experimental value of 97%. Exchange of the hydroxydiphenylmethane group in the ligand for a CH_2OH unit leads to a substantial loss in selectivity. Thus the hydroxydiphenylmethane group, although it is not a permanent stereogenic center, exerts a critical influence on the course of the asymmetric reaction due to its fixation in a chiral reactive conformation.[16] Changing from prolinol to diphenylprolinol auxiliaries also results in an increase in stereoselectivity[19] in the addition of dialkylzinc to aldehydes,[13b] Reformatsky reactions,[17] and pinacol-type coupling of 2-formylbenzamides.[18] Even the usually very efficient RAMP/SAMP hydrazone method (RAMP, SAMP = (*R*)- and (*S*)-*N*-amino-2-(methoxymethyl)pyrrolidine) can be improved in individual cases through replacement of the methoxymethyl group by the diphenylmethoxymethyl side chain.[13a]

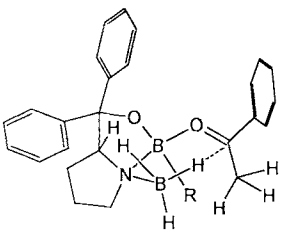

27

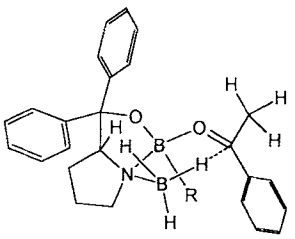

28

With increasing frequency, chiral oxazaborolidines are proving to be the reagents of choice for the enantioselective reduction of prochiral carbonyl compounds. Their unusual efficiency is taken into account by the description "chemzymes",[11d] a term that is, however, not undisputed.[20]

German version: *Angew. Chem.* **1996**, *108*, 565–568

Keywords: aldol reactions · asymmetric syntheses · sulfoxides · reductions · titanium compounds

[1] A. K. Beck, B. Bastani, D. A. Plattner, W. Petter, D. Seebach, H. Braunschweiger, P. Gysi, L. LaVecchia, *Chimia* **1991**, *45*, 238–244, and references therein.

[2] Review: R. Dahinden, A. K. Beck, D. Seebach in *Encyclopedia of Reagents for Organic Synthesis* (Ed.: L. A. Paquette), Vol. 3, Wiley, Chichester, **1995**, pp. 2167–2170.

[3] a) D. Seebach, D. A. Plattner, A. K. Beck, Y. M. Wang, D. Hunziker, *Helv. Chim. Acta* **1992**, *75*, 2171–2209; b) Y. N. Ito, X. Ariza, A. K. Beck, A. Bohác, C. Ganter, R. E. Gawley, F. N. M. Kühnle, J. Tuleja, Y. M. Wang, D. Seebach, *ibid.* **1994**, *77*, 2071–2110.

[4] a) F. Toda, *Top. Curr. Chem.* **1988**, *149*, 211–238; E. Weber, N. Dörpinghaus, C. Wimmer, Z. Stein, H. Krupitsky, I. Goldberg, *J. Org. Chem.* **1992**, *57*, 6825–6833; F. Toda, M. Miyamoto, S. Kikuchi, *J. Chem. Soc. Chem. Commun.* **1995**, 621–622; F. Toda, K. Tanaka, T. Okada, *ibid.* **1995**, 639–640; b) G. Wulff, S. Gladow, B. Kühneweg, S. Krieger, *Macromol. Symp.*, **1996**, *101*, 359–362.

[5] M. Braun, R. Devant, *Tetrahedron Lett.* **1984**, *25*, 5031–5034; M. Braun, *Angew. Chem.* **1987**, *99*, 24–37; *Angew. Chem. Int. Ed. Engl.* **1987**, *26*, 24–37.

[6] M. Braun, S. Gräf, *Org. Synth.* **1993**, *72*, 38–47.

[7] a) H. Sacha, D. Waldmüller, M. Braun, *Chem. Ber.* **1994**, *127*, 1959–1968; b) M. Braun, H. Sacha, D. Galle, A. El-Alali, *Tetrahedron Lett.* **1995**, *36*, 4213–4216.

[8] H. B. Kagan, F. Rebiere, *Synlett* **1990**, 643–650.

[9] V. K. Singh, *Synthesis* **1992**, 605–617, and references therein.

[10] S. Itsuno, M. Nakano, K. Miyazaki, H. Masuda, K. Ito, A. Hirao, S. Nakahama, *J. Chem. Soc. Perkin Trans. 1* **1985**, 2039–2044, and references therein.

[11] a) E. J. Corey, R. K. Bakshi, S. Shibata, *J. Am. Chem. Soc.* **1987**, *109*, 5551–5553; b) E. J. Corey, R. K. Bakshi, S. Shibata, C.-P. Chen, V. K. Singh, *ibid.* **1987**, *109*, 7925–7926; c) E. J. Corey, S. Shibata, R. K. Bakshi, *J. Org. Chem.* **1988**, *53*, 2861–2863; d) E. J. Corey, J. O. Link, *Tetrahedron Lett.* **1989**, *30*, 6275–6278.

[12] A. V. Rama Rao, M. K. Gurjar, P. A. Sharma, V. Kaiwar, *Tetrahedron Lett.* **1990**, *31*, 2341–2344; S. Walbaum, J. Martens, *Tetrahedron: Asymmetry* **1991**, *2*, 1093–1096; *ibid.* **1993**, *4*, 637–640; R. Berenguer, J. Garcia, M. Gonzàlez, J. Vilarrasa, *ibid.* **1993**, *4*, 13–16; J. G. H. Willems, F. J. Dommerholt, J. B. Hammink, A. M. Vaarhorst, L. Thijs, B. Zwanenburg, *Tetrahedron Lett.* **1995**, *36*, 603–606.

[13] a) D. Enders, V. Bhushan, *Tetrahedron Lett.* **1988**, *29*, 2437–2440; b) K. Soai, A. Ookawa, T. Kaba, K. Ogawa, *J. Am. Chem. Soc.* **1987**, *109*, 7111–7115.

[14] D. J. Mathre, A. S. Thompson, A. W. Douglas, K. Hoogsteen, J. D. Carroll, E. G. Corley, E. J. J. Grabowski, *J. Org. Chem.* **1993**, *58*, 2880–2888; see also: P. Y. Chavant, M. Vaultier, *J. Organomet. Chem.* **1993**, *455*, 37–46.

[15] D. K. Jones, D. C. Liotta, I. Shinkai, D. J. Mathre, *J. Org. Chem.* **1993**, *58*, 799–801; see also: V. Nevalainen, R. Uggla, M. R. Sundberg, *Tetrahedron: Asymmetry* **1995**, *6*, 1431–1440, and references therein.

[16] For similar effects of geminal diaryl groups in ligands of late transition metals, see: B. M. Trost, D. J. Murphy, *Organometallics* **1985**, *4*, 1143–1145.

[17] K. Soai, Y. Kawase, *Tetrahedron: Asymmetry* **1991**, *2*, 781–784.

[18] R. Annunziata, M. Benaglia, M. Cinquini, F. Cozzi, P. Giaroni, *J. Org. Chem.* **1992**, *57*, 782–784.

[19] The hydroxydiphenylmethyl group does not, however, always effect an increase in stereoselectivity. An example for this are 1,3-dipolar cycloadditions: Y. H. Kim, S. H. Kim, D. H. Park, *Tetrahedron Lett.* **1993**, *34*, 6063–6066.

[20] D. Seebach, *Angew. Chem.* **1990**, *102*, 1363–1409; *Angew. Chem. Int. Ed. Engl.* **1990**, *29*, 1320–1367, and references therein.

 © VCH Verlagsgesellschaft mbH, D-69451 Weinheim, 1996 0570-0833/96/3505-0522 $ 15.00+.25/0

Pyridinium Ions Adjacent to Oxirane Rings: Useful Intermediates for the Stereospecific Synthesis of β-Hydroxy Ketones**

Yousef Al-Abed, Noshena Naz, Khalid Mohammed Khan, and Wolfgang Voelter*

Dedicated to Professor Ivar Ugi on the occasion of his 65th birthday

Chiral β-hydroxy carbonyl compounds are interesting building blocks for natural product synthesis.[1, 2] They are typically prepared by 1,2-rearrangement of epoxysilylethenes under Lewis acid conditions.[3] We have made use of the unlimited amounts of carbohydrates available from the "chiral pool" and report here on a simple procedure for the introduction of enantiomerically pure β-carbonyl hydroxy functions in the pyranose ring.

In studies directed toward the development of chiral building blocks for synthesis[4] our research group has frequently used the epoxypyranosides benzyl-2,3-anhydro-β-L-ribopyranoside (**1**) and benzyl-2,3-anhydro-α-D-ribopyranoside (**2**). We describe here a one-pot procedure for converting epoxyhydroxy functions in compounds such as these into β-carbonyl hydroxy functions. The strategy relies on the introduction of a pyridinium ion adjacent to the oxirane ring, which facilitates opening of the epoxy ring with formation of an *N*-vinylpyridinium derivative. Subsequent reduction with $NaBH_4$ yields an *N*-alkyl-1,2,5,6-tetrahydropyridine derivative,[5] which can be hydrolyzed under acidic conditions to yield a β-hydroxy ketone (Scheme 1).

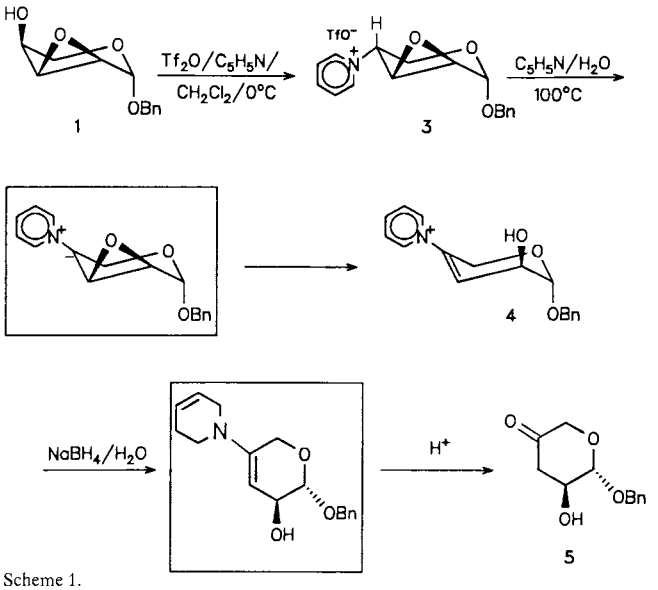

Scheme 1.

[*] Prof. Dr. W. Voelter, Dr. Y. Al-Abed, N. Naz, Dr. K. M. Khan
Abteilung für Physikalishe Biochemie
des Physiologisch-chemischen Instituts der Universität
Hoppe-Seyler-Strasse 4, D-72076 Tübingen (Germany)
Fax: Int. code +(7071)29-3361

[**] This work was supported by the Fonds der Chemischen Industrie and the German Academic Exchange (doctoral stipend for Y. A.-A.).

In a representative procedure **1** was treated with one equivalent of trifluoromethanesulfonic anhydride in pyridine at room temperature for 3 h to give the pyridinium salt **3** in quantitative yield. When a solution of **3** in pyridine was diluted with the same amount of water and heated at reflux for 3 h, **4** was obtained. The solvent was removed under reduced pressure and the residue taken up in water, treated with $NaBH_4$ at 0 °C for 2 h, acidified with 0.1 N HCl, and extracted with ethyl acetate. The extract was concentrated to dryness and the residue was purified by column chromatography to provide the desired β-hydroxy ketone **5** in 82% yield.

The structure of **4** was confirmed unequivocally by ^1H and ^{13}C NMR spectra (Table 1). The chemical shifts of the pyridinium protons are similar to those in **3**; the signal of the olefinic proton is at $\delta = 6.54$, and those of the sp^2 C atoms are at $\delta = 140.8$ and 127.0. Since no vicinal coupling is observed for the C-5 protons, the pyridinium residue must be linked to C-4. The lowfield shift of the anomeric C atom ($\delta = 99.7$; the C-1 signal of **3** is at $\delta = 94.7$) also indicates that the oxirane ring is cleaved.

Table 1. Selected ^1H and ^{13}C NMR data for compounds **3**–**5**.

3: ^1H NMR(400 MHz, [D$_6$]DMSO): $\delta = 9.07$ (d, 2 H, $J = 5.7$ Hz, H^{α}-Py), 8.67 (dd, 1 H, $J = 7.8$ Hz, H^{γ}-Py), 8.22 (dd, 2 H, $J = 7.3$, 7.0 Hz, H^{β}-Py), 7.44–7.30 (m, 5 H, aromat. H), 5.34 (dd, 1 H, $J = 6.2$, 5.9 Hz, H-4), 5.16 (s, 1 H, H-1), 4.80 (d, 1 H, $J = 11.8$ Hz, OC*H*HPh), 4.66 (d, 1 H, $J = 11.8$ Hz, OCH*H*Ph), 3.93 (dd, 1 H, $J = 12.3$, 5.4 Hz, H-5), 3.88 (dd, 1 H, $J = 11.9$, 7.5 Hz, H-5), 3.88 (d, 1 H, $J = 4.0$ Hz, H-3), 3.50 (d, 1 H, $J = 3.5$ Hz, H-2); ^{13}C NMR (100 MHz, [D$_6$]DMSO): $\delta = 146.5$ (C^{γ}-Py), 144.5 (C^{α}-Py), 137.1–127.7 (aromat. C), 128.4 (C^{β}-Py), 120.6 (CF_3SO_3, q, $J = 322.4$, 644.8 Hz), 94.7 (C-1), 70.1 (OCH_2Ph), 61.4 (C-4), 59.2 (C-5), 50.9 (C-3), 50.5 (C-2)

4: ^1H NMR (400 MHz, [D$_6$]DMSO): $\delta = 9.20$ (d, 2 H, $J = 5.7$ Hz, H^{α}-Py), 8.72 (dd, 1 H, $J = 7.8$ Hz, H^{γ}-Py), 8.22 (dd, 2 H, $J = 7.6$, 6.8 Hz, H^{β}-Py), 7.50–7.30 (m, 5 H, aromat. H), 6.54 (d, 1 H, $J = 4.3$ Hz, H-3), 5.87 (d, 1 H, $J = 6.2$ Hz, OH), 4.85 (d, 1 H, $J = 2.3$ Hz, H-1), 4.78 (d, 1 H, $J = 12.0$ Hz, OC*H*HPh), 4.67 (s, 2 H, C-5,5'H), 4.61 (d, 1 H, $J = 12.0$ Hz, OCH*H*Ph), 4.10 (br. s, 1 H, H-2); ^{13}C NMR (100 MHz, [D$_6$]DMSO): $\delta = 147.5$ (C^{γ}-Py), 143.7 (C^{α}-Py), 140.8 (C-4), 137.5–126.4 (aromat. C), 128.9 (C^{β}-Py), 127.0 (C-3), 120.8 (CF_3SO_3, q, $J = 322.0$, 644.0 Hz), 99.7 (C-1), 70.1 (OCH_2Ph), 64.2 (C-2), 59.4 (C-5)

5: ^1H NMR (400 MHz, $CDCl_3$): $\delta = 7.40–7.30$ (m, 5 H, aromat. H), 4.86 (d, 1 H, $J = 2.6$ Hz, H-1), 4.84 (d, 1 H, $J = 11.7$ Hz, OC*H*HPh), 4.64 (d, 1 H, $J = 11.7$ Hz, OCH*H*Ph), 4.16 (m, 1 H, H-2), 4.16 (d, 1 H, $J = 16.6$ Hz, H-5), 3.99 (d, 1 H, $J = 16.6$ Hz, H-5'), 2.90 (dd, 1 H, $J = 16.8$, 4.6 Hz, H-3), 2.58 (d, 1 H, $J = 16.8$, 4.4 Hz, H-3'), 2.0 (br. s, 1 H, OH); ^{13}C NMR (100 MHz, $CDCl_3$): $\delta = 205.9$ (C-4), 136.8–128.1 (aromat. C), 98.1 (C-1), 70.1 (OCH_2Ph), 68.6 (C-2), 68.1 (C-5), 43.1 (C-3)

The formation of **4** can be explained by the abstraction of the acidic proton at C-4 in **3** by the pyridine base. The transition state is presumably an ylide structure stabilized by the pyridinium residue, which leads to opening of the epoxy ring and simultaneously to introduction of a double bond in the pyranose ring.

The reduced form of **4** could not be isolated despite numerous attempts. However, when the reduction was conducted in D_2O and the ^1H NMR spectrum recorded before workup in acidic medium, the occurence of the olefinic proton signal and simultaneous disappearence of the pyridinium proton signals was observed. Moreover, the NMR spectra indicate that the opening of

the epoxy ring occurs with retention of configuration at C-2. This is illustrated by the 3-deoxyketoses **5** and **6**. The geminal coupling constants $J_{2,3}$ for **5** are 4.4 and 4.6 Hz, and for **6**, 5.0 and 8.3 Hz. This indicates that in **5** the OH group at C-2 is axial, whereas in **6** it is equatorial. The carbonyl signals of compounds **5** and **6** are at $\delta = 205.9$.

The same procedure was used to convert **2** and **7**–**9** into **6**, **5**, **10**, and **11**, respectively, in yields of 71–84% (Table 2). The reaction is not limited to carbohydrates as the transformation of **12** into **13** indicates.

Table 2. Products and yields for the reaction of epoxyhydroxy compounds with 1) Tf_2O/pyridine/CH_2Cl_2, 2) water/pyridine (1/1), 100 °C, 3) $NaBH_4$/water.

Starting material	Product	Yield [%]
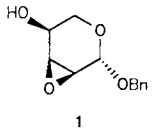 **1**	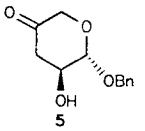 **5**	82
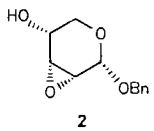 **2**	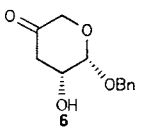 **6**	80
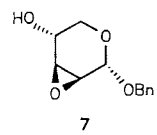 **7**	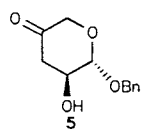 **5**	84
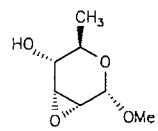 **8**	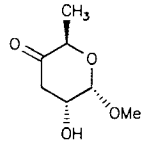 **10**	76
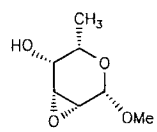 **9**	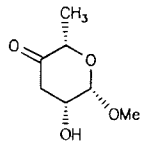 **11**	71
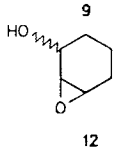 **12**	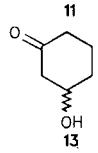 **13**	82

Received: September 8, 1995 [Z8381IE]
German version: *Angew. Chem.* **1996**, *108*, 581–582

Keywords: carbohydrates · chiral reagents · 3-deoxyketoses · β-hydroxy carbonyl compounds · *N*-vinylpyridinium derivatives

[1] a) P. A. Pieper, Z. Guo, H.-W. Liu, *J. Am. Chem. Soc.* **1995**, *117*, 5158–5159; b) S. Hanessian, *Adv. Carbohydr. Chem. Biochem.* **1966**, *21*, 143; c) N. Williams, J. Wander in *The Carbohydrate Chemistry and Biochemistry, Vol. 1B* (Ed.: W. Pigman, D. Horton), Academic Press, New York, **1980**, p. 761.

[2] a) S. Masamune, W. Choy, J. S. Petersen, L. R. Sita, *Angew. Chem.* **1985**, *97*, 1–31; *Angew. Chem. Int. Ed. Engl.* **1985**, *24*, 1–30; b) S. J. Danishefsky, *Aldrichimica Acta* **1986**, *19*, 59–68; c) S. Hanessian, *Total Synthesis of Natural Products: The Chiron Approach*, Pergamon, Oxford, **1983**.

[3] a) K. Maruoka, J. Sato, H. Yamamoto, *Tetrahedron* **1992**, *48*, 3749–3762; b) K. Maruoka, T. Ooi, S. Nagahara, H. Yamamoto, *ibid.* **1991**, *47*, 6983–6998; c) K. Maruoka, T. Ooi, H. Yamamoto, *J. Am. Chem. Soc.* **1989**, *111*, 6431–6432; d) K. Suzuki, M. Miyazawa, G. Tsuchihashi, *Tetrahedron Lett.* **1987**, *28*, 3515–3518; e) M. Shimazaki, H. Hara, K. Suzuki, G. Tsuchihashi, *ibid.* **1987**, *28*, 5891–5894.

[4] a) Y. Al-Abed, T. H. Al-Tel, C. Schröder, W. Voelter, *Angew. Chem.* **1994**, *106*, 1568–1570; *Angew. Chem. Int. Ed. Engl.* **1994**, *33*, 1499–1501; b) T. H. Al-Tel, Y. Al-Abed, W. Voelter, *J. Chem. Soc. Chem. Commun.* **1994**, 1735–1736; c) Y. Al-Abed, T. H. Al-Tel, W. Voelter, *Tetrahedron* **1993**, *49*, 9295–9306; d) T. H. Al-Tel, Y. Al-Abed, M. S. Shekhani, W. Voelter, *Tetrahedron Lett.* **1993**, *34*, 7717–7720; e) Y. Al-Abed, F. Zaman, M. S. Shekhani, A. Fatima, W. Voelter, *ibid.* **1992**, *33*, 3305–3306.

[5] G. Decodts, G. Dressaire, Y. Langlois, *Synthesis* **1979**, 510–513.

New Cobalt Catalysts for Hydroformylations in Two-Phase Systems**

Uwe Ritter, Norbert Winkhofer, Hans-Georg Schmidt, and Herbert W. Roesky*

Dedicated to Professor Max Herberhold on the occasion of his 60th birthday

The Ruhrchemie/Rhône-Poulenc technique and the SHOP process (SHOP = Shell Higher Olefin Process) are examples of two-phase catalysis on an industrial scale.[1–3] Further evidence of the topical relevance of this theme is the recent publication of papers by Horváth et al.[4] and Cornils[5] describing new methods of two-phase catalysis. The main advantages of such systems are the ease with which the catalyst phase can be removed and the high product selectivity that results from the quasi-homogeneous reaction. Consequent benefits include low primary energy costs and reduced amounts of undesired by-products. The demand for two-phase catalysts will therefore undoubtedly grow during the years to come. Water-soluble transition metal compounds are synthesized by forming complexes of the metal with water-soluble phosphanes as donor ligands. Solubility in water is usually achieved by incorporating a sulfonic acid group in the phosphane ligand, although the use of carboxyl, ammonium, phosphonium, hydroxyl, and polyether groups has also been reported.[3] The aim of our investigations was to synthesize compounds with stable σ-bonding that are suitable for two-phase catalysis.

We now report the synthesis of a phosphane-free methylidyne-bridged cobalt carbonyl cluster and its use as a hydroformylation catalyst in a two-phase system. The parent compound is [tris(tricarbonylcobaltio)methylidyne]silanetriol (**2**), which was first described by Seyferth et al. on the basis of spectroscopic data.[6] We have been able to crystallize this compound.[7] The previously known silanetriols that have been characterized by X-ray structural analysis reveal three-dimensional frameworks linked through layers[8, 9] or through hydrogen bonds in a cagelike arrangement.[10, 11] Like $(SiMe_3)_3SiSi(OH)_3$ and $(SiMe_3)_3CSi(OH)_3$, **2** forms a cage. However, in contrast to the hexameric structures of the above-mentioned compounds, **2** forms an oval framework structure consisting of eight monomeric units (Figs. 1 and 2).

[*] Prof. Dr. H. W. Roesky, Dr. U. Ritter, Dr. N. Winkhofer, H. G. Schmidt
Institut für Anorganische Chemie der Universität
Tammannstrasse 4, D-37077 Göttingen (Germany)
Fax: Int. code +(551)39-3373

[**] This work was supported by the Fonds der Chemischen Industrie, the Deutsche Forschungsgemeinschaft, the BMBF, the Volkswagenstiftung, and Hoechst AG.

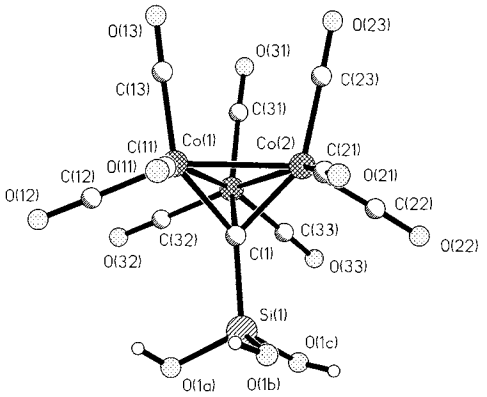

Fig. 1. The monomeric basic unit of **2** in the crystal. Bond lengths and bond angles are given in the text.

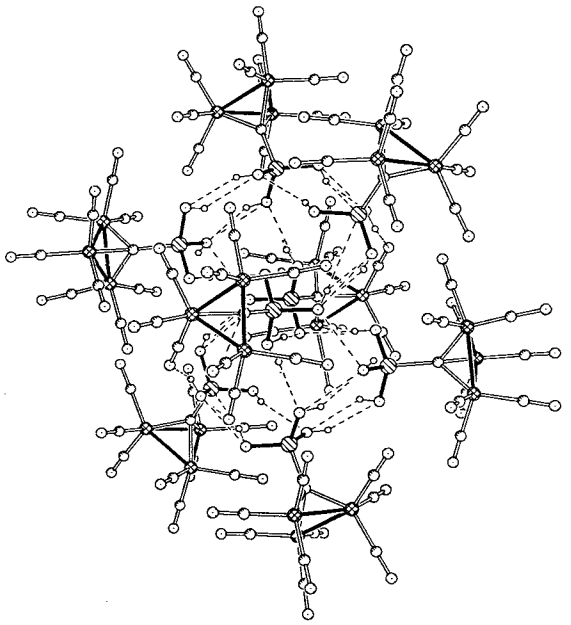

Fig. 2. In the crystal eight molecules of **2** are linked by hydrogen bonds to form a cagelike framework.

The Si–O bond lengths (161.0(5)–164.8(7) pm) and the O-Si-O angles (105.9(3)–111.7(3)°) are in agreement with corresponding values in other silanetriols.[8–10] The Co–Co bond lengths in the cluster fragments lie between 245.46(14) and 247.58(12) pm. The mean distance between the Co atoms and the apical C atoms is 190.9 pm. This value is similar to those in other tris(tricarbonylcobaltio)methylidyne compounds.[12]

The eight cobalt carbonyl fragments form the surface of the cagelike structure and shield the condensation-labile silanetriol groups. This shielding and the electron donor properties of the hydrophobic cluster fragments explain the unusual stability of the silanetriol towards condensation and its almost complete insolubility in water. However, desired modifications of the silanetriol core can be brought about by reactions at the SiOH groups. It is not possible to introduce sulfonic acid groups directly into tricobaltnonacarbonylmethylidyne derivatives.[6, 13] Instead of the intended sulfonation of the apical C atom or of organic groups bonded to it, cluster fragmentation or formation of $[(\mu^3\text{-CH})Co_3(CO)_9]$ is observed. Our investigations confirm these results. Silanols can be derivatized very simply by condensation with alcohols. Another possibility is the direct alcoholysis of the trichlorosilane **1**. The compounds **3a–c** can be obtained by this route (Scheme 1).

$$[Co_3(CO)_9CSiCl_3] + 3\,H_2O \xrightarrow[-3\,HCl]{} [Co_3(CO)_9CSi(OH)_3]$$

1 **2**

$$[Co_3(CO)_9CSiCl_3] + 3\,ROH \xrightarrow[-3\,HCl]{} [Co_3(CO)_9CSi(OR)_3]$$

1 **3a–c, 4**

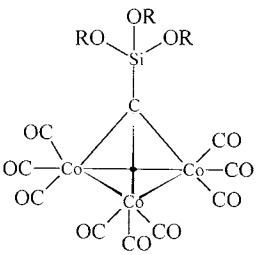

3a, $R = CH(CH_2OCH_2CH_3)_2$

3b, $R = CH_2CH_2OCH_2CH_2OCH_3$

3c, $R = CH_2CH_2(OCH_2CH_2)_2OCH_3$

4, $R = CH_2CH_2(OCH_2CH_2)_nOH$ ($n = 9$)

Scheme 1. Synthesis of **2**, **3a–c**, and **4**.

Compounds **3a–c**, like glycol-substituted phosphanes, are only slightly soluble in water. Only derivatives of the higher glycols (degree of polymerization > 16) show appreciable solubility in water.[14] Following a method comparable to the alcoholysis mentioned above, we reacted polyethylene glycol 400 with **1** to obtain **4** (Scheme 1). A solution of **4** in an excess of polyethylene glycol is completely miscible with water. However, this intensely violet-colored solution is not significantly miscible with lipophilic solvents such as hexane, hexene, and heptanal.

Hydroformylation experiments with the polymer-bound cluster units $[(\mu^3\text{-CCH}_3)Co_3(CO)_9]$ and $[(\mu^3\text{-CC}_6H_5)Co_3(CO)_9]$ and with phosphane derivatives of these compounds are described in the literature.[12, 15–17] The nature of the active species has not yet been completely elucidated and continues to be the subject of controversy. Seyferth et al.[17] and Richmond et al.,[18, 19] on the basis of IR investigations, suggest a fragmentation of the cluster, while Pittman, Jr. et al. and Balavoine et al. consider that the ease with which the compound used can be recovered indicates that the methylidyne bridge remains intact during the catalysis.[12, 15, 16]

We have investigated the catalytic activity of $[(\mu^3\text{-CSi(OH)}_3)Co_3(CO)_9]$ (**2**), two phosphane derivatives of **2**, and the polyethylene glycol compound **4** in the hydroformylation of 1-hexene. The results are given in Table 1.

Table 1. Hydroformylation of 1-hexene.

Entry	Catalyst [a]	T [°C]	p [bar] [b]	Co content [mg] [c]	Conversion [%] [d]	Time [h]	Ratio *n/iso* [e]
1	**2**	120	70	10.9	96.8	8	1.4
2	**2**	120	70	7.8	98.0	8	0.79
3	**2**	120	126	7.8	97.0	12	3.75
4	**2**	120	42	7.8	25.0	72	1.81
5	**2** [f]	120	70	11.6	98.9	8	3.2
6	**2** [g]	120	70	10.2	99.8	8	2.96
7	**4**	120	70	13.75	96.5	8	0.73
8	**4**	120	70	20.6	99.5	8	0.75
9	**4**	120	70	34	99.9	8	0.75
10	**4** [h]	120	70	34	72.9	8	0.67
11	$[Co_2(CO)_8]$	120	70	22	95.6 [i]	8	0.58

[a] Catalysis with **2** in toluene, and with **4** and $[Co_2(CO)_8]$ in polyethylene glycol. [b] Initial pressure. [c] Substrate: 2 mL 1-hexene. [d] Based on 1-hexene, ref. [21]. [e] *n/iso* ratio = 1-heptanal/(2-methylhexanal + 2-ethylpentanal). [f] With added triphenylphosphane (1:1 molar ratio to catalyst). [g] With added bis(diphenylphosphanyl)methane (1:1 molar ratio to catalyst). [h] Reused catalyst after separation of phases. [i] Chemoselectivity: 44% aldehydes/56% alcohols.

High conversions and high chemoselectivities similar to those obtained with **4** are obtained with **2** (Table 1, entries 1 and 7). However, while a decrease in the amount of **2** leads to a decrease in the regioselectivity of the products (entries 1 and 2), a change in the amount of **4** (entries 7–9) has hardly any effect on regioselectivity. As expected, the addition of phosphanes gives improved regioselectivity (entries 5 and 6). The catalyst phase can be recovered and reused many times, but shows a reduction in activity (entry 10). The formation of alcohols, which occurs as a side reaction with industrial catalytic processes, is almost completely prevented.[20] The experiments carried out with $[Co_2(CO)_8]$ in polyethylene glycol gave a product phase with a high content of alcohols, so another mechanism is occurring here (Table 1, entry 11). The conversions and selectivities obtained are comparable to results with $[(\mu^3\text{-}CH_3C)Co_3(CO)_9]$ and $[(\mu^3\text{-}C_6H_5C)Co_3(CO)_9]$ as catalysts.[12, 15] This shows that the activity induced by the metal fragment of the molecule is almost independent of the substituent on the methylidyne carbon atom. This is reflected in the fact that the frequencies of the IR vibrations of the CO groups on the cluster hardly change when substituents are introduced on the methylidyne carbon atom.[6]

A precise picture of the progress of a catalytic reaction is obtained by following the hydroformylation of 1-hexene by gas chromatography. The conversion is plotted against time in Figure 3.

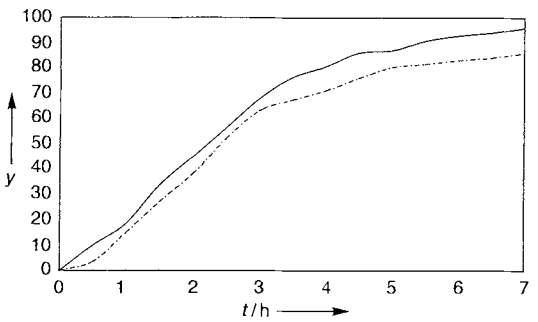

Fig. 3. Course of the hydroformylation reaction of 1-hexene catalyzed by **2** (—) and **4** (– · – · –); $T = 120\,^{\circ}C$; $p = 80$ bar; $CO:H_2 = 1:1$; 1-hexene 20 mL; catalysis with **2** in 20 mL of toluene, Co content: 110 mg; catalysis with **4** in 20 mL of polyethylene glycol 400, Co content: 130 mg. The conversion y [%] is based on all of the total C7 aldehydes formed.

The catalytic activity of the polyethylene glycol compound **4** is similar to that of **2**. With both catalysts, the reactions proceed without any significant induction phase. The similarity between the courses of the reactions indicates that their mechanisms are similar. The formation of cluster units under hydroformylation conditions cannot be excluded.

After the reaction the hydrophilic polyethylene glycol compound **4** can be recovered by simple phase separation and can then be reused. The active catalyst species cannot be determined. The dark violet color of **4** changes to a deep blue during the reaction, and this color is stable even after several catalytic cycles. Most likely polyether groups coordinate reversibly to the cobalt centers with partial displacement of CO molecules.

In contrast to the well-known water-soluble catalysts based on phosphane, the catalyst that we have been able to synthesize owes its properties as a two-phase catalyst to the presence of σ-bonded fragments. By modifying the silanol unit it should be possible to fine-tune the properties of the catalyst as desired, or combine a number of properties. The introduction of chiral substituents is currently under investigation.

Experimental Procedure

3a–c: A solution of **1** (0.574 g, 1 mmol) in 10 mL of the alcohol was stirred at 25 °C for 48 h under an atmosphere of CO. Excess alcohol was then removed by distillation under high vacuum. Compounds **3a–c** were isolated in the form of violet oils. They are not soluble in water and show IR bands typical for tris(tricarbonylcobaltio)methylidyne compounds (ν 2025(w), 2037(s), 2055(ss) cm^{-1}).

4: Chlorosilane **1** (0.574 g, 1 mmol) was taken up in polyethylene glycol 400 (10 mL) and maintained at 80 °C for 24 h under an atmosphere of CO. The sediment was filtered off; the Co content of the solution was 13.75 $g\,L^{-1}$ (determined by atomic absorption spectroscopy).

Hydroformylation of 1-hexene: The catalysis tests were carried out in a 100 mL laboratory autoclave. In a typical reaction, a solution of compound **4** in polyethylene glycol (2 mL) as prepared above (for Co content see Table 1) was added under nitrogen to 1-hexene (2 mL, 16 mmol). The autoclave was then filled with a mixture of CO and H_2 (1/1) at 70 bar, and the mixture was stirred at 120 °C for 8 h. After the reaction the phases separated within ca. 2 h. Phase separation can be accelerated by adding pentane. The product phase was separated and recovered, and the products were analyzed by gas chromatography by comparison with authentic samples and by GC-MS. The yields of aldehyde were determined by gas chromatography (DB-5, 30 m) using heptane as an internal standard. The polyethylene glycol phase containing the catalyst can be used for further catalytic cycles. Catalysis tests with **2** were carried out analogously under the conditions given in Table 1.

Received: October 19, 1995 [Z 8486 IE]
German version: *Angew. Chem.* **1996**, *108*, 591–593

Keywords: carbonyl complexes · cobalt compounds · hydroformylations · silicon compounds · two-phase catalysis

[1] a) E. G. Kuntz, Fr. Patent 2314910 (20 June 1975) Rhône Poulenc; b) B. Cornils, EP-B 0107006 (2 May 1984), Ruhrchemie AG.
[2] a) W. Keim, T. M. Shryne, R. S. Bauer, H. Chung, P. W. Glockner, H. van Zwet, DE-P 2054009 (1969), SHELL Int. Res.; b) W. Keim, *Chem. Ing. Techn.* **1984**, *56*, 850–853.
[3] a) W. A. Herrmann, C. W. Kohlpaintner, *Angew. Chem.* **1993**, *105*, 1588–1608; *Angew. Chem. Int. Ed. Engl.* **1993**, *32*, 1524–1544; b) P. Kalck, F. Monteil, *Adv. Organomet. Chem.* **1992**, *34*, 219–284.
[4] I. T. Horváth, J. Rábai, *Science* **1994**, *266*, 72.
[5] B. Cornils, *Angew. Chem.* **1995**, *107*, 1709–1711; *Angew. Chem. Int. Ed. Engl.* **1995**, *34*, 1574–1577.
[6] D. Seyferth, C. Nivert Rudie, M. Ozolins Nestle, *J. Organomet. Chem.* **1979**, *178*, 227–247.
[7] Crystallographic data for **2**: $C_{80}H_{24}Co_{24}O_{96}Si_8$, $M_r = 4160.03$, triclinic, space group $P\bar{1}$, $a = 1568.9(3)$, $b = 1585.8(3)$, $c = 1591.8(3)$ pm, $\alpha = 117.960(10)$, $\beta = 103.050(10)$, $\gamma = 90.490(10)^{\circ}$, $V = 3.3775(11)$ nm^3, $Z = 1$, $\rho_{calc.} = 2.045$ $Mg\,m^{-3}$, $F(000) = 2032$, $\lambda = 71.073$ pm, $T = 293(2)$ K, absorption coefficient = 3.043 mm^{-1}, crystal dimensions: $0.50 \times 0.40 \times 0.20$ mm^3, measured θ range 2.56–22.51°, of the 17384 reflections 8820 are independent, final R values [$I > 2\sigma(I)$]: $R1 = 0.0506$, $wR2 = 0.1333$, R values (all data): $R1 = 0.0582$, $wR2 = 0.1440$. Further details of the crystal structure determination may be obtained from the Director of the Cambridge Crystallographic Data Centre, 12 Union Road, GB-Cambridge CB2 1EZ (UK), on quoting the full journal citation.
[8] H. Ishida, J. L. Koenig, K. C. Gardner, *J. Chem. Phys.* **1982**, *77*, 5748–5751.
[9] N. Winkhofer, H. W. Roesky, M. Noltemeyer, W. T. Robinson, *Angew. Chem.* **1992**, *104*, 670–671; *Angew. Chem. Int. Ed. Engl.* **1992**, *31*, 599–601.
[10] S. S. Al-Juaid, N. H. Buttrus, R. I. Damja, Y. Derouiche, C. Eaborn, P. B. Hitchcock, P. D. Lickiss, *J. Organomet. Chem.* **1989**, *371*, 287–295.
[11] P. D. Lickiss, *Adv. Inorg. Chem.* **1995**, *42*, 240–248.
[12] G. Balavoine, J. Collin, J. J. Bonnet, G. Lavigne, *J. Organomet. Chem.* **1985**, *280*, 429–439.
[13] N. W. Duffy, B. H. Robinson, K. Robinson, J. Simpson, *J. Chem. Soc. Dalton Trans.* **1994**, 2821–2825.
[14] Y. Amrani, D. Sinou, *J. Mol. Catal.* **1984**, *24*, 231–233.
[15] R. C. Ryan, C. U. Pittman, Jr., J. P. O'Connor, *J. Am. Chem. Soc.* **1977**, *99*, 1986–1988.
[16] J. Collin, C. Jossart, G. Balavoine, *Organometallics* **1986**, *5*, 203–208.
[17] H. P. Withers, Jr., D. Seyferth, *Inorg. Chem.* **1983**, *22*, 2931–2936.
[18] M.-J. Don, H.-Y. Chien, M. G. Richmond, *J. Mol. Catal.* **1994**, *88*, 133–140.
[19] K. Yang, H.-Y. Chien, M. G. Richmond, *J. Mol. Catal.* **1994**, *88*, 159–166.
[20] G. Süss-Fink, G. Meister, *Adv. Organomet. Chem.* **1993**, *35*, 41–134.
[21] The main products detected were 1-heptanal, 2-methylhexanal, and 2-ethylpentanal. Hydrogenation of 1-hexene to hexane and of the aldehydes to alcohols was not observed. After longer reaction times, small amounts of aldehyde condensation products and oxidation products could be detected (< 6%).

The First *closo*-Monosilaborane**

Lars Wesemann* and Ulli Englert

In comparison to the thoroughly investigated carboranes[1] the study of silaboranes is still very young; until now only two of these compounds have been structurally characterized.[2, 3] Recently we were able to establish that the nucleophilic fragmentation of 1,2-dimethyl-*o*-silaborane forms **1** and thereby achieved the synthesis of the first *nido*-silaborane.[3] Here we report on the first reaction of **1**, which can be described as the first cluster construction reaction with a silaborane. Compound **1** reacts with an excess of $Et_3N \cdot BH_3$[4] in boiling bis(2-methoxyethyl) ether to form 1-methyl-1-sila-*closo*-dodecaborate(1 −) **2** in 93% yield.

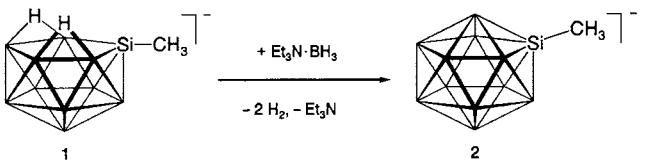

1 2

The constitution of 2 can be ascertained unequivocally from its NMR spectra. The appearance of only three signals in the ^{11}B NMR with an intensity ratio of 5:1:5 for eleven B atoms indicates that the cluster framework has fivefold symmetry. The assignment of the signals for the groups B2–B6 and B7–B11 as well as for B12 (for numbering scheme see Fig. 1) can be confirmed by the 2D ^{11}B-^{11}B NMR spectrum. Interestingly the influence of the heteroatom on the ^{11}B NMR shifts of $EB_{11}H_{11}$ in comparison to those of $[B_{12}H_{12}]^{2-}$ ($\delta = -15.3$) is especially significant for the B atom directly opposite to the heteroatom (B12).[5] This phenomenon has also been termed an "antipodal effect". In the above-mentioned example the value of the shift for B12 ($\delta = -14.6$) deviates only slightly from that for $[B_{12}H_{12}]^{2-}$. The signals for the B-bound H atoms can be assigned to the respective B groups by interpretation of the 2D ^1H-^{11}B NMR spectrum.

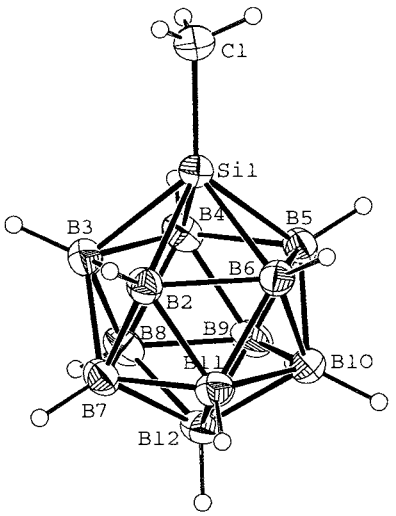

Fig. 1. Structure of the anion **2** in the crystal (PLATON representation [9], ellipsoids at the 30% probability level). Selected distances [Å], standard deviations in parentheses: Si1-C1 1.836(2), Si1-B2 2.024(2), Si1-B3 2.030(2), Si1-B4 2.025(2), Si1-B5 2.026(2), Si1-B6 2.028(2), B2-B3 1.855(3), B2-B6 1.854(3), B2-B7 1.769(3), B2-B11 1.766(3), B3-B4 1.860(3), B3-B7 1.768(3), B3-B8 1.782(4), B4-B5 1.854(3), B4-B8 1.776(3), B4-B9 1.771(4), B5-B6 1.847(3), B5-B9 1.764(3), B5-B10 1.762(3), B6-B10 1.770(3), B6-B11 1.772(3), B7-B8 1.780(3), B7-B11 1.783(3), B7-B12 1.766(3), B8-B9 1.786(4), B8-B12 1.770(4), B9-B10 1.779(4), B9-B12 1.770(3), B10-B11 1.785(3), B10-B12 1.774(3), B11-B12 1.772(3).

[*] Dr. L. Wesemann, Dr. U. Englert
Institut für Anorganische Chemie der Technischen Hochschule
Professor-Pirlet-Strasse, D-52056 Aachen (Germany)
Fax: Int. code +(241)8888-288

[**] This work was supported by the Deutsche Forschungsgemeinschaft (DFG-Schwerpunktprogramm "Polyeder").

The results of the crystal structure analysis[6] (Fig. 1) are in agreement with the structure in solution determined from spectroscopic data. The distances between the B atoms of the five-membered ring (B2–B6) capped by the Si atom are, as expected, larger [1.847(3)–1.860(3) Å] than the remaining B–B distances [1.762(3)–1.786(4) Å]. These are in turn only insignificantly longer than those in $[B_{12}H_{12}]^{2-}$ [1.755(7)–1.780(7) Å].[10] The Si–B distances are similar to those in the starting material **1**.[3]

Surprisingly many examples of the class of compounds $EB_{11}H_{11}$, to the which the title compound belongs, are already known: E = $MeAl^{2-}$,[11] RC^-,[12] $MeGe^-$,[13] $MeSn^-$,[13] Pb^{2-},[13] HN,[14] MeP,[15] As^-,[16] Sb^-,[17] S,[18] Se,[19] Te.[18] While the carbon compound homologous to **2** was synthesized as early as 1963, the higher homologues (Ge, Sn, Pb), which are formed by metathesis from $[B_{11}H_{11}]^{4-}$ and the metal dihalide, were first prepared in 1992.

Experimental Procedure

2: A solution of Et_4N-**1** (0.40 g, 1.36 mmol) and $BH_3 \cdot NEt_3$ (2.00 g, 17.4 mmol) in 5 mL of bis(2-methoxyethyl) ether was heated at reflux for 64 h. After all the volatile components were removed in vacuum, the residue was dissolved in 15 mL of THF and filtered. The product crystallized at room temperature when Et_2O was layered on top of the THF solution. Yield: 0.38 g (93%) Et_4N-**2**. Correct C, H analysis. NMR spectra at 25 °C in [D$_8$]THF: ^1H NMR (500 MHz, TMS): $\delta = 1.49$ (H7–H11, H12), 1.41 (H2–H6), 0.75 (s, SiMe), measurement and assignment of the B–H signals as crosspeaks in the 2D ^{11}B-^1H NMR spectrum; ^{11}B NMR (160 MHz, $Et_2O \cdot BF_3$): $\delta = -12.6$ (d, $J = 147$ Hz, B7–B11), −14.6 (d, $J = 134$ Hz, B12), −17.4 (d, $J = 134$ Hz, B2–B6); ^{13}C NMR (125 MHz, TMS): $\delta = -12.1$ (s, SiMe); ^{29}Si NMR (100 MHz, TMS): $\delta = -28$ (s).

Received: October 26, 1995 [Z 8500 IE]
German version: *Angew. Chem.*, **1996**, *108*, 586–587

Keywords: boron compounds · clusters · silaboranes

[1] R. N. Grimes, *Carboranes*, Academic Press, London, **1970**.
[2] D. Seyferth, K. Büchner, W. S. Rees, Jr., W. M. Davis, *Angew. Chem.* **1990**, *102*, 911–913; *Angew. Chem. Int. Ed. Engl.* **1990**, *29*, 918–920; b) D. Seyferth, K. Büchner, W. S. Rees, Jr., L. Wesemann, W. M. Davis, S. S. Bukalov, L. A. Leites, H. Bock, B. Solouki, *J. Am. Chem. Soc.* **1993**, *115*, 3586–3594.
[3] L. Wesemann, U. Englert, D. Seyferth, *Angew. Chem.* **1995**, *107*, 2435–2436; *Angew. Chem. Int. Ed. Engl.* **1995**, *34*, 2236–2238.
[4] J. S. Beck, A. P. Kahn, L. G. Sneddon, *Organometallics* **1986**, *5*, 2552–2553.
[5] S. Heřmánek, *Chem. Rev.* **1992**, *92*, 325–362.
[6] a) Single crystals of Et_3MeN-**2** were obtained from THF/Et_2O at room temperature. b) Crystal structure analysis: ENRAF-Nonius CAD4 diffractometer; $Mo_{K\alpha}$ radiation, graphite monochromator; intensity data with ω scans collected at 253 K. Et_3MeN-**2**: colorless, transparent parallelepiped, 0.60 × 0.45 × 0.40 mm, monoclinic space group $P2_1/n$ (No. 14); $a = 8.573(2)$, $b = 14.242(3)$, $c = 16.404(6)$ Å, $\beta = 105.07(3)°$, $V = 1934(1)$ Å^3, $Z = 4$, $\rho_{calcd} = 0.994$ g cm^{-1}, $\mu(Mo_{K\alpha}) = 1.03$ cm^{-1}, $F(000) = 624$; 4232 reflections with $3 < \theta < 26°$, 2816 symmetry-independent reflections with $I > \sigma(I)$ in the structure solution [7] and refinement [8] for 323 parameters; $R = 0.048$, $R_w = 0.058$, $w^{-1} = \sigma^2(F_0)$; hydrogen atoms were isotropically refined. In the cation there is orientational disorder of the methyl group versus one of the ethyl groups. This does not interfere with the packing of the crystals. c) Further details of the crystal structure determination of Et_3MeN-**2** may be obtained from the Fachinformationszentrum Karlsruhe, D-76344 Eggenstein-Leopoldshafen (Germany) on quoting the depository number CSD-404522.
[7] G. M. Sheldrick, SHELXS-86, Göttingen, **1986**.
[8] B. A. Frenz, ENRAF-Nonius, SDP, Version 5.0, **1989**.
[9] A. L. Spek, *Acta Crystallogr. Sect. A* **1990**, *46*, C34.
[10] J. A. Wunderlich, W. N. Lipscomb, *J. Am. Chem. Soc.* **1960**, *82*, 4427–4428.
[11] T. D. Getman, S. G. Shore, *Inorg. Chem.* **1988**, *27*, 3439–3440.
[12] W. H. Knoth, *J. Am. Chem. Soc.* **1967**, *89*, 1274–1275.
[13] R. W. Chapman, J. G. Kester, K. Folting, W. E. Streib, L. J. Todd, *Inorg. Chem.* **1992**, *31*, 979–983.
[14] J. Müller, J. Runsink, P. Paetzold, *Angew. Chem.* **1991**, *103*, 201; *Angew. Chem. Int. Ed. Engl.* **1991**, *30*, 175.
[15] T. D. Getman, H.-B. Deng, L.-Y. Hsu, S. G. Shore, *Inorg. Chem.* **1989**, *28*, 3612–3616.
[16] J. L. Little, S. S. Pao, K. K. Sugathan, *Inorg. Chem.* **1974**, *13*, 1752–1756.
[17] J. L. Little, *Inorg. Chem.* **1979**, *18*, 1598–1600.
[18] J. Plešek, S. Heřmánek, *J. Chem. Soc. Chem. Commun.* **1975**, 127–128.
[19] G. D. Friesen, L. J. Todd, *J. Chem. Soc. Chem. Commun.* **1978**, 349–350.

 © VCH Verlagsgesellschaft mbH, D-69451 Weinheim, 1996 0570-0833/96/3505-0527 $ 15.00+.25/0

Bis(lithiomethyl) Sulfide, An Unexpectedly Stable 1,3-Dilithiated Synthetic Building Block**

Carsten Strohmann*

Dilithio compounds can be classified as 1,1-, 1,2-, 1,3-, etc., dilithium compounds according to the distance between the metalated carbon atoms.[1] Despite their enormous synthetic potential only few 1,3-dilithio compounds are among the dilithio alkanes reported.[1] This deficit is due on one hand to facile lithium hydride β-elimination,[2, 3] and on the other to the absence of suitable synthetic methods.[1, 3] In the course of a systematic study aimed at the preparation of 1,3-dimetalated compounds of general formula $M-CH_2-E-CH_2-M$ (M = Li, MgBr, etc.; E = element of group 14–16, possibly with substituents), we prepared bis(lithiomethyl) sulfide **4**. This 1,3-dilithio compound serves as a bifunctional synthetic building block suitable for the preparation of inorganic and organic compounds containing a $-CH_2-S-CH_2-$ structural unit.

The most important strategies for the synthesis of organolithium compounds of general formula R_nE-CH_2-Li (E = element of group 14–16) are as follows: 1) hydrogen–lithium exchange, 2) halogen–lithium exchange, 3) metal–lithium exchange (each with either lithium bases or lithium metal).[1] Applying these strategies to the preparation of dilithio compounds of the general formula $Li-CH_2-E-CH_2-Li$ shows that direct metalation (first strategy) is often too slow (e.g., for $RP(CH_3)_2$)[4] or too unreactive (e.g., for $S(CH_3)_2$) for preparative purposes.[3] Halogen–lithium exchange in 1,3-dihalide compounds usually results in intramolecular lithium halide elimination after monometalation.[6] Double metal–lithium exchange therefore appeared the most suitable route, as this reaction proceeds very rapidly even at low temperatures and almost always quantitatively.[1, 7] The preparation of $MeN(CH_2Li)_2$ by tin–lithium exchange has been reported starting from $MeN(CH_2SnBu_3)_2$.[8] In case of the homologous $Me_2Si(CH_2SnPh_3)_2$ a stable cyclic stannate complex forms, and consequently only one organotin group exchanges.[1b] $Me_2C(CH_2Li)_2$ was prepared by mercury–lithium exchange.[2] The more recently reported tellurium–lithium exchange reaction[7, 9] has not yet been employed in the preparation of 1,3-dilithio compounds. To synthesize **4** we decided to attempt double tellurium–lithium or tin–lithium exchange.

The bis(tributylstannylmethyl) sulfide **2** was obtained in 92% yield by treating Bu_3SnCH_2I[10] with $Na_2S\cdot Al_2O_3$ in THF (Scheme 1) and purifying the product by Kugelrohr distillation. The analogous bis(butyltelluromethyl) sulfide **6** was synthesized analytically pure in 83% yield by treating $S(CH_2Br)_2$ (**5**)[11] with BuTeLi. Once again, purification was accomplished by Kugelrohr distillation (Scheme 2).

Treating the tellurium compound **6** with two equivalents *n*-BuLi in diethyl ether at −30 °C provided a colorless solid, which was identified by its chemical reactivity as **4**.[12] The by-product, di-*n*-butyl telluride, was removed by filtration, and, after washing with diethyl ether and drying under vacuum, **4** was obtained as a colorless powder that explosively ignites upon contact with traces of air. In the solid state **4** decomposed under argon at approximately 60 °C or explosively on impact. However, at

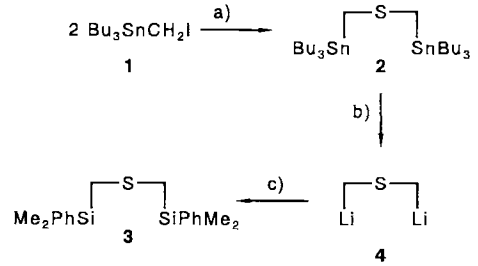

Scheme 1. Synthesis of bis(lithiomethyl)sulfide **4** by tin–lithium exchange: a) $+Na_2S\cdot Al_2O_3/-2\,NaI$; b) $+n$BuLi/ $-2\,SnBu_4$; c) $+2\,Me_2PhSiCl/-2\,LiCl$.

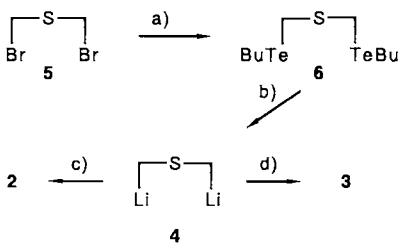

Scheme 2. Synthesis of bis(lithiomethyl) sulfide (**4**) by tellurium–lithium exchange: a) $+2$ BuTeLi/ -2 LiBr; b) $+2\,n$BuLi/ $-2\,TeBu_2$; c) $+2\,Bu_3SnCl/-2\,LiCl$; d) $+2\,Me_2PhSiCl/-2\,LiCl$.

−20 °C **4** could be stored for six months without decomposition. For preparative purposes a suspension of **4** in diethyl ether was used, as we found that after centrifugation the contaminant, di-*n*-butyl telluride, can be removed with the supernatant. An analogous transformation can be carried out in hexane as solvent. Interestingly, **4** also forms as a colorless solid by double tin–lithium exchange on **2** with *n*-BuLi in THF. No solvent has yet been found in which **4** dissolves without decomposition; determination of the structure of **4** in solution is thus not possible.[13]

The formation of **4** was confirmed by a series of control experiments: the reaction of **4**, which had been obtained from **6** by tellurium–lithium exchange, with Bu_3SnCl and $Me_2PhSiCl$ was studied, as was the reaction of **4**, which had been obtained from **2** by tin–lithium exchange, with $Me_2PhSiCl$ (cf. Schemes 1 and 2[14]). These studies were designed to answer two questions: 1. Is it indeed $LiCH_2SCH_2Li$ (**4**) that is afforded by complete metal–lithium exchange? 2. Is **4** the sole product of the metal–lithium exchange or do rearrangements also occur; rearrangements are, for example, well documented for lithiomethyl ether.[15] After separating $TeBu_2$ and $SnBu_4$, both of which are products of the metal–lithium exchange, we were able to answer the first question by showing that this exchange occurs quantitatively. Treatment of **4** with Bu_3SnCl yielded the anticipated **2** in greater than 95% yield (NMR spectroscopic studies, unseparated $TeBu_2$ as internal standard) confirming the product homogeneity of **4**, thus answering the second question.

In the solvents hexane, diethyl ether, and THF, bis(lithiomethyl) sulfide exhibits the chemical reactivity anticipated for a 1,3-dilithio compound. The observation of double tellurium–lithium exchange in both hexane and ethers is rather unusual; in contrast, 1,4-ditellura compounds react differently towards *n*-BuLi in hexane and THF.[16] The surprising stability of **4** is attributable to the fact that it forms a solid.

Additional reactions of **4** with inorganic and organic mono- and bifunctional reagents are currently being investigated. Preliminary results with analogous 1,3-dimetalated compounds consisting of main group elements other than sulfur show that the concept of double tellurium–lithium and tin–lithium ex-

[*] Dr. C. Strohmann
Institut für Anorganische Chemie der Universität
Im Stadtwald 6, D-66011 Saarbrücken (Germany)
Telefax: Int. code +(681) 302-3995

[**] This work was supported by the Deutsche Forschungsgemeinschaft. Prof. Dr. M. Veith is gratefully acknowledged for his support.

change can be extended to encompass 1,3-dilithiated compounds of general formula $Li-CH_2-E-CH_2-Li$ (E = element of group 14–16, possibly with substituents).

Experimental Procedure

2 (from starting material **1**): Bu_3SnCH_2I (20 mmol) was added to a suspension of $Na_2S \cdot Al_2O_3$ (11 mmol) in THF (30 mL). The mixture was stirred at room temperature for 16 h, after which the solvent was removed under vacuum. The residue was extracted three times with 25 mL portions of hexane. The solvent was removed and, following purification by Kugelrohr distillation (oven temperature 165 °C/ *0.001 Torr*), compound **2** was obtained in 92% yield as a colorless oil. ^1H NMR (200.1 MHz, $CDCl_3$, 25 °C, TMS): $\delta = 0.75-1.1$ (m, 12H; CH_3, $SnCH_2C$), 1.2–1.4, 1.4–1.7 (m, 42H; CCH_2C, CCH_3), 2.00 (s, 4H, $^2J(H,Sn) = 40.4$ Hz; $SnCH_2S$); ^{13}C NMR (50.3 MHz, $CDCl_3$, 25 °C, $CDCl_3$): $\delta = 9.6$ (6C, $^1J(C,^{119/117}Sn) = 329.6/315.0$ Hz; $SnCH_2C$), 13.7 (6C, CCH_3), 17.3 (2C, $^1J(C,^{119/117}Sn) = 233.7/223.2$ Hz, $^3J(C,Sn) = 30.3$ Hz; $SnCH_2S$), 27.3 (6C, $^3J(C,^{119/117}Sn) = 55.9/53.7$ Hz; $SnCH_2CH_2CH_2C$), 29.1 (6C, $^2J(C,Sn) = 20.8$ Hz; $SnCH_2CH_2C$); ^{119}Sn NMR (74.6 MHz, $CDCl_3$, 25 °C, $SnMe_4$): $\delta = -18.3$; MS (EI, 70 eV): *m/z* (%) = 640 (4) $[M^+]$, 583 (40) $[M^+ - C_4H_9]$, 527 (37) $[M^+ - C_4H_9 - C_4H_8]$, 291 (70) $[HSnBu_3^+]$, 235 (78) $[H_2SnBu_2^+]$, 179 (100) $[H_3SnBu^+]$; correct elemental analysis for $C_{26}H_{58}SSn_2$.

2 and **3** (from **6**): Under an inert atmosphere **6** (10 mmol) was dissolved in Et_2O (50 mL), and at −30 °C a solution of *n*-BuLi (20 mmol) in hexane was added. The mixture was stirred for 5 min at this temperature. Upon warming to room temperature **4** precipitated as a colorless solid. After centrifugation, the by-product $TeBu_2$ was removed with the supernatant, and the precipitate was washed with diethyl ether. This centrifugation–washing step was repeated four times. To the resulting suspension of **4** in Et_2O (approx. 30 mL) was added at −20 °C a solution of Bu_3SnCl (or $Me_2PhSiCl$ for **3**) (20 mmol), in 5 mL Et_2O. The mixture was warmed to room temperature, the solvent removed, and the mixture worked up as previously described (vide supra). Yield: 89% **2**/74% **3** (purification by Kugelrohr distillation at 155 °C oven temperature/0.001 Torr). Analogously, **3** was obtained from **2** employing THF as solvent. Yield: 84% [14].

6: Under an inert atmosphere a solution of BuTeLi was prepared by combining *tellurium* powder (12.8 g, 0.1 mol) in THF (150 mL) with a solution of *n*-BuLi (0.1 mol) in hexane (42 mL). Next, **5** (0.05 mol) dissolved in THF (5 mL) was added at −78 °C. The solution was allowed to warm to room temperature over 1 h, and volatile components were removed under vacuum. The residue was extracted with four 100 mL portions of hexane and volatile components were again removed under vacuum. Compound **6** was obtained as a colorless oil (traces of ditellurides can render the compound red) in 83% yield after Kugelrohr distillation at 135 °C oven temperature/0.001 Torr. ^1H NMR (200.1 MHz, $CDCl_3$, 25 °C, TMS): $\delta = 0.87$ (t, 6H, $^3J(H,H) = 7.2$ Hz; CCH_3), 1.34 (sextet, 4H, $^3J(H,H) = 7.3$ Hz; CCH_2CH_3), 1.73 (quin, 4H, $^3J(H,H) = 7.4$ Hz; $CH_2CH_2CH_2$), 2.72 (t, 4H, $^3J(H,H) = 7.5$ Hz; $TeCH_2C$), 3.69 (s, 4H, $^1J(H,Te) = 32.3$ Hz; $TeCH_2S$); ^{13}C NMR (50.3 MHz, $CDCl_3$, 25 °C, $CDCl_3$): $\delta = 5.0$ (2C, $^1J(C,Te) = 201.2$ Hz; $TeCH_2S$), 5.4 (2C, $^1J(C,Te) = 151.4$ Hz; $TeCH_2C$), 13.3 (2C, CCH_3), 24.9 (2C, $^3J(C,Te) = 10.7$ Hz; CCH_2CH_3), 33.9 (2C, $^2J(C,Te) = 9.8$ Hz; $TeCH_2CH_2C$); ^{127}Te NMR (63.2 MHz, $CDCl_3$, 25 °C, $TeMe_2$): $\delta = 303.4$; MS (EI, 70 eV): *m/z* (%) = 430 (2) $[M^+]$, 373 (22) $[M^+ - C_4H_9]$, 58 (100) $[C_4H_{10}^+]$; correct elemental analysis for $C_{10}H_{22}STe_2$.

Received: October 31, 1995 [Z 8517 IE]
German version: *Angew. Chem.* **1996**, *108*, 600–601

Keywords: bis(lithiomethyl) sulfide · 1,3-dilithio compounds · lithium compounds · transmetalations

[1] a) A. Krief, *Tetrahedron* **1980**, *36*, 2531–2640; b) T. Kauffmann, *Angew. Chem.* **1982**, *94*, 401–420; *Angew. Chem. Int. Ed. Engl.* **1982**, *21*, 410–429; c) A. Maercker, *Methoden Org. Chem. (Houben-Weyl) 4th ed.* **1952-**, Vol. E19d, **1993**, pp. 448–566.

[2] J. W. F. L. Seetz, G. Schat, O. S. Akkerman, F. Bickelhaupt, *J. Am. Chem. Soc.* **1982**, *104*, 6848–6849.

[3] A. Maercker, M. Theis, *Top. Curr. Chem.* **1987**, *138*, 1–61.

[4] D. J. Peterson, J. H. Collins, *J. Org. Chem.* **1966**, *31*, 2373–2376.

[5] In contrast, bis(lithiomethyl)sulfoxide and bis(lithiomethyl)sulfone can be prepared by hydrogen–lithium exchange: E. M. Kaiser, R. D. Beard, C. R. Hauser, *J. Organomet. Chem.* **1973**, *59*, 53–64.

[6] Bis(chloromethyl)dimethylsilane [1c] and bis(iodomethyl)dimethylstannane were the only 1,3-dihalogenes suitable for the preparation of 1,3-dilithio compounds: H. Schumann, R. Mohtachemi, M. Schwichtenberg, *Z. Naturforsch. B* **1988**, *43*, 1510–1513.

[7] N. Petragnani, J. V. Comasseto, *Synthesis* **1991**, 897–919.

[8] D. J. Peterson, *J. Org. Chem.* **1967**, *32*, 1717–1720.

[9] K. J. Irgolic, *Methoden Org. Chem. (Houben-Weyl) 4th ed.* **1952-**, Vol. E12b, **1990**, pp. 440–443.

[10] W. C. Still, *J. Am. Chem. Soc.* **1978**, *100*, 1481–1487.

[11] E. Weissflog, M. Schmidt, *Z. Anorg. Allg. Chem.* **1977**, *437*, 146–148.

[12] The structure depicted for **4** only reflects the reactivity of this dilithio compound and not its true structure.

[13] Discussion of the structure of 1,3-dilithiopropanes: P. von R. Schleyer, A. J. Kos, E. Kaufmann, *J. Am. Chem. Soc.* **1983**, *105*, 7617–7623.

[14] Preparation of **3**: A. Hasomi, K. Ogata, M. Ohkuma, M. Hojo, *Synlett* **1991**, 557–558.

[15] E. J. Verner, T. Cohen, *J. Am. Chem. Soc.* **1992**, *114*, 375–377.

[16] A. Maercker, H. Bodenstedt, L. Brandsma, *Angew. Chem.* **1992**, *104*, 1387–1388; *Angew. Chem. Int. Ed. Engl.* **1992**, *31*, 1339–1340.

Trapping and Imaging Molecular Dynamics by Combining Scanning Force Microscopy with Topology**

Bruno Samorì,* Carmelo Nigro, Amalia Gordano, Innocenzo Muzzalupo, and Carla Quagliariello

Scanning force microscopy (SFM) makes it possible to image molecules tightly adsorbed on flat substrates such as mica, gold, or glass.[1, 2] The SFM images contain information on the height above the surface for the molecules examined. This made it possible directly to observe and identify the chiralities of native supercoiled DNA[3, 4] and F-actin,[5] and to reveal the three-dimensional structure of chromatin fibers.[6]

The main research emphasis with SFM is now shifting from the visualization of static structures to studies of chemical processes that attempt to use this technique as a tool for investigating the dynamics and reactions of molecules loosely attached to the substrate.[2, 7, 8] Linear fragments of DNA loosely adsorbed on mica have very recently been imaged in aqueous buffer solution and their dynamics observed within the SFM time resolution, which is of the order of one minute per image.[7, 8] However, as already pointed out,[8] in this kind of experiment the motion of the scanning probe-tip could contribute to the movement when very loosely attached molecules are examined. The "ghost" of the uncertainty principle could also haunt this kind of experiment. As in the classical Heisenberg uncertainty principle, the interaction between the measuring instrument and the object of observation might be not negligible relative to the magnitude of the measurement sought.

We tailored an experiment in which subtle vibrational motions following a transient and partial desorption of chain segments of DNA molecules attached to mica were trapped and detected by combining SFM and topological restriction.

Instead of imaging the molecules continuously to catch their movement during diffusion, we monitored those processes by trapping them topologically and imaging just before and just after they had taken place.

Supercoiled pBR322 DNA plasmids were deposited on mica from a buffer solution containing 10 mM Mg^{2+} ions that induce cross-bridges between mica and DNA phosphates.[9] The sample was blown dry with nitrogen, irradiated with UV light to induce nicks, and dipped in water for different periods before being dried again and imaged with the tapping mode in air. Figure 1 shows that the molecules gradually acquire a more

[*] Prof. B. Samorì, Dr. C. Nigro, A. Gordano, Dr. I. Muzzalupo
Dipartimento di Chimica, Università della Calabria
Arcavacata di Rende (CS) I-87030 (Italy)
Fax: Int. code +(984)492044
Prof. C. Quagliariello
Dipartimento di Biologia Cellulare, Università della Calabria

[**] This work was supported by CNR (Rome) Progetto Finalizzato Biotecnologie Biostrumentazione and by Regione Emilia Romagna. We thank C. Bustamante (Eugene, OR) and G. Zuccheri for helpful comments.

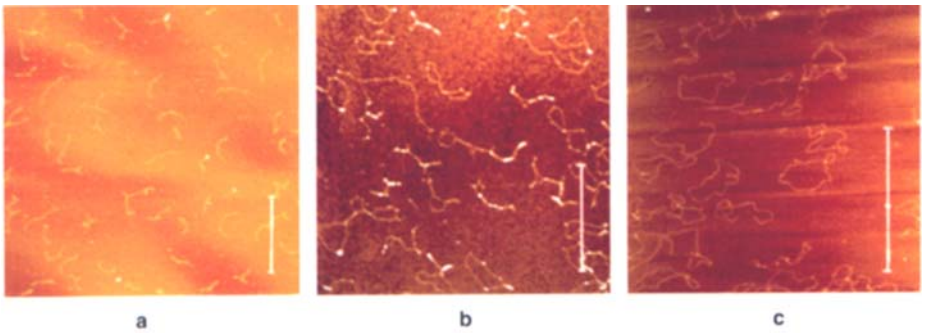

Fig. 1. SFM overview image of tightly supercoiled circular DNA molecules with either branched or unbranched shapes, deposited and dried on mica (a). When the sample is dipped in water the forces of adsorption are gradually released. Images (b) and (c) were obtained after 60 min and 12 h dipping, respectively. Bars represent 1 μm.

Fig. 2. Transient desorptions and detachments of chain segments in tightly supercoiled DNA molecules adsorbed on mica as in (a) are topologically trapped and revealed, whenever they take place, by the opening and the enlarging of loops as in (b). Detachments of increasingly larger chain segments cause the molecules to assume open circular shapes as in (c). Bars represent 100 nm.

open shape as the dipping time increases. In control experiments with nonirradiated samples the molecules maintain their tightly supercoiled shapes even after 12 h in water. As the images in Figures 1 and 2 show, the opening of the nicked molecules produces structures with open loops, which expand locally and gradually at the expense of other segments that are still very tightly supercoiled.

The chains of supercoiled circular DNA molecules are under permanent torsional strain because they have fewer duplex turns than linear DNA molecules of the same length, and because the unbroken looping of their two polynucleotide strands constricts their topology.[10] This constriction is released and the molecules are allowed to relax to open circular shapes (Fig. 1c and 2c) only when at least one of the covalent bonds in one strand is nicked so that one strand can rotate freely about the other at the nick site. In our experiment, after being nicked by the UV light[11] and ozone[12] in the irradiation box (see experimental), the DNA molecules cannot relax their supercoiling as long as they are left dried and fossilized on mica (Fig. 1a and 2a). When the samples are dipped in water, the Mg^{2+} ions anchoring the DNA chains to mica are gradually removed. Larger and larger chain segments detach from the mica and acquire the mobility required to relax their supercoiling torsional strain at the nicks induced in the strands by irradiation with UV light (Fig. 1b and 2b). The extent of the nicking thus affects the sensitivity of this approach.[13] If the frequency of the nicks along the chain is high, the supercoiling of a chain segment is relaxed whenever it moves away from the substrate. Even very minor and transient[14] motions of single adsorbed molecules, which would be very difficult to detect with any other physical technique or even with direct SFM imaging in solution, can be trapped and detected with this method without the risk that they might have been induced by the scanning tip.

Chemical topology provides permanent internal markers of any molecular event linked to bond-breakage and reunion events, no matter how evanescent the molecular structures are and how fast and transient the process is.[10] SFM imaging combined with topological restrictions can make it possible to catch those events and to study them without interfering with their dynamics.

Experimental Procedure

A 20 μL droplet of a 40 μM HEPES buffer solution containing 1 $\mu g mL^{-1}$ of supercoiled pBR322 DNA plasmid and 10 mM $MgCl_2$ was deposited on a disk of freshly cleaved ruby mica. The sample was quickly rinsed with few drops of water, blotted with filter paper, dried under a gentle flow of nitrogen, and then irradiated for 90 s in a small box with three 15 W Hg/Xe lamps. It was then immersed face-up and left for different periods in the dark in a dish with approximately 50 mL of deionized, doubly distilled water, degassed with a flow of argon. The samples were blotted and blown dry again, and then imaged under a dry nitrogen atmosphere with the tapping mode SFM (Nanoscope III, Digital Instruments, Santa Barbara, CA).

The original DNA sample was at least 95% supercoiled, as determined by agarose electrophoresis. Linear and open-circular nicked molecules were eliminated by treating the native *E. coli* pBR322 DNA samples with exonuclease III [15] in order to avoid deposition on mica of DNA molecules already relaxed.

Received: August 7, 1995 [Z 8291 IE]
German version: *Angew. Chem.* 1996, *108*, 569–570

Keywords: DNA · scanning force microscopy · topology

[1] C. Bustamante, D. Keller, G. Yang, *Curr. Opin. Struct. Biol.* **1993**, *3*, 363–372.
[2] C. Bustamante, D. A. Erie, D. Keller, *Curr. Opin. Struct. Biol.* **1994**, *4*, 750–760.
[3] B. Samorí, G. Siligardi, C. Quagliariello, A. L. Weisenhorn, J. Vesenka, C. Bustamante, *Proc. Natl. Acad. Sci. USA* **1993**, *90*, 3598–3601.
[4] B. Samorí, C. Nigro, V. Armentano, S. Cimieri, G. Zuccheri, C. Quagliariello, *Angew. Chem.* **1993**, *105*, 1482–1483; *Angew. Chem. Int. Ed. Engl.* **1993**, *32*, 1461–1463.
[5] D. Keller, F. S. Franke, *Surf. Sci.* **1993**, *294*, 409–419.
[6] S. H. Leuba, G. Yang, C. Robert, B. Samorí, K. van Holde, J. Zlatanova, C. Bustamante, *Proc. Natl. Acad. Sci. USA* **1994**, *91*, 11621–11625.
[7] M. Guthold, M. Bezanilla, D. A. Erie, B. Jenkins, H. Hansma, C. Bustamante, *Proc. Natl. Acad. Sci. USA* **1994**, *91*, 12927–12931.
[8] M. Bezanilla, B. Drake, E. Nudler, M. Kashlev, P. K. Hansma, H. Hansma, *Biophys. J.* **1994**, *67*, 2454–2459.
[9] M. Bezanilla, S. Manne, D. E. Laney, Y. L. Lyubchenko, H. G. Hansma, *Langmuir* **1995**, *11*, 655–659.
[10] A. D. Bates, A. Maxwell, *DNA Topology*, Oxford University Press, New York, **1993**.
[11] M. Matzeu, *Physica Medica* **1991**, *VII*, 3–9; R. D. Ley, R. B. Webb, *Photochem. Photobiol.* **1974**, *20*, 395–398.
[12] K. Sawadaishi, K. Miura, E. Ohtsuka, T. Ueda, K. Ishizaki, N. Shinriki, *Nucleic Acids Res.* **1985**, *13*, 7183–7194.
[13] It is most likely that a better control of the extent of the nicking can be achieved in the future by using cleavage methods that have been employed as probes of DNA structure in solution (D. M. J. Lilley, *Methods Enzymol.* **1992**, *212*, 133–139). Ozone has been found to nick pBR322 plasmids at specific sites [12].
[14] These segments are transiently released from the surface, because the number of molecules in the field of vision remains pratically constant for hours after all of them have already assumed an open shape. With a lower initial Mg^{2+} concentration the number of molecules adsorbed on mica decreases and their complete desorption is reached after shorter dipping times.
[15] S. G. Rogern, B. Weiss, *Methods Enzymol.* **1980**, *65*, 201–211.

 © VCH Verlagsgesellschaft mbH, D-69451 Weinheim, 1996 0570-0833/96/3505-0530 $ 15.00+.25/0

Programmed Self-Assembly of Copper(II)-L- and -D-Arginine Complexes with Aromatic Dicarboxylates to Form Chiral Double-Helical Structures**

Nayumi Ohata, Hideki Masuda, and Osamu Yamauchi*

Self-assembly of molecules leading to unique properties and functions has attracted a great deal of attention in recent years.[1-4] It results from an interplay of various noncovalent interactions and is often assisted by coordination to metal ions. The stereospecific assembly of molecular aggregates can be achieved by introducing chiral building blocks. Typical examples include the right-handed spiral of α-helices in proteins[5] and the right-handed double-helical structure of DNA.[6] We report here on the formation of crystalline $[Cu(L\text{-}Arg)_2](L)$ (L = *m*-phthalate (pa), 2,6-dicarboxylate (2,6-dipic)) and $[Cu(D\text{-}Arg)_2](L)$ (L = pyridine-3,5-dicarboxylate (3,5-dipic)) from copper(II), L- or D-arginine (Arg), respectively, and an aromatic dicarboxylate (L). These crystals reveal a unique hydrogen bonding network, which forms a right-handed and a left-handed double helix, respectively, depending on which arginine enantiomer was used.

Double- and triple-helical metal complexes have been shown to form for metal ions favoring tetrahedral coordination geometry such as Cu^{I}, Ag^{I}, and Ni^{II}.[7-12] The formation of such complexes is also involved in the sequence-specific DNA binding by zinc finger proteins, as revealed by X-ray studies.[13-15] The guanidinium group of arginine in proteins plays an important role in binding with carboxylate[16,17] and phosphate[18] moieties; two types (types A and B) of hydrogen bonds[19] can occur which contribute to the hydrogen bonding network. The guanidinium–carboxylate pair is ideal for bridge formation, and by using double hydrogen bonds,[19] complexes may thus form in a "programmable" way by self-assembly of the components Cu^{II}, Arg, and a dicarboxylate L.

Single crystals of $[Cu(L\text{-}Arg)_2](pa)\cdot 6H_2O$ (**1**), $[Cu(L\text{-}Arg)_2](2,6\text{-dipic})\cdot 5H_2O$ (**2**), and $[Cu(D\text{-}Arg)_2](3,5\text{-dipic})\cdot 5H_2O$ (**3**) suitable for X-ray analysis were obtained in 30–40% yields by mixing an aqueous solution containing $CuCl_2\cdot 2H_2O$ (0.171 g, 1.0 mmol) and L- or D-Arg (0.348 g, 2.0 mmol), respectively, with an alkaline (2 equiv NaOH), aqueous solution of L (L = pa, 2,6-dipic, and 3,5-dipic, respectively) and subsequent slow vapor diffusion with ethanol. The complexes **1**–**3** crystallize in the same space group, and the corresponding crystallographic parameters are very similar, although the three carboxylates L are subtly different due to the presence of the ring nitrogen and the positions of the carboxylate substituents relative to the nitrogen.[20] The crystallographic parameters of the D-enantiomer analog of **1** are similar to those of **1**.[21] The crystals of **1**–**3** contain four $[Cu(Arg)_2]^{2+}$ ions, four L^{2-} ions, and twenty or twenty-four water molecules in the unit cell, all of which are connected by a hydrogen bonding network. Figure 1a shows a view of crystallographically independent molecules in the unit cell of **1**. The Cu^{II} ion has a square-planar geometry with the two amine nitrogen atoms and two carboxylate oxygen atoms from two L-Arg molecules coordinated in the *cis* configuration. The Arg side chains of the complex ion are extended outward from the Cu^{II} coordination sphere, forming type A hydrogen bonds with the carboxylate group of an L^{2-} ion situated between the complex ions. The L^{2-} ions thus connect the Arg side chains to form an infinite chain from L^{2-}-$[Cu(L\text{-}Arg)_2]^{2+}$ units with a helical structure extended along the crystallographic *a* axis. Two such chains or strands are bound together through the hydrogen bonds between the coordinated amino groups of one strand and the L^{2-} carboxylate groups of the other strand to form a double helix. In the crystal structure one double helix thus formed is connected to a neighboring double helix through type B hydrogen bonds between the guanidinium group of one double helix and the carbonyl oxygen atoms of two carboxylate groups coordinated to a Cu^{II} ion bound in the neighboring double helix (Fig. 1b). Considering

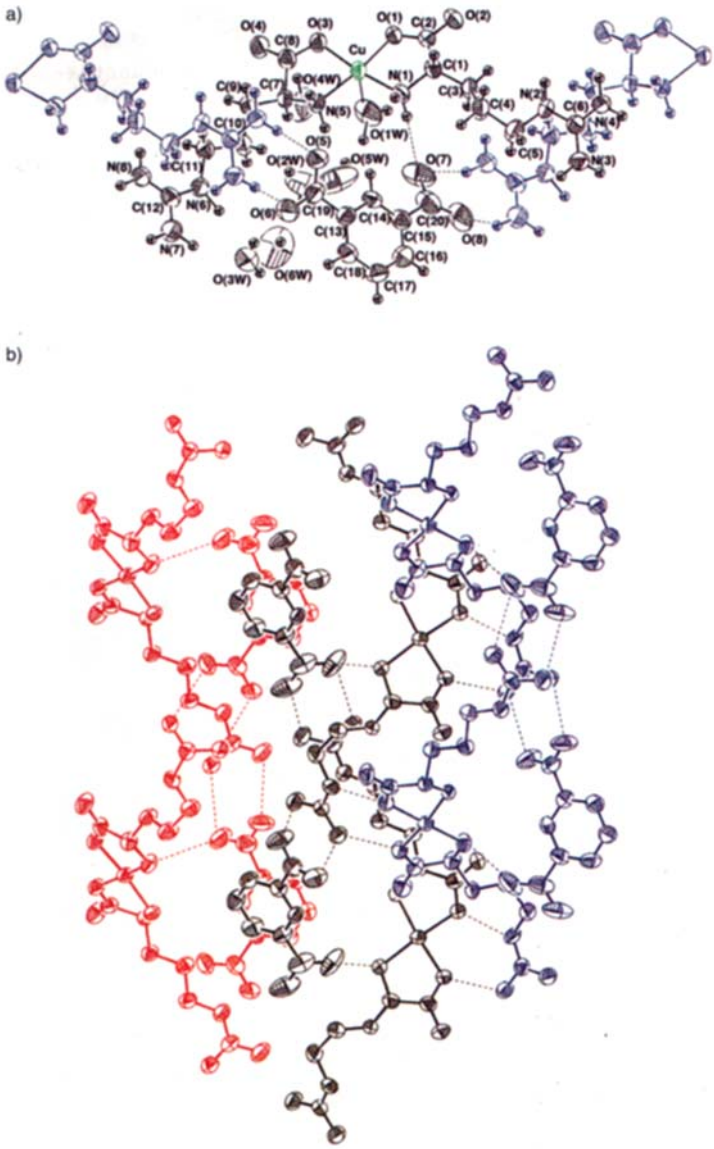

Fig. 1. a) Structure of crystallographically independent molecules in the unit cell of $[Cu(L\text{-}Arg)_2](pa)\cdot 6H_2O$ (**1**). b) Crystal structure of **1** showing the hydrogen bonds between a double helix (black) and two neighboring double helices (red and blue).

[*] Prof. Dr. O. Yamauchi, N. Ohata
Department of Chemistry, Faculty of Science
Nagoya University
Chikusa-ku, Nagoya 464-01 (Japan)
Fax: Int. code +(52)789-2953
e-mail: b42215a@nucc.cc.nagoya-u.ac.jp
Dr. H. Masuda
Department of Applied Chemistry, Nagoya Institute of Technology (Japan)

[**] This work was supported by a Grant-in-Aid for Scientific Research on Priority Areas (Bioinorganic Chemistry) from the Ministry of Education, Science, Sports, and Culture of Japan, for which we express our thanks.

that Cu^{II}–Arg complexes can usually assume both *cis* and *trans* configurations in the Cu^{II} coordination plane,[22, 23] these hydrogen bonds probably contribute to the *cis* configuration of the Cu^{II} coordination structure. The stacking of the aromatic rings of the L^{2-} ions with a mean interfacial distance of 3.49 Å leads to a further stabilization of the association between the double helices. The crystal structures of **2** and **3**, which are similar to the structure of **1**, reveal that the nitrogen atoms of 2,6-dipic and 3,5-dipic are not involved in coordination and hydrogen bonding, indicating that all the dianions L used function as bridging groups in essentially the same manner. In all three structures water molecules are not involved in the intra- and interstrand hydrogen bonding, except one water molecule which is axially coordinated with a Cu–O distance of 2.522(6), 2.387(8), and 2.385(5) Å for **1**, **2**, and **3**, respectively.

Interestingly, complexes **1** and **2** involving L-Arg form a right-handed helix, whereas complex **3** with D-Arg forms a left-handed helix (Fig. 2). This indicates that the handedness of the

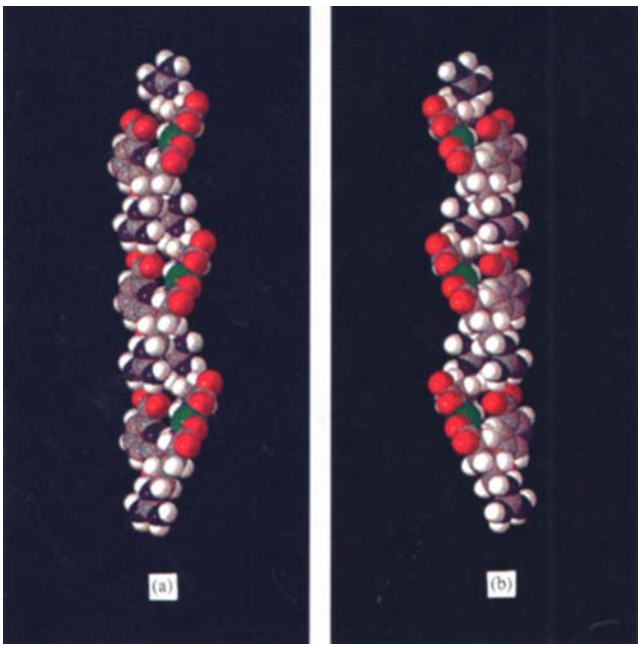

Fig. 2. Space-filling models of $[Cu(L\text{-}Arg)_2](2,6\text{-dipic})\cdot 5H_2O$ (**2**) (a) and $[Cu(D\text{-}Arg)_2](3,5\text{-dipic})\cdot 5H_2O$ (**3**) (b) showing a right-handed and a left-handed double helix, respectively, formed by intra- and interstrand hydrogen bonds. C: gray, H: white, O: red, N: blue, Cu: green.

double helices in the solid state is governed by the configuration of the α-carbon atom of the amino acids and is therefore coded in the $[Cu(L\text{-}Arg)_2]^{2+}$ and $[Cu(D\text{-}Arg)_2]^{2+}$ units, respectively. On the other hand, the *cis*-configurated complex $[Cu(L\text{-}Arg)_2](NO_3)_2\cdot 3H_2O$ does not form a double-helical structure but exhibits an infinite three-dimensional network of hydrogen bonding in which the guanidinium group, nitrate ions, and water molecules participate.[23] Weak hydrogen bonding in chiral diamine and diol motifs has recently been reported to give a triple-stranded helicate, whose helicity is dependent on the configurations of the two asymmetric carbon atoms of the diamine.[24]

The crucial difference between the structures of complexes **1**–**3** and that of $[Cu(L\text{-}Arg)_2](NO_3)_2$ lies in anionic bridging groups, L^{2-} and NO_3^-, respectively. Whereas the NO_3^- ion is small and located relatively independent of neighboring NO_3^- ions in the crystal, L^{2-} requires more space and can form two sets of spacially isolated hydrogen bonds. Therefore, the stereospecific helix formation may be regarded as "programmed" by the L^{2-} unit, which serves as a knot for the guanidinium–carboxylate bridge and reads the information of handedness coded in the $[Cu(L\text{-}Arg)_2]^{2+}$ or $[Cu(D\text{-}Arg)_2]^{2+}$ units.

These results point to the intrinsic factors for self-assembly of molecules by hydrogen bonding and for the handedness of the resulting helices, and may contribute to the understanding of organized systems in biology.

Received: October 6, 1995 [Z 8449 IE]
German version: *Angew. Chem.* **1996**, *108*, 570–572

Keywords: copper compounds · electrostatic interactions · helical structures · self-assembly

[1] J.-M. Lehn, *Angew. Chem.* **1990**, *102*, 1347–1362; *Angew. Chem. Int. Ed. Engl.* **1990**, *29*, 1304–1319.
[2] F. Vögtle, *Supromolecular Chemistry*, Wiley, Chichester, **1991**.
[3] D. B. Amabilino, J. F. Stoddart, *Pure Appl. Chem.* **1993**, *65*, 2351–2359.
[4] G. M. Whitesides, E. E. Simanek, J. P. Mathias, C. T. Seto, D. N. Chin, M. Mammen, D. M. Gordon, *Acc. Chem. Res.* **1995**, *28*, 37–44.
[5] C. Branden, J. Tooze, *Introduction to Protein Structure*, Garland, New York, **1991**.
[6] W. Saenger, *Principles of Nucleic Acid Structure*, Springer, Heidelberg, **1984**.
[7] J.-M. Lehn, A. Rigault, J. Siegel, J. Harrowfield, B. Chevrier, D. Moras, *Proc. Natl. Acad. Sci. USA* **1987**, *84*, 2565–2569.
[8] E. C. Constable, *Tetrahedron* **1992**, *48*, 10013–10059.
[9] C. Piguet, G. Bernardinelli, B. Bocquet, A. Quattropanni, A. F. Williams, *J. Am. Chem. Soc.* **1992**, *114*, 7440–7451.
[10] R. Krämer, J.-M. Lehn, A. De Cian, J. Fischer, *Angew. Chem.* **1993**, *105*, 764–767; *Angew. Chem. Int. Ed. Engl.* **1993**, *32*, 703–706 and references therein.
[11] R. F. Carina, G. Bernardinelli, A. F. Williams, *Angew. Chem.* **1993**, *105*, 1483–1485; *Angew. Chem. Int. Ed. Engl.* **1993**, *32*, 1463–1465.
[12] E. C. Constable, A. J. Edwards, P. R. Raithby, J. V. Walker, *Angew. Chem.* **1993**, *105*, 1486–1487; *Angew. Chem. Int. Ed. Engl.* **1993**, *32*, 1465–1467.
[13] N. P. Pavletich, C. O. Pabo, *Science* **1991**, *252*, 809–817.
[14] N. P. Pavletich, C. O. Pabo, *Science* **1993**, *261*, 1701–1707.
[15] L. Fairall, J. W. R. Schwabe, L. Chapman, J. T. Finch, D. Rhodes, *Nature* **1993**, *366*, 483–487.
[16] F. A. Quiocho, W. N. Lipscomb, *Adv. Protein Chem.* **1971**, *25*, 1–78.
[17] T. L. Poulos, B. C. Finzel, A. J. Howard, *Biochemistry* **1986**, *25*, 5314–5322.
[18] G. Waksman, D. Kominos, S. C. Robertson, N, Pant, D. Baltimore, R. B. Birge, D. Cowburn, H. Hanafusa, B. J. Mayer, M. Overduin, M. D. Resh, C. B. Rios, L. Silverman, J. Kuriyan, *Nature* **1992**, *358*, 646–653.
[19] D. M. Salunke, M. Vijayan, *Int. J. Peptide Protein Res.* **1981**, *18*, 348–351.
[20] Ali X-ray diffraction data were collected at 295 K with a Rigaku AFC-5R four-circle diffractometer with a rotating anode and using graphite-monochromated $Cu_{K\alpha}$ radiation ($\lambda = 1.54178$ Å) up to $2\theta_{max} = 120°$. The intensities were corrected for Lorentz and polarization effects. An empirical absorption correction, based on Ψ scans, was applied for all the crystals. The structures were solved by direct methods and refined anisotropically for non-hydrogen atoms by full-matrix least-squares methods by using reflections with $I > 3\sigma(I)$. The weighting scheme $w^{-1} = \sigma^2(F_o)$ was employed for each crystal. All calculations were performed by using the program system teXsan. All the hydrogen atoms, except for some of the water hydrogen atoms, were located from the difference Fourier maps, whose parameters were not refined. **1**: $C_{20}H_{44}N_8O_{14}Cu$, $M_r = 684.16$, orthorhombic, space group $P2_12_12_1$, $a = 13.293(4)$, $b = 30.100(7)$, $c = 7.57(1)$ Å, $V = 3027(3)$ Å^3, $Z = 4$, $\rho_{calcd} = 1.501$ g cm^{-3}, $\mu = 17.11$ cm^{-1}, $F(000) = 1444.0$, $R = 0.043$, $R_w = 0.031$ for 1953 observed reflections. **2**: $C_{19}H_{41}N_9O_{13}Cu$, $M_r = 667.13$, orthorhombic, space group $P2_12_12_1$, $a = 13.158(3)$, $b = 29.608(2)$, $c = 7.457(3)$ Å, $V = 2905(1)$ Å^3, $Z = 4$, $\rho_{calcd} = 1.525$ g cm^{-3}, $\mu = 17.53$ cm^{-1}, $F(000) = 1404.0$, $R = 0.047$, $R_w = 0.042$ for 1694 observed reflections. **3**: $C_{19}H_{41}N_9O_{13}Cu$, $M_r = 667.13$, orthorhombic, space group $P2_12_12_1$, $a = 13.158(4)$, $b = 29.596(5)$, $c = 7.464(3)$ Å, $V = 2906(3)$ Å^3, $Z = 4$, $\rho_{calcd} = 1.524$ g cm^{-3}, $\mu = 17.52$ cm^{-1}, $F(000) = 1404.0$, $R = 0.044$, $R_w = 0.039$ for 2274 observed reflections. Further details of the crystal structure investigation may be obtained from the Director of the Cambridge Crystallographic Data Centre, 12 Union Road, GB-Cambridge CB2 1EZ (UK), on quoting the full journal citation.
[21] Lattice parameters for the $[Cu(D\text{-}Arg)_2](pa)$ complex: orthorhombic, space group $P2_12_12_1$, $a = 13.331(7)$, $b = 30.10(2)$, $c = 7.545(5)$ Å, $V = 3028(3)$ Å^3.
[22] M. T. L. S. Duarte, M. A. A. F. de C. T. Carrondo, M. L. S. S. Goncalves, M. B. Hursthouse, N. P. C. Walker, H. M. Dawes, *Inorg. Chim. Acta* **1986**, *124*, 41–47.
[23] H. Masuda, A. Odani, T. Yamazaki, T. Yajima, O. Yamauchi, *Inorg. Chem.* **1993**, *32*, 1111–1118.
[24] S. Hanessian, A. Gomtsyan, M. Simard, S. Roelens, *J. Am. Chem. Soc.* **1994**, *116*, 4495–4496.

Methyltrioxorhenium(VII)-Catalyzed Epoxidation of Alkenes with the Urea/Hydrogen Peroxide Adduct

Waldemar Adam* and Catherine M. Mitchell

Selective catalytic oxidations are rapidly gaining importance in organic synthesis. The use of transition metal complexes as catalysts for such reactions is of particular interest,[1] on the one hand because of the high selectivity and the versatility of these complexes and on the other hand due to their ability to activate oxidants such as molecular oxygen and hydrogen peroxide. During the last five years, a broad spectrum of transformations of organic compounds catalyzed by the organometallic complex methyltrioxorhenium (MTO) has been reported.[2] The epoxidation of olefins with hydrogen peroxide was the first type of reaction to be described[2a-d] (Scheme 1). Although the oxidation of olefins in many cases

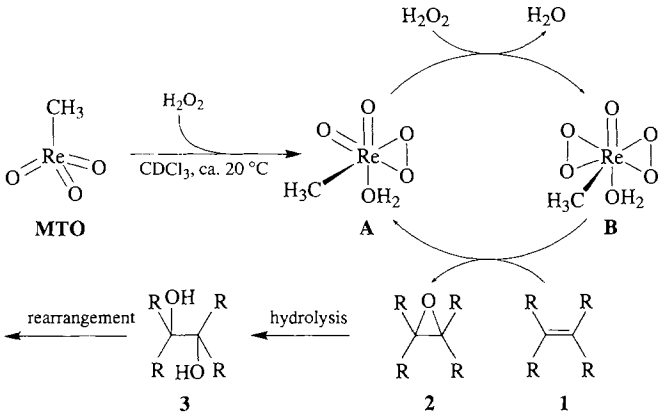

Scheme 1.

leads efficiently and selectively to the corresponding epoxides, a typical side reaction is the conversion of the hydrolytically sensitive epoxides to 1,2-diols,[2b] which sometimes undergo cleavage and rearrangement reactions (pinacol rearrangement, Hock cleavage, etc.). Such secondary reactions can now be suppressed by replacing hydrogen peroxide with the urea/hydrogen peroxide adduct (UHP) as primary oxidant. This enables epoxidations to be carried out in nonaqueous media, whereby the formation of diols and cleavage and rearrangement reactions are largely avoided. In the case of the epoxidation of chiral allylic alcohols, for the first time high diastereoselectivities (dr > 90:10) were achieved for an MTO-catalyzed reaction.

H_2O_2 adducts have already been widely employed as oxidants in organic synthesis[3] and are also particularly important in the detergent industry; one example is the peroxy salt $4Na_2SO_4 \cdot NaCl \cdot 2H_2O_2$ in neutral washing powders.[3i, 4] The only known metal-catalyzed oxidations are the epoxidation of 1,2-dihydronaphthalene with urea/hydrogen peroxide catalyzed by a Mn(salen) derivative (H_2salen = bis(salicyliden)ethylenediamine)[5] and the Mn(porphyrin)-catalyzed epoxidation of cyclooctene with various H_2O_2 adducts.[6] The adducts used in these cases include Na_2CO_3, $(CH_3)_3NO$, and $(C_6H_5)_3PO$, and also urea in one case. The urea presumably acts as a ligand; moreover, in the form of the adduct, which is present in solid and undissolved form, it also allows the H_2O_2 concentration in the reaction mixture to be exactly dosed. However, in most cases the addition of a coreactant (acetic anhydride, maleic anhydride, *para*-nitrobenzoyl chloride, *para*-nitrobenzoyl imidazolide, phthalic anhydride, tetrabutylammonium hydroxide, trifluoroacetic anhydride, etc.) is necessary for successful oxidation.

The use of additives such as amines, for instance 4,4'-dimethyl-2,2'-bipyridine, quinine, and quinchonine,[2b, 2d] has been reported for MTO-catalyzed epoxidations directly with hydrogen peroxide. Although formation of 1,2-diols is thereby suppressed, the activity of the catalyst is also diminished.[2d] When an equimolar amount of the adduct (with respect to the oxidant) is used, the conversion drops by 23% for 2,2'-bipyridine, by 60% for quinoline, and even by 96% in the case of isoquinoline. In contrast, when UHP is employed as oxidant, the respective epoxide is obtained selectively, often with high conversion.

We report here on our investigation of the MTO-catalyzed epoxidation of several selected olefins. Our results (Table 1) show that the hydrolytic ring-opening of the epoxide **2** to give the corresponding diol **3** with aqueous H_2O_2 (Table 1, entries 2 and 5) can be avoided with UHP (Table 1, entries 1 and 4). As the most striking example, the reaction of camphene (Table 1, entries 4 and 5) in the absence of urea adduct and after only 3 h

Table 1. MTO-catalyzed epoxidation of olefins with the urea/hydrogen peroxide adduct (UHP) [a].

Entry	Olefin **1**	Oxidant	*t* [h]	Conv. [%]	Epoxide [b] **2**	1,2-Diol [b, c] **3**
1	cyclohexene	UHP	18	98	99	1
2	cyclohexene	H_2O_2 (85%)	18	71	0	82 (18)
3	1-methylcyclohexene	UHP	19	88	96	4
4	camphene	UHP	30	92 [d]	≥95	0
5	camphene	H_2O_2 (85%)	3	27	0	0 (≥95)
6	styrene	UHP	19	46	≥95	0
7	α-methylstyrene	UHP	21	81	68	32
8	indene	UHP	37	51	≥95	0
9	1,1-diphenylethene	UHP	20	81	93	7
10	*trans*-stilbene	UHP	19	44	≥95	0
11	*trans*-cinnamyl alcohol	UHP	24	66	≥95 [e]	0

[a] Olefin:oxidant:MTO = 1:1:0.01 (mol ratio) in $CDCl_3$, ca. 20 °C, argon atmosphere, mass balance 100%, error ±5% of the stated values. [b] Normalized to 100% conversion. [c] Yield of the pinacol rearrangement product (aldehyde) in parentheses. [d] Traces of rearrangement products were also obtained. [e] Traces of *trans*-cinnamaldehyde were detected in the ^{1}H NMR spectrum of the crude reaction mixture.

results exclusively in cleavage and rearrangement products; however, with UHP only the desired camphene oxide is obtained, which is stable under the modified reaction conditions (conversion 92% after 30 h at room temperature (ca. 20 °C) with UHP in $CDCl_3$). In the absence of MTO no reaction takes place under otherwise identical reaction conditions. Further examples (Table 1, entries 3, 6, 8–11) illustrate the scope (<10% ring opening); considerable hydrolysis (ca. 32%) occurs only for the very hydrolytically sensitive α-methylstyrene oxide (Table 1, entry 7). Presumably the high Lewis acidity of the peroxo complexes **A** and **B** (Scheme 1) is not sufficiently buffered by the addition of urea to suppress completely such secondary reactions under the reaction conditions. Related ad-

[*] Prof. Dr. W. Adam, Dipl.-Chem. C. M. Mitchell
Institut für Organische Chemie der Universität
Am Hubland, D-97074 Würzburg (Germany)
Fax: Int. code +(931)888-4756
e-mail: adam@chemie.uni-wuerzburg.de

[**] This work was supported by the Deutsche Forschungsgemeinschaft (SFB 347 "Selektive Reaktionen metallaktivierter Moleküle"), Schwerpunktprogramm "Peroxidchemie: Mechanistische und präparative Aspekte des Sauerstofftransfers", Bayerischer Forschungsverbund Katalyse (FORKAT), and the Fonds der Chemischen Industrie. We are grateful to Prof. Dr. W. A. Herrmann for a generous supply of methyltrioxorhenium.

ditives such as amides, peptides, and amino acids, which control the hydrolysis of cyclohexene oxide in analogy to urea (not shown in Table 1), have a much more limited influence on the reaction. So far the mechanism behind the buffering effect of these additives on the Lewis acidity of Re^{VII} has not been elucidated.

In the case of electron-poor olefins such as *trans*-cinnamaldehyde, *trans*-methyl cinnamate, and 2-cyclohexenone (not shown in Table 1), the reactivity of the substrate is reduced to such an extent that the epoxidation competes with the decomposition of the catalyst. Even after approximately 20 h at about 20 °C with UHP in $CDCl_3$ hardly any conversion ($\leq 5\%$) was observed for these substrates.

To date, the diastereoselectivity of the MTO-catalyzed epoxidation has not been investigated, presumably because of the various subsequent reactions (hydrolysis, cleavage, rearrangement), which can now be avoided with UHP as oxidant. To test the selectivity, the epoxidation of chiral allylic alcohols **1a–f** to give the respective *threo*- and *erythro*-epoxy alcohols **2a–f** was carried out, for which high yields ($\geq 95\%$) were achieved (Table 2). What is noticable in Table 2 are the high diastereoselectivities (*threo*/*erythro* > 80:20) for substrates **1c–f** (Table 2, entries 3–6) in comparison with those for **1a,b** (Table 2, entries 1 and 2). It is mechanistically relevant to compare the derivatives **1a** (1,2-allylic strain), **1c** (1,3-allylic strain), and **1d** (1,2- and 1,3-allylic strain), as the diastereoselectivities in Table 2 (entries 1, 3, and 4) show. The 1,3-allylic strain[7] is decisive for the high diastereoselectivities demonstrated by results obtained with substrates **1e,f** (Table 2, entries 5 and 6); it operates in combination with the established hydroxyl group control[8] to afford the preferred *threo* isomer. These high π-facial diastereoselectivities point to pronounced interaction between the oxygen acceptor (chiral allylic alcohol) and the activated oxygen donor (diperoxorhenium complex) by the formation of hydrogen bonds.

Table 2. MTO-catalyzed oxidation [a] of chiral allylic alcohols **1** to the corresponding *threo*- and *erythro*-epoxides **2** with the urea/hydrogen peroxide adduct and comparison with the diastereoselectivities of reported epoxidations.

Entry	Allylic alcohol	*t* [h]	Conv. [%]	*threo*/*erythro* Diastereoselectivity (dr) MTO/UHP	mCPBA	$VO(acac)_2$/*t*BuOOH
1	**1a**	17	88	50:50	45:55 [b]	5:95 [b]
2	**1b**	20	81	67:33	64:36 [b]	29:71 [b]
3	**1c**	20	90	82:18	95:5 [b]	71:29 [b]
4	**1d**	25	≥95	91:9	90:10 [c]	33:67 [c]
5	**1e**	15	91	83:17	95:5 [b]	86:14 [b]
6	**1f**	17	88	95:5	90:10 [d]	

[a] Olefin:oxidant:MTO = 1:1:0.01 (mol ratio) in $CDCl_3$, ca. 20 °C, argon atmosphere, mass balance 100%, error ±5% of the stated values. [b] Ref. [9]. [c] Ref. [10]. [d] Ref. [11].

To ascertain the structural aspects of the interaction between the chiral allylic alcohol substrate and the metal-activated oxidant, a comparison with stereochemically established epoxidations such as those with peracid (*threo*-selective)[9–11] and $VO(acac)_2$/*t*BuOOH (*erythro*-selective)[9,10] is informative (Table 2). In the epoxidation of the allylic alcohol **1d** (Table 2, entry 4) as a stereochemical probe (1,2- and 1,3-allylic strain), it becomes clear that the MTO/UHP reaction proceeds through a transition state analogous to the peracid transition state *threo*-**1d**‡ and not one analogous to *erythro*-**1d**‡, the $VO(acac)_2$/*t*BuOOH transition state. Therefore it is certain that our system relies on hydrogen bond formation similar to that in epoxidations with peracids and not on direct bonding of the alcoholate to the metal complex as in the vanadium case. These are first hints on the transition state structure for the oxygen transfer in MTO-catalyzed epoxidation.

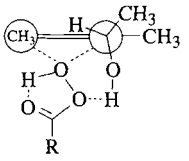

threo-**1d**‡

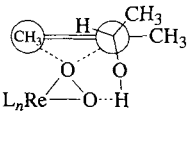

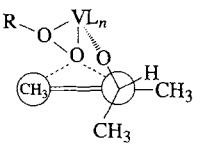

erythro-**1d**‡

One advantage of our simple MTO/H_2O_2 epoxidation of alkenes **1** with urea/hydrogen peroxide is the catalytic mode (which can be extended to the preparative scale (cf. Experimental Procedure; e.g. the epoxidation of 0.5 g of the allylic alcohol **1e** leads to the epoxide *threo*-**2e** in 67% yield [*dr* 88:12]). In addition, acid-catalyzed secondary reactions (hydrolysis, cleavage, rearrangement) are largely suppressed due to the buffering action of urea, without adversely effecting the reactivity, as is the case when amines are added.[2d] We have also established that the high *threo* diastereoselectivity for chiral allylic alcohols requires a peracid-like transition state with π-facial control of hydrogen bond formation between oxygen donor and acceptor.

Experimental Procedure

General procedure for the epoxidation of olefins: A solution of MTO (12.3 mg, 49.0 μmol, 0.01 equiv) in $CHCl_3$ (10 mL) was mixed with the urea/hydrogen peroxide adduct (940 mg, 10.0 mmol, 2.00 equiv) and stirred under an argon atmosphere at ca. 20 °C for 10 min. The olefin **1e** (500 mg, 4.99 mmol, 1.00 equiv) was added dropwise and the suspension stirred for 18 h at about 20 °C, after which 5 mL of water was added. The mixture was extracted with CH_2Cl_2 (3 × 15 mL). The combined organic phases were washed with water (2 × 5 mL) and brine (5 mL), dried over $MgSO_4$, and then concentrated at 0 °C/30 mbar. Conversion ≥95% (determined by ^1H NMR analysis). Column chromatography (silica gel, ether/hexane

 © VCH Verlagsgesellschaft mbH, D-69451 Weinheim, 1996 0570-0833/96/3505-0534 $ 15.00+.25/0

(1/1)) of the crude product yielded 391 mg (67%) of the pure epoxy allylic alcohol **2e** with a diastereoselectivity of 88:12 (*threo/erythro*).

Received: April 26, 1995
Revised version: December 8, 1995 [Z79331E]
German version: *Angew. Chem.* **1996**, *108*, 578–581

Keywords: asymmetric syntheses · catalysis · complexes with oxygen ligands · epoxidations · rhenium compounds

[1] a) R. A. Sheldon, J. K. Kochi, *Metal-Catalysed Oxidations of Organic Compounds*, Academic Press, New York, **1981**; b) H. Mimoun, *Angew. Chem.* **1982**, *94*, 750–766; *Angew. Chem. Int. Ed. Engl.* **1982**, *21*, 734–750; c) R. H. Holm, *Chem. Rev.* **1987**, *87*, 1401–1449; d) K. A. Jørgensen, *ibid.* **1989**, *89*, 431–458; e) B. Meunier, *ibid.* **1992**, *92*, 1411–1456.

[2] Epoxidation of olefins, oxidation of alkynes to α,β-unsaturated ketones or 1,2-diketones, and Baeyer–Villager rearrangement of ketones: a) W. A. Herrmann, R. W. Fischer, W. Scherer, M. U. Rauch, *Angew. Chem.* **1993**, *105*, 1209–1212; *Angew. Chem. Int. Ed. Engl.* **1993**, *32*, 1157–1160; b) W. A. Herrmann, R. W. Fischer, D. W. Marz, *ibid.* **1991**, *103*, 1706–1709 and **1991**, *30*, 1638–1641; c) H. Yu, H. Simon, *Tetrahedron* **1991**, *47*, 9035–9052; d) W. A. Herrmann, R. W. Fischer, M. U. Rauch, W. Scherer, *J. Mol. Catal.* **1994**, *86*, 243–266; e) W. A. Herrmann, R. W. Fischer, J. D. G. Correia, *ibid.* **1994**, *94*, 213–223; f) A. M. Al-Ajlouni, J. H. Espenson, *J. Am. Chem. Soc.* **1995**, *117*, 9243–9250. Oxidation of arenes to *para*-quinones: g) W. Adam, W. A. Herrmann, J. Lin, C. R. Saha-Möller, R. W. Fischer, J. D. G. Correia, *Angew. Chem.* **1994**, *106*, 2545–2546; *Angew. Chem. Int. Ed. Engl.* **1994**, *33*, 2475–2477; h) W. Adam, W. A. Herrmann, J. Lin, C. R. Saha-Möller, *J. Org. Chem.* **1994**, *59*, 8281–8283; i) W. Adam, W. A. Herrmann, C. R. Saha-Möller, M. Shimizu, *J. Mol. Catal.* **1995**, *97*, 15–20. C-H-Insertion: k) R. W. Murray, K. Iyanar, J. Chen, J. T. Wearing, *Tetrahedron Lett.* **1995**, *36*, 6415–6418. Oxidation of benzaldehydes to phenols: l) S. Yamazaki, *Chem. Lett.* **1995**, 127–128. Sulfoxidation: m) P. Huston, J. H. Espenson, A. Bakac, *Inorg. Chem.* **1993**, *32*, 4517–4523; n) W. Adam, C. M. Mitchell, C. R. Saha-Möller, *Tetrahedron* **1994**, *50*, 13121–13124; o) K. A. Vassell, J. H. Espenson, *Inorg. Chem.* **1994**, *33*, 5491–5498. Oxidation of nitrogen, phosphorus, arsenic, and antimony: p) Z. Zhu, J. H. Espenson, *J. Org. Chem.* **1995**, *60*, 1326–1332; q) M. M. Abu-Omar, J. H. Espenson, *Proc. 9th Int. Symp. Homog. Catal.* **1994**; r) M. M. Abu-Omar, J. H. Espenson, *J. Am. Chem. Soc.* **1995**, *117*, 272–280.

[3] a) G. B. Payne, P. H. Deming, P. H. Williams, *J. Org. Chem.* **1961**, *26*, 659–663; b) N. Matsumura, N. Sonoda, S. Tsutsumi, *Tetrahedron Lett.* **1970**, 2029–2032; c) C. H. Gagnieu, A. V. Grouiller, *J. Chem. Soc. Perkin Trans. 1* **1982**, 1009–1011; d) B. Ben Hassine, M. Gorsane, F. Geerts-Evrard, J. Pecher, R. H. Martin, D. Castelet, *Bull. Soc. Chim. Belg.* **1986**, *95*, 547–556; e) P. G. Cookson, A. G. Davies, N. Fazal, *J. Organomet. Chem.* **1975**, *99*, C31–C32; f) A. A. Oswald, D. L. Guertin, *J. Org. Chem.* **1963**, *28*, 651–657; g) R. D. Temple, Y. Tsuno, J. E. Leffler, *ibid.* **1963**, *28*, 2495; h) D. B. Copley, F. Fairbrother, J. R. Miller, A. Thompson, *Proc. Chem. Soc.* **1964**, 300–301; i) S. D. Cosgrove, W. Jones, *J. Chem. Soc. Chem. Commun.* **1994**, 2255–2256; urea/hydrogen peroxide (UHP): k) M. S. Cooper, H. Heaney, A. J. Newbold, W. R. Sanderson, *Synlett* **1990**, 533–535; l) W. P. Jackson, *ibid.* **1990**, 536; m) A. M. d'A. R. Gonsalves, R. A. W. Johnstone, M. M. Pereira, J. Shaw, *J. Chem. Res. Synops.* **1991**, 208–209; n) R. Balicki, L. Kaczmarek, P. Nantka-Namirski, *Liebigs Ann. Chem.* **1992**, 883–884; o) L. Astudillo, A. Galindo, A. G. Gonzalez, H. Mansilla, *Heterocycles* **1993**, *36*, 1075–1080.

[4] N. Yunosuka, S. Shigetsugu, M. Kinjiro, I. Yoshio, M. Toshio, DE-A 2 530 539, **1976** (Kao Soap Co. Ltd., Nippon Peroxide Co. Ltd.), [*Chem. Abstr.* **1976**, *84*, 152605y].

[5] T. Schwenkreis, A. Berkessel, *Tetrahedron Lett* **1993**, *34*, 4785–4788.

[6] A. M. d'A. R. Gonsalves, R. A. W. Johnstone, M. M. Pereira, J. Shaw, *J. Chem. Soc. Perkin Trans. 1*, **1991**, 645–649.

[7] a) R. W. Hoffmann, *Chem. Rev.* **1989**, *89*, 1841–1860; b) J. L. Broeker, R. W. Hoffmann, K. N. Houk, *J. Am. Chem. Soc.* **1991**, *113*, 5006–5017.

[8] W. Adam, B. Nestler, *J. Am. Chem. Soc.* **1992**, *114*, 6549–6550.

[9] B. E. Rossiter, T. R. Verhoeven, K. B. Sharpless, *Tetrahedron Lett* **1979**, *34*, 4733–4736.

[10] W. Adam, B. Nestler, *Tetrahedron Lett.* **1993**, 611–614.

[11] P. Chautemps, J.-L. Pierre, *Tetrahedron* **1976**, *32*, 549–557.

Diastereoselective Chelation-Controlled Radical Cyclization of Chiral Oxazolidinone-Derived 2-Alkenamides and Modeling of the Transition State**

Domenico Badone,* Jean-Marie Bernassau, Rosanna Cardamone, and Umberto Guzzi

The formation of carbon–carbon bonds by radical addition to alkenes is one of the most useful synthetic reactions in organic synthesis.[1] Though high α-stereoselection has been observed in radical additions to chiral acceptors, such as α,β-unsaturated amides and imides,[2] a high degree of β-stereoselection is difficult to achieve and remains a challenge. Recently Curran et al. introduced an auxiliary, derived from Kemp's triacid, that provides high β-diastereoselectivity in radical addition and annulation reactions.[3] However, several steps are required for the preparation of the auxiliary, and development of easier methodologies is still required.

We now report that the radical cyclization of **1a,b** bearing the oxazolidinone chiral auxiliary R′ gives **2** with good diastereoselectivity in the presence of a Lewis acid (Scheme 1). β-Tetralines like **2**, **3**, and their derivatives are valuable compounds in pharmaceutical research.[4]

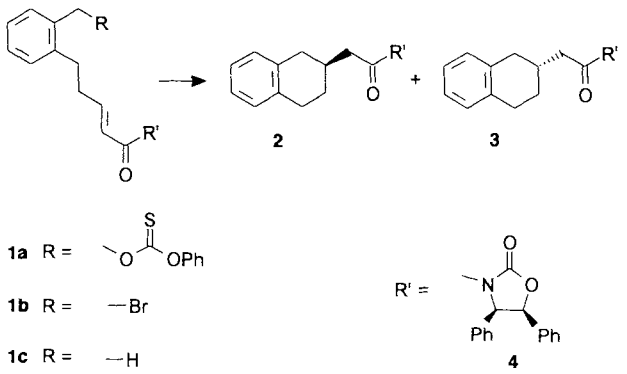

Scheme 1. Radical cyclization of **1a,b**.

Asymmetric 1,4-additions of organometallic reagents to chiral α,β-unsaturated *N*-acyloxazolidinones has been studied, and they show excellent diastereoselectivity.[5] Scheme 2 outlines the synthesis of key intermediates **5** and **6**.[6] Coupling of **5** and **6** (DMAP, $CHCl_3$, 60 °C, 8 h) followed by acid hydrolysis of THP ether (AcOH, THF/H_2O, 50 °C, 8 h) gave the single diastereoisomer **7** ($E:Z$ >99:1) in 50% overall yield. Synthesis of **1a,b** was easily carried out (Scheme 3).

Radical generation and cyclization were obtained by three different reaction conditions: addition by syringe pump (3.4 mL h^{-1}) of TTMS and AIBN in C_6H_6 to a solution of **1a,b** (9×10^{-3} M) in C_6H_6 at 80 °C (A);[7] addition by syringe pump (3.4 mL h^{-1}) of SmI_2 in THF (0.1 M) to **1b** (9×10^{-3} M) in THF/HMPA 95/5 at 25 °C (B);[8] stirring of a solution of **1b** (10^{-2} M),

[*] Dr. D. Badone, Dr. R. Cardamone, Dr. U. Guzzi
Research Center Sanofi-MIDY
Via Piranesi 38, I-20137 Milan (Italy)
Telefax: Int. +(2)7394453
Dr. J.-M. Bernassau
Sanofi Research Montpellier (France)

[**] In this communication the following abbreviations are used: AIBN = azobis(isobutyronitrile), DMAP = 4-(dimethylamino)pyridine, HMPA = hexamethylphosphoric triamide, PTC = phase-transfer catalysis, PTSA = *para*-toluenesulfonic acid, THP = tetrahydro-2*H*-pyran-2-yl, TTMS = tris(trimethylsilyl)silane.

 © VCH Verlagsgesellschaft mbH, D-69451 Weinheim, 1996 0570-0833/96/3505-0535 $ 15.00+.25/0

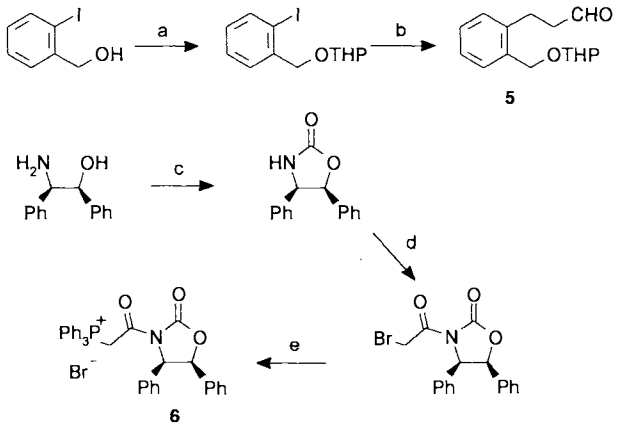

Scheme 2. Synthesis of **5** and **6**. a) 3,4-dihydro-2H-pyran, PTSA, CH_2Cl_2, 25 °C, 12 h (93%); b) allyl alcohol, $KHCO_3$, nBu_4NBr, $Pd(OAc)_2$ (2%), DMF, 90 °C, 2 h (87%); c) 1,1'-carbonyldiimidazole, THF, reflux, 3 h (70%); d) *n*BuLi, THF, −78 °C, 15 min, then $BrCH_2COBr$, -78 °C, 2 h (85%); e) Ph_3P, benzene, reflux, 3 h (90%).

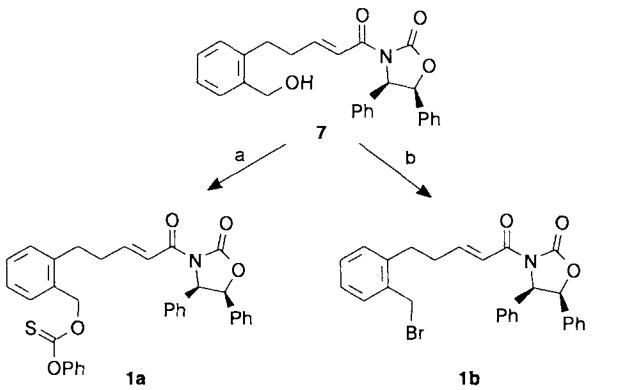

Scheme 3. Synthesis of **1a,b**. a) ClCSOPh, pyridine, CH_2Cl_2, 0 °C, 2 h (65%); b) PBr_3, pyridine, benzene, 50 °C, 30 min, (95%).

nBu_3SnH, and Et_3B (10%) in toluene at 0 °C for 13 h (C).[9] The absolute configuration at the newly formed stereocenter of **2** was determined by comparison with the spectral data (^1H NMR, ^{13}C NMR) of a sample of **2** synthesized from known (*S*)-(−)-methyl 1,2,3,4-tetrahydronaphth-2-yl carboxylate.[10]

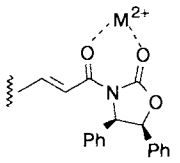

Fig. 1. Possible chelated *syn*-conformation of **1a,b**.

Good yields were obtained, but only modest diastereoselectivity (Table 1, entries 1–3).[11] The reversed diastereoselectivity observed when the cyclization was performed with SmI_2 (Table 1, compare entry 2 with entry 1) suggested that the Sm center was weakly or partially coordinated to the 1,3-dicarbonylic system (Fig. 1). Few stereoselective chelation-controlled radical reactions have been described, so we decided to test this idea with our substrate **1b**, using a Lewis acid with better coordinating properties than SmI_2.[12] Thus, cyclization of **1b** with method A in the presence of one equivalent of $MgBr_2 \cdot Et_2O$ gave an 82:18 mixture of **2** and **3** in fairly good yield (45%).[13] As shown in Table 1, no diastereoselectivity was obtained in the presence of $Ti(OiPr)_4$, in accord with reported results.[12b] When $ZnCl_2$ and $Sn(OTf)_2$ were employed, we obtained almost exclusively the product of Friedel–Crafts alkylation of the solvent (benzene) with **1b**.

Table 1. Radical cyclization of **1a,b**.

No.	Substrate	Method [a]	Lewis acid	**2**:**3** [b]	Yield [%] [c]
1	**1a**	A	none	45:55	75
2	**1b**	B	none	60:40	46
3	**1b**	C	none	50:50	60
4	**1b**	A	$Ti(OiPr)_4$	50:50	60
5	**1b**	A	$MgBr_2 \cdot Et_2O$	82:18	45

[a] For methods A–C see text. [b] The ratio was determined by ^{13}C NMR. [c] Yields of isolated products.

No simple stereochemical rationale for the observed diastereoselectivities (Table 1, compare entries 5 and 2 with entry 1) can be offered.[14] Compared to analogous Michael-like radical additions,[12b,e] which may be rationalized in an straightforward manner, the situation here is more complex. In order to gain insight into the key factors guiding the stereochemical course and possibly to improve the diastereomeric ratio, we decided to model the transition state by using a specifically developed "radical force-field".[15] The modeled transition state is shown schematically in Figure 2. Atom types of the

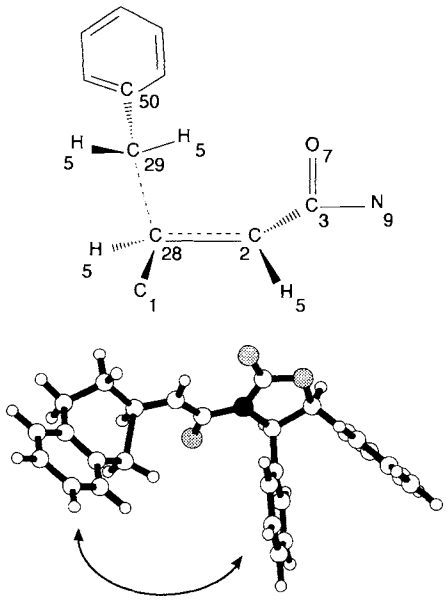

Fig. 2. Top: model of the transition state for the cyclization of **1a,b**. The numbers indicate the atom types used in the force field calculations. Bottom: van der Waals arene–arene attractive interaction in the structures of the transition states **A** and **B**.

MM2 force field were used in the calculations. The Spellmeyer–Houk parameter set for intramolecular alkenyl radical cyclizations proved to be a convenient starting point.[16] In this model the incoming radical center is defined as MM2 type 29 with type 1 (C_{sp^3}-hybridized C atom) atom equivalence.

However, radical cyclization of **1a,b** involved a benzylic radical, which is stiffer and reacts more slowly with alkenes than simple alkyl radicals, because "it resists pyramidalization more strongly than other species".[17] For this reason, we chose to change the atom type equivalence for the radical center from atom type 1 to atom type 2 (C_{sp^2}-hybridized C atom). This means that any undefined parameters corresponding to the radical carbon atom were assigned values equal to analogous parameters for type 2 atoms. The newly developed list of parameters is then as follows: For bond stretching, type 29-28 has bond length $L_0 = 2.14$ Å[18] and 50-29 has $L_0 = 1.39$ Å with the original force constants. For torsional parameters type 29-28-2-3 has the potentials $V_1 = 0$, $V_2 = -25.0$, $V_3 = 0$ by

analogy with Houk's parameters for type 29-28-2-5. Types 28-2-3-7 and 28-2-3-9 have $V_1 = 0$, $V_2 = 6.25$, $V_3 = 0$. This large V_2 term resulted in an overestimation of the rotational barrier around the X-C2-C3-Y bond, but it fits the experimental data better than smaller terms. These modifications generated a force field that modeled a Spellmeyer–Houk-like transition state in which the radical center is pyramidal.

The diastereoselectivity of the radical cyclization of **1a** (Table 1, entry 1) was computed by first calculating all possible minimum-energy transition conformations. We found eight structures. When included in a Boltzmann distribution calculation at a reaction temperature of 80 °C, four have energies within 3 kcal mol^{-1} of the transition state of lowest energy. Prediction of the diastereomeric ratio was in very good agreement with the experimental result (Fig. 3). Careful comparison of

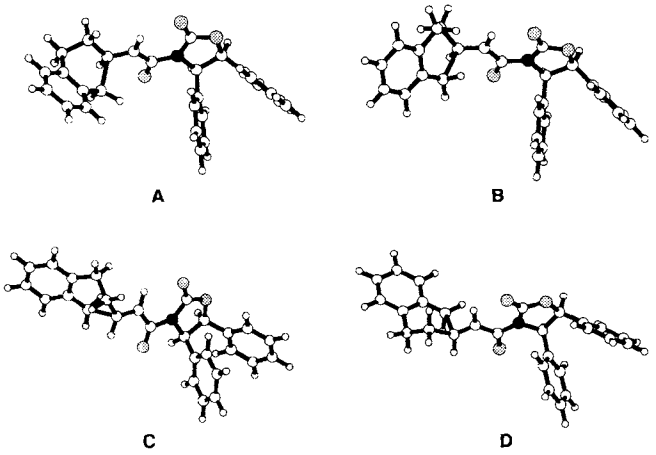

Fig. 3. Four models of the transition structures for the radical cyclization of **1a**. Experimentally determined ratio $R:S = 55:45$. Calculated ratio $R:S = 59:41$. The difference in energy between the structure **A** and **B**, **C**, and **D** are +0.02, +0.22, and +0.24 kcal mol^{-1}, respectively.

individual components of the total energies revealed that the van der Waals potential was the main difference in energy (-0.22 kcal mol^{-1} between **A** and **D**!). Detailed analysis of the van der Waals interactions between various atom groups of **A**–**D** showed an important attractive arene–arene interaction in conformations **A** and **B** (Fig. 2).[19] Therefore, the observed diastereoselectivity can be ascribed to attractive van der Waals interactions, and steric factors seem to play a secondary role.

Next, we computed the diastereoselectivity in radical cyclization of *syn*-1,3-dicarbonylic conformers to mimic the rigid system that is presumably formed in the presence of a Lewis acid (Fig. 1). The relative energies of the four structures obtained indicated that the diastereoisomer **2** was favored, and the diastereomeric ratio (81:19) calculated for **2**:**3** was in good agreement with the experimental data (Table 1, entry 5). Attractive van der Waals interactions between arenes, as for cyclization of **1a**, were again the major intraatomic forces responsible for the observed energy differences (Fig. 4).

In conclusion, according to the performed calculations, oxazolidinone group efficiently controls the *syn*- and *anti*-conformations of the amide linkage (Fig. 3), but the steric shielding of the 4-phenyl substituent plays only a minor role, and the diastereoselectivity is probably rather the result of attractive van der Waals interactions. We are currently conducting additional experiments to identify a suitable chiral auxiliary.

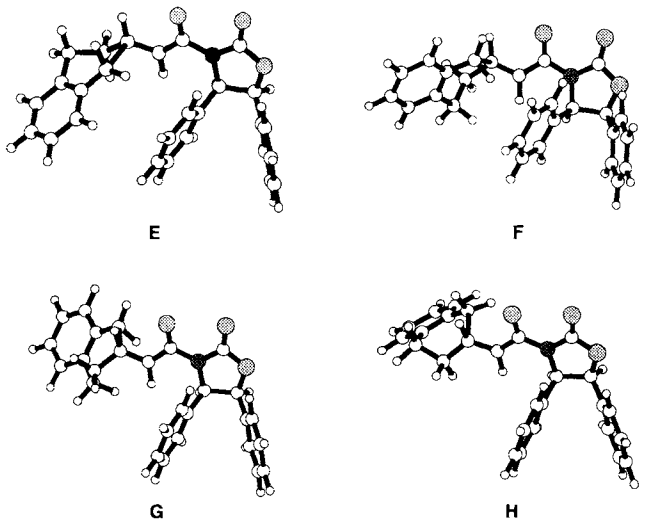

Fig. 4. Models of the transition states for the radical cyclization of *syn*-1,3-dicarbonylic conformer of **1b**. Experimentally determined ratio $R:S = 18:82$. Calculated ratio $R:S = 19:81$. The difference in energy between the structure **E** and **F**, **G**, and **H** are +0.08, +1.03, and +1.12 kcal mol^{-1}, respectively.

Received: May 16, 1995 [Z 7994 IE]
German version: *Angew. Chem.* **1996**, *108*, 575–578

Keywords: asymmetric syntheses · force field calculations · oxazolidinones · radicals · tetralines

[1] D. P. Curran, *Synthesis* **1988**, 417, 489; C. Thebtaranonth, Y. Thebtaranonth, *Tetrahedron* **1990**, *46*, 1385; C. P. Jasperse, D. P. Curran, T. L. Fevig, *Chem. Rev.* **1991**, *91*, 1237.

[2] D. P. Curran, W. Shen, J. Zhang, T. A. Heffner, *J. Am. Chem. Soc.* **1990**, *112*, 6738; N. A. Porter, D. M. Scott, I. J. Rosenstein, B. Giese, A. Veit, H. G. Zeitz, *ibid.* **1991**, *113*, 1791; N. A. Porter, I. J. Rosenstein, R. A. Breyer, J. D. Bruhnke, W.-X. Wu, A. T. McPhail, *ibid.* **1992**, *114*, 7664; B. Giese, U. Hoffmann, M. Roth, A. Veit, C. Wyss, M. Zehnder, H. Zipse, *Tetrahedron Lett.* **1993**, *34*, 2445; A. Veit, R. Lenz, M. E. Seiler, M. Neuburger, M. Zehnder, B. Giese, *Helv. Chim. Acta* **1993**, *76*, 441.

[3] J. G. Stack, D. P. Curran, S. V. Geib, J. Rebek Jr., P. Ballester, *J. Am. Chem. Soc.* **1992**, *114*, 7007.

[4] A. Bianchetti, L. Manara, *Br. J. Pharmacol.* **1990**, *100*, 831; USA Pat. Appl. USP 5130339.

[5] K. Rück, H. Kunz, *Synthesis* **1993**, 1018; E. Nicolas, K. C. Russel, V. J. Hruby, *J. Org. Chem.* **1993**, *58*, 766; E. Nicolas, K. C. Russel, J. Knollenberg, V. J. Hruby, *ibid.* **1993**, *58*, 7565.

[6] All new compounds exhibited satisfactory spectroscopic and analytical data. Yields refer to isolated compounds.

[7] C. Chatgilialoglu, *Acc. Chem. Res.* **1992**, *25*, 188.

[8] D. P. Curran, M. J. Totleben, *J. Am. Chem. Soc.* **1992**, *114*, 6050.

[9] K. Miura, Y. Ichinose, K. Nozaki, K. Fugami, K. Oshima, K. Utimoto, *Bull. Chem. Soc. Jpn.* **1989**, *62*, 143.

[10] A. Schöffs, J. P. Guetté, A. Horeau, *Bull. Soc. Chim. Fr.* **1976**, 1215; (S)-(−)-methyl 1,2,3,4-tetrahydronaphth-2-ylcarboxylate was converted into **2** in five steps: i) $NaBH_4$, MeOH, reflux; ii) PPh_3, Br_2, pyridine; iii) KCN, PTC, H_2O; iv) NaOH 25%, MeOH, reflux then HCl; v) $(CH_3)_3CCOCl$, Et_3N, THF, −78 °C then addition of *N*-lithio-4,5-diphenyloxazolidin-2-one.

[11] Diastereoselectivity was determined by ^{13}C NMR spectroscopy.

[12] a) Y. Guindon, J.-F. Lavallée, M. Llinas-Brunet, G. Horner, J. Rancourt, *J. Am. Chem. Soc.* **1991**, *113*, 9701; b) T. Toru, Y. Watanabe, M. Tsusaka, Y. Ueno, *ibid.* **1993**, *115*, 10464; c) P. Renaud, N. Moufid, L. H. Kuo, D. P. Curran, *J. Org. Chem.* **1994**, *59*, 3547; d) Y. Yamamoto, S. Onuki, M. Yumoto, N. Asao, *J. Am. Chem. Soc.* **1994**, *116*, 421; e) M. Nishida, E. Ueyama, H. Hayashi, Y. Ohtake, Y. Yamaura, E. Yanaginuma, O. Yonemitsu, A. Nishida, N. Kawahara, *J. Am. Chem. Soc.* **1994**, *116*, 6455.

[13] A minor amount of **1c** (10%) was also obtained along with several side products, each in less than 5% yield. No products of imide hydrolysis (namely, 1,2,3,4-tetrahydronaphth-2-yl carboxylic acid and oxazolidinone **H-4**) were detected in the reaction mixture. Quantitative recovery of an unchanged mixture of **2** and **3** (1:1) was obtained by refluxing for 8 h in benzene in the presence of $MgBr_2$, TTMS, and AIBN.

 © VCH Verlagsgesellschaft mbH, D-69451 Weinheim, 1996 0570-0833/96/3505-0537 $ 15.00+.25/0

[14] Since after addition of a phenyl-stabilized radical another stabilized radical formed, it is possible that cyclization is thermodynamically controlled; then the observed diastereoselectivity is the result of the relative stabilities of the cyclized radicals. In order to gain some insight into this reaction mechanism, we conducted a control experiment in which the α-bromo derivative of pure **2** (easily obtained by Evans's procedure, ref. [20]) was treated by method A. The reaction yielded **2** quantitatively, and neither the reduced ring-opened product nor **3** could be detected. This result indicates that cyclization is under kinetic control.
[15] Our model was based upon an MM + force field from HyperChem, Version 4.0 (Hypercube Inc.)
[16] D. C. Spellmeyer, K. N. Houk, *J. Org. Chem.* **1987**, *52*, 959.
[17] K. Héberger, M. Walbiner, H. Fischer, *Angew. Chem.* **1992**, *104*, 651; *Angew. Chem. Int. Ed. Engl.* **1992**, *31*, 635.
[18] H. Zipse, J. He, K. N. Houk, B. Giese, *J. Am. Chem. Soc.* **1991**, *113*, 4324.
[19] C. A. Hunter, *Angew. Chem.* **1993**, *105*, 1653; *Angew. Chem. Int. Ed. Engl.* **1993**, *32*, 1584.
[20] D. A. Evans, T. C. Britton, J. A. Ellman, R. L. Dorow, *J. Am. Chem. Soc.* **1990**, *112*, 4011.

Synthesis and NLO Properties of Polar Self-Assemblies of Molecular Pyramids Covalently Bound on Oxide Surfaces**

Xiaoguang Yang, Duncan McBranch, Basil Swanson, and DeQuan Li*

The construction of artificial supramolecular architectures on surfaces is currently of great interest and represents an important aspect of the chemistry of self-assembly processes,[1] because self-assembly offers rational design and construction of highly ordered mesoscale structures with defined chemical functionalities and physical properties. The preparation of polar molecular superstructures is particularly challenging and is an important endeavor since polar molecular compounds are essential for the development of materials with second-order nonlinear optical (NLO) properties. Several approaches such as the Langmuir–Blodgett technique, liquid crystals, and electric field poled polymers have been reported to generate molecular-based materials with organized polar architecture.[2, 3] However, the orientation in these materials is maintained by weak bonding or steric hindrance, which results in metastable structures with the loss of polar alignment over time. Recent developments in self-assembly and host–guest chemistry offer a novel route to ordered materials through the design and synthesis of new molecular building blocks, templates, and substructures that can be organized into supramolecular assemblies. The synthetic approach here is to fix dipole orientation by structural interlocking of NLO chromophores into cone-shaped "supermolecules", and then to utilize them to build polar self-assembled monolayers. In this communication, we report on the molecular design of calixarene-based NLO molecular "pyramids", their self-assembly on oxide surfaces, and their spectroscopic second-order NLO properties.

Organic NLO chromophores are typically π-conjugated molecules with a D-π-A structure, where D and A are electron donor and acceptor, respectively, and π is a π-conjugated segment or sensitizer. This structural feature has been widely used to attain large values of the molecular second-order nonlinear susceptibility β. By tethering these linear molecular units together through methylene bridges, a calixarene-based NLO chromophoric pyramid is derived.[4] Reinhoudt et al. have recently reported the study of poled neat calixarene films and calixarene-doped polymeric films for second-order nonlinear optics.[5] To achieve an optimum molecular value of β, the orientation of each D-π-A unit should be fixed in nearly the same direction. Therefore, we based our approach on the synthesis of a calix[4]arene with a frozen "cone" conformation by substitution at the lower rim with ethoxyethyl groups (Scheme 1). Similar procedures have been employed for the synthesis of bowl-shaped calixarene-based liquid crystals.[6, 7] The upper rim of the calixarene was then functionalized for the incorporation of pyridyl units (Scheme 1). Compounds **1a** and **1b** were synthesized according to literature procedures.[8, 9] Reduction of the nitrocalixarene **1b** gave the *p*-aminocalix[4]arene **1c** in 79% yield. The condensation of **1c** with 4-pyridylcarboxaldehyde gave the desired cone-shaped chromophoric precursor **2**. The total mass of compound **2** with a protonated pyridyl group (M + H) was determined by matrix-assisted laser desorption/ionization mass spectrometry (LDIMS). All of the compounds were characterized by ^{1}H NMR and IR spectroscopy. The ^{1}H NMR spectrum of **2** in $CDCl_3$ confirmed that it has a rigid cone conformation in which the D-π-A dipolar units are aligned in the same direction, since two doublets (J = 12 Hz) were observed for the equatorial and axial methylene protons.[4] The long ethoxyethyl groups prevent flip-over of the individual NLO units in **2**, and

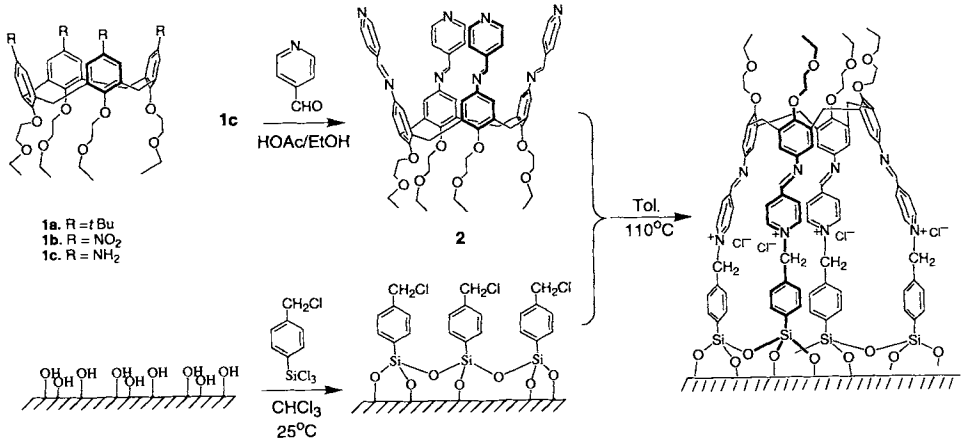

Scheme 1. Synthesis of surface building blocks (calix[4]arene-based molecular pyramids) and strategy for the construction of self-assembled monolayers. Tol = toluene.

[*] Dr. D. Li, Dr. X. Yang, Dr. D. McBranch, Dr. B. Swamson
Chemical Sciences and Technology Division
Los Alamos National Laboratory
Los Alamos, NM 87545 (USA)
Fax: Int. code +(505)665-2992

[**] This research was performed under the auspices of the Department of Energy. The authors acknowledge the support of the Center for Materials Science at Los Alamos National Laboratory and the Laboratory Directed Research and Development program. X. Y. acknowledges the support of a Los Alamos Director's Postdoctoral Fellowship. We thank Mr. Johnny E. Anderson for performing matrix-assisted laser desorption mass spectrometry.

the cone conformation is virtually frozen. Because of the rigid structure and fixed dipole orientation of the molecular building block, it is expected that the self-assembled monolayer (SAM) of **2** will have higher alignment and better thermal and structural stability than SAMs from single chromophoric units.

The construction of covalently bonded self-assembled monolayers of **2** is based on the methodologies reported by Li et al.[10] Silicon wafer and fused silica substrates were treated with the silane coupling agent *p*-chloromethylphenyltrichlorosilane in either toluene or chloroform for 24 h, followed by an incubation of silylated substrate in 1 mM of compound **2** in toluene at 110 °C for three days to quaternize the pyridyl groups on **2** (Scheme 1). Under these conditions, compound **2** is stable and no decomposition was observed. The monolayer was thoroughly cleaned by sonication in $CHCl_3$, followed by vigorous rinsing with $CHCl_3$ to remove any noncovalently bonded surface species. The self-assembled monolayers consisting of the pyramidlike imine derivative of calix[4]stilbazole were characterized by surface-polarized FTIR spectroscopy (Fig. 1a) by using internal attenuated total reflection (ATR) (Ge hemisphere crystal with *p*-polarization at 45° of incidence).[11] The formation of covalent C–N bonds between **2** and the silane anchoring layer was revealed by the presence of pyridinium species ($\tilde{\nu} = 1638\ cm^{-1}$ in Fig. 1b) on

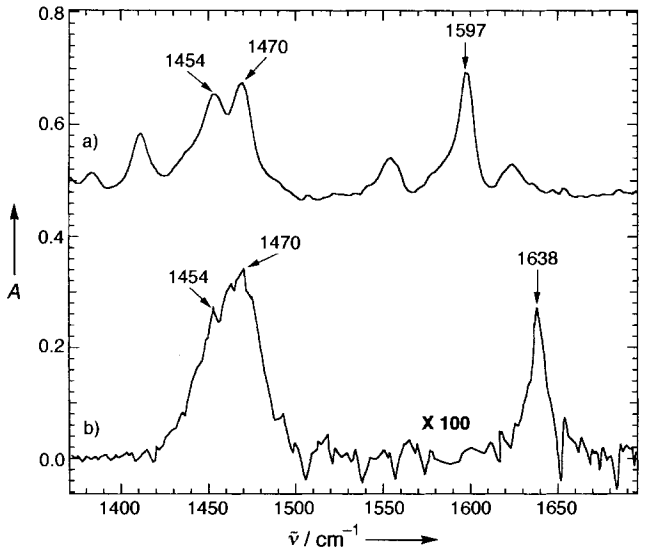

Fig. 1. a) FTIR spectrum of compound **2** (KBr disk). b) Surface FTIR spectrum of a monolayer of **2** on a Si (100) surface, with *p*-polarized light incident at 45°. The baseline was corrected to zero absorbance and offset for display purposes.

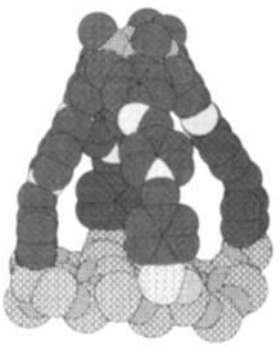

Fig. 2. A space-filling model of a self-assembled, calix[4]arene-based monolayer on an idealized silica surface.

the surface.[12] A space-filling model of **2** on the surface is shown in Figure 2 in which the ethoxyethyl groups are replaced by methyl groups for clarity. The fact that no pyridine mode at 1597 cm^{-1} was observed indicated that the surface quaternization was complete; thus no dangling stilbazole imine structures were left in the self-assembled monolayer (Fig. 1a). The advantages of four-point C–N attachment are that the molecular orientation angle is fixed by the cone configuration and does not depend on the surface coverage. However, the alignment in films of single-poled chromophores relies on steric interplay among chromophores, that is, lower coverage results in poorer alignment.[13b] The average molecular orientation angle ψ is defined as the angle of the dipole moment of the chromophore with respect to the surface normal. The electronic absorption spectrum of the monolayer exhibits a characteristic charge transfer transition at 380 nm, which is typical for pyridinium compounds and confirms that the Schiff base structure is intact; this indicates a successful quaternization reaction. The absorption peak of the monolayer at 380 nm is red-shifted in comparison with the absorption of **2** in solution (350 nm), which is also consistent with the presence of stronger electron-withdrawing groups (pyridinium vs. pyridyl group) in the film. The surface coverage[13] of **2** was found to be 0.92 molecules per nm^2, which corresponds to a densely packed monolayer consisting of calix[4]stilbazole pyramids with bases of about $10 \times 10\ Å^2$, as derived from a space-filling model (Fig. 2).

To study the molecular orientation and the NLO response on the surface, the spectroscopic second harmonic generation (SHG) was measured on the quaternized monolayers of **2**. These measurements were performed by using a mode-locked Ti-sapphire laser in either femtosecond (150 fs autocorrelation width) or picosecond (2 ps width) mode with 100 MHz repetition rate, for fundamental wavelengths between 890 nm and 750 nm. The angular dependence of the SHG for picosecond pulsed excitation has been discussed elsewhere;[11, 14] results obtained by using femtosecond pulses to generate *p*-polarized SHG from both *p*- and *s*-polarized fundamental are shown in Figure 3a for

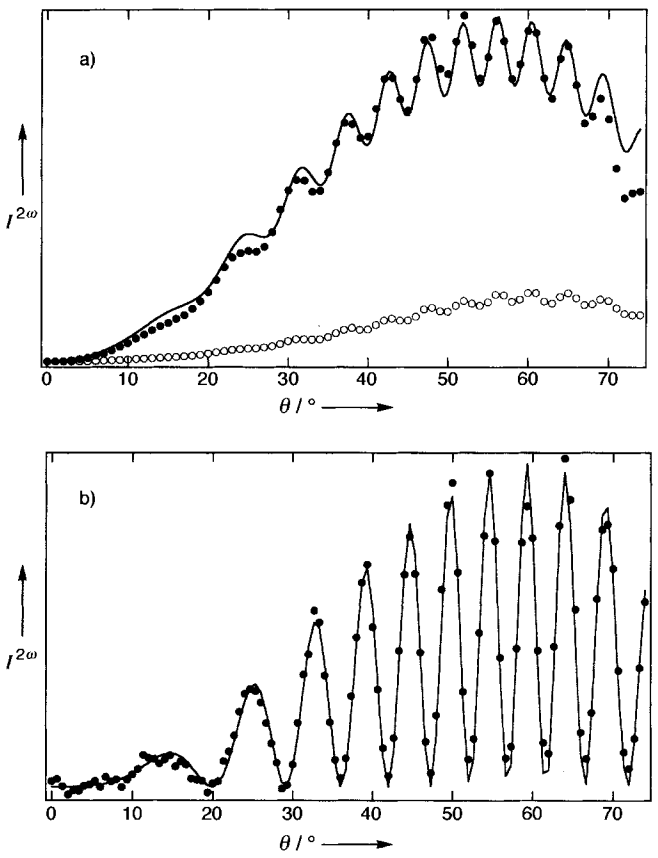

Fig. 3. a) SHG signal versus incident angle for *p*-polarized SHG from both *p*- (dots) and *s*-polarized (circles) fundamental at a wavelength of 862 nm and 150 fs pulsewidth. The solid line is the best theoretical fit to the measured values. b) The *p*-polarized SHG from *p*-polarized fundamental (dots) at a wavelength of 890 nm and 2 ps pulsewidth, and best fit (solid line).

 © VCH Verlagsgesellschaft mbH, D-69451 Weinheim, 1996 0570-0833/96/3505-0539 $ 15.00+.25/0

a fundamental wavelength of 862 nm. An average molecular orientation of $\psi \approx 35 \pm 5°$ was deduced by modeling the angular-dependent SHG response ($n_{film} = 1.7$, n = refractive index); an absolute magnitude of $d_{33} \approx 80\ pm\ V^{-1}$ for monolayers of **2** was deduced by calibrating to reference Y-cut quartz. The solid lines in Figure 3 are best fits to an expression developed in reference [13], modulated by an interference term, which has the same physical origin and angular dependence as the well-known Maker fringes in bulk samples.[15] We performed an experiment at 890 nm in picosecond mode to verify that complete destructive interference is observed in these films (Fig. 3b). This proves that the two films on opposite sides are identical. In Figure 3a, however, the amplitude of the fringes is much smaller, due to the increased spectral width of the femtospecond pulses; complete destructive (or constructive) interference cannot be achieved across the entire pulse spectrum. For the fused silica samples (1 mm) considered here, effects of pulse walk-off due to mismatched group velocities of the fundamental and SH pulses can be neglected.

Figure 4 shows the measured values of d_{33} plotted against the fundamental wavelength for monolayer films of **2** together with

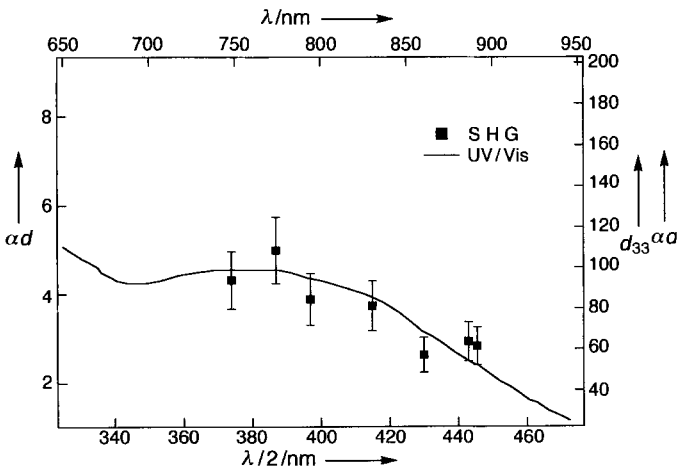

Fig. 4. Second-order nonlinear susceptibility d_{33} in $pm\ V^{-1}$ (solid squares) versus fundamental wavelength (top and right axes) or second harmonic wavelength (bottom and right axes) along with the linear absorption spectrum αd (solid line) vs. wavelength (bottom and left axes) for a self-assembled monolayer of **2**. The lowest two-photon resonance is at 390 nm corresponding to 780 nm in the d_{33} dispersion.

the linear absorption spectrum αd taken from the same sample; α is the linear absorption coefficient and d is the film thickness. The nonlinear optical spectrum closely resembles the linear optical absorption spectrum, which is fairly featureless. The wavelength dependence (fundamental $\lambda = 890-750$ nm; harmonic $\lambda = 445-375$ nm) indicates a gradual increase of d_{33} as the fundamental moves to shorter wavelength, consistent with normal refractive index dispersion in this spectral region approaching the charge transfer resonance at 390 nm. Figure 4 reveals that the charge transfer resonance is fairly broad; the measured value for d_{33} at the longest wavelength (60 $pm\ V^{-1}$ at 890 nm) is still somewhat resonance-enhanced. We find a value of $d_{33} \approx 110\ pm\ V^{-1}$ at $\lambda = 775$ nm, which indicates a nearly twofold two-photon resonant enhancement at the peak of the charge transfer band.

To summarize, we have made a significant step forward in the construction of supramolecular materials by demonstrating the formation of self-assembled monolayers with pyramidlike molecular building blocks. Structural interlocking through the bridging methylene groups among the D-π-A units yields films with extremely large second-order nonlinearities ($d_{33} \approx 60\ pm\ V^{-1}$; $\lambda = 890$ nm), and robust molecular dipole alignment. It is expected that the multilayer films synthesized from pyramidlike molecules would have similarly attractive properties. We are currently pursuing calixarene building blocks in which both rims are functionalized in an attempt to construct multilayer molecular films for nonlinear optical studies.

Experimental Procedure

1c: A suspension of 5,11,17,23-tetranitro-25,26,27,28-tetrakis(2-ethoxyethoxy)-calix[4]arene (**1b**) (0.88 g, 0.98 mmol), hydrazine monohydrate (4 mL), and a catalytic amount of Raney nickel in methanol (50 mL) was heated to reflux for 3 h. The reaction mixture was filtered and the solvent was removed. The residue was dissolved in CH_2Cl_2 and washed with 2 M NaOH (10 mL), H_2O (10 mL), and brine (10 mL) until the aqueous phase was neutral. The organic phase was then dried over $MgSO_4$. After filtration, the solvent was removed to give **1c** (600 mg; yield: 79%). IR (KBr): $\tilde{\nu}$ = 3421, 3345, 3212 (N-H), 2966, 2860 (C-H), 1598, 1464, 1445, 1215, 1114 (CC) cm^{-1}. ^1H NMR (300 MHz, $[D_1]CDCl_3$, 25°C, TMS): δ = 6.04 (s, 8H, Ar*H*), 4.32, 2.99 (d, $^2J(H,H) = 12$ Hz, 8H, $ArCH_2Ar$), 3.97 (t, 8H, OCH_2CH_2), 3.78 (t, 8H, OCH_2CH_2O), 3.49 (q, 8H, OCH_2CH_3), 3.18 (b, 8H, $ArNH_2$), 1.18 (t, 12H, OCH_2CH_3).

2: Compound **1c** (0.2 g, 0.26 mmol) was dissolved in EtOH (10 mL) and two drops of glacial acetic acid and 4-pyridinecarboxyaldehyde (0.11 g, 1.04 mmol) were added. The resulting yellow solution was heated to reflux at 78°C for 20 h. The solvent was then removed in vacuum and the residue was recrystallized from toluene and hexane. Yield: 0.16 g. IR (KBr): $\tilde{\nu}$ = 3027, 2968, 2923, 2860 (C-H), 1595, 1553, 1471, 1452, 1410, 1211, 1116 (CC and NC), 1054, 887, 807 cm^{-1}. ^1H NMR (300 MHz, $[D_1]CDCl_3$, 25°C, TMS): δ = 8.55, 7.49 (AB d, 16H, $^2J(H,H) = 6$ Hz, Py*H*), 8.12 (s, 8H, Ar*H*), 6.71 (s, 4H, C*H*N), 4.63, 3.23 (AB d, $^2J(H,H) = 12$ Hz, 8H, $ArCH_2Ar$), 4.20 (t, 8H, OCH_2CH_2), 3.85 (t, 8H, OCH_2CH_2O), 3.55 (q, 8H, OCH_2CH_3), 1.21 (t, 12H, OCH_2CH_3). Matrix-assisted LDIMS, *m/z* (%): 1129 (100) [$M^+ > H$], 1038 (54) [$M + H -$ pyCH], 947 (24) [$M^+H -$ 2pyCH].

Received: July 13, 1995 [Z 8205 IE]
German version: *Angew. Chem.* **1996**, *108*, 572–575

Keywords: calixarenes · monolayers · NLO materials · nonlinear optics

[1] J.-M. Lehn, *Science* **1993**, *260*, 1762.
[2] G. L. Ashwell, P. D. Jackson, W. A. Crossland, *Nature* **1994**, *368*, 438.
[3] M. Eich, G. C. Bjorklund, D. Y. Yoon, *Polym. Adv. Tech.* **1990**, *1*, 189.
[4] C. D. Gutsche, *Calixarenes*, Royal Society of Chemistry, **1989**.
[5] a) E. Kelderman, L. Derhaeg, G. J. T. Heesink, W. Verboom, J. F. J. Engbersen, N. F. Hulst, A. Persoons, D. N. Reinhoudt, *Angew. Chem.* **1992**, *104*, 1107; *Angew. Chem. Int. Ed. Engl.* **1992**, *31*, 1075; b) E. Kelderman, G. J. T. Heesink, L. Derhaeg, T. Verbiest, P. T. A. Klaase, W. Verboom, J. F. J. Engbersen, N. F. Hulst, K. Clays, A. Persoons, D. N. Reinhoudt, *Adv. Mater.* **1993**, *5*, 925.
[6] B. Xu, T. M. Swager, *J. Am. Chem. Soc.* **1993**, *115*, 1159.
[7] T. Komri, S. Shinkai, *Chem. Lett.* **1993**, 1455.
[8] S. -K. Chang, I. Cho, *J. Chem. Soc. Perkin Trans. 1*, **1986**, 211.
[9] W. Verboom, A. Durie, R. J. M. Egberink, Z. Asfari, D. N. Reinhoudt, *J. Org. Chem.* **1992**, *57*, 1313.
[10] D. Li, M. A. Ratner, T. J. Marks, C. H. Zhang, J. Yang, G. K. Wong, *J. Am. Chem. Soc.* **1990**, *112*, 7389.
[11] D. Li, B. I. Swanson, J. M. Robinson, Mark A. Hoffbauer, *J. Am. Chem. Soc.* **1993**, *115*, 6975.
[12] D. Li, C. T. Buscher, B. I. Swanson, *Chem. Mater.* **1994**, *6*, 803.
[13] a) The surface coverage is determined according $\Gamma_{surf} = \frac{2 A_{surf}}{3 \varepsilon_{soln} \sin^2 \psi}$, where A_{surf} is the absorbance of the monolayer thin film, ε_{soln} is the solution extinction coefficient of the chromophore, and ψ is the molecular orientation angle. See reference [13b] for details; b) C. T. Buscher, D. McBranch, D. Li, *J. Am. Chem. Soc.*, in press.
[14] a) H. E. Katz, G. Scheller, T. M. Putvinski, M. L. Schilling, W. L. Wilson, C. E. D. Chidsey, *Science* **1991**, *254*, 1485; b) T. Zhang, C. Zhang, G. K. Wong, *J. Opt. Soc. Am. B.* **1990**, *7*, 902.
[15] P. D. Maker, R. W. Terhune, M. Nisenoff, C. M. Savage, *Phys. Rev. Lett.* **1962**, *8*, 21.

 © VCH Verlagsgesellschaft mbH, D-69451 Weinheim, 1996 0570-0833/96/3505-0540 $ 15.00+.25/0

Formation of a Porous Zirconium Oxo Phosphate with a High Surface Area by a Surfactant-Assisted Synthesis**

Ulrike Ciesla, Stefan Schacht, Galen D. Stucky, Klaus K. Unger, and Ferdi Schüth*

The synthesis of MCM-41, a silica with a hexagonal arrangement of cylindrical pores, the sizes of which are adjustable from 2 to 10 nm, and related materials[1] has stimulated a considerable amount of interest in this new class of mesoporous materials. Shortly after its synthesis, different mechanisms were developed to explain the formation of this porous material.[2] The mechanism suggested by Monnier et al.[2a] implies the possibility of substituting the silicate with other metal oxides to prepare a wide range of mesostructured oxidic materials. Subsequently, mesostructured surfactant composites of tungsten oxide, antimony oxide, and other metal oxides have been synthesized.[3, 4] However, a major problem of these non-siliceous materials is the removal of the template: It was neither possible to remove the surfactant by conventional methods like calcination or extraction nor by oxygen plasma calcination without destroying the pore structure. An exception is the recently described mesoporous TiO_2, in which the hexagonal pore structure remains stable even after calcination, but the BET surface area is only about 200 $m^2 g^{-1}$.[5] The thermal instability of the mesostructured metal oxide composites is probably due to the different oxo chemistry of the metals in comparison with silicon. For instance, the walls in the tungsten oxide surfactant composite are formed by Keggin ions, and a complete condensation seems improbable.[6] Another reason is probably the existence of several relatively stable oxidation states of the metal centers. Thus, during the calcination, reduction by the surfactant and/or oxidation by air oxygen could occur leading to structural collapse.

We have chosen zirconium as the metal species because it has only one stable oxidation state and exhibits a pronounced polyoxo ion chemistry in aqueous solutions.[7] Here we present two different syntheses leading to zirconia compounds with high surface areas and regular pore systems, in which either zirconium sulfate or zirconium propoxide is used as the Zr source.

The syntheses were carried out in aqueous solution at 373 K with a surfactant—unless otherwise stated hexadecyltrimethylammonium bromide—as template and a zirconium compound. We initially used $Zr(SO_4)_2 \cdot 4H_2O$ as Zr source. Zirconium sulfate forms polymeric $[Zr(OH)_2SO_4OH_2]$ units in water that are capable of crosslinking through sulfate bridges.[8] Charge interactions between the sulfate groups and the positively charged surfactant headgroups lead to the formation of the $ZrO_x(SO_4)_{2-x}$ surfactant composite.

The X-ray diffraction (XRD) pattern of the colorless solid product shows three reflections at very low angles (Fig. 1, trace A). These reflections correspond to d spacings of 4.06 nm, 2.37 nm, and 2.04 nm. Three reflections are usually not sufficient to index a pattern; however, in analogy to MCM-41 these reflections can be indexed as (100), (110), and (200), assuming a hexagonal unit cell. There are no more reflections in the X-ray diffraction pattern at higher angles. Only around 30° (2θ) a broad halo can be distinguished which is typical for amorphous material and which can also be detected in the siliceous MCM-41 material. Whether this halo is due to large amorphous regions or to disorder in the pore walls, as discussed for MCM-41, is at present uncertain. All available structural data suggest that the zirconia compound prepared as described above has a structure that is similar to MCM-41.[9] We believe that the structure possesses a hexagonal arrangement of cylindrical pores that are filled with surfactant. The pore walls consist of $ZrO_x(SO_4)_{2-x}$. The rodlike pores build up a two-dimensional system with no long-range order in the *c* direction—similar to the pure surfactant liquid crystal.

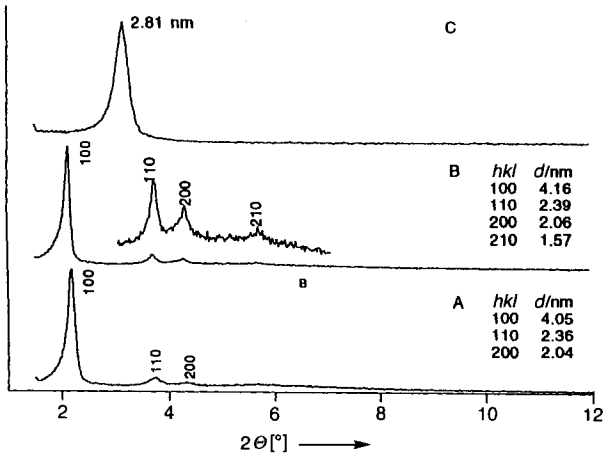

Fig. 1. X-ray diffraction pattern of the zirconium oxide compound synthesized with zirconium sulfate as Zr source. As-synthesized containing surfactant (A), after treatment with phosphoric acid (B), and sample after calcination at 773 K (C).

Thermal treatment of such samples in air at 773 K for five hours leads to a collapse of the ordered pore structure which is noticeable in the loss of intensity or disappearance of the low angle reflections. This may be due to incomplete condensation of the walls because of the very low pH value during the synthesis.

To stabilize the structure the as-synthesized surfactant composite was treated with phosphoric acid solution. During this treatment the uncondensed Zr–OH groups probably react with the phosphate ions, leading to complete crosslinking. The XRD pattern of this sample shows four sharp reflections, which, in comparison to the reflections of the untreated sample, are shifted to lower angles (Fig. 1, trace B and Table 1). This pattern can also be indexed assuming a hexagonal unit cell as (100), (110), (200), and (210) reflections. After calcination (6 h at 773 K) a

Table 1. Summary of the properties of the zirconium oxide synthesized with zirconium sulfate as Zr source.

Surfactant	*d* spacing (100) [a] [nm]	*d* spacing (100) [b] [nm]	BET surface area [$m^2 g^{-1}$]	Pore volume [$cm^3 g^{-1}$]
C_{16}	4.16	2.81	230	0.122
C_{18}	4.62	3.38	320	0.153
C_{20}	4.90	3.86	390	0.218

[a] After H_3PO_4 treatment. [b] After calcination at 773 K.

[*] Prof. Dr. F. Schüth, Dipl.-Chem. U. Ciesla, Dipl.-Chem. S. Schacht
Institut für Anorganische Chemie der Universität
Marie-Curie-Strasse 11, D-60439 Frankfurt (Germany)
Fax: Int. code +(69)798-292-60
Prof. Dr. G. D. Stucky
Chemistry Department, University of California at Santa Barbara (USA)
Prof. Dr. K. K. Unger
Institut für Anorganische und Analytische Chemie der Universität Mainz (Germany)

[**] This work was supported by the Deutsche Forschungsgemeinschaft (SCHU 744/8-1), the Fonds der Chemischen Industrie, the U. S. National Science Foundation (DMR 95-20971), and the NATO Research Grant Programme (CRG.950169). We thank Dr. B. Matthiasch and U. Junges for the chemical analysis and W. Jacobs for recording the IR spectra.

 © VCH Verlagsgesellschaft mbH, D-69451 Weinheim, 1996 0570-0833/96/3505-0541 $ 15.00+.25/0

porous material is obtained that shows only one reflection, which has a d spacing of 2.81 nm (Fig. 1, trace C). The higher order reflections are no longer observed which is probably due to a decrease in the long-range order of the hexagonal pore arrangement. Nevertheless, nitrogen adsorption measurements (see below) show that the pores still exist in the calcined material.

Variation of the chain length of the surfactant changes the dimensions of the system: If trimethyl(octadecyl) or icosyltrimethyl ammonium bromide is used, the corresponding reflections are shifted to lower angles, both for the as-synthesized product and the calcined form (Table 1). Similar results have also been obtained for MCM-41. Moreover, nitrogen adsorption measurements at 77 K show that the surface areas increase with longer surfactant chain length. From nitrogen adsorption analysis, Brunauer–Emmett–Teller (BET) surface areas of 230 $m^2 g^{-1}$ for the sample synthesized with C_{16}-surfactant, 320 $m^2 g^{-1}$ for that with the C_{18}-surfactant, and 390 $m^2 g^{-1}$ for the sample prepared with the C_{20}-surfactant can be calculated. To the best of our knowledge these are the highest surface areas obtained for zirconia. In a recently described surfactant-assisted synthesis for zirconia by M. J. Hudson et al., BET surface areas up to 329 $m^2 g^{-1}$ were obtained.[10] However, these materials do not possess a regular pore system, neither in the as-synthesized nor in the calcined form.

Figure 2 shows the nitrogen isotherms for the samples synthesized with C_{16}-surfactant (Fig. 2A), C_{18}-surfactant (Fig. 2B), and C_{20}-surfactant (Fig. 2C). The difference in the position of

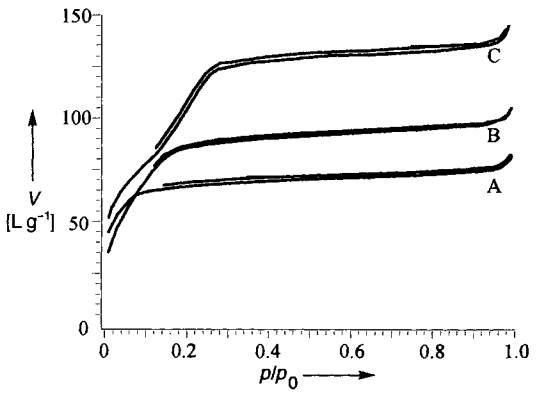

Fig. 2. Nitrogen adsorption isotherms at 77.4 K for calcined and post-treated samples synthesized with hexadecyltrimethylammonium bromide (A), trimethyl(octadecyl)ammonium bromide (B), and icosyltrimethylammonium bromide (C).

the steep increase in the volume adsorbed is apparent from the isotherms. The increase for the sample synthesized with C_{16}-surfactant is at low pressure and thus is an indication for the presence of micropores, whereas the step of the isotherm for the C_{20}-surfactant sample is around a relative pressure of 0.2. N_2 isotherms of this type are typical for pores with sizes between micro- and mesopores. Similar adsorption isotherms have been described for MCM-41 with pore sizes of 2.5 nm;[11] however, in this case the step in the isotherm was obtained at a slightly higher relative pressure of $p/p_0 = 0.3$. Therefore a pore diameter of 2 nm can be estimated for the zirconium compound. However, the pore size determination by nitrogen adsorption measurements is not very precise in this region because BJH analysis (BJH = Barrett–Joyner–Halenda) does not yield reliable data and other algorithms do differ in their results. The relatively small pore diameter seems to be inconsistent with the d spacings determined by X-ray diffraction which would be 3.5 nm for MCM-41. This is probably due to the existence of thicker walls in the zirconia material than in the silicate MCM-41. The structural parameters obtained by analysis of the nitrogen adsorption are in good agreement with the data from X-ray diffraction: An increase of the lattice parameter corresponds to an increase of the pore diameter, the pore volume, and the BET surface area.

The sulfur content of the calcined sample determined by X-ray fluorescence analysis is less than 1 wt%, the phosphorus content about 10 wt%. From this a nominal wall composition of 45 wt% zirconium oxide (based on ZrO_2), 54 wt% zirconium phosphate (based on $Zr_3(PO_4)_4$), and only 0.5–1 wt% zirconium sulfate (based on $Zr(SO_4)_2$) can be calculated.

Starting from zirconium propoxide, the synthesis is carried out analogous to the acidic synthesis of MCM-41 developed by Huo et al,[4] in which strong HCl acidic surfactant solutions are used. In contrast to the MCM-41 synthesis, the addition of $(NH_4)_2SO_4$ is necessary for the formation of the corresponding zirconia surfactant composite. After isolation and drying of the product at 363 K, three reflections were observed in the XRD pattern (4.51 nm, 2.60 nm, and 2.24 nm); however, the intensities of the latter two corresponding to the (110) and (200) reflections are very weak (Fig. 3 trace A). The reason for the broad signal at 6–8° (2θ) is not yet clear.

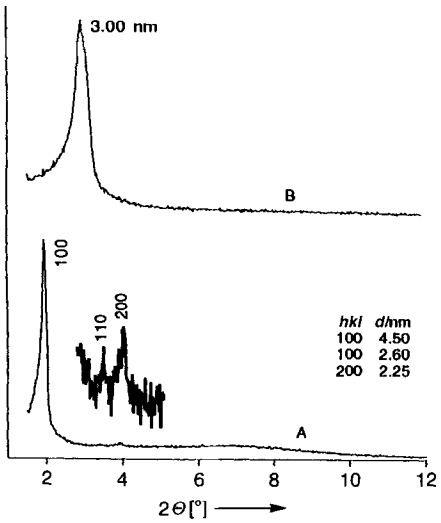

Fig. 3. X-ray diffraction pattern of the zirconium oxide compound synthesized with zirconium propoxide as Zr source; as-synthesized (A) and after calcination at 773 K (B).

In contrast to the material from zirconium sulfate, it is possible to calcine the material from zirconium propoxide at 773 K without the structure collapsing. However, also in this case the (100) reflection is shifted to higher angles (Fig. 3, trace B) and the intensity decreases. The (110) and (200) reflections disappear completely. The nitrogen adsorption isotherm is typical for a microporous material; the BET surface area can be calculated to 280 $m^2 g^{-1}$. The sulfur content of this zirconia after calcination at 500 °C is about 2 wt%; thus, this material essentially consists of zirconium oxide.

The fact that the samples contain sulfur even after calcination is interesting for potential applications. The sulfur remains in the calcined products in form of sulfate groups which could be detected by IR spectroscopy. Zirconias are important as catalysts and catalyst supports. Sulfated zirconias are used as super

 © VCH Verlagsgesellschaft mbH, D-69451 Weinheim, 1996 0570-0833/96/3505-0542 $ 15.00+.25/0

acidic catalysts in isomerization reactions. High surface areas are often the main requirement of such materials. The new zirconias prepared by surfactant-controlled syntheses show interesting structures and could become important for technical applications.

Experimental Procedure

Synthesis with $Zr(SO_4)_2 \cdot 4H_2O$: Hexadecyltrimethylammonium bromide (2.5 g, 6.87 mmol) was dissolved in H_2O (85 g), and $Zr(SO_4)_2 \cdot 4H_2O$ (4.55 g, 0.0128 mol) dissolved in H_2O (15 g) was added. This led to a colorless solid precipitate. The mixture was stirred for 2 h at room temperature and then heated to 100 °C for two days in a closed polypropylene beaker. The precipitate was filtered and dried at 100 °C. The dried precipitate was stirred in a phosphoric acid solution (0.87 M 0.87 M) for 2 h, then filtered and dried again at 100 °C. The colorless product was then calcined at 500 °C for 5 h. S-content after calcination: 1–2 wt%, P-content after H_3PO_4 treatment and calcination: 10 wt%.

Synthesis with $Zr(OC_3H_7)_4$: Hexadecyltrimethylammonium bromide (2.5 g, 6.87 mmol) was dissolved in a solution of water (115 g) and HCl (24.4 g) (37 wt%). After the hydrolysis products had dissolved, $(NH_4)SO_4$ (2.04 g, 0.0155 mol) in water (23 g) was added and the mixture was stirred at room temperature for 1 h. The initially clear solution was then heated at 100 °C for two days. The colorless precipitate was filtered, dried, and calcined at 500 °C for 5 h. S-content after calcination: 1–2 wt%. The as-synthesized samples contain 40–50 wt% surfactant, as detected by thermogravimetric analysis between 200 and 600 °C.

X-ray diffraction: Scintag PADX diffractometer with nitrogen-cooled Ge-detector. $Cu_{K\alpha}$ radiation ($\lambda = 1.54056$ nm), step 0.02°, scan 2.4 s.

Nitrogen adsorption measurements: Micromeritics ASAP 2000, 77.4 K, equilibration time: 60s.

Received: September 6, 1995 [Z83701E]
German version: *Angew. Chem.* 1996, *108*, 597–600

Keywords: mesoporous materials · surfactants · zeolites · zirconium compounds

[1] C. T. Kresge, M. E. Leonowicz, W. J. Roth, J. C. Vartuli, J. S. Beck, *Nature* **1992**, *359*, 710; J. S. Beck, J. C. Vartuli, W. J. Roth, M. E. Leonowicz, C. T. Kresge, K. D. Schmitt, C. T-W. Chu, D. H. Olson, E. W. Sheppard, S. B. McCullen, J. B. Higgins, J. L. Schlenker, *J. Am. Chem. Soc.* **1992**, *114*, 10834.

[2] a) A. Monnier, F. Schüth, Q. Huo, D. Kumar, D. Margolese, R. S. Maxwell, G. D. Stucky, M. Krishnamurty, P. Petroff, A. Firouzi, M. Janicke, B. F. Chmelka, *Science* **1993**, *261*, 1299; b) Q. Huo, D. L. Margolese, U. Ciesla, D. Demuth, P. Feng, T. E. Gier, P. Sieger, A. Firouzi, B. F. Chmelka, F. Schüth, G. D. Stucky, *Chem. Mater.* **1994**, *6*, 1176; c) S. Inagaki, Y. Fukushima, K. Kuroda, *J. Chem. Soc. Chem. Commun.* **1993**, 680; d) C. Y. Cheng, S. L. Burkett, H.-X. Li, M. E. Davis, *Micropor. Mater.* **1993**, *2*, 27.

[3] U. Ciesla, D. Demuth, R. Leon, P. Petroff, G. D. Stucky, K. Unger, F. Schüth, *J. Chem. Soc. Chem. Commun.* **1994**, 1387.

[4] Q. Huo, D. L. Margolese, U. Ciesla, P. Feng, T. E. Gier, P. Sieger, R. Leon, P. M. Petroff, F. Schüth, G. D. Stucky, *Nature* **1994**, *368*, 317.

[5] D. M. Antonelli, J. Y. Ying, *Angew. Chem.* **1995**, *107*, 2202; *Angew. Chem. Int. Ed. Engl.* **1995**, *34*, 2014.

[6] A. Stein, M. Fendorf, T. P. Jarvie, K. T. Mueller, A. J. Benesi, T. E. Mallouk, *Chem. Mater.* **1995**, *7*, 304.

[7] C. J. Brinker, G. W. Scherer, *Sol-Gel Science*, Academic Press, New York, **1990**.

[8] J. Livage, M. Henry, C. Sanchez, *Prog. Solid State Chem.* **1988**, *18*, 259.

[9] The mesoporous silicates could also only be characterized by X-ray diffraction, chemical analysis, and nitrogen adsorption measurements, sometimes assisted by transmission electron microscopy (TEM) and ^{29}Si and ^{27}Al MAS NMR. The reason for this is nature of the material itself: It has no order in the walls and therefore diffraction methods are limited, except for the information about the periodicity of the pore system. TEM analysis gives only selective information about the particle but not about the whole sample. By using TEM we detected hexagonal pore arrangements in the zirconium compounds. However, X-ray diffraction and nitrogen adsorption appear to us to be more important than TEM for the characterization of the structure.

[10] J. A. Knowles, M. J. Hudson, *J. Chem. Soc. Chem. Commun.* **1995**, 2083.

[11] P. Llewellyn, Y. Grillet, F. Schüth, H. Reichert, K. K. Unger, *Micropor. Mater.* **1994**, *3*, 345.

Generation of a Heterocyclic 1,3-Cyclopentanediyl Radical Cation by Chemically Induced Electron Transfer Oxidation and Pulse Radiolysis**

Waldemar Adam,* Thomas Kammel, and Steen Steenken*

Although the chemistry of 1,3-diradicals derived from cyclic azoalkanes and their corresponding strained hydrocarbons (housane ≡ bicyclo[2.1.0]pentane) has been extensively studied,[1] their electron transfer oxidation[2, 3] was investigated only recently. The reaction of 1,3-disubstituted bicyclo[2.1.0]pentanes with catalytic amounts of the oxidant tris(4-bromophenyl)aminium hexachloroantimonate ($TBA^{\cdot+}SbCl_6^-$) led to the corresponding cyclopentenes after 1,2-hydrogen or -alkyl migration in the intermediary 1,3-radical cations [Eq. (a)].[4]

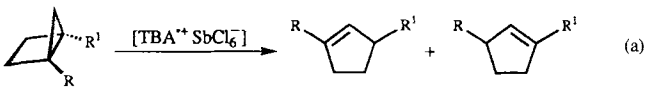

(a)

Since no examples of heterocyclic analogues of these distonic 1,3-radical cations were known, it was of interest, particularly with regard to the reaction mechanism, to investigate the chemical behavior of these systems. Arnold et al.[5] had synthesized the urazole-substituted azoalkanes (urazole = 1,2,4-triazolidine-3,5-dione) by Diels–Alder reaction of 4-phenyl-1,2,4-triazoline-3,5-dione (PTAD) with substituted isopyrazoles. Direct photolysis of these azoalkanes led to the corresponding housanes. The latter are suitable precursors for the desired heterocyclic 1,3-radical cations. By replacing PTAD with 4-methyl-1,2,4-triazoline-3,5-dione (MTAD), the solubility of the radical cation was significantly improved, which allowed a thorough examination of these urazole-annelated azoalkanes and their corresponding housanes.[6] Moreover, it is known from the work of Nelsen et al.[7] that substituted hydrazine derivatives yield stable radical cations upon oxidation at the nitrogen atoms. Consequently, it was of interest to assess the effect of heteroatoms on the mechanism of the chemically induced electron transfer (CET) reaction of these housanes. Herein, we report on the generation and spectroscopic detection of the first urazole-bridged 1,3-radical cation and its unusual chemical transformations.

Direct photolysis of azoalkane **1** (Scheme 1, path a) led exclusively to the corresponding housane **2**.[8] The latter is heat and acid labile and rearranges subsequently to the olefin **3** (Scheme 1, pathways c and d). In contrast to carbocyclic bicyclo[2.1.0]pentane derivatives (heteroatom-free housanes) [Eq. (a)], stoichiometric amounts of tris(4-bromophenyl)-aminium hexachloroantimonate are necessary for the CET reaction of **2** (Scheme 1, path e). The CET product **4**[9] could only

[*] Prof. Dr. W. Adam, Dipl.-Chem. T. Kammel
Institut für Organische Chemie der Universität Würzburg
Am Hubland, D-97074 Würzburg (Germany)
Fax: Int. code +(931) 888-4756
e-mail: adam@chemie.uni-wuerzburg.de
Prof. Dr. S. Steenken
Max-Planck-Institut für Strahlenchemie
Stiftstrasse 34–36, D-45470 Mülheim an der Ruhr (Germany)

[**] This work was supported by the Volkswagenstiftung [Photoelektronentransferchemie (PET) von Azoalkanen und gespannten Kohlenwasserstoffen]. We thank Dipl.-Chem. H. M. Harrer for performing the PM3 calculations and M. Toubartz for experimental assistance with the pulse radiolyses at the Max-Planck-Institut, Mülheim an der Ruhr.

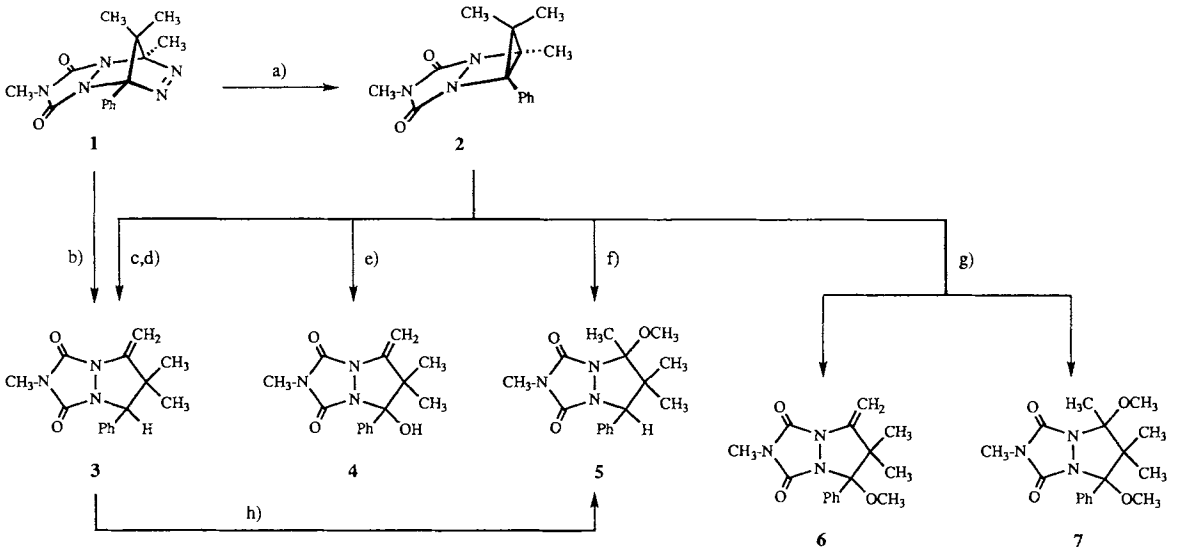

Scheme 1. Synthesis and transformations of the housane **2**. a) Photolysis, 364-nm line of argon ion laser, $CDCl_3$ or CH_2Cl_2 as solvent, $-10\,^{\circ}C$, 100% conversion (^1H NMR); b) thermolysis, 110 °C, 52%; c) thermolysis, 70 °C, 98%; d) CF_3COOH (0.25 molar equiv), $CDCl_3$, 0 °C, 70%; e) $TBA^{\bullet+}SbCl_6^-$ (1 molar equiv), 2,6-di-*tert*-butylpyridine (2 molar equiv), 0 °C, 80%; f) $TBA^{\bullet+}SbCl_6^-$ (1 molar equiv), 2,6-di-*tert*-butylpyridine (2 molar equiv), methanol (200 molar equiv), 81%; g) $TBA^{\bullet+}SbCl_6^-$ (2 molar equiv), 2,6-di-*tert*-butylpyridine (4 molar equiv), methanol (200 molar equiv), **5** (16%) and **6** (19%); when about 10 molar equiv of base were used, **7** was isolated in less than 2% yield, along with **5** in 47% yield; h) CF_3COOH (ca. 0.1 molar equiv) and methanol (ca. 100 molar equiv) gave a 41:59 mixture of **3** and **5** (^1H NMR), while 2,6-di-*tert*-butylpyridinium salt (1.0 molar equiv) and methanol (ca. 20 molar equiv) led to a 13:87 mixture of **3** and **5** (^1H NMR).

be detected and isolated when the oxidation was performed in the presence of a base to avoid acid catalysis. The intermediary dimer of the corresponding monoradical **(2 − H)•** was identified under these conditions (Scheme 2) by NMR spectroscopy.[10] Upon workup and silica gel chromatography, the dimer reacts further to give the hydroxylated monoolefin **4** when oxygen or water are present. When the CET reaction was performed in the presence of methanol as nucleophilic scavenger, the products

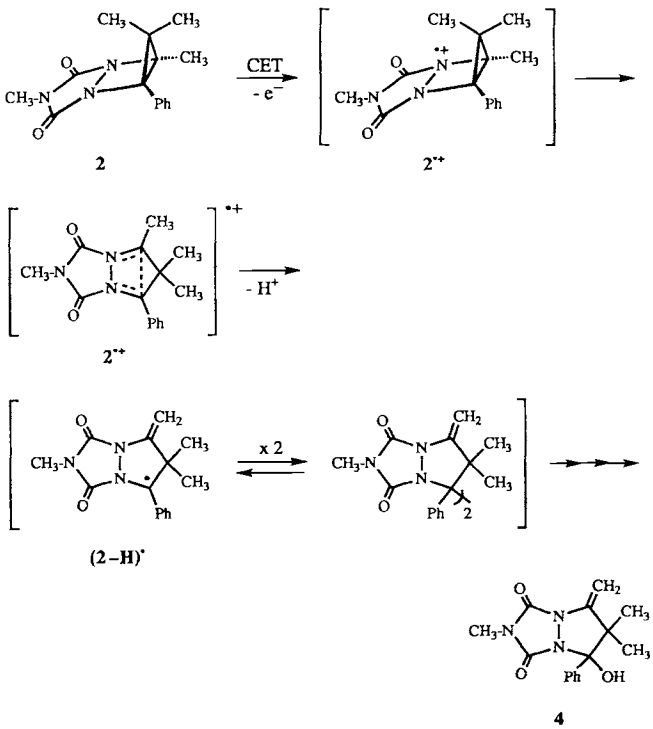

Scheme 2. Mechanism of the oxidation of **2** initiated by chemical electron transfer (CET).

5–7 were observed. When stoichiometric amounts of $TBA^{\bullet+}SbCl_6^-$ were used, the only product was the monoether **5** (Scheme 1, path f). Addition of two equivalents of CET oxidant led to **5–7**, besides spectroscopically unidentified material (Scheme 1, path g). To avoid the acid-catalyzed rearrangement of housane **2** to the monoolefin **3** caused by the protons released during the CET reaction, the oxidations were performed in the presence of an excess of the base 2,6-di-*tert*-butylpyridine.[11] When a large excess of base was used, the double-trapping product **7** was observed, which establishes the double oxidation of the housane **2** unequivocally.

Comparison of the results for the urazole-bridged systems (Scheme 1) with those for the corresponding carbocylic bicyclo[2.1.0]pentenes [Eq. (a)][4] clearly indicates the significant influence of the heteroatom on the chemistry of distonic 1,3-radical cations. In the first place, the CET reaction does not proceed catalytically,[4] but stoichiometric amounts are necessary, as observed by Nelsen et al.[7] for substituted hydrazine derivatives. In addition, the 1,3-radical cation is not stabilized by rearrangement to the olefinic radical cation followed by electron back transfer. Instead, deprotonation leads to the formation of an exocyclic double bond, a process which Shono et al.[12] have observed upon anodic oxidation of substituted cyclopropane derivatives. Presumably, the carbonyl function in the urazole moiety facilitates deprotonation, because the proton is directly released to the carbonyl group, a favorable process for which a six-membered transition state applies. A control experiment established the conversion of **3** to the monoether **5** (Scheme 1, path h); thus, the latter trapping product is formed from the olefin **3**. In addition, **2** is so sensitive towards acids that even the 2,6-di-*tert*-butylpyridinium ion rearranges it to the monoolefin **3**. The ene-ether product **6** is formed by oxidation of the monoradical **(2 − H)•** to the corresponding cation, which subsequently is trapped by methanol. The ene-ether **6** oxidation product as well as the bis-ether **7** double-trapping product were only observed when two molar equivalents of $TBA^{\bullet+}SbCl_6^-$ were added.

In addition, semiempirical PM3 calculations were performed to assess whether the initial ionization occurs from the hy-

 © VCH Verlagsgesellschaft mbH, D-69451 Weinheim, 1996 0570-0833/96/3505-0544 $ 15.00+.25/0

drazine moiety or the cyclopropane central bond. The results clearly establish that especially in the puckered conformation most of the positive charge is located at the two nitrogen atoms of the hydrazine bond in the urazole-bridged 1,3-radical cation $\mathbf{2}^{\bullet+}$. As a consequence, the initially formed radical cation is generated by abstraction of an electron from one of these nitrogen atoms (Scheme 2).[13] After relaxation to the planar conformation, most of the charge is relocated at the two carbon atoms C-1 and C-3. Compared with the carbocyclic derivatives,[4] the charge is delocalized to a larger extent in the radical cation $\mathbf{2}^{\bullet+}$ and thereby the urazole moiety suppresses the usually observed 1,2-methyl migration.

The formation of the radical cation $\mathbf{2}^{\bullet+}$ was spectroscopically established by time-resolved pulse radiolysis of azoalkane **1** in *n*-butyl chloride as solvent. First, a transient with maxima at ca. 280 and 330 nm was observed, which was relatively unreactive toward molecular oxygen. This species transformed with a rate constant $k = 4 \times 10^5\,s^{-1}$ into a second intermediate having a narrow absorption band with $\lambda_{max} = 325$ nm, which reacted efficiently with oxygen. The initially formed transient most probably corresponds to the radical cation $\mathbf{2}^{\bullet+}$, which upon deprotonation yields the radical $(\mathbf{2} - \mathrm{H})^{\bullet}$. This interpretation was confirmed by comparison with pulse radiolyses of analogous systems.[14]

In summary, the present novel results establish that the heterocyclic 1,3-radical cation $\mathbf{2}^{\bullet+}$ can conveniently be generated by chemical oxidation of the corresponding housane **2** by using stoichiometric amounts of tris(4-bromphenyl)aminium hexachloroantimonate. Instead of 1,2-alkyl migration, as is usually observed for carbocyclic 1,3-radical cations,[4] the analogous urazole-bridged derivative $\mathbf{2}^{\bullet+}$ reacts further through deprotonation by transferring the proton to the well-located carbonyl function. This unprecedented stabilization process of 1,3-radical cations enhances our knowledge about such short-lived, highly reactive intermediates.

Received: July 19, 1995 [Z 8228 IE]
German version: *Angew. Chem.* **1996**, *108*, 582–584

Keywords: electron transfer · radical cations · reactive intermediates

[1] a) W. Adam, O. DeLucchi, *Angew. Chem.* **1980**, *92*, 815; *Angew. Chem. Int. Ed. Engl.* **1980**, *29*, 762; b) P. S. Engel, *Chem. Rev.* **1980**, *80*, 99.

[2] a) T. A. Zona, J. L. Goodman, *J. Am. Chem. Soc.* **1993**, *115*, 4925; b) C. J. Rhodes, H. Agirbas, M. Lindgren, O. N. Antzutkin, *J. Chem. Soc. Perkin Trans. 2* **1993**, 2135; c) P. S. Engel, D. M. Robertson, J. N. Scholz, H. J. Shine, *J. Org. Chem.* **1992**, *57*, 6178; d) T. A. Zona, J. L. Goodman, *Tetrahedron Lett.* **1992**, *33*, 6093; e) T. A. Karatsu, H. Hotta, A. Kitamura, *J. Chem. Soc. Chem. Commun.* **1991**, 1451; f) P. S. Engel, A. K. M. M. Hoque, J. N. Scholz, H. J. Shine, K. H. Whitmire, *J. Am. Chem. Soc.* **1988**, *110*, 7880; g) F. Williams, Q.-X. Guo, P. A. Petillo, S. F. Nelsen, *ibid.* **1988**, *110*, 7887; h) F. Gerson, X.-Z. Qin, *Helv. Chim. Acta* **1988**, *71*, 1498; i) S. C. Blackstock, J. K. Kochi, *J. Am. Chem. Soc.* **1987**, *109*, 2484; j) P. S. Engel, A. Kitamura, D. E. Keys, *J. Org. Chem.* **1987**, *52*, 5015; k) *J. Am. Chem. Soc.* **1985**, *107*, 4964; l) H. Abdallah, R. Grée, R. Carrié, *Can. J. Chem.* **1985**, *63*, 3031; m) J. Martelli, R. Grée, *J. Chem. Soc. Chem. Commun.* **1980**, 355.

[3] a) W. Adam, C. Sahin, J. Sendelbach, H. Walter, G.-F. Chen, F. Williams, *J. Am. Chem. Soc.* **1994**, *116*, 2576; b) W. Adam, J. Sendelbach, *J. Org. Chem.* **1993**, *58*, 5316; c) *ibid.* **1993**, *58*, 5310; d) W. Adam, U. Denninger, R. Finzel, F. Kita, H. Platsch, H. Walter, G. Zang, *J. Am. Chem. Soc.* **1992**, *114*, 5027; e) W. Adam, H. Walter, G.-F. Chen, F. Williams, *ibid.* **1992**, *114*, 3007; f) W. Adam, M. Dörr, *ibid.* **1987**, *109*, 1570.

[4] W. Adam, C. Sahin, *Tetrahedron Lett.* **1994**, *35*, 9027.

[5] a) A. B. Evnin, D. R. Arnold, *J. Am. Chem. Soc.* **1968**, *90*, 5330; b) D. R. Arnold, A. B. Evnin, P. H. Kasai, *ibid.* **1969**, *91*, 784; c) A. B. Evnin, D. R. Arnold, L. A. Karnischky, E. Strom, *ibid.* **1970**, *92*, 6218.

[6] W. Adam, K. Goller, T. Kammel, K. Peters, *J. Org. Chem.* **1995**, *60*, 308.

[7] a) S. F. Nelsen, Y. Kim, F. A. Neugebauer, C. Krieger, R. Siegel, M. Kaftory, *J. Org. Chem.* **1991**, *56*, 1045; b) S. F. Nelsen, Y. Wang, *ibid.* **1994**, *59*, 3082; c) X.-Z. Qin, T. C. Pentecost, J. T. Wang, F. Williams, *J. Chem. Soc. Chem. Commun.* **1987**, 450.

[8] Spectroscopic data for housane **2**: ^{1}H NMR ($CDCl_3$, 200 MHz): $\delta = 0.87$ (s, 3H), 1.57 (s, 3H), 1.78 (s, 3H), 3.08 (s, 3H), 7.27–7.34 (m, 2H), 7.38–7.44 (m, 3H); ^{13}C NMR ($CDCl_3$, 50 MHz): $\delta = 8.9$ (q), 13.3 (q), 18.9 (q), 26.2 (q), 30.4 (s), 63.1 (s), 65.4 (s), 127.9 (s), 128.7, 129.7, 130.3 (d), 160.9 (s), 161.9 (s); MS (70 eV): *m/z* (%) = 272 [$M+1^+$] (5), 271 [M^+] (34), 256 [$M^+ - CH_3$] (18), 199 (22), 184 (8), 143 (23), 132 (7), 105 (100), 77 (31), 51 (6), 41 (6); IR (CCl_4): $\tilde{\nu} = 2950$, 2930, 1780, 1720, 1435, 1385, 1265, 1175, 1075, 1030, 695 cm^{-1}; UV (CH_2Cl_2): λ_{max} (lg ε) = 228 nm (3.729).

[9] Spectroscopic data for the CET product **4**: ^{1}H NMR ($CDCl_3$, 200 MHz): $\delta = 0.88$ (s, 3H), 1.27 (s, 3H), 3.02 (s, 3H), 4.13 (s, 1H, OH), 4.49 (d, $J_{gem.} = 2.10$ Hz, 1H), 5.34 (d, $J_{gem.} = 2.10$ Hz, 1H), 7.39–7.44 (m, 3H), 7.50–7.60 (m, 2H); ^{13}C NMR ($CDCl_3$, 50 MHz): $\delta = 17.5$ (q), 25.3 (q), 27.6 (q), 53.5 (q), 87.3 (t), 96.3 (s), 127.0, 128.2, 129.4 (d), 135.8 (s), 145.9 (s), 150.0 (s), 154.5 (s); MS (70 eV): *m/z* (%) = 287 [M^+] (6), 269 [$M^+ - H_2O$] (1), 106 (8), 105 [Ph_2CO^+] (100), 77 [$C_6H_5^+$] (27), 70 (3), 51 (11); IR (KBr): $\tilde{\nu} = 3320$, 2920, 2870, 1740, 1670, 1620, 1430, 1370, 1340, 1155, 1050, 835, 755 cm^{-1}; $C_{15}H_{17}N_3O_3$ (287.3): calc. C 62.70, H 5.96, N 14.62; obs. C 62.90, H 5.72, N 14.38.

[10] Spectroscopic data for the dimer: ^{1}H NMR ($CDCl_3$, 200 MHz): $\delta = 0.96$ (s, 6H), 1.44 (s, 6H), 3.12 (s, 6H), 4.58 (d, $J_{gem.} = 2.30$ Hz, 2H), 5.43 (d, $J_{gem.} = 2.30$ Hz, 2H), 7.05–7.45 (m, 10H); ^{13}C NMR ($CDCl_3$, 50 MHz): $\delta = 19.6$ (q), 25.5 (q), 27.1 (q), 57.4 (q), 88.1 (t), 97.6 (s), 127.9, 128.0, 129.7 (d), 135.6 (s) 144.3 (s), 149.4 (s), 152.9 (s).

[11] During the CET reaction, the 2,6-di-*tert*-butylpyridinium hexachloroantimonate ($C_{13}H_{22}N^+SbCl_6^-$) was observed and isolated.

[12] a) T. Shono, Y Matsumara, *Bull. Chem. Soc. Jpn.*, **1975**, *48*, 2861; b) M. Klehr, H. J. Schäfer, *Angew. Chem.* **1975**, *87*, 173; *Angew. Chem. Int. Ed. Engl.* **1975**, *24*, 247.

[13] W. Adam, T. Kammel, unpublished results. Cyclic voltammetry of analogous substrates established, as expected, irreversible oxidation for the urazole-bridged systems. Comparison with the corresponding carbocyclic derivatives revealed that the oxidation occurs at one of the nitrogen atoms of the urazole moiety.

[14] In addition, laser flash photolyses of the azoalkane **1** (excitation wavelengths 248 und 408 nm) confirmed that the transients observed in the pulse radiolysis do not correspond to 1,3-diradical intermediates.

Sibyllimycine, 5,6,7,8-Tetrahydro-3-methyl-8-oxo-4-azaindolizidine, a Novel Metabolite from *Thermoactinomyces* sp.**

Doris Hafenbradl, Martin Keller,* Karl O. Stetter, Peter Hammann,* Frank Hoyer, and Herbert Kogler

For a few years it has been known that hot, volcanic springs contain thermophilic and hyperthermophilic organisms.[1] These organisms have been studied intensively owing to possible applications in biotechnology, for example as producers of heat-stable enzymes. However, it is not known whether thermophilic or hyperthermophilic organisms are able to produce novel natural products and active compounds. Therefore we tried to collect and selectively enrich potential secondary metabolite producing organisms such as organisms from the family *Bacillaceae* from hot springs. Several thermophilic actinomyces were isolated from hydrothermal sources for the first time, for example from a 60 °C hot spring at Lake Tanganyika in Cape Banza (Africa). Previously *Thermoactinomyces* were isolated only from self-heating biotopes like hay, compost, and soil.[2] *Thermoactinomyces* belong to the family of the *Bacil-*

[*] Dr. M. Keller, Dipl.-Biol. D. Hafenbradl, Prof. Dr. K. O. Stetter
Lehrstuhl für Mikrobiologie der Universität
Universitätsstrasse 31, D-93053 Regensburg (Germany)
Fax: Int. code +(941)943-2403
e-mail: martin.keller@biologie.uni-regensburg.de
Priv.-Doz. Dr. P. Hammann, Dr. H. Kogler
Allgemeine Pharma Forschung, Hoechst AG (Germany)
Dipl.-Ing. F. Hoyer
Tierärztliche Hochschule Hannover (Germany)

[**] This work was supported by the Fonds der Chemischen Industrie (grant to K. O. S.).

 © VCH Verlagsgesellschaft mbH, D-69451 Weinheim, 1996 0570-0833/96/3505-0545 $ 15.00+.25/0

laceae and are assigned to the *Actinomycetales* based on their morphological similarities.[3] So far within the genus *Thermoactinomyces* six different species have been described.[2] Only *Thermoactinomyces vulgaris* is known give rise to two natural products, namely 5-deoxyguanosine[4] and thermorubine.[5]

To test whether the new isolates are able to produce novel natural products we subjected them to chemical screening and compared the results.[6] The isolate CB21 from a hot spring at Lake Tanganyika attracted our attention because of its pattern of metabolites. For further characterization the new isolate CB21 was cultivated in a 50 L fermenter at 60 °C and was harvested in fractions over five days. After the mycel was removed, the culture filtrate was concentrated with Amberlite XAD-16. Among the diverse metabolites we were particularly interested in a compound that appeared at the third fermentation day and stained yellow with anisaldehyde (solvent system $CHCl_3$/MeOH 30/1, $R_f = 0.5$, HPTLC plates, Merck). This compound was obtained from the concentrated supernatant by flash chromatography (silica gel, $CHCl_3$). Final chromatography on Sephadex LH-20 with acetone as eluent yielded in 4 mg of a colorless powder.

The molecular formula $C_8H_{10}N_2O$ was determined unequivocally by quantitative elemental analysis (C 64.9, H 6.7, N 18.5%) and a mass spectrum (m/z [$(M+H)$]$^+$ = 151.08). The spectroscopic data (see Table 1) was interpreted systematically by stepwise exclusion of possible structures.[7–9] Structure **1** was supported by the assigned ^1H-^{13}C through-space coupling constants (Fig. 1); however, application of statistically reliable criteria for interpretation of spectroscopic data did not lead to an unequivocal structure assignment.[9] Therefore the proposed structure **1** was verified by synthesis.

4-Methylimidazole (**2**) was treated with acetanhydride for 1.5 h at 100 °C,[10–12] then alkylated with 4-bromobutyronitrile (Scheme 1, Table 2). The two *N*-alkyl compounds **3a** and **3b** were purified by chromatography on silica gel (solvent system $CHCl_3$/MeOH 25/1). Deprotonation of **3b** with two equivalents of BuLi led to ring closure. Sibyllimycine (**1**) was obtained by hydrolysis of the imine with 4 M HCl. The physical properties of the synthetic compound **1** are identical to those of the compound isolated from the culture ($\Delta\delta(^{13}C) < 0.5$ ppm). After confirmation of the cyclic structure by synthesis, the position of the methyl group was secured by NOE experiments (Table 1).

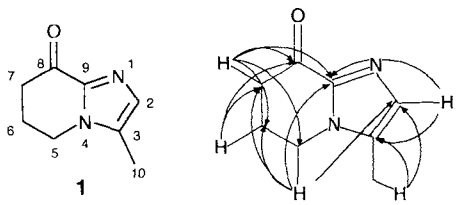

Fig. 1. Structural formula of sibyllimycine (**1**) and ^1H-^{13}C through-space couplings.

Table 2. Selected physical and spectroscopic data for compounds **1**, **3a**, and **3b**.

1: colorless crystals; m.p. 122–123 °C (toluene); $R_f = 0.20$ ($CHCl_3$/MeOH 20/1); IR (KBr): $\tilde{\nu} = 1679\ cm^{-1}$ (C=O); UV/Vis: λ_{max} ($CHCl_3$) = 297 (24481), 240 nm (9379); C,H,N analysis calcd for $C_8H_{10}N_2O$ (150.18): C 64.98, H 6.71, N 18.65; found: C 64.85, H 6.70, N 18.52 [b]

3a: colorless oil; $R_f = 0.16$ (silica gel, $CHCl_3$/MeOH 20/1); IR (neat): $\tilde{\nu} = 2247\ cm^{-1}$ (CN); ^1H NMR ($CDCl_3$): $\delta = 2.09$ (dddd, $J = 6.7$ Hz, 2H; 2′-H), 2.21 (d, $J = 1$ Hz, 3H; CH_3), 2.31 (dd, $J = 6.8$ Hz, 2H; 3′-H), 4.04 (dd, $J = 6.7$ Hz, 2H; 1′-H), 6.65 (d, $J = 1$ Hz, 1H; 5-H), 7.38 (br.s, 1H; 2-H); ^{13}C NMR: $\delta = 13.29$ (CH_3), 13.95 (C-3′), 26.37 (C-2′), 44.49 (C-1′), 114.77 (C-5), 118.16 (CN), 135.96 (C-2), 138.68 (C-4)

3b: colorless oil; $R_f = 0.13$ ($CHCl_3$/MeOH 20/1); IR (neat): $\tilde{\nu} = 2246\ cm^{-1}$ (CN); ^1H NMR (300 MHz, $CDCl_3$): $\delta = 2.09$ (dddd, $J = 6.7$ Hz, 2H; 2′-H), 2.22 (d, $J = 1$ Hz, 3H; CH_3), 2.36 (dd, $J = 6.7$ Hz, 2H; 3′-H), 4.02 (dd, $J = 6.7$ Hz, 2H; 1′-H), 6.76 (d, $J = 1$ Hz, 1H; 4-H), 7.43 (br.s, 1H; 2-H); ^{13}C NMR: $\delta = 8.81$ (CH_3), 13.95 (C-3′), 26.02 (C-2′), 42.34 (C-1′), 118.16 (CN), 126.69 (C-5), 126.91 (C-4), 136.39 (C-2)

[a] The ^1H NMR spectra were recorded at 300 MHz, the ^{13}C NMR spectra at 300 MHz. [b] The ^1H and ^{13}C NMR data for **1** are in Table 1.

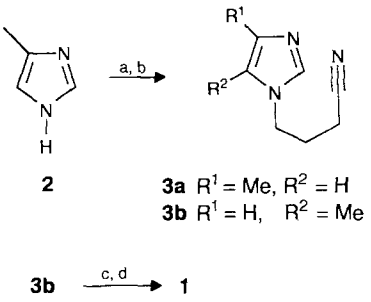

Scheme 1. Synthesis of 5,6,7,8-tetrahydro-3-methyl-8-oxo-4-azaindolizidine (**1**). Reagents and reaction conditions: a) 1.0 equiv **2**, 1.1 equiv Ac_2O, PhH, 100 °C, 1.5 h. b) 1.2 equiv $Br(CH_2)_3CN$, 160 °C, 16 h; then H_2O, room temperature (RT), 1 h, **3a**: 4%, **3b**: 52%. c) 2.0 equiv *n*BuLi, *n*-hexane, THF, −50 °C, then RT, 18 h; d) 4 M HCl, **1**: 92%. For important physical data for **1** and **3** see Tables 1 and 2.

Sibyllimycine (**1**) has no known structural analogues from natural sources. Currently we are examining its pharmacological activity by extensive biological screening. The pattern of

Table 1. NMR spectroscopic data for sibyllimycine (**1**).

	1 ($c = 4$ mg mL^{-1})	Synthetic **1** ($c = 15$ mg mL^{-1})						
^{13}C NMR:				$^1J_{C,H}$/Hz			$^nJ_{C,H}$/Hz (partner)	
C-8	187.33	187.33		–	6.0 (7-H)		6.5 (6-H)	
C-9	143.13	143.66		–	10.1 (2-H)		2.2 (5-H_2)	1.0 (7-H_2)
C-2	130.38	130.86		189.6 (2-H)	4.1 (10-H_3)		0.9 (5-H_2)	
C-3	133.34	133.89		–	6.9 (10-H_3)		14.8 (2-H)	
C-5	43.66	44.18		143.1 (5-H_2)	3.2 (6-H_2)		5.3 (7-H_2)	
C-7	37.51	38.03		129.9 (7-H_2)	3.8 (6-H_2)		5.2 (5-H_2)	
C-6	24.03	24.55		131.6 (6-H_2)	3.8 (5-H_2)		3.9 (7-H_2)	
C-10	9.18	9.68		129.0 (10-H_3)				
^1H NMR:			multiplicity	$^nJ_{H,H}$/Hz in $CDCl_3$ (partner)			NOE/% (partner)	
2-H	7.037	7.04	sext	0.8 (5-H_2)	0.8 (10-H_3)		4 (10-H_3)	
5-H_2	4.142	4.14	t	5.8 (6-H_2)	0.4 (10-H_3)	0.8 (2-H_2)	1 (7-H_2)	3 (10-H_3)
7-H_2	2.689	2.692	dd	5.9 (6-H)	6.5 (6-H′)		1 (5-H_2)	
6-H_2	2.349	2.344	ddt	5.8 (5-H_2)	5.9 (7-H)	6.5 (7-H′)		
10-H_3	2.300	2.304	dt	0.8 (2-H)	0.4 (5-H_2)		4 (2-H)	3 (5-H_2)

 © VCH Verlagsgesellschaft mbH, D-69451 Weinheim, 1996 0570-0833/96/3505-0546 $ 15.00+.25/0

metabolites of the new isolates established by chemical screening gives good evidence for further novel compounds. The screening of organisms from extreme biotopes previously not closely examined seems to be a successful approach to finding new potentially active metabolites.

Received: June 30, 1995
Revised version: December 15, 1995 [Z8151IE]
German version: *Angew. Chem.* **1996**, *108*, 589–591

Keywords: heterocycles · natural products · sibyllimycine · thermophilic bacteria

[1] K. O. Stetter in *Frontiers of Life* (Eds.: J. Tran Than Van, K. Tran Than Van, J. C. Mounolou, J. Schneider, C. McKay), Editions Frontières, Gif-sur-Yvette, Frankreich, **1992**, pp. 195–219.
[2] J. Lacey in *Bergey's Manual of Systematics* (Eds.: S. M. E. Williams, S. T. Holt), Williams and Wilkins, Baltimore, **1981**, pp. 2573–2585.
[3] E. Stackebrandt, C. R. Woese, *Curr. Microbiol.* **1981**, *5*, 197–202.
[4] B. G. Isaac, S. W. Ayer, L. J. Letendre, R. J. Stonard, *J. Antibiot.* **1991**, *44*, 729–732.
[5] F. Aragozzini, R. Craveri, E. Maconi, G. S. Ricci, C. Scolastico, *J. Chem. Soc.* **1988**, *17*, 1865–1867.
[6] S. Grabley, J. Wink, A. Zeeck in *Jahrbuch Biotechnologie* (Ed.: P. Präve), Hanser, München, **1990**, pp. 379–390.
[7] L. M. Masinter, N. S. Sridharan, J. Lederberg, D. H. Smith, *J. Am. Chem. Soc.* **1974**, *96*, 7702–7723.
[8] I. P. Bangov, S. Simova, D. Cabrol-Bas, I. Laude, *J. Chem. Inf. Comput. Sci.* **1994**, *34*, 546–557.
[9] We removed a description of our deduction of the proposed structural from this communication on the request of a referee, who considered the structure to be obvious from the spectoscopic data. Our novel approach to this structure elucidation will be published separately.
[10] C. Kashima, Y. Harada, A. Hosomi, *Heterocycles* **1993**, *35*, 433–440.
[11] U. Gebert, B. von Kerékjárto, *Liebigs Ann. Chem.* **1974**, 644–654.
[12] a) F. Wingler, *Methoden Org. Chem. (Houben-Weyl) 4th ed. 1952–*, Vol. VII/2a, **1973**, p. 618; b) U. Schöllkopf, *ibid.*, Vol. XIII/1, **1970**, p. 188.

Phosphaalkyne Hydrometalation: Synthesis of $[RuCl(P{=}CH\,tBu)(CO)(PPh_3)_2]$**

Robin B. Bedford, Anthony F. Hill,* and Cameron Jones*

The notional similarity between alkynes (RC≡CR) and phosphaalkynes (P≡CR) raises the question of metal-mediated transformations of the reactive P≡C linkage.[1] To date, the majority of such studies have focused on oligomerizations, effected by organometallic substrates which bear essentially "innocent" co-ligands.[2, 3] We have previously described the interaction of P≡C*t*Bu (**1**) with a transition metal alkylidyne which proceeded by a metathesis of Mo≡C and P≡C triple bonds.[4] Subsequently it was shown that **1** could also be induced to couple with the metal–carbon multiple bonds in alkylidene[5] and vinylidene complexes.[6] Given that one of the most fundamental activation processes of alkynes by metal centers is the hydrometalation reaction to provide σ-vinyl complexes, it is noteworthy that the hydrometalation of **1** has remained prior to this report one of the "holy grails" of phosphaalkyne chemistry. Our studies on alkyne hydrometalation have centered on the complex $[RuHCl(CO)(PPh_3)_3]$ (**2**) and its derivatives,[7] and in this report we discuss the extension of this chemistry to **1**. This leads to the formation of stable coordinatively unsaturated σ-phosphaalkenyl complexes in a reaction completely and reassuringly analogous to those of alkynes. Furthermore such compounds are shown to be precursors to a range of complexes of otherwise unstable phosphaalkenes.

Treatment of a solution of **2** in dichloromethane with **1** leads to the clean formation of an orange-red complex, spectroscopic data (Table 1) for which are consistent with the formulation $[RuCl(P{=}CH\,tBu)(CO)(PPh_3)_2]$ (**3**) (Scheme 1). The ^{31}P NMR spectrum shows a doublet for the phosphane ligands (δ = 33.9, $^2J(P_2,P)$ 10.0 Hz) and a triplet (δ = 450.4, $^2J(P_2,P)$ 10.0 Hz) in an area considered typical of phosphaalkenyl ligands[6, 8] (although such a simple and non-kinetically stabilized derivative has not been previously reported). The alkenic proton appears as a doublet of triplets (δ = 7.12) with a large coupling ($^2J(P,H)$ = 16.9 Hz) to the adjacent phosphorus atom and a

Table 1. Selected spectroscopic data for the complexes $[Ru(P{=}CH\,tBu)Cl(CO)_n(PPh_3)_2]$; n = 1 (**3**) and 2 (**4a**).

	3	**4a**
IR (nujol [cm^{-1}]): ν(CO)	1929	2024, 1975
phosphaalkenyl		
NMR (CD_2Cl_2, 25 °C)		
$^{31}P\{^1H\}$: δRuPPh$_3$	33.9	22.1
δ(RuP=C)	450.4	369.5
$J(P_2,P)$ [a]	10.0	[b]
$^{13}C\{^1H\}$: δ(RuCO) [$J(P_2,C)$] [a]	202.4 [15.2]	198.7 [b], 193.0 [b]
δ(RuP=C) [J(P,C)] [a]	184.9 [58.9]	196.8 [62.5]
$\delta C(CH_3)_3$ [J(P,C)] [a]	40.8 [10.7]	41.8 [b]
$\delta C(CH_3)_3$ [J(P,C)] [a]	30.8 [14.3]	15.1 [b]
FAB-MS (nba matrix) [c]	940(64) [M^+ + nba]	940(41) [M^+ − CO + nba]
m/z (%) [assignment]:	791(9) [M − H$^+$]	819(18) [MH^+]
	–	789(2) [M^+ − H − CO]
	689(24)	689(24)
	[MH^+ − HPCH*t*Bu]	[MH^+ − HPCH*t*Bu − CO]

[a] Coupling in Hz. [b] Coupling not resolved. [c] nba = nitrobenzyl alcohol.

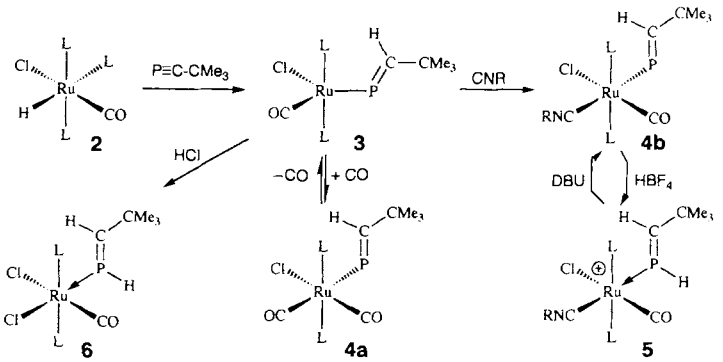

Scheme 1. Phosphaalkyne hydroruthenation. R = 2,6-$Me_2C_6H_3$; L = PPh_3.

[*] Dr. A. F. Hill, Dr. R. B. Bedford
Department of Chemistry
Imperial College of Science, Technology and Medicine,
South Kensington, London SW7 2AY (UK)
Fax: Int. code +(171)-594-5804
e-mail: a.hill@ic.ac.uk
Dr. C. Jones,
Department of Chemistry
University of Wales, Swansea
Singleton Park, Swansea SA2 8PP (UK)
e-mail: c.a.jones@swansea.ac.uk

[**] This research was supported by the Engineering and Physical Sciences Research Council, the Royal Society, and the Nuffield Foundation.

smaller coupling to the phosphorus atoms of the phosphane ligands ($^4J(P_2,H) = 2.8$ Hz). The gross molecular formulation is confirmed by FAB mass spectrometry; the mass spectrum shows in addition to a molecular ion, fragmentations for the loss of the phosphaalkenyl ligand as well as the formation of a nitrobenzyl alcohol adduct.

The recently reported transformation of a phosphaalkyne-(hydrido)iron complex to a fluoro(phosphaalkene) complex[9] is a process which could plausibly proceed by a hydroferration of the coordinated phospaalkyne, akin to the result reported here. Other than this report the remaining examples of phosphaalkenyl complexes are limited to those featuring kinetically stabilizing substituents[8a] or the metallacyclic complexes $[OsP{=}C(CF_3)O(CO)_2(PPh_3)_2]$[8b] and $[RhP{=}CtBuC(=CH_2)Cl(PiPr_3)_2]$.[6]

The implied coordinative unsaturation at ruthenium raises the questions of σ-π coordination of the phosphaalkenyl ligand and the possibility of ligand addition reactions. The former may be discounted as this would render the phosphane ligands diastereotopic, a possibility not supported by ^{31}P NMR data. The latter, however, provides a point of interest and this was subsequently investigated. The complex **3** rapidly reacts with CO under ambient conditions to provide the pale yellow complex **4a** (see Scheme 1), the stereochemistry of which follows unequivocally from spectroscopic data, whilst the gross molecular composition follows from FAB-MS data. Complex **4a** readily decarbonylates both in solution and in the solid state to reform **3**. This observation points to a substantial *trans* effect for the phosphalkenyl ligand, although this has not been previously appreciated since the majority of prior examples are of the "piano-stool" variety. A similar reaction occurs with 2,6-$Me_2C_6H_3NC$ to provide **4b**; however, in this case ligand addition is not as readily reversible. The phosphorus center in the free phosphalkyne **1** is typically electrophilic; however, hydroruthenation reverses this polarity making the phosphorus nucleophilic. This is reflected in the clean protonation of **4b** with $HBF_4 \cdot OEt_2$ to afford the cationic phosphaalkene complex **5**. The site of protonation is unambiguously established by the appearance of a doublet of triplets in the proton-coupled ^{31}P NMR spectrum at $\delta = 164.3$ ($J(P,P) = 45.0$, $J(P,H) = 376.4$ Hz), which collapses to a triplet in the proton-decoupled spectrum, and a doublet of doublet of triplets in the ^1H NMR spectrum at $\delta = 5.73$ ($^1J(P,H) = 375.8$; $^3J(H,H) = 20.5$ Hz; $^3J(P_2,H)$ discernable but not resolved) due to the phosphorus-bound proton. This protonation is readily reversed upon treatment with a non-nucleophilic base such as 1,8-diazabicyclo[5.4.0]undec-7-ene (DBU). These transformations in effect represent the unprecedented metal-mediated hydrogenation of a phosphaalkyne to a phosphaalkene.

The reaction of **3** with HCl also proceeds to a give a neutral phosphaalkene complex **6** (see Scheme 1). This raises questions about the bonding in **3** in that coordinative unsaturation in phosphaalkenyl complexes is normally accommodated by linearization of the M-P-C linkage, a process which renders the phosphorus center electrophilic. Clearly the phosphorus center in **3** is nucleophilic. Thus, we suggest the possibility that in metal centers that combine high d-occupancies and coordinative unsaturation the linearization of phosphaalkenyl ligands is not necessarily favored. In this context we note the isoelectronic relationship between the ligands -P=CR_2, -NO, and -NNR. The complex $[OsCl(NO)(CO)(PPh_3)_2]$ requires a linear nitrosyl on effective atomic number (EAN) grounds but actually features a bent and nucleophilic nitrosyl ligand as illustrated by the facile and reversible hydrochlorination to provide $[OsCl_2(HNO)(CO)(PPh_3)_2]$ (Scheme 2).[10] We therefore suggest

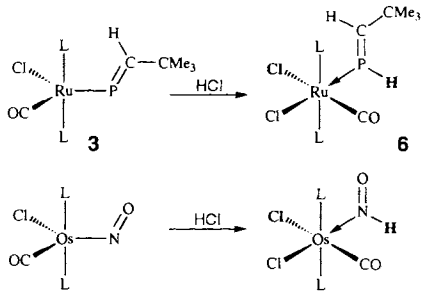

Scheme 2. Nitrosyl and phosphaalkenyl hydrochlorination. L = PPh_3.

that the arguments used to rationalize the geometries of late transition metal nitrosyl complexes[11] may equally well find application in the developing chemistry of phosphaalkenyl ligands.

Experimental Procedure

3: A solution of $[RuHCl(CO)(PPh_3)_3]$ (1.00 g, 1.05 mmol) in dichloromethane (50 mL) was treated with P≡C*t*Bu (0.43 mL, about 2.4 equivalents) and stirred for 1 h and then freed of volatiles. The residue was recrystallized (CH_2Cl_2/Et_2O) to provide **3**. Yield 0.76 g (92%). Anal. found C 62.5, H 6.2%. $C_{42}H_{40}ClOP_3Ru$ requires C 63.8, H 5.1%.

Note: The hydrometalation of adamantylphosphaalkyne proceeds under analogous conditions to those described above; however, the product could not be isolated in greater than about 90% purity due to its high solubility.

4a: Carbon monoxide was passed through a solution of **3** (0.15 g, 0.19 mmol) in dichloromethane (4 mL) for 2 min. Addition of diethyl ether (20 mL) and cooling to −10 °C for 12 h provided **4a**. Yield 0.13 g (84%). Analytical data not obtained due to rapid decarbonylation in the solid state.

4b: A solution of **3** (0.15 g, 0.19 mmol) in dichloromethane (5 mL) was treated with 2,6-$Me_2C_6H_3NC$ (0.03 g, 0.23 mmol) and stirred for 5 min and then freed of volatiles. The residue was crystallized from a mixture of dichloromethane and diethyl ether to provide **4b**. Yield 0.12 g (69%). Anal. found C 65.0, H 5.7, N 1.5%. $C_{51}H_{49}ClONP_3Ru \cdot 0.5CH_2Cl_2$ requires C 65.3, H 5.3, N 1.5%.

Received: October 11, 1995 [Z 8462 IE]
German version: *Angew. Chem.* **1996**, *108*, 587–589

Keywords: metalations · multiple bonds · phosphaalkynes · phosphorus compounds · ruthenium compounds

[1] For a recent review of the organometallic chemistry of phosphaalkynes see J. F. Nixon, *Chem. Ind.* **1993**, *11*, 404.

[2] Recent reports on the simple coordination chemistry of phosphaalkynes include S. I. Al-Resayes, C. Jones, M. J. Maah, J. F. Nixon, *J. Organomet. Chem.* **1994**, *468*, 107; J. Grobe, D. Le Van, M. Hegemann, B. Krebs, M. Lage, *Chem. Ber.* **1993**, *126*, 63; P. Binger, T. Wettling, R. Schneider, F. Zurmuhlen, U. Bergstrasser, J. Hoffmann, G. Maas, M. Regitz, *Angew. Chem.* **1991**, *103*, 208; *Angew. Chem. Int. Ed. Engl.* **1991**, *30*, 207.

[3] Reports on the metal-mediated oligomerization of phosphaalkynes include: P. Binger, J. Haas, P. Betz, C. Kruger, *Chem. Ber.* **1995**, *128*, 737; G. Brauers, M. Green, C. Jones, J. F. Nixon, *J. Chem. Soc. Chem. Commun.* **1995**, 1125; D. Bohm, F. Knoch, S. Kummer, U. Schmidt, U. Zenneck, *Angew. Chem.* **1995**, *107*, 251; *Angew. Chem. Int. Ed. Engl.* **1995**, *34*, 198; R. M. Matos, J. F. Nixon, J. Okuda, *Inorg. Chim. Acta* **1994**, *222*, 13; P. B. Hitchcock, C. Jones, J. F. Nixon, *Angew. Chem.* **1994**, *106*, 478; *Angew. Chem. Int. Ed. Engl.* **1994**, *33*, 463; F. G. N. Cloke, K. R. Flower, P. B. Hitchcock, J. F. Nixon, *J. Chem. Soc. Chem. Commun.* **1994**, 489; P. B. Hitchcock, M. J. Maah, J. F. Nixon, M. Green, *J. Organomet. Chem.* **1994**, *466*, 153; R. Milczarek, W. Russeler, P. Binger, K. Jonas, K. Angermund, C. Kruger, M. Regitz, *Angew. Chem.* **1987**, *99*, 957; *Angew. Chem. Int. Ed. Engl.* **1987**, *26*, 908; A. R. Barron, A. H. Cowley, *ibid.* **1987**, *99*, 956 and **1987**, *26*, 907.

[4] A. F. Hill, J. A. K. Howard, T. P. Spaniol, F. G. A. Stone, J. Szameitat, *Angew. Chem.* **1989**, *101*, 213; *Angew. Chem. Int. Ed. Engl.* **1989**, *28*, 210.

[5] K. H. Dötz, A. Tiriliomis, K. Harms, *Tetrahedron* **1993**, *49*, 5577.

[6] P. Binger, J. Haas, A. T. Herrmann, F. Langhauser, C. Krüger, *Angew. Chem.* **1991**, *103*, 316; *Angew. Chem. Int. Ed. Engl.* **1991**, *30*, 310.

[7] For a recent review of alkyne hydroruthenation see A. F. Hill, in *Comprehensive Organometallic Chemistry II, Vol 7*, (Eds.: E. W. Abel, F. G. A. Stone, G. Wilkinson) Pergammon Press, Oxford (UK) **1991**.

 © VCH Verlagsgesellschaft mbH, D-69451 Weinheim, 1996 0570-0833/96/3505-0548 $ 15.00+.25/0

[8] a) D. Gudat, E. Niecke, W. Malisch, U. Hofmockel, S. Quashie, A. H. Cowley, A. M. Arif, B. Krebs, M. Dartmann, *J. Chem. Soc. Chem. Commun.* **1985**, 1687; S. J. Goede, H. P. van Schaik, F. Bickelhaupt, H. Kooijman, A. L. Spek, *Organometallics* **1992**, *11*, 3844; L. Weber, T. Matzke, R. Boese, *Chem. Ber.* **1990**, *123*, 739; L. Weber, K. Reizig, R. Boese, M. Polk, *ibid.* **1986**, *5*, 1098; L. Weber, K. Reizig, G. Meine, *Z. Naturforsch. B* **1985**, *40*, 1698; L. Weber, K. Reizig, R. Boese, M. Polk, *Angew. Chem.* **1985**, *97*, 583; *Angew. Chem. Int. Ed. Engl.* **1985**, *24*, 604; b) D. S. Bohle, G. R. Clark C. E. F. Rickard, W. R. Roper, *J. Organomet. Chem.* **1988**, *353*, 355.

[9] P. B. Hitchcock, M. F. Lemos-Manida-Meidine, J. F. Nixon, A. J. L. Pombeiro, *J. Organomet. Chem.* **1991**, *402*, C23.

[10] R. D. Wilson, J. A. Ibers, *Inorg. Chem.* **1979**, *18*, 336; K. Laing, W. R. Roper, *J. Chem. Soc. Chem. Commun.* **1968**, 1556.

[11] R. Hoffmann, M. M. L. Chen, M. Elian, A. Rossi, D. M. P. Mingos, *Inorg. Chem.* **1974**, *13*, 2666.

Synthesis of a "Molecular Pinwheel": [3.3.3.3.3.3]-(1,2,3,4,5,6)Cyclophane**

Youichi Sakamoto, Naomi Miyoshi, and Teruo Shinmyozu*

[3_6](1,2,3,4,5,6)Cyclophane **1**, a compound we have long sought[1, 2] and one of the final target molecules in the field of [3.3]cyclophane chemistry, has finally been synthesized and characterized. We expect **1** to have fascinating chemical and structural features. A photochemical isomerization of **1** to the propella[3_6]prismane **2** (Scheme 1) has been predicted based on

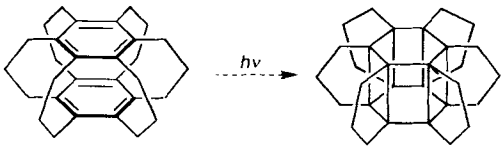

1 **2**

Scheme 1. Predicted photochemical isomerization of **1** to the propella[3_6]prismane **2**.

semiempirical MO calculations,[3] and a correlated inversion of the six trimethylene chains, which resemble six blades of a pinwheel, is expected in solution (Scheme 2).[4]

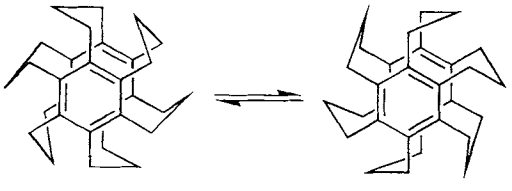

1a **1b**

Scheme 2. Predicted most stable conformations and correlated inversion of the six trimethylene bridges of **1**.

[*] Prof. Dr. T. Shinmyozu
Institute for Fundamental Research of Organic Chemistry (IFOC)
Kyushu University
Hakozaki 6-10-1, Fukuoka 812 (Japan)
Fax: Int. code +(92)-641-0915
e-mail: shinmyo@ms.ifoc.kyushu-u.ac.jp
Y. Sakamoto, N. Miyoshi
Department of Chemistry, Faculty of Science
Kyushu University, Fukuoka 812 (Japan)

[**] Multibridged [3_6]cyclophanes, Part 3. We gratefully acknowledge financial support by the Grant-in-Aid for Scientific Research (no. 06453042) and the Grant-in-Aid for Scientific Research on Priority Area of New Development of Organic Electrochemistry (no. 06226264) from the Ministry of Education, Science and Culture, Japan. Part 2: ref. [2].

The synthesis of the highly strained [2_6](1,2,3,4,5,6)cyclophane **3**, named "superphane", was accomplished by Boekelheide et al. in 1979,[5] and the work opened the new field of superphane chemistry.[6] Since then syntheses, novel structures, and chemical properties of various superphanes such as **3** by Hopf et al.,[7] [4_5](1,2,3,4,5)ferrocenophane (superferrocenophane) by Hisatome et al.,[8] metal-capped [3_4](1,2,3,4)cyclobutadienophane by Gleiter et al.,[9] and [2_4](2,3,4,5)thiopenophane (superthiophenophane) by Tashiro et al.[10] have been reported.

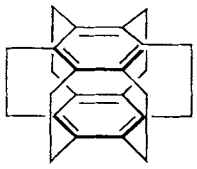

3

In our efforts toward the stepwise synthesis of **1** starting from the [3_3](1,3,5)cyclophane **4**[4c] (Scheme 3), we reported

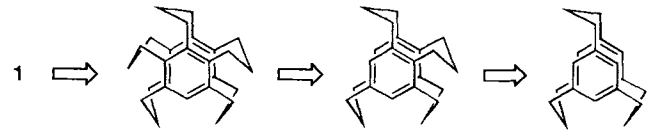

1 **6** **5** **4**

Scheme 3. The stepwise synthetic approach.

the syntheses of the [3_4](1,2,3,5)cyclophane **5**[1] and the [3_5](1,2,3,4,5)cyclophane **6**,[2] in which the key reaction for the construction of a trimethylene bridge was the acid-catalyzed condensation between the acetyl group and the pseudogeminally substituted chloromethyl group. Recently we developed an alternative method using aldol condensation between the acetyl group and a pseudogeminally substituted formyl group, in place of chloromethyl group. This reaction proceeds in very high yields, and the resultant enones can be readily reduced to give trimethylene bridges. Since the precursors of **1** are now available in multigram quantities, we set about the synthesis of **1** from the [3_5]cyclophane **6** (Scheme 4).[2]

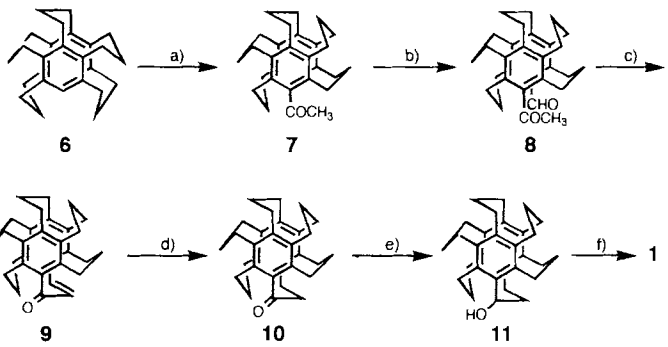

6 **7** **8** **9** **10** **11**

Scheme 4. Synthetic route to **1** from **6**. a) $(CH_3CO)_2O$, $AlCl_3$, CS_2, reflux, 3 d, **7**: 52% (based on recovered **6**); b) CH_3OCHCl_2, $AlCl_3$, CH_2Cl_2, room temperature (RT), 3 h, **8**: quantitative; c) 3N aqueous NaOH, THF, CH_3OH, reflux, 82 h, **9**: 92% (based on recovered **8**); d) H_2, PtO_2, $CHCl_3$-CH_3OH, RT, 41 h, **10**: quantitative; e) SmI_2, 1N aqueous KOH, THF, RT, 30 min; f) $AlCl_3$, $LiAlH_4$, THF, reflux, 12 h, **1**: 61% (based on **10**).

Formylation of the acetyl compound **7**, prepared by treatment of **6** with acetic anhydride in the presence of $AlCl_3$ (52%), quantitatively provided the pseudogeminally substituted compound **8**. Intramolecular aldol condensation of **8** under alkaline conditions afforded the enone **9** (92%), which was readily hydrogenated in the presence of catalytic amounts of PtO_2 to give the ketone **10** quantitatively. We initially attempted to reduce

 © VCH Verlagsgesellschaft mbH, D-69451 Weinheim, 1996 0570-0833/96/3505-0549 $ 15.00+.25/0

the carbonyl group of **10** to give us **1** directly; however, the reaction did not proceed at all by using either $LiAlH_4$-$AlCl_3$[11] or triethylsilane[12] as the reducing agents. Thus, we studied the reduction of the carbonyl group **10** via the hydroxyl compound **11**. Reduction of the carbonyl group of **10** by $LiAlH_4$ in refluxing THF or by *n*-Bu_4NBH_4 in dichloromethane[13] resulted in the complete recovery of the starting ketone **10**. Finally we chose SmI_2 in THF,[14, 15] since this reagent is a potentially powerful reducing agent toward a variety of functional groups, particularly in the presence of acids or bases.[16] In fact, the reduction of the extremely inert carbonyl group of **10** to alcohol **11** was accomplished with SmI_2 in THF in the presence of 1 N aqueous KOH. The resultant alcohol **11** was readily reduced by $LiAlH_4$-$AlCl_3$ to give the desired compound **1** as colorless crystals which decomposed above 358 °C (yield 61% from **10**).

In the ^{1}H NMR spectrum (270 MHz, $CDCl_3$, 22 °C, TMS: $\delta = 2.41-2.51$ (m, 12H; $CH_2CH_2CH_2$), 3.19 (t, $J = 7.3$ Hz, 24H; $CH_2CH_2CH_2$)), two groups of well-averaged proton signals are observed for the trimethylene bridges. The proton-decoupled ^{13}C NMR spectrum (90 MHz, $CDCl_3$, 22 °C, TMS) shows three singlets at $\delta = 20.5$ (t, $CH_2CH_2CH_2$), 28.2 (t, $CH_2CH_2CH_2$), and 135.4 (s, aromatic). The multiplicity of the signals (in parentheses) is determined by the off-resonance decoupled ^{13}C NMR spectrum. These NMR data are consistent with the proposed, highly symmetrical structure of **1** and its dynamic nature (Scheme 2). Elemental analysis and mass spectral data (MS (70 eV): M^+ $m/z = 396$) are also in good agreement with the calculated values for **1**. The spectroscopic data of the intermediates **7**–**11** are listed in Table 1.

Table 1. Spectroscopic data for the intermediates **7**–**11** [a].

7: ^{1}H NMR: $\delta = 2.12$ (s, 3H, $COCH_3$), 2.22–2.80 (m, 14H, $CH_2CH_2CH_2$), 3.05–3.22 (m, 16H, $CH_2CH_2CH_2$), 7.02 (s, 1H, ArH); IR (KBr): $\tilde{\nu} = 1692$ cm^{-1} (C=O); MS: m/z 398 [M^+]

8: ^{1}H NMR: $\delta = 2.08$ (s, 3H, $COCH_3$), 2.11–2.65 (m, 12H, $CH_2CH_2CH_2$), 3.08–3.29 (m, 16H, $CH_2CH_2CH_2$), 3.54–3.63 (m, 2H, $CH_2CH_2CH_2$), 10.59 (s, 1H, CHO); IR (KBr): $\tilde{\nu} = 1694$ cm^{-1} (C=O), 1671 cm^{-1} (C=O); MS: m/z 426 [M^+]

9: ^{1}H NMR: $\delta = 2.11-2.57$ (m, 10H, $CH_2CH_2CH_2$), 2.72–3.28 (m, 20H, $CH_2CH_2CH_2$), 6.78 (d, $J = 11.9$ Hz, 1H), 7.74 (d, $J = 11.9$ Hz, 1H); IR (KBr): $\tilde{\nu} = 1647$ cm^{-1} (C=O); MS: m/z 408 [M^+]

10: ^{1}H NMR: $\delta = 2.01-2.60$ (m, 10H, $CH_2CH_2CH_2$), 2.76–3.43 (m, 24H, $CH_2CH_2CH_2$ and CH_2CH_2CO); IR (KBr): $\tilde{\nu} = 1674$ cm^{-1} (C=O); MS: m/z 410 [M^+]

11: ^{1}H NMR: $\delta = 1.94-2.16$ (m, 6H, $CH_2CH_2CH_2$), 2.42–2.56 (m, 2H, $CH_2CH_2CH_2$), 2.69–3.09 (m, 16H, $CH_2CH_2CH_2$), 3.26–3.54 (m, 10H, $CH_2CH_2CH_2$), 4.19–4.31 (m, 1H, CH_2CH_2CHOH), 5.75–5.82 (m, 1H, CH_2CH_2CHOH); IR (KBr): $\tilde{\nu} = 3416$ cm^{-1} (OH); MS: m/z 412 [M^+]

[a] ^{1}H NMR: Jeol JNX-EX 270 spectrometer; standard: TMS; solvent: $CDCl_3$; IR: Hitachi Nicolet I-5040 FT-IR spectrometer; MS: Jeol JMS-SX/SX102A tandem mass spectrometer (EI, 70 eV).

In conclusion, we have synthesized **1** by using the newly developed aldol condensation of **8** as the key reaction for introducing the final trimethylene bridge. An X-ray crystal structure analysis of **1** is in progress, as are studies on the dynamic behavior of the compound and its photochemical properties.

Received: October 19, 1995 [Z8485IE]
German version: *Angew. Chem.* **1996**, *108*, 585–586

Keywords: aldol condensations · arenes · cyclophanes · strained rings superphanes

[1] T. Shinmyozu, S. Kusumoto, S. Nomura, H. Kawase, T. Inazu, *Chem. Ber.* **1993**, *126*, 1815–1818.
[2] T. Shinmyozu, M. Hirakida, S. Kusumoto, M. Tomonou, T. Inazu, J. M. Rudzinski, *Chem. Lett.* **1994**, 669–672.
[3] O. J. Cha, E. Osawa, S. Park, *J. Mol. Struct.* **1993**, *300*, 73–81.
[4] a) K. Sako, T. Hirakawa, N. Fujimoto, T. Shinmyozu, T. Inazu, H. Horimoto, *Tetrahedron Lett.* **1988**, *29*, 6275–6278; b) K. Sako, T. Meno, H. Takemura, T. Shinmyozu, T. Inazu, *Chem. Ber.* **1990**, *123*, 639–642; c) T. Meno, K. Sako, M. Suenaga, M. Mouri, T. Shinmyozu, T. Inazu, H. Takemura, *Can. J. Chem.* **1990**, *68*, 440–445; d) K. Sako, T. Shinmyozu, H. Takemura, M. Suenaga, T. Inazu, *J. Org. Chem.* **1992**, *57*, 6536–6541.
[5] Y. Sekine, M. Brown, V. Boekelheide, *J. Am. Chem. Soc.* **1979**, *101*, 3126–3127; Y. Sekine, V. Boekelheide, *ibid.* **1981**, *103*, 1777–1785.
[6] For reviews, see: a) V. Boekelheide, *Acc. Chem. Res.* **1980**, *13*, 65–70; b) V. Boekelheide in *Cyclophanes I*, (Ed.: F. Vögtle), Springer, Berlin, **1983**, pp. 87–139; c) F. Vögtle, *Cyclophan-Chemie*, B. G. Teubner, Stuttgart, **1990**, pp. 266–310; c) J. Kleinschroth, H. Hopf, *Angew. Chem.* **1982**, *94*, 485–496; *Angew. Chem. Int. Ed. Engl.* **1982**, *21*, 469–480; d) H. Hopf in *Cyclophanes, Vol. 2* (Eds.: P. M. Keehn, S. M. Rosenfeld), Academic Press, New York, **1983**, pp. 521–572; e) R. Gleiter, D. Kratz, *Acc. Chem. Res.* **1993**, *26*, 311–318.
[7] S. El-tamany, H. Hopf, *Chem. Ber.* **1983**, *116*, 1682–1685.
[8] a) M. Hisatome, J. Watanabe, K. Yamakawa, Y. Iitaka, *J. Am. Chem. Soc.* **1986**, *108*, 1333–1334; b) Review: M. Hisatome, K. Yamakawa, *Yuki Gosei Kagaku Kyokaishi* **1990**, *48*, 319.
[9] a) R. Gleiter, M. Karcher, M. L. Ziegler, B. Nuber, *Tetrahedron Lett.* **1987**, *28*, 195–198; b) R. Gleiter, M. Karcher, *Angew. Chem.* **1988**, *100*, 851–852; *Angew. Chem. Int. Ed. Engl.* **1988**, *27*, 840–841; c) Review: R. Gleiter, *ibid.* **1992**, *104*, 29–46 and **1992**, *31*, 27–44.
[10] M. Takeshita, M. Koike, H. Tsuzuki, M. Tashiro, *J. Org. Chem.* **1992**, *57*, 4654–4658.
[11] a) R. F. Nystron, C. R. A. Berger, *J. Am. Chem. Soc.* **1958**, *80*, 2896–2898; b) K. T. Potts, D. R. Liljegren, *J. Org. Chem.* **1963**, *28*, 3202–3205; c) J. H. Brewster, H. O. Bayer, S. F. Osman, *ibid.* **1964**, *29*, 110–115; d) J. H. Brewster, H. O. Bayer, *ibid.* **1964**, *29*, 116–121.
[12] a) D. N. Kursanov, Z. N. Parnes, N. M. Loim, *Synthesis* **1974**, 633–651; b) O. D. Dailey Jr., *J. Org. Chem.* **1987**, *52*, 1984–1989; c) M. P. Doyle, C. T. West, S. J. Donnelly, C. C. McOsker, *J. Organomet. Chem.* **1976**, *117*, 129–140.
[13] D. J. Raber, W. C. Guida, *J. Org. Chem.* **1976**, *41*, 690–696.
[14] P. Girard, J. L. Namy, H. B. Kagan, *J. Am. Chem. Soc.* **1980**, *102*, 2693–2698.
[15] Review: J. Inanaga, *Rev. Heteroat. Chem.*, **1990**, *3*, 75–86, and references therein.
[16] Y. Kamochi, T. Kudo, *Yuki Gosei Kagaku Kyokaishi* **1994**, *52*, 285.

Synthesis and Structure of a Digallane with Tris(trimethylsilyl)silyl and Chloro Substituents**

Gerald Linti* and Wolfgang Köstler

Organoelement compounds of divalent gallium containing a gallium–gallium bond have been structurally investigated predominantly as tetraorgano derivatives such as $\{[(Me_3Si)_2CH]_2Ga\}_2$[1] and $[Aren_2Ga]_2$[2, 3] (Aren = 2,4,6-triisopropylphenyl, 2,4,6-tris(trifluoromethyl)phenyl). Gallium(II) halides with a metal–metal bond, either in the form of donor adducts like $Ga_2Cl_4 \cdot 2$dioxane[4] or as hexahalogeno digallates $[Ga_2Cl_6]^{2-}$,[5] have been known for a longer period. However, no digallanes containing two different substituents, such as $R_2Ga_2Cl_2$, have been isolated to date. These would, however, as an inspection of the corresponding boron compounds reveals,[6] be ideal starting materials for the synthesis of novel gallium(II) derivatives. Compounds containing gallium–silicon bonds have been rarely studied;[7–9] the stabilization and isolation of some metal(I) and metal(II) derivatives of Group 13 elements was achieved by using sterically demanding silyl substituents:

[*] Dr. G. Linti, Dipl.-Chem. W. Köstler
Institut für Anorganische Chemie der Universität
Engesserstrasse Geb. 30.45, D-76128 Karlsruhe (Germany)
Fax: Int. code +(721)608-4854
e-mail: linti@achpc9.chemie.uni-karlsruhe.de

[**] The Chemistry of Gallium Compounds, Part VII. This work was supported by the Deutsche Forschungsgemeinschaft and the Fonds der Chemischen Industrie. We thank Prof. Dr. H. Schnöckel for his support, and Prof. Dr. D. Fenske and Prof. Dr. P. Klüfers for collecting diffractometer data sets. Part VI: Ref. [11].

$[MSiR_3]_4$ (M = Al, R = *t*Bu;[10] M = Ga, R = $SiMe_3$[11]), $\{[(SiMe_3)Si]_2Tl\}_2$.[12] We report here on the use of the tris(trimethylsilyl)silyl group (hypersilyl) for the preparation of silyl-substituted digallanes.

If mixed-valent gallium (I,III) chloride is allowed to react with lithium tris(trimethylsilyl)silanide·3THF[13] [Eq. (a)] in a molar

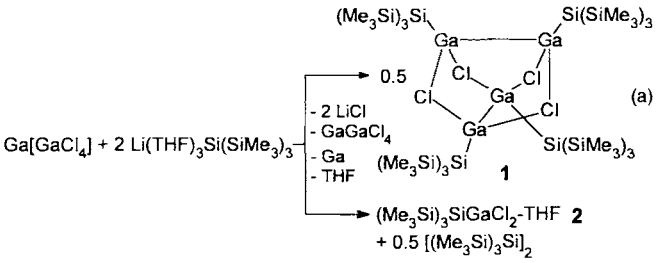

ratio of 1:1, among other products, colorless crystals of the dimeric dichlorobis(hypersilyl)digallane **1** are isolated. The formation of this compound of the type $R_2Ga_2Cl_2$ is surprising, because such compounds were considered to be unstable towards a disproportionation into gallium and gallium(III) derivatives.[1] $[(Me_3Si)_3SiGa]_4$ was neither isolated nor detected by NMR spectroscopy. Additional products in the nonuniform reaction [Eq. (a)] are **2**, which will not be discussed here further, gallium metal, and the disilane $[(Me_3Si)_3Si]_2$ (molar ratio of disilane to **2** = 1:2). According to ^{1}H NMR spectroscopic investigations of the reaction mixtures, the ratio in which the compounds **1** and **2** are formed is sensitive to the exact reaction conditions and varies between 1:1 and 1:3 (ratio of integrals in the ^{1}H NMR spectrum). This suggests that a redox reaction competes with the substitution. Compound **1** probably originates via intermediary formed Ga_2Cl_4·2THF, since **1** is formed in high yield in the reaction of two molar equivalents of lithium tris(trimethylsilyl)silanide·3THF with Ga_2Cl_4·2dioxane [Eq. (b)].

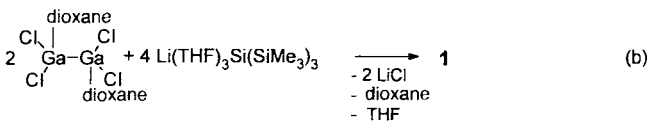

If two or more molar equivalents of lithium tris(trimethylsilyl)silanide·3THF are used in a reaction analogous to Equation (a), [Eq. (c)] compound **1** was not detected; in this

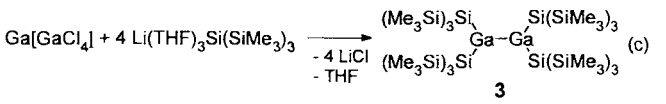

case **3** is isolated as the major gallium-containing product. Compound **3** is also formed as a by-product in the synthesis of $[(Me_3Si)_3SiGa]_4$ (**4**) from three equivalents of lithium tris(trimethylsilyl)silanide·3THF and Ga_2Cl_4·2dioxane.

The analysis of the crystal structure[14] of **1** (Fig. 1) shows a cage comprising four gallium and four chlorine atoms, in which the four gallium atoms are situated at the corners of a bisphenoid (Fig. 2). Pairs of gallium atoms are bonded to each other (d_{Ga-Ga} = 250.5 pm (average)). These bond lengths are typical for digallanes with four bulky organo substituents (d_{Ga-Ga} = 247–255 pm).[1–3] According to a preliminary crystal structure

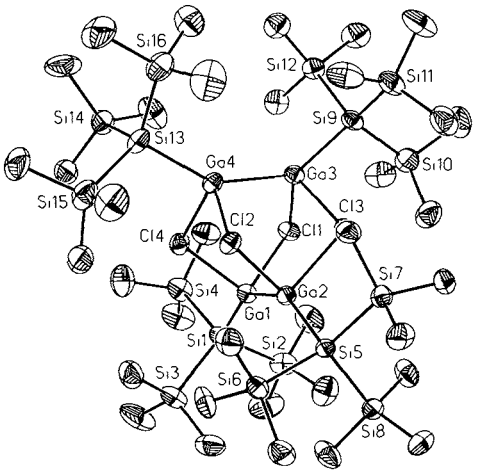

Fig. 1. Crystal structure of **1** (ORTEP, 30% probability ellipsoids). The hydrogen atoms are omitted for clarity. Selected bond lengths [pm] and angles [°]: Ga(1)–Ga(2) 250.14(10), Ga(3)–Ga(4) 250.93(12), Ga-Cl 238.9(2)–240.1(2), Ga-Si 239.0(2)–240.2(2); Si-Ga-Ga 145.02(7)–146.76(7), Ga-Cl-Ga 99.85(6)–100.54(7), Cl-Ga-Cl 91.02(7)–92.28(7), Cl-Ga-Ga 100.31(6)–102.33(6), Cl-Ga-Si 100.79(9)–103.71(7).

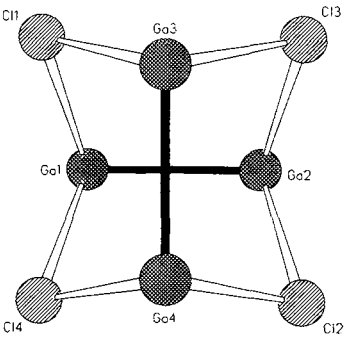

Fig. 2. Frame of the gallium and chlorine atoms in **1**.

determination, compound **3** has a Ga–Ga bond that is 9 pm longer (d_{Ga-Ga} = 259.9(4) pm) than that in **1**, and a nearly orthogonal arrangement of the Si_2Ga planes (interplanar angle: 80°). Compound **4** also has longer Ga–Ga distances (d_{Ga-Ga} = 258.4(2) pm),[11] which can be attributed to the sterically demanding hypersilyl groups. The other four edges of the bisphenoid are too long (d_{Ga-Ga} = 365–369 pm) for Ga–Ga interactions, and are instead bridged by four chlorine atoms, forming a square (d_{Cl-Cl} = 345 pm). The Ga–Cl distances in the nearly symmetric Ga-Cl-Ga bridges (d_{Ga-Cl} = 240.1 pm (average)) are similar in length to those, for example, in dimeric Mes_2GaCl (d_{Ga-Cl} = 240.7(1), 238.4(1) pm),[15] but shorter than those in $[(\eta^1\text{-}C_5Me_5)_2GaCl]_2$ (d_{Ga-Cl} = 243.2(7), 249.9(8) pm).[16] Significantly shorter Ga–Cl bridging distances are observed ($d_{Ga-Cl(bridging)}$ = 229 pm) in Ga_2Cl_6.[17]

The Ga–Si distances in **1** (d_{Ga-Si} = 239.8 pm (average)) lie in the expected range and are nearly equal the sum of covalent radii of the participating elements. They are markedly shorter than the Ga–Si distance in the sterically strained $tmp_2GaSi(SiMe_3)_3$ (d_{Ga-Si} = 246.8(2) pm)[9] (tmp = 2,2,6,6-tetramethylpiperido) and comparable to those in $[(Me_3Si)_3SiGa]_4$[11] (d_{Ga-Si} = 240.6(2) pm). The bond angles centered at the silicon atoms bonded to gallium approach the tetrahedral angle. The very wide Ga-Ga-Si angles (145°) are striking, and for the planar arrangement of the Ga_2Si_2 units (torsional angle Si1-Ga1-Ga2-Si5: 1.3°) this allows the lowest steric strain between the hypersilyl groups. Compound **1** can be considered as a product of the partial oxidation of tetrahedrally built **4** (Scheme 1); the preformed structure of the gallium frame remains essentially intact. An isomeric structure (**5**) with double chlorine bridges, typical for dimeric diorganogallium chlorides, would have—according to simple MM+ force field calcula-

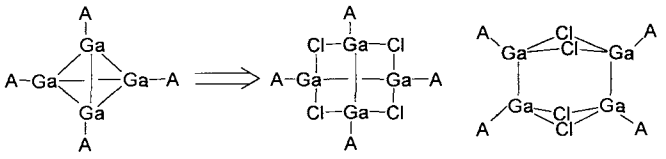

4 1 5

Scheme 1. A = $Si(SiMe_3)_3$.

tions—short Cl–Cl distances (less than 300 pm) between the parallel, nonplanar Ga_2Cl_2 rings and would evidently suffer from a high ring strain.

The dichlorobis(hypersilyl)digallane opens manifold possibilties for the synthesis of new gallium(II) compounds, in particular, heterocycles containing a Ga_2 unit.

Experimental Procedure

1: A suspension of $Ga[GaCl_4]$ (0.48 g, 1.68 mmol) in pentane (10 mL) was combined at −78 °C with a solution of $Li(THF)_3Si(SiMe_3)_3$ (0.79 g, 1.68 mmol) in pentane (15 mL). After slow warming to room temperature, the mixture was stirred overnight and all volatiles were removed from the red solution in vacuum. The residue was taken up in pentane (10 mL) and filtered. Colorless plates of **2** (0.20 g, 24%) crystallized from the solution at −30 °C; then after reducing the volume of the mother liquor, colorless prisms of **1** (0.21 g; 35% relative to $Li(THF)_3Si(SiMe_3)_3$) subsequently crystallized; m. p. >180 °C (decomp.). **1**: ^{1}H NMR (C_6D_6): $\delta = 0.44$; ^{13}C NMR (C_6D_6): $\delta = 3.5$. MS (70 eV, EI, ^{69}Ga): *m/z* (%): 1053 (4) $[Ga_3[Si(SiMe_3)_3]_3Cl_3]^+$, 667 (11) $[Ga_2[Si(SiMe_3)_3]_2Cl]^+$, 598 (1) $[Ga[Si(SiMe_3)_3]_2Cl]^+$, 583 (12) $[Ga[Si(SiMe_3)_3]_2Cl - Me]^+$, 563 (6) $[Ga[Si(SiMe_3)_3]_2]^+$, 351 (1) $[GaSi(SiMe_3)_3Cl]^+$, 316 (80) $[GaSi(SiMe_3)_3]^+$, 73 (100) $[SiMe_3]^+$. **2**: ^{1}H NMR (C_6D_6): $\delta = 3.72$ (m, 4H, OCH_2), 1.10 (m, 4H, CH_2), 0.38 (s, 27H, $SiMe_3$); ^{13}C NMR (C_6D_6): $\delta = 69.1$ (OCH_2), 25.8 (CH_2), 2.8 ($SiMe_3$). MS (70 eV, EI, ^{69}Ga): *m/z* (%): 386 (0.5) [M − THF]$^+$, 371 (0.5) [M − THF − Me]$^+$, 351 (15) [M − THF − Cl]$^+$, 247 (90) $[Si(SiMe_3)_3]^+$, 73 (100) $[SiMe_3]^+$.

3: Compound **3** was synthesized analogously to **1** from $Ga[GaCl_4]$ (0.25 g, 0.88 mmol) and $Li(THF)_3Si(SiMe_3)_3$ (0.83 g, 1.75 mmol). Yield: 0.22 g **3** (49%). ^{1}H NMR (C_6D_6): $\delta = 0.35$; ^{13}C NMR (C_6D_6): $\delta = 3.1$. MS (70 eV, EI, ^{69}Ga): *m/z* (%) 563: (10) $[Ga[Si(SiMe_3)_3]_2]^+$, 73 (100) $[SiMe_3]^+$.

Received: November 8, 1995 [Z8534IE]
German version: *Angew. Chem.* **1996**, *108*, 593–595

Keywords: digallanes · gallium compounds

[1] a) W. Uhl, *Angew. Chem.* **1993**, *105*, 1449–1461; *Angew. Chem. Int. Ed. Engl.* **1993**, *32*, 1386; b) W. Uhl, M. Layh, T. Hildenbrand, *J. Organomet. Chem.* **1989**, *364*, 289.

[2] X. He, R. A. Bartlett, M. M. Olmstead, K. Ruhlandt-Senge, B. E. Sturgeon, P. P. Power, *Angew. Chem.* **1993**, *105*, 761; *Angew. Chem. Int. Ed. Engl.* **1993**, *32*, 717.

[3] R. D. Schluter, A. H. Cowley, D. A. Atwood R. A. Jones, M. R. Bond, C. J. Carraro, *J. Am. Chem. Soc.* **1993**, *115*, 2070.

[4] J. C. Beamish, R. W. H. Small, I. J. Worrall, *Inorg. Chem.* **1979**, *18*, 220.

[5] K. L. Brown, D. Hall, *J. Chem. Soc. Dalton Trans.* **1973**, 1843. [6] See for example H. Fussstetter, H. Nöth, W. Winterstein, *Chem. Ber.* **1977**, *110*, 1931.

[7] L. Rösch, H. Neumann, *Angew. Chem.* **1980**, *92*, 62; *Angew. Chem. Int. Ed. Engl.* **1980**, *19*, 55.

[8] A. M. Arif, A. H. Cowley, T. M. Elkins, R. A. Jones, *J. Chem. Soc. Chem. Commun.* **1986**, 1776.

[9] R. Frey, G. Linti, K. Polborn, *Chem. Ber.* **1994**, *127*, 101.

[10] a) N. Wiberg in *Frontiers in Organosilicon Chemistry* (Eds.: A. B. Bassingdale, P. P. Gaspar), The Royal Society of Chemistry, Cambridge, **1991**, p. 263; b) U. Schneider, R. Ahlrichs, H. Horn, A. Schäfer, *Angew. Chem.* **1992**, *104*, 327; *Angew. Chem. Int. Ed. Engl.* **1992**, *31*, 353.

[11] G. Linti, *J. Organomet. Chem.*, submitted.

[12] S. Henkel, K.-W. Klinkhammer, W. Schwarz, *Angew. Chem.* **1994**, *106*, 721; *Angew. Chem. Int. Ed. Engl.* **1994**, *33*, 681.

[13] a) H. Gilman, C. L. Smith, *J. Organomet. Chem.* **1968**, *14*, 91; b) G. Gutekunst, A. G. Brook, *J. Organomet. Chem.* **1982**, *225*, 1; c) A. Heine, R. Herbst-Irmer, G. M. Sheldrick, D. Stalke, *Inorg. Chem.* **1993**, *32*, 2694.

[14] Details of the crystal structure determination of **1**: Crystal size: 0.30 × 0.15 × 0.15 mm, orthorhombic, space group $Pca2_1$, $a = 3606.3(6)$, $b = 1472.6(1)$, $c = 3253.7(3)$ pm, $V = 17.279(6)$ nm^3, $Z = 8$, $\rho_{calcd} = 1.085$ g cm^{-3}, $\mu = 1.60$ mm^{-1}, 64041 measured reflections in $2\theta = 4–52°$, STOE IPDS, $Mo_{K\alpha}$ radiation. Structure solution with direct methods, 28580 (23486 with $F > 4\sigma(F)$) unique reflections were used in the full-matrix refinement of 1172 parameters against F^2. $R_1 = 0.057$, $wR_2 = 0.186$ (all data), hydrogen atoms with riding model, max. residual electron density 0.725 e Å^{-3}. TWIN parameter for racemic twinning set. In one of the two independent molecules in the asymmetric unit, one of the hypersilyl groups is disordered in such a way that two silicon positions are observed for each of the three trimethylsilyl groups, but no split positions are seen for the carbon atoms. The two molecules do not markedly differ in terms of their bond lengths and angles. Both molecules (neglecting the disorder) are correlated by a pseudo center of inversion in (0, 0.25, −0.14). Refinement of the structure in space group *Pcab* (no. 61, *Pbca*) did result in a R_1 value of 0.20. The advice of Prof. Dr. H. Bärnighausen is gratefully acknowledged. Details of the crystal structure determination of **3**: The examined crystals were of very low diffracting intensity. Therefore the present X-ray structure determination only confirms the constitution of **3**, but allows no further discussion of the structure. Crystal size: 0.20 × 0.20 × 0.04 mm, monoclinic, space group $P2_1/c$, $a = 2324.6(10)$, $b = 1285.6(2)$, $c = 2304.9(5)$ pm, $\beta = 101.69(3)°$, $V = 6.745(3)$ nm^3, $Z = 4$, $\rho_{calcd} = 1.11$ g cm^{-3}, $\mu = 1.11$ mm^{-1}. Programs used are Siemens SHELXTL Plus (PC) and SHELXL93 (PC). Further details of the crystal structure investigation of **1** may be obtained from the Fachinformationszentrum Karlsruhe, D-76344 Eggenstein-Leopoldshafen (Germany), on quoting the number CSD-404582.

[15] M. A. Petrie, P. P. Power, H. V. R. Dias, K. Ruhlandt-Senge, K. M. Waggoner, R. J. Wehmschulte, *Organometallics* **1993**, *12*, 1086.

[16] O. T. Beachley, Jr., R. B. Hallcock, H. M. Zhang, J. L. Atwood, *Organometallics* **1985**, *4*, 1675.

[17] A. F. Wells, *Structural Inorganic Chemistry*, 5th ed., Clarendon Press, Oxford **1984**.

$Na_{14}Ba_{14}CaN_6$—A Nanodispersion of a Salt in a Metal**

Ulrich Steinbrenner and Arndt Simon*

Subnitrides of sodium and barium have recently been discovered. These compounds contain discrete Ba_6N octahedra in $Na_{16}Ba_6N$[1] as well as chains of face-sharing $Ba_{6/2}N$ octahedra in $NaBa_3N$[2] and Na_5Ba_3N.[3] The bond between barium and nitrogen is ionic, whereas that between barium and sodium is metallic.

The replacement of sodium by potassium as well as the introduction of additional potassium into a sodium-barium subnitride seemed a logical extension of this work. The reaction with NaK alloy (Na:K = 3:1) and barium (which had been pretreated with nitrogen in the ratio Ba:N = 3:1) led to a rather unexpected result: a few brittle crystals isolated from the liquid had the composition "$Na_{14}Ba_{14}KN_6$" according to X-ray structure analysis. The subnitride cluster unit of this structure is shown in Fig. 1a. The atom in the cluster can easily be refined as potassium. However, since potassium nitrides are unknown,[4] the coordination of nitrogen atoms to potassium is rather uncommon. All attempts to synthesize a compound of the composition above in high yield were unsuccessful.

A refinement of the X-ray data with calcium instead of potassium gave slightly better *R* values,[5] and subsequent attempts to synthesize $Na_{14}Ba_{14}CaN_6$ by specific addition of calcium were indeed successful.[6] The compound formed in approximately 65% yield together with $NaBa_3N$ and Ba_2N. A quantitative synthesis of the new compound $Na_{14}Ba_{14}CaN_6$ has not yet been achieved, probably because of the low solubility of Ca (added in small pieces) in NaK alloy and because of the generally low reaction rate.[7]

[*] Prof. Dr. A. Simon, Dipl.-Chem. U. Steinbrenner
Max-Planck-Institut für Festkörperforschung
Heisenbergstrasse 1, D-70569 Stuttgart (Germany)
Fax: Int. code +(711)689-1642

[**] We thank Dr. T. Braun, O. Buresch, Dr. J. Köhler, Dr. R. Pöttgen, and Dr. R. Ramlau for experimental assistance and discussions.

The spurious formation of $Na_{14}Ba_{14}CaN_6$ in the reaction performed without added Ca has an interesting interpretation. The barium used, which had been distilled in high vacuum, still contained 0.3(1) wt% Ca according to AAS analysis (AAS = atomic absorption spectrometry). Virtually all the calcium impurity was incorporated into the solid subnitride. An EDX analysis (EDX = energy dispersive X-ray spectroscopy) verifies that calcium is trapped in $Na_{14}Ba_{14}CaN_6$ crystals.[8]

From a structural point of view, the $Ba_{14}CaN_6$ cluster extends the series of previously known subnitride and suboxide clusters (Fig. 1). While the M_6A octahedra in $Na_{16}Ba_6N$ remain

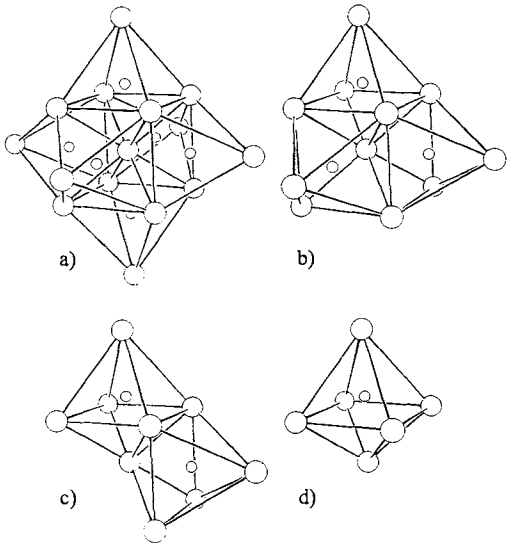

Fig. 1. The $Ba_{14}CaN_6$ cluster (a) in $Na_{14}Ba_{14}CaN_6$ and its schematic fragmentation into $M_{11}A_3$ (b), M_9A_2 (c), and MA_6 fragments (d) (see text). Drawn from the center outwards, the $Ba_{14}CaN_6$ cluster consists of a central Ca atom, an octahedron of N atoms, a cube of Ba^i atoms, and an octahedron of Ba^a atoms.

discrete, in Rb_9O_2[9] two of them share a face to form the M_9A_2 cluster;[10] in $Cs_{11}O_3$[11] three octahedra are connected through common faces to form the $M_{11}A_3$ cluster. The $M_{15}A_6$ cluster in $Na_{14}Ba_{14}CaN_6$ results from six analogously connected octahedra. Consequently, the central calcium atom is surrounded by an octahedron of N atoms and a cube of Ba atoms (Ba^i). Six additional Ba atoms (Ba^a) cap the faces of this cube. In the structure of $Na_{14}Ba_{14}CaN_6$ the clusters are arranged in the cubic close packing scheme. The tetrahedral voids of the packing are occupied by eight of the fourteen Na atoms in two Na tetrahedra whose edges are bridged by the six remaining Na atoms. Remarkably, the octahedral voids of the cluster packing remain empty.

The Ca–N distance of 257(1) pm in the cluster (Fig. 1a) is about 14 pm longer than corresponding distances in comparable structures (Ca_2N: 243 pm,[12] α-Ca_3N_2: 246 pm,[13] Ca_3NAu: 241 pm[14]). On the other hand the Ba^a–N distance of 250(1) pm is 25 pm shorter (Ba_2N: 276 pm,[15] $NaBa_3N$: 273 pm[2]), and the Ba^a–Na distances (440 pm and 451 pm) are somewhat longer than Ba–N or Ba–Na distances in comparable structures ($NaBa_3N$: 420 pm and 450 pm, Na_2Ba: 432 pm,[16] NaBa: 410 pm and 435 pm[17]). The distance between Ba^i and N is 276 pm. The striking differentiation in the Ba–Ba distances (Ba^i–Ba^i: 379 pm, Ba^i–Ba^a: 416 pm) is also found in the cluster chain Ba_3N in $NaBa_3N$ and Na_5Ba_3N (365 pm and 408 pm), in contrast to the intermetallic phases NaBa (449 pm and 459 pm) and Na_2Ba (452 pm) in which this differentiation does not occur. The Na–Na distances are 401(1) pm between atoms in the Na tetrahedra and 366 pm to the bridging Na atoms (Na_5Ba_3N: 370 pm to 410 pm, Na_2Ba: 370 pm, NaBa: 366 pm and 387 pm).

The band structure calculated with the Extended-Hückel approximation shows a distinct separation in energy between the sharp, localized levels of the N atoms and a broad band consisting of Na and Ba orbitals, which extends beyond the Fermi level. A Mulliken population analysis resulted in highly negatively charged nitrogen atoms, which can be interpreted as N^{3-} ions. Calcium and barium supply the electrons needed to form these ions. The Ca and Ba^i atoms have a higher positive charge than the Ba^a atoms, which indicates that especially the Ba^a atoms are responsible for the bonding between the cluster and the Na matrix. Both the cluster unit itself and the Na atoms may be considered neutral.

On the basis of a purely electrostatic model the shift of the nitride ions out of the centers of the Ba_5CaN octahedra, which is responsible for the long Ca–N distances, is a result of the mutual repulsion of the highly charged N^{3-} ions. A similar displacement is found for the O^{2-} ions in the suboxide structures $Cs_{11}O_3$[11] and Rb_9O_2.[9] In the latter the anions are situated 31 pm from the centers of the octahedra. This model also explains the trigonal distorsion of the Ba_6N octahedra in $NaBa_3N$[2] and Na_5Ba_3N,[3] which results in the two different Ba–Ba distances in the Ba_3N chains.

The plausible assumption that the bonds within the cluster are predominantly ionic and that it is embedded in a metallic matrix leads to a formal description of the bonding as $[Na_{14}Ba_6][Ba_8^{2+}Ca^{2+}N_6^{3-}]$. In this model one part of the structure forms a metallic $Na_{14}Ba_6$ matrix, which contains discrete, finely dispersed unit cells of the hypothetical perovskite type "$BaCaN_3$". $Na_{14}Ba_{14}CaN_6$ may be considered a nanodispersion of a salt in a metal.

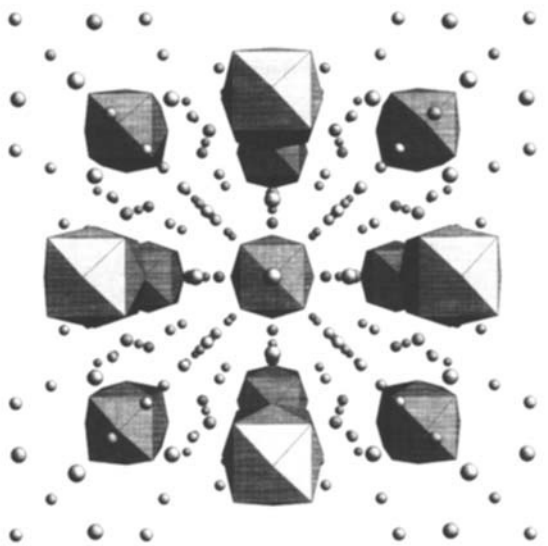

Fig. 2. A schematic view of the structure of $Na_{14}Ba_{14}CaN_6$: a dispersion of ionic Ba_8CaN_6 units in a metallic matrix of sodium and barium. The shaded polyhedra represent Ca-centered Ba_8 cubes whose faces are all capped by N atoms.

It is interesting to note that the amount of sodium is variable. So far we synthesized four different, strictly stoichiometric phases $Na_nBa_{14}CaN_6$ with $n = 14$, 17, 21 and 22. According to X-ray analysis all these phases contain the described $Ba_{14}CaN_6$ cluster in different Na environments.[20]

Received: November 17, 1995 [Z85621E]
German version: *Angew. Chem.* **1996**, *108*, 595–597

 © VCH Verlagsgesellschaft mbH, D-69451 Weinheim, 1996 0570-0833/96/3505-0553 $ 15.00+.25/0

Keywords: barium compounds · calcium compounds · nitrides · solid-state structures

[1] G. J. Snyder, A. Simon, *Angew. Chem.* **1994**, *106*, 713; *Angew. Chem. Int. Ed. Engl.* **1994**, *33*, 689.
[2] P. E. Rauch, A. Simon, *Angew. Chem.* **1992**, *104*, 1505. *Angew. Chem. Int. Ed. Engl.* **1992**, *31*, 1519.
[3] G. J. Snyder, A. Simon, *J. Am Chem. Soc.* **1995**, *117*, 1996.
[4] Nitrides M_3N of the alkali metals Na, K, Pb, and Cs have been mentioned, but could not be characterized: F. Fischer, F. Schröter, *Ber.* **1910**, *43*, 1465; R. Suhrmann, K. Clusius, *Z. Anorg. Allg. Chem.* **1926**, *152*, 52; F. Blatter, E. Schumacher, *J. Less Common Met.* **1986**, *115*, 307.
[5] Structural analysis of $Na_{14}Ba_{14}CaN_6$: space group *Fm3m*, $a = 1789.54(6)$ pm, $Z = 4$, $\rho_{calcd} = 2.745\ g\,cm^{-3}$, N in 24*e* ($x = 0.8563(4)$), Ca in 4*a*, Na1 in 24*d*, Na2 in 32*f*, ($x = 0.3292(2)$), Ba^a in 24*e* ($x = 0.71644(3)$), Ba^i in 32*f* ($x = 0.10577(1)$), *R1* = 0.0283 ("$Na_{14}Ba_{14}KN_6$": 0.0287, "$Na_{14}Ba_{14}ScN_6$": 0.0283), *wR2* = 0.0452 ("$Na_{14}Ba_{14}KN_6$": 0.0453, "$Na_{14}Ba_{14}ScN_6$": 0.0471) for 512 reflections and 17 parameters. $F(000) = 4000$, CAD-4 diffractometer, $\omega - \theta$ scan, θ range from 2 to 24°, $Ag_{K\alpha}$ radiation, absorption correction: ψ scan. Further details of the crystal structure investigation may be obtained from the Fachinformationszentrum Karlsruhe, D-76344 Eggenstein-Leopoldshafen (Germany) on quoting the depository number CSD-404430.
[6] Under an inert argon atmosphere distilled Ba (555.6 mg, 4.046 mmol), distilled Ca (11.6 mg, 0.289 mmol), NaN_3 dried under high vacuum (37.6 mg, 0.578 mmol), and Na–K alloy (1223.8 mg, 69 atom%) were sealed in a tantalum ampoule. To prevent oxidation of the tantalum, the ampoule was additionally sealed in a *Duran* glass ampoule. This ampoule was heated to 400 °C at $20\ K\,h^{-1}$. After 24 h at this temperature, the ampoule was cooled at $1\ K\,h^{-1}$ to 120 °C and annealed at this temperature for 3 months. Excess alloy was removed from the metal slurry in a press (about 5 kbar). The product was a brittle metallic substance, two-thirds of which consisted of $Na_{14}Ba_{14}CaN_6$. All manipulations were performed in a glovebox under argon.
[7] Experiments with Ca_2N or Ca–Ba alloy as calcium source are in progress.
[8] Standardless EDX point analysis on a $Na_{14}Ba_{14}CaN_6$ crystal gave a Ca:Ba ratio of 1:15.8.
[9] A. Simon, *Z. Anorg. Allg. Chem.* **1977**, *431*, 5.
[10] A (anion): N or O.
[11] A. Simon, E. Westerbeck, *Z. Anorg. Allg. Chem.* **1977**, *428*, 187.
[12] E. T. Keve, A. C. Skapski, *Inorg. Chem.* **1968**, *7*, 1757.
[13] P. Y. Laurent, J. Lang, M. T. LeBihan, *Acta Crystallogr. Sect. B* **1968**, *24*, 494.
[14] J. Jäger, D. Stahl, P. C. Schmidt, R. Kniep, *Angew. Chem.* **1993**, *105*, 738. *Angew. Chem. Int. Ed. Engl.* **1993**, *32*, 709.
[15] T. Künzel, Dissertation, University of Stuttgart, **1980**.
[16] G. J. Snyder, A. Simon, *Z. Naturforsch. B* **1994**, *49*, 189.
[17] G. J. Snyder, A. Simon, *J. Chem. Soc. Dalton Trans.* **1994**, 1159.
[18] Band structure calculations [21,22] have been performed with the program package EHMACC/EHPC/EHPP [23] using relativistic *single-zeta* orbitals and orbital energies [24] (N 2s: $H_{ii} = -26.253$ eV, $\zeta = 1.886$; N 2p: $H_{ii} = -13.829$ eV, $\zeta = 1.728$; Na 3s: $H_{ii} = -4.962$ eV, $\zeta = 0.833$; Na 3p: $H_{ii} = -2.975$ eV, $\zeta = 0.611$; Ca 4s: $H_{ii} = -5.342$ eV, $\zeta = 1.071$; Ca 4p: $H_{ii} = -3.561$ eV, $\zeta = 0.891$; Ba 6s: $H_{ii} = -4.440$ eV, $\zeta = 1.279$; Ba 6p: $H_{ii} = -2.991$ eV, $\zeta = 1.059$). The results yield a sharp band of N 2s character (−27.0 to −26.0 eV), another sharp band of N 2p character (−14.4 to −13.4 eV), and a diffuse band (starting at −8.0 eV) with Na and Ba character, which extends beyond the Fermi level. Obviously, the bond energies found for the N 2s and N 2p bands are too high [25]. This is not surprising, since the nitride ions in the subnitrides can not be treated satisfactorily within the Extended-Hückel approximation. A similar band structure calculation for $NaBa_3N$ results in a bond energy of 9.7 eV for the N 2p levels. In contrast, the UP spectra of the N 2p levels in this substance show that the experimental bond energy is only 2.0 eV [25]. The result corresponds with UPS measurements of the alkali metal suboxides, which show photoemission from the O 2p levels at 2.7 eV.[26]
[19] Without charge iteration the band structure calculation results in the following Mulliken charges: N −2.77, Ba^i +1.58, Ba^a +1.14, Ca +1.43, Na1 −0.24, Na2 −0.38.
[20] A. Simon, U. Steinbrenner, *J. Chem. Soc. Dalton Trans.*, in press.
[21] R. Hoffmann, *J. Chem. Phys.* **1963**, *39*, 1397.
[22] R. Hoffmann, W. N. Lipscomb, *J. Chem. Phys.* **1962**, *36*, 2179.
[23] QCPE program EHMACC of M. H. Whangbo, M. Evain, T. Hughbanks, M. Kertesz, S. Wijeyesekera, C. Wilker, C. Zheng, R. Hoffmann.
[24] J. P. Desclaux, *At. Data Nucl. Data Tables* **1973**, *12*, 311.
[25] U. Steinbrenner, Diplomarbeit, University of Stuttgart, **1994**.
[26] G. Ebbinghaus, A. Simon, *Chem. Phys.* **1979**, *43*, 117.

Corrigendum

In the communication "Selective Catalysis on Silicon Dioxide with Substrate-Specific Cavities" by W. F. Maier and J. Heilmann (*Angew. Chem. Int. Ed. Engl.* **1994**, *33*, 471–473) the reaction rate of 7 $mmol\,h^{-1}\,g^{-1}$ (p. 472, last paragraph) should be corrected to 0.07 $mmol\,h^{-1}\,g^{-1}$. In addition the specification of 1.0 g of catalyst **A** used in this experiment is missing.

 © VCH Verlagsgesellschaft mbH, D-69451 Weinheim, 1996 0570-0833/96/3505-0554 $ 15.00+.25/0

A Magnum Opus in Stereochemistry

Stereochemistry of Organic Compounds. By *E. L. Eliel* and *S. H. Wilen*. Wiley, Chichester, 1994. 1267 pp. $ 80.00/£ 29.95.—ISBN 0-471-01670-5/0-471-05446-1

In 1962 Eliel's book *Stereochemistry of Carbon Compounds* appeared. It summarized the status quo at that time in organic stereochemistry, and for a long time was the standard work on the subject. More than thirty years later the author has now brought out a second book, and since the information on the topic has burgeoned in the last three decades, he sought the help of two co-authors, Samuel H. Wilen and Lewis N. Mander. The structure of the thoroughly revised and updated book follows that of the previous work. Thus its strengths lie in the updated representation of the classical approaches to static stereochemistry. New directions in stereochemistry, for instance molecular dynamics or conformational analysis of peptides and oligonucleotides, are treated only lightly in the new book. In the foreword the authors point out that these days complete coverage of organic stereochemistry is no longer possible in one book. One has to make a selection, and where the focus lies depends on the point of view of the authors. For Eliel the emphasis is on the physical-organic aspects of stereochemistry.

The book is divided into 14 chapters. Chapter 1 (Introduction) serves to delineate the extent of the material, gives a historical outline of organic stereochemistry, and explains the concepts of polarimetry and optical rotation. Chapter 2 (Structure) defines structure from the view of organic chemistry with its subdivisions of constitution, configuration, and conformation, and touches upon experimental determination of structure and predictions of structure by calculations. A concluding subsection explains the most common molecular models, without, however, showing pictures of them. Chapter 3 (Stereoisomers) and Chapter 4 (Symmetry) present the distinction between enantiomers and diastereomers, as well as the classification of molecular structures according to symmetry arguments. In Chapter 5 (Configuration) absolute and relative configuration are defined. Chapter 6 (Properties of Stereoisomers. Stereoisomer Discrimination) and Chapter 7 (Separation of Stereoisomers. Resolution. Racemization) cover the physical properties of stereoisomers and stereoisomer mixtures. Both chapters are not only full of important information about chiroptic methods and NMR spectroscopic, kinetic, and calometric procedures, but also give the reader an outstanding overview of the present state of the art of stereoisomer separation. The ensuing Chapter 8 (Heterotopic Ligands and Faces) treats the distinction between homotopic, enantiotopic, and heterotopic ligands and surfaces as well as their spectroscopic and chemical consequences. The next three chapters, 9 (Stereochemistry of Alkanes), 10 (Conformation of Acyclic Molecules), and 11 (Configuration and Conformation of Cyclic Molecules), offer a contextually updated discussion of conformation analysis, which is, however related to the first edition of 1962 in its structure.

In Chapter 12 (Stereoselective Synthesis) the "guest author" Lewis M. Mander presents stereoselective synthesis in a compressed form. A caveat at the beginning of the chapter deals with the correct use of the terms stereoselective and stereospecific, and an introduction into the stereochemical classification of reactions. This is followed by a selection of the most important methods of stereoselective synthesis of alkenes. Finally Mander provides examples on the control of diastereoselective reactions, including a short overview on chiral auxiliaries. Then the well-written presentation of nucleophilic additions to carbonyl takes up a large portion of the chapter. The subsequent section deals with pericyclic transformations. The stereochemical course of radical reactions, methods for enantioselective synthesis, and examples of double stereocontrol conclude the chapter on stereoselective synthesis. The reader can certainly find many well-chosen examples in this chapter. Nevertheless, Mander himself correctly points out that for a more thorough review the reader should study the multivolume work *Asymmetric Synthesis*. One could also add *Comprehensive Organic Synthesis*, or the new volumes of Houben-Weyl's *Stereoselective Synthesis*, that, however, had not yet appeared when Eliel's work was published.

In Chapter 13 (Chiroptical Properties) the most important chiroptic methods and the applications are presented. Besides chiral allenes, alkylidenecycloalkanes, spiranes, and biphenylene, the concluding Chapter 14 (Chiralty in Molecules Devoid of Chiral Centers) also treats molecular propellers, helical structures, molecules with planar chirality, and cyclostereoisomers. Each chapter contains an extensive reference section, covering the literature to 1993. At the end of the book is a glossary with about 230 definitions and explanations of important concepts and common abbreviations. The detailed subject index is a useful reference.

To whom can I recommend this book? Every chemistry library should have the new "Eliel/Wilen/Mander" besides the old "Eliel" as reference work. Everyone interested in stereochemistry will find the desired information in the fields of characterization and separation of stereoisomers, and those who seek the historical roots and development in all aspects of organic stereochemistry, will have their research rewarded in the new "Eliel". Whether students on a tight budget will find the purchase worthwhile must be left to each individual case. In view of the extent of the material, students might have difficulty sifting out the important aspects for a beginner. The new book is not a typical textbook because it does not concentrate on principles in a skillful didactic manner. It is a useful compendium of stereochemical knowledge.

Ulrich Koert
Fachbereich Chemie der Universität
Marburg (Germany)

This section contains book reviews and a list of new books received by the editor. Book reviews are written by invitation from the editor. Suggestions for books to be reviewed and for book reviewers are welcome. Publishers should send brochures or (better) books to Dr. Illenora Beckmann, Redaktion Angewandte Chemie, Postfach 101161, D-69451 Weinheim, Federal Republic of Germany. The editor reserves the right of selecting which books will be reviewed. Uninvited books not chosen for review will not be returned.

 © *VCH Verlagsgesellschaft mbH, D-69451 Weinheim, 1996* *0570-0833/96/3505-0555 $ 15.00+.25/0*

Friedrich Hund,
aged 85,
at the lectern
(Photo: Ruth Müller, Göttingen)

Friedrich Hund and Chemistry

Werner Kutzelnigg*

Friedrich Hund, one of the few physicists still alive of the generation that pioneered quantum mechanics, celebrates his 100th birthday this year. This is an occasion to recall how much chemistry owes to him. The important contributions of Hund to theoretical chemistry will not be presented in a primarily historical context—the cooperation of Hund and Mulliken during the development of MO theory will, however, be duly discussed—but the stress will be on the impact of the concepts introduced by Hund on theoretical chemistry today. Nearly all methods of quantum chemical calculations presently in use have a first step based on Hund's MO theory. Hund recognized that the use of delocalized molecular orbitals does not necessarily conflict with a description of a molecule in terms of localized bonds. Moreover, he formulated conditions for localizability that are still pertinent today. The classification of the spectra of diatomic molecules by Hund in 1925 was virtually definitive. Recently Hund's rules, which, among other things, make predictions about the energetic ordering of states with different spin multiplicities within the same electronic configuration, have aroused renewed interest. The concept of atomic states of natural and unnatural parity plays a key role in this context. Hund's first two rules for atomic states have been found to be special cases of more general rules. Molecules can violate Hund's first rule through spin polarization and through the preference of different equilibrium geometries of the singlet and triplet states.

Keywords: history of chemistry · Hund, Friedrich · Hund's rules · MO theory

1. Introduction

Few physicists of the generation that pioneered quantum mechanics have played as important a role for chemistry as Friedrich Hund, who celebrates his hundredth birthday this year. His name is omnipresent in "Hund's rules"[1–3] and "Hund's coupling cases".[4, 5] The fact that Hund,[6] together with Mulliken,[7] laid the foundations of MO theory is also widely known. Hund's localization criteria[8] are probably only familiar to the readers of my textbooks[9] (in particular Vol. 2) and students who have had assignments on this topic.

This article reviews the above-mentioned contributions not from the angle of science history, but in terms of the role played by Hund's concepts in current theoretical chemistry.

2. Biographical Details

Friedrich Hund was born on February 4, 1896, in Karlsruhe. He studied in Göttingen and Marburg to become a high school teacher of mathematics, physics, and geography. Fortunately he changed his mind and decided to pursue an academic career. He obtained his doctorate in 1922 in Göttingen and while working as Max Born's assistent completed his habilitation in 1925. Already two years later he became associate professor at Rostock and a further two years later full professor in Leipzig, where Heisenberg and Debye were among his colleagues. He spent the winter of 1926/27 with Niels Bohr in Copenhagen as a visiting scientist, and in 1929 was a visiting professor at Harvard University. Further stations of his career included Jena in 1946, and Frankfurt in 1951, before, in 1956 he returned to Göttingen to take the chair once held by his mentor, Max Born. In 1965 Friedrich Hund became Professor Emeritus. He lectured until beyond his 90th birthday, primarily on the history of physics from the viewpoint of a contemporary witness. At the age of 95 he gave his farewell lecture at Göttingen on "What I Have Not Found".

Those of Hund's publications that are relevant to chemistry stem from the years 1925 to 1933. The particularly important papers on MO theory were written around 1927. For the breakthrough of MO theory, the cooperation with Robert S. Mulliken was of crucial importance. This aspect will be outlined in the next chapter.

Hund fulfilled the criteria that would have enabled him to serve as the "seed crystal" in Germany for a theoretical chemistry based on quantum mechanics. When I asked him many years later why he did not take this opportunity, he answered with his well-known humility that his knowledge of chemistry had been insufficient to take on this task. On another occasion

[*] Prof. Dr. Werner Kutzelnigg
Lehrstuhl für Theoretische Chemie
Ruhr-Universität Bochum
D-44780 Bochum (Germany)
Fax: Int. code +234-7094109
e-mail: werner.kutzelnigg@rz.ruhr-uni-bochum.de

 © VCH Verlagsgesellschaft mbH, D-69451 Weinheim, 1996 0570-0833/96/3506-0573 $ 15.00+.25/0

he said—and here his humility is somewhat less apparent—that he dealt with a topic only until all fundamental questions had been answered. He has repeatedly commented on his role in the early days of quantum chemistry.[10, 11] Hund speaks of the early history of quantum mechanical theories of chemical bonding, when the primary goal was a qualitative understanding, as "the happy days when the cream had not yet been scooped off the top".[10] In answer to my question, Hund might have also correctly pointed out that the German chemistry community in the 30s, and even later, was hardly ready to accept a physics-based theory. Erich Hückel, another pioneer of theoretical chemistry in Germany, had painful experiences in this field. His theory of π-electron systems[13, 14], which is based on Hund's MO theory, was scarcely appreciated by chemists in Germany, even though his brother Walter—an established chemist—worked hard to bridge the gap between theory and the chemistry of the day. Only in the 1960s, after Hückel's MO theory had become popular in England,[15] France,[16] and the United States,[17] did it become accepted in Germany. Robert Mulliken, who saw the foundation of theoretical chemistry as one of his most important tasks,[18] found much more favorable conditions in the United States, as the chemistry community there was less bound by tradition and, hence, more flexible. From hindsight, Hund's departure from chemistry in the early 1930s might not have been a mistake in the long run, especially as there remained enough for him to do in physics. But this is not the topic of this article and is being appraised elsewhere.[12] Suffice it to say that Hund's experience with the quantum theory of molecules could be applied to solids, for an understanding of which chemical knowledge was not so important.

Now a few remarks on my personal contacts with Friedrich Hund: I first met him in Paris in 1962 where he was giving a lecture at the Cité universitaire. By chance, I met him again the following weekend in Chartres, where we had the opportunity for a longer conversation. When I came to Göttingen at the end of 1964, I listened with great enthusiasm to a lecture of Hund on the history of quantum theory. Hund was a member of my habilitation committee, and of course the most prominent one. In 1976 I was asked by Jürgen Hinze to give a lecture at a symposium honoring Hund and Mulliken's 80th birthdays (Fig. 1) in Bielefeld. I titled it "Hund's Localization Criteria and Their Relevance to Chemistry". I had apparently coined that term and Hund did not appear to be too pleased. The gist of his

Fig. 1. Professors Mulliken (left) and Hund (right) on July 8, 1976, in Göttingen, Germany. (Photograph by courtesy of the *Neuen Westfälischen* newspaper.)

complaint was that he minded less being mentioned in the name index of a scientific publication than in the subject index. His place in the subject indexes of physics, however, was already well established by then.

I remember one detail from a conversation with Friedrich Hund particularly well. He explained to me that in order to understand a physical problem, he first examined it in the framework of classical physics. Then he would apply the correspondence principle. I responded that I had grown up with quantum mechanics, that classical mechanics and the correspondence principle were rather foreign to me, and that I rather regarded classical theory as a limiting case of quantum theory. Hund replied that this was a good reason for the mandatory retirement age for professors and that he would reach his in two years.

Hund is a particularly friendly and also a tolerant man. Nevertheless, he is very critical and cannot be easily fooled. His "stupid questions" after lectures at the "Physikalisches Kolloquien" in Göttingen were much feared, because they could be quite penetrating.

3. Hund and Mulliken

The cooperation between Hund and Mulliken, who were of the same age, proved particularly fruitful for the theory of chemistry. Actually, this was no conventional cooperation, for

Werner Kutzelnigg, born on September 10, 1933 in Vienna, studied chemistry in Bonn (Vordiplom in 1954) and Freiburg (Diplom 1958). He obtained his doctorate with R. Mecke in 1960, working on IR spectroscopy. He was a postdoctoral fellow in Paris with B. Pullmann and G. Berthier (1960–1963), and in Uppsala with P. O. Löwdin (1963/64). He completed his habilitation in Göttingen in 1967. From 1970–1973 he was H2/H3 professor at the TU Karlsruhe. Since 1973 he has been H4/C4 professor at the Ruhr-Universität Bochum. His research interests are in theoretical chemistry, in particular the development of new methods, with the emphasis on electron correlation in molecules, relativistic quantum chemistry, magnetic properties of molecules, theory of chemical bonding, intermolecular forces, and formal and mathematical aspects of theories.

as far as I know there are no joint publications by Hund and Mulliken. As an aside, neither Hund nor Mulliken had coauthors for most of their fundamental papers. Their cooperation consisted mainly of a mutual stimulation, in sometimes similar and sometimes complementary ideas. The two scientists met several times and, in a way, always at the right time. Mulliken has written nicely about these encounters.[19] Reading Mulliken's memoirs one is surprised at the ease with which he, in European terms merely a young "Privatdozent", approached the leading figures in his field, and not just his peers in terms of age and experience like F. Hund. Perhaps this unconventional behavior was tolerated because he was an American, whereas it would not have been accepted from a European. Recently Hund also commented in some detail on his cooperation with Mulliken in an introduction to Mulliken's autobiography *Life of a Scientist*.[20] Mulliken had made several trips to Europe during each of which he visited a number of countries such as England, France, Denmark, Germany, Switzerland, the Netherlands, Austria, and Italy. The itinerary of his first European trip in 1925 included Göttingen, where he met Hund for the first time. Hund had just finished his paper "Zur Deutung einiger Erscheinungen in den Molekel-Spektren",[4] in which he introduced the coupling cases later named after him, and was working on his book on atomic spectra.[3] Two years later Mulliken was in Göttingen again, and the cooperation with Hund on molecular spectra continued, also during a hiking trip to the Black Forest. Mulliken's publication "Assignment of Quantum Numbers for Electrons in Molecules", Part I and II,[7] appeared in 1928. He stated that the main ideas and methods were those that had been previously successfully applied by Hund.[6] However, he went beyond Hund's approach. He sent Hund a copy of the manuscript, upon which Hund answered that it overlapped closely with a paper that he had just finished. He did not want to duplicate anything and therefore left out all those details from his own manuscript[21] that he considered Mulliken had dealt with in his work. In the summer of 1929 Hund, Heisenberg, and Dirac were guests in Chicago, where Mulliken had recently been appointed full professor. In 1930 Mulliken traveled to Europe again and spent a large part of his time in Leipzig as Hund's guest. Erich Hückel was also in Leipzig during this period. In 1930 Hückel's publication "Die Quantentheorie der Doppelbindungen" appeared[13] and in 1931 his habilitation paper "Elektronenkonfiguration des Benzols und verwandter Verbindungen".[14] Hückel expressly built upon Hund's work. Mulliken was again in Leipzig in 1932/33, after which he and Hund did not meet again until 1953, when Hund was Professor at Frankfurt University.

Attempts to disentangle Hund's and Mulliken's contributions to the development of molecular orbital (MO) theory might attribute to Hund a primary interest in the fundamental physical concepts, whereas Mulliken was concerned with the actual application to problems of molecular spectra and to the theory of chemical bonding. Hund much more than Mulliken was involved in comparing alternative approaches. One should also not forget the contributions of other scientists, in particular Herzberg[22] and Lennard-Jones,[23] to the development of MO theory. At about the same time as MO theory was developed, another approach to the theory of molecules was proposed primarily by F. London.[24] It came to be known as the theory of spin valence, and is based on the idea of constructing the wave function of a molecule from those of the separate atoms. This is a generalization of the successful Heitler–London approach for the H_2 molecule (which will be discussed briefly in Chapter 4).[25] A related approach came from Heitler and Rumer,[26] and an important paper by Wigner and Witmer should also be mentioned in this context.[27] Another method based on the Heitler–London approach for H_2 is the valence bond (or HLSP method) of Slater[28] and Pauling,[29] in which Heitler–London type pair functions are assigned to the individual bonds.

While the theory of spin valence never became very popular, the valence bond (VB) theory turned out to be a serious competitor of MO theory. It was so successful, because it could be viewed as the visualization of the concept of mesomerism, which was then very popular in chemistry. Moreover, Mulliken's comprehensive papers[18, 31] were relatively difficult to read, in contrast to those of his opponent Linus Pauling,[29, 30] who quickly swayed chemists toward his theory. This is not the place to review critically the role of Pauling in the development of theoretical chemistry. Pauling certainly had a profound knowledge of quantum mechanics, but he was not averse to easy success, and did not always mind dubious simplifications; in critical situations, he relied more on his chemical intuition than on rigorous theory. It is in part due to Pauling's influence that the breakthrough of the MO theory took such a long time.

While today we use the terms molecular orbital theory or MO theory, coined by Mulliken, Hund referred less spectacularly to a "Zuordnungsschema" (correlation scheme).[6, 21] A key concept in his theory is what is now generally called a correlation diagram. Hund was the first to realize that molecules can be constructed from molecular orbitals, even if he did not yet use that term. He correctly classified the molecular one-electron states according to symmetry and correctly gave occupation schemes for molecular configurations. Instead of looking for a way to calculate the molecular orbitals explicitly, Hund essentially proposed interpolating them from the states of the united atom and those of the isolated atoms by means of a correlation diagram. From these diagrams (Fig. 2) one can see which MOs are bonding[22] and which antibonding ("loosening"). Coulson[32] said of a similar correlation diagram[9, 31] that it deserved a place next to the periodic system of the elements in every chemical institute.

The proposal to represent molecular orbitals as linear combinations of atomic orbitals (LCAO) goes back to Lennard-Jones.[23] Such an approach had previously been used by Pauling[33] for the H_2^+ ion. At this point, it might be noteworthy that the first quantitative MO calculations for diatomic molecules were performed at the end of the 1950s at the Mulliken Institute in Chicago by Clemens Roothan and coworkers.[34]

In 1966 Mulliken received the Nobel Prize in Chemistry for his work on MO theory. He repeatedly stressed that he would have liked to share this honor with his friend Hund. Erich Hückel would have also been a worthy corecipient.

Mulliken[19] mentioned that he never could understand why Hund (like, by the way, Sommerfeld) used the term "die Molekel", while all other German-speaking colleagues referred

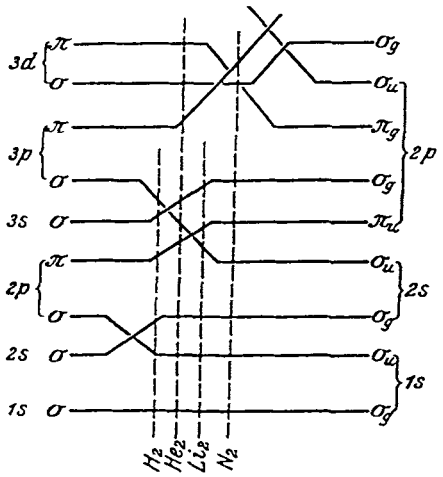

Fig. 2. Correlation diagram for the one-electron states in a homonuclear diatomic molecule (from Ref. [6d]).

to "das Molekül". A purist ought to argue that the correct German equivalent of the Latin "molecula" or French "la molecule" should be "die Molekel" in analogy to the Latin word "particula" (in French "la particule" and in German "die Partikel"), and in contrast to "calculus" ("le calcul" and "der Kalkül"). How "molecula" became "das Molekül" is hard to comprehend. Anyway, terminology has become established and "die Molekel" sounds artificial. An analogous situation arises in English: why is the word "molecule" and not "molecle"?

4. The Theory of Molecular Orbitals (MO Theory)

Even though Hund did not formulate MO theory—at least in his first papers—in terms of the LCAO approximation, this approach should be discussed here in this article, because it allows a clear comparison with the valence-bond method. Both the VB and the MO theory of molecules start with the theory of atoms. In the VB approximation, one attempts to construct the wave function of a molecule directly from those of the individual atoms. In MO theory, on the other hand, one regards the molecule as a unit and attempts to describe it like an atom, with the difference that several nuclei are present rather than one. In the older German literature the term "Methode der Molekülzustände" (method of molecular states) was popular for a while. The direct translation of Mulliken's term molecular orbital (Molekülorbital) is now standard, even in German. It is useful to recapitulate briefly the difference between the VB and MO descriptions using the H_2 molecule as example.

In view of the present special occasion I repeat something here that a reader of *Angewandte Chemie* is expected to be familiar with. More details can be found in my textbooks.[9] A look at overviews from the 1930s can also be recommended, in particular the book by Hellmann[35] and the article by VanVleck and Sherman.[36]

Let a and b be wave functions of the two isolated hydrogen atoms. In VB theory (which in this case is identical to the approach by Heitler and London),[25] one first formulates the product $a(\vec{r}_1)b(\vec{r}_2)$—which would be exact for noninteracting atoms. One then realizes that $a(\vec{r}_2)b(\vec{r}_1)$ is an equivalent description and that, for reasons of symmetry, the wave function must be either a (+) or a (−) linear combination of these two primitive product functions. The term $\vec{r}_1$ stands for the spatial coordinates of the first electron, $\vec{r}_2$ for those of the second electron. Hence there are, starting from the 1s functions of the isolated hydrogen atoms, two approximate wave functions for the molecule (Eq. (a)), where $N_\pm$ is a normalization factor, which is

$$\psi_\pm(1,2) = N_\pm\{a(\vec{r}_1)b(\vec{r}_2) \pm b(\vec{r}_1)a(\vec{r}_2)\} \quad \text{(a)}$$

different for the two functions. If these two wave functions are used to calculate the energy expectation value as a function of the internuclear distance R, as was first done by Heitler and London,[25] one obtains two potential curves. One of them is bonding and therefore describes the ground state of the H_2 molecule, while the other one is repulsive for all internuclear distances and does not represent a bonding state. Qualitatively, the bonding potential curve (E_{HL}) of the ground state of the H_2 molecule is rather similar to the exact potential curve (E_{ex}, Fig. 3).

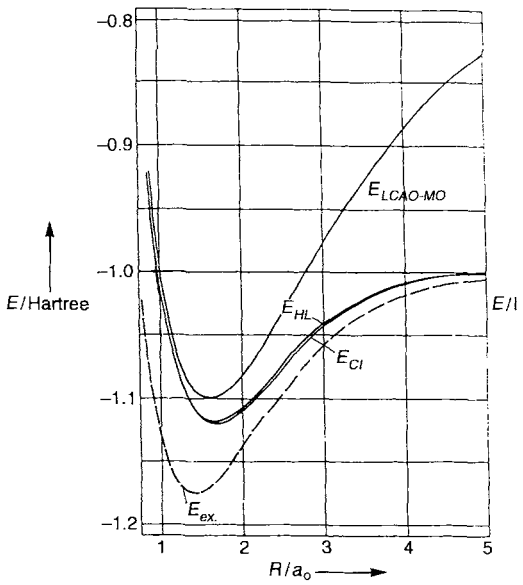

Fig. 3. Potential curves of the H_2 ground state according to the Heitler–London approximation, the LCAO-MO approximation, and the CI approximation, as well as the exact curve.

As mentioned above, in MO theory one regards the H_2 molecule as a unit. It is then described by a configuration of molecular orbitals, just like the He atom is approximated by a configuration of atomic orbitals. Corresponding to the ground state configuration of the He atom of $1s^2$, the ground state configuration of H_2 is $1\sigma_g^2$. Hence, the lowest-lying molecular orbital $1\sigma_g$ is doubly occupied. This molecular orbital is represented by a linear combination of the orbitals a and b of the isolated hydrogen atoms [Eq. (b)]. An antibonding MO $1\sigma_u$ can be constructed analogously [Eq. (c)]. The factors N_g and N_u serve to normal-

$$1\sigma_g(\vec{r}) = N_g\{a(\vec{r}) + b(\vec{r})\} \quad \text{(b)}$$

$$1\sigma_u(\vec{r}) = N_u\{a(\vec{r}) - b(\vec{r})\} \quad \text{(c)}$$

ize each MO to 1. Hence, the MO wave function of the H_2 ground state is given by equation (d).

$$\psi(\vec{r}_1,\vec{r}_2) = \sigma_g(\vec{r}_1)\sigma_g(\vec{r}_2) \quad \text{(d)}$$

A calculation of the energy expectation value as a function of the distance R between the two H atoms yields again a potential curve ($E_{LCAO\ MO}$) with a minimum in the vicinity of the actual equilibrium separation of the H_2 molecule. That is, the MO approach also describes the bonding (Fig. 3).

A comparison of the VB and MO functions for the H_2 ground state shows that the VB function is significantly better (Fig. 3). Both functions exhibit a minimum in the vicinity of the actual equilibrium separation in the H_2 molecule, but only the VB wave function behaves correctly for large distances, that is, the energy converges to the sum of the energies of two H atoms. The MO energy shows a physically unreasonable behavior at large internuclear separations; it is much too large. This defect of MO theory can be corrected, as the following discussion shows.

As is the case for atoms, molecular states may only be described by a single configuration (such as $1\sigma_g^2$) if this configuration is clearly separated in energy from other possible configurations. For large internuclear distances, however, the configurations $1\sigma_g^2$ and $1\sigma_u^2$ have nearly the same energy (and the same overall symmetry, $^1\Sigma_g^+$; the configuration $1\sigma_g 1\sigma_u$ has a different overall symmetry, $^1\Sigma_u^+$, and does not mix in). In this case, one must not use a single configuration to describe the molecule, but rather a linear combination of both configurations [Eq. (e)].

$$\psi(\vec{r}_1,\vec{r}_2) = c_1\sigma_g(\vec{r}_1)\sigma_g(\vec{r}_2) + c_2\sigma_u(\vec{r}_1)\sigma_u(\vec{r}_2) \quad \text{(e)}$$

This is called configuration interaction (CI). The potential curve that belongs to the MO-CI wave function (e) (E_{CI} in Fig. 3) gives the correct behavior for $R \rightarrow \infty$ and is overall a slightly better approximation for the exact potential curve than the VB approach. A proponent of the VB approximation would not give up at this stage, but would point out that a further improvement of the VB approach is also feasible. This consists of adding ionic structures, such as $a(\vec{r}_1)a(\vec{r}_2)$ and $b(\vec{r}_1)b(\vec{r}_2)$, where, in a sense, both electrons are located on the same atom. Indeed it can be shown that the MO approach with full configuration interaction and the VB approximation including all ionic structures are exactly equivalent.[37]

Once one proceeds beyond the H_2 molecule to more complex molecules, the MO approach does have some advantages over the VB description. Specifically, these are:

a) While the simple VB description fails for an ion-pair molecule, such as LiH, the ionic bond results naturally from MO theory. The valence MO of LiH is localized primarily on the H atom, that is, the MO description reflects the idea that a Li^+ and a H^- is present, between which there exists a Coulombic attraction. The VB theory, however, requires the inclusion of ionic structures even at the lowest level of approximation.

b) MO theory automatically yields the tetravalent nature of the carbon atom, for example in CH_4, while the VB approximation requires additional assumptions: in particular, a "valence state" is to be formed initially, and the atomic orbitals must hybridize before the chemical bond can be described.[28–30] Neither the concept of a valence state nor that of hybridization is required within the MO approximation.

c) Delocalized bonds, such as in benzene or even in H_3^+, follow automatically from the MO approach—the molecular orbitals are delocalized over the entire molecule—while in VB theory, one has to postulate the resonance of several valence structures. Hückel,[13, 14] in particular, recognized the potential of MO theory in this area and contributed greatly to its popularization (even if this occurred only relatively late in Germany).

d) The classification of the spectra of molecules, as well as the description of optical transitions, is much more straightforward with the MO theory than with the VB approach. The description of spectral transitions as excitations from an occupied to an unoccupied MO is often a good approximation. This is one of the reasons why Hund and Mulliken, who initially studied the analysis of molecular spectra, preferred MO theory.

e) The similarity in physical properties of isosteric compounds like N_2 and CO is readily understood on the basis of MO theory, whereas this is rather more difficult in the VB approach.[22]

f) MO theory can be much more easily and better handled than VB theory when it comes to practical calculations. Certainly, to Mulliken this argument was as important as statement d), because he was interested in real calculations of molecular structures.

g) Woodward and Hoffmann[38] intentionally based their theory of the orbital-symmetry control of electrocyclic reactions on MO theory. They employed correlation diagrams similar to those used by Hund, with the difference that the correlation was not between separated and united atoms, but between starting materials and products of a chemical reaction.

From Hund's point of view, a weak point of the Heitler–London approximation, which forms the basis of the method of spin valence[24] as well as of the VB method, was that it was originally formulated as a perturbation theory. The noninteracting atoms represented the unperturbed system. The interaction of the atoms is a rather unusual perturbation, as it also entails a change in symmetry. The extension of perturbation theory to the next higher order[39] caused unexpected difficulties, which were understood only later.[40–43] It is now known that such a perturbation approach does not converge except for H_2^+ and H_2,[40, 44, 45] even if the first order exists and is well defined.

One has to accept a certain hierarchy of approximation steps for both MO and VB theory. In the early days, it only appeared feasible to formulate theories with minimal basis sets.

The considerations about the H_2 molecule given above are based on such a minimal basis set, which is constructed from the *1s* orbitals of both the two H atoms. For the CH_4 molecule a minimal set for the C atom would include the orbitals 1s, 2s, $2p_x$, $2p_y$, and $2p_z$. Minimal basis sets never played an important role in ab initio MO calculations. The results obtained in this way are too inaccurate, and the extra effort with an enlarged basis set, for instance of the double-zeta kind (with about twice as many functions than the minimal set), is not all that much

bigger. In qualitative approaches or in a semiempirical version of the theory (where the integrals are not solved but used as adjustable parameters), one often employs minimal basis sets, for example in the CNDO (complete neglect of differential overlap) approximation[46] or in EHT (extended Hückel theory).[47]

While the semiempirical variant of MO theory is more or less consistent, there were fundamental difficulties with semiempirical VB theory, which were related to the nonorthogonality of VB structures. It was often incorrectly assumed that these structures were, in fact, orthogonal. One then attempted to compensate for this error by using physically unrealistic values for the exchange integrals (these exchange integrals in VB theory are not to be confused with the true two-electron exchange integrals that will play a role in the discussions in Chapter 6).[36] In an ab initio version of VB theory, it was necessary to explicitly account for the overlap integrals between valence structures, which lead to significant practical difficulties. This was one of the reasons why ab initio VB calculations have only played a marginal role. It was also unclear for a long time how a VB approximation using a non-minimal basis set should be formulated.

The MO calculations usually performed today employ basis sets that have very little in common with the atomic orbitals of the original LCAO-MO approximations. They can, however, be systematically enlarged to approach a complete basis set, and all occurring integrals can be readily evaluated.[48] This approach led to the SCF approximation or molecular Hartree–Fock theory, which began its conquest of this field in the 1960s. If one is interested not only in geometries close to the equilibrium structure, but also in the behavior at large distances from it—in which case MO theory becomes invalid in the single-configuration approximation—the SCF approximation has to be improved by including configuration interaction (CI).[49] In practical terms this is often difficult, but does not present any fundamental problems these days.

There have been repeated attempts to revive the VB approximation. Recently, the modern valence-bond theory has been propagated, in particular by Gerratt.[50] In this approach, one retains the formal structure of the VB functions; however, the atomic orbitals are not those of isolated atoms, but are strongly deformed. They are determined by the requirement that the total energy becomes minimized (similar to the MOs in ab initio SCF theory). For quite some time now, Goddard[51] has preferred the generalized valence bond (GVB) method. The term "generalized" is somewhat misleading, because the GVB structures are chosen to be orthonormal, which is a loss of generality relative to the original VB structures.

Nowadays, the choice between MO and VB has become obsolete. For precise calculations one uses the MO-CI method, which includes the VB approximation as a special case, or CI-like methods of the coupled-cluster (CC) type.[52] If very high accuracy is desired, neither MO-CI nor CC procedures are sufficient, and one has to employ wave functions that depend explicitly on the interelectronic coordinates.[53–56]

It should be realized that ab initio MO theory, including its improvements such as CI and CC, have a serious rival in density function theory.[57] This theory has been very popular in solid-state physics for some time, but is now also conquering chemistry. In essence, however, this alternative approach is also based on the MO concept. Only the electron interaction is evaluated differently from the usual ab initio methods. At least, one can interpret density function theory in this manner. Formally, the exchange interaction of MO theory (including self-exchange) is replaced by an exchange-correlation function. This has the effect of partially compensating for the errors of MO theory and of approximating correlation effects.

From today's vantage point, one can say that the MO approximation, proposed by Hund and Mulliken in 1927, has become fully accepted and the method of choice, although for a long time the VB approximation of Heitler, London, Slater, and Pauling was the more popular. Nowadays, MO theory is the basis for the qualitative understanding of the chemical bond and the properties of molecules, as well as the first step in sophisticated ab initio calculations.

5. Hund's Localization Criteria

The molecular orbitals of MO theory are generally delocalized over the entire molecule. The crystal orbitals in a solid behave similarly. In many cases, this delocalization is unavoidable and physically significant, for example in the case of metallic bonds. In other cases, however, delocalization conflicts with physical or chemical intuition. There are molecules and even crystals where the indications are that the bonds are localized. Hund was one of the first to recognize that there is no inherent contradiction between a localized and a delocalized description. The important issue is that some situations can be described with localized or delocalized functions, while others only correspond to the delocalized description. Diamond would be an example of the first case, sodium metal an example of the second.

In 1931 Hund[8] succeeded in formulating criteria that indicate when an equivalent localized formulation can be valid in addition to the always applicable delocalized description. The equivalence of the two approaches—if the localization criteria are satisfied—has a simple explanation, which was pointed out much later, in particular by Lennard-Jones et al.[58] A wave function in the form of a single Slater determinant is invariant with respect to a unitary transformation of the occupied orbitals. This is best explained with the example of the BeH_2 molecule.[9]

This linear, symmetrical molecule has in its ground state the MO configuration $1\sigma_g^2 2\sigma_g^2 1\sigma_u^2$, where the $1\sigma_g$ MO is essentially identical to the 1s AO (K shell AO) of Be, and $2\sigma_g$ and $1\sigma_u$ are symmetry adapted and delocalized over the entire molecule. In the LCAO approximation (that is, using a minimal basis set), $2\sigma_g$ and $1\sigma_u$ can be approximated by equations (f) and (g).

$$2\sigma_g = c_1 h_1 + c_2 s + c_1 h_2 \quad \text{(f)}$$

$$1\sigma_u = c_3 h_1 + c_4 p - c_3 h_2 \quad \text{(g)}$$

Here, h_1 and h_2 represent the 1s AOs of the two H atoms, while s stands for the 2s orbital and p for the $2p_z$ orbital of Be (z is the molecular axis). The symbols $c_1 - c_4$ are coefficients.

Contour diagrams of the $2\sigma_g$ and $1\sigma_u$ MOs resulting from a MO-SCF calculation are depicted in Figure 4a. If one assumes that s and p are equally capable of forming bonds to the H

atoms—which implies that $c_1 \approx c_3$ and $c_2 \approx c_4$—and takes into consideration that the total wave function does not change when $2\sigma_g$ and $1\sigma_u$ are replaced by linear combinations, for example φ_1 and φ_2 according to Equations (h) and (i), one can

$$\varphi_1 = \frac{1}{\sqrt{2}}(2\sigma_g + 1\sigma_u) \approx c_1\sqrt{2}\, h_1 + \frac{c_2}{\sqrt{2}}(s+p) \quad \text{(h)}$$

$$\varphi_2 = \frac{1}{\sqrt{2}}(2\sigma_g - 1\sigma_u) \approx c_1\sqrt{2}\, h_2 + \frac{c_2}{\sqrt{2}}(s-p) \quad \text{(i)}$$

now recognize that φ_1 and φ_2 are two approximately localized two-center molecular orbitals. Only the 1s AO of one H atom and one sp hybrid orbital of Be participates in each MO. This means that in this case a localized description is possible. Figure 4b shows the contour diagrams of the localized MOs φ_1 and

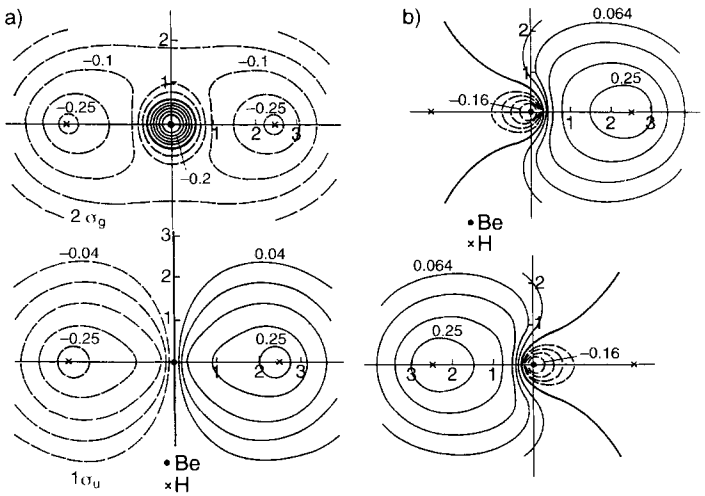

Fig. 4. Contour diagrams of the MOs of the BeH_2 molecule: a) canonical (delocalized), b) equivalent (localized) (from ref. [9]). The axes represent the distance from the Be core in units of a_0.

φ_2. The localization criteria that Hund formulated can be illustrated for this example. For each atom, three numbers have to be identical: 1) the number r of bound neighbors, 2) the number n of available valence electrons, and 3) the number t of valence atomic orbitals participating in the bonding. In BeH_2 these three numbers are 2 for the Be atom and 1 for each H atom.

The requirement that r, n, and t must be equal is a necessary condition for localization, which can be seen when one arbitrarily changes one of them. Let us assume, for example, that s and p do not participate equally in the bond, because, for example, p is too high in energy or overlaps poorly with h_1 and h_2. The conditions $c_1 \approx c_3$ and $c_2 \approx c_4$ would then no longer be valid, and the equivalent MOs φ_1 and φ_2, which could still be constructed according to Equations (h) and (i), would no longer represent two-center orbitals, but rather a four-electron, three-center bond. This is approximately the case in MgH_2, where the 3p orbital is much less involved in bonding than the 2p orbital in BeH_2. In this case, Mg only provides one valence AO. Of course, BeH_2 as well as MgH_2 fall between the limiting cases of systems with two-center bonds and those with a four-electron, three-center bond. BeH_2, however, is closer to the first case, whereas MgH_2 is closer to the second one.

Let us now remove an electron from BeH_2 and form the ion BeH_2^+! Now Be only provides one valence electron and Hund's localization criteria are no longer satisfied. Indeed, now the MO $2\sigma_g$ is doubly occupied, while $1\sigma_u$ is only singly occupied. One can still construct the localized MOs according to Equations (h) and (i), but there is no configuration of localized MOs that would be equivalent to $2\sigma_g^2 1\sigma_u$. Hence, BeH_2^+ can only be described as delocalized.

Further examples can be found in my textbook.[9] There one can also read how the localization criteria must be modified when semipolar or multiple bonds are present. The possibility that three critical numbers cannot be uniquely assigned is also discussed there.

Methane (CH_4) and diamond are examples of systems that can be described by localized two-center bonds: the three numbers r, n, t are equal to 4 for each C atom. The situation is different for benzene or graphite. If one looks at the σ-system, all three numbers are equal to 3. In the case of the π-system, however, two neighbors are present in benzene and three in graphite, while per carbon atom only one electron and one p-AO are available. Hence, a description using localized π-bonds is not possible. An extreme case in terms of non-fulfillment of the Hund's localization criteria is illustrated by a cubic-closest-packed lattice of atoms with one valence electron per atom. The number of neighbors is 12, the number of available valence orbitals is 4 (s, p_x, p_y, p_z), and the number of available valence electrons per atom is 1. Of course, it is a characteristic of the metallic bond that it cannot be described by localized two-center bonding.

6. Hund's Rules

Friedrich Hund's name appears in the literature probably most frequently in connection with Hund's rules. This is somewhat surprising as these rules originate from one of Hund's earliest scientific publications: "Zur Deutung verwickelter Spektren, insbesondere der Elemente Scandium bis Nickel"[1] ("On the interpretation of complex spectra, particularly of the elements scandium to nickel") from 1925. The quantum mechanical tools to interpret these spectra were then available in rudimentary form only. One was aware, for example, that the angular momentum in the central field is a constant of motion, and the Pauli principle was known. Quantum mechanics enabled the possible terms for a given electronic configuration to be stated, but it was necessary to resort to empirical analyses of spectra to order them in terms of energy. Hund made the remarkable observations that (as quoted from ref. [1]) (1) the energetically lowest lying term of an electron configuration always has the highest possible spin multiplicity (2) among the terms with the highest spin multiplicity, the one with the largest angular momentum quantum number L appears to be lowest in energy.

Hund later formulated these rules in somewhat more precise terms,[3] but did not give a quantum mechanical explanation. He did not state under which conditions these rules are valid, even though one can conclude from the context that they apply to energetically low-lying configurations with at most one open shell with $l > 0$, that is, for example to 1s2p or $1s^2 2s^2 2p^4$. For

such configurations, Hund's rules hold surprisingly well. Those who have criticized Hund's rules have often intentionally assumed that they are valid almost unconditionally in order to find many exceptions.

A few years after the publication of Hund's rules, Slater presented his theory of the spectra of complex atoms.[59] If one restricts this theory to two-electron configurations with only a single angular momentum L, one immediately notes that, in agreement with Hund's rules, the triplet state is lower in energy than the singlet state. Slater, however, also found configurations, albeit having more than one open shell with $l>0$, that apparently contradicted Hund's rules, while his theory was in accord with experimental results. Slater therefore declared Hund's rules obsolete. Hund himself no longer mentioned them in his 1933 review article for the Handbuch der Physik.[60] Despite their popularity, Hund's rules are mentioned almost by the way in textbooks on the electronic structures and spectra of atoms,[61-63] and caution is advised when applying them.

Hund also formulated a third rule,[2, 3] which is less commonly associated with his name. This rule concerns the spin–orbit interaction and predicts whether a normal or an inverted multiplet is present. Even though the explanation of this rule requires relativistic quantum mechanics, which did not yet exist in 1925, Hund quite correctly traced this third rule to a magnetic interaction between angular momentum and electron spin.

It is remarkable that Hund's first two rules have enjoyed continuous popularity until now, and that one usually turns to them first when the ordering of energy levels in a configuration needs to be predicted. Apparently the prevailing opinion is that Hund's rules are based on some fundamental physical principle, even if one does not fully understand it. Particularly for the theory of molecules Hund's first rule has become invaluable, though Hund did not initially consider this aspect (the second rule does not apply to molecules).

In order to understand Hund's rules, it is useful to look at the special case mentioned above where only the first rule is relevant, because a configuration then has, for example, only a single value of L (like in a 1s2s or 1s2p configuration) or because L is not defined (as in molecules). We shall limit the discussion to a two-electron system (or a system with two electrons outside a closed shell). For the configuration $\varphi_1\varphi_2$, a singlet and a triplet wave function can be constructed; the spin-independent parts are given by (j) and (k) and the corresponding energies by (l) and (m) where h_1 and h_2 are single-electron contributions,

$$^1\psi = \frac{1}{\sqrt{2}}[\varphi_1(1)\varphi_2(2) + \varphi_2(1)\varphi_1(2)] \quad \text{(j)}$$

$$^3\psi = \frac{1}{\sqrt{2}}[\varphi_1(1)\varphi_2(2) - \varphi_2(1)\varphi_1(2)] \quad \text{(k)}$$

$$^1\mathrm{E} = h_1 + h_2 + (11|22) + (12|21) \quad \text{(l)}$$

$$^3\mathrm{E} = h_1 + h_2 + (11|22) - (12|21) \quad \text{(m)}$$

(11|22) is a Coulomb integral, and (12|21) is an exchange integral. It can now be shown that such exchange integrals are always positive.[64, 65] This directly implies that ^3E is lower than ^1E.

In this proof, it was assumed that the two states can be described exactly by (j) and (k) and that the orbitals φ_1 and φ_2 are the same for both states. Both assumptions are only approximately justified.[66, 67] It can be shown[65, 67] that $^3E<{}^1E$ remains valid if one allows different orbitals for the two states. Even though in such an improved description the difference between (l) and (m) is no longer equal to twice the exchange integral (12|21), this integral remains the critical quantity that determines the energetic ordering. If one deviates from the single-configuration description, $^3E<{}^1E$ is no longer rigorously valid, that is, electron correlation effects (not accounted for in the single-configuration model) can lead to violations of Hund's first rule. These kinds of violations are rather rare, however. The violations of Hund's first rule due to the spin polarization[68] are more interesting. These arise for certain molecules, but rarely for atoms, and will be discussed in more detail at the end of this chapter.

At this point, it is tempting to see an analogy between the singlet and triplet functions (j, k) of an atom and the VB wave functions (a) of an H_2 molecule. A fundamental difference, however, lies in the fact that the two functions φ_1 and φ_2 in Equations (j) and (k) are orthogonal, so that the energy difference between ^1E and ^3E according to Equations (l) and (m) is given by a genuine two-electron exchange integral. Such integrals are positive, so ^3E must be lower in energy than ^1E. The atomic orbitals a and b of the VB function for H_2 are not orthogonal, but overlap strongly, and this overlap is at the very origin of the bonding. Furthermore, the exchange integrals of the VB approximation still contain single-particle contributions. All this leads to the a bonding singlet state lower in energy than the antibonding triplet state. This has nothing to do with Hund's rule. One of the conditions for its validity is the orthogonality of the involved atomic or molecular orbitals.

Things become more complicated when several values of L are possible for a configuration, that is, when both of Hund's rules must be considered.

The simplest example is the configuration p^2, for which the energetic ordering of the possible terms is $^3P<{}^1D<{}^1S$. The fact that ^3P is lowest in energy is apparently in agreement with Hund's first rule, but is not immediately obvious in light of the considerations discussed above. One could come to the conclusion that the relationship $^1D<{}^1S$ is a manifestation of Hund's second rule. The energetic ordering of terms for a d^2 configuration, $^3F<{}^1D<{}^3P<{}^1G<{}^1S$, indicates that this is indeed premature. As required by Hund's first rule, a triplet term, ^3F, is lowest in energy, and the second rule applies as well inasmuch as $^3F<{}^3P$. The ordering indicates, however, that the second rule does not apply to terms other than those with the highest multiplicity (in this case, not for the singlet terms, as ^1D lies lower than ^1G). It is rather strange that Hund's second rule should apply to the triplet, but not the singlet terms. Things get even more intriguing when we consider states with two open shells, like pp′ (for example 2p3p) or pd configurations. For pp′, there are singlet and triplet terms for P, D, and S. The lowest-lying term in this case is ^1P, a clear violation of both Hund's first and second rules.

This was known to some extent in the late 1920s. Russell and Meggers[68] formulated the alternating rule especially for two-electron states: Among the two-electron terms from two open

shells with minimum and maximum total angular momentum quantum numbers defined according to (n) and (o), something

$$L_{max} = l_1 + l_2 \quad (n)$$

$$L_{min} = |l_1 - l_2| \quad (o)$$

similar to Hund's first rule holds for L_{max} and L_{min}, as well as $L_{max} - 2$, $L_{max} - 4$, ... $L_{min} + 2$, that is, the triplet is lower in energy than the singlet, while for $L_{max} - 1$, $L_{max} - 3$ etc., the order is inverted, and the singlet lies below the triplet. Hence, for pp' configurations $^3D < {}^1D, {}^1P < {}^3P$, and $^3S < {}^1S$. This rule does not, however, predict why ^1P is the lowest of all states.

There have been attempts to make the alternating rule plausible, but a convincing explanation has only been given recently.[65] The key lies in the distinction between states of natural and unnatural parity.

The parity of an atomic state is defined as its behavior upon the coordinate transformation $\vec{r} \rightarrow -\vec{r}$. It is readily apparent that orbitals with $l = 0, 2, 4$ (that is, s,d,g...) have even parity, while those with $l = 1, 3, 5$ (that is, p,f,h...) have odd parity. For a multielectron atom, the parities of the orbitals must be multiplied. Hence the configuration p^2 has even parity, the configuration p^3 odd parity, d^2 and d^3 are both even, dp is odd, etc.

While for one-electron states, every angular momentum l has exactly one associated parity, both parities (even and odd) are possible for each L for multielectron states. It is useful to label states like S_g, P_u, D_g, etc. as having natural parity, while S_u, P_g, D_u, etc. are labeled as states of unnatural parity.[69] For one-electron states, only natural parity is possible, that is, s_g, p_u, d_g, etc. Among the states of configuration d^2 (which are all even), ^1S_g, ^1D_g, and ^1G_g have natural parity, whereas ^3P_g, ^3F_g have unnatural parity. In this case, all triplet states show unnatural parity. For the configuration dd', however, ^1S_g, ^3S_g, ^1D_g, ^3D_g, ^1G_g, and ^3G_g have natural parity, and ^1P_g, ^3P_g, ^1F_g, ^3F_g have unnatural parity. The alternating rule can now be formulated as follows: Among the terms of a two-electron configuration with the same L, the triplet state is lower in energy for states of natural parity, while the singlet state is lower in energy for states of unnatural parity.

This statement has been rigorously proven, under the assumption that the states could be described by a single configuration.[65] The proof contains several complicated and nontrivial steps and will not be given here. However, a fundamental physical concept that forms the basis for the alternating rule will be presented here.

A discussion of the analytical behavior of the solutions of a two-electron Schrödinger equation reveals that in the limit $r_{12} \rightarrow 0$ (r_{12} is the interelectronic distance), there are exactly three possibilities:[69]

1) $\psi(r_{12}) \sim r_{12}^0$ = const: relative s wave
2) $\psi(r_{12}) \sim r_{12}$: relative p wave
3) $\psi(r_{12}) \sim r_{12}^2$: relative d wave

Case 1 is realized for a singlet state of natural parity, case 2 for a triplet state (either natural or unnatural parity), and case 3 for a singlet state of unnatural parity. If one plots the probability density that the distance between the electrons is close to $r_{12} = 0$ (Fig. 5), one recognizes the typical correlation cusp for case 1, the well-known Fermi hole that keeps the electrons apart, for case 2, and--and this is the surprising feature--an even broader symmetry hole for case 3.

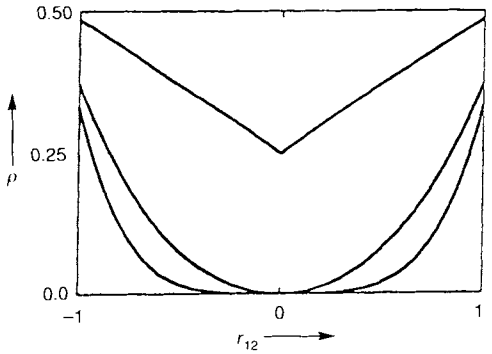

Fig. 5. Schematic representation of the probability density ρ for finding two electrons at a distance r_{12} for a singlet state of natural parity (top), a triplet state (center), and a singlet state of unnatural parity (bottom).

In a singlet state of unnatural parity, the electrons avoid each other even more strongly than in a triplet state, which results in a reduction of the electron–electron repulsion (assuming that both states have the same orbitals). This makes it at least plausible why the energy of such a state is lower than that of the corresponding triplet state.

Hund's 100th birthday stimulated me to continue earlier joint work with J. D. Morgan and think in more detail about Hund's rules,[65, 69] concentrating mainly on their physical foundation, range of validity, and extension to situations where they do not apply in their original form.[70]

This collaboration was the source of some surprising results, which confirmed that, up to now, no rigorous explanation of Hund's second rule has been attempted. Details can be found in a publication on this topic.[70] The pertinent results are the following:

1) The ordering of the mean values of the energy for the singlet and triplet terms of a two-electron configuration for the same angular momentum quantum number L (as functions of L) is governed by two effects:

a) the electrostatic interaction of the non-totally symmetric parts of the orbital density, which are dominated by quadrupole-like charge densities. This interaction is determined by the coefficient $a_2(L)$ of Slater's theory.[59] This $a_2(L)$ is a fourth-order polynomial in L. The minimum of $a_2(L)$, for sufficiently large l_1 and l_2, is found when (p) is valid.[70]

$$L + \tfrac{1}{2} \approx (l_1 + l_2 + 1)/\sqrt{2} \quad (p)$$

b) the short-range electrostatic interaction, which is markedly smaller for states of unnatural parity than for those of natural parity, as only for the former does the probability that $\vec{r}_1/r_1 = \vec{r}_2/r_2$ vanish.[70]

2) The alternating rule determines how the singlet–triplet mean values are split into a singlet and a triplet term.[65, 68]

The energetic ordering of $^3P < {}^1D < {}^1S$ for p^2 configurations and $^3F < {}^1D < {}^3P < {}^1G < {}^1S$ for d^2 configurations follows directly from these new rules. One finds, however, that, for example for an h^2 configuration, Hund's second rule no longer applies (the ground state is not ^3M with $L = 9$, but ^3K with $L = 7$). It also follows that the ground state for a 2p3d configura-

tion is ^1P. Our analysis suggests that it is somewhat accidental that Hund's second rule apparently applies well to triplet states of two-electron atoms, but not to the singlet states.

Interestingly, Hund's rules in their original form are valid for the ground states of nearly all atoms for which Z is small enough to allow the states to be described by L and S. A remarkable exception is Ce, which has a ground state configuration $\ldots 4f5s^2 5p^6 5d$, the ground state being ^1G_u, in agreement with the alternating rule.[65]

Before concluding this section, a few words are in order about Hund's rules for molecules. Its importance for chemistry can, for example, be illustrated by the observation that a review article by Berson on metaquinoid compounds[71] contains a separate chapter about Hund's rules. Apart from linear molecules, such as O_2 (for which the terms are $^3\Sigma_g^- < {}^1\Delta_g < {}^3\Sigma_g^+$), only Hund's first rule plays a role for molecules. It applies surprisingly well, but there is a remarkable class of exceptions, which was analyzed in particular by Kollmar and Staemmler.[72]

Cyclobutadiene is the classic example for a violation of Hund's first rule as a consequence of spin polarization. In this molecule with a planar, square structure, the bonding π-MO φ_1 is fully, that is, doubly, occupied, while the degenerate π-MOs φ_2 and φ_3 are half-occupied, with two of four possible electrons. These MOs are represented in Figure 6. In terms of Hund's rule,

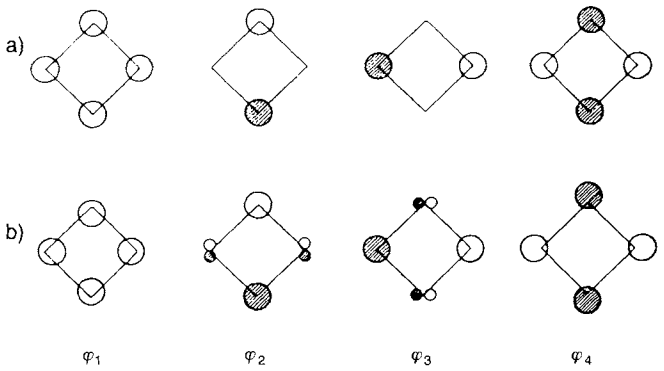

Fig. 6. Schematic representation of the π MOs of cyclobutadiene according to ref. [72] without (a) and with (b) d-function participation.

the exchange integral between the two degenerate π-MOs φ_2 and φ_3 is responsible for the singlet–triplet splitting. As these two MOs overlap only minimally (this is a special characteristic of the fourfold symmetry), the exchange interaction is also extraordinarily small. The spin polarization of the doubly occupied bonding MO by the singly occupied, degenerate MOs, on the other hand, is relatively big. This spin polarization can be understood on referring to Figure 7.

In a first approximation, the MO φ_1 is doubly occupied, that is, $\varphi_1\alpha$ and $\varphi_1\beta$ are each singly occupied. If the electron in MO φ_2 has, for example, α-spin, then $\varphi_1\alpha$ and $\varphi_1\beta$ experience a different field and become spin polarized. This is taken into account by replacing $(\varphi_1\alpha)(\varphi_1\beta)$ with $(\varphi_1'\alpha)(\varphi_1''\beta)$, that is, a single MO φ_1 is replaced by two different MOs φ_1' and φ_2''. The singly occupied φ_3-MO leads similarly to a spin polarization. The total spin polarization depends upon whether φ_2 and φ_3 are coupled to a singlet or a triplet. In the former case (Fig. 7a), a spin polarization is possible for which φ_1' and φ_1'' are linear

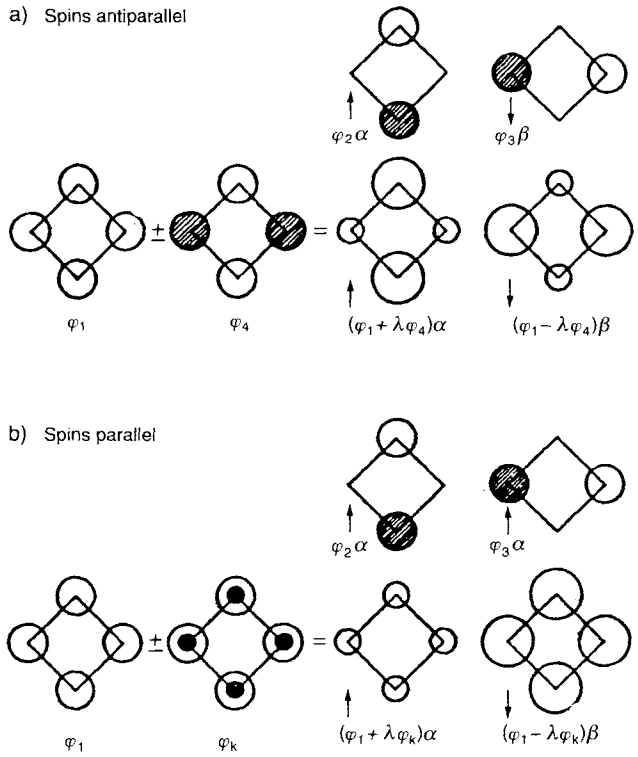

Fig. 7. Explanation of the spin polarization in cyclobutadiene according to ref. [72].

combinations of the π-MOs φ_1 and φ_4. This is particularly effective because φ_4 is low in energy. If φ_2 and φ_3 are coupled to a triplet, there is only a spin polarization by mixing in an MO of the same symmetry as φ_1 formed from the $3p_z$ AO. This leads only to a small energetic stabilization. Overall, this spin polarization, and the ensuing lowering of the energy, is larger for the singlet state than for the triplet state. This effect overcompensates for the exchange effect, so that the singlet state ends up lower in energy than the triplet state.

Actually, the situation for the cyclobutadiene molecule is even more complicated, because in addition to the above-mentioned effect, which counteracts Hund's rule, there is a second effect in the same direction. It is, namely, possible to lower the energy of the singlet state by distorting the C_4 frame from a square into a rectangular structure. This distortion, termed a pseudo-Jahn-Teller effect, does not effect the triplet state. If one compares the lowest-lying singlet and triplet states in their respective equilibrium geometries, one finds that the singlet state is distinctly lower in energy than the triplet state, and the pseudo-Jahn-Teller stabilization becomes more important than the spin polarization (which is the deciding factor if one compares identical geometries).

The fact that for two states of the same configuration sometimes the triplet and sometimes the singlet state is lower in energy is generally not only connected to Hund's rule, but also related to the mechanisms that dictate the equilibrium geometry of the two states.

The classic example for the singlet–triplet competition is the CH_2 species. The potential energy diagrams of the lowest triplet and singlet states as a function of the HCH angle are shown in Figure 8a. From the Walsh diagram in Figure 8b it can be seen that the highest doubly occupied MO, $1\pi_u$ is doubly degenerate

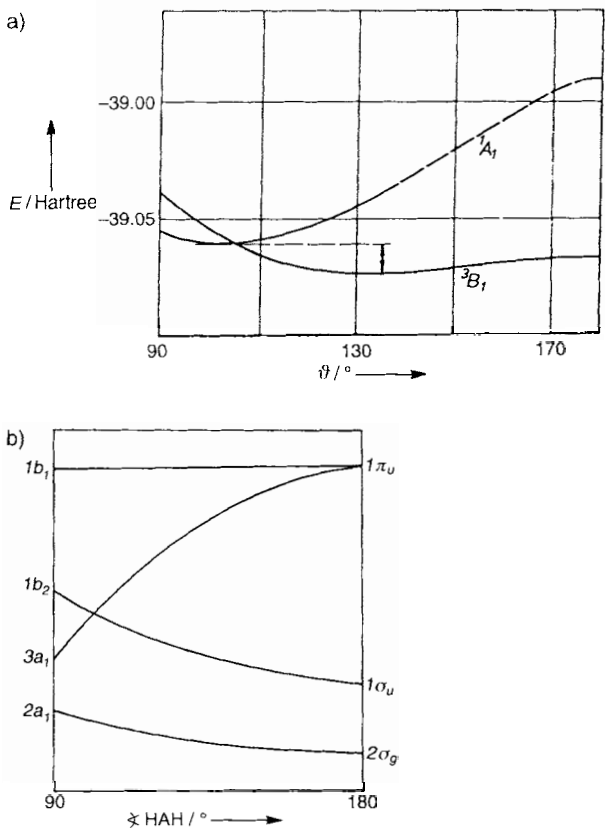

Fig. 8. a) Potential energy curves of the lowest singlet and triplet states of CH_2 as functions of the HCH angle ϑ (from ref. [9]). b) Walsh diagram for AH_2 molecules. For a bent geometry, $2a_1$, $1b_2$, and $3a_1$ are each doubly occupied in lowest singlet state of CH_2

in the limiting case of linear geometry. According to Hund's rule, for this geometry the triplet state lies lower, provided this degenerate MO is occupied. For HCH angles close to 90°, the difference in energy between the two components $1b_1$ and $3a_1$ of the original $1\pi_u$-MOs is so large, that, following the Aufbau principle, the lower-lying $3a_1$ MO prefers to be doubly occupied, and the ground state is a singlet. For angles between these extremes the Aufbau principle competes with Hund's rules. This leads to different equilibrium geometries for the singlet and the triplet state. The actual difference in energy between the two minima is rather small. There is no longer any doubt that the $^3CH_2$ is approximately 10 kcal mol^{-1} more stable than $^1CH_2$.[9, 73]

I hope that this presentation of Hund's rules has shown that they still are of great importance today, although they are only rules and not theorems. In each instance where they do not apply, a physically remarkable effect is involved. The study of actual or apparent violations of Hund's rules allows a better understanding of the physics of atoms and molecules.

7. Hund's Coupling Cases

For Hund's coupling cases we can be brief. These cases deal with the classification of band spectra of diatomic molecules, which Hund, in his fundamental papers,[4, 5] essentially accomplished. His formulation is still the basis for the analysis of these spectra today, as Herzberg's book makes plain.[74] These coupling cases are less interesting for a regular chemist than for a molecular spectroscopist. They are only relevant for those diatomic molecules that have a nonzero angular momentum about the molecular axis or a nonzero spin, like, for example, O_2 and NO.

One can characterize the state of a molecule in which the nuclei and electrons move by a few angular-momentum-like quantities,[74] such as

J = total angular momentum
N (or R) = angular momentum of the nuclear motion (perpendicular to the nuclear axis)
L = electronic angular momentum
Λ = projection of L onto the molecular axis
S = electron spin
Σ = projection of the spin onto the molecular axis
J_a = $L + S$ = total electronic angular momentum
Ω = $\Lambda + \Sigma$ = projection of J_a onto the molecular axis

In a strict sense only the total angular momentum J is a constant of motion—and, hence, suitable for the classification of states.

If in the Hamiltonian the interaction terms between different partial angular momenta are small, other quantities can also be regarded as almost good quantum numbers and can be used to characterize states. For light atoms, for example, the spin–orbit interaction is small and one can characterize atomic states to a good approximation by J, L, and S, where L and S primarily determine the energy level, while J only leads to a small splitting. This is referred to a Russell-Saunders (or LS) coupling. For molecules there are correspondingly more possibilities.

Hund's coupling case a) assumes that the interaction between nuclear and electronic motion is weak, but also that the motion of the electrons is referred to the nuclear axis, even in a rotating molecule. Here the projection Ω of the electronic angular momentum (including spin) onto the nuclear axis is well-defined. Ω and the nuclear rotation N couple to give the total angular momentum J. Figure 9 shows that a rotational progression is built up on each fine structure level.

In case b) the coupling of the spin to the molecular axis is negligibly small. This case occurs frequently when L = 0. Here

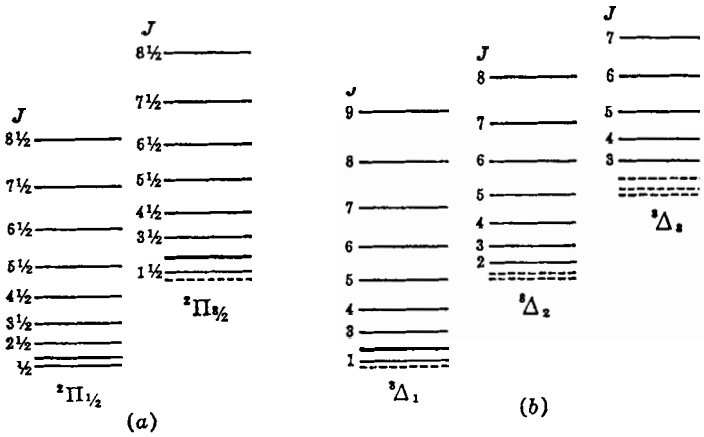

Fig. 9 Term scheme for the Hund coupling case a) for a diatomic molecule (according to ref. [74]) for a ^2P (a) and a ^3D state (b).

L and N couple to give a total angular momentum K without spin contribution. Interaction with spin then leads to a fine structure splitting of the rotational levels. Hence, one finds rotational progressions with fine structure splitting of each rotational level (Fig. 10).

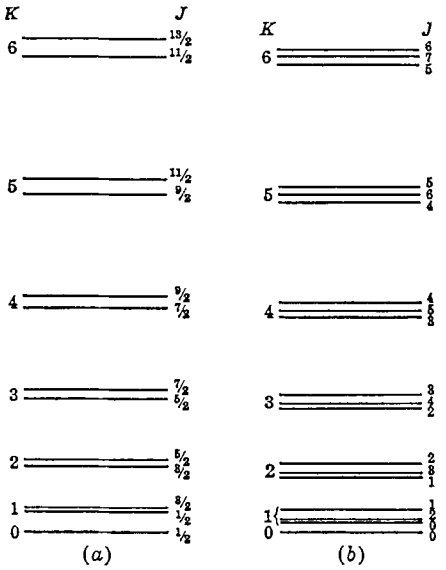

Fig. 10. Term scheme for the Hund coupling case b) (according to ref. [74]) for a ^2S (a) and a ^3S state (b).

The coupling cases c), d), and e) are less important. In case c) the interaction between L and S is stronger than the interaction with the molecular axis. This occurs particularly for molecules with at least one very heavy atom. In case d) the interaction between L and the molecular axis is weak, but the interaction with the rotational axis is strong. Case e) resembles d), but the interaction between L and S is strong and must be considered first.

In practice, transitions between the different coupling cases become important. These have been extensively discussed by Herzberg.[74]

8. Qualitative or Quantitative Theory?

Upon reading Hund's original papers,[1-6, 8, 21] one always realizes that he strives for simplicity and clarity. This is equally true for his textbooks[75] and other papers.[76] Instead of long mathematical derivations, one finds readily visualizable arguments. In the early days a nomenclature different from the present was used, but this does not make the reading difficult (for example, atomic quantum numbers were half-integral). For Hund, apparently "understanding" enables one to present a simple image of reality that is also convincing to a nonexpert. In view of this attitude of Hund it is questionable whether modern numerical ab initio quantum chemistry, which is based on the MO theory founded by Hund, can claim him as one of its fathers. Mulliken's position in this respect leaves no doubt. He not only encouraged numerical calculations, but also performed them himself after his retirement, at IBM in San José. He is certainly a pioneer of ab initio theory.

Did Hund then prefer qualitative to quantitative theory? In this context, a critical assessment of the progress of modern numeric quantum chemistry is in order. The solution of the Schrödinger equation for an atom or molecule with many electrons to any desired degree of accuracy seemed hopeless in the pioneering era of quantum mechanics; today it is feasible. Dirac[77] once stated that all of chemistry is in the Schrödinger equation, but that its solution was so difficult that it would never be achieved. With hindsight one can say that Dirac could not anticipate the advances in computer technology. Nevertheless, he did suggest that techniques should be developed to approximate solutions of the Schrödinger equation "without too much computation", which one can interpret as the suggestion to adjust the level of approximation to the available computer power.

As an alternative to the previous definition of understanding, one could also argue that understanding means that one can make predictions. While the simple qualitative theories available in the early days of quantum chemistry succeeded in explaining experimental observations, predictions based on them were uncertain at best, and even risky. Nowadays, however, in many areas reliable predictions are possible. Present-day computer chemistry is popularly caricaturized as a black box theory. Basically the black box predicts the same results that would be obtained from an experiment, if this could be performed, but gives no information about what happens between input and output. A long time ago, E. P. Wigner[78] argued that such a black box – if it were available, which it was not at the time – would hardly contribute to our understanding. This opinion, together with a manifest, and often irrational, disdain for numerical theory was very popular in researchers of Wigner's generation (there are no indications of this in F. Hund's work). I believe this is based on a misunderstanding.

On one hand, such a black box can give useful information that is not accessible by experiment. Theory, on which, after all, the black box is founded, can look at situations that are inaccessible to experiment. Theory can focus on a single molecule, while experiment usually has to deal with an ensemble of molecules under certain external conditions of pressure, temperature, etc. Theory can easily prepare a single quantum state of a molecule. It can study extremely short-lived molecules, even transition states of chemical reactions. It can artificially suppress certain mechanisms (such as hyperconjugation or d-orbital participation), and much more. All this means that the black box furnishes a lot of information that allows a better interpretation or classification of experimentally observed phenomena.

There is also a further aspect. The approaches used in modern quantum chemical calculations are rarely of a brute force type lacking transparency between input and output. To some extent Monte Carlo-type methods belong to this group. Most methods, however, are based on initial assumptions, which are successively improved. For instance, one usually starts with MO theory and then improves it by means of configuration interaction. It is often meaningful to notice that a certain observation can already be explained in the framework of MO theory, and that nothing crucial changes upon inclusion of configuration interaction. On the other hand, there are phenomena that can only be accounted for beyond the MO approximation, namely, those that depend strongly on the electron correlation. Likewise,

some experimental results can be understood in terms of a nonrelativistic theory, while others require a relativistic approach. Similarly, one can distinguish between effects that can be rationalized within the framework of the Born–Oppenheimer approximation while others cannot be explained within this approximation. It is thus generally possible to define models, that is, simplified theoretical approaches, and to specify phenomena that are understandable on the basis of a particular model. Without doubt some phenomena have simple explanations, while other empirical observations are the result of the interplay of several different, often opposing contributions. For those, it may be extremely difficult to give qualitative explanations. Many physical effects can finally be fully explained in different, and at first glance contradictory, ways that are nevertheless equivalent. W. H. E. Schwarz has given some convincing examples.[79] One has, of course, to face the argument that this approach for explaining chemical observations requires a certain hierarchy of approximations, which makes it somewhat arbitrary. But one can also consider other types of hierarchies or look for explanations that are independent of the chosen hierarchy, for example, in terms of observables only. Whether one should dispense with nonobservables altogether is a matter of discussion.

Even though the mere laconic statement that the explanation of a chemical finding lies in the Schrödinger equation certainly does not impart any understanding, modern quantum chemistry does contribute to the explanation by providing not only the black box, but also models, illustrations, and concepts, whose importance should not be underestimated.

At this point a few comments on reductionism are in order. In the present context, reductionism means, in simplified form, that chemistry can be derived from physics. This concept is plausible according to modern knowledge, but it is not entirely undisputed. The question of reductionism was not relevant for Hund, because for him molecules were objects of physics and therefore subject to physical explanations. If one wants to enter a realm of chemistry that is not just the theory of the physical properties of molecules, it makes sense to ask whether there are intrinsically chemical qualities that do not arise from quantum mechanics. Primas, among others, has dealt with this question.[80] He has pointed out, that reductionism is already relevant within physics in the context of the derivation of thermodynamics from statistical mechanics. Even though this derivation is correct and useful, thermodynamics can also be defined axiomatically without any reference to the statistical derivation. Thermodynamics contains qualities that are not a direct consequence of its atomistic, statistical mechanics derivation. The thermodynamic functions are, for example, classical, that is, commuting variables, that have no place in the framework of quantum theory. Whether there can be an axiomatic basis for chemistry, as for thermodynamics, and what the classical variables corresponding to the thermodynamic functions would look like, is yet unknown.

A famous example of a classical concept that has no place in quantum theory –at least in that of stationary states—is the chirality of molecules. There is an apparent paradox, namely that stationary states must be adapted to the symmetry of the Hamiltonian operator, so chiral molecules should not exist at all. Hund[81] has resolved this apparent paradox by pointing out that stationary states are only realized if the time scale of the measurement is large relative to the time for the tunneling between the nonstationary states of two optical isomers, which may even be larger than the age of the universe. Then stationary states are not realized.

It is questionable whether it is possible to specify more precisely some of the simplified concepts that are rather popular in qualitative theoretical chemistry, such as resonance or electronegativity, in order to use them, like the thermodynamic functions, without having to rely on their derivation from quantum mechanics. I regard it unlikely that drastically simplified theories, which often contain semiempirical corrections, can contribute more to the understanding of chemistry than exact quantum chemical calculations, since the predictive power of such simplified theories is small. However, the last word may not yet have been said in this context.

From Friedrich Hund we can learn to separate the essential from the marginal aspects and to search for simple explanations even for very complex phenomena, without, of course, forcing theory beyond its limits.

My thanks are due to D. Herschbach for suggesting that I write this article, to W. Lüttke for many valuable suggestions, to V. Staemmler as well as C. van Wüllen for reviewing the manuscript, and to E. Heilbronner for constructive comments. I am grateful to D. D. Morgan for helping with the English version.

Received: October 6, 1995 [A136IE]
German version: *Angew. Chem.* **1996**, 629
Translated by Dr. W. C. Wilisch, Ansbach (Germany)

[1] F. Hund, *Z. Phys.* **1925**, *33*, 345.
[2] F. Hund, *Z. Phys.* **1925**, *33*, 855.
[3] F. Hund, *Linienspektren und periodisches System der Elemente*, Springer, Berlin, **1927**.
[4] F. Hund, *Z. Phys.* **1926**, *36*, 45.
[5] F. Hund, *Z. Phys.* **1926**, *36*, 657; *ibid.* **1927**, *42*, 93; *ibid.* **1928**, *52*, 601.
[6] a) F. Hund, *Z. Phys.* **1926**, *36*, 257; b) *ibid.* **1927**, *40*, 742; c) *ibid.* **1927**, *43*, 788; d) *ibid.* **1930**, *63*, 719.
[7] R. S. Mulliken, *Phys. Rev.* **1928**, *32*, 186, 761.
[8] F. Hund, *Z. Phys.* **1931**, *73*, 1, 565; *ibid.* **1932**, *74*, 1.
[9] W. Kutzelnigg, *Einführung in die Theoretische Chemie, Vol. 1: Quantenchemische Grundlagen*, VCH, Weinheim, **1992**; *Vol. 2: Die chemische Bindung*, 2nd ed., VCH, Weinheim, **1994** (first editions **1975** and **1978**, respectively).
[10] F. Hund, *Angew. Chem.* **1977**, *89*, 89; *Angew. Chem. Int. Ed. Engl.* **1977**, *16*, 87.
[11] „Wie haben die Physiker die Chemie verstanden?": F. Hund, *Phys. Bl.* **1973**, *29*, 310.
[12] J. Hajdu, *Z. Phys.*, in press.
[13] E. Hückel, *Z. Phys.* **1930**, *60*, 423.
[14] E. Hückel, *Z. Phys.* **1931**, *70*, 204.
[15] C. A. Coulson, *Proc. R. Soc. London A* **1938**, *164*, 383; *ibid.* **1939**, *169*, 413; C. A. Coulson, G. S. Rushbrooke, *Proc. Cambridge Philos. Soc.* **1940**, *36*, 193; C. A. Coulson, H. C. Longuet-Higgins, *Proc. R. Soc. London A* **1947**, *191*, 39; *ibid.* **1948**, *193*, 456.
[16] B. Pullman, A. Pullman, *Les théories électroniques de la chimie organique*, Masson, Paris, **1952**.
[17] A. Streitwieser, *Molecular Orbital Theory for Organic Chemistry*, Wiley, New York, **1961**.
[18] R. S. Mulliken, *J. Chem. Phys. Phys. Chim. Biol.* **1949**, *46*, 497, 675.
[19] R. S. Mulliken, *J. Chem. Phys.* **1965**, *43*, S2.
[20] R. S. Mulliken, *Life of a Scientist: An Autobiographical Account of the Development of Molecular Orbital Theory with an Introductory Memoir by Friedrich Hund*, Springer, New York, **1989**.
[21] F. Hund, *Z. Phys.* **1928**, *51*, 759.
[22] G. Herzberg, *Z. Phys.* **1929**, *57*, 601.
[23] J. E. Lennard-Jones, *Trans. Faraday Soc.* **1929**, *25*, 668.
[24] F. London, *Z. Phys.* **1928**, *46*, 455; *ibid.* **1928**, *50*, 24; *ibid.* **1930**, *63*, 245.
[25] W. Heitler, F. London, *Z. Phys.* **1927**, *44*, 455.
[26] W. Heitler, G. Rumer, *Z. Phys.* **1931**, *68*, 12.
[27] E. Wigner, E. E. Witmer, *Z. Phys.* **1928**, *51*, 859.
[28] J. C. Slater, *Phys. Rev.* **1931**, *37*, 481.

[29] L. Pauling, *J. Am. Chem. Soc.* **1931**, *53*, 1367.
[30] L. Pauling, *The Nature of the Chemical Bond*, Cornell University Press, Ithaka, **1938**.
[31] R. S. Mulliken, *Rev. Mod. Phys.* **1930**, *2*, 60, 506; *ibid.* **1931**, *3*, 89; *ibid.* **1932**, *4*, 1.
[32] C. A. Coulson in *Molecular Orbitals in Chemistry, Physics and Biology* (Eds.: B. Pullman, P. O. Löwdin), Academic Press, New York, **1964**.
[33] L. Pauling, *Chem. Rev.* **1928**, *5*, 173.
[34] C. C. J. Roothaan, *Rev. Mod. Phys.* **1960**, *32*, 179; C. C. J. Roothaan, L. M. Sachs, A. W. Weiss, *ibid.* **1960**, *32*, 194; B. J. Ransil, *ibid.* **1960**, *32*, 239; P. E. Cade, K. D. Sales, A. C. Wahl, *J. Chem. Phys.* **1966**, *44*, 1973.
[35] H. Hellmann, *Einführung in die Quantenchemie*, F. Deuticke, Leipzig/Wien, **1937**.
[36] J. H. van Vleck, A. Sherman, *Rev. Mod. Phys.* **1935**, *7*, 167.
[37] J. C. Slater, *Phys. Rev.* **1930**, *35*, 509; *J. Chem. Phys.* **1951**, *19*, 220.
[38] R. B. Woodward, R. Hoffmann, *The Conservation of Orbital Symmetry*, Verlag Chemie, Weinheim, **1970**.
[39] R. Eisenschitz, F. London, *Z. Phys.* **1930**, *60*, 491.
[40] P. Claverie, *Int. J. Quantum Chem.* **1971**, *5*, 273.
[41] W. Kutzelnigg, *Int. J. Quantum Chem.* **1978**, *14*, 101.
[42] W. Kutzelnigg, *J. Chem. Phys.* **1980**, *73*, 343.
[43] D. M. Chipman, J. D. Bowman, J. O. Hirschfelder, *J. Chem. Phys.* **1973**, *59*, 2830.
[44] W. Kutzelnigg, *Chem. Phys. Lett.* **1992**, *195*, 77.
[45] W. H. Adams, *J. Math. Chem.* **1992**, *10*, 1.
[46] J. A. Pople, D. P. Santry, *Mol. Phys.* **1963**, *7*, 269.
[47] R. Hoffmann, *J. Chem. Phys.* **1963**, *39*, 1397.
[48] S. F. Boys, *Proc. Soc. London A* **1950**, *200*, 542.
[49] I. Shavitt in *Modern Theoretical Chemistry, Vol. III, Methods of Electronic Structure Theory* (Ed.: H. F. Schaefer III), Plenum, New York, **1977**, p. 129.
[50] J. Gerratt, *Adv. At. Mol. Phys.* **1971**, *7*, 141; P. B. Karadakov, J. Gerratt, D. L. Cooper, M. Raimondi, *J. Chem. Phys.* **1992**, *97*, 7637.
[51] W. A. Goddard, *Phys. Rev.* **1967**, *157*, 73, 81, 93.
[52] F. Coester, H. Kümmel, *Nucl. Phys.* **1960**, *17*, 477; J. Cizek, *J. Chem. Phys.* **1966**, *45*, 4256; R. J. Bartlett, *J. Phys. Chem.* **1989**, *93*, 1697; W. Kutzelnigg, *Theor. Chim. Acta* **1991**, *80*, 349.
[53] E. A. Hylleraas, *Z. Phys.* **1928**, *48*, 469; *ibid.* **1928**, *51*, 150.
[54] S. A. Alexander, H. J. Monkhorst, R. Roeland, K. Szalewicz, *J. Chem. Phys.* **1990**, *93*, 4230; R. Bukowski, B. Jeziorski, K. Szalewicz, *ibid.* **1994**, *100*, 1366.
[55] W. Kutzelnigg, W. Klopper, *J. Chem. Phys.* **1991**, *94*, 1985; R. Röhse, W. Klopper, W. Kutzelnigg, *ibid.* **1993**, *99*, 8830; J. Noga, W. Kutzelnigg, *ibid.* **1994**, *101*, 7738; W. Klopper, *ibid.* **1995**, *102*, 6168.
[56] V. Cencek, J. Komasa, J. Rychlewski, *Chem. Phys. Lett.*, **1995**, *246*, 417.
[57] W. Kohn, L. J. Sham, *Phys. Rev. A* **1965**, *140*, 1133.
[58] J. E. Lennard-Jones, *Proc. Soc. London A* **1949**, *198*, 1, 14; J. E. Lennard-Jones, J. A. Pople, *ibid.* **1950**, *202*, 166; *ibid.* **1951**, *210*, 190; G. G. Hall, J. E. Lennard-Jones, *ibid.* **1950**, *202*, 155, 336; *ibid.* **1951**, *205*, 357.
[59] J. C. Slater, *Phys. Rev.* **1929**, *34*, 1293.
[60] „Allgemeine Quantenmechanik des Atom- und Molekelbaus": F. Hund in *Handbuch der Physik, Band 24/1* (Eds.: H. Geiger, K. Scheel), 2nd ed., Springer, Berlin, **1933**, p. 36.
[61] E. U. Gondon, G. H. Shortley, *The Theory of Atomic Spectra*, Cambridge University Press, **1935**.
[62] M. Weissbluth, *Atoms and Molecules*, Academic Press, New York, **1978**.
[63] R. D. Cowan, *The Theory of Atomic Structure and Spectra*, University of California Press, Berkeley, **1981**.
[64] G. Racah, *Phys. Rev.* **1943**, *62*, 460.
[65] J. D. Morgan, W. Kutzelnigg, *J. Phys. Chem.* **1993**, *97*, 2415.
[66] D. A. Katriel, *J. Chem. Phys.* **1972**, *56*, 4236; R. Pauncz, D. A. Katriel, *Adv. Quantum Chem.* **1977**, *10*, 143.
[67] J. P. Colpa, *Mol. Phys.* **1974**, *28*, 581.
[68] H. N. Russell, W. F. Meggers, *Bur. Stand. (U.S.) Sci. Pap.* **1927**, *22*, 364.
[69] W. Kutzelnigg, J. D. Morgan, *J. Chem. Phys.* **1992**, *96*, 4484.
[70] W. Kutzelnigg, J. D. Morgan, *Z. Phys.*, in press.
[71] J. A. Berson in *The Chemistry of the Quinoid Compounds* (Eds.: S. Patai, Z. Rappoport), Wiley, New York, **1988**, p. 455.
[72] H. Kollmar, V. Staemmler, *J. Am. Chem. Soc.* **1977**, *99*, 3586; *Theor. Chim. Acta* **1978**, *48*, 223.
[73] D. C. Comeau, I. Shavitt, P. Jensen, P. R. Bunker, *J. Chem. Phys.* **1989**, *90*, 6491.
[74] G. Herzberg, *Spectra of Diatomic Molecules*, Van Nostrand, Princeton, **1950**.
[75] F. Hund, *Materie als Feld*, Springer, Berlin, **1954**; „Quantenmechanik der Atome": F. Hund in *Handbuch der Physik, Band 36* (Ed.: S. Flügge), Springer, Berlin, **1956**, p. 1; *Theorie des Aufbaus der Materie*, Teubner, Stuttgart, **1961**; *Geschichte der Quantentheorie*, Bibliographisches Institut, Mannheim, **1967**; *Grundbegriffe der Physik*, Bibliographisches Institut, Mannheim, **1969**; *Geschichte der physikalischen Begriffe*, Bibliographisches Institut, Mannheim, **1972**.
[76] F. Hund, *Z. Elektrochem.* **1957**, *61*, 891; *Stud. Gen.* **1965**, *18*, 174.
[77] P. A. M. Dirac, *Proc. Soc. London A* **1929**, *123*, 713.
[78] E. P. Wigner, F. Seitz in *Solid State Physics, Vol. 1* (Eds.: F. Seitz, D. Turbull), Academic Press, New York, **1955**, p. 97.
[79] W. H. E. Schwarz, S. Y. Chu, F. Mark, *Mol. Phys.* **1983**, *46*, 603.
[80] „Chemistry, Quantum Mechanics, and Reductionism": H. Primas, *Lect. Notes Chem.* **1981**, *24*.
[81] F. Hund, *Z. Phys.* **1927**, *43*, 805.

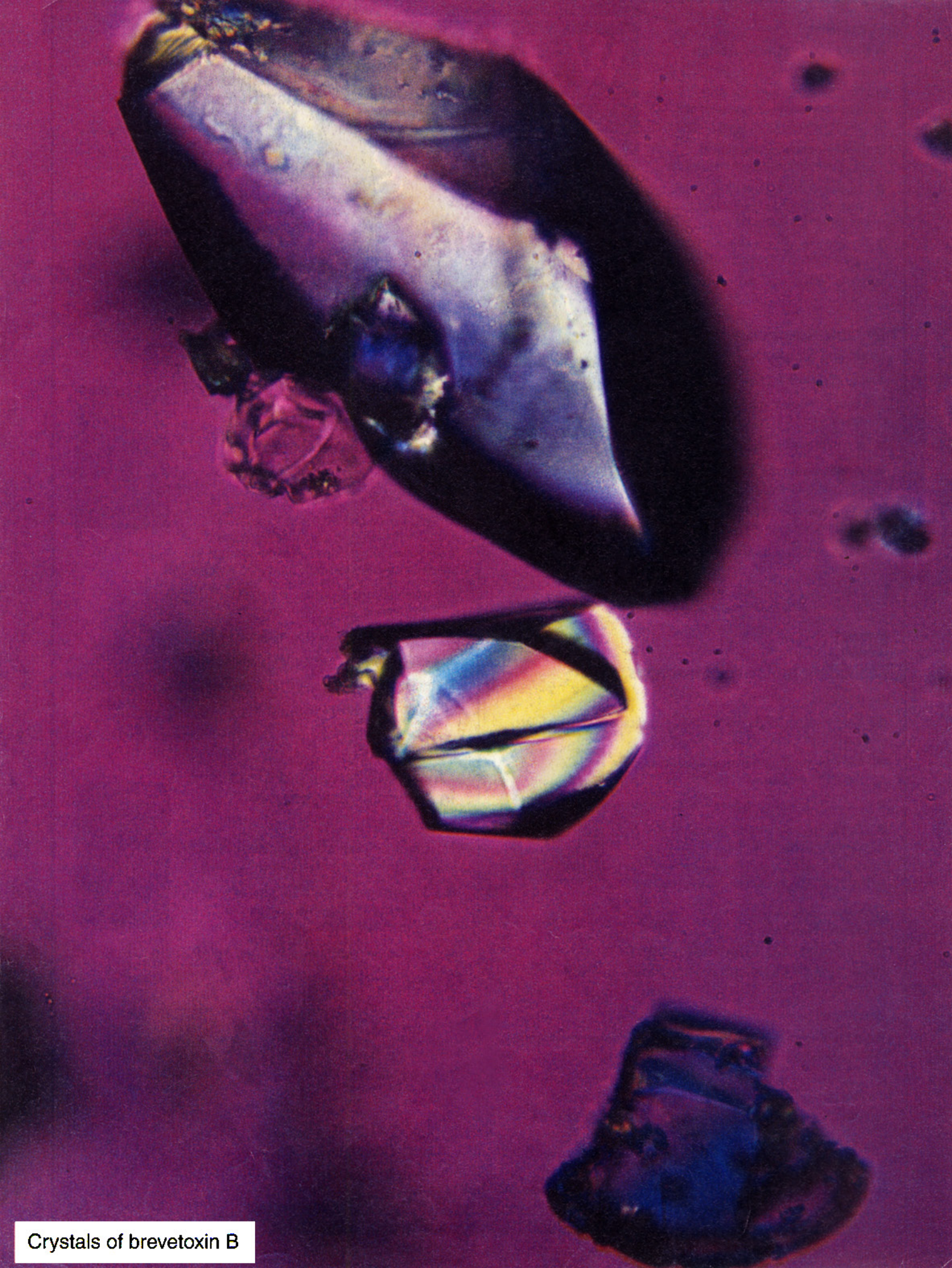

Crystals of brevetoxin B

The Total Synthesis of Brevetoxin B: A Twelve-Year Odyssey in Organic Synthesis

Kyriacos Costa Nicolaou*

Dedicated to Professor Elias J. Corey on the occasion of his 65th birthday

The total synthesis of brevetoxin B has been achieved recently after a long search for a suitable pathway. This twelve-year odyssey[1] in synthetic organic chemistry was marked by several strategic and tactical routes, and resulted in numerous new synthetic methods. This article is a behind-the-scenes account of the total synthesis of brevetoxin B, from its origins at the University of Pennsylvania to its completion at the University of California, San Diego, and The Scripps Research Institute, La Jolla, California.

Keywords: brevetoxin B · natural products · total syntheses

1. Introduction

One day in November 1981, while scanning through the latest issue of the chemistry journal with the gray cover, I came to an abrupt halt on page 6773. There it was: the imposing and beautifully complex structure of brevetoxin B (**1**) (Fig. 1).[2] Only rarely before or since, has the structure of a molecule, natural or designed, evoked in me the same feeling of awe and admiration. My instincts as a synthetic chemist were, no doubt, responsible for the pause, after which I immediately proceeded to read the entire paper, something I rarely do nowadays I have to admit. The paper by Lin, Clardy, Nakanishi, et al.[2] began with the gloomy lines: "A dense growth, or bloom, of dinoflagellates can occur under certain favorable conditions, causing a phenomenon descriptively known as 'red tide'. Blooms of the dinoflagellate *Ptychodiscus brevis* Davis (*Gymnodinium breve* Davis) have caused massive fish kills, mollusk poisoning, and human food poisoning along the Florida coast and in the Gulf of Mexico..." and ended with an appropriately striking statement: "Brevetoxin B is made up of a single carbon chain locked into a rigid ladder-like structure consisting of 11 contiguous trans-fused ether rings. There is no precedent for this extraordinary structure, and in addition, a plausible biogenetic scheme is not obvious..." (see Fig. 1 for structure and computer-generated models).

It was love at first sight! I was intrigued, challenged, and excited by brevetoxin's exquisite and fascinating regularity. I was attracted by the opportunity I recognized in the molecule for the discovery and development of new reactions and novel synthetic strategies, and by its important and deadly biological activity (vide infra), and simply by the sheer thought that I had

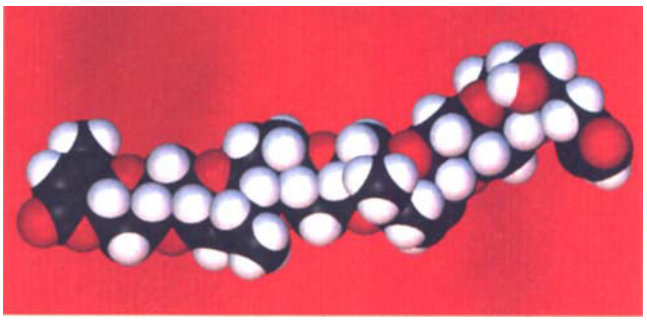

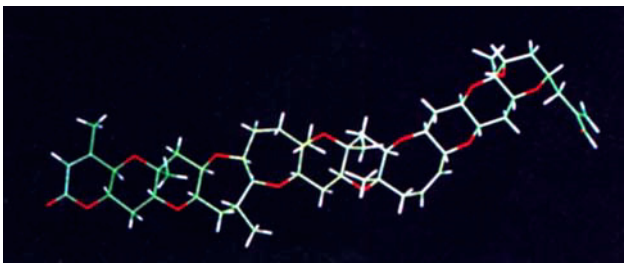

Fig. 1. Structural formula (middle) and computer-generated models of brevetoxin B (**1**).

[*] Prof. Dr. K. C. Nicolaou
Department of Chemistry, The Scripps Research Institute
10666 N. Torrey Pines Road, La Jolla, CA 92037 (USA)
Fax: Int. code +(619)554-6738
and
Department of Chemistry and Biochemistry
University of California, San Diego
9500 Gilman Drive, La Jolla, CA 92093 (USA)

 © VCH Verlagsgesellschaft mbH, D-69451 Weinheim, 1996 0570-0833/96/3506-0589 $ 15.00+.25/0

no idea how to even begin to synthesize it! I considered the wealth of new insights and findings my students and I would encounter in our journey to this formidable target. But worries also crept into my mind, leaving me in a difficult dilemma: What if we never finish the synthesis? What if we end up chasing an elusive goal while our competitors make progress in other, more attainable projects? It would clearly be a treacherous and risky project, I concluded, but surely, just like the Odyssey,[1] an adventurous and, it was hoped, rewarding journey.

Still vacillating whether to commit ourselves to the total synthesis of such a formidable target, I opted to postpone the final decision until I heard from the National Institutes of Health (NIH), where a proposal would be dispatched as soon as we had formulated a synthetic plan. This way, I would not only buy more time to think about taking such a gamble, but also I would benefit from the comments of other, more senior colleagues evaluating my plans. This maneuver, of course, carried the risk that the project could end abruptly as a major embarrassment if the study section members found my plans totally ridiculous.

Before proceeding with the "synthetic odyssey," it is interesting at this point to review briefly the history of the "red tides," the catastrophic phenomena with which brevetoxin B (**1**) is associated.

2. History of the Red Tides

"...and the waters that were in the river were turned to blood. And the fish that was in the river died; and the river stank and the Egyptians could not drink of the water of the river..."

Exodus 7:20–21

This passage in the Bible describes an occurrence in roughly 1000 BC which could be the first recorded incident of a "red tide" phenomenon. Red tide is the common name given to vast blooms of single-celled algae[3–6] called phytoplankton, which constitute the base of the marine food chain. Although only a few dozen of the approximately 5000 species of algae known today are implicated in toxin production, the red tide phenomenon can be catastrophic to marine life, including fish, shellfish, and mammals such as dolphins and whales. Humans can also be endangered by the red tides through eating poisonous seafood and general environmental pollution. The name red tide is derived from the color of some of these blooms, which is due to the dense growth of algae containing the carotenoid pigment peridinin.[7] In the broader sense, however, the term red tide is used to describe all such phenomena in which brown or green colorations are observed or even cases without visible discoloration. These catastrophes are quite common today and occur periodically in most parts of the world, causing major environmental, economic, and health problems. Figure 2 shows dramatic pictures from four red tides near the Japanese coast, and Figure 3 shows fish killed during an outbreak of a red tide off the coast of Florida.

The first modern-day incident of human poisoning with shellfish contaminated by a red tide was recorded in 1793 when Captain George Vancouver and his crew landed in British Columbia in the area known today as Poison Cove. Captain Vancouver noted that the native Indians considered it dangerous to eat shellfish when the seawater was colored by algae blooms.

A famous red tide incident, which has been repeated every year ever since, was the October 1972 outbreak in which a massive bloom stretched from Maine to Massachussets on the east coast of the United States. The outbreak followed a September hurricane that originated in the Gulf of Mexico and presumably carried the poisonous algae with it to the New England coast. 1972 was also a disastrous year for Japanese fisheries. In a severe red tide occurrence an estimated $ 500 million worth of caged yellowtail fish were killed in the Seto Inland Sea.

The story of the fourteen humpback whales that suddenly died off the coast of Cape Cod, Massachussetts in 1987 is, perhaps, one of the most striking events due to a red tide.[3,4] Investigators later traced the cause of death of the whales to the saxitoxins, a group of powerful biotoxins produced by the algae *Alexandrium tamarense*, which had been eaten by mackerel, the main food of the humpback whales. At about the same time that year, and in two different incidents along the coast of North Carolina, several hundred people were poisoned from bathing in the ocean and consuming local seafood. The victims complained of diarrhea, dizziness, respiratory problems, eye irritation, and other symptoms, which all pointed to neurotoxic poi-

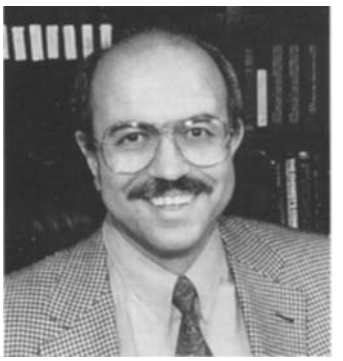

K. C. Nicolaou was born in Cyprus and received his Ph.D. degree from the University of London under the direction of F. Sondheimer and P. Garratt. After postdoctoral work at Columbia University with T. Katz and at Harvard University with E. J. Cory, in 1976 he joined the faculty at the University of Pennsylvania, where he was promoted to Rhodes-Thompson Professor of Chemistry. In 1989 he accepted joint appointments as Professor of Chemistry at the University of California, San Diego and as Darlene Shiley Professor of Chemistry and Chairman of the Department of Chemistry at The Scripps Research Institute. His awards include a Guggenheim Fellowship, a Humboldt Senior American Scientist Award, the American Chemical Society Award for Creative Work in Synthetic Organic Chemistry, the American Chemical Society's Gunther Award, the Dr. Paul Janssen Prize for Creativity in Organic Synthesis, and the Nichols medal. He has received honorary degrees from the Universities of Pennsylvania, London, and Athens. Nicolaou's research interests focus on chemical synthesis, molecular design and recognition, and the biological function of molecules. He is the author of 350 publications, 45 patents, and two books. A new textbook by Nicolaou, "Classics in Total Synthesis: Targets, Strategies, Methods" (Coauthor: E. J. Sorensen) was published by VCH in January 1996.

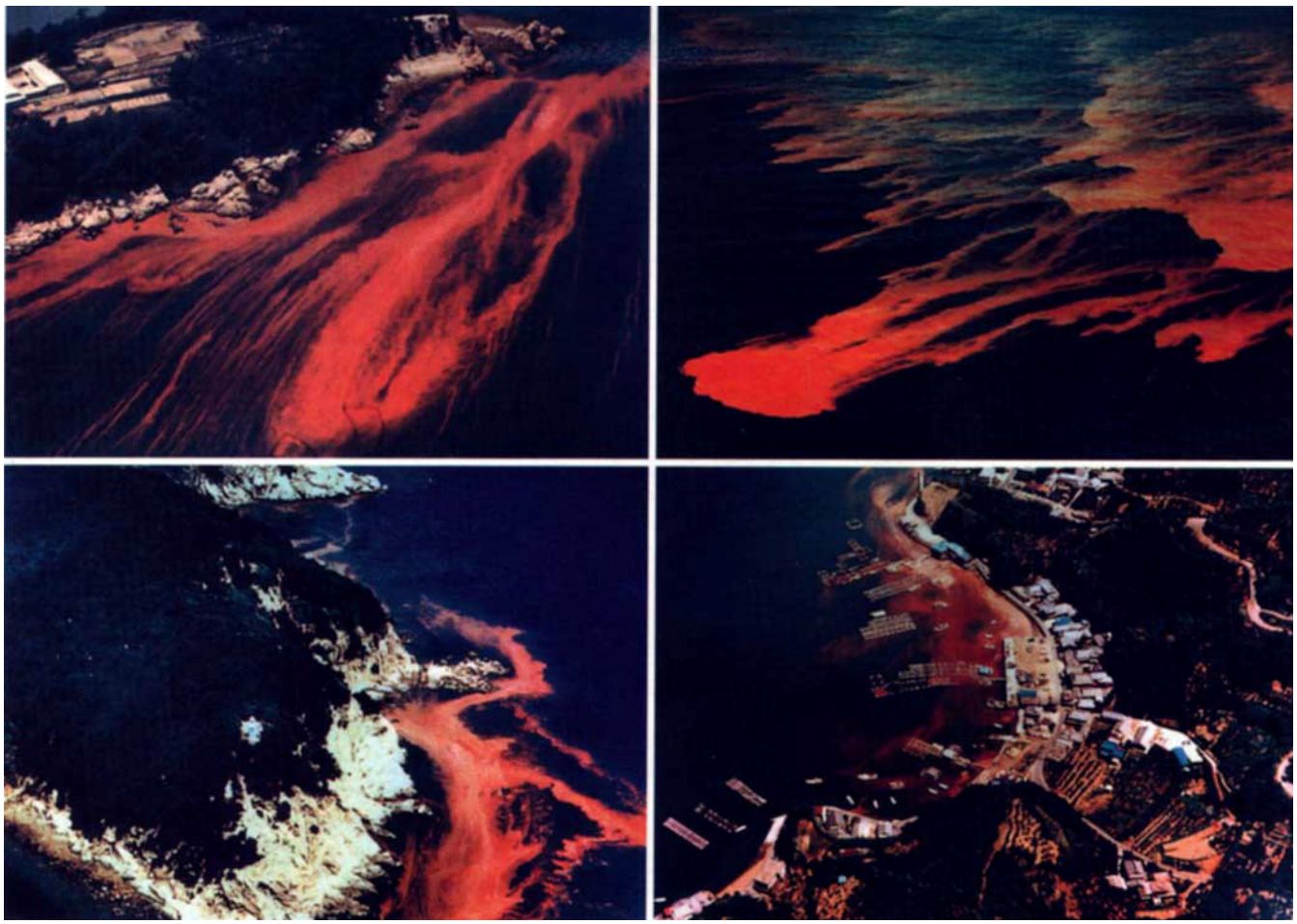

Fig. 2. Top left: A red tide on June 16, 1974, near Otafu Island, Okayama Prefecture, Japan. Top right: A red tide on May 6, 1976, approaching the coast of Oshima Island, Tokushima Prefecture, Japan. Bottom left: A red tide on May 8, 1976, off the coast of Matsushima Island, one of the Ieshima Islands, Hyogo Prefecture, Japan. Bottom right: A red tide on August 18, 1983, in Araihanatsu Bay, Japan, which resulted in a massive kill of caged fish.

soning. Yet another mass poisoning in 1987 erupted in Canada with patients complaining of vomiting, diarrhea, disorientation, and abdominal cramps. In some cases, permanent short-term memory loss was also observed. This outbreak was traced to mussels from Prince Edward Island that apparently were contaminated with marine toxins from red tide blooms of a *Pseudonitzschia* species. The same type of algae were responsible for a 1991 incident near Monterey, California, in which hundreds of sick and dying pelicans were found on the beaches. In both of these last cases domoic acid, a potent paralytic toxin secreted by the phytoplankton, was implicated as the causative agent.

Fig. 3. Fish killed by a ride tide that occurred off the coast of Florida.

Another devastating red tide incident hit the east coast of the United States between 1987 and 1988, right after the humpback whales had been poisoned. On that occasion, 740 bottlenose dolphins were found washed up along the Atlantic coast from New Jersey to Florida. Scientists later determined that the dolphins were probably the victims of yet another species of algae, *Gymnodinium brevis*, the producers of the lethal brevetoxins. Such incidents clearly demonstrate the great danger to the environment through poisoning in the food chain.

The frequency of these oceanic catastrophes has increased alarmingly in recent years because of environmental pollution and shipping practices that tend to spread and facilitate algal growth. Recent scientific evidence links the production of powerful biotoxins by the algae to a defense-related mechanism against their natural predators. However, alternative sources of these biotoxins, for example, bacteria residing in or on such

algae cannot, as yet, be ruled out. Regardless of the origins and reasons behind the biogenesis of these toxins, scientists agree that coastal pollution provides the necessary nutrients and creates the favorable conditions required for rapid and frequent proliferation of these algae and is, perhaps, responsible for the increase of these incidents during the last few decades. It is noteworthy, for example, that in Tolo Harbor in Hong Kong between 1976 and 1986, the frequency of appearance of the red tides increased eightfold as the human population and activities along the coastal area increased sixfold. Similar dramatic effects have been observed in Japan. Uncontrolled transfer of contaminated seawater and microorganisms from one area to another by oil tankers and other naval vessels may also be equally responsible for the appearance of new algal colonies in previously unaffected areas. Studies revealed that certain conditions of temperature (10–33 °C), salinity (levels of 27–37%), and sunlight (duration and intensity) are important factors favoring algal proliferation. Furthermore, analysis of satellite photographs of the coastal areas of Florida and hydrographic measurements implicated currents in red tide blooms.[8] Even more intriguing are the findings involving nutritional factors. For example, high concentrations of chelated iron discharged from the Peace River in Florida proved very crucial to the initiation of algal blooms and can be used as an index to predict the occurrence of red tides near Tampa, Florida. Heavy rains carrying soil rich in organic chelates to the ocean is also thought to stimulate growth of algae. Gibberellic acid, a plant hormone, has also been implicated as a promoter of red tides.[8]

Of particular danger is the way these microorganisms suddenly spread and colonize certain areas. A number of these species encapsulate themselves inside hard shells, called cysts, and move around in the oceans in a dormant state until they encounter favorable conditions, when they germinate and proliferate rapidly, causing massive blooms. The worldwide losses due to red tides and related phenomena such as *ciguatera* are devastating to marine life and human health; the ecological damage and economic loss may exceed hundreds of millions of dollars annually. Clearly these unicellular marine organisms, like viruses and bacteria, can endanger some of the largest and most sophisticated creatures of our planet, including humans, through the food chain.

Realizing the danger from and the significance of red tides, scientists have devoted increasing attention in recent years to understanding and controlling this phenomenon. Working together, chemists and biologists have isolated and identified a number of marine biotoxins and their phytoplankton sources. Among them are tetrodotoxin[9] (from the puffer fish), palytoxin[10] (from the coral *Palythoa toxica*), the saxitoxins[11] (from *Alexandrium*), domoic acid[12] (from *Pseudonitzschia*), ciguatoxin[13] and maitotoxin,[14] cause of the *ciguatera* phenomenon (both from *Gambierdiscus toxicus*), and the brevetoxins[15] (from *Gymnodinium breve*).

Brevetoxin B (**1**) was the first of these marine toxins to be reported, and is perhaps the most prominent member of the brevetoxin family of biotoxins[15] because of its complex structure and biological activity. Isolated and characterized in 1981,[2] brevetoxin B is lethal to fish and highly harmful to humans. This compound exerts its damaging effects by acting on the voltage-sensitive domains of sodium channels, which are situated in the membranes of the cells.[5, 6] The brevetoxins are thought to be responsible for massive fish kills in the Gulf of Mexico, along the Atlantic coast, and in many other regions of the world, and for many mass poisonings of humans caused by consumption of seafood. The symptoms in human victims include a tingling sensation in the mouth and digits, disruption of coordination (ataxia), hot–cold reversal of temperature sensation, dilated pupils (mydriasis), brachycardia, diarrhea and, occasionally, respiratory problems. Poisoning with these symptons is commonly known as neurotoxic shellfish poisoning (NSP), paralytic shellfish poisoning (PSP), amnesic shellfish poisoning (ASP), diarrhetic shellfish poisoning (DSP), and ciguatera seafood poisoning (CSP).[3–6]

3. Total Synthesis

3.1. Planning the Initial Strategy

We now return to brevetoxin B (**1**) and the dilemma it posed as a target for total synthesis. As decided, a proposal on the total synthesis of brevetoxin B was developed and dispatched to the NIH on January 24, 1982, and the long and anxious wait for a response began. In the meantime, the challenging structure of the molecule attracted two young and ambitious first-year graduate students at the University of Pennsylvania, where the project was initiated. Chan-Kou (Jack) Hwang and Mark Duggan in their innocence and naïvete expected to complete the total synthesis together in their Ph.D. theses within three years. I did not discourage them, even though, of course, I suspected differently, and in the summer of 1982, after completion of their course work, they embarked on the project with great enthusiasm and no shortage of ideas.

Soon thereafter, the "pink sheet" (summary statement) from the NIH arrived with the verdict from the study section ("the jury"). An incredible and very pleasing score of 1.45 (on a scale of 5, in which 1 is the best) worked magic on our morale. This score was much better than I had expected even in my wildest dreams, particularly in view of the miserable performances I had become accustomed to in my previous experiences with the NIH. I was wondering what had happened until I carefully examined the list of study section members. Among them were Yoshito Kishi from Harvard University, Stephen Hanessian from the University of Montreal, and Larry Overman from the University of California, Irvine, masterful chemists, whose opinions I valued highly. Twelve years later, when we finally reached the island of "Ithaca",[1] we remembered these pioneers and saluted their contributions to the field of total synthesis, an area of research that they had championed and whose future they continue to shape. Despite its highly encouraging score, however, the summary statement ended with a gloomy estimation: "This is a clever approach to a novel, biologically interesting molecule, whose stereochemical complexities have been reduced to the synthesis of appropriate allylic alcohols, their epoxidation, and the regioselective opening of these epoxides. The overall plan is remarkably convergent but it is high risk." Work began in earnest and funding started on January 1, 1983.

At this juncture, it will be constructive to briefly review the initial plan, as flawed as it was, to help us reconstruct and follow the story chronologically. Inspection of the structure of brevetoxin B (**1**) led immediately to the first exciting recognition that this formidable structure could be reduced, by virtue of its regularity, to single polyepoxide precursors (Scheme 1). Equipped with an initiator at one side of the structure and a terminator at the other side of the structure, these polyepoxides could, in principle, be considered as potential precursors to brevetoxin B (**1**). The following verbatim abstract from the original proposal of 1982 conveys accurately our thoughts and reservations on this possibility at the time:

"In theory a 'zip reaction' as indicated by the arrows (Scheme 1) and accompanied by the expected inversions could lead to brevetoxin B (**1**) in a single step under 'favorable conditions'. Synthetically, however, there are two serious problems with such an approach, at least with the present state of the art. The first problem is the lack of regioselectivity (or 'ringselectivity') in the consecutive opening of these epoxides. Indeed, either under basic or acidic conditions, some of these epoxides can safely be predicted to open in the undesired fashion giving rise to the wrong size rings. The second problem with this one-step approach is the difficulty in synthesizing stereoselectively such a polyepoxide precursor due to the absence of any 'handles' adjacent to the epoxide functionalities that may be used to direct epoxide formation and also the reactivity of the epoxide unit that may preclude long sequences involving polyepoxides. Thus, it is unlikely that such a 'zip', one-step generation of brevetoxin B will succeed in the laboratory under presently known chemical means."

Fearing that no graduate student would ever undertake such a risky, one-step approach (not to mention the reaction of the NIH study section!), I had included a more realistic strategy to brevetoxin B in the proposal. This second plan depended on a convergent strategy involving intermediates **3**–**5** (Scheme 1). The synthesis and utilization of these intermediates as originally conceived are outlined in Schemes 2 and 3. Key to the success of these proposals were the postulates that base-induced openings of hydroxyepoxides would prefer pathways involving nucleophilic attacks on secondary rather than tertiary centers and on epoxide positions being activated by adjacent double bonds. The latter epoxide openings, in which the carbon centers are

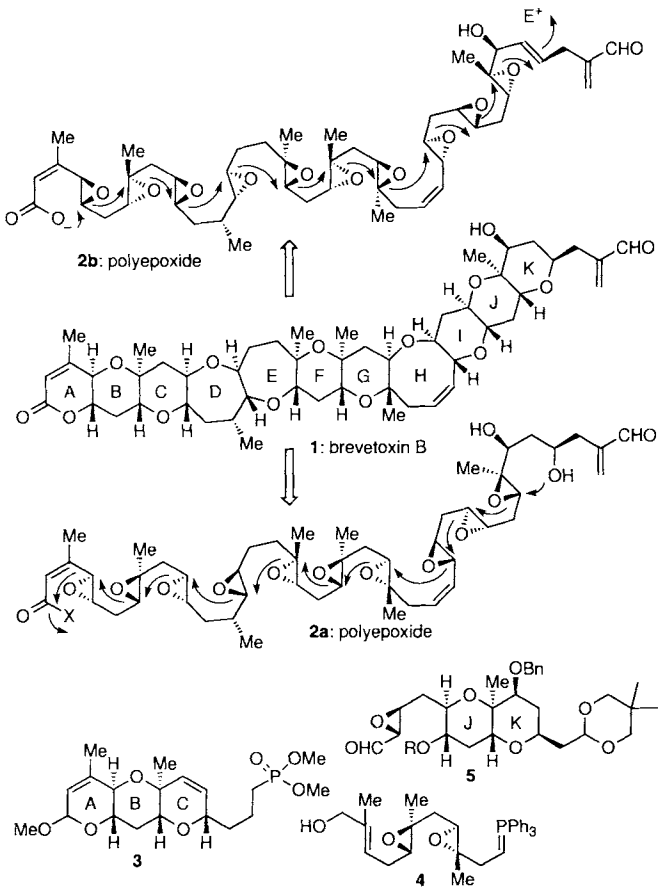

Scheme 1. February 1982. Proposal to NIH. Top: Generation of brevetoxin B (**1**) from polyepoxides **2a** and **2b** by a zip reaction. Bottom: Retrosynthetic analysis of brevetoxin B (**1**) leading to compounds **3**–**5**.

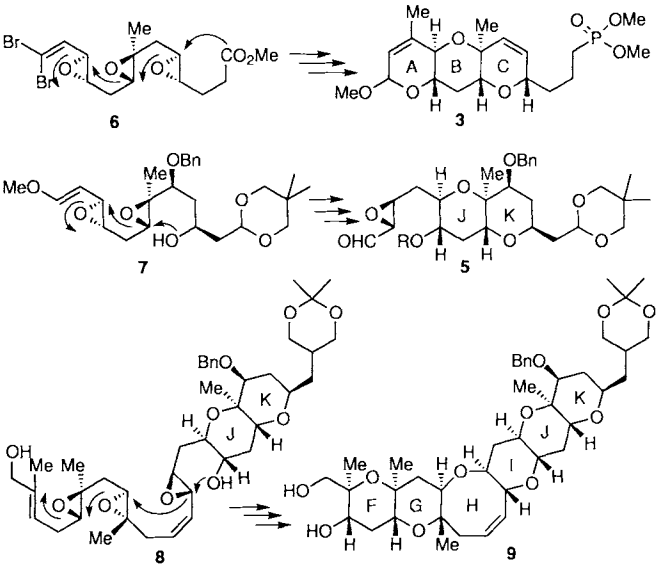

Scheme 2. February 1982. Proposal to NIH. Proposed synthesis of the ABC, JK, and FGHIJK ring systems relying on polyepoxides.

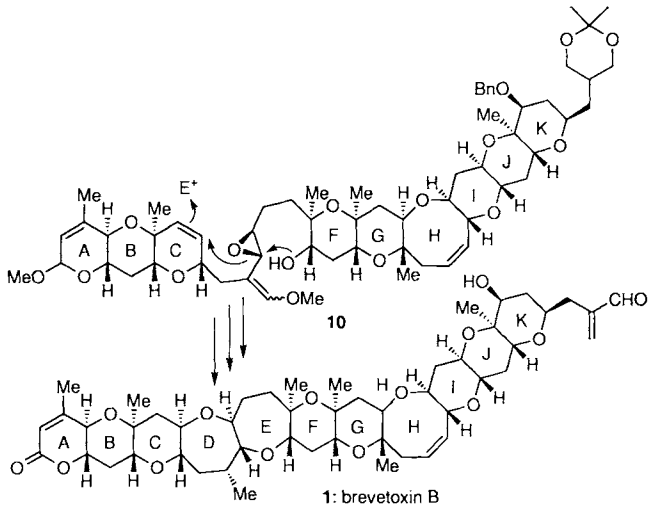

Scheme 3. Febrary 1982. Proposal to NIH. Proposed construction of the DE ring system of brevetoxin B (**1**).

activated by adjacent electron density, would also proceed under acid catalysis. These concepts needed development and verification with model studies, but one could take comfort in the success of prior related work.

3.2. The Tetrahydropyran Problem

According to the original plan, the first objective of the brevetoxin project was to develop the necessary methodology for the regioselective and stereospecific construction of the tetrahydropyran systems of the target. The results of the model studies in this direction were remarkably successful and involved simple chemical principles and manipulations (Scheme 4). The basic

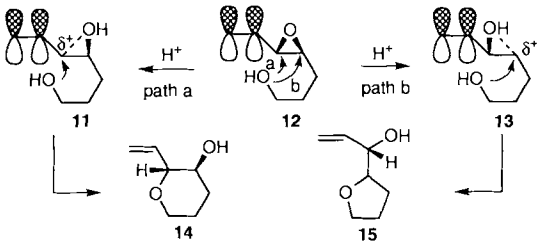

Scheme 4. The basic concept behind the regio- and stereospecific ring closure leading to tetrahydropyrans. The orbital with developing electron deficiency is stabilized by conjugation with a π orbital in the same plane; path a: 6-*endo* ring closure; path B: 5-*exo* ring closure.

concept here was to utilize the p orbitals of an adjacent double bond to bias the location of the incipient positive charge and, thereby favor formation of the desired six-membered ring. Combination of this new chemistry[16] with the then recently discovered Sharpless asymmetric epoxidation reaction[17] allowed the quick assembly of the polycyclic building blocks required for the synthesis of brevetoxin B. Thus, the project moved forward, and in a relatively short time we were in a position to proceed to the next stage.

3.3. The Oxocene Problem

While the coupling reactions of the tetrahydropyran segments proceeded smoothly, the oxocene ring proved more than equal to its reputation as a notoriously difficult system to construct and, thus, became a major obstacle. Although we had no illusions regarding the construction of medium-sized rings, the initial failures we encountered were frustrating. First to fail was the projected hydroxy-diepoxide opening cascade shown in Scheme 5a. Then came the disappointment of the failure of the intramolecular Michael reaction depicted in Scheme 5b. Finally, a timely report by Schreiber et al.[18] prompted us to try the ring expansion shown in Scheme 5c, but again to no avail.

After several other conventional approaches also failed, we decided that it was time to go back to the drawing board, for we then realized that the strain in the oxocene region of the molecule would not allow us easy passage. A new method for the construction of eight-membered ring ethers, based on consecutive [2 + 2]cycloaddition and cyclobutene opening reactions, was tested successfully with a model system (Scheme 6a).[19]

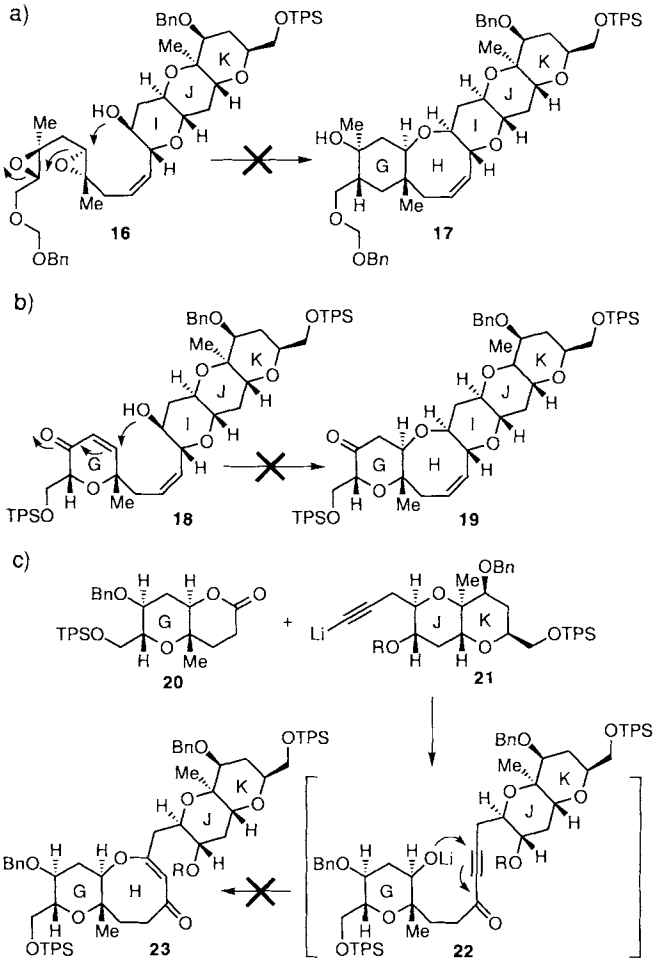

Scheme 5. Unsuccessful attempts to synthesize the oxocene ring of brevetoxin B (1) by: a) polyepoxide opening, b) conjugate addition c) ring expansion following a report by Schreiber et al. [18].

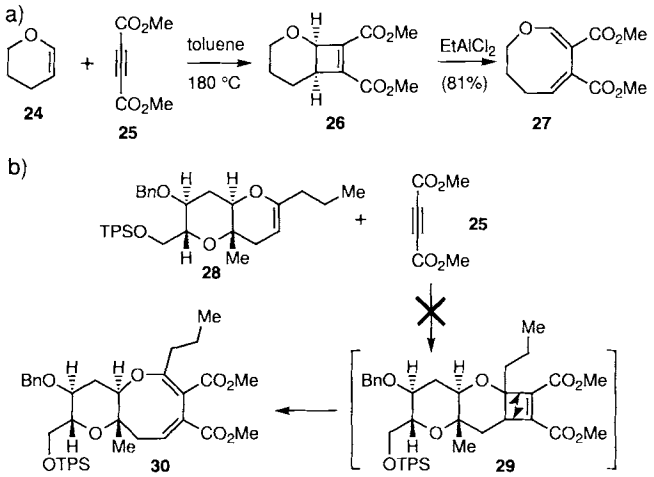

Scheme 6. Synthesis of oxocenes by [2 + 2]cycloaddition and cyclobutene ring opening. a) Successful model study; b) unsuccessful attempt with substrates resembling brevetoxin B (1).

However, a more realistic system did not undergo this newly developed reaction (Scheme 6b), presumably for steric reasons. Our initial excitement faded quickly, but in rethinking the problem we found a radically different solution.

The new concept focused on the attack of a highly reactive, perhaps polar species to overcome the strain and entropic barri-

ers encountered during the formation of the oxocene ring system of brevetoxin B. It was clear that, despite the favorable effect of the (*Z*) double bond of the ring-forming chain, considerable driving force was still needed before ring closure could be realized. A hydroxydithioketal was chosen as a potential progenitor of a hydroxysulfonium species (e.g. **32**, Scheme 7),

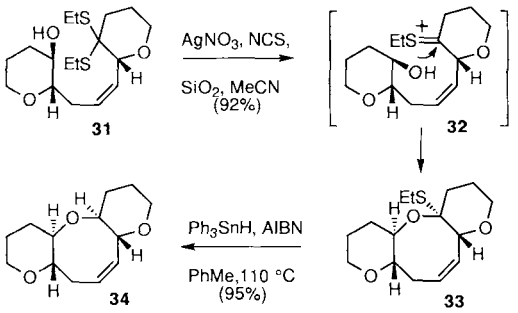

Scheme 7. Hydroxydithioketal strategy for the synthesis of oxocene systems.

which was expected to undergo rapid intramolecular reaction leading to the oxocene ring system. The remaining ethylthio group was expected to be easily excised from the product (**33**, Scheme 7) and replaced with a hydrogen atom docking in from the desired face. These predictions proved delightfully correct, and graduate students Mark Duggan and Jack Hwang proceeded to execute successfully the designed experiments with characteristic speed and precision (Scheme 7). This method proved to be remarkably efficient and quite general in scope.[20] It is certainly a prime candidate for the honor of "best reaction in the brevetoxin odyssey", for so crucial and effective was its role in the final outcome of the venture.

3.4. The Bis(oxepane) Problem

With powerful methods of constructing six- and eight-membered ether rings at our disposal, we turned our attention to the third and final problem, the annelated bis(oxepane) ring system of brevetoxin B. The hydroxyepoxide and the hydroxydithioketal methods appeared, based on model system studies, to be reasonably promising for this task, but the opportunity to develop yet another method for synthesizing medium-sized heterocycles was too tempting to pass. It was in this spirit and context that we postponed a final drive towards the target molecule in order to explore yet another important idea for the synthesis of bicyclic compounds. The concept of bridging macrocycles to form bicycles was thus born (Scheme 8).

Particularly appealing was the idea of utilizing the easily accessible macrodilactones as potential precursors, which would give bridged bicyclic systems through radical coupling reactions. Unfortunately, however, such couplings proved unsuccessful in forming the desired bicyclic systems under electron transfer conditions due to facile and rapid ring openings induced by the negative charge on the generated alkoxide species. In retrospect, this was not so surprising, considering the ring strain of the cyclic frameworks formed and the relatively low nucleophilicity of oxygen towards added trapping agents that

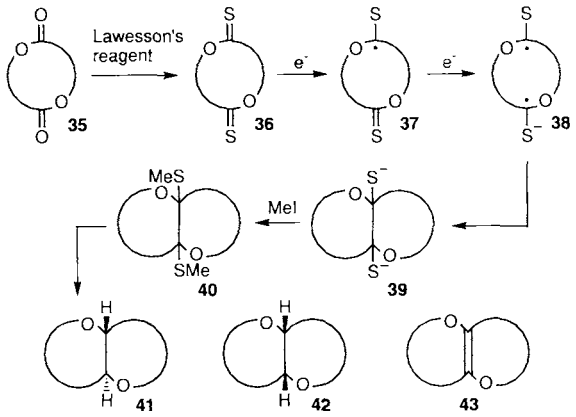

Scheme 8. The concept behind bridging macrocycles to give bicycles.

could have prevented such ruptures. In pondering over these difficulties, we immediately thought of replacing oxygen with sulfur as a more appropriate element. The relatively low reduction potential of the C=S group, the ability of sulfur to stabilize a negative charge, and its high nucleophilicity, coupled with the multitude of possibilities in sulfur chemistry for further chemical manipulations indicated that macrodi(thiolactones) like **36** should be ideal candidates for the conceptualized bridging reaction (Scheme 8). Convinced of the soundness of the new idea, Jack and Mark rushed to the laboratory to execute the designed sequences. It was not long before the first successful experimental results on the bridging of macrocycles to give bicycles were at hand (Scheme 9).[21] Realizing what a gold mine we had struck, we immediately took time to test the generality of the new reaction and explore the chemistry of the products (Scheme 9). Furthermore, a photo-induced version of this

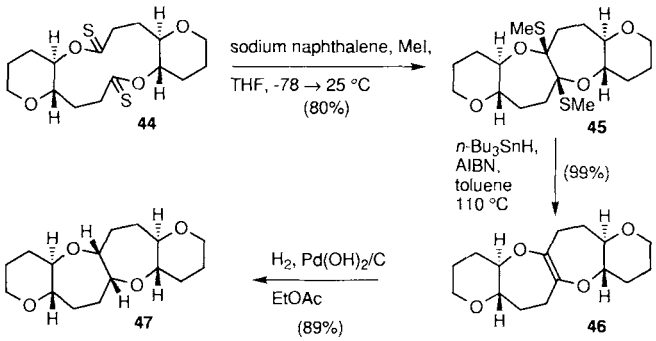

Scheme 9. Bridging macrocycles to give bicycles: first successful experiments with macrodi(thiolactones).

bridging process was developed, which led to the first, exquisitely beautiful and crystalline 1,2-dithietane (Scheme 10).[22] So aesthetically pleasing were the crystals (Fig. 4) of this compound that I took them home to show my wife, Georgette, and my daughter, Colette, whose immediate reaction upon seeing them was: "They look like gemstones, like topaz. Can we make rings with them?" "No, they are too fragile," I explained, "But thanks for the idea." The first stable 1,2-dithietane became known as dithiatopazine.

We shall return to further explorations of the di(thiolactone) bridging chemistry later, but first we will proceed to the applica-

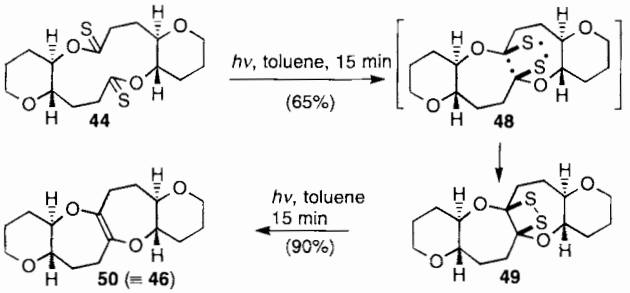

Scheme 10. Photo-induced bridging of macrodi(thiolactones) via dithiatopazine **49**, the first stable 1,2-dithietane.

Fig. 4. Crystals of dithiatopazine **49**.

tion of this powerful reaction to the problem at hand, the construction of the entire skeleton of brevetoxin B (**1**). The newly discovered bridging reaction would be reserved for the final C–C bond formation to give the bis(oxepane) system (**52** → **53**, Scheme 11). The synthesis of the requisite precursor **51** proceeded smoothly and swiftly as summarized in Scheme 11. The tetrahydropyran-containing fragments were constructed through hydroxyepoxide ring closures and related chemistry and elaborated according to the sequence of steps [1] → [2] → [3] → [4] as indicated in structure **51** (Scheme 12). The euphoria generated by the speed and efficiency of the sequences leading to **51** was, however, soon to dwindle, as we shall see.

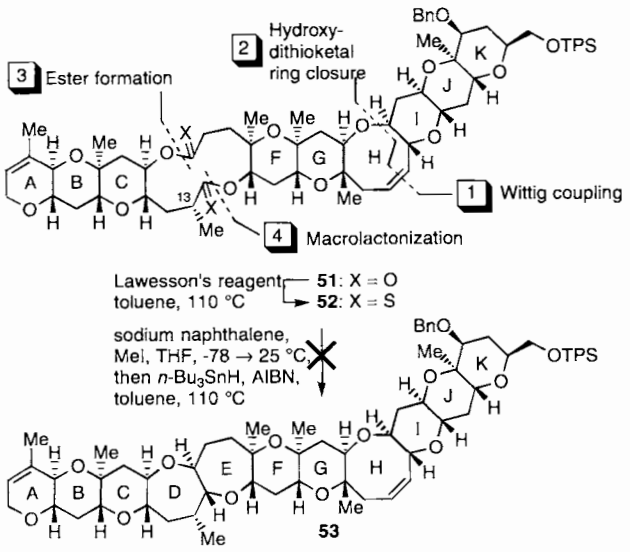

Scheme 11. When applied to the synthesis of brevetoxin, the bridging of macrodi(thiolactones) fails.

First, it was the miserably low-yielding conversion of the dilactone functionality into the corresponding di(thiolactone) system using Lawessons's reagent (**51** → **52**, Scheme 11) that brought the operations to a virtual halt.[23] Several other known Lawesson-type reagents also gave disappointing results, and no conditions could be found to increase the yield of this difficult step. Then the bridging reaction, attempted on the meager amounts of di(thiolactone) **52** obtained, proved equally problematic, leading to mixtures of products in low yields. In both instances, the steric hindrance of the C-13 methyl group adjacent to one of the reaction sites was to blame. That seemingly innocent methyl group, perfectly positioned to thwart our advance, was almost certainly responsible for this failure. Furthermore, we became convinced that, had that methyl group not been there, brevetoxin B (**1**) could have been reached in short order. But the methyl group was there, and we decided to face the challenge rather than opt for the easy way out, the synthesis of 13-norbrevetoxin B, that some suggested. We believed in the promise of new chemistry that such a challenge would bring. We were not disappointed for, as we shall see, much more adventure was ahead before we reached the real "Ithaca". For a start, a number of new Lawesson-type reagents were designed, synthesized, and tested in order to overcome the steric hindrance around the resisting carbonyl group.[24] Despite the novelty and effectiveness of these reagents in model systems, however, progress could not be made along this bridging pathway.

Having failed to construct the final C–C bond of the brevetoxin B framework by bridging the 12-membered macrocycle, we then opted for a stepwise construction of the two oxepane rings, a decision that we suspected would detract from the elegance of the synthesis. Again, instead of attempting to apply known reactions for this task, we proceeded to design new synthetic technology for the synthesis of oxepane systems. Scheme 12 summarizes a new route to oxepanes from

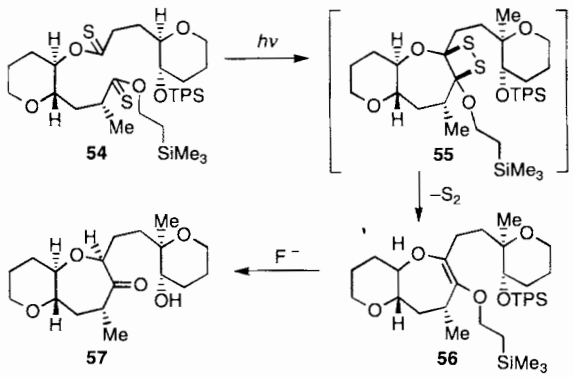

Scheme 12. Bridging of di(thioesters) for construction of oxepane systems.

di(thioesters) by photo-induced radical coupling followed by sulfur extrusion and selective enol hydrolysis.[23, 25] For our purpose, however, a second method for oxepane synthesis was needed, which would immediately follow the construction of the first oxepane ring. Such a strategy was tailor-made for the brevetoxin structure (Scheme 13) and quickly demonstrated in the laboratory with simple model systems (Scheme 14a).[23, 26] Although, the initially demonstrated method was successfully

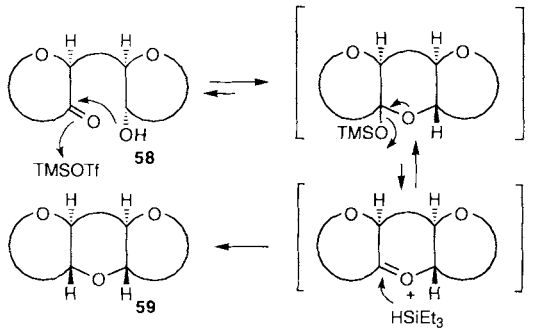

Scheme 13. General strategy for bis(oxepane) formation through TMSOTf-induced cyclization of hydroxyketones.

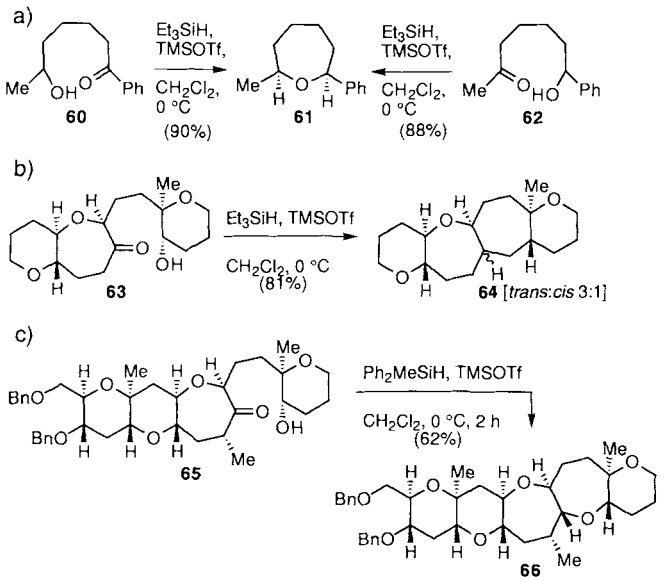

Scheme 14. TMSOTf-induced cyclizations of hydroxyketones for the construction of oxepanes and bis(oxepanes).

applied to a number of more complex systems (Schemes 14b and 14c), these efforts were again destined to fail as we approached the real system.[23, 26] The first bitter surprise came when we subjected the advanced hydroxyketone **67** (Scheme 15)

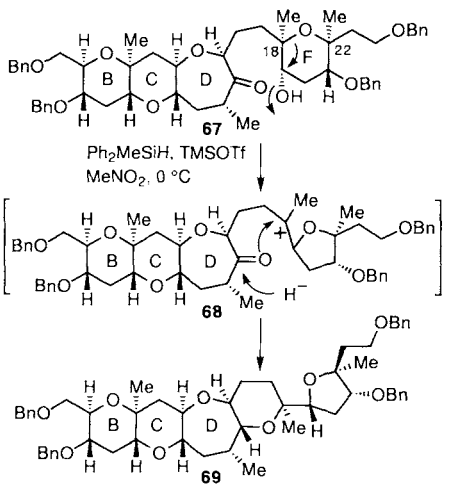

Scheme 15. Hydroxyketone cyclizations: applications to more advanced brevetoxin intermediates fail.

to the ring closure conditions. We did not obtain the expected bis(oxepane) system; we soon realized (and confirmed by X-ray crystallography) that a drastic rearrangement had accompanied the reductive ring closure of the carbonyl oxygen onto an incipient carbenium ion (Scheme 15).[23] Once again our problems could be traced to methyl groups, those at C-18 and C-22 (brevetoxin B (**1**) numbering) which, owing to steric repulsion (1,3-diaxial interactions), facilitate collapse of the six-membered ring to which they are attached, leading to a conveniently stabilized tertiary carbocation and, thence, to the observed reductive cyclization product **69** (Scheme 15). This was a novel

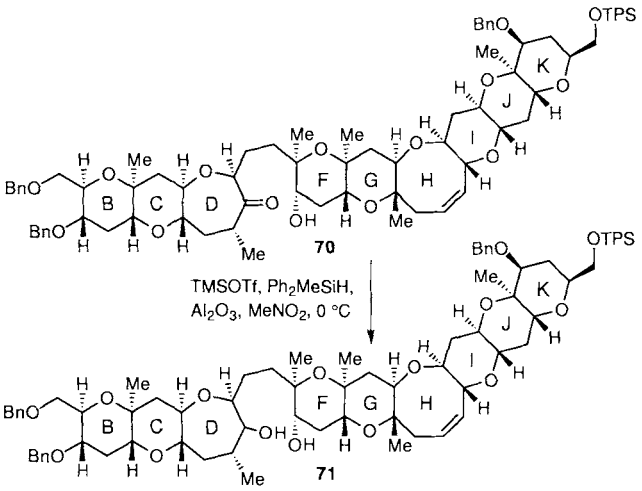

Scheme 16. Attempts to close the E-ring by reductive hydroxyketone cyclization fail.

ring contraction, but we had no use for it in our quest for brevetoxin B (**1**). A second, and more ambitious approach relying on the reductive hydroxyketone cyclization was designed and tested (Scheme 16).[23] Again, the skeleton of brevetoxin B, only one C–O bond away, eluded us; we were left with a dihydroxy by-product and pondered our misfortunes. Further explorations along these lines led to more frustrations, and the plan of constructing the bis(oxepane) system by this strategy was abandoned. The new chemistry was the only gleanings from the failed first and second approaches to the bis(oxepane) unit. In the long run, this was not a bad deal, of course, considering the wealth of chemistry that was discovered.

In the meantime, members of the group were devoting considerable time to exploring the novel chemistry of dithiatopazine **49** (Scheme 10) and devising new synthetic transformations that made use of the properties of the thiolactone functionality. It is instructive to briefly survey this chemistry here, for the exercise serves to focus attention on an important aspect of total synthesis: the exploitation of the opportunities encountered in such endeavors to discover, invent, and develop new chemistry. The reactions shown in Schemes 17–19 are representative of the wealth of designed and serendipitously discovered chemistry during this phase of the program. Thus, several novel and unexpected rearrangements and ring systems were encountered (Schemes 17 and 18),[22] and numerous new methods for the construction of cyclic ethers were developed (Scheme 19).[27, 28] Having collected this "merchandise and gems in foreign lands,"

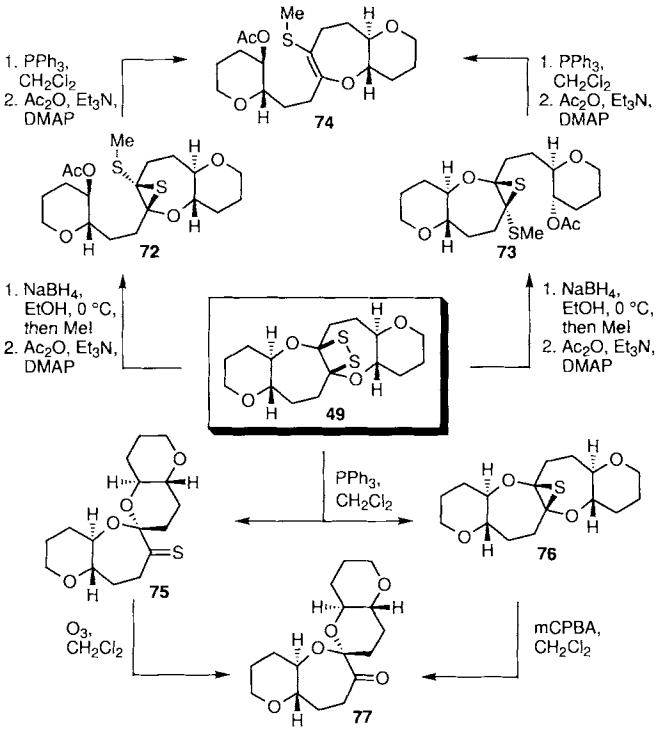

Scheme 17. Novel chemistry of dithiatopazine **49**.

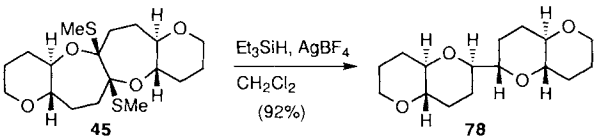

Scheme 18. Novel rearrangement of polycyclic ether frameworks, which could be useful for the synthesis of maitotoxin.

we were still not completely content, for back in our minds was still "Ithaca" and how to get there.

3.5. Moving to the West Coast and Planning a New Strategy

Our repeatedly thwarted attempts to construct the final bonds around the bis(oxepane) region of brevetoxin B left us scrambling for new ideas and led us to consider a less convergent approach towards the ABCDE framework. By now it was the middle of 1989 and the group was preparing to move from Philadelphia to La Jolla, where new laboratories were awaiting for us at The Scripps Research Institute and the University of California, San Diego. Our recent setbacks on the project, coupled with the move to California and the new exciting projects that were taking shape in the group, resulted in a brief lull in activity, and for a while no major assaults were launched on brevetoxin B (**1**). It was at about the same time that Shimizu et al. reported the structure of hemibrevetoxin B (**91**), a tetracyclic

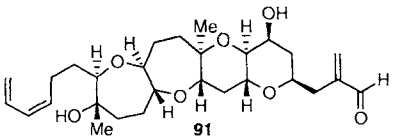

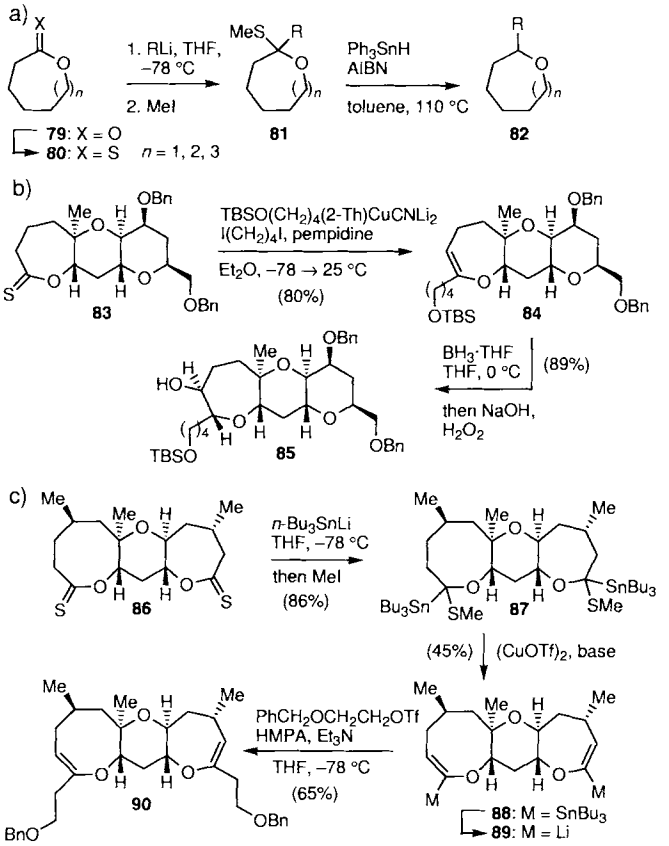

Scheme 19. Nucleophilic additions to thiolactones: a) synthesis of cyclic ethers; b) synthesis of medium-sized cyclic ethers (for application to the synthesis of hemibrevetoxin B (**91**) see ref. [30]); c) bidirectional synthesis of medium-sized cyclic ethers (for application to the synthesis of brevetoxin A see ref. [28]).

"little sister" of brevetoxin B (**1**).[29] With this considerably less complex target a new brevetoxin team was recuited and trained. By 1992 we had completed the first total synthesis of hemibrevetoxin B (**91**).[30] Most importantly, we had tested some new strategies, morale was high, and we were now poised for the final campaign towards the real prize, brevetoxin B (**1**).

The new strategy for the total synthesis of brevetoxin B (**1**) was designed to take advantage of the regioselective and stereospecific reactions shown in Scheme 20[31, 32] to form the tetrahydropyran ring systems of the molecule and was based on the retrosynthetic analysis shown in Scheme 21. This convergent approach relied on the hydroxydithioketal cyclization as the "anchor" reaction to complete the brevetoxin B skeleton by forming the oxocene ring at the final stages of the sequence. The

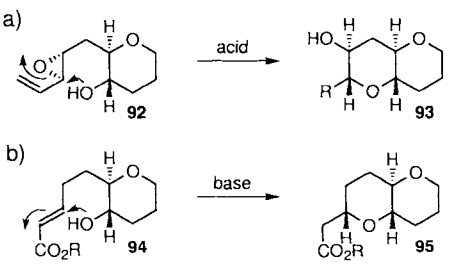

Scheme 20. Crucial synthetic transformations for the regio- and stereospecific ring closure of the tetrahydropyran systems of brevetoxin B (**1**).

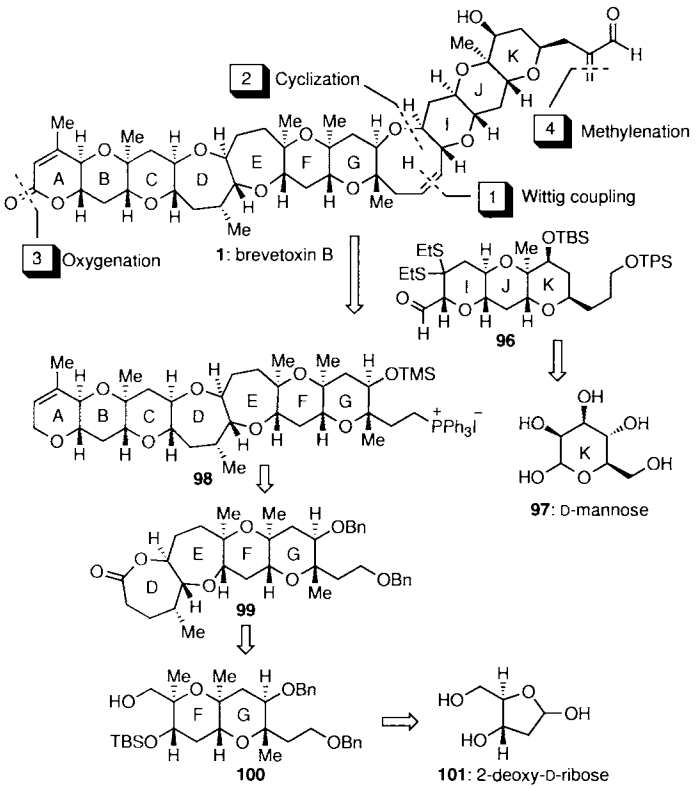

Scheme 21. A new approach: strategic bond disconnections and retrosynthetic analysis of brevetoxin B (**1**).

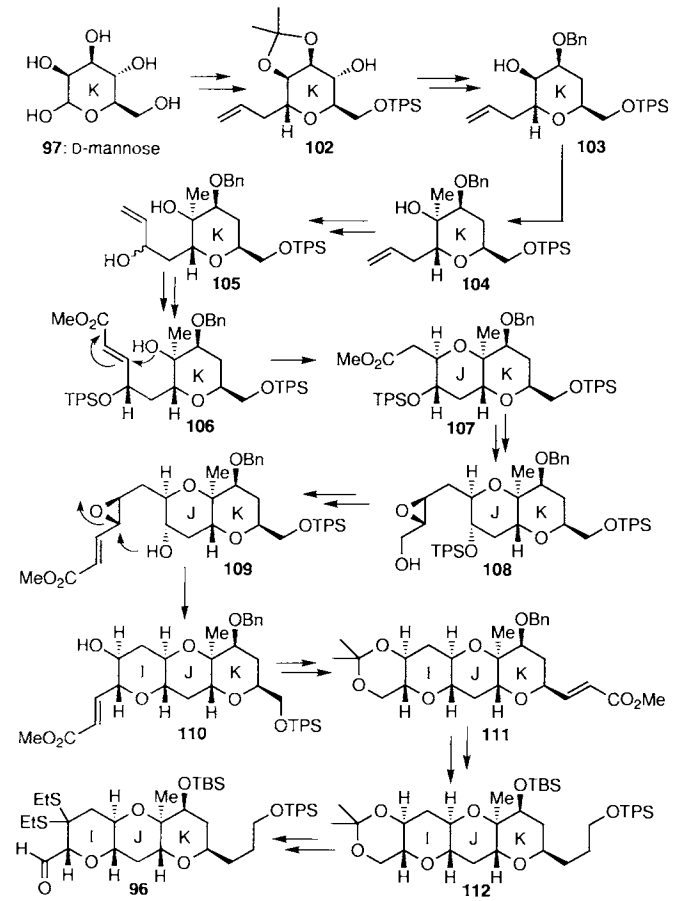

Scheme 22. Synthesis of the IJK framework from D-mannose.

aldehyde **96** (IJK segment) and the phosphonium salt **98** (ABCDEFG segment) were chosen as advanced intermediates. While the IJK framework **96** was to be derived from D-mannose (**97**), the more complex ABCDEFG ring system **98** was traced back to 2-deoxy-D-ribose (**101**) via key intermediates **99** (DEFG system) and **100** (FG system).

The construction of the IJK aldehyde **96** proceeded smoothly following the sequence K → JK → IJK as summarized in Scheme 22.[33] The synthesis of the DEFG lactone **99** also proceeded along a linear route according to which each ring was fused onto the previous one in the direction F → FG → EFG → DEFG (Schemes 23[34] and 24[35, 36]). Since our dreams of optimum convergency had been ruined, we deliberately chose these linear approaches; mundane as they may seem at first, they later proved their worth.

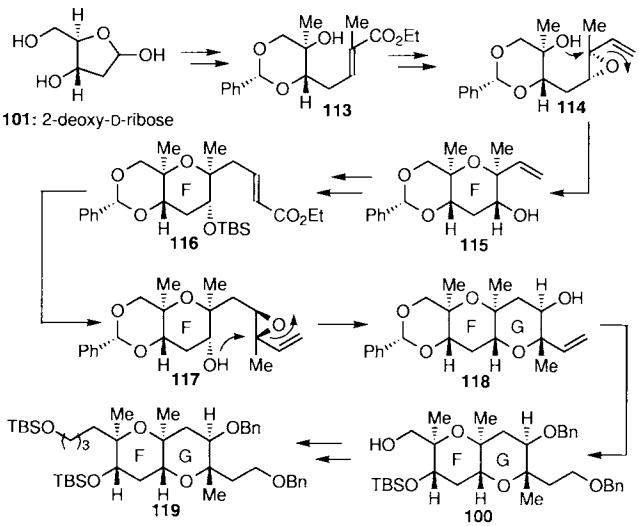

Scheme 23. Synthesis of the FG ring framework from 2-deoxy-D-ribose.

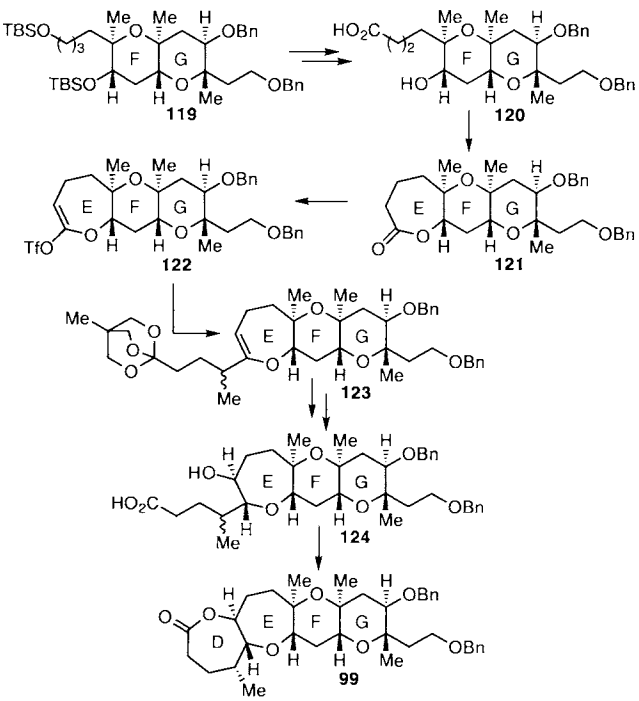

Scheme 24. Synthesis of the DEFG ring framework.

Despite the dividends of our stepwise approach, we were still intrigued by possible convergency in the synthesis, and once again we took a risk, namely, a shortcut for the installment of the next two rings resulting in the BCDEFG system. Thus, in our first approach towards this goal, ring B, as aldehyde **125**, was to be coupled to a suitable derivative of the DEFG ring system (Scheme 25) and the coupling product elaborated in

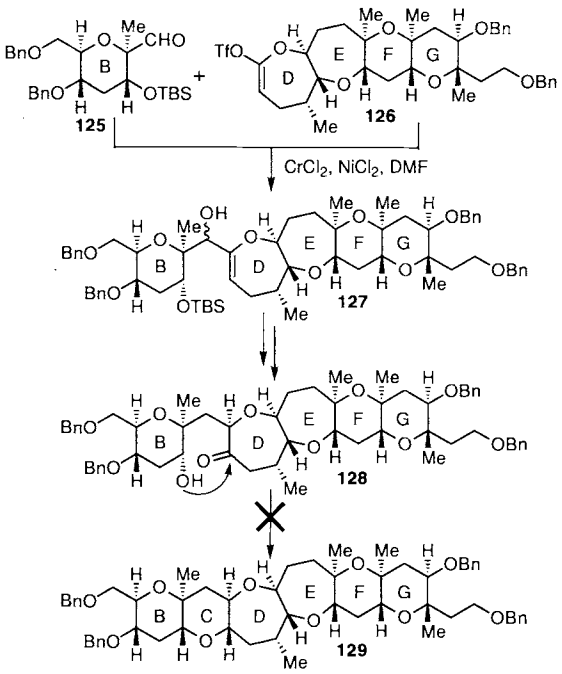

Scheme 25. Convergent approach to the BCDEFG fragment based on reductive hydroxyketone cyclization fails.

preparation for ring closure and construction of ring C. The first order of business was to find ways to effect the coupling of aldehyde **125** to lactone **99** (Scheme 24). A literature search revealed that enol triflates derived from ketones participate in Cr/Ni-induced couplings with aldehydes,[37] an encouraging finding for our intentions. Extending this coupling reaction to include trifluoromethylsulfonyl ketene acetals derived from lactones was a reasonable proposition. Postdoctoral fellow Emmanuel Theodorakis was the first to demonstrate this reaction using the aldehyde and triflate partners shown in Scheme 25.[35, 36] Later this reaction proved to be crucial for the success of the project, and it is sure to find widespread applications in other areas of synthesis.

Having secured the requisite coupling product **127** (Scheme 25), we then proceeded to implement the rest of the plan towards closing ring C. The first option called for deoxygenation of the newly generated hydroxyl group followed by reductive cyclization of the hydroxyketone **128**, which was arrived at by hydroboration, oxidation, and desilylation. For reasons still unknown, this ring closure could not be effected under a variety of conditions, leading us to abandon it as part of the sequence. The second strategy (Scheme 26) began with oxidation of the newly generated hydroxyl group in **127**, followed by intramolecular attack of the liberated secondary alcohol onto the formed enone (**130**) through a Michael-type reaction (see also Scheme 5b). Again this approach met with stubborn resistance at the closure of ring C. The molecule would not give in

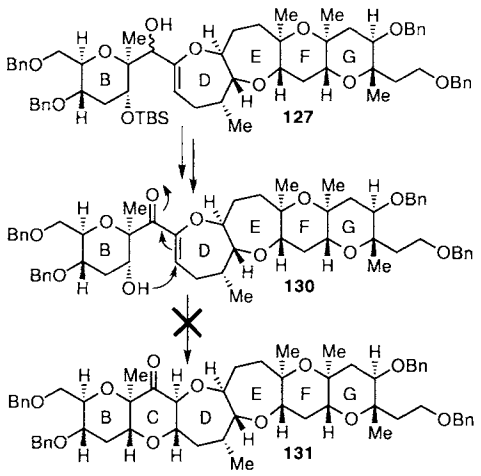

Scheme 26. Convergent approach to the BCDEFG fragment based on intramolecular conjugate addition fails.

to convergency! This was the last stroke, and we decided once and for all to abandon our dreams of convergence for the construction of this region of brevetoxin B. Nature had sent us enough messages and we learned the hard way that linearity has its place in total synthesis after all! From this point on there would be no more risky shortcuts, and we proceeded with the idea of one ring fusion at a time. The distinction of convergency would be reserved for the construction of the oxocene ring.

In the meantime, a courageous member of the team, postdoctoral fellow Jörg Tiebes, supported by his teammates (and behind my back!) started work on a shorter version of brevetoxin B, which we later called "truncated brevetoxin B" (AFGHIJK) **148** (Scheme 30). Lacking the trouble-causing BCDE ring system, this molecule was an easier target. The rationale behind this excursion was twofold. First we would have the opportunity to explore the final stages of the projected total synthesis, particularly the construction of the oxocene ring, and the completion of the two ends. Second, a paper just published by the groups of Baden and Gawley[38] proposed an interesting hypothesis regarding an essential length for the "cigar-shaped" brevetoxins in order for them to bind to their receptors. The designed truncated brevetoxin B **148** seemed just the right molecule to test this hypothesis. I also suspected an attempt for a "quick strike" by Jörg, whose time on the project was running out. Pressed by impending job interviews in Germany, he may have wished for a nice publication and at least partial success before leaving California. Be that as it may, I did not object to the operation and work intensified on the truncated compound in parallel to the latest, totally linear strategy towards the ABCDEFG segment of the real target, brevetoxin B (**1**). We shall first follow the path leading to the original target.

The plans now called for fusing ring C onto ring D of the DEFG lactone fragment. In the first step the newly developed Cr/Ni-coupling process mentioned previously was proposed to attach the required side chain, and then appropriate manipulations would effect ring closure. Scheme 27 outlines one of our early attempts to build the polycyclic framework CDEFG following this general approach. Thus, coupling of acetonide aldehyde **132** with lactone-derived enol triflate **126**, followed by a standard deoxygenation and deprotection protocol led to the triol **134**, which was projected as a substrate for a Fetizon oxida-

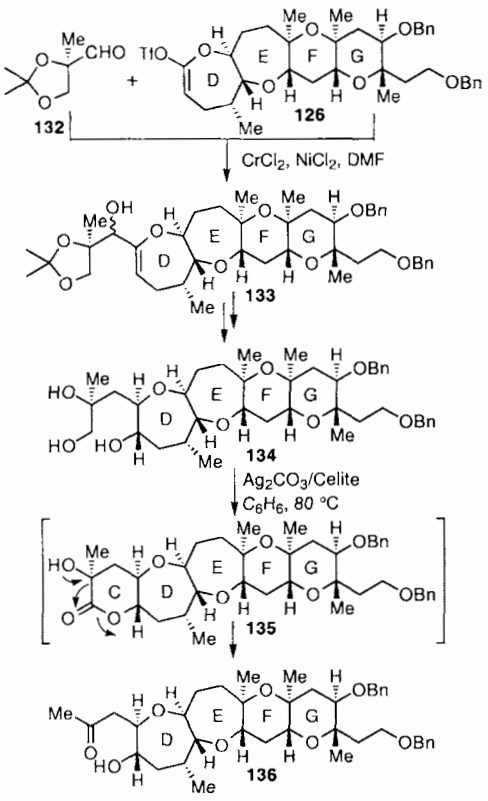

Scheme 27. Attempts to fuse a functionalized C-ring onto the DEFG ring system leads to unexpected decarbonylation.

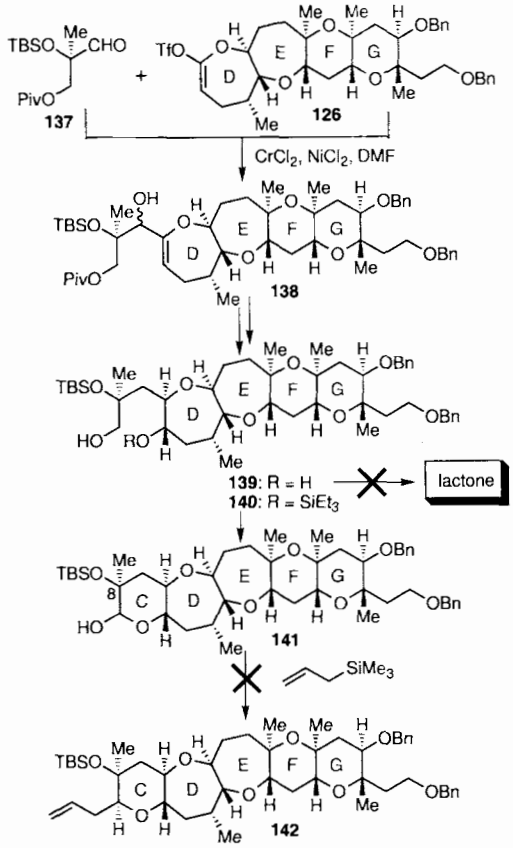

Scheme 28. Attempts to functionalize C-ring of **141** fail.

tion to afford the corresponding α-hydroxy-δ-lactone **135** (Scheme 27). However, despite much precedent from other laboratories,[39] the Fetizon reaction did not furnish the desired product. Rather, it surprised us with the unexpected formation of methyl ketone **136** (Scheme 27) as the sole product. This rather bizarre outcome could be explained by the mechanism proposed in Scheme 27, which involves spontaneous loss of carbon monoxide from the postulated hydroxylactone intermediate **135**. The logical solution to this problem was to protect the tertiary alcohol in order to prevent the collapse of the intermediate hydroxylactone **135**. This scheme required the utilization of the differentially protected aldehyde **137** in the coupling reaction with enol triflate **126** (Scheme 28). The new sequence proceeded according to plan until we encountered a different obstacle: the Fetizon oxidation of diol **139** did not lead to lactone formation, presumably due to steric hindrance of the bulky neighboring groups. We then tried a stepwise approach to the lactol via the silyl ether **140**. But again, attempts to attach an allyl chain at the anomeric center of lactol **141** did not prove fruitful (Scheme 28). We were pretty convinced that this latest series of defeats could once more be ascribed to a simple methyl group, this time the one situated at C-8 (brevetoxin B numbering). We now know that these methyl groups are the fiercest defenders of fortress brevetoxin B (**1**)!

Armed with another idea (Scheme 29), postdoctoral fellow Floris Rutjes was back in the front line attempting to overcome what seemed to be one of the last barriers to the total synthesis. According to this latest strategy towards the ABCDEFG ring system, an α,β-unsaturated ester at the end of the side chain on ring D of the DEFG compound was to serve as a Michael acceptor for the hydroxyl group attached to the adjacent oxepane system (Scheme 29). On June 2, 1994, this objective was achieved with complete stereoselectivity and in high yield! At that point we knew that the most stubbornly resistant region of brevetoxin B, the CDEFG framework, was captured. Yet we were still uncertain about the configuration of the newly formed stereogenic center at C-7 in **144**. Our fears were soon dispelled, however, when X-ray crystallographic analysis of a later intermediate revealed the proper configuration of all stereocenters, including the C-7. In the meantime, further good news was coming in from Jörg Tiebe's campaign directed at the truncated

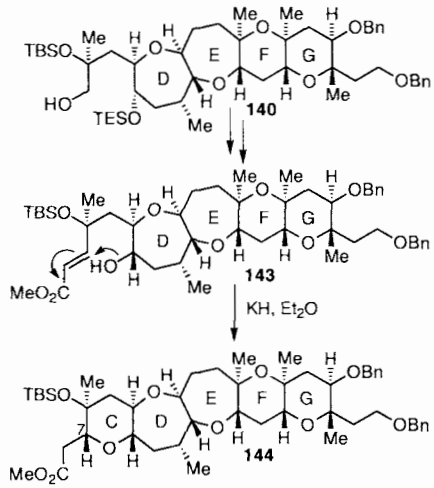

Scheme 29. June 2, 1994. Ring closure of the completely functionalized C-ring by intramolecular conjugate additions yields the long-sought CDEFG ring framework.

brevetoxin B **148**. Let us then now return to that campaign and see how the goal was reached and what we learned.

Scheme 30 summarizes the synthesis of truncated brevetoxin B **148** (AFGHIJK), which proceeded amazingly well and beyond our wildest expectations.[33] Considering the many torturous setbacks we experienced on our main front, this smooth

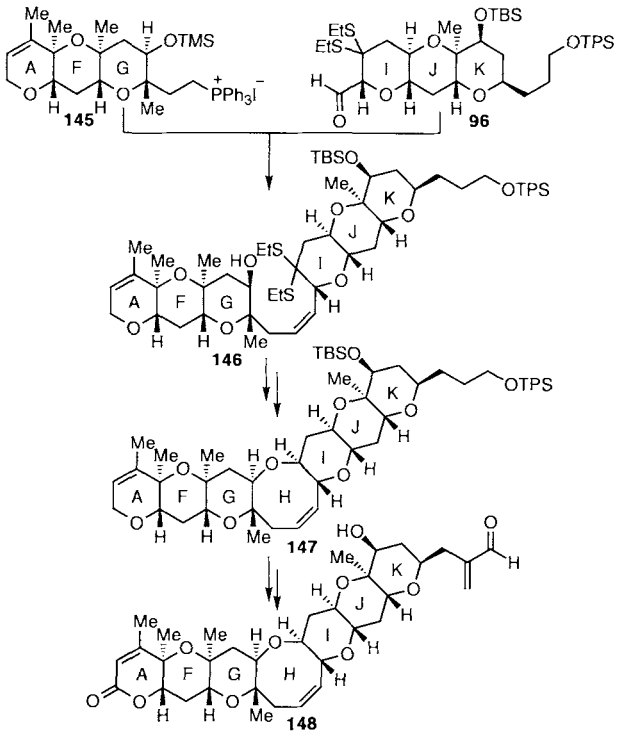

Scheme 30. May 10, 1994. Total synthesis of truncated brevetoxin B **148**. This model study furnished essential information about the final stages of the total synthesis of brevetoxin B (**1**).

sequence was certainly refreshing and helped us to establish an important beachhead for the conquest. This was perhaps the greatest testament to the effectiveness by which the "bis(oxepane) phalanx" and its adjacent rings and methyl groups defended the fortress for so long. The synthesis of truncated brevetoxin B **148**, completed on May 10, 1994, was highly valuable, because we then knew how the final triumphant march to brevetoxin B would proceed. We now could almost see brevetoxin B (**1**) far away on the horizon. To quote from Homer's Odyssey (Book I, v. 281):[1] "*... it looked like a shield lying on the misty face of the water.*"

3.6. The Final Stage

At the beginning of the summer of 1994 the final brevetoxin B team, consisting of Emmanuel A. Theodorakis (Greece), Floris P. J. T. Rutjes (Netherlands), Jörg Tiebes (Germany), Edouard Untersteller (France), and Mitsunobu Sato (Japan), was poised for the final assault on brevetoxin B (**1**) and the "homecoming to Ithaca". Projections were made that by the end of August 1994 we would reach our destination and submit the papers for publication early in September. I was convinced that these five men would carry out their mission as planned, for by then I was well aware of their talents and commitment. As it happened, however, one more August would come and go before we would arrive at "Ithaca". In my calculations, I had neglected a small detail, a detail that became an important factor, and one that "Poseidon" would exploit at our expense and inflict one more delay before the final success...

> "*It is the earth encircler Poseidon who, ever relentless, nurses a grudge because of the Cyclops, whose eye he blinded; ... For his sake Poseidon, shaker of the earth, although he does not kill Odysseus, yet drives him back from the land of his fathers.*"
> Book V, v. 68, 69, and 74, 75[1]

During the summer of 1994, when the final campaign towards brevetoxin B was taking place, the World Cup in Soccer was hosted in the U. S., and all the members of the brevetoxin B team were either European or Japanese! Placing such soccer fanatics on the team for this highly demanding operation was rather unfortunate. Well, you can never think of everything in total synthesis! Brevetoxin B (**1**) could not, however, escape for much longer, and before the end of the fall in that year it was destined to yield to the enthusiasm and pressure of these relentless professionals. Needless to say, this victory was to serve well as a consolation to each one of them for their countries' not winning the World Cup!

The completion of the synthesis of the ABCDEFG ring framework as the phosphonium salt **98**, proceeded smoothly and swiftly (Scheme 31). An X-ray crystallographic analysis on

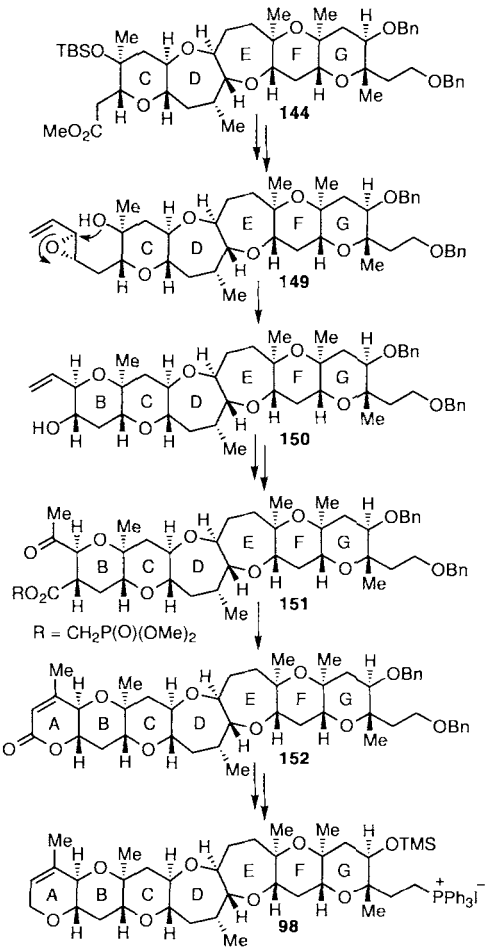

Scheme 31. Linearity and fusion of the ABCDEFG ring system.

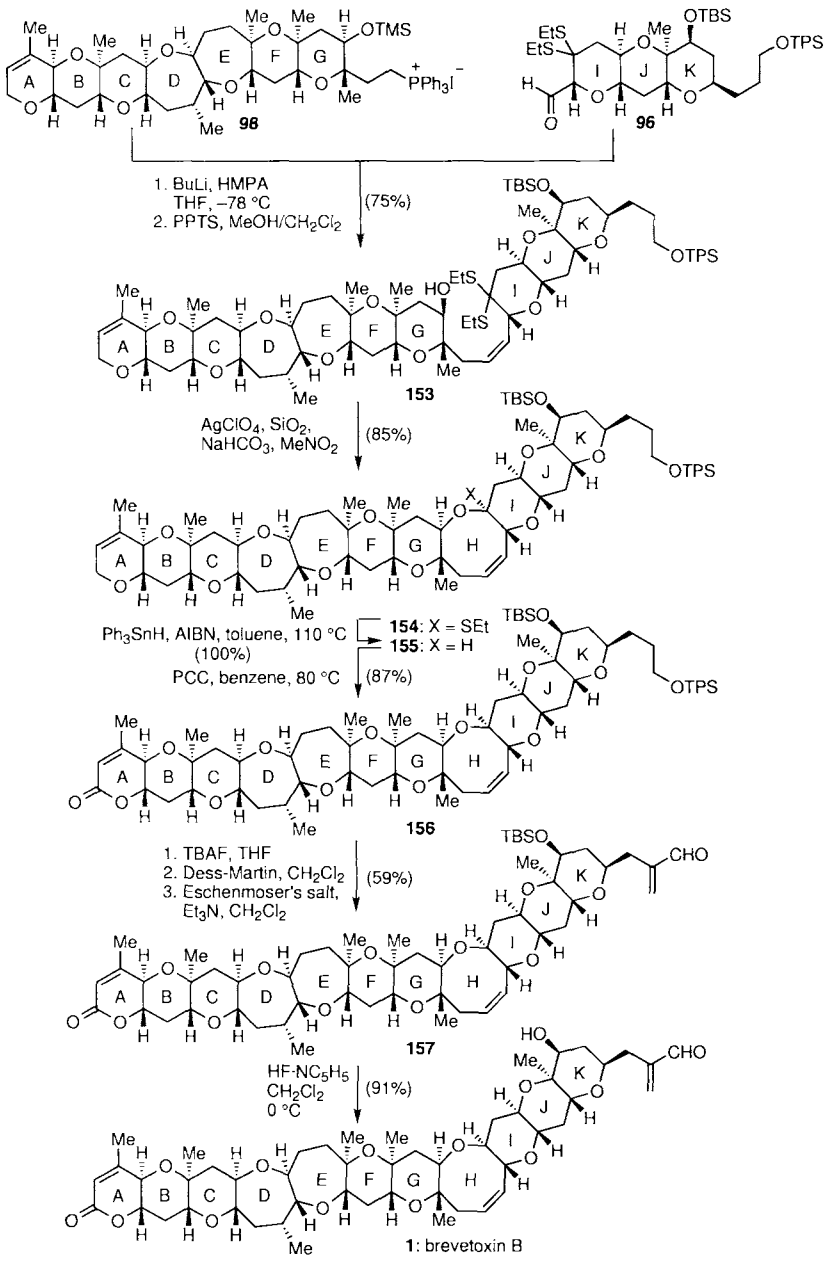

Scheme 32. Convergency and final stages of the total synthesis.

the iodide precursor of **98** confirmed its structure. Scheme 32 details the final stages of the total synthesis of brevetoxin B (**1**). As anticipated, both the coupling of the two segments and the oxocene formation proceeded extremely well, leading to compound **155**. We celebrated the long-sought victory of completing the skeleton of brevetoxin B! Before euphoria overwhelmed the group, on October 1, 1994, a day-by-day schedule was drawn on the wall between the fumehoods of Floris and Emmanuel, where the front work was being carried out. This timetable was to end on October 20, 1994, the day I was scheduled to fly from Copenhagen, Denmark, to Athens, Greece.

My trip to Europe took me to Lünd on the southern tip of Sweden, where Professors Salo Gronowitz and Torbjörn Frejd met me at the airport with the bad news that on their way they had hit a "kronjort" (red deer), which caused considerable harm to both the animal and the car. The deer was "sacrificed" later that evening by the authorities, and, for the next two days I was driven by Torbjörn in a hardly functioning car, a fortuitous experience I must admit, and one that I enjoyed very much, since it gave me the chance to spend more time inside the car than outside, where it was bitterly cold! After an exceedingly pleasant visit, which included two exquisite meals on venison, I crossed the Öresund channel to Copenhagen on the morning of October 20th and boarded a flight to Athens. There, I was met at the airport by Elias Couladouros and Demetris Papahatjis, two of my former students, who now teach and do research in Athens. They immediately took me to "Dionysos," a cafe below the Akropolis, for an afternoon drink. From there I could see the Parthenon, the temple of Athene, standing majestically and radiating serene contentment and wisdom through its beautiful architecture. Perhaps she, Athene, had a secret victorious message for me—at least so I wished!

Comfortable, but anxious, back at the Hilton Hotel later on that evening, I received, a fax from my students just before midnight with the news of the completed total synthesis of brevetoxin B (**1**), accompanied by the first ^{1}H NMR spectrum of the synthetic brevetoxin B. (A sample of the authentic, natural material from Dan Baden and Bob Gawley would arrive the following week.) It was a great moment for me and certainly for my students, and my first reaction was to thank God in a heartfelt silent prayer for helping us reach our target. Since my departure from California on October 15, I had intentionally not communicated with the brevetoxin team. The tension was simply too high, and besides, I suspected that they would do better without my interference—and they did!

Poseidon, however, would have the last word! As if to take vengeance one last time, the ruler of the sea unleashed a major storm the next day, and Athens suffered the worst floods in forty years!

Figure 5 shows the ^{1}H and ^{13}C NMR spectra of synthetic and natural samples of brevetoxin B (**1**), Figure 6 presents some of the beautiful crystals of synthetic brevetoxin B, and Figure 7 depicts results of the X-ray crystallographic analysis (ORTEP representation). There is little need to attempt to describe the thrill, contentment, and happiness we had at the moment of final success. Figure 8 tells it all! Particularly pleasing for me was the fact that I was able to provide these students and postdoctoral fellows, and those before them, the opportunity to be independent, to learn, create, imagine, and succeed; and all those things they accomplished and more! My pride in them cannot be described in words, but will always remain a precious part of my reward as a teacher.

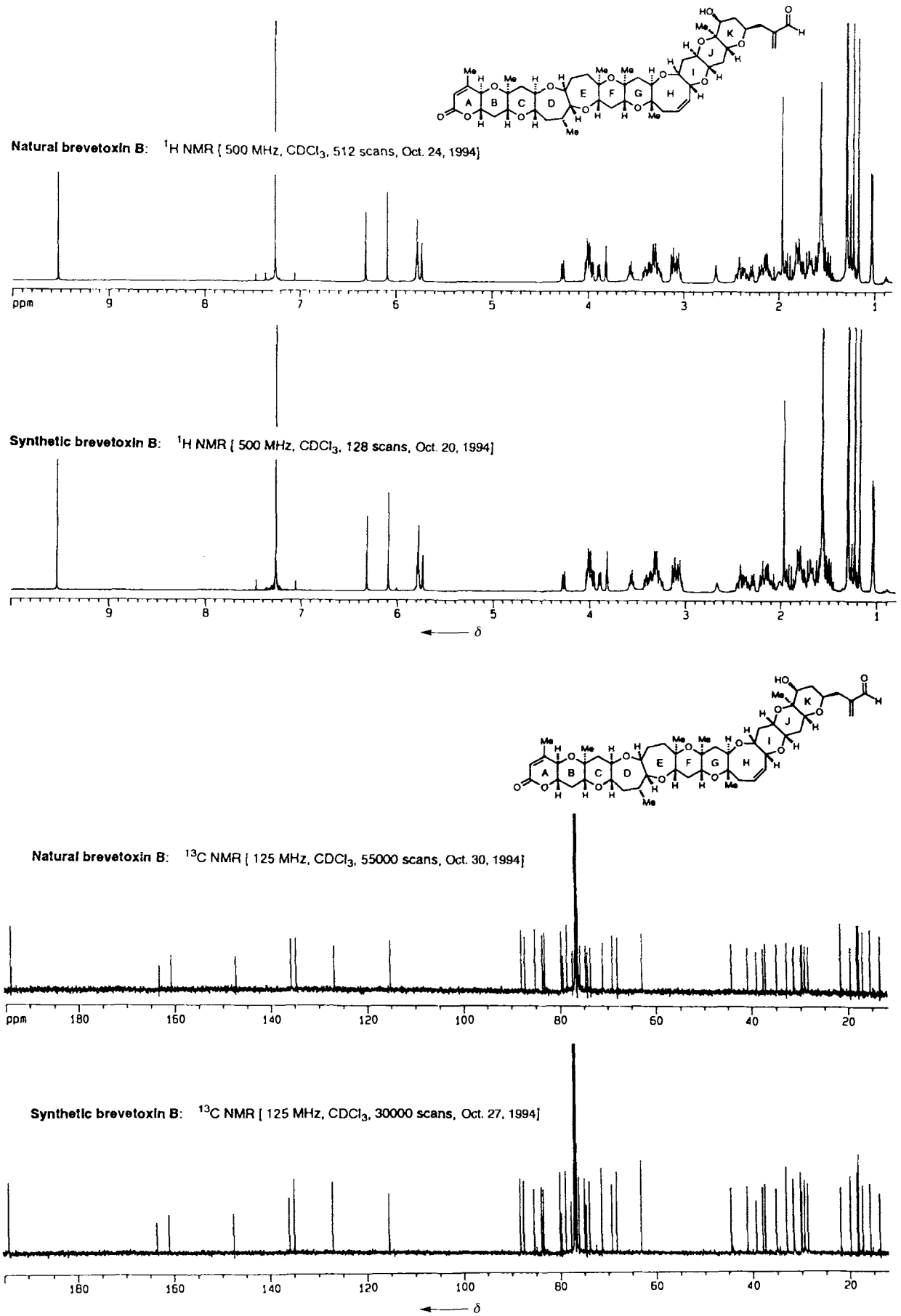

Fig. 5. ^{1}H (top) and ^{13}C NMR spectra (bottom) of synthetic and natural brevetoxin B (1).

Fig. 6. Crystals of synthetic brevetoxin B (**1**).

Fig. 7. X-ray crystal structure of synthetic brevetoxin B (**1**) (ORTEP representation). The crystallographic analysis was carried out by Dr. Raj Chadha at The Scripps Research Institute.

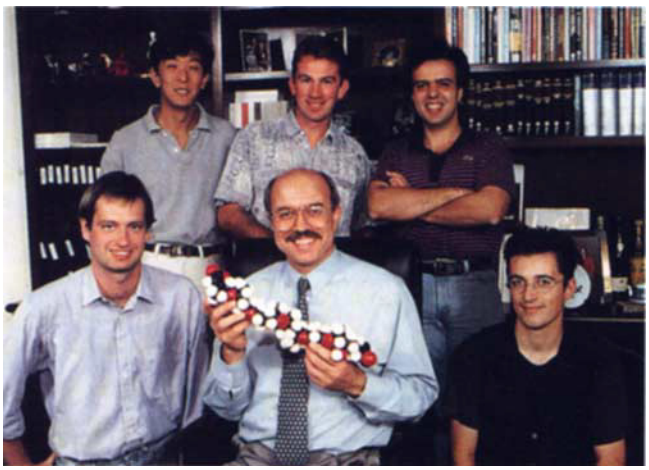

Fig. 8. The final brevetoxin B team (clockwise from bottom left to right): Jörg Tiebes, Mitsunobu Sato, Floris Rutjes, Emmanuel Theodorakis, and Edouard Untersteller. Center front holding a model of the target molecule: K. C. Nicolaou.

4. Epilogue

It is hoped that with its light style this article has made abundantly clear, and in an enjoyable way, the many findings along the way to brevetoxin B (**1**) and their potential value to future basic and applied research.[40] Lest there are skeptics remaining, here is an appropriate and beautiful poem to help us understand what it was and should be all about. The modern Greek poet C. P. Cavafy points out in his poem "Ithaca" that it is not the destination that finally matters the most, but rather what one observes, discovers, and accumulates on the way.[41]

Ithaca

When you start on your journey to Ithaca,
Then pray that the road is long,
Full of adventure, full of knowledge,
Do not fear the Lestrygonians
And the Cyclopes and the angry Poseidon.
You will never meet such as these on your path,
If your thoughts remain lofty, if a fine
Emotion touches your body and your spirit.
You will never meet the Lestrygonians,
The Cyclopes and the fierce Poseidon,
If you do not carry them within your soul,
If your soul does not raise them up before you.

Then pray the road is long.
That the summer mornings are many,
That you will enter ports seen for the first time
With such pleasure, with such joy!
Stop at Phoenician markets,
And purchase fine merchandise,
Mother-of-pearl and corals, amber and ebony,
And pleasurable perfumes of all kinds,
Buy as many pleasurable perfumes as you can;
Visit host of Egyptian cities,
To learn and learn from those who have knowledge.
Always keep Ithaca fixed in your mind.
To arrive there is your ultimate goal.
But do not hurry the voyage at all.
It is better to let it last for long years;
And even to anchor at the isle when you are old,
Rich withal that you have gained on the way,
Not expecting that Ithaca will offer you riches.

Ithaca has given you the beautiful voyage.

Without her you would never have taken the road.
But she has nothing more to give you.

And if you find her poor, Ithaca has not defrauded you.
With the Great Wisdom you have gained,
with so much experience,
You must surely have understood by then what Ithacas mean.

C. P. Cavafy

The great British novelist Robert Lewis Stephenson said it much more succinctly: "It is better to travel in hope than to arrive." There is no denying that exercises such as the one described, as torturous as they are, provide invaluable opportunities for strengthening the mind, skills, and character. This story, like the personal accounts written earlier on the total syntheses of calicheamicin[42] and taxol,[43] describes the strategies, exhilarations, frustrations, and behind-the-scenes maneuvers often encountered in the total synthesis of complex molecules, and are meant to be light, entertaining, and educational to both practitioners and students of the art.

It is perhaps appropriate to conclude this article with some thoughts regarding the state of the art of total synthesis today. The polycyclization of polyepoxides following a zip-type mech-

anism (Scheme 1) proposed in 1982, intriguing as it might be, is still a far-off dream for synthetic chemists. Another, distant dream is the "magical zipping" approach to brevetoxin B involving a poly(thioxooxamacrocycle) such as **158** shown in Scheme 33, an idea that arose from the bridging reactions dis-

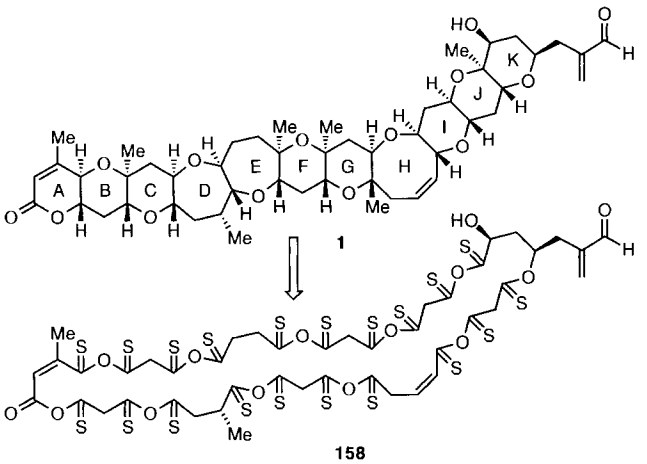

Scheme 33. A "magical zipping" approach to brevetoxin B (**1**).

covered during this campaign. Developing new synthetic methods for such transformations is the challenge of tomorrow, while elucidating the mechanism by which nature makes this compound remains another exciting odyssey. Finally, the merging of the chemistry and biology of natural products such as the brevetoxins through chemical synthesis is also destined to provide further fuel for the field of total synthesis.

I am deeply indebted to my talented collaborators, all of whom worked on the brevetoxin B project with the outmost enthusiasm, dedication, and persistence (listed alphabetically): Y. Abe, R. A. Awartani, K. Bal Reddy, T. Bleckman, E. A. Couladouros, S. A. DeFrees, M. E. Duggan, H.-M. He, C.-K. Hwang, D. A. Nugiel, D. R. Reddy, F. P. J. T. Rutjes, F. Sato, M. Sato, J. Shin, E. A. Theodorakis, J. Tiebes, E. Untersteller, X.-Y. Xiao, and Z. Yang. I am also grateful to Dee H. Huang, Gary Siuzdak, and Raj Chadha from The Scripps Research Institute, and George Furst, John Dykins, and Pat Carroll from the University of Pennsylvania for their superb and invaluable assistance with NMR (D. H. H. and G. F.), mass spectroscopy (G. S. and J. D.), and X-ray crystallography (R. C. and P. C.). I am particularly grateful to Emmanuel Theodorakis and Floris Rutjes for their assistance in the preparation of this article. This research was carried out at the University of Pennsylvania, The Scripps Research Institute, and the University of California, San Diego, and was supported financially by The National Institutes of Health, the University of Pennsylvania, The Scripps Research Institute, the University of California, San Diego, the ALSAM Foundation (USA), Dainippon Pharmaceutical Co., Ltd. (Japan), Glaxo (USA), Hoffmann La Roche (USA), Merck Sharp & Dohme (USA), Pfizer (USA), Rhone-Poulenc Rorer (USA), Schering Plough (USA), and Smith Kline Beecham (USA), and through fellowships by Rhone-Poulenc Rorer (C.-K. H.), the Netherlands Organization for Scientific Research (NWO) (F. P. J. T. R.), the Deutsche Forschungsgemeinschaft (J. T.), the Agricultural University of Athens (E. A. C.), Unitika, Ltd. (M. S.), and Rhone-Poulenc Rorer, S. A. (E. U.).

Received: March 30, 1995 [A 111 IE]
German version: *Angew. Chem.* **1996**, *108*, 644–664

[1] *The Odyssey of Homer*, translated by R. Lattimore, Harper Perenial, New York, **1975**. Homer's *Odyssey*, one of the western world's first two poems (the *Iliad* is the other), is the tale of the adventures, wanderings, and exploits of Odysseus, a Greek hero of the Trojan war, as he attempts to reach Ithaca, his home island where his wife Penelope awaits him. During his journey Odysseus has an incredible series of adventures and setbacks caused by the anger of the god Poseidon, whose son Odysseus had blinded. Finally, assisted by his patroness, the goddess Athene, Odysseus returns home to Ithaca to find and punish the suitors, evil men who tried to win his wife's hand and who squandered his wealth and corrupted his servants while he was away. Telemachus, Odysseus' son, who had his own share of adventures while growing up, facing the suitors and, looking for his father, joins him in glory and wisdom as they reestablish their throne on Ithaca. Besides Odysseus, other main characters of *Odyssey* are as follows:
Telemachus: The son of Odysseus, who is just entering manhood, is highly conscious of his duties as a prince successor to the throne and protector of his mother as well as the need to live up to his father's reputation as a hero. His actions waver between the immature and the well-thought over as he searches for the truth about his father and desperately appeals to others for help. It is not until towards the end of the story that he exhibits great courage, skills, and confidence and one feels that he is, indeed, the son of Odysseus.
Athene: She is the daughter of Zeus, goddess of wisdom, and patroness of arts and crafts. Odysseus is her favorite and protegé and she is his heroine, even though she is a goddess. She plays a leading role in all important events in the narrative, and her spirit and power always influence and assist Odysseus and Telemachus in their difficult moments. A friend and a confidant to Odysseus, she enjoys winning him over and her relationship with him, while the hero adores her and finds special comfort, companionship, and understanding in her.
Poseidon: Younger brother to Zeus, god of the sea and of earthquakes, father of Polyphenus the one-eyed Cyclops whom Odysseus blinds. As a ruler of the sea and natural phenomena, Poseidon is able to place many obstacles in front of Odysseus, whom he despises. Poseidon, however, is unable to hold out against the combined pressure of the other gods, particularly Athene, of whom Odysseus is a favorite, and so eventually relents, but not before he repeatedly unleashes his anger.
The Cyclops, Scylla, and The Sirens: Some of the superhuman and monstrous characters of the tale who inflicted tremendous tortures and blows at Odysseus and his men, before he finally overcame them.
The Suitors: The evil noblemen of Ithaca who attempt to undermine Odysseus, win the hand of his queen, Penelope, and corrupt his palace servants. They succeed partly, wasting away a great deal of Odysseus fortune, but he eventually prevails and punishes them.
Ithaca: The island kingdom of Odysseus, most likely located somewhere off the western coast of Greece and the destination of the hero in this adventure. It is interesting to compare places, events, and characters from the Odyssey to those of modern-day total synthesis, an excercise left to the imagination of the reader!

[2] Y.-Y. Lin, M. Risk, S. M. Ray, D. Van Engen, J. Clardy, J. Golik, J. C. James, K. Nakanishi, *J. Am. Chem. Soc.* **1981**, *103*, 6773; see also: M. S. Lee, D. J. Repeta, K. Nakanishi, M. G. Zagorski, *ibid.* **1986**, *108*, 7855.

[3] D. M. Anderson, *Sci. Am.* **1994**, No. 8, 62, and references therein.

[4] D. M. Anderson, A. W. White, *Oceanus* **1992**, *35*, 55.

[5] V. L. Trainer, R. A. Edwards, A. M. Szmant, A. M. Stuart, T. J. Mende, D. G. Baden in *Marine Toxins: Origin, Structure and Molecular Pharmacology* (Eds.: H. Shenwood, G. Strichartz), ACS Symp. Ser. **1990**, *418*, 166.

[6] V. L. Trainer, D. G. Baden, W. A. Catterall, *J. Biol. Chem.* **1994**, *269*, 19904.

[7] H. H. Strain, W. A. Svec, K. Atlzemüller, M. C. Grandolfo, J. J. Katz, H. Kjøsen, S. Norgård, S. Liaaen-Jensen, F. T. Haxo, P. Wegfahrt, H. Rapoport, *J. Am. Chem. Soc.* **1971**, *93*, 1823.

[8] D. G. Baden, *Int. Rev. Cytol.* **1983**, *82*, 99–150.

[9] Isolation and structure elucidation: R. B. Woodward, *Pure Appl. Chem.* **1964**, *9*, 49; T. Goto, Y. Kishi, S. Takahashi, Y. Hirata, *Tetrahedron* **1965**, *21*, 2059; K. Tsuda, S. Ikuma, M. Kawamura, K. Tachikawa, K. Sakai, C. Tamura, O. Amakasu, *Chem. Pharm. Bull.* **1964**, *12*, 1357; Synthesis: Y. Kishi, M. Aratani, T. Fukuyama, F. Nakatsubo, T. Goto, S. Inoue, H. Tanino, S. Sugiura, H. Kakoi, *J. Am. Chem. Soc.* **1972**, *94*, 9217.

[10] Isolation: R. E. Moore, P. J. Scheuer, *Science* **1971**, *172*, 495; Structure elucidation and synthesis: R. E. Moore, G. Bartolini, *J. Am. Chem. Soc.* **1981**, *103*, 2491; D. Uemara, K. Ueda, Y. Hirata, *Tetrahedron Lett.* **1981**, *22*, 2781; R. W. Armstrong, J.-M. Beau, S. H. Cheon, W. J. Christ, H. Fujioka, W.-H. Ham, L. D. Hawkins, H. Hin, S. H. Kang, Y. Kishi, M. J. Martinelli, W. W. McWorther, M. Mizuno, M. Nakata, A. E. Stutz, F. X. Talamas, M. Taniguchi, J. A. Tino, K. Ueda, J. Uenishi, J. B. White, M. Yonaga, *J. Am. Chem. Soc.* **1989**, *111*, 7530.

[11] Isolation: E. J. Schantz, J. D. Mold, D. W. Stanger, J. Shavel, F. J. Riel, J. P. Bowden, J. M. Lynch, R. S. Wyler, B. Riegel, H. Sommer, *J. Am. Chem. Soc.* **1957**, *79*, 5230, 5235; Structure elucidation: E. J. Schantz, V. E. Ghazarossian, H. K. Schnoes, F. M. Strong, J. P. Springer, J. O. Pezzanite, J. Clardy, *ibid.* **1975**, *97*, 1238; J. Bordner, W. E. Thiessen, H. A. Bates, H. Rapoport, *ibid.*

1975, *97*, 6008; Synthesis: H. Tanino, T. Nakata, T. Kaneko, Y. Kishi, *ibid.* **1977**, *99*, 2818; P. A. Jacobi, M. J. Martinelli, S. Polanc, *ibid.* **1984**, *106*, 5594.

[12] Isolation: K. Daigo, *J. Pharm. Soc. Jpn.* **1959**, *79*, 350; Structure elucidation and synthesis: Y. Ohfune, M. Tomita, *J. Am. Chem. Soc.* **1982**, *104*, 3511.

[13] See for example: T. Yasumoto, M. Murata, *Chem. Rev.* **1993**, *93*, 1897.

[14] Isolation: P. J. Scheuer, W. Takahashi, J. Tsutsumi, T. Yoshida, *Science* **1976**, *155*, 1267; Structure elucidation: M. Murata, A.-M. Legrand, Y. Ishibashi, T. Yasumoto, *J. Am. Chem. Soc.* **1989**, *111*, 8927.

[15] Isolation: T. Yasumoto, R. Bagnis, J. P. Vernoux, *Bull. Jpn. Soc. Sci. Fish.* **1976**, *42*, 359; Structure elucidation: M. Murata, H. Naoki, S. Matsunaga, M. Satake, T. Yasumoto, *J. Am. Chem. Soc.* **1994**, *116*, 7098.

[16] K. C. Nicolaou, M. E. Duggan, C.-K. Hwang, P. K. Somers, *J. Chem. Soc. Chem. Commun.* **1985**, 1359; K. C. Nicolaou, C. V. C. Prasad, P. K. Somers, C.-K. Hwang, *J. Am. Chem. Soc.* **1989**, *111*, 5330; K. C. Nicolaou, C. V. C. Prasad, P. K. Somers, C.-K. Hwang, *ibid.* **1989**, *111*, 5335.

[17] T. Katsuki, K. B. Sharpless, *J. Am. Chem. Soc.* **1980**, *102*, 5976.

[18] S. L. Schreiber, S. E. Kelly, *Tetrahedron Lett.* **1984**, *25*, 1757.

[19] K. C. Nicolaou, C.-K. Hwang, M. E. Duggan, K. B. Reddy, *Tetrahedron Lett.* **1987**, *28*, 1501.

[20] K. C. Nicolaou, M. E. Duggan, C.-K. Hwang, *J. Am. Chem. Soc.* **1986**, *108*, 2468; K. C. Nicolaou, C. V. C. Prasad, C.-K. Hwang, M. E. Duggan, C. Veale, *ibid.* **1989**, *111*, 5321.

[21] K. C. Nicolaou, C.-K. Hwang, M. E. Duggan, B. K. Reddy, B. E. Marron, D. G. McGarry, *J. Am. Chem. Soc.* **1986**, *108*, 6800; K. C. Nicolaou, C.-K. Hwang, B. E. Marron, S. A. DeFrees, E. Couladouros, Y. Abe, P. J. Carroll, J. P. Snyder, *ibid.* **1990**, *112*, 3040.

[22] K. C. Nicolaou, C.-K. Hwang, M. E. Duggan, P. J. Carroll, *J. Am. Chem. Soc.* **1987**, *109*, 3801; K. C. Nicolaou, C.-K. Hwang, S. A. DeFrees, N. A. Stylianides, *ibid.* **1988**, *110*, 4868; K. C. Nicolaou, S. A. DeFrees, C.-K. Hwang, N. Stylianides, P. J. Carroll, J. P. Snyder, *ibid.* **1990**, *112*, 3029.

[23] K. C. Nicolaou, C.-K. Hwang, M. E. Duggan, D. A. Nugiel, Y. Abe, K. Bal Reddy, S. A. DeFrees, D. R. Reddy, R. A. Awartani, S. R. Conley, F. P. J. T. Rutjes, E. A. Theodorakis, *J. Am. Chem. Soc.*, **1995**, *117*, 10227.

[24] K. C. Nicolaou, D. G. McGarry, P. K. Somers, B. H. Kim, W. W. Ogilvie, G. Yiannikouros, C. V. C. Prasad, C. A. Veale, R. R. Hark, *J. Am. Chem. Soc.* **1990**, *112*, 6263.

[25] K. C. Nicolaou, C.-K. Hwang, D. A. Nugiel, *Angew. Chem.* **1988**, *100*, 1413; *Angew. Chem. Int. Ed. Engl.* **1988**, *27*, 1362.

[26] K. C. Nicolaou, C.-K. Hwang, D. A. Nugiel, *J. Am. Chem. Soc.* **1989**, *111*, 4136.

[27] K. C. Nicolaou, D. G. McGarry, C. A. Veale, P. K. Somers, G. T. Furst, *J. Am. Chem. Soc.* **1987**, *109*, 2504; K. C. Nicolaou, C. V. C. Prasad, W. W. Ogilvie, *ibid.* **1990**, *112*, 4988.

[28] K. C. Nicolaou, D. G. McGarry, P. K. Somers, *J. Am. Chem. Soc.* **1990**, *112*, 3696.

[29] A. V. Krishna Prasad, Y. Shimizu, *J. Am. Chem. Soc.* **1989**, *111*, 6479.

[30] K. C. Nicolaou, K. R. Reddy, G. Skokotas, F. Sato, X.-Y. Xiao, *J. Am. Chem. Soc.* **1992**, *114*, 7935; K. C. Nicolaou, K. R. Reddy, G. Skokotas, F. Sato, X.-Y. Xiao, C.-K. Hwang, *ibid.* **1993**, *115*, 3558.

[31] For cyclizations of hydroxyketones see: K. C. Nicolaou, M. E. Duggan, C.-K. Hwang, *J. Am. Chem. Soc.* **1989**, *111*, 6666, 6676.

[32] K. C. Nicolaou, C.-K. Hwang, M. E. Duggan, *J. Am. Chem. Soc.* **1989**, *111*, 6682.

[33] K. C. Nicolaou, J. Tiebes, E. A. Theodorakis, F. P. J. T. Rutjes, K. Koide, M. Sato, E. Untersteller, *J. Am. Chem. Soc.* **1994**, *116*, 9371.

[34] K. C. Nicolaou, D. A. Nugiel, E. Couladouros, C.-K. Hwang, *Tetrahedron* **1990**, *46*, 4517.

[35] K. C. Nicolaou, E. A. Theodorakis, F. P. J. T. Rutjes, J. Tiebes, M. Sato, E. Untersteller, X.-Y. Xiao, *J. Am. Chem. Soc.* **1995**, *117*, 1171; K. C. Nicolaou, F. P. J. T. Rutjes, E. A. Theodorakis, J. Tiebes, M. Sato, E. Untersteller, *ibid.* **1995**, *117*, 1173.

[36] K. C. Nicolaou, E. A. Theodorakis, F. P. J. T. Rutjes, M. Sato, J. Tiebes, X.-Y. Xiao, C.-K. Hwang, M. E. Duggan, Z. Yang, E. A. Couladouros, F. Sato, J. Shin, H.-M. He, T. Bleckman, *J. Am. Chem. Soc.* **1995**, *117*, 10239; K. C. Nicolaou, F. P. J. T. Rutjes, E. A. Theodorakis, J. Tiebes, M. Sato, E. Untersteller, *ibid.* **1995**, *117*, 10252.

[37] K. Takai, M. Tagashira, T. Kuroda, K. Oshima, K. Utimoto, H. Nozaki, *J. Am. Chem. Soc.* **1986**, *108*, 6048; Y. Kishi, *Pure Appl Chem.* **1989**, *61*, 313.

[38] K. S. Rein, D. G. Baden, R. E. Gawley, *J. Org. Chem.* **1994**, *59*, 2101; K. S. Rein, B. Lynn, R. E. Gawley, D. G. Baden, *ibid.* **1994**, *59*, 2107.

[39] M. Fetizon, M. Golfier, J.-M. Louis, *Tetrahedron* **1975**, *31*, 171; see for example: S. Masamune, L. D.-L. Lu, W. P. Jacobson, T. Kaiho, T. Toyoda, *J. Am. Chem. Soc.* **1982**, *104*, 5523.

[40] For a didactic presentation of the synthesis of brevetoxin (and syntheses of many other complex natural products) see: K. C. Nicolaou, E. J. Sorensen, *Classics in Total Synthesis: Targets, Strategies, Methods*, VCH, Weinheim, **1996**, p. 731 ff.

[41] C. P. Cavafy, *The Complete Poems of Cavafy*, Translated by R. Dalven, Harcourt, Brace & World, New York, **1991**, p. 36.

[42] K. C. Nicolaou, *Angew. Chem.* **1993**, *105*, 1462; *Angew. Chem. Int. Ed. Engl.* **1993**, *32*, 1377.

[43] K. C. Nicolaou, R. K. Guy, *Angew. Chem.* **1995**, *107*, 2247; *Angew. Chem. Int. Ed. Engl.* **1995**, *34*, 2079.

Oxygen Activation by Mononuclear Non-Heme Iron Proteins**

Alexandre L. Nivorozhkin and Jean-Jacques Girerd*

Mono- and dinuclear non-heme iron centers are frequently present in the active centers of enzymes that catalyze oxidations.[1] However, in the past more effort has been focused on enzymes with dinuclear than those with mononuclear iron centers—at the last International Conference on Bioinorganic Chemistry (ICBIC-7) last year in Lübeck, 26 contributions were devoted to dinuclear iron proteins and only 13 to the mononuclear ones. Nevertheless, interest in mononuclear iron enzymes is rapidly growing in biology and chemistry.[2] The amazingly diverse functional properties of the mononuclear iron enzymes from lipid oxidation (lipid dioxygenases, LO) through oxidations of arenes (arene dioxygenases, catechol dioxygenases, pteridine-dependent enzymes) to the synthesis of isopenicillin (isopenicillin N synthase, IPNS) and oxidation of nonactivated C–H bonds (α-keto acid dependent enzymes) undoubtedly make this a worthwhile field of research from which both industry and medicine can apparently benefit. An important topic of research in this field is bleomycin (BLM), a naturally occurring iron-containing glycopeptide, which like cisplatin is successful as an anti-cancer drug.

Studies on the sequence-specific oxidative cleavage of DNA by BLM[3] and the investigation of synthetic model complexes were particulary instructive for understanding the key features of the oxygen activation steps and of the mechanism of the catalytic oxidation by activated mononuclear iron complexes. The latest results[4] leave no doubts that the formation of the spectroscopically detected BLM transient mononuclear peroxo species, "activated BLM", is one of the primary steps of the oxygen activation. The debates on the reactivity mechanism are still continuing. The involvement of the radical species OH· can probably be excluded, but ferryl species are frequently discussed even though they have never been detected spectroscopically. One of the most impressive results obtained by using BLM mimics[4a] is that the DNA cleavage pathway is essentially determined by the metal-binding domain; metal complexes without a polypeptide tail with specific dithiazole terminus, which is believed to be decisive for binding to DNA, display a very similar cleavage pattern to that of BLM. This fact may have important consequences for finding other distinct simple synthetic iron complexes with an activity which could rival that of BLM.[5a] Iron complexes with aminopyridine ligands[5b,c] have been reported to display a DNA cleavage activity only ten times lower than that of BLM.[5b] Studies on these and other aminopyridine iron complexes as well as on bipyridine iron complexes[5d–g] provide reliable spectroscopic evidence for the occurrence of the Fe^{III}-peroxo transient species with characteristics similar to those of "activated BLM".

Knowledge of the atomic structure of the active site is one of the key requirements for elucidating an enzymatic reaction mechanism. Recently achieved milestones are the crystal structure analyses of several important mononuclear non-heme iron proteins: extradiol dioxygenase, IPNS, and lipid dioxygenase.

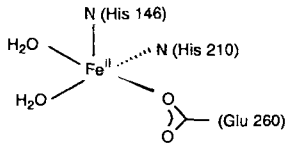

2,3-dihydroxybiphenyl 1,2-dioxygenase

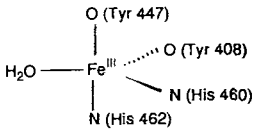

intradiol dioxygenase

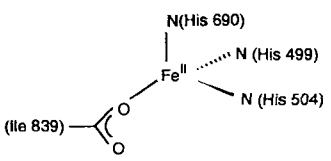

(Amzel et al.)

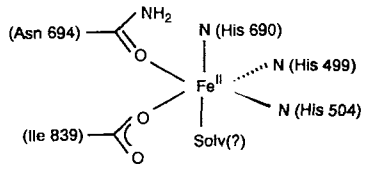

(Axelrod et al.)

soybean lipoxygenase L-1

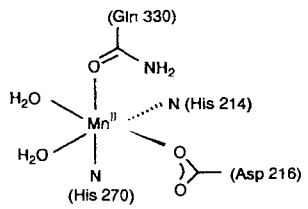

isopenicillin N synthase

[*] Dr. J.-J. Girerd, Dr. A. L. Nivorozhkin
Laboratoire de Chimie Inorganique
URA CNRS 420, Bat. 420, Université Paris-Sud
F-91405 Orsay (France)
Fax: Int. code +(1) 69 85 55 36

[**] We are grateful to Dr. J. T. Bolin, Purdue University, USA, for providing us a preprint of his paper to *Science* (see ref. [9a]) and to Dr. B. Meunier, Toulouse, France, for fruitful discussions. We acknowledge the financial support of the group Elf Aquitaine.

 © VCH Verlagsgesellschaft mbH, D-69451 Weinheim, 1996 0570-0833/96/3506-0609 $ 15.00+.25/0

The lipid oxidation catalyzed by lipoxygenase (oxygenation of a *cis,cis*-1,4-diene to a conjugated 1-hydroperoxodiene) appears chemically to be one of the most simple transformations. The structure of the enzyme active site reported by Amzel et al.[6a] at the 2.5 Å resolution contains a Fe^{II} center (bound to three histidine nitrogens and a monodentate terminal carboxylate) in a distorted tetrahedral geometry similar to that found for the iron superoxide dismutase. This finding is contrary to all previous spectroscopic results, which indicated an octahedral geometry. The authors confidently excluded other ligating groups such as water or hydroxide ions, and envisaged an essential role for an Asn residue close to the iron center in stabilizing a probable iron–peroxo intermediate. Nevertheless, an X-ray structure analysis of an isomeric form of the same enzyme published by Axelrod et al.[6b] reveals the presence of a five-coordinate iron center with a monodentate-bound asparagine residue. This has been confirmed by a recent spectroscopic study.[6c] The first step of the lipid oxidation is the generation of a carbon-centered radical, which is subsequently attacked by oxygen to form a 1-OOH species. Regio- and stereoselectivity of this process indicates an absence of hydroxy radicals in the course of the oxidation. Experiments with substrates in anaerobic conditions revealed that the ferric form of the enzyme is responsible for the primary hydrogen abstraction step. Characteristic changes in the UV/Vis spectrum indicate the formation of the iron–peroxo intermediates in presence of oxygen and substrate. Based on this observation, Nelson et al. recently proposed a novel reaction mechanism for LO.[7a] Mascharak et al.[7b] have described model iron complexes that show activity similar to that of BLM and form unambiguously detected iron–peroxo species; these complexes react with linoleic and arachidonic acid in the presence of O_2 or H_2O_2 to afford very efficiently 1-OOH products with good stereoselectivity.

IPNS catalyzes a fairly sophisticated reaction in penicillin biosynthesis—transformation of the linear tripeptide (δ-(L-α-aminoadipoyl)-L-cysteinyl-D-valine) (ACV) into isopenicillin N. Unlike other non-heme oxidases, IPNS does not require electron donors or oxidized cofactors. The X-ray structure analysis of a Mn^{II}-substituted IPNS reveals[8] a metal center in an octahedral environment with two histidine nitrogens, one monodentate carboxylate, one O-bound amido group, and two water molecules. This structure is in good agreement with spectroscopic data; thus, almost no revision of the proposed multistep reaction mechanism, which was based mainly on experiments with substrate analogs and isotopic labeling, is required. The development of biomimetic model complexes to clarify the enzyme–substrate interaction modes and to verify the occurrence of a transient ferryl species should now be the aims of bioinorganic chemists.

The features of the active site of 2,3-dihydroxybiphenyl 1,2-dioxygenase,[9a] an extradiol dioxygenase, which along with intradiol dioxygenase controls two metabolic pathways of catechol degradation, were also successfully predicted by spectroscopy, as a subsequent X-ray analysis has shown. Consistent with spectral data by Solomon, Lipscomb et al.,[9b,c] the enzyme contains a square-pyramidal Fe^{II} center bound to two histidine nitrogen atoms, a terminal monodentate carboxylate, and two water molecules that are probably exchanged for a chelated substrate in the catalytic cycle. A distinct feature of extradiol dioxygenase is that the oxidation state of the iron center is conserved for all the reaction steps. Very few mechanistic studies have been carried out,[9d] and up to date no biomimetic complexes possessing extradiol cleavage activity are known. The results of the X-ray structure analysis[9a] now provide a good starting point to investigate the reaction mechanism and to compare it with the well-studied intradiol cleavage oxidation. Knowledge of the rich chemistry of the iron–phenolato complexes facilitated the elucidation of the reaction mechanism[10a] of intradiol–dioxygenase, in the active site of which the iron center is bound to two tyrosine and two histidine residues and a water molecule or a hydroxide anion, as a refined X-ray structure has recently shown[10b,c]. Several synthetic complexes that can catalyze the intradiol cleavage have also been reported.[11] The most efficient systems surprisingly contain only nitrogen ligands, whereas the phenolato complexes are inhibited after the catechol–semiquinone oxidation step, which thus provides evidence for direct attack of the oxygen on the aromatic ring.

Three classes of nonheme iron enzymes for which the structure of the active site as well as the catalytic mechanism are poorly understood are arene dioxygenases and pterin-dependent and α-keto acid dependent enzymes. They are strongly dependent on the cofactors that deliver the electrons for oxygen reduction. Far less is known with respect to pertubations at the metal center in the mechanism of arene dioxygenases.[12a,b] Putative peroxo intermediates similar to "activated BLM" may be involved in the catalytic cycle of these dioxygenases and putidamonooxin[12c] (oxygen activation component of 4-methoxybenzoate monooxygenase). Arene dioxygenases and putidamonooxin contain a mononuclear iron center and a Rieske iron–sulfur cluster as cofactors. The mechanism of pterin-dependent metalloenzymes (tyrosine, phenylalanine, and tryptophan hydroxylase) is still unresolved: Is the iron–peroxo species the primary transient species or is it a secondary product generated by initially produced hydroperoxy-pterin?[13a] Hydroxylation of a metal-bound phenol in a simple synthetic iron complex, which had been treated with *m*-chloroperbenzoic, was observed by Kitajima et al.[13b] The first model complexes of α-keto acid dependent, Fe^{II}-containing dioxygenases were reported by L. Que et al.[14a,b] The hitherto best model complex was synthesized by J. Valentine et al.[14c] and was capable of reproducing the complete reactivity of the enzyme: oxygenation of the substrate (epoxidation of cyclohexene and stilbene) with concomitant oxygenation and decarboxylation of the iron-bound benzoylformate to benzoic acid. These results open favorable perspectives for modeling complicated catalytic reactions involving cofactor transformations. The simple biomimetic modeling of the oxygen activation has, however, a general problem, namely the formation of μ-peroxo dimers.[15]

Taking into account the diverse and complex interactions between the active site and substrate, which are often modulated further by participation of cofactors, one can hardly expect a unified view of the reaction mechanism and the active oxygenating species for mononuclear non-heme iron proteins. Nevertheless the intensive research over the last few years has revealed that the non-heme iron enzyme probably reacts via a peroxo intermediate, thus different from iron porphyrins for which high-valent iron–oxo species are the predominant intermediate.

German version: *Angew. Chem.* **1996**, *108*, 665–667

 © VCH Verlagsgesellschaft mbH, D-69451 Weinheim, 1996 0570-0833/96/3506-0610 $ 15.00+.25/0

Keywords: bioinorganic chemistry · bleomycin · iron compounds · non-heme iron proteins · O_2 activation

[1] A. L. Feig, S. Lippard, *Chem. Rev.* **1994**, *94*, 759.
[2] "Iron Proteins with Mononuclear Active Site": L. Que in *Encyclopedia of Inorganic Chemistry, Vol. 4* (Ed.: R. B. King), Wiley, Chichester, **1994**, p. 1859.
[3] J. Stubbe, J. W. Kozarich, *Chem. Rev.* **1987**, *87*, 1107.
[4] a) R. J. Guajardo, S. E. Hudson, S. J. Brown, P. Mascharak, *J. Am. Chem. Soc.* **1993**, *115*, 7971; b) J. W. Sam, X.-J. Tang, J. Peisach, *ibid.* **1994**, *116*, 5250; c) T. E. Westre, K. E. Loeb, J. M. Zaleski, B. Hedman, K. O. Hodgson, E. I. Solomon, *ibid.* **1995**, *117*, 1309.
[5] a) G. C. Silver, W. C. Trogler, *J. Am. Chem. Soc.* **1995**, *117*, 3983; b) A. L. Nivorozhkin, P. Mialane, J.-J. Girerd, G. Blondin, A. Rabion, G. Pratviel, M. Slany, F. Godde, B. Meunier, T. A. Mattioli, P. Soubayrol, *Inorg. Chem.* **1995**, submitted; c) I. Bernal, I. M. Jensen, K. B. Jensen, C. J. McKenzie, H. Toftlund, *J. Chem. Soc. Dalton Trans.* **1995**, 3667; d) Y. Zang, T. E. Elgren, Y. Dong, L. Que, *J. Am. Chem. Soc.* **1993**, *115*, 811; e) S. Menage, E. Wilkinson, L. Que, M. Fontecave, *Angew. Chem.* **1995**, *107*, 198; *Angew. Chem. Int. Ed. Engl.* **1995**, *34*, 203; f) M. Lubben, A. Meetsma, E. C. Wilkinson, B. Feringa, L. Que, *ibid.* **1995**, *107*, 1610 and **1995**, *34*, 1512; g) J. Kim, E. Larka, E. C. Wilkinson, L. Que, *ibid.* **1995**, *107*, 2191 and **1995**, *34*, 2048.
[6] a) J. C. Boyington, B. J. Gaffney, L. M. Amzel, *Science* **1993**, *260*, 1483; b) W. Minor, J. Steczko, J. T. Bolin, Z. Otwinowski, B. Axelrod, *Biochemistry* **1993**, *32*, 6320; c) M. A. Pavlosky, Y. Zhang, T. E. Westre, Q.-F. Gan, E. G. Pavel, C. Campochiaro, B. Hedman, K. O. Hodgson, E. I. Solomon, *J. Am. Chem. Soc.* **1995**, *117*, 4316.
[7] a) M. J. Nelson, R. A. Cowling, S. P. Seitz, *Biochemistry* **1994**, *33*, 4966; b) R. J. Guajardo, P. K. Mascharak, *Inorg. Chem.* **1995**, *34*, 802.
[8] P. L. Roach, I. J. Clifton, V. Fülöp, K. Harlos, G. J. Barton, J. Hajdu, I. Andersson, C. J. Schofield, J. E. Baldwin, *Nature* **1995**, *375*, 700.
[9] a) S. Han, L. D. Eltis, K. N. Timmis, S. W. Muchmore, J. T. Bolin, *Science* **1995**, *270*, 976; b) P. A. Mabrouk, A. M. Orville, J. D. Lipscomb, E. I. Solomon, *J. Am. Chem. Soc.* **1991**, *113*, 4053; c) L. Shu, Y.-M. Chiou, A. M. Orville, M. A. Miller, J. D. Lipscomb, L. Que, *Biochemistry* **1995**, *34*, 6649; d) J. Sanvoisin, G. J. Langley, T. D. H. Bugg, *J. Am. Chem. Soc.* **1995**, *117*, 7836.
[10] a) A. M. Orville, J. D. Lipscomb, *J. Biol. Chem.* **1993**, *268*, 8596; b) D. H. Orlendorf, J. D. Lipscomb, P. C. Weber, *Nature* **1988**, *336*, 403; c) D. H. Orlendorf, A. W. Orville, J. D. Lipscomb, *J. Mol. Biol.* **1994**, *244*, 586.
[11] a) H. G. Jang, D. D. Cox, L. Que, *J. Am. Chem. Soc.* **1991**, *113*, 9200; b) Y.-M. Chiou, L. Que, *Inorg. Chem.* **1995**, *34*, 3577; c) W. O. Koch, H.-J. Krüger, *Angew. Chem.* **1995**, *107*, 2928; *Angew. Chem. Int. Ed. Engl.* **1995**, *107*, 2671.
[12] a) G. T. Gassner, D. P. Ballou, G. A. Landrum, J. W. Whittaker, *Biochemistry* **1993**, *32*, 4820; b) E. G. Pavel, L. J. Martins, W. R. Ellis, E. E. Solomon, *Chem. Biol.* **1994**, *1*, 173; c) P. Wende, I.-H. Bernhardt, K. Pfleger, *Eur. J. Biochem.* **1989**, *181*, 189.
[13] a) T. Dix, S. J. Benkovic, *Acc. Chem. Res.* **1988**, *21*, 101; b) N. Kitajima, M. Ito, H. Fukui, Y. Moro-oka, *J. Am. Chem. Soc.* **1993**, *115*, 9335.
[14] a) Y.-M. Chiou, L. Que, *J. Am. Chem. Soc.* **1992**, *114*, 7567; b) Y.-M. Chiou, L. Que, *ibid.* **1995**, *117*, 3999; c) E. H. Ha, R. Y. N. Ho, J. F. Kisiel, J. S. Valentine, *Inorg. Chem.* **1995**, *34*, 2265.
[15] N. Kitajima, N. Tamura, H. Amagai, H. Fukui, Y. Moro-oka, Y. Mizutani, T. Kitagawa, R. Mathur, K. Heerwegh, C. A. Reed, C. R. Randall, L. Que, K. Tatsumi, *J. Am. Chem. Soc.* **1994**, *116*, 9071.

The Dimeric Steroid–Pyrazine Marine Alkaloids: Challenges for Isolation, Synthesis, and Biological Studies**

Arasu Ganesan

Dedicated to Professor Clayton Heathcock on the occasion of his 60th birthday

Isolation of Cephalostatins and Ritterazines

Since 1955 the American National Cancer Institute (NCI) has conducted a massive search for compounds with antitumor activity. Between 1955 and 1980 alone, some 130000 plant and animal extracts were screened, with the major success story being the discovery of taxol from the Pacific yew tree. This highlight covers a family of steroids also discovered by the NCI efforts.

In 1974 extracts of the tiny (ca. 5 mm) marine tube worm *Cephalodiscus gilchristi* collected off the coast of South Africa were found to be active in the NCI's primary assay, the murine lymphocytic leukemia P388. Fifteen years of relentless research by Pettit's group culminated in the isolation of 139 mg of the major bioactive component, cephalostatin 1, from 166 kg wet weight of the tube worm, and its structural elucidation.[1] This stage was summarized[2] as follows: "Interest in such a powerfully antileukemic agent as cephalostatin 1 ... has prompted Americans to dive extensively at a depth of 20 meters to collect *C. gilchristi* in open seawaters controlled by the white shark."

Cephalostatin 1 is extremely potent against P388, with an ED_{50} value of 10^{-7} to 10^{-9} $\mu g\,mL^{-1}$. Over the years, the Pettit group has characterized[3] sixteen other cephalostatins, all containing the novel structural framework of two steroid units linked at the A ring by a pyrazine (Scheme 1). The "right half" is identical in fifteen of the alkaloids, while cephalostatin 12 is a C_2-symmetric homodimer.

In 1994 a steroid–pyrazine dimer was reported[4] from an unexpected source. Fusetani's group isolated ritterazine A, which has an ED_{50} of 10^{-3} $\mu g\,mL^{-1}$ against P388, from the tunicate *Ritterella tokioka* collected off the coast of Japan. Twelve other ritterazines have since been described[5] (Scheme 2), including one homodimer, ritterazine K. A possible mechanism accounting for the rearranged "right half" in some of the ritterazines may involve protonation of the double bond in the D ring followed by either a 1,2 Wagner - Meerwein shift or retro-Prins ring opening and alternative Prins ring closure (Scheme 3).

The compounds from *C. gilchristi* and *R. tokioka* are clearly related (ritterazine K, for example, contains the "left half" of cephalostatin 7), although the same alkaloid has yet to be identified from both species. The presence of these compounds in two phyla suggests they may be produced by a symbiotic microorganism.

[*] Dr. A. Ganesan
Centre for Natural Product Research, Institute of Molecular and Cell Biology
National University of Singapore
10 Kent Ridge Crescent, Singapore 119260 (Singapore)
Fax: Int. code +(779)1117
e-mail: mcbgane@nus.sg

[**] The author wishes to thank Dr. Christopher Larson of the Salk Institute in San Diego, USA, for helpful discussions.

 © VCH Verlagsgesellschaft mbH, D-69451 Weinheim, 1996 0570-0833/96/3506-0611 $ 15.00+.25/0

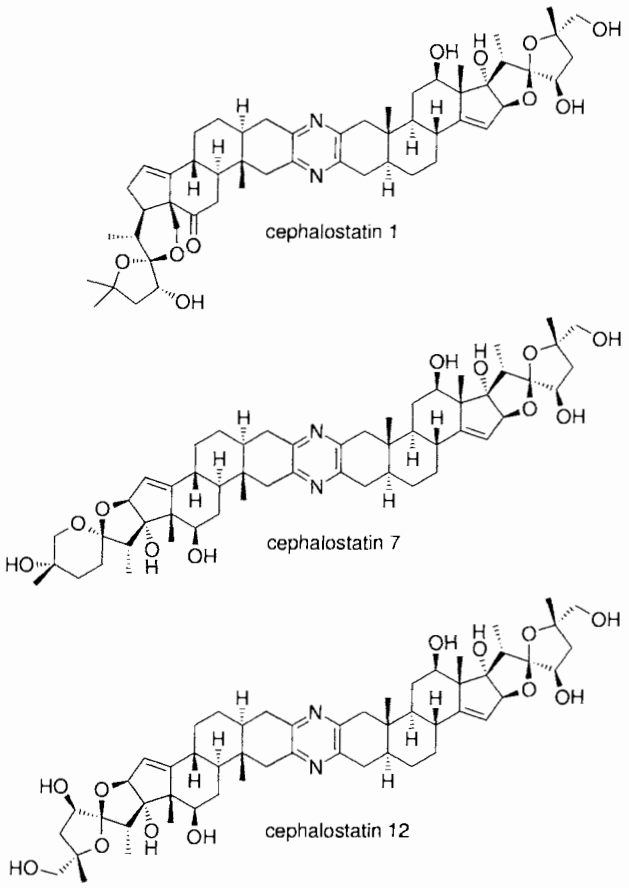

Scheme 1. Three of the seventeen known cephalostatins.

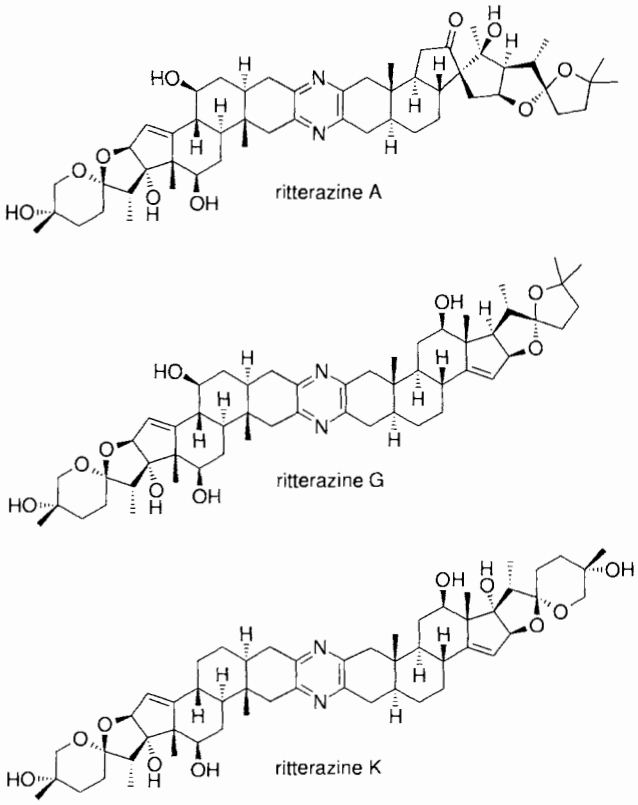

Scheme 2. Three of the thirteen known ritterazines.

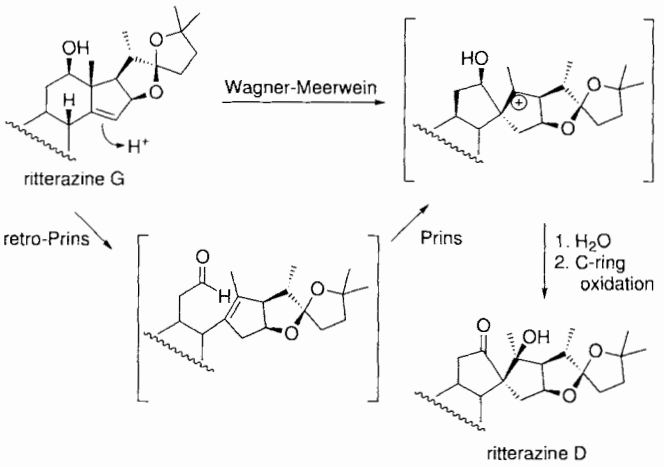

Scheme 3. Possible mechanism for the rearrangement of ritterazine G to give ritterazine D.

Synthetic Studies

Initial synthetic attention focused on preparation[6] of symmetrical steroid–pyrazine dimers by the classical condensation of α-amino ketones (Scheme 4). Interestingly, dimer **1** is itself weakly cytotoxic, with an ED_{50} around 10 μg mL^{-1} against tumor cell lines.

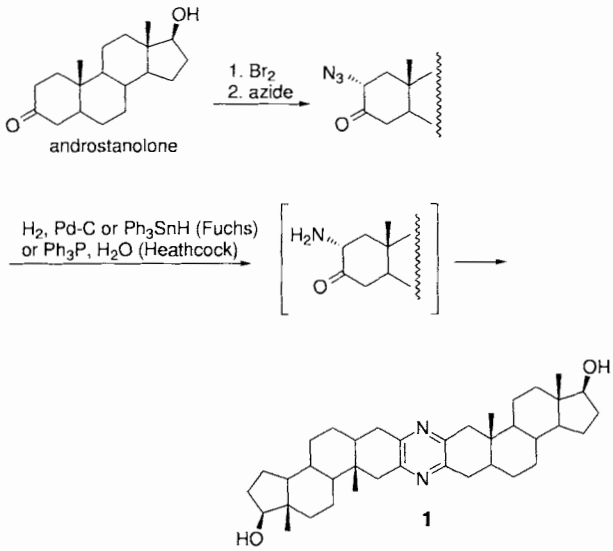

Scheme 4. Synthesis of symmetrical steroid–pyrazine dimers.

Smith and Heathcock[6b] achieved the synthesis of unsymmetrical dimers (most of these natural products fit this category) (Scheme 5). At 90 °C, α-amino oxime ether **2** and α-acetoxy ketone **3** preferentially react with each other to give intermediates that aromatize to give pyrazine **4** at higher temperature. The two-stage protocol is necessary as the α-amino oxime ether condenses with itself at 140 °C.

Introduction of asymmetry into a homodimer was demonstrated by Winterfeldt and co-workers (Scheme 6).[7] Commercially available hecogenin acetate was transformed into ketone **5** following literature precedents, and dimerized to give **6**. Eno-

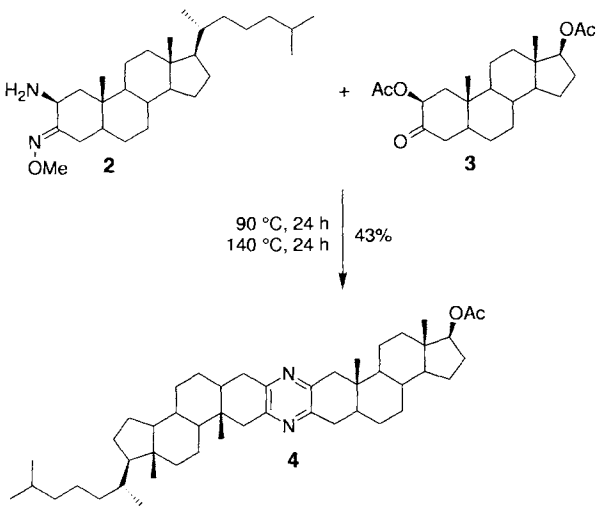

Scheme 5. Smith and Heathcock's synthesis of an unsymmetrical steroid–pyrazine dimer.

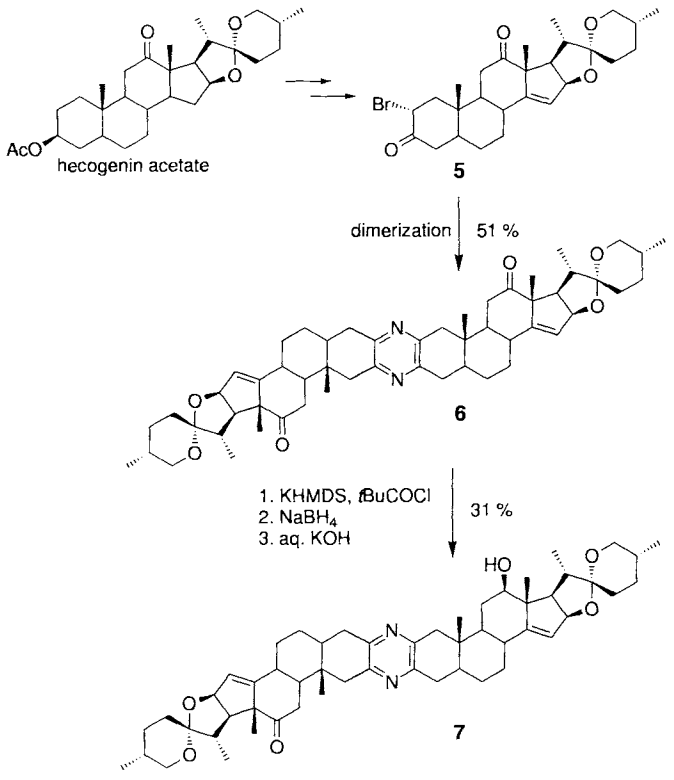

Scheme 6. Selective manipulation of a symmetrical dimer into an unsymmetrical dimer by Winterfeldt et al.

lization and trapping yielded a statistical mixture of separable asymmetric mono- and symmetric bis-enol esters. The former was reduced and hydrolyzed to afford dimer **7**, which has the C-ring oxygenation pattern and D-ring double bond of cephalostatin 1.

So far, all the publications related to total synthesis have been from Fuchs's group, who first reported[8] a symmetrical dimer corresponding to the "right half" of cephalostatin 1 but lacking the D-ring double bond. In fact, this dimer is the tetrahydro derivative of cephalostatin 12, whose existence had yet to be disclosed at that time.

The synthesis began with a derivative of hecogenin acetate, which already contains all the carbons needed. Classical Marker ring opening of the sapogenin spiroketal gave **8** (Scheme 7), which was carried forward to **9**. Acid-catalyzed cyclization of **9**

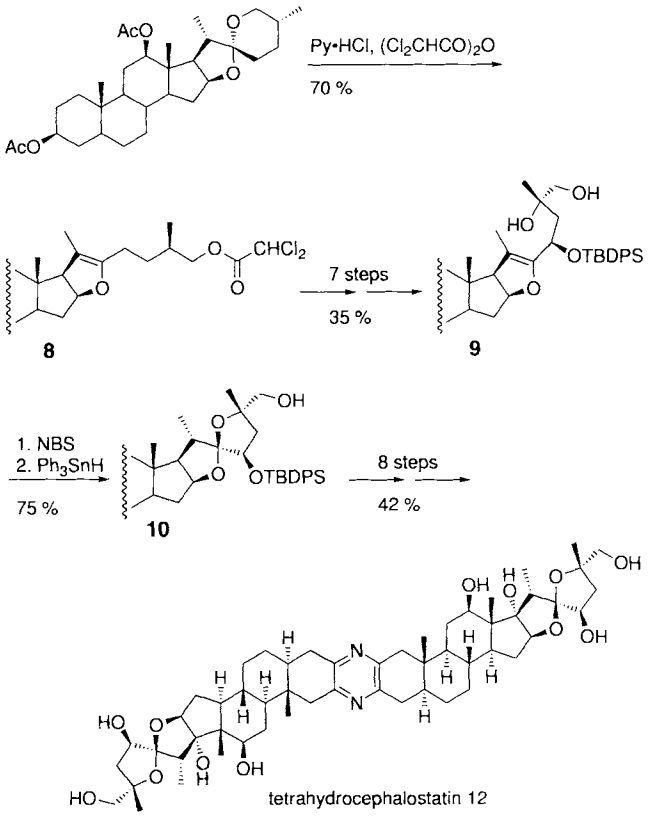

Scheme 7. Synthesis of tetrahydrocephalostatin 12 by Fuchs et al.

yielded a mixture of 5/5 and 6/5 spiroketals epimeric to the natural product. In general, for cephalostatin intermediates the ratio of spiroketal products is highly sensitive to the specific substitution pattern. The natural products also reflect this fine balance: there are three pairs of ritterazines differing only in spiroketal configuration. In this case, the desired product **10** was obtained from **9** by electrophilic bromination and halogen removal. Dimerization afforded tetrahydrocephalostatin 12, whose biological activity was not described.

Recent communications from the Fuchs group have climaxed[9] in the total synthesis of three alkaloids in this family. The presence of the D-ring double bond and C-17 hydroxyl group necessitated a different route from that for tetrahydrocephalostatin 12. First, Marker side chain degradation of hecogenin acetate gave enone **11** (Scheme 8). The D-ring functionality was introduced, and ring E constructed by intramolecular Wadsworth–Emmons reaction of **12**. The rest of the side chain was reintroduced by methallyl stannane addition to **13** yielding **14**.

The two diastereomers of **14** were separated, and individually processed to eventually yield monomers **15** and **16**. In the grand finale, a 1:1 mixture of the α-azido ketones was reduced to give roughly the expected 1:2:1 mixture of three dimers, with the heterodimer predominating. Separation and deprotection afforded the natural products. Fuchs et al. suggest that similar

 © VCH Verlagsgesellschaft mbH, D-69451 Weinheim, 1996 0570-0833/96/3506-0613 $ 15.00+.25/0

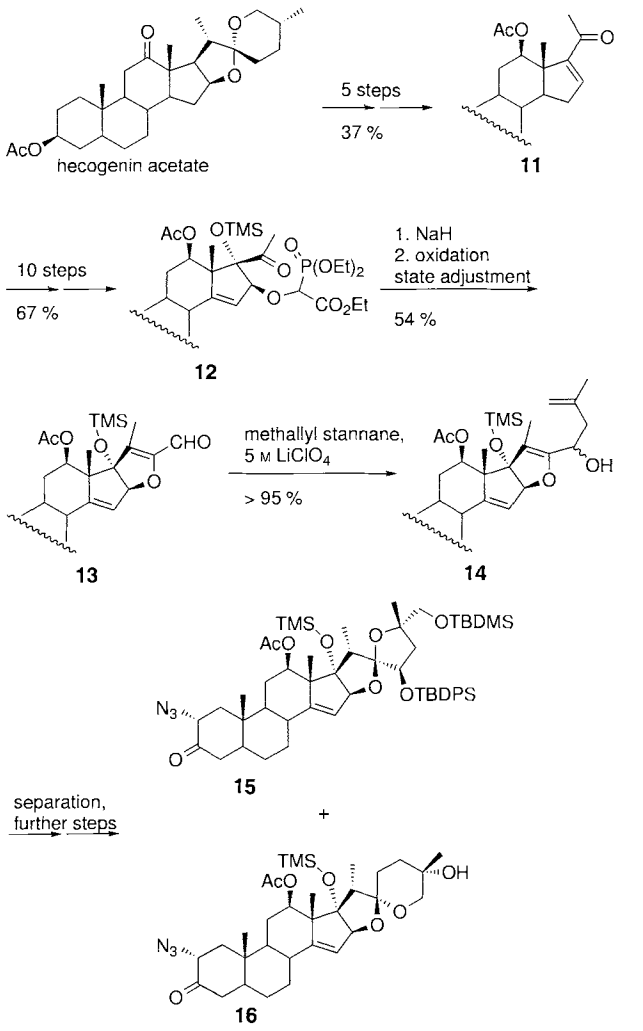

Scheme 8. Synthesis of cephalostatin 7, cephalostatin 12, and ritterazine K by Fuchs et al.

statistical coupling occurs in nature, which implies that ritterazine K is also produced by *C. gilchristi*. Indeed, examination of residual material in the Pettit group identified a compound in microgram quantities with the same chromatographic profile.

This work represents a milestone in the synthesis of complex marine natural products. At the same time, it reflects on the state of organic synthesis, which some consider to be a fully mature science. While total synthesis is *effective*, in the sense that any stable compound can probably be made, it is seldom *efficient*. This is particularly true for targets containing a multiplicity of oxygenated functional groups. The preparation of the two halves required over 20 steps from hecogenin acetate, the majority of which involve functional group interchange and protecting group manipulations. Clearly, there is much left for organic chemists to do in the next century!

The Fuchs group has also prepared[10] the "left half" of cephalostatin 1 without the D-ring double bond, hoping to determine the importance of the latter functional group. In this synthesis (Scheme 9), the angular methyl group of keto alcohol **17** (obtained from hecogenin acetate) was functionalized by Meystre's hypoiodite method and oxidized to yield **18**. Further reactions via intermediates **19** and **20** afforded **21**, which will presumably be carried forward to an α-azido ketone suitable for coupling with **15**.

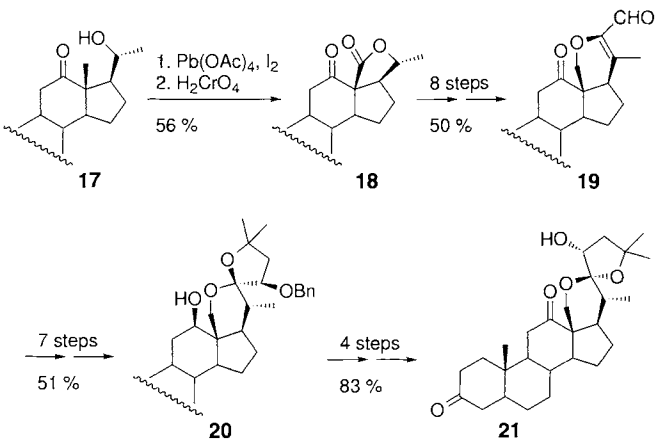

Scheme 9. Synthesis of a precursor to the "left half" of dihydrocephalostatin 1 by Bhandaru and Fuchs.

Biological Studies

These alkaloids do not contain functional groups commonly associated with cytotoxicity such as alkylation sites, Michael acceptors, intercalators, or redox-active quinones, and their scarcity has hindered investigation of the mechanism of action. An early proposal,[11] taking into account the steroidal and dimeric nature of the alkaloids, was that these compounds span the lipid bilayer (cephalostatin 1 is 30 Å long) and perturb the eukaryotic cell membrane. Later, Fuchs considered[6a] that they may be enzyme inhibitors that form hydrogen bonds with a specific target. More recently, he has suggested[10a] that a process similar to that in Scheme 3 (vide infra) may occur in vivo, in which protonation or epoxidation of the D-ring double bond generates reactive electrophilic intermediates. The advantage for the alkaloids to be dimeric is also unclear. An analogy may be drawn with the potent immunosuppressive agent FK 506, where a synthetic dimer has unique properties.[12]

Steroids have important roles in providing membrane rigidity, as components of lipoproteins, and as ligands that dimerize a superfamily of nuclear hormones, resulting in gene transcription or repression. The effects of steroids can also be indirect, for example, in triggering apoptosis (programmed cell death), while the antiinflammatory glucocorticoids have recently been shown to interfere with signal transduction in addition to binding their hormone response element.[13] The determination of the precise target of the cephalostatins and ritterazines may require large-scale preparation of simpler analogs of the natural products.

Random screening continues to be an important source of leads for drug discovery. The cephalostatins and ritterazines highlight the power of screening natural product extracts in the

search for novel, complex lead structures over the screening of synthetic combinatorial libraries currently in fashion. At the present time, libraries are constructed by short sequences of synthetic transformations, whereas natural products are the result of much longer and more creative pathways.

German version: *Angew. Chem.* **1996**, *108*, 667–671

Keywords: alkaloids · cephalostatins · ritterazines · total syntheses

[1] G. R. Pettit, M. Inoue, Y. Kamano, D. L. Herald, C. Arm, C. Dufresne, N. D. Christie, J. M. Schmidt, D. L. Doubek, T. S. Krupa, *J. Am. Chem. Soc.* **1988**, *110*, 2006–2007.
[2] F. Pietra, *A Secret World: Natural Products of Marine Life*, Birkhäuser, Basel, **1990**, p. 149.
[3] Most recent publication: G. R. Pettit, J.-P. Xu, J. M. Schmidt, *Bioorg. Med. Chem. Lett.* **1995**, *5*, 2027–2032.
[4] S. Fukuzawa, S. Matsunaga, N. Fusetani, *J. Org. Chem.* **1994**, *59*, 6164–6166.
[5] Most recent publication: S. Fukuzawa, S. Matsunaga, N. Fusetani, *Tetrahedron* **1995**, *51*, 6707–6716.
[6] a) Y. Pan, R. L. Merriman, L. R. Tanzer, P. L. Fuchs, *Bioorg. Med. Chem. Lett.* **1992**, *2*, 967–972; b) C. H. Heathcock, S. C. Smith, *J. Org. Chem.* **1994**, *59*, 6828–6839.
[7] A. Kramer, U. Ullmann, E. Winterfeldt, *J. Chem. Soc. Perkin Trans. 1* **1993**, 2865–2867.
[8] J. U. Jeong, P. L. Fuchs, *J. Am. Chem. Soc.* **1994**, *116*, 773–774.
[9] J. U. Jeong, S. C. Sutton, S. Kim, P. L. Fuchs, *J. Am. Chem. Soc.* **1995**, *117*, 10157–10158.
[10] a) S. Bhandaru, P. L. Fuchs, *Tetrahedron Lett.* **1995**, *36*, 8347–8350; b) *ibid.* **1995**, *36*, 8351–8354.
[11] A. Ganesan, C. H. Heathcock, *Chemtracts Org. Chem.* **1988**, *1*, 311–312.
[12] D. J. Austin, G. R. Crabtree, S. L. Schreiber, *Chem. Biol.* **1994**, *1*, 131–136.
[13] J. Marx, *Science* **1995**, *270*, 232–233.

Crystal Structure Analysis of a Synthetic Non-Heme Diiron–O_2 Adduct: Insight into the Mechanism of Oxygen Activation**

Yanhong Dong, Shiping Yan, Victor G. Young, Jr., and Lawrence Que, Jr.*

Dedicated to the memory of Nobumasa Kitajima

Dioxygen binding and activation are key processes carried out by a number of metalloproteins, including those of an emerging subclass with non-heme diiron active sites.[1] For example, the diiron active site of hemerythrin (Hr)[2] functions to bind O_2 reversibly in invertebrates, while those of methane monooxygenase (MMO)[3] and ribonucleotide reductase (RNR)[4] activate dioxygen to carry out their respective functions. Interestingly, Hr has a histidine-rich active site (five His and two Asp/Glu residues), while MMO and RNR have carboxylate-rich diiron sites (two His and four Asp/Glu residues). One goal of our research efforts has been to understand the principles underlying nature's choice of ligands for such proteins. Coordination chemists have obtained important insights into the nature and reactivity of the bound O_2 from studies of synthetic metal–dioxygen complexes;[5] in particular, the crystal structure analyses of O_2 adducts of biomimetic heme and dicopper complexes have yielded crucial structural information.[6–8] However, no crystal structure analysis of a synthetic nonheme diiron–O_2 adduct has thus far been reported, though several such complexes have been characterized in solution.[9, 10] We report here on the first crystal structure analysis of a nonheme diiron–O_2 adduct which provides the first structural details on a (μ-1,2-peroxo)diiron unit. Furthermore some novel features of this structure prompted us to carry out kinetic experiments that have shed light on the stability of the O_2 adduct and show how the ligand environment can modulate the reactivity of the O_2 adduct in nonheme diiron enzymes.

We previously reported that the diiron(II) complex **1** binds O_2 irreversibly at $-60\,^{\circ}C$ in CH_2Cl_2 to afford a metastable blue adduct **1**-O_2[10a, b, 11] that has a proposed structure similar to

$[Fe_2(N\text{-Et-hptb})(O_2CC_6H_5)]^{2+}$ **1**

$[Fe_2(\mu\text{-}1,2\text{-}O_2)(N\text{-Et-hptb})(\mu\text{-}O,O'\text{-}O_2CC_6H_5)]^{2+}$ **1**-O_2

that recently reported for $[Co_2(O_2)(tpdb)(O_2CC_6H_5)]^{2+}$.[12] We surmised that the benzoate bridge present in the precursor was retained upon binding of O_2, since the peroxo-to-iron(III) charge transfer (CT) band was blue shifted when the benzoate was substituted with the more basic propionate.[10b] Furthermore the lifetime of this adduct could be extended by the addition of Ph_3PO. This enhanced stability has allowed us to grow crystals of the O_2 adduct at $-40\,^{\circ}C$ over a period of several weeks.[13]

The crystal structure analysis (Fig. 1) revealed that the O_2 adduct has a (μ-alkoxo)diiron core supported by a μ-1,2-dioxygen bridge; the Fe–Fe separation is 3.462(2) Å. The Fe–μ-O_{alkoxo} bond length is 1.991(3) Å, typical of those found in related (μ-alkoxo)diiron(III) complexes.[14] The dioxygen moiety coordinates in a *cis* μ-1,2 fashion, and the O–O bond is 1.416(7) Å long. This distance is consistent with the reduction

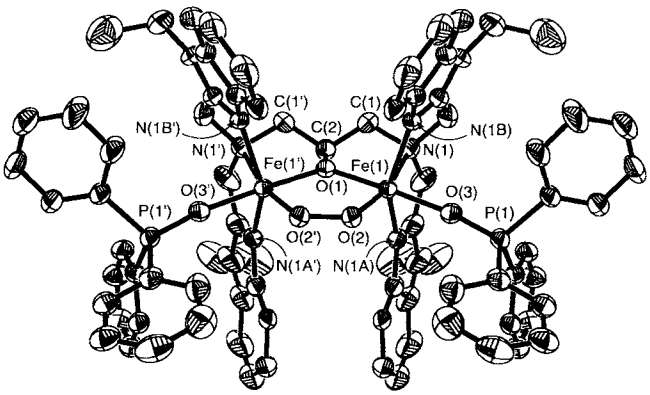

Fig. 1. Crystal structure of $[Fe_2(\mu\text{-}1,2\text{-}O_2)(N\text{-Et-hptb})(Ph_3PO)_2]^{3+}$ (ORTEP plot showing 30% probability thermal ellipsoids). Selected bond lengths [Å] and angles [°]: Fe1–O1 1.991(3), Fe1–O2 1.880(4), Fe1–O3 2.035(4), Fe1–N1 2.364(5), Fe1–N1A 2.082(4), Fe1–N1B 2.094(4), O2–O2' 1.416(7), Fe1···Fe1' 3.462(3); Fe1-O1-Fe1' 120.8(3), Fe1-O2-O2' 122.97(10), O1-Fe1-O2 86.5(2), O1-Fe1-N1 78.0(2), O2-Fe1-O3 90.4(2), N1-Fe1-O3 105.2(2), O1-Fe1-N1A 93.7(2), O1-Fe1-N1B 97.7(2).

of O_2 to peroxide upon coordination, as was first indicated by resonance Raman data.[10a] For comparison, $[Fe_6(\mu\text{-}O)_2(\mu_4\text{-}O_2)(O_2CC_6H_5)_{12}(OH_2)_2]$, the only previously structurally characterized synthetic iron peroxide complex, has an O–O bond length of 1.480(12) Å,[15] while dicopper–O_2 adducts such as $[Cu_2(Tp^{iPr2})_2(\mu\text{-}\eta^2\text{:}\eta^2\text{-}O_2)]$ and $[Cu_2(tpa)_2(\mu\text{-}trans\text{-}1,2\text{-}O_2)]^{2+}$ have O–O bond lengths of 1.412(12) and 1.432(6) Å, respectively.[7, 8] The Fe–O_{peroxo} bonds are 1.880(4) Å long, a value consistent with the basicity of the peroxide ligand. Comparably short Fe–O bonds (1.88–1.91 Å) are found for complexes with terminal Fe^{III}–OH and Fe^{III}–OCH_3 groups.[16] Thus, in agreement with the spectroscopic studies, the structure analysis shows that O_2 binding to **1** converts it into an adduct with a (μ-alkoxo)(μ-1,2-peroxo)diiron(III) core.

The iron coordination spheres are completed by the nitrogen atoms of the N-Et-hptb ligand and the oxygen atoms of two phosphane oxides. As are typical of tripodal ligands of this type, the tertiary amine nitrogens have the longest metal–ligand bond lengths and coordinate *trans* to the most basic ligand in the complex, the peroxide in this case. The pendant benzimidazole rings on each iron are coordinated *trans* to each other, perpendicular to the plane defined by the two iron centers, the alkoxide, and the peroxo bridge. To our surprise, the benzoate bridge is absent in the crystalline O_2 adduct; instead two triphenylphosphane oxide ligands are coordinated *trans* to the alkoxo bridge. The Fe–O bonds to the two Ph_3PO ligands are 2.035(4) Å long, a distance which is typical of such bonds.[17] The presence of these Ph_3PO ligands is the key to the enhanced stability of this O_2 adduct.

$[Fe_2(\mu\text{-}1,2\text{-}O_2)(N\text{-Et-hptb})(Ph_3PO)_2]^{3+}$ is stable for months at $-40\,^{\circ}C$, but decomposes at $30\,^{\circ}C$ within an hour to form a diiron(III) product. The decay of the characteristic peroxide-to-iron(III) CT band of the O_2 adduct follows first-order kinetics over at least five half-lives ($k_1 = 1.1 \times 10^{-3}\,s^{-1}$). The decomposition of the O_2 adduct presumably occurs by cleavage of the O–O bond which would result in the oxidation of the iron(III) centers to a higher oxidation state. In view of the symmetry of the diiron complex, we favor homolysis of the O–O bond, leading to the generation of a diiron(IV) unit as shown in Figure 2.

According to the proposed mechanism, the O–O bond cleavage should be enhanced by the substitution of the neutral phosphane oxide ligands by the more electron-donating anionic benzoate. The increased electron density provided to the metal

[*] Prof. L. Que, Jr., Dr. Y. Dong, Prof. S. Yan, Dr. V. G. Young, Jr.
Department of Chemistry, University of Minnesota
207 Pleasant St. SE, Minneapolis, MN 55455 (USA)
Fax: Int. code +(612)624-7029
e-mail: que@chemsun.chem.umn.edu

[**] This work was supported by the National Institutes of Health (GM-38767).

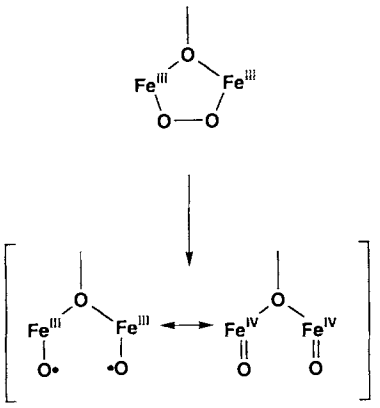

Fig. 2. Proposed mechanism for the decomposition of the (μ-1,2-peroxo)diiron(III) intermediate.

centers would promote the cleavage of the O–O bond and stabilize the resulting high valent oxidation state. Indeed **1**-O_2 decomposes within seconds at 30 °C. The decay rate can be modulated by the introduction of substituents on the bridging benzoate and shows an excellent correlation with Hammett σ values (Fig. 3). The ρ value of -1.1 indicates a process that is

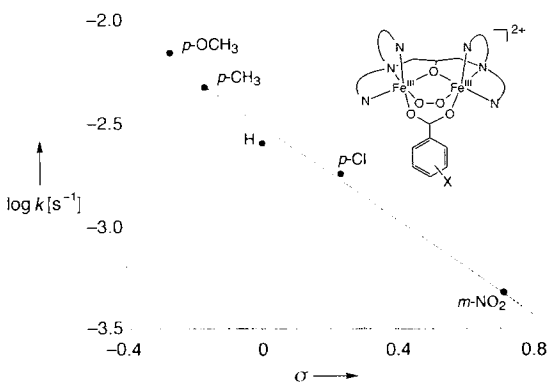

Fig. 3. Hammett plot for the decomposition rates of a series of O_2 adducts of the type $[Fe_2(\mu\text{-}1,2\text{-}O_2)(N\text{-Et-hptb})(O_2CC_6H_4\text{-}X)]^{2+}$ in CH_3CN at -10 °C ($\rho = -1.1$).

accelerated by electron-donating groups. While earlier studies on diiron–O_2 complexes have concentrated on the Fe–O_2 bond formation reaction and its reversibility,[10c, 18] this investigation has focused on the factors that affect the integrity of the O–O bond and its activation, and provides a quantitative basis for the mechanism proposed in Figure 2. A similar "push" effect is observed for the cleavage of the O–O bond in heme–peroxy acid complexes, leading to the formation of higher valent iron–oxo species, when electron-donating ligands are introduced.[19] We have also examined the temperature dependence of the decomposition of **1**-O_2 and obtained activation parameters, $\Delta H^{\ddagger} = 15.5 \pm 0.8$ kcal mol^{-1} and $\Delta S^{\ddagger} = -11 \pm 5$ cal mol^{-1} K^{-1}, which are consistent with values associated with the cleavage of the O–O bond in other O_2 adducts.[20]

The studies described here contribute insights into nature's design of non-heme diiron active sites for controlling dioxygen chemistry. They clearly demonstrate that the amount of electron density contributed by the ligands can modulate the reactivity of the O_2 adduct. The histidine-rich active site of the dioxygen carrier hemerythrin helps maintain the integrity of the O–O bond, thereby contributing to reversibility of O_2 binding. The presence of a larger number of anionic carboxylate ligands in the diiron sites of MMO and RNR activates the O–O bond and provides access to the higher valent iron states that are needed to carry out the hydrogen abstraction reactions associated with their respective functions. Indeed rapid kinetic studies of these enzymes have provided evidence for the participation of transient intermediates with high-valent iron centers that derive from peroxodiiron(III) species in their reaction cycles.[21, 22] Although other factors undoubtedly come into play, the functional differences between hemerythrin, on the one hand, and MMO and RNR, on the other, can now be rationalized in light of the ligand–reactivity relationships we have uncovered through the determination of the crystal structure of this non-heme diiron–O_2 adduct.[23]

Received: December 14, 1995 [Z 8645 IE]
German version: *Angew. Chem.* **1996**, *108*, 673–676

Keywords: bioinorganic chemistry · iron compounds · non-heme iron proteins · O_2 activation · peroxo complexes

[1] a) *Active Oxygen in Biochemistry* (Eds.: J. S. Valentine, C. S. Foote, A. Greenberg, J. F. Liebman), Chapman & Hall, New York, **1995**; b) A. L. Feig, S. J. Lippard, *Chem. Rev.* **1994**, *94*, 759–805; c) L. Que, Jr. in *Bioinorganic Catalysis* (Ed.: J. Reedijk), Marcel Dekker, New York, **1993**, pp. 347–393.

[2] a) R. E. Stenkamp, *Chem. Rev.* **1994**, *94*, 715–726; b) M. A. Holmes, I. L. Trong, S. Turley, L. C. Sieker, R. E. Stenkamp, *J. Mol. Biol.* **1991**, *218*, 583–593.

[3] a) J. D. Lipscomb, *Annu. Rev. Microbiol.* **1994**, *48*, 371–399; b) A. C. Rosenzweig, C. A. Frederick, S. J. Lippard, P. Nordlund, *Nature* **1993**, *366*, 537–543; c) A. C. Rosenzweig, P. Nordlund, P. M. Takahara, C. A. Frederick, S. J. Lippard, *Chem. Biol.* **1995**, *2*, 409–418.

[4] a) J. Stubbe, *Adv. Enzymol.* **1989**, *63*, 349–419; b) P. Nordlund, H. Eklund, *J. Mol. Biol.* **1993**, *232*, 123–164.

[5] a) E. C. Niederhoffer, J. H. Timmons, A. E. Martell, *Chem. Rev.* **1984**, *84*, 137–203; b) A number of review articles on metal–dioxygen complexes can also be found in a special thematic issue of *Chemical Reviews*: *Chem. Rev.* **1994**, *94*, 567–856.

[6] a) G. B. Jameson, F. S. Molinaro, J. A. Ibers, J. P. Collman, J. I. Brauman, E. Rose, K. S. Suslick, *J. Am. Chem. Soc.* **1980**, *102*, 3224–3237; b) G. B. Jameson, G. A. Rodley, W. T. Robinson, R. R. Gagne, C. A. Reed, J. P. Collman, *Inorg. Chem.* **1978**, *17*, 850–857; c) M. Schappacher, L. Ricard, J. Fischer, R. Weiss, E. Bill, R. Montiel-Montoya, H. Winkler, A. X. Trautwein, *Eur. J. Biochem.* **1987**, *168*, 419–429.

[7] Z. Tyeklár, R. R. Jacobson, N. Wei, N. N. Murthy, J. Zubieta, K. D. Karlin, *J. Am. Chem. Soc.* **1993**, *115*, 2677–2689.

[8] N. Kitajima, K. Fujisawa, C. Fujimoto, Y. Moro-oka, S. Hashimoto, T. Kitagawa, K. Toriumi, K. Tatsumi, A. Nakamura, *J. Am. Chem. Soc.* **1992**, *114*, 1277–1291.

[9] a) N. Kitajima, H. Fukui, Y. Moro-oka, Y. Mizutani, T. Kitagawa, *J. Am. Chem. Soc.* **1990**, *112*, 6402–6403; b) N. Kitajima, N. Tamura, H. Amagai, H. Fukui, Y. Moro-oka, Y. Mizutani, T. Kitagawa, R. Mathur, K. Heerwegh, C. A. Reed, C. R. Randall, L. Que, Jr., K. Tatsumi, *ibid.* **1994**, *116*, 9071–9085; c) N. Kitajima, N. Tamura, M. Tanaka, Y. Moro-oka, *Inorg. Chem.* **1992**, *31*, 3342–3343.

[10] a) S. Ménage, B. A. Brennan, C. Juarez-Garcia, E. Münck, L. Que, Jr., *J. Am. Chem. Soc.* **1990**, *112*, 6423–6425; b) Y. Dong, S. Ménage, B. A. Brennan, T. E. Elgren, H. G. Jang, L. L. Pearce, L. Que, Jr., *ibid.* **1993**, *115*, 1851–1859; c) Y. Hayashi, T. Kayatani, H. Sugimoto, M. Suzuki, K. Inomata, A. Uehara, Y. Mizutani, T. Kitagawa, Y. Maeda, *ibid.* **1995**, *117*, 11220–11229.

[11] Abbreviations used: N-Et-hptb = *N,N,N',N'*-tetrakis[2'-(1'-ethylbenzimidazolyl)]-1,3-diamino-2-hydroxypropane; tpa = tris(2-pyridylmethyl)amine; tpdb = *N,N,N',N'*-tetrakis(2-pyridylmethyl)-1,4-diamino-2-hydroxybutane; Tp^{iPr_2} = hydrotris(3,5-diisopropyl-1-pyrazolyl)borate.

[12] T. Kayatani, Y. Hayashi, M. Suzuki, A. Uehara, *Bull. Chem. Soc. Jpn.* **1994**, *67*, 2980–2989.

[13] Crystals of the diiron–O_2 adduct were grown from an acetonitrile solution prepared by the reaction of 10 mM $\{Fe_2(N\text{-Et-hptb})(OBz)\}(BF_4)_2$ (containing 50 mM Ph_3PO) with O_2 at -40 °C, which was then layered with cold diethyl ether. Crystal data for $[Fe_2(O_2)(N\text{-Et-hptb})(Ph_3PO)_2](BF_4)_3 \cdot 3CH_3CN$: $C_{85}H_{88}B_3F_{12}Fe_2N_{13}O_5P_2$, $M_r = 1805.75$, crystal dimensions $0.45 \times 0.45 \times 0.08$ mm, monoclinic, space group $P2_1/m$, $a = 13.0808(2)$, $b = 25.3452(1)$, $c = 15.0328(2)$ Å, $\beta = 98.344(1)°$, $V = 4931.1(1)$ Å^3, $Z = 2$, $\rho_{calcd} = 1.216$ g cm^{-3}, $2\theta_{max} = 48.26°$, $Mo_{K\alpha}$ radiation ($\lambda = 0.71073$ Å), $T = 173(2)$ K. Data were collected by using the Siemens SMART system and the structure was solved by direct methods. Full-matrix least squares refinement on F^2 using SHELXTL-Plus V 5.0 (Siemens Industrial Automation, Inc., Madison, WI) converged with final $R1 = 0.0943$ and $wR2 = 0.2559$ for 7696 ($R_{int} = 0.0669$) independent reflections with $I > 2\sigma(I)$ and 594 parameters and 148 restraints. The SQUEEZE program (A. L. Spek, *Acta Crystallogr. Sect. A* **1990**, *46*, C34) was used to correct the reflection data for the diffuse scattering due to disordered solvent. Further details of the crystal structure may be obtained from the

Director of Cambridge Crystallographic Data Center, 12 Union Road, GB-Cambridge CB2 1EZ (UK) on quoting the full journal citation.
[14] Q. Chen, J. B. Lynch, P. Gomez-Romero, A. Ben-Hussein, G. B. Jameson, C. J. O'Connor, L. Que, Jr., *Inorg. Chem.* **1988**, *27*, 2673–2681.
[15] W. Micklitz, S. G. Bott, J. G. Bentsen, S. J. Lippard, *J. Am. Chem. Soc.* **1989**, *111*, 372–374.
[16] a) Y. Dong, H. Fujii, M. P. Hendrich, R. A. Leising, G. Pan, C. R. Randall, E. C. Wilkinson, Y. Zang, L. Que, Jr., B. G. Fox, K. Kauffmann, E. Münck, *J. Am. Chem. Soc.* **1995**, *117*, 2778–2792; b) A. Hazell, K. B. Jensen, C. J. McKenzie, H. Toftlund, *Inorg. Chem.* **1994**, *33*, 3127–3134; c) A. Caneschi, A. Cornia, A. C. Fabretti, D. Gatteschi, W. Malavasi, *ibid.* **1995**, *34*, 4660–4668.
[17] a) F. Tomi, H. L. K. Wah, M. Postel, *New J. Chem.* **1988**, *12*, 289–292; b) D. Zirong, S. Bhattacharya, J. K. McCusker, P. M. Hagen, D. N. Hendrickson, C. G. Pierpont, *Inorg. Chem.* **1992**, *31*, 870–877; c) E. Durcanska, T. Glowiak, E. Gyepes, I. Ondrejkovivcova, G. Ondrejovic, *Acta Fac. Rerum. Nat. Univ. Comenianeac. Chim.* **1991**, *39*, 3; d) X. Feng, S. G. Bott, S. J. Lippard, *J. Am. Chem. Soc.* **1989**, *111*, 8046–8047.
[18] A. L. Feig, S. J. Lippard, *ibid.* **1994**, *116*, 8410–8411.
[19] K. Yamaguchi, Y. Watanabe, I. Morishima, *J. Am. Chem. Soc.* **1993**, *115*, 4058–4065.
[20] a) D.-H. Chin, G. N. L. Mar, A. L. Balch, *J. Am. Chem. Soc.* **1980**, *102*, 4344–4349; b) S. Mahapatra, J. A. Halfen, E. C. Wilkinson, L. Que, Jr., W. B. Tolman, *ibid.* **1994**, *116*, 9785–9786. c) O. M. Reinaud, K. H. Theopold, *ibid.* **1994**, *116*, 6979–6980.
[21] a) S.-K. Lee, J. C. Nesheim, J. D. Lipscomb, *J. Biol. Chem.* **1993**, *268*, 21569–21577; b) K. E. Liu, A. M. Valentine, D. Wang, B. H. Huynh, D. E. Edmondson, A. Salifoglou, S. J. Lippard, *J. Am. Chem. Soc.* **1995**, *117*, 10174–10185.
[22] a) J. M. Bollinger, Jr., D. E. Edmondson, B. H. Huynh, J. Filley, J. Norton, J. Stubbe, *Science* **1991**, *253*, 292–298; b) N. Ravi, J. M. Bollinger, Jr., B. H. Huynh, D. E. Edmondson, J. Stubbe, *J. Am. Chem. Soc.* **1994**, *116*, 8007–8014; c) J. M. Bollinger, Jr., W. H. Tong, N. Ravi, B. H. Huynh, D. E. Edmondson, J. Stubbe, *ibid.* **1994**, *116*, 8015–8023; d) J. M. Bollinger, Jr., W. H. Tong, N. Ravi, B. H. Huynh, D. E. Edmondson, J. Stubbe, *ibid.* **1994**, *116*, 8024–8032.
[23] **Note added in proof** (February 21, 1996): After this paper was accepted, Ookubo et al. reported the crystal structure of a reversible diiron–O_2 adduct with a structure similar to that of **1**-O_2 proposed in Figure 3 (T. Ookubo, H. Sugimoto, T. Nagayama, H. Masuda, T. Sato, K. Tanaka, Y. Maeda, H. Okawa, Y. Hayashi, A. Uehara, M. Suzuki, *J. Am. Chem. Soc.* **1996**, *118*, 701–702). The structure of one other O_2 adduct $[Fe_2(Tp^{iPr2})_2(O_2CCH_2Ph)_2(O_2)]$ has also been solved by K. Kim, and S. J. Lippard (S. J. Lippard, personal communication).

Synthesis of Flavin-Containing Model Compounds for DNA Photolyase Mediated DNA Repair**

Thomas Carell,* Robert Epple, and Volker Gramlich

Irradiation of cells with UV light causes severe genome damage.[1] In double-stranded DNA, the major alteration is the formation of *cis-syn* cyclobutane pyrimidine dimers by [2+2]cycloaddition.[2] In single-stranded DNA, a second isomer, the *trans-syn* configured species is also formed, but to a lesser extent. These photoproducts are known to induce various forms of skin cancer, such as basal and squamous cell carcinomas, and to cause cell death.[2] Since it was established that the ozone layer, which shields the earth from harmful solar UV radiation, is becoming depleted, rising skin cancer incidents are predicted.[3] This situation has stimulated renewed interest in the mechanisms used by organisms to remove sunlight-induced DNA lesions from the genome. One widespread DNA repair system employs a single enzyme, the flavin-containing DNA photolyase, to revert *cis-syn* cyclobutane pyrimidine dimers to their pyrimidine precursors in a process initiated by sunlight (300–500 nm).[4] It is widely accepted that the essential event in the repair reaction is a light-induced electron transfer from a reduced flavin cofactor, tightly bound by the enzyme, to the cyclobutane pyrimidine dimer moiety within the DNA double strand.

Through the synthesis and investigation of model compounds that are able to mimic crucial steps of a complex biological process, important aspects of the underlying reaction sequence can be investigated.[5] The few model compounds prepared to study photolyase-mediated DNA repair consist predominantly of pyrimidine photodimers covalently linked to electron-rich aromatic systems such as indole or dimethoxybenzene derivatives.[6, 7] Although, reduced and deprotonated flavins have been shown to reverse the cyclobutane formation if they are added to a solution containing photodimers and subsequently irradiated,[8] no functionally active model compounds containing both, biologically relevant reduced flavins and pyrimidine photodimers have been prepared.[9, 10] To investigate the requirements for an efficient cleavage of pyrimidine photodimers mediated by reduced flavins, we prepared the series of model compounds **1**–**3**. The parent compound **1** contains

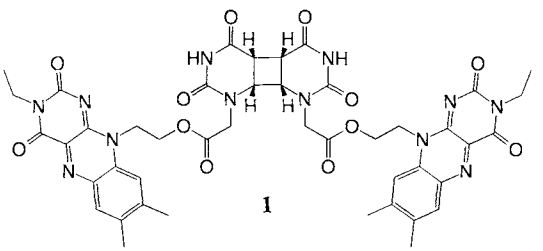

1

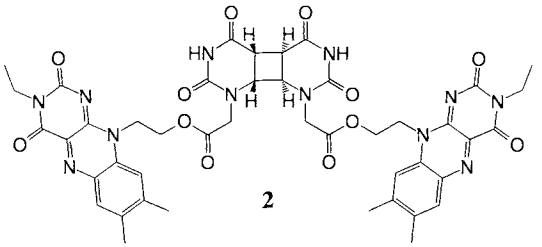

2

two riboflavin derivatives covalently attached to a cyclobutane uracil photodimer with *cis-syn* configuration. Since photolyases were shown to also split thymine photodimers with *trans-syn* configuration (but only at high enzyme concentration) two other derivatives, **2** and **3**, containing uracil dimers with *trans-syn* and *trans-anti* geometry, respectively, were prepared to investigate if these structural alterations effect the splitting efficiency.[11]

The uracil photodimers were prepared without a methyl group or an additional linking chain at the imide nitrogens, since such substitution was found to dramatically reduce splitting efficiencies.[9] To counter potentially poor solubility, the flavins were ethylated at the N-3 positions. Rather flexible ethyl chains were chosen as the connecting elements between the flavin subunits and the pyrimidine photodimer to allow the flavins to adopt conformations with van der Waals contacts to the cyclobutane moiety.

[*] Dr. T. Carell, R. Epple
Laboratorium für Organische Chemie, ETH-Zentrum
Universitätstrasse 16, CH-8092 Zürich (Switzerland)
Fax: Int. code +(1)632 1109
e-mail: tcarell@org.chem.ethz.ch
Dr. V. Gramlich
Institut für Kristallographie und Petrographie, ETH-Zentrum, CH-8092 Zürich (Switzerland)

[**] This work was supported by Hoffmann-La Roche, Basel. We thank the German Stiftung Stipendien-Fonds des Verbandes der Chemischen Industrie for a Liebig-Stipendium to T. C., Prof. F. Diederich for his generous support of this research, and Dr. R. Thomas for carefully reading the manuscript.

While the dicarboxylic acid **10** with *trans-syn* geometry had been described,[7] all other pyrimidine dimers depicted in Scheme 1, including **5** and **12** with the biologically relevant *cis-syn* structure, were unknown. We found that all four possible

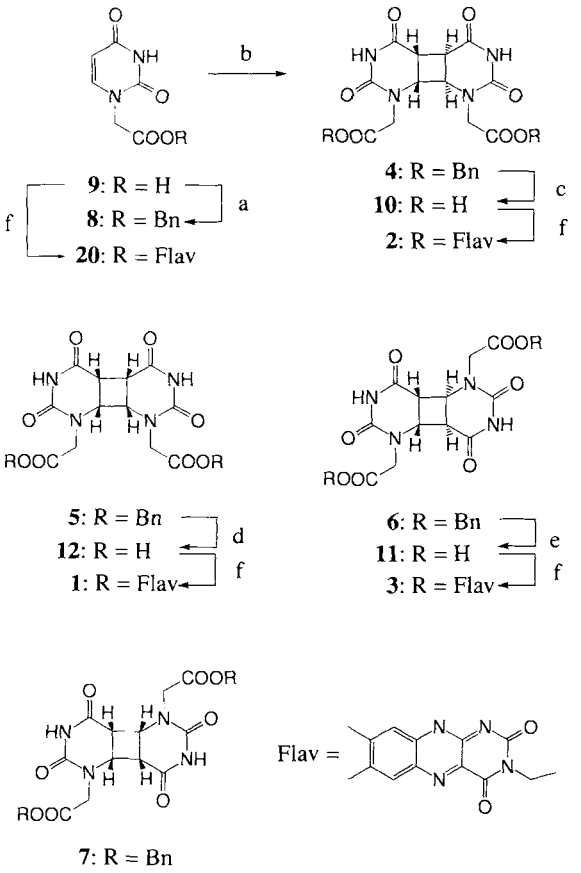

Scheme 1. Synthesis of the four cyclobutane uracil photodimer isomers **4**–**7** and the debenzylated compounds **10**–**12**. a) $C_6H_5CH_2OH$, carbonyldiimidazole, DMF, 20 °C, 95%; b) $h\nu > 290$ nm, acetone, 2 h, 20 °C, **4**: 18%, **6**: 30%, **5**: 5%, **7**: 2.5%; c) 1 N NaOH, 3.5 h, 20 °C then conc. HCl to pH 1, 86%; d) Pd/C (10%), H_2, EtOH, 20 °C; quant.; e) conc. HCl, 3 h reflux, 70%; f) **13**, DMF, BOP, Et_3N, 12 h, 20 °C.

cyclobutane uracil dimers can be prepared as their benzyl esters **4**–**7**. Irradiation of the benzyl ester **8**, which is readily available through esterification of **9**[12] with benzyl alcohol, in 2 g portions in acetone for 2 h in a pyrex reaction vessel with a medium-pressure mercury lamp yielded predominantly the four dimers **4**–**7**. They can be separated by a combination of chromatography and selective precipitation. The *trans-anti* isomer **6** is insoluble in acetone and can be separated in excellent purity from the reaction suspension by filtration (600 mg). Concentration of the filtrate and trituration with ice-cold chloroform caused precipitation of approximately half of the *trans-syn* isomer **4** (350 mg) present. After filtration, the residual solution was concentrated and the remaining oil treated sequentially with ether and boiling toluene to remove nonpolar impurities. The remaining two isomers, the *cis-syn* compound **5** (100 mg) and the *cis-anti* compound **7** (50 mg), were isolated from the residual powdery material by flash-chromatography (SiO_2-H, $CHCl_3$/MeOH).

The structures of **4**–**7** were assigned based on their ^{1}H NMR spectra (Table 1) and by X-ray crystal structure analyses of the two dibenzyl esters **4** and **5** (Fig. 1).[13] The crystal structures confirmed the *trans-syn* configuration of the cyclobutane ring in **4** and the *cis-syn* configuration of the cyclobutane ring in **5**.[13]

Table 1. Selected physical data of the four cyclobutane pyrimidine dimers **4**–**7** and the three model compounds **1**–**3** [a].

4: m.p. 216 °C; IR (KBr): $\tilde{\nu}$(C=O) = 1689 cm^{-1}; ^{1}H NMR (300 MHz, $(CD_3)_2SO$): δ = 3.43 (d, J = 8.3 Hz, 2H), 4.11 (s, 4H), 4.38 (d, J = 8.3 Hz, 2H), 5.07 (d, J = 12.6 Hz, 2H), 5.15 (d, J = 12.6 Hz, 2H), 7.35 (s, 10H), 10.71 (s, 2H, NH); ^{13}C NMR (125 MHz, $(CD_3)_2SO$): δ = 169.6, 169.2, 151.6, 135.5, 128.3, 128.0, 127.7, 66.0, 59.3, 48.4, one signal covered by $(CD_3)_2SO$; FAB$^+$-MS: m/z: 521 (MH^+, calc. for $C_{26}H_{24}N_4O_8$ 521.2)

5: m.p. 180–183 °C; IR (KBr): $\tilde{\nu}$(C=O) = 1744, 1696 cm^{-1}; ^{1}H NMR (300 MHz, $(CD_3)_2SO$): δ = 3.74 (m, 2H), 4.00 (d, J = 17.4 Hz, 2H), 4.21 (m, 2H), 4.27 (d, J = 17.4 Hz, 2H), 5.15 (s, 4H), 7.36 (s, 10H), 10.58 (s, 2H, NH); ^{13}C NMR (125 MHz, $(CD_3)_2SO$): δ = 168.6, 167.0, 152.6, 135.6, 128.3, 128.0, 127.7, 66.0, 55.0, 47.2, 38.1; FAB$^+$-MS: m/z: 521 (MH^+ calc. for $C_{26}H_{24}N_4O_8$ 521.2)

6: m.p. 268 °C; IR (KBr): $\tilde{\nu}$(C=O) = 1733, 1717, 1684 cm^{-1}; ^{1}H NMR (300 MHz, $(CD_3)_2SO$): δ = 3.76 (dd, J_1 = 5.4, J_2 = 9.1 Hz, 2H), 4.02 (d, J = 17.8 Hz, 2H), 4.22 (d, J = 17.8 Hz, 2H), 4.34 (dd, J_1 = 5.4, J_2 = 9.1 Hz, 2H), 5.17 (s, 4H), 7.36 (s, 10H), 10.69 (s, 2H, NH); ^{13}C NMR (125 MHz, $(CD_3)_2SO$): δ = 168.4, 168.3, 151.1, 135.6, 128.3, 128.0, 127.8, 66.1, 52.9, 46.2, 43.0; FAB$^+$-MS: m/z: 521 (MH^+ calc. for $C_{26}H_{24}N_4O_8$ 521.2)

7: m.p. 227–230 °C; IR (KBr): $\tilde{\nu}$(C=O) = 1712 cm^{-1}; ^{1}H NMR (300 MHz, $(CD_3)_2SO$) d = 3.79 (dd, J_1 = J_2 = 8.7 Hz, 2H), 3.89 (d, J = 17.9 Hz, 2H), 4.38 (dd, J_1 = J_2 = 8.7 Hz, 2H), 4.43 (d, J = 17.9 Hz, 2H), 5.17 (s, 4H), 7.37 (s, 10H), 10.66 (s, 2H, NH); ^{13}C NMR (125 MHz, $(CD_3)_2SO$): d = 168.6, 167.4, 151.5, 135.7, 128.3, 128.0, 127.7, 66.0, 48.2, 46.9, 44.1; FAB$^+$-MS: m/z: 521 (MH^+ calc. for $C_{26}H_{24}N_4O_8$ 521.2)

1: m.p. 180 °C (decomp.); IR (KBr): $\tilde{\nu}$(C=O) = 1703, 1647 cm^{-1}; ^{1}H NMR (500 MHz, $(CD_3)_2SO$): δ = 1.14 (t, J = 7.2 Hz, 6H), 2.38 (s, 6H), 2.49 (s, 6H), 3.57 (m, 2H), 3.67 (d, J = 17.3 Hz, 2H), 3.86 (q, J = 7.1 Hz, 4H), 4.00 (d, J = 17.3 Hz, 2H), 4.13 (m, 2H), 4.50 (m, 4H), 4.80 (m, 2H), 5.00 (m, 2H), 7.83 (s, 2H), 7.91 (s, 2H), 10.48 (s, 2H, NH); ^{13}C NMR (125 MHz, $(CD_3)_2SO$): δ = 168.6, 166.9, 159.1, 154.7, 152.6, 149.2, 147.0, 136.3, 136.1, 134.1, 131.1, 131.0, 116.1, 61.2, 54.8, 46.9, 42.8, 38.2, 36.0, 20.7, 18.8, 12.8; FAB$^+$-MS: m/z: 933 (MH^+ calc. for $C_{44}H_{44}N_{12}O_{12}$ 933.3)

2: m.p. 159 °C (decomp.); IR (KBr): $\tilde{\nu}$(C=O) = 1706, 1650 cm^{-1}; ^{1}H NMR (500 MHz, $(CD_3)_2SO$): δ = 1.14 (t, J = 7.1 Hz, 6H), 2.37 (s, 6H), 2.47 (s, 6H), 3.35 (d, J = 8.3 Hz, 2H), 3.90 (q, J = 7.1 Hz, 4H), 3.95 (d, J = 17.7 Hz, 2H), 4.12 (d, J = 17.7 Hz, 2H), 4.31 (d, J = 8.3 Hz, 2H), 4.50 (m, 4H), 4.87 (m, 4H), 7.83 (s, 2H), 7.85 (s, 2H), 10.62 (s, 2H, NH); ^{13}C NMR (125 MHz, $(CD_3)_2SO$): δ = 169.5, 169.3, 158.9, 154.6, 151.4, 149.0, 146.8, 136.1, 135.9, 133.9, 131.0, 130.8, 115.9, 61.1, 58.8, 47.9, 42.6, 38.1, 35.9, 20.5, 18.6, 12.8; FAB$^+$-MS: m/z: 933 (MH^+ calc. for $C_{44}H_{44}N_{12}O_{12}$ 933.3)

3: m.p. 170–172 °C; IR (KBr): $\tilde{\nu}$(C=O) = 1706, 1656 cm^{-1}; ^{1}H NMR (500 MHz, $(CD_3)_2SO$): δ = 1.13 (t, J = 7.0 Hz, 6H), 2.38 (s, 6H), 2.50 (s, 6H), 3.47 (dd, J_1 = 5.3, J_2 = 9.2 Hz, 2H), 3.82 (d, J = 17.7 Hz, 2H), 3.90 (q, J = 7.1 Hz, 4H), 3.99 (d, J = 17.7 Hz, 2H), 4.13 (dd, J_1 = 5.2 Hz, J_2 = 9.3 Hz, 2H), 4.53 (m, 4H), 4.92 (m, 4H), 7.89 (s, 2H), 7.90 (s, 2H), 10.56 (s, 2H, NH); ^{13}C NMR (125 MHz, $(CD_3)_2SO$): δ = 168.4, 168.0, 159.0, 154.5, 150.9, 149.0, 146.7, 136.2, 135.8, 133.9, 131.0, 130.9, 116.1, 61.2, 52.7, 46.1, 42.9, 42.6, 35.9, 20.6, 18.7, 12.8 FAB$^+$-MS: m/z: 933 (MH^+ calc. for $C_{44}H_{44}N_{12}O_{12}$ 933.3)

[a] All new compounds described were fully characterized by ^{1}H and ^{13}C NMR spectroscopy, FT-IR spectroscopy, and FAB$^+$ mass spectrometry.

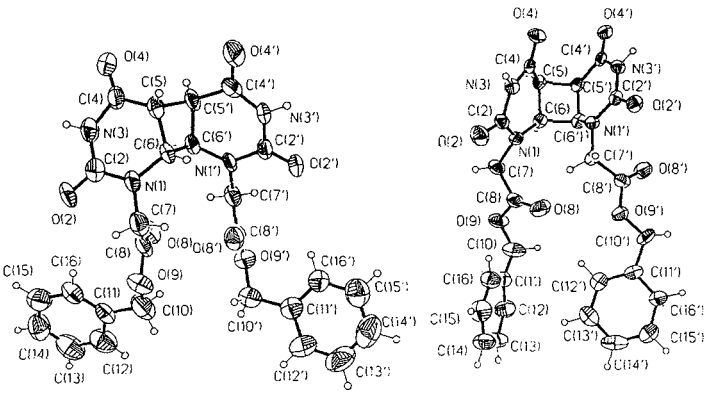

Fig. 1. Crystal structures of the dibenzyl esters **4** (*trans-syn*) and **5** (*cis-syn*) [13].

The structures of the remaining isomers **6** and **7** were assigned on the basis of their differing coupling patterns for the four cyclobutane protons in their ^{1}H NMR spectra.[14] Since only **7** featured two overlapping doublets of doublets for the four cyclobutane protons, each caused by two *cis* couplings of similar magnitude (in one case between C(5)-H and C(6)-H, C(6′)-H and in the second between C(6)-H and C(5)-H, C(5′)-H), **7** was assigned the *cis-anti* structure. Compound **6** exhibited two doublets of doublets for the four protons, caused by *trans* coupling between C(5)-H and C(6′)-H and between C(5′)-H and C(6)-H) and *cis* coupling between C(5)-H and C(6)-H and between C(5′)-H and C(6′)-H, and thus **6** was assigned the *trans-anti* structure.

The isomer **4** was deprotected to give **10** with 1 N sodium hydroxide. Cleavage of the benzyl ester in **6** to give **11** was achieved with concentrated hydrochloric acid and debenzylation of the *cis-syn* isomer **5** to afford **12** was found to be optimal through catalytic hydrogenation in ethanol. The hydroxyethyl-substituted flavin **13**, required for the preparation of the model compounds **1**–**3**, was synthesized in six steps from commercially available 4,5-dimethyl-2-nitroaniline (**14**) as depicted in Scheme 2.

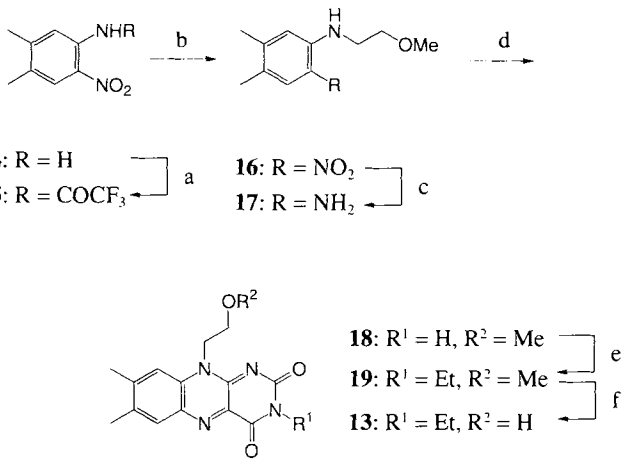

Scheme 2. Synthesis of the flavin building block **13**. a) $(CF_3CO)_2O$, 2 h, 20 °C, 90%; b) $BrCH_2CH_2OCH_3$ [15], K_2CO_3, DMF, 100 °C then 90 min reflux, 89%; c) Pd/C (10%), H_2, CH_3COOH, 20 °C (yield not determined); d) alloxane monohydrate, boric acid, 3 h, 20 °C, 70%; e) CH_3CH_2I, K_2CO_3, DMF, 11 h, 20 °C, 83%; f) BBr_3, CH_2Cl_2, 4.5 h, 0 °C, 81%.

The esterification of **13** with the cyclobutane uracil dimers **10**–**12** was achieved by using the strong carboxyl-activating Castro's reagent (benzotriazol-1-yloxytris(dimethylamino)-phosphonium hexafluorophosphate, BOP).[16] All three model compounds **1**–**3** were obtained as orange powders after chromatography (SiO_2-H, $CHCl_3$/MeOH). As a reference compound, the product of the cyclobutane splitting reaction, **20**, was prepared by esterification of **13** with **9** (Scheme 1). All spectroscopic data of the model compounds **1**–**3** (Table 1) are consistent with the proposed structures. The positive ion FAB mass spectra gave a strong molecular ion peak for $[M\mathrm{H}]^+$ at $m/z = 933$; a high-resolution scan of this molecular ion peak confirmed the elemental composition of these compounds ($C_{44}H_{44}N_{12}O_{12}$). Apart from the splitting pattern of the signals for protons of the cyclobutane ring, the ^{1}H NMR spectra of the **1**–**3** are very similar. All three feature the same coupling characteristics of their four cyclobutane protons as determined for their corresponding dibenzyl esters. This indicates that the harsh debenzylation conditions caused no isomerization of the cyclobutane moieties. The ^{13}C NMR spectra of the model compounds showed the requisite peaks. All three model compounds are sufficiently soluble in a variety of different solvents, enabling the planned splitting experiments and further spectroscopic studies.

In the initial splitting experiments solutions of **1**–**3** in chloroform were irradiated with light at 254 nm to study the cleavage reaction under conditions in which the flavin units do not participate. The irradiation at 254 nm caused the awaited partial conversion of **1**–**3** into **20** and established a photosteady monomer–dimer state. Compound **20** is the only product formed as shown by TLC. We found that at this wavelength, the *trans-syn* isomer **2** cleaved approximately 1.5 times faster than the *cis-syn* compound **1**. Negligible opening of the cyclobutane ring was observed for the *trans-anti* species **3**.[17] To discover if the compounds are able to mimic the biological repair reaction, they were dissolved in ethyleneglycol, acetonitrile, or dioxane and the flavins were reduced by additon of an 0.05 M aqueous sodium dithionite solution (inert gas atmosphere). Upon addition the strong flavin fluorescence immediately disappeared, indicating complete reduction of the flavin unit. Alternatively, the flavins were reduced by addition of an aqueous solution of sodium ethylenediamine tetraacetate and subsequent irradiation with white light.[18] Our preliminary experiments show that the *cis-syn* compound **1** and the *trans-syn* compound **2**, when reduced, cleanly yield the reference compound **20** upon irradiation with either white light or light at 366 nm. Under all conditions employed, the cyclobutane substructure of the *cis-syn* model compound **1** cleaved significantly faster than in the *trans-syn* species **2**. In the case of compound **3**, as with irradiation at 254 nm, only a very slow cleavage could be detected. Without prior reduction of the flavins, no cleavage reaction in any of the three model compounds was observed. In other control experiments in which the dibenzyl ester compounds **4** and **5** were irradiated in the presence of the reduced model compound **1**, only cleavage of the model compound and not of the benzyl esters was observed, indicating that the cleavage reaction of the cyclobutane moiety is an intramolecular process.

The reluctance of the *trans-anti* isomer **3** to cleave can be explained by the lack of mesomeric stabilization of the intermediate radicals by an adjacent carbonyl group.[2c, 19] We propose that the difference in cleavage rate between the two isomers **2** and **1** is related to the greater accessibility of the cyclobutane ring for the flavin units in **1**.

Both **1** and **2** mimic the photoreactivation process, and to our knowledge they are the first functionally active model compounds for the DNA photolyase mediated repair reaction. We are currently in the process of investigating the structural requirements of this repair process through detailed studies of splitting efficiencies of these and further analogues.

Received: October 30, 1995 [Z 8510 IE]
German version: *Angew. Chem.* **1996**, *108*, 676–679

Keywords: DNA repair · electron transfer · flavins · nucleobases · photolyases

[1] E. C. Friedberg, G. C. Walker, W. Siede, *DNA Repair and Mutagenesis*, ASM Press, Washington, **1995**; T. Lindahl, *Nature (London)* **1993**, *362*, 709–715; F. Hutchinson, *Photochem. Photobiol* **1987**, *45*, 897–903.

[2] a) J.-S. Taylor, *Acc. Chem. Res.* **1994**, *27*, 76–82; b) *J. Chem. Educ.* **1990**, *67*, 835–841; c) T. P. Begley, *Acc. Chem. Res.* **1994**, *27*, 394–401; d) P. F. Heelis, R. F. Hartman, S. D. Rose, *Chem. Soc. Rev.* **1995**, 289–297; e) T. Carell, *Angew. Chem.* **1995**, *107*, 2697–2700, *Angew. Chem. Int. Ed. Engl.* **1995**, *34*, 2491–2494.

[3] J. C. van der Leun, *J. Photochem. Photobiol. B: Biol.* **1988**, *1*, 493–496.

[4] S.-T. Kim, A. Sancar, *Photochem. Photobiol.* **1993**, *57*, 895–904, A. Sancar, *Biochemistry* **1994**, *33*, 1–9. For the crystal structure of the *E. coli* photolyase see: H.-W. Park, S.-T. Kim, A. Sancar, J. Deisenhofer, *Science* **1995**, *268*, 1866–1872.

[5] *Tetrahedron Symposia-in-Print 39 Tetrahedron* **1989**, *45*, 4669–4902; H. Dugas, *Bioorganic Chemistry*, 3rd ed., Springer, Heidelberg, **1996**.
[6] D. G. Hartzfeld, S. D. Rose, *J. Am. Chem. Soc.* **1993**, *115*, 850–854; R. Austin, S. McMordie, T. P. Begley, *ibid.* **1992**, *114*, 1886–1887; *J. Photochem. Photobiol. B: Biol.* **1992**, *12*, 179–191; S. T. Kim, R. F. Hartman, S. D. Rose, *Photochem. Photobiol.* **1990**, *52*, 789–794; J. R. Van Camp, T. Young, R. F. Hartman, S. D. Rose, *ibid.* **1987**, *45*, 365–370; for a review see: P. F. Heelis, S.-T. Kim, T. Okamura, A. Sancar, *J. Photochem. Photobiol. B: Biol.* **1993**, *17*, 219–228.
[7] For an investigation of *trans-syn* pyrimidine dimer splitting mediated by catalytic antibodies see: J. R. Jacobsen, A. G. Cochran, J. C. Stephans, D. S. King, P. G. Schultz, *J. Am. Chem. Soc.* **1995**, *117*, 5453–5461; A. G. Cochran, R. Sugasawara, P. G. Schultz, *ibid.* **1988**, *110*, 7888–7890.
[8] M. Schuman Jorn, *J. Am. Chem. Soc.* **1987**, *109*, 3133–3136; R. F. Hartman, S. D. Rose, *ibid.* **1992**, *114*, 3559–3560.
[9] R. F. Hartman, S. D. Rose, *J. Org. Chem.* **1992**, *57*, 2302–2306; S. E. Rokita, C. T. Walsh, *J. Am. Chem. Soc.* **1984**, *106*, 4589–4595.
[10] M. S. Goodman, S. D. Rose, *J. Am. Chem. Soc.* **1991**, *113*, 9380–9382.
[11] S.-T. Kim, K. Malhotra, C. A. Smith, J.-S. Taylor, A. Sancar, *Biochemistry* **1993**, *32*, 7065–7068.
[12] S. Y. Wang, J. C. Nnadi, D. Greenfeld, *Tetrahedron Lett.* **1970**, 5913–5921; A. S. Jones, P. Lewis, S. F. Withers, *Tetrahedron* **1973**, *29*, 2293–2296.
[13] The crystal structures were solved by direct methods (SHELXTL PLUS) and refined by full-matrix least-squares analysis using experimental weights (heavy atoms anisotropic; H atoms riding model, fixed isotropic). Further details of the crystal structure investigations are available on request from the Director of the Cambridge Crystallographic Data Centre, University Chemical Laboratory, 12 Union Road, GB-Cambridge CB2 1EZ (UK), on quoting the full journal citation. *trans-syn* isomer **4**: colorless platelets ($HCOOH/H_2O$); $C_{20}H_{24}N_4O_8$, $M_r = 520.5$; triclinic space group $P\bar{1}$, $\rho_{calc} = 1.321\ g\,cm^{-3}$, $Z = 2$, $a = 9.042(16)$, $b = 11.342(16)$, $c = 13.66(3)$ Å, $\alpha = 91.99(17)$, $\beta = 109.28(12)$, $\gamma = 96.87(13)$, $V = 1309(4)$ Å^3, $Mo_{K\alpha}$ radiation, 2040, 2431 unique reflections. Final $R(F) = 0.0576$, $wR(F) = 0.0772$ for 368 variables and 1304 observed reflections with $F > 4.0\sigma(F)$. *cis-syn* isomer **5**: colorless platelets ($EtOH \cdot H_2O$); $C_{20}H_{24}N_4O_8$, $M_r = 520.5$; monoclinic space group $C2/c$, $\rho_{calc} = 1.471\ g\,cm^{-3}$, $Z = 8$, $a = 52.69(9)$, $b = 7.809(13)$, $c = 11.516(16)$ Å, $\beta = 96.80(13)$, $V = 4702(13)$ Å^3, $Mo_{K\alpha}$ radiation, 2040, 2086 unique reflections. Final $R(F) = 0.0468$, $wR(F) = 0.0645$ for 343 variables and 1356 observed reflections with $F > 4.0\sigma(F)$.
[14] E. Fahr, P. Maul, K.-A. Lehner, D. Schentzow, *Z. Naturforsch. B* **1972**, *27*, 1481–1484.
[15] R. O. Roblin, J. O. Lampen, J. P. English, Q. P. Cole, J. R. Vaughten, *J. Am. Chem. Soc.* **1945**, *67*, 290–294.
[16] B. Castro, G. Evin, C. Selve, R. Seyer, *Synthesis* **1977**, 413.
[17] For previously reported differences in splitting efficiencies see: E. Ben-Hur, I. Rosenthal, *Photochem. Photobiol.* **1970**, *11*, 163–168.
[18] D. B. McCormick, *Photochem. Photobiol.* **1977**, *26*, 169–182.
[19] E. Schaumann, R. Ketcham, *Angew. Chem.* **1982**, *94*, 231–253; *Angew. Chem. Int. Ed. Engl.* **1982**, *21*, 225–247; for reductive cycloreversions see: [2c,7] and references cited therein; M. Horner, S. Hünig, *Liebigs Ann. Chem.* **1982**, *8*, 1409–1422; R. J. Robbins, D. Falvey, *J. Org. Chem* **1993**, *58*, 3616–3618.

Polymerization of Ethylene Oxide with Alkyllithium Compounds and the Phosphazene Base "*t*Bu-P_4"**

Beate Esswein and Martin Möller*

The ring opening anionic polymerization of ethylene oxide occurs via alkoxide ions as a "living polymerization".[1] The rate of polymerization depends on the association and formation of ion pairs, which is still important even at the low concentrations of growing ends and in highly polar solvents such as hexamethylphosphortriamide (HMPT).[2]

The rates of monomer addition can differ by several orders of magnitude for the different states of the reaction solution.[1] Strong dipole interactions of the ion pairs compete successfully with the solvation of the cation,[2] and the alkoxides of the smaller alkali metal cations like Li^+ and Na^+ form unreactive associates. Li^+ ions show the strongest association behavior because of their tendency to form covalent bonds.[3] No propagation reaction occurs, even though poly(ethylene oxide) itself is known to interact strongly with Li^+ ions.[4]

Complexation of the alkali metal cation by cryptands[5] has been shown to shift the equilibrium towards the reactive free anions and leads to simple polymerization kinetics for ethylene oxide.[6–8] The dissociation constant K_{Diss} has been determined to be 3×10^{-7} for a mixture of RO^-K^+ and [2.2.2]cryptand[3] compared to 1.8×10^{-10} for RO^-K^+[9] alone in THF at 20 °C. Although the ions are complexed, they are slightly less or just as reactive in the polymerization of oxirane as the corresponding noncomplexed ion pairs[3, 10] (Table 1). In the RO^-K^+ complex

Table 1. Propagation constants k_p for ion pairs and free anions for the polymerization of ethylene oxide in THF [10].

Monomer	k_p for counterion [$M^{-1}\,s^{-1}$]				k_p [$M^{-1}\,s^{-1}$]
	Li^+	Na^+	K^+	Cs^+	free anion
ethylene oxide	–	–	0.05	0.12	1.7
ethylene oxide + [2.2.2]cryptand	–	–	0.025	0.09	

with [2.2.2]cryptand an interionic distance of only 4.6 Å has been deduced according to the Fuoss equation.[10] This value is significantly smaller than that for cryptated living poly(propylene sulfide)[11] and for cryptated tetraphenylborides in THF,[12] indicating that the K^+ is not placed in the cavity, or that the oxy anion can penetrate into the cavity of the cryptand.

In the case of Li^+ alkoxides, neither we nor others observed efficient polymerization.[13] This was also the case when we employed an even more efficient complexing agent for Li^+ ions, the spherand first synthesized by Cram.[14] We know of only one report on the successful polymerization of oxirane with BuLi in the presence of *N,N,N',N'*-tetramethylethylenediamine (tmeda), which, however, does not give data on the degree of polymerization, polydispersity, or yield.[15]

We addressed the question of whether the recently developed, extremely strong phosphorazene bases[16, 17] can efficiently complex lithium ions and facilitate polymerization of ethylene oxide through formation of lithium alkoxides. The base "*t*Bu-P_4" fulfills an important criterium of a cryptand: the polar amino groups are located inside the globular molecule, and the outer shell is formed by the alkyl substituents. The free volume inside the molecule might be sufficient to host the rather compact Li^+ ion. We recently reported on the application of the protonated polyiminophosphazene base [H-*t*Bu-P_4]$^+$ for the initiation of the anionic polymerization of ethylene oxide.[18]

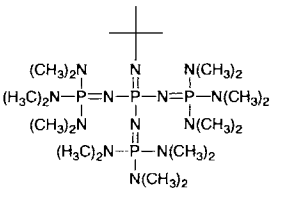

Table 2 summarizes the results of the homopolymerization of ethylene oxide in THF with BuLi/*t*Bu-P_4 as the initiator system. Good yields of poly(ethylene oxide) (> 80% after precipitation) with low polydispersity were obtained. The molecular weights determined by GPC correspond well with the theoretical molecular weights (M_n(th.) = 2200, 6600, and 22000).

[*] Prof. Dr. M. Möller, Dipl.-Chem. B. Esswein
Institut für Organische Chemie III der Universität
Albert-Einstein-Allee 11, D-89069 Ulm (Germany)
Fax: Int. code +(731) 502-2883
e-mail: martin.moeller@chemie.uni-ulm.de

[**] We thank Prof. Dr. S. Boileau, College de France, Paris, for fruitful discussions, and Dr. U. Werz and U. Ziegler for conducting the NMR experiments.

Table 2. Molecular weights and polydispersities D of poly(ethylene oxides) (PEOs) obtained with tBu-P_4 and BuLi as initiator system; GPC data were determined in chloroform at room temperature.

	PEO 1	PEO 2	PEO 3
Solvent	THF	THF	THF
Yield [a]	81%	89%	84%
M_n (th.) [g mol^{-1}]	2200	6600	22000
M_n [g mol^{-1}] [b]	1900	5900	18100
M_w [g mol^{-1}] [b]	2800	6900	23300
D	1.08	1.16	1.28

[a] After precipitation. [b] Relative to polyethylene glycol standards.

Furthermore, a diblock copolymer of poly(styrene-β-ethylene oxide) (theoretically 100 styrene and 300 ethylene oxide monomer units) was synthesized in toluene at room temperature (Table 3). First, styrene was polymerized with sBuLi as the initiator. After three hours a small sample was taken, and the molecular weight was determined by gel permeation chromatography (GPC) before ethylene oxide and tBu-P_4 were added to the living polystyrene solution. The diblock copolymer was characterized by GPC and ^{1}H NMR measurements. The theoretically expected molecular weight and composition agreed rather well with the experimental results (Table 3). The block copolymer could be dissolved in water as well as in toluene, indicating micelle formation. Transmission electron microscopy demonstrated microphase separation of the two incompatible blocks.

Table 3. Molecular weights and polydispersities D of the polystyrene (PSt) block and the poly(styrene-β-ethylene oxide) (PSt-β-EO) block copolymer prepared with tBu-P_4/sBuLi as initiator system; GPC data of the block copolymer are determined in chloroform, the data for the styrene block in toluene.

	PSt Block	P(St-β-EO)
Yield [a]	–	75%
M_n (th.) [g mol^{-1}]	10400	23600
M_n [g mol^{-1}] [b]	12000	20900
M_w [g mol^{-1}] [b]	13000	24000
D	1.09	1.15
Block length (th.)	100	100:300 (PS:EO)
Block length: ^{1}H NMR [c]	–	115:215 (PS:EO)

[a] After precipitation. [b] Relative to polystyrene standards. [c] Determined in $CDCl_3$, relative to TMS.

The results demonstrate that the phosphorazene bases can efficiently complex lithium ions. This interpretation was confirmed by the results of ^{7}Li NMR studies with lithium octanolate in [D_8]toluene (Fig. 1). While pure lithium octanolate in toluene gives rise to a ^{7}Li NMR peak at $\delta = 0.68$, addition of tBu-P_4 resulted in a split signal with a maximum at $\delta = 0.81$. This change in the chemical shift indicates an altered structure of the Li–alkoxide ion pair. Yet it is not clear why the spectrum of a solution with tBu-P_4 shows different ^{7}Li NMR signals. Preliminary polymerization experiments with varying Li^+/tBu-P_4 ratios demonstrate that all lithium alkoxides are equally reactive, thus indicating that the splitting of the Li NMR signal cannot be attributed to a slow exchange between the complexed and the uncomplexed state.

We conclude that the phosphazene base can form a [Li–tBu-P_4]$^+$ complex that suppresses ion pair association. The activation of lithium alkoxides by tBu-P_4 for the polymerization of ethylene oxide is rather remarkable in view of the negative results with the [2.1.1]cryptand and the spherand. Detailed NMR and kinetic investigations on the exact nature of the interaction are currently in progress.

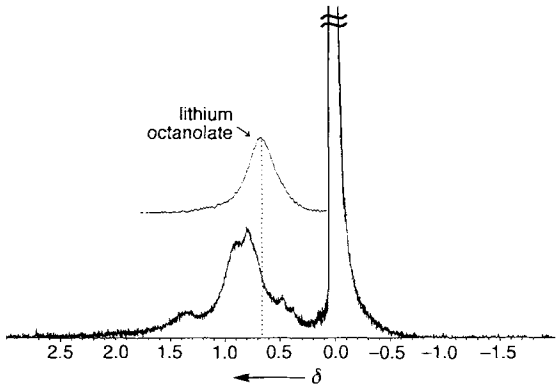

Fig. 1. ^{7}Li NMR spectrum of lithium octanolate and tBu-P_4 in [D_8]toluene.

Experimental Procedure

Materials: Ethylene oxide (Linde 2.7) was dried over CaH_2 and distilled into an ampoule. tBu-P_4 (1.0 M solution in hexane from Fluka), BuLi (Aldrich, 1.6 M in hexane), sBuLi (Aldrich, 1.4 M in cyclohexane), acetic acid (Merck), and dibutylmagnesium (Aldrich, 1.0 M in heptane) were used without further purification. THF and toluene (Merck p.a.) were freshly distilled from sodium–benzophenone ketyl under argon. Styrene (Aldrich, 99%, GC) was distilled twice, first from CaH_2 and then from dibutylmagnesium directly into an ampoule with a PTFE stopcock. Petroleum ether (Merck, technical grade) and diethyl ether (Merck, technical grade) were distilled. Reactions were performed on a high-vacuum line. The apparatus was dried by several heating and evacuation cycles, and flushed with argon.

Homopolymerization: Freshly distilled THF (100 mL) was cooled to −78 °C and 10 mL (200 mmol) of ethylene oxide was introduced from an ampoule. After addition of 250 μL (0.4 mmol) of BuLi, the reaction mixture was stirred for 30 min at −78 °C. To this solution was added 0.4 mL (0.4 mmol) of tBu-P_4, and the mixture was stirred for 48 h at room temperature. The reaction was quenched with 0.1 mL of acetic acid, and the solvent was removed under vacuum. The residue was dissolved in some THF and precipitated by addition of diethyl ether. The polymer was obtained as a white powder and was dried under vacuum. Yield: 7.4 g (84%). ^{1}H NMR: $\delta = 3.61-3.65$ (CH_2-O).

Block copolymerization: Styrene (8 mL, 70 mmol) was introduced from an ampoule into a flask containing 80 mL of freshly distilled toluene. After addition of 600 μL (0.70 mmol) of sBuLi, the reaction mixture was stirred for 3 h at room temperature. Then the solution was cooled to −78 °C and 11 mL (220 mmol) of ethylene oxide was introduced from an ampoule. The reddish color disappeared immediately. The reaction mixture was stirred for another 2 h, then 720 μL (0.72 mmol) of tBu-P_4 was added. The reaction mixture was stirred for further 48 h at room temperature. Subsequently the reaction was quenched with 0.1 mL of acetic acid, the solvent evaporated, and the residue dissolved in THF. The polymer was precipitated in petroleum ether and collected as a white powder, which was dried under vacuum. Yield: 12.8 g (75%). ^{1}H NMR: $\delta = 3.61-3.65$ (CH_2O) 7.16–6.20 (aromat. C-H), 2.06–1.14 (aliphat. C-H).

Characterization: GPC measurements were carried out with chloroform as solvent, using Waters microstyragel columns (pore size 10^5, 10^4, and 10^3 Å). Molecular weights were determined by universal calibration and are relative to narrow polystyrene and polyethylene glycol standards. A dual detection system consisting of a differential refractometer (Waters model 410) and a differential viscometer (Viscotek model H502, GPC-Win software) was employed. ^{1}H NMR spectra were performed in $CDCl_3$ on a Bruker AC 200 spectrometer at 200 MHz. Chemical shifts are relative to TMS. ^{7}Li NMR spectroscopy was performed in [D_8]toluene on a Bruker AMX 500 spectrometer at 194.4 MHz. A 4 M solution of $LiClO_4$ in D_2O was used as external standard.

Received: August 29, 1995 [Z 8354IE]
German version: *Angew. Chem.* **1996**, *108*, 703–705

Keywords: alkoxides · cryptands · ethylene oxide · phosphazenes · polymerizations

[1] S. Boileau in *Comprehensive Polymer Science, Vol. 3* (Eds.: G. Allen, J. C. Bevington), Pergamon, Oxford, **1985**.
[2] C. C. Price, M. K. Akkapeddi, *J. Am. Chem. Soc.* **1972**, *94*, 3972.
[3] H. F. Mark, N. M. Bikales, C. G. Overberger, G. Menges, J. I. Kroschwitz, *Encycl. Polym. Sci. Eng., 1985–, Vol. 2*, **1985**.

[4] C. J. Chang, R. F. Kiesel, T. E. Hogen-Esch, *J. Am. Chem. Soc.* **1973**, *95*, 8446.
[5] B. Dietrich, J.-M. Lehn, J. P. Sauvage, *Tetrahedron Lett.* **1969**, *34*, 2885.
[6] P. Sigwalt, S. Boileau, *J. Polym. Sci. Polym. Symp.* **1978**, *62*, 51.
[7] A. Deffieux, S. Boileau, *Polymer* **1977**, *18*, 1047.
[8] S. Boileau, A. Deffieux, D. Lassalle, F. Menezes, B. Vidal, *Tetrahedron Lett.* **1978**, 1767.
[9] A. A. Solovyanov, K. S. Kazanskii, *Vysokomol. Soedin Ser. A* **1972**, *14*, 1063, 1071.
[10] "Use of Cryptates in Anionic Polymerization of Heterocyclic Compounds": S. Boileau, *A. C. S. Symp. Ser. 166*, **1981**.
[11] P. Hemery, S. Boileau, P. Sigwalt, *J. Polym. Sci. Polym. Symp.* **1975**, *52*, 189.
[12] S. Boileau, P. Hemery, J. C. Justice, *J. Solution Chem.* **1975**, *4*, 873.
[13] S. Boileau (College de France, Paris), private communication.
[14] D. J. Cram, T. Kaneda, R. C. Helgeson, G. M. Lein, *J. Am. Chem. Soc.* **1979**, *101*, 6752.
[15] K. Gonsalves, M. D. Rausch, *J. Polym. Sci. Polym. Chem. Ed.* **1986**, *24*, 1419.
[16] R. Schwesinger, H. Schlemper, *Angew. Chem.* **1987**, *99*, 1212; *Angew. Chem. Int. Ed. Engl.* **1987**, *26*, 1167.
[17] R. Schwesinger, *Nachr. Chem. Tech. Lab.* **1990**, *38*, 1214.
[18] B. Esswein, N. M. Steidl, M. Möller, *Makromol. Chem. Rapid Commun.* **1996**, *17*, in press.

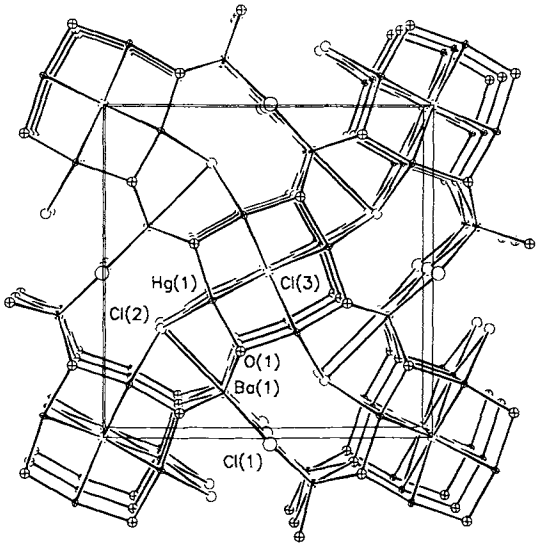

Fig. 1. ORTEP view of the structure of **1** along the crystallographic *c* axis.

Synthesis and Structure Determination of $BaHg_2O_2Cl_2$ by Powder X-ray Diffraction: Isolated Hg_4O_4 Squares**

William T. A. Harrison,* Lumei Liu, and Allan J. Jacobson

A great deal of work has been recently been reported on layered, high-T_c, mercury-based superconductors,[1-4] all of which contain isolated, linear O-Hg^{II}-O "dumbbell" units. During our own synthetic investigations of barium- and mercury-based phases, we observed the formation of $BaHg_2O_2Cl_2$ **1**, the new phase described below. Single crystals of $BaHg_2O_2Cl_2$ could not be synthesized under the reaction conditions employed, but the structure[5] was determined by ab initio methods from medium-resolution laboratory powder X-ray diffraction data.[6] This phase, which contains isolated squares of Hg_4O_4 units, is the first well-characterized barium mercury oxide chloride.

The structure of **1** (Table 1, Fig. 1) is built up from distorted squares of alternating mercury and oxygen atoms. The Hg atoms occupy the sides of the squares, and the O atoms the corners: d(Hg–O) = 2.03(3) Å and 2.09(4) Å; θ(O-Hg-O) = 169.0(2)°; θ(Hg-O-Hg) = 101.1(2)°. These perfectly flat Hg_4O_4 units are aligned in the *ab* plane. Four long Hg–Cl bonds (d > 3.03 Å) to two Cl(2) and two Cl(3) atoms complete a grossly squashed HgO_2Cl_4 octahedron. Four of these distorted octahedra share edges [through two Cl(3) atoms] and faces [through one O(1) and two Cl(3) atoms]. They are bonded into infinite columns in the *c*-direction through the Cl(3) atoms (Fig. 2), which are bonded to eight Hg atoms in elongated cubic coordination. The columns are crosslinked in the *ab* plane by Cl(2) atoms, which bond to four Hg atoms and one Ba atom in square-pyramidal geometry (apical atom Ba). The minimum Hg–Hg separation is 3.182(4) Å, across the corner of the Hg_4O_4 square.

Table 1. Atomic position parameters for **1**.

Atom	W [a]	x	y	z	U_{iso} [Å^2]
Hg(1)	8*j*	0.5789(3)	0.3272(3)	1/2	0.0078 [b]
Ba(1)	4*g*	0.3648(4)	0.1352	0	0.0084 [b]
Cl(1)	2*c*	1/2	0	1/2	0.02(1)
Cl(2)	4*g*	0.673(2)	0.172	0	0.014(6)
Cl(3)	2*a*	0	0	0	0.002(80)
O(1)	8*j*	0.228(3)	0.089(3)	1/2	0.001(100)

[a] Wyckoff letter from International tables. [b] U_{eq} [Å^2] = $\frac{1}{3}\sum_i\sum_j U_{ij} a_i^* a_j^* \mathbf{a}_i \mathbf{a}_j$.

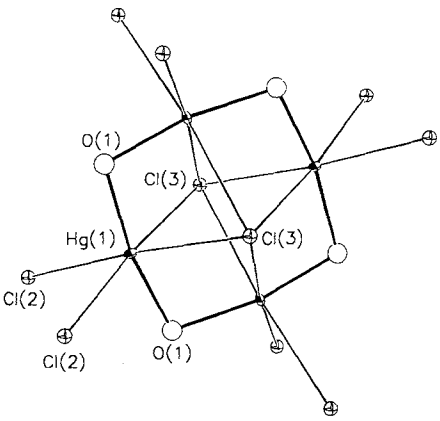

Fig. 2. Detail of the structure of **1** showing an Hg_4O_4 square.

The Ba(1) and Cl(1) atoms complete the $BaHg_2O_2Cl_2$ structure; Ba(1) coordinates to three Cl atoms and four O atoms (Fig. 3, Table 2) in capped trigonal-prismatic geometry [d(Ba–Cl) = 3.119(4)–3.22(2) Å; d(Ba–O) = 2.74(2) Å]. As a result the bond angles at O(1), which is surrounded by two Ba and two Hg atoms, are fairly close to those of a regular tetrahedron, despite the gross disparity in Ba–O and Hg–O bond lengths. Finally, the Cl(1) atom (square-planar coordination) bonds to four adjacent Ba atoms. If these Ba, O, and Cl atoms were considered in isolation, then a pattern of isolated double "fishbones" propagating along the *c*-direction would result.

[*] Dr. W. T. A. Harrison
Department of Chemistry, University of Western Australia
Nedlands, WA 6907 (Australia)
Fax: Int. code +(9) 380-1005
e-mail: wtah@chem.uwa.edu.au
L. Liu, Prof. A. J. Jacobson
Center for Superconductivity and Department of Chemistry
University of Houston, Houston, TX 77204-5641 (USA)

[**] This work was partially funded by the National Science Foundation.

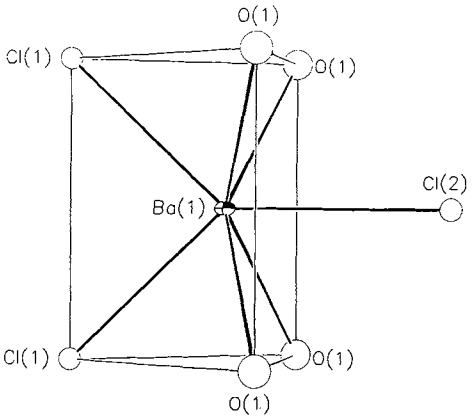

Fig. 3. The capped prismatic coordination of the barium atom in **1**.

Table 2. Bond lengths [Å] and angles [ ] in **1**.

Hg(1)–Cl(2) × 2	3.030(4)	Hg(1)–Cl(3) × 2	3.107(2)
Hg(1)–O(1)	2.09(3)	Hg(1)–O(1)	2.03(3)
Ba(1)–Cl(1) × 2	3.119(4)	Ba(1)–Cl(2)	3.22(2)
Ba(1)–O(1) × 4	2.74(2)		
Cl(2)–Hg(1)–Cl(2)	90.1(2)	Cl(2)–Hg(1)–Cl(3)	91.16(9)
Cl(2)–Hg(1)–Cl(3)	175.0(4)	Cl(2)–Hg(1)–O(1)	99.1(7)
Cl(2)–Hg(1)–O(1)	88.7(7)	Cl(3)–Hg(1)–Cl(3)	87.22(6)
Cl(3)–Hg(1)–O(1)	85.5(6)	Cl(3)–Hg(1)–O(1)	86.5(6)
O(1)–Hg(1)–O(1)	169(2)		
Cl(1)–Ba(1)–Cl(1)	86.8(2)	Cl(1)–Ba(1)–Cl(2)	136.59(6)
Cl(1)–Ba(1)–O(1)	70.2(5)	Cl(1)–Ba(1)–O(1)	137.4(7)
Cl(2)–Ba(1)–O(1)	74.1(6)	O(1)–Ba(1)–O(1)	102.9(9)
O(1)–Ba(1)–O(1)	68.1(1)	O(1)–Ba(1)–O(1)	148(2)
Ba(1)–Cl(1)–Ba(1)	86.8(2)	Ba(1)–Cl(1)–Ba(1)	93.2(2)
Ba(1)–Cl(1)–Ba(1)	180		
Hg(1)–Cl(2)–Hg(1)	90.1(2)	Hg(1)–Cl(2)–Hg(1)	86.7(2)
Hg(1)–Cl(2)–Hg(1)	160.6(7)	Hg(1)–Cl(2)–Ba(1)	80.3(4)
Hg(1)–Cl(3)–Hg(1)	87.22(6)	Hg(1)–Cl(3)–Hg(1)	61.59(4)
Hg(1)–Cl(3)–Hg(1)	118.41(4)	Hg(1)–Cl(3)–Hg(1)	92.78(6)
Hg(1)–Cl(3)–Hg(1)	180		
Hg(1)–O(1)–Hg(1)	101(2)	Hg(1)–O(1)–Ba(1)	112.2(8)
Hg(1)–O(1)–Ba(1)	114.5(8)	Ba(1)–O(1)–Ba(1)	102.9(9)

Assuming the usual oxidation states of barium, chlorine, and oxygen, charge balancing requires that all the mercury atoms in **1** are present as Hg^{II}. Thus, we may assume that all the Hg^{I} centers in the Hg_2Cl_2 starting material have been oxidized to Hg^{II} by the barium peroxide. This electroneutrality requirement for Hg^{II} is consistent with the presence of the pseudo-linear O-Hg-O units in $BaHg_2O_2Cl_2$ and the minimum Hg–Hg separation (3.182 Å). Phases containing Hg^{I} have a typical minimum Hg–Hg separation of roughly 2.5 Å,[7] which is much less than the distance of 3.18 Å observed in **1**. Assuming that **1** contains solely Hg^{II}, the isolated Hg_4O_4 units are formally electronically neutral.

The isolated Hg_4O_4 squares in **1** are unique in mercury(II)-containing systems. Many mercury/oxygen-containing phases such as $BaHgO_2$,[3] $CdHgO_2$,[8] and the superconductor phases noted above contain isolated dumbbell-shaped $O\text{-}Hg^{II}\text{-}O$ groups, in which the oxygen atoms are associated with only one nearby mercury cation. Other Hg^{II}/O-containing phases such as $Hg(OHg)_4Br_2$[9] contain infinite chains of alternating mercury and oxygen atoms as $[\text{-O-Hg-}]_\infty$ units, in which each oxygen atom is associated with two nearby Hg^{II} neighbors. $Hg_6O_4Cl_4$[10] contains also contains $[\text{-O-Hg-}]_\infty$ units, but they are linked into double chains, which involves some three-coordinate (to Hg) oxygen atoms. The recently reported phase $Hg_3O_2CrO_4$[11] contains novel, infinite sheets of edge-sharing six-rings of mercury(II) and oxygen (two-coordinate Hg, three-coordinate O), which surround isolated $[Cr^{VI}O_4]^{2-}$ tetrahedra.

In summary, the new phase $BaHg_2O_2Cl_2$ **1** has been prepared and structurally characterized from powder X-ray diffraction data. The precision of the refined atomic parameters is quite satisfactory, based on the X-ray powder refinement. The thermal factors for Cl(3) and O(1) are small, but their uncertainties are large. The crystal chemistry of **1** is consistent with the presence of solely Hg^{2+} centers in this phase. Novel Hg_4O_4 squares are present in $BaHg_2O_2Cl_2$.

Experimental Procedure

$BaHg_2O_2Cl_2$ was synthesized by the reaction of BaO_2 and Hg_2Cl_2 in the mole ratio 2:3. The reactants were intimately mixed and then sealed in a Pyrex tube under vacuum (10^{-3} Torr), which was then heated to 360 °C for three days. After reaction, one end of the tube was cooled to ambient temperature and the excess Hg_2Cl_2 removed by sublimation. The pure $BaHg_2O_2Cl_2$ product was recovered as an ivory-colored, microcrystalline powder, which yielded a powder X-ray diffraction pattern unlike those of the starting materials or known Hg/Ba phases. X-ray microanalysis (EDAX) indicated an approximate Ba:Hg:Cl ratio of 1:2:2.

The crystal structure of $BaHg_2O_2Cl_2$ was determined ab initio from laboratory X-ray powder diffraction data (Scintag automated diffractometer, $Cu_{K\alpha}$ radiation; $\lambda = 1.5418$ Å). The primitive tetragonal powder pattern of $BaHg_2O_2Cl_2$ was indexed using TREOR90, and possible space groups were determined by inspection. Starting positions for Ba, Hg, and two Cl atoms in space group *P4/mbm* (No. 127) were determined by using the direct methods program SIRPOW90. These initial atomic positions were optimized by Rietveld refinement (program GSAS) against powder X-ray data. The other atoms (one Cl, one O) were easily found from difference Fourier syntheses and added to the model. Refinement of 30 profile and atomic parameters converged to final residuals of $R_p = 0.097$, $R_{wp} = 0.138$, $R_{F^2} = 0.0621$, and $\chi^2 = 1.77$. The final Rietveld profiles are shown in Figure 4.

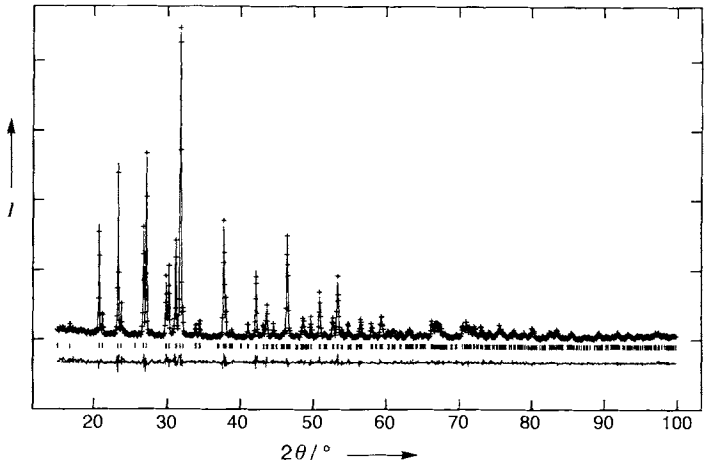

Fig. 4. Final observed (crosses), calculated (line), and difference profiles for the Rietveld refinement of **1**. Allowed reflection positions are indicated by tick marks.

Received: September 19, 1995 [Z 8410 IE]
German version: *Angew. Chem.* **1996**, *108*, 687–689

Keywords: barium compounds · mercury compounds · structure elucidation · superconductors · X-ray powder diffraction

[1] S. N. Putilin, E. V. Antipov, O. Chmaissem, M. Marezio, *Nature (London)* **1993**, *362*, 226.
[2] A. Schilling, M. Cantoni, J. D. Gao, H. R. Ott, *Nature (London)* **1993**, *363*, 56.
[3] O. Chmaissem, Q. Huang, S. N. Putilin, M. Marezio, A. Santoro, *Physica C* **1993**, *212*, 259.
[4] L. W. Finger, R. M. Hazen, R. T. Downs, R. L. Meng, C. W. Chu, *Physica C* **1994**, *226*, 216, and references therein.

[5] $BaHg_2O_2Cl_2$: $M_r = 641.42$, tetragonal, $P4/mbm$ (No. 127), $a = 11.8442(5)$, $c = 4.2865(2)$ Å, $V = 601.33(6)$ Å^3, $Z = 4$, $F(000) = 1064$.
[6] A. Le Bail, H. Duroy, J. L. Fourquet, *Mater. Res. Bull.* **1988**, *23*, 447; W. T. A. Harrison, T. E. Gier, G. D. Stucky, *Angew. Chem.* **1993**, *105*, 788; *Angew. Chem. Int. Ed. Engl.* **1993**, *32*, 724.
[7] A. F. Wells, *Structural Inorganic Chemistry*, Oxford University Press, New York, **1984**, p. 917.
[8] T. Hansen, H. Müller-Buschbaum, *Z. Anorg. Allg. Chem.* **1995**, *620*, 1137.
[9] K. Aurivillius, *Ark. Kemi.* **1965**, *23*, 469.
[10] K. Aurivillius, C. Stålhandske, *Acta Crystallogr. Sect. B* **1978**, *34*, 79.
[11] T. Hansen, H. Müller-Buschbaum, L. Walz, *Z. Naturforsch. B* **1995**, *50*, 47.

Magneto-Structural Correlations in Dinuclear d^1-d^1 Complexes: Structure and Magnetochemistry of Two Ferromagnetically Coupled Vanadium(IV) Dimers**

Winfried Plass*

The magnetic properties of molecular compounds have attracted considerable interest in recent years because of their relevance for the understanding of magnetically coupled active sites in metalloproteins as well as their potential applications as magnetic materials.[1] An important aspect of this research area is devoted to magneto-structural correlations. For some dinuclear systems it was possible to establish quantitative magneto-structural relationships,[2] among which the dihydroxo-bridged dicopper(II) complexes (d^9–d^9) are the most thoroughly investigated examples. However, little is known about other systems containing transition metal centers with an $S = 1/2$ ground state, in particular, well-characterized dinuclear oxovanadium(IV) complexes for which a structural-magnetic correlation has been established are rather rare.[3, 4]

For dimeric oxovanadium(IV) complexes only two arrangements are reported to yield a ferromagnetic interaction, namely a series of tartrate complexes[3a–d] composed of two square pyramidal coordinated oxovanadium(IV) centers bridged through the carbon backbone of the ligands and a fluoride-bridged complex containing two octahedrally coordinated oxovanadium(IV) centers.[3e] A common feature of both structure types is the almost linear arrangement of the two oxovanadium(IV) groups in an antiparallel orientation. As a consequence the two magnetic orbitals (d_{xy}) are more or less perpendicular to the dimer axis. In contrast, all other reported dimeric oxovanadium(IV) complexes exhibit an antiferromagnetic exchange interaction.[4, 5]

In this context the question arises whether it is possible to design ligand environments to introduce specific magnetic properties to dinuclear d^1–d^1 systems containing two oxovanadium(IV) centers. This can be achieved most easily for a dinuclear system composed of two octahedrally coordinated oxovanadium(IV) centers bridged by one shared edge leading to the formation of a $\{VO(\mu_2\text{-}OR)_2VO\}^{2+}$ core, since the three remaining coordination sites—with either facial or meridional arrangement—can be blocked at each center by chelating ligands which force the two oxo groups into specific configurations as shown in Scheme 1. The resulting classification is not limited to octahedrally coordinated oxovanadium(IV) centers but is also applicable to dimers containing centers with a square pyramidal coordination environment, although the missing donor atom in the *trans* position to the oxo group at the vanadium(IV) center restricts the possible arrangements to the *syn*- and *anti*-orthogonal as well as the twist configuration (cf. Scheme 1). Hitherto, structurally and magnetically characterized examples of dimeric vanadium(IV) complexes containing a $\{VO(\mu_2\text{-}OR)_2VO\}^{2+}$ core have only been reported for the two orthogonal configurations depicted in Scheme 1.[4a–e]

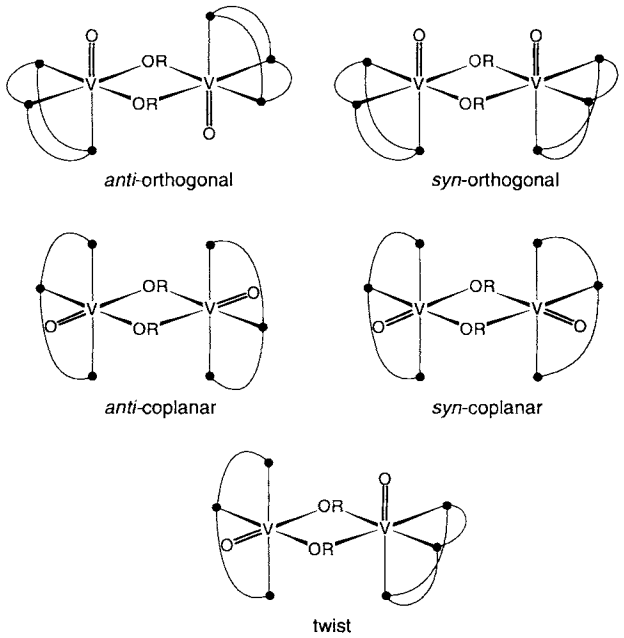

Scheme 1. Possible configurations of a $\{VO(\mu_2\text{-}OR)_2VO\}^{2+}$ core in complexes consisting of two edge-sharing octahedrally coordinated oxovanadium(IV) centers. The configurations are classified according the orientation of the V=O groups with respect to the plane defined by the two vanadium centers and the two bridging oxygen atoms (orthogonal, coplanar, twist) and the orientation of the two V=O groups (*syn*, *anti*).

By utilizing the trivalent, pentadentate Schiff base ligand *N*-salicyclidene-2-(bis(2-hydroxyethyl)amino)ethylamine (H_3sabhea) it has now been possible to synthesize the first examples of dimeric vanadium(IV) complexes with an *anti*-coplanar and a twist configuration, **1** and **2**, respectively. The reaction

$[\{VO(Hsabhea)\}_2]$ **1**

$[\{VO(Hsabhea)\}\{VO(acac)(HOMe)\}(\mu_2\text{-}OMe)]$ **2**

of $[VO(acac)_2]$ (Hacac = 2,4-pentanedione) with H_3sabhea in chloroform yields the neutral complex **1** as a green microcrystalline solid which is insoluble in most organic solvents.[6] Complex **1** is only sparingly soluble in hot *N*,*N*-dimethylformamide (DMF) and completely reprecipitates at temperatures below 90 °C. These solubility properties, which are also observed for other N,O chelating ligands,[5a, 8] are probably why only one X-ray crystallographically characterized neutral oxovanadium(IV) complex with an amino alcohol ligand has been reported.[4c] When the reaction was performed in methanol, however,

[*] Dr. W. Plass
Fakultät für Chemie der Universität
Lehrstuhl für Anorganische Chemie I
Postfach 100131, D-33501 Bielefeld (Germany)
Fax: Int. code + (521)106-6003
e-mail: winfried.plass@post.uni-bielefeld.de

[**] This work was supported by the Deutsche Forschungsgemeinschaft, the Fonds der Chemischen Industrie, and the Herbert Quandt-Stiftung der VARTA AG. I am thankful to Dr. R. Sessoli, Florence, for measuring the magnetic susceptibility data and to Prof. Dr. A. Müller for his continuous support.

 © VCH Verlagsgesellschaft mbH, D-69451 Weinheim, 1996 0570-0833/96/3506-0627 $ 15.00+.25/0

a crystalline material containing the neutral complexes **1** and **2** was formed depending on the $[VO(acac)_2]$ to ligand ratio.

The X-ray crystal structure analyses[9] of the isolated compounds **1** · 2 MeOH, **1** · MeOH, and **2** · MeOH reveal the dimeric molecular structure of the neutral oxovanadium(IV) complexes **1** (Fig. 1 top, cf. ref. [10]) and **2** (Fig. 2 top). The prearranged

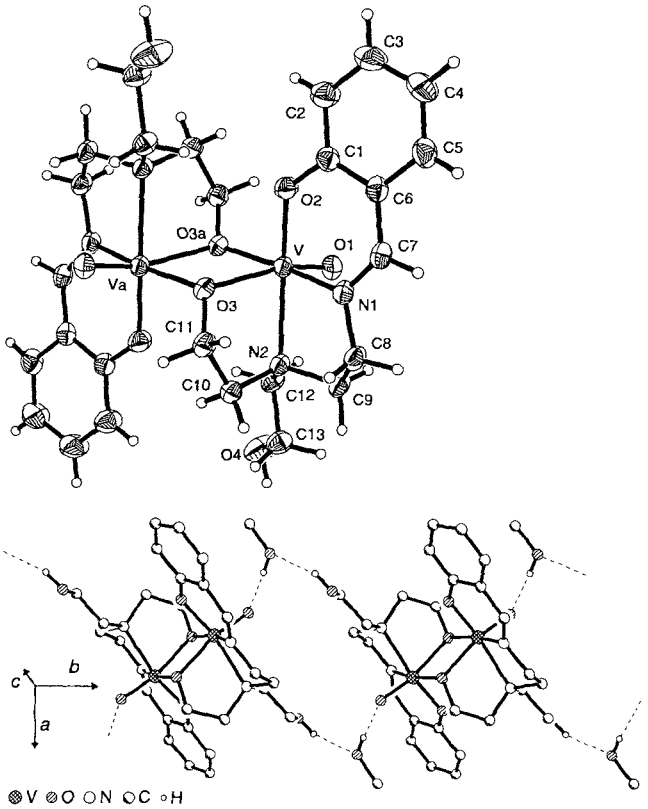

Fig. 1. Top: Molecular structure of the neutral dimer **1** in crystals of **1** · 2 MeOH. The two halves of the molecule are related by a crystallographic inversion center (indicated by the letter a in the atomic numbering scheme). Thermal ellipsoids of the non-hydrogen atoms are drawn at the 50% probability level. Pertinent bond lengths [pm] and angles [°]: V–O1 162.6(2), V–O2 193.8(2), V–O3 207.9(2), V–O3a 203.6(2), V–N1 212.1(2), V–N2 227.1(2); O1-V-O2 104.98(9), O1-V-O3 159.29(8), O1-V-O3a 96.03(8), O1-V-N1 94.91(9), O1-V-N2 89.51(9), O3-V-O3a 73.03(7). Bottom: Representation of the chains parallel to the [010] axis formed by the association of **1** (only the chain formed by one enantiomer is shown) through hydrogen bonding to methanol molecules (O5) in crystals of **1** · 2 MeOH. Relevant distances: O4–O5 277.7, O5–O1 275.0 pm.

meridional orientation for three donor sets of the H_3sabhea ligand (N1, N2, and O2; see Fig. 1 top and Fig. 2 top) provides the necessary condition for the formation of either a coplanar or twist configuration. In addition the deprotonated oxygen atom of one of the hydroxyethyl groups (O3) is coordinated to the oxovanadium(IV) center thereby generating a {VO(Hsabhea)} fragment with a five-coordinate vanadium center, which in the case of **1** is dimerized to give centrosymmetric molecular structure with O3 and O3a in the μ_2-bridging positions. In **2** the {VO(Hsabhea)} fragment (V1) is linked to a $\{VO(acac)(HOMe)\}^+$ fragment (V2) through the oxygen atom O3 of the former and an additional coordinating methoxide (O5). The observed *anti* configuration for the V=O group of the latter fragment (V2) and the phenolate oxygen (O2) at the $\{VO(\mu_2\text{-}OR)_2VO\}^{2+}$ core is favored by the formation of an intramolecular hydrogen bond between O2 and O7 (see Fig. 2). The different configuration of the $\{VO(\mu_2\text{-}OR)_2VO\}^{2+}$ core found for **1**

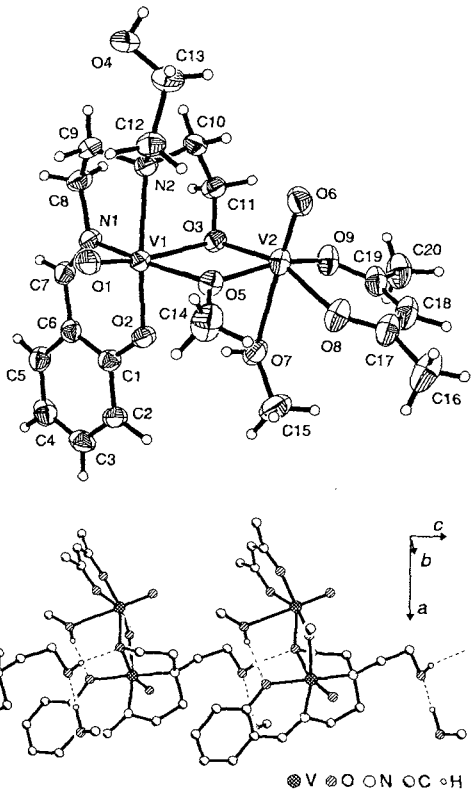

Fig. 2. Top: Molecular structure of the neutral complex **2** in crystals of **2** · MeOH. Thermal ellipsoids of the non-hydrogen atoms are drawn at the 50% probability level. Pertinent bond lengths [pm] and angles [°]: V1–O1 160.6(2), V1–O2 196.0(2), V1–O3 216.3(2), V1–O5 201.2(2), V1–N1 207.5(3), V1–N2 222.9(3), V2–O6 159.9(3), V2-O3 201.4(2), V2-O5 197.2(2), V2-O7 245.7(3), V2-O8 199.5(3), V2-O9 198.9(3); O1-V1-O2 106.12(11), O1-V1-O3 163.91(10), O1-V1-O5 99.07(11), O1-V1-N1 97.66(12), O1-V1-N2 91.69(11), O3-V1-O5 73.35(9), O3-V2-O6 104.00(12), O5-V2-O6 101.13(12), O6-V2-O7 177.46(12), O6-V2-O8 99.41(13), O6-V2-O9 99.40(13), O3-V2-O5 77.55(9), V1-O3-V2 101.01(9), V1-O5-V2 108.02(10). Bottom: Representation of the chains parallel to the [001] axis formed by the association of **2** through hydrogen bonding in crystals of **2** · MeOH (the methanol molecule (O10) forms a terminal hydrogen bond). Relevant distances: O3–O4 276.1 (intermolecular, chain), O2–O7 267.5 (intramolecular), O4–O10 276.7 pm.

and **2** and the asymmetric structure of the latter are consistent with the vibrational spectra observed for **1** · 2 MeOH and **2** · MeOH.[11] The neutral complexes **1** and **2** form hydrogen-bridged chains in crystals of **1** · 2 MeOH (see Fig. 1 bottom; for **1** · MeOH cf. ref. [10]) and **2** · MeOH (see Fig. 2 bottom) due to the pendant hydroxyethyl group of the constituent {VO(Hsabhea)} fragment. The presence of both intra- and intermolecular hydrogen bonds in **2** · MeOH is consistent with the observation of two bands at distinctively different energies for the ν(OH) stretching vibrations in the IR spectrum.[11]

The X-band ESR powder spectra of **1** · 2 MeOH and **2** · MeOH recorded at room temperature show broad structured bands with no detectable hyperfine structure at $g = 1.984$ (peak to peak separation: 20 mT, total width: 200 mT, shoulders at 294 and 395 mT) and $g = 1.989$ (peak to peak separation: 50 mT, total width: 250 mT, shoulders at 269 and 423 mT, and two small additional signals at 210 and 500 mT), respectively, and a band at half-field from the forbidden $\Delta m_s = 2$ transition at approximately 160 mT. The spectral data are consistent with an $S = 1$ spin system that exhibits a small zero-field splitting, as typically observed for other dimeric vanadium(IV) compounds with intramolecular interactions.[12] In addition no marked temperature dependence of the ESR spectra was detected, and even at 5 K the signals did not lose intensity; only the width of the band observed for **1** · 2 MeOH decreased by about 20 mT.

 © VCH Verlagsgesellschaft mbH, D-69451 Weinheim, 1996 0570-0833/96/3506-0628 $ 15.00+.25/0

These observations are indicative of intramolecular ferromagnetic interactions in the exchange-coupled d^1-d^1 systems of **1** and **2** and thus of a triplet ground state.

The magnetic susceptibility χ of polycrystalline samples of **1** · 2MeOH and **2** · MeOH was measured in a temperature range of 4–250 K with a SQUID magnetometer with an applied field of $H = 10$ kOe. The temperature dependence of the product $\chi_M T$ is shown in Figure 3. At temperatures above 150 K

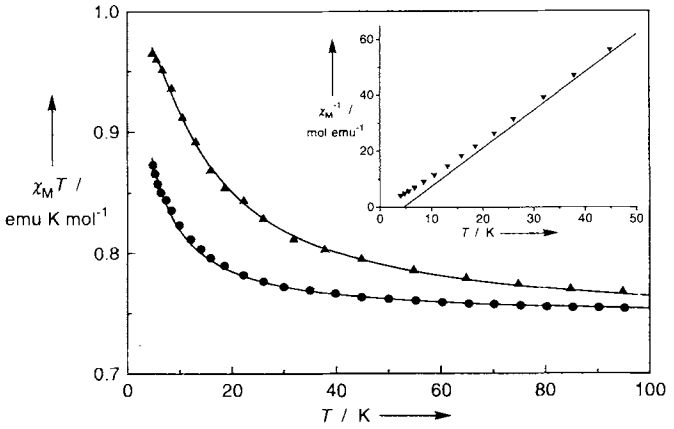

Fig. 3. Temperature dependence of the product of the molar magnetic susceptibility with temperature for **1** · 2MeOH (exp., ●) and **2** · MeOH (exp., ▲). The solid lines represent the calculated values (see text). The inset shows χ_M^{-1} vs temperature for **2** · MeOH, yielding a Curie–Weiss temperature of 4.6 K (for **1** · 2MeOH a Curie–Weiss temperature of 1.3 K is obtained).

the susceptibility data obeys the Curie–Weiss law (see inset in Fig. 3), and $\chi_M T$ is close to the expected spin-only value for two independent vanadium(IV) centers per molecule. The observed increase of $\chi_M T$ upon cooling is in accord with intramolecular ferromagnetic interactions in the oxovanadium(IV) dimers **1** and **2**. A quantitative analysis of the susceptibility data (corrected for diamagnetic contributions by using Pascal constants) under the assumption of an isotropic interaction by using the Heisenberg–Dirac–Van Vleck Hamiltonian $\hat{H} = -J\hat{S}_1 \cdot \hat{S}_2$[1d] was used to describe the temperature dependence of the product $\chi_M T$. As shown in Figure 3, good fits to the experimental data were attained for the magnetic parameters $g = 1.99$ and $J = +3.1$ cm^{-1} for **1** · 2MeOH and $g = 1.98$ and $J = +10.6$ cm^{-1} for **2** · MeOH.[13]

Density functional calculations using the broken-symmetry formalism were performed for the neutral complexes **1** and **2**.[14] The comparison of the results obtained by restricted and unrestricted Hartree–Fock–Slater (RHFS and UHFS, respectively) calculations as well as the fact that the magnetic orbitals based on broken-symmetry UHFS calculations are largely localized (see Scheme 2) indicate the presence of weak interactions between the two vanadium(IV) centers. For such weakly interacting dimers (i.e. $S_{ab}^2 \ll 1$; S_{ab} is the overlap integral between the magnetic orbitals) spin-projection techniques within the broken-symmetry formalism allow the isotropic interaction parameter to be determined according to $J = 2[E_B - E(S=1)]$,[15] where E_B is the energy of the broken-symmetry state. The calculated singlet–triplet splittings of +46 and +65 cm^{-1} for **1** and **2**, respectively, although somewhat too large when compared to the experimental values, are in line with their observed ferromagnetic behavior.

A qualitative interpretation of the magnetic interactions in transition metal dimers is usually given by the well-known

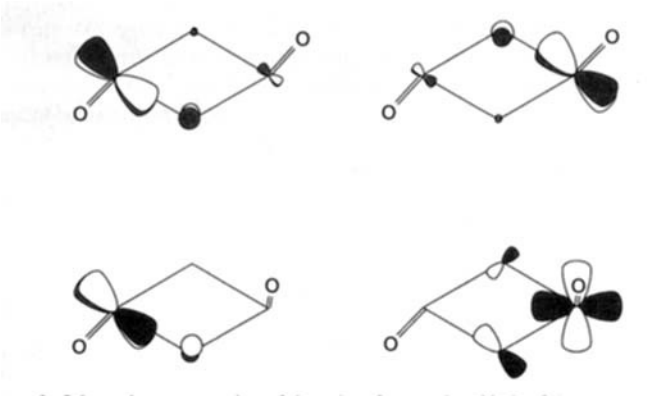

Scheme 2. Schematic representation of the pairs of magnetic orbitals of the complexes **1** (top) and **2** (bottom) derived from broken-symmetry density functional calculations. (Only contributions from atoms of the $\{VO(\mu_2\text{-}OR)_2VO\}^{2+}$ core are depicted.)

Goodenough–Kanamori rules,[16] which are based on the interaction between pairs of natural magnetic orbitals. Since the unpaired electron in oxovanadium(IV) complexes generally resides in a metal-centered orbital with d_{xy} character (with the oxo group oriented along the z axis), the five configurations outlined in Scheme 1 impose specific interactions between the corresponding magnetic orbitals. For the two orthogonal configurations either a direct interaction or a superexchange mechanism between the magnetic orbitals can be expected to be operative, yielding rather strong antiferromagnetic coupling. In fact this is in agreement with the observed magnetic behavior of all compounds reported to possess such a core configuration.[4a–e] Although a dinuclear complex with a *syn*-coplanar configuration has not yet been synthesized, similar orbital interactions are possible and suggest that such dimers should also exhibit antiferromagnetic coupling. The situation is different for the *anti*-coplanar and twist configuration where neither a direct interaction nor a superexchange mechanism can be effective. In general, ferromagnetic interactions are expected if the magnetic orbitals are orthogonal. Such orthogonality may be strict—in the sense that it is imposed by symmetry—as observed for some copper-containing heterodinuclear complexes,[17] or accidental as found for several dimeric copper(II) and nickel(II) complexes.[18] For the twist configuration a case of accidental orthogonality can be expected, which is in accord with the observed ferromagnetic coupling for **2** and the magnetic orbitals obtained from broken-symmetry UHFS calculations (see Scheme 2). Whereas for complexes with *anti*-coplanar configuration such as **1**, the accidental orthogonality (cf. Scheme 2) is certainly dependent on the structural parameters of the $\{VO(\mu_2\text{-}OR)_2VO\}^{2+}$ core and, moreover, the overlap between the two magnetic orbitals is expected to be rather small. Therefore an alternative mechanism might be invoked to explain the ferromagnetic coupling. Such a mechanism might be the "crossed interaction" between singly occupied and empty orbitals at either transition metal center, a mechanism that has already been used to justify the ferromagnetic interaction observed for some manganese(III)-containing dimeric complexes.[19] A possible crossed pathway for an *anti*-coplanar configuration of the $\{VO(\mu_2\text{-}OR)_2VO\}^{2+}$ core is depicted in Scheme 3.

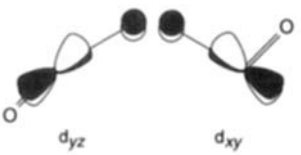

Scheme 3. Sketch of the interaction between a singly occupied d_{xy} atomic orbital and an empty d_{yz} atomic orbital located at the vanadium centers in an *anti*-coplanar arrangement as found in **1**. The interaction is mediated by the p_y atomic orbital of the bridging oxygen towards which both d atomic orbitals are delocalized.

The neutral complexes **1** and **2** are the first edge-sharing octahedral oxovanadium(IV) dimers that exhibit ferromagnetic interactions between the metal centers. These examples show that it is possible to enforce specific magnetic properties on such systems through the choice of ligand employed. Furthermore, the correlation between the structure of a $\{VO(\mu_2\text{-}OR)_2VO\}^{2+}$ core and the related magnetic properties has been demonstrated. Consequently this magneto-structural correlation facilitates the differentiation between configurational arrangements in corresponding dimeric complexes and, moreover, allows the interpretation of magnetic interactions in larger vanadium(IV) clusters with similar structural features.

Experimental Procedure

The syntheses were carried out under an argon atmosphere using Schlenk line techniques, and the solvents were purified prior to use. The ligand H_3sabhea was synthesized as described previously [7].

1: H_3sabhea (1.00 g, 4.0 mmol) dissolved in $CHCl_3$ (15 mL) was added to a solution of $[VO(acac)_2]$ (1.02 g, 4.0 mmol) in $CHCl_3$ (50 mL) at room temperature. After the addition a green precipitate was observed and the resulting suspension was stirred for 12 h (or alternatively heated to reflux for 1 h) to complete the reaction. The green microcrystalline solid **1** was isolated by filtration, washed twice with $CHCl_3$, and dried in vacuo (2.05 g, 85%). Analysis for $C_{26}H_{36}N_4O_8V_2$: calcd: C, 49.22; H, 5.72; N, 8.83; found: C, 49.38; H, 5.81; N, 8.69.

1 · MeOH and **1** · 2MeOH: A solution of H_3sabhea (1.80 g, 7.2 mmol) in methanol (5 mL) was added to $[VO(acac)_2]$ (0.37 g, 1.4 mmol) dissolved in methanol (10 mL). The resulting deep green solution was allowed to stand at room temperature. After 2–3 d green crystals of **1** · MeOH (plates) and **1** · 2MeOH (prisms) began to grow and could be harvested after two weeks to yield a total amount of 0.25 g (80%). The crystals of **1** · MeOH and **1** · 2MeOH could be separated by hand according their shape and were obtained approximately in a 1:1 ratio. Analysis for $C_{28}H_{44}N_4O_{10}V_2$ (**1** · 2MeOH): calcd: C, 48.14; H 6.35; N, 8.02; found: C, 47.98; H, 6.39; N, 8.15. Analysis for $C_{27}H_{40}N_4O_9V_2$ (**1** · MeOH): calcd: C, 48.66; H, 6.05; N, 8.41; found: C, 48.72; H, 6.13; N, 8.45.

2 · MeOH: To a solution of $[VO(acac)_2]$ (1.24 g, 4.7 mmol) in methanol (20 mL) was added H_3sabhea (0.60 g, 2.3 mmol) dissolved in methanol (5 mL). After the mixture had been allowed to stand at room temperature for 3–4 d dark brownish green (almost black) crystals of **2** · MeOH formed. After a period of two weeks the crystals of **2** · MeOH were collected by filtration to yield 0.43 g (32%). Analysis for $C_{21}H_{36}N_2O_{10}V_2$: calcd: C, 43.61 H, 6.27; N, 4.84; found: C, 43.90; H, 6.31, N, 4.84.

Received: September 22, 1995 [Z 8419 IE]
German version: *Angew. Chem.* **1996**, *108*, 699–703

Keywords: density functional calculations · electronic structure · magnetic properties · structure elucidation · vanadium compounds

[1] a) *Magneto-Structural Correlations in Exchange Coupled Systems* (Eds.: R. D. Willet, D. Gatteschi, O. Kahn), Reidel, Dordrecht, **1985**; b) *Magnetic Molecular Materials* (Eds.: D. Gatteschi, O. Kahn, J. S. Miller, F. Palacio), Kluwer, Dordrecht, **1991**; c) O. Kahn, Y. Pei, Y. Journaux in *Inorganic Materials* (Eds.: D. W. Bruce, D. O'Hare), Wiley, Chichester, **1992**, p. 59; d) O. Kahn, *Molecular Magnetism*, VCH Publishers, New York, **1993**.

[2] a) V. H. Crawford, H. W. Richardson, J. R. Wasson, D. J. Hodgson, W. E. Hatfield, *Inorg. Chem.* **1976**, *15*, 2107; b) S. M. Gorun, S. J. Lippard, *ibid.* **1991**, *30*, 1625; c) A. Niemann, U. Bossek, K. Wieghardt, C. Butzlaff, A. X. Trautwein, B. Nuber, *Angew. Chem.* **1992**, *104*, 345; *Angew. Chem. Int. Ed. Engl.* **1992**, *31*, 311; d) K. K. Nanda, L. K. Thompson, J. N. Bridson, K. Nag, *J. Chem. Soc. Chem. Commun.* **1994**, 1337.

[3] a) G. O. Carlisle, G. D. Simpson, *J. Mol. Struct.* **1975**, *25*, 219; b) M. V. Hanson, C. B. Smith, G. O. Carlisle, *Inorg. Nucl. Chem. Lett.* **1975**, *11*, 865; c) V. H. Crawford, W. E. Hatfield, R. E. Tapscott, *J. Mol. Struct.* **1977**, *38*, 141; d) J. T. Wrobleski, M. R. Thompson, *Inorg. Chim. Acta* **1988**, *150*, 269; e) M. Mohan, M. R. Bond, T. Otieno, C. J. Carrano, *Inorg. Chem.* **1995**, *34*, 1233.

[4] a) K. Wieghardt, U. Bossek, K. Volckmar, W. Swiridoff, J. Weiss, *Inorg. Chem.* **1984**, *23*, 1387; b) A. Neves, K. Wieghardt, B. Nuber, J. Weiss, *Inorg. Chim. Acta* **1988**, *150*, 183; c) X-ray structure: C. J. Carrano, C. M. Nunn, R. Quan, J. A. Bonadies, V. L. Pecoraro, *Inorg. Chem.* **1990**, *29*, 945; $\chi(T)$: A. Syamal, E. F. Carey, L. J. Theriot, *ibid.* **1973**, *12*, 245; d) G. Huan, J. W. Johnson, A. J. Jacobson, D. P. Goshorn, J. S. Merola, *Chem. Mater.* **1991**, *3*, 539; e) S. L. Castro, M. E. Cass, F. J. Hollander, S. L. Bartley, *Inorg. Chem.* **1995**, *34*, 466; f) J. T. Wrobleski, *ibid.* **1988**, *27*, 946.

[5] a) A. Syamal, *Coord. Chem. Rev.* **1975**, *16*, 309; b) H. Toftlund, S. Larsen, K. S. Murray, *Inorg. Chem.* **1991**, *30*, 3964; c) J. C. Dutton, K. S. Murray, E. R. T. Tiekink, *Inorg. Chim. Acta* **1989**, *166*, 5; d) H. Okawa, I. Ando, S. Kida, *Bull. Chem. Soc. Jpn.* **1974**, *47*, 3041; e) M. J. Heeg, J. L. Mack, M. D. Glick, R. L. Lintvedt, *Inorg. Chem.* **1981**, *20*, 833; f) D. Collison, D. R. Eardley, F. E. Mabbs, A. K. Powell, S. S. Turner, *ibid.* **1993**, *32*, 664.

[6] Suspensions of **1** in organic solvents are readily air-oxidized to form the corresponding oxovanadium(V) complex in quantitative yield [7]. Cyclic voltammetry studies on the oxovanadium(V) complex show an irreversible reduction process at -903 mV (10^{-3} M in DMF, 0.1 M nBu$_4$NClO$_4$, scan rate: 50 mVs^{-1}).

[7] W. Plass, *Z. Anorg. Allg. Chem.* **1994**, *620*, 1635.

[8] A. A. Diamantis, J. M. Frederiksen, M. A. Salam, M. R. Snow, E. R. T. Tiekink, *Aust. J. Chem.* **1986**, *39*, 1081.

[9] Data for crystal structure analyses: a) **1** · 2MeOH: $C_{28}H_{44}N_4O_{10}V_2$, M = 698.6, crystal dimensions 0.2 × 0.3 × 0.4 mm, monoclinic, $P2_1/c$, a = 1102.5(3), b = 1009.6(3), c = 1407.9(3) pm, β = 95.22(2)°, V = 1.5606(7) nm^3, Z = 2, ρ_{calcd} = 1.487 g cm^{-3}, $F(000)$ = 732, T = 188 K, λ = 71.073 pm, $\mu(Mo_{K\alpha})$ = 0.660 mm^{-1}, ω-scan, range $4 < 2\theta < 54°$, 3721 measured, 3389 independent (R_{int} = 0.028), 3381 used reflections, 276 parameters, $R1(F > 4\sigma(F))$ = 0.045, $wR2$ = 0.121 (all data). b) **1** · MeOH: $C_{27}H_{40}N_4O_9V_2$, M = 666.5, crystal dimensions 0.1 × 0.3 × 0.4 mm, monoclinic, $P2_1/c$, a = 2049.9(3), b = 978.5(2), c = 1423.0(3) pm, β = 92.14(1)°, V = 2.8523(9) nm^3, Z = 4, ρ_{calcd} = 1.552 g cm^{-3}, $F(000)$ = 1392, T = 188 K, λ = 71.073 pm, $\mu(Mo_{K\alpha})$ = 0.716 mm^{-1}, ω-scan, range $4 < 2\theta < 50°$, 4402 measured, 4025 independent (R_{int} = 0.021), 4010 used reflections, 383 parameters, $R1(F > 4\sigma(F))$ = 0.086, $wR2$ = 0.240 (all data). c) **2** · MeOH: $C_{21}H_{36}N_2O_{10}V_2$, M = 578.4, crystal dimensions 0.3 × 0.4 × 0.6 mm, monoclinic, $C2/c$, a = 4056.7(6), b = 854.2(2), c = 1514.8(3) pm, β = 90.30(2)°, V = 5.249(2) nm^3, Z = 8, ρ_{calcd} = 1.464 g cm^{-3}, $F(000)$ = 2416, T = 188 K, λ = 71.073 pm, $\mu(Mo_{K\alpha})$ = 0.766 mm^{-1}, ω-scan, range $4 < 2\theta < 54°$, 6039 measured, 5700 independent (R_{int} = 0.040), 5677 used reflections, 404 parameters, $R1(F > 4\sigma(F))$ = 0.057, $wR2$ = 0.157 (all data). Instrumentation and conditions: The data were collected on a Siemens R3m/V diffractometer by using graphite-monochromated $Mo_{K\alpha}$ radiation. Lorentz and polarization corrections were applied to the data. An absorption correction based on azimuthal Ψ scans was made for **1** · 2MeOH and **2** · MeOH. The structures were solved by direct methods (SHELXTL PLUS); full-matrix least-squares refinement of the function $\Sigma w(F_o^2 - F_c^2)^2$ (G. M. Sheldrick, SHELXL-93, Universität Göttingen, **1993**). For **1** · 2MeOH and **2** · MeOH the hydrogen atoms of the CH_3 groups were refined by using a rotating group model, whereas all other hydrogen atoms were located from the difference fourier map and refined isotropically. For **1** · MeOH all hydrogen atoms were refined by using the appropriate riding model. Further details of the crystal structure investigations may be obtained from the Fachinformationszentrum Karlsruhe, D-76344 Eggenstein-Leopoldshafen (Germany), on quoting the depository numbers CSD-404246 (**1** · 2MeOH), CSD-404247 (**1** · MeOH), and CSD-404248 (**2** · MeOH).

[10] The neutral complex **1** is isolated in two different crystalline compounds **1** · 2MeOH and **1** · MeOH [9]. The structural parameters of the two symmetry-independent molecules of **1** in **1** · MeOH are, within the uncertainty limits, the same as those observed in crystals of **1** · 2MeOH (see legend to Fig. 1). Differences are observed for the packing of **1** in both crystal structures. In **1** · 2MeOH all molecules of **1** are involved in the formation of chains along the [010] direction through hydrogen bonding through methanol molecules (see Fig. 1 bottom), whereas in **1** · MeOH only one of the two independent molecules forms such hydrogen-bonded chains along the [010] direction.

[11] Additional characteristic physical data: for **1** · 2MeOH: IR (Nujol mull): $\tilde{\nu}$ = 3430 (m, br, ν(OH)), 1629 (vs, ν(C=N)), 921 cm^{-1} (vs, ν(V=O)); Raman (λ_e = 514.5 nm): 1630 (vs, ν(C=N)), 922 cm^{-1} (s, ν(V=O)); Vis (solid-state reflection) and NIR (KBr pellet, transmission): 20800 (sh), 16400, 11900 cm^{-1}; for **2** · MeOH: IR (Nujol mull): 3410 (m, br, ν(OH)), 3240 (m, br, ν(OH)), 1632 (vs, ν(C=N)), 972 (vs, ν(V=O), V2 see Fig. 2 top), 955 cm^{-1} (vs, ν(V=O), V1 see Fig. 2 top); Raman (λ_e = 514.5 nm): 1631 (vs, ν(C=N)), 971 (w, ν(V=O), V2), 952 cm^{-1} (w, ν(V=O), V1); Vis (solid-state reflection) and NIR (KBr pellet, transmission): ν = 21300 (sh), 17500, 13500 (sh), 11100 cm^{-1}.

[12] a) A. Ozarowski, D. Reinen, *Inorg. Chem.* **1986**, *25*, 1704; b) A. Bencini, D. Gatteschi, *Electron Paramagnetic Resonance of Exchange Coupled Systems*, Springer, Berlin, **1990**; c) F. E. Mabbs, D. Collison, *Electron Paramagnetic Resonance of d Transition Metal Compounds*, Elsevier, Amsterdam, **1992**.

[13] If in addition intermolecular interactions are taken into account in the numerical analysis of the susceptibility data of **1** · 2MeOH and **1** · MeOH according to the equation

$$\chi_M = 2Ng^2\beta^2\left[kT - \frac{2zJ'}{3 + \exp(-J/kT)}\right]^{-1}\,[3 + \exp(-J/kT)]^{-1}$$

(A. P. Ginsberg, M. E. Lines, *Inorg. Chem.* **1972**, *11*, 2289), the following parameters are obtained: g = 1.99, J = +3.8 cm^{-1}, and zJ' = −0.15 cm^{-1} for **1** · 2MeOH and g = 1.99, J = +11.1 cm^{-1}, and zJ' = −0.06 cm^{-1} for **2** · MeOH. According to the rather small intermolecular exchange parameters zJ', magnetic interactions between dimers in **1** · 2MeOH and **1** · MeOH seem not to play an important role.

[14] Program package ADF, version 1.1.3, Department of Theoretical Chemistry, Vrije Universiteit, Amsterdam, **1994**; E. J. Baerends, D. E. Ellis, P. Ros, *Chem.*

Phys. **1973**, *2*, 41; G. te Velde, E. J. Baerends, *J. Comput. Phys.* **1992**, *99*, 84. Computational details: A local spin density approximation (S. H. Vosko, L. Wilk, M. Nusair, *Can. J. Phys.* **1980**, *58*, 1200) was used in connection with the self-interaction correction of Stoll et al. (H. Stoll, C. M. E. Pavlidou, H. Preuss, *Theor. Chim. Acta* **1978**, *49*, 143) and a gradient correction to the exchange part of the potential (A. D. Becke, *Phys. Rev. A* **1988**, *38*, 3098). Frozen core approximation with the following Slater-type-orbital (STO) basis sets for the valence shells: V, double-ζ for 3s, 3p, and 4s and triple-ζ for 3d; O, N, and C, double-ζ for 2s and 2p; H double-ζ for 1s. A set of auxiliary s, p, d, f, and g type STOs centered on the different atoms was used to fit the electronic density.

[15] a) L. Noodleman, J. G. Norman Jr., *J. Chem. Phys.* **1979**, *70*, 4903; b) L. Noodleman, *ibid.* **1981**, *74*, 5737.

[16] A. P. Ginsberg, *Inorg. Chim. Acta Rev.* **1971**, *5*, 45.

[17] a) O. Kahn, J. Galy, Y. Journaux, J. Jaud, I. Morgenstein-Badarau, *J. Am. Chem. Soc.* **1982**, *104*, 2165; b) K. K. Nanda, S. Mohanta, S. Ghosh, M. Mukherjee, M. Helliwell, K. Nag, *Inorg. Chem.* **1995**, *34*, 2861.

[18] O. Kahn, *Struct. Bonding (Berlin)* **1987**, *68*, 89.

[19] R. Hotzelmann, K. Wieghardt, U. Flörke, H. J. Haupt, D. C. Weatherburn, J. Bonvoisin, G. Blondin, J. J. Girerd, *J. Am. Chem. Soc.* **1992**, *114*, 1681.

$[\{Na^+(thf)_2\}_4(rubrene^{4-})]$: Crystallization and Structure Determination of a Contact-Ion Quintuple for the First π-Hydrocarbon Tetraanion**

Hans Bock,* Katayoun Gharagozloo-Hubmann, Christian Näther, Norbert Nagel, and Zdenek Havlas

Dedicated to Professor Herbert W. Roesky on the occasion of his 60th birthday

The insertion of electrons into π-hydrocarbons C_xH_y releases less energy than is needed for electron expulsion, and within the total energy scale for the molecular states, the resulting molecular anions $[C_xH_y]^{n-}$ are located below the ground state of the uncharged molecule,[1] in contrast to the molecular cations $[C_xH_y]^{n+}$. Single-electron reductions generate radical anion salts, which can be either solvent-separated $[Met^+_{solv}][C_xH_y]^{\bullet -}$ or solvent-shared contact ion pairs $[Met^+(C_xH_y)^{\bullet -}]_{solv}$, and the structural changes upon transition from the neutral molecule to the radical anion are only small.[1, 2] In contrast, two electron reductions to either solvent-separated or solvent-shared contact ion triples $[Met^+_{solv}]_2[C_xH_y]^{2-}$ or $[Met_2^+(C_xH_y)^{2-}]_{solv}$ usually cause severe structural distortions.[1] For instance, in ethylene derivatives $R_2C{=}CR_2$, on reduction of the neutral molecule to the dianion the double bond is stretched to a single one, around which the two molecular halves twist;[1] allenes $R_2C{=}C{=}CR_2$ are folded at their central C center and protonated;[1] and six-membered benzene rings can be deformed into a "boat" conformation.[4] Although up to four consecutive reversible one-electron oxidations are observed in cyclic voltammetric studies,[1] a single-electron reduction of benzene can be achieved only under extremely aprotic conditions at the potential range limit. Extensive Chemical Abstracts Service (CAS) and Cambridge Structural Database searches gave no hint of known structures of π-hydrocarbon trianions or tetraanions.[6]

Much to our surprise, therefore, the structure determination of the product of rubrene reduction at a sodium metal mirror[7] proved the existence of the first π-hydrocarbon tetraanion (Fig. 1).

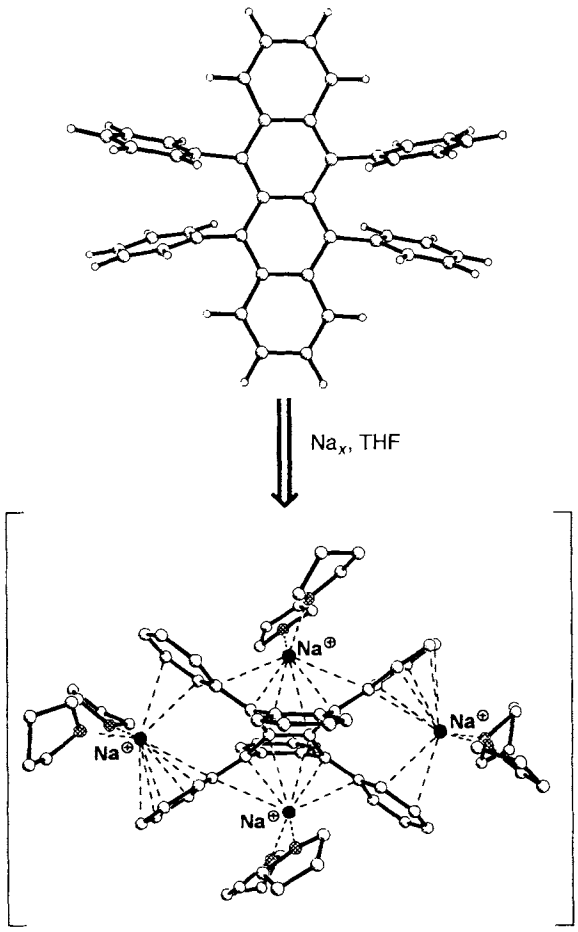

Fig. 1. Structural changes on the fourfold reduction of rubrene at a sodium metal mirror to form the contact-ion quintuple of its tetraanion.

In the tetrakis[bis(tetrahydrofuran)sodium]-5,6,11,12-tetraphenyltetracene (triclinic, $P\bar{1}$, $Z = 1$), the four Na^+ countercations, each doubly solvated by THF, are located in two different positions: either above and below the central tetracene skeleton or between the peripheral bis(phenyl) pincers. The central Na^+ ions are eightfold coordinated with shortest $Na^+ \cdots C^{\delta -}$ contacts of between 260 and 263 to the two phenyl-substituted carbon centers and longer ones of 272 pm to the tetracene carbon centers. Other contacts, namely to the *ipso* centers of the two phenyl rings that face each other, exceed 290 pm. The $Na^+ \cdots O_{THF}$ contacts of 227 pm are short.[8] The peripheral Na^+ centers exhibit a higher coordination number of 10: one of the C_6 rings is η^6-coordinated and the other one only η^2, because the spatial arrangement of the phenyl substituents of the tetracene does not allow a symmetrical dibenzene sodium sandwich.[1] The contact distances $Na^+ \cdots C^{\delta -}$ range from 277 to 293 pm for the η^6-coordinated ring and from 275 to 284 pm for the η^2 one.

The incorporation of four electrons into rubrene, the tetracene skeleton of which is planar,[9] causes drastic structural

[*] Prof. Dr. H. Bock, Dipl.-Chem. K. Gharagozloo-Hubmann, Dr. C. Näther, Dipl.-Chem. N. Nagel
Chemische Institute der Universität
Marie-Curie-Strasse 11, D-60439 Frankfurt am Main (Germany)
Dr. Z. Havlas
Institute of Organic Chemistry and Biochemistry of the Czech Academy of Sciences
Flemingovo Nam 2, CS-16610 Prague (Czech Republic)

[**] Interactions in Crystals, Part 100. This project has been supported by the Adolf-Messer-Stiftung, the Deutschen Forschungsgemeinschaft, the State of Hesse (Germany), and the Fonds der Chemischen Industrie. Part 99: H. Bock, C. Näther, N. Nagel, *Angew. Chem.* and *Angew. Chem. Int. Ed. Engl.*, submitted.

distortions: The tetraanion is bent at the phenyl substitution centers 5/12 and 6/11, in each case by 43°(!) (Fig. 2, top). Numerous short bonds are elongated and long ones shortened (Fig. 2, bottom). In detail, the central CC bond length in the

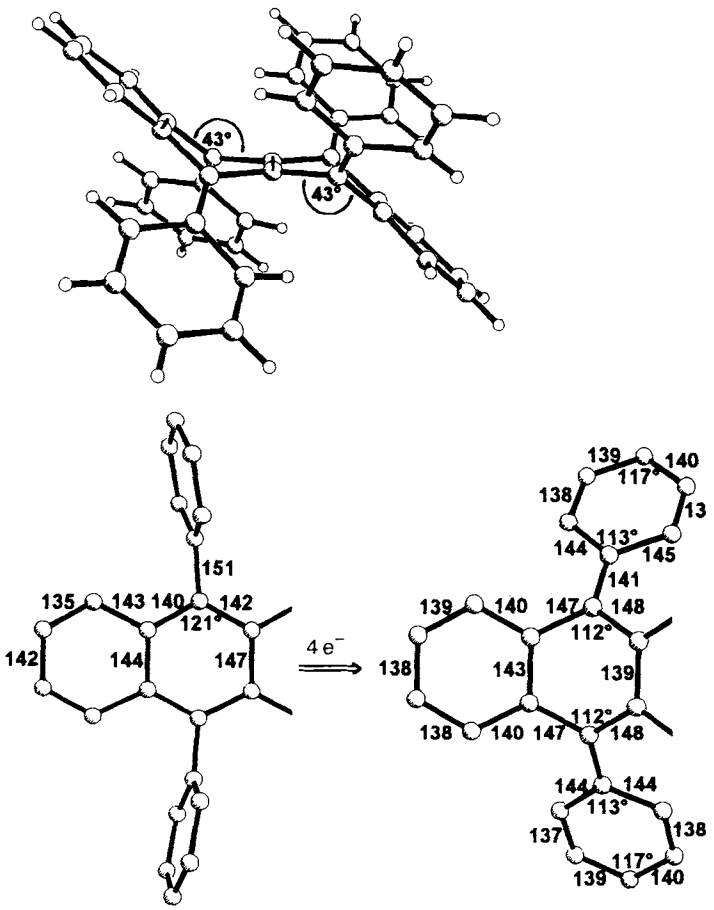

Fig. 2. Molecular structure of the rubrene tetraanion. Top: side view. Bottom: comparison with rubrene.

tetraanion is cut by 8 pm(!) from 147 to 139 pm, and the four adjacent CC bonds are increased by 6 pm(!) from 142 to 148 pm. Both bent six-membered rings exhibit record angle compressions from 121 to 112°(!), which together with the quinoid ring distortions—the CC bond connecting the rings is shortened from 151 pm by 10 pm(!) to 141 pm, and the *ipso* angle reduced to 113°[1]—indicate where most of the fourfold negative surplus charge is localized.

Tetraanions such as the one reported above are supposed to be an excellent testing ground for calculations that employ highly correlated wavefunctions. Meanwhile we estimated from the experimental structural parameters within the MNDO approximation both the charge distribution as well as the heats of formation. This method revealed the following: 1) The four negative charges are unexpectedly distributed rather uniformly over the entire molecule: on average -0.62 for the phenyl rings and -0.60 each for the six-membered tetracene rings (counting the central CC bonds twice). Expectedly, rather high single charges of -0.22 are predicted for each of the four C centers at which the framework bends. 2) The heat of formation for the eightfold THF-solvated tetrasodium salt is calculated to be $\Delta H_f^{MNDO} = -2520$ kJ mol^{-1} versus $\Delta H_f^{MNDO} = +1076$ kJ mol^{-1} for neutral rubrene. Subtracting the total contribution of -521 kJ mol^{-1} from the four $[Na^+(thf)_2]$ countercations yields for the rubrene tetraanion $\Delta H_f^{MNDO} = -1992$ kJ mol^{-1} and still $\Delta\Delta H_f^{MNDO} = +916$ kJ mol^{-1} for the electron affinity (rubrene + 4 e$^-$ → rubrene^{4-}); that is, about 2.4 eV per electron.

Despite all rationalization attempts, the fourfold rubrene reduction at a sodium metal mirror remains strange: Presumably only two electrons are initially incorporated, which generate a contact-ion triple with two Na^+ countercations above and below the tetracene skeleton and simultaneously bend the dianion to such an extent that two more electron transfer steps to the peripheral bis(phenyl) Na-subunits become feasible.

Whatever the microscopic reduction pathway to the contact-ion quintuple of the rubrene tetraanion might be, our report should stimulate the search for further three- or four-electron incorporation into unsaturated hydrocarbons! Under comparable conditions the reduction of anthracene in THF at a potassium metal mirror generates the first contact ion septuple of $[\{K^+(thf)\}_4(anthracene)_3^{4-}]_\infty$, which despite its extreme air-sensitivity, could be structurally characterized down to an *R*1 value of only 0.043 [11].

Received: October 4, 1995 [Z 8440 IE]
German version: *Angew. Chem.* **1996**, *108*, 720–722

Keywords: reductions · rubrene · structure elucidation · tetraanions

[1] H. Bock, K. Ruppert, C. Näther, Z. Havlas, H.-F. Herrmann, C. Arad, I. Göbel, A. John, J. Meuret, S. Nick, A. Rauschenbach, W. Seitz, T. Vaupel, B. Solouki, *Angew. Chem.* **1992**, *104*, 564; *Angew. Chem. Int. Ed. Engl.* **1992**, *31*, 550, and references therein.

[2] a) H. Bock, C. Arad, C. Näther, Z. Havlas, *J. Chem. Soc. Chem. Commun.* **1995**, in press; b) H. Bock, C. Näther, Z. Havlas, A. John, C. Arad, *Angew. Chem.* **1994**, *106*, 1823; *Angew. Chem. Int. Ed. Engl.* **1994**, *33*, 1755, and references therein.

[3] H. Bock, C. Näther, K. Ruppert, Z. Havlas, *J. Am. Chem. Soc.* **1992**, *114*, 6907.

[4] H. Bock, M. Ansari, N. Nagel, Z. Havlas, *J. Organomet. Chem.* **1995**, *499*, 63, and references therein, in particular A. Sekiguchi, K. Ebata, C. Kabuto, H. Sakurai, *J. Am. Chem. Soc.* **1991**, *113*, 1464.

[5] J. Heinze, *Angew. Chem.* **1984**, *96*, 823; *Angew. Chem. Int. Ed. Engl.* **1984**, *23*, 831, and references therein.

[6] The literature searches were carried out on 28. 9. 1995.

[7] Preparation and single crystal growth of $[\{Na(thf)_2\}_4(C_{42}H_{28})]$: freshly cut sodium (40 mg, 1.74 mmol) was weighed into a Schlenk trap, dried at 10^{-3} mbar, and distilled to form a metal mirror on the trap walls. Under argon dried 5,6,11,12-tetraphenyltetracene (rubrene) (50 mg, 0.094 mmol) was added, as well as 10 mL thoroughly dried tetrahydrofuran. The Schlenck trap was fixed in a diagonal position so that the rubrene solution covered the metal mirror. After 2 d almost black crystals with a green luster grew from the dark-green colored solution. Crystal structure determination: Black blocks, $C_{42}H_{28}Na_4 \cdot 4\,C_4H_8O$ ($M_r = 1201.44$), $a = 1139.4(1)$, $b = 1295.8(1)$, $c = 1301.9(1)$ pm, $\alpha = 99.02(1)$, $\beta = 108.07(1)$, $\gamma = 109.31(1)°$, $V = 1650.9 \times 10^6$ pm^3 ($T = 150$ K), $\rho_{calcd} = 1.208$ g cm^{-3}, triclinic, $P\bar{1}$ (No. 2), $Z = 1$, Siemens P4 four-circle diffractometer, $Mo_{K\alpha}$ radiation, $\mu = 0.10$ mm^{-1}, 7233 registered reflections within $3° \le 2\theta \le 54°$, of which 6885 are independent and used for refinement ($R_{int} = 0.0241$). Structure solution by direct methods and difference Fourier technique (SHELXS-86), refinement versus F^2 (SHELXL-93), 436 parameters, $w = 1/[\sigma^2(F_o^2) + (0.0717\,P)^2 + 1.02\,P]$, R for 5066 $F_o > 4\,\sigma(F_o) = 0.0588$, wR_2 (for all 6885 data) = 0.1627, GOOF = 1.023, residual electron density 0.29/−0.26 e Å^{-3}. All positions C, O, and Na were refined anisotropically; all H were positioned in geometrically ideal sites and refined with individual isotropic displacement parameters ($[U_{iso} = 1.2 \times U_{eq}(CH/CH_2)]$; $[U_{iso} = 1.5 \times U_{eq}(CH_3)]$ within a riding model. Further details of the crystal structure determinations may be obtained from the Fachinformationszentrum Karlsruhe, D-76344 Eggenstein-Leopoldshafen (Germany), on quoting the depository number CSD-404813.

[8] H. Bock, C. Näther, Z. Havlas, A. John, C. Arad, *Angew. Chem.* **1993**, *105*, 931; *Angew. Chem. Int. Ed. Engl.* **1993**, *32*, 875.

[9] I. Bulgarovskaya, V. Vozzhennikov, S. Aleksandrov, V. Belsky, *Latv. PSR Zinat. Akad. Vestis Khim. Ser.* **1983**, *53*.

[10] Z. Havlas, S. Nick, H. Bock, *Int. J. Quantum Chem.* **1992**, *44*, 449; cf. also [*1–3*].

[11] H. Bock, T. Hauck, C. Näther, unpublished, cf. T. Hauck, Dissertation, Universität Frankfurt, **1995**.

Novel Neutral and Anionic Rhodium Complexes Containing Imido Ligands**

Cristina Tejel, You-Mao Shi, Miguel A. Ciriano*, Andrew J. Edwards, Fernando J. Lahoz, and Luis A. Oro*

The interest in the chemistry of transition metal imido complexes has grown substantially in recent years.[1] These compounds are believed to be intermediates in many important catalytic processes such as propene ammoxidation,[2] nitrile reduction,[3] imide group transfer,[4] and reduction and carbonylation of nitroarenes,[5] and they are models for the Haber ammonia synthesis. Whereas the majority of complexes with imido ligands contain early transition metals in high oxidation states, few imido complexes are known for the late transition metals in low oxidation states.[6] Dinuclear amido–imido tautomers, which are stabilized by dppm bridging ligands (dppm = methylenebis(diphenylphosphane)), are the only examples of such complexes with rhodium in a low oxidation state.[6a] We report here on the first neutral and anionic clusters of rhodium bridged by imido ligands. These novel compounds, which contain diene and carbonyl groups as ancillary ligands, possess new, interesting bonding and structural features.

Reactions of equimolar amounts of the complexes $[\{Rh(\mu\text{-}Cl)(diene)\}_2]$ with a solution of *para*-toluidine and butyllithium (in a 1:2 molar ratio) in diethyl ether at room temperature afforded complexes of the type $[Rh_4(\mu\text{-}N\text{-tolyl})_2(diene)_4]$ (diene = 1,5-cyclooctadiene (cod) (**1**), tetrafluorobenzobarrelene (tfb) (**2**)) as dark red crystalline solids in high yields. Characterization of the new complexes as imido clusters was based on spectroscopic data and an X-ray crystal structure analysis.[7] In the neutral tetranuclear complex **1** (Fig. 1) two *para*-tolylimido ligands cap either side of a trirhodium triangle through their nitrogen atoms, while the ring of the phenyl group of one of these ligands coordinates an isolated [Rh(cod)] fragment. Three remaining cyclooctadiene ligands are each bound to a rhodium atom of the trinuclear triangular core, which consists of two clearly bonded edges and one slightly longer, apparently nonbonded edge. Discounting the metal–metal interactions, each rhodium atom in the trimetallic core, is essentially square-planar coordinated. The molecular structure of **1** found in the crystal is also maintained in solution. The ^1H NMR spectra of **1** and **2** reveal the presence of two types of phenyl rings, each showing a well-defined A_2B_2 pattern, one of which, as a result of the π coordination to the fourth Rh atom, is shifted to higher field by approximately 1 ppm. Furthermore, signals for two types of diene ligands appear in the ratio 3:1, which are attributed to the ligands at the trimetallic core and to that bonded to the isolated rhodium atom, respectively. Complex **1** is the first example of an μ_3-imido rhodium system. Within **1**, the average Rh–N bond lengths differ significantly (0.04 Å) between the two face-capping ligands, unlike in comparable examples such as $[Os_3(NC_6H_5)_2(CO)_9]$,[8] where they are essentially equivalent. The η^5-cyclohexadienyl-like coordination of the imido ligand to the fourth rhodium atom follows from the deviation of the *ipso* carbon from the ring plane by 17.4(4)° and from the Rh–C_{ipso} distance which is 0.294 Å longer than the average Rh–C distance for this ligand. Associated with this peculiar η^5 coordination is a dramatic shortening of the C_{ipso}–N bond, indicative of clear partial C–N double bond character.[9] These data suggest a charge delocalization from the nitrogen atom into the ring. Furthermore, attempts to isolate pentanuclear complexes by coordination of mononuclear cationic species such as $[Rh(cod)S_x]BF_4$ (S = solvent) at the free phenyl group have proved unsuccessful, since **1** lacks coordination sites with sufficient electron density. However, the imido nitrogen atom still possesses nucleophilic character, since complexes **1** and **2** react slowly with methanol to give the known methoxo complexes $[\{Rh(\mu\text{-}OMe)(diene)\}_2]$ and *para*-toluidine.

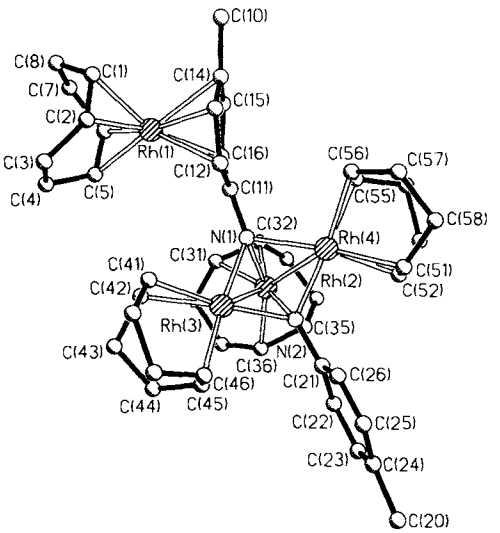

Fig. 1. Molecular structure of **1**. Selected interatomic distances [Å] and angles [°]: Rh(2)-Rh(3) 2.765(1), Rh(2)-Rh(4) 2.774(1), Rh(3)···Rh(4) 3.108(1), Rh(2)-N(1) 2.107(3), Rh(2)-N(2) 2.112(3), Rh(3)-N(1) 2.088(3), Rh(3)-N(2) 2.058(3), Rh(4)-N(1) 2.139(3), Rh(4)-N(2) 2.043(3), N(1)-C(11) 1.355(5), N(2)-C(21) 1.422(6), Rh(1)-C(12)/C(16) 2.224–2.375(5). Rh(1)···C(11) 2.576(11), Rh(3)-Rh(2)-Rh(4) 68.27(3), Rh(2)-Rh(3)-Rh(4) 56.00(2), Rh(2)-N(1)-Rh(3) 82.5(1), Rh(2)-N(1)-Rh(4) 81.6(1), Rh(3)-N(1)-Rh(4) 94.7(1), C(11)-N(1)-Rh(2) 138.2(3), C(11)-N(1)-Rh(3) 130.8(3), C(11)-N(1)-Rh(4) 114.1(3), Rh(2)-N(2)-Rh(3) 83.0(1), Rh(2)-N(2)-Rh(4) 83.8(1), Rh(3)-N(2)-Rh(4) 98.6(1), C(21)-N(2)-Rh(2) 138.1(3), C(21)-N(2)-Rh(3) 119.7(3), C(21)-N(2)-Rh(4) 122.2(3).

Complexes **1** and **2** can be considered, in a simplified way, to be related to the known species $[Rh(cod)BPh_4]$, where the trimetallic core takes the role of the BPh_4^- ion. However, in our case the η^5 coordination of the imido ligand seems to be nonlabile when compared with π-coordinated arene ligands in corresponding complexes of rhodium.[10] With this in mind, the preparation of μ_3-imido anionic complexes, for example $[Rh_3(\mu\text{-}N\text{-tolyl})_2(tfb)_3]^-$, requires the formation of very stable cations such as $[Rh(CN\mathit{t}Bu)_4]^+$. Thus, reaction of **2** with excess $CN\mathit{t}Bu$ leads to the rupture of the Rh-π-cyclohexadienyl interaction, yielding the anionic imidorhodium cluster $[Rh_3(\mu\text{-}N\text{-tolyl})_2(tfb)_3][Rh(CN\mathit{t}Bu)_4]$ **3** (Scheme 1). Complex **3** is isolated as a yellow crystalline solid in 75% yield and shows the expected spectroscopic features. Thus, the anion is detected in the negative ion FAB mass spectrum, and the *para*-tolylimido groups are equivalent in the ^1H and $^{13}C\{^1H\}$ NMR spectra (Table 1). Furthermore, the *ortho* carbon atoms give rise to quartets in the $^{13}C\{^1H\}$ NMR spectrum because of coupling with three equivalent Rh nuclei, while the *ipso* carbon atoms give a broad singlet. Complex **3** is the first characterized anionic imido complex of rhodium which, despite the low oxidation state of the

[*] Dr. M. A. Ciriano, Prof. L. A. Oro, Dr. C. Tejel, Dr. Y.-M. Shi, Dr. A. J. Edwards, Dr. F. J. Lahoz
Departamento de Química Inorgánica
Instituto de Ciencia de Materiales de Aragón
Universidad de Zaragoza-C.S.I.C., E-50009-Zaragoza (Spain)
Fax: Int. code + (76)761143

[**] We thank the Dirección General de Investigación Científica y Técnica (DGICYT) for financial support (Projects PB94-1186 and PB92-86-C2) and for a fellowship to Y.-M. S. (on leave from Dalian Institute of Chemical Physics, Chinese Academy of Sciences) and the European Community Human Capital and Mobility Program (CT93-0347) for a fellowship to A. J. E.

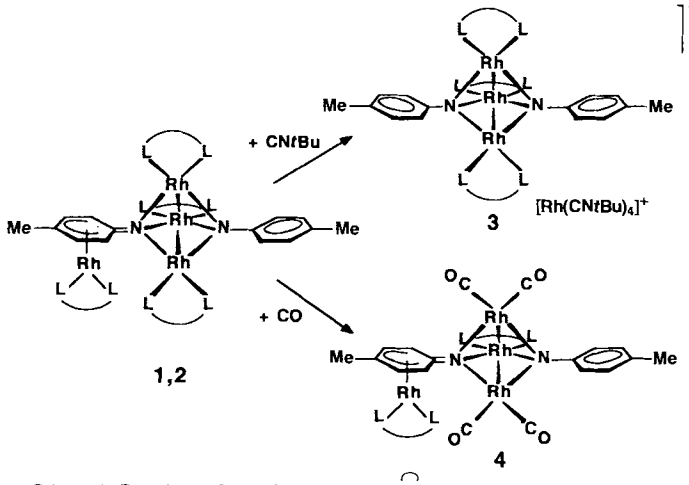

Scheme 1. Reactions of complexes **1** and **2**. L L = diene ligand: cod (**1**, **4**), tfb (**2**, **3**).

Table 1. Selected physical data of complexes **1**–**4** [a].

1: ^{1}H NMR (CD_2Cl_2, 298 K): δ = 6.61 (δ_A, 2H, Ph), 6.32 (δ_B, J_{AB} = 8.4 Hz, 2H, Ph), 5.60 (δ_A, 2H, Ph^a), 5.36 (δ_B, J_{AB} = 7.0 Hz, 2H, Ph^a), 4.18 (br. s, 4H, =CH^a), 3.54 (br. s, 12H, =CH), 2.44 (m, 12H, CH_2), 2.33 (m, 4H, CH_2^a), 2.17 (s, 3H, Me), 2.08 (s, 3H, Me^a), 2.01 (d, 8.24, 4H, CH_2^a), 1.84 (d, 7.69, 12H, CH_2); ^{13}C{^{1}H} NMR (CD_2Cl_2, 298 K): δ = 166.7 (br. s, *ipso*-C, Ph), 161.5 (br. s, *ipso*-C, Ph^a), 130.0 (C4, Ph), 126.8 (C3, Ph), 125.2 (q, J(Rh,C) = 1 Hz, C2, Ph), 107.5 (d, J(Rh,C) = 2 Hz, C4, Ph^a), 101.7 (d, J(Rh,C) = 3 Hz, C3, Ph^a), 94.0 (m, C2, Ph^a), 77.0 (d, J(Rh,C) = 13 Hz, =CH), 73.4 (br. s, =CH^a), 31.9 (CH_2), 31.1 (CH_2^a), 20.4 (Me), 18.6 (Me^a); MS (FAB$^+$): *m/z* (%): 1054 (M^+, 5), 843 (M^+ − Rh(cod), 48)

2: ^{1}H NMR (CD_2Cl_2, 298 K): δ = 6.46 (δ_A, 2H, Ph), 5.96 (δ_A, 2H, Ph^a), 5.82 (δ_B, J_{AB} = 8.20 Hz, 2H, Ph), 5.34 (δ_B, J_{AB} = 7.1 Hz, 2H, Ph^a), 5.53 (br. s, 6H, HC), 5.04 (br. s, 2H, HC^a), 3.62 (br. s, 4H, =CH^a), 3.19 (br. s, 6H, =CH), 3.06 (br. s, 6H, =CH), 1.97 (s, 3H, Me), 1.91 (s, 3H, Me^a); ^{19}F NMR (CD_2Cl_2, 298 K): δ = −146.6 (m, 2F^a), −148.9 (m, 6F), −158.7 (m, 2F^a), −162.1 (m, 6F); MS (FAB$^+$): *m/z* (%): 1526 (M^+, 10), 1197 (M^+ − Rh(tfb), 30)

3: IR (Nujol): $\tilde{\nu}$ = 2156 (s) cm^{-1} (CN); ^{1}H NMR (CD_2Cl_2, 298 K): δ = 6.43 (δ_A, 4H, Ph), 6.05 (δ_B, J_{AB} = 8.2 Hz, 4H, Ph), 5.42 (br. s, 6H, HC), 2.95 (br. s, 12H, =CH), 1.98 (s, 6H, Me), 1.53 (t, 36H, CN*t*Bu); ^{19}F NMR (CD_2Cl_2, 298 K): δ = −150.2 (m, 6F), −164.1 (m, 6F); ^{13}C{^{1}H}-NMR (CD_2Cl_2, 298 K): δ = 163.7 (br. s, *ipso*-C, Ph), 140.2 (C4, Ph), 137.5 (m, tfb), 130.5 (m, tfb) 129.0 (m, tfb), 126.9 (C3, Ph), 121.5 (q, ^3J(Rh,C) = 1 Hz, C2, Ph), 45.2 (d, J(Rh,C) = 10 Hz, =CH, tfb), 39.9 (CH, tfb), 30.5 (CN*t*Bu), 20.4 (Me); MS (FAB$^-$): *m/z* (%): 1197 (anion of **3**, 78); MS (FAB$^+$): *m/z* (%): 435 (cation of **3**, 100); Λ_m (aceton) = 61.8 S cm^2 mol^{-1}

4: IR (CH_2Cl_2): $\tilde{\nu}$ = 2035 (m, CO), 2016 (s, CO), 1960 (s) cm^{-1} (CO). ^{1}H NMR ($CDCl_3$, 298 K): δ = 7.03 (δ_A, 2H, Ph), 6.79 (δ_B, J_{AB} = 8.3 Hz, 2H, Ph), 6.16 (δ_A, 2H, Ph^a), 6.01 (δ_B, J_{AB} = 7.1 Hz, 2H, Ph^a), 4.25 (m, 4H, =CH^a), 2.92 (m, 2H, =CH), 2.66 (m, 2H, =CH), 2.40 (m, 4H, H_2C), 2.24 (m, 4H, H_2C), 2.17 (s, 3H, Me), 2.07 (s, 3H, Me^a), 2.06 (m, 4H, H_2C), 1.66 (m, 4H, H_2C); ^{13}C{^{1}H} NMR (CD_2Cl_2, 298 K): δ = 191.3 (d, J(Rh,C) = 65 Hz, CO), 191.2 (d, J(Rh,C) = 71 Hz, CO), 160.9 (br. s, *ipso*-C, Ph), 155.0 (br. s, *ipso*-C, Ph^a), 130.3 (C4, Ph), 127.6 (C3, Ph), 124.7 (q, ^3J(Rh,C) = 1 Hz, C2, Ph), 108.7 (d, J(Rh,C) = 3 Hz, C4, Ph^a), 103.5 (d, J(Rh,C) = 3 Hz, C3, Ph^a), 99.0 (dq, ^1J(Rh,C) = 3, ^3J(Rh,C) = 1 Hz, C2, Ph^a), 80.7 (d, J(Rh,C) = 13 Hz, =CH^a), 76.9 (d, J(Rh,C) = 14 Hz, =CH), 75.5 (d, J(Rh,C) = 12 Hz, =CH), 31.9 (H_2C^a), 31.2 (H_2C), 31.0 (H_2C), 20.4 (Me), 18.4 (Me^a); MS (FAB$^+$): *m/z* (%): 950 (M^+, 87), 922 (M^+ − CO, 66), 894 (M^+ − 2CO, 17), 866 (M^+ − 3CO, 20), 838 (M^+ − 4CO, 70)

[a] The new compounds give satisfactory C,H,N, elemental analyses; the superscript a denotes the η^5-(μ-N-*p*-tolyl)Th(diene) fragment; H,H-COSY experiments, and high-resolution processing of the ^{13}C{^{1}H} NMR spectra were used for accurate assignments.

metals and the high electronic density (hard-base character) of the imido ligand, is surprisingly stable. Substitution of the ancillary ligands in the periphery of the trinuclear core of **1** by carbon monoxide reveals the inequivalence of the metals within this triad. Thus, reaction of **1** with carbon monoxide at room temperature leads to [Rh_4(μ-N-tolyl)$_2$(CO)$_4$(cod)$_2$] (**4**) (Scheme 1), which is isolated in 90% yield as a yellow microcrystalline solid. Further studies on the reactivity of the electron-rich complexes **3** and **4** are in progress.

In conclusion, neutral and anionic imidorhodium(I) clusters are feasible and stable and could possibly be intermediates in the catalytic reduction and carbonylation of nitroarenes by Rh complexes.

Experimental Procedure

General synthesis of **1** and **2**: Solid [{Rh(μ-Cl)(diene)}$_2$] (0.5 mmol) was added to a solution of *para*-toluidine (0.5 mmol) and butyllithium (1.0 mmol) in diethyl ether at room temperature to give a dark red solid. Further extraction with dichloromethane and work up yielded the complexes **1** and **2** as crystalline solids.

Received: September 15, 1995
Revised version: December 11, 1995 [Z 8404 IE]
German version: *Angew. Chem.* **1996**, *108*, 707–709

Keywords: arene complexes · clusters · complexes with nitrogen ligands · rhodium compounds

[1] D. E. Wigley, *Prog. Inorg. Chem.* **1994**, *42*, 239, and references therein; W. A. Nugent, J. M. Mayer, *Metal-Ligand Multiple Bonds*, Wiley, New York, **1988**.
[2] E. A. Maatta, Y. J. Du, *J. Am. Chem. Soc.* **1988**, *110*, 8249, and references therein.
[3] a) M. Bakir, P. E. Fanwick, R. A. Walton, *Inorg. Chem.* **1988**, *27*, 2016; b) S. H. Han, G. L. Geoffroy, *Polyhedron* **1988**, *7*, 2331.
[4] a) P. J. Walsh, A. M. Baranger, R. G. Bergman, *J. Am. Chem. Soc.* **1992**, *114*, 1708; b) D. A. Evans, M. M. Faul, M. T. Bilodeau, *J. Org. Chem.* **1991**, *56*, 6744.
[5] a) F. Ragaini, S. Cenini, F. Demartin, *Organometallics* **1994**, *13*, 1178; b) J. D. Gargulak, W. L. Gladfelter, *J. Am. Chem. Soc.* **1994**, *116*, 3792.
[6] a) Rhodium complexes: Y.-W. Ge, F. Peng, P. R. Sharp, *J. Am. Chem. Soc.* **1990**, *112*, 2632; b) iridium complexes: C. Ye, P. R. Sharp, *Inorg. Chem.* **1995**, *34*, 55; D. A. Dobbs, R. G. Bergman, *Organometallics* **1994**, *13*, 4594; M. K. Kolel-Veetil, K. J. Ahmed, *Inorg. Chem.* **1994**, *33*, 4945, and references therein; c) recent ruthenium and osmium compounds: A. K. Burrel, A. J. Steedman, *J. Chem. Soc. Chem. Commun.* **1995**, 2109; D. L. Ramage, G. L. Geoffroy, A. L. Rheingold, B. S. Haggerty, *Organometallics* **1992**, *11*, 1242.
[7] Crystal data for **1**: $C_{46}H_{62}N_2Rh_4 \cdot C_4H_8O$, M_r = 1126.74, monoclinic, space group $P2_1/n$ (No. 14), a = 17.912(4), b = 12.419(2), c = 20.649(4) Å, β = 105.41(3)°, V = 4428(2) Å^3, Z = 4, ρ_{calcd} = 1.690 g cm^{-3}, F(000) = 2288, λ = 0.71073 Å, T = 173.0(2) K, μ($Mo_{K\alpha}$) = 1.504 mm^{-1}. Data were collected on a Stoe AED diffractometer by using an oil-coated rapidly cooled crystal of dimensions 0.29 × 0.23 × 0.18 mm mounted directly from solution (T. Kottke, D. Stalke, *J. Appl. Crystallogr.* **1993**, *26*, 615). A total of 5665 unique reflections were collected by the $2\theta/\omega$ method ($3.5 \le 2\theta \le 45.0$). The structure was solved by direct methods (SHELXTL PLUS, G. M. Sheldrick, Siemens Analytical X-ray Instruments, Inc., Madison, WI **1990**) and refined by full-matrix least-squares on F^2 (SHELXL-93; G. M. Sheldrick, Göttingen, 1993) to R_1 = 0.0264 [$F > 4\sigma(F)$, for 4830 reflections] and R_2 = 0.0716 (all data) [$R_1 = \sum||F_o| - |F_c||/\sum|F_o|$, $R_2 = \{\sum w(F_o^2 - F_c^2)^2/\sum wF_o^4\}^{1/2}$, $w = 1/[\sigma^2(F_o^2) + (xP)^2 + yP]$($x$ = 0.0358, y = 8.1612), $P = (F_o^2 + 2F_c^2)/3$]. A THF molecule was located and found to be disordered over two sites, these were modelled at 50% occupancy. All non-hydrogen atoms were refined anisotropically, with the exception of disordered oxygen and carbon atoms in the THF solvate molecule. All hydrogen atoms riding on sp^2 carbon atoms were located and allowed to freely refine isotropically, the remaining hydrogen atoms were fixed in idealized positions with thermal parameters (1.2 times that of the corresponding parent carbon atom). Largest peak and hole in the final difference map 0.528 and −0.362 e Å^{-3}. Further details of the crystal structure investigation are available on request from the Director of the Cambridge Crystallographic Data Centre, 12 Union Road, GB-Cambridge, CB21EZ (UK), on quoting the full journal citation.
[8] J. A. Smieja, W. L. Gladfelter, *Inorg. Chem.* **1986**, *25*, 2667.
[9] R. Usón, L. A. Oro, D. Carmona, M. A. Esteruelas, C. Foces-Foces, F. H. Cano, S. García-Blanco, A. Vázquez de Miguel, *J. Organomet. Chem.* **1984**, *273*, 111.
[10] M. Aresta, E. Quaranta, A. Albinati, *Organometallics* **1993**, *12*, 2039; R. Usón, L. A. Oro, C. Foces-Foces, F. H. Cano, S. García-Blanco, M. Valderrama, *J. Organomet. Chem.* **1982**, *229*, 293.

Double Oxygen Atom Centered Rhodium–Gold Clusters**

Hui Shan and Paul R. Sharp*

Main group atom centered gold clusters such as $[(Ph_3PAu)_nC]^{(n-4)+}$ ($n = 5$, 6), $[(Ph_3PAu)_5N]^{2+}$, and $[(Ph_3PAu)_4S]^{2+}$ are remarkable because of their unexpected stability and the "hypercoordinate" nature of the central atom.[1] A major contributory factor to the stability of these clusters is the bonding interaction between the gold(I) atoms of the clusters ("aurophilicity"[2]). Here we describe the synthesis and characterization of related clusters which are stabilized by Au–Rh interactions as well Au–Au interactions. In addition, these new clusters contain not one main group atom center but two and show oxygen in an unusual trigonal pyramidal geometry.

In previous work we observed that oxo/halide exchange occurred between the gold oxo complexes $[(LAu)_3(\mu\text{-O})]BF_4$ and the gold halide complexes L'AuCl [Eq. (a), L and L' = phosphane].[3] We have discovered that this type of exchange

$$[(LAu)_3(\mu\text{-O})]BF_4 + L'AuCl \rightleftharpoons [(L'Au)(LAu)_2(\mu\text{-O})]BF_4 + LAuCl \quad (a)$$

reaction also occurs for other metal halide systems. Thus, the reactions of $[\{Rh(diene)(\mu\text{-Cl})\}_2]$ (diene = 1,5-cyclooctadiene (cod), norbornadiene (nbd)) with two equivalents of $[(Ph_3PAu)_3(\mu\text{-O})]BF_4$ give the orange-yellow to yellow products **1** [Eq. (b), diene = cod, nbd].

$$[\{Rh(dien)(\mu\text{-Cl})\}_2] + 2[(Ph_3PAu)_3(\mu\text{-O})]BF_4 \longrightarrow [\{(dien)Rh[(\mu\text{-O}(AuPPh_3)_2]\}_2][BF_4]_2 + 2\,Ph_3PAuCl \quad (b)$$

^{1}H NMR spectra for **1** show resonances for a single type of diene and PPh_3 ligand. ^{31}P NMR spectra show a single sharp resonance at $\delta = 25$ very near the position found for the parent complex $[(Ph_3PAu)_3(\mu\text{-O})]BF_4$ ($\delta = 27$).[4] This data and the formula for **1** suggested a highly symmetric structure with four-coordinate oxygen atoms in an approximately tetrahedral geometry. The X-ray structure analysis of **1**, diene = nbd, revealed a surprising result:[5] the dication (Fig. 1) consists of a planar $[(nbd)Rh(\mu\text{-O})_2Rh(nbd)]^{2-}$ array in which two Ph_3PAu^+ groups are coordinated to each oxygen atom. One of the Ph_3PAu^+ groups (Au1) is in the $[(nbd)Rh(\mu\text{-O})_2Rh(nbd)]^{2-}$ plane, while the other (Au2) is orthogonal to the plane. This results in a trigonal pyramidal coordination geometry for the oxygen atoms.[6] An examination of the metal–metal distances suggests the reason for this unusual geometry. The out-of-plane, axial, gold atom (Au2) bonds with the in-plane gold atom (Au1) and with the two rhodium atoms (Fig. 1). The Au–Au distance of 3.008 Å is typical of Au–Au distances observed in all-gold main group atom centered clusters and in other gold compounds where "aurophilic" interactions occur.[1, 2] The Rh–Au distances (3.020 and 2.984 Å) are similar to those observed in

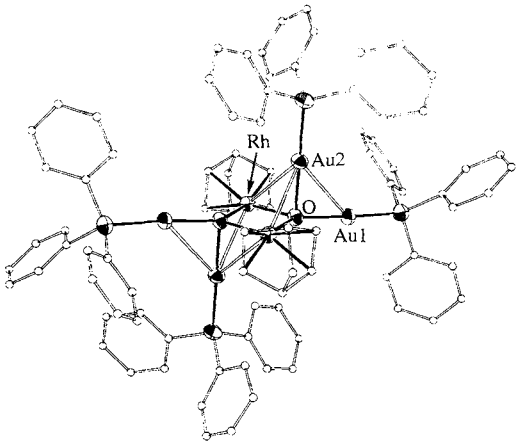

Fig. 1. Crystal structure of the dication of **1**, diene = nbd; ORTEP drawing (50% ellipsoids for non-carbon atoms, hydrogen atoms excluded). The dication is located on a center of symmetry.

compounds where long Au–M (M = Rh, Ir, Pt) bonds are found.[7] The metal–metal interactions in **1** appear to be responsible for the unusual oxygen coordination geometry and indicate a close relationship to the main group atom centered clusters of gold. Complex **1** is the first heteronuclear cluster of this type containing a central oxygen atom[8] and the first to involve two main group atom centers. Finally, **1** should be compared to the recently reported cluster $[(LAu)_4O]^{2+}$ (L = $(2\text{-}CH_3C_6H_4)_3P$).[9] In this all-gold oxygen-centered cluster, the oxygen atom is in a more common tetrahedral environment and although Au···Au interactions are present they are longer (3.359 Å) than those in **1** as required for the more symmetric distribution of the metal atoms.

In conclusion, **1** is a novel double oxygen atom centered cluster in which the unusual trigonal pyramidal oxygen coordination geometry is maintained by Au–Au and Au–Rh bonds. Other examples of unusual main group atom centered clusters containing gold and other transition metals may be expected by exchange reactions similar to that in Equation (b).

Experimental Procedure

1, (diene = 1,5-cod): A solution of $[\{Rh(cod)(\mu\text{-Cl})\}_2]$ (40.2 mg, 0.0815 mmol) in THF (10 mL) was vigorously stirred with solid $[(Ph_3PAu)_3(\mu\text{-O})]BF_4$ (241 mg, 0.0163 mmol). The mixture became an almost clear red-orange solution within 5 minutes and meanwhile an orange-yellow solid gradually precipitated. After the mixture had been stirred for 15 minutes, the orange-yellow product was isolated by filtration, washed with THF and then ether, and dried in vacuo. Yield: 190 mg (94.9%). Elemental analysis: calcd (found): C 42.88 (42.72), H 3.43 (3.36); ^{1}H NMR (300 MHz, $CDCl_3$, 22 °C): δ = 7.34–7.59 (m, 30H, Ph), 3.93 (br, 4H, CH), 2.08 (br, 4H, CH_2), 1.65 (d, t, 4H, CH_2, J(H,H) = 8.4 Hz, J'(H,H) = 5.5 Hz); ^{31}P NMR (121.2 MHz, CH_2Cl_2, 22 °C, ext H_3PO_4 ref): δ = 25; IR (thin film on NaCl plate): ν = 3075–2829 (m, CH), 1482, 1437 (m, C=C), 1104 (s), 1060 cm^{-1} (br, s, B-F).

1, (diene = nbd): A solution of $[\{Rh(nbd)(\mu\text{-Cl})\}_2]$ (46.1 mg, 0.100 mmol) in THF (10 mL) was vigorously stirred with solid $[(Ph_3PAu)_3(\mu\text{-O})]BF_4$ (296 mg, 0.200 mmol). The mixture became an almost clear orange solution within 5 minutes and meanwhile a yellow solid gradually precipitated. After the mixture had been stirred for 15 minutes, the yellow product was isolated by filtration, washed with THF and then ether, and dried in vacuo. Yield: 230 mg (94.5%). Elemental analysis: calcd (found): C 42.46 (41.50), H 3.15 (2.98); ^{1}H NMR (250 MHz, $CDCl_3$, 22 °C): δ = 7.36–7.59 (m, 30H, Ph), 3.75 (m, 4H, CH), 3.66 (br, 2H, CH), 1.12 (br, 2H, CH_2); ^{31}P NMR (101.3 MHz, CH_2Cl_2, 22 °C, ext H_3PO_4 ref): δ = 25. IR (thin film on NaCl plate): ν = 3060–2860 (m, CH), 1480, 1438 (m, C=C), 1104 (m), 1063 cm^{-1} (br, s, B-F).

Received: October 11, 1995 [Z8464IE]
German version: *Angew. Chem.* **1996**, *108*, 716–717

Keywords: aurophilicity · clusters · gold compounds · rhodium compounds

[*] Prof. P. R. Sharp, H. Shan
Department of Chemistry
University of Missouri
Columbia, MO 65211 (USA)
e-mail: chemprs@showme.missouri.edu

[**] Late Transition Metal Oxo and Imido Complexes, Part 17. This work is supported by the Division of Chemical Sciences, Office of Basic Energy Sciences, Office of Energy Research, U. S. Department of Energy (DE-FG02-88ER13880). Grants from the National Science Foundation provided a portion of the funds for the purchase of the X-ray (CHE-9011804) and NMR (grant no. 8908304 and 9221835) equipment. We thank Johnson Matthey for loans of precious metal salts. Part 16: J. J. Li, W. Li, P. R. Sharp, *Inorg. Chem.* **1996**, *35*, 604.

 © VCH Verlagsgesellschaft mbH, D-69451 Weinheim, 1996 0570-0833/96/3506-0635 $ 15.00+.25/0

[1] F. Scherbaum, A. Grohmann, B. Huber, C. Kruger, H. Schmidbaur, *Angew. Chem.* **1988**, *100*, 1602; *Angew. Chem. Int. Ed. Engl.* **1988**, *27*, 1544; F. Scherbaum, A. Grohmann, G. Müller, H. Schmidbaur, *ibid.* **1989**, *101*, 464 and **1989**, *28*, 463; E. Zeller, H. Beruda, A. Kolb, P. Bissinger, J. Riede, H. Schmidbaur, *Nature (London)* **1991**, *352*, 141; F. Canales, M. C. Gimeno, P. G. Jones, A. Laguna, *Angew. Chem.* **1994**, *106*, 811; *Angew. Chem. Int. Ed. Engl.* **1994**, *33*, 769.

[2] H. Schmidbaur, *Gold Bull.* **1990**, *32*, 11–21.

[3] Y. Yang, P. R. Sharp, *Inorg. Chem.* **1993**, *32*, 1946–1951.

[4] A. N. Nesmeyanov, E. G. Perevalova, Y. T. Struchkov, M. Y. Antipin, K. I. Grandberg, V. P. Dyadchenko, *J. Organomet. Chem.* **1980**, *201*, 343–349.

[5] Crystal data for **1**·2THF at 22 °C: Crystals from THF, 0.33 × 0.13 × 0.05 mm, triclinic, $P\bar{1}$, $a = 11.430(3)$, $b = 11.985(4)$, $c = 17.712(6)$ Å, $\alpha = 79.43(2)$, $\beta = 83.46(2)$, $\gamma = 73.62(2)°$, $V = 2283(1)$ Å^3, $Z = 1$, $\rho_{calcd} = 1.87$ g cm^{-3}, $\mu = 7.23$ mm^{-1}, Enraf-Nonius CAD-4 diffractometer, θ-2θ scans ($2\theta < 46°$, 6579 reflections measured, 6337 independent), graphite monochromated $Mo_{K\alpha}$ radiation ($\lambda = 0.70930$ Å). NRCVAX programs were used for all calculations: E. J. Gabe, Y. Le Page, J.-P. Charland, F. L. Lee, P. S. White, *J. Appl. Cryst.* **1989**, *22*, 384–387. Data were corrected for absorption (empirical method, trans. range: 62.7–100%). The structure was solved by direct methods. Least squares refinement based on F_0 with riding hydrogen atoms and all non-hydrogen and non-solvent atoms anisotropic converged to $R = 0.037$ and $R_w = 0.044$ with 4572 reflections ($I > 2.5\sigma I$) and 473 parameters. The top four residual peaks (1.50 to 0.94 e Å^{-3}) were found in the region of the BF_4 ion. Selected distances and angles (atoms labeled with an "a" are inversion related): Au1–Au2 3.008(1), Au2–Rh 3.020(1), Au2–Rh_a 2.984(1), Au1–O 2.026(7), Au2–O 2.083(7), Rh–O 2.118(7), Rh–O_a 2.095(7); Au1-Au2-Rh 72.88(3), Au1-Au2-Rh_a 80.04(3), Rh-Au2-Rh_a 65.74(3), Au2-Rh-$Au2_a$ 114.26(4), O-Rh-O_a 78.6(3), Au1-O-Au2 94.1(3), Au1-O-Rh 119.6(3), Au1-O-Rh_a 138.5(4), Au2-O-Rh 91.9(3), Au2-O-Rh_a 91.1(3), Rh-O-Rh_a 101.4(3). Further details of the crystal structure investigation may be obtained from the Director of the Cambridge Crystallographic Data Centre, 12 Union Road, GB-Cambridge, CB2 1EZ (UK), by quoting the full literature citation.

[6] $[Cu_{10}O_2(Mes)_6]$ (Mes = mesityl) is the only other complex we have found with a trigonal pyramidal oxygen atom coordination geometry: M. Hakansson, M. Ortendahl, S. Jagner, M. P. Sigalas, O. Eisenstein, *Inorg. Chem.* **1993**, *32*, 2018–2024.

[7] Hon-Kay Yip, Hsui-Mei Lin, Yu Wang, Chi-Ming Che, *J. Chem. Soc. Dalton Trans.* **1993**, 2939; C. E. Briant, D. I. Gilmour, D. M. P. Mingos, *ibid.* **1986**, 835; A. L. Balch, J. K. Nagle, D. E. Oram, P. E. Reedy Jr. *J. Am. Chem. Soc.* **1988**, *110*, 454; A. L. Balch, V. J. Catalano, M. M. Olmstead, *ibid.* **1990**, *112*, 2010; J. C. Jeffery, P. A. Jelliss, F. G. A. Stone, *Inorg. Chem.* **1993**, *32*, 3943; A. L. Balch, B. J. Davis, M. M. Olmstead, *ibid.* **1989**, *28*, 3148; A. L. Balch, V. J. Catalano, M. M. Olmstead, *ibid.* **1990**, *29*, 585; A. L. Balch, E. Y. Fung, M. M. Olmstead, *ibid.* **1990**, *29*, 3203.

[8] Heteronuclear boron- and carbon-centered gold clusters are known. For examples see: A. G. Cowie, B. F. G. Johnson, J. Lewis, P. R. Raithby, *J. Chem. Soc. Chem. Commun.* **1984**, 1710; K. S. Harpp, C. E. Housecroft, A. L. Rheingold, M. S. J. Shongwe, *ibid.* **1988**, 965; C. E. Housecroft, A. L. Rheingold, *Organometallics*, **1987**, *6*, 1332; C. E. Housecroft, M. S. J. Shongwe, A. L. Rheingold, *ibid.* **1989**, *8*, 2651; A. K. Chipperfield, C. E. Housecroft, A. L. Rheingold, *ibid.* **1990**, *9*, 681; S. M. Draper, C. E. Housecroft, A. L. Rheingold, *J. Organomet. Chem.* **1992**, *435*, 9.

[9] H. Schmidbaur, S. Hofreiter, M. Paul, *Nature (London)* **1995**, *377*, 503.

Hexalithiated Hexakis(cyclohexylamino)-cyclotriphosphazene; a $(Li^+)_{12}$ Cage Containing Puckered $[NP(NCy)_2]_3^{6-}$ Ions**

Alexander Steiner* and Dominic S. Wright

Highly charged anionic systems are well known in inorganic solid-state chemistry. The extensive class of silicates contains a variety of anionic host lattices from mononuclear $[SiO_4]^{4-}$ units to polymeric networks.[1] Recently a number of isoelectric lithium phosphorus nitrides have been described.[2] Further examples are anionic main group element clusters in Zintl phases.[3] In contrast, highly charged anions have rarely been investigated in molecular species. Compared with dimetalated organic compounds far less is known about coordination compounds containing triply or more highly charged anions.[4, 5] A structurally characterized example of the latter is the tetralithiated dibenzyl(methyl)phosphane, which exists as a TMEDA-solvated (TMEDA = *N*,*N*,*N*′,*N*′-tetramethylethylenediamine) dimer in the solid state.[4] Metalated organonitrogen species up to trianions are widely used as shielding ligands towards metal centers.[6] However, metal complexes containing more highly charged organonitrogen anions, to our knowledge, have not been structurally characterized to date.

A large number of organometallic phosphazene compounds[7] and metallophosphazenes[8] have been described, owing to the high stability of their partially delocalized P–N skeletons.[9] As a precursor for producing a highly charged organonitrogen ligand system, we chose hexakis(cyclohexylamino)triphosphazene $[NP(NHCy)_2]_3$ (Cy = cyclohexyl), which contains six potentially acidic N–H functions. The deprotonation of $[NP(NHCy)_2]_3$ with *n*BuLi (molar ratio 1:6) in the presence of TMEDA in toluene yields **1**. Crystals of **1** proved unsuitable for X-ray structure analysis; however, crystallization of **1** from THF/hexane afforded X-ray quality crystals of **2** (see also Experimental Procedure).

$[\{NP(NLiCy)_2\}_3(tmeda)_3]$ **1**

$[\{[NP(NLiCy)_2]_3(thf)_2\}_2] \cdot 2.5\,THF$ **2**

A low-temperature X-ray study[10] of **2** shows it to have a centrosymmetric dimeric cage structure, in which twelve Li cations are complexed by two chair-shaped $[NP(NCy)_2]_3^{6-}$ ions and by four thf donor molecules (Fig. 1). The central core of the molecule is that of an approximately D_{3d}-symmetric polyhedron, formed by the interaction of the ring-N and equatorially substituted NCy groups of the two $[NP(NCy)_2]_3^{6-}$ ions with six Li centers. Each metal center is coordinated by a bidentate

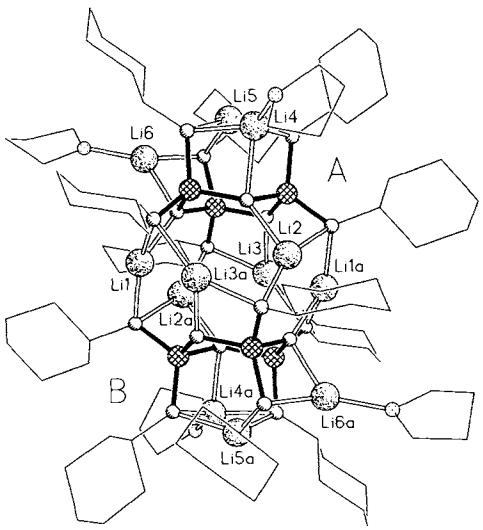

Fig. 1. Crystal structure of **2**. Hydrogen atoms have been omitted for clarity. Selected bond lengths [Å] and angles [°] (average): P–N(Ring) 1.66, P–N(eq) 1.63, P–N(ax) 1.64, Li(1,2,3)–N(ringA) 2.01, Li(1,2,3)–N(eqA) 2.02, Li(1,2,3)–N(eqB) 2.01, Li(4)–N(ax) 2.04, Li(4)–N(ring) 2.12, Li(4)–O(thf) 1.94, Li(5)–N(ax) 2.05, Li(6)–N(ring) 2.04, Li(6)–N(ax) 1.96, Li(6)–O(thf) 1.90; N(ring)–P–N(ring) 110, N(eq)–P–N(ax) 118, N(ring)–P–N(eq) 106, N(ring)–P–N(ax) 108, P–N(ring)–P 120.

[*] Dr. A. Steiner, Dr. D. S. Wright
University Chemical Laboratory
Lensfield Road, GB-Cambridge CB2 1EW (UK)
Fax: Int. code +(1223)/336-362

[**] We thank the European Union (fellowship for A. S.), the Engineering and Physical Sciences Research Council (D. S. W.), the Royal Society (D. S. W.) and the Nuffield Foundation (D. S. W.). Cy = cyclohexyl.

N(ring)–P–N(eq)-chelate system [N(ring)–Li 1.971(8)–2.054(8), N(eq)–Li 1.979(8)–2.067(8) Å] from one anion and by a further N(eq) interaction [N(eq)–Li 1.973(8)–2.070(9) Å] from the other anion. The remaining lithium cations are accommodated at the other P_3N_3 faces of each of the hexaanions. While Li5 is coordinated in a tridentate manner by all three axial NCy groups [N(ax)–Li5 2.028(8)–2.076(8) Å], Li6 is tricoordinated by a N(ax)–P–N(ring) chelate system [N(ax)–Li6 1.957(8), N(ring)–Li6 2.038(8) Å] and by a thf donor molecule [O2–Li6 1.904(8) Å]. Li4 is the only tetracoordinate metal center in **2**; it is coordinated by two axial nitrogen atoms [N(ax)–Li4 2.027(8)–2.044(9) Å], one ring nitrogen atom [N(ring)–Li4 2.124(8) Å], and by a further thf molecule [O1–Li4 1.936(8) Å]. All N–Li distances in **2** are similar to those found in other lithiated phosphazenes.[11]

In addition to the electrostatic stabilization of each hexaanion in **2** by tight ion-pairing with nine Li counterions, delocalization of the negative charge from the substituent nitrogen on to the ring nitrogen centers can be assumed. The central phosphazene ring shows marked distortion from planarity into a chair conformation and all P–N distances throughout the whole anion are in the same range [P–N(ring) 1.651(3)–1.674(3), P–N(eq) 1.624(4)–1.637(4), P–N(ax) 1.638(3)–1.652(3) Å]. In contrast, cyclotriphosphazene skeletons of neutral hexaamino-substituted derivatives are planar or only slightly chair-shaped and their P–N(ring) distances are about 0.06 Å shorter than their terminal P–N distances.[12] While the terminal N–P–N angles in the neutral species are far more acute than their ring N–P–N angles, the N(eq)–P–N(ax) angles [116.9(2)–119.7(2)°] in **2** are significantly wider than the N–P–N ring angles [108.2(2)–111.1(2)°].

In the IR spectrum of **1** the phosphazene P=N–P stretching band (1016 cm^{-1}) shows a strong red shift in the hexaanion compared to neutral hexaaminocyclotriphosphazenes (typical stretching frequencies 1170–1195 cm^{-1}).[8] This shift is greater than that in lithium complexes with uncharged N-phosphazene ligands[13] and indicates weakening of the P–N(ring) bonds in **1**, while the terminal P–N bonds are strengthened as a result of the electron excess. The change in charge distribution upon lithiation is also indicated by the high-field shift of the ^{31}P NMR resonance of **1** ($\delta = -55.0$ in **1**; cf. $-50 < \delta < +50$ in cyclic phosphazenes and metallophosphazenes relative to 85% H_3PO_4[8, 9]).

The hexalithiated hexaaminophosphazene **2** is a molecular analogue of lithium phosphorus nitrides, which exist as polymeric ionic lattice compounds.[2] However, in contrast to the latter the high solubility of **2** in aprotic solvents promises an extensive chemistry of this highly charged anionic system in solution. Transmetalation reactions of **2** with main group metal and transition metal halides looks promising and may lead to a large number of interesting multinuclear metal complexes.

Experimental Procedure

All experiments were carried out under a dry argon atmosphere by using Schlenk techniques and a glove box. Solvents were dried over Na/benzophenone and distilled prior to use. $[NP(NCy)_2]_3$ was prepared as described in the literature [14].

1: *n*BuLi (9 mL, 13.5 mmol, 1.5 M solution in hexane) was added at 0 °C over 15 min to a solution of $[NP(NCy)_2]_3$ (1.4 g, 1.93 mmol) in TMEDA (1.5 mL) and toluene (15 mL). The resulting orange solution was stirred for 2 h at room temperature. During this time a yellow precipitate was formed. This was separated by filtration, and the solid washed twice with hexane (10 mL). Yield: 1.6 g (75%). Decomp. >250 °C; IR (Nujol): ν [cm^{-1}] = 1586, 1290, 1253, 1154, 1136, 1016, 908, 841, 791, 729; ^1H NMR (25 °C, [D$_8$]THF): δ = 3.01 (m, CH, 6 H), 2.25 (s, N–CH_2, 12 H), 2.11 (s, N CH_3, 36 H), 1.0–1.7 (m, CH_2, 60 H); ^{31}P NMR (25 °C, [D$_8$]THF, relative to 85% H_3PO_4): $\delta = -55.0$.

2: When **1** was stored for three weeks at 3 °C in THF/hexane single crystals of **2** suitable for X-ray structure analysis were obtained in low yield.

Received: October 4, 1995 [Z 8446IE]
German version: *Angew. Chem.* **1996**, *108*, 712–714

Keywords: lithium compounds · nitrogen compounds · phosphazenes · polycycles

[1] F. Liebau, *Structural Chemistry of Silicates*, Springer, Berlin, **1985**.
[2] W. Schnick, *Angew. Chem.* **1993**, *105*, 846; *Angew. Chem. Int. Ed. Engl.* **1993**, *32*, 806.
[3] a) H. G. von Schnering, *Angew. Chem.* **1981**, *93*, 44; *Angew. Chem. Int. Ed. Engl.* **1981**, *20*, 33; b) J. D. Corbett, *Chem. Rev.* **1985**, *85*, 383.
[4] M. A. Beswick, D. S. Wright, *Comprehensive Organometallic Chemistry II, Vol. I*, Pergamon, Oxford, **1995**, p. 1.
[5] M. Winkler, M. Lutz, G. Müller, *Angew. Chem.* **1994**, *106*, 2372; *Angew. Chem. Int. Ed. Engl.* **1994**, *33*, 2279.
[6] a) A. J. Edwards, M. A. Paver, P. R. Raithby, M.-A. Rennie, C. A. Russell, D. S. Wright, *Angew. Chem.* **1994**, *106*, 1334; *Angew. Chem. Int. Ed. Engl.* **1994**, *33*, 1277; b) D. J. Brauer, H. Bürger, G. R. Liewald, *J. Organomet. Chem.* **1986**, *308*, 119; c) D. J. Brauer, H. Bürger, G. R. Liewald, J. Wilke, *ibid.* **1985**, *287*, 305; d) M. Schubart, B. Findeis, L. H. Gade, W.-S. Li, M. McPartlin, *Chem. Ber.* **1995**, *128*, 329; e) L. H. Gade, N. Mahr, *J. Chem. Soc. Dalton Trans.* **1993**, 489; f) M. Veith, *Angew. Chem.* **1987**, *99*, 1; *Angew. Chem. Int. Ed. Engl.* **1987**, *26*, 1.
[7] H. R. Allcock, J. L. Desorcie, G. H. Riding, *Polyhedron* **1987**, *6*, 119.
[8] a) M. Witt, H. W. Roesky, *Chem. Rev.* **1994**, *94*, 1163; b) H. W. Roesky, *Synlett* **1990**, 651.
[9] H. R. Allcock, *Chem. Rev.* **1972**, *72*, 315.
[10] Crystallographic data for **2**: $C_{108}H_{204}Li_{12}N_{18}O_9P_9$, M_r = 2168.00, monoclinic, space group *C2/c*, a = 33.662(7), b = 17.424(3), c = 25.871(6) Å, β = 125.86(3), V = 12297(4) Å^3, Z = 4, ρ_{calcd} = 1.171 Mg m^{-3}, $F(000)$ = 4704, λ = 0.71073 Å, T = 153 K, $\mu(Mo_{K\alpha})$ = 0.146 mm^{-1}. Data were collected on a Stoe AED diffractometer using an oil-coated, rapidly cooled crystal [15] of dimensions 0.5 × 0.5 × 0.4 mm. Of a total of 8115 collected reflections, 8014 were unique. The structure was solved by direct methods [16] and refined by full-matrix least squares against F^2 [17] to final values of $R1$ ($F > 4\sigma(F)$) = 0.067 and $wR2$ (all data) = 0.178; largest peak and hole in the final difference Fourier map were 0.377 and −0.382 e Å^{-3}. Additionally there are 2.5 noncoordinated THF molecules in the crystallographic asymmetric unit of which one is disordered over two positions. All non-hydrogen atoms were refined by using anisotropic displacement parameters, and hydrogen atoms were set geometrically. Further details of the crystal structure investigation can be obtained from the Director of the Cambridge Crystallographic Data Centre, 12 Union Road, GB-Cambridge CB2 1EZ, UK on quoting the full journal citation.
[11] a) A. Steiner, D. Stalke, *Inorg. Chem.* **1993**, *32*, 1977; b) A. Recknagel, A. Steiner, M. Noltemeyer, S. Brooker, D. Stalke, F. T. Edelmann, *J. Organomet. Chem.* **1991**, *414*, 327; c) J. F. van de Maelen Uria, S. K. Pandey, H. W. Roesky, G. M. Sheldrick, *Acta Crystallogr. Sect. C* **1994**, *50*, 671.
[12] a) T. S. Cameron, B. Borecka, W. Kwiatkowski, *J. Am. Chem. Soc.* **1994**, *116*, 1211; b) H. Jacobs, R. Kirchgässner, *Z. Anorg. Allg. Chem.* **1990**, *581*, 125; c) F. Golinski, H. Jacobs, *ibid.* **1994**, *620*, 965.
[13] A. Steiner, D. Stalke, *Angew. Chem.* **1995**, *107*, 1908; *Angew. Chem. Int. Ed. Engl.* **1995**, *34*, 1752.
[14] S. K. Ray, R. A. Shaw, *J. Chem. Soc.* **1961**, 872.
[15] T. Kottke, D. Stalke, *J. Appl. Crystallogr.* **1993**, *26*, 615.
[16] G. M. Sheldrick, SHELXS-86, program for crystal structure solution, Göttingen, **1986**.
[17] G. M. Sheldrick, SHELXL-93, program for crystal structure refinement, Göttingen, **1993**.

 © VCH Verlagsgesellschaft mbH, D-69451 Weinheim, 1996 0570-0833/96/3506-0637 $ 15.00+.25/0

π-Dimers of End-Capped Oligopyrrole Cation Radicals**

J. A. E. H. van Haare, L. Groenendaal, E. E. Havinga, R. A. J. Janssen,* and E. W. Meijer

The conductivity of doped polymers with conjugated π-electron systems is directly related to their redox states and part of it has been rationalized in terms of polarons (cation radicals) and bipolarons (dications) migrating along the conjugated chain.[1] The general understanding of the electronic structure and redox states of semiconducting polymers has benefited from studies on well-defined conjugated oligomers that allow functional properties to be investigated as a function of (effective) conjugation length.[2-7] In recent years, numerous studies have addressed the redox states of oligothiophenes,[2-5] and it was found that in addition to cation radicals and dications, spinless π-dimers of cation radicals can be formed.[3-5] These interchain cation radical π-dimers have been proposed as an alternative to diamagnetic bipolarons as an explanation for the weak ESR signal for highly oxidized polythiophenes.[3-5] Although several organic ion radicals form π-complexes in solution, dimerization has never been reported for conjugated oligomers other than oligothiophenes. The availability of well-defined oligopyrroles[8] makes such a study possible for one of the most interesting conducting polymers: polypyrrole.

α-Oligopyrroles with phenyl end caps (PhPy$_n$Ph, n = 2, 3, 4) exhibit two chemically reversible one-electron oxidation waves (Table 1).[9] The chemical stability of the first two oxidation states of PhPy$_n$Ph is a result of the phenyl end caps, which prevent polymerization over the α-positions. The successive electrochemical oxidation of the oligomers to cation radicals (PhPy$_n$Ph$^{\bullet+}$) and dications (PhPy$_n$Ph^{2+}) at controlled potentials was monitored by in-situ UV/Vis/NIR absorption spectroscopy (Fig. 1). Several optical transitions, listed in Table 1, are observed. The number and relative ordering of the absorption bands closely resembles the spectral characteristics of oxidized oligothiophenes.[2-5] For the oligopyrrole cation radicals two bands (M1 and M2) appear at low and high energy, respectively. Each of the M1 and M2 bands has an associated second transition (D1 and D2), shifted to higher energy by about 0.3 eV. These second transitions are attributed to π-dimers of oligopyrrole cation radicals. In contrast, for the oligopyrrole dications, only a single electronic transition (DC) is observed, with one or two associated vibronics at higher energy. Each of the optical transitions (N, M1, M2, D1, D2, and DC; Table 1) shifts to lower energy for longer oligomers, in accord with an approximately linear dependence with the inverse length of the oligomer (taken as $1/m$; where $m = n + 2$ is the total number of aromatic rings).[9]

Table 1. Electrochemical data [a] and optical transition energies [b] of redox states of PhPy$_n$Ph oligopyrroles.

	$n = 2$ E [eV]	$n = 3$ E [eV]	$n = 4$ E [eV]
E_1^0	0.37	0.13	0.01
E_2^0	1.05	0.60	0.37
N	3.05	2.89	2.78
M1 [c]	1.60, 1.79	1.32	1.13
M2	2.55	2.26	2.10
D1	1.91	1.65	1.39
D2	2.86	2.63	2.42
DC [c]	2.21, 2.34	1.88, 2.05, (2.23)	1.58, 1.70, (1.88)

[a] Potentials in CH_2Cl_2/NBu_4PF_6 (0.1 M) solution at 100 mVs^{-1} and oligomer concentration c = 0.1–1.0 mM vs SCE, internally calibrated vs Fc/Fc$^+$. [b] Transitions of redox states labeled as follows: N: neutral oligomer; M1, M2: monomer cation radical; D1, D2: dimer of cation radicals; DC: dication. [c] Second and third entries are attributed to different vibronics of the same electronic transition.

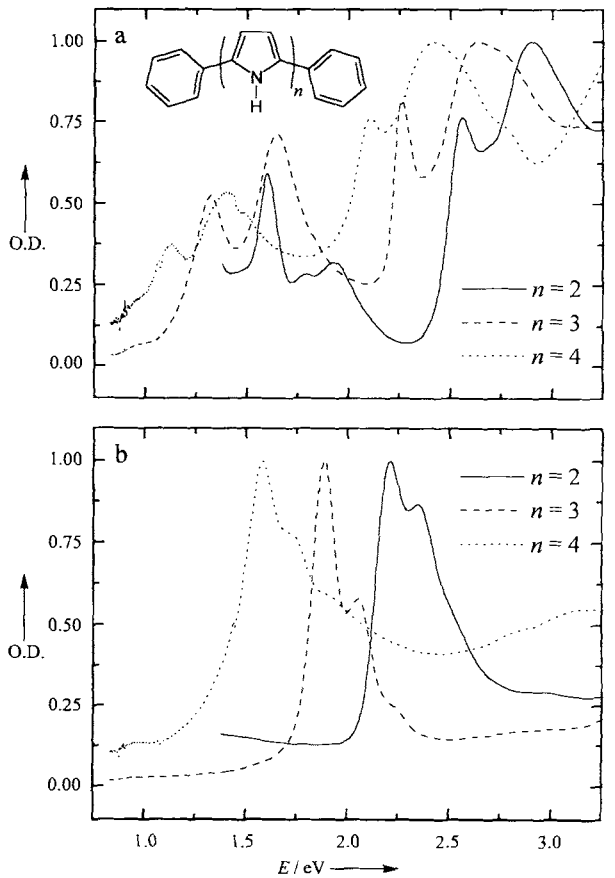

Fig. 1. Normalized electronic spectra obtained after electrochemical oxidation of PhPy$_n$Ph to the corresponding cation radicals (a) and dications (b). Spectra were recorded in a CH_2Cl_2/NBu_4PF_6 (0.1 M) solution at room temperature with 0.1 mm path length and an oligomer concentration c = 0.1–1.0 mM.

The various bands can be assigned to specific transitions using the molecular symmetry of PhPy$_n$Ph. Assuming an all-*transoid* conformation of the bonds between pyrrole rings, the molecular symmetry is either C_{2h} (n = 2, 4) or C_{2v} (n = 3). The symmetry of the frontier π orbitals is given in Figure 2a; the dipole-allowed transitions among these orbitals are indicated. Since these excitations are all polarized along the oligomer chain axis they are expected to be intense.[10] The π-interaction between two cation radicals to give a π-dimer will cause a splitting of frontier orbitals into bonding (+) and antibonding (−) levels (Fig. 2b). In this dimer the D1 (− ← −) and D2 (+ ← +) transitions (originating from the states M1 and M2, respectively, in the cation radical) are dipole-allowed and polarized along the

[*] Dr. R. A. J. Janssen, J. A. E. H. van Haare, L. Groenendaal, Dr. E. E. Havinga,[+] Prof. E. W. Meijer
Laboratory of Organic Chemistry, Eindhoven University of Technology
P. O. Box 513, NL-5600 MB Eindhoven (The Netherlands)
Fax: Int. code +(40)2451036
e-mail: tgtorj@chem.tue.nl

[+] Also at Philips Research Laboratories, Eindhoven (The Netherlands)

[**] We thank Prof. P. Bäuerle and Dr. S. Scheib, Universität Würzburg, Germany, for providing us with the spectroelectrochemical cell used in this study. Philips Research is gratefully acknowledged for an unrestricted research grant.

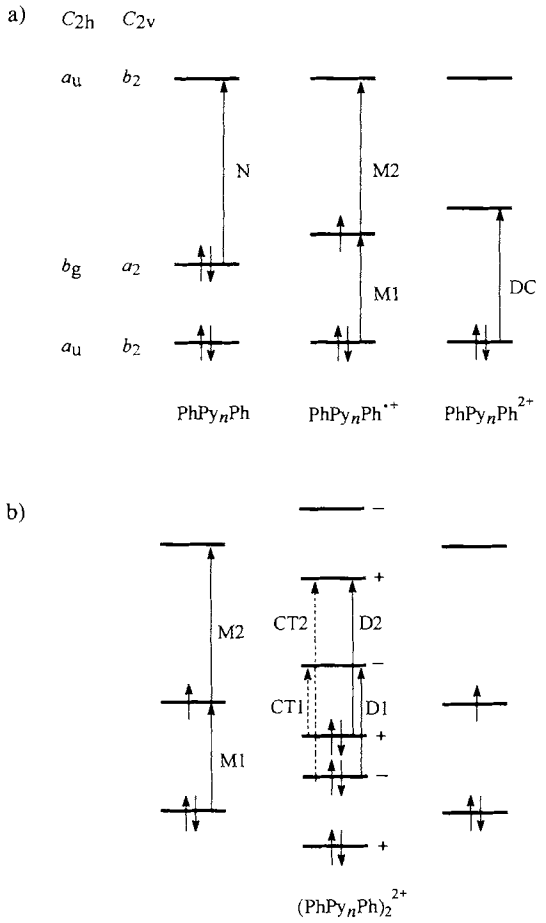

Fig. 2. Schematic energy diagram and symmetry of the frontier orbitals for the neutral, cation radical, and dication states of $PhPy_nPh$ (a), and cation radical π-dimers (b). Dipole-allowed transitions are indicated. Experimentally D1 and D2 exhibit an additional blue shift as a result of a Davydov interaction.

long axis of the oligomer. Experimentally the D1 and D2 transitions are shifted to higher energy than M1 and M2 by about 0.3 eV, comparable with shifts found for oligothiophene cation radical dimers[4] and other π-radical ion dimers.[11] Such a blue shift is a well-known phenomenon for ionic π-dimers and has been attributed to the interaction between transition dipole moments on the adjacent cation radicals (Davydov shift),[11] although other phenomena may contribute such as different splittings of frontier orbitals upon dimerization. In addition to D1 and D2, two charge transfer transitions CT1 and CT2 are possible in the π-dimer, polarized along the short axis connecting the two cation radicals. As a consequence, the CT1 and CT2 bands are expected to be less intense than D1 and D2.

The temperature dependence of the electronic spectrum of $PhPy_2Ph^{\bullet+}$ (Fig. 3), obtained by chemical oxidation with iron(III) chloride ($FeCl_3$), reveals that the intensities of the M1 and M2 bands decrease at lower temperatures in favor of the intensities of the D1 and D2 bands. These changes with temperature are reversible and consistent with the proposed equilibrium between two oligopyrrole cation radicals and their π-dimer.

The in situ electrochemical or chemical ($FeCl_3$) oxidation of $PhPy_nPh$ to the cation radical produces a strong ESR signal at $g = 2.0025$. A subsequent decrease of ESR signal intensity is observed upon further oxidation, leading to the loss of the signal after complete conversion of the cation radical to the (diamagnetic) dication. Highly resolved ESR spectra of the oligopyrrole cation radicals can be obtained by oxidizing the $PhPy_nPh$

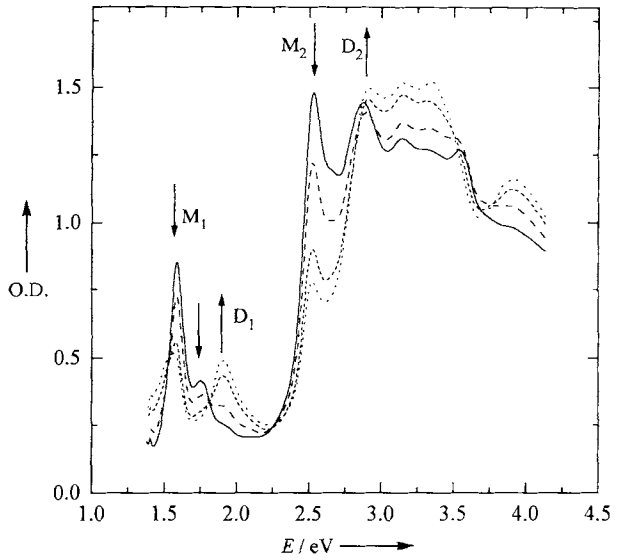

Fig. 3. Electronic spectrum of $PhPy_2Ph^{\bullet+}$ cation radicals, obtained by oxidation with $FeCl_3$ in CH_2Cl_2 solution between 295 and 245 K ($c = 0.2$ mM, path length 10 mm). The arrows mark the decay of the M1 and M2 transitions and the increase of D1 and D2 transitions with decreasing temperature.

oligomers in a 1:1 mixture of CH_2Cl_2 and trifluoroacetic acid (TFA).[12] Figure 4 shows the ESR spectrum of $PhPy_2Ph^{\bullet+}$ in CH_2Cl_2/TFA. The ESR spectrum is fully symmetric, indicating the formation of a single doublet species and arguing against the presence of different conformations of the $PhPy_2Ph^{\bullet+}$ cation radical (e.g. *s-transoid* and *s-cisoid*), as has been found for oligothiophene cation radicals.[13] The intensity of the ESR signal decreases by one order of magnitude upon lowering the temperature from 295 K to 200 K (Fig. 4). This temperature dependence is reversible and in agreement with the expected behavior for an equilibrium between two oligopyrrole cation radicals and a diamagnetic π-dimer.[14]

In conclusion we have shown that phenyl end-capped oligopyrroles can be oxidized reversibly to the corresponding

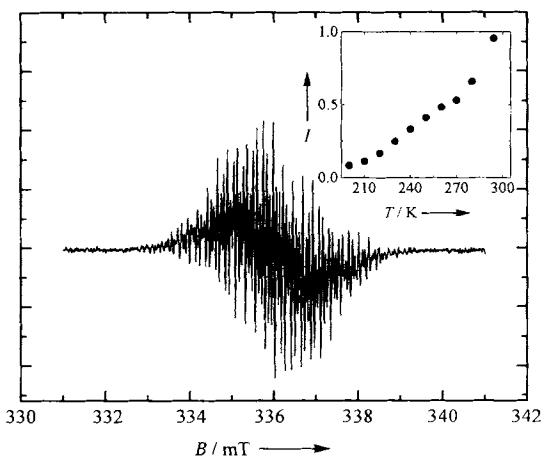

Fig. 4. ESR spectrum of the $PhP_2Ph^{\bullet+}$ cation radical generated by dissolving $PhPy_2Ph$ (0.4 mM) in CH_2Cl_2/TFA (1:1) at 295 K. The inset shows the temperature dependence of the ESR intensity. The ESR spectrum can be simulated by using the following parameters $a_H(4H) = 0.614$, $a_H(2H) = 0.853$, $a_H(4H) = 0.328$, $a_H(2H) = 0.703$, $a_H(2H) = 0.395$, $a_H(2H) = 0.470$, and $DH_{pp} = 0.03$ mT. These couplings are tentatively assigned to *o*-PhH, *p*-PhH, *m*-PhH, C3H, C4H, and NH based on a semiempirical quantum chemical calculation using the PM3 Hamiltonian.

cation radicals and dications. Variable temperature UV/Vis/NIR and ESR spectra give direct evidence for the π-dimerization of oligopyrrole cation radicals. The results on oligopyrroles are in full analogy to π-dimerization of oligothiophene cation radicals.[3–5] Therefore, the present results together with those on oligothiophenes, give credence to the proposition that π-dimers have an important role as interchain conducting entities for conducting polymers in general.

Experimental Procedure

The preparation of $PhPy_nPh$ oligomers and conditions for cyclic voltammetry have been described elsewhere [9]. All experiments were conducted under rigorously inert conditions. UV/Vis/NIR spectroelectrochemical data were obtained with a Perkin Elmer Lambda 9 spectrophotometer in CH_2Cl_2/NBu_4PF_6 (0.1 M) solution with a thin-layer cell consisting of two ITO glasses separated by a spacer of 0.1 mm as the optical transparent working electrode, a platinum disk as a counter electrode, and an Ag/AgCl wire as reference electrode [4]. ESR spectra were recorded on a Bruker ER200D SRC X-band spectrometer with a ER4111 variable temperature unit.

Received: November 10, 1995 [Z 8542 IE]
German version: *Angew. Chem.* **1996**, *108*, 696–699

Keywords: π-dimers · electrochemistry · oligopyrroles · polymers

[1] A. J. Heeger, S. Kivelson, J. R. Schriefer, W. P. Su, *Rev. Mod. Phys.* **1988**, *60*, 781; Y. Lu, *Solitons and Polarons in Conducting Polymers*, World Scientific, Singapore, **1988**.
[2] Z. Xu, D. Fichou, G. Horowitz, F. Garnier, *J. Electroanal. Chem.* **1989**, *267*, 339; D. Fichou, G. Horowitz, Z. Xu, F. Garnier, *Synth. Met.* **1990**, *39*, 243.
[3] M. G. Hill, K. R. Mann, L. L. Miller, J.-P. Penneau, *J. Am. Chem. Soc.* **1992**, *114*, 2728; M. G. Hill, J.-P. Penneau, B. Zinger, K. R. Mann, L. L. Miller, *Chem. Mater.* **1992**, *4*, 1106; B. Zinger, K. R. Mann, M. G. Hill, L. L. Miller, *ibid.* **1992**, *4*, 1113.
[4] P. Bäuerle, U. Segelbacher, A. Maier, M. Mehring, *J. Am. Chem. Soc.* **1993**, *115*, 10217; P. Bäuerle, U. Segelbacher, K. U. Gaudl, D. Huttenlocher, M. Mehring, *Angew. Chem.* **1993**, *105*, 125; *Angew. Chem Int. Ed. Engl.* **1993**, *32*, 76.
[5] G. Zotti, G. Schiavon, A. Berlin, G. Pagani, *Chem. Mater.* **1993**, *5*, 620; *Synth. Met.* **1993**, *61*, 81.
[6] E. E. Havinga, I. Rotte, E. W. Meijer, W. ten Hoeve, H. Wynberg, *Synth. Met.* **1991**, *41–43*, 473; W. ten Hoeve, H. Wynberg, E. E. Havinga, E. W. Meijer, *J. Am. Chem. Soc.* **1991**, *113*, 5887.
[7] G. Zotti, S. Martina, G. Wegner, A.-D. Schlüter, *Adv. Mater.* **1992**, *4*, 798.
[8] S. Martina, V. Enkelmann, A.-D. Schlüter, G. Wegner, *Synth. Met.* **1991**, *41-43*, 403; S. Martina, V. Enkelmann, A.-D. Schlüter, G. Wegner, *ibid.* **1992**, *51*, 299; L. Groenendaal, H. W. I. Peerlings, E. E. Havinga, J. A. J. M. Vekemans, E. W Meijer, *ibid.* **1995**, *69*, 467.
[9] J. A. E. H. van Haare, L. Groenendaal, H. W. I. Peerlings, E. E. Havinga, R. A. J. Janssen, E. W. Meijer, *Chem. Mater.* **1995**, *7*, 1984.
[10] J. Cornil, D. Beljonne, J. L. Brédas, *J. Chem. Phys.* **1995**, *103*, 842; R. A. J. Janssen, D. Moses, N. S. Sariciftci, *ibid.* **1994**, *101*, 9519.
[11] J. B. Torrance, B. A. Scott, B. Welber, F. B. Kaufman, P. E. Seiden, *Phys. Rev. B* **1979**, *19*, 730, and references therein.
[12] The UV/Vis/NIR spectrum of $PhPy_nPh$ in CH_2Cl_2/TFA exhibits the same transitions as observed after electrochemical or chemical oxidation with $FeCl_3$.
[13] C. Alemán, E. Brillas, A. G. Davies, L. Fajari, D. Giró, L. Juliá, J. J. Pérez, J. Rius, *J. Org. Chem.* **1993**, *58*, 3091; B. Kirste, P. Tian, G. Kossmehl, G. Engelmann, W. Jugelt, *Magn. Reson. Chem.* **1995**, *33*, 70.
[14] From the one order of magnitude decrease of the ESR intensity it is possible to estimate the enthalpy of dimerization to be on the order of $\Delta H^0 = -25$ to $-35\ kJ\ mol^{-1}$. Further studies on the equilibrium and thermodynamic parameters are currently in progress.

Solid-Phase, Parallel Syntheses by Ugi Multicomponent Condensation**

Paul A. Tempest, S. David Brown, and Robert W. Armstrong*

Dedicated to Professor Ivar Ugi on the occasion of his 65th birthday

The combinatorial synthesis of chemical libraries of small organic molecules represents a new tool for investigating the effects of structure on biological activity.[1] Recent efforts have focused on the solid-phase syntheses of a core set of atoms (or a pharmacophore), in which diversity is introduced sequentially at each step of a linear synthesis.[2] The theoretical number of compounds that can be generated in these libraries is related to the number of steps required for their synthesis and the availability of chemical starting compounds (inputs) for each step. An alternative strategy for the generation of chemical libraries involves the use of multicomponent condensation reactions (MCCs).[3] MCC-derived compounds require a single synthetic transformation. The potential size of these libraries is dependent on the number of components in the MCC and their availability—not on the number of synthetic steps. Described herein is the solid-phase synthesis of a library of α-acylamino amides by a four-component condensation (4CC) and a strategy for increasing the structure diversity of one of its inputs by a pre-MCC condensation of two substrates in solution.

The Ugi 4CC is ideally suited for the construction of chemical libraries based on the α-acylamino amide core structure (Scheme 1).[4] When the synthesis is conducted on a solid support, libraries of structurally diverse mono- and disubstituted α-amino acids may be obtained. While any of the four inputs (aldehyde, carboxylic acid, isonitrile, and amine) can be tethered covalently to a solid support, we chose to use an immobilized amino group since a variety of amino-functionalized matrices are readily available. A secondary amide results upon cleavage from the solid support.

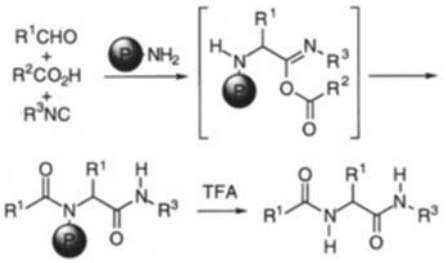

Scheme 1. A 4CC reaction on solid support (P) to generate compounds with an α-acylamino core.

A 96-member library was generated (12 acids, 8 aldehydes, 1 amine, and 1 isocyanide were the starting compounds) in a 96-well microtiter plate with a distribution of one product per well. The inputs of this library were chosen so that a substituent effect analysis of the 4CC reaction on solid support could

[*] Prof. R. W. Armstrong, P. A. Tempest, S. D. Brown
Department of Chemistry and Biochemistry
University of California, Los Angeles
Los Angeles, CA 90095-1569 (USA)
Fax: Int. code +(310)825-0767

[**] This research was supported by NIH grant GM-20080. We thank Dr. Edmund J. Moran, Ontogen Corp., Carlsbad, CA, for discussions of experimental details.

 © VCH Verlagsgesellschaft mbH, D-69451 Weinheim, 1996 0570-0833/96/3506-0640 $ 15.00+.25/0

be obtained with a single plate (96 individual reactions). For the reaction, 0.014 mmole of Rink-amine[5] resin per well in $MeOH/CH_2Cl_2$ (1/2) served as the amine input, and methylisocyanoacetate (10 equiv) as the single isocyanide input. The carboxylic acids **1**–**12** (10 equiv) and aldehydes **A**–**H** (10 equiv) used for construction of the library are shown in Scheme 2.

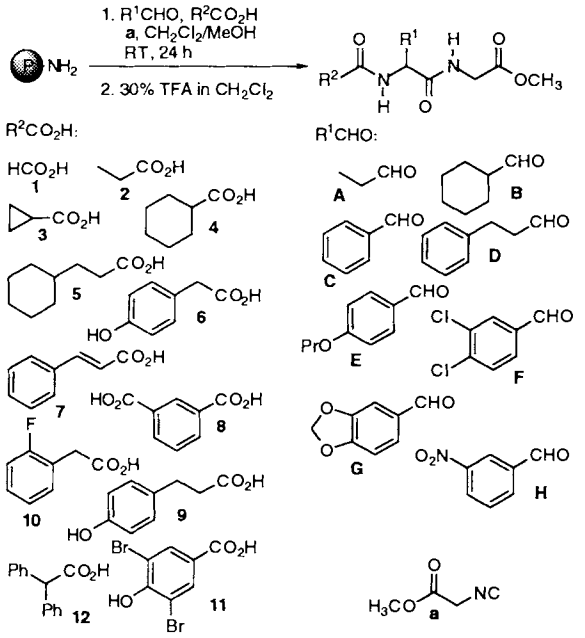

Scheme 2. Carboxylic acid and aldehyde inputs for the synthesis of a compound library.

After stirring for 24 h, the products were cleaved from the resin; 1–3 mg of predicted product was obtained as the single component in 88 wells. In parallel with solution reactions, the product yields were most sensitive to the structure of the aldehyde inputs (Table 1). Reactions with aliphatic aldehydes and those containing electron-donating groups exhibit good overall yields, compared to the reactions of aldehydes with electron-withdrawing groups (**F** and **H**) even in the presence of large excess of reagents or repeated addition of fresh reagents. For the carboxylic acid inputs, the reactions involving phenolic derivatives **6**, **9**, and **11** gave generally low yields, owing in part to their precipitation from solution over the 24 h reaction period. Four reactions were carried out on larger scale (0.12 mmol) and afforded products in the following yields[6]: **7Ba**, 30 mg, 69%; **8Ea**, 40 mg, 80%; **10Aa**, 26 mg, 68%; and **12Da**, 41 mg, 77%. Similar yields are observed for the solution reactions. Analysis by ^{13}C and ^1H NMR revealed >90% purity.

Table 1. Yields [%] based on the support-bound amine for the three steps a) deprotection of the amine, b) four-component condensation with the carboxylic acids **1**–**12**, aldehydes **A**–**H**, and the isonitrile **a**, and c) cleavage from the resin with TFA.

	1	2	3	4	5	6	7	8	9	10	11	12
A	59	95	95	79	95	45	95	95	85	17	8	51
B	67	14	70	59	52	41	64	71	42	2	9	37
C	81	65	77	57	93	23	71	68	21	2	4	36
D	58	65	95	79	95	98	96	90	93	91	64	50
E	42	86	37	64	61	70	80	76	25	4	78	54
F	46	30	14	11	30	0	48	31	0	35	28	26
G	55	94	46	52	64	33	66	70	0	5	47	33
H	5	0	0	24	45	0	0	30	5	0	21	18

We next addressed the issue of the limited commercial availability of isocyanides as starting materials for the Ugi reaction. For the purpose of library generation, this greatly reduces the structural diversity of this input (and size of the library). The generation of diverse structures would require substantial synthetic effort. The approach described herein represents a general strategy for the generation of input diversity by the solution condensation of two or more subunits prior to the solid-phase synthesis of the library. α-Lithiated benzylisocyanide (1 equiv) was treated with a small excess (1.1 equiv) of methyl iodide, benzyl bromide, and cyclohexyl bromide to afford respective isocyanides **c**–**e**.[7] Each crude reaction mixture was concentrated and, along with isocyanide **b**, used without purification to generate a library on solid support by the Ugi 4CC reaction (3 carboxylic acids, 3 aldehydes, 4 isocyanides, 1 amine). This array afforded all 36 products distributed as one compound per well in a microtiter plate (Scheme 3, Table 2). Four reactions

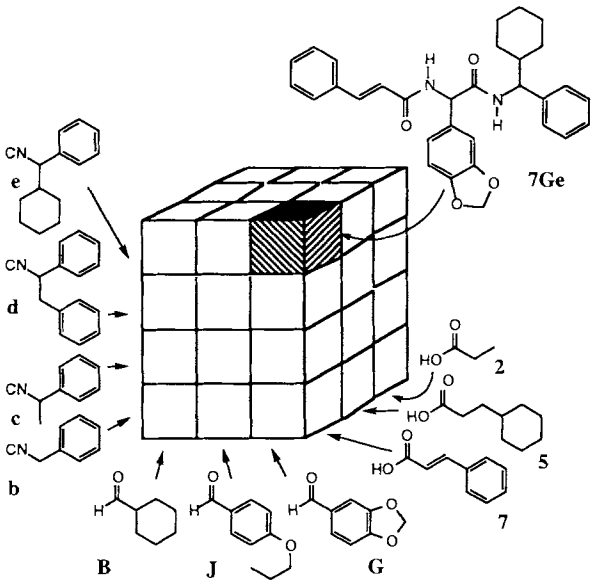

Scheme 3. Chemical inputs and a selected product of the 4CC, in which three inputs are varied. The code used to identify the products consists of the designations of the inputs.

Table 2. Yields [%] based on the support-bound amine for the three steps a) deprotection of the amine, b) four-component condensation with the carboxylic acids **2**, **5**, and **7**, aldehydes **I**–**K**, and isonitriles **b**–**e**, and c) cleavage from the resin with TFA.

	2	5	7		2	5	7
I, b	55	11	10	**I, d**	38	40	31
J, b	55	50	31	**J, d**	50	40	55
K, b	51	30	19	**K, d**	32	40	28
I, c	31	40	50	**I, e**	40	30	30
J, c	42	52	50	**J, e**	18	30	23
K, c	38	31	30	**K, e**	10	30	20

were performed on larger scale, affording the condensation products in the following yields: **7Jb**, 51 mg, 61%; **7Jc**, 37 mg, 43%; **7Jd**, 38 mg, 37%; **7Je**, 31 mg, 31%. Even though unpurified isocyanides were used in the 4CC reaction, the observed purity of the products was still >90%.

We have described the parallel syntheses of a combinatorial library on solid support based on the Ugi 4CC. We generated

isocyanides otherwise not commercially available by quenching α-lithiated isocyanides with alkyl halides, thus improving the diversity of the isocyanide input. In addition, condensation of the isocyanide input in solution prior to library generation effectively produces a "5CC" library on the solid support. This strategy has been extended to the synthesis of ethanolamine libraries effectively containing six components.[8]

Experimental Procedure

Synthesis of a library in 96-well microtiter plate: Rink FMOC-amide resin (2.88 g, 0.46 mmol g^{-1}) was deblocked with piperidine and partitioned equally into a 96-well polyethylene microtiter plate. Each of the eight aldehydes (1 M in CH_2Cl_2, 138 μL, 10 equiv) and twelve carboxylic acids (1 M in CH_3OH, 138 μL, 10 equiv) was added to the appropriate wells such that each column contained a different aldehyde and each row contained a different carboxylic acid. After 30 min methyl isocyanoacetate (1 M in CH_2Cl_2, 138 μL, 10 equiv) was added to all the wells. The plate was capped for 24 h then allowed to evaporate to dryness. The resin was transferred to a 96-well filtration apparatus and washed liberally with methanol and CH_2Cl_2. The products were removed from the resin and washed into a second 96-well plate with TFA in CH_2Cl_2 (2 × 600 μL), then rinsed with CH_2Cl_2 (200 μL) and CH_3OH (200 μL). The solvents were then removed in a reduced-pressure oven.

7Ba: ^{1}H NMR (400 MHz, $CDCl_3$, 25 °C): δ = 1.17 (br. m, 6H), 1.64 (br. m, 5H), 3.73 (s, 3H), 4.00 (d, J = 17.5 Hz, 1H,), 4.11 (d, J = 17.5 Hz, 1H,), 4.56 (br. s, 1H), 6.53 (br. m, 1H), 7.32–7.66 (m, 8H); ^{13}C NMR (125 MHz, $CDCl_3$, 25 °C): δ = 25.70, 25.75, 25.88, 25.98, 28.35, 28.85, 29.43, 40.35, 41.18, 52.28, 52.36, 58.34, 119.75, 127.93, 128.21, 128.79, 128.90, 129.94, 134.45, 142.25; IR (film): $\tilde{\nu}$ = 3277, 2928, 2853, 1753, 1653, 1618 cm^{-1}; FAB HRMS (calcd/found): 359.1971/359.1975 [(M + H)$^+$].

8Ea: ^{1}H NMR (400 MHz, $CDCl_3$, 25 °C): δ = 1.02 (t, J = 7.3 Hz, 3H), 1.79 (m, 2H), 3.61 (s, 2H), 3.69 (s, 3H), 3.88 (t, J = 6.5 Hz, 2H,), 3.92 (m, 2H), 5.52 (br. s, 1H), 6.62 (br. s, 1H), 6.82 (d, J = 7.3 Hz, 2H,), 6.98 (br. s, 1H), 7.08 (m, 2H), 7.25 (br. d, 4H); ^{13}C NMR (125 MHz, $CDCl_3$, 25 °C): δ = 10.52, 22.53, 36.50, 41.41, 52.44, 56.57, 69.52, 114.92, 115.44, 115.66, 124.45, 124.48, 128.60, 129.11, 129.25, 129.33, 131.65, 131.69, 159.24, 159.75, 169.62, 169.77, 170.53; IR (film): $\tilde{\nu}$ = 3287, 1761, 1641, 1514 cm^{-1}; FAB HRMS (calcd/found): 417.1826/17.1822 [(M + H)$^+$].

Received: September 13, 1995 [Z83961E]
German version: *Angew. Chem.* **1995**, *108*, 689–691

Keywords: amino acids · combinatorial chemistry · multicomponent reactions · solid-phase syntheses

[1] See also: a) M. A. Gallop, R. W. Barrett, W. J. Dower, S. P. A. Fodor, E. M. Gordon, *J. Med. Chem.* **1994**, *37*, 1233–1251; b) E. M. Gordon, R. W. Barrett, W. J. Dower, S. P. A. Fodor, M. A. Gallop, *ibid.* **1994**, *37*, 1385–1401.

[2] a) B. A. Bunin, J. A. Ellman, *J. Am. Chem. Soc.* **1992**, *114*, 10997–10998; b) S. H. Dewitt, J. S. Kiely, C. J. Stankovic, M. C. Schroeder, *Proc. Natl. Acad. Sci. USA* **1993**, *90*, 6909–6913; c) M. J. Plunkett, J. A. Ellman, *J. Am. Chem. Soc.* **1995**, *117*, 3306–3307; d) E. K. Kick, J. A. Ellman, *J. Med. Chem.* **1995**, *38*, 1427–1430; e) S. M. Hutchins, K. T. Chapman, *Tetrahedron Lett.* **1995**, *36*, 2583–2586; f) D. A. Campbell, J. C. Bermak, T. S. Burkoth, D. V. Patel, *J. Am. Chem. Soc.* **1995**, *117*, 5381–5382.

[3] G. Possner, *Chem. Rev.* **1986**, *86*, 831–844.

[4] The potential of generating large numbers of structural analogs by this reaction was addressed by I. Ugi in *Isonitrile Chemistry* (Ed.: I. Ugi), Academic Press, London, **1971**. For a strategy for the solution-phase synthesis of a library, see: I. Ugi, A. Domling, W. Horl, *Endeavour* **1994**, *18*, 115–123.

[5] H. T. Rink, *Tetrahedron Lett.* **1994**, *18*, 115–123.

[6] Reactions were performed in analogy to that with isonitrile **a**; yields are based on equiv. of FMOC amine on Rink resin.

[7] W. A. Böll, F. Gerhart, A. Nürrenbach, U. Schöllkopf, *Angew. Chem.* **1970**, *82*, 482–483; *Angew. Chem. Int. Ed. Engl.* **1970**, *9*, 458–459.

[8] Condensation of α-lithiated benzyl isocyanide with benzaldehyde followed by addition of acetic anhydride affords a three-input isocyanide, which can be used without purification in the solid-phase 4CC reaction.

Continuous Asymmetric Synthesis in a Membrane Reactor

Udo Kragl* and Claus Dreisbach

Decoupling the residence time of catalyst and reactants in a reactor can be achieved by immobilization of the catalyst. The aim is to achieve a high total turnover number or an easy recovery of the catalyst for repeated use, or to enable the use of continuously operated reactors.[1] The latter offers the advantage of better controlled reaction conditions; for instance, if the steady state is reached, concentrations of reactants are constant with time. To address these problems homogeneous catalysts are most often anchored to insoluble supports. The main problems related to this approach are the nonuniform and partly unknown structures of the resulting heterogeneous catalysts, mass transport limitation due to hindered diffusion, and a low catalytic activity. In addition, there have been attempts to recover catalysts by using membrane processes such as ultrafiltration or reverse osmosis.[2, 3] Examples in hydroformylation,[4, 5] hydrogenation,[6] or reduction of NAD(P)$^+$[7] have been reported. But no data for industrial processes that use this approach have yet been published. In contrast, in biotechnology, enzyme membrane reactors, where the soluble enzyme is retained behind an ultrafiltration membrane, are used on a scale of 100 tons per year for the synthesis of fine chemicals.[8] The advantage of this method is that fresh catalyst can be supplemented even in the continuous process, which is difficult for a fixed bed reactor.

For the example of the enantioselective addition of diethylzinc **2** to benzaldehyde **1**, we here describe the continuous asymmetric synthesis in a membrane reactor using the homogeneously soluble catalyst **4**. The α,α-diphenyl-L-prolinol used as chiral ligand was coupled to a copolymer made from 2-hydroxyethyl methacrylate and octadecyl methacrylate (molecular weight 96000 g mol^{-1})[9] in order that it can be retained by an ultrafiltration membrane within the reaction vessel. The reac-

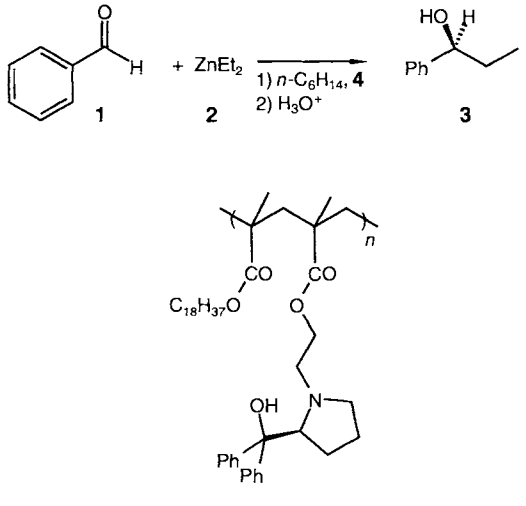

[*] Dr. U. Kragl, Dr. C. Dreisbach[+]
Forschungszentrum Jülich GmbH, Institut für Biotechnologie
D-52425 Jülich (Germany)
Fax: Int. code +(2461)61-3870
e-mail: u.kragl@kfa-juelich.de

[+] New address: Bayer AG, Leverkusen (Germany)

[**] This work was supported by the Deutsche Forschungsgemeinschaft. We thank Bayer AG, Leverkusen, for a sample of the copolymer and Hoechst AG, Frankfurt, for the ultrafiltration membranes.

tion chosen is very suitable for process development, as it occurs only in the presence of the catalyst. Leakage of the catalyst from the reactor would cause a decrease in conversion due to a lowered volumetric activity but not a change in the enantiomeric excess of the product.

For a stable continuous process high retention of the catalyst is required. The solvent-stable polyaramide ultrafiltration membrane Hoechst Nadir UF PA20[10] retains more than 99.8% of **4**. The enantiomeric excess of **3** that can be achieved with the soluble polymer-bound α,α-diphenyl-L-prolinol is somewhat lower than that achieved with the noncoupled ligand (80% compared to 97%[11]). For polymer-supported ligands *ee* values between 10 and 92% are reported; the majority of values are below 80%.[12a] An enantiomeric excess of 94% has been reported for the addition of diethylzinc to 4-chlorobenzaldehyde with this type of catalyst in a flow-through reactor.[12b]

For the addition of **2** to **1** catalyzed by **4** in a batch reactor, the enantiomeric excess of **3** is strongly influenced by the ratio of the starting materials.[13] A surplus of **2** yields the (*S*)-alcohol, whereas a surplus of **1** surprisingly yields the (*R*)-alcohol. The reason for this behavior of **4** may be the coupling of the polymer to the nitrogen atom of the prolinol. Attempts to verify this by replacing the polymer with less bulky analogues were not successful. The resulting catalysts were either insoluble or inactive. Experiments with a constant amount of catalyst but varying amounts of reactants reveal that the ratio between catalyst and reactants has only a minor influence.

The enantiomeric excesses achieved are similar in the batch reactor and the continuously operated membrane reactor. Figure 1 shows the change in the enantiomeric excess as function of

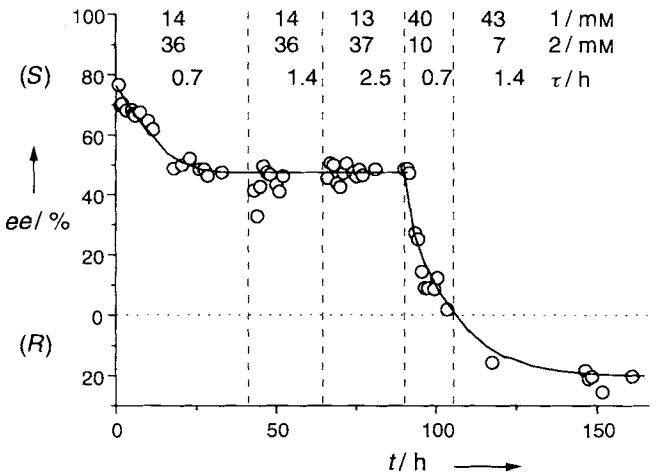

Fig. 1. Change in the enantiomeric excess of **3** with time for the addition of **2** to **1** in a continuously operated membrane reactor. Conditions: c(**4**) 10 g L^{-1}; concentrations of reactants and the residence time τ are given in the figure; solvent: *n*-hexane; 0 °C.

time. Different residence times τ and starting material ratios were used. For the given concentrations of 14 mM of **1** and 36 mM of **2**, an enantiomeric excess of about 50% was reached for **3** in the continuous process. The higher values at the beginning of up to 80% are caused by the start-up conditions of a high excess of **2**. With the same concentrations similar values for the enantiomeric excess can be reached in a batch reactor as well.[13] Because of the limited reaction rate of the addition of **2** to aldehydes, the maximum conversion that could be reached at a residence time of 2.5 hours was 30%. Higher concentrations of **4** are not possible due to its limited solubility at 0 °C. In contrast to ligands coupled to insoluble polymers, where the reaction rate is reduced to 20% by the immobilization,[12a] the ligand bound to the soluble polymer is as active as before. The residence time in the continuous reactor has no influence on the enantiomeric excess in the conversion range from 7 to 30%. However, the enantiomeric excess reached in the batch reactor depends on the time elapsed and therefore on the conversion.[13] An excess of **1** yields the (*R*)-alcohol with up to 20% *ee*. But the conversion based on the limiting compound **2** of 12% is quite low. For all operating conditions used, the undesirable reduction of the aldehyde to the corresponding alcohol is negligible. Although almost stoichiometric amounts of catalyst and aldehyde are present (10 g L^{-1} catalyst, corresponding to 5 mmol L^{-1} of ligand), high chemoselectivities of between 89 and 96% were obtained.

The values for conversion and the enantiomeric excesses reached here are not yet sufficient for preparative use. The big advantage of this approach is the increase of the total turnover number for the chiral ligand. By varying the ratio of concentrations and the duration of continuous operation, the total turnover number for **4** has been raised by a factor of 10 from 50 to 500.[14] No deactivation of the catalyst was observed within seven days, which indicates that, in principle, longer operating times are possible for the reactor. To reach a total turnover number of 500 in batch experiments without any recovery of the catalyst its concentration has to be reduced from 2 to 0.2 mol%. Such low concentrations of chiral ligands are still seldom used in asymmetric synthesis. It should be possible, in principle, to convert a reaction with stoichiometric amounts of catalyst into a catalytic reaction by decoupling the residence time of catalyst and reactants in a continuously operated reactor. Besides an increase of the total turnover number, poor selectivity may be improved by high catalyst concentrations.

Recently dendrimers have been described that act as homogeneous catalysts.[15] These catalysts may be used in the reactor configuration described above. Since a steadily increasing number of solvent-stable membranes are now available for ultrafiltration and nanofiltration, the recovery of homogeneous catalysts becomes possible with methods already established in biocatalytic reactions such as 'repetitive batch'[16] or continuously operated reactors.

Experimental Procedure

The synthesis of **4** has been described elsewhere [13]. As reactor a flat membrane cell (volume 10 mL, membrane diameter 62 mm) made from polypropylene was used with stirring, as described for enzymatic reactions [17]. Connections were made with PEEK capillaries used for high performance liquid chromatography (HPLC). To ensure inert conditions substrate and product flasks were kept under argon. Additionally, the whole set-up was kept under argon in a box made from Plexiglas. The ultrafiltration membrane (Nadir UF PA 20, Hoechst AG, Frankfurt, Germany) was conditioned with dry *n*-hexane as described by the supplier. Catalyst **4** (100 mg) was dissolved in *n*-hexane (10 mL) and pumped into the reactor, which was subsequently rinsed with dry *n*-hexane for 12 h. The temperature was set to 0 °C. Solutions of **1** and **2** (50 mM each) in *n*-hexane were pumped separately into the reactor by means of two piston pumps P500 from Pharmacia (Freiburg, Germany). Different residence times and concentration ratios were obtained by varying the flow rate of the pumps. To determine the enantiomeric excess and conversion, aliquots (0.5 mL) of solution were collected at the reactor outlet and hydrolyzed with NH_4Cl solution. The samples were analyzed by GC (carrier gas H_2, 105 °C isothermal, injector 240 °C) on a permethylated β-cyclodextrin column (CS-Chromatographieservice, Langerwehe, Germany).

Received: October 9, 1995
Revised version: December 22, 1995 [Z8456IE]
German version: *Angew. Chem.* **1996**, *108*, 684–685

Keywords: asymmetric syntheses · immobilization · homogeneous catalysis · membrane filtration · membrane reactors

 © VCH Verlagsgesellschaft mbH, D-69451 Weinheim, 1996 0570-0833/96/3506-0643 $ 15.00+.25/0

[1] The total turnover number is defined as amount product formed per amount catalyst consumed.
[2] For filtration processes, see *Membrane Handbook* (Eds.: W. S. W. Ho, K. K. Sirkar), Chapman & Hall, New York, **1992**; R. Reidy, *Profile of the International Filtration and Separation Industry*, Elsevier, Oxford, **1993**.
[3] For a short review, see U. Kragl, C. Dreisbach, C. Wandrey in *Applied Homogeneous Catalysis* (Eds.: B. Cornils, W. A. Herrmann), VCH, Weinheim, in press.
[4] E. Bayer, V. Schurig, *Angew. Chem.* **1975**, *87*, 484–485; *Angew. Chem. Int. Ed. Engl.* **1975**, *14*, 493–494.
[5] U. Meyer-Blumenroth, J. Schneider in *Preprints des Aachener Membrankolloquiums*, VDI, Düsseldorf, **1991**, pp. 329–352.
[6] L. W. Gosser, W. H. Knoth, G. W. Parshall, *J. Mol. Catal.* **1977**, *2*, 253–263.
[7] E. Steckhan, S. Herrmann, R. Ruppert, J. Thömmes, C. Wandrey, *Angew. Chem.* **1990**, *102*, 445–447; *Angew. Chem. Int. Ed. Engl.* **1990**, *29*, 388–390.
[8] Reviews: A. S. Bommarius in *Biotechnology, Vol. 3: Bioprocessing* (Eds.: H.-J. Rehm, G. Reed, A. Pühler, P. Stadler, G. Stephanopoulos), VCH, Weinheim, **1993**, pp. 427–466; U. Kragl in *Industrial Enzymology*, 2nd ed. (Eds.: T. Godfrey, S. West), Macmillan, Hampshire, **1996**.
[9] The copolymer contains 0.75 mmol hydroxyl groups per gram polymer and the modified polymer about 0.53 mmol α,α-diphenyl-L-prolinol per g polymer.
[10] Now only a hydrophilic version of the membrane is commercially available (PAH20), which may be conditioned accordingly.
[11] K. Soai, S. Niwa, *Chem. Rev.* **1992**, *92*, 833–856.
[12] a) S. Itsuno, J. M. J. Fréchet, *J. Org. Chem.* **1987**, *52*, 4140–4142; b) S. Itsuno, Y. Sakurai, K. Ito, T. Mauyama, S. Nakahama, J. M. J. Fréchet, *ibid.* **1990**, *55*, 304–310.
[13] C. Dreisbach, G. Wischnewski, U. Kragl, C. Wandrey, *J. Chem. Soc. Perkin Trans. 1* **1995**, 875–878.
[14] For all calculations a conversion of 30% was used, as found for the continuously operated reactor for a residence time of 2.5 h. The total turnover number for the continuous reactor was calculated only under these conditions. Based on the amount of product formed during the whole operating time of the reactor, the total turnover number is higher than 2 000.
[15] J. W. J. Knapen, A. W. van der Made, J. C. de Wilde, P. W. N. M. van Leeuwen, P. Wijkens, D. M. Grove, G. van Koten, *Nature* **1994**, *372*, 659–663; H. Brunner, G. Net, *Synthesis* **1995**, 423–426.
[16] U. Kragl, A. Gödde, C. Wandrey, W. Kinzy, J. J. Cappon, J. Lugtenburg, *Tetrahedron: Asymmetry* **1993**, *4*, 1193–1202.
[17] U. Kragl, D. Gygax, O. Ghisalba, C. Wandrey, *Angew. Chem.* **1991**, *103*, 854–855; *Angew. Chem. Int. Ed. Engl.* **1991**, *30*, 827–828; G. F. Herrmann, U. Kragl, C. Wandrey, *ibid.* **1993**, *105*, 1399–1400, and **1993**, *32*, 1342–1343.

Polarized π-Electron Systems in a Chemically Generated Electric Field: Second-Order Nonlinear Optical Properties of Ammonium/Borate Zwitterions**

Christoph Lambert,* Stefan Stadler, Grant Bourhill, and Christoph Bräuchle

Second- and third-order nonlinear optical materials play an important role in future optoelectronic technology.[1] Among the second-order effects studied are second harmonic generation (SHG) and the electrooptic or Pockels' effect. Efforts are therefore directed at increasing the first-order hyperpolarizability β, which is the molecular property responsible for these effects. The compounds commonly employed are donor–acceptor substituted π-electron systems **A** with polarized electron distribution that exhibit internal charge transfer (CT) bands in the UV/Vis spectrum, such as *p*-aminonitrobenzene (*p*NA), 4-amino-4'-nitrotolane (ANT), and 4-*N*,*N*-dimethylamino-4'-nitrostilbene (DANS).

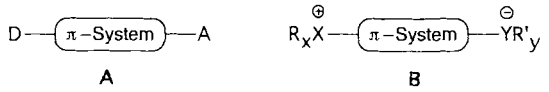

A **B**

The two-level model [Eq. (a)],[2] derived from a sum over states (SOS) approximation of the hyperpolarizability,

$$\beta_0 \propto \mu_{eg}^2 (\mu_e - \mu_g)/\tilde{\nu}_{eg}^2 \qquad \text{(a)}$$

shows that the CT transition energy ($\tilde{\nu}_{eg}$), the difference between exited- and ground-state dipole moment (μ_e and μ_g), and the transition dipole moment (μ_{eg}) govern the magnitude of the static first-order hyperpolarizability (β_0). The trivial approach to increasing β_0 is to lower the transition energy $\tilde{\nu}_{eg}$, for example, by increasing the conjugation length (*p*NA → DANS) (which will also alter μ_{eg} and $\mu_e - \mu_g$).[3] However, because this leads to less transparent molecules, the use of these systems for SHG applications is hampered by self-absorption of the second harmonic.[4] For this reason, we tried to maximize the $\mu_e - \mu_g$ difference by designing transparent zwitterionic systems **B** that show a very high ground-state dipole moment and are expected to have a small dipole moment in the first excited singlet state.

The general synthetic procedure for compounds **1**–**4** is similar for all derivatives and is outlined for **1** in Scheme 1.[5] All zwitterions are air stable but hygroscopic crystalline compounds that dissolve readily in polar nonhydrogen-bonding solvents such as THF (least polar) and MeCN (most polar). In these zwitterions the π-electron systems benzene, tolane, stilbene, and diphenylbutadiene have onium and at substituent groups along

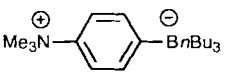

1

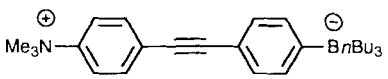

2

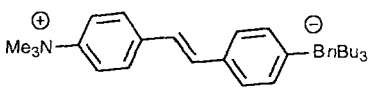

3

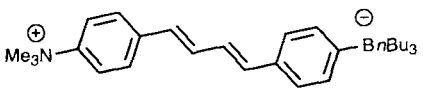

4

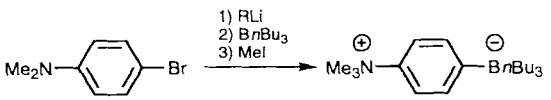

1 (b)

[*] Dr. C. Lambert
Institut für Organische Chemie der Universität
Universitätsstrasse 31, D-93040 Regensburg (Germany)
Fax: Int. code +(941)943-4984
Dipl.-Chem. S. Stadler, Dr. G. Bourhill, Prof. Dr. C. Bräuchle
Institut für Physikalische Chemie der Universität
Sophienstrasse 11, D-80333 München (Germany)

[**] We are grateful to the Fonds der Chemischen Industrie (Liebig grant to C. L.), to the Deutsche Forschungsgemeinschaft for financial funding and especially to Prof. J. Daub for his kind support at Regensburg. We thank M. Kollmannsberger for technical assistance.

the molecular z axis. These onium and at groups generate an electric field and consequently polarize the π-electron systems[6] much in the same way as a combination of push- and pull-substituents do, but by an inductive and/or field effect rather than by a mesomeric effect.[7] Since the onium and at groups are not conjugated with the π-electron systems, the internal CT transition of the zwitterions are expected to be at shorter wavelengths than those of analogous push–pull-substituted compounds. Indeed, for all zwitterions we observed CT bands in the UV spectra (see Table 1); the wavelengths of the CT bands and the extinction coefficients increase with the size of the π-system, but even in THF the former are substantially smaller than those of analogous NMe_2/NO_2-substituted species (for example in $CHCl_3$: *p*NA 348, ANT 380, DANS 430 nm[8, 9]).

Table 1. Comparison of calculated (AM1) and experimental optical data: absorption maximum (λ_{max}), extinction coefficient (ε), AM1-computed static hyperpolarizability ($\beta_{\mu 0}$), and hyperpolarizability at 1064 nm (β_μ), as well as the total isotropic averaged hyperpolarizabilities (β_0 and β) from HRS measurements.

	MeCN				Et_2O	THF	Et_2O
	AM1 λ_{max} [nm]	exp. λ_{max}[nm] ($\varepsilon \times 10^3$)	AM1 $-\beta_\mu(-\beta_{\mu 0})$ [10^{-30} esu]	exp.[a] $\beta(\beta_0)$ (1064nm) [10^{-30} esu]	AM1 λ_{max} [nm]	exp. λ_{max}[nm] ($\varepsilon \times 10^3$)	AM1 $-\beta_\mu(-\beta_{\mu 0})$ [10^{-30} esu]
1	266	237(7.9)	5(4)	7(5)	272	253[b](5.8)	5(4)
2	286	329(27.1)	50(34)	38(19)	316	349(23.5)	75(46)
3	302	349(33.7)	50(32)	84(38)	344	373(27.3)	94(50)
4	341	371(47.1)	103(55)	153(69)	411	400(39.4)	310(109)

[a] Error ± 15%. [b] In Et_2O.

All zwitterions investigated show strong negative solvatochromism, that is, the CT wavelengths decrease with increasing solvent polarity (Table 1): the shift of λ_{max} for solutions of **1**–**4** in MeCN and in THF is 1740–2670 cm^{-1}. The negative solvatochromism is indicative of a high ground-state dipole moment and a small excited-state dipole moment.[10] Indeed, AM1 calculations[11] of the zwitterions in the gas phase predict huge μ_g (**1** 20.0, **2** 44.5, **3** 41.9, **4** 47.1 D) and small μ_e (**1** 4.2, **2** 6.3, **3** 9.4, **4** 13.0 D). Although the dipole moment difference $\mu_e - \mu_g$ of the zwitterions might be overestimated by AM1 calculations,[16] it is substantially higher than those of comparable push–pull-substituted compounds [$(\mu_e - \mu_g)_{exp.}$ of *p*NA is 8.6, ANT 9.5, and DANS 18.2 D[17]].

How can charge transfer excitation in the zwitterionic systems be rationalized? AM1 calculation of the difference of Coulson charges of the ground and singlet excited state (calculated with the pairs and singles excitation CI (PECI) method) of, for example, **4** in the gas phase demonstrates the z-polarized charge transfer very well (Fig. 1). From the difference electron populations one can see that the negative charge located in the ground state at the BR_3Ph^- group is partially transferred to the phenyl ring adjacent to the ammonium group upon excitation. The charge transfer *within* the diphenylbutadiene moiety occurs solely in the π system; the σ electrons are not influenced.

Using the self consistent reaction field (SCRF) method implemented in the VAMP program, we calculated the CT bands of the zwitterions in MeCN and in Et_2O (the calculations for THF cannot be performed, but Et_2O has a similar permittivity). The agreement between observed and calculated CT bands is quite good (see Table 1), and the negative solvatochromic shift is also reproduced very well. This encouraged us to calculate the first-order hyperpolarizability β_μ at zero frequency (static hyperpolarizability) and 1064 nm excitation wavelength with an SOS method and using the SCRF approximation to model the solvent influence on β_μ. We found consistently higher β_μ values in Et_2O than in MeCN, which is predominantly due to the lower CT energy of the zwitterions in Et_2O (see Eq. a). The total isotropic averaged hyperpolarizability β[18] has been measured in MeCN by Hyper-Rayleigh scattering (HRS)[19] at 1064 nm with *p*NA as an external reference (β_μ(1064nm) = 29.2×10^{-30} esu in MeCN[8]); β_0 values have been calculated from these values by the two-level model approximation.[2] The agreement with the theoretical data is amazingly good, especially because neither the AM1 nor the SCRF method are parametrized to reproduce UV data (as are, for example, CNDO/S and INDO/S).[1f]

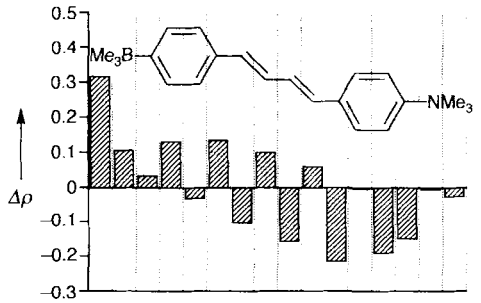

Fig. 1. Coulson charge differences $\Delta\rho$, calculated with the AM1 approximation, between the ground state and the first excited singlet state of an analogue of **4** (*n*-butyl groups are replaced by methyl groups). The charge differences refer to the sum of charges of all heavy atoms and hydrogen atoms drawn in each column. A positive charge difference indicates loss of negative charge upon excitation.

The β_0 values observed are similar to $\beta_{\mu 0}$ of analogous NMe_2/NO_2- or NH_2/NO_2-substituted systems (*p*NA 7.6, ANT 19, DANS 55×10^{-30} esu[9]). Although direct comparison with these literature data is hampered by different measurement techniques and different reference compounds the trends of β_0 in the zwitterion series is the same as for the push–pull-substituted analogues.

In conclusion, we have shown in this study that onium and at groups can polarize π-electron systems; the resulting main group organometallic zwitterions exhibit z-polarized CT bands as do comparable push–pull-substituted compounds. However, these zwitterions are more transparent than their push–pull analogues, which should promote application in SHG devices. Nonetheless, the first-order hyperpolarizability of the zwitterions is about the same as that of analogous donor–acceptor-substituted species. In addition, the high ground-state dipole moment of the zwitterions should favor the alignment of these derivatives in polymer films in order to obtain enhanced macroscopic SHG and electrooptic effects (note the very high $\mu\beta_0$ value of, for example **4**: about 3250×10^{-48} esu). Furthermore, it might be possible to introduce chiral ligands to boron or to nitrogen to induce a noncentrosymmetric space group in the crystalline state. These topics are currently under investigation.

Received: October 5, 1995
Revised version: December 7, 1995 [Z 8447 IE]
German version: *Angew. Chem.* **1996**, *108*, 710–712

Keywords: boron compounds · nonlinear optics · semiempirical calculations · zwitterions

[1] For general introductions to nonlinear optics see, for example, a) P. N. Prasad, D. J. Williams, *Nonlinear Optical Effects in Molecules and Polymers*, Wiley, New York, **1991**; b) *Principles and Applications of Nonlinear Optical Materials* (Eds.: R. W. Munn, C. N. Ironside), Blackie, Glasgow, **1993**; c) *Organic Materials for Photonics* (Ed.: G. Zerbi), North-Holland, Amsterdam, **1993**; d) T. J. Marks, M. A. Ratner, *Angew. Chem.* **1995**, 107, 167; *Angew. Chem. Int. Ed. Engl.* **1995**, *34*, 155; e) N. J. Long, *ibid.* **1995**, 107, 37 and **1995**, *34*, 21; f) D. R. Kanis, M. A. Ratner, T. J. Marks, *Chem. Rev.* **1994**, *94*, 195.

[2] J. L. Oudar, D. S. Chemla, *J. Chem. Phys.* **1977**, *66*, 2664.
[3] S. R. Marder, D. N. Beratan, L.-T. Cheng, *Sience* **1991**, *252*, 103.
[4] D. M. Burland, R. D. Miller, C. A. Walsh, *Chem. Rev.* **1994**, *94*, 31.
[5] See also G. Wittig, W. Herwig, *Chem. Ber.* **1955**, *88*, 962. Synthetic procedures for **1–4**, as well as X-ray structures of **1** and **4**, will be published elsewhere.
[6] S. R. Marder, C. B. Gorman, F. Meyers, J. W. Perry, G. Bourhill, J.-L. Bredas, B. M. Pierce, *Science* **1994**, *265*, 632.
[7] The NLO properties of some betaines have been studied earlier: B. F. Levine, C. G. Bethea, E. Wasserman, L. Leenders, *J. Chem. Phys.* **1978**, *68*, 5042; A. Dulic, C. Flytzanis, *Opt. Commun.* **1978**, *25*, 402; M. S. Paley, J. M. Harris, *J. Org. Chem.* **1991**, *56*, 568. However, the π polarization in the compounds studied (pyridinium phenoxides, merocyanines) is mainly caused by mesomeric rather than inductive effects as in **1–4**. This simplified view disregards the fact that the nitrogen and boron alkyl substituents in **1–4** also may interact with the π system by hyperconjugation.
[8] M. Stähelin, D. M. Burland, J. E. Rice, *Chem. Phys. Lett.* **1992**, *191*, 245.
[9] a) L.-T. Cheng, W. Tam, S. H. Stevenson, G. R. Meredith, G. Rikken, S. R. Marder, *J. Phys. Chem.* **1991**, *95*, 10631; b) L.-T. Cheng, W. Tam, S. R. Marder, A. E. Stiegman, G. Rikken, C. W. Spangler, *ibid.* **1991**, *95*, 10643.
[10] C. Reichardt, *Solvents and Solvent Effects in Organic Chemistry*, 2nd ed., VCH, Weinheim, **1990**, p. 289.
[11] The AM1 calculations were performed with the VAMP 5.01. program [12]. An analogue of compound **4** was calculated: the *n*-butyl groups were replaced by methyl groups. The excited states were calculated at the geometry of the ground states with the PECI = 10 [13]. The UV transitions and hyperpolarizabilities were computed with the SCRF method in order to model the influence of the solvent [14]. The hyperpolarizability β_μ was calculated with the SOS method at zero and at 1.16 eV excitation energy (1064 nm) [13]. β_μ is the projection of the β tensor on the dipole moment vector. To compare the calculated β_μ values with the experimental values, they must be divided by 3, since the SOS approximation refers to β based on a perturbation theory, whereas β of the experimental reference compound is differently defined [8,15].
[12] VAMP, Version 5.01, G. Rauhut, A. Alex, J. Chandrasekhar, T. Steinke, T. Clark, Erlangen, **1993**.
[13] T. Clark, J. Chandrasekhar, *Isr. J. Chem.* **1993**, *33*, 435.
[14] G. Rauhut, T. Clark, T. Steinke, *J. Am. Chem. Soc.* **1993**, *115*, 9174.
[15] A. Willetts, J. E. Rice, D. M. Burland, D. P. Shelton, *J. Chem. Phys.* **1992**, *97*, 7590.
[16] While ground state dipole moments are usually well reproduced by the AM1 method, there is no information available on the reliability of excited state dipole moments calculated with the PECI method; see J. J. P. Stewart in *Reviews in Computational Chemistry, Vol. 1* (Eds.: K. B. Lipkowitz, D. B. Boyd), VCH, Weinheim, **1991**, p. 45; N. Matsuzawa, D. A. Dixon, *J. Phys. Chem.* **1992**, *96*, 6232; J. O. Morley, *ibid.* **1994**, *98*, 13182.
[17] a) A. E. Stiegman, E. Graham, K. J. Perry, L. R. Khundkar, L.-T. Cheng, J. W. Perry, *J. Am. Chem. Soc.* **1991**, *113*, 7658; b) N. G. Bakhshiev, M. I. Knyazhanskii, V. I. Minkin, O. A. Osipov, G. V. Saidov, *Russ. Chem. Rev.* **1969**, *38*, 740.
[18] Although β measured in the HRS experiment is the averaged isotropic value it corresponds to β_μ in dipolar molecules where the largest β component lies parallel to the CT direction; see G. J. T. Heesink, A. G. T. Ruiter, N. F. van Hulst, B. Bölger, *Phys. Rev. Lett.* **1993**, *71*, 999; E. Hendrickx, C. Clays, A. Persoons, C. Dehu, J. L. Bredas, *J. Am. Chem. Soc.* **1995**, *117*, 3547.
[19] A description of the specific experimental set-up used in this study and the data analysis can be found in S. Stadler, F. Feiner, C. Bräuchle, S. Brandl, R. Gompper, *Chem. Phys. Lett.* **1995**, *245*, 292. For general introductions into HRS measurements, see K. Clays, A. Persoons, *Phys. Rev. Lett.* **1991**, *66*, 2980; *Rev. Sci. Instrum.* **1992**, *63*, 3285; K. Clays, A. Persoons, L. De Maeyer, *Adv. Chem. Phys.* **1994**, *85*, 455. The chromophores were checked for fluorescence prior to HRS measurements. In addition, the spectral purity of the HRS signal was investigated with a set of narrow bandpass filters of varying transmission peak wavelength (500, 532, and 570 nm). Only at the wavelength of the second harmonic (532 nm) could a signal be detected. Thus, we can exclude the possibility of broadband contributions such as hot-two-photon- or three-photon-induced fluorescence. For **3** we found an unusually strong bathochromic shift of $\lambda_{cut-off}$ at higher number densities (15.71×10^{18} cm^{-3}). For **4** we found a positive deviation from a linear correlation between the SHG signal and the number density above about 2.5×10^{18} cm^{-3} (these data have been omitted in the data evaluation of β). Both effects might indicate aggregation at these very high concentrations. It is currently not known to which extent these aggregation effects influence the HRS signal, for example, by correlated scattering.

Automated Solid Phase Synthesis of Platinated Oligonucleotides via Nucleoside Phosphonates**

Jürgen Schliepe, Ulrich Berghoff, Bernd Lippert, and Dieter Cech*

Platinum compounds, in particular, *cis*-diamminedichloroplatinum(II) (cisplatin, CDDP) and several of its derivatives, are widely used nowadays in the treatment of a number of tumour diseases.[1] The cancerostatic activity of these compounds is directly related to their reaction with cell DNA, and the formation of covalent adducts.[2] On the basis of numerous studies with model nucleobases, nucleosides, nucleotides, and short DNA fragments, we now believe that we understand the fundamental aspects of these interactions.[3] Till now, studies of the platination of oligonucleotides have been carried out exclusively with presynthesized samples.[4] To our knowledge, there has been no report to date of any platinated oligonucleotide that was obtained by direct inclusion of a platinated nucleotide building block in an automated DNA synthesis, though this route offers clear advantages with respect to possible synthetic variations.

We describe herein the automated synthesis of *trans*-$(NH_3)_2$-Pt^{II}-modified oligonucleotides via a 3′-phosphitylated platinum nucleoside synthon. Initial studies showed that it is necessary to carry out the phosphitylation before the platination. For reasons of greater stability, we chose to use phosphonates[5] in this procedure, rather than the more usual phosphoramidites.[6] Till now, we have concentrated on the reaction of the 5′-dimethoxytritylated thymidine-3′-phosphonate **1** with *trans*-$[(NH_3)_2PtCl_2]$ (TDDP) (Scheme 1). Compound **1** was synthe-

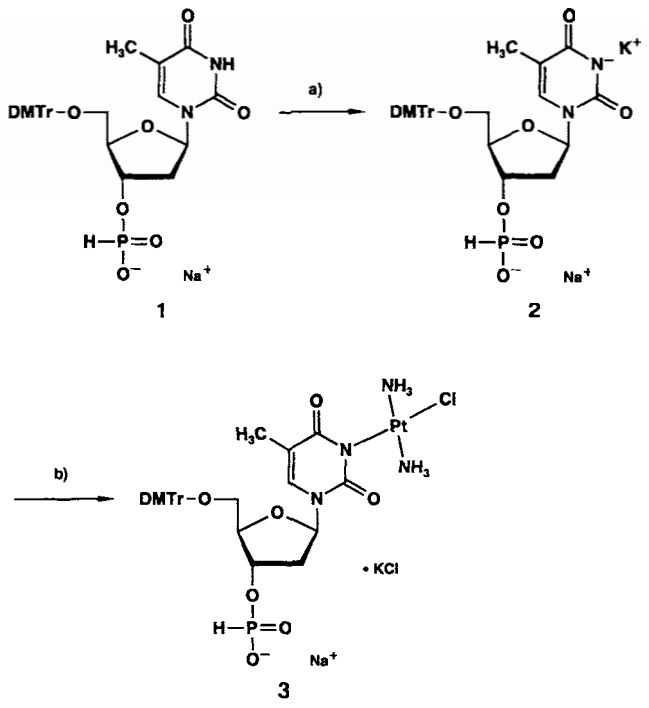

1 2 3

Scheme 1. DMTr = dimethyoxytrityl; a) +1 equiv KOH, H_2O; b) +1 equiv TDDP, *N*,*N*-dimethylformamide (DMF).

[*] Prof. Dr. D. Cech, Dipl.-Chem. J. Schliepe
Fachbereich Chemie der Humboldt-Universität
Hessische Strasse 1-2, D-10099 Berlin (Germany)
Fax: Int. code +(30)2397 2479
Dipl.-Chem. U. Berghoff, Prof. B. Lippert
Fachbereich Chemie der Universität Dortmund (Germany)

[**] This work was supported by the Deutsche Forschungsgemeinschaft

sized as previously reported,[7] deprotonated with KOH[8] to give **2**, and subsequently treated with *trans*-$[(NH_3)_2PtCl_2)]$ to afford the Pt complex **3**.[9] Complex **3** was characterized by elemental analysis, as well as by ^1H NMR, ^{195}Pt NMR, and IR spectroscopy.[10] The ^{195}Pt NMR signal of **3** ($\delta = -2265$, $[D_7DMF]$) lies in the expected region for a PtN_3Cl coordination sphere,[11] and its chemical shift is also clearly distinct from that of free *trans*-$[(NH_3)_2PtCl_2)]$ and its DMF solvolysis products. The thymine H6 resonance signal of **3** is shifted upfield compared to that of **1**, as expected, and is obscured by the resonance signals of the dimethoxytrityl group.[12] However, its existence can be unambiguously proven by $^1H,^1H$-COSY experiments (coupling to the $C(5)CH_3$ of the thymine). The formulation of **3** as a KCl adduct is based on the analytical data[10] and is possibly due to the tendency of N3-platinated thymine or uracil to take up further cations at O4 or O5, respectively, as described several times in the past.[13]

The modified oligodeoxyribonucleotides 5′-d(CXCA) and 5′-d(ATAGTAXACAGA), with X = *trans*-$[(NH_3)_2Pt^{II}]$-T were synthesized by using **3** and an automated synthesizer (Gene Assembler, Pharmacia).[14] The coupling of **3** to the unmodified nucleotides was carried out following usual synthesis protocols. To improve the yield, **3** and the following phosphonate in the elongation cycle were added in two- to threefold excess. The yields were estimated to be 98.3% per coupling step and 85.2% in overall yield (by measurement of DMTr release). Following the final cycle, the oligonucleotides were cleaved from the carrier and purified by reversed-phase high-performance liquid chromatography (RP-HPLC).[15] The yields of platinated product were about 30% (estimated from the HPLC signal intensities, Fig. 1) based on the yields obtained from similar syntheses with

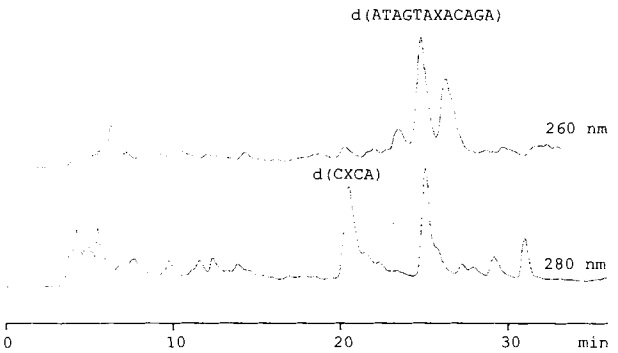

Fig. 1. HPL chromatograms of the oligonucleotides d(CXCA) and d(ATAGTAXACAGA) (X = Pt-T), before purification [15].

unmodified oligonucleotides. Although the yields for the individual coupling steps and the estimated overall yield was in the region expected for standard oligonucleotide syntheses, the low yields of isolated product point to numerous side reactions during cleavage and workup, which still need to be optimized. Deplatination of the sensitive oligonucleotides presumably plays a large role here. The *trans*-$(NH_3)_2TPt^{II}(py)$ unit which is produced during the synthetic cycle remains unchanged during deprotection with NH_3; substitution by NH_3, as for Cl-containing compounds, does not occur.[16] Matrix-assisted laser desorption ionization mass spectrometry (MALDI-MS) revealed the molecular ion at 3985.0, as calculated for the platinated 12-mer; 3984.7 for *trans*-$[(NH_3)_2Py\{d(ATAGTATACAGA)$-N3-T(7)$\}Pt]^+$. The non-occurrence of the triammine complex was confirmed by a comparison of the retention times (HPLC) of the platinum-modified nucleoside obtained after enzymatic hydrolysis with synthetically produced $[(NH_3)_3(N3\text{-}T)Pt]^+$.[17] The *trans*-$(NH_3)_2Pt^{II}$ structure is also retained after deprotection with NaOH. The platinated 4-mer gave monoisotope peaks of m/z 1439.8 ($z = 1$) and m/z 720.9 ($z = 2$) in the ion spray mass spectra. This also corresponds to the pyridine-coordinated platinum complex (m/z 1440).

The synthesized platinated oligonucleotides were investigated by gel electrophoresis before and after deplatination.[18] As expected, the platinated oligonucleotides showed a shift in comparison with the unmodified oligonucleotides,[19] which was no longer observed after treatment with cyanide (Fig. 2). Enzy-

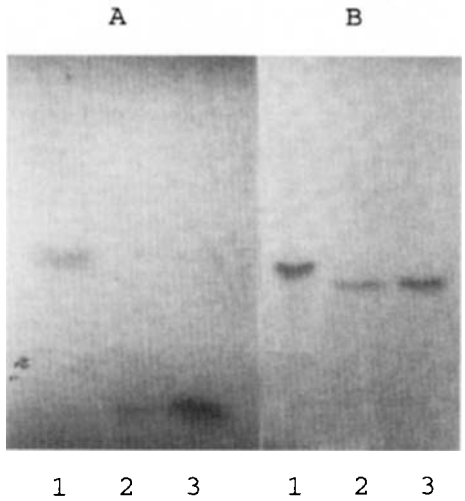

Fig. 2. A) Gel electrophoresis of d(CXCA) before (lane 1) and after deplatination (lane 2), and of d(CTCA) (lane 3); B) gel electrophoresis of d(ATAGTAXACAGA) before (lane 1) and after deplatination (lane 2), and of d(ATAGTATACAGA) (lane 3) [18].

matic hydrolysis under the usual conditions[20] showed the expected total composition in the HPL chromatogram of the oligonucleotides (Fig. 3).[21] The peaks at 27.1 and 2.6 min. are

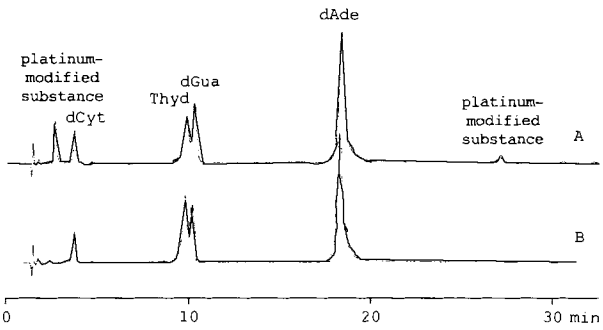

Fig. 3. Enzymatic hydrolysis of the modified 12-mer (A) and of the unmodified 12-mer (B) with 0.2 u snake venom phosphodiesterase and 2 u alkaline phosphatase, as described in ref [20].

an indication of the successful incorporation of the platinated thymidine. The latter peak can be assigned to the platinated thymidine on the basis of its polarity. However, the platinum-modified material appears initially as a peak at 27.1 min., which is degraded with time and reappears as a peak at 2.6 min. Presumably the first peak can be assigned to a platinated dinucleotide containing the incorporated platinated thymidine, that is, the modification evidently leads to a reduction in the enzymatic

hydrolysis rate. Such products are known for the enzymatic hydrolysis of modified oligonucleotides.[22] The presence of Pt in the synthetic oligonucleotides was shown qualitatively with $SnCl_2$ (thin layer chromatography) and electrochemically.[23] Quantitative Pt analysis by atomic absorption spectroscopy (AAS) yielded a value of 1.05 Pt per tetramer or dodecamer.

The medium-term aim of our studies is to synthesize platinated oligonucleotides that are able to react with target sequences in DNA or RNA via the metal ion. Such reactions cannot be expected with the coordinately saturated platinum oligonucleotides described here. They could then lead to the development of useful chemical nucleic acid probes and/or antisense and antigen reagents.[24]

Received: August 18, 1995
Revised version: November 27, 1995 [Z 8322 IE]
German version: *Angew. Chem.* **1996**, *108*, 705–707

Keywords: cytostatics · DNA synthesis · oligonuleotides · platinum compounds

[1] M. E. Heim in *Metal Complexes in Cancer Chemotherapy* (Ed.: B. K. Keppler), VCH Weinheim, **1993**, pp. 9 ff.

[2] S. E. Sherman, S. J. Lippard, *Chem. Rev.* **1987**, *87*(5), 1153–1181; W. I. Sundquist, S. J. Lippard, *Coord. Chem. Rev.* **1990**, *100*, 293–322; E. Holler in *Metal Complexes in Cancer Chemotherapy* (Ed.: B. K. Keppler), VCH, Weinheim, **1993**, pp. 37 ff; J. Reedijk, A. M. J. Fichtinger-Schepman, A. T. van Oosterom, P. van de Putte, *Struct. Bonding (Berlin)* **1987**, *67*, 53–89.

[3] B. Lippert, *Prog. Inorg. Chem.* **1989**, *37*, 1–97; S. Yao, J. P. Plastaras, L. G. Marzilli, *Inorg. Chem.* **1994**, *33*, 6061–6077; G. Admiraal, M. Alink, C. Altona, F. J. Dijt, C. J. van Garderen, R. A. G. de Graaff, J. Reedijk, *J. Am. Chem. Soc.* **1992**, *114*, 930–938.

[4] C. A. Lepre, K. G. Strothkamp, S. J. Lippard, *Biochemistry* **1987**, *26*, 5651–5657; L. J. Naser, A. L. Pinot, S. J. Lippard, J. M. Essigmann, *ibid.* **1988**, *27*, 4357–4367; C. A. Lepre, L. Chassot, C. E. Costello, S. J. Lippard, *ibid.* **1990**, *29*, 811–823; K. M. Comess, C. E. Costello, S. J. Lippard, *ibid.* **1990**, *29*, 2102–2110; D. P. Bancroft, C. A. Lepre, S. J. Lippard, *J. Am. Chem. Soc.* **1990**, *112*, 6860–6871; V. Brabec, M. Sip, M. Leng, *Biochemistry* **1993**, *32*, 11676–11681; V. Brabec, M. Leng, *Proc. Natl. Acad. Sci. USA* **1993**, *90*, 5345–5349; J. M. Malinge, C. Perez, M. Leng, *Nucleic Acids Res.* **1994**, *22*, 3834–3839.

[5] B. C. Froehler, M. D. Matteucci, *Tetrahedron Lett.* **1986**, *27*, 469–472; B. C. Froehler, P. G. Ng, M. D. Matteucci, *Nucleic Acids Res.* **1986**, *14*, 5399–5407; P. J. Garreg, T. Regberg, J. Stawinski, R. Stroemberg, *Chem. Scr.* **1986**, *26*, 59–61.

[6] M. J. Gait in *An Introduction to Modern Methods of DNA Synthesis* (Ed.: M. J. Gait), IRL Press, Oxford, **1984**, pp. 1–22.

[7] R. A. Jones in *Preparation of Protected Desoxyribonucleosides* (Ed.: M. J. Gait), IRL Press, Oxford, **1984**, p. 23–34; H. Takaku, S. Yamakage, O. Sakatsume, M. Ohtsuki, *Chem. Lett.* **1988**, *10*, 1675–1678.

[8] Synthesis in analogy to that of thymine: C. J. L. Lock, P. Pilon, B. Lippert, *Acta Crystallogr. Sect. B* **1979**, *35*, 2533–2537; the Na salt analogous to **2** has in the meantime also been synthesized and converted to **3**.

[9] Method: Compound **2** (206 mg, 0.3 mmol) was made anhydrous by repeated distillation in vacuo with anhydrous pyridine, and was then treated with *trans*-$[(NH_3)_2PtCl_2]$ (90 mg, 0.3 mmol) in DMF (1.5 mL) (5 h 50 °C, 3 d 22 °C). After removal of the DMF in vacuo, MeOH (6 mL) was added, filtered after 24 h, and the filtrate reduced to dryness. After reprecipitation in acetone, the product **3** (255 mg, 86 %) was used without further purification.

[10] Satisfactory elemental analysis for C, H, N, Cl; Proof of Na and K by scanning electron microscopy (SEM); IR (KBr): ν(Pt-Cl) 330 cm^{-1}; ^1H NMR ([D$_7$]DMF): δ (**3**) = 1.47 (s, 3H, 5-CH_3), 2.28–2.41 (m, 2H, H-2′,H-2″), 3.26–3.44 (m, 2H, H-5′,H-5″), 3.80 (s, 6H, CH_3O), 3.89 (b, 6H, $(NH_3)_2$Pt), 4.15 (m, 1H, H-4′), 4.95 (m, 1H, H-3′), 6.41 (m, 1H, H-1′), 6.79 (d, $J(^{31}P,^1H)$ = 577 Hz, 1H, H-P), 6.93–7.53 (m, 13H, DMTr), 7.50 according to ^1H-^1H-COSY (s, 1H, H-6); ^{195}Pt NMR ([D$_7$]DMF): δ = −2265 relative to $[PtCl_6]^{2-}$. The NMR measurements were carried out on Bruker-AC 200; -AM 300- as well as -DRX-400-approaches.

[11] T. G. Appleton, A. J. Bailey, K. J. Barnham, J. R. Hall, *Inorg. Chem.* **1992**, *31*, 3077–3082 and references therein.

[12] ^1H NMR ([D$_7$]DMF): δ (**1**) = 1.46 (s, 3H, 5-CH_3), 2.44–2.47 (m, 2H, H-2′,H-2″), 3.23–3.46 (m, 2H, H-5′,H-5″), 3.80 (s, 6H, CH_3O), 4.21 (m, 1H, H-4′), 4.99 (m, 1H, H-3′), 6.36 (m, 1H, H-1′), 6.78 (d, $J(^{31}P,^1H)$ = 582 Hz, 1H, H-P), 6.94–7.52 (m, 13H, DMTr), 7.65 (s, 1H, H-6), 11.42 (s, 1H, 3-NH).

[13] O. Renn, B. Lippert, I. Mutikainen, *Inorg. Chim. Acta* **1994**, *218*, 117–120 and references therein.

[14] P. J. Garreg, I. Lindt, T. Regberg, J. Stawinski, R. Strömberg, *Tetrahedron Lett.* **1986**, *27*, 4051–4054.

[15] Synthesis of the 12-mer: for the unmodified monomers nucleoside phosphonates from Millipore were used, deprotection with conc. NH_3 (7 h 50 °C); purification with RP–HPLC (Nucleosil 100, C18, 7 μm; 15–25 % MeOH gradient in 0.1 M NH_4OAc over 30 min) and ion exchange–HPLC. Synthesis of the 4-mer: PAC-dA (Pharmacia) was used as carrier, for the unmodified dC *i*Bu-dC-H-phosphonate was synthesized (by standard procedures), deprotection with 0.17 M NaOH for 1–2 days, purification analogous to that of the 12-mer, but using a 10–20 % MeOH gradient in 0.1 M NH_4OAc over 30 min.

[16] R. Pfab, P. Jandik, B. Lippert, *Inorg. Chim. Acta* **1982**, *66*, 193–204.

[17] Synthesis of *trans*-$[(NH_3)_2Cl(N_3\text{-}T)Pt]$ analogous [9], conversion of $[(NH_3)_3(N3\text{-}T)Pt]^+$ by reaction with NH_3 (conc.) for 30 min. at 90 °C and removal of the excess NH_3 (conc.) in vacuo.

[18] Deplatination in 0.05 M Tris·HCl, pH = 8.0 with 0.3 M NaCN at 50 °C for 24 h, gel electrophoresis in 40 % acrylamide/bisacrylamide + 7 M urea.

[19] Synthesis of the unmodified standard nucleotides with the Gene Assembler (Pharmacia), using the amidite method with the corresponding standard reagents from Pharmacia, deblocking with conc. ammonia (6 h, 50 °C), desalting of the 4-mer with Sephadex G-10, and of the 12-mer with Sephadex G-25 (Pharmacia).

[20] S. Schmidt, C.-D. Pein, H.-J. Fritz, D. Cech, *Nucleic Acids Res.* **1992**, *20*, 2421–2426.

[21] The number of bases of the platinated 12-mer compared as integration areas with those of the unmodified oligonucleotides (calculated, theoretical): A (6.0, 6); C (1.1, 1); G (2.1, 2); T 2.2, 2).

[22] A. Eastman, M. M. Jennerwein, D. L. Nagel, *Chem. Biol. Interact.* **1988**, *67*, 71–80.

[23] E. Merck, *Anfärbereagentien für Dünnschicht- und Papier-Chromatographie, Darmstadt*, **1980**, p. 109; J. Wang, J. Zadeii, M. S. Lin, *J. Electroanal. Chem.* **1987**, *237*, 281–287.

[24] O. Krizanovic, M. Sabat, R. Beyerle-Pfnür, B. Lippert, *J. Am. Chem. Soc.* **1993**, *115*, 5538–5548.

The First "Charm Bracelet" Conjugated Polymer: An Electroconducting Polythiophene with Covalently Bound Fullerene Moieties**

Tiziana Benincori, Elisabetta Brenna, Franco Sannicolò,* Licia Trimarco, Gianni Zotti, and Piero Sozzani

A great deal of effort is currently being directed towards the design and realization of functionalized "intelligent" materials:[1] the synthesis of polymers containing fullerene moieties in either the main or side chains[2, 3] and which show peculiar electrical[4] and electrochemical[5] properties is a challenging topic in this field of research. We report here the first conjugated conducting "charm bracelet" polymer,[6] consisting of fullerene moieties linked to a highly ordered polythiophene backbone. One of the potential interests in associating a p-type conjugated polythiophene and an n-type fullerene lies in the possibility of charge transfer between these two moieties, as recently shown by Heeger and Wudl et al., who, however, prepared and studied heterogeneous blends of C_{60} and poly(3-alkylthiophenes) only.[7]

[*] Prof. F. Sannicolò, Dr. T. Benincori, Dr. E. Brenna, Dr. L. Trimarco, Prof. P. Sozzani
Dipartimento di Chimica Organica e Industriale
Centro CNR Sintesi e Stereochimica Speciali Sistemi Organici
Università degli Studi di Milano
Via Golgi 19, I-20133 Milano (Italy)
Fax: Int. code + (2) 2364369
e-mail: staclaus@icil64.cilea.it.
Dr. G. Zotti
Istituto di Polarografia ed Elettrochimica Preparativa del CNR, Padova (Italy)

[**] This work was supported by CNR - Progetto Strategico Materiali Innovativi.

Our aim was to connect a C_{60} unit to a suitable thiophene monomer, through stable and possibly rigid bonds capable of exchanging electronic information between the two moieties, and then to anodically oxidize the resulting system to give a conducting polymer. The plan was designed on the basis of the well-documented[8] reactivity of C_{60} towards diazoalkanes and on the possibility of obtaining the 4-diazocyclopenta[2,1-*b*:3,4-*b'*]dithiophene **2** from 4*H*-cyclopenta[2,1-*b*:3,4-*b'*]dithiophene (**1**), a 2,2'-bithiophene monomer recently made accessible

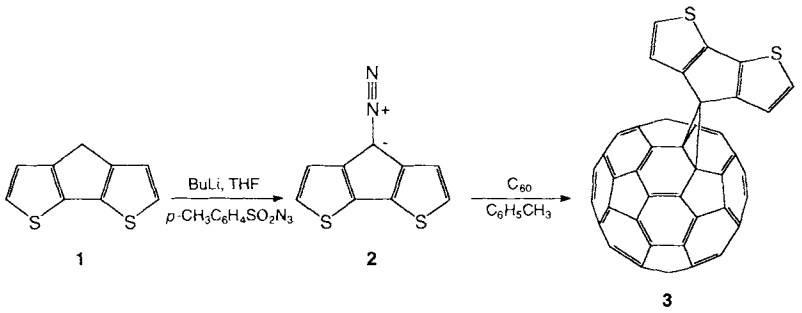

Scheme 1. Synthesis of the cyclopentadithiophene fullerene adduct **3**

through a simple and reproducible route.[9] The cyclopentadithiophene structure satisfactorily answered all the synthetic, geometric, and electronic requirements:

1. The cyclopentadithiophene **1** could give, at least in theory, a diazo derivative capable of reacting with C_{60}, just as fluorene does.[6]
2. The planar cyclopentadithiophene can be electrochemically polymerized to give a material endowed with good electrical conductivity ($\sigma = 40\ S\,cm^{-1}$) and extended conjugation (λ_{max} of the neutral polymer: 545 nm).[9]
3. The C_{2v} symmetry of **1** and the homotopism of the positions involved in the polymerization process would be preserved in the adduct: this is a prerequisite for regioselective polymerization.
4. The diameter of C_{60}[5] and the distance between the two α-carbon atoms[10] of cyclopentadithiophene involved in the polymerization process are of similar length: thus polymerization would not be prevented by steric factors.
5. The cyclopropane bonds, connecting the C_{60} and the cyclopentadithiophene units, are known to exhibit a high π character.[11] This would allow conjugative interaction between the polythiophene chain and the fullerene pendants.

We converted **1** into the stable diazo derivative **2** by using the "diazo transfer reaction"[12] (Scheme 1), and then allowed **2** to react with one equivalent of C_{60} in toluene at room temperature for 12 hours. This led to the thermodynamically favored adduct **3**, which has the structure of a closed 6,6-bridged methanofullerene (elemental analysis, MS, ^1H and ^{13}C CP-MAS NMR, and UV spectroscopy).[13] The ^1H NMR spectrum of **3** showed only two doublets, which were assigned to the α and β thiophene hydrogen atoms. This provided evidence for the addition of the cyclopentadithiophene moiety across a 6,6 ring junction. The ^{13}C CP-MAS spectrum of **3** contained a signal at $\delta = 45.9$, which corresponds to the sp^3 carbon atom in position 4 of the cyclopentadithiophene system ($\delta = 31$ in **1**). A signal at $\delta = 76.1$ was assigned to the two homotopic carbon atoms of C_{60} involved in the cyclopropane ring formation. The signals of the α and β carbon atoms of the cyclopentadithiophene system at $\delta = 123.3$ and 127.7 were not markedly affected by substitution ($\delta = 122.7$ and 124.2 in **1**). The signals at $\delta = 139.5$ and 147.5 result from the superimposition of thiophene ($\delta = 138.4$ and 147.4 in **1**) and fullerene carbon atoms. A complex pattern of signals, in which two main peaks emerge at $\delta = 143.1$ and 144.6, was assigned to the C_{60} moiety. Furthermore, the UV spectrum resembled those of other fullerene cyclopropane derivatives,[14] showing a characteristic absorption band at 434 nm.

The electrochemical behavior of **3** was first examined in a 5×10^{-5} M toluene/acetonitrile (5/1) solution. The cathodic cyclic voltammogram (Fig. 1) showed three one-electron reversible processes, typical of C_{60} derivatives, at -0.82, -1.21, and -1.73 V, close to the potential values reported for C_{60}.[15] In the anodic scan, **3** was irreversibly oxidized with no polymerization.

The electrochemical oxidation of **3** was then investigated in a 2×10^{-4} M chlorobenzene solution. In the first anodic scan ($0.1\ Vs^{-1}$), **3** displayed a two-electron irreversible oxidation peak at 1.05 V related to the cyclopentadithiophene moiety. This peak is 0.55 V more positive than the oxidation potential of the parent compound **1**;[9] this is attributed to the electron-withdrawing properties of the fullerene substituent. The oxidation of C_{60} and its derivatives is described[16] at potential values 2.3–2.4 V more positive than the first reduction step. The continuous cycling of

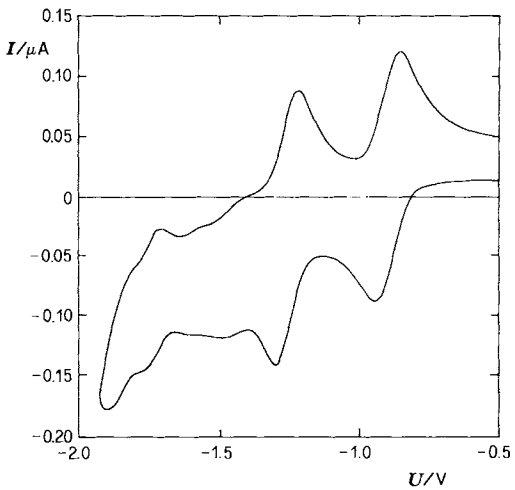

Fig. 1. Cathodic cyclic voltammogram of **3** in toluene/acetonitrile 5/1. Scan rate: $0.1\ Vs^{-1}$.

the potential at the oxidation peak developed the redox response of the polymer growing on the anode (Fig. 2, left).

The anodic and cathodic cyclic voltammograms of poly-**3** were investigated in acetonitrile. The polythiophene backbone was reversibly oxidized at 0.1 and 0.5 V (Fig. 2, right), whereas the corresponding poly-**1** showed a redox system centered at 0.0 V.[9] The charge involved is about 50% of that needed for a one-electron exchange, measured in reduction. Thus, oxidation corresponds to about 0.25 electrons per thiophene ring, a value which is usually found for polythiophenes. The side chain C_{60} substituents were reversibly reduced in three steps at -0.88, -1.38, and -1.85 V (Fig. 3).

The neutral film appeared as a violet deposit, showing an absorption maximum at 440 nm and a shoulder at 600 nm

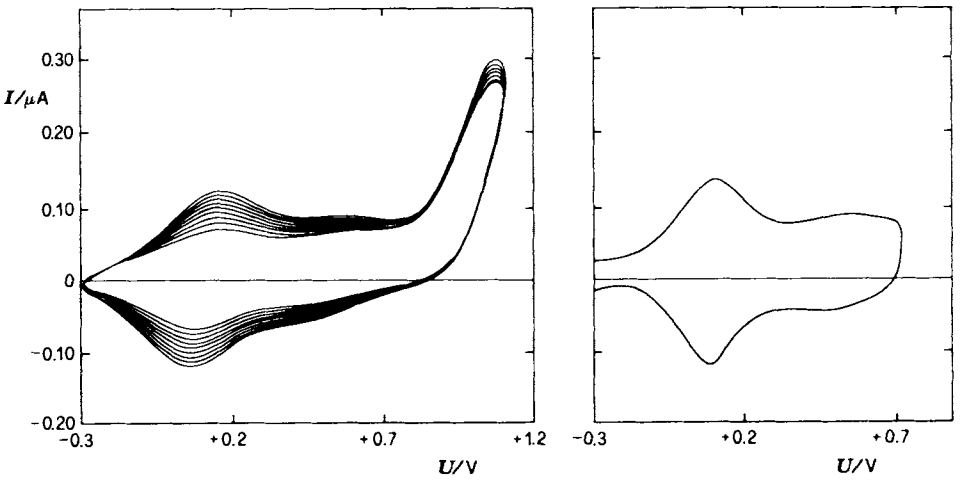

Fig. 2. Left: Repetitive cyclic voltammogram of **3** in chlorobenzene. Scan rate: 0.1 Vs^{-1}. Right: Anodic cyclic voltammogram of poly-**3** in acetonitrile. Scan rate: 0.1 Vs^{-1}.

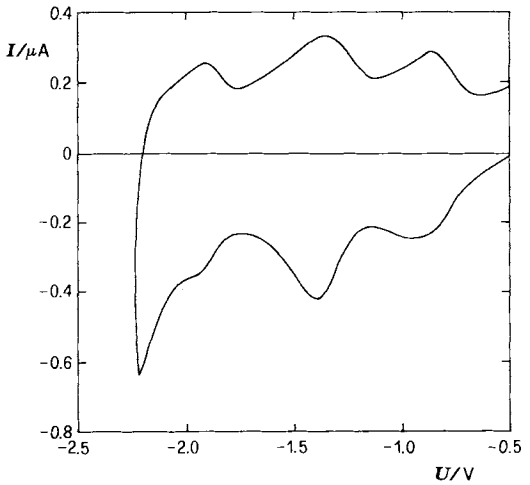

Fig. 3. Cathodic cyclic voltammogram of poly-**3** in acetonitrile. Scan rate: 0.1 Vs^{-1}.

(Fig. 4). This shoulder was assigned to the low-energy transitions of fullerene,[17] vibronically enhanced in the solid state.[18] The band at 440 nm, interpreted as the UV conjugation band of the polythiophene chain, is blue shifted in comparison with the corresponding band of poly-**1** (λ_{max} of the neutral polymer: 545 nm). This blue shift is better interpreted on the basis of a low polymerization degree, due to the very low solubility of **3**, than as the effect of the twisting of the polythiophene backbone.

Poly-**3** is the first conjugated polymer that contains covalently bound fullerene moieties as functional groups. Cyclic voltammetry has shown that both the polythiophene backbone and the C_{60} substituents retain, unaltered, their peculiar electrochemical behavior, though new properties are expected from their interaction. Work is in progress on the following aspects: 1. Characterization of the conductivity of the p-dopable polythiophene that is associated to the n-dopable fullerene pendants. 2. Study of the intermolecular photoinduced electron transfer between the C_{60} units and the conjugated polythiophene chain, as already described for C_{60}-doped polythiophenes.[19, 7]. 3. Copolymerization of **3** with a thiophene derivative carrying solubilizing groups, in order to obtain a more easily characterizable material with a lower loading of C_{60}.

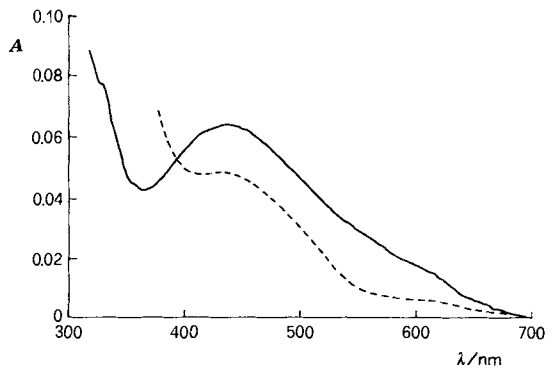

Fig. 4. UV spectrum of neutral poly-**3** on ITO electrode (—); UV spectrum of C_{60} on ITO electrode (- - -).

Experimental Procedure

2: A solution of BuLi (1.6 M) in *n*-hexane (2.0 mL) was added dropwise to a solution of **1** (0.500 g, 2.8 mmol) in THF (10 mL) at −10 °C under nitrogen. After 15 min the reaction mixture was added to a solution of *p*-toluenesulfonylazide (0.600 g, 3.0 mmol) in THF (10 mL) at −30 °C. After evaporation of THF at reduced pressure, the residue was treated with petroleum ether and filtered. The diazo compound **2** precipitated as a red solid (0.497 g, 87% yield; m.p. 65–67 °C (decomp)) upon concentration of the clear filtrate under reduced pressure. ^{1}H NMR (300 MHz, $CDCl_3$): δ = 7.2 (d, J = 5 Hz, 2H), 7.1 (d, J = 5 Hz, 2H); IR (Nujol): $\tilde{\nu}$ = 2099 (N_2) cm^{-1}. Anal. for $C_9H_4N_2S_2$: calc. C 52.92, H 1.97, N 13.71, S 31.39; found C 52.77, H 1.67, N 13.52, S 31.12.

3: **2** (0.051 g, 0.25 mmol) was added to a solution of C_{60} (0.178 g, 0.25 mmol) in toluene (200 mL) at room temperature. After 12 h, removal of the solvent under reduced pressure left a solid residue which was washed with diethyl ether to give the adduct **3** (0.112 g, 50% yield). ^{1}H NMR (300 MHz, $CS_2/CDCl_3$): δ = 7.60 (d, J = 5 Hz, 2H), 7.13 (d, J = 5 Hz, 2H); ^{13}C CP-MAS NMR (75.5 MHz, spinning speed: 4.5 kHz, contact time: 1.5 ms, TMS): main resonances at δ = 45.9, 76.1, 123.3, 127.4, 139.5, 143.1, 144.6, 147.5; FAB-MS (4-nitrobenzylalcohol): m/z 720 [$M^+ - C_9H_4S_2$], 176 [$C_9H_4S_2^+$]; UV/Vis (cyclohexane): λ_{max} = 209, 258, 328, 404, 434 nm; thermally stable up to 500 °C (DSC, in nitrogen atmosphere). Anal. for $C_{69}H_4S_2$: calc. C 92.40, H 0.45, S 7.15; found C 92.32, H 0.51, S 7.07.

Electrochemical experiments were performed at 25 °C, under nitrogen, in a three electrode cell, with a platinum working electrode (0.003 cm^2) and counterelectrode. The reference electrode was silver/0.1 M silver perchlorate in acetonitrile (0.34 V vs saturated calomel electrode). The supporting electrolyte was 0.1 M tetrabutylammonium perchlorate. Polymeric films for electronic spectroscopy were grown on indium tin oxide (ITO) sheets (0.8 × 2.5 cm; sheet resistance: 20 Ω/square).

Received: October 16, 1995 [Z 8478 IE]
German version: *Angew. Chem.* **1996**, *108*, 718–720

Keywords: conductivity · cyclic voltammetry · fullerenes · polymers · polythiophenes

[1] F. Garnier, *Angew. Chem. Adv. Mater.* **1989**, *1*, 117; *Angew. Chem. Int. Ed. Engl. Adv. Mater.* **1989**, *28*, 517.
[2] For a classification of fullerene polymers: A. Hirsch, *Adv. Mater.* **1993**, *5*, 859.
[3] a) T. Suzuki, Q. Li, K. C. Khemani, F. Wudl, Ö. Almarsson, *J. Am. Chem. Soc.* **1992**, *114*, 7300; b) S. Shi, K. C. Khemani, Q."Chan" Li, F. Wudl, *ibid.* **1992**, *114*, 10656; c) D. Loy, R. Assink, *ibid.* **1992**, *114*, 3977; d) A. M. Rao, P. Zhou, F. Wang, G. T. Hager, J. M. Holden, Y. Wang, X. X. Lee, P. C. Eklund, D. S. Cornett, M. A. Duncan, I. J. Amster, *Science* **1993**, *259*, 955; e) N. Tokahasi, H. Dock, N. Matsuzawa, M. Ata, *J. Appl. Phys.* **1993**, *74*, 5790;.
[4] M. Fedurco,D. A. Costa,A. L. Balch,W. R. Fawcett, *Angew. Chem.* **1995**, *107*, 220; *Angew. Chem. Int. Ed. Engl.* **1995**, *34*, 194.

 © VCH Verlagsgesellschaft mbH, D-69451 Weinheim, 1996 0570-0833/96/3506-0650 $ 15.00+.25/0

[5] H. L. Anderson, C. Boudon, F. Diederich, J. P. Gisselbrecht, M. Gross, P. Seiler, *Angew. Chem.* **1994**, *106*, 1691; *Angew. Chem. Int. Ed. Engl.* **1994**, *33*, 1628.
[6] F. Wudl, *Acc. Chem. Res.* **1992**, *25*, 157.
[7] a) N. S. Sariciftci, L. Smilowitz, A. J. Heeger, F. Wudl, *Science* **1992**, *258*, 1474; b) L. Smilowitz, N. S. Sariciftci, R. Wu, C. Gettinger, A. J. Heeger, F. Wudl, *Phys. Rev. B* **1993**, *47*, 13835; c) B. Kraabel, C. H. Lee, D. McBranch, D. Moses, N. S. Sariciftci, A. J. Heeger, *Chem. Phys. Lett.* **1993**, *213*, 389; d) C. H. Lee, G. Yu, D. Moses, N. S. Sariciftci, A. J. Heeger, *Phys. Rev. B* **1993**, *48*, 15425; e) C. H. Lee, A. J. Janssen, N. S. Sariciftci, A. J. Heeger, *ibid.* **1994**, *49*, 5781.
[8] F. Diederich, L. Isaacs, P. Douglas, *Chem. Soc. Rev.* **1994**, 243.
[9] T. Benincori, E. Brenna, F. Sannicolò, L. Trimarco, G. Moro, D. Pitea, T. Pilati, G. Zerbi, G. Zotti, *J. Chem. Soc. Chem. Commun.* **1995**, 881.
[10] T. Pilati, *Acta Crystallogr. Sect. C* **1995**, *51*, 690.
[11] R. Hoffmann, R. B. Davidson, *J. Am. Chem. Soc.* **1971**, *93*, 5699; T. Tsuji, T. Shibata, Y. Hienuki, S. Nishida, *J. Am. Chem. Soc.* **1978**, *100*, 1806; A. de Meijere, *Angew. Chem.* **1979**, *91*, 867; *Angew. Chem. Int. Ed. Engl.* **1979**, *18*, 809.
[12] W. von E. Doering, C. H. De Puy, *J. Am. Chem. Soc.* **1953**, *75*, 5955.
[13] No satisfactory ^{13}C NMR spectrum could be obtained due to insolubility, as observed in other similar cases: see, for example, T. Suzuki, Q. Li, K. C. Khemani, F. Wudl, Ö. Almarsson, *Science* **1991**, *254*, 1186.
[14] A. B. Smith III, R. M. Strongin, L. Brard, G. T. Furst, W. J. Romanow, K. G. Owens, R. J. Goldschmidt, R. C. King, *J. Am. Chem. Soc.* **1995**, *117*, 5492.
[15] D. Dubois, K. M. Kadish, S. Flanagan, R. E. Haufler, L. P. F. Chibante, L. J. Wilson, *J. Am. Chem. Soc.* **1991**, *113*, 4364.
[16] T. Suzuki, Y. Maruyama, T. Akasaka, W. Ando, K. Kobayashi, S. Nagase, *J. Am. Chem. Soc.* **1994**, *116*, 1359.
[17] J. P. Hare, H. W. Kroto, R. Taylor, *Chem. Phys. Lett.* **1991**, *177*, 394.
[18] A. Skumanich, *Chem. Phys. Lett.* **1991**, *182*, 486.
[19] S. Morita, A. A. Zachidov, T. Kawai, H. Araki, K. Yoshino, *Jpn. J. Appl. Phys.* **1992**, *31*, L890.

Stereoselective Solid-Phase Synthesis of Cyclopentane and Cyclohexane Derivatives by Two-Component Domino Reactions: Generation of Combinatorial Libraries**

Lutz F. Tietze* and Adrian Steinmetz

Dedicated to Professor Burchard Franck on the occasion of his 70th birthday

Despite some remarkable successes in rational drug design for the development of novel substances with interesting biological activity, one cannot neglect the importance of random screening for the identification of new lead structures. For this reason the generation of libraries of chemical compounds is of great significance. Due to the availibility of screening assays for testing the biological activity of compounds, in which only minimal amounts are needed, the area of combinatorial chemistry has developed. With this approach a huge number of products are accessible by manifold combination of different substrates, mostly by the use of solid-phase reactions.[1] Although many examples for the synthesis of biopolymers exist,[2-4] there are only a few reports on the generation of small-molecule libraries.[5-12] Herein, we describe a two-component domino reaction[13] on a solid support for the generation of diversomer libraries.

Commercially available Merrifield resin **1** (2.58 mmole of Cl per gram of resin, 2% DVB, Acros) was treated with disodium 1,3-propanediolate **2** (2 equiv, 85 °C, 24 h, DMF) and then quenched with with water to give **3**. By this procedure a spacer with a free hydroxyl group was introduced to guarantee enhanced reactivity of the substrates bound to the polymer (Scheme 1). To estimate the number of free hydroxyl groups, the

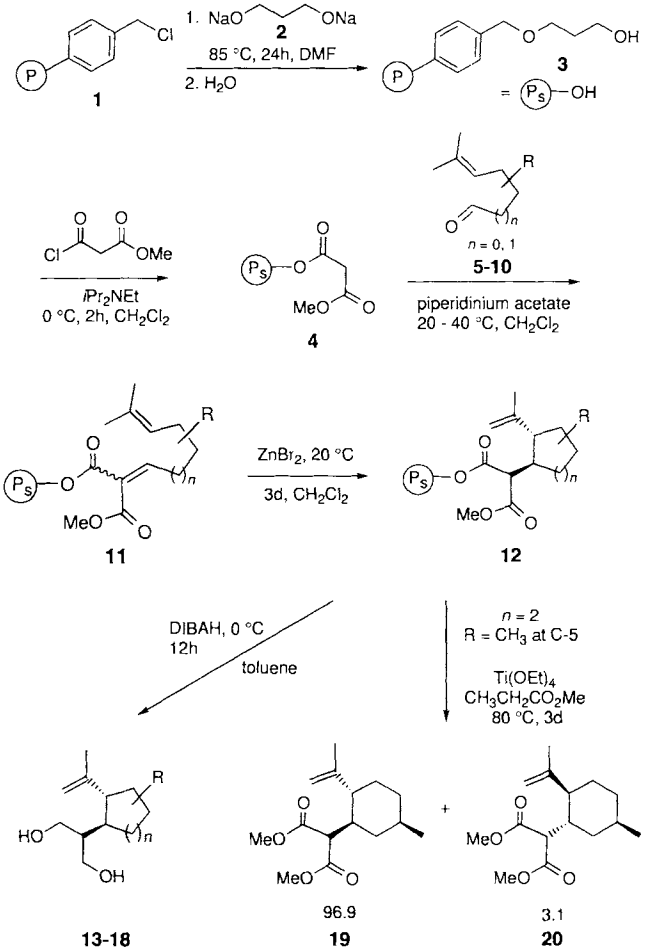

Scheme 1. Synthesis of the malonate-functionalized polymer **4** and reactions with aldehydes **5**–**10** to give the cycloalkanes **13**–**20**. Ⓟ = polymer, Ⓡ = spacer-modified polymer.

spacer-functionalized resin **3** was treated with 3,5-dinitrobenzoyl chloride in pyridine to afford the corresponding immobilized ester. Measurement of the nitrogen content by elemental analysis indicated 0.75 mmole of hydroxyl groups per gram of resin. Compound **3** was then transformed into the malonate-functionalized polymer **4**, which was needed for the subsequent domino Knoevenagel–ene reaction, by treatment with malonic acid methyl ester chloride (2 equiv iPr_2NEt, 0 °C, 2 h, CH_2Cl_2). The two-component domino reaction was performed by condensation of **4** with the Δ^5 and Δ^6 unsaturated aldehydes **5**–**10** (3 equiv) in the presence of catalytic amounts of piperidinium acetate (0.1–0.2 equiv, 20 °C, 1–3 h, CH_2Cl_2) and subsequent addition of $ZnBr_2$ (1.1 equiv, 20 °C, 3 d, CH_2Cl_2). Generally, the primary Knoevenagel reaction yielding **11** proceeded without the addition of any drying agents; however, condensation of α-substituted aldehydes required added sodium sulfate and elevated temperatures (40 °C). The subsequent intramolecular ene reaction led to the cyclopentane and cyclohexane derivatives **12**, which can be cleaved from the support providing the products **13**–**18**,[14] and **19** and **20**, respectively. Thus, the reduction of **12** with diisobutylaluminum hydride (4 equiv, 0 °C, 12 h, toluene)

[*] Prof. Dr. L. F. Tietze, Dipl.-Chem. A. Steinmetz
Institut für Organische Chemie der Universität
Tammanstrasse 2, D-37077 Göttingen (Germany)
Fax: Int. code +(551)39-9476

[**] This work was supported by BASF and the Fonds der chemischen Industrie.

resulted in the generation of the corresponding diols **13**–**18**, whereas transesterification in dry methyl propionate in the presence of titanium(IV) ethoxide (1 equiv, 80 °C, 3 d)[15] afforded the substituted methyl malonates **19** and **20**. In both transformations the products were obtained in good yield and high purity as well as with excellent simple and induced diastereoselectivity (Table 1). The yields based on the number of free hydroxyl groups on the polymer range from 41 to 61% and the cleaved products had purities of about 90%. The linkage to the polymeric support seems not to influence the simple and induced diastereoselectivity of the ene reaction.[13, 16] This is surprising when one assumes that the alkylidene intermediates exist as *E*/*Z* mixtures. In each case the *trans*-1,2-disubstituted cyclohexanes were formed with a simple diastereoselectivity of *ds* > 99:1 and the corresponding *trans*-1,2-disubstituted cyclopentanes with *ds* = 98.5:1.5. For the reaction with the α-substituted aldehydes **5** and **8**, the induced diastereoselectivity was *ds* > 99:1, whereas for the reaction of the β-substituted aldehyde **7** an induced diastereoselectivity of *ds* = 96.9:3.1 was found. As expected, employing the geminally disubstituted aldehydes **9** and **10** resulted in only a low induced diastereoselectivity.

Table 1. Yields and diastereoselectivities of the reactions of polymer-bound malonate **4** with aldehydes **5**–**10** giving products **13**–**18**.

Substrate	Major product	Yield [%] [a]	*trans*:*cis* [b]
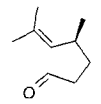 **5**	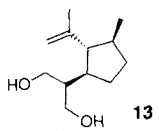 **13**	61	98.5:1.5
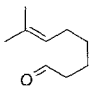 **6**	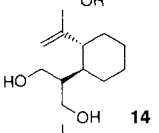 **14**	63	>99:1
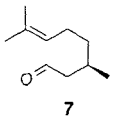 **7**	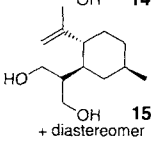 **15** + diastereomer 97.2 : 2.8	61	>99:1
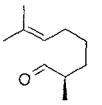 **8**	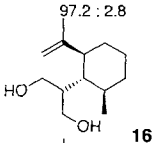 **16**	59	>99:1
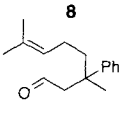 **9**	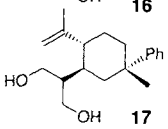 **17** + diastereomer 78 : 22 [c]	51	>99:1
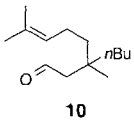 **10**	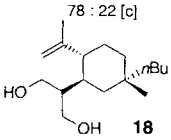 **18** + diastereomer 58 : 42	48	>99:1

[a] The overall yield is based on the concentration of free hydroxyl groups in **3**. [b] Determined by GC analysis of the silylated crude products. [c] The major product was assigned based on the assumption of a chair-like transition structure [16, 17] and the preferred orientation of the geminal substituents [18].

The transformations on solid support have significant advantages over those in solution. Since products are obtained with higher purity, chromatographic separation is unnecessary. Furthermore, isomerization of the double bond in the initially formed alkylidene 1,3-dicarbonyl compounds, which is frequently observed for reactions in solution, does not occur. Also the possible intramolecular carbonyl ene reaction of the aldehydes is of little importance since the free alcohols formed are removed when the polymer-bound products are washed.

The good yields, the high purity of the products, and the simple procedure for the reaction sequence described here make its application for the synthesis of combinatorial libraries very attractive. Therefore we synthesized a sample library by simultaneous Knoevenagel condensation of an equimolar mixture containing the aldehydes **5**–**10** and polymer-bound malonate **4** (0.15 equiv of each aldehyde for 1 equiv of malonate) followed by $ZnBr_2$-initiated ene reaction and reductive cleavage of the products from the resin. To analyze the mixture of the resulting diols **13**–**18**, they were transformed into the corresponding bis(trimethylsilyl) ethers and examined by gas chromatography. It was found that the purity was greater than 90% and all compounds occurred in similar ratio (with the exception of **16** which showed a concentration of only 7%) in an overall yield of about 45%.

A major advantage of this procedure is the possibility of conducting the synthesis without the "split and combine" technique. Moreover, it can be carried out on readily available and inexpensive Merrifield resin. We are currently investigating the increase of diversity by studying the cleavage of the products using different alcohols and amines and the implementation of a three-component reaction on a solid support.

Received: October 30, 1995 [Z8512IE]
German version: *Angew. Chem.* **1996**, *108*, 682–683

Keywords: cascade reactions · combinatorial chemistry · ene reactions · multicomponent reactions · solid-phase syntheses

[1] J. Alper, *Science* **1994**, *264*, 1399–1401.
[2] M. R. Pavia, T. K. Sawyer, W. H. Moos, *Bioorg. Med. Chem. Lett.* **1993**, *3*, 387–396.
[3] M. A. Gallop, R. W. Barret, W. J. Dower, S. P. A. Fordor, E. M. Gordon, *J. Med. Chem.* **1994**, *37*, 1232–1251.
[4] R. S. Youngquist, G. F. Fuentes, M. P. Lacey, T. Keough, *J. Am. Chem. Soc.* **1995**, *117*, 3900–3906.
[5] B. A. Bunin, J. A. Ellman, *J. Am. Chem. Soc.* **1992**, *114*, 10997–10998.
[6] S. Hobbs DeWitt, J. S. Kiely, C. J. Stankovic, M. C. Schroeder, D. M. Reynolds Cody, M. R. Pavia, *Proc. Natl. Acad. Sci USA* **1993**, *90*, 6909–6913.
[7] M. J. Kurth, L. A. Ahlberg Randall, C. Chen, C. Melander, R. B. Miller, *J. Org. Chem.* **1994**, *59*, 5862–5864.
[8] T. Carell, E. A. Winter, A. Bashir-Hashemi, J. Rebek, Jr., *Angew. Chem.* **1994**, *106*, 2159–2162; *Angew. Chem. Int. Ed. Engl.* **1994**, *33*, 2059–2061.
[9] C. Chen, L. A. Ahlberg Randall, R. B. Miller, A. D. Jones, M. J. Kurth, *J. Am. Chem. Soc.* **1994**, *116*, 2661–2662.
[10] S. M. Dankwardt, S. R. Newman, J. L. Krstenansky, *Tetrahedron Lett.* **1995**, *35*, 4923–4926.
[11] D. W. Gorden, J. Steele, *Bioorg. Med. Chem. Lett.* **1995**, *5*, 47–50.
[12] E. M. Gordon, R. W. Barret, W. J. Dower, S. P. A. Fordor, M. A. Gallop, *J. Med. Chem.* **1994**, *37*, 1385–1401.
[13] a) L. F. Tietze, U. Beifuss, *Angew. Chem.* **1993**, *105*, 137–170; *Angew. Chem. Int. Ed. Engl.* **1993**, *32*, 131–163; b) L. F. Tietze, *Chem. Rev.* **1996**, *96*, 115–136.
[14] **13**: ^{1}H NMR (200 MHz, $CDCl_3$): δ = 0.89 (d, *J* = 6 Hz; 3H, 3'-CH_3), 0.96–1.89 (m; 7H, remaining protons on ring), 1.68 (m_c; 3H; 1''-CH_3), 1.98 (m_c; 1H), 2.38 (s br; 2H, OH), 3.53–3.93 (m; 4H, 1-H_2, 3-H_2), 4.82 (m_c; 2H, 1''-H_2).
[15] P. Schnurrenberger, M. F. Züger, D. Seebach, *Helv. Chem. Acta* **1982**, *65*, 1197–1201.
[16] a) L. F. Tietze, U. Beifuss, M. Ruther, *J. Org. Chem.* **1989**, *54*, 3120–3129; b) L. F. Tietze, U. Beifuss, M. Ruther, A. Rühlmann, J. Antel, G. M. Sheldrick, *Angew. Chem.* **1988**, *100*, 1200–1201; *Angew. Chem. Int. Ed. Engl.* **1988**, *27*, 1186–1187; c) L. F. Tietze, U. Beifuss, *ibid.* **1985**, *97*, 1067–1068 bzw. **1985**, *24*, 1042–1043.
[17] L. F. Tietze, H. Geissler, J. Fennen, T. Brumby, S. Brand, G. Schulz, *J. Org. Chem.* **1994**, *59*, 182–191.
[18] E. L. Eliel, M. Manoharan, *J. Org. Chem.* **1981**, *46*, 1959–1962.

 © VCH Verlagsgesellschaft mbH, D-69451 Weinheim, 1996 0570-0833/96/3506-0652 $ 15.00+.25/0

Addition of Organic 1,3-Dipolar Compounds across a Heterobinuclear Bond between Early and Late Transition Metals: Mechanism of Nitrogen Loss from an Organoazido Complex To Form a Bridging Imido Complex**

Tracy A. Hanna, Anne M. Baranger, and Robert G. Bergman*

Organic azides are commonly used in transition metal chemistry as sources of :NR moieties to form metal imido complexes.[1-3] When a metal–metal bond is exposed to an organic azide, for example, the product is usually a complex with a bridging imido group.[4, 5] However, in spite of the frequent use of this methodology, little mechanistic information is available on either the mono-[6, 7] or binuclear versions of this reaction. In this paper we report: a) that both azides and diazo compounds add smoothly, and without N_2 loss, to the polarized metal–metal bond in an early–late heterobinuclear (ELHB) complex, to yield new heterobinuclear adducts that have very similar solid-state structures; b) the diazo compound adduct is inert to both heat and light, but thermolysis of the azide complexes leads smoothly to N_2 and the corresponding ELHB bridging imido complexes; c) studies involving isotope labeling, kinetics, and substituent effects reveal a mechanism in which electron-withdrawing substituents stabilize the transition state for imido complex formation.

Addition of phenyl azide to $[Cp_2Zr(\mu\text{-}NtBu)IrCp^*]$ (**1**)[8, 9] resulted in immediate formation of dark green **2** in 75% yield (Fig. 1). Similarly, addition of ethyl diazoacetate to **1** produced the dark green diazo adduct **3** in 59% yield. Both reactions proceed without loss of N_2. X-ray diffraction studies of **2** and **3** have been carried out, and their solid-state structures are remarkably similar.[10, 11] As shown in Figure 1, both are end-on (terminal) adducts, and the terminal nitrogen atom and phenyl or carboxylate groups are oriented *anti* to one another. The phenyl azido ligand of **2**, the diazo ligand of **3**, and the heteronuclear cores in both complexes are planar, and in both molecules the $IrZrN_2$ core and RXN_2 fragments lie in the same plane. The nitrogen–nitrogen distances in **2** are intermediate between single- and double-bond distances, showing some electron delocalization across the ligand. Likewise, the N2-N3-N4 angle is 111° rather than the 120° that would be expected for an sp^2 nitrogen center. In **3** the N–N distance (1.30 Å) is shorter than that of a typical single bond, consistent with electron delocalization, but the N2-N3-C25 angle of 119° is closer to the sp^2 standard. The C25–N3 bond length of 1.33 Å is also indicative of some delocalization (for example, C–N of pyridine is 1.338 Å). There is no sign of the formation of the more sterically hindered isomers in either compound.[12-17]

Irradiation of azide adduct **2** and diazo adduct **3** in a quartz vessel for 12 hours at room temperature led to only a trace of the product formed by nitrogen loss. Complex **3** also did not undergo clean thermal decomposition. However, thermolysis of **2** at 75 °C readily caused nitrogen loss and quantitative formation (NMR determination) of the diimido complex **4** (43% yield of isolated product). The structure of this material has also been determined by X-ray diffraction (Fig. 2). In contrast to **2** and **3**, in **4** the $ZrIrN_2$ core is slightly buckled. The metal–nitrogen distances are very similar to one another and typical for complexes with bridging imido ligands.[2, 18-20]

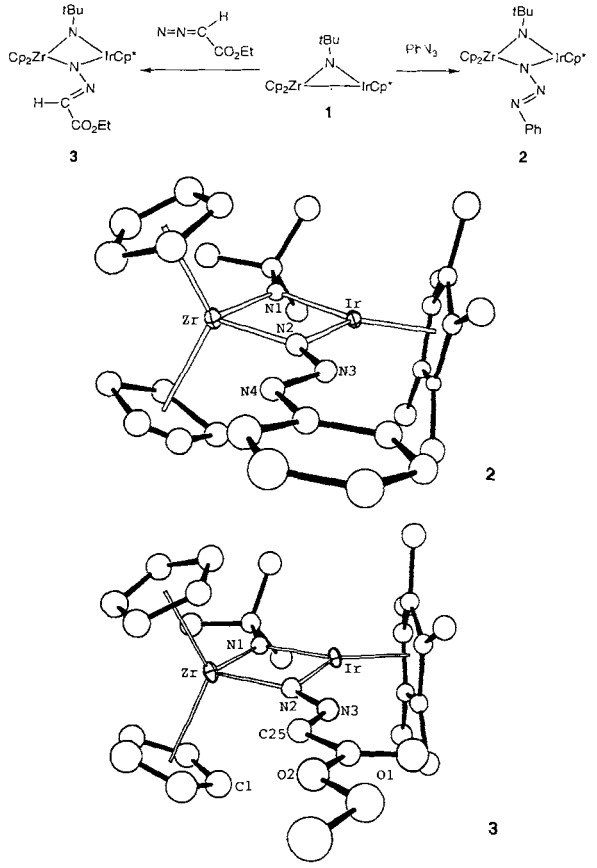

Fig. 1. Formation of **2** and **3** from **1** (top) and ORTEP diagrams showing the structures of complexes **2** and **3** (bottom) (Cp = C_5H_5; Cp* = C_5Me_5). Disorder in one of the Cp rings of complex **2** is not shown. Selected intramolecular distances [Å] and angles [°] for **2**: Ir–Zr 2.938(1), Ir–N1 1.983(9), Ir–N2 2.072(10), Zr–N1 2.076(10); Zr–N2 2.027(10), N1-Ir-N2 88.4(4), N1-Zr-N2 87.2(4), Ir-N1-Zr 92.7(4), Ir-N2-Zr 91.6(4), N2–N3 1.320(13), N3–N4 1.331(13), N4–C25 1.417(15), N2-N3-N4 111.1(9), N3-N4-C25 111.6(10). For **3** Ir–Zr: 2.922(1), Ir–N1 1.948(9), Ir–N2 2.096(7), Zr–N1 2.071(7), Zr–N2 2.020(7), N1-Ir-N2 88.8(3), N1-Zr-N2 87.6(3), Ir-N1-Zr 93.2(3), Ir-N2-Zr 90.4(3), N2–N3 1.304(10), N3–C25 1.331(12), N2-N3-C25 119.2(7), N3-C25-C26 115.2(8).

The smooth thermal conversion of **2** to **4** provided us with an opportunity to investigate the mechanism of this N_2-loss reaction. The kinetics of N_2 loss from **2** were followed by ^1H NMR spectroscopy from 75 to 105 °C. The rate law was rigorously first order at all temperatures. A plot of $\ln k/T$ vs. $1/T$ (Fig. 3) provided the following activation parameters for the thermolysis: $\Delta H^{\ddagger} = 29 \pm 1$ kcal mol^{-} and $\Delta S^{\ddagger} = 0 \pm 2$ e.u. The activation entropy indicates little gain or loss of geometrical restriction in the transition state and is consistent with the exchange studies in suggesting that dissociation of PhN_3 is unlikely. Complex **2** labeled with ^{15}N at the phenyl-substituted nitrogen was prepared by treating the starting Zr–Ir complex **1** with $Ph-{}^{15}N{=}N{=}N$. Upon thermolysis the corresponding isotopically labeled arylimido complex **4**-^{15}N was obtained, with no evidence of the presence of unlabeled **4**.

[*] Prof. R. G. Bergman, T. A. Hanna, Dr. A. M. Baranger
Department of Chemistry, University of California
Berkeley, CA 94720 (USA)
Fax: Int. code +(510)642-7714
e-mail: rgberg@violet.berkeley.edu

[**] We acknowledge Dr. F. J. Hollander, Director of the X-ray Diffraction Facility (CHEXRAY) at the University of California, Berkeley, for solving the crystal structures of compounds **2**, **3**, and **4**, and Professors T. Don Tilley and K. N. Raymond for helpful discussions. Support for this work was provided by the National Science Foundation (Grant no. CHE-9113261). We are also grateful to the Johnson Matthey Aesar/Alpha Corporation for a generous loan of iridium trichloride.

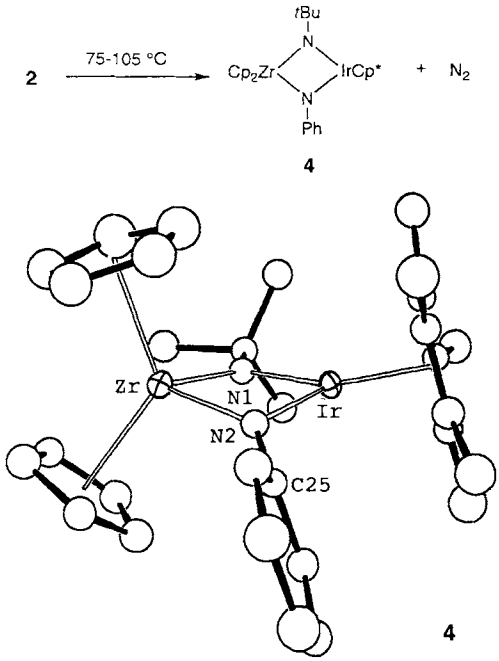

Fig. 2. Formation of complex **4** from complex **2** (top) and ORTEP diagram showing the structure of complex **4**. Selected intramolecular distances [Å] and angles [°]: Ir–Zr 2.900(1), Ir–N1 1.977(7), Ir–N2 2.066(7), Zr–N1 2.055(7), Zr–N2 1.985(7); N1-Ir-N2 87.1(3), N1-Zr-N2 87.2(3), Ir-N1-Zr 92.0(3), Ir-N2-Zr 91.4(3).

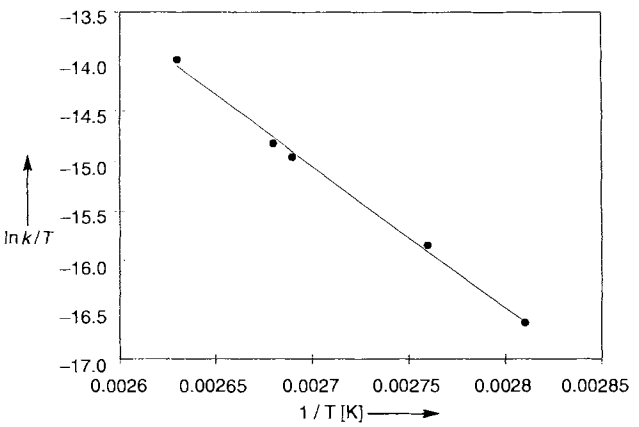

Fig. 3. Eyring plot for the loss of nitrogen from **2** to form **4**.

A crossover experiment [Eq. (a), Cp′ = $EtMe_4Cp$] established that the nitrogen loss proceeds without fragmentation of the heterobimetallic core. Thermolysis of a mixture of **2**-^{15}N and **2**-Cp′ led to **4**-^{15}N and **4**-Cp′ but no crossover products (**4**-Cp′,^{15}N or **4**).[21] The possibility of reversible loss of RN_3 from adduct **2** was investigated by addition of excess *p*-$CF_3C_6H_4N_3$ and *p*-NMe_2-C_6H_4-N_3 to solutions containing **2** [Eq. (b)]. Only **4** was formed; neither exchange product was observed at temperatures up to 75 °C.

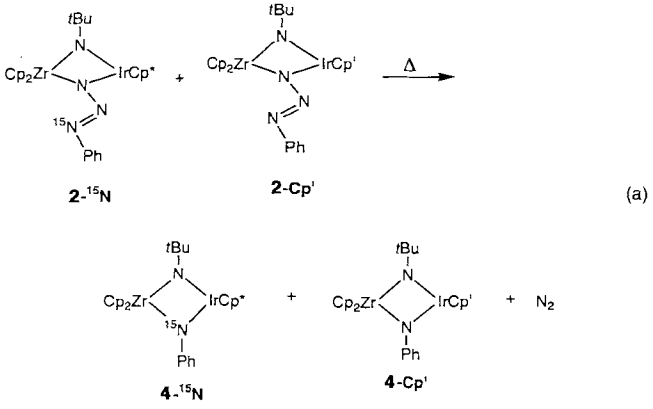

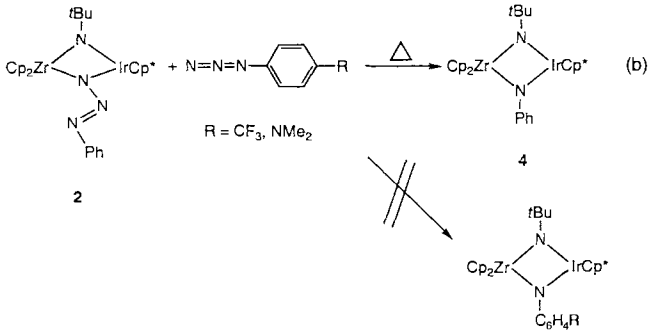

To examine the effect of electron density changes on the N_2 loss, we measured the rate of decomposition of several ArN_3 complexes in which the *para* substituent on the aryl group was varied. A linear Hammett plot was constructed from these data; this yielded an ρ value of +0.4, which indicates that electron-withdrawing substituents exert a modest activating effect upon the reaction rate. This is somewhat surprising, because we expected that the rate-determining step of the reaction would involve nucleophilic attack of the phenyl-substituted azide nitrogen atom at the zirconium center.

The overall mechanism illustrated in Scheme 1 is most consistent with our observations. Because the N–Ph group is located

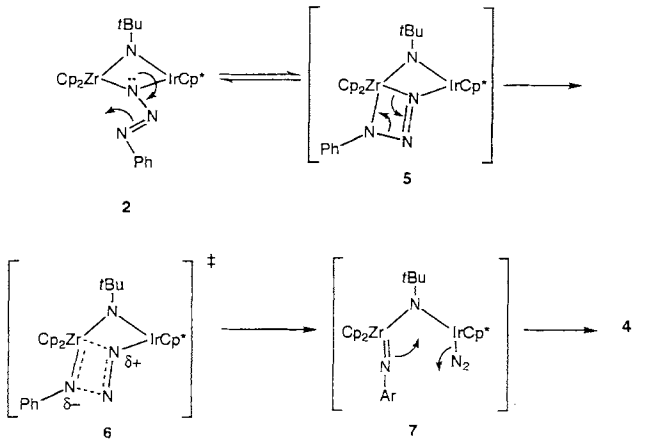

Scheme 1. Proposed mechanism for the loss of nitrogen from **2** to form **4**.

close to the Zr center in the starting material, we suggest (as initially assumed) that Zr–N bond formation involving nucleophilic attack of the N atom at the Zr center is the first step in the reaction. However, to account for the aryl substituent effects we suggest that this step is rapid and reversible, probably taking place over a relatively low barrier and leading to intermediate **5**. The second step of the reaction, which proceeds via the rate-determining transition state **6**, involves cleavage of the Zr–N and N–N bonds to give intermediate **7**. This species then undergoes fast N_2 dissociation and recyclization to give the final product **4**. The electronic effect supports a partial negative charge on the aryl nitrogen in the transition state **6**, as shown.

 © VCH Verlagsgesellschaft mbH, D-69451 Weinheim, 1996 0570-0833/96/3506-0654 $ 15.00+.25/0 Angew. Chem. Int. Ed. Engl. 1996, 35, No. 6

Experimental Procedure

General laboratory procedures were as described previously [9]. Commercial reagents were used, except for phenyl azide [22] and **1** [8,9], which were prepared by published procedures.

2: PhN_3 (34.8 mg, 0.293 mol) in toluene (3 mL) was added to a solution of **1** (201 mg, 0.325 mol) in toluene (5 mL). The color changed immediately to dark green. Dark green **2** (162 mg, 120 mmol, 75%) was crystallized directly from the reaction mixture at −30 °C. ^1H NMR ([D$_8$]THF) δ = 1.69 (s, 9H), 1.80 (s, 15H), 5.76 (s, 10H), 6.92 (t, J = 7.33 Hz, 1H), 7.26 (t, J = 7.25 Hz, 2H), 7.60 (m, 2H); $^{13}C\{^1H\}$ NMR ([D$_8$]THF) δ = 10.7, 35.9, 71.1, 90.8, 108.7, 120.9, 122.4, 129.2, 156.0; IR ([D$_8$]THF) $\tilde{\nu}$ = 3419 (br), 2917, 1590, 1477, 1376, 1343, 1229, 1182, 787, 673 cm^{-1}. Elemental analysis: Calcd. for $C_{30}H_{34}IrN_4Zr$: C 48.75, H 5.32, N 7.58. Found: C 48.43, H 5.35, N 7.20.

3: Ethyl diazoacetate (21.9 μL, 0.208 mol) in toluene (5 mL) was added to a solution of **1** (110 mg, 0.177 mol) in toluene (15 mL); the color changed immediately to dark green. The reaction mixture was concentrated in vacuo to approximately 2 mL and cooled to −30 °C to obtain dark green **3** (77 mg, 0.105 mol, 59%). ^1H NMR ([D$_8$]THF) δ = 1.30 (t, J = 7.12 Hz, 3H), 1.47 (s, 15H), 1.50 (s, 9H), 4.49 (q, J = 7.12 Hz, 2H), 5.61 (s, 10H), 7.29 (s, 1H); $^{13}C\{^1H\}$ NMR ([D$_8$]THF) δ = 9.9, 15.1, 35.3, 59.0, 69.9, 91.0, 107.5, 121.0, 166.2; IR (Nujol) $\tilde{\nu}$ = 3103, 2996, 1674, 1425, 1479, 1338, 1116, 1022, 788, 694, 553 cm^{-1}. Elemental analysis: Calcd. for $C_{28}H_{40}N_3O_2IrZr$: C 45.81, H 5.49, N 5.72. Found: C 45.67, H 5.43; N 5.68.

4: Complex **2** (159 mg, 0.215 mol) was dissolved in toluene (15 mL) and loaded into an airtight reaction bomb. The solution was heated to 75 °C for one week, and then the volatile materials were removed in vacuo. The solid was recrystallized from a mixture of hexanes to obtain dark green **4** (66 mg, 0.093 mmol, 43%). ^1H NMR ([D$_8$]THF) δ = 1.53 (s, 15H), 1.70 (s, 9H), 5.62 (s, 10H), 6.75 (m, 1H), 6.81 (m, 2H), 7.18 (m, 2H); $^{13}C\{^1H\}$ NMR ([D$_8$]THF) δ = 11.0, 36.1, 68.9, 88.6, 109.5, 120.0, 125.3, 128.3, 167.9; IR ([D$_8$]THF) $\tilde{\nu}$ = 3103, 3062, 2967, 2912, 1584, 1482, 1379, 1352, 1284, 800, 691 cm^{-1}. HRMS (EI) m/z: calcd. for $C_{30}H_{39}IrN_2Zr$: 710.1790 (M^+); found: 710.1782 (M^+).

Received: August 30, 1995 [Z 83551E]
German version: *Angew. Chem.* **1996**, *108*, 693–696

Keywords: complexes with imido ligands · diazo compounds · iridium compounds · zirconium compounds

[1] D. E. Wigley, *Prog. Inorg. Chem. Vol. 42* (Ed.: K. D. Karlin), Wiley, New York, **1994**, p. 239.
[2] W. A. Nugent, B. L. Haymore, *Coord. Chem. Rev.* **1980**, *31*, 123.
[3] S. Cenini, G. L. Monica, *Inorg. Chim. Acta* **1976**, *18*, 279.
[4] R. S. P. Coutts, J. R. Surtees, *Aust. J. Chem.* **1966**, *19*, 387.
[5] W. A. Herrmann, B. Menjon, E. Herdtweck, *Organometallics* **1991**, *10*, 2134.
[6] G. Proulx, R. G. Bergman, *J. Am. Chem. Soc.* **1995**, *117*, 6382.
[7] M. G. Fickes, W. M. Davis, C. C. Cummins, *J. Am. Chem. Soc.* **1995**, *117*, 6384.
[8] A. M. Baranger, F. J. Hollander, R. G. Bergman, *J. Am. Chem. Soc.* **1993**, *115*, 7890.
[9] A. M. Baranger, R. G. Bergman, *J. Am. Chem. Soc.* **1994**, *116*, 3822.
[10] Further details of the crystal structure investigations are available on request from the Director of the Cambridge Crystallographic Data Centre, 12 Union Road, GB-Cambridge CB21EZ (UK), on quoting the full journal citation.
[11] A referee expressed concern about several of the difficulties we encountered in solving the structure of complex **2**. We therefore re-analyzed the structure after receiving the reviews of the paper. One cyclopentadienyl ring is disordered; as an alternative to the modeling method used in the first report (fixed B_{iso} constant, refined occupancies), this part of the structure was modeled with nine atomic carbon positions to give a total occupancy of 5.0 carbons. In the new analysis the metal atoms and all four nitrogen atoms have been refined anisotropically, but we were not able to refine the carbon atoms of the complex with anisotropic thermal parameters, because these always yielded solutions in which one or more carbon atoms had nonpositive, definite thermal tensors. Inspection of the data revealed that there were many reflections in the data set with F_o significantly greater than F_{calc}, both for low and high intensity reflections, indicating some minor problem of unknown nature with the data set. The 29 reflections with worst agreement between F_o and F_{calc} were removed from the least squares refinement. With these adjustments, the structure refined with R = 0.037, wR = 0.039 and GOF = 1.29. We have consulted with Prof. K. N. Raymond about the overall reliability of the structure. Both he and Dr. Hollander agree that there may be some minor error in the final metrical parameters but there is very little chance that the atom connectivity is incorrect.
[12] Some representative examples of structurally characterized metal–metal bridging organodiazo complexes are given in Refs. [13–20].
[13] R. K. Minhas, J. J. H. Edema, S. Gambarotta, A. Meetsma, *J. Am. Chem. Soc.* **1993**, *115*, 6710.
[14] G. M. Arvanitis, J. Smegal, I. Meier, A. C. C. Wong, J. Schwartz, D. Van Engen, *Organometallics* **1989**, *8*, 2717.
[15] M. D. Curtis, L. Messerle, J. J. D'Errico, W. M. Butler, M. S. Hay, *Organometallics* **1986**, *5*, 2283.
[16] M. H. Chisholm, K. Folting, J. C. Huffman, A. L. Ratermann, *Inorg. Chem.* **23**, **1984**, *23*, 2303.
[17] W. A. Herrmann, *J. Organomet. Chem.* **1983**, *250*, 319.
[18] W. A. Nugent, R. L. Harlow, *Inorg. Chem.* **1979**, *18*, 2030.
[19] D. A. Dobbs, R. G. Bergman, *J. Am. Chem. Soc.* **1993**, *115*, 3836.
[20] M. K. Kolel-Veetil, M. Rahim, A. J. Edwards, A. L. Rheingold, K. J. Ahmed, *Inorg. Chem.* **1992**, *31*, 3877.
[21] The products were identified by ^1H NMR, ^{13}C NMR, and mass spectrometry.
[22] P. A. S. Smith, J. H. Boyer, *Org. Synth.* **1951**, *31*, 14.

Pr[MOE-DO3A], a Praseodymium Complex of a Tetraazacyclododecane: An In Vivo NMR Thermometer

K. Roth,* G. Bartholomae, H. Bauer, T. Frenzel, S. Kossler, J. Platzek, B. Radüchel, and H.-J. Weinmann

As most biochemical reaction cascades are exothermic, the spatial temperature distribution within a living organism directly reflects local metabolic activity. NMR spectroscopy is an ideal technique for measuring in vivo tissue temperature because it is noninvasive. Potential applications of an in vivo NMR thermometer could be the detection and localization of tumors, inflammations, and infarctions. Furthermore, an in vivo NMR thermometer would be of invaluable help in hyperthermia treatment of malignant tumours,[1,2] where the amount of heat applied depends on the actual temperature in the region of interest and its surroundings. Unfortunately, none of the various existing thermometers developed for high-resolution NMR studies is suitable for in vivo studies because the majority of the reference compounds are not soluble in water and/or are toxic.[3–8] To the best of our knowledge, only perfluorotributylamine has been used as a temperature probe in an in vivo system.[9] However, the application of this compound is very limited, because as perfluorotributylamine is not miscible with water, small bubbles of the pure substance have to be injected into the region of interest.

We have developed a new type of highly water-soluble in vivo NMR temperature probes based on paramagnetic lanthanide chelate complexes. This class of compounds is closely related to the gadolinium-based contrast agents used routinely in clinical magnetic resonance imaging. These complexes are suitable temperature probes based on the following considerations. The chemical shift δ_{obs} of a nucleus in a paramagnetic compound is given by Equation (a).[10,11] The diamagnetic term, δ_{dia}, is small

$$\delta_{obs} = \delta_{dia} + \delta_{con} + \delta_{dip} \quad (a)$$

and virtually temperature-independent, whereas the other terms, δ_{con} and δ_{dip}, vary strongly with temperature.[12,13] The contact term, δ_{con}, describes the through-bond transfer of electron spin density from the lanthanide ion to the observed nucle-

[*] Prof. Dr. K. Roth
Dahlem Konferenzen der Freien Universität Berlin
Thielallee 66, D-14195 Berlin (Germany)
Fax: Int. code +(30)84109103
e-mail: dahlem@zedat.fu-berlin.de
G. Bartholomae, Dr. H. Bauer, Dr. T. Frenzel, S. Kossler, Dr. J. Platzek, Dr. B. Radüchel, Dr. H.-J. Weinmann
Forschungslaboratorien der Schering AG
D-13342 Berlin (Germany)

us; the dipolar term, δ_{dip}, describes the through-space interaction between the dipolar magnetic field centered at the lanthanide ion and the observed nucleus.

In the course of our studies of paramagnetic lanthanide chelate complexes[14] we have examined the applicability of many chelates as NMR thermometers. Pr[MOE-DO3A] **3**, the praseodymium complex of 10-(2-methoxyethyl)-1,4,7,10-tetraazacyclododecane-1,4,7-triacetate,[15] proved to be the most promising compound.

Complex **3** was synthesized by alkylating the chromium tricarbonyl complex (**1**) of cyclene[16] with 2-methoxyethyl bromide, resulting in the monoalkylated product **2**. Reaction of **2**

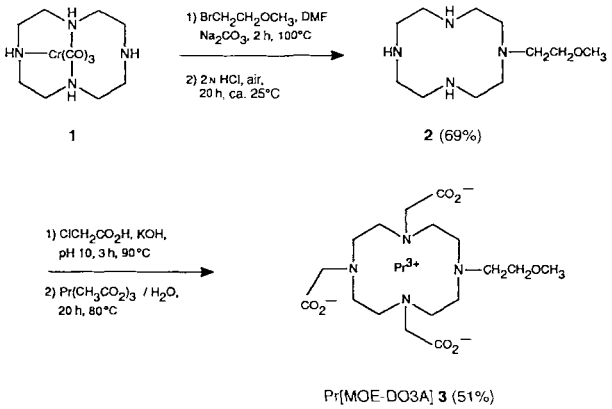

with monochloroacetic acid[17] and complex formation with praseodymium triacetate yielded **3**. Thermodynamically, complex **3** is very stable ($\lg K = 19.2 \pm 0.1$[18]); its high tolerance in mice (LD_{50} (mouse) $= 12.5$ mmol kg^{-1}) is comparable to that of the gadolinium chelates used routinely as contrast media in diagnostic imaging.

The great number of signals in the ^{1}H NMR spectrum (Fig. 1) of a solution of **3** in D_2O is the result of the chirality of the complex. In the solid state the praseodymium ion in **3** is ninefold coordinated, as in other related lanthanide complexes.[19–21]

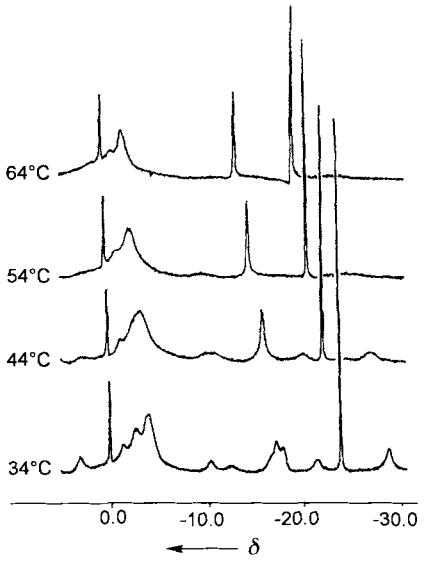

Fig. 1. High-resolution 250 MHz ^{1}H NMR spectrum of a 5 mM solution of **3** in D_2O at several temperatures. The chemical shift scale is referenced to the residual proton signal of D_2O ($\delta = 0$). For each spectrum 64 FIDs were accumulated with a repetition time of 0.5 s. No time-domain filter functions were applied.

Due to intramolecular racemization in solution, the ^{1}H NMR spectrum shows line-broadening effects with varying temperature. Unlike all other signals, however, the line width of the methoxy group signal at approximately $\delta = -24$ (relative to water) remains virtually unchanged in the temperature range studied. It is this temperature-sensitive signal ($\Delta\delta = 0.131$ ppm K^{-1}) that forms the basis for the temperature determination.

The detection of weak ^{1}H NMR signals from compounds in the millimolar concentration range in an in vivo system is much more difficult, due to the presence of the strong signal arising from water in tissue. The large dynamic range of $1:10^5$ leads to an additional noise contribution because of the limited resolution of the analog-to-digital converter.[22] Since the frequency difference between the protons of the methoxy group of Pr[MOE-DO3A] and the protons of the water tissue is relatively large (24 ppm), the strong water signal can be suppressed very effectively through various techniques such as selective excitation of the signal of interest, selective saturation of the water signal, and use of low-pass audiofilters, which are standard in every NMR spectrometer or imager.

The chemical shift of the methoxy protons of **3** varies linearly with temperature within the range relevant to clinical situations. The temperature calibration curve was determined with a solution of the complex in bovine plasma, which approximates the extracellular matrix where **3** is distributed in vivo. Other physiological parameters such as pH (± 1.0 pH unit) and the concentration of the complex (between 0.2 and 10 mmol L^{-1}) do not change the calibration curve within experimental error. The calibration curve can be obtained from a least-square fit (correlation coefficient = 0.998) and is given by Equation (b).

$$T[°C] = 210.2 - 7.634\,\delta_{obs} \qquad (b)$$

In a first in vivo application of the new NMR thermometer we monitored the body temperature of a rat during anesthesia. Thirty minutes after anesthetization, one mmole of **3** per kilogram body weight was administered intravenously. The NMR spectrum was measured by using a surface coil positioned over the liver. In this arrangement, the NMR signal originated only from liver tissue (lower spectrum in Fig. 2). To demonstrate the response of the NMR thermometer, the animal's body temperature was raised a few degrees with a heated waterbed (upper spectrum in Fig. 2).

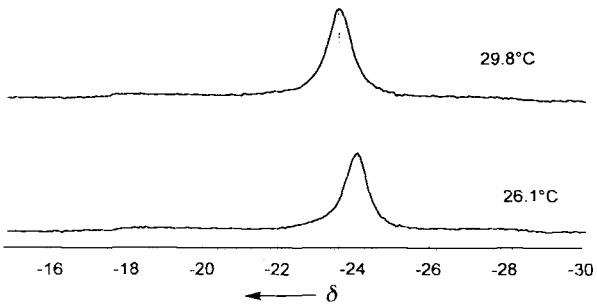

Fig. 2. In vivo ^{1}H NMR spectra of the liver of an anaesthetized rat after intravenous administration of 1 mmol of **3** per kg of body weight. The ^{1}H NMR signal of the methoxy group was excited with a frequency-selective 4 ms Gauss pulse and detected by using a surface coil (2 cm diameter) placed above the liver of the animal. 1500 FIDs with a repetition time of 0.16 s were accumulated, resulting in a total measurement time of about 4 min. The temperature was determined from the chemical shift (with respect to tissue water) according to Equation (b). These calculated values agreed closely with those measured directly with a rectal thermocouple. Upper spectrum: anesthesized rat with additional heating (waterbed at 44 °C). Lower spectrum: anesthesized rat without additional heating.

Although the volume selection in this first in vivo demonstration was achieved with a simple surface coil, **3** can be used as a thermometer in other, more sophisticated localization schemes.[23] Since the a transversal relaxation time (T_2) of the methoxy protons is approximately 10 ms, short spin-echo pulse sequences may be used for volume selection. The longitudinal relaxation time (T_1) of the methoxy protons is 47 ms in bovine plasma, which allows short repetition times. The high sensitivity and precision of the Pr[MOE-DO3A] thermometer could be used to generate images representing temperature distribution[24] in order to identify and localize regions of abnormal metabolic activity or to monitor temperature during thermal energy therapy (for instance, laser-induced interstitial thermotherapy, hyperthermia).

Received: July 12, 1995
Revised version: December 12, 1995 [Z8204IE]
German version: *Angew. Chem.* **1996**, *108*, 691–693

Keywords: chelate ligands · in vivo NMR spectroscopy · lanthanide compounds · NMR spectroscopy

[1] J. L. Meyer, *Cancer Res.* **1984**, *44*, 4745s–4751s.
[2] L. F. Fajardo, *Cancer Res.* **1984**, *44*, 4826s–4835s.
[3] M. L. Martin, J.-J. Delpuech, G. J. Martin, *Practical NMR Spectroscopy*, Heyden, London, **1980**.
[4] R. K. Gupta, P. Gupta, *J. Magn. Reson.* **1980**, *40*, 587–589.
[5] G. L. Levy, J. T. Bailey, D. A. Wright, *J. Magn. Reson.* **1980**, *37*, 353–356.
[6] P. E. Peterson, *Anal. Chem.* **1978**, *50*, 298–303.
[7] M. J. Forster, D. G. Gillies, R. W. Matthews, *J. Magn. Reson.* **1985**, *65*, 497–500.
[8] K. Roth, *Magn. Reson. Chem.* **1987**, *25*, 429–431.
[9] B. A. Berkowitz, J. T. Handa, C. A. Wilson, *NMR Biomed.* **1992**, *5*, 65–68.
[10] R. S. Drago, J. I. Zink, R. M. Richman, W. D. Perry, *J. Chem. Educ.* **1974**, *51*, 371–376, 464–467.
[11] C. N. Reilley, B. W. Good, J. F. Desreux, *Anal. Chem.* **1975**, *47*, 2110–2116.
[12] B. Bleaney, *J. Magn. Reson.* **1972**, *8*, 91–100.
[13] R. M. Golding, P. Pyykkö, *Mol. Phys.* **1973**, *26*, 1389–1396.
[14] S. Hoeft, K. Roth, *Chem. Ber.* **1993**, *126*, 869–873.
[15] Patent application DE-A 4318369, **1994**.
[16] J.-J. Yaouanc, N. LeBris, G. LeGall, J.-C. Clement, H. Handel, H. des Abbayes, *J. Chem. Soc. Chem. Commun.* **1991**, 206–207.
[17] H. Stetter, W. Frank, *Angew. Chem.* **1976**, *88*, 760; *Angew. Chem. Int. Ed. Engl.* **1976**, *15*, 686.
[18] E. Brücher, E. Toth, private communication.
[19] J. P. Dubost, J. M. Leger, M. H. Langlois, D. Meyer, M. Schaefer, *C. R. Acad. Sci. Ser. 2*, **1991**, *312*, 349–354.
[20] M. R. Spirlet, J. Rebizant, J. F. Desreux, M. F. Loncin, *Inorg. Chem.* **1984**, *23*, 359–363.
[21] C. A. Chang, *Eur. J. Solid State Inorg. Chem.* **1991**, *28*, 237–241.
[22] B. J. Kimber, K. Roth, J. Feeney, *Anal. Chem.* **1981**, *53*, 1026–1030.
[23] G. B. Matson, M. W. Weiner in *Magnetic Resonance Imaging* (Eds.: D. D. Stark, W. G. Bradley), The C. V. Mosby Company, St. Louis, USA, **1988**.
[24] L. D. Hall, S. L. Talagal, *J. Magn. Reson.* **1985**, *65*, 501–505.

Characterization of Reactive Intermediates in Palladium-Catalyzed Arylation of Methyl Acrylate (Heck Reaction)**

John M. Brown* and King Kuok (Mimi) Hii

Among palladium-catalyzed reactions available to the synthetic organic chemist, the Heck reaction has enjoyed widespread use. This stems in part from the variety of circumstances in which coupling occurs with high yield and regioselectivity,[1] and in part from successful application to asymmetric synthesis.[2] The coupling reaction often requires forcing conditions, and optimization has proceeded by empirical methods, with a bewildering variation of base, solvent, and catalysts. Since mechanistic information is rather lacking, we have begun a project with an emphasis on the characterization of true catalytic intermediates in solution for the case of a bis(phosphane)palladium catalyst.

Much recent work employed organotriflate electrophiles[3] or organohalides in the presence of silver salts, which has led to the presumption that cationic palladium intermediates are involved. In the first instance we studied the addition of aryl triflates to the organopalladium complex **1**, which had been

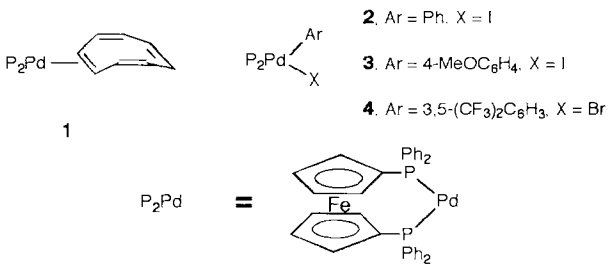

previously used in mechanistic work on catalytic cross-coupling.[4] The reaction is fairly slow at −25 °C and did not give rise to the desired product (vide infra). For this reason the fully characterized aryl halide complexes **2**–**4** were treated with silver triflate in THF at −78 °C, and the products examined by ^{31}P NMR after removal of silver salts by low-temperature centrifugation. In each case an AB quartet was observed in the range −60° to −35 °C, although only the product from **4** was stable at higher temperatures. In that case rapid isolation at 0 °C gave a yellow ionic solid (specific molar conductivity, Λ_m = 4.91 $S cm^{-1} mol^{-1}$ (THF, −20 °C))[5] with an electrospray MS (*m*/*z* 873) that corresponds to the $Ar\{P_2Pd\}^+$ ion with the predicted isotope pattern. In all three cases the low-temperature ^{31}P NMR spectrum in THF exhibited characteristic broadening of both signals, more evident in the high-field partner. The reaction with complex **2** was investigated in most detail. On cooling from −40 °C, the ^{31}P NMR spectrum at 101.3 MHz in THF broadened and then separated below the coalescence region of about −70 °C into two distinct AB systems: At −98 °C the chemical shifts for spin system (A) were δ_P = 35.4 and 13.5

[*] Dr. J. M. Brown, Dr. K. K. Hii
Dyson Perrins Laboratory
South Parks Road, Oxford OX1 3QY (UK)
Fax: Int. code +(1865)275674
e-mail: bjm@vax.ox.ac.uk

[**] We thank EPSRC for postdoctoral support (to K. K. H.) and Johnson-Matthey for the loan of palladium salts. We are grateful to Professor P. J. Stang for his insights into Pd triflate chemistry and Professor A. Jutand for an exchange of information. Dr. R. T. Aplin was very helpful in the obtention of electrospray MS.

(J = 30 Hz), and those for spin system (B) δ_P = 34.8 and 16.0 (J = 30 Hz); the ratio of signal intensities was about 1:2. Assuming a dissociative exchange mechanism we calculated a rate constant k_{ex} of 800 s^{-1} at −70 °C (Fig. 1). The identity of the second complex was defined by addition of H_2O to the sample,

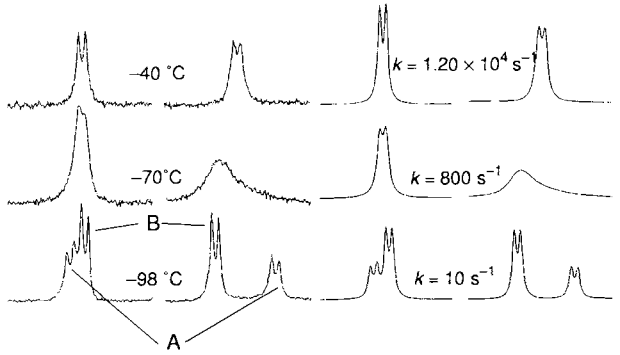

Fig. 1. The observed (left) and simulated (right) $^{31}P\{^1H\}$ NMR spectra for the equilibrium between solvate complexes **5** and **6**; simulation was carried out with the program gNMR.

which shifts the equilibrium towards spin system (A). These observations are consistent with a fast exchange between solvates **5** and **6** (giving rise to signals (A) and (B) respectively, Scheme 1). Since the concentration of H_2O is low, its binding

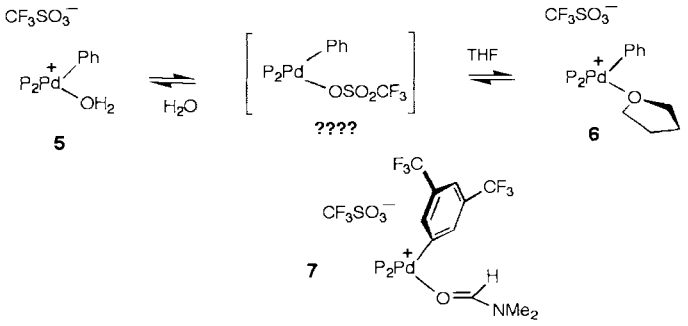

Scheme 1. Solvation equilibria for arylpalladium cations.

constant to Pd is concomitantly high:[6] $K_{aq} \approx 500$ M^{-1} has been estimated from the titration of the THF solution of the triflate derived from **2** with 1% H_2O in THF. When dimethylformamide (DMF) (1–3 μL) was added to a sample of the triflate salt derived from **4** (0.02 M in THF) at −78 °C, a single nondynamic species, (δ_P = 15.3 and 37.1, J = 27 Hz) was observed, which can be attributed to structure **7**. An important recent study of the addition of aryl triflates to $[(PPh_3)_nPd^0]$ complexes concluded that the main species produced was an ionic *trans*-$[Ar(PPh_3)_2Pd^+]$ complex; the existence of strongly bound DMF complexes was noted.[7]

Alkenes, including norbornene, methyl acrylate, 2,3-dihydrofuran, and 2,5-dihydrofuran, reacted with the triflate complexes at low temperatures. For the most part, this was manifested by changes in the ^{31}P NMR first to form a new AB quartet, and then by decomposition around −30 °C. The most clear-cut results were obtained with an excess of methyl acrylate. At −60 °C, there is a slow pseudo-first-order conversion of complex **6** ($k_{obs} = 2.35 \times 10^{-4}$ s^{-1} with 20-fold excess of methyl acrylate; **5**:**6** = 1:3) into a new species A (δ_P = 42.5, 20.8, J = 33 Hz). The rate is slower at lower concentrations of methyl acrylate, and also when H_2O (1.5 equiv) is added, indicating a pre-equilibrium competition between alkene and solvent for the labile coordination site.[8] If the sample is then warmed to −40 °C, a further transformation takes place, which results in the formation of **B** (δ_P = 41.4 and 20.6, J = 37 Hz). This intermediate is in turn converted into C (δ_P = 40.4 and 17.5, J = 35 Hz), and that product is stable to 0 °C. Electrospray MS of **C** isolated as the bromide (m/z 746) indicated the basic structural elements ($H_2C{=}CHCO_2Me$ and $\{P_2Pd\}H^+$). Direct electrospray MS whilst **A** was still present indicated the structural elements $H_2C{=}CHCO_2Me$ and $\{P_2Pd\}Ph^+$. The ^1H NMR spectrum indicated concomitant formation of *E*-methyl cinnamate as the only organic product at −40 °C, which was confirmed by its isolation.

In order to identify the various transient species, a new synthesis of [3-^{13}C] methyl acrylate was developed (Scheme 2).[9]

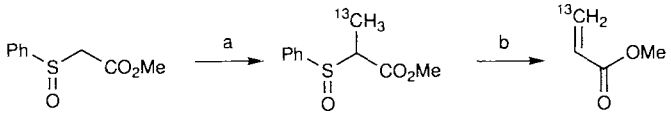

Scheme 2. Synthesis of ^{13}C-labeled methyl acrylate. a) NaH, 1,3-dimethylhexahydro-2-pyrimidinone (DMPU), THF, 0 °C then $^{13}CH_3I$, 51% yield; b) 125 °C, 2 h, 74% yield.

Reaction of an excess of this labeled compound with complex **6** (Scheme 3) clearly showed that **A** was the Pd alkyl **8** ($\delta(^{13}C)$ = 35.3, $J_{C,P}$ = 4 Hz for the ^{13}C nucleus *trans* to the P atom). In similar manner complex **B** was shown to have structure **9** (δ = 13.6; $J_{C,P}$ = 5 Hz), and **C** to be the regioisomeric complex **10** (δ = 30.8; $J_{C,P}$ = 85 Hz). Complexes **8** and **9** both disappear rapidly when 2,4,6-trimethylpyridine is added to the solution at the appropriate stage, but complex **10** is robust to this treatment. The rearrangement is intermolecular and occurs via the unobserved hydride complex **12**, since addition of unlabeled methyl acrylate to the reaction after **8** had disappeared led to the equilibrium distribution of ^{13}C-label in the ultimate product **10**. No other species except *E*-methyl cinnamate (δ = 145.5) were detectable by ^{13}C NMR spectroscopy. Two ^{31}P NMR spectra

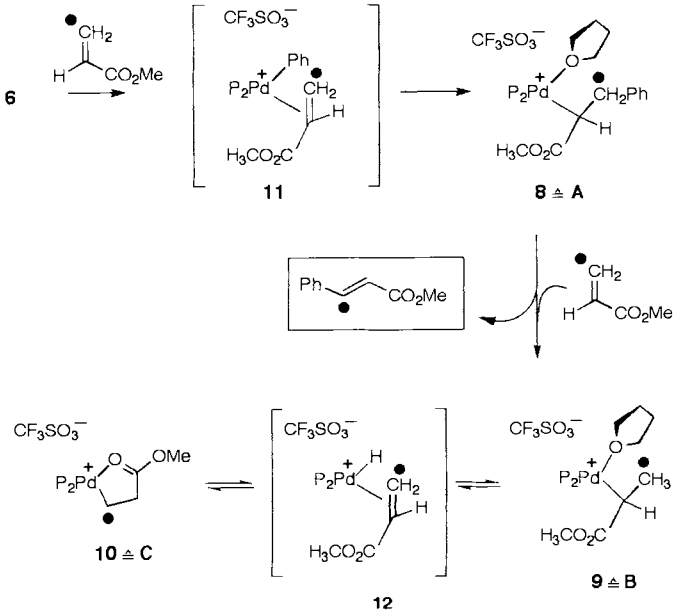

Scheme 3. Heck intermediates observed by heteronuclear NMR spectroscopy. The complex **12** exchanges acrylate ligands with the acrylate pool. The labeled C atom is indicated as ·C.

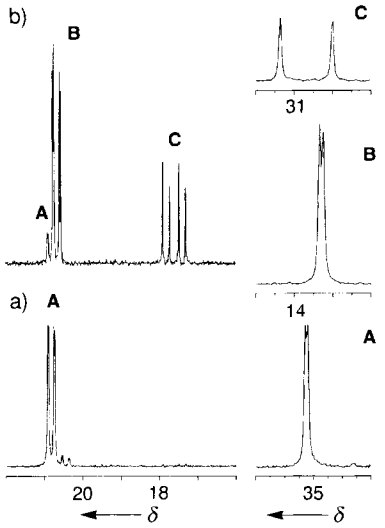

Fig. 2. Left : the high-field region of the $^{31}P\{^1H\}$ NMR spectrum of the reaction between the solvate species **5**/**6** and 3-$\{^{13}C\}$ methyl acrylate a) after about 2 h at −60 °C and b) after warming to −40 °C and holding for a further hour. The $^{13}C\{^1H\}$ NMR spectra of the three intermediates **A**–**C** recorded in the same experiment are reproduced on the right.

recorded in the course of a single experiment are shown in Figure 2; at −40 °C the separation of the stages **A** through **B** to **C** is less clear than at −60 °C.

With this information in hand, the structure of the initial species formed from complex **1** and 3,5-$(CF_3)_2C_6H_3OTf$ was investigated. At −30 °C, the now familiar AB type ^{31}P NMR spectrum ($\delta_P = 12.6$ and 32.8, $J = 29$ Hz) developed cleanly over an hour, and the electrospray MS in MeOH indicated that the probable structure of the new complex was **13** (*m/z* 873; $\{P_2Pd\}^+ + Ar + C_8H_8 + MeOH$). In this case the initially formed migration product is stabilized by the absence of a feasible β-elimination pathway.

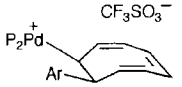

13

These observations clarify several features of the Heck reaction catalyzed by bis(phosphane)palladium complexes:

a) The Pd aryl triflate complex, already shown to be cationic in the PPh_3 series, is also ionized in chelate complexes, and solvent molecules rapidly exchange at the labile coordination site.

b) Traces of water can alter the composition of the initial ionic Pd complex, since its binding constant is high. Influences of water on the Heck reaction have been noted.[10]

c) The putative η^2-alkene complex **11** cannot be observed at −60 °C, thus putting a conservative upper limit of $\Delta G^{\neq} \approx 14$ kcal mol^{-1} on the barrier for the C–C bond-forming step under these conditions. In a search for intermediates in the Pd-catalyzed copolymerization of propene and CO, complexes **14** and **15** were characterized by low-temperature NMR spectroscopy, and $\Delta G^{\neq}$ values of 18.5 and 19.4 kcal mol^{-1} were measured for respective migration of Me and Et groups.[11]

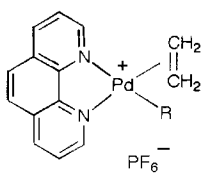

14, R = CH_3

15, R = C_2H_5

d) The aryl migration is completely regiospecific; the only product is *E*-methyl cinnamate, the expected outcome of a Heck reaction. The elimination step generates an unseen Pd–H intermediate, which adds regiospecifically to methyl acrylate to give a new alkyl complex **9**.

e) The initially formed complex **9** then rearranges cleanly to the more stable, primary alkyl regioisomer, for which a chelate form with coordinated ester carbonyl group is likely (**10**).[12] A precedent for such a rearrangement by reversible β-hydride transfer to Pd has already been established, although the precursor of the stable alkyl complex was not observed in the previous case.[13] In addition, a Pt analogue of complex **10** formed by Pt–H insertion into methyl acrylate has been demonstrated.[14]

In summary, a key intermediate of the Heck reaction was characterized in a catalytically viable system, and the alkene elimination step then observed directly. A stoichiometric amount of base is widely employed in catalysis, and its likely function is seen to be the deprotonation of a hydridopalladium complex to regenerate the oxidative addition precursor; otherwise this may intercept the alkene as observed here. Future work will endeavour to clarify the role of base, to define the enantioselective variant, and to pursue the elusive η^2-alkene complex, which could not be observed here.

Experimental Procedure

The ^{13}C-labeled methyl 2-phenylsulfinylpropanoate was prepared as an (*R*R**)/(*R*S**) mixture from $^{13}CH_3I$ according to the general procedure in Ref. [9] and purified by chromatography on silica (1:1 ethyl acetate:petroleum). Yield 51%, ^{13}C NMR (125.7 MHz, $CDCl_3$, 25 °C) $\delta = 8.6, 9.3$, ($^1J(C,H) = 131$, $^2J(C,H) = 3.5$ Hz from ^1H NMR). Thermolysis was carried out in a Kugelrohr apparatus at 125 °C for 2 h under A. Yield 74%, $\delta_C = 130.8$, $^1J(C,H) = 160$, 160.6, $^2J(C,H) \approx 0$ Hz.

Received: October 31, 1995 [Z85161E]
German version: *Angew. Chem.* **1996**, *108*, 679–682

Keywords: catalysis · Heck reactions · NMR spectroscopy palladium compounds

[1] Recent reviews: A. de Meijere, F. E. Meyer, *Angew. Chem.* **1994**, *106*, 2473–2506; *Angew. Chem. Int. Ed. Engl.* **1994**, *33*, 2379–2411; W. Cabri, I. Candiani, *Acc. Chem. Res.* **1995**, *28*, 2–7; for an application in taxol total synthesis, see J. J. Masters, J. T. Link, L. B. Snyder, W. B. Young, S. J. Danishefsky, *Angew. Chem.* **1995**, *107*, 1886–1888; *Angew. Chem. Int. Ed. Engl.* **1995**, *34*, 1723–1726.

[2] K. Kondo, M. Sodeoka, M. Shibasaki, *J. Org. Chem.* **1995**, *60*, 4322–4323; Y. Sato, M. Mori, M. Shibasaki, *Tetrahedron: Asymmetry* **1995**, *6*, 757–766; F. Ozawa, A. Kubo, Y. Matsumoto, T. Hayashi, E. Nishioka, K. Yanagi, K. Moriguchi, *Organometallics* **1993**, *12*, 4188–4196; A. Ashimori, T. Matsuura, L. E. Overman, D. J. Poon, *J. Org. Chem.* **1993**, *58*, 6949–6951.

[3] Recent examples: K. Ohrai, K. Kondo, M. Sodeoka, M. Shibasaki, *J. Am. Chem. Soc.* **1994**, *116*, 11737–11748; F. Guillier, F. Nivoliers, A. Godard, F. Marsais, G. Queguiner, M. A. Siddiqui, V. Snieckus, *J. Org. Chem.* **1995**, *60*, 292–296; E. D. Edstrom, Y. Wei, *ibid.* **1995**, *60*, 5069–5076; Y. Q. Mu, R. A. Gibbs, *Tetrahedron Lett.* **1995**, *36*, 5669–5672; T. Takahashi, H. Koga, H. Sato, T. Ishizawa, N. Taka, *Heterocycles* **1995**, *41*, 2405–2408.

[4] J. M. Brown, P. J. Guiry, *Inorg. Chim. Acta* **1994**, *220*, 249–259.

[5] Conductivities were measured with a digital conductivity meter (PTI-18) with platinum electrodes. The value was found to be comparable to that obtained for a THF solution of [(dppf)Rh(nbd)][OTf] at the same temperature ($\Lambda_m = 6.98$ S cm^{-1} mol^{-1}).

[6] For an X-ray structure of a aquapalladium complex, see P. J. Stang, D. H. Cao, G. T. Poulter, A. M. Arif, *Organometallics* **1995**, *14*, 1110–1114.

[7] A. Jutand, A. Mosleh, *Organometallics* **1995**, *14*, 1810–1817.

[8] When an excess of methyl 2-butenoate was added to a solution of **6** in THF at −60 °C, no changes were observed in the ^{31}P NMR spectrum, which shows that complexation of the ester carbonyl group was not important.

[9] B. M. Trost, K. K. Leung, *Tetrahedron Lett.* **1975**, 4197.

[10] For example, T. Jeffery, *Tetrahedron Lett.* **1994**, *35*, 3051–3054; J. S. Kiji, T. Okano, T. Hasegawa, *J. Mol. Catal. A* **1995**, *97*, 73–77; N. A. Bumagin, V. V. Bykov, L. I. Sukhomlinova, T. P. Tolstaya, I. P. Beletskaya, *J. Organomet. Chem.* **1995**, *486*, 259–262; related observations on Pd-catalyzed aldol reactions: M. Sodeoka, K. Ohrai, M. Shibasaki, *J. Org. Chem.* **1995**, *60*, 2648–2649.

[11] L. K. Johnson, C. M. Killian, M. Brookhart, *J. Am. Chem. Soc.* **1995**, *117*, 6414–6415.

[12] For analogous intermediates in the Pd-catalyzed copolymerization of alkenes and CO, see K. Nozaki, N. Sato, H. Takaya, *J. Am. Chem. Soc.* **1995**, *117*, 9911–9912, and references therein.

[13] J. M. Brown, J. J. Perez-Torrente, N. W. Alcock, H. J. Clase, *Organometallics* **1995**, *14*, 207–213.

[14] R. J. Hinkle, P. J. Stang, A. M. Arif, *Organometallics* **1993**, *12*, 3510–3516.

The First Rotational Isomers of Stable Selenoaldehydes and Their η^1-Tungsten Complexes**

Nobuhiro Takeda, Norihiro Tokitoh, and Renji Okazaki*

In recent decades much attention has been paid to the chemistry of thiocarbonyl[1] and selenocarbonyl[2] compounds. Selenoaldehydes, however, have been very little explored because they are highly reactive and difficult to prepare. Some selenoaldehydes stabilized by mesomeric effects due to heteroatoms such as nitrogen and sulfur[3] or by coordination to transition metals[2, 4, 5] have been isolated. The only known stable, electronically unperturbed selenoaldehyde, 2,4,6-tri-*tert*-butylselenobenzaldehyde, is stabilized kinetically by a bulky substituent.[6] In addition, some transient selenoaldehydes have been reported.[7]

Recently, we succeeded in synthesizing rotational isomers of 2,4,6-tris[bis(trimethylsilyl)methyl]thiobenzaldehydes as stable compounds[8] by the desulfurization of the corresponding cyclic polysulfides TbtCHS$_n$ (n = 5, 8).[9] This synthesis takes advantage of an efficient steric protecting group, 2,4,6-tris[bis(trimethylsilyl)methyl]phenyl, which we will refer to Tbt. We now report here on 1) the synthesis of stable selenoaldehydes **1a** and **1b** (the rotational isomer of **1a**), 2) an equilibrium among 1,3-diselenetane **2** and the seleoaldehydes **1a** and **1b**, and 3) the synthesis of η^1-selenoaldehyde complexes **3a** and **3b** and the structure of **3a**, the first η^1-selenoaldehyde complex characterized by X-ray crystallography.

Deselenation of cyclic polyselenide TbtCHSe$_n$ **4**[10] with excess triphenylphosphane at room temperature resulted in the formation of the corresponding selenoaldehyde **1a** (greenish yellow solution), which was identified based on its spectroscopic data (δ_H(CHSe) = 16.06, δ_C(CHSe) = 237.6, $^1J_{CH}$(CHSe) = 161.2 Hz, δ_{Se} = 2075, λ_{max} = 792 nm; Scheme 1, Table 1). This deselenation of cyclic polyselenides with a trivalent phosphorous reagent is a novel synthetic approach to selenocarbonyl compounds. The isolation of **1a** was unsuccessful; concentration of the reaction solution resulted in the complete conversion of **1a** into the head-to-tail dimer **2** (79%). Like reactive selenoaldehydes generated in situ,[7] **1a** reacted with 2,3-dimethyl-1,3-butadiene and mesitonitrile oxide to afford the corresponding cycloadducts **5** (53%) and **7**[12] (60%), respectively (Scheme 1). The formation of **5** and **7** indicates that **1a** still has a high reactivity toward these reagents in spite of its severe steric congestion, which prohibits its dimerization in a dilute solution for several hours. This is in sharp contrast to the fact that 2,4,6-tri-*tert*-butylselenobenzaldehyde is too crowded to produce the corresponding cycloadducts.[13]

When a solution of **2** was heated at 45 °C, the formation of **1a** and its isomer **1b** (rotation of the bis(trimethylsilyl)methyl (disyl) group at the 2-position[14]) was evident in the ^{1}H NMR and UV/Vis spectra (**2**:**1a**:**1b** = 1:8:3). In another experiment **1a** was trapped when **2** was treated with 2,3-dimethyl-1,3-butadiene at 60 °C giving the [4 + 2] cycloadduct **5** (81%) (Scheme 2). A few years ago Erker et al. reported a similar formation of monomeric selenobenzophenone from the corresponding 1,3-diselenetane, although the monomer was not isolated.[15] It is interesting that only **5**, which was formed from **1a**, was obtained in spite of the equilibrium among **1a**, **1b**, and **2**; this indicates that the two rotamers have different reactivities. Heating the solution at 100 °C in the absence of the trapping agent resulted in the quantitative formation of benzoselenolane **6**. The formation of **1b**, which was not observed in the deselenation at room temperature, suggests the occurrence of the thermal isomerization **1a** → **1b** in solution at 45 °C. Selenoaldehyde **1b** was isolated from the equilibrium mixture by flash column chromatography on silica gel at −20 °C under nitrogen atmosphere (Table 1). It is noteworthy that in **1b** the signal of the methine proton in one *o*-disyl group is at much lower field (δ = 5.87)

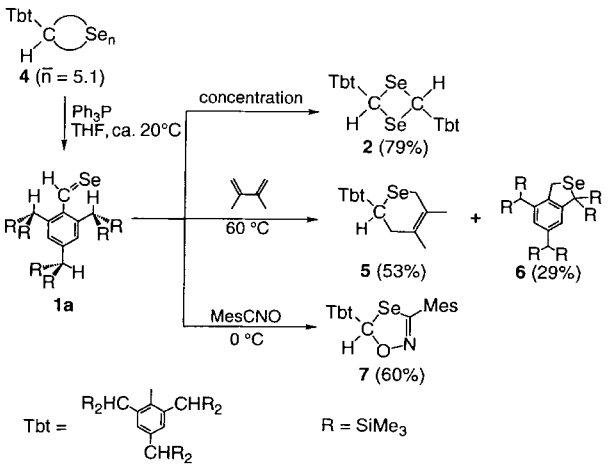

Scheme 1. Synthesis and reactions of selenoaldehyde **1a**.

Table 1. Selected spectroscopic data for compounds **1** and **3**. ^{1}H NMR: 500 MHz, $CDCl_3$, 27 °C, TMS; ^{13}C NMR: 125 MHz, $CDCl_3$, 27 °C, TMS; ^{77}Se NMR: 95 MHz, $CDCl_3$, 27 °C, Me_2Se; UV/Vis: hexane; IR: KBr.

1a: ^{1}H NMR: δ = 0.02 (s, 36H), 0.09 (s, 18H), 1.47 (s, 1H), 3.24 (s, 1H), 3.59 (s, 1H), 6.34 (s, 1H), 6.46 (s, 1H), 16.06 (s, 1H); ^{13}C NMR: δ = 0.4 (q), 0.7 (q), 24.9 (d), 25.4 (d), 33.0 (d), 237.6 (d, ^1J(C,H) = 161.2 Hz, C=Se); the signals of the aromatic C atoms could not be assigned due to overlap with signals from Ph_3P and Ph_3P=Se; ^{77}Se NMR: δ = 2075; UV/Vis: λ_{max} = 792 nm; HRMS (70 eV): *m/z* found: 644.2457, calcd for $C_{28}H_{60}Si_6{}^{80}Se$: 644.2476.

1b: m.p. 195–202 °C (decomp); ^{1}H NMR: δ = 0.00 (s, 18H), 0.06 (s, 18H), 0.08 (s, 18H), 1.48 (s, 1H), 1.75 (s, 1H), 5.87 (s, 1H), 6.37 (2 × s, 2H), 15.51 (s, 1H); ^{13}C NMR: δ = 0.4 (q), 0.5 (q), 1.0 (q), 22.2 (d), 33.4 (d), 35.3 (d), 127.0 (d), 131.0 (d), 141.7 (s), 150.8 (s), 151.7 (s), 152.5 (s), 233.2 (d, ^1J(C, H) = 156.5 Hz, C=Se); ^{77}Se NMR: δ = 1893; UV/Vis: $\lambda_{max}(\varepsilon)$ = 828 nm (38); HRMS (70 eV): *m/z* found: 644.2490, calcd for $C_{28}H_{60}Si_6{}^{80}Se$: 644.2476.

3a: deep blue crystals; m.p. 187–189 °C (decomp); ^{1}H NMR: δ = 0.05 (s, 18H), 0.07 (s, 18H), 0.10 (s, 18H), 1.55 (s, 1H), 3.14 (s, 1H), 3.36 (s, 1H), 6.38 (s, 1H), 6.49 (s, 1H), 13.97 (s, 1H); ^{13}C NMR: δ = 0.4 (q), 0.8 (q), 27.5 (d), 27.7 (d), 34.9 (d), 124.1 (d), 129.0 (d), 141.9 (s), 150.4 (s), 150.8 (s), 154.1 (s), 198.4 (s, ^1J(C,W) = 128.2 Hz, *cis*-CO), 202.1 (s, ^1J(C,W) = 160.2 Hz, *trans*-CO), 227.4 (d, ^1J(C,H) = 162.0 Hz, C=Se); ^{77}Se NMR: δ = 1184; UV/Vis: λ_{max} (ε) = 603 nm (18000); IR: $\tilde{\nu}$ = 2061, 1931, 1908 cm^{-1} (C=O); HRMS (70 eV): *m/z* found: 968.1708, calcd for $C_{33}H_{60}O_5Si_6{}^{80}SeW$: 968.1731.

3b: deep blue crystals; m.p. 171–172 °C (decomp); ^{1}H NMR: δ = 0.04 (s, 18H), 0.08 (s, 18H), 0.11 (s, 18H), 1.52 (s, 1H), 1.80 (s, 1H), 4.69 (s, 1H), 6.37 (s, 1H), 6.40 (s, 1H), 13.33 (s, 1H); ^{13}C NMR: δ = 0.5 (q), 0.8 (q), 1.3 (q), 25.8 (d), 34.3 (d), 35.9 (d), 127.7 (d), 130.9 (d), 142.5 (s), 150.0 (s), 150.8 (s), 152.0 (s), 198.1 (s, ^1J(C,W) = 127.2 Hz, *cis*-CO), 201.9 (s, *trans*-CO), 224.0 (d, ^1J(C,H) = 166.2 Hz, C=Se); ^{77}Se NMR: δ = 1162; UV/Vis: λ_{max} (ε) = 595 nm (21000); IR: $\tilde{\nu}$ = 2066, 1986, 1947, 1929, 1911, 1895 cm^{-1} (C=O).

[*] Prof. Dr. R. Okazaki, N. Takeda, Prof. Dr. N. Tokitoh
Department of Chemistry, Graduate School of Science
The University of Tokyo
7-3-1 Hongo, Bunkyo-ku, Tokyo 113 (Japan)
Fax: Int. code +(3)5800-6899
e-mail: okazaki@chem.s.u-tokyo.ac.jp

[**] This work was partly supported by the Sumitomo Foundation (N. T.) and by a Grant-in-Aid for Scientific Research (No. 05236102) from the Ministry of Education, Science and Culture, Japan. We are grateful to Shin-etsu Chemical Co. and Tosoh Akzo Co. for the generous gifts of chlorosilanes and alkyllithiums, respectively.

 © VCH Verlagsgesellschaft mbH, D-69451 Weinheim, 1996 0570-0833/96/3506-0660 $ 15.00+.25/0

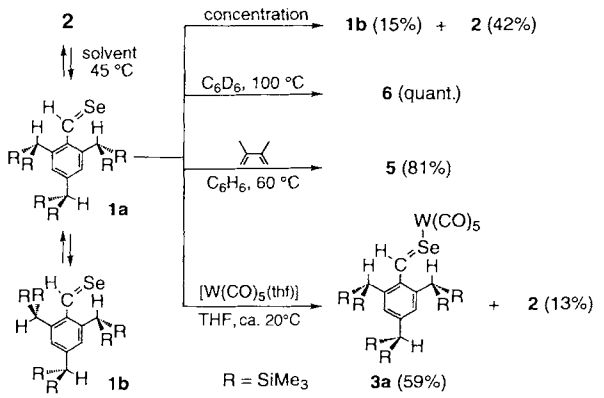

Scheme 2. Synthesis of selenoaldehydes **1a** and **1b** from 1,3-diselenetane **2**.

than that of the other ($\delta = 1.75$). This can be explained by the strong anisotropic effect of the C=Se bond, which is directed toward the methine hydrogen in the former *o*-disyl group in order to avoid steric interactions with the trimethylsilyl groups of the latter *o*-disyl group. In the solid state **1b** is stable even in air, whereas in solution it slowly isomerizes at room temperature to give **1a**, which then dimerizes to afford **2** as a precipitate. The higher stability of **1b** as a monomer indicates that the *o*-disyl groups of **1b** prevent the dimerization of the selenoformyl group more efficiently than those of **1a**; in **1b** one of the *o*-disyl groups is rotated in such a way that the bulky trimethylsilyl groups face the selenoformyl group.

The reaction of **1a**, generated from **2**, with $[W(CO)_5(thf)]$ gave the corresponding η^1-selenoaldehyde tungsten complex **3a** as stable, deep blue crystals (Scheme 2, Table 1). The structure of **3a** was established by X-ray crystallographic analysis (Fig. 1).[16] Although some η^1-selenoaldehyde complexes have

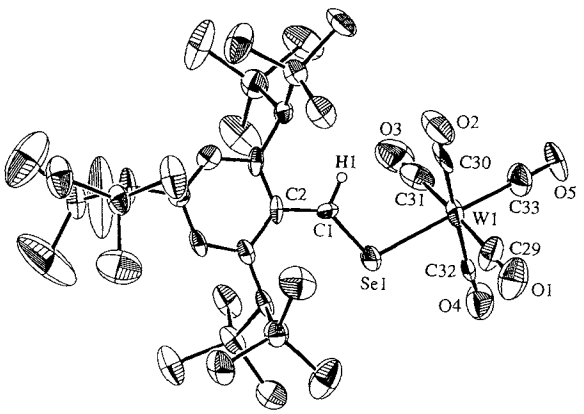

Fig. 1. X-ray crystal structure of **3a** (ORTEP drawing with thermal ellipsoids at 30% probability for non-hydrogen atoms). Selected bond lengths [Å] and angles [°]: C1–Se1 1.783(15), C1–C2 1.44(2), W1–Se1 2.638(2), W1–C29 1.95(2), W1–C30 1.97(2), W1–C31 1.93(2), W1–C32 2.02(2), W1–C33 2.01(2), O1–C29 1.19(2), O2–C30 1.14(2), O3–C31 1.17(2), O4–C32 1.17(2), O5–C33 1.13(2); Se1-C1-C2 136(1), W1-Se1-C1 107.8(4), Se1-W1-C29 87.8(6), Se1-W1-C30 91.4(5), Se1-W1-C31 89.2(6), Se1-W1-C32 89.8(5), Se1-W1-C33 178.9(6).

been synthesized,[4] this is the first to be characterized by X-ray structure analysis. The C–Se bond in **3a** (1.783(15) Å) is significantly shorter than a C–Se single bond (1.970 Å)[17] and the C–Se bond in pentacarbonyl(η^2-selenobenzaldehyde)tungsten (1.864 Å),[4a] and rather close to the length of the C–Se double bond in selenoketones (1,5-dimethyl-3,7-dithiabicyclo[3.3.1]-nonaneselone: 1.774 Å,[18] 4,4′-dimethoxyselenobenzophenone: 1.790 Å[19]). This result indicates weak coordination of the selenoformyl group to the metal in **3a**.

The rotational isomer **1b** was also treated with $[W(CO)_5(thf)]$ to afford the corresponding η^1-selenoaldehyde tungsten complex **3b** [Eq. (a)], which showed satisfactory spectral data

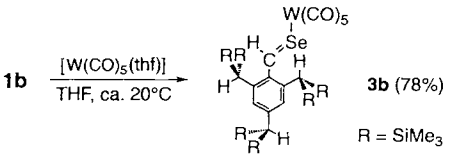

(a)

(Table 1). Complex **3b** is stable in the solid state even in air; however, in solution, it isomerized almost completely to **3a** over several days. This is probably because repulsion between the $[W(CO)_5]$ moiety and the trimethylsilyl groups makes **3b** less stable than **3a**, which does not have such repulsion. It is interesting that as free selenoaldehydes **1b** is isolable but **1a** is not, whereas both complexes **3a** and **3b** are isolable, but **3a** is much more stable than **3b**.

Experimental Procedure

1a, 2: A solution of **4** (26.2 mg, 0.0273 mmol) in THF (10 mL) was added dropwise over 5 min to a solution of Ph_3P (36.7 mg, 0.140 mmol) in THF (5 mL) at room temperature. After stirring for 45 min, the resulting greenish yellow solution containing **1a** was concentrated to dryness under reduced pressure. Distilled hexane (5 mL) was added to the residue and evaporated to remove remaining THF. After hexane (5 mL) was added and evaporated again, a small amount of benzene was added to the pale yellow residue, and insoluble **2** (13.8 mg, 0.0107 mmol, 79%) was removed by filtration. The filtrate was concentrated to dryness, hexane was added to the residue, and insoluble $Ph_3P=Se$ (35.7 mg, 0.105 mmol, 94%) was removed by filtration. The NMR and UV/Vis spectra of **1a** were recorded after the reaction had been performed in $CDCl_3$ and hexane, respectively.

1b: When a suspension of **2** (31.2 mg, 0.0242 mmol) in THF (25 mL) was heated at 45 °C for 17 h under an argon atmosphere, the reaction mixture turned greenish yellow. After evaporation of the solvent, degassed pentane was added to the residue and evaporated to remove the remaining THF. The residue was again dissolved in pentane and insoluble material was filtered off under argon. The filtrate was purified by flash column chromatography (SiO_2, pentane, at −20 °C under nitrogen) to afford **1b** (4.7 mg, 0.0073 mmol, 15%) as a greenish yellow powder. All other fractions were combined and dissolved in hexane, and then insoluble **2** (17.0 mg, 0.0132 mmol, 54%) was recovered by filtration.

Received: October 9, 1995 [Z8457IE]
German version: *Angew. Chem.* **1996**, *108*, 714–716

Keywords: rotational isomers · selenium compounds · tungsten compounds

[1] F. Duss in *Comprehensive Organic Chemistry, Vol. 3* (Eds.: D. H. R. Barton, W. D. Ollis), Pergamon, Oxford, **1979**, p. 373.

[2] P. D. Magnas in *Comprehensive Organic Chemistry, Vol. 3* (Eds.: D. H. R. Barton, W. D. Ollis), Pergamon, Oxford, **1979**, p. 491; C. Paulmier, *Selenium Reagents and Intermediates in Organic Synthesis*, Pergamon, Oxford, **1986**, p. 58; F. S. Guziec, Jr., in *The Chemistry of Organic Selenium and Tellurium compounds, Vol. 2* (Ed.: S. Patai), Wiley, New York, **1987**, p. 215.

[3] D. H. Reid, R. G. Webster, S. Mckenzie, *J. Chem. Soc. Perkin Trans. 1* **1979**, 2334.

[4] a) H. Fischer, S. Zeuner, J. Riede, *Angew. Chem.* **1984**, *96*, 707; *Angew. Chem. Int. Ed. Engl.* **1984**, *23*, 726; b) H. Fischer, S. Zeuner, H. G. Alt, *J. Organomet. Chem.* **1985**, *289*, C21; c) H. Fischer, S. Zeuner, U. Gerbing, J. Riede, C. G. Kreiter, *ibid.* **1989**, *377*, 105; d) M. Muraoka, T. Yamamoto, K. Enomoto, T. Takeshima, *J. Chem. Soc. Perkin Trans. 1* **1989**, 1241; e) H. G. Raubenheimer, G. J. Kruger, L. Linford, C. F. Marais, R. Otte, J. T. Z. Hatingh, A. Lombard, *J. Chem. Soc. Dalton Trans. 1* **1989**, 1565.

[5] W. Paul, H. Werner, *Angew. Chem.* **1983**, *95*, 333; *Angew. Chem. Int. Ed. Engl.* **1983**, *22*, 316; C. E. L. Headford, W. R. Roper, *J. Organomet. Chem.* **1983**, *244*, C53; W. A. Herrmann, J. Weichmann, R. Serrano, K. Blechschmitt, H. Pfisterer, M. L. Ziegler, *Angew. Chem.* **1983**, *95*, 331; *Angew. Chem. Int. Ed. Engl.* **1983**, *22*, 314; A. F. Hill, W. R. Roper, J. M. Waters, A. H. Wright, *J. Am.*

Chem. Soc. **1983**, *105*, 5939; L. Hofmann, H. Werner, *J. Organomet. Chem.* **1983**, *255*, C41; H. Werner, W. Paul, *Angew. Chem.* **1984**, *96*, 68; *Angew. Chem. Int. Ed. Engl.* **1984**, *23*, 58; W. A. Herrmann, J. Rohrmann, A. Schäfer, *J. Organomet. Chem.* **1984**, *265*, C1; J. H. Shin, G. Parkin, *Organometallics* **1995**, *14*, 1104.

[6] R. Okazaki, N. Kumon, N. Inamoto, *J. Am. Chem. Soc.* **1989**, *111*, 5949.

[7] K. Okuma, Y. Komiya, I. Kaneko, Y. Tachibana, E. Iwata, H. Ohta, *Bull. Chem. Soc. Jpn.* **1990**, *63*, 1653; P. T. Meinke, G. A. Krafft, *J. Am. Chem. Soc.* **1988**, *110*, 8671; M. Segi, S. Nakajima, S. Suga, S. Murai, S. Ryu, A. Ogawa, N. Sonoda, *ibid.* **1988**, *110*, 1976; G. Erker, R. Hock, R. Notle, *ibid.* **1988**, *110*, 624; J. Nakayama, K. Akimoto, M. Hoshino, *J. Phys. Org. Chem.* **1988**, *1*, 53; G. W. Kirby, A. N. Tretheway, *J. Chem. Soc. Chem. Commun.* **1986**, 1152; R. Okazaki, A. Ishii, N. Inamoto, *ibid.* **1986**, 71, and references therein.

[8] N. Tokitoh, N. Takeda, R. Okazaki, *J. Am. Chem. Soc.* **1994**, *116*, 7907.

[9] N. Tokitoh, N. Takeda, T. Imakubo, M. Goto, R. Okazaki, *Chem. Lett.* **1992**, 1599; *Bull. Chem. Soc. Jpn.* **1995**, *68*, 2757.

[10] TbtCHSe$_n$ **4** was prepared by the reaction of TbtCHN$_2$[9] with $(C_5H_5)_2TiSe_5$[11] in the presence of a catalytic amount of CuCl at room temperature. **4** was obtained as an inseparable mixture of compounds with different numbers of selenium atoms, the average number of which was determined to be 5.1 by elemental analysis.

[11] A. Shaver, J. M. McCall, *Organometallics* **1984**, *3*, 1823.

[12] Compound **7** gradually decomposes to TbtCHO and MesNCSe at room temperature.

[13] S. Watanabe, T. Kawashima, R. Okazaki, unpublished results.

[14] The structures of **1a** and **1b** in solution were determined by $^1H\{^1H\}$ nuclear Overhauser effect (NOE) experiments, the results of which were similar to those for TbtCHS[8]. For rotational isomerization of sterically congested, substituted benzenes, see: J. Siegel, A. Gutiérrez, W. B. Schweizer, O. Ermer, K. Mislow, *J. Am. Chem. Soc.* **1986**, *108*, 1569; J. S. Lomas, V. Bry-Capdeville, *J. Chem. Soc. Perkin Trans. 2* **1994**, 459, and references therein.

[15] G. Erker, R. Hock, C. Krüger, S. Werner, F. G. Klärner, U. Artschwager-Perl, *Angew. Chem.* **1990**, *102*, 1082; *Angew. Chem. Int. Ed. Engl.* **1990**, *29*, 1067.

[16] Crystallographic data for **3a**: $C_{33}H_{60}O_5SeSi_6W$, $M = 968.16$, triclinic, space group $P\bar{1}$, $a = 12.859(3)$, $b = 16.680(7)$, $c = 11.748(6)$ Å, $\alpha = 107.67(3)$, $\beta = 97.32(3)$, $\gamma = 95.50(3)^\circ$, $V = 2357(1)$ Å^3, $Z = 2$, $\rho_{calcd} = 1.364$ g cm^{-3}, $\mu = 34.09$ cm^{-1}. The final cycle of full-matrix least-squares refinement was based on 2776 observed reflections [$I < 3.00\sigma(I)$] and 415 variable parameters with R (R_w) = 0.054 (0.032). Further details of the crystal structure investigation may be obtained from the Director of the Cambridge Crystallographic Data Centre, 12 Union Road, GB-Cambridge CB21EZ (UK), on quoting the full journal citation.

[17] F. H. Allen, O. Kennard, D. G. Watson, L. Brammer, A. G. Orpen, R. Taylor, *J. Chem. Soc. Perkin Trans. 2* **1987**, S1.

[18] P. R. Brooks, J. A. Counter, R. Bishop, E. R. T. Tiekink, *Acta Crystallogr. Sect. C* **1991**, *47*, 1939.

[19] K. Okuma, K. Kojima, I. Kaneko, Y. Tsujimoto, H. Ohta, Y. Yokomori, *J. Chem. Soc. Perkin Trans. 1* **1994**, 2151.

Enantioselective Cycloisomerization of 1,6-Enynes Catalyzed by Chiral Diphosphane–Palladium Complexes

Andreas Goeke, Masaya Sawamura, Ryoichi Kuwano, and Yoshihiko Ito*

The cycloisomerization of 1,6-enynes in the presence of Pd^0, acetic acid, and phosphane ligands reported by Trost opened elegant pathways to 1,3- and 1,4-dienes, which are difficult to produce using other methods. 1,3-Dienes with exocyclic double bonds are suitable for Diels–Alder reactions.[1, 2] Of particular interest is the formation of the Alder–ene type 1,4-diene, since the construction of a stereogenic center offers an economical access to optically active five-membered carbo- and heterocycles, which occur abundantly in natural products. To date, only two examples of asymmetric induction have been reported utilizing 1) optically active carboxylic acids in conjunction with Pd^0[3] and 2) chiral phosphanes for the double stereodifferentiation of optically active substrates.[4] We now demonstrate that chiral diphosphane–Pd complexes effectively catalyze this interesting cycloisomerization, furnishing 1,4-dienes in medium to high enantioselectivities.

Although phosphane ligands reduce the rate of the cyclization, they are crucial for smooth conversion and for minimizing side reactions. Pd complexes with (*S,S*)-(*R,R*)-TRAP ligands **4**[5] were found to be particularly effective for the cyclization of **1a** (R = SiMe$_3$) at room temperature [Eq. (a), Table 1]. In-

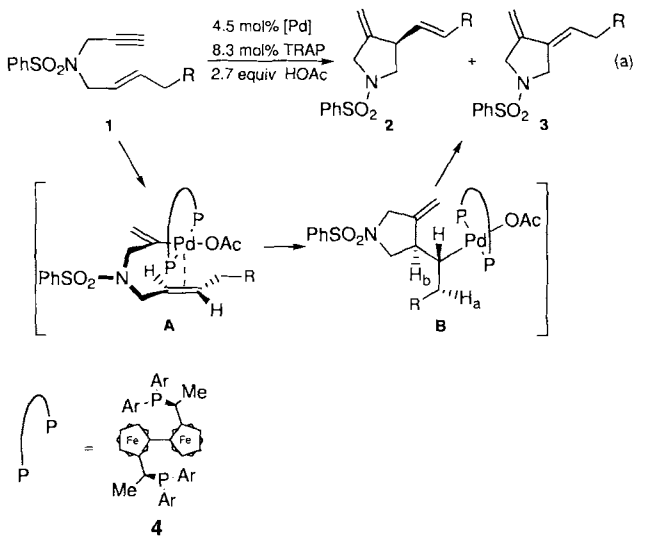

Table 1. Enantioselective cycloisomerization of 1,6-enynes **1a** (R = SiMe$_3$) catalyzed by TRAP–palladium complexes [a].

Entry	TRAP **4** (Ar) [b]	Product **2a** Yield [%] [c]	*ee* [%] [d]	Config. [e]
1	**4a** (C_6H_5)	77	36	(*R*)
2	**4b** (*p*-$CH_3OC_6H_4$)	71	34	(*R*)
3	**4c** (*p*-ClC_6H_4)	66	41	(*R*)
4	**4d** (*p*-FC_6H_4)	70	40	(*R*)
5	**4e** (*p*-$F_3CC_6H_4$)	72	48	(*R*)
		66[f]	58[f]	(*R*)[f]
		24[g]	76[g]	(*R*)[g]
6	**4f** (*m*-$F_3CC_6H_4$)	61	10	(*R*)
7	**4g** (3,5-$(CF_3)_2C_6H_3$)	60	10	(*R*)
8	**4h** (2-furyl)	76	4	(*R*)

[a] Reactions were carried out in benzene at 40 °C for 5 h; **1a**:[$Pd_2(dba)_3$]·$CHCl_3$:**4**:HOAc = 100:2.25:8.3:180. [b] (*S,S*)-(*R,R*)-configurated TRAPs were used. [c] Yield after purification by chromatography. [d] Determined by HPLC with Chiralcel OJ. [e] Assigned based on elution behavior on chiral HPLC analogous to that of **2e** (Table 2, entry 5). [f] 25 °C for 12 h. [g] 0 °C for 24 h with 2.7 equiv of acetic acid; starting material was recovered.

creasing the electron-withdrawing ability of the ligand P-aryl substituents (**4a**, **4b** < **4c**, **4d** < **4e**) resulted in higher selectivities and also higher reactivities. With **4e** cyclization occurred even at 0 °C (76% *ee*, 24% yield), whereas the reaction with **4a** did not occur at this temperature. On the other hand, ligands **4f–h** did not lead to better results. For the *meta*-substituted TRAPs **4f** and **4g**, steric bulk is assumed to account for these

[*] Prof. Dr. Y. Ito, Dr. A. Goeke, R. Kuwano
Department of Synthetic Chemistry and Biological Chemistry
Faculty of Engineering, Kyoto University
Sakyo-ku, Kyoto 606-01 (Japan)
Fax: Int. code +(75)753-5668
Dr. M. Sawamura
Department of Chemistry, School of Science
The University of Tokyo, Hongo, Bunkyo-ku, Tokyo 113 (Japan)

 © VCH Verlagsgesellschaft mbH, D-69451 Weinheim, 1996 0570-0833/96/3506-0662 $ 15.00+.25/0

results. In addition, optically active *cis*-chelating phosphanes such as CHIRAPHOS,[6] DIOP,[7] BPPFA,[8] and PPFA[8] only led to selectivities of 6–15% *ee* with conversions of 56–85%. Moreover, with BINAP[9] and the electron-donating EtTRAP[10] no conversion occurred even at 80 °C. Neither isomerization to the constitutional isomer **3** nor racemization, which may be responsible for low enantiomeric excesses of the cyclization products, was observed on treatment of **2** with $[Pd(PPh_3)_4]$ under the reaction conditions.

The regioselective formation of 1,4-dienes **2** can be explained by the relative ease of the β-elimination of H_a over H_b in the proposed palladium(II) intermediate **B**. The β-elimination of H_a, however, is affected by steric and electronic factors and leads to mixtures of 1,4- (**2**) and 1,3-dienes (**3**) in most cases.[2, 3] When a silylallyl unit[11] serves as the alkene component, the 1,4-dienes are formed selectively due to the kinetically enhanced acidity of the CH group α to silicon. The configuration of the double bond in **2** was always *E* (*E*:*Z* > 50:1), indicating that the cis-β-elimination took place out of the sterically less congested conformation. Although the reaction mechanism remains highly speculative, we believe the *trans*-chelation of the TRAP ligands to the palladium atom to be essential for the enantioselectivity-determining step. This premise is supported by the observation of only two doublets at $\delta = 21.4$ and 38.3 ($J = 455$ Hz) in the ^{31}P NMR spectrum (81 MHz, C_6D_6, **4a** as ligand, 30 °C) of the catalyst system under conditions similar to the reaction conditions described in Table 1.

Results of the cycloisomerization of various 1,6-enynes (**1a–i**) with (*S*,*S*)-(*R*,*R*)-*p*-$CF_3C_6H_4$-TRAP (**4e**) are summarized in Table 2. The replacement of one of methyl substituents of the

Table 2. Enantioselective cycloisomerization of 1,6-eneynes **1** catalyzed by the palladium complex of *p*-$CF_3C_6H_4$-TRAP **4e** [a].

Entry	R (**1**)	*T* [°C]	**2**:**3**[b]	Yield [%]	*ee* [%][c] (Config.)[d]
1	$SiMe_3$ (**1a**)	0	>98:2	24	76 (*R*)
2[e]	$SiMe_2Ph$ (**1b**)	0	>98:2	27	66 (*R*)
3[f]	CH_2SiMe_3 (**1c**)	25	3.5:1	68	95 (*R*)
4	$C_2H_4SiMe_3$ (**1d**)	35	>15:1	71	65 (*R*)
5	Me (**1e**)	35	8.1:1	71	34 (*R*)[h]
6	Et ((*E*)-**1f**)	35	8.9:1	74	69 (*R*)
7[g]	Et ((*Z*)-**1f**)	35	>15:1	66	59 (*S*)
8	C_5H_{11} (**1g**)	35	6.8:1	73	67 (*R*)
9	CH_2Ph (**1h**)	35	5:1	75	75 (*R*)
10	CH_2CHMe_2 (**1i**)	35	>15:1	80	53 (*R*)

[a] See Experimental Procedure; reaction time 24 h. [b] Determined by ^1H NMR spectroscopy. [c] Determined for all compounds by HPLC using Chiralcel OJ. For the determination of the *ee* value, **3** was removed by treatment with an excess of *N*-phenylmaleimide in CH_2Cl_2. [d] Assigned based on elution behavior on chiral HPLC analogous to that of **2** (R = Me). [e] Reaction time 48 h. [f] Reaction time 20 h. [g] *Z*:*E* = 96:4.

silicon atom with a phenyl group had only a limited influence on both the reactivity and enantioselectivity (entries 1, 2). The preferential formation of 1,4-dienes in substrates bearing a silylallyl group was extinguished in substrates having a homoallyl (**1c**, entry 3) or an even more remote silyl group (**1d**, entry 4), leading to some 1,3-diene formation. Interestingly, when steric congestion was relieved by placing the silyl group on a remote position, the enantioselectivity increased considerably, peaking at 95% *ee*. However, steric reasons alone cannot account for this observation, since *ee* values obtained with substrates having alkyl or phenyl substituents at the homoallylic position (**1g–i**) were lower (entries 8–10). It is important to note that the product of (*Z*)-**1f** has opposite configuration to that of substrate (*E*)-**1f** (entries 6, 7). Therefore, the use of diasteriomerically pure enynes is a prerequisite for obtaining high enantioselectivities.

The enantioselectivity was also sensitive towards the sulfonamide groups. The idea of stabilizing the conformation of intermediate **A** by the introducing bulkier sulfonamide groups was not tenable, since the selectivities continuously decreased (data not shown). Moreover, the reaction of an enyne carrying a methanesulfonamide group (R = $SiMe_3$) proceeded with very low enantioselectivity (0 °C 11% *ee*). This low selectivity may indicate that the substituent on the sulfonamide group may be primarily electronic.

Experimental Procedure

A solution of $[Pd_2(dba)_3]\cdot CHCl_3$ (2.2 mg, 2.25 mol%) (dba = dibenzylideneacetone) and *p*-$CF_3C_6H_4$-TRAP **4e** (8.6 mg, 8.1 mol%) in toluene (0.5 mL) was stirred under N_2 at 25 °C for 30 min. Acetic acid was added (15 mg), and after 5 min **1c** (31.0 mg, 0.093 mmol, entry 3 in Table 2) was added, and the mixture was stirred for 20 h. The solvent was evaporated in vacuo and the residue purified by preparative thin-layer chromatography (silica gel, hexane/EtOAc 5/1) affording **2c** and **3c** as a mixture (**2c**:**3c** = 3.5:1, 21.1 mg, 68%). For the determination of the enantioselectivity **3c** was removed by stirring the above mixture in CH_2Cl_2 (1 mL) with phenyl maleimide (ca. 10 equiv). Purification by preparative thin-layer chromatography (silica gel, hexane/EtOAc 5/1) afforded pure **2c** (95% *ee* (*R*), Chiralcel OJ, $[\alpha]_D^{23} = +31.9$ (*c* = 0.31 in $CHCl_3$)).

Received: September 30, 1995 [Z84371E]
German version: *Angew. Chem.* **1996**, *108*, 686–687

Keywords: asymmetric syntheses · complexes with phosphorus ligands · cyclizations · enynes · palladium compounds

[1] For a review: a) B. M. Trost in *Studies in Natural Product Chemistry. Stereoselective Synthesis, Vol. 8* (Ed.: Atta-ur-Rahman), Elsevier, Amsterdam, **1991**, pp. 277–282; b) B. M. Trost, *Acc. Chem. Res.* **1990**, *23*, 34–42.

[2] a) B. M. Trost, G. J. Tanoury, M. Lautens, C. Chan, D. T. MacPherson, *J. Am. Chem. Soc.* **1994**, *116*, 4255–4267; b) B. M. Trost, D. L. Romero, F. Rise, *ibid.* **1994**, *116*, 4268–4278; c) B. M. Trost, M. Lautens, C. Chan, D. J. Jebaratnam, T. Mueller, *ibid.* **1991**, *113*, 636–644; d) B. M. Trost, M. Lautens, *ibid.* **1985**, *107*, 1781–1783.

[3] B. M. Trost, D. C. Lee, F. Rise, *Tetrahedron Lett.* **1989**, *30*, 651–654.

[4] B. M. Trost, B. A. Czeskis, *Tetrahedron Lett.* **1994**, *35*, 211–214.

[5] (*R*,*R*)-(*S*,*S*)-TRAP = (*R*,*R*)-2,2″-Bis[(*S*)-1-(diarylphosphanyl)ethyl]-1,1″-biferrocene: a) M. Sawamura, H. Hamashima, M. Sugawara, R. Kuwano, Y. Ito, *Organometallics*, **1995**, *14*, 4549–4558; b) M. Sawamura, H. Hamashima, Y. Ito, *Tetrahedron: Asymmetry* **1991**, *2*, 593–596.

[6] CHIRAPHOS = 2,3-bis(diphenylphosphanyl)butane: M. Fryzuk, B. J. Bosnich, *J. Am. Chem. Soc.* **1977**, *99*, 6262–6267.

[7] DIOP = 2,3-*O*-isopropylidene-2,3-dihydroxy-1,4-bis(diphenylphosphanyl)-butane: H. B. Kagan, T.-P. Dang, *J. Am. Chem. Soc.* **1972**, *94*, 6429–6433.

[8] BPPFA = *N*,*N*-dimethyl-1-[1,2-bis(diphenylphosphanyl)ferrocenyl]ethylamine, PPFA = 1-[1-(dimethylamino)ethyl]-2-(diphenylphosphanyl)ferrocene: T. Hayashi, T. Mise, M. Fukushima, M. Kagotani, N. Nagashima, Y. Hamada, A. Matsumoto, S. Kawakami, M. Konishi, K. Yamamoto, M. Kumada, *Bull. Chem. Soc. Jpn.* **1980**, *53*, 1138–1151.

[9] BINAP = 2,2′-bis(diphenylphosphanyl)-1,1′-binaphthyl: A. Miyashita, A. Yasuda, H. Takaya, K. Toriumi, T. Ito, T. Souchi, R. Noyori, *J. Am. Chem. Soc.* **1980**, *102*, 7932–7934.

[10] R. Kuwano, M. Sawamura, J. Shirai, M. Takahashi, Y. Ito, *Tetrahedron Lett.* **1995**, *36*, 5239–5242.

[11] Allylsilane has already been used in an asymmetric intramolecular Heck reaction: L. F. Tietze, R. Schimpf, *Angew. Chem.* **1994**, *106*, 1138–1139; *Angew. Chem. Int. Ed. Engl.* **1994**, *33*, 1089–1090.

[12] For the determination of both the enantiomeric excess and absolute configuration, the sulfonamide group was converted into a *tert*-butoxycarbonyl (Boc) group [Li/NH_3, −78 °C; $(Boc)_2O/Et_3N$]. The optical rotation of the resulting carbamate ($[\alpha]_D^{20} = +12.9$ (*c* = 0.35 in $CHCl_3$)) was compared with the reported value for the (*S*)-configurated carbamate (>96% *ee*) ($[\alpha]_D^{20} = -37.3$ (*c* = 0.55 in $CHCl_3$)): W. Oppolzer, T. N. Birkinshaw, G. Bernardinelli, *Tetrahedron Lett.* **1990**, *31*, 6995–6998).

 © VCH Verlagsgesellschaft mbH, D-69451 Weinheim, 1996 0570-0833/96/3506-0663 $ 15.00+.25/0

Structure Made Crystal Clear

Structure Correlation. Vols. 1 and 2. Edited by *H.-B. Bürgi* and *J. D. Dunitz*. VCH Verlagsgesellschaft, Weinheim, 1994; 888 pp., hardcover, DM 398.00.—ISBN 3-527-29042-7

In less than 100 years, our concept of a chemical substance has reversed from the thermodynamicist view of a statistical ensemble of independent entities with internal energies unrelated to the peculiarities of molecular structure, to the stereochemical/quantum chemical picture of a structurally definable chemical (molecular) entity with a specific relationship between molecular geometry and internal energy. Indeed, as strongly the chemist of today would cling as strongly to a CPK model or ORTEP diagram for reassurance that his chemical intuition was still valid, as Mach in 1880 rejected the consideration that modeling molecular structure could give rise to any chemical insight. This peculiar change in philosophy was made technologically possible by Bragg at the turn of the century; it was conceptually founded by Pauling's (the grandfather of structure-correlation) exposé on "The Nature of the Chemical Bond"; and, it was finally embossed on the chemist's "tabula rasa" by high gloss and sumptuously seductive images provided by modern computer generated molecular graphics. The structural molecular hypothesis has been so successful that it is now taken for granted by virtually every branch of natural science.

Since Pauling's revolutionary work, the silos for structural data have been filled relentlessly. The fiduciary structural correlations shown by Pauling with 0.1% of the present available data still hold fast. In the last 20 years, however, the concepts of structural correlation have evolved beyond structure-structure correlations, primarily due to the work of Hans-Beat Bürgi and Jack D. Dunitz, to permit extremely detailed and enlightening studies on chemical dynamics (Structure-Energy and Structure-Activity Correlations). The combined expansion of data-base size and application of statistical methods has driven structure correlation theory to have a major impact on small molecular chemical physics, solid-state chemistry, and biochemical mechanism and action. Much of this work has been dispersed so widely in the chemical literature as to dilute the fundamental message. The task of bringing to order the many tiles of this mosaic is nothing less than gargantuan. Nonetheless, Bürgi and Dunitz have succeeded in creating a magnificent mural of molecular structure correlation in their recent two volume set from VCH.

"Structure Correlation" by Bürgi and Dunitz covers the entire field in a didactic, yet research-motivated style. The four parts of this two volume set break down the subject into digestible sections: 1) *Basics*—the "handyman's" guide to getting started in structure correlation; 2) *Molecular Structure and Reactivity*—demonstration of the principles and the kinds of chemical intuition that can be derived; 3) *Crystal Packing*—a view separating the forest from the trees in solid-state chemistry; 4) *Proteins and Nucleic Acids*—biochemical insight from an ordered look at biomolecular structure. As a (self) teaching tool, this collection will empower the structural chemist to tackle the most important problems at the heart of materials and biomolecular technology. As a reference it will provide researchers from all facets of molecular science with a compass to facilitate their structural investigations.

1) *Basics*: The first part of the series contains five well written chapters which, with some mathematical background (or fundamental references) will give the reader the necessary foundations in structure correlation theory. Chapters 1 and 2 cover fundamental quantitative specification of structures and structural distortions. The discussion of coordinate systems and symmetry arguments starts at an entry level that will be useful in course work. Chapter 3 provides an excellent overview of the hows and whys of the various available crystallographic data bases. Statistical packages accompany several databases, and Chapter 4 covers many of the common types of analysis that can be done with these packages and the significance of these analyses to structural correlation studies. Chapter 5 introduces the reader to chemical questions that can be addressed by the structure correlation method. The concept of the potential energy surface and the physical parameters that can be derived from knowing this surface are discussed with select chemical examples. As this first part of five chapters is strongly oriented toward newcomers to the field, I list here some small typographical errors to alert the reader that it is not a glitch in their own algebraic manipulations. For example, page 5, the block matrix formula entry for column 3, row 2 should be A_{23} not A_{33}; page 47, Figure 2.9, the line numbering would be more consistent if the ends were swapped on the last four linear projections; page 53, Table 2.6, the operation $R_{AB}s(xz)$ in the left column should be R_{AB}; page 168, lines 14–15, the sentence should read "The eigenvector, associated with the smallest eigenvalue of f, points in the direction..."; page 196, line 5, the equation should read $q_0 = (Dr_{10}^2 + Dr_{20}^2)^{1/2}$. These are trivial matters and in no way detract from the desirability of the book.

2) *Molecular Structure and Reactivity*: The second part begins to expand the concepts and applications of structural correlation. The chapter on organic addition and elimination reactions, by Cieplak, is an exhaustive and scholarly treatise, but does not have the same teaching value as some others. It is a wonderfully detailed collection of the subtleties of reactions at trigonal carbon, but one wonders if the depth and detail are warrented in the present context. Chapter 7 by Bürgi and Shklover depicts the classical art of structure-correlation theory. Working from data on the structural distortions of primarily inorganic compounds, they show the similarity of reactions based on coordination number rather than atom type. These early examples established the generality of the methods. The chapter by

This section contains book reviews and a list of new books received by the editor. Book reviews are written by invitation from the editor. Suggestions for books to be reviewed and for book reviewers are welcome. Publishers should send brochures or (better) books to Dr. Illenora Beckmann, Redaktion Angewandte Chemie, Postfach 101161, D-69451 Weinheim, Germany. The editor reserves the right of selecting which books will be reviewed. Uninvited books not chosen for review will not be returned.

Auf der Heyde on transition metal complexes is very well written and gives the reader a good perspective how to use statistical methods to extract order from (greatly simplified) clusters of data. Cluster analysis and principle coordinate analysis are techniques to which the average chemist is exposed; however, Auf der Heyde does an excellent job showing the usefulness of such methods in studies of ligand field exchanges and rearrangements. The final chapter of Volume 1 by Schweizer on conformational analysis is also a classic in the field. The conformational analysis of polyaryl X compounds and medium ring systems is one of the proving grounds for structure correlation analysis. Schweizer clearly presents these classic studies.

3) *Crystal Packing*: Part 3 comprises three chapters which really display the power of structural correlation theory to elucidate molecular interactions when linked to a database like that of CCDB. The chapter by Brown builds directly on Pauling's fundamental work; this chapter demonstrates how elegantly the Pauling's bond-length/bond-order relationship applies to a wide variety of systems. Indeed, this is really the basis of the original structural correlation ideas. The following chapter, by Bernstein, Etter, and Leiserowitz, on hydrogen bonding is one of the best in the collection. Although I found their original definition for the existence of a hydrogen bond to be cyclic (a hydrogen bond exists when there is evidence for the existence of a bond involving a hydrogen atom) they present a practical scheme for describing and organizing hydrogen bonding patterns as well as a number of useful energetic thumb rules for predicting the hierarchy of hydrogen-bonded aggregates. This chapter would be improved if standard chemical structural formula accompanied the many packing diagrams which contain no atomic or bonding labels, and it would be nice if they consistently used their network notation to annotate all of the exemplary figures. Figure 11.15 on page 459 has the labels for part a and part b reversed. The chapter by Gavzzoti describes the substantial advances that have been made toward the derivation of a consistent force field for crystal environments. This chapter is perhaps one of the most important for future developments in computational crystal engineering. The formulae in the chapter often used the same capital letters to mean different things which makes the reading a little bit cumbersome, but the ideas are well worth the effort. Table 12.2 must have some numbers for F switched or wrong, particularly those for tetraphenylmethane, adamantane, and DABCO.

4) *Proteins and Nucleic Acids*: Part 4 contains a series of chapters on biological structure, which except for Chapter 13 by Klebe do not fully blend into the style of the book. The chapter on steroids is more an expose than a lesson. The chapter of protein structural motifs is not easily accessible to the nonspecialist; this chapter could have been a jewel with a few more pages of background, and a conscientious attempt to define terms and jargon rather than just citing literature and expecting the readers to fend themselves. Blundell's contribution was for me interesting but of such small scope that I felt it might well have been included with a broader discussion. Indeed, a combined chapter containing the principles of Chapters 15, 16, and 17 from a generalist's perspective would have been more fitting for the book. Ultimately, although this final section of four chapters is competent, it reads like an afterthought rather than an integral part of the structural correlation field.

In summary, I feel all of the contributing authors did a splendid job; however, the diversity of topics is such that few readers will remain "riveted" throughout the whole 18 chapters. Indeed, in this day of interdisciplinary hype, it is a pleasure finally to read a book that truly captures the spirit of boundary-free research. Thus, I would call "Structure Correlation" by Bürgi and Dunitz a "must have" for anyone interested in molecular structure. My copy stands on my shelf of most accessed books.

Jay S. Siegel
Department of Chemistry
University of California—San Diego
La Jolla, CA (USA)

High Resolution NMR in the Solid State. Fundamentals of CP/MAS. By *E. O. Stejskal* and *J. D. Memory*. Oxford University Press, Oxford, 1994. 189 pp., hardcover £ 30.00.—ISBN 0-19-507380-0

The subject of high-resolution solid-state NMR, including all fundamental aspects of NMR of solids, has been thoroughly treated in several excellent monographs. However, these books have been written by physicists in language which is often not at all familiar to chemists. At the other extreme, a number of fairly oversimplified, purely qualitative introductions to solid-state NMR have appeared, aiming at the chemists' approach by trying to more or less completely avoid "unloved" topics such as mathematics and quantum mechanics. In between these two extremes there exists a large gap: the attempt to provide a bridge between these two worlds is, by its very nature, an extremely difficult task, like trying to square the circle. The task is so difficult because there simply is no purely qualitative approach to high-resolution solid-state NMR which would do justice to the subject. This difficulty of translating and communicating between the worlds of physics and chemistry is almost certainly the reason why no such "intermediate" textbooks on CP/MAS NMR have appeared on the otherwise well supplied NMR book market. On the other hand, a textbook on CP/MAS NMR at that level would certainly represent a much needed commodity, especially since many fascinating and challenging applications of high-resolution solid-state NMR methodology in the field of chemistry remain to be explored. Any serious effort to make the principles of CP/MAS NMR more accessible to the chemistry community is therefore to be welcomed.

The book by Steijskal and Memory represents a quite successful attempt at squaring the circle. From every page in this book it is obvious that it has resulted from long experience of teaching the subject to undergraduate and graduate students. The strategy follows a step-by-step method, starting with the introduction of the basic principles of NMR in Chapter 1. This introduction also includes a brief explanation of the density matrix formalism which is absolutely necessary. This explanation should certainly provide a golden bridge for readers more familiar with solution-state NMR; the example chosen is the polarization transfer experiment in solution using the DEPT sequence. Naturally, an introduction compressed into approximately ten printed pages can only outline the general idea, but all important references for further reading are given.

Chapter 2 is devoted to cross-polarization (CP) in the solid state and follows "traditional" descriptions within the framework of a thermodynamic approach, introducing the concept of spin temperature. For this chapter too all important key references are given in the bibliography. Although it is implicitly clear that this approach to explaining CP under Hartmann–Hahn matching conditions is only valid for a rigid lattice with an abundant spin reservoir as the source of magnetization, a more explicit statement about the limitations of the thermodynamic approach would seem necessary. Also, given the strategy of starting out

 © VCH Verlagsgesellschaft mbH, D-69451 Weinheim, 1996 0570-0833/96/3506-0666 $ 15.00+.25/0

from a familiar solution-state polarization transfer experiment in Chapter 1, a mention of Hartmann–Hahn CP in solution via *J*-coupling would probably have helped the reader to appreciate the unified picture of gradual changes of NMR behavior all the way from non-viscous liquids to rigid solids.

Chapters 3 and 4 deal with spin–spin interactions and with magic angle spinning (MAS), including a very brief encounter with average Hamiltonian theory. Again, this is a topic of fundamental importance for the understanding of MAS spectra, and for a more thorough understanding the reader will need to refer to the original literature. Finally, Chapter 5 is concerned with spectrometer and probe design. It is probably a matter of taste whether one considers such technicalities as an important aspect of the fundamentals of CP/MAS. Personally I would tend to agree with the authors that such a chapter should be included: tuned rf circuits and the principles of construction of double resonance probes are of vital practical importance. A short description of the basic features may, therefore, help to bridge yet another gap. I feel that this chapter will help to improve communication between "users" and engineers and technicians. The collected appendices at the end of the book are too short to be useful.

In summary, I can recommend this book as a useful, solid guide to the "secrets" of CP/MAS for all readers who would tend to be frightened by physics monographs, but nevertheless want a deeper understanding than merely being able to extract an isotropic chemical shift from a CP/MAS spectrum. Armed with this book, with the desire to *understand*, and with access to the library (for the literature cited in the bibliographies), every chemist should be able to master the basics of high-resolution solid-state NMR.

Angelika Sebald
Bayerisches Geoinstitut
Universität Bayreuth
Bayreuth (Germany)

The Chemistry of Organophosphorus Compounds. Volume 3. Phosphonium Salts, Ylides and Phosphoranes. (Series: The Chemistry of Functional Groups. Series editor: *S. Patai.*) Edited by *F. R. Hartley*. Wiley, Chichester, 1994. 442 pp., hardcover £ 120.00.—ISBN 0-471-93057-1

Volumes 1 and 2 of this four-volume series on the chemistry of organophosphorus compounds appeared in 1990 and 1992; the third volume has now been published. A survey of this nature covering the still rapidly advancing field of organophosphorus chemistry is very welcome, especially since other works in this area, such as the handbook edited by G. M. Kosolapoff and L. Maier, are now over twenty years old.

It was noted earlier in reviews of the two previous volumes (*Angew. Chem. Int. Ed. Engl.* **1991**, *30*, 1046; *ibid.* **1993**, *32*, 1215) that a clear plan for the work as a whole did not seem to emerge. This third volume does little to alter that view, but it is at least internally consistent. It covers the phosphonium ylides and phosphonium salts, together with the closely related phosphoranes containing a five-coordinated pentacovalent phosphorus atom. The final chapter ("Chemical Analysis of Organophosphorus Compounds", by H. Feilchenfeld) does not really fit into the context of the rest of the volume, and is not directly related to the preceding chapters. It is in itself a very welcome contribution, but would perhaps have been better placed at the beginning of the series, or alternatively it could have been delayed until the last volume.

The book contains six contributions altogether on the ylides and phosphoranes, all written by recognized experts in their fields. Chapter 1 (D. G. Gilheaney) and Chapter 4 (S. M. Bachrach and C. I. Nitsche) are concerned with bonding and structure in phosphonium ylides, phosphonium salts, and phosphoranes. These two fundamental chapters deal with similar subjects, but differ in their lengths and in the depth of the treatment. A certain degree of overlapping is evident.

The longest chapters are those concerned with the preparation, properties, and reactions of phosphonium salts (Ch. 2, H. J. Cristau and F. Plenat) and with phosphoranes (Ch. 3, R. Burgada and R. Setton). Chapter 5 (K. S. V. Santhanam) deals with the electrochemistry of ylides, phosphonium salts, and phosphoranes, and Chapter 6 (M. Dankowski) with the photochemistry of these classes of compounds.

Concluding the book, Chapter 7 describes the chemical analysis of organophosphorus compounds, giving an overview of the available methods, from the classical wet-chemical methods to the various instrumental methods (gas chromatography, mass spectrometry, etc.). The very important method of NMR spectroscopy, especially the application of ^{31}P NMR methodology to phosphorus compounds, is not included (although it is true that this has recently been covered by other authors). Chapter 7 alone contains over 400 literature references.

The book provides a detailed coverage of the field of phosphonium ylides, phosphonium salts, and phosphoranes in about 350 pages of closely printed text. For each of these classes of compounds several hundred well-chosen references are listed (original papers, review articles, and monographs), giving the reader easy access to the literature. However, only a few of these refer to publications from 1990 onwards. Also there are many instances where insufficient care has been taken with the references. It is disconcerting when the same author's name appears with two, or even three, different spellings, and these garbled names then reappear in the author index, sometimes immediately adjacent to each other and sometimes widely separated.

Despite some shortcomings of the kind mentioned above, this third volume in the series edited by Hartley is an indispensable addition to the literature for all organophosphorus chemists, and the final volume is awaited with interest. Finally, this review would be incomplete without a comment which unfortunately nowadays applies all too often, namely that although the book should be in the departmental library of every organophosphorus chemist, its high price is likely to discourage any wider circulation.

Reinhard Schmutzler
Institut für Anorganische und
Analytische Chemie
der Technischen Universität
Braunschweig (Germany)

Understanding and Manipulating Inorganic Materials with Scanning Probe Microscopes

Charles M. Lieber,* Jie Liu, and Paul E. Sheehan

Scanning probe microscopies, such as scanning tunneling microscopy and atomic force microscopy, are uniquely powerful tools for probing the microscopic properties of surfaces. If these microscopies are used to study low-dimensional materials, from two-dimensional solids such as graphite to zero-dimensional nanostructures, it is possible to elucidate atomic-scale structural and electronic properties characteristic of the bulk of a material and not simply the surface. By combining such measurements with chemical synthesis or direct manipulation it is further possible to elucidate relationships between composition, structure, and physical properties, thus promoting an understanding of the chemical basis of material properties. This article illustrates that the combination of scanning probe microscopies and chemical synthesis has advanced our understanding of charge density waves, high-temperature superconductivity, and nanofabrication in low-dimensional materials. This new approach to studying materials has directly contributed to our knowledge of how metal dopants interact with charge density waves and elucidated the local crystal chemistry of complex copper oxides, microscopic details of the superconducting states in materials with a high superconducting transition T_c, and new approaches to the fabrication of multicomponent nanostructures. Coupling scanning probe microscopy measurement and manipulation with chemical synthesis should provide an approach to understanding material properties and creating complex nanostructures in general.

Keywords: atomic force microscopy · low-dimensional materials · nanosyntheses · scanning tunneling microscopy · superconductivity

1. Introduction

An important goal of condensed matter research is to understand how microscopic or atomic level structural and electronic characteristics of a solid determine observable properties like superconductivity and magnetism. This goal is motivated by the recognition that such an understanding will enable scientists to design bulk solids and nanostructures having predictable properties rationally. For chemists, instrumental methodologies that provide a real-space picture of the connectivity of atoms in a solid or of the local electronic structure are perhaps most appealing, since our training in chemistry typically focuses on the direct analysis of the properties of isolated molecules and macromolecules and not the inverse (that is, reciprocal space) analysis of periodic ensembles of atoms and molecules. Furthermore, real-space probes are required to assess the intrinsic structural and electronic properties of very small material structures that are a focus of the burgeoning area of nanotechnology.

Scanning tunneling microscopy (STM), atomic force microscopy (AFM), and other scanning probe microscopies (SPMs) are uniquely powerful tools for probing the microscopic properties of materials.[1-12] STM can be used to probe the surface structure and electronic states of conducting and semiconducting materials directly on the atomic scale,[1-3,9] while AFM can be used to assess the structure and elastic properties of insulators, semiconductors, and conductors at the nanometer scale.[2,4-6,10-12] SPMs are also effective tools for manipulating matter on the atomic to nanometer scales and for constructing individual nanostructures.[9-11,13,14] Additionally, these techniques represent one of the best approaches for relating nanoscale structures to the world we can visualize.

SPMs are, by their very nature, highly surface-sensitive techniques. The ability to probe the uppermost layers of a material is an important advantage in studies of very small supported structures, such as nanocrystals on surfaces, and in fundamental investigations of growth and catalysis on metal and semiconductor surfaces.[15-17] Surface sensitivity can, however, be a severe limitation in studies designed to probe the bulk properties of a material. For example, the coordinatively unsaturated surface atoms of three-dimensional (3D) solids typically adopt a different geometrical arrangement from those in the bulk (that is, they reconstruct). However, highly anisotropic materials—for example, layered solids possessing strong covalent bonding

[*] Prof. C. M. Lieber, J. Liu, P. E. Sheehan
Department of Chemistry and Division of Applied Sciences
Harvard University, Cambridge, MA 02138 (USA)
Fax: Int. code +(617) 496-5442

 © VCH Verlagsgesellschaft mbH, D-69451 Weinheim, 1996 0570-0833/96/3507-0687 $ 15.00+.25/0

in two-dimensional (2D) sheets with weak noncovalent bonds holding these layers together—cleave preferentially along planes defined by the weak noncovalent bonds. The coordination of atoms at the surface cleavage plane in such low-dimensional solids is similar to that in the bulk, since the covalent bonding is unchanged, and thus these surfaces do not reconstruct. SPM studies of such low-dimensional materials offer the opportunity of probing atomic level structural and electronic properties that are representative of the bulk of a material.

Low-dimensional solids offer a great richness and complexity of physical phenomena that make them generally an important focal point of condensed matter research. For example, many two-dimensional and one-dimensional metal chalcogenide materials exhibit complex charge density wave and spin density wave phases, and furthermore, the layered structure of the copper oxide superconductors is central to the high-temperature superconductivity that these materials exhibit. This review highlights first the application of SPM techniques to understanding fundamental properties of low-dimensional inorganic materials that exhibit charge density wave and superconducting states. By utilizing these microscopies often combined with systematic chemical modifications, new and unique insight into the properties of these materials has been gained that goes far beyond that obtained with more conventional approaches. Secondly, this review will also focus on the use of SPMs to manipulate inorganic systems. Direct manipulation of atoms and clusters enables the construction of new low-dimensional materials—nanostructures—that can then be investigated by SPM techniques in a nonperturbative mode.

2. Background: Scanning Probe Microscopies

2.1. Scanning Tunneling Microscopy

The scanning tunneling microscope was invented by Binnig and Rohrer in the early 1980s[1] and is now a widely used tool in many fields of research.[1-16] Here we briefly review key features of STM and the theoretical underpinning necessary to understand the investigations discussed below. The basic design of a scanning tunneling microscope is illustrated in Figure 1.

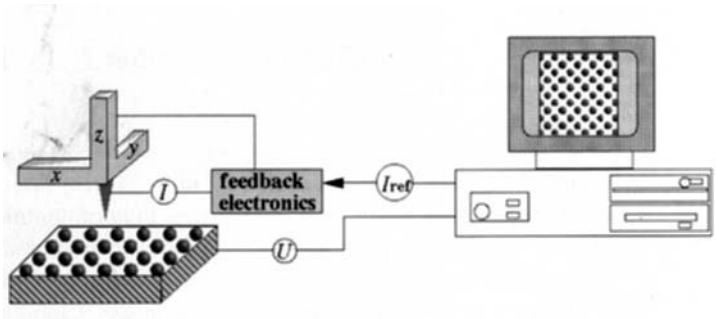

Fig. 1. Schematic diagram of a scanning tunneling microscope.

The essential components include a sharp metal tip, which acts as the local probe, a sample with a conducting surface, a system for positioning the probe in the x, y, and z directions that uses piezoceramic drivers, a feedback loop for controlling the separation between tip and sample with subangstrom precision, and an overall controller that drives the scanner while recording the surface image.

C. M. Lieber

J. Liu

P. E. Sheehan

Charles M. Lieber obtained his early education in New Jersey. He completed a B. A. with honors in chemistry in 1981 at Franklin and Marshall College, earned his Ph.D. at Stanford University under the direction of N. S. Lewis, and carried out postdoctoral research at the California Institute of Technology under H. B. Gray. He is currently a Professor at Harvard University, where he is a member of the Chemistry Department and Division of Applied Sciences. His research integrates several disciplines, including inorganic, physical and materials chemistry, condensed matter physics, and materials science. His research group has been using scanning probe microscopies and other new techniques combined with materials synthesis to understand and control the fundamental properties of materials.

Jie Liu was born in Shandong, China, in 1968. He received his B. Sc. and M. S. degrees from Shandong University in 1987 and 1990. He is currently a graduate student in Professor Lieber's research group at Harvard, investigating the structural and electronic properties of low-dimensional materials, including high-T_c superconductors and transition metal dichalcogenides.

Paul E. Sheehan was raised and educated in North Carolina. He received his B. S. in Materials Science in 1993 from the University of North Carolina-Chapel Hill. He is currently a graduate student in Professor Lieber's research group at Harvard, pursuing the mechanics and tribology of nanoscale structures.

The underlying basis for the operation of the microscope is electron tunneling between a sharp metal tip and a conducting sample.[1-3] When the tip and sample are brought sufficiently close (5–10 Å), their wave functions can overlap. If a bias voltage U is then applied to the sample, a tunneling current I will flow between the sample and tip. Electrons will tunnel from filled electronic states in the tip to empty states in the sample when U is positive, and from filled sample states to empty tip states when U is negative. The tunneling current that flows when U is applied varies exponentially with the tip–sample separation, and for typical work functions decreases tenfold for an increase of one angstrom in separation. The strong exponential dependence of the tunneling current on distance enables STM to achieve high vertical resolution. An atomic resolution map of the surface can then be generated by rastering the tip over the sample with control in the angstrom range provided by the piezoceramic positioners. Under favorable conditions, a vertical resolution of hundredths of an angstrom and a lateral resolution of about one angstrom can be achieved.

There are two principal modes of surface imaging with the STM: constant current and constant height. In the constant current mode, the feedback loop controls the vertical position of the tip above the sample so that I is equal to a reference current at all coordinates on the surface. Features in constant current mode images thus correspond to vertical displacements of the positioner needed to maintain a constant tunneling current. In constant height mode imaging the tip height above the surface is constant, and images correspond to the variation of I with position. Since the feedback loop does not respond to rapid height variations in this mode, it is possible to scan at a higher rate than in the constant current mode. The constant height mode is, however, limited to flat samples.

To interpret STM data requires an understanding of the response of the tunneling current to a number of factors, including applied voltage, tunneling barrier height, and the sample's electronic structure.[2e, 3] As first discussed by Tersoff and Hamann, an expression for I can be readily derived by using perturbation theory to treat the interaction between sample and tip wave functions.[18] In the limit of small bias voltage and low temperature this treatment yields Equation (a), where M_{st} is the tunneling matrix element between wave functions on the tip (Ψ_t) and sample (Ψ_s). As shown by Bardeen,[19] the tunneling matrix element can be written as Equation (b), where the integral corresponds to a surface within the barrier region between the sample and tip. To evaluate M_{st} in a way that the resulting expression for I can be compared quantitatively to STM images in general (that is, not for one specific choice of sample and tip) requires several approximations. Tersoff and Hamann showed that by assuming that the tip forms a locally spherical potential well with only s-wavefunctions, I could be expressed as (c).

$$I = (2\pi/\hbar)e^2 U \sum |M_{st}|^2 \delta(E_s - E_f)\delta(E_t - E_f) \quad (a)$$

$$M_{st} = (\hbar^2/2m) \int (\Psi_t^* \nabla \Psi_s - \Psi_s \nabla \Psi_t^*) dS \quad (b)$$

$$I \sim \sum_s |\Psi_s(r_0)|^2 \delta(E_s - E_f) \quad (c)$$

By definition the summation is the local density of sample electronic states, $\rho(r_0,E)$, at the center of curvature of the tip (d).

Thus, constant current images correspond simply to contours of constant density of sample electronic states.

$$\rho(r_0,E) \equiv \sum_s |\Psi_s(r_0)|^2 \delta(E_s - E_f) \quad (d)$$

It is useful to consider the effect of the approximations made in deriving (d). Treatment of the tip's potential as spherical is reasonable, because although the experimental tip shape is generally unknown, it probably terminates in a cluster of atoms; that is, the tip is approximately spherical. The s-wavefunction approximation for the tip is even more significant, because it leads to a cancellation in Equation (b) which makes I dependent only on the square of the sample wavefunction with no contribution from the tip. Tersoff has examined more general descriptions of the tip and found that constant current images still correspond to contours of constant density of sample electronic states for metals.[20, 21] STM images of semiconductor surfaces at low U could, however, deviate significantly from this simple picture, since only a small pocket of the surface Brillouin zone contributes to the tunneling. This deviation is limited, however, to the lowest Fourier component of the image, and thus the model of the tip approximated by an s-wavefunction may still be used in many cases to interpret images at higher bias voltages. While these results indicate that the assumptions used to derive (d) are reasonable, it is important to develop further theoretical models so that data can be quantitatively interpreted.[6, 22]

The dependence of the tunneling current on applied bias voltage, which corresponds to tunneling spectroscopy, can probe the local density of electronic states versus energy, since I is proportional to the local density of states. For finite voltages (c) can be rewritten as (e), where $T(E,eU)$ is the transmission probability that takes into account the energy-dependent wavefunction decay. This expression incorporates the assumption that the density of tip states does not vary significantly with energy. In the limit of small bias, dI/dU is proportional to the density of states; however, for finite bias the exponential dependence of $T(E,eU)$ on U becomes important. This exponential dependence can be effectively removed by normalizing dI/dU by U/I[23] [expression (f)].

$$I \sim \int \rho(r,E) T(E,eU) dE \quad (e)$$

$$(U/I)dI/dU \sim \text{LDOS} \quad (f)$$

Comparisons of the local density of states data obtained by STS with photoemission and inverse photoemission results show that the approximations made in arriving at (f) are reasonable.

2.2. Atomic Force Microscopy

The atomic force microscope, which was invented several years after STM,[10] is now perhaps the most widely used probe microscopy technique.[4-6, 11, 12, 24] The underlying basis for

force microscopy is similar to a simple profilometer;[25] that is, the forces on a probe tip attached to a cantilever are detected and plotted as a sample is scanned beneath the tip. The magnitude of the load in force microscopy is, however, many orders of magnitude smaller than those applied with a conventional profilometer: 10^{-13} to 10^{-6} versus 10^{-4} N. The combination of small loads with sharp tips enables AFM to image at close to atomic resolution. Importantly, force microscopy can, in principle, be used to probe the structure of any solid material, be it a conductor, an insulator, or a living cell, since this technique relies solely on the mechanical interaction between the tip and sample.

The basic design of a modern force microscope is illustrated schematically in Figure 2. The essential components that differ

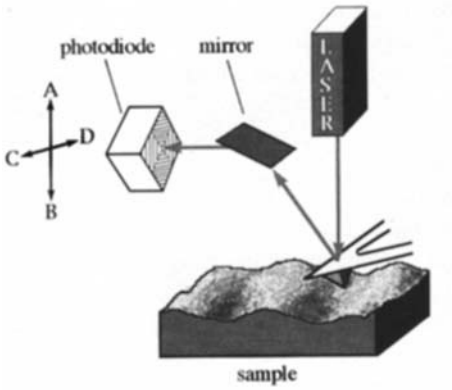

Fig. 2. Illustration of a force microscope that utillizes optical detection.

from those shown for the tunneling microscope (Fig. 1) include an integral tip-cantilever assembly and optical detection system that measures the cantilever deflection. Since the cantilever (spring) deflection is linearly related to the force, the experimental signal is a measure of the force. In operation, variations in the cantilever position, which result from sample topography and/or differing sample–tip interaction, lead to a deflection of the laser beam on a quadrant photodiode detector. By measuring the vertical (A–B) and horizontal (C–D) displacements on the photodiode it is possible to extract both normal and lateral forces. Furthermore, if the normal and lateral spring constants of the cantilever are known, it is possible to quantify these forces from the measured cantilever displacements.[24]

There are several common modes of imaging in contact-mode force microscopy, including constant normal force and lateral force. In the constant-force mode, which is analogous to constant-current mode of STM, the feedback loop controls the vertical position of the sample so that the cantilever displacement and hence normal force is constant at all points on the surface. Features in images recorded in constant-force mode thus correspond to vertical displacements of the positioner needed to maintain a set force between the cantilever–tip assembly and sample surface. In the lateral-force mode, the frictional or lateral force between the tip and sample is mapped as a function of x, y coordinates for a constant applied load. Thus, the constant-force mode of imaging provides a good measure of surface structure, while the lateral-force mode provides indirect information about variations in surface composition (reflected by variations in friction).

3. Quasi-Two-Dimensional Transition Metal Dichalcogenides

3.1. Basic Structure

The dichalcogenides of transition metals of Groups IV, V, and VI have layered structures in which the transition metal (M) occupies either octahedral or trigonal prismatic sites between two layers of hexagonal close packed chalcogenide atoms (X). The X-M-X sandwiches are then stacked in a direction perpendicular to the chalcogenide layer to complete the structure.[26] The octahedral coordination of Ta atoms in 1T-TaS_2[*] is schematically shown in Figure 3. In general, the X-M-X layers are held together by strong covalent or ionic bonding, whereas the interactions holding the layers together are much weaker dispersion forces. These materials cleave readily between the weakly bonded layers to yield free surfaces that are structurally and electronically similar to the bulk material.[7, 8, 26–29]

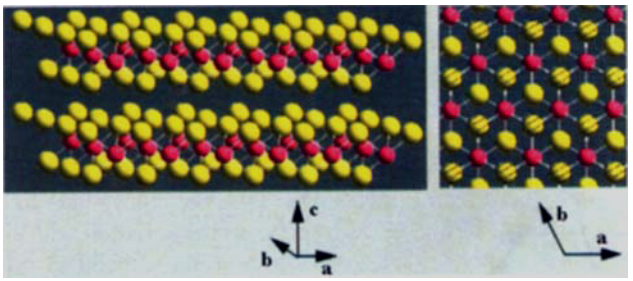

Fig. 3. Schematic side view (left) and top view (right) of 1T-TaS_2. White bonds between yellow sulfur and magenta tantalum atoms highlight the octahedral coordination of tantalum. In the top view, the upper sulfur layer (solid yellow), tantalum, and lower sulfur layer (yellow with black lines) are superimposed.

3.2. Charge Density Waves

The d^1 transition metal dichalcogenide materials exhibit rich temperature-dependent structural and electronic properties. Electronically, the partially filled t_{2g} conduction band in a d^1 system should give rise to metallic conductivity. Indeed, at high temperatures the compound 1T-TaS_2 is metallic; however, on cooling below 543 K 1T-TaS_2 exhibits four distinct temperature-dependent charge density wave (CDW) states.[8, 27, 28] A schematic diagram of the CDW and atomic lattice in 1T-TaS_2 is shown in Figure 4. In general, CDWs are found in low-dimensional systems that exhibit significant Fermi surface nesting (nesting refers to the condition that a piece of the solid's Fermi surface may be translated and superimposed on another piece by a wave vector $\boldsymbol{q}$). Fermi surface nesting leads to a divergence

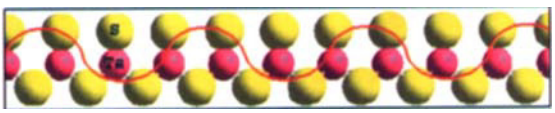

Fig. 4. Cross sectional view of a CDW (sinusoidal red line) in a single layer of TaS_2.

[*] The notation 1T indicates the polytype in which all tantalum atoms are octahedrally coordinated.

in the electronic susceptibility at the q, and through electron–phonon coupling can yield a stable periodic modulation of the atomic lattice and of the electron density in the conduction bond; that is, a CDW. The wavelength (λ) of the CDW is governed by q. Since λ is determined by the Fermi surface size through q, it might not correspond to an integral number of lattice constants (na). In the case where $\lambda \neq na$ the CDW is called incommensurate; however, when $\lambda = na$ it is commensurate.

Prior to the advent of STM the structure of the CDW phases in TaS_2 and other materials had been investigated by X-ray and electron diffraction methods. These techniques showed in 1T-TaS_2 that the high temperature CDW was incommensurate, and that for $T < 183$ K the CDW rotated 13.9° relative to the atomic lattice to become commensurate.[27–29] The real-space structures of these phases are illustrated schematically in Figure 5.

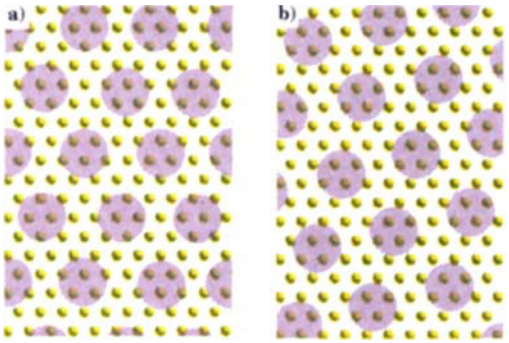

Fig. 5. Schematic top views of the incommensurate (a) and commensurate (b) CDW phases in 1T-TaS_2. The CDW maxima are indicated by pink-shaded circles and the atomic lattice by yellow spheres.

The CDW superlattice of both phases has a regular hexagonal symmetry. In the incommensurate phase the peaks of CDW are located randomly relative to the atomic lattice. In the commensurate phase, the CDW superlattice rotates 13.9° relative to the atomic lattice and expand by 2% with the result that each CDW maximum is oriented over a similar atomic lattice site. Unfortunately it was not possible to resolve the structures of the intermediate-temperature nearly-commensurate and triclinic nearly-commensurate CDW phases by means of diffraction techniques. These two phases had been suggested to exhibit either uniformly incommensurate structures or domainlike structures.[30, 31]

The first application of STM to CDWs was carried out by Coleman and co-workers in 1985.[32] Significantly, this work showed that the charge modulation of a CDW and atomic lattice could be viewed simultaneously in real space. In addition, comparison of early STM data with previous diffraction results demonstrated that the surface-sensitive STM experiment truly reflected the bulk properties of 1T-TaS_2.[32, 33] The ability of STM to determine simultaneously both CDW and atomic lattice positions has subsequently been exploited to resolve the complicated structural details of the intermediate-temperature CDW phases in TaS_2 that previously could not be determined by diffraction techniques.[6, 7, 34–38]

STM studies of the real-space structure of TaS_2 at room temperature showed that the nearly-commensurate CDW phase adopts a novel, hexagonal, domainlike structure, in which there is a periodic variation in the CDW amplitude that occurs on a wavelength much larger than the CDW wavelength λ (Fig. 6).[34] In images of large areas the CDW maxima (Fig. 6a, filled white circles) define a regular hexagonal superlattice with an average wavelength that is consistent in diffraction and STM measurements. The amplitude of the CDW maxima further exhibits a larger periodic modulation that defines domains consisting of relatively high-amplitude CDW maxima separated by lower amplitude domain boundaries. The roughly circular, high-amplitude domains are arranged in a hexagonal superstructure with a period of approximately 70 Å at room temperature. Hence, the nearly-commensurate CDW exhibits a fascinating hierarchy of structures: the hexagonal atomic lattice with period 3.35 Å, the fundamental hexagonal CDW lattice with period of about 12 Å, and the hexagonal domain superlattice with period 70 Å.

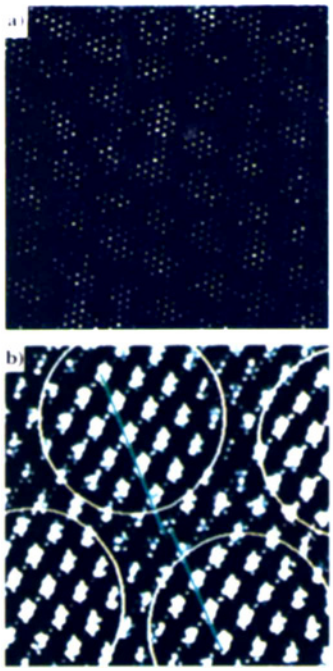

Fig. 6. STM images of 1T-TaS_2 at room temperature: a) 50×50 nm^2 surface showing CDW maxima and domains; b) atomic-resolution imge of four domains.

Images with atomic resolution of the nearly-commensurate phase have provided further insight into the complex structure of the domain phase; four domains are highlighted by white circular lines in Figure 6b. This image shows well-defined phase shifts of one atomic lattice period between the CDWs in adjacent domains:[34, 35, 38] the green lines indicating the CDW directions in adjacent domains have a one-atom mismatch. The abrupt changes in CDW phase are clear in real-space images, but are quite difficult to detect in diffraction measurements. Furthermore, the high-resolution images show a similar arrangement of atoms at each CDW maximum within a domain, thus indicating that the CDW is approximately commensurate (see for example, schematic representation in Fig. 5) in the domains. Because the actual angle between the atomic lattice and CDW superlattice can be measured, such images also enable the issue of commensurability to be addressed quantitatively. Significantly, these measurements showed the angle within single domains was that expected for a commensurate CDW (approximately 13.9°). Taken together, these STM studies unambiguously resolved the long standing controversy about the structure of the nearly-commensurate CDW phase in 1T-TaS_2.

Temperature-dependent SPM measurements are also important for probing CDW phases in the transition metal dichalcogenides further, since temperature variations can be used to assess melting and other phase transitions.[33, 35, 36] STM studies of the nearly-commensurate phase in 1T-TaS_2 first demonstrated the power of such measurements.[35] Images recorded

between 200 and 350 K exhibit the hexagonal CDW domain structure described above. The period of the domain structure was found to undergo a remarkable and unexpected change with temperature decreasing from 100 Å at 200 K to approximately 60 Å at 350 K (Figs. 7a–c). At still higher temperatures, there is an abrupt loss of the domain structure as the true incommensurate phase is formed (Fig. 7d). Significantly, the decrease in domain size appears similar to a second-order melting transition as the sample temperature is raised; however, it is important to point out that this corresponds to melting of an electronic (CDW) lattice and not the atomic lattice.

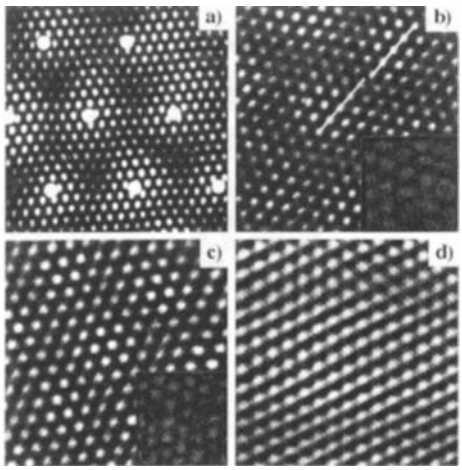

Fig. 7. STM images of 1T-TaS_2 recorded at sample temperatures of 242 (a), 298 (b), 349 (c), and 357 K (d). The imaged surfaces are 30×30 (a), 17.5×17.5 (b), and 15.5×15.5 nm^2 (c and d). The insets in b) and c) are 30×30 nm^2. The domain center positions for an ideal hexagonal structure are marked with white dots in a).

3.3. Role of Metal Substitution

From a chemist's perspective one of the most exciting areas of SPM-related materials research is that focusing on understanding how chemical substitutions or doping affect the structural and electronic properties of a solid at the atomic level. In the specific case of materials with CDWs, the crucial issue is to understand how a CDW interacts with the metal impurities doped into the atomic lattice, since the nature of the interaction between impurities and a CDW controls both the static and dynamic properties of the CDW state.[39–45] CDW pinning can, in general, be classified as either strong or weak depending on the competing energetics of the CDW–impurity interaction and the CDW deformation energy (Fig. 8).[39, 41, 42] In strong pinning, the impurity's potential dominates the CDW elastic energy and pins the phase of the CDW at each impurity site. In weak pinning, the CDW breaks up into constant phase regions that are pinned collectively by impurities. Despite the fundamentally different structural manifestations of strong and weak pinning, there has been considerable controversy concerning the nature of pinning in CDW systems.[39–49] This controversy has been due in large part to the lack of data characterizing the evolution of CDW structure with impurity doping. Real-space imaging of the CDW structure in doped materials by STM has, however, addressed and resolved directly the important issue of strong versus weak pinning.[8, 50–57]

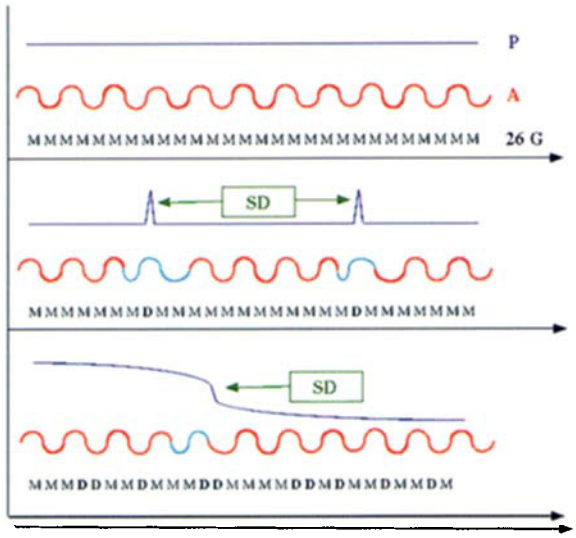

Fig. 8. Plots of the CDW phase and amplitude as a function of lattice position for a perfect one-dimensional lattice (top), a lattice containing strong pinning impurities (middle), and a lattice containing weak pinning impurities (bottom). A = CDW amplitude, L = lattice, P = CDW phase, SD = structural defect. D in the lattice represents dopant molecules.

We have investigated the effect of impurities through systematic studies of metal-substituted tantalum disulfide, $M_xTa_{1-x}S_2$, where M atoms randomly replace Ta sites in the lattice.[50–57] In principle, substitution of isoelectronic Nb^{IV} for Ta^{IV} centers represents the weakest perturbation on the potential that is possible with metal substitution, and thus serves as the best test of the weak pinning regime. The effect of Nb-substitution on the macroscopic transport properties of these $Nb_xTa_{1-x}S_2$ materials has been assessed by variable-temperature resistivity measurements.[27, 28] Nb-substitution (and other metal substitutions) decreases the transition temperature from the high-temperature incommensurate CDW state to the lower temperature nearly-commensurate state. Qualitatively, the suppression in the transition temperature can be rationalized by assuming that the incommensurate state is stabilized by impurity pinning. Structural studies of these same materials with electron diffraction confirmed that the Nb-impurities pin the incommensurate CDW, but could not provide information about the nature of pinning.[27] STM images do, however, provide direct insight into the structural effects and mechanism of pinning.

STM images of $Nb_xTa_{1-x}S_2$ single crystals with values of x ranging from 0 to 0.07 are shown in Figure 9. The images were recorded at the elevated temperatures of 380 K ($x = 0$), 340 K ($x = 0.04$), and 315 K ($x = 0.07$) to ensure that the samples were in the incommensurate state, where the CDW interacts only weakly with the underlying lattice.[53, 57] Pure TaS_2 exhibits a nearly perfect hexagonal CDW lattice that is characteristic of the known incommensurate state in this material. In contrast, substitution with niobium causes disorder in the CDW lattice. The images of the Nb-doped materials exhibit areas in which the CDW lattice has hexagonal order and regions containing defects. These defects introduce disorder into the CDW lattice. The predominant defects observed in the samples in which $x(Nb) < 0.07$ are dislocations. Dislocations are formed by the insertion of extra half rows of CDW sites in the lattice. Importantly, there is a significant strain field associated with the dislo-

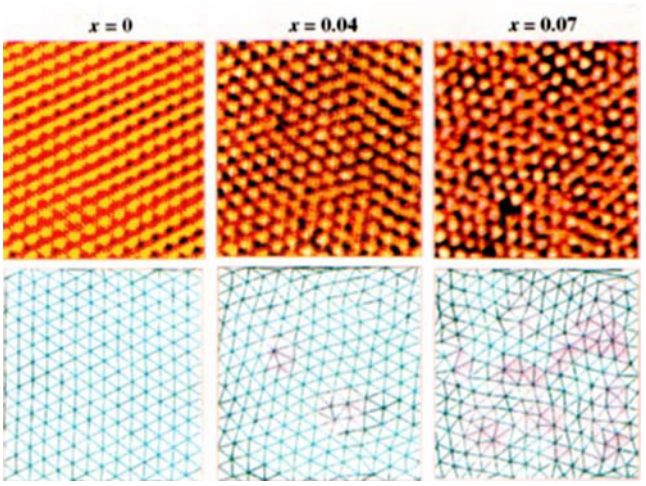

Fig. 9. STM images of the $Nb_xTa_{1-x}S_2$ crystals recorded at 380 ($x = 0$, 340 ($x = 0.04$) and 315 K ($x = 0.07$). Delaunay triangulations are shown below the corresponding STM images.

cations.[58] The CDW can relax the strain field by locally deforming through positional shifts and rotations, although these deformations introduce disorder into the lattice. In the samples containing higher impurity concentrations (x(Nb) ≥ 0.07) STM images exhibit extended defects. The CDW lattice in these latter samples exhibits significant disorder, and regions of hexagonal order and positional order extend only several lattice constants. Nevertheless, it is important to note that the disorder does not appear to destroy the orientational order of the CDW lattice. The presence of relatively long-range orientational order can be seen qualitatively by sighting down the rows of the CDW lattice: this shows that the average direction is defined regardless of the Nb impurity concentration.

To examine in more detail the order of a lattice it has been instructive to analyze the images quantitatively. The quantitative analysis involves defining the location (x, y coordinates) of each CDW maxima and the nearest neighbors in the lattice. Once the lattice points are determined, the Voronoi diagram, which uniquely defines the nearest neighbors of all lattice points, is computed for the lattice.[59] To highlight defects in the lattice we triangulate the Voronoi diagram by drawing "bonds" from all CDW lattice points to their nearest neighbors.[55, 57, 59] This resulting plot is termed the Delaunay triangulation. For the CDW lattice, fully coordinated sites are indicated by six bonds, while topological defects containing a smaller or greater number of bonds are highlighted by shading. The triangulated images are shown below their corresponding STM images in Figure 9; the topological defects are shaded pink. These data demonstrate clearly that the pure 1T-TaS_2 CDW lattice is defect free and that the number of topological defects increases with increasing Nb impurity concentration. Significantly, analysis of the average spacing between topological defects shows that it is much greater than the average spacing between Nb impurities, and thus this analysis unambiguously shows that the pinning by Nb atoms is a weak or collective effect.[8]

It is also possible to obtain further insight into the changing order in this system by calculating the translational [$G_T(r)$] and orientational [$G_6(r)$] correlation functions for a two-dimensional lattice.[8, 55, 59, 60] Significantly, analyses of $G_T(r)$ and $G_6(r)$ as a function of the Nb impurity concentration show that 1) for $x = 0$, both $G_T(r)$ and $G_6(r)$ exhibit long-range order; 2) for $0 < x \leq 0.04$, $G_T(r)$ decays exponentially (which indicates short-range order), and $G_6(r)$ exhibits long-range order; and 3) for $x \geq 0.07$, $G_T(r)$ and $G_6(r)$ decay exponentially. The existence of long-range orientational order but short-range translational order was an important observation, because it showed the existence of a hexatic glass state in these doped materials.[55, 59, 60] Hence, these microscopic STM studies led to the unexpected discovery that the CDW lattice evolves from a crystalline state in the pure solid through a hexatic glass state to a liquid-like amorphous state as the impurity concentration increases.

A very different impurity pinning effect has been observed in our STM studies of titanium-doped $TaSe_2$.[54] The CDW state in 1T-$TaSe_2$ is commensurate at all experimentally accessible temperatures, and each CDW maximum is located on a similar symmetric Ta atom site (Fig. 5b) effectively pinning the CDW to the underlying atomic lattice. The driving force for the commensurate state is an electrostatic interaction between the Ta ions and the CDW. In the incommensurate state, this electrostatic pinning term would be zero. The strong interaction between the CDW and atomic lattice that exists in the commensurate state suggests that the added pinning effect of metal impurities should be quite different than observed in the above studies of $Nb_xTa_{1-x}S_2$. STM images recorded on a series of $Ti_xTa_{1-x}Se_2$ single crystals with $x = 0$, 0.02, and 0.04 support this idea (Fig. 10). The CDW lattices observed in samples containing

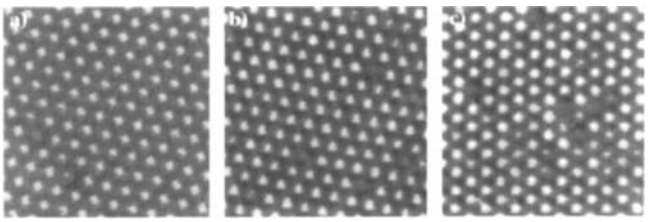

Fig. 10. STM images ($13.5 \times 13.5\,nm^2$) of $TaSe_2$ (a), $Ti_{0.02}Ta_{0.98}Se_2$ (b), and $Ti_{0.04}Ta_{0.96}Se_2$ samples (c) recorded at room temperature.

titanium impurities exhibit a regular hexagonal structure that is similar to the pure sample. The overall order in the CDW lattice of the Ti-doped materials thus differs significantly from that observed in the $Nb_xTa_{1-x}S_2$ materials where the niobium impurities create substantial disorder in the CDW superlattice. The images of the Ti-doped materials do, however, exhibit localized regions where the CDW amplitude is suppressed relative to the surrounding CDW maxima. In addition, we have shown that the density of these localized defects increases linearly with the titanium impurity concentration. These data and the highly localized nature of the CDW defects represent solid evidence for strong pinning.

The studies of $Nb_xTa_{1-x}S_2$ and $Ti_xTa_{1-x}Se_2$ demonstrate the power of STM in elucidating complex structural problems in these CDW materials. It is also possible that detailed spectroscopic studies of single CDW defects at strong pinning sites will provide unique information relating to the microscopic details of CDW formation. In particular, it should be possible to probe the symmetry properties of the CDW gap by probing electron

scattering at CDW defect sites. Careful analysis of the symmetry and decay of the charge density around the defects, which is measured in voltage-dependent STM images, should provide unique information about the Fermi surface topography and scattering in these materials.

4. Copper Oxide Superconductors

4.1. $Bi_2Sr_2Ca_{n-1}Cu_nO_{2n+4}$ Materials: The Incommensurate Superstructure

The copper oxide superconductors are highly anisotropic materials containing two-dimensional copper oxide planes as a key structural element.[61-63] The other components of these materials determine the overall structural anisotropy, chemical complexity, and ultimately the superconducting transition temperatures T_c of these materials. Among the high-temperature superconductors now known, the $Bi_2Sr_2Ca_{n-1}Cu_nO_{2n+4}$ family of materials ($n = 1-3$) are the most anisotropic and probably best suited to surface-sensitive experiments. The $n = 2$ compound, $Bi_2Sr_2CaCu_2O_8$ (BSCCO-2212), is structurally representative of this family and consists of two-dimensional repeat units containing 2-BiO, 2-SrO, Ca, and 2-CuO_2 layers (Fig. 11).[61a, 63, 64]

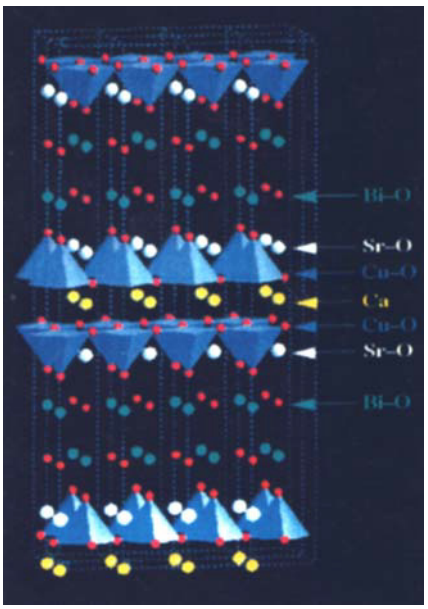

Fig. 11. Structural model of $Bi_2Sr_2CaCu_2O_8$.

The average structure of BSCCO-2212 obtained from diffraction studies is quite straightforward, although in reality these materials exhibit a wide range of structural complexities.[64, 65] For example, BSCCO-2212 shows considerable disorder in the atomic structure of the BiO layer, oxygen nonstoichiometry, and exchange of metals between the idealized layers shown in Figure 11. The detailed nature of such local disorder is intrinsically difficult to address by conventional diffraction techniques, as are the electronic consequences of these structural variations. A complete picture of the microscopic properties of these materials is, however, almost certainly necessary to understand high-temperature superconductivity, since the structural disorder has a dimensionality similar to the coherence length of the superconducting electron pairs. Moreover, the complex high-T_c materials can also serve as models to understand the role of intricate compositional and structural variations that are present in multicomponent materials in general.

The crystallographic separation between adjacent BiO layers in BSCCO is quite large (greater than 3 Å) and as such provides a natural cleavage plane in crystals of these materials.[63, 64] Because covalent bonds are not broken when cleaving crystals between the weakly interacting BiO layers, the BiO surface layer does not reconstruct; hence, STM experiments probe properties similar to that found in the bulk.[66-68] STM images of cleaved BSCCO-2212 crystal surfaces exhibit structure on several length scales (Fig. 12). Of particular interest has been the one-dimen-

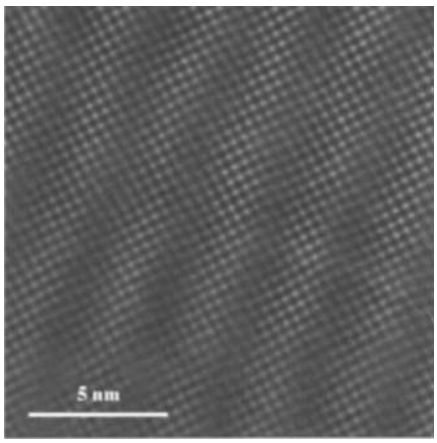

Fig. 12. STM image of $Bi_2Sr_2CaCu_2O_8$ exhibiting the one-dimensional superstructure and BiO layer atomic lattice.

sional superstructure modulation of period 27 Å that occurs along the a axis. A number of models have been proposed to explain the origin of this unique structural modulation in BSCCO, including 1) lattice mismatch between the BiO and CuO layers; 2) extra oxygen atoms substituted into the BiO layer, which causes it to buckle periodically; and 3) periodic Cu or Sr substitution for Bi in the BiO layer.[64, 66, 67, 69, 70] At least three problems intrinsic to these materials have hampered efforts based on diffraction to elucidate the origin of this superstructure. Firstly, the superstructure period is incommensurate with respect to the lattice. Secondly, the BiO layer has considerable disorder, and thirdly, the X-ray and electron scattering cross sections for oxygen are significantly smaller than for Bi.[65, 70]

STM is not limited by these problems and has provided unique insight into the origin and effects of this modulation.[66-68] Real space STM images such as Figure 12 show that the superstructure period is not a sinusoidal modulation; the period varies randomly from 22 to 27 Å.[67] These results demonstrated that the superstructure could not be due simply to BiO/CuO lattice mismatch (which would yield a sinusoidal modulation), but must have a random substitutional component that caused local fluctuations in the superstructure period. Further evidence for the importance of substitution in determin-

ing the properties of the superstructure will be discussed below with relation to metal substitution and oxygen doping.

The atomic structure in images of the BiO layer (for example, Fig. 12) has tetragonal symmetry with a period of 3.8 Å. This distance is consistent with both the average Bi–Bi and O–O distances determined by crystallography; that is, alternate atomic sites, either Bi or O, are imaged by STM. Because only one site is imaged by STM, such data cannot be used to define unambiguously the complete atomic structure associated with the superstructure modulation. The images at atomic resolution do show, however, that there can be significant positional disorder in the BiO layer. We have suggested that this disorder reflects inhomogeneity at the atomic level in the material. Hence, one possible application of STM is the improvement crystal quality achieved by monitoring order in the real-space atomic structure as a function of crystal growth conditions.

4.2. Chemical Inhomogeneity in $Tl_2Ba_2Ca_2Cu_3O_{10}$

The ability of SPM techniques to monitor growth-dependent local atomic order in these complex systems and thereby provide insight into observable properties at a microscopic level is general. Studies of the $Tl_2Ba_2C_{n-1}Cu_nO_{2n+4}$ family of materials ($n = 2, 3$) have clearly illustrated this point.[71, 72] These materials are derived from the Bi family simply by replacing Bi with Tl and Sr with Ba.[61, 63] In general, the average atomic structures of the Tl-based materials are similar to those of the Bi family, although there are several important differences: 1) the Tl materials do not exhibit a regular one-dimensional superstructure and 2) the bonding between adjacent TlO layers is significantly stronger.[61, 63, 73] Despite the stronger bonding between the TlO double layers, crystals of $Tl_2Ba_2CaCu_2O_8$ and $Tl_2Ba_2Ca_2Cu_3O_{10}$ cleave predominantly between the TlO double layers to expose a TlO surface in a manner analogous to that for BSCCO.[71, 72]

The correlation of the microscopic studies by means of STM with macroscopic conductivity measurements have been particularly interesting. Temperature-dependent resistivity measurements made on $Tl_2Ba_2Ca_2Cu_3O_{10}$ crystals grown under various conditions showed strikingly different T_c values (Fig. 13).[72] Crystals grown from a flux containing a Tl:Ba:Ca:Cu ratio of 4:1:3:6 exhibited a broad superconducting transition and a low

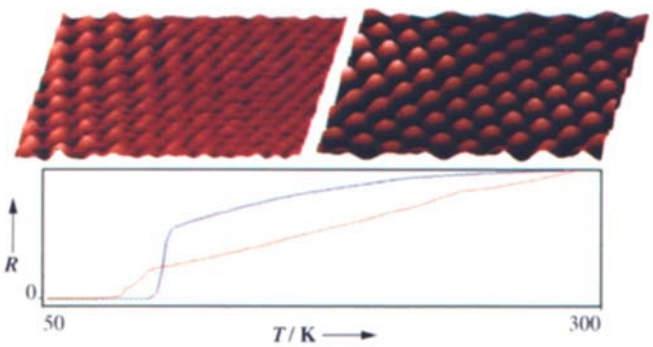

Fig. 13. Top: STM images $Tl_2Ba_2Ca_2Cu_3O_{10}$ crystals grown from 4:3:1:6 (left) and 4:3:1:10 Tl:Ba:Ca:Cu mixtures (right). Bottom: Temperature-dependent resistivity measurements made on $Tl_2Ba_2Ca_2Cu_3O_{10}$ crystals grown under these conditions. R = resistivity.

T_c of 72 K. In contrast, crystals grown from a flux containing a Tl:Ba:Ca:Cu ratio of 4:1:3:10 had a sharp T_c of 110 K. Despite the large differences in T_c, X-ray diffraction and the analysis of the composition showed that these two types of crystals had the same average structure and composition.[61a, 73, 74] The origin of these differences in T_c were, however, readily traced from atomic resolution STM measurements (Fig. 13). The STM images showed clearly that the lower T_c $Tl_2Ba_2Ca_2Cu_3O_{10}$ crystals had pronounced atomic structural disorder, while images of the higher T_c materials exhibited a very regular atomic lattice.[72] These results thus indicate that difference in the macroscopic parameter T_c are due to localized, microscopic variations in the structure of the $Tl_2Ba_2Ca_2Cu_3O_{10}$ samples.

4.3. Metal Substitution: Probing Local Crystal Chemistry

SPM techniques have also been used to probe the effects on the microscopic level of metal substitution in high-T_c copper oxide materials.[7a, 67, 75, 76] In the case of Pb-substituted BSCCO crystals ($Pb_xBi_{2-x}Sr_2CaCu_2O_8$), STM is an especially good probe, since lead primarily replaces bismuth in the BiO layers. The Pb-doped crystals can be cleaved to expose a Bi(Pb)O layer directly at the surface (Fig. 14).[67] STM images

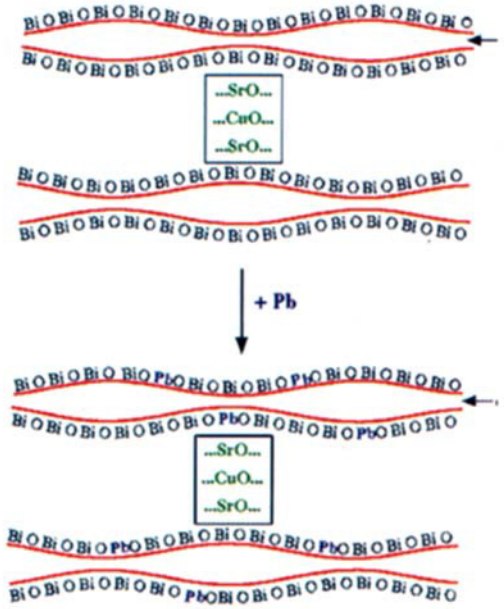

Fig. 14. Schematic illustration of Pb-substitution into the BiO layer of BSCCO-2212. The arrows indicate cleavage planes.

of the Bi(Pb)O layer of Pb-doped BSCCO-2212 single crystals are shown in Figure 15. Images of pure ($x = 0$) BSCCO-2212 crystals exhibit the one-dimensional, incommensurate superstructure that is characteristic of the BSCCO materials.[67, 75] As Pb atoms are substituted for Bi atoms in these crystals, however, the superstructure exhibits increasing disorder. STM images of materials with $x \leq 0.2$ show that the one-dimensional superstructure is less regular than in Pb-doped BSCCO as evidenced by the random displacements along the a axis.[67] The distortions of the superlattice have been attributed to the random substitution of lead for bismuth in the Bi(Pb)O planes and

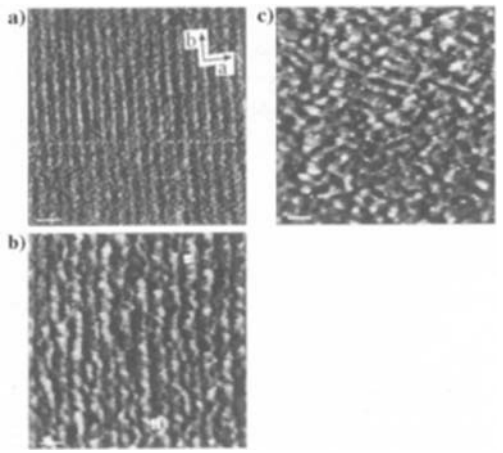

Fig. 15. STM images of $Bi_2Sr_2CaCu_2O_8$ (a), $Pb_{0.3}Bi_{1.7}Sr_2CaCu_2O_8$ (b), and $Pb_{0.5}Bi_{1.5}Sr_2CaCu_2O_8$ (c). The underlying a and b cell axes are indicated in a). The white bar corresponds to 5 nm in these images. The tiny arrows in b) indicate two locations where the superstructure fluctuates significantly from its average position.

the differences between PbO and BiO bonding. Significantly, distortions in the superstructure imaged directly by STM explain the decrease in correlation length reported in diffraction studies of these materials;[77] that is, random fluctuations along the a axis (due to Pb-substitution) reduces the scattering coherence. The suggestion that Pb-substitution distorts the superlattice has been further supported by STM images of samples containing high concentrations of lead (Fig. 15c), since these images exhibit a highly disordered superstructure modulation.

The STM structural data have also provided an understanding of observed variations in the critical current density (J_c) that occur with Pb-substitution. Studies of J_c in Pb-doped BSCCO-2212 have shown that the substitution of lead causes reproducible and significant enhancements in J_c.[78] While it is well known that crystal "defects" can enhance pinning of the fluxlines in superconductors, thereby increasing J_c, the nature of these defects are often not well understood. In the case of Pb-doped BSCCO, the STM images suggest that it is the Pb-induced disorder that enhances flux pinning.

STM studies of crystals of Pb-doped BSCCO-2201, $Pb_xBi_{2-x}Sr_2CuO_6$ single crystals have shown similar results and have been used to develop a new approach for understanding the local disorder probed by SPM measurements.[76] Images of Pb-doped BSCCO-2201 crystals exhibit increasing disorder as the concentration of Pb atoms is increased (Fig. 16). To quantify the order in these crystals and to compare the results to those obtained by electron diffraction we have used the two-dimensional structure factor $S_{2D}(k)$ ($S_{2D}(k) = |\rho(k)|^2$, where $\rho(k)$ is the Fourier transform of the atom density calculated from STM images as function of Pb concentration (Fig. 17). Consideration of this analysis has shown several significant points. Firstly, for samples with intermediate Pb concentrations the comparison of $S_{2D}(k)$ and real-space images with in-plane electron diffraction patterns show that the multiple superlattices inferred from electron diffraction[77] are due to harmonics of the principle superlattice period (Figs. 16b, 17b, e). Secondly, at higher Pb concentrations this same comparison demonstrates that the absence of the one-dimensional superstructure inferred from electron diffraction[79] is due to extreme disorder in this

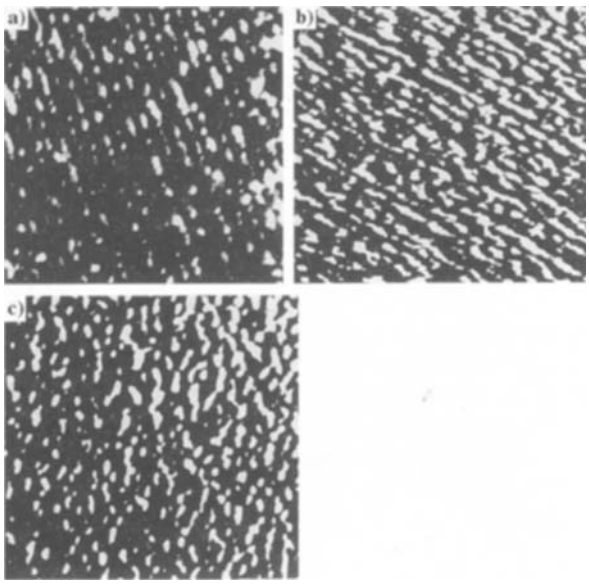

Fig. 16. Images ($60 \times 60\ nm^2$) of $Bi_2Sr_2CuO_6$ (a), $Pb_{0.15}Bi_{1.85}Sr_2CuO_6$ (b), and $Pb_{0.3}Bi_{1.7}Sr_2CuO_6$ (c).

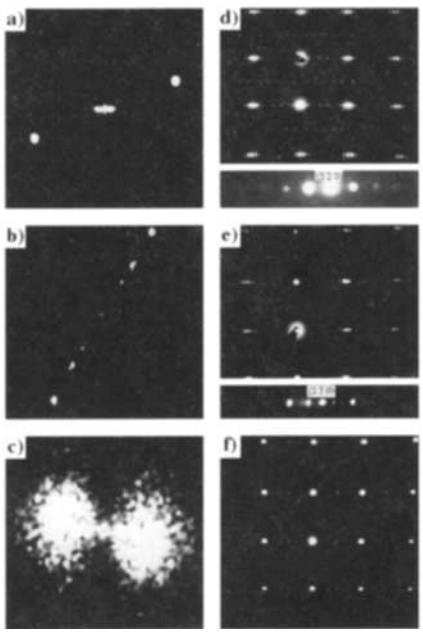

Fig. 17. a)–c): Two-dimensional Fourier transform power spectra of the STM images in Figure 16. d)–f): Electron diffraction patterns recorded on same Pb-doped samples.

structural modulation. Thirdly, it is possible to use the calculated $S_{2D}(k)$ to define a correlation length for the superlattice. More generally, the approach of calculating $S_{2D}(k)$ from real-space images enables the quantitative determination of local crystalline order and should thus be of great utility in materials science (for example, in comparing local microstructures and optimizing growth conditions).

4.4. Oxygen Doping: Probing Local Electronic Structure

It is widely recognized that oxygen doping plays a key role in determining the properties of oxide superconductors.[61, 62] The results from a number of studies have shown that variations in

oxygen concentration change the average carrier concentration and thereby the superconducting transition temperature. X-ray photoemission spectroscopy (PES) studies of BSCCO-2212 crystals doped at high oxygen pressure showed that the density of states near the Fermi level increases with increasing oxygen concentration.[80] To explain this increase in the density of states it has been suggested that oxygen doping transforms the BiO structural element into a metallic layer. The PES interpretation is complicated, however, by the fact that this technique probes several unit cells in depth. STM is uniquely suited to elucidating the origin of high-pressure doping, since it can probe directly the surface BiO layer's electronic states with little contribution form the underlying CuO_2 planes.

STM spectroscopy data obtained on as-grown and oxygen-annealed BSCCO crystals exhibit distinctly different $I-U$ behavior for the different oxygen treatments (Fig. 18),[81-83] attributable to distinctly different electronic structures near the

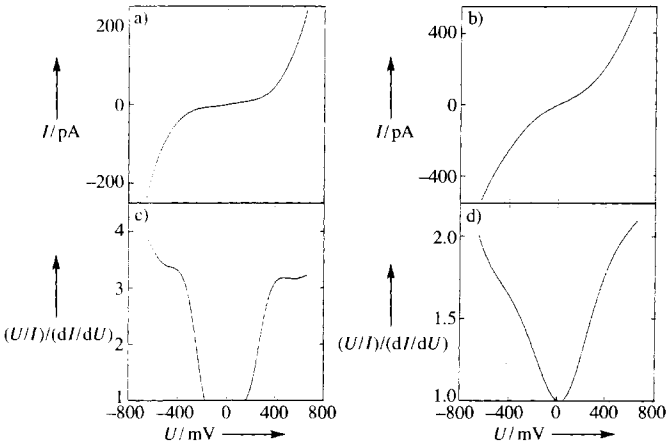

Fig. 18. Current versus voltage data (a, b) and normalized conductivity curves (c, d) obtained on as-grown (a, c) and oxygen-annealed (b, d) BSCCO-2212 single crystal samples.

Fermi level. The as-grown crystals exhibit a low current within ± 200 mV of E_f and relatively sharp increases in I beyond these points, while the oxygen-annealed samples show a smooth increase in I for all U. Indeed, the normalized conductivity $(U/I)\mathrm{d}I/\mathrm{d}U$ shows that there is a 330 mV gap in BiO layer density of states for the as-grown sample, but no obvious gap for the oxygen-annealed sample. The absence of a gap in the oxygen-annealed samples suggests that oxygen doping introduces impurity states into the gap or causes the BiO layer to become metallic.

STM imaging of the BiO layer atomic structure has provided additional information helping to resolve these two possibilities.[82] Atomic resolution images of the as-grown and oxygen-annealed samples exhibit the same surface atomic structure (Fig. 19). The lattices for the samples have periods of 3.8 ± 0.2 Å that corresponds to either the Bi–Bi or O–O distances. The observation of alternate lattice sites for a range of bias conditions indicates that the BiO layer is semiconducting in both as-grown and oxygen-annealed crystals. These structural results combined with the spectroscopic measurements thus suggest that the BiO layer's density of states increases with oxygen annealing, although this layer does not become metallic.

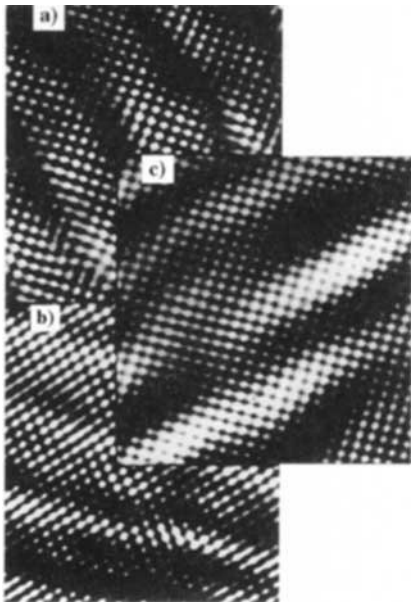

Fig. 19. STM images (10×10 nm^2) recorded on BSCCO crystals. Sample preparation: a) as-grown, b) annealed under 12 atm oxygen, and c) annealed under 150 atm oxygen.

4.5. The Superconducting Energy Gap

The spectroscopic capabilities of STM have also been exploited by many research groups to study the superconducting state of the high-T_c copper oxide materials.[84] The emphasis in this work has been to probe the superconducting energy gap (2Δ) and low-energy excitations in these materials, since this information is essential to understanding the mechanism of superconductivity. In the conventional Bardeen, Cooper, and Schrieffer (BCS) model of superconductivity, there is a complete gap in the density of electronic states as the temperature approaches 0, and the magnitude of 2Δ has the universal value of $3.53\,kT_c$.[85] For conventional superconductors these predictions have agreed well with measurements of the density of states by tunneling spectroscopy.[84, 86] In the case of the copper oxide materials, however, tunneling spectroscopy measurements have led to suggested values of 2Δ between 0 and $12\,kT_c$, although recent studies have converged towards an energy scale of $5-8\,kT_c$.[84, 87-90] It is likely that material inhomogeneity, such as oxygen nonstoichiometry, have been responsible for many of the apparently conflicting measurements of 2Δ by tunneling spectroscopy,[88-91] since the short coherence lengths of the copper oxide materials make these measurements especially susceptible to local variations in the superconducting properties. Indeed, spatially resolved spectroscopy measurements have shown clear evidence for variations in 2Δ associated with structural inhomogeneity.[88, 89]

To delineate the intrinsic versus extrinsic features of the superconducting energy gap in the high-T_c materials we have reported systematic measurements on carefully annealed BSCCO-2212 samples with T_c values ranging from 79 to 92 K. The STM spectroscopy measurements exhibited values of 2Δ that were uniform over the sample surfaces (Fig. 20). The $I-U$ curves recorded on crystals with T_c values of 79, 86, and 92 K all exhibit similar features including a relatively flat low-current

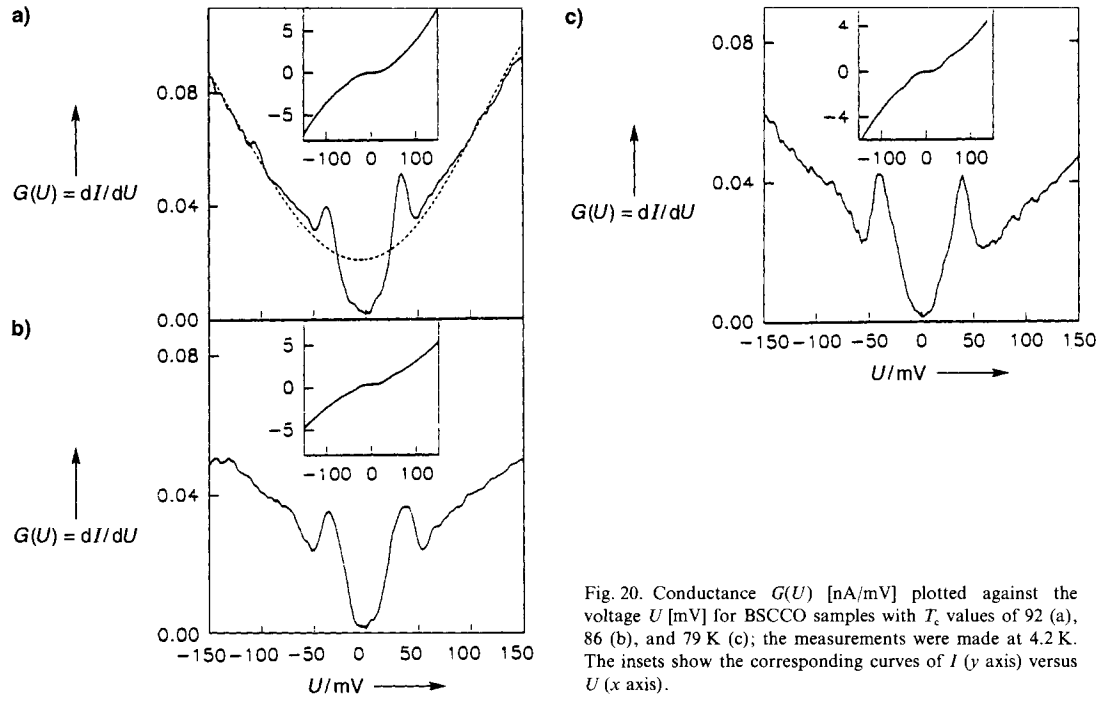

Fig. 20. Conductance $G(U)$ [nA/mV] plotted against the voltage U [mV] for BSCCO samples with T_c values of 92 (a), 86 (b), and 79 K (c); the measurements were made at 4.2 K. The insets show the corresponding curves of I (y axis) versus U (x axis).

region about $U = 0$ and pronounced conductance onsets at $\pm(20-25)$ mV. These features agree qualitatively with those expected for a superconducting gap. Clear insight into the electronic spectrum of the BSCCO samples in the superconducting state was obtained from the conductance $G(U)$, since it is proportional to the density of states N_S. The $G(U)$ vs. U curves obtained on the samples with T_c values varying from 79 to 92 K all showed similar features (Fig. 20). Reproducible features reported in these tunneling spectra include excitations within the gap region for $|U| > 0$ and well-defined conductance peaks. Significantly, the magnitudes of 2Δ determined from this data are similar, irrespective of the sample T_c.[90] These results demonstrate that 2Δ does not scale with T_c as found previously with conventional superconductors and thus have important implications regarding the mechanism of superconductivity.[90]

These data have also afforded the opportunity to examine in detail the quasi-particle excitations within the gap region (Fig. 21). Such an analysis is important, since it can provide insight into the symmetry of the energy gap function. Several models have been used to fit the tunneling spectroscopy data including the broadened BCS s-wave, the gapless, and the d-wave models. The broadened BCS function (g) does not provide

$$\frac{N_S}{N_N} = \mathrm{Re}\left\{\frac{\varepsilon}{\sqrt{\varepsilon^2 - \Delta^2}}\right\} \qquad (g)$$

($\varepsilon = eV - i\Gamma$, where V is the applied voltage and Γ a broadening parameter that reflects the finite lifetimes of quasi-particles)

a good fit of the experimental data, since it cannot simultaneously have sharp conductance peaks and excitations within the gap (Fig. 21 a). Hence, it is not expected to provide new insight into the physics of pairing. Alternatively, strong pair-breaking can lead to quasi-particle excitations within the gap. The long-dashed line in Figure 21 b was fit using a small amount of pair breaking ($\alpha = \Gamma/\Delta = 0.05$, where α is the pair-breaking parameter), while the short-dashed line corresponds to the behavior expected for a gapless superconductor ($\alpha = 1$). For s-wave symmetry pairing, previous theoretical studies have shown that as inelastic scattering is increased, the conductance peaks broaden and the observed gap ω_g gets smaller, but until the "gapless" regime is reached, no quasi-particle excitations should be observed within the gap.[92] In the context of s-wave pairing, this description is inconsistent with the observation of sharp conductance peaks.

The fact that $G(U)$ is strongly peaked around $\pm\Delta$ and decreases gradually to a minimum at $U = 0$ strongly suggests that there are nodes in the gap function. A function with d-wave symmetry (for example, $d_{x^2-y^2}$: $\Delta(k) \sim \cos k_x a - \cos k_y a$) is one that will have nodes and also has the symmetry that in several theoretical models is a prerequisite for pairing. Significantly, good agreement was obtained by fitting the energy-dependent density of states predicted for gap functions with d-wave symmetry to the tunneling spectroscopy data (Fig. 21 c, d).[90] The fit in Figure 21 c corresponds to the function of N_S/N_N expected for a pure d-wave symmetry gap, while that in Figure 21 d corresponds to the specific d-wave pairing model of

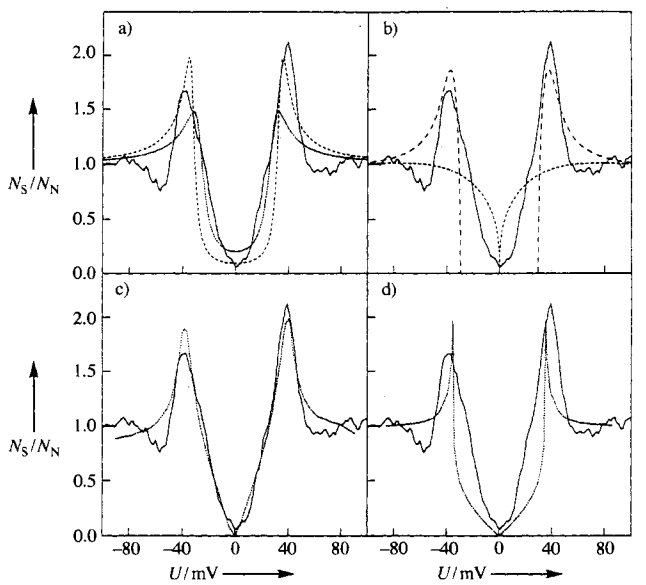

Fig. 21. Curve fitting to typical normalized conductance N_S/N_N versus voltage U data. In all cases the solid curve corresponds to the experimental data and the dashed lines to the fits. The fits were made with Equation (a), varying Δ and Γ in a) and α in b). The curve in c) represents a pure d-wave superconductors, and that in d) the d-wave model of Monthoux, Balatsky, and Pines.

Monthoux, Balatsky, and Pines.[93] Hence, the tunneling data strongly support the idea of an anisotropic gap function, but does not distinguish conclusively between d-wave and anisotropic s-wave models.

4.6. Magnetic Flux-Lines

When a type-II superconductor, such as a material of the copper oxide family, is placed in a sufficiently large field, magnetic flux penetrates through the sample in the form of quantized magnetic flux-lines called vortices.[95, 96] In the absence of crystal defects and pinning the vortices are expected to be arranged in a hexagonal lattice that minimizes the repulsive interaction between lines. This hexagonal structure was recorded beautifully in STM images of flux-line arrays in $NbSe_2$ (Fig. 22).[97] In contrast, when pinning is present, the flux-line lattice structure will change to maximize the pinning interaction, and defects are balanced against the elastic deformation energy expended to distort the lattice.[95, 96]

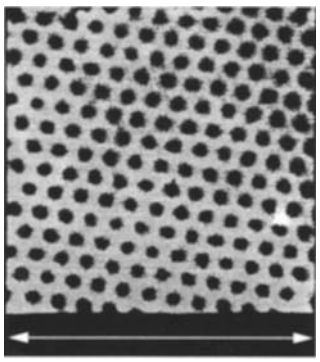

Fig. 22. STM image of the magnetic flux-line lattice in $NbSe_2$ at a field of 1 Tesla. The data were recorded at 1.8 K [97]. The arrow represents 6000 Å.

Surface and bulk defects can play an important role in pinning magnetic flux-lines in high-T_c materials.[95, 96, 98, 99] Because flux-line pinning determines to large extent the magnitude of J_c in superconductors (and therefore possible applications), an understanding of pinning is central to much work in the high-T_c field. Several techniques, including Bitter decoration and neutron diffraction, have been used to study the structure of flux-line lattices in the copper oxide materials.[95, 98] While both of these techniques have provided significant insight into the structure of flux-line lattices, they have not been able to provide direct information about the defects that pin the flux-lines. A new approach that we have developed combining conventional Bitter decoration and AFM has yielded significant insight into this critical area.[100] Bitter decoration is a well-established technique for highlighting reproducibly large numbers of flux-lines, and when combined with AFM, enables us to image the decorated flux-line positions and map out surface defects with a resolution of nanometers. Typical AFM images obtained on BSCCO single crystals that had been decorated in a magnetic field of 33 G are shown in Figure 23. Two distinct types of structures are seen in these images: the magnetic flux-line positions, which appear as small circular spots, and surface steps that appear as lines running through each image. Analysis of the surface topography demonstrates that these steps have heights of 30, 100, and 300 nm. Importantly, we have shown that the flux-line lattice structure can differ significantly depending on the surface step height.[100]

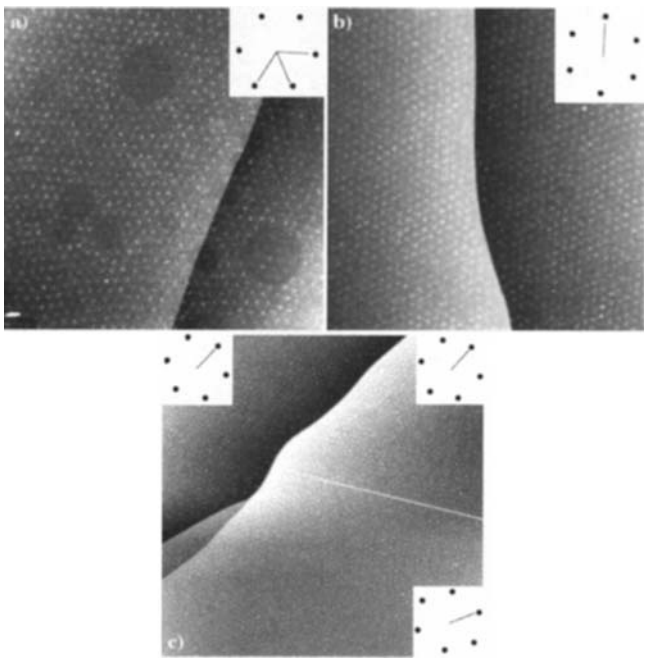

Fig. 23. AFM images recorded on a BSCCO crystal that was decorated at 4.2 K in a magnetic field of 33 Gauss. See text for further details.

The flux-line lattice orientation is seen most clearly in two-dimensional Fourier transform power spectra (2DFT) of selected regions of these images. The 2DFT, which are plotted as insets in each of the figures, each exhibit six diffraction spots characteristic of the hexagonal symmetry of the flux-line lattice and orientation defined by the reciprocal lattice vectors. In Figure 23a, the flux-line lattice orientation is independent of the surface step as is clearly evident when comparing the flux-line lattice reciprocal lattice vectors with the step direction. In Figure 23b, which contains a larger step, the 2DFT shows that a principle axis of the flux-line lattice is aligned preferentially along the straight section of the step. The overall orientation of the flux-line lattice is not perturbed, however, by the curvature in the step at the bottom of the image. The structure of the flux-line lattice in Figure 23c, which contains the largest step, is more complex and interesting. On the lower surface terrace in the upper left of the image, the 2DFT shows that the flux-line lattice orientation is pinned to the step direction. The flux-line lattice in the upper right portion of the image is also pinned in this same orientation. However, the 2DFT demonstrates that the flux-line lattice orientation in the lower part of the image is rotated relative to the upper part. This rotation follows the change in step direction that occurs at the bottom of the image. Significantly, the two distinct flux-line lattice orientations lead to the formation of a grain boundary in the lattice that is indicated by the white line running across the right side of this image. We have developed a model to understand the propagation of these grain boundaries through a sample by considering the pinning energy associated with the surface step and the energy required to elastically deform the flux-lattice.[98] Importantly, using the AFM data it has been possible to demonstrate that the grain boundaries propagate completely through the superconductor samples and thus influence significantly the bulk structure of the flux-line lattice.

5. Manipulation of Matter

5.1. New Nanomaterials Using SPMs

SPM techniques can, in addition to probing the microscopic properties of low-dimensional materials, be used to create new low-dimensional materials—nanostructures. SPM techniques are particularly powerful in nanoscale research, since they can be exploited for both the synthesis and the characterization of a material.[13, 14, 101-113] For example, STM has been used to assemble individual iron atoms into circular structures on a copper metal surface, and to show that the resulting structure exhibited properties of quantum confinement.[111]

The simplicity and flexibility of SPM techniques are a significant advantage for the synthesis and characterization of nanostructures. STM and AFM tips may be coated with thin films of almost any material thereby enabling researchers to control interactions and reactions at substrate surfaces.[114, 115] Experiments may also be carried out in vacuum or in ambient or fluid environments. Such flexibility is not possible in other top down lithography techniques.

5.2. General Approaches to Manipulation

SPM techniques have been used extensively to modify surfaces at the atomic to nanometer scale.[13, 14, 101-113] While modification of a surface in and of itself does not constitute the preparation of a nanostructure, an understanding of the processes involved in modification and manipulation are needed to prepare new structures rationally. Below we describe several processes that have been employed in STM and AFM studies.

Two general types of processes that have been used for STM-based manipulation involve the parallel or perpendicular motion of atoms and clusters (Fig. 24).[14a] In parallel processes, manipulated material is not removed from a surface but rather slid to a particular surface location. In perpendicular processes, however, the probe tip is used to pick up material from the surface and then redeposit it at another location. Parallel processes rely on either electric fields or chemical forces to slide atoms. An electric field emanating from a STM tip induces a dipole in adsorbates that attract them to the tip.[14a, 107] When this attraction is greater than the potential barrier associated with the dipole's moving across a surface, the adsorbate will move towards the tip. An advantage of this technique is that it enables both sample manipulation and the measurement of the dipole moment of an adsorbate. A second parallel process exploits short range attractive interactions between the probe tip and adsorbate to overcome the barrier to surface motion.

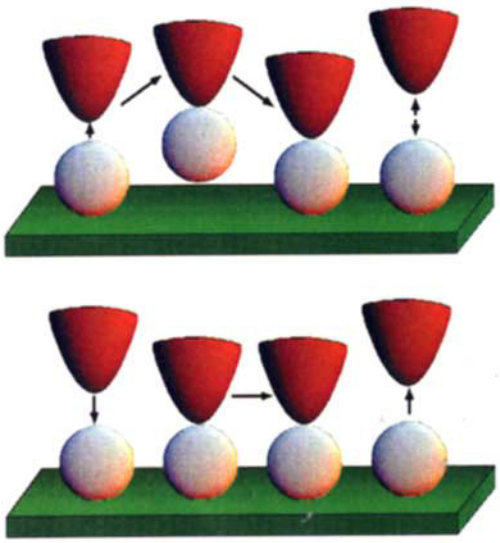

Fig. 24. Schematic diagram illustrating perpendicular (top) and parallel (bottom) manipulation processes.

The principal perpendicular processes are field evaporation and transfer-on-contact. The simpler of the two is transfer-on-contact whereby the tip is lowered onto an atom or cluster so that tip interacts strongly with the surface adsorbate.[14] As the tip is lifted from the surface, it carries the atom or cluster with it. At a desired location the tip is again lowered until the atom or cluster transfers back to the surface. The second type of perpendicular process involves field evaporation or chemically assisted field evaporation.[14, 106, 109] Field evaporation occurs when a large positive bias is applied to the sample (or tip) causing positive cluster ions to evaporate and ideally redeposit on the tip (or sample). An important example of this approach has been the selective removal and deposition small silicon clusters on the surface of crystalline silicon.[106]

AFM modification and manipulation processes are generally more direct than those for the STM. Manipulation based on force microscopy typically involves direct mechanical interactions between the probe tip and substrate. Force microscopy has been used to manipulate materials both by nanomachining[104, 110, 116] and sliding.[112, 113] In nanomachining, the AFM removes atoms from the surface through fatigue wear.[110, 117] For example, the pattern of letters "MoO_3" shown in Figure 25 was machined in a MoO_3 nanocrystal with an AFM probe tip.

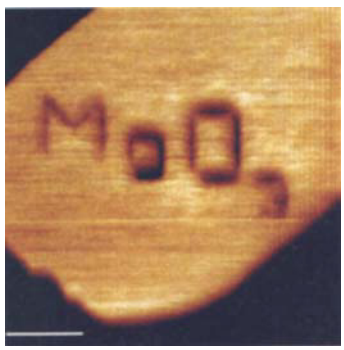

Fig. 25. AFM image engraved with "MoO_3". The pattern of letters was machined in a MoO_3 nanocrystal using the AFM probe tip.

The mechanics of the interaction between tip and sample that is relevant to nanomachining are illustrated in Figure 26. The tip elastically deforms due to the applied load, where the dashed line in the figure shows the shape of the nondeformed tip. A detailed view of the stresses felt by the sample are shown in the zoom of the tip–sample contact region (Fig. 26, right). The upper half of the zoom shows that the pressure distribution felt by the surface, while the lower half shows the stresses in the sample. The maximum stress occurs at a depth of $0.48/a$ below the surface, where a is proportional the radius of curvature of the tip. Under sufficient stress the sample will plastically deform, bonds will break, and material will be lost. All the material in the region may be removed by scanning the tip over it several times. Practical considerations limit the materials that may be machined in this way. The material should be softer than the tip and should not

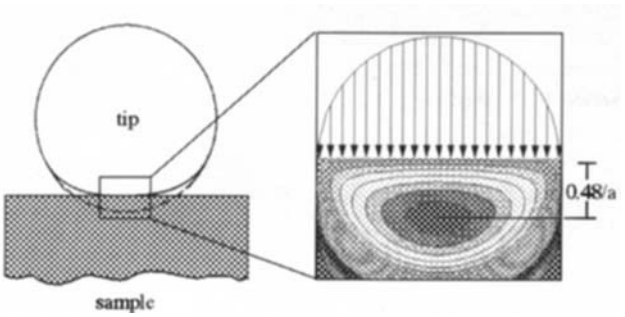

Fig. 26. Illustration of an AFM tip in contact with a surface. Left: The tip elastically deforms on the surface. Right: The arrows represent the pressure experienced by the surface and the gray hatched regions the stresses in the surface. See text for further details.

have of low friction coefficient. A soft material is needed, so that the tip may reproducibly modify the sample and not be modified itself, while a high friction coefficient ensures high interfacial shear and hence large transfer of energy.

The second means of AFM manipulation involves sliding small islands of material on a surface with the AFM's tip.[112, 113] A particularly interesting example of sliding is the phenomenon of lattice-directed sliding that we have recently discovered while manipulating nanocrystals of MoO_3 on MoS_2.[113] MoO_3 nanocrystals can be grown on the surface of MoS_2 by controlled thermal oxidation.[110] When these nanocrystals are pushed with an AFM tip, they move along only one of the lattice directions of the underlying MoS_2 substrate. The motion of two distinct MoO_3 nanocrystals are illustrated in the sequence of images shown in Figure 27a–c.[113] A composite view of these three images and the underlying MoS_2 atomic lattice (Fig. 27d) shows that these two nanocrystals move at a 60° angle with respect to each other and that this motion is along two distinct directions of the MoS_2 lattice. Under most conditions the MoO_3 nanocrystal will slide on this predetermined path indefinitely. The nanocrystals path can be changed, however, by applying a large torque using the tip. Hence, by combining lattice directed sliding with nanomachining it should be possible to construct complex multicomponent nanostructures.

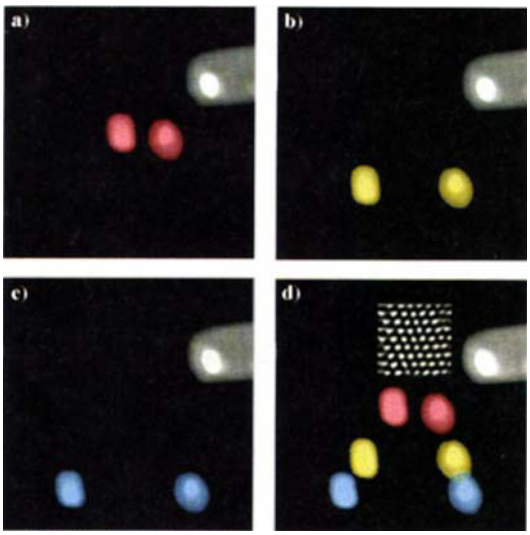

Fig. 27. AFM images showing the lattice-directed sliding of two MoO_3 nanocrystals on a MoS_2 surface. The red (a), white (b), and blue (c) colors correspond to the initial, intermediate, and final positions of the nanocrystals, respectively. d) Depicts a superposition of a), b), and c). The inset shows the atomic lattice of MoS_2.

5.3. Nanostructures

We now turn to two exciting examples of complex nanostructures that have been *synthesized* with the STM and AFM. One of the most elegant structures created with STM is the "quantum corral" built by Eigler and co-workers (Fig. 28).[111] Using a low-temperature (4 K) STM operating in ultrahigh vacuum, they slid 48 Fe atoms into a 14.3 nm ring on a Cu(111) surface. This ring of atoms acted as a hard wall, reflecting electrons trapped in a two-dimensional state at the surface of the copper substrate. The quantum-mechanical interference between these electrons created circular regions of high and low electron density (Fig. 28d).[111] Structures like the quantum corral, though currently limited to low temperature and high vacuum, are solid steps forward in quantum electronics research.

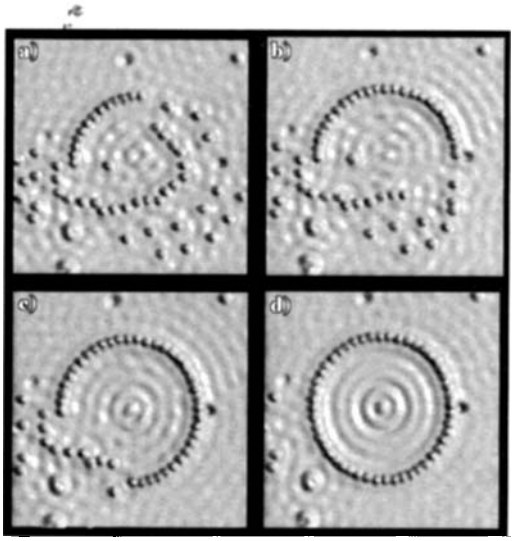

Fig. 28. Steps a)–d) in the formation of a quantum corral [111]. The corral has a radius of 14.3 nm and was created with parallel processes in STM manipulation. In d) the surface electron waves scatter from the Fe atoms leaving fringes.

We have used AFM to create an interlocking nanostructure that is stable at room temperature by combining nanomachining and lattice-directed sliding to manipulate MoO_3 nanocrystals on MoS_2 (Fig. 29).[113] Initially, nanomachining is used to define a notch in crystal 2 (Fig. 29b) and a rectangular latch in crystal 1 (Fig. 29c). Lattice-directed sliding is used to move crystal 2 to crystal 1 (Fig. 29c) and then move the latch into the notch of crystal 2 (Fig. 29d). The smaller crystallite is thereby locked into place by the latch. The preferred lattice-directed sliding directions of the small crystallite and the latch are different, which prevents the small crystallite from moving. The latch itself is prevented from rotating by the large crystallite. An interesting feature of this system is the reversibility of the connection. The smaller nanocrystal may be locked into place, unlocked, manipulated, and then relocked. This is exactly what has oc-

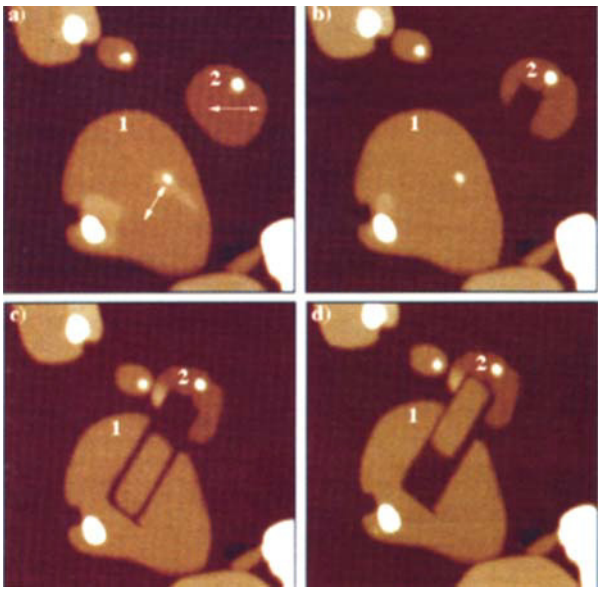

Fig. 29. AFM images illustrating the fabrication and final structure of three interlocking MoO_3 nanocrystals. See text for further details.

curred in Figures 29 c and d. This locking mechanism can, however, readily resist motion, relative to the larger crystal, of the small nanocrystal along its preferred sliding direction. Hence, the lock can be used as a structure to facilitate the fabrication of larger, more complicated systems that include, for example, electronically distinct oxide pieces. In addition, such a mechanical latch corresponds to the basic components needed to construct a nano logic gate.

6. Summary and Outlook

The combination of scanning probe microscopies and chemical synthesis has significantly advanced the understanding of charge density waves, high-temperature superconductivity, and nanofabrication in low-dimensional materials. This new approach to studying materials has directly elucidated the structure of complex charge density wave phases and how metal dopants interact with charge density waves in two-dimensional metal dichalcogenide solids. The real-space picture of atomic and charge density wave lattices provided by STM transforms the diffuse structural view based on diffraction into one that has demonstrated clearly the theoretical concept of weak pinning and has led to discovery of new phases not yet understood theoretically. The coupling of STM with synthesis has also illuminated complex structural disorder in two distinct classes of copper oxide superconductors, thus providing an understanding of observed variations in the bulk transition temperature and critical current density. The methods developed to quantify structural disorder in these studies—termed local crystallography—provide an approach for preparing pure and doped crystals that are homogeneous on a nanometer scale and should be of general utility in the future. Application of this approach to the superconducting state has elucidated details of the electronic excitations important in defining the mechanism of superconductivity and also the structure of magnetic flux-line arrays that are crucial to most technological applications. Such studies are, however, still in their infancy and will require additional work to broaden their impact. Lastly, the combination of scanning probe microscopy measurement and manipulation with chemical synthesis has provided a novel route to the fabrication of nanostructures (which represent the ultimate dimensional reduction in materials). Selective synthesis yields nanocrystals that have, through fundamental studies of friction and wear, been selectively modified and manipulated using force microscopy into interlocking, multicomponent structures. By using this strategy it should be possible to extend nanostructure complexity, and importantly, to readily investigate the physical properties of any new structure created with the probe microscope. More generally, the studies outlined in this review provide a clear pathway to unify work on bulk low-dimensional materials and nanostructures and our understanding of these solids, and in so doing they promise to expand our knowledge and our ability to conceive of new materials for the future.

Received: August 18, 1995 [A 132 IE]
German version: *Angew. Chem.* **1996**, *108*, 748–768

[1] G. Binnig, H. Rohrer, C. Gerber, E. Weibel, *Phys. Rev. Lett.* **1982**, *49*, 57–60.
[2] Introductions: a) *Scanning Tunneling Microscopy* (Eds.: J. A. Stroscio, W. J. Kaiser), Academic Press, New York, **1993**; b) *Scanning Tunneling Microscopy I* (Eds.: H.-J. Guntherodt, R. Wiesendanger), Springer, New York, **1992**; c) *Scanning Tunneling Microscopy II* (Eds.: R. Wiesendanger, H.-J. Guntherodt), Springer, New York, **1992**; d) *Scanning Tunneling Microscopy III* (Eds.: R. Wiesendanger, H.-J. Guntherodt), Springer, New York, **1993**; e) C. J. Chen, *Introduction to Scanning Tunneling Microscopy*, Oxford University Press, New York, **1993**.
[3] G. Binnig, H. Rohrer, *Sci. Am.* **1985**, *256*, 50–56; C. F. Quate, *Phys. Today* **1986**, *39*, 26–33; G. Binnig, H. Rohrer, *Angew. Chem.* **1987**, *99*, 622–631; *Angew. Chem. Int. Ed. Engl.* **1987**, *26*, 606–614; P. K. Hansma, J. Tersoff, *J. Appl. Phys.* **1987**, *61*, R1–R23; Y. Kuk, P. J. Silverman, *Rev. Sci. Instrum.* **1989**, *60*, 165–180; J. E. Griffith, G. P. Kochanski, *Annu. Rev. Mater. Sci.* **1990**, *20*, 219–244; Ph. Avouris, *J. Phys. Chem.* **1990**, *94*, 2246–2256.
[4] J. Frommer, *Angew. Chem.* **1992**, *104*, 1325–1357; *Angew. Chem. Int. Ed. Engl.* **1992**, *31*, 1298–1328.
[5] P. K. Hansma, V. B. Elings, O. Marti, C. E. Bracker, *Science* **1988**, *242*, 209–242.
[6] S. N. Magonov, M.-H. Whangbo, *Adv. Mater.* **1994**, *6*, 355–371.
[7] C. M. Lieber, *Chem. Eng. News* **1994**, *72*, 28–41; X. L. Wu, C. M. Lieber, *Prog. Inorg. Chem.* **1991**, *39*, 431–510; C. M. Lieber, X. L. Wu, *Acc. Chem. Res.* **1991**, *24*, 170–177.
[8] H. Dai, C. M. Lieber, *Annu. Rev. Phys. Chem.* **1993**, *44*, 237–263.
[9] J. A. Golovchenko, *Science* **1986**, *232*, 48–53; R. M. Tromp, R. J. Hamers, J. E. Demuth, *Science* **1986**, *234*, 304–309.
[10] G. Binnig, C. F. Quate, C. Gerber, *Phys. Rev. Lett.* **1986**, *56*, 930–933.
[11] D. Sarid, *Scanning Force Microscopy*, Oxford University Press, New York, **1994**.
[12] B. Drake, C. B. Prater, A. L. Weisenhorn, S. A. C. Gould, T. R. Albrecht, C. F. Quate, D. S. Cannell, H. G. Hansma, P. K. Hansma, *Science* **1989**, *243*, 1586–1589; D. Ruger, P. Hansma, *Phys. Today* **1990**, *October*, 23–30; S. M. Hues, R. J. Colton, E. Meyer, H.-J. Guntherodt, *MRS Bull.* **1993**, *18*, 41–49; C. F. Quate, *Surf. Sci.* **1994**, *299/300*, 980–995.
[13] *Technology of Proximal Probe Lithography* (Eds.: C. R. K. Marrian), SPIE Optical Engineering Press, Bellingham, WA, **1993**; *Atomic and Nanometer-Scale Modification of Materials: Fundamentals and Applications* (Ed.: Ph. Avouris), Kluwer, Boston, **1993**.
[14] a) J. A. Stroscio, D. M. Eigler, *Science* **1991**, *254*, 1319–1326; Ph. Avouris, *Acc. Chem. Res.* **1994**, *27*, 159–165; b) Ph. Avouris, *ibid.* **1995**, *28*, 95–102.
[15] J. C. Patrin, J. H. Weaver, *Phys. Rev. B* **1993**, *48*, 17913–17921; D. Rioux, R. J. Pechman, M. Chander, J. H. Weaver, *ibid.* **1994**, *50*, 4430–4438.
[16] K. Koguchi, T. Matsumoto, T. Kawai, *Science* **1995**, *267*, 71–73.
[17] M. Kanai, T. Kanai, K. Motui, X. D. Wang, T. Hashizume, T. Sakurai, *Surf. Sci.* **1995**, *329*, L619–623; X. D. Wang, T. Hashizume, T. Sakurai, *Mod. Phys. Lett. B* **1994**, *8*, 1597–1626.
[18] J. Tersoff, D. R. Hamann, *Phys. Rev. Lett.* **1983**, *50*, 1998–2001; J. Tersoff, D. R. Hamann, *Phys. Rev. B* **1985**, *31*, 805–813; J. Tersorff, N. D. Lang in Ref. [2a], 1–29.
[19] J. Bardeen, *Phys. Rev. Lett.* **1961**, *6*, 57–59.
[20] J. Tersoff, *Phys. Rev. B* **1990**, *41*, 1235–1238.

[21] J. Tersoff, *Phys. Rev. B* **1989**, *40*, 11990–11993.
[22] N. D. Lang, *Phys. Rev. Lett.* **1986**, *56*, 1164–1167; H. J. Unger, *Comput. Mater. Sci.* **1994**, *2*, 357–365.
[23] R. M. Feenstra, J. A. Stroscio, A. P. Fein, *Surf. Sci.* **1987**, *181*, 295–306.
[24] E. Meyer, H. Heinzelmann in Ref. [2c], 99–149.
[25] E. C. Teague, G. E. Scire, S. M. Baker, S. W. Jensen, *Wear* **1982**, *83*, 1.
[26] J. A. Wilson, A. D. Yoffe, *Adv. Phys.* **1969**, *18*, 193–335; R. M. A. Lieth, J. C. J. M. Terhell in *Preparation and Crystal Growth of Materials with Layered Structures* (Ed.: R. M. A. Lieth), D. Reidel Publishing Co., Dordrecht, **1977**, p. 141.
[27] J. A. Wilson, F. J. DiSalvo, S. Mahajan, *Adv. Phys.* **1975**, *24*, 117–201.
[28] F. J. DiSalvo in *Electron-Phonon Interactions and Phase Transitions* (Ed.: T. Riste), New York, **1977**.
[29] R. L. Withers, J. A. Wilson, *J. Phys. C: Solid State Phys.* **1986**, *19*, 4809–4845.
[30] K. Nakanishi, H. Takatera, Y. Yamada, H. Shiba, *J. Phys. Soc. Jpn.* **1977**, *43*, 1509–1517; K. Nakanishi, H. Shiba, *ibid.* **1977**, *43*, 1839–1847.
[31] C. B. Scruby, P. M. Williams, G. S. Parry, *Philos. Mag.* **1975**, *31*, 255–275; G. Brusdeylins, C. Heimlich, J. P. Toennies, *Surf. Sci.* **1989**, *211/212*, 98–105.
[32] R. V. Coleman, B. Drake, P. K. Hansma, G. Slough, *Phys. Rev. Lett.* **1985**, *55*, 394–397.
[33] R. V. Coleman, B. Giambattista, P. K. Hansma, A. Johnson, W. W. McNairy, C. G. Slough, *Adv. Phys.* **1988**, *37*, 559–644.
[34] Xian Liang Wu and Charles M. Lieber, *Science* **1989**, *243*, 1703–1705.
[35] Xian Liang Wu and Charles M. Lieber, *Phys. Rev. Lett.* **1990**, *64*, 1150–1153.
[36] R. E. Thomson, U. Walter, E. Ganz, J. Clarke, A. Zettl, *Phys. Rev. B* **1988**, *38*, 10734–10743.
[37] B. Giambattista, C. G. Slough, W. W. McNairy, R. V. Coleman, *Phys. Rev. B* **1990**, *41*, 10082–10103; C. G. Slough, W. W. McNairy, R. V. Coleman, J. Garnaes, C. B. Prater, P. K. Hansma, *ibid.* **1990**, *42*, 9255–9258.
[38] B. Burk, R. E. Thomson, A. Zettl, J. Clarke, *Phys. Rev. Lett.* **1991**, *66*, 3040–3043.
[39] G. Grunner, *Rev. Mod. Phys.* **1988**, *60*, 1129–1181; G. Grunner, A. Zettl, *Phys. Rep.* **1985**, *119*, 117–232.
[40] F. J. DiSalvo, J. A. Wilson, B. G. Bagley, J. V. Waszczak, *Phys. Rev. B* **1975**, *12*, 2220–2235.
[41] H. Fukuyama, P. A. Lee, *Phys. Rev. B* **1978**, *17*, 535–548.
[42] P. A. Lee, T. M. Rice, *Phys. Rev. B* **1979**, *19*, 3970–3980.
[43] S. N. Coppersmith, *Phys. Rev. Lett.* **1990**, *65*, 1044–1047.
[44] J. R. Tucker, *Phys. Rev. B* **1989**, *40*, 5447–5459.
[45] J. Bardeen, *Phys. Rev. Lett.* **1990**, *64*, 2297–2299.
[46] E. Sweetland, C.-Y. Tsai, B. A. Wintner, J. D. Brocker, R. E. Thorne, *Phys. Rev. Lett.* **1990**, *65*, 3165–3168.
[47] J. R. Tucker, *Phys. Rev. Lett.* **1990**, *65*, 270–273.
[48] J. C. Gill, *Phys. Rev. Lett.* **1990**, *65*, 271–272.
[49] R. E. Thorne, J. McCarten, *Phys. Rev. Lett.* **1990**, *65*, 273.
[50] X. L. Wu, P. Zou, C. M. Lieber, *Phys. Rev. Lett.* **1988**, *61*, 2604–2607.
[51] H. Chen, X. L. Wu, C. M. Lieber, *J. Am. Chem. Soc.* **1990**, *112*, 3326–3332.
[52] X. L. Wu, C. M. Lieber, *J. Am. Chem. Soc.* **1989**, *111*, 2731–2733.
[53] H. Dai, H. Chen, C. M. Lieber, *Phys. Rev. Lett.* **1991**, *66*, 3183–3186.
[54] X. L. Wu, C. M. Lieber, *Phys. Rev. B* **1990**, *41*, 1239–1242.
[55] H. Dai, C. M. Lieber, *Phys. Rev. Lett.* **1992**, *69*, 1576–1579.
[56] X. Wu, P. Zhou, C. M. Lieber, *Nature* **1988**, *335*, 55–57.
[57] H. Dai, C. M. Lieber, *J. Phys. Chem.* **1993**, *97*, 2362–2367.
[58] F. R. N. Nabarro, *Theory of Dislocations*, Dover, New York, **1967**.
[59] D. R. Nelson, M. Rubinstein, F. Spaepen, *Philos. Mag. A* **1982**, *46*, 105–126.
[60] B. I. Halperin, D. R. Nelson, *Phys. Rev. Lett.* **1978**, *41*, 121–124; D. R. Nelson, B. I. Halperin, *Phys. Rev. B* **1979**, *19*, 2457–2484.
[61] B. Raveau, C. Michel, M. Hervieu, D. Groult, *Crystal Chemistry of High-Tc Superconducting Copper Oxides*, Springer, Berlin, **1991**; *Chemistry of Superconductor Materials* (Ed.: T. A. Vanderah), Noyes Publications, Park Ridge, New Jersey, **1991**.
[62] A. W. Sleight, *Science* **1988**, *242*, 1519–1527; I. K. Schuller, J. D. Jorgensen, *Mater. Res. Soc. Bull.* **1989**, *14*, 27–30.
[63] C. N. R. Rao, B. Raveau, *Acc. Chem. Res.* **1989**, *22*, 106–113; B. Raveau, C. Michel, *Annu. Rev. Mater. Sci.* **1989**, *19*, 319–339; H. Müller-Buschbaum, *Angew. Chem.* **1989**, *101*, 1503–1524; *Angew. Chem. Int. Ed. Engl.* **1989**, *28*, 1472–1493; R. J. Cava, *Science* **1990**, *247*, 656–662.
[64] Y. Gao, P. Lee, P. Coppens, M. A. Subramanian, A. W. Sleight, *Science* **1988**, *241*, 954–956; C. Patterson, P. D. Hatton, R. J. Nelmes, X. Chu, Y. F. Yan, Z. X. Zhao, *Supercond. Sci. Technol.* **1990**, *3*, 297–301.
[65] P. Lee, Y. Gao, H. S. Sheu, V. Petricek, R. Restori, P. Coppens, A. Darovskikh, J. C. Phillips, A. W. Sleight, M. A. Subramanian, *Science* **1989**, *244*, 62–63.
[66] M. D. Kirk, J. Nogami, A. A. Baski, D. B. Mitzi, A. Kapitulnik, T. H. Geballe, C. F. Quate, *Science* **1988**, *242*, 1673–1675.
[67] X. L. Wu, Z. Zhang, Y. L. Wang, C. M. Lieber, *Science* **1990**, *248*, 1211–1214.
[68] C. K. Shih, R. M. Feenstra, G. V. Chandrashekhar, *Phys. Rev. B* **1991**, *43*, 7913–7922; A. Chang, Y. M. Ivanchenko, Z. Y. Rong, E. L. Wolf, *Surf. Sci.* **1992**, *274*, L504–L508; K. Ikeda, K. Takamuku, K. Yamaguchi, R. Itti, N. Koshizuka, *J. Mater. Res.* **1992**, *7*, 1060–1062.
[69] Y. Yamamoto, M. Onoda, E. Takayama-Muromachi, F. Izumi, *Phys. Rev. B* **1990**, *42*, 4228–4239; V. Petricek, Y. Gao, P. Lee, P. Coppens, *ibid.* **1990**, *42*, 387–392.
[70] H. W. Zandbergen, W. A. Groen, F. C. Mijlhoff, G. van Tendeloo, S. Amelinckx, *Physica C* **1988**, *156*, 325–354; H. W. Zandbergen, W. T. Fu, G. van Tendeloo, S. Amelinckx, *J. Cryst. Growth* **1989**, *96*, 716–725; O. Eibl, *Physica C* **1991**, *175*, 419–434.
[71] X.-L. Wu, C. M. Lieber, D. S. Ginley, R. J. Baughman, *Appl. Phys. Lett.* **1989**, *55*, 2129–2131; Z. Zhang, C. M. Lieber, D. S. Ginley, R. J. Baughman, B. Morosin, *J. Vac. Sci. Technol. B* **1991** *9*, 1009–1012.
[72] Z. Zhang, C.-C. Chen, C. M. Lieber, B. Morosin, D. S. Ginley, E. L. Venturini, *Phys. Rev. B* **1992**, *45*, 987–992.
[73] D. E. Cox, C. C. Torardi, M. A. Subramanian, J. Gopalakrishnan, A. W. Sleight, *Phys. Rev. B* **1988**, *38*, 6624–6630; C. C. Torardi, M. A. Subramanian, J. C. Calabrese, J. Gopalakrishnan, K. J. Morrissey, T. R. Askew, R. B. Flippen, U. Chowdhry, A. W. Sleight, *Science* **1988**, *240*, 631–634.
[74] D. S. Ginley, B. Morosin, R. J. Baughman, E. L. Venturini, J. E. Schirber, J. F. Kwak, *J. Crystal Growth* **1988**, *91*, 456–462; B. Morosin, R. J. Baughman, D. S. Ginley, J. E. Schirber, E. L. Venturini, *Physica C* **1990**, *161*, 115–124; B. Morosin, D. S. Ginley, E. L. Venturini, R. J. Baughman, C. P. Tigges, *ibid.* **1991**, *172*, 413–422.
[75] Z. Zhang, Y. L. Wang, X. L. Wu, J.-L. Huang, C. M. Lieber, *Phys. Rev. B* **1990**, *42*, 1082–1085.
[76] J. Liu, C. M. Lieber, *Inorg. Chim. Acta*, in press.
[77] C. H. Chen, D. J. Werder, G. P. Espinosa, A. S. Cooper, *Phys. Rev. B* **1989**, *39*, 4686–4689; J. Schneck, L. Pierre, J. C. Toledano, C. Daguet, *ibid.* **1989**, *39*, 9624–9627.
[78] Y. L. Wang, X. L. Wu, C.-C. Chen, C. M. Lieber, *Proc. Natl. Acad. Sci.* **1990**, *87*, 7058–7061.
[79] C. C. Torardi, E. M. McCarron, P. L. Gai, J. B. Parise, J. Ghoroghchian, D. B. Kang, M.-H. Whangbo, J. C. Barry, *Physica C* **1991**, *176*, 347–356; K. Yanagisawa, Y. Matsui, K. Shoda, E. Takayama-Muromachi, S. Horiuchi, *ibid.* **1992**, *196*, 34–42.
[80] B. O. Wells, Z.-X. Shen, D. S. Dessau, W. E. Spicer, C. G. Olson, D. B. Mitzi, A. Kapitulnik, R. S. List, A. Arko, *Phys. Rev. Lett.* **1990**, *65*, 3056–3059; b) Z.-X. Shen, D. S. Dessau, B. O. Well, C. G. Olson, D. B. Mitzi, L. Lombado, R. S. List, A. J. Arko, *Phys. Rev. B* **1991**, *44*, 12098–12101.
[81] X. L. Wu, Y. L. Wang, Z. Zhang, C. M. Lieber, *Phys. Rev. B* **1991**, *43*, 8729–8732.
[82] Z. Zhang, C. M. Lieber, *Phys. Rev. B* **1992**, *46*, 5845–5848.
[83] Z. Zhang, C. M. Lieber, *J. Phys. Chem.* **1992**, *96*, 2030–2038.
[84] J. R. Kirtley, *Int. J. Mod. Phys. B* **1990**, *4*, 201–237; T. Haegawa, H. Ikuta, K. Kitazawa in *Physical Properties of High Temperature Superconductors III* (Ed.: D. M. Ginsberg), World Scientific Publishing, River Edge, NJ, **1992**, p. 525.
[85] J. Bardeen, L. N. Cooper, J. R. Schrieffer, *Phys. Rev.* **1957**, *108*, 1175–1204.
[86] I. Giaever, K. Megerle, *Phys. Rev.* **1961**, *122*, 1101–1111.
[87] Z. Zhang, C. M. Lieber, *Phys. Rev. B* **1993**, *47*, 3423–3426; Y. Li, J. Liu, C. M. Lieber, *Phys. Rev. Lett.* **1993**, *70*, 3494–3497.
[88] E. L. Wolf, A. Chang, Z. Y. Rong, Y. M. Ivanchenko, F. Lu, *J. Supercond.* **1994**, *7*, 355–360.
[89] C. Renner, O. Fischer, *Phys. Rev. B* **1995**, *51*, 9208–9218.
[90] J. Liu, Y. Li, C. M. Lieber, *Phys. Rev. B* **1994**, *49*, 6234–6238.
[91] J.-X. Liu, J.-C. Wan, A. M. Goldman, Y. C. Chang, P. Z. Jiang, *Phys. Rev. Lett.* **1991**, *67*, 2195–2198; H. J. Tao, A. Chang, F. Lu, E. L. Wolf, *Phys. Rev. B* **1992**, *45*, 10622–10632.
[92] K. Maki in *Superconductivity* (Ed.: R. D. Parks), Dekker, New York, **1969**, p. 1035.
[93] P. Monthoux, A. V. Balatsky, D. Pines, *Phys. Rev. Lett.* **1991**, *67*, 3448–3451; P. Monthoux, A. V. Balatsky, D. Pines, *Phys. Rev. B* **1992**, *46*, 14803–14817.
[94] C. Jiang, J. P. Carbotte, R. C. Dynes, *Phys. Rev. B* **1993**, *47*, 5325–5331.
[95] D. J. Bishop, P. L. Gammel, D. A. Huse, C. A. Murray, *Science* **1992**, *255*, 165–172; D. A. Huse, M. P. A. Fisher, D. S. Fisher, *Nature* **1992**, *358*, 553–559.
[96] R. P. Huebener, *Magnetic Flux Structures in Superconductors*, Springer, New York, **1979**.
[97] H. F. Hess, R. B. Robinson, R. C. Dynes, J. M. Valles, J. V. Waszczak, *Phys. Rev. Lett.* **1989**, *62*, 214–216; H. F. Hess, C. A. Murray, J. V. Waszczak, *Phys. Rev. B* **1994**, *50*, 16528–16540.
[98] H. Dai, J. Liu, C. M. Lieber, *Phys. Rev. Lett.* **1994**, *72*, 748–751.
[99] H. Dai, S. Yoon, J. Liu, R. C. Budhani, C. M. Lieber, *Science* **1994**, *265*, 1552–1556; S. Behler, P. Jess, A. Baratoff, H. J. Guntherodt, *Physica C* **1994**, *235–240*, 2703–2704.
[100] S. Yoon, H. Dai, J. Liu, C. M. Lieber, *Science* **1994**, *265*, 215–218.
[101] F. Grey, *Adv. Mater.* **1993**, *5*, 704–710.
[102] P. Bedrossian, D. M. Chen, K. Mortensen, J. A. Golovchenko, *Nature* **1989**, *342*, 258–260.
[103] Y. Utsugi, *Nature* **1990**, *347*, 747–749; H. J. Mamin, D. Rugar, *Appl. Phys. Lett.* **1992**, *61*, 1003–1005; A. Sato, Y. Tsukamoto, *Nature* **1993**, *363*, 431–432.

[104] E. Garfunkel, G. Rudd, D. Novak, S. Wang, G. Ebert, M. Greenblatt, T. Gustafsson, S. H. Garofalini, *Science* **1989**, *246*, 99–100; S. Miyake, *Appl. Phys. Lett.* **1994**, *65*, 980–982.
[105] D. M. Eigler, E. K. Schweizer, *Nature* **1990**, *344*, 524–526; D. M. Eigler, P. S. Weiss, E. K. Schweizer, N. D. Lang, *Phys. Rev. Lett.* **1991**, *66*, 1189–1192.
[106] I.-W. Lyo, Ph. Avouris, *Science* **1991**, *253*, 173–176; C. T. Salling, M. G. Lagally, *ibid.* **1994**, *265*, 502–506; A. Kobayashi, F. Grey, R. S. Williams, M. Aono, *ibid.* **1993**, *259*, 1724–1726.
[107] L. J. Whitman, J. A. Stroscio, R. A. Dragoset, R. J. Celotta, *ibid.* **1991**, *251*, 1206–1210.
[108] C. M. Lieber, Y. Kim, *Thin Solid Films* **1991**, *206*, 355–359; Y. Kim, J.-L. Huang, C. M. Lieber, *Appl. Phys. Lett.* **1991**, *59*, 3404–3406; E. Delawski, B. A. Parkinson, *J. Am. Chem. Soc.* **1992**, *114*, 1661–1667.
[109] J.-L. Huang, Y.-E. Sung, C. M. Lieber, *Appl. Phys. Lett.* **1992**, *61*, 1528–1530; S. Akari, R. Moller, K. Dransfeld, *ibid.* **1991**, *59*, 243–245.
[110] Y. Kim, C. M. Lieber, *Science* **1992**, *257*, 375–377; C. M. Lieber, Y. Kim, *Adv. Mater.* **1993**, *5*, 392–394.
[111] M. F. Crommie, C. P. Lutz, D. M. Eigler, *Science* **1993**, *262*, 218–220.
[112] R. Lüthi, E. Meyer, H. Haefke, L. Howald, W. Gutmannsbauer, H.-J. Güntherodt, *Science* **1994**, *266*, 1979–1982.
[113] P. E. Sheehan, C. M. Lieber, *Science*, submitted.
[114] C. D. Frisbie, L. F. Rozsnyai, A. Noy, M. S. Wrighton, C. M. Lieber, *Science* **1994**, *265*, 2071–2073; A. Noy, C. D. Frisbie, L. F. Rozsnyai, M. S. Wrighton, C. M. Lieber, *J. Am. Chem. Soc.* **1995**, *117*, 7943–7951.
[115] W. T. Muller, D. L. Klein, T. Lee, J. Clarke, P. L. McEuen, P. G. Schultz, *Science* **1995**, *268*, 272–273; S. J. O'Shea, R. M. Atta, M. E. Welland, *Rev. Sci. Instrum.* **1995**, *66*, 2508–2512.
[116] J. Hu, X.-D. Xiao, D. F. Ogletree, M. Salmeron, *Surf. Sci.* **1995**, *327*, 358–370.
[117] U. Landman, W. D. Luedtke, N. Burnham, R. J. Colton, *Science* **1990**, *248*, 454–461.

EVENTS

IRaP 96

2nd International Symposium on Ionizing Radiation and Polymers

Nov. 3-8, 1996, Saint-François, Guadeloupe, FWI

IRaP96 is the second symposium of an international series devoted to ionizing radiation effects in polymers. IRaP conferences bring together scientists from research, universities and industries involved in radiation polymer science. Their aim is to facilitate the exchange of knowledge and information in this cross-disciplinary field and to promote innovative industrial applications. The topics will cover fundamental process, surface and bulk modifications, advanced materials and technological applications. Furthermore, IRaP96 will highlight the influence of ionizing radiation on the modification of chemical and physical properties (e.g. electrical, mechanical, optical, tribological, diffusion...). In addition to electron, photon and ion beam effects, studies with lasers and cluster beams in polymers will be included.

The program consists of keynote lectures, invited and contributed talks, and posters.

A particular attention is given to new materials which can find applications in medecine, biology, biotechnology, defense, environmental protection, and energy saving.

For more information and registration (before September the 15th), please contact:

Dr. Natacha BETZ
Chairwoman of IRaP 96 organizing committee
DRECAM/SRSIM/LPI
CEA/Saclay
F - 91191 Gif sur Yvette Cedex
tel.: (33) 1 69 08 48 34 ; fax : (33) 1 69 08 96 00
e-mail : betz@drecam.cea.fr.; irap@drecam.cea.fr

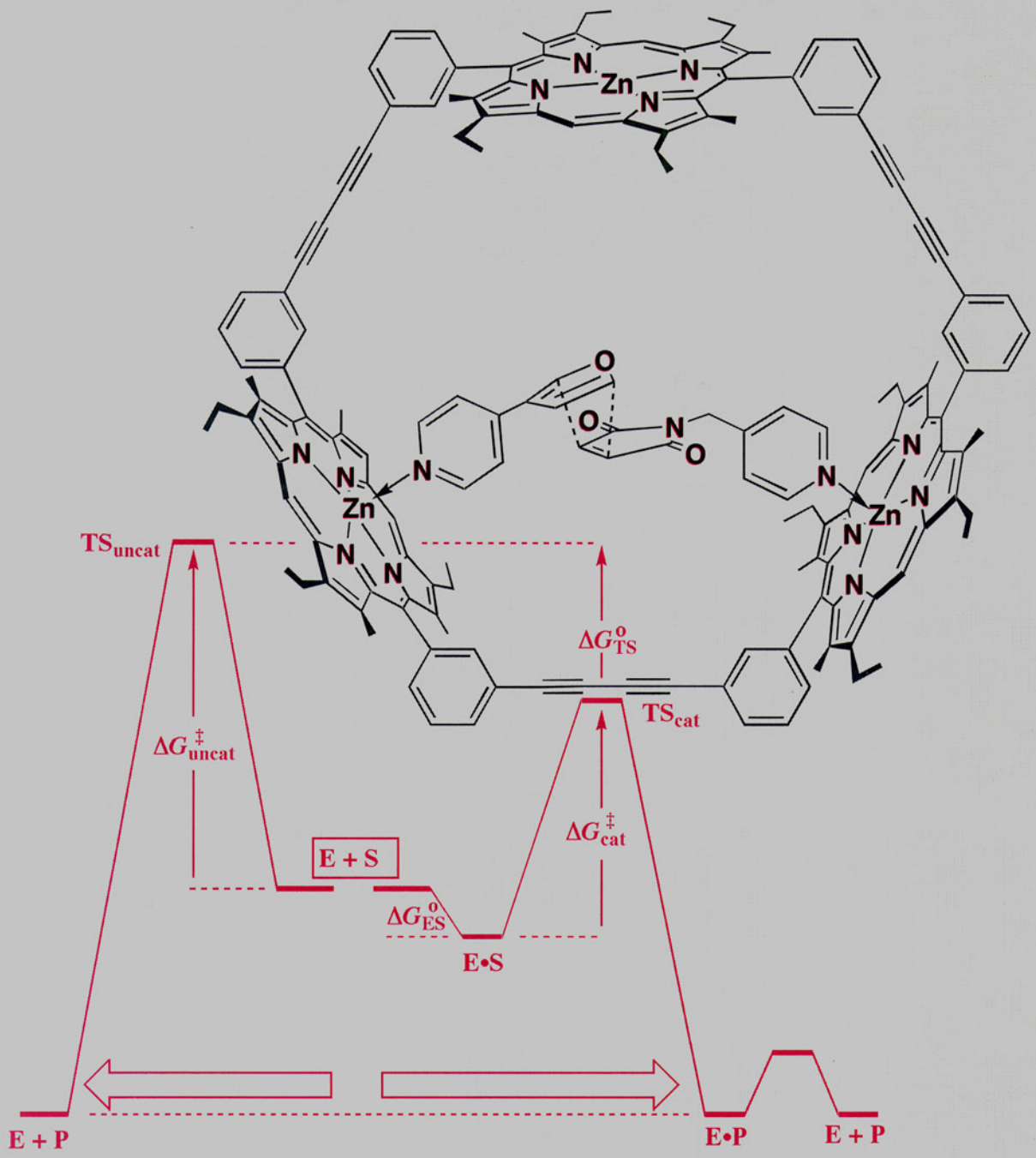

A prerequisite for the catalytic efficiency of a synthetic enzyme is that it stabilize the transition state.

Enzyme Mechanisms, Models, and Mimics

Anthony J. Kirby*

"One of the great intellectual challenges presented to Science by Nature is a proper understanding of how enzymes work. At one level we can 'explain' enzyme catalysis— what an enzyme does is bind, and thus stabilize, selectively the transition state for a particular reaction.[1] But our current level of understanding fails the more severe, practical test that of designing and making artificial enzyme systems with catalytic efficiencies which rival those of natural enzymes." This was the introduction to a recent Highlight in *Angewandte Chemie*,[2] prompted by the appearance of a paper[2] that appeared to defy established ideas, by claiming artificial enzyme systems that did indeed attain catalytic efficiency rivaling that of natural enzymes. The "pepzymes" of Atassi and Manshouri[3] were relatively small (29-residue) peptides modeled on the active site structures of trypsin and chymotrypsin by "surface simulation." One was claimed to hydrolyze the simple trypsin "substrate" *N*-tosyl-L-arginine methyl ester with k_{cat} and K_m values comparable to those of the native enzyme, and also to hydrolyze the peptide bonds of test proteins to give comparable peptide profiles. This extraordinary result provoked as much skepticism as excitement, and several groups tried to reproduce the results. They failed, comprehensively.[3, 4] Some specific reasons why this failure came as no surprise have been summarized by Matthews et al.[5] This review examines the problems involved in the design of enzyme mimics in more general terms, with the emphasis specifically on the efficiency of catalysis.

Keywords: catalytic antibodies · enzymatic catalysis · enzyme mimics · molecular recognition

1. Introduction: Approaches to Artificial Enzymes

Quite apart from the intellectual challenge, a proper understanding of how enzymes work holds out the promise of artificial catalysts more robust than proteins and available for practically any organic reaction of interest. How far this is a practical proposition at the present time is an important question. To begin to answer the question, and to read the literature critically, we need to understand first of all what the term "artificial enzyme" currently means.

Real enzymes are more than just highly evolved catalysts: they also recognize and respond to molecules other than their specific substrate and product, as part of the control mechanisms of the cell. The evolution of artificial enzymes is at a much more primitive stage, with efficient catalysis the primary objective. Systems are known that model various other functions, including potential control mechanisms. But to be useful as an industrial catalyst, for example, an artificial enzyme does not need sophisticated built-in feedback control or high substrate specificity. A stable molecule that is an efficient catalyst for a key target reaction in a chemical reactor will not be required to select its substrate from many hundreds in the same solution, as enzymes routinely must in the cell. So the sensible design strategy is minimalist: just those features of enzymes that are essential for catalytic efficiency are considered. This review adopts the same strategy.

We first discuss enzyme mechanism in rather general terms, to identify and define their key features. We then go on to enzyme models, systems designed to reproduce specific features of enzyme reactions, and so test basic ideas on enzyme mechanism. Finally we discuss enzyme mimics, the most successful of which combine more than one of the key features identified previously and catalyze reactions by mechanisms that are demonstrably enzyme-like. An enzyme mimic that can do all this, *and* achieve turnover, deserves to be called an artificial enzyme. (If it also proves to be of practical utility it certainly will be.)

2. Enzyme mechanisms

2.1. Molecular Recognition of Transition States

What an enzyme does is bind, and thus stabilize, selectively, the transition state for a particular reaction.[7–9] So the problem can be defined in terms of the molecular recognition of transition states.[10] First we need to recall a few familiar terms.

[*] Prof. A. J. Kirby
University Chemical Laboratory
GB-Cambridge CB2 1EW (UK)
Fax: Int. code +(1223)-336362
e-mail: AJK1 *a* cus.cam.ac.uk

Experimentally the characteristic feature of an enzyme-catalyzed reaction is that it follows saturation or Michaelis–Menten kinetics[1] characteristic of a mechanism involving formation of an enzyme–substrate complex (**E·S**) as the first step [Eq. (a)].

$$\mathbf{E} + \mathbf{S} \underset{k_{-1}}{\overset{k_1}{\rightleftharpoons}} \mathbf{E \cdot S} \xrightarrow{k_2\,(k_{cat})} \mathbf{E \cdot P} \overset{\text{fast}}{\rightleftharpoons} \mathbf{E} + \text{products} \qquad \text{(a)}$$

Note that almost any enzyme reaction is a great deal more complicated than this, but the equation describes reactions catalyzed by enzyme models and mimics very well.

If the substrate concentration is high enough, the catalyst becomes saturated. Under these conditions the rate is determined solely by k_2 (usually called k_{cat}), and the reaction is first order (in enzyme concentration). The substrate concentration that gives half this maximum rate is called K_m. At sufficiently low substrate concentrations the first step becomes rate determining and the reaction is second order (rate $= k_1[\mathbf{E}][\mathbf{S}]$; for further details see ref. [1]).

It is important to have a feel for what these parameters mean:

- k_{cat} is the first-order rate constant for the reaction of the bound substrate. It can be compared directly with those of other first-order reactions, for example intramolecular reactions, and allows estimates of the effective molarity (see Section 3.1) within the complex if the mechanism is known. It is easy to interpret: bigger is better.
- K_m is a measure of binding, generally of all enzyme-bound species, but of the substrate in the simplest case, when the binding step is a rapid preequilibrium (i.e. $k_{-1} \gg k_2$). K_m then becomes equal to the dissociation constant of the catalytic complex [**E·S**] and is easy to interpret: smaller values correspond to tighter binding.
- k_{cat}/K_m is the apparent second-order rate constant at very low substrate concentrations; under these conditions it is a useful measure of the overall efficiency of the catalyst, *including the binding step*. It can be compared with other second-order rate constants. (Competitive catalytic chemists like it because it gives big numbers.)

So far we have not considered the transition state explicitly. This is done most simply with an energy profile diagram for enzyme-catalyzed and uncatalyzed reactions of a substrate **S** (Fig. 1). The two transition states of interest are $\mathbf{TS}_{cat}$ for the catalyzed reaction and $\mathbf{TS}_{uncat}$ for the reaction in the absence of the catalyst. Molecular recognition of the transition state is

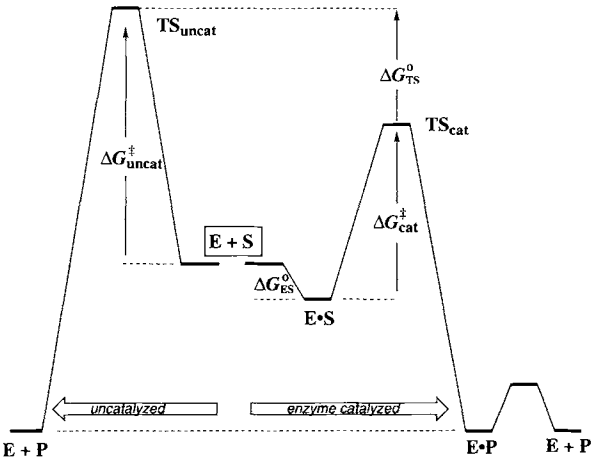

Fig. 1. Energy profiles for both enzyme-catalyzed (left to right) and uncatalyzed (right to left) reactions of a substrate **S**. The ordinate represents (qualitatively) the Gibbs free energy, the abscissa the progress along a theoretical reaction coordinate. (Note that the route via **E·S** is the unique low-energy pathway from starting materials to transition state.)

measured by its free energy of binding $-\Delta G^0_{TS}$, which is derived simply from Figure 1 by applying Equations (b) and (c). We

$$\Delta G^{\ddagger}_{uncat} + \Delta G^0_{ES} = \Delta G^{\ddagger}_{cat} + \Delta G^0_{TS} \qquad \text{(b)}$$

$$-\Delta G^0_{TS} = \Delta G^{\ddagger}_{cat} - (\Delta G^{\ddagger}_{uncat} + \Delta G^0_{ES}) \qquad \text{(c)}$$

will use this parameter in the later stages of this review to compare the efficiencies of different sorts of enzyme mimics (see Tables 4 and 5). Note, also in the simplest case, that in terms of rate and equilibrium constants $k_{cat}/k_{uncat} = K_M/K_{TS}$; in other words, the rate acceleration due to transition state binding is given by the stronger binding of the transition state compared with the ground state.

2.2. Passive Versus Dynamic Binding

It is helpful for the analysis to distinguish two sorts of binding relevant to transition states: *passive binding*, referring to ordinary molecular recognition through hydrogen bonding, hydrophobic interactions, and the like, and *dynamic binding*. Dynamic binding refers to interactions between catalyst and substrate *at the reaction center*. These interactions are of crucial importance

Anthony John Kirby was born in Welwyn Garden City (UK), on the railway line between Cambridge and London (which he has been able to use ever since). He graduated and received his Ph.D. from the University of Cambridge in 1962, then spent a decisive postdoctoral year (1963–1964) with William P. Jencks at Brandeis University, Waltham, MA (USA), where he learned the value of a systematic approach to the problems of bioorganic mechanism. Since 1964 he has been at the University Chemical Laboratory in Cambridge, where he is currently Professor of Bioorganic Chemistry. His research interests focus on enzymes and chemical descriptions of their catalytic activity.

for catalysis, because they are the most obvious difference between the binding of the substrate and that of the transition state. They differ from the interactions involved in passive binding, because they change substantially as bonds are made and broken, and because they are generally stronger than the interactions involved in ordinary molecular recognition.

Before we discuss dynamic binding any further it should be stressed that there is no clear-cut distinction between the two sorts of binding. A real example will illustrate the point (Fig. 2). Fersht and his co-workers used site-directed mutagenesis in a series of elegant experiments to identify the amino acid side

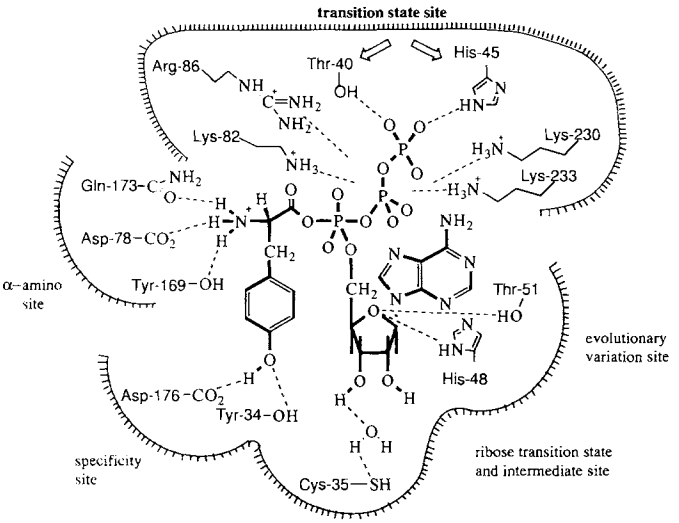

Fig. 2. Binding interactions of the transition state in the tyrosyl tRNA synthetase reaction [11]. The substrate is in bold. I am grateful to Alan Fersht for this updated version.

chains involved in binding and catalysis in the tyrosyl *t*RNA synthetase reaction.[11] Several amino acids identified as involved in binding in the transition state but not in the enzyme–substrate complex (e.g. Thr40 and His45) are clearly not interacting directly with the reaction center. They act primarily to position the terminal phosphate of ATP, helping to set up the favorable geometry for the reaction at the α-phosphate center, but they are not involved directly in bond making or breaking. The actual binding at these sites is thus more passive than dynamic. For purposes of the analysis we use the simple definition of dynamic binding given above, as referring specifically to interactions at the reaction center between catalyst and transition state.

To illustrate dynamic binding we take the familiar reaction catalyzed by a serine protease such as chymotrypsin (Fig. 3a),[1] in which a general base **B** (the imidazole of His57 in the case of α-chymotrypsin) assists the attack of a nucleophilic OH group (of Ser195) at the carbonyl carbon center of the amide substrate. A backbone amide NH group provides further assistance, acting in effect as a general acid (**HA**). (Because it is familiar the process looks easy, but amide cleavage is one of the most daunting challenges for man-made catalysts, and so far we are not even close.) In the transition state for this step (Fig. 3b) at least six bonds are being made and broken, probably simultaneously, and it is not obvious where transition state binding starts and

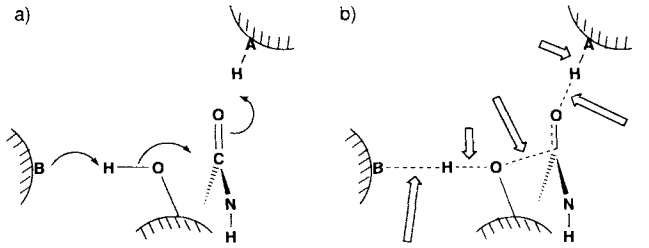

Fig. 3. a) Schematic representation of the mechanism of the first step, an acylation, in a serine protease reaction. For clarity only the amide group of the substrate is shown. b) The transition state for the reaction in (a). The arrows indicate bonds being formed and broken, corresponding to dynamic binding interactions between the enzyme and the transition state.

finishes, since in this case the nucleophile is part of the enzyme. But the details are unimportant: the important point is that the "binding" of the transition state by the enzyme involves more than ordinary molecular recognition. These *dynamic* interactions at the reaction center involve partially formed or broken covalent bonds (marked by arrows in Fig. 3b). These interactions, this "dynamic binding," can be substantially stronger than the individual interactions involved in ordinary molecular recognition, and so can make a major contribution to catalytic efficiency. We need to know how strong these interactions can be and understand the factors that can make them so strong in the enzyme situation. This information is most easily obtained from model systems.

3. Enzyme Models

3.1. Intramolecular Reactions

The only simple reactions that can rival their enzyme-catalyzed counterparts in rate are intramolecular reactions such as cyclizations, and specifically intramolecular nucleophilic reactions. Making the reaction of interest part of a thermodynamically favorable cyclization can produce systems in which the extraordinarily stable groups of structural biology (amides, glycosides, and phosphate esters typically have half-lives of many tens of years under physiological conditions near pH 7) can be cleaved in seconds or less. An early example is the cyclization of **1**, in which an ordinary aliphatic amide is forced into close proximity with a COOH group[12] [Eq. (d)]. A more recent case, which models enzyme reactions in which the OH group of a tyrosine side chain acts as a nucleophile, is the cyclization of phosphate diester **2**, which reacts in this case as the anion[13] [Eq. (e)].

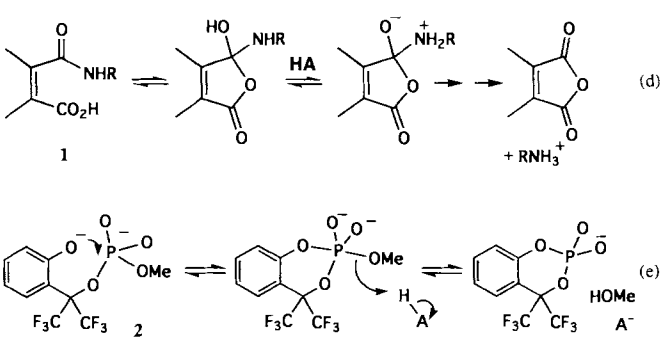

The efficiency of intramolecular catalysis[14] is conveniently measured in terms of the effective molarity (EM) of the catalytic group.[15] The EM is the ratio of the first-order rate constant for the intramolecular reaction and the second-order rate constant for the intermolecular reaction that proceeds by the same mechanism under the same conditions. The EM has the dimensions of molarity and is easy to understand as the nominal concentration of the catalytic group that would be required in the equivalent intermolecular process to match the rate of the intramolecular reaction. (In the examples cited, which have EMs greater than 10^{10} M, this is *purely* nominal.) EMs can tell us how catalytic efficiency relates to structure in systems designed to bring functional groups together in close proximity, just as the same functional groups are brought together in an enzyme–substrate complex.

Two generalizations are of major importance:

1. Catalysis can be highly efficient in cyclization reactions, which involve the formation of bonds between heavy (non-hydrogen) atoms. EMs of 10^8–10^9 M can be attained even in flexible systems,[16] and higher figures are possible in systems in which ground state strain is relieved as part of the reaction. The EM of the carboxyl group in the cyclization of **1**, for example, is over 10^{13} M.[12] (Enzymes cannot exert the sorts of very strong nonbonding interactions that can be built into synthesized structures like **1**, because proteins are fairly flexible. But studies of such rigid systems give us access to mechanistic information about the reactions of relevant functional groups proceeding at rates comparable to those of the corresponding enzyme-catalyzed processes.) There has been much discussion of the origins of the rate enhancements in these systems; at least a dozen theories have been proposed,[15] ranging from orbital steering to the spatiotemporal hypothesis.[17] Some of these provide useful guidance for system design, but the fundamental requirement for a high (kinetic) EM is a thermodynamically favorable cyclization with no stereoelectronic impediment to the reaction.[18]

2. Intramolecular reactions involving rate-determining proton transfer, for example general acid and general base catalyzed reactions, are far less efficient, with EMs generally less than about 10 M.[15] For instance, the EM of the carboxylate group in half-esters **3** of dialkylmalonic acids, which are hydrolyzed by general base catalysis because cyclization is strongly disfavored, ranges from less than 1 M up to 60 M[19] [Eq. (f)].

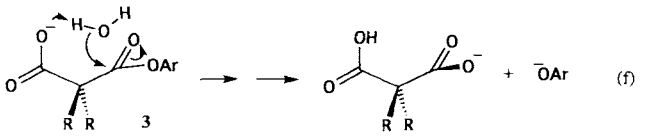

(f)

Though the highest EM measured for intramolecular general base catalysis, 60 M is tiny compared with figures easily attained in nucleophilic reactions. For several years this dichotomy presented a serious problem, since proton transfer is the most common enzyme-catalyzed reaction. It is scarcely possible to carry out an ionic reaction in water without involving a proton transfer at some point. The model reactions with **1** and **2** make the point. They are fast because the nucleophilic reaction is very favorable, but in both cases the rate is now limited by a proton transfer step; a general acid is required to take the reaction forward from the high-energy intermediate. Note that though the rate constant for proton transfer is very high, the *rate* of a particular step depends also on the concentration of the reactant, and the concentration of a high-energy intermediate is by definition very low. Even intrinsically very fast reactions can thus be rate determining under these circumstances.

There is no doubt that enzymes catalyze proton transfers efficiently. Thus the reasonable conclusion is that the models, not the enzymes, are deficient. Recent work suggests a solution. Efficient intramolecular proton transfer reactions (EMs up to at least 10^6 M) are found to be possible in systems specially designed to form strong intramolecular hydrogen bonds. In the best known case, which provided the initial clue, derivatives **4** of salicylic acid—acetals, phosphates, even ethers—lose a stable "electrofuge" X^+ in a reaction involving protonation of the X-substituted oxygen atom and formation of the salicylate monoanion. Anion **5** is stabilized by over 20 kJ mol^{-1} in water

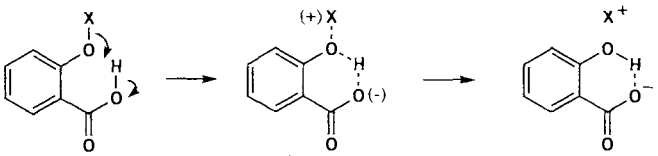

by the intramolecular hydrogen bond, and so too is transition state **4**‡. Since hydrogen bonding is much weaker in the starting material, this amounts to selective stabilization of the transition state. The result is an exceptionally rapid reaction, corresponding to an effective molarity of up to 10^4 M for the COOH group.

This provides a general basis for efficient proton transfer catalysis, and several new efficient systems have been devised recently.[20] Perhaps most interesting is the extension to reactions involving proton transfer to and from carbon atoms. Enolizations, for example, are key steps in enzyme-catalyzed aldol condensations. Proton transfer to and from carbon centers is known to be intrinsically slow, and in enzyme reactions efficient catalysis is needed here more than for proton transfers to O and N centers, which are already reasonably fast (usually diffusion-controlled in the thermodynamically favorable direction). Efficient catalysis is clearly available, as shown by the example of mandelate racemase,[21] which removes a proton from the α-carbon of the mandelate anion [Eq. (g)]. Gerlt and Gassman[22]

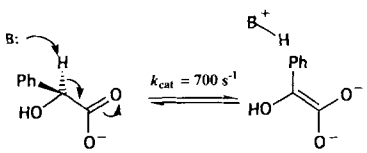

(g)

have proposed that the enolate intermediate, and the transition state leading to it, are stabilized by "short strong hydrogen bonds" to the negatively charged oxygen. These have the effect of increasing the effective acidity of the proton to be removed, which otherwise would be very weakly acidic, with $pK_a > 25$.

This idea is consistent with the effects of the strong (and so by definition short) intramolecular hydrogen bonds identified

above as the source of high effective molarities in general acid or base catalysis. Furthermore, recent work on enol ethers suggests that even C–H protons can become acidic enough to become involved in strong hydrogen bonding in enolization reactions. Thus enol ether **7** is based on compound **8**, which is known to

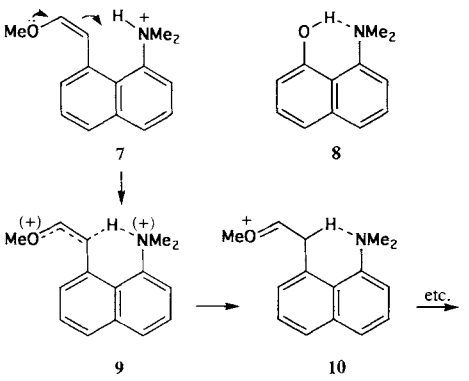

be stabilized by a strong intramolecular hydrogen bond ($pK_a(OH) = 14.9$). The effective molarity of the dimethylammonium group in the reaction of **7** (half-life 10 s at 39 °C) is of the order of 10^6 M (the figure is approximate since the corresponding intermolecular reaction is too slow to measure) and is consistent with very effective selective stabilization of the transition state.[23] This is ascribed to the strong intramolecular hydrogen bonding indicated in transition state **9**. C–H protons are normally too weakly acidic to be involved in hydrogen bonds in aqueous solution, but a simple calculation shows that the C–H proton in the intermediate **10** is in fact strongly acidic (at least as strong as H_3O^+!) and expected to be stabilized by hydrogen bonding to an available basic center.

The structural requirements for hydrogen bonding of this sort strong enough to be significant in water—are very precise, which is why relevant systems are only now being identified. Such precision is, however, no problem in enzyme–substrate interactions, where precise group–group interactions in three dimensions may be presumed to be the norm. We conclude that the key requirement for efficient proton transfer catalysis is dynamic binding of the proton during transfer in a strong transition state hydrogen bond. Note that this may very well be stronger than the corresponding hydrogen bond in either starting material or product: hydrogen bonds are primarily electrostatic and the charge distribution around the central proton changes continuously as bond making or breaking proceeds. It is not easy to estimate just how strong such dynamic binding might be at this stage in the work, but the evidence from the systems so far available suggests figures of at least 30–40 kJ mol^{-1} in water.

To maintain high catalytic efficiency enzymes must provide catalysis for each individual step of a reaction, and not just the rate-determining step. The majority of enzyme models, on the other hand, are designed simply to catalyze the slowest chemical step; however, models are known in which two different intramolecular groups catalyze separate steps of the same reaction. The proton transfer involved in the hydrolysis of the amide group of **1**, for example, is catalyzed by a second carboxyl group, as in the β-amino acid derivative **11**, efficiently enough that the proton transfer step is no longer rate determining[24] [Eq. (h)].

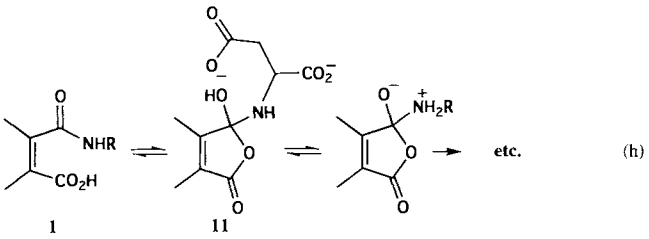

(h)

Reactions involving the concerted action of two catalytic groups on the same step of a reaction are more elusive—and more interesting. A simple example is the lactonization of the aspirin analogue **12**, for which the EM of the carboxylate and hydroxyl groups are the same as for the hydrolysis of aspirin and the lactonization of 4-hydroxybutyric acid (13 and 500 M, respectively).[25] Here a two-step mechanism with separate proton transfer and bond-forming steps is possible, but the concerted process is preferred [Eq. (i)].

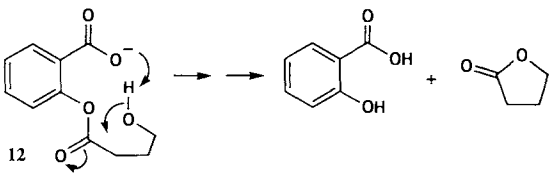

(i)

This, like most known examples, involves an activated system with a good (phenolic) leaving group. Enzymes, on the other hand, and thus also the most interesting potential artificial enzymes, must deal with unactivated systems and often have to displace poor leaving groups (e.g. the OH groups of aliphatic alcohols and sugars). Of special current interest is the possibility of synergy, or cooperativity in concerted reactions of such systems. The idea arises naturally when one considers reactions like glycoside cleavage. Glycosidases like lysozyme catalyze this chemically very difficult reaction (at pH 7) by way of a mechanism involving two carboxyl groups, one in the COOH and one in the COO^- form. Since a glycosyl carbenium ion is probably too unstable to exist in the presence of a nucleophile, a simple S_N1 process looks unlikely. A double displacement mechanism (with the initial displacement by carboxylate, acting as a nucleophilic catalyst) would explain the observed retention of configuration at C1 of the glycosyl residue,[26] and is known to be involved in some cases. The problem is explaining the high rate of this normally very difficult process. A possible solution is that nucleophilic attack and general acid catalysis of the departure of the leaving group act efficiently in concert, as in structure **13**. We know that both general acid and nucleophilic catalysis can be efficient if the leaving group is good enough. The question is: can efficient nucleophilic catalysis make a poor leaving group good

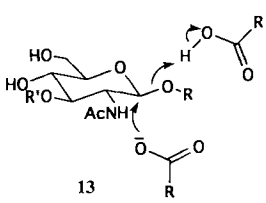

enough *in the transition state* to support efficient general acid catalysis? And, can efficient general acid catalysis make the leaving group good enough to trigger even more efficient nucleophilic catalysis? If the answer to both questions is yes, the result will be a group transfer reaction more efficient than the sum of the parts.[27]

3.2. Passive Binding and Molecular Recognition

It is, at least in principle, simple enough to design a system with two groups on the same molecule in a desired geometrical relationship. But enzymes must first recognize and bind their substrate(s) to set up the correct geometry. The binding process is a major problem in the development of artificial enzymes.

The principles involved in binding are well understood from work on small-molecule systems. To understand the interplay between binding and reactivity it is convenient to recognize three important classes of association. In order of decreasing strength these are covalent, weak covalent (primarily hydrogen bonding), and noncovalent (hydrophobic and electrostatic).

3.2.1. Covalent Binding

The strongest single interaction possible between two molecules is of course the formation of a covalent bond, and acyl, glycosyl, and phosphoryl intermediates, for example, are often involved in enzyme-catalyzed group transfer reactions. Reactions with other active site functional groups then become intramolecular, with close control of geometry, and we have seen that intramolecular catalysis can be highly efficient. However, true catalysis is only possible if the formation of the covalent bond is readily reversible; otherwise the catalytic cycle is not complete.

Reversible formation of covalent bonds is particularly important in enzyme reactions involving active site metal cations. The suggested mechanism for the reaction of metalloproteinase carboxypeptidase A (Scheme 1) is an example. At the end of the

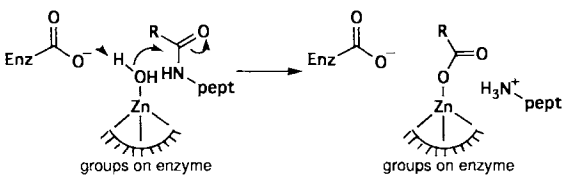

Scheme 1. Proposed mechanism for the reaction of the metalloprotease carboxypeptidase A. Enz = enzyme, Pept = peptide chain.

process the $RCOO^-$ group cleaved from the N-terminus of the peptide diffuses away from the metal and is replaced by an new water molecule from the solvent; the catalytic cycle can then start anew. The metal in this mechanism helps to solve two problems. Hydrolytic enzymes must use water as a nucleophile at some stage, but binding and positioning such a small molecule presents a problem. This is neatly resolved by attaching water as a ligand to the active site metal, which in turn increases the chemical reactivity of the water molecule, because the pK_a of bound H_2O is reduced. The reactivity of the water molecule can also be fine-tuned because it now depends not only on the metal concerned but also on the number, type, and arrangement of the other ligands. We will not discuss metal ion catalysis explicitly in this review; interested readers are referred to a book on the subject.[28] But the study of metal ion catalysis clearly has a great deal to offer in the design of enzyme mimics.

3.2.2. Hydrogen Bonding

A hydrogen bond is much weaker than a covalent bond, although it retains definite directional preferences.[29] The strength of a single hydrogen bond is very sensitive to its environment and is typically of the order of 5–20 kJ mol^{-1}—too weak to support significant association at room temperature. Multiple H-bonding can lead to observable, but strongly medium-dependent association, as shown by the equilibrium constants K_{ass} for the formation of the familiar carboxylic acid dimer **14** [Eq. (j)]. Carboxylic acids almost always crystallize in

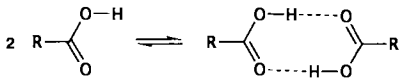

(j)

14

the dimeric form, and dimers also form in solution in chloroform (K_{ass} = 4000 M^{-1}). But in water K_{ass} is only 0.1 M^{-1}: each proton and lone pair of the monomer is strongly solvated by hydrogen bonding to water molecules and dimerization is suppressed. Of course any sort of association in solution is in direct competition with solvation, and water is very good at solvating ions and H-bond donors and acceptors. Thus multiple H-bonding is the basis of protein secondary structures like the α-helix, but isolated α-helices are only marginally stable in water,[30] and the stability of protein structures depends on additional, noncovalent interactions. A simple illustration comes from the work of Hamilton et al. on H-bonding receptors for dicarboxylic acids.[31]

The diamide **15** binds glutaric acid strongly in chloroform (K_{ass} = 60 000 M^{-1}) but not in dimethyl sulfoxide (DMSO).[31] However, the bisguanidinium system **17**, which has the same number of hydrogen bonds, is almost as good a receptor (K_{ass} = 50 000 M^{-1}) in DMSO containing 5% tetrahydrofuran, and binding is still measurable in the presence of 25% D_2O.[32] The main difference is that the strongly basic guanidine group is protonated by COOH, so hydrogen bonding is reinforced by electrostatic attraction.

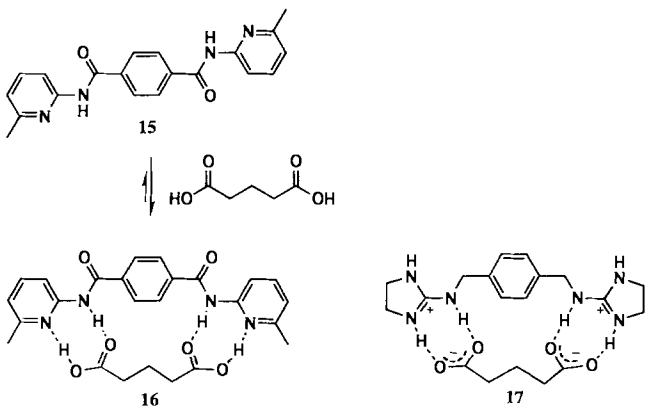

15

16

17

The strength of multiple H-bonding interactions is also subject to more subtle influences, as shown by the big difference between the two apparently similar triply H-bonded systems shown in Scheme 2.[33] These differ in the sequence of H-bond

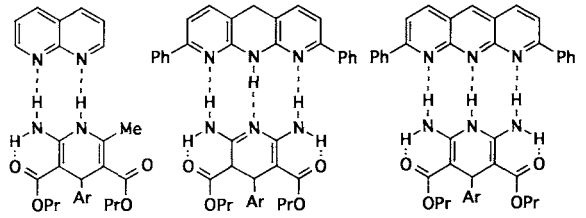

Scheme 2. Systems held together by multiple hydrogen bonds with different sequences of the H-bond acceptors (**A**) and donors (**D**).

acceptor (**A**) and donor (**D**) groups. Remarkably the binding of all-acceptor to all-donor systems is so strongly preferred that the third hydrogen bond does not increase K_{ass} at all if it is introduced in the wrong place. Clearly multiple hydrogen bonding includes an element of specificity and provides the possibility of strong, geometrically defined association.

3.2.3. *Noncovalent Interactions*

Electrostatic[34] and hydrophobic interactions[35] play essential, complementary[36] roles in determining the three-dimensional structures of proteins,[30] and of protein–ligand complexes in general. Their roles in host–guest interactions have been extensively documented. However, the forces involved are not intrinsically strongly directional, and they can be used to set up specific geometries only in combination. This problem may have been underestimated, partly because it is avoided in the cyclodextrins, which are perhaps the most studied models for hydrophobic binding.[37] In some cases cyclodextrins are rather effective as enzyme mimics (see Section 4.1), partly because they carry large numbers of hydroxyl groups in all directions around the cavity. Consequently, a bound substrate does not have to assume a specific orientation for proximity to a OH group.

It should be clear, even from this brief summary, why enzymes use an array of complementary noncovalent binding interactions to bring their substrate into productive association with the catalytic apparatus of the active site. However, defining the structure of the enzyme–substrate complex—as can be done with some confidence when good three-dimensional structures of complexes with substrate analogues are available—does not necessarily tell us more about the reaction than the structure of the starting materials.

3.3. The Strength of Dynamic Binding

The key transformation of the enzyme–substrate complex into the enzyme–transition state complex (see Fig. 1) is conveniently described by Scheme 3. The binding process first brings

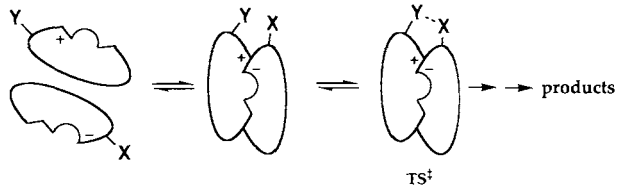

Scheme 3. Formation of an enzyme–substrate complex and its conversion into the enzyme–transition state complex. **TS*** = transition state.

the functional groups X and Y into close enough proximity for reaction to be favored. This process may include some activation of the ground state, for example by binding in a reactive conformation.[16] It will certainly include desolvation of reacting polar groups. Any polar functional group is strongly solvated, and thus stabilized, in water. (One way of looking at the selective stabilization of the transition state is in terms of specific "solvation" of the reactants by the enzyme active site, which replaces the random solvation by the solvent.) The subsequent formation of the transition state **TS*** involves partial bond formation between X and Y. The driving force for bond formation comes partly from the intrinsic chemical reactivity of the groups concerned and partly from the way the groups are brought together; it is this second factor that controls efficiency.

The clear message from the work on intramolecular reactions is that a prerequisite for efficient catalysis is a stable platform. Table 1 shows how tighter binding of the reacting groups in a

Table 1. Strength of dynamic binding based on effective molarities for intramolecular cyclizations.

	EM [M]	$\Delta\Delta G^*$ [kJ mol^{-1}]
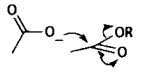	1	0
	220	13
	5×10^4	27
	3×10^9	54
	4×10^{12}	(73)

simple cyclization reaction leads to higher effective molarities. This treatment allows for the intrinsic chemical reactivity of the reacting groups. When expressed as free energy differences, the EMs give a measure of the strength of dynamic binding in each system. (The comparison is with the corresponding intermolecular process in the presence of 1 M acetate; thus $\Delta\Delta G^*$ is a conservative estimate for a reaction under physiological conditions, where concentrations are much lower.) Simply bringing the reacting groups together on the same molecule makes productive encounters more probable, but the most efficient systems are those in which multivalent bonding eliminates conformational flexibility and a transition state-like geometry is prescribed. This

sort of information has been available for many years for cyclization reactions, but recent work on the efficiency of intramolecular proton transfer reactions reveals a similar pattern. Table 2 shows data for a series of acetal hydrolysis reactions for which intramolecular general acid catalysis is particularly efficient. (Note that for the great majority of general acid or base catalyzed reactions the EMs are of the order of 1 M or less ($\Delta\Delta G^{\neq} \leq 10\,kJ\,mol^{-1}$) and show no strong dependence on structure.)

Table 2. Strength of dynamic binding for intramolecular proton transfer.

	$\Delta\Delta G^{\neq}$ [kJ mol^{-1}]
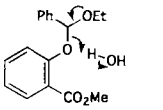	0
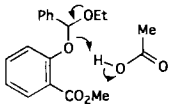	10
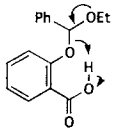	28
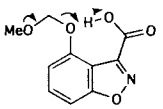	ca. 36

In Table 2 the comparison with the spontaneous hydrolysis reaction gives a quantitative idea of the effectiveness of an external general acid and is a common way of measuring k_{cat}/k_{uncat}. The intrinsic chemical reactivity of the catalytic group depends most strongly on the bond being formed, so varies most for nucleophilic reactions, which are generally the most efficient intramolecular reactions. For example, the $\Delta\Delta G^{\neq}$ parameter for nucleophilic catalysis (Table 1) can be compared with that for the hydrolysis of *p*-nitrophenyl acetate at 25 °C.[38] The strength of dynamic binding is only about 5 kJ mol^{-1} for acetate, which has to displace a more basic leaving group, but rises to 36 kJ mol^{-1} for imidazole and to 47 kJ mol^{-1} for the reaction with the thiolate group of mercapto acetate. So the most efficient intramolecular general acid group of Table 2 is still less efficient than the best intermolecular nucleophiles. The efficient systems in Table 2 all depend on the formation of a strong intramolecular hydrogen bond in the initial product, and, as discussed in Section 3.1, this gives an indication of the potential strength of the binding of the transferred proton in the transition state. The most efficient system in Table 2 (last entry) is hydrolyzed 16 times faster than the corresponding acetal of salicylic acid. The naphthylamine system **7** discussed in Section 3.1 is probably more efficient still in terms of EM.

3.4. Cooperativity in Binding and Catalysis

The simple general conclusions that emerge from work on models are that efficient catalysis depends on tight binding, and that the geometrical requirements are particularly stringent for proton transfer catalysis. The effect can be regarded as an extension to transition states of a familiar phenomenon, which appears as high equilibrium constants (thermodynamic EMs) for certain cyclization reactions,[15] as the chelate effect on the stability of metal complexes,[39] and as cooperativity in binding processes.[30] The stronger the binding interaction between two systems, the stronger a given additional interaction can be, for example between the groups X and Y in Scheme 3; this applies to dynamic as well as to passive binding. Furthermore the effect can be reciprocated—the development of bonding between X and Y can strengthen the original binding interaction. We will go on to discuss some of the most interesting enzyme mimics in the light of these ideas.

4. Enzyme Mimics

Enzyme mimics catalyze reactions by mechanisms that are demonstrably enzyme-like. The minimum requirement is that the reactions concerned should involve an initial binding interaction between the substrate and the catalyst. This gives rise to Michaelis–Menten kinetics, and reactivity is measured in terms of the familiar parameters k_{cat} and K_m. Since these systems are relatively simple, we can discuss the binding of the transition state in terms of Figure 1 (Section 2) and **E** can denote either enzyme or enzyme mimic. The key parameter for discussion is ΔG^0_{TS} [Eqs. (b), (c)]. Further details of the treatment can be found in the excellent review by Tee.[40] ΔG^0_{TS} is the difference in energy between the transition state for the catalyzed reaction and that for the reaction in water (or other aqueous mixed solvent). Since this takes no account of the intrinsic reactivity of the catalytic group,[41] the effective molarity of the catalytic group, which makes this allowance and is a more specific measure of the efficiency of the system at bringing groups together, is also quoted where the data are available and the mechanism is known.

4.1. Catalysis by Cyclodextrins

Cyclodextrins—familiar, readily available, stable, water-soluble cyclic oligomers of α-D-glucose—have proved the most enduringly popular enzyme mimics (Section 3.2.3). Their central hydrophobic cavity is lined with CH groups and glycosidic oxygen atoms, and carries arrays of functional hydroxyl groups on both rims. The full structural formula (e.g. **18** for α-cyclodextrin) is usually represented in simplified form (e.g. **19**), often showing only the single functional group of interest, as in **20**

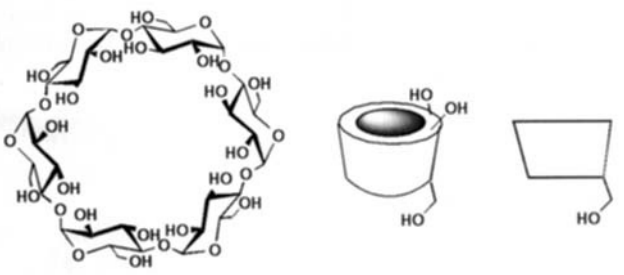

18 **19** **20**

(which like **19** does not specify the oligomer). The torus is slightly more open on the side of the secondary OH groups. This, plus some steric hindrance by the primary 6'-CH_2OH groups on the other face, makes this face more accessible to hydrophobic guests, which can bind in the cavity if they are of the right size.[37]

The unmodified cyclodextrins are themselves good functional enzyme mimics, catalyzing various relatively rapid reactions, like the hydrolysis of nitrophenyl esters, in reactions that show Michaelis–Menten kinetics. The mechanism typically involves nucleophilic attack by the secondary OH groups, which have pK_a values of 12–12.5 and so are present in the reactive anionic form in higher concentration than hydroxide ion. This nucleophilic reaction is inefficient for *p*-substituted benzene derivatives because the ester group is bound near the central axis of the cavity, so that the reacting groups cannot come easily come into close proximity if binding is reasonably tight. In this situation general base catalysis can compete, and is the main route for the reactions of some 4-nitrobenzoate (pNB) esters (**21**, α-cyclodextrin).[42] Though relatively inefficient (EM per OH group < 0.1 M), this general base catalyzed reaction is true

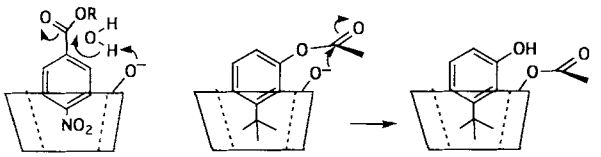

21 **22** **23**

catalysis, at least by one criterion: the catalytic group is unchanged and immediately available for further reaction. The nucleophilic mechanism on the other hand, which is favored for aryl acetates with substituents in the *meta* position of the aromatic ring, gives the acylated cyclodextrin **23** as the initial product. The EM per OH group is less than 1 M even for the most efficient reaction of this sort (**22** → **23**) with *m-tert*-butylphenyl acetate.[37] The subsequent hydrolysis of this intermediate ester, which is usually less reactive than the original substrate, then becomes rate determining. The hydrophobic part of the product is also bound, so product inhibition is a problem. The problem is typically circumvented by using an excess of the cyclodextrin: thus the observed "catalysis" does not involve turnover.

The binding of the substrate is not very strong in these systems (K_{ass} is 295 and 500 M^{-1} for **21** and **23**, respectively, and typically less than 10^3 M^{-1}), so the most obvious way to improve efficiency is to improve binding. This can be done by modification of the cyclodextrin, but the synthesis required can be a major undertaking, and this approach has not produced large rate accelerations.[40] However, cyclodextrins of three sizes are available—α-, β-, and γ-cyclodextrins, with cavity diameters of about 5, 7, and 9 Å, respectively—and these show clear binding specificities. Thus *m-tert*-butylphenyl acetate binds more strongly to β-cyclodextrin, and transition state binding is also improved (Table 3). In fact Tee[40] has shown that a simple linear free relationship exists between substrate and transition state binding for the hydrolysis of series of similar esters, and that transition state binding is more sensitive (slope greater than unity) to structural change for these reactions. This is specific, quantitative evidence justifying the simple approach to improved design, which aims at improved substrate binding. The experimental results described below provide more, convincing evidence.

The easier way to improve binding (not available to enzymes!) is to modify the substrate. This approach is based on the principle that in these simple systems tighter binding should increase the EM of the catalytic hydroxyl groups as well as the passive binding of the substrate, and thus make possible the desired net increase in transition state binding. Most successful are systems based on adamantane and ferrocene, designed by Breslow to optimize fit in the hydrophobic cavity of β-cyclodextrin.[43–45] These systems are based on models of the transition state (tetrahedral carbonyl C atom) in nucleophilic attack by the OH groups of the cyclodextrin on the *p*-nitrophenyl ester group of the substrate; after the reaction the acyl group remains bound, rather than the leaving group. The adamantyl derivative **24** binds strongly but probably mostly unproductively, with the *p*-nitrophenyl ester group inside the cavity,[43] that is, the wrong way around. This is a common problem not unknown in reac-

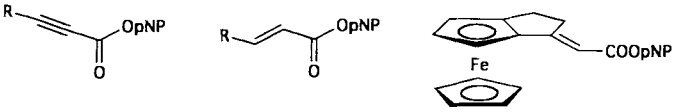

24, R = 1-adamantyl
25, R = ferrocenyl (Fc)

26, R = Fc

27

Table 3. Reactivity and transition state binding data for reactions conducted in the presence of cyclodextrins (CDs).

CD	Substrate	k_{cat} [s^{-1}]	EM [M]	K_{ass} [M^{-1}]	k_{cat}/k_{uncat}	ΔG^0_{ES} [kJ mol^{-1}]	ΔG^0_{TS} [kJ mol^{-1}]
α	pNB-CH_2CF_3[a]	8.8×10^{-4}	<0.1[b]	294	4.4	14	18
α	*m*-*t*BuC$_6$H$_4$OAc[c]	0.13	0.4	500	260	15	29
β	*m*-*t*BuC$_6$H$_4$OAc[c]	0.12	0.3	7700	250	22	36
β	**24**[d]	8.4×10^{-2}	7[e]	3300	2150	20	39
β	**25**[d]	0.4	480[e]	200	1.4×10^5	13	43
β	**26**[d]	0.21	1100[e]	143	7.5×10^5	12	46
β	**27**[d]	9.2×10^{-2}	2×10^4[e]	175	5.9×10^6	13	51
32	**24**[d]	6.8×10^{-3}	–	7×10^4	2.2×10^5	28	58
30	**29**[f]	1.4×10^{-3}	7[g]	5555	360	21	36

[a] At pH 8.6, 16 °C [42]. [b] The authors' figure, after several extrapolations, is about 5 M. [c] At pH 10.6, 25 °C [37]. [d] Measured at 30 °C in DMSO/water (60/40), because of low substrate solubility; pH ≈ 10 (pH ≈ 7 in water). [e] Approximate values, estimated from the original data; considered accurate within an order of magnitude. The figures are more accurate relative to each other. [f] **29** is a phosphodiester. Data measured at 25 °C at the pH-optimum of 6.3. [g] Compared with catalysis by *N*-methylimidazole under the same conditions.

tions of enzymes with synthetic substrates. With ferrocenyl derivatives this problem does not arise; the ferrocene nucleus fits snugly in the cavity of β-cyclodextrin (though this is not reflected in particularly strong "enzyme"–substrate binding). Varying the geometry of a rigidly attached side chain produced the series of esters **25**–**27**, which showed accelerations of 10^5 to 10^6 (Table 3).[43,44] The acceleration comes specifically from improved transition state binding. The relatively weak binding of the ground states of **25**–**27** indicates that dynamic binding—partial formation of a C–O bond—in the transition state reinforces the passive binding of the ferrocenyl unit within the cavity, as discussed in Section 3.4.

The effective molarities attained in the most efficient of these reactions are moderate compared with those available in efficient intramolecular reactions, and not high enough to support catalysis of the hydrolysis of unactivated (ethyl or methyl) esters, or amides near pH 7. To improve reactivity—though not necessarily efficiency—still further, cyclodextrins can be functionalized with groups more reactive at pH 7 than hydroxyl. Most interesting are the more specific enzyme mimics this strategy makes available. The functional groups may be those of coenzymes[45] or match those in the active site of a particular enzyme.[46] Breslow et al. has described β-cyclodextrins **28** carrying two imidazole groups, which may be arranged in three different ways on the rim of a β-cyclodextrin: on glucose units that are adjacent (**AB**), one apart (**AC**), or two apart (**AD**). The imidazole groups on the three isomers have different geometries of interaction with a bound substrate or transition state; if both groups in one isomer are involved in catalysis its efficiency will reflect the strength of dynamic binding. Both imidazoles appear to be involved in the hydrolysis of the (doubly activated) cyclic phosphodiester **29**; one is in the conjugate acid form, as indicated by pH optima near pH 7. The **AB** isomer is clearly the most efficient, by factors of about 4 and 6 and over **AC** and **AD**, respectively (which are themselves not much better than the monoimidazole derivative). A proton inventory study[47] suggests that the mechanism involves concerted general acid and general base catalysis, as sketched in structure **29**/**30**. This mechanism is likely to be involved in the reactions of ribonucleases, but has not been achieved previously in models.

Although catalysis is not particularly efficient (Table 3), the degree of organization implicit in the mechanism shown in **29**/**30** begins to approach that involved in enzyme reactions, and can in principle provide suggestive evidence about geometric preferences, which can be related to fundamental stereoelectronic effects. Thus the higher efficiency of the **AB** isomer of **28** in the hydrolysis of **29** is relevant to the stereoelectronic preferences for displacement at the phosphorus center of phosphodiesters.[48] In the same vein the bisimidazole derivatives **28** also catalyze the enolization of the ketone **31** (R = H), but in this case the **AD** isomer is most effective; this could imply stereoelectronic preferences for the proton transfer (though the reactivity is only about twice that of the monoimidazole-substituted cyclodextrin).[49] This work has recently been extended to the intramolecular aldolization of the related substrate **31** with R = $(CH_2)_4CHO$.[50]

An alternative approach to improved binding, which is normal in interactions between enzyme and substrate, and enzyme and transition state, is to introduce a second binding site. This has the further advantage of making available an improved degree of organization that allows specific provision for stereoelectronic preferences, and provides one of the most promising ways towards more efficient enzyme mimics. Breslow et al.,[51] amongst others,[52] have joined two β-cyclodextrins with various linkers and find that the binding of molecules with two hydrophobic groups is improved, as expected. When the linker includes a catalytic group this improved binding can be converted into catalysis.[53,54] Thus the Cu^{2+} complex **32** (M = Cu^{2+}) is an efficient catalyst for the hydrolysis of the

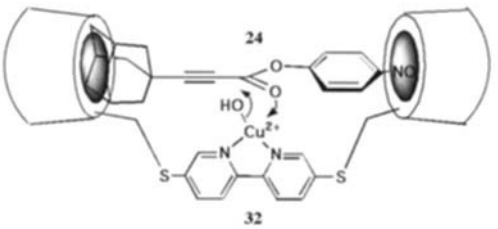

32

adamantanyl ester **24**. This reaction was a problem for the cyclodextrin monomer because the ester was bound the wrong way round (see above).[52] Complex **32** binds both ends of **24**, the ester group is presented to the reactive Cu–OH unit, and the reaction is effectively intramolecular. In contrast to the reaction with free hydroxide, catalysis is most efficient near pH 7, because the pK_a of the bound water is 7.15. The overall process represents true catalysis: not only can the metal exchange the bound carboxylate for water (see Scheme 1), the bifunctional binding of the substrate is sufficiently stronger than that of the two halves produced on ester cleavage that they are released into solution fast enough for turnover to be observed.[52]

4.2. Synthetic Hosts

The challenge of understanding enzyme catalysis and the quest for artificial enzymes have been powerful driving forces for the rapid developments in host–guest chemistry, and in molecular recognition in general. These fields have been thoroughly reviewed. The discussion here is limited to a handful of particularly instructive, and occasionally successful, cases designed specifically as catalysts. These fall naturally into two classes: systems that bind mostly single substrates *and* react with them, and those, which we will discuss first, that bind two (or more) substrates which can *then* react with each other. (More sophisticated still as an enzyme mimic would be a system that binds two separate reactants and actively catalyzes the reaction between them; the reverse of a reaction like the hydrolysis of **24** catalyzed by **32** above would make a good target.)

4.2.1. Synthetic Hosts as Matchmakers

One function of enzymes that can be achieved rather successfully in models is the binding, and thus bringing together of two reactants in the active site. To get them to react together is more difficult, but model builders have reported some notable successes. Nevertheless, to achieve catalysis with turnover remains a major problem. Its origin is the same effect that *permits* turnover in the cleavage of **24** catalyzed by **32**. A simple system that binds the transition state better than the ground state is likely to bind the product at least as well, and the formation of a bond—or a partial bond—between two bound reactants, other things being equal, inevitably strengthens the binding interaction with the host.

β-Cyclodextrin can accommodate small diene–dienophile combinations, and thus transition states for Diels–Alder reactions.[55] Catalysis is not very efficient compared with the already accelerated reaction in water, reflecting relatively weak substrate binding. A synthetic model with much improved binding is the (substrate-free) porphyrin trimer **33** described by Sanders et al.[56] This host binds symmetrical di- and tripyridyl systems very strongly, and substituted monomeric pyridines well enough to accelerate the Diels–Alder reaction between suitable guests when they are bound inside the cavity. The binding controls the stereochemistry of the reaction (shown in **33**) well enough to reverse the normal kinetic selectivity, so that the *exo* adduct is produced up to 1000 times faster than the corresponding *endo* isomer (which is the kinetic product in the absence of the macrocycle). This acceleration corresponds to a reasonable EM of about 20 M, but the system is not catalytic because of product inhibition.

The porphyrin trimer host in **33** similarly catalyzes the acetylation of 4-hydroxymethylpyridine (**34**) by acetylimidazole.[57]

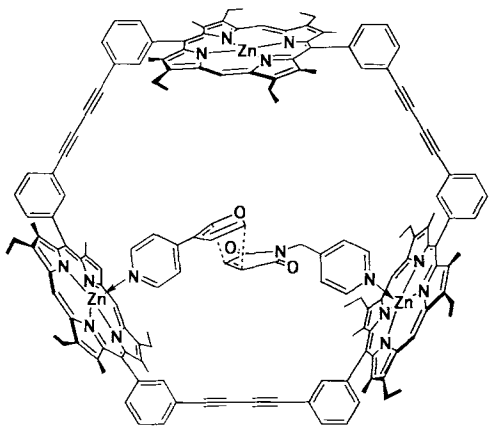

33

Here the two reactants are bound as before, but now the extra bond is present only in the transition state **35** (and the related tetrahedral intermediate). The two products (**36**) are thus not strongly bound, and turnover is possible. Catalysis is not highly efficient; the EM is estimated at 2 M, and the turnover per trimer is about 25 per week (in toluene at 70 °C[58]). But the potential for selective binding of the transition state is illustrated by the strong binding of the dipyridyl **37**, which acts as a competitive inhibitor of the acyl transfer reaction. (K_{ass}(**37**) = 2.3×10^7 M^{-1}; for comparison: K_{ass}(pyridine) = 1.8×10^3 M^{-1}, K_{ass}(*N*-acetylimidazole) = 360 M^{-1}. These values are similar to those in Table 3 obtained for binding to cyclodextrins.) Presumably neither the geometry nor the charge distribution in transition state **35** matches the preferences of the cavity as well as **37**.

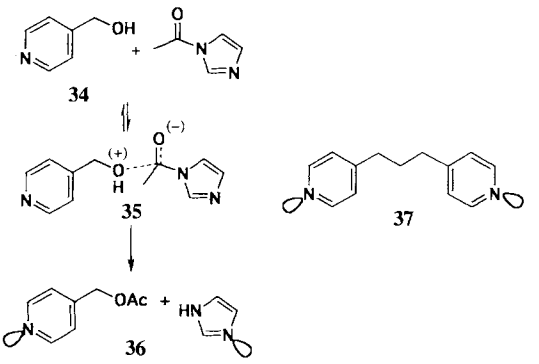

34 **35** **36** **37**

Similar problems arise with Rebek's host **38**, designed to catalyze the aminolysis of the (highly reactive) *p*-nitrophenyl ester

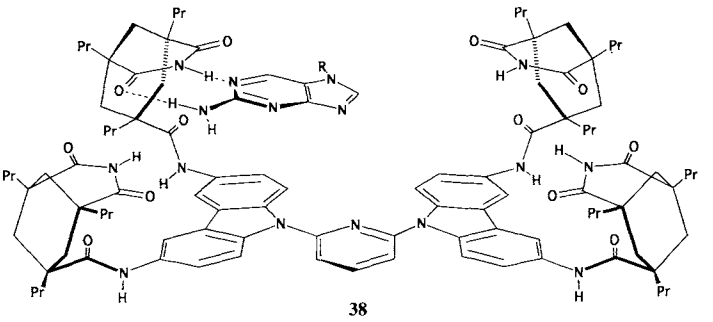

38

39 by 5-aminoadenosine (**40**).[59] **38** and systems like it bind adenine derivatives[60] as shown, with K_{ass} up to 10^6 M^{-1} in chloroform, by a combination of hydrogen bonding to the Kemp triacid imide and dispersion interactions between the aromatic systems (stacking interactions), which would be strengthened in a water-soluble version. The dimeric system **38** (with various central spacers providing a range of convergent binding sites) is designed to bring together two adenine derivatives. **38** is the most effective catalyst of the series in promoting the reaction of **39** with **40**, achieving a 160-fold acceleration (k_{cat}/k_{uncat} at 25 °C in chloroform containing an excess of triethylamine). However, the observed acceleration applies only to the initial stages of the reaction. The amide product, with two adenine groups now covalently attached to each other, binds more strongly than the reactants, thus inhibiting the later stages of the

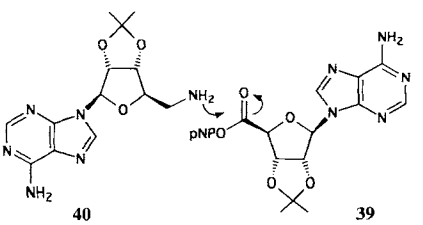

40 **39**

reaction and precluding turnover.[61] Even this fastest reaction is relatively inefficient, with an estimated effective molarity of 35 mM, and it seems evident that the reactants are not bound predominantly in the optimal geometry for reaction.[62] In more recent work on the simple *n*-butylaminolysis of **39** in the presence of a series of functionalized monomeric hosts, an acceleration of up to 100-fold is obtained for the benzoate derivative **41**.[61] The carboxylate group of **41** is evidently better than triethylamine alone in replacing the second molecule of amine involved in intermolecular aminolysis reactions in non-hydroxylic solvents.

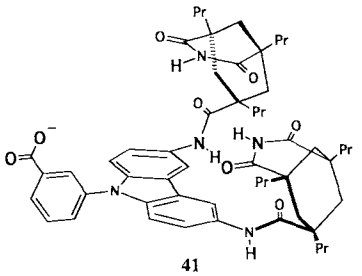

41

One of the biggest challenges in this area is to devise catalysts for the S_N2 reaction, which is known to have strict stereoelectronic requirements for a linear transition state. Since, by definition, a new bond is formed between two reactants, problems with product inhibition are virtually certain. Host **42** was designed by Kelly et al. as a template for reactants that can form three hydrogen bonds to each aminopyridone system.[63] The reactants were the aminomethyl- and bromomethylnaphthyridine derivatives **43** and **44**, respectively,

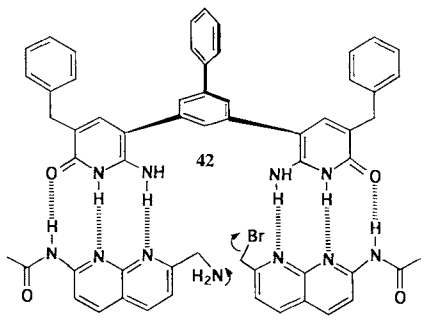

43 **44**

which bind strongly ($K_{ass} > 10^4\ M^{-1}$) to the aminopyridone structure (and turned out to have the advantage that the product ammonium ion precipitated from solution). However, the rate acceleration observed was only sixfold, and turnover could not be demonstrated. This disappointing result points up a number of problems. A minor one is that the two binding sites are identical, allowing nonproductive binding of two identical reactant molecules. Reactivity was indeed improved by the expected factor of 2 by changing one binding site. More fundamental is the conclusion that the host does not bind the transition state effectively, and that what is in effect a cyclization reaction is evidently not favored thermodynamically.

In one system enhanced transition state binding has been shown to provide a significant rate acceleration for an S_N2 reaction. Dougherty and his co-workers[64] have shown that the water-soluble host **45** binds positively charged hydrophobic guests particularly well. For example, K_{ass} for the *N*-methylquinolinium cation **46** is $1.4 \times 10^6\ M^{-1}$, but for the neutral but isosteric 4-methylquinoline it is some 100 times weaker. Macrocycle **45** also catalyzes the formation of **46** from bound quinoline [Eq. (k)]. The reaction with methyl iodide (which is not itself bound) is 80 times faster than in the absence of **45** (Table 4), and in water at pH 9 the transition state is bound almost as tightly as product **46**. Of particular interest is the observation that the transition state is in some cases bound more strongly than product, and this led to the discovery that dealkylation of a cationic aromatic guest can also be catalyzed. For the demethylation of the sulfonium compound **47** [Eq. (l)] in the presence of a modified host k_{cat}/k_{uncat} is 9.[64] Clearly binding does not depend simply on charge: possibly the higher polarizability of the transition state allows a better electronic match to the cavity of the host.

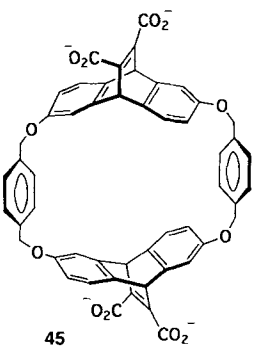

45

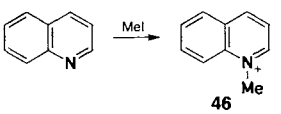

46 (k)

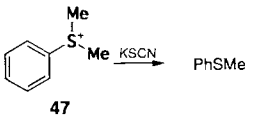

47 (l)

Table 4. Data for the reactivity and transition state binding in reactions with synthetic enzyme mimics.

Host	Reaction (see Text)	k_{cat} [s^{-1}]	EM [M]	k_{cat}/k_{uncat}	$-\Delta G^{\circ}_{TS}$ [kJ mol^{-1}]	$-\Delta G^{\circ}_{TS}$ [kJ mol^{-1}]
33[a]	Diels–Alder	5.8×10^{-4}	20		17.5, 15.5	
33[a]	acetyl transfer	6×10^{-5}	2		18.6, 14.5	
38[a]	ester aminolyse	3.5×10^{-3}	0.035	(160)	ca. 27 (×2)	
42	S_N2	–	–	6	23	27
45	S_N2 (reaction (k))	1.9×10^{-3}	–	80	25	35
45	S_N2 (reaction (l))	1.1×10^{-3}	–	9.4	19	27
49[a]	intramolecular aminolysis of ATP	1.1×10^{-3}	–	500	23	43
50[a]	intramoleular ester thiolysis	8.8×10^{-2}	6760	$>10^4$	22	46
51[a]	intramolecular general base catalysis	1.1×10^{-4}	>20	290	16	30
52	intramolecular ester thiolysis	6×10^{-4}	–	240	>50	65
53	intramolecular ester aminolysis	8.5×10^{-3}	–	472	18	33
Oxaldie	decarboxylation	6.7×10^{-3}		10^3–10^4	13	33±3

[a] Substrate-free host compound.

4.2.2. Synthetic Hosts with Built-In Functionality

A rational approach to catalyst design is to optimize the binding arrangements for the substrate of interest, then add the catalytic functionality in the right place. In practice this is not so easy, because in the dynamic situation in solution guests often do not bind exclusively where the designer plans (or even suspects). But the approach has had some notable successes, based—as would be expected—on multiple host–guest binding interactions. Early attempts based on crown ethers and cryptands[65] often achieved significant rate accelerations, though not high efficiency or true catalysis, when a reactive nucleophile like thiolate was built in. Recent trends are typified by dithiol **48** devised by Koga et al.,[66] which is based on a simpler dithiol that can be used to synthesize peptide bonds.[67]

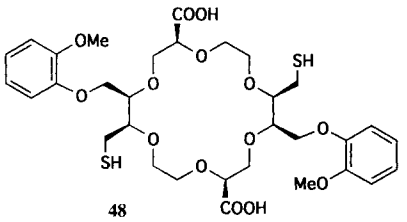

48

Early work, by Cram and Lehn in particular, had shown that crown ethers bind the ammonium group of amino acid derivatives, and that bound activated esters will acylate groups like SH attached to the crown. Loading **48** with first one then a second α-amino acid (as thioesters) allows (not very efficient) intramolecular aminolysis and the formation of the dipeptide, as the thioester. The COOH groups in **48** were added in the hope that they would catalyze the slow intramolecular aminolysis step. In fact they quenched it.

Perhaps the most elegant system of this sort is Lehn's cryptand **49**, which binds polyphosphate anions by a combination of electrostatic interactions and multiple hydrogen bonds. The cryptand is nucleophilic by virtue of the ring nitrogens, only four of which are protonated at pH 7, and can catalyze in vitro the key biological phosphate transfer reaction from ATP by way of an intermediate phosphoramidate [Eq. (m)].[68] The hydrolysis of ATP is catalyzed by this mechanism and accelerated by a factor of 500 at pH 7. This system remains one of the most efficient enzyme mimics (Table 4).

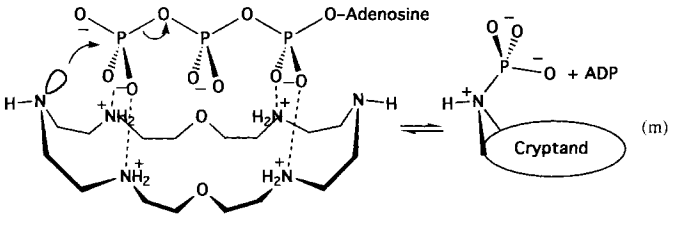

49 (m)

Alone, even multiple hydrogen bonding is not enough to bind a substrate in water, but H-bonding hosts with built-in functionality can work well in organic solvents. Hamilton et al. has added SH groups to his hydrogen-bonding receptors, which bind barbiturates in a well-defined orientation. The dithiol **50** binds and rapidly cleaves the 2,4-dinitrophenyl ester as shown ($k_{cat}/k_{uncat} > 10^4$, in CH_2Cl_2 at 25 °C) in the presence of 2,6-lutidine as a nonnucleophilic base.[69] This is not catalysis—the receptor is used in considerable excess and the product is its thioester—but the reaction is efficient, with an EM of 6760 M for the SH groups as nucleophiles. This is consistent with both the basic requirement for tight, properly orientated binding, and with the observation that SH groups attached by more flexible linkers are much less efficient.[69]

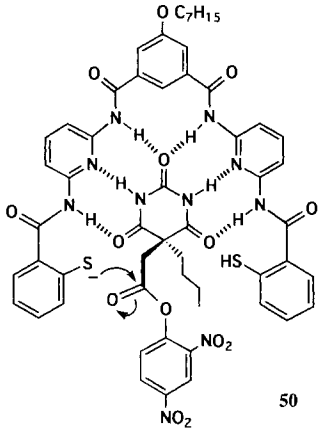

50

Similar principles were considered in the design of new enzyme mimics that facilitate phosphodiester cleavage. The most highly developed is the host compound in **51**, which binds phosphodiester anions with its two alkylguanidinium groups by hydrogen bonding reinforced by electrostatic attraction. This interaction mimics the well-established role of the alkylguanidinium group of arginine at the active sites of various nucleases. The model reaction is the intramolecular cyclization of *p*-nitrophenyl 2-hydroxypropyl phosphate. The phosphate group is doubly activated by virtue of the good leaving group and the intramolecular nucleophile (itself a model for the nucleophilic 2′-hydroxyl group of ribose in the ribonuclease reaction). The reaction requires a general base. The most effective of several tried[70] was the dimethylaminoethyl group shown in **51**, which improves the acceleration observed from 14- to 290-fold (in acetonitrile at 25 °C, in the absence of the built-in tertiary amino group but with added 2,6-lutidine). The EM for the dimethylamino group (correcting for the difference in pK_a between the catalytic group and lutidine using pK_a values in water and a β-value of 0.67[71]) is over 20 M, which would be unusually good for simple intramolecular general base catalysis by the dimethylaminoethyl group. But the monocations of ethylene diamines are known to be particularly effective catalysts for the cleavage of phosphodiesters, probably by a mechanism involving an electrostatic contribution to dynamic binding.[72]

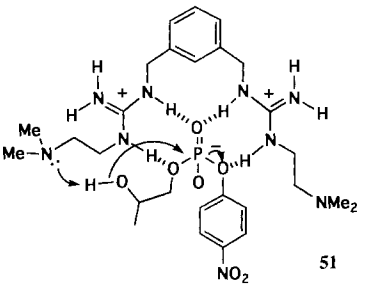

51

Perhaps the most highly developed synthetic hosts are Cram's spherands, based on three urea subunits linked by electron-rich anisyl rings. These hosts bind ammonium ions such as $Me_3CNH_3^+$ in a tripodal orientation to the three urea C=O groups, as shown by crystal structures of complexes. Binding can be very strong, with K_{ass} values up to 10^9 M^{-1},[73] and attaching a carefully placed hydroxyl group gave system **52**, which was a far better nucleophile towards the bound *p*-nitrophenyl ester of L-alanine **53** than the model compound **54** under the same conditions. (Adding an imidazole group in an attempt to generate a more faithful chymotrypsin mimic gave a more reactive system, but now the imidazole acted as a nucleophile rather

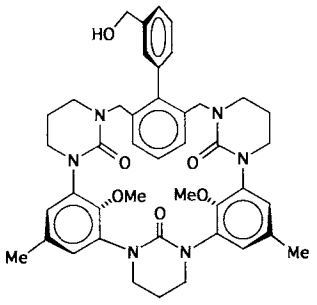

52

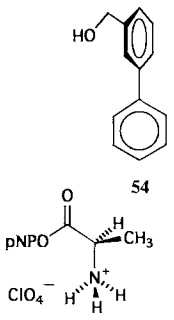

54

53

than a general base catalyst for the hydroxide reaction. This will always happen unless the reaction with the better nucleophile is prevented by the geometry of the system.) The rate accelerations observed in this work are impressive: under the given conditions $(k_{cat}/k_{uncat})K_{ass}$ is of the order of 10^{11} for the second-order reaction. (Here, too, **52** is not a true catalyst: it is used in excess and turnover is not possible because the reactive OH group is esterified in the reaction.) An effective molarity cannot be estimated, because the reaction within the complex involves the anion of the benzylic alcohol (pK_a unknown), whereas the comparison reaction with **54** was not detectable under the conditions ($CDCl_3$ containing 0.15% DMF, buffered with a tertiary amine and its salt). So the figure of 10^{11} comes from the low estimate of the upper limit for this reaction and the high value of K_{ass}. However—as Cram et al. make clear[74]—the very high rate acceleration does not mean that the system shows high absolute reactivity, for reasons already discussed.[58] To put the figures in perspective, the absolute rate of the reaction of the bound substrate **53** (k_{cat}) is reached for the alkaline hydrolysis in water of this reactive ester between pH 7 and 8.[75]

Diederich et al.[76] have reported work with phenol-capped cationic cyclophanes similar to macrocycle **55** with R,R = $-CH_2NEtCH_2-$, which are acylated by bound naphthyl acetates in predominantly aqueous solutions. At pH 8 the most effective system gives a ratio $(k_{cat}/k_{uncat})K_{ass}$ of about 6×10^5. This value is smaller than the figures attained by Cram et al. discussed above but reflects the somewhat higher k_{cat} values. (K_{ass}, at about 1500 M^{-1}, is much less favorable than that for the binding of amino acid esters by **52** in $CDCl_3$.) The phenolate anion serves as the nucleophile, and deacylation is fast enough at pH 8 and low host concentration for some turnover to be observed. The reaction in the presence of 10^{-5} M host is 20–30% faster than the background reaction.

As found by Cram et al., the nucleophilic hydroxyl group is not a great asset in these model systems, and the most effective catalyst of this sort, the anionic macrocycle **55** (R = COO^-), has two imidazoles in place of the phenol. Both binding and solubility are reduced, so that saturation kinetics are no longer observed. But the hydrolysis of **56** (in phosphate buffer, pH 8, with 25% DMSO) is now some ten times faster than the background rate for the hydrolysis of this ester,[77] corresponding to an EM of 1.3 M per imidazole.

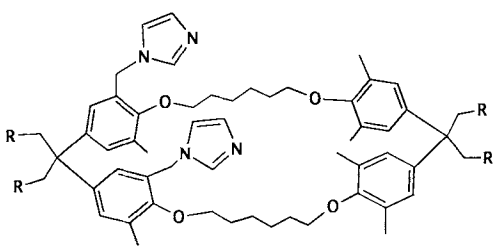

55

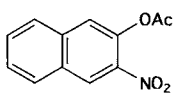

56

Diederich et al. have also attached the functional groups of coenzymes to their cationic cyclophanes to produce representative members of a major class of enzyme mimics of this sort.[78] For example, the thiazolium heterocycle of thiamine has been attached to cyclodextrins,[79] crown ethers,[80] and cyclophanes; flavin has been built in to a crown ether;[81] and pyridoxal, which was attached with long alkyl chains in a supramolecular assembly with a synthetic peptide–lipid bilayer containing histidine, has been shown to catalyze transamination.[82] These systems show accelerations ranging from a few percent to several hundred-fold, but the reactions are multistep and catalytic efficiency is not readily analyzed in detail.

A more specific use of synthetic peptides as catalysts has been reported by Benner and his group,[83] who based the design of a synthetic decarboxylase on the known properties of proteins and the mechanism of amine-catalyzed decarboxylation of β-keto acids. Their enzyme mimics are 14-residue peptides (oxaldie 1 and 2, Scheme 4) based on leucine and lysine. The amino acid

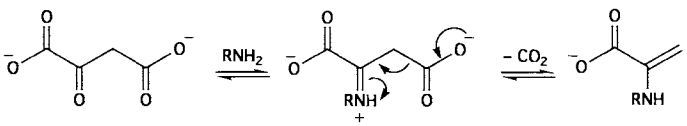

Oxaldie 1: H_2NLeuAlaLysLeuLeuLysAlaLeuAlaLysLeuLeuLysLysCONH$_2$

Scheme 4. Decarboxylation of oxaloacetate catalyzed by an enzyme mimic. R = lysine side chain.

sequence is intended to favor α-helix formation, and thus the mimics are expected to exist in water in protein-like conformations, with a hydrophobic core and a hydrophilic exterior. They catalyze the decarboxylation of oxaloacetate by the expected mechanism shown; the cationic lysine side chains are presumably involved in binding the carboxylates of both the substrate and transition state (acetoacetate, with a single COO^- group, is not a substrate). Michaelis–Menten kinetics are observed and imine formation is 10^3 to 10^4 times faster than with simple amine catalysts. Activity does indeed seem to depend on the degree of α-helix formation. Given the relative ease of peptide synthesis, and current progress in our understanding of protein folding, we may expect to see renewed activity in the area of designed peptide catalysts.

4.3. Catalytic Antibodies

Catalytic antibodies (or abzymes)[84] are currently the most successful enzyme mimics, though they too fall far short of enzymes in terms of catalytic efficiency. They are proteins raised in a biological system specifically against transition state analogues (haptens) for the reaction of interest. Consequently, the problems of design and synthesis involve in principle only small molecules on a scale familiar to the organic chemist. Under the right conditions the immune system responds to the transition

state analogue by producing vast numbers of antibodies that recognize and bind to it—literally an exercise in the molecular recognition of transition states. The primary limitations are the accuracy of the hapten as a model for the transition state and the effectiveness of screening the large numbers of antibodies produced for catalysis. (Standard immunological methods screen very efficiently for *binding*.)

Though their specificity and potentially regio- and enantioselectivity are good, current catalytic antibodies are not much more efficient than other enzyme mimics. They are quite good at catalyzing easy reactions, like the hydrolysis of *p*-nitrophenyl esters, and have been reported to catalyze the hydrolysis of benzyl[85] and other alkyl esters,[86] but not that of ordinary amides at a useful rate.[87] Catalysis of the hydrolysis of activated esters is rather reliably obtained with suitable, usually phosphonate haptens (e.g. **57**), which model the structure of the tetrahedral transition states [Eq. (n)] involved. In this rather

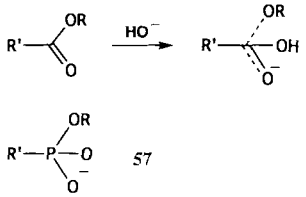

(n)

57

basic strategy the nucleophile comes from the solvent and the hapten is a rather approximate analogue as far as charge is concerned. For this reason more efficient catalysis should be possible when both reactants are recognized and bound, or when a nucleophilic group is located in the abzyme binding site.

Antibodies designed to catalyze the formation of a bond between two bound substrates suffer from the same problems of product inhibition as other enzyme mimics. Thus Schultz's antibodies raised against hapten **58** catalyzed transesterification of the activated ester **60** with **59** (when T = thymidyl the reaction

Hapten:

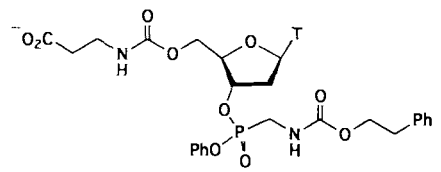

58

Substrates:

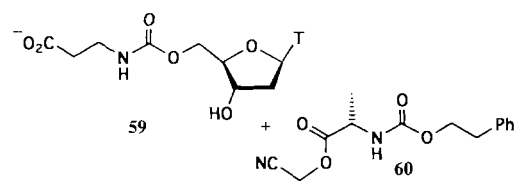

59 60

is a model for the aminoacylation of tRNA)[88] with high efficiency (EM $\approx 10^5$ M). But the product ester binds strongly to the antibody ($K_{diss} = 18$ nM) and thus inhibits turnover. The comparison with Rebek's synthetic enzyme mimic **38**, which catalyzes an ester aminolysis reaction between two very similar reactants, shows that the EM is some 10^6 times higher for the abzyme-catalyzed reaction (Tables 4 and 5). The product amide—and no doubt the transition state also—is bound much more weakly by the synthetic host.

This problem can be avoided by careful hapten design in favorable cases. Thus Hilvert's antibody catalyzing the Diels–Alder reaction of tetrachlorothiophene dioxide **61** and *N*-ethylmaleimide achieves turnover because the initial adduct **62** rapidly loses SO_2 to give the bicyclic product **63**.[89] Catalysis results simply from productive binding (an EM > 110 M is estimated). The hapten **64** is a reasonable transition state analogue but geometrically very different from the final product.

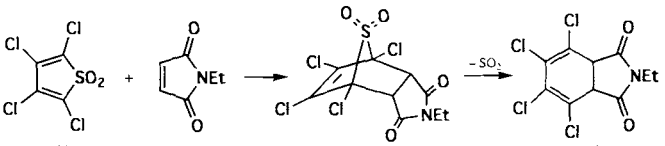

61 62 63

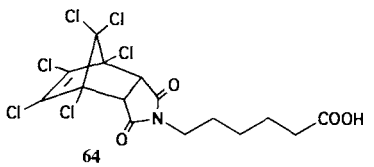

64

More ambitious systems with catalytic groups built in can in principle be obtained by careful hapten design. Building a charged group into the hapten could—and occasionally does—elicit a charged group of opposite sign in the antibody, which might act as a general acid or base, or as a nucleophile. The cleavage of compound **65**[90] is of particular interest because it involves general base catalysis, typically an inefficient intramolecular process, as already discussed. Like the heterocyclic substrate, the hapten is [5.6]-fused, and as a 2-aminobenzimidazole it is protonated at physiological pH and thus elicits a complementary anionic group as part of the binding site of antibodies generated against it. Two antibodies out of >1000 that bound the hapten catalyzed the E2 reaction of substrate **65** [Eq. (o)] with notably high efficiency (EM = 5000–6000 M, with

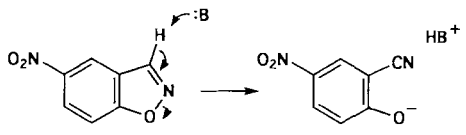

(o)

65

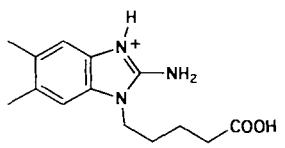

66

proton transfer rate-determining) and good turnover, since the product is geometrically and electrostatically very different from the hapten.

An alternative strategy is to introduce a functional group into an existing catalytic antibody by protein engineering. As might be expected, site-directed mutagenesis of enzymes does not nor-

mally improve the efficiency of reactions with natural substrates. But catalytic antibodies, which have no significant evolutionary history and rarely even a functional group in the active site, are expected to be more promising candidates. The evidence available is insufficient to confirm this judgement. Benkovic and his group used site-directed mutagenesis to probe the mechanism of action of their antibody 43C9, which accelerates the hydrolysis of a *p*-nitroanilide by a factor of 10^6.[91] The mechanism is thought to involve nucleophilic catalysis by a histidine imidazole, and indeed replacing the relevant histidine by glutamine eliminates catalysis. Of seven mutations, made for various reasons, none improved catalytic efficiency.

In a similar study Schultz and his co-workers[92] used a mechanistically simpler antibody, which was known to bind phosphorylcholine (**67**) and to catalyze the hydrolysis of the carbonate **68**. Of seven mutants, one, in which a tyrosine residue shown not to be catalytically active was replaced by imidazole, led to an eightfold increase in k_{cat}. The new functionality is thought not to be ideally placed for catalysis, but it is a good nucleophile close enough to attack the C=O group of the substrate (EM ≈ 11 M).

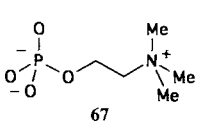

67

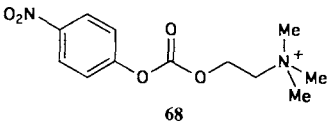

68

Finally, just as with a synthetic host, it is possible to introduce a functional group chemically into an abzyme. To do this with precision requires a good understanding of the three-dimensional arrangements at the binding site. But targeting this site is not difficult in principle by using affinity labeling. Pollack and Schultz used this technique to introduce a nucleophilic thiol group into the binding site of an antibody that binds 2,4-dinitrophenyl compounds, and they were able to attach an imidazole to the SH group by disulfide exchange.[93] The semisynthetic catalytic antibody produced was a rather good catalyst for the hydrolysis of activated esters with a suitably positioned 2,4-dinitrophenyl group (Table 5). The data in Tables 4 and 5 show that catalytic antibodies are generally more efficient than synthetic enzyme mimics, when some of the best catalysts of each type acting on similar substrates are compared (absolute values of k_{cat} and k_{cat}/k_{uncat}). Both sorts of catalysts suffer from similar problems of product inhibition, so that turnover is currently a major limitation to their utility. This limitation is magnified by both the absolute rates and the rate accelerations that can be achieved. Thus transition state binding for the hydrolysis of the unactivated amide in Table 5 is almost as good as that achieved by Schultz's mutant enzyme for the hydrolysis of the carbonate ester **68**. But the amide is so intrinsically unreactive that the actual rates obtained are hardly detectable.

5. Summary and Outlook

The comparison of enzyme mimics with real enzymes is sobering. Table 6 presents a small set of data taken from a recent paper of Radzicka and Wolfenden.[94] The k_{cat} values are larger by at least two orders of magnitude than those in Table 5 for catalysis by abzymes. The rates of the enzyme-catalyzed reactions are in the practically useful range and may not seem too great a challenge for improved design of enzyme mimics. But the big difference lies in the values of k_{cat}/k_{uncat} and transition state stabilization ($-\Delta G^0_{TS}$): for slow reactions—like those of the extraordinarily stable groups of structural biology (see Section 1)—the enzyme reactions are more efficient by up to ten orders of magnitude in k_{cat}/k_{uncat} and 60 kJ mol^{-1} in transition state binding.[95]

This is a measure of the intellectual challenge of this field of research. For some practical applications, particularly in synthesis, the prospect of useful catalysts is by no means so remote. We have concentrated in this review on systems where reliable kinetic information is available, rather than on reactions of

Table 6. Selected data on the reactivity and transition state binding in enzyme-catalyzed reactions [94].

Enzyme	k_{cat} [s^{-1}]	k_{cat}/k_{uncat}	$-\Delta G^0_{ES}$ [a] [kJ mol^{-1}]	$-\Delta G^0_{TS}$ [kJ mol^{-1}]
OMP decarboxylase	39	1.4×10^{17}	35	133
staphylococcal nuclease	95	5.6×10^{14}	29	113
adenosine deaminase	370	2.1×10^{12}	26	96
carboxyl peptidase A	578	1.9×10^{11}	23	88
triosephosphate isomerase	4300	10^9	27	78
carboanhydrase	10^6	7.7×10^6	12	51
chorismate mutase	50	1.9×10^6	25	61

[a] Since the values are based on K_m values, they cannot be compared directly with most of the data in Tables 3–5.

Table 5. Data for the reactivity and transition state binding in reactions with abzymes.

Reaction (see Text)	k_{cat} [s^{-1}]	EM [M]	k_{cat}/k_{uncat}	$-\Delta G^0_{ES}$ [kJ mol^{-1}]	$-\Delta G^0_{TS}$ [kJ mol^{-1}]	Lit.
carbonate (**67**) hydrolysis	7×10^{-3}		770	21	37	[96]
carbonate (**67**) hydrolysis by mutant abzyme	0.095	11	10^4	16	39	[92]
phenyl ester hydrolysis	3.72		2.2×10^4	20	45	[97]
phenyl acetate hydrolysis	8.2×10^{-2}		2.5×10^5	19	50	[98]
p-nitrobenzyl ester hydrolysis	0.12		2.6×10^5	20	51	[85]
aryl arylacetate ester hydrolysis	20		6.2×10^6	16	55	[99]
ester exchange (**59** + **60**)	0.24	5.5×10^4		17.8, 20.5	47	[88]
hydrolysis of unactivated amide	1.7×10^{-7}		132	19	34	[87]
hydrolysis of activated amide	0.46		2.5×10^5	19	50	[91]
proton transfer from C atom	0.66	6100	2.1×10^4	22	47	[90]

immediate interest to the organic chemist. But most useful synthetic reactions are by definition not very slow, and catalysts that lead to excellent chemo- and regioselectivity, and even good diastereo- and enantioselectivity must be of potential interest.[100] Synthetically useful differences between pathways rely on only rather small differences in activation energy (about 7 kJ mol^{-1} for a 95% preference). So enzyme mimics, and especially antibody catalysis, remains an area of definite promise and of much current activity.

Received: July 21, 1995 [A 1241E]
German version: *Angew. Chem.* **1996**, *108*, 770–790

[1] A. R. Fersht, *Enzyme Structure and Mechanism*, 2nd ed., Freeman, New York, **1985**.
[2] A. J. Kirby, *Angew. Chem.* **1994**, *106*, 573–576; *Angew. Chem. Int. Ed. Engl.* **1994**, *33*, 551–553.
[3] M. Z. Atassi, T. Manshouri, *Proc. Natl. Acad. Sci. USA* **1993**, *90*, 8282–8286.
[4] D. R. Corey, M. A. Phillips, *Proc. Natl. Acad. Sci. USA* **1994**, *91*, 4106–4109.
[5] J. A. Wells, W. J. Fairbrother, J. Otlewski, M. Lagowski, J. Burnier, *Proc. Natl. Acad. Sci. USA* **1994**, *91*, 4110–4114.
[6] B. W. Matthews, C. S. Craik, H. Neurath, *Proc. Natl. Acad. Sci. USA* **1994**, *91*, 4103–4105. Coincidentally, but also significantly, the second example of remarkably effective catalysis of amide hydrolysis discussed in ref. [2] has also recently been shown not to be true catalysis; W. K. Fife, S. Liu, *Angew. Chem.* **1995**, *107*, 2946–2948; *Angew. Chem. Int. Ed. Engl.* **1995**, *34*, 2718–2720.
[7] This very general statement, due originally in this form to Pauling and refined by Jencks [8], is now widely accepted, though—as one would hope—not uncritically [9].
[8] W. P. Jencks, *Catalysis in Chemistry, Enzymology*, McGraw-Hill, New York, **1969**.
[9] F. M. Menger, *Biochemistry* **1992**, *31*, 5368–5373.
[10] A. J. Kirby, *Philos. Trans. R. Soc. London A* **1993**, *345*, 67–76.
[11] A. R. Fersht, *Biochemistry* **1987**, *26*, 8031–8037.
[12] A. J. Kirby, P. W. Lancaster, *J. Chem. Soc. Perkin Trans. 2* **1972**, 1206.
[13] K. N. Dalby, A. J. Kirby, F. Hollfelder, *J. Chem. Soc. Perkin Trans. 2* **1993**, 1269.
[14] Intramolecular reactions may be catalytic, in the sense that they accelerate the reaction and the catalytic group is eventually regenerated unchanged, but they do not normally achieve turnover.
[15] A. J. Kirby, *Adv. Phys. Org. Chem.* **1980**, *17*, 183–278.
[16] W. P. Jencks, *Adv. Enzymol.* **1975**, *37*, 219.
[17] F. M. Menger, *Acc. Chem. Res.* **1985**, *18*, 28–33.
[18] The entropy term is always more favorable for an intramolecular process (the basis of the description of enzymes as "entropy traps"). But this factor is common to all intramolecular processes and does not vary a great deal for many favorable reactions. In contrast, the entbalpy term can depend strongly on the way the reacting groups are brought together. See L. Mandolini, *Adv. Phys. Org. Chem.* **1986**, *22*, 1.
[19] A. J. Kirby, G. J. Lloyd, *J. Chem. Soc. Perkin Trans. 2* **1976**, 1753.
[20] A. J. Kirby, J. M. Percy, *J. Chem. Soc. Chem. Commun.* **1987**, 1774; *J. Chem. Soc. Perkin Trans. 2* **1989**, 907–912; A. J. Kirby, A. Parkinson, *J. Chem. Soc. Chem. Commun.* **1994**, 707–708.
[21] J. A. Landro, J. A. Gerlt, J. W. Kozarich, C. W. Koo, V. J. Shah, G. L. Kenyon, D. J. Neidhart, S. Fujita, J. R. Clifton, G. A. Petsko, *Biochemistry* **1994**, *33*, 635–643; G. L. Kenyon, J. A. Gerlt, G. A. Petsko, J. W. Kozarich, *Acc. Chem. Res.* **1995**, *28*, 178–186.
[22] J. A. Gerlt, P. G. Gassman, *J. Am. Chem. Soc.* **1993**, *115*, 11552–11568.
[23] A. J. Kirby, F. O'Carroll, *J. Chem. Soc. Perkin Trans. 2* **1994**, 649–656.
[24] A. J. Kirby, R. S. McDonald, C. R. Smith, *J. Chem. Soc. Perkin Trans. 2* **1974**, 1495.
[25] A. J. Kirby, G. J. Lloyd, *J. Chem. Soc. Perkin Trans. 2* **1974**, 637.
[26] A. J. Kirby, *Crit. Rev. Biochem.* **1987**, *22*, 283.
[27] This sort of concerted process was often described and sometimes tested in the early research on the subject, but in practice the two catalytic groups generally turned out to act on separate steps of model reactions. With the availability of systems showing more efficient general acid or base catalysis it becomes possible to design a new generation of test systems containing unactivated groups.
[28] I. Bertini, H. B. Gray, S. J. Lippard, J. S. Valentine, *Bioinorganic Chemistry*, Interscience Books, Mill Valley, CA, **1994**. For a more focused review see: J. Chin, *Acc. Chem. Res.* **1991**, *24*, 145–152.
[29] R. Taylor, O. Kennard, *Acc. Chem. Res.* **1984**, *17*, 320–326.
[30] T. E. Creighton, *Proteins*, 2nd ed., Freeman, New York, **1993**.
[31] F. Garcia-Tellado, S. Goswami, S.-K. Chang, S. J. Geib, A. D. Hamilton, *J. Am. Chem. Soc.* **1990**, *112*, 7393–7394.
[32] E. Fan, S. A. Vanarman, S. Kincaid, A. D. Hamilton, *J. Am. Chem. Soc.* **1993**, *115*, 369–370.
[33] S. C. Zimmerman, T. J. Murray, *Philos. Trans. R. Soc. London A* **1993**, *345*, 49–56. The importance of the secondary electrostatic interactions thought to be responsible for these differences was identified computationally: J. Pranata, S. G. Wierschke, W. L. Jorgensen, *J. Am. Chem. Soc.* **1991**, *113*, 2810–2819.
[34] D. Bashford, *Curr. Opin. Struct. Biol.* **1991**, *1*, 175–184.
[35] N. Muller, *Acc. Chem. Res.* **1990**, *23*, 23–28.
[36] Hydrogen bonding and electrostatic interactions are stronger in the absence of water solvent, hydrophobic interactions are stronger when it is present [8].
[37] For nicely complementary accounts of the basics of this area see: M. Komiyama, M. L. Bender, *Cyclodextrin Chemistry*, Springer, Berlin, **1978**; F. Cramer in *The Lock and Key principle* (Ed.: J.-P. Behr), Wiley, Chichester, **1994**, p. 1.
[38] W. P. Jencks, J. Carriuolo, *J. Am. Chem. Soc.* **1960**, *82*, 1778–1786.
[39] R. Breslow, *Rec. Trav. Chim.* **1994**, *113*, 493–498.
[40] O. S. Tee, *Adv. Phys. Org. Chem.* **1994**, *29*, 1.
[41] This difference is implicit in the different scales of Tables 1 and 2, as already discussed.
[42] M. Komiyama, S. Inoue, *Bull. Chem. Soc. Jpn.* **1980**, *53*, 3334–3337; M. Komiyama, H. Hirai, *Chem. Lett.* **1980**, 1251–1254.
[43] R. Breslow, M. F. Czarniecki, J. Emert, H. Hamaguchi, *J. Am. Chem. Soc.* **1980**, *102*, 762–770.
[44] R. Breslow, G. Trainor, A. Ueno, *J. Am. Chem. Soc.* **1983**, *105*, 2739–2744.
[45] R. Breslow, *Adv. Enzymol.* **1986**, *58*, 1–60; D. Hilvert, R. Breslow, *Bioorg. Chem.* **1984**, *12*, 206; R. Breslow, P. J. Duggan, J. P. Light, *J. Am. Chem. Soc.* **1992**, *114*, 3982–3983.
[46] V. T. D'Souza, M. L. Bender, *Acc. Chem. Res.* **1987**, *20*, 146–152.
[47] E. Anslyn, R. Breslow, *J. Am. Chem. Soc.* **1989**, *111*, 8931–8932.
[48] R. Breslow, *Acc. Chem. Res.* **1987**, *20*, 146–152.
[49] R. Breslow, A. Graff, *J. Am. Chem. Soc.* **1993**, *115*, 10988–10989.
[50] J. M. Desper, R. Breslow, *J. Am. Chem. Soc.* **1994**, *116*, 12081–12082.
[51] R. Breslow, N. Greenspoon, T. Guo, R. Zarzycki, *J. Am. Chem. Soc.* **1989**, *111*, 8296–8297; R. Breslow, S. Chung, *ibid.* **1990**, *112*, 9659–9660.
[52] I. Tabushi, Y. Kuroda, K. Shimokawa, *J. Am. Chem. Soc.* **1979**, *101*, 1614; K. Fujita, S. Ejima, T. Imoto, *J. Chem. Soc. Chem. Commun.* **1984**, 1277; T. Akiike, Y. Nagano, Y. Yamamoto, A. Nakamura, H. Ikeda, A. Ueno, F. Toda, *Chem. Lett.* **1994**, 1089–1092.
[53] R. Breslow, B. Zhang, *J. Am. Chem. Soc.* **1992**, *114*, 5882–5883.
[54] T. Akiike, Y. Nagano, Y. Yamamoto, A. Nakamura, H. Ikeda, A. Ueno, F. Toda, *Chem. Lett.* **1994**, 1089–1092.
[55] D. Rideout, R. Breslow, *J. Am. Chem. Soc.* **1980**, *102*, 7816–7817; H.-J. Schneider, N. K. Sangwan, *Angew. Chem.* **1987**, *99*, 924–925; *Angew. Chem. Int. Ed. Engl.* **1987**, *26*, 896–897.
[56] C. J. Walter, H. L. Anderson, J. K. M. Sanders, *J. Chem. Soc. Chem. Commun.* **1993**, 458.
[57] L. G. Mackay, R. S. Wylie, J. K. M. Sanders, *J. Am. Chem. Soc.* **1994**, *116*, 3141–3142.
[58] Note the slow absolute rate: most synthetic hosts are only soluble in organic solvents, and ionic reactions—especially those involving proton transfers—are generally much slower than in water. Efficiency can be measured in the usual way, but a very low k_{uncat} can mean that even highly efficient catalysis may not bring the absolute rate up to the level of k_{uncat} in water.
[59] I. Huc, J. Pieters, J. Rebek, Jr., *J. Am. Chem. Soc.* **1994**, *116*, 10296–10297.
[60] M. M. Conn, G. Deslongchamps, J. de Mendoza, J. Rebek, Jr., *J. Am. Chem. Soc.* **1993**, *115*, 3548–3557.
[61] R. J. Pieters, I. Huc, J. Rebek, Jr., *Chem. Eur. J.* **1995**, *1*, 183–192.
[62] Menger et al. have questioned the formation of the termolecular complex in studies of a system closely related to substrate-free **38**. These authors have demonstrated accelerated aminolysis for an active naphthoate ester that cannot form hydrogen bonds as adenine can: F. M. Menger, A. V. Eliseev, N. A. Khanjin, M. J. Sherrod, *J. Org. Chem.* **1995**, *60*, 2870–2878.
[63] T. R. Kelly, G. J. Bridger, C. Zhao, *J. Am. Chem. Soc.* **1990**, *112*, 8024–8034.
[64] A. McCurdy, L. Jimenez, D. A. Stauffer, D. A. Dougherty, *J. Am. Chem. Soc.* **1992**, *114*, 10314–10321.
[65] For a recent review see: A. M. Reichwein, W. Verboom, D. N. Reinhoudt, *Rec. Trav. Chim.* **1994**, *113*, 343–349.
[66] S. Sasaki, Y. Takase, K. Koga, *Tetrahedron Lett.* **1990**, *30*, 6051.
[67] K. Koga, *Pure. Appl. Chem.* **1988**, *60*, 539–548.
[68] M. W. Hosseini, J.-M. Lehn, K. C. Jones, K. E. Plute, K. B. Mertes, M. P. Mertes, *J. Am. Chem. Soc.* **1989**, *111*, 6330–6335.
[69] P. Tecilla, V. Jubian, A. D. Hamilton, *Tetrahedron* **1995**, *51*, 435–448.
[70] P. Tecilla, A. Veronese, R. P. Dixon, A. D. Hamilton, *Angew. Chem.* **1995**, *107*, 1334–1337; *Angew. Chem. Int. Ed. Engl.* **1995**, *34*, 1237–1239.
[71] A. M. Davis, A. D. Hall, A. Williams, *J. Am. Chem. Soc.* **1988**, *110*, 5105–5108.
[72] K. N. Dalby, F. Hollfelder, A. J. Kirby, *J. Chem. Soc. Chem. Commun.* **1992**, 1770; *Pure Appl. Chem.* **1994**, *66*, 687–694.
[73] D. J. Cram, J. M. Cram, *Container Molecules and Their Guests*, Royal Society of Chemistry, Cambridge, **1994**, Chapter 4.

[74] D. J. Cram, H. E. Katz, I. B. Dicker, *J. Am. Chem. Soc.* **1984**, *106*, 4987–5000.
[75] Estimate based on the data of G. Aksnes, P. Frøyen, *Acta Chem. Scand.* **1967**, *21*, 1507–1510.
[76] F. Diederich, G. Schürrmann, I. Chao, *J. Org. Chem.* **1988**, *53*, 2744–2757.
[77] I. Chao, F. Diederich, *Rec. Trav. Chim.* **1993**, *112*, 335–338.
[78] D. R. Benson, R. Valentekovich, S.-W. Tam, F. Diederich, *Helv. Chim. Acta* **1993**, *76*, 2034–2060; S.-W. Tam-Chang, L. Jimenez, F. Diederich, *ibid.* **1993**, *76*, 2616–2639; L. Jimenez, F. Diederich, *Tetrahedron Lett.* **1989**, *30*, 2759–2762; H.-D. Lutter, F. Diederich, *Angew. Chem.* **1986**, *98*, 1125–1127; *Angew. Chem. Int. Ed. Engl.* **1986**, *25*, 1125–1127; F. Diederich, H.-D. Lutter, *J. Am. Chem. Soc.* **1989**, *111*, 8438–8446.
[79] R. Breslow, E. Kool, *Tetrahedron Lett.* **1988**, *29*, 1635–1638.
[80] Y. Yano, M. Kimura, K. Shimaoka, H. Iwasaki, *J. Chem. Soc. Chem. Comm.* **1986**, 160–161.
[81] S. Shinkai, Y. Ishikawa, H. Shinkai, T. Tsuno, H. Makashima, K. Ueda, O. Manabe, *J. Am. Chem. Soc.* **1984**, *106*, 1801–1808.
[82] J. Kikuchi, Z. Zhangand Y. Murakami, *Chem. Lett.* **1994**, 1559–1562.
[83] K. Johnsson, R. K. Allemann, H. Widmer, S. Benner, *Nature (London)* **1993**, *365*, 530–532.
[84] P. G. Schultz, *Angew. Chem.* **1989**, *101*, 1336; *Angew. Chem. Int. Ed. Engl.* **1989**, *28*, 1283; U. K. Pandit, *Rec. Trav. Chim.* **1993**, *112*, 431. "Catalytic Antibodies": *Ciba Found. Symp.* **1991**, *159*; S. J. Benkovic, *Annu. Rev. Biochem.* **1992**, *61*, 29–54.
[85] D. S. Tawfik, B. S. Green, R. Chap, M. Sela, Z. Eshhar, *Proc. Natl. Acad. Sci. USA* **1993**, *90*, 373–377.
[86] S. J. Pollack, P. Hsiun, P. G. Schultz, *J. Am. Chem. Soc.* **1989**, *111*, 5961–5962; T. Nakatani, R. Umeshita, J. Hiratake, A. Shinzaki, T. Suzuki, H. Nakajima, J. Oda, *Bioorg. Med. Chem. Lett.* **1994**, *2*, 457–468.
[87] M. T. Martin, T. S. Angeles, R. Sugasawara, N. I. Aman, A. D. Napper, M. J. Darsley, R. I. Sanchez, P. Booth, R. C. Titmas, *J. Am. Chem. Soc.* **1994**, *116*, 6508–6512.
[88] J. R. Jacobsen, J. R. Prudent, L. Kochersperger, S. Yonkovich, P. G. Schultz, *Science* **1992**, *256*, 365–367.
[89] D. Hilvert, K. W Hill, K. D. Narel, M.-T. M. Auditor, *J. Am. Chem. Soc.* **1989**, *111*, 9261. Braisted and Schultz reported a similar result: A. C. Braisted, P. G. Schultz, *J. Am. Chem. Soc.* **1992**, *114*, 7431
[90] S. N. Thorn, R. G. Daniels, M.-T. M. Auditor, D. Hilvert, *Nature (London)* **1995**, *373*, 228–230.
[91] J. D. Stewart, V. A. Roberts, N. R. Thomas, E. D. Getzoff, S. J. Benkovic, *Biochemistry* **1994**, *33*, 1994–2003.
[92] D. Y. Jackson, J. R. Prudent, E. P. Baldwin, P. G. Schultz, *Proc. Natl. Acad. Sci. USA* **1991**, *88*, 58–62.
[93] S. J. Pollack, P. G. Schultz, *J. Am. Chem. Soc.* **1989**, *111*, 1929–1931.
[94] A. Radzicka, R. Wolfenden, *Science* **1995**, *267*, 90–93.
[95] An important measure of the efficiency of catalysis by abzymes is the extent to which hapten binding is expressed as useful transition state binding. For a recent discussion see: J. D. Stewart, S. J. Benkovic, *Nature (London)* **1995**, *375*, 388–391.
[96] S. J. Pollack, J. W. Jacobs, P. G. Schultz, *Science* **1986**, *234*, 1570–1573.
[97] J. Guo, W. Huang, T. S. Scanlan, *J. Am. Chem. Soc.* **1994**, *116*, 6062–6065.
[98] M. T. Martin, A. D. Napper, P. G. Schultz, A. G. Rees, *Biochemistry* **1991**, *30*, 9757–9761.
[99] A. Tramontano, A. A. Ammann, R. A. Lerner, *J. Am. Chem. Soc.* **1988**, *110*, 2282–2286.
[100] A. J. Kirby, *Acta Chem. Scand.*, in press.

Time is money...

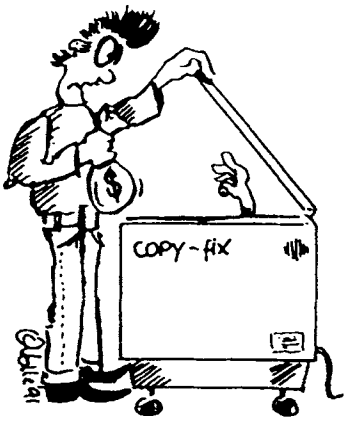

Save both by starting a personal subscription to *Angewandte Chemie* (now with *Chemistry - A European Journal*). At 9¢ per page you can't go wrong. With your own private copy you can read the "hot" articles before they cool, and waste less time in front of the copier.

Order now!
An order form can be found on the last page of this issue.

Nucleophilic Carbenes: An Incredible Renaissance

Manfred Regitz*

Carbenes **1** can be considered typical representatives of reactive intermediates and have found a broad range of applications in synthetic chemistry. Their impressive reactivity is comprehensively documented in two thick volumes of a standard reference series on organic synthesis.[1] As a result of the deficit of electrons they have electrophilic character, provided that the two substituents R are not electron donors. If this is not the case as, for example in the system **3A** ↔ **3B**, the donor groups enforce

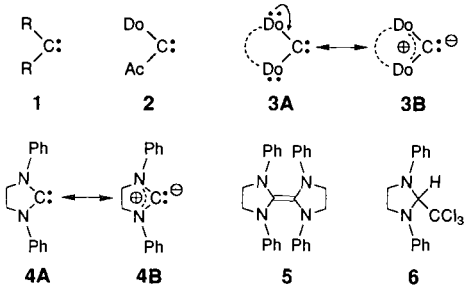

nucleophilic character at the carbene center. The ambiphilic carbenes **2** having both a donor and an acceptor substituent occupy a position between carbenes **1** and **3**. Only carbenes of type **3** can be isolated as stable compounds ("carbenes in a bottle"), and these were realized for the first time just a few years ago.[2]

The beginnings of the chemistry of nucleophilic carbenes **3** date back to the early 1960s and are associated with the name H.-W. Wanzlick.[3] At that time species of the type **4A** ↔ **4B** were examined; precursors of **4** include the dimeric and electron-rich olefin **5** and imidazolidine **6** (thermal α-elimination of chloroform). By means of cross-coupling experiments, however, it was shown that **5** is not in equilibrium with the two carbene units **4**.[4] On the other hand, it is certain that the C–C double bond of **5** is cleaved in reactions with electrophiles with liberation of **4**.[5] The carbene-stabilizing influence of the donor groups of **4** was clearly recognized and an even larger effect was correctly predicted for structurally related carbenes of type **7** owing to the participation of the "aromatic resonance structures" (**7A** ↔ **7B** ↔ **7C** ↔ **7D**);[3a] however, serious attempts to isolate carbenes of types **4** and **7** were not undertaken until 1991.

[*] Prof. Dr. M. Regitz
Fachbereich Chemie der Universität
Erwin-Schrödinger-Strasse, D-67663 Kaiserslautern (Germany)
Fax: Int. code +(631)205-3921

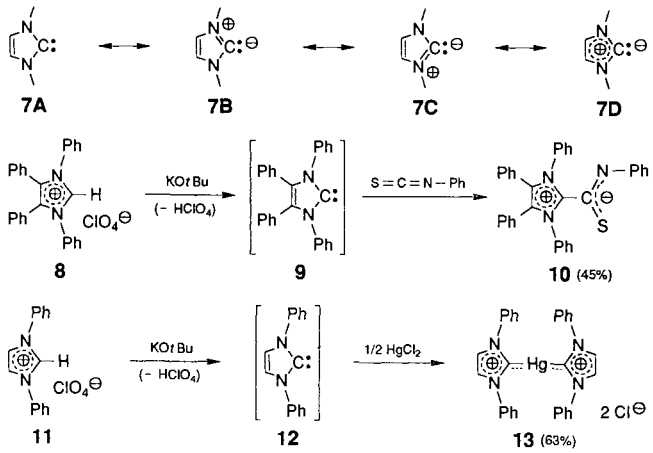

Even so, H.-W. Wanzlick and co-workers did demonstrate in 1970 that imidazolium salts such as **8** and **11** are deprotonated by potassium *tert*-butoxide to furnish carbenes **9** and **12**, respectively, which were then trapped (but not isolated). With phenyl isothiocyanate as trapping agent, the zwitterion **10**[6] was isolated, and treatment with mercury acetate gave the carbene complex **13**.[7] Thus, the first opportunity to isolate stable carbenes of the type **7**, to which **9** and **12** also belong, was missed. Just this principle was used almost two decades later by A. J. Arduengo et al.[8] to isolate electronically stabilized, nucleophilic carbenes for the first time.

When bis(1-adamantyl)imidazolium chloride (**14a**) was deprotonated with sodium hydride in tetrahydrofuran in the presence of a catalytic amount of dimethyl sulfoxide anion, **15a** precipitated as a colorless, crystalline, and thermally stable compound.[8] The crystal structure analysis unequivocally confirmed this result; in the ^{13}C NMR spectrum the lowfield position of the signal for the carbene carbon atom (δ = 211.4) is characteristic. A singlet ground state for imidazolylidene (**15**, $R^1 = R^2 = H$) was determined from ab initio MO calculations;[9] the dominating carbene character was deduced from neutron diffraction studies and crystal structure analysis of perdeuterated **15b**.[10]

In addition to the obvious steric effects, electronic factors are considered responsible for the stability of **15a**. These include π-electron transfer from the electron-rich π system of the heterocyclic ring (see resonance structures **7A**–**7D**) into the p orbital of the carbene carbon atom that is perpendicular to the ring plane.[2, 8]

 © VCH Verlagsgesellschaft mbH, D-69451 Weinheim, 1996 0570-0833/96/3507-0725 $ 15.00+.25/0

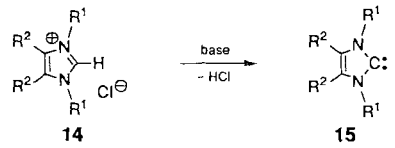

14 15

14 → 15	R^1	R^2	Reaction conditions	Yield [%]
a	1-adamantyl	H	NaH, THF, 25 °C DMSO (cat.)	96
b	Me	Me	NaH, THF, 25 °C tBuOK (cat.)	89
c	Me	H	NaH, THF, 25 °C tBuOK (cat.)	–
d	mesityl	H	tBuOK, THF, 25 °C	84
e	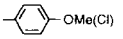	H	tBuOK, THF, 25 °C	45 (43)

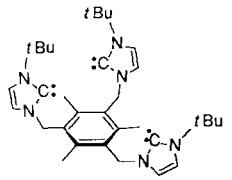

16

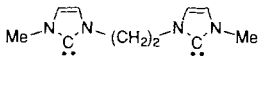

17 (≥ 95%)

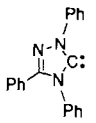

18 (100%)

The importance of steric effects was without doubt overestimated initially. This is apparent when one considers that stable carbenes of the same type can also be obtained by deprotonation of imidazolium salts bearing less bulky substituents in the 1- and 3-positions (**14b–e** → **15b–e**).[11] These species also exhibit characteristic ^{13}C NMR signals (δ = 213.7–219.7) for the carbene carbon atom.

Polyfunctional derivatives also open interesting perspectives for the chemistry of stable carbenes. The developments were initiated by the synthesis of the triscarbene **16** (^{13}C NMR: δ = 215.2), in which the imidazolylidene units are attached to a benzene ring. This compound was prepared by deprotonating the corresponding trisimidazolium salt with sodium hydride/*tert*-butoxide.[12] The biscarbene **17** is also stable and accessible by the same method except that sodium hydride in liquid ammonia/tetrahydrofuran is used as the deprotonating agent.[13] Advantages of this alternative method, which also provides access to **15c**, are low reaction temperatures (– 50 °C) and short reaction times. The series of stable, nucleophilic carbenes was extended by incorporating an additional nitrogen atom in the five-membered ring. 1,2,4-Triazol-5-ylidene **18** (^{13}C NMR: δ = 214.6 (C-5)) is obtained in quantitative yield by the thermal α-elimination of methanol from 5-methoxy-1,3,4-triphenyl-4,5-dihydro-1*H*-1,2,4-triazole.[14]

N. Kuhn and co-workers reported on a similarly successful synthesis of imidazolylidenes in 1993 which was completely independent of the above-mentioned examples. They condensed aldol **19** with thioureas **20a–c** to furnish imidazole-2(3*H*)-thiones **21a–c**, which were subsequently reduced with metallic potassium in tetrahydrofuran to give carbenes **22a–c** (**22a** ≡ **15b**).[15] The scope of this elegant method has not yet been fully explored.

The climax of the current developments is the isolation by A. J. Arduengo and co-workers of the first of the imidazolidin-2-ylidenes originally postulated by H.-W. Wanzlick. The stable, nucleophilic carbene **24** was obtained by deprotonation of the bis(mesityl)imidazolium chloride **23** with potassium hydride.[16]

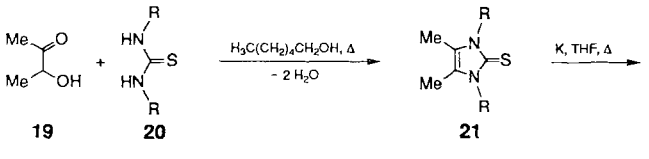

19 20 21

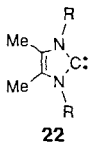

22

20, 21, 22a R = Me (95%)
b R = Et (96%)
c R = *i*Pr (93%)

A ^{13}C NMR signal at δ = 244.5 (relatively low field in comparison to the analogous signal of compounds of type **7**) and a crystal structure analysis conclusively confirmed the monomeric nature of the molecule.[16]

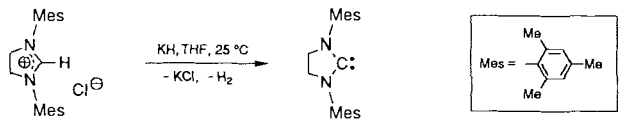

23 24 (72%)

In spite of their thermodynamic stability, nucleophilic carbenes exhibit an undeniable tendency to increase their coordination number and covalency state. For example, **22a–c** undergo smooth addition of elemental selenium at 20 °C to furnish **25a–c**[17] and of tellurium at 0 °C to give **26a–c**[18] in yields of ≥84%; the latter species can be considered to be imidazolium chalcogenides. Reactions with the carbon electrophile CS_2 lead to the stable, red zwitterions **27a–c** (69–82%).[19, 20]

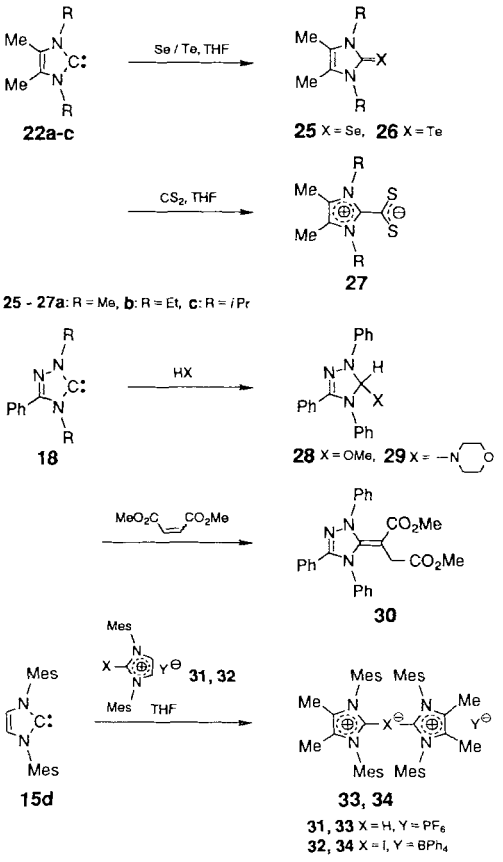

22a-c

25 X = Se, **26** X = Te

27

25 - 27a: R = Me, b: R = Et, c: R = *i*Pr

18

28 X = OMe, **29** X = –N O

30

15d

33, 34

31, 33 X = H, Y = PF_6
32, 34 X = I, Y = BPh_4

1,2,4-Triazolylidene **18** undergoes insertion into the H–X bond of protic nucleophiles with quantitative formation of triazolines **28** and **29**.[14, 21] Compound **18** reacts with dimethyl fumarate or maleate to furnish the methylenetriazoline **30**.[22] It is assumed that the initial step is a [2 + 1]cycloaddition to give a cyclopropane, and that subsequent ring opening and [1,2]-hydrogen shift lead to **30**.[14]

The coordinative unsaturation of stable carbenes is also reflected in the reaction of **15d** with imidazolium salts: the bis(carbene) - hydrogen complex **33** is formed with the salt **31**. A significant structural feature of **33** is the C-H-C moiety.[23] Analogously, reaction of **15d** with the iodoimidazolium salt **32** gives rise to the bis(carbene) - iodine complex **34**.[24, 25] In both cases the bond angle at the bridging atom X deviates only slightly from 180°.[23, 24]

In contrast to the organic chemistry of the stable, nucleophilic carbenes, which is still rather modest, the perspectives for the coordination chemistry of the same compounds have developed much more rapidly; this will be illustrated by a selection of carbene complexes of differing stoichiometries.

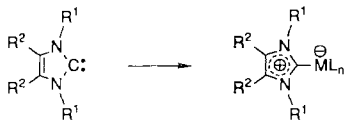

15, 22 **35**

35	R^1	R^2	ML_n	Ref.
a	1-Ad	H	$MgEt_2$	[26]
b	Me	Me	BH_3	[27]
c	Me	Me	BF_3	[27]
d	Mes	H	AlH_3	[28]
e	*i*Pr	Me	$SiCl_4$	[29]
f	Mes	H	GeI_2	[30]
g	Et	Me	$TiCl_4$	[31]
h	Me	Me	$Cr(CO)_5$	[32, 33]
i	Me	H	$Fe(CO)_4$	[32]
j	Me	H	$Ni(CO)_3$	[32]
k	Mes	H	$ZnEt_2$	[26]
l	Me	H	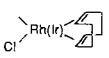	[34]
m	Me	Me	$Sm(Cp^*)_2$	[35, 36]

The formation of these complexes is based on the pronounced Lewis base character of the carbenes **15** and **22**. Lewis acids with main group elements as the central atom such as diethylmagnesium, borane, boron trifluoride, aluminum hydride, silicon tetrachloride (→ formation of hypervalent silicon), and germanium diiodide undergo addition as such or in the form of "stabilized adducts" to furnish the carbene complexes **35a–f** in high yields.[26–30] In principle, Lewis acids of the transition metals behave analogously: titanium tetrachloride (→ formation of hypervalent titanium) is incorporated as readily as the pentacarbonylchromium, tetracarbonyliron, tricarbonylnickel, and diethylzinc fragments to furnish the carbene complexes **35g–k**.[26, 31–33] Finally, carbene complexes with chloro(1,5-cyclooctadiene)-rhodium and -iridium (**35l**)[13] as well as bis(pentamethylcyclopentadienyl)samarium (**35m**)[34, 35] can be prepared easily.

The structures of the nickel and platinum[36] as well as the copper and silver complexes,[37] in which two nucleophilic carbene ligands are coordinated to the central atom, are similar to the structures of compounds **33** and **34** described previously, which have hydrogen or iodine as bridging elements. Two or three carbene ligands can also be incorporated in complexes containing chromium, molybdenum, or tungsten as the central atom.[38] Nucleophilic carbenes such as **15c** are coordinated by transition metal halides and oxides as well. Titanium(IV), hafnium(IV), vanadium(II), niobium(IV), and tantalum(IV) complexes of the general formula $[MX_nL_m]$ as well as rhenium complexes of the type $[MeReO_3L_2]$ (L = carbene ligand) have been isolated and their structures elucidated.[39] Beryllium–carbene complexes (1:3) are also known.[40]

The chemistry of stable (nucleophilic) carbenes has also had an impact on other, totally different fields, as will be shown in the following examples. The formyl anion character of a lithium derivative of 4-*tert*-butylthiazole, which exists in crystalline form as a complex with glyme (**36**), has been reported;[41] the synthetic potential of this species has been mentioned but not yet fully exploited.

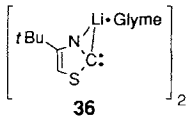

36

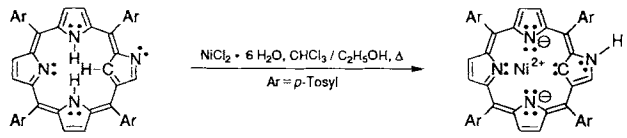

37 **38**

Nucleophilic carbenes also play a significant role as complex ligands in the chemistry of the "N-confused" porphyrins **37**. Complex **38**, accessible from **37** and nickel(II) chloride, can be viewed as an Ni-stabilized carbene.[42] Ab initio and LDF (low density functional) calculations are in accord with this description.[42]

The applications of the carbene–palladium complexes **39** and **40** in homogeneous catalysis are completely new and their full

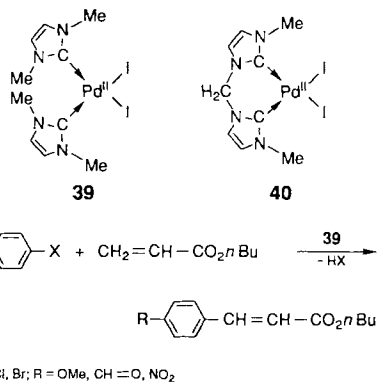

perspectives cannot yet be predicted. In a model study, this new structural principle for catalysts was investigated for the Heck reaction of aryl halides with *n*-butyl acrylate.[43] Both palladium complexes can be obtained from the corresponding imidazolium salts and palladium(II) acetate. Complex **39** is exceptionally stable towards heat, oxygen, and moisture; these are favorable characteristics for its use as a catalyst under extreme conditions. The palladium complex **40** is less suitable for the Heck reaction since it begins to decompose in solution at 70 °C.

The advantage of this novel structural principle for catalysts is the formation of active species stable for long periods even at the higher temperatures still necessary for the activation of chlorine atoms.[43] The addition of a reducing agent to **39** and the

independent generation of the active species, presumably the palladium(0) compound [Pd(carbene)$_2$], allow the Heck reaction to proceed without an induction period; deposition of palladium has not been observed.[43]

We wait with interest to see how the chemistry of the nucleophilic, stable carbenes will develop: surprises may be just around the corner. In addition, the exploration of the chemistry of the higher homologues (silylenes, germylenes with similar environments) will be a journey into uncharted territory.[44, 45]

German version: *Angew. Chem.* **1996**, *108*, 791–794

Keywords: carbene complexes · carbenes · imidazolylidenes

[1] *Houben-Weyl, Methoden der Organischen Chemie*, E19b (Ed.: M. Regitz), Thieme, Stuttgart, **1989**.
[2] Short review: M. Regitz, *Angew. Chem.* **1991**, *103*, 691; *Angew. Chem. Int. Ed. Engl.* **1991**, *30*, 674; and references therein
[3] a) Reviews: H.-W. Wanzlick, *Angew. Chem.* **1962**, *74*, 129; *Angew. Chem. Int. Ed. Engl.* **1962**, *1*, 75; b) R. W. Hoffmann, *ibid.* **1968**, *80*, 823 and **1968**, *7*, 754; c) J. Hocker, R. Merten, *ibid.* **1972**, *84*, 1022 and **1972**, *11*, 964.
[4] For a short review, see: N. Wiberg, *Angew. Chem.* **1968**, *80*, 809; *Angew. Chem. Int. Ed. Engl.* **1968**, *7*, 766.
[5] D. M. Lemal, R. A. Lovald, K. J. Kawano, *J. Am. Chem. Soc.* **1964**, *86*, 2518; W. Krasuski, D. Nikolaus, M. Regitz, *Liebigs Ann. Chem.* **1982**, 1451.
[6] H.-W. Wanzlick, H.-J. Schönherr, *Liebigs Ann. Chem.* **1970**, *731*, 176.
[7] H.-J. Schönherr, H.-W. Wanzlick, *Chem. Ber.* **1970**, *103*, 1037.
[8] A. J. Arduengo III, R. L. Harlow, M. Kline, *J. Am. Chem. Soc.* **1991**, *113*, 361.
[9] D. A. Dixon, A. J. Arduengo III, *J. Phys. Chem.* **1991**, *95*, 4180.
[10] A. J. Arduengo III, H. V. R. Dias, D. A. Dixon, R. L. Harlow, W. T. Kloster, T. F. Koetzle, *J. Am. Chem. Soc.* **1994**, *116*, 6812.
[11] A. J. Arduengo III, H. V. R. Dias, R. L. Harlow, M. Kline, *J. Am. Chem. Soc.* **1992**, *114*, 5530.
[12] H. V. R. Dias, W. Jin, *Tetrahedron Lett.* **1994**, *35*, 1365.
[13] W. A. Herrmann, M. Elison, J. Fischer, C. Köcher, G. R. J. Artus, *Chem. Eur. J.* **1996**, *2*, issue 7.
[14] D. Enders, K. Breuer, G. Raabe, J. Runsink, J. H. Teles, J.-P. Melder, K. Ebel, S. Brode, *Angew. Chem.* **1995**, *107*, 1119; *Angew. Chem. Int. Ed. Engl.* **1995**, *34*, 1021.
[15] N. Kuhn, T. Kratz, *Synthesis* **1993**, 561.
[16] A. J. Arduengo III, J. R. Goerlich, W. J. Marshall, *J. Am. Chem. Soc.* **1995**, *117*, 11027.
[17] N. Kuhn, G. Henkel, T. Kratz, *Z. Naturforsch. B* **1993**, *48*, 973.
[18] N. Kuhn, G. Henkel, T. Kratz, *Chem. Ber.* **1993**, *126*, 2047.
[19] N. Kuhn, H. Bohnen, G. Henkel, *Z. Naturforsch. B* **1994**, *49*, 1473.
[20] The formation of the zwitterion from **4** and CS_2 has been described: W. Krasuski, D. Nikolaus, M. Regitz, *Liebigs Ann. Chem.* **1982**, 1451.
[21] For the corresponding reaction with HCl, see: R. Boese, D. Bläser, N. Kuhn, *Z. Kristallogr.* **1994**, *209*, 837.
[22] For the analogous reactions with **4** and **5**, see: M. Regitz, D. Nikolaus, unpublished; D. Nikolaus, Dissertation, Universität Kaiserslautern, **1982**.
[23] A. J. Arduengo III, S. F. Gamper, M. Tamm, J. C. Calabrese, F. Davidson, H. A. Craig, *J. Am. Chem. Soc.* **1995**, *117*, 572.
[24] A. J. Arduengo III, M. Tamm, J. C. Calabrese, *J. Am. Chem. Soc.* **1994**, *116*, 3265.
[25] For carbene–pentafluoroiodobenzene and carbene–I_2 complexes, see: A. J. Arduengo III, M. Kline, J. C. Calabrese, F. Davidson, *J. Am. Chem. Soc.* **1991**, *113*, 9704; N. Kuhn, T. Kratz, G. Henkel, *J. Chem. Soc. Chem. Commun.* **1993**, 1778.
[26] A. J. Arduengo III, H. V. R. Dias, F. Davidson, R. L. Harlow, *J. Organomet. Chem.* **1993**, *462*, 13.
[27] N. Kuhn, G. Henkel, T. Kratz, J. Kreutzberg, R. Boese, A. H. Maulitz, *Chem. Ber.* **1993**, *126*, 2041.
[28] A. J. Arduengo III, H. V. R. Dias, J. C. Calabrese, F. Davidson, *J. Am. Chem. Soc.* **1992**, *114*, 9724.
[29] N. Kuhn, T. Kratz, D. Bläser, R. Boese, *Chem. Ber.* **1995**, *128*, 245.
[30] A. J. Arduengo III, H. V. R. Dias, J. C. Calabrese, F. Davidson, *Inorg. Chem.* **1993**, *32*, 1541.
[31] N. Kuhn, T. Kratz, D. Bläser, R. Boese, *Inorg. Chim. Acta* **1995**, *99*, 1.
[32] K. Öfele, W. A. Herrmann, D. Mihalios, M. Elison, E. Hertweck, W. Scherer, J. Mink, *J. Organomet. Chem.* **1993**, *459*, 177.
[33] N. Kuhn, T. Kratz, R. Boese, D. Bläser, *J. Organomet. Chem.* **1994**, *470*, C8.
[34] H. Schumann, M. Glanz, J. Winterfeld, H. Hemling, N. Kuhn, T. Kratz, *Chem. Ber.* **1994**, *127*, 2369; for an analogous Yb complex, see H. Schumann, M. Glanz, J. Winterfeld, H. Hemling, N. Kuhn, T. Kratz, *Angew. Chem.* **1994**, *106*, 1829; *Angew. Chem. Int. Ed. Engl.* **1994**, *33*, 1733.
[35] A. J. Arduengo, M. Tamm, S. J. McLain, J. C. Calabrese, F. Davidson, W. J. Marshall, *J. Am. Chem. Soc.* **1994**, *116*, 7927.
[36] A. J. Arduengo III, S. F. Gamper, J. C. Calabrese, F. Davidson, *J. Am. Chem. Soc.* **1994**, *116*, 4391.
[37] A. J. Arduengo III, H. V. R. Dias, J. C. Calabrese, F. Davidson, *Organometallics* **1993**, *12*, 3405.
[38] K. Öfele, W. A. Herrmann, D. Mihalios, M. Elison, E. Herdtweck, T. Priermeier, P. Kiprof, *J. Organomet. Chem.* **1995**, *494*, 1.
[39] W. A. Herrmann, K. Öfele, M. Elison, F. E. Kühn, P. W. Roesky, *J. Organomet. Chem.* **1994**, *480*, C7.
[40] W. A. Herrmann, O. Runle, G. Artus, *J. Organomet. Chem.* **1995**, *501*, C1.
[41] G. Boche, C. Hilf, K. Harms, M. Marsch, J. W. Lohrenz, *Angew. Chem.* **1995**, *107*, 509; *Angew. Chem. Int. Ed. Engl.* **1995**, *34*, 487.
[42] A. Ghosh, *Angew. Chem.* **1995**, *107*, 1117; *Angew. Chem. Int. Ed. Engl.* **1995**, *34*, 1028.
[43] W. A. Herrmann, M. Elison, J. Fischer, C. Köcher, G. R. J. Artus, *Angew. Chem.* **1995**, *107*, 2602; *Angew. Chem. Int. Ed. Engl.* **1995**, *34*, 2371.
[44] A. J. Arduengo III, H. Bock, H. Chen, M. Denk, D. A. Dixon, J. C. Green, W. A. Herrmann, N. L. Jones, M. Wagner, R. West, *J. Am. Chem. Soc.* **1994**, *116*, 6641.
[45] B. Gehrhus, M. F. Lappert, J. Heinicke, R. Boese, D. Bläser, *J. Chem. Soc. Chem. Commun.* **1995**, 1931.

 © VCH Verlagsgesellschaft mbH, D-69451 Weinheim, 1996 0570-0833/96/3507-0728 $ 15.00+.25/0

Additions to Functionalized Arenes with Concurrent Dearomatization

Thorsten Bach*

The six-membered aromatic ring of benzene and its derivatives is a C_6 unit that may be used as an alicyclic synthetic building block if the conjugated π system can be successfully broken up. The fascination of such a reaction rests on its high economy and its simple elegance, as demonstrated by two examples from the annals of organic synthesis. Woodward conceived the introduction of the angular methyl group to tetralin **1** by a Reimer–Tiemann reaction and subsequent dehalogenation of intermediate **2** [Eq. (a)].[1] This work was related to earlier observations by Auwers et al. that cyclohexadienones form as side products in the reaction of *ortho*- and *para*-alkylated phenols with $CHCl_3$/NaOH.[2] The Adler reaction,[3] which was discovered in the beginning of the 1970s, was chosen by Corey et al. as a key step in the synthesis of ovalicin to construct the spirocyclic product **4** from the salicylic alcohol **3** in a single step [Eq. (b)].[4]

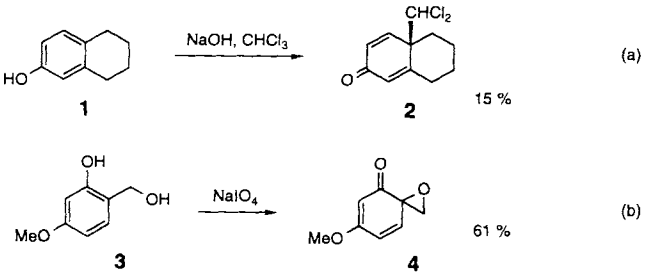

Modern dearomatization reactions,[5] which will be presented in this account, often utilize transition metal complexation to activate the arene. For example, the tendency for C-alkylations in phenols can be enhanced by η^2-complexation with Os^{II} fragments, which bind selectively to C-2 and C-3.[6] An intermolecular addition to Michael acceptors becomes possible due to the partial localization of the π-electron density in racemic complexes such as **5**. 2,5-Cyclohexadienones are formed in a process that is thermodynamically favored by the enhanced π-acidity of these ligands [Eq. (c), only one enantiomer is shown].[7] The addition proceeds stereoselectively from the face of the six-membered ring opposite to the metal. In general, *para*-substituted products such as **6** are formed predominantly; however, the regioselectivity can be shifted to preferential *ortho*-addition at C-6 upon Lewis acid catalysis. Anilines were shown to react in an analogous fashion.[8]

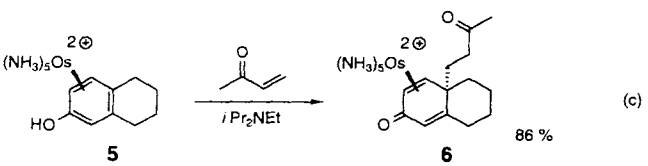

[*] Dr. T. Bach
Organisch-chemisches Institut der Universität Münster
Orléansring 23, D-48149 Münster (Germany)
Fax: Int. code +(251)83-9772
e-mail: bachta uni-muenster.de

In contrast to this method, in which the nucleophilicity of an arene is increased by η^2-complexation, several dearomatization reactions can be conducted on η^6-arene complexes.[9] The most prominent examples are found in the area of the corresponding $Cr(CO)_3$ complexes. Nucleophilic attack on the electrophilic arene occurs readily, and under carefully controlled conditions the reaction may be completed by subsequent quenching with an electrophile to yield a cyclohexadiene. During the conversion of a monosubstituted benzene a stereogenic center is generated on the six-membered ring whose absolute configuration is determined by the enantiotopic position of the nucleophilic attack.[10] If the substituent attached to the arene is chiral, both the *ortho* and the *meta* carbon atoms are diastereotopic and a differentiation by achiral reagents is feasible. Based on these considerations Kündig et al. developed a chelation-induced, diastereoselective *ortho*-alkylation of complex **7** as exemplified in Equation (d).[11] The product **8** is formed with excellent diastereomeric excess (>98% *de*).[12]

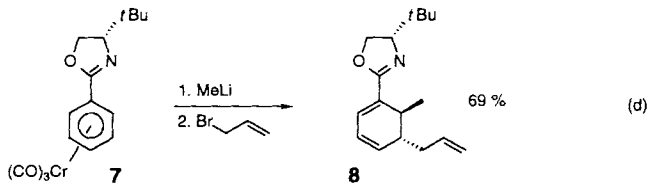

The oxazoline auxiliary employed by Kündig et al. is reminiscent of the pioneering work by Meyers in the field of asymmetric addition to 1- or 2-(dihydrooxazolyl)naphthalenes.[13] In the case of a 1-substituted naphthalene selective addition of nucleophiles at the 2-position proceeds with excellent diastereofacial selectivities, provided the oxazoline is chiral. Similar addition reactions were conducted on naphthalenes bearing a carbonyl or a carboxyl substituent in 1-position.[14] A recent result reported by the group of H. Yamamoto shows that even acceptor-substituted benzene derivatives can be dearomatized under suitable conditions.[15] For a successful reaction the complexation of the carbonyl group in aromatic aldehydes or ketones such as acetophenone (**9**) by the sterically demanding Lewis acid aluminum tris(2,6-diphenylphenoxide) (ATPH) is mandatory. A deoxygenated mixture of toluene and THF (1/1) serves as the solvent. Since the *ortho* positions and the carbonyl group are shielded by the Lewis acid, an enolate is formed by 1,6-addition of the alkyl lithium species. Under carefully chosen workup conditions (conc. HCl) the cyclohexadiene **10** can be isolated [Eq. (e)]. Slight modification of the reaction conditions

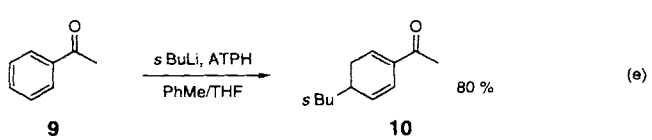

 © VCH Verlagsgesellschaft mbH, D-69451 Weinheim, 1996 0570-0833/96/3507-0729 $ 15.00+.25/0

(workup with acetic acid or reaction in CH_2Cl_2) leads to the formation of the aromatic substitution product.[16]

All of the methods previously mentioned rely on conventional electrophilic or nucleophilic reagents. To close, a reaction will be addressed that proceeds by an enzymatic transformation. The oxidation of monosubstituted arenes by mutant strains of *Pseudomonas putida* leads to enantiomerically pure diols[17] such as **11**, which are widely used starting materials for the synthesis of alkaloids and carbohydrates.[18] In a recent example diol **11** is transformed into the central six-membered ring of (+)-pancratistatin (**12**) [Eq. (f)]; the diol's stereochemical information

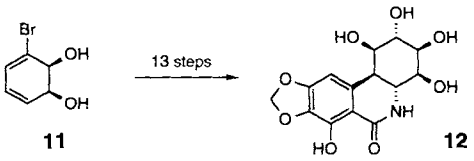

11 **12** (f)

and its C–C connectivity are essential.[19] The aromatic residue in **12** was attached in the form of an *ortho*-metalated arene to an aziridine by nucleophilic substitution. The aziridine, in turn, was generated regio- and diastereoselectively from diol **11**. In the synthesis of (+)-deoxypancratistatin a structurally related mixed higher-order cuprate was employed for this purpose.[20]

The enzyme-catalyzed dihydroxylation of disubstituted iodobenzenes proceeds with high regioselectivity at their unsubstituted *ortho* and *meta* carbon atoms [**13** → **14**, Eq. (g)]. After

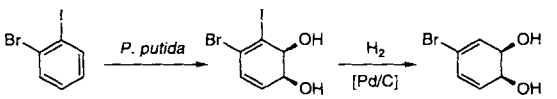

13 **14** **15** 65 % (g)

the directing power of the iodine substituent has been used, it can be removed by catalytic hydrogenolysis on palladium. This sequence was applied to the synthesis of *cis*-3,4-dihydrodiols such as **15** and also to the preparation of the (2*R*,3*R*) enantiomers[21] of *cis*-2,3-dihydrodiols, which cannot be obtained by conventional oxidation with *Pseudomonas putida*.[22]

The methods presented here were selected to show some recent developments in the field of dearomatization reactions. Besides regio- and diastereoselectivity as criteria for synthetic efficiency, the preparation of enantiomerically pure compounds and the formation of C–C bonds are further goals. The ubiquitous occurrence of six-membered rings in natural products and biologically relevant molecules should be a sufficient reason to search for improvements on the existing methods and to develop novel dearomatization reactions.

German version: *Angew. Chem.* **1996**, *108*, 795–796

Keywords: arene complexes · cyclohexadienes · dearomatizations · electrophilic additions · nucleophilic additions

[1] R. B. Woodward, *J. Am. Chem. Soc.* **1940**, *62*, 1208–1211.
[2] K. Auwers, G. Keil, *Ber. Dtsch. Chem. Ges.* **1902**, *35*, 4207–4217.
[3] E. Adler, S. Brasen, H. Miyake, *Acta Chem. Scand.* **1971**, *25*, 2055–2069; H.-D. Becker, T. Bremholt, E. Adler, *Tetrahedron Lett.* **1972**, 4205–4208.
[4] E. J. Corey, J. P. Dittami, *J. Am. Chem. Soc.* **1985**, *107*, 256–257.
[5] Further references to many dearomatization reactions can be found in: L. N. Mander, *Synlett* **1991**, 134–144.
[6] W. D. Harman, M. Sekine, H. Taube, *J. Am. Chem. Soc.* **1988**, *110*, 5725–5731.
[7] M. E. Kopach, W. D. Harman, *J. Am. Chem. Soc.* **1994**, *116*, 6581–6592.
[8] J. Gonzalez, M. Sabat, W. D. Harman, *J. Am. Chem. Soc.* **1993**, *115*, 8857–8858.
[9] For further references, see: a) M. F. Semmelhack in *Comprehensive Organic Synthesis, Vol. 4* (Ed.: B. Trost), Pergamon, Oxford, **1991**, pp. 517–549; b) E. P. Kündig, A. Ripa, R. Liu, G. Bernardinelli, *J. Org. Chem.* **1994**, *59*, 4773–4783.
[10] For reactions of chiral nucleophiles with achiral $Mn(CO)_3$–arene complexes in which enantiotopic positions are differentiated, see: W. H. Miles, H. R. Brinkman, *Tetrahedron Lett.* **1992**, *33*, 589–592, and references therein.
[11] E. P. Kündig, A. Ripa, G. Bernardinelli, *Angew. Chem.* **1992**, *104*, 1115–1117. *Angew. Chem. Int. Ed. Engl.* **1992**, *31*, 1071–1073.
[12] Selective reaction of cationic $Mn(CO)_3$–arene complexes at one of the two diastereotopic *meta* positions is facilitated by a chiral C_2-symmetric 2,5-dimethylpyrrolidine substituent (70–90% *de*): A. J. Pearson, P. Y. Zhu, W. J. Youngs, J. D. Bradshaw, D. B. McConville, *J. Am. Chem. Soc.* **1993**, *115*, 10376–10377; A. J. Pearson, M. C. Milletti, P. Y. Zhu, *J. Chem. Soc. Chem. Commun.* **1995**, 853–854.
[13] Reviews: a) M. Reuman, A. I. Meyers, *Tetrahedron* **1985**, *41*, 837–860; b) T. G. Gant, A. I. Meyers, *ibid.* **1994**, *50*, 2297–2360.
[14] K. Tomioka, M. Shindo, K. Koga, *Tetrahedron Lett.* **1990**, *31*, 1739–1740. Enantioselective variant: K. Tomioka, M. Shindo, K. Koga, *ibid.* **1993**, *34*, 681–682.
[15] K. Maruoka, M. Ito, H. Yamamoto, *J. Am. Chem. Soc.* **1995**, *117*, 9091–9092.
[16] It has been known for some time that aryl phenyl ketones with a very bulky aryl group (e.g. 2,3,5,6-tetramethylphenyl) are substituted by Grignard reagents in *para* position: R. C. Fuson, B. C. McKusick, *J. Am. Chem. Soc.* **1943**, *65*, 60–64.
[17] Review: a) H. A. J. Carless, *Tetrahedron: Asymmetry* **1992**, *3*, 795–826; b) H. Waldmann, T. Pohl in *Enzyme Catalysis in Organic Synthesis, Vol. 2* (Eds.: K. Drauz, H. Waldmann), VCH, Weinheim, **1995**, pp. 701–704.
[18] a) S. V. Ley, *Pure Appl. Chem.* **1990**, *62*, 2031–2034; b) T. Hudlicky, *ibid.* **1994**, *66*, 2067–2070.
[19] X. Tian, T. Hudlicky, K. Königsberger, *J. Am. Chem. Soc.* **1995**, *117*, 3643–3644.
[20] X. Tian, R. Maurya, K. Königsberger, T. Hudlicky, *Synlett* **1995**, 1125–1126.
[21] When the priority of the substituent in 1-position of the cyclohexadiene is less than O, the configuration is designated (2*S*,3*R*).
[22] D. R. Boyd, N. D. Sharma, S. A. Barr, H. Dalton, J. Chima, G. Whited, R. Seemayer, *J. Am. Chem. Soc.* **1994**, *116*, 1147–1148.

 © VCH Verlagsgesellschaft mbH, D-69451 Weinheim, 1996 0570-0833/96/3507-0730 $ 15.00+.25/0

Directed Self-Assembly of Chiral, Optically Active Macrocyclic Tetranuclear Molecular Squares**

Peter J. Stang* and Bogdan Olenyuk

Dedicated to Professor Cheves T. Walling on the occasion of his 80th birthday

Chiral macromolecules play an essential role in biology and chemistry and are key constituents of all living organisms. The structural elegance and complexity of proteins and nucleic acids evolved by nature have been intriguing subjects for numerous investigations for over a century. The design and study of various artificial models of complex biological systems have largely been developed in the last three decades and now represent one of the major frontiers of modern supramolecular chemistry. Among the many systems investigated, the most intriguing are the chiral macrocycles: crown ethers,[1] cyclophanes,[2] cyclodextrins,[3] and calixarenes.[4] Molecular recognition studies in these model systems provide insights into not only fundamental concepts of noncovalent interactions, occlusion phenomena, and chiral recognition, but also into enzymatic processes. The exact molecular architecture of these compounds, as manifested in their precise shape, size, conformation, and configuration, is critical to their function.[5]

Recently, conformationally more rigid macrocycles, with unique geometric features, commonly referred to as molecular squares, have emerged. To date, three distinct types of these assemblies are known: those with a main-group element (polyvalent iodine) at the corners,[6] transition metal based systems,[7] and hybrid species, incorporating both polyvalent iodine and transition metals.[8]

Their high-yielding, facile, and rapid preparation as well as air and thermal stability make molecular squares interesting targets for investigations of inclusion phenomena, host–guest interactions, and potentially even biomimetic studies.[9] Therefore, the application of the self-assembly phenomenon in an attempt to create hitherto unknown symmetrical yet chiral metallamacrocycles was particularly interesting and challenging.

The de novo design of chiral macromoleculecular assemblies, due to their conformational rigidity, required an alternative approach to that used for the preparation of the achiral square-shaped species. Whereas the spatial orientation of the donor atoms (e.g. nitrogens) of the bidentate ligand may remain 180° relative to each other, the ligand should possess C_{2h} symmetry, as opposed to the D_{2d}- or D_{2h}-symmetrical diaza ligands used in all molecular squares assembled to date.[7, 8] Although several such bidentate ligands are feasible, 2,6-diazaanthracene (daa) and 2,6-diazaanthracene-9,10-dione (daad) seemed to be among the most suitable. Moreover, upon formation of the conformationally rigid tetranuclear assembly, these ligands must be restricted in rotation around the metal–nitrogen bonds and remain orthogonal to the transition metal coordination plane.

Because six diastereomers may be formed in complexes with such ligands (Fig. 1), the separation of the diastereomers of these tetranuclear species was expected to be very difficult. The solution to this problem was unexpectedly simple: the components of the assembly are defined, which under appropriate conditions would generate exclusively one enantiomer; in other words, the internal properties of the components are used to achieve stereoselective self-assembly.

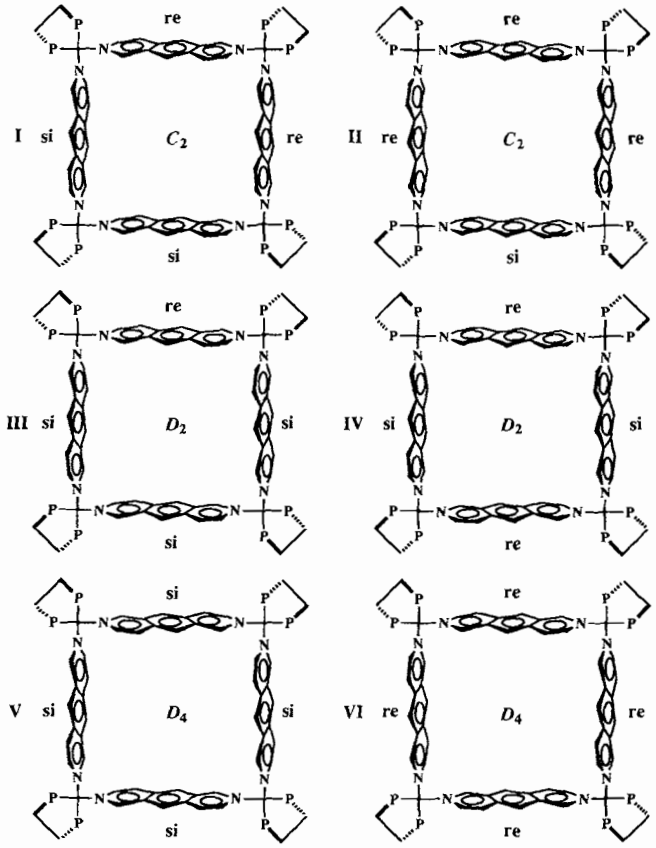

Fig. 1. Schematic representation of the symmetries of all possible diastereomeric cyclic tetranuclear complexes incorporating chiral transition metal bisphosphane *R*-(+)-binap units and the C_{2h}-symmetric ligand daa. Each face of the diaza ligands is labeled according to the π stacking rules [13a].

The reaction of the chiral, square-planar (around the metal) *R*-(+)-binap palladium(II) and platinum(II) bis(triflate) complexes **1** and **2** (binap = *P*, *o'*-(1,1'-binaphthyl-2,2'-diyl)bis-(diphenylphosphane)) with 2,6-diazaanthracene (daa) **3** in acetone at room temperature gives excellent yields of the self-assembled, single, diastereomeric, stable products **4** and **5**, respectively (Scheme 1), as assessed by NMR techniques. Chiral molecular squares **4** and **5** are air-stable (albeit hygroscopic), microcrystalline solids with high decomposition points. In spite of both the large charge (+8) and relatively high molecular mass (ca. 5000), these molecules are remarkably soluble in polar organic solvents such as acetone, nitromethane, and methanol.

The spectroscopic data and, especially the fact that the ^{31}P NMR spectra of **4** and **5** each show only a single signal, indicate that all the phosphorus atoms are equivalent, and hence these molecules must be highly symmetrical. In particular, the singlet in the ^{31}P NMR spectra of **4** and **5** indicates that the orientation of the two coordinated diaza ligands is *anti* (structures **V** and **VI**, Fig. 1) with respect to *each* square-planar metal center, because the molecules with *syn*-oriented ligands (structures **I**–**IV**) have different, lower symmetry. Also the *syn* orientation of the ligands would reveal itself in the ^{31}P NMR spectrum as a set of AB-type doublets due to the desymmetrization of the two neighboring binap P atoms. Therefore, the ^{31}P NMR spectra of the C_2-symmterical isomers **I**–**III** (Fig. 1) would contain a singlet and

[*] Prof. Dr. P. J. Stang, B. Olenyuk
Department of Chemistry, The University of Utah
Salt Lake City, UT 84112 (USA)
Fax: Int. code +(801)581-8433

[**] This work was supported by the National Science Foundation. We thank Prof. Jay S. Siegel for useful discussions and Johnson-Matthey for the generous loan of platinum salts.

 © VCH Verlagsgesellschaft mbH, D-69451 Weinheim, 1996 0570-0833/96/3507-0732 $ 15.00+.25/0

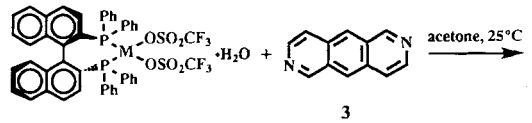

1, M = Pd
2, M = Pt

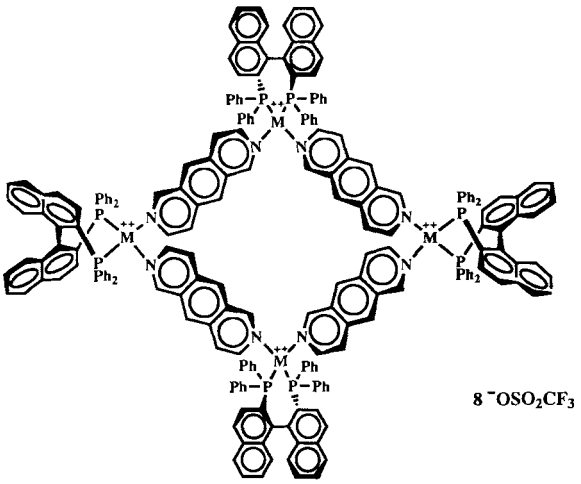

4, M = Pd, 86%, $[\alpha]_D = +441$ (CH_3COCH_3)
5, M = Pt, 84%, $[\alpha]_D = +237$ (CH_3COCH_3)

Scheme 1.

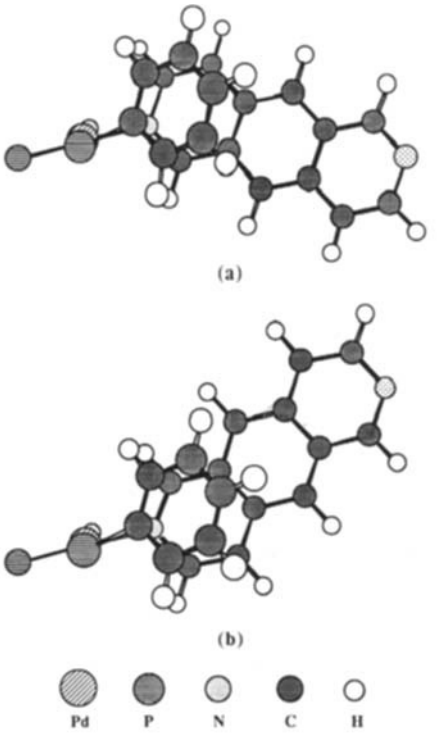

Fig. 2. Model of a fragment of molecular square **4** obtained from MM2 calculations, indicating the geometry of the arene–heteroarene stacking. Favored (a) and disfavored (b) rotamers are shown from the same viewing angle.

an AB-type doublet, whereas the D_2-symmetrical square **IV** would give rise to only an AB-type doublet. Moreover, had the other *anti* diastereomer (structure **V**, Fig. 1) been formed as well, its ^{31}P NMR signal would have been a separate singlet. This assertion is based on our previous studies of the mononuclear palladium(II) and platinum(II) complexes of *R*-(+)-binap, **1** and **2**, respectively, and isoquinoline.[10] Three different isomers formed due to restricted rotation about the metal–nitrogen bond: two C_2-symmetrical *anti* isomers (one of them as the major product) and one unsymmetrical *syn* isomer, with readily detectable chemical shift differences of $\Delta\delta = 0.2-0.8$ in the ^{31}P NMR spectra.[10] In the ^{31}P NMR spectra of the $[Pd(R\text{-}(+)\text{-binap})(C_{12}H_8N_2)]_4[OTf]_8$ **4** recorded between -80 and $+80$ °C no line broadening or signal splitting was evident, which ruled out isomerization, and therefore confirmed that at least within this temperature range, all diaza ligands are indeed restricted in rotation. Hence, **4** and **5** are each formed, within the limits of NMR detection, in diastereomerically pure form (structure **VI**, Fig. 1) with complete asymmetric induction in a conformationally rigid manner. MM2 force field calculations[11] indicate that the preferred formation of the chiral tetranuclear molecular square with the symmetrical all-*anti* orientation, *R,S,S* configuration[12] of each metal center, and D_4 symmetry (structure **VI**, Fig. 1) is likely a consequence of electronic factors. Although in the absence of strong charge transfer the preferred alignment of aryl rings is normally edge-to-face,[13] the face-to-face arene–heteroarene stacking in these squares is the result of the enforced proximity of the daa units and the binap phenyls. The spatial disposition of the P-phenyl rings of the chelate ligands and the metal-daa groups is sustained by the rigid binaphthyl backbone, and in the preferred diastereomer **VI** the dipole of the neighboring daa is forced away from the centroid of the nearest P-phenyl ring. This interaction (Fig. 2a) is favored over the alternative (Fig. 2b), where the dipole is in proximity to the P-phenyl centroid, and likely accounts for the preferred formation of only one diastereoisomer.

Use of 2,6-diazaanthracene-9,10-dione **6** (daad) as a ligand for the assembly of optically active molecular squares **7** and **8** (Scheme 2) results in highly symmetrical, chiral major products by asymmetric induction. However, small but detectable amounts of additional diastereomers are formed in each case, as evident in the ^{31}P NMR spectrum of **8** (Fig. 3). In other words,

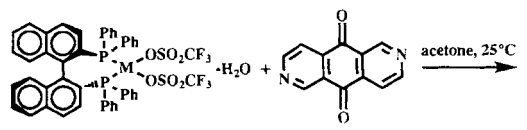

1, M = Pd
2, M = Pt

6

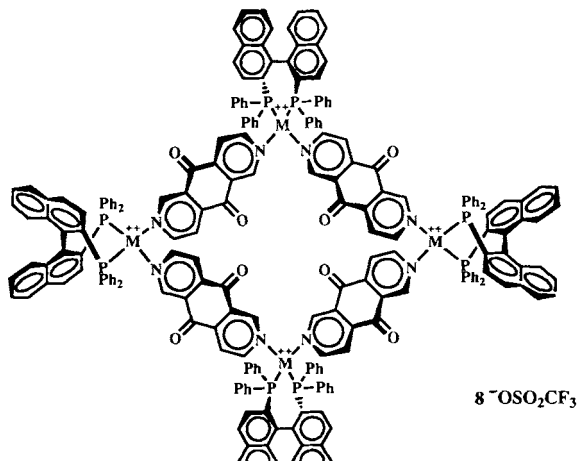

7, M = Pd, 94%, $[\alpha]_D = +395$ (CH_3COCH_3)
8, M = Pt, 89%, $[\alpha]_D = +154$ (CH_3NO_2)

Scheme 2.

 © VCH Verlagsgesellschaft mbH, D-69451 Weinheim, 1996 0570-0833/96/3507-0733 $ 15.00+.25/0

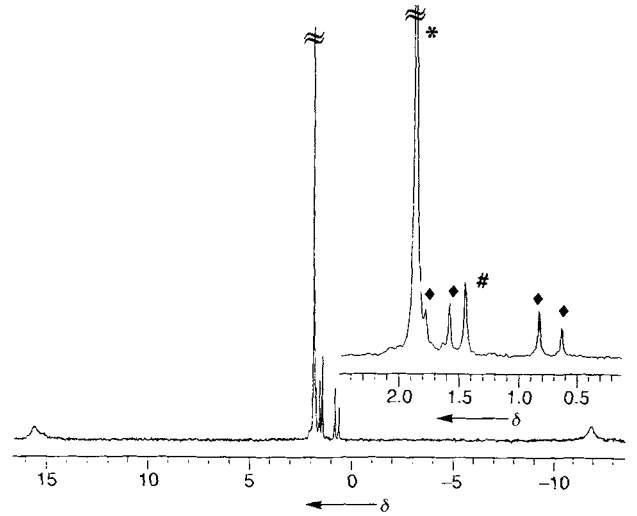

Fig. 3. Proton-decoupled ^{31}P NMR spectrum of molecular square **8** (*, #: *anti* isomers, ♦: *syn* isomer).

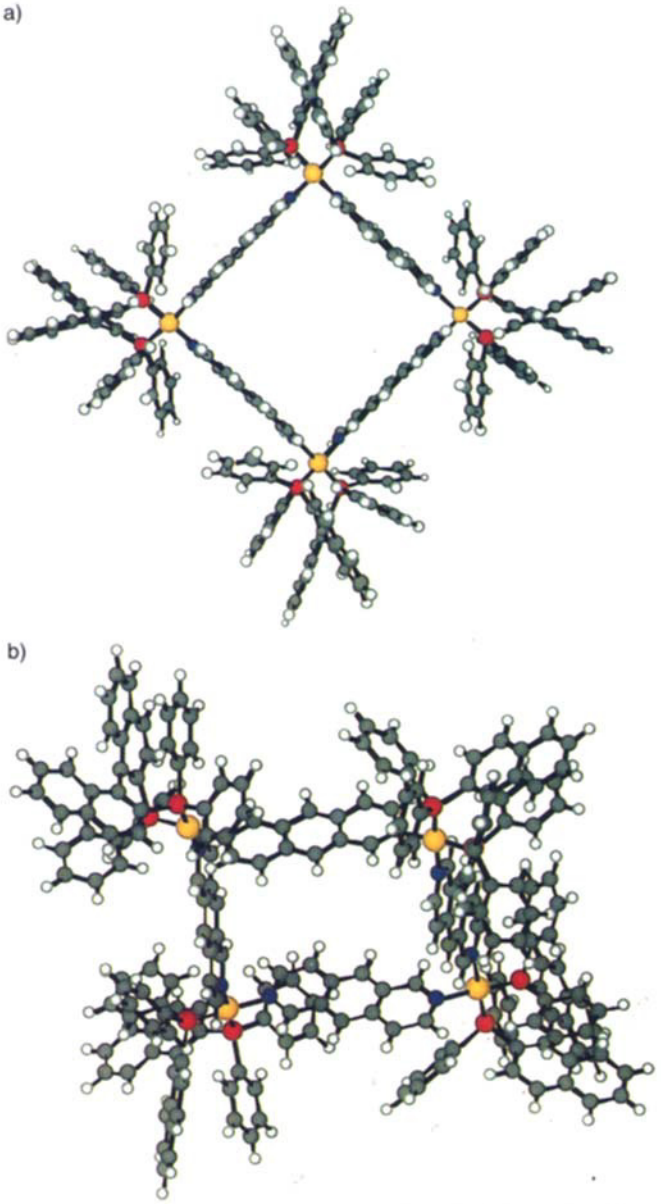

Fig. 4. Ball-and-stick model of molecular square **4**. Note the the large cavity evident in the top view (a) and the elements of helicity in the side view (b).

asymmetric induction is incomplete; only 81% of the major diastereomer of **7** and 72% of that of **8** are formed. These observations support our hypothesis concerning the conformations of **4** and **5**.

Electrospray (ES) mass spectrometric data for **8** show the presence of the doubly charged $[M-2\,^{-}OTf]^{2+}$ and quadruply charged $[M-4\,^{-}OTf]^{4+}$ ions with m/z ratios of 2503 and 1177, respectively. These signals correspond to the loss of two and four triflate anions, but the cationic part of the molecule remains intact, as assessed by the analysis of the isotopic distributions. These novel chiral species possess a large molecular-sized cavity in a unique combination with the elements of molecular helicity (Fig. 4).

The synthesis was also carried out with the other enantiomer of the chiral platinum bisphosphane complex (ligand: *S*-(−)-binap). Use of the opposite enantiomer in asymmetric induction predicts formation of the mirror image product. Indeed, interaction of [Pt(*S*-(−)-binap)(H_2O)($OTf)_2$] **9** with **6** results in the formation of the opposite enantiomeric product, molecular square **10** (Scheme 3). The physical and NMR spectroscopic

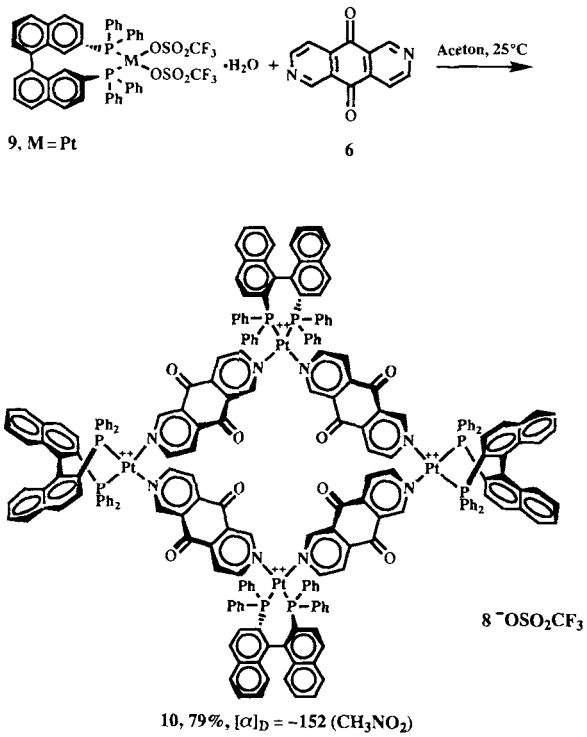

Scheme 3.

data of **10** are identical with those of **8**, but its optical rotation (within experimental error) is opposite. The mirror image relationship of **8** and **10** is confirmed by the circular dichroism (CD) spectra displayed in Figure 5 along with the CD spectrum of the palladium analogue **7**.

In summary, a new class of supramolecular assemblies, molecular squares that are chiral due to molecular helicity, can be readily constructed by self-assembly and coordination between the chiral square-planar Pd^{II} and Pt^{II} bisphosphane triflate complexes and appropriate achiral bidentate diaza ligands as building blocks. Asymmetric induction through a chiral bisphosphane (binap) auxiliary chelated to the metal center, and restricted rotation about the metal–nitrogen bond of the heteroarene ligand bond play a vital role in the stereoselective for-

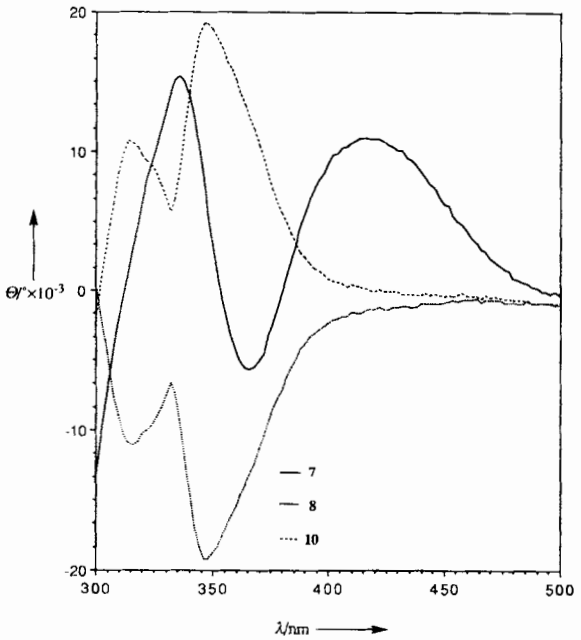

Fig. 5. CD spectra of the molecular squares **7**, **8**, and **10**.

mation of these cyclic, symmetrical, yet chiral species. The possible use of these chiral molecular squares as model systems in biomimetic studies, for asymmetric catalysis, and in other potential applications are currently under investigation.

Experimental Procedure

Preparation of **4**, **5**, **7**, **8**, and **10**: Schlenk techniques and dry N_2 were employed. A solution of 0.051 mmol of daa or daad in 8 mL of dry acetone was charged with 0.050 mmol of the appropriate chiral palladium(II) or platinum(II) triflates **1**, **2** [10], or **9** [14], and the solution was stirred under nitrogen for 30 min. Diethyl ether was then added and the precipitate was collected, washed with diethyl ether, and dried in vacuo.

4: Yield: 86%; m.p. 268–270 °C (decomp); $[\alpha]_D = +441$ ($c = 0.015$, acetone, 20 °C); ^{1}H NMR (300 MHz, [D$_6$]acetone, 25 °C, TMS): $\delta = 9.71$ (s, 8H, daa H-1 and H-5), 8.66 (d, $J = 6.8$ Hz, daa H-3 and H-7), 8.34 (s, 8H, daa H-9 and H-10), 8.16 (t, $J = 9.0$ Hz, 8H, binap), 8.06 (t, $J = 7.6$ Hz, 8H, binap), 7.87 (m, 16H, binap +daa H-4 and H-8), 7.55 (t, $J = 8.0$ Hz, 8H, binap), 7.44 (d, $J = 6.6$ Hz, 8H, binap), 7.14 (m, 24H, binap), 6.87 (t, $J = 7.3$ Hz, 8H, binap), 6.46 (d, $J = 8.5$ Hz, 8H, binap); ^{13}C{^{1}H} NMR (75 MHz, [D$_6$]acetone, 25 °C, TMS): $\delta = 160.2$ (s), 141.3 (t), 140.2 (s), 135.7 (overlapping m), 134.2 (t), 132.7 (s), 132.5 (s), 131.6 (s), 131.1 (t), 130.2 (m), 130.0 (s), 129.8 (s), 129.5 (s), 129.4 (s), 128.2 (s), 127.8 (s), 127.7 (s), 125.0 (t), 124.9 (s), 121.3 (q), 120.2 (t); ^{31}P{^{1}H} NMR (121 MHz, [D$_6$]acetone, 25 °C, H_3PO_4): $\delta = 27.42$ (s); ^{19}F NMR (282 MHz, [D$_6$]acetone, 25 °C, $CFCl_3$): $\delta = -75.7$ (s, CF_3SO_3); IR (neat): $\tilde{\nu}$ [cm^{-1}]: 1259, 1159, 1097, 1029 (all OTf); Anal. calcd for $C_{232}H_{160}N_8S_8P_8O_{24}F_{24}Pd_4 \cdot 3H_2O$: C 57.06, H 3.43, N 2.29, S 5.25; found: C 56.94, H 3.44, N 2.31, S 5.28.

5: Yield: 84%; m.p. 365–367 °C (decomp); $[\alpha]_D = +237$ ($c = 0.0082$, acetone, 20 °C); ^{1}H NMR (300 MHz, [D$_6$]acetone, 25 °C, TMS): $\delta = 9.86$ (s, 8H, daa H-1 and H-5), 8.66 (d, $J = 6.4$ Hz, daa H-3 and H-7), 8.47 (s, 8H, daa H-9 and H-10), 8.13 (t, $J = 10.0$ Hz, 8H, binap), 8.07 (t, $J = 7.7$ Hz, 8H, binap), 7.86 (m, 16H, binap +daa H-4 and H-8), 7.51 (t, $J = 7.9$ Hz, 8H, binap), 7.19–7.07 (m, 32H, binap), 6.87 (t, $J = 7.4$ Hz, 8H, binap), 6.45 (d, $J = 8.5$ Hz, 8H, binap; ^{13}C{^{1}H} NMR (75 MHz, [D$_6$]acetone, 25 °C, TMS): $\delta = 160.5$ (s), 141.2 (t), 140.7 (s), 135.7 (t), 135.6 (s), 134.2 (t), 132.5 (s), 131.7 (s), 131.0 (t), 130.3 (s), 129.7 (s), 129.1(s), 128.1 (s), 127.4 (t), 125.6 (s), 123.4 (t), 123.0 (t), 121.3 (q), 120.2 (t); ^{31}P {^{1}H} NMR (121 MHz, [D$_6$]acetone, 25 °C, H_3PO_4): $\delta = 0.63$ (s, ^{195}Pt satellites, J(Pt,P) = 3277 Hz); ^{19}F NMR (282 MHz, [D$_6$]acetone, 25 °C, $CFCl_3$): $\delta = -75.3$ (s, CF_3SO_3); IR (neat): $\tilde{\nu}$ [cm^{-1}]: 1248, 1152, 1092, 1028 (all OTf). Anal. calcd for $C_{232}H_{160}N_8S_8P_8O_{24}F_{24}Pt_4 \cdot 6H_2O$: C 52.65, H 3.28, N 2.12, S 4.85; found: C 52.39, H 3.47, N 2.15, S 4.96.

7: Yield: 94%; m.p. 254–256 °C (decomp); $[\alpha]_D = +395$ ($c = 0.05$, acetone, 20 °C); ^{1}H NMR (300 MHz, [D$_6$]acetone, 25 °C, TMS): $\delta = 9.46$ (d, $J = 4.8$ Hz, 8H, daad), 8.89 (s, 8H, daad), 8.20 (t, $J = 9.0$ Hz, 8H, binap), 8.12–8.01 (m, 8H, binap), 7.86 (m, 16H, binap), 7.65 (d, $J = 5.3$ Hz, 8H, binap), 7.57 (t, $J = 7.0$ Hz, 8H, binap), 7.33 (t, $J = 6.0$ Hz, 16H, binap), 7.28–6.92 (m, 24H, binap), 6.43 (d, $J = 8.7$ Hz, 8H, binap); ^{13}C{^{1}H} NMR (75 MHz, [D$_6$]acetone, 25 °C, TMS): $\delta = 178.0$ (s), 155.8 (s), 152.2 (s), 150.3 (s), 141.3 (t), 138.9 (s), 135.9 (s), 135.6 (s), 135.4 (s), 135.2 (s), 134.2 (s), 132.9 (s), 131.3 (s), 130.4 (t), 130.1 (s), 129.1 (s), 128.5 (s), 127.9 (s), 124.9 (t), 123.1 (t), 122.5 (s), 121.3 (q), 119.8 (t); ^{31}P{^{1}H} NMR (121 MHz, [D$_6$]acetone, 25 °C, H_3PO_4): $\delta = 27.43$ (s); ^{19}F NMR (282 MHz, [D$_6$]acetone, 25 °C, $CFCl_3$): $\delta = -75.6$ (s, CF_3SO_3); IR (neat): $\tilde{\nu}$ [cm^{-1}]: 1695 (C=O), 1245, 1149, 1027 (all OTf); Anal. calcd for $C_{232}H_{152}N_8S_8P_8F_{24}O_{32}Pd_4 \cdot 3H_2O$: C 55.69, H 3.18, N 2.24, S 5.13; found: C 55.69, H 3.22, N 2.27, S 5.07.

8: Yield: 89%; m.p. 320–322 °C (decomp); $[\alpha]_D = +154$ ($c = 0.011$, CH_3NO_2, 20 °C). ^{1}H NMR (300 MHz, [D$_6$]acetone, 25 °C, TMS): $\delta = 9.50$ (d, $J = 5.0$ Hz, 8H, daad), 9.06 (s, 8H, daad), 8.30–8.03 (m, 16H, binap), 7.83 (m, 16H, binap), 7.74 (d, $J = 6.0$ Hz, 8H, binap), 7.51 (t, $J = 7.3$ Hz, 8H, binap), 7.32 (t, $J = 6.8$ Hz, 16H, binap), 7.22 (t, $J = 7.1$ Hz, 8H, binap), 7.17–6.98 (m, 16H, binap), 6.40 (d, $J = 8.6$ Hz, 8H, binap); ^{13}C{^{1}H} NMR (75 MHz, [D$_6$]acetone, 25 °C, TMS): $\delta = 177.6$ (s), 155.8 (s), 156.4 (s), 152.7 (s), 141.4 (t), 138.9 (s), 139.2 (s), 135.8 (s), 135.6 (s), 135.5 (s), 134.3 (s), 133.0 (s), 132.9 (s), 131.4 (t), 130.3 (s), 130.2 (s), 129.8 (s), 129.2 (s), 128.4 (s), 128.1 (s), 127.6 (s), 124.5 (t), 123.9 (s), 123.6 (s), 123.5 (t), 121.3 (q), 119.9 (t); ^{31}P{^{1}H} NMR (121 MHz, [D$_6$]acetone, 25 °C, H_3PO_4): $\delta = -1.25$ (s, ^{195}Pt satellites, J(Pt,P) = 3340 Hz, major *anti* isomer), -1.65 (s, ^{195}Pt satellites, J(Pt,P) = 3340 Hz, minor *anti* isomer), -1.90 (dd, $J = 24$, 115 Hz, ^{195}Pt satellites, J(Pt,P) = 3340 Hz, *syn* isomer); ^{19}F NMR (282 MHz, [D$_6$]acetone, 25 °C, $CFCl_3$): $\delta = -75.3$ (s, CF_3SO_3); IR (neat): $\tilde{\nu}$ [cm^{-1}]: 1695 (C=O), 1250, 1152, 1092, 1028 (all OTf); Anal. calcd for $C_{232}H_{152}N_8S_8P_8F_{24}O_{32}Pt_4 \cdot 4H_2O$: C 51.83, H 3.00, N 2.08, S 4.77; found: C 51.68, H 2.98, N 2.21, S 4.73.

10: Yield: 79%; m.p. 320–322 °C (decomp); $[\alpha]_D = -152$ ($c = 0.0045$, CH_3NO_2, 25 °C). The ^{1}H and ^{31}P NMR spectra of **10** were found to be identical to those of **8**.

Received: October 2, 1995
Revised version: December 13, 1995 [Z 8439 IE]
German version: *Angew. Chem.* **1996**, *108*, 798–802

Keywords: chirality · complexes with nitrogen ligands · helical structures · supramolecular chemistry

[1] a) E. P. Kyba, M. G. Siegel, L. R. Sousa, G. D. Y. Sodah, D. J. Cram, *J. Am. Chem. Soc.* **1973**, *95*, 2691; b) E. P. Kyba, K. Koga, L. R. Sousa, M. G. Siegel, D. J. Cram, *ibid.* **1973**, *95*, 2692; c) R. C. Helgeson, K. Koga, J. M. Timko, D. J. Cram, *ibid.* **1973**, *95*, 3021; d) R. C. Helgeson, J. M. Timko, D. J. Cram, *ibid.* **1973**, *95*, 3023; e) G. W. Gokel, D. J. Cram, *J. Chem. Soc. Chem. Commun.* **1973**, 481; f) W. D. Curtis, D. A. Laidler, J. F. Stoddart, J. H. Jones, *ibid.* **1975**, 833; g) *ibid.* **1975**, 835; h) J.-M. Girodeau, J.-M. Lehn, J.-P. Sauvage, *Angew. Chem.* **1975**, *87*, 813; *Angew. Chem. Int. Ed. Engl.* **1975**, *14*, 764; i) M. P. Mack, R. P. Hendrixson, R. A. Palmer, R. G. Ghirardelli, *J. Am. Chem. Soc.* **1976**, *98*, 7830; j) S. C. Peacock, L. A. Domaier, F. C. A. Gaeta, R. C. Helgeson, J. M. Timko, D. J. Cram, *ibid.* **1978**, *100*, 8190; k) O. Kaneko, N. Matsuura, K. Kimura, T. Shono, *Chem. Lett.* **1979**, 369; l) S. C. Peacock, D. M. Walba, F. C. A. Gaeta, R. C. Helgeson, D. J. Cram, *J. Am. Chem. Soc.* **1980**, *102*, 2043; m) G. D. Y. Sodah, D. J. Cram, *ibid.* **1979**, *101*, 3035; n) G. D. Malpass, Jr., R. A. Palmer, R. G. Ghirardelli, *Tetrahedron Lett.* **1980**, *21*, 1489; o) M. P. Mack, R. P. Hendrixson, R. A. Palmer, R. G. Ghirardelli, *J. Org. Chem.* **1983**, *48*, 2029; p) J. F. Stoddart in *Topics in Stereochemistry, Vol. 17* (Eds.: E. Eliel, S. Wilen), Wiley, New York, **1987**, p. 207; q) D. Gu, B. D. Kenney, W. W. Brown, *Tetrahedron Lett.* **1994**, *35*, 681.

[2] a) Y. Murakami, I. Kikuchi, T. Ohno, O. Hayashida, M. Kojima, *J. Am. Chem. Soc.* **1990**, *112*, 7672; b) Y. Murakami, T. Ohno, O. Hayashida, Y. Hisaeda, *Chem. Lett.* **1991**, 1595; c) F. Diederich, *Cyclophanes*, The Royal Society of Chemistry, Cambridge, UK, **1991**; d) Y. Murakami, O. Hayashida, T. Ito, Y. Hisaeda, *Pure Appl. Chem.* **1993**, *65*, 551; e) Y. Murakami, O. Hayashida, K. Ono, Y. Hisaeda, *ibid.* **1993**, *65*, 2319; f) F. Vögtle, *Cyclophane Chemistry*, Wiley, Chichester, **1993**; g) Y. Murakami, O. Hayashida, Y. Nagai, *J. Am. Chem. Soc.* **1994**, *116*, 2611.

[3] a) S. Hamai, T. Ikeda, A. Nakamura, H. Ikeda, A. Ueno, F. Toda, *J. Am. Chem. Soc.* **1992**, *114*, 6012; b) G. Wulff, S. Kubik, *Carbohydr. Res.* **1992**, *237*, 1; c) M. Suzuki, M. Kajtar, J. Szejtli, M. Vikman, E. Fenyvesi, *ibid.* **1992**, *223*, 71; d) M. Suzuki, M. Kajter, I. Szeitli, M. Vikman, E. Fenyuesi, L. Szente, *ibid.* **1991**, *214*, 25; e) G. Patonay, I. M. Warner, *J. Inclusion Phenom. Mol. Recognit. Chem.* **1991**, *11*, 313.

[4] a) T. Arimura, S. Shinkai, *Bull. Chem. Soc. Jpn.* **1991**, *64*, 1896; b) T. Arimura, H. Kawabata, T. Matsuda, T. Muramatsu, H. Satoh, K. Fujio, O. Manabe, S. Shinkai, *J. Org. Chem.* **1991**, *56*, 301; c) *Calixarenes: A Versatile Class of Macrocyclic Compounds* (Eds.: J. Vicens, V. Bohmer), Kluwer, Dordrecht, **1990**; d) C. D. Gutsche, *Calixarenes*, The Royal Society of Chemistry, Cambridge, UK, **1989**; e) T. Arimura, H. Kawabate, S. Edamitsu, S. Shinkai, O. Manabe, T. Muramatsu, M. Tashiro, *Chem. Lett.* **1987**, 2269; f) S. Shinkai, T. Arimura, H. Satoh, O. Manabe, *J. Chem. Soc. Chem. Commun.* **1987**, 1495.

[5] a) J.-M. Lehn, *Supramolecular Chemistry: Concepts and Perspectives*, VCH, New York, **1995**; b) D. J. Cram, J. M. Cram, *Container Molecules and Their Guests*, The Royal Society of Chemistry, Cambridge, UK, **1994**.

[6] P. J. Stang, V. V. Zhdankin, *J. Am. Chem. Soc.* **1993**, *115*, 9808.

[7] a) P. J. Stang, D. H. Cao, S. Saito, A. M. Arif, *J. Am. Chem. Soc.* **1995**, *117*, 6273; b) C. M. Drain, J.-M. Lehn, *J. Chem. Soc. Chem. Commun.* **1994**, 2313; c) P. J. Stang, J. A. Whiteford, *Organometallics* **1994**, *13*, 3776; d) P. J. Stang, D. H. Cao, *J. Am. Chem. Soc.* **1994**, *116*, 4981; e) M. Fujita, Y. J. Kwon, S. Washizu, K. Ogura, *ibid.* **1994**, *116*, 1151; f) H. Rauter, E. C. Hillgeris, A. Erxleben, B. Lippert, *ibid.* **1994**, *116*, 616; g) M. Fujita, S. Nagao, M. Iida, K. Ogura, *ibid.* **1993**, *115*, 1574; h) M. Fujita, J. Yazaki, K. Ogura, *ibid.* **1990**, *112*, 5645.

[8] a) P. J. Stang, K. Chen, *J. Am. Chem. Soc.* **1995**, *117*, 1667; b) P. J. Stang, K. Chen, A. M. Arif, *ibid.* **1995**, *117*, 8793.

[9] a) C. A. Hunter, *Angew. Chem.* **1995**, *107*, 1181; *Angew. Chem. Int. Ed. Engl.* **1995**, *34*, 1079; b) D. S. Lawrence, T. Jiang, M. Levett, *Chem. Rev.* **1995**, *95*, 2229.

[10] P. J. Stang, B. Olenyuk, A. M. Arif, *Organometallics* **1995**, *14*, 5281. For another example of restricted rotation, see also J. M. Brown, J. J. Pérez-Torrente, N. W. Alcock, *ibid.* **1995**, *14*, 1195.

[11] a) U. Burkett, N. L. Allinger, *Molecular Mechanics*, American Chemical Society, Washington, D. C., **1982**; b) T. Clark, *Computational Chemistry*, Wiley, New York, **1985**.

[12] The *R,S,S* configuration around each metal center was assigned by using the standard Canh-Ingold-Prelog conventions for the assignment of atropoisomeric chirality and treating the *trans*-P-M-N′ as one pair of substituents about the Pt-N axis: V. Prelog, G. Helmchen, *Angew. Chem.* **1982**, *94*, 614; *Angew. Chem., Int. Ed. Engl.* **1982**, *21*, 567. Note that the first letter (*R*) refers to the configuration of the binap ligand.

[13] a) F. Cozzi, J. S. Siegel, *Pure Appl. Chem.* **1995**, *67*, 683; b) C. A. Hunter, *Chem. Soc. Rev.* **1994**, *23*, 101.

[14] The bistriflate complex **9** was prepared in analogy to the synthesis of complex **2** by the reaction of [Pt(*S*-(-)-BINAP)Cl_2] with AgOTf.

Cuprates as Selective Metalating Reagents for Aromatic Halides

Yoshinori Kondo, Tetsuji Matsudaira, Junko Sato, Naoko Murata, and Takao Sakamoto*

Ate complexes such as cuprates have been used as versatile reagents for selective carbon-carbon bond forming reactions; however, little attention has been paid to halogen-metal exchange reactions using ate complexes.[1] With the aim of developing a new facile method for the preparation of arylcuprates, we investigated the halogen-copper exchange reaction of aromatic halides using cuprates. [$Li_2Cu(CN)Me_2$] was found to be an excellent metalating reagent. We describe here the application of this metalating method for the asymmetric synthesis of precursors of the CC-1065/duocarmycin pharmacophore with high enantiomeric purity.

Organocopper complexes are the organotransition metal reagents most widely used as soft nucleophiles in organic synthesis.[2] Organocopper and organocuprate reagents are employed for carbon-carbon bond formation owing to their characteristic reactivities in conjugate additions to α,β-unsaturated carbonyl compounds, in substitution reactions, and in carbometalations of carbon-carbon triple bonds. Although these reagents tolerate a wide range of electrophilic functional groups, the formation of functionalized organocopper reagents is not promising, because transmetalation of organolithium or Grignard reagents is typically required. Functionalized organocopper reagents have been prepared by transmetalation of functionalized organozinc compounds[3] and by direct oxidative addition of active copper to organic halides.[4]

[*] Prof. Dr. T. Sakamoto, Prof. Dr. Y. Kondo, T. Matsudaira, J. Sato, N. Murata
Department of Heterocyclic Chemistry
Faculty of Pharmaceutical Sciences, Tohoku University
Aobayama, Aoba-ku, Sendai 980-77 (Japan)
Fax: Int. code +(22)217-6864
e-mail: j23396@cctu.cc.tohoku.ac.jp

Since the first preparation of [$LiCuMe_2$][5] a number of Gilman-type reagents of the general formula [$LiCuR_2$] have been used in organic syntheses, and recently higher order, mixed cuprates [$Li_2Cu(CN)R_2$] have been reported to show high reactivity toward a variety of organic substrates.[6] During our recent studies on arene and heteroarene chemistry,[7] we became interested in developing methods for preparing mixed arylcuprates with functional groups from haloarenes by halogen-copper exchange. The halogen-metal exchange reaction is one of the most useful processes for the preparation of metalated arenes such as the lithium[8] and magnesium[9] compounds. However, use of other organometallic compounds other than organolithiums and organomagnesiums for the halogen-metal exchange reaction seems to be rather limited. Although the possibility of halogen-copper exchange has been suggested in the coupling reaction of aryl halides with cuprates,[10] the reactions of organocopper intermediates with electrophiles are still unexplored from the viewpoint of synthetic chemistry.

Cuprate **2a** was prepared by reaction of iodobenzene (**1a**) with [$Li_2Cu(CN)Me_2$] in THF at $-40\,^{\circ}C$ for 2.5 h (Table 1).

Table 1. Formation of cuprates **2a-c** by halogen-metal exchange and addition to benzaldehyde. RT = room temperature.

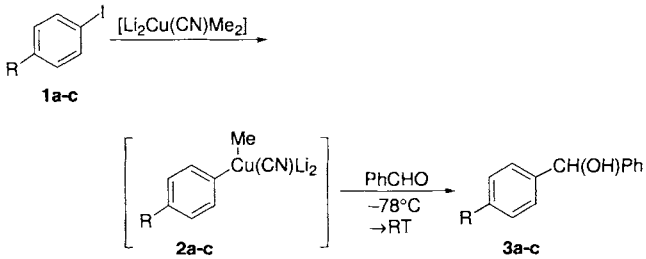

	R	Solvent	T [°C]	t [h]	Yield [%]
a	H	THF	−40	2.5	89
a	H	Et_2O	−40	2.5	56
b	OMe	THF	−20	2	59
c	CO_2Me	THF	−78	4	56

Subsequent reaction with benzaldehyde at $-78\,^{\circ}C$ gave benzhydrol **3a** in 89% yield. Yields were moderate when Et_2O was employed as solvent. Other mixed cuprates such as [$LiCuMe_2$], [$Li_2CuMe_2(SCN)$], [$Li_2Cu(C{\equiv}CPh)(CN)Me$], and [$Li_2Cu(C_4H_3S)(CN)Me$] ($C_4H_3S$ = thienyl) were found to be less reactive than [$Li_2Cu(CN)Me_2$], and benzhydrol **3a** was obtained in 12-32% yield under otherwise identical reaction conditions. The halogen-copper exchange reaction of *p*-iodoanisole (**1b**) with [$Li_2Cu(CN)Me_2$] seemed to be slower than the reaction of iodobenzene. Satisfactory results were obtained when the metalation was conducted at $-20\,^{\circ}C$. A *p*-methoxycarbonyl group (**1c**) was tolerated in the halogen-copper exchange reaction, and the intermediary copper reagent **2c** reacted with benzaldehyde to give the alcohol **3c**. For better yields the metalation was conducted at $-78\,^{\circ}C$.

The high reactivity of the cuprates formed in this halogen-copper exchange reaction in 1,2-addition reactions encouraged us to investigate other classical reactions for carbon-carbon bond formation. The conjugate addition of the phenylcuprate **2a** to 2-cyclohexenone afforded 3-phenylcyclohexanone (**4**) in 61% yield without additional reagents (Scheme 1). The reaction of **2a** with 1,2-epoxycyclohexane gave *trans*-2-phenylcyclohexanol (**5**) in 53% yield in the absence of additives.

 © VCH Verlagsgesellschaft mbH, D-69451 Weinheim, 1996 0570-0833/96/3507-0736 $ 15.00+.25/0

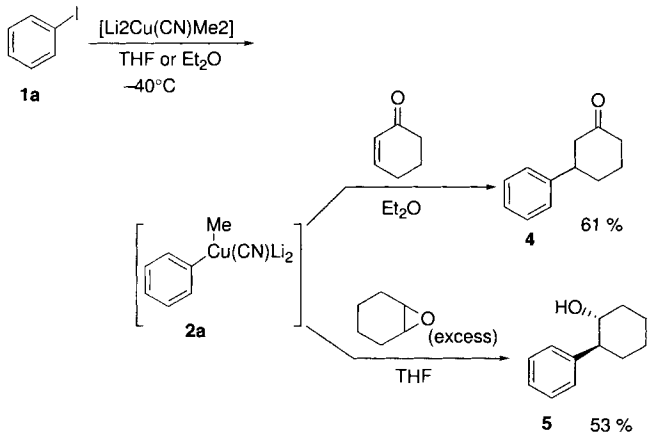

Scheme 1. 1,4-Addition and epoxide opening with cuprate **2a**, which is formed from **1a**.

The halogen–copper exchange reaction of aryl halides with $[Li_2Cu(CN)Me_2]$ is a new method for the preparation of functionalized arylcuprates. To determine the structure of the arylcopper intermediate, arylcuprate **6**, which was obtained by halogen–copper exchange reaction of methyl *p*-iodobenzoate (**1c**), was hydrolyzed and oxidized with oxygen (Scheme 2). The hydrolysis of **6** in aqueous NH_4Cl at −40 °C gave methyl benzoate (**7**) in 85% yield; formation of methyl *p*-methylbenzoate (**8**) was not observed. In the halogen–copper exchange process MeI is probably produced and may be scavenged by another equivalent of $[Li_2Cu(CN)Me_2]$. The resulting [LiCu(CN)Me] is less reactive to electrophiles than $[Li_2CuAr(CN)Me]$ is. Oxidation of **6** by bubbling oxygen through the reaction mixture at −78 °C gave coupling product **8** in 76% yield. These results suggest the arylcopper intermediate is a mixed higher order species.[11]

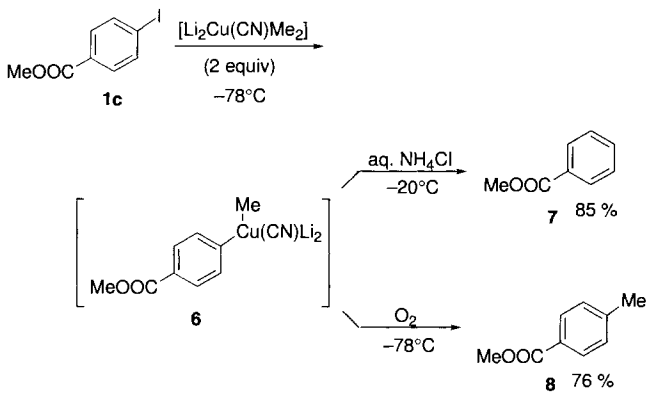

Scheme 2. Hydrolysis and oxidation of cuprate **6**, which is formed from **1c**.

Our interest next focused on the application of the method to the synthesis of biologically active molecules. CC-1065[12a] and duocarmycins A[12b] and SA[12c] are potent antitumour antibiotics, and they have been synthetic targets for many synthetic chemists in connection with the mechanism of their biological activity.[13, 14] They contain a common spirocyclic subunit, and 3-hydroxymethyl-2,3-dihydroindoles and 3-hydroxy-1,2,3,4-tetrahydroquinolines are considered to be key precursors for the synthesis of the spirocyclic pharmacophore (Scheme 3).

In connection with our recent studies on the synthesis of CC-1065/duocarmycin pharmacophores[15] we became interested in the asymmetric synthesis of 3-hydroxymethyl-2,3-dihydroindoles and 3-hydroxy-1,2,3,4-tetrahydroquinolines. If these precursors are available in enantiomerically pure form, asymmetric synthesis of the pharmacophore should be straightforward.

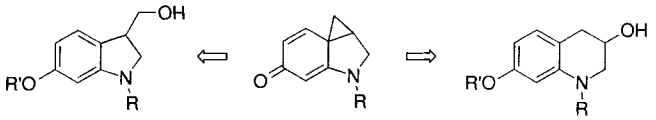

Scheme 3. Retrosynthetic analysis of the spirocyclic pharmacophore of CC-1065 and the duocarmycins leading back to 3-hydroxymethyl-2,3-dihydroindole and 3-hydroxy-1,2,3,4-tetrahydroquinoline precursors.

The intramolecular ring opening of epoxyorganometallic compounds is of interest in particular with regard to the regioselectivity of subsequent cyclizations.[16] We investigated the synthesis of a precursor of the CC-1065/duocarmycin pharmacophore by intramolecular ring opening of epoxyarylmetal ate complexes. The chiral epoxide **9** was chosen as a substrate and the regioselectivity of the cyclization was investigated. When **9** was treated with *n*BuLi at −90 °C, the 5-*exo* cyclization product[17] **10** was formed in 43% yield without loss of enantiomeric purity (Table 2, Entry 1). At higher temperature the yield of the product decreased dramatically (Entry 2). The reaction of **9** with lithium trimethylzincate at −50 °C gave the 5-*exo* product **10** in 40% yield and the 6-*endo* product **11** in 57% yield. Reaction with the zincate obtained from three equivalents of MeLi and $[Zn(SCN)_2]$[18] furnished the 5-*exo* product **10** as the main product together with the 6-*endo* product **11** (Entry 3).[16] The reactions of **9** with cuprates (Entries 4,5) showed reverse regioselectivity, and the 6-*endo* product **11** was obtained exclusively when $[Li_3Cu(CN)Me_3]$[19] was used as the metalating reagent. In general, enantiomeric purity was unchanged after the ring opening; the only exception was the 5-*exo* product **10** in the reaction of **9** with $[Li_2Cu(CN)Me_2]$.

Table 2. Synthesis of the precursors **10** and **11** of the CC-1065/duocarmycin pharmacophore.

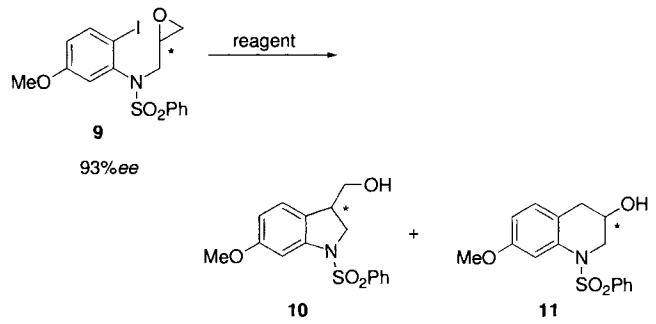

Entry	Reagent	T [°C]	Yield [%] (*ee* [%] [a]) **10**	**11**
1	*n*BuLi	−90	43 (93)	0
2	$[LiZnMe_3]$	−50	40 (91)	57 (91)
3	$[Li_3ZnMe_3(SCN)_2]$	−78	72 (90)	15 (91)
4	$[Li_2Cu(CN)Me_2]$	−78	6 (78)	62 (90)
5	$[Li_3Cu(CN)Me_3]$	−78	0	73 (92)

[a] The enantiomeric excesses were determined with a Chiralcel OD-H column.

We do not yet have enough experimental data for discussing the origin of this diverse selectivity in the cyclization which

depends on the metalating reagent. However, the coordination of the oxygen atoms of the epoxide and sulfonyl groups to the metals of the ate complex is considered to be important in determining the direction of cyclization.

We have described a new method for the synthesis of enantiomerically pure 3-hydroxmethyl-2,3-dihydroindole and 3-hydroxyl-1,2,3,4-tetrahydroquinoline. The reagents of choice for the regioselective ring closure are $[Li_3ZnMe_3(SCN)_2]$ for the 5-*exo* cyclization and $[Li_3Cu(CN)Me_3]$ for the 6-*endo* cyclization.

Experimental Procedure

General procedure for halogen–copper exchange reaction followed by reaction with an electrophile: MeLi (1.04 M solution in Et_2O; 3.84 mL, 4 mmol) was added to a suspension of dry CuCN (179 mg, 2 mmol) in THF or Et_2O (5 mL) at −78 °C, and the mixture was stirred at −40 °C for 30 min. Then an aryl iodide (1 mmol) in THF or Et_2O (1 mL) was added and the reaction mixture stirred at −40 °C for 1 h. The mixture was cooled to −78 °C before an electrophile (2 mmol or excess) was added. The mixture was gradually warmed to room temperature over 12 h. The reaction mixture was quenched with aqueous NH_4Cl (2 mL) and the solvent removed in vacuo. The residue was diluted with H_2O (30 mL), and the mixture was extracted with $CHCl_3$ (3 × 30 mL). The combined organic layers were dried over anhydrous $MgSO_4$. After purification by silica gel column chromatography, the crude material was recrystallized or distilled under reduced pressure.

Reaction of **8** with $[Li_2Cu(CN)Me_2]$: Under Ar atomosphere, MeLi (1.03 M solution in Et_2O, 1.46 mL, 1.5 mmol) was added to the mixture of 90% CuCN (74.6 mg, 0.75 mmol) and dry THF (3 mL) at −78 °C. The mixture was warmed to −40 °C and stirred for 30 min. The mixture was cooled to −78 °C and a solution of **9** (223 mg, 0.50 mmol) in dry THF (5 mL) was added dropwise. The mixture was allowed to warm to room temperature and was stirred for 12 h. After evaporation of the solvent, the residue was diluted with H_2O (30 mL) and was extracted with CH_2Cl_2 (3 × 50 mL). The combined extracts were dried over $MgSO_4$ and the solvent was removed under reduced pressure. The residue was purified by silica gel column chromatography (EtOAc/hexane (1/1)) to give a viscous oil (**10**: 9.5 mg, 6%, 78% *ee*) and a colorless solid (**11**: 98.1 mg, 62%, 90% *ee*). **10**: viscous oil; ^{1}H NMR (300 MHz, $CDCl_3$, TMS): δ = 1.87–2.06 (br. s, 1H), 3.20–3.32 (m, 2H), 3.47–3.56 (m, 1H), 3.81 (s, 3H), 3.88 (dd, 1H, J = 4.6, 11.0 Hz), 3.97 (dd, 1H, J = 8.8, 11.0 Hz), 6.53 (dd, 1H, J = 2.2, 8.1 Hz), 7.00 (d, 1H, J = 8.1 Hz), 7.26 (d, 1H, J = 2.2 Hz), 7.44 (dd, 2H, J = 7.3, 7.3 Hz), 7.55 (t, 1H, J = 7.3 Hz), 7.82 (d, 2H, J = 7.3 Hz); MS: *m/z*: 319 [M^+]. **11**: m.p. 113 °C; ^{1}H NMR (300 MHz, $CDCl_3$, TMS): δ = 1.79 (d, 1H, J = 5.1 Hz), 2.45 (dd, 1H, J = 6.4, 15.9 Hz), 2.70 (dd, 1H, J = 4.6, 15.9 Hz), 3.57–3.68 (m, 1H), 3.78 (s, 3H), 3.98–4.07 (m, 2H), 6.67 (d, 1H, J = 8.4 Hz), 6.93 (d, 1H, J = 8.4 Hz), 7.30 (s, 1H), 7.41–7.47 (m, 2H), 7.55 (t, 1H, J = 7.3 Hz), 7.73 (d, 2H, J = 7.7 Hz); MS: *m/z*: 319 [M^+]; $[\alpha]_D^{23}$ = −50.0 (c = 3.09, $CHCl_3$).

Received: August 7, 1995 [Z 8288 IE]
German version: *Angew. Chem.* **1996**, *108*, 818–820

Keywords: asymmetric syntheses · cuprates · copper compounds · metalations

[1] Lithium trimethylzincate can be used to metalate aromatic halides having electrophilic functional groups: Y. Kondo, N. Takazawa, C. Yamazaki, T. Sakamoto, *J. Org. Chem.* **1994**, *59*, 4717–4718.

[2] a) G. H. Posner, *Org. React.* **1972**, *19*, 1–113; b) *ibid.* **1975**, *22*, 253–400; c) B. H. Lipshutz, S. Sengupta, *ibid.* **1992**, *41*, 135–631; d) *Comprehensive Organometallic Chemistry, Vol. 2* (Eds.: G. Wilkinson, F. G. A. Stone, E. W. Abel), Pergamon, Oxford, **1982**; e) G. Van Koten, J. G. Noltes in ref. [2d], pp. 709–763; e) W. Curruther in ref. [2d], pp. 685–722.

[3] a) L. Zhu, R. M. Wehmeyer, R. D. Rieke, *J. Org. Chem.* **1991**, *56*, 1445–1453; b) L. Zhu, R. D. Rieke, *Tetrahedron Lett.* **1991**, *32*, 2865–2866; c) P. Knochel, S. A. Rao, *J. Am. Chem. Soc.* **1990**, *112*, 6146–6148; d) P. Knochel, *ibid.* **1990**, *112*, 7431–7433; e) S. A. Rao, P. Knochel, *ibid.* **1991**, *113*, 5735–5741; f) P. Wipf, *Synthesis* **1993**, 537–557; g) P. Knochel, R. D. Singer, *Chem. Rev.* **1993**, *93*, 2117–2188.

[4] a) G. W. Ebert, R. D. Rieke, *J. Org. Chem.* **1984**, *49*, 5281–5282; b) *ibid.* **1988**, *53*, 4482–4488; c) R. D. Rieke, R. M. Wehmeyer, T.-C. Wu, G. W. Ebert, *Tetrahedron* **1989**, *45*, 443–454; d) R. D. Rieke, B. T. Dawson, D. E. Stack, D. E. Stinn, *Synth. Commun.* **1990**, *20*, 2711–2721; e) G. W. Ebert, J. W. Cheasty, S. S. Tehrani, E. Aouad, *Organometallics* **1992**, *11*, 1560–1564; f) R. D. Rieke, D. E. Stack, B. T. Dawson, T.-C. Wu, *J. Org. Chem.* **1993**, *58*, 2483–2491; g) G. W. Ebert, D. R. Pfennig, S. D. Suchan, T. A. Donovan, Jr., *Tetrahedron Lett.* **1993**, *34*, 2279–2282.

[5] H. Gilman, R. G. Jones, L. A. Woods, *J. Org. Chem.* **1952**, *17*, 1630–1634.

[6] a) B. H. Lipshutz, R. S. Wilhelm, D. M. Floyd, *J. Am. Chem. Soc.* **1981**, *103*, 7672–7674; b) B. H. Lipshutz, J. A. Kozlowski, R. S. Wilhelm, *ibid.* **1982**, *104*, 2305–2307; c) *J. Org. Chem.* **1983**, *48*, 546–550; d) B. H. Lipshutz, R. S. Wilhelm, J. A. Kozlowski, D. Parker, *ibid.* **1984**, *49*, 3928–3938; e) B. H. Lipshutz, R. S. Wilhelm, J. A. Kozlowski, *ibid.* **1984**, *49*, 3938–3942; f) *Tetrahedron*, **1984**, *40*, 5005–5038; g) B. H. Lipshutz, *Synthesis*, **1987**, 325–341.

[7] a) T. Sakamoto, Y. Kondo, N. Murata, H. Yamanaka, *Tetrahedron Lett.* **1992**, *33*, 5373–5374; b) *Tetrahedron*, **1993**, *49*, 9713–9720; c) T. Sakamoto, Y. Kondo, N. Takazawa, H. Yamanaka, *Heterocycles* **1993**, *36*, 941–942; d) *Tetrahedron Lett.* **1993**, *34*, 5955–5956.

[8] a) B. J. Wakefield, *The Chemistry of Organolithium Compounds*, Pergamon, Oxford, **1974**; b) *Organolithium Method*, Academic Press, London, **1988**.

[9] a) C. Tamborski, G. J. Moore, *J. Organomet. Chem.* **1971**, *26*, 153–156; b) H. H. Paradies, M. Gorbing, *Angew. Chem.* **1969**, *81*, 293; *Angew. Chem. Int. Ed. Engl.* **1969**, *8*, 279.

[10] a) H. O. House, D. G. Koepsell, W. J. Campbell, *J. Org. Chem.* **1972**, *37*, 1003–1011; b) G. M. Whitesides, W. F. Fischer, Jr., J. S. San Filippo, Jr., R. W. Bashe, H. O. House, *J. Am. Chem. Soc.* **1969**, *91*, 4871–4882; c) F. Babdri, L. DiNunno, S. Florio, G. Marchese, F. Naso, *J. Organomet. Chem.* **1979**, *166*, 265–270.

[11] Although the structure of $[Li_2Cu(CN)R_2]$ is still uncertain and is a controversial issue, the synthetic potential of these organocopper species should be distinguished from that of the Gilman-type lower order cuprates. For recent discussion on the structure of cyanocuprates see a) J. P. Snyder, D. P. Spangler, J. R. Behling, *J. Org. Chem.* **1994**, *59*, 2665–2667; b) B. H. Lipshutz, E. L. Ellsworth, T. J. Siahaan, *J. Am. Chem. Soc.* **1988**, *110*, 4834–4835; c) S. H. Bertz, *ibid.* **1990**, *112*, 4031–4032; d) B. H. Lipshutz, S. Sharma, E. L. Ellsworth, *ibid.* **1990**, *112*, 4032–4034.

[12] a) C. G. Chidester, W. C. Krueger, S. A. Mizsak, D. J. Duchamp, D. G. Martin, *J. Am. Chem. Soc.* **1981**, *103*, 7629; b) I. Takahashi, K. Takahashi, M. Ichimura, M. Morimoto, K. Asano, I. Kawamoto, F. Tomita, H. Nakano, *J. Antibiot.* **1988**, *41*, 1915; c) M. Ichimura, T. Ogawa, K. Takahashi, E. Kobayashi, I. Kawamoto, T. Yasuzawa, I. Takahashi, H. Nakano, *ibid.* **1990**, *43*, 1037.

[13] CC-1065 synthesis: a) D. L. Boger, R. S. Coleman, *J. Am. Chem. Soc.* **1988**, *110*, 1321–1323; b) *ibid.* **1988**, *110*, 4796–4807; c) R. C. Kelly, I. Gebhard, N. Wicnienski, P. A. Aristoff, P. D. Johnson, D. G. Martin, *ibid.* **1987**, *109*, 6837–6838.

[14] Duocarmycin synthesis: a) D. L. Boger, K. Machiya, *J. Am. Chem. Soc.* **1992**, *114*, 10056–10058; b) D. L. Boger, K. Machiya, D. L. Hertog, P. A. Kitos, D. Holmes, *ibid.* **1993**, *115*, 9025–9036; c) H. Muratake, I. Abe, M. Natsume, *Tetrahedron Lett.* **1994**, *35*, 2573–2576.

[15] T. Sakamoto, Y. Kondo, M. Uchiyama, H. Yamanaka, *J. Chem. Soc. Perkin Trans. 1* **1993**, 1941–1942.

[16] a) W. E. Parham, C. K. Bradsher, *Acc. Chem. Res.* **1982**, *15*, 300–305; b) C. K. Brasher, D. C. Reames, *J. Org. Chem.* **1978**, *43*, 3800–3802; c) L. A. Last, E. R. Fretz, R. M. Coates, *ibid.* **1982**, *47*, 3211–3219; d) M. P. Cook, Jr., I. N. Houpis, *Tetrahedron Lett.* **1985**, *26*, 3643–3646; e) J. H. Babler, W. E. Bauta, *ibid.* **1984**, *25*, 4323–4324; f) I. R. Hardcastle, P. Quale, E. L. M. Ward, *ibid.* **1994**, *35*, 1747–1748; g) K. L. Dhawan, B. D. Gowland, T. Durst, *J. Org. Chem.* **1980**, *45*, 924–926; h) R. D. Rieke, D. E. Stack, B. T. Dawson, T.-C. Wu, *ibid.* **1993**, *58*, 2483–2491.

[17] J. E. Baldwin, *J. Chem. Soc. Chem. Commun.* **1976**, 734–736.

[18] We are currently studying the nature of organozinc compounds derived from $[Zn(SCN)_2]$ and organolithiums; the difference in the reactivity of $[LiZnMe_3]$ and $[Li_3ZnMe_3(SCN)_2]$ was observed. Details of these new organozinc derivatives will be reported elsewhere soon.

[19] The formula $[Li_3Cu(CN)Me_3]$ indicates a mixture of CuCN (1 equiv) and MeLi (3 equiv); however, the reactivity described in the present study suggests that $[Li_3Cu(CN)Me_3]$ is not a mixture of $[Li_2Cu(CN)Me_2]$ and and MeLi.

 © VCH Verlagsgesellschaft mbH, D-69451 Weinheim, 1996 0570-0833/96/3507-0738 $ 15.00+.25/0

An Unprecedented Example of Pt_4Ag_3 Cluster Formation: Synthesis and Crystal Structure of $[Pt_2(dppy)_4(\mu_3\text{-}S)_2Ag_3(\mu_3\text{-}S)_2Pt_2(dppy)_4]^{3+}$**

Vivian Wing-Wah Yam,* Phyllis Kok-Yan Yeung, and Kung-Kai Cheung

The chemistry of soluble metal–sulfur complexes has been of considerable interest for a number years.[1] Recently, we showed that a tetranuclear d^{10} copper(I) cluster containing a μ_4-sulfido moiety exhibits rich photophysical and photochemical properties.[2] This together with our enormous efforts on the design of luminescent polynuclear d^8 and d^{10} metal complexes[2, 3] prompted us to extend our studies to polynuclear d^8 metal–sulfur clusters.[3a, b] We report herein on the novel reaction of a dimeric $[Pt_2(\mu\text{-}S)_2(dppy)_4]$ complex (dppy = 2-diphenylphosphanopyridine) with silver(I) that gives a heptanuclear heterometallic complex, which contains a triangular Ag_3 unit and direct Pt–Ag bonding interactions. Although there have been reports on clusters containing triangular d^{10}-M_3 fragments,[4] those of the coinage metals are mostly held together by polyhydrido complexes of late transition metals.[4, 5] Herein we report the X-ray crystal structure and luminescent behavior of the heptanuclear complex **1**, which contains a non-hydrido bridged Ag_3 unit. Furthermore, the synthesis and photophysical behavior of the related tetranuclear complex **2** dppm = bis(diphenylphosphano)methane) is also described.

$[Pt_2(dppy)_4(\mu_3\text{-}S)_2Ag_3(\mu_3\text{-}S)_2Pt_2(dppy)_4](PF_6)_3$ **1**

$[Pt_2(dppy)_4(\mu_3\text{-}S)_2Ag_2(dppm)](BF_4)_2$ **2**

Reaction of $[Pt_2(\mu\text{-}S)_2(dppy)_4]$ with $[Ag(MeCN)_4]PF_6$ in the molar ratio of 2:3 in THF/MeCN (v/v 1:1) in an inert atmosphere of nitrogen, followed by recrystallization from MeCN/Et_2O gave the heptanuclear complex **1** as yellow crystals in about 50% yield;[6] the identity of **1** has been confirmed by single-crystal X-ray diffraction.[7] Attempted synthesis of the pentanuclear complex cation $[Pt_2(dppy)_4(\mu_3\text{-}S)_2Ag(\mu_3\text{-}S)_2Pt_2(dppy)_4]^+$ by reacting $[Pt_2(\mu\text{-}S)_2(dppy)_4]$ with $[Ag(MeCN)_4](PF_6)$ in a molar ratio of 2:1 was, however, unsuccessful: the reaction afforded **1**; however, in slightly lower yield. This was surprising since an analogous reaction of $[Pt_2(\mu\text{-}S)_2(PPh_3)_4]$ with silver(I) afforded the complex cation $[Ag_2\{Pt_2(\mu_3\text{-}S)_2(PPh_3)_4\}_2]^{2+}$.[8] On the other hand, reaction of $[Pt_2(\mu\text{-}S)_2(dppy)_4]$ with $[Ag_2(dppm)_2(MeCN)_2](BF_4)_2$ in the molar ratio of 1:1 in THF/MeCN (v/v 1:1) in an inert atmosphere of nitrogen, followed by recrystallization from MeCN/Et_2O gave the desired tetranuclear complex **2**. The structure of **1** (Fig. 1) consists of an isosceles triangle of Ag atoms sandwiched between two $[Pt_2(\mu\text{-}S)_2(dppy)_4]$ units, leading to an overall barrel-shaped structure. The Ag(1)–Ag(2) and Ag(2)–Ag(2*) distances of 2.854(3) and 3.042(4) Å, respectively, may indicate weak Ag–Ag interactions, since the Ag–Ag distance in metallic silver is 2.889(6) Å[9] and other reported Ag–Ag distances where bonding is considered to occur range from 2.740 to 3.085 Å;[5a, 10] however, examples of structures with metal atoms at fairly close proximity but without any appreciable bonding interaction between them are also known. The Pt(1)–Ag(2) distance of 2.824(2) Å is also indicative of Pt–Ag bonding.[11] No Pt–Ag bonding is observed in the related complex cation $[Ag_2\{Pt_2(\mu_3\text{-}S)_2(PPh_3)_4\}_2]^{2+}$ (Pt···Ag 3.450(3)–3.905(3) Å).[8] Upon coordination to the Ag_3 unit, the $[Pt_2(\mu\text{-}S)_2(dppy)_4]$ ligand changes the conformation of the Pt_2S_2 four-membered ring from a flat square-planar geometry,[3a] unusual for this class of compounds, to a hinged square-planar geometry, in which the dihedral angle opens from 0 to 132.6°. The Pt(1)–Pt(2) distance of 3.23 Å in **1** is shorter than that in the parent complex $[Pt_2(\mu\text{-}S)_2(dppy)_4]$ (3.555(1) Å).[3a] The S···S separation of 3.11 Å is slightly longer than that in $[Pt_2(\mu\text{-}S)_2(dppy)_4]$ (3.005(2) Å). The Ag(1)-Ag(2)-Ag(2*) and Ag(2)-Ag(1)-Ag(2*) angles of 57.79(5) and 64.41(10)° are close to the value of 60° expected for an equilateral triangle, as observed in a related Ag_3 cluster.[5a] Although as yet we have not determined the X-ray structure of complex **2**, it is likely that the nitrogen atom on the dppy ligand coordinates to the Ag atom to give three-coordinate Ag atoms (Scheme 1).

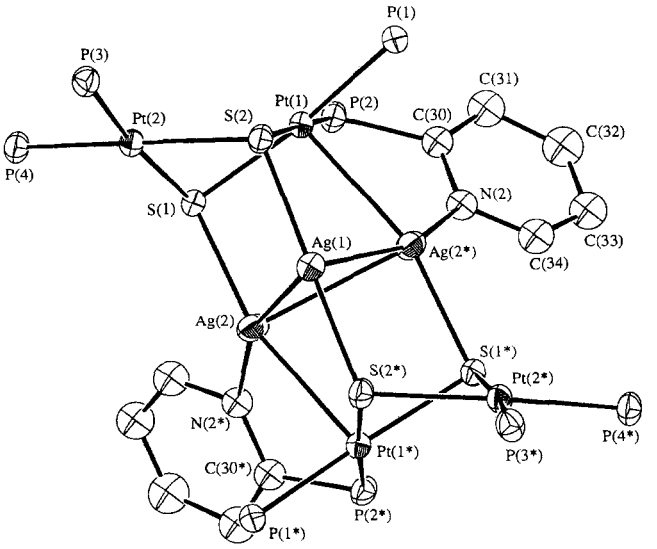

Fig. 1. Perspective drawing of the cation of complex **1** with the atomic numbering scheme. Phenyl and non-coordinating pyridyl rings on the phosphorus atoms have been omitted for clarity. Thermal ellipsoids are shown at the 30% probability levels. Symmetry related atoms (*) have coordinates at $(-x, y, (1/2)-z)$. Selected bond lengths [Å] and angles [°]: Pt(1)–Ag(2*) 2.824(2), Ag(1)–Ag(2) 2.854(3), Ag(2)–Ag(2*) 3.042(4), Pt(1)–S(1) 2.339(6), Pt(1)–S(2) 2.353(6), Pt(2)–S(1) 2.359(6), Pt(2)–S(2) 2.350(6), Ag(1)–S(2) 2.430(6), Ag(2)–S(1) 2.489(6), Ag(2)–N(2*) 2.38(2), Pt···Pt* 3.23, S···S* 3.11; Ag(2)-Ag(1)-Ag(2*) 64.41(10), Ag(1)-Ag(2)-Ag(2*) 57.79(5), S(2)-Ag(1)-S(2*) 178.9(3), S(1)-Ag(2)-Pt(1*) 164.5(2), S(1)-Ag(2)-N(2*) 102.9(5), Pt(1)-Ag(2*)-N(2) 83.9(5), Pt(1)-S(1)-Pt(2) 86.8(2), Pt(1)-S(1)-Ag(2) 98.4(2), Pt(1)-S(2)-Pt(2) 86.7(2), Pt(1)-S(2)-Ag(1) 99.3(2).

The UV/Vis spectra of complexes **1** and **2** show a low-energy absorption band at about 400 nm. Excitation of solid samples of **1** and **2** at $\lambda > 350$ nm at 77 K shows long-lived luminescence at about 560–660 nm (Table 1). An emission lifetime of about 1.5 μs was measured for a solid sample of **2** at room temperature. The long lifetime of the excited state suggests that the

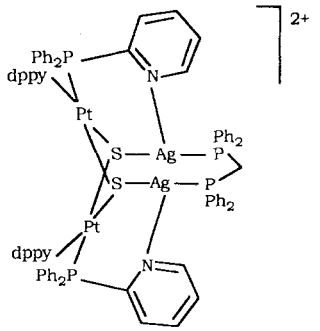

Scheme 1. Proposed structure for the complex cation in **2**.

[*] Dr. V. W. W. Yam, P. K. Y. Yeung, Dr. K. K. Cheung
Department of Chemistry
The University of Hong Kong
Pokfulam Road, Hong Kong (Hong Kong)
Fax: Int. code +2857-1586
e-mail: wwyam@hkucc.hku.hk

[**] V. W.-W. Y. acknowledges financial support from the Research Grants Council, the Croucher Foundation, and The University of Hong Kong. P. K.-Y. Y. acknowledges the receipt of a postgraduate studentship, administered by The University of Hong Kong. dppy = 2-diphenylphosphanopyridine.

Table 1. Photophysical data for complexes **1** and **2**.

Complex	Medium	T [K]	λ_{em} [nm]	τ_0 [μs]
1	solid	298	560	<0.1
	solid	77	560, 635 sh	
	glass [a]	77	560, 630 sh	
	MeCN	298	600	<0.1
2	solid	298	630	1.5 ± 0.2
	solid	77	660	
	glass [a]	77	630	

[a] EtOH:MeOH (4:1, v/v).

emission is most likely associated with a spin-forbidden transition. Similar findings have been observed in the parent complex $[Pt_2(\mu\text{-}S)_2(dppy)_4]$.[3a] Presumably the origin of these transitions is derived from the $[Pt_2(\mu\text{-}S)_2(dppy)_4]$ core. Since the low-energy absorption bands at about 370–400 nm and the emission at about 630 nm are only observable in the parent complex $[Pt_2(\mu\text{-}S)_2(dppy)_4]$ and complexes **1** and **2**, and not in $[Pt(dppy)_2Cl_2]$, we suggest that the origin of these low-energy transitions does not lie in dppy intraligand (IL) nor in metal-to-ligand charge transfer (d(Pt) → π*(dppy), MLCT) transitions. As the sulfido moiety is a good σ-donor, it is likely that the low-energy emitting state arises from states bearing a large amount of ligand-to-metal charge transfer (LMCT) character characteristic of the platinum–sulfur core.[3a] However, for complexes **1** and **2** we cannot exclude the possibility that the emission originates from silver-centered d-s/S → Ag LMCT. In contrast to $[Pt_2(\mu\text{-}S)_2(dppy)_4]$ and complex **2**, complex **1** also emits at about 560 nm in the solid state and in EtOH/MeOH glass. The band at 560 nm may arise from the Ag_3/Ag–S or the Pt–Ag metal-centered cluster core. Silver thiocarbamate clusters have been shown to exhibit low-temperature emissive behavior at similar energies, thought to originate from metal-centered cluster d-s/LMCT.[12] Interestingly, $[Pt_2(dppy)_4(\mu_3\text{-}S)_2Cu_2(dppm)](PF_6)_2$, a complex related to **2**, emits at about 695 nm at 77 K in the solid state.[13] The red shift in emission energy relative to that of **2** may be suggestive of an emitting state bearing a large sulfur-to-metal LMCT character. Assuming that the first quasireversible oxidation couple of **2** at +0.53 V and the first irreversible oxidation wave of **1** at +0.66 V (vs the ferrocenium–ferrocene couple) are metal-centered in nature, excited state reduction potentials $E^\circ(\{Pt_2Ag_2\}^{3+/2+*})$ and $E^\circ(\{Pt_4Ag_3\}^{4+/3+*})$ of about −1.09 and −0.96 V, respectively, versus the saturated calomel electrode (zero spectroscopic energy $E_{o-o} \approx 2.00$ eV) are estimated.

Preliminary work shows that **2** reacts photochemically with alkyl halides.[14] Comparison of the relative quantum yields using a series of structurally related alkyl halides such as CBr_4, $CHBr_3$, and their chloro analogues shows that the reactivity appears to follow the trend of the reduction potentials of the halides. This suggests a photoredox mechanism for the reactions.

Received: September 13, 1995 [Z 8395 IE]
German version: *Angew. Chem.* **1996**, *108*, 839–841

Keywords: clusters · platinum compounds · silver compounds

[1] T. Shibahara, *Coord. Chem. Rev.* **1993**, *123*, 73; A. Müller, B. Krebs, *Sulfur. Its Significance for Chemistry, for the Geo-, Bio- and Cosmosphere and Technology*, Elsevier, Amsterdam, **1984**; R. H. Holm, S. Ciurli, J. A. Weigel, *Prog. Inorg. Chem.* **1991**, *38*, 1; A. Müller, E. Diemann in *Comprehensive Coordination Chemistry, Vol. 2* (Ed.: G. Wilkinson), Pergamon, Oxford, **1987**, pp. 515–550.

[2] V. W. W. Yam, W. K. Lee, T. F. Lai, *J. Chem. Soc. Chem. Commun.* **1993**, 1571.

[3] a) V. W. W. Yam, P. K. Y. Yeung, K. K. Cheung, *J. Chem. Soc. Chem. Commun.* **1995**, 267; b) *J. Chem. Soc. Dalton Trans.* **1994**, 2587; c) V. W. W. Yam, L. P. Chan, T. F. Lai, *Organometallics* **1993**, *12*, 2197; d) *J. Chem. Soc. Dalton Trans.* **1993**, 2075; e) V. W. W. Yam, W. K. Lee, T. F. Lai, *Organometallics* **1993**, *12*, 2383; f) V. W. W. Yam, W. K. Lee, *J. Chem. Soc. Dalton Trans.* **1993**, 2097; g) V. W. W. Yam, S. W. K. Choi, *ibid.* **1994**, 2057.

[4] See for example, D. Imhof, L. M. Venanzi, *Chem. Soc. Rev.* **1994**, 185; R. J. Puddephatt, L. Manojlovic-Muir, K. W. Muir, *Polyhedron* **1990**, *9*, 2767.

[5] See for example, a) A. J. Amoroso, J. C. Jeffrey, P. L. Jones, J. A. McCleverty, E. Psillakis, M. D. Ward, *J. Chem. Soc. Chem. Commun.* **1995**, 1175; b) A. Albinati, F. Demartin, P. Janser, L. F. Rhodes, L. M. Venanzi, *J. Am. Chem. Soc.* **1989**, *111*, 2115; c) A. Albinati, J. Eckert, P. Hofmann, H. Rüegger, L. M. Venanzi, *Inorg. Chem.* **1993**, *32*, 2377; d) F. Bachechi, J. Ott, L. M. Venanzi, *J. Am. Chem. Soc.* **1985**, *107*, 1760; e) T. H. Lemmen, J. C. Huffman, K. G. Caulton, *Angew. Chem.* **1986**, *98*, 267; *Angew. Chem. Int. Ed. Engl.* **1986**, *25*, 262; f) L. F. Rhodes, J. C. Huffman, K. G. Caulton, *J. Am. Chem. Soc.* **1985**, *107*, 1759.

[6] **1**: Elemental analysis: Calcd for $1 \cdot 2H_2O$ (found) (%): C 42.87 (42.95), H 3.05 (3.01), N 2.94 (2.73); UV/Vis (MeCN): $\lambda = 394$ nm (2900 $L\,mol^{-1}\,cm^{-1}$); positive FAB-MS: ion cluster at m/z: 1742 $[M-2PF_6]^{2+}$, 1114 $[M]^{3+}$; ^1H NMR (270 MHz, CD_3CN, 298 K): $\delta = 6.5$–8.5 (m, 112H, dppy); molar conductivity (298 K, Me_2CO): 410 $\Omega^{-1}\,cm^2\,mol^{-1}$ (3:1 electrolyte). **2**: elemental analysis: calcd (found) (%): C 49.04 (49.37), H 3.46 (3.35), N 2.74 (2.55); UV/Vis (MeCN): $\lambda = 394$ nm (1225 $L\,mol^{-1}\,cm^{-1}$); positive FAB-MS: ion cluster at m/z: 2198 $[M-BF_4]^+$, 2111 $[M-2BF_4]^+$, 1055 $[M-2BF_4]^{2+}$; ^1H NMR (270 MHz, CD_3CN, 298 K): 3.64 (hept., 2H, CH_2), 7.0–8.0 (m, 72H, Ph and 3,4,5-pyH), 8.18 (d, 4H, 6-pyH).

[7] **1**: monoclinic, space group $C2/c$ (no. 15), $a = 27.611(3)$, $b = 22.392(5)$, $c = 29.384(3)$ Å, $\beta = 104.025(9)°$, $V = 17625(5)$ Å^3, $Z = 4$, $\rho_{calcd} = 1.435\,g\,cm^{-3}$, $\mu(Mo_{K\alpha}) = 36.83\,cm^{-1}$, $F(000) = 7392$; $R = 0.059$ for 6283 reflections with $I > 3.0\sigma(I)$; Rigaku AFC7R diffractometer with graphite monochromatized $Mo_{K\alpha}$ radiation ($\lambda = 0.71073$ Å); ω-2θ scan. The structure was solved by Patterson and Fourier methods and subsequent refinement by full-matrix least squares using the MSC-Crystal Structure Package TeXsan on a Silicon Graphics Indy computer. Crystallographic data (excluding structure factors) for the structure(s) reported in this paper have been deposited with the Cambridge Crystallographic Data Centre as supplementary publication no. CCDC-179-3. Copies of the data can be obtained free of charge on application to The Director, CCDC, 12 Union Road, Cambridge CB2 1EZ, UK (fax: Int. code +(1223) 336-033; e-mail: teched@chemcrys.cam.ac.uk).

[8] C. E. Briant, T. S. A. Hor, N. D. Howells, D. M. P. Mingos, *J. Organomet. Chem.* **1983**, *256*, C15.

[9] R. W. G. Wyckoff *Crystal Structures, Vol 1*, 2nd ed., Wiley, New York, **1963**, p.10. From the unit cell edge, 4.086 Å, the internuclear distance of 2.88 Å is calculated.

[10] See for example, P. J. M. W. L. Birker, G. C. J. Verschoor, *J. Chem. Soc. Chem. Commun.* **1981**, 322.; N. W. Alcock, P. Moore, P. A. Lampe, K. F. Mock, *J. Chem. Soc. Dalton Trans.* **1982**, 207; N. C. Baenziger, A. W. Struss, *Inorg. Chem.* **1976**, *15*, 1807; W. Beesk, P. G. Jones, H. Rumpel, E. Schwarzmann, G. M. Sheldrick, *J. Chem. Soc. Chem. Commun.* **1981**, 664; G. W. Eastland, M. A. Mazid, D. R. Russell, M. C. R. Symons, *J. Chem. Soc. Dalton Trans.* **1980**, 1682; H. Dietrich, W. Storck, G. J. Manecke, *J. Chem. Soc. Chem. Commun.* **1982**, 1036.

[11] R. Usón, J. Forniés, B. Menjón, F. A. Cotton, L. R. Falvello, M. Tomás, *Inorg. Chem.* **1985**, *24*, 4651.

[12] P. C. Ford, A. Vogler, *Acc. Chem. Res.* **1993**, *26*, 220.

[13] V. W. W. Yam, P. K. Y. Yeung, unpublished results.

[14] The photoreactivity studies were performed by irradiating degassed samples of **2** (4×10^{-4} mol L^{-1}) with various alkyl halides (in the concentration range of 0.05–0.85 mol L^{-1}) in acetone with an Oriel 200 W mercury (xenon) lamp equipped with a water lens to remove IR radiation and a UV cutoff filter to allow only light of $\lambda > 350$ nm to pass through. The UV/Vis spectral changes during the course of the reaction were monitored by using a Hewlett-Packard HP8452A diode array spectrophotometer. Comparison of the relative quantum yields using a series of structurally related alkyl halides revealed the following trend in reactivity: $CBr_4 \gg CHBr_3 \geq CCl_4 \gg CHCl_3 \approx CH_2Br_2 \approx CH_2Cl_2$.

Synthesis and Characterization of the Novel Iron Carbonyl Tellurium Chloride Cluster $[Fe_2(CO)_6(\mu\text{-}Cl)(\mu\text{-}TeCl)_2]_2[\eta^2,\mu_2,\mu_2\text{-}Te_2Cl_{10}]$, and Its Decomposition to the Zintl Ion Complex $[Fe_2(CO)_6(\eta^2, \mu_2,\mu_2\text{-}Te_4)(\mu\text{-}TeCl_2)]$**

Jeffrey R. Eveland and Kenton H. Whitmire*

Dedicated to Professor Dr. Herbert W. Roesky on the occasion of his 60th birthday

Clusters comprising transition metal carbonyls and phosphanes with heavy chalcogenide main group elements have been studied in several groups, particularly in the last decade. This work has shown these types of compounds to have a very rich and varied chemistry, and compounds of new structural types continue to be produced.[1] The types of compounds observed have ranged from simple complexes and small clusters[2-5] through polynuclear clusters with large cage structures.[6] In addition, some very novel complexes of polychalcogenide (Zintl) ions with transition metals have been produced in recent years.[1d, e] However, such compounds containing intact chalcogenide–halogen bonds have been conspicuously absent, with the exception of one recent report.[7] In an attempt to oxidize the square-pyramidal cluster $[Te_2Fe_3(CO)_9]$ to a cationic species which would be isoelectronic to the known Group 15 compound $[Bi_2Fe_3(CO)_9]$.[8] we studied its reactivity toward SO_2Cl_2 and $SOCl_2$, which are known to oxidize main group centers.[9] Rather than oxidation to $[Te_2Fe_3(CO)_9]^{2+}$, we observed a complex halogenation reaction that gave some very interesting new compounds. Here we report the synthesis and structural characterization of the iron carbonyl tellurium chloride cluster **1**, and its decomposition to the complex **2**, which contains both a novel dibridging Te_4 unit and a linear $TeCl_2$ moiety.

$[Fe_2(CO)_6(\mu\text{-}Cl)(\mu\text{-}TeCl)_2]_2[\eta^2,\mu_2,\mu_2\text{-}Te_2Cl_{10}]$ **1**

$[Fe_2(CO)_6(\eta^2,\mu_2,\mu_2\text{-}Te_4)(\mu\text{-}TeCl_2)]$ **2**

The reaction of $[Te_2Fe_3(CO)_9]$ (**3**) with SO_2Cl_2 (or $SOCl_2$) in CH_2Cl_2 gives **1** cleanly. It may be isolated as an orange solid in 89% yield based on Te and 40% based on Fe, indicating that tellurium is the limiting agent in the reaction. Compound **1** is reasonably stable in solution, and may be recrystallized from CH_2Cl_2 by cooling a concentrated solution to $-20\,^{\circ}C$, or by solvent diffusion with hexanes. Allowing a solution of **1** to stand for a week to ten days gives complex **2** as a crystalline orange solid in 73% yield based on Te and 44% based on Fe. Complex **2** dissolves in CH_3CN, but is extremely unstable in solution; the half-life is approximately three minutes. It is, however, stable over long periods of time in the solid state. Carbon monoxide analyses of compounds **1** and **2** gave results consistent with the formulas derived from the crystal structure determinations.[10] The ^{13}C NMR spectrum of **1** at room temperature shows two resonances for the carbonyl ligands ($\delta = 204.1$ and 194.8) with relative peak areas of approximately 1:2, respectively. These resonances are within the expected regions for carbonyl ligands in cluster molecules, but the resonance at about $\delta = 195$ is at very high field for CO ligands bound to iron. These signals are quite sharp, indicating that little or no exchange of the carbonyl ligands in the two environments takes place at room temperature. Attempts to obtain ^{125}Te spectra were unsuccessful, probably due to the presence of the quadrupolar Cl nuclei, but fluxional processes cannot be ruled out.

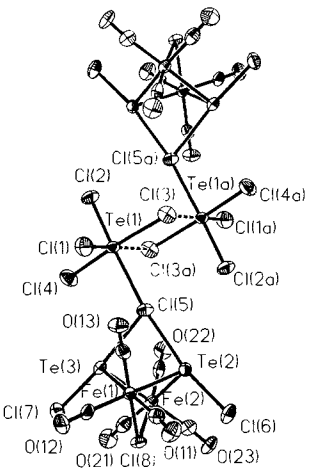

Fig. 1. Crystal structure of **1** showing 50% probability thermal ellipsoids and the atom labeling scheme. Important bond lengths [Å] and angles [°]: Te(1)–Cl(1) 2.343(2), Te(1)–Cl(2) 2.341(2), Te(1)–Cl(3) 2.716(2), Te(1)–Cl(3A) 2.858(2), Te(1)–Cl(4) 2.376(2), Te(1)–Cl(5) 2.829(2), Te(2)–Cl(5) 2.857(2), Te(2)–Cl(6) 2.401(2), Te(3)–Cl(5) 2.860(2), Te(3)–Cl(7) 2.409(2), Te–Fe av 2.604(2), Fe–Cl(8) av 2.334(2); *cis* Cl-Te(1)-Cl av 89.98(8), *trans* Cl-Te(1)-Cl av 176.11(7), Te(1)-Cl(5)-Te(2) 171.35(9), Te(1)-Cl(5)-Te(3) 114.10(7), Te(2)-Cl(5)-Te(3) 73.63(5), Te-Fe-Te av 82.26(4), Te-Fe-Cl(8) av 84.17(6), Cl(5)-Te(2,3)-Cl av 171.92(7), Fe-Te-Fe av 75.70(4), Fe(1)-Cl(8)-Fe(2) 86.41(6).

The solid-state structure of **1** (Fig. 1)[10a] consists of two $[\{Fe_2(CO)_6(\mu\text{-}Cl)(\mu\text{-}TeCl)_2\}]^+$ units, linked by coordination of the two μ-Te atoms to a chloro ligand of the $[Te_2Cl_{10}]^{2-}$ complex ion, producing an unusual triply bridging chloride ion (Cl(5)). The iron centers have approximate octahedral coordination, while the tellurium atoms have a coordination environment which may best be described as trigonal bipyramidal; a stereochemically active lone pair of electrons occupies an equatorial site. The terminal chloro ligands are tilted slightly away from the cluster core and toward Cl(5), giving a smaller Cl-Te-Cl(5) angle (av 171.92(7)°). The most likely cause of this effect is steric repulsions between the terminal chloro ligands and the carbonyl ligands on the iron centers. The coordination around Te(1) is very nearly octahedral; only very slight distortions are observed. Octahedral coordination by halogeno ligands is observed for tellurium in many of its complexes,[11] but this type of arrangement has not been observed in molecular organo-transition metal compounds, although some very interesting main group tellurium chloride compounds in which the Te has square-pyramidal geometry have been reported.[12] Te(1) retains a lone pair of electrons which does not appear to be stereochemically active but may exert an influence on the Te–Cl bond lengths. The Te–Fe (av 2.604(2) Å)[2-5] and Fe–Cl (av 2.334(2) Å)[13] distances are within the expected range.

The angles around Cl(5) are unusual in that the angles are severely distorted from the anticipated pyramidal configuration. The Cl atom resides in a planar environment (sum of angles at Cl(5) = 359.1°), but the angles are very asymmetric, as can be seen in Figure 1. The most remarkable feature is the nearly linear Te(1)-Cl(5)-Te(2) angle, which may result from repulsions between the cluster unit and the other chloro ligands on the $[Te_2Cl_{10}]^{2-}$ group.

The Te–Cl bond lengths to the terminal chloro ligands in the cluster unit (Te(2)–Cl(6) and Te(3)–Cl(7)) are within the normal bonding range (av 2.405 Å),[11, 14] as are those for the chloro ligands terminally bound to the tellurium atoms of the central $[Te_2Cl_{10}]^{2-}$ unit (av 2.353(2) Å). The Te(1)–Cl(3) and Te(1)–Cl(3a) distances are much longer (2.716(2) and 2.858(2) Å, respectively). The observed asymmetry in these bonds is not surprising, since bridging ligands are quite often

[*] Prof. Dr. K. H. Whitmire, J. R. Eveland
Department of Chemistry, Rice University
Houston, TX USA 77251-1892
Fax: Int. code +(713)285-5155
e-mail: whitmir@pop.rice.edu

[**] The authors wish to thank the National Science Foundation and the Robert A. Welch foundation for financial support of this research.

unequally shared between the two centers; however, one of the contacts under such circumstances is usually a normal bonding length. The greater length of the two bonds here may be caused by the presence of a lone pair of electrons on Te(1). Nearly equal sharing of the chloro ligands between the two tellurium centers is an effect also observed in other inorganic halides of tellurium. The distances between the Te atoms and the μ_3-chloro ligand Cl(5) are also long and nearly equal; only the Te(1)–Cl(5) distance is slightly shorter (2.829(2) Å) than the others (av 2.859(2) Å).

Compound **1** contains many more chloro ligands than may be accounted for by the reaction stoichiometry relative to SO_2Cl_2, so it is clear that the halogenated solvent, CH_2Cl_2, plays a key role in the production of this cluster. The fate of the methylene unit of the solvent molecule was not traced in the reaction. The structural relationship between the starting cluster $[Te_2Fe_3(CO)_9]$ and **1** gives no obvious indication of the mechanism of this reaction, but in spite of the loss of a considerable amount of iron (detected spectrophotometrically as $FeCl_2$), most of the tellurium in the starting material is retained in the isolated product. Similarly, the mechanistic route in the transformation from **1** to **2** by necessity involves the loss of chloro ligands and some iron species, perhaps through the initial dissociation of the central $[Te_2Cl_{10}]^{2-}$ ion from the cluster.

Compound **2** exists in the solid state[10b] as discrete molecules; two crystallographically unique molecules are present per asymmetric unit (Fig. 2). These molecules are very similar in

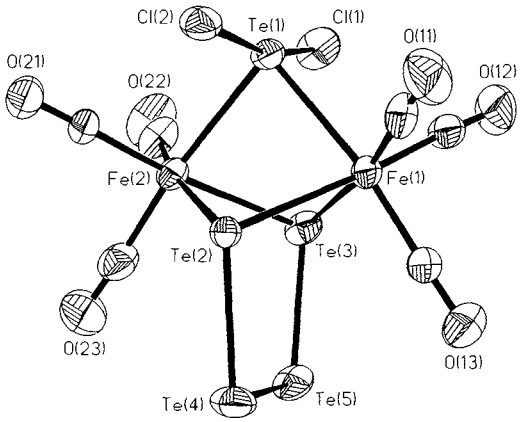

Fig. 2. Crystal structure of **2** showing 50% probability thermal ellipsoids and the atom labeling scheme. Important bond distances [Å] and angles [°]: Te–Fe av 2.624(2), Te(2)–Te(4) 2.744(2), Te(3)–Te(5) 2.730(2), Te(4)–Te(5) 3.738(2), Te(1)–Cl(1) 2.549(4), Te(1)–Cl(2) 2.705(3), Fe-Te-Fe av 81.94(7), Fe-Te(1)-Cl(1) av 96.2(1), Fe-Te(1)-Cl(2) av 92.94(9), Cl(1)-Te(1)-Cl(2) 167.9(1), Te(2)-Te(4)-Te(5) 99.12(5), Te(3)-Te(5)-Te(4) 96.26(5), Te(1)-Fe-Te av 81.08(7), Te(2)-Fe-Te(3) av 82.83(6). For the other unique molecule in the asymmetric unit, the values are: Te–Fe av 2.618(2), Te(7)–Te(9) 2.734(1), Te(8)–Te(10) 2.739(1), Te(9)–Te(10) 2.740(2), Te(6)–Cl(3) 2.579(3), Te(6)–Cl(4) 2.662(3), Fe-Te-Fe av 81.46(6), Fe-Te(6)-Cl(3) av 94.86(9), Fe-Te(6)-Cl(4) av 92.65(9), Cl(3)-Te(6)-Cl(4) 170.0(1), Te(7)-Te(9)-Te(10) 98.85(4), Te(8)-Te(10)-Te(9) 96.79(5), Te(6)-Fe-Te av 81.38(6), Te(7)-Fe-Te(8) av 83.33(5)

structure, but some bond lengths and angles differ by slightly more than 3σ. There are two $[Fe(CO)_3]^+$ fragments doubly bridged by a $[Te_4]^{2-}$ unit and also bridged by an unusual $TeCl_2$ moiety. An unusual feature of this complex is the presence of both oxidized ($TeCl_2$) and reduced (Te_4^{2-}) tellurium. The bridging $TeCl_2$ unit has a trigonal-bipyramidal arrangement of electron pairs with the lone pair occupying an equatorial site, as observed for the iron-bound tellurium atoms in **1**. Since the Te center of the $TeCl_2$ unit apparently retains lone pairs of electrons, it is best considered as Te^{4+} and serves as a one-electron donor to each iron atom. Each iron atom attains an 18-electron configuration without formation of an Fe–Fe bond.

The square Te_4 unit bridges symmetrically between the two iron centers through two terminal atoms of the ring. The Te-Te-Te angles in the Te_4^{2-} chain (av 97.69(5)°) are slightly larger than 90°, which is normal for a metal-bound E_4 unit as has been established in a number of mononuclear complexes. The Te–Te distances within the Te_4 unit are within the normal range for a metal-bound tellurium ring[15] and are all approximately equal within experimental error. To our knowledge, the only other compounds reported to have an E_4 unit bridging two metals are $[Cp^*_2M_2(\mu\text{-Se})(\eta^2,\mu_2,\mu_2\text{-Se}_4)]$ (M = Co, Rh; Cp* = C_5Me_5).[16]

The Cl-Te-Cl angle is nearly linear (167.9(1)°) and the Te-Cl distances are quite asymmetric. For the first molecule in the asymmetric unit, one Te–Cl distance is similar to that observed in inorganic tellurium chlorides,[11,13] but the other (Te(1)–Cl(2)) is considerably longer. The lengths of the Te–Cl distances in the second molecule (2.579(3) and 2.662(3) Å) show less asymmetry. There are no short intermolecular contacts under about 3.8 Å which could account for this effect.

The coordination spheres around the iron atoms are quite regular; the angles are very near to 90° (av 93.1(7)°). Te–Fe bond parameters (av 2.624(2) Å) are within the range normally observed for bridging tellurium–iron bonding interactions.

Experimental Procedure

1: $[Te_2Fe_3(CO)_9]$ (1.50 g, 2.22 mmol) was weighed into a Schlenk flask and dissolved in CH_2Cl_2 (80 mL). SO_2Cl_2 (0.36 mL, 4.5 mmol, 0.60 g) was added by syringe, and the solution stirred for one hour. The deep orange solution was then filtered through diatomaceous earth and the solvent removed in vacuo. The solid was washed with Et_2O (3 × 20 mL) and dried under vacuum to give analytically pure **1** (yield 1.25g, 89% based on Te). The solid was recrystallized by dissolution in CH_2Cl_2 (30 mL) and cooling at −20 °C for two days, giving bright orange platelike crystals of **1**. Compound **1** is soluble in THF, CH_2Cl_2, and CH_3CN, partially soluble in acetone, and insoluble in hexanes, diethyl ether, and toluene. The compound is unstable in strongly coordinating solvents such as CH_3CN. IR (ν(CO) [cm^{-1}], CH_2Cl_2): 2115 (w), 2101 (vs), 2085 (w), 2072 (m), 2049 (ms). ^{13}C NMR (62.90 MHz, CD_2Cl_2, 295 K): δ = 204.1, 194.8 (s, CO). Analysis of CO content by digestion of compounds with $[C_6H_5NH]Br_3$ in CH_2Cl_2 and subsequent quantitation of liberated CO with a Toepler pump. Anal. calcd. for **1**: 1.08 mmol CO; found: 1.07 mmol CO.

2: **1** (0.500 g, 0.528 mmol) was weighed into a Schlenk flask and dissolved in CH_2Cl_2 (30 mL). The solution was allowed to stand for one week at room temperature, yielding a mixture of deep orange block-shaped crystals of **2** and a black powder. The powder was partially removed by swirling the solution followed by decanting the fine powder suspension. This was repeated several times with fresh CH_2Cl_2 to give nearly pure **2**. The crystals were separated manually from the remainder of the dark powder to give analytically pure **2** (yield 0.227 g, 73% based on Te). Compound **2** is insoluble in all common organic solvents except CH_3CN, but is extremely unstable in solution. IR (ν(CO) [cm^{-1}], CH_3CN): 2075 (vs), 2036 (m). Analysis of CO content by digestion of compounds with $[C_6H_5NH]Br_3$ in CH_2Cl_2 and subsequent quantitation of liberated CO with a Toepler pump. Anal. calc. for **2**. 0.82 mmol CO; found. 0.80 mmol CO.

Received: October 25, 1995 [Z.8497IE]
German version: *Angew. Chem.* **1996**, *108*, 841–843

Keywords: carbonyl complexes · clusters · halogen compounds · iron compounds · tellurium compounds

[1] Reviews: a) N. A. Compton, R. J. Errington, N. C. Norman, *Adv. Organomet. Chem.* **1990**, *31*, 91; b) K. H. Whitmire, *J. Coord. Chem.* **1988**, *17*, 95; c) W. A. Herrmann, *Angew. Chem.* **1986**, *98*, 57; *Angew. Chem. Int. Ed. Engl.* **1986**, *25*, 56; d) M. C. Kanatzidis, S.-P. Huang, *Coord. Chem. Rev.* **1994**, *130*, 509; e) L. C. Roof, J. W. Kolis, *Chem. Rev.* **1993**, *93*, 1037.

[2] a) E. J. Voss, C. L. Stern, D. F. Shriver, *Inorg. Chem.* **1994**, *33*, 1087; b) P. Mathur, B. Manimaran, M. M. Hossain, R. Shanbag, J. Murthy, I. S. Saranathan, C. V. V. Satyanarayana, M. M. Bhadbhade, *J. Organomet. Chem.* **1995**, *490*, 173; c) S. Hüffner, K. Polborn, W. Beck, *Organometallics* **1995**, *14*, 953.

[3] a) D. A. Lesch, T. B. Rauchfuss, *Organometallics* **1982**, *1*, 499; b) A. L. Rheingold, R. L. Ostrander, P. Mathur, *Acta Crystallogr. Sect. C* **1993**, *49*, 1741.

[4] a) S. Schulz, M. Andruh, T. Pape, T. Heinze, H. W. Roesky, L. Häming, A. Kuhn, R. Herbst-Irmer, *Organometallics* **1994**, *13*, 4004; b) C. S. Strouse, L. F. Dahl, *J. Am. Chem. Soc.* **1971**, *93*, 6032; c) P. Braunstein, A. Tiripicchio, M. Tiripicchio Camellini, E. Sappa, *Inorg. Chem.* **1981**, *20*, 3586; d) K. Fischer, W. Deck, M. Schwarz, H. Vahrenkamp, *Chem. Ber.* **1985**, *118*, 4946; e) L. E. Bogan, Jr., T. B. Rauchfuss, A. L. Rheingold, *J. Am. Chem. Soc.* **1985**, *107*, 3843; f) W. A. Herrmann, J. Rohrmann, C. Hecht, *J. Organomet. Chem.* **1985**, *290*, 53; g) R. E. Bachman, K. H. Whitmire, *Organometallics* **1993**, *12*, 1988; h) R. E. Bachman, K. H. Whitmire, J. W. van Hal, *Organometallics* **1995**, *14*, 1792.

[5] a) G. Cetini, P. L. Stanghellini, R. Rosetti, O. Gambino, *J. Organomet. Chem.* **1968**, *15*, 373; b) D. A. Lesch, T. B. Rauchfuss, *Inorg. Chem.* **1981**, *20*, 3583; c) H. Schumann, M. Magerstädt, J. Pickardt, *J. Organomet. Chem.* **1982**, *240*, 407; d) B. W. Eichhorn, R. W. Haushalter, J. S. Merola, *Inorg. Chem.* **1990**, *29*, 728; e) G. Gervasio, *J. Organomet. Chem.* **1993**, *445*, 147; f) L. C. Roof, D. M. Smith, G. W. Drake, W. T. Pennington, J. W. Kolis, *Inorg. Chem.* **1995**, *34*, 337.

[6] a) J. G. Brennan, T. Siegrist, Y.-U. Kwon, S. M. Stuczynski, M. L. Steigerwald, *J. Am. Chem. Soc.* **1992**, *114*, 10334; b) D. Fenske, J.-C. Steck, *Angew. Chem.* **1993**, *105*, 254; *Angew. Chem. Int. Ed. Engl.* **1993**, *32*, 238; c) S. Pohl, U. Opitz, *ibid.* **1993**, *105*, 950 and **1993**, *32*, 863; d) S. Dehnen, D. Fenske, *ibid.* **1994**, *106*, 2369 and **1994**, *33*, 2287; e) D. Fenske, A. Fischer, *ibid.* **1995**, *107*, 340 and **1995**, *34*, 307.

[7] L. E. Bogan, Jr., T. B. Rauchfuss, A. L. Rheingold, *Inorg. Chem.* **1985**, *24*, 3722.

[8] M. W. Churchill, J. C. Fettinger, K. H. Whitmire, *J. Organomet. Chem.* **1985**, *284*, 13.

[9] S. Wallenhauer, K. Seppelt, *Angew. Chem.* **1994**, *106*, 1044; *Angew. Chem. Int. Ed. Engl.* **1994**, *33*, 976.

[10] a) Crystal structure data for **1**. $C_6Cl_8Fe_2O_6Te_3$: $M = 946.16$, monoclinic, space group $P2_1c$ (no. 14), $Z = 4$, $a = 16.401(3)$, $b = 10.549(2)$, $c = 14.035(3)$ Å, $\beta = 115.13(3)°$, $V = 2198.4(7)$ Å^3, $\rho_{calcd} = 2.859$ g cm^{-3}, $Mo_{K\alpha}$, $\lambda = 0.71069$ Å, $\mu = 6.213$ mm^{-1}. A total of 2406 independent reflections were collected on a Rigaku AFC5S diffractometer at 223(2) K with θ between 2.37 and 22.49° using 2θ-ω scans, and an absorption correction by azimuthal (ψ) scans was applied. The structure was solved by direct methods (Siemens SHELXTL-PC) and refined (SHELXL-93, G. M. Sheldrick) by full-matrix least-squares on F^2 to final residuals of $R = 0.0255$ (F) and $wR = 0.0647$ (F^2) for observed data ($I > 2\sigma(I)$), and GOF = 1.064; b) crystal structure data for **2**. $C_{12}Cl_4Fe_4O_{12}Te_{10}$: $M = 1977.32$, triclinic, space group $P\bar{1}$ (no. 2), $Z = 2$, $a = 9.045(2)$, $b = 13.684(3)$, $c = 17.961(4)$ Å, $\alpha = 72.74(3)°$, $\beta = 82.19(3)°$, $\gamma = 75.15(3)°$, $V = 2047.7(8)$ Å^3, $\rho_{calcd} = 3.207$ g cm^{-3}, $Mo_{K\alpha}$, $\lambda = 0.71069$ Å, $\mu = 8.673$ mm^{-1}. A total of 6428 independent reflections were collected on a Rigaku AFC5S diffractometer at 223(2) K with θ between 2.24 and 25.00°, and an absorption correction by azimuthal (ψ) scans was applied. The structure was solved by direct methods and refined by full-matrix least-squares on F^2 to final residuals of $R = 0.0418$ (F) and $wR = 0.1167$ (F^2) for observed data ($I > 2\sigma(I)$), and GOF = 0.994. Further details of the crystal structure investigation may be obtained from the Fachinformationszentrum Karlsruhe, D-76344 Eggenstein-Leopoldshafen (Germany), on quoting the depository number CSD-59195.

[11] a) A. C. Hazell, *Acta Chem. Scand.* **1966**, *20*, 165; b) P. H. Collins, M. Webster, *Acta Crystallogr. Sect. B* **1972**, *28*, 1260; c) B. Krebs, B. Buss, D. Altena, *Z. Anorg. Allg. Chem.* **1971**, *386*, 257; d) B. Buss, B. Krebs, *Inorg. Chem.* **1971**, *10*, 2795.

[12] a) J. Münzenberg, M. Noltemeyer, H. W. Roesky, *Chem. Ber.* **1989**, *122*, 1915; b) H. W. Roesky, A. Mazzah, D. Hesse, M. Noltemeyer, *ibid.* **1991**, *124*, 519.

[13] a) E. Solari, F. Corazza, C. Floriani, A. Chiesi-Villa, C. Guastini, *J. Chem. Soc., Dalton Trans.* **1990**, 1345; b) D. K. Mills, Y. M. Hsaio, P. J. Farmer, E. V. Atnip, J. H. Reibenspies, M. Y. Darensbourg, *J. Am. Chem. Soc.* **1991**, *113*, 1421; c) F. A. Cotton, R. L. Luck, K.-A. Son, *Inorg. Chim. Acta* **1991**, *179*, 11; d) F. Bitterer, D. J. Brauer, F. Dörrenbach, F. Gol, P. C. Knüppel, O. Stelzer, C. Krüger, Y.-H. Tsay, *Z. Naturforsch. B* **1991**, *46*, 1131; e) K. R. Dunbar, A. Quillevéré, *Angew. Chem.* **1993**, *105*, 298; *Angew. Chem. Int. Ed. Engl.* **1993**, *32*, 293; f) A. Winter, L. Zsolnai, G. Huttner, *J. Organomet. Chem.* **1982**, *232*, 47.

[14] R. Kniep, D. Mootz, A. Rabenau, *Angew. Chem.* **1973**, *85*, 504; *Angew. Chem. Int. Ed. Engl.* **1973**, *12*, 499.

[15] a) S. C. O'Neal, W. T. Pennington, J. W. Kolis, *Inorg. Chem.* **1990**, *29*, 3134; b) W. A. Flomer, J. W. Kolis, *ibid.* **1989**, *28*, 2513; c) M. A. Ansari, C. H. Mahler, G. S. Chorghade, Y.-J. Lu, J. A. Ibers, *ibid.* **1990**, *29*, 3832; d) T. B. Rauchfuss, S. Dev, S. R. Wilson, *ibid.* **1992**, *31*, 153; e) M. G. Kanatzidis, S.-P. Huang, *ibid.* **1989**, *28*, 4667.

[16] a) H. Brunner, W. Meier, B. Nuber, J. Wachter, M. L. Ziegler, *Angew. Chem.* **1986**, *98*, 907; *Angew. Chem. Int. Ed. Engl.* **1986**, *25*, 907; b) H. Brunner, N. Janietz, W. Meier, J. Wachter, E. Herdtweck, W. A. Herrmann, O. Serhadli, M. L. Ziegler, *J. Organomet. Chem.* **1988**, *347*, 237.

Formation of Stable DNA Loops by Incorporation of Nonpolar, Non-Hydrogen-Bonding Nucleoside Isosteres**

Xiao-Feng Ren, Barbara A. Schweitzer, Charles J. Sheils, and Eric T. Kool*

Hairpin loops are ubiquitous structures found in folded RNA and DNA sequences in nature. Recent reports have noted special stability for certain loop sequences. For example, RNA tetranucleotide loops (tetraloops) having the sequence GNRA and UUCG are more stable than other tetraloops and are highly conserved in nature.[1, 2] DNA tetraloops having the sequence GAAA, in certain contexts, are unusually stable in duplex DNA;[3] in triplex structures the loop sequence CTTTG has been reported to be especially stable as well.[4] In most or all of these cases, structural study has either implicated or identified intraloop hydrogen bonds between bases and/or phosphates as important structural features. It has long been recognized, however, that hydrogen bonds in aqueous solution are weak. In this regard a detailed study of hydrogen bonding in the GAAA tetraloop in RNA concluded that single hydrogen bonds contribute relatively little to the overall stability.[5] While less well understood, base stacking is also known to be at least as important a contribution to nucleic acid stability as hydrogen bonding.[6–8] Studies of loop structures in RNA and DNA have not generally addressed the relative importance of base stacking and hydrogen bonding in stabilizing such loops.

We have undertaken a program to design and synthesize non-hydrogen-bonding nucleoside analogues to be used as probes of the biological noncovalent interactions of oligonucleotides and nucleic acids in general.[9] We now describe the incorporation of three such isosteres into DNA loops, and we have found that such substitutions can lead to significant stabilization of double- and triple-helical folded structures in DNA.

Nucleosides **1** (F), **2** (B), and **3** (D) were designed to act as nearly perfect isosteres for the natural nucleosides thymidine (T) and deoxyadenosine (A) (Fig. 1). However, in contrast to the natural nucleosides, analogues **1**–**3** have little or no hydrogen bonding capability.[9] Compounds **1**–**3** are considerably more hydrophobic and less polar than the natural structures, and evidence from dangling-base studies in our laboratory indicate that they are more efficient at base stacking as well.[9b, 10] To test the effects of their properties on folded DNA structures, we incorporated **1**–**3** at loop positions into DNA hairpin-forming sequences and evaluated the thermal and thermodynamic stabilities of the folded structures.

Nucleosides **1**–**3** were synthesized by using previously described methods.[9] The primary products of coupling of the bases of **1** and **2** with the α-chlorodeoxyribose toluoyl ester synthon are α-anomers,[11] which were converted to β-anomers by acid-catalyzed epimerization.[11b] Compounds **1**–**3** were unknown previous to our reports, although two other substituted indole nucleoside derivatives have recently been described.[12] The coupling of **1**–**3** in oligodeoxynucleotides using standard phosphoramidite chemistry was efficient, with stepwise yields of >95% (trityl cation monitoring). For comparison we also syn-

[*] Prof. E. T. Kool, X.-F. Ren, B. A. Schweitzer, C. J. Sheils
Department of Chemistry, University of Rochester
Rochester, NY 14627 (USA)
Fax: Int. code +(716)473-6889
e-mail: etk@etk.chem.rochester.edu

[**] This work was supported by the National Institutes of Health (GM 52956). E. T. K also acknowledges a Camille and Henry Dreyfus Teacher-Scholar Award and an Alfred P. Sloan Foundation Fellowship.

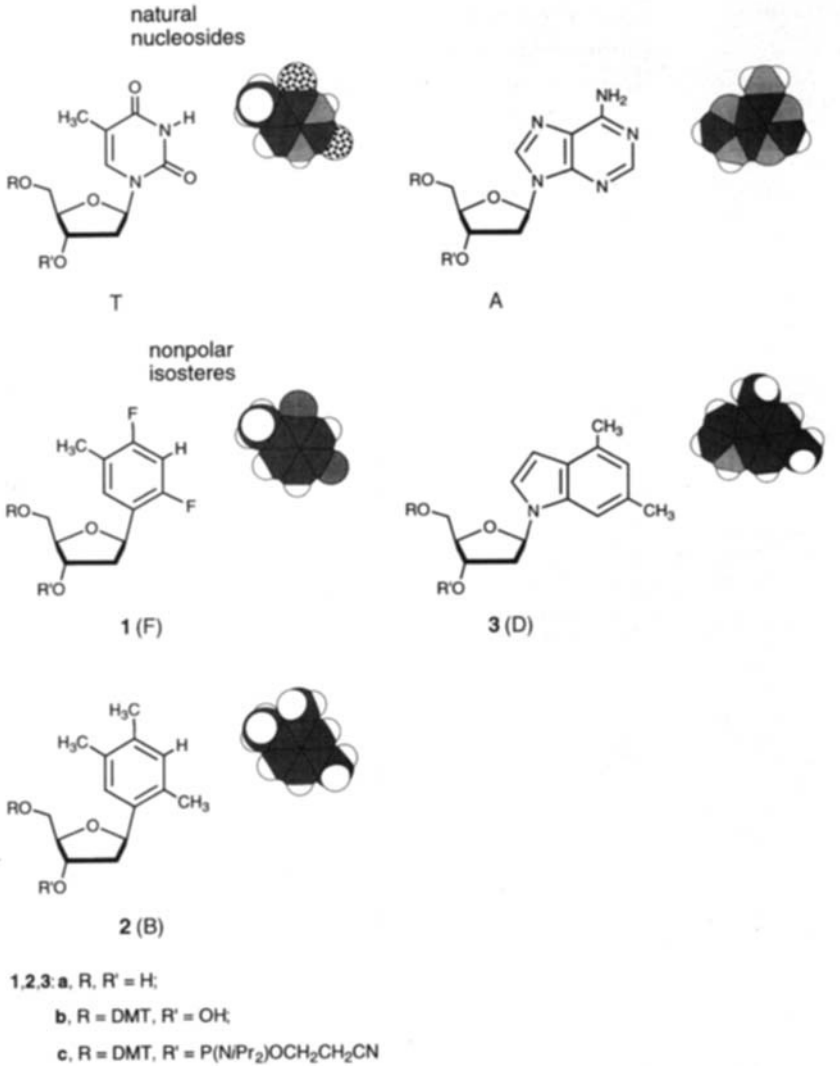

Fig. 1. Structural formulas and space-filling models of nonpolar nucleoside isosteres **1** (F), **2** (B), and **3** (D). Also shown are the structures of the natural nucleosides thymidine and deoxyadenosine.

Table 1. Effects of natural and nonnatural nucleosides in tetranucleotide loops on the stability of double-stranded DNA hairpin structures at pH 7.0 [a].

Sequence	T_m [°C]	$-\Delta G^\circ_{60}$ [kcal mol^{-1}]
thymidine and analogues		
5'-GCAATTGC^{T}T 3'-CGTTAACG$_{T}$T	67.7(0.6)	1.3(0.1)
5'-GCAATTGC^{F}F 3'-CGTTAACG$_{F}$F	78.5(0.5)	3.6(0.3)
5'-GCAATTGC^{B}B 3'-CGTTAACG$_{B}$B	78.4(0.5)	3.1(0.3)
deoxyadenonsine and analogues		
5'-GCAATTGC^{A}A 3'-CGTTAACG$_{A}$A	62.9(0.4)	0.4(0.2)
5'-GCAATTGC^{D}D 3'-CGTTAACG$_{D}$D	67.2(1.2)	1.1(0.1)

[a] Conditions: 100 mM NaCl, 10 mM phosphate (pH 7.0); DNA concentration: 5.0 μM. The sequences with the natural nucleotides are the same as those described in ref. [13]. Data shown are averages; error limits are given in parentheses.

thesized analogous sequences containing the corresponding natural nucleosides at the same positions (see Tables 1 and 2).

We first studied the effects of **1** (F), **2** (B), and **3** (D) in a duplex DNA hairpin loop, by using two self-complementary sequences of eight base pairs bridged by a tetranucleotide loop consisting of four identical residues. Previous studies of this sequence by Breslauer et al.[13] showed that, of sequences containing A_4, C_4, G_4, and T_4 loops, the most stable was the T_4 case, and the least stable, the A_4 case. We studied the properties of sequences containing F_4, B_4, and D_4 loops, and we synthesized the natural T_4 and A_4 analogues for comparison.

Table 1 shows data obtained for the duplex hairpin sequences. Buffer conditions were pH 7.0 (10 mM phosphate) with 100 mM NaCl. All five sequences gave melting transitions that were independent of concentration, confirming the expected hairpin structure as opposed to intermolecular complexes. The data show that the modified hairpin sequences containing **1** (F) and **2** (B) are significantly more stable than the T_4 analogue. The melting temperature (T_m) for the modified F_4 sequence, which contains difluorotoluene nucleosides, is 78.5 °C, or 10.8 °C higher than that of the T_4 loop structure, which is the most stable tetraloop containing four identical natural nucleosides.[13] The four hairpin structures with natural nucleosides (A_4, T_4, C_4, G_4) have T_m values lying in a narrow range between 62 and 68 °C.[13] Free energy values obtained by curve fitting show that the modified loop containing **1** is thermodynamically more stable than the most stable natural loop (the T_4 loop) (Table 1). Similarly, the B_4 hairpin sequence, with trimethylphenyl nucleosides, is almost as stable as the sequence with the F_4 loop.

Interestingly, just as the pyrimidine isosteres give more stable loops than a natural pyrimidine, we find that the purine analogue **3** is more stabilizing than its deoxyadenosine counterpart ($\Delta T_m = 4.5$ K). As was reported by Breslauer et al.,[13] we find that the T_4 loop is more stabilizing than the A_4 loop. Moreover, we find that the nonnatural pyrimidine isosteres **1** and **2** are more stabilizing than the purine isostere **3**. This difference in the natural hairpin structures has been attributed to cross-loop hydrogen bonding. Since in the nonnatural cases this difference cannot be due to hydrogen bonding, it seems likely that steric differences in the pyrimidine and purine analogues may play an important role both in the natural and nonnatural cases.

Because the nonpolar thymidine isostere **1** was found to be the better stabilizing of the two analogues and because it is the best isosteric substitution, we tested it in a triple helix bridging loop. Such folded triplex-forming oligonucleotides are finding increasing use as ligands for single-stranded nucleic acids.[14] The stability of the loops in such a complex depends largely on the nature of the first and last bases in the loop.[4] The nucleoside **1** was therefore placed at these positions in a pentanucleotide loop bridging the pyrimidine strands in an eight-base triplex. For comparison we synthesized the natural T_5-bridged triplex (see Table 2). We examined both 5'- and 3'-type loop orientations[4] at pH 7.0 with 100 mM NaCl and 10 mM $MgCl_2$.

The nonpolar nucleoside **1** gives complexes that are both thermally and thermodynamically more stable than structures containing the natural nucleosides (Table 2). For example, the hydrophobic nucleoside F gives complexes that are 4.8–5.4 K more thermostable than the T,T-substituted oligonucleotides, and

 © VCH Verlagsgesellschaft mbH, D-69451 Weinheim, 1996 0570-0833/96/3507-0744 $ 15.00+.25/0

Table 2. Effects of varying the first and last nucleotides in the loop on the stability of triplexes formed between 21-nucleotide pyrimidine DNAs and complementary 8-nucleotide purine DNA strands at pH 7.0 [a].

Complex with 5′ loop	T_m [°C]	$-\Delta G^\circ_{25}$ [kcal mol^{-1}]	Complex with 3′ loop	T_m [°C]	$-\Delta G^\circ_{25}$ [kcal mol^{-1}]
T T C T T T T C T T -3′ T G A A A A G A A -3′ T T C T T T T C T T -5′	27.2	8.8	5′- T T C T T T T T C T T 5′- A A G A A A A G T 3′- T T C T T T T C T T	25.6	8.4
T F C T T T T C T T -3′ T G A A A A G A A -3′ T F C T T T T C T T -5′	32.6	10.6	5′- T T C T T T T C F T 5′- A A G A A A A G T 3′- T T C T T T T C F T	32.4	10.6

[a] Conditions: 100 mM NaCl, 10 mM $MgCl_2$, 10 mM Na-PIPES (pH 7.0); DNA concentration: 2.0 μM per strand. Errors: ±5 °C in T_m and ± 10% in free energy.

free energies are 1.8–2.2 kcal mol^{-1} more favorable. Previous studies carried out with natural bases in this loop[4] have shown that the T,T case is intermediate in stability; the C,C loop is the least stable and the G,G loop the most stable. The G,G loop was found to be more stable than the T,T analogue by 1.5 kcal mol^{-1}.[4] Thus our F,F loop is more stable than all four cases doubly substituted with the natural bases.

Previous studies have described the use of simple nonnucleotide linkers as loop replacements in nucleic acids.[15] Such loops are often less stabilizing than natural nucleotide loops; this may be due both to the greater rigidity of nucleotide loops relative to the highly flexible nonnucleotide linkers and to favorable base stacking interactions in natural loops, which are missing in simple linkers. The nucleoside analogues in this study are designed to stabilize nucleic acid helices as a result of both rigidity and base stacking. In contrast to natural DNAs, loops containing nucleosides **1**–**3** have the added advantage of being resistant to degradation by nucleases (data not shown). In addition, such nonpolar nucleosides have been shown to pair with low affinity and low specificity with natural sequences[9b] and thus would not interfere with the expected pairing in biological systems.

The present results on the incorporation of hydrophobic nucleoside analogues in oligonucleotide loops show that in general these compounds are significantly stabilizing. Because they do not undergo measurable hydrogen bonding interactions,[9b] it would seem that the best explanation for this behavior is superior base stacking propensity. This suggests a general strategy for stabilizing nucleic acid complexes containing loops: the use of arenes instead of natural bases, especially at positions adjacent to the helix, where stacking interactions are expected to make the greatest contributions. Although the present compounds cannot form stabilizing cross-loop hydrogen bonds, they may have favorable hydrophobic or van der Waals interactions. Detailed structural and physical studies will be necessary to investigate the specific origins of this stability.

Experimental Procedure

Epimerization of α-anomers of **1a** and **2a** (bis-*p*-toluoyl esters) to β-anomers.

1a: To a solution of the α-anomer of the bis-*p*-toluoyl ester of compound **1a** (synthesis described in ref. [9a]) (780 mg, 1.62 mmol) in toluene (50 mL) was added a catalytic amount of benzenesulfonic acid (ca. 10%), one drop of concentrated H_2SO_4, and two to four drops of H_2O. The reaction mixture was stirred vigorously at reflux for 4–6 h, and the mixture was then poured into 5% aqueous $NaHCO_3$ (50 mL) and extracted with EtOAc (3 × 50 mL). The combined organic layers were dried over anhydrous $MgSO_4$ and concentrated to dryness. Silica column chromatography (eluent 8/1 → 2/1 hexanes/EtOAc) of the crude mixture gave 430 mg of **1a** (β-epimer, 46% yield). ^{1}H NMR ($CDCl_3$): δ = 8.02 (2H, d, J = 8.0 Hz), 7.97 (2H, d, J = 8.0 Hz), 7.30–7.37 (1H, m, obscured), 7.31 (2H, d, J = 8.0 Hz), 7.25 (2H, d, J = 8.0 Hz), 6.75 (1H, dd, J = 8.0, 8.0 Hz), 5.64 (1H, br d, J = 5.8 Hz), 5.47 (1H, dd, J = 5.1, 10.8 Hz), 4.78 (1H, dd, J = 3.8, 11.8 Hz), 4.66 (1H, dd, J = 3.7, 11.8 Hz), 4.54 (1H, m), 2.64 (1H, m), 2.46 (3H, s), 2.43 (3H, s), 2.23 (1H, m), 2.17 (3H, s); ^{13}C NMR ($CDCl_3$): δ = 13.8 (d), 22.0 (d), 40.1, 64.9, 74.9, 83.0, 103.0 (t), 120.1 (d), 124.5 (d), 127.3 (d), 128.6, 128.8 (d), 128.9 (d), 144.0 (d), 156.5 (d), 158.0 (d), 155.9 (d), 162.3 (d), 166.1 (d); HRMS (FAB, 3-nitrobenzyl alcohol matrix, M + H$^+$): calcd for $C_{28}H_{26}F_2O_5$ 481.1827, found 481.1853.

2a (β-epimer, 54% yield). ^{1}H NMR ($CDCl_3$): δ = 8.02 (2H, d, J = 8.0 Hz), 7.97 (2H, d, J = 8.0 Hz), 7.30–7.37 (1H, m, obscured) 7.32 (2H, br d, J = 10.7 Hz), 7.31 (2H, br d, J = 11.2 Hz), 7.24 (1H, s), 6.95 (1H, s), 5.65 (1H, br d, J = 5.6 Hz), 5.42 (1H, dd, J = 5.0, 10.8 Hz), 4.76 (1H, dd, J = 3.9, 11.8 Hz), 4.70 (1H, dd, J = 3.6, 11.8 Hz), 4.55 (1H, m), 2.56 (1H, m), 2.46 (3H, s), 2.43 (3H, s), 2.31 (3H, s), 2.23 (3H, s), 2.18 (1H, m), 2.13 (3H, s); ^{13}C NMR ($CDCl_3$): δ = 18.2, 19.5, 22.1 (d), 41.0, 65.0, 82.5, 126.2, 127.0 (d), 128.6 (d), 128.8 (d), 132.1 (d), 135.5, 136.2, 141.4, 144.5, 165.5, 166.0; HRMS (FAB, 3-nitrobenzyl alcohol matrix, M^+): calcd for $C_{30}H_{32}O_5$ 472.2250, found 472.2234.

Conversion of nucleoside bis-*p*-toluoyl esters of **1a**, **2a** to phosphoramidite derivatives **1c**, **2c**: The hydrolysis of the bis-*p*-toluoyl esters, subsequent conversion to 5′-O-dimethoxytrityl derivatives, and 3′-O-phosphitylation in preparation for automated DNA synthesis were carried out by using the same methods previously described for the α-isomers [9b]. Analytical data for these compounds were in complete accord with their assigned structures [11b].

Oligonucleotide synthesis: DNA oligonucleotides were synthesized on an Applied Biosystems 392 instrument by using standard β-cyanoethylphosphoramidite chemistry [16]. Methods for deprotection, tritylation, and phosphitylation of nucleosides **3a**–**c** were as described previously [9b]. Oligomers were purified by preparative gel electrophoresis with 20% denaturing polyacrylamide (detection at 260 nm). Molar extinction coefficients for sequences containing the natural nucleosides were calculated by the nearest neighbor method [17]. The molar extinction coefficients measured for nucleosides **1**, **2**, and **3** were 1200, 851, and 6362, respectively; molar absorptivities for oligonucleotides containing these residues were derived as previously described [9b]. Oligodeoxynucleotides were obtained after purification as the sodium salts. Intact incorporation of residues **1**–**3** was confirmed by synthesis of short oligomers of sequence 5′-T-X-T (where X = **1**, **2**, or **3**). The ^{1}H NMR spectra (500 MHz) indicated the presence of the intact aromatic ring structures with the expected integration relative to thymine C-5 protons and methyl groups. Enzymatic degradation analysis could not be performed because the nonnatural residues were found to inhibit enzymatic cleavage.

Thermal denaturation studies: Buffers used for optical melting experiments were 100 mM NaCl, 10 mM Na-phosphate (for duplex hairpins) or 100 mM NaCl, 10 mM $MgCl_2$, 10 mM Na-PIPES (1,4-piperazine(bisethanesulfonate)) (for triplexes). The buffer pH is that of a 1.4x stock solution at 25 °C containing the buffer and salts. After the solutions were prepared they were heated to 90 °C and allowed to cool slowly to room temperature prior to the melting experiments.

The melting studies were carried out in Teflon-stoppered quartz cells (1 cm pathlength) under nitrogen atmosphere on a Varian Cary 1 UV/Vis spectophotometer equipped with a thermoprogrammer. Absorbance was monitored at 260 nm while temperature was increased at a rate of 0.5 °C min^{-1}; a slower heating rate with this instrument does not affect the results. In all cases the complexes displayed sharp, apparently two-state melting transitions. Melting temperatures (T_m) were determined by computer fit of the first derivative of absorbance with respect to $1/T$. Uncertainty in individual T_m values is estimated at ±0.5 K. Free energy values were derived by computer-fitting the denaturation data with an algorithm employing linear sloping baselines by using the two-state approximation for melting [7]. Uncertainty in individual free energy measurements is estimated at ±5 to 10%.

Received: April 4, 1995
Revised version: December 27, 1995 [Z 7865 IE]
German version: *Angew. Chem.* **1996**, *108*, 834–837

Keywords: base stacking · DNA · hydrogen bonds · nucleosides · triple helices

[1] D. R. Groebe, O. C. Uhlenbeck, *Nucleic Acids Res.* **1988**, *16*, 11725–11735.
[2] H. A. Heus, A. Pardi, *Science* **1991**, *253*, 191–194.
[3] I. Hirao, Y. Nishimura, Y. Tagawa, K. Watanabe, K. Miura, *Nucleic Acids Res.* **1992**, *20*, 3891–3896.
[4] S. Wang, M. A. Booher, E. T. Kool, *Biochemistry* **1994**, *33*, 4639–4644.
[5] J. SantaLucia, R. Kierzek, D. H. Turner, *Science* **1992**, *256*, 217–219.
[6] C. R. Cantor, P. R. Schimmel, *Biophysical Chemistry, Part III: The Behavior of Biological Macromolecules*, W. H. Freeman, San Francisco, **1980**, pp. 1117–1133.
[7] M. Petersheim, D. H. Turner, *Biochemistry* **1983**, *22*, 256–263.
[8] M. Senior, R. A. Jones, K. J. Breslauer, *Biochemistry* **1988**, *27*, 3879–3885.
[9] a) B. A. Schweitzer, E. T. Kool, *J. Org. Chem.* **1994**, *59*, 7238–7242; b) *J. Am. Chem. Soc.* **1995**, *117*, 1863–1872.
[10] X.-F. Ren, B. A. Schweitzer, C. J. Shiels, N. C. Chaudhuri, E. T. Kool, unpublished.
[11] a) N. C. Chaudhuri, E. T. Kool, *Tetrahedron Lett.* **1995**, *36*, 1795–1798; *ibid.* **1995**, *36*, 4910; b) X.-F. Ren, N. C. Chaudhuri, E. T. Kool, unpublished.
[12] a) R. S. Coleman, Y. Dong, J. C. Arthur, *Tetrahedron Lett.* **1993**, *34*, 6867–6870; b) D. Loakes, D. M. Brown, *Nucleic Acids Res.* **1994**, *22*, 4039–4043.

[13] M. M. Senior, R. A. Jones, K. J. Breslauer, *Proc. Natl. Acad. Sci. USA* **1988**, *85*, 6242–6246.

[14] a) L. E. Xodo, G. Manzini, F. Quadrifoglio, G. A. van der Marel, J. H. van Boom, *Nucleic Acids Res.* **1991**, *19*, 5625–5631; b) E. T. Kool, *J. Am. Chem. Soc.* **1991**, *113*, 6265–6266; c) G. Prakash, E. T. Kool, *J. Chem. Soc. Chem. Commun.* **1991**, 1161–1162; *ibid.* **1994**, 646; d) C. Giovannangeli, T. Montenay-Garestier, M. Rougée, M. Chassignol, N. T. Thuong, C. Hélène, *J. Am. Chem. Soc.* **1991**, *113*, 7775–7776; e) G. Prakash, E. T. Kool, *ibid.* **1992**, *114*, 3523–3528; f) M. Salunkhe, T. Wu, R. L. Letsinger, *ibid.* **1992**, *114*, 8768–8772; g) D. J. D'Souza, E. T. Kool, *J. Biomol. Struct. Dyn.* **1992**, *10*, 141–152; h) S. Rumney, E. T. Kool, *Angew. Chem.* **1992**, *104*, 1686–1689; *Angew. Chem. Int. Ed. Engl.* **1992**, *31*, 1617–1619; i) T. A. Perkins, J. L. Goodman, E. T. Kool, *J. Chem. Soc. Chem. Commun.* **1993**, 215–217; j) C. Giovannangeli, N. T. Thuong, C. Hélène, *Proc. Natl. Acad. Sci. USA* **1993**, *90*, 10013–10017; k) S. M. Gryaznov, D. H. Lloyd, *Nucleic Acids Res.* **1993**, *21*, 5909–5915; l) R. H. E. Hudson, M. J. Damha, *Nucleic Acids Symp. Ser.* **1993**, *29*, 97–99; m) D. J. D'Souza, E. T. Kool, *Bioorg. Med. Chem. Lett.* **1994**, *4*, 965–970; n) S. Wang, E. T. Kool, *Nucleic Acids Res.* **1994**, *22*, 2326–2333; o) S. Wang, E. T. Kool, *J. Am. Chem. Soc.* **1994**, *116*, 8857–8858; p) E. R. Kandimal, S. Agrawal, *Gene* **1994**, *149*, 115–121; q) D. M. Noll, J. L. O'Rear, C. D. Cushman, P. S. Miller, *Nucleosides Nucleotides* **1994**, *13*, 997–1005; r) T. L. Trapane, M. S. Christopherson, C. D. Roby, P. O. P. Ts'o, D. Wang, *J. Am. Chem. Soc.* **1994**, *116*, 8412–8413; s) R. Bandaru, H. Hashimoto, C. Switzer, *J. Org. Chem.* **1995**, *60*, 786–788; t) N. C. Chaudhuri, E. T. Kool, *J. Am. Chem. Soc.* **1995**, *117*, 10434–10442.

[15] a) M. Durand, K. Chevrie, M. Chassignol, N. T. Thuong, J. C. Maurizot, *Nucleic Acids Res.* **1990**, *18*, 6353–6359; b) M. Durand, S. Peloille, N. T. Thuong, J. C. Maurizot, *Biochemistry* **1992**, *31*, 9197–9204; c) M. Y.-X. Ma, L. S. Reid, S. C. Climie, W. C. Lin, R. Kuperman, M. Sumner-Smith, R. W. Barnett, *ibid.* **1993**, *32*, 1751–1758; d) M. J. Doktycz, T. M. Paner, A. S. Benight, *Biopolymers* **1993**, *33*, 1765–1777; e) J. B. Thomson, T. Tuschl, F. Eckstein, *Nucleic Acids Res.* **1993**, *21*, 5600–5603; f) F. Benseler, D. Fu, J. Ludwig, L. W. McLaughlin, *J. Am. Chem. Soc.* **1993**, *115*, 8483–8484; g) S. Rumney IV, E. T. Kool, *ibid.* **1995**, *117*, 5635–5646.

[16] a) S. L. Beaucage, M. H. Caruthers, *Tetrahedron Lett.* **1981**, *22*, 1859–1862; b) N. D. Sinha, J. Biernat, H. Köster, *ibid.* **1983**, *24*, 5843–5846.

[17] P. N. Borer in *Handbook of Biochemistry and Molecular Biology, Vol. 1*, 3rd ed. (Ed.: G. D. Fasman), CRC Press, Cleveland, OH, USA, **1985**, p. 589.

1,3-Didehydrobenzene (*m*-Benzyne)**

Ralph Marquardt, Wolfram Sander,* and Elfi Kraka*

Of the three isomeric didehydrobenzenes, only 1,2-didehydrobenzene (**1**) has been characterized unequivocally by direct spectroscopic methods.[1] The only derivative of **2** that has been characterized by matrix IR spectroscopy is 2,4-didehydrophenol.[2] Early reports on the UV/Vis spectroscopic characterization of **2** and **3** are questionable, since the reaction conditions and reported properties suggest that a more stable isomer, such as enediyne **4**, was observed.

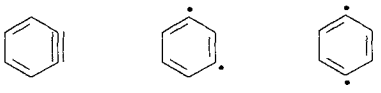

1 **2** **3**

A barrier of only 19.8 kcal mol^{-1} was determined for the ring opening of **3** by Roth et al.,[3] which compares well with barriers of 19.4 and 20.5 kcal mol^{-1} for this reaction calculated at the CCSD(T) level of theory by Kraka and Cremer.[4, 5] Flash vacuum pyrolysis of both 1,3-diiodobenzene (**5**)[6] and isophthaloyl diiodide (**6**)[7] produced **4** as the principal product, which suggests that **2** also undergoes thermal ring opening to give **4** (Scheme 1).

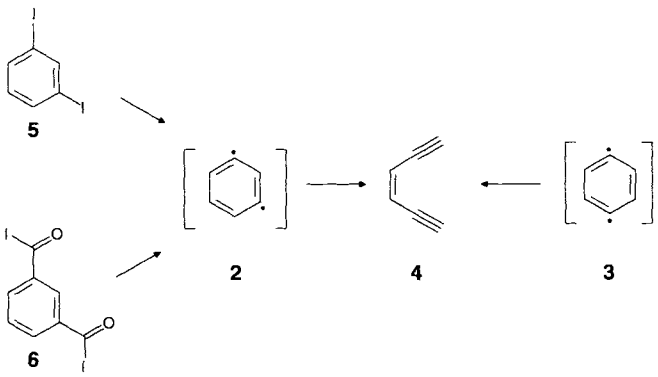

Scheme 1. Thermochemistry of 1,3-diiodobenzene (**5**) and isophthaloyl diiodide (**6**).

Squires et al. determined the heats of formation of the arynes **1**–**3** from collision-induced dissociation measurements to be 106.6 ± 3.0, 122.0 ± 3.1, and 137.3 ± 3.3 kcal mol^{-1}, respectively.[8, 9] These thermodynamic data have been confirmed by Kraka and Cremer [4, 5] and Lindh et al.[10] using high-level ab initio methods. Here we describe the matrix isolation and IR spectroscopic characterization of 1,3-didehydrobenzene (**2**), generated from two independent precursors.

UV photolysis ($\lambda > 305$ nm) of matrix-isolated[11] [2.2]metaparacyclophane-2,9-dione (**7**)[12] results in the formation of carbon monoxide, *p*-xylylene (**8**),[13] and a new compound with an intense IR absorption at 547 cm^{-1} and several weak absorptions (Scheme 2, Table 1). The new compound was stable toward prolonged irradiation at 248 nm, and based on the comparison of the IR spectrum obtained experimentally with the ab initio calculated IR spectrum (vide infra) it was assigned the structure of **2** (Fig. 1).

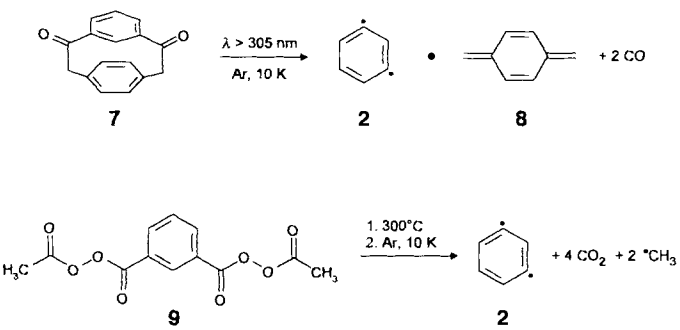

Scheme 2. Photochemistry of [2.2]metaparacyclophane-2,9-dione (**7**) and thermochemistry of isophthaloyl diacetyl peroxide (**9**).

Flash vacuum pyrolysis (300 °C) of isophthaloyl diacetyl peroxide (**9**)[14] with subsequent trapping of the products in argon at 10 K produced carbon dioxide and methyl radicals (Scheme 2).[15] In addition, the same intense IR absorption at 547 cm^{-1} assigned to **2** was observed. Annealing of the matrix at 30–35 K resulted in the loss of the methyl radicals and a simultaneous decrease in intensity of the absorptions assigned to **2**. In solid argon at temperatures above 30 K the diffusion of

[*] Prof. Dr. W. Sander, Dipl.-Chem. R. Marquardt
Lehrstuhl für Organische Chemie II der Universität
D-44780 Bochum (Germany)
Fax: Int. code +(234) 709-4353
Prof. Dr. E. Kraka
Department of Theoretical Chemistry
University of Göteborg
Kemigården 3, S-41296 Göteborg (Sweden)
Fax: Int. code +(31) 772-2933

[**] This work was supported by the Deutsche Forschungsgemeinschaft and the Fonds der Chemischen Industrie as well as the Swedish Natural Science Research Council (NFR) and the Swedish Institute (SI). We owe special thanks to the Nationellt Superdatorcentrum (NSC), Linköping, Sweden, for a generous allotment of computer time.

Table 1. IR spectroscopic data for 1,3-didehydrobenzene (**2**).

Entry [a]	CCSD(T)/6-31G(d,p) $\tilde{\nu}$ [cm^{-1}] [b]	I [c]	Sym. [d]	assignment [e]	Argon, 10 K $\tilde{\nu}$ [cm^{-1}]	I [c]
24	3289	5	a_1	CH stretch	3037 [f]	5
23	3256	7	a_1	CH stretch		
22	3251	12	b_1	CH stretch		
21	3210	22	a_1	CH stretch		
20	1706	4	a_1	CC stretch		
19	1544	18	b_1	HCC deformation + CC stretch	1486	15
18	1454	14	a_1	CC stretch + HCC deformation	1402	15
11	975	28	b_1	HCC deformation	936	25
7	818	10	b_2	CH wagging	824	20
6	743	54	b_2	CH wagging	751	45
5	545	100	b_1	ring deformation	547	100
2	386	6	a_1	ring deformation		
1	367	4	b_2	boat, out of plane [g]		

[a] Number of calculated vibrations (ab initio); only vibrational frequencies with relative intensities (I) greater than 1 are listed. [b] Calculated frequencies are unscaled. [c] Relative intensities based on the most intense band (100). [d] Symmetry of vibrations obtained from the calculated spectrum. [e] The assignment of experimental and calculated vibrations is based on band positions and relative intensities. [f] Because of overlapping bands, only one CH stretching absorption could be identified. Note that $\tilde{\nu}_{24}$ scaled with 0.92 yields a value of 3026 cm^{-1}.

small molecules (such as CH_3) is rapid, and thus radical recombinations become possible. We were not able to identify the products formed during annealing the matrix; however, this method allowed for the identification of several weak absorptions of **2**.

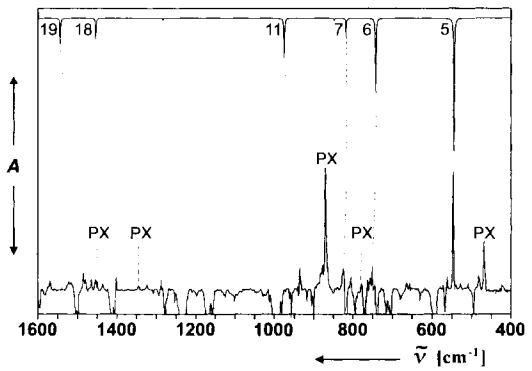

Fig. 1. Bottom: IR difference spectrum showing the photolysis ($\lambda > 305$ nm, argon, 10 K) of matrix-isolated [2.2]metaparacyclophane-2,9-dione (**7**). Bands of **7** which disappear upon irradiation point downwards; bands of **2** and **8** which appear upon irradiation point upwards; PX: bands assigned to *p*-xylylene (**8**). Top: IR spectrum of **2** calculated at the CCSD(T)/6-31G(d,p) level.

Energy and geometry of **2** (Fig. 2) were determined at the CCSD(T)/6-31G(d,p) level of theory using analytical energy gradients.[4, 5] According to these calculations **2** is a planar distorted hexagon. The CCSD(T) method is known to provide a reliable description of the energetics of dehydrobenzenes[4, 5] as well as of the vibrational spectrum of 1,2-didehydrobenzene (**1**).[1 6] It should be noted that despite previous claims, neither HF, GVB(1), and MP2, nor CCSD lead to a reasonable description of the vibrational spectrum of dehydrobenzenes, which is due to the necessity of both large dynamic correlation corrections and a significant coverage of multireference effects in these cases.

In the presence of other didehydrobenzenes, **2** can be identified by the strong ring deformation motion at 547 cm^{-1}, which in the cases of the *o*- and *p*-isomer appears in the IR spectrum at 470 (exp. 472) and 727 cm^{-1}, respectively.[1 6] Comparison of the IR spectrum calculated at the CCSD(T) level of theory with the IR spectra of the decomposition products of **7** and **9** allows for the identification of several weak absorptions due to **2**

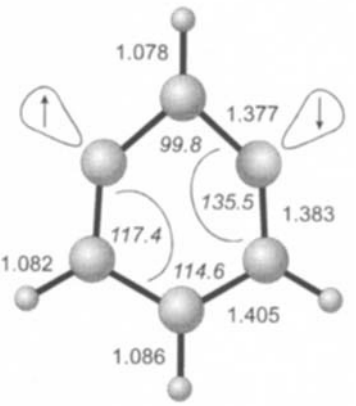

Fig. 2. CCSD(T)/6-31G(d,p) geometry, heat of formation ΔH_f, and dipole moment μ of **2**. Bond lengths in Å, bond angles (in italics) in degrees.

(Table 1, Fig. 1), which result from CH wagging (824 and 751 cm^{-1}, Table 1) as well as ring stretch and CH deformation motions (936, 1402, 1486 cm^{-1}, Table 1). Depending on the overlap with bands from other molecules (**8**, etc.), these absorptions can be also used to identify **2**.

In conclusion, we have synthesized *m*-benzyne from two precursors and characterized this species spectroscopically for the first time. The experimental and theoretical IR spectra are in excellent agreement and demonstrate that IR spectra of diradicals with limited multireference character can be calculated with experimental accuracy at the CCSD(T) level of theory.

Received: November 2, 1995 [Z8520IE]
German version: *Angew. Chem.* **1996**, *108*, 825–827

Keywords: ab initio calculations · 1,3-didehydrobenzene · diradicals · photolysis · thermolysis

[1] a) J. G. Radziszewski, B. A. J. Hess, R. Zahradnik, *J. Am. Chem. Soc.* **1992**, *114*, 52–57; b) O. L. Chapman, K. Mattes, C. L. McIntosh, J. Pacansky, G. V. Calder, G. Orr, *ibid.* **1973**, *95*, 6134–6135; G. Maier, W. Mayer, H.-A. Freitag, H. P. Reisenauer, R. Askani, *Chem. Ber.* **1981**, *114*, 3935.
[2] G. Bucher, W. Sander, E. Kraka, D. Cremer, *Angew. Chem.* **1992**, *104*, 1225–8; *Angew. Chem. Int. Ed. Engl.* *31*, 1230–1233.
[3] W. R. Roth, H. Hopf, C. Horn, *Chem. Ber.* **1994**, *127*, 1765–1779.
[4] E. Kraka, D. Cremer, *J. Am. Chem. Soc.* **1994**, *116*, 4929–4936.
[5] E. Kraka, D. Cremer, *Chem. Phys. Lett.* **1993**, *216*, 333–340.
[6] I. P. Fisher, F. P. Lossing, *J. Am. Chem. Soc.* **1963**, *85*, 1018–1019.
[7] R. Marquardt, *Diplomarbeit*, Technical University of Braunschweig, **1993**.

 © VCH Verlagsgesellschaft mbH, D-69451 Weinheim, 1996 0570-0833/96/3507-0747 $ 15.00+.25/0

[8] P. G. Wenthold, J. A. Paulino, R. R. Squires, *J. Am. Chem. Soc.* **1991**, *113*, 7414–7415.
[9] P. G. Wenthold, R. R. Squires, *J. Am. Chem. Soc.* **1994**, *116*, 6401–6412.
[10] R. Lindh, T. J. Lee, A. Bernhardsson, B. Joakim Persson, G. Karlstroem, *J. Am. Chem. Soc.* **1995**, *117*, 7186–7194.
[11] Irradiations were carried out by using Osram HBO 500 W mercury high-pressure arc lamps in Oriel housings equipped with quartz optics and suitable cut-off filters. For a description of the matrix apparatus see: W. W. Sander, *J. Org. Chem.* **1989**, *54*, 333–339.
[12] V. Boekelheide, P. H. Anderson, T. A. Hylton, *J. Am. Chem. Soc.* **1974**, *96*, 1558–1564.
[13] *p*-Xylylene (**8**) was identified by comparison with authentic matrix-isolated material, see: O. L. Chapman, J. W. Johnson, R. J. McMahon, P. R. West, *J. Am. Chem. Soc.* **1988**, *110*, 501–509.
[14] Isophthaloyl diacetyl peroxide (**9**) was prepared by the reaction of benzene-1,3-dicarboperoxoic acid with acetyl chloride in $CHCl_3$ in the presence of pyridine. Benzene-1,3-dicarboperoxoic acid was obtained by a method similar to that described by Baeyer et al. for the synthesis of benzene-1,4-dicarboperoxoic acid see: A. Baeyer, V. Villiger, *Chem. Ber.* **1901**, *34*, 762–767.
[15] J. Pacansky, J. Bargon, *J. Am. Chem. Soc.* **1975**, *97*, 6896–6897.
[16] E. Kraka, D. Cremer, unpublished results.

Synthesis and Structure of Gallium Siloxane Cages: Model Substances for Gallium-Containing Silicates**

Andreas Voigt, Ramaswamy Murugavel, Emilio Parisini, and Herbert W. Roesky*

Dedicated to Professor Kurt Dehnicke on the occasion of his 65th birthday

Silicates are used as catalysts in a number of industrial processes.[1–3] The breakthrough of zeolites, in particular, into technical applications is due to their easily variable characteristics such as form-selectivity, acidity, and temperature stability. The acidity, and the catalytic properties associated with it, can be altered by isomorphic substitution of Si or Al atoms of the zeolite lattice with other elements. In general, these solids have only been characterized by X-ray powder diffraction. As a result, the local structure at the catalytic center is not known. It is therefore appropriate to use model compounds in order to describe this structure more clearly.[4–9]

Titanium-containing zeolites (TS1 and TS2) are employed in oxidation reactions such as the epoxidation of olefins and the oxidation of nonactive hydrocarbons.[10–13] The synthesis of model compounds for titanium-containing zeolites would make it possible to throw light on the catalytically active species.[7, 9]

Gallium-containing zeolites are used as dehydrogenation catalysts.[1] Successful dehydrogenation of C2 to C5 alkanes occurs with Ga-theta-1-zeolite.[14] Other catalysts (Ga-ZSM-5, 30 Ga MFI) afford aromatic products in high yields upon the dehydrocyclization reaction of propene.[15, 16]

[*] Prof. Dr. H. W. Roesky, Dipl.-Chem. A. Voigt, Dr. R. Murugavel, Dr. E. Parisini
Institut für Anorganische Chemie der Universität
Tammannstrasse 4, D-37077 Göttingen (Germany)
Fax: Int. code +(551)39-3373

[**] This work was supported by the Deutsche Forschungsgemeinschaft, the Fonds der Chemischen Industrie, the Bundesministerium für Bildung und Forschung, and the Hoechst AG. R. M. thanks the Alexander von Humboldt Foundation and E. P. the European Union for postdoctoral stipends (ERB CHBG 940731).

Our work concentrates on the synthesis of heterosiloxanes as model compounds for metal-containing zeolites.[6–9, 17] We report here on the synthesis of soluble gallium siloxane cages and the first single crystal X-ray structure determination of such a species.

Several methods have been described for the synthesis of gallium siloxanes.[18, 19] The most favorable are the addition of silanolates or silanols to gallium trichloride or the reaction of silanols with alkylgallium compounds. As has been shown by the synthesis of aluminum siloxanes, the reaction of alkylaluminum compounds with silanetriols, accompanied by elimination of alkane, is a simple and elegant method to obtain aluminum siloxanes.[8, 20, 21] Therefore, **1** and **2** were allowed to react with trimethylgallium. Depending on the stoichiometry used, the gallium siloxanes **3**, **4**, **5**, and **6** could be obtained (Scheme 1). They are soluble in common organic solvents (diethyl ether, THF, *n*-hexane, toluene).

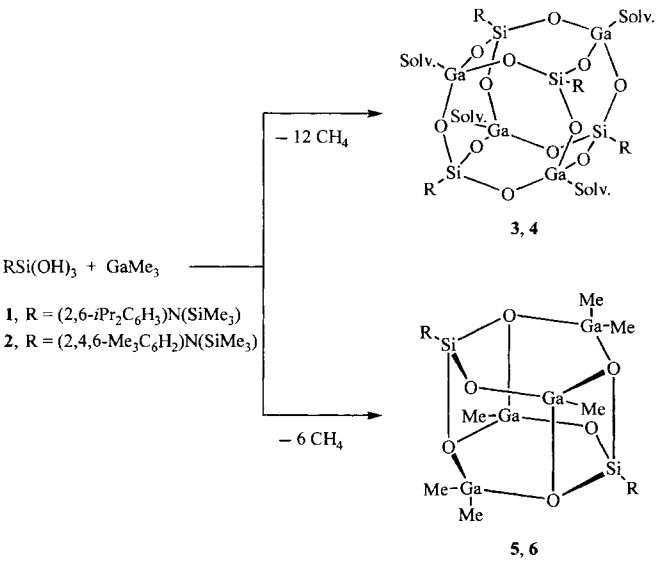

Scheme 1. Synthesis of **3**–**6** from **1** and **2**. Solv. = 1,4-dioxane.

The compounds **3** and **4** were formed on addition of one equivalent of trimethylgallium to a suspension of **1** or **2**, respectively, in *n*-hexane/1,4-dioxane (10/1). A donor solvent is necessary for this reaction, and methane is spontaneously released during the addition. In order to carry the reaction to completion, the mixture is heated at reflux until gas evolution ceases. Single crystals for an X-ray structure analysis have not yet been obtained for either compound **3** or **4**. They are both very soluble in common organic solvents (diethyl ether, THF, toluene, pentane) and have been fully characterized by IR and NMR spectroscopy, mass spectrometry, and elemental analysis. The IR spectra show no free OH bands, and the signals in the mass spectrum can be unambiguously assigned. Furthermore, the ^{1}H NMR spectra show one signal each[22] for the protons of the 1,4-dioxane molecule coordinated to the Ga atom. The relative intensity (1/1) of the signals for the silanetriol ligand and the dioxane enables the unequivocal determination of the number of Ga atoms. For **3** and **4** we assume a cubic ground structure, which has also been found in compounds formed by the reaction of silanetriols with alkylaluminum compounds.[8, 21]

When **1** and **2** are allowed to react with trimethylgallium in a 1:2 molar ratio in *n*-hexane/1,4-dioxane (10/1), the compounds **5** and **6**, respectively, are obtained. The framework of these polyhedra shows a Si–Ga ratio of 1:2. During the synthesis of the two

different structures (**3**,**4** and **5**,**6**), a white solid is observed which could not be isolated. We suppose that an eight-membered Ga-O-Si ring with free OH groups on the Si atoms is first formed. This is insoluble in the reaction mixture and therefore precipitates out.[23] In the formation of **5** and **6** the ring presumably folds and reacts with a further equivalent of trimethylgallium, finally forming **5** and **6** (Scheme 2).

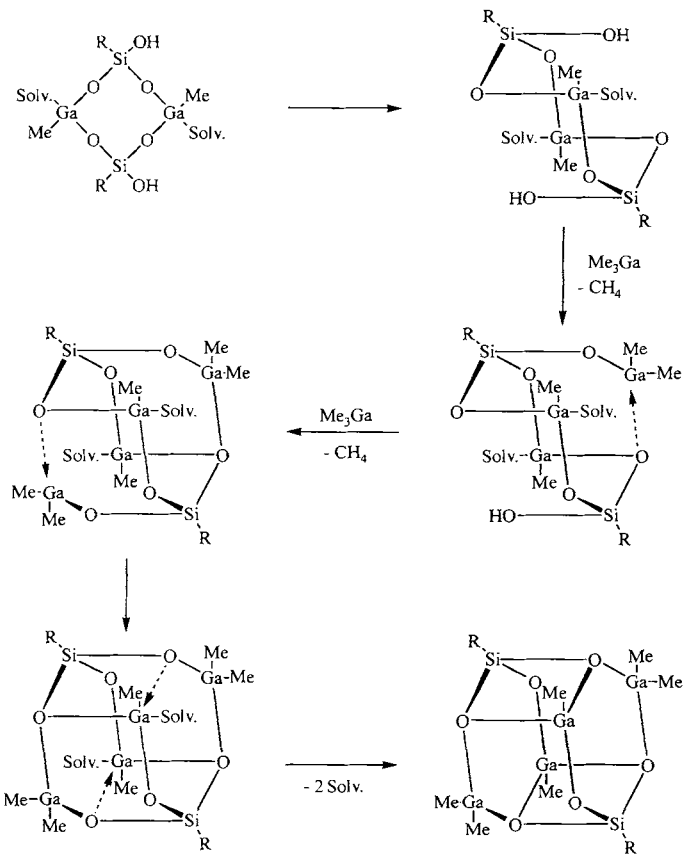

Scheme 2. Postulated reaction pathway for the synthesis of **5** and **6**. Solv. = 1,4-dioxane.

Suitable single crystals of **5** and **6** were obtained at room temperature within several hours from a mixture of *n*-hexane/THF (5/1). The X-ray structure analyses of **5** and **6** show $Ga_4O_6Si_2$ polyhedra, which can be described as six-sided prisms. The basic surfaces consist of six-membered Ga_2SiO_3 rings, which are connected to each other by four oxygen atoms—two from each ring. All the six-membered rings are in a boat configuration. In contrast, the four-membered rings are completely planar. As the bond lengths and angles in **5** and **6** are very similar, only the structure of **5** will be described here (Fig. 1).

Compound **5** shows two Si–O bonds of different lengths; the longer of the two (1.670 Å) is part of the four-membered ring. Likewise, two Ga–O bond lengths can be detected. The η^3-Ga–O bonds (1.96 Å) are considerably longer than the η^2-Ga–O bonds (1.82 Å). This difference affects the angle in the polyhedron: the expected tetrahedral angle at the Si atom is reduced to 94.2°. The angles at the μ^3 oxygen atom are also smaller (94°), whereas the tetrahedral angles at the Ga atoms vary over a wide range (77.2–129.1°). Especially noticeable is the positioning of the two Si atoms, the two N atoms the Ga atoms (Ga1, Ga1A) and the O atoms (O1, O1A). They all lie in a plane, which is perpendicular to the plane formed by the atoms Ga2, Ga2A, O1, O1A, O2, and O2A.

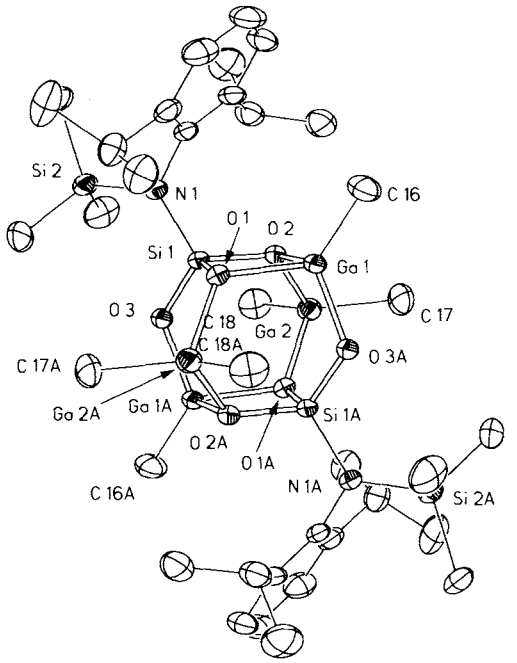

Fig. 1. Structure of **5** in the crystal. Selected bond lengths [Å] and angles [°]: Si1-O1 1.668(2), Si1-O2 1.671(2), Si1-O3 1.599(2), Ga1-O1 1.957(2), Ga1-O2 1.960(2), Ga1-O3A 1.824(2), Ga2-O1A 1.966, Ga2-O2 1.973(2); O1-Ga1-O2 77.24(8), O1-Ga1-O3A 103.38(9), O2-Ga1-O3A 103.15(9), O2-Ga2-O1A 92.37(9), C17-Ga2-C18 129.1.

The synthesis and structural characterization of the gallium siloxane compounds presented here provide an important contribution towards explaining the bonding in these systems. The Si–N and the Ga–C bonds are easy to cleave hydrolytically, which makes these molecules promising precursors for the synthesis of gallium-containing silicates under the mild conditions used for sol–gel techniques.

Experimental Procedure

3 and **4**: A solution of $GaMe_3$ (3.00 mmol) in *n*-hexane (5 mL) was slowly added at room temperature to a suspension of **1** [24] or **2** [24] (3.00 mmol) in *n*-hexane (30 mL) and 1,4-dioxane (3 mL). Afterwards the reaction mixture was stirred for 10 min at room temperature and then heated at reflux for 1 h. Compounds **3** and **4** were obtained in quantitative yields upon removal of the volatiles in vacuum. **3**: M.p. 205–211 °C; ^{1}H NMR (200 MHz, C_6D_6): δ = 0.08 (s, 36H, Si(CH_3)$_3$), 1.18 (m, 48H, CH(CH_3)$_2$), 3.45 (m, 8H, CH(CH$_3$)$_2$), 3.70 (s, 32H, OCH_2), 7.05 (m, 12H, aromat.); ^{29}Si NMR (50 MHz, C_6D_6): δ = −77.9 (s, SiO_3), 3.5 (s, $SiMe_3$); IR (KBr, Nujol): $\tilde{\nu}$ = 1497, 1318, 1250, 1182, 1052, 971, 905, 840, 802, 754, 688, 597 cm^{-1}; MS(EI): *m*/*z*: 1928 [M^+]; elemental analysis: $C_{76}H_{136}Ga_4N_4O_{20}Si_8$; calcd. C 47.34, H 7.05, N 2.90; found C 47.0, H 6.8, N 3.1. **4**: M.p. 198–202 °C; ^{1}H NMR (200 MHz, C_6D_6): δ = 0.26 (s, 36H, Si(CH_3)$_3$), 2.01 (s, 12H, CH_3), 2.11 (s, 24H, CH_3), 3.30 (s, 32H, OCH_2), 6.65 (s, 8H, aromat.); ^{29}Si NMR (50 MHz, C_6D_6): δ = −76.8 (s, SiO_3), 5.0 (s, $SiMe_3$); IR (KBr, Nujol): $\tilde{\nu}$ = 1606, 1303, 1258, 1214, 1153, 1049, 971, 889, 840, 800, 754, 589, 470 cm^{-1}; MS(EI): *m*/*z*: 1730 [M^+ − 2CH$_3$]; elemental analysis: $C_{60}H_{104}Ga_4N_4O_{20}Si_8$; calcd. C 42.26, H 6.15, N 3.29; found C 41.9, H 6.4, N 3.3.

5 and **6**: A solution of $GaMe_3$ (6.00 mmol) in *n*-hexane (5 mL) was quickly added at room temperature to a suspension of **1** or **2** (3.00 mmol) in *n*-hexane (30 mL)/1,4-dioxane (3 mL). The solution was then heated at reflux. During the reaction a white solid precipitates out. The reaction mixture was heated for an additional hour until a clear solution was obtained. Within 12 h crystals were formed that were suitable for single-crystal X-ray structure analysis. Further concentration of the solutions provided **5** and **6** in nearly quantitative yields. **5**: M.p. 223–227 °C; ^{1}H NMR (400 MHz, C_6D_6): δ = − 0.62 (s, 6H, Ga(CH_3)), 0.15 (s, 12H, Ga(CH_3)$_2$), 0.30 (s, 18H, Si(CH_3)$_3$), 1.21, 1.26 (d, ^3J(H,H) = 6.9 Hz, 24H, CH(CH_3)$_2$), 3.65 (sept, ^3J(H,H) = 6.9 Hz, 4H, CH(CH$_3$)$_2$), 7.05 (m, 6H, aromat.); ^{29}Si NMR (50 MHz, THF, C_6D_6): δ = − 65.4 (s, SiO_3), 6.7 (s, $SiMe_3$); IR (KBr, Nujol): $\tilde{\nu}$ = 1321, 1253, 1515, 1186, 1076, 1025, 959, 933, 843, 810, 743, 689, 544 cm^{-1}; MS(EI): *m*/*z*: 1018 [M^+]; elemental analysis: $C_{36}H_{70}Ga_4N_2O_6Si_4$; calcd. C 42.49, H 6.88, N 2.75;

found C 42.1, H 7.0, N 3.1. **6**: M.p. 255–258 C; ^{1}H NMR (200 MHz, C_6D_6): $\delta = -0.52$ (s, 6H, Ga(CH_3)), 0.14 (s, 12H, Ga(CH_3)$_2$), 0.27 (s, 18H, Si(CH_3)$_3$), 2.08 (s, 6H, CH_3), 2.34 (s, 12H, CH_3), 6.78 (s, 4H, aromat.); ^{29}Si NMR (50 MHz, C_6D_6): $\delta = -66.9$ (s, SiO_3), 8.7 (s, $SiMe_3$); IR (KBr, Nujol): $\tilde{\nu}$ = 1302, 1208, 1150, 1015, 989, 956, 892, 822, 723, 629, 546, 465 cm^{-1}; *MS(EI)*: *m/z*: 919 [$M^+ - CH_3$]; elemental analysis: $C_{30}H_{58}Ga_4N_2O_6Si_4$; calcd. C 38.58, H 6.26, N 3.00; found C 38.4, H 6.3, N 3.0.

Crystal structure data for **5**: $C_{36}H_{70}Ga_4N_2O_6Si_4$, M_r = 1018.18, triclinic, space group $P\bar{1}$, a = 10.233(2), b = 10.298(2), c = 13.975(3) Å, α = 94.20(3), β = 104.58(3), γ = 117.68(3), V = 1230.7(4) Å^3, Z = 1, ρ_{calcd} = 1.374 g cm^{-3}, $F(000)$ = 528, λ = 0.71073 Å, T = 193(2) K, $\mu(Mo_{K\alpha})$ = 2.30 mm^{-1}. The intensities were measured by a Stoe-Siemens-AED four-circle diffractometer on a crystal with the dimensions 0.50 × 0.30 × 0.25 mm^3 in the range of $5 \leq 2\theta \leq 50$ using the Learnt Profile Method [25]. From the 4342 collected reflections 4339 were independent, and 4329 were used in the structure refinement. $R1 = \sum|F_o - F_c|/\sum F_o$ = 0.0395($F > 4\sigma F$), $wR2 = [w(F_o^2 - F_c^2)^2/\sum wF_o^4]^{1/2}$ = 0.1295 (total data) for $w^{-1} = \sigma^2(F_o^2) + (g_1 \times P)^2 + (g_2 \times P)$ with $P = (F_o^2 + 2F_c^2)/3$ and g_1 = 0.0754 and g_2 = 0.9659; minimum/maximum residual electron density: 1.072/−1.294 eÅ^{-3}. Crystal structure data for **6**: $C_{30}H_{58}Ga_4N_2O_6Si_4$, M_r = 934.02, monoclinic, space group $P2_1/n$, a = 11.484(2), b = 12.707(3), c = 15.674(3) Å, β = 107.71(3)°, V = 2178.9(7) Å^3, Z = 2, ρ_{calcd} = 1.424 g cm^{-3}, $F(000)$ = 960, λ = 0.71073 Å, T = 193(2) K, $\mu(Mo_{K\alpha})$ = 2.59 mm^{-1}. The intensities were measured by a Stoe-Siemens-AED four-circle diffractometer on a crystal with the dimensions 0.60 × 0.30 × 0.20 mm^3 in the range $5 \leq 2\theta \leq 50$ using the Learnt Profile Method.[25] From the 4627 collected reflections 3820 were independent and 3819 were used in the structure refinement. $R1 = \sum|F_o - F_c|/\sum F_o$ = 0.0384($F > 4\sigma F$), $wR2 = [w(F_o^2 - F_c^2)^2/\sum wF_o^4]^{1/2}$ = 0.1260 (total data) for $w^{-1} = \sigma^2(F_o^2) + (g_1 \times P)^2 + (g_2 \times P)$ with $P = (F_o^2 + 2F_c^2)/3$ and g_1 = 0.0495 and g_2 = 2.1870; minimum/maximum residual electron density: 0.706/−0.642 eÅ^{-3}. Both structures were solved by direct methods (SHELXS-90) [26] and refined with all data by the least squares fit method on F^2 (SHELXL-93) [27]. All non-hydrogen atoms were anisotropically refined. The hydrogen atoms were added in idealized positions and included in the refinement. Crystallographic data (excluding structural factors) for the structures reported in this paper have been deposited at the Cambridge Crystallographic Data Centre as supplementary publication no. CCDC-179-1 and CCDC-179-2. Copies of the data can be obtained free of charge on application to The Director, CCDC, 12 Union Road, GB-Cambridge CB2 1EZ, UK (Fax: Int. code +1223/336-033; e-mail: teched@chemcrys.cam.ac.uk).

Received: November 6, 1995 [Z 8526 IE]
German version: *Angew. Chem.*, **1996**, *108*, 823–825

Keywords: cage compounds · gallium compounds · silicon compounds

[1] W. Hölderich, M. Hesse, F. Näumann, *Angew. Chem.* **1988**, *100*, 232; *Angew. Chem. Int. Ed. Engl.* **1988**, *27*, 226.
[2] R. L. Schneider, R. F. Howe, K. L. Waters, *J. Catal.* **1983**, *79*, 298.
[3] M. Ichikawa, L. R. Rao, A. Fukuoka in *Catalytic Science and Technology*, *Vol. 1*, VCH, Weinheim, **1991**.
[4] F. J. Feher, T. A. Budzichowski, K. J. Weller, *J. Am. Chem. Soc.* **1989**, *111*, 7288.
[5] F. J. Feher, K. J. Weller, *Organometallics* **1990**, *9*, 2638.
[6] N. Winkhofer, H. W. Roesky, M. Noltemeyer, W. T. Robinson, *Angew. Chem.* **1992**, *104*, 670; *Angew. Chem. Int. Ed. Engl.* **1992**, *31*, 599.
[7] N. Winkhofer, A. Voigt, H. Dorn, H. W. Roesky, A. Steiner, D. Stalke, A. Reller, *Angew. Chem.* **1994**, *106*, 1414; *Angew. Chem. Int. Ed. Engl.* **1994**, *33*, 1352.
[8] V. Chandrasehkar, R. Murugavel, A. Voigt, H. W. Roesky, H.-G. Schmidt, M. Noltemeyer, *Organometallics*, **1996**, *15*, 918.
[9] A. Voigt, R. Murugavel, V. Chandrasekhar, N. Winkhofer, H. W. Roesky, I. Usón, H.-G. Schmidt, *Organometallics*, in press.
[10] G. Perego, G. Ballussi, C. Corno, M. Tamarasso, F. Buonomo, A. Esposito in *Stud. Surf. Sci. and Catal.* **1986**, *28*, 129.
[11] P. Kumar, V. R. Hegde, B. Pandey, T. Ravindranathan, *J. Chem. Soc. Chem. Commun.* **1993**, 1553.
[12] D. R. C. Huybrechts, L. De Bruycker, P. A. Jacobs, *Nature* **1990**, *345*, 240.
[13] T. Tatsumi, M. Nakamura, S. Negishi, H. Tominaga, *J. Chem. Soc. Chem. Commun.* **1990**, 476.
[14] L. S. Marchenko, D. Z. Levin, V. A. Plakhotnik, E. S. Mortikov, *Izv. Akad. Nauk. SSSR Ser. Khim.* **1986**, 94; *Bull. Acad. Sci. USSR Div. Chem. Sci. (Engl. Transl.)* **1986**, *35*, 81.
[15] T. Inui, Y. Makino, F. Okazumi, A. Miyamoto, *J. Chem. Soc. Chem. Commun.* **1986**, 571.
[16] G. Giannetto, A. Montes, N. S. Gnep, A. Florentino, P. Cartraud, M. Guisnet, *J. Catal.* **1993**, *145*, 86.
[17] A. Haoudi-Mazzah, H.-G. Schmidt, M. Noltemeyer, E. Irmer, R. Herbst-Irmer, *Z. Naturforsch. B* **1991**, *46*, 584.
[18] H. Schmidbaur, *Angew. Chem.* **1965**, *77*, 206; *Angew. Chem. Int. Ed. Engl.* **1965**, *4*, 201.
[19] H. Schmidbaur, W. Findeiss, *Chem. Ber.* **1966**, *99*, 2187.
[20] M. L. Montero, I. Usón, H. W. Roesky, *Angew. Chem.* **1994**, *106*, 2198; *Angew. Chem. Int. Ed. Engl.* **1994**, *33*, 2103.
[21] M. L. Montero, A. Voigt, M. Teichert, I. Usón, H. W. Roesky, *Angew. Chem.* **1995**, *107*, 2761; *Angew. Chem. Int. Ed. Engl.* **1995**, *34*, 2504.
[22] Two signals are expected for a coordinated 1,4-dioxane. That only one signal is observed is probably due to fast exchange.
[23] The IR spectrum of this compound shows one OH band at 3379 cm^{-1}. A similar eight-membered ring is formed in the reaction of a silanetriol with an alkylaluminum compound [20].
[24] R. Murugavel, V. Chandrasekhar, A. Voigt, H. W. Roesky, H.-G. Schmidt, M. Noltemeyer, *Organometallics* **1995**, *14*, 5298.
[25] W. Clegg, *Acta Crystallogr. Sect. A* **1983**, *39*, 158.
[26] G. M. Sheldrick, *Acta Crystallogr. Sect. A* **1990**, *46*, 467.
[27] G. M. Sheldrick, SHELXL-93, Göttingen, **1993**.

Wittig Olefination of Lactones

Mohammed Lakhrissi and Yves Chapleur*

The formation of carbon–carbon double bonds from carbonyl compounds by the Wittig reaction and its variants,[1] or Peterson olefination,[2] has become an invaluable method in organic synthesis. However, enol ether formation from an ester by olefination has hardly been reported. Carbonyl groups of esters are much less reactive in the Wittig reaction than those of aldehydes or ketones, and only a few cases dealing with intramolecular reactions of this type have appeared.[3] More recently the Tebbe methylenation of lactones and esters has been described.[4] Several applications to the synthesis of C-methylene glycosides have been reported.[5]

Direct olefination at the anomeric center of sugars is an interesting way to introduce a carbon chain, which can be in turn chemically manipulated. We have been interested in such a transformation for several years now and have developed the dichloroolefination of lactones and esters using phosphorus-based chemistry.[6] This new reaction on ester carbonyl groups led to interesting developments in carbohydrate chemistry such as stereocontrolled methylation and methylenation of the anomeric center.[7, 8] However, a direct route from lactones **I** to C-glycosylidene compounds **II** (Scheme 1) remains to be found.

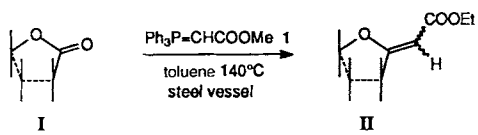

I **II**

Scheme 1.

In an effort to open such a new route, we investigated the direct Wittig olefination of esters by stabilized phosphoranes and now report our preliminary results. Some C-glycosylidene sugars such as **II**, a precursor of chiral cyclopentanones, have been prepared by a stepwise procedure.[9]

We reasoned that by analogy with the dichloromethylenation reaction of lactones, which proceeds at room temperature for aldehydes and ketones but needs to be performed at higher

[*] Dr. Y. Chapleur, Dr. M. Lakhrissi
Laboratoire de Méthodologie et Synthèse Enantiospécifique de Biomolécules, associé au CNRS
Institut Nancéien de Chimie Moléculaire
Université Henri Poincaré-Nancy I, B. P. 239, F-54506 Vandoeuvre (France)
Fax: Int. code +8391 24 79
e-mail: ychapleu@meseb.u-nancy.fr

temperature on lactones, the reaction of a lactone with a stabilized phosphorane should require more drastic conditions than those routinely used for aldehydes and ketones.

Attempts to treat methoxycarbonylmethylene(triphenyl)-phosphorane **1** with lactone **2** at reflux in tetrahydrofuran or toluene failed completely. However heating a toluene solution of these compounds at 140 °C in a sealed vessel for 24 hours gave an excellent yield of the expected olefins (*E*)-**3** and (*Z*)-**3** as a 1.6:1 mixture (Entry 1 in Table 1). The structure of these olefins was clearly established by mass spectrometry and ^1H and ^{13}C NMR spectroscopy. The configuration at the double bond was tentatively assigned on the basis of the chemical shifts of the vinylic (H-2) and H-4 protons (octitol numbering; *E* isomer: $\delta = 5.5$ and 5.75, respectively; *Z* isomer: both protons appear between $\delta = 5.0$ and 5.1). The difference in chemical shifts observed for the vinylic protons in the *E* and *Z* isomers ($\Delta\delta \approx 0.5$) fits well with the values observed for the vinylic protons in 1-C-methylene glycosides.[8]

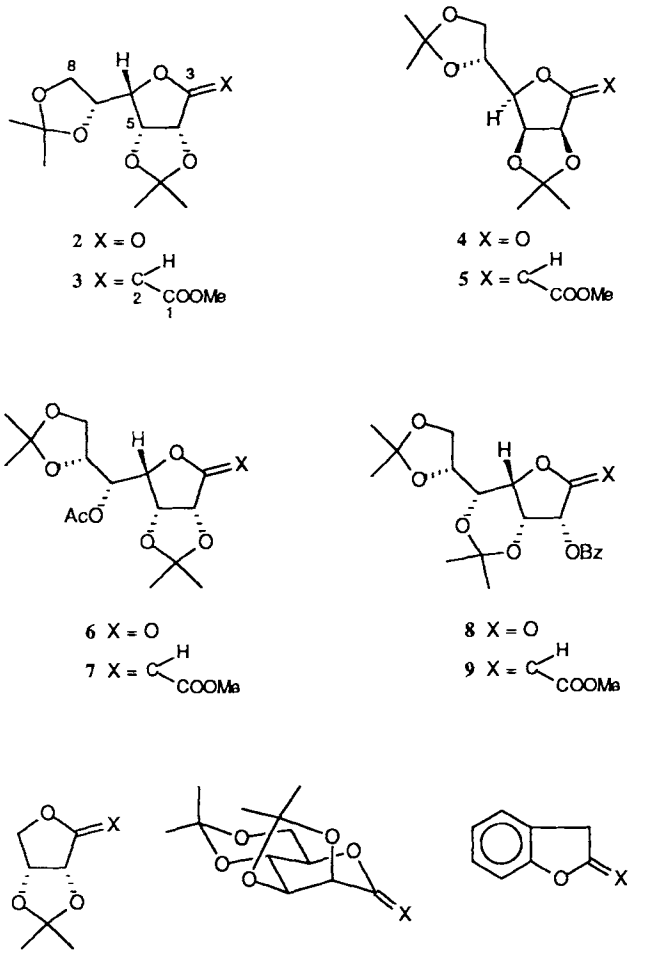

Table 1. Wittig olefinations of lactones.

Entry	Starting material	Product	*E*/*Z* ratio	*t* [h]	Yield [%]
1	**2**	(*E*)-**3**, (*Z*)-**3**	1.6:1	24	90
2	**4**	(*E*)-**5**, (*Z*)-**5**	1.1:1	24	80
3	**6**	(*E*)-**7**, (*Z*)-**7**	1.4:1	16	69
4	**8**	(*E*)-**9**		48	27
5	**10**	(*E*)-**11**, (*Z*)-**11**	1:1	17	56
6	**12**	(*E*)-**13**, (*Z*)-**13**	3:1	15	71
7	**14**	(*E*)-**15**		4	58

The reaction proceeded equally well for the mannono-1,4-lactone **4**, which gave a mixture of (*E*)-**5** and (*Z*)-**5** in a 1.1:1 ratio (Entry 2). It is noteworthy that this Wittig reaction tolerates the presence of an acetate group remote to the lactone carbonyl of compound **6** (Entry 3). The reaction was also possible with a lactone having a benzoate group at C-2 such as in compound **8**. A single olefinic compound (*E*)-**9** was isolated albeit in low yield (Entry 4). However, the acetate analogue of **8** could not be efficiently transformed into olefins and led to numerous products. We had previously demonstrated that the presence of esters at position 2 of a lactone was also troublesome in the dichloromethylenation reaction. Finally the six-membered ring lactone **12** derived from D-mannose was treated under the same conditions and gave a 3:1 mixture of olefins (*E*)-**13** and (*Z*)-**13** as seen from NMR data (Entry 6). Another interesting reaction was the alkylidenation of lactone **14** which gave olefin (*E*)-**15** as a single isomer in 58% yield together with another yet unidentified side-product.

The reaction of D-ribono-1,4-lactone derivatives protected at the primary position either with an acetate or a methoxy methyl ether failed. Tetra-*O*-benzyl-D-gluconolactone also failed to react under these conditions and was recovered unchanged. These failures should be explained by the steric hindrance induced on both faces of the lactone ring by the protective groups at C-2 and C-5/C-6 of the starting lactone.

In conclusion, this new application of the Wittig reaction proceeds with poor stereochemical control of the double bond configuration with 1,4-lactones, whereas a better stereocontrol was observed with a 1,5-lactone. Although it is still limited to bicyclic sugar lactones, interesting results have been obtained with an aromatic lactone. Further studies are currently underway to determine the scope and limitations of this reaction with other substrates and using other Wittig reagents. Obviously the olefins obtained in this way might be extremely useful starting compounds to access a variety of highly functionalized C-glycosides by subsequent 1,4-addition, reduction etc.

Experimental Procedure

Typical synthesis: (*E*)-**3**/(*Z*)-**3**: A solution of the lactone **2** (258 mg, 1 mmol) and the triphenylphosphorane **1** (670 mg, 2 mmol) in toluene (10 mL) was placed in a standard stainless steel vessel under an argon atmosphere and heated for 24h at 140 °C. After cooling, the solvent was removed under vacuum, and the residue was taken up in dichloromethane and placed on a silica gel column. Elution with a 3:2 mixture of hexane/ethyl acetate gave analytically pure olefins (*E*)-**3** and (*Z*)-**3**. (*E*)-**3**: 170 mg, 56%; $[\alpha]_D^{20} = -108$ ($c = 0.3$, $CHCl^3$); $\nu_{max} = 1716$, 1666 cm^{-1}; ^1H NMR ($CDCl_3$, 250 MHz, octitol numbering, see formula): $\delta = 1.40$ (s, 6H, $2CH_3$), 1.47 (s, 6H, $2CH_3$), 3.70 (s, 3H, OCH_3), 3.75 (dd, $J(8,8') = 9$, $J(7,8) = 6.5$ Hz, 1H, H-8), 4.18 (dd, $J(5,6) = 4.5$, $J(6,7) = 8$ Hz, 1H, H-6), 4.25 (dd, $J(7,8') = 7.5$ Hz, 1H, H-8'), 4.42 (m, 1H, H-7), 4.74 (dd, $J(4,5) = 6.5$ Hz, 1H, H-5), 5.54 (d, $J(2,4) = 1.5$ Hz, 1H, H-2), 5.78 (dd, 1H, H-4); ^{13}C NMR: $\delta = 25.24$ (CH_3), 26.01 (CH_3), 26.61 (CH_3), 26.93 (CH_3), 51.03 (OCH_3), 65.66 (C-8); 75.21, 76.49, 81.72, 87.43 (C-4 to C-7), 92.13 (C-2), 110.26, 114.46 ($2 \times C(CH_3)_2$), 165.57 (C-3), 168.54 (C=O); EI-MS: $m/z = 314$ ($M^{+\cdot}$), 299, 283, 243, 185, 167, 101, and 43.

(*Z*)-**3**: 106 mg, 34%; $[\alpha]_D^{20} = -139$ ($c = 0.2$, $CHCl_3$); $\nu_{max} = 1709$, 1659 cm^{-1}; ^1H NMR ($CDCl_3$, 250 MHz): $\delta = 1.35$ (s, 3H, CH_3), 1.38 (s, 3H, CH_3), 1.42 (s, 3H, CH_3), 1.45 (s, 3H, CH_3), 3.70 (s, 3H, OCH_3), 3.75 (dd, $J(7,8) = 6$, $J(8,8') = 9$ Hz, 1H, H-8), 4.12 (dd, $J(7,8') = 8$ Hz, 1H', H-8'), 4.44 (m, 2H, H-6,7), 5.12 (d, $J(2,4) = 1.5$ Hz, 1H, H-4), 4.65 (dd, $J(4,5) = 6$, $J(5,6) = 3$ Hz, 1H, H-5), 5.15 (dd, 1H, H-4); ^{13}C NMR: $\delta = 25.22$ (CH_3), 25.98 (CH_3), 26.58 (CH_3), 26.90 (CH_3), 50.98 (OCH_3), 65.64 (C-8), 75.18, 76.48, 81.69, 87.42 (C-4 to C-7), 92.08 (C-2), 110.26, 114.25 ($2 \times C(CH_3)_2$) 165.57 (C-3), 168.58 (C=O). EI-MS: m/z: 314 ($M^{+\cdot}$), 299, 243, 181, 167, 101, 43.

Received: November 27, 1995 [Z8594IE]
German version: *Angew. Chem.* **1996**, *108*, 833–834

Keywords: carbohydrates · lactones · synthetic methods · Wittig reactions

[1] A. Maercker, *Org. React.* **1965**, *14*, 270–490; E. Vedejs, M. J. Peterson, *Top. Stereochem.* **1994**, *21*, 1–157.
[2] D. J. Ager, *Org. React.* **1990**, *38*, 1–224.
[3] A. J. Dugan, M. A. Adams, P. J. Brynes, J. Meinwald, *Tetrahedron Lett.* **1978**, 4323–4326; J. Brennan, P. J. Murphy, *ibid.* **1988**, *29*, 2063–2066.
[4] S. H. Pine, *Org. React.* **1993**, *43*, 1–91.
[5] C. S. Wilcox, G. W. Long, H. Suh, *Tetrahedron Lett.* **1984**, *25*, 395–398; T. V. RajanBabu, G. S. Reddy, *J. Org. Chem.* **1986**, *51*, 5458–5461; M. H. Ali, P. M. Collins, W. G. Overend, *Carbohydr. Res.* **1990**, *205*, 428–434; R. Csuk, B. I. Glanzer, *Tetrahedron* **1991**, *47*, 1655–1664; V. Faivre-Buet, I. Eynard, H. Ntede Nga, G. Descotes, A. Grouiller, *J. Carbohydr. Chem.* **1993**, *12*, 349–356; E. Untersteller, Y. C. Xin, P. Sinaÿ, *Tetrahedron Lett.* **1994**, *35*, 2537–2540.
[6] Y. Chapleur, *J. Chem. Soc. Chem. Commun.* **1984**, 449–450; A. Bandzouzi, M. Lakhrissi, Y. Chapleur, *J. Chem. Soc. Perkin Trans. 1* **1992**, 1471–1473; M. Lakhrissi, Y. Chapleur, *Synlett* **1991**, 583–587; *J. Org. Chem.* **1994**, *59*, 5752–5757.
[7] A. Bandzouzi, Y. Chapleur, *Carbohydr. Res.* **1987**, *171*, 13–24; *J. Chem. Soc. Perkin Trans. 1* **1987**, 661–664.
[8] M. Lakhrissi, A. Bandzouzi, Y. Chapleur, *Carbohydr. Lett.* **1995**, 307–314.
[9] B. M. Trost, T. A. Runge, *J. Am. Chem. Soc.* **1981**, *103*, 7559–7572.

Superconductivity in Intercalated and Substituted $Y_2Br_2C_2$

Michael Bäcker, Arndt Simon,* Reinhard K. Kremer, Hans-Jürgen Mattausch, Richard Dronskowski, and Jean Rouxel

The superconductors $(RE)_2X_2C_2$ (RE = nonmagnetic rare earth element; X = Cl, Br, I) are model systems for an understanding of superconductivity in terms of chemistry.[1, 2] So far the yttrium compounds were investigated in detail.[3, 4]

The structures are characterized by planar slabs X-Y-Y-X with closest packing of the atoms in the slab and van der Waals forces between the X atoms of adjacent slabs. All octahedral voids within the Y–Y double layer are occupied by C_2 units.[5] $Y_2Cl_2C_2$ and $Y_2I_2C_2$ crystallize in a different structure type to $Y_2Br_2C_2$; the difference lies in the stacking sequence of the slabs. The monoclinic cells of the two types exhibit angles of $\beta \approx 93°$ (1s phase)[6] and $\beta \approx 100°$ (3s phase).

Within the Zintl–Klemm concept the chemical bonding is approximated by the formula $(Y^{3+})_2(X^-)_2C_2^{4-}$. However, due to C_2-π^* and Y-d mixing electron delocalization and conductivity in two-dimensions results. In contrast, the compound Y_2Br_2C $(Y_2^{3+})(Br^-)_2C^{4-}$ with a single C atom is a semiconductor as expected. According to our view, superconductivity of $Y_2X_2C_2$ is due to the tendency of pairwise occupation of quasimolecular C_2-π^* states at the Fermi level E_F, that is, a situation near to electronic localization. This assumption is corroborated by band structure calculations.[3]

Fundamentally, the electronic and, hence, the superconducting properties can be varied chemically in the following ways: I A change of the lattice dimensions by isoelectronic substitution leads to a variation in the degree of covalency in the C–Y bonds. The change can be performed a) in the center of the slab by substitution of Y by other (nonmagnetic) RE elements or b) in the periphery by exchange with the differently sized X atoms. II The Fermi level can be shifted relative to the C_2-π^* level by a) substitution of Y by Ca (lowering E_F) and Y by Th (raising E_F) within the slabs, or by b) intercalation of acceptors or donors into the gap between the slabs.

As detailed investigations with method Ib on $Y_2(Cl,Br)_2C_2$, $Y_2(Cl,I)_2C_2$ and $Y_2(Br,I)_2C_2$ show,[3, 7] the transition temperature T_c increases from 2.30 K for $Y_2Cl_2C_2$ to 5.05 K for $Y_2Br_2C_2$, has a maximum at 11.20 K for $Y_2Br_{0.4}I_{1.6}C_2$, and again decreases towards $Y_2I_2C_2$ (T_c = 9.85 K). It is interesting to note that the changes of the structure (1s → 3s → 1s form) are not reflected in the T_c values. This result indicates that the origin of superconductivity is to be sought in the central Y-C_2-Y part of the slab. Chemical changes introduced with methods Ib and IIb do not influence this central region significantly, whereas changes with Ia and IIa cause lattice defects in this part.

In particular, the intercalation of alkali metals (that is, route IIb) allows a well-defined variation of the carrier concentration in the $Y_2X_2C_2$ slab. As a complication the halides, in contrast to chalcogenides, intercalate only with difficulty.[8, 9, 10] A topochemical reaction is possible with a solution of sodium and potassium in THF in the presence of benzophenone and naphthalene, respectively.[11, 12] First results of intercalation reactions with $Y_2Br_2C_2$, which was chosen because of its well-defined superconducting transition, are summarized in Table 1.[13]

As expected, the incorporation of sodium in $Y_2Br_2C_2$ leads to an expansion along [001]. Moreover, a transition[15] from the 3s to the 1s phase is found. After the reaction with benzophenone sodium is complete at room temperature[16] the X-ray powder diagram shows only diffuse lines except for the narrow 00l reflections. Annealing of a pressed pellet at 400 °C for one week yields X-ray diagrams with reflections sufficiently sharp for a Rietveld refinement.[17] A projection of the structure of $Na_{0.23}Y_2Br_2C_2$[19] is shown in Figure 1. The sodium content

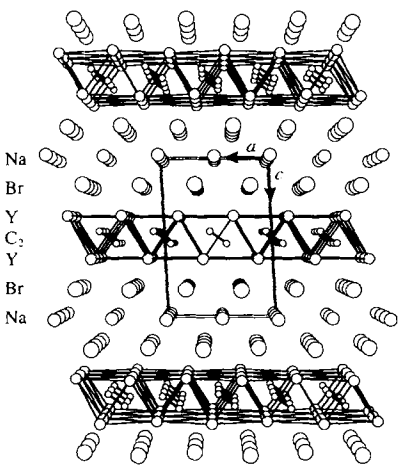

Fig. 1. Structure of $Na_{0.23}Y_2Br_2C_2$ as central projection along [010].

was determined by the refinement. The other phases $Na_xY_2Br_2C_2$ characterized in Table 1 were prepared by annealing of appropriate mixtures of $Na_{0.23}Y_2Br_2C_2$ and $Y_2Br_2C_2$. On the basis of lattice constants the product of the reaction of $Y_2Br_2C_2$ with naphthalenesodium contains more than 0.23 Na atoms per formula unit. However, an unambiguous refinement of the site occupancy factor for Na is not possible for this phase. The experiments give evidence for the increase of T_c by an injection of electrons into the $Y_2Br_2C_2$ slab. The degree of order is important, as an increased T_c after annealing of the samples clearly indicates.

When increasing E_F by partial substitution of Y^{3+} by Th^{4+} ions, disorder is introduced into the central part of the slab. As shown in Table 2,[13] T_c decreases with increasing Th content.

[*] Prof. Dr. A. Simon, Dipl.-Chem. M. Bäcker, Dr. R. K. Kremer, Dr. H. J. Mattausch, Dr. R. Dronskowski
Max-Planck-Institut für Festkörperforschung
Heisenbergstrasse 1, D-70569 Stuttgart (Germany)
Fax: Int. code +(0711) 689-1642
e-mail: micha@vaxff2.mpi-stuttgart-mpg.de

Prof. Dr. J. Rouxel
University of Nantes (France)

Table 1. Lattice constants [Å] and transition temperatures T_c [K] of sodium yttrium carbide bromide.

Composition	Reagents [a]	T_c [b]	T_c [c]	a	b	c	β [°]
$Y_2Br_2C_2$			5.05	6.958(1)	3.767(1)	9.932(1)	99.97(1)
$Na_{0.06(1)}Y_2Br_2C_2$	Na/Bzph		5.40	6.999(2)	3.755(1)	10.209(3)	93.26(3)
$Na_{0.12(1)}Y_2Br_2C_2$	Na/Bzph		5.65	7.009(1)	3.748(1)	10.308(1)	93.07(1)
$Na_{0.12(1)}Y_2Br_2C_2$	Na/Bzph		5.90	7.020(1)	3.745(1)	10.349(1)	93.02(2)
$Na_{0.23(1)}Y_2Br_2C_2$	Na/Bzph	5.6	6.2	7.061(1)	3.724(1)	10.464(1)	92.96(1)
$Na_xY_2Br_2C_2$	Na/Naph	6.0		7.081(2)	3.727(1)	10.509(1)	92.83(2)

[a] Bzph = benzophenone, Naph = naphthalene. [b] As prepared. [c] Annealed.

Table 2. Lattice constants [Å] and transition temperatures T_c [K] of thorium yttrium carbide bromide and $Y_2Br_2C_2$.

Composition	T_c	a	b	c	β [°]
$Y_2Br_2C_2$	5.05	6.958(1)	3.767(1)	9.932(1)	99.97(1)
$Th_{0.1}Y_{1.9}Br_2C_2$	4.70	6.984(1)	3.772(1)	9.949(1)	100.05(1)
$Th_{0.2}Y_{1.8}Br_2C_2$	4.15	7.014(2)	3.774(1)	9.964(3)	100.09(2)
$Th_{0.3}Y_{1.7}Br_2C_2$	3.65	7.038(1)	3.776(1)	9.979(1)	100.29(1)
$Th_{0.4}Y_{1.6}Br_2C_2$	3.60	7.061(3)	3.776(1)	9.983(2)	100.36(1)

This result appears to contradict the intercalation experiment and must be interpreted in terms of an overcompensation effect. The T_c increase due to increased carrier concentration is outweighed by the T_c decrease due to the introduced disorder.

The corresponding substitution of Y by Ca has not yet been achieved.

Received: November 29, 1995 [Z 8604 IE]
German version: *Angew. Chem.* **1996**, *108*, 837–839

Keywords: intercalation compounds · superconductivity · yttrium compounds

[1] A. Simon, *Angew. Chem.* **1987**, *99*, 602; *Angew. Chem. Int. Ed. Engl.* **1986**, *26*, 579.
[2] A. Simon, H. J. Mattausch, R. Eger, R. K. Kremer, *Angew. Chem.* **1991**, *103*, 1209; *Angew. Chem. Int. Ed. Engl.* **1991**, *30*, 1188.
[3] A. Simon, A. Yoshiasa, M. Bäcker, R. Henn, C. Felser, R. K. Kremer, H. J. Mattausch, *Z. Anorg. Allg. Chem.* **1996**, *622*, 123.
[4] R. W. Henn, R. K. Kremer, W. Schnelle, A. Simon, *Phys. Rev. Lett.*, submitted.
[5] U. Schwanitz-Schüller, A. Simon, *Z. Naturforsch. B*, **1985**, *40*, 710.
[6] H. J. Mattausch, H. Borrmann, A. Simon, *Z. Kristallogr.* **1994**, *209*, 281.
[7] M. Bäcker, Diplom thesis, Universität Düsseldorf, **1994**.
[8] R. Schöllhorn, *Angew. Chem.* **1980**, *92*, 1015; *Angew. Chem. Int. Ed. Engl.* **1980**, *19*, 983.
[9] J. D. Corbett, in *Intercalation Chemistry* (Eds.: M. Whittingham, A. Jacobson), Academic Press, New York, **1980**, Chap. 11.
[10] J. E. Ford, J. D. Corbett, S. J. Hwu, *Inorg. Chem.* **1983**, *22*, 2789.
[11] J. R. Kennedy, A. Simon, *Inorg. Chem.* **1991**, *30*, 2564.
[12] D. W. Murphy, P. A. Christian, *Science* **1979**, *205*, 651.
[13] Lattice constants were obtained from Guinier–Simon films [14] and subsequent least-squares refinement (for $Na_{0.23}Y_2C_2Br_2$ from Rietveld refinement). Onset transition temperatures were taken from magnetic susceptibility measurements (MPMS magnetometer; Fa. Quantum Design).
[14] A. Simon, *J. Appl. Crystallogr.* **1970**, *3*, 11.
[15] J. Rouxel, *J. Chim. Phys.* **1986**, *83*, 841.
[16] For intercalation reactions in the presence of benzophenone or naphthalene, benzophenone (130 mg, 0.71 mmol) and freshly cut sodium (50 mg, 2.2 mmol) or naphthalene (90 mg, 0.71) and sodium (30 mg, 1.3 mmol) were added to $Y_2C_2Br_2$ (200 mg, 0.55 mmol) in a 100 mL Schlenk flask. After introducing 40 mL freshly distilled THF, the mixture was stirred for 5 days at room temperature. The reaction mixture was filtered and washed several times with THF before the excess of agglomerated Na was removed. All operations were carried out under an inert atmosphere (argon). The color of the intercalated crystals intensifies from bronze ($Y_2C_2Br_2$) to deep copper red.
[17] X-ray powder diagrams were measured at room temperature with an INEL powder diffractometer (0.2 mm capillary; $Cu_{K\alpha1}$ radiation; $6.72° \geq 2\theta \geq 113.70°$; step rate 0.03°). Rietveld refinement was carried out with the program DBW 9006 [18] for two phases with YOBr as minority phase. The profile matching of the 3567 data points was performed with a pseudo-Voigt function and 19 parameters, of which 7 global (1 instrumental parameter, 5 profile parameter, 1 asymmetry parameter) and 11 + 1 local parameters (1 overall scale parameter, 1 parameter for preferred orientation, 4 for the lattice constants, 4 positional parameters, 1 site occupation parameter for $Na_{0.23}Y_2C_2Br_2$; 1 overall scale parameter for YOBr). Thermal vibrations were neglected. The C positions were calculated for $d(C-C) = 1.3$ Å and fixed. The residual values are $R_p = 0.076$, $R_{wp} = 0.105$ and $R_{Bragg}(I) = 0.057$ for $Na_{0.23}Y_2C_2Br_2$ and $R_{Bragg}(I) = 0.076$ for YOBr, the goodness of fit $GOF = 2.97$.
[18] D. W. Wiles, R. A. Young, *J. Appl. Crystallogr.* **1981**, *14*, 148.
[19] The obtained positions (lattice constants in Table 2) for $Na_{0.23}Y_2C_2Br_2$ in the space group $C2/m$ (No. 12) are Na in *2a* with site occupancy factor *SOF* of 0.116(6); Y in *4i* with $x = 0.3540(6)$, $z = 0.3680(3)$; Br in *4i* with $x = 0.6861(6)$, $z = 0.1780(3)$, and C in *4i* (not refined) with $x = 0.081$, $z = 0.470$. The sample contained 92.8(9)% $Na_{0.23}Y_2C_2Br_2$. The lattice and positional parameters for YOBr were taken from Ref. [20] and were not refined.
[20] I. Mayer, S. Zolotov, F. Kassierer, *Inorg. Chem.* **1965**, *11*, 1637.

Stoichiometric Dependence of the Long-Established Reaction of Butyllithium with Pyridine: A Hidden Secondary Reaction That Produces a Pyridine Adduct of a Lithiodihydropyridine**

William Clegg, Lorraine Dunbar, Lynne Horsburgh, and Robert E. Mulvey*

Over 60 years ago Ziegler first recognized the value of alkyllithium compounds in converting pyridine to 2-alkyl-substituted derivatives.[1] However, only recently has the reactive intermediate in such processes, a solvated nitrogen–lithium adduct **1**, been isolated and studied directly.[2]. Examination of the adduct **1**[2] revealed that addition is accompanied by bis(pyridine) solvation of the nitrogen-attached metal center, which requires a *n*-butyllithium: pyridine ratio of 1:3. As reported here, by using more than a threefold molar excess of the heterocycle, we have uncovered a remarkable secondary reaction which, despite the age of and considerable attention given to this chemistry, had previously gone unnoticed. Formally the new reaction involves reduction of pyridine by lithium hydride, though it is certain that the conventional ionic solid does not form during the process. The isolated product **2**, characterized both in the crystal and in solution, is a novel bis(pyridine)-dihydropyridyllithium dimer.

Earlier work[2] established that the solid adduct **1** was susceptible to LiH elimination even at ambient temperature. Here, by preparing it in situ in hexane solution warmed to near boiling

[*] Prof. R. E. Mulvey, L. Dunbar
Department of Pure and Applied Chemistry
University of Strathclyde
GB-Glasgow, G1 1XL (UK)
Fax: Int. code +(141) 552 0876
Prof. W. Clegg, L. Horsburgh
Department of Chemistry
University of Newcastle
GB-Newcastle upon Tyne, NE1 7RU (UK)

[**] This work was supported by the UK Engineering and Physical Science Research Council and by the Carnegie Trust (sponsors of an undergraduate vacation scholarship to L. D.). We express our sincere gratitude to a very thorough referee for assistance in the interpretation of the X-ray structural results.

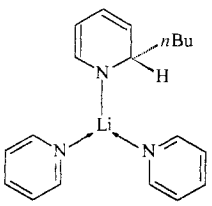

1

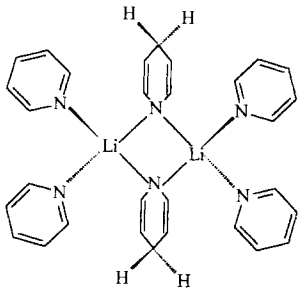

2

for three minutes, this process would presumably accelerate. Critically, however, the dark wine red solution still maintained its homogeneity (i.e., with no visible signs of LiH precipitation). The introduction of further pyridine at this stage (making seven equivalents overall per equivalent of *n*-BuLi) followed by allowing the solution to slowly cool from this elevated temperature, produced yellow-orange crystals of **2**.[3] This adduct is noticeably more robust than **1**, which begins to degrade immediately following isolation; **2** is stable indefinitely in the absence of air and moisture. The byproduct of this reaction is 2-*n*-butylpyridine. Significantly, no reaction was observed when a suspension of lithium hydride in pyridine (more than 15 molar equivalents in a small amount of hexane) was heated vigorously for five hours, reflecting the formidable barrier presented by the high lattice energy of the ionic solid.

The molecular constitution of **2** gives it the distinct advantage of being soluble in arenes, a property denied conventional lithium hydride because of its extended face-centred cubic lattice structure. ^{1}H NMR spectroscopic studies of **2** in [D_6]benzene[4] revealed a 1:1 mixture of 1,2-dihydro- and 1,4-dihydropyridyl anions as well as four normal pyridine molecules. Lithium tetrakis(*N*-dihydropyridyl)aluminate,[5] a reducing agent which exhibits novel selectivity towards certain ketones, is known to contain a similar mixture of dihydropyridyl anions, though they are reported to be bound to aluminum and not to lithium. Each distinct type of proton in **2** gives rise to an individual resonance signal in the ^{1}H NMR spectrum, generally well-separated from each other, thus making assignments straightforward.[4]

Consistent with this solution data, a dinuclear arrangement is found for crystalline **2** by an X-ray diffraction study.[6] This structure (Fig. 1) shows that the anions occupy the bridging positions, while the neutral ligands bind terminally, as is the norm in complexed lithium dimers. While other neutral ligands such as THF have occasionally been reported in bridging roles to lithium,[7] it is significant that to date no such cases have been found for pyridine. Two of the terminal pyridine ligands exhibit twofold disorder, but this could be resolved and refined with the assistance of restraints. The geometries of the terminal pyridine ligands compare favorably with those of the forty-four neutral pyridine ligands bonded to lithium (covering seventeen crystal structures) presently contained in the Cambridge Structural Database: the mean geometry in the database is shown in Figure 2.

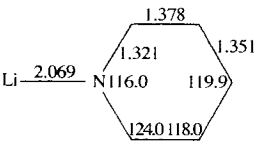

Fig. 2. Mean bond lengths [Å] and angles [°] in Li-bound pyridine ligands. The data were taken from the Cambridge Structural Database.

Though the two central N atoms (N(1), N(2)) bridge the Li centers they form slightly shorter bonds to lithium (mean length, 2.069 Å) than their terminal counterparts (mean length, 2.098 Å), reflecting the anionic nature of the central pyridine ligands. These bridging ligands have geometries consistent with 1,4-dihydropyridyl anions, as evidenced by a comparison with the structure of bis(1,4-dihydro-1-pyridyl)-bis(pyridine)zinc(II),[8] which also contains neutral, terminally bound pyridine ligands: in particular, the positions of the C=C double bonds [C24–C25, C21–C22 and C11–C12, C14–C15] are clearly indicated by the pattern in bond lengths (see legend to Fig. 1). Presumably, in view of the mixture of 1,2-dihydro- and 1,4-dihydropyridyl anions found in solution, the latter must crystallize preferentially in **2**.

One possible explanation for the formation of **2** is the intramolecular mechanism depicted in Scheme 1. The incoming "excess" pyridine molecule in solvating (or attempting to solvate) the Li^+ center sets up a six-membered cyclic intermediate. Hydride transfer then occurs driven by the electron-poor, $\delta+$ nature of the pyridine C atoms and aided by the electron-donating character of the 2-butyl substituent in **1**. Thus LiH never actually forms in this formal LiH reduction process. Complex **2** could undergo a similar elimination process but the absence of an electron-donating group in the 2-position—where two H atoms reside—makes it less favorable, hence the reason why **2** is more stable than **1**.

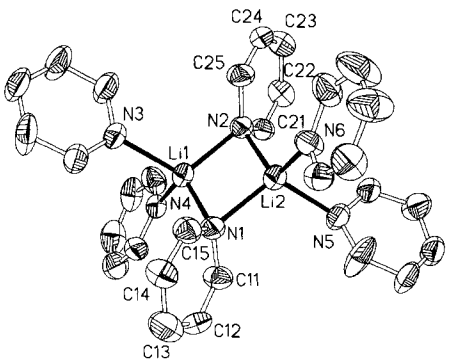

Fig. 1. Molecular structure of **2** with important atoms labeled (thermal ellipsoid plot (30% probability)). Hydrogen atoms and minor disorder components are omitted for clarity. Seleeted bond lengths [Å] and angles [°]: Li1-N1 2.070(10), Li1-N2 2.047(9), Li2-N1 2.088(10), Li2-N2 2.069(10), Li1-N3 2.104(9), Li1-N4 2.081(8), Li2-N5 2.106(10), Li2-N6 2.102(9); Li1-N1-Li2 74.8(3), Li1-N2-Li2 75.7(4), N1-Li1-N2 105.4(4), N1-Li2-N2 104.1(4), N3-Li1-N4 100.7(4), N5-Li2-N6 102.2(4); within bridging ligands: N-C 1.373(7)–1.412(7), C=C 1.288(8)–1.338(8), C-C 1.387(9)–1.453(10).

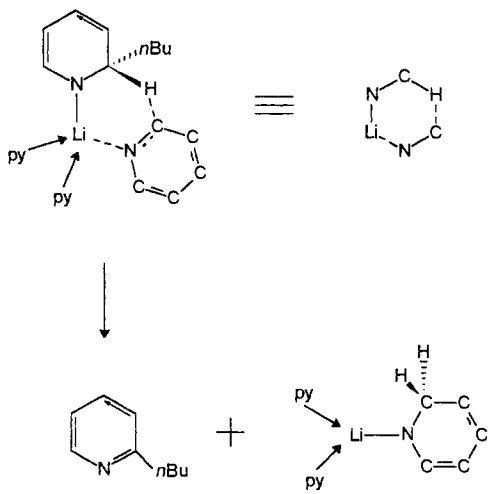

Scheme 1. Part of the postulated mechanism of the synthesis of the bis(pyridine)-dihydropyridyllithium dimer. py = pyridine.

 © VCH Verlagsgesellschaft mbH, D-69451 Weinheim, 1996 0570-0833/96/3507-0754 $ 15.00+.25/0

Experimental Procedure

2: The preparation was performed in a Schlenk tube under a dry argon blanket. *n*-Butyllithium (10 mmol in hexane) was added to a chilled volume of pyridine (30 mmol). The mixture was allowed to warm to ambient temperature, leading to an orange precipitate. Dissolution occurred on gently rewarming the mixture and additional pyridine (40 mmol) was then added. Immersing the solution in a water bath maintained at 50 °C led to the growth of transparent orange crystals of **2** [3]. Decomp. from 90 °C. Satisfactory C, H, Li, N analyses. Single crystals suitable for X-ray crystallography were examined and mounted under an inert oil.

Received: October 12, 1995
Revised version: December 27, 1995 [Z 8467 IE]
German version: *Angew. Chem.* **1996**, *108*, 815–816

Keywords: dihydropyridine · heterocycles · hydride transfer · lithium compounds · structure elucidation

[1] K. Ziegler, H. Zeiser, *Chem. Ber.* **1930**, *63*, 1847; B. J. Wakefield, *Organolithium Methods*, Academic Press, London, **1988**, pp. 58–62.

[2] a) D. Barr, R. Snaith, R. E. Mulvey, D. Reed, *Polyhedron* **1988**, *7*, 665; b) D. R. Armstrong, R. E. Mulvey, D. Barr, R. Snaith, D. Reed, *J. Organomet. Chem.* **1988**, *350*, 191.

[3] Yield of first crop, obtained without recourse to subambient cooling (based on initial amount of alkyllithium), 85%; decomp. from 90 °C. Elemental analysis for C, H, Li, N gave the formula $C_{30}H_{32}Li_2N_6$.

[4] ^{1}H NMR spectrum (400 MHz, [D$_6$]benzene, 300 K, TMS) 1,2-dihydro ligand: δ = 4.28 (*H1*, *H1'*, 2H, d), 4.77 (*H2*, 1H, m), 6.76 (*H3*, 1H, m), 5.56 (*H4*, 1H, td), 7.36 (*H5*, 1H, dm); 1,4-dihydro ligand: δ = 6.68 (*H1*, *H5*, 2H, dm), 4.61 (*H2*, *H4*, 2H, m), 4.16 (*H3*, *H3'*, 2H, m), neutral pyridine ligands: δ = 6.63 (βH, 8H, m), 6.89 (γH, 4H, m), 8.77 (αH, 8H, m).

[5] P. T. Lansbury, J. O. Peterson, *J. Am. Chem. Soc.* **1963**, *85*, 2236.

[6] Crystal data for **2**: $C_{30}H_{32}Li_2N_6$, M = 490.5, orthorhombic, $Pna2_1$, a = 17.808(4), b = 10.849(2), c = 14.579(3) Å, V = 2816.6(10) Å^3, Z = 4, ρ_{calcd} = 1.157 g cm^{-3}, $\lambda(Cu_{K\alpha})$ = 1.54184 Å, μ = 0.535 mm^{-1}, $F(000)$ = 1040. Measurements were made at 160 K on a Stoe-Siemens diffractometer with an Oxford Cryostream cooler from a crystal of size 0.8 × 0.6 × 0.5 mm^3. Structure solution was by direct methods and refinement by full-matrix least squares on F^2. 2693 reflections measured, 2611 unique (R_{int} = 0.0147), 435 refined parameters, $wR2 = \{\sum[w(F_o^2 - F_c^2)^2] / \sum[w(F_o^2)^2]\}^{1/2}$ = 0.1958, conventional R = 0.0598 for F values of 2030 reflections having $F_o^2 > 2\sigma(F_o^2)$, goodness of fit S = 1.052 on F^2, largest peak hole 0.229 −0.168 e Å^{-3}. Twofold disorder of orientation was resolved and refined for two terminal pyridine ligands, with occupancy factors 0.771:0.229(8) and 0.52:0.48(2); relatively high displacement parameters for many of the carbon atoms indicates possible further unresolved disorder in the ligands. Restraints for similarity of geometry and on displacement parameters were applied to the terminal ligands to aid the disorder refinement, but the bridging ligands were refined freely. Hydrogen atoms were geometrically positioned and constrained with a riding model; other atoms were refined anisotropically. The absolute structure (polar axis direction) could not be reliably determined. Crystallographic data (excluding structure factors) for the structure(s) reported in this paper have been deposited with the Cambridge Crystallographic Data Centre as supplementary publication no. CCDC-179-4. Copies of the data can be obtained free of charge on application to The Director, CCDC, 12 Union Road, Cambridge CB2 1EZ, UK (fax: Int. code +(1223) 336-033; e-mail: teched@chemerys.cam.ac.uk).

[7] W. Clegg, L. Horsburgh, F. M. Mackenzie, R. E. Mulvey, *J. Chem. Soc. Chem. Commun.* **1995**, 2011.

[8] A. L. Spek, *Cryst. Struct. Comm.* **1982**, *11*, 1621. For a related structure of a lithiobenzoquinoline derivative see: W. N. Setzer, P. von R. Schleyer, W. Mahdi, H. Dietrich, *Tetrahedron* **1988**, *44*, 3339.

Diazodi(4-pyridyl)methane and Diazophenyl-(4-pyridyl)methane as Photoresponsive Ligands for Metal–Carbene Hetero-Spin Systems

Noboru Koga,* Yoichiro Ishimaru, and Hiizu Iwamura*

Diphenylcarbene with a triplet ground state has served as an important building block in the construction of molecules and molecular assemblies with high spin multiplicities.[1, 2] Thus the connection of n carbene units through *meta*-phenylene, 1,3,5-benzenetriyl, and other ferromagnetic coupling units gives rise to various polycarbenes with $S = n$ ground states; in the series the highest spin state reported so far is $S = 9$.[3] Efforts to increase the number of aligned spins have, however, been hampered by the development of antiferromagnetic intra- and/or interchain interactions between the carbene centers assembled in high local concentration; chemical bonds appear to be formed in the extreme case.[4] Our last recourse is a strategy of assembling carbene centers in a rigid polymeric metal complex. We report here on the ligation of the pyridyl nitrogens of diazodi-(4-pyridyl)methane (**1**) with coordinatively doubly unsaturated paramagnetic metal ions and on the photolysis of the resulting complex.

The 1:1 complex [Mn(hfac)$_2$(**1**)] was obtained as orange rectangular prisms from a solution of anhydrous manganese(II) bis(hexafluoroacetylacetonate) [Mn(hfac)$_2$] and **1** in *n*-heptane/CH_2Cl_2 containing a small amount of methanol. The 1:2 complex [Mn(hfac)$_2$(**2**)$_2$] was also prepared analogously as a reference complex by using two mole equivalents of diazophenyl(4-pyridyl)-methane (**2**). X-ray crystal structure analysis of [Mn(hfac)$_2$(**2**)$_2$] shows that the two pyridyl nitrogens are ligated in *trans* form to a manganese ion (Fig. 1). The Mn–N and Mn–O bond lengths are 2.28 and 2.15 Å, respectively; the coordination geometry is an elongated octahedron. Considering that **1** is a bismonodentate ligand and forms a 1:1 complex with [Mn(hfac)$_2$] in contrast with the monodentate ligand **2**, we may assume that the two pyridyl nitrogens of **1** are coordinated to two different manganese ions to produce a one-dimensional chain.[5]

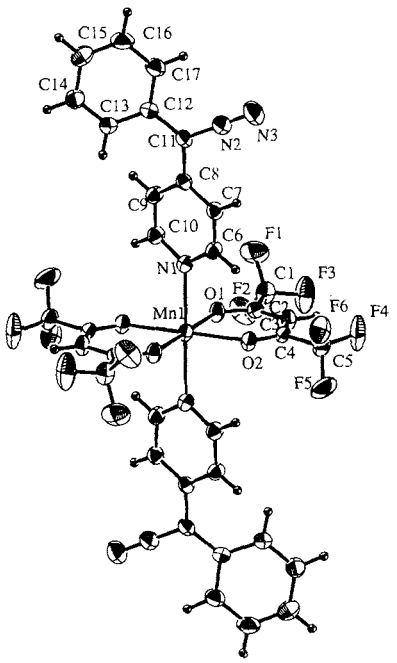

Fig. 1. ORTEP drawing of the X-ray crystal structure of [Mn(hfac)$_2$(**2**)$_2$] (ellipsoids at 30% probability).

[*] Prof. Dr. N. Koga, Y. Ishimaru
Faculty of Pharmaceutical Science, Kyushu University
Maidashi, Higashi-ku, Fukuoka 812-82 (Japan)
Prof. Dr. H. Iwamura
Institute for Fundamental Research in Organic Chemistry
Kyushu University
Hakozaki, Higashi-ku, Fukuoka 812-81 (Japan)
Fax: Int. code +(92)641-0915

[**] This work was supported by a Grant-in-Aid on Priority-Area-Research "Photoreaction Dynamics" from the Ministry of Education, Science and Culture, Japan (No. 07228104).

Before irradiation, the $\chi_{mol}T$ values of finely crystalline samples of [Mn(hfac)$_2$(**2**)$_2$] and [Mn(hfac)$_2$(**1**)] were nearly constant in the range 2–300 K, and the values of 4.44 and 4.14 emu K mol^{-1} at 300 K, respectively, were close to the theoretical spin-only value of 4.37 emu K mol^{-1} expected for paramagnetic samples with $S = 5/2$. When the samples were irradiated with a xenon lamp ($\lambda > 400$ nm),[6] the $\chi_{mol}T$ values for both changed with irradiation time and remained constant after 18 h (Fig. 2). When the temperature was increased from 2 to

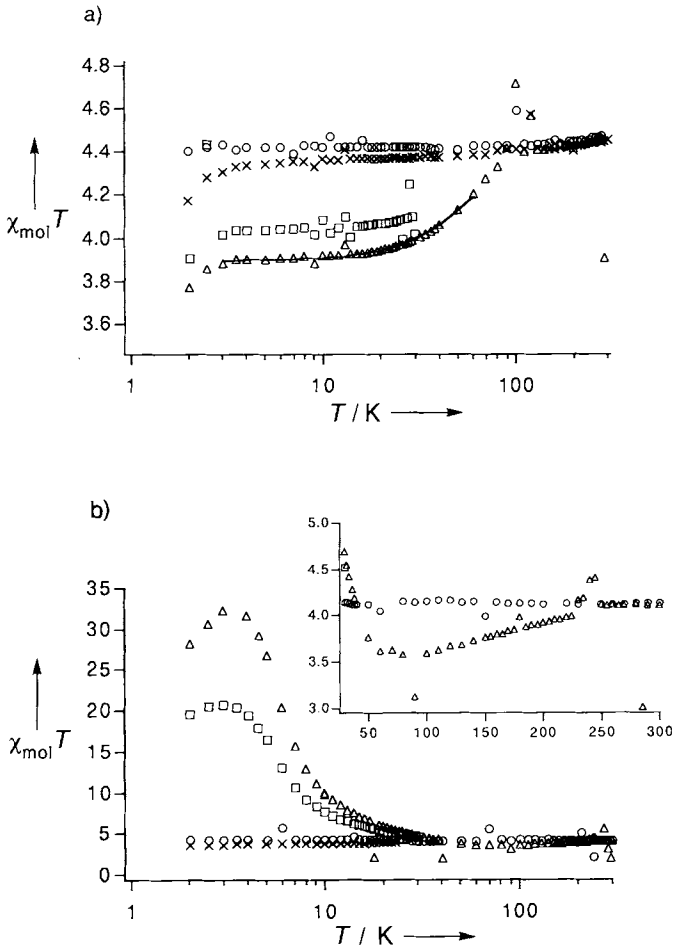

Fig. 2. The temperature dependence of $\chi_{mol}T$ [emu K mol^{-1}], the product of the "molar" magnetic susceptibility and temperature per formula unit of crystalline samples of a) [Mn(hfac)$_2$(**2**)$_2$] and b) [Mn(hfac)$_2$(**1**)] before (○) and after irradiation for 2 h (□) and 18 h (△), and then after maintaining the samples at 300 K for one hour (×). The changes for [Mn(hfac)$_2$(**1**)] are also given in inset in (b). The solid curve in (a) is the curve calculated based on the linear three-spin system with optimized parameters (see Experimental Procedure).

300 K in the dark after the photolysis, the $\chi_{mol}T$ values of [Mn(hfac)$_2$(**2**)$_2$] remained nearly constant at 3–20 K, gradually increased until approximately 90 K, and then corresponded exactly to those before irradiation. The 1:1 complex [Mn(hfac)$_2$(**1**)], showed strongly contrasting behavior under similar conditions. As the temperature was increased from 2 K, $\chi_{mol}T$ values increased, reached a maximum of 32.2 emu K mol^{-1} at 3 K, rapidly decreased to a shallow minimum of 3.58 emu K mol^{-1} at approximately 80 K, and then gradually increased up to 230 K. An abrupt change in the $\chi_{mol}T$ value was observed at 230 K, above which it retraced the horizontal line recorded before irradiation. For both complexes, subsequent measurements of the $\chi_{mol}T$ values at 2–300 K of samples that had been left at 300 K for an hour showed temperature-independent horizontal lines overlapping with those before irradiation.

The temperature-independent $\chi_{mol}T$ values before irradiation and after irradiation followed by annealing at >90 and >230 K for [Mn(hfac)$_2$(**2**)$_2$] and [Mn(hfac)$_2$(**1**)], respectively, are characteristic of magnetically dilute d^5 manganese(II) centers; both the diazo ligands **2** and **1**, and the annealed carbene ligands are insulating magnetic couplers. The $\chi_{mol}T/T$ plot after photolysis of [Mn(hfac)$_2$(**2**)$_2$] revealed that the two generated carbene centers interact with the manganese ion antiferromagnetically.[7] The temperature dependence ($T < 230$ K) of the $\chi_{mol}T$ values after photolysis of [Mn(hfac)$_2$(**1**)] is best interpreted in terms of the formation of a ferrimagnetic chain[5] composed of alternating units of triplet di(4-pyridyl)carbenes and d^5 manganese(II) ions. As the temperature is lowered, the antiferromagnetic coupling of the unpaired electrons of the manganese ion ($S = 5/2$) and the carbene center ($S = 2/2$) becomes stronger than kT and leads to a minimum in the $\chi_{mol}T/T$ plot, similar to behavior in a number of hetero-spin systems.[8, 9] The correlation over increasing length along the ferrimagnetic chain leads to the increases in $\chi_{mol}T$;[9] the correlation length at 3 K is estimated to be the ordering over about 40 units. The decrease in $\chi_{mol}T$ below 3 K is mostly due to the antiferromagnetic interchain interaction and partly to the saturation of magnetization under the field of 500 Oe used for the measurement. The discontinuous change of the $\chi_{mol}T$ value at 230 K and its temperature independence after annealing at 300 K indicate that the triplet carbene units undergo chemical reaction back to diamagnetic products at temperatures higher than 230 K and clearly imply the role of the di(4-pyridyl)carbene as a spin source and magnetic coupler.

It is worth noting that while the carbene species generated in the crystal of [Mn(hfac)$_2$(**2**)$_2$] disappeared at approximately 90 K, those in the crystal of [Mn(hfac)$_2$(**1**)] survived temperatures as high as roughly 200 K. The free carbenes from **1** and **2** in a 2-methyltetrahydrofuran matrix ($|D/hc| = 0.434$, $|E/hc| = 0.020$ cm^{-1} from **1**)[10] started to disappear at 60–80 K as observed by EPR spectroscopy.

It is concluded that the photochemical generation of the triplet carbene centers induces polarization of the π electrons on the pyridine rings, which in turn effects the coupling of magnetically isolated, unpaired 3d electrons of the Mn ions[11] along the one-dimensional chain (Scheme 1). In the present communication we have described the first example of the photochemical generation of a ferrimagnetic chain. This system is a prototype of a molecular optomagnetic recording device, in which only the irradiated domain of the nonmagnetic or weakly magnetic material becomes strongly magnetic, just as the irradiated portions of photoresists become functional for printing circuit elements.[12]

Experimental Procedure

1 [10]: A solution of di(4-pyridyl) ketone [13] (0.11 g, 0.60 mmol) and 1 mL of 85% hydrazine hydrate in 2 mL of ethanol was heated at reflux for ca. 12 h. The cooled reaction mixture was treated with ice water and the colorless precipitate was collected and dried over $CaCl_2$ under vacuum to give 0.11 g (0.56 mmol) of the corresponding hydrazone in 93% yield. To a solution of 0.11 g (0.56 mmol) of the hydrazone in 1 mL of *n*-hexane and 0.2 mL of dichloromethane was added 0.15 g of yellow HgO and a drop of saturated sodium hydroxide solution in ethanol. The mixture was stirred vigorously for 12 h with careful exclusion of light. The filtrate was concentrated under vacuum to give an orange solid, which was recrystallized from *n*-pentane/dichloromethane to give 0.02 g (17%) of **1** as red crystals. IR (KBr): $\tilde{\nu} = 2060$ cm^{-1}; UV/Vis (CH_2Cl_2): $\lambda = 304$, 484 nm; ^{1}H NMR ($CDCl_3$, 270 MHz): $\delta = 8.60$ (dd, 4H, $J = 4.6$, 1.6 Hz), 7.21 (dd, 4H, $J = 4.6$, 1.6 Hz); Anal. calcd for $C_{11}H_8N_4$: C 67.33, H 4.11, N 28.56; found: C 67.24, H 4.44, N 28.94.

2: This compound was obtained in 51% yield from 4-benzoylpyridine as described in the literature [14].

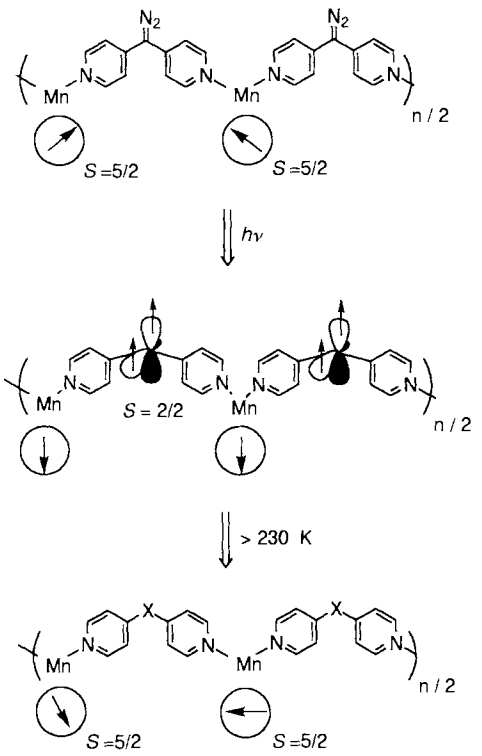

Scheme 1. Exchange coupling in [Mn(hfac)$_2$(**1**)] and the resulting complexes generated by irradiation (loss of N_2) and annealing at higher temperature. X = nonmagnetic carbon center. The hfac ligands are omitted for clarity.

[Mn(hfac)$_2$(**1**)] and [Mn(hfac)$_2$(**2**)$_2$]: A solution of **1** in CH_2Cl_2 was mixed with an equimolar solution of [Mn(hfac)$_2$] in *n*-heptane containing a small amount of methanol. For the preparation of the latter complex, two mole equivalents of **2** was used. The mixtures were kept in a refrigerator to give orange rectangular prisms.

[Mn(hfac)$_2$(**1**)]: Anal. calcd for $C_{21}H_{12}N_4O_4F_{12}Mn$: C 37.80, H 1.81, N 8.40; found: C 38.08, H 1.74, N 8.11. Owing to the limited quality of the single crystal (orthorhombic, space group *Pbca* for [Mn(hfac)$_2$(**1**)]) and its sensitivity to X-ray irradiation, we could not improve the residuals beyond $R = 0.244$ and $R_w = 0.121$.

[Mn(hfac)$_2$(**2**)$_2$]: Anal. calcd for $C_{34}H_{22}N_6O_4F_{12}Mn$: C 47.40, H 2.57, N 9.76; found: C 47.45, H 2.51, N 9.89. The following crystal parameters were obtained: monoclinic, space group $P2_1/c$ (No. 14), $a = 12.432(3)$, $b = 6.739(4)$, $c = 22.192(3)$ Å, $\beta = 104.87(1)°$, $V = 1797(1)$ Å^3, $Z = 3$, $\rho_{calcd} = 1.267$ g cm^{-1}, $R = 0.039$, $R_w = 0.026$.

Magnetic measurement: Finely crystalline samples of [Mn(hfac)$_2$(**1**)] and [Mn(hfac)$_2$(**2**)$_2$] (each ca. 0.5 mg) were measured on a SQUID susceptometer/magnetometer before and after irradiation with a 300 W xenon lamp through an optical fiber [8] at or below 5 K. Light in the range $770 > \lambda > 400$ nm obtained by a combination of a Kenko L-42 sharp-cut filter and an OCLI B cold mirror was used. The light intensity at the inside edge of the optical fiber was ca. 35 mW. The degree of the photolysis was estimated to be 68 and 25% for [Mn(hfac)$_2$(**1**)] and [Mn(hfac)$_2$(**2**)$_2$], respectively, by comparing the absorptivity of the diazo groups at 2072 cm^{-1} for [Mn(hfac)$_2$(**1**)] and 2060 cm^{-1} for [Mn(hfac)$_2$(**2**)$_2$] before and after the photolysis. The progress of the photolysis was found not to be even; visual inspection proved that the irradiated side of the crystalline samples suffered higher decomposition on photolysis than the unirradiated side. Therefore the production of the carbene species on the irradiated side of the crystals is judged to be higher than these figures. The temperature dependence of the magnetic susceptibility per formula unit of [Mn(hfac)$_2$(**1**)] and [Mn(hfac)$_2$(**2**)$_2$] was investigated under constant fields of 500 and 5000 Oe below and above 70 K, respectively. For a more quantitative analysis of the observed $\chi_{mol}T$ values for [Mn(hfac)$_2$(**2**)$_2$], the Hamiltonian $\boldsymbol{H} = -2J(\boldsymbol{S}_1\boldsymbol{S}_M + \boldsymbol{S}_M\boldsymbol{S}_2)$, which describes the linear three-spin system revealed by the X-ray crystal structure analysis, was employed. The resulting equation derived for χ_{mol} containing photolysis factor F, Weiss temperature θ, and Landé factor g, was fitted to the experimental data (after 18 h irradiation, between 3–60 K) by a least squares method. The best fitting parameters were $J/k_B = -17.8 \pm 0.4$ K, $\theta = -0.011 \pm 0.007$ K, $g = 2.06 \pm 0.01$, and $F = 18.0 \pm 0.1$%. The corresponding curve is included in Figure 2.

Received: August 21, 1995
Revised version: November 28, 1995 [Z 8329 IE]
German version: *Angew. Chem.* **1996**, *108*, 802–804

Keywords: carbenes · magnetic properties · manganese compounds · spin coupling

[1] a) K. Itoh, *Chem. Phys. Lett.* **1967**, *1*, 235–238; b) E. Wasserman, R. W. Murray, W. A. Yager, A. M. Trozzolo, G. Smolinsky, *J. Am. Chem. Soc.* **1967**, *89*, 5076–5078; c) N. Mataga, *Theor. Chim. Acta* **1968**, *10*, 372–376.
[2] a) Y. Teki, T. Takui, K. Itoh, H. Iwamura, K. Kobayashi, *J. Am. Chem. Soc.* **1986**, *108*, 2147–2156; b) A. Izuoka, S. Murata, T. Sugawara, H. Iwamura, *ibid.* **1987**, *109*, 2631–2639; c) N. Koga, H. Iwamura, *Nippon Kagaku Kaishi* **1989**, 1456–1462; d) I. Fujita, Y. Teki, T. Takui, T. Kinoshita, K. Itoh, F. Miko, Y. Sawaki, H. Iwamura, A. Izuoka, T. Sugawara, *J. Am. Chem. Soc.* **1990**, *112*, 4074–4075; e) N. Nakamura, K. Inoue, H. Iwamura, T. Fujioka, Y. Sawaki, *ibid.* **1992**, *114*, 1484–1485; f) K. Matsuda, N. Nakamura, K. Takahashi, K. Inoue, N. Koga, H. Iwamura, *ibid.* **1995**, *117*, 5550–5560.
[3] N. Nakamura, K. Inoue, H. Iwamura, *Angew. Chem.* **1993**, *105*, 900–901; *Angew. Chem. Int. Ed. Engl.* **1993**, *32*, 872–874.
[4] K. Matsuda, N. Nakamura, K. Inoue, N. Koga, H. Iwamura, *Chem. Eur. J.* **1996**, *2*, 259–264.
[5] Unrefined X-ray crystal and molecular structure data for [Mn(hfac)$_2$(**1**)] suggest that the two pyridyl nitrogens of **1** are coordinated to two different manganese ions to produce the one-dimensional chain as shown in Scheme 1.
[6] A full description of the photolysis system using an optical fiber will be published elsewhere.
[7] $J/k_B = -17.8 \pm 0.4$ K (see Experimental Procedure).
[8] a) M. Kitano, N. Koga, H. Iwamura, *J. Chem. Soc. Chem. Commun.* **1994**, 447–448; b) Y. Ishimaru, K. Inoue, N. Koga, H. Iwamura, *Chem. Lett.* **1994**, 1693–1696.; c) M. Kitano, Y. Ishimaru, K. Inoue, N. Koga, H. Iwamura, *Inorg. Chem.* **1994**, *33*, 6012–6019.
[9] G. R. Eaton, S. S. Eaton, *Acc. Chem. Res.* **1988**, *21*, 107–113; A. Caneschi, D. Gatteschi, J. Laugier, P. Rey, R. Sessoli, *Inorg. Chem.* **1988**, *27*, 1553–1557; A. Caneschi, D. Gatteschi, J. P. Renard, P. Rey, R. Sessoli, *ibid.* **1989**, *28*, 1976–1980; A. Caneschi, D. Gatteschi, P. Rey, *Prog. Inorg. Chem.* **1991**, *39*, 331–429; A. B. Burdukov, V. I. Ovcharenko, V. N. Ikorski, N. V. Pervukhina, N. V. Podberezskaya, I. A. Grigor'ev, S. V. Larionov, L. B Volodarsky, *Inorg. Chem.* **1991**, *30*, 972–976; A. Caneschi, A. Dei, D. Gatteschi, *J. Chem. Soc. Chem. Commun.* **1992**, 630–631; A. Caneschi, P. Chiesi, L. David, F. Ferraro, D. Gatteschi, R. Sessoli, *Inorg. Chem.* **1993**, *32*, 1445–1453; K. Inoue, H. Iwamura, *J. Am. Chem. Soc.* **1994**, *116*, 3173–3174; K. Inoue, H. Iwamura, *J. Chem. Soc. Chem. Commun.* **1994**, 2273–2274.
[10] M. Ono, M. Sc. Thesis, The University of Tokyo, **1991**.
[11] The 1:1 copper complex [Cu(hfac)$_2$(**1**)], which was prepared similarly, gave an analogous $\chi_{mol}T/T$ profile in which carbene and copper interacted *ferro*magnetically.
[12] For practical applications, sensitivity to oxygen and thermal reactivity of triplet carbenes are serious disadvantages and should be overcome.
[13] A. Murray, III, W. H. Langham, *J. Am. Chem. Soc.* **1952**, *74*, 6289–6295.
[14] C. Murray, C. Wentrup, *J. Am. Chem. Soc.* **1975**, *97*, 7467–7480.

Selective Cation Movement across Lipid Bilayers Containing Brevetoxin B**

Stefan Matile* and Koji Nakanishi

The structures of a large number of polyether marine toxins with ladderlike skeletons are rapidly being elucidated.[1] One of the earliest identified toxins of this type is brevetoxin B (BTX-B), the "red tide" toxin produced by dinoflagellates.[2] However, despite the great interest in and importance of polyether marine toxins, the nature of their activity still remains largely unknown. In the case of BTX-B, specific binding to voltage-sensitive sodium channels (VSSC) implied that activation of VSSC

[*] Dr. S. Matile, Prof. K. Nakanishi
Columbia University, Department of Chemistry
New York, NY 10027 (USA)
Fax: Int. code +(212)932-8273
e-mail: matile@chem.columbia.edu

[**] We thank Dr. J. Decatur for assistance in NMR measurements and Prof. N. Berova, Dr. N. Sakai, and Prof. P. N. R. Usherwood for discussions. This work was supported by the U. S. National Institutes of Health (AI 10187) and the Schweizerischer Nationalfonds zur Förderung der wissenschaftlichen Forschung (S. M.).

is the mode of action of brevetoxins.[3] The results described in the following have disclosed a second, entirely new view regarding its mode of action: brevetoxin B presumably increases ion movement through cell membranes by transmembrane self-assembly.

Incorporation of macromolecular polyoxyethylene derivatives[4] into lipids has been shown to result in cation transport rates comparable to those of ion channels formed by natural and synthetic oligopeptides or antifungal macrolides.[5] Because of the polyether structure as well as the rigid skeleton of BTX-B with a length of approximately 30 Å, which corresponds to the thickness of lipid bilayers,[5a] the possibility of transmembrane BTX-B channel formation was suspected. Thus, ion movement across large unilamellar egg phosphatidylcholine (PC) vesicles containing 0.3 mol% BTX-B was investigated (Scheme 1).

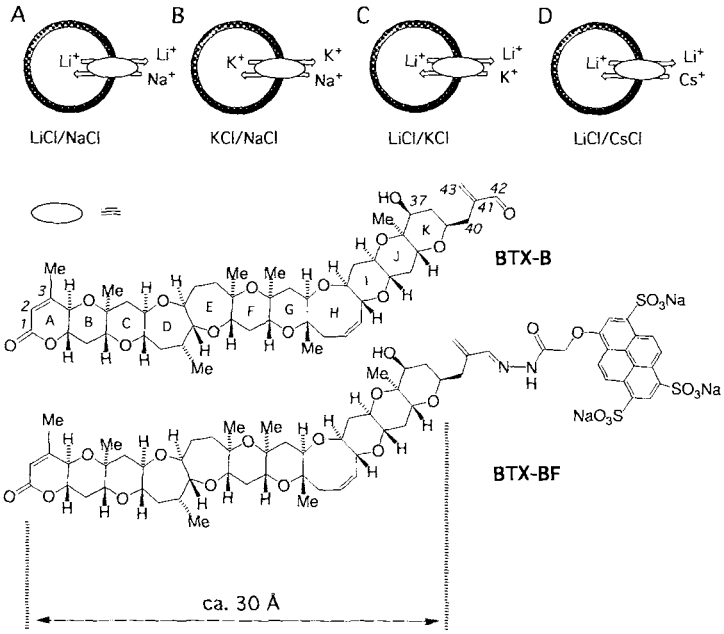

Scheme 1. Structures of BTX-B and fluorescent ("cascade blue")-labeled brevetoxin B (BTX-BF). Schematic representation of the gradient systems used for ion transport kinetics: egg PC vesicles containing 0.3 mol% BTX-B or BTX-BF in aqueous LiCl (A, C, D) or KCl (B) diluted with isoosmolar NaCl (A, B), KCl (C), or CsCl (D). Thus, in (A) a sodium gradient from outside to inside the vesicle and a lithium gradient of opposite direction are established.

Transport rates were estimated by $^{23}Na/^{7}Li$ NMR spectroscopy[6] according to the system designed by Lehn and coworkers,[4a] which has the advantage that the intravesicular sodium concentration can be monitored in a noninvasive manner (Fig. 1).

Fig. 1. ^{23}Na NMR spectra of egg PC vesicles containing 0.3 mol% BTX-B measured a) immediately after establishment of the Na^+/Li^+ gradient and b) 1 h later. The added shift reagent leads to an upfield shift of the signal of the cations outside the vesicle: in the ^{23}Na NMR spectrum anisochronous Na^+_{in} and Na^+_{out} each give rise to one signal.

The observed transport rates of the ions were found to be sensitive to temperature of vesicle formation, cholesterol concentration, and ion size (Fig. 2, Table 1). The most dramatic

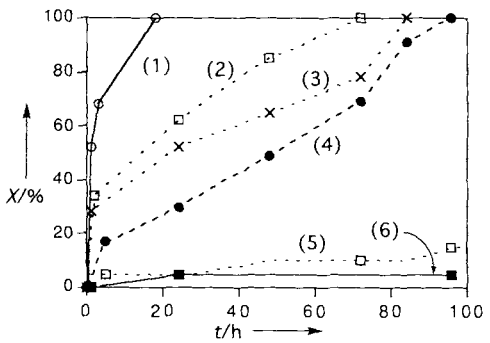

Fig. 2. Sodium ion influx into egg PC vesicles containing 0.3 mol% BTX-B (BTX-BF) (X is the proportion of exchanged cations; for conditions see Table 1). In control experiments in the absence of BTX-B (BTX-BF) no Na^+ entry was detected over the same time period.

Table 1. Conditions for the ion transport studies (1)–(6) represented in Figure 2 [a].

	(1)	(2)	(3)	(4)	(5)	(6)
Toxin	BTX-B	BTX-BF	BTX-B	BTX-B	BTX-BF	BTX-B
Dialysis temperature	RT	RT	RT	4 °C	4 °C	RT
Cholesterol [%]	50	50	0	0	50	50
Gradient	LiCl/NaCl	LiCl/NaCl	LiCl/NaCl	LiCl/NaCl	LiCl/NaCl	KCl/NaCl

[a] RT = room temperature.

rate increase was achieved with vesicles containing 50% cholesterol (curve 1). Since the addition of cholesterol reduces lipid/BTX-B dynamics, the observed rate increase implies ion transport through membrane-spanning channels (a "channel-like" mechanism) and not by a carrier mechanism.[7] Moreover, apparent first-order rate constants for Na^+ entry comparable to $k = 0.69 \pm 0.2\ h^{-1}$ have so far been observed only for amphotericin B measured in the same[4d] and gramicidin ion channels in a similar system.[5b] Cation selectivity was investigated by exchanging the lithium gradient for a potassium gradient (Scheme 1 B); the latter yielded very moderate transmembrane ion exchange (Fig. 2, curve 6). The decrease in the intensity and the broadening of the Li^+_{in} peak in the ^{7}Li NMR spectrum[4b] in the presence of sodium, potassium, and cesium gradients (Scheme 1 A, C, D, respectively) gave the selectivity order of $Na^+, Li^+ > K^+ > Cs^+$; even after two weeks, no Cs^+_{in} was detectable in the ^{133}Cs NMR spectrum.

Fluorescence labeling (BTX-BF) resulted in reduced rate constants (Fig. 2, curve 2) accompanied by a blue-shifted emission maximum in lipid-bound BTX-BF compared to the emission of BTX-BF in the absence of lipids (Fig. 3). A similar blue-shifted emission maximum (406 nm) in the micelle-forming, amphiphilic steroidal C-3 "cascade blue"[8] derivative strongly indicates that this effect is caused by self-assembly of BTX-BF in lipid bilayers and not by environmental influences on a single fluorophore at the lipid/water interface.[9] The blue-shifted emission of aggregated "cascade blue" can be explained, for example, by relaxation from the Franck–Condon excited state, which is "frozen in" by restricted molecular motion.[10] Upon treatment of the 100 mM LiCl stock solution with isoosmolar HCl (100 mM HCl, pH 1), the emission maxima of lipid-bound

 © VCH Verlagsgesellschaft mbH, D-69451 Weinheim, 1996 0570-0833/96/3507-0758 $ 15.00+.25/0 Angew. Chem. Int. Ed. Engl. 1996, 35, No. 7

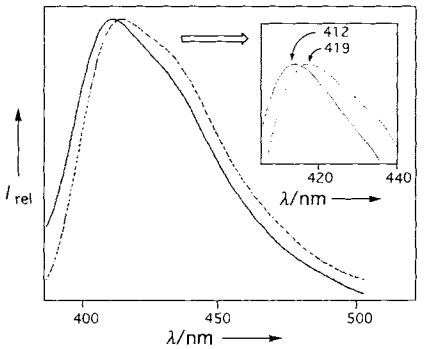

Fig. 3. Emission spectra of BTX-BF in 100 mM LiCl, 10 mM Tris, pH 7.4, incorporated into egg PC vesicles (solid line) and without egg PC vesicles (dashed line); excitation 360 nm.

and free BTX-BF both shift to 416 nm. Protonation of the nitrogen moieties of the extra- as well as the intravesicular fluorescence labels shows them to be at the lipid surface, and thus the BTX-B skeleton to be oriented perpendicular to the lipid surface[9] (Fig. 4).

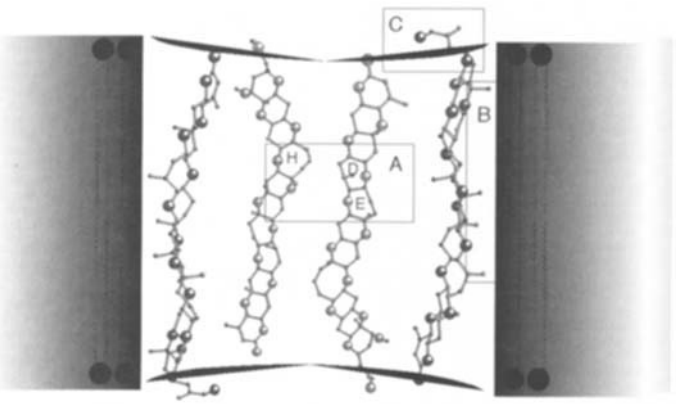

Fig. 4. Presentation of six cylindrically arranged BTX-B molecules (MacroModel V4.5 [12]; the specification of six molecules is hypothetical). The two BTX-B molecules in the front are not shown, and the carbon atoms are reduced and the oxygen atoms enlarged for clarity. The crown ether like arrangement of oxygen atoms, the stiff *trans*-fused rings with intermittent flexible D-, E-, and H-rings (A), the axial methyl groups (B), and the terminal K-ring substituents (C), all which are conserved motifs in brevetoxins and ciguatera toxins, probably play a crucial role for activity. Cholesterol is not shown here because we interpret that its role is to reduce the lipid/BTX-B dynamics rather than to interact in a specific manner with BTX-B.

Transmembrane self-assembly of BTX-B and selective cation transport via a "channel-like" mechanism[7] are consistent with the model structure shown in Figure 4. Consequently, a second mode of action of BTX has to be considered: cation movement across cell membranes mediated by transmembrane self-assembly of BTX-B itself. In view of the similar structures of polyether marine toxins,[1] it is possible that transmembrane cation transport is a general mode of action. In particular, maitotoxin[1a] may be considered as a covalently linked brevetoxin assembly; its enhanced toxicity could then be rationalized by reduced critical micelle concentration. The observed sensitivity of brevetoxin B channel formation to temperature, presence or absence of cholesterol, etc., suggests that in vivo, penetration into specific cell membranes and self-assembly stabilization may also be governed by the presence or absence of membrane proteins. Further investigations, in particular structural studies of transmembrane BTX self-assemblies[9] and single-channel measurements, will be reported in due course.

Experimental Procedure

BTX-BF was prepared according to ref. [8]. Following the method of Reynolds et al. [11], fresh egg yolk PC (15 mg), octyl β-D-glucopyranoside (90 mg), BTX-B or BTX-BF (60 nmol), and in some experiments (see Fig. 2) cholesterol (3.9 mg) were dissolved in 5 mL of chloroform/methanol (2/1) and the solution evaporated to a thin film. After complete removal of organic solvents, the residue was dissolved in 1 mL of 100 mM LiCl (Scheme 1 A, C, D) or KCl (Scheme 1 B), 10 mM tri(hydroxymethyl)aminomethane (Tris), pH 7.4. The resulting clear solution was dialyzed against 100 mM LiCl (Scheme 1 A, C, D) or KCl (Scheme 1 B), and 10 mM Tris, pH 7.4 (3 × 800 mL, 4 °C or room temperature (see Fig. 2)). The lipid concentration of the resulting vesicle solution was estimated by measuring the phosphate content after digestion, and the BTX-B/BTX-BF concentration by quantitative reversed-phase HPLC (detection at 210 nm/400 nm). The concentration of lipid-bound BTX-BF was further monitored by fluorescence spectroscopy by comparing the emission with known concentrations of free BTX-BF. Chromatography of the resulting vesicle solution on Sephadex G-25 or Sepharose CL 4B did not change the vesicle composition. To 300 μL of the vesicle solution were added 240 μL of 100 mM NaCl (Scheme 1 A), KCl (Scheme 1 C), or CsCl (Scheme 1 D), 10 mM Tris (pH 7.4), and 100 μL of shift reagent (10 mM $DyCl_3$, 30 mM $(Me_4N)_5P_3O_{10}$, 10 mM Tris, pH 7.4).

Received: October 2, 1995 [Z.8438IE]
German version: *Angew. Chem.* **1996**, *108*, 812–814

Keywords: brevetoxins · fluorescence labeling · ion channels · lipids · self-assembly

[1] a) T. Yasumoto, M. Murata, *Chem. Rev.* **1993**, *93*, 1897, and references therein; b) H. Ishida, A. Nozawa, K. Totoribe, N. Muramatsu, H. Nukaya, K. Tsuji, K. Yamaguchi, T. Yasumoto, H. Kaspar, N. Berkett, T. Kosuge, *Tetrahedron Lett.* **1995**, *36*, 725.

[2] a) Y. Y. Lin, M. Risk, S. M. Ray, D. Van Engen, J. Clardy, J. Golik, J. C. James, K. Nakanishi, *J. Am. Chem. Soc.* **1981**, *103*, 6773; b) Y. Shimizu, H. Bando, H.-N. Chou, G. Van Dyne, J. C. Clardy, *J. Chem. Soc. Chem. Commun.* **1986**, 1656.

[3] R. E. Gawley, K. S. Rein, G. Jeglitsch, D. J. Adams, E. A. Theodorakis, J. Tiebes, K. C. Nicolaou, D. G. Baden, *Chem. Biol.* **1995**, *2*, 533, and references therein.

[4] a) M. J. Pregel, L. Jullien, J.-M. Lehn, *Angew. Chem.* **1992**, *104*, 1695; *Angew. Chem. Int. Ed. Engl.* **1992**, *31*, 1637; b) A. Nakano, Q. Xie, J. V. Mallen, L. Echegoyen, G. W. Gokel, *J. Am. Chem. Soc.* **1990**, *112*, 1287; c) J.-H. Fuhrhop, U. Liman, *ibid.* **1984**, *106*, 4643; d) E. Stadler, P. Dedek, K. Yamashita, S. L. Regen, *ibid.* **1994**, *116*, 6677, and references therein.

[5] a) D. B. Datta, *A Comprehensive Introduction to Membrane Biochemistry*, Floral, Madison, **1987**; b) M. M. Pike, S. R. Simon, J. A. Balschi, C. S. Springer Jr., *Proc. Natl. Acad. Sci. USA* **1982**, *79*, 810; c) M. R. Ghadiri, J. R. Granja, L. K. Buehler, *Nature* **1994**, *369*, 301, and references therein.

[6] R. K. Gupta, P. Gupta, *J. Magn. Reson.* **1982**, *47*, 344, and references in [4a–c].

[7] Excellent discussions about the semantic problems surrounding use of the term "channel" are given in references [4].

[8] J. E. Whitaker, R. P. Haugland, P. L. Moore, P. C. Hewitt, M. Reese, R. P. Haugland, *Anal. Biochem.* **1991**, *198*, 119.

[9] Structural studies of self-assemblies and ionophoric properties of BTX-B/porphyrin conjugates in the presence and absence of cations lipid bilayers by circular dichroism fully corroborate this conclusion: S. Matile, N. Berova, K. Nakanishi, unpublished results.

[10] E. L. Wehry, in *Practical Fluorescence. Theory, Methods, and Techniques* (Ed.: G. G. Guilbault), Dekker, New York, **1973**, pp. 124–131.

[11] L. T. Mimms, G. Zampighi, Y. Nozaki, C. Tanford, J. A. Reynolds, *Biochemistry* **1981**, *20*, 833.

[12] F. Mohamadi, N. G. J. Richards, W. C. Guida, R. Liskamp, C. Caufield, G. Chang, T. Hendrickson, W. C. Still, *J. Comput. Chem.* **1990**, *11*, 440.

Spontaneous Formation of Chirality in J-Aggregates Showing Davydov Splitting

Umberto De Rossi,* Siegfried Dähne, Stefan C. J. Meskers, and Harry P. J. M. Dekkers

Dedicated to Professor Heinz A. Staab on the occasion of his 70th birthday

The origin of optical activity on earth continues to be a main topic of interest in science. In the absence of chiral auxiliaries or applied external forces, all known synthetic procedures yield racemates, 1:1 mixtures of the enantiomers, in accordance with the principle of parity. Thus, the existence of a multitude of optically active compounds in the biosphere is hard to understand. Processes leading to spontaneous formation of chirality, besides mechanisms such as surface-controlled catalysis with enantiomorphic crystals, are thought to be responsible. Famous examples are the crystallization of 1,1'-binaphthyl[1] and sodium chlorate.[2]

We report on two new model systems, benzimidocyanines **1** and **2**[3] with long alkyl chains, which spontaneously show optical activity due to aggregation of the achiral monomers to form chiral J-aggregates. J-aggregates are of great importance for the study of biologically relevant processes because they serve as model systems for energy migration in antennae systems.[4] Additionally, aggregation phenomena in general play an important role in nature.[5]

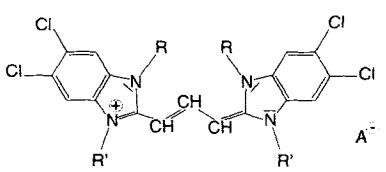

1 : R', R' = $(CH_2)_3CO_2H$; R, R = C_8H_{17}, A = Br

2 : R', R' = $(CH_2)_3CO_2H$; R, R = $C_{12}H_{25}$, A = Br

Cyanine dyes show a great tendency to self-associate. The aggregates formed can be distinguished by UV/Vis spectroscopy because either one sharp absorption band is red-shifted relative to that in the absorption spectrum of the monomer (J-aggregates) or one broad absorption band is blue-shifted (H-aggregates). Their spectroscopic properties can be understood qualitatively on the basis of the exciton model formulated by McRae and Kasha.[6] While the parallel arrangement of monomers with only *one* molecule per unit cell leads to the formation of *one* aggregate band, interaction of two, not translationally equivalent molecules produces a splitting of the absorption band (Davydov splitting), which depends on the angle of the transition dipole moments and the distance between the molecules.[7] In accordance with the principle of parity, circular dichroism (CD) of J-aggregates has to date been observed only under the influence of external chiral disturbances.[8, 9]

[*] U. De Rossi, Prof. Dr. S. Dähne
Bundesanstalt für Materialforschung und -prüfung
Laboratorium für zeitaufgelöste Spektroskopie
Rudower Chaussee 5, D-12489 Berlin (Germany)
Fax: Int. code +(30)6392-5787

S. C. J. Meskers, Dr. H. P. J. M. Dekkers
Leiden Institute of Chemistry
Gorlaeus Laboratories, Leiden University
P. O. Box 9502, NL-2300RA Leiden (The Netherlands)

[**] Energy Migration Phenomena in J-Aggregates, Part 7. These results were first presented on March 8, 1996 at the University of Eindhoven, Institute of Organic Chemistry. This work was supported by the Deutsche Forschungsgemeinschaft (Sonderforschungsbereich 337) and the Fonds der Chemischen Industrie. The model dyes **1** and **2** were synthesized by M. Lisk, Max-Planck-Institut für Kolloid- und Grenzflächenforschung [3]. To check the presented results model system **1** was prepared by a second, independent route. We thank Prof. Saenger (Freie Universität Berlin) for access to a CD spectrometer. Part 6: U. De Rossi, S. Dähne, M. Lindrum, *Langmuir*, in press.

A solution of monomeric **1** in methanol has an absorption maximum at 523 nm and is, as expected, optically inactive. Strong aggregation of the dye is observed in 0.01 N NaOH, and the two absorption maxima at 604 nm and 575 nm are attributed to Davydov splitting (Fig. 1a, thin line). In contrast to the solution of the monomer, that of the aggregate is optically active; its CD spectrum shows a well-resolved couplet with a Davydov splitting energy of 835 cm^{-1} (Fig. 1a, thick line). The lack of orientation dependence of the ΔA values of **1** prove that the optical activity is not due to experimental errors such as linear dichroism[10] or light scattering. The origin of the CD band at 565 nm is unknown and will not be discussed further here. The measured CD amplitudes depend on the preparation of the sample and reach a maximum value of 3×10^{-4} for a concentration of 1×10^{-4} mol L^{-1} of the monomer in NaOH and a cuvette of 0.1 cm thickness (Fig. 1b, broken line). When the dye is dissolved in monomeric form in ethanol, and this solution is treated with a threefold excess of 0.01 N aqueous NaOH, ΔA increases a further, five- to tenfold, although the aggregation is strongly suppressed by the large proportion of ethanol in the solvent mixture (Fig. 1b, solid line). This is confirmed by the occurrence of large ΔA values for a series of dye solutions in NaOH when the concentration of J-aggregates is low.

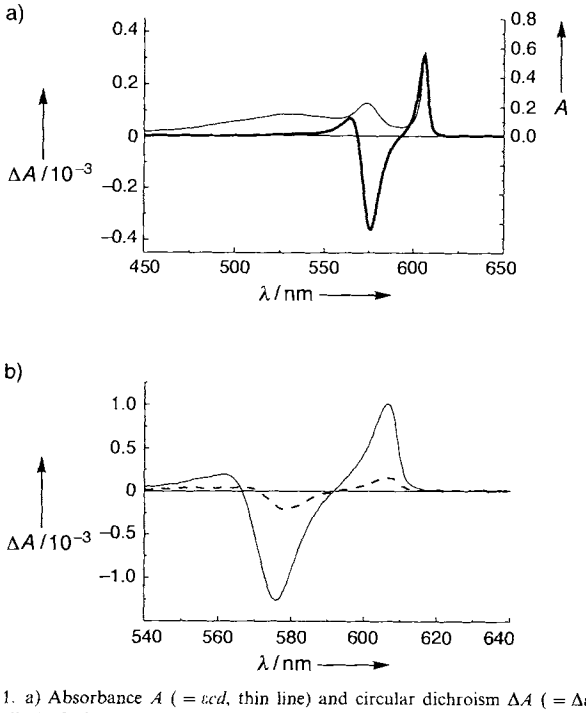

Fig. 1. a) Absorbance A ($= \varepsilon cd$, thin line) and circular dichroism ΔA ($= \Delta\varepsilon cd$, thick line) of **1** in 0.01 N NaOH. b) Dependence of the ΔA values on sample preparation. Dissolving **1** directly in 0.01 N NaOH (– – –) leads to lower amplitudes than the addition of NaOH to a solution of the dye in ethanol (——).

Optically active anions such as tartrate significantly influence the aggregation behavior. Addition of 50 vol% of a saturated solution of sodium (+)-tartrate in 0.01 N NaOH changes the sign of the originally positive couplet of the aggregate solution (Fig. 2b, thin line) and simultaneously increases the ΔA value (Fig. 2b, thick line). The blue shift that appears in the absorption spectrum is evident in the CD spectrum as well and is attributed to a change of the effective dielectric constant. Addition of a (+)-tartrate solution always induces a negative couplet, while addition of a (–)-tartrate solution results in a positive couplet, regardless of the sign of the couplet of the starting solution.

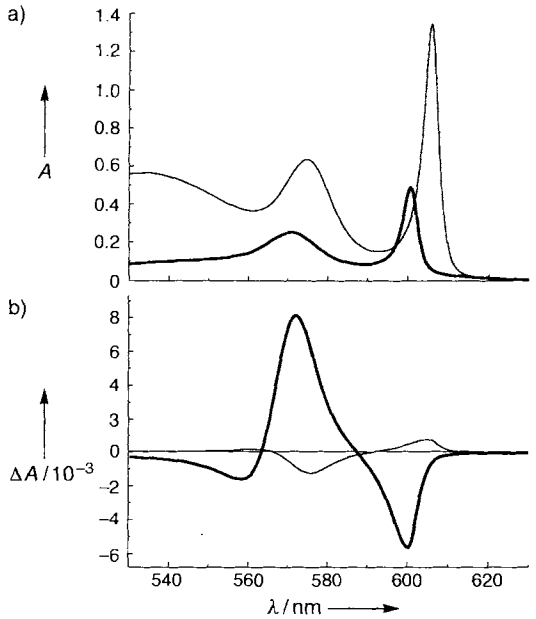

Fig. 2. Effect of added (+)-tartrate solution in NaOH on the a) absorption and b) CD spectrum of 1. Addition of 50 vol% (+)-tartrate solution (thick line) shifts the absorption of the starting solution (thin line) and changes the sign of the CD couplet.

The spontaneous formation of chirality in an achiral system seems to contradict the principle of parity, but the evaluation of 27 experiments, in which aggregation of the dye in an ethanolic solution was induced by addition of NaOH, gave a statistical distribution of 15 positive and 12 negative couplets (Fig. 3).

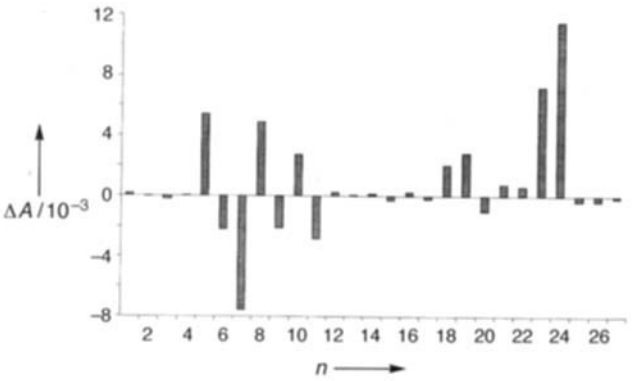

Fig. 3. Distribution of the signs and the CD amplitudes of J-aggregates of model system **1** determined for 27 experiments. The concentration of the monomer in all the experiments described is 1.7×10^{-6} mol L^{-1}. n = experiment number.

Chiral interferences of remaining preagglomerates or adsorbed species on the cuvette surface were excluded by using very low dye concentrations (1.7×10^{-6} mol L^{-1}) and new cuvettes for each experiment.

A clue to the mechanism favoring the formation of an excess of one enantiomer could be derived from the temperature dependence of the CD and absorption spectra. According to the absorption spectra, an increase in temperature shifts the equilibrium between the aggregate and the monomer in the direction of the monomer (steady decrease of the absorption of the J-band, Fig. 4). In constrast, the CD spectra display a two-step temperature dependence. ΔA remains constant below approxi-

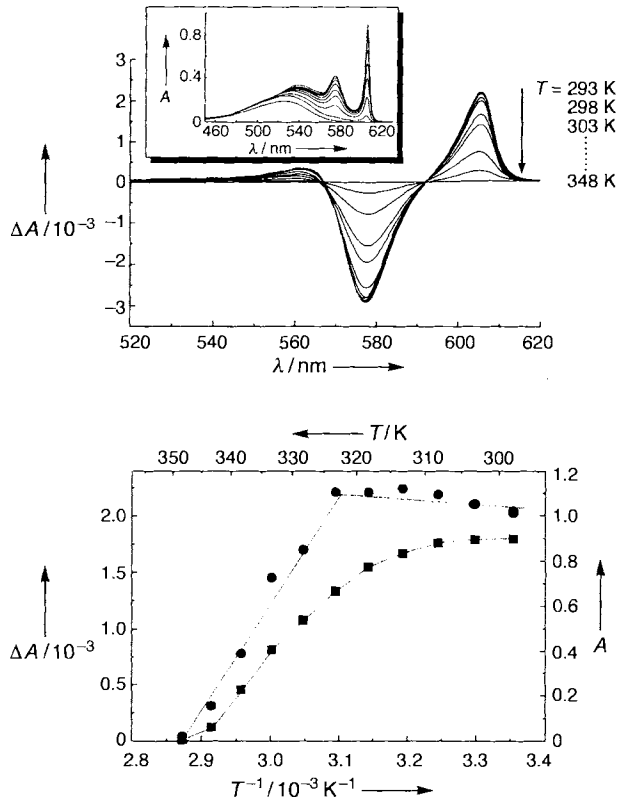

Fig. 4. Top: Absorption spectrum (insert) and CD spectrum of **1** in the temperature region of 293 to 348 K. Bottom: Temperature dependence of the absorption intensity at 604 nm (■) and the CD amplitude (●) of **1**.

mately 320 K and decreases drastically above this temperature. This behavior is reversible and leads to the conclusion that the solution consists of both racemic and enantiomeric aggregates. Racemic aggregates, in other words aggregates consisting of both dextro- and levorotatory subunits, do not contribute to the CD signal and are thus only detectable in the absorption spectrum. In comparison, enantiomerically pure aggregates give both a CD signal and an absorption band and can be detected by both spectroscopic methods. If one assumes that the enantiomerically pure aggregates are more stable than the racemic, as is observed for 1,1'-binaphthyl,[11] the racemic aggregates should be the first to dissociate when the temperature is increased. This behavior should only diminish the absorption of the J-band and should not affect the amplitude of the CD signal. The diminution of both the absorption and the CD signal above 320 K is ascribed to the dissolution of the enantiomerically pure aggregates.

At room temperature model systems **1** and **2** have the same properties. The absorption spectrum of a solution of the monomer **2** in methanol has a maximum at 523 nm. The dye forms aggregates in 0.01 N NaOH as evidenced by absorption maxima at 578 nm and 606 nm and a couplet at the same wavelengths in the CD spectrum. Samples prepared under different conditions yield ΔA values comparable to those of **1**.

However, between 270 and 300 K model system **2** exists in two different types of aggregates showing two distinct J-absorption bands. These two aggregate structures can be reversibly transformed into each other. The aggregate formed on cooling a solution of **2** has an absorption maximum at 595 nm (Fig. 5a). The CD spectrum of a solution containing both aggregate types displays only the already observed couplet of aggregate J_2 (Fig. 5b). Even at higher absorption of the aggregate J_1, no

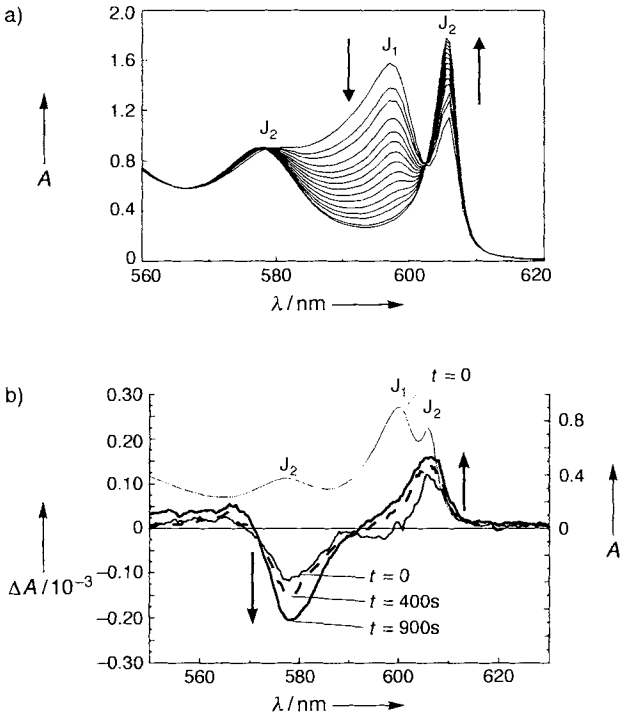

Fig. 5. a) UV/Vis spectra recorded during the transformation of aggregate J_1 into J_2 at room temperature. A spectrum was recorded every 300 s; the sample had been cooled to 270 K for 30 min prior to measurement. b) Absorption spectrum (thin line) and CD spectrum (thick lines) of a solution containing both aggregate species at $t = 0$. The increase of the absorption of J_2 with time (not shown) is accompanied by an increase in the ΔA values (CD spectra at $t = 400$ and 900 s).

circular dichroism is detectable for the band at 595 nm, which suggests that this aggregate form is achiral. At room temperature aggregate J_2 is formed again and the CD signal increases (Fig. 5b).

To the best of our knowledge, this is the first example for spontaneous formation of chirality through aggregation. If one regards J-aggregation as a first step towards crystallization, then the observed phenomena are comparable to the formation of chirality from racemic mixtures (e.g. 1,1'-binaphthyl) or achiral substances (e.g. sodium chlorate). From a theoretical point of view, the formation of an enantiomeric excess cannot be excluded;[12] the probability of this formation is a consequence of a Gaussian distribution. The effect has been proved experimentally for the crystallization of sodium chlorate,[2b] where the observed equimolecular formation of both enantiomers simply has the highest probability.

So far, only speculations can be made on the complicated dynamics of the coupled reactions of formation, growth, and possible decomposition of crystal nuclei. The occurrence of statistical fluctuations during the first phase of the crystal nucleation could lead to an accidental excess of one enantiomeric species. This excess depends on the number of crystal nuclei formed and explains the decrease in ΔA with increasing J-aggregate absorption and the strong variation of ΔA for samples prepared by different procedures. If the size of the aggregate exceeds a critical value, fracture into smaller fragments could be the consequence. These fragments would then serve as crystal nuclei for new aggregates of the same chirality, which would result in an autocatalytic increase in the selection of *one* enantiomeric species.

The absorption and CD spectra give some important evidence for the structure of the aggregates, too. The appearance of two absorption bands suggests the coupling of two nontranslationally equivalent molecules arranged in a herringbone-type structure. Following exciton theory,[7] the ratio of the oscillator strengths of the absorptions of **1** at 575 and 604 nm allows an estimation of the angle α between the two transition dipole moments; this angle is roughly 50°. Calculations based on the model of extended dipoles confirm that an aggregate with $\alpha = 50°$ should give rise to two J-bands red-shifted relative to the monomer spectrum.[13]

The CD spectra also support a herringbone-type structure. Because coplanar arrangement of the molecules would lead to an achiral aggregate structure giving no CD signal, the observed CD spectra allows the conclusion that the planes of the two facing molecules are tilted against each other by the dihedral angle δ along the axis of the herringbone structure. A possible model for the structure taking into account interactions both between the single dye molecules and between the long alkyl substituents is shown in Figure 6. Similar structures have been proposed for a chiral dye dimer incorporated into cyclodextrins[14] as well as for a chiral dye whose cyclohexane ring is substituted with two pentamethinecyanine chromophores in *ortho* position.[15]

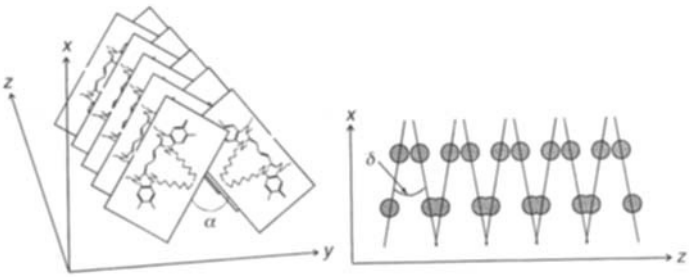

Fig. 6. Front (left) and side view (right) of the proposed structure of aggregates of **1**. α designates the angle between the transition dipole moments of the aggregated molecules of **1**. The dihedral angle δ indicates the tilting of two facing molecules within the herringbone structure. – : chromophore, ○: octyl chain.

On assumption that the presented model resembles the real structure, the *g*-factor can be estimated by applying exciton theory ($g = 4R/D$, R = rotational strength, D = dipole strength).[16] Comparison of the calculated value of 10^{-3} to 10^{-2} with the measured *g*-factors ($= \Delta A/A$) shows that the optical purity of the aggregates lies within the range of 10–100%. Such high values support the assumption of an autocatalytic process during the spontaneous formation of optical active J-aggregates.

The results described here indicate a new and promising way of designing chiral supramolecular structures from achiral substances by combination of two principles, the self-association of organic dyes and the hydrophobic interaction between long alkyl chains.

Received: September 25, 1995
Revised version: January 22, 1996 [Z 8423 IE]
German version: *Angew. Chem.* **1996**, *108*, 827–830

Keywords: chirality · circular dichroism · cyanines · dyes · J-aggregates

[1] R. E. Pincock, K. R. Wilson, *J. Am. Chem. Soc.* **1971**, *93*, 1291–1292; K. R. Wilson, R. E. Pincock, *ibid.* **1975**, *97*, 1474–1478.

[2] a) F. S. Kipping, W. J. Pope, *J. Chem. Soc. Trans.* **1898**, *73*, 606–617; b) J. M. McBride, R. L. Carter, *Angew. Chem.* **1991**, *103*, 298–300; *Angew. Chem. Int. Ed. Engl.* **1991**, *30*, 293–295; D. K. Kondepudi, K. L. Bullock, J. A. Digits, J. K. Hall, J. M. Miller, *J. Am. Chem. Soc.* **1993**, *115*, 10211–10216.

[3] a) U. De Rossi, J. Moll, M. Spieles, G. Bach, S. Dähne, J. Kriwanek, M. Lisk, *J. Prakt. Chem.* **1995**, *337*, 203–208; b) A. Pawlik, U. De Rossi, S. Dähne, unpublished results.
[4] T. V. Dracheva, V. I. Novoderezhkin, A. P. Razjivin, *Chem. Phys.* **1995**, *194*, 223–235; W. Kühlbrandt, *Nature* **1995**, *374*, 497–498.
[5] T. Goto, T. Kondo, *Angew. Chem.* **1991**, *103*, 17–33; *Angew. Chem. Int. Ed. Engl.* **1991**, *30*, 17–33.
[6] E. G. McRae, M. Kasha in *Physical Processes in Radiation Biology* (Eds.: L. Augenstein, R. Mason, B. Rosenberg), Academic Press, New York, **1964**, p. 23.
[7] E. G. McRae, M. Kasha, *J. Chem. Phys.* **1958**, *28*, 721–722.
[8] J. K. Maurus, G. Bird, *J. Phys. Chem.* **1972**, *76*, 2982–2986.
[9] E. Daltrozzo, G. Scheibe, K. Gschwind, F. Haimerl, *Photogr. Sci. Eng.* **1974**, *18*, 441–450.
[10] F. D. Saeva, G. R. Olin, *J. Am. Chem. Soc.* **1977**, *99*, 4848–4850.
[11] K. R. Wilson, R. E. Pincock, *Can. J. Chem.* **1977**, *55*, 889–894.
[12] S. F. Mason in *Circular Dichroism Principles and Applications* (Eds.: K. Nakanishi, N. Berova, R. W. Woody), VCH, Weinheim, **1994**, p. 48.
[13] S. Kirstein, H. Möhwald, *J. Chem. Phys.* **1995**, *103*, 826–833.
[14] V. Buss, *Angew. Chem.* **1991**, *103*, 889–890; *Angew. Chem. Int. Ed. Engl.* **1991**, *30*, 869–870.
[15] D. Gargiulo, F. Derguini, N. Berova, K. Nakanishi, N. Harada, *J. Am. Chem. Soc.* **1991**, *113*, 7046–7047.
[16] I. Tinoco, *Radiat. Res.* **1963**, *20*, 133–139.

Organic Reactions Classified by Neural Networks: Michael Additions, Friedel–Crafts Alkylations by Alkenes, and Related Reactions**

Lingran Chen and Johann Gasteiger*

Organic reactions are influenced by many factors: the structures of the starting materials, reagents, and catalysts as well as reaction conditions such as temperature, solvent, pressure, and light. Each of these factors can be considered as a separate coordinate spanning a multidimensional space, and in this sense a chemical reaction is an event in this type of multidimensional space. Chemists have largely gained their knowledge on organic reactions from observations on a series of reactions; common and differentiating features were sought in order to assign reactions to classes, which were frequently named after the principal discovers, for example Wittig reaction, Michael addition, and Beckmann rearrangement. Clearly, such a one-dimensional classification scheme can only insufficiently account for the variety of observations on chemical reactions.

We will show here that a set of chemical reactions can be projected by a self-organizing neural network into a two-dimensional map. A reaction consists of a point in such a map, and the distance between two points reflects how similar two reactions are. Different types of similarities between reactions can be represented by projection into different directions of the two-dimensional map.

The human brain generates two-dimensional maps in the visual, auditory, and somatosensory cortex from corresponding sensory information obtained from the environment. The self-organizing neural network method developed by Kohonen[1] models this feature of the human brain.[2] In this network the basic processing units, the artificial neurons, are arranged in two dimensions and thus "maps" are obtained of the analyzed information.

Clearly, an enormous range of variations exists for organic reactions, and a map reflecting this broad spectrum of possibilities would be large indeed. To illustrate the potential of our method we will therefore limit the discussion to a set of reactions having an important feature in common: the reaction center, the set of atoms and bonds directly involved in the bond rearrangement during reaction. The reaction scheme chosen is the addition of a C–H bond to a C=C bond (Table 1) and includes such important reaction types as Michael additions, Friedel–Crafts alkylations by alkenes, and free radical additions to alkenes.

Table 1. Electronic variables for characterizing the reaction centers of the reactions discussed [a].

Electronic variables	C=C		+ H–C → H–C–C–C				
	1	2	4	3	4	1	2	3
α_i				×			
q_{tot}		×		×			
χ_σ	×			×			
χ_π	×			×			

[a] For definitions of the symbols refer to the text.

A set of 120 reactions was obtained by a search with the reaction retrieval system ISIS Host[3] in the 1991 version of the ChemInform-RX data base.[4] As the changes in the structures of the starting materials are the most decisive influences on a chemical reaction, we concentrated in this investigation only on these structural influences. The question is then, how should the structures be coded? Clearly, lists of functional groups around the reaction center cannot be the best method, because this list would be quite extensive. Actually, chemists have already tackled the problem of having to compare diverse functional groups and have generalized the influence of functional groups with concepts such as partial charges and inductive/field, resonance, and polarizability effects. Methods for the empirical calculations of these effects developed in our group[5–8] were used to calculate the influence of functional groups on the atoms of the reaction center. Specifically, σ- and π-electronegativities, χ_σ and χ_π, were considered at atoms C-1 and C-3, the total charges, q_{tot}, on atoms C-2 and C-3, and the effective polarizability, α_i, on C-3 (see Table 1).

These seven variables were used to describe each individual reaction of the data set and used as input to the Kohonen neural network. This network projects a seven-dimensional space into a map consisting of 12 × 12 neurons. Each neuron has as many weights as there are input variables for each object; in our case there are seven. A reaction s will be mapped into that neuron c that has weights w_{ji} most similar to the input variables x_{si} of the reaction considered [Eq. (a)]. After each input of a reaction the

$$c \leftarrow \min\left\{\sum_{i=1}^{7}(w_{ji}-x_{si})^2\right\} \quad j = 1-144 \qquad \text{(a)}$$

weights of all neurons are adjusted such as to make them more similar to the input variables. However, this adjustment is largest for the winning neuron c and decreases with increasing distance of a neuron from this central neuron. Reactions that have similar electronic variables will thus be mapped into the

[*] Prof. J. Gasteiger, Dr. L. Chen
Computer-Chemie-Centrum
Institut für Organische Chemie der Universität Erlangen-Nürnberg
Nägelsbachstrasse 25, D-91052 Erlangen (Germany)
Fax: Int. code +(9131)85-6566
e-mail: gasteiger@eros.ccc.uni-erlangen.de

[**] This work was supported by the Alexander-von-Humboldt-Stiftung (scholarship to L.C.). We thank MDL Information Systems providing us with ISIS Host and, together with Fachinformationszentrum Chemie, Berlin, for giving access to the ChemInform-RX reaction data base.

same or adjacent neurons. In our case quite a few neurons obtained several reactions (up to five), indicating a high degree of similarity for those reactions. A number of neurons (78) did not obtain any reaction at all.

To visualize the results of the self-organization of the 120 reactions in the Kohonen network, the reactions were inspected by chemists and assigned to appropriate reaction types, which were identified by symbols (Table 2). The neurons were labeled with these symbols to indicate which reaction was projected into which neuron. The results are shown in Figure 1.

Table 2. Assigned reaction types, associated symbols (see Fig. 1), and the number of reaction instances.

	Reaction type	No. of reactions	Reaction index
A	Michael addition	75	1–14, 24–84
B	misassigned reaction center	1	85
C	Friedel–Crafts alkylation by alkenes	18	15–23, 86–92, 115, 116
D	electron transfer reaction	1	93
E	photochemical addition of an acyl radical to an electron-poor olefin	1	94
F	photoinduced alkylation	4	95–97, 101
G	$H^{\bullet}$ transfer reaction	3	98–100
H	reaction with special mechanism	1	102
I	hydride abstraction reaction	3	103–105
J	Nazarov reaction	5	106–110
K	allylation of an oxo ester and subsequent anti-Markovnikov addition of HBr[a]	1	111
L	palladium-catalyzed hexatrienolate cyclization[a]	3	112–114
M	condensation reaction	1	117
N	photoinitiated radical addition to crown ethers	3	118–120

[a] Two-step reaction.

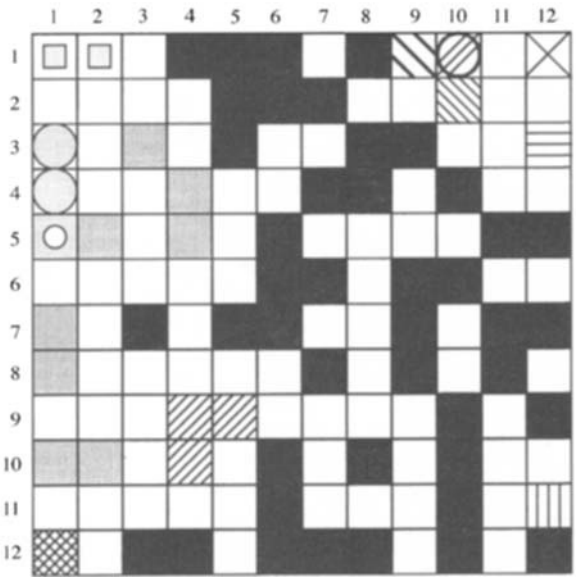

Fig. 1. Kohonen feature map obtained for the classification of 120 reactions. White boxes represent empty neurons; boxes with an × denote conflict neurons. The symbols are defined in Table 2.

Quite a few neurons obtained several reactions, which were always of the same type, indicating the power of the Kohonen network in perceiving similarities of different reactions. Only one neuron, neuron (12,1) stored conflicting information: it contained both a condensation reaction and a reaction that had been coded in the data base with a wrong reaction center.

Michael additions comprised the bulk of the reactions, and consequently the Kohonen network reserved the largest area for this reaction type. The more specialized reaction types and those with only a few members were pushed to the edges of the map. It is quite remarkable that the reaction types assigned by a chemist were also perceived by a Kohonen network, which used the specified physicochemical variables of the reaction center as criteria for assigning reactions; in the Kohonen network the individual reactions of one type were collected in the same region of the map.

Even within the area of one reaction type the site in which a reaction is located contains a lot of chemical information. Figure 2 shows the part of the map of Figure 1 containing Michael

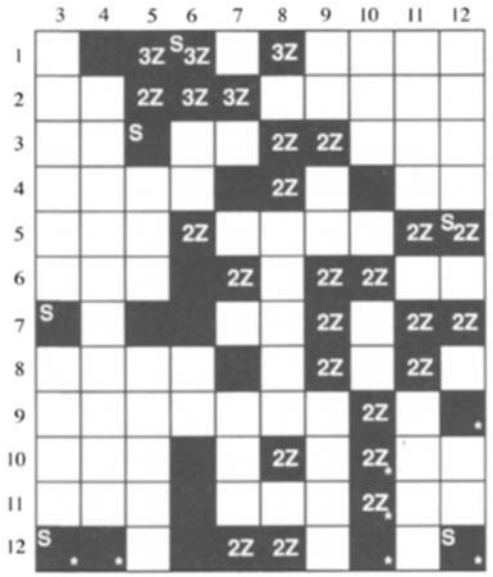

Fig. 2. Detailed analysis of the cluster of Michael additions in the Kohonen feature map in Fig. 1. The neurons marked with 2Z and 3Z were mapped by Michael additions in which the reacting H–C bonds are activated by two or three strongly electron-withdrawing groups, respectively. The neurons marked with * indicate Michael additions in which the reacting C=C bonds are activated by two strongly electron-withdrawing groups. The neurons marked with S were mapped by special Michael additions.

additions. Additional labels give further information on the individual reactions. Reactions that have only one (no label), two (2Z), or three (3Z) electron-withdrawing groups at the reacting H–C bond are quite well separated. By the same token, reactions that have two strongly electron-withdrawing groups (*) at the C=C bond are separated from those that have only one (no label). An important advantage of a two-dimensional map is that structural variations at both reacting bonds, the C–H and the C=C bonds, can be indicated simultaneously. Furthermore, also within a reaction type such as Michael additions the more special examples (S) are found at the edges of the map.

We will now discuss some of the special Michael additions in more detail. Scheme 1 shows the reactions mapped into neurons (6,1), (3,7), (3,12), and (12,12). Whereas in most Michael additions a H–C bond is activated by groups that exert a –M effect, the three reactions mapped into neuron (6,1) show that the

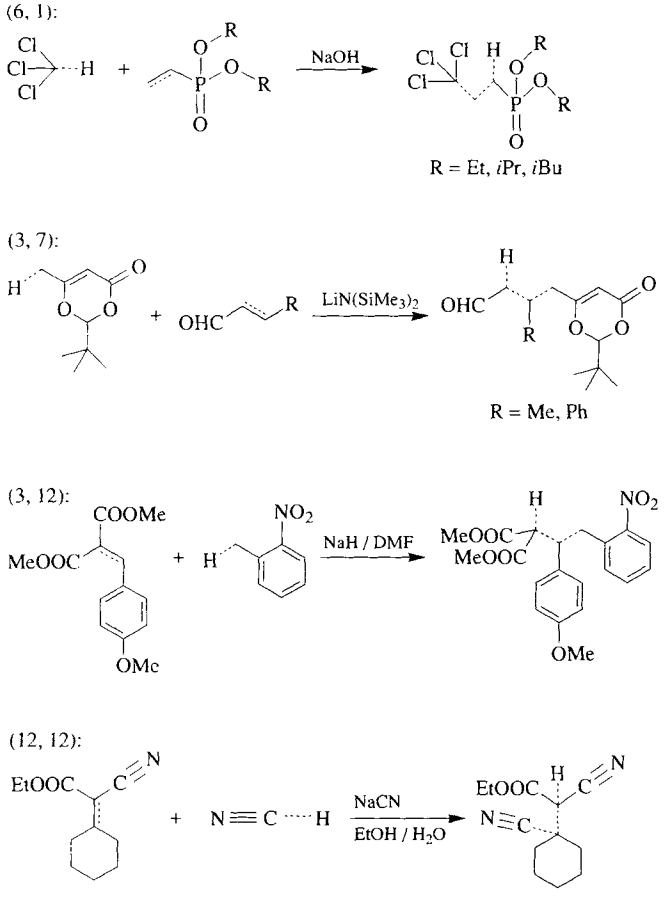

Scheme 1. Michael additions mapped into neurons (6,1), (3,7), (3,12) and (12,12). The bonds denoted by dashed lines are those broken or made in the reaction.

carbanion initiating a Michael addition can also be stabilized by three groups exerting a $-I$ effect.[9] The two reactions in neuron (3,7) are quite unique: the CH_3 group reacting is activated by an ester group that exerts its influence through conjugation across a double bond.[10] A CH_3 group also reacts in the reaction stored in neuron (3,12), but it is activated by an *ortho*-nitro substituent on the phenyl group.[11] Clearly, a common feature in the last two reactions is that a CH_3 group is activated by an electron-withdrawing group in conjugation; however, this effect is transmitted across different π systems. Thus, it is gratifying that these two special Michael additions end up in similar regions of the map (neuron (3,7) and (3,12)).

The reaction in neuron (12,12) is the only Michael addition[12] in this set of reactions in which a $H-C_{sp}$ bond reacts; all other cases involve a $H-C_{sp^3}$ bond. This reaction thus extends the scope of Michael additions and is stored at the borderline of the area of this reaction type.

One of the exciting features of the Kohonen network is that in classifying the reactions, the network automatically gains chemical knowledge from those reaction instances. This "trained" network can then be used to predict reaction types of the unknown reactions. To illustrate this point, the 120 reactions of the previous data set were divided into two groups. The 60 reactions with odd indices (see Table 2) were used as the training set, the other 60 reactions as test set. The result is quite impressive: The reaction types of 95 % (57 instances) of the reactions in the test set were correctly predicted. The reason for two undecided cases and one wrong case is very simple: these three special reactions are not represented in the training set. In fact, all three of these reactions were mapped into empty neurons at the edges of the map.

The two-dimensional Kohonen feature maps can show the relationships of the chemical reactions under investigation, point out the major reaction types, present their scopes, and indicate also unusual reactions. Thus, they allow the chemist to order observations on chemical reactions in an intuitively more appealing and chemically more significant manner.

Received: October 6, 1995 [Z84501E]
German version: *Angew. Chem.* **1996**, *108*, 844–846

Keywords: Kohonen maps · Michael additions · neural networks · reaction classification

[1] a) T. Kohonen, *Biol. Cybern.* **1982**, *43*, 59–69; b) *Self-Organization and Associative Memory*, 3rd ed., Springer, Berlin, **1989**.
[2] J. Zupan, J. Gasteiger, *Neural Networks for Chemists: An Introduction*, VCH, Weinheim, **1993**; J. Gasteiger, J. Zupan, *Angew. Chem.* **1993**, *105*, 510–536; *Angew. Chem. Int. Ed. Engl.* **1993**, *32*, 503–527.
[3] ISIS Host is available from MDL Information Systems, Inc., San Leandro, CA, USA.
[4] a) A. Parlow, C. Weiske, J. Gasteiger, *J. Chem. Inf. Comput. Sci.* **1990**, *30*, 400–402; b) ChemInform-RX data base: Produced by Fachinformationszentrum Chemie, Berlin, Germany, available from MDL Information Systems Inc., San Leandro, CA, USA.
[5] J. Gasteiger, M. Marsili, *Tetrahedron* **1980**, *36*, 3219–3228.
[6] J. Gasteiger, H. Saller, *Angew. Chem.* **1985**, *97*, 699–701; *Angew. Chem. Int. Ed. Engl.* **1985**, *24*, 687–689.
[7] M. G. Hutchings, J. Gasteiger, *Tetrahedron Lett.* **1983**, *24*, 2541–2544.
[8] J. Gasteiger, M. G. Hutchings, *J. Chem. Soc. Perkin Trans. 2* **1984**, 559–564.
[9] O. A. Kolyamshin, V. V. Kormachev, Y. N. Mitrasov, *Zh. Obshch. Khim.* **1990**, *60*, 2170–2171.
[10] D. Seebach, U. Mißlitz, P. Uhlmann, *Chem. Ber.* **1991**, *124*, 1845–1852.
[11] D. M. Floyd, R. V. Moquin, K. S. Atwal, S. Z. Ahmed, S. H. Spergel, J. Z. Gougoutas, M. F. Malley, *J. Org. Chem.* **1990**, *55*, 5572–5579.
[12] G. Griffiths, H. Mettler, L. S. Mills, F. Previdoli, *Helv. Chim. Acta* **1991**, *74*, 309–314.

Schellman Motif in Dehydrooligopeptides: Crystal and Molecular Structure of Boc-Val-ΔPhe-Leu-Phe-Ala-ΔPhe-Leu-OMe**

Kanagalaghatta Ramabhatta Rajashankar, Suryanarayanarao Ramakumar, Tapas Kumar Mal, Ratan Mani Jain, and Virander Singh Chauhan*

In the last few years it has become increasingly apparent that peptides containing α,β-didehydrophenylalanine residues (ΔPhe) exhibit preferential secondary structural features both in the solid state and in solution.[1–13] Introduction of ΔPhe residues in peptide sequences results in β-turns[14] and helical structures.[1–13] Recently we observed a novel β-bend ribbon structure in a pentapeptide containing two ΔPhe residues.[12] In longer peptides containing several ΔPhe residues 3_{10}-helical structures dominate.[5–8, 10] In a recent example an α-helical

[*] Prof. V. S. Chauhan, T. K. Mal, Dr. R. M. Jain
International Center for Genetic Engineering and Biotechnology
NII Campus, Aruna Asaf Ali Marg
New Delhi-110067 (India)
Fax: Int. code +(11)6862316
K. R. Rajashankar, Prof. S. Ramakumar
Department of Physics, Indian Institute of Science
Bangalore-560012 (India)

[**] We thank the Department of Science and Technology (DST), India, for financial support, the Department of Biotechnology (DBT), India, for access to facilities, and Prof. K. K. Tiwari for encouragement. K. R. R. thanks Council of Scientific and Industrial Research (CSIR), India, for a fellowship.

conformation was observed in a pentapeptide containing a single ΔPhe residue.[13] Apparently the final conformation of any ΔPhe peptide depends upon the number and position of ΔPhe residues as well as the nature of the amino acids flanking them.

Amino acids such as ΔPhe and Aib,[15-17] which do not occur in natural proteins, have proved to be useful in generating secondary structural motifs and may be useful in the de novo synthesis of protein mimics.[18] In proteins most of the helices terminate with a reversal of helix sense at the C-terminus; the helix-breaking residue adopts an α_L conformation ($\phi = +50°$, $\psi = +30°$) conformation.[19-25] This conformation generally results in the formation of a 6 → 1 hydrogen bond accompanied by a 5 → 2 hydrogen bond. The 6 → 1 and 5 → 2 hydrogen bonded turn motif in which the fifth residue adopts an α_L conformation has been referred to as a Schellman motif.[25] This conformation, which may be useful in designing helix-terminating motifs, has been identified recently in the crystal structures of oligopeptides containing multiple aminoisobutyric acid (Aib) residues.[26-28] We report here on the crystal and molecular structure of the dehydroheptapeptide **1**, which also exhibits a

Boc-Val-ΔPhe-Leu-Phe-Ala-ΔPhe-Leu-OMe **1**

helical structure terminated by a Schellman motif at the C-terminus. A comparison of the structure of **1** with the crystal structure of Boc-Leu-Phe-Ala-ΔPhe-Leu-OMe,[11] a fragment thereof, highlights the versatility of ΔPhe residues in designing structural motifs.

Heptapeptide **1** was synthesized by conventional solution-phase procedures using a fragment condensation approach.[7] In the characterization of **1** by X-ray structure analysis[29] three standard reflections, which were monitored at regular intervals during data collection, did not vary significantly in their intensities, implying crystal and electronic stability.

In the molecular structure shown in Figure 1 a number of features are evident. The Boc group assumes a double-transoid conformation (relative to O1–C5 and C5–N1) as indicated by the torsion angles θ^1 and ω^0 (Table 1). This particular conformation enables the O2(Boc) atom to participate in the first 4 → 1 intramolecular hydrogen bond.[31] The urethane moiety adopts the generally preferred planar conformation.[31] The value of the dihedral angle $\theta^{1\prime}$ indicates that the C5–O2 bond is *syn*-planar with C4–O1 bond. The three methyl carbon atoms of the Boc group are staggered with respect to O1–C5 bond [$\theta^{2,1} = -60.6(6)°$, $\theta^{2,2} = 63.7(6)°$, and $\theta^{2,3} = -179.4(6)°$]. As expected, the side chains of both ΔPhe residues are planar, as indicated by the dihedral angle χ^1. The side chain conformation of residues Val [g^-t], Phe [$g^-(g^-g^+)$] and Leu [$g^-(g^-t)$] and

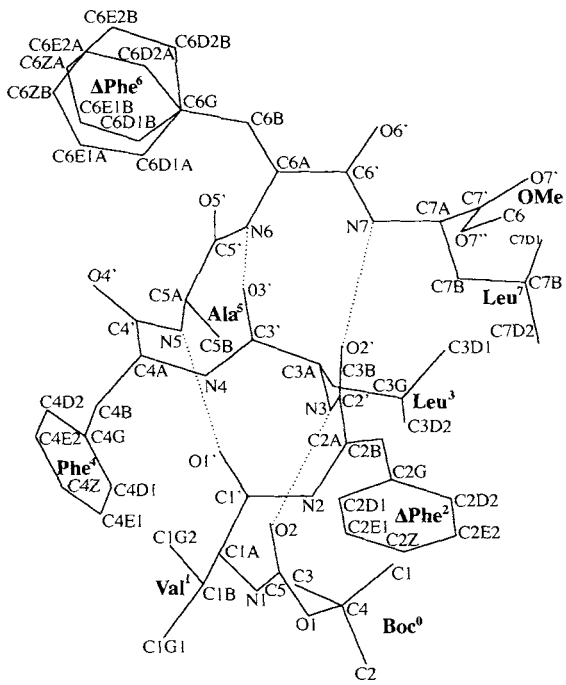

Fig. 1. Molecular structure of **1** in the crystal. The dotted lines indicate the intramolecular N–H···O hydrogen bonds. The two positions of the disordered benzene ring in ΔPhe[6] are also shown.

[$t(g^+t)$] is consistent with the observed conformation in peptide crystal structures[32] (Table 1). The two Leu side chains adopt two different conformations.

The molecule is characterized by a mixed $3_{10}/\alpha$-helix at the N-terminus comprising the first five residues, Boc-Val-ΔPhe-Leu-Phe-Ala. This helix is stabilized by three intramolecular N–H···O hydrogen bonds. Two of these are 4 → 1 type [N3···O2 and N6···O3′] and leads to type III β-bends,[14] and one is 5 → 1 type [N5···O1′] and results in an α-turn[33] (Table 2). α-Turns are quite rare in dehydropeptides. We

Table 2. Parameters of the hydrogen bonds in **1**.

Donor (D)	Acceptor (A)	D···A [Å]	H···A [Å]	D–H···A [°]	Symmetry
N3	O2	3.053(3)	2.303(3)	145.7(3)	x, y, z
N5	O1′	2.929(3)	2.268(3)	133.7(3)	x, y, z
N6	O3′	3.177(4)	2.348(4)	161.8(3)	x, y, z
N7	O2′	3.064(3)	2.334(3)	141.9(4)	x, y, z
N1	O7′	2.960(5)	2.163(5)	154.3(3)	$-x+1, y-1/2, -z$
N2	O6′	2.860(3)	2.073(3)	151.9(3)	$-x+1, y-1/2, -z$

Table 1. Selected torsion angles from the crystal structure of **1** [a].

Angle	Val ($i=1$)	ΔPhe ($i=2$)	Leu ($i=3$)	Phe ($i=4$)	Ala ($i=5$)	ΔPhe ($i=6$)	Leu ($i=7$)
ϕ_i	−52.8(5)	−54.2(4)	−75.2(4)	−62.7(4)	−83.7(4)	95.7(4)	−62.6(4)
ψ_i	−40.1(4)	−31.4(5)	−40.3(4)	−22.7(4)	−9.5(5)	−3.6(5)	−39.3(5) [b]
ω_i	−179.2(3)	176.2(3)	172.7(3)	−179.7(3)	−178.8(3)	−177.6(3)	178.3(5) [b]
$\chi_i^{1,1}$	−62.5(5)	−7.9(6)	−67.5(4)	−69.0(4)		−5.4(7)	−167.9(4)
$\chi_i^{1,2}$	173.3(3)						
$\chi_i^{2,1}$ [c]		−54.9(6)	−57.5(6)	−77.1(5)		−10.2(12)	61.7(7)
						−34.7(8)	
$\chi_i^{2,2}$ [c]		128.7(5)	176.9(4)	102.4(4)		157.6(6)	−176.9(4)
						151.1(7)	

[a] For the Boc group: $\omega_0 = -175.7(3)$, $\theta^1 = -176.2(4)$, $\theta^{1\prime} = 4.6(6)$, $\theta^{2,1} = -60.7(6)$, $\theta^{2,2} = 63.7(6)$, and $\theta^{2,3} = -179.3(5)°$. [b] ψ_7 = N7-C7A-C7′-O3, ω_7 = C7A-C7′-O3-C6. [c] The two values correspond to the disordered positions of the benzene ring in ΔPhe[6].

recently found an α-helical conformation in the crystal structure of the dehydropentapeptide Boc-Val-ΔPhe-Ala-Leu-Gly-OMe.[13] In **1** the NH group of the fourth residue, Phe^4, does not participate in any hydrogen bonds. [The strongest interaction of N4 is characterized by N4···O1′ = 3.053(3) Å, H···O1′ = 2.668(3) Å, and N4–H···O = 108.7(2)°]. The average main chain torsion angles for the first five residues are $\phi = -65.7°$ and $\psi = -28.8°$, which corresponds to a helical conformation and is in agreement with the values observed for the helical modules in peptides and proteins.[34–36] The sixth residue, ΔPhe^6, adopts an unusual left-handed α-helical conformation (α_L) as evident from its backbone dihedral angles (Table 1). The α_L conformation of ΔPhe^6 encourages the formation of a 6→1 hydrogen bond between NH of Leu^7 and CO of ΔPhe^2. This 6→1 hydrogen bond along with the 5→2 hydrogen bond between NH of ΔPhe^6 and CO of Leu^3 leads to a Schellman motif.[25]

The packing mode of the peptide molecules in the crystal is illustrated in Figure 2. The helical part of the peptide molecule

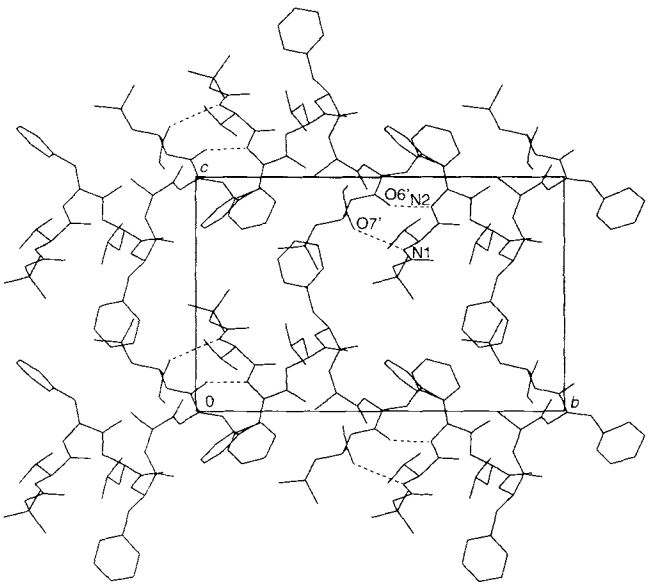

Fig. 2. Crystal packing of **1**; view down the crystallographic *a* axis. The dashed lines indicate the intermolecular N–H···O hydrogen bonds.

is approximately parallel to the crystallographic *b* axis. As the helix axis is along this axis, the neighboring helices are parallel. The helices related by the 2_1 screw axis interact through head-to-tail N–H···O hydrogen bonds (Table 2). The geometries of the hydrogen bond donor and acceptor do not match very well. Hence helical rods, a frequent feature observed in helical peptides,[10, 15] do not form. Instead a slightly zigzagged pattern of peptide molecules is evident along crystallographic *b* axis.

The Schellman motif at the C-terminus of the helix is not surprising in light of the fact that helices in proteins generally terminate with a Schellman motif.[19–25] Also, ΔPhe^6 at position 5 of the Schellman motif[25] is well suited to adopt the left-handed helical conformation since as an achiral residue it can exhibit helical conformations of either sense. The residue adopting the α_L conformation is frequently Gly, and less often Asn, in Schellman motifs of proteins.[19–25] Heptapeptide **1** provides an example wherein a residue with a rigid and bulky side chain is accommodated in the α_L position of the Schellman motif.[25] This might suggest that the achiral nature of the residue occupying the α_L position is more important than the size of the side chain. However, more studies with model peptides are needed to confirm this hypothesis. It has also been observed in proteins that positions 1 and 6 in the Schellman motif[25] are frequently occupied by hydrophobic residues.[19, 21, 25] In **1** these positions are occupied by ΔPhe and Leu, respectively, which are highly hydrophobic.

In oligopeptides containing ΔPhe residues helical structures are generally stabilized. For example, the structure of Boc-Leu-Phe-Ala-ΔPhe-Leu-OMe (**2**), which we recently solved,[11] shows a 3_{10}-helical conformation. Though **2** occurs as a fragment in the present peptide, its conformations in these two cases are different. The reason for this discrepency is not clear. The maximization of intramolecular hydrogen bond interactions is not likely to be a decisive factor, since a perfect $3_{10}/\alpha$-helical conformation would provide a greater number of well-matched helical hydrogen bonds than observed in **1**. Even the crystal packing considerations also do not explain this unusual conformation at the C-terminus of **1**. It is likely that the intramolecular nonbonding interactions play a main role in determining the final conformation. In fact the distances C7D2–C2D2 (4.08 Å), C7B–C2B(4.07 Å), and C7D2–C2B (4.11 Å) indicate significant nonbonding interactions between residues ΔPhe^2 and Leu^7. The residues at these positions are known to show nonbonding interactions in proteins as well.[25]

Experimental Procedure

Synthesis of **1**: The Boc group of the pentapeptide **2** [11] (1.5 g, 2.075 mmol) was removed by treatment with trifluoroacetic acid in dichloromethane (1:1, 20 mL) at room temperature for 30 min. The excess acid was removed in vacuo and the residue triturated with anhydrous ether and filtered. To a solution of Boc-Val-ΔPhe-azlactone (1.12 g, 3.11 mmol) in CH_2Cl_2 (20 mL) was added deprotected **2** and triethylamine (0.3 mL). The reaction mixture was stirred for 72 h at room temperature. After removal of solvent in vacuo, the residue was dissolved in ethyl acetate and washed with saturated $NaHCO_3$ solution, water, and saturated NaCl solution, and dried over Na_2SO_4. Evaporation of solvent in vacuo gave the desired heptapeptide. Yield: 1.5 g (76 %): m.p. 162–164 °C; R_f ($CHCl_3$:CH_3OH 9:1) = 0.93, R_f (*n*-butanol:acetic acid:water 4:1:1) = 0.97. ^{1}H NMR (500 MHz, $CDCl_3$): δ = 8.35 (1H, s, NH(ΔPhe^6)), 7.90 (1H, s, NH(ΔPhe^2)), 7.66 (1H, d, NH(Phe^4)), 7.64 (1H, d, NH(Ala^5)), 7.38 (1H, d, Leu^7), 7.32 (1H, d, Leu^3), 7.31–7.22 (17H, m, aromatic protons of ΔPhe^6, ΔPhe^2, Phe^4, C$^\beta$H (ΔPhe^6 and ΔPhe^2)), 5.03 (1H, s, NH(Val^1)), 4.73 (1H, br, C$^\alpha$H(Leu^7)), 4.47 (1H, br, C$^\alpha$H(Ala^5)), 4.45 (1H, br, C$^\alpha$H(Phe^4)), 4.13 (1H, br, C$^\alpha$H(Leu^3)), 3.84 (1H, br, C$^\alpha$H(Val^1)), 3.68 (3H, s, OCH_3), 3.45 (1H, d, C$^\alpha H_A$(Phe^4)), 3.07 (1H, t, C$^\beta H_B$(Phe^4)), 2.24 (1H, br, C$^\beta$H(Val^1)), 1.79 (2H, br, C$^\beta$H(Leu^7)), 1.77 (1H, br, C$^\gamma$H(Leu^7)), 1.59 (2H, br, C$^\beta$H(Leu^3)), 1.58 (1H, br, C$^\gamma$H(Leu^3)), 1.45 (9H, s, 3×CH_3 (Boc)), 1.12 (6H, dd, C$^\delta H_3$(Val^1)), 0.96 (6H, dd, C$^\delta H_3$(Leu^3)), 0.79 (6H, dd, C$^\delta H_3$(Leu^7)). Crystals suitable for X-ray structure analysis were grown by slow evaporation of a solution of **1** in methanol and water at 4 °C.

Received: October 13, 1995
Revised version: December 28, 1995 [Z84731E]
German version: *Angew. Chem.* **1996**, *108*, 807–810

Keywords: dehydroamino acids · oligopeptides · Schellman motif

[1] O. Pieroni, A. Fissi, C. Pratesi, P. A. Temussi, F. Ciardelli, *Biopolymers* **1993**, *33*, 1.
[2] A. Tuzi, M. R. Ciajolo, G. Guarino, P. A. Temussi, A. Fissi, O. Pieroni, *Biopolymers* **1993**, *33*, 1111.
[3] M. R. Ciajolo, A. Tuzi, C. R. Pratesi, A. Fissi, O. Pieroni, *Int. J. Peptide Protein Res.* **1991**, *38*, 539.
[4] V. Busetti, M. Crisma, C. Toniolo, S. Salvadori, G. Balboni, *Int. J. Biol. Macromol.* **1992**, *14*, 23.
[5] M. R. Ciajolo, A. Tuzi, C. R. Pratesi, A. Fissi, O. Pieroni, *Biopolymers* **1990**, *30*, 911.
[6] K. K. Bhandary, V. S. Chauhan, *Biopolymers* **1993**, *33*, 209.
[7] V. S. Chauhan, K. K. Bhandary, *Int. J. Peptide Protein Res.* **1992**, *39*, 223.
[8] R. M. Jain, M. Singh, V. S. Chauhan, *Tetrahedron* **1994**, *50*, 907.
[9] H. C. Patel, T. P. Singh, V. S. Chauhan, P. Kaur, *Biopolymers* **1990**, *29*, 509.

[10] K. R. Rajashankar, S. Ramakumar, V. S. Chauhan, *J. Am. Chem. Soc.* **1992**, *114*, 9225.
[11] K. R. Rajashankar, S. Ramakumar, T. K. Mal, R. M. Jain, V. S. Chauhan, *Biopolymers* **1995**, *35*, 141.
[12] K. R. Rajashankar, S. Ramakumar, T. K. Mal, V. S. Chauhan, *Angew. Chem.* **1994**, *106*, 1048; *Angew. Chem. Int. Ed. Engl.* **1994**, *33*, 970.
[13] K. R. Rajashankar, S. Ramakumar, R. M. Jain, V. S. Chauhan, *J. Am. Chem. Soc.* **1995**, *117*, 10129.
[14] C. M. Venkatachalam, *Biopolymers* **1968**, *6*, 1425.
[15] I. L. Karle, P. Balaram, *Biochemistry* **1990**, *29*, 6747.
[16] C. Toniolo, E. Benedetti, *Macromolecules* **1991**, *24*, 4004.
[17] G. R. Marshall, E. E. Hodgkin, D. A. Langs, G. D. Smith, J. Zabrocki, M. T. Leplawy, *Proc. Natl. Acad. Sci. USA* **1990**, *87*, 487.
[18] W. F. DeGrado, *Adv. Protein Chem.* **1988**, *39*, 51.
[19] C. Schellman in *Protein Folding* (Ed.: R. Jaenicke), Elsevier, Amsterdam, **1980**, pp. 53–61.
[20] E. N. Baker, R. E. Hubbard, *Prog. Biophys. Mol. Biol.* **1984**, *44*, 97.
[21] E. J. Milner-White, *J. Mol. Biol.* **1988**, *199*, 503.
[22] H. A. Nagarajaram, R. Sowdhamini, C. Ramakrishnan, P. Balaram, *FEBS Lett.* **1993**, *321*, 79.
[23] J. S. Richardson, D. C. Richardson, *Science* **1988**, *240*, 1648.
[24] R. Preissner, P. Bork, *Biochem. Biophys. Res. Commun.* **1991**, *180*, 660.
[25] R. Aurora, R. Srinivasan, G. D. Rose, *Science* **1994**, *264*, 1126.
[26] E. Benedetti, B. Di Blasio, V. Pavone, C. Pedone, A. Santini, A. Bavoso, C. Toniolo, M. Crisma, L. Sartore, *J. Chem. Soc. Perkin Trans. 2* **1990**, 1829.
[27] R. Bosch, G. Jung, H. Schmitt, W. Winter, *Biopolymers* **1985**, *24*, 961.
[28] I. L. Karle, J. L. Flippen-Anderson, K. Uma, P. Balaram, *Int. J. Peptide Protein Res.* **1993**, *42*, 401.
[29] Structure analysis of **1** ($T = 295$ K): Data were collected from a dry crystal mounted on a glass fiber by using a Enraf–Nonius CAD4 diffractometer. $M_r = 966.2$ ($C_{53}H_{71}N_7O_{10}$), monoclinic, space group $P2_1$, $a = 10.953(2)$, $b = 20.065(2)$, $c = 12.862(2)$ Å, $\beta = 95.1(1)°$, $V = 2815.3(7)$ Å^3, $Z = 2$, $\rho_{calcd} = 1.14$ g cm^{-3}; $Cu_{K\alpha}$ radiation, $\lambda = 1.5418$ Å, $\mu = 6.109$ cm^{-1}; $F(000) = 1036.0$, $2\theta = 130°$, ($\omega - 2\theta$) scans; 4926 independent reflections, of which 4674 with $|F_o| > 4\sigma(|F_o|)$ were considered as independent. Lorentz and polarization corrections were applied to the data, but no absorption correction was made. The structure was determined using the direct methods employing the SHELXS86 [29] computer program and full-matrix least-squares refinement was carried out using the software SHELXL93 [30]. All non-hydrogen atoms were refined anisotropically. The hydrogen atoms fixed on the basis of stereochemistry were used only for structure factor calculations. The atoms of the benzene ring in residue ΔPhe^6 (except C6G) were found to be disordered between two positions (see Fig. 1). These five atoms were refined isotropically with the effective occupancy adding up to 1. Final *R*-values (based on $|F_o|$) for the observed reflections 0.046, for all reflections 0.048, (based on *I*) for all reflections 0.136, GoF = 1.049. Crystallographic data (excluding structure factors) for the structure described in this paper have been deposited with the Cambridge Crystallographic Data Centre as supplementary publication no. CCDC-179-5". Copies of the data can be obtained free of charge on application to The Director, CCDC, 12 Union Road, Cambridge CB21EZ, UK (fax: Int. code +(1223)336-033; e-mail: teched*@* chemcrys.cam.ac.uk).
[30] a) G. M. Sheldrick, *Crystallographic Computing, Vol. 3*, Oxford University Press, New York, **1985**, pp. 175; b) *Acta Crystallogr. Sect. A* **1990**, *46*, 467.
[31] E. Benedetti, C. Pedone, C. Toniolo, G. Nemethy, M. S. Pottle, H. A. Scheraga, *Int. J. Peptide Protein Res.* **1980**, *16*, 156.
[32] E. Benedetti, G. Morelli, G. Nemethy, H. Scheraga, *Int. J. Peptide Protein Res.* **1983**, *22*, 1.
[33] C. Toniolo, *Crit. Rev. Biochem.* **1980**, *9*, 1.
[34] E. Benedetti, B. Di Blasio, V. Pavone, C. Pedone, C. Toniolo, M. Crisma, *Biopolymers* **1992**, *32*, 453.
[35] C. Toniolo, E. Benedetti, *Trends Biochem. Sci.* **1992**, *16*, 50.
[36] D. J. Barlow, J. M. Thornton, *J. Mol. Biol.* **1988**, *201*, 601.

Chlorine Tetraoxide**

Hinrich Grothe and Helge Willner*

The existence of the ClO_4 radical, one of the simplest chlorine oxides ClO_x ($x = 1-4$), has not yet been unequivocally established. Yet it has been postulated as a reactive intermediate in several reactions and should be a binary compound of fundamental significance. ClO_4 is probably an intermediate in the photochemical formation of Cl_2O_7 from Cl_2 and O_3,[1] as well as in the thermal decomposition of Cl_2O_6[2] and Cl_2O_7,[3] and in the anodic oxidation of ClO_4^- ions.[4] An indication of the existence of ClO_4 was obtained from ESR measurements on $KClO_4$ crystals that had been irradiated with X-rays.[5] However, the assignment and analysis of the ESR signals is still controversial.[6,7] The formation enthalpy of the endothermic ClO_4, derived from mass spectrometric and kinetic measurements on Cl_2O_7, amounts to 200–270 kJ mol^{-1}.[8,9]

The successful synthesis and spectroscopic identification of ClO_3 in the vacuum thermolysis of $ClOClO_3$ and matrix isolation of the products[10] encouraged us to generate a ClO_4 radical in the same way. For this purpose a sample of Cl_2O_6 (or Cl_2O_7) in a U-tube was cooled to -35 (or -105 °C) such that the partial pressure was roughly 10^{-3} mbar. Neon or argon was passed over the cold sample to give a 1:500 mixture of starting material and noble gas. This gas stream was thermolyzed at 230 °C (410 °C) at the orifice of the nozzle. Under these conditions 95 % of the molecules decay within a few milliseconds. The construction of the vacuum thermolysis and the matrix isolation apparatus is described elsewhere.[11] IR and UV/Vis spectra of the matrix-isolated thermolysis products were recorded. The proportion of decayed starting material was calculated by comparison with reference spectra of pure matrix-isolated starting material. In a total of 25 experiments we found five new bands in the IR spectra of the thermolysis products of Cl_2O_6 and Cl_2O_7 (Fig. 1, Table 1). These reproducible bands belonging to an

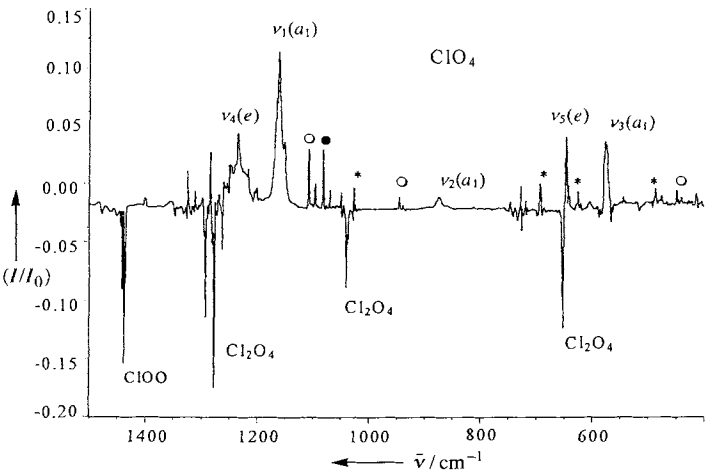

Fig. 1. Difference spectrum before and after the photolysis ($\lambda > 495$ nm) from the IR spectra of the thermolysis products of Cl_2O_6 isolated in a neon matrix. The bands of ClO_4 point upwards and those of the photolysis products downwards. Some noncompensated bands disrupt the spectrum. Bands arising from the by-products OClO (o), ClO_3 (•), and the starting material Cl_2O_6 (*) are labeled. Cl_2O_4 is formed in the photolysis of Cl_2O_6 [2].

[*] Prof. Dr. H. Willner, Dipl.-Chem. H. Grothe
Institut für Anorganische Chemie der Universität
Callinstrasse 9, D-30167 Hannover (Germany)
Fax: Int. code +(511)762-3006

[**] This work was supported by the Deutsche Forschungsgemeinschaft and by the Fonds der Chemischen Industrie.

Table 1. Wavenumbers $\tilde{\nu}$ [cm^{-1}], intensities (in parentheses), and assignments of the fundamental vibrations of ClO_4, ClO_3F, and SO_3F radical.

$^{35}Cl^{16}O_4$ [b]	$^{35}Cl^{18}O_4$ [b]	ClO_3F [c]	SO_3F [d]	Assignment [a] XO_3Y
1234 (s)	1196 (s)	1315.6 (vs)	1177.4 (m)	$\nu_4(e) = \nu_{as}(XO)$
1161 (vs)	1118 (vs)	1062.3 (m)	1053.0 (s)	$\nu_1(a_1) = \nu_s(XO)$
874 (w)	832 (w)	712.4 (s)	832.8 (s)	$\nu_2(a_1) = \nu(XY)$
646 (m)	609 (m)	588.3 (m)	601 (w)	$\nu_5(e) = \delta_{as}$
576 (m)	548 (m)	547.5 (w)	531.2 (m)	$\nu_3(a_1) = \delta_s$
		405.9 (w)	366 (vw)	$\nu_6(e) = \rho$

[a] Assignment for point group C_{3v}. [b] In Ne matrix. [c] In Ne matrix [14]. [d] In Ar matrix [15].

unknown chlorine oxide are remarkable because their full width at half maximum is up to 10 cm^{-1}. This partly obscures the $^{35/37}Cl$ isotopic pattern, which is typical of species with one Cl atom. Since the relative intensities of the bands were the same in all experiments and since the bands decreased uniformly after photolysis of the matrix (tungsten–halogen lamp, cutoff filter, $\lambda > 495$ nm), all bands must belong to one single species. By IR spectroscopy we identified only ClOO as a product of the photolysis; it is probably formed by the primary decomposition of ClO_4 to give OClO and O_2 and subsequent photoisomerization of OClO.[12] In the UV/Vis spectra ClO_4 shows a wide absorption band ranging from 380 to 510 nm (maximum at 425 nm) with vibrational fine structure. The intensity of this band on photolysis decreases in the same fashion as the infrared bands of ClO_4. Below 380 nm the UV spectrum is obscured by the bands of ClO_3, ClO_2, and the starting material.

ClO_2 and ClO_3 are the most important by-products formed in the thermolysis of Cl_2O_6 and Cl_2O_7, respectively. Thus the primary decomposition can be described according to Equations (a) and (b), and the new bands can be assigned to the

$$Cl_2O_6 \longrightarrow ClO_4 + ClO_2 \quad (a)$$

$$Cl_2O_7 \longrightarrow ClO_4 + ClO_3 \quad (b)$$

ClO_4 radical. Experiments with $Cl_2{}^{18}O_6$ and the calculation of the vibrational frequencies with the program NORCOR[13] verify the existence of ClO_4. There are numerous possibilities for the arrangement of atoms in a ClO_4 molecule and for its symmetry. Based on the mode of formation, it can be assumed that ClO_4 has a tetrahedral or distorted tetrahedral structure with T_d, C_{3v}, C_{2v}, or C_s symmetry. Therefore two, six, eight, or nine corresponding bands can be expected in the range of fundamental vibrations in the IR spectrum. Comparison of the five new vibrations with the fundamentals of the similarly built $FClO_3$ and the isosteric FSO_3 radical clearly indicates a ClO_4 molecule with C_{3v} symmetry (Table 1). We have not yet been able to detect the missing $\nu_6(e)$ vibration, which is expected as a weak band around 400 cm^{-1}.

Our assignment of the bands to the vibrational modes is supported by the product rule for the mode a_1. The wavenumbers of the three a_1 vibrations of $^{35}Cl^{16}O_4$ and $^{35}Cl^{18}O_4$ were used to calculate the quotient of the wavenumber products (observed: 1.311; calculated: 1.308). In addition, a normal coordinate analysis of the vibrational data was performed with the bond lengths listed and a bond angle of 116° between the short ClO bonds of OClO. The results are three strong (8.7×10^2 $N m^{-1}$) and one weak ClO bond (5.3×10^2 $N m^{-1}$). The correlation of the force constant with the bond length (Fig. 2) leads to the structure of the ClO_4 radical shown in Figure 3.

The distortion of the ClO_4 radical to C_{3v} symmetry is dynamic (Jahn–Teller effect). One electron switches from an antibonding σ* orbital of one ClO bond to that of another, resulting in the broadening of the IR bands.

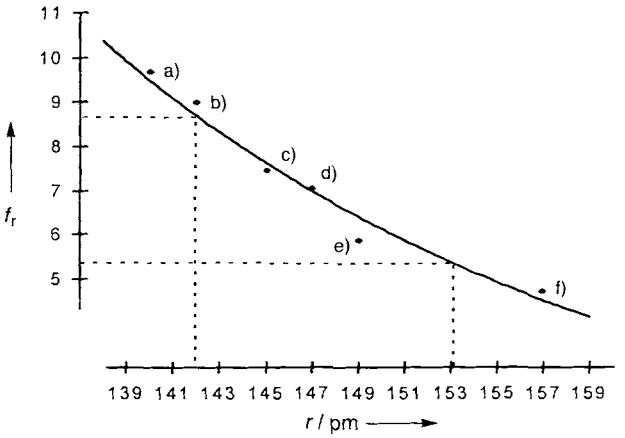

Fig. 2. Plot of the length of the Cl–O versus the force constant in 10^2 $N m^{-1}$ for the Cl–O bond for a) $FClO_3$, b) $FClO_2$, c) ClO_4^-, d) OClO, e) ClO_3^-, and f) ClO. An exponential function was fitted to the data. The broken lines relate the force constants of the ClO_4 radical with the corresponding bond lengths.

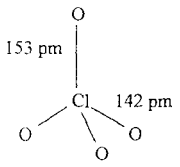

Fig. 3. Structure of ClO_4.

The ClO_4 radical completes the series of mononuclear binary chlorine oxides known, which can combined formally to give the binuclear species Cl_2O_2, Cl_2O_3, Cl_2O_4, Cl_2O_6, and Cl_2O_7. We have demonstrated that the primary thermal decay of two binuclear chlorine oxides yields the corresponding mononuclear radicals, with a preference for the formation of OClO. The chemistry of NO_x is analogous: the radicals NO, NO_2, and NO_3 participate in the formation and the decomposition of N_2O_3, N_2O_4, and N_2O_5, respectively.

Received: October 26, 1995 [Z8499IE]
German version: *Angew. Chem.* **1996**, *108*, 816–818

Keywords: chlorine compounds · IR spectroscopy · matrix isolation

[1] R. Simonaitis, J. Heicklen, *Planet. Space Sci.* **1975**, *23*, 1567–1567.
[2] M. Jansen, G. Schatte, K. M. Tobias, H. Willner, *Inorg. Chem.* **1988**, *27*, 1703–1706.
[3] R. V. Figini, E. Coloccia, H. J. Schumacher, *Z. Physik. Chem.* **1958**, *14*, 32–58.
[4] H. Schmidt, J. Noack, *Z. Anorg. Allgem. Chem.* **1958**, *296*, 262–272.
[5] J. R. Morton, *J. Chem. Phys.* **1966**, *45*, 1800–1802.
[6] J. R. Byberg, J. K. Jensen, *J. Chem. Phys.* **1970**, *52*, 5902–5910.
[7] J. R. Byberg, *J. Phys. Chem.* **1995**, *99*, 13392–13396.
[8] A. J. Colussi, M. A. Grela, *J. Phys. Chem.* **1993**, *97*, 3775–3779.
[9] V. I. Alekseev, T. S. Zyubina, A. S. Zyubin, A. V. Bafuev, *Bull. Acad. Sci. USSR. Div.Chem. Sci. Engl. Transl.* **1989**, *38*, *10*, 2092–2096.
[10] H. Grothe, H. Willner, *Angew. Chem.* **1994**, *106*, 1581–1582; *Angew. Chem. Int. Ed. Engl.* **1994**, *33*, 1482–1484.
[11] G. A. Argüello, H. Grothe, M. Kronenberg, H. Willner, H.-G. Mack, *J. Phys. Chem.* **1995**, *99*, 17525–17531.
[12] H. S. P. Müller, H. Willner, *J. Phys. Chem.* **1993**, *97*, 10589–10598.
[13] D. Christen, *J. Mol. Struct.* **1978**, *48*, 101.
[14] K. O. Christe, E. C. Curtis, W. Sawodny, H. Härtner, G. Fogarasi, *Spectrochim. Acta, Part A* **1981**, *37*, 549–556.
[15] E. M. Suzuki, J. W. Nibler, *J. Molec. Spectrosc.* **1975**, *58*, 201–215.

Electronic Structure of Non-Heme High-Valent Oxoiron Complexes with the Unprecedented $[Fe_2(\mu\text{-}O)_2]^{3+}$ Core**

Abhik Ghosh, Jan Almlöf, and Lawrence Que, Jr.*

The chemistry of dioxygen activation at non-heme diiron centers in enzymes such as ribonucleotide reductase and methane monooxygenase has recently attracted significant attention.[1, 2] For the latter enzyme, a transient intermediate, "compound Q", which is kinetically competent to hydroxylate methane, has been characterized by Mössbauer spectroscopy as a coupled diiron(IV) species.[2] Our synthetic efforts to model such high-valent intermediates have resulted in two complexes with the general formula $[LFe(\mu\text{-}O)_2FeL](ClO_4)_3$ [**1**: L = tris(2-pyridylmethyl)amine (tpa); **2**: L = tris(5-methyl-2-pyridylmethyl)amine (tpa′)], which contain the unprecedented high-valent $[Fe_2(\mu\text{-}O)_2]^{3+}$ core.[3, 4] The EPR spectra of intermediates **1** and **2** are indicative of a quartet spin state ($S = 3/2$), and the Mössbauer spectral parameters are very similar to those of compound Q.[4] Though the iron centers in the $[Fe_2(\mu\text{-}O)_2]^{3+}$ core can naively be assigned the formal oxidation states III and IV, Mössbauer spectra of **1** and **2** show that the two iron centers are identical. To gain insight into the electronic structure of these novel species, we have carried out first-principles quantum chemical calculations on **1** (C_{2h}) and report our results herein.

The large size of the molecules of interest severely limits the choice of an appropriate theoretical method. Transition metal complexes are generally poorly described at the Hartree–Fock level, while standard ab initio correlated methods require prohibitive amounts of computer time and memory. In contrast, density functional theory (DFT)[5, 6] is attractive, owing to its computational expediency and because it implicitly includes the effects of electron correlation. Local density functional (LDF) calculations, including a geometry optimization, were performed on **1**[7] (excluding the perchlorate ions) with a C_{2h} symmetry constraint, to take advantage of the experimentally established indistinguishability of the iron centers. Of the various electronic configurations examined, the configuration with the lowest energy had three unpaired electrons with parallel spins, consistent with the experimentally observed quartet spin states of **1** and **2**.[4]

The optimized structure of **1** (Fig. 1) provides valuable structural information on the novel high-valent $Fe_2(\mu\text{-}O)_2$ core of **1** and **2**. The two symmetry-distinct Fe–O vectors are 1.77 and 1.83 Å in length; the shorter one is *trans* to the nitrogen atom of the aliphatic amino group of tpa. The exceptionally short Fe–Fe separation (2.83 Å) and the compressed Fe-O-Fe angle (105.1°) are a consequence of the Fe_2O_2 core structure and reminiscent of analogous features in the ions $[(tpa)Mn^{III}(\mu\text{-}O)_2Mn^{IV}(tpa)]^{3+}$,[10] $[(tpa'')Fe^{III}(\mu\text{-}O)(\mu\text{-}OH)Fe^{III}(tpa'')]^{3+}$ [tpa″ = tris(6-methyl-2-pyridylmethyl)amine],[11] and $[(tpa'')Fe^{III}(\mu\text{-}O)_2Fe^{III}(tpa'')]^{2+}$.[12] The Fe–N distances in the Fe_2O_2 plane of **1** are 1.95 and 2.03 Å; the longer bond is associated with the more weakly bound nitrogen atom of the aliphatic amino group, while the Fe–N distances outside the Fe_2O_2 plane are 1.91 Å. These Fe–N distances are significantly shorter than those in high-spin Fe^{III} tpa complexes,[1] but are in excellent agreement with those in low-spin $[Fe^{III}(tpa')(acac)](ClO_4)_3$ (acac = 2,4-pentanedionate).[14]

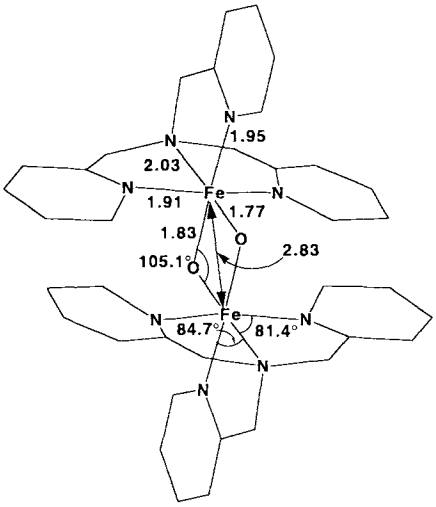

Fig. 1. Optimized geometry in the core of **1**; distances in [Å], angles in [°].

The optimized geometry of **1** can be compared with experimental EXAFS data (Fe K-edge) on the related complex **2**.[4] The best EXAFS fit for **2** consists of one Fe–N/O vector at 1.76 Å, three Fe–N/O vectors at 1.94 Å, two Fe–N/O vectors at 2.17 Å, and one Fe–Fe vector at 2.89 Å. Our optimized geometry is in good agreement with the presence of shells at 1.76, 1.94, and 2.89 Å in the EXAFS fit, but does not reproduce the shell at 2.17 Å. At present, it is not clear whether this discrepancy reflects a limitation of our calculation or of the EXAFS analysis. Overall, despite minor discrepancies, the optimized structure of **1** and experimental data agree quite well.

Figure 2 depicts the energy level diagram of the frontier molecular orbitals (MOs) of **1** that have predominant Fe 3d character.[15] While the symmetries of the frontier orbitals may be predicted from qualitative arguments alone, we obtained

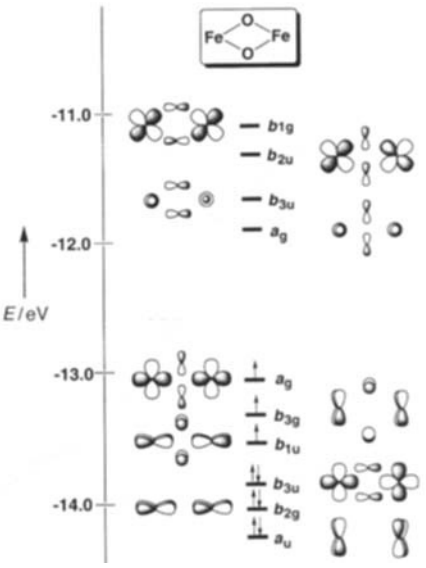

Fig. 2. Shapes and energy level diagram of the canonical MOs constituting the 3d band of **1**. The irreducible representations refer to the D_{2h} point group, which is the maximum possible symmetry of the $[Fe_2O_2]$ unit. E = orbital energy.

[*] Prof. Dr. L. Que, Jr., Dr. A. Ghosh,[+] Prof. Dr. J. Almlöf[†]
Department of Chemistry, University of Minnesota
Minneapolis, MN 55455 (USA)
Fax: Int. code +(612)624-7029

[+] New address: Department of Chemistry
Institute of Mathematical and Physical Sciences (IMR)
University of Tromsø
Breivika, N-9037 Tromsø (Norway)

[†] Deceased January 17, 1966

[**] This work was supported by the Minnesota Supercomputer Institute (computer time on a Cray C90 computer), the National Institutes of Health (grant GM-38767 to L. Q.), the National Science Foundation (grant CHE-9223782 to J. A.), and Biosym Technologies, Inc., San Diego, CA.

their orbital energies and occupancies directly from our calculations. Occupation of these MOs with the nine 3d electrons of the formally $[Fe^{III}Fe^{IV}]$ dinuclear center according to Hund's rule results in the configuration shown, which is as expected on the basis of the large HOMO–LUMO gap (> 1 eV). This configuration has three unpaired electrons, in agreement with the EPR measurements. The six singly or doubly occupied MOs depicted in Figure 2 are exactly those derived from symmetric and antisymmetric combinations of the three $3d_\pi$ ("t_{2g}-type") AOs of the two irons. Similarly, the unoccupied MOs shown in Figure 2 can be recognized as based on Fe $3d_\sigma$ ("e_g") AOs. Thus, the quartet spin state of **1** appears to be a direct result of a substantial t_{2g}–e_g band gap.[16]

Some further insight into the electronic structure of the $[Fe_2(\mu\text{-}O)_2]^{3+}$ group can be obtained from the Mulliken population analysis results, including gross AO populations and gross AO spin populations (Table 1). As might be expected from Figure 2, the Fe $3d_\pi$ or "t_{2g}-type" AOs (d_{xz}, d_{yz}, and $d_{x^2-y^2}$) have larger Mulliken populations than the $3d_\sigma$ or "e_g-type" AOs (d_{xy} and d_{z^2}). Thus, the very small population of the Fe $3d_{z^2}$ AO is consistent with this notion. The Fe d_{xy} $3d_\sigma$ AO, on the other hand, has a significant population of 0.68, but this results solely from partial iron character of subfrontier, predominantly oxygen-based MOs with Fe–O bonding character, which reflects the essentially covalent nature of the interaction between the high-valent iron centers and the oxide ions. Relatively large Fe $3d_\sigma$ AO populations have also been found in other calculations on low-spin high-valent oxoiron species such as Fe^{IV}=O porphyrin complexes which have Fe $3d_{z^2}$ (the Fe=O vector defines the z axis) AO populations of 0.73–0.76.[17] However, the Fe $3d_\sigma$ AOs contribute only to doubly occupied MOs and thus do not carry any spin population. Overall, to the extent that spin states can be assigned to individual atoms in a polynuclear complex, the calculations predict that the iron centers in **1** may be described as low-spin. This is an important insight since the majority of known iron tpa or methyl-substituted tpa complexes have high-spin configurations.[13, 14]

Table 1. Gross electron and spin populations of AOs of **1** [a].

	Fe "t_{2g}" MOs			Fe "e_g" MOs		O		
AO	d_{xz}	d_{yz}	$d_{x^2-y^2}$	d_{xy}	d_{z^2}	p_x	p_y	p_z
AO population	1.63	1.59	1.48	0.68	0.04	1.93	1.36	1.77
AO spin population	0.36	0.39	0.41	0.00	0.00	0.00	0.11	0.23

[a] AO = atomic orbital, MO = molecular orbital.

The three unpaired electrons of **1** are nearly fully localized on the Fe_2O_2 core, and distributed in a 4:1 ratio between the Fe and O atoms, which have spin populations of 1.16 and 0.34, respectively. Clearly, the iron or oxygen atoms do not have integral spin populations, which shows that the bonding in the $[Fe_2O_2]^{3+}$ core has substantial covalent character. Thus, purely ionic formulations[4] of the electronic structure of **1**, such as $Fe^{III}(O^{2-})_2Fe^{IV} \leftrightarrow Fe^{IV}(O^{2-})_2Fe^{III}$ or $Fe^{III}(O^{\bullet})(O^{2-})Fe^{III} \leftrightarrow Fe^{III}(O^{2-})(O^{\bullet})Fe^{III}$ are simplistic. An interesting point of similarity between the LDF spin density distributions of the present $[Fe_2O_2]^{3+}$ complexes and Fe^{IV}=O porphyrins is that in both classes of compounds, the spin density is confined to the Fe and O atoms with essentially none delocalized over to the organic ligand(s) constituting the rest of the molecule. Moreover, the spin populations of the iron centers are nearly identical (ca. 1.2) in the $[Fe_2O_2]^{3+}$ complexes and Fe^{IV}=O porphyrins.[6] The spin population of the oxygen atom in an Fe^{IV}=O unit is about 0.8;[6] that is about half an electron spin higher than the spin population of each oxygen atom in the $[Fe_2O_2]^{3+}$ group. Thus, the $[Fe_2O_2]^{3+}$ unit is electronically equivalent to a one-electron reduced dimerized pair of $[Fe^{IV}$=O$]^{2+}$ groups; the decrease in spin population takes place exclusively on the two oxygen atoms (Fig. 3).

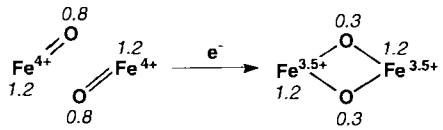

Fig. 3. Populations of unpaired spins (in italics) in the $[Fe{=}O]^{2+}$ and $[Fe_2O_2]^{3+}$ units.

This bonding scheme is qualitatively consistent with the unusual Mössbauer spectral parameters of these species. The low-spin configurations of the iron centers in **1** are consistent with the low Mössbauer isomer shifts of these species (ca. 0.13 mm s^{-1}). In addition, the populations of the three $3d_\pi$ AOs of each iron are quite similar, suggesting a highly isotropic electron spin distribution around each iron center, which may explain the perplexingly low Mössbauer quadrupole splittings of **1** and **2** (ca. 0.5 mm s^{-1}).

These calculations also provide some insight into the Raman-active vibrations of the $[Fe_2O_2]^{3+}$ core. For simplicity, we have used a D_{2h}-symmetric model of **1**, $[(py)_4Fe(\mu\text{-}O)_2Fe(py)_4]^{3+}$ **3** (py = pyridine) to construct the following three-coordinate potential energy surface. The potential energy V is calculated by Equation (a), where where r_1 is the Fe–Fe distance, r_2 is the

$$V = A(\Delta r_1)^2 + B(\Delta r_2)^2 + C(\Delta r_1)(\Delta r_2) + D(\Delta\theta)^2 \quad \text{(a)}$$

O–O distance, θ is the angle between the Fe–Fe and O–O vectors, and Δ indicates deviations from equilibrium values.[18, 19] This potential energy was used to perform a standard vibrational analysis using an $[Fe_2O_2]$ four-atom model. The normal modes are schematized (with some exaggeration) in Figure 4,

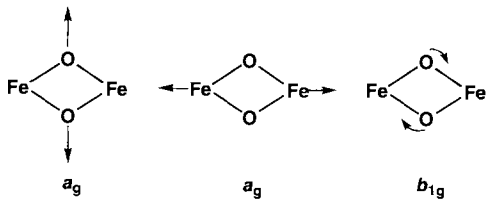

Fig. 4. Schematic representation of the calculated normal modes of the $[Fe_2O_2]$ unit of **3**.

and calculated frequencies and isotope shifts are given in Table 2. One of the a_g normal modes (712.6 cm^{-1}) exhibits significant oxygen isotope sensitivity (^{18}O shift of −39 cm^{-1}), which corresponds to the experimentally observed feature at 666 cm^{-1} in the resonance Raman spectra of **1** and **2**.[4] The experimentally observed ^{18}O shifts of −29 to −32 cm^{-1} are in good qualitative agreement with theory, especially in view of the point group symmetries of **1** and **2** (C_{2h}) versus that of **3** (D_{2h}).[19] Table 2 also predicts that this mode should be insensitive to iron isotope substitution, as qualitatively suggested by Figure 4; experiments are underway to verify this prediction.

In summary, DFT calculations have provided full structural and some vibrational data on $[Fe_2O_2]^{3+}$ complexes. A conceptual framework has also emerged for understanding key electronic and structural (EPR and Mössbauer) properties of these

Table 2. Calculated frequencies [cm^{-1}] and isotope shifts (in parentheses [Δcm^{-1}]) of the Raman-active normal modes of the $[Fe_2O_2]$ unit of **3**.

Symmetry	$^{56}Fe_2{}^{16}O_2$	$^{56}Fe_2{}^{18}O_2$	$^{54}Fe_2{}^{16}O_2$	$^{58}Fe_2{}^{16}O_2$
a_g	712.6 (0.0)	673.4 (−39.2)	713.1 (0.5)	712.1 (−0.5)
a_g	445.3 (0.0)	444.2 (−1.1)	453.2 (7.9)	437.8 (−7.5)
b_{1g}	577.6 (0.0)	549.4 (−28.2)	579.1 (1.5)	576.1 (−1.5)

species. Our success in studying high-valent oxoiron compounds with DFT promises a bright future for DFT applications to such areas as the interaction of dioxygen with iron-containing enzymes and the electronic structure of novel reactive intermediates such as compound Q of methane monooxygenase.

Received: October 27, 1995 [Z8508IE]
German version: *Angew. Chem.* **1996**, *108*, 846–849

Keywords: ab initio calculations · electronic structure · geometry optimizations · iron compounds

[1] a) L. Que, Jr., in *Bioinorganic Catalysis* (Ed.: J. Reedijk), Dekker, New York, **1993**, p. 347; b) A. L. Feig, S. J. Lippard, *Chem. Rev.* **1994**, *94*, 759.
[2] a) S.-K. Lee, B. G. Fox, W. A. Froland, J. D. Lipscomb, E. Münck, *J. Am. Chem. Soc.* **1993**, *115*, 6450; b) S.-K. Lee, J. C. Nesheim, J. D. Lipscomb, *J. Biol. Chem.* **1993**, *268*, 21569; c) K. E. Liu, D. Wang, B. H. Huynh, D. E. Edmondson, A. Salifoglou, S. J. Lippard, *J. Am. Chem. Soc.* **1994**, *116*, 7465.
[3] Solution-phase spectroscopic characterization of **1**: R. A. Leising, B. A. Brennan, L. Que, Jr., B. G. Fox, E. Münck, *J. Am. Chem. Soc.* **1991**, *113*, 3988. This paper incorrectly proposed a mononuclear structure for **1**.
[4] Spectroscopic characterization of solid **2**: ($\delta = 0.13\ mm\,s^{-1}$ and $\Delta E_Q = 0.53\ mm\,s^{-1}$): Y. Dong , H. Fujii, M. P. Hendrich, R. A. Leising, G. Pan, C. R. Randall, E. Wilkinson, Y. Zang, L. Que, Jr., B. G. Fox, K. Kauffmann, E. Münck, *J. Am. Chem. Soc.* **1995**, *117*, 2778.
[5] For a review of chemical applications of DFT, see: T. Ziegler, *Chem. Rev.* **1991**, *91*, 651.
[6] For DFT calculations on oxo(porphyrinato)iron(IV) complexes, see: A. Ghosh, J. Almlöf, L. Que, Jr. *J. Phys. Chem.* **1994**, *98*, 11004.
[7] The calculations were carried out with the DMOL program [8], employing the local exchange-correlation potential of Hedin and von Barth [9] and double-ζ plus polarization basis sets.
[8] B. Delley, *J. Chem. Phys.* **1990**, *92*, 508.
[9] U. von Barth, L. Hedin, *J. Phys. C* **1972**, *5*, 1629.
[10] K. Wieghardt, *Angew. Chem.* **1989**, *101*, 1179; *Angew. Chem. Int. Ed. Engl.* **1989**, *28*, 1153.
[11] Y. Zang, G. Pan, L. Que, Jr., B. G. Fox, E. Münck, *J. Am. Chem. Soc.* **1994**, *116*, 3653.
[12] Y. Zang, Y. Dong, L. Que, Jr., K. Kauffmann, E. Münck, *J. Am. Chem. Soc.* **1995**, *117*, 1169.
[13] a) S. Yan, D. D. Cox, L. L. Pearce, C. Juarez-Garcia, L. Que, Jr., *Inorg. Chem.* **1989**, *28*, 2507; b) R. E. Norman, R. C. Holz, J. H. Zhang, C. J. O'Connor, S. Menage, L. Que, Jr., *Inorg. Chem.* **1990**, *29*, 4629; c) R. C. Holz, T. E. Elgren, L. L. Pearce, J. H. Zhang, C. J. O'Connor, L. Que, Jr., *Inorg. Chem.* **1993**, *32*, 5844.
[14] Y. Dong, L. Que, Jr. unpublished results.
[15] The Kohn–Sham orbitals in DFT are often similar to their counterparts in Hartree–Fock theory, and their treatment in the computational schemes is nearly indistinguishable. Thus, in spite of the formal lack of a many-electron wavefunction, an analysis of the LDF MOs permits us to construct a qualitative framework for understanding the electronic structure and spin state of **1**.
[16] The terms "e_g-type" and "t_{2g}-type" are used to loosely describe MOs whose amplitudes or shapes, near the approximately octahedral metal centers, resemble rigorous e_g and t_{2g} d AOs of centers with perfect O_h local symmetry. The terms d_σ and d_π are used synonymously with "e_g-type" and "t_{2g}-type", respectively, and do not refer to the molecular mirror plane of **1**.
[17] a) S. Yamamoto, J. Teraoka, H. Kashiwagi, *J. Chem. Phys.* **1988**, *88*, 303; b) S. Yamamoto, H. Kashiwagi, *Chem. Phys. Lett.* **1988**, *145*, 111.
[18] A series of single-point calculations on **3** were performed with various values of r_1, r_2, and θ; all other internal coordinates were fixed at their optimized values. The potential energy surface was obtained by multi-variable least-squares fitting of the data sets $V(r_1, r_2, \theta)$ (where V is the molecular total energy) with a polynomial including up to quadratic terms. The calculated values of $\partial^2 V/\partial r_1^2$ ($= 2A$), $\partial^2 V/\partial r_2^2$ ($= 2B$), and $\partial^2 V/\partial r_1 \partial r_2$ ($= C$) are 0.22226, 0.15013, and 0.03338 Hartree $Bohr^{-2}$, respectively, and $\partial^2 V/\partial \theta^2$ ($= 2D$) is 1.48105 Hartree $radian^{-2}$; all force constants were evaluated at the equilibrium geometry.
[19] The force constants $\partial^2 V/\partial r_1 \partial \theta$ and $\partial^2 V/\partial r_2 \partial \theta$ are required by symmetry to be zero in **3** but not in **1** or **2**.

Self-Assembly of an Artificial Light-Harvesting Antenna: Energy Transfer from a Zinc Chlorin to a Bacteriochlorin in a Supramolecular Aggregate**

Hitoshi Tamiaki,* Tomohiro Miyatake, Rikukei Tanikaga, Alfred R. Holzwarth,* and Kurt Schaffner

In recent years many supramolecular assemblies with novel chemical and material properties have been shown to form by self-organization of identical or complementary building blocks.[1] We have studied extensively the self-assembly of metallochlorins ((17,18-dihydroporphyrinato)metal complexes) in nonpolar organic solvents[2–4] and have demonstrated that these in vitro homoaggregates have the same structure as aggregates of bacteriochlorophyll *c* and *d* (Scheme 1) present in

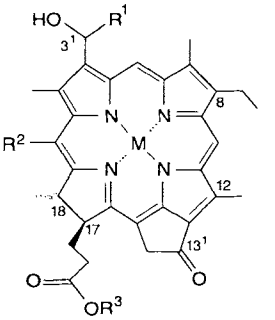

BChlc, M = Mg, $R^{1,2} = CH_3$, R^3 = stearyl

BChld, M = Mg, $R^1 = CH_3$, R^2 = H, R^3 = farnesyl

1, M = Zn, $R^{1,2}$ = H, $R^3 = CH_3$

Scheme 1. Bacteriochlorophylls(BChl) *c* and *d* and zinc chlorin model **1**; numerous other structural variants are encountered in vivo, which differ in the alkyl substituents at C-8 and C-12, and in R^3 [15].

natural chlorosomes. These aggregates, the light-harvesting system of green bacteria,[5] are notably the first photosynthetic antenna system known not to require a protein for the pigment organization.[6–8] The understanding of the principles of the interactions (for example hydrogen bonding, van der Waals, $\pi-\pi$, and electrostatic interactions) responsible for the self-assembly of both in vitro and in vivo supramolecular aggregates of metallochlorins can now be exploited in various ways. One of the possibilities is to construct artificial photoactive devices capable of performing a useful task.

We describe in the following a supramolecular system, in which efficient transfer of singlet excitation energy occurs from about 50–100 aggregated zinc chlorins to a single metal-free bacteriochlorin. It is the first example of a functional self-

[*] Prof. Dr. H. Tamiaki, T. Miyatake, Prof. Dr. R. Tanikaga
Department of Bioscience and Biotechnology
Faculty of Science and Engineering, Ritsumeikan University
Kusatsu, Shiga 525-77 (Japan)
Fax: Int. code +(775)612-659
e-mail: tamiaki@bkc.ritsumei.ac.jp
Prof. Dr. A. R. Holzwarth, Prof. Dr. K. Schaffner
Max-Planck-Institut für Strahlenchemie
Postfach 101365, D-45413 Mülheim an der Ruhr (Germany)
Fax: Int. code +(208)306-3951
e-mail: holzwartha@mpi-muelheim.mpg.d400.de

[**] This work was supported by the Japanese Ministry of Education, Science and Culture (Grants-in-Aid for Scientific Research no. 05808052 and 06808057), the Mazda Foundation, the Yazaki Memorial Foundation for Science and Technology, and the Nissan Science Foundation.

assembled unit that mimics the function of a natural photosynthetic antenna and represents the first step en route to a potential photoactive device.

Zinc chlorins possessing 3^1-hydroxyl and 13^1-ketone functions readily aggregate in nonpolar organic solvents such as hexane. These aggregates have been judged to be good structural models for bacteriochlorophyll *c* and *d* aggregates formed in both nonpolar solvents and in native chlorosomes.[2-4, 9]

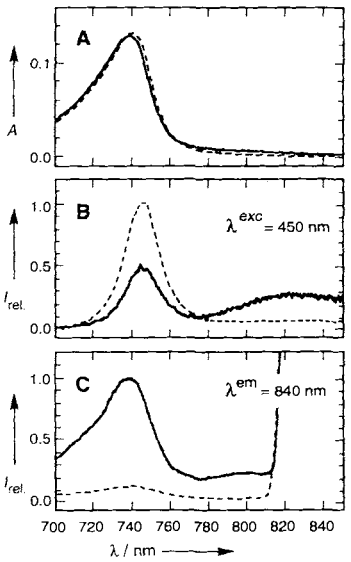

Fig. 1. Visible absorption (A), corrected fluorescence (B), and corrected fluorescence excitation spectra (C) of **1** (- - -) and a 50:1 mixture of **1** and **3** (—) in THF/hexane (1/99 v/v).

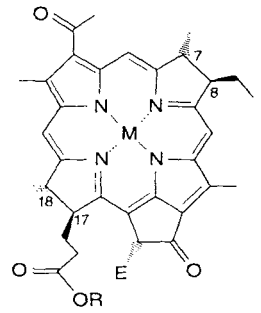

BChla, M = Mg, E = CO_2CH_3, R = phytyl

2, M = 2 H, E = H, R = CH_3

Scheme 2. Bacteriochlorophyll(BChl) *a* and the metal-free bacteriochlorin model compound **2**.

The absorption of zinc chlorin **1**[3] is red-shifted on conversion from the monomeric form (λ_{max} = 647 nm, in THF) to the aggregate (λ_{max} = 740 nm, in THF/hexane (1/99)),[4] and the fluorescence of the aggregate peaks at approximately 750 nm (Figs. 1A and B). Addition of a small amount of metal-free bacteriochlorin **2**[10] (a 7,8,17,18-tetrahydroporphyrin; Scheme 2) effects neither a change in the 740-nm absorption of aggregate **1** nor in its 750-nm emission, although monomeric **2** (λ^{abs}_{max} = 755 nm) should be a suitable acceptor in terms of exothermic energy transfer conditions—similar to bacteriochlorophyll *a*, which in chlorosomes traps the light energy absorbed by the core bacteriochlorophyll *c* and *d* aggregates.[11] The failure of **2** to quench excited aggregate **1** can be explained by a large mean donor–acceptor distance; **2** is not capable of coaggregating with **1** because it lacks both a central metal and a 3^1-hydroxyl group. (The concentration of **1** is only 2.5×10^{-6} M. Taking into account that several thousand zinc chlorin molecules (**1**) may form an aggregate, the average distance to an acceptor (**2**) will be far too large for the efficient operation of any kind of energy transfer mechanism.)

In contrast, quite a different result is obtained when the chromophoric systems of **1** and **2** are linked covalently, as in compound **3**. When a solution of a 50:1 mixture of **1** and **3** in THF is diluted with hexane, the 740-nm absorption of aggregate **1** is accompanied by a proportionate weak absorption of **3** growing in at around 800 nm (Fig. 1A). In the fluorescence spectrum, the 750-nm emission of aggregate **1** (*hν'* in Fig. 2) is decreased to about 50% of the intensity of that in the absence of **3**, and a new broad emission appears instead at around 820 nm (Fig. 1B; *hν''* in Fig. 2). The fluorescence excitation spectrum (Fig. 1C) of the

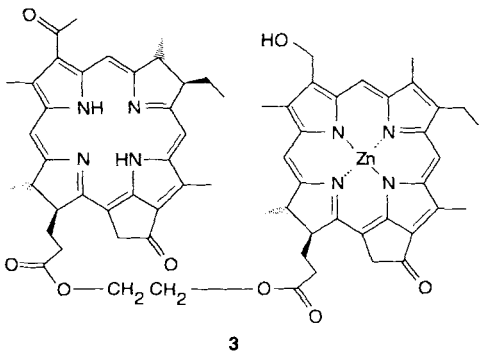

3

mixture shows that an appreciable part of this new fluorescence, which is attributable to the bacteriochlorin chromophore of **3**, arises by way of excitation of the aggregate **1** (cf. the 740-nm excitation band). This then clearly documents intrasupramolecular energy transfer from singlet-excited aggregate **1** to the bacteriochlorin moiety of **3** (Fig. 2). The de-

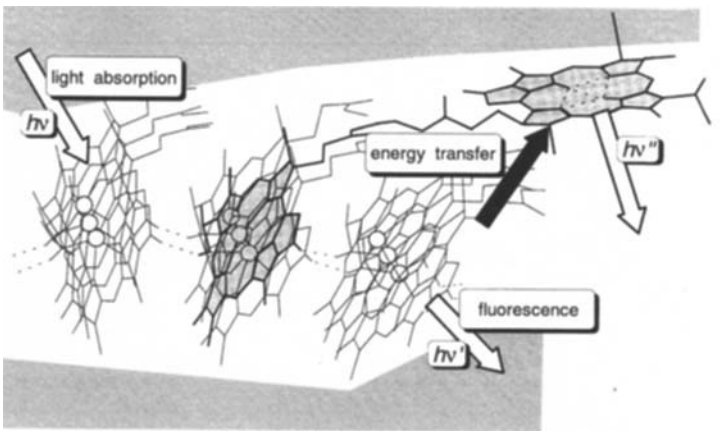

Fig. 2. Representation of the intrasupramolecular energy transfer from a singlet-excited aggregate of **1** (nonshaded stack) to the metal-free bacteriochlorin moiety of **3** (shaded molecule): ○, zinc atom; - - -, C=O···H–O hydrogen bond; the solvation sphere (nonpolar solvent, lipid, detergent) is indicated by the shaded area enveloping the stacked aggregate. This picture represents a section of the three-dimensional arrangement of an aggregate adopted from molecular modeling results [8a].

crease in the donor fluorescence by a factor of about two is close to that expected theoretically for a rapidly established energy transfer equilibrium between the donor and (long-lived) acceptor states.[12] This indicates that the energy transfer is fast as well as highly efficient.

The seemingly low quenching effect of 50% would not limit the maximal yield of energy usage in a potential electron transfer device, since the electron transfer yield would primarily depend on the ratio of the rate constants of, for example, a useful electron transfer reaction and of nonradiative relaxation of the system. We note, furthermore, that the rates of radiationless deactivation in the natural chlorosomes and in artifical bacteriochlorophyll aggregates are similarly high, leading to excited-state lifetimes in the order of 10 to 100 ps in systems without an acceptor.[13] Nevertheless, this does not harm in any way the efficient light-harvesting function of natural chlorosomes.

An even more efficient energy transfer than that in nonpolar organic solvent is achieved by providing the heteroaggregate **1**·**3** with a higher order solvation sphere: while aqueous solutions of

1·**3** with either α-lecithin (a lipid) or Triton X-100 (a nonionic detergent) give absorption and emission spectra qualitatively similar to those shown in Figure 1, the quenching of the donor fluorescence by energy transfer is substantially increased, up to 80–90%. This suggests that embedding the heteroaggregate in a nonpolar lipid or detergent sphere either increases the size of the aggregates or—perhaps even more likely—invokes efficient interaggregate energy transfer like that in natural chlorosomes.[11] Both possibilities increase the probability that an energy acceptor (**3**) is available to the excited donor aggregate (**1**).

In conclusion, in vitro zinc chlorin aggregates are not only adequate model systems for in vivo bacteriochlorophyll *c* and *d* aggregates in the chlorosomal core in terms of their supramolecular structure,[2–4] but also enable the self-assembly of efficient functional units for heterogeneous energy transfer.

Experimental Procedure

Following literature procedures [3,14] compound **3** was synthesized by condensation of pyropheophorbide *d* with 2-hydroxyethyl bacteriopyropheophorbide *a*, followed by selective reduction of the 3-formyl group and equally selective zinc metalation of the pyropheophorbide half of the molecule. HPLC chromatography gave pure **3** as a dark purple solid. M.p. > 300 °C. ^{1}H NMR ($CDCl_3$/CD_3OD 7/3): δ = 9.13, 8.95, 8.61, 8.14, 8.04, 8.02 (6 s, 1H each; meso-CH), 5.40 (s, 2H; CH_2-3), 4.88, 4.72, 4.64, 4.42 (4 d, ^2J(HH) = 20 Hz, 1H each; CH_2-13^2), 4.05–4.15 (m, 1H), 3.65–3.97 (m, 8H), 3.29–3.49 (m, 3H), 3.81, 3.25, 2.96, 2.93, 2.81 (5 s, 3H each; CH_3), 1.77–2.28 (m, 10H), 1.53, 1.43, 1.34 (3 d, ^3J(HH) = 7 Hz, 3H each; CH_3), 1.39, 0.83 (2 t, ^3J(HH) = 7 Hz, 3H each; CH_3); UV/Vis (THF): λ_{max} (I_{rel}): 751 (0.49; Q_y band of metal-free bacteriochlorin moiety *a*), 678 (0.08), 647 (0.68; Q_y of zinc chlorin moiety), 605 (0.11), 566 (0.06), 530 (0.22), 424 (0.90), 387 (0.69), 359 nm (1.00); MS (FAB): *m/z*: 1178 (M^+ for ^{64}Zn).

Received: October 31, 1995 [Z8515IE]
German version: *Angew. Chem.* **1996**, *108*, 810–812

Keywords: chlorins · chlorosomes · energy transfer · self-assembly · supramolecular chemistry

[1] L. Julien, J. Canceill, B. Valeur, E. Bardezz, J.-M. Lehn, *Angew. Chem.* **1994**, *106*, 2582; *Angew. Chem. Int. Ed. Engl.* **1994**, *33*, 2438; V. Balzani, F. Scandola, *Supramolecular Photochemistry*, Ellis Horwood, New York, **1991**, p. 355.

[2] H. Tamiaki, A. R. Holzwarth, K. Schaffner, *J. Photochem. Photobiol. B* **1992**, *15*, 355; H. Tamiaki, S. Takeuchi, R. Tanikaga, S. T. Balaban, A. R. Holzwarth, K. Schaffner, *Chem. Lett.* **1994**, 401.

[3] H. Tamiaki, M. Amakawa, Y. Shimono, R. Tanikaga, A. R. Holzwarth, K. Schaffner, *Photochem. Photobiol.* **1996**, *63*, 92.

[4] P. Hildebrandt, H. Tamiaki, A. R. Holzwarth, K. Schaffner, *J. Phys. Chem.* **1994**, *98*, 2192; H. Tamiaki, A. R. Holzwarth, K. Schaffner, *Photosynth. Res.* **1994**, *41*, 245.

[5] H. Zuber, R. A. Brunisholz in *Chlorophylls* (Ed.: H. Scheer), CRC Press, Boca Raton, FL, **1991**, p. 627.

[6] A. R. Holzwarth, K. Griebenow, K. Schaffner, *Z. Naturforsch. C* **1990**, *45*, 203; K. Griebenow, A. R. Holzwarth, K. Schaffner, *ibid.* **1990**, *45*, 823; P. Hildebrandt, K. Griebenow, A. R. Holzwarth, K. Schaffner, *ibid.* **1990**, *46*, 228; T. S. Balaban, A. R. Holzwarth, K. Schaffner, G.-J. Boender, H. J. M. de Groot, *Biochemistry* **1995**, *34*, 15259.

[7] Review: A. R. Holzwarth, K. Griebenow, K. Schaffner, *J. Photochem. Photobiol. A* **1992**, *65*, 61; H. Tamiaki, *Coord. Chem. Rev.* **1996**, *147*, in press.

[8] For the structure of the bacteriochlorophyll *c* aggregates in the chlorosomal core see: a) A. R. Holzwarth, K. Schaffner, *Photosynth. Res.* **1994**, *41*, 225; b) J. Chiefari, K. Griebenow, F. Fages, N. Griebenow, T. S. Balaban, A. R. Holzwarth, K. Schaffner, *J. Phys. Chem.* **1995**, *99*, 1357.

[9] M. I. Bystrova, I. N. Mal'gosheva, A. A. Krasnovskii, *Mol. Biol.* **1979**, *13*, 440; K. M. Smith, L. A. Kehres, J. Fajer, *J. Am. Chem. Soc.* **1983**, *105*, 1387; D. C. Brune, T. Nozawa, R. E. Blankenship, *Biochemistry* **1987**, *26*, 8644.

[10] H. Falk, G. Hornaert, H.-P. Isenring, A. Eschenmoser, *Helv. Chim. Acta* **1975**, *58*, 2347.

[11] M. G. Müller, K. Griebenow, A. R. Holzwarth, *Biochim. Biophys. Acta* **1993**, *1144*, 161; S. Savikhin, P. I. van Noort, Y. Zhu, S. Lin, R. E. Blankenship, W. S. Struve, *Chem. Phys.* **1995**, *194*, 245.

[12] If we make the reasonable assumption that the rates of energy transfer between donor and acceptor are fast relative to the rates of nonradiative relaxation in either system, and that the nonradiative donor relaxation is essentially unaffected by the binding of the acceptor, then an energy transfer equilibrium will be established between donor and acceptor. Taking into account the energy differences as judged by the absorption spectra, and the donor/acceptor ratio, one can estimate that the donor fluorescence should be quenched by about 60%, in good agreement with the experiment.

[13] T. P. Causgrove, D. C. Brune, R. E. Blankenship, J. M. Olson, *Photosynth. Res.* **1990**, *25*, 1; A. R. Holzwarth, M. G. Müller, K. Griebenow, *J. Photochem. Photobiol. B* **1990**, *5*, 457.

[14] M. R. Wasielewski, W. A. Svec, *J. Org. Chem.* **1980**, *45*, 1969.

[15] K. M. Smith, *Photosynth. Res.* **1994**, *41*, 23; F. Fages, N. Griebenow, K. Griebenow, A. R. Holzwarth, K. Schaffner, *J. Chem. Soc. Perkin Trans. 1* **1990**, 2791.

Hexaterphenylyl- and Hexaquaterphenylylbenzene: The Behavior of Chromophores and Electrophores in a Restricted Space**

Menno A. Keegstra, Steven De Feyter, Frans C. De Schryver, and Klaus Müllen*

Oligo-*para*-phenylenes and poly-*para*-phenylenes are classical chromophores and redox systems.[1] Because of their electroluminescent properties, they have been used often recently as active components in light-emitting diodes,[2] but they can also be employed to investigate the influence of chain length and geometry on charging processes.[1a, 3] For both applications, it would be desirable to have model compounds that contain several identical oligomer building blocks in a restricted space. We therefore directed our attention to the aesthetically appealing benzene derivatives hexa-*p*-terphenylylbenzene (**1**) and hexa-*p*-quaterphenylylbenzene (**2**). Formally, the star-shaped compound **1** can be regarded as being constructed of three septiphenyl chains with one benzene unit in common. However, the interplanar angle makes an arrangement of six electronically coupled terphenylyl chains a more plausible structure.[4] We describe the synthesis and the electrophoric and chromophoric properties of **1** and **2**.

As a synthesis of **1** by formation of aryl–aryl bonds to a central benzene unit did not seem to be a promising approach, the method of choice was a cyclotrimerization of suitable derivatives of diphenylacetylene. It is well known that hexaphenylbenzene can be formed from diphenylacetylene in the presence of a transition metal catalyst.[5] However, the rigid diterphenylylacetylene **3** to be used as the starting material must contain alkyl groups to increase its solubility. These must be *tert*-alkyl groups to shield the *ortho* positions in the alkylbenzene **7**, as shown in Scheme 1.

Bromination of **7** is followed by a Suzuki coupling[6] with 4-biphenylboric acid.[7] The terphenyl **9** formed can be brominated regioselectively in the 4″ position, and this bromide (**10**) is

[*] Prof. Dr. K. Müllen, Dr. M. A. Keegstra
Max-Planck-Institut für Polymerforschung
Ackermannweg 10, D-55128 Mainz (Germany)
Fax: Int. code +(6131)379350
Dipl.-Chem. S. De Feyter, Prof. Dr. F. C. De Schryver
Department of Chemistry, Katholieke Universiteit Leuven (Belgium)

[**] This work was supported by the Human Capital and Mobility Program "Conjugated ladder-type oligomers and polymers containing fused six- and five-membered rings" of the European Commission (CHRX-CT93-0148). The Belgian authors thank the Ministry of Science for its support through IUAP-16 and IUAP-40, the Belgian "Nationaal Fonds voor Wetenschappelijk Onderzoek" (S. D. F.).

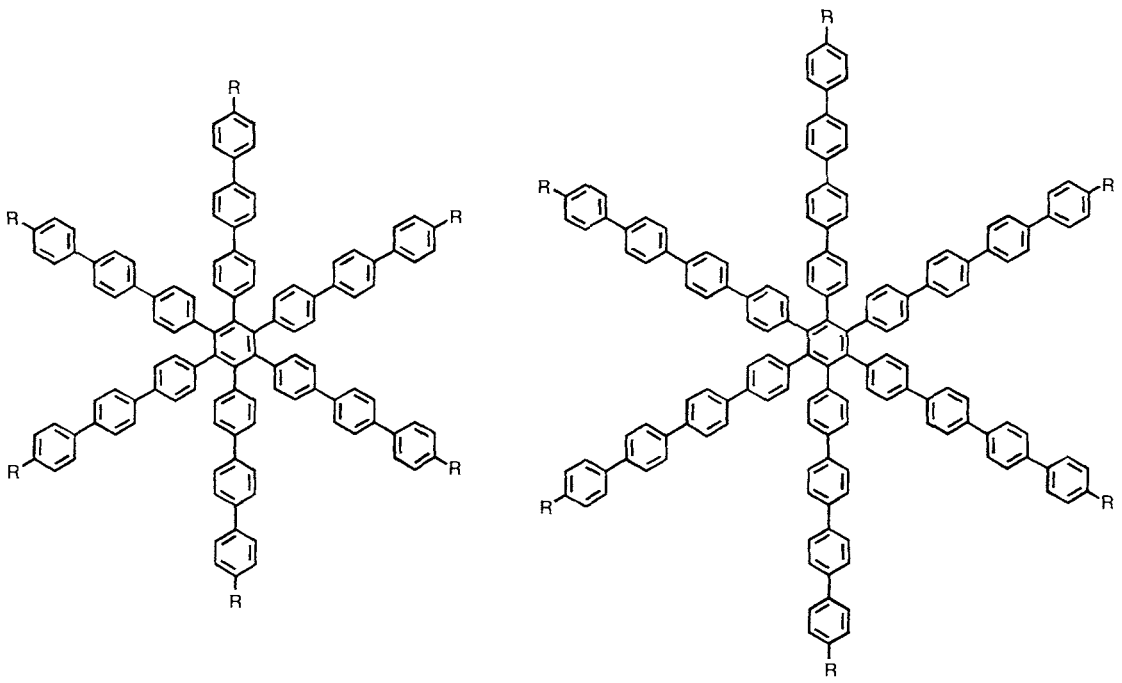

1 R = $C(CH_3)_2C_{14}H_{29}$ 2

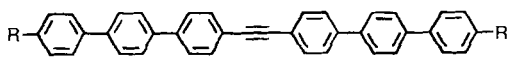

3

then subjected to a three-step synthesis sequence to give the disubstituted acetylene **3**.[8, 9] All the reactions can be carried out on a 0.5 mol scale, and compounds **5**–**8** are obtained in an analytically pure state without further purification, while the other compounds can be purified by recrystallization from acetone.

Acetylene **3** is converted into **1** by a palladium(II)-catalyzed trimerization.[5] The solubility of **1** in common solvents is excellent, unlike that of the starting compound **3**. The expected twisting of the terphenyl units at an angle of about 65° to the central benzene ring in **1**[4] probably hinders close packing of the molecules in the solid state, and this explains the good solubility of **1** compared with that of **3**. Selected physical and spectroscopic data for **1**, **2**, and **3** are given in Table 1.

The low solubility of the acetylene precursor means that one cannot assume that cyclotrimerization would give successful results with larger systems. Hexaquaterphenylylbenzene **2**, a homologue of **1**, was therefore synthesized by a Suzuki reaction of hexa(4-iodophenyl)benzene[10] with terphenylboric acid **13**[11] (Scheme 2). As 4-(1,1-dimethylpentadecyl)-*p*-quaterphenyl is formed as a by-product of the reaction, it can be deduced that, under the reaction conditions used, cleavage of the bond to the central benzene ring occurs.

The behavior of **1** and **2** as multielectrophore and multichromophore π systems was investigated by cyclovoltammetric, ESR/ENDOR-spectroscopic, and optical methods. The electro-

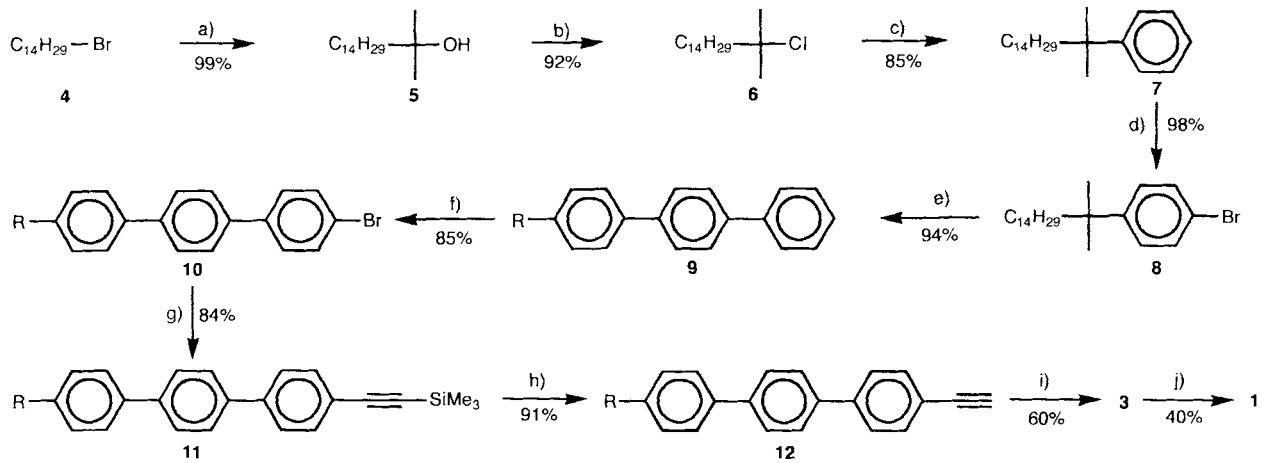

Scheme 1. Synthesis of **1**. R = $C(CH_3)_2C_{14}H_{29}$. a) 1. Mg/diethyl ether, 3 h; 2. acetone, 0 °C; b) 10 equiv. 37% HCl(aq)/CH_2Cl_2, room temperature (RT), 18 h; c) $FeCl_3$, RT, benzene, 18 h; d) Br_2, Fe, RT, CH_2Cl_2, 18 h; e) $C_6H_5C_6H_4B(OH)_2$, 1% $[Pd(PPh_3)_4]$, 2.0 M $NaHCO_3$(aq)/THF, 66 °C, 18 h; f) Br_2, Fe, RT, CH_2Cl_2, 18 h; g) trimethylsilylacetylene, 3% $[PdCl_2(PPh_3)_2]$, 6% PPh_3, 6% CuI, 80 °C, piperidine, 3 h; h) KF, DMF/H_2O, RT, 18 h; i) **10**, 3% $[PdCl_2(PPh_3)_2]$, 6% PPh_3, 6% CuI, 80 °C, piperidine, 18 h; j) $[PdCl_2(PhCN)_2]$, 80 °C, toluene, 20 h.

 © VCH Verlagsgesellschaft mbH, D-69451 Weinheim, 1996 0570-0833/96/3507-0775 $ 15.00+.25/0

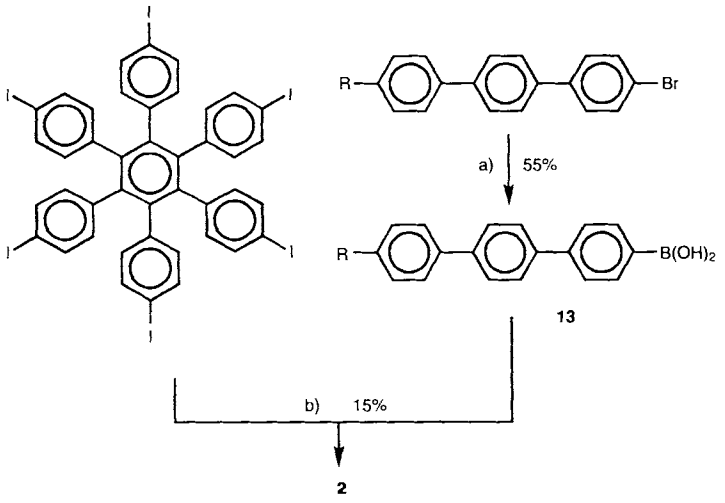

Scheme 2. Synthesis of **2**. R = $C(CH_3)_2C_{14}H_{29}$; a) 1. *n*BuLi, RT, ether, 4 h; 2. $B(OMe)_3$, −70 °C; b) 1% $[Pd(PPh_3)_4]$, 2.0 M $NaHCO_3$(aq), THF, 66 °C, 18 h.

Table 1. Selected physical and spectroscopic data for **1**–**3**.

1: MS (FD, 8 kV): *m/z*: 2884.3 $[M^+]$; ^{1}H NMR (300 MHz, $CDCl_3$, 30 °C): δ = 0.85 (t, ^3J = 6.7 Hz, 3H), 0.99–1.27 (m, 24H), 1.28 (s, 6H), 1.57–1.64 (m, 2H), 6.99 (d, ^3J = 8.3 Hz, 2H), 7.22 (d, ^3J = 8.3 Hz, 2H), 7.34 (d, ^3J = 8.5 Hz, 2H), 7.48–7.55 (m, 6H).

2: MS (FD, 8 kV): *m/z*: 3336.3 $[M^+]$; ^{1}H NMR (300 MHz, $CDCl_3$, 30 °C): δ = 0.86 (t, ^3J = 6.5 Hz, 3H), 0.99–1.28 (m, 24H), 1.31 (s, 6H), 1.54–1.66 (m, 2H), 7.05 (d, ^3J = 7.9 Hz, 2H), 7.22 (d, ^3J = 8.2 Hz, 2H), 7.38 (d, ^3J = 8.0 Hz, 2H), 7.52–7.62 (m, 10H).

3: MS (FD, 8 kV): *m/z*: 959.9 $[M^+]$; ^{1}H NMR (300 MHz, $CDCl_3$, 30 °C): δ = 0.86 (t, ^{3}J = 6.8 Hz, 3H), 1.02–1.31 (m, 24H), 1.32 (s, 6H), 1.52–1.64 (m, 2H), 7.40 (d, ^{3}J = 8.2 Hz, 2H), 7.57 (d, ^3J = 8.3 Hz, 2H), 7.63 (m, 4H), 7.68 (m, 4H); UV/Vis (CH_2Cl_2): λ_{max} = 332 nm.

chemical reduction of **1** (THF, 0.05 M Bu_4NPF_6, Au electrode, v = 100 mV s^{-1}, 258 K) under cyclovoltammetric control indicates a fivefold charge on the system ($E^{1-3}_{1/2}$ = −2.56 V, E^4_{pc} = −3.12 V, E^5_{pc} = −3.24 V, where pc = peak in the cathodic cycle).[12] The ready formation of the trianion indicates minimal coulombic repulsion, that is, a localization of the individual charges on the terphenyl units. Comparison of the first reduction potential with that of *p*-terphenyl ($E^1_{1/2}$ = −2.60 V, E^2_{pc} = −2.92 V) confirms the conclusion that considerably decoupled terphenyl redox units are present in **1**. It is worth noting that the ENDOR spectrum of the radical monoanion of **1** (K^+, THF, 260 K) shows a maximum hyperfine coupling constant a_h of 0.023 mT. Thus, there is effective delocalization over the entire π system brought about by an electron transfer between the terphenyl redox units that is rapid relative to the measurement time scale. UV/Vis spectroscopic observation of the reduction of **1** with potassium (K^+, THF, 260 K) reveals a monoanion (λ_{max} = 990, 780, 487 nm) and a dianion (λ_{max} = 1060, 720 nm). However, further charging under these conditions leads to the decomposition of **1**. The appearance of terphenyl radical anions shows that the aryl–aryl bond is cleaved to some extent.

Table 2. Optical properties of **1**, **2**, **9**, and **14** [a].

Compd	λ_{max} (abs) [nm] [b]	ε [L mol^{-1}cm^{-1}]	λ_{max} (em) [nm] [c]	Quantum yield [g]
1	305	2.5×10^5	360–380 [d]	0.66
2	316	3.2×10^5	425 [e], 385, 374 [f]	0.93
9	285	3.6×10^4	364, 346, 332	0.99
14	299	4.7×10^4	390 [e], 367, 354	0.96

[a] Solvent CH_2Cl_2, 298 K. [b] No fine structure. [c] Excitation wavelengths corresponding to absorption maxima. [d] Broad, fine structure at 77 K. [e] Shoulder. [f] Further splitting on temperature reduction. [g] Relative error 10%.

To describe the optical properties of **1** and **2**, model substances (alkyl-substituted terphenyl **9** and *p*-quaterphenyl **14**) were used as for comparison (Table 2). The bathochromic shift in the absorption and emission spectra of **1** and **2** relative to **9** and **14**, respectively, is not consistent with the picture of completely independent oligophenyl chromophores in **1** and **2**. However, in view of the high local concentration of these chromophores, the molecular extinction coefficients of **1** and **2** are remarkably higher than those of **9** and **14**, respectively (six to seven times). It is also interesting that the fluorescence quantum yields of the star-shaped compounds **1** and **2** are only slightly smaller than those of the model substances. Furthermore, the similarity between the fluorescence spectra of the film and those of the solution excludes the formation of aggregates in the solid state.

The absence of excimer formation, the high fluorescence quantum yields, the good solubility, and the low crystallization tendency make **1** and **2** extremely good potential materials for light-emitting diodes.[13] Their electroluminescence properties will be reported elsewhere.

Received: November 23, 1995 [Z8583IE]
German version: *Angew. Chem.* **1996**, *108*, 830–833

Keywords: chromophores · cyclotrimerizations · electrophores · oligo-*para*-phenylenes

[1] a) A. Bohnen, W. Heitz, K. Müllen, H.-J. Räder, R. Schenk, *Makromol. Chem.* **1991**, *192*, 1679–1693; b) G. Grem, G. Leditzky, B. Ullricht, G. Leising, *Adv. Mater.* **1992**, *4*, 36–37; c) W. Ried, D. Freitag, *Angew. Chem.* **1968**, *80*, 932–942; *Angew. Chem. Int. Ed. Engl.* **1968**, *7*, 835.

[2] a) G. Grem, G. Leising, *Synth. Met.* **1993**, *55–57*, 4105–4110; b) G. Grem, V. Martin, F. Meghdadi, C. Poor, J. Sturm, J. Stampfl, S. Tasch, G. Leising, *ibid.* **1995**, *71*, 2193–2194; c) Y. Sakon, T. Ohnuma, M. Hashimoto, S. Saito, T. Tsutsui, C. Adachi (Ricoh Co., Ltd., Japan), US 5077142, **1990** [*Chem. Abstr.* **1991**, *117*, 16862]; d) J. Salbeck, lecture at the conference: *Light Emitting Polymers, IOP Condensed Matter and Materials Physics Conference* **1994**, University of Warwick.

[3] a) H. Gregorius, W. Heitz, K. Müllen, *Adv. Mater.* **1993**, *5*, 279–281; b) M. Baumgarten, K. Müllen, *Top. Curr. Chem.* **1994**, *169*, 1–103.

[4] J. C. J. Bart, *Acta Crystallogr. Sect. B* **1968**, *24*, 1277–1287.

[5] a) H. Fiege, K.-D. Gundermann, C. Grundmann, *Methoden Org. Chem. (Houben-Weyl) Vol V/2b*, 4th ed., **1981** p. 63; b) C. Pugh, V. Percec, *J. Mater. Chem.* **1991**, *1*, 765–773; c) A. Stabel, P. Herwig, K. Müllen, J. P. Rabe, *Angew. Chem.* **1995**, *107*, 1768–1770; Angew. Chem. Int. Ed. Engl. **1995**, *34*, 1609–1611.

[6] N. Miyaura, T. Yanagi, A. Suzuki, *Synth. Commun.* **1981**, *11*, 513–519.

[7] I. U. Rau, M. Rehahn, *Acta Polymer.* **1994**, *45*, 3–13.

[8] M. Alami, F. Ferri, G. Linstrumelle, *Tetrahedron Lett.* **1993**, *34*, 6403–6406.

[9] *Reagents for Organic Synthesis Vol. 10* (Ed.: M. Fieser), Wiley, New York, **1982**, p. 325.

[10] J. A. Hyatt, *Org. Prep. Proced. Int.* **1991**, *23*, 460–463.

[11] M. Rehahn, A.-D. Schlüter, G. Wegner, *Makromol. Chem.* **1990**, *191*, 1991–2003.

[12] The determination of the threefold charge transfer in the first redox stage was carried out by comparing the peak currents of **1** with that of an exactly known amount of ferrocene. The result was confirmed by computer calculations using program M271 of the company EG & G, Munich.

[13] J. Huber, K. Müllen, J. Salbeck, H. Schenk, U. Scherf, T. Stehlin, R. Stern, *Acta Polymer.* **1994**, *45*, 244–247.

The Cycloaddition Way to Glycosyl Transfer**

Giuseppe Capozzi, Angelos Dios, Richard W. Franck,* Aloma Geer, Cecilia Marzabadi, Stefano Menichetti, Christina Nativi, and Maria Tamarez

Dedicated to the memory of William S. Johnson

A century of glycosyl transfer chemistry can be summarized, with a few exceptions, by Equation (a), in which the anomeric

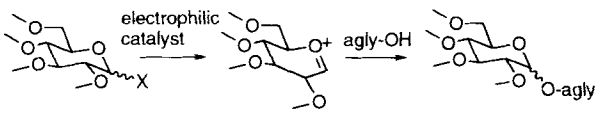

(a)

carbon of a sugar is activated to become electrophilic whereupon it bonds to a nucleophilic aglycone.[1] The extent and subtlety of glycosidation methodology rests on the development of diverse activation methods and the control of stereochemistry in the formation of the glycoside bond. This communication outlines our successful application of a different concept for glycosyl transfer, a cycloaddition method depicted in general form in Equation (b). Thus, a diene with heteroatoms at its

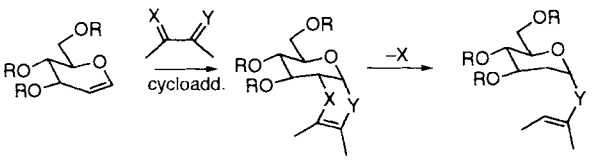

(b)

termini undergoes cycloaddition to a glycal followed by ring-opening of the adduct at the heteroatom not at the glycosidic position.

This sequence would yield a glycoside without reverting to traditional glycoside chemistry. Our approach has its antecedents in two earlier reports of cycloadditions to glycals. Inverse electron demand Bradsher cycloadditions of isoquinolinium salts to glycals demonstrated both the ease and high stereoselectivity of these cycloadditions [Eq. (c) DNP = 2,4-dinitrophenyl].[2] Of course, the products formed are not glycosides since the new bonds are C–C linkages.

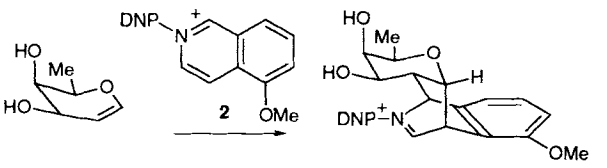

(c)

1 3

[*] Prof. R. W. Franck, A. Dios, A. Geer, Dr. C. Marzabadi, M. Tamarez
Department of Chemistry, Hunter College/CUNY
695 Park Avenue, New York, NY 10021 (USA)
Fax: Int. code +(212)772-5332
e-mail: rfranck@shiva.hunter.cuny.edu
Prof. G. Capozzi, Dr. S. Menichetti, Dr. C. Nativi
Centro CNR "Chimica dei Composti Eterocicli"
Dipartimento di Chimica Organica, Università di Firenze (Italy)

[**] The research conducted at Hunter College was supported in part by the National Institutes of Health (grants GM51216, RR03037 (RCMI support for the NMR and X-ray facilities), and GM08176) (MBRS for M. T.) and by the PSC-CUNY. The Firenze group was supported by MURST.

At about the same time, the light-catalyzed [4 + 2]cycloaddition of azodicarboxylates to glycals to form oxadiazenes was reported.[3] The reaction was usually highly stereoselective and when followed by catalyzed ring-opening at the anomeric carbon and reduction of the hydrazo group, the reaction sequence led to an elegant synthesis of glycosides of 2-aminosugars [Eq. (d); TBDMS = *tert*-butyldimethylsilyl].

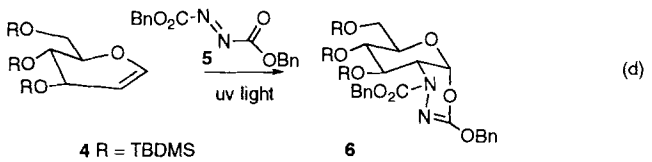

(d)

4 R = TBDMS 6

The heterodiene system that led to the development of our new method is the diacylthione **9**, which is generated in situ with a weak base from the phthalimidosulfenyl precursor **8**. In turn, **8** is easily formed from pentanedione and phthalimidosulfenyl chloride [Eq. (e)].[4]

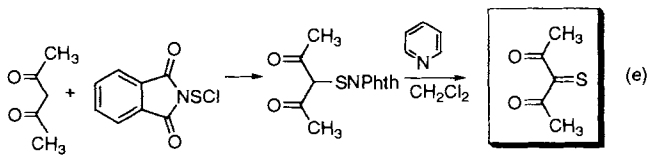

(e)

7 8 9

The results of our exploratory work are summarized in Table 1; the corresponding formulas are in Scheme 1. In a typical experiment 3-phthalimidosulfenylpentanedione (**8**) was mixed with a glycal and an equivalent of pyridine or lutidine in CH_2Cl_2 at room temperature. Workup generally afforded pure crystalline products after straightforward chromatographic removal of phthalimide, unreacted glycal, and residual pyridine or lutidine. One interesting feature of the cycloaddition is the qualitative correlation of reactivity with the HOMO–LUMO gap of the reactants.[5] The cycloaddition appears to be a reaction with

Table 1. Results of cycloadditions of diacylthione **9** (LUMO −1.62 eV) to glycals.

Entry	Dienophile [a]	ΔE(HOMO–LUMO) [eV] v [b]	Adduct	Yield [%]
1	**10** (−9.53)	7.91 slow $t_{1/2}$: 3 d	**11**	80
2	**12** (−9.53)	7.91 slow $t_{1/2}$: 3 d	**13**	54
3	**14** (−9.17)	7.55 moderate $t_{1/2}$: 12 h	**15**	73
4	**16** (−9.50)	7.88 slow $t_{1/2}$: 3 d	**17**	68
5	**18** (−9.74)	8.12 no reaction		
6	**19** (−9.39)	7.77 moderate $t_{1/2}$: 1 d	**20**	74 3.6α/1β
7	**21** (−9.35)	7.73 moderate $t_{1/2}$: 1 d	**22**	42 1α/3β

[a] Numbers in parentheses are LUMO energies [eV]. [b] Apparent rate.

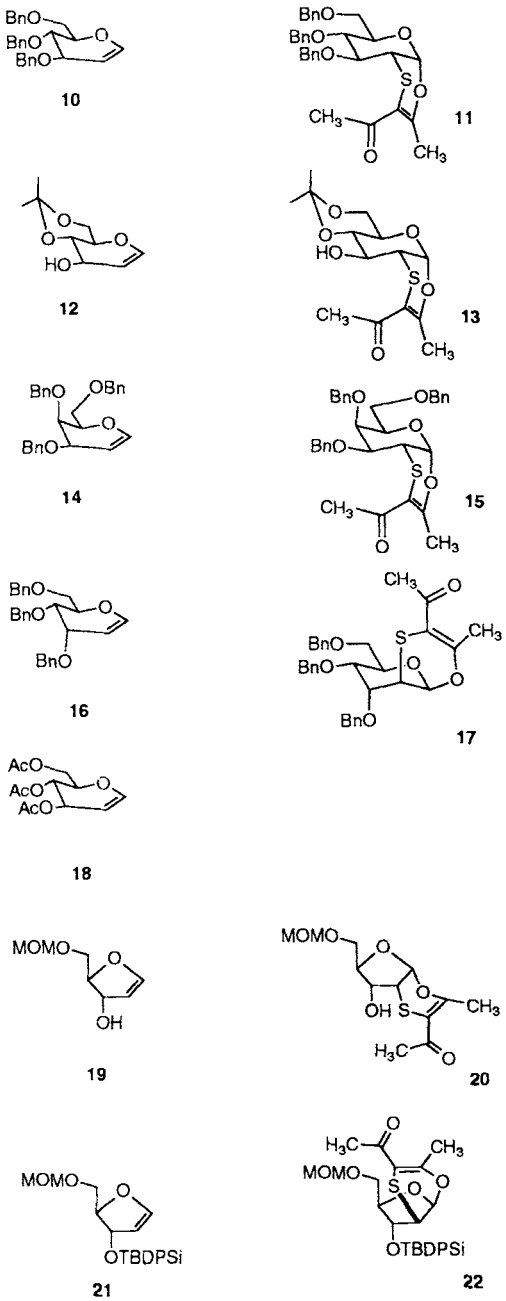

Scheme 1. Structural formulas of the compounds listed in Table 1. MOM = methoxymethyl; TBDPSi = *t*-butyldiphenylsilyl.

inverse electron demand, since the smallest differences in energy are between the HOMO of the glycal dienophile and the low-lying LUMO of the heterodiene. Table 1 includes the pertinent energy levels as computed at the AM1 level with the SPARTAN program package.[6] In this reaction the sugar may be either protected or unprotected; however, acetates lower the HOMO of the glycal so that it adds to only very reactive acylthiones (cf. entry 5 in Table 1 and entry 2 in Table 2). The stereochemistry of the adducts conforms with our earlier proposal[7] that the glycal π bond is polarized below the plane except in the allal case (entry 4 in Table 1) where both the polarization and the obvious steric effects direct the cycloaddition above the plane. The NMR spectra of the crude products before chromatography do not give evidence for stereoisomeric adducts [with the exception of furanoid glycals, entries 6 and 7 in

Table 2. Results of cycloadditions of diacylthione **24** (LUMO -2.22 eV) to glycals.

Entry	Dienophile [a]	ΔE(HOMO-LUMO) [eV] v [b]	Adduct [c]	Yield [%]
1	**10** (-9.53)	7.31 moderate $t_{1/2}$: 1 d	**25**	43
2	**18** (-9.74)	7.52 moderate $t_{1/2}$: 1 d	**26**	50
3	**14** (-9.17)	6.95 fast $t_{1/2}$: 1 h	**27**	52
4	**16** (-9.50)	7.28 moderate $t_{1/2}$: 1 d	**28**	50

[a] Numbers in parenthesese are LUMO energies [eV]. [b] Apparent rate. [c] For formulas, see Scheme 2.

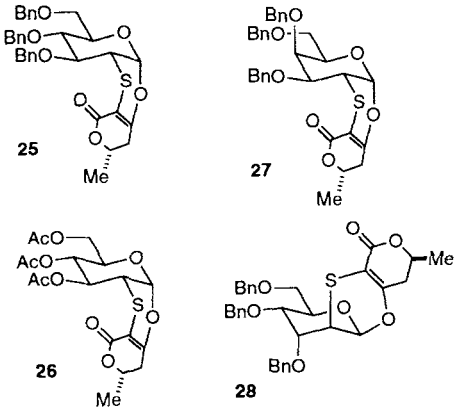

Scheme 2. Structural formulas of the compounds listed in Table 2.

Table 1, and the reaction of diene **30** derived from barbiturate summarized in Equation (g)]. But conclusive proof that no stereoisomeric adducts are formed can be drawn only after comparison of the spectra with those of independently prepared compounds. For entries 2 and 4 in Table 1, the stereochemistry has been confirmed by X-ray crystal structure determinations. Table 2 presents the results obtained with cyclic diacylthione **24**, which is generated in situ according to Equation (f). Since **24**

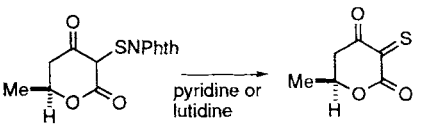

(f)

23 **24** (-2.22 ev)

has a lower lying LUMO, it is somewhat more reactive than the pentanedione-derived thione. The barbituric acid derived thione **30** affords a 9/1 mixture of α and β adducts in 64% combined yield [Eq. (g)].

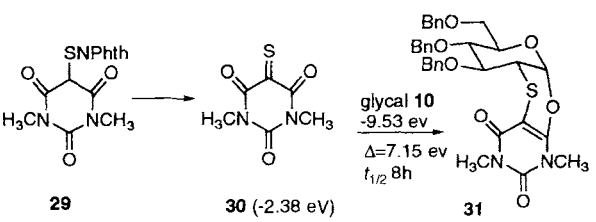

(g)

29 **30** (-2.38 eV) **31**

 © VCH Verlagsgesellschaft mbH, D-69451 Weinheim, 1996 0570-0833/96/3507-0778 $ 15.00+.25/0

To illustrate our scheme for glycoside synthesis without conventional glycoside chemistry, we have treated cycloadducts **25** and **27** from Table 2 with W-2 Raney nickel at room temperature to yield glycosides **32** and **33** in 45% and 31% yield, respectively (Scheme 3). This conversion is quite sensitive to the age of the

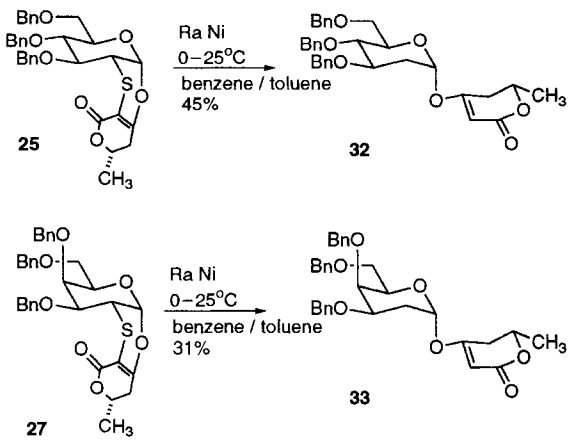

Scheme 3.

catalyst; reduction of the enol ether double bond is a persistent problem.[8] A survey of desulfurization catalysts has not yet been carried out, but it is our goal to obtain yields for the second step at least equal to those of our cycloaddition.

Our cycloaddition concept is an easily accessible approach for highly stereoselective glycosyl transfer and is orthogonal to conventional carbohydrate methodology. Further goals are to employ heterodienes with elements other than sulfur and oxygen at the termini.[9] We are also developing subsequent reactions at the anomeric carbon of our novel cycloadducts.

Received: November 9, 1995 [Z8536IE]
German version: *Angew. Chem.* **1996**, *108*, 805–807

Keywords: cycloadditions · glycals · glycosides · thiones

[1] a) K. Toshima, K. Tatsuta, *Chem. Rev.* **1993**, *93*, 1503–1531; b) R. R. Schmidt in *Comprehensive Organic Synthesis, Vol. 6* (Eds.: B. M. Trost, I. A. Fleming, E. Winterfeldt), Pergamon, Oxford, **1991**, pp. 33–64, and references therein.

[2] R. B. Gupta, R. W. Franck, *J. Am. Chem. Soc.* **1989**, *111*, 7668–7670.

[3] a) Y. Leblanc, B. J. Fitzsimmons, J. P. Springer, J. Rokach, *J. Am. Chem. Soc.* **1989**, *111*, 2995–3000; b) in a more recent report, thermal cycloaddition was used to form the same system: A. Toepfer, R. R. Schmidt, *Carbohydr. Res.* **1993**, *247*, 159–164.

[4] a) G. Capozzi, C. Nativi, S. Menichetti, A. Rosi, G. Valle, G., *Tetrahedron* **1992**, *48*, 9023–9029; b) G. Capozzi, S. Menichetti, C. Nativi, A. Rosi, R. W. Franck, *Tetrahedron Lett.* **1993**, *34*, 4253-4256; c) G. Capozzi, R. W. Franck, S. Menichetti, M. Mattioli, C. Nativi, G. Valle, *J. Org. Chem.* **1995**, *60*, 6416–6426. This paper reports the reaction of entry 1 in Table 1 as one example among many cycloadditions of the versatile diene **9**.

[5] R. Sustmann, I. Siangouri-Feulner, *Chem. Ber.* **1993**, *126*, 1241–1245.

[6] SPARTAN is an integrated software package for quantum chemical calculations produced by Wavefunction, Inc., Irvine CA.

[7] R. W. Franck, N. Kaila, M. Blumenstein, A. Geer, X.-L. Huang, J. J. Dannenberg. *J. Org. Chem.* **1993**, *58*, 5335–5337.

[8] The reduced yield in the conversion of **27** to **33** is due to the fragmentation of the organonickel species back to tribenzyl galactal.

[9] a) Aspects of this work were reported at the ACS Meeting, Anaheim, CA, April 2–6, 1995, CARBO 033 and ORG 483. b) An application of this concept to form 2-deoxyaryl glucosides has been reported: G. Capozzi, C. Falciani, S. Menichetti, C. Nativi, R. W. Franck, *Tetrahedron Lett.* **1995**, *36*, 6755–6758.

Synthesis of *cis*-Enediynes from 1,5-Diynes by Rearrangement of an Allylic Double Bond**

Wei-Min Dai,* Kin Chiu Fong, Hiroshi Danjo, and Sei-ichi Nishimoto

Until the discovery of the class of enediyne antitumor antibiotics[1, 2] in 1985 and shortly thereafter, the benzenoid diradical derived from the cycloaromatization of enediynes, discovered in 1971–1972,[3] had not received much attention for potential application in biomedical science. During recent years numerous enediynes have been synthesized,[1a] and their ability to damage DNA[4] and kill cancer cells has been demonstrated.[5] Synthesis of pro-enediyne compounds[6] is a new direction of enediyne studies. Introduction of a double bond into 1,5-diynes has been achieved by elimination[7] of mono- or diols under reductive, basic, acidic, or neutral conditions. Oxidation[8a] and photochemical processes[8b] have been also used. In this communication, we report for the first time[9] the synthesis of acyclic *cis*-enediynes **2** from 1,5-diynes **1** by an allylic double bond migration (Scheme 1).

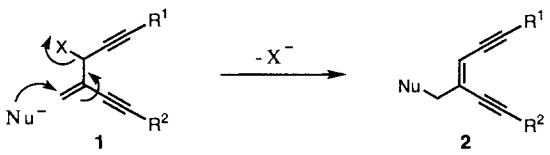

Scheme 1. Synthesis of enediyne **2** from 1,5-diyne **1** by rearrangement of the allylic double bond. Nu = nucleophile.

The enyne aldehydes **5** and **7** were synthesized by the Pd^0-mediated cross coupling reaction of **3**[10] with acetylene derivatives **4** and **6**, respectively (Scheme 2). Addition of $Li-C\equiv CR^2$ to **5** or **7** at −80 °C provided the 1,5-diynes **8a–h** in good yield (Table 1). Formation of the methanesulfonate (mesylate) of **8c** (CH_3SO_2Cl, NEt_3, THF, −80 to 0 °C) was initially attempted. However, only the rearranged allylic alcohol **9c** was isolated. This result suggested that the mesylate was too unstable to be isolated.[11] It decomposed to **9c** after exposure to moisture or aqueous work up. We also noted a set of signals at δ = 5.45 (s) and 5.99 (s), in addition to the signals [δ = 5.19 (s) and 5.99 (s)] of **9c** in the ^{1}H NMR spectrum of the crude product. However, these peaks disappeared after purification by flash column chromatography over silica gel. We suspected that this mysterious compound was the putative allylic chloride formed by attack of chloride ion at the γ position of the mesylate. The chemical yield of **9c** was improved by using $(i\text{Pr})_2\text{NEt}$ and quenching the reaction with aqueous $NaHCO_3$

[*] Dr. W.-M. Dai, K. C. Fong
Department of Chemistry
The Hong Kong University of Science and Technology
Clear Water Bay, Kowloon (Hong Kong)
Fax: Int. code +2358-1594
e-mail: chdai@usthk.ust.hk
H. Danjo, Prof. Dr. S.-i Nishimoto
Laboratory of Excited-State Hydrocarbon Chemistry
Division of Energy and Hydrocarbon Chemistry
Graduate School of Engineering
Kyoto University, Sakyo-ku, Kyoto 606-01 (Japan)

[**] This work was supported by a UGC Competitive Earmarked Research Grant [HKUST 212/93E] from the Hong Kong Research Grants Council. Financial support from the Department of Chemistry, HKUST, is also acknowledged. H. Danjo and Professor S. Nishimoto interpreted the DNA cleavage assay. *m*CPBA = *meta*-chloroperbenzoic acid. NOE = nuclear Overhauser effect.

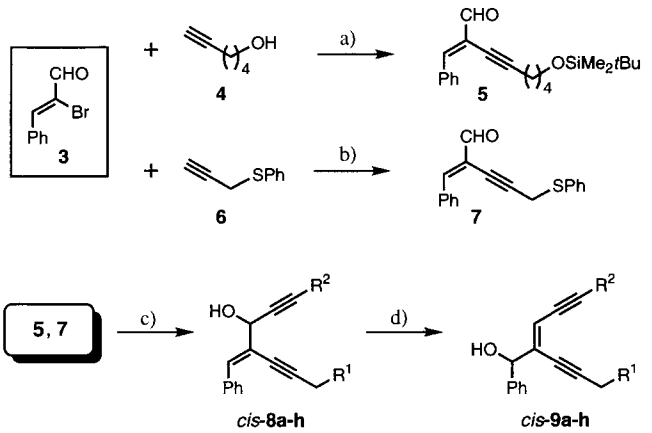

Scheme 2. Synthesis of *cis*-enediynes **9a–h**. a) **4**, 5 mol% $[Pd(PPh_3)_4]$, 10 mol% CuI, Et_3N, THF, 20 °C, 1 h; $tBuMe_2SiCl$, imidazole, DMF, 20 °C, 24 h, 70% based on **3**; b) **6**, 5 mol% $[Pd(PPh_3)_4]$, 10 mol% CuI, Et_3N, CH_3CN, 20 °C, 1 h, 84%; c) Li-C≡CR^2, THF, −80 °C, 30 min; d) CH_3SO_2Cl, $(iPr)_2NEt$, THF, −80 °C, 1 h; aqueous $NaHCO_3$ solution, −80 °C. R^1 and R^2: see Table 1.

Table 1. Yields of compounds **8a–h** and **9a–h**.

R^1	R^2	Yield [%]	
		8	**9**
$-(CH_2)_3OSiMe_2tBu$	$SiMe_3$	**8a** 74	**9a** 50
$-(CH_2)_3OSiMe_2tBu$	Ph	**8b** 75	**9b** 57 [a]
$-(CH_2)_3OSiMe_2tBu$	CH_2OTHP	**8c** 75	**9c** 60
$-(CH_2)_3OSiMe_2tBu$	CH_2SPh	**8d** 92	**9d** 83
-SPh	H	**8e** 87	**9e** 50 [b]
-SPh	$SiMe_3$	**8f** 70	**9f** 65
-SPh	Ph	**8g** 78	**9g** 58 [c]
-SPh	CH_2OTHP	**8h** 81	**9h** 60

[a] 90:10 mixture of *cis*-**9b** and *cis*-**8b**. [b] 95:5 mixture of *cis*-**9e** and its *trans* isomer. [c] 80:5:10:5 mixture of *cis*-**9g**, *trans*-**9g**, *cis*-**8g**, and *trans*-**8g**.

solution at −80 °C. Rearrangement of the allylic alcohols **8** turned out to be a general reaction. Table 1 lists the yields of the eight enediynes isolated. Compounds **9a,c,d,f,h** were formed in the high regio- and stereoselectivity that might be expected for an S_N2' reaction mechanism of *syn* attack[12] at the γ position.[13] The transition state **A** in Scheme 3 illustrates the favorable pathway leading to *cis*-**9**. A similar transition state **B** that would afford *trans*-**9** is destabilized by the strain of the

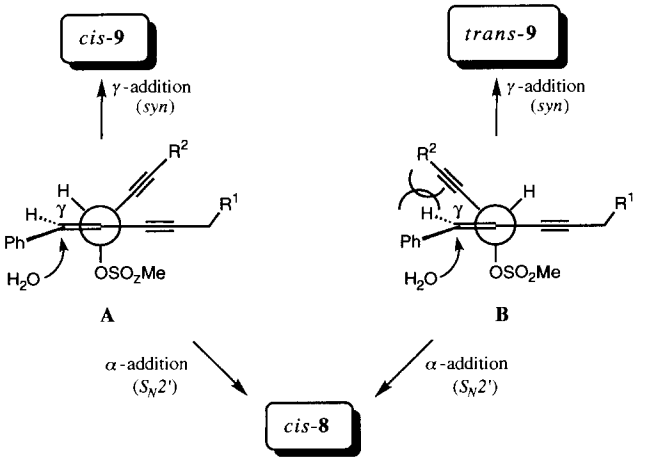

Scheme 3. Postulated transition states **A** and **B** of the allylic rearrangement. Both transition states can add H_2O at the γ and α positions (S_N2' and S_N2, respectively). The γ addition is shown.

allyl system, which interacts with the acetylene substituent (-C≡CR^2). A small fraction (5%) of *cis*-**9e**, where R^2 is H, was formed through **B**. The *anti* attack of a nucleophile at the α position is also possible.[13] We observed 10% of the α addition product for **8b** that was formed via **A**. In this case the α addition product should be the enantiomer of the starting alcolhol *cis*-**8b**. Only for one substrate, **8g**, were four isomers *cis*-**9g**, *trans*-**9g**, *cis*-**8g**, and *trans*-**8g** isolated; *cis*-**9g** was the major component (80%) (Table 1). Since addition of H_2O to the mesylate could not produce *trans*-**8g** via transition states **A** and **B** either by γ or by α addition, an alternative mechanism involving a stabilized allylic cation might account for the product distribution.[14]

The migration of the allylic double bond causes the chemical shifts of the vinyl and methine protons in **9** to differ significantly from those of **8**. The signals of the vinyl protons in **9a–h** move to high field ($\Delta\delta$ ranges between 0.67 and 0.84), while those for the methine protons (with the exception of those of **9b** and **9g**) shift downfield by $\Delta\delta$ = 0.19–0.45. Nuclear Overhauser effect (NOE) experiments confirmed the configuration of the double bond in **9**. Irradiation at the vinyl proton of **10a** (Scheme 4) gave

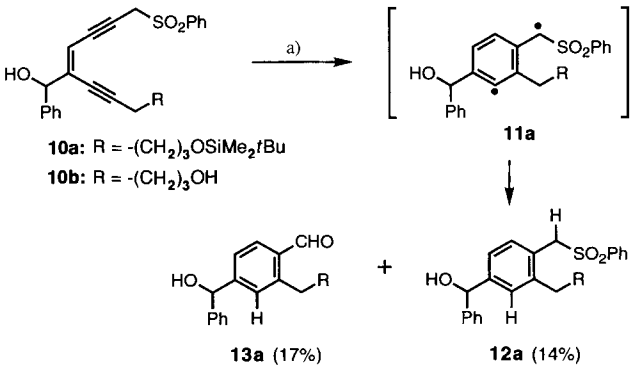

Scheme 4. Base-induced cycloaromatization of **10a**. a) Et_3N, degassed benzene/1,4-cyclohexadiene (10:1), 20 °C, 24 h.

8.8% enhancement of the signal for the methine proton but did not affect the the protons of the aromatic ring. Further evidence supporting the *cis* configuration of **9** was provided by a base-induced cycloaromatization (Scheme 4) of the sulfone **10a** prepared by oxidation of **9d** (*m*CPBA, CH_2Cl_2).[15] All these results verified unequivocally the assigned structures for **9**. We examined the DNA cleavage by **10b** with ΦX174 Form I DNA. The agarose gel picture shown in Figure 1 indicated that the proportion of single strand cleavage product (Form II DNA) increased with increasing amount of **10b**. About 40% Form I DNA was converted into Form II DNA at concentration of 5.0 mM (Lane 6).

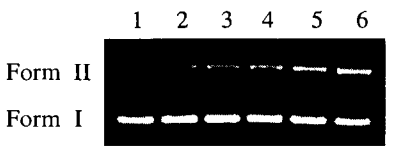

Fig. 1. Results of DNA cleavage by **10b**. ΦX174 Form I DNA (50 μM/bp) was incubated for 72 h at 37 °C with **10b** in TEA buffer solution (pH 8.5) containing 20% DMSO and analyzed by electrophoresis (1% agarose gel, ethidium bromide stain). Lane 1: DNA control without incubation; lanes 2–6: DNA with 0.1, 0.5, 1.0, 2.0, and 5.0 mM **10b**, respectively.

In summary, an efficient synthesis of acyclic *cis*-enediynes has been established for the first time by migration of an allylic double bond into 1,5-diyne. The S_N2' reaction pathway proceeded with remarkably high stereoselectivity to provide the *cis* isomers. Rearrangement of the allylic double bond in the mesylate intermediate of **8** by other nucleo-

philes such as alcohols and thiols were also performed and provided the *cis*-enediynes as major products.

Received: November 20, 1995 [Z8565IE]
German version: *Angew. Chem.* **1996**, *108*, 821–822

Keywords: enediynes · rearrangements · sulfones

[1] Reviews: a) K. C. Nicolaou, W.-M. Dai, *Angew. Chem.* **1991**, *103*, 1453; *Angew. Chem. Int. Ed. Engl.* **1991**, *30*, 1387; b) M. D. Lee, G. A. Ellestad, D. B. Borders, *Acc. Chem. Res.* **1991**, *24*, 235; c) I. H. Goldberg, *ibid.* **1991**, *24*, 191.

[2] a) Structures of neocarzinostatin chromophore, calicheamicin γ_1^I, esperamicin A_1, and dynemicin A: see references cited in [1a]; b) structure of kedarcidin chromophore: J. E. Leet, D. R. Schroeder, S. J. Hofstead, J. Golik, K. L. Colson, S. Huang, S. E. Klohr, T. W. Doyle, J. A. Matson, *J. Am. Chem. Soc.* **1992**, *114*, 7946; J. E. Leet, D. R. Schroeder, D. R. Langley, K. L. Colson, S. Huang, S. E. Klohr, M. S. Lee, J. Golik, S. J. Hofstead, T. W. Doyle, J. A. Matson, *ibid.* **1993**, *115*, 8432; c) structure of C-1027 chromophore: K. Yoshida, Y. Minami, R. Azuma, M. Sakei, T. Otani, *Tetrahedron Lett.* **1993**, *34*, 2637; d) structures of artifacts of the chromophore isolated from maduropeptin: D. R. Schroeder, K. L. Colson, S. E. Klohr, N. Zein, D. R. Langley, M. S. Lee, J. A. Matson, T. W. Doyle, *J. Am. Chem. Soc.* **1994**, *116*, 9351.

[3] a) R. G. Bergman, *Acc. Chem. Res.* **1973**, *6*, 25; b) R. R. Jones, R. G. Bergman, *J. Am. Chem. Soc.* **1972**, *94*, 660; c) N. Darby, C. V. Kim, J. A. Salaun, K. W. Shelton, S. Takada, S. Masamune, *J. Chem. Soc. Chem. Commun.* **1971**, 1516.

[4] First example of DNA cleavage by synthetic enediynes: a) K. C. Nicolaou, G. Zuccarello, Y. Ogawa, E. J. Schweiger, T. Kumazawa, *J. Am. Chem. Soc.* **1988**, *110*, 4866; b) K. C. Nicolaou, G. Zuccarello, C. Reimer, V. A. Estevez, W.-M. Dai, *ibid.* **1992**, *114*, 7360.

[5] Cytotoxicity of synthetic enediynes: a) K. C. Nicolaou, W.-M. Dai, S.-C. Tsay, V. A. Estevez, W. Wrasidlo, *Science* **1992**, *256*, 1172; b) K. C. Nicolaou, W.-M. Dai, S.-C. Tsay, W. Wrasidlo, *BioMed. Chem. Lett.* **1992**, *2*, 1155; c) K. C. Nicolaou, Y. P. Hong, W.-M. Dai, Z.-J. Zeng, W. Wrasidlo, *J. Chem. Soc., Chem. Commun.* **1992**, 1542; d) M. D. Wittman, J. F. Kadow, D. R. Langley, D. M. Vyas, W. C. Rose, W. Solomon, N. Zein, *BioMed. Chem. Lett.* **1995**, *5*, 1049.

[6] Review: M. E. Maier, *Synlett* **1995**, 13.

[7] a) A. G. Myers, P. S. Dragovich, *J. Am. Chem. Soc.* **1992**, *114*, 5859; b) H. Audrain, T. Skrydstrup, G. Ulibarri, D. S. Grierson, *Synlett* **1993**, 20; c) M. Shibuya, Y. Sakai, Y. Naoe, *Tetrahedron Lett.* **1995**, *36*, 897; d) M. Yoshimatsu, H. Yamada, H. Shimizu, T. Kataoka, *J. Chem. Soc. Chem. Commun.* **1994**, 2107; e) M. F. Semmelhack, J. Gallagher, *Tetrahedron Lett.* **1993**, *34*, 4121; M. F. Semmelhack, J. J. Gallagher, W.-D. Ding, G. Krishnamurthy, R. Babine, G. A. Ellestad, *J. Org. Chem.* **1994**, *59*, 4357; f) R. S. Huber, G. B. Jones, *Tetrahedron Lett.* **1994**, *35*, 2655.

[8] a) M. E. Maier, T. Brandstetter, *Tetrahedron Lett.* **1991**, *32*, 3679; b) J. M. Nuss, M. M. Murphy, *Tetrahedron Lett.* **1994**, *35*, 37.

[9] After we began our current project in 1992, an intramolecular allylic migration was proposed for the action of the artifacts of the chromophore isolated from maduropeptin. See ref. [2d].

[10] Compound **3** was prepared from cinnamaldehyde (Br_2 followed by treatment with Et_3N). Its structure was confirmed by an X-ray crystallographic analysis.

[11] The corresponding acetate of **8a** was isolated and exhibited good stability at room temperature.

[12] The *anti* addition of nucleophiles will give the enantiomeric product of *syn* addition in the reaction under consideration.

[13] J. March, *Advanced Organic Chemistry*, 3rd. ed., Wiley, New York, **1985**, p. 289.

[14] We performed the allylic rearrangment of **8** under acidic conditions and obtained the four *cis* and *trans* isomers of **8** and **9**. The major component was *cis*-**9**.

[15] a) Y. Sakai, Y. Bando, K. Shishido, M. Shibuya, *Tetrahedron Lett.* **1992**, *33*, 957; b) M.-J. Wu, C.-F. Lin, J.-S. Wu, H.-T. Chen, *ibid.* **1994**, *35*, 1879.

Corrigenda

In the review "Electronegativity and Molecular Properties" by D. Bergmann and J. Hinze (*Angew. Chem. Int. Ed. Engl.* **1996**, *35*, 150–163), Equation (49) should read as follows:

$$D_{AB} = \frac{1}{(1 + |Q_A Q_B|)}\left[\frac{1}{2}(D_{AA} + D_{BB}) + c_3 \frac{(\chi_A - \chi_B)^2}{4(\eta_A + \eta_B)} + c_4 \frac{Q_A Q_B}{d_{AB}}\right] \qquad (49)$$

Furthermore, three corrections are necessary in Table 5: $c_3 = 18.36 \frac{\text{kcal}}{\text{mol eV}}$, $c_4 = -751.98 \frac{\text{kcal Å}}{\text{mol e}^2}$, and the bond dissociation energy of N(te) should be 87.2 kcal mol^{-1}.

In the communication "Single-Chain Polyprenyl Phosphates Form 'Primitive' Membranes" by G. Ourisson et al. (*Angew. Chem. Int. Ed. Engl.* **1996**, *35*, 177–180) the structure of Nile Red was incorrectly given as that of 9-methylanthracene, as in the catalog (Molecular Probes) from which Nile Red was ordered. The excitation and emmission wavelengths given in the communication and correct.

 © VCH Verlagsgesellschaft mbH, D-69451 Weinheim, 1996 0570-0833/96/3507-0781 $ 15.00+.25/0

An Orgy of Organic Synthesis

Encyclopedia of Applied Physics. Vols. 1–12, Accelerators to Optics. Edited by *G. L. Trigg*. VCH Verlagsgesellschaft, Weinheim/VCH Publishers, New York, 1991–1995. Hardcover DM 450.00/398.00 (single/set) per volume.—ISBN 1-56081-058-0 (set)

So far, we have reached Volume 12 (Nuclear Waste Management to Optics, Underwater) in this massive undertaking published by VCH and sponsored by the American Institute of Physics, the Deutsche Physikalische Gesellschaft, the Japan Society of Applied Physics, and the Physical Society of Japan. Now we have come more than halfway through the alphabet since Accelerators, Linear first saw the light of day in 1991, and successive volumes of about 600 pages each have provided us with a rich fare of 300 articles, with another 200 to come. I have to declare an interest, for I act as an editorial consultant. However, that has given me some insight into the care and attention to quality that has gone into this enormous work. Each article has been commissioned from an expert or a small team; the outline plan is assessed, as is the final typescript. A cumulative index appears with approximately every third volume, and the final volume will contain the complete index. The index is necessary, partly because in a work spread over so many years and written by so many hands, some articles have to be renamed to let them fall later in the alphabet than they were first expected.

Many articles conclude with a glossary of terms, which is very helpful. They all list the works cited and include a list of further reading. However, I did detect some references to books published in the early 1960s, which suggest a somewhat moribund field (or perhaps author). There is a smattering of colored plates. Some articles conclude with lists of research opportunities and major outstanding problems: few authors can be expected to be so generous with their ideas.

I shall direct part of this review at the content of the *Encyclopedia* that is likely to be of immediate interest to chemists. Most readers of this journal will no doubt wonder anxiously whether "applied physics" might merely include "chemistry" as an article, and leave it at that. That is not the case. Although Volume 3 (Calibration and Maintenance to Collective Phenomena in Solids) does contain Chemical Analysis, Chemical Kinetics, and Chemical Reactions, there is a healthy emphasis on chemistry throughout the twelve volumes currently available. Indeed, of the 300 articles before me, about 30 are unarguably of direct interest to chemists, and many more provide useful peripheral information or contain chemistry buried within. For instance, there are articles on air pollution, atoms, conformational analysis, crystallography, diffraction, electrochemistry, fullerenes, glasses, laser photochemistry, molecules, and nucleic acids.

It must be admitted that some of these articles, particularly those on ostensibly chemical topics contributed by physicists (although a good number of chemists have also contributed), do have a rather physics spin on them. However, that can be viewed as providing a healthy shift in perspective, and affords a way of letting a chemist see how a physicist views the topic. Who knows, the shift in perspective might even stimulate a fruitful shift in a chemist's attitude. On the other hand, the ostensibly physical articles provide a bridge for traveling in the opposite direction: they are moderately succinct summaries of concepts from a wide range of physics, and many of these core topics are essential to a chemist's understanding of instrumentation and the properties of materials and fields. A chemist is much more likely to want this set of volumes for the doorway they provide into applied physics than for the descriptions they give of the more elementary aspects of chemistry. Here the user will be well rewarded, for the articles are up-to-date and cover topics that chemists are likely to want to know about, at least superficially.

I do have some minor criticisms. With well over 500 authors at work, there is inevitably a variability in clarity of exposition. Some authors have been too restricted by the compass of their articles, and too much information, or just too much raw mathematics has been included for it to be readily digestible. On the other hand, some articles are really first class: they give compact, insightful summaries of the state of their topic. Secondly, there is a wide variability in the standard of illustration: some illustrations seem to have been done by amateurs with stencils; others are fine computer graphics; lettering sizes are all over the place.

Half the pleasure of an encyclopedia is in gaining information on the topic of interest; the other half is the luck of serendipitous discovery. These volumes have been slowly spreading along my shelves for about four years, and it is always a pleasure to learn about tuning handbells and their vibrational modes when one should actually be turning up information on nanophase materials (in Volume 11, Mössbauer Effect to Nuclear Structure), or to learn about explosives when I should have been making notes on excitons (in Volume 6, Electronic Circuits to Fusion, Magnetic Confinement).

It would be too much to expect individuals to buy the entire projected 20 volumes or so of the complete encyclopedia, and too frustrating for ownership to extend to no more than one or two favored volumes. An encyclopedia of this breadth is an all-or-none question of ownership. Nevertheless, it is certainly an obligation for libraries to make this span of readily accessible and up-to-date knowledge available to their readers. At the very least, such a work provides a starting point for deeper penetration of the literature; at its best, it provides just enough information to satisfy an immediate need. Libraries should certainly buy this set, and chemistry libraries in particular will find their money well spent.

Peter W. Atkins
Lincoln College
Oxford University
Oxford (UK)

This section contains book reviews and a list of new books received by the editor. Book reviews are written by invitation from the editor. Suggestions for books to be reviewed and for book reviewers are welcome. Publishers should send brochures or (better) books to Dr. Illenora Beckmann, Redaktion Angewandte Chemie, Postfach 101161, D-69451 Weinheim, Federal Republic of Germany. The editor reserves the right of selecting which books will be reviewed. Uninvited books not chosen for review will not be returned.

Classics in Total Synthesis. Targets, Strategies, Methods. By *K. C. Nicolaou* and *E. J. Sorensen*, VCH, Weinheim, **1996**. pp. 798, Paperback DM 78.00—ISBN 3-527-29132-4, Hardcover DM 128.00—ISBN 3-527-29284-5

This very attractive book by Nicolaou—a master of the synthesis of complex molecules—and Sorensen is a hymn of praise to the high art of total synthesis. In this book the classical syntheses are, of course, discussed, like Woodward's reserpine and strychnine syntheses, Corey's and Stork's prostaglandin synthesis, and Woodward's and Eschenmoser's vitamin B_{12} synthesis. Three quarters of the book, however, cover the syntheses of the eighties and nineties. The syntheses are arranged chronologically. The good selection of increasingly more complex natural product syntheses illustrates very well the enormous advances that have been made in the last twenty years. In almost 800 pages the syntheses of about forty significant target molecules are described in a very engaging style. The work of Nicolaou is represented by six syntheses, together with that of other important natural product chemists in the USA, such as Corey, Still, Schreiber, Evans, and Danishefsky. Also interesting are the three industrial syntheses (by Merck, Hoffmann-LaRoche, and Takasago), which, with respect to the academic research, have a different status. For this reason other criteria determined their retrosyntheses.

For every natural product an overview of its biological properties, its significance, and its history is given in a short introduction. Potential problems and difficulties for the total syntheses are already mentioned at this juncture, which considerably facilitates the understanding of the retrosynthesis. Key reactions for the total synthesis are thoroughly discussed in this introduction. For example, in the case of rapamycin (Chapter 31) the Heck reaction, the Suzuki reaction, the Stille reaction, and the Sonogashira reaction are presented in detail. In the case of the palytoxin synthesis by Kishi the $NiCl_2/CrCl_2$-catalyzed coupling reaction is discussed, and in the chapter on zaragossic acid the most important features of the Sharpless dihydroxylation are covered. The reader is familiarized with the mechanism of these reactions as well as with the scope of their application. The retrosynthetic analysis always follows the introduction, and every reaction step is exhaustively discussed and the synthesis strategy presented very clearly. Finally the synthesis is described as it was actually performed. The conditions of the most important key reactions are given in detail, and the stereochemical and mechanistic aspects of these steps are thoroughly discussed. In this section the usefulness of many reagents is briefly explained, with the result that for each synthesis many important concepts and techniques of organic chemistry are covered. Moreover, an appendix on catalytic asymmetric synthesis is offered. This additional information increases the pedagogic value of the book even more and turns it into a valuable organic chemistry textbook. It contains aspects of sugar chemistry, radical chemistry, short but detailed explanations of the Cram–Felkin–Anh and the Baldwin rules, etc. The text is illustrated by many schemes that depict the reactions in excellent diagrams. The whole book is extremely reader-friendly and will without doubt become a best-seller. It is appropriate for undergraduate students as well as for graduate students. In addition it is eminently suitable for a course of special lectures on syntheses of natural products.

In summary, this book can and must be highly recommended. Its content provides an excellent picture of modern natural products chemistry. It will fire many chemists with enthusiasm for total synthesis and organic chemistry. In the light of its overwhelming content, its price of only about 80 DM for the softcover edition is more than reasonable.

Paul Knochel
Fachbereich Chemie
der Universität Marburg

Adventures of a Chemist Collector. By *A. Bader*. Weidenfeld and Nicholson, London, 1995. 288 pp., hardcover £ 14.99, $ 25.00.—ISBN 0-297-83461-4

Alfred Bader is a remarkable and compassionate *Mensch* (human being), whose visits with his wife Isabel through the years as roving ambassador for the Aldrich Chemical Company (now Sigma-Aldrich), the world's largest supplier of research chemicals, have made him a familiar figure, welcomed on university campuses and in industrial laboratories alike. In keeping with Bader's genuine interest in people, which is reflected on almost every page, his autobiography, characteristically dedicated to Isabel, is as much concerned with other persons, especially those who have helped or influenced him in his career, as it is with himself.

It is an engrossing and romantic love story; it tells of his love for one woman, Isabel, who finally became his wife after a separation of a third of a century; of his love for what he calls the ABC of his life—art collecting, the Bible, and chemistry, to which he has made so many valuable contributions; of his love for a city, Milwaukee, Wisconsin, to which he has remained faithful despite opportunities to relocate; of his love for a company, Aldrich, which he cofounded at age 27 and with which his name is still synonymous in spite of his unjust and undeserved expulsion as director; and his love of philanthropy and public service, by which he has tried to repay his debt to society and to persons and institutions who have helped him, and for which he received the American Chemical Society's 1995 Charles Lathrop Parsons Award "for his unprecedented innovation, ... for his vision and dedication as a chemist, ... but most of all for his unflagging ambassadorship to the international chemical community, which he has helped to mold into a truly global village".

This volume is also reminiscent of the biblical Book of Job—the saga of a moral, upright man whose triumph over tragedy, injustice, and adversity without bitterness or loss of faith is an inspiring tribute to the resilience of the human spirit.

Alfred Robert Bader was born in Vienna on April 28, 1924, the son of Alfred and Elisabeth Bader (née Serényi). The Baders were middle-class Jews, and the Serényis were devout Hungarian Catholic aristocrats. His father either committed suicide or was murdered two weeks after Alfred, called Bobby as a child, was born. Because his mother was left with almost nothing to support herself, Alfred, and his sister Marion during the extraordinary inflation raging in post-World War I Austria, he was adopted by his paternal aunt Gisela Reich, whom he regarded as his mother ("Muttili"). Although his sister received a strict Catholic upbringing, he was brought up with a love of Judaism, which has served as "a cornerstone of [his] life". He attended the *Sperlgymnasium*, a high school close to his home, from 1934 until July 1938 when, following the *Anschluss*, Jewish students above the age of 14 were not permitted to attend class.

Although the rest of his immediate family remained behind, in December 1938 Alfred emigrated to England with thousands of other Jewish children. He attended the East Hove Senior School for Boys, followed by the Brighton Technical Col-

 © VCH Verlagsgesellschaft mbH, D-69451 Weinheim, 1996 0570-0833/96/3507-0784 $ 10.00+.25/0

lege until he turned 16, whereupon he was interned as an enemy alien, first in England and then in a Canadian prisoner-of-war camp. On November 2, 1941, after Martin Wolff, "the first father figure in [his] life", agreed to sponsor him, he was released, and that same month he entered Queen's University at Kingston, Ontario, where he majored in engineering chemistry. Receiving a $ 30 scholarship, he said to himself: "If ever I could, I would establish such scholarships", a promise that he later fulfilled to an extraordinary degree.

Bader obtained practical industrial experience in formulating lacquers during summer jobs at the Murphy Paint Company in Montreal. A $ 50 Scholarship in Public Speaking led him to join the debating society, and he admits: "I have enjoyed public speaking and debating ever since." His experience at Queen's University taught him that "there are two kinds of Christians, those to whom Christianity is just an empty shell and those to whom love, respect and care for neighbors are reality". In 1945 he received his B.Sc. and the medal in chemistry. He then spent an additional year at Queen's, earning an M.Sc. working on fatty acid chemistry.

Although accepted by the University of Zürich and the Eidgenössische Technische Hochschule (ETH), in September 1947 Bader entered Harvard University, because it offered him a fellowship. In only two and a half years he received his Ph.D. for research on naphthoquinones under Louis Fieser's supervision. Rather than accept a junior teaching position at the University of New Brunswick or continue at Harvard, on January 15, 1950, he moved to Milwaukee to work with the Pittsburgh Plate Glass Company (now PPG), which had purchased Murphy Paint, because he "wanted to start [his] own family and that seemed more important to [him] at the time than learning a good deal more chemistry". His starting salary, $ 400 per month, was the lowest received by any Harvard Ph.D. in chemistry. From these humble beginnings Bader was to become an internationally renowned and successful millionaire chemist, collector, and philanthropist.

On July 14, 1949, during a trip from Quebec to Liverpool, England on the S. S. Franconia, Bader met Isabel Overton, daughter of a deeply religious Protestant family from Kirkland Lake, Ontario, and nine days later he proposed to her despite their differences in religion. Isabel accepted a position teaching English and history at a private school for girls at Bexhill-on-Sea, England, and in letter 79 (1950) of the 408 letters that she wrote to Bader, who has preserved and numbered them, she wrote that she did not think their marriage would work and that she would not write to him again or answer any further letters. In the spring of 1950 he met Helen Ann Daniels ("Danny"), a Protestant girl who had converted to Judaism, long before he proposed to her on May 20, 1952. She differed from Isabel in "that she wanted to marry [him] and have a Jewish home and family". The two were married in July, and their two sons David and Daniel were born in 1958 and 1961. In 1975 Bader began having repeated frightening nightmares about Isabel's father. He learned that Isabel had never married, and the two resumed their correspondence. Danny requested a divorce, which took place in 1981. Bader provided for her well, and in 1982 he married Isabel. Danny died of ovarian cancer in November 1989.

On August 17, 1951, Bader and his friend Jack Eisendrath, a Milwaukee attorney, incorporated the Aldrich Chemical Company, named after Eisendrath's fiancée Betty Aldrich. Each of them contributed half the required capital of $ 500. The fledgling company's first product was methylnitrosonitroguanidine (MNNG), which Bader had learned to make while working for his M.Sc. at Queen's. All operations were first carried out in Eisendrath's office and then in a garage rented for $ 25 per month. According to Bader, "the greatest problem every entrepreneur faces is how to find really good employees", and he is proud of the fact that "with one minor exception, no union ever threatened us, and we never had a strike". Realizing that Aldrich could not succeed if it sold only what he knew how to make, Bader decided to combine production with resale, particularly of imports. He began his practice of spending several months every year "travelling in Europe, visiting small and medium-sized chemical companies, inquiring what we might purchase from them". He devotes an entire chapter to these visits, and he states: "Suppliers have been vital to Aldrich. Knowing them personally, understanding them and working with them fueled our growth." He similarly devotes a chapter to "Friends and Competitors".

Most of the sales of the rapidly growing company were for catalog items, and from Aldrich's inception Bader paid special attention to its catalogs and publications, including *Aldrichimica Acta*, which, appearing three or four times per year with its familiar cover usually adorned with an old master painting, has become a collector's item in itself. Aldrich established the American Chemical Society Award for Creative Work in Synthetic Organic Chemistry, and Bader established awards with the Royal Society of Chemistry and the Chemical Institute of Canada. By publication in the *Acta* the prize papers reached an audience greater than that for any chemical journal (by the 1980s more than 200000 copies of each *Acta* issue were distributed worldwide). Aldrich also participated in a number of joint ventures, some successful and some not. These included ALFA Inorganics and Aldrich-Boranes, formed at Nobel laureate Herbert C. Brown's suggestion. Aldrich made its first public stock offering in 1965, and by the late 1960s Bader realized that the greatest growth in chemical research lay in the field of biochemistry. In August 1975 Sigma, the leading supplier of biochemicals, and Aldrich, the leading supplier of organics, merged to form Sigma-Aldrich, with Dan Broida of Sigma as chairman of the board and Bader as president. Today the company employs more than 5000 employees with sales of $ 851 million.

The management styles of Sigma and Aldrich were very different, and Bader's difficulties with his successors at Sigma-Aldrich revolved almost entirely around how to treat people. Sigma-Aldrich's chief executive officer, Tom Cori, the only child of Nobel medicine laureates Carl and Gerty Cori, once told Bader: "Alfred, the problem with you is that you want to be liked, even loved. I don't have a single friend in the world, not one". In contrast, many of Aldrich's suppliers and customers had become Bader's good personal friends. He regarded himself as "a useful link between academics and our company", and he believed that "people are the key to success in every venture".

In May 1991 Bader retired but served as chairman emeritus (without pay beginning in 1992). Matters reached a crisis stage on November 20, 1991, when Cori and David Harvey, the chief operating officer, met with Bader in London and demanded that he sign a letter of resignation. Bader, who had always railed at injustice directed toward others and "enjoy[ed] fights when I know or think I know, I am right", refused. The purported reason for his dismissal was that he was "betting against the company". Although he was the only major stockholder never to have sold any of his Sigma-Aldrich stock, in August 1991 Bader had decided to give 10000 of his 3.66 million shares of stock, a mere 0.33% of his holdings (he is still the largest individual shareholder), to Queen's University. To maximize the gift to his alma mater, instead of selling these

 © VCH Verlagsgesellschaft mbH, D-69451 Weinheim, 1996 0570-0833/96/3507-0785 $ 10.00+.25/0

shares outright he wrote a call option, which he regarded as "betting with the company" because he expected the shares to rise in value. Ironically, that same month Cori, Harvey, and Peter Gleich, the vice-president, sold outright 10000, 7000, and 5000 shares, respectively, much larger proportions (about 10%) of their holdings. Bader's use of an option resulted in Queen's University recovering about $ 60000 more than Cori had received for the same number of shares.

In April 1992 Bader distributed an open letter to chemists detailing what soon became known as "the Sigma-Aldrich affair", which quickly became a *cause célèbre*. Articles appeared in *Chemical & Engineering News*, *Chemistry in Britain*, various newspapers, and even *Forbes*, a respected business magazine. The international chemical community was shocked, and Bader and journal editors received letters of support from all over the world, several of which are reproduced in the book ("I never realized how many friends I had", he wrote). Supporters also telephoned or met with Cori, who refused to relent or discuss the issue.

In addition to being justifiably angry, Bader characteristically reacted with sorrow, regret, and concern for the company: "I regard it as a pity that an intelligent, able CEO should have been willing to deprive himself, his team and the company of several more years of effective, valuable help with new products, customer relations, purchasing and other profit and growth producing activities, and that the board supported him." Moreover, although he writes about the present policy of "management by fear", he harbors no enmity for the company, and, with his typical optimism, he predicts for it a rosy future: "I am confident... that Sigma-Aldrich has so many good things going for it, including many very able people, that with some needed reinforcement of top management, it will continue to be a leader in its industry". For several weeks after his dismissal Bader was unable to sleep, but just as the gross injustices of his youth failed to daunt his indomitable spirit, he is well on the road to recovery: "I sleep well now, but once or twice a week I dream that Isabel and I are visiting an old academic friend who is suggesting a new reagent."

Since his childhood years in Vienna, when he bought and sold stamps, Bader has been an inveterate collector. In the middle 1950s he began to "rescue" research samples from various sources that otherwise might have been lost. Eventually this collection, now numbering more than 60000 samples, became known as the Alfred Bader Chemical (ABC) Library (now renamed the Sigma-Aldrich Library)—of immense value for generations of future researchers as well as "a great way to study the history of chemistry". Bader's collection of paintings, first Dutch and Flemish 17th-century and now "biblical subjects by Rembrandt students and truly great works by as yet unidentified artists", is well known. A long chapter details his career as a collector. Another describes 18 of his "trophies of the hunt" in the art world with plates of these paintings; of one of these he writes: "I have spent hundreds of hours studying it in our living room and have often carried it into our bedroom for a last look before putting my arms around Isabel and falling asleep". Separate chapters deal with art collector Efim Schapiro and John Whalley, an artist whom Bader supported. Bader also offers pertinent and amusing anecdotes about his experiences in the art world, including problems involved in donating and appraising paintings.

After his dismissal from Sigma-Aldrich in May 1992, Bader had to move the dozens of paintings hung in the Aldrich offices to his own gallery, and he now spends about a third of his time dealing in paintings, a third writing and lecturing, and a third trying to help chemists, particularly in small companies ("My life's work was to be a chemist helping chemists"). At Queen's University Bader and Isabel recently endowed a Bader Chair in Art History to begin in 1995 and contributed $ 2 million as seed money for an art museum extension. They also established prizes, scholarships, and awards for students in Canada, the United States, Great Britain, and the Czech Republic. In 1986 Bader also established the ACS's Alfred Bader Award in Bioinorganic or Bioorganic Chemistry. He recently donated £ 6 million to Queen's University to purchase and renovate Herstmonceux Castle in Sussex as an international study center. He concludes his copiously illustrated book, which will fascinate not only chemists, business students, art historians, collectors, and Bader aficionados, with a question and an answer that aptly summarize his long career of dedicated service to others: "The one serious problem posed by such a gift is the challenge: what can we do for an encore? But with Isabel's vision, and if the Lord gives us time, we will find other great things to do with our money, which we neither want to use for ourselves nor can take with us."

George B. Kauffman, Laurie M. Kauffman
California State University
Fresno, CA (USA)

Principles of Organic Synthesis. 3rd Edition. By *R. O. C. Norman* and *J. M. Coxon*. Blackie/Chapman and Hall, London, 1993. 811 pp., paperback £ 22.50.—ISBN 0-7514-0126-9

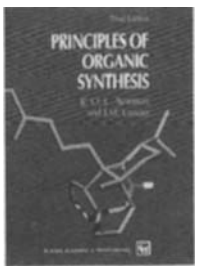

Like the two previous editions (1968 and 1978), this book is intended "for those who have had no more than a brief introduction to organic chemistry". Beginning with the essential concepts of mechanistic theory, Norman and Coxon instruct their readers in the methods and planning of organic syntheses. They deliberately avoid describing the methods used to verify reaction mechanisms, nor do they reproduce experimental details. Exercise problems are included at the end of each chapter.

The first part of the book consists of five chapters dealing with the fundamentals of general chemistry (thermodynamics, chemical bonding, and kinetics), followed by a brief account of the most important types of organic reaction mechanisms, and ending with a discussion of stereochemistry. The second part is much longer, consisting of 17 chapters in which the different types of reaction mechanisms form the starting point for describing synthetic methods based on these mechanisms. Apart from Chapter 22 the material in this part of the book is mainly organized under the various mechanisms, and only to a small extent according to synthetic strategies. Three chapters on the formation of carbon–carbon bonds (using polar organometallic compounds and with acids or bases as catalysts) are followed by chapters on pericyclic reactions and the formation of carbon–nitrogen bonds. Next comes a thoroughly conventional treatment of arene chemistry (electrophilic and nucleophilic substitutions and aromatic diazonium salts), rearrangements, photochemistry, free radicals, oxidation, reduction, and heterocyclic compounds with five- and six-membered rings. In accordance with their importance in modern organic synthesis, compounds of phosphorus, sulfur, silicon, and boron as reagents are treated in a separate chapter, and another is devoted to organometallic compounds of transition elements. These two chapters, together with the final one (Chapter 22), which describes in detail some well-chosen natural products syntheses, form the most topical and interesting part of the book.

 © VCH Verlagsgesellschaft mbH, D-69451 Weinheim, 1996 0570-0833/96/3507-0786 $ 10.00+.25/0

On comparing this book with the previous edition which appeared 15 years earlier, it is seen that only one complete new chapter has been added, namely that on transition metal reagents. Also the selection of examples of natural products syntheses in the last chapter has been brought up to date, and the sections on silicon compounds, peptide syntheses, and the preparation of "preformed enolates" using lithium diisopropylamide have been considerably enlarged. By far the greater part of the material has simply been carried over from the previous edition, at least as regards information content, and sometimes even word-for-word. This hardly seems to do justice to the rapid developments that have occurred in synthetic methods in the last two decades. Thus, in common with many other general textbooks, this book mainly provides a survey of classical preparative organic chemistry, structured according to reaction mechanisms. On the other hand, the *principles* of organic synthesis, announced in the title, are scarcely covered. It is only in the accounts of nine examples of natural products syntheses that the reader learns something about the rational planning of a synthesis, at least in rudimentary form. The inadequacy of the treatment is illustrated by the fact that the concept of retrosynthetic analysis does not appear until Chapter 21 (pp. 679–681), where it receives a mere two pages.

The book cannot be said to fully reflect the current state of research. This can be seen, for example, in the treatment of the synthesis of enantiomerically pure compounds. The Sharpless–Katsuki epoxidation merits less than twenty lines of text (pp. 589–590), and the only method given for enantioselective reduction of "symmetrical" (i.e. achiral) ketones is the reaction with pinanyl-9-BBN (pp. 653–654). The diastereoselective (not "enantioselective") alkylation of Davies-Liebeskind enolates is included (p. 572), but other methods such as the Evans aldol method and the asymmetric hydrogenation using Wilkinson catalysts are not mentioned, revealing some lack of balance in the choice of topics. Another very significant shortcoming is that, apart from Chapter 22, there are no references to original publications, and even the suggestions for further reading that were included in the second edition have now been dropped.

The book is unlikely to offer new perspectives to synthetic chemists in universities or industry, but seems more suitable for providing students starting a degree course in chemistry with a readily understandable survey of the repertoire of (mainly classical) synthetic methods.

Manfred Braun
Institut für Organische
und Makromolekulare Chemie
der Universität Düsseldorf (Germany)

Ziegler Catalysts. Recent Scientific Innovations and Technical Improvements. Edited by *G. Fink, R. Mülhaupt* and *H. H. Brintzinger*. Springer, Berlin, 1995. 511 pp., hardcover DM 198.00.—ISBN 3-540-58225-8

This book contains an impressive collection of papers presented at an international symposium held in honor of Karl Ziegler. The symposium, entitled "Forty Years of Ziegler Catalysts", took place in September 1993 at the University of Freiburg. The organizers, who have also edited this book, were Professors R. Mühlhaupt of the Materials Research Center in Freiburg, G. Fink of the Max-Planck-Institut für Kohlenforschung, Mülheim/Ruhr, and H. H. Brintzinger of the University of Konstanz.

In 1953 Karl Ziegler and his coworkers discovered the "Aufbaureaktion" for the oligomerization of ethene. This subsequently led to the low-pressure process for high-molecular-mass polyethene, using a mixture of aluminum alkyls and titanium tetrachloride as the catalyst. This discovery was the starting point for a period of rapid development in the field of olefin polymerization, providing alternatives to the older high-pressure process for polymerization of ethene, an area of activity that continues up to the present day.

Examples of some of the new developments described in the book are recent results on the nickel-ylide-catalyzed polymerization of acetylene (Storzewski), CO–alkene copolymerization using palladium(II) catalysts (Drent, Chien, and coworkers), and the synthesis of functionalized polymers by ring-opening polymerization (ROMP) reactions (Feast et al.). However, the main themes are the classical Ziegler–Natta catalysis using heterogeneous titanium(III) catalysts and polymerization using metallocene complexes with well-defined molecular structures. In the first article, characteristically entitled "Karl Ziegler—The Last Alchemist", G. Wilke briefly surveys the scientific contributions made by Ziegler and his collaborators and describes the development of the "Aufbaureaktion" for making polyethene. Following the discovery that the oligomerization of ethene was affected by the presence of transition metals (the "nickel effect"), further research led to another success: Giulio Natta and his team discovered that propene could be polymerized stereoselectively using Ziegler catalysts. The contributions of Ziegler and Natta were recognized in 1963 by the award of a Nobel Prize. The second article also presents a historical view; here Heinz Martin, a colleague of Ziegler who worked alongside him for many years, discusses the patenting aspects of Ziegler's work, including the successes and failures that occurred during forty years of Ziegler catalysis. This is followed by an article in which Rolf Mühlhaupt, under the title "Novel Polyolefin Materials and Processes: Overview and Prospects", gives a concise account of developments in the field of Ziegler catalysis and takes the reader up to the current state of knowledge of the relevant science and technology. The comprehensive bibliography with this article helps the reader to seek out the most significant publications on Ziegler catalysis. In the fourth contribution H. Sinn and his coauthors shed some light on the subject of methylaluminumoxanes. Although these compounds have been in use for many years as activators for metallocene catalysts, their structures have still not been fully elucidated.

It would be pointless to try to summarize the contents of every article. It is enough to add that the reader will find here a collection covering the latest developments both in conventional supported catalysts and in metallocenes. The excellent presentations of the individual topics are supported by a detailed subject index and comprehensive bibliographies, which give quick access to the desired information. The book can be thoroughly recommended not only for specialists in metal-catalyzed polymerization but also for everyone with interests in this area.

Bernhard Rieger, Ulf Dietrich
Abteilung für Organische Chemie III
der Universität Ulm (Germany)

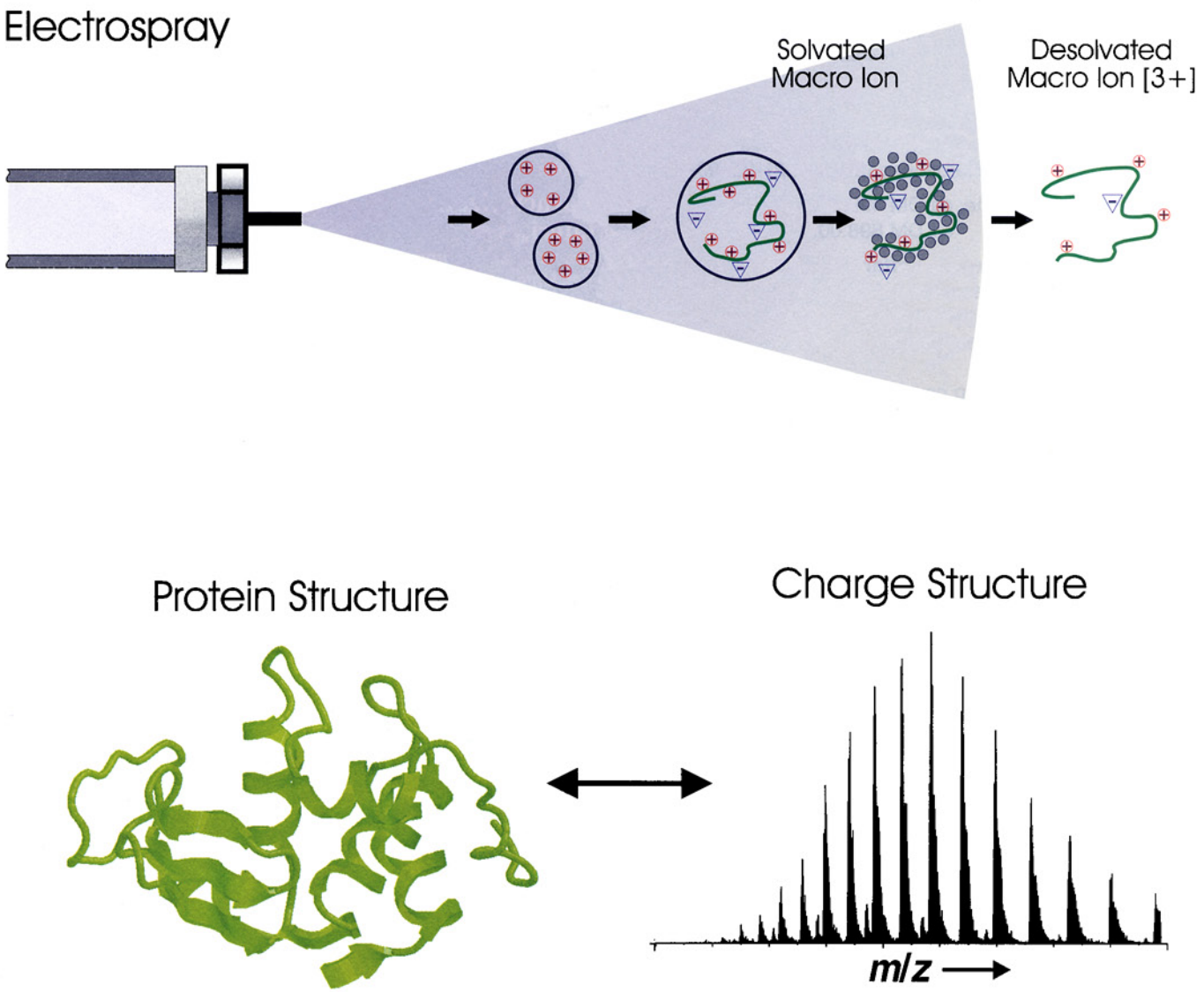

Schematic illustration of the electrospray ionization and formation of desolvated macro ions (top), and of the relation between macromolecular structure and ion-charge structure in the electrospray mass spectrum (bottom).

Electrospray Mass Spectrometry of Biomacromolecular Complexes with Noncovalent Interactions—New Analytical Perspectives for Supramolecular Chemistry and Molecular Recognition Processes

Michael Przybylski* and Michael O. Glocker

The development of "soft" ionization methods in recent years has enabled substantial progress in the mass spectrometric characterization of macromolecules, in particular important biopolymers such as proteins and nucleic acids. In contrast to the still existing limitations for the determination of molecular weights by other ionization methods such as fast atom bombardment and plasma desorption, electrospray ionization (ESI) and matrix-assisted laser desorption have provided a breakthrough to macromolecules larger than 100 kDa. Whereas these methods have been successfully applied to determine the molecular weight and primary structure of biopolymers, the recently discovered direct characterization by ESI-MS of complexes containing noncovalent interactions ("noncovalent complexes") opens new perspectives for supramolecular chemistry and analytical biochemistry. Unlike other ionization methods ESI-MS can be performed in homogeneous solution and under nearly physiological conditions of pH, concentration, and temperature. ESI mass spectra of biopolymers, particularly proteins, exhibit series of multiply charged macromolecular ions with charge states and distributions ("charge structures") characteristic of structural states in solution, which enable a differentiation between native and denatured tertiary structures. In the first part of this article, fundamental principles, the present knowledge about ion formation mechanism(s) of ESI-MS, the relations between tertiary structures in solution and charge structures of macro-ions in the gas phase, and experimental preconditions for the identification of noncovalent complexes are described. The hitherto successful applications to the identification of enzyme–substrate and –inhibitor complexes, supramolecular protein– and protein–nucleotide complexes, double-stranded polynucleotides, as well as synthetic self-assembled complexes demonstrate broad potential for the direct analysis of specific noncovalent interactions. The present results suggest new applications for the characterization of supramolecular structures and molecular recognition processes that previously have not been amenable to mass spectrometry; for example, the sequence-specific oligomerization of polypeptides, antigen–antibody complexes, enzyme– and receptor–ligand interactions, and the evaluation of molecular specificity in combinatorial syntheses and self-assembled systems.

Keywords: macromolecules · mass spectrometry · noncovalent interactions · self-assembly · supramolecular chemistry

1. Introduction

The development of efficient "soft" ionization methods has led to significant advances of mass spectrometry for the direct characterization of macromolecules, particularly important classes of biopolymers such as proteins and nucleic acids.[1–3] Intact molecular ions of higher molecular weight compounds were first obtained in the 1970s by field desorption mass spectrometry (FD-MS).[4] Since the 1980s bombardment by primary particles with energies in the keV range (fast atom bombardment mass spectrometry (FAB-MS) or LSIMS[5]) and ^{252}Cf-plasma desorption mass spectrometry (PD-MS) enabled sensitive and accurate molecular weight determinations of polypeptides and smaller proteins.[6,7] In the past years electrospray ionization (ESI)[8] and matrix-assisted laser desorption-ionization (MALDI)[9] have provided a breakthrough in macromolecular mass spectrometry with the successful analysis of molecular weights greater than 100000 Da. ESI-MS and MALDI-MS have now generally overcome previous limitations in the mass spectrometric analysis of polymers.[10,11]

Although little or no fragmentation of macromolecular ions[12] occurs, soft ionization MS methods have already found broad application in the analysis of primary structures of

[*] Prof. Dr. M. Przybylski, Dr. M. O. Glocker
Fakultät für Chemie der Universität
Postfach 5560 M731, D-78434 Konstanz (Germany)
Fax: Int. code +(7531)88-3097
e-mail: Michael.Przybylski@uni-konstanz.de

 © VCH Verlagsgesellschaft mbH, D-69451 Weinheim, 1996 0570-0833/96/3508-0807 $ 15.00+.25/0

biopolymers. Thus, in addition to collision-induced fragmentation and tandem-MS analysis (for example with FAB-MS[13]), the combination with specific chemical (for example enzymatic) degradation reactions has been successfully applied to sequence determinations of proteins.[14] In particular, the direct mass spectrometric analysis of proteolytic peptide mixtures (peptide mapping)[15] has led to numerous applications in structure–function studies of proteins, such as the identification of post-translational modifications with covalent bonds,[16] the determination of epitope sequences in antigen–antibody complexes,[17] and the characterization of isoenzymes[18] and recombinant proteins.[19]

Beyond the elucidation of primary structures, the application of mass spectrometry to the characterization of tertiary structures and supramolecular complexes[20] has previously not been considered feasible. In a few cases dependence of the fragmentation on tertiary structure has been found, for instance the specific fragmentation in FAB mass spectra of α-helical polypeptides[21] and the strong ion suppression effects in PD mass spectra of proteins upon denaturation on the nitrocellulose (NC) sample target,[14a, 22] which indicates that some "native-like" structure is required for obtaining macromolecular ions.[6b] This situation has been changed drastically by the most recent development of electrospray–ionization mass spectrometry. A number of studies by ESI-MS in the last three years have identified supramolecular complexes of biopolymers, as well as specific noncovalent complexes with low molecular weight constituents.[23, 24] In contrast to other ionization methods in which predominantly singly charged ions are produced from liquid (FAB)[7] or solid matrices (PD, MALDI[6, 11]), continuous series of multiply charged macro-ions are obtained by ESI-MS,[8, 25] with distributions of charges characteristic of the solution structure ("charge structure"; see Section 2).[10, 24–26] Moreover, ESI-MS can be readily carried out with aqueous solutions at nearly physiological solution conditions, thus enabling comparison with other methods of structure determination such as NMR spectroscopy.[27]

The direct mass spectrometric characterization of noncovalent macromolecular complexes opens new perspectives for analysis in supramolecular chemistry in which methods with molecular specificity and sensitivity are needed.[28] Unlike other characterization methods, ESI-MS is applicable to relatively impure samples and multicomponent mixtures and is compatible with microanalytical separation techniques.[10] Although the mechanism of ion formation in ESI-MS has not yet been elucidated in detail, a number of different noncovalent interactions (ionic, hydrophobic) have already been successfully characterized. In this article, the results hitherto obtained are discussed primarily in the context of biochemistry and supramolecular chemistry. The current state of the development of the ESI method with regard to the ion formation pathways and their correlation with solution structures is summarized first. In the subsequent sections, applications to noncovalent complexes of biopolymers and synthetic self-assembled complexes are described, followed by a comparison with potential applications of other mass spectrometric methods. Since the development of ESI-MS is still new, this article will not attempt to present an overview; instead, its main goal is to stimulate further evaluation of its analytical potential for the characterization of supramolecular complexes in conjunction with established methods of structure determination.

M. Przybylski

M. O. Glocker

Michael Przybylski, born in 1948 in Berlin, studied chemistry at the University of Mainz and received his PhD in 1975 with H. Ringsdorf with a dissertation on the synthesis and metabolism of polymeric sulfonamides. After two years as visiting research scientist at the National Cancer Institute, NIH, Bethesda, USA, with biochemical studies of antifolate cytostatic agents, he returned to the University of Mainz, where he finished his habilitation in 1985 on the development and bioanalytical application of mass spectrometry for the structure elucidation of natural products and chemotherapeutic agents. Since 1987 he has been Professor of Analytical Chemistry at the University of Konstanz. He was guest professor at the Universities of Odense, Budapest, and Szeged, received the St. Denis research award, and is author of more than 160 original publications. His research areas are the structure and function of lipid-modified peptides and proteins, structure elucidation and degradation of cell surface protens, xenobiotic peptide conjugates, and mass spectrometry of biomacromolecules in which he focuses on mass spectrometric techniques combined with protein-chemical methods for the characterization of tertiary structures, antigenic determinants, and supramolecular complexes.

Michael O. Glocker, born in 1960 in Altheim, studied chemistry at the University of Konstanz and received his PhD in 1990 with J. C. Jochims with a dissertation of nitrilium salts as reactive intermediates. After two years with M. L. Deinzer at the Oregon State University, Corvallis, USA, working on the structure elucidation of macrophage colony-stimulating proteins and natural and chemically modified phytoalexins, he returned to the University of Konstanz in 1992. He is research associate and habilitand at present, received a habilitation stipend from the DFG in 1994, and is author of more than 30 original publications. His research areas are the protein-chemical and mass spectrometric characterization of tertiary structures of proteins and folding pathways mediated by disulfide bridges, and the structure elucidation of natural and recombinant cytokines.

2. Electrospray Mass Spectrometry of Biomacromolecules

2.1. Formation of Macromolecular Ions by Electrospray Ionization

Initial pioneering studies on the electrospray ionization of large molecules were performed more than twenty years ago by Dole et al.[29] However, the development of ESI-MS was initiated only in 1988 with the introduction of efficient ionization sources suitable for quadrupole mass spectrometers.[8, 10, 30] Two types of electrospray ionization sources frequently used in commercial quadrupole mass analyzers are shown schematically in Figure 1. A sample solution is pumped, typically at flow rates of 2–10 $\mu L\,min^{-1}$, through a fused silica microcapillary (often coated with polyimide), whose end is supported in a stainless steel capillary needle. Charged aerosol droplets are electrosprayed by means of an electrical potential (about 2–5 kV) between the needle tip and a cylindrical counterelectrode (nozzle) and dispersed into the ionization region.[10] Gas-phase macromolecular ions of different charges (cations and anions with different charge numbers) are formed by a process formerly referred to as "field-ion evaporation",[31] which leads to the rapid decrease of droplet size ("nanodroplets") and to desolvation. An important parameter for the desolvation of macro-ions is the small (about 10–100 V) potential difference between the nozzle and a second skimmer-type repeller electrode ("declustering" potential ΔCS[10, 23]).

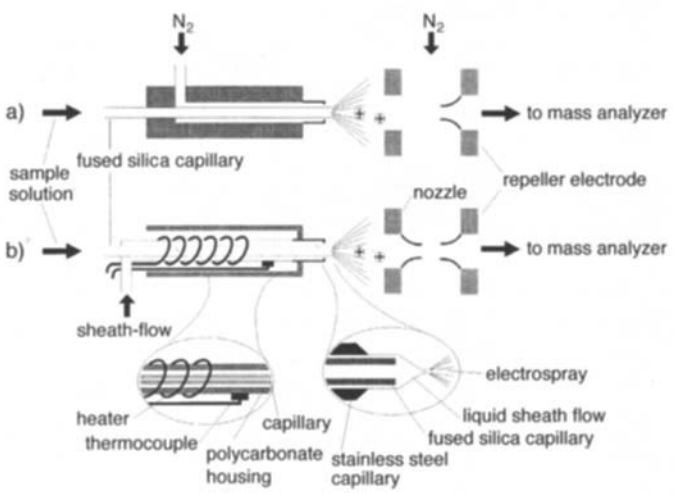

Fig. 1. Schematic representation of electrospray ion sources used in commercial quadrupole mass spectrometers. a) Ion spray source with countercurrent gas (for example, Sciex-API III [30]); b) thermally assisted ESI source without countercurrent gas flow (for example, Vestec A201) [33]. The inserts show a liquid sheath-flow configuration of the inlet capillary (bottom right) [35] and a thermostated capillary heater (bottom left), which controls the temperature of the sample delivery probe to about 20–80 °C [37].

In ionization sources operated at nearly atmospheric pressure and ambient temperature, the desolvation can be assisted pneumatically by ion–molecule reactions by means of a countercurrent flow of an inert "curtain" gas such as nitrogen ("ion-spray" source; Fig. 1a).[30, 32] In a second thermally assisted type of ion source,[33] a nozzle-repeller interface with slight heating of the droplets (typically 40–45 °C) is employed without a countercurrent gas (Fig. 1b). Both ion sources have been used in ESI-MS studies of a wide range of macromolecules and successfully applied to supramolecular complexes. A countercurrent gas was considered to support particularly mild desolvation conditions and has been employed in the majority of studies of noncovalent complexes;[23] however, no advantage of either type of ionization source has yet been demonstrated. An additional coaxial liquid sheath flow through an annular capillary, originally employed to provide suitable interface conditions for online coupling of capillary electrophoresis with ESI-MS,[10, 34, 35, 36] is advantageous for providing specific solution conditions (for example, pH, buffer salts) for the analysis of noncovalent complexes (see Section 2.3). The standard sample delivery probe has been further modified by addition of a thermostated microheater (schematically shown in Fig. 1b).[17c, 24, 37] This probe enables precise temperature control of the inlet capillary to between approximately 20–80 °C and thus provides suitable preconditions to study temperature-dependent equilibria of supramolecular complexes.

Typical features of ESI-MS are illustrated in Figure 2 by the positive ion spectra of bovine ribonuclease A and S, and negative ion spectra of two synthetic oligodeoxyribonucleotides. Acidic aqueous solutions, with an organic cosolvent (for example, 5–10% methanol) to provide stable electrospray conditions, have been widely employed in ESI-MS studies of peptides and proteins.[8, 10, 38] Under these conditions the spectrum of RNase A shows a homogeneous series of multiply protonated molecular ions, with the most abundant $[M+9H]^{9+}$ charge state (Fig. 2a, top). The molecular weight ($M_r = 13682$) is accurately determined from the m/z values for the successive charge numbers.[10, 39] A second ion series of lower abundance is also observed with a mass increment of 98 Da, which is due to a single additional phosphate ion, specifically bound to the S-protein and S-peptide chains of RNase A.[40] The spectrum of RNase S, which comprises the noncovalent complex of the S-protein and S-peptide constituents,[41] in acidic solution (pH 3) shows only the $[M+nH]^{n+}$ ions of the dissociated components; two series of A/B ion doublets (Fig. 2a, bottom) result from the inhomogeneous enzymatic cleavage into the S-peptide (1–19/20) and the S-protein (20/21–124).[42] However, the molecular ions of the intact RNase S complex in aqueous solution at pH 7 have been identified,[43] which is consistent with the known stability of the complex at physiological pH conditions.[44]

In contrast to proteins, oligo- and polynucleotides have mainly been studied by negative ion ESI-MS.[10, 45] The formation of the (formally deprotonated) polyanions is strongly dependent on the counterions present. For example, the spectrum of a 24-mer oligonucleotide recognition sequence of the GCN4 transcriptional activator from yeast,[46] obtained from the purified polyammonium salt,[45] shows a homogeneous series of $[M-nH]^{n-}$ polyanions, indicating complete removal of the ammonium counterions in the desolvation process (Fig. 2b). However, the preparation of homogeneous polyammonium salts is difficult for polynucleotides with increasing chain lengths.[47, 48] The presence of alkali ions leads to the formation of complex molecular ion adducts with strongly decreased sensitivity (see Fig. 2b).[38, 49] Efficient purification techniques to remove contaminating counterions must, therefore, be devel-

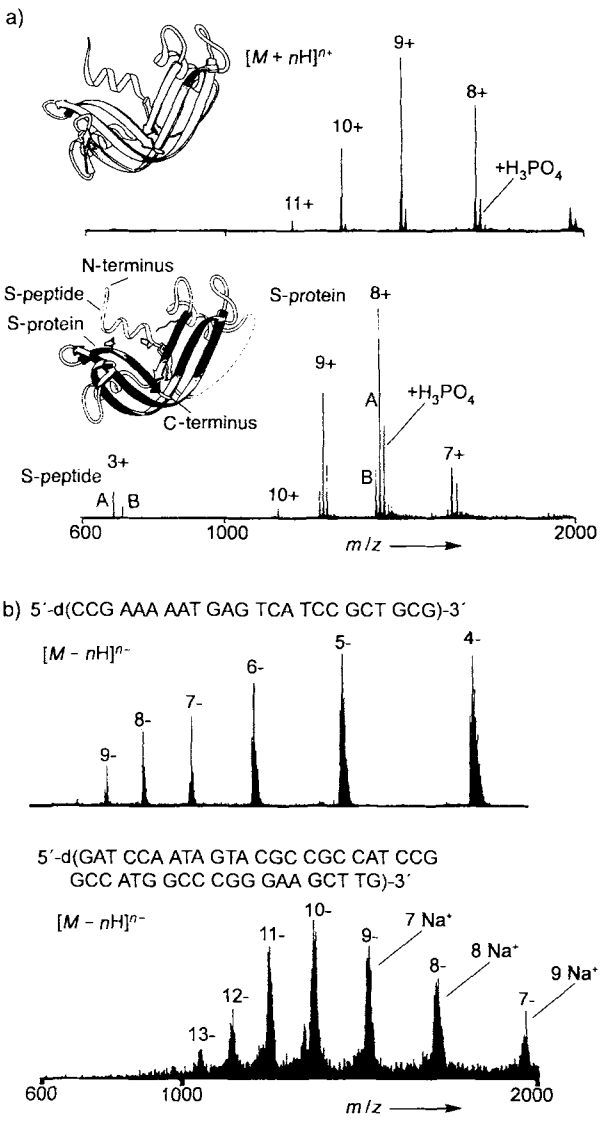

Fig. 2. a) Positive ion ESI mass spectra of bovine RNase A (top; $M_r = 13682$) and RNase S (bottom; $M_r = 11534$) in a mixture of aqueous acetic acid (2%) and methanol (9/1, pH 3). b) Negative ion ESI mass spectra of a synthetic 24-mer oligonucleotide (top, $M_r = 7347$) and a 44-mer (bottom, $M_r = 13504$). Sample solutions of about 0.1 $\mu g \mu L^{-1}$ in acetonitrile: 5 mM ammonium acetate (1/1) (pH 7.5) were introduced through the fused silica inlet capillary with a Harvard microinfusion pump at 4 $\mu L\,min^{-1}$.

oped as a critical step for the analysis of high molecular weight DNA. Accurate molecular weight determinations have so far been limited to sequences of approximately 80 bases.[45, 49]

A qualitative model for the formation of macromolecular ions by electrospray that is compatible with the mechanism discussed by Smith et al.,[23] Fenn,[50] and Röllgen et al.[51] is depicted in Figure 3. The first, generally accepted step in this model is the formation of microdroplets close to the Rayleigh charge limit,[31, 52] which are rapidly reduced to small solvated macro-ions ("nanodroplets"[23]). Coulombic forces in combination with effects of the ESI interface conditions[53] (cf. Fig. 1), analyte charge, temperature, and solvent (solvent proton affinities[54]) have been discussed as major factors influencing the ESI process. A "charge-residue" model, which has not yet been elucidated in detail, has been postulated by Smith et

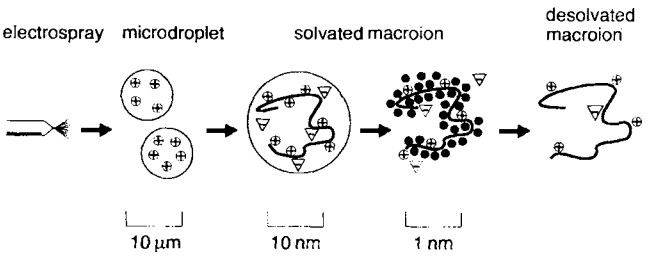

Fig. 3. Schematic representation of macromolecular ion formation from electrosprayed droplets according to the "charge-residue" model of desolvation [23]. ⊕ positive charge sites, ▽ negative charge sites, • solvent molecules. In this example the desolvated ion has a 3 + charge.

al.[23] to explain the formation of desolvated ions. However, direct ion emission from the liquid cone tip (Taylor cone[55]) to which the electrical field is applied has been discussed recently as an alternative mechanism to the original "ion evaporation".[31] This model qualitatively explains the "survival" of noncovalent complexes and is consistent with several features in ESI mass spectra such as remaining specific counterions but removal of other "original" solute components (like NH_3, CH_3COOH).[10, 54, 56] It also appears to be consistent with the observation of charge states and distributions of macro-ions characteristic of structural states in solution (see Section 2.2). Since a rapid adiabatic "cooling" can be assumed to accompany desolvation of charged droplets,[51] the time scale of the ESI process may also suggest that a precondition for observing supramolecular complexes is the maintenance of intact structural elements under kinetically controlled conditions. The still limited experimental approaches to elucidate the ESI mechanism, and their application to the characterization of biomacromolecular structures in solution, are discussed in Sections 2.2 and 2.3.

2.2. Correlation of Charge Structures of Protein Molecular Ions with Tertiary Structures in Solution

Generally, ESI mass spectra show a steady increase of the charge states of ions with increasing molecular weight. The number of charged groups in solution has been found to be a dominant factor determining the maximum charge numbers of macromolecular ions.[10, 38, 57] Initial ESI-MS studies of proteins were mainly carried out with moderately to strongly acidic solutions. Under these conditions, a rough correlation of the number of basic residues (Lys, Arg) with the maximum charge states of protonated ions was observed. However, recent pH-dependent studies provided evidence for a correlation of structural states in solution with the charge distribution ("charge structure"[26]) of multiply protonated molecular ions.[56] As an example, ESI spectra of native hen egg-white lysozyme (HEL) and irreversibly denatured HEL by reduction of disulfide bonds and alkylation are compared in Figure 4. The spectrum of native HEL (Fig. 4a) exhibits a most abundant $[M+9H]^{9+}$ ion and a maximum charge state of 11+, the characteristic charge distribution of the molecular ions showing only little pH dependence.[24, 58] By contrast, the spectrum of the denatured protein shows a significant shift of the ion distribution to higher charge states (Fig. 4b). This result is consistent

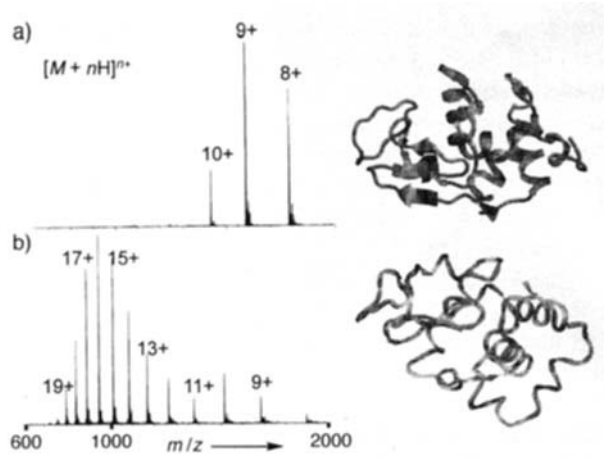

Fig. 4. ESI mass spectra of a) native hen egg-white lysozyme ($M_r = 14307$) and b) DTT-reduced, 4-pyridylethylated lysozyme ($M_r = 15154$) [64]. The structural representations of native and denatured lysozyme were taken from the Brookhaven National Laboratory protein structure data bank. Sample solutions: 0.1 $\mu g \mu L^{-1}$ in a mixture of aqueous acetic acid (2%) and methanol (95/5, pH 3).

with the unfolded, extended surface of the protein as illustrated in Figure 4 by the ribbon diagrams of the tertiary structure.

Similar results have been obtained from comparison of spectra from solutions of native proteins and proteins after denaturation by reduction of disulfide bridges,[10, 59, 60] thermal denaturation,[61] and denaturation induced by solvent changes.[62] Furthermore, they are in agreement with ESI-MS determinations of the extent of deuterium exchange of labile protons, which yield characteristic differences of deuterium incorporation for native and denatured proteins.[58, 63] For example, approximately 50% of the labile H were exchanged for D in the native HEL, but nearly 90% for the reduced protein after 4 hours deuteration in aqueous D_2O.[60, 64] Results of deuterium incorporation for several model proteins are summarized in Table 1 and are in good agreement with NMR data of H/D exchange kinetics of rapidly exchangeable protons.[65] Moreover, ESI-MS studies of exchange kinetics over extended periods, initially carried out by Katta and Chait with bovine ubiquitin,[63] revealed a substantial proportion of slowly exchangeable protons, which is also consistent with NMR data of nativelike protein structures in solution.[65, 66] Additional information on the relationship between solution structures and desolvated molecular ions has been derived from H/D exchange studies of ions from native and denatured proteins in the gas phase, which show opposite reactivities (Table 1). The higher deuterium incorporation for ions of native proteins was explained by Coulomb effects in the compact native structure.[67, 68]

The present model studies clearly indicate that tertiary structure states in solution are reflected in the charge structures of gas-phase molecular ions. However, they do not provide evidence for conservation of tertiary structures in molecular ions in the gas phase.[23] More detailed information about structures of gas-phase macromolecular ions may be derived from charge structures and localization of charge sites on macro-ions by chemical reactions in situ in a reaction system consisting of two ESI capillaries (Y-tube[10, 36]), and by employing the sheath-flow inlet system[36, 69] (cf. Fig. 1). For reactions of proteins with triethylamine or similar bases a significant reduction in the charge numbers on the molecular ions was demonstrated. This observation is well explained by proton transfer; for example, a shift from the 18 + charged ion to a most abundant $[M+9H]^{9+}$ ion was observed for myoglobin.[10, 70]

An alternative approach for probing tertiary structure differences in solution is the comparative ESI-MS analysis of protein derivatives obtained by selective chemical modification.[24, 71] Acylation of lysine- and N-terminal amino groups was used to neutralize basic protonation sites selectively in proteins with known structures, and the extent and sites of partial modifications were identified by molecular weight determinations and mass spectrometric peptide mapping analysis.[60] The charge distributions of molecular ions of partially acetylated RNase A are similar to those of the native protein; in contrast, a significant charge reduction was found upon succinylation.[60] On H/D exchange similar extents of deuterium were incorporated in partially modified and native proteins (see Table 1), and no structural differences between the protein derivatives were detected by ORD/CD spectra.[72] Furthermore, ESI spectra of acetylated myoglobins (Myo) provided the molecular ions of the intact heme–protein complexes under mild desolvation conditions (see Fig. 6). Direct evidence for the conservation of tertiary structures has been recently obtained for partially acylated derivatives of the ion-channel protein porin from *R. capsulatus* by mass spectrometry and X-ray crystallography; a tetrasuccinylated porin was crystallized as an intact trimeric complex isomorphous to the native protein.[73] An example showing that charge structures of molecular ions can reveal even detailed structural differences in solution is the selective modification of arginine residues by 1,2-cyclohexanedione, which yields N^7,N^8-(dihydroxycyclohexanediyne) adducts (DHCH-Arg)[24, 71] (Fig. 5). The DHCH-Arg modification of

Table 1. H/D exchange studies by ESI-MS of native and denatured proteins in solution and in the gas phase.

H/D exchange in solution [a]				gas phase H/D exchange [b]			
protein	state	%D [c]	Ref.	protein	state	%D [c]	Ref.
lysozyme	native	52	[60]	proinsulin	native	17	[68]
lysozyme	reduced +4VP-alkylated [d]	89	[64]	proinsulin	reduced	9	[68]
lysozyme	glycine-amidated [e]	54	[64]	α-lactalbumin	native	45	[68]
lysozyme	glycine-amidated +4VP-alkylated	86	[64]	α-lactalbumin	reduced	36	[68]
cytochrome c	native	48	[63]				
cytochrome c	denatured	91	[63]				

[a] H/D exchange reactions performed for 12 h at 20 °C in D_2O / 1% deuteroacetic acid. [b] Gas-phase H/D exchange at experimental conditions described in ref. [68]. [c] % of labile protons deuterated. [d] Lysozyme after DTT-reduction and alkylation with 4-vinylpyridine. [e] Lysozyme carboxamidated by carbodiimide / glycine-methylester coupling [64].

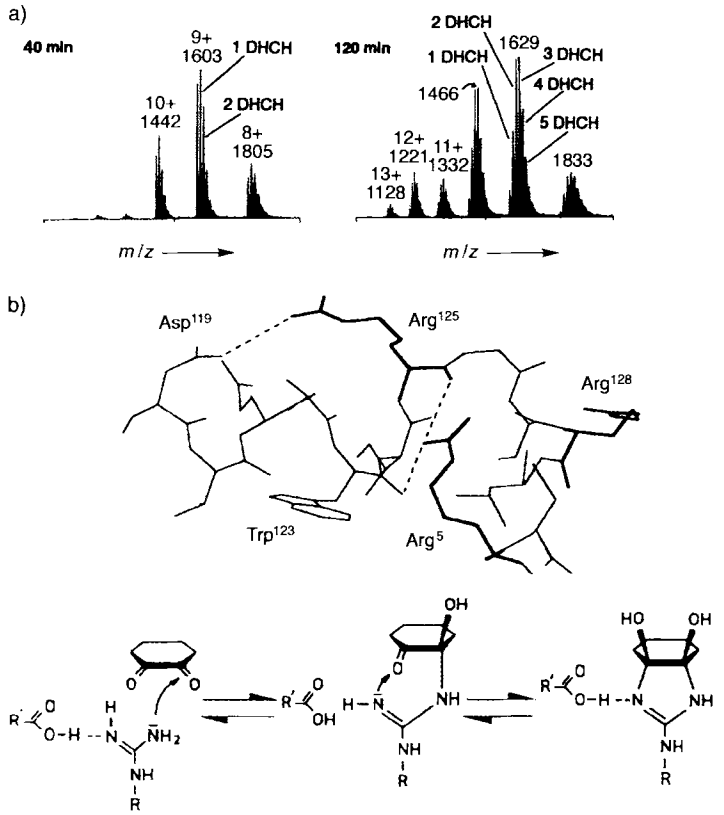

Fig. 5. a) ESI mass spectra of DHCH-Arg-modified hen egg-white lysozyme (HEL); b) tertiary structure of HEL around the Arg-5 and Arg-125 residues and reaction pathway of the arginine modification by 1,2-cyclohexanedione. Native HEL was treated with a 50-fold excess of 1,2-cyclohexanedione in sodium borate (pH 8.5) and protein derivatives isolated at different time intervals [71]. The solvent used for the ESI-MS analysis was a mixture of aqueous acetic acid (2%) and methanol (95/5). From ref. [71].

lysozyme, monitored directly by ESI-MS, showed molecular ion distributions of protein derivatives identical to that of native HEL until four specific Arg residues were modified.[24] All four Arg residues modified under these conditions were found to have suitable intramolecular proton acceptor residues in their microenvironment[71] (shown in Fig. 5b by the partial structures around Arg^5 and Arg^{125} residues). By contrast, ESI spectra of protein derivatives with a higher extent of modification (obtained after extended reaction times) showed additional higher charge-state ions, indicative of gradual unfolding and denaturation (Fig. 5a).

These initial results indicate that further studies probing the effect of defined chemical modifications of structures in solution on electrosprayed molecular ions might be useful. In situ chemical and enzymatic reactions of proteins using the sheath-flow system for delivery of reactant solutions (cf. Fig. 1) can be employed in model studies under conditions similar to those in physiological solutions.[24] An example is the pH-dependent renaturation and formation of the intact heme–protein myoglobin (Fig. 6), one of the first noncovalent complexes detected by ESI-MS.[10, 74] At pH 6, the intact heme–Myo complex is identified by a most abundant $[M+9H]^{9+}$ ion, whereas under increasingly acidic conditions (pH 4) partial dissociation of the complex leads to the doublet series of multiply protonated heme–protein (HP) and apoprotein (AP) ions; at pH 2 only high charge-state ions of AP are observed together with the ion (m/z 616) of the Fe^{III}–porphyrin prosthetic group (Fig. 6a–c). Nearly identical molecular ion distributions were found under comparable solution conditions for the isolated apoprotein. The most abundant peak for the renatured AP was also $[M+9H]^{9+}$ at pH 6 (Fig. 6d–f). In situ reconstitution with a heme–porphyrin solution finally yielded the $[M+9H]^{9+}$ ion of the intact heme–protein (Fig. 6g).

These results and further model studies provide strong evidence for a correlation between charge structures of ions in ESI-MS and solution structures of noncovalent biopolymer complexes.[23, 24] It must be borne in mind that mainly highly charged ions within the mass range of quadrupole analyzers have been studied so far. Thus, the characterization of ions with low charge state (high m/z) and their possible energy differences and higher stabilities of the supramolecular complexes should be interesting in further studies[75, 76] (see Section 3.2); the required ESI sources suitable for time-of-flight and magnetic sector instruments have recently become available.[77]

2.3. Preconditions for the Characterization of Supramolecular Complexes

In addition to the instrumental conditions described in Section 2.1, several analytical preconditions must be fulfilled to enable the direct characterization of supramolecular complexes of biomacromolecules: in particular, specific complexes and unspecific aggregation products must be distinguishable, as well as noncovalent complexes and covalent adducts. The formation of unspecific association products may, in principle, occur in solution or under the electrospray conditions. Corresponding artifact ions (for example, dimeric "cluster ions") are formed with other ionization methods such as FAB-MS and MALDI-MS,[5, 9, 11] but have not been observed by ESI-MS at typical sample concentrations (micromolar solutions).[10] Unspecific association products in ESI spectra of biomacromolecules have been observed with different solution components such as buffers, surfactants, and counterions.[10, 76] The ion abundances of such adducts depend mainly on their relative binding strengths (for example, for hydrophobic interactions in proteins; see Section 3.2 with examples of leucine zipper polypeptides). An analytically relevant example of adducts of lysozyme with sodium dodecylsulfate (SDS) is shown in Figure 7. Adduct ions with up to ten dodecylsulfate anions, leading to a substantial shift of charge distributions and overlapping of protonated molecular ions, have been found at low SDS concentrations.[78] In the light of the broad application of SDS-gel electrophoresis (SDS-PAGE) for protein separation, contamination by SDS and suitable purification techniques are of importance for ESI-MS analyses of proteins. While only little success has been achieved with classical purification techniques (for example, ion-pair extraction),[45, 79] an efficient isolation procedure by direct electroelution from SDS-PAGE has been recently developed for ESI-MS of proteins.[79]

Noncovalent complex formation, for example, between enzyme and specific substrate or inhibitor components, was detected in initial model studies by a specific increase in molecular weight for the complex ions (see Section 3.1).[23]

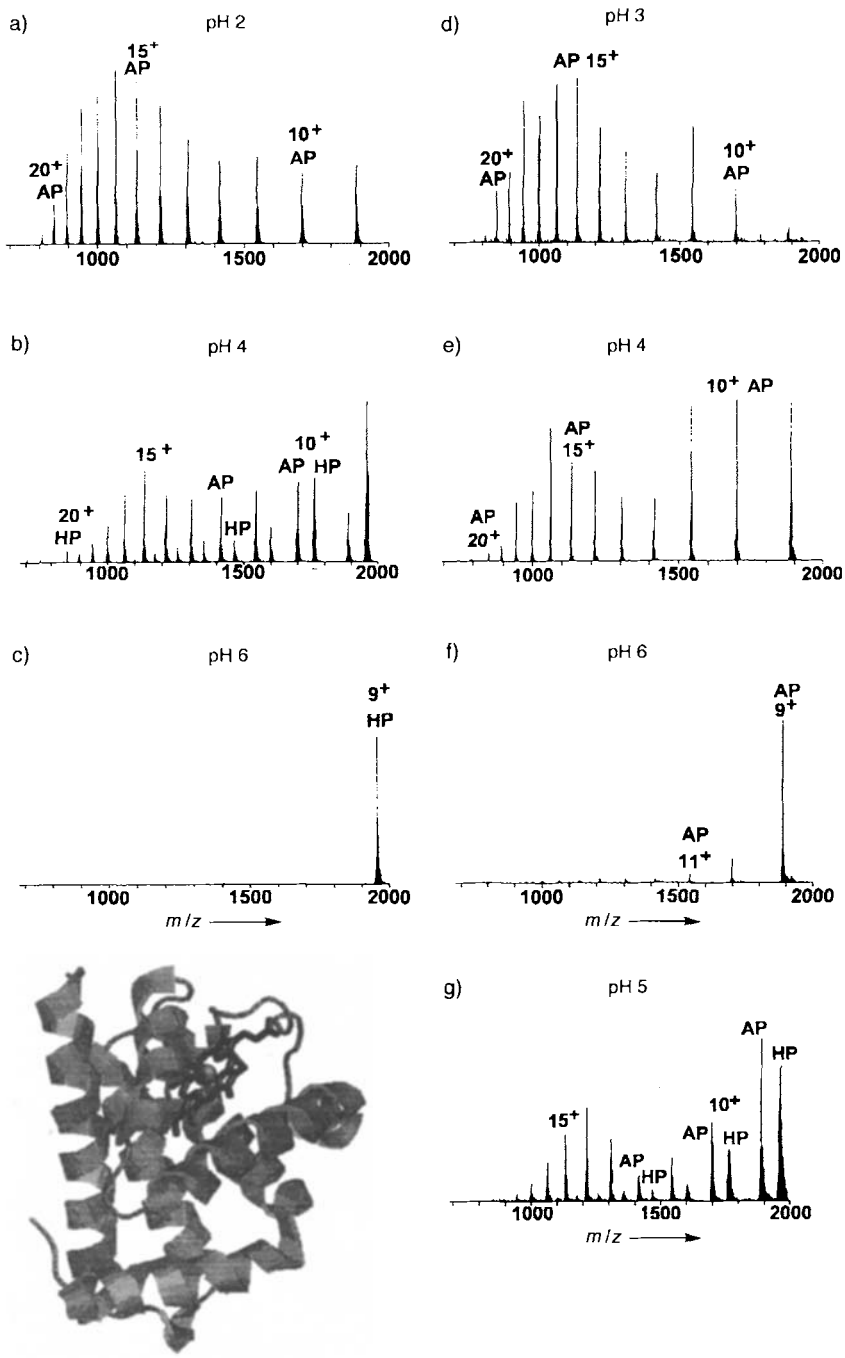

Fig. 6. ESI mass spectra of heme–protein complex of horse heart myoglobin (HP) at several pH values (left) and pH-dependent renaturation of apoprotein (AP, right). a)–c) Spectra after dissociation by acidification with acetic acid/ammonium acetate (5 mM) buffer; d)–f) spectra after renaturation of the apoprotein (ammonium acetate); g) spectrum after reconstitution of heme–myoglobin by addition of heme–porphyrin (pH 5). The solvent used was a mixture of ammonium acetate (5 mM) and methanol (95/5). The representation of the compact tertiary structure of the intact heme–protein (bottom left) was obtained from the Brookhaven National Laboratory crystallographic data base. From ref. [24].

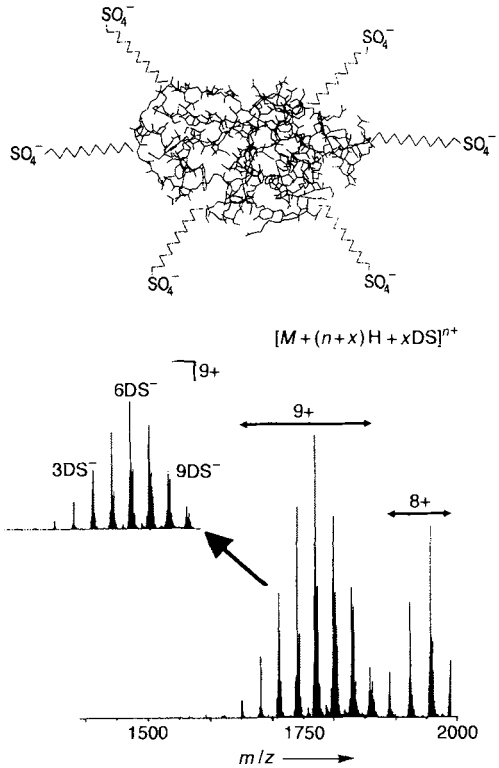

Fig. 7. Top: Structural model of a complex of HEL with six dodecylsulfate ions (DS). Bottom: ESI mass spectrum of dodecylsulfate-contaminated HEL isolated from SDS-polyacrylamide gel electrophoresis by electroelution [79] and expansion of the series of 9+ charged $[M+(n+x)H+xDS]^{n+}$ ions. Solvent: a mixture of acetic acid (2%) and methanol (9/1).

However, the unequivocal distinction between specific noncovalent interaction and covalent binding may be considerably more difficult in analytical applications and may require the detailed characterization of structure and binding mechanism of the complex. The ESI-MS analysis of the complexation of HEL with oligosaccharide substrates and with structural analogs that are inhibitors illustrates this problem.[80] The reaction of HEL with the substrate, hexa-β-(1–4)-*N*-acetylglucosamine (NAG_6), was monitored directly by ESI-MS and revealed the rapid formation (and subsequent disappearance) of the enzyme–substrate complex ions ($M_r = 15542$). During the reaction ions were detected that were attributable to a complex of HEL with the tetraglucosamine hydrolysis product (NAG_4), which binds with a similar affinity to the active hydrolytic site of the enzyme.[81] Competition experiments with several oligosaccharide substrates known to bind at different subsites of the hydrolytic center[72,82] and with a high-affinity inhibitor (oligo-*N*-acetylchitotetraose) provided evidence for the formation of specific noncovalent complexes. Furthermore, the enzyme–substrate complex in this study could be completely dissociated (that is, abundances of complex ions diminished) by using stronger desolvation conditions (increasing declustering potential ΔCS). However, a different behavior was observed in a study of oligosaccharide complexes with a lysozyme mutant in which one of the active-site residues, Asp-52, had been replaced by Ser (D52S-HEL), resulting in a complete loss of enzymatic activity albeit comparable nonproductive substrate binding.[83] The D52S mutant yielded complex ions with the NAG_6 substrate and the NAG_4 product that could not be dissociated by changes of solvent or ion-desolvation conditions (Fig. 8). Based on the molecular

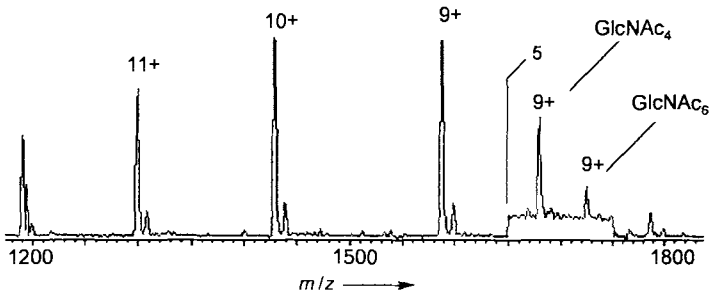

Fig. 8. ESI mass spectrum of adducts of the lysozyme mutant, D52S-HEL with oligo-β-(1-4)-*N*-acetylglucosamine. The expanded peaks are attributable to the $[M+9\,H]^{9+}$ ions of the HEL-$GlcNAc_4$ and HEL-$GlcNAc_6$ adducts. From ref. [83].

weight identified, a covalent complex by formation of a hemiacetal between the Ser-52 residue and the reducing sugar bond of the product (NAG_4) at the active subsite was proposed.[83, 84]

The unequivocal differentiation of noncovalent and covalent macromolecular complexes by molecular weight determination may be difficult with low resolution quadrupole mass analyzers and may require additional chemical studies and/or separation techniques to complement the ESI-MS analysis. The formation of both a noncovalent complex and covalent adducts has been identified in a recent study of the binding of glutathione (GSH) to a recombinant bacterial glutathione-S-transferase (GST) expressed in *E. coli*.[85] ESI spectra of GST after isolation by affinity chromatography on GSH-sepharose in the presence of GSH revealed two major series of molecular ions indicating the addition of two and three GSH molecules to the protein (Fig. 9, center).[86] A substantial part of the bound GSH could not be removed by dialysis; a homogeneous series of $[M+nH]^{n+}$ ions and exact molecular weight of the free enzyme ($M_r = 26\,898$) was obtained only after repeated reduction with dithiotreitol (DTT) and dialysis (Fig. 9, bottom). Mass spectrometric peptide mapping analyses identified the covalent adducts as mixed disulfides (for example, linked through the Cys-138 residue;[16, 86] see Fig. 9, top).

Table 2 summarizes experimental parameters and criteria for the identification of noncovalent complexes and their effects on the ion formation in ESI mass spectra. An essential precondition is a specific or at least predominant stoichiometry of the complex ions in comparison to the ions of the components in solution. The complex formation may be modified by changing the stoichiometry of solution components, and by modification of the ESI-MS conditions (interface temperature; declustering potential).[23] However, further evidence can be obtained by competition experiments with different complex components, and by analysis of the specificity of pH or concentrations changes. Changes of solution conditions may significantly influence the ion formation in ESI spectra, for example, by changes of the charge-state distributions. Equilibria of complex formation have been quantitatively characterized by means of ion abundance ratios in most recent studies (see Section 3.1). Thus at present, comparison with conventional analytical techniques such as ultracentrifugation and native gel electrophoresis is still important for the analysis of noncovalent complexes by ESI-MS.

Several recent studies have demonstrated that the modification of the electrospray conditions for the desolvation of ions and collision-induced dissociation can be effectively used to determine the gas-phase stability of ions of noncovalent complexes and to identify possible artifact products.[10] Important parameters of ESI-MS that affect the conservation of noncovalent complexes are the type of countercurrent gas, the temperature of the ionization chamber, and the residence time of the ion (extraction potential) in the desolvation region.[23, 24] Mild desolvation conditions enable a direct identification of solvent ad-

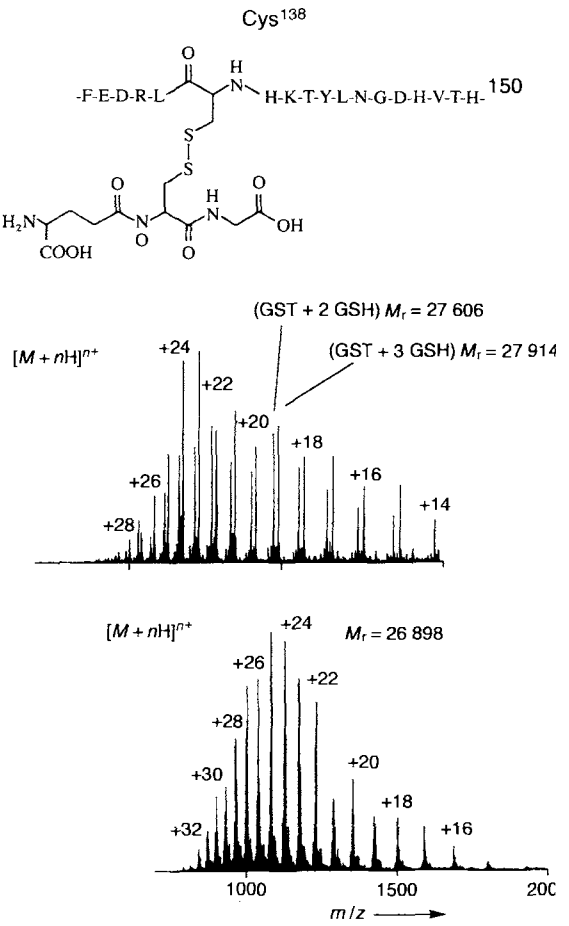

Fig. 9. ESI mass spectrometric characterization of recombinant glutathione-S-transferase (*S. japonicum*), expressed in *E. coli* and isolated by affinity chromatography on glutathione-sepharose. Top: The partial sequence of the tryptic peptide with the Cys-138-mixed glutathionyl disulfide adduct identified by proteolytic digestion and mass spectrometric peptide mapping [86a]. Center: Spectrum of GST isolated in the presence of excess GSH. Bottom: Spectrum of GST ($M_r = 26\,898$) obtained after DTT-reduction and repeated dialysis.

Table 2. Criteria and ESI-MS parameters for the identification of supramolecular complexes.

Criteria indicating the presence of noncovalent complexes	ESI-MS techniques for complex dissociation
specific complex stoichiometry/ equilibrium of complex components	change of solution stoichiometry increase of interface temperature increase of declustering voltage ΔCS
competition of complex components	chemical modification, specific mutation of components
specificity of solution conditions	pH change, change of buffer, concentration change
gas-phase stability of complex ions	increase of declustering voltage, collision-induced dissociation (countercurrent gas)

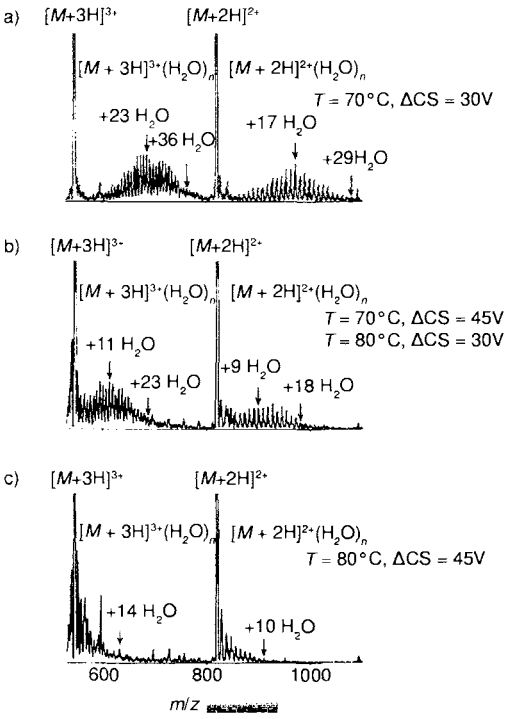

Fig. 10. ESI mass spectra of somatostatin ($M_r = 1638$) and water adducts at different temperatures T and declustering voltages (a–c). The major offscale peaks represent the nonsolvated doubly and triply protonated molecular ions. From ref. [23].

ducts. In one example, up to 40 H_2O molecules were observed in the spectrum of adducts of the polypeptide somatostatin and water under conditions of incomplete desolvation (Fig. 10). These adducts could be dissociated by increasing the ΔCS potential or by increasing the interface temperature.[23, 87] Thus, the lowest possible ΔCS potential appears to provide the mildest conditions for the survival of macromolecular complexes; high ΔCS values (> 100 V) have been shown to induce fragmentation of even covalent bonds.[10, 24]

3. Applications of Electrospray Mass Spectrometry to the Characterization of Supramolecular Complexes of Biomacromolecules

3.1. Protein Complexes with Low Molecular Weight Ligands

The first applications of ESI-MS to the characterization of noncovalent protein complexes with low molecular weight ligands were reported within a short period of time.[23, 88, 89] Examples of complexes with ligands such as enzyme substrates, cofactors, and inhibitors, the protein:ligand stoichiometries, and the charge states of specific complex ions are summarized in Table 3 (see also Figures 6 and 9). The complexes hitherto identified encompass different binding types such as ionic and hydrogen bonds, coordinative binding, and predominantly hydrophobic interactions. Furthermore, the wide range of dissociation constants for complexes of known structures and binding properties (about 10^{-11}–10^{-7} M) suggests a broad potential for applications of ESI-MS.

In most proteins examined so far the molecular weight differences between protein and protein–ligand complexes have been

Table 3. Protein complexes with low molecular weight ligands identified by ESI-MS.

Protein	M_r [a]	Ligand	Complex			Ref.
			M_r [b]	Charge [c] state	Stoichiometry [d]	
rubredoxin	5937	Fe^{III}	5989	4+	1:1	[90]
ferredoxin	10828	$Fe^{III}S$	11178	4+	1:4	[90]
HIV-nucleocapsid	6444	Zn^{II}	6576	6+	1:2	[91]
lysozyme	14305	$GlcNac_6$ [e]	15544	8+	1:1	[88]
lysozyme	14305	TACL [f]	15136	8+	1:1	[88]
myoglobin	16951	Fe-heme	17568	9+	1:1	[24, 72]
ras-oncogen [g]	18852	GDP	19295	9+	1:1	[89]
HIV-1-protease [h]	10747	JG-365 [i]	22345	10+	2:1	[92]
aldose-reductase	35779	NADPH	36527	33+	1:1	[93]

[a] Molecular weight of apoprotein form. [b] Average molecular weight determined from $[M+nH]^{n+}$ ions of protein complex. [c] Charge state of most abundant $[M+nH]^{n+}$ ion of complex. [d] Protein:ligand stoichiometry determined. [e] Hexa-*N*-acetylglucosamine. [f] Tetra-*N*-acetylchitotetraose-δ-lactone. [g] Recombinant human ras-oncogen (1–166) sequence. [h] Synthetic [$Aba^{67, 95}$]-HIV-1 protease [94]. [i] Synthetic peptide inhibitor, (Ac-Ser-Leu-Asn-Phe-ψ[CH(OH)CH_2N]-Pro-Ile-Val).

sufficiently large to enable the unequivocal determination of molecular weights (charge numbers) and complex stoichiometries (see Table 3). However, the accuracy and resolution of the mass determination amenable to quadrupole instruments limit the analysis of high molecular weight proteins (greater than about 50000 Da). Such applications may require high-mass analyzers or instruments providing isotopic resolution (see Section 3.2). Despite these limitations, specific complexes have been identified for a number of model proteins, such as heme–proteins and complexes with oligonucleotide cofactors. Some examples also demonstrated the ability of ESI-MS to characterize more complex binding structures that have not been accessible by conventional methods, such as the complexation of two Zn^{II} ions at two binding sites of the HIV-nucleocapsid polypeptide.[91] An interesting application has been reported by Baca and Kent in studies of synthetic peptide inhibitors of the HIV-1 protease.[92] A synthetic mutant ($Aba^{67}C$, $Aba^{95}C$; see Table 3) of the HIV-protease was shown by the specific molecular ions to form a ternary protease–inhibitor complex comprising two protein subunits and the peptide inhibitor.[95] This result revealed the active, *dimeric* form of the enzyme, which contributes one aspartate residue of each subunit to the catalytic center.[96]

In nearly all protein complexes studied so far, the charge-state distributions of complex ions shift to substantially lower charge (higher m/z) numbers than those observed for the free protein[23] (see Table 3). Corresponding "neutralization" effects have been found for biopolymer complexes, for complexes with low molecular weight ligands, as well as for synthetic supramolecular complexes. For instruments with limited m/z range, this effect may lead to significant problems in the detection of the most abundant complex ions.[24] (see Sections 3.2 and 3.3). As little is known about the effect of complex formation on the charge structure of protein ions from conventional analytical methods, systematic model studies by ESI-MS are required. Furthermore, in some protein complexes with metal ions as ligands it is difficult to identify the oxidation state of the ligand from the charge distribution of complex ions (that is, to ascertain whether the charge state observed was modified under the electrospray conditions).[23, 88] In a study of protein–iron complexes van Dorsselaer et al. obtained exact mass determinations of protonated molecular ions, which identified the Fe^{III}–

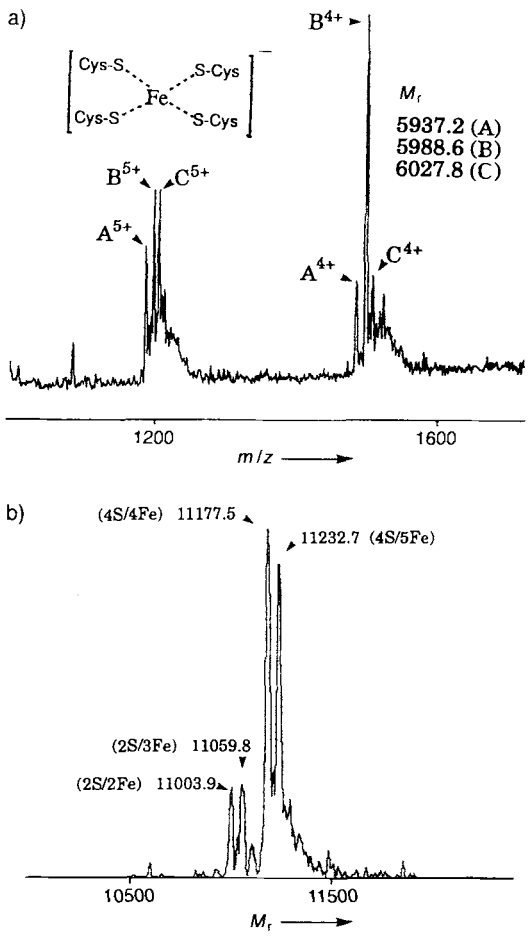

Fig. 11. ESI mass spectrometric identification of protein–iron–cysteine thiolate complexes. a) Spectrum of rubredoxin in H_2O/methanol (1/1). A = aporubredoxin, B = holorubredoxin, C = holorubredoxin–potassium adduct. b) Reconstructed spectrum of complexes of ferrexodin and the ferric ion after transformation to the mass scale. From ref. [90].

rubredoxin complex with four cysteine-thiolate ligands and the tetraferritetrathiolatoferredoxin complex (Fig. 11); the charge numbers present in the molecular ions of these complexes clearly reflected the authentic oxidation states in solution.[90] By contrast, oxidation of Fe^{II} to Fe^{III} porphyrin under the ESI-MS conditions has been suggested for the heme–protein complexes of the α- and β-chains of hemoglobin.[88a]

The aim of ESI-MS analyses of protein complexes so far has primarily been the qualitative identification of the specific complex ions. Only a few initial studies of the pH-, temperature-, and concentration-dependence of complex formation have been carried out, as exemplified by the pH-dependent spectra of myoglobin (Fig. 6) and the characterization of the RNaseS complex.[24, 43] The mass spectrometric determination of thermodynamic stabilities and complex formation constants in solution (as estimated by Ogorzalek-Loo et al. for RNaseS[43]) are only at the initial stage. However, first investigations suggest such applications for ESI-MS. For example, the formation constants of crown-ether ([18]crown-6) complexes with alkali metal ions have been directly determined from intensity ratios in the ESI mass spectra of the complex ions and agree well with published data; furthermore, the intensities of the complex ions correlated with the solvation energies of crown-ether complexes.[97a] Likewise, the formation constants for complexes of crown-ether modified peptides with alkali metal ions obtained from the molecular ion intensities in ESI-MS agreed with those obtained by calorimetric methods.[97b] These most recent results indicate that the further development of ESI-MS for the quantitative determination of equilibrium constants for noncovalent complexes is promising, for example, by using crown-ether derivatives for selective "ion-labeling".[97]

3.2. Identification of Supramolecular Protein Complexes

As pointed out in Section 2.3, the identification of supramolecular complexes requires the differentiation of specific complex ions from unspecific noncovalent association. Initial studies on proteins have, therefore, been carried out on dimers of known structure that lead to the formation of specific molecular ions (in contrast to unspecific oligomeric "cluster" ions in FAB and MALDI spectra[5, 11]). The principle for the identification of dimeric complexes by a multiply charged ion series is schematically shown in Figure 12 for a leucine zipper protein. Generally, an oligomer composed of identical polypeptide chains is unequivocally identified by a molecular ion with a non-integer charge number when divided by the number of complex components.[24, 45b] Therefore, all leucine zipper homodimers are characterized by odd charged molecular ions; an identical principle applies to duplex-oligonucleotides from single strands with identical base composition (see Section 3.3).

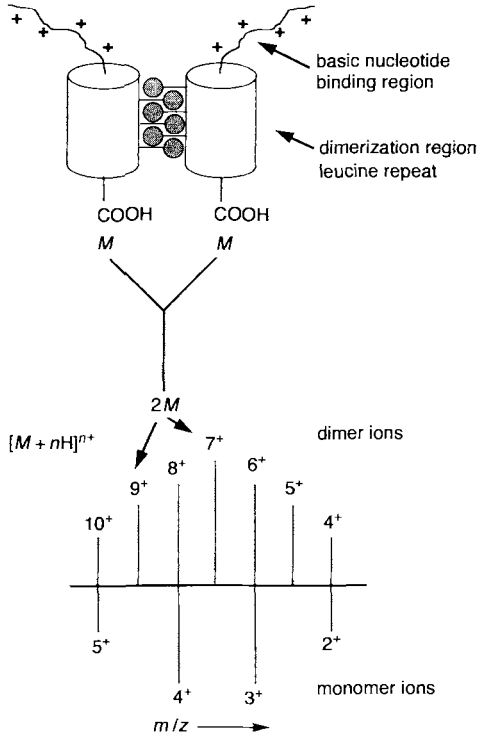

Fig. 12. Schematic structure of leucine zipper polypeptides, and principle of the identification of homodimers by odd-charged $[M + nH]^{n+}$ ion series. The even-charged ions of the dimer are superimposed by the corresponding ions of the monomer (shown downwards) on the m/z scale.

Several classes of leucine zipper proteins have attracted interest recently because of their significance in transcription regulation as well as their structure and specificity in DNA recognition, which has not been elucidated in detail.[98, 99] Leucine zipper structural elements, consisting of regular heptad repeats of leucine residues followed by basic DNA-binding units (see Figures 12 and 13), have been identified in a number of transcription activator proteins[46] and recently in ribosomal RNA-binding proteins.[100] Probably the best known leucine zipper is the GCN4 transcription activator from yeast (GCN4-leucine zipper[46]), which consists of a double-stranded α-helical coiled coil with a 4–3 heptad sequence of hydrophobic and polar residues. Although binding of a specific DNA sequence (palindrome-nucleotide; see Figure 17) has been shown to induce the dimerization and to stabilize the complementary protein conformation,[98, 101] stable dimers of leucine zipper polypeptides have been prepared.[102] Several leucine zipper polypeptides have been characterized by spectroscopic methods (CD, NMR[102, 103]) and the GCN4 sequence by X-ray crystallography.[104] However, since many structural details and general prerequisites for the specificity of protein–nucleotide complexes are still unresolved, the possibility of a direct mass spectrometric characterization has found considerable interest.

First ESI mass spectra of dimeric complexes have been reported by Li et al. for a synthetic leucine zipper peptide.[105] Specific odd-charge $[M+5H]^{5+}$ and $[M+7H]^{7+}$ ions of the dimers could be detected; however, their intensities are low relative to the most abundant even-charged ions of the monomer, which suggests that the stability of the complexes with hydrophobic interactions is low under the ESI conditions. Their identification, however, was ascertained by tandem-ESI-MS analysis upon collision-induced dissociation of the $[M+5H]^{5+}$ ions.[106] Systematic studies based on the sequences of naturally occurring coiled coils have been carried out on a series of synthetic polypeptides containing both leucine zipper dimerization regions and the basic DNA-binding regions.[24, 107, 108] The ESI spectrum of a GCN4 polypeptide at low declustering potential ($\Delta CS \approx 5$–10 V, Fig. 13) displayed an intense peak for the 5+ charged molecular ion of the dimer (M_2) at m/z 1616 ($M_r = 8078$, $(2\times4039+5)/5 = 1616.6$). The ions at m/z 1347 and 1010 can originate from either the monomer or the dimer ($M^{3+}/(M_2)^{6+}$ and $M^{4+}/(M_2)^{8+}$, respectively; see also Fig. 14). The $[M+5H]^{5+}$ ion of the dimer completely disappeared upon dissociation at higher ΔCS (60 V), thus confirming the noncovalent complex; the intensities of the 3+ and 4+ ions of the monomer remained unchanged (Fig. 13, bottom right). In accord with these results, the intensities of the dimeric ion increased at higher concentration (about 100 μM), whereas a change in the temperature of the inlet capillary (30–70 °C) showed only little effect on the monomer/dimer ratio.[108a] Under the conditions employed the dimer could not be formed quantitatively; subsequent studies attributed this to partial dissociation of leucine zipper complexes at the polar capillary surface.[108]

The success of ESI-MS in characterizing supramolecular leucine zipper complexes could be demonstrated in further studies on "coiled coil" polypeptides, one of which ("coil-Ser", see Fig. 14) forms a triple-standed coiled coil according to its crystal structure.[109] Trimeric complexes of "coil-Ser" and related

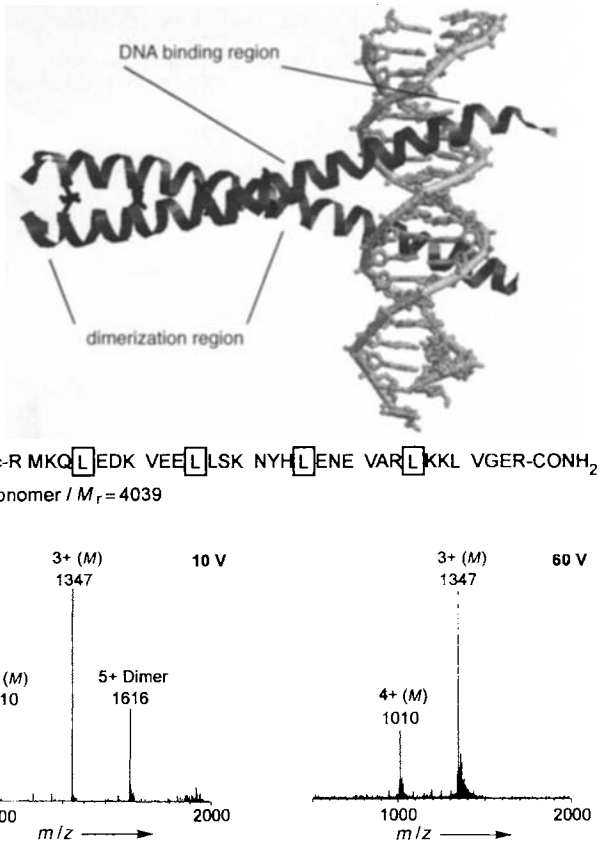

Fig. 13. Bottom: ESI mass spectra of leucine zipper polypeptide GCN4-p1 at 10 V (left) and 60 V (right) declustering voltage. The 5+ charged molecular ion of the homodimer is only observed at ΔCS = 10 V. Spectra were obtained by injection of 5 μL of a 50 μM peptide solution in a solvent mixture of ammonium acetate (2 mM) and methanol (9/1) with pH 6. Top: The structure of the GCN4 leucine zipper protein is taken from the Brookhaven National Laboratory data base (from Ref. [46]).

polypeptides were identified by ESI-MS by their specific $(M_3)^{5+}$ ions, and their presence was confirmed by sedimentation equilibrium analysis.[107] Moreover, the analytical potential of ESI-MS was demonstrated recently by the first identification of homo- and heteromeric complexes in hybridization experiments of polypeptides comprising different sequence variants.[107, 108a] As example, Figure 14 shows ESI mass spectra of an equimolar mixture of two sequence variants (LZ/LZ12A; LA) in which ions characteristic of the heterodimer, AL^{4+}, and both possible heterotrimers, ALL^{5+} and AAL^{5+}, were detected in addition to the homomeric complexes. In contrast to the ESI mass spectra obtained with a quadrupole mass analyzer (Fig. 14a), isotopic resolution and direct assignment of the dimeric and trimeric complex ions was achieved on a double focusing magnetic sector instrument (Fig. 14b).[108a] Thus, the 4+ charged homodimer ion and the 2+ charged monomer were differentiated directly by the mass differences of the isotopic multiplets at m/z 1633 and 1654 ($\Delta m = 0.25$). Likewise, the trimeric $(M_3)^{5+}$ complex ions were ascertained by the correct isotopic distribution ($\Delta m = 0.2$). Under these conditions it was even possible to demonstrate that hybridization of GCN4-polypeptide and "coil-Ser" leucine zippers produced both dimeric and trimeric heteromers,[107] consistent with the results of spectroscopic studies of fluorescence-labeled polypeptides.[110]

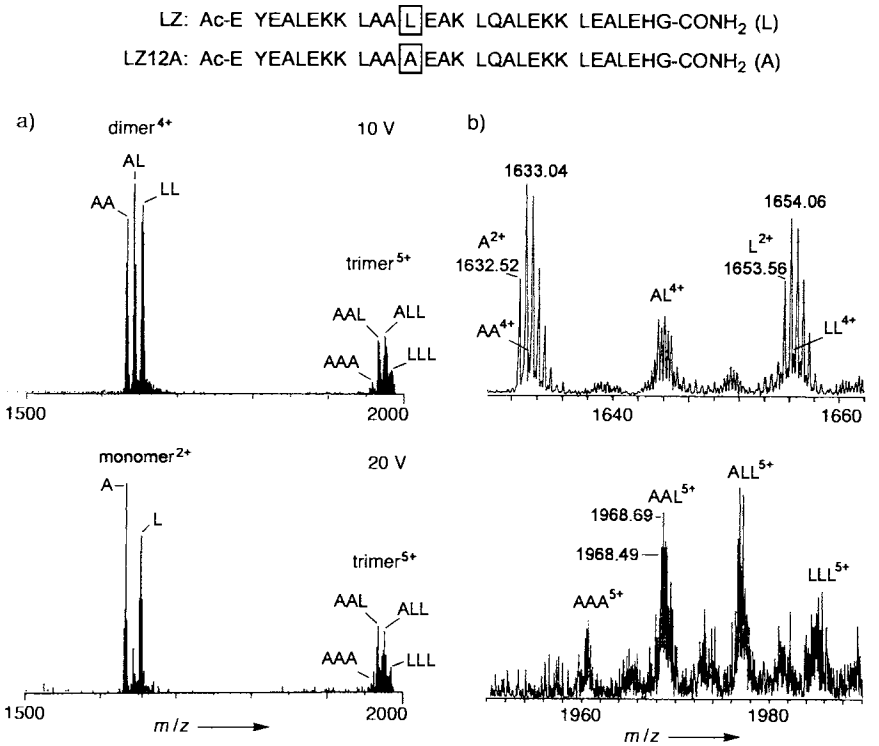

Fig. 14. ESI mass spectra of dimeric and trimeric heteromers obtained from an equimolar mixture (0.1 mM) of peptides LZ and LZ12A [108a]. a) Spectra of dimeric (4+) and trimeric (5+) complexes recorded with a quadrupole mass spectrometer at $\Delta CS = 10$ V (top) and 20 V (bottom). b) Spectrum of dimers (top) and trimers (bottom) on a magnetic sector-field instrument at a mass resolution of about 7000, showing the isotopic resolution for the 4+ and 5+ charged complex ions.

Dimeric complexes of several other DNA- and RNA-binding proteins have been recently characterized by ESI-MS, for instance the RNA-binding autoantigen L7[100] and the nuclear matrix protein SAF-A.[111] A further application has been found in the structure elucidation of the lipid-analogue SP-C protein from lung surfactant, which exerts important biochemical functions in the lung alveolar system.[112–114] A recombinant variant has been developed for the therapy of respiratory distress syndrome.[115] The SP-C protein, which has an extremely hydrophobic α-helical domain (without analogy to the leucine zipper motif) and a palmitoylated N-terminal sequence,[116, 117] was identified by ESI-MS as a specific dimeric complex.[113] This result contributed essentially to the formulation of a structural model for the insertion and stabilization of the palmitoylated SP-C in the lipid alveolar surface layer.[113, 115] In these applications, a considerable problem, particularly for the characterization of complexes with hydrophobic interactions, was the strong tendency of protein complexes to adsorb at the polar fused-silica inlet capillary.[24] Increased stabilities of complex ions and improvements in the characterization of pH- and concentration-dependent equilibria has recently been obtained by using polyacrylamide-coated capillaries,[118] yielding a correlation of ion intensities and stabilities of "coiled coil" polypeptide complexes.[107, 108a] However, a general problem is the decrease in charge numbers for ions of protein complexes relative to the complex components (cf. Section 3.1); for example, the leucine zipper dimers and trimers yielded maximum charge numbers of 5+, while the sum of charge numbers of the monomers is 8+ and 12+, respectively (see Figures 13 and 14). Such charge effects are most characteristic for protein–nucleotide complexes (see Section 3.3), leading to increasing demands on instrumentation (sector or time-of-flight analyzers).[119]

Despite these present limitations, first mass spectra of intact quaternary structures of high molecular weight proteins have been reported. Model studies have been carried out on proteins with a known specific association of subunits in solution, such as dimeric hemoglobin and the tetrameric complexes of avidin and streptavidin, two of the most stable known quaternary structures. A further successful application was the characterization of the cell-recognition lectin, concanavalin A (Con A), with a high-mass quadrupole analyzer[23] (Fig. 15; M_r of the subunit 25500). Abundant ions of the dimer and tetramer with charge states between 14+ and 22+ (m/z region around 4500) were identified from aqueous solution at pH 6.7, in good agreement with the known pH-dependent stability of Con A.[120] At elevated temperature or in acidic solution complete dissociation of the complex into the subunits was established by the appearance of monomer ions at m/z lower than 2000 (charge numbers to about 18+; Figure 15b). Crucial evidence for the specific identification of the quaternary structures in this study was the absence of ions in the spectrum due to nonspecific association products such as trimers and the reversibility of the complex formation upon pH and temperature changes. As expected, the relative decrease of charge numbers is most pronounced for ions of the tetramer, while the denatured monomer shows highly charged ions. Recent studies indicate that ESI time-of-flight instru-

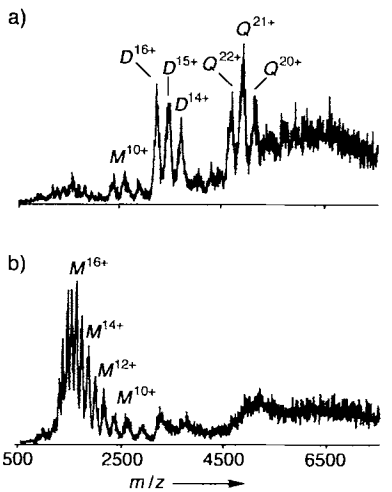

Fig. 15. ESI mass spectrometric identification of dimeric and tetrameric con A with an extended mass range quadrupole mass spectrometer. a) Spectrum of Con A in 10 mM ammonium acetate (pH 6.7); D = duplex, Q = quadruplex ion series. b) Dissociation of the quaternary structure at elevated temperature (185 °C); M = ion series of monomeric subunits. From Ref. [23].

mentation is well suited to determine charge numbers of ions within a broad m/z range for quaternary structures with multiple subunits.[121]

3.3. Characterization of Double-Stranded Oligonucleotides and Higher Order Nucleotide Complexes

Because of the problems in obtaining homogeneous polyanions in the presence of alkali salts, most studies of oligo- and polynucleotides have been carried out with the ammonium salts[45, 49, 122] (cf. Section 2.1; Figure 2b); identical conditions have been applied to the characterization of supramolecular complexes (however, see Figure 18). In the negative-ion ESI mass spectra of DNA and RNA sequences, the $[M - nH]^{n-}$ ions were not significantly pH-dependent from pH 4 to 8.[24, 122a, 123] In contrast to proteins, no clear relation between charge structures of polyanions and structural states in solution has been observed; ion abundances are affected by organic cosolvents and by differences in base composition.[123] However, charge numbers of negative ions are considerably lower for double-stranded complexes than for the complementary single-strand sequences (see Fig. 17). As pointed out in Section 3. 1. for protein complexes, double-stranded oligonucleotides are unambiguously distinguished from isobaric single-strand sequences by the odd-charged duplex polyanions, as illustrated in Figure 16 by an

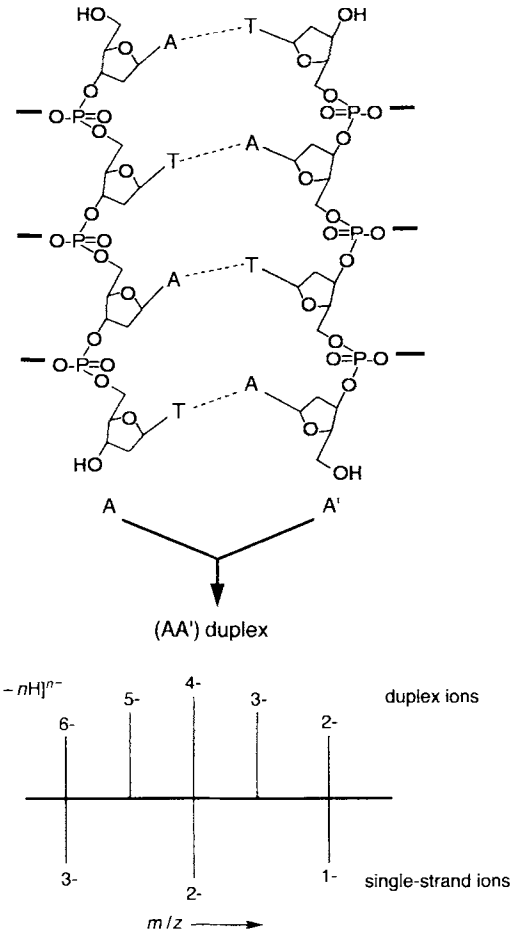

Fig. 16. Scheme illustrating the identification of double-stranded polynucleotides by odd-charged duplex polyanions $[M - nH]^{n-}$ (cf. Fig. 12).

A/T-duplex, while isotopic resolution would be required for the assignment of even-charged complex ions.

First successful investigations of double-stranded synthetic oligonucleotides with conventional quadrupole mass spectrometers have been reported by several authors.[45, 122a] Duplex-specific ions have been identified for self-complementary (isobaric) oligonucleotides, as well as for sequences of different base compositions (see Table 4). ESI mass spectra of the hybridization product of two recognition sequences of the GCN4 leucine zipper (GCN4-U/-L[125]) with a central pseudo-palindromic binding region are illustrated in Figure 17. Among the anions with charges of 8 − to 10 −, the duplex is specifically identified by the $[M - 9H]^{9-}$ ion ($M_r = 14707$; Fig. 17a), whereas the even-charged ions do not enable a direct differentiation because of the small differences in molecular weight in the single-strand sequences ($M_r = 7360$ and 7347; $\Delta m = 13$; see Table 4); however, the quantitative formation of the duplex was ascertained by gel electrophoresis.[45, 126] Analyses of the single-stranded sequences and further model studies also provided evidence for the direct identification of mixtures of duplex and single-strand oligonucleotides.[24, 122b] Thus, the spectrum of the partially dissociated GCN4-U/-L duplex shows the duplex-specific ions (9 −, 11 −), as well as the $[M - nH]^{n-}$ ions of the single-strand sequences with significantly higher *relative* charge numbers (Fig. 17 b). The direct analysis of single-strand/duplex mixtures provides the basis for the determination of duplex melting temperatures by ESI-MS; first model studies have been performed and compared with conventional methods.[127] For the GCN4-U/-L duplex, a melting temperature of 59 °C was obtained with the temperature-controlled sample delivery probe ($T_m = 64$ °C by UV spectroscopic determination).[45a] ESI-MS studies of hybridization products of different synthetic oligodeoxyribonucleotides are summarized in Table 4. For most products studied so far, the molecular weight of the duplex determined by ESI-MS was higher than that calculated

Table 4. Identification of double-stranded oligodeoxynucleotides by negative-ion ESI mass spectrometry.

Oligonucleotide [a]	M_r [b] Single strands	Duplex	m/z	Duplex ions [c] Charge state [d]	M_r [e]	Ref.
dC_4G_4	2411/ 2411	4822	1607	3	4824	[124b]
$d(T)_8/d(A)_8$	2371/ 2443	4814	1624	3	4872	[124b]
$d(T)_{10}/d(A)_{10}$	2980/ 3070	6050	1209	5	6052	[45a]
d(20mer)I/II	5827/ 6410	12237	2446 [f]	5	12297	[124a]
GCN4-L/-U	7360/ 7347	14707	1638	9	14714	[24, 45a]
GCN4II-low/-up	11898/12073	23971	1843	11	23997	[45a]

[a] Oligonucleotide sequences: dC_4G_4 = self-complementary 5'-dCCCCGGGG-3'; d(20mer)I/II = 5'-dCCTTCCTCCCTCTCTCCTCC-3', 3'-GGAAGGAGGGAGAGAGGAGG-5'; GCN4-L/-U = 5'-dCGCAGCGGATGACTCATTTTTCGG-3', 3'-dGCGTCGCCTACTGAGTAAAAAGCC-5'; GCN4II-low/-up = 5'-dAATTCCACCTAGCGGATGACTTACTTTTTTTCTTAGCGA-3'; 5'-dAGCTTCGCTAAGAAAAAAGTAAGTCATCCGCTAGGTGG-3'. Synthetic oligonucleotides were prepared in automated DNA synthesizers with phosphoramidite chemistry [45,47]. [b] Monoisotopic molecular weights without counterions. [c] $[M - nH]^{n-}$ ions of the duplex. [d] Most abundant charge states within an m/z range of approximately 2000. [e] Average molecular weight determined from duplex ion signals for different charge states. [f] Duplex ion detected with a quadrupole mass analyzer with extended mass range.

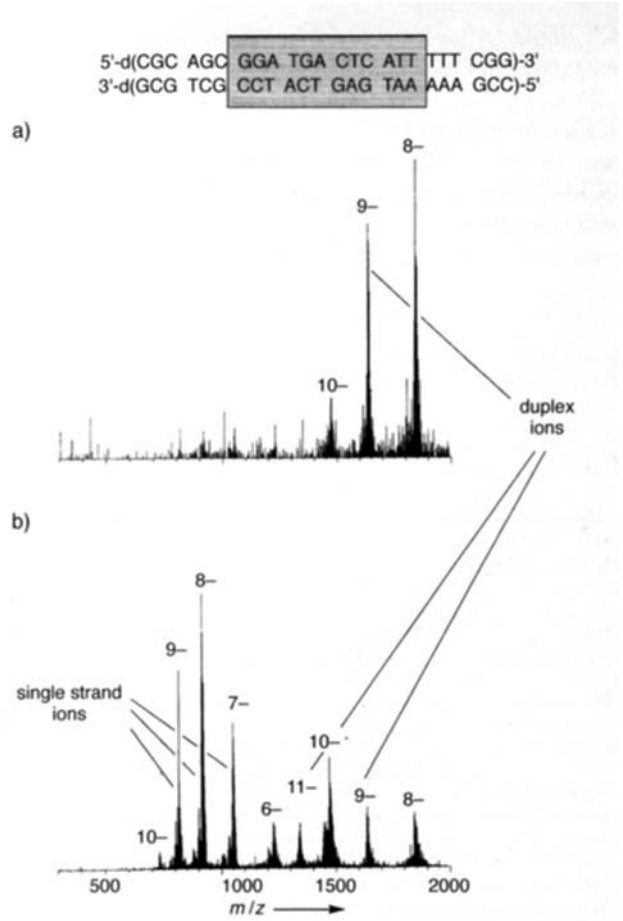

Fig. 17. Identification of the double-stranded 24-mer recognition sequence of the GCN4 leucine zipper protein. a) Negative-ion spectrum of the purified GCN4-L/-U hybridization product in 10 mM ammonium acetate. b) Spectrum of the partially dissociated product after lyophylization and redissolution in 1 mM ammonium acetate [45]. Solvent mixture: 5 mM ammonium acetate containing NH_3/acetonitrile 1/1 (pH 9). The central pseudo-palindrome is depicted in the shaded box. See Ref. [24].

from the single-strand sequences (without counterions), since the formation of homogeneous $[M - nH]^{n-}$ ion series essentially depends on the purity of the ammonium salts (cf. Section 2.1). As expected, the charges of all oligonucleotide duplex ions are significantly lower than the sum of charges of the single-strand ions. For example, the most abundant duplex ion of a 20-mer hybridization product ($M_r = 12200$[124a]) was observed at m/z 2446 (see Table 4); hence the ions of high molecular weight complexes (found up to m/z 2000) probably represent only a fraction with high charge numbers. Moreover, Light-Wahl et al.[122, 124] suggested that duplex ions with low charge have higher relative stabilities, which may result from the stabilizing effect of remaining counterions.

The results hitherto obtained with double-stranded complexes are encouraging, taking into consideration that little knowledge is yet available about ion compositions and structures in ESI spectra of oligo- and polynucleotides. A number of applications can be envisaged for the characterization of supramolecular complexes for which no specific methods are available at present. Examples are sequence determinations by hybridization products (rather than by mass spectrometric analysis of sequential fragment ions from single-stranded oligonucleotides[128]), the characterization of duplex products of chemically modified nucleotides without the use of radioactive labeling techniques,[129] and the analysis of "antisense" oligonucleotides[130] and intercalation complexes; the characterization of oligonucleotide complexes with actinomycin D and distamycin has been reported recently.[131] Of particular interest should be applications to supramolecular complexes formed by hybridization additional or alternative to the Watson–Crick base pairing, such as Hogsteen complexes and nucleotide-specific triplex structures.[132, 133] That higher-order nucleotide complexes can be studied by ESI-MS has been demonstrated recently by Goodlett et al. with the identification of a quadruplex of the guanine-rich oligonucleotide, d($CGCG_3GCG$) $(dG4)_4$,[134] formed by "quartet" pairing of the central guanine bases, alternative to the intramolecular Watson–Crick base pairing.[135, 136] Negative-ion ESI mass spectra of the complex were obtained in sodium phosphate buffer (required to stabilize the quadruplex by insertion of the alkali metal counterions into the G-base stacks[135]), and under particularly mild desolvation conditions by using sulfur hexafluoride as a sheath gas[137] (Fig. 18). Although the presence of alkali salt caused

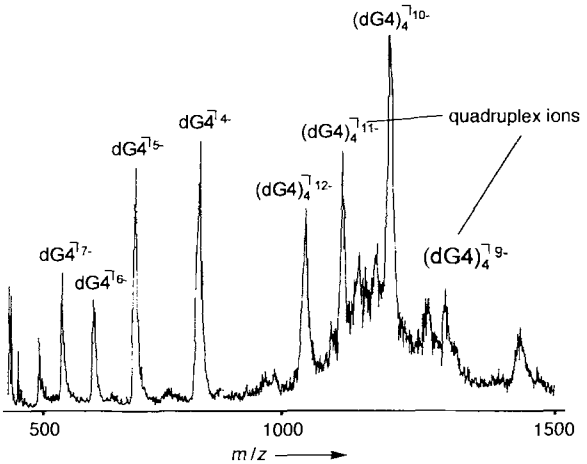

Fig. 18. Identification of the tetramer of 5'-d(CGCGGGGGCG)-3' (dG4) by negative ion ESI-MS. A 0.9 mM solution of dG4 was prepared in 10 mM sodium phosphate (pH 7.6) and 0.1 mM ethylenediamintetraacetic acid (EDTA); spectra were obtained with sulfur hexafluoride as a sheath gas. Ions specific for the quadruplex are labeled $(dG4)_4$. From ref. [134].

considerable peak broademing by multiply sodiated polyanions, unambiguous identification of the quadruplex was obtained by the characteristic *odd-charge* state ions, $(dG4)_4^{11-}$ and $(dG4)_4^{9-}$.

In principle, the successful characterization of supramolecular complexes of proteins as well as oligonucleotides prepares the way for the direct analysis of protein–nucleotide interactions. For protein complexes with mono- and dinucleotides and related cofactors, the conditions of positive-ion ESI-MS of proteins are applicable[89, 93] (cf. Table 3). In studies of the nucleotide-binding region of the elongation factor EF-Tu from *T. thermophilus*,[138] the protein complexes with GDP and GTP were identified as homogeneous $[M + nH]^{n+}$ ion series, and their presence was confirmed by chemical and spectrospopic results.[139] However, protein complexes with high molecular weight DNA and RNA sequences (leucine zipper proteins, EF-Tu/tRNA complex[138]) did not yield highly charged ions.[108a]

Thus, the analysis of protein–nucleic acid complexes with multiple ionic interactions and neutralization by counterions appears to be limited to high-molecular weight ions, so future applications will essentially depend on the development of high-mass analyzers.

4. ESI-MS Characterization of Synthetic Supramolecular Complexes

The synthesis of supramolecular complexes from synthetic self-assembling components and their structural and functional characterization has recently evolved as a most exciting research area.[140–143] A wide range of supramolecular structures such as synthetic helicates, catenanes,[144] and host–guest complexes[145] have been developed, both as model systems for natural self-association processes[146] and as complexes with new supramolecular structures.[147] The isolation and purification of supramolecular complexes often present particular difficulties, and only in a few cases could the complete spectroscopic characterization and crystallographic structure determination be undertaken.[141] Frequently, a major analytical problem is the characterization of reaction pathways leading to the formation of specific complexes in multicomponent mixtures;[148] here mass spectrometric methods have recently found increasing application.[148, 149]

Examples of ESI mass spectra of supramolecular complexes from building blocks of rotaxanes, catenanes, and helicates are summarized in Table 5. For nearly all complexes hitherto analyzed, appropriate electrospray conditions and high ion intensities were obtained with organic (aprotic) solvents. In most cases the charge states of complex ions were derived either from the presence of metal ions[153, 154] or by the formal loss of one or several counterions.[149] Thus, for catenane complexes composed of 4,4′-bipyridyl derivatives and different macrocyclic and aromatic polyether ligands, molecular ions that had lost up to four PF_6^- counterions were detected.[149] The corresponding multiply charged series enables the dimers to be identified by a principle analogous to that applied to the multiply protonated ion series of protein complexes (cf. Section 3.2). Several catenanes and rotaxanes shown in Table 5 have also been successfully analyzed by FAB-MS[149, 150] (see Section 5). Comparative studies of catenanes[155] showed that FAB-MS gives predominantly singly charged ions; thus ESI-MS offers advantages for the analysis of higher molecular weight complexes (greater than 3000 Da). For example, Bitsch et al.[152] detected multicyclic complexes with molecular weights over 7000 Da and containing up to seven interlocked catenane rings by ESI-MS.

Furthermore, ESI-MS has been recently demonstrated as an efficient tool for the direct analysis of mixtures of self-assembling components. For example, double-stranded complexes of oligo-(2,2′-bipyridyl)-ether derivatives were identified with copper(I) ions, whereas triplex helicates are furnished upon insertion of nickel(II) ions.[151] An elegant example has been the ESI mass spectrometric characterization of a polynuclear self-assembly complex of a bis(isoquinoline) (L1) and a hexaphenylhexaazatriphenylene ligand (L2) with $CuPF_6$[149] (Fig. 19). ESI mass spectra of aliquots from an equimolar mixture of the two ligands upon titration with 2.5 equivalents of $CuPF_6$ established the identity of the three-component complex **1** due to the specific triply charged ion $[(L1)(L2)Cu_3^I]^{3+}$ (m/z 616). The composition of the fully assembled complex was ascertained by collisionally activated dissociation and tandem ESI-MS analysis, which yielded fragment ions from the components $[(L1)Cu_2]^{2+}$ (m/z 547) and $[(L2)Cu]^+$ (m/z 753) (Fig. 19b). In addition, protonated ions arising from complexes with one and two Cu^I ions inserted into the "partially capped" complexes (**2** and **3**, respectively) were detected as by-products. The ion intensities of the complex species determined by ESI-MS showed good agreement with the relative amounts deduced from spectrophotometric titration.[156] These results suggest that the formation of supramolecular complexes can be directly analyzed under thermodynamic equilibrium conditions. However, the extent to which the formation of complexes from multicomponent reaction mixtures can be quantitatively analyzed remains to be established in further studies.[148, 157]

5. Comparison of ESI-MS with Other Ionization Methods

The successful development of ESI-MS suggests the potential application of other "soft" ionization MS methods for the analysis of supramolecular complexes. With the exception of a few previous studies such as FAB-MS of polysaccharide–lipid complexes,[158] no systematic investigations of noncovalent interactions with biopolymers have yet been performed by FAB-MS,

Table 5. ESI mass spectrometric identification of supramolecular complexes from synthetic self-assemblying components.

	complex components			supramolecular complex		
complex type	ligand components	metal/counterion [a]	M_r [b]	association	charge state [c]	Ref.
catenane	4,4′-bipyridyl; macrocyclic polyether	–/PF_6^-	2525	dimer	3+	[149]
rotaxane	bis(porphyrin)phenanthroline (spacer); macrocyclic polyether	Cu^I/PF_6^- Au^{III}/PF_6^-	2986	1:1 complex	2+	[150]
helicate	oligo(2,2′-bipyridyl)ether derivative	Cu^I/ClO_4^-	1659	double helicate	3+	[151]
		Ni^{II}/ClO_4^-	2419	triple helicate	6+	
catenane	phenanthroline; (*cyclo*)-oligoacetylene derivative	Cu^I/BF_4^-	4444	pentacatenane	4+	[152]
			5557	hexacatenane	5+	
			6668	heptacatenane	6+	

[a] Metal- and counterion employed in the preparation of the self-assembled complexes. [b] Molecular weights refer to the neutral complexes (including counterions). [c] Most abundant charge states of observed complex ions.

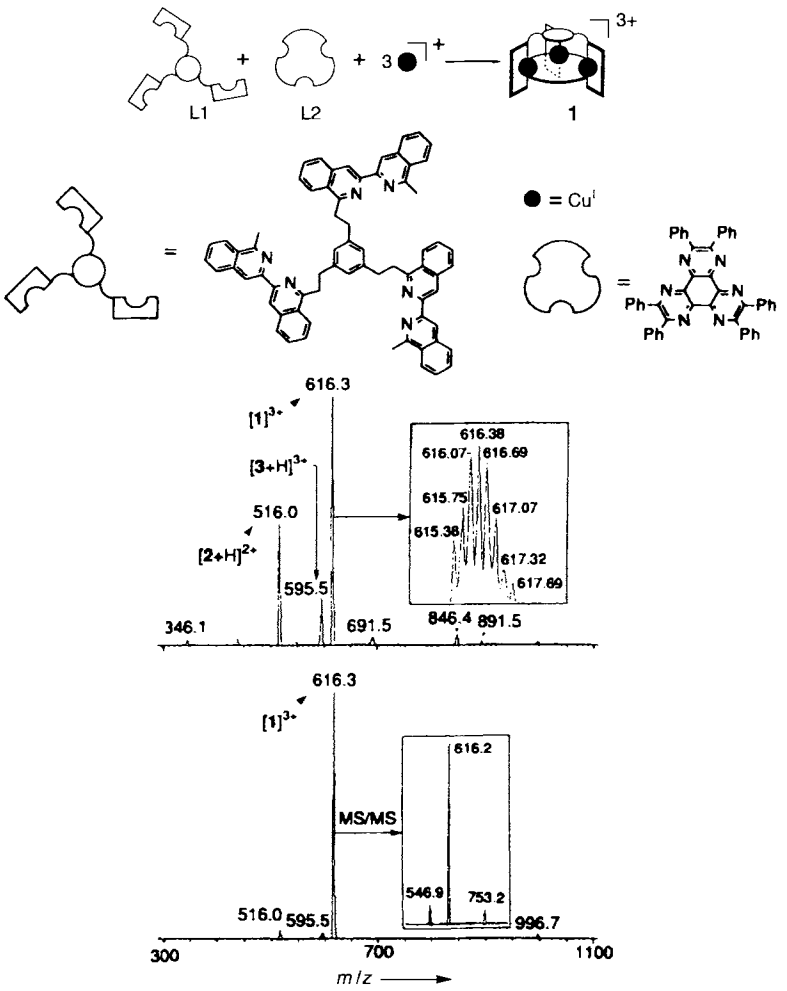

Fig. 19. ESI mass spectrometric identification of the three-component self-assembly complex **1** between tris(bisisoquinoline) (L1) and hexaphenylhexaazatriphenylene (L2) ligands and three Cu^{I} ions. Spectra were recorded of acetonitrile/CH_2Cl_2 (1/1) solutions after titration of an equimolar mixture of L1 and L2 with 2.5 (top spectrum) and 6 equivalents (bottom spectrum) of $CuPF_6$. From Ref. [148].

PD-MS, and MALDI-MS. Comparison of these techniques with ESI-MS on biopolymer complexes with defined structures in solution are difficult, because different sample preparation procedures are used in other ionization methods. Only in FAB-MS are sample solutions used;[5] PD-MS is mainly performed with solid samples, and special conditions are required for solubilization (for example, for the analysis of chemical reactions in situ on the sample target).[7, 15, 159] For nearly all applications of MALDI-MS solid samples were prepared by admixture of a large excess of matrix;[11, 160, 161] no information is currently available about the structural state of macromolecules under these conditions.

A number of synthetic supramolecular complexes such as catenanes and rotaxanes have been identified by FAB-MS in organic solvents (mainly with 3-nitrobenzyl alcohol as matrix).[155, 162, 163] The positive-ion FAB spectra of oligocatenanes from macrocyclic polyethers (cf. Table 5) exhibit abundant molecular cations arising from loss of one of the PF_6^- counterions; ring-opening and elimination of bipyridinium units are the major fragmentaions.[162b] The main limitations for the application of FAB-MS are the limited molecular weight range accessible, the variation of sample concentration by solvent evaporation, and the instability of many coordination complexes in polar solvents. However, first successful studies have been carried out in aqueous solutions with glycerol as matrix.[97, 163, 164] For example, semirotaxane complexes of β-cyclodextrins (β-CD) have been identified in aqueous glycerol solutions through their abundant $[M+H]^+$ ions, as illustrated in Figure 20 by a 1:1 complex of β-CD and 11-aminoundecane-4′-triphenylmethylanilide.[163] Studies of semirotaxanes by ESI-MS for comparison also afforded predominantly the formation of singly charged complex ions.[164] A major obstacle for the analysis of biomacromolecular complexes by FAB-MS is the problem of preparing sample solutions with the same conditions as in physiological solutions. Thus, negative-ion FAB spectra of duplex oligonucleotides did not provide ions indicative of double-stranded products, but only molecular ions of the single-stranded chains and fragments, some of which are sequence-specific;[45] likewise, studies with PD-MS did not yield ions of double-stranded oligonucleotides. However, the recent identification of specific Cu^{II} complexes of the oligopeptide angiotensin[165, 166] by PD-MS from aqueous solution at carefully controlled pH indicates that progress in the analysis of noncovalent complexes by FAB-MS and PD-MS can be expected by improved matrix and sample preparation procedures.[164, 166, 167]

The major problems at present preventing the analysis of supramolecular complexes by MALDI-MS are the harsh, denaturing sample preparation conditions and the formation of unspecific "cluster" ions and matrix adducts.[161, 168, 169] The formation of unspecific adduct ions is illustrated in Figure 21 by UV-MALDI spectra of cytochrome C and an IgG monoclonal antibody,[11] which show ions of dimeric and

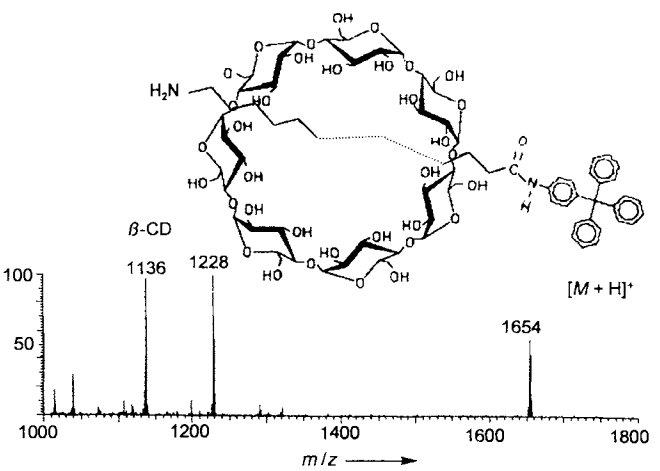

Fig. 20. FAB mass spectrum of the semirotaxane complex of β-CD with 11-aminodecane-4′-triphenylmethylanilide. Solvent: methanol; matrix: 3-nitrobenzyl alcohol [163].

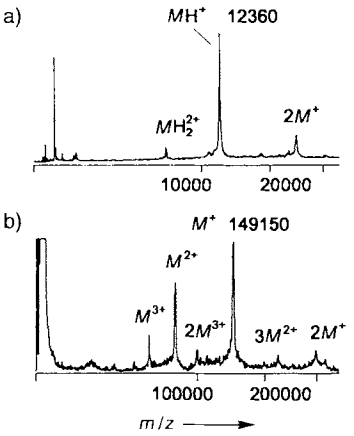

Fig. 21. MALDI mass spectra of a) porcine cytochrome C in 2,5-dihydroxybenzoic acid matrix (337 nm) and b) a mouse IgG monoclonal antibody against a human lymphokine in nicotinic acid matrix (266 nm). From Ref. [11].

trimeric aggregates in addition to the singly and doubly charged molecular ions, without relevance to a quaternary structure. In most cases the samples are incorporated into a strongly acidic matrix with suitable absorption properties (for example, benzoic and cinnamic acid derivatives for UV-MALDI-MS[161, 168]). Under these conditions, complete denaturation of protein structures and dissociation of specific interactions must generally be expected. Accordingly, initial attempts to characterize noncovalent complexes did not yield reproducible results, or yielded only dissociation products (for example, for heme-proteins[169]).[168a, 170] A number of new matrices for UV-MALDI-MS that can be crystallized from aqueous solutions at pH 2–8[171] have recently been developed, but their feasibility for the analysis of supramolecular complexes has not yet been tested. For the characterization of noncovalent interactions, the mild desorption conditions of IR-MALDI-MS with liquid matrices[172] might be more promising than the analysis of solid, crystalline samples. Of particular interest has been the recent observation of multiply charged ion series in IR-MALDI spectra of proteins, for example, of immunoglobuline antibodies.[161] In conclusion, despite single observations of specific complex ions (for example, for the ion channel protein porin[161]), the feasibility of MALDI-MS for supramolecular complexes has not yet been demonstrated. The elucidation of matrix chemistry and desorption mechanism(s) will be of crucial importance for further development.

6. Conclusions and Perspectives

Although introduced only in the past few years as a method for molecular weight and primary structure determination of biopolymers, the ability of ESI-MS to provide information on tertiary structures and specific noncovalent interactions of macromolecules in solution is presently adding a new dimension beyond the characterization of *primary structures* as the classical domain of mass spectrometry. The hitherto successful applications open new perspectives for the direct analysis of supramolecular complexes and molecular recognition processes. Furthermore, they demonstrate that the ESI-mass spectrometric identification of molecular constitution and composition, and of binding specificities of supramolecular complexes provides complementary information to the structure determination by spectroscopic methods and by crystal structure analysis.[173–176]

Considering that for ESI-MS—like other soft ionization methods—little more than qualitative models are available yet on the mechanism of ion formation and transfer from solution to the gas phase, the analytical potential indicated by the present results appears promising.[23, 50, 177] Whereas the detection of electrostatic interactions between charged macromolecules can, in principle, be anticipated,[110, 177] molecular specificity has also been demonstrated with complexes comprising types of binding such as hydrogen-bond and hydrophobic interactions. Moreover, it must be borne in mind that the present investigations have been primarily carried out on ions with high charge states and at low resolution; high-mass ESI-MS instrumentation suitable for the characterization of supramolecular complexes by ions with low charge states has only recently become available.[23, 119] The most recently developed ESI ion-cyclotron resonance (ICR) instruments[178] are particularly promising, especially for the identification of complex ions of high mass *and* at high resolution and for the characterization of gas-phase structures of macromolecular ions. Of primary importance for future applications will be the development of improved sample delivery systems to control the conditions of formation of supramolecular complexes (pH, temperature) in solution and the conditions of desolvation. Although useful correlations between structural states in solution and charge structures of ions in the gas phase have been shown, the structural characterization of gas-phase macromolecular ions is in its infancy, and it is still speculative to postulate a conservation of solution structures. However, first investigations by a combination of ESI-MS and NMR spectroscopy have already provided useful complementary results in the characterization of solution structures, for example, in H/D-exchange studies.[179]

The full potential and limitations of ESI-MS for the analysis of supramolecular complexes cannot yet be evaluated, particularly with regard to the quantitative characterization of equilibria of noncovalent complexes. However, a number of new applications are clearly emerging, for example, the identification of sequence-specific oligomerization products of helical polypeptides,[180] the characterization of antigen-antibody interactions,[181, 182] the characterization of specific enzyme- and receptor-ligand interactions even from complex mixtures such as those obtained from combinatorial peptide syntheses,[183] and the study of specificity in synthetic supramolecular complexes.[184, 185] Further development should stimulate the growing interdisciplinary application of ESI mass spectrometry.

We are indebted to our co-workers for their enthusiasm, ideas, and many discussions throughout the investigations reported in this article: Dr. Detlev Suckau, Dr. Klaus Schneider, Dr. Andrea Schäfer, Dr. Per F. Nielsen, Dr. Michal Svoboda, Dr. Claudia Maier, Dipl.-Ing. Klaus Hägele, Dipl.-Chem. Winfried Fiedler, Dipl.-Chem. Christoph Borchers, Dipl.-Chem. Petra Mayer, Dipl.-Chem. Jürgen Kast, Dr. Kerstin Seidel, Dipl.-Chem. Rainer Schuhmacher, Dr. Wolfgang Weinmann, Dr. Martin Kussmann, Dipl.-Chem. Ingrid G. Kaufmann, Dipl.-Chem. Stephan Witte, Dipl.-Chem. Volker Schnaible, Dipl.-Chem. Andreas Wattenberg, Dipl.-Chem. Martina Schuhmacher, Dipl.-Chem. Marcus Macht, and Dipl.-Chem. Sebastian Bauer. We are grateful to Professors K. P. Schäfer, K. Klemm, A. L. Burlingame, F. W. Röllgen, C. Stürmer, U. Krawinkel, G. Spiteller, M. Speinzl, P. Roepstorff, and W. Welte for helpful discussions, advice, and encouragement, particularly concerning new application areas. Furthermore, we thank A. van Dorsselaer, K. Tomer, M. L. Deinzer, G. Jung, F. W. McLafferty, M. Mák, and R. Frank, for making manuscripts and

many unpublished results available to us. M. P. thanks the state of Baden-Württemberg for support, and particularly Professor B. Penke for his hospitality and many discussions during a guest stay at the A. Szent-György-University, Szeged. We gratefully acknowledge the generous financial support by the Deutsche Forschungsgemeinschaft, Bundesministerium für Forschung und Technologie, Fonds der chemischen Industrie, the European Community within the EU-network "Peptide and Protein Structure Elucidation by Mass Spectrometry", Byk Gulden Konstanz, and Boehringer Mannheim.

Received: April 9, 1994
Revised version: October 19, 1995 [A 621E]
German version: *Angew. Chem.* **1996**, *108*, 878–899

[1] *Biological Mass Spectrometry* (Eds.: A. L. Burlingame, J. A. McCloskey), Elsevier, Amsterdam, **1990**.
[2] K. Biemann, S. A. Martin, *Mass Spectrom. Rev.* **1987**, *6*, 1.
[3] A. L. Burlingame, T. A. Baillie, D. H. Russel, *Anal. Chem.* **1992**, *64*, 467.
[4] H. D. Beckey, *Principles of Field-Ionization and Field Desorption Mass Spectrometry*, Pergamon, Oxford, **1977**.
[5] a) M. Barber, R. S. Bordoli, R. D. Sedgwick, A. N. Tyler, *J. Chem. Soc. Chem. Commun.* **1981**, 325; b) W. Aberth, K. M. Straub, A. L. Burlingame, *Anal. Chem.* **1982**, *54*, 2029; c) M. Przybylski, *Z. Anal. Chem.* **1983**, *315*, 402. d) Liquid secondary-ion mass spectrometry (LSIMS) has been used throughout recent literature as a synonym for FAB-MS.
[6] a) B. Sundquist, R. D. Macfarlane, *Mass Spectrom. Rev.* **1985**, *4*, 421; b) R. J. Cotter, *Anal. Chem.* **1988**, *60*, 781.
[7] G. P. Jonsson, A. B. Hedin, P. L. Hakanson, B. U. R. Sundquist, B. G. S. Save, P. F. Nielsen, P. Roepstorff, K. E. Johansson, I. Kamensky, M. S. L. Lindberg, *Anal. Chem.* **1986**, *58*, 10843.
[8] J. B. Fenn, M. Mann, C. K. Meng, S. F. Wong, C. M. Whitehouse, *Science* **1989**, *246*, 46.
[9] a) M. Karas, F. Hillenkamp, *Anal. Chem.* **1988**, *60*, 2299; b) F. Hillenkamp, M. Karas, A. Ingendoh, B. Stahl in *Biological Mass Spectrometry* (Eds.: A. L. Burlingame, J. A. McCloskey), Elsevier, Amsterdam, **1990**, p. 49.
[10] R. D. Smith, J. A. Loo, R. R. Orgorzalek-Loo, M. Busman, H. R. Udseth, *Mass Spectrom. Rev.* **1991**, *10*, 359.
[11] M. Karas, U. Bahr, U. Gießmann, *Mass Spectrom. Rev.* **1991**, *19*, 335.
[12] Ions derived from an *intact* macromolecule, for example, by protonation (such as $[M+H]^+$), frequently called "quasimolecular ions", are generally termed *molecular ions* to simplify assignments.
[13] K. Biemann in *Protein Sequencing - A Practical Approach* (Eds.: J. B. C. Findley, M. J. Geisow), IRL, Oxford, **1989**, p. 99.
[14] a) P. Roepstorff, P. F. Nielsen, K. Klarskov, P. Hørjup, *Biomed. Environ. Mass Spectrom.* **1988**, *16*, 9; b) P. F. Nielsen, B. Landis, M. Svoboda, K. Schneider, M. Przybylski, *Anal. Biochem.* **1990**, *191*, 302; c) K. Biemann, *Biomed. Environ. Mass Spectrom.* **1988**, *16*, 99; d) B. T. Chait, F. H. Field, *Biochem. Biophys. Res. Commun.* **1986**, *134*, 420.
[15] a) P. F. Nielsen, K. Schneider, D. Suckau, B. Landis, M. Przybylski in *Mass Spectrometry of Large Non-Volatile Molecules* (Eds.: E. Hilf, A. Tuczynski), World Sci., Singapur, **1990**, p. 194; b) C. Fenselau, *Adv. Mass Spectrom.* **1995**, *13*, 129.
[16] a) J. T. Stults, W. J. Henzel, J. H. Bourell, P. R. Griffin in Ref. [1], p. 599; b) M. Svoboda, M. Przybylski, J. Schreurs, A. Miyajima, K. Hogeland, M. Deinzer, *J. Chromatogr.* **1991**, *562*, 403; c) M. O. Glocker, B. Arbogast, J. Schreurs, M. L. Deinzer, *Biochemistry* **1993**, *32*, 482.
[17] a) D. Suckau, J. Köhl, G. Karwarth, K. Schneider, M. Casaretto, D. Bitter-Suermann, M. Przybylski, *Proc. Natl. Acad. Sci. USA* **1990**, *87*, 9848; b) D. Suckau, Dissertation, Universität Konstanz, **1991**; c) M. Przybylski, W. Fiedler, M. Macht, M. O. Glocker, *Mass Spectrom. Rev.* **1996**, in press.
[18] C. Gauss, J. Klein, K. Post, D. Suckau, K. Schneider, H. Thomas, F. Oesch, M. Przybylski, *Environ. Health Perspect.* **1990**, *88*, 57.
[19] H. R. Morris, F. M. Grier, *Trends Biotechnol.* **1988**, *6*, 140.
[20] The term supramolecular complex is used in this article for a general designation of noncovalent complexes formed by specific association of a macromolecule or low molecular weight self-assembly components.
[21] M. Przybylski, I. Manz, P. Fonrobert, I. Dietrich, H. Brückner, *Adv. Mass Spectrom. B* **1986**, *10*, 1519.
[22] K. Schneider, Dissertation, Universität Konstanz, **1991**.
[23] R. D. Smith, K. J. Light-Wahl, *Biol. Mass Spectrom.* **1993**, *22*, 493.
[24] M. Przybylski, *Adv. Mass Spectrom.* **1995**, *13*, 257.
[25] R. Feng, Y. Konishi, *J. Am. Soc. Mass Spectrom.* **1993**, *4*, 638.
[26] As a working definition, the charge state series and distribution of ions characteristic of a macromolecule is termed charge structure in this article.
[27] a) L. J. Smith, M. J. Sutcliffe, C. Refield, C. M. Dobson, *Biochemistry* **1991**, *30*, 986; b) H. Rode, *Methods Enzymol.* **1989**, *176*, 446.
[28] F. Vögtle, *Supramolekulare Chemie*, Teubner, Stuttgart, **1992**.
[29] a) M. Dole, L. L. Mack, R. L. Hines, R. C. Mobley, L. D. Ferguson, M. B. Alice, *J. Chem. Phys.* **1968**, *49*, 2240; b) G. A. Clegg, M. Dole, *Biopolymers* **1971**, *10*, 821.
[30] A. P. Bruins, T. R. Covey, J. D. Henion, *Anal. Chem.* **1987**, *59*, 2642.
[31] J. V. Iribarne, B. A. Thompson, *J. Chem. Phys.* **1976**, *64*, 2287.
[32] T. R. Covey, R. F. Bonner, B. I. Sushan, J. D. Henion, *Rapid Commun. Mass Spectrom.* **1988**, *2*, 249.
[33] M. H. Allen, M. L. Vestal, *J. Am. Soc. Mass Spectrom.* **1992**, *3*, 18.
[34] M. Mann, *Org. Mass Spectrom.* **1990**, *25*, 575.
[35] R. D. Smith, H. R. Udseth, C. J. Barinaga, C. G. Edmonds, *J. Chromatogr.* **1991**, *559*, 197.
[36] R. D. Smith, C. J. Barinaga, H. R. Udseth, *Anal. Chem.* **1988**, *60*, 1948.
[37] W. Fiedler, M. Macht, M. O. Glocker, I. Kaufmann, M. Przybylski, *Protein Sci.* **1995**, *4*, Suppl. 1, 122.
[38] R. D. Smith, J. A. Loo, C. G. Edmonds, C. J. Barinaga, H. R. Udseth, *Anal. Chem.* **1990**, *62*, 882.
[39] a) M. Mann, C. K. Meng, J. B. Fenn, *Anal. Chem.* **1989**, *61*, 1702; b) M. H. Allen, T. W. Hutchens, *Rapid Commun. Mass Spectrom.* **1992**, *6*, 308.
[40] C. Michinson, R. L. Baldwin, *Proteins* **1986**, *1*, 23.
[41] I. Kato, C. B. Anfinson, *J. Biol. Chem.* **1969**, *244*, 1004.
[42] J. A. Loo, C. G. Edmonds, R. D. Smith, M. P. Lacey, T. Keough, *Biomed. Environ. Mass Spectrom.* **1990**, *19*, 286.
[43] R. R. Ogorzalek-Loo, D. R. Goodlett, R. D. Smith, J. A. Loo, *J. Am. Chem. Soc.* **1993**, *115*, 4391.
[44] A. A. Schreier, R. L. Baldwin, *Biochemistry* **1977**, *16*, 4203.
[45] a) J. Kast, Diplomarbeit, Universität Konstanz, **1993**; b) J. Kast, M. Przybylski, E. Dürr, H. Wendt, H. R. Bosshard, *Protein Sci.* **1995**, *4*, 105.
[46] T. E. Ellenberger, C. J. Brandle, K. Struhl, S. C. Harrison, *Cell* **1992**, *71*, 1223.
[47] J. W. Efcavitch, L. J. McBride, J. S. Eadie in *Biophosphates and Their Analogues/Synthesis, Structure, Metabolism and Activity* (Eds.: K. S. Bruzik, W. J. Stec), Elsevier, Amsterdam, **1990**, p. 205.
[48] B. A. Connolly, B. V. L. Potter, F. Eckstein, A. Pingoud, L. Grotjahn, *Biochemistry* **1984**, *23*, 3443.
[49] J. T. Stults, J. C. Marsters, *Rapid Commun. Mass Spectrom.* **1991**, 5, 359.
[50] J. B. Fenn, *J. Am. Soc. Mass Spectrom.* **1993**, *4*, 524.
[51] a) U. Lüttgens, F. W. Röllgen, *Proc. 39th Conf. Am. Soc. Mass Spectrom. Allied Topics* **1991**, 439; b) G. Schmelzeisen-Redeker, L. Bütfering, F. W. Röllgen, *Int. J. Mass Spectrom. Ion Processes* **1989**, *90*, 139; c) F. W. Röllgen, U. Lüttgens, T. Dülcks, U. Giessmann, *Proc. 41st Conf. Am. Soc. Mass Spectrom. Allied Topics* **1993**, 1.
[52] S. F. Wong, C. K. Meng, J. Fenn, *J. Phys. Chem.* **1988**, *10*, 368.
[53] A. L. Rockwood, M. Busman, R. D. Smith, *Int. J. Mass Spectrom. Ion Processes* **1991**, *111*, 103.
[54] B. E. Winger, K. J. Light-Wahl, R. D. Smith, *J. Am. Soc. Mass Spectrom.* **1992**, *3*, 624.
[55] R. Guevremont, J. C. Y. Le Blanc, K. M. W. Siu, *Org. Mass Spectrom.* **1993**, *28*, 1345.
[56] a) S. K. Chowdhury, V. Katta, B. T. Chait, *J. Am. Chem. Soc.* **1990**, *112*, 9012; b) K. W. M. Siu, R. Guevremont, J. C. Y. Le Blanc, R. T. O'Brien, S. S. Berman, *Org. Mass Spectrom.* **1993**, *29*, 570; c) R. Guevremont, K. W. M. Siu, J. C. Y. Le Blanc, S. S. Berman, *J. Am. Soc. Mass Spectrom.* **1992**, *3*, 216.
[57] J. A. Loo, C. G. Edmonds, H. R. Udseth, R. D. Smith, *Anal. Chem.* **1990**, *62*, 693.
[58] a) C. Borchers, Diplomarbeit, Universität Konstanz, **1992**; b) M. O. Glocker, C. Borchers, M. Przybylski, unpublished.
[59] M. Svoboda, A. Bauhofer, P. Schwind, E. Bade, I. Rasched, M. Przybylski, *Biochim. Biophys. Acta* **1994**, *1206*, 35.
[60] M. O. Glocker, C. Borchers, W. Fiedler, D. Suckau, M. Przybylski, *Bioconjugate Chem.* **1994**, *5*, 583.
[61] a) J. C. Y. Le Blanc, D. Beuchemin, K. W. M. Siu, R. Guevremont, S. S. Berman, *Org. Mass Spectrom.* **1991**, *26*, 831; b) A. U. Mirza, S. K. Cohen, B. T. Chait, *Anal. Chem.* **1993**, *65*, 1.
[62] a) V. Katta, B. T. Chait, *J. Am. Chem. Soc.* **1991**, *113*, 8534; b) J. A. Loo, R. R. Ogorzalek-Loo, H. R. Udseth, C. G. Edmonds, R. G. Smith, *Rapid Commun. Mass Spectrom.* **1991**, *5*, 101.
[63] a) V. Katta, B. T. Chait, *Proc. 39th Conf. Am. Soc. Mass. Spectrom. Allied Topics* **1991**, 1247; b) *Rapid Commun. Mass Spectrom.* **1991**, *5*, 214.
[64] a) M. O. Glocker, E. Dürr, C. Borchers, M. Przybylski, *Proc. 42nd Conf. Am. Soc. Mass. Spectrom. Allied Topics* **1994**, 793; b) R. Schuhmacher, Diplomarbeit, Universität Konstanz, **1993**.
[65] a) K. Wüthrich, *NMR of Proteins and Nucleic Acids*, Wiley-Interscience, New York, **1986**; b) C. K. Woodward, L. M. Ellis, A. Rosenberg, *J. Biol. Chem.* **1975**, *250*, 440.
[66] a) F. M. Hughson, P. E. Wright, R. L. Baldwin, *Science* **1990**, *249*, 1544; b) H. Roder, G. A. Elore, S. W. Englander, *Nature* **1988**, *355*, 700.
[67] D. Suckau, Y. Si, S. C. Beu, M. W. Senko, J. P. Quinn, F. M. Wampler, F. W. McLafferty, *Proc. Natl. Acad. Sci. USA* **1993**, *90*, 790.
[68] B. E. Winger, K. J. Light-Wahl, A. L. Rockwood, R. D. Smith, *J. Am. Chem. Soc.* **1992**, *114*, 5897.

[69] a) R. R. Ogorzalek-Loo, H. R. Udseth, J. L. Fulton, R. D. Smith, *Rapid Commun. Mass Spectrom.* **1992**, *6*, 159; b) R. R. Ogorzalek-Loo, H. R. Udseth, R. D. Smith, *J. Am. Soc. Mass Spectrom.* **1992**, *3*, 695.

[70] S. A. McLuckey, G. J. Van Berkel, G. L. Glish, *J. Am. Chem. Soc.* **1990**, *112*, 5668.

[71] a) D. Suckau, M. Mak, M. Przybylski, *Proc. Natl. Acad. Sci. USA* **1992**, *89*, 5630; b) M. Przybylski, C. Borchers, D. Suckau, M. Mak, M. Jetschke in *Peptides 1992* (Eds.: C. H. Schneider, A. N. Eberle), Escom, Amsterdam, **1993**, p. 83.

[72] T. Imoto, L. N. Johnson, A. C. T. North, D. C. Phillips, J. A. Rupley in *The Enzymes, Vol. 7* (Ed.: P. D. Boyer), Academic Press, New York, **1972**, p. 666.

[73] a) M. Przybylski, M. O. Glocker, U. Nestel, V. Schnaible, K. Diederichs, J. Weckesser, M. Schad, A. Schmid, W. Welte, R. Benz, *Protein Sci.* **1996**, in press; b) V. Schnaible, Diplomarbeit, Universität Konstanz, **1995**.

[74] a) V. Katta, B. T. Chait, *J. Am. Chem. Soc.* **1991**, *113*, 8534; b) R. Feng, Y. Konishi, Proc. *40th Conf. Am. Soc. Mass Spectrom. Allied Topics* **1992**, 1635.

[75] B. E. Winger, K. J. Light-Wahl, R. R. Ogorzalek-Loo, H. R. Udseth, R. D. Smith, *J. Am. Soc. Mass Spectrom.* **1993**, *4*, 536.

[76] R. D. Smith, K. J. Light-Wahl, B. E. Winger, J. A. Loo, *Org. Mass Spectrom.* **1992**, *27*, 811.

[77] a) R. B. Cody, J. Tamura, J. W. Finch, B. D. Musselman, *J. Am. Soc. Mass Spectrom.* **1994**, *5*, 194; b) A. N. Verentchikov, W. Ens, K. G. Standing, *Anal. Chem.* **1994**, *66*, 126.

[78] W. Weinmann, M. Przybylski, C. E. Parker, K. B. Tomer, *Proc. 41st Conf. Am. Soc. Mass Spectrom. Allied Topics* **1993**, 743.

[79] a) M. Schuhmacher, M. Wunderlin, M. Przybylski, *Proc. 43rd Conf. Mass Spectrom. Allied Topics* **1995**, 618; b) M. Schuhmacher, Diplomarbeit, Universität Konstanz, **1994**.

[80] B. Ganem, Y. T. Li, H. J. D. Henion, *J. Am. Chem. Soc.* **1991**, *113*, 7818.

[81] M. Schindler, Y. Assaf, N. Sharon, D. M. Chipman, *Biochemistry* **1977**, *16*, 423.

[82] S. J. Perkins, L. N. Johnson, D. C. Philips, R. A. Dwek, *Biochem. J.* **1981**, *193*, 553.

[83] K. J. Lumb, R. T. Aplin, S. E. Radford, D. B. Archer, D. J. Jeenes, N. Lambert, D. A. MacKenzie, C. M. Dobson, G. Lowe, *FEBS Lett.* **1992**, *296*, 153.

[84] a) C. C. F. Blake, L. N. Johnson, G. A. Mair, A. C. T. North, D. C. Philips, V. R. Sarma, *Proc. R. Soc. London Ser. B* **1967**, *167*, 378; b) C. B. Post, M. Karplus, *J. Am. Chem. Soc.* **1986**, *108*, 1317.

[85] a) D. B. Smith, K. M. Davern, P. G. Board, W. U. Tin, E. G. Garcia, G. F. Mitchel, *Proc. Natl. Acad. Sci. USA* **1986**, *83*, 8703; b) A. Ruppel, R. Burger, R. Dell, H. J. Diesfeld, J. E. Shi, D. Wei, *Immunobiology* **1986**, *83*, 8703.

[86] a) M. R. Jetschke, M. O. Glocker, C. Adomat, M. Przybylski, *Proc. Int. ISSX-Workshop Glutathione S-transferases* **1995**, *7*, 73; b) C. Adomat, Diplomarbeit, Universität Konstanz, **1993**; c) M. Przybylski, M. O. Glocker, *Bioconjugate Chem.* **1996**, in press.

[87] M. H. Allen, I. A. S. Lewis, *Rapid Commun. Mass Spectrom.* **1989**, *3*, 255.

[88] a) Y. T. Li, Y. L. Hsieh, J. D. Henion, B. Ganem, *J. Am. Soc. Mass Spectrom.* **1993**, *4*, 631; b) Y. T. Li, Y. L. Hsieh, H. K. Lim, J. Henion, B. Ganem, *Proc. 41st Conf. Am. Soc. Mass Spectrom. Allied Topics* **1993**, 262.

[89] E. C. Huang, B. N. Pramanik, A. Tsarbopoulos, P. Reichert, A. K. Ganguly, P. P. Trotta, T. L. Nagabushan, *J. Am. Soc. Mass Spectrom.* **1993**, *4*, 624.

[90] M. Jaquinod, E. Leize, N. Potier, A. M. Albrecht, A. Shanzer, A. Van Dorsselaer, *Tetrahedron Lett.* **1993**, *34*, 2771.

[91] A. Surovoy, D. Waidelich, G. Jung in *Peptides 1992*, (Eds.: C. H. Schneider, A. N. Eberle), Escom, Amsterdam, **1993**, p. 563.

[92] M. Baca, B. H. Kent, *J. Am. Chem. Soc.* **1992**, *114*, 3992.

[93] M. Jaquinod, N. Potier, K. Klarskov, J. M. Reymann, O. Sovokine, S. Kiefer, P. Barth, V. Andriantomanga, J. F. Biellmann, A. Van Dorsselaer, *Eur. J. Biochem.* **1996**, in press.

[94] J. Schneider, S. B. H. Kent, *Cell* **1988**, *54*, 363.

[95] P. F. Alewood, R. I. Brinkworth, R. J. Dancer, B. Garnham, A. Jones, S. B. H. Kent, *Tetrahedron Lett.* **1992**, *33*, 977.

[96] P. L. Darke, C. T. Leu, L. J. Davis, J. C. Heimbach, R. E. Diehl, W. S. Hill, R. A. F. Dixon, I. S. Sigal, *J. Biol. Chem.* **1989**, *264*, 2307.

[97] a) E. Leize, A. Jaffrezic, A. Van Dorsselaer, *J. Mass Spectrom.* **1996**, in press; b) P. Kopf, Diplomarbeit, Universität Konstanz, **1995**.

[98] M. A. Weiss, T. Ellenberger, C. R. Wobbe, J. P. Lee, S. C. Harrison, K. Struhl, *Nature* **1990**, *347*, 575.

[99] K. T. O'Neil, R. H. Hoess, W. F. DeGrado, *Science* **1990**, *249*, 774.

[100] P. Hemmerich, A. von Mikecz, F. Neumann, O. Sözeri, G. Wolff-Vorbeck, R. Zoebelein, U. Krawinkel, *Nucleic Acids Res.* **1993**, *21*, 223.

[101] E. E. Blatter, Y. W. Ebright, R. H. Ebright, *Nature* **1992**, *359*, 650.

[102] C. Cohen, D. A. D. Perry, *Proteins Struct. Funct. Gen.* **1990**, *7*, 1.

[103] T. G. Oas, L. P. McIntosh, E. K. O'Shea, F. W. Dahlquist, P. Kim, *Biochemistry* **1990**, *29*, 2891.

[104] E. K. O'Shea, J. D. Klemm, P. S. Kim, T. Alber, *Science* **1991**, *254*, 539.

[105] Y. T. Li, Y. L. Hsieh, J. D. Henion, M. W. Senko, F. W. McLafferty, B. Ganem, *J. Am. Chem. Soc.* **1993**, *115*, 8409.

[106] S. C. Beu, M. W. Senko, J. P. Quinn, F. M. Wampler, F. W. McLafferty, *J. Am. Soc. Mass Spectrom.* **1993**, *4*, 557.

[107] H. Wendt, E. Dürr, R. M. Thomas, M. Przybylski, H. R. Bosshard, *Protein Sci.* **1995**, *4*, 1563.

[108] a) M. Przybylski, J. Kast, M. O. Glocker, E. Dürr, H. R. Bosshard, S. Nock, M. Sprinzl, *Toxicol. Lett.* **1995**, *82/83*, 567–575; b) T. Fligge, Diplomarbeit, Universität Konstanz, **1995**.

[109] B. Lovejoy, S. Choe, D. Cascio, D. K. McRorie, W. F. DeGrado, D. Eisenberg, *Science* **1993**, *259*, 1288.

[110] H. Wendt, C. Berger, A. Baici, R. M. Thomas, H. R. Bosshard, *Biochemistry* **1995**, *34*, 4097.

[111] a) M. Przybylski, M. O. Glocker, C. Maier, C. Borchers, E. Dürr, W. Fiedler, J. Kast, H. Wendt, H. R. Bosshard in *Peptides 1994* (Ed.: H. L. S. Maia), Escom, Leiden, **1995**, p. 42; b) S. Witte, F. Neumann, U. Krawinkel, M. Przybylski, *J. Biol. Chem.* **1996**, submitted.

[112] C. Maier, K. Müller, K. Baumeister, E. Bauer, E. Hannappel, R. Nave, K. Melchers, E. Sturm, W. Gernandt, U. Krüger, K. P. Schäfer, M. Przybylski, *Proc. 41st Conf. Am. Soc. Mass Spectrom. Allied Topics* **1993**, 351.

[113] M. Przybylski, C. Maier, K. Hägele, E. Bauer, E. Hannappel, R. Nave, K. Melchers, U. Krüger, K. P. Schäfer in *Peptides: Chemistry, Structure and Biology* (Eds.: R. S. Hodges, J. A. Smith), Escom, Leiden, **1994**, p. 338.

[114] T. E. Weaver, J. A. Whitsett, *Biochem. J.* **1991**, *273*, 249.

[115] J. F. Lewis, A. H. Jobe, *Am. Rev. Resp. Dis.* **1993**, *147*, 218.

[116] T. Voss, K. P. Schäfer, P. F. Nielsen, A. Schäfer, C. Maier, E. Hannappel, J. Maaßen, B. Landis, K. Klemm, M. Przybylski, *Biochim. Biophys. Acta* **1992**, *1138*, 261.

[117] a) A. Schäfer, P. F. Nielsen, T. Voss, E. Hannappel, C. Maier, J. Maaßen, E. Sturm, K. Klemm, K. P. Schäfer, M. Przybylski in *Peptides 1990* (Eds.: E. Giralt, D. Andreu), Escom, Leiden, **1991**, p. 350; b) T. Curstedt, J. Johansson, P. Persson, A. Eklund, B. Robertson, B. Löwenadler, H. Jörnvall, *Proc. Natl. Acad. Sci. USA* **1990**, *87*, 2985.

[118] a) W. Weinmann, C. E. Parker, K. Baumeister, C. Maier, K. B. Tomer, M. Przybylski, *Electrophoresis* **1994**, *15*, 118; b) W. Weinmann, C. Maier, K. Baumeister, M. Przybylski, C. E. Parker, K. B. Tomer, *J. Chromatogr.* **1994**, *664*, 271.

[119] B. L. Schwartz, J. E. Bruce, G. A. Anderson, S. A. Hofstadler, A. L. Rockwood, R. D. Smith, A. Chilkoti, P. S. Stayton, *J. Am. Soc. Mass Spectrom.* **1995**, *6*, 459.

[120] D. F. Senear, D. C. Teller, *Biochemistry* **1981**, *20*, 3076.

[121] A. Verentchikov, W. Ens, K. G. Standing, *Proc. 41st Conf. Am. Soc. Mass Spectrom. Allied Topics* **1993**, 4.

[122] a) M. Claeys, L. Dillen, E. L. Esmans, *Adv. Mass Spectrom.* **1995**, *13*, 521; b) F. W. McLafferty, M. W. Senko, D. P. Little, T. D. Wood, P. B. O'Conner, J. P. Speir, R. A. Chorush, N. L. Kelleher, *ibid.* **1995**, *13*, 115.

[123] S. A. McLuckey, G. J. Van Berkel, G. L. Glish, *J. Am. Soc. Mass Spectrom.* **1992**, *3*, 60; b) K. Bleicher, E. Bayer, *Biol. Mass Spectrom.* **1994**, *23*, 320; c) S. C. Pomerantz, J. A. Kowalak, J. A. McCloskey, *J. Am. Soc. Mass Spectrom.* **1993**, *4*, 204.

[124] a) K. J. Light-Wahl, D. L. Springer, B. E. Winger, C. G. Edmonds, D. G. Camp, B. D. Thrall, R. D. Smith, *J. Am. Chem. Soc.* **1993**, *115*, 803; b) B. Ganem, Y. T. Li, J. D. Henion, *Tetrahedron Lett.* **1993**, *34*, 1445.

[125] V. Saudek, H. S. Pasley, T. Gibson, H. Gausepohl, R. W. Frank, A. Pastore, *Biochemistry* **1991**, *30*, 1310.

[126] A. Paulus, J. I. Ohms, *J. Chromatogr.* **1990**, *507*, 113.

[127] D. R. Goodlett, C. C. Hardin, M. Corregan, R. D. Smith, *Proc. 41st Conf. Am. Soc. Mass Spectrom. Allied Topics* **1993**, 258.

[128] a) L. Grotjahn, L. C. E. Taylor, *Org. Mass Spectrom.* **1985**, *20*, 146; b) S. A. McLucky, S. Habibi-Goudarzi, *J. Am. Chem. Soc.* **1993**, *115*, 12085.

[129] a) J. Sambrook, E. F. Fritsch, T. Maniatis, *Molecular Cloning*, Cold Spring Harbor Laboratory Press, New York, **1989**; b) J. Meinkoth, G. Wahl, *Anal. Biochem.* **1984**, *138*, 267; c) A. G. Polson, P. F. Crain, S. C. Pomerantz, J. A. McCloskey, B. L. Bass, *Biochemistry* **1991**, *30*, 11507; d) E. Bruenger, J. A. Kowalak, Y. Kuchino, J. A. McCloskey, H. Mizuchima, K. O. Stetter, P. F. Crain, *FASEB J.* **1993**, *7*, 196.

[130] E. Uhlmann, A. Peymann, *Chem. Rev.* **1990**, *90*, 544.

[131] a) Y. L. Hsieh, Y.-T. Li, J. D. Henion, B. Ganem, *Biol. Mass Spectrom.* **1994**, *23*, 272; b) D. C. Gale, D. R. Goodlett, K. J. Light-Wahl, R. D. Smith, *J. Am. Chem. Soc.* **1994**, *116*, 6027.

[132] H. E. Moser, P. B. Dervan, *Science* **1987**, *238*, 645.

[133] M. D. Distefano, P. B. Dervan, *Proc. Natl. Acad. Sci. USA* **1993**, *90*, 1779.

[134] D. R. Goodlett, D. G. Camp, C. C. Hardin, M. Corregan, R. D. Smith, *Biol. Mass Spectrom.* **1993**, *22*, 181.

[135] C. C. Hardin, T. Watson, M. Corregan, C. Bailey, *Biochemistry* **1992**, *31*, 833.

[136] J. R. Williamson, M. K. Raghuramunan, T. R. Cech, *Cell* **1989**, *59*, 871.

[137] M. G. Ikonomou, A. T. Blades, P. Kebarle, *Anal. Chem.* **1991**, *63*, 1989.

[138] M. Sprinzl, *Trends Biol. Sci.* **1994**, *19*, 245.

[139] M. O. Glocker, S. Nock, M. Sprinzl, M. Przybylski, *Proc. 43rd Conf. Am. Soc. Mass Spectrom. Allied Topics* **1995**, 1330.

[140] a) E. C. Constable, *Angew. Chem.* **1991**, *103*, 418; *Angew. Chem. Int. Ed. Engl.* **1991**, *30*, 407; b) *Nature* **1990**, *346*, 314.

[141] a) J.-M. Lehn, *Angew. Chem.* **1990**, *102*, 1347; *Angew. Chem. Int. Ed. Engl.* **1990**, *29*, 1304; b) P. Baxter, J.-M. Lehn, A. DeCian, J. Fischer, *ibid.* **1993**, *105*, 92 bzw. **1993**, *32*, 69.

[142] a) D. Philp, J. F. Stoddart, *Synlett* **1991**, 445; b) J. F. Stoddart, *Angew. Chem.* **1992**, 104, 860; *Angew. Chem. Int. Ed. Engl.* **1992**, *31*, 846.
[143] H. Ringsdorf, B. Schlarb, J. Venzmer, *Angew. Chem.* **1988**, *100*, 117; *Angew. Chem. Int. Ed. Engl.* **1988**, *27*, 113.
[144] a) C. O. Dietrich-Buchecker, J. P. Sauvage, *Chem. Rev.* **1987**, *87*, 795; b) C. O. Dietrich-Buchecker, B. Frommberger, I. Luer, J. P. Sauvage, F. Vögtle, *Angew. Chem.* **1993**, *105*, 1526; *Angew. Chem. Int. Ed. Engl.* **1993**, *32*, 1434.
[145] a) J. F. Stoddart, *Guest-Host Molecular Interactions: from Chemistry to Biology*, Wiley, Chichester, **1991**, pp. 5–22; b) C. Seel, F. Vögtle, *Angew. Chem.* **1992**, *104*, 542; *Angew. Chem. Int. Ed. Engl.* **1992**, *31*, 528.
[146] U. Koert, M. M. Harding, J.-M. Lehn, *Nature* **1990**, *346*, 339.
[147] J. S. Nowick, Q. Feng, T. Tjivikua, P. Ballester, J. Rebek, Jr., *J. Am. Chem. Soc.* **1991**, *113*, 8831.
[148] E. Leize, A. Van Dorsselaer, R. Krämer, J.-M. Lehn, *J. Chem. Soc. Chem. Commun.* **1993**, 990.
[149] P. R. Ashton, C. L. Brown, J. R. Chapman, R. T. Gallagher, J. F. Stoddart, *Tetrahedron Lett.* **1992**, *33*, 7771.
[150] J. C. Chambron, V. Heitz, J. P. Sauvage, *J. Chem. Soc. Chem. Commun.* **1992**, 1131.
[151] R. Krämer, J.-M. Lehn, A. Marquis-Rigault, *Proc. Natl. Acad. Sci. USA* **1993**, *90*, 5394.
[152] F. Bitsch, C. O. Dietrich-Buchecker, A. K. Khemiss, J. P. Sauvage, A. Van Dorsselaer, *J. Am. Chem. Soc.* **1991**, *113*, 4023.
[153] V. Katta, S. K. Chowdhury, B. T. Chait, *J. Am. Chem. Soc.* **1990**, *112*, 5348.
[154] S. R. Wilson, A. Yasmin, Y. Wu, *J. Org. Chem.* **1992**, *57*, 6941.
[155] a) P. R. Ashton, T. T. Goodnow, A. E. Kaifer, M. V. Reddington, A. M. Z. Slawin, N. Spencer, J. F. Stoddart, C. Vincent, D. J. Williams, *Angew. Chem.* **1989**, *101*, 1404; *Angew. Chem. Int. Ed. Engl.* **1989**, *28*, 1396; b) P. R. Ashton, D. Philp, J. F. Stoddart, *J. Chem. Soc. Chem. Commun.* **1992**, 1124.
[156] A. Pfeil, J.-M. Lehn, *J. Chem. Soc. Chem. Commun.* **1992**, 838.
[157] E. C. Constable, *Tetrahedron* **1992**, *48*, 10013.
[158] C. E. Ballou, A. Dell, *Carbohydr. Res.* **1985**, *140*, 139.
[159] K. Schneider, P. F. Nielsen, D. Suckau, M. Przybylski in *Mass Spectrometry of Large Non-Volatile Molecules* (Eds.: E. Hilf, A. Tuczynski), World Sci., Singapur, **1990**, p. 176.
[160] a) F. Hillenkamp, M. Karas, *Methods Enzymol.* **1990**, *193*, 280; b) R. Beavis, B. T. Chait, *Rapid Commun. Mass Spectrom.* **1989**, *3*, 323; c) M. Karas, U. Bahr, A. Ingendoh, F. Hillenkamp, *Angew. Chem.* **1989**, *101*, 805; *Angew. Chem. Int. Ed. Engl.* **1989**, *28*, 760.
[161] A. Overberg, A. Hassenbürger, F. Hillenkamp in *Mass Spectrometry in the Biological Sciences* (Eds.: M. Gross, G. Sindona), Kluwer, Dordrecht, **1994**, p. 181.
[162] a) J. P. Sauvage, *Acc. Chem. Res.* **1990**, *23*, 319; b) D. B. Amabilino, P. R. Ashton, A. S. Reder, N. Spencer, J. F. Stoddart, *Angew. Chem.* **1994**, *106*, 450; *Angew. Chem. Int. Ed. Engl.* **1994**, *33*, 433.
[163] a) M. Born, H. Ritter, *Makromol. Chem. Rapid Commun.* **1991**, *121*, 471; b) K. Hägele, M. Born, H. Ritter, M. Svoboda, M. Przybylski, *Abstr. 12th Int. Mass Spectrom. Conf.* **1991**, 196.
[164] M. Svoboda, Dissertation, Universität Konstanz, **1993**.
[165] B. D. Reverend, F. Liman, C. Livera, L. D. Pettit, S. Pyburn, H. Kozlowski, *J. Chem. Soc. Dalton Trans.* **1988**, 887.
[166] R. D. Macfarlane, Z. H. Hu, S. Song, E. Pittenauer, E. R. Schmid, G. Allmaier, J. O. Metzger, W. Tuczynski, *Biol. Mass Spectrom.* **1994**, *3*, 117.
[167] G. Allmaier, E. Pittenauer, E. R. Schmid, *Org. Mass Spectrom.* **1991**, *26*, 804.
[168] a) D. L. Smith, Z. Zhang, *Mass Spectrom. Rev.* **1994**, *13*, 411; b) R. C. Beavis, *Org. Mass Spectrom.* **1992**, *27*, 653.
[169] a) W. Weinmann, C. E. Parker, L. E. Deterding, D. Papac, J. Hoyes, M. Przybylski, K. B. Tomer, *J. Chromatogr.* **1994**, *680*, 353; b) A. Wattenberg, Diplomarbeit, Universität Konstanz, **1995**.
[170] M. J. F. Suter, W. T. Moore, T. B. Farmer, J. S. Cottrell, R. M. Caprioli in *Techniques in Protein Chemistry III* (Ed.: H. Angeletti), Academic Press, New York, **1992**.
[171] M. C. Fitzgerald, G. R. Parr, L. M. Smith, *Anal. Chem.* **1993**, *65*, 3204.
[172] a) A. Overberg, M. Karas, U. Bahr, R. Kaufmann, F. Hillenkamp, *Rapid Commun. Mass Spectrom.* **1990**, *4*, 293; b) A. Overberg, M. Karas, F. Hillenkamp, *ibid.* **1991**, *5*, 128.
[173] E. A. Merritt, S. Sarfaty, F. van den Akker, C. L'Hoir, J. A. Martial, W. G. J. Hol, *Protein Sci.* **1994**, *3*, 166.
[174] J. Drenth, *Principles of Protein X-Ray Crystallography*, Springer, New York, **1994**.
[175] A. Bax, *Annu. Rev. Biochem.* **1989**, *58*, 223.
[176] Y. Hagihara, Y. Tany, Y. Goto, *J. Mol. Biol.* **1994**, *237*, 336.
[177] P. Kebarle, L. Tang, *Anal. Chem.* **1993**, *65*, 972A.
[178] J. P. Speir, M. W. Senko, D. P. Little, J. A. Loo, F. W. McLafferty, *J. Mass Spectrom.* **1995**, *30*, 39.
[179] A. Miranker, C. V. Robinson, J. E. Radford, R. T. Aplin, C. M. Dobson, *Science* **1993**, *262*, 896.
[180] M. A. Lemmon, J. M. Flanagan, H. R. Treutlein, J. Zhang, D. M. Engelman, *Biochemistry* **1992**, *31*, 12719.
[181] A. Plückthun, *Immun. Rev.* **1992**, *130*, 152.
[182] R. E. Bird, K. D. Hardman, J. W. Jacobson, S. Johnson, B. M. Kaufman, S. M. Lee, T. Lee, S. H. Pope, G. S. Riordan, M. Whitlow, *Science* **1988**, 242, 423.
[183] a) K. Falk, O. Rötschke, S. Stefanovic, G. Jung, H. G. Rammensee, *Nature* **1991**, *351*, 290; b) J. W. Metzger, K. H. Wiesmüller, V. Gnau, J. Brünjes, G. Jung, *Angew. Chem.* **1993**, *105*, 901; *Angew. Chem. Int. Ed. Engl.* **1993**, *32*, 894.
[184] J.-M. Lehn, M. Mascal, A. DeCian, J. Fischer, *J. Chem. Soc. Chem. Commun.* **1990**, 479.
[185] F. H. Kohnke, J. P. Mathias, J. F. Stoddart in *Molecular Recognition: Chemical and Biochemical Problems* (Ed.: S. M. Robert), The Royal Society of Chemistry, Cambridge, **1989**, p. 233.

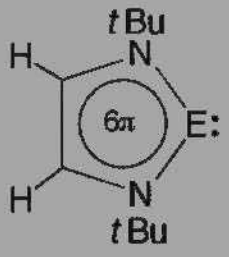

E = Si, Ge

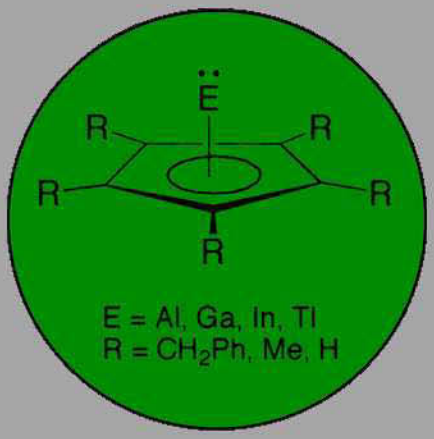

E = Al, Ga, In, Tl
R = CH_2Ph, Me, H

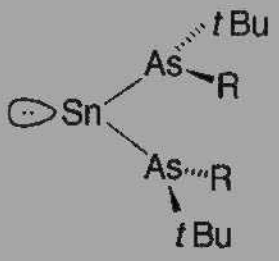

R = *i* $Pr_3C_6H_2$

R^2 = 2,4,6-$(CF_3)_3C_6H_2$

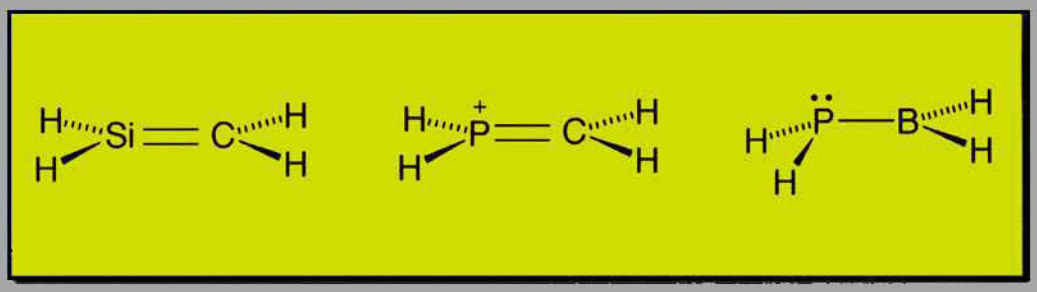

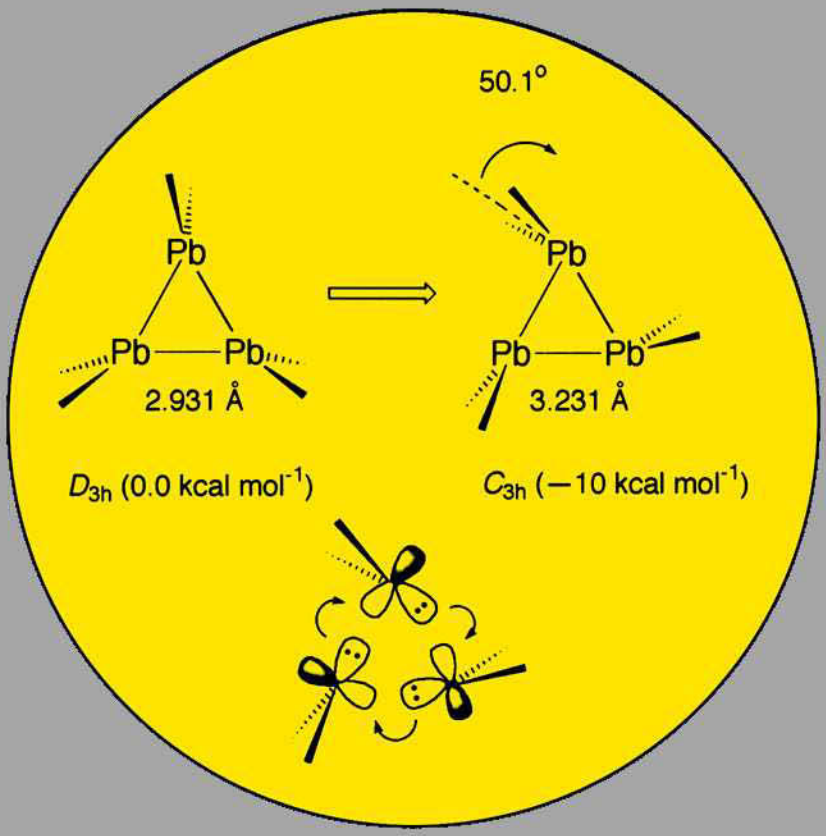

A wealth of main group element compounds that resemble olefins, carbenes, and small carbon rings, and yet exhibit their own quite individual chemistry are reported by M. Driess and H. -J. Grützmacher.

Main Group Element Analogues of Carbenes, Olefins, and Small Rings

Matthias Driess* and Hansjörg Grützmacher*

Dedicated to Professor Herbert W. Roesky on the occasion of his 60th birthday

For a long time methylene ($:CH_2$), ethylene ($H_2C=CH_2$), and cyclopropane [$(CH_2)_3$] were considered as compounds whose higher main group homologues or analogues could not be synthesized. One consequence of the failure of earlier experiments was, for example, the "double bond rule" which was introduced over twenty years ago and is still often quoted. Although it does not dispute the existence of multiple bonding between elements, it states that it leads to very kinetically unstable species. This interpretation of the double bond rule has long since been surpassed due to improved experimental and quantum chemical methods which have allowed the synthesis of main group analogues of methylene, ethylene, and cyclopropane that are kinetically stable in solution and the solid state at room temperature. In the following review recent advances in the synthesis of these compounds will be referenced, and the concepts, which were developed by a systematic study, will be laid out. In doing so, a detailed description of the complex reactivity of the individual classes of compounds will be avoided in order to highlight the basic principles. These can then be used to approximately predict reactivity and characteristics of new compounds. There are significant differences between formally and even structurally analogous compounds with elements from the higher rows as compared to their "lighter" homologues. For example, while every chemist is familiar with the planar D_{2h} symmetrical structure of $H_2C=CH_2$ as the only "significant" isomer, it must be accepted that Sn_2H_4 has four isomers that are separated by very small energy differences. For *cis/trans* isomerism of olefins only the rotation of the C–C double bond needs to be considered, but there are three possible mechanisms for the disilene derivatives $R^1RSi=SiR^1R$. In the last century cyclopropane was considered to be not producible and this provided the impetus for Baeyer's strain theory. Investigations into small silicon cycles, which were discovered much later, show that this theory has more validity for these rings. As a result of the collected data, it is slowly becoming clearer that precisely the carbon compounds once seen as mere models are in reality the "exotic" compounds. Rules with broader applications can be developed by studying the compounds made up of main group elements.

Keywords: carbene analogues · double bond systems · main group element compounds · small rings

1. Introduction

It is the endeavor of every scientist to order his findings and to add to the current body of knowledge. The development of the periodic system of the elements in 1869 by Mendeleev and Meyer is a result of this effort in chemistry and has proven itself as a capable concept of lasting value. From this time comes, for example, the established concept of homologous elements. This defines elements with the same number of valence electrons as forming a family (element group) in which the individual elements and their compounds exhibit similar chemical and physical properties. This "early" periodic system as an ordering principle was based on the experimental methods available at that time. In other words, the capabilities of the systemization were (and have remained) in direct relationship to technical developments and the experimenter's manual skill. The then accepted model led, at the beginning of this century, to attempts to extend the chemistry of the classical main group elements, carbon, nitrogen, and oxygen, to their higher homologues. Investigations were therefore carried out into making silicon analogues of classes of compounds known from organic chemistry such as alkanes, cycloalkanes, and olefins. Despite the decades of continual failure in the search for such compounds, the persistent confidence of many research groups has led to the solution of many synthetic problems. In addition, a symbiotic relationship between experimental and theoretical chemistry has provided an essential improvement in our basic understanding of bonding

[*] Priv.-Doz. Dr. M. Driess
Anorganisch-chemisches Institut der Universtität
Im Neuenheimer Feld 270, D-69120 Heidelberg (Germany)
Fax: Int. code +(6221) 54 41 97
e-mail: dp0@ix.uni-heidelberg.de

Prof. Dr. H. Grützmacher[+]
Institut für Anorganische und Analytische Chemie der Universität
Albertstrasse 21, D-79104 Freiburg (Germany)

[+] New address: Laboratorium für Anorganische Chemie der Eidgenössischen Technischen Hochschule ETH-Zentrum
Universitätsstrasse 6, CH-Zürich (Switzerland)
Fax: Int. code +(1) 632 1090
e-mail: gruetz@elwood.ethz.ch

 © VCH Verlagsgesellschaft mbH, D-69451 Weinheim, 1996 0570-0833/96/3508-0829 $ 15.00+.25/0

theory. However, in applying the homologue concepts, the dramatic changes that occur in character upon replacement of one carbon center with a silicon (semi-metal) or even a tin (metal) center have sometimes been overlooked. Since characteristics of various materials can be analyzed by using an appropriate spectroscopic measurement of energy exchanges, the classical two-dimensional periodic system can be extended to a third dimension to include energy values. For this, L. C. Allen chose spectroscopic electronegativity, χ_{spec}, as a characteristic value for each element. It can be experimentally determined from the atomic ionization potentials and proves itself to be compatible with the electronegativity scales established by Pauling and Allred-Rochow.[1] Based on the three-dimensional periodic system much information including the transition from nonmetals [for example: χ_{spec} 4.193 (F)-2.253 (P)] to "metalloids" B, Si, Ge, As, Sb, Te [χ_{spec} 2.211 (As)-1.916 (Si)] and metals [$\chi_{spec} < 1.824$] is well defined. The significant changes in χ_{spec} that occur upon going from the elements in the second row ($n = 2$) to the homologues in higher rows ($n > 2$) are also clarified. This corresponds to the differences in material character between formally comparable compounds. In addition, this extension of the periodic system provides a physical basis for the long known "diagonal relationship" between elements, which becomes apparent from the similar spectroscopic electronegativities (for example: B (2.051) → Si (1.916) and C (2.544) → P (2.253); compare with the larger difference in the electronegativities $\Delta\chi_{spec}$ for the respective homologous elements Al (1.613) and Si). By using selected main group element compounds analogous to carbenes, olefins, and cycloalkanes, we would like to try and point out the similarities and, more importantly, the differences the homologous substance classes may show.

2. The Concept: The Carter-Goddard-Malrieu-Trinquier (CGMT) Model for Describing Distortions in Multiply Bonded Systems

In the following review molecular compounds of main group elements that are formed from carbene-analogous fragments will be discussed. It is therefore useful to present a model developed by Carter and Goddard III as well as Malrieu and Trinquier, which allows a correlation of the singlet-triplet excitation energy of these fragments with several characteristics of the complete molecule.

In a computational experiment, a molecule $XYE=E^1X^1Y^1$ (E = central atom, X,Y,X^1,Y^1 = arbitrary substituents) with a double bond was homolytically cleaved into two fragments EXY and $E^1X^1Y^1$.[2] In this process, the σ and π bonds, by removal of spin-pairing, were broken and the fragments EXY and $E^1X^1Y^1$ thus exist in a *triplet state* (Fig. 1).

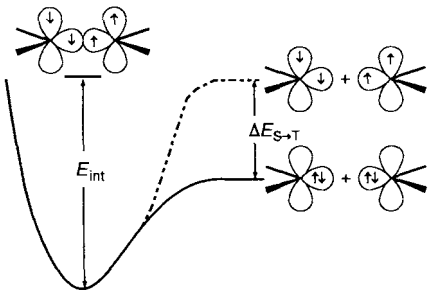

Fig. 1. Schematic representation of the dissociation of a planar, double bond system into two triplet carbene fragments [2a]. E_{int} corresponds to the C=C bond energy for C_2H_4 (172 ± 2 kcal mol^{-1}). $\Delta E_{S\rightarrow T}$ is the singlet-triplet excitation energy of the carbene fragments, which in this case is positive (the fragments have a singlet ground state).

Matthias Driess was born in 1961 in Eisenach/Thüringen, studied chemistry from 1981 to 1985 in Heidelberg, and obtained his Ph.D. in 1988 under the supervision of Professor W. Siebert. After a one-year post-doctoral position with Professor R. West in Madison, Wisconsin (USA), he returned to Heidelberg and started his habilitation in 1990 which he finished in 1993. Since then he has been a Privatdozent at the Anorganisch-chemisches Institut, Heidelberg.

Hansjörg Grützmacher was born in 1959 in Hamburg, studied chemistry from 1978 to 1984 in Göttingen, and obtained his Ph.D. in 1986 under the supervision of Professor H. W. Roesky. After a one-year post-doctoral position with Dr. G. Bertrand at the CNRS-LCC in Toulouse he started his habilitation in 1987 with Professor W. Sundermeyer in Heidelberg which he finished in 1992. In the same year he accepted a position as a C3 professor in Freiburg and in 1995 took up an offer as a distinguished professor at the ETH Zürich.

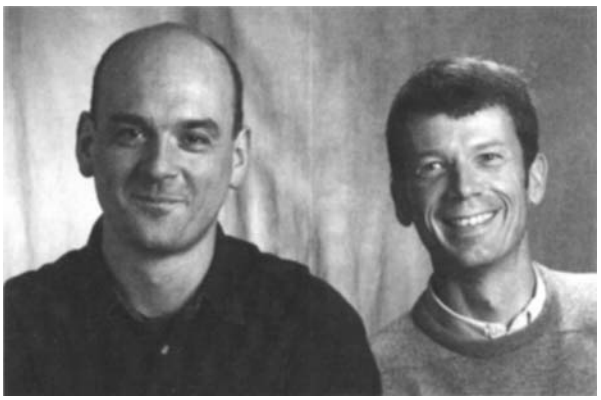

M. Driess H. Grützmacher

The authors of this contibution have been friends since their habilitation time in Heidelberg and have been mainly involved with main group element compounds and their significance in simple, useful bonding concepts ("chemical rules of thumb"). Both received the ADUC prize for young scientists and were further distinguished with the Ruprecht-Karls-Preis der Universität Heidelberg (M. D.), the Freudenberg-Preis der Akademie der Wissenschaften zu Heidelberg (H. G.), a Winnacker award (H. G.), the Carl-Duisberg-Gedächtnis-Preis der GDCh (H. G.), and a Dozentenstipendium (award) from the Fonds der Chemischen Industrie (M. D.).

In general the *ground state* of these fragments can be either a triplet or a singlet state. By using differently substituted alkenes $XYC{=}C^1X^1Y^1$, Carter and Goddard III showed that the C=C double bond energy E_{TBE} can be obtained from the intrinsic C=C bond energy E_{int} of ethylene (172 ± 2 kcal mol^{-1}) minus the sum of the singlet–triplet excitation energy $\Sigma\Delta E_{S\rightarrow T}$ of the fragments EXY and $E^1X^1Y^1$ [Eq. (a)].

$$E_{TBE} = E_{int} - \Sigma\Delta E_{S\rightarrow T} \qquad \text{(a)}$$

Difluorocarbene CF_2 has a singlet ground state that is about 46.5 kcal mol^{-1} more stable than the triplet state. Thus, E_{TBE} is $172 - 2\,(46.5) = 79$ kcal mol^{-1} and in excellent agreement with the experimentally determined value of 76.3 ± 3 kcal mol^{-1}. Equation (a) is also suitable for estimating the singlet–triplet excitation energy of carbenes from experimentally available double bond energies. EXY fragments with a central atom E from a higher row have a singlet ground state that can be considerably more stable than the triplet state (see below). Since the intrinsic bond energy of the E–E double bond decreases with increasing atomic number, this leads to the curious observation that an E - E double bond can have a lower dissociation energy than an E–E single bond.[3] In other words, the dissociation energy alone is not an appropriate criterion for characterizing a multiply bonded system.

This model from Carter and Goddard III, which correlates the bond energy E_{TBE} with the excitation energy $\Delta E_{S\rightarrow T}$ of the fragment EXY, was extended by Trinquier and Malrieu to enable predictions to be made about the *geometry* of a doubly bonded system depending on the $\Delta E_{S\rightarrow T}$ values of the fragments EXY and $E^1X^1Y^1$. Here the dissociation of a multiply bonded system was not considered. Instead the *combination* of the fragments, as a function of the spin state, was investigated by calculating the total energy of the systems $EXY + E^1X^1Y^1$ as well as the geometric parameters r and θ.[4] The latter describe the E-E^1 distance (r) and the angle (θ) of the two orthogonally placed fragments EXY, $E^1X^1Y^1$ (Fig. 2).

A relative energy scale was plotted on the abscissa, whose origin corresponds to the energy content of two carbene fragments in the *singlet* state. Curve a corresponds to the combination of two carbene fragments with a triplet ground state [$\Delta E_{S\rightarrow T} < 0$]. Curve b represents the combination of two carbene fragments with excited triplet states and is shifted by the value $\Sigma\Delta E_{S\rightarrow T}$ with respect to curve a. The differently shaped curve c results from the interaction of two singlet state carbene fragments. The trace of curves a and b can be described as follows. When the distance r between two separated triplet carbenes is reduced to the equilibrium distance r_{eq}, the system first gains σ bonding energy E_σ as a result of the overlap of the two oppositely positioned spins in the singly occupied p orbitals of the fragments EXY. Thereafter, a tipping action, described by θ, of the fragments away from each other takes place. This leads to a maximal stabilization of the two triplet carbene fragments at an angle $\theta = 0°$. The total energy gain in the resulting "classical" planar doubly bonded system corresponds to the interaction energy $E_{\sigma+\pi}$ which was approximated by Malrieu and Trinquier using experimental or calculated dissociation energies. Another trace is shown by curve c, which describes the approach of two singlet state carbene fragments. There is no observed change in energy in the system upon approaching the distance r_{eq} as there is no bond formation. Furthermore the repulsive interaction due to the unoccupied p orbitals of the fragments in their *trans* orientation with respect to each other is negligible. Only in the second step during which the fragments are tilted is there an interaction. This reaches a maximum at about 45° since the effective electron density from the lone pairs of electrons of the singlet EXY fragments is delocalized in the p(π) acceptor orbitals. This description of a "double bond" as a doubled donor–acceptor bond matches that used by Lappert et al. in 1976.[5] This interaction becomes increasingly destabilized with decreasing angle θ, since the lone pairs of electrons repel each other (two-center–four-electron interaction). The depth of the potential well in curve c also corresponds to approximately half of the interaction energy $E_{\sigma+\pi}$.

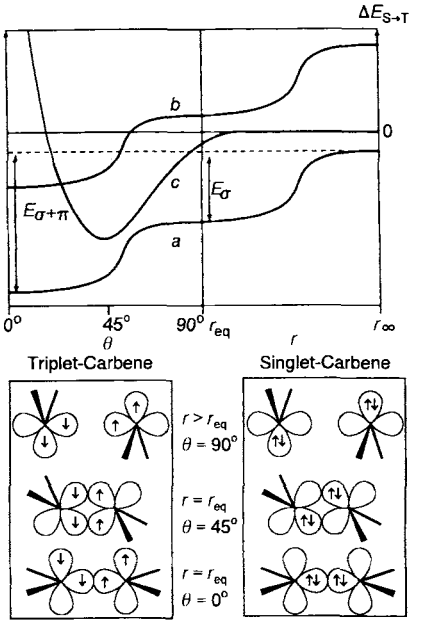

Fig. 2 Schematic interaction diagram of two carbenes or carbene analogues EXY as a function of the positional parameter r (distance) and θ (bending angle) [2b–d]. Curve *a* describes the interaction of two carbene fragments with a triplet ground state. The parallel curve *b* shows the interaction of two carbene fragments with excited triplet states. Curve *c* describes the interaction of two singlet state carbene fragments and has its start at the arbitrarily placed origin of the energy scale ($2\Delta E_{S\rightarrow T}$ (singlet) = 0). For an explanation of $E_{\sigma+\pi}$ and E_σ see text. The orbital interaction of triplet and singlet carbene fragments for different bending angles and distances is shown schematically at the bottom.

The extent of deviation of a doubly bonded system from planarity as well as the vibration energy that must be expended for the *trans* bending of the two fragments EXY and $E^1X^1Y^1$ is dependent on the respective positioning of the curves. In general, the following rules apply: a "classical" planar doubly bonded system is expected according to inequality (b), a "nonclassical"

$$\Sigma\Delta E_{S\rightarrow T} < 1/2E_{\sigma+\pi} \qquad \text{(b)}$$

structure with deviations from planarity according to inequality (c). In other words carbene fragments with a triplet ground state ($\Sigma\Delta E_{S\rightarrow T} < 0$), which form thermodynamically stable double

$$\Sigma\Delta E_{S\rightarrow T} > 1/2E_{\sigma+\pi} \qquad \text{(c)}$$

bonds ($1/2E_{\sigma+\pi} \gg 0$), lead to a coplanar ordering of the fragments. Double bonds that are formed from fragments with a singlet ground state ($\Sigma\Delta E_{S\rightarrow T} > 0$), and whose bond energies $E_{\sigma+\pi}$ are very small, show a nonplanar (*trans*-bent) orientation of the fragments with respect to each other. As we will show, these predictions have been confirmed without exception. The limiting cases in which the sum of the excitation energies $\Sigma\Delta E_{S\rightarrow T}$ is almost as large as half of the bond energy $1/2E_{\sigma+\pi}$ are of interest. Such compounds can adopt different molecular geometries as a result of minor changes (for example, crystal packing and substituent effects).

π-Donor substituents, such as F, OR, or NR_2 groups, stabilize singlet carbene fragments by interaction of the occupied p orbitals (lone pairs of electrons) on the heteroatom with the formally unoccupied p orbitals on the carbene center (Fig. 3).

Fig. 3. Representation of the π* MO of a carbene fragment with π-donor substitution (for example, NR_2, OR, F) which, instead of combining with an unoccupied pπ orbital of a carbene fragment without π-donor sustituents (see Figs. 1 and 2), combines with a second carbene fragment to describe the interaction with an occupied *n*σ orbital. π-Donors cause first an increase in the electron density on the carbene center E and thereby a repulsive interaction upon a lowering of r and second a decrease in the depth of the potential well (compare $E_{\sigma-\pi}$ in Section 2) with variation of $\theta < 90°$; thus this fragment prefers a nonclassical structure [2b].

In addition, the singlet ground state of a carbene can be lowered even further in energy by σ acceptors. This can be explained clearly in the framework of the VSEPR model as a reduction in the X-E-Y angle and an increase in the s character of the lone pair of electrons on the carbene center (see also Section 3). Since the substituents used also influence the dissociation energy of the E–E double bond, inequalities (b) and (c) must be modified. A bent ordering of the π-conjugated fragments would be expected when the relationship (d) is valid,

$$\Sigma\Delta E_{S\rightarrow T} > 1/2E_{\sigma+\pi}\,[1 + (q^1 + q^2)/2] + \alpha q^1 q^2 = f(E_{\sigma+\pi}) \qquad \text{(d)}$$

$$f = 1/2[1 + (q^1 + q^2)/2] + \alpha q^1 q^2 \qquad \text{(d')}$$

in which f is defined according to (d') and where q^1 and q^2 are calculated net charges of the p(π) orbital on the carbene fragments EXY and $E^1X^1Y^1$, respectively, and the proportionality factor α can be estimated to within 200 kcal mol^{-1}. Due to the factor f, the value on the right-hand side of the relationship (d) becomes smaller and the sum of the excitation energy $\Delta E_{S\rightarrow T}$ in π-donor substituted singlet carbene fragments rises simultaneously. The result is, for example, that (partial) fluorination of a doubly bonded system leads to a drastic change in the molecular geometry. This is shown by a comparison of $H_2Si{=}CH_2$ with $F_2Si{=}CH_2$, $H_2Si{=}CF_2$, and $F_2Si{=}CF_2$. Silanediyl H_2Si: has a singlet ground state ($\Delta E_{S\rightarrow T}$ = 21 kcal mol^{-1}) and H_2C: has a triplet ground state ($\Delta E_{S\rightarrow T}$ = −9 kcal mol^{-1}) so that, by assuming a bond energy $E_{\sigma+\pi}$ of about 105 kcal mol^{-1}, inequality (b) is fulfilled and silaethene shows a "classical" planar molecular core. Substitution of hydrogen by fluorine (π-donor) stabilizes the singlet states of the carbene fragments enormously (F_2C: $\Delta E_{S\rightarrow T}$ = 46.5 kcal mol^{-1}; F_2Si: $\Delta E_{S\rightarrow T}$ = 73 kcal mol^{-1}). As a result, the relationship (d) is fulfilled for $F_2Si{=}CH_2$, $H_2Si{=}CF_2$, $F_2Si{=}CF_2$, or even $F_2Si{=}SiF_2$ and no planar molecular structure is expected. A small weakness of the CGMT model must, however, be mentioned. For a given molecular formula, it does not provide a detailed description of the molecular structure associated with a global minimum on the potential energy surface. Therefore, the potential surface must be carefully analyzed by ab initio methods.[6]

The calculation for the E_2H_4 molecules (E = C, Si, Ge, Sn, Pb) provides five minima on the potential surface with the structures **A**–**E** (Fig. 4).

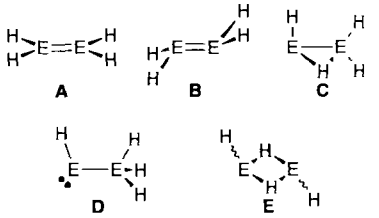

Fig. 4 Possible isomers **A**–**E** for E_2H_4 [6].

For E = C, only the planar, "classic" isomer **A** with C–C double bonding is found as a minimum. One isomer with E=E multiple bonding was also localized as a minimum for E = Si, Ge, and Sn albeit that it is present in the *trans*-bent conformation **B**, which corresponds to the global minimum for E = Si and Ge. No minima representing the conformations **A** or **B** were found for Pb_2H_4. In general, Trinquier showed that a $E{-}E^1$ multiply bonded system, whether it be planar or bent, could only exist when the sum of the singlet–triplet excitation energy is smaller than the bonding energy $E_{\sigma+\pi}$. If instead inequality (e) is valid, the $E{=}E^1$ bond is lost to

$$\Sigma\Delta E_{S\rightarrow T} \geq E_{\sigma+\pi} \qquad \text{(e)}$$

give a more favorable isomer without a direct $E{-}E^1$ connection. Therefore, for example, for the molecules Pb_2H_4 and Si_2F_4, four-membered rings with bridging H and F centers, respectively, are the most stable (isomer **E**) (with $\Delta E_{S\rightarrow T}$ = 37 kcal mol^{-1} for PbH_2[15] and $E_{\sigma+\pi}$ = 50–60 kcal mol^{-1} for Pb=Pb, Equation (e) is fulfilled).[6a]

Except for C_2H_4, the doubly bonded isomer **E** (that can be present in *cis* or *trans* forms which are distinguished by very small energy differences) was found as the local minimum on the potential energy surface of all the heavier homologues and represents the global minimum for Sn_2H_4 and Pb_2H_4. In addition, the carbene-analogous isomer **D** was found as a minimum on the E_2H_4 potential surface for E = Si, Ge, Sn, Pb. For Sn_2H_4 and Pb_2H_4, isomer **C**, in which one hydrogen bridges the E–E single bond, also appears as a local minimum. All four isomers **B**–**E** correspond to minima on the Sn_2H_4 potential energy surface and fall within a narrow range of 10 kcal mol^{-1}![6b]

The CGMT model can also be applied to cumulated multiply bonded systems. If a CO, CS, or an isocyanide group is a constituent of the multiple bond, the relationship (f), in which f' is defined by Equation f', is valid for predicting a bent molecular geometry.[2b] It accounts for the altered acceptor character of the π* orbital of this unit, as compared to a p(π)-acceptor orbital of an electronically unchanged EXY fragment (Fig. 5).

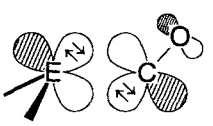

Fig. 5 Schematic interaction of a singlet carbene with CO for $\theta = 45°$ [2b].

$$\Sigma\Delta E_{S\rightarrow T} > E_{\sigma+\pi}\,[3/4 + q^1 + q^2)/8 + \alpha q^1 q^2 = f' E_{\sigma+\pi} \qquad \text{(f)}$$

$$f' = [3/4 + (q^1 + q^2)/8 + \alpha q^1 q^2 \qquad \text{(f')}$$

Using inequality (f) a linear geometry was calculated for ketene $H_2C=C=O$, which is in agreement with experimental results, and a bent structure for $H_2Si=C=O$.

Recently Jacobsen and Ziegler investigated a series of homonuclear doubly bonded systems $XYE=E^1X^1Y^1$ by using density-functional theory (DFT).[3b] In particular they studied the interaction between two triplet fragments ^3EXY and $^3E^1X^1Y^1$. They divided the bonding energy into individual terms that allowed them to separately investigate the steric factors, such as the difference in the geometry of free and bound EXY and $E^1X^1Y^1$ fragments, repulsive interactions of occupied orbitals (Pauli repulsion), and attractive electrostatic interactions of electronic factors (singlet–triplet excitation energies $\Delta E_{S\rightarrow T}$ of the fragments and exchange energy that is released upon formation of two triplet fragments with α and β spins). The essential findings of this bond analysis are that there is indeed multiple bonding between the carbene-analogous fragments with central atoms from higher rows and that the π component of these multiple bonds in molecules with *trans*-bent geometry is of greater importance than in molecules with planar geometry.

The deviation from a planar $XYE=E^1X^1Y^1$ molecule can also be described as a second-order Jahn–Teller distortion. Its importance increases for the higher homologues of ethene due to a smaller energy gap between the HOMO and LUMO.[3b, 5b] Upon *trans*-bending of the central framework, the bonding (p-p)π orbital (HOMO) enters into a stabilizing interaction with the antibonding (p-p)σ^* orbital (LUMO +1) of the $E-E^1$ bond. Simultaneously, the bonding (p-p)σ orbital (HOMO – 2) can mix with the (p-p)π^* orbital (LUMO) of the $E=E^1$ bond and cause destabilization of the (p-p)σ orbital. The interaction of these orbitals becomes stronger the smaller the energy difference between them. In ethene, the destabilization of the bonding (p-p)σ orbital as a result of *trans*-bending is larger than the stabilization of the (p-p)π orbital. Therefore, C_2H_4 remains planar. In contrast, in the higher homologues, which have weaker $E-E^1$ bonds and smaller (p-p)π/(p-p)σ^* orbital energy differences, the reduction of the energy of the bonding (p-p)π orbitals due to *trans*-bending is not compensated for and these molecules are *trans*-bent. Since the GCMT model provides for unrestricted, definitive bonding between carbene-analogous fragments and the double-bonded systems and small rings which are made from them, it will often be referred to in the current article. The following maxims have been formulated:

1) The geometry of a molecule with a multiple bond, defined by the equilibrium distance r_{eq} and the angle θ, which shows deviation from a planar geometry, can be conclusively determined from the singlet–triplet excitation energy $\Delta E_{S\rightarrow T}$ of the fragments formed by bond cleavage. Fragments with a singlet ground state favor *trans*-bent geometries.

2) The stability of the singlet state increases with increasing atomic number at the central atom E in EXY.

3) The dissociation energy of a multiply bonded system is also dependent on the excitation energy $\Delta E_{S\rightarrow T}$ of the fragment. The more stable the singlet state of the fragments EXY and $E^1X^1Y^1$, the lower is the dissociation energy of the doubly bonded system $XYE=E^1X^1Y^1$. It can even be lower than that of the $E-E^1$ single bond energy.

4) The higher the atomic number at the central atom E, the stronger is the deviation of the doubly bonded system from a planar geometry and the longer is the $E=E^1$ bond. This is because the repulsive steric interaction increases with a larger angle θ. It is, however, in general true that *trans*-bending of the fragments of a doubly bonded system with central atoms from the higher rows stabilizes the system to a greater degree than bond lengthening destabilizes it. In other words, the slope of the potential curve is much steeper for the variation of angle θ than for the distance r. With increasing atomic number at the central atom E, the distance r can be varied over a wide range depending on the substituents X and Y. As a result, a discussion of the double bond length has little meaning.

5) The sustituents X and Y display a strong influence on the character of the multiply bonded system. Isolable compounds that contain sterically demanding substituents can only be compared to the compounds EH and EH_2 with limitations. Larger substituents lead to a widening of the X-E-Y angle and therefore to a lowering in the energy of the triplet state as compared to that of the singlet state in the EXY fragment. Consequently, large groups can lead to a flattening in the geometry of an $E=E^1$ doubly bonded system and a shortening of the $E=E^1$ distance (see below for examples).

6) With increasing difference in electronegativity (expressed as the difference in the spectroscopic electronegativity χ_{spec} by Allen)[1] between the central atoms, multiple bonding within a class of compounds for a given central atom E becomes more stable; this means $C=O>C=N>C=C$; $Si=O>Si=N>Si=C$ but $C=O>Si=O$.[7]

7) A multiply bonded system with an $E=E^1$ bond is unstable with respect to an isomer without direct $E=E^1$ bonding when the sum of the singlet–triplet excitation energy of the fragments is larger than the bonding energy $E_{\sigma+\pi}$. A large difference in electronegativity $\Delta\chi_{spec}$ between the central atom E and substituent centers X and Y leads to a preference for isomers with bridging X or Y centers, respectively. This is because the E–X or E–Y bond has increasingly ionic character. A difference in $\Delta\chi_{spec}$ (E,X,Y) of about 0.48 can be estimated as a limiting value. Thus, the boron atoms in the B_2H_2 molecule (which has a triplet ground state!)[7] are connected by a classical B=B double bond. In contrast the most stable isomers of the homologous molecules E_2H_2 with the more electropositive elements E = Al, Ga, In, Tl form four-membered rings with hydrogen-bonded metal centers (see Scheme 10) [$\Delta\chi_{spec}(H,E)\geq 0.544$].

3. The Building Blocks: Carbene-Analogous Fragments with Group 13 to Group 15 Centers

For the directed synthesis of $E-E^1$ multiply bonded systems or the preparation of heterocycles with direct $E-E^1$ bonding by combination of EXY and $E^1X^1Y^1$ fragments, a broad palette of isolable fragments of this kind is desirable.[8] The carbene-analogous fragments with a central atom from the third or higher row ($n>2$) have a singlet ground state. In Figure 6a the singlet–triplet excitation energies $\Delta E_{S\rightarrow T}$ of several HE and H_2E fragments are graphically presented.

Whenever possible, precisely determined, average experimental values from gas-phase investigations were used for the production of Figure 6a or when these values were not available, energies calculated by extensive ab initio methods were used (see

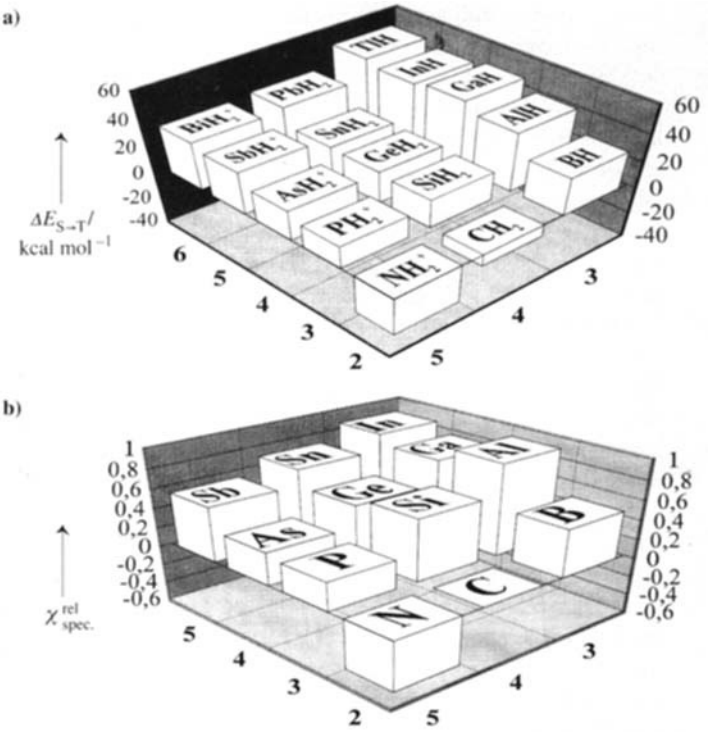

Fig. 6. a) Graphic representation of the singlet–triplet excitation energy $\Delta E_{S\to T}$ [kcal mol^{-1}] for carbene-analogous fragments with central atoms from Groups 13–15: BH (calc.): 27.7 [14a], 31.9 [14b]; AlH (calc.): 42.7 [14a]; GaH (exp.): 49.6 [9]; InH (exp.): 47.0 [9]; TlH (exp.): 50.7 [9]; CH_2 (exp.): -9.0 ± 0.1 [10]; SiH_2 (exp.): 21.0 [11]; GeH_2 (calc.): 23 [3b,15]; SnH_2 (calc.): 24 [15], 23 [3b]; PbH_2 (calc.): 37 [15], 34.2 [3b]; NH_2^+ (exp.): -30.2 [12]; PH_2^+ (exp.): 16.4 [13]; AsH_2^+ (calc.): 22.0 [16]; SbH_2^+ (calc.): 31.0 [16]; BiH_2^+ (calc.): 35.0 [16]. b) Graphic representation of the relative spectroscopic electronegativity χ_{spec}^{rel} based on $\chi_{spec}^{rel}(C) = 0$. The following values for χ_{spec} (in Pauling units [1]) were taken from ref. [1]: B 2.051; Al 1.613; Ga 1.756; In 1.656; C 2.544; Si 1.916; Ge 1.994; Sn 1.824; N 3.066; P 2.253; As 2.211; Sb 1.984.

legend to Fig. 6a). For a better comparison with $\Delta E_{S\to T}$, electronegativity values shown in Figure 6b are given relative to the carbon atom ($\chi_{spec}^{rel}(C) = 0$), that is, relative electronegativities χ_{spec}^{rel} of the main group elements E are graphically portrayed ($\chi_{spec}^{rel}(E) = 2.544 - \chi_{spec}(E)$).[1]

From the listed fragments, only CH_2 and NH_2^+ have a triplet ground state. Within a series of homologous fragments, the value of $\Delta E_{S\to T}$ like that of $\chi_{spec}(E)$ changes drastically upon going from a central atom of the second row to the third row. This jump can be readily explained by the "reluctance to hybridize" shown by elements in the higher rows ($n > 2$). The X-E-Y valence angle of a carbene fragment in a triplet state is larger than that of one in a singlet state ($^3CH_2$: $133.84\pm0.05°$; $^1CH_2$: 100°).[17] As a result, the s contribution in the hybrid orbitals is larger for the triplet state, when such a description is employed for the X–E and Y–E bonds. This assumes an effective hybridization of the s and p atomic orbitals (AO) of the central atom in the framework of the applied mathematical model. For this the comparable, expected values $\langle r \rangle$ (equivalently meaningful as the spatial expansion) of the s and p AOs calculated by quantum mechanics are decisive. Only for elements in the second row do s and p electrons show approximately the same spatial extension because the core electrons occupy the 1s level exclusively. For the elements from the higher rows the *n*p valence electrons ($n > 2$) are spatially separated from the *n*s valence electrons due to Pauli repulsion from the $(n-1)$p electrons in the lower lying shell. Therefore these elements are "reluctant to hybridize".[18, 3a] The H-E-H bond angle in carbene-analogous fragments containing an element E from higher than the second row and with a singlet ground state decreases within a group (for example SiH_2: 92.7°, GeH_2: 91.5°, SnH_2: 91.1°, PbH_2: 90.5°),[15] that is the lone pair of electrons on the central atom E has increasing s AO character.

In view of the hybridization model, the correlation of the spectroscopic electronegativity χ_{spec} with the excitation energy $\Delta E_{S\to T}$ of the fragments EH and EH_2 expressed by the resemblance of the plots shown in Figure 6 can be explained. For electronegative elements E, the energy needed for the s, p hybridization is more than compensated as result of the high E–X valence bond energy E_b. This is because the E–X valence bond energy E_b rises with increasing s AO contribution to the bonding hybrid orbital for electronegative elements ($E_b(C(sp)-H) > E_b(C(sp^2)-H > E_b(C(sp^3)-H)$; but $E_b(Si(sp)-H) \approx E_b(Si(sp^2)-H \approx E_b(Si(sp^3)-H)$).[3a] The valence bond energy E_b is proportional to the ionization potential I_b of the valence orbitals used in describing the bond.[19] These potentials I_b are largest for the more electronegative elements, just as for atomic ionization energies chosen for the calculation of $\chi_{spec}(E)$.

In the past few years several inert carbenes and carbene analogues have been synthesized in which the hydrogen atoms in the compounds shown in Figure 6a have been replaced by bulky organic groups or heteroatoms. As yet, the only carbene analogues, which are monomeric also in the solid state, with a Group 13 element were found in the solid modification of $Tl[C_5(CH_2Ph)_5]$ (**1**)[20a] and in the sandwich compound Tl(1,3-$B_2C_3Me_5$)CoCp (Cp = C_5H_5).[20b] In these compounds the thallium center is η^5 coordinated and can therefore be perceived as a *nido* cluster with $(n + 2)$ core electron pairs according to the Wade–Mingos–Rudolph rules. The same is true for [AlCp*] (**2**) (Cp* = C_5Me_5), [GaCp*] (**3**), [InCp] (**4**), [InCp*] (**5**), [TlCp] (**6**), and [TlCp*] (**7**) which are present as monomers in dilute solutions and/or the gas phase; thus, gas-phase structures of **3**–**7** could be determined.[21, 22] In the crystal, however, many of

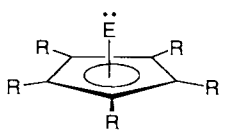

	1	2	3	4	5	6	7
E	Tl	Al	Ga	In	In	Tl	Tl
R	CH_2Ph	Me	Me	H	Me	H	Me

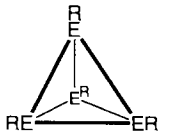

	8	9	10
E	B	Ga	In
R	*t*Bu	$C(SiMe_3)_3$	$C(SiMe_3)_3$

the cyclopentadienides with Group 13 elements with a formal oxidation state of +1 are oligomers (for example $[(AlCp^*)_4]$[23] and $[(InCp^*)_6]$[22]). The alkyl-substituted diyls with Group 13 elements known to date form tetramers in the solid state. Examples include $[(BtBu)_4]$ (**8**),[25] $[\{GaC(SiMe_3)_3\}_4]$ (**9**),[26] and $[\{InC(SiMe_3)_3\}_4]$ (**10**).[27] These clusters with only *n* core electron pairs do not obey the Wade–Mingos–Rudolph rules![28] From these compounds, only the gallium compound **9** dissociates to monomers in dilute solutions or in the gas phase. As a result, it was recently possible to determine the gas phase structure of $[GaC(SiMe_3)_3]$ as the first monomeric alkylgallium(I) compound (Fig. 7).[29] The Ga–C bond is, despite the steric over-

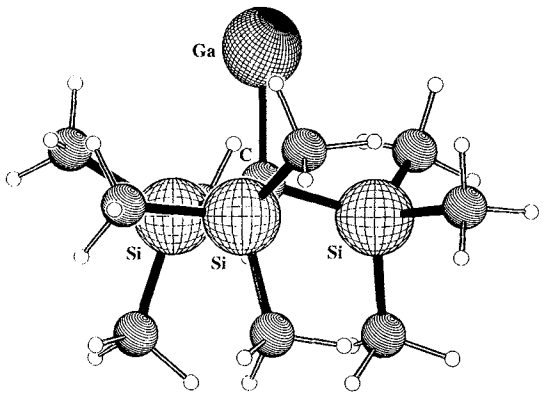

Fig. 7. Structure of monomeric **9** in the gas phase [29]. d(Ga-C) 2.964(17) Å; Ga-C-Si angle 106.2(9)°.

load in monomeric **9**, as expected shorter than that in pentamethylcyclopentadienylgallium (**3**), [**9**: 2.06(2) Å; **3**: 2.405(4) Å]. Since many of the tetrameric clusters $[(RE)_4]$ dissociate readily in solution to the monomers, they are a suitable source of carbene-analogous Group 13 diyls. Thus, Cp*Al (**2**) reacts smoothly with selenium or tellurium to give the heterocubanes **11** (Scheme 1).[30]

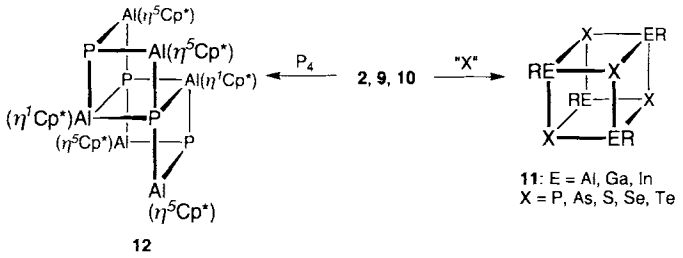

12

Scheme 1. Synthesis of **11** and **12** from **2**, **9**, and **10**.

P_4 reacts with **2** to give the polycyclic cage compound $[(Cp^*Al)_6P_4]$ (**12**) in which the Al centers connected to three phosphorus atoms are η^1 bonded to the Cp* ring, while the Al centers connected to only two phosphorus centers are η^5 bonded to Cp*. In contrast, in **11** all Al centers are η^5 bound to the Cp* groups. The reactions of the gallium (**9**) and indium (**10**) clusters with phosphorus, arsenic, selenium, or tellurium also lead to the heterocubanes **11** ($R = C(SiMe_3)_3$).[32]

Noteworthy is the synthesis of stable carbenes. Bertrand et al. successfully synthesized the first singlet carbene stabilized by heteroatoms **14** by pyrolysis of the diazo compound **13** (Scheme 2).[33]

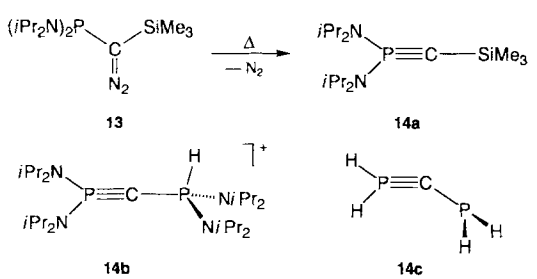

Scheme 2. Synthesis of **14a,b,c**.

The structure of compound **14a** has not yet been experimentally determined but it was recently possible to establish the structure of the phosphonium salt $[(iPr_2N)_2P{\equiv}C{-}PH(N\text{-}iPr_2)_2](O_3SCF_3)$ (**14b**).[34] The cation is closely related to **14a** because of the isoelectronic relationship between R_2Si and R_2P^+. In **14b** the $(iPr_2N)P-C$ distance (1.548(4) Å) is shorter than the other P-C distance, which could only be inaccurately determined as 1.605–1.616(5) Å due to disorder of the phosphonium group $[(iPr_2N)_2HP]^+$. The P-C-P angle is about 165° and is, like the P-C distance, in agreement with the value calculated for the $[(H_2N)_2P{\equiv}C\text{-}PH(NH_2)]^+$ ion.[35] Earlier ab initio calculations carried out for $(H_2N_2)P{\equiv}C\text{-}SiH_3$ also showed that the P-C-Si angle of 175.9° is widened in comparison to the structural characteristics described above for singlet carbenes (smaller bond angles at the carbon atom). Therefore these compounds are best described as λ^5-phosphaacetylenes,[36] even though the reactivity of **14a** is very similar to that of a nucleophilic λ^3-phosphanylcarbene.[37] An explanation for the ambivalent reactivity of **14a** as λ^5-phosphaacetylene and λ^3-phosphanylcarbene is offered by theoretical investigations of the diphosphanylcarbene derivative $H_2P{\equiv}C{-}PH_2$ (**14c**), which has not yet been synthesized. The conformation with lowest energy does not have equivalent P-C distances (1.533 Å, 1.765 Å; P-C-P angle 160.5°). As a result, it is considered as a λ^5-phosphaacetylene with polar P^+-C^- multiple bonding. However, the diphosphanylcarbene with equivalent P-C distances (1.719 Å) and considerably smaller P-C-P angle (131.4°) is only 5.7 (SCF) or 14.8 kcal mol^{-1} (MP2) richer in energy. Therefore the ambivalent reactivity of this class of compounds is understandable.[35]

In 1991 Arduengo III et al. extended the investigations on nucleophilic carbenes studied by Wanzlick et al. in the 1960s[38] and reported on the synthesis of the isolable carbenes **16**, in which the carbene center is stabilized by incorporation within an imidazole ring.[39] The synthesis of these compounds is remarkably simple and involves deprotonation of the imidazolium salts **15** with KOtBu or removal of sulfur from 2-thio-imidazolidones **17** with potassium (Scheme 3).[40]

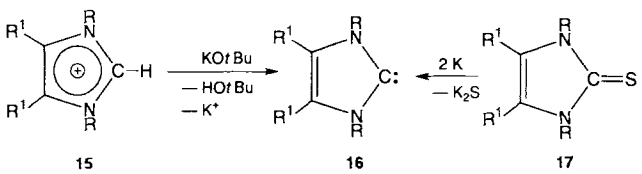

Scheme 3. Synthesis of **16** from **15** or **17**.

The imidazol-2-ylidene **16** has, as expected, a singlet ground state. In the molecular structure determined by single-crystal X-ray crystallography, a small N-C-N angle of about 102° (the corresponding N-C-N angle in **17** is about 109°) and symmetric, relatively long C-N distances (ca. 1.37 Å in **16**, ca. 1.32 Å in **17**) were observed. Reactivity studies prove the nucleophilic character of these carbenes since stable adducts are formed with Lewis acids such as BH_3,[41a] AlH_3,[41b] I^+ ions,[41c] or metal cations.[41d–f] The isolation of a relatively stable triplet carbene was also recently described.[41h]

Inert silicon compounds with a two-coordinate silicon atom (silylenes or silanediyls) have until recently only been studied in

a low-temperature matrix.[8c, 42] They have already been proven to be intermediates in photochemical and thermal decomposition reactions by many trapping reactions.[43] The stable silylene (silanediyl) **19** was also synthesized by a remarkably simple method in 1994. At first glance it is closely related to the above-mentioned stable carbene **16** (Scheme 4).[44]

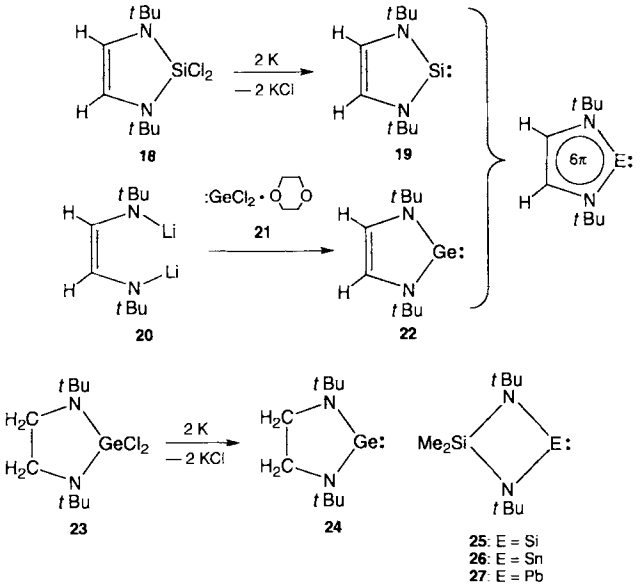

Scheme 4. Synthesis of **19**, **22**, and **24**.

The germylene (germanediyl) **22** had already been synthesized by a method similar to that for **19** and is also exceptionally stable.[45] The N-E-N bond angles at the C, Si, and Ge centers in **16**, **19** and **22**, respectively, decrease, as expected, in the given order: $102° > 95.4° > 84.8°$. The volatility of the structurally analogous compounds **16**, **19**, and **22** allowed photoelectron (PE) spectra to be recorded. Their interpretation with the help of density function theory (DFT) clarified interesting differences in the electronic bonding behavior.[46] While according to this study in the carbenes **16** the HOMO is represented by the lone pair of electrons on carbon (σ-C), in the silanediyl **19** and in the germanediyl **22** it is described by a π orbital from the imidazole ring that is formed from the out-of-phase combination of the C=C π orbital with the p orbitals on nitrogen and Si or Ge, respectively (Fig. 8). It has to be stressed, however, that ab initio calculations of $(HC)_2(NH)_2C$: give a different orbital ordering which corresponds to the one found for silanediyls or germanediyls.[46b–d]

With increasing atomic number, the ionization from the σ-Si and the σ-Ge orbital, which in **19** and **22** is the HOMO-1, requires increasingly higher energy and the energy difference between the HOMO and HOMO-1 increases [**19**: 8.21 eV, Δ(HOMO − [HOMO-1]) = 1.09 eV; **22**: 8.60 eV, Δ(HOMO − [HOMO-1]) = 1.78 eV]. The silanediyl **19** and the germanediyl **22** owe their unusual stability to cyclic 6π-electron delocalization, a "trick" which has already proven itself in the synthesis of other low-coordinate main group element compounds.[47] This clarifies, in particular, the comparison with the significantly more reactive germanediyl **24**, in which the germanium forms the building block for a saturated five-membered GeN_2C_2 ring,[45] and the silanediyl $Me_2Si(NtBu)_2Si$: (**25**) which could

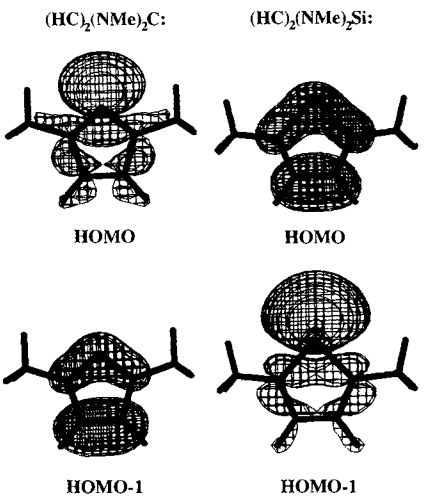

Fig. 8. SPARTAN plots of the HOMO and HOMO-1 for the *N*-methyl derivatives $(HC)_2(NMe)_2C$: (left) and $(HC)_2(NMe)_2Si$: (right) that were calculated with DFT methods as model compounds for **16** and **19** (C. Marchand, H. Grützmacher, unpublished results). The results are in agreement with the reported DFT calculations of **16** and **19** in ref. [46].

only be detected up to 77 K in a matrix.[42a] In both of these systems such a delocalization is not possible. The synthesis of the saturated cyclic diaminocarbene $(H_2C)(MesN)_2C$:[41g] and $(H_2C)_2(tBuN)_2Si$:[42e] has also been achieved recently. The PE spectra of **19** and **22** were interpreted to indicate the presence of formal Si(0) and Ge(0) chelate complexes with the corresponding diazabutadiene ligands.[46] The homologues **26** and **27**, which could be isolated, are closely related to **25**.[48] By using PE spectroscopy and ab initio calculations, it was also proven for **26** and **27** that the HOMO cannot be described by a σ-Sn or σ-Pb orbital, as would be expected for a singlet carbene analogue. The HOMO is a π-N^+N^- orbital that actually represents the antisymmetric combination of the p orbitals on the nitrogen center.[49] A series of frontier orbitals that deviate from those for a singlet carbene were observed as well for the long known, acyclic, PE spectroscopically investigated amides $[R(Me_3Si)N]_2Sn$: (**29a,b**) and $[R(Me_3Si)N]_2Pb$: (**30a,b**) (**a**: R = Me_3Si; **b**: R = *t*Bu).[50] In these amides the HOMO is described as a b_2 orbital which is essentially an out-of-phase combination of the p orbitals of the lone pairs of electrons on the nitrogen atoms. With these amides, it is therefore not a question of isolobal analogues of singlet carbenes. This analogy has been suggested for **24** and **25** because of their reactivity but it has yet to be proven by PE spectroscopic and quantum chemical investigations.

Alkyl- or aryl-substituted diyls with Group 14 elements are without doubt analogous to singlet carbenes and are significantly more reactive than the above-mentioned aminodiyls **19**, **22**, **26**, and **27**. The synthesis of an isolable monomeric alkyl- or aryl-substituted silanediyl has not been successful but a series of comparable, stable germanediyls, stannanediyls, and plumbanediyls have been isolated and studied in the past few years (Scheme 5).

As early as 1976 Lappert et al. synthesized the alkyl-substituted diyls **28**–**30**; however, they are monomeric only in solution and in the gas phase and dimerize upon crystallization (see below).[54] Therefore the gas phase structures of the germanium and tin compounds were determined.[51] As is expected for dia-

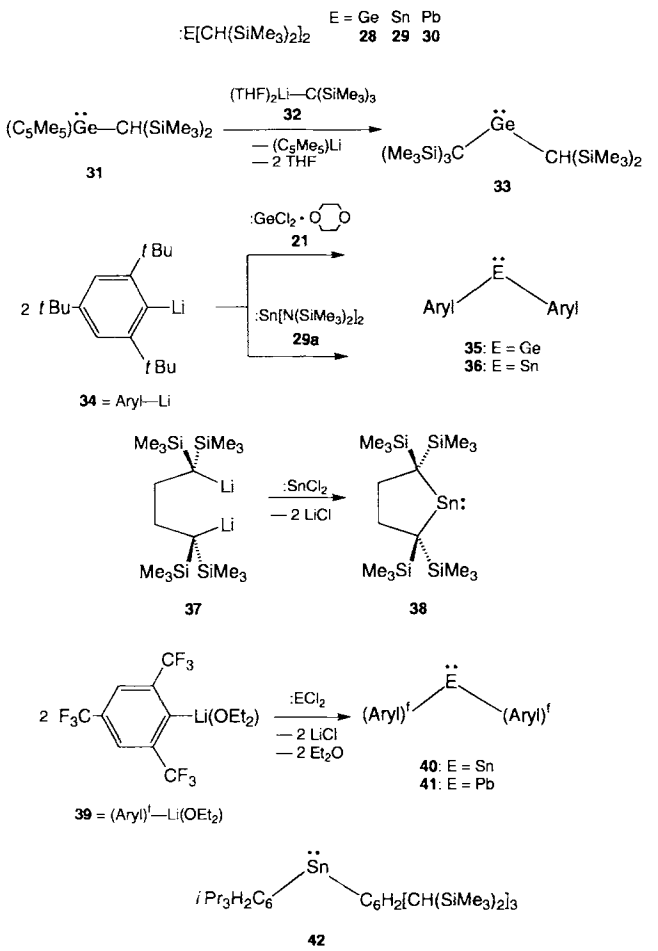

Scheme 5. Synthesis of germanediyls, stannanediyls, and plumbanediyls.

magnetic carbene analogues, the bond angle at the central atom is small (E = Ge: 107(2)°; E = Sn: 97(2)°) and lies within the range observed for acyclic germanediyls and stannanediyls with amino, phenolato, and thiolato substitutents (111–85.4°). Naturally, in the cyclic derivatives the bond angle is smaller (for example 73.2° in **26**; see also the above-mentioned angles for **16**, **19**, and **22**).

The dialkylgermanediyl **33** (C-Ge-C angle 111.3(2)°), which is monomeric even in the solid state, was synthesized by exchange of the η^2-π-bound Cp* group in **31** (C-Ge-Cp* angle 106.9(2)°) with the very sterically demanding $C(SiMe_3)_3$ group.[52] The 2,4,6-tBu$_3$C$_6$H$_2$ group (supermesityl = Mes*) is suitable as a bulky aryl substituent for the synthesis of the diarylgermanediyl **35**, which is inert below 20 °C. Extended heating (> 20 °C) of **35** in solution as well as in the solid state leads to insertion of the germanium atom into a C–H bond of the *ortho*-positioned tBu group and formation of a germa-indane derivative.[53] In contrast, the diarylstannanediyl **36** (C-Sn-C angle 103.6(1)°), which is formed by ligand exchange from the bis(amino)stannanediyl :Sn[N(SiMe$_3$)$_2$]$_2$ **29a** and 2,4,6-tBu$_3$C$_6$H$_2$Li, is also stable under an inert atmosphere even at room temperature. However, isomerization presumably to [(2,4,6-tBu$_3$C$_6$H$_2$)Sn(CH$_2$C-(Me)$_2$-3,5-tBu$_2$C$_6$H$_3$)] also occurs here in solution at 50 °C.[54] The synthesis of the cyclic dialkylstannanediyl **38** (C-Sn-C angle 86.7(2)°), which is monomeric even in the solid state, was only reported recently.[55] The diarylstannanediyl **40** (C-Sn-C angle

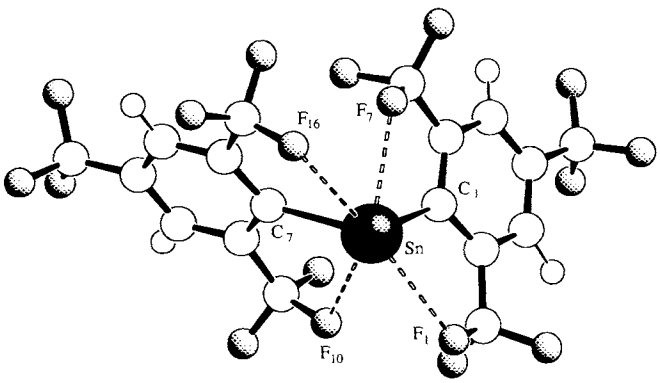

Fig. 9. Molecular structure of **40** in the crystal (yellow modification with monomeric units; Sn–Sn > 6 Å) [56]. Bond lengths [Å] and and angle [°]: Sn–C1 2.278(5), Sn–C7 2.284(5), Sn–F1 2.833(4), Sn–F7 2.663(4), Sn–F10 2.681(4), Sn–F16 2.807(4); C1-Sn-C7 98.3(1).

98.3(1)°) and plumbanediyl **41** (C-Pb-C angle 94.5(1)°) are special cases since in these compounds the low-coordinate main group metal centers are protected against oligomerization by metal–fluorine contacts (Fig. 9).[56, 57]

The metal–fluorine distances for **40** are about 25% shorter than the sum of the van der Waals radii and, because of the temperature dependence of the unusually large $^{119/117}$Sn–^{19}F coupling (> 240 Hz), could probably also be stable in solution. The diarylstannanediyl **42** substituted with the sterically demanding 2,4,6-[(Me$_3$Si)$_2$CH]$_3$C$_6$H$_2$ group has until now only been characterized in solution and exists, as expected, as a monomer.[58] An interesting comparison can be made between the above-mentioned amino-substituted diyls **19**, **22**, and **24**–**27** and the structurally characterized phosphanyl- and arsanyl-substituted germanediyls (**44**), stannanediyls (**45**, **48**), and plumbanediyls (**46**) (Scheme 6).[59] The P-E-P and As-Sn-As angles in these compounds also lie in the expected range for singlet carbene analogues (95.0–98.8°).

Since the inversion barrier for the pyramidal phosphorus and arsenic center (Σ°(P,As) = 315–320°) is significantly higher

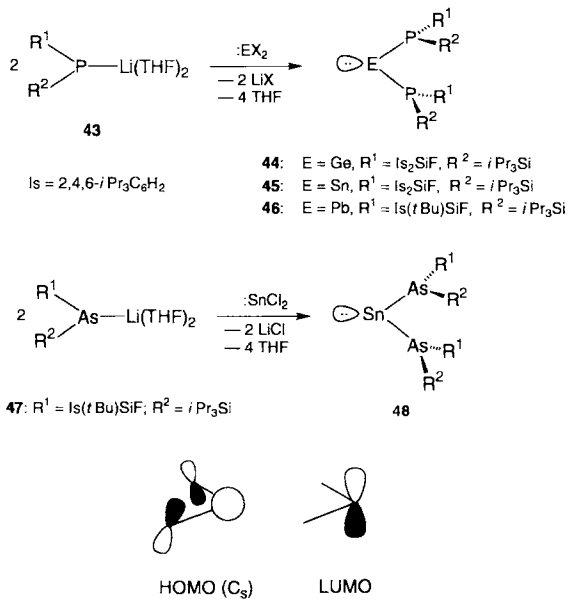

Scheme 6. Synthesis of phosphanyl- and arsanyl-substituted germanediyls, stannanediyls, and plumbanediyls.

than that for the trigonal-planar coordinated nitrogen center ($\Sigma°(N) = 360°$) in the amino-substituted silanediyls, germanediyls, and stannanediyls, the diyls **44**–**46** and **48** are only slightly "stabilized" by π interactions with the lone pairs of electrons on the phosphorus or arsenic centers.

The *ns* atomic orbital of the main group metal center E (E = Ge, $n = 4$; E = Sn, $n = 5$; E = Pb, $n = 6$) provides a larger contribution to the HOMO of the compounds (Scheme 6), which can therefore better considered as (isolobal) analogues to singlet carbenes than as amino-substituted diyls that have an allyl-type HOMO. By the replacement of the electronegative amino with phosphino or arsino substituents the energy difference between the HOMO and the LUMO becomes smaller. Also this σ effect makes the phosphanyl- and arsanyl-substituted carbene analogues more similar to the parent compounds EH_2. This has been proven by the UV/Vis spectra of the intense green and yellow/brown solutions of compounds **44**–**46** and **48**. The lowest electronic excitation energy deviates less from the calculated S_1 transition for the EH_2 molecules (for example SnH_2: 2.50 eV, **45**: 1.92 eV). In contrast, the comparable acyclic aminostannanediyls such as **29a,b** are yellow (S_1: **29a**: 3.18 eV; **29b**: 2.86 eV). The incorporation of the even stronger electron-donating $Si(SiMe_3)_3$ ("hypersilyl") group into stannanediyls and plumbanediyls has been achieved by Klinkhammer and Schwarz (Scheme 7).[60]

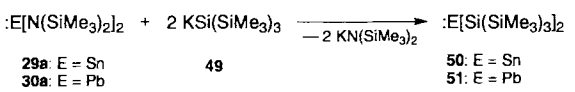

Scheme 7. Synthesis of **50** and **51**.

The reaction of the amides :E[N(SiMe$_3$)$_2$] (**29a**: E = Sn; **30a**: E = Pb) with solvent-free KSi(SiMe$_3$)$_3$ in *n*-pentane led to intensively colored solutions [UV/Vis (λ[nm]): 838, 559 (**50**); 1056, 620 (**51**)] from which the stannanediyl **50** and the plumbanediyl **51** were obtained as black crystals. Both compounds are present as monomers in solution but **50** dimerizes in the solid state to give a remarkable distannene (see **87d** in Section 4.1.). The molecular structure of the plumbanediyl **51**, which is also monomeric in the solid state, is shown in Figure 10.

Particularly notable in **51** are the unusually large Si-Pb-Si angles (between 113.6 and 115.7° for four symmetry-independent molecules) that deviate significantly from the smaller angles of other plumbanediyls (**30a**: 103.6(7)°; **41**: 94.5(1)°; **46**: 98.78(4)°). Silyl substitutents destabilize the singlet ground state of a carbene to a greater extent than the first excited singlet state and cause a red shift in this S_1 electronic transition.[61] Moreover, steric interactions restrict the opening of the Si-Pb-Si angle and decrease the HOMO–LUMO energy difference (S_1: 1.17 eV) in **51** further.

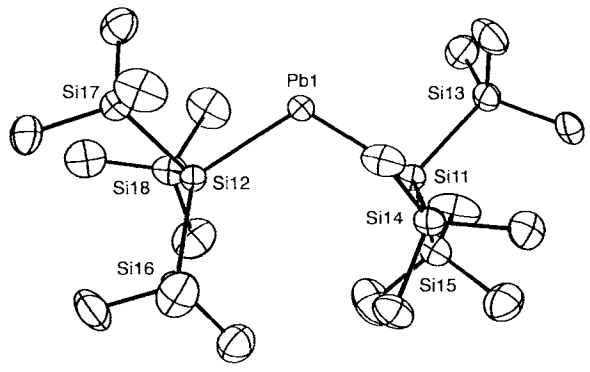

Fig. 10. Molecular structure of **51** in the crystal [60]. Bond lengths [Å] and angle [°] for one of the four symmetry-independent molecules: Pb1–Si11 2.700(3), Pb1–Si12 2.704(3); Si11-Pb1-Si12 113.56(10).

From the cationic carbene analogues H_2E^+ (see Fig. 6) with Group 15 elements (E = N, P, As, Sb, Bi), no stable alkyl or aryl derivatives have yet been described. Nevertheless, the synthesis of divalent, cationic species was possible by applying a few "tricks" which have been mentioned above: a) stabilization by π-donor substituents with nitrogen or sulfur centers, b) stabilization by π delocalization in π-conjugated ring systems, and c) stabilization by cyclopentadienyl groups (Scheme 8).

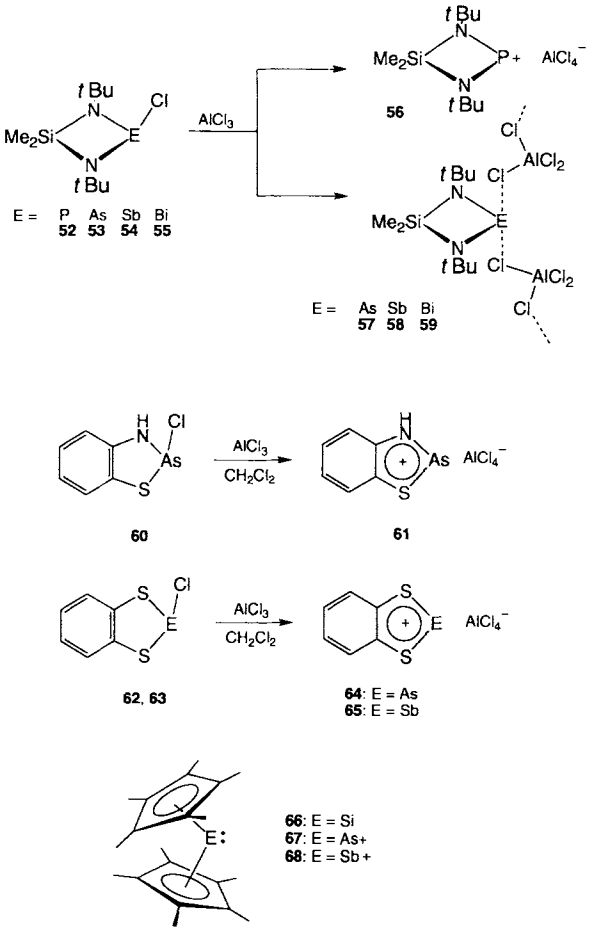

Scheme 8. Synthesis of **57**–**59**, **61**, **64** and **65**. Structures of **66**–**68**.

In this manner Veith et al. used the Me$_2$Si(N*t*Bu)$_2$ ligand system, whose applicability was already proven in the synthesis of the stannanediyl **26**, for the formation of compounds **56**–**59**. These compounds are accessible by chloride abstraction from the derivatives **52**–**55** with $AlCl_3$.[62] However, only the phosphenium salt **56** was proven to be a discrete ion pair in the crystal. In the case of the stibenium and bismuthenium salts **58** and **59** the cations are bridged to the $AlCl_4$ units through a chloride substituent. Compounds **56**–**59** are remarkably soluble in benzene, and, as shown by cryoscopic measurements, are present as monomeric cation–$AlCl_4$ ion pairs or, in the case of

the bismuth compound **59**, as dimeric ion pairs $[\{Me_2Si(NtBu)_2Bi\}_2(AlCl_4)_2]$. The interaction of the *t*BuN units as π donors with the main group element E with a formal electron sextet in the planar heterocycles $Me_2Si(NtBu)_2E$ **26** and **56–59** can be indirectly inferred from the Si–N distances and the N-Si-N angles. It increases in the following order: $Me_2Si(NtBu)_2Sn < [Me_2Si(NtBu)_2Bi]^+ < [Me_2Si(NtBu)_2Sb]^+ \ll [Me_2Si(NtBu)_2P]^+$.

"Stabilized" phosphenium ions, $[XYP]^+$, in which at least one group is X,Y = NR_2, SR, or Cp*, have been well investigated.[63] In contrast, arsenium ions have not been so well studied. The structurally characterized compound **61** was synthesized by Burford et al. (Scheme 8).[64] The low- coordinate arsenic center is bound within a delocalized 10π-electron system. The As–N and As–S distances are very short and the HOMO of the cation is not represented by the lone pair of electrons on arsenic. It is therefore questionable whether this compound, as well as the comparable dithiaarsolium and dithiastibolium salts **64** and **65**, can be described as analogues of singlet carbenes (see also the discussion of the silanediyl **19** and germanediyl **22**). In the cations $[(Cp^*)_2E]^+$ (**67**: E = As, **68**: E = Sb) the E centers are multihapto bound, and, therefore, within the confines of the definition applied here they do not belong to the carbene analogues shown in Figure 6, as is the case for the above-mentioned Cp derivative with Group 13 elements or the silicocene **66**.[65] A possible interesting access to cations with low-coordinate antimony or bismuth centers has been described by Dehnicke et al. (Scheme 9).[66]

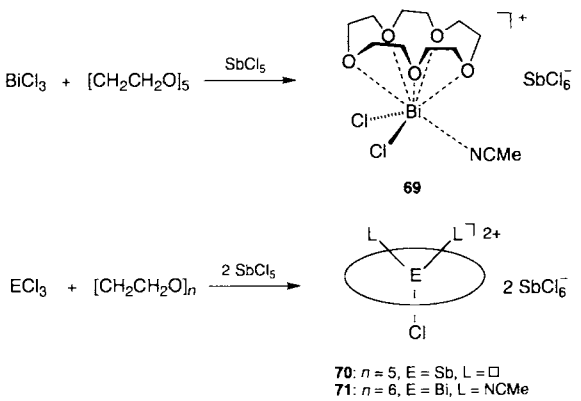

Scheme 9. Synthesis of **69**–**71**. L = □ denotes the absence of the NCMe ligands in the case of antimony.

The reaction of $SbCl_3$ or $BiCl_3$ with the strong Lewis acid $SbCl_5$ as chloride acceptor led to the successful complexation of the cations $[BiCl_2]^+$ and $[ECl_2]^+$ in the presence of crown ether. The size of the crown determines the complex formation. Hence, the $[BiCl_2]^+$ complex **69** is obtained with [15]crown-5, while using [18]crown-6 provides the $[BiCl]^{2+}$ complex **71**. In the latter the Bi center is enveloped by a crown ether which has reformed into the shape of a bowl. Two acetonitrile molecules, which are absent in the case of the antimony complex **70**, complete the coordination sphere of the bismuth center in **71** (coordination number 9). It has yet to be tested whether the $[BiCl_2]^+$ or $[ECl]^{2+}$ fragments can be transferred to another substrate in solution.

The numerous carbenes and carbene-analogous fragments presented here provide a broad palette of compounds by which the characteristics of not only symmetrical, but particularly asymmetrical multiply bonded systems $XYE{=}E^1X^1Y^1$ of the main group elements can be studied. It must be taken into consideration that the above-mentioned experimental tricks provide inert compounds with molecular structures that correspond to the expectations for singlet analogues (X-E-Y <120°). They can, however, be electronically very different.

4. The Dimers: Classical and Nonclassical Doubly Bonded Systems

The molecules with the general formula $EE^1XX^1YY^1$ can, in many cases, actually be synthesized by combining the carbene fragments EXY and $E^1X^1Y^1$. Since the isolation of the first diphosphene Mes*P=PMes* by Yoshifuji et al. and the first disilene by West et al. in 1981, many reviews have reported on multiple bonding between elements from the higher rows.[67] Therefore we will only discuss recent advances in order to illustrate the GCMT concept.

4.1. Compounds with Symmetrical E–E Double Bonds

Within the framework of the GCMT model, application of the inequalities (b)–(e) presented in Section 2 to XE=EX and $X_2E{=}EX_2$ molecules, in connection with the values given in Table 1, allows for the prediction that only diborenes and olefins should contain "classical" molecular structures with "ordinary" σ and (p-p)π bonds as defined by the valence bond model. Choosing a value for $E_{\sigma+\pi}$ is complicated. Several authors quote the dissociation energy ΔE_{TBE} for which data exist from only a few experiments and usually the values must be obtained from calculations. Other authors apply values calculated by quantum mechanics that show some deviations. In each case, the calculated values vary considerably depending on the calculation method. The values that are listed in Table 1, and which form the basis of our discussion, are those that were used by Malrieu and Trinquier and can vary by about ±20%.

As yet a diborene derivative has not been synthesized successfully. Attempts to obtain the diborene **73** by dehalogenation with Na/K alloy of the sterically substituted borane **72** only led to the diborane(6) derivative **74** (Scheme 10).[70]

MO calculations on the parent compound HB=BH show a linear arrangement with a triplet ground state.[71] As a result **73** is a plausible intermediate in the formation of **74**. The calculated B–B distance (1.53 Å) in HB=BH is about 12% shorter than a B–B single bond and therefore reflects the trend observed for carbon compounds (C=C: 1.34 Å; C–C: 1.54 Å).

The two-electron reduction with lithium metal of the diborane(4) compounds **75a,b**, which can be viewed as isoelectronic analogues of ethylene dications, proceeds cleanly to give the diborata dianions **76** and **77**, respectively (Scheme 10).[72] The distinct shortening of the B–B distance by 4.1% and 4.9% in **76** and **77**, respectively, as well as the flattening of the molecular form compared to **75a** and **75b** is attributed to partial B–B π multiple bonding. Despite the evident analogy between

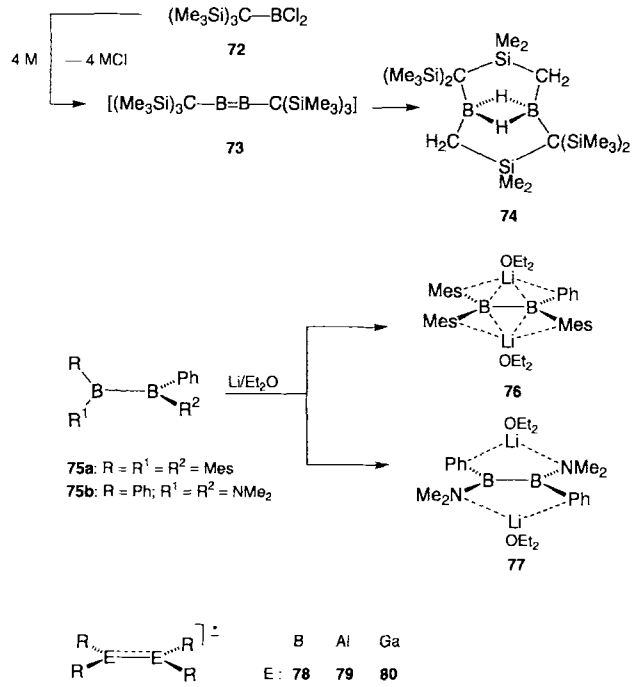

Scheme 10. Synthesis of borane, alane, and gallane derivatives.

Table 1. Sums of the singlet–triplet excitation energies $\Sigma\Delta E_{S\rightarrow T}$, halves of the dissociation energies $1/2\Delta E_{TBE}$ [a], halves of the interaction energies $1/2D^{\circ}$ (0 K) [a], the molecular structures in the electronic ground state, and the designation of the inequalities presented in Section 2. All energies in kcal mol^{-1}; pl = planar, r = ring, f = folded.

Compound	$\Sigma\Delta E_{S\rightarrow T}$	$1/2\Delta E_{TBE}$	$1/2D^{\circ}$	Structure	Inequality
HB=BH	55 [c]		76 [b]	pl	(b)
HAl=AlH	85		43 [b]	r	(e)
HGa=GaH	99		39 [b]	r	(e)
HIn=InH	94		38 [b]	r	(e)
HTl=TlH	101		30 [b]	r	(e)
$H_2C=CH_2$	−18	86	95 [a]	pl	(b)
$H_2Si=SiH_2$	42	32	52 [a]	pl or f	(b, c)
$H_2Ge=GeH_2$	46	21	48 [a]	f	(c)
$H_2Sn=SnH_2$	48	15	41 [a]	f	(c)
$H_2Pb=PbH_2$	74 [d]	5	43 [a]	r	(e)
$H_2Si=CH_2$	12	55	70 [a]	pl	(b)
$H_2Ge=CH_2$	14	43	59 [a]	pl	(b)
$H_2Sn=CH_2$	15	33	50 [a]	pl	(b)
$H_2Pb=CH_2$	28 [d]	23	45 [a]	pl [d] or f	(b, c)
$H_2Ge=SiH_2$	44	22 [e]		f	(c)

[a] ΔE_{TBE} corresponds to half of the total bonding energy and can partially be obtained from experimentally (C_2H_4, Si_2H_4) determined dissociation energies for the dissociation of $H_2E=EH_2$ into two EH_2 fragments in the ground state. These values were assumed by Malrieu and Trinquier as values for $E_{\sigma+\pi}$ [2b]. The values given in parentheses for $1/2D^{\circ}$ are taken from calculations by Treboux and Barthelat [b] as well as by Jacobsen and Ziegler. They are calculated from half the dissociation energy of the dissociation of a double bond system into two triplet carbene fragments (the so-called snapping energy) and therefore do not correspond to ΔE_{TBE} [3b]. Karnie and Apeloig calculated $\Delta E_{TBE} = E_{\sigma+\pi} - \Sigma\Delta E_{S\rightarrow T}$ and obtained instead of inequality (c) in Section 2 the inequality $\Sigma\Delta E_{S\rightarrow T} > \Delta E_{TBE}$ as a criterion for a *trans*-bent double bond. Thereby, in contrast to experiment and ab initio calculations, a planar structure was predicted for $H_2Si=SiH_2$ and $H_2Ge=GeH_2$ [68]. [b] Values corresponding to the dissociation of HE=EH in the triplet state $^3\Sigma_g^-$, which only for E = B corresponds to the ground state, into two HE fragments in the triplet state ($^3\Pi$) [14a]. [c] We used $\Delta E_{S\rightarrow T}$ = 27.7 kcal mol^{-1} for BH (Treboux and Barthelat) [14a]. Pople and Schleyer give $\Delta E_{S\rightarrow T}$ = 31.9 kcal mol^{-1} [14b]. [d] For PbH_2, a value of 37 kcal mol^{-1} was found for $\Delta E_{S\rightarrow T}$ by Balasubramanian by considering relativistic effects and electron correlation [15]. This is the value which we use. Jacobsen and Ziegler obtained $\Delta E_{S\rightarrow T}$ = 34 kcal mol^{-1} with DFT methods so that $\Sigma\Delta E_{S\rightarrow T}$ = 68 kcal mol^{-1} ($H_2Pb=PbH_2$) and 25 kcal mol^{-1} ($H_2Pb=CH_2$). These authors predict a planar structure for $H_2Pb=CH_2$ [3b]. [e] Ref. [69]. These authors calculate $1/2\Delta E_{TBE}(Si_2H_4)$ = 26 kcal mol^{-1} and $1/2\Delta E_{TBE}(Ge_2H_4)$ = 18 kcal mol^{-1}.

$R_2C=CR_2$ and $[R_2B=BR_2]^{2-}$, any comparative discussion must not ignore the $Li(OEt_2)$ groups bound in the diborata dianion. Therefore, **76** and **77** can also be viewed as diborane(6) derivatives in which the bridging H atoms have been replaced by Li centers. The B–B distances in **76** (1.636(11) Å) and **77** (two halves of symmetry-independent molecules are in the unit cell 1.623(8), 1.631(9) Å) correspond to those calculated for $Li_2B_2H_4$, for which the most stable conformation is planar (B=B: 1.613 Å).[73] The isomer of $Li_2B_2H_4$ in which the Li centers above and below the H_2BBH_2 plane are placed above the B–B bond is 14.9 kcal mol^{-1} higher in energy and has a slightly longer B–B bond (1.629 Å). In the experimentally determined structures of **76** and **77** the Li centers are above and below the R_2BBR_2 plane but are not located over the B–B vector. In each case, the coordination of the Li centers contributes significantly to the stability of these compounds. The attempted twofold reduction of tetraalkyl-substituted diboranes(4) to diborates, in which coordination of the Li centers to aryl carbon or nitrogen centers is impossible, led only to the radical monoanion **78**.[74a] The homologous radical anions **79** and **80** of the corresponding dialane(4) and digallane(4) were recently synthesized and characterized by ESR spectroscopy and, in part, by structural analysis.[74b–e] Also here, attempts to synthesize the dianions were unsuccessful.[74f] Finally, the high thermodynamic stability of the dilithium diborates **76** and **77** was confirmed by calculating the value for the energy released upon dimerization of monomeric $LiBH_2$ units (117.9 kcal mol^{-1}).[73] Consequently these synthetic building blocks, which are of great value in boron chemistry, must be protected by very large substituents.

The values for $\Delta E_{S\rightarrow T}$ and $1/2D^{\circ}$ listed in Table 1 show that, according to inequality (e) and maxim 7 (Section 2), the higher homologues of H_2B_2 should be most stable in an isomeric form without E–E bonding. Also quantum mechanical calculations predict the four-membered ring **F** (Scheme 11) to be the most stable isomer for the molecular formula E_2H_2 (E = Al, Ga, In, Tl).[14a, 75] For E = Al, Ga, and In the isomers **G**, **H**, and **I** were also found as local minima on the singlet potential energy surface. They are increasingly stable in the given order within a relatively narrow energy range of about 25 kcal mol^{-1}. For Tl_2H_2 the calculations provided only the isomers **F** and **G** as minima on the potential energy surface.

Interestingly, Schumann et al. found that in the solid state structures, the cyclopentadienyl derivatives of In(I) **81** and Tl(I) **82** form "dimers" with extremely long E–E distances (3.63 Å) (Scheme 11).[76]

The vectors from the E centers to the center of the C_5R_5 rings (R = CH_2Ph) form an angle θ of 43.5° (E = In) or 48.2° (E = Tl) with the E–E vectors, as expected from the GCMT model. The interaction between the In and Tl centers in **81** and **82**, respectively, is, however, extraordinarily weak and is evidently only observed in solids. This can be ascertained from the yellow color of crystals of **81** and **82**, since crystals in which molecules of **82** exist as monomers without a Tl–Tl interaction (see **1** in Section 2) are colorless.[20] The four-membered rings **83** and **84** with two-coordinate In and Tl centers, which correspond to isomer **F**, were synthesized by Roesky et al. (Scheme 11).[77] These compounds are dimers of the EOR fragments with π-donor substitution and correspond to the structures expected

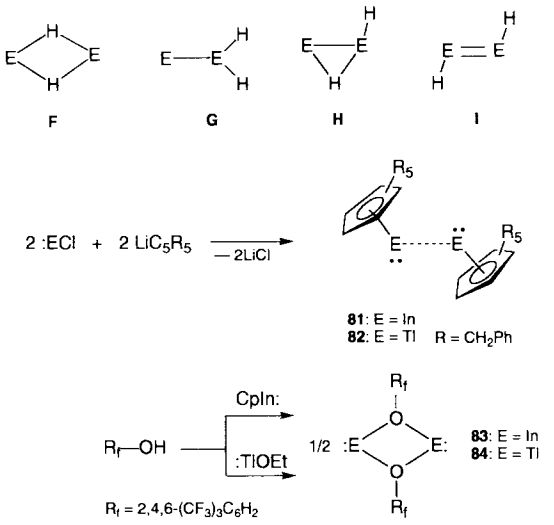

Scheme 11.

from the GCMT model. The low degree of association is attributed to the *ortho*-positioned CF_3 groups that shield the low-coordinate In and Tl centers (compare the cubic tetramer $[(TlOMe)_4]$[78]).

While a prediction of the molecular form of olefins (planar), digermenes **86a–c** (bent), distannenes **87a–d** (bent), and diplumbenes (ring) is relatively facile with the GCMT model (see Table 1), an evaluation of disilenes such as **85a–i** is difficult because here $\Sigma\Delta E_{S\rightarrow T}$ is on the same order of magnitude as $1/2E_{\sigma+\pi}$ and therefore both planar as well as *trans*-bent structures are possible. Indeed this makes the investigation of such systems particularly exciting, since the electronic and structural character can be varied within a large range by the choice of substituents. Several bonding parameters for the compound classes **85–87** are listed in Table 2.[79]

A comparison of the recently characterized disilenes **85f**[80] and **85g–i**[81] with the previously known compounds **85a–e** shows that disilenes, in agreement with the predictions from the GCMT model, can exist in a planar as well as a weakly bent form. However, no systematic influence of the substituents on the character could be recognized. It must be kept in mind that the energy required to convert $H_2Si{=}SiH_2$, which has a *trans*-bent structure according to extensive ab initio calculations,[3b, 68, 69] to a planar form is very small (<1 kcal mol^{-1}). The observation that the silylated disilenes **85g** and **85i** are bent despite steric strain is contradictory to the theoretical view of SiH_3-substituted compounds held up to now. The observed deviation may be due to hyperconjugative interactions between the Si=Si π bond and σ^* orbitals on the SiR_3 groups, which have a higher group electronegativity. In solution several disilenes including **85a**, **85g,h** are thermochromic. This is attributed to increased thermal occupation of a strongly twisted state ($\varphi >> 0°$; see Scheme 12) by which the longest wavelength absorption band experiences a bathochromic shift.[81]

The digermenes known are, as predicted by the GCMT model, without exception *trans*-bent although also here, as in **85a–i**, the E–E distances and angle θ vary. An even stronger variation of these parameters is observed for the distannenes **87a–d**, which is not surprising due to the decreasing bond strength that accompanies the higher atomic number and the calculated, flat potential energy surface for the lengthening of the E–E distance. At this point, a comparison with the "most crowded known olefin" *Z*-(*t*BuMe$_2$Si)(Me$_3$Si)C=C(*t*BuMe$_2$Si)(Me$_3$Si) is instructive. With a twist angle of $\varphi = 60°$, the C=C bond (1.369 Å) in this compound is lengthened by only about 2% with respect to the reference value (1.34 Å).[82] Olefins can be labeled as molecules with "hard" double bonds, while disilenes, digermenes, and distannenes have "soft" double bonds.[81] Also in agreement with the GCMT model is the average bending angle which increases in the order disilene–digermene–distannene, θ: $4° < 27° < 44°$. It should be mentioned once more that the energy potentials for the bending angle θ and, particularly, for the lengthening of the E=E bond are very flat. As was explained above using Figure 4, several constitutional isomers of the molecule E_2H_4 (E = Si, Ge, Sn, Pb) are localized as minima on the singlet potential energy surface. For Sn_2H_4 there are four isomers (**B–E**) that vary in energy content by a maximum of 10 kcal mol^{-1} since the Sn–H and Sn–Sn bond energies as well as the angle deformation energy are very low. Under this aspect, it is not surprising that a wide range of conformational isomers have been observed for distannenes in the solid state.

The distannene **87a** [83] synthesized in 1976 by Lappert et al. has a Sn–Sn distance (2.77 Å) that lies in the range of a single bond (2.81 Å) and a bending angle θ of 41°. The C-Sn-C angle in **87a** (109.2°) is, as expected from the VSEPR model, slightly

Table 2. Selected bonding parameters for $XX^1E{=}EYY^1$ molecules (E = Si, Ge, Sn). The bending angle θ is the angle that is formed between the XX^1E or YY^1E plane and the E–E bond. The angle φ describes the twisting about the E–E bond [a].

E		X,X^1	Y,Y^1	d(E–E) [Å]	θ [°]	ϕ [°]
Si	**85a**	Mes	Mes	2.16	10–18	3–12
	E-**85b**	*t*Bu	Mes	2.14	0	0
	E-**85c**	1-Ad	Mes	2.14	3	0
	85d	2,6-Et$_2$C$_6$H$_3$	2,6-Et$_2$C$_6$H$_3$	2.14	0	10
	85e	2,4,6-*i*Pr$_3$C$_6$H$_2$	2,4,6-*i*Pr$_3$C$_6$H$_2$	2.14	0	3
	E-**85f**	Tbt	Mes	2.23	–	–
	85g	*i*Pr$_2$MeSi	*i*Pr$_2$MeSi	2.23	5.4	0
	85h	*t*BuMe$_2$Si	*t*BuMe$_2$Si	2.20	0.1	8.9
	85i	*i*Pr$_3$Si	*i*Pr$_3$Si	2.25	10.2	0
Ge	**86a**	2,6-Et$_2$C$_6$H$_3$	2,6-Et$_2$C$_6$H$_3$	2.21	12	10
	86b	(Me$_3$Si)$_2$CH	(Me$_3$Si)$_2$CH	2.35	32	0
	Z-**86c**	Mes	2,6-*i*Pr$_2$C$_6$H$_3$	2.30	36	7
Sn	**87a**	(Me$_3$Si)$_2$CH	(Me$_3$Si)$_2$CH	2.77	41	0
	87b	2,4,6-(CF$_3$)$_3$C$_6$H$_2$	2,4,6-(CF$_3$)$_3$C$_6$H$_2$	3.63	46	0
	87c	2-*t*Bu-4,5,6-Me$_3$C$_6$H	2-*t*Bu-4,5,6-Me$_3$C$_6$H	2.91	21, 64	10.6
	87d	(Me$_3$Si)$_3$Si	(Me$_3$Si)$_3$Si	2.82	29	63.2

[a] Ad = adamantyl; Mes = mesityl; Tbt = 2,4,6-[(Me$_3$Si)$_2$CH]$_3$C$_6$H$_2$.

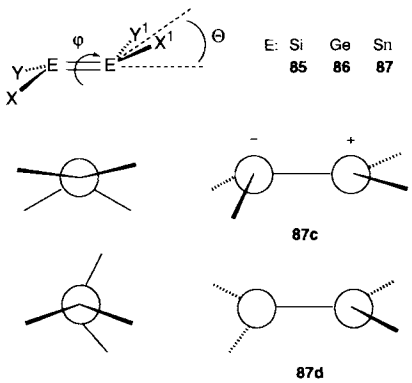

larger than that in the monomer **29** (97(2)°), in which the lone pair of electrons on tin leads to a reduction of the angle. In **87b** the angle θ is 46° and the Sn–Sn distance is increased to 3.63 Å. At most this can be considered as a very weak Sn–Sn interaction, although it can be optically observed. As with the "dimeric" [CpTl] and [CpIn] compounds **81** and **82**,[76] the crystals of **87b** are red, while those of the monomeric stannanediyl **40** are yellow. In a cocrystallizate of the stannanediyl **40** with stannocene [Cp_2Sn] the Sn–Sn distance is even further increased to 4.0 Å, and the crystals of this mixture are orange.[84]

Noteworthy distortions have been observed in the molecular structures of the distannenes **87c**[85] and **87d**[60] (Table 2). In **87c** the two R_2Sn fragments are rotated by an φ angle of 10.6° with respect to one another, the Sn–Sn distance (2.91 Å) is significantly longer than a single bond and both fragments show extremely different bending angles θ. The authors therefore described **87c** as a donor–acceptor complex in which the more strongly pyramidalized Sn center (64.4°) has a negative partial charge and the other less strongly pyramidalized center (21.4°) has a positive partial charge. This description corresponds formally to a dipolar resonance structure $[R_2Sn^+-Sn^-R_2] \leftrightarrow [R_2Sn^- - Sn^+R_2]$ which is by definition not observable. Here one electron from the 5s orbital of one stannanediyl must be promoted to a 5p orbital of the other. This formulation has been discussed by Lappert et al.[5] within the framework of resonance theory and was later used by Pauling for the description of the bonding in olefin-analogous compounds.[86] In **87d** the silylated stannanediyl fragments are strongly rotated with respect to one another ($\varphi = 63.2°$); thus, the authors suggest the possibility of thermal excitation into the triplet state, which is then more stable than the singlet state for olefins rotated by 90°. The Sn–Sn distance (2.82 Å) is shorter than that in **82c**. The bending angle θ in **87d** (28.6°) is smaller than that expected for $H_2Sn{=}SnH_2$ (46–51°).[3b, 87] This is attributed to the silyl substitution, which favors a flattening of the coordination sphere at the Sn center, as well as the sterically demanding $(Me_3Si)_3Si$ groups.

In solution the disilenes, digermenes, and distannenes display varied *cis–trans* isomerization behavior. Three possibilities are shown in Scheme 12.

The classical pathway A in Scheme 12 corresponds to rotation of the E–E bond in which the E=E π bond is broken and the molecule, in a singlet transition state, is rotated by $\varphi = 90°$ about the E–E bond. In addition dissociation into two singlet

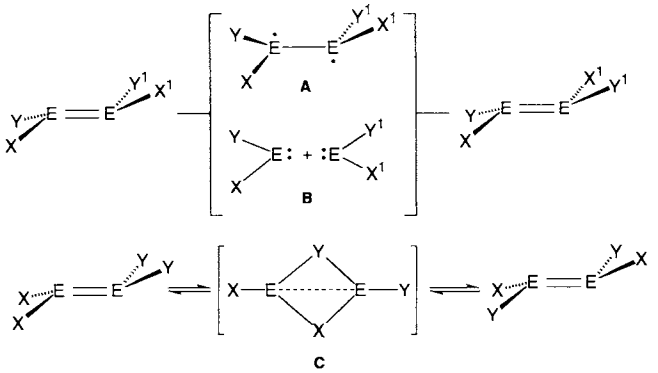

Scheme 12. Isomerizations of disilenes, digermenes, and distannenes.

ER_2 fragments (pathway B) can occur; recombination then provides the *cis* and *trans* isomers. Experimentally, the *cis–trans* isomerization along pathway A has been proven for a series of 1,2-diaryl-1,2-dialkyldisilenes. An activation enthalpy of 25–28 kcal mol^{-1} has been determined for rotation about the Si=Si bond. This is in agreement with the calculated values. The thermal dissociation, on the other hand, requires much more energy (52–58 kcal mol^{-1}) but has been proven recently for the first time for the extremely sterically substituted disilene **85f**.[80] For digermenes only the energetically preferred classical *cis–trans* isomerization by pathway A has as yet been observed. In contrast only dissociation into two stannanediyls has been seen for distannenes. In the case of **87a** and **87c** the monomer–dimer equilibrium has been experimentally proven,[88] while the distannenes **87b** and **87d** evidently exist as monomers in solution.

An interesting alternative to pathways A and B has been suggested by West et al. for tetraaryl disilenes.[89] Isomerization pathway C has a doubly bridged intermediate. The evaluation of the kinetic data provided an activation enthalpy of only 15 ± 2 kcal mol^{-1}. Indeed such a mechanism, a dyotropic rearrangement, is not impossible in light of the many energetically similar E_2H_4 isomers **B**–**E** mentioned in Section 2 (Fig. 4), and consequently, it should be discussed as the preferred "nonclassical" mechanism for digermenes and particularly for distannenes with aryl substitutents.

Doubly bridged structures such as in **88**, **89**,[90] **90a,b**,[91] and **92a,b**[92] are the most stable isomers for dimers of stannanediyls, plumbanediyls, and arsenium ions when they are substituted with heteroatoms bearing lone pairs of electrons (Scheme 13).

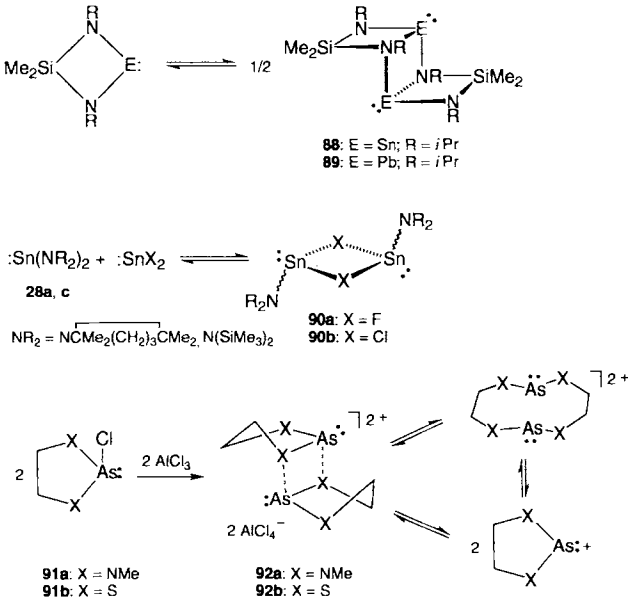

Scheme 13. Synthesis of **88**–**92**.

Owing to the rise in the excitation energy $\Delta E_{S\rightarrow T}$ upon substitution with R_2N, F, or Cl and the weakness of the Sn=Sn or Pb=Pb bond the inequality (e) in the GCMT model is satisfied, and there is no direct E–E bonding in the dimers. In solution the cyclic dimers **88** and **89** as well as **92a,b** are in equilibrium with

the monomers. This has been proven by trapping reactions.[48, 93] The doubly chloro-bridged **90b**, which is found as *cis–trans* isomers in the solid state and in solution (see the discussion for Figure 4), is a dimer in solution. The fluoro-bridged dimer **90a** is in equilibrium with the trimer $[(R_2N)SnF]_3$. It is noteworthy that to our knowledge no phosphorus analogues of **92a,b** are known. In an unsuccessful search for dications $[R_2P{=}PR^1{}_2]^{2+}$, which are isoelectronic with disilenes, diphosphanes were subjected to electrochemical oxidation reactions. In the case of the amino-substituted diphosphane $(i\mathrm{Pr}_2N)_2P{-}PR_2$ decomposition of even the radical monocation takes place with formation of the phosphenium ion $[(i\mathrm{Pr}_2N)_2P]^+$ and the symmetrical diphosphane $R_2P{-}PR_2$ ($R = i\mathrm{Pr}_2N$, *t*Bu). This finding impressively demonstrates the stability of monomeric, amino-substituted phosphenium ions.[94] In contrast monoamino-substituted disilenes such as $(Me_3Si)_2NMesSi{=}SiMesN(SiMe_3)_2$ are known and are described as having a Si=Si double bond that is less stable than that in aryl- and alkyl-substituted compounds.[95]

4.2. Compounds with Asymmetrical Double Bonds

Silaethene **93**,[96] methylenephosphonium ion **94**,[97] and phosphanylborane **95**[98] are isoelectronic but not isostructural

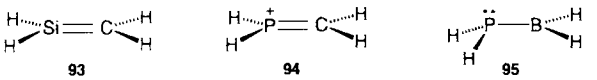

with one another. Methylenephosphonium salts **97a–c** (**97a**: R = H, R′ = $SiMe_3$; **97b**: R = R′ = $SiMe_3$; **97c**: R = R′ = aryl), which are comparable to olefins (Scheme 14), can be synthesized from the di(*tert*-butyl)-*P*-chloro-phosphorus ylides

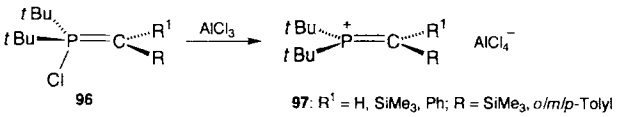

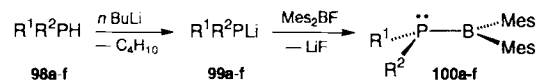

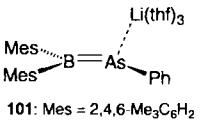

Scheme 14. Synthesis of **97** and **100a–f**.

96a–c by chloride abstraction with $AlCl_3$. Just as with silaethene **93**, these compounds have a classical molecular framework (Fig. 11) with trigonal-planar coordination at the phosphorus and carbon centers involved in the P=C bond. This bond has a typical length of 1.68 Å which is about 10% shorter than a P–C single bond (≈ 1.85 Å).

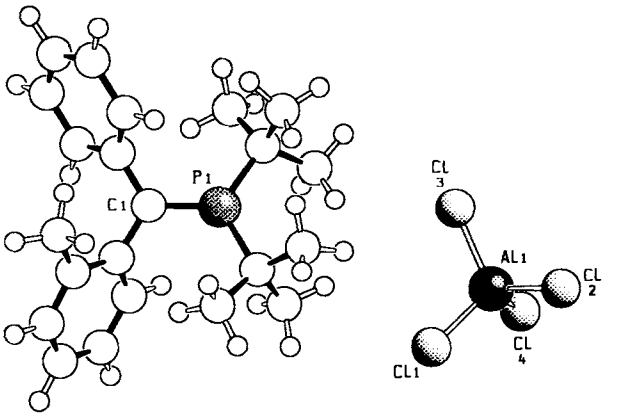

Fig. 11. Molecular structure of **97c** in the crystal [97a]. P1–C1 bond length 1.680(8) Å, shortest cation–anion contact 2.83 Å.

The observed molecular structures of **97c** is as expected by the GCMT model since the following is valid: $\Sigma\Delta E_{S\to T} \approx 7.4\ \mathrm{kcal\,mol^{-1}} < 1/2E_{\sigma+\pi} \approx 25\ \mathrm{kcal\,mol^{-1}}$. The twisting angle φ varies from 11° in **97a** to about 22° in **97c**. The isoelectronic substitution of C^+ in methylenephosphonium ions by a boron center leads to phosphanylboranes such as **100a–f**. These can be synthesized from the phosphanides **99a–f** and Mes_2BF. Although the excitation energy $\Delta E_{S\to T}$ for $[BH_2]^-$ and the bond energy $E_{\sigma+\pi}$ of a B=P bond are not known, it is expected that $\Sigma\Delta E_{S\to T} > 1/2E_{\sigma+\pi}$ is valid since both fragments $[PH_2]^+$ and $[BH_2]^-$ should have a singlet ground state and the P–B bond is weak. As a result the molecular framework in phosphanylboranes should be bent, which has been confirmed by ab initio calculations on **94**[99] and by the experimentally determined molecular structures of **100a–f**.[98] A bond length of 1.93 Å would be expected for a P–B single bond. In the *trans*-bent ground state of $H_2P{-}BH_2$ ($\theta(P) = 70°$; $\theta(B) = 6°$) the calculated B–P distance is 1.901 Å. The flattening of $H_2P{-}BH_2$ requires only 5.9 kcal mol^{-1} (compare the inversion barrier for $PH_3 \approx 38\ \mathrm{kcal\,mol^{-1}}$)[100] and the B–P bond is shortened by about 5% to 1.807 Å. The experimentally determined structures of the differently substituted phosphanylboranes **100a–f** can be considered as conformers with differently pyramidalized phosphorus centers (angle θ) and different degrees of rotation about the B–P bond (angle φ) which are "frozen" in the solid state (Table 3).

The degree to which these parameters influence the B–P bond length can be easily seen. Short distances are found in **100a–c**, in which the sterically demanding substituents flatten the coordination sphere of the three-coordinate phosphorus center, which prefers a pyramidal environment, and therefore forces the

Table 3. Selected structural parameters of phosphanylboranes [98]. The bending angle θ is the angle that is formed between the R^1R^2P plane and the B–P bond. The angle φ describes the twisting about the B–P bond.

	R^1	R^2	d(B-P) [Å]	θ [°]	ϕ [°]
100a	*t*Bu	*t*Bu	1.839	26.9	14.5
100b	*t*Bu	*t*Bu	1.843	8.9	21.8
100c	Mes	Mes	1.839	2.2	2.8
100d	Ph	Ph	1.859	42.1	2.4
100e	H	1-Ad	1.897	61.6	7.5
100f	$(Et_2O)Li$	1-Ad	1.823	16.1	13.8

formation of a (p-p) π bond (maxim 5, Section 2). A relatively broad variation in the angles θ (2–27°) and φ (3–15°) can be tolerated without noticeable influence on the B–P distance. Only when bending angles > 40° and twisting angles of more than 20° occur, is there a significant lengthening of the B–P bond.

The lithiated compound **100f** and the analogous (lithio)arsaboraethene **101**[101] are exceptional. They show the shortest B–P and As–P distances, respectively, observed in a molecular compound of this type. Lithium is only weakly bonded to the pnicogen atom, which does indeed have a pyramidal coordination sphere ($\Sigma°(P) = 357.4°$; $\Sigma°(As) = 341.4°$). The carbon atoms that are directly bound to the boron or the pnicogen atom all lie in one plane so that the P=B or P=As double bond is here fully formed. As a result, relatively high rotation barriers ($\Delta G^{\neq} > 20$ kcal mol^{-1}) about the B=E bond (E = P, As) were estimated for these compounds by NMR spectroscopy.

The diborylcarbene **103** can be combined with germanediyls or stannanediyls to form germaethenes and stannanethenes, respectively. Single-crystal X-ray structure analyses were also carried out for **104**[102a] and **105**[102b] (Scheme 15).

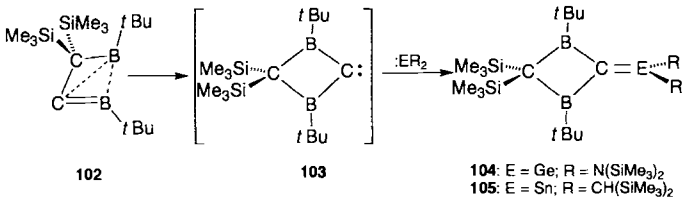

102 **103** **104**: E = Ge; R = $N(SiMe_3)_2$
105: E = Sn; R = $CH(SiMe_3)_2$

Scheme 15. Synthesis of **104** and **105** from **102**.

The Ge=C and Sn=C bond lengths (**104**: 1.827 Å; **105**: 2.025 Å) are in good agreement with calculated values (Ge=C: 1.814 Å; Sn=C: 2.063 Å)[87] about 8% and 6%, respectively, shorter than the corresponding single bond lengths (compare the corresponding shortening of about 13% for olefins and about 9% for silaethenes). In **104** and **105** the two carbene-analogous fragments are relatively strongly rotated with respect to each other (**104**: $\varphi = 36°$; **105**: $\varphi = 61°$), and the germanium, the tin, and unexpectedly even the carbon centers are pyramidal (**104**: $\theta(Ge) = 1.7°$, $\theta(C) = 4.8°$; **105**: $\theta(Sn) = 5.0°$, $\theta(C) = 16.0°$). In contrast, the germaethene **106** (Scheme 16) synthesized by Escudié et al. is planar (Ge=C: 1.801 Å)[103] and corresponds to the structure expected from the GCMT model.

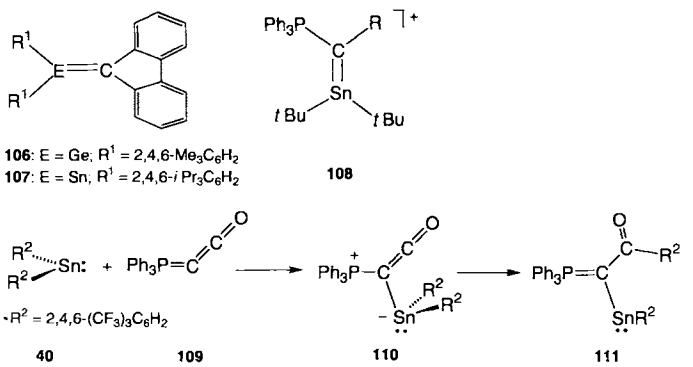

106: E = Ge; $R^1 = 2,4,6\text{-}Me_3C_6H_2$
107: E = Sn; $R^1 = 2,4,6\text{-}i\,Pr_3C_6H_2$ **108**

$R^2 = 2,4,6\text{-}(CF_3)_3C_6H_2$

40 **109** **110** **111**

Scheme 16.

The molecular structure of the analogous stannaethene **107**[104] has not yet been investigated. Ab initio calculations at various levels predict a planar structure for $H_2Ge{=}CH_2$ and a planar[3b] (DFT, RHF, or MP2 level) or a slightly more stable bent structure[87] (MCSCF level) for $H_2Sn{=}CH_2$. In general, very little is known about stannaethenes; their existence has been considered plausible mainly as intermediates such as **108**.[105] Reaction of the ketene ylide **109** and the stannanediyl **40** leads to the adduct **110**. Subsequent migration of an aryl group provides the compound **111**.[106] The central Sn–C bond is about 0.1 Å shorter than a Sn–C single bond, and all the substituents of this bond lie in a plane. Thereby at least a few criteria for the presence of a Sn=C multiple bond have been fulfilled.

The synthesis of the carbene adducts **112**[107] and **113a,b**[108] is similar to that of **104** and **105** in that also here a stable carbene is combined with a carbene-analogous fragment (Scheme 17).

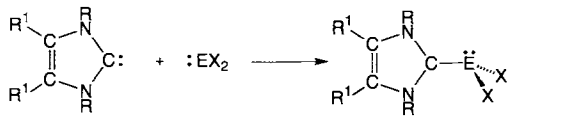

16

112: E = Ge, X = I
113a: E = Sn, X = Cl
113b: E = Sn, X = 2,4,6-$i\,Pr_3C_6H_2$

Scheme 17. Synthesis of **112** and **113a,b**.

However, carbene **16** has an energetically low-lying singlet state and is therefore not electrophilic like **103** but rather nucleophilic. It is therefore not surprising that the products **112** and **113a,b** are very different from **104** and **105**. Noteworthy is the strong pyramidalization of the coordination sphere at the main group metal (**112**: $\Sigma°(Ge) = 290°$; **113a**: $\Sigma°(Sn) = 282°$; **113b**: $\Sigma°(Sn) = 309°$) as well as the large extent to which the two halves of the molecule are twisted with respect to one another. In addition, the long Ge–C and Sn–C distances (Ge–C: 2.102 Å; Sn–C: 2.290 Å and 2.379 Å) refute double bond character; thus, these compounds are better described as Lewis acid–base adducts since, as has been proven for **113**, they dissociate to their components in solution. The molecular structures obtained for **112** and **113a,b** can be considered as models for the *least motion* attack of one singlet carbene on another.[107] The combination of two carbene fragments shown schematically in Figure 2 is then only a purely theoretical model.

Special consideration must be given to the fact that it has not yet been possible to synthesize an isolable heteronuclear $XYE{=}E^1X^1Y^1$ multiply bonded system with two Group 14 E and E^1 centers from the higher rows ($n > 2$). These compounds should have especially interesting characteristics. Indeed, the digermasilacyclopropane **114** decomposes thermally (105 °C, 7 h) or photochemically ($\lambda = 254$ nm) to give the dimesitylgermanediyl **116**, the more stable of the two conceivable diyls, and the germasilaethene **115**; however, the latter has not yet been proven since it undergoes spontaneous 1,2-mesityl group migration to form the silylated germanediyl **117** (Scheme 18).

The germanediyls **116** and **117** were proven by reaction with $HSiEt_3$, the trapping reagent typically used for these species.[109] In the meantime, it has also been suggested that tetra-

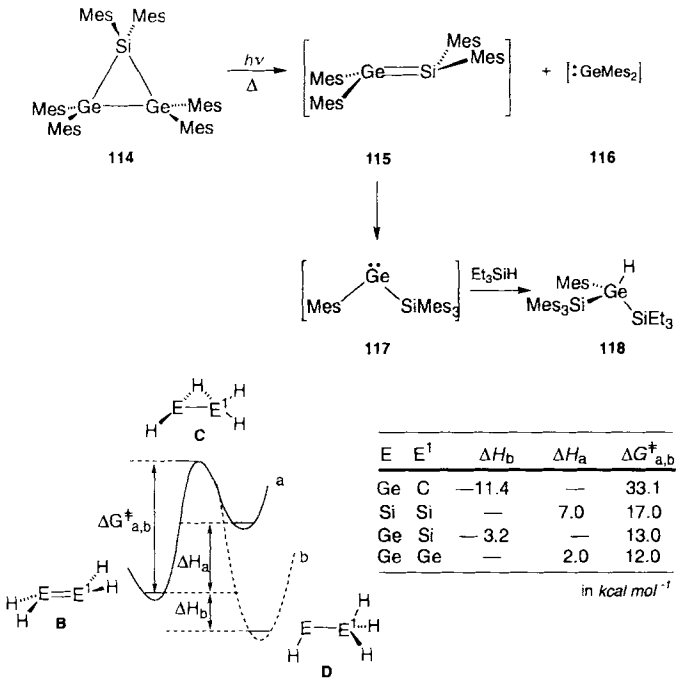

E	E¹	ΔH_b	ΔH_a	$\Delta G^{\ddagger}_{a,b}$
Ge	C	−11.4	—	33.1
Si	Si	—	7.0	17.0
Ge	Si	−3.2	—	13.0
Ge	Ge	—	2.0	12.0

in *kcal mol*$^{-1}$

Scheme 18. Top: Fragmentation of **114**. Bottom: The energy diagram for the rearrangement of doubly bonded compounds **B** via the hydrogen-bridged transition states **C** to the ethanediyl compounds **D**. Gibbs free energy ($\Delta G^{\ddagger}$), exothermic reaction enthalpy (ΔH_b) and endothermic reaction enthalpy (ΔH_a).

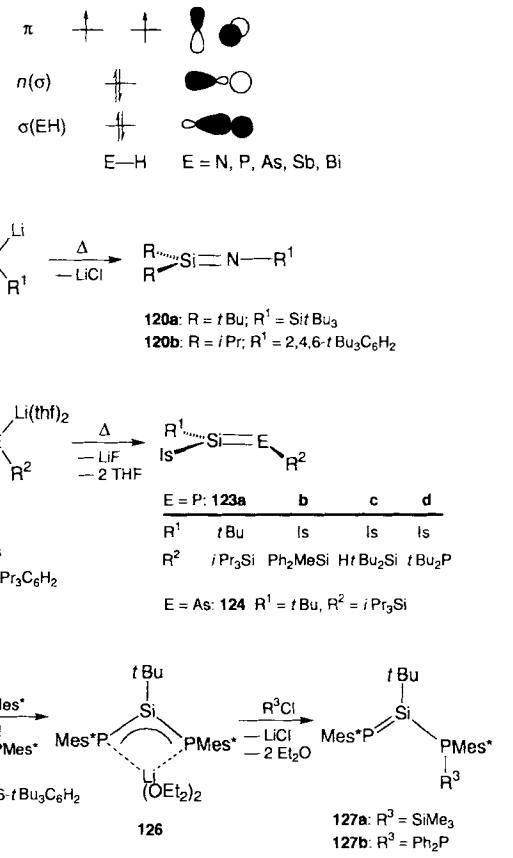

Scheme 19. Top: The EHT orbital energy diagram for E–H carbene analogues. Bottom: Synthesis of **120a,b**, **123a–d**, and **127a,b**.

mesityldigermene $Mes_2Ge{=}GeMes_2$, just like **115**, can thermally or photochemically rearrange to give $MesGe{-}GeMes_3$.[110] As is the case with digermenes, a germasilaethene should also have a *trans*-bent structure.[69, 87] The unsuccessful attempt to make a stable germasilaethene by the above-mentioned method can be explained by a quantum chemical study. This revealed that the rearrangement of a germasilaethene to a silylgermanediyl is an exothermic process with a relatively low activation energy. The same is true for the approximately isoenergetic pair digermene/germylgermanediyl. On the other hand, the thermodynamically favored rearrangement of a germaethene to a germanediyl is blocked by a high activation energy (Scheme 18).[111] The transition state for this rearrangement corresponds to the singly bonded, bridged isomer **C** in Figure 4. The same isomer is found as a local minimum on the singlet potential energy surface for Sn_2H_4 and Pb_2H_4. This example further substantiates the variety of possible isomers on the E_2H_4 potential surface (Fig. 4), which, in turn, makes the experimental search for these isomers exciting and full of promise!

The fragments PH, AsH, SbH, and BiH, which are not shown in Figure 6, are like CH_2, in contrast to the protonated species $[EH_2]^+$, present in a triplet ground state. This observation is simply understood, at least for PH and AsH, by using the qualitative EHT orbital energy level diagram shown in Scheme 19. In contrast to the BH or AlH species with four valence electrons which are present in the singlet ground state (Fig. 6), the π level that lies energetically higher than the nσ orbitals is occupied by two electrons in the six-electron systems PH and AsH. For P and As the magnetic quantum number *l* is still a "good quantum number", which means that the spin-orbit coupling can be ignored. As a result, according to Hund's rule, the more stable state has a maximum total spin $S = 2s + 1 = 3$ (for example $PH(^3\Sigma) \rightarrow PH(^1\Delta) = 21.7\ kcal\,mol^{-1}$).[9] For the higher homologues SbH and, in particular, BiH this simple approximation is no longer valid but these molecules are in the triplet state too.[112] A valence electron configuration in which, from the viewpoint of localized electrons, the central atom has two lone pairs of electrons is avoided. According to the GCMT model, the molecular structures of the higher homologues of the imine $H_2E{=}E^1H$ (E = Si, Ge, Sn, Pb; E^1 = P, As, Sb, Bi) should be planar. That is essentially in agreement with experimental results and ab initio calculations.[113–117] Compounds **120a,b**,[118] **123a–d**,[119] **124** [119b, 120] and **127a,b** [121] were synthesized by thermal elimination of LiCl or LiF, respectively (Scheme 19).

The iminosilane **120a**, phosphasilene **123a** (Fig. 12) and arsasilene **124** are planar ($\Sigma^\circ(Si) = 360^\circ$), as are the longer known phosphagermenes.[67d] The $E{=}E^1$ bonds (Si=N: 1.568 Å; Si=P: 2.062–2.094 Å; Si=As: 2.164 Å; Ge=P: 2.138–2.144 Å) are about 8% shorter than the corresponding single bond lengths.

An exception is the phosphanyl-substituted phosphasilene **127b** whose Si atom is slightly pyramidalized ($\Sigma^\circ(Si) = 356.7^\circ$).[121] While the angles at the phosphorus centers of the Si=P bonds in **123a** and **127b** (112.8°; 104.2°) and the Ge=P bonds in phosphagermenes (102.6°; 107.5°) as well as the angle at the arsenic center in **124** (110.9°) are strongly bent, the nitrogen atom in the *N*-silylated iminosilane **120a** is linearly coordinated (177.8°). This effect is again based on the "reluctance to hybridize" found for the elements phosphorus and arsenic.[116] A parallel is seen in phosphanes and arsanes, which have more

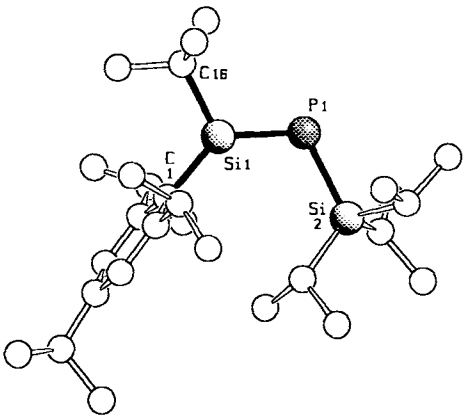

Fig. 12. Molecular structure of **123a** in the crystal [119b]. Bond lengths [Å] and angles [°]: P1–Si1 2.062(1), P1–Si2 2.255(1); Si1-P1-Si1 112.79(4), C1-Si1-C16 113.36(9), C1-Si1-P1 131.99(9), C16-Si1-P1 114.59(7).

strongly pyramidalized structures than amines.[122] The observed deviations from the calculated structures of the parent compounds $H_2Si{=}NH$ (Si-N-H: 122.8°) and $H_2Si{=}PH$ (Si-P-H: 93.7°) are attributed to the replacement of the H atoms with bulky, more electropositive silyl groups (compare NH_3 (pyramidal) and $N(SiH_3)_3$ (planar)).

Calculations of the potential energy surface of H_2SiNH provide a further surprise. The isomeric silylnitrene $H_3Si\text{-}N{:}$ is a local minimum that is 18 kcal mol^{-1} more stable than $H_2Si{=}NH$.[117] The rearrangement of $H_2Si{=}NH$ to $H_3Si\text{-}N{:}$ is, however, hindered by a high energy barrier (60 kcal mol^{-1}). In contrast, $H_2Si{=}PH$ is more stable than the isomeric phosphanediyl $H_3Si\text{-}P{:}$.[117] For the phosphanyl- and arsanyl-substituted germanediyls, stannanediyls, and plumbanediyls shown in Section 3, Scheme 6, the rearrangement in Equation (g) was investigated by quantum mechanical methods.

$$(H_2P)_2E{:} \rightarrow HP{=}E(PH_2)H \quad (E = Si, Ge, Sn, Pb) \qquad (g)$$

It was determined that for E = Si and Ge double bond isomers are favored, while for E = Sn and Pb the carbene-analogues are lower in energy.[59] In all cases the activation energy for the rearrangement process is considerable (30–70 kcal mol^{-1}) and thus allows the directed synthesis of the isomers possible.

The synthesis of thiones **131**[123] (E = Si), **132a**[124] (E = Ge), and **133**[126] (E = Sn), which are monomeric in the solid state, as well as the germaselenones **132b**[125] has clearly shown that by carefully choosing sufficiently bulky ligands and the correct synthetic routes, even the compounds which were only known as oligomers can be obtained as doubly bonded systems (Scheme 20). The E=E^1 distances in these compounds are about 7–10% shorter than the corresponding E–E^1 single bonds.

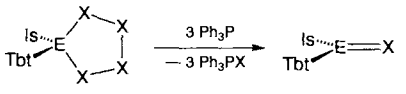

Is = 2,4,6-*i*Pr$_3$C$_6$H$_2$ Tbt = 2,4,6-[(Me$_3$Si)$_2$CH]$_3$C$_6$H$_2$

	128	129a	129b	130		131	132a	132b	133
X:	S	S	Se	S	X:	S	S	Se	S
E:	Si	Ge	Ge	Sn	E:	Si	Ge	Ge	Sn

Scheme 20. Synthesis of **131**–**133** from **128**–**130**, respectively.

4.3. Cumulated Multiply Bonded Systems

Within the framework of the GCMT model, Inequality (f) (Section 2) is valid for cumulated doubly bonded systems XYE = $(E)_n{=}EXY$. Despite the high excitation energy $\Delta E_{S\rightarrow T}$ for C≡O (≈139 kcal mol^{-1}), the estimation predicts a planar molecular structure for ketene $H_2C{=}C{=}O$ due to the large energy term $f'(E_{\sigma+\pi})$ (for factor f' see [Eq. (f)] in Section 2). Since the H_2Si and C≡O fragments are in a singlet ground state and the Si=C bond is considerably weaker, a *trans*-bent molecular structure is expected for $H_2Si{=}C{=}O$.[2b] Results from ab initio calculations show a Si–C distance of 1.938 Å, which is about 3.5% longer than a Si–C single bond, and an angle θ of 88.6°. The C=O distance (1.137 Å) in the bent molecule is slightly shorter than in free C≡O (1.150 Å); the calculated C≡O stretching frequency is shifted to higher wavenumbers by 8 cm^{-1}.[127] Silanediyl–CO complexes have been experimentally detected in frozen hydrocarbon matrices. Their structures have been controversially discussed [**135a–e**: bent;[128a] **135a**: planar[128b]] (Scheme 21).

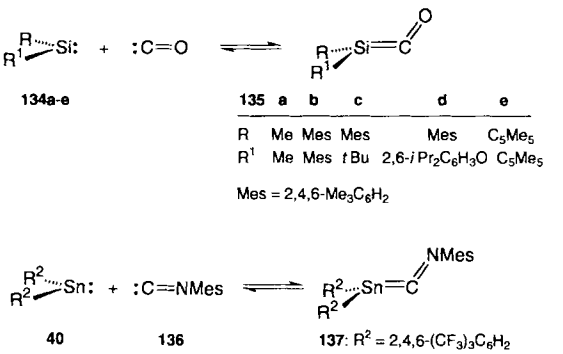

Scheme 21. Synthesis of **135** and **137**.

C≡O is very weakly bound in these complexes. As a result, upon melting the matrix, disilenes are obtained as products of the dimerization of silanediyls, which are formed upon decomposition of the silaketenes. Also the silicocene **66** forms a weak complex with C≡O, which has been observed by IR spectroscopy in liquid xenon at 1.5 bar CO pressure.[129] In [Cp*$_2$Si(CO)] and in **135a**, which has been investigated by Arrington et al., the C≡O stretching frequencies appear at significantly lower wavenumbers ($\Delta\nu$(CO) = 78 cm^{-1} and 181 cm^{-1}, respectively) than the calculated values. This is more consistent with the formation of a classical Si=C=O double bond and a linear molecular structure.

The silanediyl–C≡O complexes can be compared to the stannaketenimine **137**. The latter is the only complex of this form that has been characterized by X-ray structure analysis (Fig. 13).[130]

In analogy to the results for $H_2Si(CO)$, the Sn–C distance (2.397(3) Å) in the stannanediyl-isocyanide complex **137** is about 4% longer than the Sn–C distance between the tin atom and the *ipso*-carbon centers of the aryl rings (2.31 Å); the bending angle θ is 153.9(2)° and the C=N stretching frequency of the isonitrile ligand is shifted by 48 cm^{-1} to higher wavenumbers. The dissociation enthalpy (7.07 ± 0.09 kcal mol^{-1}) and entropy (90 ± 1 e.u.)

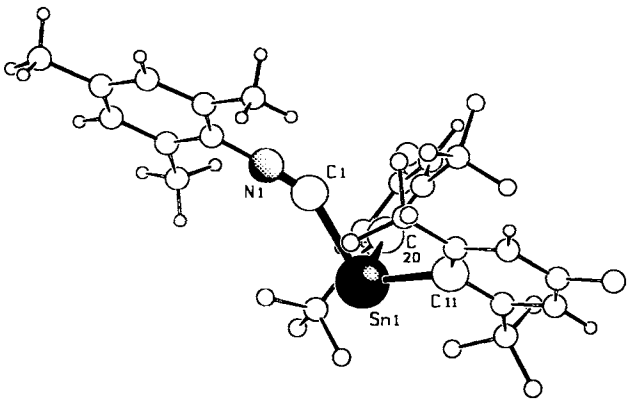

Fig. 13. Molecular structure of **137** in the crystal [130]. Bond lengths [Å] and angles [°]: Sn1-C1 2.397(3), Sn1-C11 2.306(2), Sn1-C20 2.314(3), C1-N1 1.158(3); N1-C1-Sn1 153.9(2), C1-Sn1-C11 104.9(1), C1-Sn1-C20 83.4(1), C11-Sn1-C20 102.6(1).

could be determined by temperature-dependent ^{119}Sn NMR spectroscopy. By using these values an equilibrium constant K of 0.33 mol L^{-1} at 298 K was calculated. This indicated that at this temperature about 45% of the stannaketenimine has already decomposed.

The examples discussed in this section prove that the GCMT model is generally suitable for predicting the molecular structure of dimers from carbene-analogous fragments with central atoms from the higher rows. However no ad hoc conclusions can be made about the number of possible conformational isomers and, in particular, their energetic relationship to one another. Here the method of choice has been and remains ab initio calculations. In the next section, we will discuss trimers and strained polycycles that can be constructed from carbene-analogous fragments. Thereby it will be made clear that, in particular, the fragmentation behavior of such rings can be understood and predicted by using the $\Delta E_{S\rightarrow T}$ values that are graphically shown in Figure 6.

5. Heterocyclopropanes: Trimers from Carbene Analogues and Related Heterobicyclo[1.1.0]butanes of the Main Group Elements

Cyclopropanes have something in common with the above-mentioned multiply bonded systems in that their ability to exist was originally disputed.[131] Hence they were always something special. "Acute" angles (60°) are found between the nucleus–nucleus axes that deviate considerably from the "normal" bond angles at the CR_2 groups acting as ring members. This places great angular (Baeyer) strain on the molecules.[132] Moreover, the substituents on the ring members are forced into ecliptic positions from which there is no deviation and thereby cause additional torsional strain.[133] As a result, these small rings are reactive. The C–C single bond in cyclopropane is about 20 kcal mol^{-1} weaker than a normal C–C single bond (84 kcal mol^{-1}).[134] If the electron density of the E–E bond in the small rings $(ER_2)_n$ is experimentally determined within the framework of the available methods and models, the maxima are not found along the nucleus–nucleus bond axes, rather outside of them.[135] Therefore these molecules are described as having bent bonds (banana bonds), and the angles, which include the pathways of maximum electron density (MED) between the nuclei of the ring members, are now 78° in cyclopropane.[136]

The previous sections have shown that in general it is possible to systematically describe the molecular structures and several characteristics of E=E and E=E^1 bonds of the main group elements on the basis of carbene-analogous fragments. This concept can also be applied without restrictions to cyclopropane and its analogues as well as to heterobicyclo[1.1.0]butanes. By doing so the occasionally lower stability or higher reactivity of such systems becomes understandable. Conversely, this concept allows one to predict which electronic structure the carbene-analogous fragments $:ER_2$ must have in order to build a stable ("more stable") heterocyclopropane. This is exemplified in the known series of heterocyclopropanes with Group 14 elements as framework atoms. They can be photolytically and/or thermally broken down to molecules with E=E or E=E^1 double bonds and carbene analogues; thus, they are versatile synthetic building blocks (see Scheme 18 and ref. [67e]). Due to this reactivity, they correspond to the general bond description of mixed E_2Y rings with E and Y as ring members as defined by the Dewar–Chatt–Duncanson model. These can, for example, be described as π complexes from one E=E unit and a carbene analogue Y (Scheme 22).[133c]

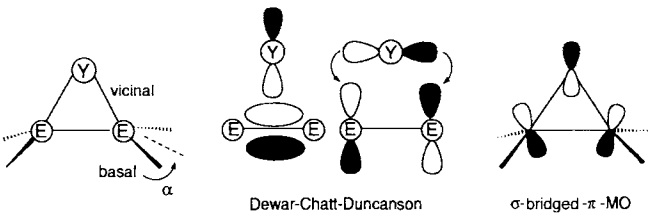

Scheme 22. Bond formation in E_2Y rings.

With increasing electronegativity on Y, a shortening of the basal E–E bond and an increase in the angle α is observed. This is a measure of the leveling of the planarity of the coordination geometry of the basal ring centers. This phenomenon can be summarized as a result of reduced back-bonding from an occupied, symmetry-adapted Y orbital into the π* orbital of the E=E unit. On the other hand, it is possible to explain the molecular structure and stability of three-membered rings by the strong dependence of the total energy on the energy variance of a "σ-bridged π orbital" upon alteration of the molecular shape.[137] Without this arbitrary subdivision into molecular orbitals an analysis of the Laplacian distribution of the total electron density reveals depletion and concentration of charge. Within this mathematical model, a short E–E distance corresponds with a strongly bent path of the valence electron density which can be bent concavely (towards the ring exterior) as well as convexly (towards the ring interior).[138]

In the following, a comparison of cyclopropane with the homonuclear and mixed heterocyclopropanes that contain carbon, silicon, germanium, tin, lead, and phosphorus as framework atoms will be presented. It will be shown that their description as trimers of carbene analogues provides an explanation for their varying ring strain and reactivity.

5.1. Description of Homonuclear Three-Membered Rings as Formal Trimers of Carbene Analogues: Cyclopropanes Versus Heterocyclopropanes with Si, Ge, Sn, Pb, and P as Framework Atoms

First a few fundamental differences in the molecular characteristics of cyclopropane and analogous homonuclear three-membered rings with Si, Ge, Sn, Pb, and P as ring building blocks will be discussed.[139, 140] Cyclopropanes **138** have been known for a long time. Numerous experimental and theoretical investigations have brought to light that these ring systems are unique in comparison to other three-membered rings. Its olefin-like reactivity is attributed to the relatively large p character of the C–C framework bonds. The unexpectedly low ring strain (**138a** ca. 27 kcal mol^{-1}), which corresponds to that of cyclobutane (C_4H_8 ca. 25 kcal mol^{-1}) despite the small bond angles, is achieved by the six equivalent and particularly strong C–H bonds. They offer compensation for the angle strain, since the strain energy is defined as the difference in the heat of formation between strained and unstrained molecules calculated incrementally. The C–C bonds of the ring, as mentioned above, can be described by the banana bonding orbitals as interpreted by the Coulson–Moffitt model.[141] This is analogous to the formulation of ethene with bent bonds. This description corresponds to that provided by Baeyer in which ethene is perceived as the first representative of strained $(CH_2)_n$ rings.[142]

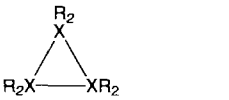

X	R = H	R = Alkyl, Aryl	R = Silyl
C	**138a**	**138b**	**138c**
Si	**139a**	**139b**	**139c**
Ge	**140a**	**140b**	—
Sn	**141a**	**141b**	—
Pb	**142a**	—	—

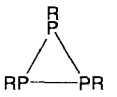

143: R = H, Alkyl, Silyl

A comparison of cyclopropane **138a** with cyclotrisilane **139a** and other homologues reaffirms that carbon shows "exotic" unprecedented bonding behavior. According to theoretical investigations, carbon forms equivalently strong σ and π bonds as a direct result of its ability to hybridize, an ability not shown by silicon and the other homologues. In addition, the bond strength of the E–E bonds intrinsically decreases, and carbon is clearly more electronegative than its homologues (Fig. 6b).[143, 18, 3a] Consequently, the hypothetical cyclotrisilane **139a**, the cyclotrigermane **140a**, and the cyclotristannane **141a**, which show approximately the same strain energy, are about 10 kcal mol^{-1} more strained than cyclopropane (HF/6-31G*), while the cyclotriplumbane **142a** (ca. 7 kcal mol^{-1} more strained than **138a**) even prefers a structure in which the PbH_2 fragments are rotated in the same direction about the C_3 axis (Scheme 23).

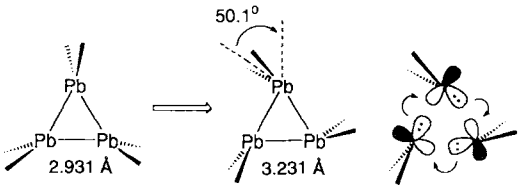

Scheme 23.

This molecule with C_{3h} symmetry is 10 kcal mol^{-1} more stable (MP4/DZ//HF/DZ) than the higher symmetry form with D_{3h} symmetry.[139] The distortion of the hypothetical cyclotriplumbane **142a** from the D_{3h} to C_{3h} structure is evidently based on an intrinsically weak interaction between three $:PbH_2$ particles and has thereby the same origin as the *trans*-bending in nonclassical double bonds.

According to calculations the bonds between the electropositive silicon centers in cyclotrisilanes have a large degree of s-orbital character,[143b] while the bonds to the more electronegative substituents show high p-orbital participation (see the rules from Bent and the VSEPR model). In the case of $(t\mathrm{Bu}_2\mathrm{Si})_3$ (**114b**: R = *t*Bu) an increase in the Si–Si distance of 7%, as compared to the parent compound **139a**, has actually been observed, which leads to a minor destabilization of the three-membered ring. The calculated bonding behavior in cyclotriphosphanes **143** is basically different since the localized lone pair of electrons on the phosphorus atom shows a high degree of s-orbital character and, as a result, the degree of p-orbital participation in the P–P bond is high. Accordingly, experimental and theoretical investigations show that cyclotriphosphanes **143** are about 10 kcal mol^{-1} less strained than cyclopropanes **138**.[145] The low ring strain in **143** is not unexpected since ring strain essentially originates from Pauli repulsion betweeen the geminal E–E bonds which are pushed together by small interior ring angles. A high s-orbital character in these bonds—like in **139**—causes a strongly antibonding σ/σ* delocalization.[146] The ring strain and, as far as is known, the varying reactivity of compounds of the type **138–142** can also be interpreted on the basis of the ground state of the carbene-like $:ER_2$ fragments which can be thought of as forming the three-membered ring. Calculations from Nagase show that the stabilization of three $:EH_2$ particles (E = Si, Ge, Sn, Pb) sharply decreased with increasing atomic number upon formation of the three-membered rings **139a–142a**.[139a] This is attributed to the increased stability of the singlet ground state of the carbene homologues and the decreased E–E bond energy. The much lower thermal stability of hexafluorocyclopropane (**138d**) than **138a** is also attributed to the different ground states of the respective carbenes. Compound **138d** decomposes even at 160 °C into difluorocarbene with a singlet ground state, which is about 46.5 kcal mol^{-1} more stable that the triplet state, and tetrafluoroethene,[147] while **138a** does not isomerize to propene until 400 °C.[148] Ab initio calculations from Nagase have shown that the stability of the three-membered rings with Group 14 elements is increased markedly by substitution, which reduces the singlet–triplet separations $E_{S\rightarrow T}$ for the carbene analogues.[139a] As mentioned above, this is accomplished by electropositive silyl substituents; thus, for example, the singlet–triplet difference in $:SiH_2$ (21 kcal mol^{-1}) is reduced to 4 kcal mol^{-1} in $:Si(SiH_3)_2$. Thereby the cyclotrisilane **139c** has the same ring strain as cyclopropane **138a**! Exceptional reactivity is shown by the cyclotrisilane **139** with $2\text{-}(Me_2NCH_2)C_6H_4$

substituents on silicon. Under thermal stress it does not dissociate into the corresponding disilene and silanediyl but instead forms three silanediyl fragments.[144b]

5.2. Molecular Structures of Selected Three-Membered E_2X Rings (E = Si, Ge, Sn; X = ER_2, NR, O, S, Se, Te) Determined Experimentally

The three-membered rings containing a main group element from a higher row that have been synthesized until now have sterically bulky substituents that hinder decomposition of reactive three-membered rings and formation of thermally favored higher ER_2 oligomers.[67e] The E–E distances *d* and their percentage change Δd(E–E) as a function of the third ring building block X are listed in Table 4.

Table 4. Bond lengths *d*(E E) [Å] and the percentage shortening Δd(E–E) [%] in three-membered E_2X rings.

	X	*d*(E–E)	Δd(E–E)
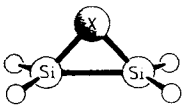	R_2Si	2.398 [a]	0
	O	2.227	7.1
	RN	2.230	7.0
	H_2C	2.272	5.3
	S	2.289	4.6
	Se	2.303	4.0
	Te	2.337	2.5
	Cp_2W	2.260	5.7
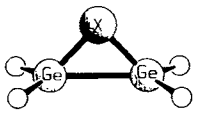	R_2Ge	2.558 [a]	0
	RN	2.379	7.0
	H_2C	2.379	7.0
	S	2.383	6.8
	Se	2.398	6.2
	Te	2.435	4.8
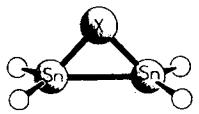	R_2Sn	2.901 [a]	0
	RN	2.709	6.6
	Te	2.827	2.5

[a] Average values for aryl-substituted cyclotrisilanes, trigermanes, and tristannanes (see ref. [67e]).

It must, however, be kept in mind that substituting an ER_2 fragment with X can also result in considerable changes in the steric interactions between the substituents. Therefore the parameters obtained may not be compared with the calculated changes in the parent compound. Hence the E–E bonds given in Table 4, which are used as a reference, are about 2–4% longer in the experimentally investigated, sterically hindered cyclotrisilanes, cyclotrigermanes, and cyclotristannanes $(ER_2)_3$ than in those calculated for $(EH_2)_3$.

The above-mentioned effects become very clear. Electronegative building blocks X such as O and RN lead to a significant shortening of the basal E–E bonds on the same order of magnitude as going from E–E to E=E bonds. For the planar ring $(H_2Sn)_2NH$, in which the difference in electronegativities $\Delta\chi_{spec}$ = 3.066 – 1.824 = 1.242 is very large, a quantum mechanical analysis of the electron density was conducted. The results are shown in Figure 14a as a contour plot.[149]

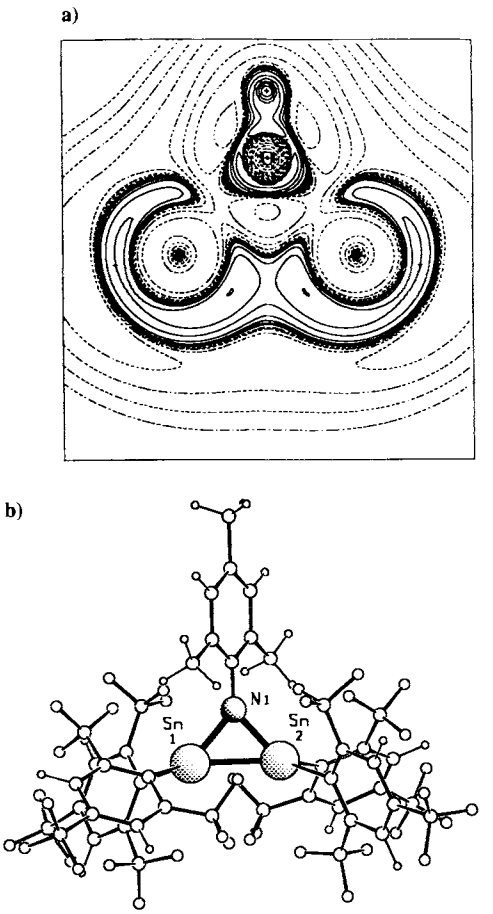

Fig. 14 a) Graphic representation of Laplacian ∇^2 of the electron density of $(H_2Sn)_2NH$ [149]. Solid lines show higher charge density, dashed lines show lower charge density. b) Molecular structure of **152** in the crystal [150]. Bond lengths [Å] and angles [°]: Sn1–Sn2 2.709(2), Sn1–N1 2.079(11), Sn2–N1 2.074(16); Sn1-N1-Sn2 81.4(4), N1-Sn1-Sn2 49.2(4), Sn1-Sn2-N1 49.4(3).

The geometry-optimized, calculated structural data [*d*(Sn–Sn): 2.746 Å; *d*(Sn–N): 2.019 Å] are in good agreement with the results of a single-crystal structure analysis of **152** (Fig. 14b and Scheme 27).[150] The Laplacian distribution clearly shows that azadistanniridines can be viewed as cyclic N-donor-Sn_2-acceptor compounds with a concavely bent Sn–Sn bond. This description is contrary to the Dewar–Chatt–Duncanson formalism in so far as that this would describe the three-membered ring as a complex of one nitrene RN: as an acceptor and a distannene $R_2Sn{=}SnR_2$ as a donor.

5.3. Fragmentation Behavior of Mixed Heterocyclopropanes

In this section the fragmentation behavior of several selected heterocyclopropanes is presented. The results reveal that the description of the three-membered rings as trimers of carbene analogues is a useful concept for predicting this fragmentation behavior. It explains, for example, the experimental finding that the aryl-substituted cyclotristannane $(Is_2Sn)_3$ (Is = 2,4,6-triisopropylphenyl) **141b** fragments even at 20 °C into [Is_2Sn:] **144** and the corresponding distannane **145** (Scheme 24).[151, 152]

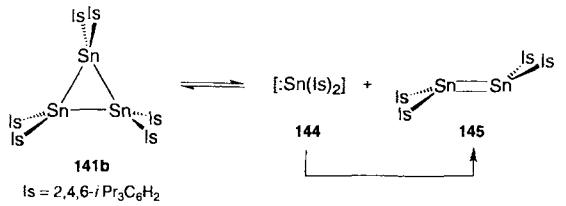

Scheme 24. Fragmentation of **141b** into **144** and **145**.

The analogous [2 + 1]cycloreversion reactions of cyclotrisilanes **139b** and cyclotrigermanes **140b** are also possible by photolysis. This means that these systems are valuable sources of the corresponding $:ER_2$ and $R_2E{=}ER_2$ compounds.

It is expected that fragmentation of a three-membered ring XYZ into the olefin-like molecule X=Y and the carbene-like molecule Z: occurs in such a way as to form the most stable multiply bonded system and carbene analogue (Scheme 25, Table 5).

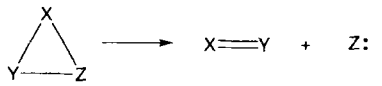

Scheme 25. Fragmentation of heterocyclopropanes. The resulting carbene analogue exists in the singlet state.

Table 5. Fragmentation of C_2E and CE_2 rings. ΔE_{elec} [kcal mol^{-1}] is the change in the electronic energy between the starting material and products. The heterocarbene exists in the singlet state.

	ΔE_{elec}
$SiC_2H_6 \rightarrow H_2C{=}CH_2 + H_2Si:$	47.5
$SiC_2H_6 \rightarrow H_2C{=}SiH_2 + H_2C:$	120.5
$GeC_2H_6 \rightarrow H_2C{=}CH_2 + H_2Ge:$	48.4
$GeC_2H_6 \rightarrow H_2C{=}GeH_2 + H_2C:$	114.8
$Si_2CH_6 \rightarrow H_2C{=}SiH_2 + H_2Si:$	64.7
$Si_2CH_6 \rightarrow H_2Si{=}SiH_2 + H_2C:$	127.2
$Ge_2CH_6 \rightarrow H_2C{=}GeH_2 + H_2Ge:$	48.4
$Ge_2CH_6 \rightarrow H_2Ge{=}GeH_2 + H_2C:$	106.5

This expectation is supported by ab initio calculations of the fragmentation of C_2E and CE_2 three-membered rings (E = Si, Ge) [140, 153, 154] and is discussed here by using several examples.

Silacyclopropanes such as **146** fragment upon heating into the intermediate silanediyl and the corresponding olefin; the silanediyl **147** can be transferred to another olefin even at 70 °C (Scheme 26).[155, 156]

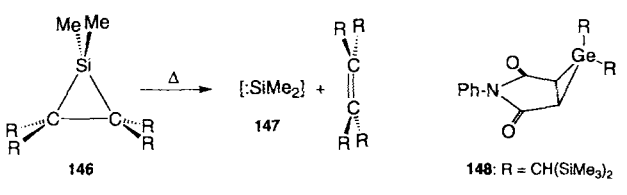

Scheme 26. Fragmentation of **146** and structure of **148**.

Because of the weaker Ge–C bond and the increased stability of germanediyls, an experimental trick was needed to synthesize a stable germirane. This was recently accomplished by Ando et al. who synthesized the germirane **148**; its stability is attributed to the electron-poor maleinimine group and the weakened C–C π bond in free maleinimine.[157] It has not yet been possible to synthesize a stannirane; moreover, there is still no evidence that this system exists in equilibrium in solution with its components, an olefin and a stannanediyl. By applying the trick used for the synthesis of **148**, namely the destabilization of the decomposition products of the three-membered ring, a stannacyclopropene was obtained as an unsaturated ring with a SnC_2 framework from R_2Sn and a highly strained cyclic acetylene (R = $(Me_3Si)_2CH$).[158] In solution this three-membered heterocycle is in equilibrium with its components, whereas the comparable silacyclopropenes and germacyclopropenes are considerably more thermally stable.[159] The sterically substituted disilacyclopropane **149** is relatively stable and decomposes only photochemically. Here the silanediyl **150** and the silaethene **151** are formed as intermediates which could be identified by trapping reactions (Scheme 27).[160]

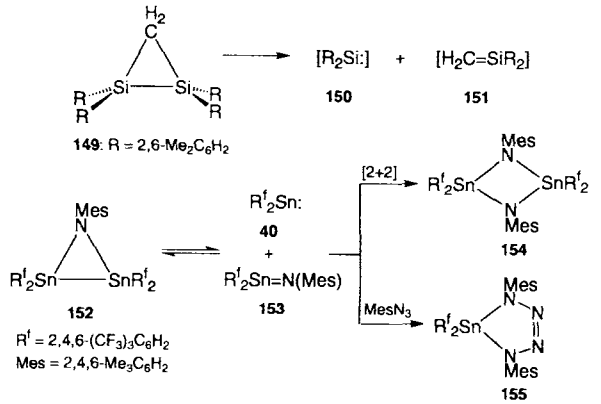

Scheme 27. Fragmentation of **149** and **152**.

In contrast, the azadistanniridine **152** decomposes even at room temperature into the stannanediyl **40**, which can be added to mesitylazide in a 2:1 ratio to reform **152**, and the stannanimine **153** (Scheme 27).[150] The stannanimine **153**, unlike **40**, cannot be detected by ^{119}Sn NMR spectroscopy in the presence of **152**; however, it can be isolated in the form of the dimeric diazadistannetidine **154**. With an excess of mesitylazide **153** can be trapped as the tetraazastannole **155**.

While E_2X three-membered rings (E = C, Si, Ge, Sn; X = O, S, Se, Te) with Se and Te as framework atoms are likewise very unstable for E = C because of the relatively strong C=C bond, several stable derivatives for systems with E = Si, Ge, and Sn have been synthesized in the past few years.[67e, 152] The elimination of selenium or tellurium is, however, also a possibility with these three-membered rings, and as a result of the [2 + 1]cycloreversion they provide relatively weak doubly bonded systems. For example, fragmentation of silaphosphatellurane **156**[119] (Fig. 15) or of the isotypical arsenic analogue[119b] in the presence of a cyclophosphanes provides phosphanetellurides and the corresponding free phosphasilene or arsasilene, respectively.[161]

A remarkably different thermal fragmentation is shown by the three-membered ring systems **L** and **M**, which are formed by the [2 + 1]cycloaddition of $E{=}E^1$ bonds (E = Si; E^1 = Si, P, As) to organoazides and diazoalkane derivatives (Scheme 28).[162] The first compound of this type was **157** which was also structurally characterized (Fig. 16).[162c]

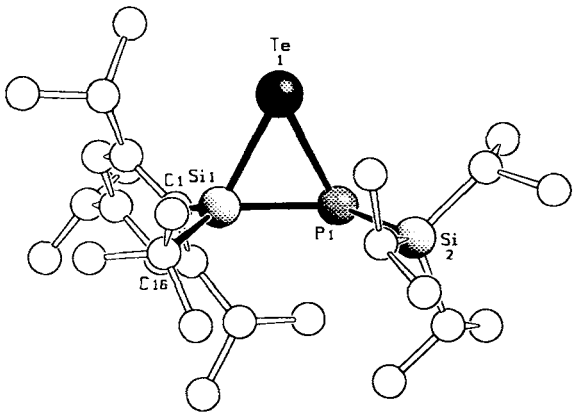

Fig. 15. Molecular structure of **156** in the crystal [119d]. Bond lengths [Å] and angles [°]: Te1–P1 2.524(2), Te1–Si1 2.496(2), P1–Si1 2.235(2); P1-Te1-Si1 52.88(5), Te1-P1-Si1 62.90(6), Te1-Si1-P1 64.22(6), Si1-P1-Si2 123.07(7), Si2-P2-Te1 105.41(7).

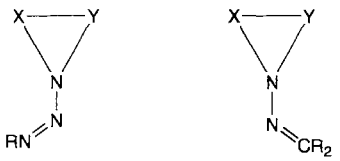

L: X = SiR_2; Y = R_2Si, RP, RAs M: X = SiR_2; Y = R_2Si, RP, RAs

Scheme 28.

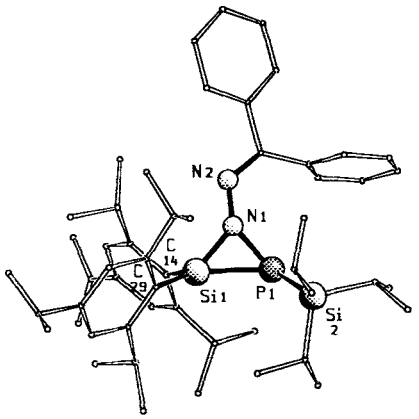

Fig. 16. Molecular structure of **157** in the crystal [162c]. Bond lengths [Å] and angles [°]: P1–Si1 2.237(2), P1–Si2 2.298(2), P1–N1 1.817(3), Si1–N1 1.729(3), N1–N2 1.375(4); Si1-P1-N1 49.2(1), Si1-P1-Si2 112.9(1), P1-Si1-N1 52.7(1), P1-N1-Si1 78.2(1), C1-N2-N1 124.3(2).

The three-membered ring **157** isomerizes upon heating because of its reactive side chain to give the [2 + 3]cycloadduct **158**. In addition the silaphosphiridine **159** is formed by elimination of N_2. The heterocycle **159** fragments upon heating to 110 °C but not into silanediyl and phosphaalkene but instead goes selectively to the rearrangement product **160** (Scheme 29). This example shows that the reactivity of such three-membered rings can be decisively influenced by bulky organic substituents.

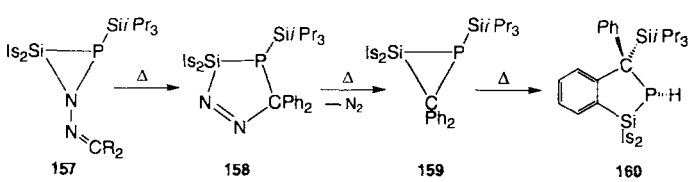

157 **158** **159** **160**

Scheme 29. Fragmentation of **157**.

5.4. Structure and Ring Strain of Tetrasilabicyclo[1.1.0]-butanes and Tetraphosphabicyclo[1.1.0]butanes

The relatively large ring strain in cyclotrisilanes **139** in comparison to cyclopropanes **138** and cyclotriphosphanes **143** has notable consequences for the electronic structures of the corresponding bicyclo[1.1.0]butanes. From ab initio calculations on the parent compound of tetrasilabicyclo[1.1.0]butane it was ascertained that the compound exists in the two forms **161a** and **161b**, which can be referred to as bond stretch isomers. Isomer **161b** is 17 kcal mol^{-1} more stable than **161a** and represents a singlet diradical with an extremely long Si–Si bridgehead bond (2.731 Å in **161b** vs. 2.343 Å in **161a**). The isomers are separated from one another by a very small barrier of 0.12 kcal mol^{-1}.[163]

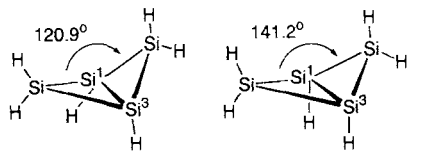

161a Si^1—Si^3 2.343 Å **161b** Si^1—Si^3 2.731 Å

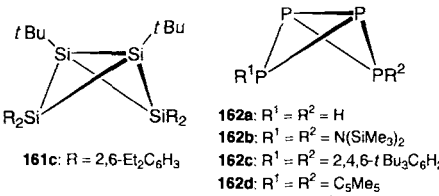

161c: R = 2,6-$Et_2C_6H_3$

162a: $R^1 = R^2 = H$
162b: $R^1 = R^2 = N(SiMe_3)_2$
162c: $R^1 = R^2 = 2,4,6\text{-}t\,Bu_3C_6H_2$
162d: $R^1 = R^2 = C_5Me_5$
162e: $R^1 = H$, $R^2 = SnMe_3$

The molecule evidently rids itself of its high ring strain by bond stretching, that is it prefers a cyclobutane-like structure which in the case of silicon is particularly low in ring strain. Calculation of the strain energy did in fact show that **161** is about 7 kcal mol^{-1} less strained than bicyclo[1.1.0]butane.[164] The structural characterization of the sterically substituted derivative **161c** shows a relatively short Si–Si bridgehead bond (2.373(3) Å); thus, this compound corresponds to the isomeric form **161a**.[165]

In contrast, the tetraphosphabicyclo[1.1.0]butane **162a**, the derivatives (**162b–e**) of which have already been synthesized,[166] has a structure similar to bicyclo[1.1.0]butane.[167] However, in contrast to the latter, **162a** shows scarcely any ring strain.[145c] The P–P bridgehead bond shows a high degree of π character, which is strengthened by the influence of π-donor substituents on the peripheral P atoms. The HOMO has a_1 symmetry and lies only slightly higher in energy than the HOMO-1 with b_1 symmetry (Fig. 17). Compound **162** can therefore

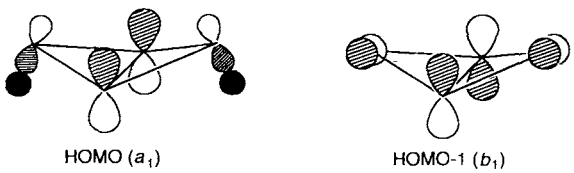

HOMO (a_1) HOMO-1 (b_1)

Fig. 17 Graphic representation of the HOMO (a_1) and the HOMO-1 (b_1) in tetraphosphabicyclo[1.1.0]butane **162** [145c].

be formally described as a donor–acceptor complex of P_2 and two phosphanediyl fragments :PR in terms of the Dewar–Chatt–Duncanson model. This is in agreement with the relatively short P–P distance in the P_2 bridge (ca. 2.12 Å); this value lies between that for a P=P (2.00 Å) and a P–P (2.21 Å) bond.

The comparably high stability of the P–P bridgehead bond is lost in this system when the :PR fragments at the peripheral positions are replaced by other carbene-analogous fragments with electropositive central atoms such as boron or silicon. In this case the ordering of the frontier orbitals is reversed and has, as discussed below, a drastic influence on the structure of such systems.

5.5. Mixed Heterobicyclo[1.1.0]butanes with a P_2 and As_2 Bridge

Recently the first B_2P_2-bicyclo[1.1.0]butane derivative **163** was reported; it contains an unusually long P–P bond (2.349(2) Å).[168] This increase in comparison to the P–P bond in diphosphanes and tetraphosphabicyclo[1.1.0]butanes **162b,c** is attributed to the σ-donor character of boron and the ring strain. The hybrid silicon-containing bicycles **164**[169] and **165**[170] with a P_2 or As_2 bridge show, as expected, the same effect.

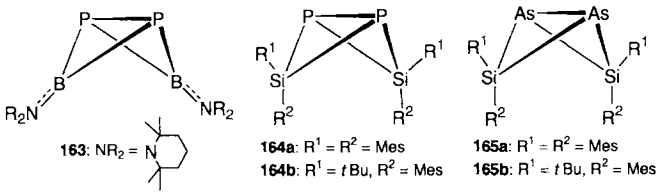

The strikingly long As–As distance (2.602(3) Å) in **165b** (Fig. 18) is only comparable with that in Realgar As_4S_4 (2.59 Å) (ca. 6% longer than in diarsanes). Ab initio calculations on the parent systems $X_2(SiH_2)_2$ (X = P, As) show that the X–X bond has no diradical character, unlike the case with the tetrasilabicyclo[1.1.0]butanes **161**, but instead, the X atoms are strongly negatively polarized and repel each other.[170]

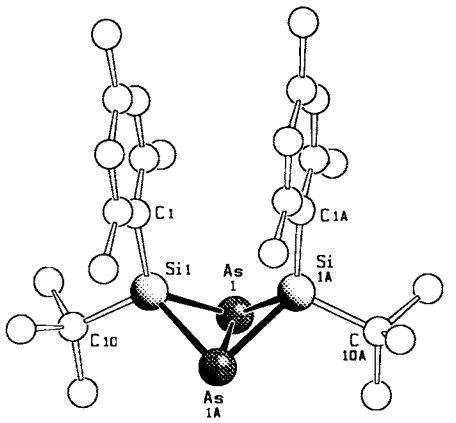

Fig. 18. Molecular structure of **165b** in the crystal [170]. Bond lengths [Å] and angles [°]: As–As 2.602(3), As1–Si1 2.355(3); Si1-As1-Si1A 84.3(1), As1A-As1-Si1 56.5(1), As-Si1-As1A 67.1(1).

Particularly interesting is the isomerization of the *exo,endo* butterfly molecules **164b*** and **165b*** to the *exo,exo*-configurated compounds **164b** and **165b**, respectively. This gave the first indications of the readiness of these compounds to fragment into silanediyl and X_2Si fragments (X = P, As), and thereby parallels the reactivity seen for the strained three-membered rings with Si framework atoms (Scheme 30).

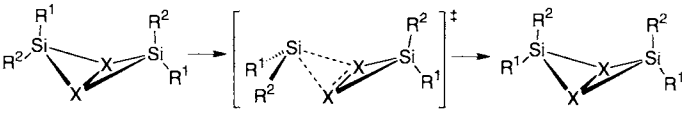

164b* (*exo, endo*): X = P
165b* (*exo, endo*): X = As

164b (*exo, exo*): X = P
165b (*exo, exo*): X = As

Scheme 30. Isomerization of **164b*** and **165b***.

While **164b*** can be converted easily through an inversion of configuration at the silicon center into the *exo,exo* form **164b** by heating (40 °C, 2 h) or irradiation with a lightbulb (200 W, 20 min), the arsenic analogue **165b*** isomerizes significantly slower (7 d irradiation). For energetic reasons the inversion should proceed over a silanediyl–P_2Si complex as transition state. The different behavior of **164b*** and **165b*** is attributed to the unfavorable As–As π interaction in the transition state. Calculations on the isomerization process provided the surprising result that the parent compound $(H_2Si)_2X_2$ (X = P, As) has a relatively high inversion barrier which lies significantly higher in energy than the dissociation limit to H_2SiX_2 and silanediyl (X = P: SCF: 62.5 kcal mol^{-1}; MP2: 71 kcal mol^{-1}). Parent systems and derivatives with bulky substituents are therefore also in this case not comparable with one another[170] (see Maxim 5 in Section 2) since the potential energy surface of the Si_2X_2 framework can be strongly "deformed" by the substituents.

An experimental indication for the extrusion of a silanediyl from the Si_2P_2 bicyclus **164a** is offered by its thermolysis in which the Si_3P_2 bicyclus **166a** and elemental phosphorus are formed.[171] In the presence of a trapping reagent such as 2,3-dimethylbutadiene, thermolysis provides the expected silol derivative **167** (Scheme 31).

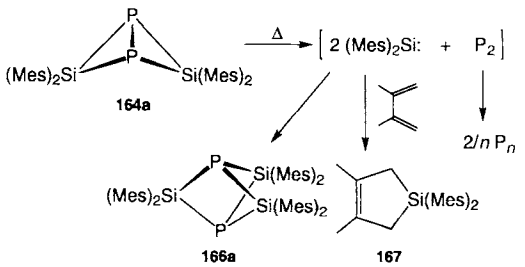

Scheme 31. Fragmentation of **164a** and trapping reaction with 2,3-dimethylbuta-1,3-diene.

The readiness of such butterfly molecules to fragment into a carbene-analogous molecule and X_2 (X = P, As) increases, as expected, when silicon is replaced by germanium or tin. It is therefore understandable that after photochemical reductive elimination of Hg from **168**, which has proven to be an excellent method for the synthesis of **164a,b** and **165a,b**,[172] the SiP_2Sn

bicyclus **169** could not be detected. Instead the bicyclus **166b** is formed as the silicon-containing product together with the distannene **145**, which is in equilibrium with the stannanediyl **144**. The latter compounds can be trapped by reaction with 2,3-dimethylbutadiene under formation of the stannole **170** (Scheme 32).

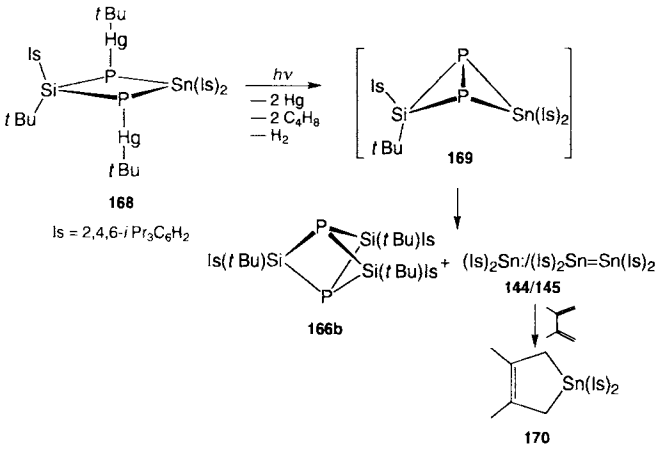

Scheme 32. Fragmentation of **168**.

6. Summary and Outlook

In the current article, an effort has been made to show a correlation between the atomic characteristics of the main group elements (expressed as their spectroscopic electronegativity), the characteristics of reactive fragments HE, H_2E, and $[H_2E]^+$ produced by addition of hydrogen or protons to the elemental atoms, and the characteristics of the compounds constructed from these fragments. In doing so, three classical objects of study in traditional organic chemistry, namely methylene ($:CH_2$), ethene ($CH_2=CH_2$), and cyclopropane [$(CH_2)_3$], were chosen as models for formally analogous main group element compounds. These classical, substance classes with interesting electronic properties have in the past provided us with the now familiar bonding theory, structure chemical concepts, and reactivity principles. Can these ideas be applied to homologous and analogous main group element compounds without further thought? The answer is no. The chemistry of carbon is that of an "exotic" element and is determined by its position in the periodic table. As an element from the second row, it is especially "willing to hybridize" since the element–carbon bond has a high bonding energy which compensates for the considerable "promotion energy" required by this mathematical model. As an element with intermediate electronegativity, carbon almost always forms bonds with high covalent character in molecular compounds (see for example organolithium compounds on the one hand and organofluorine compounds on the other). This characteristic is not seen to such an extent in any other element. A comparison of methylene with the corresponding fragments with main group elements from higher rows already reveals the special position held by carbon. Most of the carbene-analogous fragments have, as a result of their "reluctance to hybridize", a singlet ground state. The ability of carbon to form σ and π bonds of high energy, explains the planarity of olefins. This ability even increases with increasing s orbital participation in the mathematical function used to describe bonding, the valence hybrid orbital. The higher homologues show, within the framework of perturbation theory, an increasing tendency to form *trans*-bent structures. This is a result of a second-order Jahn–Teller distortion.

A concept developed by Malrieu and Trinquier is particularly suitable for predicting the molecular structure of multiply bonded systems of the main group elements. Here the singlet–triplet excitation energies $\Delta E_{S\rightarrow T}$ of the fragments determine the character of the dimers formed from them. Multiply bonded systems have a molecular structure that deviates from planarity or linearity when the sum of the excitation energy $\Sigma\Delta E_{S\rightarrow T}$ is larger than the term $f(E_{\sigma+\pi})$ (with $1/2<f<1$). When $\Sigma\Delta E_{S\rightarrow T}>E_{\sigma+\pi}$ is also valid, a constitutional isomer without direct E–E bonding is predicted for the dimers of the carbene-analogous fragments. Until now no exceptions have been found for the rules derived from the GCMT model. The common ideas taken from carbon chemistry that a "double bond" actually has a higher bonding energy than a single bond or that bond lengths are an analytical criterion for the presence of multiple bonding cannot be transferred to homologous and analogous compounds of the main group elements from the higher rows. Even the preferred bonding theory held up to now of noncylindrical electron density in a double bond, which can be approximated mathematically by a σ and a π bond, is (again) in question for molecules with *trans*-bent structures (see ref.[141c]).

The fragmentation behavior of three-membered rings containing main group elements, in particular, can be advantageously understood and predicted with the concept of describing these cycles as trimers of carbene-analogous fragments. It is almost curious that the observation that Baeyer's strain theory, which was based on the investigations of cycloalkanes, shows more validity for the series of cyclosilanes completed almost 100 years later. Due to the desire to transfer known principles in carbon chemistry to formally analogous main group element compounds, in view of the homologue idea, the uniqueness of the chemistry of the element carbon has been made clear. In the same manner, similar characteristics shown by other compound classes have been recognized. On this basis, fragments such as RE and R_2E can be specifically used for the "design" of molecules with predictable characteristics for many areas of research, for example in materials science where the thermal behavior and fragmentation pattern of precursor molecules plays a large role.

However, there remains much to be done. For example, the search for constitutional isomers of a given molecular formula is particularly exciting. And we think that in this case asymmetrical multiply bonded systems with metalloid main group elements deserve special consideration. For example, it seems that the search for a compound with the formula R_3EE^1 (E = Si, Ge, Sn; E^1 = Al, Ga, In) is worthwhile. The question is will such compounds be "nonclassical" multiply bonded systems $R_2E=E^1R_2$, R-bridged rings and cage compounds, or substituted carbene analogues $:E^1-ER_3$? For several alkoxides such as $Sn(OtBu)_3In$ or $Sn(OtBu)_3Tl$ (R = O*t*Bu) cage structures with three bridging alkoxide groups (not unexpected within the framework of the GCMT model; compare Scheme 11) have been obtained;[178] however, alkyl- or aryl-substituted compounds of this sort have yet to be synthesized. The building

blocks are known (see Section 3), they just need to be "mixed together". Many characteristics of the compounds presented in this article have not yet been investigated. This is especially true for the redox behavior and the related changes in the molecular structure of the (radical) cations and anions in comparison to the corresponding carbon compounds.[173, 174] In addition to an improvement in the bonding theory model, much development in experimental technique is needed.

In conclusion the following must be mentioned: although the chemistry of elements that are "reluctant to hybridize" has been presented here, this behavior must not necessarily apply to the researchers that work in this area. Exactly the attitude "let's see what the neighbors are doing" has allowed this field of research to become what it is, interdisciplinary.

This work was supported by the Deutschen Forschungsgemeinschaft (SFB 247) and the Fonds der Chemischen Industrie. We thank our mentors Professors. G. Bertrand, G. Huttner, H. W. Roesky, W. Siebert, W. Sundermeyer, and R. West as well as our co-workers Dr. U. Heim, Dr. H. Schönberg, Dr. U. Winkler, and Dipl.-Chem. S. Rell, who participated on several of the projects presented here, for their continual support. We especially thank Dr. H. Pritzkow who conducted almost all of the X-ray crystal structure analyses for us. We thank Dr. U. Fleischer, Prof. G. Frenking, and Prof. R. Janoschek for quantum mechanical calculations, and Mrs. Christina Marchand for her assistance in preparing the figures.

Received: July 28, 1995 [A126IE]
German version: *Angew. Chem.* **1996**, *108*, 900–929
Translated by Anuradha Gunale, Heidelberg (Germany)

[1] L. C. Allen, *J. Am. Chem. Soc.* **1989**, *111*, 9003.
[2] a) E. A. Carter, W. A. Goddard III, *J. Phys. Chem.* **1986**, *90*, 998; b) G. Trinquier, J.-P. Malrieu, *J. Am. Chem. Soc.* **1987**, *109*, 5303; c) J.-P. Malrieu, G. Trinquier, *ibid.* **1989**, *111*, 5916; d) G. Trinquier, J.-P. Malrieu in *The chemistry of functional groups, Suppl. A: The chemistry of double-bonded functional groups, Vol. 2, Part 1* (Ed.: S. Patai), Wiley, Chichester, **1989**, p. 1.
[3] a) R. Janoschek, *Chem. Unserer Zeit* **1988**, *21*, 128; b) H. Jacobsen, T. Ziegler, *J. Am. Chem. Soc.* **1994**, *116*, 3667.
[4] The authors could show that a description with the MO formalism provided the corresponding prediction.
[5] a) P. J. Davidson, D. H. Harris, M. F. Lappert, *J. Chem. Soc. Dalton Trans* **1976**, 2268; b) D. E. Goldberg, P. B. Hitchcock, M. F. Lappert, K. M. Thomas, A. J. Thorne, T. Fjeldberg, A. Haaland, B. E. R. Schilling, *ibid.* **1986**, 2387.
[6] a) G. Trinquier, *J. Am. Chem. Soc.* **1990**, *112*, 2130; b) G. Trinquier, *ibid.* **1991**, *113*, 144.
[7] P. von R. Schleyer, *Pure Appl. Chem.* **1987**, *59*, 1647.
[8] Reviews on silanediyls, germanediyls, and plumbanediyls: a) W. P. Neumann, *Chem. Rev.* **1991**, *91*, 311; b) M. Veith, O. Recktenwald, *Top. Curr. Chem.* **1982**, *104*, 1; c) G. Raabe, J. J. Michl, *Chem. Rev.* **1985**, *85*, 419.
[9] K. P. Huber, G. Herzberg, *Molecular Spectra and Molecular Structure, IV. Constants of Diatomic Molecules*, Van Nostrand Reinhold, New York, **1979**.
[10] a) D. G. Leopold, K. K. Murray, A. E. S. Miller, W. C. Lineberger, *J. Chem. Phys.* **1985**, *83*, 489; b) A. R. W. McKeller, P. R. Bunker, T. J. Sears, K. M. Evenson, R. J. Saykally, S. R. Langhoff, *ibid.* **1983**, *79*, 5251.
[11] J. Berkowitz, J. P. Greene, H. Cho, B. Rucic', *J. Chem. Phys.* **1987**, *86*, 1235.
[12] S. T. Gibson, J. P. Greene, J. Berkowitz, *J. Chem. Phys.* **1985**, *83*, 4319.
[13] J. Berkowitz, H. Cho, *J. Chem. Phys.* **1989**, *90*, 1.
[14] a) G. Treboux, J.-C. Barthelat, *J. Am. Chem. Soc.* **1993**, *115*, 4870; b) J. A. Pople, P. von R. Schleyer, *Chem. Phys. Lett.* **1986**, *129*, 279.
[15] K. Balasubramanian, *J. Chem. Phys.* **1988**, *89*, 5731.
[16] K. Balasubramanian, *J. Chem. Phys.* **1989**, *91*, 2443.
[17] a) P. R. Bunker, P. Jensen, *J. Chem. Phys.* **1983**, *79*, 1124; b) I. Shavitt, *Tetrahedron* **1985**, *41*, 1531.
[18] a) W. Kutzelnigg, *Angew. Chem.* **1984**, *96*, 262; *Angew. Chem. Int. Ed. Engl.* **1984**, *23*, 272.
[19] R. Ahlrichs, C. Ehrhardt, *Chem. Unserer Zeit* **1985**, *19*, 120.
[20] a) H. Schumann, C. Janiak, M. A. Khan, J. J. Zuckerman, *J. Organomet. Chem.* **1988**, *354*, 7; b) K. Stumpf, H. Pritzkow, W. Siebert, *Angew. Chem.* **1985**, *97*, 64; *Angew. Chem. Int. Ed. Engl.* **1985**, *24*, 71.
[21] A. Haaland, K.-G. Martinsen, H. V. Volden, D. Loos, H. Schnöckel, *Acta Chem. Scand.* **1994**, *48*, 172 and references therein; A. Haaland, K.-G. Martinsen, S. A. Shlykov, H. V. Volden, C. Dohmeier, H. Schnöckel, *Organometallics* **1995**, *14*, 3116.
[22] O. T. Beachley Jr., R. Blom, M. R. Churchill, K. Faegri Jr., J. C. Fettinger, J. C. Pazik, L. Victoriano, *Organometallics* **1989**, *8*, 346.
[23] C. Dohmeier, C. Robl, M. Tacke, H. Schnöckel, *Angew. Chem.* **1991**, *103*, 594; *Angew. Chem. Int. Ed. Engl.* **1991**, *30*, 564.
[24] Compare with: P. Paetzold, *Angew. Chem.* **1991**, *103*, 559; *Angew. Chem. Int. Ed. Engl.* **1991**, *30*, 544.
[25] P. Paetzold, T. Mennekes, P. Paetzold, R. Boese, D. Bläser, *Angew. Chem.* **1991**, *103*, 199; *Angew. Chem. Int. Ed. Engl.* **1991**, *30*, 173.
[26] W. Uhl, W. Hiller, M. Layh, W. Schwarz, *Angew. Chem.* **1992**, *104*, 1378; *Angew. Chem. Int. Ed. Engl.* **1992**, *31*, 1364.
[27] W. Uhl, R. Graupner, M. Layh, U. Schütz, *J. Organomet. Chem.* **1995**, *493*, C1.
[28] U. Schneider, R. Ahlrichs, H. Horn, A. Schäfer, *Angew. Chem.* **1992**, *104*, 327; *Angew. Chem. Int. Ed. Engl.* **1992**, *31*, 353.
[29] W. Uhl, U. Schütz, A. Haaland, K.-G. Martinsen, H. V. Volden, W. Kaim, E. Waldhoer, *Organometallics*, **1996**, *15*, 1146.
[30] S. Schulz, H. W. Roesky, H. J. Koch, G. M. Sheldrick, D. Stalke, A. Kuhn, *Angew. Chem.* **1993**, *105*, 1828; *Angew. Chem. Int. Ed. Engl.* **1993**, *32*, 1729.
[31] C. Dohmeier, H. Schnöckel, C. Robl, U. Schneider, R. Ahlrichs, *Angew. Chem.* **1994**, *106*, 225; *Angew. Chem. Int. Ed. Engl.* **1994**, *33*, 199.
[32] W. Uhl, R. Graupner, M. Pohlmann, S. Pohl, W. Saak, *Chem. Ber.* **1996**, *129*, 143.
[33] A. Igau, H. Grützmacher, A. Baceiredo, G. Bertrand, *J. Am. Chem. Soc.* **1988**, *110*, 6463 and references therein.
[34] M. Soleihavoup, A. Baceiredo, O. Treutler, R. Ahlrichs, M. Nieger, G. Bertrand, *J. Am. Chem. Soc.* **1992**, *114*, 10959.
[35] O. Treutler, R. Ahlrichs, M. Soleihavoup, *J. Am. Chem. Soc.* **1993**, *115*, 8788.
[36] D. A. Dixon, K. D. Dobbs, A. J. Arduengo III, G. Bertrand, *J. Am. Chem. Soc.* **1991**, *113*, 8782.
[37] G. Alcaraz, U. Wecker, A. Bacereido, F. Dahan, G. Bertrand, *Angew. Chem.* **1995**, *107*, 1358; *Angew. Chem. Int. Ed. Engl.* **1995**, *34*, 1246.
[38] Review: H.-W. Wanzlick, *Angew. Chem.* **1962**, *74*, 129; *Angew. Chem. Int. Ed. Engl.* **1962**, *1*, 75.
[39] a) A. J. Arduengo III, R. L. Harlow, M. Kline, *J. Am. Chem. Soc.* **1991**, *113*, 361; b) A. J. Arduengo III, H. V. Rasika Dias, R. L. Harlow, M. Kline, *ibid.* **1992**, *114*, 5530.
[40] N. Kuhn, T. Kratz, *Synthesis* **1993**, 561.
[41] a) N. Kuhn, G. Henkel, T. Kratz, J. Kruezberg, R. Boese, A. H. Maulitz, *Chem. Ber.* **1993**, *126*, 2041; b) A. J. Arduengo III, H. V. Rasika Dias, J. C. Calabrese, F. Davidson, *J. Am. Chem. Soc.* **1992**, *114*, 9724; c) A. J. Arduengo III, M. Tamm, J. C. Calabrese, *ibid.* **1994**, *116*, 3625; d) A. J. Arduengo III, S. F. Gamper, J. C. Calabrese, F. Davidson, *ibid.* **1994**, *116*, 4391 and references therein; e) A. J. Arduengo III, H. V. Rasika Dias, F. Davidson, R. L. Harlow, *J. Organomet. Chem.* **1993**, *462*, 13; f) A. J. Arduengo III, S. F. Gamper, M. Tamm, J. C. Calabrese, F. Davidson, H. A. Craig, *J. Am. Chem. Soc.* **1995**, *117*, 572; g) A. J. Arduengo III, J. R. Görlich, W. J. Marshall, *J. Am. Chem. Soc.* **1995**, *117*, 11027; h) H. Tomioka, T. Watanabe, K. Hirai, K. Furukawa, K. Itoh, *ibid.* **1995**, *117*, 6376.
[42] a) M. Veith, E. Werle, R. Lisowsky, R. Löppe, H. Schnöckel, *Chem. Ber.* **1992**, *125*, 1375; b) G. R. Gillette, G. Noren, R. West, *Organometallics* **1990**, *9*, 2925 and references therein; c) W. Sander, A. Patyk, G. Bucher, *J. Mol. Struct.* **1990**, *222*, 21; d) G. Maier, J. Glatthaar, H. P. Reisenauer, *Chem. Ber.* **1989**, *122*, 2403; e) M. Denk, R. West, R. Hayashi, Silylenes, Stable and Unstable in *Organosilicon Chemistry* (Eds.: N. Auner, J. Weis), VCH, Weinheim, **1995**, p. 251.
[43] a) W. P. Neumann, *Nachr. Chem. Tech. Lab.* **1982**, *30*, 190 and references therein; b) P. P. Gaspar, *React. Intermed.* **1981**, *2*, 335; c) G. Maier, H. P. Reisenauer, K. Schoettler, U. Wessolek-Kraus, *J. Organomet. Chem.* **1989**, *366*, 25 and references therein.
[44] M. Denk, R. Lennon, R. Hayashi, R. West, A. V. Belyakov, H. P. Verne, A. Haaland, M. Wagner, N. Metzler, *J. Am. Chem. Soc.* **1994**, *116*, 2691.
[45] W. A. Herrmann, M. Denk, J. Behm, W. Scherer, F.-R. Klingan, H. Bock, B. Solouki, M. Wagner, *Angew. Chem.* **1992**, *104*, 1489; *Angew. Chem. Int. Ed. Engl.* **1992**, *31*, 1485.
[46] a) A. J. Arduengo III, H. Bock, H. Chen, M. Denk, D. A. Dixon, J. C. Green, W. A. Herrmann, N. L. Jones, M. Wagner, R. West, *J. Am. Chem. Soc.* **1994**, *116*, 6641; b) C. Heinermann, W. Thiel, *Chem. Phys. Lett.* **1994**, *217*, 11; c) C. Heinermann, W. A. Herrmann, W. Thiel, *J. Organomet. Chem.* **1994**, *475*, 73; d) C. Böhme, G. Frenking, *J. Am. Chem. Soc.* **1996**, *118*, in press.
[47] See for examples the arenes EC_5H_5 (E = P, As, Sb, Bi); review: P. Jutzi, *Angew. Chem.* **1975**, *87*, 269; *Angew. Chem. Int. Ed. Engl.* **1975**, *14*, 232; see also ref. [67i].
[48] M. Veith, *Angew. Chem.* **1987**, *99*, 1; *Angew. Chem. Int. Ed. Engl.* **1987**, *26*, 1.
[49] M. V. Andreocci, C. Cauletti, S. Stranges, B. Wrackmeyer, C. Stader, *Z. Naturforsch. B* **1991**, *46*, 39.
[50] a) D. H. Harris, M. F. Lappert, J. B. Pedley, G. J. Sharp, *J. Chem. Soc. Dalton Trans.* **1976**, 945.

[51] T. Fjeldberg, A. Haaland, B. E. R. Schilling, M. F. Lappert, A. J. Thorne, *J. Chem. Soc. Dalton Trans.* **1986**, 1551.

[52] a) P. Jutzi, A. Becker, H. G. Stammler, B. Neumann, *Organometallics* **1991**, *10*, 1647; b) P. Jutzi, A. Becker, C. Leue, H. G. Stammler, B. Neumann, *ibid.* **1991**, *10*, 3838 and references therein.

[53] L. Lange, B. Meyer, W.-W. du Mont, *J. Organomet. Chem.* **1987**, *329*, C17.

[54] M. Weidenbruch, J. Schlaefke, A. Schäfer, K. Peters, H. G. von Schnering, H. Marsmann, *Angew. Chem.* **1994**, *106*, 1938; *Angew. Chem. Int. Ed. Engl.* **1994**, *33*, 1846.

[55] M. Kira, R. Yauchibara, R. Hirano, C. Kabuto, H. Sakurai, *J. Am. Chem. Soc.* **1991**, *113*, 7785.

[56] H. Grützmacher, H. Pritzkow, F. T. Edelmann, *Organometallics* **1991**, *10*, 23.

[57] S. Brooker, J.-K. Buijink, F. T. Edelmann, *Organometallics* **1991**, *10*, 25.

[58] N. Tokitoh, M. Saito, R. Okazaki, *J. Am. Chem. Soc.* **1993**, *115*, 2065.

[59] M. Driess, R. Janoschek, H. Pritzkow, S. Rell, U. Winkler, *Angew. Chem.* **1995**, *107*, 1746; *Angew. Chem. Int. Ed. Engl.* **1995**, *34*, 1614.

[60] K. W. Klinkhammer, W. Schwarz, *Angew. Chem.* **1995**, *107*, 1448; *Angew. Chem. Int. Ed. Engl.* **1995**, *34*, 1334.

[61] Compare with a) Y. Apeloig, M. Karni, *J. Chem. Soc. Chem. Commun.* **1985**, 1048; b) S. G. Bott, P. Marshall, P. E. Wagenseller, Y. Wong, R. T. Conlin, *J. Organomet. Chem.* **1995**, *499*, 11.

[62] M. Veith, B. Bertsch, V. Huch, *Z. Anorg. Allg. Chem.* **1988**, *559*, 73.

[63] Reviews: a) M. Sanchez, M. R. Mazières, L. Lamandé, R. Wolf in *Multiple Bonds and Low Coordination in Phosphorus Chemistry* (Eds.: M. Regitz, O. J. Scherer), Thieme, Stuttgart, **1990**, pp. 129–149; b) A. H. Cowley, R. A. Kemp, *Chem. Rev.* **1985**, *85*, 367; cyclopendienyl derivatives: Cp^*PNHR^+, $Cp^*PCH(SiMe_3)_2^+$; c) D. Gudat, M. Nieger, E. Nicke, *J. Chem. Soc. Dalton Trans.* **1989**, 693; d) D. Gudat, E. Niecke, B. Krebs, M. Dartmann, *Chimia* **1985**, *39*, 277.

[64] a) N. Burford, B. W. Royan, *J. Am. Chem. Soc.* **1989**, *111*, 3746; b) N. Burford, B. W. Royan, *J. Chem. Soc. Chem. Commun.* **1989**, 19; c) N. Burford, A. I. Dipchand, B. W. Royan, P. S. White, *Inorg. Chem.* **1990**, *29*, 4938.

[65] P. Jutzi, D. Kanne, C. Krüger, *Angew. Chem.* **1986**, *98*, 163; *Angew. Chem. Int. Ed. Engl.* **1986**, *25*, 164; P. Jutzi, T. Wippermann, C. Krüger, H. J. Kraus, *Angew. Chem.* **1983**, *95*, 244; *Angew. Chem. Int. Ed. Engl.* **1983**, *22*, 250.

[66] M. Schäfer, G. Frenzen, B. Neumüller, K. Dehnicke, *Angew. Chem.* **1992**, *104*, 354; *Angew. Chem. Int. Ed. Engl.* **1992**, *31*, 334.

[67] Reviews: Group 13: a) A. Berndt, *Angew. Chem.* **1993**, *105*, 1034; *Angew. Chem. Int. Ed. Engl.* **1993**, *32*, 985; 4. Group 14: b) G. Raabe, J. Michl, *Chem. Rev.* **1985**, *85*, 419; c) A. G. Brook, K. M. Bains, *Adv. Organomet. Chem.* **1986**, *25*, 1; c) R. West, *Angew. Chem.* **1987**, *99*, 1231; *Angew. Chem. Int. Ed. Engl.* **1987**, *26*, 1201; d) J. Barrau, J. Escudié, J. Satgé, *Chem. Rev.* **1990**, *90*, 283; e) T. Tsumaraya, S. A. Batcheller, S. Masamune, *Angew. Chem.* **1991**, *103*, 916; *Angew. Chem. Int. Ed. Engl.* **1991**, *30*, 902. This article also refers to further reviews on silanediyls, germanediyls, and stannanediyls; Group 15: f) *Multiple Bonds and Low Coordination in Coordination Phosphorus Chemistry* (Eds.: M. Regitz, O. Scherer), Thieme, Stuttgart, **1990**; g) A. H. Cowley, *Acc. Chem. Res.* **1984**, *17*, 386; h) E. Niecke, D. Gudat, *Angew. Chem.* **1991**, *103*, 251; *Angew. Chem. Int. Ed. Engl.* **1991**, *30*, 217; i) M. Driess, *Chem. Unserer Zeit* **1993**, *27*, 141.

[68] M. Karnie, Y. Apeloig, *J. Am. Chem. Soc.* **1990**, *112*, 8589.

[69] R. S. Grev, H. F. Schaeffer III, K. M. Baines, *J. Am. Chem. Soc.* **1990**, *112*, 9458.

[70] T. Mennekes, P. Paetzold, R. Boese, *Angew. Chem.* **1990**, *102*, 909; *Angew. Chem. Int. Ed. Engl.* **1990**, *29*, 899.

[71] a) C. Jouany, J. C. Barthelat, J. P. Daudey, *Chem. Phys. Lett.* **1987**, *136*, 52; b) D. R. Armstrong, *Theor. Chim. Acta* **1981**, *60*, 159; c) J. D. Dill, P. von R. Schleyer, J. Pople, *J. Am. Chem. Soc.* **1975**, *97*, 3402.

[72] a) A. Moezzi, M. M. Olmstead, P. P. Power, *J. Am. Chem. Soc.* **1992**, *114*, 2715; b) A. Moezzi, R. A. Bartlett, P. P. Power, *Angew. Chem.* **1992**, *104*, 1075; *Angew. Chem. Int. Ed. Engl.* **1992**, *31*, 1082.

[73] E. Kaufmann, P. von Ragué Schleyer, *Inorg. Chem.* **1988**, *27*, 3987.

[74] a) H. Klusik, A. Berndt, *Angew. Chem.* **1981**, *93*, 903; *Angew. Chem. Int. Ed. Engl.* **1981**, *20*, 870; b) Al-Al: W. Uhl, A. Vester, W. Kaim, J. Poppe, *J. Organomet. Chem.* **1993**, *454*, 9; c) C. Pluta, K.-R. Pörschke, C. Krüger, K. Hildenbrand, *Angew. Chem.* **1993**, *105*, 451; *Angew. Chem. Int. Ed. Engl.* **1993**, *32*, 388; d) Ga-Ga: X. He, R. A. Bartlett, M. M. Olmstead, K. Ruhlandt-Senge, B. E. Sturgeon, P. P. Power, *Angew. Chem.* **1993**, *105*, 761; *Angew. Chem. Int. Ed. Engl.* **1993**, *32*, 717; e) review: W. Uhl, *Angew. Chem.* **1993**, *105*, 1449; *Angew. Chem. Int. Ed. Engl.* **1993**, *32*, 1386; f) W. Uhl, A. Vester, D. Fenske, G. Baum, *J. Organomet. Chem.* **1994**, *464*, 23.

[75] a) P. Schwerdtfeger, *Inorg. Chem.* **1991**, *30*, 1660; compare with: b) C. Janiak, R. Hoffmann, *Angew. Chem.* **1989**, *101*, 1706; *Angew. Chem. Int. Ed. Engl.* **1989**, *28*, 1688.

[76] a) H. Schumann, C. Janiak, J. Pickardt, U. Bömer, *Angew. Chem.* **1987**, *99*, 788; *Angew. Chem. Int. Ed. Engl.* **1987**, *26*, 789; b) H. Schumann, C. Janiak, F. Görlitz, J. Loebel, A. Dietrich, *J. Organomet. Chem.* **1989**, *363*, 243.

[77] M. Scholz, M. Noltemeyer, H. W. Roesky, *Angew. Chem.* **1989**, *101*, 1419; *Angew. Chem. Int. Ed. Engl.* **1989**, *28*, 1383; H. W. Roesky, M. Scholz, M. Noltemeyer, F. T. Edelmann, *Inorg. Chem.* **1989**, *28*, 3829.

[78] M. Veith, *Chem. Rev.* **1990**, *90*, 1 and references therein.

[79] For synthesis and reactivity see also [67d, e] and M. F. Lappert, *Main Group Met. Chem.* **1994**, *117*, 183.

[80] N. Tokitoh, H. Suzuki, R. Okazaki, K. Ogawa, *J. Am. Chem. Soc.* **1993**, *115*, 10428.

[81] M. Kira, T. Maruyama, C. Kabuto, K. Ebata, H. Sakurai, *Angew. Chem.* **1994**, *106*, 1575; *Angew. Chem. Int. Ed. Engl.* **1994**, *33*, 1498.

[82] H. Sakurai, K. Ebata, C. Kabuto, Y. Nakadaira, *Chem. Lett.* **1987**, 301.

[83] P. J. Davidson, M. F. Lappert, *J. Chem. Soc. Chem. Commun.* **1973**, 317.

[84] H. Grützmacher, F. Pauer, D. Stalke, unpublished results.

[85] M. Weidenbruch, H. Kilian, K. Peters, H. G. von Schnering, H. Marsmann, *Chem. Ber.* **1995**, *128*, 983.

[86] L. Pauling, *Proc. Natl. Acad. Sci. USA* **1983**, *80*, 3871.

[87] T. L. Windus, M. S. Gordon, *J. Am. Chem. Soc.* **1992**, *114*, 9559.

[88] a) K. W. Zilm, G. A. Lawless, R. M. Merrill, J. M. Millar, G. G. Webb, *J. Am. Chem. Soc.* **1987**, *109*, 7236; b) M. F. Lappert, *Silicon, Germanium, Tin, Lead Compd.* **1986**, *9*, 129.

[89] H. B. Yokelson, D. A. Siegel, A. J. Millevolte, J. Maxka, R. West, *Organometallics* **1990**, *9*, 1005.

[90] a) M. Veith, *Z. Naturforsch. B* **1978**, *33*, 1; b) B. Wrackmeyer, K. Horchler, H. Zhou, M. Veith, *ibid.* **1989**, *44*, 288; c) B. Wrackmeyer, C. Strader, K. Horchler, H. Zhou, *Inorg. Chim. Acta* **1990**, *176*, 205.

[91] a) R. W. Chorley, P. B. Hitchcock, B. S. Jolly, M. F. Lappert, G. A. Lawless, *J. Chem. Soc. Chem. Commun.* **1991**, 1302; b) R. W. Chorley, D. Ellis, P. B. Hitchcock, M. F. Lappert, *Bull. Soc. Chim. France* **1992**, *129*, 599.

[92] N. Burford, T. M. Parks, B. W. Royan, B. Borecka, T. S. Cameron, J. F. Richardson, E. J. Gabe, R. Hynes, *J. Am. Chem. Soc.* **1992**, *114*, 8147 and references therein.

[93] N. Burford, T. M. Parks, P. K. Bakshi, T. S. Cameron, *Angew. Chem.* **1994**, *106*, 1332; *Angew. Chem. Int. Ed. Engl.* **1994**, *33*, 1267.

[94] J. Niemann, W. W. Schoeller, V. von der Gönna, E. Niecke, *Chem. Ber.* **1991**, *124*, 1563.

[95] M. J. Michalczyk, R. West, J. Michl, *J. Am. Chem. Soc.* **1984**, *106*, 821.

[96] a) N. Wiberg, G. Wagner, G. Müller, *Angew. Chem.* **1985**, *97*, 220; *Angew. Chem. Int. Ed. Engl.* **1985**, *24*, 229; b) G. Raabe, J. Michl in *The Chemistry of Organic Silicon Compounds* (Eds.: S. Patai, Z. Rappoport), Wiley, Chichester, **1989**, chapter 17 and references therein.

[97] a) U. Heim, H. Pritzkow, H. Schönberg, H. Grützmacher, *J. Chem. Soc. Chem. Commun.* **1993**, 673; b) H. Grützmacher, H. Pritzkow, *Angew. Chem.* **1991**, *103*, 721; *Angew. Chem. Int. Ed. Engl.* **1991**, *30*, 709; c) A. Igau, A. Baceiredo, H. Grützmacher, H. Pritzkow, G. Bertrand, *J. Am. Chem. Soc.* **1989**, 6853.

[98] a) D. C. Pestana, P. P. Power, *J. Am. Chem. Soc.* **1991**, *113*, 8426; b) P. P. Power, *Angew. Chem.* **1990**, *102*, 527; *Angew. Chem. Int. Ed. Engl.* **1990**, *30*, 449.

[99] T. L. Allen, A. C. Schreiner, H. F. Schaefer III, *Inorg. Chem.* **1990**, *29*, 1930.

[100] J. M. Lehn, B. Munsch, *Mol. Phys.* **1972**, *23*, 91.

[101] M. A. Petrie, S. C. Shoner, H. V. Rasika Dias, P. P. Power, *Angew. Chem.* **1990**, *102*, 1061; *Angew. Chem. Int. Ed. Engl.* **1990**, *102*, 1033.

[102] a) H. Meyer, G. Baum, W. Massa, A. Berndt, *Angew. Chem.* **1987**, *99*, 790; *Angew. Chem. Int. Ed. Engl.* **1987**, *26*, 798; b) H. Meyer, G. Baum, W. Massa, S. Berger, A. Berndt, *ibid.* **1987**, *99*, 559 bzw. **1987**, *26*, 546.

[103] M. Lazraq, J. Escudié, C. Couret, J. Satgé, M. Dräger, R. Dammel, *Angew. Chem.* **1988**, *100*, 885; *Angew. Chem. Int. Ed. Engl.* **1988**, *27*, 828.

[104] G. Anselme, H. Ranaivonjatovo, J. Escudié, C. Couret, J. Satgé, *Organometallics* **1992**, *11*, 2748.

[105] a) H. Grützmacher, H. Pritzkow, *Organometallics* **1991**, *10*, 938 and references therein; b) N. Wiberg, K. S. Vasisht, *Angew. Chem.* **1991**, *103*, 105; *Angew. Chem. Int. Ed. Engl.* **1991**, *30*, 93; review: J. Escudié, C. Couret, H. Ranaivonjatovo, G. Anselme, G. Delpon-Lacaze, M.-A. Chaubon, A. Kandri Rodi, J. Satgé, *Main Group Metal. Chem.* **1994**, *17*, 33.

[106] H. Grützmacher, W. Deck, H. Pritzkow, M. Sander, *Angew. Chem.* **1994**, *106*, 467; *Angew. Chem. Int. Ed. Engl.* **1994**, *33*, 456.

[107] A. J. Arduengo III, H. V. Rasika Dias, J. C. Calabrese, F. Davidson, *Inorg. Chem.* **1993**, *32*, 1541.

[108] a) N. Kuhn, T. Kratz, D. Bläser, R. Boese, *Chem. Ber.* **1995**, *128*, 245; b) A. Schäfer, M. Weidenbruch, W. Saak, S. Pohl, *J. Chem. Soc. Chem. Commun.* **1995**, 1157.

[109] a) K. M. Baines, J. A. Cooke, *Organometallics* **1992**, *11*, 3487; b) K. M. Baines, J. A. Cooke, *Organometallics* **1991**, *10*, 3419.

[110] K. M. Baines, J. A. Cooke, J. J. Vittel, *J. Chem. Soc. Chem. Commun.* **1992**, 1484.

[111] R. S. Grev, H. F. Schaeffer III, *Organometallics* **1992**, *11*, 3489.

[112] Review: K. Balasubramanian, *Chem. Rev.* **1989**, *89*, 1801.

[113] P. J. Bruna, V. Krumbach, S. D. Peyerimhoff, *Can. J. Chem.* **1985**, *63*, 1594.

[114] M. W. Schmidt, P. N. Truong, M. S. Gordon, *J. Am. Chem. Soc.* **1987**, *109*, 5217.

[115] P. von R. Schleyer, D. Kost, *J. Am. Chem. Soc.* **1987**, *109*, 5227.

[116] W. W. Schoeller in *Multiple Bonds and Low Coordination in Phosphorus Chemistry* (Eds.: M. Regitz, O. J. Scherer), Thieme, Stuttgart, **1990**, p. 12.

[117] M. Driess, R. Janoschek, *J. Mol. Struc. (THEOCHEM)* **1994**, *313*, 129.

[118] a) N. Wiberg, K. Schurz, G. Fischer, *Angew. Chem.* **1985**, *97*, 1058; *Angew. Chem. Int. Ed. Engl.* **1985**, *24*, 1053; b) M. Hesse, U. Klingebiel, *ibid.* **1986**, *98*, 638 bzw. **1986**, *25*, 649; c) N. Wiberg, K. Schurz, G. Müller, J. Riede, *ibid.* **1988**, *100*, 979 *ibid.* **1988**, *27*, 935.

[119] a) M. Driess, *Angew. Chem.* **1991**, *103*, 979; *Angew. Chem. Int. Ed. Engl.* **1991**, *30*, 1022; b) M. Driess, S. Rell, H. Pritzkow, *J. Chem. Soc. Chem. Commun.* **1995**, 253; c) Compare with the review: F. Bickelhaupt in *Multiple Bonds and Low Coordination in Phosphorus Chemistry* (Eds.: M. Regitz, O. J. Scherer), Thieme, **1990**, p. 287; M. Driess, *Adv. Organomet. Chem.* **1996**, *39*, 193; M. Driess, *Coord. Chem. Rev.* **1995**, *145*, 1; d) **156** is isotypical with the arsenic analogue [119 b]; Further details of the crystal structure investigation may be obtained from the Fachinformationszentrum Karlsruhe, D-76344 Eggenstein-Leopoldshafen (Germany), on quoting the depository number CSD-404655.

[120] M. Driess, H. Pritzkow, *Angew. Chem.* **1992**, *104*, 350; *Angew. Chem. Int. Ed. Engl.* **1992**, *31*, 316.

[121] H. R. G. Bender, E. Niecke, M. Nieger, *J. Am. Chem. Soc.* **1993**, *115*, 3314.

[122] A simple, comprehensive arguement within the framework of perturbation theory is described: W. Cherry, N. Epiotis, W. T. Borden, *Acc. Chem. Res.* **1977**, *10*, 167.

[123] H. Suzuki, N. Tokitoh, S. Nagase, R. Okazaki, *J. Am. Chem. Soc.* **1994**, *116*, 11578.

[124] N. Tokitoh, T. Matsumoto, K. Manmaru, R. Okazaki, *J. Am. Chem. Soc.* **1993**, *115*, 8855.

[125] T. Matsumoto, N. Tokitoh, R. Okazaki, *Angew. Chem.* **1994**, *106*, 2418; *Angew. Chem. Int. Ed. Engl.* **1994**, *33*, 2339.

[126] N. Tokitoh, M. Saito, R. Okazaki, *J. Am. Chem. Soc.* **1993**, *115*, 2065.

[127] T. P. Hamilton, H. F. Schaeffer III, *J. Chem. Phys.* **1989**, *90*, 1031; J. Hrušák, R. Srinivas, D. K. Böhme, H. Schwarz, *Angew. Chem.* **1991**, *103*, 1396; *Angew. Chem. Int. Ed. Engl.* **1991**, *30*, 1323.

[128] a) M.-A. Pearsall, R. West, *J. Am. Chem. Soc.* **1988**, *110*, 7228; b) C. A. Arrington, J. T. Petty, S. E. Payne, W. C. K. Haskins, *ibid.* **1988**, *110*, 6240.

[129] M. Tacke, Ch. Klein, D. J. Stufkens, A. Oskam, P. Jutzi, E. A. Bunte, *Z. Anorg. Chem.* **1993**, *619*, 865.

[130] H. Grützmacher, S. Freitag, R. Herbst-Irmer, G. S. Sheldrick, *Angew. Chem.* **1992**, *104*, 459; *Angew. Chem. Int. Ed. Engl.* **1992**, *31*, 437.

[131] V. Meyer, *Justus Liebigs Ann. Chem.* **1876**, *180*, 192.

[132] A. von Baeyer, *Ber. Dtsch. Chem. Ges.* **1885**, *18*, 2278.

[133] Reviews: a) K. B. Wiberg, *Angew. Chem.* **1986**, *98*, 312; *Angew. Chem. Int. Ed. Engl.* **1986**, *25*, 312; b) A. de Meijere, *ibid.* **1979**, *91*, 867 bzw. **1979**, *18*, 809; c) A. Greenberg, J. L. Liebman, *Strained Organic Compounds*, Academic Press, New York, **1978**, S. 280 and references therein.

[134] E. W. Schlag, B. S. Rabinovitch, *J. Chem. Phys.* **1960**, *32*, 5996.

[135] R. Boese, *Chem. Unserer Zeit*, **1989**, *23*, 77 und zit. Lit.

[136] R. F. Bader, Y. Tal, S. G. Anderson, T. T. Nguyen-Dang, *Isr. J. Chem.* **1980**, *19*, 8.

[137] C. Liang, L. C. Allen, *J. Am. Chem. Soc.* **1991**, *113*, 1878.

[138] a) R. F. W. Bader, P. J. MacDougall, C. D. H. Lau, *J. Am. Chem. Soc.* **1984**, *106*, 1594; b) D. Cremer, E. Kraka, *ibid.* **1985**, *107*, 3800; D. Kremer, E. Kraka, *ibid.* **1985**, *107*, 3811; T. Clark, G. W. Spitznagel, R. Close, P. von R. Schleyer, *ibid.* **1984**, *104*, 4412; Highlight: H. Grützmacher, *Angew. Chem.* **1992**, *104*, 1358; *Angew. Chem. Int. Ed. Engl.* **1992**, *31*, 1329.

[139] Compare with a) S. Nagase, *Polyhedron* **1991**, *11*, 1299; b) S. Nagase, K. Kobayashi, M. Nagashima, *J. Chem. Soc. Chem. Commun.* **1992**, 1302.

[140] D. A. Horner, R. S. Grev, H. F. Schaefer III, *J. Am. Chem. Soc.* **1992**, *114*, 2093.

[141] a) C. A. Coulson, W. E. Moffitt, *J. Chem. Phys.* **1947**, *15*, 151; a) C. A. Coulson, W. E. Moffitt, *Philos. Mag.* **1949**, *40*, 1; c) J. G. Hamilton, W. E. Palke, *J. Am. Chem. Soc.* **1993**, *115*, 4159, and references therein.

[142] A. von Baeyer, *Ber. Dtsch. Chem. Ges.* **1885**, *18*, 2269.

[143] a) W. W. Schoeller, T. Dabisch, *J. Chem. Soc. Chem. Commun.* **1985**, 1706; b) W. W. Schoeller, T. Dabisch, *Inorg. Chem.* **1987**, *26*, 1081.

[144] a) A. Schäfer, M. Weidenbruch, K. Peters, H. G. von Schnering, *Angew. Chem.* **1984**, *96*, 311; *Angew. Chem. Int. Ed. Engl.* **1984**, *23*, 302; M. Weidenbruch, *Chem. Rev.* **1995**, *95*, 1479; b) J. Belzner, *J. Organomet. Chem.* **1992**, *430*, C51.

[145] a) R. Gleiter, M. C. Böhm, M. Baudler, *Chem. Ber.* **1981**, *114*, 1004; b) M. Baudler, K. Glinka, *Chem. Rev.* **1993**, *93*, 1623; c) W. W. Schoeller, V. Staemmler, P. Rademacher, E. Niecke, *Inorg. Chem.* **1986**, *25*, 4382; d) M. Häser, R. Ahlrichs, H. Schiffer, *Theor. Chim. Acta* **1989**, 75.

[146] S. Inagaki, K. Yoshikawa, Y. Hayano, *J. Am. Chem. Soc.* **1993**, *115*, 3706.

[147] J. M. Birchall, R. Fields, R. N. Haszeldine, D. W. Roberts, *J. Chem. Soc. C* **1973**, 1071.

[148] R. Breslow, *Molecular Rearrangements*, Wiley, New York, **1963**, Part 1, Chapter 4.

[149] G. Frenking, unpublished results.

[150] H. Grützmacher, H. Pritzkow, *Angew. Chem.* **1991**, *103*, 976; *Angew. Chem. Int. Ed. Engl.* **1991**, *30*, 1017.

[151] S. Masamune, L. R. Sita, *J. Am. Chem. Soc.* **1985**, *107*, 6390.

[152] M. Weidenbruch, *Novel Ring Systems from Cyclotrisilanes and Cyclotristannanes* in *The Chemistry of Inorganic Ring Systems Vol. 14* (Ed.: R. Steudel), Studies in Inorganic Chemistry, Elsevier, **1992**, p. 51.

[153] J. A. Boatz, M. S. Gordon, *J. Phys. Chem.* **1989**, *93*, 3025.

[154] D. B. Kitchen, J. E. Jackson, L. C. Allen, *J. Am. Chem. Soc.* **1990**, *112*, 3408.

[155] a) Me_2Si: D. Seyferth, R. L. Lambert, *J. Am. Chem. Soc.* **1972**, *94*, 9246; D. Seyferth, D. P. Duncan, S. C. Vick, *J. Organomet. Chem.* **1977**, *125*, C5; D. Seyferth, D. P. Duncan, M. L. Shannon, E. W. Goldman, *Organometallics* **1984**, *3*, 574.

[156] tBu_2Si: P. Boudjouk, V. Samaraweera, R. Sooriyakumaran, J. Chrisciel, K. R. Anderson, *Angew. Chem.* **1988**, *100*, 1406; *Angew. Chem. Int. Ed. Engl.* **1988**, *27*, 1355.

[157] W. Ando, H. Ohgaki, Y. Kabe, *Angew. Chem.* **1994**, *106*, 723; *Angew. Chem. Int. Ed. Engl.* **1994**, *33*, 659.

[158] L. R. Sita, R. D. Bickerstaff, *J. Am. Chem. Soc.* **1988**, *110*, 5208.

[159] Compare with a) D. Seyferth, D. C. Annarelli, D. P. Duncan, *Organometallics* **1982**, *1*, 1288; b) M. P. Egorov, S. P. Kolesnikov, Yu. T. Struchkov, M. Yu. Antiin, S. V. Sereda, O. M. Nefedov, *J. Organomet. Chem.* **1985**, *290*, C27; c) A. Krebs, J. Berndt, *Tetrahedron Lett.* **1983**, *24*, 4083 and references therein.

[160] S. Masamune, S. Murakami, H. Tobita, *J. Am. Chem. Soc.* **1983**, *105*, 7776.

[161] M. Driess, unpublished results.

[162] a) Addition to Si=Si: G. R. Gillette, R. West, *J. Organomet. Chem.* **1990**, *394*, 45; b) H. Piana, U. Schubert, *ibid.* **1988**, *348*, C19; c) addition an Si=P, Si=As: . Driess, H. Pritzkow, *Angew. Chem.* **1992**, *104*, 775; *Angew. Chem. Int. Ed. Engl.* **1992**, *31*, 751; d) M. Driess, H. Pritzkow, S. Rell, U. Winkler, *Organometallics*, **1996**, in press; see also [119b].

[163] a) P. von R. Schleyer, A. F. Sax, J. Kalcher, R. Janoschek, *Angew. Chem.* **1987**, *99*, 374; *Angew. Chem. Int. Ed. Engl.* **1987**, *26*, 364; b) T. Dabisch, W. W. Schoeller, *J. Chem. Soc. Chem. Commun.* **1986**, 869; c) W. W. Schoeller, T. Dabisch, T. Busch, *Inorg. Chem.* **1987**, *76*, 4383; d) S. Collins, R. Dutler, R. Rauk, *J. Am. Chem. Soc.* **1987**, *109*, 2564.

[164] J. A. Boatz, M. S. Gordon, *J. Phys. Chem.* **1988**, *92*, 3037.

[165] R. Jones, D. J. Williams, Y. Kabe, S. Masamune, *Angew. Chem.* **1986**, *98*, 176; *Angew. Chem. Int. Ed. Engl.* **1986**, *25*, 173.

[166] a) E. Niecke, R. Rüger, B. Krebs, *Angew. Chem.* **1982**, *94*, 553; *Angew. Chem. Int. Ed. Engl.* **1982**, *21*, 544; b) R. Riedel, H.-D. Hausen, E. Fluck, *Angew. Chem.* **1985**, *97*, 1050; *Angew. Chem. Int. Ed. Engl.* **1985**, *24*, 1056; c) E. Fluck, R. Riedel, H.-D. Hausen, G. Heckmann, *Z. Anorg. Allg. Chem.* **1987**, *551*, 85; d) P. Jutzi, T. Wippermann, *J. Organomet. Chem.* **1985**, *287*, C5; e) M. Baudler, B. Wingert, *Z. Anorg. Allg. Chem.* **1992**, *611*, 50.

[167] W. W. Schoeller, C. Lerch, *Inorg. Chem.* **1983**, *22*, 2992.

[168] a) P. Kölle, G. Linti, H. Nöth, K. Polborn, *J. Organomet. Chem.* **1988**, *7*; b) R. T. Paine, H. Nöth, *Chem. Rev.* **1995**, *95*, 343.

[169] a) M. Driess, A. D. Fanta, D. Powell, R. West, *Angew. Chem.* **1989**, *101*, 1087; *Angew. Chem. Int. Ed. Engl.* **1989**, *28*, 1038; b) A. D. Fanta, R. P. Tan, N. M. Comerlato, M. Driess, D. R. Powell, R. West, *Inorg. Chim. Acta* **1992**, *198–200*, 733; c) M. Driess, H. Pritzkow, M. Reisgys, *Chem. Ber.* **1991**, *124*, 1923.

[170] a) M. Driess, R. Janoschek, H. Pritzkow, *Angew. Chem.* **1992**, *104*, 449; *Angew. Chem. Int. Ed. Engl.* **1992**, *31*, 460; b) R. P. Tan, N. M. Comerlato, D. R. Powell, R. West, *ibid.* **1992**, *104*, 1251; *ibid.* **1992**, *31*, 1217.

[171] A. D. Fanta, M. Driess, D. Powell, R. West, unpublished results.

[172] M. Driess, *Phosphorus, Sulfur, and Silicon* **1992**, *64*, 39.

[173] See for example the review: H. Bock, K. Ruppert, C. Näther, Z. Havlas, H.-F. Herrmann, C. Arad, I. Göble, A. John, J. Meuret, S. Nick, A. Rauschenbach, W. Seitz, T. Vaupel, B. Solouki, *Angew. Chem.* **1992**, *104*, 564; *Angew. Chem. Int. Ed. Engl.* **1992**, *31*, 550.

[174] V. Ya. Lee, A. A. Basova, I. A. Matchkorovskaya, V. I. Faustov, M. P. Egorov, O. M. Nefedov, R. D. Rakhimov, K. P. Butin, *J. Organomet. Chem.* **1995**, *499*, 27 and references therein.

Separation, Characterization, and Fraction Collection in the Nanoliter Domain with Capillary Electrophoresis

Aran Paulus*

In a relatively short time capillary electrophoresis (CE) has advanced to become a new analytical tool with broad applicability. Commercial instrumentation (Fig. 1) has been available

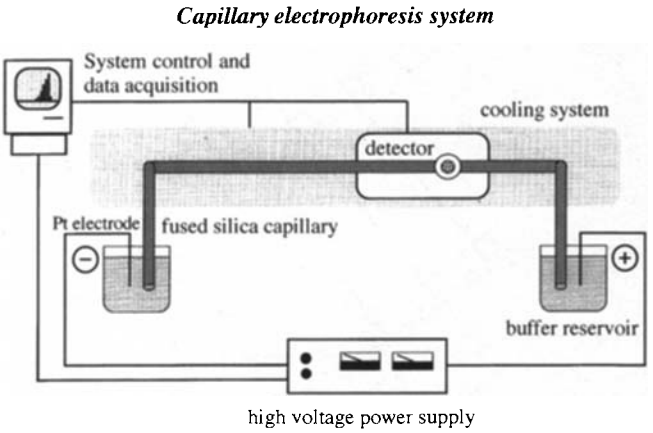

Fig. 1. Schematic representation of a commercial CE instrument. Fused silica capillary: internal diameter 50–100μm, length 20–50 cm; power supply: 0 to ±30 kV; detector: UV- or laser-induced fluorescence; temperature control: 15–60 °C.

only since the end of 1988, but a variety of analytical problems has been solved in capillaries with an inner diameter of 50 to 100 μm and 20 to 50 cm in length. Charged as well as uncharged analytes, inorganic ions, and small organic molecules, as well as complex biopolymers such as peptides, proteins, DNA fragments, and carbohydrates, have been separated by CE under suitable conditions.[1] Especially the extremely high separation efficiency, unparalleled by any other separation technique, added to the appeal of CE. Additional benefits include miniaturization, separation speed, automation, and flexibility in the choice of separation modes.

The majority of CE applications operates with capillaries filled with buffer. By applying an electrical field, an electroosmotic flow (EOF) is generated. In contrast to the parabolic flow profile of a pressure-driven HPLC flow, the EOF is characterized by a plug flow profile, which does not contribute to band broadening and therefore results in higher separation efficiencies. The number of theoretical plates depends only on the diffusion coefficient of the analyte. It can range from several hundred thousand to several million. As the total volume of a CE capillary is a few microliters, the injection volumes are in the order of a few nanoliters. CE has therefore been labeled a nanoseparation technique. The application of an electrical field of 200 to 500 $V\,cm^{-1}$ results in separation times ranging from 5 to 30 min.

The EOF-generated mass transport is supplemented by the electrophoretic mobility. In the presence of an electrical field the electrophoretic mobility causes an additional acceleration or deceleration of the ionic components of the sample according to their charge and mass. The separation mechanism of CE in its simplest form, the capillary zone electrophoresis (CZE), is based on differences in the charge-to-mass ratio of the analytes. Electrophoretic size separations, important for the analysis of DNA fragments and proteins, can be adapted to the CE format by using sieving matrices such as gels or polymer solutions in the capillaries. Capillary gel electrophoresis (CGE) is especially valuable in industrial biotechnology for analysis of recombinant proteins and antisense oligonucleotides because of its high separation efficiency and degree of automation.[2]

Using CZE conditions, neutral analytes would migrate with the EOF. By adding sodium dodecyl sulfate (SDS) to the buffer, micelles are formed, which act like a pseudostationary phase mobilized by the EOF. In the presence of micelles, neutral analytes partition between the aqueous buffer phase and the micellar phase and can thus be separated according to their hydrophobicity.[3] Alternatively, it is possible to fill the capillary with an HPLC stationary phase and to utilize chromatographic interactions with the EOF in the electrical field. This approach is an attractive alternative to microcolumn HPLC and is currently actively pursued as electrochromatography. Compared to HPLC, electrochromatography has its appeal in its high separation efficiencies and miniaturization.[4]

For a number of laboratories, a new analytical technique is only accessible after the introduction of commercial instrumentation. The majority of users will be busy with the solution of practical problems on available machines. However, commercialization also consolidates instrumental standards. Nevertheless, the stormy instrumental development in CE is not yet over, as demonstrated by the literature of the last year. A year ago, the direct coupling of CE with NMR spectroscopy was reported.[5] By using a 5 nL NMR sample cell made of a copper wire

[*] Dr. A. Paulus
Ciba Analytical Research, K-127.162
CH-4002 Basel (Switzerland)
Fax: Int. code +(61)696-4504
e-mail: 100064.242@Compuserve.com

wrapped around the fused silica capillary, NMR spectra with a signal line width of 11 Hz were recorded on-line from CE separations. When these results were published, the author's prophetic comment read: "The described method of miniaturization must be continued to derive a NMR resolution under the described measuring conditions which is close to values attainable by conventional acquisition system." This is exactly what has happened.

In a recent publication, Sweedler at al. report on NMR signal line widths of 0.6 Hz with the same experimental set-up, made possible through a stabilization of the magnetic field around the sample. By flushing the NMR sample compartment with Fluorinert FC-43, a fluid with a magnetic susceptibility between that of copper and heavy water, magnetic field in homogeneities could be suppressed. In this way, the mass sensitivity was improved 130-fold relative to that for conventional 5mm NMR tubes. Even the recording of 2D COSY spectra was possible with the nanoliter NMR sample cell. With an acquisition time of 1 min, 19 ng (56 pmol) sucrose was detected.

Although a direct coupling of NMR with CE is not described in this work, what only two years ago would have sounded impossible now seems feasible: the coupling of a high efficiency separation technique with an information-rich detection method. A CE-band containing picograms of sample migrates within 10 to 20 s passed the detection window. Both acquisition time and sensitivity of NMR spectroscopy are still one order of magnitude off that obtainable with optimal CE with UV detection. Nevertheless, an operational CE–NMR coupling for separation and immediate structural assignment in complex biological and environmental samples is no longer merely a pipe dream.

CE is not limited to separation and characterization of complex sample mixtures. In another paper from Sweedler's group,[7] the miniaturized dimensions of CE have been exploited for nanoliter kinetic assays. Instead of using a capillary, the long sides of two microscope slides were glued together at a distance of 40 μm to form a rectangular separation channel. Each short, open side was immersed in a buffer reservoir. If a capillary to dispense the sample is moved along one open side with the help of a micropositioner, sample injection is continuous and perpendicular to the direction of the separation. The dispenser capillary was filled with 200 nL of a mixture consisting of two amino acids and the derivatization agent naphthalene dialdehyde. Within minutes the reaction yields fluorescent products. Since the reaction is terminated when the reaction partners are separated in the electrical field, the reaction kinetics can be followed as a function of the movement of the dispenser capillary. This approach allows the measurement of rate constants, even if several reaction processes occur simultaneously with a time constant of 1 s in nL volumes. Such a set-up can conceivably be used for tracking biochemical processes such as protein biosynthesis directly in the cellular environment.

An important current instrumental development in CE for further miniaturization and integration of sample pretreatment is microchip CE. In this approach a lithographic process, familiar from microelectronics, is used to fabricate channels into quartz or glass plates. The channel dimensions are similar to those in fused silica capillaries. The advantages of planar or integrated CE include small overall dimensions with short separation channels, the simplicity with which channels can be connected for the integration of sample pretreatment or post separation routines, and the option for multiplexing with several parallel channels. With channels with effective lengths of only 5 cm, a power supply capable of delivering 10 kV is sufficient to generate high electric fields of up to 2000 Vcm^{-1}. Separation efficiency and resolution increase with increasing applied electric field. Since at the same time analysis times decrease, the microchip offers a simple method for fast, highly efficient separations. For example, 5000 theoretical plates per second were achieved in less than 1 min.[9]

Connecting fused silica capillaries for sample pretreatment or transfer of separated sample constituents in subsequent reservoirs introduces dead volumes. Any dead volume in micro columns is detrimental, since the prior separation is destroyed through mixing effects. This problem is circumvented with a microchip: the layout of the lithographic mask (Fig. 2) enables

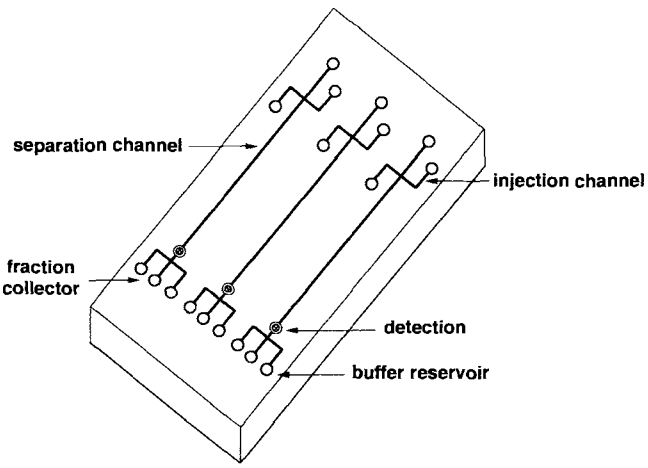

Fig. 2. Schematic representation of a planar integrated CE on a microchip. Channel dimensions: about 10 μm deep, 30 μm wide; length of separation channel: 2 to about 5 cm; chip dimensions: 10 × 5 × 0.5 cm.

any connections to be made without additional dead volumes. Ramsey's group was able to demonstrate the integration of precolumn derivatization of amino acids with phthalaldehyde in a 1 nL reaction volume on a microchip.[10]

The ultimate goal of chemists and biochemists is not only the separation and characterization of complex mixtures, but also, if at all possible, the isolation of a component of the sample for further reactions and investigations. However, in many separation techniques good separations and preparative amounts of samples very often have mutually exclusive criteria. As stated above, it is virtually impossible to handle the nanoliter volumes from CE outside the capillaries. Fortunately, the microchip approach also offers an alternative. C. S. Effenhauser et al. were able to demonstrate a functional picoliter fraction collector.[11] Using a microchip layout with crossing channels after the detection point, the authors separated antisense oligonucleotide mixtures in a polyacrylamide filled channel. By switching the electrical field, they could direct a part of the sample, ideally one component, into a reservoir to separate it from all other components. Single molecule detection is possible today with fluores-

cence detection techniques.[1,2] With that in mind, this combination triggers intriguing possibilities for chemists and biochemists: Single molecules can conceivably be separated, collected, and manipulated on a chip, and possibly even made to undergo chemical reactions. Chemistry with single molecules could soon be reality.

German version: *Angew. Chem.* **1996**, *108*, 931–933

Keywords: analytical methods · capillary electrophoresis · miniaturization

[1] A selection of review articles and monographs: J. W. Jorgenson, K. D. Lukacs, *Science* **1983**, *222*, 266–272; M. J. Gordon, X. Huang, S. L. Pentoney, Jr., R. N. Zare, *ibid.* **1988**, *242*, 224–228; A. G. Ewing, R. A. Wallingford, T. M. Olefirowicz, *Anal. Chem. A* **1989**, *61*, 292–303; H. Engelhardt, W. Beck, J. Kohr, T. Schmitt, *Angew. Chem.* **1993**, *105*, 659–680; *Angew. Chem. Int. Ed. Engl.* **1993**, *32*, 629–649; S. F. Y. Li, *Capillary Electrophoresis* (*J. Chromatogr. Libr. 52*) Elsevier, Amsterdam **1992**; *Capillary Electrophoresis Technology* (*Chromatogr. Sci. Ser. 64*) (Ed.: N. A. Guzman) Dekker, New York, **1993**; *Handbook of Capillary Electrophoresis* (Ed.: J. P. Landers) CRC Press, Boca Raton, FL, USA, **1993**.

[2] B. L. Karger, A. S. Cohen, A. Guttman, *J. Chromatogr.* **1989**, *492*, 585–614; G. J. M. Bruin, A. Paulus, *Anal. Methods Instrum.* **1995**, *2*, 3–26.

[3] S. Terabe, K. Otsuka, K. Ichikawa, A. Tsuchiya, T. Ando, *Anal. Chem.* **1984**, *56*, 113–116.

[4] J. H. Knox, I. H. Grant, *Chromatographia* **1991**, *32*, 317–328; N. W. Smith, M. B. Evans, *ibid.* **1994**, *38*, 649–657; K. Schmeer, B. Behnke, E. Bayer, *Anal. Chem.* **1995**, *67*, 3656–3658; B. Behnke, E. Grom, E. Bayer, *J. Chromatogr. A* **1995**, *716*, 207–213.

[5] K. Albert, *Angew. Chem.* **1995**, *107*, 699–701; *Angew. Chem. Int. Ed. Engl.* **1995**, *34*, 641–642.

[6] D. L. Olson, T. L. Peck, A. G. Webb, R. L. Mangin, J. V. Sweedler, *Science* **1995**, *270*, 1967–1969.

[7] Y. M. Liu, J. V. Sweedler, *J. Am. Chem. Soc.* **1995**, *117*, 8871–8872.

[8] D. J. Harrison, K. Fluri, K. Seiler, Z. Fan, C. S. Effenhauser, A. Manz, *Science* **1993**, *261*, 895–897; C. S. Effenhauser, A. Manz, H. M. Widmer, *Anal. Chem.* **1993**, *65*, 2637–2642.

[9] C. S. Effenhauser, A. Paulus, A. Manz, H. M. Widmer, *Anal. Chem.* **1994**, *66*, 2949–2953.

[10] S. C. Jacobson, R. Hergenroeder, A. W. Moore, Jr., J. M. Ramsey, *Anal. Chem.* **1994**, *66*, 4127–4132.

[11] C. S. Effenhauser, A. Manz, H. M. Widmer, *Anal. Chem.* **1995**, *67*, 2284–2287.

[12] M. Eigen, R. Riegler, *Proc. Natl. Acad. Sci USA* **1994**, *91*, 5740–5746; S. Nie, D. T. Chiu, R. N. Zare, *Science* **1994**, *266*, 1018–1020.

Superlattices, Thin Films, and Materials Design—A Mechanistic Approach

Robert Schöllhorn*

The area of thin films is rapidly developing into a key technology with applications ranging from electronic materials (semiconductors, superconductors, optoelectronics etc.) to chemical sensor systems. A variety of deposition techniques for the preparation of single layers and superlattices is now available, extending from molecular beam epitaxy to chemical vapor deposition. While physicists are focussing their attention on the detection of new quantum phenomena associated with the constrained morphology in nanorange dimensions, it appears that a new avenue is opening here for solid-state chemistry through the controlled synthesis of complex metastable structures. A particularly interesting example in this line is represented by the approach documented in recent work by D. C. Johnson and coworkers which concerns the preparation of new compositionally modulated layered transition metal dichalcogenide structures characterized by the use of a rational synthesis strategy that involves a topological model for kinetic trapping and directed interfacial growth.[1–3]

Superlattices are defined here as multilayer thin films with long-range structural coherence perpendicular to the basal plane which are prepared by time sequential deposition of components. In the area of molecular solids the formation of ordered multilayer systems with complex arrays of subunits has become an established art (for example, Langmuir–Blodgett and polymer films).[4, 5] The deposition of multilayers of metals/alloys,[6] covalent semiconductor materials,[7] and oxometalate superconductors[8] are well known for nonmolecular solids; however, there are only a few reports on other materials. The usual method of preparation is to deposit these phases under conditions that lead directly to the final product.

A different philosophy underlies the approach used by Johnson et al. for the controlled chemical synthesis of complex metastable chalcogenide structures by superlattice precursors. The concept used is based on a two-step process. In the first step a multilayer structure is prepared by modulated sequential deposition of the chemical elements required. This structure is subsequently transformed by low-temperature thermal conversion under defined conditions into a crystalline superlattice compound with compositional modulation. The formation of the heterostructure is not based on conventional epitaxial growth but on kinetic trapping of the desired structure by the specific solid-state reaction mechanism.

Layered transition metal dichalcogenides MX_2 of the CdI_2 or MoS_2 structure type were selected for investigations on this reaction model. These chalcogenides are interesting for several reasons. Their electronic properties vary from insulator to metal and superconductor behavior; charge density waves have been studied extensively with these layered phases.[9, 10] Their topotactic reactivity is exceptional;[11, 12] in terms of application they are of interest, for example as electrode materials for secondary batteries and photoelectrochemical cells, as solid lubricants, and in heterogeneous catalysis. Their physical and chemical properties can be modified by isomorphous replacement of lattice cations and anions.

[*] Prof. Dr. R. Schöllhorn
Institut für Anorganische und Analytische Chemie, Sekr. C 2
Technische Universität Berlin
Strasse des 17. Juni 135, D-10623 Berlin (Germany)
Fax: Int. code +(30) 314-21106
e-mail: schoe@wap0209.chem.tu-berlin.de

 © VCH Verlagsgesellschaft mbH, D-69451 Weinheim, 1996 0570-0833/96/3508-0859 $ 15.00+.25/0

Experimental investigations were initially carried out on the *binary* Nb/Se system by X-ray diffraction and differential scanning calorimetry; these demonstrated the oriented formation of the binary chalcogenide $NbSe_2$ as a result of the nucleation and growth of the product along the planar interfaces of the modulated precursor phase. The major parameters for reaction control were the diffusion length (layer thickness in the precursor state), the annealing temperature, and the annealing time. With appropriate reaction parameters a variation of the Nb/Se ratio (i.e. metal or chalcogen excess relative to the 1:2 stoichiometry) had no influence on the formation of stoichiometric $NbSe_2$, in spite of the potential competition by neighboring binary phases thermodynamically stable under these conditions. This is in perfect agreement with the assumption of a low-temperature solid-state reaction with kinetic control.

If the mechanism of the interfacial nucleation with oriented crystal growth of kinetic products (Fig. 1) is correct, it should be

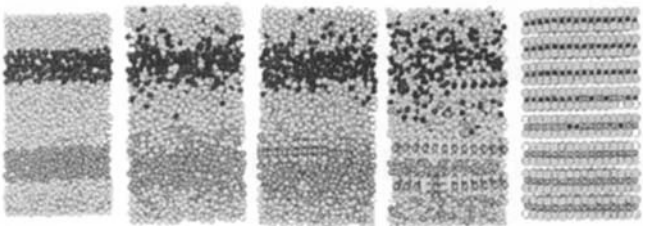

Fig. 1. The reaction pathway for the formation of chalcogenide superlattices: low-temperature thermal transformation of amorphous chalcogenide precursor multilayers, comprising layers of niobium (black spheres) and titanium atoms (gray spheres), each separated by intervening layers of selenium atoms (white spheres) (left), by interfacial nucleation and oriented growth into the desired crystalline product superlattice after annealing (right).

possible to prepare new metastable heterostructures containing ternary compounds with modulated composition perpendicular to the direction of the thin film basal plane. X-ray and DSC studies on the Ti/Nb/Se system in the stoichiometric ratio used for the formation of MX_2 layers demonstrated a persistence of the precursor thin film composition modulation in the course of the low-temperature annealing process and a continuous oriented growth of the product phase. An experiment with a precursor superlattice sequence corresponding to 6(Ti/2 Se)–6(Nb/2Se) yielded a remarkable result: the X-ray pattern of the product phase displayed all of the calculated 62 Bragg reflections of the desired superlattice (Fig. 2). The high quality of the reflections allowed a Rietveld analysis that confirmed the correlation between the precursor heterostructure sequence and the superlattice ordering of the final product. As expected high-temperature annealing of the product phase leads to quantitative conversion into the thermodynamically stable, solid solution phase with short periodicity and identical layer units of the composition $Ti_{0.5}Nb_{0.5}Se_2$.

The novel concept for the controlled low-temperature solid-state synthesis of metastable phases by thin-layer precursors modulated in the nanometer range—characterized by the competition in time windows between short-scale diffusion and heterogeneous interface nucleation with oriented growth of a metastable product phase—has thus been successfully applied by the authors for the controlled preparation of novel transition

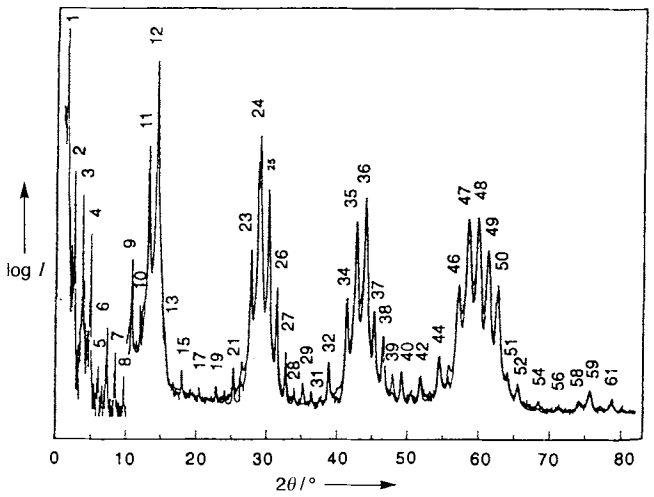

Fig. 2. X-ray diffractogram of a dichalcogenide superlattice with a modulation sequence corresponding to six $NbSe_2$ and six $TiSe_2$ layer units. All 62 Bragg reflections of the desired superlattice are shown.

metal dichalcogenide structures. A new dimension is given here for modifying the interesting physical and topochemical properties of these materials. Transition metal dichalcogenides belong to the category of van der Waals type layered solids; their structural morphology and bonding anisotropy naturally should favor the directed interfacial growth mechanism. A large variety of related layered compounds with similar or more complex layered structures or stoichiometry are known to which this concept could be extended (e.g. transition metal dihalides, phosphorous chalcogenides, sulfide carbides etc.). It seems most likely that this synthesis strategy can similarly be applied to the preparation of metastable framework solids characterized by strongly anisometric structures, such as layer-type perovskites. The limit of application of this concept may be reached with structurally isometric solids, in which coherent directed nucleation and growth at interfaces appears to be less probable. Further aspects of general interest related to this concept are the investigation of dynamic interface processes (in situ diffraction studies), nucleation phenomena, and the transformation mechanisms of amorphous phases in low-temperature solid-state reactions whose investigation with bulk material is frequently problematic.

It is important to note in this context a further line of progress achieved recently concerning modulated materials. Present techniques for the preparation of pristine thin films of nonmolecular solids are based essentially on physical or chemical vacuum techniques in which atoms, molecules or cluster aggregates are deposited from the vapor phase onto solid substrates (i.e. gas/solid processes). A basically different approach is the use of *electrochemical* techniques for thin film preparation (i.e. fluid–solid conversion). There are several advantages associated with this technique: a) the strong tendency of electrochemically deposited materials—including isometric systems—for epitaxial growth, b) the possibility of working with systems not suited for vacuum deposition, c) suppression of interdiffusion between layers (room temperature), and d) precise control of deposition by current density (kinetics) and electrode potential (variable energy scale). Whereas the electrochemical deposition of multilayer systems of metals/alloys and semiconductors[13] has been

well investigated in the last decade, recent work by Switzer and coworkers appears to be the first successful attempt to obtain superlattices from a complex ternary inorganic material by the electrochemical deposition technique.[14]

The major subject of these investigations was the ternary Tl/Pb/O system with a fluorite type structure and a large variation in stoichiometry. By pulsed-current or pulsed-potential deposition from electrolytes with appropriate ionic composition, superlattices with a modulation layer unit thickness of 3 nm could be prepared. X-ray and scanning tunneling microscopy studies confirmed the high quality of the superlattice architecture. The modulation wave lengths were in the order of mean free path dimensions of electrons. The material is a degenerate n-type semiconductor whose high electronic conductivity, which lies in the order of that of metals, is combined with the optical properties of a semiconductor; it is of interest with respect to quantum optical, electronic, and optoelectronic functions.

A further remarkable recent result from the work by Switzer et al. is the pulsed anodic electrodeposition of nanometer-scale modulated "defect chemistry superlattices" of thallium(III) oxide (Fig. 3).[15] The modulation parameters here are intrinsic anion vacancies and cation Frenkel type defects. It could be shown that the defect chemistry of Tl_2O_3 is a function of the applied electrode potential: high overpotentials were found to induce oxygen vacancy defects (Tl_2O_{3-y}), whereas low overpotentials favor excess Tl ions on interstitial sites of the lattice (i.e. $Tl_xTl_2O_3$).

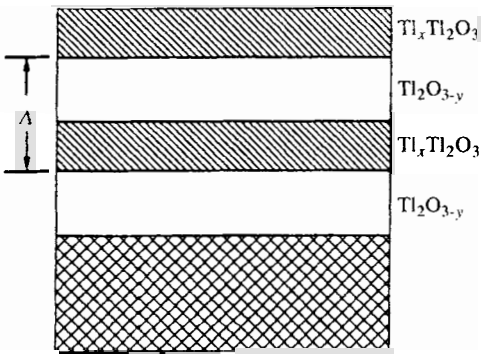

Fig. 3. Scheme of defect modulation in a thallium(III) oxide superlattice obtained by anodic pulsed deposition. Substrate = stainless steel. Λ = Periodicity of layer sequence.

The examples of recent work presented here underline the increasing involvement of chemistry in the area of nonmolecular materials artificially modulated on the nanometer scale, and the potential of low-temperature solid-state processes and controlled materials design. In comparison with the impressive rapid progress in "supramolecular chemistry" it now seems that some keys to doors are becoming available, providing access to a comparable tailoring approach in the domain of nonmolecular solids.

German version: *Angew. Chem.* **1996**, *108*, 933–935

Keywords: electrochemistry · materials design · superlattices · thin films

[1] M. Noh, J. Thiel, D. C. Johnson, *Science* **1995**, *270*, 1181.
[2] T. Novet, D. C. Johnson, L. Fister, *Adv. in Chem. Ser.* **1995**, *245*, 425.
[3] L. Fister, T. Novet, C. A. Grant, D. C. Johnson in *Advances in the Synthesis and Reactivity of Solids, Vol. 2* (Ed.: T. E. Mallouk), JAI Press, London, **1994**, p. 155.
[4] R. H. Tredgold, *J. Mater. Chem.* **1995**, *5*, 1095.
[5] M. Seufert, M. Schaub, G. Wenz, G. Wegner, *Angew. Chem.* **1995**, *107*, 363; *Angew. Chem. Int. Ed. Engl.* **1995**, *34*, 340.
[6] I. K. Schuller, *Solid State Commun.* **1994**, *92*, 141.
[7] A. Ourmazd, M. Scheffler, M. Heinemann, J. L. Rouviere, *MRS Bull.* **1992**, *17*, 24.
[8] D. Neerinck, K. Temst, M. Baert, E. Osquigil, C. van Hasendonck, Y. Bruynserade, A. Gilabert, I. K. Schuller, *Phys. Rev. Lett.* **1991**, *67*, 2577.
[9] J. A. Wilson, A. D. Yoffe, *Adv. Phys.* **1969**, *18*, 193.
[10] F. Lévy, *Intercalated Layered Materials*, D. Reidel, Dordrecht, **1979**.
[11] A. J. Jacobson in *Solid State Chemistry: Compounds* (Eds.: A. K. Cheetham, P. Day), Clarendon, Oxford, **1992**, p. 183.
[12] R. Schöllhorn in *Progress in Intercalation Research* (Eds.: W. Müller-Warmuth, R. Schöllhorn), Kluwer, Dordrecht/Boston, **1994**, p. 1.
[13] K. Rajeshwar, *Adv. Mater.* **1992**, *4*, 23.
[14] J. A. Switzer, R. J. Phillips, T. D. Golden, *Appl. Phys. Lett.* **1995**, *66*, 819; J. A. Switzer, T. D. Golden, *Adv. Mater.* **1993**, *5*, 474; J. A. Switzer, R. J. Phillips, R. P. Raffaele in *Supramolecular Architecture* (Ed.: T. Bein), ACS Symposium Series 499, Amer. Chem. Soc., Washington, **1992**, p. 244.
[15] R. A. van Leeuwen, C. J. Hung, D. R. Kammler, J. A. Switzer, *J. Phys. Chem.* **1995**, *99*, 15247; J. A. Switzer, C. J. Hung, B. E. Breyfogle, M. G. Shumsky, R. van Leeuwen, T. D. Golden, *Science* **1994**, *264*, 1573.

 © VCH Verlagsgesellschaft mbH, D-69451 Weinheim, 1996 0570-0833/96/3508-0861 $ 15.00+.25/0

Anions Stabilized by β-Nitro Groups: The Acidity and *ortho*-Metalation of Nitrocubanes—Penta- and Hexanitrocubanes**

Kirill Lukin, Jianchang Li, Richard Gilardi, and Philip E. Eaton*

Nitro groups are powerfully electron withdrawing. On both resonance and inductive scales they are more potent than any other uncharged functionality.[1,2] Anions with α-nitro substituents are highly stabilized by resonance delocalization of charge; an α-nitronate (the *aci*-nitro anion) is 10^{+10} times less basic than a ketone enolate.[3] The acidity of carboxylic acids is increased about one thousandfold by the inductive effect of an α-nitro group.[4] We show here that nitro substituents have a dramatic effect on the acidity and chemistry of cubanes.

Cubane uses an s-rich orbital to bond substituents. Thus, cubyl hydrogens are more acidic than those on more usual hydrocarbons; for example, cubane is approximately 60000 times more acidic than cyclohexane.[5] Experiments with mono- and 1,4-dinitrocubanes, designed to probe for substituent-enhanced acidity (refer to the effects of amide substituents[6]) were entirely frustrated by the ease with which base destroys these compounds. Not even the simplest exchange reaction could be achieved. If one can use transient colorations as an indicator, single electron transfer mechanisms probably intervened and somehow unraveled the cubane framework; nothing of substance could be isolated. It is possible that an anion was formed, but that β-elimination of nitrite then occurred. Although this happens readily with enolizable β-nitro ketones and the like,[7] elimination of nitrite is much less likely here, for the product would be a cubene. Cubenes are anti-Bredt olefins, highly pyramidalized and difficult to access, but they do give isolable products.[8]

1,3,5,7-Tetranitrocubane (**1**), first made here in 1992 and now much more easily available,[9,10] has four identical hydrogen atoms each surrounded by three nitro groups (the molecule has pseudo-tetrahedral symmetry). The possibility of deprotonating to an anion (**2**) much stabilized by the inductive electron-withdrawing effects (− I effect) of three vicinal (β) nitro groups and, perhaps more importantly, by coordination of the electron-rich oxygen atoms of these groups with the counterion seemed particularly attractive. Indeed, we have found that the acidity of the cubane hydrogen atoms is so enhanced in **1** that their exchange can be effected rapidly even with bases as mild as sodium methoxide in methanol. Thus, reaction of [H_4]-**1** with 0.125 M CD_3ONa in CD_3OD for 45 minutes at room temperature, followed by quenching with hydrochloric acid and extraction with EtOAc, gave [D_4]-**1** in 87% yield. The reverse experiment, that is, reaction of [D_4]-**1** with CH_3ONa in CH_3OH, returned [H_4]-**1**.

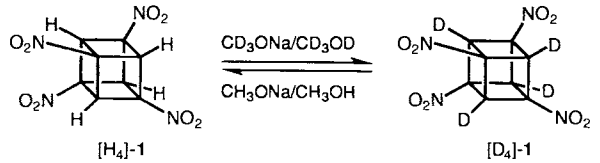

[H_4]-**1** [D_4]-**1**

The anion that must intervene in these exchanges exists at only very low concentration in methanolic CH_3ONa. It could not be detected in this milieu by NMR spectroscopy, nor did we have any success trapping it with electrophiles other than acid. However, ^{1}H NMR examination of the reaction of **1** with sodium bis(trimethylsilyl)amide in [D_8]THF at −75 °C showed clearly the formation of the salt Na-**2**: ^{1}H NMR $\delta = 5.54$ (s). This salt is stable for hours at −75 °C, but it decomposes rapidly above −50 °C.

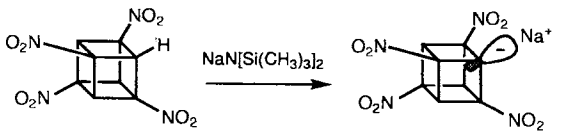

1 Na-**2**

We could estimate the pK_a of **1** from low temperature proton NMR measurements on equilibrium mixtures with various bases. Almost complete metalation (salt formation) occurs in THF with one equivalent of sodium bis(trimethylsilyl)amide, but none with α-lithiobenzyl cyanide. As the pK_a in THF of bis(trimethylsilyl)amine is 25.8[11] and that of benzyl cyanide is 18.7,[12] the pK_a of **1** must be between about 20 and 24.5. We have narrowed this to between 20.5 and 22.5 by noting that **1** is partially converted into its anion by 1.5 equivalents of potassium *tert*-butoxide (the pK_a of *tert*-butyl alcohol in THF is given as 21.6[13]).

The salt of tetranitrocubane can be used to achieve further substitution on the cubane framework. For example, reaction of Na-**2** in THF at −75 °C with carbon dioxide followed by neutralization gave the tetranitrocubane carboxylic acid **3** in 85%

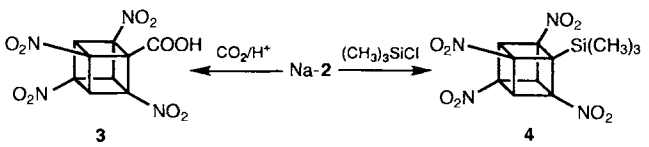

3 **4**

yield (characterized as its methyl ester: ^{1}H NMR: $\delta = 3.84$ (s, 3H), 6.22 (s, 3H); ^{13}C NMR: $\delta = 54.3$ (OCH_3), 67.0 (3C, CH), 72.0, 73.4, 75.2 (3C, CNO_2), 159.9 (C=O)). Quenching **2** with chlorotrimethylsilane gave the tetranitro(trimethylsilyl)cubane **4** in 80% yield (^{1}H NMR: $\delta = 0.16$ (s, 9H), 6.07 (s, 3H); ^{13}C NMR: $\delta = -3.3$ (3C, $SiCH_3$), 67.8 (3C, CH), 71.7, 74.4 (3C, CNO_2), 75.5). These conversions are the first to our knowledge of substitutions by way of "*ortho*-metalations" in which the nitro group activates a β C–H bond and stabilizes the resulting anion.[14]

When a larger excess of sodium bis(trimethylsilyl)amide was used in these reactions, yet more highly substituted cubanes were obtained. Treatment of **1** with five equivalents of base followed by quenching with carbon dioxide and neutralization gave a 70:30 mixture of **3** with **5**, the tetranitro diacid (charac-

[*] Prof. P. E. Eaton, Dr. K. Lukin
Department of Chemistry, The University of Chicago
5735 S. Ellis Avenue, Chicago, IL 60637 (USA)
Fax: Int. code +(312) 702-2053
Dr. J. Li
Geo-Centers Inc.
762 Route 15 South, Lake Hopatcong, NJ 07849 (USA)
Dr. R. Gilardi
Laboratory for the Structure of Matter
The Naval Research Laboratory, Washington, D.C. 20375 (USA)

[**] We are grateful to Dr. Ravi Shankar and Dr. Gene Wicks for their initial studies of lower nitrocubanes and to Dr. Eric Punzalan and Dr. A. Bashir-Hashemi for samples of **1**. This work was supported by The U.S. Army Research, Development and Engineering Center (Geo-Centers) and the Office of Naval Research.

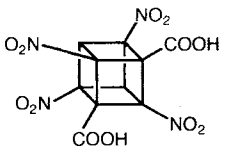

5

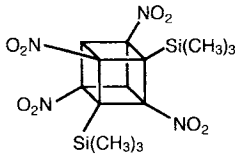

6

terized as its dimethyl ester: ^{1}H NMR: $\delta = 3.90$ (s, 6H), 6.34 (s, 2H); ^{13}C NMR: $\delta = 54.5$ (2C, OCH_3), 66.3 (2C, CH), 72.5 (2C), 74.4 (2C), 76.5 (2C), 159.3 (2C, C=O)). Similarly, the use of three equivalents of base followed by reaction with chlorotrimethylsilane gave a 20:80 mixture of **4** with **6**, the bissilylated product (^{1}H NMR: $\delta = 0.19$ (s, 18H), 6.10 (s, 2H); ^{13}C NMR: $\delta = -3.2$ (6C, CH_3), 67.1 (2C, CH), 72.7 (2C), 75.4 (2C), 75.8 (2C)). We are reasonably certain that **5** and **6** result from sequential anion formations from **3** and **4**. There is no evidence from the low temperature NMR study for dianion formation from **1**.

As anions derived from **1** are trapped effectively with simple electrophiles, we hoped that reaction with electrophilic nitrating reagents would allow us access to more highly nitrated cubanes. Such cubanes are predicted to be powerful, shock-insensitive, high-density explosives.[15] Until now the most highly nitrated cubane known was **1**, obtained from the corresponding tetraacid by oxidation of the derived amine, an approach not applicable to cubanes with vicinal nitro groups.[9, 10]

As best we can determine, there are no firm examples of successful direct nitration of localized (non-resonance-stabilized) organometallic compounds of alkali metals reported.[16, 17] In line with this, we were quite unsuccessful in nitrating salts of **1** with NO_2BF_4, acetyl nitrate, tetranitromethane, amyl nitrate, or similar reagents.[18] However, condensation of excess N_2O_4 into a frozen solution of anion **2** in THF at $-196\,^\circ$C followed by warming produced a 60:40 mixture of 1,2,3,5,7-pentanitrocubane (**7**) and **1**. This strongly suggests that N_2O_4 effects oxidation of **2** to the radical, which then either abstracts a hydrogen atom from the solvent (THF) giving **1** or reacts with N_2O_4 to give **7** (Scheme 1).

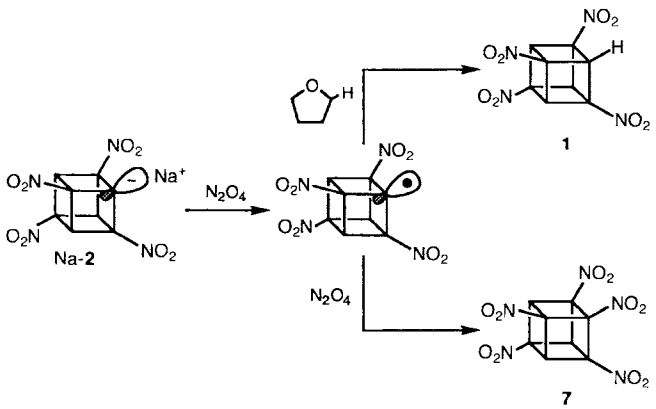

Scheme 1. Reaction of N_2O_4 with Na-**2**.

Pentanitrocubane **7**, the first cubane containing vicinal nitro groups, is colorless and highly crystalline (^{1}H NMR ([D$_6$]acetone): $\delta = 6.43$ (s); ^{13}C NMR: $\delta = 66.5$ ($C_{4,6,8}$-H), 72.8 (C_7-NO_2), 78.8 ($C_{1,3,5}$-NO), 93.0 (C_2-NO_2)). Differential scanning calorimetry (20 °C min^{-1}) indicated a stability similar to earlier polynitrocubanes,[9] decomposition setting in above 250 °C.

The detailed structure of **7** was obtained by single-crystal X-ray analysis.[19] Comparison to that of tetranitrocubane **1**[9] showed that the fifth nitro group in **7**, even though surrounded by three others, causes no significant disturbance in molecular geometry—bond angles and lengths are essentially unperturbed. Molecules of **7** close-pack in the crystal; each oxygen has nine non-bonded O···O contacts shorter than 3.0 Å of which four are between 2.75 and 2.92 Å. This close packing leads to a density of 1.96 gcm^{-3} at 21 °C, a value exceeded by few other CHNO compounds.

Our methodology for nitration of **1** by ortho-metalation can be extended to nitration of pentanitrocubane **7** via its salt Na-**8**. Thus, formation of anion **8** from **7** with sodium bis(trimethylsilyl)amide followed by nitration with N_2O_4 gave a 30:70 mixture of 1,2,3,4,5,7-hexanitrocubane (**9**) and pentanitrocubane **7**, presumably via a radical intermediate (cf. Scheme 1).

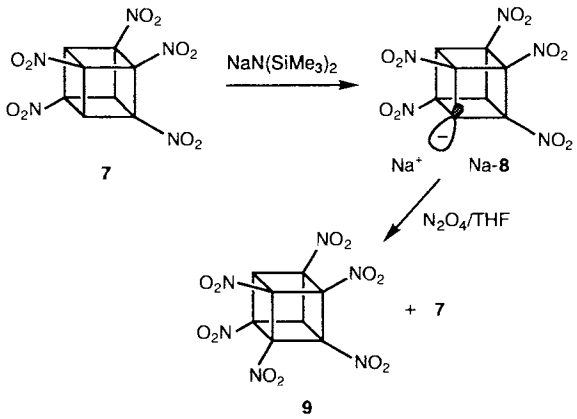

The separation of these two polynitrocubanes is very difficult. Nonetheless, we obtained enough of **9** to identify it unambiguously: ^{1}H NMR ([D$_6$]acetone): $\delta = 6.73$ (s); ^{13}C NMR: $\delta = 65.0$ ($C_{6,8}$-H), 78.9 ($C_{1,7}$-NO_2), 83.1 ($C_{3,5}$-NO_2), 91.0 ($C_{2,4}$-NO_2). The assignment was confirmed fully by X-ray analysis of the crystalline bis-acetonitrile solvate of **9**.[20]

Received: October 12, 1995
Revised version: January 25, 1996 [Z 8469/8470 IE]
German version: *Angew. Chem.* **1996**, *108*, 938–940

Keywords: carbanions · cubanes · *ortho*-metalation · nitro compounds

[1] C. Gardner, E. C. Lupton, *J. Am. Chem. Soc.* **1968**, *90*, 4328.
[2] R. W. Taft, I. S. Lewis, *J. Am. Chem. Soc.* **1958**, *80*, 2436.
[3] R. G. Pearson, R. L. Dillon, *J. Am. Chem. Soc.* **1953**, *75*, 2439.
[4] H. L. Finkleiner, M. Stiles, *J. Am. Chem. Soc.* **1963**, *85*, 616.
[5] R. Dixon, A. Streitwieser, P. G. Williams, P. E. Eaton, *J. Am. Chem. Soc.* **1991**, *113*, 357.
[6] Review: P. E. Eaton, *Angew. Chem.* **1992**, *104*, 1447; *Angew. Chem. Int. Ed. Engl.* **1992**, *31*, 1421.
[7] N. Ono in *Nitro Compounds. Recent Advances in Synthesis and Chemistry* (Eds.: H. Feuer, A. T. Nielsen), VCH Publishers, New York, **1980**, p. 86.
[8] P. E. Eaton, M. Maggini, *J. Am. Chem. Soc.* **1988**, *110*, 7230.
[9] P. E. Eaton, Y. Xiong, R. Gilardi, *J. Am. Chem. Soc.* **1993**, *115*, 10195.
[10] For recent improvements in the synthesis of **1**, see a) A. Bashir-Hashemi, *Angew. Chem.* **1993**, *105*, 585; *Angew. Chem. Int. Ed. Engl.* **1993**, *32*, 612; b) R. L. Hertzler, P. E. Eaton, *Abstr. Pap. Am. Chem. Soc.* **1993**, paper 128.
[11] R. R. Fraser, T. S. Mansour, S. Savard, *J. Org. Chem.* **1985**, *50*, 3232.
[12] R. R. Fraser, T. S. Mansour, S. Savard, *Can. J. Chem.* **1985**, *63*, 3505.
[13] C. A. Brown, *J. Chem. Soc. Chem. Commun.* **1974**, 680.
[14] Even the anion of 1,3,5-trinitrobenzene has not been obtained by direct proton abstraction. It and other *o*-nitrophenyl anions have been made by lithium-for-bromine exchanges below $-100\,^\circ$C. Such anions have been trapped by carboxylation. For details, see: G. Köbrich, P. Buck, *Chem. Ber.* **1970**, *103*, 1412; P. Buck, G. Köbrich, *ibid.* **1970**, *103*, 1420.

 © VCH Verlagsgesellschaft mbH, D-69451 Weinheim, 1996 0570-0833/96/3508-0865 $ 15.00+.25/0

[15] a) E. E. Gilbert, U.S. Army Research Development and Engineering Center, Picatinny, NJ, private communication, **1979**; b) J. Alster, O. Sandus, R. Genter, N. Slagg, J. P. Ritchie, M. J. S. Dewar, paper at the Working Group Meeting on High-Energy Molecules, **1981**; c) A. P. Marchand, *Tetrahedron* **1988**, *44*, 2377.

[16] J. Thiele, *Ber. Dtsch. Chem. Ges.* **1907**, *33*, 666.

[17] a) H. Feuer in *The Chemistry of Amino, Nitroso and Nitro Compounds and Their Derivatives, Supplement F* (Ed.: S. Patai), Wiley, New York, **1982**, p. 805; b) for an interesting special example, see M. E. Sitzmann, L. A. Kaplan, I. Angers, *J. Org. Chem.* **1977**, *42*, 563.

[18] Similarly, poor results were obtained with nitrosylating reagents.

[19] Crystal data of **7**: monoclinic ($P2_1/c$), $a = 6.637(3)$, $b = 23.275(14)$, $c = 7.860(5)$ Å, $\beta = 113.21(5)^\circ$, $V = 115.8(11)$ Å^3, $Z = 4$, $\rho_{calcd} = 1.959$ g cm^{-3}. The thin-plate crystal was small ($0.01 \times 0.35 \times 0.40$ mm), leading to a somewhat weak set of diffraction intensities, and thus low precision in the numerical results. Of 1542 collected reflections [$\lambda(Cu_{K\alpha}) = 1.54178$ Å, $T = 294(2)$ K, $\theta/2\theta$ scan mode, $2\theta_{max} = 96^\circ$], 1051 were unique, and 684 with $I > 2\sigma(I)$ were used for refinement. Lorentz, polarization, and absorption corrections (integration, $T_{max} = 0.98$, $T_{min} = 0.72$) were applied to data. The structure was solved and refined using SHELX programs (G. M. Sheldrick, SHELXS86 and SHELXL93, University of Göttingen, Germany). Full-matrix least squares on F^2 refinement varied 218 parameters: atom coordinates and anisotropic thermal parameters for all non-H atoms and isotropic thermal parameters for hydrogen atoms. Final $R = 0.0668$, $wR2 = 0.1647$ with final difference Fourier excursions of 0.294 and -0.302 e Å^{-3} [20b].

[20] a) Crystal data of **9** · 2MeCN: monoclinic, $C2/c$, $a = 13.0102(7)$, $b = 7.7242(6)$, $c = 18.0758(12)$ Å, $\beta = 95.404(7)^\circ$, $V = 1808.4(2)$ Å^3, $Z = 4$, $\rho_{calcd} = 1.676$ g cm^{-3}. The asymmetric unit comprises half of **9** and one acetonitrile molecule; a crystallographic twofold axis passes through the centers of the di- and tetra-substituted faces of the cube. Crystal size $0.36 \times 0.6 \times 0.75$ mm. Of 1567 collected reflections ($\lambda(Cu_{K\alpha}) = 1.54178$ Å, $T = 223(2)$ K, $\theta/2\theta$ scan mode, $2\theta_{max} = 115^\circ$), 1241 were unique ($I > 2\sigma(I)$), and were used for refinement. Lorentz, polarization, and absorption corrections (integration, $T_{max} = 0.65$, $T_{min} = 0.47$) were applied to data. The structure was solved and refined as described above. Final $R = 0.0407$, $wR2 = 0.1062$ with final difference Fourier excursions of 0.278 and -0.186 e Å^{-3}. The indicated precision in the numerical results is about four times higher than that for **7**; the appearance of bonding-electron density peaks in the final electron density map indicated above-average diffraction quality. b) Crystallographic data (excluding structure factors) for the structures reported in this paper have been deposited with the Cambridge Crystallographic Data Centre as supplementary publication no. CCDC-179-6. Copies of the data can be obtained free of charge on application to The Director, CCDC, 12 Union Road, Cambridge CB2 1EZ, UK (fax: Int. code +(1223) 336-033; e-mail: teched@chemcrys.cam.ac.uk).

Stable Tin and Lead Derivatives of Nitrocubanes: Their Formation and Use in Multiple Functionalization**

Kirill Lukin, Jianchang Li, Richard Gilardi, and Philip E. Eaton*

The discovery that 1,3,5,7-tetranitrocubane (**1**) is acidic enough to permit preparation of its monosodium salt led us to attempt making polymetallic derivatives with metals forming more covalent bonds.[1]

Trialkyl(amino)stannanes can metalate weak acids such as acetonitrile and cyclopentadiene.[2] The mechanism of such metalations is not known, but we suspect it is not simple. Nonetheless, as the p*K*a of cyclopentadiene is not unlike that of methanol, and we already knew that methoxide in [D_1]methanol was basic enough to effect D-for-H exchange on **1**, it seemed possible that an aminostannane could metalate **1**. Indeed, reaction of **1** with excess (diethylamino)trimethylstannane[3] proved to be very smooth and easily followed by ^{1}H NMR ([D_8]THF, 20 °C). After 15 min, more than 50% of **1** was converted into the monotin derivative ($\delta = 5.94$ (s)). Another singlet ($\delta = 5.99$) corresponding to the ditin compound grew to its maximum (60% yield) in about 1.5 hours. A further singlet ($\delta = 6.05$) for the tritin derivative rose to a maximum (70% yield) after 7.5 h. After 48 hours all signals from cubane hydrogen atoms were gone, and the formation of the tetratin compound **2** was complete. On a preparative scale (0.1 mmol), reaction of **1** with seven equivalents of the base in THF at room temperature for 24 hours resulted in 80% yield of 1,3,5,7-tetranitro-2,4,6,8-tetrakis(trimethylstannyl)cubane (**2**), a stable, white solid, easily purified by column chromatography.[4]

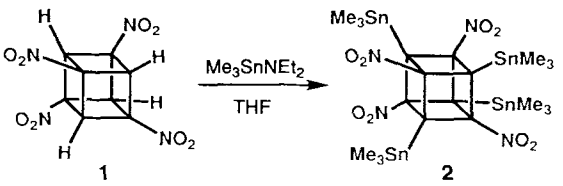

Single-crystal X-ray structural analysis of **2** (Fig. 1) confirmed the assigned structure and revealed disorder amongst the nitro groups.[5] This is noteworthy, as commonly the intermolecular electrostatic interactions amongst highly polar nitro groups of nitro compounds, including other nitrocubanes,[6] result in a high degree of ordering. Apparently the bulky trimethylstannyl groups of **2** serve as 'umbrellas,' distancing the nitro groups of adjacent molecules and thus reducing their interactions. The closest intermolecular approaches of oxygen atoms in **2** are greater than 5.5 Å, whereas in tetranitrocubane **1** each of the four nitro groups is less than 3.0 Å from a nitro group atom on a neighboring molecule in the crystal.

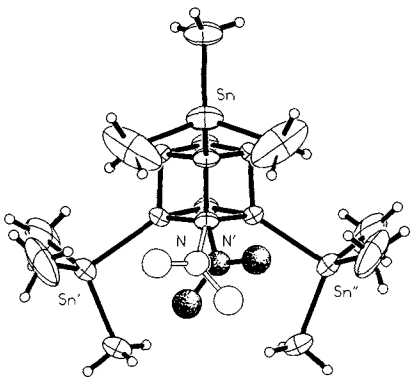

Fig. 1. The molecular structure of crystalline **2**. Anisotropic thermal ellipsoid envelopes are shown at the 25% population density level. For clarity, only one nitro group and the three closest stannyl groups are shown. The observed disorder (55:45) of the nitro groups is illustrated by the shaded (primed) and unshaded constituent atoms.

The general order for the rate of cleavage of carbon–tin bonds with electrophiles is ethynyl > phenyl > vinyl > methyl > butyl and thus correlates apparently with the acidity of the

[*] Prof. P. E. Eaton, Dr. K. Lukin
Department of Chemistry, The University of Chicago
5735 S. Ellis Avenue, Chicago, IL 60637 (USA)
Dr. J. Li
Geo-Centers Inc.
762 Route 15 South, Lake Hopatcong, NJ 07849 (USA)
Dr. R. Gilardi
Laboratory for the Structure of Matter
The Naval Research Laboratory Washington, D.C. 20375 (USA)

[**] We are grateful to our colleague Prof. Larry Sita for a stimulating conversation about tin amides. We thank Dr. Eric Punzalan for samples of **1**. This work was supported by The U.S. Army Research, Development and Engineering Center (Geo-Centers) and by the Office of Naval Research.

corresponding hydrocarbons.[7] Considering the increased acidity of tetranitrocubane, we quite expected that the cubyl–tin bond in compound **2** would be cleaved first by electrophiles. This is not the case. Reactions of **2** with various electrophiles (e.g. Br_2, $Hg(OAc)_2$, NO_2BF_4) under mild conditions resulted only in cleavage of methyl–tin bonds, leaving the cubyl–tin bonds intact.[8] Attempts to achieve complete cleavage of all carbon–tin bonds in **2** under forcing conditions were unsuccessful. Heating with liquid bromine (5 hours, 50 °C) only resulted in the cleavage of more tin–methyl bonds. We conclude that the tetranitrocubyl group resembles highly electron-deficient groups such as trifluoromethyl and pentachlorophenyl, whose bonds to tin are resistant to electrophiles.[9, 10]

As much of the chemistry of organolead compounds is different from that of other elements of Group IV-A,[11] we examined cubylplumbanes. [Bis(trimethylsilyl)amino]triethylplumbane[12] metalates tetranitrocubane **1** easily. Experiments monitored by NMR spectroscopy showed that the first metalation was much faster than that with the aminostannanes and was complete under comparable conditions after 1 minute at room temperature. Each subsequent metalation was slower, making possible selective synthesis and isolation of **3**–**6**, the four possible lead derivatives of **1**: the yield of the isolated monolead compound **3** was 40%, the dilead compound **4** 65%, the trilead compound **5** 80%, and the tetralead compound **6** 60%.[13] All are white, air-stable solids, somewhat sensitive to light.

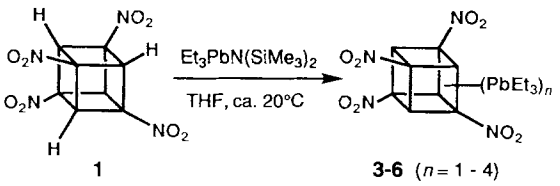

1 **3-6** (n = 1 - 4)

The reaction of the tetralead compound **6** with bromine was followed by ^{1}H NMR spectroscopy. In the beginning the order of cleavage of carbon–lead bonds was like that observed for the carbon–tin bonds in tetranitrocubylstannanes: one ethyl group was cleaved from each lead atom with formation of bromoethane. However, unlike the tin case, the cleavage by bromine continued readily, resulting ultimately in precipitation of lead bromide and formation of 2,4,6,8-tetrabromo-1,3,5,7-tetranitrocubane (**7**), isolated in 65% yield from a preparation on a 20 mmol scale.[14] The structure was confirmed by single-crystal X-ray diffraction analysis.[5, 6] Iodination of **6**, although slower than bromination, produced the corresponding tetraiodotetranitrocubane **8**, isolated in 50% yield.[15]

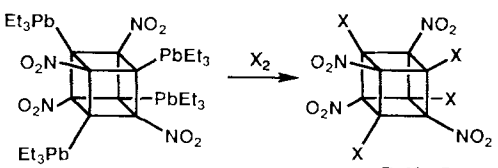

6 **7**; X = Br **8**; X = I

Although nitrodemetalation is a highly desirable reaction for organic synthesis, only a few specialized examples are known,[16] and none proved applicable to conversion of tetranitrocubyl tin or lead derivatives to more highly nitrated cubanes. Nitroso-demetalation has been applied somewhat more generally,[17] but never successfully to the cleavage of all four carbon–lead bonds in a tetraalkylplumbane.[18] Nonetheless, reaction of monolead derivative **3** of tetranitrocubane in dichloromethane at −15 °C with N_2O_4 gave lead nitrate cleanly (75% yield of isolated product; identification by IR spectroscopy). The two new organic products each had one singlet (δ = 6.32 and 6.41) in the ^{1}H NMR spectrum. Although their instability precluded identification, we suggest that they are the geometric isomers of the dimers of nitrosotetranitrocubane (**9**, unseen) and in equilibrium with it. Ozonolysis of the mixture in acetone/dichloromethane (1/5) produced pentanitrocubane **10** (higher than 90% yield by NMR spectroscopy, 70% after isolation), identical to that obtained from nitration of the sodium salt of tetranitrocubane.[1]

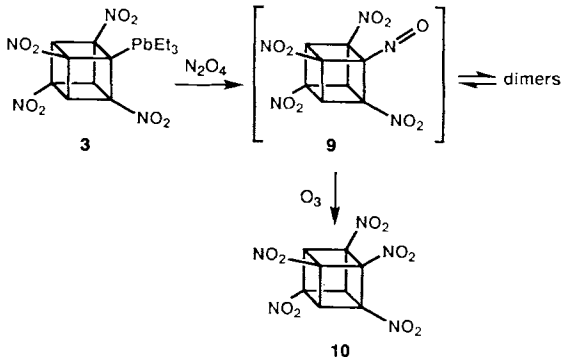

3 **9** **10**

Under the same conditions reaction of dilead compound **4** with N_2O_4 followed by ozonolysis gave a 40% yield of an isolated mixture of pentanitrocubane **10**[19] with hexanitrocubane **11** (40:60). The latter was separated by careful crystallization from 95/5 chloroform/acetonitrile and identified by comparison to an authentic sample.[1]

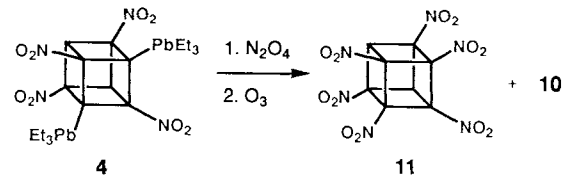

4 **11**

We have so far been unsuccessful in obtaining yet more highly nitrated cubanes from more highly metalated precursors, but our efforts continue, and we expect ultimate success.

Received: October 12, 1995 [Z 8471IE]
German version: *Angew. Chem.* **1996**, *108*, 940–942

Keywords: cubanes · lead compounds · *ortho*-metalation · nitro compounds · tin compounds

[1] K. Lukin, J. Li, R. Gilardi, P. E. Eaton, *Angew. Chem.* **1996**, *108*, 938; *Angew. Chem. Int. Ed. Engl.* **1996**, *35*, 864.
[2] Review: M. F. Lappert, P. P. Power, A. R. Sanger, R. C. Srivastava, *Metal and Metalloid Amides*. Ellis Horwood, Chichester, **1980**, p. 847.
[3] K. Jones, M. F. Lappert, *J. Chem. Soc.* **1965**, 1944.
[4] **2**: ^{1}H NMR (CD_2Cl_2): δ = 0.27; ^{13}C NMR (CD_2Cl_2): δ = −9.0, 75.6, 76.7.
[5] a) Crystal data of **2**: tetragonal ($I\bar{4}$), $a = b = 11.5163$ (3), $c = 12.9457$ (8) Å, $V = 1716.9$ (2) Å^3, $Z = 2$, $\rho_{calcd} = 1.809$ g cm^{-3}. Due to fourfold molecular symmetry, the asymmetric unit comprises just a quarter of **2**. Crystal size: 0.20 × 0.30 × 0.36 mm. Of 2293 reflections collected [$\lambda(Cu_{K\alpha}) = 1.54178$ Å, $T = 294$ (2) K, $\theta/2\theta$ scan mode, $2\theta_{max} = 75°$], 2096 were unique, and 2095 with $I > \sigma(I)$ were used for refinement. Lorentz, polarization, and absorption corrections (integration, $T_{max} = 0.61$, $T_{min} = 0.47$) were applied to data. The structure was solved and refined using SHELX programs [G. M. Sheldrick,

SHELXS 86 and SHELXS 93, University of Göttingen, Germany]. Full-matrix least squares refinement on F^2 varied 85 parameters: atom coordinates and anisotropic thermal parameters for all non-H atoms and isotropic thermal parameters for hydrogen atoms. Final $R = 0.0513$, $wR2 = 0.1271$ with final difference Fourier excursions of 0.749 and -0.629 e Å^{-3}. b) Crystallographic data (excluding structure factors) for the structure reported in this paper have been deposited with the Cambridge Crystallographic Data Centre as supplementary publication no. CCDC-179-8. Copies of the data can be obtained free of charge on application to The Director, CCDC, 12 Union Road, GB-Cambridge CB2 1EZ (fax: Int. code +(12 23/3 36-0 33; e-mail: teched@chemcrys.cam.ac.uk).

[6] P. E. Eaton, Y. Xiong, R. Gilardi, *J. Am. Chem. Soc.* **1993**, *115*, 10195.

[7] For a review, see for example M. Gielen, J. Nasielski in *Organotin Compounds, Vol. 3* (Ed.: A. K. Sawyer), Marcel Dekker, New York, **1972**, p. 625.

[8] The formation of CH_3X and a single cubane-containing product displaying a singlet in ^{1}H NMR spectrum suggested that one methyl group was cleaved from each tin atom in **2**. We did not attempt further characterization of these compounds. Cubyl–tin bonds are cleaved easily by KF in aqueous methanol.

[9] a) D. C. Chambers, H. C. Clark, C. J. Willis, *Can. J. Chem.* **1961**, *39*, 131; b) S. N. Bhattacharya, A. S. Pakdaman, *Indian J. Chem. A* **1989**, *28*, 1888.

[10] Similar reactivity was observed for the mono- und bis(tri-*n*-butylstannyl) derivatives.

[11] Review: P. G. Harrison in *Comprehensive Organometallic Chemistry, Vol. 2* (Ed.: G. Wilkinson), Pergamon Press, Oxford, **1982**, p. 629.

[12] a) W. P. Neumann, K. Kühlein, *Tetrahedron Lett.* **1966**, 3419; b) O. J. Scherer, M. Schmidt, *J. Organomet. Chem.* **1961**, *1*, 49.

[13] **3**: ^{1}H NMR (CD_2Cl_2): $\delta = 1.49$ (t, $J = 8$ Hz, 9H), 1.94 (q, $J = 8$ Hz, 6H), 5.88 (s, 3H); ^{13}C NMR (CD_2Cl_2): $\delta = 13.9$, 18.1, 67.5, 71.2, 73.6, 79.1. – **4**: ^{1}H NMR (CD_2Cl_2): $\delta = 1.49$ (t, $J = 8$ Hz, 18H), 1.90 (q, $J = 8$ Hz, 12H), 5.90 (s, 2H); ^{13}C NMR (CD_2Cl_2): $\delta = 13.9$, 17.6, 68.4, 73.8, 76.3, 81.2. – **5**: ^{1}H NMR (CD_2Cl_2): $\delta = 1.48$ (t, $J = 8$ Hz, 27H), 1.84 (q, $J = 8$ Hz, 18H), 5.91 (s, 1H); ^{13}C NMR (CD_2Cl_2): $\delta = 13.9$, 17.2, 69.5, 76.8, 79.4, 82.8. – **6**: ^{1}H NMR (CD_2Cl_2): $\delta = 1.48$ (t, $J = 8$ Hz, 36H), 1.80 (q, $J = 8$ Hz, 24H); ^{13}C NMR (CD_2Cl_2): $\delta = 13.9$, 16.9, 80.3, 84.3.

[14] **7**: ^{13}C NMR ([D$_6$]acetone): $\delta = 64.6$, 81.6.

[15] **8**: ^{13}C NMR ([D$_6$]acetone): $\delta = 38.4$, 74.6.

[16] a) R. J. Schmitt, J. C. Bottaro, R. Malhotra, C. D. Bedford, *J. Org. Chem.* **1987**, *52*, 2294; b) V. Jager, J.-C. Motte, H. G. Viehe, *Chimia* **1975**, *29*, 516; c) E. J. Corey, H. Estreicher, *Tetrahedron Lett.* **1980**, *21*, 1113; d) G. A. Olah, C. Rochin, *J. Org. Chem.* **1987**, *52*, 702.

[17] a) S. Uemura, A. Toshimitsu, M. Okamo, *J. Chem. Soc. Perkin Trans. 1* **1978**, 1076; b) E. Müller, H. Metzger, *Chem. Ber.* **1956**, *89*, 396; c) P. Tarrant, D. E. O'Connor, *J. Org. Chem.* **1964**, *29*, 2012.

[18] K. C. Williams, D. W. Imhoff, *J. Organomet. Chem.* **1972**, *42*, 107.

[19] Presumably formed by oxidation of the anion to a cubyl radical and H atom abstraction from the solvent (cf. Ref. [1]).

Heterometallic Polymeric Cluster Compounds Derived from Tetrathiotungstate and Silver(I): Syntheses and Crystal Structures of $\{[AgWS_4]\}_n[NH_4]_n$ and $\{[W_4Ag_5S_{16}]\}_n[M(DMF)_8]_n$ (M = Nd and La)**

Qun Huang, Xintao Wu,* Quanming Wang, Tianlu Sheng, and Jiaxi Lu

Polymeric transition metal chalcogenides have attracted a great deal of attention because they have many useful properties that are derived from their low-dimensional structures.[1] Tetrathiometalates MS_4^{2-} (M = Mo, W), which are versatile reactants, have been used extensively for the syntheses of a variety of transition metal sulfides, including some polymeric structures.[2] Since the first polymeric M-Ag-S complex (PPh_4)-$AgMoS_4$ (linear chain) was identified by Müller et al. by resonance Raman spectroscopy in 1985,[3] only one report on such polymeric species has appeared.[4] Recently we obtained several W-Ag-S polymeric cluster complexes from the ammonium tetrathiotungstate/silver nitrate system, for example $\{[AgWS_4]\}_n$-$[H_3NC(CH_2OH)_3 \cdot H_2O]_n$[5] (double chain), which has a novel polymeric cluster anion double-chain structure and a hydrogen-bonded chain cation supermolecular structure; thus Ag^+ and WS_4^{2-} can self-assemble in different ways to form polymeric complexes with different configurations. We report herein on the syntheses and structures of polymeric cluster complexes **1**–**3** (DMF = *N*,*N*-dimethylformamide); in **2** and **3**, neodymium(III) and lanthanum(III) cations, respectively, were encapsulated into the one-dimensional W-Ag-S anion polymer.

$\{[AgWS_4]\}_n[NH_4]_n$ **1**

$\{[W_4Ag_5S_{16}]\}_n[M(DMF)_8]_n$ **2**, M = Nd; **3**, M = La

Lanthanoid complexes have many useful properties and have therefore found a large number applications,[6] for example as catalysts and luminescent materials. Lehn described that in the solid state europium(III) and terbium(III) cryptates can convert light energy extremely efficiently.[7] Encapsulation of such lanthanoid complexes into low-dimensional metal sulfides will possibly lead to materials with interesting properties.

The syntheses were all performed at room temperature in air.[8] Complex **1** was obtained by reacting ammonium tetrathiotungstate, silver nitrate, and D,L-valine (1:1:1) in DMF and H_2O. In contrast, complex **2** was produced by reacting ammonium tetrathiotungstate, silver nitrate, neodymium nitrate, and *p*-nitroaniline (2:4:1:2) in DMF and CH_3CN, and complex **3** was synthesized analogously to complex **2** except that lanthanum nitrate was used instead of neodymium nitrate. These three polymeric complexes were all synthesized by self-assembly, which represents an attractive route to molecular materials with novel solid-state properties.[9] In the synthesis of **1**, the addition of amino acid may prevent the formation of a dark AgS precipitate and support the polymerization of W-Ag-S. The above-mentioned syntheses imply that the valence of cation can influence the structure of W-Ag-S polymers obtained in this reaction system; for example, in the syntheses of **2** and **3**, trivalent cations Nd^{III} and La^{III} induced the formation of $[(W_4Ag_5S_{16})^{3-}]_n$ with trivalent anion cluster fragments as cyclic units. It is also expected that divalent and tetravalent cations can induce the formation of new structures of W-Ag-S polymers.

Complexes **1** and **2** were characterized by X-ray single-crystal analyses;[10, 11] the complexes crystallize in the tetragonal $I\bar{4}$ space group and the triclinic $P\bar{1}$ space group, respectively. The linear-chain structure of the anion of **1** is similar to that found in reference [4]; thus only details of the structure of **2** will be given here. However, it should be noted that the W–Ag bond length (2.928(1) Å) in **1** is much shorter than the values found in other W–Ag–S complexes reported previously (e.g. 2.948(1) Å in $\{[AgWS_4]\}_n[MePyH]_n$[4] (py = pyridine), 2.971(2) Å in $[(PPh_3)_3Ag_2WS_4 \cdot 0.8\,CH_2Cl_2]$,[12] and 2.997(2) Å in $[(PPh_3)_4Ag_4W_2S_8]$[13]); this suggests that Ag → WS_4 electron delocalization and much stronger continuous metal–metal interactions are present in this linear chain.[3] The ORTEP drawing of a section of the anion of **2** is shown in Figure 1. This one-dimensional polymeric anion is oriented along the crystallographic *c* axis, and can be regarded as octanuclear cyclic cluster fragments $[W_4Ag_4S_{16}]^{4-}$ linked through Ag^+ ions. In a $[W_4Ag_4S_{16}]^{4-}$

[*] Prof. X.-T. Wu, Q. Huang, Q.-M. Wang, T.-L. Sheng, J.-X. Lu
State Key Laboratory of Structural Chemistry
Fujian Institute of Research on Structure of Matter
Chinese Academy of Sciences, Fuzhou, Fujian 350002 (China)
Fax: Int. code +(591) 3714946

[**] This research was supported by grants from the State Key Laboratory of Structural Chemistry, Fujian Institute of Research on Structure of Matter, Chinese Academy of Sciences, the National Science Foundations of China and the Provincial Science Foundations of Fujian. DMF = *N*,*N*-dimethylformamide.

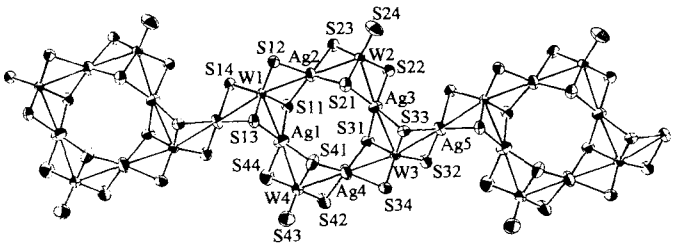

Fig. 1. ORTEP diagram of a section of the crystal structure of the one-dimensional polymeric complex **2** (50% displacement ellipsoids). Selected distances [Å] and angles [°]: W–Ag (av) 2.964(3), W–S_t (av) 2.128(11), W–(μ_2-S) (av) 2.190(9), W–(μ_3-S) (av) 2.248(9), Ag–S (av) 2.542(10); S-W-S (av) 109.4(4), S-Ag-S (av) 109.8(3), W-S-Ag (av) 76.6(3), Ag-S-Ag (av) 104.7(2), W-Ag-W (av) 173.1(1), Ag1-W1-Ag2 88.12(9), Ag1-W1-Ag5a 80.0(1), Ag2-W1-Ag5a 168.0(1), Ag2-W2-Ag3 87.39(9), Ag3-W3-Ag4 86.59(9), Ag3-W3-Ag5 80.53(9), Ag4-W3-Ag5 166.7(2), Ag1-W4-Ag4 88.6(1).

fragment, the W atoms form an approximate square, in which the Ag atoms nearly lie along the edges. The metals (W and Ag) reside in distorted tetrahedral environments; the S-W-S angles range from 106.4(4) to 113.6(5)°, and the S-Ag-S angles from 91.2(4) to 127.7(3)°. Since there are three kinds of sulfur atoms present in the anion, namely, terminal sulfur atoms, μ_2-S atoms, and μ_3-S atoms, the W–S lengths range from 2.123 to 2.268 Å. The mean W–S_t, W–(μ_2-S), and W–(μ_3-S) lengths are 2.128, 2.190, and 2.248 Å, respectively. In comparison, in discrete WS_4^{2-} ions the W–S_t length is 2.177 Å,[2a] whereas in $[WS_4Ag_3(PPh_3)_3\{S_2P(OCH_2CH_3)_2\}]$ the W–S_t, W–(μ_2-S), and W–(μ_3-S) lengths are 2.144(3), 2.217(2), and 2.242(3) Å, respectively.[14] The average W–Ag distance of 2.964 Å in complex **2** is shorter than those in $[(PPh_3)_3Ag_2WS_4 \cdot 0.8\,CH_2Cl_2]$[12] (2.971 Å) and $[WS_4Ag_3(PPh_3)_3\{S_2P(OCH_2CH_3)_2\}]$[14] (3.080 Å), but much longer than that in complex **1** (2.928 Å).

Each Nd^{III} cation in **2** is coordinated by eight DMF molecules; the average Nd–O bond length is 2.43 Å. These simple complex ions $[Nd(DMF)_8]^{3+}$, which function as larger trivalent cations, crystallize with the one-dimensional cluster anions $[(W_4Ag_5S_{16})^{3-}]_n$ from the solution. Figures 2 and 3 show the packing viewed along the *b* and *c* axes, respectively. As shown in Figure 3, the $[Nd(DMF)_8]^{3+}$ ions, which are well separated from each other and from cluster anions, are positioned between the cluster anion chains, and are arranged linearly along these chains. The distance between two neighboring Nd atoms along these chains (i.e. along the crystallographic *c* axis) is 12.608 Å.

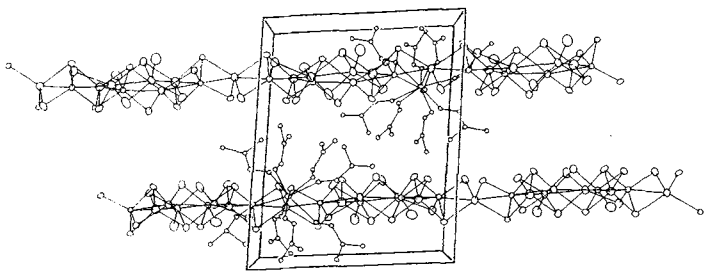

Fig. 2. Packing drawing of **2** viewed along *b* axis.

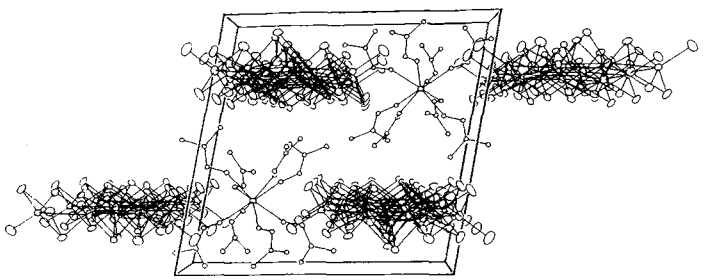

Fig. 3. Packing drawing of **2** viewed along *c* axis.

Experimental Procedure

1: To a solution of $AgNO_3$ (0.17 g, 1 mmol) and D,L-valine (0.12 g, 1 mmol) in H_2O (3 mL) was added a solution of $(NH_4)_2WS_4$ (0.35 g, 1 mmol) in DMF (5 mL). The dark precipitate was filtered off; 0.17 g of orange-red crystals of **1** were obtained by layering the orange-red filtrate with *n*-pentane and methanol.

2: A solution of $AgNO_3$ (0.68 g, 4 mmol), $Nd(NO_3)_3 \cdot 6H_2O$ (0.44 g, 1 mmol), and *p*-nitroaniline (0.28 g, 2 mmol) in CH_3CN (15 mL) was added to a solution of $(NH_4)_2WS_4$ (0.70 g, 2 mmol) in DMF (5 mL). The dark precipitate was filtered off; 0.30 g of red crystals of **2** were obtained by allowing the red filtrate to stand in air for one day.

3: A procedure similar to that for the synthesis of **2** was employed except that $La(NO_3)_3 \cdot 6H_2O$ was used instead of $Nd(NO_3)_3 \cdot 6H_2O$. Allowing the red filtrate to stand in air for one day gave 0.30 g of red crystals of **3**.

All the above complexes gave satisfactory elemental analyses [8].

Received: October 18, 1995 [Z 8484 IE]
German version: *Angew. Chem.* **1996**, *108*, 985–987

Keywords: chalcogenides · clusters · lanthanide compounds · silver compounds · tungsten compounds

[1] a) D. W. Murphy, P. A. Christian, *Science* **1979**, *205*, 651; b) M. S. Whittingham, *Prog. Solid State Chem.* **1978**, *12*, 41; c) R. R. Chianelli, T. A. Pecoraro, T. R. Halbert, H. W. Pan, E. I. Stiefel, *J. Catal.* **1984**, *86*, 226.

[2] a) A. Müller, E. Diemann, R. Jostes, H. Bögge, *Angew. Chem.* **1981**, *93*, 957; *Angew. Chem. Int. Ed. Engl.* **1981**, *20*, 934; b) C. E. Holloway, M. Melnik, *Rev. Inorg. Chem.* **1993**, *13*, 233; c) X.-T. Wu, P.-C. Chen, S.-W. Du, N.-Y. Zhu, J.-X. Lu, *J. Clust. Sci.* **1994**, *5(2)*, 265.

[3] a) A. Müller, W. Jaegermann, W. Hellmann, *J. Mol. Struct.* **1983**, *100*, 559; b) A. Müller, W. Hellmann, *Spectrochim. Acta A* **1985**, *41*, 359.

[4] J.-P. Lang, J.-G. Li, S. Bao, X.-Q. Xin, *Polyhedron* **1993**, *12*, 801.

[5] Q. Huang, X.-T. Wu, T.-L. Sheng, Q.-M. Wang, *Inorg. Chem.* **1995**, *34*, 4931.

[6] a) M. L. Steigerwald, *Chem. Mater.* **1989**, *1*, 52; b) J.-C. G. Bünzli in *Lanthanide Probes in Life* (Eds.: J.-C. G. Bünzli, G. R. Choppin), Elsevier, Amsterdam, **1989**.

[7] J. M. Lehn, *Angew. Chem.* **1990**, *102*, 1347; *Angew. Chem. Int. Ed. Engl.* **1990**, *29*, 1304.

[8] Compound **1** is soluble in DMF, in contrast **2** and **3** are insoluble in common solvents. Elemental analysis for **1**: W 41.36, S 29.06, N 3.38. Calcd.: W 41.97, S 29.28, N 3.20. Elemental analysis for **2**: found: C 11.89, H 2.19, N 4.68. Calcd.: C 11.45, H 2.24, N 4.45. Elemental analyses for **3**: found: C 11.78, H 2.18, N 4.59. Calcd: C 11.48, H 2.25, N 4.46. IR (KBr pellet): $\tilde{\nu}$ [cm^{-1}] = W-(μ_2-S): 439.7 for **1**; 1647.1, 677.0, 495.7, 472.5, 461.0, 455.2, 441.7, 426.2 and 412.7 for **2**; 1647.1, 675.1, 495.7, 472.5, 461.0, 455.2, 441.7, 426.2 and 412.7 for **3**.

[9] S. D. Christin, S. Subramanian, L. K. Thompson, M. J. Zaworotko, *J. Chem. Soc. Chem. Commun.* **1994**, 2563.

[10] Crystal data for **1**: $WS_4Ag \cdot NH_4$, $M = 438.01$, tetragonal, dimensions: $0.30 \times 0.20 \times 0.10$ mm; space group $I\bar{4}$, $a = 7.994(2)$, $c = 5.855(2)$ Å, $V = 373.9(2)$ Å^3, $Z = 2$, $\rho_{calcd} = 3.89\,g\,cm^{-3}$, $\lambda(Mo_{K\alpha}) = 0.71069$ Å, $\mu(Mo_{K\alpha}) = 19.27\,cm^{-1}$. The intensity data were collected at room temperature on a Rigaku AFC5R diffractometer. 341 absorption-corrected reflections with $I > 3.0\sigma(I)$ of the 367 unique reflections were used to solve the structure by using the MolEN program [15]. Atoms were all refined anisotropically. The structure and that of its enantiomorph were refined with full-matrix least-squares; the absolute configuration was assigned to the form with the better of two sets of agreement factors (R, R', and GOF). No attempt was made to locate hydrogen atoms. The final cycle of full-matrix least-squares refinement was converged with $R = \sum(|F_o| - |F_c|)/\sum|F_o| = 0.045$ and $R' = [\sum w(|F_o| - |F_c|)^2/\sum w|F_o|^2]^{1/2} = 0.055$ [16].

[11] Crystal data for **2**: $W_4Ag_5S_{16} \cdot C_{24}H_{56}N_8O_8Nd$, $M = 2516.78$, triclinic, dimensions: $0.35 \times 0.20 \times 0.17$ mm; space group $P\bar{1}$, $a = 16.104(9)$, $b = 16.328(4)$, $c = 12.608(2)$ Å, $\alpha = 94.23(2)$, $\beta = 94.47(3)$, $\gamma = 100.19(3)°$, $V = 3240(2)$ Å^3, $Z = 2$, $\rho_{calcd} = 2.58\,g\,cm^{-3}$, $\lambda(Mo_{K\alpha}) = 0.71069$ Å, $\mu(Mo_{K\alpha}) = 100.1\,cm^{-1}$. The intensity data were collected at room temperature on a Rigaku AFC5R diffractometer. 4106 absorption-corrected reflections with $I > 3.0\sigma(I)$ of the 11396 unique reflections were used to solve the structure by using the MolEN program [15]. Metal and sulfur atoms were refined an-

isotropically. No attempt was made to locate hydrogen atoms. The final cycle of full-matrix least-squares refinement was converged with $R = \sum(|F_o| - |F_c|)/\sum|F_o| = 0.056$ and $R' = [\sum w(|F_o| - |F_c|)^2/\sum w|F_o|^2]^{1/2} = 0.063$. The first five residual peaks in the final difference F-map are ghosts of heavy atoms [16].

[12] A. Müller, H. Bögge, E. Koniger-Ahlborn, *Z. Naturforsch. B* **1979**, *34*, 1698.

[13] A. Müller, H. Bögge, E. Koniger-Ahlborn, *J. Chem. Soc. Chem. Commun.* **1978**, 739.

[14] S.-W. Du, N.-Y. Zhu, P.-C. Chen, X.-T. Wu, *J. Mol. Struct.* **1993**, *291*, 167.

[15] MolEN, An Interactive Structure Solution Procedure, Enraf-Nonius, Delft, The Netherlands (1990).

[16] Further details of the crystal structure investigations may be obtained from the Fachinformationszentrum Karlsruhe, D-76344 Eggenstein-Leopoldshafen (Germany), on quoting the depository number CSD-59267.

The First C_2-Symmetric, Chiral Monomethine Dye—An Apparent Violation of the Helicity Rule for Optical Rotation**

Lutz Eggers, Volker Buss,* and Gerald Henkel

Dedicated to Professor Fritz P. Schäfer on the occasion of his 65th birthday

Steric interactions prevent the chromophore in the monomethine cyanine **1**[1] from attaining the planar geometry preferred by conjugated π systems: the X-ray structure of the tetrafluoroborate salt of **1**[2] reveals a twisted *cis,cis* conformation with an angle of 43° between the two indolenine end groups. In solution the two oppositely twisted forms equilibrate rapidly: the barrier to interconversion, determined by dynamic ^{1}H NMR spectroscopy,[3] is 50.0 kJ mol^{-1}.

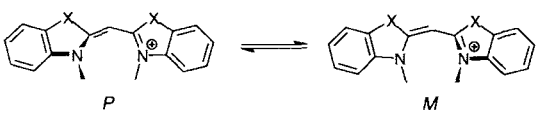

X = $C(CH_3)_2$ **1**
X = $C(CH_3)C_3H_7$ **2**

In an achiral environment, the two interconverting conformations are enantiomers and cannot be distinguished. Chiral interaction, for example the introduction of a chiral group into the molecule, should remove the degeneracy, converting the oppositely twisted enantiomers into diastereomers, and render them susceptible to chiroptical methods. To this end, we have synthesized the chirally substituted symmetrical monomethine cyanines (*R,R*)-**2** and (*S,S*)-**2** and determined the absolute configuration by X-ray analysis. The observed Cotton effects apparently contradict established rules for optical rotation.

The key intermediates in the synthesis of **2** are the chiral 2-methylene indolines **3**, which were obtained by dimethylation of 2-methyl-3-propylindole[4] and subsequent resolution of the enantiomers with di-*O*-benzoyltartaric acid, a method recently described by Reichardt et al.[5] Reaction with their respective hydroximinium salts **4**[1, 6] yielded both enantiomers of **2**, which after recrystallization from ethanol/diethyl ether proved to be diastereomerically pure[7] (Scheme 1).

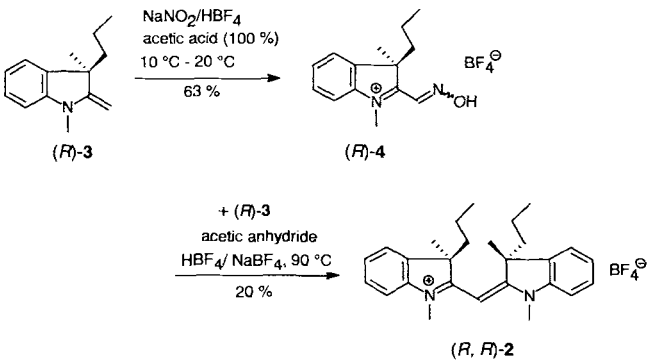

Scheme 1. Syntheses of the monomethine (*R,R*)-**2**.

The structure of what turned out to be (*R,R*)-**2** was determined by single-crystal X-ray analysis of the perchlorate (Fig. 1).[8] In the crystal the molecule adopts a twisted *cis,cis* configuration along the conjugated chain of five atoms from N(1) to N(1′). The overall structure is thus very similar to the one reported for **1**.[2]

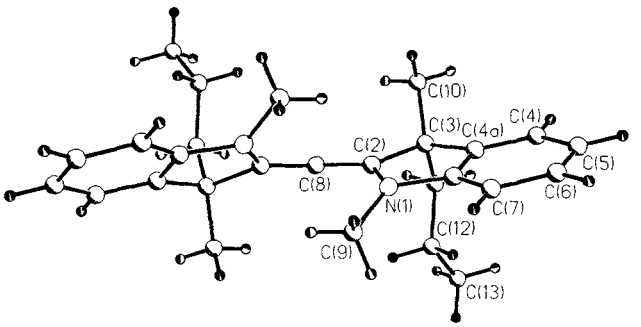

Fig. 1. Crystal structure of (*R,R*)-**2** as perchlorate. Selected bond lengths [pm]: N(1)–C(2) 138.9, C(2)–C(8) 139.0, N(1)–C(7a) 142.7, C(2)–C(3) 152.9. Selected dihedral angles [°]: C(2)-C(8)-C(2′) 129.07, C(2)-C(3)-C(4a) 101.5.

The dihedral angle between the essentially planar indolenine groups and the central plane formed by carbon atoms C(2)-C(8)-C(2′) is 26.8° compared to 21° and 27° in **1**. The out-of-plane deformation of the chromophore is caused by the two *N*-methyl groups that are bent away from each other but still have a nearest H–H distance of only 275.6 pm.

The absolute configuration of the two chiral centers C(3) and C(3′) is identical, which means that the integrity of the chiral center of **3** was conserved throughout the conversion into **2**. There is, of course, another element of chirality present in **2**, namely, the twist of the two indoline rings against each other. The sense of twist in (*R,R*)-**2** is positive: looking along the axis C(2)–C(2′), the front group has to be turned clockwise to eclipse the bonds N(1)–C(2) and N(1′)–C(2′). Consequently a *P*-helical[9] conformation is assigned to this enantiomer in the solid state. In (*S,S*)-**2**, this rotation has to be anticlockwise, so the conformation is *M*.

The UV/Vis spectra of (*R,R*)- and (*S,S*)-**2** are identical, as expected. Position (438 nm) and intensity ($\lg \varepsilon = 4.57$) of the cyanine band resemble that of **1** and other monomethine cyanines.[10] The CD spectra of (*R,R*)- and (*S,S*)-**2** (Fig. 2) exhibit

[*] Prof. PhD V. Buss, Dr. L. Eggers
Fachgebiet Theoretische Chemie der Universität
Lotharstrasse 1, D-47048 Duisburg (Germany)
Fax: Int. code +(203) 379-2772
e-mail: theobuss@uni-duisburg.de

Prof. Dr. G. Henkel
Fachgebiet Festkörperchemie der Universität Duisburg

[**] This work was supported by the Deutsche Forschungsgemeinschaft. For the opportunity to use NMR facilities, we thank Prof. Dr. W. Grahn, Braunschweig.

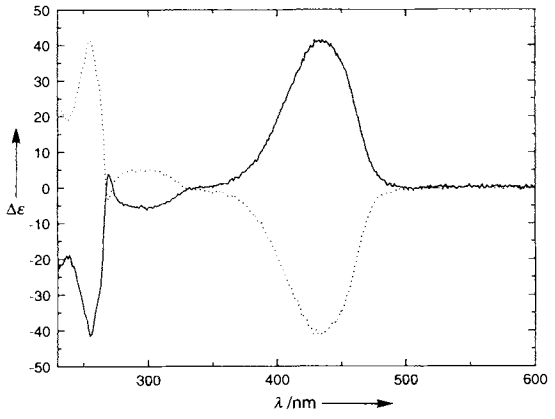

Fig. 2. CD spectra of (*R,R*)-**2** ($c = 4.425 \times 10^{-5}$ mol L^{-1} (····)) and (*S,S*)-**2** ($c = 3.94 \times 10^{-5}$ mol L^{-1} (——)) in ethanol/methanol 4/1 at 23 °C.

perfect mirror symmetry showing that the optical purity of the enantiomers, which were synthesized essentially independently of each other, is very high. The most prominent CD absorption occurs in the region of the cyanine band, where its maximum coincides exactly with the maximum of the UV/Vis band. Another CD absorption around 250 nm is probably due to excitations of the indolenine end groups coupled through the cyanine chromophore.

In solutions of **1**, rapid interconversion (on the NMR time scale[3]) of the enantiomers leads to a racemic mixture of the *P*- and *M*-helical conformation. Likewise, a fast equilibrium between the *M* and *P* form is established in **2**, which for this mixture of diastereomers can, however, never be 1:1. Lower temperatures should shift the equilibrium towards the more stable diastereomer, an effect that should be observable in the CD spectra.

The temperature-dependence of the CD spectra of (*R,R*)-**2** (Fig. 3) shows that this assumption is correct. Lowering the

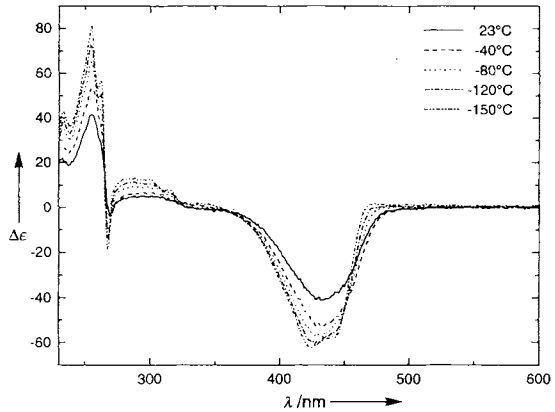

Fig. 3. Temperature-dependent CD spectra of (*R,R*)-**2** in ethanol/methanol 4/1; $c = 4.425 \times 10^{-5}$ mol L^{-1}; temperatures from 23 °C to −150 °C.

temperature to −150 °C increases the amplitudes of all bands by about one half. Analysis of the data in terms of an equilibrium between the *P* and *M* diastereomers[11] fails to converge with meaningful results. Additional data, preferably at elevated temperatures, would probably improve the analysis. However, if as an additional restraint, the two components are assumed to have comparable, but opposite strengths, the model yields a free energy difference of 4 kJ mol^{-1}, but with a correlation coefficient of only 0.85. Whatever the exact numbers, the only plausible interpretation of the spectra is a shift of the equilibrium at low temperature towards the diastereomer with negative rotatory strength at the long-wavelength cyanine band. It is probable, but by no means imperative, that this more stable conformation also corresponds to the structure found in the X-ray analysis for (*R,R*)-**2**, which means that it has a *P*-helically twisted chromophore.

With their delocalized π-electrons constrained to move on a helical path, twisted cyanine dyes are paradigmatic of inherently chiral, open chain π systems, just as the helicenes are for aromatic compounds.[12] For inherently chiral chromophores the sign of the Cotton effect is determined by the screw sense of the transition charge density[13]—which is definitely positive in the case of (*R,R*)-**2**. Does the observed negative rotatory strength for a cyanine with *P*-helical twist violate this rule?

CNDO/S calculations for the chromophore (N(1) to N(1')) of (*R,R*)-**2** with coordinates taken from the X-ray structure show that this is not the case. The calculated rotational strength is -174×10^{-40} cgs units, the experimental value from the integrated area under the CD band at −150 °C is -188×10^{-40} cgs units, a more than satisfactory agreement. The apparent discrepancy with what one would expect on the basis of helical charge movement is resolved by a component analysis. The calculated rotatory strength *R* is the sum of two contributions, $R_\parallel$ corresponding to the component parallel to the helix axis (Fig. 4) and $R_\perp$ to the component perpendicular to this axis

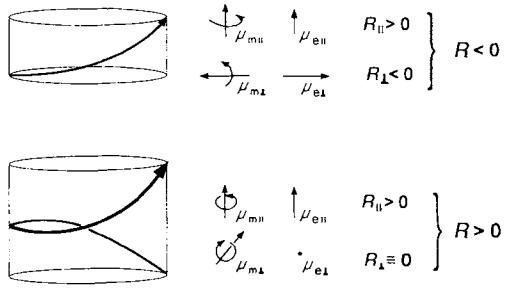

Fig. 4. Rotational strength of electronic charge movement with *P*-helical screw sense and its dependence on helix length. The magnetic moments μ_m are obtained from the charge rotation and the right-hand-rule, the electric moments μ_e from the charge translation. The rotatory strength *R* (that is, the scalar product of these vectors) is positive when the vectors point in the same direction and negative when they point in opposite directions. Top: The positive parallel component of *R* is more than cancelled by the negative contribution of the perpendicular component, leading to an overall negative *R* and negative Cotton effect. Bottom: helix with one complete turn. The perpendicular component is approximately zero because of the (approximately) vanishing perpendicular electric transition moment, leading to a positive *R* and positive Cotton effect.

(which is not the C_2 symmetry axis!). These components are obtained, respectively, as the products of the parallel and perpendicular components of the electric and magnetic transition moments. The calculated values are +3 for $R_\parallel$ and -177×10^{-40} cgs units for $R_\perp$. Because of the much larger contribution of the perpendicular component, the total rotatory strength is negative.[14]

It is evident that the sign and magnitude of the rotatory strength are strongly dependent on the particular structural parameters of the helix. Increasing the twist of the chromophore, which corresponds to a greater turn on the helical path, will lead to a larger parallel component of the electric moment and thus to an increase of the positive contribution to *R*. Likewise, increasing the length of the twisted chromophore will result in a smaller perpendicular component of the electric

transition moment and a decrease of the negative contribution to R. Figure 4 illustrates what happens after one turn of the helix is complete. Because of the very small perpendicular electric transition moment the rotatory strength is now derived exclusively from the parallel component of R, which for a P helix is, of course, positive.

We conclude that the negative rotatory strength of the P-helical cyanine dye (R,R)-**2** is not a violation, but rather a confirmation of the rules that connect the screw sense of helical charge movement with the sign of the observed Cotton effect.

Received: September 18, 1995
Revised version: November 22, 1995 [Z 8408 IE]
German version: *Angew. Chem.* **1996**, *108*, 973–975

Keywords: chirality · circular dichroism · dyes · helices · monomethines

[1] R. Kuhn, A. Winterstein, G. Balser, *Ber. Dtsch. Chem. Ges.* **1930**, *63*, 3176–3184.
[2] R. Allmann, T. Debaerdemaeker, *Cryst. Struct. Commun.* **1976**, *5*, 211–214.
[3] W. Grahn, H.-H. Johannes, J. Rheinheimer, B. Knieriem, E. U. Würthwein, *Liebigs Ann.* **1995**, 1003–1009.
[4] M. P. Prochazka, L. Eklund, R. Carlson, *Acta Chem. Scand.* **1990**, *44*, 610–613.
[5] C. Reichardt, U. Budnik, K. Harms, G. Schäfer, J. Stein, *Liebigs Ann.* **1995**, 329–340.
[6] W. Grahn, *Liebigs Ann. Chem.* **1981**, 107–121.
[7] Based on the sufficient chemical shift difference between the (equivalent) 3- and 3′-methyl protons in (S,S)- and (R,R)-**2** and the (enantiotopic) methyl protons in the meso-product (R,S)-**2**.
[8] X-ray structure determination for (R,R)-**2**: Siemens P4RA four-circle diffractometer, $Mo_{K\alpha}$ radiation ($\lambda = 0.71073$ Å), graphite monochromator, rotating anode, scintillation counter, 150 K, empirical absorption correction, SHELXTL-PLUS programs, direct methods, full-matrix least-squares refinement; $C_{27}H_{35}N_2O_4Cl$, formula weight 487.02, tetragonal, space group $P4_32_12$, $a = 7.998(2)$, $c = 40.070(20)$ Å, $V = 2563.20$ Å^3, $Z = 4$, $\rho = 1.262$ g cm^{-3}, $\mu(Mo_{K\alpha}) = 1.47$ mm^{-1}, transmission range 0.934–0.871; crystal dimensions $0.47 \times 0.18 \times 0.16$ mm, ω scan, $2\theta_{max} = 54°$, 4440 reflections measured ($\pm h, +k, +l$; Flack parameter −0.05(13) for the correct space group), 1740 independent reflections used for final refinement, $R(R_w) = 0.0598$ (0.0573) for 1302 observed reflections ($I > 2\sigma(I)$), 183 variables, all non-hydrogen atoms anisotropic, H atoms at idealized positions (one common isotropic temperature factor), one scaling parameter, one isotropic extinction parameter. Further details of the Crystallographic data (excluding structure factors) for the structure reported in this paper have been deposited with the Cambridge Crystallographic Data Centre as supplementary publication no. CCDC-179-6. Copies of the data can be obtained free of charge on application to The Director, CCDC, 12 Union Road, Cambridge CB2 1EZ, UK (fax: Int. code +(1223) 336-033; e-mail: teched@chemcrys.cam.ac.uk).
[9] V. Prelog, G. Helmchen, *Angew. Chem.* **1982**, *94*, 614–631; *Angew. Chem. Int. Ed. Engl.* **1982**, *21*, 567–583.
[10] J. Fabian, H. Hartmann, *Light Absorption of Organic Colorants*, Springer, Berlin, **1980**, p. 172ff.
[11] a) W. W. Wood, W. Fickett, J. G. Kirkwood, *J. Chem. Phys.* **1952**, *20*, 561–568; b) A. Moscowitz, K. M. Wellman, C. Djerassi, *J. Am. Chem. Soc.* **1963**, *85*, 3515–3516.
[12] V. Buss, K. Kolster, *Chem. Phys.*, in press.
[13] a) O. E. Weigang in *Fundamental Aspects and Recent Developments in ORD and CD* (Eds.: F. Ciardelli, P. Salvadori), Heyden, London, **1973**, p. 61ff.; b) E. Charney, *The Molecular Basis of Optical Activity*, Wiley, New York, **1979**, p. 223ff.; c) for the optical rotation of a free electron constrained to move on a helix, see I. Tinoco, Jr., R. W. Woody, *J. Chem. Phys.* **1964**, *40*, 160–165.
[14] Positive and negative components also contribute to the twisted *cis*-diene chirality, as discussed by the late G. Snatzke in *Chirality—From Weak Bosones to the α-Helix* (Ed.: R. Janoschek), Springer, Berlin, **1992**, p. 59ff.

Formation of a Novel μ-Nonasulfido Ligand and Its Degradation into a μ-Disulfido Ligand at a Diiridium Center**

Masayuki Nishio, Hiroyuki Matsuzaka, Yasushi Mizobe, and Masanobu Hidai*

The reactivity of complexes containing two or more metals in close proximity is now attracting significant attention, since activation and reactions of substrates at the multimetallic center in these complexes may lead to novel reactions that are not possible at the monometallic center. We have recently shown that thiolato-bridged diruthenium complexes can undergo unique transformations of various substrates such as terminal alkynes and hydrazines.[1] These studies have subsequently been extended to the preparation of the related thiolato-bridged dirhodium and diiridium complexes. Thereby we have found that the Ir^{II} complex **1**[2] (Cp* = η^5-C_5Me_5) reacts with S_8 to give the dinuclear Ir^{III} complex **2** that contains a novel μ-S_9 ligand. Herein we report on the synthesis and characterization of **2** as well as on its reaction with $NaBPh_4$ that leads to the paramagnetic diiridium μ-S_2 complex **3**.

[Cp*Ir(μ-S*i*Pr)$_2$IrCp*] **1**

[Cp*Ir(μ-S*i*Pr)$_2$(μ-S_9)IrCp*] **2**

[Cp*Ir(μ-S*i*Pr)$_2$(μ-S_2)IrCp*][BPh_4] **3**

Treatment of **1** with excess S_8 (S/Ir ≈ 5) in toluene at room temperature gave an orange precipitate of **2**, which was crystallized from $CHCl_3$/hexane and isolated as an orange crystalline solid in 38% yield (Scheme 1). The structure of **2** was deter-

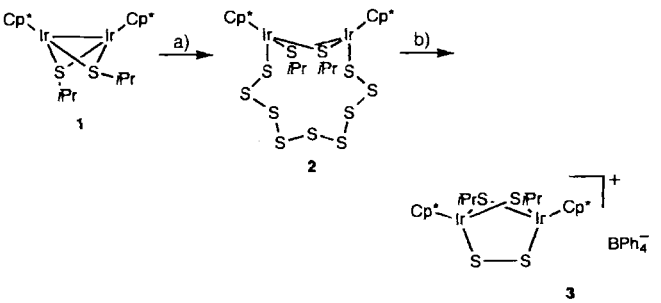

Scheme 1. Reagents and conditions; a) S_8, toluene, room temperature; b) $NaBPh_4$, CH_2Cl_2/THF, room temperature.

mined by X-ray analysis (Fig. 1).[3] The most remarkable feature of **2** is a unique bridging nonasulfido chain, which is bonded at each end to an Ir atom.

Although polysulfido ligands are ubiquitous in various metal complexes,[4] the nonasulfido ligand is, to our knowledge, that with the longest sulfur chain, and the known examples are limited to the monometallic complexes $[MS_9]^-$ (M = Ag,[5] Au[6]). The present reaction differs significantly from that of the related Ru complexes [Cp*Ru(μ-SR)$_2$RuCp*] with S_8, in which

[*] Prof. M. Hidai, M. Nishio, Dr. H. Matsuzaka, Dr. Y. Mizobe
Department of Chemistry and Biotechnology
Graduate School of Engineering, The University of Tokyo
Hongo, Tokyo 113 (Japan)
Fax: Int. code +(3) 5800-6945

[**] This work was supported by the Ministry of Education, Science and Culture of Japan. M. N. acknowledges the JSPS Research Fellowships for Young Scientists.

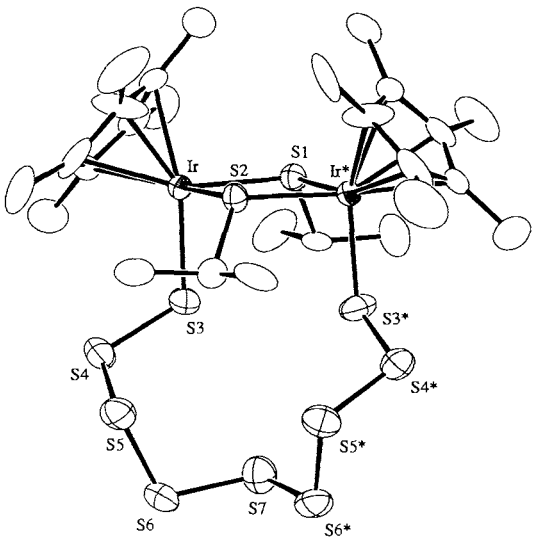

Fig. 1. Crystal structure of **2**. Selected bond lengths [Å], angles [°], and torsion angles [ ]: Ir···Ir* 3.702(1), Ir-S(1) 2.393(4), Ir-S(2) 2.366(4), Ir-S(3) 2.360(4), S(3)-S(4) 2.048(7); S(4)-S(5) 2.062(7), S(5)-S(6) 2.051(6), S(6)-S(7) 2.048(7), Ir-S(3)-S(4) 114.3(2), S(3)-S(4)-S(5) 108.5(3), S(4)-S(5)-S(6) 105.5(3), S(5)-S(6)-S(7) 106.4(3), S(6)-S(7)-S(6)* 109.4(5); Ir-S(3)-S(4)-S(5) 107.7(3), S(3)-S(4)-S(5)-S(6) 84.0(3), S(4)-S(5)-S(6)-S(7) 80.5(4), S(5)-S(6)-S(7)-S(6)* 94.2(4).

the μ-S_2 complexes [Cp*Ru(μ-SR)$_2$(μ-S_2)RuCp*] (R = *i*Pr,[7] *t*Bu[8]) are formed exclusively.

The structure of **2** contains a crystallographically imposed mirror plane that bisects the Ir–Ir vector. The interatomic distance between the two Ir atoms (3.702(1) Å) suggests the absence of any direct metal–metal interaction. The $Ir_2S(1)S(2)$ core is almost planar, and the two *i*Pr groups attached to these sulfur atoms adopt a *cis* configuration. The metrical parameters in the μ-S_9 ligand (S–S distances, 2.048(7)–2.062(7) Å; S-S-S angles, 105.5(3)–109.4(5)°) are not unusual and are comparable to those in S_8[9] and $[MS_9]^-$ (M = Ag, Au). The heptasulfido array from S(4) to S(4)* is bent towards the S(2) thiolato ligand; therefore, the two *i*Pr groups are nonequivalent in the solid state.

In accordance with this structure, the ^{1}H NMR spectrum of **2** recorded at −40 °C exhibits two doublets at δ = 0.83 and 1.16 and two septets at δ = 1.87 and 2.20 assignable to the two *i*Pr groups, together with a singlet at δ = 1.54 for the methyl protons in the Cp* ligands. Upon warming the sample to room temperature, the *i*Pr methyl resonances coalesced to one broad singlet, while the Cp* singlet remained essentially unchanged presumably indicating the fluxional nature of the μ-S_9 ligand at the higher temperatures.

Interestingly, treatment of **2** with $NaBPh_4$ (3 equiv) in CH_2Cl_2/THF at room temperature resulted in the degradation of the μ-S_9 ligand. This was accompanied by the one-electron oxidation of the dimetallic center leading to the formal Ir^{III}/Ir^{IV} complex **3**. The fate of the eliminated "S_7^-" unit could not be clarified. The product **3**, which was isolated as dark green crystals in 44% yield, is paramagnetic; its EPR spectrum (CH_2Cl_2) shows a broad singlet at $g \approx 2.07$. The structure of **3** was confirmed by X-ray analysis.[3] As shown in Figure 2, the cation in **3** has a dinuclear structure, in which two Cp*Ir units are bridged by one S_2 and two S*i*Pr ligands. The Ir(1)Ir(2)S(1)S(2) core in **3** is puckered with a dihedral angle of about 143.1° around the S–S vector, while the Ir(μ-S_2)Ir moiety is essentially planar (Ir(1)-S(3)-S(4)-Ir(2) torsion angle, 0.9(3)°); the Ir–S (disulfido) distances (Ir(1)–S(3), 2.334(3); Ir(2)–S(4), 2.389(4) Å) fall in the expected range for Ir–S single bonds.[10] The S–S distance in the disulfido ligand of 1.997(5) Å is substantially shorter than

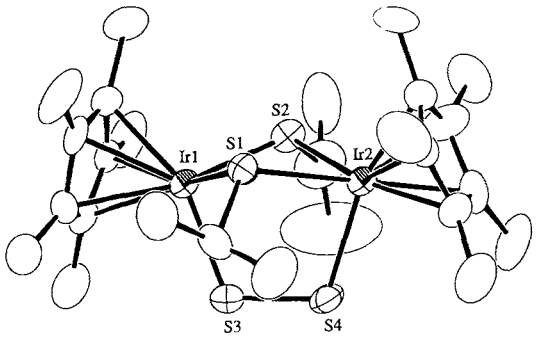

Fig. 2. Crystal structure of the cation in **3**. Selected bond lengths [Å] and angles [°]: Ir(1)···Ir(2) 3.5559(6), Ir(1)-S(1) 2.384(3), Ir(1)-S(2) 2.263(4), Ir(1)-S(3) 2.334(3), Ir(2)-S(1) 2.463(3), Ir(2)-S(2) 2.384(3), Ir(2)-S(4) 2.389(4), S(3)-S(4) 1.997(5); Ir(1)-S(3)-S(4) 108.8(2), Ir(2)-S(4)-S(3) 109.7(2).

that in HSSH (2.055 Å),[9] and comparable to those of η^1:η^1-S_2 ligands in known diruthenium complexes.[7, 11] The distance between the two Ir atoms (3.5559(6) Å) implies the absence of a metal–metal bonding interaction. Since no significant difference is observed in the coordination environment around each Ir atom, it can be assumed that the unpaired electron is delocalized over the two Ir atoms and the μ-S_2 ligand.

Presumably, the degradation involves the heterolytic cleavage of the S–S bond in the μ-S_9 ligand induced by interaction with Na^+. To obtain some insights into this reaction, the redox properties of **2** and **3** were examined by cyclic voltammetry.[12] The cyclic voltammogram of **3** reveals two reversible and one irreversible waves at $E_{1/2}$ = −0.45 and +0.66 V, and E_p = +1.3 V, respectively, assignable to the redox couples $[Ir^{III}/Ir^{III}]/[Ir^{III}/Ir^{IV}]$, $[Ir^{III}/Ir^{IV}]/[Ir^{IV}/Ir^{IV}]$, and $[Ir^{IV}/Ir^{IV}]/[Ir^{IV}/Ir^{V}]$, respectively. In contrast, the cyclic voltammogram of **2** exhibits one irreversible wave at E_p = +0.58 V, assignable to a one-electron oxidation process which appears to correlate with the degradation reaction of the ligand. Thus, the cyclic voltammogram of the oxidation product generated at this potential is essentially similar to that of **3**, showing two reversible waves at $E_{1/2}$ = −0.44 and +0.65 V. This finding strongly suggests that the species generated from **2** by electrochemical oxidation is quite unstable and is rapidly converted into the cation [Cp*Ir(μ-S*i*Pr)$_2$(μ-S_2)IrCp*]$^+$ by degradation of the μ-S_9 ligand.

Experimental Procedure

2: To a solution of **1** (541 mg, 0.672 mmol) in toluene (20 mL) was added S_8 (200 mg, 0.780 mmol), and the mixture was stirred at room temperature for 12 h. An orange solid precipitate was filtered off and dried in vacuo. Recrystallization from $CHCl_3$/hexane gave **2** as an orange crystalline solid (282 mg, 38.4%). C,H analysis: calcd: C 28.55, H 4.05; found: C 28.54, H 4.10.

3: To a solution of **2** (75 mg, 0.069 mmol) in CH_2Cl_2 (20 mL) was added $NaBPh_4$ (70 mg, 0.20 mmol) in THF (15 mL), and the mixture was stirred at room temperature for three days. After removal of the solvent in vacuo, the resulting dark green solid was extracted with CH_2Cl_2. Addition of hexane to the concentrated extract gave **3** as dark green needles (33 mg, 44%). C,H analysis: calcd: C 50.53, H 5.43; found: C 50.00, H 5.58.

Received: December 4, 1995 [Z 8609 IE]
German version: *Angew. Chem.* **1996**, *108*, 979–981

Keywords: iridium compounds · sulfides

[1] M. Hidai, Y. Mizobe, H. Matsuzaka, *J. Organomet. Chem.* **1994**, *473*, 1, and references therein; S. Kuwata, Y. Mizobe, M. Hidai, *Inorg. Chem.* **1994**, *33*, 3619; M. Nishio, H. Matsuzaka, Y. Mizobe, T. Tanase, M. Hidai, *Organometallics* **1994**, *13*, 4214; H. Matsuzaka, Y. Takagi, Y. Ishii, M. Nishio, M. Hidai, *ibid.* **1995**, *14*, 2153.

[2] Complex **1** was prepared by sodium amalgam reduction of [Cp*(Cl)Ir(μ-S*i*Pr)$_2$IrCp*Cl] derived from the reaction of [Cp*(Cl)Ir(μ-Cl)$_2$IrCp*Cl] with *i*PrSH. Details of the synthesis and structures of [Cp*Ir(μ-SR)$_2$IrCp*] will be reported elsewhere.

[3] Crystal structure analyses of **2** and **3**: Intensity data were collected on a Rigaku AFC7R diffractometer equipped with a graphite monochromator by using $Mo_{K\alpha}$ radiation ($\lambda = 0.7107$ Å) at room temperature, and corrected for Lorentz polarization effects and for absorption (ψ scans). Structure solution and refinements were performed by using the TEXSAN program package [13]. All non-hydrogen atoms were refined anisotropically by using full-matrix least-squares techniques. Hydrogen atoms were included at their calculated positions with fixed parameters. Crystal data for **2**: crystals from CH_2Cl_2/ether, crystal dimensions $0.15 \times 0.10 \times 0.60$ mm, monoclinic, $Z = 2$, $P2_1/m$, $a = 9.2698(9)$, $b = 19.217(1)$, $c = 10.149(2)$ Å, $\beta = 92.77(1)^\circ$, $V = 1811.0(3)$ Å^3, $\rho_{calcd} = 2.006$ g cm^{-3}, $\mu = 80.1$ cm^{-1}, $F(000) = 1060$, $2\theta_{max} = 55^\circ$ ($\omega - 2\theta$ scan), 4588 measured reflections, 4282 of which were independent, $R = 0.069$ and $R_w = 0.051$ for 184 variables and 2742 observed reflections [$I > 3.0\sigma(I)$], residual electron density $+6.26/-3.49$ e Å^{-3} (around Ir atom). Crystal data for **3**: crystal dimensions $0.20 \times 0.10 \times 0.90$ mm, monoclinic, $Z = 2$; $P2_1$; $a = 15.720(2)$, $b = 9.679(2)$, $c = 16.565(3)$ Å, $\beta = 103.93(1)^\circ$, $V = 2446.3(7)$ Å^3, $\rho_{calcd} = 1.613$ g cm^{-3}, $\mu = 56.5$ cm^{-1}, $F(000) = 1174$, $2\theta_{max} = 55^\circ$ ($\omega - 2\theta$ scan), 6156 measured reflections, 5947 of which were independent, $R = 0.038$ and $R_w = 0.021$ for 512 variables and 4775 observed reflections [$I > 3.0\sigma(I)$], residual electron density $+1.54/-1.03$ e Å^{-3}. Crystallographic data (excluding structure factors) for the structures reported in this paper have been deposited with the Cambridge Crystallographic Data Centre as supplementary publication no. CCDC-179-7. Copies of the data can be obtained free of charge on application to The Director, CCDC, 12 Union Road, Cambridge CB2 1EZ, UK (fax: int. code +(1223) 336-033; e-mail: teched@chemcrys.cam.ac.uk).

[4] M. Draganjac, T. B. Rauchfuss, *Angew. Chem.* **1985**, *97*, 745; *Angew. Chem. Int. Ed. Engl.* **1985**, *24*, 742; J. Wachter, *ibid.* **1989**, *101*, 1645 and **1989**, *28*, 1613; A. Müller, E. Dietman, *Adv. Inorg. Chem.* **1987**, *31*, 89.

[5] A. Müller, M. Römer, H. Bögge, E. Krickemeyer, M. Zimmermann, *Z. Anorg. Allg. Chem.* **1986**, *534*, 69.

[6] G. Marbach, J. Strähle, *Angew. Chem.* **1984**, *96*, 229; *Angew. Chem. Int. Ed. Engl.* **1984**, *23*, 246.

[7] Y. Mizobe, M. Hosomizu, S. Kuwata, J. Kawabata, M. Hidai, *J. Organomet. Chem.*, in press; Y. Mizobe, M. Hosomizu, J. Kawabata, M. Hidai, *J. Chem. Soc. Chem. Commun.* **1991**, 1226.

[8] A. Hörnig, C. Rietmann, U. Englert, T. Wagner, U. Kölle, *Chem. Ber.* **1993**, *126*, 2609.

[9] B. Meyer, *Chem. Rev.* **1976**, *76*, 367.

[10] A. Venturelli, T. B. Rauchfuss, *J. Am. Chem. Soc.* **1995**, *116*, 4824; M. Herberhold, G.-X. Jin, W. Milus, *Chem. Ber.* **1995**, *128*, 557; M. Herberhold, G.-X. Jin, A. L. Rheingold, *ibid.* **1991**, *124*, 2245; D. A. Dobbs, R. G. Bergman, *Inorg. Chem.* **1994**, *33*, 5329.

[11] J. Amarasekera, T. B. Rauchfuss, S. R. Wilson, *Inorg. Chem.* **1987**, *26*, 3328; D. Sellmann, P. Lechner, F. Knoch, M. Moll, *J. Am. Chem. Soc.* **1992**, *114*, 922; M. Kawano, C. Hoshino, K. Matsumoto, *Inorg. Chem.* **1992**, *31*, 5185.

[12] In $CH_2Cl_2/[n\text{Bu}_4\text{N}][BF_4]$. Scan rate: 0.05 V sec^{-1} (for **2**); 0.2 V sec^{-1} (for **3**). Reference electrode: saturated calomel electrode (SCE).

[13] TEXSAN: Crystal Structure Analysis Package; Molecular Structure Corp., **1985** and **1992**.

The Influence of Substituents on the Formation of Liquid Crystals Induced by Hydrogen Bonds**

Henry Bernhardt, Wolfgang Weissflog, and Horst Kresse*

Pauling pointed out as early as the late 1930s that the physiological importance of hydrogen bonding exceeds that of any other structural property.[1] Hydrogen bonds are directional and offer one of the most effective ways to selectively influence the properties of organic materials by self-assembly of the building blocks.[2] Hydrogen bonds can also play a very important role in the formation of liquid crystalline phases. Lyotropic liquid crystals are essentially stabilized by the interaction of amphiphilic molecules with protic solvents such as water through hydrogen bonding. Thermotropic liquid crystals are formed by self-assembly of anisotropic, often rodlike molecules. These molecules may be replaced by hydrogen-bonded associates of identical or different components, as is the case for 4-*n*-alkoxybenzoic acids. The characterization of mixed associates formed from 4-substituted benzoic acids was first accomplished by Kresse et al. by dielectric investigations.[3, 4] In the meantime, liquid crystals in which intermolecular hydrogen bonding plays a key role in the formation have developed into an interesting area of research.[5] Associates formed from benzoic acid and pyridine derivatives, which were introduced by Kato, Fréchet et al.,[6, 7] have proven to be very promising examples.

It is also possible to form thermotropic mesophases from molecules whose shape differs significantly from a rodlike form. For instance, there are mesogens that are laterally alkyl- or aryl-substituted or terminally branched to a large extent.[8] So far, our attempts to model such mesogens by associates that are linked by hydrogen bonds have resulted in liquid crystalline aggregates in only a few cases.[9] We report here on the influence of the strength of hydrogen bonds on the induction of liquid crystalline properties by using the simple model system pyridine–benzoic acid as an example.

The formation of a single associate between a carboxylic acid and a pyridine derivative is primarily affected by the acidity of the acid (H donor) and the basicity of the pyridine derivative (H acceptor). When a specific pyridine derivative is used, the strength of the hydrogen bonds is dependent only on the acidity of the respective acid. Thus, we investigated the association behavior of 4-(4-*n*-hexyloxyphenyl)pyridine[10] towards substituted benzoic acid derivatives.

Based on inductive and mesomeric effects, different substituents in various positions of the benzoic acid generally determine not only the strength of the hydrogen bonds, but also the thermal stability of liquid crystalline phases. If the strength of the hydrogen bonds is to be correlated with the mesophase behavior in our pyridine–benzoic acid system, the influence of both steric and polar effects on the mesogenic properties has to be eliminated. Thus, we synthesized the benzoates **1** containing an analogous substitution pattern,[11] and compared their mesophase behavior (Table 1) with that of the corresponding associates **2** formed by hydrogen bonding (Table 2). The stabil-

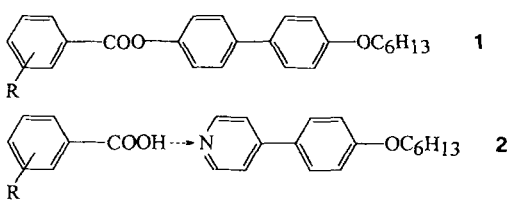

1 **2**

Table 1. Phase behavior of the substituted benzoic esters **1**; listed values are the clearing temperatures in °C [a]. Dots and dashes stand for existing and nonexisting phases, respectively.

1	R	C	S_E	S_c	S_A	N	I
a	*p*-$C_7H_{15}NH$	171	–	–	–	203	
b	*p*-$C_6H_{13}O$	119	–	(115)	–	184	
c	H	122	–	–	–	135	
d	*p*-$ClCH_2$	145	–	–	202	–	–
e	*m*-F	134	135	–	149	–	
f	*m*-NO_2	122	–	–	133	135	

[a] C = crystal; S = smectic phase; N = nematic phase; I = isotropic liquid.

[*] Prof. Dr. H. Kresse, Dipl.-Chem. H. Bernhardt
Fachbereich Chemie, Institut für Physikalische Chemie der Universität
Mühlpforte 1, D-06108 Halle (Germany)
Fax: Int. code +(345) 552-7156
Priv.-Doz. Dr. W. Weissflog
Max-Planck-Arbeitsgruppe "Flüssigkristalline Systeme"
Mühlpforte 1, D-06108 Halle (Germany)

[**] This work was supported by the Deutsche Forschungsgemeinschaft.

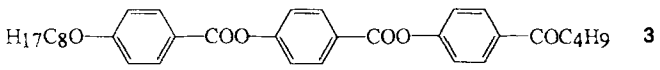

3

Table 2. Phase behavior of the hydrogen-bonded associates **2**. All temperatures in C. Dots and dashes stand for existing and nonexisting phases, respectively.

2	R	C	S_c	S_A	N	I
a	*p*-C-H_{15}NH	125	–	–	( ) (109)	
b	*p*-$C_6H_{13}O$	83	( ) (74)	130	134.5	
c	H	63	–	103	–	
d	*p*-$ClCH_2$	234	–	( ) (172)		
e	*m*-F	51	–	102.5	–	
f	*m*-NO_2	61	–	73	–	

ity of the resulting liquid crystalline state is usually assessed by the clearing temperatures; the nature of the resulting phase types was not considered.

The 1:1 associates **2** were prepared from equimolar amounts of the pure components by fusing, subsequent mixing, and crystallization. The transition temperatures and the phase behavior were determined with a heatable polarizing microscope, and were verified by calorimetric measurements (DSC 7, Perkin-Elmer). The number of suitable benzoic acid derivatives is unfortunately rather low due to the high melting points of many derivatives. Nevertheless, the substituents used allowed the Hammett constant to be varied over a wide range.

A representative phase diagram is shown in Figure 1 for the system 4-(4-*n*-hexyloxyphenyl)pyridine/3-fluorobenzoic acid.

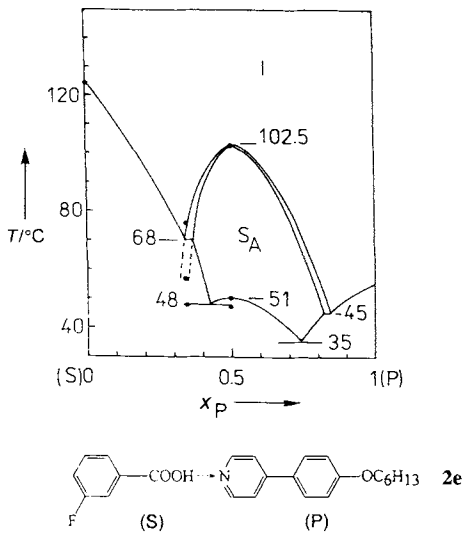

2e

Fig. 1. Phase diagram of 3-fluorobenzoic acid (S) and 4-(4-*n*-hexyloxyphenyl)-pyridine (P).

The formation of a compound in the solid state can be identified by the presence of two eutectic points. In this case mesophases are generally induced by association of two non-liquid crystalline components. The determination of the clearing point of the associate **2d** in the metastable region proved problematic, since the associate could not be supercooled sufficiently. Therefore, a so-called virtual clearing point was determined by linear extrapolation upon admixing of the liquid crystalline compound **3** (K 135 S_A 217 N 218 I) (Fig. 2). This procedure can be justified considering the linearity of the transition temperatures S_A/I in the range $0.25 \leq x_3 \leq 0.75$, which also indicates the chemical similarity of the substance classes **2** and **3**.

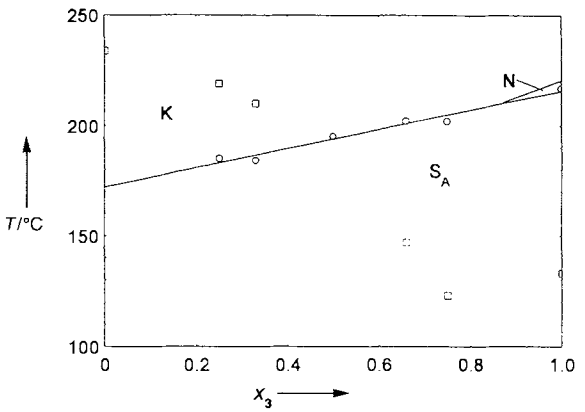

Fig. 2. Determination of the virtual clearing point of the associate **2d** by admixing of compound **3**. The circles indicate the transition temperatures S_A/I and S_A/N, the squares indicate the ends of the melting ranges.

The transition temperatures of the single associates **2a**–**2f** are summarized in Table 2 and can be compared to the mesophase behavior of the corresponding benzoates of 4-*n*-hexyloxy-4′-hydroxybiphenyl **1a**–**1f** (Table 1). The differences in the clearing points of the respective pairs (i.e. $T_{2a} - T_{1a} = \Delta T = -94$ K) were plotted against the Hammett constants σ of the substituents of the benzoic acids (Fig. 3).[12] Because of its large

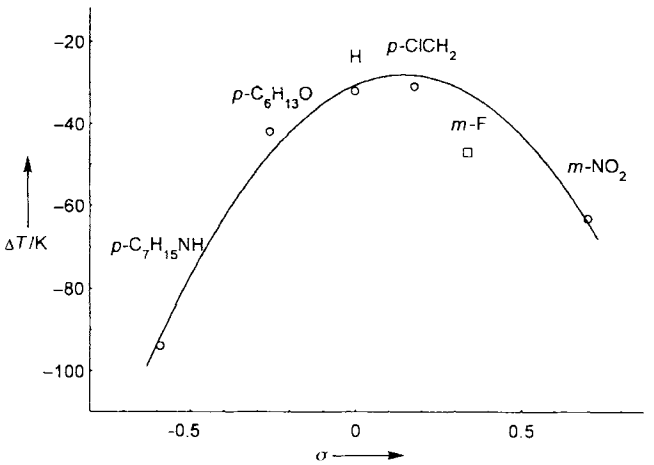

Fig. 3. The clearing point differences ΔT as a function of the Hammett constant and weighted quadratic curve for the substituents indicated by circles.

error, the value for R = *m*-F was not used in the determination of the weighted quadratic curve. Larger differences $|\Delta T|$ indicate a reduced tendency of the associates to form a liquid crystalline state. The investigated system exhibits a maximum of the stability of the liquid crystalline state for weakly electron-withdrawing substituents. An increase in the clearing point differences for small σ values reflects the reduced ability of the acids to make the acidic proton available for hydrogen bonding. Higher σ values lead to stronger hydrogen bonding; however, deviations from the 180° arrangement, no longer meet the steric requirements for the formation of thermotropic mesophases. The increasing charge separation leads to ionic pyridinium salts, which are potentially interesting as lyotropic liquid crystals.

For pyridines of similar basicity, such as 4-alkyl- and 4-alkoxypyridines, esters of 4-hydroxypyridine, and substituted stilbazoles, enantiotropic liquid crystalline associates with 4-*n*-

 © VCH Verlagsgesellschaft mbH, D-69451 Weinheim, 1996 0570-0833/96/3508-0875 $ 15.00+.25/0

alkyl- and 4-*n*-alkoxybenzoic acids are known.[6, 7, 13] The substituent constants of the benzoic acids employed deviate only slightly from the optimal value in Figure 3 which suggests that they show a principally identical association behavior. For less basic pyridines, such as isonicotinates, it can be assumed that similar dependencies apply, but the optimal acidity of the respective acid should be shifted in this case. By systematically varying the acidity, it should be possible to find optimal mixing partners for any pyridine derivative. Thus, this method provides a simple way to model covalent liquid crystalline compounds by hydrogen-bonded molecules. The goal of developing novel liquid crystals using hydrogen-bonded associates can be achieved more efficiently by taking electronic substituent effects into consideration.

Received: November 13, 1995 [Z8543IE]
German version: *Angew. Chem.* **1996**, *108*, 966–968

Keywords: associates · hydrogen bonds · liquid crystals · substituent effects

[1] L. Pauling, *Die Natur der chemischen Bindung*, Verlag Chemie, Weinheim, **1962**, p. 418.
[2] M.-J. Brienne, J. Gabard, J.-M. Lehn, I. Stibor, *J. Chem. Soc. Chem. Commun.* **1989**, 1868.
[3] H. Kresse, S. König, D. Demus, *Wiss. Z. Martin-Luther-Univ. Halle-Wittenberg*, Math.-Naturwiss. Reihe **1978**, *27*, 47–52.
[4] H. Kresse, N. K. Sharma, W. Weissflog, *Krist. Tech.* **1981**, *16*, 101.
[5] C. M. Paleos, D. Tsiourvas, *Angew. Chem.* **1995**, *107*, 1839–1855; *Angew. Chem. Int. Ed. Engl.* **1995**, *34*, 1696–1712.
[6] T. Kato, H. Kihara, T. Uryu, S. Ujiie, K. Iimura, J. M. J. Fréchet, U. Kumar, *Ferroelectrics* **1993**, *148*, 161–167.
[7] T. Kato, H. Kihara, U. Kumar, T. Uryu, J. M. J. Fréchet, *Angew. Chem.* **1994**, *106*, 1728–1729; *Angew. Chem. Int. Ed. Engl.* **1994**, *33*, 1644–1645.
[8] D. Demus, *Liq. Cryst.* **1989**, *5*, 75–100.
[9] H. Kresse, A. Treybig, A. Kolbe, W. Weissflog, *SPIE* **1995**, *2372*, 222–226.
[10] Synthesized by Suzuki coupling of hexyloxyphenylboronic acid with 4-bromopyridine and $[Pd(PPh_3)_4]$.
[11] Synthesized by esterification of the benzoic acids with 4-hexyloxy-4′-hydroxybiphenyl in the presence of *N*,*N*′-dicyclohexylcarbodiimide.
[12] H. A. Staab, *Einführung in die Theroetische Organische Chemie*, 3rd edition, Verlag Chemie, Weinheim, **1962**, p. 584.
[13] T. Kato, M. Fukumasa, J. M. J. Frechet, *Chem. Mater.* **1995**, *7*, 368–372.

Carbene Complexes of Divalent Chromium**

Alexander C. Filippou,* Dirk Wössner, Bernhard Lungwitz, and Gabriele Kociok-Köhn

Dedicated to Professor Max Herberhold on the occasion of his 60th birthday

Numerous mononuclear chromium(0) carbene complexes have been synthesized since their discovery by E. O. Fischer.[1] These compounds have achieved a certain status in organometallic chemistry and in organic synthesis.[2, 3] In comparison, carbene complexes of chromium in higher oxidation states are quite rare. Several Cr^I carbene complexes have been prepared by oxidation of Cr^0 precursors[4] and by transmetalation of $[(tmeda)CrCl_2]$ (tmeda = *N*,*N*,*N*′,*N*′-tetramethylethylenediamine) with $LiCH_2Ph$.[5] In contrast, carbene complexes of divalent chromium have not been described previously, although analogous molybdenum(II) and tungsten(II) complexes are well known.[6] We report here the synthesis, structure, and reactions of the first chromium(II) carbene complexes.

The reaction of **1a**[7] with one equivalent of anhydrous HCl (or HBr) in pentane at −50 °C provided the chromium(II) aminocarbene complexes **2a** and **3** selectively [Eq. (a); the filled

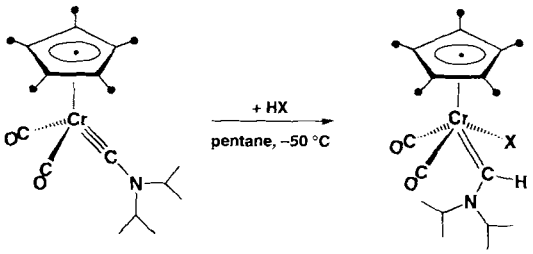

(a)

1a **2a**, X = Cl; **3**, X = Br

circles on the cyclopentadiene ligand represent methyl groups]. These products were isolated as red solids, which decompose on melting at 57 and 47 °C, respectively. In solution below 0 °C they decompose to give a mixture of **1a** and blue, carbonyl-free, paramagnetic products of unknown composition. Complexes **2a** and **3** thus display a significantly lower thermal stability than the analogous tungsten complexes $[Cp^*(CO)_2(X)W{=}C(H)NEt_2]$ ($Cp^* = C_5Me_5$; X = Cl, Br, I) (m.p. 137–150 °C).[6h] The same approach can be used to prepare the red, thermally labile aminocarbene complex $[Cp(CO)_2(Cl)Cr{=}C(H)NiPr_2]$ **2b** from HCl and $[Cp(CO)_2Cr{\equiv}CNiPr_2]$ **1b**.

When the halogeno ligand in **2a** and in **3** is abstracted with $TlPF_6$ in the presence of isocyanides, phosphanes, or phosphites, thermally stable aminocarbene complexes of divalent chromium are obtained, as demonstrated by the selective conversion of **2a** into **4a** and **5** [Eq. (b)], and by the synthesis of the

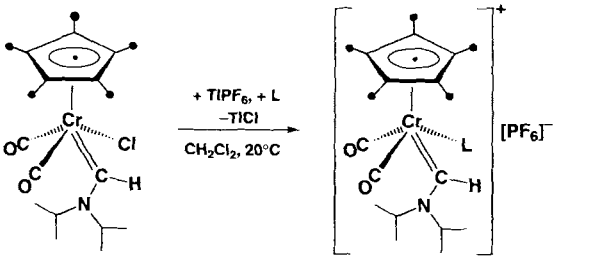

(b)

2a **4a**, L = EtNC; **5**, L = P(OMe)$_3$

cyclopentadienyl complexes $[Cp(CO)_2(L)Cr{=}C(H)NiPr_2]PF_6$ (**4b**: L = EtNC; **6**: L = *t*BuNC; **7**: L = PMe_3) from **2b**. These compounds also provide access to more electron-rich Cr^{II} carbene complexes by substitution of a carbonyl ligand. For example, the reaction of **4a** with EtNC yields the salt **8** [Eq. (c)]. The cationic Cr^{II} carbene complexes were isolated as yellow (**4a**, **4b**, **5**, **6**, **7**) and brown (**8**), thermally stable solids.

The composition and structures of **2**–**8** were supported by the results of elemental analyses, IR and NMR spectroscopy, and mass spectrometry (Table 1). In the IR spectra of the Cr^{II}

[*] Prof. Dr. A. C. Filippou, Dipl.-Chem. D. Wössner, Dr. B. Lungwitz, Dr. G. Kociok-Köhn
Institut für Anorganische und Allgemeine Chemie der Humboldt-Universität
Hessische Strasse 1–2, D-10115 Berlin (Germany)
Fax: Int. code +(30)28468639
e-mail: filippou@chemie.hu-berlin.de

[**] This work was supported by the Volkswagenstiftung, the Deutsche Forschungsgemeinschaft, and the Fonds der Chemischen Industrie.

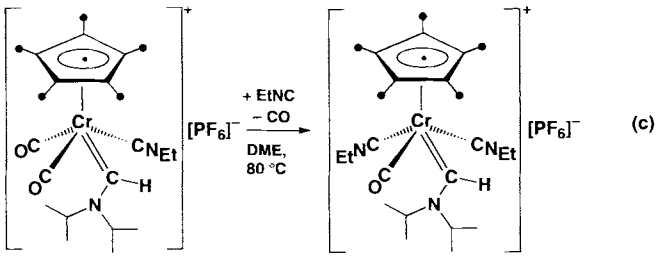

4a 8

Table 1. Selected spectroscopic data for complexes **2**–**8** [a, b].

2a: m.p. 57 °C (decomp); IR (CH_2Cl_2, −40 °C): $\tilde{\nu}$ [cm^{-1}] = 1942 vs, 1856 vs (CO); 1527 m ($C_{carbene}$-N); ^1H NMR (CD_2Cl_2, −15 °C): δ = 1.14 (d, 3H, $CHMe_A$), 1.23 (d, 3H, $CHMe_B$), 1.24 (d, 3H, $CHMe_C$), 1.34 (d, 3H, $CHMe_D$), 1.70 (s, 15H, C_5Me_5); 3.87 (sept., 1H, $CHMe_{A,B}$), 4.24 (sept., 1H, $CHMe_{C,D}$), 11.29 (s, 1H, Cr=CH); $^{13}C\{^1H\}$ NMR (CD_2Cl_2, −15 °C): δ = 9.7 (C_5Me_5), 19.4, 21.3, 24.0, 24.2 (2 × $CHMe_2$), 51.4, 60.7 (2 × $CHMe_2$), 104.1 (C_5Me_5), 260.3 (Cr=C; ^1J(C,H) = 129.5 Hz), 260.5, 263.8 (CO); EI-MS (70 eV): *m/z*: 355 [M^+ − HCl], 327 [M^+ − HCl − CO], 312 [M^+ − HCl − *i*Pr], 299 [M^+ − HCl − 2CO], 284 [M^+ − HCl − *i*Pr − CO], 256 [M^+ − HCl − 2CO − *i*Pr], 214 [M^+ − HCl − 2CO − *i*Pr − MeC(H)=CH_2], 187 [M^+ − HCl − 2CO − *i*Pr − MeC(H)=CH_2 − HCN].

2b: IR (CH_2Cl_2, −40 °C): $\tilde{\nu}$ [cm^{-1}] = 1960 vs, 1875 vs (CO); 1535 m ($C_{carbene}$-N); ^1H NMR (CD_2Cl_2, −80 °C): δ = 12.31 (s, 1H, Cr=CH); $^{13}C\{^1H\}$ NMR (CD_2Cl_2, −80 °C): δ = 254.2 (Cr=C; ^1J(C,H) = 135.5 Hz), 258.6, 261.4 (CO).

3: m.p. 47 °C (decomp); IR (THF, −40 °C): $\tilde{\nu}$ [cm^{-1}] = 1944 vs, 1862 vs (CO); 1522 m ($C_{carbene}$-N); ^1H NMR (CD_2Cl_2, −50 °C): δ = 11.31 (s, 1H, Cr=CH); $^{13}C\{^1H\}$ NMR (CD_2Cl_2, −50 °C): δ = 258.0 (Cr=C; ^1J(C,H) = 135.7 Hz), 259.8, 262.4 (CO).

4a: m.p. 122 °C (decomp); IR: $\tilde{\nu}$ [cm^{-1}] = 2157 m (C≡NEt); 1971 vs, 1918 s (CO); 1534 m ($C_{carbene}$-N); ^1H NMR (CD_2Cl_2, −20 °C): δ = 10.94 (s, 1H, Cr=CH); $^{13}C\{^1H\}$ NMR (CD_2Cl_2, −20 °C): δ = 170.3 ($CNCH_2CH_3$), 245.7, 247.9 (CO), 253.7 (Cr=C).

4b: m.p. 101 °C (decomp); IR: $\tilde{\nu}$ [cm^{-1}] = 2170 m (C≡NEt); 1986 vs, 1933 s (CO); 1537 m ($C_{carbene}$-N); ^1H NMR: δ = 11.75 (s, 1H, Cr=CH); $^{13}C\{^1H\}$ NMR: δ = 166.1 ($CNCH_2CH_3$), 244.9, 246.4 (CO), 249.2 (Cr=C, ^1J(C,H) = 146.0 Hz).

5: m.p. 157 °C (decomp); IR: $\tilde{\nu}$ [cm^{-1}] = 1963 vs, 1901 s (CO); 1528 m ($C_{carbene}$-N); ^1H NMR (CD_2Cl_2, −20 °C): δ = 3.72 (d, ^3J(H,P) = 11.0 Hz, 9H, $P(OMe)_3$), 10.46 (s, 1H, Cr=CH); $^{13}C\{^1H\}$ NMR (CD_2Cl_2, −20 °C): δ = 246.3 (d, ^2J(C,P) = 13.6 Hz, CO), 248.9 (d, ^2J(C,P) = 72.9 Hz, CO), 251.0 (d, ^2J(C,P) = 69.5 Hz, Cr=C); $^{31}P\{^1H\}$ NMR: δ = −143.7 (sept., ^1J(P,F) = 717 Hz, PF_6), 183.8 ($P(OMe)_3$).

6: m.p. 59 °C (decomp); IR: $\tilde{\nu}$ [cm^{-1}] = 2144 s (C≡N*t*Bu); 1982 vs, 1928 s (CO); 1537 m ($C_{carbene}$-N); ^1H NMR: δ = 11.91 (s, 1H, Cr=CH); $^{13}C\{^1H\}$ NMR: δ = 167.0 ($CNMe_3$), 244.2, 246.5 (CO), 251.7 (Cr=C).

7: IR: $\tilde{\nu}$ [cm^{-1}] = 1969 vs, 1900 s (CO); 1517 m ($C_{carbene}$-N); ^1H NMR (CD_2Cl_2, −20 °C): δ = 1.55 (d, ^2J(P,H) = 9.6 Hz, 9H, PMe_3), 11.56 (s, 1H, Cr=CH); $^{31}P\{^1H\}$ NMR: δ = 34.8 (PMe_3).

8: IR: $\tilde{\nu}$ [cm^{-1}] = 2144 vs, 2122 s, 2099 m (C≡NEt); 1895 vs (CO); 1509 m ($C_{carbene}$-N); ^1H NMR: 10.94 (s, 1H, Cr=CH); $^{13}C\{^1H\}$ NMR: δ = 179.7, 183.7 (2 × $CNCH_2CH_3$), 254.1 (CO), 263.7 (Cr=C; ^1J(C,H) = 132.7 Hz).

[a] Correct elemental analyses were obtained for **2a**, **3**, **4a**, **4b**, and **5**. [b] IR spectra (Bruker IFS-55 spectrometer) in CH_2Cl_2 at room temperature, if not specified otherwise; NMR spectra (Bruker AM-300 spectrometer) in CD_2Cl_2 at room temperature, if not specified otherwise; the δ_H and δ_C values are relative to the residual signal of the solvent, the δ_P values are relative to 85% H_3PO_4 solution as external standard; the ^3J(H,H) coupling constants in the isopropyl groups are 6.1 Hz; mass spectra: *m/z* values relative to the ^{52}Cr isotope.

aminocarbene complexes an absorption band of medium intensity is observed between 1509 and 1537 cm^{-1} and attributed to the $\tilde{\nu}(C_{carbene}\text{-}N)$ stretching vibration. This indicates the strong π conjugation of the amino group with the Cr–C double bond.[3f, 8] The number and relative intensities of the $\tilde{\nu}$(CO) bands of **2**–**7** and of the $\tilde{\nu}$(C≡NEt) bands of **8** provide evidence for the lateral arrangement of these ligands in the coordination sphere. In the ^1H NMR spectra of **2**–**8** an extremely lowfield singlet (δ = 10.46–12.31) is observed for the proton bound to the carbene carbon.[6c, 9] Accordingly, the carbene carbon resonances of **2**–**8** (δ = 249.2–263.7) are split into a doublet in the proton-coupled ^{13}C NMR spectra. The ^1J(C,H) coupling constants of 129.5 and 146.0 Hz are in the range found for "nondistorted" secondary carbene complexes.[6a–c, 9a]

The crystal structure of carbene complex **4a** was determined by X-ray diffraction (Fig. 1).[10, 11] The Cr–$C_{carbene}$ bond

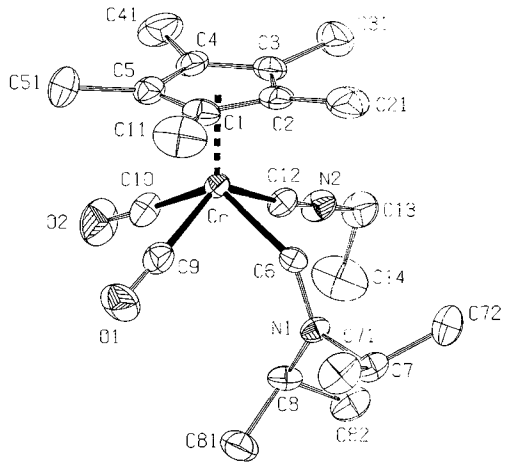

Fig. 1. Crystal structure of the cation in **4a** (PLATON plot). Selected bond lengths [Å] and angles [°]: Cr-C6 203.3(5), Cr-C9 184.4(5), Cr-C10 186.1(5), Cr-C12 198.0(5), Cr-$Cp^*_{centroid}$ 186.12(7), C6-N1 130.4(6), C7-N1 151.9(6), C8-N1 148.7(6), C12-N2 115.1(6); Cr-C6-N1 138.0(3), Cr-C12-N2 174.1(4), C6-Cr-C9 74.9(2), C6-Cr-C10 125.0(2), C6-Cr-C12 80.9(2), C9-Cr-C10 77.3(2), C9-Cr-C12 125.6(2), C10-Cr-C12 78.2(2).

(203.3(5) pm) is somewhat shorter than that found in octahedral Cr^0 aminocarbene complexes[3f] and, as expected, considerably longer then the Cr–$C_{carbyne}$ bond in **1b** (172.8(8) pm). The short $C_{carbene}$–N bond (130.4(6) pm) reflects the double bond character of this bond, which was also evident in the spectroscopic data.[8, 12] The plane of the aminocarbene ligand passing through the atoms Cr, C6, N1, C7, and C8 is almost perpendicular to the Cp* ring plane (dihedral angle between the best planes 85.9(2)°).

Compounds **2**–**8** are the first isolated and characterized Cr^0 aminocarbene complexes. Heteroatom-free derivatives should also be accessible by the route described above, as preliminary results of protonation reactions of chromium phenylcarbyne complexes show. Future studies are aimed to extend this synthetic strategy to Cp-free chromium carbene complexes and to determine their role in chromium-mediated C–C bond forming reactions.[13]

Experimental Procedure

2a: A solution of **1a** (0.355 g, 1.00 mmol) in 20 mL of pentane was cooled to −50 °C, treated by dropwise addition of a 1 M solution of HCl in diethyl ether (1 mL, 1.00 mmol), and stirred for 15 min. A red precipitate formed. The supernatant slightly yellow solution was decanted off and the precipitate washed twice with cold (−50 °C) pentane. Yield: 0.39 g (quantitative), red microcrystalline powder, m.p. 57 °C (decomp).

4a: A solution of **2a** (0.39 g, 1.00 mmol) in 20 mL of CH_2Cl_2 was cooled to −78 °C and treated with EtNC (0.060 g, 0.08 mL, 1.09 mmol) and $TlPF_6$ (0.35 g, 1.00 mmol). The reaction mixture was warmed to 0 °C and stirred for 1 h. The resulting yellow suspension was treated with diethyl ether, the Tl salts were removed by filtration, the filtrate was concentrated to a few mL, and **4a** was precipitated by addition of Et_2O/pentane (1/1). The yellow precipitate was dissolved in a minimum amount of THF and the product precipitated again by addition of Et_2O. Yield: 0.50 g (90%), yellow powder, m.p. 122 °C (decomp).

8: A solution of **4a** (0.265 g, 0.48 mmol) in 20 mL of 1,2-dimethoxyethane was treated with EtNC (0.030 g, 0.04 mL, 0.54 mmol) and heated at 80 °C until the $\tilde{\nu}$(CO) bands of **4a** at 1963 and 1906 cm^{-1} were no longer observed in the IR spectrum of the reaction solution (12 h). The solvent was removed in vacuo, the

residue purified by chromatography on silanized silica gel at −10 °C, and the product eluted with Et_2O/CH_2Cl_2 (5/1). Yield: 0.20 g (72%), brown powder.

Received: December 4, 1995 [Z8611IE]
German version: *Angew. Chem.* **1996**, *108*, 981–983

Keywords: carbene complexes · carbyne complexes · chromium compounds · protonations

[1] E. O. Fischer, A. Maasböl, *Chem. Ber.* **1967**, *100*, 2445.
[2] The carbene group is considered as a neutral two-electron ligand in all the complexes.
[3] a) E. O. Fischer, *Pure Appl. Chem.* **1970**, *24*, 407; b) D. J. Cardin, B. Cetinkaya, M. F. Lappert, *Chem. Rev.* **1972**, *72*, 545; c) F. A. Cotton, C. M. Lukehart, *Prog. Inorg. Chem.* **1972**, *16*, 487; d) E. O. Fischer, *Angew. Chem.* **1974**, *86*, 651; e) F. J. Brown, *Prog. Inorg. Chem.* **1980**, *27*, 1; f) K. H. Dötz, H. Fischer, P. Hofmann, F. R. Kreißl, U. Schubert, K. Weiss, *Transition Metal Carbene Complexes*, VCH, Weinheim, **1983**; g) K. H. Dötz, *Angew. Chem.* **1984**, *96*, 573; *Angew. Chem. Int. Ed. Engl.* **1984**, *23*, 587; h) K. S. Chan, G. A. Peterson, T. A. Brandvold, K. L. Faron, C. A. Challener, C. Hyldahl, W. D. Wulff, *J. Organomet. Chem.* **1987**, *334*, 9; i) R. Aumann, *Angew. Chem.* **1988**, *100*, 1512; *Angew. Chem. Int. Ed. Engl.* **1988**, *27*, 1456; j) L. S. Hegedus, *Pure Appl. Chem.* **1990**, *62*, 691; k) H. Rudler, M. Audouin, E. Chelain, B. Denise, R. Goumont, A. Massoud, A. Parlier, A. Pacreau, M. Rudler, R. Yefsah, C. Alvarez, F. Delgado-Reyes, *Chem. Soc. Rev.* **1991**, *20*, 503; l) W. A. Herrmann, J. L. Hubbard, I. Bernal, J. D. Korp, B. L. Haymore, G. L. Hillhouse, *Inorg. Chem.* **1984**, *23*, 2978.
[4] a) M. F. Lappert, R. W. McCabe, J. J. MacQuitty, P. L. Pye, P. I. Riley, *J. Chem. Soc. Dalton Trans.* **1980**, 90; b) M. F. Lappert, *J. Organomet. Chem.* **1988**, *358*, 185.
[5] S. Hao, J.-I. Song, P. Berno, S. Gambarotta, *Organometallics* **1994**, *13*, 1326.
[6] a) J. H. Wengrovius, R. R. Schrock, M. R. Churchill, H. J. Wasserman, *J. Am. Chem. Soc.* **1982**, *104*, 1739; b) S. J. Holmes, D. N. Clark, H. W. Turner, R. R. Schrock, *ibid.* **1982**, *104*, 6322; c) F. R. Kreißl, W. J. Sieber, M. Wolfgruber, *J. Organomet. Chem.* **1984**, *270*, C45; d) J. A. K. Howard, J. C. Jeffery, J. C. V. Laurie, I. Moore, F. G. A. Stone, A. Stringer, *Inorg. Chim. Acta* **1985**, *100*, 23; e) V. A. Osborn, M. J. Winter, *J. Chem. Soc. Chem. Comm.* **1985**, 1744; f) A. Mayr, M. F. Asaro, M. A. Kjelsberg, K. S. Lee, D. Van Engen, *Organometallics* **1987**, *6*, 432; g) H. Adams, N. A. Bailey, G. W. Bentley, C. E. Tattershall, B. F. Taylor, M. J. Winter, *J. Chem. Soc. Chem. Comm.* **1992**, 533; h) B. Lungwitz, A. C. Filippou, *NATO ASI Ser. Ser. C*, **1993**, *392*, 249.
[7] A. C. Filippou, K. Wanninger, C. Mehnert, *J. Organomet. Chem.* **1993**, *461*, 99.
[8] a) E. Moser, E. O. Fischer, *J. Organomet. Chem.* **1969**, *16*, 275; b) M. F. Lappert, *ibid.* **1975**, *100*, 139; c) W. K. Dean, W. A. G. Graham, *Inorg. Chem.* **1977**, *16*, 1061; d) E. O. Fischer, D. Himmelreich, R. Cai, H. Fischer, U. Schubert, B. Zimmer-Gasser, *Chem. Ber.* **1981**, *114*, 3209.
[9] a) H. Fischer, S. Zeuner, K. Ackermann, *J. Chem. Soc. Chem. Comm.* **1984**, 684; b) C. Borel, L. S. Hegedus, J. Krebs, Y. Satoh, *J. Am. Chem. Soc.* **1987**, *102*, 1101.
[10] Crystal structure analysis of **4a**: $C_{22}H_{35}CrF_6N_2O_2P$, M_{rel} = 556.49; yellow rectangular prisms (1.0 × 0.5 × 0.3 mm) obtained from CH_2Cl_2/Et_2O by diffusion at −30 °C; orthorhombic, space group $P2_12_12_1$ (No. 19), a = 8.214(3), b = 14.391(4), c = 22.509(10) Å, (24 reflections, $2\theta_{min./max.}$ = 28.55°/29.66°), V = 2661(2) Å^3, Z = 4, ρ_{calcd} = 1.389 g cm^{-3}, $\mu(Mo_{K\alpha})$ = 0.54 mm^{-1}, $F(000)$ = 1160, λ = 71.073 pm, T = 193(2) K, STOE-STADI4 four-circle diffractometer, ω-2θ scan, 3° ≦ 2θ ≦ 50° (0 ≦ h ≦ 9, 0 ≦ k ≦ 17, 0 ≦ l ≦ 26); 2706 measured reflections, of which 2681 were unique; 2662 with $I > 2\sigma(I)$ were used in the refinement. After data reduction and correction for Lorentz and polarization effects, the Cr position was determined by Patterson methods (SHELX-86). The initial coordinates for the light atoms were determined by subsequent difference Fourier syntheses (SHELXL93) (R = 8%). The Cr, C, N, and O atoms were refined anisotropically, whereas the H atoms were placed in idealized positions with d(C–H) = 98 pm and U_{iso} = 0.08 Å^2. The refinement converged at R = 0.044, ($wR(F^2)$ = 0.110, GOF = 1.023 (SHELXL93), min./max residual electron density −0.265/0.459 e Å^{-3}, 312 parameters). The hydrogen atom H6 bound to the carbene C atom was refined isotropically. Satisfactory refinement of the structural model was possible only by assuming a racemic twin (volume ratio of the twin 0.54(4), SHELXL93). Further details of the crystal structure investigation may be obtained from the Fachinformationszentrum Karlsruhe, D-76344 Eggenstein-Leopoldshafen (Germany) on quoting the depository number CSD-404 543.
[11] A. L. Spek, PLUTON-92, PLATON-93, graphics program, University of Utrecht (The Netherlands), **1992** and **1993**; *Acta Crystallogr. Sect. A* **1990**, *46*, C34.
[12] a) C. Sandorfy in *The Chemistry of the Carbon-Nitrogen Double Bond* (Ed.: S. Patai), Interscience, London, **1970**, p. 2; b) R. Allmann in *The Chemistry of the Hydrazo, Azo and Azoxy Groups* (Ed.: S. Patai), Interscience, London, **1975**, p. 27.
[13] a) A. Mayr, C. M. Bastos, *Prog. Inorg. Chem.* **1992**, *40*, 1; b) A. C. Filippou in *45 Jahre Fonds der Chemischen Industrie* (Ed.: Verband der Chemischen Industrie), Frankfurt, **1995**, p. 209.

Propargylation of Carbonyl Compounds by Umpolung of Propargylpalladium Complexes with Diethylzinc

Yoshinao Tamaru,* Sachio Goto, Akihiro Tanaka, Masamichi Shimizu, and Masanari Kimura

π-Allylpalladium complexes are versatile intermediates, which serve not only as allylic electrophiles toward hard and soft carbon nucleophiles[1] but also as allylic nucleophiles toward carbonyl compounds.[2] In constrast, the use of propargylpalladium complexes as intermediates is rather limited: Their reaction with hard carbon nucleophiles such as alkyl-, aryl-, ethynylmagnesium and -zinc compounds generally provides allenes;[3] however, their reaction with soft carbon nucleophiles has not been fully elucidated yet.[4] Moreover, to our knowledge, no reports have appeared that indicate that propargylpalladium complexes serve as nucleophiles toward carbonyl compounds. We report here preliminary results that reveal for the first time that propargylpalladium complexes undergo a nucleophilic addition to carbonyl compounds to provide homopropargyl alcohols **2** selectively [Eq. (a)].

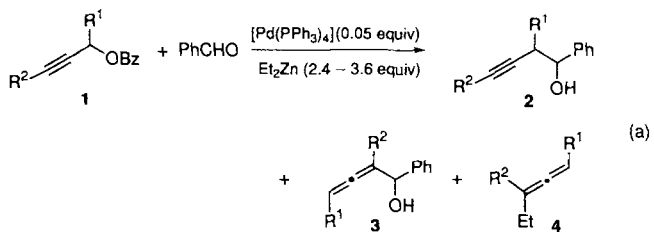

(a)

The propargylation of carbonyl compounds proceeded smoothly at room temperature by stirring a solution of a propargylic benzoate **1** (1.2 mmol), a carbonyl compound (1.0 mmol), diethylzinc (2.4–3.6 mmol), and tetrakis(triphenylphosphane)palladium (0.05 mmol) in THF under nitrogen. Results for the reactions with benzaldehyde are summarized in Table 1.[5, 6]

The parent compound **1a** (run 1), 1-substituted compounds **1b–d** (runs 2–7), and the 1,3-disubstituted propargyl benzoate **1h** (run 11) reacted with benzaldehyde to provide homopropargyl alcohols **2** selectively, whereas 3-substituted propargyl benzoates **1e–g** (runs 8–10) reacted to give allenyl alcohols **3** in addition to homopropargyl alcohols **2**. The ratio of **3** to **2** markedly depends on the kind of R^2 substituents, ranging from 72/28 for **3e**/**2e** (R^2 = Me, run 8) to 0/100 for **3g**/**2g** (R^2 = $SiMe_3$, run 10).

Surprisingly, cross-coupling products, ethylallenes **4**, were either not detected at all, or obtained only as minor products (run 6). The propargylation presented here showed poor stereoselectivity: **2b**, **2c**, and **2h** formed as mixtures of the *syn* and *anti* isomers in a ratio of about 1:1.

All the reactions were examined under the conditions specified in footnote [a] in Table 1 and have not been optimized yet. The yields may be improved by modification of the conditions (e.g., 70% in THF alone vs. 90% in a mixture of benzene/THF, run 2 and footnote [d] in Table 1). Propargylic substrates with

[*] Prof. Dr. Y. Tamaru, S. Goto, A. Tanaka, M. Shimizu, Dr. M. Kimura
Department of Applied Chemistry, Faculty of Engineering
Nagasaki University, 1-14 Bunnkyo, Nagasaki 852 (Japan)
Fax: Int. code +(958)47-9008
e-mail: +tamaru@net.nagasaki-u.ac.jp

Table 1. Palladium-catalyzed propargylations of benzaldehyde according to Equation (a).

Run	I	mmol Et_2Zn	t [h] [a]	Products (Yield [%]) [b]
1	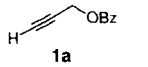 **1a**	3.6	7	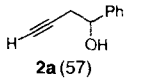 **2a** (57)
	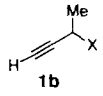 **1b**			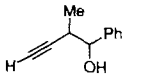
2 [d]	X = OBz	3.6, [3.6]	3, [1]	**2b** (70) [c], [90]
3	X = OTs	3.6	1.5	**2b** (55) [c]
4	X = OCO_2Me	3.6	7	**2b** (72) [c]
5	X = Br	3.6	0.2	**2b** (88) [c]
6	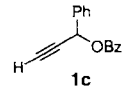 **1c**	3.6	1	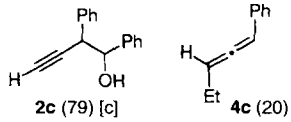 **2c** (79) [c] **4c** (20)
7	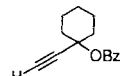 **1d**	3.6	2.5	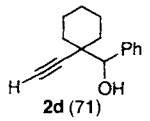 **2d** (71)
8	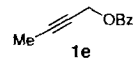 **1e**	2.4	24	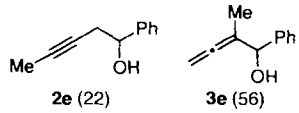 **2e** (22) **3e** (56)
9	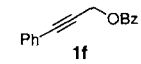 **1f**	2.4	75	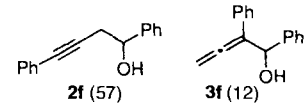 **2f** (57) **3f** (12)
10	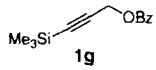 **1g**	2.4	96	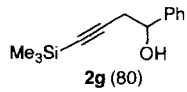 **2g** (80)
11	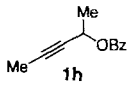 **1h**	2.4	30	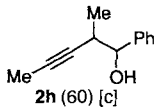 **2h** (60) [c]

[a] Reaction conditions: **1** (1.2 mmol), benzaldehyde (1.0 mmol), diethylzinc (indicated amount), $[Pd(PPh_3)_4]$ (0.05 mmol) in THF (5 mL) at room temperature under N_2. [b] Yields for the spectroscopically homogeneous products based on the amounts of benzaldehyde used. [c] Mixture of *syn* and *anti* isomers in a ratio of about 1:1. [d] The conditions and yields for a reaction carried out in benzene/THF (5 mL/1.6 mL) are given in square brackets.

various leaving groups other than benzoate can be utilized with similar efficiency (runs 3–5).

The reaction time required for the complete conversion of benzaldehyde (TLC monitoring) ranges from about 10 min (run 5) to 96 h (run 10), and seems to be correlated with two factors: 1) the accessibility of the acetylenic C3 carbon atom to palladium(0), which is restricted by the steric bulk of the R^2 substituent (runs 8–11); 2) the ease of a heterolytic cleavage of the C1–X bond, which depends on the nature of the leaving group X and of the R^1 substituent (runs 2–7).

The present novel palladium-catalyzed propargylation of carbonyl compounds may be rationalized according to Scheme 1, under the assumption that both the transformation of **II** to a mixture of **III** and **IV**[7] and the reactions of these two with benzaldehyde[8] proceed much faster than the reductive elimination of **II** to provide **4**.[3] At present, the metal complex fragment M of **III** and **IV** has not been specified; however, M = ZnX

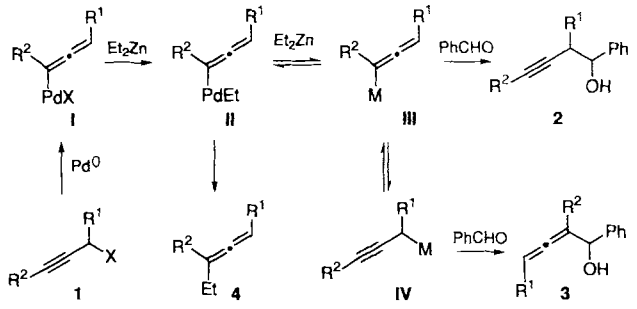

Scheme 1. Mechanistic rationale for the propargylation and allenylation of benzaldehyde according to Equation (a).

(X = OBz, Br, etc.) is unlikely, judging from the formation of **2b**, **2c**, and **2h** with low stereoselectivity.[9]

The selective formation of the alcohols **2** (runs 1–5, 7, 11) may be attributed to the preponderance of **III** (with C_{sp^2}–M bonding) over **IV** (with C_{sp^3}–M bonding) in the equilibrium shown in Scheme 1. The dramatic change in the ratios of **2**/**3** for the reactions of a series of 3-substituted propargyl benzoates (runs 8–10) may owe its origin to a steric destabilization of **III** for R^2 = Ph and Me groups and to an electronic stabilization of **III** for $R^2 = Me_3Si$.

Extensive studies are in progress to clarify the detailed reaction mechanism and the scope of this technique for the umpolung of propargylpalladium intermediates, which may open new perspectives in organic synthesis.

Experimental Procedure

2b (run 2, Table 1): To a solution of $[Pd(PPh_3)_4]$ (0.05 mmol) and **1b**, X = OBz (1.2 mmol) in dry THF (5 mL) under nitrogen were successively added benzaldehyde (1.0 mmol) and diethylzinc (3.6 mmol, 2 M solution in THF) by syringe. The mixture was stirred at room temperature for 3 h, then diluted with ethyl acetate (40 mL). The mixture was washed successively with 2 M HCl (10 mL), aqueous $NaHCO_3$ (2 × 10 mL), and brine (10 mL). The organic phase was dried ($MgSO_4$) and concentrated, and the residue was purified by flash chromatography on silica gel (hexane/ethyl acetate gradient) to afford 112 mg (70%) of **2b** as a mixture of diastereomers (55:45): B.p. (0.43 Torr): 80 °C; IR (neat): $\tilde{\nu}$ = 3400, 3300, 2110, 1050, 1030 cm^{-1}; ^1H NMR (400 MHz, $CDCl_3$, TMS): δ (major isomer) = 1.10 (d, J = 7.0 Hz, 3H), 2.21 (d, J = 2.6 Hz, 1H), 2.80 (d quint, J = 2.6, 7.0 Hz, 1H), 4.51 (br. d, J = 7.0 Hz, 1H), 7.25 - 7.44 (m, 5H); δ (minor isomer) = 1.23 (d, J = 7.0 Hz, 3H), 2.12 (d, J = 2.6 Hz, 1H), 2.89 (d quint, J = 2.6, 7.0 Hz, 1H), 4.74 (br. d, J = 7.0 Hz, 1H), 7.25–7.44 (m, 5H). C, H analysis for $C_{11}H_{12}O$: calcd. C 82.46, H 7.55; found C 82.53, H 7.68.

Received: December 19, 1995 [Z8667IE]
German version: *Angew. Chem.* **1996**, *108*, 962–963

Keywords: carbon–carbon coupling · homopropargyl alcohols · propargylpalladium · umpolung

[1] S. A. Godleski in *Comprehensive Organic Synthesis, Vol. 4* (Eds.: B. M. Trost, I. Fleming, M. F. Semmelhack), Pergamon, Oxford, **1991**, pp. 585–661; R. F. Heck, *Palladium Reagents in Organic Synthesis*, Academic Press, London, **1985**.

[2] Umpolung by transmetalation with diethylzinc: a) Y. Tamaru, A. Tanaka, K. Yasui, S. Goto, S. Tanaka, *Angew. Chem.* **1995**, *107*, 862–864; *Angew. Chem. Int. Ed. Engl.* **1995**, *34*, 787–789; b) K. Yasui, Y. Goto, T. Yajima, Y. Taniseki, K. Fugami, A. Tanaka, Y. Tamaru, *Tetrahedron Lett.* **1993**, *34*, 7619–7622; c) umpolung by reduction with metal: Y. Masuyama, Y. Nimura, Y. Kurusu, *Tetrahedron Lett.* **1991**, *32*, 225–228; Y. Masuyama, J. P. Takahara, Y. Kurusu, *J. Am. Chem. Soc.* **1988**, *110*, 4473–4474; d) umpolung by electrochemical reduction: P. Zhang, W. Zhang, T. Zhang, Z. Wang, W. Zhou, *J. Chem. Soc. Chem. Commun.* **1991**, 491–492; S. Torii, H. Tanaka, T. Katoh, K. Morisaki, *Tetrahedron Lett.* **1984**, *25*, 3207–3208; e) umpolung by substitution with heteroatoms: J. P. Takahara, Y. Masuyama, Y. Kurusu, *J. Am. Chem. Soc.* **1992**, *114*, 2577–2586; S. Matsubara, K. Wakamatsu, Y. Morizawa, N. Tsuboniwa, K. Oshima, H. Nozaki, *Bull. Chem. Soc. Jpn.* **1985**, *58*, 1196–1199.

[3] E. Keinan, E. Bosch, *J. Org. Chem.* **1986**, *51*, 4006–4016; C. J. Elsevier, P. M. Stehouwer, H. Westmijze, P. Vermeer, *ibid.* **1983**, *48*, 1103–1105; K. Ruitenberg, H. Kleijn, C. J. Elsevier, J. Meijer, P. Vermeer, *Tetrahedron Lett.* **1981**, *22*, 1451–1452; T. Jeffery-Luong, G. Linstrumelle, *ibid.* **1980**, *21*, 5019–5020.

[4] C.-C. Su, J.-T. Chen, G.-H. Lee, Y. Wang, *J. Am. Chem. Soc.* **1994**, *116*, 4999–5000; J. Tsuji, H. Watanabe, I. Minami, I. Shimizu, *ibid.* **1985**, *107*, 2196–2198.
[5] All the products listed in Table 1 were properly characterized by spectroscopic methods (IR, 400 MHz ^{1}H NMR, high-resolution MS) and elemental analyses.
[6] Ketones seem to react equally well. For example, the reaction of **1b** (X = OBz) with acetophenone under the same conditions as that of run 2 in Table 1 (THF, 29 h) provided 3-methyl-2-phenyl-4-pentyn-2-ol in 58% yield.
[7] The complexes of **III** and **IV** with M = ZnEt and $ZnEt_2^-$ may be generated via a similar transition state to that proposed for an allyl group migration of π-allylpalladium to Zn^{2+} [2a].
[8] E. J. Corey, K. A. Cimprich, *J. Am. Chem. Soc.* **1994**, *116*, 3151–3152; J. A. Marshall, J. Perkins, *J. Org. Chem.* **1994**, *59*, 3509–3511; H. Yamamoto in *Comprehensive Organic Synthesis, Vol. 2* (Eds.: B. M. Trost, I. Fleming, C. H. Heathcock), Pergamon, Oxford, **1991**, pp. 81–98.
[9] **III** with M = ZnCl provides *anti*-**2** with high selectivity: G. Zweifel, G. Hahn, *J. Org. Chem.* **1984**, *49*, 4565–4567.

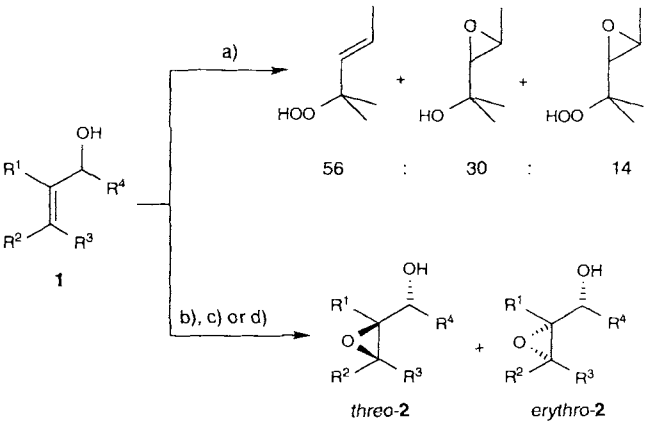

Scheme 1. Heterogeneous TS-1- and homogeneous $Ti(OiPr)_4$-catalyzed epoxidations of the allylic alcohols **1** and side reactions for TS-1. a) For **1f**: TS-1 (100 wt%), H_2O_2 (30%), H_2O, 50 °C, 3 h, conversion > 95%, m.b. ≤ 50%. m.b. = mass balance. b) For **1f**: TS-1 (100 wt%), H_2O_2 (85%), $MgSO_4$, acetone, reflux, 20 h, conversion 90%, yield > 95%. c) TS-1 (50%), UHP (1 equiv), acetone, 50 °C, 14–20 h, conversion > 95%, yield 76–97%, m.b. > 76%. d) $Ti(OiPr)_4$, *t*BuOOH (1.2 equiv), CH_2Cl_2, 16 h, conversion > 85%, yield 82–95%, m.b. > 80%.

Chemo- and Diastereoselective Epoxidation of Chiral Allylic Alcohols with the Urea Hydrogen Peroxide Adduct, Catalyzed by Titanium Silicate 1**

Waldemar Adam,* Rajiv Kumar, T. Indrasena Reddy, and Michael Renz

Titanium silicates belong to the class of heterogeneous oxidation catalysts that oxidize a variety of organic compounds with aqueous hydrogen peroxide as relatively cheap oxygen source. Titanium silicate 1 (TS-1), the titanium analog of the ZSM-5 zeolite, can be recycled many times without losing its activity and catalyzes CH insertions,[1] epoxidations,[2] and arene[3] and heteroatom oxidations of amines[4] and sulfides.[5]

The high reactivity of the catalyst can also be a disadvantage, for example, in the product selectivity of epoxidations. For α-methylstyrene only 15% of the epoxide is obtained; the rest undergoes further reactions like epoxide opening and rearrangements.[6] An important aim is the control of diastereoselectivity. In spite of the many investigations in this research field, only little has been reported. Tatsumi et al.[2d] describe the epoxidation of some chiral allylic alcohols, but neglect to comment on the diastereoselectivity. The only known examples are the diastereoselective epoxidation of two cyclic allylic alcohols.[7]

In continuation of our studies on selective catalytic oxyfunctionalizations of organic substrates,[8] we report herein the first diastereoselective epoxidations of acyclic systems and compare their efficiency and diastereoselectivities with relevant known methods. The epoxy alcohols of defined configuration are useful building blocks for oxyfunctionalized natural products.[9]

When, as usually practiced, dilute, aqueous hydrogen peroxide solution is used, migration and/or substitution of the hydroxy group was observed (Scheme 1, path a). These undesirable reactions most likely derive from allyl-stabilized cationic intermediates.[10] If 85% H_2O_2 is employed in the presence of $MgSO_4$, or if it is filtered over this salt prior to use, the desired epoxide **2f** was obtained in 85% yield (Scheme 1, path b). Thus, whereas the presence of water usually makes no difference in epoxidations because TS-1 is known to be hydrophobic, in the case of the allylic alcohols it causes undesirable side reactions. The potentially explosive concentrated hydrogen peroxide can be replaced by the easier to handle and safer, anhydrous crystalline urea adduct of hydrogen peroxide (urea hydrogen peroxide, UHP). The epoxy alcohols were obtained in similarly high yields and high product selectivity (Scheme 1, path c). Only traces of the C–H insertion product, namely the ketone, were detected, and in no case do the above-mentioned troublesome side reactions occur. The allylic alcohols **1** were consumed completely in 12 to 24 h to form the epoxy alcohols **2**, which were isolated in 72 to 95% yields.

To compare the diastereoselectivities of the heterogeneous TS-1 zeolite with those of a homogeneous titanium catalyst in solution, we chose the *t*BuOOH (TBHP) and $Ti(OiPr)_4$ oxidation system (Sharpless epoxidation without tartrate; Scheme 1, path d). The diastereoselectivities of the oxidants UHP/TS-1 and TBHP/$Ti(OiPr)_4$, and for comparison also *meta*-chloroperbenzoic acid (*m*-CPBA) and TBHP/$VO(acac)_2$, are shown in Table 1.

With the UHP/TS-1 oxidant, substrate-specific selectivities are obtained when 1,3-allylic strain (caused by the substituents R^3 and R^4) is present in the substrate. For the allylic alcohol **1f**, for example, the *threo* isomer was obtained essentially exclusively (entry 6, Table 1), while the alcohols **1d** and **1h** also show relatively high *threo* selectivity (entries 4 and 8). Substrates with R^1 and R^3 substituents, for example **1e** and **1g**, still give high *threo* selectivities (entries 5 and 7), which indicates that the R^1 substituent exercises no significant influence on the diastereoselectivity. The allylic alcohol **1b** exhibits no diastereoselectivity (entry 2), like substrates without R^1 and R^3 substituents (**1a** and **1c**, entries 1 and 3).

The substrate **1f** shows a high *threo* selectivity with the oxidant *m*-CPBA (entry 6). In this case, the coordination of the substrate to the peracid through hydrogen bonding is optimal for oxygen transfer when the dihedral angle (O–C–C=C) of the allylic alcohol is 120° (see structure **E**, Fig. 1).[12] The two possible diastereomeric transition states are then energetically sufficiently differentiated by 1,3-allylic strain so that one predominates and one epoxide diastereomer results preferentially.

[*] Prof. Dr. W. Adam, Dr. T. I. Reddy, Dipl.-Chem. M. Renz
Institut für Organische Chemie der Universität
Am Hubland, D-97074 Würzburg (Germany)
Fax: Int. code +(931)888-4756
e-mail: adam@chemie.uni-wuerzburg.de
Dr. R. Kumar
Catalysis Division, National Chemical Laboratory, 411008 Pune (India)

[**] This research was supported by the Deutsche Forschungsgemeinschaft (SFB 347: "Selektive Reaktionen Metall-aktivierter Moleküle") and the Fonds der Chemischen Industrie.

Table 1. Comparison of the diastereomeric ratios (d.r.) for the epoxidations of the allylic alcohols **1** with the UHP/TS-1, TBHP/$Ti(OiPr)_4$, *m*-chloroperbenzoic acid (*m*-CPBA) and TBHP/$VO(acac)_2$ oxidants. Hacac = acetylacetone

Entry			UHP/ TS-1/ Acetone [a] d.r. [d]	TBHP/ $Ti(OiPr)_4$/ CH_2Cl_2 [b] d.r. [d]	*m*-CPBA/ CH_2Cl_2 d.r. [e]	TBHP/ $VO(acac)_2$/ C_6H_6 [c] d.r. [e]
1		**1a**	65:35	71:29	60:40	20:80
2		**1b**	50:50	22:78	45:55	5:95
3		**1c**	65:35	66:34	64:36	29:71
4		**1d**	80:20	91:9	95:5	71:29
5		**1e**	81:19	83:17	90:10	33:67
6		**1f**	95:5	95:5	95:5	86:14
7		**1g**	90:10	95:5	90:10	
8		**1h**	80:20	95:5	90:10 [f]	78:22

[a] The TS-1 was synthesized by the published procedure with a Si:Ti ratio of about 29 [15], that is, 50 wt% TS-1 represent 2.5 mol% based on the allylic alcohol; all reactions were monitored by TLC to more than 95% conversion; after 12–24 h the oxiranemethanols were isolated in 72–95% yields; traces of the enones were detected in the ^1H NMR spectra of the crude reaction mixture. [b] Carried out by a modified procedure [16]; $Ti(OiPr)_4$ was used in stoichiometric amounts. [c] $VO(acac)_2$ was used in a catalytic amount (0.5 mol%). [d] Diastereomeric ratios (d.r.) of *threo*:*erythro* products determined by ^1H NMR analysis of the characteristic signals in the crude reaction mixture; error ±5% of the stated values. [e] Substrates **1a**–**d**, see ref. [17], substrate **1e** ref. [12]; [f] $CDCl_3$ as solvent.

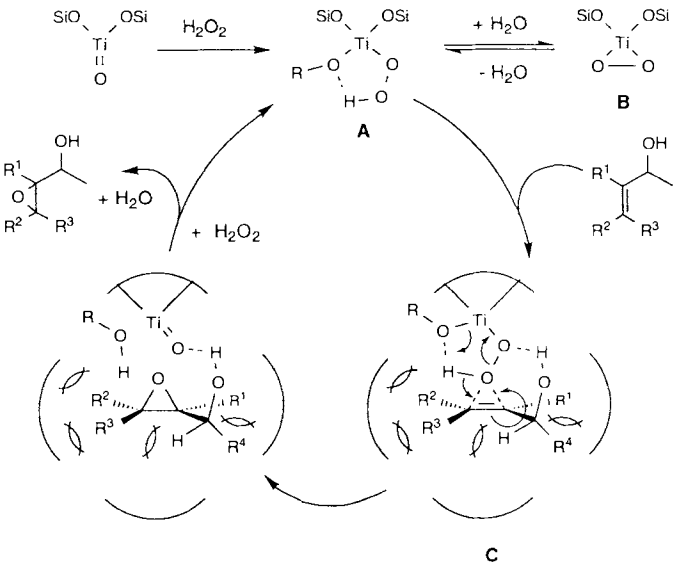

Scheme 2. Catalytic cycle and structures of the titanium peroxide intermediates **A** and **B** and of the transition state **C** for the oxygen transfer of the UHP/TS-1 oxidant.

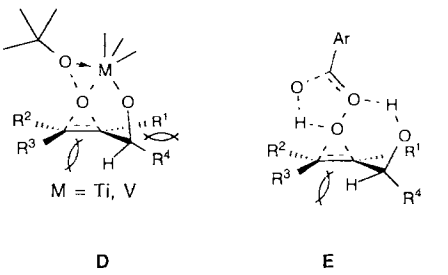

Fig. 1. Transition states for the epoxidations with the oxidants *t*BuOOH/$Ti(OiPr)_4$ or *t*BuOOH/$VO(acac)_2$ (**D**) and *m*-CPBA (**E**).

On the basis of solvent and acid/base effects on the reaction kinetics, the active species for the TS-1 epoxidation is postulated to be similar to peracids (**A**, Scheme 2)[2c, 11, 13] and not to the titanium peroxo complex (**B**, Scheme 2). Consequently, hydrogen bonding between the oxidant and the substrate also operates for the TS-1 epoxidations, and the oxygen is transfered at an optimal dihedral angle of 120° in the allylic alcohol (**C**, Scheme 2). This analogy to the transition state for the oxygen transfer of *m*-CPBA rationalizes the observed identical selectivities; however, the advantage of the UHP/TS-1 oxidant over *m*-CPBA is its catalytic nature (Scheme 2) and the H_2O_2 oxygen source.

As with *m*-CPBA, 1,2-allylic strain is ineffective, as illustrated by substrate **1b**, for which no *erythro* selectivity was obtained with either oxidant (entry 2, Table 1). *Erythro* selectivity would be expected if the dihedral angle were 40°, as it is in the epoxidations of allylic alcohols by the TBHP/$VO(acac)_2$ oxidant (**D**, Fig. 1).[14] The stereochemical probe with both 1,2- and 1,3-allylic strain, namely the alcohol **1e**, which for the vanadium oxidant gives preferentially the *erythro* diastereomer, confirms the similarity between the *m*-CPBA and UHP/TS-1 oxidants in view of the pronounced *threo* selectivity (entries 5 and 7).

Only the substrates **1d** and **1h** (entries 4 and 8), which do not possess *trans* substituents, deviate from this trend. Whereas in the case of *m*-CPBA the *threo* epoxy alcohols are obtained due to the 1,3-allylic strain, the diastereoselectivity for the heterogeneous Ti system drops significantly—surely a zeolite framework effect. We propose that the majority of the molecules will usually react through transition state **C**; however, for *cis* olefins, the sterically less hindered side of the double bond allows additional, less selective attack on the oxygen atom to be transfered in the activated complex. Such unselective possibilities are presumably prevented by steric interactions of the R^2 or R^3 substituents with the zeolite lattice. Alternatively, it is also possible that the less stereoselective Ti peroxo complex **B** is involved in the oxygen transfer, a pathway that is less likely for more sterically hindered substrates such as **1f** and **1g** (entries 6 and 7).

The heterogeneous UHP/TS-1 oxidant differs from the homogeneous TBHP/$Ti(OiPr)_4$ system in several points. A necessary condition for stereocontrolled oxygen transfer in the homogeneous system is coordination of the allylic alcohol to the metal center by means of an alcoholate bond, as suggested by the fact that unfunctionalized olefins are only slowly oxidized and in poor stereoselectivity. Furthermore, the dihedral angle for the TBHP/$Ti(OiPr)_4$ system has to be smaller than 120° because, in contrast to the UHP/TS-1 system, 1,2-allylic strain causes significant *erythro* selectivity (entry 2), but it must be larger than the 40° for the TBHP/$VO(acac)_2$ oxidant because for the stereochemical probe with both 1,2- and 1,3-allylic strain, the latter dominates (entries 5 and 7). Surprisingly, in contrast to the vanadium oxidant, the homogeneous titanium oxidant is very sensitive to 1,3-allylic strain and the *threo* epoxy alcohols are obtained essentially exclusively (entries 4, 6, and 8).

Thus, the heterogeneous UHP/TS-1 oxidant conforms mechanistically to *m*-CPBA, which would be expected in view of the similar active species for the oxygen transfer (cf. transition states **C** and **E**). Hydrogen bonding coupled with 1,3-allylic strain provides the high *threo* diastereoselectivity, as exemplified in substrate **1f**, and 1,2-allylic strain has no significant effect (cf. derivative **1b**). However, mechanistic similarities to the homogeneous TBHP/Ti(O*i*Pr)$_4$ oxidant are also evident, because the latter also displays high *threo* selectivities, but it differs from the UHP/TS-1 oxidant for substrate **1b**, for which TBHP/Ti(O*i*Pr)$_4$ shows significant *erythro* selectivity in view of the greater importance of 1,2-allylic strain. Moreover, besides these mechanistic insights, it should be emphasized that the UHP/TS-1 oxidant is an environmentally acceptable, safe, and mild oxidant for the epoxidation of allylic alcohols. In this way, side reactions that are observed with dilute, aqueous hydrogen peroxide are avoided, and the use of the potentially explosive, concentrated hydrogen peroxide is circumvented.

Experimental Procedure

A solution of 200 mg (2.00 mmol) of the allylic alcohol **1f** in 10 mL acetone was added dropwise to a suspension of 184 mg (2.00 mmol) UHP and 100 mg (50 wt%) TS-1 in 10 mL acetone at room temperature (about 20 °C). The mixture was held at reflux for 20 h, filtered at room temperature through a glass filter, the residue was washed with acetone (2 × 10 mL), and the solvent was removed in a rotoevaporator (35 °C, 20 Torr). The crude product was analyzed by NMR spectroscopy and the *threo*/*erythro* diastereomeric ratio of the sole product was determined to be 95/5 at a conversion of 90%.

Received: October 9, 1995 [Z 8455 IE]
German version: *Angew. Chem.* **1996**, *108*, 944–947

Keywords: asymmetric epoxidations · epoxidations · catalysis · zeolites

[1] a) D. R. C. Huybrechts, L. DeBruycker, P. A. Jacobs, *Nature* **1990**, *345*, 240–242; b) T. Tatsumi, M. Nakamura, S. Negishi, H. Tominaga, *J. Chem. Soc. Chem. Commun.* **1990**, 476–477; c) M. R. Boccuti, K. M. Rao, A. Zecchina, G. Leofanti, G. Petrini, *Stud. Surf. Sci. Catal.* **1988**, *48*, 133–144; d) B. Notari, *ibid.* **1988**, *60*, 413–425; e) M. G. Clerici, *Appl. Catal.* **1991**, *68*, 249–261.

[2] a) T. Tatsumi, M. Nakamura, K. Yuasa, H. Tominaga, *Chem. Lett.* **1990**, 297–298; b) T. Tatsumi, M. Nakamura, H. Tominaga, *ibid.* **1989**, 419–420; c) M. G. Clerici, P. Ingallina, *J. Catal.* **1993**, *140*, 71–83; d) T. Tatsumi, M. Yako, M. Nakamura, Y. Yuhara, H. Tominaga, *J. Mol. Catal.* **1993**, *78*, L41–L45; e) A. Bhaumik, R. Kumar, P. Ratnasamy, *Stud. Surf. Sci. Catal.* **1994**, *84*, 1883–1888.

[3] a) M. Taramasso, G. Perego, B. Notari, SNAM Progetti S. p. A *US-A* **1983**, 4410501 [*Chem. Abstr.* **1982**, *96*, 37802w]; b) A. V. Ramaswamy, S. Sivasanker, P. Ratnasamy, *Microporous Mater.* **1994**, *2*, 451–458.

[4] a) P. Roffia, M. Padovan, E. Moretti, G. De Alberti, Montedipe S. p. A *EP-A* **1987**, 208311 [*Chem. Abstr.* **1987**, *106*, 155944s]; b) P. Roffia, G. Leofanti, A. Cesana, M. Mantegazza, M. Padovan, G. Petrini, S. Tonti, V. Gervasutti, R. Varagnolo, *Chim. Ind. (Milan)* **1990**, *72*, 598–603; c) J. S. Reddy, P. A. Jacobs, *J. Chem. Soc. Perkin Trans. 1* **1993**, 2665–2666.

[5] R. S. Reddy, J. S. Reddy, R. Kumar, P. Kumar, *J. Chem. Soc. Chem. Commun.* **1992**, 84–85.

[6] J. S. Reddy, U. R. Khire, P. Ratnasamy, R. B. Mitra, *J. Chem. Soc. Chem. Commun.* **1992**, 1234–1235.

[7] R. Kumar, G. C. G. Pais, B. Pandey, P. Kumar, *J. Chem. Soc. Chem. Commun.* **1995**, 1315–1316.

[8] a) W. Adam, B. Nestler, *J. Am. Chem. Soc.* **1992**, *114*, 6549–6550; b) W. Adam, B. Nestler, *ibid.* **1993**, *115*, 7226–7231; c) W. Adam, B. Nestler, *Angew. Chem.* **1993**, *105*, 767–769; *Angew. Chem. Int. Ed. Engl.* **1993**, *32*, 733–735; d) W. Adam, M. Richter, *Acc. Chem. Res.* **1994**, *27*, 57–62; e) W. Adam, K. Peters, M. Renz, *Angew. Chem.* **1994**, *106*, 1159–1161; *Angew. Chem. Int. Ed. Engl.* **1994**, *33*, 1107–1108; f) W. Adam, C. M. Mitchell, *Angew. Chem.* **1996**, *108*, 578–581; g) W. Adam, F. Prechtl, M. J. Richter, A. K. Smerz, *Tetrahedron Lett.* **1993**, *34*, 8427–8430; h) W. Adam, F. Prechtl, M. J. Richter, A. K. Smerz, *Tetrahedron Lett.* **1995**, *36*, 4991–4994; i) W. Adam, A. K. Smerz, *Tetrahedron* **1995**, *51*, 13039–13044.

[9] a) P. A. Bartlett, *Tetrahedron* **1980**, *36*, 1–72; b) B. Meunier, *Chem. Rev.* **1992**, *92*, 1411–1456; c) Organic Peroxygen Chemistry (Ed.: W. A. Herrmann), (*Top. Curr. Chem.* **1993**, *164*); d) P. Besse, H. Veschambre, *Tetrahedron* **1994**, *50*, 8885–8927; e) A. Pfenninger, *Synthesis* **1986**, 89–116; f) M. G. Finn, K. B. Sharpless in *Asymmetric Synthesis, Vol. V* (Ed.: J. D. Morrison), Academic Press, Orlando, FL, **1985**.

[10] a) A. I. Biaglow, R. J. Gorte, D. White, *J. Chem. Soc. Chem. Commun.* **1993**, 1164–1166; b) D. Fârcaşiu, *ibid.* **1994**, 1801–1802; c) T. Xu, J. Zhang, E. J. Munson, J. F. Haw, *ibid.* **1994**, 2733–2735; d) M. L. Cano, V. Fornés, H. García, M. A. Miranda, J. Pérez-Prieto, *ibid.* **1995**, 2477–2478.

[11] C. B. Khouw, C. B. Dartt, J. A. Labinger, M. E. Davis, *J. Catal.* **1994**, *149*, 195–205.

[12] a) A. H. Hoveyda, D. A. Evans, G. C. Fu, *Chem. Rev.* **1993**, *93*, 1307–1370; b) W. Adam, B. Nestler, *Tetrahedron Lett.* **1993**, *34*, 611–614.

[13] A. Corma, M. A. Camblor, P. Esteve, A. Martínez, J. Pérez-Pariente, *J. Catal.* **1994**, *145*, 151–158.

[14] K. B. Sharpless, T. R. Verhoeven, *Aldrichimica Acta* **1979**, *12*, 63–74.

[15] A. Thangaraj, S. Sivasanker, *J. Chem. Soc. Chem. Commun.* **1992**, 123–124.

[16] T. Katsuki, K. B. Sharpless, *J. Am. Chem. Soc.* **1980**, *102*, 5974–5976.

[17] B. E. Rossiter, T. R. Verhoeven, K. B. Sharpless, *Tetrahedron Lett.* **1979**, 4733–4736.

Silolyl Anions and Silole Dianions: Structure of [K([18]crown-6)$^+$]$_2$[$C_4Me_4Si^{2-}$]**

William P. Freeman, T. Don Tilley,* Glenn P. A. Yap, and Arnold L. Rheingold*

Silolyl anions [C_4R_4SiR']$^-$ have been the focus of recent experimental[1, 2] and theoretical[3, 4] investigations. These studies are concerned with characterizing the structural and chemical properties of these novel π-electron systems, which may possess some degree of aromaticity. Theoretical studies suggest a significant amount of delocalization for the free $C_4H_4SiH^-$ anion, and NMR data obtained by Hong and Boudjouk for the lithium and sodium derivatives of [$Ph_4C_4Si(t$Bu)]$^-$ in THF indicate some delocalization of the negative charge in the ring.[2] We have recently reported the metal π-complex (η^5-C_5Me_5)Ru[η^5-$C_4Me_4SiSi(SiMe_3)_3$], which appears to have significantly delocalized electron density in the C_4Si ring, as shown by NMR spectroscopy.[5]

After the initial report by Joo and co-workers on the generation of the silole dianion $C_4Ph_4Si^{2-}$, a number of investigations described further properties for such species and their usefulness as intermediates in the synthesis of silole derivatives.[6] Based on somewhat downfield-shifted ^{29}Si NMR resonances, these species appear to have at least some delocalization of negative charge in the five-membered ring.[6b, c] The dilithium derivative [$Li(thf)_2$][$Li(thf)_3$][η^5,η^1-C_4Ph_4Si], recently described by West and co-workers, appears to have a delocalized structure based on the equivalent C–C distances in the C_4Si ring.[6d] Calculations support this view,[6d, 7] and Schleyer et al. have predicted that the "free" silole dianion $C_4H_4Si^{2-}$ would be highly aromatic and form dilithium, disodium, and dipotassium salts with the metals bound in an η^5-fashion to both sides of the ring.[7] Here we report on a silole dianion of the latter type, which is isoelectronic with tetramethylthiophene and has an aromatic $C_4Me_4Si^{2-}$ ring.

Reduction of $C_4Me_4SiBr_2$[8] with three equivalents of potassium in THF gives a solution of dianion **1** (Scheme 1), as deter-

[*] Prof. Dr. T. D. Tilley, W. P. Freeman
Department of Chemistry
University of California, Berkeley
Berkeley, CA 94720-1460 (USA)
Fax: Int. code +(510) 642-8940
Prof. Dr. A. L. Rheingold, G. P. A. Yap
Department of Chemistry
University of Delaware
Newark, DE 19716 (USA)

[**] This research was supported by the National Science Foundation. We thank Greg Mitchell for helpful discussions, and Prof. P. von R. Schleyer for a preprint of ref. [7].

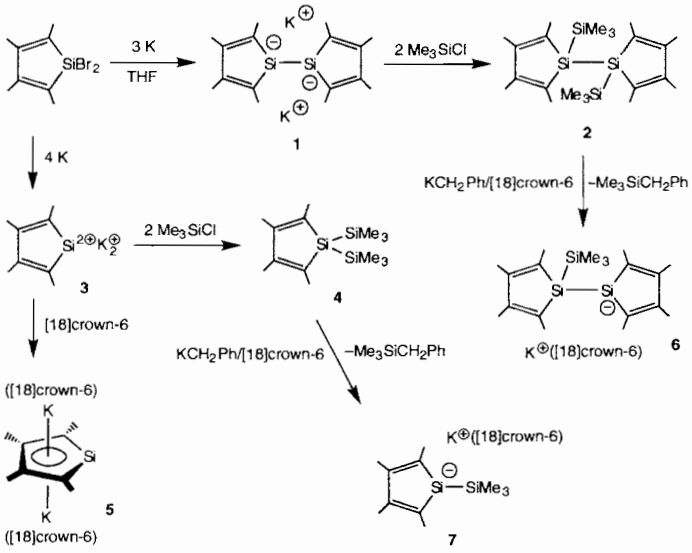

Scheme 1. Synthetic routes to silolyl anions and the silole dianion **5**.

mined by subsequent quenching with Me_3SiCl to produce the tetrasilane **2**. The latter compound was isolated in 60% yield as colorless crystals. A similar reaction sequence was used by Hong et al. to prepare $C_4Ph_4Si(SiMe_3)-Si(SiMe_3)C_4Ph_4$.[6b] Reduction of $C_4Me_4SiBr_2$ with four equivalents of potassium produces THF solutions of dianion **3** (Scheme 1), which was converted to the known[6c] silole **4** by reaction with Me_3SiCl. In the presence of [18]crown-6, this reduction gives complex **5**, which was isolated in crystalline form by slow, gas-phase diffusion of pentane into a solution of **5** in tetrahydrofuran.

Figure 1 provides a view of the molecular structure of **5**.[9] The very slight bond length alternation in the C_4Si ring (C(25)–C(26) = 1.40(1) Å; C(27)–C(28) = 1.38(1) Å; C(26)–C(27) = 1.44(1) Å) is consistent with considerable delocalization of π-electron density. Calculations by Schleyer et al. indicate that $C_4H_4Si^{2-}$ would have even more equivalent C–C distances.[7]

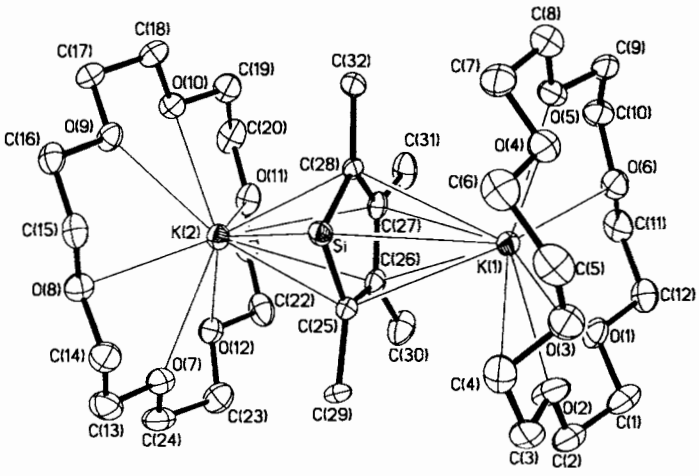

Fig. 1. Molecular structure of **5**. Selected interatomic distances [Å] and angles [°]: C(25)–C(26) 1.40(1), C(26)–C(27) 1.44(1), C(27)–C(28) 1.38(1), Si–C(25) 1.830(8), Si–C(28) 1.851(8), K(1)–C(25) 3.139(8), K(1)–C(26) 2.980(8), K(1)–C(27) 2.986(7), K(1)–C(28) 3.138(7), K(1)–Si 3.387(3), K(2)–C(25) 3.161(8), K(2)–C(26) 3.085(8), K(2)–C(27) 3.060(8), K(2)–C(28) 3.149(8), K(2)–Si 3.364(3); C(25)-Si-C(28) 87.2(4), Si-C(25)-C(26) 113.7(6), C(25)-C(26)-C(27) 112.2(7), C(26)-C(27)-C(28) 114.3(7), C(27)-C(28)-Si 112.6(6).

For comparison, much greater C–C bond length differences have been observed for the siloles $C_4Ph_4SiCl_2$ (1.35(1) Å; 1.54(1) Å),[7] $C_4Me_4SiCl_2$ (1.356(4) Å; 1.515 (6) Å),[6c] and $C_4Ph_4SiMe_2$ (averages: 1.36 Å; 1.51 Å).[10] The Si–C distances in **5** (1.85 (1) and 1.83 (1) Å) are surprisingly close to those observed in the latter silole derivatives (1.83(1),[7] 1.834(3),[6c] and 1.87(1)[10] Å, respectively). The K–C distances range from 2.980(8) to 3.161(8) Å, and are therefore similar to the average K–C bond lengths in $K[C_5H_4SiMe_3]$ (3.00(2) Å)[11] and $K[C_5(CH_2Ph)_5]$ (3.04(4) Å).[12] Each potassium atom is about 0.1 Å closer to the adjacent carbon atoms C(26) and C(27) than to C(25) and C(28). The K–Si distances (3.387(3) and 3.364(3) Å) are longer than the average K–C bond length, by about 0.3 Å. This difference is somewhat less than the difference in covalent radius between carbon and silicon (ca. 0.4 Å).[13] For comparison, the K–Si distances in β-$KSiH_3$ range from 3.56 to 3.86 Å.[14]

We recently reported the synthesis of germolyl anions by nucleophilic cleavage of Si–Ge bonds with benzylpotassium, and the crystal structure analysis of the "free" germolyl anion $[C_4Me_4GeSi(SiMe_3)_3]^-$ which has a highly pyramidalized germanium center.[15] As shown in Scheme 1, this method also works for the synthesis of silolyl anions **6** and **7**. Interestingly, the ^{29}Si NMR resonances for these anions (**6**: $\delta = -53.43$; **7**: $\delta = -41.52$) are shifted upfield relative to the corresponding resonances for the parent siloles (**1**: $\delta = -34.71$; **4**: $\delta = -34.26$). This trend is opposite to that reported by Hong and Boudjouk for the silolyl anions $M[C_4Ph_4Si(tBu)]$ (M = Li, Na) formed from $C_4Ph_4Si(tBu)-Si(tBu)C_4Ph_4$; their ^{29}Si NMR resonances are shifted downfield relative to those of the starting material ($\Delta\delta = 22.5$). The latter observation was interpreted in terms of delocalization of negative charge onto the silolyl anion ring.[2] Based on NMR data, it appears that this is not the case for anions **6** and **7**. The difference between these systems may be attributed to phenyl vs. methyl substitution in the rings, and/or to different degrees of interaction between the alkali metal ion and the silolyl ring. Goldfuss and Schleyer have suggested that η^5 bonding of an Li^+ ion to $C_4H_4SiH^-$ increases delocalization in the C_4Si ring.[4b] Ongoing investigations are intended to address these issues.

Experimental Procedure

2: Tetrahydrofuran (100 mL) was added to a Schlenk flask containing $C_4Me_4SiBr_2$ (0.62 g, 2.3 mmol) and small potassium chunks (0.27 g, 6.9 mmol). After stirring the reaction mixture at room temperature for 10 days, the red reaction solution was cooled to −78 °C, and then Me_3SiCl (1.50 mL, 11.8 mmol) was added. After warming the solution to room temperature, the volatile material was removed, and the resulting colorless oil was extracted into pentane (3 × 40 mL). Concentration and cooling (−78 °C) allowed crystallization of the product in 60% yield. Elemental analysis for $C_{22}H_{42}Si_4$: calcd: C 63.06, H 10.12; found: C 62.89, H 10.24. ^1H NMR (400 MHz, [D_6]benzene): $\delta = 0.13$ (s, 18H, $SiMe_3$), 1.87, 2.12 (s, 12H, CMe). $^{13}C\{^1H\}$ NMR (100.6 MHz, [D_6]benzene): $\delta = -0.61$ ($SiMe_3$), 14.81, 15.74 (*CMe*), 131.83, 150.11 (*C*Me). $^{29}Si\{^1H\}$ NMR (59.6 MHz, INEPT, [D_6]benzene): $\delta = -34.71$ (s, C_4Me_4Si), −13.24 (s, $SiMe_3$).

4: The procedure for the preparation of **2** was followed; however, four equivalents of potassium per equivalent of $C_4Me_4SiBr_2$ were used. The product was isolated as a spectroscopically pure [6c], colorless oil by simply removing the pentane extraction solvent (75% yield). ^1H NMR (400 MHz, [D_6]benzene): $\delta = 0.19$ (s, 18H, $SiMe_3$), 1.84, 2.01 (s, 6H, CMe). $^{13}C\{^1H\}$ NMR (100.6 MHz, [D_6]benzene): $\delta = -0.34$ ($SiMe_3$), 14.65, 15.38 (*CMe*), 130.99, 149.81 (*C*Me). $^{29}Si\{^1H\}$ NMR (59.6 MHz, INEPT, [D_6]benzene): $\delta = -34.26$ (s, C_4Me_4Si), −14.83 (s, $SiMe_3$).

5: Tetrahydrofuran (50 mL) was added to a flask containing $Me_4C_4SiBr_2$ (0.050 g, 1.9 mmol), [18]crown-6 (0.49 g, 1.9 mmol), and small potassium chunks (0.22 g, 5.65 mmol). The solution was stirred for three days, and then the product was crystallized by vapor diffusion of pentane into the red solution of the dianion. Complex **5** formed as red crystals in 5% yield after four days (yield not optimized). Elemental analysis for $C_{32}H_{60}K_2SiO_{12}$: calcd: C 51.71, H 8.15; found: C 49.12, H 7.94. ^1H NMR (400 Mz, [D_6]benzene) $\delta = 2.81$, 3.27 (s, 6H, CMe), 3.47 (broad s, 24H, [18]crown-6).

6: To an NMR tube was added **2** (0.020 g, 0.048 mmol), [18]crown-6 (0.013 g, 0.048 mmol), [D$_6$]benzene (0.3 mL), and KCH_2Ph (0.006 g, 0.05 mmol), and the NMR tube was shaken for 20 minutes. During this time the insoluble benzylpotassium reacts to give an orange solution of the silole anion. ^{1}H NMR (400 MHz; [D$_6$]benzene): $\delta = 0.44$ (s, 9H, $SiMe_3$), 2.08, 2.39 (s, 6H, $C_4\mathit{Me}_4Si-SiMe_3$), 2.33, 2.65 (s, 6H, $C_4\mathit{Me}_4Si^-K^+$), 3.24 (s, 24H, [18]crown-6). $^{13}C\{^1H\}$ NMR (100.6 MHz, [D$_6$]benzene): $\delta = 0.60$ (s, $SiMe_3$), 14.60, 16.45 (s, $C_4\mathit{Me}_4Si-SiMe_3$), 15.71, 18.43 (s, $C_4\mathit{Me}_4Si^-K^+$), 69.95 (s, [18]crown-6), 137.23, 143.80 (s, $C_4Me_4Si-SiMe_3$), 138.49, 149.08 (s, $C_4\mathit{Me}_4Si^-K^+$). $^{29}Si\{^1H\}$ NMR (59.6 MHz, INEPT, [D$_6$]benzene): $\delta = -53.43$ (s, $C_4Me_4\mathit{Si}^-K^+$), -25.47 (s, $C_4Me_4\mathit{Si}-SiMe_3$), -13.49 (s, $C_4Me_4Si-\mathit{Si}Me_3$).

7: To an NMR tube was added **4** (0.010 g, 0.034 mmol), [18]crown-6 (0.009 g, 0.034 mmol), [D$_6$]benzene (0.3 mL), and KCH_2Ph (0.005 g, 0.034 mmol). The tube was shaken for 20 min . The resulting orange solution was identified by NMR spectroscopy as the product **7**. ^{1}H NMR (400 MHz; [D$_6$]benzene): $\delta = 0.57$ (s, 9H, $SiMe_3$), 2.34, 2.67 (s, 6H, $C_4\mathit{Me}_4Si$), 3.20 (s, 24H, [18]crown-6). $^{13}C\{^1H\}$ NMR (100.6 MHz, [D$_6$]benzene): $\delta = 2.50$ (s, $SiMe_3$), 15.55 , 18.34 (s, $C_4\mathit{Me}_4Si$), 70.05 (s, [18]crown-6), 135.76, 149.60 (s, C_4Me_4Si). $^{29}Si\{^1H\}$ NMR (59.6 MHz, INEPT, [D$_6$]benzene): $\delta = -41.52$ (s, $C_4Me_4\mathit{Si}$), -11.00 (s, $SiMe_3$).

Received: November 23, 1995 [Z8586IE]
German version: *Angew. Chem.* **1996**, *108*, 960–962

Keywords: aromaticity · cyclopentadienides · heterocycles · silicon compounds · silole derivatives

[1] J. Dubac, A. Laporterie, G. Manuel, *Chem. Rev.* **1990**, *90*, 215; E. Colomer, R. J. P. Corriu, M. Lheureux, *ibid.* **1990**, *90*, 265; H. Grützmacher, *Angew. Chem.* **1995**, *107*, 323; *Angew. Chem. Int. Ed. Engl.* **1995**, *34*, 295.
[2] J.-H. Hong, P. Boudjouk, *J. Am. Chem. Soc.* **1993**, *115*, 5883.
[3] M. S. Gordon, P. Boudjouk, F. Anwari, *J. Am. Chem. Soc.* **1983**, *105*, 4972; J. R. Damewood, Jr., *J. Org. Chem.* **1986**, *51*, 5028.
[4] a) P. von R. Schleyer, P. K. Freeman, H. Jiao, B. Goldfuss, *Angew. Chem.* **1995**, *107*, 332; *Angew. Chem. Int. Ed. Engl.* **1995**, *34*, 337; b) B. Goldfuss, P. von R. Schleyer, *Organometallics* **1995**, *14*, 1553.
[5] W. P. Freeman, T. D. Tilley, A. L. Rheingold, *J. Am. Chem. Soc.* **1994**, *116*, 8428.
[6] a) W.-C. Joo, J.-H. Hong, S.-B. Choi, H.-E. Son, C. H. Kim, *J. Organomet. Chem.* **1990**, *391*, 27; b) J.-H. Hong, P. Boudjouk, S. Castellino, *Organometallics* **1994**, *13*, 3387. c) U. Bankwitz, H. Sohn, D. R. Powell, R. West, *J. Organomet. Chem.* **1995**, *499*, C7; d) R. West, H. Sohn, U. Bankwitz, J. Calabrese, Y. Apeloig, T. Mueller, *J. Am. Chem. Soc.* **1995**, *117*, 11608.
[7] B. Goldfuss, P. von R. Schleyer, F. Hempel, *Organometallics*, submitted.
[8] P. J. Fagan, W. A. Nugent, *J. Am. Chem. Soc.* **1988**, *110*, 2310.
[9] Crystal data for **5**: $C_{32}H_{60}K_2O_{12}Si$, monoclinic, $P2_1/n$, $a = 10.599(2)$, $b = 22.534(4)$, $c = 16.897(3)$ Å, $\beta = 92.26(2)^\circ$, $V = 4032(1)$ Å^3, $Z = 4$; $\mu(Mo_{K\alpha}) = 3.18$ cm^{-1}, $T = 243$ K. Of 5196 data collected (max $2\theta = 42^\circ$), 4325 were independent and used in the F^2 refinement of 424 variables. $R(F) = 0.0764$ [$I > 2\sigma(I)$], $R(wR2) = 0.2741$ (all data). SHELXTL (version 5.2) was used for data processing. Further details of the crystal structure investigation are available on request from the Director of the Cambridge Crystallographic Data Centre, 12 Union Road, GB-Cambridge CB2 1EZ (UK), on quoting the full journal citation.
[10] L. Párkányi, *J. Organomet. Chem.* **1981**, *216*, 9.
[11] P. Jutzi, W. Leffers, B. Hampel, S. Pohl, W. Saak, *Angew. Chem.* **1987**, *99*, 563; *Angew. Chem., Int. Ed. Engl.* **1987**, *26*, 583.
[12] J. Lorbeth, S.-H. Shin, S. Wocadlo, W. Massa, *Angew. Chem.* **1989**, *101*, 793; *Angew. Chem., Int. Ed. Engl.* **1989**, *28*, 735.
[13] L. Pauling, *The Nature of the Chemical Bond*, 3rd ed., Cornell University Press, Ithaca, NY, **1960**, p. 224.
[14] G. Becker, H.-M. Hartmann, O. Mundt, W. Schwarz, *Z. Anorg. Allg. Chem.* **1989**, *572*, 75.
[15] W. P. Freeman, T. D. Tilley, F. P. Arnold, A. L. Rheingold, P. K. Gantzel, *Angew. Chem.* **1995**, *107*, 2029; *Angew. Chem. Int. Ed. Engl.* **1995**, *34*, 1887.

N-Acyl Enamines in the Paternò–Büchi Reaction: Stereoselective Preparation of 1,2-Amino Alcohols by C–C Bond Formation**

Thorsten Bach*

In the Paternò–Büchi reaction of terminal heteroatom-substituted alkenes with aldehydes, oxetanes are formed that carry the substituent X either in the 3- or in the 4-position depending on the regioselectivity of the photocycloaddition (Scheme 1).[1]

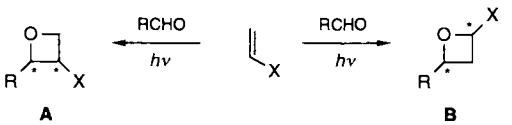

Scheme 1. The regioisomeric oxetanes **A** and **B** (1,2- and 1,3-connectivity, respectively, of the groups R and X) that can be formed by the photocycloadditon of an aldehyde to a heteroatom(X)-substituted alkene.

If the electronic properties of the $^3n\pi^*$ state, which is to a large extent responsible for the photochemical reactivity of many carbonyl compounds, are taken into consideration a preference for products of type **A** is expected. The 1,2-connectivity of functional groups in oxetane **A** reflects the nucleophilic character of the carbonyl carbon atom and is thus a hallmark for the photochemically induced reversal of the polarity of the carbonyl group. However, only in a few cases does the reaction of monosubstituted alkenes proceed with sufficient regioselectivity. One example are vinyl sulfides,[2] which, in contrast to the O-analogous vinyl ethers,[3] deliver the photocycloaddition products with good selectivity.

A further problem not yet solved for terminal alkenes concerns the simple diastereoselectivity of the C–C bond formation. Since numerous reactions have been reported that ring-open oxetanes of type **A** at the least substituted C-4 position under retention of the C–C bond formed in the course of the photocycloaddition,[4] the simple diastereoselectivity achieved in the Paternò–Büchi reaction can be transferred potentially to acyclic target molecules.

In view of the importance of 1,2-amino alcohols,[5] for example as enzyme inhibitors,[6] we looked for suitable N-substituted alkenes that may add selectively to carbonyl compounds. Compounds in which the donor activity of the nitrogen atom is reduced are for example N-acylated enamines (enamides), which can be prepared readily from imines **1** [Eq. (a)].[7] The

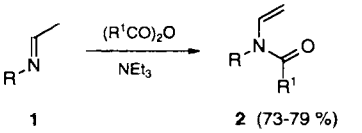

1 **2** (73–79 %)

a, R = Pr, R^1 = Me
b, R = Bn, R^1 = Me
c, R = Bn, R^1 = O*t*Bu (a)

[*] Dr. T. Bach
Organisch-chemisches Institut der Universität
Orléansring 23, D-48149 Münster (Germany)
Fax: Int. code +(251)83-9772
e-mail: bacht@uni-muenster.de

[**] This project was supported by the Fonds der Chemischen Industrie, the Gesellschaft zur Förderung der Westfälischen Wilhelms-Universität, and the Dr. Otto Röhm-Gedächtnisstiftung. Thanks are due to Mrs. K. Busse, Dr. J. Lauterwein, and Dr. T. Fox for their help with the NOE studies. The continuing support of Prof. Dr. D. Hoppe is gratefully acknowleged.

other compounds under scrutiny *N*-vinyl pyrrolidone (**2d**) and *N*-vinyl acetamide[8] (**2e**) are either commercially available or can be synthesized following published procedures.

Substrates of this kind have not yet been employed in stereoselective Paternò–Büchi reactions. Only studies on heterocyclic enamides[9] and 2-aminopropenenitriles[10] have been reported previously. For our irradiation experiments acetonitrile was found to be the solvent of choice, and benzaldehyde was employed as the carbonyl compound. The photocycloadditions generate the products in very good yields with remarkable regio- and diastereoselectivities [Eq. (b),[11] Table 1]. In the reactions with alkenes **2a** and **2b** one of the four possible isomers was isolated (as a racemic mixture) in diastereomerically pure form. The relative configuration of the products was most readily demonstrated on the oxetanes **3d**/**4d** since there are no rotamers to complicate the NOE studies; thus, the assignment of major and minor diastereoisomer are unambiguous for this particular case. The results of NOE measurements were consistent with the structures of the major diastereoisomers **3c** and **3e** shown in Equation (b). Unfortunately some compounds decomposed at elevated temperature; thus NOE studies on oxetanes **3b** and **4b** which had to be carried out at 373 K remained inconclusive. Based on analogy arguments the relative configuration for the depicted products appears very likely. The amino substituent and the phenyl group in the major diastereoisomer are consequently oriented *cis* to each other.

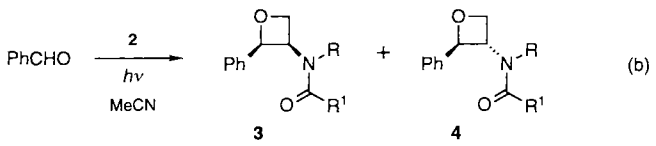

3 4

Table 1. Yields, regioisomeric (r.r.) and diastereomeric ratios (d.r.) in the photocycloaddition of benzaldehyde to *N*-acyl enamine **2** carried out in acetonitrile at room temperature [Eq. (b)].

Enamine	R	R^1	*t* [h] [a]	Yield [%] [b]	r.r. [c]	d.r.(**3**:**4**) [d]
2a	Pr	Me	14	70 [e]	>95:5	>90:10
2b	Bn	Me	14	73 [e]	97:3	89:11
2c	Bn	O*t*Bu	14	77 [f]	94:6	87:13
2d		$-(CH_2)_3-$	18	82 [f]	92:8	88:12
2e	H	Me	120 [g]	58 [f, g]	>95:5	79:21

[a] Irradiation time. [b] Isolated yields obtained by using two equivalents of the alkene. [c] Determined by GLC analysis of the crude product. [d] Determined by ^{1}H NMR spectroscopic analysis of the crude product. [e] Yield of pure diastereoisomer **3**. [f] Yield of the diastereomeric mixture **3** and **4**. [g] Slow reaction due to the formation of an amorphous precipitate. The yield relative to converted benzaldehyde is 79%.

The photocycloaddition procedure can also be applied to β-substituted alkenes. The cyclic enamide **5**[12] reacts with benzaldehyde to yield the bicyclic compound **6** [Eq. (c)], whose relative configuration was elucidated by NOE studies. The regioselectivity of the carbonyl attack in this reaction was less pronounced than in the cases described earlier. The yield of desired oxetane **6** was therefore lower than for β-unsubstituted compounds. The facile Pd-catalyzed hydrogenolytic ring opening[13] provides a straightforward access to excellent yields of pyrrolidine derivatives such as **7**, which carry an arylmethyl in the 2-position and a *cis*-oriented hydroxy group in the 3-position. Related natural products of this kind exert antifungal[14] and antibiotic activity.[15]

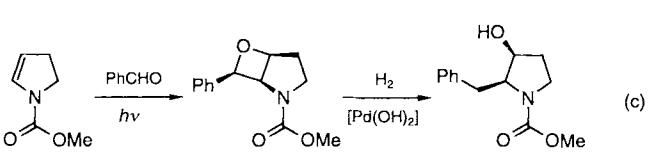

5 6 (56 %) 7 (94 %)

Further experiments as to the origin of the high regio- and diastereoselectivity are in progress. With regard to regioselectivity possible explanations can be based on previous work[2] as already mentioned. To understand the high degree of simple diastereoselectivity it is appealing to consider the preferred intersystem crossing (ISC) conformations of an intermediate 1,4-triplet biradical.[16] This picture may, however, become more complex if the retro cleavage of a 1,4-biradical can effectively compete with the ring closure step. Temperature-dependent measurements of the simple diastereoselectivity may provide us with additional information related to this issue.[17] Studies concerned with the influence of the aldehyde substrate and with the facial diastereoselectivity of the reaction are under way.

Experimental Procedure

Benzaldehyde (159 mg, 1.5 mmol, 152 µL) and **2** (3.0 mmol) were dissolved in acetonitrile (10 mL) in a quartz tube. This mixture was irradiated for the period of time *t* given in Table 1 (λ = 300 nm; light source: Rayonet RPR 3000). The course of the reaction was monitored by TLC and GLC. Upon complete conversion of the aldehyde the solvent was evaporated in vacuo. The regioisomeric ratio (*r.r.*) was determined by GLC analysis of the crude product mixture, the simple diastereoselectivity (*d.r.*) by ^{1}H NMR spectroscopic analysis. The excess enamide was separated from the desired oxetane by column chromatography (flash chromatography; eluent: cyclohexane/ethyl acetate mostly as a gradient 90/10 to 60/40). A complete separation of the diastereoisomers **3a** and **4a** and **3b** and **4b** was possible by chromatography.

Received: November 24, 1995 [Z 8593 IE]
German version: *Angew. Chem.* **1996**, *108*, 976–977

Keywords: asymmetric syntheses · enamines · oxetanes · Paternò–Büchi reactions · photochemistry

[1] Recent reviews on the Paternò–Büchi reaction: a) J. Mattay, R. Conrads, R. Hoffmann in *Methoden Organ. Chem. (Houben-Weyl) 4th ed. 1952 , Band E 21c*, **1995**, pp. 3133–3178; b) J. A. Porco, S. L. Schreiber in *Comprehensive Organic Synthesis, Vol. 5* (Ed. B. Trost), Pergamon Press, Oxford, **1991**, pp. 151–192; c) H. A. J. Carless in *Synthetic Organic Photochemistry* (Ed.: W. M. Horspool), Plenum, New York, **1984**, pp. 425–487; d) G. Jones II in *Organic Photochemistry Vol. 5*, (Ed.: A. Padwa), Dekker, New York, **1981**, pp. 1–123.

[2] N. Khan, T. H. Morris, E. H. Smith, R. Walsh, *J. Chem. Soc., Perkin Trans. 1* **1991**, 865–870. Further references concerning regioselective Paternò–Büchi reactions of monosubstituted alkenes can be found therein.

[3] a) S. H. Schroeter, C. M. Orlando Jr., *J. Org. Chem.* **1969**, *34*, 1181–1187; b) Y. Araki, J. I. Nagasawa, Y. Ishido, *Carbohydr. Res.* **1981**, *91*, 77–84.

[4] Some recent examples: H. Xianming, R. M. Kellogg, *Tetrahedron: Asymmetry* **1995**, *6*, 1399–1408; P. Crotti, L. Favero, F. Macchia, M. Pineschi, *Tetrahedron Lett.* **1994**, *35*, 7089–7092; M. Chini, P. Crotti, L. Favero, F. Macchia, *ibid.* **1994**, *35*, 761–764.

[5] M. T. Reetz, *Angew. Chem.* **1991**, *103*, 1554–1573; *Angew. Chem. Int. Ed. Engl.* **1991**, *30*, 1531–1546, and references therein.

[6] Reviews: a) J. Gante, *Angew. Chem.* **1994**, *106*, 1780–1802; *Angew. Chem. Int. Ed. Engl.* **1994**, *33*, 1699–1720; b) B. Weidmann, *Chimia* **1991**, *45*, 367–376; c) J. R. Huff, *J. Med. Chem.* **1991**, *34*, 2305–2314.

[7] a) H. Breederveld, *Recl. Trav. Chim. Pays-Bas* **1960**, *79*, 401–407; b) O. Meth-Cohn, K. T. Westwood, *J. Chem. Soc., Perkin Trans. 1*, **1984**, 1173–1182.

[8] R. C. Schulz, H. Hartmann, *Monatsh. Chem.* **1961**, *92*, 303–309.

[9] a) Aromatic heterocycles: D. R. Julian, G. D. Tringham, *J. Chem. Soc. Chem. Commun.* **1973**, 13; T. Nakano, C. Rivas, C. Perez, J. M. Larrauri, *J. Heterocyclic Chem.* **1976**, *13*, 173–174; C. Rivas, R. A. Bolivar, *ibid.* **1976**, *13*, 1037–1040; T. Nakano, W. Rodríguez, S. Z. de Roche, J. M. Larrauri, C. Rivas, C. Perez, *ibid.* **1980**, *17*, 1777–1780; b) oxazoline derivatives: K.-H. Scholz, H.-G. Heine, W. Hartmann, *Tetrahedron Lett.* **1978**, *17*, 1467–1470; M. Weuthen, H.-D. Scharf, J. Runsink, *Chem. Ber.* **1987**, *120*, 1023–1026; M. Weuthen, H.-D. Scharf, J. Runsink, R. Vassen, *ibid.* **1988**, *121*, 971–976.

[10] D. Döpp, H. R. Memarian, M. A. Fischer, A. M. J. van Eijk, C. A. G. O. Varma, *Chem. Ber.* **1992**, *125*, 983–984; D. Döpp, M.-A. Fischer, *Recl. Trav. Chim. Pays-Bas* **1995**, *114*, 498–503.

[11] In all equations only one enantiomer is arbitrarily shown.
[12] G. A. Kraus, K. Neuenschwander, *J. Org. Chem.* **1981**, *46*, 4791–4792.
[13] a) T. Bach, *Tetrahedron Lett.* **1994**, *35*, 1855–1858; b) T. Bach, *Liebigs Ann.* **1995**, 1045–1053.
[14] (+)-Preussin: R. E. Schwartz, J. Liesch, O. Hensens, L. Zitano, S. Honeycutt, G. Garrity, R. A. Fromtling, J. Onishi, R. Monaghan, *J. Antibiot.* **1988**, *41*, 1774–1779.
[15] (−)-Anisomycin: B. A. Sobin, F. W. Tanner, *J. Am. Chem. Soc.* **1954**, *76*, 4053.
[16] Review: A. G. Griesbeck, H. Mauder, S. Stadtmüller, *Acc. Chem. Res.* **1994**, *27*, 70–75.
[17] For the relationship of temperature-dependent diastereoselectivities and mechanistic implications in Paternò-Büchi reactions, see: H. Buschmann, H.-D. Scharf, N. Hoffmann, M. W. Plath, J. Runsink, *J. Am. Chem. Soc.* **1989**, *111*, 5367–5373.

Polybenzoid C_{54} Hydrocarbons: Synthesis and Structural Characterization in Vapor-Deposited Ordered Monolayers**

Markus Müller, Jörg Petersen, Rainer Strohmaier, Christian Günther, Norbert Karl, and Klaus Müllen*

Basic research aimed at developing molecular electronic devices tends to focus more and more on thin—if possible epitaxially ordered—organic films. Such films are produced preferentially under high-vacuum conditions by vapor deposition onto well-characterized substrate surfaces, with careful control of deposition rate, substrate temperature, and film thickness. This development requires organic compounds that vaporize without decomposition, but for applications they must also have a negligible vapor pressure at room temperature, that is, they must have strong intermolecular binding forces. Moreover, suitable molecules must have a shape and symmetry that allows two-dimensional close packing.[1, 2] With the aim of producing adsorbate films composed of molecules that resemble larger sections of graphite layers, we here describe a structure-specific synthesis of the extended polybenzoid hydrocarbons **3** and **13** and report the study of the ordered adsorbate films of **3** by electron diffraction analysis and scanning tunneling microscopy (STM). Evaluation of the shape of larger molecules by ultrahigh-resolution STM and special diffraction methods becomes increasingly important as their characterization by classical spectroscopic methods is impaired by decreasing solubility.

Polybenzoid arenes that can be represented by at least one Kekulé form that consists only of electron sextets as a mesomeric limiting structure[3] can be obtained—as has been described previously—by a cycloaddition–cyclodehydrogenation sequence (Scheme 1).[4] Starting from the ene–diene component **1**, a double intramolecular Diels–Alder cycloaddition and dehydrogenation leads to the phenylene-bridged bistriphenylene derivative **2**, which exists as two rotamers **2a** and **2b**. Therefore the synthesis sequence described[4] must lead to the two isomers **3** and **4** as cyclodehydrogenation products.

[*] Prof. Dr. K. Müllen, Dipl.-Chem. M. Müller
Max-Planck-Institut für Polymerforschung
Ackermannweg 10, D-55128 Mainz (Germany)
Fax: Int. code +(6131)379-100
Dipl.-Phys. J. Petersen, Dipl.-Phys. R. Strohmaier
1. Physikalisches Institut der Universität Stuttgart (Germany)
Dipl.-Phys. C. Günther, Prof. Dr. N. Karl
3. Physikalisches Institut der Universität Stuttgart (Germany)

[**] This work was supported by the Bundesministerium für Bildung und Forschung ("Molecular Electronics" project) and by the Deutsche Forschungsgemeinschaft (in the Collaborative Research Center 329 "Physical and Chemical Foundations of Molecular Electronics).

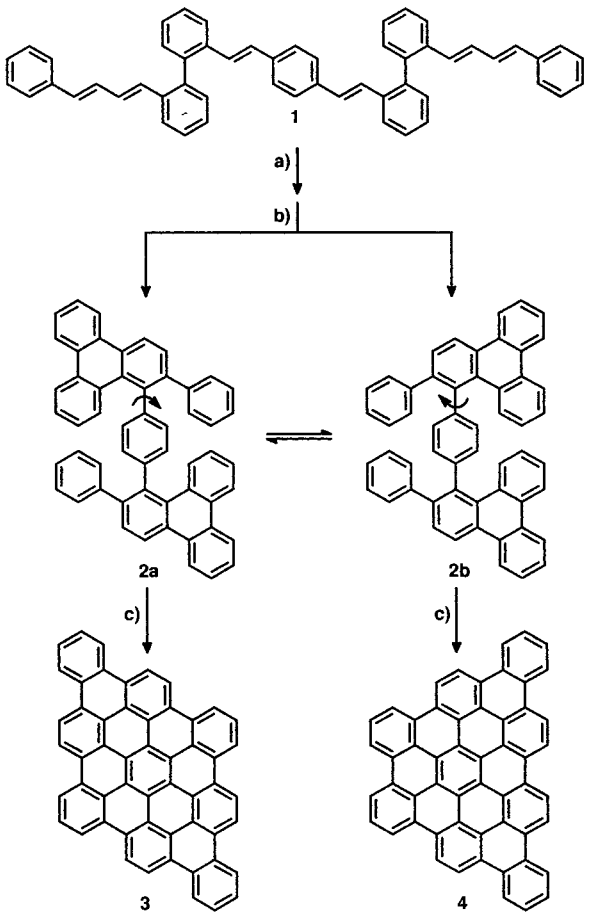

Scheme 1. a) 100 °C in toluene. b) DDQ; 140 °C in 1,1,2,2-tetrachloroethane. c) $AlCl_3/CuCl_2$; room temperature in carbon disulfide. For spectroscopic data see Table 1.

Table 1. Physical and spectroscopic data for **3**, **5**, **7**, **10**, **12**, and **13**.

3: MS (FD, 8 kV): *m/z* (%): 670 (100) $[M^+]$, 335 (21) $[M^{2+}]$; MS (LD-TOF): *m/z* (%): 670 (100) $[M^+]$ (calibrated with C_{60} and C_{70}); UV/Vis (vapor-deposited film on quartz): λ_{max} = 202, 241, 285, 392, 486, 521 nm; m.p. >300 °C

5: ^{1}H NMR (500 MHz, $[D_2]$1,1,2,2-tetrachloroethane, 30 °C): δ = 7.89 (d, ^3J(H,H) = 7.9 Hz, 2H; H6, H6″, terphenyl, outer), 7.65 (s, 2H; H3′, H6′, terphenyl, central), 7.44–7.32 (m, 8H), 7.27–7.08 (m, 18H), 6.97 (d, ^3J(H,H) = 16.3 Hz, 2H; olefinic AB system), 6.93 (m_c, 2H; BC, olefinic ABCD system), 6.82 (d, ^3J(H,H) = 16.3 Hz, 2H; olef. AB system), 6.77 (m_c, 2H; BC, olefinic ABCD system), 6.57 (d, ^3J(H,H) = 15.1 Hz, 2H; AD, olefinic ABCD system), 6.56 (d, ^3J(H,H) = 15.4 Hz, 2H; AD, olefinic ABCD system); MS (FD, 8 kV): *m/z* (%): 690 (100) $[M^+]$; m.p. (decomp.) >80 °C

7: ^{1}H NMR (500 MHz, $[D_2]$1,1,2,2-tetrachloroethane, 130 °C): δ = 8.94 (s, 2H; H1, H1′), 8.58 (d, ^3J(H,H) = 8.5 Hz, 2H; H6, H6′), 8.47 (d, ^3J(H,H) = 7.9 Hz, 2H; H5, H5′), 7.63 (d, ^3J(H,H) = 8.4 Hz, 2H; H7, H7′), 7.51 (dd, ^3J(H,H) = 7.7 Hz, ^3J(H,H) = 7.2 Hz, 2H; H4, H4′), 7.34–7.28 (m, 8H; H3, H3′, 4H *m*-phenyl-1, 2H *p*-phenyl-1), 7.24 (d, ^3J(H,H) = 7.2 Hz, 4H; 4H *o*-phenyl-1), 7.17–7.13 (m, 8H; H2, H2′, 4H *m*-phenyl-2, 2H *p*-phenyl-2), 6.99 (d, ^3J(H,H) = 7.5 Hz, 4H; 4H *o*-phenyl-2); MS (FD, 8 kV): *m/z* (%): 682 (100) $[M^+]$; m.p. >300 °C

10: (crude mixture) MS (FD, 8 kV): *m/z* (%): 690 (100) $[M^+]$

12: ^{1}H NMR (500 MHz, $[D_2]$1,1,2,2-tetrachloroethane, 130 °C): δ = 9.79 (s, 2H; H1, H1′), 8.92 (d, ^3J(H,H) = 8.4 Hz, 2H; H6, H6′), 8.78 (d, ^3J(H,H) = 8.4 Hz, 2H; H2, H2′), 7.74 (d, ^3J(H,H) = 8.4 Hz, 2H; H7, H7′), 7.62 (d, ^3J(H,H) = 7.9 Hz, 2H; H5, H5′), 7.49 (dd, ^3J(H,H) = 8.3 Hz, ^3J(H,H) = 7.6 Hz, 2H; H3, H3′), 7.21–7.13 (m, 16H; 4H *o*-phenyl-1, 4H *m*-phenyl-1, 2H *p*-phenyl-1, 4H *m*-phenyl-2, 2H *p*-phenyl-2), 7.08 (d, ^3J(H,H) = 7.9 Hz, 4H; 4H *o*-phenyl-2), 7.01 (dd, ^3J(H,H) = 7.9 Hz, ^3J(H,H) = 7.6 Hz, 2H; H4, H4′); MS (FD, 8 kV): *m/z* (%): 682 (100) $[M^+]$, 341 (16) $[M^{2+}]$; m.p. >300 °C

13: MS (FD, 8 kV): *m/z* (%): 674 (100) $[M^+]$; MS (LD-TOF): *m/z* (%): 674 (100) $[M^+]$ (calibrated with C_{60} and C_{70}); m.p. >300 °C

In view of this problem, we decided on a new synthesis route that is structure-specific. If the 1,4-di(2′-iodo-*trans*-styryl)-benzene[4] needed to form the ene–diene component **1** as the central building block is replaced by 1,4-dibromo-2,5-di-*trans*-styrylbenzene (**8**), double hetero-aryl–aryl coupling with **9** leads to the *para*-terphenyl derivative **5**. This opens up a new cycloaddition–cyclodehydrogenation route (Scheme 2) which, in contrast to the earlier route (Scheme 1), no longer permits rotation of the two outer phenyl rings about the central *para*-terphenyl unit after the double intramolecular [4+2] cycloaddition to **6**. Consequently, the formation of a different isomer of the cyclodehydrogenation product **3** is prevented.

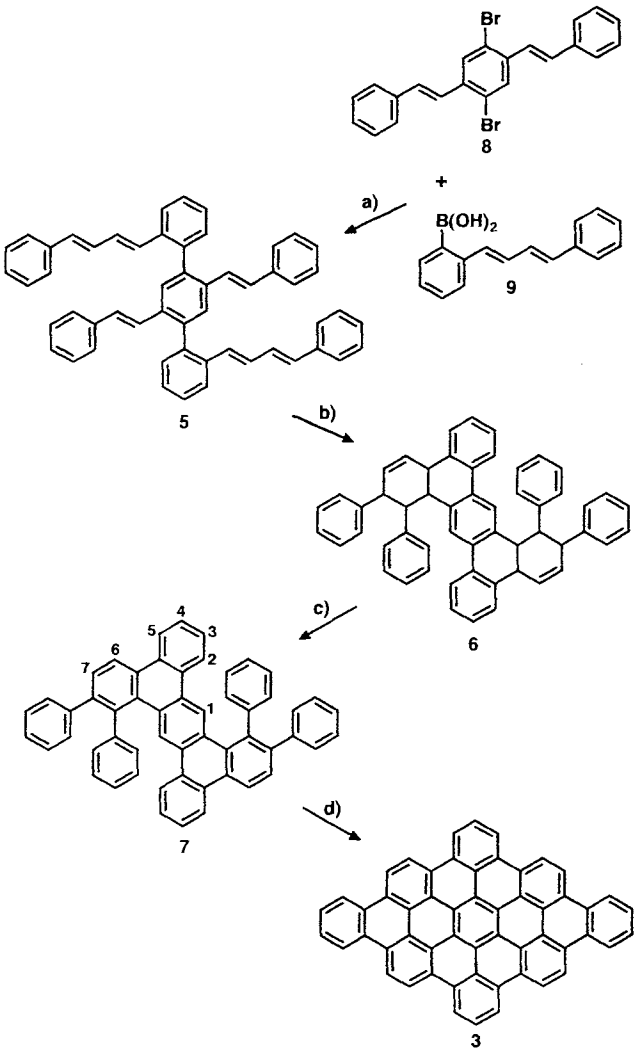

Scheme 2. a) Tetrakis(triphenylphosphane)palladium(0); reflux in toluene/ethanol/water mixture (50:25:25 vol%); exclusion of light. b) 135 °C in 1,1,2,2-tetrachloroethane. c) DDQ; 135 °C in 1,1,2,2-tetrachloroethane. d) $AlCl_3/CuCl_2$; room temperature in carbon disulfide. For spectroscopic data see Table 1.

Unlike the ene–diene component **1**, the *para*-terphenyl derivative **5**, which takes part in the double intramolecular Diels–Alder reaction, is not synthesized by aryl–aryl coupling involving zincates, but from boronates, in accordance with the method of Suzuki.[5] Here, the distyrylbenzene **8** is treated with 2-(4′-phenyl-*trans*,*trans*-buta-1′,3′-dienyl)phenylboronic acid (**9**) in 92% yield to form **5**. The formation of **8** proceeds very readily by a double Wittig reaction of benzaldehyde with α,α′-bis(triphenylphosphonio)-2,5-dibromo-*para*-xylene dibromide, and the preparation of the boronic acid **9** proceeds via the known 2′-iodo-1,4-diphenyl-*trans*,*trans*-buta-1,3-diene[4] by lithiation with *n*-butyllithium followed by transmetalation with the trimethyl ester of boric acid.

In the aryl–aryl coupling according to Suzuki to give **5**, no intramolecular [4+2] cycloaddition takes place even after a reaction time of several days in a mixture of toluene, ethanol, and water (50:25:25 vol%) at boiling point (about 100 °C). However, the double intramolecular Diels–Alder reaction of **5** takes place quantitatively in [D_2]1,1,2,2-tetrachloroethane at 135 °C within 1 h (monitored by NMR). On the laboratory scale, the yield for the double [4+2] cycloaddition is 98%. The mixture of isomers of **6** caused by of the formation of eight new chirality centers is not separated. Instead, dehydrogenation of the cyclohexene structures of the crude mixture of **6** formed by the cycloaddition is carried out with 2,3-dichloro-5,6-dicyano-1,4-benzoquinone (DDQ). All the isomers lead to the tetraphenyltetrabenzoanthracene derivative **7** (96% yield).

The oxidative cyclodehydrogenation of **7** is carried out with copper dichloride and aluminum trichloride in carbon disulfide at room temperature (99% yield). The removal of twelve hydrogen atoms can be demonstrated by field desorption (FD) and laser desorption time-of-flight (LD-TOF) mass spectrometry, which show that six new aryl–aryl bonds are formed, with complete planarization of the four phenyl substituents of **7** in the plane of the tetrabenzoanthracene structure. However, unlike the cyclization of **2**, this leads exclusively to the formation of the polybenzoid arene tribenzo-[*hi*,*o*,*uv*]triphenylene[2,1,12,11-*bcdef*]ovalene (**3**)[6] with $D_{2h}(2/mmm)$ symmetry.

The versatility of the cycloaddition–cyclodehydrogenation route described here is shown by the ability to form not only the *para*-terphenyl derivative **5** but also the *para*-terphenyl derivative **10** in which the positions of the styryl and phenylbutadienyl substituents are reversed relative to those in the ene–diene compound **5** (Scheme 3).

The preparation of **10** is also achieved by a double hetero-aryl–aryl coupling of the Suzuki type, in which 1,4-dibromo-2,5-di(4′-phenyl-*trans*,*trans*-buta-1′,3′-dienyl)benzene (**14**) is treated with *trans*-stilbene-2-boronic acid **15**. The formation of the dibromobenzene **14** proceeds in analogy to the synthesis of **8** by the double Wittig reaction of *trans*-cinnamic aldehyde with α,α′-bis(triphenylphosphonio)-2,5-dibromo-*para*-xylene dibromide, and the preparation of the stilbeneboronic acid **15** proceeds in analogy to the synthesis of **9** from 2-iodo-*trans*-stilbene.

Because of its low solubility in the usual solvents, the crude product **10** of the Suzuki reaction is not purified by column chromatography. Instead, it is separated from the inorganic palladium catalyst residues by a Soxhlet extraction with 1,1,2,2-tetrachloroethane, during which the double intramolecular [4+2] cycloaddition of **10** also takes place. The mixture of isomers of **11** is dehydrogenated with DDQ without prior purification (as in the case of the mixture of isomers of **6**), to form the tetraphenyltetrabenzoanthracene derivative **12**, which is then recrystallized several times from 1,1,2,2-tetrachloroethane (53% yield over all reactions).[7]

In the oxidative cyclodehydrogenation of **12** with copper dichloride and aluminum trichloride (98% yield), only eight hydrogen atoms can be removed because of the positions of the four phenyl substituents, so that only four new aryl–aryl bonds are formed, as can be shown by LD-TOF mass spectrometry. As in the synthesis of the arene **3**, the intramolecular Diels–Alder reaction prevents the rotation of the outer phenyl rings of the central *para*-terphenyl unit of **10** after the first cycloaddition stage. The synthesis therefore leads exclusively to the formation of the polybenzoid hydrocarbon **13**, which has $C_{2h}(2/m)$ symmetry.

 © VCH Verlagsgesellschaft mbH, D-69451 Weinheim, 1996 0570-0833/96/3508-0887 $ 15.00+.25/0

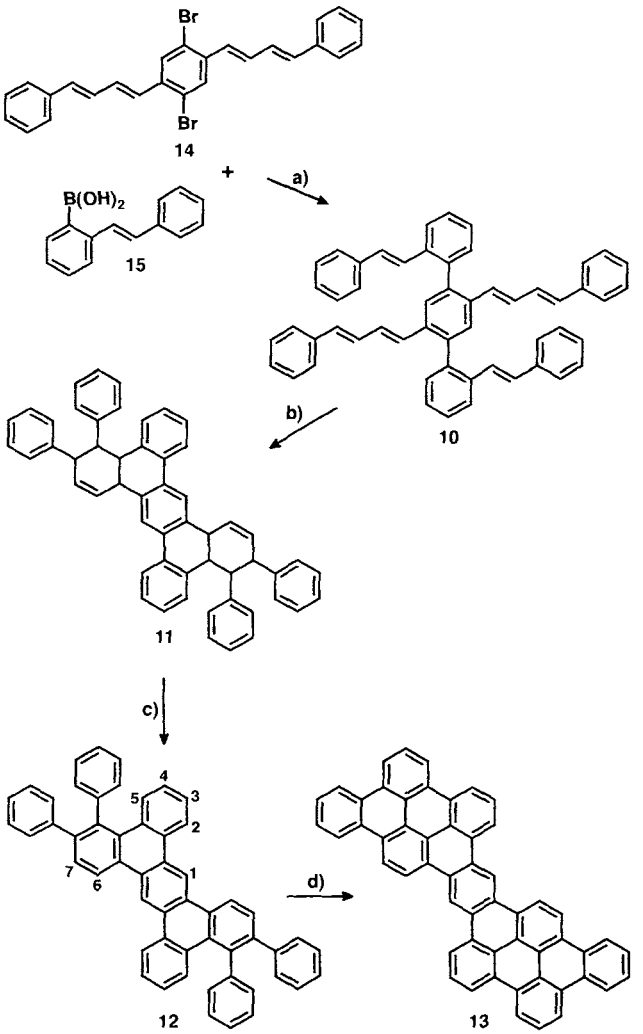

Scheme 3. a) Tetrakis(triphenylphosphane)palladium(0); reflux in toluene/ethanol/water mixture (50/25/25 vol%); exclusion of light. b) 135 °C in 1,1,2,2-tetrachloroethane. c) DDQ; 135 °C in 1,1,2,2-tetrachlorethane. d) $AlCl_3/CuCl_2$; room temperature in carbon disulfide. For spectroscopic data see Table 1.

For structural characterization of **3** and for the production of thin films by vacuum vapor deposition, the crude product was first subjected to a fractionating high vacuum sublimation in a fused silica tube using a temperature step program. At an evaporation temperature of 600 °C, a bright orange, microcrystalline material (maximum crystal size $100 \times 10 \times 1\ \mu m^3$) deposited, which displayed an orange-red fluorescence in high yield when irradiated with UV light.

For investigations by low-energy electron diffraction (LEED), a monomolecular film (approximately 3 Å thick) of **3** was deposited at a rate of 20 $Å\,h^{-1}$ onto a freshly cleaved (0001) surface of a single crystal of the layer chalcogenide MoS_2 (molybdenite) pretreated by heating to 450 °C for about 5 min in ultrahigh vacuum (UHV). Film thickness was monitored by a vibrating quartz balance. Only with very low energy electrons (in the region of 10 eV) could useful electron diffraction diagrams be obtained displaying the very small reciprocal lattice vectors 0.071(3) and 0.105(3) $Å^{-1}$. Taking into account the directions of the latter and their multiplication (induced by the substrate symmetry, with the consequence of multiple domain formation), the very large unit mesh $a = 14.2(5)$ Å, $b = 14.2(5)$ Å, $\gamma = 84.9(1.4)°$ in direct space was derived, with an area of 201 $Å^2$. The appearance of discrete diffraction spots indicates a well-ordered growth of **3** on the MoS_2 substrate. The large unit mesh with an area that corresponds closely to the (estimated) van der Waals area of the planar molecule **3** indicates a close-packed arrangement ($Z = 1$) of molecules that lie flat (cf. Ref. [8]). In situ thermodesorption spectroscopy with detection by mass spectrometry showed that the molecular mass of the molecules that could be resublimed from the monomolecular film was 670 u, in agreement with the formula $C_{54}H_{22}$.

For direct investigation of the molecular size and shape by scanning tunneling microscopy (STM) (see Ref. [2]), a suitably prepared sample was removed from the UHV and scanned in air. The STM images obtained thus clearly showed molecules of rhombic shape and of the expected size (Fig. 1). Here, too, the molecules were found to lie flat on the substrate surface. The intermolecular distances in the STM image are, however, somewhat larger than those that correspond to the close molecular packing concluded from the LEED patterns. One should be aware, however, that the LEED image reflects the dominant packing across a large surface area (about 1 mm^2), whereas the STM image gives very local information. It is known from STM investigations of monolayers of other systems that competition between intermolecular interactions (tending to give close pack-ing) and strongly ordering local interactions with the substrate can lead to more than one structure.[9]

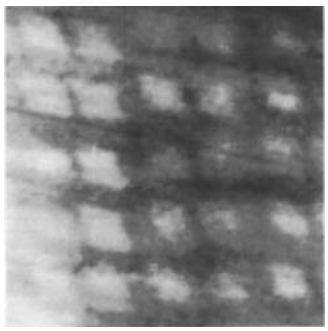

Fig. 1. STM image of a nominally 3 Å thick vapor-deposited layer of **3** on a (0001) face of a MoS_2 single crystal, taken in constant height mode (bias: +1.8 V at the sample; tunneling current: 90 pA; image area: 100 Å × 100 Å). A regular arrangement of rhombic molecules can be discerned.

With the compound **3**, we were successful in synthesizing a large aromatic molecule with remarkable thermal stability, high fluorescence yield, and high symmetry that allows dense surface coverage; these properties render **3** an extremely useful and promising model system for further investigations aimed at the development of a molecular electronics system on the basis of ultrathin epitaxial organic films.

Received: November 23, 1995 [Z 8584 IE]
German version: *Angew. Chem.* **1996**, *108*, 947–950

Keywords: cycloadditions · cyclodehydrogenations · graphite sections · polycycles · scanning tunneling microscopy

[1] U. Zimmermann, N. Karl, *Surf. Sci.* **1992**, *268*, 296–306.
[2] C. Ludwig, B. Gompf, W. Glatz, J. Petersen, W. Eisenmenger, M. Möbus, U. Zimmermann, N. Karl, *Z. Phys. B* **1992**, *86*, 397–404.
[3] E. Clar, *The Aromatic Sextet*, Wiley, London, **1972**.
[4] M. Müller, H. Mauermann-Düll, M. Wagner, V. Enkelmann, K. Müllen, *Angew. Chem.* **1995**, *107*, 1751–1754; *Angew. Chem. Int. Ed. Engl.* **1995**, *34*, 1583–1586.
[5] N. Miyaura, T. Yanagi, A. Suzuki, *Synth. Commun.* **1981**, *11*, 513–519; A. Suzuki, *Acc. Chem. Res.* **1982**, *15*, 178–184.
[6] J. R. Dias, *J. Chem. Inf. Comput. Sci.* **1993**, *33*, 117–127; *Handbook of Polycyclic Hydrocarbons – Part A: Benzenoid Hydrocarbons*, Elsevier, Amsterdam, **1987**.
[7] The intermediates previously mentioned had only been characterized by mass spectrometry. Therefore, a thorough investigation by NMR spectroscopy (^1H, ^{13}C, $^1H,^1H$-COSY, $^1H,^1H$-NOESY) of **12** was carried out. Although the number of the signal groups was the same as for the analogous compound **7** in the ^1H NMR spectrum, there was a considerable difference in the chemical shift of comparable signal groups of **7** and **12**.
[8] R. Strohmaier, C. Ludwig, J. Petersen, B. Gompf, W. Eisenmenger, *Surf. Sci.* **1994**, *318*, L1181–L1185.
[9] C. Ludwig, R. Strohmaier, J. Petersen, B. Gompf, W. Eisenmenger, *J. Vac. Sci. Technol.* **1994**, *B12*, 1963.

Copper(I)-Promoted Stille Cross-Coupling of Stannyl Enol Ethers with Enol Triflates: Construction of Complex Polyether Frameworks**

K. C. Nicolaou,* Mitsunobu Sato, Neil D. Miller, Janet L. Gunzner, Johanne Renaud, and Edouard Untersteller

The polyether marine natural products are a remarkable class of compounds whose complexity and structural diversity continue to impress and fascinate synthetic chemists.[1] Their scarcity and striking biological actions dictate their total synthesis and the design, chemical synthesis, and biological evaluation of novel structural analogs. Fundamental to these studies is the development of new synthetic methods for the construction of such systems.[2] Amongst the remaining challenges in this area is a ready access to the unusual bistetrahydropyran systems represented by the ring pairs K–L, O–P, and V–W of maitotoxin[3] (Scheme 1). We report here a highly efficient and practical method for the construction of such units through the copper-promoted Stille cross-coupling of cyclic stannyl enol ethers with cyclic enol triflates.

A potential solution to the synthetic problem posed by the maitotoxin fragments K–L, O–P, and V–W and by other complex natural products would be to cross-couple the glycal partners **I** and **II** and then functionalize the resultant diene **III** appropriately (Scheme 2). Despite the existence of precedent[4] for carbon–carbon bond forming reactions involving Pd^0-catalyzed cross-coupling of stannyl glycals with vinyl or aryl derivatives, the development of a successful procedure for the cross-coupling of appropriate glycal partners proved problematic due to low reaction rates and formation of homodimers[5] (e.g. **IV** and **V**, Scheme 1). As a simple model system, we chose to examine the cross-coupling of enol triflate **1** with trimethylstannyl enol ether **2**. A series of experiments were carried out to optimize reaction conditions for the selective formation of the heterocoupling product **3**. As seen from Table 1 the Pd^0-catalyzed cross-

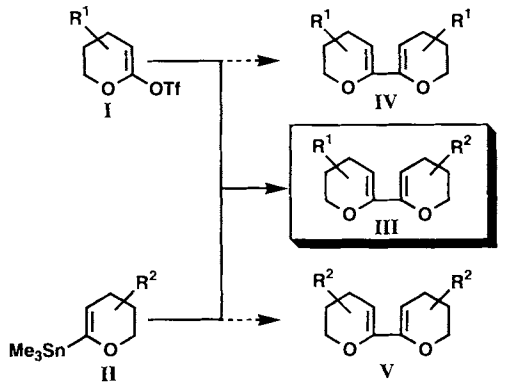

Scheme 2. Cross-coupling of enol triflates with stannyl enol ethers.

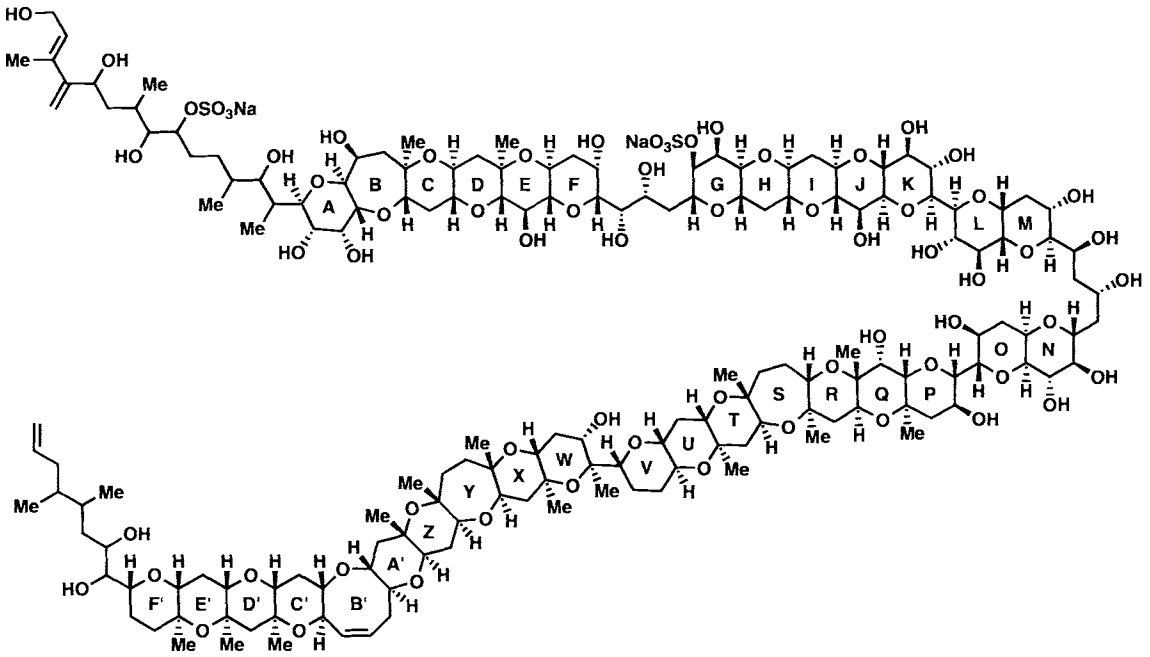

Scheme 1. Structural formula of maitotoxin.

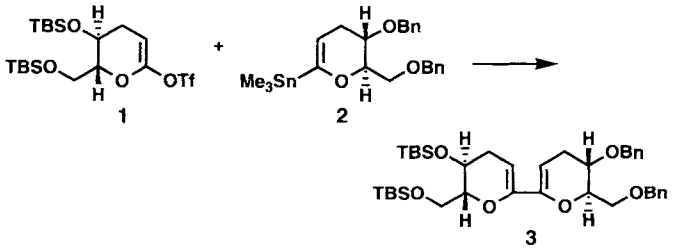

[*] Prof. Dr. K. C. Nicolaou, M. Sato, Dr. N. D. Miller, J. L. Gunzner, Dr. J. Renaud, Dr. E. Untersteller
Department of Chemistry, The Scripps Research Institute
10666 N. Torrey Pines Road, La Jolla, CA 92037 (USA)
and
Department of Chemistry and Biochemistry
University of California San Diego
9500 Gilman Drive, La Jolla, CA 92093 (USA)

[**] We thank Drs. Dee H. Huang and Gary Siuzdak for their assistance with NMR spectroscopy and mass spectrometry, respectively. Financial support provided by the National Institutes of Health, USA, the ALSAM Foundation, Merck, Pfizer, Hoffmann La Roche, Amgen, and the Unitika Ltd., Co. (Japan) is gratefully acknowledged.

coupling of enol triflate **1** and stannyl enol ether **2** is best carried out in the presence of CuCl (2.0 equiv) and potassium carbonate (2.0 equiv) in THF at 25 °C giving the desired bisglycal **3** in 80% yield. The role of CuCl was particularly crucial for the success of this reaction.[6] Whether the CuCl acts as a scavenger of free triphenylphosphane ligands or whether a discrete organocuprate is formed as a result of a Sn/Cu transmetalation is open to conjecture.[6a]

Table 1. Conditions for the cross-coupling of **1** with **2** in the presence of a palladium(0) catalyst [a].

Entry	Ratio 1:2	Additives (equiv)			Conditions		Yield [%] [b]
1	1.1				THF	25 °C, 78 h	43
2	1.1	LiCl	(3.0)		THF	Δ, 12 h	53
3	1.2	$ZnCl_2$	(3.0)		THF	25 °C, 8 h	51
4	1.1	CuCl	(2.0)		THF	Δ, 12 h	49
5	1.1	CuCl	(2.0)	Et_3N (2.0)	THF	Δ, 12 h	61
6	1.2	CuCl	(2.0)	Et_3N (2.0)	THF	25 °C, 0.5 h	73
7	1.2	CuCl	(0.1)	K_2CO_3 (2.0)	THF	25 °C, 27 h	45
8	1.2	CuCl	(0.5)	K_2CO_3 (2.0)	THF	25 °C, 2 h	69
9	1.2	CuCl	(1.0)	K_2CO_3 (2.0)	THF	25 °C, 1.75 h	70
10	1.2	CuCl	(1.5)	K_2CO_3 (2.0)	THF	25 °C, 1.6 h	71
11	1.2	CuCl	(2.0)	K_2CO_3 (2.0)	THF	25 °C, 1 h	80
12	1.2	CuCl	(4.0)	K_2CO_3 (2.0)	THF	25 °C, 0.5 h	67
13	1.2	CuCN	(2.0)	K_2CO_3 (2.0)	THF	25 °C, 24 h	52
14	1.2	CuBr	(2.0)	K_2CO_3 (2.0)	THF	25 °C, 3 h	68
15	1.2	CuI	(2.0)	K_2CO_3 (2.0)	THF	25 °C, 36 h	53
16	1.2	$CuCl_2$	(2.0)	K_2CO_3 (2.0)	THF	25 °C, 12 h	0
17	1.2	CuCl	(2.0)	K_2CO_3 (2.0)	THF	25 °C, 96 h	[c]
18	1.2	CuCl	(2.0)	K_2CO_3 (2.0)	DMSO	25 °C, 1 h	33
19	1.2	CuCl	(2.0)	K_2CO_3 (2.0)	NMP [d]	25 °C, 2 h	38
20	1.2	CuCl	(2.0)	K_2CO_3 (2.0)	dioxane	25 °C, 72 h	21

[a] Catalyst: 0.1 equivalents of freshly prepared $[Pd(PPh_3)_4]$. [b] By-products from the homocoupling of **1** and **2** were also obtained in yields of 5–20%. [c] Reaction without palladium catalyst. After 96 h only trace amounts of **3** were detected. [d] NMP = *N*-Methyl-2-pyrrolidinone.

An application of the developed methodology to the maitotoxin-related intermediate **17** is shown in Scheme 3. Thus, the readily accessible building blocks **9** and **16** were coupled smoothly under the optimum $[Pd(PPh_3)_4]$/CuCl/K_2CO_3 conditions to afford the targeted intermediate **17** in 83% yield. The

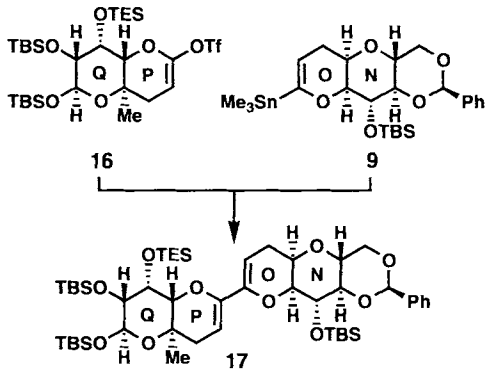

Scheme 3. Synthesis of intermediate **17**, which is related to the NO–PQ system of maitotoxin. Reagents and conditions: 1.0 equiv stannyl enol ether **9**, 1.2 equiv enol triflate **16**, 0.1 equiv $[Pd(PPh_3)_4]$, 2.0 equiv CuCl, 2.0 equiv K_2CO_3, THF, 25 °C, 1 h, 83%.

Table 2. Palladium(0)/copper(I)-mediated coupling of enol triflates with stannyl enol ethers to give complex cyclic polyether frameworks [a].

Entry	Enol triflate	Stannyl enol ether	Coupling product	Yield [%] [b]
1	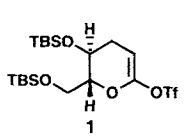 **1**	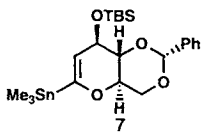 **7**	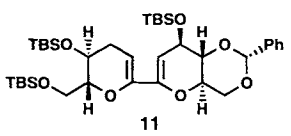 **11**	71
2	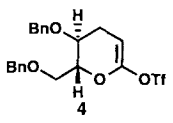 **4**	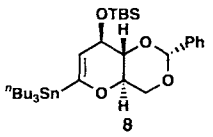 **8**	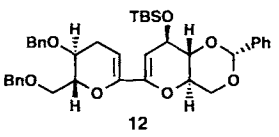 **12**	70
3	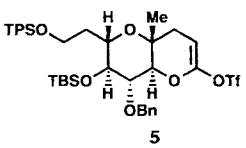 **5**	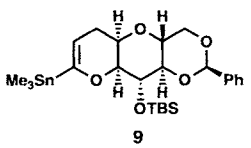 **9**	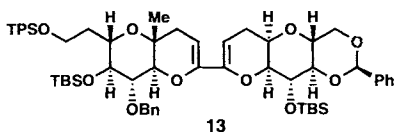 **13**	79
4	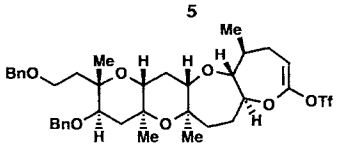 **6**	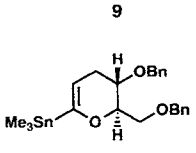 **2**	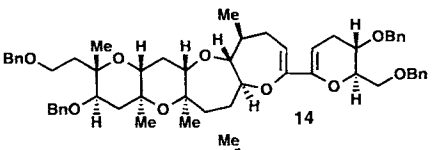 **14**	77
5	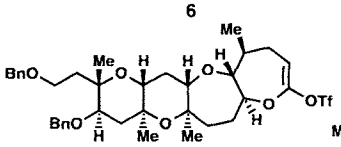 **6**	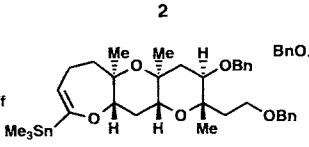 **10**	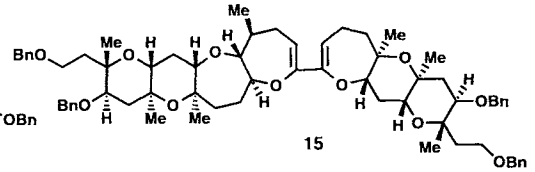 **15**	81

[a] Conditions: 1.0 equiv stannyl enol ether, 1.2 equiv enol triflate, 0.1 equiv $[Pd(PPh_3)_4]$, 2.0 equiv CuCl, 2.0 equiv K_2CO_3, THF, 25 °C, 1–2 h. [b] By-products (5–10%) arising from homocoupling of both reaction partners were obtained in all reactions.

Table 3. Selected physical data for compounds **15** and **17**.

15: colorless foam; $R_f = 0.25$ (silica gel, 20% ether, 20% CH_2Cl_2 in petroleum ether); $[\alpha]_D^{22} = -11.1$ ($c = 1.0$, in $CHCl_3$); IR (film): $\tilde{\nu}_{max} = 2939, 2876, 1629, 1496, 1454, 1380, 1284, 1206, 1070, 1028, 890, 804, 735, 697\ cm^{-1}$; ^1H NMR (500 MHz, $CDCl_3$): $\delta = 7.37$–7.26 (m, 20H, Ar-H), 5.60 (dd, $J = 6.0, 6.5$ Hz, 1H, =CH), 5.45 (dd, $J = 3.5, 8.5$ Hz, 1H, =CH), 4.57 (d, $J = 11.5$ Hz, 2H, 2CHHPh), 4.47 (s, 2H, CH_2Ph), 4.46 (s, 2H, CH_2Ph), 4.40 (d, $J = 11.5$ Hz, 2H, 2CHHPh), 3.70–3.58 (m, 6H, CH-O), 3.56–3.45 (m, 2H, CH-O), 3.40–3.32 (m, 3H, CH-O), 3.13 (dd, $J = 7.5, 8.5$ Hz, 1H, CH-O), 2.30–1.72 (m, 19H, CHH and CH), 1.67–1.58 (m, 1H, CHH or CH), 1.50–1.37 (m, 3H, CHH and CH), 1.34 (s, 3H, CH_3), 1.32 (s, 3H, CH_3), 1.28 (s, 3H, CH_3), 1.27 (s, 3H, CH_3), 1.26 (s, 3H, CH_3), 1.21 (s, 3H, CH_3), 1.11 (d, $J = 7.0$ Hz, 3H, CH_3); ^{13}C NMR (125 MHz, $CDCl_3$): $\delta = 154.0, 153.4, 138.5, 138.5, 138.4, 128.3, 128.2, 127.6, 127.5, 127.4, 127.4, 108.1, 106.3, 90.7, 85.8, 83.4, 83.3, 78.4, 78.0, 77.7, 73.2, 73.1, 73.0, 72.3, 71.0, 66.0, 40.8, 40.3, 40.3, 39.7, 37.4, 31.3, 29.2, 29.0, 24.6, 21.2, 20.1, 19.9, 19.9, 19.8, 19.3, 17.5, 17.4$; HRMS (FAB): calcd for $C_{76}H_{86}O_{11}$ as $(M + Cs^+)$ 1199.5224, found 1199.5254

17: colorless oil; $R_f = 0.47$ (silica gel, 10% ether in petroleum ether); $[\alpha]_D^{22} = -36.3$ ($c = 0.4$, in CH_2Cl_2); IR (film): $\tilde{\nu}_{max} = 2928, 2856, 1631, 1463, 1377, 1255, 1158, 1099, 1022, 838, 778, 745, 697\ cm^{-1}$; ^1H NMR (500 MHz, $CDCl_3$): $\delta = 7.50$–7.48 (m, 2H, Ar-H), 7.39–7.35 (m, 3H, Ar-H), 5.52 (s, 1H, CHPh), 5.25 (dd, $J = 2.5, 6.0$ Hz, 1H, =CH), 5.20 (dd, $J = 4.0, 4.0$ Hz, 1H, =CH), 5.18 (d, $J = 7.5$ Hz, 1H, CH-O), 4.44–4.41 (m, 1H, CH-O), 4.31–4.28 (m, 2H, CH-O), 4.09–4.07 (m, 1H, CH-O), 4.01 (dd, $J = 6.0, 8.0$ Hz, 1H, CH-O), 3.90–3.84 (m, 1H, CH-O), 3.69 (dd, $J = 10.0, 10.0$ Hz, 1H, CH-O), 3.63 (dd, $J = 8.0, 10.0$ Hz, 1H, CH-O), 3.43 (d, $J = 2.5$ Hz, 1H, CH-O), 3.34 (dd, $J = 2.5, 7.5$ Hz, 1H, CH-O), 2.51–2.45 (m, 1H, CHH), 2.34–2.25 (m, 2H, CHH), 1.98 (dd, $J = 6.0, 17.0$ Hz, 1H, CHH), 1.41 (s, 3H, CH_3), 0.99 (t, $J = 8.0$ Hz, 9H, CH_2CH_3), 0.94 (s, 9H, tBu), 0.94 (s, 9H, tBu), 0.88 (s, 9H, tBu), 0.69 (dq, $J = 3.0, 8.0$ Hz, 6H, CH_2CH_3), 0.14 (s, 3H, CH_3), 0.13 (s, 3H, CH_3), 0.12 (s, 3H, CH_3), 0.11 (s, 3H, CH_3), 0.07 (s, 3H, CH_3), 0.04 (s, 3H, CH_3); ^{13}C NMR (125 MHz, $CDCl_3$): $\delta = 146.2, 144.4, 137.3, 128.9, 128.1, 126.2, 101.7, 97.0, 93.1, 91.5, 83.1, 77.9, 77.5, 74.6, 73.0, 71.3, 70.5, 69.8, 67.1, 64.0, 39.3, 26.2, 26.1, 26.1, 25.8, 23.2, 19.2, 18.3, 18.3, 18.2, 6.9, 5.1, 3.6, −3.9, −4.1, −4.2, −4.3, −4.6, −4.8$; HRMS (FAB): calcd for $C_{49}H_{86}O_{10}Si_4$ $(M + Cs^+)$ 1079.4352, found 1079.4385

important physical data for compounds **15** and **17** are summarized in Table 3.

We have developed a practical and highly efficient method for the cross-coupling of enol triflates and stannyl enol ethers to afford complex bisglycals, a class of valuable synthetic intermediates.[7] We have, furthermore, demonstrated the applicability of this method to the synthesis of cyclic polyethers through the construction of several complex polyether frameworks, including a fragment related to the NO–PQ system of maitotoxin.[8, 9]

Received: December 18, 1995 [Z 8661 IE]
German version: *Angew. Chem.* **1996**, *108*, 952–955

Keywords: maitotoxin · natural products · polyethers · Stille couplings

[1] a) M. J. Garson, *Chem. Rev.* **1993**, *93*, 1699; b) T. Yasumoto, M. Murata, *ibid.* **1993**, *93*, 1897; c) D. J. Faulkner, *Nat. Prod. Rep.* **1984**, *1*, 251.

[2] a) C. J. Moody, M. J. Davies, *Stud. Nat. Prod. Chem.* **1992**, *10*, 201; b) K. C. Nicolaou, C. V. C. Prasad, P. K. Somers, C.-K. Hwang, *J. Am. Chem. Soc.* **1989**, *111*, 5330, 5335; c) K. C. Nicolaou, C. V. C. Prasad, C.-K. Hwang, M. E. Duggan, C. A. Veale, *ibid.* **1989**, *111*, 5321; d) K. C. Nicolaou, P. K. McGarry, P. K. Somers, B. H. Kim, W. W. Ogilvie, G. Yiannikouros, C. V. C. Prasad, C. A. Veale, R. R. Hark, *ibid.* **1990**, *112*, 6263; e) K. C. Nicolaou, C.-K. Hwang, B. E. Marron, S. A. DeFrees, E. A. Couladouros, Y. Abe, P. J. Carroll, J. P. Snyder, *ibid.* **1990**, *112*, 3040.

[3] a) M. Satake, S. Ishida, T. Yasumoto, M. Murata, H. Utsumi, T. Hinomoto, *J. Am. Chem. Soc.* **1995**, *117*, 7019; b) M. Murata, H. Naoki, S. Matsunaga, M. Satake, T. Yasumoto, *ibid.* **1994**, *116*, 7098; c) for the syntheses of the L–M and N–O fragments of maitotoxin, see: M. Sasaki, T. Nonomura, M. Murata, K. Tachibana, *Tetrahedron Lett.* **1994**, *35*, 5023.

[4] a) J. K. Stille, *Angew. Chem.* **1986**, *98*, 504; *Angew. Chem. Int. Ed. Engl.* **1986**, *25*, 508; b) T. Mitchell, *Synthesis* **1992**, 803; c) for a comprehensive review of C-glycoside synthesis, including approaches relying on Pd-catalyzed reactions, see: M. H. D. Postema, *C-Glycoside Synthesis*, CRC, Boca Raton, FL, **1995**.

[5] G.-J. Boons, D. A. Entwistle, S. V. Ley, M. Woods, *Tetrahedron Lett.* **1993**, *34*, 5649; for a mechanistic discussion of homodimer formation see: R. W. Friesen, R. W. Loo, C. F. Sturino, *Can. J. Chem.* **1994**, *72*, 1262.

[6] For leading references on the copper-facilitated Stille coupling, see: a) V. Farina, S. Kapadia, B. Krishnan, C. Wang, L. S. Liebeskind, *J. Org. Chem.* **1994**, *59*, 5905; b) J. R. Falck, R. K. Bhatt, Y. Jianhua, *J. Am. Chem. Soc.* **1995**, *117*, 5973 and references therein; c) the intramolecular coupling of vinyltrialkylstannanes with vinyl halides using stoichiometric CuCl has been reported: E. Piers, T. Wong, *J. Org. Chem.* **1993**, *58*, 3609.

[7] a) S. J. Danishefsky, K. F. McClure, J. T. Randolph, R. B. Ruggeri, *Science* **1993**, *260*, 1307; b) D. M. Gordon, S. J. Danishefsky, *Carbohydr. Res.* **1990**, *206*, 361.

[8] For a titanium-mediated approach to cyclic polyether structures see: K. C. Nicolaou, M. H. D. Postema, C. F. Claiborne, *J. Am. Chem. Soc.* **1996**, *118*, 1565.

[9] All new compounds exhibited satisfactory spectroscopic and exact mass data. Yields refer to spectroscopically and chromatographically homogeneous materials.

The "Bare" Uranyl(2+) Ion, UO_2^{2+}**

Hans H. Cornehl, Christoph Heinemann, Joaquim Marçalo, António Pires de Matos,* and Helmut Schwarz*

Dedicated to Professor Hubert Schmidbaur on the occasion of his 60th birthday

Uranium has attracted particular attention, not only among scientists, ever since the fateful development of nuclear technology some 50 years ago. The linear uranyl moiety UO_2^{2+} is the leitmotif in the coordination chemistry of this element, and thus both experimental[1] and theoretical[2] methods were extensively employed to study UO_2^{2+} and derived molecules[3] in terms of their structural, electronic, and spectroscopic properties. However, despite the abundant information available on UO_2^{2+} ions in solution and in the solid state, to the best of our knowledge neither the existence nor the basic thermochemical data of isolated UO_2^{2+} ions, unperturbed by the presence of counterions and bulk effects, has been established so far (for the available data[4] on UO_x^{y+} ($x = 0$–2, $y = 1, 2$), see Table 1).[5] We are

Table 1. ΔH_f [kcal mol^{-1}] for UO_x^{y+}.

	U^{y+}	UO^{y+}	UO_2^{y+}	Ref.
$y = 0$	127	6 ± 2	-111 ± 1	[4a]
$y = 1$	270	135	14	[4a]
$y = 2$	544 ± 12	-		[4b]

[*] Prof. Dr. H. Schwarz, Dipl.-Chem. H. H. Cornehl, Dr. C. Heinemann
Institut für Organische Chemie der Technischen Universität
Strasse des 17. Juni 135, D-10623 Berlin (Germany)
Fax: Int. code +(30)314-21102
e-mail: schw0531@zrzsp5.chem.tu-berlin.de
Dr. A. Pires de Matos, Dr. J. Marçalo
Instituto Tecnólogico e Nuclear, Departamento de Química
Estrada Nacional 10, P-2686 Sacavém Codex (Portugal)
Fax: Int. code +(1)994-1455
e-mail: pmatos@dms01.ineti.pt.

[**] This work was supported by the Bundesministerium für Bildung und Forschung (German–Portuguese cooperation in science and technology, Project No. X182.6), the Deutsche Forschungsgemeinschaft (Program "Relativistic Effects"), the Fonds der Chemischen Industrie, the Junta Nacional de Investigaçao Cientifica e Tecnológica, and the European Science Foundation (REHE program).

studying the gas-phase chemistry of f-block elements[6] and here communicate the first experimental observation and thermochemical characterization of isolated UO_2^{2+} ions using two different mass-spectrometric techniques. In addition, we report ab initio calculations of singly and doubly charged uranium dioxide UO_2, which corroborate the deduced thermochemical data and provide information on the underlying electronic structures.

Our first set of experiments involved the generation of UO_2^{2+} by ion–molecule reactions of laser-generated doubly charged atomic uranium cations with various oxygen donors at thermal energies. This was achieved in a Fourier transform ion cyclotron resonance (FTICR) mass spectrometer. Thus, UO_2^{2+} can be generated by the reaction of U^{2+} with molecular oxygen according to the two-step process depicted in Scheme 1. While the

$$U^{2+} \xrightarrow[-O]{+O_2} UO^{2+} \xrightarrow[-O]{+O_2} \boxed{UO_2^{2+}} \xrightarrow[-O_2]{+O_2} UO_2^+$$

Scheme 1.

primary formation of UO^{2+} from U^{2+}/O_2 occurs with collisional efficiency ($k_{obs} = k_{ADO}$, the collision rate calculated from average-dipole-orientation (ADO) theory[7]), the secondary reaction of UO^{2+} with O_2 to yield the uranyl dication UO_2^{2+} is more than one order of magnitude slower ($k_{obs} = 4\%\ k_{ADO}$). In a tertiary step, the so-formed uranyl dications undergo electron transfer with O_2 to yield singly charged uranium dioxide and O_2^+ as the final reaction products ($k_{obs} = 35\%\ k_{ADO}$).

$$U^{2+} \xrightarrow[-CO]{+CO_2} UO^{2+} \xrightarrow[-CO]{+CO_2} UO_2^{2+}$$

Scheme 2.

Oxidation of U^{2+} can also be achieved with carbon dioxide (Scheme 2) or nitrous oxide (Scheme 3). In the case of CO_2, the oxidation stops at the stage of diatomic UO^{2+}. In the U^{2+}/N_2O reaction mixture, both the primary and the secondary reaction proceed at the collisional limit, but the charge transfer decay of UO_2^{2+} is significantly slower ($k_{obs} = 3\%\ k_{ADO}$). Besides the formation of UO^{2+}, the U^{2+}/N_2O reaction also yields singly charged UN^+ [3d, 8] with loss of NO^+, consistent with the lower ionization energy (IE) of NO (IE = 9.3 eV) relative to that of N_2 (IE = 15.1 eV), which is lost as a neutral species in the oxidation pathway.

$$U^{2+} \xrightarrow{+N_2O} \begin{cases} \xrightarrow[80\%]{-N_2} UO^{2+} \xrightarrow[-N_2]{+N_2O} \boxed{UO_2^{2+}} \xrightarrow[-N_2O]{+N_2O} UO_2^+ \\ \xrightarrow[20\%]{-NO^+} UN^+ \xrightarrow{+N_2O} \end{cases}$$

Scheme 3.

The observed reactions allow a "bracketing interval" for $\Delta H_f^\circ(UO_2^{2+})$ to be deduced, since only exothermic or thermoneutral reactions can occur under the experimental conditions chosen. From the U^{2+}/CO_2 reaction, a lower bound of 127 kcal mol^{-1} for the bond dissociation energy (BDE) of UO^{2+} can be derived, which translates into $\Delta H_f^\circ(UO^{2+}) <$ 489 kcal mol^{-1}. Formation of UO_2^{2+} from UO^{2+}/O_2 requires BDE$(OU^{2+}-O) >$ 119 kcal mol^{-1}; thus $\Delta H_f^\circ(UO_2^{2+}) <$ 430 kcal mol^{-1}. Finally, the observed charge transfer between N_2O and UO_2^{2+} yields a lower bound of $\Delta H_f^\circ(UO_2^{2+}) >$ 311 kcal mol^{-1}; thus $\Delta H_f^\circ(UO_2^{2+}) = 371 \pm 60$ kcal mol^{-1}, corresponding to a second ionization energy of 15.4 ± 2.6 eV for uranium dioxide. A noteworthy conclusion from the derived thermochemistry is that both UO^{2+} and UO_2^{2+} are thermodynamically stable dications, that is, the molecular dications lie energetically below the lowest dissociation limits (for UO^{2+}: $\Delta H_f^\circ(U^{2+}) + \Delta H_f^\circ(O) = 604 \pm 12$ kcal mol^{-1}; for UO_2^{2+}: $\Delta H_f^\circ(UO^+) + \Delta H_f^\circ(O^+) = 509$ kcal mol^{-1}, $\Delta H_f^\circ(UO^{2+}) + \Delta H_f^\circ(O) < 549$ kcal mol^{-1}). Thus, metastable decays of the doubly charged species into singly charged fragments by "Coulomb explosions"[9] cannot occur without excitation from the ground state.

In view of the relatively large error bars, the experimentally derived thermochemical data were theoretically cross-checked using the coupled cluster method (CCSD) with a quasi-relativistic ab initio pseudopotential for uranium. The second ionization energy of UO_2 was computed, since via $\Delta H_f(UO_2^+)$ it directly leads to the central thermodynamic quantity $\Delta H_f(UO_2^{2+})$. UO_2^+ is derived from closed-shell UO_2^{2+} (see the MO diagram in Fig. 1) by addition of one electron into either of the uranium-

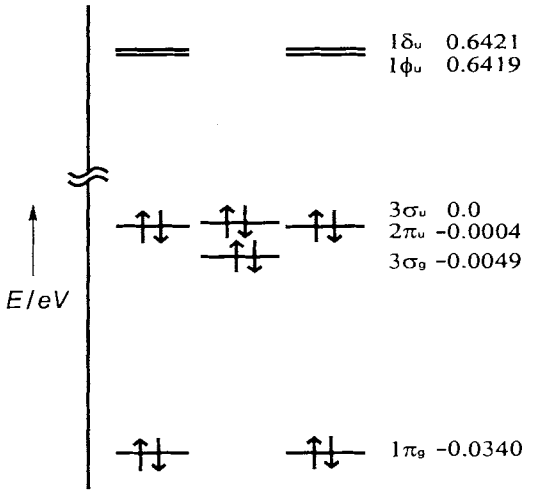

Fig. 1. Hartree–Fock frontier molecular orbital scheme for UO_2^+ and UO_2^{2+}. The occupation shown corresponds to the $^1\Sigma_g^+$ ground state of UO_2^{2+} and the $^2\Delta_u$ and $^2\Phi_u$ states of UO_2^+ arise upon addition of a single electron into either the $1\delta_u$ or the $1\phi_u$ orbital, respectively.

centered nonbonding $1\delta_u$ or $1\phi_u$ orbitals, which have pure atomic 5f character. The remaining frontier MOs are bonding combinations between the uranium 7s, 6d, 6p, and 5f as well as oxygen 2s and 2p atomic orbitals.[10] Calculated U–O equilibrium distances for the low-lying states of UO_2^+ and the $^1\Sigma_g^+$ ground state of UO_2^{2+} are given in Table 2. In the ΛS coupling scheme, UO_2^+ adopts a $^2\Phi_u$ ground state with an adiabatic excitation energy of 0.1 eV to the $^2\Delta_u$ term. The uranium–oxygen distances (Table 2) in the two lowest electronic states of UO_2^+ are 0.06–0.07 Å longer than in the uranyl dication. Upon ionization of UO_2^+ to UO_2^{2+}, the Mulliken charge q(U) of uranium increases by 0.61 e (UO_2^+, $^2\Phi_u$, $q(U) = +2.32$; UO_2^{2+}, $q(U) = +2.93$), less than

Table 2. Optimized U–O bond lengths [Å] for UO_2^+ and UO_2^{2+} as well as calculated [a] vertical energies E_v [eV] for the process $UO_2^+ \rightarrow UO_2^{2+} + e^-$.

	UO_2^+	UO_2^+	UO_2^{2+}
r(U–O)	1.753	1.766	1.697
E_v	15.05	14.63	-

[a] Total energy differences, corrected for spin–orbit effects, which stabilize the lowest electronic states of UO_2^+ by 0.36 eV ($^2\Phi_u$) and 0.20 eV ($^2\Delta_u$), respectively [2c].

the 1.0 e expected from the character of the singly occupied highest molecular orbital of UO_2^+. The associated reorganization of the uranium–oxygen interaction is reflected in the compositions of the bonding molecular orbitals, which acquire more uranium 5f character at the cost of oxygen 2p contributions[10] upon formation of UO_2^{2+} from UO_2^+. The higher partial charge of uranium accounts for the shorter bonds in UO_2^{2+}.

Table 2 lists the calculated second ionization energies for UO_2. Spin-orbit coupling was not included explicitly in the quantum-chemical calculations; however, in the closed-shell species UO_2^{2+} it vanishes in the first approximation. The spin–orbit stabilization of UO_2^+ can be estimated according to Figure 2: The $5f_\phi$ and $5f_\delta$ orbitals split into the $5f_{\phi 7/2}/5f_{\phi 5/2}$ and

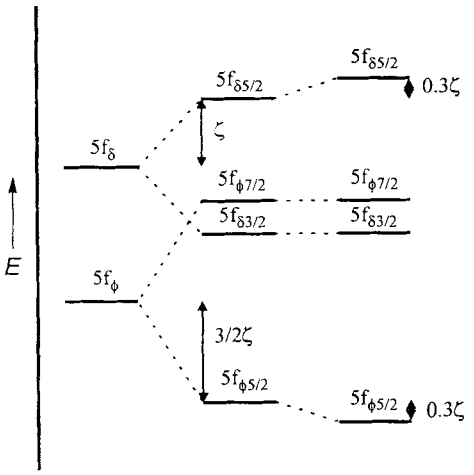

Fig. 2. Spin–orbit effects for $5f_\phi$ and $5f_\delta$ orbitals in UO_2^{2+} according to Ref. [2c].

$5f_{\delta 5/2}/5f_{\delta 3/2}$ pairs, of which the 5/2 components undergo further interaction such that the lowest $5f_{\phi 5/2}$ orbital lies $1.8\zeta(U) = 0.36$ eV lower than the unperturbed $5f_\phi$ level ($\zeta(U)$ is the 5f spin–orbit coupling constant in uranium), while the stabilization of the lowest $5f_{\delta 3/2}$ amounts to $1.0\zeta(U) = 0.2$ eV.[2c] Including this correction, the predicted vertical ionization energies for the ground and first excited state of UO_2^+ are 15.05 eV and 14.63 eV, respectively.[11] Since due to the larger correlation energy in UO_2^+ the calculated ionization energies will be slightly too low, the exact value for the second ionization energy of UO_2 is expected to be in the upper half of the experimentally determined bracketing interval of 15.4 ± 2.6 eV.

In a second, independent mass spectrometric experiment, we observed UO_2^{2+} cations in "charge-stripping" (CS) collisions between singly charged UO_2^+ ions, generated by fast-atom bombardment (FAB),[12] with O_2 targets at 8 keV kinetic energy (laboratory frame). The main products of these energetic UO_2^+/O_2 collisions are the singly charged fragments UO^+ and U^+ arising from collision-induced dissociation (CID) of the parent ion. The uranyl dication, along with the more abundant atomic and diatomic cations U^{2+} and UO^{2+}, is also produced in this event, but the CS process is about a hundred times less efficient than the competing CID channels (Fig. 3). This surprisingly low efficiency is possibly related to the spatially compact nature of the singly occupied molecular orbital of UO_2^+, a hypothesis that is currently under study in our laboratories.[13]

Experimental Procedure

Ion–molecule reactions at thermal energies were studied in Sacavém with an Extrel FTMS-2001 Fourier transform ion cyclotron resonance mass spectrometer, in which U^{2+} ions were generated by laser desorption/laser ionization by focusing the

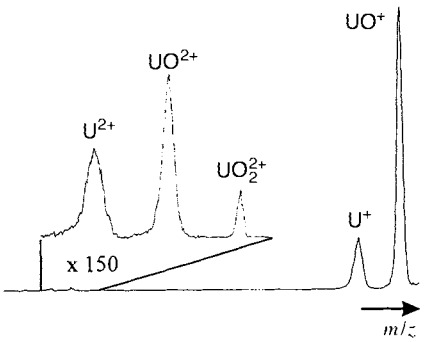

Fig. 3. B(2)-scan "charge-stripping" mass spectrum of UO_2^+ mass-selected by means of B(1) and E(1); oxygen (70% transmission) was used as a collision gas.

beam of a Nd:YAG laser (GCR-11, Spectra Physics, Mountain View, CA; $\lambda = 1064$ nm) onto a pure uranium metal piece, mounted on the solids probe close to the ICR cell. Thermalization of the ions and removal of excess energy was achieved by collisions with argon present at 5×10^{-7} mbar. The reactant gases were admitted to the cell through a leak valve. Reaction pathways were elucidated by MS_2MS and double-resonance techniques. Rate constants k (reported relative to the collision rate k_{ADO} [7]) were derived from the pseudo-first-order decay of the reactant ion and have an estimated accuracy of $\pm 30\%$. The "charge-stripping" experiments were performed in Berlin with a modified VG ZAB-HF AMD 604 four-sector mass spectrometer of BEBE configuration (B stands for magnetic and E for electric sectors), which has been described elsewhere [14]. In brief, UO_2^+ ions were generated by fast atom bombardment (FAB) of a suspension of uranyl acetate in sulfolane, accelerated to 8 keV kinetic energy, mass-selected with B(1)E(1), and collided with oxygen (50–80% transmission).

Ab initio pseudopotential (PP) calculations were performed with the quasi-relativistic 60-core electron uranium PP and the associated (12s11p10d8f) [8s7p6d4f] valence basis set by Küchle et al. [15] augmented by two g-type polarization functions (exponents: 1.2649 and 0.5060). A (14s9p4d)/[6s5p3d] atomic natural orbital (ANO) basis set was used for oxygen [16]. Spin-restricted Hartree–Fock computations were followed by spin-restricted coupled-cluster calculations covering all single and double excitations to account for electron correlation (CCSD, [17]) with correlation of all explicitly treated electrons except for the 5s, 5p, and 5d electrons of uranium and the 1s electrons of oxygen), as implemented in MOLPRO94 [18]. The geometries were optimized stepwise by calculating several points close to the minima on the potential energy surfaces (with omission of the g-functions on uranium in the PP calculations). Second ionization energies are not corrected for zero-point vibrational energies.

Received: October 13, 1995
Revised version: December 11, 1995 [Z 8482 IE]
German version: *Angew. Chem.* **1996**, *108*, 950–952

Keywords: ab initio calculations · mass spectrometry · thermodynamics · uranium compounds

[1] *Gmelin Handbook of Inorganic Chemistry, U Suppl. Vol. A6*. Springer, Berlin, **1992**.

[2] Selected references: a) E. M. van Wezenbeek, E. J. Baerends, J. G. Snijders, *Theor. Chim. Acta* **1991**, *81*, 129; b) P. Pyykkö, Y. Zhao, *Inorg. Chem.* **1991**, *30*, 3787; c) E. M. van Wezenbeek, Dissertation, Free University of Amsterdam, **1991**; d) R. G. Denning, *Struct. Bonding* **1992**, *79*, 215.

[3] a) T. J. Tague Jr., L. Andrews, R. D. Hunt, *J. Phys. Chem.* **1993**, *97*, 10920; b) R. D. Hunt, J. T. Yustein, L. Andrews, *J. Chem. Phys.* **1993**, *98*, 6070; c) P. Pyykkö, J. Li, N. Runeberg, *J. Phys. Chem.* **1994**, *98*, 4809; d) C. Heinemann, H. Schwarz, *Chem. Eur. J.* **1995**, *1*, 7.

[4] a) Thermochemical data are taken from: S. G. Lias, J. F. Liebman, R. D. Levin, S. A. Kafafi, *NIST Standard Reference Database, Positive Ion Energetics*, Version 2.01, January **1994**; b) a compilation of thermochemical data of actinide compounds is given in: D. L. Hildenbrand, L. V. Gurvich, V. S. Yungman, *The Chemical Thermodynamics of Actinide Elements and Compounds, Part 13 – The Gaseous Actinide Ions*, International Atomic Energy Agency, Wien, **1985**; c) atomic energy levels of actinides: J. Blaise, J.-F. Wyart, *Energy Levels and Atomic Spectra of the Actinides* in *International Tables of Selected Constants 20*. Tables Internationales de Constantes, Paris, **1992**.

[5] a) An earlier report applicable to the "bare" uranyl cation concerns the ion pair $UO_2^{2+}:O_2^{2-}$, which is observed in reactions of uranium atoms with O_2 in solid argon at 12 K: R. D. Hunt, L. Andrews, *J. Phys. Chem.* **1993**, *98*, 3690; b) the second ionization energy of UO_2 has been estimated as 12.0 ± 0.2 eV based on a Born–Haber cycle and an estimate for the lattice energy of UO_2F_2: Y. Marcus, *J. Inorg. Nucl. Chem.* **1975**, *37*, 493.

[6] a) H. H. Cornehl, C. Heinemann, D. Schröder, H. Schwarz, *Organometallics* **1995**, *14*, 992; b) C. Heinemann, H. H. Cornehl, H. Schwarz, *J. Organomet. Chem.* **1995**, *501*, 201; c) J. Marçalo, A. Pires de Matos, W. J. Evans, *Organometallics* **1995**, *15*, 345.
[7] T. Su, M. T. Bowers, *Int. J. Mass. Spectrom. Ion Phys.* **1973**, *12*, 347.
[8] a) K. A. Gingerich, *J. Chem. Phys.* **1967**, *47*, 2192; b) P. B. Armentrout, R. V. Hodges, J. L. Beauchamp, *ibid.* **1977**, *66*, 4683.
[9] a) K. Lammertsma, P. von R. Schleyer, H. Schwarz, *Angew. Chem.* **1989**, *101*, 1313; *Angew. Chem. Int. Ed. Engl.* **1989**, *28*, 1321; b) L. M. Roth, B. S. Freiser, *Mass. Spectrom. Rev.* **1991**, *10*, 303; c) D. Mathur, *Phys. Rep.* **1993**, *225*, 193.
[10] Compositions of the Hartree–Fock molecular orbitals in a) UO_2^{2+} ($^1\Sigma_g^+$): $3\sigma_u$: 42% (2p(O), 16% 6p(U), 42% 5f(U); $2\pi_u$: 83% 2p(O), 7% 6p(U), 10% 5f(U); $3\sigma_g$: 70% 2p(O), 6% 2s(O), 12% 7s(U), 12% 6d(U); $1\pi_g$: 91% 2p(O), 9% 6d(U); b) UO_2^+ ($^2\theta_u$): $3\sigma_u$: 50% 2p(O), 20% 6p(U), 30% 5f(U); $2\pi_u$: 90% 2p(O), 5% 6p(U), 5% 5f(U); $3\sigma_g$: 76% 2p(O), 4% 2s(O); 10% 7s(U), 10% 6d(U); $1\pi_g$: 92% 2p(O), 8% 6d(U).
[11] The adiabatic ionization energies $UO_2^+ \rightarrow UO_2^{2+}$ are only slightly lower than the vertical values (15.00 and 14.66 eV for $^2\Phi_u$ and $^2\Delta_u$, respectively).
[12] FAB of uranyl salts has been extensively investigated: T. J. Kemp, K. R. Jennings, P. A. Reed, *J. Chem. Soc. Dalton Trans.* **1995**, 885.
[13] Preliminary measurements of the kinetic energy loss of the incident UO_2^+ beam (Q_{min} value) point to the preferential population of an electronically excited (MO-occupation $3\sigma_u^1 1\delta_u^1$ or $3\sigma_u^1 1\phi_u^1$, see Refs. [1,2]) rather than the ground state of UO_2^{2+} in the charge-stripping collisions.
[14] a) R. Srinivas, D. Sülzle, T. Weiske, H. Schwarz, *Int. J. Mass Spectrom. Ion Processes* **1991**, *107*, 368; b) R. Srinivas, D. Sülzle, W. Koch, C. H. DePuy, H. Schwarz, *J. Am. Chem. Soc.* **1991**, *113*, 5970.
[15] W. Küchle, M. Dolg, H. Stoll, H. Preuss, *J. Chem. Phys.* **1994**, *100*, 7535.
[16] P.-O. Widmark, B. J. Persson, B. O. Roos, *Theor. Chim. Acta* **1991**, *79*, 419.
[17] P. J. Knowles, C. Hampel, H.-J. Werner, *J. Chem. Phys.* **1993**, *99*, 5219.
[18] MOLPRO is a package of ab initio programs written by H.-J. Werner, P. J. Knowles, with contributions from J. Almlöf, R. D. Amos, M. J. O. Deegan, S. T. Elbert, C. Hampel, W. Meyer, K. Peterson, R. Pitzer, A. J. Stone, P. R. Taylor.

Combination of the Fe_4S_4 and M-CN-Fe Redox Functions**

Nianyong Zhu, Jürgen Pebler, and Heinrich Vahrenkamp*

The ubiquity of the Fe_4S_4 ferredoxin as an electron-transfer agent in biological systems[1] and its skillful modeling by inorganic chemists[2] have made it a popular object of teaching and research. We became attracted to this compound in the context of our studies on the redox and mixed-valence properties of polynuclear complexes with M-CN-M′ cyanide links,[3] specifically those containing metallocyanides attached to metal clusters.[4] We assumed that the combination of the two redox-active functions, Fe_4S_4 and M-CN-Fe, would lead to new electronic and electron-transfer properties, and herein we report some results of our attempts to verify this assumption.

The target compounds **1** and **2** are easily accessible by using salts of the anionic $[Fe_4S_4Cl_4]^{2-}$ cluster as starting compounds; this is also a suitable reference for physical measurements and structural comparisons.[5] Combination with $[(CO)_5W-CN]^-$ and $[Cp(CO)_2Mn-CN]^-$ ions in CH_2Cl_2 and with [(dppe)-CpFe-CN] (dppe = 1,2-bis(diphenylphosphanino)ethane and $[(Ph_3P)_2CpRu-CN]$ in acetone leads to chloride substitution and formation of the octanuclear $[Fe_4S_4(NC-M)_4]$ cluster ions. Layering their solutions, containing the appropriate counterions, with hexane results in a slow precipitation of **1a,b** and **2a,b** in 80–90% yield. Compounds **1a** and **1b** are stable even at elevated temperatures, while **2a** and **2b** decompose slowly at room temperature.

$(Ph_4P)_2[Fe_4S_4\{NC-W(CO)_5\}_4]$ **1a** $\quad [Fe_4S_4\{NC-FeCp(dppe)\}_4](PF_6)_2$ **2a**

$(Et_4N)_2[Fe_4S_4\{NC-Mn(CO)_2Cp\}_4]$ **1b** $\quad [Fe_4S_4\{NC-RuCp(PPh_3)_2\}_4](SbF_6)_2$ **2b**

The constitutions of **1a** and **1b** were confirmed by X-ray structure determinations. Figure 1 shows the cluster anion of **1a**.[6] The anion is highly symmetrical; a crystallographic twofold axis passes through the centers of two opposing faces of the Fe_4S_4 cube. All bond lengths of the cluster constituents Fe_4S_4 and Fe-NC-W fall within the range known from Fe_4S_4 and Fe-NC-M reference compounds.[2, 3, 7]

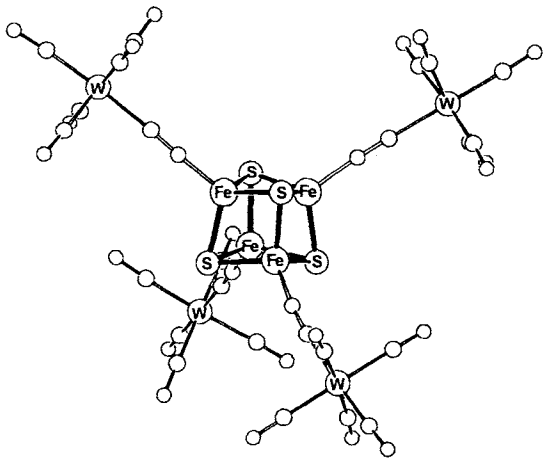

Fig. 1. Crystal structure of the anion of **1a**. Average bond lengths [Å]: Fe–Fe 2.733±0.012, Fe–S 2.275±0.025, Fe–N 1.915±0.005, N–C 1.16±0.005, W–C(CN) 2.143±0.001.

Compounds **1** and **2** are deeply colored, show a characteristic ν(CN) band in the IR spectrum, and their electrochemistry is governed by a reversible one-electron reduction and an irreversible multielectron oxidation (Table 1). Considering the difference of four charge units between the cluster ions **1** and **2**, the difference between their redox potentials is rather small.

Table 1. Vibrational frequencies $\tilde{\nu}$ [cm^{-1}], oxidation and reduction potentials E [V], and UV/Vis absorptions λ [nm] and extinction coefficients ε [$L\,mol^{-1}\,cm^{-1}$].

Cmpd.	$\tilde{\nu}_{CN}$ [a]	E_p (ox) $E_{1/2}$ (red) [b]	λ_{max} [c] (ε)	λ_{IT} [c] (ε)
1a	2034 m	+1.0	273	506
		−0.46	(51000)	(17500)
1b	2015 s	+0.4	272	602
		−0.76	(18000)	(15000)
2a	2016 s	+0.7	<250	526
		−0.64	(>70000)	(12000)
2b	2023 s	+1.2	<250	440
		−0.57	(>40000)	(11000)

[a] As KBr disk. [b] In CH_2Cl_2, vs. Ag/AgCl. The peak potential is given for the oxidation (ox) and the half-wave potential for the reduction (red). [c] In CH_2Cl_2.

[*] Prof. Dr. H. Vahrenkamp, M Sc N. Zhu
Institut für Anorganische und Analytische Chemie der Universität
Albertstrasse 21, D-79104 Freiburg (Germany)
Fax: Int. code +(761)203-6001
Prof. Dr. J. Pebler
Fachbereich Chemie der Universität
Hans-Meerwein-Strasse, D-35032 Marburg (Germany)
Fax: Int. code +(6421)28-8917

[**] This work was supported by the Graduiertenkolleg "Systeme mit ungepaarten Elektronen" and by the Landes-Schwerpunktprogramm "Molekulare Elektrochemie".

The electronic spectra of **1** and **2** (Table 1) differ significantly from those of the reference compounds $[Fe_4S_4Cl_4]^{2-}$[5] and $[Fe_4S_4(SR)_4]^{2-}$.[8] While the intense absorption of the latter in the upper visible or near UV range, assigned to intracore charge transfers,[9] appears in the near UV for **1** and **2** as well, the lower visible or near IR range, which shows only weak features for the reference compounds, is dominated by intense and very broad bands for **1** and **2** (Fig. 2). The UV/Vis absorptions assignable

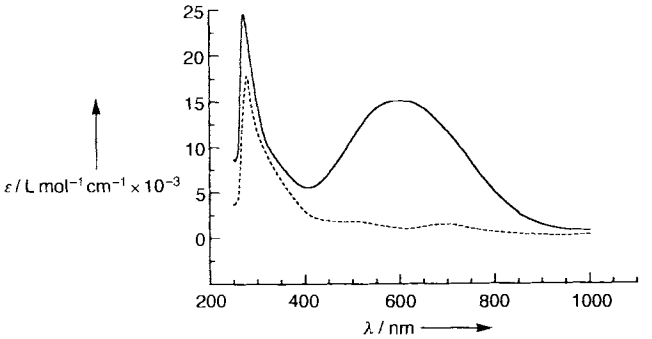

Fig. 2. UV/Vis/NIR spectra of **1b** (—) and $(PPN)_2[Fe_4S_4Cl_4]$ (- - -) in CH_2Cl_2. PPN = bis(triphenylphosphane)iminium.

to the cyanometal units with ε values around 2000 are completely hidden by these bands. We assign the broad bands to intervalence transfer (IT) transitions from the cyanometal unit to the Fe_4S_4 core. This assignment is consistent with the observation that solutions of the trianionic cluster, which is obtained by one-electron reduction of **1a** with cobaltocene, show the IT band at higher energy (466 nm, $\varepsilon = 14000$ L mol^{-1}cm^{-1}).

To further elucidate the electronic nature of the clusters, magnetic measurements were performed for **1a** with a Squid magnetometer. Figure 3 shows the surprising result. At very low tem-

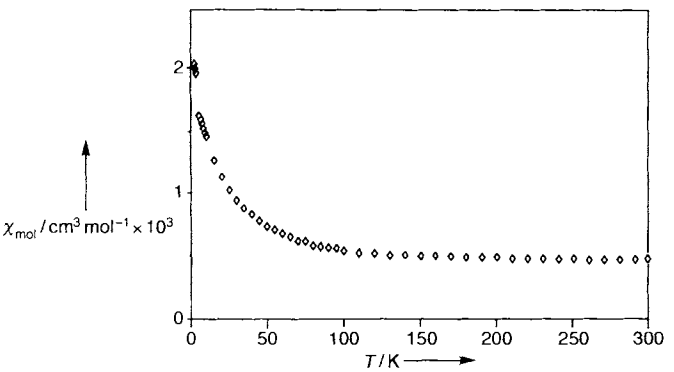

Fig. 3. Temperature dependence of the magnetic susceptibility of **1a**.

peratures an apparent rise of the susceptibility indicates the presence of a paramagnetic impurity that has also been observed in all reference compounds.[5, 10] Between 120 and 300 K, however, χ_{mol} is practically temperature-independent which, to our knowledge, has not been observed for any other synthetic or biological $Fe_4S_4X_4$ derivative. The remaining temperature-independent paramagnetism (TIP) of about 480×10^{-6} cm^3 mol^{-1} lies in the range reported for $[Fe_4S_4Cl_4]^{2-}$ and $[Fe_4S_4(SPh)_4]^{2-}$ ions.[5, 10] If the TIP term is taken as a correction term as has been done for the reference compounds, cluster **1a** and possibly **1b**, **2a**, and **2b** are essentially diamagnetic. In terms of the description of the bonding and the spin–spin interaction for $Fe_4S_4X_4$ species[9, 11] this means that there is very strong antiferromagnetic coupling between the iron atoms with J values well above -300 cm^{-1}. Consequently, the energy gap between the $S' = 0$ ground state and the ladder of excited states is so large that the latter are unaccessible at room temperature.

In accordance with this picture compound **1a** is EPR-silent. Its Mössbauer spectrum recorded at 4.2 K shows a very well resolved doublet with $\delta = 0.333(8)$ mm s^{-1} relative to Fe metal and $\Delta E^Q = 1.06(1)$ mm s^{-1}. These values indicate a delocalized electronic state for the cluster with chemically equivalent iron atoms in the oxidation state +2.5, and the data from the Mössbauer spectrum of **1a** are again very similar to those of other symmetrical $[Fe_4S_4X_4]^{2-}$ compounds.[5, 10, 12]

Thus, while the overall electronic behavior of our new Fe_4S_4 derivatives corresponds to that of known compounds, their strong antiferromagnetic coupling and their intervalence transfer properties pose new questions. It remains to be quantified to what extent the electron-transfer properties of the M-CN-Fe units in **1** and **2** can be exploited, and whether the large separation of the magnetic ground and excited states caused by the cyanometal "ligands" can be related to the preference for the low-spin state caused by cyanide ligands in ordinary complexes.

Received: November 15, 1995 [Z85541E]
German version: *Angew. Chem.* **1996**, *108*, 984–985

Keywords: complexes with cyano ligands · electron transfer · iron–sulfur clusters · magnetic properties

[1] W. Kaim, B. Schwederski, *Bioanorganische Chemie*, Teubner, Stuttgart, **1995**, chapter 7; S. J. Lippard, J. M. Berg, *Principles of Bioinorganic Chemistry*, University Science Books, Mill Valley, **1994**, chapter 9.

[2] For recent review articles see R. H. Holm, S. Ciurli, J. A. Weigel, *Prog. Inorg. Chem.* **1990**, *38*, 1–74; R. H. Holm, *Adv. Inorg. Chem.* **1992**, *38*, 1–71.

[3] N. Zhu, H. Vahrenkamp, *J. Organomet. Chem.* **1994**, *472*, C5–C7; *Angew. Chem.* **1994**, *106*, 2166–2167; *Angew. Chem. Int. Ed. Engl.* **1994**, *33*, 2090–2091.

[4] B. Oswald, A. K. Powell, F. Rashwan, J. Heinze, H. Vahrenkamp, *Chem. Ber.* **1990**, *123*, 243–250. N. Zhu, P. Hauser, J. Heinze, H. Vahrenkamp, *J. Cluster Sci.* **1995**, *6*, 147–162.

[5] G. B. Wong, M. A. Bobrik, R. H. Holm, *Inorg. Chem.* **1978**, *17*, 578–584. M. G. Kanatzidis, W. R. Dunham, W. R. Hagen, D. Coucouvanis, *J. Chem. Soc. Chem. Commun.* **1984**, 356–358.

[6] Crystal data for **1a**: space group $C2/c$, $a = 27.743(6)$, $b = 16.906(3)$, $c = 19.169(4)$ Å, $\beta = 92.75(3)°$, 4996 reflections, 532 parameters, $R = 0.048$. Further details of the crystal structure investigation may be obtained from the Fachinformationszentrum Karlsruhe, D-76344 Eggenstein-Leopoldshafen (Germany), on quoting the depository number CSD-404693.

[7] The possibility of CN inversion, that is the presence of Fe-CN-W links in **1a**, cannot be excluded as we have observed such inversions before and as C and N cannot be distinguished crystallographically.

[8] P. V. DePamphilis, B. A. Averill, T. Herskovitz, L. J. Que, R. H. Holm, *J. Am. Chem. Soc.* **1974**, *96*, 4159–4167.

[9] A. Aizman, D. A. Case, *J. Am. Chem. Soc.* **1982**, *104*, 3269–3279.

[10] E. J. Laskowski, R. B. Frankel, W. O. Gillum, G. C. Papefthymiou, J. Renaud, J. A. Ibers, R. H. Holm, *J. Am. Chem. Soc.* **1978**, *100*, 5322–5337.

[11] G. C. Papefthymiou, E. J. Laskowski, S. Frota-Pessoa, R. B. Frankel, R. H. Holm, *Inorg. Chem.* **1978**, *21*, 1723–1728.

[12] M. G. Kanatzidis, N. C. Baenzinger, D. Coucouvanis, A. Simopoulos, A. Kostikas, *J. Am. Chem. Soc.* **1984**, *106*, 4500–4511.

[5 + 2]Cycloaddition of Cyclic *N*-Phosphino-1-azadienes: Synthesis, Structure, and Reactivity of the First Seven-Membered Iminophosphorane**

José Barluenga,* Miguel Tomás, Klaus Bieger, Santiago García-Granda, and Rafael Santiago-García

Despite the importance of seven-membered carbocycles, the [5 + 2]cycloaddition reaction has been little developed,[1] and in most cases cationic pentadienyl species are involved.[2] The synthesis of seven-membered heterocycles by 1,5-dipolar cycloadditions is unknown, as far as we are aware;[3] to date only the intramolecular trapping of a vinylthiocarbonyl-*S*-sulfide (1,5-dipole) with an alkene has been reported.[4] The particular chemical properties of phosphorus in compounds led us to investigate α,β-unsaturated *N*-phosphino-substituted imines (*N*-phosphino-1-azadienes) as possible 1,5-dipoles. Our considerations were supported by recent findings in which *N*-phosphino imines[5] and various phosphino 1,3-dipoles[6] were found to react with activated alkenes and alkynes as 1,3- and 1,4-dipoles, respectively. We report herein that 1,2-dihydro-1,3,2-diazaphosphinine **2** actually undergoes [5 + 2]cycloaddition with dimethyl acetylenedicarboxylate (DMAD) leading to novel phospha-heterocycles, as well as on the novel structure and reactivity of these products.[7]

Compound **2** (^{31}P NMR: δ = 57.9) was readily prepared in quantitative yield by condensation of the 4-amino-1-azadiene **1** with dichloro(diisopropylamino)phosphane according to a known procedure (Scheme 1).[8] Treatment of **2** with DMAD in ether at −20 °C afforded a single reaction product (^{31}P NMR: δ = 48.2), which was characterized as the bicyclo[3.2.1]-2,8-diaza-1-phospha-1,3,6-octatriene **4**, and has a new type of iminophosphorane structure.[9] This unprecedented 1,5-dipolar cycloaddition most probably involves nucleophilic attack of the phosphorus center at the electrophilic alkyne, leading to the zwitterionic intermediate **3** followed by 1,7-electrocyclization to give **4** (Scheme 1).

To establish unambiguously the structure of **4**, an X-ray structure analysis was carried out on crystals grown from ether/hexane at −20 °C (Fig. 1).[10] The C4–C6 distance (228.05 pm) is significantly shortened, and the C4-C5-C6 angle (96.1°) as well as the pyramidalization of C7 (sum of angles: 353.9°) suggest an equilibrium between the valence isomers **4** and **4'** in the solid state.[11]

Compound **4** is not thermally stable and rearranges quantitatively (^{31}P NMR spectroscopy) at room temperature in solution (CH_2Cl_2, Et_2O) leading to the new cyclic phosphorus ylide **5** (^{31}P NMR: δ = 56.5) (Scheme 2).[12] Furthermore, we have tested the reactivity of **4** towards electrophiles such as chlorodifluoroacetic acid and methyl iodide. Interestingly, protonation and methylation occurred readily (CH_2Cl_2 at −20 °C) at the carbon adjacent to the phosphorus atom to deliver **6** (E = H) (^{31}P NMR: δ = 46.4) and **7** (E = Me) (^{31}P NMR: δ = 48.5),

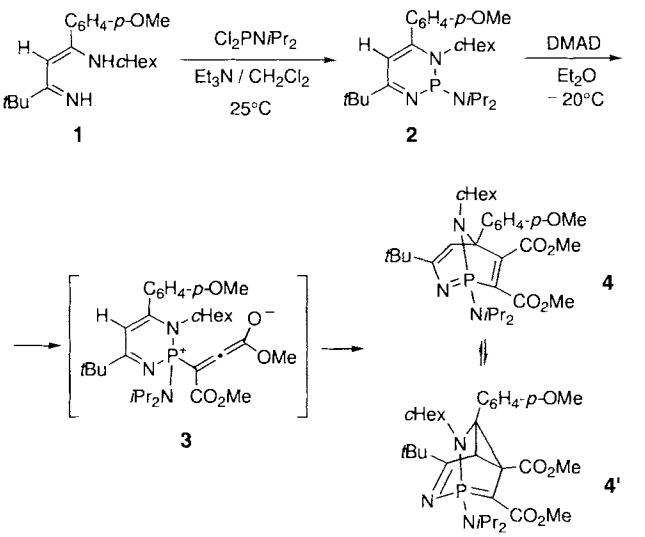

Scheme 1. Synthesis of diazaphosphinine **2** and the phosphorus-containing bi- and tricyclic compounds **4** and **4'**, respectively.

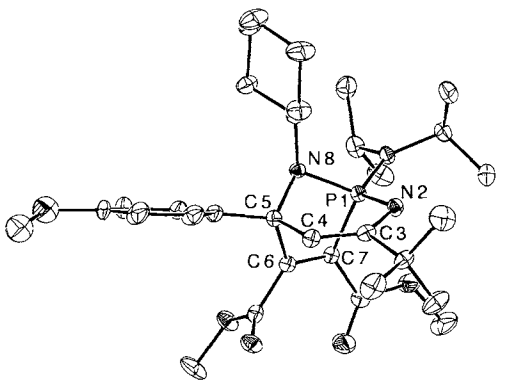

Fig. 1. Crystal structure of **4**. Selected bond lengths [pm] and bond angles [°]: P1–N2 159.7(3), P1–N8 167.8(3), P1–C7 177.2(3), N2–C3 138.7(4), C3–C4 136.6(5), C4–C5 153.2(4), C5–C6 153.5(4), C5–N8 150.1(4), C6–C7 135.1(4); C4-C5-C6 96.1(2), P1-C7-C6 104.6(1), P1-C7-CO, 127.3(2), C6-C7-CO 122.0(3).

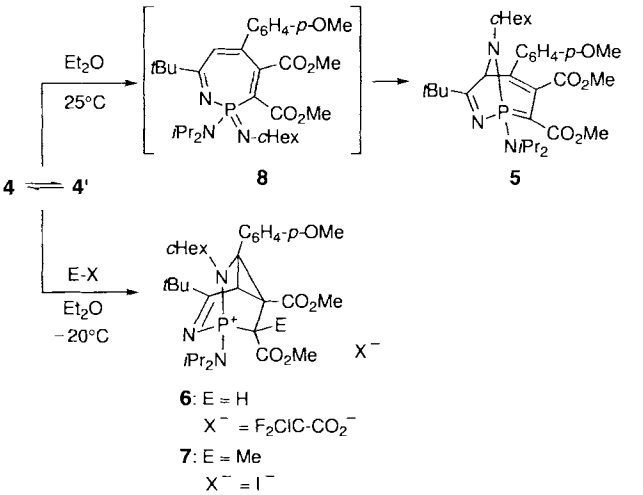

Scheme 2. Formation of phosphorus ylide **5** and phosphonium salts **6** and **7** from **4** and **4'**.

respectively (Scheme 2). These transformations seem to proceed through the valence isomer species **4'**. Thus, the formation of **5** is conceivable by cyclopropane cleavage of **4'** to form intermediate **8**, followed by Michael addition.[13] The trapping reactions of the ylidic carbon atom of **4'** to give the novel phosphonium

[*] Prof. Dr. J. Barluenga, Dr. M. Tomás, Dr. K. Bieger
Instituto Universitario de Química Organometálica Enrique Moles
Unidad Asociada C. S. I. C.
Universidad de Oviedo
Julián Clavería, 8; E-33071, Oviedo (Spain)
Fax: Int. code +(8) 510 34 50
Dr. S. García-Granda, R. Santiago-García
Departamento de Química Física y Analítica (Spain)

[**] This work was supported by DGICYT (Project PB92-1005) and the European Community (Fellowship to K. B.; Contract No. ERBCHBICT941732). The X-ray crystal structure analyses were carried out by S. G.-G. and R. S.-G.

salts **6** and **7** occur stereoselectively, which can be explained easily by the steric hindrance of one of the sides of the molecule by ester and *tert*-butyl groups (see Fig. 1).

Compound **6** cocrystallized in ether together with one molecule of chlorodifluoroacetic acid and the structure was determined by X-ray crystallography (Fig. 2).[10]

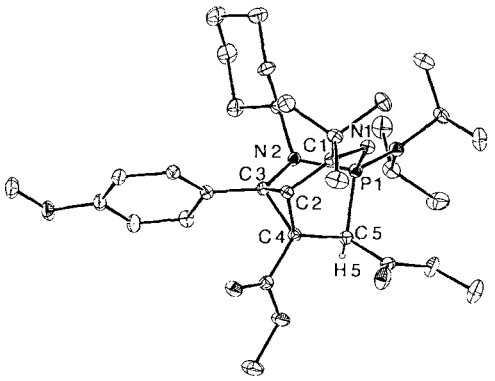

Fig. 2. Crystal structure of **6**. Selected bond lengths [pm] and bond angles [°]: P1–N1 163.9(6), P1–N2 165.8(6), P1–C5 180.9(7), N1–C1 130.8(8), C1–C2 147.6(9), C2–C3 157.4(9), C2–C4 153.4(9), N2–C3 146.3(8), C3–C4 151.7(9), C4–C5 151.3(9); C4-C2-C3 58.4(4); C4-C3-C2 59.5(4); C2-C4-C3 62.1(4).

In summary, we have reported the first [5 + 2]heterocycloaddition of a neutral species, namely a masked phosphorus-containing 1,5-dipole, as well as unusual rearrangements of the resulting bicyclic iminophosphorane. The interatomic distances and angles determined by X-ray structure analysis suggest a norcaradiene–cycloheptatriene type rearrangement **4** $\rightleftharpoons$ **4′** *in the solid state*. Moreover, it is worth noting that all transformations reported here result in the isolation of new, unusual structures (**4**–**7**) in high yields.

Experimental Procedure

Aminoazadiene **1** [14] (4.85 g, 15.4 mmol) was added slowly at 0 °C to a solution of dichloro(diisopropylamino)phosphane (3.12 g, 15.4 mmol) in CH_2Cl_2/NEt_3 (20 mL/5 mL). After the mixture had been stirred for 6 h at 20 °C, the solvent and excess amine were removed under reduced pressure, the residue was treated with ether, and the salts were filtered off. Dihydrophosphinine **2** (^{31}P NMR: δ = 57.9) was obtained as a yellow oil after evaporation of the solvent (6.40 g, 94%) and used without further purification.

A solution of DMAD (0.45 g, 3.2 mmol) in ether (5 mL) was added to a well-stirred solution of **2** (1.41 g, 3.2 mmol) in ether (30 mL) at −20 °C. The mixture was kept at −20 °C for 12 h. Then compounds **4**–**7** were prepared as follows: 1) Evaporation of the solvent at reduced pressure and treatment of the residue with hexane at −20 °C afforded **4** [1.5 g, 80%; ^{31}P NMR: δ = 48.2; m.p. 106–109 °C (decomp)] as yellow-orange crystals. 2) The reaction mixture was left at room temperature for 24 h, the solution was concentrated under vacuum, and the residue crystallized from hexane/ether to afford **5** [1.4 g, 75%; ^{31}P NMR: δ = 56.5; m.p. 134–136 °C (decomp)] as yellow crystals. 3) The reaction mixture was stirred at −20 °C with an excess of chlorodifluoroacetic acid or methyl iodide for 15 min. Removal of solvents and crystallization of the residue from ether gave compounds **6**·ClF_2CCO_2H [1.8 g, 66%; ^{31}P NMR: δ = 46.4; m.p. 115 °C (decomp)] and **7** [1.7 g, 73%; ^{31}P NMR: δ = 48.5; m.p.: 165–170 °C (decomp)] as colorless crystals.

Selected ^{13}C NMR data (75 MHz): **4**: ([D_8]THF, −30 °C): δ = 167.1 (s, N-*C*=C), 166.1 (d, ^3J(P,C) = 18.0 Hz, C=O), 165.6 (d, ^2J(P,C) = 13.0 Hz, C=O), 161.9 (s, C_{Ar}), 137.5 (d, ^2J(P,C) = 11.3 Hz, PC*C*), 133.9 (s, $C_{Ar}H$), 132.6 (d, ^3J(P,C) = 9.5 Hz, *C*C_{Ar}), 131.0 (s, $C_{Ar}H$), 115.9 (s, $C_{Ar}H$), 114.0 (s, $C_{Ar}H$), 96.5 (d, ^1J(P,C) = 129.2 Hz, P*C*), 84.6 (d, ^3J(P,C) = 13.2 Hz, C H), 67.2 (d, ^2J(P,C) = 13.2 Hz, *C*C_{Ar}), 56.6 (s, OCH_3 + NC H), 53.4 (s, OCH_3), 52.8 (s, OCH_3), 48.9 (d, ^2J(P,C) = 8.6 Hz, NC H), 48.3 (s, NC H), 40.5 (d, ^3J(P,C) = 22.3 Hz, CMe_3), 36.6 (s, CH_2), 33.3 (s, CH_2), 30.8 (s, 3CH_3), 29.3 (s, CH_2), 29.0 (s, CH_2), 27.7 (s, CH_2), 27.2 (s, CH_3), 25.7 (s, CH_3), 22.6 (s, CH_3), 22.1 (s, CH_3).

5: ($CDCl_3$, 25 °C): δ = 181.4 (d, ^2J(P,C) = 5.6 Hz, C=N), 169.4 (d, ^3J(P,C) = 19.4 Hz, C=O), 165.2 (d, ^2J(P,C) = 10.4 Hz, C=O), 157.3 (s, C_{Ar}), 135.1 (d, ^3J(P,C) = 13.2 Hz, PCC*C*), 131.7 (s, C_{Ar}), 130.2 (s, $C_{Ar}H$), 112.8 (s, $C_{Ar}H$), 104.6 (d, ^2J(P,C) = 2.1 Hz, PC*C*), 62.3 (d, ^2J(P,C) = 20.1 Hz, NC H), 54.6 (s, OCH_3), 53.4 (d, ^2J(P,C) = 2 Hz, C H), 52.3 (d, ^1J(P,C) = 148.4 Hz, PC), 51.0 (s, OCH_3), 49.8 (s, OCH_3), 47.8 (d, ^2J(P,C) = 5.6 Hz, NC H), 37.2 (d, ^3J(P,C) = 20.8 Hz, N=*C*C), 32.4 (d, 6.3 Hz, CH_2), 29.5 (s, CH_2), 28.1 (s, 3 × CH_3), 26.1 (s, CH_2), 26.0 (s, CH_2), 25.4 (s, CH_2), 22.7 (d, ^3J(P,C) = 2.1 Hz, 2 × CH_3), 22.6 (s, 2 × CH_3).

7: ($CDCl_3$, 25 °C): δ = 205.3 (d, ^2J(P,C) = 8.6 Hz, C=N), 165.8 (s, CO), 164.2 (d, ^3J(P,C) = 13.3 Hz, CO), 160.1 (s, C_{Ar}), 132.4 (s, $C_{Ar}H$), 130.2 (s, $C_{Ar}H$), 120.4 (d, ^3J(P,C) = 8.6 Hz, C_{Ar}), 114.5 (s, $C_{Ar}H$), 113.1 (s, $C_{Ar}H$), 57.8 (d, ^2J(P,C) = 10.2 Hz, NC), 56.1 (s, NC H), 55.0 (s, OCH_3), 53.2 (s, OCH_3), 53.0 (s, OCH_3), 49.7 (b, 2 × NC H), 43.9 (d, ^3J(P,C) = 19.6 Hz, N=*C*C), 40.5 (d, ^1J(P,C) = 72.8 Hz, PC), 38.9 (s, P*C*C), 34.9 (d, ^3J(P,C) = 28.2 Hz, C H), 32.6 (d, CH_2), 30.4 (d, CH_2), 26.9 (s, 3 × CH_3), 25.8 (s, CH_2), 25.4 (s, CH_2), 23.8 (s, CH_3), 20–23 (b, 4 × CH_3), 15.6 (d, ^2J(PC) = 7.1 Hz, PC*C*H$_3$).

Received: October 31, 1995 [Z 8518 IE]
German version: *Angew. Chem.* **1996**, *108*, 977–979

Keywords: cycloadditions · nitrogen compounds · phosphoranes · phosphorus ylides

[1] a) P. A. Wender, H. Takahashi, B. Witulski, *J. Am. Chem. Soc.* **1995**, *117*, 4720; b) P. A. Wender, L. Siggel, J. M. Nuss in *Comprehensive Organic Synthesis*, *Vol. 5*, (Eds.: B. M. Trost, I. Fleming), Pergamon, New York, **1991**, p. 645.

[2] a) P. A. Wender, J. L. Mascareñas, *J. Org. Chem.* **1991**, *56*, 6267; b) A. Rumbo, L. Castedo, A. Mouriño, J. L. Mascareñas, *ibid.* **1993**, *58*, 5585; c) T. A. Engler, M. A. Letavic, K. D. Combrink, F. Takusagawa, *ibid.* **1990**, *55*, 5810.

[3] a) A. Padwa, T. Kumagai, A. D. Woolhouse, *J. Org. Chem.* **1983**, *48*, 2330; b) R. Huisgen, *Angew. Chem.* **1980**, *92*, 979; *Angew. Chem. Int. Ed. Engl.* **1980**, *19*, 947.

[4] a) T. Saito, M. Nagashima, T. Karakasa, S. Motoki, *J. Chem. Soc. Chem. Commun.* **1992**, 411.

[5] a) A. Schmidpeter, W. Zeiss, *Angew. Chem.* **1971**, *83*, 398; *Angew. Chem. Int. Ed. Engl.* **1971**, *10*, 396; b) G. Veneziani, R. Réau, F. Dahan, G. Bertrand, *J. Org. Chem.* **1994**, *59*, 5927.

[6] a) T. Facklam, O. Wagner, H. Heydt, M. Regitz, *Angew. Chem.* **1990**, *102*, 316; *Angew. Chem. Int. Ed. Engl.* **1990**, *29*, 314; b) J. Tejeda, R. Réau, F. Dahan, G. Bertrand, *J. Am. Chem. Soc.* **1993**, *115*, 7880; c) M. Granier, A. Baceiredo, M. Nieger, G. Bertrand, *Angew. Chem.* **1990**, *102*, 1185; *Angew. Chem. Int. Ed. Engl.* **1990**, *29*, 1123; d) F. Castan, M. Granier, T. A. Straw, A. Baceiredo, K. B. Dillon, G. Bertrand, *Chem. Ber.* **1991**, *124*, 1739.

[7] For a recent reference concerning synthesis of complex phosphaheterocycles, see for example: H. Heydt, U. Bergstrasser, R. Fässler, E. Fuchs, N. Kamel, T. Mackewitz, G. Michels, W. Rösch, M. Regitz, P. Mazerolles, C. Laurent, A. Faucher, *Bull. Soc. Chim. Fr.* **1995**, *132*, 652.

[8] a) J. Barluenga, J. Jardón, F. Palacios, V. Gotor, *Synthesis* **1985**, 309; b) See also: R. Sonnenburg, I. Neda, A. Fischer, P. G. Jones, R. Schmutzler, *Chem. Ber.* **1995**, *128*, 627.

[9] Some examples of four-, five-, and six-membered iminophosphoranes are known. A. W. Johnson, *Ylides and Imines of Phosphorus*, J. Wiley, New York, **1993**.

[10] Crystal data. Compound **4**: $C_{32}H_{48}N_3O_5P_1$, M_r = 585.72, monoclinic, space group $P2_1/c$, a = 16.126(6), b = 20.451(4), c = 10.311(2) Å, β = 102.09(3)°, V = 3325(2) Å^3, Z = 4, ρ_{calcd} = 1170 Mg m^{-3}, $Mo_{K\alpha}$ radiation (graphite crystal monochromator, λ = 0.71073 Å), μ = 0.124 mm^{-1}, $F(000)$ = 1264, T = 200(2) K. Final conventional R = 0.052 and $wR2$ = 0.133 for 2783 observed reflections and 466 variables. The function minimized was $[\Sigma w(F_o^2 - F_c^2)^2/[\Sigma w(F_o^2)^2]]^{1/2}$, $w = 1/[\sigma^2(F_o^2) + (0.0926P)^2]$ with $\sigma(F_o^2)$ from counting statistics and $P = Max\ (F_o^2, 0) + 2F_c^2)/3$. Compound **6**: $C_{34}H_{40}F_2Cl_1N_3O_7P_1 \cdot C_2H_1F_2Cl_1O_2$, M_r = 846.66, monoclinic, space group $P2_1/n$, a = 11.345(11), b = 15.750(7), c = 24.284(10) Å, β = 92.47(6)°, V = 4335(5) Å^3, Z = 4, ρ_{calcd} = 1.297 Mg m^{-3}, $Mo_{K\alpha}$ radiation (graphite crystal monochromator, λ = 0.71073 Å), μ = 0.255 mm^{-1}, $F(000)$ = 1776, T = 293(2) K. Final conventional R = 0.085 and $wR2$ = 0.234 for 2905 observed reflections and 499 variables. The function minimized was $[\Sigma w(F_o^2 - F_c^2)^2/[\Sigma w(F_o^2)^2]]^{1/2}$, $w = 1/[\sigma^2(F_o^2) + (0.1551P)^2 + (7.35P)]$ with $s(F_o^2)$ from counting statistics and $P = (Max\ (F_o^2, 0) + 2F_c^2)/3$. Crystallographic data (excluding structure factors) for the structures reported in this paper have been deposited with the Cambridge Crystallographic Data Centre as supplementary publication no. CCDC-179-9. Copies of the data can be obtained free of charge on application to The Director, CCDC, 12 Union Road, Cambridge CB2 1EZ, UK (fax: int. code +(1223) 336-033; e-mail: teched@chemcrys.cam.ac.uk).

[11] This phenomenon has been established for substituted semibullvalenes and barbaralanes wherein Cope rearrangements take place. In these cases the nonbonding interatomic distances are generally in the range of 220–230 pm. See: a) L. M. Jackman, A. Benesi, A. Mayer, H. Quast, E.-M. Peters, K. Peters, H. G. von Schnering, *J. Am. Chem. Soc.* **1989**, *111*, 1512; b) H. Quast, J. Carlsen, R. Janiak, E.-M. Peters, K. Peters, H. G. von Schnering, *Chem. Ber.* **1992**, *125*, 955; c) H. Quast, M. Witzel, E.-M. Peters, K. Peters, H. G. von Schnering, *Liebigs Ann.* **1995**, 725.

[12] Structure **5** was established by an X-ray determination. S. García-Granda, R. Santiago-García, unpublished results.

[13] A retro-Michael reaction/Michael re-addition sequence also accounts for the formation of **5** from **4**.

[14] a) H. Hoberg, J. Barluenga, *Synthesis* **1970**, 142; b) G. Wittig, S. Fischer, M. Tanaka, *Liebigs Ann. Chem.* **1973**, 1075.

 © VCH Verlagsgesellschaft mbH, D-69451 Weinheim, 1996 0570-0833/96/3508-0897 $ 15.00+.25/0

Mixed-Metal Triple-Decker Sandwich Complexes with the Porphyrin/Phthalocyanine/Porphyrin Ligand System**

Porphyrin and porphyrin–phthalocyanine double-decker sandwich complexes $[M(p)_2]$ and [M(p)(pc)] can be expanded to symmetric and asymmetric triple-decker sandwich complexes of the form $[M_2(p)_3]$, $[M_2(p)_2(pc)]$, and $[M_2(pc)_2(p)]$ (M = trivalent metal ion; p = porphyrin dianion, pc = phthalocyanine dianion).[1–4] The electronic structures of these triple-decker molecules have been probed by means of the electrochemical, magnetic, and spectroscopic properties of their neutral and one-electron oxidized and reduced states. UV/Vis and electrochemical studies and magnetic susceptibility measurements indicate that upon oxidation of the [(tpp)M(pc)M(tpp)] (tpp = tetraphenylporphyrin dianion) complexes in which no Ce^{III} center is present ($M = La^{III}$, Gd^{III}), the phthalocyanine dianion is preferentially oxidized to the radical monoanion.[5] In contrast, magnetic studies and X-ray photoelectron spectroscopy show that in [(tpp)Ce(pc)Ce(tpp)], one Ce^{III} center is oxidized to Ce^{IV}.[4b]

We have now synthesized and characterized the following mixed-metal complexes: [(tpp)M(pc)M′(tpp)] (**1**(M,M′)), containing no oxidizable metal (M = La, M′ = Y) or one oxidizable metal (M = Ce, M′ = Gd, Lu, Y), and [(tpp)Ce(pc)-Gd(oep)] (**2**(Ce,Gd), oep = octaethylporphyrin dianion). The complex **2**(Ce,Gd) is the first heteronuclear triple-decker sandwich complex with mixed ligands that has been analyzed by a crystal structure determination. The structural formulas of the ligands and a diagrammatic representation of the triple-decker complex is shown in Scheme 1. Electrochemical studies of these mixed-metal sandwich complexes lead to two different linear correlations of the first oxidation potentials with the mean ionic radii of the metals ($[r_i(M) + r_i(M')]/2$) that depend on the presence or absence of an oxidizable Ce^{III} ion.

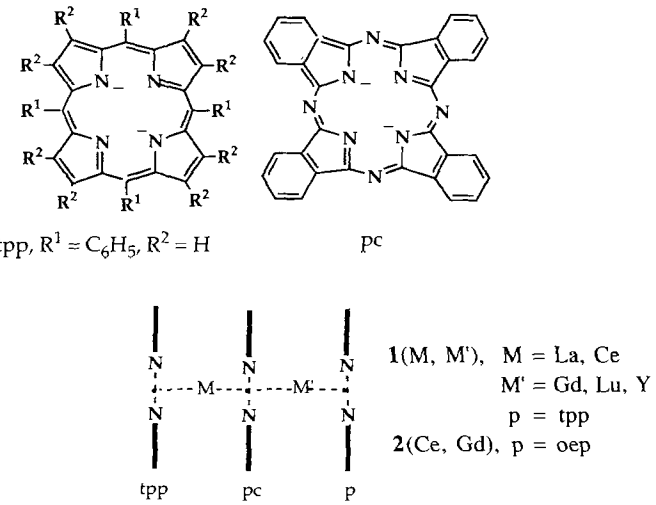

Scheme 1. Structural formulas of the p and pc ligands and a schematic representation of the triple-decker complexes **1** and **2**.

The synthesis of the heteroleptic, heteronuclear complexes **1**(M,M′) is described in the experimental procedure. However, all attempts to grow suitable crystals of these complexes for X-ray crystal structure analysis failed. Instead we therefore synthesized the Ce^{III}/Gd^{III} derivative with tetraphenylporphyrin, phthalocyanine, and octaethylporphyrin as ligands. This compound yielded crystals of composition **2**(Ce,Gd)·$2C_6H_5Cl$,[6] which contain discrete molecules of **2**(Ce,Gd) (Fig. 1).[7] The triple-decker molecules do not exhibit any bonding interactions with one another nor with the chlorobenzene molecules of solvation. As shown in Figure 1, both the Ce and Gd atoms are

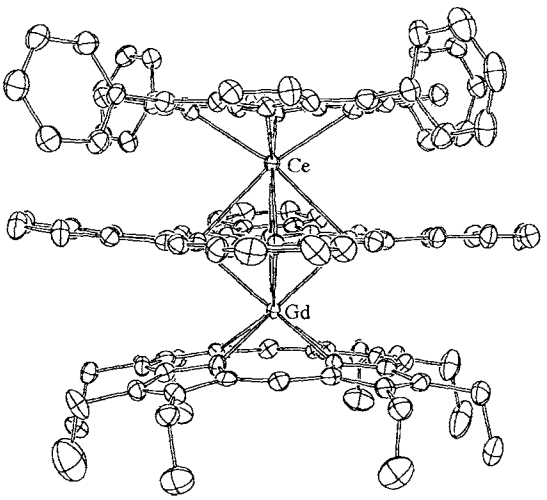

octacoordinated. The outer oep and central pc rings are rotated by an angle of 44.8(4)° relative to their eclipsed orientation. Consequently, the coordination polyhedron of the Gd atom is a slightly distorted square antiprism. In contrast, the outer tpp and central pc rings are almost eclipsed, the rotation angle being only 5.0(1)°. Therefore, the coordination polyhedron of the Ce^{III} ion is a slightly distorted cube. The displacements of the metals relative to the four pyrrole-nitrogen and isoindole-nitrogen mean planes of the macrocycles are as follows: Ce–tpp = 1.330(4), Ce–pc = 1.987(4), Gd–pc = 1.775(4), and Gd–oep = 1.190(4) Å. The outer tetraphenylporphyrin and octaethylporphyrin rings adopt conformations that are domed towards the Gd and Ce cations.[8] The phthalocyanine ring is also domed, with the result that the mean plane of its four isoindole–nitrogens lies closer to the Gd cation than the mean plane through the inner 24 atoms of the ring framework.[8] This particular conformation of the pc ring arises probably both because the ionic radius of Gd^{III} is smaller than that of Ce^{III} and because π–π interactions between the oep and pc are stronger than those between the tpp and pc rings. It had been previously noticed that the π–π interactions in $[Zr(oep)_2]$ were stronger than those in $[Zr(tpp)_2]$.[9–11]

The UV/Vis spectra of all the complexes **1**(M,M′) (M = La, M′ = Y; M = Ce, M′ = Gd, Lu, or Y) and **2**(Ce,Gd) obtained in solution are very similar to each other (see Experimental Procedure) and to the spectra of triple-decker systems with two identical metals **1**(M,M) (M = La, Ce, Pr, Nd, Eu, Gd).[4b]

Laboratoire de Cristallochimie et de Chimie Structurale (UA 424)
Institut Le Bel, Université Louis Pasteur
4, rue Blaise Pascal, F-67070 Strasbourg (France)
Fax: Int. code +(88)415363

[**] We thank Professor Jack Fajer of the Department of Applied Science, Brookhaven National Laboratory, Upton, NY (USA), for valuable discussions and helpful comments and Prof. Dr. Roger Guilard, Université de Bourgogne (France), for a sample of octaethylporphyrin. This work was supported by the Centre National de la Recherche Scientifique (UA 424).

 © VCH Verlagsgesellschaft mbH, D-69451 Weinheim, 1996 0570-0833/96/3508-0898 $ 15.00+.25/0

They are also similar to those displayed by thin films of **1**(Ce,Ce) obtained by sublimation under vacuum.[12] These spectral properties thus confirm that the triple-decker sandwich structures, observed in the solid state for **2**(Ce,Gd) and **1**(Ce,Ce),[4a] are retained in solution for both series of complexes **1**(M,M′) and **1**(M,M). The redox behavior of the mixed-metal complexes **1**(M,M′) was determined by cyclic voltammetry (CH_2Cl_2, 0.1 M NBu_4PF_6). The cyclic voltammograms of these species parallel those of the systems with two identical metals.[4b] All the complexes belonging to the two series **1**(M,M′) and **1**(M,M) undergo three reversible oxidations and two reversible reductions. Moreover, as shown in Figure 2a and 2b, the first oxidation potentials

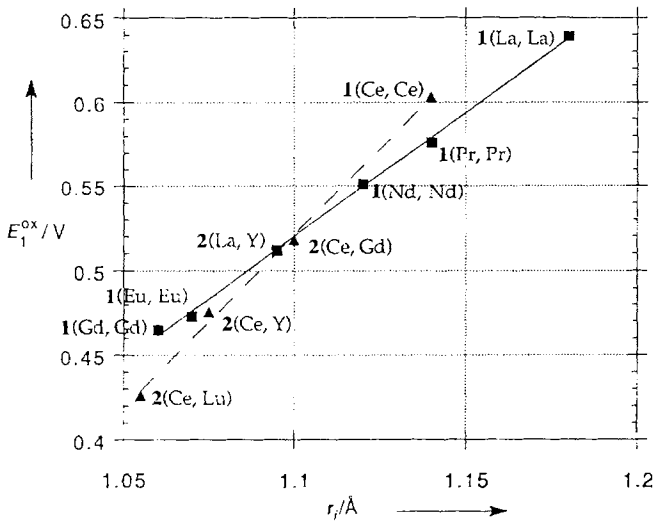

Fig. 2. Correlation between the first oxidation potentials E_1^{ox} of the triple-decker sandwich complexes **1**(M,M′) and **1**(M,M) and the mean ionic radii of M and M′ or the ionic radii of M: ▲ cerium-containing complexes, ■ cerium-free complexes.

(E_1^0) of the mixed-metal complexes **1**(M,M′) examined to date also show a linear correlation with the mean ionic radii of their metal cations. However, as in the complexes containing two identical metal cations **1**(M,M), the slopes of the correlations depend on the presence or absence of a Ce^{III} metal center. These results thus confirm that the presence or absence of an oxidizable Ce^{III} metal ion controls whether the first oxidation occurs at the central atom or the ligand.[4b, 5]

Experimental Procedure

1(M,M′) and **2**(Gd,Ce): A solution of the metal acetylacetonate [M′(acac)$_3$·nH$_2$O] and the metal-free porphyrin H_2p (H_2tpp or H_2oep) (about 0.10 mmol) in 1,2,4-trichlorobenzene was heated at reflux in a three-neck flask for four hours under argon. After cooling, a solid sample (about 0.07 mmol) of a heteroleptic sandwich complex [(tpp)M(pc)] (M = La, Ce) was added, and the resulting mixture was heated at reflux for another eight hours under argon. After cooling, a crude solid was precipitated by addition of pentane. This solid was then extracted several times with dichloromethane. The extracts were combined, and the resulting solution was concentrated under vacuum and then chromatographed on a silica gel column (3/18 cm). Elution with toluene yielded successively some porphyrin H_2p and the olive green triple-decker complex [(tpp)M(pc)M′(tpp)] **1**(M,M′) or [(tpp)Ce(pc)Gd(oep)] **2**(Ce,Gd), which were precipitated by addition of pentane.

1(Ce, Gd): yield 112 mg (79%); correct C,H,N elemental analysis; MS (FAB^+): m/z (%) = 2034 (100) [M^+]; UV/Vis (CH_2Cl_2) λ_{max} [nm] (lgε) = 354 (5.4), 418 (5.6), 490 (5.2), 553 (5.1), 605 (5.1).

2(Ce, Gd): yield 110 mg (81%); correct C,H,N elemental analysis; MS (FAB^+): m/z (%) = 1954 (100) [M^+]; UV/Vis (CH_2Cl_2) λ_{max} [nm] (lgε) = 351 (5.4), 395 (5.3), 420 (5.4), 465 (4.8), 516(5.2), 595 (4.8).

1(Ce, Lu): yield 91 mg (64%). Correct C,H,N elemental analysis; MS (FAB^+): m/z (%) = 2052 (100) [M^+]; UV/Vis (CH_2Cl_2) λ_{max} [nm] (lgε) = 350 (5.5), 413 (5.6), 424 (5.6), 489 (5.3), 558 (5.1), 608 (5.2).

1(Ce, Y): yield 96 mg (70%); correct C,H,N elemental analysis; MS (FAB^+): m/z (%) = 1966 (100) [M^+]; UV/Vis (CH_2Cl_2) λ_{max} (lgε) = 350 (5.5), 415 (5.6), 424 (5.6), 488 (5.3), 558 (5.1), 607 (5.2).

1(La, Y): yield 94 mg (69%); correct C,H,N elemental analysis; MS (FAB^+): m/z (%) = 1965 (100) [M^+]; UV/Vis (CH_2Cl_2) λ_{max} (lgε) = 350 (5.5), 414 (5.6), 424 (5.6), 487 (5.3), 558 (5.2), 607 (5.3); ^{1}H NMR (300 MHz, $CDCl_3$, 25 °C, TMS): δ = 10.3 (d, 4H), 9.48 (m, 8H), 8.44 (m, 8H), 8.35 (t,4H), 7.75 (t, 4H), 7.71 (s,8H), 7.51 (t, 4H), 7.37 (t, 4H), 7.11 (t, 4H), 6.94 (s, 8H), 6.84 (t, 4H), 6.57 (d, 4H), 6.30 (d, 4H), 5.48 (d, 4H).

Received: October 16, 1995
Revised version: January 26, 1996 [Z 8476 IE]
German version: *Angew. Chem.* **1996**, *108*, 942–944

Keywords: lanthanide compounds · phthalocyanines · porphyrinoids · sandwich complexes

[1] a) J. W. Buchler, B. Scharbert, *J. Am. Chem. Soc.* **1988**, *110*, 4272–4276; b) J. W. Buchler, H. G. Kapellmann, M. Knoff, K. L. Lay, S. Pfeifer, *Z. Naturforsch. B* **1983**, *38*, 1339–1345; c) J. W. Buchler, P. Hammerschmitt, I. Kaufeld, J. Löffler, *Chem. Ber.* **1991**, *124*, 2151–2159.

[2] D. Chabach, M. Tahiri, A. De Cian, J. Fischer, M. El Malouli-Bibout, R. Weiss, *J. Am. Chem. Soc.* **1995**, *117*, 8548–8556.

[3] a) J. W. Buchler, M. Knoff in *Optical Properties and Structure of Tetrapyrroles* (Eds.: G. Blauer, H. Sund), De Gruyter, Berlin, **1985**, pp. 91–105; b) J. W. Buchler, K. Elsässer, M. Kihn-Botulinski, B. Scharbert, S. Tansil, *ACS Symp. Ser.* **1986**, *321*, 94–104; c) J. W. Buchler, A. De Cian, J. Fischer, M. Kihn-Botulinski, H. Paulus, R. Weiss, *J. Am. Chem. Soc.* **1986**, *108*, 3652–3659; d) J. W. Buchler, A. De Cian, J. Fischer, M. Kihn-Botulinski, R. Weiss, *Inorg. Chem.* **1988**, *27*, 339–345; e) J. W. Buchler, M. Kihn-Botulinski, J. Löffler, M. Wicholas, *ibid.* **1989**, *28*, 3770–3772; f) J. W. Buchler, M. Kihn-Botulinski, J. Löffler, B. Scharbert, *New J. Chem.* **1992**, *16*, 545–553.

[4] a) D. Chabach, M. Lachkar, A. De Cian, J. Fischer, R. Weiss, *New J. Chem.* **1992**, *16*, 431–433; b) D. Chabach, Doctoral Thesis, Université Louis Pasteur de Strasbourg, January **1994**.

[5] T. H. Tran-Thi, T. Mattioli, D. Chabach, A. De Cian, R. Weiss, *J. Phys. Chem.* **1994**, *34*, 8279–8288.

[6] Crystal data for **2**(Ce,Gd)·2(C_6H_5Cl): $C_{112}H_{88}N_{16}CeGd \cdot 2C_6H_5Cl$, M = 2180.5, triclinic, space group $P\bar{1}$, a = 17.212(5), b = 19.777(6), c = 15.050(5) Å, α = 91.10(2), β = 104.46(2), γ = 89.63(2)°, V = 4959.8 Å^3, ρ_{calcd} = 1.460 g cm^{-3}, Z = 2, $\mu(Cu_{K\alpha})$ = 36.18 cm^{-1} (graphite monochromator). A total of 10922 reflections were collected at −100 °C with a Philips PW 1100/16 automatic diffractometer. The resulting data set was analyzed with the Enraf-Nonius SDP/VAX package. The structure was solved with the heavy atom method and refined to $R(F)$ = 0.046 ($Rw(F)$ = 0.074) using 8056 reflections with $I > 3\sigma(I)$. Crystallographic data (excluding structure factors) for the structure reported in this paper have been deposited with the Cambridge Crystallographic Data Centre as supplementary publication no. CCDC-179-10. Copies of the data can be obtained free of charge on application to The Director, CCDC, 12 Union Road, Cambridge CB2 1EZ, UK (fax: int. code +(1223) 336-033; e-mail: teched@chemcrys.cam.ac.uk).

[7] ORTEP II: C. K. Johnson, **1976**, ORNL-5138.

[8] The separations between the mean planes through the coordinated nitrogen atoms and the mean planes through the inner 24 atoms of the framework of the oep, tpp, and pc rings are 0.208(4), 0.196(4), and 0.077(4) Å, respectively.

[9] R. D. Shannon, C. T. Prewitt, *Acta Crystallogr. Sect. B* **1969**, *25*, 828–829

[10] a) K. Kim, W. S. Lee, H. J. Kim, S. H. Cho, G. S. Girolami, P. A. Gorlin, K. S. Suslick, *Inorg. Chem.* **1991**, *30*, 2652–2656; b) J. W. Buchler, A. De Cian, J. Fischer, P. Hammerschmitt, R. Weiss, *Chem. Ber.* **1991**, *124*, 1051–1058.

[11] J. W. Buchler, A. De Cian, S. Elschner, J. Fischer, P. Hammerschmitt, R. Weiss, *Chem. Ber.* **1992**, *125*, 107–115.

[12] T. Fournier, *Doctoral Thesis*, Université de Paris IX, **1994**.

Direct Observation of Enantiomorphous Monolayer Crystals from Enantiomers by Scanning Tunneling Microscopy

Forrest Stevens, Daniel J. Dyer, and David M. Walba*

Pasteur's brilliant observation, using optical microscopy, that crystals of a salt of "racemic acid" actually existed in two enantiomorphous forms[1] not only uncovered the existence of enantiomers, but indeed stimulated the development of modern structural theory. The direct (without resorting to diffraction techniques) observation of supermolecular chirality and the relationship between supermolecular chirality and molecular structure have fascinated chemists ever since. Starting with early studies of the morphology of chiral crystals by optical microscopy, the scale for the observation of chiral supermolecular assemblies has been approaching that of the molecules themselves. McConnell and Weis first recorded the formation of chiral crystalline monolayer domains in Langmuir films of enantiomerically pure lipids by epifluorescence optical microscopy.[2] More recently, chiral monolayers have been observed at molecular resolution by scanning probe microscopy. Thus, chiral symmetry breaking from achiral[3] and racemic[4] molecules has been detected in Langmuir films by atomic force microscopy (AFM), and enantiomorphous monolayer domains from achiral liquid crystal (LC) molecules on graphite have been observed by scanning tunneling microscopy (STM).[5] In related work, amino acids have been spontaneously resolved by crystallization in two dimensions at the air–water interface.[6]

We report here on the molecular resolution STM observation of enantiomorphous images of crystal monolayers grown from pure enantiomers. Furthermore, a racemic mixture of the same molecules produced images of co-existing enantiomorphic domains indistinguishable from those obtained from the enantiomerically pure materials, providing strong evidence for chiral symmetry breaking to give a two-dimensional (2-D) conglomerate. These results suggest a complete 2-D analog of Pasteur's famous system.

The experiments were performed on enantiomerically enriched and racemic biphenylbenzoates **1**. These have one tetra-

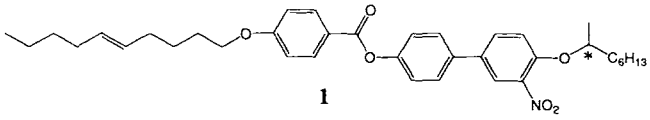

1

hedral stereogenic center (indicated by an asterisk). Both enantiomers were prepared in approximately 99% *ee*; the racemate was also prepared.[7] All three compounds were liquid crystalline with a smectic A phase at room temperature.

Each STM sample was prepared by placing a small amount (<1 mg) of the liquid crystal on a freshly cleaved surface of highly oriented pyrolytic graphite. Scanning tips were prepared from mechanically cut 0.025 cm platinum/iridium (80:20) wire. Images were recorded in air at room temperature using a commercially available STM (Nanoscope II, Digital Instruments, Inc.) with tip positive bias.

[*] Prof. D. M. Walba, F. Stevens, Dr. D. J. Dyer
Department of Chemistry and Biochemistry and
Optoelectronic Computing Systems Center
Campus Box 215, University of Colorado
Boulder, CO 80309-0215 (USA)
Fax: Int. code +(303) 492-5894
e-mail: walba@colorado.edu

[**] This work was supported by the National Science Foundation (Grants DMR-9202312 and DMR-9224168).

The images obtained for monolayers of either enantiomer varied somewhat in appearance, probably due to variations in the STM tip. However, by using autocorrelation analysis (see below)[8] the measured unit cell dimensions for all the images obtained were the same within experimental error. Thus, while polymorphism has been observed with similar molecules,[9] enantiomerically pure **1** apparently produces only one monolayer crystal structure.

When the images were of sufficient quality to resolve the molecules, similar structures were always observed, as illustrated in Figure 1 for samples of (*S*)-**1** (Fig. 1A) and (*R*)-**1** (Fig. 1B).

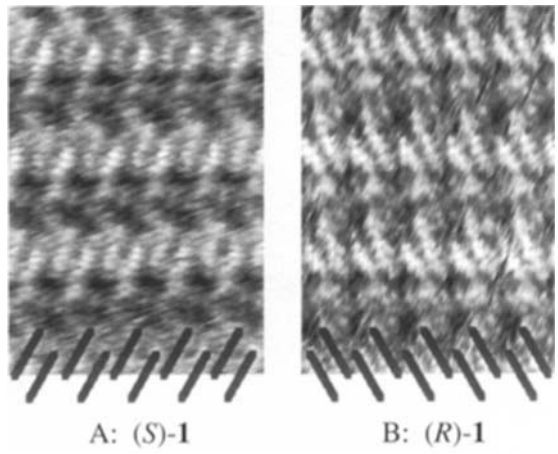

Fig. 1. Enantiomorphous images obtained from (*S*)-1 (A) and (*R*)-**1** (B). The dimensions of the image are 8 nm × 11.5 nm; the gray bars representing the bright regions in the images are 16 Å in length on this scale. These images are raw data, rotated and cropped from the original 15 × 15 nm (400 × 400 data points) scans to aid in the comparison. The scanning parameters were: A: 400 mV, 1 nA; B: 300 mV, 1 nA.

The unit cell dimensions are the same within experimental error, but examination of the images shows that they are clearly enantiomorphous. Images of monolayer crystals grown from both enantiomers exhibit well-defined rows of tilted, rod-shaped bright regions (i.e. areas of enhanced tunneling efficiency), but the bright rods are tilted in opposite directions for the enantiomers.

While the precise mechanisms involved in imaging of organic monolayers overlying conducting surfaces is not known, it is well established that aromatic molecular units image brightly, while aliphatic units are darker.[10, 11] This is the case whether the surface is biased negatively or positively relative to the tip. In the present case the bright regions are approximately 16 Å in length, consistent with the size and shape of the biphenylbenzoate aromatic units. In the monolayers formed from the (*S*) liquid crystal, the cores are tilted about 30° clockwise from the row normal (Fig. 1A), while the monolayers formed from the (*R*) liquid crystal show the cores tilted counterclockwise by a similar amount (Fig. 1B). For the purposes of the present discussion, the image type in Figure 1A, obtained from (*S*)-**1**, will be denoted (+) for clockwise, while that obtained from (*R*)-**1** will be denoted (−) for counterclockwise.

In all cases where monolayer chirality could be resolved, the handedness of the images was coupled to the configuration of the molecules. Out of nine attempts to image (*S*)-**1** six gave monolayer crystals providing images with clearly distinguishable (+) chirality, while in six separate sessions (*R*)-**1** gave discernible (−) images. Hundreds of images were recorded in these sessions, and in no case was observable (+) chirality associated with (*R*)-**1** or (−) chirality associated with (*S*)-**1**. Thus, it can be

stated with a high degree of certainty that molecular chirality is transferred to a chiral supermolecular packing mode, which in turn gives rise to chiral images by STM.

When monolayer crystals are grown from racemic **1**, the formation of a racemic monolayer might be expected by analogy with three-dimensional (3-D) organic crystals, which show some tendency to form racemic crystals rather than conglomerates. However, in a total of eight imaging sessions with racemic **1**, (+) images were observed six times, (−) images were observed seven times, and in four separate cases domain walls between regions of opposite chirality were observed, as illustrated in Figure 2. While Eckhardt et al[4] have used AFM to observe

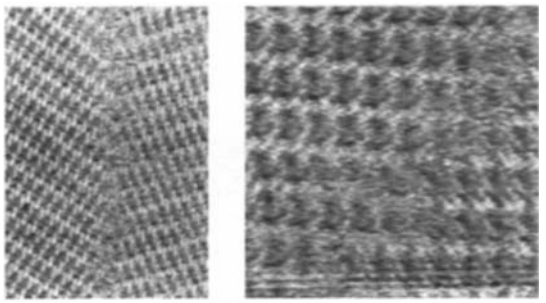

Fig. 2. Co-existing enantiomorphous images obtained from racemic **1**. Image A shows an area of dimensions 27 nm × 38 nm, and image B shows a 15 nm × 15 nm area. These images are raw data, cropped from originals of 50 × 50 nm and 20 × 20 nm, respectively. The scanning parameters were: A: 300 mV, 1 nA; B: 600 mV, 1 nA.

enantiomorphous domains in a racemic material, they did not have access to the corresponding enantiomerically pure material and so could not compare the structures formed by the racemate to structures formed by pure enantiomers, as we have done.

Observation of enantiomorphous domains from the racemic material by STM could result from two different mechanisms: 1) The racemic material could spontaneously resolve into monolayer crystals of pure (*R*) and pure (*S*) material forming a 2-D conglomerate. 2) Both enantiomorphous domains could be composed of racemate—an example of formation of chiral supermolecular structures from "achiral" pairs of enantiomeric molecules. In both cases the enantiomorphous domains represent enantiomeric monolayer crystal structures; in the latter case the enantiomeric domains are composed of mixtures of (*R*) and (*S*) molecules, while in the former case the domains are composed of homochiral molecules (it is not possible to physically separate the domains to measure optical activity in solution, as Pasteur did, to distinguish between these two possibilities). Of course, the crystals formed by these two mechanisms must be diastereomeric.

If resolution occurs and the monolayer crystal domains are enantiomerically pure, the chiral images observed from the racemic material must be identical to those obtained from one or the other of the pure enantiomers. On the other hand, if the monolayer crystals are racemic, the observed images should be different from those of the pure enantiomers, though due to the limits of the STM technique the racemic crystal could fortuitously produce images indistinguishable from those derived from the pure enantiomers.

Autocorrelation was used to calculate unit cells for monolayer crystals grown from enantiomerically pure and racemic **1**. Tip drift often caused "up" scans to be stretched, while "down" scans were compressed, or vice versa. To compensate for this effect, whenever possible consecutive up and down scans were taken and their unit cells averaged. Only these "pair averaged" values were used in the analysis.

Over one hundred pairs of images were analyzed for each material (the two enantiomers and the racemate), and the unit cells from both the pure enantiomers and from the racemate were found to be the same within experimental error.[12] This strongly suggests that the racemate forms a 2-D conglomerate of enantiomerically pure monolayer crystals upon adsorption on graphite—these enantiomerically pure crystals are identical to those obtained from the pure enantiomers. This is similar to the results obtained by Nassoy et al[13] who used grazing incidence X-ray diffraction to show that the unit cells in monolayers of D,L, and racemic myristoyl-alanine were identical. However, they were unable to resolve domains within the racemate or to obtain images of the structures with molecular resolution.

We have used STM to observe monolayers formed by both enantiomers of a chiral material, and the corresponding racemate. The pure enantiomers gave monolayer crystals that produced chiral 2-D images by STM, and enantiomeric molecules delivered enantiomorphic images reproducibly. The racemic material produced monolayer crystals showing both chiralities in two dimensions, and the domains were indistinguishable from images obtained from enantiomerically pure material. This strongly suggests that the racemate forms a 2-D conglomerate of enantiomerically pure monolayer crystals on the graphite surface.

Received: November 2, 1995 [Z8521IE]
German version: *Angew. Chem.* **1996**, *108*, 955–957

Keywords: chirality · liquid crystals · scanning tunneling microscopy · symmetry

[1] L. Pasteur, *C. R. Hebd. Seances Acad. Sci. Paris* **1848**, *26*, 535–539.
[2] R. M. Weis, H. M. McConnell, *Nature* **1984**, *310*, 47–49.
[3] R. Viswanathan, J. A. Zasadzinski, D. K. Schwartz, *Nature* **1994**, *368*, 440–443.
[4] C. J. Eckhardt, N. M. Peachy, D. R. Swanson, J. M. Takacs, M. A. Khan, X. Gong, J.-H. Kim, J. Wang, R. A. Uphaus, *Nature* **1993**, *362*, 614–616.
[5] D. P. E. Smith, *J. Vac. Sci. Technol. B* **1991**, *9*, 1119–1125.
[6] I. Weissbuch, M. Berfeld, W. Bouwman, K. Kjaer, J. Als-Nielsen, M. Lahav, L. Leizerowitz, poster presented at 7th International Symposium on Chiral Discrimination (ISCD 7) Jerusalem; *J. Am. Chem. Soc.*, submitted.
[7] The synthesis and novel ferroelectric liquid crystalline properties of compounds **1** will be described elsewhere. The enantiomerically enriched samples were prepared from (*R*)- and (*S*)-2-octanol (Aldrich, >99% *ee*).
[8] W. O. Saxton, J. Frank, *Ultramicroscopy* **1977**, *2*, 219–227.
[9] F. Stevens, D. J. Dyer, D. M. Walba, *Langmuir*, **1996**, *12*, 436–440.
[10] D. P. E. Smith, H. Hörber, C. Gerber, G. Binnig, *Science* **1989**, *245*, 43–45.
[11] D. M. Walba, F. Stevens, D. C. Parks, N. A. Clark, M. D. Wand, *Science* **1995**, *267*, 1144–1147.
[12] Average unit cell metrics observed for compounds **1** by autocorrelation analysis were as follows. (*S*)-**1**: [0] = 1.61 ± 0.06 nm, [1] = 3.16 ± 0.14 nm, angle = 88 ± 6°; (*R*)-**1**: [0] = 1.65 ± 0.08 nm, [1] = 3.17 ± 0.13 nm, angle = 88 ± 6°; (*rac*)-**1**: [0] = 1.60 ± 0.06 nm, [1] = 3.08 ± 0.12 nm, angle = 87 ± 6°.
[13] P. Nassoy, M. Goldmann, O. Bouloussa, F. Rondelez, *Phys. Rev. Lett.* **1995**, *75*, 457–460.

Synthesis of Thiophosphoryl Derivatives of Proline: Building Blocks for Phosphanyl-Substituted Peptides with β-Turns

Scott R. Gilbertson* and Robert V. Pawlick

Natural proteins bind metal atoms for two purposes.[1-3] One is the control and stabilization of protein structure. A number amino acids[4-18] with potential ligands for metals have been incorporated into or at the end of peptide sequences. In these peptides metal complexation has been used to stabilize secondary structure[4-10] or to connect two or more peptides.[11-14] The second role metal atoms play in protein chemistry is based on reactivity of the metal,[19] which may be involved in a variety of reactions such as oxidation, electron transport, protein hydrolysis, and oxygen binding. While much has been accomplished in the use of unnatural amino acids to bind metals to stabilize peptide secondary structure, little work has done in the area of designing and building artificial peptides that contain catalytically active metal systems.[20] For this reason we undertook the development of amino acids that contain phosphanyl groups. The ability to bind transition metals into peptides with phosphanyl groups will make a variety of organometallic chemistry accessible.[21-23] Potentially, peptide structure can then be used to control reactions not usually associated with biological systems such as hydrogenation,[24a] hydroformylation,[25] and cycloisomerization reactions.[26, 27] With a variety of phosphanyl amino acids available one should be able to use metal–phosphane coordination to control peptide structure as well as control reactivity by positioning metals such as rhodium, ruthenium, palladium, and platinum in unique steric environments. In this paper we report on the synthesis of thiophosphorylprolines **1** and **2** by standard peptide coupling methods; their incorporation, along with another phosphanyl-substituted amino acid, into a peptide with a β-turn structural motif; the reduction of the thiophosphoryl group to give the free phosphanes; and the binding of rhodium to this structurally unique ligand.[4, 5, 28] The secondary structures of both the uncomplexed and the metalated peptide were characterized by 2D NMR spectroscopy.

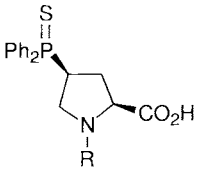

1 R = FMOC
2 R = *t*BOC

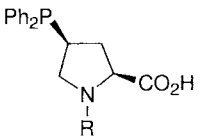

3 R = FMOC
4 R = *t*BOC

The original approach to the synthesis of the desired proline derivative was to protect the amino and carboxyl groups of 4-hydroxyproline, convert the hydroxyl group into a good leaving group, and replace this by nucleophilic displacement with a phosphane.[29-31] Our initial attempts using hydroxyproline, in which the ester was protected with a variety of protecting groups, failed. We believe that owing to the high nucleophilicity of the diphenylphosphanide anion, the ester group did not survive the reaction conditions. The next approach attempted was to perform the nucleophilic substitution on a protected hydroxyprolinol and then oxidize the primary hydroxyl group to the carboxlic acid. This route has proven successful despite the potential problem of oxidation of the phosphane sulfide to a phosphane oxide.

Amino acids **1** and **2** were synthesized from readily available 4-hydroxyproline (Scheme 1). Reaction of the ethyl ester of

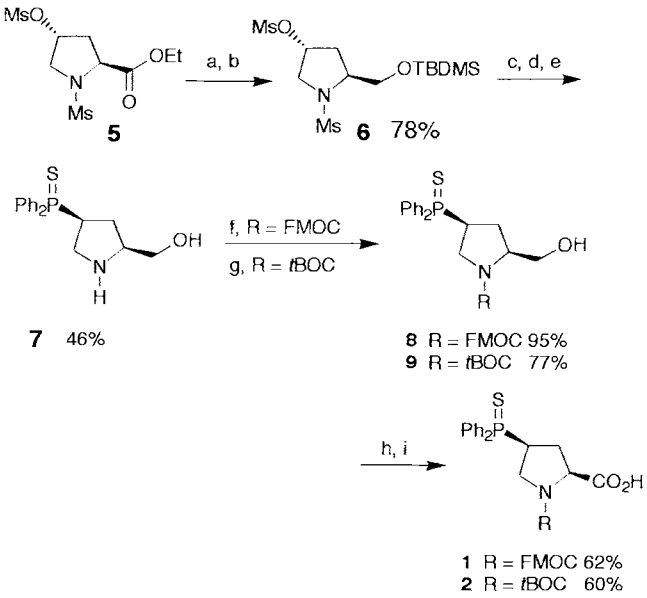

Scheme 1. a) $NaBH_4$, LiCl, THF/EtOH, 78%; b) TBDMSOTf, lutidine, CH_2Cl_2, 90%; c) Ph_2PNa, THF; d) RedAl, DME, reflux; e) $Na_2S_2O_3$, MeOH, H_2O; f) FMOCOSu, $NaHCO_3$, acetone/H_2O; g) $(BOC)_2O$, $NaHCO_3$, dioxane/H_2O; h) Swern oxidation; i) PDC, DMF.

4-hydroxyproline with two equivalents of methanesulfonyl chloride in triethylamine gave the bis(mesyl) ethyl ester **5**. Compound **5** was reduced to the alcohol and the hydroxyl group was protected by silylation with *tert*-butyldimethylsilyl trifluorosulfonate (TBDMSOTf) to afford **6**. Reaction with sodium diphenylphosphanide displaced the mesylate at the 4-position with inversion of that chiral center.[31] Reaction with sodium bis(2-methoxyethoxy)aluminum hydride (RedAl) in dimethoxyethane (DME) removed both the *N*-mesyl and the silyl group. Treatment with sodium thiosulfate in water/methanol formed the air-stable thiophosphoryl amino alcohol **7**.[32, 33] Reaction with *N*-(9-fluorenylmethoxycarbonyloxy)succinimide (FMOCOSu) yielded the FMOC-protected amino alcohol **8**, whereas reaction with di-*tert*-butyl dicarbonate gave the *tert*-butylcarbonyl (BOC) protected amino alcohol **9**.[34] The remaining reactions in the sequence proceeded smoothly on both the FMOC- and the BOC-protected intermediates. Swern oxidation[35, 36] followed by oxidation with pyridinium dichlorochromate (PDC)[37, 38] provided the desired N-protected thiophosphoryl amino acids **1** and **2** in good yields.

The incorporation of phosphanyl-substituted amino acids into peptides with stable secondary structure is critical to the goal of using peptide secondary structure to control the reactivity of catalytic transition metals. One of the motives for the synthesis of a phosphane-containing proline derivative was to be able to incorporate rhodium and ruthenium atoms into β-turn structural motifs. Recently Imperiali et al. demonstrated that the tetrapeptide Ac-Val-Pro-D-Ser-His-NH_2 shows a significant

[*] Prof. S. R. Gilbertson, R. V. Pawlick
Department of Chemistry, Washington University
Campus Box 1134, One Brookings Drive
St. Louis, MO 63130 (USA)
Fax: Int. code +(314)935-4481
e-mail: srg@wuchem.wustl.edu

[**] We gratefully acknowledge Mallinckrodt Chemicals Inc., the Washington University High-Resolution NMR Facility (partially supported by NIH 1S10R02004), and the Washington University Mass Spectrometry Resource Center (partially supported by NIH RR00954).

proportion of type II β-turn conformation in DMSO or aqueous solution.[39] Additionally, it has been shown that β-turn structures are favored when a proline residue is in the $i+1$ position.[40] For these reasons we chose to synthesize tetramer **10** (Val-Ppp(S)-Pps(S)-Ala).[41] A second phosphane-containing amino acid, diphenylphosphanylalanine (Pps), is located in the $i+2$ position of the target peptide (Scheme 2).[32] Molecular

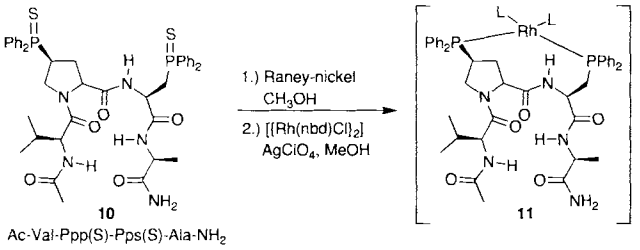

Scheme 2. Synthesis of the peptide–phosphane ligand from **10** and formation of the phosphane–rhodium complex **11**. Ppp(S) = 4-(diphenylthiophosphoryl)proline, Pps(S) = diphenylthiophosphorylalanine, Ppp = 4-(diphenylphosphanyl)-proline, Pps = diphenylphosphanylalanine.

modeling indicated that when peptide **10** is in a turn conformation the thiophosphoryl groups are on the same face of the molecule and properly positioned to bind transition metals (see Fig. 1).

The NOESY spectra of **10** in $CDCl_3$ and DMF indicate that the predominate conformation is a type II β-turn. In particular, NOE interactions observed between $d_{\alpha N}(i+1,i+2)$ (A), $d_{NN}(i+2,i+3)$ (B), $d_{N\alpha}(i+2,i+2)$ (C), and $d_{\alpha N}(i+1,i+3)$ (D) are indicative of a type II β-turn structure. Furthermore, interactions E and F between the side chains at positions i (valine) and $i+3$ (alanine) are additional evidence for a β-turn structure. This assignment of secondary structure is supported by a ^3J coupling constant of 5.5 Hz between $(i+2)$NH and $(i+2)\alpha$H.[42] We were moderately surprised the peptide would form a β-turn as its major conformation, given that this secondary sturcture positions the large diphenylthiophosphoryl groups on the same face of the turn structure (Fig. 1). That the structure appears to be a type II β-turn is also interesting; only a limited number of peptides with type II β-turns having L-amino acids in the $i+1$ and $i+2$ positions are known.[43]

Reaction of peptide **10** with Raney nickel converted the thiophosphoryl groups into free phosphanes. The resulting bidentate ligand was then treated with $[Rh(nbd)]^+$ (nbd = norbornadiene), which was generated by reaction of $[\{Rh(nbd)Cl\}_2]$ and $AgClO_4$, to give the rhodium–peptide complex **11** (Scheme 2).

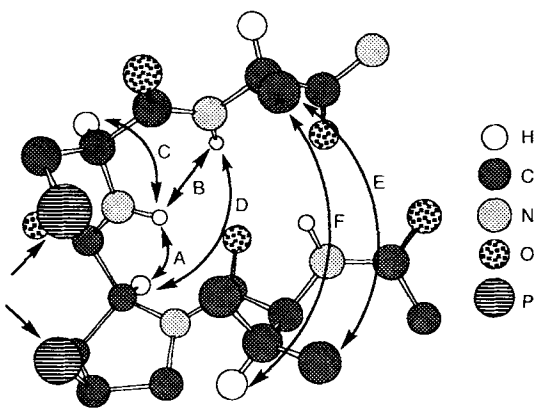

Fig. 1. NOE interactions (double-headed arrows) observed for **10** and **11**: A) $d_{\alpha N}$(Ppp, Pps); B) d_{NN}(Pps, Ala); C) $d_{N\alpha}$(Pps, Pps); D) $d_{\alpha N}$(Ppp, Ala); E) $d_{\alpha\beta}$(Val, Ala); F) $d_{\beta\beta}$(Val, Ala). The phenyl groups of the thiophosphoranes and the protons of the valine and alanine side chains have been omitted for clarity. Note that the two thiophosphoryl groups are located on the same face of the β-turn (arrows).

Metal complexation to the phosphane ligands was easily followed by ^{31}P NMR spectroscopy. Coupling of rhodium (spin = 1/2) to the P atoms of the peptide clearly indicated metal chelation. The NOESY NMR experiments indicated that the rhodium peptide complex **11** has a type II reverse turn structure. As in **10**, NOE interactions A–F (Fig. 1) were observed in **11**.

The ability to incorporate phosphanyl groups into various peptide structures allows for the facile synthesis of a wide variety of phosphane ligands with unique secondary structures. It should now be possible to incorporate phosphanyl groups into virtually any type of peptide structure attainable by peptide synthesis. In principle, a large number of ligands can be synthesized and screened for unique structural characteristics, useful reactivity, and important biological activity. We are currently using commercially available technology to build libraries of ligands and are then screening their reactivity. Phosphanyl-containing peptides might be used to immobilize catalytically active metals in membranes or on surfaces, thus leading to new types of catalyst systems. We are beginning to use this chemistry to synthesize polymer-bound metal ligand systems with the goal of developing well-defined polymer-bound catalysts.

Experimental Procedure

Selected spectroscopic data for **1**, **2**, **10**, and **11**.

1: ^1H NMR (300 MHz, $CDCl_3$): δ = 7.92–7.79 (m, 4H), 7.7–7.63 (m, 2H), 7.59–7.42 (m, 8H), 7.38–7.16 (m, 4H), 4.5–4.36 (m, 2H), 4.34–4.04 (m, 2H), 3.83–3.61 (m, 2H), 3.3 (m, 1H), 2.55 (m, 1H), 2.29 (m, 1H); ^{13}C NMR (75 MHz, $CDCl_3$) (major rotational isomer): δ = 176.5, 154.8, 143.7, 143.3, 141.2, 132.0, 131.6 (d, J(C,P) = 7.1 Hz), 131.3, 131.0 (d, J(C,P) = 9.9 Hz), 128.9 (d, J(C,P) = 11.4 Hz), 127.6, 124.8 (d, J(C,P) = 10.3 Hz), 119.8, 67.9, 59.2 (d, J(C,P) = 10.5 Hz), 47.8 (d, J(C,P) = 31 Hz), 46.9, 38.5 (d, J(C,P) = 60.4 Hz), 30.4; ^{31}P NMR (120 MHz, $CDCl_3$): δ = 44.19 (major rotational isomer), 44.08 (minor isomer); IR (film): $\tilde{\nu}$ = 3060 (br.), 2955 (w), 2881 (w), 1751 (m), 1724 (m), 1706 (s), 1479 (m), 1451 (m), 1436 (s), 1426 (m), 1320 (m), 1170 (m), 1102 cm^{-1} (m); LRFABMS: *m/z* (%): 554 (MH^+, 70), 336 (15), 307 (27), 219 (25), 179 (87); HRFABMS: *m/z* calcd for $C_{32}H_{29}NO_4PS$: 554.1555, found 554.1552.

2: ^1H NMR (300 MHz, $CDCl_3$): δ = 7.91–7.84 (m, 6H), 7.54–7.44 (m, 6H), 4.32 (m, 1H), 3.75–3.65 (m, 2H), 3.33 (m, 1H), 2.55 (m, 1H), 2.29 (m, 1H), 1.41 (s, 9H); ^{13}C NMR (125 MHz, $CDCl_3$): δ = 177.1, 157.1, 154.7, 153.3, 131.9 (d, J(C,P) = 4.7 Hz), 131.1 (d, J(C,P) = 17.6 Hz), 131.1 (d, J(C,P) = 17.6 Hz), 131.0 (d, J(C,P) = 13.8 Hz), 131.0 (d, J(C,P) = 15.1 Hz), 128.8 (d, J(C,P) = 12.3 Hz), 81.0, 60.4, 59.0 (d, J(C,P) = 9.9 Hz), 47.3 (d, J(C,P) = 7.5 Hz), 37.7 (d, J(C,P) = 60.3 Hz), 31.5, 28.1, 27.9, 14.1; ^{31}P NMR (120 MHz, $CDCl_3$): δ = 44.13 (major isomer), 43.94, 45.35 (minor isomer); IR (film): $\tilde{\nu}$ = 3055 (br.), 3004 (w), 2981 (w), 2932 (w), 1700 (s), 1696 (s), 1419 (s), 1399 (s), 1159 cm^{-1} (s); LRFABMS: *m/z* (%): 432 (MH^+, 22), 376 (88), 332 (31), 219 (64), 154 (100); HRFABMS: *m/z* calcd for $C_{22}H_{27}NO_4PS$: 432.1398, found 432.1401.

10: ^1H NMR (500 MHz, $CDCl_3$): δ = 8.3 (d, J(H,H) = 5.5 Hz, 1H), 7.91–7.80 (m, 8H), 7.58–7.36 (m, 13H), 6.90 (s, 1H), 6.74 (s, 1H), 5.8 (s, 1H), 4.42 (m, 1H), 4.29 (m, 1H), 4.21–4.18 (m, 2H), 4.1 (dd, J(H,H) = 10.3 Hz, 1H), 3.69 (dd, J(H,H) = 7.3, 9.7 Hz, 1H), 3.37 (m, 1H), 3.26–3.19 (m, 2H), 2.3 (dddd, J(H,P) = 12.1, J(H,H) = 10.5, 9.5, 9.5 Hz, 1H), 2.04 (m, 1H), 1.96 (br. s, 4H), 1.30 (d, J(Me-H,H) = 7.3 Hz, 3H), 0.89 (d, J(Me-H,H) = 6.1 Hz, 3H), 0.86 (d, J(Me-H,H) = 6.7 Hz, 3H), see Table 1 for signal assignment; ^{13}C NMR (75 MHz, $CDCl_3$): δ = 175.4, 172.2, 171.2, 170.9, 170.5, 170.3, 132.6, 132.0, 132.7, 131.2, 131.1, 130.9, 130.8, 131.1, 129.0, 128.9, 128.8, 128.7, 128.6, 128.5, 62.1, 62.01, 56.7, 51.0, 49.2, 48.7, 39.2 (d, J(C,P) = 59.9 Hz), 31.6 (d, J(C,P) = 55.9 Hz), 29.9, 29.5, 22.6, 19.2, 18.2, 16.8; ^{31}P NMR (120 MHz, $CDCl_3$): δ = 42.1, 38.66; LRFABMS: *m/z* (%): 868 ($M+K^+$, 25), 852 ($M+Na^+$, 100), 830 (58); HRFABMS: *m/z* calcd for $C_{42}H_{50}N_5O_5P_2S_2$: 830.2728, found 830.2709.

11: ^1H NMR (500 MHz, $CDCl_3$): for chemical shifts and assignments see Table 2; ^{31}P NMR (120 MHz, CD_3OD): δ = 31.28 (d, J(Rh,P) = 168.8 Hz, 1P), 22.37 (d, J(Rh,P) = 168.8 Hz, 1P); LRFABMS: *m/z* (%): 992 (47), 960 (M^+, 50), 874 (100), 776 (35); HRFABMS: *m/z* calcd for $C_{49}H_{52}N_5O_5P_2Rh$: 960.2890, found 960.2888.

Table 1. Assignment of the ^1H NMR signals of **10** (2D NMR).

Residue	α	β_1	β_2	γ_1	γ_2	δ_1	δ_2	Amide
Val	4.17	1.95	-	0.89	0.86	-	-	6.88
Ppp(S)	4.26	2.29	2.05	3.35	-	4.1	3.69	-
Pps(S)	4.42	3.22	3.22	-	-	-	-	8.29
Ala	4.2	1.29	-	-	-	-	-	7.55

Table 2. Assignment of the ^{1}H NMR signals of **11**.

Residue	α	β_1	β_2	γ_1	γ_2	δ_1	δ_2	Amide
Val	4.37	1.98	–	0.92	0.92	–	–	8.41
Ppp	4.28	2.28	2.18	3.46	–	4.46	4.05	–
Pps	4.49	3.05	2.80	–	–	–	–	7.94
Ala	4.20	1.26	–	–	–	–	–	7.66

Received: November 20, 1995 [Z 8569 IE]
German version: *Angew. Chem.* **1996**, *108*, 963–966

Keywords: complexes with phosphorus ligands · peptides · phosphanes · rhodium compounds

[1] L. D. Pettit, J. E. Gregor, H. Kozlowski, *Perspectives on Bioinorganic Chemistry, Vol. 1*, JAI Press, Greenwitch, CT (USA), **1991**, pp. 1–41.
[2] A. V. Xavier, *Frontiers in Bioinorganic Chemistry*, VCH, New York, **1986**.
[3] C. B. Anfinsen, J. T. Edsall, F. M. Richards, D. S. Eisenberg, *Advances in Protein Chemistry*, Academic Press, New York, **1991**.
[4] B. Imperiali, S. L. Fisher, *J. Am. Chem. Soc.* **1991**, *113* 8527.
[5] B. Imperiali, S. L. Fisher, *J. Org. Chem.* **1992**, *57*, 757.
[6] J. P. Schneider, J. W. Kelly, *J. Am. Chem. Soc.* **1995**, *117*, 2533.
[7] F. Ruan, Y. Chen, P. B. Hopkins, *J. Am. Chem. Soc.* **1990**, *112*, 9403.
[8] M. R. Ghadiri, C. Chong, *J. Am. Chem. Soc.* **1990**, *112*, 1630.
[9] M. R. Ghadiri, A. K. Fernholz, *J. Am. Chem. Soc.* **1990**, *112*, 9633.
[10] F. Ruan, Y. Chen, K. Itoh, T. Sasaki, P. B. Hopkins, *J. Org. Chem.* **1991**, *56*, 4347.
[11] M. R. Ghadiri, M. A. Case, *Angew. Chem.* **1993**, *105*, 1663; *Angew. Chem. Int. Ed. Engl.* **1993**, *32*, 1594.
[12] M. Lieberman, T. Sasaki, *J. Am. Chem. Soc.* **1991**, *113*, 1470.
[13] M. R. Ghadiri, C. Soares, C. Choi, *J. Am. Chem. Soc.* **1992**, *114*, 825.
[14] K. S. Akerfeldt, R. M. Kim, D. Camac, J. T. Groves, J. D. Lear, W. F. DeGrado, *J. Am. Chem. Soc.* **1992**, *114*, 9656.
[15] T. Handel, W. F. DeGrado, *J. Am. Chem. Soc.* **1990**, *112*, 6710.
[16] B. A. Krizek, B. T. Amann, V. J. Kilfoil, D. L. Merkle, J. M. Berg, *J. Am. Chem. Soc.* **1991**, *113*, 4518.
[17] F. H. Arnold, B. L. Haymore, *Science* **1991**, *252*, 1796.
[18] S. F. Michael, V. J. Kilfoil, M. H. Schmidt, B. T. Amann, J. M. Berg, *Proc. Natl. Acad. Sci. USA* **1992**, *89*, 4796.
[19] W. Ando, Y. E. Moro-oka, *The Role of Oxygen in Chemistry and Biochemistry*, Elsevier, Amsterdam **1988**.
[20] D. L. Merkle, M. H. Schmidt, J. M. Berg, *J. Am. Chem. Soc.* **1991**, *113*, 5450.
[21] G. L. Baker, S. J. Fritschel, J. R. Stille, J. K. Stille, *J. Org. Chem.* **1981**, *46*, 2954.
[22] G. Parrinello, J. K. Stille, *J. Am. Chem. Soc.* **1987**, *109*, 7122.
[23] S. E. Tunney, J. K. Stille, *J. Org. Chem.* **1987**, *52*, 748.
[24] a) H. Takaya, T. Ohta, R. Noyori in Lit. [24b], S. 1–39; b) *Catalytic Asymmetric Synthesis* (Ed.: I. Ojima), VCH, New York, **1993**.
[25] G. Consiglo in ref. [24b], pp. 273–302.
[26] L. McKinstry, T. Livinghouse, *Tetrahedron* **1994**, *50*, 6145.
[27] B. M. Trost, G. J. Tanoury, M. Lautens, C. Chan, D. T. MacPherson, *J. Am. Chem. Soc.* **1994**, *116*, 4255.
[28] G. E. Schulz, R. H. Schirmer, *Principles of Protein Structure*, Springer, New York, **1988**.
[29] *Organic Phosphorus Compounds, Vol. 1* (Eds.: G. M. Kosolapoff, L. Maier), Wiley, New York, **1972**.
[30] F. R. Hartley, *The Chemistry of Organophosphorus Compounds, Vol. 1*, Wiley, Chichester, **1990**.
[31] J. K. Stille, H. Su, P. Brechot, G. Parrinello, L. S. Hegedus, *Organometallics* **1991**, *10*, 1183.
[32] S. R. Gilbertson, G. Chen, M. McLoughlin, *J. Am. Chem. Soc.* **1994**, *116*, 4481.
[33] P. Bartlett, R. E. Davis, *J. Am. Chem. Soc.* **1958**, *80*, 2513.
[34] M. Bodanszky, A. Bodanszky, *The Practice of Peptide Synthesis*, Springer, Berlin, **1984**.
[35] J. G. Moffatt in *Oxidation, Vol. 2* (Eds.: R. L. Augustine, D. J. Trecker), Marcel Dekker, New York, **1971**, pp. 1–64.
[36] J. D. Albright, L. Goldman, *J. Am. Chem. Soc.* **1967**, *89*, 2416.
[37] E. J. Corey, G. Schmidt, *Tetrahedron Lett.* **1979**, 399.
[38] W. M. Coates, J. R. Corrigan, *Chem. Ind. (London)* **1969**, 1594.
[39] B. Imperiali, S. L. Fisher, R. A. Moats, T. J. Prins, *J. Am. Chem. Soc.* **1992**, *114*, 3182.
[40] C. M. Wilmont, J. M. Thornton, *J. Mol. Biol.* **1988**, *203*, 221.
[41] The peptide was synthesized by standard methods (coupling of components with 1-ethyl-3-[3-(dimethylamino)propyl]carbodiimide (EDC) and deprotections with trifluoroacetic acid (TFA)).
[42] A. Aubry, M. T. Cung, M. Marraud, *J. Am. Chem. Soc.* **1985**, *107*, 7640.
[43] While the number of peptides with type II β-turns having amino acids other than glycine or a D-amino acid in the $i+2$ positon is limited, this type of structure is by no means impossible. There are many well-characterized type II β-turns with L-amino acids in the $i+2$ postion. Since the energy difference between type I and type II turns is small, conformational preferences are sensitive to a number of effects.

Studies on the Asymmetric Synthesis of *Stemona* Alkaloids: Total Synthesis of (−)-Stenine**

Yoshiki Morimoto,* Maki Iwahashi, Koji Nishida, Yuji Hayashi, and Haruhisa Shirahama

Extracts from the roots and rhizomes of stemonaceous plants (*Stemona* and *Croomia*) have long been used in China and Japan as cough remedies for humans and as anthelmintics for domestic animals. A number of related *Stemona* alkaloids have been isolated from these extracts and their structures have been determined, mostly by X-ray diffraction studies.[1] The most prototypical members of this family of alkaloids are stenine (**1**), tuberostemonine (**2**), and tuberostemonine A (**3**),[2] and of these **2**, in particular, has been shown to possess inhibitory activity

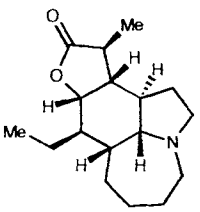

1

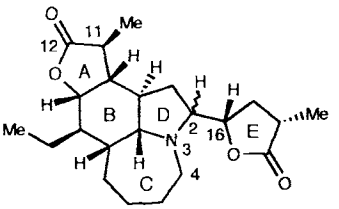

2 2α-H
3 2β-H

on the excitatory transmission at the crayfish neuromuscular junction.[3] These pharmacological properties indicate that some of the effects of the crude extracts may be attributable to **2** and that this alkaloid may be a useful tool in the field of neuropharmacology. These and other types of *Stemona* alkaloids have recently been the subject of several studies[4] because of their stimulating structures and prominent physiological activities, and the total synthesis of (±)-stenine (**1**) has already been accomplished by Hart and Chen.[4b] In the course of our investigations into the asymmetric syntheses of these alkaloids, we now report the highly stereocontrolled total synthesis of (−)-stenine (**1**).[5, 6]

The retrosynthetic analysis of these alkaloids is outlined in Figure 1. Recently we developed an efficient synthetic proto-

[*] Dr. Y. Morimoto, M. Iwahashi, K. Nishida, Prof. Dr. Y. Hayashi
Department of Chemistry, Faculty of Science, Osaka City University, Sumiyoshiku, Osaka 558 (Japan)
Fax: Int. code +(6)605-2522
e-mail: h1391@ocugw.cc.osaka-cu.ac.jp
Prof. Dr. H. Shirahama
Department of Chemistry, School of Science
Kwansei Gakuin University, Uegahara, Nishinomiya 662 (Japan)

[**] We thank Prof. M. Haruna (Meijo University) for generously supplying a copy of the ^{1}H NMR spectrum of natural stenine. This work was partly supported by the Saneyoshi Scholarship Foundation and a Grant-in Aid for Scientific Research from the Ministry of Education, Science, and Culture of Japan.

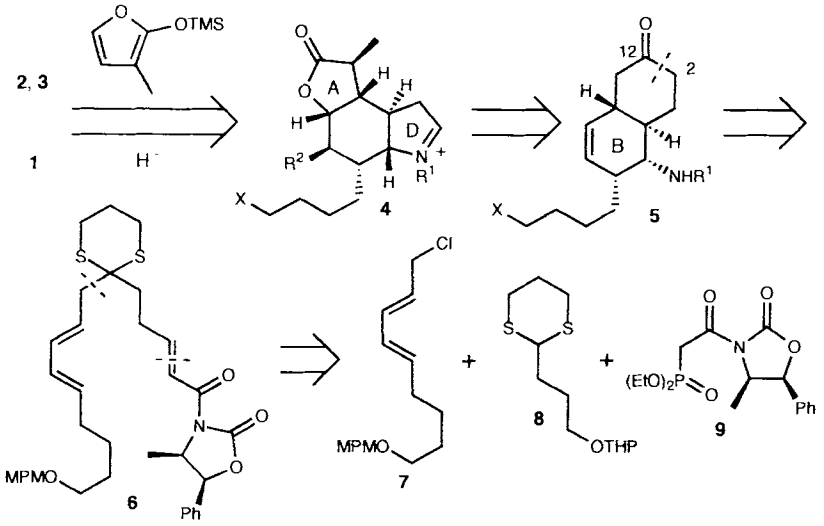

Fig. 1. Retrosynthetic analysis of the *Stemona* alkaloids **1**–**3**. MPMO = 4-methoxyphenylmethyloxy, THP = tetrahydropyranyl; TMS = trimethylsilyl.

col[4i,j] of the D,E ring system, based on the stereoselective addition of 3-methyl-2-trimethylsilyloxyfuran to an *N*-acyliminium ion.[7] In the context of these results, disconnections of the 2,16 and 3,4 bonds designated the iminium ion **4** as a conceivable common intermediate of these alkaloids. It was anticipated that the tricyclic ring system **4** would be prepared from the bicyclic ketone **5** by oxidative cleavage of the 2,12 bond, followed by cyclization of A and D rings. An intramolecular asymmetric Diels–Alder reaction[8] of the (*E*,*E*,*E*)-triene **6**, containing Evans' chiral auxiliary,[9] was considered to be the most efficient method for simultaneously constructing the decalin skeleton and the four stereogenic centers on the B ring in **5**. The desired Diels–Alder precursor **6** was to be assembled, in turn, by convergent coupling of three fragments (dienyl chloride **7**, dithiane **8**, and chiral phosphonate **9**).

We began the synthesis by alkylation of the dithiane **8**[10] with the readily available dienyl chloride **7**.[12] Subsequent removal of the tetrahydropyranyl group provided the alcohol **10**, which was oxidized with SO_3·Py. The modified Horner–Emmons reaction[14] of the resulting aldehyde with the chiral phosphonate **9**[15] afforded the (*E*,*E*,*E*)-triene **6** in good overall yields (Scheme 1). The key reaction—the intramolecular asymmetric Diels–Alder reaction of **6**—proceeded smoothly at −20 °C in the presence of 1.3 equivalents of dimethylaluminum chloride as a Lewis acid to produce the bicyclic compound **11** in good diastereoselectivity and complete *endo* selectivity (**11**: antipode of B ring = 10:1).[9,16] Sequential manipulation of the Diels–Alder adduct **11** (that is, 1) hydrolysis of the 1,3-dithiane, 2) removal of the chiral oxazolidinone,[17] 3) reduction of the resulting thiol ester to aldehyde,[18] and 4) oxidation of the aldehyde with sodium chlorite) furnished the carboxylic acid **13** in high overall yields. The introduction of a nitrogen functionality to **13** to give **14** was carried out by the modified Curtius rearrangement according to the Shioiri's method[19] in the presence of a catalytic amount of copper(I) chloride.[20]

The next stage involved the oxidative cleavage of the 2,12 bond in ketone **14** (Scheme 2). The regioselective enolization of **14** was performed under thermodynamically controlled conditions[16] to predominantly yield the preferred trimethylsilyl enol ether **15** ($\Delta^{2,12}$: $\Delta^{11,12}$ = 6:1). Treatment of **15** with 1.1 equivalents of *m*-chloroperbenzoic acid and subsequent oxidative cleavage of the resulting α-alkoxy ketone with orthoperiodic acid afforded an intermediary carboxylic acid derivative, in situ iodolactonization of which stereoselectively formed the A,B,D ring system **16**. After protection of the hemiacetal in **16**, an appropriately functionalized α-alkoxycarbamate **17** was constructed by stereocontrolled allylation and methylation at the convex side of the molecule by applying Hart's procedure.[4b] Concurrent reduction of the acetal group and of the *p*-methoxybenzyl ether in **17** with an excess of triethylsilane in the presence of boron trifluoride etherate in acetonitrile at 0 °C gave the alcohol **18** in good yield. The allylic group in **18** was converted to an ethyl group by a Lemieux–Johnson oxidation, followed by formation of the dithiolane, and desulfurization with Raney nickel to provide the alcohol **19**, which was transformed to the iodide **20** by using the approach commonly applied for azepane ring formation. Finally, the C ring was constructed by removal of the methoxycarbonyl group with trimethylsilyl iodide,[4b] followed by consecutive intramolecular *N*-alkylation of the corresponding amine in refluxing acetonitrile to afford (−)-stenine (**1**) ($[\alpha]_D^{23}$ = −27.5 (c = 0.523 in MeOH), ref.[2a] $[\alpha]_D$ = −30.2 (in MeOH)). The spectroscopic (^{1}H NMR, ^{13}C NMR, IR) and mass spectrometric data of synthetic

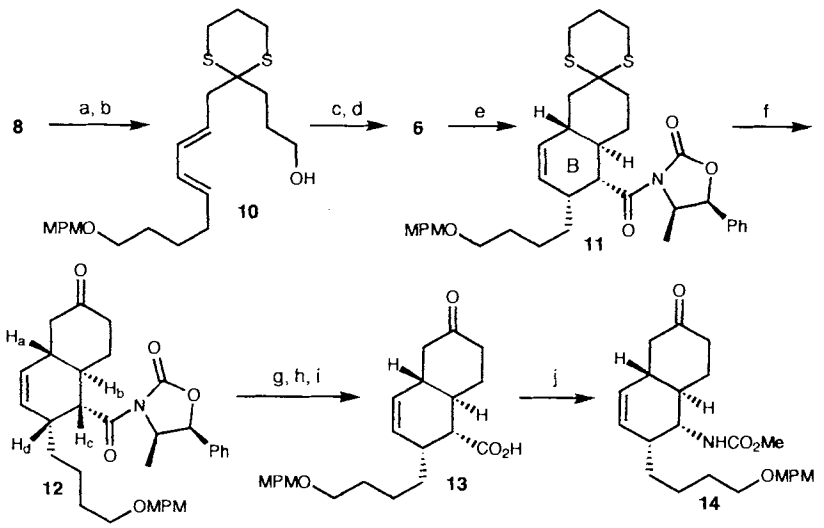

Scheme 1. a) *n*BuLi, THF, −25 °C, 4 h, then **7**, hexamethylphosphoric triamide (HMPA), −78 °C → room temperature (RT), 20 h; b) 0.1 equiv *p*-TsOH·H_2O, MeOH/THF (7:3), RT, 1.5 h, 68% (3 steps); c) SO_3·Py, dimethyl sulfoxide (DMSO), Et_3N, CH_2Cl_2, 0 °C → RT, 2 h, 85%; d) **9**, LiCl, Et_3N, THF, 0 °C → RT, 24 h, 90%; e) 1.3 equiv Me_2AlCl, CH_2Cl_2, −20 °C, 72 h, 85%; f) $AgNO_3$, *N*-chlorosuccinimide (NCS), CH_3CN/H_2O (4:1), 0 °C, 20 min, 80%; g) LiSEt, THF, 0 °C, 1.5 h, 91%; h) Et_3SiH, 10% Pd-C, acetone, 0 °C → RT, 1.5 h, 100%; i) $NaClO_2$, NaH_2PO_4, 2-methyl-2-butene, *t*BuOH/H_2O (5:2), 0 °C → RT, 1 h, 100%; j) diphenylphosphoryl azide (DPPA), Et_3N, DMF, 60 °C, 30 min, then 10 equiv MeOH, 0.2 equiv CuCl, RT, 40 h, 82%.

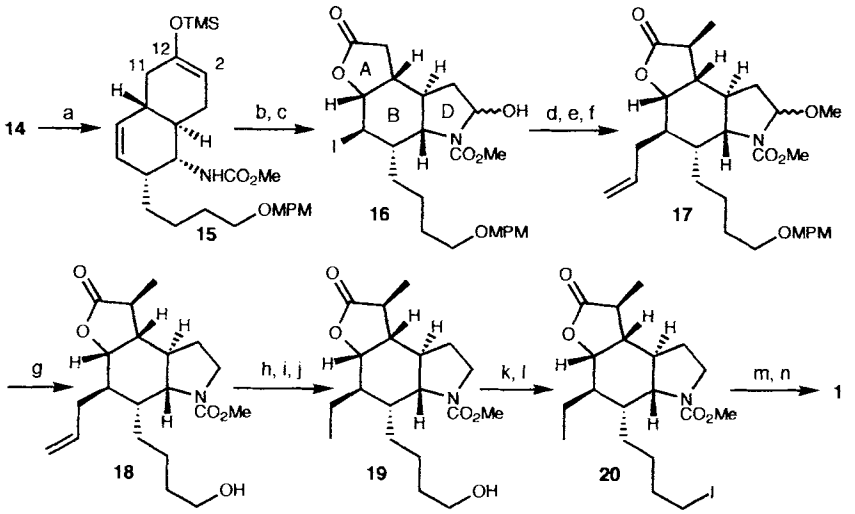

Scheme 2. a) TMSCl, NaI, Et_3N, CH_3CN, 50 °C, 3 h; b) 1.1 equiv *m*-chloroperoxybenzoic acid (*m*-CPBA), hexane/CH_2Cl_2 (2:1), −15 °C → RT, 2 h; c) H_5IO_6, THF/H_2O (2:1), RT, 2 h, then I_2, $NaHCO_3$, RT, 40 h, 50% (3 steps); d) 0.05 equiv camphorsulfonic acid (CSA), $CH(OMe)_3$, MeOH, CH_2Cl_2, RT, 1 h, 90%; e) 3 equiv allyltributyltin, 0.15 equiv azobis(isobutyronitrile) (AIBN), toluene, 80 °C, 4 h, 80%; f) lithium diisopropylamide (LDA), HMPA, THF, −78 °C, 30 min, then MeI, −78 °C, 1.5 h, 73%; g) 5 equiv Et_3SiH, 2.2 equiv $BF_3 \cdot OEt_2$, CH_3CN, 0 °C, 50 min, 82%; h) cat. OsO_4, $NaIO_4$, THF/H_2O (2:1), RT, 1 h, 75%; i) 1,2-ethanedithiol, $BF_3 \cdot OEt_2$, CH_2Cl_2, −15 °C, 45 min, 81%; j) Raney Ni (W-2), EtOH, reflux, 2 h, 85%; k) methanesulfonyl chloride (MsCl), Et_3N, CH_2Cl_2, 0 °C, 30 min, 88%; l) NaI, acetone, reflux, 2 h, 98%; m) 10 equiv trimethylsilyl iodide (TMSI), CH_2Cl_2, RT, 5 h; n) CH_3CN, reflux, 1 h, 70% (2 steps).

(−)-stenine (**1**) was consistent with the ^{1}H NMR spectrum of natural stenine (**1**) and with the data reported for (±)-stenine (**1**).[4b]

In summary, the highly stereocontrolled total synthesis of (−)-stenine (**1**) has been accomplished, in which the key features are an intramolecular asymmetric Diels–Alder reaction of the triene **6** prepared in a convergent fashion from three readily available components **7**, **8**, and **9** and efficient construction of the tricyclic A,B,D ring system **16**. These concepts are currently being applied to the asymmetric synthesis of tuberostemonine (**2**).

Received: November 27, 1995 [Z 8598 IE]
German version: *Angew. Chem.* **1996**, *108*, 968–970

Keywords: alkaloids · asymmetric syntheses · (−)-stenine · total syntheses

[1] a) M. Gotz, O. E. Edwards in *The Alkaloids, Vol. IX* (Ed.: R. H. F. Manske), Academic Press, New York, **1967**, p. 545; b) M. Gotz, G. M. Strunz in *Alkaloids: MTP International Review of Sciences, Series One, Vol. IX* (Ed.: K. Wiesner), Butterworth, London, **1973**, p. 143.

[2] a) S. Uyeo, H. Irie, H. Harada, *Chem. Pharm. Bull.* **1967**, *15*, 768–770; b) H. Harada, H. Irie, N. Masaki, K. Osaki, S. Uyeo, *Chem. Commun.* **1967**, 460–462; c) O. E. Edwards, G. Feniak, K. L. Handa, *Can. J. Chem.* **1962**, *40*, 455–462; d) W.-H. Lin, Y. Ye, R.-S. Xu, *J. Nat. Prod.* **1992**, *55*, 571–576.

[3] H. Shinozaki, M. Ishida, *Brain Res.* **1985**, *334*, 33–40.

[4] For total syntheses of the *Stemona* alkaloids, see: a) D. R. Williams, D. L. Brown, J. W. Benbow, *J. Am. Chem. Soc.* **1989**, *111*, 1923–1925; b) C.-Y. Chen, D. J. Hart, *J. Org. Chem.* **1993**, *58*, 3840–3849; c) D. R. Williams, J. P. Reddy, G. S. Amato, *Tetrahedron Lett.* **1994**, *35*, 6417–6420. For some synthetic approaches toward the *Stemona* alkaloids, see: d) M. Haruna, T. Kobayashi, K. Ito, *Tennen Yuki Kagoubutsu Toronkai Koen Yoshishu* **1985**, *27*, 200–207 [*Chem. Abstr.* **1986**, *105*, 79195k]; e) L. Xiang, A. P. Kozikowski, *Synlett* **1990**, 279–281; f) S. F. Martin, J. W. Corbett, *Synthesis* **1992**, 55–57; g) R. L. Beddoes, M. P. H. Davies, E. J. Thomas, *J. Chem. Soc. Chem. Commun.* **1992**, 538–540; h) P. Wipf, Y. Kim, *Tetrahedron Lett.* **1992**, *33*, 5477–5480; i) Y. Morimoto, K. Nishida, Y. Hayashi, H. Shirahama, *ibid.* **1993**, *34*, 5773–5776; j) Y. Morimoto, M. Iwahashi, *Synlett* **1995**, 1221–1222.

[5] Since our manuscript was submitted to this journal, another total synthesis of (−)-stenine (**1**) has been reported by Wipf et al., see: P. Wipf, Y. Kim, D. M. Goldstein, *J. Am. Chem. Soc.* **1995**, *117*, 11106–11112.

[6] It is worthwhile noting Overman's work in the field of enantioselective synthesis of the complicated alkaloids. For example, see the following recent papers: a) L. E. Overman, M. H. Rabinowitz, P. A. Renhowe, *J. Am. Chem. Soc.* **1995**, *117*, 2657–2658 and references therein; b) C. Y. Hong, N. Kado, L. E. Overman, *ibid.* **1993**, *115*, 11028–11029 and references therein; c) S. D. Knight, L. E. Overman, G. Pairaudeau, *ibid.* **1993**, *115*, 9293–9294 and references therein.

[7] For another example closely related to this methodology, see ref. [4f]. We thank Prof. S. F. Martin (The University of Texas, Austin) for providing us with a reprint.

[8] For a review of intramolecular Diels–Alder reactions, see: E. Ciganek in *Organic Reactions, Vol. 32* (Ed.: W. G. Dauben), Wiley, New York, **1984**, p. 1. For a review of asymmetric Diels–Alder reactions, see: W. Oppolzer, *Angew. Chem.* **1984**, *96*, 840–854; *Angew. Chem. Int. Ed. Engl.* **1984**, *23*, 876–889.

[9] D. A. Evans, K. T. Chapman, J. Bisaha, *J. Am. Chem. Soc.* **1988**, *110*, 1238–1256.

[10] The dithiane **8** was prepared from 2-(3-hydroxypropyl)-1,3-dithiane [11] by THP protection.

[11] Y. Wu, E. Ohlsson, *Acta Chem. Scand.* **1993**, *47*, 422–424.

[12] The dienyl chloride **7** was prepared in five steps from commercially available 1,5-pentanediol by the following conventional sequence: a) NaH, MPMCl, 73%; b) Swern oxidation, 89% [13]; c) lithium diisopropylamide (LDA), triethyl 4-phosphonocrotonate, hexamethylphosphoric triamide (HMPA), THF, 70%; d) diisobutylaluminum hydride (DIBALH), 98%; e) *n*BuLi, MsCl, THF.

[13] A. J. Mancuso, S.-L. Huang, D. Swern, *J. Org. Chem.* **1978**, *43*, 2480–2482.

[14] M. W. Rathke, M. Nowak, *J. Org. Chem.* **1985**, *50*, 2624–2626.

[15] The chiral phosphonate **9**, $[\alpha]_D^{28} = +16.4$ ($c = 0.560$ in $CHCl_3$), was prepared in quantitative yield from the Evans' chiral oxazolidinone [9] by the following sequence: a) *n*BuLi, $BrCH_2COCl$, THF, −78 °C; b) $(EtO)_3P$, benzene, reflux.

[16] The stereochemistry of **11** was assigned as shown on the basis of the diagnostic coupling constants in the ^{1}H NMR spectrum of **12** (J(a,b) = 11.6 Hz, J(b,c) = 11.0 Hz, J(c,d) = 5.5 Hz). For a similar example of complete *endo* selectivity in an intramolecular Diels–Alder reaction, see: K. Narasaka, M. Saitou, N. Iwasawa, *Tetrahedron: Asymmetry* **1991**, *2*, 1305–1318 and references therein.

[17] R. E. Damon, G. M. Coppola, *Tetrahedron Lett.* **1990**, *31*, 2849–2852. It was found that direct hydrolysis of this carboximide using LiOH or LiOOH resulted in cleavage of oxazolidinone ring.

[18] T. Fukuyama, S.-C. Lin, L. Li, *J. Am. Chem. Soc.* **1990**, *112*, 7050–7051.

[19] T. Shioiri, K. Ninomiya, S. Yamada, *J. Am. Chem. Soc.* **1972**, *94*, 6203–6205.

[20] M. E. Duggan, J. S. Imagire, *Synthesis* **1989**, 131–132.

Multicomponent Molecular Systems Incorporating Porphyrins and Copper(I) Complexes: Simultaneous Synthesis of [3]- and [5]Rotaxanes**

Nathalie Solladié, Jean-Claude Chambron, Christiane O. Dietrich-Buchecker, and Jean-Pierre Sauvage*

Multiporphyrinic assemblies are of special interest as structural and functional mimics of the photosynthetic reaction center.[1] Porphyrins have also been used as building blocks for

[*] Dr. J.-P. Sauvage, N. Solladié, Dr. J.-C. Chambron, Dr. C. O. Dietrich-Buchecker
Laboratoire de Chimie Organo-Minérale, UA 422 au CNRS
Faculté de Chimie, Université Louis Pasteur
F-67000 Strasbourg (France)
Fax: Int. code +88 60 73 12

[**] This work was supported by the CNRS. N. S. thanks the Ministry of Education for a fellowship (MRE). We thank Dr. R. Graff and J.-D. Sauer for recording the NMR spectra. A. Dupont-Gervais and Dr. A. Van Dorsselaer are acknowledged for the ES-MS spectra.

constructing novel structures and topologies such as catenanes[2-4] and rotaxanes.[5] We have recently synthesized a family of porphyrin-stoppered rotaxanes,[6] the prototype of which consists of a central copper(I) complex coordinated to two 2,9-diphenyl-1,10-phenanthroline (dpp) units. One these units is included in a ring and the other is threaded through the ring and bears at its two ends a gold(III) porphyrin acting as an electron acceptor (A) and a zinc(II) porphyrin (electron donor D). Ultrafast photoinduced electron transfer between D (singlet excited state) and A was shown to occur, with a strong superexchange contribution from the central copper(I) complex.[7]

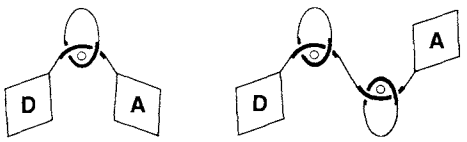

Scheme 1. Representation of a [2]- (left) and a [3]rotaxane (right) with different terminal porphyrin groups, which function as either electron donors (D) or electron acceptors (A).

The most straightforward approach to increasing the lifetime of the charge separated state is to increase the distance between D and A while keeping a strong coupling between both components. It was thus hoped that by increasing the number of rings coordinated to Cu^{I} centers and interspersed between the terminal porphyrins, fast forward electron transfer between D and A would still take place, whereas the back electron transfer reaction between the redox products (D^{+} and A^{-}) would be significantly slowed.

We report here the synthesis of a [3]rotaxane, whose organic backbone is indeed similar to that shown on the right-hand side of Scheme 1, as well as the preparation of an unexpected compound obtained in the same condensation reaction as that affording the [3]rotaxane. This compound is a [5]rotaxane with one central and two terminal porphyrins in the open-chain fragment, which is threaded through four rings (Scheme 2).

The strings of the [5]rotaxanes $\mathbf{3}^{4+}$ and $\mathbf{4}^{4+}$ contain three porphyrins but, in contrast to some recent interesting examples of linearly arranged multiporphyrinic compounds,[8-12] each porphyrinic unit is separated from its next neighbor by a long, multifunctional spacer. Noteworthy is the length of the central string. It contains a total of 83 atoms and should be approximately 60 Å long in an extended conformation.

The synthetic strategy is based on the threading of two rings onto the same two-chelate string (Scheme 3). The driving force behind this reaction is the coordination of all the dpp chelates to copper(I) centers.[13] Since appropriate end functions were previously introduced in the string, porphyrinic stoppers can be constructed. As previously shown with similar compounds,[13] the threading step (Scheme 3a) can be quantitative. The second step (Scheme 3b) can involve formation of terminal porphyrins only (upper route) or entail construction of both terminal and bridging porphyrin units (lower route).

1,10-Phenanthroline was treated with the C4-lithiated derivative of 2,2-dimethylpropane-1,3-diyl-protected benzaldehyde[14]

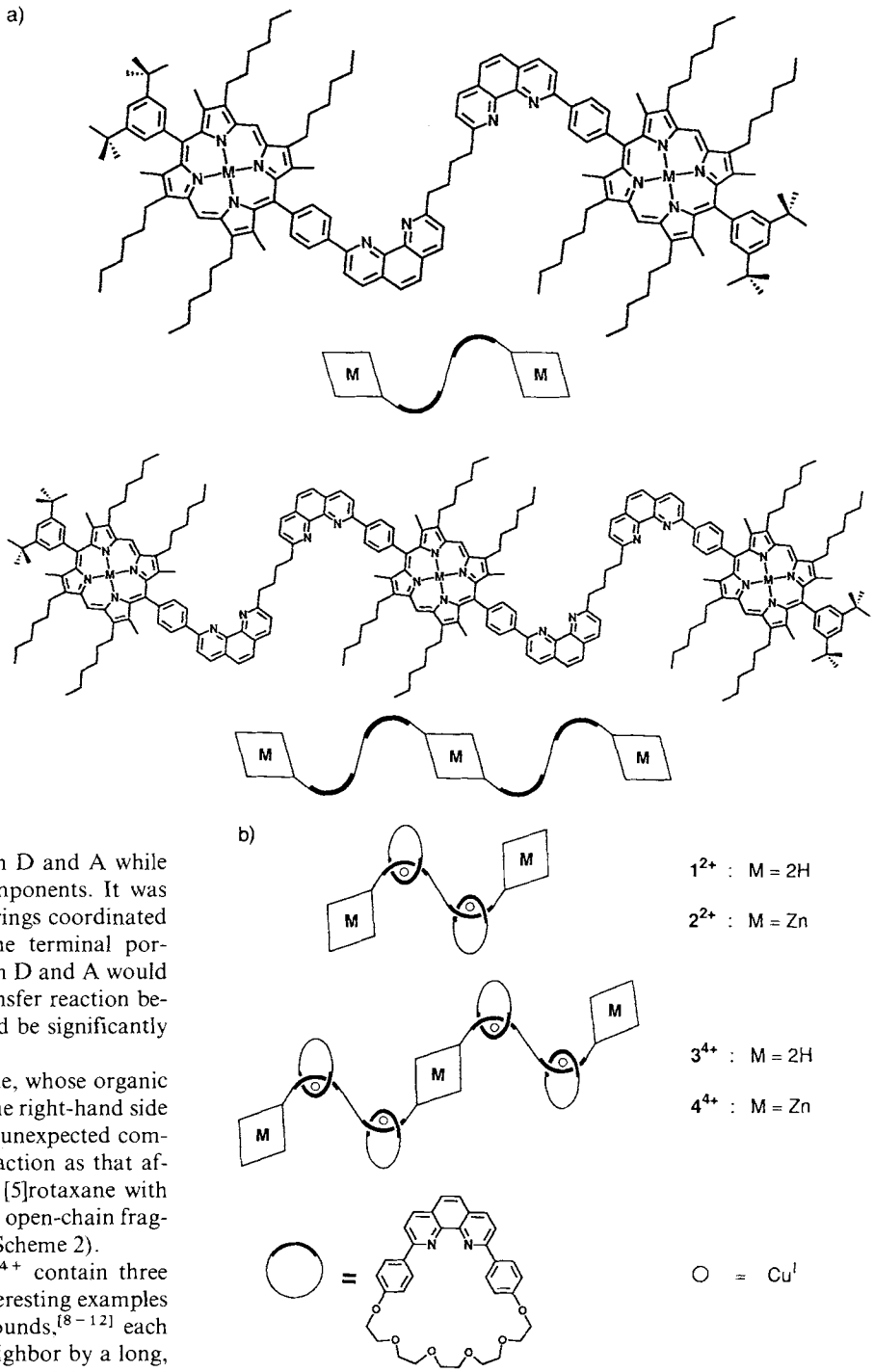

Scheme 2. a) Chemical formulae of the molecular strings constructed in the course of the rotaxane synthesis. b) Schematic representations of the [3]rotaxanes ($\mathbf{1}^{2+}$, $\mathbf{2}^{2+}$) and [5]rotaxanes ($\mathbf{3}^{4+}$, $\mathbf{4}^{4+}$). The porphyrin groups are symbolized by diamonds. Note that the ring used in the threading process is a 30-membered ring.

at 0 °C in THF under argon. Following a classical procedure,[15] after hydrolysis and reoxidation with MnO_2, **5** was isolated in pure form in 71% yield. Compound **6** was obtained by treating **5** with 1,4-dilithiobutane[16] under similar conditions, eventually leading to the dialdehyde **7** after deprotection (73% overall yield from **5**). The difunctional string **7** can be prepared readily on a multigram scale. Macrocycle **8** is one of the most frequently used cyclic building blocks in our group.[17] The threading step

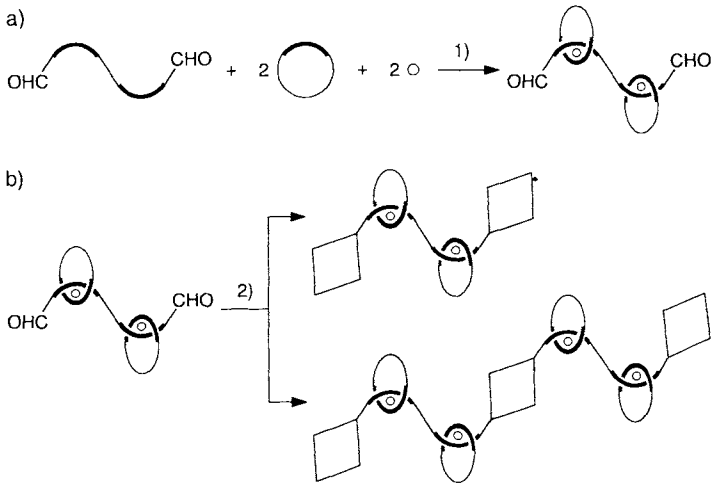

Scheme 3. Synthetic strategy for making porphyrin-stoppered polyrotaxanes. a) The starting dialdehyde molecular string has two phenanthroline units for binding; the macrocycle is also able to bind the metal (small open circle) while being threaded by the string. The threading step (1) is assumed to be spontaneous and will thus not require any additional reagent. b) The porphyrin-forming reaction (2) requires the proper reagents and can, in principle, be directed mostly towards the construction of porphyrins stoppers or of both terminal and bridging porphyrins.

(Scheme 3a) was carried out by first mixing equimolar amounts of $[Cu(CH_3CN)_4]^+PF_6^-$ and **8** and then adding 0.5 equivalents of **7** (CH_2Cl_2/CH_3CN, room temperature). The dication $\mathbf{9}^{2+}$ was obtained quantitatively, as indicated by ^1H NMR spectroscopy. It was treated with the 2,2′-methylenedipyrrole derivative **10**[18] and 3,5-di-*tert*-butylbenzaldehyde (**11**)[19] under experimental conditions analogous to those originally described by Lindsey et al.[20] and also utilized with other copper(I)-containing threaded complexes.[4, 6] The three components, $\mathbf{9}^{2+}$, **10**, and **11**, in a molar ratio of 1:10:8 were treated with CF_3COOH at room temperature in CH_2Cl_2. The porphyrinogen intermediates were reoxidized with chloranil and the final products separated by repeated column chromatography. Compound $\mathbf{1}^{2+}$ was obtained in surprisingly high yield (34%) considering that two porphyrins have to be formed more or less simultaneously. In addition, $\mathbf{3}^{4+}$ was also isolated in pure form (8%) and characterized. The new compounds were characterized by high-resolution ^1H NMR spectroscopy and electrospray mass spectrometry (ES-MS). Figure 1 shows the ES-MS spectrum of a representative product, [5]rotaxane $\mathbf{3}^{4+}$.

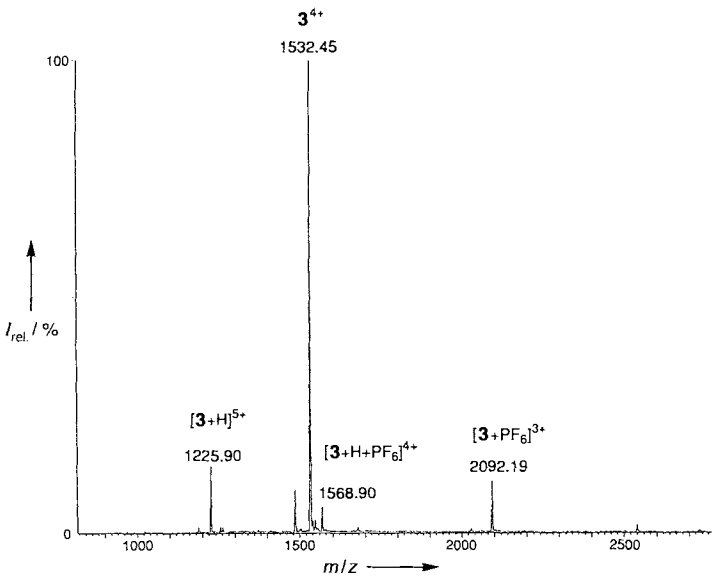

Fig. 1. ES mass spectrum of $\mathbf{3}^{4+}\cdot 4PF_6^-$ (M_r = 6711.78). The spectrum was recorded on a VG BioQ triple-quadrupole mass spectrometer with a m/z range of 4000 (VG Bio Tech Ltd., Altrincham, UK). The accelerating cone voltage (V_c) [21] was set at 20 V to minimize fragmentation. The sample in CH_2Cl_2 was infused in the mass spectrometer with a syringe pump with a continuous flow of 5 μL min^{-1}.

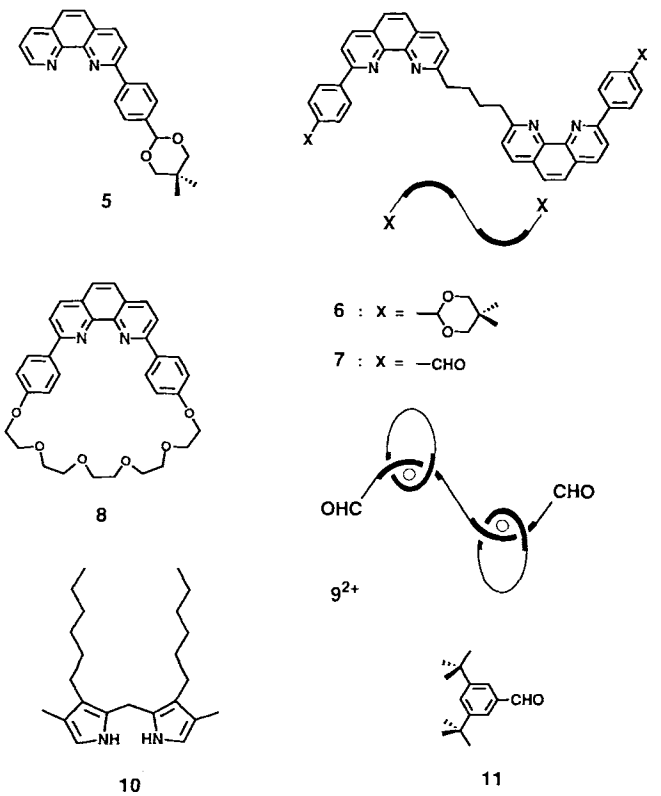

To induce vectorial electron transfer in these polyrotaxanes on irradiation it will be necessary to desymmetrize the molecules and, in particular, to selectively metalate the different porphyrinic sites of each compound. The copper(I) complex subunits are also expected to participate in energy and electron transfer processes. Preliminary emission measurements show that relatively efficient quenching of free-base or zinc porphyrin fluorescence by the copper(I) complex components takes place.

Experimental Procedure

$\mathbf{9}^{2+}$: A solution of $[Cu(CH_3CN)_4]^+PF_6^-$ (2 equiv) in acetonitrile under argon was added by cannula and at room temperature to a stirred solution of **8** (2 equiv) in dichloromethane. The mixture turned orange instantaneously, indicating the formation of $[Cu\cdot\mathbf{8}\cdot(CH_3CN)_2]^+PF_6^-$. The reaction mixture was stirred for 20 min at room temperature, then a solution of bisphenanthroline **7** (1 equiv) in dichloromethane was added. The solution turned dark red immediately. After the solution was stirred for ca. 12 h under argon at room temperature, the solvents were removed under vacuum to afford crude $\mathbf{9}^{2+}\cdot 2PF_6^-$ ($\mathbf{7}\cdot(\mathbf{8})_2\cdot(Cu^+)_2$) in quantitative yield.

$\mathbf{1}^{2+}\cdot 2PF_6^-$ and $\mathbf{3}^{4+}\cdot 4PF_6^-$: A solution of $\mathbf{9}^{2+}\cdot 2PF_6^-$ (0.398 g, 0.18 mmol), **11** (0.32 g, 1.47 mmol), and **10** (0.627 g, 1.83 mmol) in dichloromethane (180 mL) was treated with four drops of trifluoroacetic acid and then stirred overnight at room temperature and under argon. Chloranil (1.39 g, 5.65 mmol) was added and the reaction mixture refluxed for 1.5 h. After cooling, the crude reaction mixture was neutralized with 10% sodium carbonate (80 mL). The resulting organic phase (200 mL) was washed three times with water, stirred for ca. 12 h with 6.5% KPF_6 (200 mL), washed again twice with water, and concentrated to dryness. The residue (1.1 g) was purified by repeated column chromatography on alumina. Elution with

 © VCH Verlagsgesellschaft mbH, D-69451 Weinheim, 1996 0570-0833/96/3508-0908 $ 15.00+.25/0

0.5% methanol in dichloromethane afforded pure $\mathbf{1}^{2+}\cdot 2PF_6^-$ (240 mg, 34%). Elution with 1.5% methanol in dichloromethane afforded pure $\mathbf{3}^{4+}\cdot 4PF_6^-$ (50 mg, 8%).

$\mathbf{1}^{2+}\cdot 2PF_6^-$: Dark red solid. ^{1}H NMR (400 MHz, CD_2Cl_2): δ = 10.16 (s, 4H), 9.08 (d, 2H, J = 8.3 Hz), 8.67 (d, 2H, J = 8.3 Hz), 8.49 (d, 2H, J = 9.0 Hz), 8.46 (d, 4H, J = 8.3 Hz), 8.23 (d, 2H, J = 9.0 Hz), 8.22 (d, 2H, J = 8.2 Hz), 8.00 (s, 4H), 7.96 (d, 4H, J = 8.2 Hz), 7.89 (d, 4H, J = 1.7 Hz), 7.86 (s, 2H), 7.71 (d, 4H, J = 7.9 Hz), 7.56 (d, 4H, J = 8.0 Hz), 7.26 (d, 8H, J = 8.6 Hz), 7.25 (d, 2H, J = 8.1 Hz), 6.11 (d, 8H, J = 8.6 Hz), 3.97 (t, 8H, J = 7.7 Hz), 3.87 (s, 8H), 3.78 (t, 8H), 3.72 (m, 16H), 3.56–3.51 (m, 16H), 2.46 (s, 12H), 2.19 (q, 8H, J = 7.8 Hz), 2.04 (q, 8H, J = 7.8 Hz), 1.75 (m, 20H), 1.71 (s, 12H), 1.51 (s, 36H), 1.51 (m, 16H), 1.40 (m, 16H), 0.95 (t, 12H, J = 7.3 Hz), 0.92 (t, 12H, J = 7.3 Hz), 0.36 (t, 4H), −2.61 (br. s, 2H), −2.70 (br. s, 2H); FAB-MS: m/z (%): 3896.8 (5) $[M + H]^+$, 3750.2 (75) $[M - PF_6^-]^+$, 3037.4 (100) $[M - 2PF_6^- - 8 - 2H^+]^+$.

$\mathbf{3}^{4+}\cdot 4PF_6^-$: Dark red solid. ^{1}H NMR (500 MHz, CD_2Cl_2): δ = 10.16 (s, 4H), 10.06 (s, 2H), 9.08 and 9.07 (2d, 4H, J = 8.2 Hz), 8.68 and 8.67 (2d, 4H, J = 8.0 Hz), 8.49 (d, 4H, $J \approx 10.2$ Hz), 8.47 (d, 8H, $J \sim 8.6$ Hz), 8.24 and 8.23 (2d, 4H, $J \approx 9.3$ Hz), 8.22 and 8.21 (2d, 4H, $J \approx 8.7$ Hz), 8.01 (s, 8H), 7.97 and 7.96 (2d, 8H, J = 8.2 Hz), 7.89 (d, 4H, J = 1.8 Hz), 7.85 (t, 2H, J = 1.7 Hz), 7.70 (d, 8H, $J \approx 8.0$ Hz), 7.56 (d, 4H, J = 7.8 Hz), 7.51 (d, 4H, J = 7.8 Hz), 7.25 and 7.24 (2d, 16H, J = 8.5 Hz), 7.24 (obscured, 4H), 6.11 and 6.10 (2d, 16H, J = 8.5 Hz), 3.97 (t, 8H, J = 7.8 Hz), 3.87 (s, 16H), 3.71 (m, 48H), 3.54 (m, 32H), 2.46 (s, 12H), 2.19 (q, 8H, J = 7.6 Hz), 2.02 (m, 16H), 1.74 (m, 32H), 1.71 (s, 12H), 1.68 (s, 12H), 1.54 (m, 24H), 1.50 (s, 36H), 1.41 (m, 24H), 0.92 (m, 36H), 0.32 (t, 8H), −2.62, −2.72 and −2.84 (3 br. s, 6H); ES-MS: m/z (%): 1532.51 (100) $[M - 4PF_6^-]^{4+}$.

Received: October 23, 1995 [Z 8492 IE]
German version: *Angew. Chem.* **1996**, *108*, 957–960

Keywords: copper compounds · electron transfer · macrocycles · porphyrinoids · rotaxanes

[1] A few representative examples, among many other systems, can be found in the following publications: J. P. Collman, C. M. Elliott, T. R. Halbert, B. S. Tovrog, *Proc. Natl. Acad. Sci. USA* **1977**, *74*, 18; A. Helms, D. Heiler, G. McLendon, *J. Am. Chem. Soc.* **1992**, *114*, 6227; D. Gust, T. A. Moore, A. L. Moore, L. Leggett, S. Lin, J. M. DeGraziano, R. M. Hermant, D. Nicodem, P. Craig, G. R. Seely, R. A. Nieman, *J. Phys. Chem.* **1993**, *97*, 7926; X. Zhou, K. Shing Chan, *J. Chem. Soc. Chem. Comm.* **1994**, 2493.

[2] M. J. Gunter, M. R. Johnston, *J. Chem. Soc. Chem. Comm.* **1992**, 1163; M. J. Gunter, D. C. R. Hockless, M. R. Johnston, B. W. Shelton, A. H. White, *J. Am. Chem. Soc.* **1994**, *116*, 4810.

[3] M. Momenteau, F. Le Bras, B. Loock, *Tetrahedron Lett.* **1994**, *35*, 3289.

[4] J.-C. Chambron, V. Heitz, J.-P. Sauvage, *Bull. Soc. Chim. Fr.* **1995**, *132*, 340.

[5] P. R. Ashton, J. F. Stoddart, M. S. Tolley, J. W. Wheeler, M. R. Johnston, *J. Chem. Soc. Chem. Comm.* **1992**, 1128; H. W. Gibson, M. K. Bheda, P. T. Engen, *Prog. Polym. Sci.* **1994**, *19*, 843.

[6] J.-C. Chambron, V. Heitz, J.-P. Sauvage, *J. Chem. Soc. Chem. Commun.* **1992**, 1131; *J. Am. Chem. Soc.* **1993**, *115*, 12378.

[7] J.-C. Chambron, A. Harriman, V. Heitz, J.-P. Sauvage, *J. Am. Chem. Soc.* **1993**, *115*, 6109, 7419.

[8] T. Nagata, A. Osuka, K. Maruyama, *J. Am. Chem. Soc.* **1990**, *112*, 3054.

[9] M. J. Crossley, P. L. Burn, *J. Chem. Soc. Chem. Commun.* **1991**, 1569.

[10] H. L. Anderson, *Inorg. Chem.* **1994**, *33*, 972.

[11] J. L. Sessler, V. Capuano, *Tetrahedron Lett.* **1993**, *34*, 2287; *Angew. Chem.* **1990**, *102*, 1162; *Angew. Chem. Int. Ed. Engl.* **1990**, *29*, 1134.

[12] R. W. Wagner, J. S. Lindsey, *J. Am. Chem. Soc.* **1994**, *116*, 9759.

[13] J.-C. Chambron, C. O. Dietrich-Buchecker, J.-F. Nierengarten, J.-P. Sauvage, *J. Chem. Soc. Chem. Commun.* **1993**, 801; J.-C. Chambron, C. O. Dietrich-Buchecker, J.-F. Nierengarten, J.-P. Sauvage, N. Solladié, A.-M. Albrecht-Gary, M. Meyer, *New. J. Chem.* **1995**, *19*, 409.

[14] J. A. Marshall, G. A. Flynn, *Synth. Commun.* **1979**, *9*, 123.

[15] C. O. Dietrich-Buchecker, P. A. Marnot, J.-P. Sauvage, *Tetrahedron Lett.* **1982**, *23*, 5291; C. O. Dietrich-Buchecker, J.-P. Sauvage, J.-P. Kintzinger, P. Maltèse, C. Pascard, J. Guilhem, *New J. Chem.* **1992**, *16*, 931.

[16] R. West, E. G. Rochow, *J. Org. Chem.* **1953**, *18*, 1739; J. X. McDermott, J. F. White, G. Whitesides, *J. Am. Chem. Soc.* **1976**, *98*, 6529.

[17] C. O. Dietrich-Buchecker, J.-P. Sauvage, *Tetrahedron Lett.* **1983**, *24*, 5091; *Tetrahedron* **1990**, *46*, 503.

[18] R. Young, C. K. Chang, *J. Am. Chem. Soc.* **1985**, *107*, 898.

[19] M. S. Newman, L. F. Lee, *J. Org. Chem.* **1972**, *37*, 4468.

[20] J. S. Lindsey, H. C. Hsu, I. C. Schreiman, *Tetrahedron Lett.* **1986**, *27*, 4969.

[21] A. P. Bruins, T. R. Covey, J. D. Henion, *Anal. Chem.* **1987**, *59*, 2642.

Synthesis of Boron-Rich Lysine Dendrimers as Protein Labels in Electron Microscopy**

Britta Qualmann,* Michael Manfred Kessels,* Hans-Jürgen Musiol, Walter Daniel Sierralta, Peter Wilhelm Jungblut, and Luis Moroder

Currently, interest is growing in the design and synthesis of boron-rich compounds suitable for boron neutron capture therapy of cancer (BNCT)[1] and increasingly also for new electron microscopic techniques like electron energy loss spectroscopy (EELS) and electron spectroscopic imaging (ESI).[2] In all these applications high topical concentrations of boron and reactive handles are required in the molecule for selective conjugation of carborane clusters to molecules that recognize the biological target.

Previous studies clearly revealed the limitations of multiple attachments of small boron-containing molecules to carrier proteins. In the case of antibodies the solubility and immunoreactivity was impaired.[3] Randomly boronated polymers such as poly-D,L-lysine,[4] poly-L-ornithine,[5] dextranes,[6] and starburst dendrimers[7] are inherently heterogeneous and compelled the synthesis of more defined molecules, for example of peptides containing carboranyl amino acids.[8] The main difficulties encountered in this approach derived from the slow and incomplete coupling of carboranyl amino acids at the C- and particularly the N-terminus due to steric hindrance by the bulky 1,2-dicarbadodecaborane moiety. Moreover, both the intermediates and the final products had very low solubilities.[8]

We expected that the handicaps of these linear constructs could possibly be overcome by the use of spherical dendritic molecules built up of lysines (that is, poly-(α,ε-L-Lys)[9]) carrying the carborane clusters at the outer surface. Such lysine dendrimers would offer the advantage of a single acylation step for a multiple attachment of carboranyl amino acids and should ensure quantitative derivatization, since the spherically arranged amino functions of the dendrimers are known to be fully accessible.[10]

Since these carborane-dotted spheres have to be grafted to a defined locus of the carrier protein, for example through the thiol function of antibody fragments (Fab'), the two constructs **A** and **B**, whose structures are shown in Figure 1, were designed to fulfill the following requirements:

1) A boron load high enough to exceed the boron ESI detection limit in biological probes has to be achieved. Though not yet defined for boron, 80 incorporated boron atoms were expected to suffice. This can be obtained with a heptalysine tree (second generation dendrimer), which enables simultaneous incorporation of eight carboranyl amino acids, yielding a dendrimer with 80 clustered boron atoms at its outer sphere. The resulting rather compact, ball-like molecules with a radius of about 12–14 Å, similar to the value of 11.4 Å calculated for the third generation poly-(α,ε-L-Lys),[11] represent marker compounds of defined and homogeneous size and would be most valuable tools in immunocytochemistry based on ESI.[12]

[*] Dipl.-Biochem. B. Qualmann, Dipl.-Biochem. M. M. Kessels, Dr. W. D. Sierralta, Prof. Dr. Dr. P. W. Jungblut
Max-Planck-Institut für Experimentelle Endokrinologie
Feodor-Lynen-Strasse 7–9, D-30625 Hannover (Germany)
Fax: Int. code +(511)5359-203
H.-J. Musiol, Prof. Dr. L. Moroder
Max-Planck-Institut für Biochemie, Martinsried (Germany)

[**] The authors thank Dr. C. Eckerskorn, Max-Planck-Institut für Baier and Dr. G. Paulus, Shimadzu, Duisburg, for the MALDI-MS measurements.

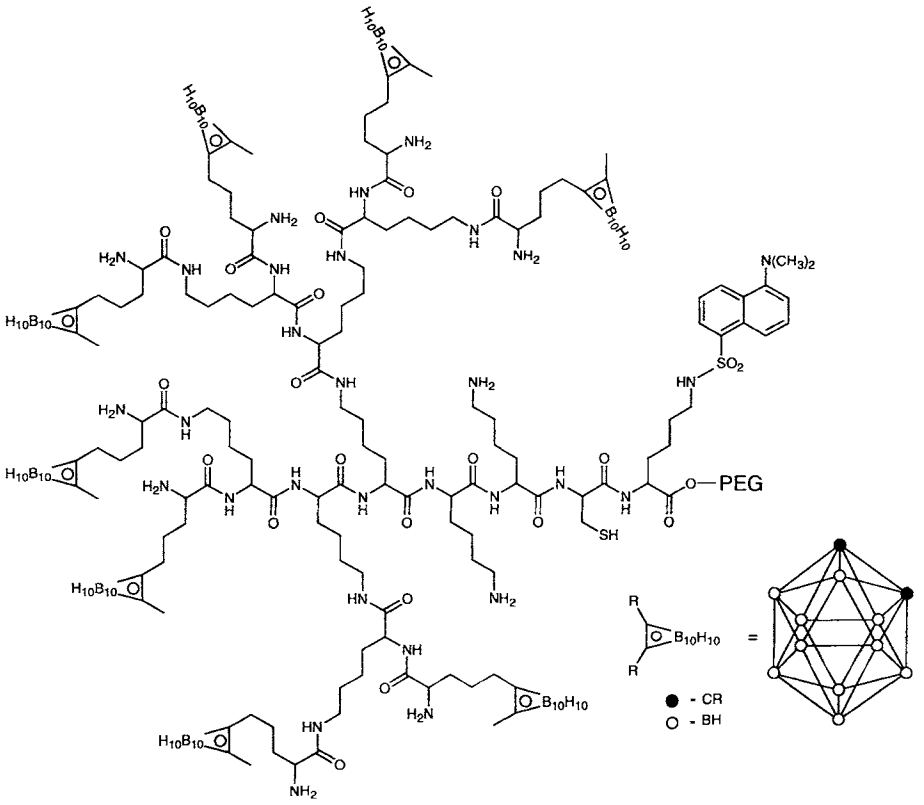

Fig. 1. Structure of the poly-(α,ε-L-Lys) dendrimer **B**. Peptide **A** lacks the polyether moiety at the C-terminus of **B**. PEG = polyethylene glycol (with $\bar{x}$ = 68 glycol units).

2) A reactive handle, like the thiol function of a Cys residue, linked to the terminus of a flexible spacer must be fully accessible to guarantee the selective grafting of the carborane-dotted spheres to defined loci of targeting molecules.
3) A fluorescent probe, in the present case ε-*N*-dansyl-lysine, must be incorporated to allow spectroscopic monitoring of the coupling rate of the boron-rich markers to targeting proteins.
4) The solubility in water must be improved. Increased water-solubility of the hydrophobic boron-rich moiety was expected from the hydrophilic positively charged Lys–Lys spacer and—in the case of peptide **B**—from an additionally attached PEG-tail. Pegylation of peptides is known to strongly enhance the solubility of both protected and unprotected peptides[13] and has recently been found to increase the critical micellar concentration of amphiphiles markedly.[14]

In syntheses of compounds with potential use in BNCT published recently, a dendritic polyalcoholic structure was linked with a single carborane cluster,[15a] or carboranyl groups were introduced into a dendritic micelle;[15b] none of these compounds can be coupled specifically to proteins.

The two peptidic protein marker constructs **A** and **B** presented here were synthesized according to standard procedures of solid-phase peptide synthesis with the Fmoc/*t*Bu strategy (Fmoc = 9-fluorenylmethoxycarbonyl) and using pegylated polystyrene resins. This type of resin was expected to prevent a hydrophobic collapse of the dendrimers by increasing their solvation,[16] and to allow direct generation of the desired compounds with and without the PEG chain. In the final acylation step of the lysine-tree we used (*S*)-5-(2-methyl)-1,2-dicarba-*closo*-dodecaborane(12)-1-yl)-2-amino pentanoic acid[17] (L-MeCBA), for which we have recently developed a highly efficient and convenient new synthesis, as carboranyl amino acid.[18] Cleavage and deprotection of the resin-bound fully protected peptide constructs from TentaGel S-PHB and TentaGel PAP led to compounds **A** and **B** in 88 and 81% yield, respectively. In the HPLC investigation compound **A** showed a dominant product peak of the expected mass according to electron-impact mass spectrometry (EI-MS) (3679.0; calcd. $[M^+]$ = 3679.2 for $C_{139}H_{306}N_{30}O_{22}S_2B_{80}$), which indicates complete incorporation of the eight L-MeCBA residues. For compound **B** HPLC again revealed a main product peak. Mass determinations by FAB-MS (FAB = fast atom bombardment) and EI-MS failed because of the known difficulties encountered in mass spectrometry with pegylated peptides;[19] the spectrum of MALDI-MS (MALDI = matrix-assisted laser desorption/ionization) showed a bell-shaped distribution corresponding to the presence of varying molecular weights of polyethyleneglycol and an apex at 6649.7 Da, which corresponds fairly well with the theoretical value (6675 Da) and is in full agreement with previous MALDI-MS measurements on pegylated peptides.[20]

Compounds **A** and **B** exhibited good solubilities in several polar organic solvents like DMF and alcohols as well as in aqueous organic mixtures, which enabled their conjugation to the thiol group of Fab'. Yields, however, were moderate in the case of **A**, whereas the reaction of compound **B** proceeded smoothly with both 1,4-di-[3'-(2'-pyridyldithio)-propionamido)]butane or bismaleimidohexane as crosslinkers. The high yields of labeled Fab' obtained in the latter case are likely to be due to the good water solubility of marker peptide **B**.

The properties of these two new markers were expected to be superior to those of the sequential polypeptides synthesized by us in previous experiments (the undecapeptide[8c] consisting of alternating racemic carboranyl amino acids and serines as well as a lysine residue for attachment to Fab' through heterobifunctional reagents). In EELS experiments using a Zeiss 902 electron microscope with an integrated energy loss spectrometer, the novel Fab'-(**A**,**B**) conjugates gave sharp signals for the Fab'-**B** conjugate (Fig. 2). The small immunoreagents carrying the antigen-combining site at one end and the boron-rich dendritic marker at the opposite end of the molecule have also been used in immunocytochemical investigations with ESI. First results show high resolution properties[21, 22] and confirm the validity of the new approach in terms of exceeding the detection limits with the 80 boron atom label and of sufficient solubility induced by pegylation of the marker moiety. This innovative approach could represent an interesting route even for the construction of covalently attachable multiple gold or other labels; furthermore, homogeneous functional dendrimers carrying a reactive handle like the constructs described here may be valuable carriers for drug targeting.

Experimental Procedure

Synthesis of **A** and **B**: Fmoc-Lys(Dansyl)-OH [23] was coupled in about 20 h to TentaGel S-PHB or TentaGel PAP (Rapp Polymere, Tübingen, Germany) in DMF

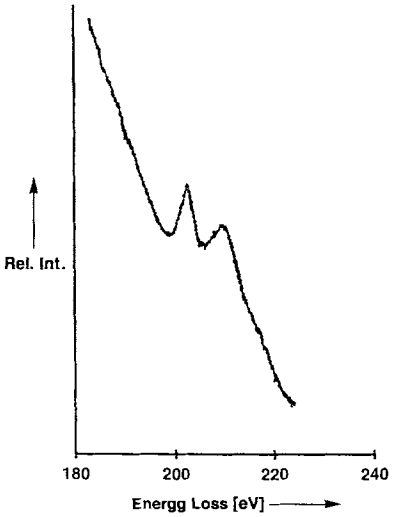

Fig. 2. Electron energy loss spectrum of an immunoprobe containing peptide **B**, adsorbed from an aqueous solution (0.5 mg mL^{-1}) onto nitrocellulose-coated gold grids. The sharp boron absorption edge at an energy loss of 197 eV originates in the element-specific inelastic scattering of outer shell electrons recorded with the electron detector of an energy filter transmission electron microscope (EFTEM) connected to a digital compensation X/Y plotter (Zeiss EM 902, operated at 80 kV; objective aperture 90 μm; spectrometer entrance aperture 100 μm; beam current 30 μA; slit width 1–2 eV; scan speed 1.6 eV s^{-1}; magnification 30000).

by preactivation with O-(7-benzotriazol-1-yl)1,1,3,3-tetramethyluronium tetrafluoroborate (TBTU) (5 min) and addition of 4-dimethylaminopyridine (DMAP). Free hydroxymethylphenoxy linker was capped with acetic acid anhydride. Resin loading was 0.079 mmol g^{-1} TentaGel S-PHB and 0.106 mmol g^{-1} TentaGel PAP as determined spectrophotometrically from the fluorene/piperidine adduct upon Fmoc removal with 20% piperidine in DMF. Chain elongation was carried out with Fmoc-Cys(Trt)-OPfp/HOBt and twice with Fmoc-Lys(Boc)-NCA in DMF with fourfold molar excesses of acylating agents. The lysine tree was constructed by three successive couplings with fourfold molar excesses of Fmoc-Lys(Fmoc)-OH by the TBTU/HOBt/DIEA (1:1:2, DIEA = diisopropylethylamine; HOBt = 1-hydroxybenzotriazole hydrate) procedure [24]. In the case of incomplete couplings (Kaiser's test) reacylation with twofold molar excesses of acylating agents were performed. Finally, Boc-MeCBA-OH [25] was coupled to the dendrimer with HATU/DIEA (1:2, HATU = O-(7-azabenzotriazol-1-yl)-1,1,3,3-tetramethyluronium hexafluorophosphate (PerSeptive Biosystems, Wiesbaden, Germany)) [26] until Kaiser's test was negative. Compound **A** was cleaved from TentaGel S-PHB with 95% aqueous trifluoroacetic acid (TFA) and 2% triethylsilane at room temperature for 2 h, and compound **B** from TentaGel PAP with TFA containing 5% thioanisol and 1% triethylsilane at room temperature for 20 h. The resins were filtered off and the filtrates evaporated to small volumes. The peptides were isolated by precipitation with argon-saturated methyl *tert*-butyl ether/petroleum ether (2:1) (**A**) and additional lyophilization from degassed argon-saturated water (**B**). HPLC was performed on C8 Nucleosil 300; eluent: linear gradient (30 min) from a 5:95 to a 80:20 mixture of CH_3CN and 2% H_3PO_4; flow rate: 1 mL min^{-1}; detection: UV at 210 nm; R_t of **A** = 24.35 min; R_t of **B** = 21.75 min.

Received: August 29, 1995
Revised version: January 15, 1996 [Z 8345 IE]
German version: *Angew. Chem.* **1996**, *108*, 970–973

Keywords: boron compounds · dendrimers · electron microscopy · peptides · solid-phase synthesis

[1] a) M. F. Hawthorne, *Angew. Chem.* **1993**, *105*, 997–1033; *Angew. Chem. Int. Ed. Engl.* **1993**, *32*, 950–984; b) C. Morin, *Tetrahedron* **1994**, *50*, 12521–12569.
[2] F. P. Ottensmeyer, *J. Ultrastruct. Res.* **1984**, *88*, 121–134.
[3] a) F. Alam, A. H. Soloway, J. E. McGuire, R. F. Barth, W. E. Carey, D. Adams, *J. Med. Chem.* **1985**, *28*, 522–525; b) E. Mizusawa, H. L. Dahlman, S. J. Bennett, D. M. Goldenberg, M. F. Hawthorne, *Proc. Natl. Acad. Sci. USA* **1982**, *79*, 3011–3014.
[4] a) R. F. Barth, N. Mafune, F. Alam, D. M. Adams, A. H. Soloway, G. E. Makroglou, O. A. Oredipe, T. E. Blue, Z. Steplewski, *Strahlenther. Onkol.* **1989**, *165*, 142–145; b) R. F. Barth, A. Fazul, A. H. Soloway, D. M. Adams, Z. Steplewski, *Hybridoma* **1986**, *5*, 43–50.
[5] S. R. Tamat, A. Patwardhan, D. E. Moore, A. Kabral, K. Bradstock, P. Hersey, B. J. Allen, *Strahlenther. Onkol.* **1989**, *165*, 145–147.
[6] a) R. Abraham, R. Müller, D. Gabel, *Strahlenther. Onkol.* **1989**, *165*, 148–151; b) M. L. Petterson, M.-N. Courel, N. Girard, R. Abraham, D. Gabel, M. Thellier, B. Delpech, *J. Immunol. Methods* **1990**, *126*, 95–102.
[7] R. F. Barth, D. M. Adams, A. H. Soloway, F. Alam, M. V. Darby, *Bioconjugate Chem.* **1994**, *5*, 58–66.
[8] a) A. Varadarajan, M. F. Hawthorne, *Bioconjugate Chem.* **1991**, *2*, 242–253; b) R. R. Kane, R. H. Pak, M. F. Hawthorne, *J. Org. Chem.* **1993**, *58*, 991–992; c) A. Leusch, P. W. Jungblut, L. Moroder, *Synthesis* **1994**, 305–308.
[9] R. G. Denkewalter, J. Kolc, W. J. Lukasavage (Allied Corp.), US-A 4289872, **1981** [*Chem. Abstr.* **1985**, *102*, 79324q].
[10] a) T. P. Tam, *Proc. Natl. Acad. Sci. USA* **1988**, *85*, 5409–5413; b) D. N. Posnett, H. McGrath, J. P. Tam, *J. Biol. Chem.* **1988**, *263*, 1719–1725.
[11] S. M. Aharoni, C. R. Crosby, E. K. Walsh, *Macromolecules* **1982**, *15*, 1093–1098.
[12] a) M. Bendayan, R. F. Barth, D. Gingras, I. Londoño, P. T. Robinson, F. Alam, D. M. Adams, L. Mattiazi, *J. Histochem. Cytochem.* **1989**, *37*, 573–580; b) M. M. Kessels, B. Qualmann, F. Klobasa, W. D. Sierralta, *Cell Tissue Res.* **1996**, in press.
[13] a) M. Mutter, H. Oppliger, A. Zier, *Makromol. Chem. Rapid Commun.* **1992**, *13*, 151–157; b) A. Zier, D. Ryan, M. Mutter, *Tetrahedron Lett.* **1994**, *35*, 1039–1042.
[14] T. M. Chapman, G. L. Hillyer, E. J. Mahan, K. A. Shaffer, *J. Am. Chem. Soc.* **1994**, *116*, 11195–11196.
[15] a) H. Nemoto, J. Cai, Y. Yamamoto, *J. Chem. Soc. Chem. Commun.* **1994**, 577–578; b) G. R. Newkome, C. N. Moorefield, J. N. Keith, G. R. Baker, G. H. Escamilla, *Angew. Chem.* **1994**, *106*, 701–703; *Angew. Chem. Int. Ed. Engl.* **1994**, *33*, 666–668.
[16] E. Bayer, *Angew. Chem.* **1991**, *103*, 117–133; *Angew. Chem. Int. Ed. Engl.* **1991**, *30*, 113–129.
[17] S. Sjöberg, M. F. Hawthorne, P. Lindström, J. Malmquist, J. Carlsson, A. Andersson, O. Pettersson, *Advances in Neutron Capture Therapy* (Eds.: R. F. Barth, D. E. Carpenter, A. H. Soloway), Plenum, New York, **1993**, pp. 269–272.
[18] M. M. Kessels, B. Qualmann, *J. Prakt. Chem.*, **1996**, 89–91.
[19] M. Dey, J. A. Castoro, C. L. Wilkins, *Anal. Chem.* **1995**, *67*, 1575–1579.
[20] A. M. Felix, Y.-A. Lu, R. M. Campbell, *Int. J. Peptide Protein Res.* **1995**, *46*, 253–264, and references therein.
[21] B. Qualmann, M. M. Kessels, P. W. Jungblut, W. D. Sierralta, *5th European Workshop on Electron Spectroscopic Imaging, Diffraction und Analysis Techniques*, Freiburg, Germany, **1995**, Abstr. 39.
[22] B. Qualmann, M. M. Kessels, F. Klobasa, P. W. Jungblut, W. D. Sierralta, *J. Microsc.*, **1996**, in press.
[23] Fmoc-Lys(Dansyl)-OH was obtained in 96% yield by reaction of Fmoc-Lys-OH with dansyl chloride in aqueous dioxane ($NaHCO_3$ as auxilliary base) and workup by distribution between 5% $KHSO_4$ and AcOEt and precipitation with petroleum ether; homogeneous on TLC (HAc/*n*BuOH/H_2O/pyridine 29/15/6/5), R_f 0.80; ^{1}H NMR and ^{13}C NMR spectra are consistent with the structure; FAB-MS: $[M+H^+]$ = 602.1 (602.7 calcd. for $C_{33}H_{36}N_3SO_6$).
[24] R. Knorr, A. Trzeciak, W. Bannwarth, D. Gillessen, *Tetrahedron Lett.* **1989**, *30*, 1927–1930.
[25] H-L-MeCBA-OHxHCl [18] was converted into H-L-MeCBA-OH in dichloromethane with propylene oxide and isolated by crystallization from MeOH in 81% yield; homogeneous on TLC (AcOEt/*n*BuOH/HAc/H_2O 5/3/1/1; R_f = 0.6); FAB-MS: $[M+H^+]$ = cluster of peaks centered around 274.4 (274.4 calc. for $C_8H_{24}B_{10}NO_2$); the ^{1}H NMR spectrum is consistent with the assigned structure. H-L-MeCBA-OH was converted to Boc-L-MeCBA-OH by reaction with $(Boc)_2O$ in DMF (DIEA as auxilliary base). The reaction mixture was worked up by distribution between AcOEt and 5% $KHSO_4$. The organic phase was evaporated and the residue crystallized on standing in the cold; yield 95%; homogeneous on TLC (AcOEt/*n*BuOH/HAc/H_2O 5/3/1/1, R_f = 0.95), ($CHCl_3$/cyclohexane/HAc 9/9/2, R_f = 0.45); ^{1}H NMR (500 MHz, $CDCl_3$) δ = 1.4–2.8 (10H, BH), 1.47 (s, 9H, $(CH_3)_3$), 1.65–1.77 (m, 2H and 1H, γ-CH_2 and β-CH_2), 1.85–1.95 (m, 1H, β-CH_2), 2.02 (s, 3H, carb.-CH_3), 2.16–2.22 and 2.26–2.30 (2 × m, 2 × 1H, δ-CH_2), 4.31–4.38 (m, 1H, α-CH), 5.00–5.05 (d, 1H, NH); ^{13}C NMR (75 MHz, $CDCl_3$): δ = 23.18 (carb.-CH_3), 25.34 (γ-CH_2), 28.34 ($(CH_3)_3$), 32.17 (β-CH_2), 34.45 (δ-CH_2), 52.44 (α-CH), 69.77 ($C(CH_3)_3$), 74.90 and 80.56 (2 × $C_{carb.}$), 155.60 (OCN), 175.62 (COOH); FAB-MS: clusters of peaks centered around 374.7 (10%) $[M+H^+]$, 318.6 (90%) $[M - t\text{Bu} + 2H^+]$, 274.6 (65%) $[M - \text{Boc} + 2H^+]$ and 228.5 (40%) $[M - (\text{Boc and } CO_2) + 2H^+]$; $[M+H^+]$ 374.7 calcd. for $C_{13}H_{32}O_4NB_{10}$.
[26] L. A. Carpino, *J. Am. Chem. Soc.* **1993**, *115*, 4397–4398.

Shocking Colors

Electrochromism. Fundamentals and Applications. By *P. M. S. Monk, R. J. Mortimer* and *D. R. Rosseinsky*. VCH Verlagsgesellschaft, Weinheim, 1995. 216 pp., hardcover DM 168.00.— ISBN 3-527-29063-X

When a compound has two or more redox states with different absorption spectra in the visible region, a color change occurs on oxidation or reduction. The color can be switched by electron transfer, and this behavior is known as electrochromism. This general definition serves as the starting point for the treatment of electrochromic phenomena by Monk, Mortimer and Rosseinsky, three British physical chemists. The task that they address is multifaceted and demanding. On the one hand they aim to establish the fundamentals that enable the reader to understand the striking electrochromic phenomena observed and to interpret the results of spectroscopic and electrochemical experiments on electrochromic compounds, while on the other hand they set out to describe and explain existing or potential technological applications. The book is intended both for those already working in the area and for newcomers. Furthermore, the authors have set out not only to look at the topic from a chemical standpoint but also to serve the needs of physicists, materials scientists, and engineers. Despite having deliberately restricted the literature coverage (the 12 chapters contain slightly over a thousand references), it is almost inevitable that the attempt to fulfill these aims in a book of 200 or so pages encounters problems.

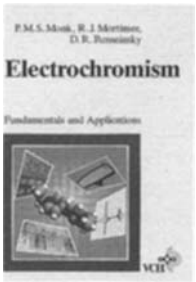

The book is divided into three main parts dealing in turn with the fundamentals, existing applications (electrochromic devices, ECDs), and interesting current work and future developments. Part I ("Introduction") consists of three chapters. First the concept of electrochromism is defined, and its capabilities are compared with those of other related technologies (LCDs, LEDs, etc.), taking as an example the application in a commercial device, an "intelligent" rear-view mirror for cars. Another potential application in the same area is also mentioned: a "smart window". Chapter 1 concludes with various definitions relating to the chemistry, physics, and applications of electrochromic devices.

Chapter 2 contains an introduction to the elementary processes that occur in electrochemical reactions and form the basis of electrochromism. Beginning with a description of the galvanic cell the authors develop the concept of the potential (however, on p. 25 they describe the use of the silver wire pseudo-reference electrode, which in my opinion should be avoided, whereas they ignore reference systems such as that based on ferrocene/ferricinium ion). Voltammetry is then discussed, enabling the potential to be related to the dynamics, kinetics, and charge-transfer processes at an electrode surface. Electrochromic materials are then classified according to the solubilities of the different redox states. The sign convention generally used for the potential in electrochemistry is not simple, but the authors do not exactly clarify it by choosing an example which they themselves describe as "an unusual use, even an abuse". It is, of course, important that the potential E of the working electrode in a voltammetry cell must be related to a reference electrode, but the same does not apply to the voltage increase rate dE/dt (p. 29). It would have been useful to extend the discussion of cyclic voltammograms to include not only dissolved but also adsorbed species, since redox-active particles on the electrode surface play an important role in the later parts of the book. On the whole this chapter seems to be the least successful.

Chapter 3 briefly describes the essential principles and components of an electrochromic device (ECD), including the arrangement of the electrodes, the electrolyte, and the production of electrochromic films. The development of the principles into a practical system is discussed, taking the rear-view mirror mentioned earlier as an example.

Part II ("Electrochromic Systems") consists of seven chapters in which the authors present a survey of the most important classes of substances whose electrochromic properties have been or are being investigated: metal oxides, phthalocyanines, Prussian blue and related compounds, bipyridylium systems, electroactive conducting organic polymers, and various other inorganic and organic materials. These are treated in the style of a review article, with numerous literature references (which according to the preface cover publications up to late summer, 1994). For reasons of space alone many of the results can receive no more than a brief mention. Nevertheless, the authors have managed to provide the reader with a good impression of the enormous variety of electrochromic systems (for example, every optical "redox indicator" is in principle an electrochromic substance, as pointed out on p. 122). Throughout this there are frequent references to the problems in developing such systems into practical ECDs and ways in which these might be solved. Where necessary, references to publications containing contradictory views are juxtaposed, but only rarely are such results critically evaluated. The authors do not conceal the fact that for many of the reaction mechanisms described the details are not yet thoroughly understood, or that many unanswered questions remain with regard to applications.

Part III ("Elaborations") concludes the book with two chapters on polyelectrochromic systems (those with more than two colors) and on photoelectrochromism (where the electrochemical reaction occurs only under the action of light). These discussions also bring in possible future applications, such as electrochromic four-color printing.

This section contains book reviews and a list of new books received by the editor. Book reviews are written by invitation from the editor. Suggestions for books to be reviewed and for book reviewers are welcome. Publishers should send brochures or (better) books to Dr. Illenora Beckmann, Redaktion Angewandte Chemie, Postfach 101161, D-69451 Weinheim, Federal Republic of Germany. The editor reserves the right of selecting which books will be reviewed. Uninvited books not chosen for review will not be returned.

I found relatively few printing errors (examples: on p. XXII the correct abbreviation for the supporting electrolyte tetra-*n*-butylammonium perchlorate is TBAP, not "TPAP"; on p. 28, line 11, and p. 32, line 8, the brackets are incorrectly printed; on p. 31 "Sevcik" should be Ševčic; in Equation (8.1) "+." appears as a superscript; on p. 176, first line of Section 10.1.4, "Würster salts" should be Wurster salts). Here and there it appears that bits of a sentence have been lost, as in "...have performed ellipsometric studies the proton injection into... films..." (p. 64, 11th line from bottom), and in "...thiophene units are chemically bonded rather than by physically mixed" (p. 163, bottom line). In Figure 9.1 some symbols in the margin have been cut off, and on page 177 the formula shows a pyrazole derivative instead of a pyrazoline. A few other inaccuracies or minor faults are the following: in the list of abbreviations it would have been better to keep the entries in strictly alphabetical order (bottom of p. XXII and top of p. XXIII); in the discussion of cyclic voltammograms (p. 32) the term "reversibility" should not be confused with "superimposability"; the unit of the standard exchange current i_0 (pp. 32/33) is given as $\mu A cm^{-2}$, but this unit applies instead to the current *density*; the technique of chronoamperometry mentioned in Table 2.1 is not explained; in Figure 6.1 the potential is given relative to an "SSCE" reference electrode but this is not explained; Figure 8.4 is not referred to in the text; in Section 8.4.2 under the title "Pulsed Potentials" the experiments described instead use "pulses of current"; aniline derivatives (p. 143) are, of course, not heterocyclic compounds, and *o*-toluidine (p. 147) is not an *N*-substituted aniline; Table 9.11 does not give the dihedral angle on which the absorption maximum and the oxidation potential are said to depend.

As to whether this book is suitable for "anyone wishing to enter the field" (consider the targeted readership!), I have to admit to some doubts. To meet the needs of beginners some revision of the foundation chapters in Part I would certainly be necessary, and in Part II the literature would have to be more critically evaluated and classified. On the other hand, the scientist already engaged in work on electrochromic systems, whether in basic research or in applications, will overlook these flaws and the minor errors mentioned above. The latter reader will find in Part II a rich source of references to advanced work.

Bernd Speiser
Institut für Organische Chemie
der Universität Tübingen (Germany)

Chemical Kinetics of Solids. By *H. Schmalzried.* VCH Verlagsgesellschaft, Weinheim, 1995. 433 pp., hardcover DM 298.00.—ISBN 3-527-29094-X

In this latest book H. Schmalzried, author of the successful *Solid State Reactions* (which went to three editions), updates the treatment by including the developments that have taken place in solid state kinetics in recent years. These include important advances in the use of in-situ methods of investigation, an increasing emphasis on the importance of materials science, and a growth in chemists' awareness of the formal theory of nonequilibrium systems and its applications. The author's objective is to give a systematic account of the many different types of solid state processes, and therefore the emphasis is on deriving and explaining the physicochemical concepts, illustrated by appropriate limiting cases, rather than describing a large number of complex reactions. He adopts a phenomenological approach; readers interested in the underlying statistical theory are referred to the relevant literature.

The book can be broadly divided into three parts. The first five chapters present the fundamentals. An introduction is followed by a phenomenological description of the thermodynamics of point defects, taking into account the special characteristics of the crystalline phase with the restrictions imposed on it through the introduction of structure elements (in particular the irregular structure elements of vacant sites and interstitial atoms). Here the author also introduces the chemical potential of the structure elements according to the Schottky model. The special conditions for crystal growth and transport at dislocations and grain boundaries are then described, followed by the fundamentals of irreversible thermodynamics, diffusion, transport in ionic crystals and across phase boundaries, and rate equations for homogeneous reactions. Next the author discusses the relationship between kinetics and dynamics, including the basic essentials of linear response theory, of the transition state, and of the Brownian motion. Here it becomes evident that one should not mistake the work for a textbook; for example, the treatment of irreversible thermodynamics in only three pages can do no more than direct the novice to read up on the subject more fully elsewhere.

The second part consists of ten chapters dealing on the one hand with classical cases of heterogeneous reactions and on the other hand with modern aspects of solid state kinetics. Chapters 6 and 7 treat cases in which the formation of the reaction products increases the spatial separation between the reactants, as for example in the oxidation of metals. Chapter 8 is concerned with solids in a thermodynamic potential gradient, and Chapter 9 with internal reactions. Chapters 10–12 are concerned with reactions at and through phase boundaries, morphology, and phase transformations. Chapter 13 discusses solid state reactions occurring in the presence of radiation, which are important in photographic processes and in the design of nuclear reactors, for example. Chapter 14 deals with the special features of solid state reactions occurring under mechanical stress, and Chapter 15 with the kinetics of certain special solids (silicates, fast ionic conductors, hydrides, layer crystals, polymers).

Finally, Chapter 16 forms an appendix giving an overview of in-situ methods for studying the kinetics of solid state reactions. Here the author addresses the fundamental problem that many of the processes determining the kinetics of the solid state occur at quite high temperatures, whereas measurements are generally carried out ex-situ, i.e., after quenching. The quenching inevitably alters the condition of the system, often introducing a certain amount of ambiguity into the results. Here Schmalzried gives a (brief) description of the capabilities of modern in-situ methods, thereby helping to stimulate their wider use and further development. The list includes thermodynamic methods (thermogravimetry, thermomanometry, thermovolumetry, thermal analysis), electrochemical methods (time- and space-resolved measurements of chemical potentials using miniaturized galvanic cells), nuclear spectroscopic methods (NMR, Mössbauer), electron spectroscopy (UV, VIS, IR, X-ray), and neutron diffraction and scattering. However, rather than giving a detailed introduction to these experimental techniques the author describes examples to show how they can be used for in-situ measurements.

In *Chemical Kinetics in Solids* one is impressed by the breadth of coverage of all relevant aspects of the kinetics of solid state reactions, illustrated by instructive examples (which, as expected, reflect the author's areas of interest to some extent). The length has almost doubled compared with that of *Solid State Reactions*, but nevertheless the treatment remains very succinct and demands thorough concentration from the reader. For the interested newcomer the book offers an excellent insight into the field, with up-to-date lists of references at the ends of the individual

 © VCH Verlagsgesellschaft mbH, D-69451 Weinheim, 1996 0570-0833/96/3508-0914 $ 15.00+.25/0

chapters and a well-prepared index, while for the scientist already working in solid state kinetics it is likely to become the standard work of reference.

Dirk Wilmer
Institut für Physikalische Chemie
der Universität Münster (Germany)

Monosaccharides. Their Chemistry and their Roles in Natural Products. By *P. M. Collins* and *R. J. Ferrier*. Wiley, Chichester, 1995. 574 pp., paperback £ 22.50.—ISBN 0-471-95343-1

The forerunner of this book was published by Penguin Books Ltd. (Harmondsworth, Great Britain) under the title *Monosaccharide Chemistry*. After a long interval the authors have now brought out this up-to-date monograph on the chemistry of monosaccharides, enlarged to include the whole area of carbohydrates. It is not intended solely for specialists in the field of monosaccharides, but is designed to have a broader appeal to everyone concerned with organic chemistry. Thus, the authors rightly point out that "parts of the book can be looked on as portrayals of modern general organic chemistry with monosaccharides as model systems". To support this they describe the development of carbohydrates chemistry since the 1970s, to which not only carbohydrates chemists but also "mainstream organic chemists" have made fundamental contributions.

A short introduction, in which the authors discuss the contributions made by E. Fischer, Haworth, Hudson and Lemieux to carbohydrates chemistry, is followed by a second chapter of 50 pages dealing with the structural aspects of monosaccharides and their biosynthesis. Although this is intended primarily for chemists about to begin serious work in the field for the first time, it also serves as a useful "refresher course" for those already experienced in carbohydrates chemistry. Chapter 3 then discusses the reactions occurring at the anomeric center of aldoses and ketoses, subdivided into the reactions of free sugars, glycosyl esters, and *O*-protected glycosyl halides. Chapter 4 is concerned with reactions at non-anomeric carbon atoms, beginning with nucleophilic substitutions and ring-opening reactions of oxiranes, followed by the synthesis and reactions of deoxy-, aminodeoxy-, thio-, and deoxyhalogen-sugars. This chapter also covers the chemistry of anhydro-sugars, ring contractions of monosaccharides, branched sugars, dicarbonyl compounds and unsaturated sugars (glycals, 6-deoxy-5-enopyranoses, and "isolated alkenes", i.e. monosaccharides with double bonds at other positions). Chapter 5 is concerned with reactions of the hydroxy groups and the resulting products. First the different reactive properties of the anomeric, primary, and secondary OH groups are described. Other topics discussed here are the kinetic anomeric effect and the selective substitution of hydroxy groups using organotin compounds. The reaction products are classified as ethers, esters (with sub-sections on enzymatic acylation and deacylation reactions, orthoesters, carbonates and their derivatives, sulfonates, chlorosulfonates, sulfites, phosphates, nitrates, borates, boronates, and borinates), and acetals. This chapter ends with a detailed discussion of glycol cleavage. Two chapters cover topics that one would perhaps not expect from the book's title. Chapter 6 deals with the synthesis, structures, and biological functions of oligosaccharides. These are then considered from a different standpoint in Chapter 8 on natural products, which also covers polysaccharides, glycoproteins, proteoglycans, glycolipids, other glycosides (including also nucleosides and their analogs together with nucleotides and nucleic acids), and cyclitols. Chapter 7 describes syntheses of enantiomerically pure "non-carbohydrates" from monosaccharides, with some well-chosen examples (methods using carbohydrates as chiral auxiliaries, and conversion of carbohydrates into other products). The appendix includes a concise survey of the literature on monosaccharides and a very brief note on nomenclature rules, referring to D. Horton's *Tentative Rules for Carbohydrate Nomenclature, Part I*, originally published in 1969 and now superseded by a revised edition (1995). Also included here is a list of trivial names of sugar derivatives, mainly of microbiological origin, and some ^{1}H and ^{13}C NMR data for monosaccharides and their peracetates.

Notable features of the book are the detailed discussions of reaction mechanisms (that of the Ferrier reaction provides a fitting illustration for the dust-cover) and of the unique aspects of the reactions of monosaccharides that result from their structures. In their presentation of structural formulas the authors have unfortunately been more concerned with "economy" than with esthetic quality. Also they have been very sparing in mentioning researchers' names in the text; for example, in Chapter 6.6 on the synthesis of oligosaccharides one would at least have expected a mention of H. Paulsen. This very convenient book contains over a thousand literature citations extending up to 1993, and although these unfortunately do not include authors' names they ensure that it is a valuable reference source. Because of the excellent layout and reasonable price it can also be thoroughly recommended as a student textbook.

Klaus Peseke
Fachbereich Chemie
der Universität Rostock (Germany)

 © *VCH Verlagsgesellschaft mbH, D-69451 Weinheim, 1996* *0570-0833/96/3508-0915 $ 15.00+.25/0*

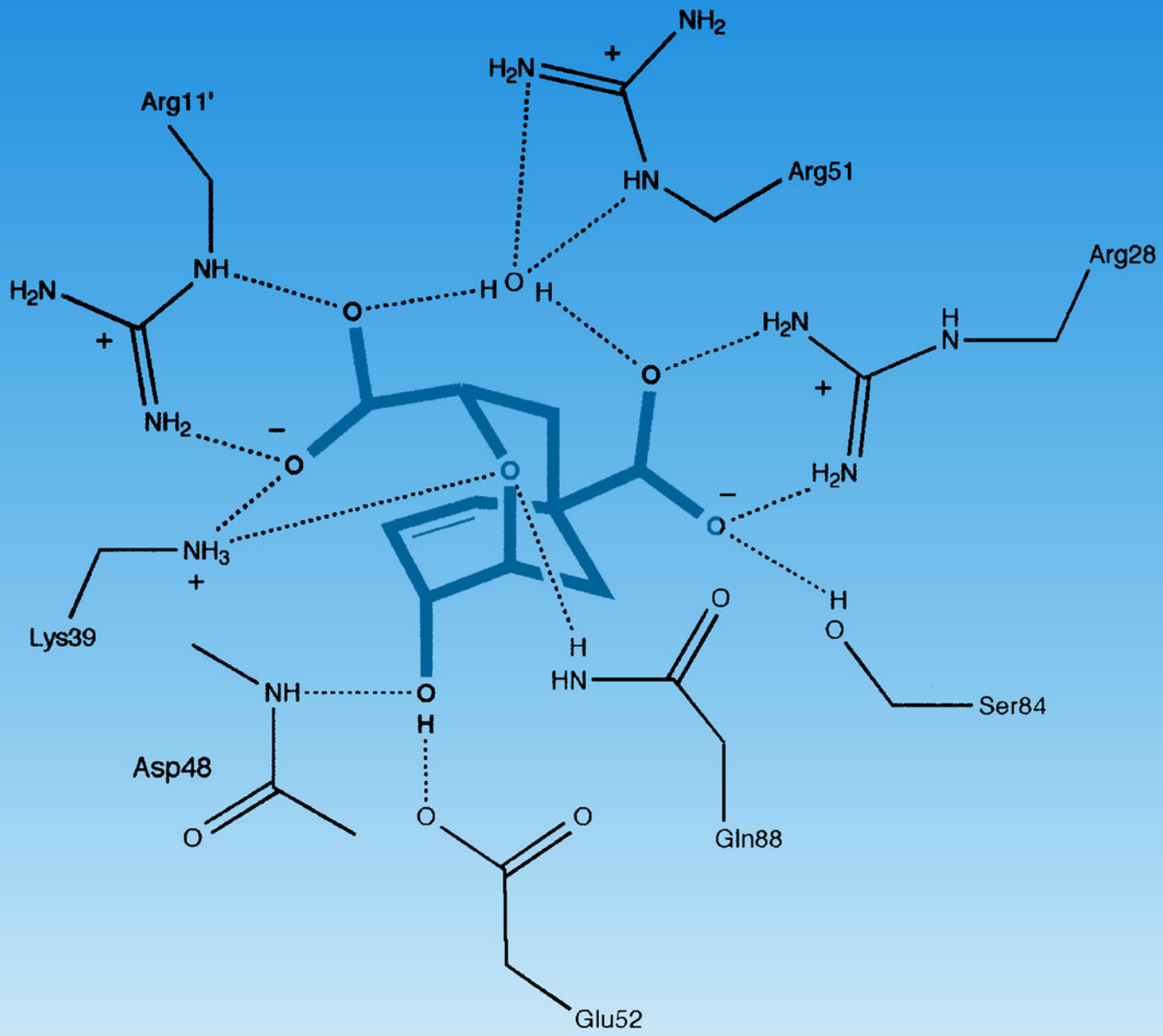

What significance the binding of a substrate molecule (dark blue) to the active site of chorimate mutase has for the mechanism of the Claisen rearrangement is reported by Bruce Ganem.

The Mechanism of the Claisen Rearrangement: Déjà Vu All Over Again

Bruce Ganem*

The great baseball player Yogi Berra, who is quoted in the title, succinctly described what it meant to learn something that others had long ago appreciated. The mechanism by which the enzyme chorismate mutase accelerates the Claisen rearrangement of chorismic acid has for many years perplexed and intrigued chemists and biochemists. Yet classical effects of solvents and catalysts, which were largely ignored by the chemical community, not only provided important clues about the mechanism of the enzyme, but put the Claisen rearrangement in a new perspective. Whereas chorismic acid once seemed exceptional because it rearranged so rapidly under physiological conditions, it is now clear that even allyl vinyl ether rearranges at room temperature in aqueous solution. While the ability of the enzyme to accelerate the rearrangement of chorismate by a factor of 10^6 was once considered extraordinary, catalysis by trivalent aluminum compounds matches, and in some cases exceeds, those rate enhancements. Therefore, it really should not be surprising to learn that Nature has independently evolved several structurally distinct solutions to the design of enzyme catalysts for the rearrangement of chorismic acid.

Keywords: allyl vinyl ethers · Claisen rearrangement · enzymatic catalysis · rearrangements

1. Introduction

The Claisen rearrangement of allyl vinyl ethers, which was first described in 1912, is the earliest recorded example of a [3,3]-sigmatropic reaction.[1] In its simplest form, the rearrangement is exemplified by the transformation of allyl vinyl ether **1** to 4-pentenal **2** (Scheme 1).[2] Together with its all-carbon counterpart, the Cope rearrangement, these two reactions are pericyclic processes in which, by definition, bond breaking and bond making occur through a cyclic array of interacting orbitals. With their highly ordered transition states, the Claisen and Cope rearrangements are especially useful in creating and controlling new stereocenters. Because the Claisen rearrangement also generates a new carbonyl group, it has become one of the most widely used methods of stereoselective C–C bond formation in synthetic chemistry. Several elegant transformations such as the Johnson orthoester,[3] Eschenmoser amide acetal,[4] and Ireland ester enolate[5] rearrangements rely on the [3,3]-sigmatropic rearrangement of substituted allyl vinyl ethers and variants thereof.

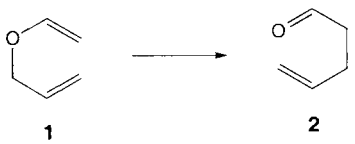

1 **2**

Scheme 1. Claisen rearrangement of allyl vinyl ether **1** to 4-pentenal **2**.

The Claisen rearrangement also enjoys the distinction of being the only example of a pericyclic reaction observed in primary metabolism. Moreover, this biological Claisen is subject to enzyme catalysis.[6] The chorismate ion **3** (Scheme 2), the free acid of which is a key intermediate in the shikimic acid pathway, undergoes a Claisen rearrangement leading to the prephenate ion **4**, the free acid of which is an intermediate in the biosynthesis of phenylalanine and tyrosine. The enzyme chorismate mutase, which is found widely in bacteria, fungi, and plants, catalyzes the rearrangement of **3** to **4** by more than a millionfold.[7, 8]

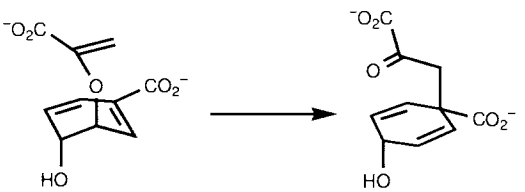

3 **4**

Scheme 2. Claisen rearrangement of the chorismate ion **3** to the prephenate ion **4**.

It is this apparently unique ability to accelerate a pericyclic reaction that has made chorismate mutases so interesting. Pericyclic processes are thought to proceed by concerted reaction

[*] Prof. B. Ganem
Department of Chemistry
Baker Laboratory, Cornell University
Ithaca, NY 14853-1301 (USA)
Fax: Int. code +(607)255-6318
e-mail: bg18@cornell.edu

mechanisms. with simultaneous, but not necessarily synchronous, bond making and bond breaking.[9] While the bonds undergoing chemical change might not necessarily be broken or formed to the same extent at every stage along the reaction coordinate, the changes must occur together in a single kinetic step, and there can be no discrete intermediates. For that reason, pericyclic reactions have always been elusive to study by the usual tools of mechanistic chemists. Interest in chorismate mutases has thus been fueled by the notion that somehow Nature may have gleaned, through evolution, important insights into the rearrangements of allyl vinyl ethers that have otherwise eluded chemists.

In fact, however, the history of research on the aliphatic Claisen rearrangement over the past eighty-odd years has been replete with provocative clues to the mechanism. Appreciable solvent effects and significant levels of catalysis have been reported, although until very recently, these important chemical insights went largely unnoticed in inquiries into the mechanism. The solid-state structure determinations of chorismate mutases from *Bacillus subtilis* (BsCM)[10] and *Escherichia coli* (EcCM)[11] have been instrumental in bringing this area of chemistry into sharper focus.[12]

2. Background

To appreciate the evolution of current thinking about the mechanism of the aliphatic Claisen rearrangement, about the rearrangement of chorismate to prephenate ions, and about the properties of chorismate mutase, some historical background is important. In particular, it is worth reviewing what mechanistic features of pericyclic processes distinguish them from their polar or radical counterparts.

2.1. Sigmatropic Rearrangements

The Claisen rearrangement is a classic example of a [3,3]-sigmatropic rearrangement, one of five categories of pericyclic processes defined by Woodward and Hoffmann.[13] The [3,3]-sigmatropic rearrangement of allyl vinyl ether occurs with a negative activation entropy[14, 15] and negative activation volume.[16] The reaction displays first-order kinetics,[14, 15] and no crossover products are observed.[17] The bond reorganization leading to **2** proceeds through a chair (or chairlike) transition state of contiguous p orbitals,[18, 19] and the stereochemical course of rearrangement is consistent with orbital symmetry rules.

The same hallmarks of a [3,3]-sigmatropic reaction have been noted in the nonenzymatic rearrangement of chorismate ions, including negative activation entropy,[7] first-order kinetics, and chair transition state geometry.[20] Interestingly, the inherent (i. e. uncatalyzed) rate of rearrangement of **3** (H_2O, 75 °C, pH 5) is about 4200 times as fast as that of allyl vinyl ether in dibutyl ether at the same temperature.[21] The mutase-catalyzed rearrangement of chorismate ions also proceeds with a transition state of chairlike geometry,[22] but the entropy of activation in the mutase-assisted process is nearly zero,[8] suggesting that the conformation of the substrate is severely restricted in the enzyme–substrate (E–S) complex.[23] This conformational control undoubtedly contributes to the observed catalysis. The enzyme also lowers the activation enthalpy of rearrangement by about 5 kcal mol^{-1}, which indicates that the protein plays some additional role in catalysis (vide infra).

2.2. Concerted Rearrangements

The Claisen rearrangement is generally regarded as a concerted, but asynchronous, pericyclic process.[9] Secondary deuterium kinetic isotope effects (KIEs) reported by Gajewski on the parent, allyl vinyl ether **1**, indicate that C–O bond breaking proceeds somewhat ahead of C–C bond making, as might be expected in a diradical transition state like **5** (Scheme 3).[24]

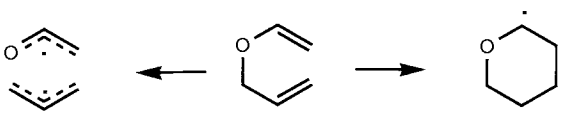

5 **1** **6**

Scheme 3. Diradical transition state **5** and diyl transition state **6** for the Claisen rearrangement of allyl vinyl ether **1**.

Bruce Ganem earned a BA degree in chemistry from Harvard College in 1969. In 1972 he received his PhD degree in organic chemistry at Columbia University, then served as a National Institutes of Health Postdoctoral Fellow at Stanford University before joining the faculty of the Department of Chemistry at Cornell in 1974. His broad scientific interests lie at the emerging interfaces of organic and biological chemistry with biochemistry, biotechnology, and molecular medicine. He has held numerous lectureships around the world, and is the author of over 180 scientific papers as well as numerous popular articles about science and science education. He has also served on the advisory or editorial boards of several professional journals.
Profesor Ganem has been the recipient of both A. P. Sloan and J. S. Guggenheim Foundation Fellowships. His awards include the Camille and Henry Dreyfus Teacher–Scholar Award, an Eli Lilly Young Scientist Award, the American Cyanamid Award for the Advancement of the Art and Science of Chemical Synthesis, the Clark Distinguished Teaching Award at Cornell, and the 1996 Arthur C. Cope Scholar Award of the American Chemical Society. He is a member of the Scientific Advisory Board of LeukoSite, and has served as a consultant for American Cyanamid, Cambridge Neurosciences, Cordis Corporation, Ciba-Geigy, Exxon Chemical, Genencor International, Magainin Pharmaceuticals, Parke-Davis Pharmaceuticals, Purdue Pharma, the Teltech Resource Network, and Union Carbide Corporation.

Based on MNDO/3 calculations, however, Dewar has argued that C–C bond formation is more advanced than C–O cleavage, which implies more diyl character (e. g. **6**) in the transition state.[25] Recent ab initio calculations at the MP2/6-31G level indicate a transition structure with appreciable C–O bond breaking (as observed experimentally by Gajewski), but markedly different from Dewar's MNDO calculation.[26]

The nonenzymatic rearrangement of chorismate ions is also a concerted asynchronous rearrangement.[27] Secondary tritium isotope effects using both C5 and C9 double-labeled **3** indicate an asymmetric transition state in which C–O bond breaking is substantially more advanced than C–C bond making. Several ab initio calculations of the uncatalyzed transition structure have been reported,[7, 28] of which the most recent[29] best rationalizes the experimentally observed asychronous bond breaking. An experimental study of kinetic isotope effects on the enzymatic reaction was less revealing: no isotope effect was observed in the mutase-catalyzed rearrangement of C5/C9-labeled **3**.[27] Nevertheless, the catalyzed and uncatalyzed processes might still involve similar mechanisms, since isotope effects on an enzyme-promoted pericyclic process could be masked by some other, earlier, rate-limiting event.

2.3. Solvent and Catalyst Effects

While not an axiom of pericyclic reaction theory, it is generally true that pericyclic processes are, in contrast to most polar and radical reactions, relatively insensitive to solvent.[30, 31] For example, the Cope rearrangement of 1,5-dienes is not influenced by changes in solvent polarity.[32, 33] Also as a consequence of their concertedness, pericyclic reactions are usually not catalyzed by acids, bases, or other agents. Nevertheless, there are exceptions. Certain 1,5-dienes do undergo Cope rearrangement with catalysis by transition metal species.[34, 35] However, the catalyzed processes likely involve transient cyclohexylmetal cations[36] or bis-π-allylmetal complexes,[37] and are thus no longer concerted.[38]

The aliphatic Claisen rearrangement seems to differ from conventional pericyclic processes in its long history of sensitivity to solvents and catalysts. Indeed, both solvent effects and catalysis are more the rule than the exception in Claisen systems. Yet chemists have been reluctant to acknowledge these well-documented reports, perhaps because solvent and catalyst effects seem inconsistent with the mechanistic lore of pericyclic processes. How catalysts might accelerate even the simplest Claisen rearrangements is not known, and the effect of catalysis on reaction mechanism remains poorly understood.[38] At the same time, it should be noted that no evidence has been presented which suggests that accelerated Claisen rearrangements represent anything other than true pericyclic reactions.[39]

This review examines the effect of solvents on the rearrangement of **1** and other aliphatic Claisen systems, including the nonenzymatic rearrangement of chorismate. Known examples of catalysis of aliphatic Claisen rearrangements are also considered. In the case of biological systems, the catalytic sites of two known chorismate mutases are reviewed, as elucidated by recent X-ray diffraction studies on BsCM and EcCM. The clear commonalities that emerge provide the framework for a consistent, coherent mechanistic rationale of solvent and catalyst effects on the aliphatic Claisen rearrangement.

3. Discussion

3.1. Solvent Effects on Claisen Rearrangement Rates

The earliest indications of solvent effects in Claisen processes, detected in allyl aryl ethers almost sixty years ago, set an important precedent for the influence of solvent on aliphatic rearrangements. Kincaid and Tarbell[40] investigated the rearrangement of allyl p-tolyl ether **7** to 2-allyl-4-methyl phenol **8** (Scheme 4). The rate was found to increase with time as concen-

7 8

Scheme 4. Claisen rearrangement of allyl *p*-tolyl ether **7** to 2-allyl-4-methyl phenol **8**.

trations of phenol **8** increased. Measured in separate experiments, the rearrangement of **7** in a 4:1 mixture of **8**:**7** was four times faster than that in neat **7**. Such autocatalysis is not observed in aliphatic Claisen systems because the enol tautomer of the initally formed carbonyl compound is a minor component at equilibrium. To test for simple acid catalysis, both acetic and chloroacetic acids were added; however, no rate enhancements were detected.

In 1958, White et al. measured rate constants for the rearrangement of **7** at 181 °C in five different solvents (Table 1, column 1) and observed a distinct acceleration in solvents of higher polarity.[41] Although no mechanistic rationale was presented, the authors noted that the sevenfold rate difference was comparable in magnitude to that observed in a well-known polar reaction: the N-alkylation of tertiary amines with methyl iodide (Menschutkin reaction) run in benzene/nitrobenzene mixtures.

Appearing jointly with the report by White et al. was an independent study by Goering and Jacobson in which rate constants for the rearrangement of **7** were measured in twelve solvents at 184 °C (Table 1, column 2). A significant solvent effect was observed, with the rearrangement of **7** some 30 times faster in phenol than in decalin.[42] The more rapid rates in hydroxylic solvents led Goering and Jacobson to suggest, for the first time, a correlation with the solvent's hydrogen bonding ability. That idea, though challenged, ultimately provided an important clue to solvent effects in aliphatic Claisen rearrangements.

Twelve years later, the concept that solvents influenced the rate of Claisen rearrangements had still not gained wide acceptance in the chemical community, as was evident from this introduction to a 1970 study by White and Wolfarth:[43]

"The Claisen rearrangement has often been cited as a reaction insensitive to solvent effects, in spite of the fact that early studies indicated that this was probably not so."

Table 1. Influence of the solvent on the rate constants k of the Claisen rearrangement of allyl p-tolyl ether **7**.

Solvent	k [10^5 s^{-1}][41] $T = 181.1 \pm 0.1$ °C	k [10^5 s^{-1}][42] $T = 184.45$ °C	k [10^6 s^{-1}][43] $T = 170$ °C
none (gas phase)			1.01
n-octane	0.80		
tetradecane			3.01
decalin		1.56 ± 0.01	
di-*n*-butyl ether			3.27
n-decylamine			4.52
diethylene glycol diethyl ether			5.33
diphenyl ether		2.08 ± 0.01	
diphenylmethane		2.12 ± 0.02	
acetophenone		2.41 ± 0.12	
propylene carbonate			9.42
2-octanol			9.65
adiponitrile	2.47		10.5
methyl salicylate		2.45 ± 0.01	
N,*N*-dimethylaniline		2.46 ± 0.04	
benzonitrile		2.49 ± 0.03	
sulfolane			10.7
1-decanol			11.1
tetrahydrothiophene dioxide	3.14		
diethylene glycol monoethyl ether	4.39	3.6 ± 0.3	17.9
diethylene glycol monoethyl ether + 10% LiCl	5.96		
1-octanol		9 ± 2	
octanoic acid			24.2
2-aminoethanol			27.1
benzyl alcohol		9.7 ± 1	
ethylene glycol		18 ± 1	67.3
p-cresol			73.1
phenol		45 ± 1	103
ethanol/water (28.5%)			107
p-chlorophenol			303

White and Wolfarth examined the rearrangement of **7** to **8** at 170 °C both in the gas phase and in 17 solvents of different polarities (Table 1, column 3). A substantial solvent effect leading to a 300-fold variation in rate was observed, with rates generally faster in hydrogen bonding solvents, as had been noted by Goering and Jacobson.[42]

In addition to solvent effects, both the White and Goering groups found that *para*-substituents influenced the rate of allyl phenyl ether rearrangements (Table 2). Twentyfold differences

Table 2. Rate constants k [$10^6 s^{-1}$] for the rearrangement of *para*-substituted allyl phenyl ethers at $T = 181$ °C [46].

Solvent	Substituents in *para* position			
	NO_2	Br	CH_3	OCH_3
tetradecane	2.34	5.98	7.94	28.3
diethylene glycol monoethyl ether	10.3	27.7	44.2	91.6
ethanol/water (28.5%)	90.9	134	233	621

in rate were noted, with electron-donating groups (OCH_3, NH_2) being moderately accelerating and electron-withdrawing groups (NO_2, CN) mildly retarding. Substituent effects on the rates of aliphatic Claisen[2b] and Cope rearrangements[44] have also been observed. Because the effects of substituents in aliphatic and aromatic systems were sometimes contradictory, they have generated much discussion and debate.

It is now evident that the *apparent* effects of substituents in aromatic systems may result from competing phenomena that greatly complicate direct comparisons with corresponding aliphatic systems. First, as has already been noted, aromatic Claisen systems produce phenols that can catalyze the [3,3]-sigmatropic step,[40] thus making every rearrangement subject to a solvent effect. Since *para*-substituents also influence phenolic acidities, the solvent effect is further obscured. Moreover, as Brønsted acids, these phenols would likely also catalyze enolization of the intermediate cyclohexadienone, and it remains unclear whether rearrangement or tautomerization is rate determining in the various solvents studied.

These same substituent effects likely also complicate the interpretation of solvent effects. Although rearrangement rates listed in Table 1 were generally faster in hydrogen bonding solvents, White and Wolfarth maintained that if hydrogen bonding were important, a correlation should be seen between rate accelerations and solvent acid dissociation constants. Yet the rearrangement of **7** in octanoic acid was slower than in *p*-chlorophenol, and rates in aqueous ethanol and in phenol were comparable. Instead, White and Wolfarth found a reasonably good correlation, which they favored in their paper, between rate and solvent polarity, as measured by Kosower's Z-factors.[45]

It should be noted that neither pK_a values nor solvent Z-factors measured at ambient temperature can easily be extrapolated to 170 °C, the temperature at which the kinetic experiments were performed. Thus, even a semiquantitative treatment of the data in Table 1 is not very reliable. Moreover, the fact that a given substituent's effect can vary from 22- to 39-fold in different solvents[46] is more than sufficient to rationalize some of the inconsistencies in the simple hydrogen-bonding model first proposed by Goering and Jacobson.[42] Only the Goering–Jacobson model explains the autocatalysis that Kincaid and Tarbell observed in rearrangements of **7**.

In 1987, the first solvent effects on aliphatic Claisen rearrangements were described in two independent publications. While there was unanimous agreement about the experimental observations, their mechanistic significance has remained open to debate.

Groups at the University of Illinois, Urbana, (Coates) and the University of Pittsburgh, (Curran) collaborated to study the effect of alkoxy substituents on aliphatic Claisen rearrangements,[47] while groups at Indiana University, Bloomington, (Gajewski) and Cornell University, Ithaca, (Carpenter, Ganem) investigated the nonenzymatic Claisen rearrangement of chorismate **3**.[48] Both groups of researchers compared the effect of solvent on the rearrangement of allyl vinyl ether (Table 3, columns 2, 3). While the Illinois/Pittsburgh team found only a modest difference between benzene and methanol, the Cornell groups measured a nearly sixtyfold rate enhancement going from dibutyl ether to 2:1 methanol:water.

Data on four other substituted acyclic allyl vinyl ethers **9**–**12** (Scheme 5) taken from both publications revealed similar solvent effects (Table 3, columns 4–7). For example, two methoxy-substituted allyl vinyl ethers, **9** and **11**, rearranged 18- and 68-fold faster, respectively, in methanol than in benzene. More extensive relative rate data on **12** collected by the Cornell groups displayed a good correlation with Dimroth's solvent E_T values[49] (Table 3, columns 1, 7), just as White and Wolfarth had concluded using a different measure of solvent polarity in the earlier aromatic Claisen studies. This trend was interpreted by

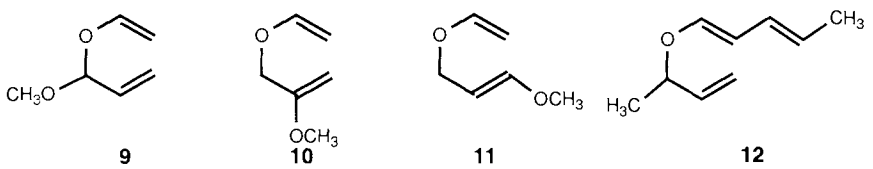

9 **10** **11** **12**

Scheme 5. Substituted acyclic allyl vinyl ethers **9**–**12**; rate constants for their rearrangements are presented in Table 3.

Table 3. Influence of the solvent on the rate constants k of the rearrangement of **1** and substituted allyl vinyl ethers [47,48].

Solvent	E_T-value [48]	**1** [47]	**1** [48]	**9** [47]	**10** [47]	**11** [47]	**12** [48]
cyclohexane	30.9						1.000
dibutyl ether	33.4		1.000				
C_6D_6	34.5	1.000		1.000	1.000	1.000	2.6 (C_6H_6)
diethyl ether	34.6						1.3
CH_3COCH_3	42.2		1.4			1.5 [D_6]acetone	3.3
CH_3SOCH_3	45.0						5.9
CD_3CN	46.0	1.5		2.1	1.5	3.2	
2-propanol	48.6						16
CH_3CH_2OH	51.9		4.0				20
CD_3OD	55.5	1.7		18		68	28 (CH_3OH)
$CH_3OH:H_2O$ (2:1)	58.0		58				117

the investigators at Illinois, Pittsburgh, and Cornell as support for a dipolar mechanism in which C–O heterolysis resulted in significant resonance-stabilized ion pair character in the rearrangement transition state.

The thermal rearrangement of chorismate **3**-H_2 the dimethyl chorismate **13**, and five additional chorismate analogs **14**–**18** (Table 4) was monitored in 2:1 $CD_3OD:D_2O$ at 75 °C to obtain the relative rates of rearrangement, and these data were cited by the Cornell researchers as additional evidence in support of a dissociative Claisen process. The observed substituent

Table 4. Relative rate constants k_{rel} for the rearrangement of chorimate analogues [48].

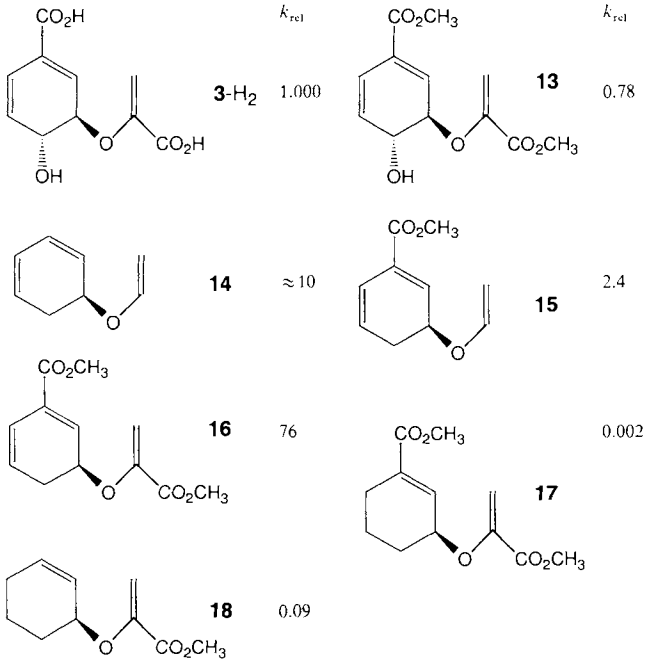

3-H_2 k_{rel} 1.000 — **13** k_{rel} 0.78

14 k_{rel} ≈10 — **15** k_{rel} 2.4

16 k_{rel} 76 — **17** k_{rel} 0.002

18 k_{rel} 0.09

effects, like solvent effects on **9**–**12**, were consistent with C–O bond heterolysis in which the developing carbocation and enolate anion experienced both σ-inductive effects exerted by the hydroxyl and carboxyl groups as well as π-delocalization effects through the disubstituted endocyclic alkene. Several other examples of aliphatic Claisen rearrangements have been reported in which observed rate enhancements could be rationalized by similar inductive and resonance effects.[50–53]

While the 20- to 120-fold solvent-induced rate accelerations for the simple allyl vinyl ethers **9**–**12** were significant, one of the most compelling findings to emerge from the study by the Cornell group was that the rearrangement of dimethyl chorismate **13** was only 18 times faster than that of allyl vinyl ether itself when both rates were measured in a mixture of methanol and water (2/1) at 75 °C. Thus for the first time, it was shown that the rapid rearrangement of chorismic acid, long thought to be an especially facile [3,3]-sigmatropic process, was in very large part attributable to the normal metabolic environment—water.[48] The practical implications and synthetic utility of this finding were quickly acknowledged, and aqueous conditions were soon shown to accelerate several synthetically important Claisen rearrangements.[54,55] Sensitive systems which would not tolerate the high temperature conditions normally required in organic solvents could be rearranged in hot water.

Although the synthetic value of aqueous Claisen rearrangements was universally acknowledged, the specific mechanism by which polar solvents enhanced the rearrangement rate remained unresolved. The Indiana group, led by Gajewski, questioned the dipolar/dissociative mechanism presented by the Pittsburgh/Illinois/Cornell groups. Gajewski argued that neither solvent[45] nor kinetic isotope[24] effects were comparable in magnitude to those observed in reactions proceeding by bona fide zwitterionic structures or tight ion pairs.

As an example, the Indiana group cited the case of a charge-separated cyclopropane opening in which changing the solvent from benzene to DMF increased the rate by 32000.[56] By contrast, the largest solvent rate enhancement in aliphatic Claisen rearrangements was a 200-fold effect on going from cyclohexane to water.[57] For solvolyses where tight ion pair formation was rate determining, typical secondary deuterium kinetic isotope effects approximated 70% of the maximum value.[58] By contrast, the nonenzymatic rearrangement of chorismate displayed only 40% of the maximum KIE.[27] Thus, Gajewski et al. concluded that whatever its structure, the transition state affected by polar hydroxylic solvents accumulated substantially less polar character than well-known zwitterions or tight ion pairs.[57]

In search of an alternative mechanistic rationale, Gajewski attempted to determine the extent to which polar solvent effects were composed of such factors as dielectric effects, solvent cohesive energy densities, hydrogen bond donating effects, and hydrogen bond accepting effects.[59] A solvent rate effect equation was derived which, for the aliphatic Claisen rearrangement, re-

vealed a specific correlation between rate and hydrogen bond donating ability of the solvent. As further evidence against an ionic transition state, secondary deuterium KIEs measured at C4 and C6 of allyl vinyl ether both in *m*-xylene and in $CD_3OD:D_2O$ mixtures indicated that bond breaking was no more extensive in aqueous media than in hydrocarbon solvents.[60]

The importance of solvent hydrogen bonding gained further credence from a Monte Carlo simulation of the effect of hydration on Claisen rearrangements carried out in 1992. Severance and Jorgensen calculated that the transition state for rearrangement of **1** in water was better hydrated than the reactant by 3.85 ± 0.16 kcal mol^{-1}.[61] Consistent with this model, the carbonyl oxygen of the product **2** would be expected to form two hydrogen bonds. The authors suggested that in the transition state, two hydrogen bonds are formed with average strengths of -4.6 kcal mol^{-1} between the oxygen atom of the vinyl ether and two water molecules. By contrast, reactant **1** displayed only a single hydrogen bond with a strength of -3.4 kcal mol^{-1}. Such enhanced hydration could account for a 600- to 700-fold rate enhancement over the Claisen rearrangement of allyl vinyl ether in the gas phase. Moreover, the computed acceleration was not attributable to zwitterionic intermediates, tight ion pairs, or other C–O bond dissociative processes. A recent simulation, modeled at the ab initio level with two explicit water molecules, reached essentially similar conclusions.[62]

A simple physical picture thus emerges for the role of enhanced solvent hydrogen bonding in accelerating the rate of Claisen rearrangements by stabilizing the transition state. Moreover, with hydrogen bonding increasing as the reactant moves towards the transition state, n-π^* conjugation in vinyl ether ground state (Fig. 1) is disrupted.[63] No dipolar or dissociative intermediate need be invoked, thus accommodating the concerns of Gajewski et al. over the magnitude of the observed solvent effects.[59, 60] With remarkable prescience, Severance and Jorgensen forecast that their results would "promote catalyst designs that incorporate two or more hydrogen-bond-donating groups positioned to interact with the oxygen in the transition state." This prediction was to be borne out with startling correctness in the detailed structure investigations of the active site of natural *E. coli* and *B. subtilis* chorismate mutases that were reported shortly thereafter.

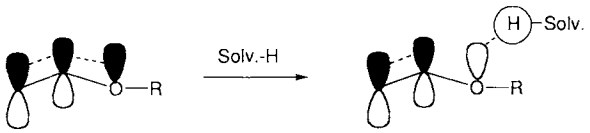

Fig. 1. Disruption of n-π^* conjugation in vinyl ethers by solvent hydrogen bonding which leads to an increase in their ground state energy. Solv. = solvent.

3.2. Chemical Catalysis of the Claisen Rearrangement

"Catalysis of the Claisen rearrangement is as old as the rearrangement itself."[2a] It was Ludwig Claisen himself who discovered in 1912 that when the allyl ether of acetoacetic ester **20** was heated in the presence of ammonium chloride, the salt noticeably enhanced the formation of C-allyl acetoacetate **21** (Scheme 6).[1] Claisen's remarkable discovery was fortuitous:

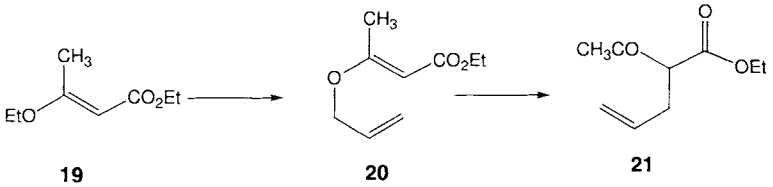

19 **20** **21**

Scheme 6. Formation and rearrangement of *O*-allyl acetoacetate **20**.

NH_4Cl was intended to catalyze the formation of **20** from **19** in an exchange reaction with allyl alcohol. However, as other synthetic approaches to allyl ethers supplanted this method, the use of ammonium chloride gradually disappeared, as did the awareness of its catalytic potential. Nevertheless, the effect of solid NH_4Cl was reinvestigated in several additional aliphatic Claisen rearrangements, and shown to cause a small, but significant, increase in rearrangement rates.[64]

A number of Brønsted and Lewis acids, and even weak acids like silica gel or Celite,[65] have since been reported to accelerate Claisen rearrangements. Developments in this area prior to 1984 have been thoroughly documented in a comprehensive review by Lutz.[38] The most promising synthetic catalysts for regio- and stereospecific rearrangements now appear to be trivalent organoaluminum reagents.[66] Very recently, Yamamoto has developed a chiral aluminum naphthoxide (*R*)-**23** (Scheme 7) that displays a cup-shaped, C_3 symmetric binding cleft whose three *p*-fluorophenyl groups effectively shield one face of the aluminum center. Catalyst (*R*)-**23** is capable of rearranging substituted allyl vinyl ethers **22** to chiral aldehydes **24** at $-78\,^{\circ}C$ with enantiomeric excesses up to 92%.[67] Like other aluminum bis- and tris-phenoxides, complex (*R*)-**23** is thought to function by coordination at the vinyl ether oxygen atom to form **25** (Scheme 7) in what has been termed a "charge-accelerated rearrangement."[38]

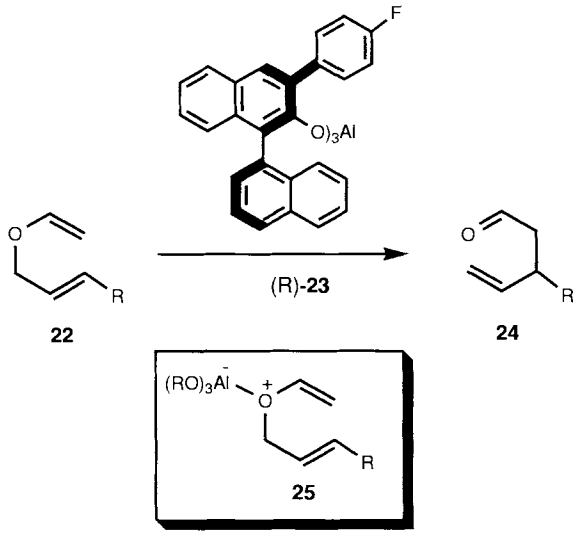

22 **24** **25**

Scheme 7. Catalysis of the rearrangement of substituted allyl vinyl ethers **2** to chiral aldehydes **24** by chiral aluminum naphthoxide (*R*)-**23**.

Charge-accelerated rearrangements occur when carbanions or carbocations attached at the allylic positions become more delocalized in the rearrangement transition structure.[68-70] Several examples of such systems reportedly undergo facile Claisen rearrangement. The dramatic rate enhancements seen are rationalized by customary arguments for the stabilization of the transition state.[38] However, zwitterions like **25** are not configured for such charge delocalization, and thus cannot accelerate the rate by lowering the enthalpy of the transition state.

Instead of invoking charge-acceleration effects, an alternative mechanism for Lewis acid catalysis may be drawn by analogy with the aqueous solvent effects heretofore described. Just as enhanced hydration of the transition state accelerated Claisen rearrangements in water, stabilization of the developing lone pairs of electrons by complexation to Lewis acids might also promote the rearrangement. Quantitative differences between the magnitude of solvent-induced and catalyst-induced rate enhancements are difficult to assess at this time, but may involve a combination of ground state and transition state effects. Qualitatively speaking, however, both aqueous solvents and Lewis acid catalysts may be viewed as exerting effects on lone pairs of electrons on oxygen that lower the activation barrier for rearrangement.

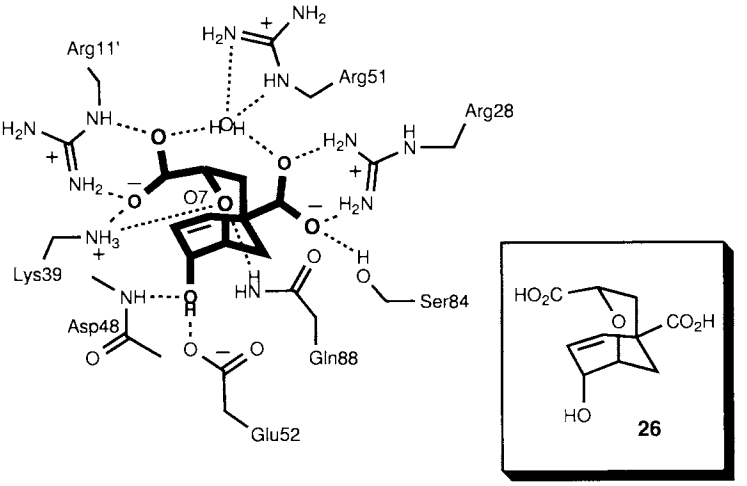

Fig. 2. Amino acid residues of the active site in EcCM, shown complexed to the dianion of the competitive inhibitor **26** (inset).

3.3. Biological Catalysis of the Claisen Rearrangement

How chorismate mutases accelerate the rearrangement of **3** remains an area of continuing debate among chemists and biochemists. Yet as this careful historical analysis of the Claisen rearrangement indicates, clues to the mechanism that were in print for eighty-odd years have largely been ignored by the chemical community. While chorismic acid was long regarded as exceptional because it rearranged so rapidly under physiological conditions, it is now clear that many allyl vinyl ethers, including **1** itself, rearrange at room temperature in aqueous solution. While the ability of the enzyme to accelerate the rearrangement of chorismate ions by a factor of 10^6 was long considered extraordinary, catalysis by trivalent aluminum compounds matches, and in some cases exceeds, those rate enhancements.[67] As with many other chemical reactions, the Claisen rearrangement is subject to a wide range of solvent and catalyst options to promote its rate. Therefore, it was not surprising to discover that Nature has independently evolved structurally distinct solutions to the design of enzyme catalysts for the rearrangement of **3**. Two very different enzymes have already been characterized.

We recently described the 2.2 Å resolution X-ray structure of the N-terminal chorismate mutase domain (residues 1-113) engineered from the bifunctional *E. coli* enzyme chorismate mutase–prephenate dehydratase (P-protein).[111] The structure was solved as a complex with inhibitor **26** (Fig. 2). Monofunctional EcCM has three helical segments (residues 6-42, 49-65, 70-100) which cause the peptide backbone to adopt a figure-4 shape. Coiled-coil and helix-helix interactions between the two longest segments create a catalytically functional, elongated homodimer whose two equivalent, elbow-shaped active sites are highly charged and completely enclosed. Although access to the active site is possible from different directions, as might be expected in the parent bifunctional enzyme, charged Arg, Asp, and Glu side chain residues shield the catalytic region from solvent on different faces of the protein (Fig. 2).

The high-resolution X-ray structure of a comparably-sized (127 residues), monofunctional *B. subtilis* chorismate mutase (BsCM) bound to **26** has also been reported.[110] While the kinetic parameters of EcCM and BsCM are similar, both the amino acid sequence and the secondary structure of BsCM are strikingly different. Standard alignment methods indicate less than 20% similarity in the EcCM and BsCM sequences. In fact, known mutases from different organisms share little sequence similarity. The peptide backbone of BsCM adopts a five-stranded mixed β-sheet containing one α-helix (residues 18-34) and a two-turn 3_{10} helix. BsCM is a symmetric trimer packed to form a pseudo-α,β-barrel; adjacent subunits form three equivalent clefts that constitute the active sites. In striking contrast to EcCM, the active site in BsCM is open and accessible to solvent (Fig. 3).

When the EcCM and BsCM active sites are compared by superimposing the atoms of bound inhibitor **26**, a common mo-

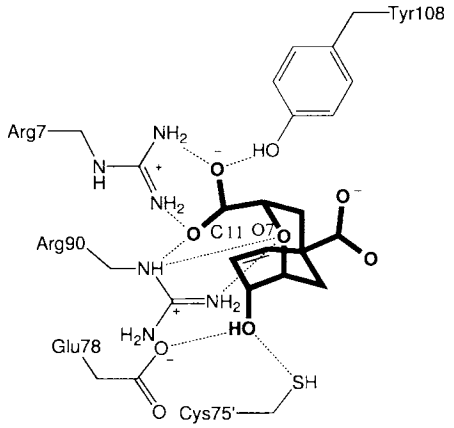

Fig. 3. Amino acid residues of the active site in BsCM, shown complexed to the dianion of the competitive inhibitor **26**.

tif emerges in the highly charged region created by the presence of adjacent, protonated residues (Lys39, Arg11′, Arg51 in EcCM; Arg90, Arg7 in BsCM).[12] This electropositive wall interacts strongly with the left flank of the chorismate ion through an elaborate network of bridging hydrogen bonds involving both O7 and the C11 carboxylate of the enol pyruvate. Besides promoting E–S complex formation through electrostatic effects, the positively charged residues in EcCM and BsCM are thought to orient and lock the chorismate ion in the requisite chair conformer for rearrangement.

At the same time, a lone pair of electrons on the oxygen atom of the vinyl ether of chorismate becomes accessible for hydrogen bonding, and in fact, each enzyme is capable of forming two hydrogen bonds with O7 of the bound inhibitor. These are precisely the hydrogen bonds predicted by Severance and Jorgensen to be important in catalyst design. In the case of EcCM, formation of the E–S complex rotates chorismate into position for hydrogen bonding with Lys39 and Gln88. In the case of BsCM, the oxygen atom of the enol ether group of the chorismate ion likewise forms two hydrogen bonds with Arg90 to promote the pericyclic rearrangement. These hydrogen bonds stabilize the transition state and reduce the activation enthalpy for rearrangement.

Thus a common mechanism is proposed for EcCM and BsCM in which a) adjacent, protonated, active site residues exert conformational control in the chorismate mutase E–S complex, and b) hydrogen bonding between active site residues and O7 of the bound chorismate ion further catalyzes the rearrangement.[12] These mechanistic ideas rationalize all available experimental data on the chorismate mutase reaction, and are consistent with the role of chemical catalysts like Lewis acids and phenols on simple Claisen rearrangements covered in this review.

It seems ironic that chorismate mutase was regarded for so long as being "unique," and that so much mystery and intrigue surrounded the enzyme's ability to catalyze a pericyclic reaction. In retrospect, X-ray structural information on BsCM and EcCM not only provided key clues about the mechanism of chorismate mutases, but also helped substantiate the role of solvent effects on aliphatic Claisen rearrangements. It thus may be worthwhile, in studying the effects of solvent on reactivity, to examine reactions where enzyme-catalyzed counterparts in Nature may provide fresh insight through X-ray crystallographic data. It is hoped that this review will also promote an appreciation of the clear commonalities of mechanism and catalysis that unite the [3,3]-sigmatropic rearrangements of allyl vinyl ethers.

Financial support by a grant from the National Institutes of Health (NIH GM24054) is gratefully acknowledged.

Received: August 16, 1995 [A 131 IE]
German version: *Angew. Chem.* **1996**, *108*, 1014–1023

[1] L. Claisen, *Ber. Dtsch. Chem. Ges.* **1912**, *45*, 3157.
[2] Reviews: a) P. Wipf in *Comprehensive Organic Synthesis, Vol. 5* (Eds.: B. M. Trost, I. Fleming, L. A. Paquette), Pergamon, New York, **1991**, p. 827ff; b) F. E. Ziegler, *Chem. Rev.* **1988**, *88*, 1423; c) S. J. Rhoads, N. R. Raulins, *Org. React.* **1975**, *22*, 1.
[3] W. S. Johnson, L. Werthemaan, W. R. Bartlett, T. J. Brocksam, T.-T. Li, D. J. Faulkner, M. R. Petersen, *J. Am. Chem. Soc.* **1970**, *92*, 741.
[4] a) A. E. Wick, D. Felix, K. Steen, A. Eschenmoser, *Helv. Chim. Acta* **1964**, *47*, 2425; b) A. E. Wick, D. Felix, K. Gschwend-Steen, A Eschenmoser, *ibid.* **1969**, *52*, 1030.
[5] a) R. E. Ireland, R. H. Mueller, *J. Am. Chem. Soc.* **1972**, *94*, 5897; b) R. E. Ireland, R. H. Mueller, A. K. Willard, *J. Am. Chem. Soc.* **1976**, *98*, 2868.
[6] E. Haslam, *Shikimic Acid Metabolism and Metabolites*, Wiley, New York, **1993**.
[7] P. R. Andrews, G. D. Smith, I. G. Young, *Biochemistry* **1973**, *12*, 3492.
[8] H. Gorisch, *Biochemistry* **1978**, *17*, 3700.
[9] T. H. Lowry, K. S. Richardson, *Mechanism and Theory in Organic Chemistry*, 3rd ed., Harper & Row, New York, **1987**, Chapter 10.
[10] Y.-M. Chook, J. V. Gray, H. Ke, W. N. Lipscomb, *J. Mol. Biol.* **1994**, *240*, 476.
[11] A. Y. Lee, P. A. Karplus, B. Ganem, J. Clardy, *J. Am. Chem. Soc.* **1995**, *117*, 3627.
[12] A. Y. Lee, J. Clardy, J. D. Stewart, B. Ganem, *Chem. and Biol.* **1995**, *2*, 195.
[13] R. B. Woodward, R. Hoffmann, *Angew. Chem.* **1969**, *81*, 797; *Angew. Chem. Int. Ed. Engl.* **1969**, *8*, 781.
[14] F. W. Schuler, G. W. Murphys, *J. Am. Chem. Soc.* **1950**, *72*, 3155.
[15] a) P. Vittorelli, T. Winkler, H.-J. Hansen, H. Schmid, *Helv. Chim. Acta* **1968**, *51*, 1457; b) H. J. Hansen, H. Schmid, *Tetrahedron* **1974**, *30*, 1959.
[16] K. R. Brower, *J. Am. Chem. Soc.* **1961**, *83*, 4370.
[17] J. W. Ralls, R. E. Lundin, G. F. Bailey, *J. Org. Chem.* **1963**, *28*, 3521.
[18] H.-J. Hansen, H. Schmid, *Chem. Br.* **1969**, *5*, 111.
[19] G. Frater, A. Habich, H.-J. Hansen, H. Schmid, *Helv. Chim. Acta* **1969**, *52*, 335, 1156.
[20] S. D. Copley, J. R. Knowles, *J. Am. Chem. Soc.* **1985**, *107*, 5306.
[21] C. J. Burrows, B. K. Carpenter, *J. Am. Chem. Soc.* **1981**, *103*, 6983.
[22] S. G. Sogo, T. S. Widlanski, J. H. Hoare, C. E. Grimshaw, G. A. Berchtold, J. R. Knowles, *J. Am. Chem. Soc.* **1984**, *106*, 2701.
[23] The same entropic restriction has been observed with a catalytic antibody exhibiting chorismate mutase activity: D. Y. Jackson, M. N. Liang, P. A. Bartlett, P. G. Schultz, *Angew. Chem.* **1992**, *104*, 196; *Angew. Chem. Int. Ed. Engl.* **1992**, *31*, 182.
[24] a) J. J. Gajewski, N. D. Conrad, *J. Am. Chem. Soc.* **1979**, *101*, 2747; b) J. J. Gajewski, N. D. Conrad, *J. Am. Chem. Soc.* **1979**, *101*, 6693; c) J. J. Gajewski, *Acc. Chem. Res.* **1980**, *13*, 142.
[25] M. J. S. Dewar, E. F. Healy, *J. Am. Chem. Soc.* **1984**, *106*, 7127.
[26] R. L. Vance, N. G. Rondan, K. N. Houk, F. Jensen, W. T. Borden, A. Komornicki, E. Wimmer, *J. Am. Chem. Soc.* **1988**, *110*, 2314.
[27] L. Addadi, E. K. Jaffe, J. R. Knowles, *Biochemistry* **1983**, *22*, 4494.
[28] P. R. Andrews, R. C. Haddon, *Aust. J. Chem.* **1979**, *32*, 1921.
[29] O. Wiest, K. N. Houk, *J. Org. Chem.* **1994**, *59*, 7582.
[30] R. W. Alder, R. Baker, J. M. Brown, *Mechanism in Organic Chemistry*, Wiley, London, **1971**, p. 239.
[31] I. Fleming, *Frontier Orbitals and Organic Chemical Reactions*, Wiley, London, **1976**, p. 32.
[32] D. C. Wigfield, S. Feiner, *Can. J. Chem.* **1970**, *48*, 855.
[33] D. C. Berndt, *J. Chem. Eng. Data* **1969**, *14*, 112.
[34] P. Heimbach, W. Brenner, *Angew. Chem.* **1967**, *79*, 814; *Angew. Chem. Int. Ed. Engl.* **1967**, *6*, 800.
[35] J. C. Trebellas, J. R. Oleckowskii, H. B. Jonassen, *J. Organomet. Chem.* **1966**, *6*, 412.
[36] a) L. E. Overman, *Angew Chem.* **1984**, *96*, 565; *Angew Chem. Int. Ed. Engl.* **1984**, *23*, 579; b) L. E. Overman, A. F. Renaldo, *J. Am. Chem. Soc.* **1990**, *112*, 3945.
[37] R. Hamilton, T. R. B. Mitchell, J. J. Rooney, *J. Chem. Soc. Chem. Commun.* **1981**, 456.
[38] Review: R. P. Lutz, *Chem. Rev.* **1984**, *84*, 205.
[39] J. V. Gray, D. Eren, J. R. Knowles, *Biochemistry* **1990**, *29*, 8872.
[40] J. F. Kincaid, D. S. Tarbell, *J. Am. Chem. Soc.* **1939**, *61*, 3085.
[41] W. N. White, D. Gwynn, R. Schlitt, C. Girard, W. Fife, *J. Am. Chem. Soc.* **1958**, *80*, 3271.
[42] H. L. Goering, R. R. Jacobson, *J. Am. Chem. Soc.* **1958**, *80*, 3277.
[43] W. N. White, E. F. Wolfarth, *J. Org. Chem.* **1970**, *35*, 2196
[44] R. K. Hill in *Comprehensive Organic Synthesis, Vol. 5*, (Eds.: B. M. Trost, I. Fleming, L. A. Paquette), Pergamon, New York, **1991**, p.785.
[45] E. M. Kosower, *J. Am. Chem. Soc.* **1958**, *80*, 3253.
[46] W. N. White, E. F. Wolfarth, *J. Org. Chem.* **1970**, *35*, 3585.
[47] R. M. Coates, B. D. Rogers, S. J. Hobbs, D. R. Peck, D. P. Curran, *J. Am. Chem. Soc.* **1987**, *109*, 1160.
[48] J. J. Gajewski, J. Jurayj, D. R. Kimbrough, M. E. Gande, B. Ganem, B. K. Carpenter, *J. Am. Chem. Soc.* **1987**, *109*, 1170.
[49] K. Dimroth, C. Reighardt, T. Siepman, F. Bohlmann, *Ann. Chem.* **1963**, *661*, 1.
[50] W. E. Childers, Jr., H. W. Pinnick, *J. Org. Chem.* **1984**, *49*, 5277.
[51] B. W. Metcalf, E. T. Jarvi, J. P. Burkhart, *Tetrahedron Lett.* **1985**, *26*, 2861
[52] G. Desimoni, G. Faita, A. Gamba, P. P. Righetti, G. Tacconi, L. Toma, *Tetrahedron* **1990**, *46*, 2165.
[53] J. J. Gajewski, K. R. Gee, J. Jurayj, *J. Org. Chem.* **1990**, *55*, 1813.
[54] P. A. Grieco, E. B. Brandes, S. McCann, J. D. Clark, *J. Org. Chem.* **1989**, *54*, 5849.

[55] A. Lubineau, J. Augé, N. Bellanger, S. Caillebourdin, *J. Chem. Soc. Perkin Trans. 1* **1992**, 1631.
[56] A. B. Chmurny, D. J. Cram, *J. Am. Chem. Soc.* **1973**, *95*, 4237.
[57] E. Brandes, P. A. Grieco, J. J. Gajewski, *J. Org. Chem.* **1989**, *54*, 515.
[58] V. J. Shiner, Jr., *ACS Sympos. Ser.* **1975**, *11*, 163.
[59] J. J. Gajewski, *J. Org. Chem.* **1992**, *57*, 5500.
[60] J. J. Gajewski, N. L. Brichford, *J. Am. Chem. Soc.* **1994**, *116*, 3165.
[61] D. L. Severance, W. L. Jorgensen, *J. Am. Chem. Soc.* **1992**, *114*, 10966.
[62] M. M. Davidson, I. H. Hillier, *J. Phys. Chem.* **1995**, *99*, 6748.
[63] H. Dodziuk, H. von Voithenberg, N. L. Allinger, *Tetrahedron* **1982**, *38*, 2811.
[64] J. W. Ralls, R. E. Lundin, G. F. Bailey, *J. Org. Chem.* **1963**, *28*, 3521.
[65] R. D. H. Murray, M. Sutcliffe, M. Hasegawa, *Tetrahedron* **1975**, *31*, 2966.
[66] K. Nonoshita, H. Banno, K. Maruoka, H. Yamamoto, *J. Am. Chem. Soc.* **1990**, *112*, 316.
[67] K. Maruoka, S. Saito, H. Yamamoto, *J. Am. Chem. Soc.* **1995**, *117*, 1165.
[68] B. K. Carpenter, *Tetrahedron* **1978**, *34*, 1877.
[69] R. Breslow, J. M. Hoffman, Jr., *J. Am. Chem. Soc.* **1972**, *94*, 2111.
[70] H.-J. Hansen, B. Sutter, H. Schmid, *Helv. Chim. Acta* **1968**, *51*, 828.

Time is money...

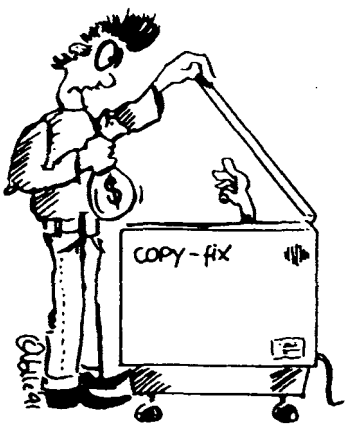

Save both by starting a personal subscription to *Angewandte Chemie* (now with *Chemistry - A European Journal*). At 9¢ per page you can't go wrong. With your own private copy you can read the "hot" articles before they cool, and waste less time in front of the copier.

Order now!
An order form can be found on the last page of this issue.

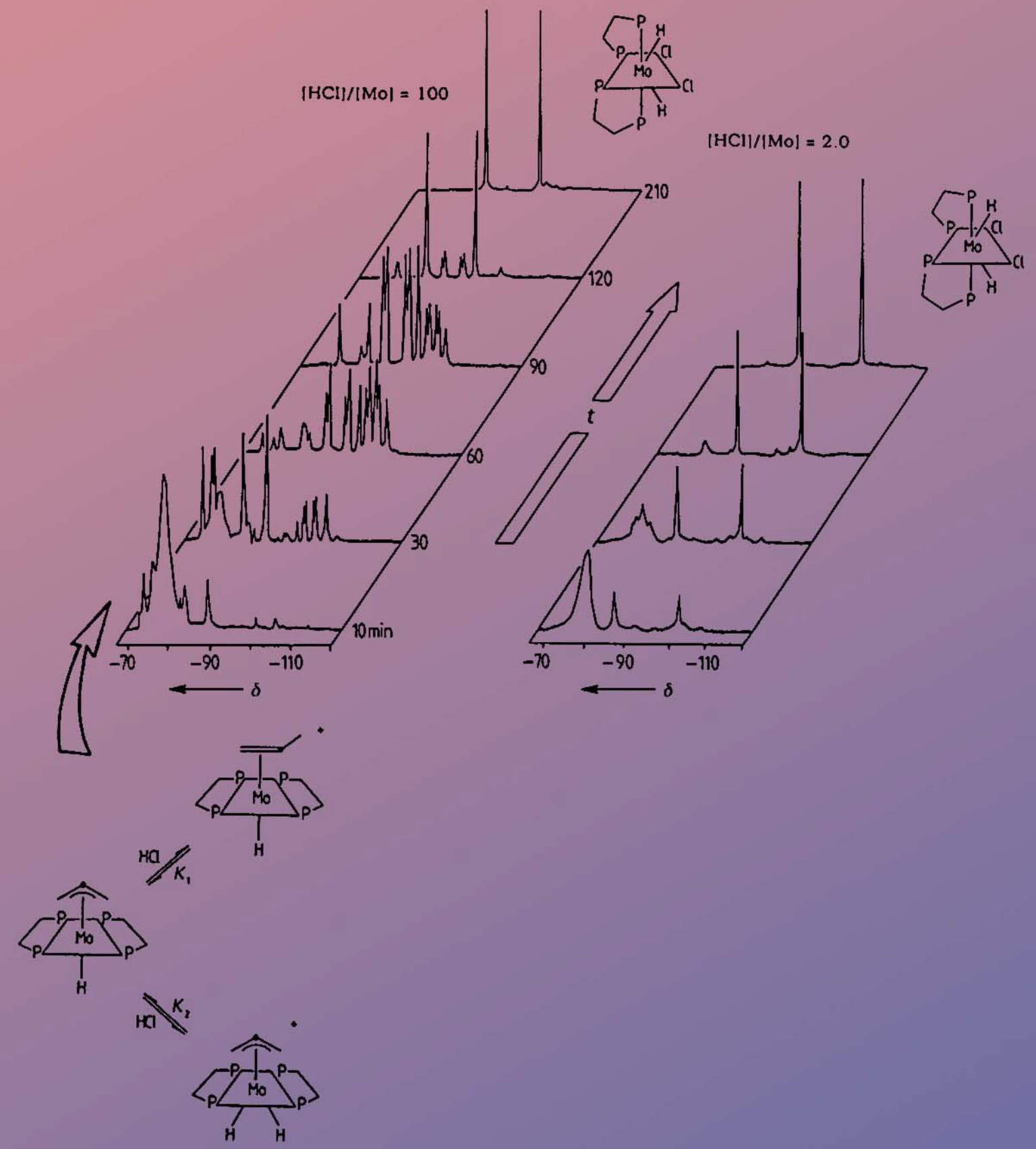

Intermediates in the protonation of a phosphane allyl molybdenum complex can be detected by ^{31}P NMR spectroscopy. For more about the kinetic analysis of protonation mechanisms for hydrocarbon transition metal complexes see the following article by R. A. Henderson.

Protonation of Unsaturated Hydrocarbon Ligands: Regioselectivity, Stereoselectivity, and Product Specificity

Richard A. Henderson*

Understanding the mechanisms of protonation of hydrocarbon ligands is fundamental to a wide range of chemistry including organic synthesis, organometallic chemistry, and even bioinorganic chemistry. Protonation at carbon or metal sites is often slow, with the result that in species containing both types of sites, initial protonation can be at either the metal or the carbon. This has fundamental consequences on the reactivity of hydrocarbon ligands, which are highlighted in this article. In particular, many reactions are apparently the result of a regioselective protonation on the basis of structural analysis of the isolated products. In fact, these products are often formed by an indirect route involving kinetically controlled protonation at the "wrong" site followed by rearrangement to form the thermodynamically controlled, apparently regioselective, product. Other aspects of the protonation mechanisms of complexes containing hydrocarbon ligands are discussed, with an emphasis on the manner in which competitive protonation at metal or ligand can be exploited to select which hydrocarbon is produced and to control the stereochemistry of the hydrocarbon.

Keywords: complexes with carbon ligands · hydrocarbons · protonation · reaction mechanisms

1. Introduction

The binding and activation of small molecules at metal sites is an area of research which is of interest to a wide range of chemists—from those involved in the simple stoichiometric reactions of inorganic compounds to those defining the elementary reactions of organometallic homogeneous catalysts, metalloenzymes, and even heterogeneous catalysts. In this article I will concentrate on the protonation of small, unsaturated hydrocarbon residues bound to relatively simple, electron-rich transition metal sites.

The chemistry of carbon residues bound to metal sites has traditionally been considered the domain of organometallic chemists; however, for many years (since the discovery of the cobalt–carbon bond in the vitamin B_{12} coenzyme)[1] it has been appreciated that bioinorganic chemistry can have an organometallic flavor.[2] Clearly in the vitamin B_{12} case, the connection between organometallic and bioinorganic chemistry is based on a structural feature. However, if some of the elementary reactions of metalloenzymes are considered, then further aspects common to organometallic and bioinorganic chemistry become evident. Examples are the 1,2-shifts associated with several types of enzymes, which are initiated by homolysis of the cobalt–carbon bond in the vitamin B_{12} coenzyme;[3] the reduction of carbon dioxide to methane by dihydrogen in methanogenic and acetogenic bacteria containing carbon monoxide dehydrogenase (in anaerobic bacteria a nickel-containing enzyme and in aerobic bacteria a molybdopterin enzyme);[4] and the mono- or dioxygenation of organic molecules by methane monoxygenase[5] and catecholases[6] (iron-containing enzymes). All involve the reaction, or intermediacy, of species containing metal–carbon bonds.

A family of enzymes that are of particular interest (at least to the author!) are the nitrogenases. These enzymes contain iron together with molybdenum or vanadium and transform dinitrogen into ammonia with the concomitant release of some dihydrogen in vivo [Eq. (1)].[7] In vitro the enzyme is capable of

$$N_2 + 8H^+ + 8e^- \longrightarrow 2NH_3 + H_2 \quad (1)$$

transforming a wide range of other small, unsaturated molecules by a sequence of electron and proton transfer reactions. The range of alternative substrates include acetylenes, cyclopropenes, azides, isonitriles, and cyanides. It is worth noting that in several of these a metal–carbon bond must be formed upon binding of the substrate. Of these substrates, the reactions of the nitrogenases with acetylene to form ethene and ethane [Eqs. (2) and (3)], respectively, warrant further comment.

$$C_2H_2 + 2H^+ + 2e^- \longrightarrow C_2H_4 \quad (2)$$

$$C_2H_2 + 4H^+ + 4e^- \longrightarrow C_2H_6 \quad (3)$$

The nitrogenases exhibit a different product specificity in their reactions with acetylene. The molybdenum-based nitroge-

[*] Dr. R. Henderson
John Innes Centre, Nitrogen Fixation Laboratory
University of Sussex, Brighton BN1 9RQ (UK)
Present address: Nitrogen Fixation Laboratory, John Innes Centre
Norwich Research Park, Colney, Norwich (UK)

nase converts acetylene into ethene exclusively, whilst the vanadium-based enzyme gives predominantly ethene but also some ethane (about 5%). In addition, both nitrogenases exhibit a stereoselectivity in their reactions with acetylene. In the presence of D_2O both enzymes give *cis*-CHDCHD as the exclusive product. The manner in which the enzyme accomplishes such stereoselectivity and product specificity by simple electron and proton transfer reactions was the inspiration of much of our own work in this area.

In this article we shall see that the fundamental mechanistic chemistry associated with the protonation of hydrocarbon residues bound to a transition metal center is a consequence of slow protonation at both metal and carbon sites. Only by understanding the basic mechanistic principles associated with protonation of simple complexes containing hydrocarbon residues can we appreciate how to harness this reactivity to accomplish stereoselective or product-specific reactions.

2. General Considerations on the Rates of Protonation

Throughout this article we shall be concerned with the protonation of unsaturated carbon residues bound to metal sites; consequently it is pertinent to start with a short, entirely general, discussion of the factors that influence the rates of protonation at various sites. This will necessarily be a "broad brush strokes" approach, and the interested reader is referred to specialist reviews of this area for a more detailed discussion.[8–10]

2.1. Rates of Proton Transfer

In general, for the simple process described by Equation (4) there is no chemical barrier for thermodynamically favorable reactions involving attachment of the proton to bases at an O,

$$H^+ + X^- \rightleftharpoons HX \tag{4}$$

N, F, or S site. The rate of the reaction is restricted only by the rate at which the two components diffuse together ($k_{diff} \approx 1 \times 10^{10}\ dm^3\,mol^{-1}\,s^{-1}$). The rate of the reverse reaction is necessarily smaller by a factor dependent on the thermodynamic driving force of the reaction, K_a, (that is, $10^{\Delta pK_a}$). If the forward reaction is not thermodynamically favorable, the rate of the reaction is dependent on the thermodynamic driving force, as given by the Brønsted relationship in Equation (5),

$$k = G_a K_a^{\alpha} \tag{5}$$

where G_a and α are constants. Thus, for the protonation of a series of structurally analogous bases, the curve of the plot of $\log k$ against $\log K_a$ initially has a slope of unity under conditions where the proton transfer is thermodynamically uphill, but levels off to a slope of zero when the proton transfer is thermodynamically favorable.

Exceptions to this general rule occur when there is a considerable change in the structure of the O, N, F, or S acid or base upon proton transfer, and then the rate is slower than the diffusion-controlled limit. For instance, the deprotonation reaction in Equation (6) is a thermodynamically favorable reaction, but

$$^-O_2NNCH_2CH_2NHNO_2 + NH_3 \rightleftharpoons {}^-O_2NNCH_2CH_2NNO_2^- + NH_4^+ \tag{6}$$

the forward rate constant ($k \approx 10^5\ dm^3\,mol^{-1}\,s^{-1}$) is five orders of magnitude slower than the diffusion-controlled limit.[11] This relatively slow rate of proton transfer indicates that there is a significant barrier to removal of the proton from the monoanionic species, which is probably associated with the delocalization of the lone pair of electrons over the NNO_2 residue.

2.2. Proton Transfer at Carbon Sites

We can consider the deprotonation of the CH_2NO_2 residue in nitroethane, as shown in Equation (7), to be the carbon ana-

$$MeCH_2NO_2 + NH_3 \rightleftharpoons MeCHNO_2^- + NH_4^+ \tag{7}$$

logue of the reaction in Equation (6).[12] The rate of this deprotonation is $k = 7 \times 10^{-3}\ dm^3\,mol^{-1}\,s^{-1}$. This example illustrates an entirely general principle: deprotonation of a carbon residue is markedly slower than deprotonation of the "analogous" nitrogen-based residue. This difference between the normal behavior exhibited by O, N, F, or S sites and carbon

Born in 1951 just outside London, Richard A. Henderson studied chemistry at University College London, receiving his PhD in 1976 under the supervision of Martin L. Tobe. After two years as postdoctoral fellow with A. Geoffrey Sykes at the University of Leeds, he moved to the Nitrogen Fixation Laboratory at the University of Sussex in October 1979. His major research interests are in mechanistic inorganic chemistry, in particular the binding of small molecules such as N_2, H_2, RNC, RCN, or unsaturated hydrocarbons to transition metal sites, and their activation towards protonation. More recently his interests have extended to the mechanisms of the reactions of iron–sulfur-based clusters. In 1993 he was the first recipient of the Royal Society of Chemistry Award in Inorganic Reaction Mechanisms.

sites is further emphasized by comparing the rates of the proton transfer reactions shown in Equations (8) and (9).[13]

$$MeCH_2NO_2 + OH \rightleftharpoons MeCHNO_2^- + H_2O \quad (8)$$

$$C_6H_5OH + OH \rightleftharpoons C_6H_5O^- + H_2O \quad (9)$$

Although phenol is a weaker acid than nitroethane, and consequently the thermodynamic driving force is larger for reaction (8), the rate of deprotonation of phenol is diffusion-controlled ($k = 1.5 \times 10^{10}\ dm^3 mol^{-1} s^{-1}$), whereas the deprotonation of nitroethane is much slower ($k = 5.2\ dm^3 mol^{-1} s^{-1}$).

There are two reasons why the rates of proton transfer involving carbon sites are slow. First, with O, N, F, or S sites, proton transfer is preceded by the formation of a hydrogen bond between the sites involved in the proton transfer, and this anchoring of the two sites facilitates the subsequent transfer of the proton. Such hydrogen bonding is much weaker in the case of carbon-based residues. Second, carbon is weakly electronegative, and thus lone pairs of electrons on a carbon atom become delocalized towards more electronegative neighboring atoms. This delocalization involves a change in the electronic structure and in the position of all the nuclei involved, and consequently results in a slow rate of proton transfer.

Clearly, if electronic and structural reorganization factors become less important in the reactions of carbon-based sites the rates of proton transfer can become fast. Thus, in the deprotonation of cyano or disulfano compounds,[14] the rates of proton transfer for thermodynamically favorable reactions are $k \approx 10^7$–$10^8\ dm^3 mol^{-1} s^{-1}$. Although these rates are still at least 100 times less than the normal diffusion-controlled limit, they are significantly faster than those normally observed with carbon-based residues. The rapidity of these reactions indicate that after deprotonation of the conjugate acid the lone pair of electrons resides predominantly on the carbon, rather than being delocalized.

2.3. Proton Transfer at Metal Sites

In general, proton transfer to and from metal sites is slow.[10, 15] The origin of this slowness is associated with the significant electronic and structural reorganization that must occur at the metal upon proton transfer. In an extensive series of studies on the rates of deprotonation of hydridic complexes by aniline, a range of reactions exhibiting a variety of thermodynamic driving forces (from exothermic to endothermic) have been studied, and a variety of rate constants have been observed: $[CoH(CO)_4]$ ($k = 1.7 \times 10^6\ dm^3 mol^{-1} s^{-1}$, $\Delta pK_a = -2.3$); $[FeH_2(CO)_4]$ ($k = 5.4 \times 10^4\ dm^3 mol^{-1} s^{-1}$, $\Delta pK_a = +0.8$); and $[OsH_2(CO)_4]$ ($k = 1.0 \times 10^{-2}\ dm^3 mol^{-1} s^{-1}$; $\Delta pK_a = +10.2$).[16] There are two features to note that are typical of proton transfer reactions at metals: first, the rates vary with the thermodynamic driving force of the reaction, and second, the rates never attain the diffusion-controlled limit.

In summary then, although the rates of protonation are usually defined by the rate of diffusion of the two components (the acid and the base), two notable exceptions are the protonation of carbon sites and the protonation of metal sites. Consequently, the difference in the rates of protonation of the ligand and the metal in the complexes containing hydrocarbon ligands may be rather small, and, depending on the system under investigation, either the metal or the hydrocarbon can be the more rapidly protonated site.

3. Regioselective Protonation of Complexes

On studying the protonation of unsaturated carbon-based residues bound to metal sites the first pertinent question, in the light of the discussion above, is, "Which site is protonated first: metal or carbon?" This is a question that cannot always be answered by synthetic chemistry. Merely to isolate the product from the reaction of an acid with any particular complex will often result in the identification of the thermodynamically controlled product. What we want to identify is the *initial* site of protonation: the kinetically controlled product. Only if the interconversion of the kinetically controlled and thermodynamically controlled products is slow will it be possible to identify the true initial site of protonation by synthetic chemistry. In order to establish unambiguously which site is protonated first, the reaction must be monitored by a sufficiently rapid method. The most commonly used technique is stopped-flow spectrophotometry, which can study reactions that take longer than about two milliseconds to complete. More conventional, and diagnostic, spectroscopy such as solution IR and multinuclear NMR spectroscopies can be used, but often low temperatures must be employed to slow these reactions sufficiently and ensure that no intermediates have avoided detection.

Protonation at the metal and the hydrocarbon can be completely isolated processes. For instance, the reaction of acids with $[Ru(\eta^5\text{-}C_5H_5)_2]$ results in protonation of the metal as shown in Scheme 1. However, at the same time, H–D exchange of the cyclopentadienyl protons occurs indicating protonation of the hydrocarbon ligands.[17] As the protonation of the metal becomes more extensive (for instance, when stronger acids or higher concentrations of acid are used), the extent of H–D exchange of the ring protons decreases. That is, protonation of the metal and hydrocarbon are competitive processes, and protonation at the metal deactivates the cyclopentadienyl ring towards protonation.

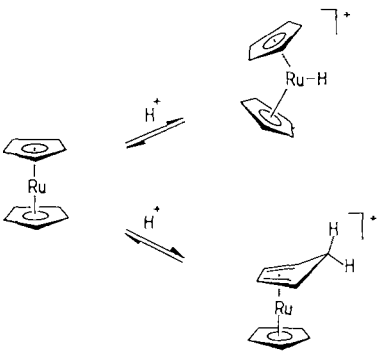

Scheme 1. The reaction of acids with $[Ru(\eta^5\text{-}C_5H_5)_2]$

However, a more common situation is that protonation at the metal or the hydrocarbon residue are not mutually independent, because of facile pathways that can transfer the proton from the metal to the carbon. This leads to another pertinent question: "What is meant by a regioselective protonation?" If we consider just the stoichiometry of the reaction and the structure of the product, then (for instance) the conversion of an alkylidyne into an alkylidene, as shown in Scheme 2, is a regioselec-

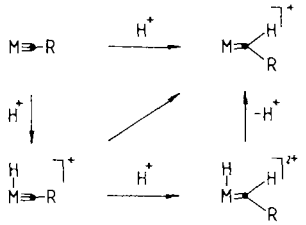

Scheme 2. The protonation of alkylidyne complexes.

tive protonation. However, if we consider the reaction mechanistically, this apparent regioselectivity could result by three pathways: direct protonation of the carbon atom, protonation of the metal followed by intramolecular migration to the carbon, or protonation of the metal followed by an acid–base catalyzed rearrangement.

We shall see in the examples that follow in this article that true regioselective protonation is rare, and initial protonation at the "wrong" site still allows formation of the product by intramolecular or acid–base catalyzed pathways. We shall also see that no generalization can be made about which site (metal or hydrocarbon) is protonated first. It appears that the energetic barriers to protonation at the metal and a coordinated carbon are rather similar, and which is protonated the faster cannot be defined a priori. In the remainder of this section we shall consider some simple stoichiometric reactions, which together illustrate the sequence of elementary reactions shown in Scheme 3.

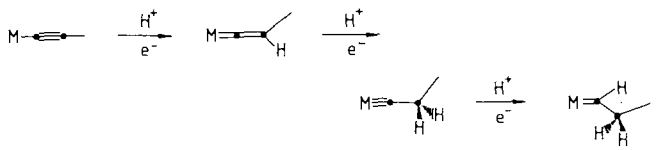

Scheme 3. A typical protonation of an alkynyl ligand to form a vinylidene.

This sequence has been chosen because each step it contains is stoichiometrically very simple, involving the addition of only a single proton, and consideration of the structure of the product would indicate the regioselective addition of a proton. However, studies on each step demonstrate that the interconversions are often mechanistically more complicated, less direct, and certainly less obvious. These studies demonstrate some useful mechanistic principles upon which we shall build in later sections.

The addition of a proton directly to its final residence, whether it be the metal or the carbon, exhibits a simple first-order dependence on the concentration of the acid. In the mechanistic studies that follow, two features are diagnostic of a more complicated mechanism: 1) a complicated rate law, and in particular a complicated dependence on the concentration of acid, and 2) the spectroscopic detection of an intermediate, the kinetically controlled product.

3.1. Protonation of an Alkynyl Ligand to a Vinylidene

This common reaction[18] is typified by the reaction of PhCCH with *fac*-[W(thf)(CO)$_3$(dppe)] (dppe = $Ph_2PCH_2CH_2PPh_2$; thf = C_4H_8O)[19] shown in Scheme 4. After the initial binding of the alkyne to the metal, rearrangement to the isomeric vinylidene complex occurs when the solution is warmed to 50 °C. Despite the prevalence of this transformation, the mechanism has not been studied in detail. However, molecular orbital calculations suggest that because of the importance

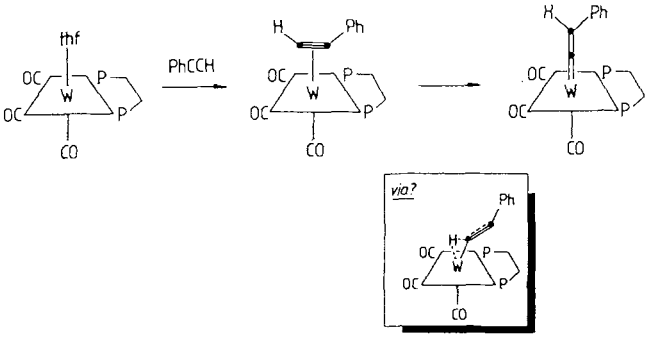

Scheme 4. Binding of PhCCH to *fac*-[W(thf)(CO)$_3$(dppe)] and rearrangement to the vinylidene complex.

of π donation from the alkyne, the rearrangement to form the vinylidene is promoted by the unfavorable four-electron, two-center bonding between the alkyne π orbitals and the filled metal d orbitals. Equally, the π complex might rearrange, because the carbon monoxide coligands render the coordinated PhCCH sufficiently acidic for the proton to be released with concomitant formation of the alkynyl species. Subsequent protonation of the alkynyl ligand at the carbon atom remote from the metal generates the vinylidene complex. Certainly, protonation of isolated alkynyl complexes gives vinylidene species, and this reaction has been studied mechanistically.

The rate of protonation of [Ru(η^5-C_5H_5)(CCMe)(PMe_3)$_2$] by [W(η^5-C_5H_5)H(CO)$_3$] shown in Equation (10)[20] is only ten

$$[Ru(\eta^5\text{-}C_5H_5)(CCMe)(PMe_3)_2] + [W(\eta^5\text{-}C_5H_5)H(CO)_3] \longrightarrow [Ru(\eta^5\text{-}C_5H_5)(CCHMe)(PMe_3)_2]^+ + [W(\eta^5\text{-}C_5H_5)H(CO)_3]^- \quad (10)$$

times faster than the rate of proton transfer from this hydrido complex to $PhNH_2$, although the alkynyl to vinylidene reaction is thermodynamically favorable by 1.5 kJ mol^{-1}, whilst the proton transfer to $PhNH_2$ is unfavorable by 1.8 kJ mol^{-1}. This relatively small difference in the rates of proton transfer indicates that, in general, the protonation of the alkynyl complex involves substantial structural and electronic reorganization.

Mulliken population analysis from molecular orbital calculations indicates that the gross atomic charge at the carbon atom remote from the metal is not significantly different for alkynyl and corresponding vinylidene species.[21] Consequently, if protonation of the alkynyl is charge-controlled and occurs at the remote carbon atom, it could be argued that protonation of the vinylidene would also occur at the remote carbon atom to form the alkylidyne. As we shall see in the next example, it is not this simple.

3.2. Protonation of a Vinylidene Ligand to an Alkylidyne

Protonation of vinylidene complexes invariably gives the corresponding alkylidyne in an apparently regioselective protonation of the remote carbon atom.[22] However, mechanistic studies on the reaction of the rhenium complex[23, 24] [Eq. (11)]

$$trans\text{-}[ReCl(CCHPh)(dppe)_2] + NHEt_3^+ \longrightarrow trans\text{-}[ReCl(CCH_2Ph)(dppe)_2]^+ + NEt_3 \quad (11)$$

demonstrate that this transformation can occur by three pathways (Scheme 5).

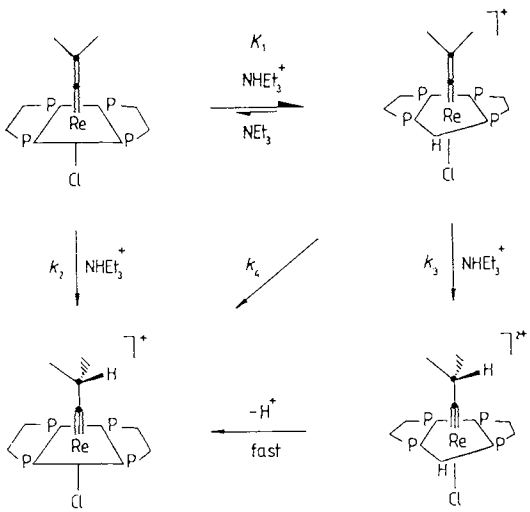

Scheme 5. Three potential pathways for the protonation of a vinylidene complex to the corresponding alkylidyne complex.

Consideration of this mechanism, assuming that k_2, k_3, and k_4 are the rate-limiting steps and that K_1 is a rapidly established protonation equilibrium, demonstrates that the rate law for the formation of the alkylidyne product is given by Equation (12).

$$k_{obs} = \frac{k_4K_1[NHEt_3^+]/[NEt_3] + (k_3K_1[NHEt_3^+]/[NEt_3] + k_2)[NHEt_3^+]}{1 + K_1[NHEt_3^+]/[NEt_3]} \quad (12)$$

Clearly, the complex acid dependence associated with this mechanism is readily distinguished from the simple first-order dependence on the concentration of acid expected for a direct protonation of the remote carbon site.

The most important feature of this mechanism is that direct, regioselective protonation of the vinylidene ligand (k_2) is slow, whilst protonation at another site, probably the metal (K_1), is rapid. It is important to emphasize that the formation of this hydride is enforced because of the difference in the rates of protonation of the carbon and metal sites. Chemical intuition tells us that this protonation must deactivate the vinylidene towards protonation by decreasing the electron density at the ligand. Nevertheless, formation of the alkylidyne subsequently occurs by both an intramolecular (k_4) and an acid-catalyzed (k_3) pathway .

In experiments with no added NEt_3, the equilibrium K_1 lies far to the right-hand side ($K_1[NHEt_3^+]/[NEt_3] \gg 1$), and the rate law is given by Equation (13). Under these conditions,

$$k_{obs} = k_4 + k_3[NHEt_3^+] \quad (13)$$

a linear dependence on the concentration of acid is observed, with a finite intercept, and the initial absorbance of the absorbance–time curve is distinctly different from that expected of *trans*-[ReCl(CCHPh)(dppe)$_2$], corresponding to the formation of the hydride within the dead time of the stopped-flow apparatus. Analysis of the data gives $k_4 = 7.3 \times 10^{-2}\,s^{-1}$, $k_4^H/k_4^D = 1.16$, and $k_3 = 9.4\,dm^3\,mol^{-1}\,s^{-1}$, $k_3^H/k_3^D = 1.35$. The acid-independent term in the rate law is associated with an intramolecular migration of the hydride ligand to the remote carbon atom. The isotope effect associated with this pathway is a consequence of the rate-limiting movement of a hydride (deuteride) whose origins are the addition of a proton (deuteron) to the metal.

In the presence of an excess of NEt_3 the position of the equilibrium, K_1, lies to the left-hand side. Consequently, $K_1[NHEt_3^+]/[NEt_3] \ll 1$, and the rate law reduces to that shown in Equation (14). From analysis of the data collected

$$k_{obs} = k_4 + \{k_3 + k_2[NEt_3]/K_1[NHEt_3^+]\}[NHEt_3^+] \quad (14)$$

under these conditions and using the previously determined value of k_4, we can calculate, $k_2/K_1 = 17.6\,dm^3\,mol^{-1}\,s^{-1}$ and $k_3 = 10.5\,dm^3\,mol^{-1}\,s^{-1}$. Furthermore, since we can estimate that K_1 is greater than 4, k_2 is larger than $70.4\,dm^3\,mol^{-1}\,s^{-1}$. The values of k_2 and k_3 both correspond to the protonation of the vinylidene ligand, but the much lower value of k_3 (corresponding to the protonation of the vinylidene ligand in *trans*-[Re(H)Cl(CCHPh)(dppe)$_2$]$^+$) confirms the earlier intuitive conclusion that initial protonation at the metal decreases the basicity of the hydrocarbon residue.

The formation of the alkylidyne complex is associated with a strong thermodynamic driving force, but kinetic factors initially result in the protonation of the "wrong" site—the rhenium center. Subsequently the complex transfers the proton from the metal to the carbon atom by both an acid-catalyzed rearrangement and a pathway (k_4) that appears to be intramolecular. Although the details of the intramolecular route have yet to be defined, it seems unlikely that the proton just "hops" from metal to the remote carbon atom. A more likely mechanism involves rate-limiting intramolecular migration to form a vinyl species, which subsequently protonates to form the corresponding alkylidene (Scheme 6). Subsequent proton loss from the carbon adjacent to the metal produces the alkylidyne complex. This type of acid-catalyzed rearrangement of vinyl species has been observed in the reactions of *trans*-[Mo(η^2-MeCCH)$_2$(dppe)$_2$] (see Section 4.1).

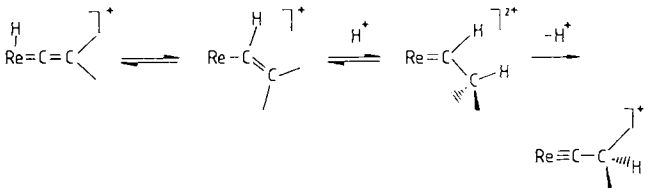

Scheme 6. Proposed mechanism for the intramolecular hydrogen transfer from the metal center to the remote carbon atom of the vinylidene complex, *trans*-[Re(H)Cl(CCHPh)(dppe)$_2$]$^+$.

In discussing this example I have stressed the details of the absorbance–time traces. The importance of establishing that the absorbance change being monitored is that expected for the reaction in question cannot be overemphasized. In addition, the observation that the initial absorbance is different from that of the reactant is indicative of the rapid formation of an intermediate. Even if the initial absorbance change had not been noticed (or, as happens in other systems, is much less marked) the experimenter would be alerted to something having occurred within the dead time of the apparatus by the kinetics of the subsequent step. An acid-independent pathway is very difficult to rationalize in such a stoichiometrically simple protonation reaction!

3.3. Protonation of an Alkylidyne Ligand to an Alkylidene

Protonation of alkylidyne complexes can occur at either the metal or the carbon atom bound to the metal, and the factors that distinguish between protonation of the two sites are rather subtle.[25] For instance, protonation of $[W(CH)L_4Cl]$ gives the hydride $[WH(CH)L_4Cl]^+$ when L_2 is $Me_2PCH_2CH_2PMe_2$ and the alkylidene $[W(CH_2)L_4Cl]^+$ when L is PMe_3.

Molecular orbital calculations[26] indicate that the HOMO in alkylidyne complexes may be metal-centered or ligand-centered, or it may be the orbital of the metal–carbon π bond. Calculations of this type also indicate that the alkylidyne residue is always negatively charged, and in particular for the fragment $MoCCH_2tBu$, the build-up of charge is at the carbon atom adjacent to the metal. If the protonation of this residue is frontier orbital controlled, then attack is at the metal (where the HOMO is centered), whereas if the protonation is charge-controlled, attack is at the carbon.[27] Studies on $[Mo(\eta^5\text{-}C_5H_5)(CCH_2tBu)\{P(OMe)_3\}_2]$ indicate that protonation is charge-controlled; the initial site of attack is the carbon atom, and subsequent formation of the hydrido species occurs by an intramolecular hydrogen shift from the alkylidene group as shown in Scheme 7. Studies on $[W(CPh)(CNtBu)Cl(CO)(PMe_3)_2]$, in

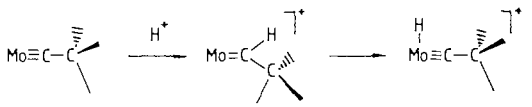

Scheme 7. Proposed mechanism for the protonation of $[Mo(\eta^5\text{-}C_5H_5)(CCH_2tBu)\{P(OMe)_3\}_2]$.

which three sites (metal, isocyanide, or alkylidyne) are potentially protonatable, indicates that the alkylidyne is protonated preferentially.[28]

It is worth noting that some alkylidene complexes can undergo rearrangement into the corresponding alkene, and in certain cases this process has been shown to be acid-catalyzed (Scheme 8).[29] The mechanism presumably involves the forma-

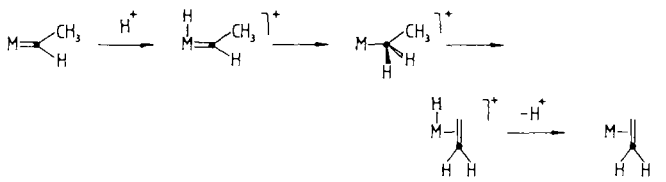

Scheme 8. Acid-catalyzed rearrangement of an alkylidene complex to form an alkene complex.

tion of a transient alkyl species, which then undergoes an intramolecular hydrogen migration from the remote carbon atom (β-hydrogen transfer) and subsequent proton release. However such rearrangements are not always acid catalyzed, as for example the intramolecular conversion of $[Re(\eta^5\text{-}C_5H_5)(CHEt)(NO)(PPh_3)]$ into $[Re(\eta^5\text{-}C_5H_5)(\eta^2\text{-}MeCHCH_2)(NO)(PPh_3)]$.[30]

There are two other examples in which apparent regioselective protonation occurs, but mechanistic studies demonstrate that the pathway is complicated. These examples will be discussed in this section, although they do not fall into any of the above headings.

3.4. Protonation of *trans*-$[\overline{Re(CH_2CCPh)Cl(dppe)_2}]$

The reaction of anhydrous HCl with the substituted coordinated allene complex, *trans*-$[\overline{Re(CH_2CCPh)Cl(dppe)_2}]$ gives an η^2-vinyl species in an apparently regioselective protonation as described by Equation (15).[31,32] This reaction exhibits a

$$trans\text{-}[\overline{Re(CH_2CCPh)Cl(dppe)_2}] + HCl \longrightarrow trans\text{-}[\overline{Re(\eta^2\text{-}CH_2CCHPh)Cl(dppe)_2}]^+ + Cl^- \quad (15)$$

simple first-order dependence on the concentration of the complex but a complicated dependence on the concentration of HCl as shown in Figure 1.[33] The complexity of this acid dependence

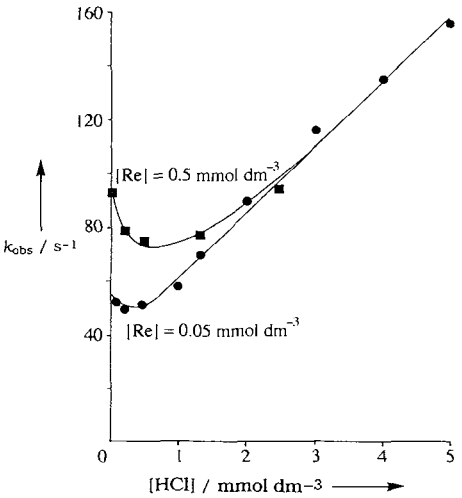

Fig. 1. Dependence of the observed rate constant k_{obs} on acid concentration for the protonation of *trans*-$[\overline{Re(CH_2CCPh)Cl(dppe)_2}]$.

is clearly inconsistent with any trivial mechanism involving direct protonation at the phenyl-substituted carbon atom, but is consistent with the mechanism shown in Scheme 9, in which the first step is the protonation of the metal ($K_1 > 80$; $k_1 \geq 1 \times 10^6\ dm^3\ mol^{-1}\ s^{-1}$) to give the hydrido species

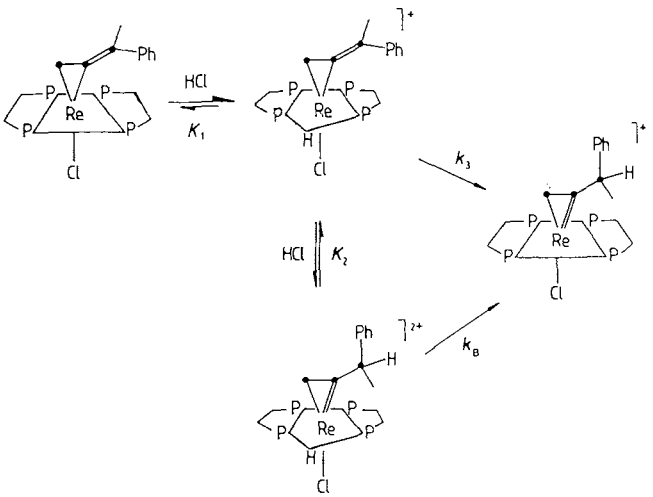

Scheme 9. Proposed mechanism of the protonation of *trans*-$[\overline{Re(CH_2CCPh)Cl(dppe)_2}]$.

$[\overline{Re(CH_2CCPh)}(H)Cl(dppe)_2]^+$, which occurs within the dead time of the stopped-flow apparatus (2 ms). This protonation would appear to be frontier orbital controlled, since extended Hückel calculations[32] indicate that the HOMO of *trans*-$[\overline{Re(CH_2CCPh)}Cl(dppe)_2]$ comprises predominantly the d_{xy}/d_{yz} orbitals on the rhenium atom (54%); the remaining electron density is divided between the phenyl-substituted carbon (36%) and the unsubstituted carbon atoms (10%) of the double bond.

The addition of the proton, albeit at the metal rather than the carbon, means that the stoichiometric requirements of reaction (15) have been met. The subsequent formation of the η^2-vinyl complex is associated with the rate law shown in Equation (16). This rate law describes two pathways: an intramolecular route ($k_3 = 94\ s^{-1}$) and an acid–base catalyzed route. The latter pathway involves rapid protonation of the hydrido complex ($K_2 = 1.37\ dm^3\ mol^{-1}$), followed by rate-limiting deprotonation of the metal by any base present in the system (k_B). The bases present in the system are the solvent (THF: $k_{THF} = 2.7\ dm^3\ mol^{-1}\ s^{-1}$), Cl^- ($k_{Cl} = 2.4 \times 10^4\ dm^3\ mol^{-1}\ s^{-1}$), and even the chloro group in HCl ($k_{HCl} = 3.4 \times 10^4\ dm^3\ mol^{-1}\ s^{-1}$).

$$k_{obs} = {}^{i}k_3 + K_2[HCl]/[Cl^-] \sum_B k_B[B]\}/(1 + K_2[HCl]/[Cl^-]) \quad (16)$$

The intramolecular pathway may be a direct, intramolecular transfer of the hydrogen from the metal to the carbon terminus. Consideration of the X-ray crystal structure of *trans*-$[\overline{Re(CH_2CCPh)}Cl(dppe)_2]$ indicates that in the intermediate $[\overline{Re(CH_2CCPh)}(H)Cl(dppe)_2]^+$ the hydrido ligand may be no more than 1.5–1.8 Å from the phenyl-substituted carbon atom—sufficiently close to permit a reasonably facile transfer.

3.5. Protonation of *trans*-$[W(\eta^2\text{-}C_2H_4)_2(dppe)_2]$

The reaction of an excess of anhydrous HX (X = Cl or Br) with *trans*-$[W(\eta^2\text{-}C_2H_4)_2(dppe)_2]$ gives the pentagonal-bipyramidal hydrido species shown in Equation (17).[34] Protonation

$$trans\text{-}[W(\eta^2\text{-}C_2H_4)_2(dppe)_2] + HX \longrightarrow [WH(\eta^2\text{-}C_2H_4)_2(dppe)_2]^+ + X^- \quad (17)$$

would appear to involve regioselective attack at the metal center. When studied on a stopped-flow spectrophotometer, the reaction clearly occurs in two distinct phases. Typical absorbance–time traces for this reaction, at high and low concentrations of acid, are shown in Figure 2. At all acid concentrations the curves are exponential, and at low concentrations of acid the initial absorbance is that of *trans*-$[W(\eta^2\text{-}C_2H_4)_2(dppe)_2]$, and the final absorbance is that of the hydride product. However, at higher concentrations of acid, although the final absorbance still corresponds to that of the hydride, the initial absorbance is now markedly lower than that of the parent complex, and at intermediate acid concentrations intermediate initial absorbances are observed. The dependence of the initial absorbance on the concentration of HX can be quantified as shown on the left-hand side of Figure 2: this analysis demonstrates that within 2 ms an equilibrium associated with the addition of a single proton to *trans*-$[W(\eta^2\text{-}C_2H_4)_2(dppe)_2]$ is established. However, this proton must have been added to the wrong position, since a further reaction (associated with the exponential decay) is required to form the hydride.

The subsequent formation of the hydrido product occurs by two pathways: one acid-independent and another showing a first-order dependence on the concentration of acid. All of this behavior is consistent with the mechanism shown in Scheme 10.

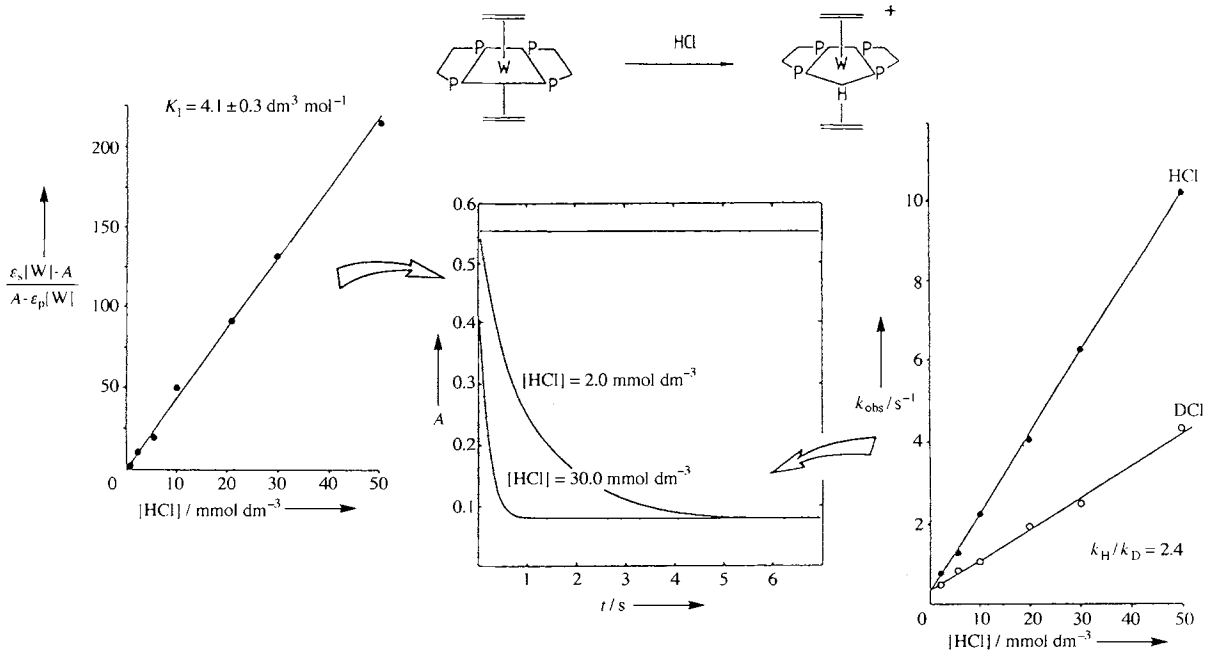

Fig. 2. The protonation of *trans*-$[W(\eta^2\text{-}C_2H_4)_2(dppe)_2]$ (top) and the experimental absorbance–time traces (bottom center). The dependence of the initial absorbance on acid concentration is depicted on the left (ε_s: extinction coefficient of the starting material, ε_p: extinction coefficient of the product, [W]: total tungsten concentration) and the plots of the observed rate constant k_{obs} against acid concentration for HCl and DCl on the right.

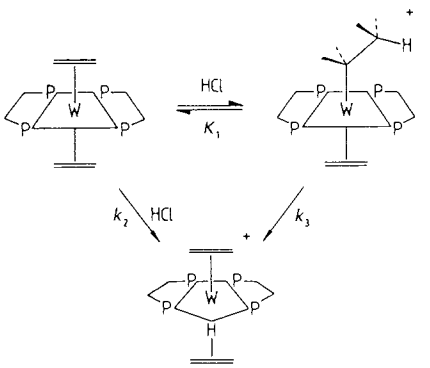

Scheme 10. Proposed mechanism for the protonation of *trans*-[W(η^2-C_2H_4)$_2$(dppe)$_2$].

Thus in a rapid equilibrium the ethene ligand is protonated ($K_1 = 4.1\ dm^3 mol^{-1}$, with HCl), which generates the ethyl species. At low concentrations of acid subsequent rate-limiting intramolecular migration of a hydrogen atom from the remote carbon atom of the ethyl ligand to the metal (β-hydrogen transfer) forms the hydrido product ($k_3 = 0.15\ s^{-1}$). At higher concentrations of acid a further pathway involving direct protonation of *trans*-[W(η^2-C_2H_4)$_2$(dppe)$_2$] at the metal contributes to the reaction. This latter pathway is associated with a significant primary isotope effect ($k_3^H/k_3^D = 2.43$).

Thus, although the stoichiometric equation indicates that the ethene ligands are innocent spectators to the reaction occurring at the metal site, mechanistic studies show that in at least one of the pathways the ethene ligands are intimately involved in transferring the proton to the metal. This noninnocent role for the ethene ligands is confirmed in the studies between *trans*-[W(η^2-C_2H_4)$_2$(dppe)$_2$] and an excess of anhydrous ^{2}HBr. Isolation of the product and its characterization by ^{2}H NMR spectroscopy showed that deuterium was incorporated both at the hydride position and in the ethene ligands.

In *trans*-[W(η^2-C_2H_4)$_2$(dppe)$_2$] the rate of protonation of the coordinated ethene can be estimated as $k_1 \geq 1 \times 10^6\ dm^3 mol^{-1} s^{-1}$, and the rate of protonation of tungsten is $k_2 = 2 \times 10^2\ dm^3 mol^{-1} s^{-1}$. Hence the rate of protonation of the carbon is at least ten thousand times faster than at the tungsten. In the analogous molybdenum system, the ethene is again protonated more rapidly than the metal but now by only a factor of 100. This less marked difference in the molybdenum complex is because the protonation at molybdenum is faster than at tungsten in analogous complexes. Studies on the proton transfer reactions of metal hydride complexes indicate that the rate constant for metal-to-metal proton transfer decreases down a group: Cr > Mo $\gg$ W.

These studies on *trans*-[M(η^2-C_2H_4)$_2$(dppe)$_2$] (M = Mo or W) define unambiguously the more rapidly protonated site. However, this is the exception rather than the rule. For instance, in the closely related propyne complex *trans*-[Mo(η^2-MeCCH)$_2$(dppe)$_2$], the propyne gives the vinyl species *trans*-[Mo(CHCHMe)(η^2-MeCCH)(dppe)$_2$]$^+$ within 2 ms. However, the proton's route to this site cannot be identified. It is possible that the proton adds either directly to the carbon site or binds initially to the metal with subsequent intramolecular migration to the carbon. In the latter case a lower limit for the rate of protonation of the metal can be estimated as $k \geq 1 \times 10^6\ dm^3 mol^{-1} s^{-1}$. This value is much faster than the rate constant for protonation of the metal site in the analogous ethene complex, but is still ten thousand times slower than the diffusion-controlled limit.

The chemistry established in this system is the foundation of the work on product specificity discussed in Section 4.

4. Using Protons as a Means of Product Control

In the discussion so far three general mechanistic principles have emerged for the protonation of complexes containing unsaturated hydrocarbons: 1) The initial site of protonation may not be the final residence of the proton. 2) Protonation can occur at both the metal and the hydrocarbon ligands. 3) Acid-catalyzed or intramolecular rearrangements can, in effect, transfer a proton between the metal and the ligand.

In the remainder of this article we shall see how these mechanistic features, and in particular that protonation can occur either the carbon or the metal, can be used to our advantage—first to control the selective production of alkane, alkene, or alkyne from alkene-based complexes, and second to control the stereochemistry of hydrocarbon products.

4.1. Protonation of *trans*-[Mo(η^2-C_2H_4)$_2$(dppe)$_2$]: Formation of Ethene and Ethane

The protonation of *trans*-[Mo(η^2-C_2H_4)$_2$(dppe)$_2$] with anhydrous HCl gives mixtures of ethane and ethene together with well-defined metal complexes. A limiting stoichiometric reaction is given by Equation (18); however, as we shall see later,

$$\textit{trans}\text{-}[Mo(\eta^2\text{-}C_2H_4)_2(dppe)_2] + 2HCl \longrightarrow \textit{trans}\text{-}[MoCl_2(dppe)_2] + C_2H_4 + C_2H_6 \quad (18)$$

this equation is only valid at relatively low concentrations of acid; at high concentrations of acid other products are formed.[35] Clearly this is a multistage reaction involving, at the very least, diprotonation of one of the ethene ligands, transfer of two electrons from the metal to the protonated ligand, release of one molecule each of ethene and ethane, and the binding of two chlorine atoms to the molybdenum center. This complexity is reflected in the stopped-flow absorbance–time trace for this reaction (Fig. 3). Three distinct stages are evident: an initial absorbance jump, complete within the dead time of the apparatus, is followed by an exponential absorbance decrease and finally an absorbance increase, which is also exponential. This trace is a kineticist's dream that can rapidly become a nightmare in trying to define what elementary reactions are associated with each stage. If we were to come "cold" to this multistage trace, there would be little chance of unambiguously identifying the steps occurring at each stage. However, the previous study on the analgous tungsten complex described in Section 3.5 has identified the characteristic behavior associated with the initial protonation of this type of complex.

The first two stages of the reaction of HCl with *trans*-[Mo(η^2-C_2H_4)$_2$(dppe)$_2$] recorded with a stopped-flow apparatus show behavior similar to that observed for the tungsten analogue (Section 3.5): an initial absorbance decrease, complete within

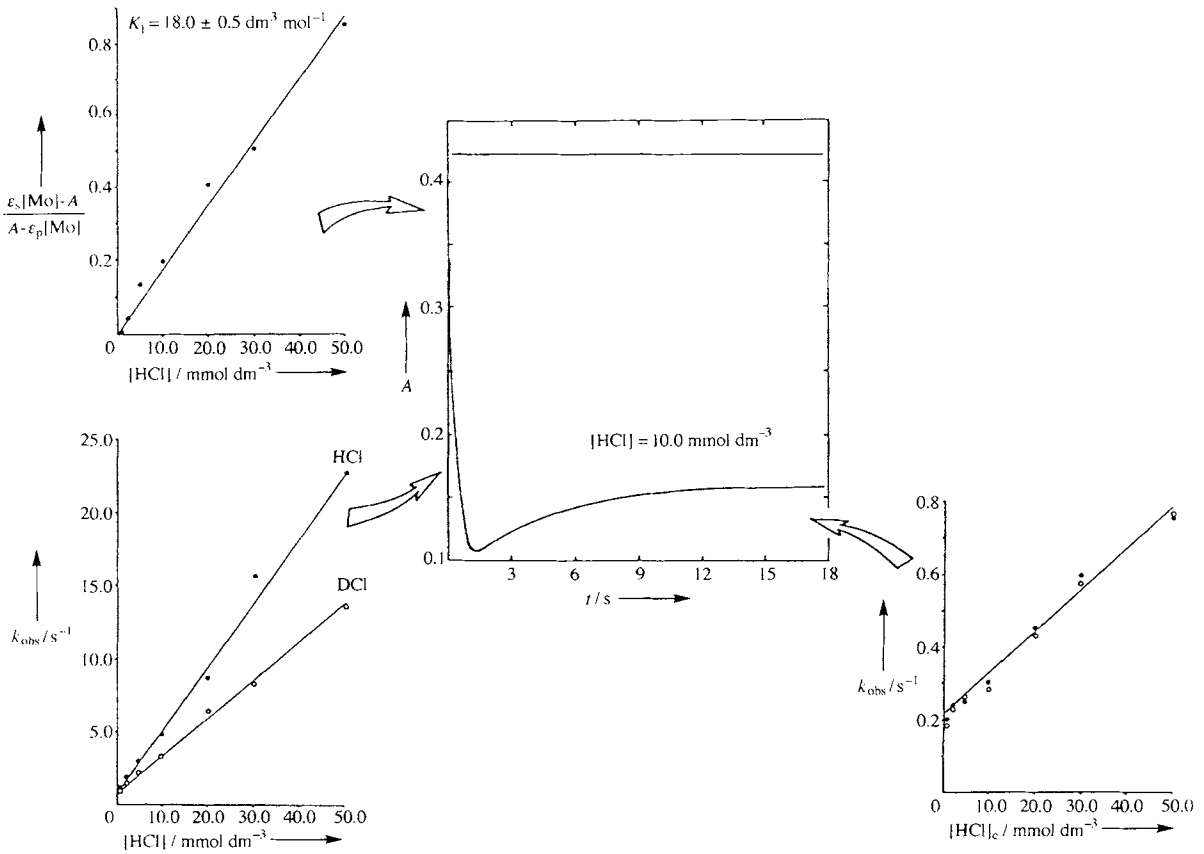

Fig. 3. The protonation of *trans*-[Mo(η^2-C_2H_4)$_2$(dppe)$_2$] to form ethene and ethane: the experimental absorbance–time trace and the dependence of the rates of relevant stages of the reaction on acid concentration ([Mo]: total molybdenum concentration, ε_s: extinction coefficient of the starting material, ε_p: extinction coefficient of the product [HCl]$_c$ = [HCl] − [Mo] (corrected acid concentration)).

2 ms, whose magnitude depends on the concentration of acid, followed by an exponential decay; the latter process shows a dependence on the concentration of HCl as illustrated in Figure 3.[34] Consequently, we can be confident that these first two phases correspond to the formation of the hydrido species [MoH(η^2-C_2H_4)$_2$(dppe)$_2$]$^+$ by two pathways: 1) rapid protonation of the ethene ligand ($K_1 = 18$ dm^{3}mol^{-1}), followed by intramolecular β-hydrogen transfer from the ethyl ligand to the metal ($k_3 + k_{-3}$) = 0.22 s^{-1}, and 2) direct protonation of the metal in *trans*-[Mo(η^2-C_2H_4)$_2$(dppe)$_2$] ($k_2 = 4.6 \times 10^2$ dm^{3}mol^{-1}s^{-1}, $k_H/k_D = 1.64$, Scheme 11). The only difference between this system and the protonation of the tungsten complex is that in this molybdenum system an equilibrium mixture of the parent complex, the ethyl complex, and the hydrido species is produced. This conclusion is consistent with previous work,[36] which showed that in solution [Mo(C_2H_5)(η^2-C_2H_4)(dppe)$_2$]$^+$ is in dynamic equilibrium with [MoH(η^2-C_2H_4)$_2$(dppe)$_2$]$^+$ and that the magnitude of the absorbance changes for these stages depend upon the acid concentration.

A further absorbance increase is observed over the last 20 seconds of the absorbance–time trace, the magnitude and rate of which depends on the concentration of acid. This stage corresponds to the protonation of the equilibrium mixture of *trans*-[Mo(η^2-C_2H_4)$_2$(dppe)$_2$], [MoH(η^2-C_2H_4)$_2$(dppe)$_2$]$^+$, and [Mo(C_2H_5)(η^2-C_2H_4)(dppe)$_2$]$^+$ to produce the dihydrido species [MoH$_2$(η^2-C_2H_4)$_2$(dppe)$_2$]$^{2+}$.

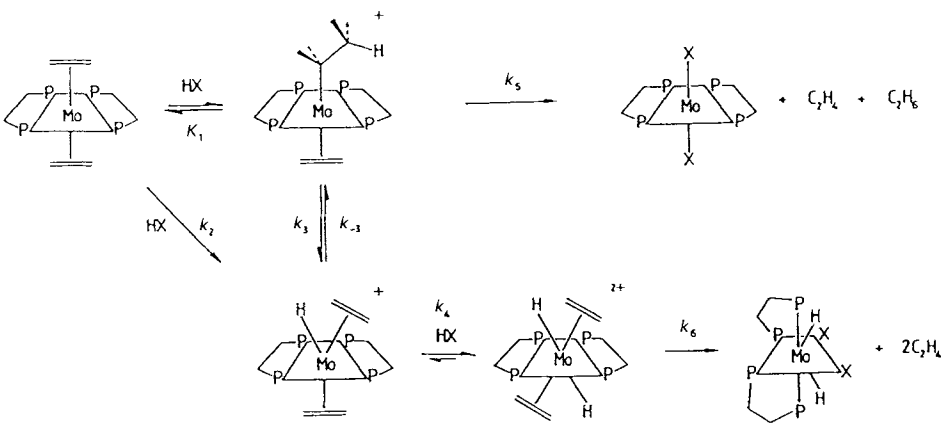

Scheme 11. Elementary reactions for the protonation of *trans*-[Mo(η^2-C_2H_4)$_2$(dppe)$_2$] to form ethene and ethane.

The kinetics of the third stage exhibits a simple two-term rate law: one term is independent of the concentration of acid and the other shows a first-order dependence on the concentration of acid. Protonation of the equilibrium mixture formed at the end of the second stage disturbs the position of this

equilibrium, and analysis of the kinetics for the third stage reveals that the term independent of the concentration of acid corresponds to $(k_3 + k_{-3})$, that is, to the sum of the rate constants for the equilibrium between $[Mo(C_2H_5)(\eta^2\text{-}C_2H_4)(dppe)_2]^+$ and $[MoH(\eta^2\text{-}C_2H_4)_2(dppe)_2]^+$. The value of $(k_3 + k_{-3})$ is already known from the analysis of the kinetics of the second stage and is in excellent agreement with the value derived from analysis of the third stage.

The discussion so far presents an internally consistent kinetic model for the early stages of the reaction of *trans*-$[Mo(\eta^2\text{-}C_2H_4)_2(dppe)_2]$, and this mechanistic behavior is reconcilable with that of the tungsten analogue. However, the identity of the intermediates has been confirmed by spectroscopic detection, isolation, and characterization. In particular the species formed at the end of the second stage has the same electronic spectrum as that of isolated $[MoH(\eta^2\text{-}C_2H_4)_2(dppe)_2]HCl_2$. However, as is typical of electronic spectra in general, this spectrum consists of rather broad peaks and is not particularly diagnostic. Certainly no structural information about the intermediate can be obtained by this method. A much better identification of the intermediates results from studying the reactions in the probe of an NMR spectrometer.

Figure 4 illustrates the course of reaction (18) as monitored by $^{31}P\{^1H\}$ NMR spectroscopy. In order to detect the intermediates, which at room temperature only have a fleeting exis

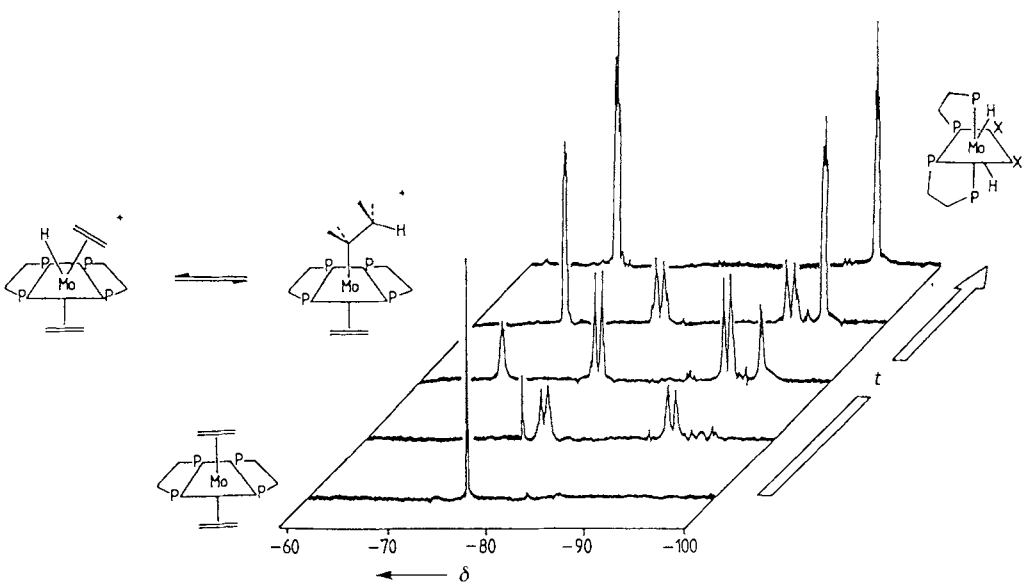

Fig. 4. The time course of the protonation of *trans*-$[Mo(\eta^2\text{-}C_2H_4)_2(dppe)_2]$ to form ethene and ethane, monitored by $^{31}P\{^1H\}$ NMR spectroscopy.

tence, the reaction is performed at relatively low concentrations of acid and low temperatures (typically $-80\,^\circ C$). The use of $^{31}P\{^1H\}$ NMR spectroscopy has the advantage that only signals associated with the complex are present, and the other components of the mixture (the acid and solvent etc.) do not complicate the spectrum. The singlet at $\delta = -78$ in the first spectrum of this series is that of the parent complex, *trans*-$[Mo(\eta^2\text{-}C_2H_4)_2(dppe)_2]$. As time passes, this peak decreases in intensity, and a new set of signals appear [$\delta = -80.0$ (d), $\delta = -92.2$ (d); $J_{P,P} = 81.8$ Hz; AA'BB' pattern]. The intensity of this pair of doublets increases, then slowly decreases as, finally, the peaks of one of the products appear. The spectrum that consists of a deceptively simple pair of doublets is that of the equilibrium mixture of $[Mo(C_2H_5)(\eta^2\text{-}C_2H_4)(dppe)_2]^+$ and $[MoH(\eta^2\text{-}C_2H_4)_2(dppe)_2]^+$ and has been observed in earlier variable temperature studies on this[36] and analogous systems.[37] However, this is the first time this spectrum has been observed for an intermediate in the protonation reactions of *trans*-$[Mo(\eta^2\text{-}C_2H_4)_2(dppe)_2]$.

This study confirms the nature of the intermediates at the end of the second stage, which was proposed on the basis of the kinetic analysis. Furthermore, at higher concentrations of acid we observe the expected contribution to the spectrum associated with the presence of $[MoH_2(\eta^2\text{-}C_2H_4)_2(dppe)_2]^{2+}$. The spectrosopic changes are similar to those shown in Figure 4, but now the spectrum of the intermediate is slightly different. It still consists of a pair of doublets, but the chemical shift separation between the doublets is smaller [$\delta = -76.2$ (d), $\delta = -92.2$ (d)], and the doublet separation itself (which is the phosphorus–phosphorus coupling constant, $J_{P,P} = 73.5$ Hz) is about 8 Hz smaller than in the spectrum observed at low concentrations of acid. The spectrum at high acid concentrations is consistent with the presence of a species that is structurally similar to that detected at low concentrations of acid, and the smaller value of $J_{P,P}$ indicates an increased protonation of the metal.[38]

$[MoH(\eta^2\text{-}C_2H_4)_2(dppe)_2]HCl_2$ has been isolated from the reaction mixture at low concentrations of acid by rapid crystallization, but attempts to isolate $[MoH_2(\eta^2\text{-}C_2H_4)_2(dppe)_2]^{2+}$ were unsuccessful, even at high concentrations of acid. The only species isolated was the monohydride, presumably because of the poorer solubility of this species and the rapidity of the monohydride–dihydride protonation equilibrium.

The multiple protonation equilibria shown in Scheme 11 are established within about 20 s. However, the evolution of both ethane and ethene (monitored by GLC) from the reaction mixture has a half-life of about 40 min. The rate of formation of either hydrocarbon is independent of the concentration of acid, but the relative proportions of ethane and ethene depend markedly on the concentration of acid (Fig. 5). Thus at relatively low concentrations of HCl one equivalent each of ethane and ethene are produced. At higher concentrations of acid the carbon mass-balance is maintained, but the proportion of ethane progressively decreases, and the proportion of ethene increases correspondingly until, at $[HCl] \approx 200$ mmol dm^{-3}, two equivalents of ethene are produced.

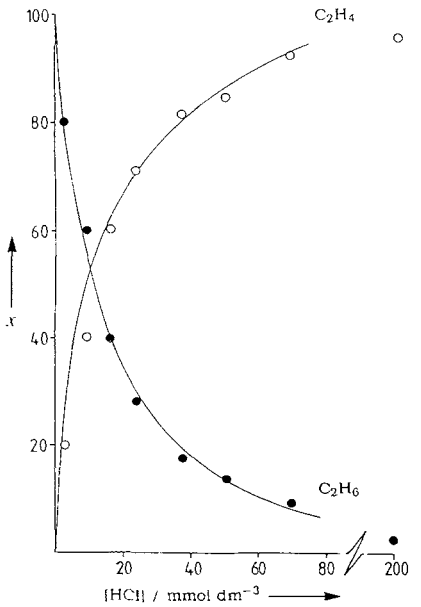

Fig. 5. Dependence of the product distribution on the acid concentration for the protonation of *trans*-$[Mo(\eta^2\text{-}C_2H_4)_2(dppe)_2]$.

The mechanism by which these hydrocarbons are formed is shown in Scheme 11. At low concentrations of HCl the predominant species in solution are the complexes of the equilibrium mixture of *trans*-$[Mo(\eta^2\text{-}C_2H_4)_2(dppe)_2]$, $[MoH(\eta^2\text{-}C_2H_4)_2(dppe)_2]^+$, and $[Mo(C_2H_5)(\eta^2\text{-}C_2H_4)(dppe)_2]^+$. Rate-limiting dissociation of the ethene ligand from $[Mo(C_2H_5)(\eta^2\text{-}C_2H_4)(dppe)_2]^+$, followed by rapid attack of chloride at the metal commits the ethyl ligand to form ethane, presumably by rapid protonation of the ethyl ligand. Thus, under these conditions, one equivalent each of ethene and ethane are produced together with *trans*-$[MoCl_2(dppe)_2]$.

At higher concentrations of HCl further protonation occurs at the metal, and $[MoH_2(\eta^2\text{-}C_2H_4)_2(dppe)_2]^{2+}$ dominates the equilibrium mixture. This further protonation at the metal labilizes both ethene ligands towards dissociation, and thus at high concentrations of acid two equivalents of ethene are produced together with $[MoH_2Cl_2(dppe)_2]$.

The product $[MoH_2Cl_2(dppe)_2]$ has been isolated and characterized. Indeed it is this species whose spectrum is observed in the last spectrum recorded in Figure 4. The product formed at low concentrations of acid, *trans*-$[MoCl_2(dppe)_2]$, has also been isolated and characterized by the common techniques, in particular by its characteristic electrochemical behavior.[39] However, this compound has a d^4 ($S = 1$) configuration and is silent in both EPR and NMR spectroscopy.

The mechanism shown in Figure 3 quantitatively predicts the hydrocarbon product distribution. Since the rate of production of both ethane and ethene is essentially the same, the composition of the hydrocarbon mixture varies with the concentration of HCl according to Equation (19), which has made allowance

$$\frac{[C_2H_6]}{[C_2H_6]+[C_2H_4]} = \frac{k_3 + k_{-3}}{(k_3 + k_{-3}) + k_4[HCl]} \qquad (19)$$

for the fact that one equivalent of ethene is produced in both pathways. All the elementary rate constants in this equation are known from the kinetic analysis. When the values are substituted into this equation the curves obtained are an excellent fit to the experimental product distribution as shown in Figure 5.

One of the most important aspects of this hydrocarbon product distribution is that it is counterintuitive. After all, in order to produce ethane by the protonation of an ethene ligand, the ethene must be supplied with two electrons and two protons. In a system such as that described here, where the two electrons are already "stored" in the metal, it would seem intuitive that the higher the concentration of acid, the more likely it is that the ethene will protonate, and hence it would be predicted that ethane would be produced preferentially at high concentrations of acid. This is the opposite to the behavior actually observed. However, the observed product distribution is readily understood when it is appreciated that protonation can occur at either the metal or the hydrocarbon, and the site that is protonated defines the hydrocarbon product.

The mechanism in Scheme 11 shows that there is no problem in protonating the ethene in these complexes (indeed it is these ligands which are protonated most rapidly), and when protonated ethane is produced. However, at high concentrations of acid further protonation of the metal occurs and results in the deactivation of the ethene ligand towards protonation and the labilization of the system to the dissociation of ethene.

Just by adding protons the product of the reaction can be controlled. The origin of this control is the sites of protonation: metal or ligand. The product of the reaction can also be controlled after the protonation step by changing the coligands on the complex as illustrated in Scheme 12. Having formed *trans*-

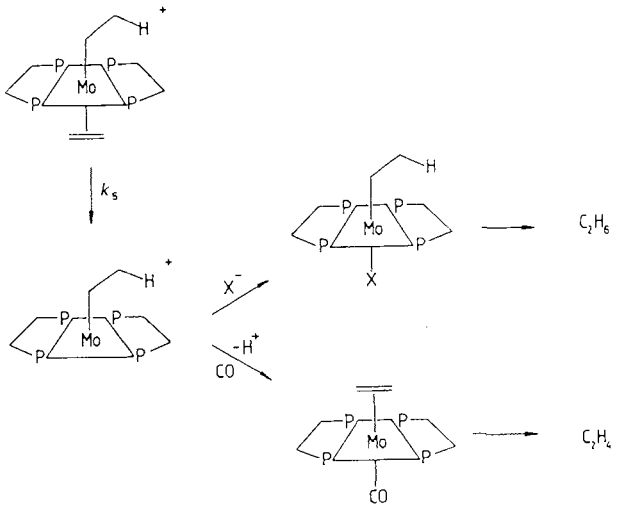

Scheme 12. Controlling the product distribution after the protonation of $[Mo(C_2H_5)(\eta^2\text{-}C_2H_4)(dppe)_2]^+$ by varying the coligands.

$[Mo(C_2H_5)(\eta^2\text{-}C_2H_4)(dppe)_2]^+$, rate-limiting dissociation of the ethene ligand is usually followed by binding of chloride. However, carbon monoxide can bind preferentially to form *trans*-$[Mo(C_2H_5)(CO)(dppe)_2]^+$. The electron-withdrawing effect of the coordinated carbon monoxide results in proton loss from the ethyl ligand, subsequent release of ethene, and ultimate formation of *trans*-$[Mo(CO)_2(dppe)_2]$. Thus, even at low concentrations of acid the system can be forced to evolve only ethene if the coordination sphere of the complex is perturbed.

Under an atmosphere of dihydrogen the situation is less clear cut, but about 20% of the hydrocarbon released at an HCl concentration of 200 mmol dm^{-3} is ethane, whereas under an atmosphere of argon no ethane is produced under these condi-

tions. It would therefore appear that dihydrogen can also bind to the vacant site generated on dissociation of ethene from $[MoH_2(\eta^2\text{-}C_2H_4)_2(dppe)_2]^{2+}$ to form a species (presumably $[MoH_4(\eta^2\text{-}C_2H_4)(dppe)_2]^{2+}$), which is sufficiently hydride-rich to produce some ethane from this route.

4.2. Protonation of *trans*-$[MoH(\eta^3\text{-}C_3H_5)(dppe)_2]$: Formation of Propene and Propyne

The protonation of any alkene other than ethene introduces another potential type of reactivity, which is a consequence of the intramolecular rearrangement possible with higher alkenes shown in Scheme 13. Only one molecule of propene will bind to

Scheme 13. The dynamic equilibrium between $[Mo(\eta^2\text{-}MeCHCH_2)(dppe)_2]$ and $[MoH(\eta^3\text{-}C_3H_5)(dppe)_2]$ illustrating the additional pathway for higher alkenes.

the $\{Mo(dppe)_2\}$ site, and variable temperature NMR spectroscopy has shown that $[Mo(\eta^2\text{-}MeCHCH_2)(dppe)_2]$ is in dynamic equilibrium with $[MoH(\eta^3\text{-}C_3H_5)(dppe)_2]$.[36] The solid state structure of this complex and the tungsten analogue has been established by X-ray crystallography.[40] The structures are essentially the same, and that of $[WH(\eta^3\text{-}C_3H_5)(dppe)_2]$ is shown in Figure 6. Two important structural features evident

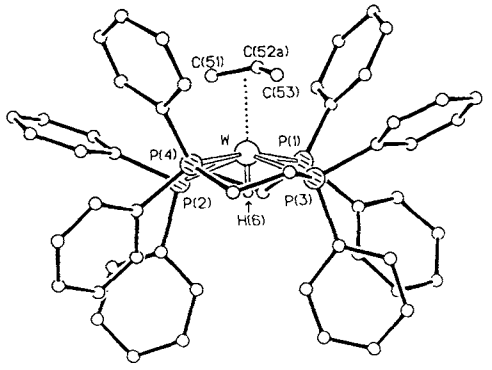

Fig. 6. The crystal structure of $[MoH(\eta^3\text{-}C_3H_5)(dppe)_2]$. Selected bond lengths [Å] and the angle of the allyl group [°]: W-P(average) 2.465 ± 0.007, W-C51 2.372(16), W-C53 2.334(14), W-C52a 2.258(30), C51-C52a 1.35(4), C53-C52a 1.23(4), W-H 1.03(9); C51-C52a-C53 139(3).

from this study are pertinent to the discussion of the reactivity of this complex. First, the hydride (which was located) is *trans* to the allyl group; but, clearly, in solution this hydride must move around the metal surface if it is to transfer intramolecularly to the allyl residue. Second, there is nothing unusual about the geometry of the allyl group: the carbon–carbon bond lengths are typical of an allyl group and the CCC angle is not flattened.

The reactivity that $[MoH(\eta^3\text{-}C_3H_5)(dppe)_2]$ exhibits in its reactions with anhydrous HCl [Eqs. (20) and (21)] led us to look for

$$trans\text{-}[MoH(\eta^3\text{-}C_3H_5)(dppe)_2] + 2HCl \longrightarrow [MoH_2Cl_2(dppe)_2] + MeCHCH_2 \quad (20)$$

$$trans\text{-}[MoH(\eta^3\text{-}C_3H_5)(dppe)_2] + 2HCl \longrightarrow [MoH_2Cl_2(dppe)_2] + H_2 + MeCCH \quad (21)$$

such a distortion in this molecule.[41] At all acid concentrations the same metal product, $[MoH_2Cl_2(dppe)_2]$ is formed. However, the hydrocarbon product is propene at low concentrations of HCl, but propyne at high concentrations of acid. That is, by protonating a complex derived from an alkene we can produce an alkyne!

In order to understand this reaction in more detail it has been studied mechanistically. Before the mechanism is discussed a further structural aspect of the work has to be clarified. The equilibrium between the propene and allyl forms of the molybdenum complex is rapid at 25.0 °C, and thus it is unclear which form is the reactive entity in the protonation reactions. Two-dimensional $\{^1H\text{-}^{13}C\}$ NMR spectroscopy has been used to assign unambiguously the peaks in the ^1H NMR spectrum that are attributable to $[Mo(\eta^2\text{-}MeCHCH_2)(dppe)_2]$ and $[MoH(\eta^3\text{-}C_3H_5)(dppe)_2]$. In this way it was established that at −40 °C the allyl species only is present. At this temperature, the system still reacts with HCl to form propyne at high concentrations of acid. This indicates that the allyl form is the reactive species, and this is confirmed in studies with the tungsten analogue.[42] *trans*-$[WH(\eta^3\text{-}C_3H_5)(dppe)_2]$ is always in the allyl form; even at +40 °C there is no sign of the propene species, and the hydride signal ($\delta = -2.8$, quintet, $J_{H,P} = 35$ Hz) is still well resolved. This complex reacts with anhydrous acid to produce propene at low concentrations of acid and propyne at high concentrations of acid.

A study of the reaction of *trans*-$[MoH(\eta^3\text{-}C_3H_5)(dppe)_2]$ with an excess of anhydrous HCl on a stopped-flow apparatus shows the same simple behavior under all conditions: an exponential absorbance–time decay.[41] The final absorbance apparently corresponds to that of the product, $[MoH_2Cl_2(dppe)_2]$ (see later discussion), but the initial absorbance is slightly lower than that expected for *trans*-$[MoH(\eta^3\text{-}C_3H_5)(dppe)_2]$. The difference between the expected and the observed initial absorbance is independent of the concentration of acid. The reaction exhibits a first-order dependence on the concentration of complex and a dependence on the concentration of HCl as described by Equation (22). These simple kinetics are to be contrasted with the

$$k_{obs} = k_3 + k_4[HCl] \quad (22)$$

hydrocarbon product distribution shown in Figure 7, which changes quite dramatically in the acid concentration range over which the kinetics are defined. At low concentrations of acid, propene is the predominant product. At higher concentrations of acid, the carbon mass-balance is maintained, but the proportion of propene decreases whilst the amount of propyne increases proportionately until at $[HCl] > 200$ mmol dm^{-3} propyne is the exclusive product. This behavior is analogous to that observed with the ethene system: the more unsaturated hydrocar-

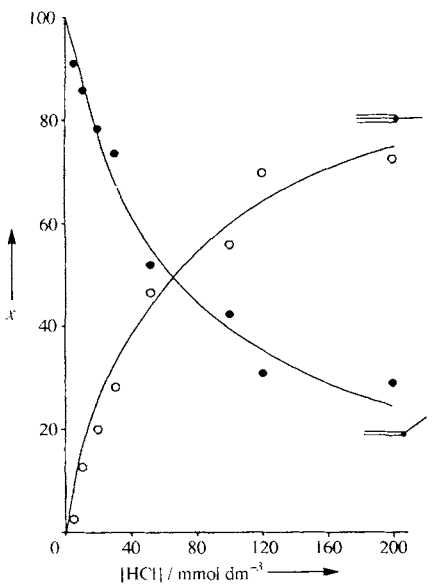

Fig. 7. The dependence of the hydrocarbon product distribution on acid concentration for the protonation of *trans*-[MoH(η^3-C_3H_5)(dppe)$_2$].

bon is formed only at the higher concentrations of acid. The mechanism of the reaction is shown in the lower portion of Scheme 14. Initial, rapid protonation of *trans*-[MoH(η^3-C_3H_5)(dppe)$_2$] at either the metal or the allyl group produces [MoH_2(η^3-C_3H_5)(dppe)$_2$]$^+$ and [MoH(η^2-MeCHCH$_2$)(dppe)$_2$]$^+$, respectively. The cationic propene complex subsequently undergoes rate-limiting dissociation of the propene ($k_3 = 4.3\,s^{-1}$) and ultimate formation of [MoH_2Cl_2(dppe)$_2$].

At low concentrations of acid, any [MoH_2(η^3-C_3H_5)(dppe)$_2$]$^+$ formed converts into [MoH(η^2-MeCHCH$_2$)(dppe)$_2$]$^+$, either by an intramolecular migration, or by proton dissociation to reform the parent allyl complex. Hence, under these conditions, one equivalent of propene is formed.

At higher concentrations of acid a further protonation of [MoH_2(η^3-C_3H_5)(dppe)$_2$]$^+$ can occur, probably at the allyl group to form [MoH_2(η^2-MeCHCH$_2$)(dppe)$_2$]$^{2+}$ (k_4 = 3.8×10^3 dm^3 mol^{-1} s^{-1}), and this commits the system to the formation of propyne. The important mechanistic point is that this second protonation labilizes the system, not to the loss of hydrocarbon but to the preferential loss of dihydrogen. It seems most likely that the dissociation of dihydrogen generates a coordinatively unsaturated, formally fourteen-electron species, [Mo(η^2-MeCHCH$_2$)(dppe)$_2$]$^{2+}$. In order to counteract this electron deficiency the metal dehydrogenates the coordinated propene to generate the formally sixteen-electron propyne species, [MoH_2(η^2-MeCCH)(dppe)$_2$]$^{2+}$, from which propyne subsequently dissociates. At high concentrations of acid, protonation of [MoH_2(η^3-C_3H_5)(dppe)$_2$]$^+$ is faster than dissociation of propene from [MoH(η^2-MeCHCH$_2$)(dppe)$_2$]$^+$, so under these conditions this propene complex converts into [MoH_2(η^3-C_3H_5)(dppe)$_2$]$^+$ and one equivalent of propyne is formed.

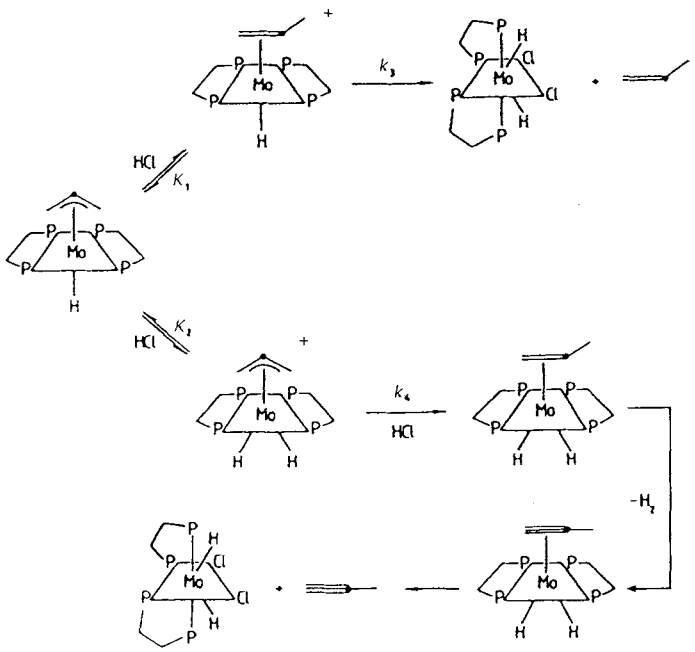

Scheme 14. Proposed mechanism for the formation of propene and propyne by the protonation of *trans*-[MoH(η^3-C_3H_5)(dppe)$_2$].

The hydrocarbon product distribution that this mechanism predicts is given by Equation (23). The elementary rate and

$$\frac{[\text{MeCCH}]}{[\text{MeCCH}] + [\text{MeCHCH}_2]} = \frac{k_4[\text{HCl}]}{k_4[\text{HCl}] + k_3(K_1/K_2)} \qquad (23)$$

equilibrium constants in this equation are known from the kinetic analysis, except for the ratio K_1/K_2. However, the best fit to the data is obtained when $K_1/K_2 \approx 50$. This is similar behavior to that observed with *trans*-[Mo(η^2-C_2H_4)$_2$(dppe)$_2$]: protonation of the hydrocarbon ligand is more favorable than protonation of the metal.

The details of how the propene and propyne are formed from [MoH(η^2-MeCHCH$_2$)(dppe)$_2$]$^+$ and [MoH_2(η^2-MeCHCH$_2$)(dppe)$_2$]$^{2+}$, respectively, are still not fully understood, and clearly more detail concerning these steps is required. The time course for the production of propene and propyne is shown in Figure 8a.[42] Propene is evolved quantitatively within about two minutes whereas it takes about an hour to produce the propyne quantatively. This indicates that the final absorbance observed in the stopped-flow experiments at high concentrations of acid is not that of [MoH_2Cl_2(dppe)$_2$], but rather corresponds to a precursor whose electronic spectrum is similar to that of the dichloro product. It seems likely that this precursor is [MoH_2(η^2-MeCCH)(dppe)$_2$]$^{2+}$, which slowly evolves propyne. In addition it is clear that dihydrogen evolution precedes propyne evolution consistent with the proposed mechanism.

Intermediates in the propyne-forming pathway have been detected by low temperature $^{31}P\{^1H\}$ NMR spectroscopy (Fig. 8b).[42] The spectra recorded for relatively low concentrations of acid are shown on the right. In the first spectrum the peak in the correct position for *trans*-[MoH(η^3-C_3H_5)(dppe)$_2$] is significantly broadened. This broadening is due in part to the low temperature, but mostly because the spectrum corresponds to the equilibrium mixture of *trans*-[MoH(η^3-C_3H_5)(dppe)$_2$], *trans*-[MoH(η^2-MeCHCH$_2$)(dppe)$_2$]$^+$, and *trans*-[MoH_2(η^3-C_3H_5)(dppe)$_2$]$^+$. As time passes this broad peak slowly decreases in intensity, and the only new peaks that appear are those of the product, [MoH_2Cl_2(dppe)$_2$]. No intermediates are detected under these conditions indicating that only short-lived species are generated on the propene-forming pathway.

At high concentrations of acid the propyne-forming pathway will dominate, and under these conditions at least three intermediates are detectable, as shown on the left of Figure 8b. As the broad peak associated with the protonation equilibria species

decreases in intensity three new sets of signals appear consecutively: the first around the initial peak, the second at high field, and the third at intermediate field. Finally, the peaks attributable to the product $[MoH_2Cl_2(dppe)_2]$ appear. To date we have not been able to identify these intermediates unambiguously, or isolate them, even at low temperatures. However, a noticeable feature of these spectra is the pairs of doublets in the last two sets of signals. This is reminiscent of the spectrum of the intermediates observed in the reaction of *trans*-$[Mo(\eta^2\text{-}C_2H_4)_2(dppe)_2]$, and it is tempting to assign these signals to the species $[MoH_2(\eta^2\text{-}MeCHCH_2)(dppe)_2]^{2+}$ and $[MoH_2(\eta^2\text{-}MeCCH)(dppe)_2]^{2+}$.

We do not understand the factors which discriminate between the evolution of dihydrogen and the evolution of a hydrocarbon upon protonation of a complex. This is a crucial aspect of the reactivity in the $[MoH(\eta^3\text{-}C_3H_5)(dppe)_2]$. Recent studies on the reaction of $[MoH_3(CCt\text{Bu})(dppe)_2]$ with anhydrous HCl shown in Equation (24) demonstrate that the rate of coupling of two-hydrogen atoms and the rate of coupling a hydrogen atom with the alkynyl differ by less than a factor of 20.

$$[MoH_3(CCt\text{Bu})(dppe)_2] + 2HCl \longrightarrow [MoH_2Cl_2(dppe)_2] + t\text{BuCCH} + H_2 \quad (24)$$

4.3. Protonation of $[MoH(\eta^3\text{-}C_4H_7)(dppe)_2]$: Dimerization of an Alkene

One of the major problems in defining the details of the formation of either propene or propyne from *trans*-$[MoH(\eta^3\text{-}C_3H_5)(dppe)_2]$ is that the two pathways operate simultaneously. It would be advantageous if the formation of one hydrocarbon product could be studied in isolation over a wide acid concentration range. The conversion of the allyl ligand into propyne must involve the removal of the hydrogen atom bound to the central carbon atom. Consequently, protonation of a complex containing a 2-alkylallyl ligand must result only in the formation of the corresponding alkene. With this in mind we attempted to prepare and study the 2-methylallyl analogue of *trans*-$[MoH(\eta^3\text{-}C_3H_5)(dppe)_2]$.

The route used to prepare $[MoH(\eta^3\text{-}C_4H_7)(dppe)_2]$ is analogous to that used for all the compounds discussed in this section, and is shown in Scheme 15.[43] Reduction of $[MoCl_4(dppe)]$ by sodium amalgam, in the presence of dppe and under an atmosphere of isobutene gives, after about 18 hours, the labile, orange complex $[Mo(\eta^2\text{-}Me_2CCH_2)_2(dppe)_2]$. This reduction takes place via a bright green intermediate, which can be isolated and shown to be the molybdenum(II), five-coordinate, sixteen-electron species. This complex contains a 2-methylallyl and a hydrido ligand as confirmed by both ^1H and ^{13}C NMR spectroscopy at room temperature. However, it seems that the 2-methylallyl ligand is sufficiently bulky that two sterically demanding dppe ligands cannot be coordinated through all four phosphorus atoms, and hence one of the dppe ligands is only monodentate. $[MoH(\eta^3\text{-}C_4H_7)(dppe)_2]$ undergoes reversible changes in the NMR spectrum when the temperature is varied. Thus, although at 25.0 °C the species is undoubtedly a 2-methylallyl complex, upon cooling an intramolecular,

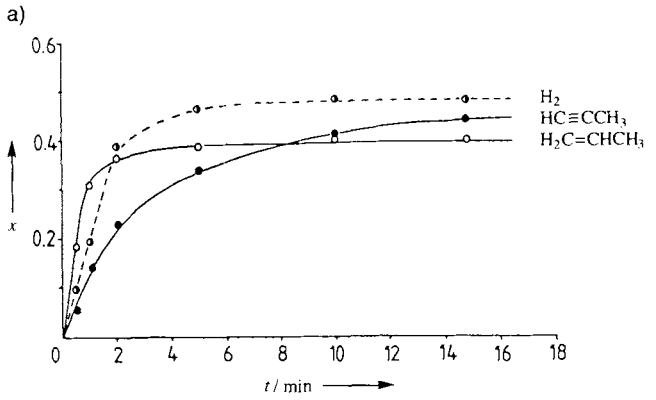

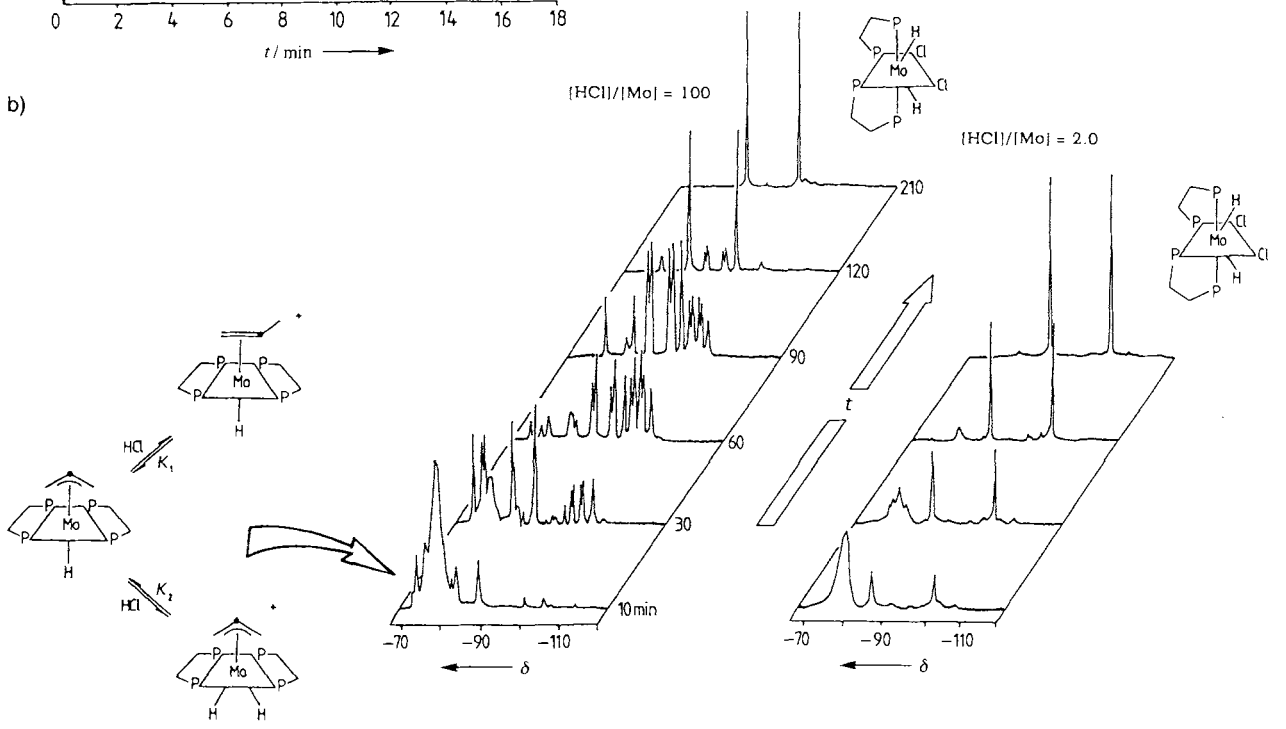

Fig. 8. a) Time course for the evolution of the products in the protonation of *trans*-$[MoH(\eta^3\text{-}C_3H_5)(dppe)_2]$ (x = moles gas per mole complex; b) time course of this reaction monitored by low temperature $^{31}P\{^1H\}$ NMR spectroscopy for [HCl]/[Mo] = 100 (left) and [HCl]/[Mo] = 2 (right).

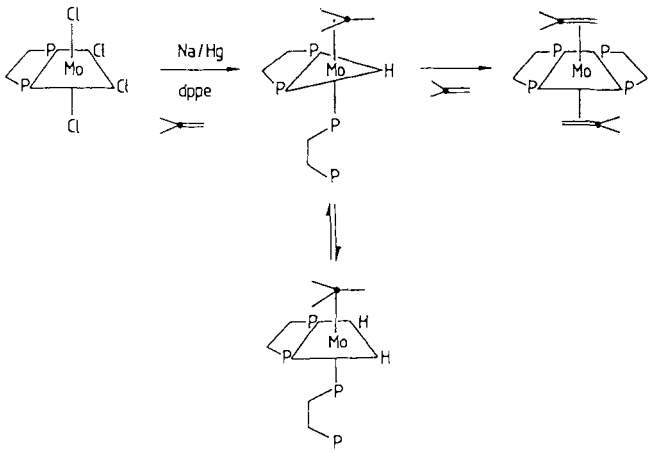

Scheme 15. Synthesis of $[MoH(\eta^3\text{-}C_4H_7)(dppe)_2]$ and its reaction with isobutene to form $[Mo(\eta^2\text{-}Me_2CCH_2)_2(dppe)_2]$.

reversible rearrangement results in the formation of the 18-electron trimethylenemethane dihydrido complex. Parenthetically, it is worth noting that the $\{Mo(dppe)_2\}$ site has been exceptional in demonstrating all the intramolecular rearrangements: alkene/$H^- \rightarrow$alkyl; allyl/$H^- \rightarrow$propene, and trimethylenemethane/$H^- \rightarrow$2-methylallyl.

Protonation of $[MoH(\eta^3\text{-}C_4H_7)(dppe)_2]$ with anhydrous HCl, at room temperature (where it is exclusively in the allyl form) proceeds according to Equation (25). $[MoH_2Cl_2(dppe)_2]$ is a product in all the systems discussed in this section, whilst the hydrocarbon results from the dimerization of isobutene.

$$[MoH(\eta^3\text{-}C_4H_7)(dppe)_2] + 2HCl \longrightarrow [MoH_2Cl_2(dppe)_2] + {}^t BuCH_2C(Me)CH_2 \quad (25)$$

A study of this reaction by the stopped-flow technique shows a single exponential trace with the final absorbance expected for $[MoH_2Cl_2(dppe)_2]$ and an initial absorbance slightly lower than that of the parent complex (Fig. 9). This initial absorbance jump is attributable to the addition of one equivalent of acid, as shown on the left-hand side of Figure 9.

The reaction reflected in the subsequent exponential absorbance–time decay exhibits a first-order dependence on the concentration of complex, but a nonlinear dependence on the concentration of HCl [Fig. 9, right-hand plot; Eq. (26)]. The mechanism of the reaction is shown in Scheme 16. Initial, rapid

$$k_{obs} = \{k_3 + k_4K_2[HCl]\}/(1 + K_2[HCl]) \quad (26)$$

protonation at the metal occurs within 2 ms to form $[MoH_2(\eta^3\text{-}C_4H_7)(dppe)_2]^+$ followed by rate-limiting intramolecular migration of the proton from the metal to the 2-methylallyl ligand ($k_3 = 0.7\ s^{-1}$) produces $[MoH(\eta^2\text{-}Me_2CCH_2)(dppe)_2]^+$. The subsequent steps can not be identified by kinetics, because they occur after the rate-limiting step, but must involve the dimerization of isobutene, and its liberation to form $[MoH_2Cl_2(dppe)_2]$. The complexity of Equation (26) is a consequence of rapid protonation of the pendant phosphorus atom ($K_2 = 52.2\ dm^3\,mol^{-1}$). Consequently the kinetics reflect the reactivity of both $[MoH_2(\eta^3\text{-}C_4H_7)(dppe)_2]^+$ and $[MoH_2(\eta^3\text{-}C_4H_7)(dppe)(dppeH)]^{2+}$ ($k_4 = 2.9\ s^{-1}$). This mechanism (in particular the rate-limiting migration steps) is able to rationalize the following kinetic observations: 1) Rate constants associated with apparently acid-

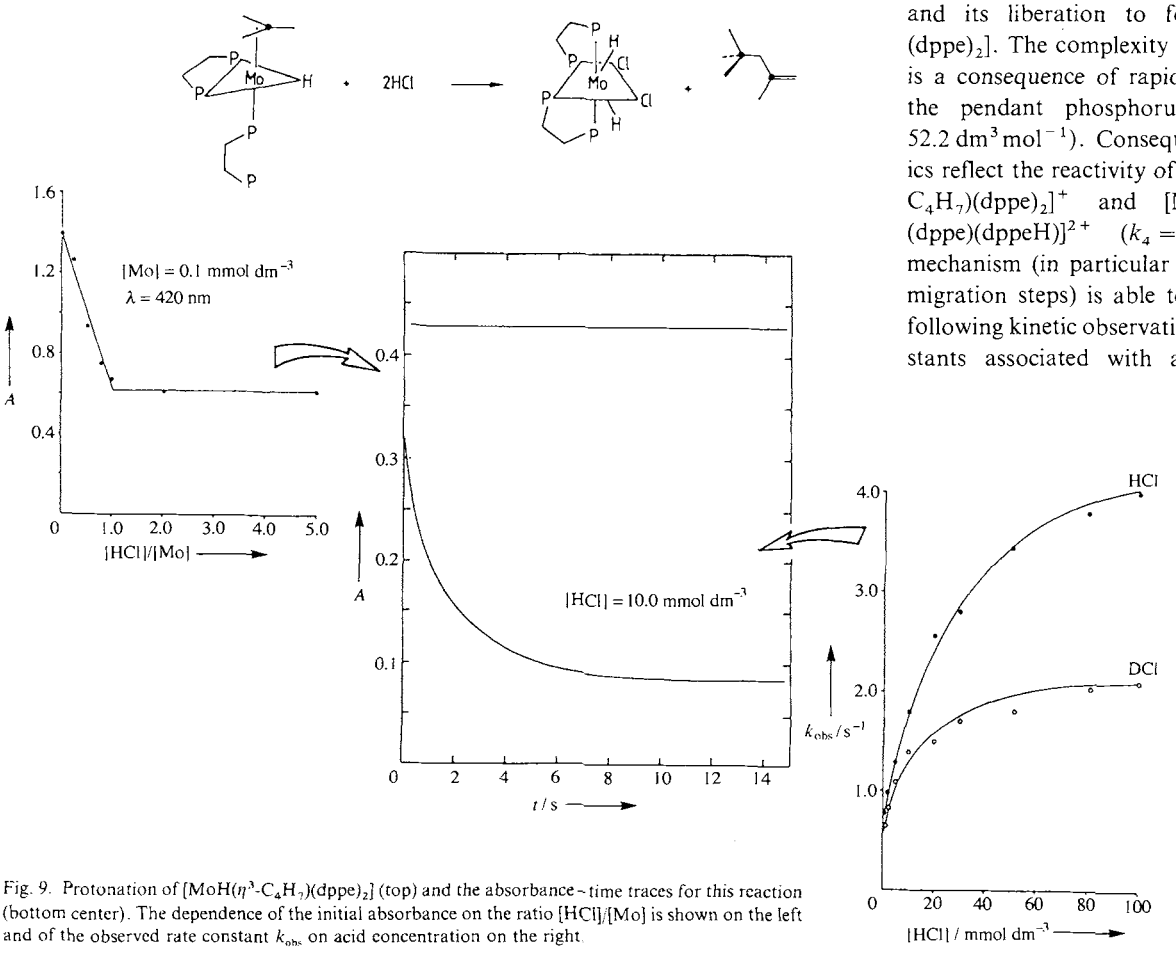

Fig. 9. Protonation of $[MoH(\eta^3\text{-}C_4H_7)(dppe)_2]$ (top) and the absorbance–time traces for this reaction (bottom center). The dependence of the initial absorbance on the ratio [HCl]/[Mo] is shown on the left and of the observed rate constant k_{obs} on acid concentration on the right.

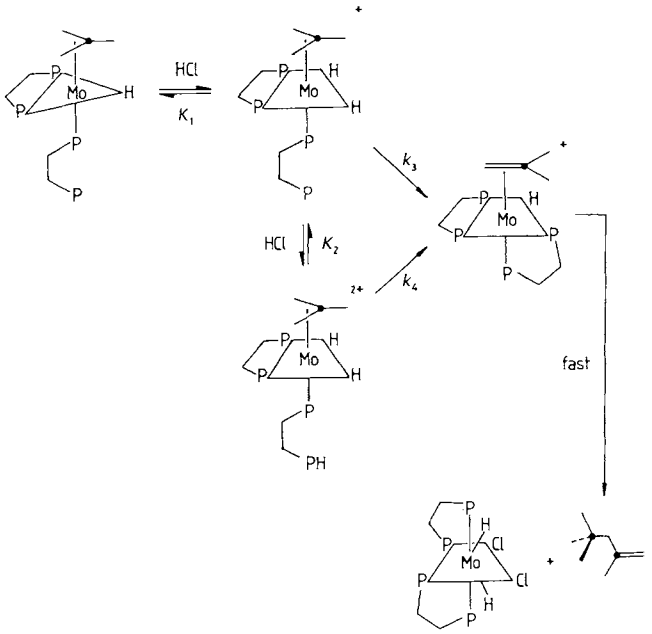

Scheme 16. Proposed mechanism for the protonation of $[MoH(\eta^3\text{-}C_4H_7)(dppe)_2]$ leading to the dimerization of isobutene.

independent steps (k_3 and k_4) exhibit primary isotope effects ($k_3^H/k_3^D = 1.27$, $k_4^H/k_4^D = 1.50$), since these elementary reactions are due to migration of hydrido groups derived from the acid. 2) The initial, rapid reaction consumes one equivalent of acid. 3) As expected, the pendant phosphorus atom is protonated by HCl. An important aspect of the mechanism is that this step is reversible, and thus, towards the end of the reaction, the phosphorus can bind to the metal whilst deprotonated.

The details of the dimerization process are not clear, but it is certainly much faster than the acid-catalyzed dimerization of free isobutene. This indicates that dimerization occurs on the metal site.

4.4. Product Control by Protonation: A Summary

In this section some relatively simple systems have been discussed that when considered together illustrate how the protonation of alkene complexes (or their rearranged analogues) can selectively give alkanes, alkenes, or alkynes as summarized in Scheme 17.

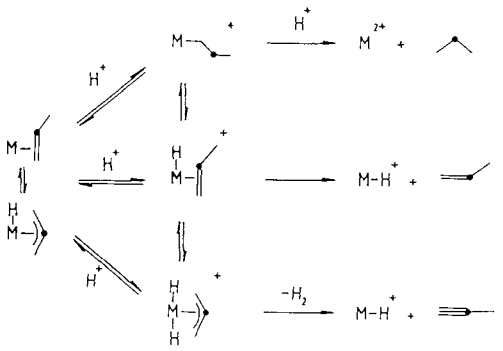

Scheme 17. Protonation of alkene complexes to give alkanes, alkenes, or alkynes, illustrating how selectivity results from protonation at the hydrocarbon or the metal.

The selectivity is a result of protonation at the hydrocarbon or the metal. Thus, protonation at the coordinated alkene gives the alkyl species, which subsequently reacts further to produce an alkane. However, further protonation of the metal occurs at higher concentrations of acid and this labilizes the system towards the release of alkene.

Alkenes higher than ethene can also rearrange on the metal site to form the allyl hydrido species, and this form is capable of producing alkynes upon protonation, if the protonation at the metal preferentially labilizes the release of dihydrogen to generate a coordinatively unsaturated site capable of dehydrogenating the bound alkene.

At first sight it seems anomalous that no propane is formed in the reaction with *trans*-$[MoH(\eta^3\text{-}C_3H_5)(dppe)_2]$. The reason for this is probably kinetic: the formation of propane is slow, and the more rapid formation of either the alkyne or the alkene occur preferentially. It would be interesting to study the products of the reaction between DCl and *trans*-$[MoH(\eta^3\text{-}C_3H_5)(dppe)_2]$ to establish whether any deuterium is incorporated specifically into the secondary carbon of the propene. This would indicate the transient existence of a propyl species that undergoes intramolecular β-hydrogen or deuterium transfer more rapidly than it can form propane.

4.5. Proton-Catalyzed Isomerization of Alkenes

A reaction which has not been observed in the reactions of alkenes bound to the $\{Mo(dppe)_2\}$ site is the acid-catalyzed rearrangements shown in Scheme 18. In principle, protonation

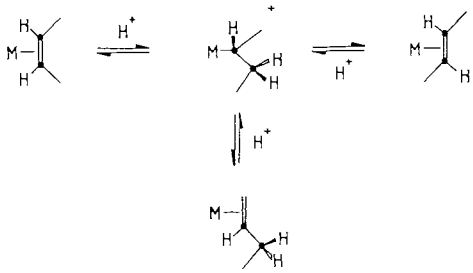

Scheme 18. Acid-catalyzed rearrangements of metal-alkene complexes.

of alkene complexes can give mixtures of *cis*- and *trans*-alkenes together with internal and terminal alkenes via intermediate alkyl species.

Acid-catalyzed *cis*–*trans* isomerization of alkenes bound to rhenium has been observed (Scheme 19).[44] Addition of acid to a solution of the *cis*-2-butene complex $[Re(\eta^5\text{-}C_5H_5)(CO)_2(\eta^2\text{-}cis\text{-}MeCHCHMe)]$ results in the formation of a 45:55 mixture of this *cis*-2-butene complex and $[Re(\eta^5\text{-}C_5H_5)(CO)_2(\eta^2\text{-}trans\text{-}MeCHCHMe)]$ within about 30 min. The proposed mechanism (Scheme 19) involves protonation of the alkene ligand to form the alkyl species, rotation about the carbon–carbon single bond, and deprotonation to generate the equilibrium mixture of alkene complexes.

The exact mechanism by which the alkene is protonated (direct attack at the carbon or via a hydrido species) is unknown, but the most important mechanistic feature is the selectivity that

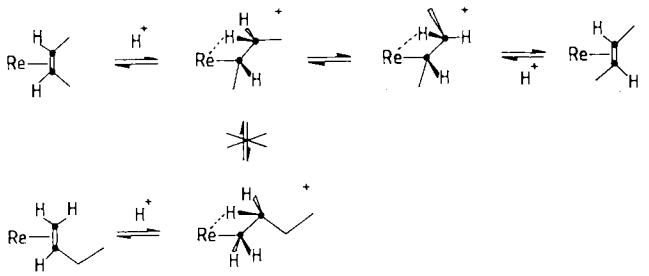

Scheme 19. Isomerization of *cis*-butene on a rhenium center.

shows that both protonation and deprotonation must occur at the same carbon atom: the postulated 2-butyl intermediate does not deprotonate to give the 1-butene complex, and similarly, protonation of the 1-butene complex does not give any 2-butene ligand. This observation can only be rationalized if the two butyl intermediates are different. It has been proposed that the protonation produces an intermediate containing a strong agostic interaction, followed by an "in place rotation" and deprotonation of the agostic alkyl group, which occurs much more rapidly than formation of a free alkyl rhenium intermediate.

A related acid-catalyzed isomerization is the equilibration of coordinated *syn* and *anti* dienes as illustrated for $[Fe(\eta^4\text{-}PhCHCHCHCHBn)(CO)_3]^+$ (Bn = $PhCH_2$) in Scheme 20.[45]

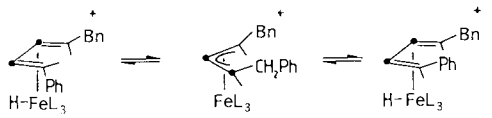

Scheme 20. Equilibration of coordinated *syn* and *anti* dienes at an iron complex. L = CO.

In this example rate-limiting protonation occurs at the metal and is associated with an exceptionally large primary isotope effect ($k_H/k_D = 27$). Intramolecular transfer of the hydrogen from the metal to the diene then forms the allyl species. Subsequent rotation about the carbon–carbon single bond followed by hydrogen migration back to the metal and deprotonation results in equilibration of the *syn* and *anti* isomers.

5. Stereoselective Protonation of Complexes

The addition of protons to coordinated hydrocarbons to produce stereoselective products has been known for some time, especially in the reactions of cyclic polyenes. Thus, as shown in Scheme 21, $[Ni(\eta^5\text{-}C_5H_5)_2]$ is protonated on the cyclopentadienyl ring stereoselectively in the *exo* position.[46] In addition the exchange of ring protons in $[Fe(\eta^5\text{-}C_5H_5)_2]$ involves *exo* attack of a proton at the cyclopentadienyl ring.[47] Subsequently, the *endo* hydrogen transfers to the metal to form $[FeH(\eta^5\text{-}C_5H_5)_2]^+$.

Whether a proton adds directly in *exo* or *endo* position in any particular system cannot be predicted, and examples of both types of addition are known. In many cases there is no clear evidence whether *exo* or *endo* attack has occurred. For instance, the protonation of $[Fe(\eta^4\text{-}C_4H_4)(CO)_3]$ is assumed to involve

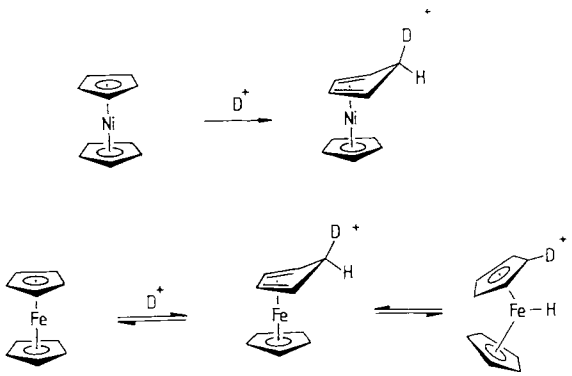

Scheme 21. Stereoselective D^+ attack at the pentadienyl ligand in $[Ni(\eta^5\text{-}C_5H_5)_2]$ and in $[Fe(\eta^5\text{-}C_5H_5)_2]$.

endo attack, since the analogous butadiene complex is protonated in this position.[48] Of course, *endo* addition may involve initial protonation of the metal followed by intramolecular migration. However, the intermediacy of a hydrido species is not essential for formation of *endo* product.

Another aspect of stereoselectivity involves the protonation of alkynes to form *cis*- or *trans*-alkenes selectively. We shall discuss this aspect in detail in this section and show how application of the kinetic principles associated with protonation at the metal or the hydrocarbon ligand outlined so far can be employed to control the stereochemistry of the product.

We saw in the Section 3 that the term regioselective is ambiguous in the sense that although the reaction may amount stoichiometrically to a regioselective protonation, the mechanism whereby this product is formed may not involve direct regioselective attack. A similar problem in terminology occurs for the stereoselectivity of products formed by protonation: the stoichiometrically stereoselective product can be formed by a variety of mechanistic pathways.

5.1. Stereoselectivity in the Protonation of Alkynes: Kinetic Control

Consideration of the protonation of a coordinated alkyne reveals that attack can occur at two faces of the alkyne: *exo* to the metal to give a *trans*-vinyl species or *endo* to the metal giving a *cis*-vinyl species.

The fundamental point is that the face of the alkyne to which the proton binds defines the configuration of the vinyl species. Provided the carbon–carbon double bond is maintained upon the addition of the second proton the resulting alkene's configuration will be defined by the position of the initial protonation: *cis*-vinyl gives a *cis*-alkene and *trans*-vinyl gives a *trans*-alkene.

Clearly if the rates of the initial *exo* and *endo* protonations are sufficiently different then a stereoselective alkene will be formed, provided intermediate isomeric vinyl species or the isomeric coordinated alkenes do not equilibrate. Both isomeric vinyl and alkene complexes can equilibrate by protonation to form alkylidene ligands and alkyl ligands, respectively. Rapid rotation about the carbon–carbon single bond in either alkylidene or alkyl ligands prior to proton loss effectively destroys any selectivity (see Section 5.2). In order to avoid this problem the system must be carefully designed.

A question that must be addressed initially is: "Can protonation of a coordinated alkyne occur stereoselectively?" To answer this question the reaction of anhydrous HCl with the symmetrical alkyne PhCCPh bound to the symmetrical site $\{V(\eta^5\text{-}C_5H_5)_2\}$ has been studied [Eq. (27)].[49] The symmetrical nature

$$[V(\eta^5\text{-}C_5H_5)_2(\eta^2\text{-PhCCPh})] + 2\,HCl \longrightarrow [V(\eta^5\text{-}C_5H_5)_2Cl_2] + PhCHCHPh \quad (27)$$

of the entire system ensures that any stereoselectivity observed is a consequence of the rates of protonation and not of the ancillary ligands' "guiding" the proton preferentially to a particular face of the alkyne. Predominantly the *cis*-alkene (85%) is formed with 15% *trans* isomer.

The reaction exhibits a first-order dependence on the concentration of complex, but the dependence on the concentration of HCl is complicated (Fig. 10). This complicated acid dependence

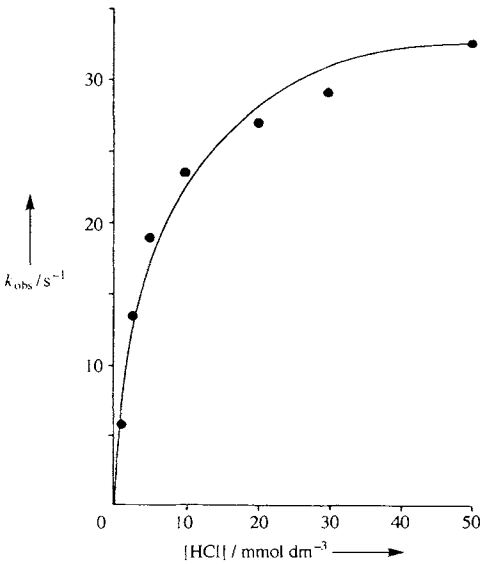

Fig. 10. Dependence of the observed rate constant k_{obs} on acid concentration for the protonation of $[V(\eta^5\text{-}C_5H_5)_2(\eta^2\text{-PhCCPh})]$.

mitigates against simple, direct proton attack at the coordinated alkyne, but rather indicates the mechanism depicted in Scheme 22 with the corresponding rate law shown in Equation (28).

$$k_{obs} = (k_2 + k_3K_1)[HCl]/(1 + K_1[HCl]) \quad (28)$$

The major pathway involves initial, rapid protonation of the metal to give $[VH(\eta^5\text{-}C_5H_5)_2(\eta^2\text{-PhCCPh})]^+$, followed by rate-limiting migration of the hydride to the alkyne necessarily producing the *cis*-vinyl species. In addition, protonation of the alkyne at the face remote from the metal produces the *trans*-vinyl species. Analysis of the data gives $(k_2 + k_3K_1) = 6.2 \times 10^3\ dm^3\,mol^{-1}\,s^{-1}$ and $K_1 = 1.56 \times 10^2\ dm^3\,mol^{-1}$. It seems likely that the carbon–carbon double bond of the vinyl ligand is retained throughout the second protonation, and hence the configuration of the final alkene is defined by the initial site of protonation of the coordinated alkyne.

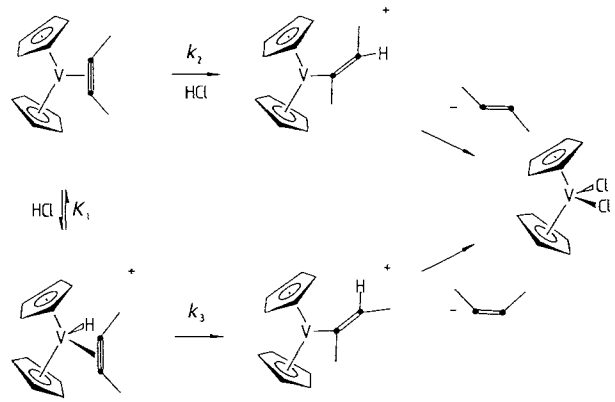

Scheme 22. Proposed mechanism for the protonation of the symmetrical complex $[V(\eta^5\text{-}C_5H_5)_2(\eta^2\text{-PhCCPh})]$.

Studies on $[Nb(\eta^5\text{-}C_5H_5)_2(CO)(CMeCH\textit{i}Pr)]$ show that protonation of the vinyl species gave an alkene of the same configuration as the vinyl ligand.[50] However, if the second protonation were to occur at the carbon atom remote from the metal, isomerization would result. Methylation of $[Nb(\eta^5\text{-}C_5H_5)_2(CO)(CMeCH\textit{i}Pr)]$ with $MeOSO_2F$ leads to an alkylidene species, which subsequently produces a mixture of alkene isomers (Scheme 23).

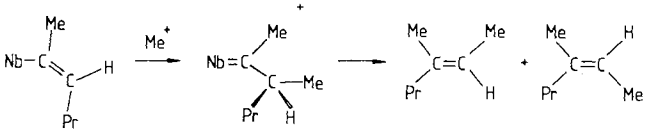

Scheme 23. Methylation of $[Nb(\eta^5\text{-}C_5H_5)_2(CO)(CMeCH\textit{i}Pr)]$ with $MeOSO_2F$ leading to a mixture of alkenes.

How then can we design the system so that the vinyl complexes do not protonate at the remote carbon atom and destroy the stereoselectivity? For protonation of vinyl complexes at either the metal or the remote carbon atom, a pair of electrons have to be supplied by the metal, and hence the formal oxidation state of the metal increases by two units. However, since $[V(\eta^5\text{-}C_5H_5)_2(PhCCHPh)]^+$ is a vanadium(IV) complex, protonation at the metal or remote carbon atom is impossible—it can only occur at the vanadium–carbon bond.

This illustrates a general way in which protonation of a complex can be controlled. Protonation of alkyne complexes where the oxidation state of the metal is less than four units from its maximum (that is, greater than +2 for V, Nb, or Ta; greater than +3 for Cr, Mo, or W, etc.) enforces the protonation of the derived vinyl species to occur at the carbon atom adjacent to the metal. In these circumstances, the configuration of the alkene product is always defined by that the vinyl species and hence by the kinetically favored site of protonation of the alkyne ligand.

Further quantitative analysis of the vanadium system in Equation (27) is possible. Since the isomeric alkene product distribution is defined by the rates of formation of the isomeric vinyl species the expression in Equation (29) can be derived,

$$\frac{[cis\text{-PhCHCHPh}]}{[cis\text{-PhCHCHPh}] + [trans\text{-PhCHCHPh}]} = \frac{k_3K_1}{k_3K_1 + k_2} \quad (29)$$

from which $k_2 = 9.3 \times 10^2\ dm^3 mol^{-1} s^{-1}$ and $k_3 = 33.8\ s^{-1}$. Since it can be estimated that $k_1 \geq 1 \times 10^6\ dm^3 mol^{-1} s^{-1}$, it is clear that the difference in the rates of protonation of the metal (to give *cis*-alkene) and alkyne (to give *trans*-alkene) would lead to essentially exclusive formation of *cis*-alkene. However, it is the relatively slow rate of intramolecular migration, together with the reversibility of the protonation at the metal that leads to the poorer stereoselectivity observed experimentally.

The reversibility of the initial protonation is another factor we have to consider in designing systems to give stereoselective alkenes. In certain circumstances, the initial site of protonation would not define the configuration of the product, for instance, if the initial protonation of the coordinated alkyne is reversible, or the favored isomeric vinyl species is protonated only slowly, whilst the minor isomeric vinyl complex protonates rapidly. However, this latter scenario seems unlikely since the isomeric vinyl species are necessarily only distinguished by the substituent on the carbon atom remote from the metal, and consequently one would expect that the rate of protonation of the carbon atom adjacent to the metal would be similar for the two isomers.

The stereoselectivity in $[V(\eta^5\text{-}C_5H_5)_2(\eta^2\text{-}PhCCPh)]$ is controlled entirely by the relative rates of protonation of the metal and the alkyne, and in this highly symmetrical complex the dominant product is the *cis*-alkene.

The nitrogenases specifically transform acetylene to *cis*-CHDCHD in vitro by a sequence of electron and proton transfer reactions.[51] Much speculation has centered around how the enzyme accomplishes this stereoselectivity.[7, 52] However, the results from this study indicate that the biological result needs little explanation: the enzyme is merely showing the normal stereoselectivity associated with this type of reaction.

In certain circumstances, stereoselective formation of alkenes by protonation of coordinated alkynes can also be accomplished under conditions of thermodynamic control. The reaction between anhydrous HX (X = Cl, Br, or BF_4) and complexes of the type *trans*-$[Mo(\eta^2\text{-alkyne})_2(dppe)_2]$ gives vinyl and alkylidyne complexes[53, 54] as shown by the examples in Equations (30) and (31), respectively. In both cases the overall stoichiometry

$$trans\text{-}[Mo(\eta^2\text{-}MeCCH)_2(dppe)_2] + HX \longrightarrow trans\text{-}[Mo(CHCHMe)X(dppe)_2] + MeCCH \quad (30)$$

$$trans\text{-}[Mo(\eta^2\text{-}MeCCH)_2(dppe)_2] + HX \longrightarrow trans\text{-}[Mo(CCH_2Me)X(dppe)_2] + MeCCH \quad (31)$$

requires the net addition of one molecule of HX, but clearly for the formation of the alkylidyne, a complex protonation/deprotonation pathway must operate. The mechanistic rationalization of how both types of products can be formed from the same reactants is shown in Scheme 24; the associated general rate law

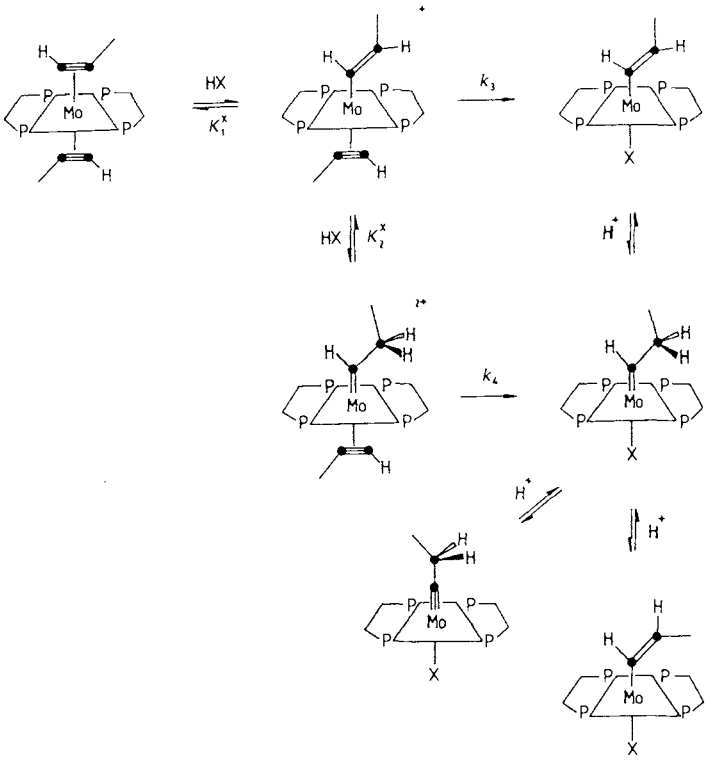

Scheme 24. Protonation of *trans*-$[Mo(\eta^2\text{-}MeCCH)_2(dppe)_2]$.

is given by Equation (32) if the dissociation of propyne is rate-limiting in both pathways.

$$k_{obs} = \frac{K_1^X[HX]\{k_3 + k_4 K_2^X[HX]\}}{1 + K_1^X[HX] + K_1^X K_2^X[HX]^2} \quad (32)$$

Initial, rapid protonation of *trans*-$[Mo(\eta^2\text{-}MeCCH)_2(dppe)_2]$ forms *trans*-$[Mo(CHCHMe)(\eta^2\text{-}MeCCH)(dppe)_2]^+$ ($K_1^{Cl} = 1.3 \times 10^2\ dm^3 mol^{-1}$) within 2 ms, which can be detected both by electronic spectroscopy and low temperature $^{31}P\{^1H\}$ NMR spectroscopy. Protonation of a propyne ligand decreases the electron density at the metal and consequently labilizes the *trans*-propyne to dissociation ($k_3 = 0.35\ s^{-1}$). Subsequent rapid binding of X^- at the site vacated by MeCCH gives the vinyl product, *trans*-$[MoX(CHCHMe)(dppe)_2]$, and at low concentrations of acid this is the exclusive product-forming pathway.

At high concentrations of acid, protonation of *trans*-$[Mo(CHCHMe)(\eta^2\text{-}MeCCH)(dppe)_2]^+$ to form *trans*-$[Mo(CHCH_2Me)(\eta^2\text{-}MeCCH)(dppe)_2]^{2+}$ can occur ($K_2^{Cl} = 3.0\ dm^3 mol^{-1}$) before dissociation of the propyne ligand. This second protonation further labilizes the *trans*-propyne ligand ($k_4 = 2.58\ s^{-1}$), which is lost in the rate-limiting step. Rapid attack by X^- and proton release from the alkylidene ligand gives either *trans*-$[Mo(CHCHMe)X(dppe)_2]$ (proton loss from the remote carbon atom) or *trans*-$[Mo(CCH_2Me)X(dppe)_2]$ (proton loss from the adjacent carbon atom).

An important mechanistic conclusion is that the product of the reaction (vinyl or alkylidyne complex) is not defined by the site of protonation but is decided by factors that have their influence after the rate-limiting step. Although the alkylidyne species has only been isolated in the reaction with $HBF_4 \cdot OEt_2$,

it seems likely that, irrespective of the acid, the equilibrium mixture of isomeric vinyl complexes, alkylidene, and alkylidyne species shown on the right-hand side of Scheme 24 is present in solution. Which product is actually isolated will depend on the magnitude of the equilibrium constants interconnecting these species, or merely the relative solubilities. It is unlikely that a fluoro ligand favors proton loss from the adjacent carbon atom whilst the chloro or bromo ligand favors proton loss from the remote carbon atom. Rather it seems more likely that the least soluble is product isolated.

The mechanism shown in Scheme 24 has important consequences for the configuration of the vinyl ligand. Irrespective of the initial site of protonation and the resulting configuration of the vinyl ligand in *trans*-[Mo(CHCHMe)(η^2-MeCCH)(dppe)$_2$]$^+$, at high concentrations of acid the reaction proceeds via the alkylidene intermediate *trans*-[Mo(CHCH$_2$Me)(η^2-MeCCH)(dppe)$_2$]$^{2+}$. Free rotation around the carbon–carbon single bond in this intermediate prior to proton loss means that any stereoselectivity introduced at the initial protonation is destroyed. However, *trans*-[Mo(CHCHMe)Br(dppe)$_2$] isolated from this reaction shows partially resolved peaks in the ^{1}H NMR spectrum, which are attributable to the vinyl ligand. Thus, the resonance at $\delta = 10.9$ is a doublet ($J_{H,H} = 8.8$ Hz), and the resonance at $\delta = 9.5$ is a multiplet. In addition the methyl signal at $\delta = 1.15$ is a doublet ($J_{H,H} = 5$ Hz). These coupling constants are consistent with a *cis*-vinyl ligand ($J^{cis}_{H,H} = 6-14$ Hz, $J^{trans}_{H,H} = 11-20$ Hz). Clearly this stereoselective formation of the *cis*-vinyl species cannot reflect a kinetic preference, but must be a consequence of a signifiant difference in the thermodynamic stability or solubility between *trans*-[Mo(*cis*-CHCHMe)Br(dppe)$_2$] and *trans*-[Mo(*trans*-CHCHMe)Br(dppe)$_2$]. That is, the stereoselectivity is thermodynamically controlled.

Thus, at least in principle, stereoselective formation of an alkene by protonation of a coordinated alkyne can be accomplished by thermodynamic control. Protonation of a particular configuration of a vinyl ligand at the carbon remote from the metal generates an alkylidene species, and subsequent deprotonation produces an equilibrium mixture of *cis* and *trans* vinyl species. Further protonation of this mixture will often result in a mixture of isomeric alkenes. However, a specific configuration of an alkene can be produced provided 1) there is a significant difference in the thermodynamic stabilities of the isomeric vinyl species and 2) protonation of the vinyl species to give the alkene is significantly slower than the rate of proton equilibration between the vinyl and alkylidene species.

It is worthwhile just briefly considering the factors that result in a significant difference in the thermodynamic stabilities of the isomeric vinyl species. Clearly the major contributors must be the size of both the vinyl substituent and the coligands of the metal. If both are bulky, one can be reasonably confident that the *trans*-vinyl residue, minimizing unfavorable steric interactions, would be the more stable thermodynamically. However, in the study on *trans*-[Mo(η^2-MeCCH)$_2$(dppe)$_2$] (with a methyl substituent) the *cis*-vinyl ligand is preferred, probably because the methyl group is buried in the surrounding coligand framework.

Finally, it should be noted that thermodynamic control of stereochemistry can only operate with alkynes other than acetylene, since the differentiation in stabilities is exclusively a consequence of the substituent on the vinyl ligand.

6. Summary and Outlook

In this review I have highlighted the mechanistic aspects associated with the protonation of unsaturated hydrocarbon residues bound to transition metal sites and emphasized how this reactivity is a natural consequence of having two sites on the same molecule that undergo slow proton transfer reactions. Three key mechanistic principles emerge with which the reactivity of these systems can be understood. 1) Protonation can occur at either the metal or the hydrocarbon ligand. 2) The initial site of attack may not be the final residence of the proton. 3) Transfer of the proton between metal and ligand can occur by intramolecular or acid-catalyzed pathways.

These principles have some important repercussions, the most fundamental of which is that protonation of complexes containing unsaturated hydrocarbons is invariably more complicated than would be imagined from inspection of the structures of the products. Consequently, a reaction can be stoichiometrically regioselective in that the product is ultimately protonated at a single site, though mechanistically the reaction might proceed by several pathways in which the complex is initially protonated at different sites.

An overall picture of the hydrocarbon-evolving transformations discussed in this article is shown in Scheme 25. This dia-

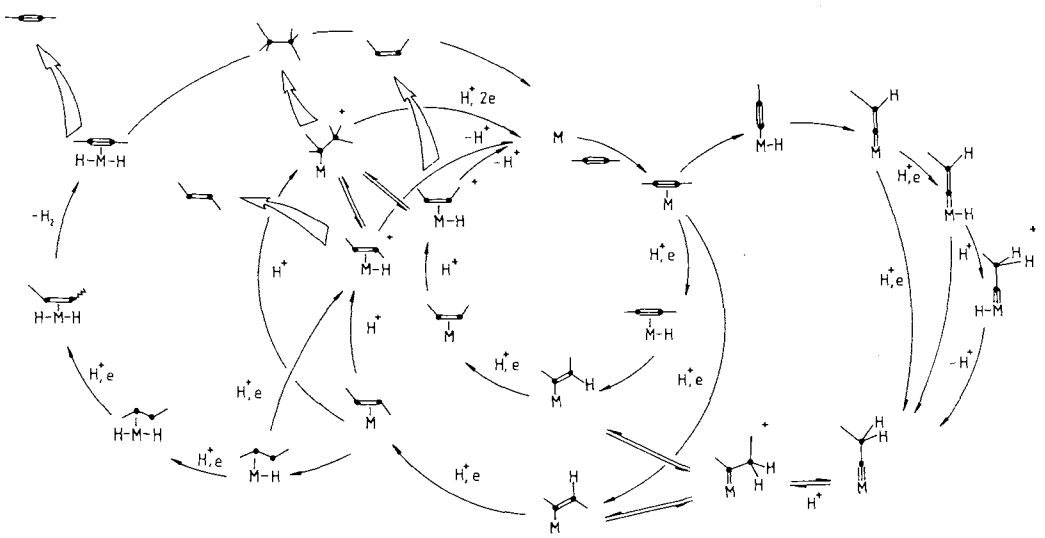

Scheme 25. Overview of all the transformations discussed in this review in which hydrocarbon ligands are released.

gram illustrates how the competitive protonation of metal and ligand can be exploited, first to control the products of the reaction and second, to control the stereochemistry of the products.

The future is still intellectually demanding. Although a lot of synthetic chemistry has resulted in a general understanding of which site is the ultimate residence of the proton, we are still a long way from understanding the mechanistic factors that discriminate between initial protonation of the metal and the hydrocarbon residue. Only if we can understand the kinetic features of this type of reaction can we hope to design complexes whose reactivity and reaction products can be defined prior to their preparation.

Finally, what about catalysis? The diagram in Scheme 25 indicates several cyclic processes established by piecing together the stoichiometric reactions discussed in this article. A feature of all the reactions discussed herein is the formation of well-defined metal-containing products. For instance, $[MoH_2Cl_2(dppe)_2]$ has been isolated from the reaction of HCl with *trans*-$[MoH(\eta^3\text{-}C_3H_5)(dppe)_2]$. In a sense, $[MoH_2Cl_2(dppe)_2]$ is "exhausted" since it has supplied electrons to protons, either to form hydride ligands or evolve dihydrogen. However, $[MoH_2Cl_2(dppe)_2]$ can be reduced under an atmosphere of propene to form *trans*-$[MoH(\eta^3\text{-}C_3H_5)(dppe)_2]$,[42] and hence, in principle, we have a catalyst, and a versatile catalyst at that, since by changing the concentration of acid used at each turnover we could selectively produce propene or propyne. Similarly, we can envisage a catalyst that selectively produces ethane or ethene based on *trans*-$[Mo(\eta^2\text{-}C_2H_4)_2(dppe)_2]$. However, in practice, there is a problem in adapting these systems to be truly catalytic because of the preferential reduction of protons to dihydrogen in any system containing an acid and a reductant. A major target in the near future must be finding solutions to this problem. After all, if nature can find ways of minimizing proton reduction in the conversion of acetylene into ethene or ethane by the nitrogenases, so can chemists!

Received: June 16, 1995 [A 119 IE]
German version: *Angew. Chem.* **1996**, *108*, 1024–1046

[1] R. A. Henderson, *J. Chem. Soc. Dalton Trans.* **1995**, 503, and references therein.
[2] P. G. Leuhert, *Proc. R. Soc. London A* **1968**, *303*, 45.
[3] P. J. Toscano, L. G. Marzilli, *Prog. Inorg. Chem.* **1984**, *31*, 105, and references therein.
[4] D. Qui, M. Kumar, S. W. Raysdale, T. G. Spiro, *Science* **1994**, *264*, 817.
[5] A. C. Rosenzweig, S. J. Lippard, *Acc. Chem. Res.* **1994**, *27*, 229.
[6] L. Que, Jr. in *Bioinorganic Catalysis* (Ed.: J. Reedijk), Marcel Dekker New York, **1993**, p. 347, and references therein.
[7] D. J. Evans, R. A. Henderson, B. E. Smith in *Bioinorganic Catalysis* (Ed.: J. Reedijk), Marcel Dekker, New York, **1993**, p. 89, and references therein.
[8] M. Eigen, *Angew. Chem.* **1963**, *75*, 489; *Angew. Chem. Int. Ed. Engl.* **1964**, *3*, 1, and references therein.
[9] R. P. Bell, *The Proton in Chemistry*, 2nd ed., Chapman and Hall, London, **1973**.
[10] K. W. Kramarz, J. R. Norton, *Prog. Inorg. Chem.* **1994**, *42*, 1.
[11] R. P. Bell, R. G. Pearson, *J. Chem. Soc.* **1953**, 3443.
[12] Ref. [9], p. 213.
[13] R. P. Bell, *Acids and Bases: Their Quantitative Behaviour*, Chapman and Hall, London, **1971**, p. 71.
[14] R. P. Bell, B. G. Cox, *J. Chem. Soc. B* **1971**, 654.
[15] R. F. Jordan, J. R. Norton, *ACS Symp. Ser.* **1982**, *198*, 403, and references therein.
[16] S. S. Krisiánsdóttir, A. J. Loendorf, J. R. Norton, *Inorg. Chem.* **1991**, *30*, 4470, and references therein.
[17] G. Cerichelli, G. Illuminati, G. Ortaggi, A. M. Giuliani, *J. Organomet. Chem.* **1977**, *127*, 357, and references therein.
[18] M. I. Bruce, A. G. Swincer, *Adv. Organomet. Chem.* **1983**, *22*, 59, and references therein.
[19] K. R. Birdwhistell, S. J. N. Burgmayer, J. L. Templeton, *J. Am. Chem. Soc.* **1985**, *107*, 4474, and references therein.
[20] R. M. Bullock, *J. Am. Chem. Soc.* **1987**, *109*, 8087.
[21] N. M. Kostic, R. F. Fenske, *Organometallics* **1982**, *1*, 974.
[22] A. Mayr, K. C. Shaefer, H. C. Huang, *J. Am. Chem. Soc.* **1984**, *106*, 1517, and references therein.
[23] A. J. L. Pombeiro, A. Hills, D. L. Hughes, R. L. Richards, *J. Organomet. Chem.* **1988**, *352*, C5.
[24] M. F. N. N. Carvalho, R. A. Henderson, A. J. L. Pombeiro, R. L. Richards, *J. Chem. Soc. Chem. Comm.* **1989**, 1796.
[25] S. J. Holmes, R. R. Schrock, *J. Am. Chem. Soc.* **1981**, *103*, 4599.
[26] N. M. Kostic, R. F. Fenske, *J. Am. Chem. Soc.* **1981**, *103*, 4677.
[27] M. Green, A. G. Orpen, I. D. Williams, *J. Chem. Soc. Chem. Comm.* **1982**, 493, and references therein.
[28] A. Mayr, C. M. Bastos, *J. Am. Chem. Soc.* **1990**, *112*, 7797.
[29] J. H. Freudenberger, R. R. Schrock, *Organometallics* **1985**, *4*, 1937.
[30] C. Roger, G. S. Bodner, W. G. Hatton, J. A. Gladysz, *Organometallics* **1991**, *10*, 3266, and references therein.
[31] D. L. Hughes, A. J. L. Pombeiro, C. J. Pickett, R. L. Richards, *J. Chem. Soc. Chem. Comm.* **1984**, 992.
[32] A. J. L. Pombeiro, D. L. Hughes, R. L. Richards, J. Silvestre, R. Hoffmann, *J. Chem. Soc. Chem. Comm.* **1986**, 1125.
[33] R. A. Henderson, A. J. L. Pombeiro, R. L. Richards, Y. Wang, *J. Organomet. Chem.* **1993**, *447*, C11.
[34] R. A. Henderson, K. E. Oglieve, *J. Chem. Soc. Chem. Comm.* **1991**, 584, and references therein.
[35] K. E. Oglieve, R. A. Henderson, *J. Chem. Soc. Dalton Trans.* **1991**, 3295, and references therein.
[36] J. W. Byrne, H. U. Blaser, J. A. Osborne, *J. Am. Chem. Soc.* **1975**, *97*, 3871.
[37] M. L. H. Green, L. L. Wong, *J. Chem. Soc. Chem. Comm.* **1988**, 677, and references therein.
[38] J. Halpern, L. Cai, P. J. Desrosiers, Z. Lim, *J. Chem. Soc. Dalton Trans.* **1991**, 717.
[39] T. Al-Salih, C. J. Pickett, *J. Chem. Soc. Dalton Trans.* **1985**, 1255.
[40] R. A. Henderson, D. L. Hughes, K. E. Oglieve, unpublished.
[41] K. E. Oglieve, R. A. Henderson, *J. Chem. Soc. Chem. Comm.* **1993**, 474.
[42] R. A. Henderson, K. E. Oglieve, unpublished.
[43] R. A. Henderson, K. E. Oglieve, *J. Chem. Soc. Dalton Trans.* **1994**, 767.
[44] C. P. Casey, C. S. Yi, *Organometallics* **1991**, *10*, 33.
[45] T. H. Whitesides, J. P. Neilan, *J. Am. Chem. Soc.* **1975**, *97*, 907.
[46] G. K. Turner, W. Kläui, M. Scotti, H. Werner, *J. Organomet. Chem.* **1975**, *102*, C9.
[47] U. T. Mueller-Westerhoff, T. J. Haas, G. F. Swiegers, T. K. Leipert, *J. Organomet. Chem.* **1994**, *472*, 229, and references therein.
[48] A. Bond, M. Green, S. H. Taylor, *J. Chem. Soc. Chem. Comm.* **1973**, 112.
[49] R. A. Henderson, D. J. Lowe, P. Salisbury, *J. Organomet. Chem.* **1995**, *489*, C22.
[50] J. A. Labinger, J. Schwartz, *J. Am. Chem. Soc.* **1975**, *97*, 1596.
[51] M. J. Dilworth, R. R. Eady, M. E. Eldridge, *Biochem. J.* **1988**, *249*, 745.
[52] G. A. Ashby, M. J. Dilworth, R. N. F. Thorneley, *Biochem. J.* **1987**, *247*, 547.
[53] A. Hills, D. L. Hughes, N. Kashef, M. A. N. D. A. Lemos, A. J. L. Pombeiro, R. L. Richards, *J. Chem. Soc. Dalton Trans.* **1992**, 1775, and references therein.
[54] R. A. Henderson, K. E. Oglieve, P. Salisbury, *J. Ghem. Soc. Dalton Trans.*, **1995**, 2479.

Organometallic "Carbon Chains": They Just Keep Getting Longer!

Uwe H. F. Bunz*

Recently a review by Beck et al.[1] and a Highlight by Lang[2] appeared in this journal in which synthesis, chemistry, and properties of novel, C_n-bridged ($n = 1-5$) homo- and heterobinuclear complexes were discussed. Complexed carbon chains can be considered as "molecular wires"[3] and represent attractive synthetic targets that allow the study of electronic, optical, and electrochemical interactions between two organometallic centers; they can also be considered as sections of the long-sought, one-dimensional carbon modification carbyne (also known as chaoite), stabilized at its ends by metal fragments.[4] Both aspects are of interest in terms of the synthetic chemistry and the materials research.

As shown in Scheme 1, the neutral rods exist in several forms **A**–**D**; those with an uneven number of C atoms occur only in form **B** (cumulene-like) or **D** (carbyne-like). However, compounds of type **A** with an even number of C atoms appear to be more stable. On oxidation of these acetylides, however, the bonding situation can change from **A** to **B** (see below).

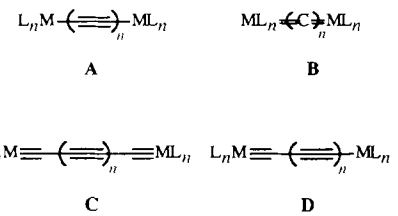

Scheme 1. Possible coordination modes of "naked" carbon chains to transition metal fragments.

In the time since the last Highlight[2] the synthesis of linear polyyne derivatives has developed rapidly through the work in the groups of Gladysz,[5] Lapinte,[6] and others;[7] thus, an update appears timely. Gladysz et al. have developed a variable synthetic route to C_n chains supported by two {Re} units ({Re} = Cp*Re(PPh$_3$)NO; Cp* = C_5Me_5).[5c]

Until 1994 only complexes were known that had between one and five C atoms between the organometallic centers. Now representatives of this type are accessible with 8, 10, 12, 16, and 20 C atoms.

[*] Dr. U. H. F. Bunz
Max-Planck-Institut für Polymerforschung
Ackermannweg 10, D-55021 Mainz (Germany)
Fax: Int. code +(6131)379-100

Syntheses

For the construction of acetylides of the form **A** with eight to twenty C atoms Gladysz et al. use a step-growth approach, in which the dimer **5** was obtained in 70% yield starting from (air

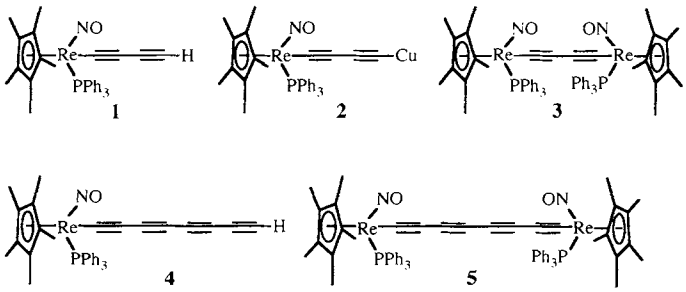

stable!)[5a] **1** by an Eglinton coupling ($Cu(OAc)_2$/pyridine/80 °C).[8a] It is amazing how the Re–C bond is so robust that it survives these comparatively harsh reaction conditions. When **1** was coupled together with the shorter homologue {Re}-C≡C-H by applying Eglinton conditions,[8a] {Re}-C≡C–C≡C–C≡C-{Re} could be isolated in 44% yield. Compound **1** is also useful in another respect. Metalation of **1** with BuLi and subsequent treatment with CuI generated the corresponding cuprate **2**. Reaction of **2** with Br-C≡C–C≡C-SiMe$_3$ in $EtNH_2$ according to a Cadiot–Chodkiewicz protocol,[8b, 9] followed by treatment with K_2CO_3 in methanol yielded the moderately sensitive species **4**. Another Eglinton coupling gave **6** in 70% yield, whereas the Eglinton coupling of {Re}-(C≡C)$_5$-H, which was synthesized analogously, led to the isolation of the decayne **7** in 41%

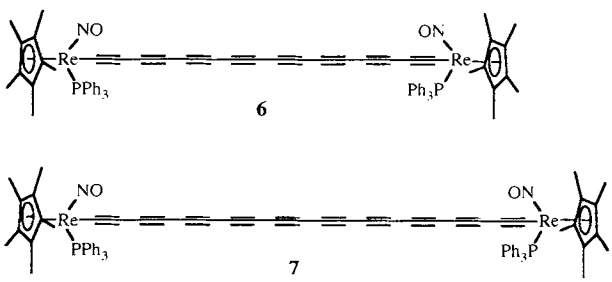

yield with a "naked" C_{20} chain. The polyynes synthesized by Gladysz are the longest organometallic carbon chains prepared to date. The synthesis of bissilyl-protected polyynes with up to 14 triple bonds was described in earlier work by Ingold and Walton;[8b] however, these were never fully characterized.

Whereas Gladysz made extensive use of copper-catalyzed couplings to produce his systems, Lapinte et al. obtained a binuclear complex bridged by a butadiyne unit through a radical dimerization:[6b] oxidation of {Fe}-C≡C-H ({Fe} = Cp*Fe(dppe); dppe = bis(diphenylphosphanyl)ethane) with ferrocenium hexafluorophosphate, led to the dimerization of the radical cation to give $[\{Fe\}=C=CH-HC=C=\{Fe\}](PF_6)_2$. KO*t*Bu reacts in THF with this dication to give the butadiyne complex **8**.

To obtain polyyne units linked to iron centers, $[Cp^*(CO)_2FeI]$ was alkynylated with Li-C≡C-C≡C-$SiMe_3$; photochemical ligand exchange with dppe and desilylation with Bu_4NF gave **10**, which was dimerized in an Eglinton coupling to afford **11** in

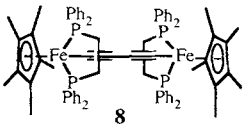

8

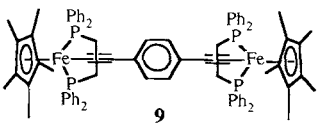

9

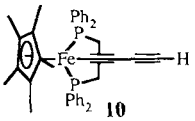

10

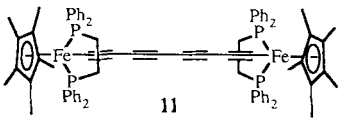

11

80% yield. Copper-catalyzed couplings also function without problems on these compounds, which in comparison to the systems prepared by Gladysz are significantly more sensitive to oxidation. It is pleasing that concepts and reactions known from the chemistry of organic alkynes can be transferred to organometallic chemistry without problems.[8, 9]

Properties

The investigation of *through-space* and *through-bond* redox interactions of organometallic fragments across C_n ligands is of fundamental interest, and the presented organometallic carbon chains are particularly suitable for such a study. The extent of the charge delocalization between the two metal centers and its effect on the bonding in the ligand in (mono)oxidized, formally mixed-valent complexes can be studied by a combination of analytical methods such as cyclic voltammetry, IR spectroscopy, and single-crystal structure analysis.

The electrochemically determined oxidation potentials of the binuclear complexes and their separation in energy as a function of the chain length and the type of organometallic fragment studied are important factors to know. A detailed investigation was made of the C_4 complex **8**, which according to cyclic voltammetry exhibits two one-electron oxidations at −0.675 and +0.045 V. The difference between the oxidation potentials (0.72 V) reveals a strong interaction along the chain between both metal centers in **8**. The radical cation of **8** was obtained in preparative quantities and a single-crystal structure analysis was carried out; **8** has a (crystallographic) inversion center, the C_4 bridge is slightly S-shaped and the C−C bonds with lengths of 1.24(1) and 1.36(1) Å predominantly retain their triple and single bond character, respectively. This somewhat unexpected result (strong electron delocalization without bond length equivalence) was supported by the IR spectroscopic data, which shows a shift of the C≡C stretching frequency to higher wavenumbers in comparison to **8**.

The oxidation product of **3**, $[\{Re\}-C\equiv C-C\equiv C-\{Re\}]^+$, described by Gladysz et al. also shows a strong electronic interaction ($E_1 = 0.11$, $E_2 = 0.64$ V, $\Delta E = 0.53$ V) between the metal centers; however, based on the IR data, for this cation a significant reduction of the bond order in comparison to that of the neutral compound must be concluded, which suggests substantial participation of the cumulene-like resonance formula $[\{Re\}=C=C=C=C=\{Re\}]^+$.

On going from **8** to the longer **11**, oxidations are now found to occur at −0.23 and +0.20 V; the difference between the oxidation potentials in **11** is 0.43 V, and thus almost twice the size as that for the rhenium analogue **5**. However, in **5**, just as in **11**, a significant shift of the C≡C stretching frequencies to lower wavenumbers occurs, which implies a significant participation of the cumulene-like resonance formula in the corresponding radical cations. Whereas **5** and **11** are similar, there are dramatic differences between **8** and **3** (see above) with regard to the bonding mode of the carbon chains that have not yet been fully explained (**A** vs. **B**).

On lengthening the carbon chain in the $\{Re\}-(C\equiv C)_n-\{Re\}$ system, the difference of the oxidation potentials ΔE between the metal centers determined by cyclic voltammetry becomes smaller (C_6: 0.38; C_8: 0.28; C_{16}: 0.1 V), and for the decayne **7** ($n = 10$) it is zero. The two Re centers in **7** are independent from each other, at least with regard to the redox properties, whereas the UV/Vis spectra still show a significant bathochromic shift of the longest wavelength maximum on transition from **6** (C_{16}) to **7** (C_{20}, 54 nm).

The synthesis and evaluation of the properties of these organometallic carbyne units will further help the elementary understanding of distance-dependent electronic interaction processes between metal centers. A study of various organometallic fragments and chain lengths such as, for example, in $(CO)_5Re-(C\equiv C)_n-Re(CO)_5$ is desirable for gaining systematic knowledge of these processes. Recent work by Lapinte et al.,[7d] in which the redox chemistry and physical properties of **9** were investigated extensively, is a step in this direction. The difference between the two oxidation potentials in **9** is 0.26 V, and is thus considerably smaller than in the geometrically similar compound **11**, in which the iron centers lie even further apart.

The following questions need to be answered: a) how large is the maximum interaction between two organometallic centers at a constant length of the C_n bridge that can be achieved by skillful manipulation of the metal fragments, and b) what is the effect of the use of other spacers (phenylene bridges, bicycles, etc.) on the difference between the oxidation potentials. In answering these questions it should be possible to distinguish between through-bond and through-space effects.

The synthesis of **7** and **11** by Gladysz et al. and Lapinte et al., respectively, has opened an area of research that in the near

future will go beyond the synthesis of these aesthetic compounds. The properties and reactions of even longer, naked carbon chains supported by organometallic fragments are eagerly awaited.

German version: *Angew. Chem.* **1996**, *108*, 1047–1049

Keywords: carbon allotropes · cumulenes · cyclic voltammetry · electron transfer · polyynes

[1] W. Beck, B. Niemer, M. Wieser, *Angew. Chem.* **1993**, *105*, 969; *Angew. Chem. Int. Ed. Engl.* **1993**, *32*, 923.

[2] H. Lang, *Angew. Chem.* **1994**, *105*, 569; *Angew. Chem. Int. Ed. Engl.* **1994**, *33*, 547, and references therein.

[3] a) J. S. Schumm, D. L. Pearson, J. M. Tour, *Angew. Chem.* **1994**, *106*, 1445; *Angew. Chem. Int. Ed. Engl.* **1994**, *33*, 1360; b) *Molecular Electronics: Science and Technology* (Ed. A. Aviram), Conf. Proc. 262, American Institute of Physics, New York **1992**; c) U. H. F. Bunz, *Angew. Chem.* **1994**, *106*, 1127; *Angew. Chem. Int. Ed. Engl.* **1994**, *33*, 1073.

[4] a) F. Diederich, *Nature* **1994**, *369*, 199; F. Diederich, Y. Rubin, *Angew. Chem.* **1992**, *104*, 1123; *Angew. Chem. Int. Ed. Engl.* **1992**, *31*, 1101; F. Diederich in *Modern Acetylene Chemistry* (Eds.: F. Diederich, P. J. Stang), VCH, Weinheim, **1995**, p. 443; b) R. J. Lagow, J. J. Kampa, H.-C Wei, S. L. Battle, J. W. Genge, D. A. Laude, C. J. Harper, R. Bau, R. C. Stevens, J. F. Haw, E. Munson, *Science*, **1995**, *267*, 362.

[5] a) J. A. Gladysz, T. A. Bartik, *Angew. Chem* **1996**, *108*, 467; *Angew. Chem. Int. Ed. Engl.* **1996**, *35*, 414; b) W. Weng, T. Bartik, J. A. Gladysz, *Angew. Chem.* **1994**, *106*, 2269; *Angew. Chem. Int. Ed. Engl.* **1994**, *33*, 2199; c) M. Brady, W. Weng, J. A. Gladysz, *J. Chem. Soc. Chem. Commun.* **1994**, 2655; d) W. Weng, T. Bartik, M. Brady, B. Bartik, J. A. Ramsden, A. M. Arif, J. A. Gladysz, *J. Am. Chem. Soc.* **1995**, *117*, 11922.

[6] a) F. Coat, C. Lapinte, *Organometallics* **1996**, *15*, 477; b) N. Le Narvor, L. Toupet, C. Lapinte, *J. Am. Chem. Soc.* **1995**, *117*, 7129; N. Le Narvor, C. Lapinte, *J. Chem. Soc. Chem. Commun.* **1993**, 357.

[7] a) P. J. Stang, R. Tykwinski, *J. Am. Chem. Soc.* **1992**, *114*, 4411; b) H. B. Fyfe, M. Mlekuz, D. Zargarian, R. Taylor, T. B. Marder, *J. Chem. Soc. Chem. Commun.* **1991**, 191; c) W. Beck, S. Mihan, unpublished results; d) N. Le Narvor, C. Lapinte, *Organometallics* **1995**, *14*, 634; e) P. J. Kim, H. Masai, K. Sonogashira, N. Hagihara, *Inorg. Nucl. Chem. Lett.* **1970**, *6*, 181.

[8] a) G. Eglinton, W. McCrae, *Adv. Org. Chem.* **1963**, *4*, 225; b) K. Sonogashira in *Comprehensive Organic Chemistry* (Ed.: B. Trost) **1991**, *3*, 551; c) R. Eastmont, T. R. Johnson, D. R. M. Walton, *Tetrahedron* **1972**, *28*, 4601.

[9] See also *Modern Acetylene Chemistry*, (Eds.: F. Diederich, P. J. Stang), VCH, Weinheim, **1995**.

Recent Developments in the Enantioselective Syntheses of Cyclopropanes

Hans-Ulrich Reissig*

The hunt for strained molecules is maintained on the one hand by the competitive ambition to find the most unusual structures and on the other by the enormous synthetic potential of small-ring compounds. Following the general trend of recent years asymmetric syntheses are at the cutting edge of this research.[1] Despite all advances the synthesis of enantiomerically and diastereomerically pure cyclopropane derivatives remains a considerable challenge, especially when particular functional groups are required. The last two years have provided little that is fundamentally new to add to the very elegant procedures based on asymmetric catalysts.[2] In the main, reaction conditions and ligands were optimized, and the scope and limitations were investigated. Most exciting were the new examples from Doyle's group who reported on the enantioselective synthesis of macrocyclic lactones by means of intramolecular carbene additions.[3] Whereas the expected intramolecular cyclopropanation to a bicyclic γ-lactone was observed with a chiral rhodium(II)-MEPY catalyst with 96% *ee* (Scheme 1), with the Evans copper complex containing a bis(oxazoline) ligand the macrocyclic lactone was strongly favored (87% *ee*). Similar, or even higher, regio- and enantioselectivities with astonishingly high yields were also found in other examples. Thus there is now a new strategy, which will certainly find practical uses, for the enantioselective synthesis of macrocycles that are otherwise accessible only with difficulty.

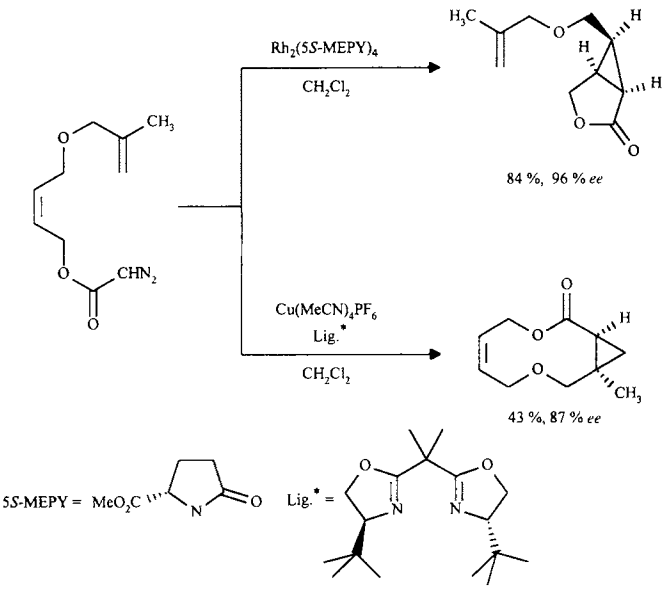

Scheme 1.

Pfaltz's semicorrin copper complexes—a real breakthrough ten years ago—can also be employed for intramolecular [2+1]-cycloadditions (Scheme 2) and achieve between 14 and 95% *ee* depending on the substrate.[4] The related, otherwise very successful, bis(oxazoline) complexes[5] (see above) do not appear to be as effective here though only one example has been investigated.

[*] Prof. Dr. H.-U. Reissig
Institut für Organische Chemie der Technischen Universität
D-01062 Dresden (Germany)
Fax: Int. code +(351)463-7030

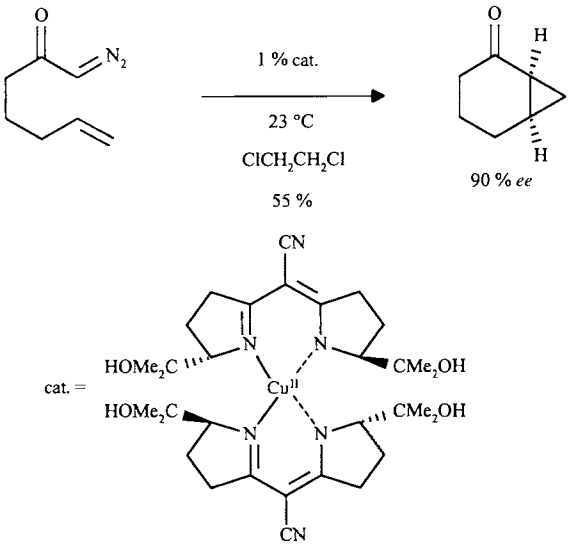

Scheme 2.

An optically active Co^{III}–salen complex was also employed for enantioselective cyclopropanation.[6] It can, however, be said that the ultimate catalyst system, which reliably delivers both high enantiomeric excess and good *cis/trans* selectivity, and which is also suitable for highly substituted and/or functionalized olefins is still a dream.

Advances, but no breakthroughs, can be seen in the several variants of the Simmons–Smith cyclopropanation.[7] Since enantioselective catalysis is developing only slowly—with respectable individual successes[8]—the auxiliary-controlled procedures are still superior.[9] In general, cyclopropane syntheses controlled by reagent-bound auxiliary groups offer a better guarantee of high enantiomeric purity than those using the more elegant asymmetric catalysts.

A beautiful new example, suitable for the synthesis of highly functionalized cyclopropane derivatives, was recently discovered by the Hanessian group.[10] Whereas in most auxiliary-controlled formal [2+1]cycloadditions[1] the auxiliary group is attached to the olefinic residue, here the chiral information is carried by a chloroallylphosphonic acid amide, such as **1**, which acts as a vinylcarbene equivalent. The reaction of the carbanion derived from **1** with α,β-unsaturated carbonyl compounds such

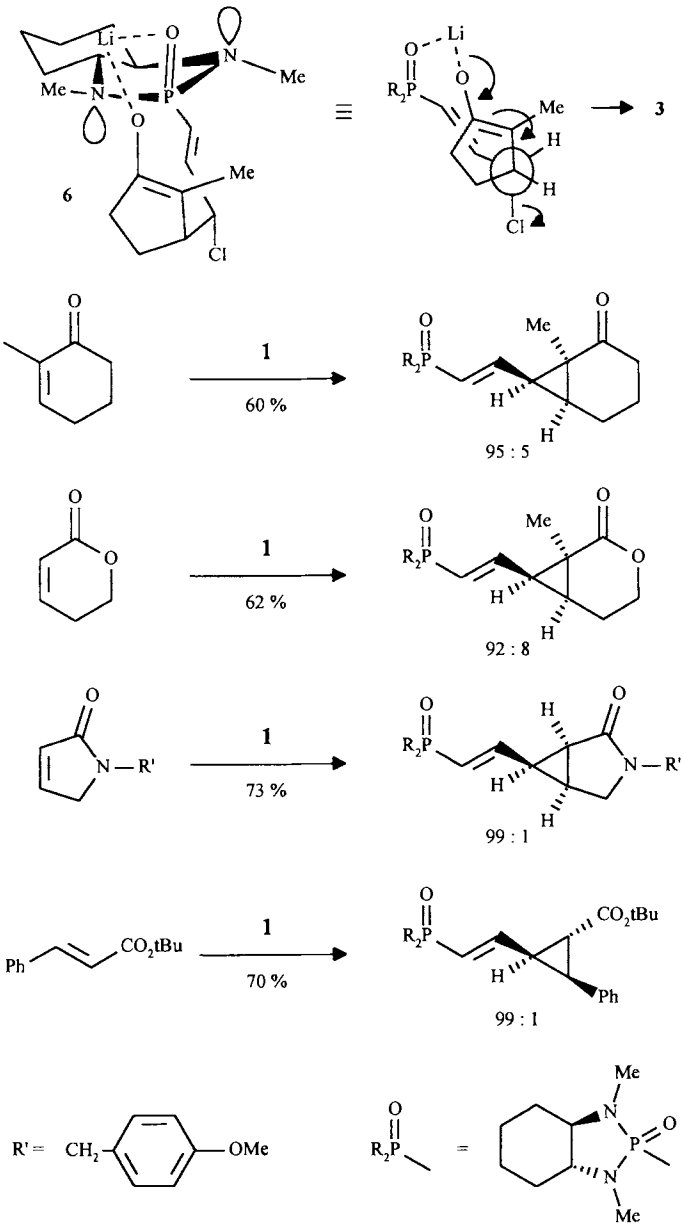

Scheme 3.

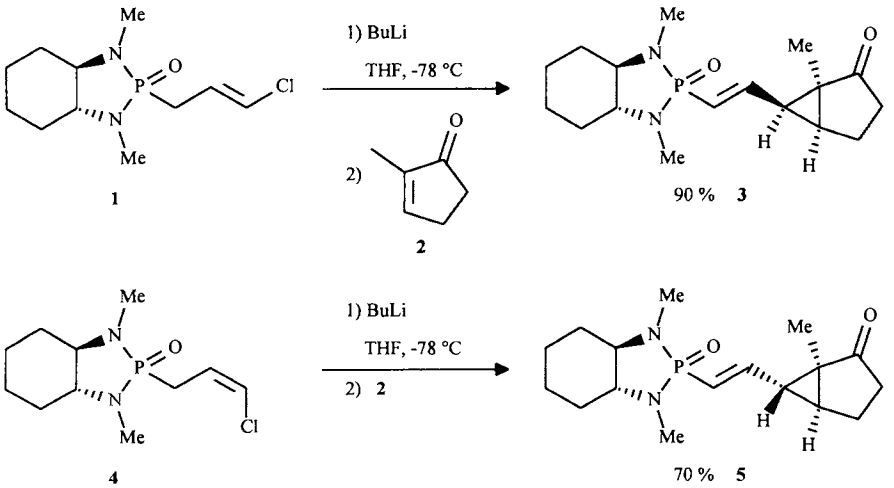

as **2** yields the diastereomerically pure bicyclo[3.1.0]hexanone derivative **3** as the *endo*-isomer (90% yield). By contrast, the reaction between the *cis*-chloroallyl derivative **4** and **2** yields the epimeric bicyclic product **5**. Mechanistically this cyclopropanation is easily understood as resulting from a Michael addition and an intramolecular S_N2 alkylation in which the intermediate **6** could account for the observed diastereoselectivity.

The method seems to be widely applicable as the examples with other cyclic enones, unsaturated lactones, lactams, and *tert*-butyl esters show (Scheme 3). The diastereoselectivities are at least 92:8 and usually much better.

 © VCH Verlagsgesellschaft mbH, D-69451 Weinheim, 1996 0570-0833/96/3509-0972 $ 15.00+.25/0 Angew. Chem. Int. Ed. Engl. 1996, 35, No. 9

After reduction of the carbonyl group with sodium borohydride and protective silylation of the resulting hydroxy group, the auxiliary is removed by ozonolysis of the alkenylphosphonamide group. By this method, or other obvious sequences, the primary products are converted into a series of enantiomerically pure, interestingly functionalized cyclopropane derivatives (Scheme 4), which should find applications as synthetic building blocks.

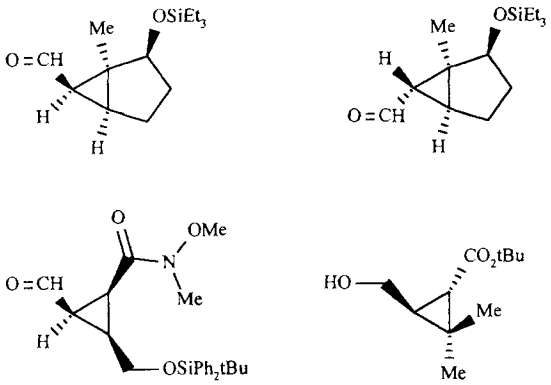

Scheme 4.

Nevertheless, ozonolysis of the alkenyl substituents destroys some of the preparative potential of the primary products; as vinylpropanes they would be interesting for many other reactions, for example, for 1,3- and 3,3-sigmatropic rearrangements.[11] It can be inferred from the footnotes of the report[10] that a Cope rearrangement of the primary product **8**, derived from the hexadienoic acid ester **7** and **1**, does actually take place at room temperature with the formation of two isomeric cycloheptadiene derivatives. No details were given about the structure of these compounds. One of the most interesting applications of the method could be the synthesis of enantiomerically pure, highly functionalized cycloheptane derivatives, since divinylcyclopropanes should be obtainable by the appropriate rearrangement of other primary products.

The results described above represent only the classical developments of organic synthesis extended and perfected; however,

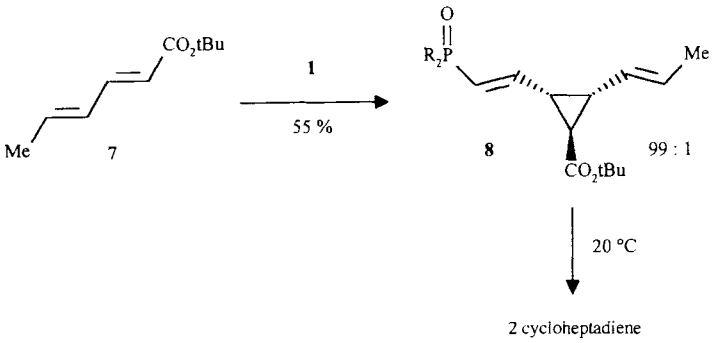

a recent publication on antibody-induced cyclopropanation could be the inauguration of what is, in principle, a new path to asymmetric cyclopropane formation (although the example is one with little preparative interest).[12]

German version: *Angew. Chem.* **1996**, *108*, 1049–1051

Keywords: asymmetric syntheses · cyclopropane derivatives · synthetic methods

[1] Comprehensive survey of diastereoselective and enantioselective [2+1]cycloadditions covering the literature up to and including 1994: H.-U. Reissig in *Stereoselective Synthesis of Organic Compounds/Methods of Organic Chemistry (Houben-Weyl), 4th ed., Vol. E21c* (Eds.: G. Helmchen, R. W. Hoffmann, J. Mulzer, E. Schaumann), Thieme, Stuttgart, **1995**, pp. 3179–3270.
[2] M. P. Doyle in *Catalytic Asymmetric Synthesis* (Ed.: I. Ojima), VCH, Weinheim, **1993**, pp. 63–99.
[3] M. P. Doyle, C. S. Peterson, D. L. Parker, Jr., *Angew. Chem.* **1996**, *108*, in press; *Angew. Chem. Int. Ed. Engl.* **1996**, *35*, in press. See also: M. P. Doyle, M. N. Protopopova, C. D. Poulter, D. H. Rogers, *J. Am. Chem. Soc.* **1995**, *117*, 7281–7282.
[4] C. Piqué, B. Fähndrich, A. Pfaltz, *Synlett* **1995**, 491–492.
[5] Short review: C. Bolm, *Angew. Chem.* **1991**, *103*, 556–558; *Angew. Chem. Int. Ed. Engl.* **1991**, *30*, 542.
[6] T. Fukuda, T. Katsuki, *Synlett* **1995**, 825–826.
[7] New review: U. Koert, *Nachr. Chem. Tech. Lab.* **1995**, *43*, 435–442.
[8] S. Kobayashi, H. Takahashi, N. Imai, K. Sakamoto, *Tetrahedron Lett.* **1994**, *35*, 7045–7048; for new aspects, see: A. B. Charette, C. Brochu, *J. Am. Chem. Soc.* **1995**, *117*, 11367–11368.
[9] Review: A. B. Charette, J.-F. Marcoux, *Synlett* **1995**, 1197–1207.
[10] S. Hanessian, D. Andreotti, A. Gomtsyan, *J. Am. Chem. Soc.* **1995**, *117*, 10393–10394.
[11] J. Salaün in *The Chemistry of the Cyclopropyl Group* (Ed.: S. Patai, Z. Rappoport), Wiley, Chichester, **1987**, pp. 809–878.
[12] T. Li, K. D. Janda, R. A. Lerner, *Nature* **1996**, *379*, 326–327.

Prototype of an Optically Responsive Molecular Switch Based on Pseudorotaxane**

Masumi Asakawa, Sayeedha Iqbal, J. Fraser Stoddart,* and Nigel D. Tinker

Supramolecular arrays in solution can often be constructed and controlled[1] by a combination of molecular recognition[2] and self-assembly[3] processes. Increasingly, the emphasis is on developing molecular systems that have technological applications in the fields of sensors,[4] devices,[5] and switches.[6] To this end, supramolecular chemistry[7] is playing an increasingly important role.

[2]Pseudorotaxanes[8] and [2]rotaxanes[9] can be assembled from cyclobis(paraquat-*p*-phenylene) as rings and 1,4-dioxy-substituted arenes as threads bearing macrocyclic polyethers at their termini. The [2]pseudorotaxanes can be readily disassembled by the addition of alkali metal cations. Here, we demonstrate how these [2]pseudorotaxanes can be used to produce an optical response on metal binding. The [18]crown-6 derivative (*R*,*S*)-**5**, containing a 1,5-dioxynaphthalene residue, can act (see Scheme 2) both as a host toward alkali metal cations and as a guest toward the tetracationic cyclophane $\mathbf{8}^{4+}$. The binding of (*R*,*S*)-**5** by $\mathbf{8}^{4+}$ can be reduced significantly by the addition of alkali metal cations, such as K^+ ions, which form complexes with [18]crown-6 derivatives.[10] In this manner, we can achieve the unthreading of the [2]pseudorotaxane (*R*,*S*)-**5**·**8**-4PF_6 by chemical means and, at the same time, encourage the self-assembly of the [2]pseudorotaxane **7**·**8**-4PF_6 lacking an [18]crown-6 stopper.

1-Benzyloxy-5-{2-(2-hydroxyethoxy)ethoxy}naphthalene (**2**) has been obtained[11] in 60% yield by the alkylation of 1-benzyloxy-5-hydroxynaphthalene[11] (**1**) with 2-(2-chloroethoxy)-ethanol under basic conditions (K_2CO_3/MeCN) (Scheme 1).[11]

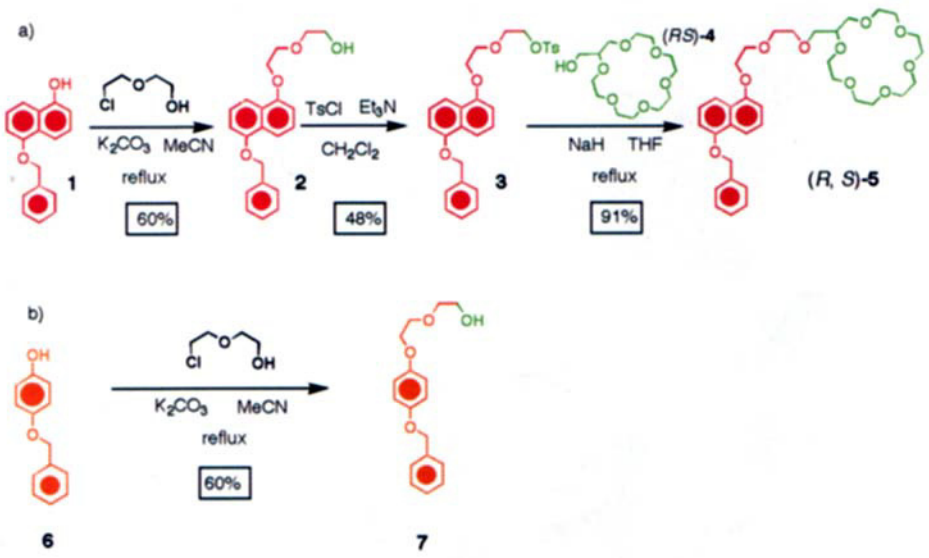

Scheme 1. The synthesis of a) the [18]crown-6 derivative (*R*,*S*)-**5** containing a 1,5-dioxynaphthalene residue and b) the 1,4-dioxybenzene derivative **7**.

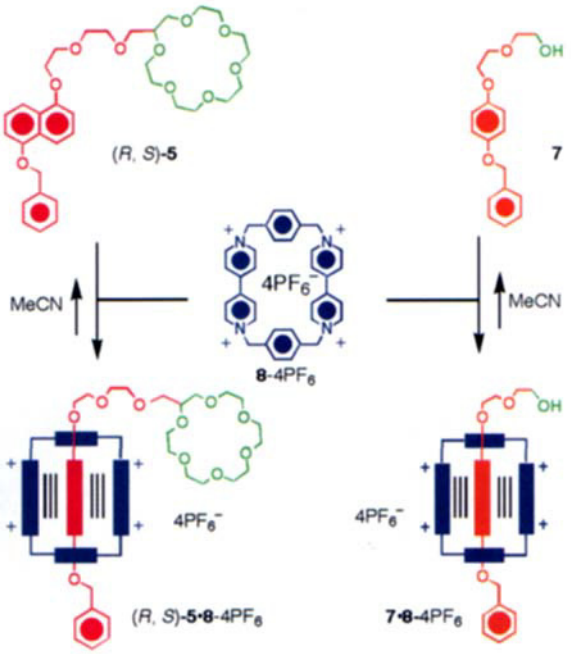

(*R*, *S*)-**5**·**8**-4PF_6	MeCN	**7**·**8**-4PF_6
purple	solution color	red/orange
530	λ_{max} / nm	475
910	K_a / M^{-1}	75
4.0	$-\Delta G°$ / kcal mol^{-1}	2.5

Scheme 2. Self-assembly of the [2]pseudorotaxanes **5**·**8**-4PF_6 and **7**·**8**-4PF_6 in MeCN.

The tosylation (TsCl/Et_3N/CH_2Cl_2) of the alcohol **2** afforded **3** (48%), which, with 1.2 molar equivalents of 2-hydroxymethyl-[18]crown-6 ((*R*,*S*)-**4**), gave the [18]crown-6 derivative (*R*,*S*)-**5** in excellent yield (91%). 1-Benzyloxy-4-{2-(2-hydroxyethoxy)ethoxy}benzene (**7**) was obtained[12] by the alkylation of 4-benzyloxyphenol (**6**) with 2-(2-chloroethoxy)ethanol under basic conditions (K_2CO_3/MeCN) in 40% yield.

UV spectrophotometric titrations monitoring the wavelength of the charge transfer (CT) band were employed[13] to evaluate the association constants K_a of the complexation of (*R*,*S*)-**5** and **7** with the tetracationic cyclophane **8**-4PF_6 in MeCN at 25 °C (Scheme 2). Mixing equimolar solutions of (*R*,*S*)-**5** and **8**-4PF_6 in MeCN results instantaneously in a deep purple color with the CT band at 530 nm, which indicates the formation of a [2]pseudorotaxane **5**·**8**-4PF_6. A K_a value of 910 M^{-1}, corresponding to a $-\Delta G°$ value of 4.0 kcal mol^{-1}, was obtained in MeCN at 25 °C with a UV titration method. Mixing equimolar MeCN solutions of **7** and **8**-4PF_6 results instantaneously in a red-orange color with the CT band centered at 475 nm, which indicates the formation of the [2]pseudorotaxane **7**·**8**-4PF_6.

[*] Prof. J. F. Stoddart, Dr. M. Asakawa, Dr. S. Iqbal
School of Chemistry, University of Birmingham
Edgbaston, GB-Birmingham B15 2TT (UK)
Fax: Int. code +(121)414-3531
Dr. N. D. Tinker
British Nuclear Fuels Plc, Springfields Works, Salwick
GB-Preston, Lancashire PR40XJ (UK)

[**] This research was supported by British Nuclear Fuels Plc, the Engineering and Physical Sciences Research Council, and the Wolfson Foundation in the UK and by the Ciba-Geigy Foundation for the Promotion of Science (Japan).

 © VCH Verlagsgesellschaft mbH, D-69451 Weinheim, 1996 0570-0833/96/3509-0976 $ 15.00+.25/0

A K_a value of $75\,M^{-1}$, corresponding to a $-\Delta G^{\circ}$ value of 2.5 kcal mol^{-1}, was obtained in MeCN at 25 °C by a UV titration method. The [18]crown-6 derivative (*R*,*S*)-**5**, containing a 1,5-dioxynaphthalene residue, has a greater propensity to bind inside the charged cavity than the 1,4-dioxybenzene derivative **7**. The tetracationic cyclophane is sufficiently small that it cannot slip[14] over the [18]crown-6 polyether residue in (*R*,*S*)-**5**, and hence the formation of the [2]pseudorotaxane **5**·**8**-4PF$_6$ can only occur by the slippage of the tetracationic cyclophane over the benzyl group of (*R*,*S*)-**5**.

Mixing equimolar proportions of (*R*,*S*)-**5**, **7**, and **8**-4PF$_6$ in MeCN results in a deep purple color with the CT band at 518 nm (Fig. 1, trace B), indicating that the tetracationic cyclophane resides mainly around the naphthalene residue of (*R*,*S*)-**5** (Scheme 3). Trace A in Figure 1 corresponds to the CT band observed for the [2]pseudorotaxane (*R*,*S*)-**5**·**8**-4PF$_6$. Addition of 10 mol equivalents of KPF$_6$ to the equimolar solution of (*R*,*S*)-**5**, **7**, and **8**-4PF$_6$ solution in MeCN resulted in a CT at 475 nm (Fig. 1, trace C), and the purple color fades. This trace

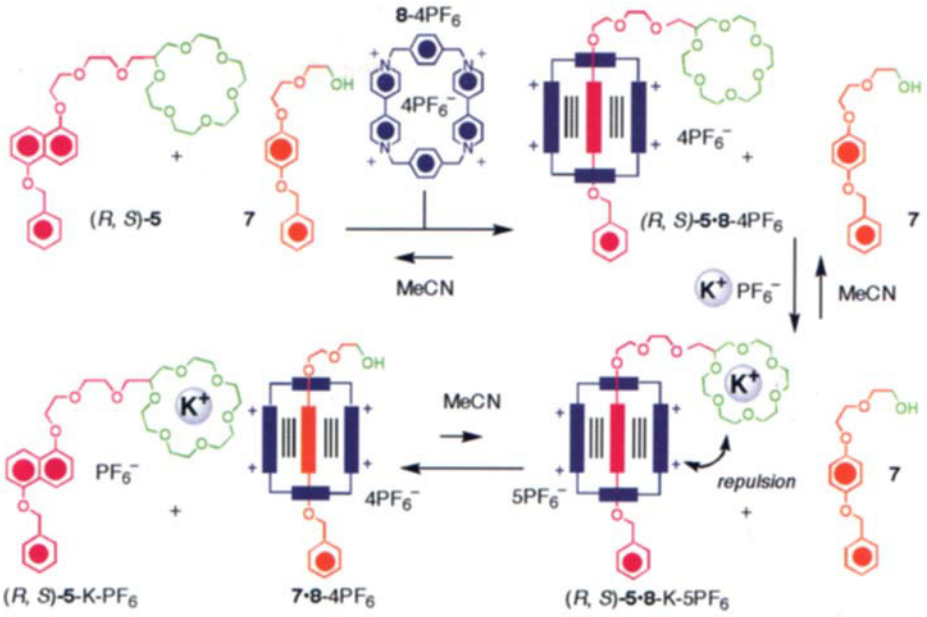

Scheme 3. The proposed mode of action of a prototypical optically responsive molecular device.

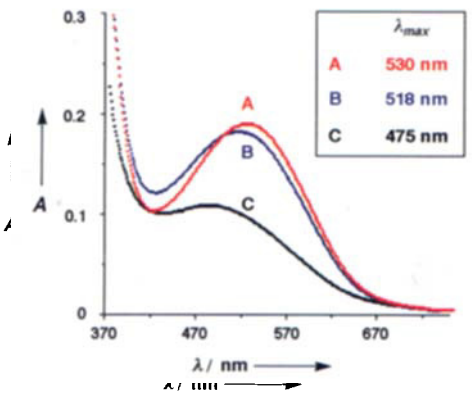

Fig. 1. UV Vis spectra showing the CT bands (concentration: 4.47×10^{-3} M in MeCN) of the[2]pseudorotaxane **5**·**8**-4PF$_6$ (A), an equimolar mixture of **5**, **7** and **8**-4PF$_6$ (B), and an equimolar mixture of **5**, **7** and **8**-4PF$_6$ upon addition of a tenfold excess of KPF$_6$ (C). *A* = absorption.

is almost identical to that found for the [2]pseudorotaxane **7**·**8**-4PF$_6$. Hence, the addition of K$^+$ ions to equimolar solutions of (*R*,*S*)-**5**, **7**, and **8**-4PF$_6$ in MeCN brings about a bathochromic shift of 43 nm.

Apparently, upon addition of an excess of KPF$_6$ to equimolar solutions of (*R*,*S*)-**5**, **7**, and **8**-4PF$_6$ in MeCN an unstable complex (*R*,*S*)-**5**·**8**-K-5PF$_6$ results (Scheme 3). Electrostatic repulsions between the bound K$^+$ ion within the [18]crown-6 terminus of the 1,5-dioxynaphthalene derivative (*R*,*S*)-**5** and the tetracationic cyclophane **8**-4PF$_6$ bring about the disassembly of the metalated complex (*R*,*S*)-**5**·**8**-K-5PF$_6$ to give the metalated derivative (*R*,*S*)-**5**-K-5PF$_6$ and the tetracationic cyclophane **8**-4PF$_6$, which forms the complex **7**·**8**-4PF$_6$ with the neutral 1,4-dioxybenzene derivative **7**. Thus a negative allosteric effect occurs in the complexation of the tetracationic cyclophane and the metal cation with the [18]crown-6 derivative (*R*,*S*)-**5** containing a naphthalene residue, that is, (*R*,*S*)-**5** can bind to either metal cations or the tetracationic cyclophane, but not to both at the same time. Very few cases[15] of negative allosteric effects have been reported.

We have shown that the alkali metal cation acts as a mediator for the negative allosteric effect, since it brings about the disassembly of the tetracationic cyclophane **8**-4PF$_6$ from (*R*,*S*)-**5**·**8**-4PF$_6$, thus enabling the formation of the [2]pseudorotaxane **7**·**8**-4PF$_6$. The net result is that a change in the absorption spectrum (that is, in the optical response) occurs upon addition of metal cations to equimolar solutions of (*R*,*S*)-**5**, **7**, and **8**-4PF$_6$ in MeCN. The development of these self-assembling systems could lead to functioning supramolecular entities that can be readily switched by chemical stimuli to give an optical response.

Experimental Procedure

(*R*,*S*)-**5**: (*R*,*S*)-**4** (64 mg, 0.22 mmol) in dry THF (20 mL) was added over a period of 20 min to a suspension of NaH (10 mg, 40 mmol) in dry THF (50 mL) under reflux. The reaction mixture was heated under reflux for a further 30 min, after which a solution of **3** (100 mg, 0.20 mmol) in dry THF (30 mL) was added over a period of 1 h. The reaction mixture was maintained under reflux for a further 24 h and then allowed to cool down to room temperature before H_2O (10 mL) was added to quench any residual NaH. The solution was then concentrated in vacuo to give a yellow oil, which was partitioned between CH_2Cl_2 and ice cold HCl (10% solution). The organic layer was separated, dried ($MgSO_4$), and concentrated in vacuo to yield a pale yellow oil (117 mg, 91%); FAB-MS: *m/z*: 637 $[M+Na]^+$, 614 $[M]^+$; ^{1}H NMR (300 MHz, $CDCl_3$): δ = 7.95–7.88 (2H, 2 × d, *J* = 8 Hz), 7.58–7.54 (2H, d, *J* = 8 Hz), 7.48–7.88 (5H, m), 6.89–6.84 (2H, 2 × d, *J* = 8 Hz), 6.75 (2H, s), 4.38–4.32 (4H, m), 4.05–3.90 (2H, m), 3.82–3.78 (2H, m), 3.70–3.55 (23H, m); ^{13}C NMR (75 MHz, $CDCl_3$): δ = 128.6, 127.9, 127.4, 125.2, 114.7, 106.0, 105.8, 78.3, 71.6, 71.3, 71.0, 70.8, 70.6, 70.1, 69.8, 68.0.

(*R*,*S*)-**5**·**8**-4PF$_6$: Mixing equimolar solutions (6.69×10^{-3} M) of (*R*,*S*)-**5** and **8**-4PF$_6$ in MeCN results in the formation of the [2]pseudorotaxane (*R*,*S*)-**5**·**8**-4PF$_6$. FAB-MS: *m/z*: 1737 $[M+Na]^+$, 1592 $[M+Na-PF_6]^+$, 1569 $[M-PF_6]^+$, 1424 $[M-2PF_6]^+$; ^{1}H NMR (300 MHz, CD_3CN): δ = 8.82–8.76 (8H, d, *J* = 8 Hz), 7.90–7.68 (5H, m), 7.63 (8H, s), 7.63–7.58 (8H, d, *J* = 8 Hz), 6.75–6.40 (4H, m), 5.74 (8H, s), 5.20 (2H, s), 4.32–4.28 (2H, m), 4.15–1.11 (2H, m), 3.95–3.91 (2H, m), 3.82–3.88 (2H, m), 3.7–3.30 (25H, m).

7·**8**-4PF$_6$: Mixing equimolar solutions (6.69×10^{-3} M) of **7** and **8**-4PF$_6$ in MeCN results in the formation of the [2]pseudorotaxane **7**·**8**-4PF$_6$. ^{1}H NMR (300 MHz,

CD_3CN): δ = 8.82–8.76 (8H, d, J = 8 Hz), 7.90–7.68 (5H, m), 7.63 (8H, s), 7.63–7.58 (8H, d, J = 8 Hz), 5.74 (8H, s), 5.20 (2H, s), 4.32–4.28 (2H, m), 4.15–1.11 (2H, m), 3.95–3.91 (2H, m), 3.82–3.88 (2H, m).

Received: October 24, 1995 [Z 8493 IE]
German version: *Angew. Chem.* **1996**, *108*, 1054–1056

Keywords: allosteric effect · cation recognition · molecular switches · pseudorotaxanes · supramolecular chemistry

[1] J.-M. Lehn, *Angew. Chem.* **1988**, *100*, 91; *Angew. Chem. Int. Ed. Engl.* **1988**, *27*, 89; G. M. Whitesides, J. P. Mathias, C. T. Seto, *Science* **1991**, *254*, 1312; G. M. Whitesides, E. E. Simanek, J. P. Mathias, C. T. Seto, D. N. Chin, M. Mammen, D. M. Gordon, *Acc. Chem. Res.* **1995**, *28*, 37.

[2] C. J. Pedersen, *Angew. Chem.* **1988**, *100*, 1053; *Angew. Chem. Int. Ed. Engl.* **1988**, *27*, 1021; J.-M. Lehn, *ibid.* **1988**, *100*, 91 and **1988**, *27*, 89; D. J. Cram, *ibid.* **1988**, *100*, 1041 and **1988**, *27*, 1009; J.-M. Lehn, *Science* **1993**, *260*, 1762; G. W. Gokel in *Crown Ethers and Cryptands* (Monographs in Supramolecular Chemistry, Ed.: J. F. Stoddart), The Royal Society of Chemistry, Cambridge, **1991**; J.-M. Lehn, *Supramolecular Chemistry – Concepts and Perspectives*, VCH, Weinheim, **1995**.

[3] J. S. Lindsey, *New J. Chem.* **1991**, *15*, 153; D. Philp, J. F. Stoddart, *Synlett* **1991**, 445; *Angew. Chem.* **1996**, *108*, No. 11; *Angew. Chem. Int. Ed. Engl.* **1996**, *35*, No. 11.

[4] M. Aizawa in *Analytical Chemistry Series, Chemical Sensors* (Eds.: T. Seiyama, K. Fueki, J. Shiokama, S. Suzuki), Elsevier, Fukuoka, **1983**, p. 683; R. B. Beswick, C. W. Pitt, *J. Colloid Interface Sci.* **1988**, *124*, 146; J. Whittal in *Photochromism, Molecules and Systems* (Eds.: H. Dürr, H. Bouas-Laurent), Elsevier, Amsterdam, **1990**, p. 467.

[5] For examples of molecular devices, see *Molecular Electronic Devices* (Ed.: F. L. Carter), Marcel Dekker, New York, **1982**; S. L. Gilat, S. H. Kawai, J.-M. Lehn, *J. Chem. Soc. Chem. Commun.* **1993**, 1439; N. P. M. Huck, B. L. Feringa, *ibid.* **1995**, 1095.

[6] Switchable catenanes and rotaxanes: P. R. Ashton, R. A. Bissell, N. Spencer, J. F. Stoddart, M. S. Tolley, *Synlett* **1992**, 914; P. R. Ashton, R. Ballardini, V. Balzani, M. Blower, M. Ciano, M. T. Gandolfi, C. H. McLean, D. Philp, L. Prodi, N. Spencer, J. F. Stoddart, M. S. Tolley, *New J. Chem.* **1993**, *17*, 68; R. A. Bissell, E. Córdova, A. E. Kaifer, J. F. Stoddart, *Nature* **1994**, *369*, 133; A. C. Benniston, A. Harriman, V. M. Lynch, *Tetrahedron Lett.* **1994**, *35*, 1473; R. Hoss, F. Vögtle, *Angew. Chem.* **1994**, *106*, 389; *Angew. Chem. Int. Ed. Engl.* **1994**, *33*, 375; P. R. Ashton, L. Pérez-García, J. F. Stoddart, A. J. P. White, D. J. Williams, *ibid.* **1995**, *107*, 607 or **1995**, *34*, 571; examples of molecular switches: S. Shinkai in *Studies in Organic Chemistry, Vol. 45: Crown Ethers and Analogous Compounds* (Ed.: M. Hiraoka), Elsevier, Amsterdam, **1992**; P. D. Beer, *Chem. Soc. Rev.* **1989**, *18*, 409; S. Nespurek, *Int. J. Electron.* **1992**, *73*, 1059; T. Saika, M. Irie, T. Shimidu, *J. Chem. Soc. Chem. Commun.* **1994**, 2123; P. D. Beer, J. P. Danks, D. Hesek, J. F. McAleer, *ibid.* **1993**, 1735; M. Shimomura, S. Aiba, S. Oguma, M. Oguchi, M. Matsute, H. Shimada, R. Kagimara, H. Emori, K. Yishiwara, K. Okuyana, T. Miyashita, A. Watanabe, M. Matsuda, *Supramol. Sci.* **1994**, *1*, 33.

[7] V. Balzani, L. De Cola, *Supramolecular Chemistry*, Kluwer, Amsterdam, **1992**; F. Vögtle, *Supramolekulare Chemie*, 2nd ed., Teubner, Stuttgart, **1991**.

[8] P. R. Ashton, S. Iqbal, J. F. Stoddart, N. D. Tinker, *J. Chem. Soc. Chem. Commun.* **1996**, 479.

[9] S. Iqbal, J. F. Stoddart, N. D. Tinker, unpublished results.

[10] *Cation Binding by Macrocycles* (Eds.: Y. Inoue, G. W. Gokel), Marcel Dekker, New York, **1990**.

[11] D. B. Amabilino, P.-L. Anelli, P. R. Ashton, G. R. Brown, E. Córdova, L. A. Gódinez, W. Hayes, A. E. Kaifer, D. Philp, A. M. Z. Slawin, N. Spencer, J. F. Stoddart, M. S. Tolley, D. J. Williams, *J. Am. Chem. Soc.* **1995**, *117*, 11142.

[12] P. L. Anelli, P. R. Ashton, R. Ballardini, V. Balzani, M. Delgado, M. T. Gandolfi, T. T. Goodnow, A. E. Kaifer, D. Philp, M. Pietraszkiewicz, L. Prodi, M. V. Reddington, A. M. Z. Slawin, N. Spencer, J. F. Stoddart, C. Vicent, D. J. Williams, *J. Am. Chem. Soc.* **1992**, *114*, 193.

[13] The association constants (K_a) of the [2]pseudorotaxanes in MeCN at 25 °C were obtained by UV titration (K. A. Connors, *Binding Constants*, Wiley, New York, **1987**). The treatment of the collected data with a nonlinear curve-fitting program UltraFit 2.11 afforded the K_a values.

[14] For references on threading, see: P. R. Ashton, M. Bělohradský, D. Philp, J. F. Stoddart, *J. Chem. Soc. Chem. Commun.* **1993**, 1269; P. R. Ashton, M. Bělohradský, J. F. Stoddart, *ibid.* **1993**, 1274; D. B. Amabilino, P. R. Ashton, M. Bělohradský, F. M. Raymo, J. F. Stoddart, *ibid.* **1995**, 745, 751.

[15] H.-J. Schneider, F. Werner, *J. Chem. Soc. Chem. Commun.* **1992**, 490; A. M. Costero, S. Rodríguez, *Tetrahedron* **1992**, *48*, 6265; J. C. Rodríguez-Ubis, O. Juanes, E. Brunet, *Tetrahedron Lett.* **1994**, *35*, 1295.

Simple Molecular Machines: Chemically Driven Unthreading and Rethreading of a [2]Pseudorotaxane

Roberto Ballardini, Vincenzo Balzani, Alberto Credi, Maria Teresa Gandolfi, Steven J. Langford, Stephan Menzer, Luca Prodi, J. Fraser Stoddart,* Margherita Venturi, and David J. Williams

The miniaturization of a "device" to the molecular level[1–5] is not only of academic interest, but can also contribute to the development of nanotechnology. Progress in constructing molecular devices may have important implications for biomimetic engineering,[6] molecular-based logic,[7] computer technologies,[8, 9] and a variety of sensory techniques.[10, 11] Molecular devices of particular interest are those displaying changes in the relative positions of their component parts – let us call them mechanical molecular machines[12–16]—as a result of the influence of some external stimulus. Here we describe the self-assembly of a novel pseudorotaxane and a very simple molecular machine, which operates by the chemically driven cyclic unthreading and rethreading processes. Pseudorotaxanes are supramolecular (multicomponent) complexes comprising at least one macrocyclic ring threaded by an acyclic component.[17] The [2]pseudorotaxane in this research is $\mathbf{1}^{2+}$ in Figure 1, obtained by self-assembly of the 2,7-dibenzyldiazoniapyrene dication $\mathbf{2}^{2+}$ with the crown ether **3** (Process I, Fig. 1).

When **2**-2PF_6 is added to a solution of **3** in MeCN, the electron-accepting dication $\mathbf{2}^{2+}$ threads itself spontaneously through the center of the macrocyclic ring **3**, which contains two 1,5-dioxynaphthalene electron-donating units. The [2]pseudorotaxane **1**-2PF_6 was characterized by mass spectrometry,[18] ^{1}H NMR spectroscopy, and X-ray crystallography.[19] The mass spectrum of **1**-2PF_6 indicates clearly the loss of one and two PF_6^- counterions from the [2]pseudorotaxane, giving rise to the $[M - PF_6]^+$ and $[M - 2PF_6]^+$ peaks at m/z 1167 and 1022, respectively. Comparison of the ^{1}H NMR spectra (Fig. 2) of the free salt **2**-2PF_6, the crown ether **3**, and the [2]pseudorotaxane **1**-2PF_6 indicates that all the protons undergo very substantial chemical shift changes ($\Delta\delta$ values of up to 0.70). X-ray crystallography reveals that $\mathbf{1}^{2+}$ crystallizes with two crystallographically independent C_i symmetric molecules in the asymmetric unit (Fig. 3). In both complexes, the π-electron-deficient diazoniapyrene component $\mathbf{2}^{2+}$ is sandwiched symmetrically between the π-electron-rich 1,5-dioxynaphthalene rings of **3** (mean interring plane separations 3.48 Å). The 1:1 complex is further stabi-

[*] Prof. J. F. Stoddart, Dr. S. J. Langford
School of Chemistry, University of Birmingham
Edgbaston, GB-Birmingham B15 2TT (UK)
Fax: Int. code +(121)414-3531

Dr. R. Ballardini, Prof. V. Balzani, A. Credi, Dr. M. T. Gandolfi, Dr. L. Prodi, Dr. M. Venturi
Dipartimento di Chimica "G. Ciamician" dell'Università and
Istituto FRAE-CNR
I-40126 Bologna (Italy)

Dr. S. Menzer, Dr. D. J. Williams
Chemical Crystallography Laboratory, Department of Chemistry
Imperial College
South Kensington, GB-London SW7 2AY (UK)

[**] This research is supported by the Engineering and Physical Sciences Research Council (EPSRC) in the UK, and CNR (Progetto Strategico Tecnologie Chimiche Innovative) and Ministero dell'Università e della Ricerca Scientifica e Tecnologica in Italy. We acknowledge the Ramsay Memorial Trust for providing S. J. L. with a Ramsay Memorial Postdoctoral Fellowship and Ciba-Geigy (Divisione Additivi) for a grant to A. C. We thank Mr. P. R. Ashton, Dr. N. Spencer, and Mr. M. S. Tolley for recording the mass spectra and ^{1}H NMR spectra of the different adducts.

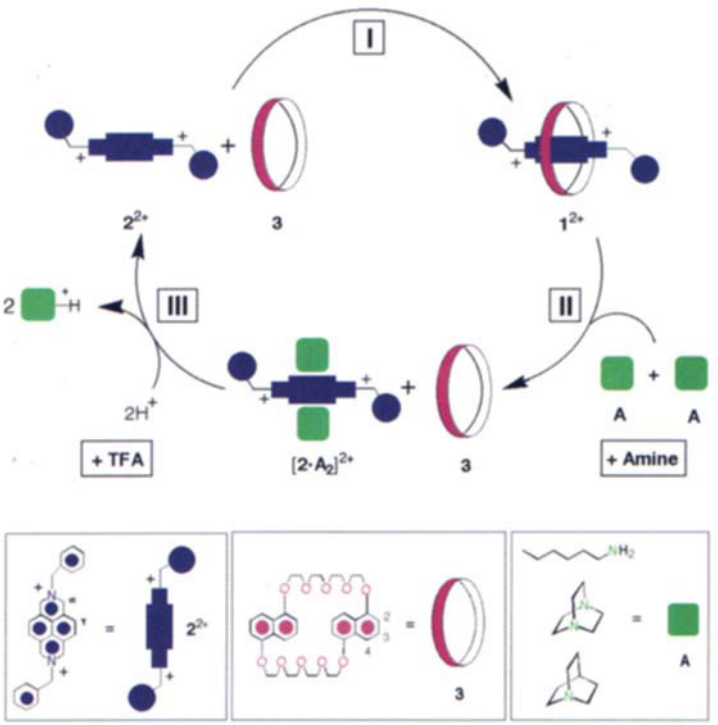

Fig. 1. Top: The chemically driven unthreading and rethreading of the [2]pseudorotaxane 1^{2+} in acetonitrile solution. Bottom: Schematic representations for the 2,7-diazoniapyrene dication 2^{2+}, the crown ether 1,5-dinaphtho-[38]crown-10 **3**, and the amines **A** (hexylamine, diazabicyclooctane (DABCO), and quinuclidine). Identification of the protons associated with 2^{2+} (Greek letters) and **3** (numbers) relate to the ^{1}H NMR assignments in Fig. 2.

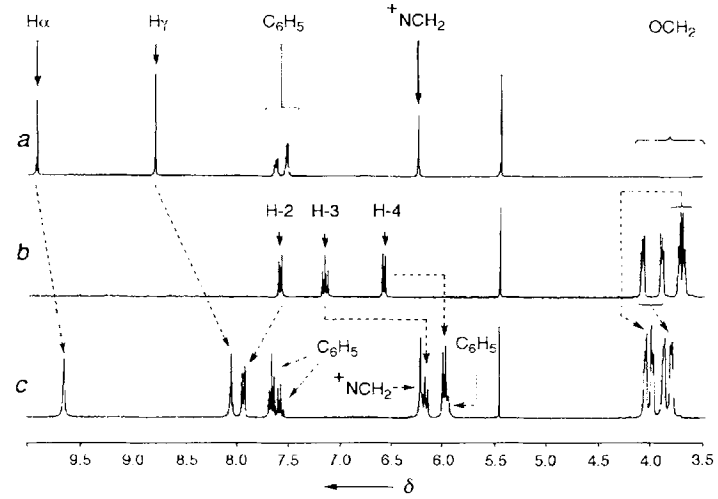

Fig. 2. 300 MHz ^{1}H NMR spectra of CD_3CN samples containing: a) 3.8 mM **2**-$2PF_6$; b) 5.2 mM **3**; and c) 3.8 mM **2**-$2PF_6$ + 3.8 mM **3**.

lized by pairs of C–H···O hydrogen bonds between one of each of the pairs of benzylic methylene protons of 2^{2+} and the central oxygen atoms of the polyether linkages in **3** (mean C···O, H···O distances, and C–H···O angles: 3.33 Å, 2.35 Å, and 176°, respectively). These hydrogen bonds are analogous to those present in the 1:1 complex formed between bis(*para*-phenylene)-[34]crown-10 (BPP34C10) and the 1,1′-dimethyl-4,4′-bipyridinium dication.[20, 21]

The absorption and emission spectra of the separated 2^{2+} and **3** components and [2]pseudorotaxane 1^{2+} are shown in Figures 4 and 5. The interaction between the π-electron donor and the π-electron acceptor leads to noticeable changes in both the

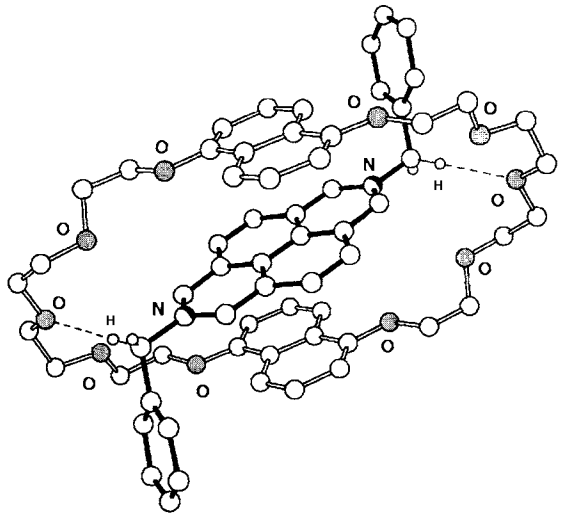
O
N
H
O
O
O

The 2,7-dibenzyldiazoniapyrene dication $\mathbf{2}^{2+}$ forms adducts with aliphatic amines, presumably as a result of a charge-transfer interaction between the electron-accepting[22] $\mathbf{2}^{2+}$ and the electron-donating amine and possibly also hydrogen bonding to the acidic protons at the α-positions in $\mathbf{2}^{2+}$. We have used a variety of amines, including 1,4-diazabicyclo[2.2.2]octane (DABCO), tributylamine, triethanolamine, quinuclidine, 1,6-diaminohexane, and hexylamine. The last one was chosen for further experiments since its adduct is reasonably stable in MeCN solution.

Formation of the adduct between hexylamine and $\mathbf{2}^{2+}$ causes the appearance of a broad CT absorption band (λ_{max} = 595 nm, $\varepsilon = 7000\,M^{-1}cm^{-1}$, trace c in Fig. 4) and a strong and broad emission band (Fig. 5). Titration of an MeCN solution of **2**-$2PF_6$ with hexylamine yielded a Job plot[23] showing the formation of a 2:1 adduct with an association constant (K_a) of the order of $10^8\,M^{-2}$. When the amine used is DABCO, the Job plot suggests that only a species with a 1:1 stoichiometry is formed.

The stability of complexes of the type $[\mathbf{2}\text{-}\mathbf{A}_2]^{2+}$ can be estimated from an experiment (Fig. 6) in which higher concentrations of the amine and the diazoniapyrene dication $\mathbf{2}^{2+}$ are used. When hexylamine **A** (4.4 equiv) is added to a solution of $\mathbf{2}^{2+}$ (5.1 mM) in CD_3CN, the solution turns dark green immediately. The ^1H NMR spectrum is not only considerably more complicated, indicating that several species are present in solution, but it also reveals a substantial loss in intensity of the arene signals. Addition of trifluoroacetic acid (TFA, 4.8 equiv) results in the loss of the intense green color, giving back the pale yellow solution. The spectrum acquired after this chemical transformation gives signals of the individual components $\mathbf{2}^{2+}$ and $\mathbf{HA}^+$ with no appreciable sign of degradation of either species. The cyclical nature of this overall transformation has been shown by repeating this experiment 50 times on the same sample without the appreciable loss of signals corresponding to $\mathbf{2}^{2+}$.

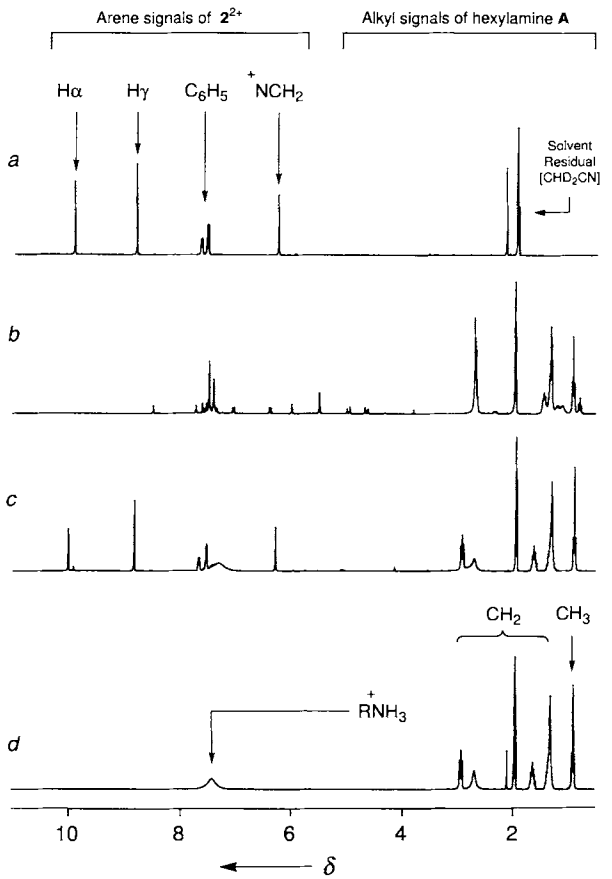

Fig. 6. 400 MHz ^1H NMR spectra of samples containing a) 5.1 mM **2**-$2PF_6$ in CD_3CN; b) after addition of 44 mL (4.4 equiv) of a 0.52 M solution of hexylamine **A** in CD_3CN to solution a); c) after subsequent addition of 64 mL (4.8 equiv) of a 0.37 M solution of TFA in CD_3CN to solution b; and d) addition of 64 mL (1.1 equiv) of a 0.37 M solution of TFA to 44 mL of a 0.52 M solution of hexylamine **A** in CD_3CN.

We have now taken advantage of the chemical affinity of aliphatic amines **A** for $\mathbf{2}^{2+}$ to unthread the component $\mathbf{2}^{2+}$ of the [2]pseudorotaxane $\mathbf{1}^{2+}$ (Process II in Fig. 1). Protonation of the amine disrupts the interactions between **A** and $\mathbf{2}^{2+}$ (Process III in Fig. 1), and so rethreading of $\mathbf{2}^{2+}$ by **3** can occur, making the whole process reversible. These chemically driven cyclic unthreading and rethreading processes exhibited by $\mathbf{1}^{2+}$ can be followed by absorption and emission spectroscopy.

In MeCN solutions containing **2**-$2PF_6$ and **3** (each 6×10^{-5} M), 80% of the species present at room temperature is the [2]pseudorotaxane $\mathbf{1}^{2+}$ (Process I in Fig. 1). Upon addition of hexylamine **A** large spectral changes take place (Figs. 4 and 5). In particular, one can observe a) the appearance of the CT absorption band of the $[\mathbf{2}\text{-}\mathbf{A}_2]^{2+}$ adduct, b) the recovery of the emission band of **3**, and c) the appearance of the emission band of $[\mathbf{2}\text{-}\mathbf{A}_2]^{2+}$. A more detailed analysis of the absorption spectrum shows also the decrease in intensity of the CT absorption band of $\mathbf{1}^{2+}$. These changes indicate the occurrence of an unthreading process with the formation of the free crown ether **3** and of the adduct $[\mathbf{2}\text{-}\mathbf{A}_2]^{2+}$ (Process II in Fig. 1). After the addition of about 20 equivalents of **A**, no further spectral changes were observed. From the recovery of the luminescence of free crown ether **3** (λ_{max} = 345 nm, Fig. 5), one can estimate that at least 60% of the [2]pseudorotaxane $\mathbf{1}^{2+}$ undergoes unthreading. On the other hand, the increase in absorption due to the formation of $[\mathbf{2}\text{-}\mathbf{A}_2]^{2+}$ (λ_{max} = 595 nm, Fig. 4) indicates that at least 80% of $\mathbf{2}^{2+}$ is present as an amine adduct. The difference in the amount of free **3** and of $\mathbf{2}^{2+}$ complexed by the amine could indicate that a small amount of $\mathbf{1}^{2+}$ gives an amine adduct without unthreading.

The unthreading process can be reversed quantitatively by the addition of TFA to the solution (Process III in Fig. 1), as shown by a) the disappearance of the absorption and emission bands of $[\mathbf{2}\text{-}\mathbf{A}_2]^{2+}$, b) the decrease of the emission intensity of **3**, and c) the reappearance of the CT absorption band of $\mathbf{1}^{2+}$. The fact that $\mathbf{1}^{2+}$, $\mathbf{2}^{2+}$, **3**, and $[\mathbf{2}\text{-}\mathbf{A}_2]^{2+}$ exhibit characteristic absorption spectra (Fig. 4), and $\mathbf{2}^{2+}$, **3**, and $[\mathbf{2}\text{-}\mathbf{A}_2]^{2+}$ are strongly emitting species (Fig. 5) allows us to follow the threading and unthreading processes in several independent ways. Although the threading/unthreading cycle shows a satisfactory chemical reversibility, its on/off switching response is not complete because, under the experimental conditions, the equilibrium (Process I in Fig. 1) is currently 80% displaced toward the [2]pseudorotaxane. We are striving, by changing the experimental conditions, to improve the efficiency of the system.

In conclusion, we have shown that the unthreading and rethreading of a [2]pseudorotaxane can be induced by chemical stimuli. The described system therefore represents a prototype at the supramolecular level for a simple molecular machine in which the changes in the relative positions of the components can be followed by readily monitorable differences in the absorption and luminescence spectra.

Experimental Procedure

2-$2PF_6$: 2,7-Diazoniapyrene [24] (75mg, 0.36 mmol) was dissolved in Me_2SO (10 mL) and benzyl bromide (2 mL) was added. The reaction mixture was stirred at 60 °C overnight. The product was then filtered and suspended in H_2O/Me_2CO (1/1, 20 mL). NH_4PF_6 (1 g) was added, and the mixture was stirred for 4 h, before being

 © VCH Verlagsgesellschaft mbH, D-69451 Weinheim, 1996 0570-0833/96/3509-0980 $ 15.00+.25/0

filtered and air-dried to yield **2**-2PF_6 (232 mg, 95%) as a yellow powder: m.p. 282 °C (decomp.); FAB-MS: *m/z* 531 $(M - PF_6)^+$, 386 $(M - 2PF_6)^+$; ^{1}H NMR (CD_3CN): δ = 6.25 (4H, s), 7.51–7.55 (6H, m), 7.62–7.67 (4H, m), 8.81 (4H, s), 9.93 (4H, s); ^{13}C NMR (CD_3CN): δ = 30.9, 67.7, 130.6, 130.7, 130.9, 131.3, 142.3. Anal.: found C 50.01, H 3.35, N 3.98, calcd for $C_{28}H_{22}N_2P_2F_{12}$: C 49.70, H 3.28, N 4.14.

1-2PF_6: Equimolar amounts (about 5 mM) of **2**-2PF_6 and **3**[25] were mixed in CD_3CN. The solution turned red instantaneously: FAB-MS: *m/z* 1167 $(M - PF_6)^+$, 1022 $(M - 2PF_6)^+$, 636 (1,5DN38C10)$^+$, 531 (DBnDAP – $PF_6)^+$; ^{1}H NMR (CD_3CN): δ = 3.75–3.81 (8H, m), 3.82–3.88 (8H, m), 3.93–4.08 (16H, m), 5.90–6.00 (6H, m), 6.15 (4H, t, *J* = 8.0 Hz), 6.23 (4H, m), 7.50–7.70 (6H, m), 7.88 (4H, d, *J* = 8.0 Hz), 8.15 (4H, s), 9.71 (4H, s); ^{13}C NMR (CD_3CN): δ = 67.4, 68.6, 70.6, 71.9, 71.9, 105.3, 112.8, 117.8, 124.5, 125.0, 125.2, 129.8, 130.6, 130.7, 131.3, 142.0, 153.4. High resolution MS: found *m/z* 1167.4315, $C_{64}H_{66}N_2O_{10}F_6P$ $(M - PF_6)$ requires *m/z* 1167.4359. Crystals suitable for X-ray structural analysis were grown by vapor diffusion of iPr_2O into an MeCN solution of a 1:1 mixture of DBnDAP[PF_6]$_2$ and 1,5DN38C10. The procedure and equipment for absorption and luminescence measurements were described previously [21].

Received: October 24, 1995 [Z 8494 IE]
German version: *Angew. Chem.* **1996**, *108*, 1056–1059

Keywords: charge-transfer complexes · molecular machines · pseudorotaxanes · supramolecular chemistry

[1] A. Aviram, *J. Am. Chem. Soc.* **1988**, *110*, 5687–5692; A. Aviram, M. Ratner, *Chem. Phys. Lett.* **1974**, *29*, 277–283.
[2] V. Balzani, L. Moggi, F. Scandola in *Supramolecular Photochemistry* (Ed.: V. Balzani), Reidel, Dordrecht, **1987**, 1–28.
[3] J.-M. Lehn, *Angew. Chem.* **1988**, *100*, 91–116; *Angew. Chem. Int. Ed. Engl.* **1988**, *27*, 90–112; *ibid.* **1990**, *102*, 1347–1362 and **1990**, *29*, 1304–1319; *Supramolecular Chemistry*, VCH, Weinheim, **1995**.
[4] *Molecular Electronic Devices* (Eds.: F. L. Carter, R. E. Siatkowsky, H. Woltjen), Elsevier, Amsterdam, **1988**.
[5] V. Balzani, F. Scandola, *Supramolecular Photochemistry*, Horwood, Chichester, **1991**, Chap. 12.
[6] K. E. Drexler, *Nanosystems: Molecular Machinery, Manufacturing, and Computation*, Wiley, New York, **1992**.
[7] A. P. De Silva, H. Q. N. Gunaratne, C. P. McCoy, *Nature* **1993**, *364*, 42–44.
[8] P. Ball, L. Garwin, *Nature* **1992**, *355*, 761–766.
[9] D. Bradley, *Science* **1993**, *259*, 890–892.
[10] R. A. Bissell, A. P. De Silva, H. Q. N. Gunaratne, P. L. M. Lynch, G. E. M. Maguire, C. P. McCoy, K. R. A. S. Sandanayake, *Top. Curr. Chem.* **1993**, *168*, 223–264.
[11] V. Balzani, F. Scandola in *Comprehensive Supramolecular Chemistry*, *Vol. 10* (Ed.: D. N. Reinhoudt), Pergamon, Oxford, **1996**, in press.
[12] P. L. Anelli, N. Spencer, J. F. Stoddart, *J. Am. Chem. Soc.* **1991**, *113*, 5131–5133; R. A. Bissell, E. Córdova, A. E. Kaifer, J. F. Stoddart *Nature* **1994**, *369*, 133–137.
[13] R. Ballardini, V. Balzani, M. T. Gandolfi, L., Prodi, M. Venturi, D. Philp, H. G. Ricketts, J. F. Stoddart, *Angew. Chem.* **1993**, *105*, 1362–1365; *Angew. Chem. Int. Ed. Engl.* **1993**, *32*, 1301–1303; P. R. Ashton, R. Ballardini, V. Balzani, A. Credi, M. T. Gandolfi, S. Menzer, L. Pérez-García, L. Prodi, J. F. Stoddart, M. Venturi, A. J. P. White, D. J. Williams, *J. Am. Chem. Soc.* **1995**, *117*, 11171–11197.
[14] P. R. Ashton, R. Ballardini, V. Balzani, M. T. Gandolfi, J.-F., Marquis, L. Pérez-García, L. Prodi, J. F. Stoddart, M. Venturi, *J. Chem. Soc. Chem. Commun.* **1994**, 177–180.
[15] M. Seiler, H. Dürr, I. Willner, E. Joselevich, A. Doron, J. F. Stoddart, *J. Am. Chem. Soc.* **1994**, *116*, 3399–3404; A. C. Benniston, A. Harriman, V. M. Lynch, *ibid.* **1995**, *117*, 5275–5291, and references cited therein; L. Zelikovich, J. Libman, A. Shanzer, *Nature*, **1995**, *374*, 790–792.
[16] A. Livoreil, C. O. Dietrich-Buchecker, J.-P. Sauvage, *J. Am. Chem. Soc.* **1994**, *116*, 9399–9400.
[17] D. Philp, J. F. Stoddart, *Synlett.* **1991**, 445–458; *Angew. Chem.* **1996**, *108*, No. 11; *Angew. Chem. Int. Ed. Engl.* **1996**, *35*, No. 11; H. W. Gibson, M. C. Bheda, P. T. Engen, *Prog. Polym. Sci.* **1994**, *19*, 843–945.
[18] Liquid secondary ion mass spectrometry (LSIMS) was carried out on a VG-Zab Spec mass spectrometer (accelerating voltage 8 kV; resolution 2000). Samples of **1**-2PF_6 were dissolved in a small volume of 3-nitrobenzyl alcohol, which had previously been coated onto a stainless steel probe tip. Spectra were recorded in the positive-ion mode at a scan speed of 5 s per decade.
[19] Crystal data for **1**-2PF_6: triclinic, a = 13.799(3), b = 14.407(4), c = 16.336(5) Å, α = 110.09(2), β = 90.33(2), γ = 91.12(2)°, V = 3049 Å^3, T = 293 K, space group $P\bar{1}$, Z = 2, ρ_{calcd} = 1.430 g cm^{-3}, μ = 15.03 cm^{-1}, 9056 independent measured, 4034 with ($|F_o| > 4\sigma|F_o|$, $\theta \leq 60$) refined to R_1 = 0.1141 and wR_2 = 0.2968. The data was collected on a Siemens P4 diffractometer with graphite monochromated $Cu_{K\alpha}$ radiation using ω scans. The structure was solved by direct methods and with the SHELXTL program package (version 5.03) (G. Sheldrick, Universität Göttingen, **1995**). Further details of the crystal structure investigation can be obtained from the Cambridge Crystallographic Data Centre, 12 Union Road, GB-Cambridge CB2 1EZ (UK) on quoting full literature citation.
[20] P. R. Ashton, D. Philp, M. V. Reddington, A. M. Z. Slawin, N. Spencer, J. F. Stoddart, D. J. Williams, *J. Chem. Soc. Chem. Commun.* **1991**, 1680–1683.
[21] P. L. Anelli, P. R. Ashton, R. Ballardini, V. Balzani, M. Delgado, M. T. Gandolfi, T. T. Goodnow, A. E. Kaifer, D. Philp, M. Pietraszkiewicz, L. Prodi, M. V. Reddington, A. M. Z. Slawin, N. Spencer, J. F. Stoddart, C. Vicent, D. J. Williams, *J. Am. Chem. Soc.* **1992**, *114*, 193–218.
[22] A. J. Blacker, J. Jazwinski, J.-M. Lehn, *Helv. Chim. Acta* **1987**, *70*, 1–12, and references therein.
[23] Z. D. Hill, P. MacCarthy, *J. Chem. Ed.* **1986**, *63*, 162–167 and references therein.
[24] S. Hünig, J. Grosse, E. F. Lier, H. Quast, *Liebigs Ann. Chem.* **1973**, 339–358.
[25] P. R. Ashton, C. L. Brown, E. J. T. Chrystal, T. T. Goodnow, A. E. Kaifer, K. P. Parry, D. Philp, A. M. Z. Slawin, N. Spencer, J. F. Stoddart, D. J. Williams, *J. Chem. Soc. Chem. Commun.* **1991**, 634–639. P. R. Ashton, E. J. T. Chrystal, J. P. Mathias, K. P. Parry, A. M. Z. Slawin, N. Spencer, J. F. Stoddart, D. J. Williams, *Tetrahedron Lett.* **1987**, *28*, 6367–6370.

Efficient Regio- and Enantioselective Mannich Reactions**

Dieter Enders,* David Ward, Johannes Adam, and Gerhard Raabe

The Mannich reaction,[1] in which an aminomethyl group is introduced in the α-position to a carbonyl function, has found a multitude of applications in organic chemistry.[2] The resulting Mannich bases are of particular interest due to their biological activity (for example, analgesic, antineoplastic, and antibiotic effects),[2] as bifunctional synthetic building blocks[2] and as precursors in the preparation of α,β-unsaturated carbonyl compounds[3] and γ-amino alcohols.[4] The introduction of separately prepared iminium salts,[5] and the use of silyl enol ethers,[6] boron enolates,[7] and enamines[8] has so extended the range of application of the reaction that regioselective aminomethylations can even be carried out in aprotic media in good yields.

While some authors have already reported on the stereoselective Mannich reaction,[9] very little is known about the enantioselective variants for the synthesis of β-amino ketones,[10] which is in sharp contrast to the plentitude of publications on its oxa analogue, the enantioselective Aldol reaction.[11] A practical procedure for highly enantioselective α-aminomethylation of ketones is, to the best of our knowledge, not yet available.

We now report an efficient, highly regio- and enantioselective synthesis of Mannich bases, starting from α-silyl ketones (*S*)-**1**, which are accessible by the SAMP/RAMP hydrazone method[12] in good yields (52–60%) and excellent enantioselectivities ($ee \geq 98\%$) (Table 1).

As illustrated in Scheme 1, the α-dimethylthexylsilyl ketones (*S*)-**1** (thexyl = 1,1,2-trimethylpropyl, abbreviated as *t*Hex in Scheme 1) are converted in quantitative yields to the (*Z*)-silyl enol ethers (*S*)-**2** ($Z:E \geq 50:1$) by treatment with lithium diisopropylamide (LDA) and chlorotrimethylsilane (TMSCl) in tetrahydrofuran/hexamethylphosphoric triamide (HMPA) at

[*] Prof. Dr. D. Enders, Dr. D. Ward, Dipl.-Chem. J. Adam, Dr. G. Raabe
Institut für Organische Chemie der Technischen Hochschule
Professor-Pirlet-Strasse 1, D-52074 Aachen (Germany)
Fax: Int. code +(241)8888127

[**] This work was funded by the Deutsche Forschungsgemeinschaft (SFB 380 and the Leibniz Prize) and by the Fonds der Chemischen Industrie. We thank the firms Degussa AG, BASF AG, Bayer AG, and Hoechst AG for gifts of chemicals. D. W. thanks the Science and Engineering Research Council, Great Britain for support (1994/1995).

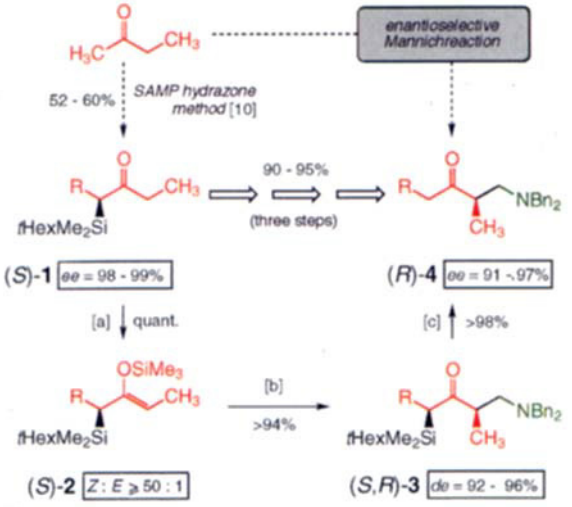

Scheme 1. Enantioselective synthesis of β-dibenzylamino ketones (*R*)-**4** by the asymmetric Mannich reaction. [a] LDA, THF, HMPA, $-70\,^{\circ}C$; TMSCl; [b] $Bn_2NCH_2OCH_3$, $BF_3 \cdot Et_2O$, CH_2Cl_2, $-95\,^{\circ}C$; [c] NH_4F, nBu_4NF, THF, $-70\,^{\circ}C$ to room temperature. *t*Hex = 1,1,2-trimethylpropyl.

Table 1. α-Dimethylthexylsilyl ketones (*S*)-**1** prepared from butanone.

1	R	Yield [a] [%]	$[\alpha]_D^{20}$ [*c*, benzene]	*ee* [b] [%]
(*S*)-**1a**	Me	57	−196.4 (0.9)	99
(*S*)-**1b**	Et	54	−191.3 (0.8)	99
(*S*)-**1c**	*n*Pr	57	−133.3 (1.5)	98
(*S*)-**1d**	*i*Bu	60	−115.3 (1.6)	98
(*S*)-**1e**	Bn	52	−77.4 (2.2)	99
(*S*)-**1f**	*p*-BrBn [c]	58	−36.4 (1.2)	99

[a] Overall yield (four steps) for the isolated α-silyl ketone starting from butanone. [b] Enantiomeric excesses were determined by gas chromatography of the corresponding alcohols by using a stationary phase consisting of β-cyclodextrin/polysiloxane. The alcohols were prepared by the reduction of the α-silyl ketones with $LiAlH_4$. [c] *p*-BrBn = *para*-bromobenzyl.

$-95\,^{\circ}C$. The formation of regioisomeric tetrasubstituted silyl enol ethers was never observed in these reactions. The high selectivity of the deprotonation to the (*Z*)-enolate in the presence of HMPA[13] is a prerequisite for a high asymmetric induction under the assumption that the bulky silyl group diastereofacially directs the introduction of the electrophilic aminomethyl group.

In previous work, the handling of the hygroscopic iminium salts was avoided by the in situ generation of the corresponding iminium ions or similar reactive species by the treatment of aminals or geminal amino ethers in the presence of Lewis acids.[7, 14] In the method described here, the alkylation of the crude silyl enol ether was carried out by reaction with dibenzylmethoxymethyl amine[15] and $BF_3 \cdot Et_2O$ in CH_2Cl_2. Aqueous workup and flash chromatography afforded the desired dibenzylaminomethyl ketones (*S*,*R*)-**3** in excellent yields (94–95%) and high diastereomeric excesses (*de* = 92 to ≥ 96%). The latter were determined by ^1H NMR spectroscopy (Table 2).

The silylated Mannich bases **3** are stable compounds, which show no tendency to epimerize or racemize and can be purified without difficulty by flash chromatography on silica gel. The use of a *tert*-butyldimethylsilyl group rather than the dimethylhexylsilyl group led to a decrease in the diastereoselectivity to as low as 81% in the case of (*S*)-**1a**, although the *Z*/*E* ratio was high and similar to that observed for (*S*)-**1a**.[16] The absolute configuration was determined by the X-ray crystal structure analysis of (*S*,*R*)-**3f** (Fig 1).[17]

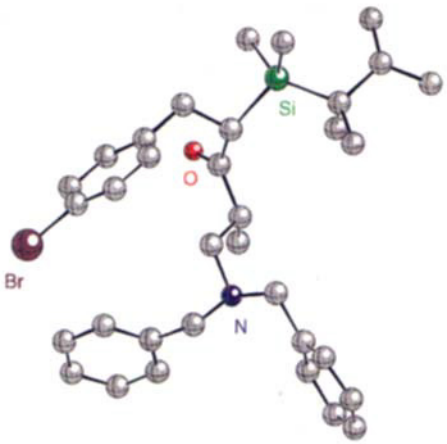

Fig. 1. X-ray crystal structure of (*S*,*R*)-**3f** (ball-and-stick model).

Table 2. α-Dimethylthexylsilyl-β-dibenzylamino ketones (*S*,*R*)-**3** prepared by aminomethylation of the silyl enol ethers (*S*)-**2**.

3	R	Yield [%]	$[\alpha]_D^{20}$ [*c*, benzene]	*de* [a] [%]
(*S*)-**3a**	Me	95	+150.1 (0.4)	92 (≥ 96 [b])
(*S*)-**3b**	Et	95	−113.7 (0.6)	≥ 96
(*S*)-**3c**	*n*Pr	95	−97.6 (0.6)	≥ 96
(*S*)-**3d**	*i*Bu	94	−71.6 (0.5)	≥ 96
(*S*)-**3e**	Bn	94	−80.6 (0.9)	≥ 96
(*S*)-**3f**	*p*-BrBn [c]	95	−32.1 (1.0)	≥ 96

[a] Determined by ^1H NMR spectroscopy (300 MHz). [b] After flash chromatography. [c] *p*-BrBn = *para*-bromobenzyl.

The α-silyl group can be removed readily at room temperature by treatment with nBu_4NF in THF, since the intermediate carbanion is stabilized as an enolate. However, this desilylation is accompanied by an almost complete racemization, the cause of which lies in the formation of basic nBu_4NOH. This problem was solved by the addition of solid NH_4F as a buffer and by carrying out the reaction at low temperatures to control the rate of formation of the base. The enantiomeric excesses (*ee* = 91–97%) of the optically active β-amino ketones (*R*)-**4** thus formed were determined by ^1H NMR spectroscopy (500 MHz) using the chiral cosolvent (*R*)-(−)-9-anthryl-2,2,2-trifluoroethanol (Table 3).

To explain the almost complete diasterofacial selectivity in the formation of (*S*,*R*)-**3**, two transition states can be discussed: On the one hand a cyclic transition state along the lines of the Zimmerman–Traxler model [$TS_{Z,S}$ (closed)][20] can be envis-

Table 3. β-Dibenzylamino ketones (*R*)-**4**, prepared by desilylation of the ketones (*S*,*R*)-**3**.

4	R	Yield [%]	$[\alpha]_D^{20}$ [*c*, benzene]	*ee* [a] [%]
(*R*)-**4a**	Me	96	−8.3 (0.6)	91
(*R*)-**4b**	Et	97	−2.5 (0.7)	93
(*R*)-**4c**	*n*Pr	98	−1.2 (0.5)	93
(*R*)-**4d**	*i*Bu	99	−2.2 (0.4)	94
(*R*)-**4e**	Bn	97	+7.2 (1.1)	97
(*R*)-**4f**	*p*-BrBn [b]	98	+9.7 (0.6)	93

[a] Determined by ^1H NMR spectroscopy (500 MHz) using a solution of (*R*)-**4** (3 mg) and (*R*)-(−)-9-anthryl-2,2,2-trifluoroethanol (10 mg) as chiral cosolvent in C_6D_6 (0.7 mL). [b] *p*-BrBn = *para*-bromobenzyl.

aged, while on the other an open transition state [$TS_{Z,S}$ (open)][21] can also be considered. In both cases the diastereoselectivity is caused by shielding of the Si-side by the bulky dimethylthexylsilyl group. The models lead, via (*S*,*R*)-**3**, to the Mannich bases **4** with *R* configuration at the newly generated stereogenic center (Scheme 2).

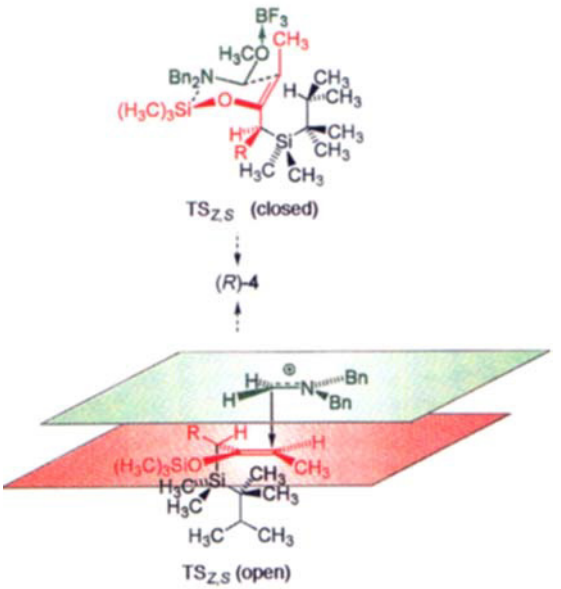

Scheme 2. Postulated transition states for the asymmetric Mannich reaction.

To summarize, it has been shown that Mannich bases can be prepared regioselectively in high enantiomeric purity and excellent overall yield by the procedure detailed here. To the best of our knowledge, this procedure is the first practical, generally applicable asymmetric Mannich reaction for the preparation of β-amino ketones. The extension of the method leading to the generation of two new stereogenic centers in the α- and β-positions is currently the object of intensive investigations.[22]

Experimental Procedure

α-Dimethylthexylsilyl ketone (*S*)-**1**: (*S*)-**1** was prepared by successive silylation and alkylation of butanone-SAMP hydrazone with chlorodimethylthexylsilane and an appropriate alkyl iodide or bromide [12].

Silyl enol ether (*S*)-**2**: A solution of LDA (1.1 mmol) in THF (10 mL, freshly prepared from *n*BuLi (0.7 mL of a 1.6 N solution) and diisopropylamine (0.15 mL) was treated with HMPA (2.5 mL) and cooled to −95 °C. To this vigorously stirred solution, a solution of (*S*)-**2** (1 mmol) in THF (1 mL) was added dropwise over a period of 5 min. Finally, TMSCl (1.2 mmol) was added in one portion. After 30 min the reaction mixture was treated with saturated aqueous $NaHCO_3$ solution (10 mL). The product was extracted with *n*-pentane (60 mL), dried over $MgSO_4$, and the solvent removed on a rotary evaporator under reduced pressure. The crude product was immediately used in the next step without further purification.

α-Dimethylthexylsilyl-α′-dibenzylaminomethyl ketone (*S*,*R*)-**3**: Dibenzylmethoxymethylamine (1.15 mmol) [15] was added to CH_2Cl_2 (10 mL) and cooled to −95 °C. The crude product (*S*)-**2**, diluted with CH_2Cl_2 (2 mL) was added dropwise to this solution. After the addition of $BF_3 \cdot Et_2O$ (1.15 mmol), the reaction mixture was allowed to warm to −70 °C. All conversions were complete within 3 h (TLC control). The reaction mixture was worked up by treatment with pH 7 buffer (5 mL), followed by extraction with CH_2Cl_2 (60 mL), drying over Na_2SO_4, removal of solvent on a rotary evaporator under reduced pressure, and flash chromatography (silica gel, diethyl ether/*n*-pentane 1:10).

α-Dibenzylaminomethyl ketone (*R*)-**4**: To a cooled (−70 °C) solution of (*S*,*R*)-**3** (1 mmol) in THF (50 mL) were added sequentially solid NH_4F (1.85 g, 50 mmol) and nBu_4NF (1.2 mL, 1 N solution in THF; 1.2 mmol). The reaction mixture was allowed to warm to room temperature, after which time pH 6 buffer (10 mL) was added and the product extracted with *n*-pentane (90 mL). After the product had been dried over Na_2SO_4, it was purified by flash chromatography (silica gel, diethyl ether/*n*-pentane 1:20).

Correct elemental analyses and satisfactory spectroscopic (NMR, IR) and spectrometric (MS) data were obtained for all new compounds.

Received: November 24, 1995 [Z85901E]
German version: *Angew. Chem.* **1996**, *108*, 1059–1062

Keywords: amino ketones · asymmetric Mannich reactions · enolates · ketones · SAMP hydrazones

[1] C. Mannich, W. Krösche, *Arch. Pharm.* **1912**, *250*, 647.
[2] Reviews: E. F. Kleinman in *Comprehensive Organic Synthesis, Vol. 2* (Eds.: B. M. Trost, I. Fleming, C. H. Heathcock), Pergamon, Oxford, **1991**, p. 893; M. Tramontini, L. Angiolini, *Tetrahedron* **1990**, *46*, 1791; M. Tramontini, *Synthesis* **1973**, 703; H. Hellmann, G. Opitz, *α-Aminoalkylierung*, Verlag Chemie, Weinheim, **1960**, p. 1; B. Reichert, *Die Mannich-Reaktion*, Springer, Berlin, **1959**, p. 1; R. Schröter in *Houben-Weyl: Methoden der Organischen Chemie, Vol. 11/1* (Ed.: E. Müller), Thieme, Stuttgart, **1957**, p. 731; H. Hellmann, G. Opitz, *Angew. Chem.* **1956**, *68*, 265; F. F. Blicke, *Org. React. (NY)* **1947**, *1*, 303; J. H. Brewster, E. L. Eliel, *ibid.* **1953**, *7*, 99.
[3] J. L. Roberts, P. S. Borromeo, C. D. Poulter, *Tetrahedron Lett.* **1977**, *18*, 1299.
[4] M. Tramontini, *Synthesis* **1982**, 605.
[5] H. Böhme, E. Mundlos, O.-E. Herboth, *Chem. Ber.* **1957**, *90*, 2003; H. Böhme, K. Hartke, *ibid.* **1960**, *93*, 1305; **1963**, *96*, 604; A. Ahond, A. Cavé, C. Kan-Fan, H.-P. Husson, J. de Rostolan, P. Potier, *J. Am. Chem. Soc.* **1968**, *90*, 5622; H. Böhme, P. Wagner, *Chem. Ber.* **1969**, *102*, 2651; H. Volz, H. H. Kiltz, *Tetrahedron Lett.* **1970**, *11*, 1917; J. Schreiber, H. Maag, N. Hashimoto, A. Eschenmoser, *Angew. Chem.* **1971**, *83*, 355; *Angew. Chem. Int. Ed. Engl.* **1971**, *10*, 330; F. Knoll, U. Krumm, *Chem. Ber.* **1971**, *104*, 31; Y. Jasor, M.-J. Luche, M. Gaudry, A. Marquet, *J. Chem. Soc. Chem. Commun.* **1974**, 253; G. Kinast, L.-F. Tietze, *Angew. Chem.* **1976**, *88*, 261; *Angew. Chem. Int. Ed. Engl.* **1976**, *15*, 239; T. A. Bryson, G. H. Bonitz, C. J. Reichel, R. E. Dardis, *J. Org. Chem.* **1980**, *45*, 524; W. N. Speckamp, H. Hiemstra, *Tetrahedron* **1985**, *41*, 4367; U. Westerwelle, R. Keuper, N. Risch, *J. Org. Chem.* **1995**, *60*, 2263.
[6] S. Danishefsky, T. Kitahara, R. McKee, P. F. Schuda, *J. Am. Chem. Soc.* **1976**, *98*, 6715; N. L. Holy, Y. F. Wang, *ibid.* **1977**, *99*, 944; N. L. Holy, R. Fowler, E. Burnett, R. Lorenz, *Tetrahedron* **1979**, *35*, 613; S. Danishefsky, M. Prisbylla, B. Lipisko, *Tetrahedron Lett.* **1980**, *21*, 805; S. Danishefsky, A. Guingant, M. Prisbylla, *ibid.* **1980**, *21*, 2033.
[7] J. Hooz, J. N. Bridson, *J. Am. Chem. Soc.* **1973**, *95*, 602; E. G. Nolen, A. Aliocco, J. Vitarius, K. McSorley, *J. Chem. Soc. Chem. Commun.* **1990**, 1532.
[8] N. Risch, A. Esser, *Z. Naturforsch. B* **1989**, *44*, 208.
[9] D. Seebach, C. Betschart, M. Schiess, *Helv. Chim. Acta* **1984**, *67*, 1593; K. Broadley, S. G. Davies, *Tetrahedron Lett.* **1984**, *25*, 1743; D. Seebach, M. Schiess, W. B. Schweizer, *Chimia* **1985**, *39*, 272; W. Oppolzer, P. Schneider, *Helv. Chim. Acta* **1986**, *69*, 1817; C. Gennari, I. Venturini, G. Gislon, G. Schimperna, *Tetrahedron Lett.* **1987**, *28*, 227; W. Oppolzer, R. Moretti, S. Thomi, *ibid.* **1989**, *30*, 5603; H. Kunz, W. Pfrengle, *Angew. Chem.* **1989**, *101*, 1041; *Angew. Chem. Int. Ed. Engl.* **1989**, *28*, 1067; H. Kunz, D. Schanzenbach, *ibid.* **1989**, *101*, 1042 and **1989**, *28*, 1068; A. R. Katritzky, P. A. Harris, *Tetrahedron* **1990**, *46*, 987; D. A. Evans, F. Urpi, T. C. Somers, J. S. Clark, M. T. Bilodeau, *J. Am. Chem. Soc.* **1990**, *112*, 8215; T. Arenz, H. Frauenrath, *Angew. Chem.* **1990**, *102*, 929; *Angew. Chem. Int. Ed. Engl.* **1990**, *29*, 932; K. T. Wanner, I. Praschak, U. Nagel, *Arch. Pharm.* **1990**, *323*, 335; E. G. Nolen, A. Aliocco, M. Broody, A. Zuppa, *Tetrahedron Lett.* **1991**, *32*, 73; H. Frauenrath, T. Arenz, G. Raabe, M. Zorn, *Angew. Chem.* **1993**, *105*, 74; *Angew. Chem. Int. Ed. Engl.* **1993**, *32*, 83; P. C. B. Page, S. M. Allin, E. W. Collington, R. A. E. Carr, *J. Org. Chem.* **1993**, *58*, 6902; N. Risch, M. Arend, *Angew. Chem.* **1994**, *106*, 2531; *Angew. Chem. Int. Ed. Engl.* **1994**, *33*, 2422; Y. Matsumura, T. Tomita, *Tetrahedron Lett.* **1994**, *35*, 3737; M. Arend, N. Risch, *Angew. Chem.* **1995**, *107*, 2861; *Angew. Chem. Int. Ed. Engl.* **1995**, *34*, 2861.
[10] N. Risch, A. Esser, *Liebigs Ann. Chem.* **1992**, 233.
[11] D. A. Evans, J. V. Nelson, T. R. Taber, *Top. Stereochem.* **1982**, *13*, 1; T. Mukaiyama, *Org. React.* **1982**, *28*, 203; C. H. Heathcock in *Asymmetric Synthesis, Vol. 3* (Ed.: J. D. Morrison), Academic Press, Orlando, FL, USA, **1984**, p. 111; S. Masamune, W. Choy, F. A. J. Kerdesky, B. Imperiali, *Angew. Chem.* **1985**, *97*, 1; *Angew. Chem. Int. Ed. Engl.* **1985**, *24*, 1; M. Braun, *ibid.* **1987**, *99*, 24 or **1987**, *26*, 24.
[12] D. Enders, B. B. Lohray, *Angew. Chem.* **1987**, *99*, 359; *Angew. Chem. Int. Ed. Engl.* **1987**, *26*, 351; D. Enders, S. Nakai, *Chem. Ber.* **1991**, *124*, 219; D. Enders, B. B. Lohray, F. Burkamp, V. Bushan, R. Hett, *Liebigs Ann.*, in press.
[13] R. E. Ireland, R. H. Mueller, A. K. Willard, *J. Am. Chem. Soc.* **1976**, *98*, 2868.
[14] A. Hosomi, S. Iijima, H. Sakurai, *Tetrahedron Lett.* **1982**, *23*, 547; H. Heaney, G. Papageorgiou, R. F. Wilkins, *J. Chem. Soc. Chem. Commun.* **1988**, 1161.
[15] Prepared by reaction of dibenzylamine with paraformaldehyde and solid K_2CO_3 in methanol at room temperature. Workup consisted of filtration of the solids and fractional distillation (b.p. 116–118 °C/0.1 Torr); T. D. Stewart, W. E. Bradley, *J. Am. Chem. Soc.* **1932**, *54*, 4172.
[16] D. Enders, D. Ward, unpublished results.

[17] Suitable single crystals were obtained by crystallization from methanol at room temperature. The substance crystallizes in the monoclinic space group $P2_1$ (no. 4) with $a = 6.644(6)$, $b = 24.243(2)$, $c = 10.688(1)$ Å and $\beta = 104.0(2)$. With a cell volume of 1670.5 Å^3, $z = 2$ and $M_{calcd} = 592.8$, the density is 1.178 g cm^{-3}. Total number of electrons per unit cell is 632. Enraf-Nonius CAD4-four-circle diffractometer, $Mo_{K\alpha}$ radiation (graphite monochromator, $\lambda = 0.71069$ Å). The structure was solved by using SHELXS86 [18] and refined with XTAL3.2 [19]. The positions of the hydrogen atoms were calculated. 3248 observed reflections [$I > 2\sigma(I)$], 343 parameters refined against F, $R = 0.061$ ($Rw = 0.035$). Maximum residual electron density ± 0.6 e A^{-3}. The absolute configuration of the newly formed stereogenic center in the α-position was determined on the basis of the known configuration in the α'-position. Crystallographic data (excluding structure factors) for the structures reported in this paper have been deposited with the Cambridge Crystallographic Data Centre as supplementary publication no. CCDC-179-11. Copies of the data can be obtained free of charge on application to The Director, CCDC, 12 Union Road, Cambridge, CB2 1EZ, UK (fax: int. code +(1223)336033; e-mail: teched@chemcrys.cam.ac.uk).

[18] G. M. Sheldrick in *Crystallographic Computing 3* (Eds.: G. M. Sheldrick, C. Krüger, R. Goodard), University Press, Oxford, **1985**, p. 175.

[19] S. R. Hall, H. D. Flack, J. M. Stewart, *XTAL3.2 Reference Manual*, Universities of Western Australia, Geneva, and Maryland, Perth, **1992**.

[20] H. E. Zimmerman, M. D. Traxler, *J. Am. Chem. Soc.* **1957**, *79*, 1920; D. Enders, B. B. Lohray, *Angew. Chem.* **1988**, *100*, 594; *Angew. Chem. Int. Ed. Engl.* **1988**, *27*, 581.

[21] I. Flemming, *Pure Appl. Chem.* **1988**, *60*, 71; B. B. Lohray, D. Enders, *Helv. Chim. Acta* **1989**, *72*, 980.

[22] J. Adam, planned Dissertation, RWTH Aachen.

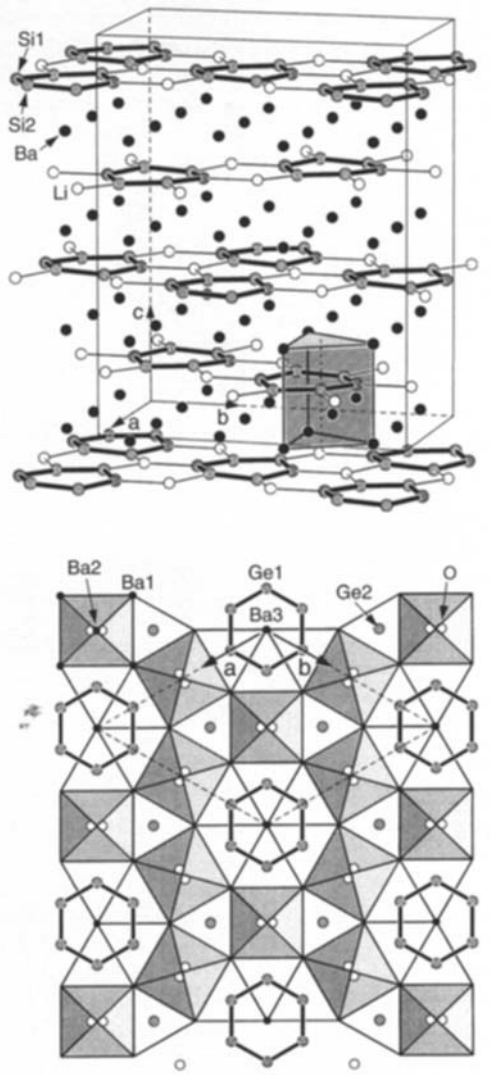

Fig. 1. Top: Crystal structure of $Ba_4Li_2Si_6$ with the weakly twisted Si_6 rings in the heterographite net $^2_\infty(Li_2Si_6)^{8-}$. The Ba atoms form slightly distorted trigonal prisms. $Ba_4Li_2Ge_6$ also crystallizes in this structure. Bottom: Projection of the $Ba_{10}Ge_7O_3$ crystal structure on its hexagonal base. In this structure, the Ge_6^{10-} anion is planar. The position Ge2 (Ge^{4-}) is statistically only half-filled; thus the O atoms are placed on either one of the two alternative positions (open circles).

Hückel Arenes with Ten π Electrons: Cyclic Zintl Anions Si_6^{10-} and Ge_6^{10-}, Isosteric to P_6^{4-} and As_6^{4-}

Hans Georg von Schnering,* Urs Bolle, Jan Curda, Karl Peters, Wilder Carrillo-Cabrera, Mehmet Somer, Martin Schultheiss, and Ulrich Wedig

Our investigations on the completely intercalated heterographite LiBC ($\cong Li^+ + (BC)^-$)[1] have revealed that very few compounds of this structure type and its derivatives do not meet the valence electron concentration (VEC) of 4 for the heterographite nets $^2_\infty(BC)^-$. A striking example is BaLiSi ($\cong Ba^{2+} + (LiSi)^{2-}$) with a VEC of 3.5.[2] Initially, this phase was described by Gladishevskij[3] as a hexagonal modification of $BaSi_2$, which with a VEC of 5 would fit even less in this family of structures. However, Axel et al.[2] showed later that this modification cannot be prepared from the elements barium and silicon, but that the compound BaLiSi is formed instead by reaction with molten LiCl. It is even more amazing that the recent edition of "Pearson's Handbook"[4] only mentions hexagonal $BaSi_2$! In the present communication we will show that the actual composition of the ternary silicide is $Ba_4Li_2Si_6$ and that an isotypic germanide, $Ba_4Li_2Ge_6$, exists as well.[5, 6] Both compounds form a stuffed derivative of the orthorhombic β-K_4P_6 structure[7] (Fig. 1, top) with complete and ordered heterographite nets $^2_\infty(Li_2Si_6)^{8-}$ and $^2_\infty(Li_2Ge_6)^{8-}$, respectively, but with a VEC of 4.25. The atoms of these nets center the trigonal Ba_6 prisms. The most remarkable structural features are isometric Si_6^{10-} and Ge_6^{10-} rings with 34 valence electrons, isosteric to P_6^{4-} and As_6^{4-},[7, 8], respectively. Both compounds are narrow-band semiconductors ($E_g \approx 80$ meV) and reveal a weak van Vleck paramagnetism.

Systematic investigations into the formation of clathrates in the Na/Ba/Ge ternary system led to the discovery of the new, unusual germanium oxide $Ba_{10}Ge_7O_3$, which formally can be considered as an oxidation product of a barium germanide. This compound was initially discovered as a byproduct in reaction mixtures accidently contaminated with traces of oxygen or moisture. However, it can be prepared in bulk by thermal decomposition of NaGe in the presence of the required amounts of BaO and Ba.[9] In the hexagonal crystal structure (Fig. 1, bottom) Ba atoms form a framework of linked monocapped trigonal prisms and tetragonal bipyramids. These polyhedra are centered either with isolated Ge atoms, with O atoms, or with Ge atoms that belong to six-membered Ge rings.[10] The electron count fulfills the Zintl–Klemm concept with the formal charge distribution according to Ba^{2+}, O^{2-}, Ge^{4-}, Ge_6^{10-}—the latter again reveals a cyclic system with 34 electrons.

[*] Prof. Dr. H. G. von Schnering, Dr. U. Bolle, Dipl.-Ing. J. Curda, Dr. K. Peters, Dr. W. Carrillo-Cabrera, Dr. M. Somer, Dipl.-Chem. M. Schultheiss, Dr. U. Wedig
Max-Planck-Institut für Festkörperforschung
Heisenbergstrasse 1, D-70569 Stuttgart (Germany)
Fax: Int. code +(711) 6891-562

In $Ba_4Li_2Si_6$ and $Ba_4Li_2Ge_6$ the six-membered rings are slightly puckered (boat conformation, torsion angle $\pm 4^\circ$, see Fig. 2) like the P_6^{4-} anion in β-K_4P_6.[7] The bond lengths are d(Si–Si) = 238.2 pm (6×) and d(Ge–Ge) = 250.8 pm (2×) and 252.0 pm (4×), whereas the endocyclic bond angles are identical within the standard deviations (119.8–119.9°). The X_6 rings are linked by Li atoms to form a heterographite net (d(Li–Si) = 266–269 pm; d(Li–Ge) = 260–266 pm). The hexagonal AlB_2 type as the assumed structure for $BaSi_2$[3] and BaLiSi[2] is still the prevailing substructure of $Ba_4Li_2Si_6$, and therefore strongly dominates the intensities of the diffraction pattern: $a = 2\,a_{hex}$, $b \cong 2\sqrt{3}\,a_{hex}$, $c = 4\,c_{hex}$. The bond lengths in such a substructure would be d(Si–Si) = d(Li–Si) = 252.4 pm and d(Ge–Ge) = d(Li–Ge) = 257.4 pm, and the shorter homoatomic bond lengths in the real structure of these compounds are thus not a stringent consequence of the crystal structure (d(Ba–Ba) = 436–483 pm, d(Ba–Si) = 340–356 pm. d(Ba–Ge) = 348–358 pm, d(Ba–Li) = 350–360 pm).

Unlike in $Ba_4Li_2Ge_6$, the Ge rings in $Ba_{10}Ge_7O_3$ are planar with significantly shorter Ge–Ge bond lengths (247.5 pm). Due to the simple hexagonal stacking, the 6/*mmm* point symmetry remains in this structure. The Ba–Ge interatomic distances are 337.6 (1×), 355.2 (2×), and 375.3 pm (6×) for the Ge ring atoms and 337.8 (3×) and 357.3 pm (6×) for isolated Ge atoms. The O atoms inside the compressed tetragonal bipyramids are shifted out of their central position towards two alternative neighboring positions, whose occupation is evidently coupled with the order at the statistically half-filled positions of the Ge^{4-} anions. This leads to a distorted tetrahedral (2+2) coordination for the O atoms with Ba–O bond lengths of 257 (2×) and 279 pm (2×).

Bonding within the 34-electron system, for example in the Si_6^{10-} anion, can be elucidated in terms of the Hückel formalism: 24 electrons form six σ bonds and six *n* electron pairs. The remaining ten electrons contribute to the π system and fill three bonding and two antibonding MOs. A more comprehensive approach to analyzing the chemical bonding is the electron localization function (ELF) proposed by Becke and Edgecombe.[11, 12] Based on the total wavefunction of a system, the ELF is a measure of the local effect of the Pauli principle within a fermion system. ELF values fall in the range between 0 and 1. Large ELF values indicate covalent bonds, *n* electron pairs, and core shells.[12]

Within the three-dimensional ELF grid of $Ba_4Li_2Si_6$, the covalent Si–Si bonds, the *n* electron pairs of the Si atoms, and the 1s shells of the Li atoms are denoted by white areas in a two-dimensional section along the mean plane of the six-membered ring, as represented in the isosurface plot of ELF = 0.68 on the left side of Figure 2. This clearly reveals the interaction between the Li and Si atoms. The ELF maxima (attractors) above and below the Si atoms are shifted towards the coplanar Li atoms and therefore indicate a polarization towards the Li atoms. As shown by the dark blue areas between the Li and Si atoms (Fig. 2), there is a distinct separation between the core and the valence regions. The *n* electron pairs of the Si atoms are polarized perpendicular to the ring plane, an effect which is obviously caused by the influence of the Li atoms in heterographite layers next to the ring (Fig. 1). This effect is presumably also responsible for the weak torsion of the six-membered rings because the crystal field symmetry at the Si_6 rings of $Ba_4Li_2Si_6$ is reduced to the point group 222-D_2. The fairly uncommon participation of the *n* electron pairs in the bond region in the Si_6 ring might lead to strong electron fluctuation between the *n* electron pairs and the covalent bonds. Quite instructive is the weighting of the electron density ρ by the ELF, as depicted on the right side of Figure 2, in which two valence electron density isosurfaces ($\rho = 0.05$, $\rho = 0.064$ e au^{-3}) are colored according to the corresponding ELF. It is apparent that the high ELF values of the Si–Si bond are associated with the larger ρ values, whereas the high ELF values of the much more diffuse *n* electron pairs are associated with the significantly smaller ρ values.

The isolated Si_6^{10-} anion can be treated formally as an aromatic system, as indicated in particular by the noncyclindrical symmetry of the ELF distribution along the Si–Si bonds. Unlike isolated unsaturated C–C bonds (e.g. like in ethene), which exhibit two ELF maxima (attractors), one above and one below the plane, the Si_6^{10-} ring, like benzene,[13] does not show this feature.

The X_6^{n-} polyanion with 34 valence electrons, which is analogous to cyclohexene, appears to be particularly stable in Zintl phases containing very electropositive metals. Thus, K_4P_6,

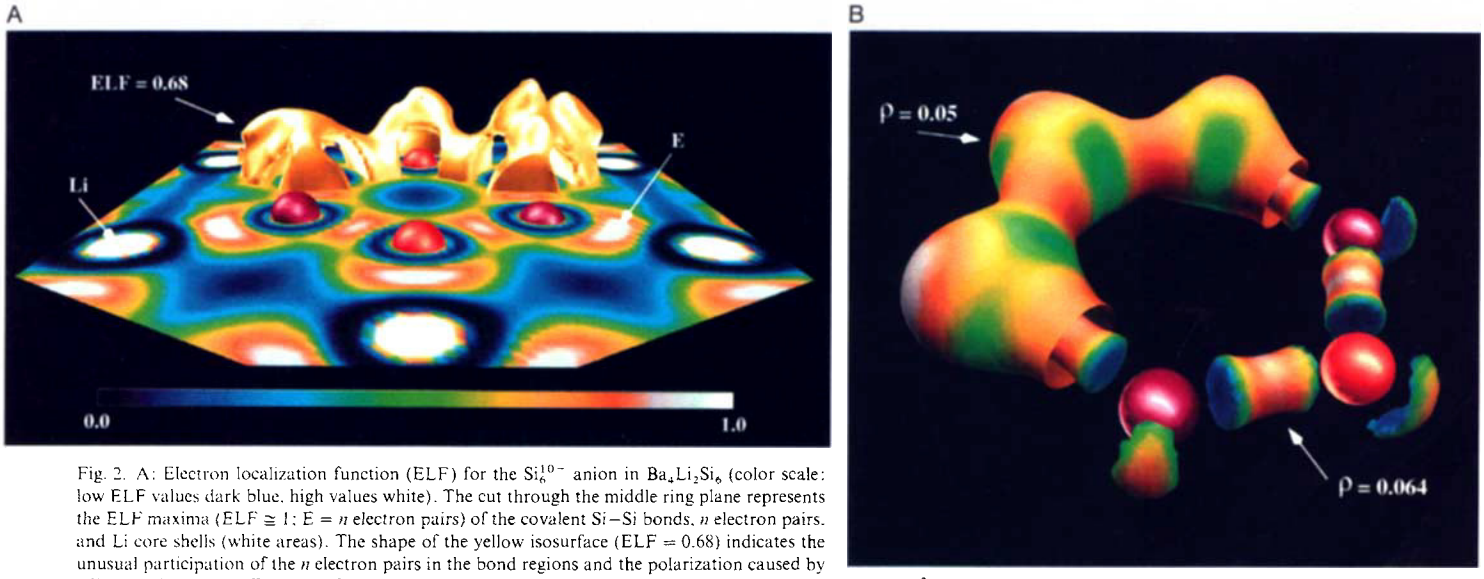

Fig. 2. A: Electron localization function (ELF) for the Si_6^{10-} anion in $Ba_4Li_2Si_6$ (color scale: low ELF values dark blue, high values white). The cut through the middle ring plane represents the ELF maxima (ELF ≅ 1; E = *n* electron pairs) of the covalent Si–Si bonds, *n* electron pairs, and Li core shells (white areas). The shape of the yellow isosurface (ELF = 0.68) indicates the unusual participation of the *n* electron pairs in the bond regions and the polarization caused by adjacent Li atoms. B: Two isosurface representations of the valence electron density ρ (0.05 and 0.064 e au^{-3}) tinted according to the corresponding ELF values (color scale in A). The regions of high ELF values of the diffuse *n* electron pairs lie at lower ρ values than those of the bonds. The Si atoms are in different colors to distinguish the different crystallographic positions.

Rb_4P_6, Cs_4P_6, and Rb_4As_6 are the only stable phases in the corresponding binary systems in which homonuclear polyanions form multiple bonds (the P–P bond length in the three hexaphosphides is 215 pm as opposed to 221 pm for a P–P single bond[7]). This stabilization effect can also be seen in the formation of $Ba_4Li_2Si_6$ and $Ba_{10}Ge_7O_3$ even under very unfavorable conditions: the former in the synthesis of $BaSi_2$ from LiCl fluxes,[3] and the latter as a byproduct in the reactions of oxygen-contaminated starting materials.[9] In this context, the existence of the radical anion P_3^{4-} (analogous to the ozonide anion) is even more remarkable. This anion occurs in the thermally unstable phase K_4P_3,[14] and can be obtained formally by cleaving a P_6^{4-} ring with four additional electrons. Thus, it appears that for the heavier group 14 and 15 elements 10 π electron Hückel arenes such as X_6^{n-} are an alternative to the formation of discrete double bonds.

Thus, it would be worthwhile to reinvestigate thoroughly all of those phases containing graphite or heterographite nets, in which the atoms of the anionic 6^3-net show VEC $\neq 4$.[15] Evidently, the formation of metallic phases can be avoided in a simple manner by variation of the stoichiometric ratio of these atoms or by formation of vacancies: $[Li_2Si_6]^{8-}$ instead of $[Li_4Si_6]^{8-}$; $[\square_2P_6]^{4-}$ instead of $[P_8]^{4-}$. $Al_4\square_2B_6$ instead of AlB_2, for instance, would be a variant containing benzene-analogous anions B_6^{12-} (6 π-electron Hückel arenes).

Received: December 21, 1995 [Z 8686 IE]
German version: *Angew. Chem.* **1996**, *108*, 1062–1064

Keywords: electron localization · germanium compounds · silicon compounds · Zintl phases

[1] M. Wörle, R. Nesper, G. Mair, M. Schwarz, H. G. von Schnering, *Z. Anorg. Allg. Chem.* **1995**, *621*, 1153.
[2] H. Axel, K. H. Janzon, H. Schäfer, A. Weiss, *Z. Naturforsch. B* **1968**, *23*, 108.
[3] E. I. Gladishevskij, *Dopovidi Akad. Nauk. Ukr. RSR* **1959**, *3*, 294.
[4] P. Villars, L. D. Calvert, *Pearson's Handbook of Crystallographic Data for Intermetallic Phases*, 2nd ed., **1991**, ASM International.
[5] $Ba_4Li_2Si_6$ and $Ba_4Li_2Ge_6$ were synthesized quantitatively by reaction of the elements in a stoichiometric ratio of 4:2.1:6 (excess Li to avoid loss at high temperatures) in arc-welded Nb ampoules under reduced Ar pressure at 1000 °C. Single crystals for X-ray structure determination were obtained by slow cooling to 400 °C and subsequent annealing at this temperature.
[6] Crystal structure of $Ba_4Li_2Si_6$: $M_r = 731.7$ g mol^{-1}; $a = 872.6(2)$, $b = 1517.4(3)$, $c = 1932.2(4)$ pm; space group *Fddd*-D_{2h}^{24} (No. 70); $Z = 8$; $V = 192.58$ cm^3 mol^{-1}, $\rho_{calcd} = 3.799$ g cm^{-3}; $N(hkl) = 677$; 575 of them with $F \geq 2\sigma(F)$, $R_{int} = 0.049$ (range of data collection $-1 \leq h \leq 11$, $-1 \leq k \leq 19$, $-1 \leq l \leq 25$); $R_{aniso} = 0.034$. Crystal structure of $Ba_4Li_2Ge_6$: $M_r = 998.78$ g mol^{-1}; $a = 890.1(1)$, $b = 1546.9(2)$, $c = 1943.0(2)$ pm; space group *Fddd*-D_{2h}^{24} (No. 70); $Z = 8$; $V = 201.38$ cm^3 mol^{-1}, $\rho_{calcd} = 4.960$ g cm^{-3}; $N(hkl) = 773$; 586 of them with $F \geq 2\sigma(F)$, $R_{int} = 0.037$ (range of data collection $-1 \leq h \leq 11$, $-1 \leq k \leq 20$, $-1 \leq l \leq 25$); $R_{aniso} = 0.038$; Siemens-P4 four-circle diffractometer (graphite monochromator, scintillation counter, $Mo_{K\alpha}$ radiation, ω scan, $3.5° \leq 2\theta \leq 55°$, 293 K); empirical absorption correction by ψ scan; program package SHELXTL. Further details of the crystal structure investigations are available on request from the Fachinformationszentrum Karlsruhe, D-76344 Eggenstein-Leopoldshafen, on quoting the depository numbers CSD-404707 ($Ba_4Li_2Si_6$) and CSD-404705 ($Ba_4Li_2Ge_6$).
[7] H.-P. Abicht, W. Hönle, H. G. von Schnering, *Z. Anorg. Allg. Chem.* **1984**, *519*, 7.
[8] W. Hönle, Dissertation, Universität Münster **1975**; W. Hönle, J. Wolf, D. Weber, H. G. von Schnering, *Collected Abstracts III^d Europ. Conf. Solid State Chem.* **1986**, *Vol. I*, p. 45.
[9] Single crystals of $Ba_{10}Ge_7O_3$ were obtained upon thermal decomposition (2 h, 450 °C, ultra high vacuum) of an oxygen-contaminated alloy of nominal composition Na_2BaGe. Polycrystalline $Ba_{10}Ge_7O_3$ is available from a reaction of BaO, Ba, and NaGe under similar decomposition conditions and subsequent annealing.
[10] Crystal structure of $Ba_{10}Ge_7O_3$: $M_r = 1929.53$ g mol^{-1}; $a = 1170.1(2)$, $c = 509.5(1)$ pm; space group $P6_3/mmm$-D_{6h}^1 (No. 191); $Z = 1$; $V = 363.79$ cm^3 mol^{-1}, $\rho_{calcd} = 5.304$ g cm^{-3}; $N(hkl) = 320$; 246 of them with $F \geq 3\sigma(F)$, $R_{int} = 0.070$ (range of data collection $0 \leq h \leq 13$, $0 \leq k \leq 13$, $0 \leq l \leq 6$); $R_{aniso} = 0.045$; Siemens-P4 four-circle diffractometer (graphite monochromator, scintillation counter, $Mo_{K\alpha}$ radiation, ω scan, $4° \leq 2\theta \leq 55°$, 293 K); empirical absorption correction via ψ scan; program package SHELXTL. Further details of the crystal structure investigation are available on request from the Fachinformationszentrum Karlsruhe, D-76344 Eggenstein-Leopoldshafen, on quoting the depository number CSD-404706.
[11] A. D. Becke, K. E. Edgecombe, *J. Chem. Phys.* **1990**, *92*, 5397.
[12] A. Savin, A. D. Becke, J. Flad, R. Nesper, H. W. Preuss, H. G. von Schnering, *Angew. Chem.* **1991**, *103*, 421; *Angew. Chem. Int. Ed. Engl.* **1991**, *30*, 409.
[13] A. Savin, B. Silvi, F. Colonna, *Can. J. Chem.*, in press.
[14] H. G. von Schnering, M. Hartweg, U. Hartweg, *Angew. Chem.* **1989**, *101*, 98; *Angew. Chem. Int. Ed. Engl.* **1989**, *28*, 56.
[15] Since the submission of this communication $Sr_4Li_2Si_6$ has been prepared. The compound also forms orthorhombic crystals ($a = 852.5(1)$, $b = 1481.2(2)$, $c = 1816(2)$ pm, space group *Fddd*) [16]. We are convinced that it is identical to the phase described by Müller et al. [17], $Sr_7Li_4Si_{10} \cong Sr_{4.2}Li_{2.4}Si_6 \approx Sr_4Li_2Si_6$, which was assumed to adopt the AlB_2 structure type with a statistical distribution of Li and Si.
[16] U. Bolle, K. Peters, W. Carrillo-Cabrera, H. G. von Schnering, unpublished.
[17] W. Müller, A. Schäfer, A. Weiss, *Z. Naturforsch. B.* **1969**, *24*, 650.

Molecular, Shell-Like Dilithium (Silyl)phosphanediide and Dilithium (Silyl)arsanediide Aggregates with an $[Li_6O]^{4+}$ Core**

Matthias Driess,* Hans Pritzkow, Stefan Martin, Stefan Rell, Dieter Fenske, and Gerhard Baum

Dedicated to Professor Kurt Dehnicke on the occasion of his 65th birthday

Dilithium derivatives of primary amines, phosphanes, and arsanes of the type $[RELi_2]_n$ (R = alkyl, aryl, silyl; E = N, P, As), which are useful nucleophilic building blocks in the element organic chemistry of nitrogen, phosphorus, and arsenic, are molecular aggregates and structurally represent an intermediate between the molecular compounds R_3E and the typical saltlike solid-state compounds Li_3E (lithium pnictides). Their structures, however, have not been well established or are not known, since these compounds have only been obtained as insoluble, X-ray amorphous solids.[1] Recently the decameric dilithium (α-naphthyl) azanediide **1**[2] and the dimeric dilithium phosphanediide-fluorosilane adduct **2**,[3] which are soluble in ether and aromatic solvents, were structurally characterized.

$[(RNLi_2)_{10}(Et_2O)_6] \cdot Et_2O$ $\quad$ $RPLi_2 \cdot 2RF$

1, R = α-$C_{10}H_7$ $\quad$ **2**, R = $SiiPr_2(2,4,6\text{-}iPr_3C_6H_2)$

We have been investigating the synthesis and structure of the dilithium (silyl)phosphanediides and arsanediides **3** which form a spherical cluster framework and are soluble as a result of their easily variable lipophilic shell.[3] Since the degree of aggregation

$[\{R_3SiELi_2\}_n]$ **3**, E = P, As; R = alkyl, aryl

[*] Priv.-Doz. Dr. M. Driess, Dr. H. Pritzkow, S. Martin, S. Rell
Anorganisch-chemisches Institut der Universität
Im Neuenheimer Feld 270, D-69120 Heidelberg (Germany)
Fax: Int. code +(6221) 54 41 97
e-mail: dp0@ix.urz.uni-heidelberg.de
Prof. Dr. D. Fenske, G. Baum
Institut für Anorganische Chemie der Technischen Universität
Engesserstrasse, D-76128 Karlsruhe (Germany)

[**] This work was supported by the Deutsche Forschungsgemeinschaft (Schwerpunktprogramm "Polyedermoleküle") and the Fonds der Chemischen Industrie.

is largely determined by the steric bulk of the triorganosilyl group, we were interested in the reactivity of **3** as a function of cluster size. We have now observed that the double lithiation of the primary silylphosphane **4** and silylarsane **6** in the presence of Li_2O results in the octameric and dodecameric aggregates **5** and **7**, respectively. Surprisingly the cavities of these compounds are filled with an octahedral $[Li_6O]^{4+}$ cluster framework. The compositions of the aggregates have been confirmed by correct elemental analyses.

Compound **5** is formed by the lithiation of **4** with two equivalents of *n*BuLi in the presence of Li_2O in toluene or Et_2O and can be isolated in 69% yield as light yellow crystals. The origin of the incorporated Li_2O has not yet been explained. Since **5** can also be produced in toluene, the hydrolysis product in commercial *n*BuLi solutions, LiOH, could be the potential source for O^{2-}. We have evidence that other Li_2O-free aggregates are formed upon rigorous exclusion of $LiOH/Li_2O$.

$$\underset{\mathbf{4}}{8\,RPH_2} \xrightarrow[-16\,C_4H_{10}]{16\,n\text{BuLi}\,Li_2O} \underset{\mathbf{5}}{[(RP)_8Li_{18}O]}$$

R = *i*Pr$_2$(Mes)Si

$$\underset{\mathbf{6}}{12\,RAsH_2} \xrightarrow[-24\,C_4H_{10}]{24\,n\text{BuLi}\,Li_2O} \underset{\mathbf{7}}{[(RAs)_{12}Li_{26}O]}$$

R = Me$_2$(*i*PrMe$_2$C)Si

A crystal structure analysis of **5**[4] revealed the presence of an aggregate with approximately 422 symmetry (Fig. 1); only the fourfold axis is required crystallographically. The twofold axes

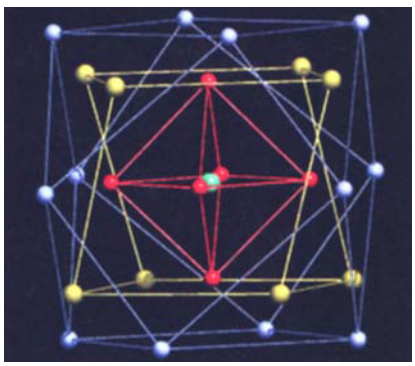

Fig. 1. Representation of the shell-like form of **5** in the crystal. For clarity the silyl groups have been omitted. OLi_6 shell = green, red, P_8 shell = yellow, Li_{12} shell = blue. Selected distances [Å]: Si–P 2.195(2), Li–P 2.39–2.46(1) for outer Li atoms, 2.56(1), 2.58(1) for inner equatorial Li atoms, 2.91(1), 2.93(1) for inner apical Li atoms, Li–O 1.81–1.90(2).

run parallel to *a* and *b* and provide pseudo symmetry. The cluster has eight formal units of dilithium phosphanediide and a Li_2O molecule. The cationic (Li centers) and anionic (P and O centers) building blocks show close packing. The structure is topologically best described as an ionogenic cluster formed by three closed shells and covered by the lipophilic silyl groups (Fig. 1). The eight P atoms comprise a strongly distorted cube, which is surrounded by a Li_{12} cuboctahedral shell and surrounds a Li_6O octahedron.

The Li centers of the Li_{12} shell each sit over an edge of the P_8 cube, whereas the Li centers of the Li_6O cluster are each located over a face. This P_8 partial structure is evidently preferred to the anti-prismatic or the bisdisphenoid ordering which are possible alternatives. An important aspect of this cluster formation is that only twelve of the total sixteen Li centers are placed on the exterior, that is on the edges, of the P_8 framework; thus, the remaining Li ions must be placed in the cavity. These four Li ions are electronically stabilized by binding to the formal O^{2-} ion of Li_2O, thus resulting in a $[Li_6O]^{4+}$ cluster. Sixfold coordination of O^{2-} by metal cations in *molecular* compounds is very unusual and has as yet only been observed in a dilithiomethane–Li_2O aggregate[5] and in a mixed lithium-barium-(*tert*-butoxide)-oxide aggregate.[6]

The Li–P distances to the external Li centers are very similar and lie in the range of 2.39–2.46(1) Å; the Li–P distances for the internal Li centers are 2.56 and 2.58(1), as well as 2.91 and 2.93(1) Å; that is, they correspond with the values observed for lithium phosphanides.[7] The Li–Li distances in the Li_{12} cuboctahedron are longer than 3 Å, and those in the Li_6O framework are significantly shorter (2.63–2.67(2) Å). It has not yet been clarified if these relatively short distances imply bonding interactions, whereas the P–P distances (>4 Å) clearly show that there are no P–P bonds present. The Li–O distances in the $[Li_6O]^{4+}$ aggregate (1.81–1.90(2) Å) are significantly shorter than in solid Li_2O (1.98 Å). In addition, the Li centers of the $[Li_6O]^{4+}$ aggregate are each coordinated by four P atoms.

The filled cluster shows a slight tendency to dissociate in solution. Cryoscopic investigations provided a degree of aggregation of $n \approx 7.7$. Crystals dissolved in benzene show three broad signals ($\nu_{1/2} = 70$–85 Hz) in the ^{31}P NMR spectrum at $\delta = -336.9$, -340.1, and -355.9 in an intensity ratio of 15:15:1. The main signals were assigned to the two different P atoms on the intact cluster, while the remaining weak signal is presumably due to an unknown dissociate. The ^7Li NMR spectrum only shows one broad signal at $\delta = 0.9$ ($\nu_{1/2} = 115$ Hz) that indicates either a fast Li exchange or only minor differences in the δ values for the various ^7Li centers. Because of the limited solubility in toluene no measurements below 0 °C were possible.

A cluster comprising three shells of platonic units is present in **7** which is topologically closely related to **5**. The As centers form a slightly distorted As_{12} icosahedron, in which all of the twenty triangular faces are each capped by a Li center (Fig. 2 left). The twenty Li centers thereby form a pentagondodecahedron as dual polyhedral framework with approximately I_h point symmetry. The remaining four Li cations are found in the cavity of the approximately spherical $[As_{12}Li_{20}]^{4-}$ framework (diameter ca. 8 Å). As in **5**, these Li ions bind to an encapsulated Li_2O molecule leading to formation of a $[Li_6O]^{4+}$ octahedral core. The formation of the approximately O_h-symmetrical cluster in the cavity of the I_h-symmetrical $[As_{12}Li_{20}]^{4-}$ aggregate is very unusual and reflects a "symmetry frustration" which is caused by the stoichiometry. The $[Li_6O]^{4+}$ octahedron is, therefore, tilted with respect to the orientation of the As_{12} icosahedron; a C_3 axis of the octahedron coincides with a C_3 axis of the Li_{20} shell.

The Li–As distances in the $As_{12}Li_{20}$ framework lie between 2.559(9)–2.76(1) Å, and are thus in the range of values obtained for lithium arsanide.[8] The Li–Li distances in the Li_{20} dodecahedron are 2.89(1) and 3.09(1) Å, whereas, like in **5**, the Li–Li distances in the Li_6O framework are significantly shorter (2.52(1)–2.81(1) Å). The large As–As distances (>4 Å) indicate that there are no As–As bonds; the Li–O distances are similar to those in **5**. The Li centers of the Li_6O framework are, as expected, still coordinated to nearby As centers (Fig. 2 right); four Li centers have relatively short distances to three As atoms each, and two Li centers are only close to two As atoms. These distances correspond to those in the $As_{12}Li_{20}$ framework. ^7Li NMR spectra measured at various temperature intervals from

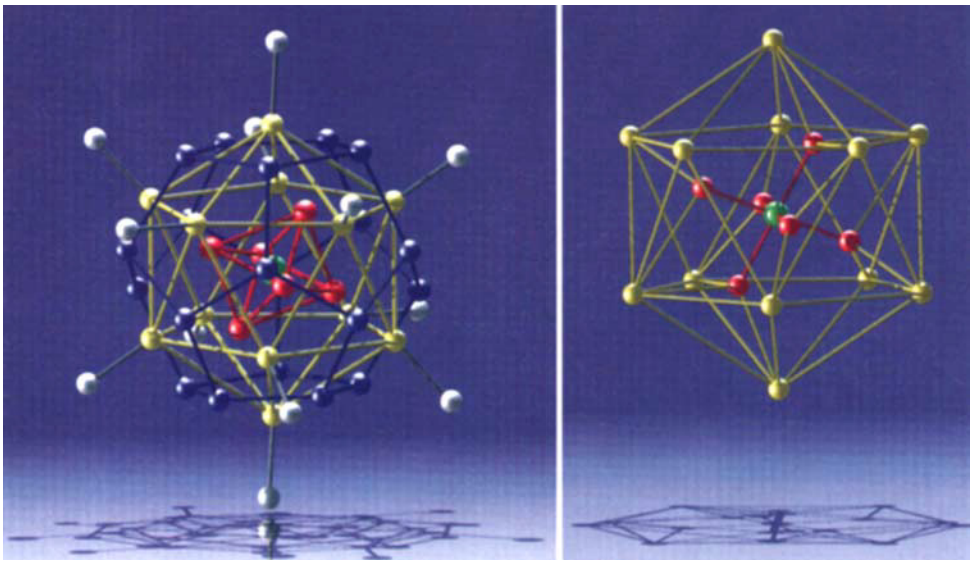

Fig. 2. Left: Representation of the shell-like form of **7** in the crystal. For clarity the organic groups have been omitted. Si = gray, As_{12} shell = yellow, Li_{20} shell = blue, OLi_6 shell = green, red. Selected distances [Å]: Si–As 2.294–2.309(2), Li–As 2.559(9)–2.76(1) for outer Li atoms, 2.55–2.63(1) for inner Li atoms coordinated to two As atoms, 2.60–2.99(1) for inner Li atoms coordinated to three As atoms, Li–O 1.85–1.90(1). Right: connection of the Li_6O octahedron (red, green) with the As centers (yellow).

−40 to 25 °C show that the structure is maintained in solution. The spectra show two sorts of Li in the Li_6O framework and one more sort of Li in the $As_{12}Li_{20}$ framework ($\delta = -1.65$ and -0.66, and 2.05, respectively, in a ratio of 1:2:10). Cryoscopic measurements gave a degree of aggregation of $n \approx 11.8$.

The question of whether other hyperlithiated cluster cations of main group elements such as $[Li_6S]^{4+}$ and $[Li_8C]^{4+}$ can be internally stabilized is currently under investigation.

Experimental Procedure

5: Compound **4** (1.3 g, 4.89 mmol) in toluene (20 mL) was allowed to react with Li_2O-containing *n*BuLi (0.63 g, 9.78 mmol, 2.5 M in hexane) at −50 °C. The yellow solution was slowly warmed to 25 °C and then concentrated in vacuum (10^{-2} Torr) to half its volume. After a few days at 25 °C, light yellow, air-sensitive crystals had formed. Yield: 0.90 g (0.39 mmol, 65%). ^{1}H NMR (300 MHz, C_6D_6): $\delta = 1.20$–1.40 (br. m, 112 H, *i*Pr), 2.11 (s, 12 H, *p*-Me), 2.14 (s, 12 H, *p*-Me), 2.76 (br., 48 H, *o*-Me), 6.72 (s, 16 H, arom. H).

7: Compound **6** (6.0 g, 27.24 mmol) was dissolved in Et_2O (90 mL) and treated with Li_2O-containing *n*BuLi (23.83 g, 54.48 mmol; 1.6 M solution in hexane) at 20 °C. The color of the solution changed upon slow warming to 25 °C from light yellow to orange. An orange-brown solid was obtained upon concentrating the solution in vacuum (10^{-2} Torr). The solid was taken up in toluene (30 mL) and gradually dissolved at 80 °C. Fractional crystallization provided orange-yellow, air-sensitive crystals. Yield: 4.80 g (1.71 mmol; 75%). ^{1}H NMR (300 MHz, C_6D_6): $\delta = 0.68$ (s, 72 H, $SiMe_3$), 1.02 (s, 72 H, CMe_3), 1.06 (d, 72 H, $CHMe_2$, J(H,H) = 6.8 Hz), 2.08 (sept., 12 H, $CHMe_2$, J(H,H) = 6.8 Hz).

Received: December 18, 1995 [Z 8658 IE]
German version: *Angew. Chem.* **1996**, *108*, 1064–1066

Keywords: arsenic compounds · clusters · lithium compounds · phosphorus compounds

[1] K. Issleib, A. Tzschach, *Chem. Ber.* **1959**, *92*, 1118; G. W. Parshall, R. V. Lindsey, Jr., *J. Am. Chem. Soc.* **1959**, *81*, 6273; G. Fritz, H. Schäfer, W. Hölderich, *Z. Anorg. Allg. Chem.* **1974**, *407*, 266; R. Appel, K. Geisler, *J. Organomet. Chem.* **1976**, *112*, 61; G. Becker, O. Mundt, M. Rössler, E. Schneider, *Z. Anorg. Allg. Chem.* **1978**, *433*, 42.

[2] D. R. Armstrong, D. Barr, W. Clegg, S. R. Drake, R. J. Singer, R. Snaith, D. Stalke, D. S. Wright, *Angew. Chem.* **1991**, *103*, 1702; *Angew. Chem. Int. Ed. Engl.* **1991**, *30*, 1707.

[3] M. Driess, S. Rell, H. Pritzkow, R. Janoschek, *Chem. Commun.* **1996**, 305.

[4] **5**: $C_{120}H_{200}Li_{18}OP_8Si_8 \cdot 2C_7H_8$, tetragonal, $P4_2/n$, $a = 22.565(11)$, $c = 16.393(8)$ Å, $V = 8347$ Å^3, $Z = 2$. The crystals are twinned (twin axis [110]). Three crystals were investigated from which two showed a 1:1 ratio of the two components, the third showed a ratio of 1:12. The results of the three refinements corresponded well with one another. There are disordered solvent molecules (toluene) in the space between the clusters. Intensity measurements: Siemens-STOE AED2 four-cycle diffractometer, $Mo_{K\alpha}$ radiation, ω scan, $T = -70$ °C, measurement range $2\theta_{max} = 47°$, 6187 independent reflections (4000 observed with $I > 2\sigma(I)$), empirical absorption correction. Structure solution with direct methods [9a], refinement with all reflections against F^2 [9b] (383 parameters, non-hydrogen atoms anisotropic, hydrogen atoms in calculated positions with the same temperature factors, toluene molecules as rigid six-membered rings isotropic), $R1 = 0.0717$, $wR2 = 0.2334$ (all data). **7**: $C_{48}H_{114}As_6Li_{13}O_{0.5}Si_6$, monoclinic, $P2_1/n$ (No. 14), $a = 19.480(2)$, $b = 19.330(2)$, $c = 19.540(2)$ Å, $\beta = 91.92°$, $V = 7353$ Å^3, $Z = 4$. Intensity measurements: Siemens-STOE IPDS diffractometer, $Mo_{K\alpha}$ radiation, $T = -100$ °C, measurement range $2\theta_{max} = 52°$, 14136 independent reflections (10481 observed with $I > 2\sigma(I)$). Structure solution with direct methods [9a], refinement with all reflections against F^2 [9b] (664 parameters, hydrogen and non-hydrogen atoms anisotropic), $R1 = 0.0607$, $wR2 = 0.1288$ (all data). Further details of the crystal structure investigations can be obtained from the Fachinformationszentrum Karlsruhe, D-76344 Eggenstein-Leopoldshafen, on quoting the depository numbers CSD-404962 (**5**) and 404961 (**7**).

[5] H.-J. Gais, J. Vollhardt, H. Günther, D. Moskau, H. J. Linder, S. Braun, *J. Am. Chem. Soc.* **1988**, *110*, 978.

[6] H. Bock, T. Hauck, C. Näther, N. Rösch, M. Staufer, O. D. Häberlen, *Angew. Chem.* **1995**, *107*, 1438; *Angew. Chem. Int. Ed. Engl.* **1995**, *34*, 1353.

[7] G. Becker, B. Eschbach, D. Käshammer, O. Mundt, *Z. Anorg. Allg. Chem.* **1994**, *620*, 29, and references therein; M. Driess, G. Huttner, N. Knopf, H. Pritzkow, L. Zsolnai, *Angew. Chem.* **1995**, *107*, 354; *Angew. Chem. Int. Ed. Engl.* **1995**, *34*, 316.

[8] A. M. Arif, R. A. Jones, K. B. Kidd, *J. Chem. Soc. Chem. Commun.* **1986**, 1440; P. B. Hitchchock, M. F. Lappert, S. J. Smith, *J. Organomet. Chem.* **1987**, *320*, C27; L. Zsolnai, G. Huttner, M. Driess, *Angew. Chem.* **1993**, *105*, 1549; *Angew. Chem. Int. Ed. Engl.* **1993**, *32*, 1439.

[9] a) G. M. Sheldrick, *SHELXS86*, Universität Göttingen, **1986**; b) G. M. Sheldrick, *SHELXL93*, Universität Göttingen, **1993**.

Solid-State Coordination Chemistry: Hydrothermal Synthesis of Layered Vanadium Oxides with Interlayer Metal Coordination Complexes**

Yiping Zhang, Jeffrey R. D. DeBord, Charles J. O'Connor, Robert C. Haushalter,* Abraham Clearfield,* and Jon Zubieta*

Layered inorganic oxides constitute a diverse class of materials most of which share the common structural feature of a cationic guest that lies between the anionic oxide layers. The largest number of examples are known for materials composed largely of main group cations like clays, but solids with transition or post-transition elements like the layered double hydroxides[1] and certain alkali metal titanates[2] are known. Layered, and three-dimensional (3-D) oxides, containing both transition and main group metal cations, such as the Zr,[3], V,[4] and Mo[5] phosphates and phosphonates, have also been studied. While many of these solids are noted for their unique characteristic of allowing a wide variety of organic or inorganic chemistries to be performed in the interlamellar region, the closed shell, diamagnetic layers serve mainly as an inert nanoscale scaffolding. In contrast to these diamagnetic layers, several lamellar vanadium oxide solids have been prepared by high-temperature syntheses as well as the intercalation of alkali metal cations,[6a] conductive organic polymers,[6b] and organic cations[6c] between the layers of V_2O_5. A one-dimensional (1-D) metavanadate chain with coordinated $Cu(NH_3)_2$ groups has also been synthesized.[7] We present here a facile, general synthetic route to an entirely new class of layered, mixed-valence vanadium oxides that possess cationic interlayer transition or post-transition metal coordination complexes. The synthesis and structural characterization of **1** (bpy = 2, 2'-bipyridine), **2** (en = ethylenediamine), **3**, and **4**, and preliminary magnetic susceptibility values for **2**–**4** are reported.

$[(bpy)_2Zn]_2[V_6O_{17}]$ **1**, $(en)_2Zn[V_6O_{14}]$ **2**
$(en)_2Cu[V_6O_{14}]$ **3**, $[(en)_2Cu]_2[V_{10}O_{25}]$ **4**

The oxides **1**–**4** are prepared in a single step by the reaction of a precursor containing a transition or post-transition element, the bidentate amine, and V_2O_5 in water at 170 °C, and are isolated as highly crystalline, thin black plates. Since no external reducing agent is employed, the amine presumably serves in this capacity. These materials, $(L_2M)_y[VO_x]$, where L = bidentate amine, M = Cu or Zn, $0.16 \leq y \leq 0.33$ and $2.33 \leq x \leq 2.83$, share common structural features of vanadium oxide layers as well as a six-coordinate interlayer cation with four of the six coordination sites occupied by N atoms from two bidentate amine ligands and two sites from O atoms of the VO layer. The layers are built up in all cases from VO_4 tetrahedra and/or VO_5 square pyramids that are connected by edge- and corner-sharing interactions.

The unprecedented structure of **1**,[8] consists of VO layers, which, when viewed parallel to [100], display a very pronounced sinusoidal ruffling with an amplitude of about 13 Å and a period of about 15 Å (Fig. 1 left). These layers are composed solely of $V^{5+}O_4$ tetrahedra each of which have a terminal vanadyl (V=O) group and share three corners with three neighboring VO_4 units (Fig. 1 right). Within each VO layer there are very large, roughly circular rings, which alternately lie in planes approximately parallel to (011) and (0$\bar{1}$1), defined by fourteen VO_4 tetrahedra with transannular V–V distances of about 13 Å. There are two $Zn(bpy)_2$ moieties per ring, on either side of the

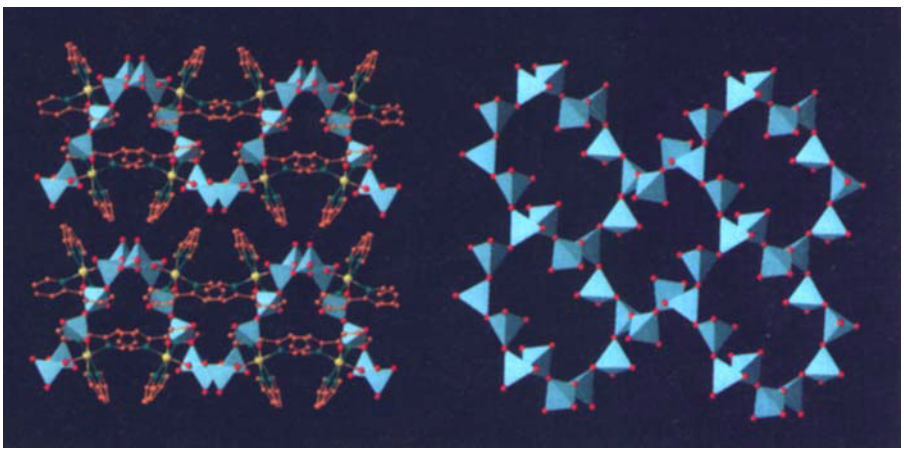

Fig. 1. Crystal structure of **1**; view parallel (left) and perpendicular (right) to the VO layers, illustrating the pronounced sinusoidal ruffling, the presence of the bpy ligands in the troughs, and the 14-ring holes within the layer.

$\bar{1}$ site in the center of the ring, each bonded in a *cis* fashion to two oxygen atoms from two second-nearest neighbor VO_4 groups on opposite sides of the ring. The bpy ligands protrude above and below the mean plane of the V_{14} ring so as to fill the troughs created from the ruffling of the layers with the organic ligands (Fig. 1 right).

The use of en as a bidentate ligand has allowed not only the isolation of new one-dimensional Cu-en-VO materials[9] but several layered solids as well. Two layered examples with en are the isotypic, mixed-valence V^{4+}/V^{5+} vanadium oxides **2**[10] and **3**.[11] Both materials contain Cu or Zn in a very distorted MO_2N_4 octahedral environment consisting of four N donor atoms, which lie approximately in a plane parallel to the VO layers (Fig. 2 left), and two *trans* O atoms from two adjacent layers, coordinated through very long M–O interactions. While this nearly square-planar coordination is not atypical for the Cu center in **3** (four N–Cu distances ≈ 2.03 Å; two O–Cu distances of 2.53 Å), it is highly unusual for the Zn center found in **2** (two N–Zn distances of 2.12 and two of 2.07 Å; two O–Zn

[*] Dr. R. C. Haushalter, Dr. Y. Zhang, Dr. J. R. D. DeBord
NEC Research Institute
4 Independence Way, Princeton, NJ 08540 (USA)
Fax: Int. code +(609)951-2481
e-mail: haushalt@research.nj.nec.com
Prof. A. Clearfield
Department of Chemistry, Texas A & M University
College Station, TX 77843 (USA)
Fax: Int. code +(409)845-2370
e-mail: clearf@acxrd.chem.tamu.edu
Prof. J. Zubieta
Department of Chemistry
Syracuse University
Syracuse, NY 13244 (USA)
Int. code +(315)-443-4070
e-mail: jazubieta@mailbox.syr.edu
Prof. C. J. O'Connor
Department of Chemistry
University of New Orleans
New Orleans, LA 70148 (USA)
e-mail: cjocm@jazz.uec.uno.edu

[**] The work at Texas A & M was supported by NSF DMR-9107715. The work at Syracuse University was supported by NSF Grant 9318824.

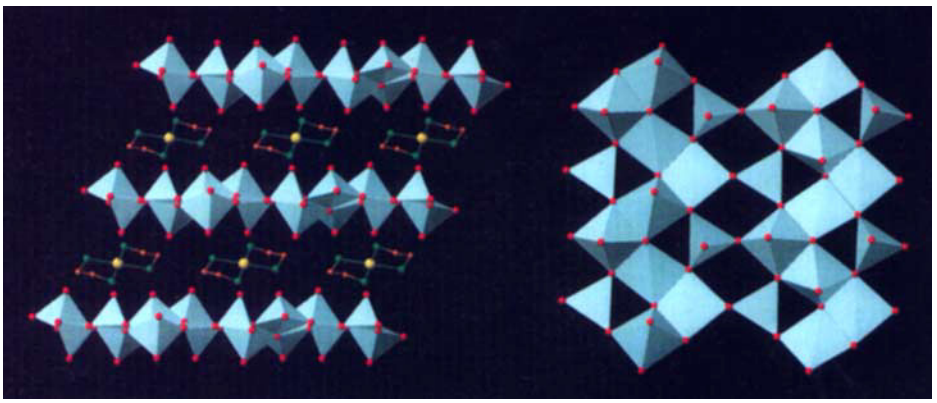

Fig. 2. Crystal structures of the isotypic compounds **2** and **3**, showing the infinite zigzag chains of edge-sharing VO_5 square pyramids and interlamellar $(en)M^{2+}$ ions. The long axial V···O bonds connecting M to the oxide layers are not shown.

distances of 2.45 Å). The VO layers in oxides **2** and **3** contain infinite zigzag chains of edge-sharing $V^{4+}O_5$ square pyramids running parallel to [010]; their terminal vanadyl groups are oriented in pairs toward opposite sides of the layer, connected together by $V^{5+}O_4$ tetrahedra (Fig. 2 right) giving a layer compostion of $[(V^{5+})_2(V^{4+})_4O_{14}]^{2-}$ according to valence sum calculations.[12] Surprisingly, in spite of the fact that 2/3 of the V atoms are in the oxidation state IV (d^1), the Zn oxide **2** does not give an ESR signal and has an anomolously low magnetic moment according to preliminary magnetization measurements (Fig. 3A), which show that $\chi = M/H$ actually decreases in the range $150 < T < 300$ K. As shown in Figure 3B, the isotypic copper compound **3** also appears to have layers with supressed magnetic moments with $\mu_{eff}(300\ K) \approx 2.2\ \mu B$ ($\mu_{eff} = [8\chi T]^{1/2}$) only slightly greater than that expected ($\approx 1.8\ \mu B$) for the Cu^{2+} ion with $S = 1/2$. Below room temperature, the moment slowly decreases and reaches the value expected for only the Cu^{2+} ion by ≈ 70 K; below this temperature $\chi^{-1}(T)$ is linear (unlike $T > 70$ K) with a θ value near zero, indicative of a paramagnet. The magnetic data for **2** and **3** suggest that either the layers have already undergone an antiferromagnetic transition above room temperature or the spins are paired within states that are delocalized within the layers. However, there is no indication of the characteristic anomaly normally associated with a transition to an antiferromagnetic state.

Changing the reaction conditions in the en-Cu^{2+}-V_2O_5 system gives rise to other vanadium oxides with ligated Cu bound to the layers such as **4**.[4] Like **2** and **3**, oxide **4** has a nearly square-planar $(en)_2Cu^{2+}$ ion bonded to two *trans* oxygen atoms from two adjacent layers (Fig. 4 left), which are formulated as $[(V^{5+})_6(V^{4+})_4O_{25}]^{4-}$ according to charge balance and valence sum calculations. The layers are built up from double strands of infinite corner-sharing strings of edge-sharing trimeric VO_5 square pyramids, which run parallel to [001] and are connected together by VO_4 tetrahedra. The double strands are in turn bridged together by additional VO_4 tetrahedra to create a layer containing ordered voids (Fig. 4 right) with transannular O···O distances of 6 Å. Magnetization data shows that $\mu(300\ K) \approx 5.5\ \mu B$, a value which is below that expected for the six unpaired spins from two Cu^{2+} and four V^{4+} ions. The magnetic moment decreases nearly linearly over the entire range $20 < T < 300$ K, and reaches a value of about 2.8 μB near 10 K, which is the magnetic moment expected for two Cu^{2+} centers each with $S = 1/2$ (Fig. 3C). Note also that below about 15 K, $\chi^{-1}(T)$ is linear with a θ value near zero, consistent with paramagnetism and the pairing of all V^{4+} spins within each layer. Thus the magnetic behavior of **4** resembles that of **3** in that the layers have magnetic moments that slowly decrease over large temperature intervals, with no characteristic anomalies indicative of a phase transition, and appear essentially diamagnetic at very low temperatures.

Thermogravimetric analysis for compounds **1**–**4** shows that the organic component leaves the materials in the 200–300 °C range under N_2 but the residues have not been characterized.

A simple single-step hydrothermal route to a new class of inorganic solid-state materials, which contain amine-ligated transition (or post-transition) metal cations situated between mixed-valence vanadium oxide layers, has been developed. Examination of these layer structures show that they are related both compositionally and structurally to the V_2O_5 starting material. The degree of reduction (V^{4+}/V^{5+}) and condensation (V:O ratio and relative amounts of edge- versus corner-sharing polyhedral connectivities) within the layers is reflected in the charge per volume ratio of the cationic interlamellar coordination complex. The extensive

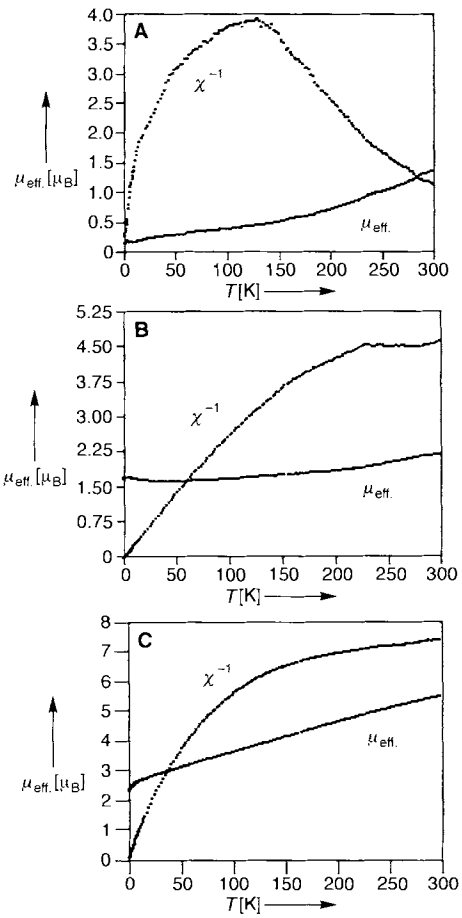

Fig. 3. Susceptibility χ [emu mol^{-1}] and effective magnetic moment μ_{eff} as a function of the temperature for the oxides **2** (A), **3** (B), and **4** (C).

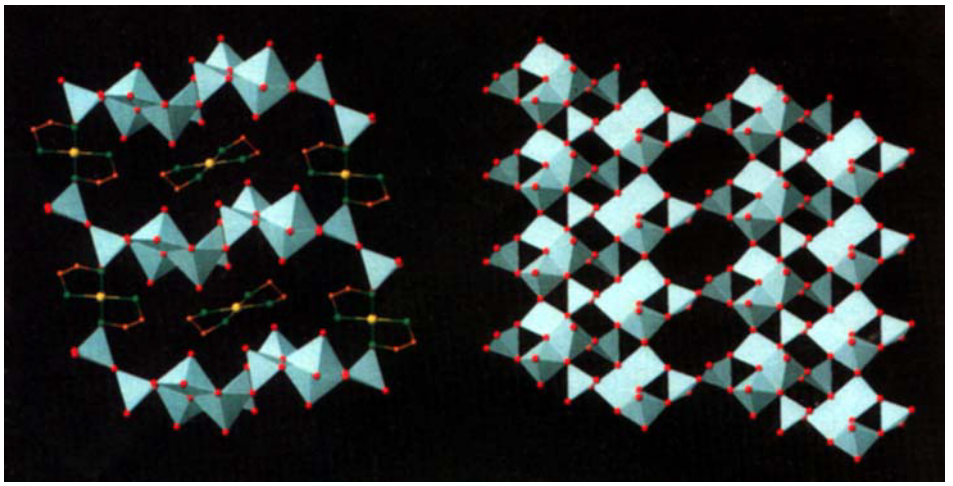

Fig. 4. Crystal structure of **4**, showing the complex layer structure composed of edge-sharing VO_5 trimers bridged together by corner-sharing into 1-D strings, which are in turn connected into the infinite 2-D layer by VO_4 tetrahedra.

edge- and corner-sharing of the vanadium-centered polyhedra in these materials strongly influence electron–electron interactions confined within the layers, which gives rise to very unusual magnetic behavior. Many more complexes of this type, in addition to the ones described here, have been prepared,[9] indicating that these materials will constitute a large class of new materials. Combining the well-studied chemistry and properties developed over the last one hundred years for coordination compounds with the heterogeneous nature, stereochemical ridgidity, and potentially variable conductivity of the mixed-valence solid-state oxide layers, suggests that it should be possible to substantially vary the properties of these materials in a relatively straightforward manner.

Experimental Procedure

The syntheses were performed in 23 mL Teflon-lined stainless steel vessels filled to 30–50% at room temperature.

1: A mixture of V_2O_5 (0.312 g), ZnO (0.049 g), H_2O (10 mL), and bpy (0.325 g) in a molar ratio of 1.0:0.35:323:1.2 was heated at 170 °C for 44 h, and then at 200 °C for 90 h. This gave 0.46 g of a solid that was a mixture of brown chunks of **1**, black rods of $VO(VO_3)_6[VO(bpy)_2]_2$, and some unidentified green powder in an approximate ratio of 4:5:1.

2: A mixture of V_2O_5 (0.192 g), ZnO (0.042 g), H_2O (10 mL), and en (0.2 mL) in a molar ratio of 1.0:0.49:524:2.82 was heated at 170 °C for 66 h. This gave 0.187 g (yield 74%) of thin black plates of **2**, which was single phase according to powder X-ray diffraction data.

3: An aliquot of en (0.28 mL) was added to a mixture of water (8 mL), $CuCl_2 \cdot 2H_2O$ (0.17 g) and V_2O_5 (0.181 g) to give a final molar ratio of $CuCl_2 \cdot 2H_2O : V_2O_5 : en : H_2O$ of 1:1:4.2:444. The mixture was heated at 170 °C for 65 h which gave a 73% yield of **3**, which was single phase according to powder X-ray diffraction data.

4: Water (8 mL) was added to a mixture of $CuCl_2 \cdot 2H_2O$ (0.51 g) and V_2O_5 (0.181 g) followed by en (0.45 mL) to give a final molar ratio of $CuCl_2 \cdot 2H_2O : V_2O_5 : en : H_2O$ of 3:1:6.7:444. The resulting mixture was heated at 170 °C for 42 h which gave **4** in about 10% yield mixed with an amorphous black powder in an approximate 1:1 ratio.

Received: October 20, 1995 [Z84901E]
German version: *Angew. Chem.* **1996**, *108*, 1067–1069

Keywords: intercalation compounds · magnetic properties · mixed-valent compounds · vanadium compounds

[1] W. Jones, M. Chibwe in *Pillared Layered Structures* (Ed.: I. V. Mitchell), Elsevier, London, **1990**, pp. 67–77; R. M. Tayor, *Clay Miner.* **1984**, *19*, 591.
[2] A. Clearfield, *Chem. Rev.* **1988**, *88*, 125.
[3] *Inorganic Ion Exchange Materials* (Ed.: A. Clearfield), CRC, Boca Raton, FL, **1982**; A. Clearfield, *Comments Inorg. Chem.* **1990**, *10*, 89.
[4] Y. Zhang, A. Clearfield, R. C. Haushalter, *J. Solid State Chem.* **1995**, *117*, 157; K.-H. Lii, L.-S. Wu, H.-M. Gau, *Inorg. Chem.* **1993**, *32*, 4153; J. T. Vaughey, W. T. Harrison, A. J. Jacobson, D. P. Goshorn, J. W. Johnson, *ibid.* **1994**, *33*, 2481; R. C. Haushalter, Z. Wang, L. M. Meyer, S. S. Dhingra, M. E. Thompson, J. Zubieta, *Chem. Mater.* **1994**, *6*, 1463; V. Soghomonian, R. C. Haushalter, Q. Chen, J. Zubieta, *Inorg. Chem.* **1994**, *33*, 1700; V. Soghomonian, R. C. Haushalter, Q. Chen, J. Zubieta, *Science* **1993**, *256*, 1596; V. Soghomonian, R. C. Haushalter, Q. Chen, J. Zubieta, *Angew. Chem.* **1993**, *105*, 601; *Angew. Chem. Int. Ed. Eng.* **1993**, *32*, 610; V. Soghomonian, R. C. Haushalter, Q. Chen, J. Zubieta, *Chem. Mater.* **1993**, *5*, 1690; V. Soghomonian, R. C. Haushalter, Q. Chen, J. Zubieta, *ibid.* **1993**, *5*, 1595.
[5] R. C. Haushalter, L. A. Mundi, *Chem. Mater.* **1992**, *4*, 31 and references therein.
[6] a) Alkali metal cations: G. Liu, J. E. Greedan, *J. Solid State Chem.* **1995**, *115*, 174; *ibid.* **1995**, *114*, 499; *ibid.* **1993**, *103*, 139; J.-C. Bouloux, J. Galy, *Acta Crystallogr. Sect. B.* **1973**, *29*, 1335; *ibid.* **1973**, *29*, 269; D. W. Murphy, P. A. Christian, F. J. DiSalvo, J. V. Waszczak, *Inorg. Chem.* **1979**, *18*, 2800; b) organic polymer intercalates: M. G. Kanatzidis, C.-G. Wu, H. O. Marcy, C. R. Kannewurf, *J. Am. Chem. Soc.* **1989**, *111*, 4139; M. G. Kanatzidis, C.-G. Wu, H. O. Marcy, D. C. DeGroot, C. R. Kannewurf, *Chem. Mater.* **1990**, *2*, 222; M. G. Kanatzidis, T. J. Marks *Inorg. Chem.* **1987**, *26*, 783; c) Y. Zhang, C. J. O'Connor, A. Clearfield, R. C. Haushalter, *Chem. Mater.* **1996**, *8*, 595.
[7] S. Aschwanden, H. W. Schmalle, A. Reller, H. R. Oswald, *Mat. Res. Bull.* **1993**, *28*, 45.
[8] a) Crystal data for **1**: monoclinic $P2_1/a$, $a = 10.573(4)$, $b = 14.736(4)$, $c = 15.503(3)$ Å, $\beta = 92.47(2)°$, $Z = 4$, $\rho_{calcd} = 1.83$ g cm^{-3}. For 2940 data with $I > 3\sigma(I)$ and 331 variables, $R(R_w) = 0.034(0.037)$. b) Further details of the crystal structure investigation may be obtained from Fachinformationszentrum Karlsruhe, D-76344 Eggenstein-Leopoldshafen (Germany, on quoting the depository number CSD-59265.
[9] J. DeBord, Y. Zhang, J. Zubieta, R. Haushalter, *J. Solid State Chem.*, in press.
[10] Crystal data for **2**: monoclinic $P2_1/n$ with $a = 9.008(4)$, $b = 6.5277(7)$, $c = 15.702(2)$ Å, $\beta = 99.70(5)°$, $Z = 4$ at 20 °C. For 1268 data with $I > 3\sigma(I)$ and 165 variables, $R(R_w) = 0.029(0.030)$ [8b].
[11] Crystal data for **3**, monoclinic $P2_1/n$ with $a = 8.934(2)$, $b = 6.558(1)$, $c = 15.694(2)$ Å, $\beta = 99.93(2)°$, $Z = 4$ at 20 °C. For 1006 data with $I > 3\sigma(I)$ and 133 variables, $R(R_w) = 0.052(0.061)$ [8b].
[12] I. D. Brown, K. K. Wu *Acta Crystallogr. Sect. B* **1976**, *32*, 1957.
[13] Crystal data for **4**: triclinic $P\bar{1}$ with $a = 8.913(3)$, $b = 15.934(4)$, $c = 6.728(8)$ Å, $\alpha = 91.12(3)$, $\beta = 106.32(3)$, $\gamma = 105.00(2)°$, $Z = 2$ at 20 °C. For 3980 data with $I > 3\sigma(I)$ and 244 variables, $R(R_w) = 0.035(0.039)$ [8b].

 © VCH Verlagsgesellschaft mbH, D-69451 Weinheim, 1996 0570-0833/96/3509-0991 $ 15.00+.25/0

$[Os_{10}(CO)_{24}\{Au(PPh_2R)\}_4]$, A Tubular Heterobimetallic Carbonyl–Osmium Cluster

Zareen Akhter, Scott L. Ingham, Jack Lewis,* and Paul R. Raithby

A large number of high nuclearity carbonyl–osmium and –ruthenium clusters have been isolated and characterized in an attempt to understand some of the properties of these compounds.[1] These clusters may be thought to lie at the interface between classical organometallic chemistry and the chemistry involved with metal surfaces. Therefore a thorough understanding of their chemical and electronic properties is of fundamental interest. One of the features that has to date characterized high nuclearity clusters of osmium and ruthenium is the presence of a closely packed array of metal atoms with high intermetal connectivity. The chemical, electronic, and photochemical properties of high nuclearity clusters can be greatly altered by the introduction of polarity within the molecule with the formation of heterobimetallic bonds.[2] To date this has been achieved by the use of redox coupling reactions between anionic carbonyl compounds and cationic metal electrophiles, and the use of mercury and gold fragments has been particularly successful.[3, 4] We now report the synthesis and characterization of a new class of bimetallic osmium–gold clusters in which the metal core has a novel *tubular* geometry, and the metal framework bonding differs from that observed in other osmium–gold systems.

The dianionic cluster $[PPN]_2[Os_{10}(CO)_{26}]$ $\{[PPN]^+ = [N(PPh_3)_2]^+\}$[5] may be readily reduced with K/Ph_2CO in THF to form the highly reduced cluster species. This species is very reactive and hence was generated in situ for further reaction with the electrophilic gold reagents of the type $[Au(PPh_2R)][NO_3]$ (where R = Ph or Me). Purification of the reaction mixture lead to the isolation of the cluster **1** in

$[Os_{10}(CO)_{24}\{Au(PPh_2R)\}_4]$ **1a**, R = Me; **1b**, R = Ph

in 30% yield.[6] The composition of **1** was initially deduced from liquid secondary ion mass spectrometry (LSIMS) and has been confirmed by a single-crystal X-ray structural analysis of **1a** (Fig. 1).[7]

The arrangement of the metal centers of **1a** may be described as two fused octahedra of osmium atoms which share a common edge and possess metal–metal bonding between their apexes. Four gold atoms cap faces of these octahedra in such a way that two adjacent triangular faces are capped at opposite ends of the cluster. However, this is not an accurate description of the osmium metal core geometry, as there appears to be little, if indeed any, metal–metal bonding across the octahedra. These osmium–osmium distances range from 3.286(2) to 3.322(2) Å and have an average value of 3.30 Å (including symmetry related distances), therefore precluding any effective direct overlap of metal orbitals and the formation of metal–metal bonding. Hence a more accurate description would be that the osmium atoms form a *tubular* cluster coordinated to two gold atoms at either end of the tube (Fig. 2). The osmium–osmium bond lengths around the tube range from 2.724(2) to 3.007(2) Å; within this range there appear to be distinctive short, medium, and long bonds. The short distances are found for bonds Os(1)–Os(2) and Os(1)–Os(3), which are 2.730(2) and 2.724(2) Å, respectively. Bonds of intermediate length (2.810(2)–2.853(2) Å) are observed for the bonds Os(2)–Os(3), Os(2)–Os(4), Os(2)–Os(5A), Os(3)–Os(4A), and Os(3)–Os(5), whereas longer metal–metal distances of 3.007(2) and 3.001(2) Å are found for Os(1)–Os(4) and Os(1)–Os(5), respectively. The reason for this apparent lack of consistency in the osmium–osmium bond lengths is unclear; however it seems feasible that the metal orbitals on Os(1) are hybridized in such a manner as to form more effective overlap with the orbitals on Os(2) and Os(3) than with the orbitals associated with Os(4) and Os(5). It is interesting to note that whilst Os(1) appears to form strong metal–metal bonds with its so-called radial orbitals, the tangential orbitals are also used to form significant osmium–osmium bonding. Thus the cluster may be visualized in terms of fused octahedra that are flattened in such a fashion that the axial–axial interactions between Os(2)···Os(3A) and Os(3)···Os(2A) are dramatically increased, with a concomitant decrease in the equato-

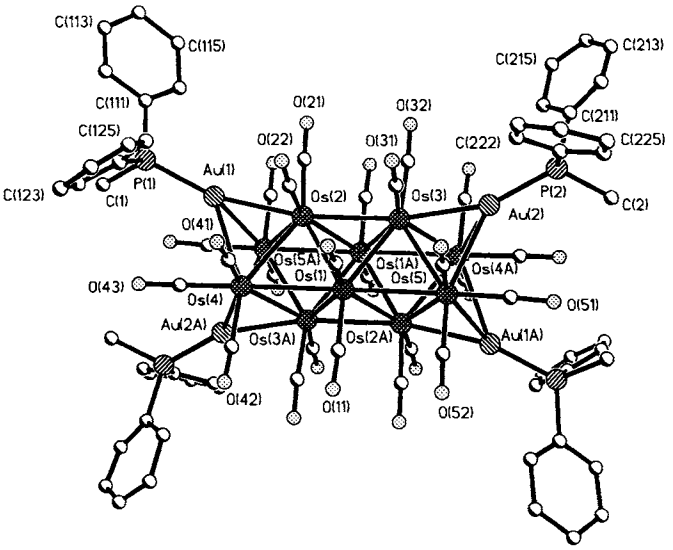

Fig. 1. X-ray crystal structure of $[Os_{10}(CO)_{24}\{Au(PPh_2R)\}_4]$ showing the core as fused octahedra of osmium atoms, which, however, are nonbonded.

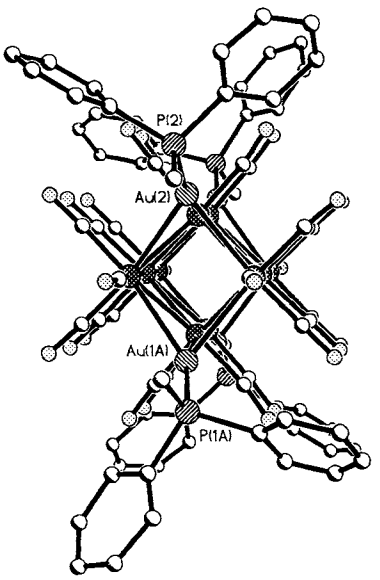

Fig. 2. X-ray crystal structure of $[Os_{10}(CO)_{24}\{Au(PPh_2R)\}_4]$ showing the tubular structure of the osmium core.

[*] Prof. the Lord Lewis, Z. Akhter, Dr. S. L. Ingham, Dr. P. R. Raithby
University Chemical Laboratory
Lensfield Road, GB-Cambridge CB2 1EW (UK)
Fax: Int. code +(1223)336-362

[**] We gratefully acknowledge the EPSRC. (S. L. I.), Cambridge Commonwealth Trust and the U. K. Committee of Vice Chancellors and Principals (Z. A.) for financial support.

rial–equatorial interactions. Indeed, both the axial–axial and equatorial–equatorial pairs of interactions of approximately 4.1 and 2.9 Å, respectively, are considerably different from those expected for an idealized Os_6 octahedron.

The gold atoms of the cluster coordinate in an asymmetric μ_3 fashion, with one strong and two weaker interactions between the gold and the three osmium atoms to which it is attached. Strong interactions are observed between Au(1)–Os(2) and Au(2)–Os(3) (metal–metal distances of 2.711(2) and 2.695(2) Å, respectively). Longer gold–osmium bond lengths are observed for Au(1)–Os(4), Au(1)–Os(5A), Au(2)–Os(4A), and Au(2)–Os(5) (between 2.924(2) and 2.943(2) Å). Hence each of the gold atoms form bonds to two osmium atoms, which are on average 0.23 Å longer than the remaining gold–osmium bond that they form. It is noteworthy that the osmium atoms with which the gold atoms interact strongly have only two carbonyl ligands attached to them and may be considered to be electron-deficient, which results in the formation of strong gold–osmium bonds. The two gold atoms at either end of the cluster are well separated (by 4.324(2) Å).

The X-ray structural determination of **1a** clearly shows that the compound exhibits a highly unusual metal core geometry, in which the osmium atoms form an unprecedented tubular array of osmium atoms. Why this cluster forms such an *open* structure is unclear and is undoubtedly due to a combination of factors. However, reduction of the cluster $[PPN]_2[Os_{10}(CO)_{26}]$ probably directs electron density in metal–metal antibonding orbitals, therefore opening up the metal core of the clusters. Subsequent addition of gold electrophiles results in the retention of these open osmium core geometries.

The cluster **1** has an overall electron count of 132 in the neutral oxidation state. This electron count cannot be obtained by the application of any of the more usual electron counting schemes, such as the Polyhedral Skeletal Electron Pair Theory for condensed polyhedra.[8] This apparent failure of electron counting schemes is not unknown for high nuclearity clusters and is due in part to the greater delocalization of the valence electrons of the metal atoms throughout the cluster as the number of metal atoms increases. The introduction of gold electrophiles to the metal cluster may also contribute to the discrepancy in the electron count, because of increased polarity introduced within the molecule on formation of the heterobimetallic bonds.

Experimental Procedure

A freshly prepared solution of potassium/benzophenone was added to $[PPN]_2[Os_{10}(CO)_{26}]$ (100 mg, 27.0 mmol) [5] dissolved in 50 mL dry, deoxygenated THF. The addition was halted when the starting material had been completely reduced, as determined by IR spectroscopy. This reduction was accompanied by a color change from dark red to brown. The solvent was then removed under vacuum, and the residue suspended in 50 mL dry, deoxygenated CH_2Cl_2. To this suspension was added an excess of the nucleophile $[Au(PPh_2R)][NO_3]$ dissolved in 10 mL CH_2Cl_2. While the mixture was stirred at room temperature for 1 h, the suspension dissolved to yield a red solution. This solution was filtered through a silica pad and the solvent removed at reduced pressure. The residue was purified by thin layer chromatography (eluent: 60% CH_2Cl_2/hexane) to yield the title compound in 30% yield.

Received: August 3, 1995 [Z8280IE]
German version: *Angew. Chem.* **1996**, *108*, 1070–1071

Keywords: carbonyl complexes · clusters · gold compounds · osmium compounds

[1] P. F. Jackson, B. F. G. Johnson, J. Lewis, M. McPartlin, W. J. H. Nelson, *J. Chem. Soc. Chem. Commun.* **1980**, 224; S. L. Ingham, J. Lewis, P. R. Raithby, *ibid.* **1993**, 166; E. Charalambous, L. H. Gade, B. F. G. Johnson, J. Lewis, M. McPartlin, H. R. Powell, *ibid.* **1990**, 688; A. J. Amoroso, L. H. Gade, B. F. G. Johnson, J. Lewis, P. R. Raithby, W. T. Wong, *Angew. Chem.* **1991**, *103*, 102; *Angew. Chem. Int. Ed. Engl.* **1991**, *30*, 107.

[2] B. F. G. Johnson, J. Lewis, W. J. H. Nelson, M. D. Vargas, D. Braga, K. Henrick, M. McPartlin, *J. Chem. Soc. Dalton Trans.* **1986**, 975; Z. Akhter, S. L. Ingham, J. Lewis, P. R. Raithby, *J. Organomet. Chem.* **1994**, *474*, 165; L. H. Gade, B. F. G. Johnson, J. Lewis, M. McPartlin, T. Kotch, A. J. Lees, *J. Am. Chem. Soc.* **1991**, *113*, 8698.

[3] V. Dearing, S. R. Drake, L. H. Gade, B. F. G. Johnson, J. Lewis, M. McPartlin, H. R. Powell, *J. Chem. Soc. Dalton Trans.* **1992**, 921.

[4] B. F. G. Johnson, J. Lewis, W. J. H. Nelson, P. R. Raithby, M. D. Vargas, *J. Chem. Soc. Chem. Commun.* **1983**, 608.

[5] A. J. Amoroso, B. F. G. Johnson, J. Lewis, P. R. Raithby, W.-T. Wong, *Angew. Chem.* **1991**, *103*, 1529; *Angew. Chem. Int. Ed. Engl.* **1991**, *30*, 1505.

[6] Spectroscopic data of **1a**: IR (CH_2Cl_2): $\tilde{\nu}$ [cm^{-1}]=2048 (vs), 2013 (vs), 1970 (w), 1957 (w). MS (negative ion LSI-MS): m/z 4181 (calcd 4180 for ^{192}Os). ^1H NMR (400 MHz, $CDCl_3$, 23 °C, TMS): δ: 7.33–7.67 (m, 40 H), 187 (d, 7.4 Hz). ^{31}P NMR (400 MHz, CH_2Cl_2, 23 °C, $P(OMe)_3$) $\delta = -77.83$ (s). Spectroscopic data of **1b**: IR (CH_2Cl_2): $\tilde{\nu}$ [cm^{-1}] = 2048 (vs), 2013 (vs), 1970 (w), 1957 (w). MS (negative ion LSI-MS): m/z 4421 (calcd 4428 for ^{192}Os). ^1H NMR (400 MHz, $CDCl_3$, 23 °C, TMS): $\delta = 7.34-7.71$ (m); ^{31}P NMR (400 MHz, CH_2CVl_2, 23 °C, $P(OMe)_3$): $\delta = -62.62$ (s).

[7] Crystallographic data of $[Os_{10}(CO)_{24}\{Au(PPh_2Me)\}_4] \cdot CH_2Cl_2$ (**1a** · CH_2Cl_2): $Au_4Os_{10}P_4O_{24}C_{76}H_{52} \cdot CH_2Cl_2$, $M = 4163.00$ (without CH_2Cl_2), monoclinic, space group $P2_1/n$ (nonstandard setting of space group No. 14), $a = 15.173(2)$, $b = 17.500(3)$, $c = 18.438(3)$ Å, $\beta = 103.25(1)$, $V = 4765(1)$ Å^3, $Z = 2$, $\rho_{calcd} = 2.960$ g cm^{-3}, $F(000) = 3756$, $\lambda(Mo_{K\alpha}) = 0.71073$ Å, $\mu(Mo_{K\alpha}) = 19.587$ mm^{-1}. Structure solution was by a combination of direct methods and Fourier techniques. Full matrix least-squares refinement on F^2_{obs} for 6251 data, 298 parameters (Os, Au, and P anisotropic) and 3 restraints converged to $wR2 = 0.1811$ (all data), conventional $R = 0.0684$ (4009 data with $F_{obs} > 4\sigma F_{obs}$). Crystallographic data (excluding structure factors) for the structure reported in this paper have been deposited with the Cambridge Crystallographic Data Centre as supplementary publication no. CCDC-179-13. Copies of the data can be obtained free of charge on application to The Director, CCDC, 12 Union Road, Cambridge CB2 1EZ, UK (fax: int. code +(1223) 336-033; e-mail: teched@chemcrys.cam.ac.uk).

[8] D. M. P. Mingos, *J. Chem. Soc. Chem. Commun.* **1983**, 706.

Reactions of a Triosmium Cluster Complex with a Side-On-Coordinated Carbene Ligand with Sulfur Compounds Resulting in the Formation of a Thioketone Complex**

Jochem U. Köhler, Jack Lewis,* and Paul R. Raithby

Transition metal clusters with π-coordinated arene ligands have been investigated extensively during the past few years.[1] Cluster compounds in which the arenes adopt a face-capping mode[1] are of special interest, because they are model compounds for the adsorption of arenes on metal surfaces.[2] It is therefore interesting to investigate the reactivity of these face-capping arene ligands. The triosmium carbonyl cluster $[Os_3(CO)_9(\mu_3:\eta^2:\eta^2:\eta^2\text{-}C_6H_6)]$ reacts with nucleophiles such as phenyllithium to form the cyclohexadienyl complex $[PPN][Os_3(CO)_9(\mu_3:\eta^2:\eta^1:\eta^2\text{-}C_6H_6Ph)]$ (**1**, PPN = $[(Ph_3P)_2N]^+$).[3] Recently we synthesized the carbene complex **2**, where the carbene ligand is coordinated side-on to a triosmium nonacarbonyl moiety, obtained by removing a hydride from the cyclohexadienyl

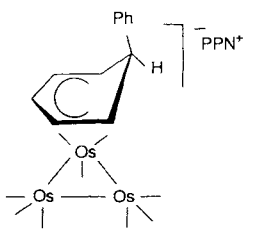

1

[*] Prof. the Lord Lewis, Dr. J. U. Köhler, Dr. P. R. Raithby
University Chemical Laboratory
Lensfield Road, GB-Cambridge CB2 1EW (UK)
Fax: Int. code +(1223)33-6343

[**] We thank the European Union for a HCM-Fellowship and the EPSRC for a grant (J. U. K.).

ligand of **1**. The carbene complex **2** can be converted easily into the cyclohexadienone complex **3** in the presence of air and a Lewis base.[4] The carbene carbon atom of complex **2** shows electrophilic behavior as we have shown with the Wittig reagent (triphenylphosphane methanylide). A C–C double bond was formed, as expected, which remains coordinated side-on to one osmium atom of the cluster **4**.[5]

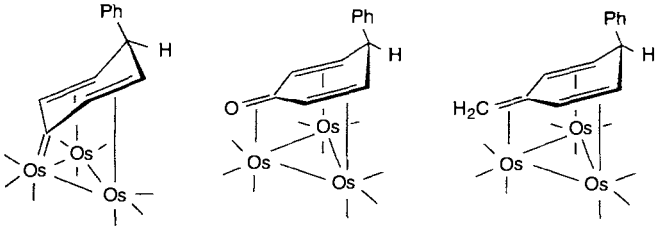

2 **3** **4**

It was of interest to see whether a C=S bond could be formed (analogous to the cyclohexadienone complex **3**) with η^2-coordination. Mononuclear Fischer carbene complexes react with elemental sulfur to form O-methylarylthiocarboxylate, which is no longer coordinated to the metal.[6] Elemental sulfur was added to a solution of the carbene complex **2** in CH_2Cl_2, and the suspension stirred for 45 minutes. No reaction occurred. A Lewis base, NEt_3, was added, and after 45 minutes of stirring at room temperature the thioketone complex **5** was obtained in 72% yield (Scheme 1). We consider that the first step of the reaction, as we proposed in the conversion of **2** into **3**,[4] is a nucleophilic attack by the base with subsequent reaction with sulfur as second step.

The thioketone complex **5** can be also be prepared by the reaction of the carbene complex with cyclohexenesulfide (Scheme 1). This reagent has been used to prepare a η^2-coordinated thioformaldehyde complex $[(\eta^5\text{-}C_5H_5)Re(NO)(PPh_3)(\eta^2\text{-}S{=}CH_2)]^+[PF_6]^-$ from the methylene complex $[(\eta^5\text{-}C_5H_5)Re(NO)(PPh_3)(=CH_2)]^+[PF_6]^-$.[7]

Apart from the signals in the phenyl region, the ^{1}H NMR spectrum of **5** shows three signals at $\delta = 4.74$ (t), 3.84 (dd), and 2.77 (d) (integration 1:2:2), indicating that the cyclohexadienyl ring is still coordinated to the triosmium triangle. The signals are shifted slightly to higher field compared to those of **3**, and the coupling constants are the same as those in **3**. In solution and in air the thioketone complex **5** converts slowly into the cyclohexanone complex **3**. ^{1}H NMR spectra recorded over several days reveal that it is not a direct conversion, as the sulfur is lost initially to form the carbene complex **2**, which then converts into **3**.

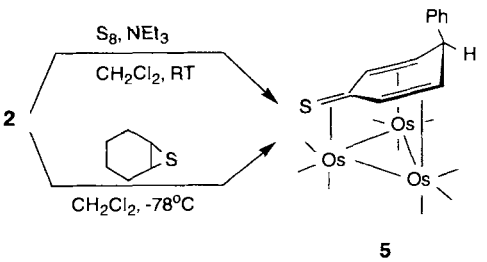

Scheme 1. Two ways to prepare the thioketone complex **5** from the carbene complex **2**. RT = room temperature.

The reactivity of the carbene complex **2** towards H_2S was investigated. The carbene complex **2** dissolved in CH_2Cl_2 did not react with H_2S. However, on the addition of 1,8-diazabicyclo[5.4.0]undec-7-ene (DBU) to abstract a proton, the color of the solution changed from orange to yellow. In the IR spectrum the carbonyl absorption bands shifted to lower wavenumbers and displayed a pattern typical for anionic triosmium cyclohexadienyl carbonyl cluster complexes (cf. **1** [3]). (A very similar IR spectrum is obtained when DBU itself interacts with the carbene complex (CH_2Cl_2): ν(CO) = 2040 (m), 2035 (sh), 1994 (vs), 1987 (vs), 1958 (m), 1934 (m), 1918 (m) cm^{-1}. This reaction is under investigation.) An anionic thiol complex **6** has been isolated as its PPN^+ salt (Scheme 2). The ^{1}H NMR spectrum is consistent with that of an anionic thiol-substituted cyclohexadienyl triosmium complex (comparable to **1**[3]): apart from the signals assigned to the phenyl groups there are four other signals assigned to the thiol ring at $\delta = 4.96$ (s) (SH), 4.56 (t), 3.93 (d), 2.31 (dd) (integration: 1:1:2:2).

Preliminary protonation of **6** with HBF_4 suggests protonation at the metal core rather than at the thiol group. The thiol group shows H/D exchange in the ^{1}H NMR spectrum on addition of deuterated methanol, as would be expected for the acidic behavior of a thiol group. Nevertheless, when the triphenylmethyl (trityl) cation is used to examine the possibility of a further hydride abstraction from the anionic complex **6**, we were surprised to isolate the thioketone complex **5** (Scheme 2). This implies that, at least formally, a hydride (H^-) has been removed from an acidic thiol group to form a thioketone group. Adding a hydride source ($Li[BHEt_3]$) to a solution of the thioketone complex **5** (which we considered to have an electrophilic center at the carbon of the thioketone group) gave the thiol complex **6**. We propose that the hydride attacks at the carbon of the thioketone group to form a thiolate group (resonance structure **A**, Scheme 3). A proton is then transferred from the carbon (via a transition state **B**) to the sulfur atom. The abstraction of the hydride may be viewed as the reverse of this reaction. We may consider that the trityl cation approaches the carbocycle remote from the metal core and polarizes the cyclohexadienyl ring towards resonance structure **C**. This implies that there is some anionic character at the carbon attached to the thiol group. A proton is then transferred from the acidic thiol group to the more basic carbanionic carbon via transition state **B** and is finally removed as a hydride by the trityl cation.

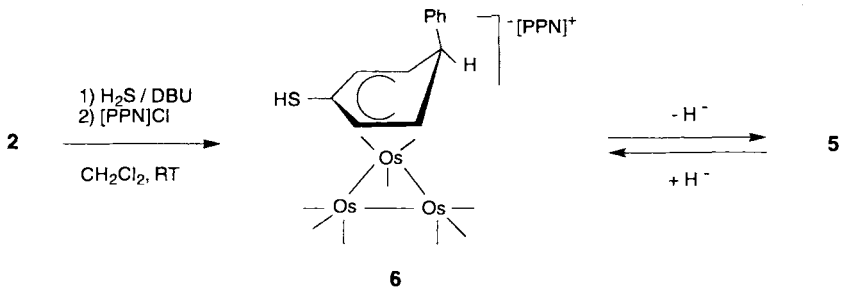

Scheme 2. Reaction of the carbene complex **2** with H_2S/DBU to form **6** and hydride abstraction with $[Ph_3C][BF_4]$ to form **5**, and back reaction of **5** to **6** with $Li[BHEt_3]$.

The system, therefore, may be considered as having formally an ambivalent thiol group. The acidic thiol group can be converted into a hydride-donating group, and the electrophilic sul-

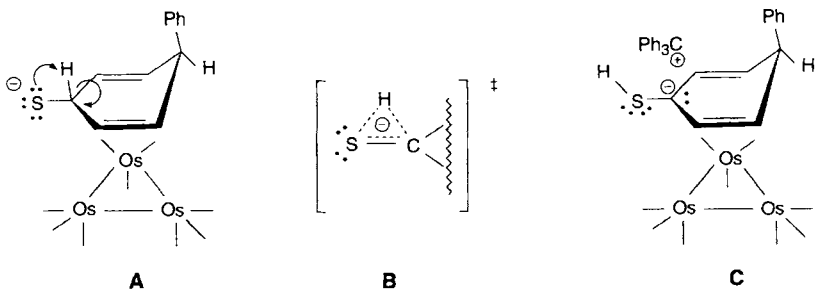

Scheme 3.

fur in the case of the thioketone can be converted into a nucleophilic group. Similar reactions may open a way to novel ligand reactions in the coordination sphere of trimetallic transition metal clusters.

Experimental Procedure

All reactions were performed under nitrogen with standard Schlenk techniques. Purification on TLC plates (CH_2Cl_2 (40%)/hexane (60%)) and filtrations were carried out under air. The products were stored under nitrogen.

5: a) Reaction of **2** with sulfur in presence of NEt_3: Elemental sulfur (8 mg) and one drop of triethylamine were added to an orange solution of **2** (31 mg) in CH_2Cl_2 (4 mL). The suspension was stirred for 45 min at room temperature and purified by TLC. Complex **5** was obtained as an orange powder (23 mg, 72%). A small amount of **3** was isolated as well. b) Reaction of **2** with cyclohexene sulfide: The orange solution of **2** (36 mg) in CH_2Cl_2 (5 mL) was cooled to $-78\,^{\circ}C$ and treated with cyclohexenesulfide (12 mg, about 3 equiv). The yellowish solution was maintained at $-78\,^{\circ}C$ for 5 min until the color had changed back to orange, and then it was warmed to room temperature. After purification on TLC 31 mg (82%) of **5** was isolated as an orange powder. c) Reaction of **6** with $[Ph_3C][BF_4]$: A solution of $[Ph_3C][BF_4]$ (11 mg, about 1.2 equiv) in CH_2Cl_2 (2 mL) was added dropwise to a yellow solution of **6** (46 mg in 3 mL CH_2Cl_2) at $-78\,^{\circ}C$. After stirring at $-78\,^{\circ}C$ for 5 min the orange solution was warmed to room temperature. The reaction solution was purified by TLC, and **5** (13 mg, 42%) was isolated as a orange powder. Cyclohexadienone complex **3** (5 mg (17%) was isolated as a side product). ^1H NMR (250 MHz, $CDCl_3$): $\delta = 7.1-7.6$ (m, 5H, Ph), 4.74 (t, $^3J(H,H) = 2.5$ Hz, 1H, *CH*-Ph), 3.84 (dd, $^3J(H,H) = 8.0$ Hz, 2.5 Hz, 2H, CH), 2.77 (d, $^3J(H,H) = 8.0$ Hz, 2H, CH); IR (CH_2Cl_2): $\tilde{\nu}$ [cm^{-1}] = 2084 (m), 2040 (sh), 2035 (vs), 2010 (m), 1987 (m), 1964 (sh); MS (positive ion FAB): *m/z*: 1014 (as calcd); elemental analysis: found (calcd): C 26.56 (24.85); H 1.21 (0.99).

6: a) Reaction of **2** with H_2S/DBU: A solution of the carbene complex **2** (19 mg) in CH_2Cl_2 (5 mL) was treated with H_2S and stirred for 5 min at room temperature. A solution of DBU·CH_2Cl_2 (1 drop DBU in 1 mL CH_2Cl_2) was added dropwise until the color changed to yellow. The solution was stirred for further 5 min, and [PPN]Cl (13 mg) was added. The solvent was evaporated, and the oily yellow residue that remained was treated with *i*PrOH (3 mL). During this procedure the product formed yellow microcrystals, which were filtered and washed with hexane (2 mL). Yield of **6**: 24 mg (79%). b) Reaction of **5** with $Li[BHEt_3]$: An orange solution of **5** (30 mg) in THF (5 mL) was cooled to $-78\,^{\circ}C$ and treated with $Li[BHEt_3]$ (0.1 mL of a 1.0 M solution in THF). After 5 min a solution of [PPN]Cl (21 mg) in *i*PrOH (2 mL) was added dropwise. The solution was stirred at $-78\,^{\circ}C$ for further 5 min and then warmed to room temperature. The solvent was evaporated, and the oily residue was treated as mentioned above. Yield of **6**: 25 mg (52%). ^1H NMR (500 MHz, $CDCl_3$): $\delta = 7.09-7.65$ (m, 35H, Ph), 4.96 (s, 1H, SH), 4.56 (t, $^3J(H,H) = 2.5$ Hz, 1H, CHPh), 3.93 (d, $^3J(H,H) = 8.2$ Hz, 2H, CH), 2.31 (dd, $^3J(H,H) = 8.3$ Hz, 2.3 Hz, 2H, CH); IR (CH_2Cl_2): $\tilde{\nu}$ [cm^{-1}] = 2044 (m), 1999 (s), 1986 (s), 1959 (m), 1934 (m), 1918 (sh); MS (negative ion FAB): *m/z*: 1015 (as calcd for anion); elemental analysis: found (calcd) C 44.12 (44.04); H 2.68 (2.64); N 0.92 (0.90); P 3.82 (3.99).

Received: September 13, 1995 [Z 8397 IE]
German version: *Angew. Chem.* **1996**, *108*, 1071–1073

Keywords: carbene complexes · clusters · complexes with sulfur ligands · osmium compounds

[1] a) H. Wadepohl, *Angew. Chem.* **1992**, *104*, 253; *Angew. Chem. Int. Ed. Engl.* **1992**, *31*, 247; b) D. Braga, P. J. Dyson, F. Grepioni, B. F. G. Johnson, *Chem. Rev.* **1994**, *94*, 1585–1620.

[2] a) G. A. Somorjai, *J. Phys. Chem.* **1990**, *94*, 1013; b) G. A. Somorjai, *Introduction to Surface Chemistry and Catalysis*, Wiley, New York, **1994**.

[3] M. A. Gallop, B. F. G. Johnson, J. Lewis, A. H. Wright, *J. Chem. Soc. Dalton Trans.* **1989**, 481–487.

[4] A. J. Edwards, M. A. Gallop, B. F. G. Johnson, J. U. Köhler, J. Lewis, P. R. Raithby, *Angew. Chem.* **1994**, *106*, 1166; *Angew. Chem. Int. Ed. Engl.* **1994**, *33*, 1093.

[5] A. J. Edwards, J. U. Köhler, J. Lewis, P. R. Raithby, *J. Chem. Soc. Dalton Trans.* **1995**, 3251.

[6] E. O. Fischer, S. Riedmüller, *Chem. Ber.* **1974**, *107*, 915–919; H. Fischer, *J. Organomet. Chem.* **1981**, *219*, C34; K. H. Dötz, W. Sturm, H. G. Alt, *Organometallics*, **1987**, *6*, 1324.

[7] W. E. Buhro, A. T. Patton, C. E. Strouse, J. A. Gladysz, F. B. McCormick, M. C. Etter, *J. Am. Chem. Soc.* **1983**, *105*, 1056–1058.

Metalated Tetra- and Penta(cyclopentadienyl)-cyclopentadienyl Compounds: Syntheses by Multiple Pd-Catalyzed Cyclopentadienylations**

Roland Boese, Gabriele Bräunlich, Jean-Pierre Gotteland, Jenn-Tsang Hwang, Carsten Troll, and K. Peter C. Vollhardt*

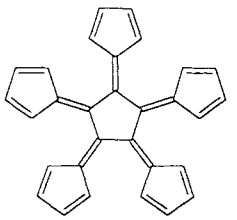

1

Penta(cyclopentadienylidene)-cyclopentane **1** constitutes the ultimate "fulvaleneradialene"[1] and, as a ligand for transition metals represents a significant target in our efforts to explore the basic chemical behavior of oligo-(cyclopentadienyl) metal compounds.[2] Apart from its potential to anchor rigidly (at least) five metals in close proximity, it also has the correct topography to provide a synthetic entry into metalated semibuckminsterfullerenes[3] or, in the dimeric form of a metallocene, to endohedral metallobuckminsterfullerenes.[4] With respect to the latter, it is noteworthy that a theoretical treatment of C_{60} (and its interactions with metal fragments) views the molecule as derived by an "implosion" of twelve cyclic C_5 units.[5]

We report that metal complexes of **1** and two regioisomers of its lower cyclopentadienyl homologs can be prepared by a remarkably simple and potentially general palladium-catalyzed reaction of iodocyclopentadienyl metal complexes[6] with cyclopentadienide.[7] Extension of this methodology to other substrates should dramatically enhance access to oligosubstituted $(\eta^5\text{-}C_5H_5)M$ systems.[8] Initially, a stepwise approach was sought, starting with the readily available[6e-h] iodocyclopenta-

[*] Prof. Dr. K. P. C. Vollhardt, Dr. G. Bräunlich, Dr. J.-P. Gotteland, Dr. J.-T. Hwang, Dr. C. Troll
Department of Chemistry, University of California at Berkeley
and
The Chemical Sciences Division, Lawrence Berkeley National Laboratory
Berkeley, CA 94720 (USA)
Fax: Int. code +(510) 643-5208
e-mail: vollhard@cchem.berkeley.edu
Prof. Dr. R. Boese
Institut für Anorganische Chemie der Universität-Gesamthochschule
Universitätstrasse 5-7, D-45117 Essen (Germany)

[**] This work was supported by the Director, Office of Energy Research, Office of Basic Energy Sciences, Chemical Sciences Division of the U. S. Department of Energy under Contract DE-AC03-76SF00098. G. B. thanks the Deutsche Forschungsgemeinschaft, J.-T. H. the Ministry of Education, Republic of China (Taiwan), and C. T. the Humboldt Foundation for postdoctoral fellowships. We are grateful to the French Ministry of Foreign Affairs for granting J. P. G. VSNA status.

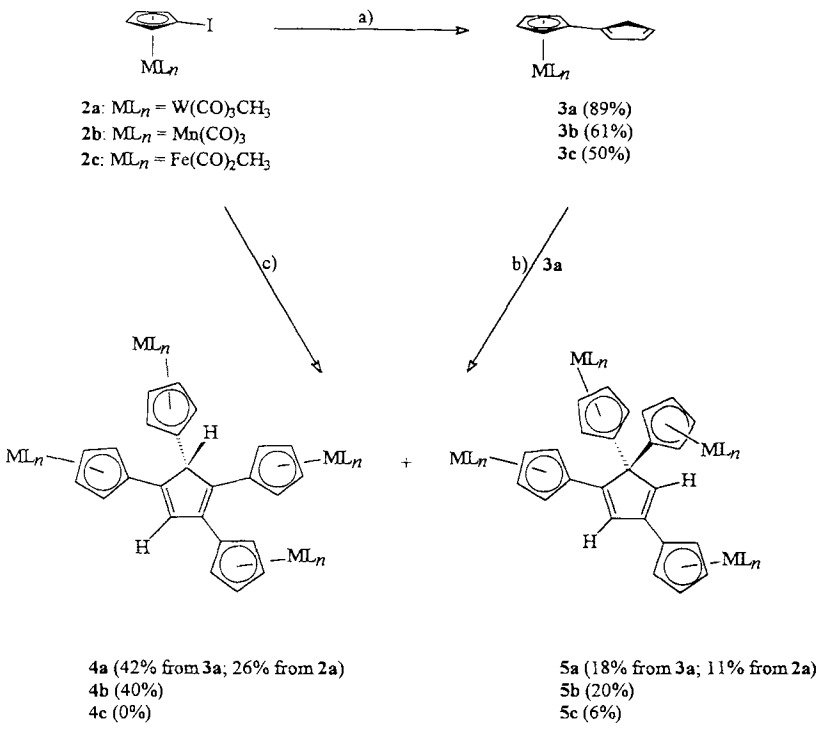

Scheme 1. a) $CpSnBu_3$ (2 equiv), 3% $[Pd(CH_3CN)_2Cl_2]$, THF (THF/DMF, 1:1, for **3b**), 23 °C, 12 h; KF_{aq} workup [11]; b) **2a** (5 equiv), 3% $[Pd(OAc)_2]$, iPr_2NEt (10 equiv), $PhCH_2(Et)_3N^+Cl^-$ (3.3 equiv), DMF, 23 °C, 52 h; c) $CpSnMe_3$ (0.3 equiv), 3% $[Pd(OAc)_2]$, NaOAc (15 equiv), $PhCH_2(Et)_3N^+Cl^-$ (5 equiv), DMF, 23 °C, 52 h.

dienyl complexes **2**, which were subjected to Pd-catalyzed single coupling with tributyl(cyclopentadienyl)stannane[9] to provide **3** as a mixture of 1,3- and 1,4-cyclopentadiene isomers (only the 1,3-isomer is shown in Scheme 1). This method is an improvement over earlier preparations of these compounds, which constitute valuable building blocks on route to (fulvalene)heterodimetal compounds.[10] Surprisingly, an attempt to effect the next step to furnish the tercyclopentadienyl system[2c] by coupling the trimethylstannyl cyclopentadienide of **3a** with **2a** (1 equiv) led instead to the 1,2,4,5-metallocyclopentadienyl-1,3-cyclopentadiene **4a** (9%), in addition to **3a** (20%).[12] The reaction conditions[13] were optimized by varying the ratio of **3a**:**2a** (1:1 to 1:10), the catalyst $[Pd_2(dba)_3]$ (dba = dibenzylideneacetone), the base (NaOAc, K_2CO_3, Na_2CO_3), the ammonium salt $[PhCH_2(Bu)_3N^+Br^-$, $Bu_4N^+Cl^-]$, added ligands (PPh_3), and reaction time (24–56 h). This allowed the isolation of **4a** and its isomer **5a** in 60% combined yield; the two compounds were separated by chromatography on silica gel (hexanes/acetone, 7/3) (Scheme 1, Table 1).[12] The following observations were made during the course of this scrutiny: 1) Complex **2a** decomposed at elevated temperatures (80 °C), thus preempting faster conversions. 2) Bases other than iPr_2NEt gave lower yields but similar product ratios (e.g., NaOAc: **4a**, 28%; **5a**, 12%; K_2CO_3: **4a**, 18%; **5a**, 6%). 3) Changing the catalyst or ammonium salt had little effect. 4) Solvent may influence the yields (e.g., with K_2CO_3, $[Pd_2(dba)_3]$, DMF: **4a**, **5a** 24%; in CH_3CN: 45%). 5) The addition of PPh_3 (0.03 equiv) either completely suppressed the emergence of **5a** (**4a**, 20%) or (0.09 equiv) the reaction altogether. 6) The direct coupling of **2a** to give **4a** and **5a** is also possible simply by using cyclopentadiene as the substrate (e.g., conditions c in Scheme 1, **4a**, 23%; **5a**, 10%). 7) An indication of the potential generality of the reaction is given by the analogous transformations of **2b** and **2c**.[12] Furthermore, the use of these metals also pinpoints some limitations; for instance, the generation of **4b** and **5b** was accompanied by that of the known $[FvMn_2(CO)_6]$ (Fv = fulvalene),[14] highlighting a reductive dimerization route that becomes predominant in the construction of **5c**, whose low yield is due to the presence of the new $[FvFe_2(CO)_4(CH_3)_2]$ (25%).[12] The latter is the only product (80%) when 20% catalyst and 3.3 equivalents of base are employed. 8) Preliminary experiments indicate that heteronuclear couplings are possible. Thus, **2b** (5 equiv) and **3a** resulted under conditions b in Scheme 1 in the so far inseparable mixture of three possible isomers of **5** (20%, 2.5:1:1) as indicated by mass, IR, and ^1H NMR spectral data. Similarly, **2c** and **3a** provided a mixture of one isomer of type **4** and two of type **5** (15%). 9) Attempted interconversion of **4a(b)** and **5a(b)** photochemically or thermally (80–160 °C) led only to decomposition.

The structural assignments of **4** and **5** are based on their distinctive spectral characteristics (Table 1); the most diagnostic are the effects of the plane of symmetry inherent in **5**, which is absent in **4**. The choice of the regiochemical disposition of the central diene unit in **4** (i.e., 1,2,4,5-substitution) is tentative, as the data do not exclude rigorously a tautomeric 1,2,3,5-substitution pattern, but appears justified on steric grounds and is the same as that formulated for 1,2,4,5-tetra-*tert*-butyl-1,3-cyclopentadiene.[15] Unfortunately, crystals of **4** suitable for X-ray analysis could not be obtained, but extensive experimentation eventually furnished such a sample for **5a** by slow diffusion of hexane vapors into a saturated toluene solution (Fig. 1).[16] The molecule is severely sterically encumbered and the central cyclopentadiene is distorted as a consequence. The structure of **5a** and molecular models of **4** also provide a rationale for the reluctance of the latter to undergo further metallocyclopentadienylation in the quest for metalated **1**, even under forcing conditions.

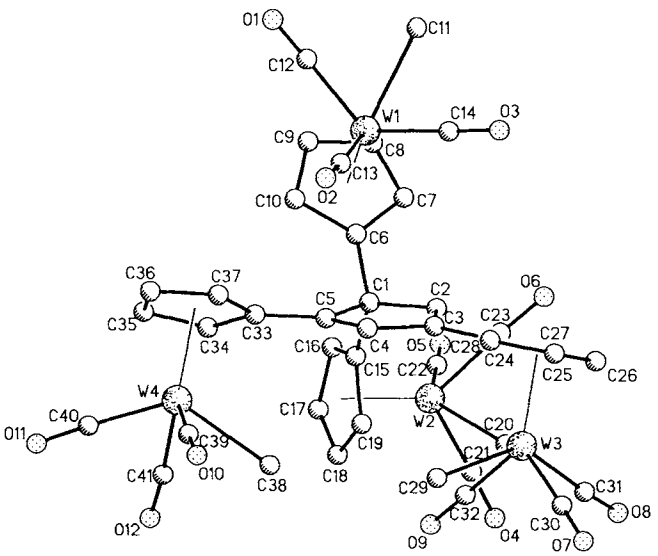

Fig. 1. Molecular structure of **5a**. Selected distances [Å] and angles [°]: C1–C2 1.514(22), C2–C3 1.310(23), C3–C4 1.428(22), C4–C5 1.323(25), C5–C1 1.562(23), C1–C6 1.527(24), C1–C15 1.563(23), C3–C24 1.459(23), C5–C33 1.433(21); C1-C2-C3 112.0(14), C2-C3-C4 107.2(15), C3-C4-C5 114.4(16), C4-C5-C1 105.7(14), C5-C1-C2 100.5(13), C6-C1-C15 108.9(13).

Chemical structural confirmation of **4a** was obtained by deprotonation with NaH (10 equiv) in THF to give the corresponding and, as expected, highly symmetrical orange Na salt **6**, which displays drastically simplified ^1H and ^{13}C NMR spectra (Table 1). Equilibration studies with cyclopentadiene ($pK_a = 15.5$) in 1,2-dimethoxyethane by ^1H NMR spectroscopy allowed the estimation of the pK_a value of **4a** as 14. The anion in **6** could be alkylated with CH_3I or CH_3CH_2I to give an inseparable mixture of 1,2,3,4,5- (minor) and 1,2,4,5,5-substituted cyclopentadiene isomers (^1H NMR), which indicates the nucleophilic reactivity of **6** at least with respect to small electrophiles. Nevertheless, since **1** could not be prepared by fivefold cyclopentadienylation according to Scheme 1, we investigated the hopefully less sterically burdened, inverse strategy given in Scheme 2.

Gratifyingly, treatment of tricarbonyl(η^5-pentaiodocyclopentadienyl)manganese (**7**)[6c] with trimethyl(cyclopentadienyl)stannane[9, 17] resulted in the desired penta(cyclopentadienyl)cyclopentadienyl complex **8** in one step in 28% yield (Scheme 2),[12] as a mixture of 1,3- and 1,4-cyclopentadiene

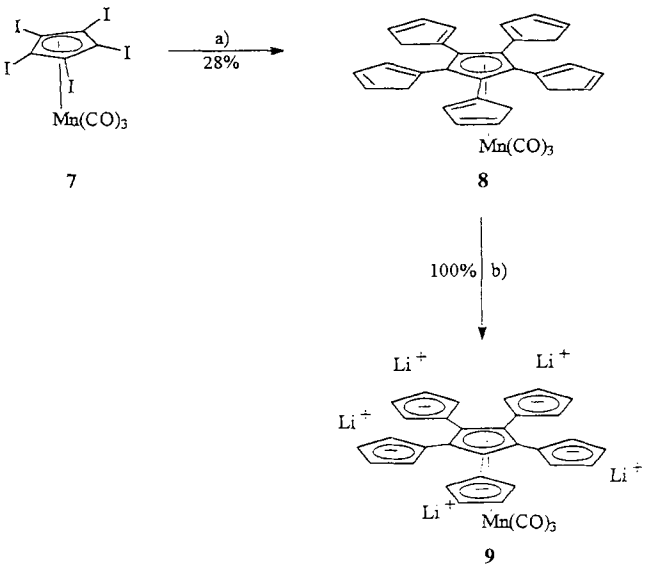

Scheme 2. a) $CpSnMe_3$ (10 equiv), 30% [$Pd(CH_3CN)_2Cl_2$], DMF, 90 °C, 15 min; b) BuLi (5 equiv), THF, 23 °C, 10 min.

tautomers. The spectral and analytical data are clearly consistent with this formulation (Table 1), and the quantity of signals in the various characteristic regions of the ^{13}C NMR spectrum are indicative of the presence of all eight possible isomers. This mixture is converged to one compound, **9**, on fivefold deprotonation. The high symmetry of **9** is strikingly evident in its NMR data, the nine proton multiplets for **8** simplifying to two AA'BB' "triplets", and the eighty signals discernible for **8** in the ^{13}C NMR spectrum reducing in number to only five in **9**.

The pentaanion in **9** is the first derivative of **1** and as such can be envisioned to function as a starting material for the construction of metalated semibuckminsterfullerenes and a multitude of organometallic clusters with novel topography. Furthermore, the facile multiple cyclopentadienylations reported here open up synthetic routes to a plethora of other oligocyclopentadienyl compounds, assembled around a perhalogenated π core.

Experimental Procedure

8: To complex **7** (1.00 g, 1.20 mmol) and [$Pd(CH_3CN)_2Cl_2$] (100 mg, 0.38 mmol) in freshly distilled DMF (10 mL, from CaH_2) was added $CpSnMe_3$ (2.70 g, 11.8 mmol) and the mixture stirred at 90 °C for 15 min. After the mixture had been cooled to 23 °C, ether (200 mL) was added, the solution washed with H_2O (3 × 100 mL), dried ($MgSO_4$), the solvent removed, and the residue filtered through silica gel (hexanes/ether, 5:1). Subsequent chomatography on silica gel (hexanes/ether, 10:1) gave a yellow fraction containing **8** (176 mg, 28%).

Received: November 29, 1995 [Z 8605 IE]
German version: *Angew. Chem.* **1996**, *108*, 1100–1102

Keywords: catalysis · complexes with carbon ligands · cyclopentadienes · cyclopentadienyl complexes

Table 1. Selected physical data for **4**, **5**, **6**, **8**, and **9** [12].

4a: orange-yellow crystals (from CH_2Cl_2/pentane), m. p. 250 °C (decomp); FAB-MS: *m/z* (%): 1450 (M^+, 15), 1348 (14), 1309 (23), 663 {$FvW_2(CO)_6$, 100}; ^1H NMR (400 MHz, C_6D_6): δ = 6.12 (s, 1H), 5.09 (m, 1H), 5.06 (m, 1H), 4.97 (m, 2H), 4.74 (m, 1H), 4.68 (m, 1H), 4.62 (m, 1H), 4.58 (m, 1H), 4.56 (m, 1H), 4.51 (m, 1H), 4.47 (m, 1H), 4.45 (m, 1H), 4.42 (m, 2H), 4.37 (m, 2H), 3.85 (s, 1H), 0.60 (s, 3H), 0.55 (s, 3H), 0.47 (s, 3H), 0.45 (s, 3H); ^1H NMR (400 MHz, [D_8]THF): δ = 6.36 (s, 1H), 5.82 (m, 2H), 5.77 (m, 2H), 5.74 (m, 1H), 5.66 (m, 1H), 5.60 (m, 3H), 5.55 (m, 2H), 5.51 (m, 1H), 5.49 (m, 2H), 5.46 (m, 2H), 4.49 (s, 1H), 0.54 [s, $J(^{183}W,^1H)$ = 3.4 Hz, 3H], 0.41 [s, $J(^{183}W,^1H)$ = 3.4 Hz, 3H], 0.40 [s, $J(^{183}W,^1H)$ = 3.4 Hz, 3H], 0.35 [s, $J(^{183}W,^1H)$ = 3.4 Hz, 3H]; $^{13}C\{^1H\}$ NMR (100 MHz, [D_8]THF): δ = 233.20, 232.92, 232.49 (2C), 219.82 (2C), 219.65 (2C), 219.12 (2C), 219.06 (2C), 146.90, 142.62, 138.84, 137.78 (CH), 113.44, 111.59, 110.92, 109.85, 97.49 (CH), 96.92 (CH), 96.44 (CH), 96.40 (CH), 96.02 (CH), 95.85 (CH), 95.77 (CH), 95.22 (CH), 94.83 (CH), 94.44 (CH), 94.35 (CH), 94.26 (CH), 93.51 (CH), 93.47 (CH), 92.98 (CH), 92.94 (CH), 57.53 (CH), −25.07, −26.87, −29.77, −29.91; IR (THF): $\tilde{\nu}$ = 2014, 1923, 1916 cm^{-1}.

5a: dark orange crystals (from toluene/hexane), m. p. 250 °C (decomp); FAB-MS: *m/z* (%): 1450 (M^+, 65), 1310 (100), 1093 (93); ^1H NMR (400 MHz, C_6D_6): δ = 6.18 (AB-q, 2H), 5.04 (t, J = 2.0 Hz, 2H), 4.97 (m, 2H), 4.91 (t, J = 2.0 Hz, 2H), 4.75 (m, 2H), 4.53 (m, 4H), 4.49 (t, J = 2.0 Hz, 2H), 4.40 (m, 2H), 0.64 (s, 3H), 0.62 (s, 3H), 0.55 (s, 6H); ^1H NMR (400 MHz, [D_8]THF): δd = 6.54 (d, J = 1.6 Hz, 1H), 6.41 (d, J = 1.6 Hz, 1H), 5.83 (t, J = 2.1 Hz, 2H), 5.67 (m, 2H), 5.59 (m, 4H), 5.57 (t, J = 2.1 Hz, 2H), 5.53 (t, J = 2.1 Hz, 2H), 5.44 (m, 2H), 5.33 (m, 2H), 0.49 [s, $J(^{183}W,^1H)$ = 3.7 Hz, 3H], 0.47 [s, $J(^{183}W,^1H)$ = 3.7 Hz, 3H], 0.41 [s, $J(^{183}W,^1H)$ = 3.7 Hz, 6H]; $^{13}C\{^1H\}$ NMR (100 MHz, [D_8]THF): δ = 230.55, 230.32, 217.37, 217.22, 217.13, 217.07, 147.07, 140.82 (CH), 137.71, 130.56 (CH), 112.47, 108.93, 105.35, 95.00 (CH), 94.47 (CH), 93.81 (CH), 93.00 (CH), 92.21 (CH), 92.03 (CH), 90.85 (CH), 90.74 (CH), 59.56, −28.64, −30.40, −33.14; IR (THF): $\tilde{\nu}$ = 2014, 1923, 1920 cm^{-1}.

4b: yellow powder (from $CHCl_3$/hexanes), m. p. 70 °C (decomp.); MS (70 eV): *m/z* (%): 874 (M^+, 16), 790 (35), 708 (100), 678 (50), 567 (23), 540 (15), 483 (36), 226 (42); ^1H NMR (300 MHz, C_6D_6): δ = 6.18 (s, 1H), 4.52 (m, 2H), 4.48 (m, 1H), 4.42 (m, 1H), 4.37 (m, 1H), 4.27 (m, 1H), 4.23 (m, 2H), 3.99 (m, 2H), 3.91 (m, 1H), 3.88 (m, 1H), 3.80 (m, 1H), 3.75 (m, 1H), 3.67 (m, 3H); $^{13}C\{^1H\}$ NMR (100 MHz, C_6D_6): δ = 224.6, 224.5, 224.4, 224.3, 143.9, 139.2, 135.1, 132.4, 98.5, 97.6, 95.9, 95.7, 87.3, 87.1, 86.5, 86.3, 83.9, 83.7, 83.3, 82.5, 82.1, 82.0, 81.7, 81.5, 81.0, 79.4, 78.1, 55.8; IR (THF): $\tilde{\nu}$ = 2011, 1932 cm^{-1}. High-resolution MS calcd for $C_{37}H_{18}O_{12}Mn_4$: 873.8320; found: 873.8304.

5b: yellow powder (from $CHCl_3$/hexanes), m. p. 69 °C (decomp); FAB-MS: *m/z* (%): 874 (M^+, 58), 790 (100), 678 (37), 652 (12), 622 (14), 567 (21), 307 (36), 289 (27), 274 (31); ^1H NMR (300 MHz, C_6D_6): δ = 6.28 (AB-q, 2H), 4.66 (t, J = 2.1 Hz, 2H), 4.56 (m, 2H), 4.40 (t, J = 2.1 Hz, 2H), 4.29 (m, 2H), 3.94 (t, J = 2.1 Hz, 2H), 3.87 (t, J = 2.1 Hz, 2H), 3.76 (m, 4H); $^{13}C\{^1H\}$ NMR (100 MHz, C_6D_6): δ = 224.9, 224.8, 224.7, 147.1, 139.3, 136.6, 130.0, 100.6, 97.4, 93.9, 88.2, 86.0, 83.1, 82.7, 82.6, 81.6, 81.2, 79.4, 57.1; IR (THF): $\tilde{\nu}$ = 2011, 1932 cm^{-1}.

6: dark orange solution; ^1H NMR (400 MHz, [D_8]THF): δ = 6.00 (s, 1H), 5.55 (t, J = 2.2 Hz, 4H), 5.24 (t, J = 2.2 Hz, 4H), 5.21 (t, J = 2.2 Hz, 4H), 5.13 (t, J = 2.2 Hz, 4H), 0.40 [s, $J(^{183}W,^1H)$ = 3.4 Hz, 3H], 0.20 [s, $J(^{183}W,^1H)$ = 3.4 Hz, 3H]; $^{13}C\{^1H\}$ NMR (100 MHz, [D_8]THF): δ = 233.91, 232.92, 220.00 (2C), 219.40 (2C), 125.95, 124.12, 122.03, 115.55, 114.11, 92.22, 91.77, 86.84, 84.99, −24.36, −26.18.

8: bright yellow powder (from ether/hexanes), m. p. 90–91 °C (decomp); MS (70 eV): *m/z* (%): 524 (M^+, 56), 440 (100); ^1H NMR (300 MHz, C_6D_6): δ = 6.48 (m, 1H), 6.26 (m, 1H), 6.13 (m, 1H), 3.11, 3.04, 2.97 (3m, ca. 1:2:1, 1H), 2.69, 2.64, 2.61 (3m, ca. 1:2:1, 1H); $^{13}C\{^1H\}$ NMR (100 MHz, [D_8]THF): δ [range (number of resolved peaks)] = 226.6–226.8(3), 138.3–139.6(14), 135.9–136.8(14), 135.2–135.4(9), 134.5 134.9(10), 132.7–133.6(9), 97.65–99.61(16), 46.56, 46.49, 42.63, 42.55, 42.46; IR (hexanes): $\tilde{\nu}$ = 2011, 1932 cm^{-1}.

9: light orange, very air- and moisture-sensitive solution; ^1H NMR (300 MHz, [D_8]THF): δ = 5.83 (t, J = 2.1 Hz, 2H), 5.51 (t, J = 2.1 Hz, 2H); $^{13}C\{^1H\}$ NMR (100 MHz, [D_8]THF, CD_3CN internal standard): δ = 230.6, 111.8, 108.2, 106.2, 104.0; IR (THF): $\tilde{\nu}$ = 1994, 1910 cm^{-1}.

 © VCH Verlagsgesellschaft mbH, D-69451 Weinheim, 1996 0570-0833/96/3509-0997 $ 15.00+.25/0

[1] For a review of radialenes, see: H. Hopf, G. Maas, *Angew. Chem.* **1992**, *104*, 953; *Angew. Chem. Int. Ed. Engl.* **1992**, *31*, 931.
[2] a) C. G. de Azevedo, R. Boese, D. A. Newman, K. P. C. Vollhardt, *Organometallics* **1995**, *14*, 4980; b) M. Tilset, K. P. C. Vollhardt, R. Boese, *ibid.* **1994**, *13*, 3146; c) R. Boese, R. Myrabo, D. A. Newman, K. P. C. Vollhardt, *Angew. Chem.* **1990**, *102*, 589; *Angew. Chem. Int. Ed. Engl.* **1990**, *29*, 549; d) P. A. McGovern, K. P. C. Vollhardt, *Synlett* **1990**, 493.
[3] a) For recent work on "buckybowls", see: A. H. Abdourazak, Z. Marcinow, A. Sygula, R. Sygula, P. W. Rabideau, *J. Am. Chem. Soc.* **1995**, *117*, 6410, and references therein; b) R. Faust, *Angew. Chem.* **1995**, *107*, 1559; *Angew. Chem. Int. Ed. Engl.* **1995**, *34*, 1429.
[4] For recent work, see: a) T. Suzuki, Y. Maruyama, T. Kato, T. Akasaka, K. Kobayashi, S. Nagase, K. Yamamoto, H. Funasaka, T. Takahashi, *J. Am. Chem. Soc.* **1995**, *117*, 9606; b) D. E. Clemmer, M. F. Jarrold, *ibid.* **1995**, *117*, 8841; c) A. Lappas, M. Kosaka, K. Tanigaki, K. Prassides, *ibid.* **1995**, *117*, 7560; d) K. B. Shelimov, M. F. Jarrold, *ibid.* **1995**, *117*, 6404; e) T. Akasaka, S. Nagase, K. Kobayashi, T. Suzuki, T. Kato, K. Yamamoto, H. Funasaka, T. Takahashi, *J. Chem. Soc. Chem. Commun.* **1995**, 1343; f) T. Akasaka, S. Nagase, K. Kobayashi, T. Suzuki, T. Kato, T. Kikuchi, Y. Achiba, K. Yamamoto, H. Funasaka, T. Takahashi, *Angew. Chem.* **1995**, *107*, 2303; *Angew. Chem. Int. Ed. Engl.* **1995**, *34*, 2139; g) T. Suzuki, Y. Maruyama, T. Kato, K. Kikuchi, Y. Nakao, Y. Achiba, K. Kobayashi, S. Nagase, *ibid.* **1995**, *107*, 1228 and **1995**, *34*, 1094; h) F. T. Edelmann, *ibid.* **1995**, *107*, 1071 and **1995**, *34*, 981.
[5] J. A. López, C. Mealli, *J. Organomet. Chem.* **1994**, *478*, 161.
[6] Related oligoethynylations of iodocyclopentadienyl metal compounds are known: a) U. H. F. Bunz, V. Enkelmann, F. Beer, *Organometallics* **1995**, *14*, 2490; b) U. H. F. Bunz, V. Enkelmann, *ibid.* **1994**, *13*, 3823; c) U. H. F. Bunz, V. Enkelmann, J. Räder, *ibid.* **1993**, *12*, 4745; d) U. H. F. Bunz, *Angew. Chem.* **1994**, *106*, 1127; *Angew. Chem. Int. Ed. Engl.* **1994**, *33*, 1073; e) E. C. Brehm, J. K. Stille, A. I. Meyers, *Organometallics* **1992**, *11*, 938; f) C. Lo Sterzo, *J. Chem. Soc. Dalton Trans.* **1992**, 1989; g) C. Lo Sterzo, J. K. Stille, *Organometallics* **1990**, *9*, 687; h) C. Lo Sterzo, M. M. Miller, J. K. Stille, *ibid.* **1989**, *8*, 2331.
[7] For related single cyclopentadienylations of haloarenes, see: a) H. M. Nugent, M. Rosenblum, *J. Am. Chem. Soc.* **1993**, *115*, 3848; b) B. M. Foxman, D. A. Gronbeck, N. Khruschova, M. Rosenblum, *J. Org. Chem.* **1993**, *58*, 4078; c) D. A. Gronbeck, S. A. Matchett, M. Rosenblum, *Tetrahedron Lett.* **1990**, *31*, 4977; d) A. Ceccon, A. Gambaro, F. Gottardi, F. Manoli, A. Venzo, *J. Organomet. Chem.* **1989**, *363*, 91; e) M.-T. Lee, B. M. Foxman, M. Rosenblum, *Organometallics* **1985**, *3*, 539; f) R. Wahren, *J. Organomet. Chem.* **1973**, *57*, 415; g) T. J. Katz, A. M. Gilgert, M. E. Hattenloch, G. Min-Min, H. H. Brintzinger, *Tetrahedron Lett.* **1993**, *34*, 3551; R. C. Larock, W. H. Gong, *J. Org. Chem.* **1990**, *55*, 407; **1989**, *54*, 2047; J.-C. Fiaud, B. Denner, J.-L. Malleron, *J. Organomet. Chem.* **1985**, *291*, 393.
[8] For reviews and recent work, see: a) N. J. Coville, K. E. du Plooy, W. Pickl, *Coord. Chem. Rev.* **1992**, *116*, 1; b) C. Janiak, H. Schumann, *Adv. Organomet. Chem.* **1991**, *33*, 291; c) J. Okuda, *Top. Curr. Chem.* **1991**, *160*, 97; d) W. E. Watts, *Comprehensive Organometallic Chemistry, Vol. 8* (Eds.: G. Wilkinson, F. G. A. Stone, E. W. Abel), Pergammon, Oxford, **1982**, p. 1013; e) K. H. Sünkel, W. Kempinger, J. Hofmann, *J. Organomet. Chem.* **1994**, *475*, 201; S. A. Kur, A. L. Rheingold, C. H. Winter, *Inorg. Chem.* **1995**, *34*, 414, and the references therein.
[9] H. P. Fritz, C. G. Kreiter, *J. Organomet. Chem.* **1964**, *1*, 323.
[10] a) A. P. Kahn, D. A. Newman, K. P. C. Vollhardt, *Synlett* **1990**, 141; b) M. H. Huffman, D. A. Newman, M. Tilset, W. B. Tolman, K. P. C. Vollhardt, *Organometallics* **1986**, *5*, 1926.
[11] a) D. Milstein, J. K. Stille, *J. Am. Chem. Soc.* **1978**, *100*, 3636; b) J. E. Leibner, J. Jacobus, *J. Org. Chem.* **1979**, *44*, 449.
[12] All new compounds gave satisfactory analytical and spectral data (see Table 1), unless mentioned otherwise.
[13] R. Rossi, A. Carpita, F. Bellina, *Org. Prep. Proc. Int.* **1995**, *27*, 129.
[14] M. D. Rausch, R. F. Kovar, C. S. Kraihanzel, *J. Am. Chem. Soc.* **1969**, *91*, 1259.
[15] G. Maier, S. Pfriem, U. Schäfer, K.-D. Malsch, R. Matusch, *Chem. Ber.* **1981**, *114*, 3965; C. G. Venier, E. W. Casserly, *J. Am. Chem. Soc.* **1990**, *112*, 2808.
[16] Crystal size $0.23 \times 0.17 \times 0.15$ mm^3, space group $P2_1/n$, scan range $3 \leq 2\theta \leq 48^\circ$, $a = 16.052(3)$, $b = 13.318(8)$, $c = 18.671(4)$ Å, $\beta = 101.85(2)^\circ$, $V = 3906(2)$ Å^3, $Z = 4$, $\rho_{calcd} = 2.459$ g cm^{-3}, $\mu = 12.06$ mm^{-1}, 6134 unique reflections at 115 K, of which 4748 were taken as observed [$F_0 \geq 4\sigma(F)$], $R = 0.0565$, $R_w = 0.0566$. Crystallographic data (excluding structure factors) for the structure reported in this paper have been deposited with the Cambridge Crystallographic Data Centre as supplementary publication no. CCDC-179-14. Copies of the data can be obtained free of charge on application to The Director, CCDC, 12 Union Road, Cambridge CB2 1EZ, UK (fax: int. code +(1223) 336-033; e-mail: teched@chemcrys.cam.ac.uk).
[17] K. Jones, M. F. Lappert, *J. Organomet. Chem.* **1965**, *3*, 295.

A Novel Heterobimetallic Layered Compound Showing Ferrimagnetism**

Jinkwon Kim,* Jin Mook Lim, Yong-Kook Choi, and Youngkyu Do*

In recent years there has been considerable research into the design of molecular magnetic materials for application in molecular electronic devices such as switches[1-3] and information recording.[4] In a search for new molecular magnetic materials, a variety of chain compounds with a magnetic ground state have been made by connecting two metal ions of unequal spin through an appropriate organic bridging unit such as oxalato,[5-7] carboxylato,[8] or cyano[9] groups. These chain compounds are models for understanding the relationship between molecular structures and magnetic properties. However, this approach toward molecular magnets based on ferrimagnetic chain compounds has some limitations, because the interchain interactions within the crystal lattice are weak. Thus it is important from a practical as well as a theoretical viewpoint to generate a magnetically ordered, two- or three-dimensional heterobimetallic compound by covalently connecting the magnetic centers.[10-13] As intercalated layered materials were recently shown to possess several remarkable properties simultaneously,[14] we directed part of our efforts toward the synthesis of heterobimetallic two-dimensional compounds containing functional branches. We now describe the synthesis, structure, and magnetic properties of compound **1**, (mtm = (bis(methylthio)-methylidene)malonate.

$[MnCu(mtm)_2(H_2O)_2(CH_3OH)_2]_n$ **1**

The reaction of equimolar amounts of MSO_4 and the dicarboxylato ligand mtm in water or alcohol leads to the formation of $[M(mtm)(solvent)_3]_n$ (M = Mn, Cu).[15] The reaction of these chain complexes in a 1:1 ratio in a water/methanol solvent mixture affords the neutral heterobimetallic complex **1**. The IR spectrum of **1** exhibits several bands from 1579 to 1527 cm^{-1} and from 1417 to 1527 cm^{-1}, characteristic regions for $\nu_a(CO_2)$ and $\nu_s(CO_2)$ bands, respectively. This observation suggests that all oxygen atoms of the carboxylato groups in **1** coordinate to metal ions in bridging modes.[16] The molecular structure of **1** established by X-ray diffraction[17] confirms with this expectation (Fig. 1).

The Cu and Mn atoms of the asymmetric unit lie on the crystallographically imposed inversion centers. All the metal atoms of the repeating unit shown in Figure 1 form the (001) plane of the unit cell, four Mn atoms being at the corners and one Cu atom at the center of the plane. The geometry around the Cu atom may be described as octahedral with a large tetragonal distortion due to the Jahn–Teller effect. The equatorial positions are occupied by four oxygen atoms of carboxylato

[*] Prof. Dr. J. Kim, J. M. Lim
Department of Chemistry
Kongju National University
Kongju, Chungnam 314-701 (South Korea)
Fax: Int. code +(416) 50-8479
Prof. Dr. Y. Do
Department of Chemistry and Center for Molecular Science
Korea Advanced Institute of Science and Technology
Teajon 305-701 (South Korea)
Prof. Dr. Y.-K. Choi
Department of Chemistry
Chonman National University (South Korea)

[**] This work was supported by Basic Science Research Institute Program administrated by Ministry of Education of Korea (BSRI 94-3429) and by Korea Science and Engineering Foundation.

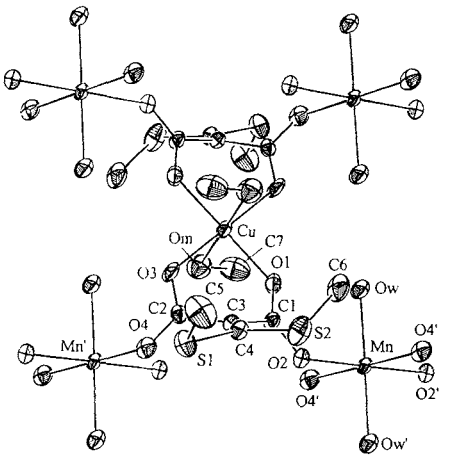

Fig. 1. Structure of the repeating unit of **1** in the crystal (ORTEP diagram, ellipsoids at 50% probability, hydrogen atoms have been omitted for clarity). Primes indicate symmetrically related atoms. Selected bond lengths [Å] and angles [°]: Cu O1 1.970(1), Cu O3 1.949(1), Cu Om 2.482(2), Mn–O2 2.215(1), Mn–O4 2.196(1), Mn Ow 2.185(1); O1-Cu-O3 92.1(1), O1-Cu-Om 85.0(1), O3-Cu-Om 83.7(1), O2-Mn-O4 93.9(1), O2-Mn-Ow 93.4(1), O4-Mn-Ow 94.6(1)

groups with moderate Cu–O bond lengths of 1.949(1) Å and 1.970(1) Å. The axial sites are occupied by two methanol molecules with very long Cu–O distances of 2.482(2) Å. The manganese atom is surrounded by four carboxylato oxygen atoms from four neighboring $[Cu(mtm)_2(CH_3OH)_2]$ units and two water molecules in a somewhat distorted octahedral arrangement. The Cu and Mn atoms are bridged by four carboxylato groups from two mtm ligands in *syn–anti* bonding modes. The separations between neighboring metal ions within the layer are 5.013 Å for Cu···Mn′ along the [110] direction and 5.317 Å for Cu···Mn along the [1$\bar{1}$0] direction.

The crystal packing structure of **1** (Fig. 2) consists of two-dimensional arrays of the $Mn^{II}Cu^{II}$ molecular unit. The resulting neutral sheets are stacked along the *c* axis through the van der Waals interactions between the sulfur atoms of SCH_3 groups that protrude perpendicularly from layers. The interlayer interactions are unique in the sense that the sulfur–sulfur interaction

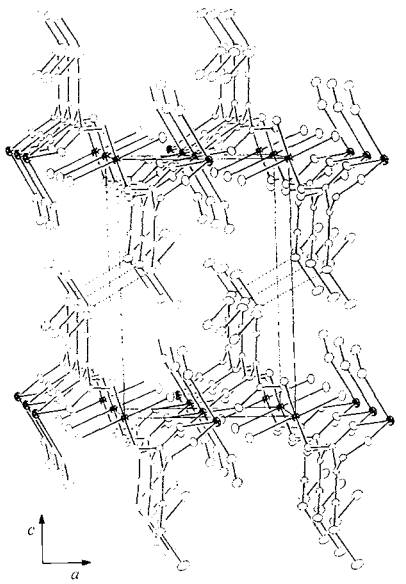

Fig. 2. Perspective view of two neighboring layers of **1**. Dashed lines indicate the shortest sulfur···sulfur interactions.

sites are connected in one dimension along the *b* direction. The shortest interlayer sulfur-to-sulfur distances of 3.479 and 3.554 Å are considerably shorter than the sum (3.60 Å) of their van der Waals radii.[18]

The magnetic behavior of **1** observed by a SQUID magnetometer at a field strength of 0.1 T is depicted as the temperature dependence $\chi_M T$ in Figure 3. The value of $\chi_M T$ remains constant at 4.50 cm^3 K mol^{-1} from room temperature down to about 100 K, and then begins to change smoothly to reach a round minimum at about 25 K (see the inset of Fig. 3), which indicates

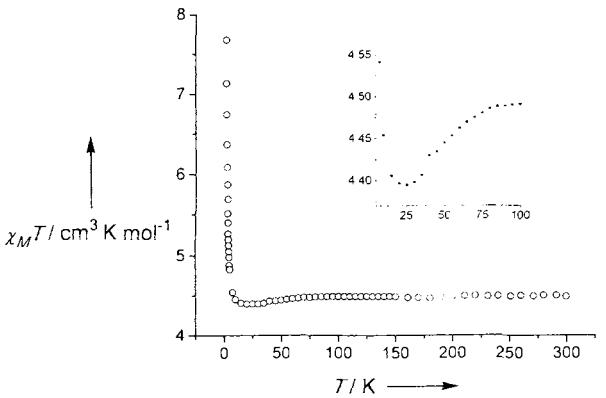

Fig. 3. Temperature dependence of $\chi_M T$ for **1**.

that the adjacent spin centers are antiferromagnetically coupled. These data fit the Curie–Weiss law $\chi = C/(T - \theta)$ with $C = 4.51$ cm^3 K mol^{-1} and $\theta = -0.72$ K. When the temperature is lowered further, $\chi_M T$ increases rapidly and reaches the value of 7.72 cm^3 K mol^{-1} at 1.8 K. The ferromagnetic-like increase of $\chi_M T$ as T is lowered below 25 K is characteristic of a ferrimagnetic material with antiferromagnetic coupling between nonequivalent nearest neighbor spin carriers. Magnetic measurements were made at temperatures as low as 1.8 K in order to characterize the three-dimensional ground state, but no critical temperature (T_c) was observed for **1**. A lower T_c might be expected for **1** considering that the carboxylato bridge in *anti-syn* bonding mode tends to result in a low T_c as seen in several two- and three-dimensional bimetallic systems.[8] The system also does not show hysteresis in field-dependent magnetization measurements (0 to 5 T) at 1.8 K.

The ligand mtm proved to be useful in linking two different metal ions to afford a ferrimagnetic layered compound. In particular the short, one-dimensional S···S interactions between two adjacent MnCu layers suggest that multifunctional layered materials might be made by modifying the alkylthio groups of the mtm ligand.

Experimental Procedure

1: Two separate equimolar mixtures of $MnSO_4 \cdot 5H_2O$ (240 mg, 1 mmol) and K_2mtm (285 mg, 1 mmol) in 10 mL of water and $CuSO_4 \cdot 5H_2O$ (250 mg, 1 mmol) and K_2mtm (285 mg, 1 mmol) in 10 mL of methanol were each stirred for 5 h at room temperature and then filtered. The two filtrates were mixed and allowed to react for 10 h at ambient temperature before filtration. Addition of Et_2O (5 mL) to the filtrate afforded green crystals of **1** in 51% yield (320 mg). Anal calcd. for $C_{14}H_{24}CuMnO_{12}S_4$: C, 26.66; H, 3.80; S, 20.33. Found: C, 26.77; H, 3.79; S, 20.24.

Received: September 12, 1995
Revised version: January 31, 1996 [Z 8394 IE]
German version: *Angew. Chem.* **1996**, *108*, 1079–1080

Keywords: copper compounds · layer compounds · magnetic properties · manganese compounds

[1] O. Kahn, J. Krober, C. Jay, *Adv. Mater.* **1992**, *4*, 718.
[2] O.-S. Jung, C. G. Pierpont, *J. Am. Chem. Soc.* **1994**, *116*, 1127.
[3] J. A. Real, E. Andrés, M. C. Muñoz, M. Julve, T. Granier, A. Bousseksou, F. Varret, *Science* **1995**, *268*, 265.
[4] C. P. Landee, M. Melville, J. S. Miller in *Magnetic Molecular Materials* (Eds.: D. Gatteschi, O. Kahn, J. S. Miller, F. Palacio), Kluwer, Dordrecht, **1991**, p. 395.
[5] A. Gleizes, M. Verdaguer, *J. Am. Chem. Soc.* **1984**, *106*, 3727.
[6] O. Kahn, Y. Pei, M. Verdaguer, J. P. Renard, J. Sletten, *J. Am. Chem. Soc.* **1988**, *110*, 782.
[7] O. Guillou, R. L. Oushoorn, O. Kahn, K. Boubekeur, P. Batail, *Angew. Chem.* **1992**, *104*, 658; *Angew. Chem. Int. Ed. Engl.* **1992**, *31*, 626.
[8] F. Sapiña, E. Coronado, D. Beltrán, R. Burriel, *J. Am. Chem. Soc.* **1991**, *113*, 7940, and references therein.
[9] M. Ohba, N. Maruono, H. Ōkawa, T. Enoki, J.-M. Latour, *J. Am. Chem. Soc.* **1994**, *116*, 11566.
[10] H. O. Stumpf, L. Ouahab, Y. Pei, D. Grandjean, O. Kahn, *Science* **1993**, *261*, 447.
[11] T. Mallah, S. Thiébaut, M. Verdaguer, P. Veillet, *Science* **1993**, *262*, 1554.
[12] W. R. Entley, G. S. Girolami, *Science* **1995**, *268*, 397.
[13] S. Decurtins, H. W. Schmalle, P. Schneuwley, J. Ensling, P. Gütlich, *J. Am. Chem. Soc.* **1994**, *116*, 9521.
[14] R. Clement, P. G. Lacroix, D. O'Hare, J. Evans, *Adv. Mater.* **1994**, *6*, 794.
[15] J. Kim, J. M. Lim, H. Yoon, H. Kang, Y. Do, unpublished.
[16] K. Nakamoto, *Infrared and Raman Spectra of Inorganic and Coordination Compounds*, 3rd ed., Wiley, New York, **1978**, p. 232.
[17] Crystal data for **1**: M = 631.06, crystal size 0.3 × 0.3 × 0.1 mm, 297 K, triclinic, space group $P\bar{1}$, $a = 7.228(1)$, $b = 7.338(2)$, $c = 11.392(1)$ Å, $\alpha = 102.70(1)$, $\beta = 91.17(1)$, $\gamma = 93.37(1)°$; $V = 592.1(2)$ Å^3, $Z = 1$, $\rho_{calcd} = 1.77$ g cm^{-3}, $F(000) = 322$, $\mu = 1.84$ mm^{-1}, Enraf-Nonius CAD4 diffractometer, $Mo_{K\alpha}$ radiation, ($\lambda = 0.71073$ Å), $2\theta_{max} = 50°$, 2003 unique reflections, 1894 observed with $F_o > 4\sigma(F_o)$. Lorenzian polarization and absorption corrections were carried out. The structure was solved by heavy atom methods (SHELXS-86); anisotropic least-squares refinement (SHELXL-93) for non-H atoms, all H atoms included in located positions; 196 parameters, $R_1 = 0.0214$ (based on F), $wR_2 = 0.0593$ (based on F^2) with $w^{-1} = \sigma^2(F_o^2) + (0.0371\,P)^2 + 0.321\,P$, where $P = (F_o^2 + 2F_c^2)/3$; $S = 1.026$; residual electron density: max = 0.31, min = −0.46 e Å^{-3}. Crystallographic data (excluding structure factors) for the structure(s) reported in this paper have been deposited with the Cambridge Crystallographic Data Centre as supplementary publication no. CCDC-179-15. Copies of the data can be obtained free of charge on application to The Director, CCDC, 12 Union Road, Cambridge CB2 1EZ, UK (fax: int. code +(1223) 336-033; e-mail: teched@chemcrys.cam.ac.uk).
[18] A. Bondi, *J. Phys. Chem.* **1964**, *68*, 441.

The First Carborane with a Distorted Cuboctahedral Structure**

Narayan S. Hosmane,* Hongming Zhang, John A. Maguire, Ying Wang, Colacot J. Thomas, and Thomas G. Gray

Dedicated to Professor William N. Lipscomb

Nearly 35 years ago, Lipscomb suggested the classical diamond–square–diamond (DSD) mechanism to explain the rearrangement of BH and CH vertices in polyhedral *closo*-boranes and -carboranes.[1] He proposed that conversion of the "carbons adjacent" 1,2-carborane (*closo*-1,2-$C_2B_{10}H_{12}$) involves six simultaneous DSD processes that give rise to a cuboctahedron, which can then collapse to give the "carbons apart" 1,7 isomer (*closo*-1,7-$C_2B_{10}H_{12}$). Diamond–square–diamond processes, or processes that are related to it, have been used in rationalizing a number of isomerizations found in boranes, carboranes, metallaboranes, and metallacarboranes.[2–6] Despite the general acceptance of the DSD process, there is not agreement on the mechanism of the isomerization of the icosahedral carboranes or on the viability of the cuboctahedron as an intermediate.[5, 7, 8] Irrespective of its specific nature, any DSD process will lead to a structure that is more open than the original, and an increase in cage electron density should stabilize such structures.[2, 9]

The two-electron reductions of *closo*-1,2-$C_2B_{10}H_{12}$ and *closo*-1,2-$(CR)_2B_4H_4$ are known to yield the corresponding "carbons apart" *nido*-carborane dianions, in which the cage carbons are on the open carborane faces and are separated by a boron atom.[10, 11] In contrast, the two-electron reduction of the "carbons adjacent" biscarborane (1,2-$C_2B_{10}H_{11})_2$ produces a much less open structure in which two of the triangular faces open to produce four-membered rings, similar to what would arise from a single DSD process.[12] This raises the question as to whether a more open, cuboctahedron-like structure could be stabilized enough for characterization if two more electrons were to be added to the 1,2-carborane precursor by replacing two two-electron BH vertices with two three-electron CR groups, thus giving a total of 28 valence electrons.

The pioneering work of Grimes et al. on Fe and Co metal-mediated oxidative ligand fusion indicates that such substitutions are possible.[13] However, none of the synthesized $(CR)_4B_8H_8$ cages (R is a less bulky Me or Et moiety) showed a cuboctahedron-like structure.[13] Thus, it is clear that in order to produce this type of carborane a different synthetic strategy is warranted. We report herein the synthesis and characterization of the first "carbons apart" tetracarbaborane, $(CSiMe_3)_4B_8H_8$, whose solid-state structure resembles a cuboctahedron.

The reinvestigation of the reaction of anhydrous $NiCl_2$ with the dilithiacarborane *closo-exo*-4,5-[(μ-H)$_2$Li(tmeda)]-1-Li(tmeda)-2,3-$(SiMe_3)_2$-2,3-$C_2B_4H_4$[14] in 1:1 stoichiometry afforded a mixture of two products, the previously reported *closo*-carborane **1**,[14, 15] which was isolated as a colorless liquid by a vacuum distillation at 25 °C, and a white crystalline solid, which was found to be a 1:1 mixture of **2** and **3** (Scheme 1). Fractional crystallization of the solid from a solution of benzene and hexane (1:1) allowed the separation of the two isomers. A neat sample of **2** was found to undergo thermal isomerization at 140–165 °C to yield **3** exclusively. The isomerization reaction showed no indication of reversibility, indicating that **3** is the more stable isomer. This conclusion is supported by ab initio molecular orbital calculations on the model compounds $C_4B_8H_{12}$ with D_{2h} and C_{2v} symmetries, in which the $SiMe_3$ groups are replaced by hydrogen atoms. These calculations show that at the 6-31G*//3-21G* level of theory the C_4B_8 cage with C_{2v} symmetry is more stable than that with D_{2h} symmetry by 124.2 kJ mol^{-1}.[16] As expected, the mass spectra,[17] IR spectra,[17] and elemental analyses (see Experimental Procedure) of **2** and **3** are identical; however, the ^{11}B and ^{13}C NMR spectra[17] are quite different. Isomer **2** exhibits a single peak in the ^{11}B NMR spectrum at $\delta = -30.18$, along with a single cage-carbon resonance in its ^{13}C NMR spectrum at $\delta = -33.32$; isomer **3** shows these resonances at $\delta = -5.57$ and $\delta = -11.41$, respectively. It is evident in the X-ray crystal structure of **2** (Fig. 1) and in a preliminary X-ray analysis of the more stable isomer **3** that while the cage-carbons might be equivalent (**2**) or nearly equivalent (**3**), there are two sets of borons in both isomers. Therefore, the appearances of single resonances in the ^{11}B NMR spectra of both compounds indicate that the C_4B_8 cages of both **2** and **3** are fluxional on an NMR time scale.

[*] Prof. Dr. N. S. Hosmane, Dr. H. Zhang, Prof. Dr. J. A. Maguire, Dr. Y. Wang, Dr. C. J. Thomas, T. G. Gray
Department of Chemistry, Southern Methodist University
Dallas, TX 75275 (USA)
Fax: Int. code +(214)768-4089
e-mail: nhosmane@mail.smu.edu

[**] This work was supported by grants from the National Science Foundation (CHE-9400672), the Robert A. Welch Foundation (N-1016), and the donors of the Petroleum Research Fund, administered by the American Chemical Society. N. S. H. is a Camille and Henry Dreyfus Scholar.

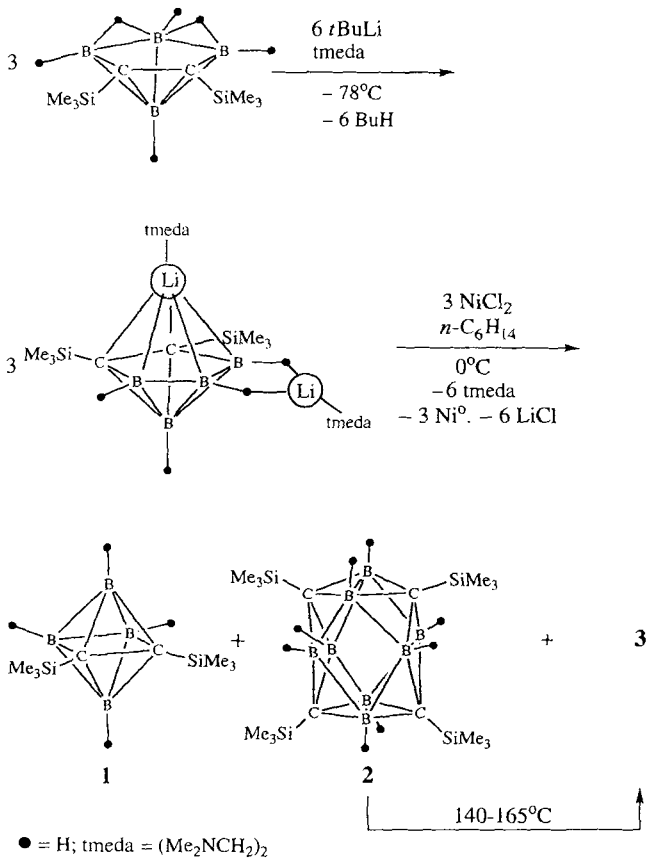

Scheme 1. Synthesis of tetracarbaborane **2** with a distorted cuboctahedral structure.

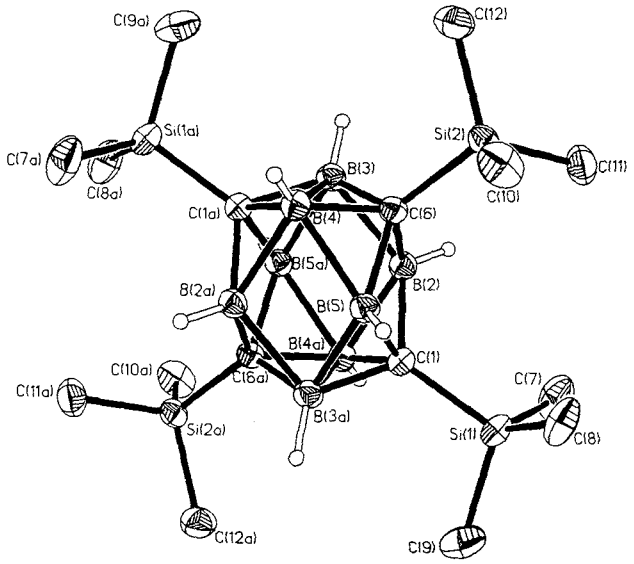

Fig. 1. Crystal structure of **2**. The H atoms of the $SiMe_3$ groups are omitted for clarity. Selected distances [Å] and angles [°]: C(1)-B(2) 1.672(3), C(1)-B(5) 1.685(3), C(1)-B(3a) 1.604(3), C(1)-B(4a) 1.596(3), B(2)-B(3) 1.879(3), B(2)-C(6) 1.682(3), B(2)-B(4a) 1.904(3), B(3)-B(4) 1.798(3), B(3)-C(6) 1.601(3), B(3)-C(1a) 1.604(3), B(3)-B(5a) 1.877(3), B(4)-B(5) 1.893(3), B(4)-C(6) 1.585(3), B(4)-C(1a) 1.596(3), B(4)-B(2a) 1.904(3), B(5)-C(6) 1.670(3), B(5)-B(3a) 1.877(3), B(2)···B(5) 2.192, B(5)···B(2a) 2.161, B(4)···B(3a) 3.072, C(1)···C(6) 2.504; B(5)-B(4)-B(2a) 69.4(1), B(3)-B(4)-B(5) 95.6(1), B(2)-B(3)-B(4) 96.4(1), B(3)-C(6)-B(5) 113.4(1), B(4)-C(6)-B(5) 71.1(1), B(2)-C(6)-B(5) 81.7(1), B(2)-C(6)-B(3) 69.8(1), B(3)-C(6)-B(4) 68.7(1).

Nevertheless, the solid-state structure of **2** (Fig. 1)[18] is that of a distorted cuboctahedron with a D_{2h}-symmetric cage,[19] reminiscent of Lipscomb's proposed intermediate structure.[1] Owing to the heteronuclear nature of the faces, the C_2B_2 rectangular faces are not planar and the B–B distances are not all equal. There are two sets of boron atoms: one of them consists of B(3), B(4), B(3a), and B(4a), and the other of B(2), B(5), B(2a), and B(5a). These could be interchanged by a dual DSD process that produces an intermediate of D_{4h} symmetry.[20]

The data available for **2** and **3** show that their structures are quite different from those of the "carbons adjacent" $(CR)_4B_8H_8$ isomers reported by Grimes et al., in which the cage-carbons are located on the same side of the cage.[13] It is of interest to note that neither **2** nor **3** could be converted to the "carbons adjacent" isomers. Moreover, the use of Grimes's methodology for the oxidative ligand fusion, involving the reaction of $FeCl_2$ with the monosodium salt of *nido*-2,3-$(SiMe_3)_2$-2,3-$C_2B_4H_6$ failed to produce the "carbons adjacent" $(CSiMe_3)_4B_8H_8$ isomers. The ^{11}B NMR spectra of the product were the same as those of **3**, thus exemplifying the role of the C(cage)-bound bulky $SiMe_3$ substituents positioned *exo* on the carborane polyhedron in determining the course of the cage fusion reaction.[21] While the mechanism for the formation of the $(CSiMe_3)_4B_8H_8$ isomers is not known, the isolation and structural characterization of **2** demonstrate that the cuboctahedron geometry in carboranes can be stabilized by increasing the total number of valence electrons in a 12-vertex cage to 28 and by introducing steric bulk on the bonding C_2B_3 faces.

Experimental Procedure

A 20.5 mmol sample of *closo-exo*-4,5-[$(\mu$-H)$_2$Li(tmeda)]-1-Li(tmeda)-2,3-$(SiMe_3)_2$-2,3-$C_2B_4H_4$ [14] was allowed to react with 20.8 mmol of anhydrous $NiCl_2$ (2.7 g) in dry benzene (20 mL) at 0 °C for 12 h, during which the color of the solution turned dark brown and some black solid started to precipitate. The heterogeneous mixture was then filtered through a frit in vacuo, the residue was washed with warm benzene (3 × 10 mL), and the washings were collected along with a filtrate. The volatile components of this pale-yellow filtrate were fractionated through a series of traps maintained at 0, −45, −78, and −196 °C, over 2 d. While solvent and tmeda condensed in the trap at −78 °C, *closo*-1,2-$(SiMe_3)_2$-1,2-$C_2B_4H_4$ (**1**) remained in the −45 °C trap (1.2 g, 5.50 mmol, 27% yield). The pale-brown residue that remained in the flask was sublimed at 110–120 °C in vacuo to give a white crystalline solid (1.0 g, 22% yield) at 0 °C. Solution NMR spectra of this substance indicated the presence of isomers **2** and **3** in equal amounts. Subsequent slow recrystallization of this solid from benzene and hexane (1/1) gave colorless plates of **2**: 0.45 g, 1.03 mmol, 10% yield; stable in air; soluble in both polar and nonpolar organic solvents; m.p. 94–95 °C; Anal for $C_{16}H_{44}B_8Si_4$: found (calculated): C 44.16 (44.15), H 10.43 (10.19), B 19.60 (19.85). The mother liquor contained predominantly isomer **3**, as identified by its ^1H, ^{11}B, and ^{13}C NMR spectra. The mother liquor was concentrated to dryness, the white residue was sublimed at 140–165 °C in vacuo over 4 h, and the resulting solid was dissolved in C_6D_6 for characterization. The NMR spectra of this solution unambiguously indicated the presence of **3** only. Vacuum resublimation of this solid at 140–165 °C yielded colorless rectangular (prismatic) crystals of **3**: 0.49 g, 1.13 mmol, 11% yield; stable in air; soluble in both polar and nonpolar organic solvents; m.p. 68 °C; Anal for $C_{16}H_{44}B_8Si_4$: found (calculated): C 44.13 (44.15), H 10.23 (10.19), B 19.71 (19.85)].

Received: November 17, 1995 [Z 8560 IE]
German version: *Angew. Chem.* **1996**, *108*, 1093–1095

Keywords: boron compounds · carboranes · rearrangements

[1] W. N. Lipscomb, D. Britton, *J. Chem. Phys.* **1960**, *33*, 275; W. N. Lipscomb, *Science* **1966**, *153*, 373.
[2] K. Wade, *Electron Deficient Compounds*, Nelson, London, **1971**.
[3] J. D. Kennedy, *Progress in Inorganic Chemistry, Vol. 34*, Wiley, New York, **1986**.
[4] D. M. P. Mingos, D. J. Wales in *Electron Deficient Boron and Carbon Clusters*, (Eds.: G. A. Olah, K. Wade, R. E. Williams), Wiley, New York, **1991**, Chapter 5, and references therein.
[5] B. M. Gimarc, D. S. Warren, J. J. Ott, C. Brown, *Inorg. Chem.* **1991**, *30*, 1598.

[6] M. L. McKee, *J. Am. Chem. Soc.* **1995**, *117*, 8001.
[7] G. M. Edvenson, D. F. Gaines, *Inorg. Chem.* **1990**, *29*, 1210.
[8] Y. V. Roberts, B. F. G. Johnson, *J. Chem. Soc. Dalton Trans.* **1994**, 759.
[9] R. Mason, K. Thomas, D. M. P. Mingos, *J. Am. Chem. Soc.* **1973**, *95*, 3802.
[10] F. Y. Lo, C. E. Strouse, K. P. Callahan, C. B. Knobler, M. F. Hawthorne, *J. Am. Chem. Soc.* **1975**, *97*, 428, and references therein.
[11] N. S. Hosmane, L. Jia, H. Zhang, J. W. Bausch, G. K. S. Prakash, R. E. Williams, T. P. Onak, *Inorg. Chem.* **1991**, *30*, 3793; H. Zhang, Y. Wang, A. K. Saxena, A. R. Oki, J. A. Maguire, N. S. Hosmane, *Organometallics* **1993**, *12*, 3933.
[12] T. D. Getman, C. B. Knobler, M. F. Hawthorne, *J. Am. Chem. Soc.* **1990**, *112*, 4593.
[13] W. M. Maxwell, V. R. Miller, R. N. Grimes, *Inorg. Chem.* **1976**, *15*, 1343; *J. Am. Chem. Soc.* **1976**, *98*, 4818; R. B. Maynard, R. N. Grimes, *ibid.* **1982**, *104*, 5983; *Inorg. Synth.* **1983**, *22*, 215; R. N. Grimes, *Adv. Inorg. Chem. Radiochem.* **1983**, *26*, 55.
[14] N. S. Hosmane, A. K. Saxena, R. D. Barreto, H. Zhang, J. A. Maguire, L. Jia, Y. Wang, A. R. Oki, K. V. Grover, S. J. Whitten, K. Dawson, M. A. Tolle, U. Siriwardane, T. Demissie, J. S. Fagner, *Organometallics* **1993**, *12*, 3001.
[15] N. S. Hosmane, R. D. Barreto, M. A. Tolle, J. J. Alexander, W. Quintana, U. Siriwardane, S. G. Shore, R. E. Williams, *Inorg. Chem.* **1990**, *29*, 2698.
[16] SPARTAN, Version 4.0, Wavefunction Inc., Irvine, CA, **1995**.
[17] **2**: ^{1}H NMR (200 MHz, C_6D_6, 295 K, TMS ext.): $\delta = 0.20-4.0$ (br., 8 H, basal and apical BH), 0.17 (br. s, 36 H, $SiMe_3$); ^{11}B NMR (64.2 MHz, C_6D_6, 295 K, $BF_3 \cdot OEt_2$ ext.): $\delta = -30.18$ (d, $^1J(B,H) = 162.1$ Hz, cage-BH); ^{13}C NMR (50.3 MHz, C_6D_6, 295 K, TMS ext.): $\delta = -1.1$ (q, $^1J(C,H) = 119.5$ Hz, $SiMe_3$), -33.32 (s, cage-C); IR (C_6H_6): $\tilde{\nu} = 2581$ (s), 2541 (m) cm^{-1} (B-H); MS: *m/z* (%): 435 (M^+, 100), 73 (Me_3Si, 60). **3**: ^{1}H NMR (200 MHz, C_6D_6, 295 K, TMS ext.): $\delta = 0.20-4.0$ (br., 8 H, basal and apical BH), 0.16 (br. s, 36 H, $SiMe_3$); ^{11}B NMR (64.2 MHz, C_6D_6, 295 K, $BF_3 \cdot OEt_2$ ext.): $\delta = -5.57$ (d, $^1J(B,H) = 146.5$ Hz, cage-BH); ^{13}C NMR (50.3 MHz, C_6D_6, 295 K, TMS ext.): $\delta = -1.4$ (q, $^1J(C,H) = 120.3$ Hz, $SiMe_3$), -11.41 (s, cage C); IR (C_6H_6): $\tilde{\nu} = 2580$ (s), 2539 (m) cm^{-1} (B-H); MS: *m/z* (%): 435 (M^+, 100), 73 (Me_3Si, 58).
[18] Crystal data for **2** ($C_{16}H_{44}B_8Si_4$, $M_r = 435.4$): monoclinic, $P2_1/n$; $a = 9.628(2)$, $b = 7.332(2)$, $c = 19.924(5)$ Å, $\beta = 93.36(2)$°, $V = 1404.0(6)$ Å^3, $Z = 2$, $\rho_{calcd} = 1.030$ Mg m^{-3}, $\mu = 0.214$ mm^{-1}; Data were collected on a Siemens R3m/V diffractometer at -43 °C ($Mo_{K\alpha}$; $2\theta = 3.5-44.0$°) and 1841 reflections) and corrected for Lorentz and polarization effects. The structure was solved by direct methods and subsequent difference Fourier synthesis using SHELXTL-Plus (G. M. Sheldrick, *Structure Determination Software Program Package*, Siemens Analytical X-ray Instruments Inc., Madison, WI (USA) **1990**). **2** has a center of symmetry at the geometric center of the cage and was refined on F with all non-H atoms anisotropically and H atoms isotropically. The final refinement converged at $R = 0.029$, $wR = 0.040$ and GOF = 1.12 for 1431 observed reflections. Further details of the crystal structure investigation may be obtained from the Fachinformationszentrum Karlsruhe, D-76344 Eggenstein-Leopoldshafen (Germany), on quoting the depository number CSD-59274.
[19] In Figure 1 the interatomic connectivities are drawn such that atoms separated by less than 2.00 Å are connected, while atoms at distances greater than 2.15 Å are considered not to interact and are not connected.
[20] According to MO calculations, this isomer is an intermediate 40.0 kJ mol^{-1} higher in energy than **2**.
[21] J. Yang, K.-J. Lu, J. A. Maguire, N. S. Hosmane, unpublished results.

The Dianion of Tetraphenylgermole is Aromatic**

Robert West,* Honglae Sohn, Douglas R. Powell, Thomas Müller, and Yitzhak Apeloig

The anions of siloles and germoles have stimulated a great deal of interest lately.[1-5] Tetraphenylgermole dianions have been studied in THF by Hong and Boudjouk,[6] who proposed a delocalized structure on the basis of the ^{13}C NMR spectrum. On the other hand, Tilley and co-workers have recently reported the X-ray structure of the germole anion, $[(MeC)_4GeSi(SiMe_3)_3]^-$, as its lithium salt **1**.[7] The structure is highly localized; the C–C bond lengths within the five-membered ring vary significantly.

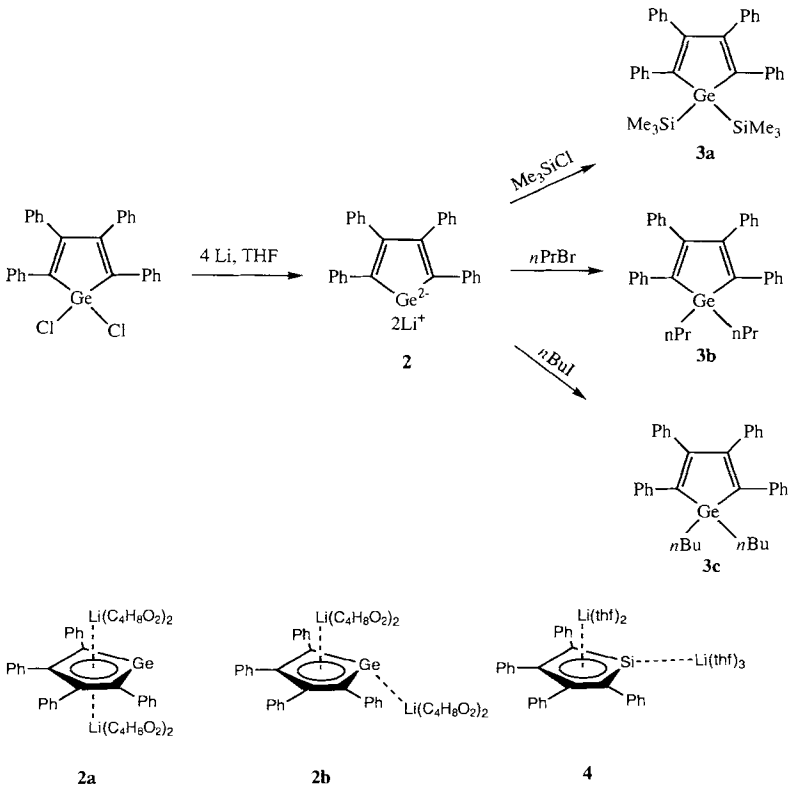

Scheme 1. Synthesis of **2** and **3a–c**.

We now report on the structure of the dilithium salt of the tetraphenylgermole dianion (**2**), which was obtained from 1,1-dichloro-2,3,4,5-tetraphenylgermole (Scheme 1). The dilithium

[*] Prof. R. West, H. Sohn, Dr. D. R. Powell
Department of Chemistry, University of Wisconsin
Madison, WI 53706 (USA)
Fax: Int. code +(608)262-6143
e-mail: west@chem.wisc.edu
Dr. T. Müller
Fachinstitut für Allgemeine und Anorganische Chemie der Humboldt Universität
Hessische Strasse 1-2, D-10115 Berlin (Germany)
Prof. Y. Apeloig
Department of Chemistry
Technion-Israel Institute of Technology
32000 Haifa (Israel)

[**] This research was supported by grants from the National Science Foundation and the Israel-US Binational Science Foundation. We thank Youngshang Pak for valuable assistance. T. M. thanks Prof. Dr. N. Auner for his interest and support of this work.

compound **2** crystallized from dioxane in two structurally distinct forms, depending upon the crystallization temperature. The crystals obtained from dioxane at $-20\,^{\circ}C$ had the composition $Li_2[(PhC)_4Ge]\cdot 5$dioxane (**2a**) and had a reverse-sandwich structure. The two lithium atoms, each coordinated to two dioxane molecules, lie above and below the C_4Ge ring within bonding distance of all five ring atoms (Fig. 1).[8] Crystals of **2** obtained at $25\,^{\circ}C$ had the composition $Li_2[(PhC)_4Ge]\cdot 5.5$ dioxane (**2b**). In **2b** one lithium atom is η^5-coordinated to the ring atoms and the other is η^1-coordinated to the germanium atom (Fig. 2).[9] In both structures the electrons within the ring are highly delocalized, which leads to nearly equal C–C bond lengths. Derivatization of solutions of **2** led to the products **3a**–**3c** (Scheme 1); thus, clearly showing the dianionic character of **2**.

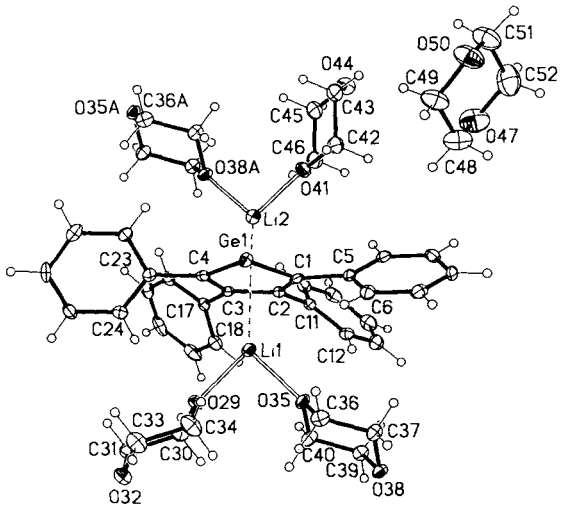

Fig. 1. Crystal structure of **2a**. Selected bond lengths [pm] and angles [°]: Ge1–Li1 273.0(5), Ge1–Li2 268.1(5), Li1–C1 238.0(6), Li1–C2 227.9(6), Li1–C3 228.8(6), Li1–C4 243.5(6), Li2–C1 240.8(6), Li2–C2 229.7(6), Li2–C3 227.8(6), Li2–C4 234.5(6), Ge1–C1 195.7(3), Ge1–C4 195.6(3), C1–C2 142.9(4), C2–C3 144.9(4), C3–C4 143.1(4); C1-Ge1-Li1 58.28(14), C1-Ge1-Li2 60.17(14), C4-Ge1-Li1 59.93(14), C4-Ge1-Li2 58.29(14), Ge1-C1-C2 114.5(2), Ge1-C4-C3 114.3(2), C1-C2-C3 113.7(3), C2-C3-C4 114.0(3), C1-Ge1-C4 83.44(12).

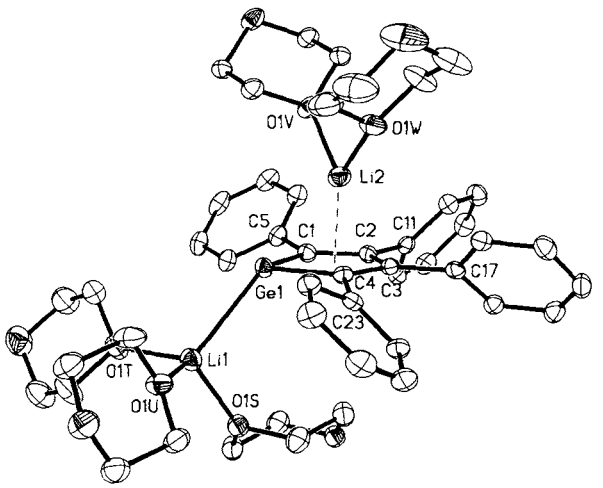

Fig. 2. Crystal structure of **2b**. Selected bond lengths [pm] and angles [°]: Ge1–Li1 261.3(3), Ge1–Li2 265.4(3), Li2–C1 235.9(4), Li2–C2 226.3(3), Li2–C3 230.8(3), Li2–C4 242.3(3), Ge1–C1 193.0(2), Ge1–C4 193.0(2), C1–C2 142.3(2), C2–C3 143.5(2), C3–C4 142.1(2); C1-Ge1-Li1 85.62(7), C1-Ge1-Li2 59.47(8), C4-Ge1-Li1 114.31(9), C4-Ge1-Li2 61.44(8), Li1-Ge1-Li2 174.48(10), Ge1-C1-C2 112.40(12), Ge1-C4-C3 112.59(12), C1-C2-C3 114.77(14), C2-C3-C4 114.62(14), C1-Ge1-C4 85.62(7).

The structure of **2b** is related to that recently published for $Li_2[(PhC)_4Si]\cdot 5$THF (**4**), which also contains η^1- and η^5-coordinated lithium centers.[5] A significant difference between the structures is that in **4** the arrangement at the silicon center is nearly planar, whereas in **2b** the η^1-coordinated lithium center is shifted to the hemisphere anti to the η^5-coordinated lithium center. The angle between the Li–Ge vector and the C-Ge-C plane is 42.9°. Intraring C–C distances for **1**, **2a**, **2b**, and **4** are given in Table 1.

Table 1. Intraring C–C distances for germole and silole anions.

	C1–C2	C3–C4	C2–C3	Ref.
1	136(6)	135(5)	146(6)	[7]
2a	142.9(4)	143.1(4)	144.9(4)	this work
2b	142.3(2)	142.1(2)	143.5(2)	this work
4	144.8(4)	142.6(4)	143.0(4)	[5]

Theoretical calculations provide some insight into the sharp differences between **1** and **2**. MO calculations reported by Tilley et al. for the anion $(H_4C_4GeSiH_3)^-$ gave a small aromatic stabilization energy (ASE) of 5.3 kcal mol^{-1}, and large differences between C–C intraring bond lengths, leading to a low Julg parameter A[10] of 0.53. Our MO calculations[11] for the $(H_4C_4Ge)^{2-}$ ion (Table 2) indicate that the C–C distances within the ring should be nearly identical; the Julg parameter is near 1. An ASE of 13.0 kcal mol^{-1} is predicted from the isodesmic reaction shown in Equation (a).[12] The MO calculations reveal

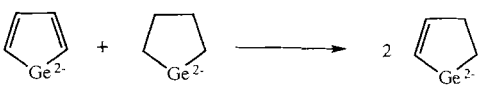

(a)

Table 2. Calculated bond lengths [pm] and Julg's parameter A for germole anions and dianions.

	C1–C2	C2–C3	C1–Ge	Li–Ge	Li–C1	Li–C2	A
$H_4C_4Ge^{2-}$	139.0	143.5	199.2				0.957
$Li_2(H_4C_4Ge)$	142.5	143.6	200.5	250.7	217.0	210.4	0.997
$Li_2(H_4C_4Ge)\cdot 4H_2O$	142.5	142.2	198.4	273.9	238.6	225.3	1.000
$H_4C_4GeSiH_3^-$ [a]	136.1	148.4					0.532

[a] Data from ref. [7].

that the $Li_2(H_4C_4Ge)$ structure in which both lithium centers are η^5 coordinated is the energy minimum; it is 25 kcal mol^{-1} (at MP2/LANL2DZ) more stable than the isomer in which one lithium center is η^1- and the other η^5-coordinated (see Table 2). Complexation of the dianion by lithium ions further increases the delocalization, as shown by the even larger values of the Julg parameter A predicted for the η^5,η^5-dilithium derivative of the $(H_4C_4Ge)^{2-}$ ion, and likewise for $Li_2(H_4C_4Ge)\cdot 4H_2O$, in which each lithium center is coordinated by two H_2O moleules. Thus both the structure for **1** (localized electrons) and that for **2** (delocalized electrons) are consistent with theory.

We note the good agreement between the experimentally determined geometry for **2a** (Fig. 1) and the calculated geometry for the model compound $Li_2(H_4C_4Ge)\cdot 4H_2O$ (Table 2), including the distances between the plane of the germole ring and the Li centers. Comparison with the calculated geometry of $H_4C_4GeLi_2$ reveals the important role of solvation in controlling the Li–germole ring distance. Thus, d(Ge–Li) and

d(C1–Li) distances in $Li_2(H_4C_4Ge)$ increase by 23.2 pm and 21.6 pm, respectively, upon coordination of two water molecules to each of the η^5-coordinated lithium ions. In contrast, solvation has practically no effect on the intraring distances.

In summary, it appears that anions of Group 14 metalloles (C_4E rings) may have either localized nonaromatic, or delocalized aromatic structures, depending on the nature of the metal E and the substituents. Further structural studies of metallole anions and dianions of this kind with different substituents will be of value in determining the factors leading to "aromaticity" in these substances.

Experimental Procedure

1,1-Dichloro-2,3,4,5-tetraphenylgermole: Diphenylacetylene (26.7 g, 150 mmol) and lithium (1.38 g, 200 mmol) were stirred in diethyl ether (150 mL) at room temperature for 3.5 h. The reaction gave a brown solution and a yellow precipitate. The solution was frozen with a bath of liquid nitrogen, after removal of lithium metal. $GeCl_4$ (25.7 mL, 300 mmol) was added by a syringe in one portion. The mixture was kept at −196 °C for 5 min before the cooling bath was removed, and the solution was allowed to warm up slowly to room temperature, and stirred for 4 h to give a yellow solution. The reaction product was extracted with diethyl ether and obtained as yellow crystals (30 g, 80%) at −10 °C. M.p. 197–199 °C. Selected data; ^{1}H NMR (300.133 MHz, $CDCl_3$): δ = 6.83–6.88 and 7.04–7.21 (br. m, 20H; Ph); $^{13}C\{H\}$ NMR (75.403 MHz, $CDCl_3$ (δ = 77.00)): δ = 149.96, 136.57, 134.66, 132.72, 129.54, 129.50, 128.36, 128.06, 127.68, 127.47; MS(EI): m/z (%): 500 (23) [M^+], 356 (78) [$M^+ - GeCl_2$]. High-resolution MS: calcd. for $C_{28}H_{20}GeCl_2$ 500.0155, found 500.0116.

2: A solution of $Ph_4C_4GeCl_2$ (10.00 g, 20 mmol) in THF (130 mL) was stirred with 4 equiv Li (0.555 g, 80 mmol) for 12 h at room temperature under an argon atmosphere. The color of the solution rapidly changed to a dark maroon. After removal of solvent, the residue, **2**, was extracted with dioxane and filtered. Orange crystals of **2b** were obtained at room temperature. Cooling of the saturated solution to −20 °C produced instead yellow crystals of **2a**. $^{13}C\{H\}$ NMR (75.403 MHz, dioxane (δ = 66.40)): δ = 165.17, 150.07, 143.83, 131.93, 129.19, 128.04, 125.89, 122.03, 119.45.

3a: An excess of trimethylchlorosilane was added slowly to a solution of **2** (20 mmol) in THF (130 mL) at 0 °C. The solution was allowed to warm to room temperature and stirred for 2 h. Then the volatiles were removed under reduced pressure. The residue was extracted with pentane (100 mL) and filtered. Yellow crystals of **3a** (quantitative yield) were obtained after the solution was concentrated and cooled to −10 °C. M.p. 114 °C. Selected data for **3a**: ^{1}H NMR (300.133 MHz, $CDCl_3$): δ = 6.76–6.89 and 6.94–7.10 (br. m, 20H, Ph), 0.16 (s, 18H, $SiCH_3$); $^{13}C\{H\}$ NMR (75.403 MHz, $CDCl_3$ (δ = 77.00)): δ = 151.55, 149.34, 142.40, 140.34, 130.61, 129.53, 127.55, 127.19, 125.54, 124.90, 0.26 ($SiMe_3$); MS(EI): m/z (%): 576 (74) [M^+], 503 (22) [$M^+ - SiMe_3$]. High-resolution MS: calcd. for $C_{34}H_{38}GeSi_2$ 576.1742, found 576.1720.

3b: Yellow crystals, quantitative yield, M.p. 78–80 °C; ^{1}H NMR (300.133 MHz, $CDCl_3$): δ = 6.75–7.10 (br. m, 20H, Ph), 1.45–1.52 (br. m, 4H, CH_2), 1.30 (t, 4H, Ge-CH_2), 0.95 (t, 6H, -CH_3); $^{13}C\{H\}$ NMR (75.403 MHz, $CDCl_3$): δ = 152.28, 143.30, 140.98, 139.65, 130.14, 128.91, 127.80, 127.35, 125.90, 125.31, 18.80, 17.58, 17.37; MS(EI): m/z (%): 516 (100) [M^+], 473 (10) [$M^+ - n$Pr], 429 (69) [$M^+ - 2n$Pr]. High-resolution MS : calcd. for $C_{34}H_{34}Ge$ 516.1882, found 516.1883.

3c: Yellow crystals, quantitative yield, M.p. 148–150 °C; ^{1}H NMR (300.133 MHz, $CDCl_3$): δ = 6.78–7.23 (br. m, 20H, Ph), 1.15–1.39 (br. m, 4H, -CH_2-), 1.00–1.15 (br. m, 4H, -CH_2-), 0.88 and 0.80 (t, 6H, -CH_3), 0.64 (t, 4H, Ge-CH_2); $^{13}C\{H\}$ NMR (75.403 MHz, $CDCl_3$): δ = 151.84, 145.40, 140.74, 139.50, 130.38, 129.46, 127.80, 127.39, 126.01, 125.54, 28.04, 25.01, 15.94, 13.44; MS(EI): m/z (%): 544 (59) [M^+], 429 (28) [$M^+ - 2n$Bu]. High-resolution MS: calcd. for $C_{36}H_{38}Ge$ 544.2197, found 544.2188.

Received: November 20, 1995 [Z 8573 IE]
German version: *Angew. Chem.* **1996**, *108*, 1095–1097

Keywords: aromaticity · germanium compounds · germoles · structure elucidation

[1] W.-C. Joo, J.-H. Hong, S.-B. Choi, H.-E. Son, *J. Organomet. Chem.* **1990**, *391*, 27.
[2] J.-H. Hong, P. Boudjouk, *J. Am. Chem. Soc.* **1993**, *115*, 5883.
[3] J.-H. Hong, P. Boudjouk, S. Castellino, *Organometallics* **1994**, *13*, 3387
[4] a) B. Goldfuss, P. von R. Schleyer, *Organometallics* **1995**, *14*, 1553; b) P. von R. Schleyer, P. K. Freeman, H. Jiao, B. Goldfuss, *Angew. Chem.* **1995**, *107*, 332; *Angew. Chem. Int. Ed. Engl.* **1995**, *34*, 337 c) B. Goldfuss, P. von R. Schleyer, F. Hampel, *Organometallics*, in press.
[5] R. West, H. Sohn, U. Bankwitz, J. Calabrese, Y. Apeloig, T. Müller, *J. Am. Chem. Soc.* **1995**, *117*, 11608.
[6] J.-H. Hong and P. Boudjouk, *Bull. Chem. Soc. Fr.* **1995**, *132*, 495.
[7] W. P. Freeman, T. D. Tilley, F. P. Arnold, A. L. Rheingold, P. K. Gantzel, *Angew. Chem.* **1995**, *107*, 2029; *Angew. Chem. Int. Ed. Engl.* **1995**, *34*, 1887.
[8] X-ray structure analysis of **2a**: $C_{28}H_{20}GeLi_2 \cdot 5C_4H_8O_2$, M_r = 795.33, triclinic, $P\bar{1}$, a = 9.9864(13), b = 13.573(2), c = 15.881(2) Å, α = 98.190(9), β = 95.827(10), γ = 109.280(9)°, V = 1985.6(4) Å^3, Z = 2, ρ_{calcd} = 1.330 Mgm^{-3}, F(000) = 836, λ = 0.71073 Å, θ = 113(2) K. A yellow single crystal (dimensions 0.40 × 0.40 × 0.10 mm) was mounted under a coating of Paratone-N. Data were collected by the ω scan method in the range of 1.50° ≤ θ ≤ 22.50° on a Siemens P4 diffractometer. Of a total of 5533 reflections, 5177 (R_{int} = 0.0310) were independent. The structure was solved by direct methods with the SHELXS-86 program and refined by the full-matrix least-squares method on using the SHELXL-93 program. $R(F)$ = 0.0370, $R_w(F^2$-all) = 0.0887. There is one lithium cation on each face of the five-membered Ge ring. Each Li is coordinated to two dioxane molecules, both of which are in chair conformations. One of the dioxane molecules that is coordinated to one lithium ion is also coordinated through its other oxygen atom to the lithium ion in another molecule. Thus these groups form infinite chains in the a direction of the crystal. There is also one dioxane molecule in a chair conformation that is not coordinated to any other group. Crystallographic data (excluding structure factors) for the structure(s) reported in this paper have been deposited with the Cambridge Crystallographic Data Centre as supplementary publication no. CCDC-179-16 and CCDC-179-17. Copies of the data can be obtained free of charge on application to The Director, CCDC, 12 Union Road, Cambridge CB2 1EZ, UK (fax: int. code +(1223) 336-033; e-mail: teched@chemcrys.cam.ac.uk).
[9] X-ray structure analysis of **2b**: $C_{28}H_{20}GeLi_2 \cdot 5.5C_4H_8O_2$, M_r = 927.48, triclinic, $P\bar{1}$, a = 12.7118 (2), b = 13.2702(2), c = 17.2801(3) Å, α = 68.293(2), β = 72.413(2), γ = 62.830(2)°, V = 2377.88(7) Å^3, Z = 2, ρ_{calcd} = 129.5 Mgm^{-3}, F(000) = 980, λ = 0.71073 Å, θ = 133(2) K. An orange single crystal (0.5 × 0.4 × 0.4 mm) was mounted under a coating of Krytox oil. Intensity data were collected by the ψ scan method (1.50° < θ < 22.50° on a Siemens P4 diffractometer equipped with a CCD area detector. From a total of 14703 measured data, 8263 were independent (R_{int} = 0.0291). The structure was solved by direct methods and refined by a full-matrix least squares method on F^2 using the SHELXTL + program. $R(F$-obs) = 0.0312, $R_w(F^2$-all) = 0.0822, S = 1.068 for 8261 data and 596 variables. One lithium ion bonds to a face of the five-membered ring and the other Li ion bonds to the Ge center directly. Dioxanes join the lithium atoms to form an infinite bonded chain [8].
[10] Julg's parameter A is a measure of the deviation of C–C bond lengths from the mean C–C bond lengths in cyclic compounds; A = 1.00 for benzene, 0 for "Kekulé benzene". A. Julg, P. Francois, *Theor. Chim. Acta* **1967**, *7*, 249; S. M. van den Kerk, *J. Organomet. Chem.* **1981**, *215*, 315
[11] Values in Table 2 were calculated by using density functional theory (B3LYP) with the polarized, triply split 6-311G* basis set augmented by diffuse functions (B3LYP/6-311 + G*). All structures were restricted to C_{2v} symmetry; Gaussian 94 was employed [13]. For comparison we calculated the structure of $H_4C_4Ge^{2-}$ at several other levels of theory using different basis sets. The predicted intraring distances and Julg parameters are: HF/6-31 + G* (C,H), ecp28mwb + diffuse (Ge): C1–C2 = 136.7 pm, C2–C3 = 144.7 pm, Ge–C1 = 201.5 pm, A = 0.835; HF/6-311 + G*: C1–C2 = 136.8 pm, C2–C3 = 144.3, Ge–C1 = 199.0, A = 0.856; MP2(fc)/6-31 + G* (C,H), ecp28mwb (Ge): C1–C2 = 142.3 pm, C2–C3 = 141.9 pm, Ge–C1 = 197.8 pm, A = 1.000. We note that RHF theory predicts a more localized structure for the dianion than does DFT theory. However, even at the HF level the structure of the dianion is predicted to be more delocalized than that of the monoanion $H_4C_4GeSiH_3^-$, as shown by the A values. MP2 calculations predict a fully delocalized structure for $H_4C_4Ge^{2-}$.
[12] This value is somewhat smaller than the ASE for the corresponding silole dianion (17.9 kcal mol^{-1} at MP2(fc)/6 + 31G*).
[13] Gaussian 94, Revision B. 3, B. G. Johnson, M. A. Robb, J. R. Cheeseman, T. Keith, G. A. Petersson, J. A. Montgomery, K. Raghavachari, M. A. Al-Laham, V. G. Zakrzewski, J. V. Ortiz, J. B. Foresman, C. Y. Peng, P. Y. Ayala, W. Chen, M. W. Wong, J. L. Andres, E. S. Replogle, R. Gomperts, R. L. Martin, D. J. Fox, J. S. Binkley, D. J. Defrees, J. Baker, J. P. Stewart, M. Head-Gordon, C. Gonzalez, J. A. Pople, Gaussian, Inc., Pittsburgh, PA, **1995**.

A Trinuclear Organoantimony Cation: Structure of $[Me_2Sb-Sb(Me_2)-SbMe_2][Me_2SbBr_2]$**

Hans Joachim Breunig,* Michael Denker, and Enno Lork

Dedicated to Professor Marianne Baudler on the occasion of her 75th birthday

Recently we reported on the binuclear adduct $Me_3Sb \rightarrow Sb(Me)I_2$ that contains a remarkably short antimony–antimony bond.[1, 2] In an attempt to prepare polynuclear adducts, we treated distibanes with organoantimony(III) halides.[1] The synthesis of a crystalline compound of the composition $Me_2SbSbMe_2 \cdot 2\,Me_2Br$ has now been accomplished by reacting dimethylantimony bromide with excess tetramethyldistibane. The X-ray structure analysis[3] revealed that instead of an uncharged Lewis acid base adduct the ionic compound **1** was obtained. The formation of **1** can be rationalized as an oxidative

$[Me_2Sb\ Sb(Me_2)\ SbMe_2][Me_2SbBr_2]$ **1**

addition of the electrophile dimethylantimony bromide to a nucleophilic antimony atom of tetramethyldistibane, and transfer of the bromide ion to a second dimethylantimony bromide molecule. Such an addition is unusual since distibanes normally react with electrophilic reagents with fission of the antimony–antimony bond.[4] For example, the reaction of tetraethyldistibane with methyl iodide gives diethylantimony iodide and diethylmethylstibane.[5]

The structure of the ions of **1** is shown in Figure 1. The cation is particularly remarkable. It consists of a chain of three

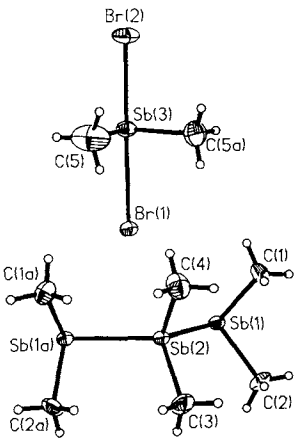

Fig. 1. Structure of **1** in the crystal. Selected bond lengths [pm] and angles [°]: Sb(1)–Sb(2) 282.03(4), Sb(1)–C(1) 215.7(5), Sb(1)–C(2) 216.1(5), Sb(2)–C(3) 212.1(8), Sb(2)–C(4) 213.1(8), Sb(3)–C(5) 213.0(7), Sb(3)–Br(2) 269.99(10), Sb(3)–Br(1) 297.72(9); Sb(1)-Sb(2)-Sb(1a) 116.19(2), C(3)-Sb(2)-C(4) 98.0(4), C(1)-Sb(1)-Sb(2) 92.4(2), C(1)-Sb(1)-C(2) 94.3(2), C(5)-Sb(3)-Br(2) 91.6(2), C(5)-Sb(3)-Br(1) 86.4(2), Br(2)-Sb(3)-Br(1) 176.98(3), C(5)-Sb(3)-C(5a) 96.7(6); dihedral angle C(1)-Sb(1)-Sb(2)-C(4) 8.59 (0.30), C(2)-Sb(1)-Sb(2)-C(5) 4.18 (0.30).

dimethylantimony groups; the two terminal groups are symmetry equivalent. Neither the tetramethyldistibane molecule nor a dimethylstibenium ion can be identified as separate units, as would have been expected for an acid–base adduct. Rather, the cation adopts the structure of a bis(dimethylstibanyl)dimethylstibonium ion. The Sb–Sb bond lengths (282.03(4) pm) are a little shorter than in crystalline tetramethyldistibane (286.2(2)[6] and 283.1(1)[7]) or in the adduct $Me_3Sb \rightarrow Sb(Me)I_2$ (285.9(1)[2]). The coordination of the central antimony atom is almost tetrahedral. The bond angles at the terminal antimony atoms of the chain are close to 90°. Analogous cationic antimony chains have not yet been described in the literature. Little is also known about neutral catenated stibanes like pentamethyltristibane. This chain compound, corresponding to the cation of **1**, has hitherto only been obtained in an equilibrium with polymeric methylantimony and tetramethyldistibane.[8, 9] However, the anion $Sb_3Ph_4^-$ has been characterized by X-ray crystallography, and the Sb–Sb bond lengths in this trinuclear compound are 276.1(1) pm,[10] thus, shorter than the corresponding distances in **1**.

The anion of **1** can be described as a trigonal bipyramid in which the bromine atoms adopt the axial positions and the lone pair of electrons and the methyl groups the equatorial positions. The antimony–bromine distances are 297.7(9) and 270.0(1) pm. These distances are considerably longer than the Sb–Br single bond lengths in solid $MeSbBr_2$ (av 257 pm).[9] The formation and structure of the anion can be explained on the basis of a bonding model[11] in which a Sb–Br σ^* orbital of Me_2SbBr serves as an acceptor orbital for the bonding of a bromide ion. The formation of four bonds by antimony(III) is not common. Related structures have been observed in the ions $[Ph_2SbCl_2]^-$[12] and $[Ph_2SbI_2]^-$.[13]

The arrangement of the ions in the crystal is shown in Figure 2. There are heavy atom contacts between the cations and

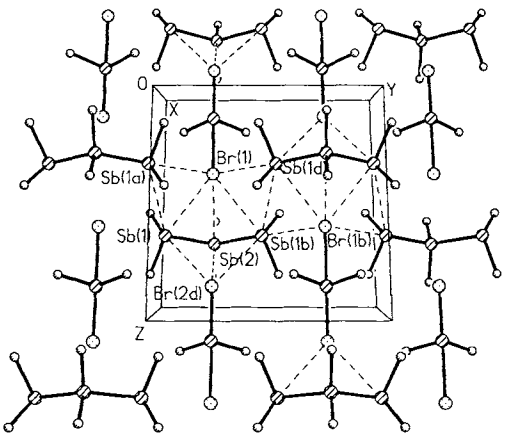

Fig. 2. Unit cell of **1**. Contact distances [pm] between the ions: Sb(1)···Br(1) 385.7, Sb(2)···Br(1) 370.4, Sb(1a)···Br(1) 385.7, Sb(2b)···Br(2) 370.9, Sb(1a)···Br(2) 379.5, Sb(1d)···Br(2) 379.5, Sb(1)···Br(1a) 346.9, Sb(1b)···Br(1a) 346.9, Sb(1)···Sb(1a) 381.5.

anions (Sb···Br 346.9–385.7 pm, Sb···Sb 381.5 pm). Particularly short contacts (Sb(1)···Br(1) 346.9 pm) exist between the terminal dimethylantimony units of two neighboring cations and a bromine atom of the anion. An estimation with the modified[14] Pauling formula[15] gives a bond order of 0.12 for these interactions. Through these weak bonds a $(Br\cdots Sb_3)_x$ zigzag chain is built up in the crystal. Consideration of the interactions between the ions also helps to explain the reactivity of **1**. A slight shift of Br(1) towards Sb(1) and an increase of the distance Sb(1)–Sb(2) corresponds to the transformation of **1** into the starting compounds $Me_2SbSbMe_2$ and Me_2SbBr. Therefore, $[Me_6Sb_3]^+$ should not be considered as an isolated cation.

The solid-state structure of **1** is not preserved in solution in benzene. The ^1H NMR spectrum shows a broad signal at room temperature with a maximum between the frequencies of pure samples of $Me_2SbSbMe_2$ and Me_2SbBr.[1] This pattern corresponds to an exchange of Me_2Sb groups between tetramethyldistibane and dimethylantimony bromide, that is a reversible

[*] Prof. Dr. H. J. Breunig, M. Denker, Dr. E. Lork
Institut für Anorganische und Physikalische Chemie (Fb 02) der Universität
Postfach 330 440, D-28334 Bremen (Germany)
Fax: Int. code +(421)218-4042
e-mail: breunig@chemie.uni-bremen.de

[**] This work was supported by the Fonds der Chemischen Industrie.

formation of **1** from $Me_2SbSbMe_2$ and Me_2SbBr. In the gas phase the components are separated. Mass spectra contain the characteristic signals of $Me_2SbSbMe_2$ and Me_2SbBr.[11] The chemical behavior justifies the description of **1** as an adduct with dative bonds.[16] The observed equivalence of the dimethylantimony groups is attributed to the inability to distinguish between dative and covalent Sb–Sb bonds in **1**. In addition to the reversible dissociation into the starting materials there are irreversible decomposition processes of **1** leading to the formation of Me_3SbBr_2, Me_3Sb, and $(MeSb)_x$. Even the formation of these products can be rationalized by consideration of the results of the structural analysis, since both the reversible and the irreversible decomposition processes may be described as reductive elimination reactions.[17]

Experimental Procedure

All operations were carried out in an argon atmosphere. Dimethylantimony bromide (0.21 g, 0.91 mmol) was added slowly to tetramethyldistibane (0.50 g, 1.65 mmol) [18] through a syringe. After the addition, a small amount of black solid material precipitated together with yellow crystals of **1** (yield 0.18 g, 51.4%). Compound **1** was stable for several days at room temperature when stored under tetramethyldistibane.

Received: November 9, 1995
Revised version: February 9, 1996 [Z8538IE]
German version: *Angew. Chem.* **1996**, *108*, 1081–1082

Keywords: antimony compounds · structure elucidation

[1] H. J. Breunig, K. H. Ebert, S. Gülec, M. Dräger, D. B. Sowerby, M. J. Begley, U. Behrens, *J. Organomet. Chem.* **1992**, *427*, 39–48.
[2] H. J. Breunig, M. Denker, K. H. Ebert, *J. Chem. Soc. Chem. Commun.* **1994**, 875–876.
[3] Crystal dimensions $0.7 \times 0.2 \times 0.15$ mm, crystal system monoclinic, space group $P2_1/m$, cell dimensions $a = 851.30(10)$ pm, $b = 1096.60(10)$ pm, $c = 1137.6(2)$ pm, $\beta = 110.510(10)^\circ$, $V = 0.9947(2)$ nm^3, $Z = 2$, $\rho_{calcd} = 2.561$ Mg m^{-3}, $2\theta_{max} = 55^\circ$, Siemens P4 four-circle diffractometer, $Mo_{K\alpha}$ radiation, $\lambda = 71.073$ pm, scan mode $\omega/2\theta$, $T = 173(2)$ K, 3198 measured reflections, 2394 independent reflections, absorption coefficient 9.367 mm^{-1}, semiempirical absorption correction from ψ scans, method of structure solution: direct methods, program used for structure solution: SHELXS-86, method of refinement: full matrix least squares refinement at F^2, program used for refinement: SHELXL-93, number of free parameters: 76, hydrogen atoms geometrically positioned and refined with a riding model, final R ($I > 2\sigma I$), $R1 = 0.0297$, $wR2 = 0.0682$. Further details of the crystal structure investigation may be obtained from the Fachinformationszentrum Karlsruhe, D-76344 Eggenstein-Leopoldshafen (Germany), on quoting the depository number CSD-404399.
[4] S. Samaan in *Methoden der Organischen Chemie, Houben-Weyl, Metallorganische Verbindungen As Sb Bi* (Ed.: H. Kropf), Thieme, Stuttgart, **1978**, p. 479.
[5] K. Issleib, H. Hamann, *Z. Anorg. Allg. Chem.* **1965**, *339*, 289–297.
[6] A. J. Ashe III, E. G. Ludwig, Jr., J. Olksyszyn, I. C. Huffman, *Organometallics* **1984**, *3*, 337.
[7] O. Mundt, H. Riffel, G. Becker, A. Simon, *Z. Naturforsch. B* **1984**, *39*, 317–322.
[8] M. Ates, H. J. Breunig, K. Ebert, S. Gülec, R. Kaller, M. Dräger, *Organometallics* **1992**, *11*, 145–150.
[9] H. J. Breunig, M. Denker, K. H. Ebert, *J. Organomet. Chem.* **1994**, *470*, 87–92.
[10] R. A. Bartlett, H. V. Rasika Dias, H. Hope, B. D. Murray, M. M. Olmstead, P. P. Power, *J. Am. Chem. Soc.* **1985**, *108*, 6921–6926.
[11] N. C. Norman, *Phosphorus, Sulfur, Silicon, Relat. Elem.* **1994**, *87*, 167–176.
[12] M. Hall, D. B. Sowerby, *J. Organomet. Chem.* **1988**, *347*, 59–70.
[13] W. S. Sheldrick, C. Martin, *Z. Naturforsch. B* **1991**, *46*, 639–646.
[14] M. Hall, M. Nunn, M. J. Begley, D. B. Sowerby, *J. Chem. Soc. Dalton Trans.* **1986**, 1231–1238.
[15] L. Pauling, *The Nature of the Chemical Bond*, 3rd ed., Cornell University Press, Ithaca, **1960**.
[16] A. Haaland, *Angew. Chem.* **1989**, *101*, 1017–1032; *Angew. Chem. Int. Ed. Engl.* **1989**, *28*, 992–1007.
[17] Compound **1** can be described as a stibonium ion of the type $[R^1_2R^2_2Sb]X$. Reductive elimination of R^1X gives $R^1R^2_2Sb$. When R^2X is eliminated $R^1_2R^2Sb$ is formed. With $R^1 = Me_2Sb$, $R^2 = Me$ and X = Br (coordinated at Me_2SbBr) the elimination of R^1X describes the reversible decomposition to Me_2SbBr and Me_4Sb_2. The irreversible decomposition of **1** with formation of Me_3SbBr_2 and $MeSb(SbMe_2)_2$ corresponds to the elimination of R^2X. The neutral tristibane gives $(MeSb)_x$ and Me_4Sb_2 on further decomposition.
[18] H. J. Breunig, V. Breunig-Lyriti, T. P. Knobloch, *Chem.-Ztg.* **1977**, *101*, 399–400.

$Na_{14}K_6Tl_{18}M$ (M = Mg, Zn, Cd, Hg) and $Na_{13.5}Sm_{0.5}K_6Tl_{18}Na$: Novel Octahedral and Centered Icosahedral Cluster Phases Related to the Mg_2Zn_{11}-Type Structure**

Zhen-Chao Dong and John D. Corbett*

Alkali-metal–thallium systems are extremely rich in phases containing thallium cluster anions,[1–7] perhaps because of both the approximate 1:1 ratio between number of atoms and cluster charge in the polyanions and the strong relativistic effect for the element Tl.[6] The use of more than one type of cation has proven to be a powerful means for tuning structural stability because of the increased flexibility for packing the cations and polyanions efficiently, thereby affording effective routes to new clusters not known in the simpler binary systems. Examples are Tl_5^{7-} (approximately D_{3h}) and Tl_9^{9-} (C_{2v}, defect icosahedron) in $Na_2K_{19}Tl_{21}$[4] and $Tl_{13}^{10-}/Tl_{13}^{11-}$ (centered icosahedra) in $Na_4A_6Tl_{13}$ (A = K, Rb, Cs) and $Na_3K_8Tl_{13}$.[6] Subsequently, $Na_{15}K_6Tl_{18}H$, a phase structurally related to $Na_4A_6Tl_{13}$, has been synthesized and shown to contain both Tl_6H^{7-} and $Tl_{12}Na^{13-}$ polyanions.[8] Wade's rules (and extended Hückel calculations) predict 14 skeletal electrons for the closed-shell octahedral Tl_8^{8-} and 26 for either the icosahedral Tl_{12}^{14-} or the centered $Tl_{12}(Na)^{13-}$. The composition $Na_{15}K_6Tl_{18}$ found by X-ray crystallography indicated a one-electron deficiency for the thallium clusters, similar to that for Tl_{13}^{10-}.[6, 7] However, the compound's contradictory Pauli-paramagnetic and ESR-silent properties, as well as the absence of cluster distortions, gave us the first hint that hydrogen was present, which was then verified by the results of subsequent syntheses and and comparisons with the structures of related phases. The amazing stabilization afforded by this small amount of hydrogen (about 0.02 wt%) further suggested a strong electronic drive for closed-shell anion configurations, and therefore opened prospects of further electronic tuning.

The most straightforward modification is the substitution of the centered Na atom within each Tl_{12} icosahedron by a dipositive cation, or partial replacement of exopolyhedral alkali-metal cations by higher valent ions. Of course, the final products are determined not only by electronic and size factors, but also by generally complex matters of phase stability. We report here the successful tuning of the $Na_{15}K_6Tl_{18}H$ phase with retention of the cubic $Pm\bar{3}$ symmetry and the formation of novel (H-free) Tl_6^{8-} (O_h) and M-centered icosahedral $Tl_{12}M^{12-}$ (T_h) clusters. These compounds turn out to be related to the long-known Mg_2Zn_{11}[9] structure and further demonstrate what kind of chemical tuning can be performed to produce new cluster species. Effects of different electron counts on the structures, as well as correlations with properties, are also briefly discussed.

Of the substitutions attempted with Zn, Cd, Hg, Mg, Ca, Sm, Eu, Yb, Ni, Pd, and Pt, only those with Zn, Cd, Hg, Mg, and Sm were successful, according to both X-ray diffraction data (with small lattice shrinkages, Table 1) and energy dispersive analysis by X-ray (EDAX) on several single crystals of each product. Guinier powder patterns for the rest showed no line shifts with

[*] Prof. J. D. Corbett, Dr. Z.-C. Dong
Ames Laboratory and Department of Chemistry
Iowa State University
Ames, IA 50011 (USA)
Fax: Int. code +(515) 294-5718

[**] This research was supported by the Office of the Basic Energy Sciences, Materials Sciences Division, U.S. Department of Energy (DOE). Ames Laboratory is operated for DOE by Iowa State University under Contract No. D-7405-Eng-82.

Table 1. Lattice constants and important distances [Å] in $Na_{15}K_6Tl_{18}H$, $Na_{14}K_6Tl_{18}M$ (M = Mg, Zn) and $Na_{13.5}Sm_{0.5}K_6Tl_{18}Na$.

Empirical formula		$Na_{14}K_6Tl_{18}Na(H)$ [a]	$Na_{14}K_6Tl_{18}Mg$	$Na_{14}K_6Tl_{18}Zn$	$Na_{13.5}Sm_{0.5}K_6Tl_{18}Na$
a [b]		11.6405(4)	11.5914(6)	11.6194(7)	11.6245(4)
Tl1–Tl1	×4	3.276(1)	3.284(2)	3.289(2)	3.283(2)
M–Tl2	×12	3.1569(5)	3.1434(8)	3.1420(8)	3.1598(7)
Tl2–Tl2	×4	3.3244(6)	3.3120(9)	3.3105(9)	3.3285(8)
	×1	3.299(1)	3.278(2)	3.277(2)	3.298(2)
$\bar{d}$(Tl1–Na)	×6	3.375(6)	3.345(9)	3.364(9)	3.361(8)
Tl1–K	×2	4.493(4)	4.449(6)	4.455(6)	4.473(6)
$\bar{d}$(Tl2–Na)	×3	3.258(6)	3.254(9)	3.258(9)	3.257(8)
Tl2–K	×3	3.700(3)	3.687(4)	3.703(4)	3.694(4)

[a] Ref. [8]. [b] Guinier data, $\lambda = 1.540\,562$ Å, $T = 23$ °C. The cell dimensions for $Na_{14}K_6Tl_{18}Cd$ and $Na_{14}K_6Tl_{18}Hg$ are 10.626(3) Å and 10.6308(6) Å, respectively.

respect to the lines for $Na_{15}K_6Tl_{18}H$ (<0.005 Å, about 6 σ), and none of the targeted substitution metals was observed in the EDAX data. Single-crystal studies[10] were carried out for $Na_{14}K_6(Tl_{18}M)$ (M = Mg, Zn) and $Na_{13.5}Sm_{0.5}K_6(Tl_{18}Na)$. The M elements in the former replace the centering Na to give icosahedral $Tl_{12}M^{12-}$ (and regular octahedral Tl_6^{8-}) while the Sm atoms in the latter partially substitute [8.3(8)%] on the exopolyhedral Na3 positions leaving the parent $Tl_{12}Na^{13-}$ but a regular and closed-shell Tl_6^{8-} (Fig. 1). The ascribed closed-

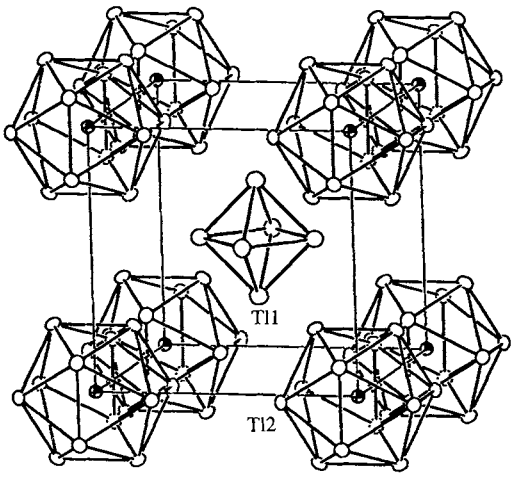

Fig. 1. Arrangement of the discrete Mg-centered icosahedral $Tl_{12}Mg^{12-}$ (T_h) and octahedral Tl_6^{8-} (O_h) anions in the unit cell of $Na_{14}K_6Tl_{18}Mg$ (90% thermal ellipsoids).

shell bonding with M is consistent with the weakly Pauli-paramagnetic property ($\chi_M = 8.5(2) \times 10^{-4}$ emu mol^{-1}) for $Na_{14}K_6(Tl_{18}M)$, where M = Mg, Zn. A Curie–Weiss-type paramagnetism for $Na_{13.5}Sm_{0.5}K_6(Tl_{18}Na)$ ($\mu_{eff} = 0.43(3)\,\mu_B$) is consistent with a trivalent Sm state (electron configuration $4f^5$) and the refined composition (the calculated magnetic moment μ_{eff} for the latter is exactly 0.43 μ_B), because the Sm^{2+} ($4f^6$) would make no contribution to the magnetic moment, because $J = 0$. In parallel with their weak Pauli paramagnetism, these compounds are expected to be poor metals in spite of their closed-shell configurations, as exemplified by the hydride phase ($\partial\rho/\rho\,\partial T \approx 0.34(1)\%\ K^{-1}$, $\rho_{290} \approx 100\ \mu\Omega$ cm). They can therefore be classified as Zintl phases that are incidentally metallic.[6, 11, 12]

It is interesting to notice the small but appreciable dimensional variations between the above phases and $Na_{15}K_6Tl_{18}H$. Lattice constants and important interatomic distances (Table 1) address how delicately different electron counts can affect both the cluster dimensions and the solvation by cations around them. First, the Tl–Tl distance in the octahedron apparently increases slightly (by 0.008(2) Å), from Tl_6H^{7-} to Tl_6^{8-}, although the cells contract (by about 0.05 Å for Mg and 0.02 Å for Zn and Sm), evidently because (polar) covalent bonding from interstitials like hydride usually increases the stabilities of clusters and decreases bond distances when no matrix effects are involved. While cation interactions with icosahedral clusters in these compounds remain basically the same, solvation of Tl_6^{8-} appears slightly stronger than that for Tl_6H^{7-} as judged from the approximately 0.02 Å shorter (Na,K)–Tl distances about the former, consistent with the cluster's higher formal charge. Second, Mg- or Zn-centered icosahedra present shorter center–surface and surface–surface distances with respect to the Na-centered cluster (by about 0.02 Å), presumably from both the stronger coulombic and covalent interactions and from the smaller sizes of Mg and Zn. The Tl–Mg distance of 3.143(1) Å compares very well with that of 3.14 Å reported in MgTl (CsCl type),[13] but the Tl–Zn distance (3.142(1) Å) is considerably longer than the 2.928(1) Å found in the Zn-centered bicapped square antiprismatic $Tl_{10}Zn^{8-}$ ion in $K_8Tl_{10}Zn$.[14] The presence of an undersized Zn atom within the icosahedron is indicated by its relatively large B_{eq} value (4.88 Å^2), and this conclusion is supported by an anomalously large, spherical residual shell (4.3 e Å^{-3} against a background near 1.6 e Å^3) found just 0.02 Å away from the central Zn site in the difference Fourier map. This is consistent with the occurrence of the same $Na_{14}K_6Tl_{18}M$ phase for the somewhat larger Cd and Hg.[15] A 3.14 Å center–surface distance appears to be about the lower limit for a thallium icosahedron.

Also noteworthy is the close structural correspondence of $Na_4K_6Tl_{13}$ (bcc, $Im\bar{3}$)[6] with the present $Na_{14}K_6Tl_{18}M$ ($Pm\bar{3}$), namely, $[(Na_8^{8+})(K_{12}^{12+})][(Tl_{13}^{10-})(Tl_{13}^{10-})]$ vs. $[(Na_8^{8+})(Na_6^{6+})(K_6^{6+})][(Tl_{12}M^{12-})(Tl_6^{8-})]$. The most substantial differences are the replacement of half the icosahedral units related by I-centering with smaller octahedra, and half of the K^+ about the latter by Na^+, and the change from a Tl atom at the center of the icosahedron to M = Mg, Zn, Cd, or Hg. Otherwise, the cation dispositions in the two phases show only slight coordinate shifts that give greater cation–anion interactions with Tl_6^{8-}. A notable contraction of the icosahedra is also observed, the center–surface distance decreasing from 3.22 Å in Tl_{13}^{10-} to 3.14 Å in $Tl_{12}M^{12-}$.

Of particular interest is the close relationship of the $Na_{14}K_6(Tl_{18}M)$ structure to the isotypic Mg_2Zn_{11}[9] (and Na_2Cd_{11}[16]), which can also be structurally formulated as $Zn_{14}Mg_6(Zn_{13}Zn_6)$ with Zn in the center of the icosahedron. Figure 2 shows the alkali-metal cation distributions around the "naked" Tl_6^{8-} (left) and $Tl_{12}M^{12-}$ (right) clusters, while Figure 3 demonstrates how these units are connected into a three-dimensional structure, here as well as for Mg_2Zn_{11} (see below). The linked network shown about the polyhedra in "salt-like" alkali-metal–thallium compounds (Fig. 3) does not imply bonding interactions among the cations, but it does highlight a different zinc substructure in the parent Mg_2Zn_{11}. The larger icosahedral units are held within a cage defined by six zigzag eight-membered rings, while the smaller octahedron is surrounded by twelve five-membered rings. The accompanying shrinkage around the octahedron to preserve suitable bonding interactions results in six extra contacts between pairs of atoms (Na or Zn, represented as gray spheres) that make the former

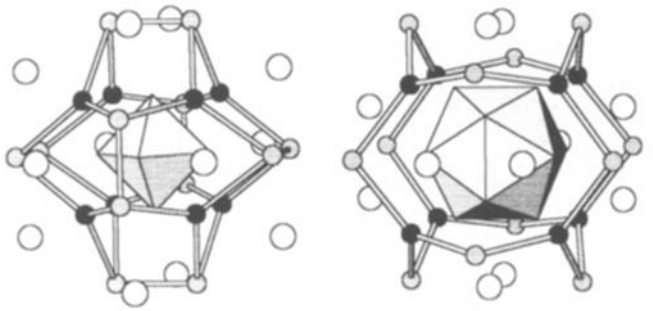

Fig. 2. Environments around the octahedral (left) and icosahedral (right) thallium clusters with the Na sites interconnected to emphasize the relationship to Mg_2Zn_{11}. The *closo*-deltahedra (large circles, and small shaded circles) represent either Tl clusters, K, and the two types of Na atoms in $Na_{14}K_6Tl_{18}M$, or Zn cluster fragments, Mg, and Zn atoms in Mg_2Zn_{11}, respectively.

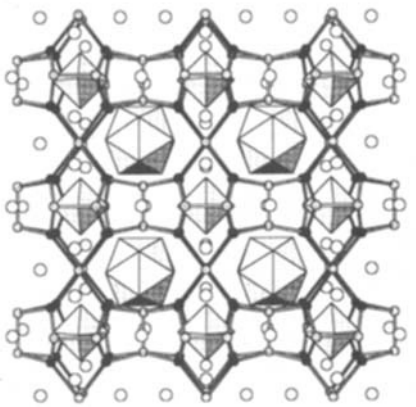

Fig. 3. View of the $Na_{14}K_6Tl_{18}M$ and Mg_2Zn_{11} structures onto [001] showing three different substructures and the interconnections among the cations between clusters. Symbols for the atoms are the same as in Fig. 2.

eight-membered ring bicyclic. Inclusion of isolated cations (represented as open circles for K or Mg) leaves all of the Tl or Zn polyhedra sheathed by 32 atoms functioning in two ways: every triangular face in both polyhedra is capped whereas each vertex is exo-bonded to one atom for the icosahedron but to two Na (or Zn) and two more distant K (Mg) for the octahedron. The eight atoms face-capping the octahedron (black circles) need special attention. These positions, always fully occupied by a single Na or Zn type, are located along the body diagonals in distorted octahedral holes defined by the neighboring polyhedral units, and so demonstrate that the octahedron and icosahedron are the only two interchangeable cluster units with suitable cubic symmetry and comparable environments.

Three different substructures are evident in Mg_2Zn_{11}: the same zinc polyhedra (octahedral Zn_6 and Zn-centered icosahedral Zn_{13}), in the holes a zinc spacer substructure (linked Zn_{14}, like Na), and solvating cations (Mg^{2+}, K^+). It is these different structural functions that afford broad chemical variability through changes in the atom types in the polyhedra, spacers, or cations. While the parent Mg_2Zn_{11} probably represents the highest condensation limit, because the two zinc substructures strongly interact with each other through homonuclear bonding, the present $Na_{14}K_6Tl_{18}M$ phase represents the opposite extreme with isolated polyhedral thallium clusters, well-separated by the solvating alkali-metal cations. Some intermediate degrees of condensation (or bonding polarity) must be also possible and are indeed observed in the isomorphous $Mg_2Al_5Cu_6$ (that is, $[(Al_{14})(Mg_6)][(Cu_{12}Al)(Cu_6)]$)[17] and $Na_2In_5Au_6$ (that is, $[(In_{14})(Na_6)][(Au_{12}In)(Au_6)]$)[18] in which Al or In atoms (in the place of Na) connect Cu or Au octahedra and icosahedra. The nature of the interactions between the linked network and polyhedra undoubtedly undergoes dramatic changes from Mg_2Zn_{11} through $Mg_2Al_5Cu_6$ to $Na_{15}K_6Tl_{18}M$ as the bonding character changes from homonuclear covalent through heteronuclear covalent to predominantly ionic. The last is mechanically the weakest in this series and extremely brittle, but it still has a metallic luster.

The title compounds are examples in which electronic tuning among closed-shell structures is successfully realized. More chemical tuning about this structure type and new octahedral and icosahedral clusters can be expected through appropriate combinations of elements from Groups 1 and 2 and Groups 11–13. In other words, dissection of a structure followed by manipulation of the numbers and types of atoms in a cluster compound may produce new cluster materials with novel properties.

Experimental Procedures

Pure phases of the title compounds were obtained through reactions of stoichiometric amounts of the constituent elements in welded Ta tubing by using the techniques described previously [4]. The surfaces of the Na chunks (99.9%, Alpha) and Tl metal bar (99.998%, Johnson-Matthey) were cleaned with a scalpel in the glovebox before use, whereas the K (99.9%, Baker, sealed under Ar), Mg turnings (99.9%, Aldrich), Zn fillings (99.9%, Fisher), and Sm granules (99.9%, Ames Lab) were used as received. In order to establish that hydrogen interstitials were not involved [8], parallel reactions were run both under vacuum (equilibration at 800 °C for 5 h followed by slow cooling to room temperature) or jacketed by fused silica tubing (equilibration at 500 °C for three days followed by annealing at 250 °C for one week) and with different heating profiles. EDAX studies were carried out on a JEOL 840A SEM with a REBEX DELTA detector with several single crystals of each phase. The single-crystal X-ray diffraction data were collected on a CAD4 diffractometer ($Mo_{K\alpha}$) at room temperature for an angle of 2θ up to 55°. Empirical absorption corrections included ψ-scans and DIFABS [19]. Magnetic susceptibility measurements were made at a field of 3 T over the range of 6–300 K with a Quantum Design MPMS SQUID magnetometer on powdered samples of $Na_{15}K_6Tl_{18}H$ (52 mg), $Na_{14}K_6Tl_{18}Mg$ (47 mg), $Na_{14}K_6Tl_{18}Zn$ (43 mg), and $Na_{13.5}Sm_{0.5}K_6Tl_{18}Na$ (50 mg) in the container type described elsewhere [16]. The raw data were corrected for the susceptibilities of the container and the diamagnetism of the cores [20] as well as for the Larmor precession contributions of the delocalized valence electrons in the clusters, as before [6, 21]. Results are shown in the supplementary material.

Received: November 21, 1995 [Z 8568 IE]
German version: *Angew. Chem.* **1996**, *108*, 1073–1076

Keywords: clusters · intermetallic compounds · thallium compounds

[1] D. A. Hansen, J. F. Smith, *Acta Crystallogr.* **1967**, *22*, 836.
[2] G. Cordier, V. Müller, *Z. Kristallogr.* **1992**, *198*, 281.
[3] Z.-C. Dong, J. D. Corbett, *J. Am. Chem. Soc.* **1993**, *115*, 11299.
[4] Z.-C. Dong, J. D. Corbett, *J. Am. Chem. Soc.* **1994**, *116*, 3429.
[5] Z.-C. Dong, J. D. Corbett, *J. Cluster Sci.* **1995**, *6*, 187.
[6] Z.-C. Dong, J. D. Corbett, *J. Am. Chem. Soc.* **1995**, *117*, 6447.
[7] G. Cordier, V. Müller, *Z. Naturforsch.* **1994**, *49 B*, 935.
[8] Z.-C. Dong, J. D. Corbett, *Inorg. Chem.* **1995**, *34*, 5709.
[9] S. Samson, *Acta Chem. Scand.* **1949**, *3*, 835.
[10] Crystal data for $Na_{14}K_6(Tl_{18}Mg)$, $Na_{14}K_6(Tl_{18}Zn)$, and $Na_{13.50(5)}Sm_{0.50(5)}K_6(Tl_{18}Na)$ (if the data differ, the values are separated by commas): cubic *Pm*3, $Z=1$, $a=11.5914(6)$, 11.6194(7), 11.6245(4) Å, $\mu=753$, 621, 621 cm^{-1}, $R_w=0.04$, 0.029, 0.03. Typical coordinates (listed for the Mg-phase are: Tl1 (6*h*): 0.2808(1), 1/2, 1/2; Tl2 (12*j*): 0, 0.15475(8), 0.25325(7); Mg (1*a*): 0, 0, 0; K (6*f*): 0.1876(8), 0, 1/2; Na2 (8*i*): 0.2812(6), x, x; Na3 (6*g*): 0.330(1), 1/2, 0. The occupancy of Sm (mixed with Na3, gray circles) in $Na_{13.5}Sm_{0.5}K_6(Tl_{18}Na)$ refined within 2σ of the listed value and was so fixed, in agreement with a closed-shell bonding model. All other positions were found fully occupied by a single atom type. Further details of the crystal structure investigations may be obtained from J. D. C. or from the Fachinformationszentrum Karlsruhe, D-76344 Eggenstein-Leopoldshafen (Germany) on quoting the depository number CSD-404694 ($Na_{15}K_6Tl_{18}H$), 404695 ($Na_{14}K_6Tl_{18}Mg$), 404696 ($Na_{14}K_6Tl_{18}Zn$), 404697 ($Na_{13.5}Sm_{0.5}K_6Tl_{18}Na$).
[11] R. Nesper, *Angew. Chem.* **1991**, *103*, 806; *Angew. Chem. Int. Ed. Engl.* **1991**, *30*, 789.

[12] J. D. Corbett in *Chemistry, Structure and Bonding of Zintl Phases and Ions* (Ed.: S. Kauzlarich), VCH, Chapter 4, in press.
[13] E. Zintl, G. Brauer, *Z. Phys. Chem.* **1933**, *20B*, 245.
[14] a) S. C. Sevov, J. D. Corbett, *Inorg. Chem.* **1993**, *32*, 1059; b) Z.-C. Dong and J. D. Corbett, unpublished.
[15] A Cd-centered Tl icosahedron has also been found in a derivative of the $Na_4K_6Tl_{13}$ structure [6]: M. M. Tillard-Charbonnel, C. H. E. Belin, A. P. Manteghetti, D. M. Flot, private communication.
[16] C.-H. Wong, C. Chieh, T.-Y. Lee, *Acta Crystallogr.* **1965**, *19*, 849.
[17] S. Samson, *Acta Chem. Scand.* **1949**, *3*, 809.
[18] U. Zachwieja, *Z. Kristallogr.* **1995**, *Suppl. Issue No. 9*, 25.
[19] N. Walker, D. Stuart, *Acta Crystallogr.* **1986**, *A39*, 158.
[20] P. W. Selwood, *Magnetochemistry*, 2nd ed., Interscience, New York, **1956**, p. 70.
[21] N. W. Ashcroft, D. N. Mermin, *Solid State Physics*; Holt, Rinehart and Winston: Philadelphia, PA, **1976**, p. 649.

A Double Calix[4]arene in a 1,3-*alternate* Conformation**

José-Antonio Pérez-Adelmar, Hervé Abraham, Concha Sánchez, Kari Rissanen, Pilar Prados,* and Javier de Mendoza*

Calixarenes offer attractive possibilities as molecular frameworks for the preparation of highly preorganized, rigid molecular receptors.[1] Double calixarenes, in which the lower rims are linked by suitable spacers (head-to-head), were recently described.[2] Some tail-to-tail (rings linked through the upper rims or *para* positions),[3] and head-to-tail[4] arrangements have also been reported. These structures have received increased attention because they display well preorganized molecular structures, most often in *cone* conformation. However, only a few examples of double calix[4]arenes in 1,3-*alternate* conformation (whose cylindrical shape features a molecular channel) are known, and they all belong to the head-to-head[5] or to the tail-to-tail[6] series. We report herein the synthesis of a 1,3-distal bridged double calix[4]arene in 1,3-*alternate* conformation, the first X-ray crystal structure of such a dimer, and a preliminary NMR study of its complexation with silver(I) ions.

The 1,3-distal O-alkylated derivative **2** was obtained from the parent *p*-H-calix[4]arene **1** (2.2 equiv potassium carbonate, 2.2 equiv 2-ethoxyethyl tosylate, acetonitrile, 2 atm, 130 °C, 74% yield). Reaction of **2** with *N*-bromosuccinimide in 2-butanone gave the dibromo compound **3** as the major component (76% yield after chromatography) and small amounts of the monobromo derivative **4** (1–4% yield). The ^1H[7] and ^{13}C NMR spectra[8] of these compounds indicate that they are in *cone* conformations.

Dibromo compound **3** was then fully O-alkylated under Reinhoudt's conditions (15 equiv cesium carbonate, 12 equiv 2-ethoxyethyl tosylate, DMF, 80 °C)[9] to give **5** as a 92:8 mixture of 1,3-*alternate* and *partial-cone* conformers from which the major 1,3-*alternate* conformer was isolated in 82% yield.

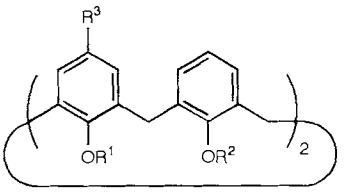

1 $R^1 = R^2 = R^3 = H$
2 $R^1 = R^3 = H$; $R^2 = CH_2CH_2OCH_2CH_3$
3 $R^1 = H$; $R^2 = CH_2CH_2OCH_2CH_3$; $R^3 = Br$
5 $R^1 = R^2 = CH_2CH_2OCH_2CH_3$; $R^3 = Br$
6 $R^1 = R^2 = CH_2CH_2OCH_2CH_3$; $R^3 = N_3$

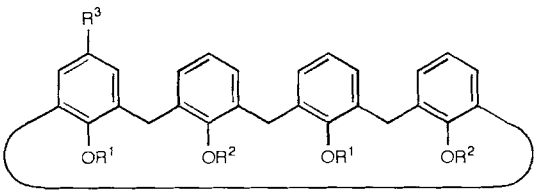

4 $R^1 = H$; $R^2 = CH_2CH_2OCH_2CH_3$; $R^3 = Br$
7 $R^1 = R^2 = CH_2CH_2OCH_2CH_3$; $R^3 = N_3$

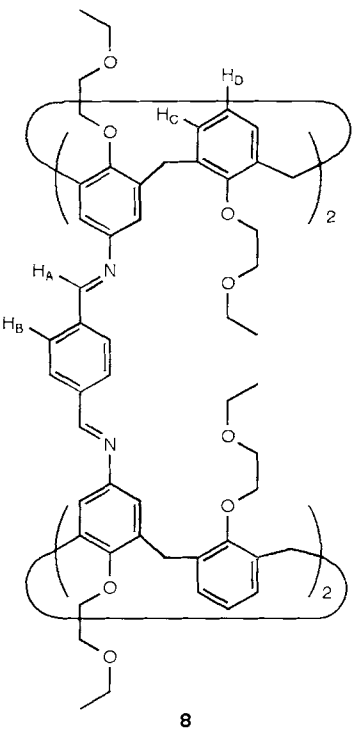

8

Bromine/lithium exchange (2.2 equiv *tert*-butyllithium, THF, −78 °C) followed by addition of tosyl azide and heating to reflux gave diazide **6** (56% yield) and small amounts of monoazide **7** (4% yield). Finally, aza-Wittig condensation of diazide **6** with terephthaldialdehyde afforded double calix[4]arene **8** in 30% yield.

In ^1H NMR spectra of compounds **5** and **8** isochronous signals at $\delta \approx 3.6$ were observed for the methylene bridge protons, even though AB systems, like those in the spectra of compounds **6** and **7**, were expected based on the substitution pattern of the aromatic rings. In the ^{13}C NMR spectra the signals of the

[*] Prof. Dr. P. Prados, Prof. Dr. J. de Mendoza, J.-A. Pérez-Adelmar, Dr. H. Abraham, Dr. C. Sánchez
Departamento de Química Orgánica
Universidad Autónoma de Madrid
Cantoblanco, E-28049 Madrid (Spain)
Fax: Int. code +(1)397-3966
Prof. Dr. K. Rissanen
Department of Chemistry, University of Jyväskylä, Jyväskylä (Finland)

[**] This work was supported by Dirección General de Investigación Científica y Técnica (DGICYT PB93 0283) and by the Finnish Academy (project no. 8588).

[12] J. D. Corbett in *Chemistry, Structure and Bonding of Zintl Phases and Ions* (Ed.: S. Kauzlarich), VCH, Chapter 4, in press.
[13] E. Zintl, G. Brauer, *Z. Phys. Chem.* **1933**, *20B*, 245.
[14] a) S. C. Sevov, J. D. Corbett, *Inorg. Chem.* **1993**, *32*, 1059; b) Z.-C. Dong and J. D. Corbett, unpublished.
[15] A Cd-centered Tl icosahedron has also been found in a derivative of the $Na_4K_6Tl_{13}$ structure [6]: M. M. Tillard-Charbonnel, C. H. E. Belin, A. P. Manteghetti, D. M. Flot, private communication.
[16] C.-H. Wong, C. Chieh, T.-Y. Lee, *Acta Crystallogr.* **1965**, *19*, 849.
[17] S. Samson, *Acta Chem. Scand.* **1949**, *3*, 809.
[18] U. Zachwieja, *Z. Kristallogr.* **1995**, *Suppl. Issue No. 9*, 25.
[19] N. Walker, D. Stuart, *Acta Crystallogr.* **1986**, *A39*, 158.
[20] P. W. Selwood, *Magnetochemistry*, 2nd ed., Interscience, New York, **1956**, p. 70.
[21] N. W. Ashcroft, D. N. Mermin, *Solid State Physics*; Holt, Rinehart and Winston: Philadelphia, PA, **1976**, p. 649.

A Double Calix[4]arene in a 1,3-*alternate* Conformation**

José-Antonio Pérez-Adelmar, Hervé Abraham, Concha Sánchez, Kari Rissanen, Pilar Prados,* and Javier de Mendoza*

Calixarenes offer attractive possibilities as molecular frameworks for the preparation of highly preorganized, rigid molecular receptors.[1] Double calixarenes, in which the lower rims are linked by suitable spacers (head-to-head), were recently described.[2] Some tail-to-tail (rings linked through the upper rims or *para* positions),[3] and head-to-tail[4] arrangements have also been reported. These structures have received increased attention because they display well preorganized molecular structures, most often in *cone* conformation. However, only a few examples of double calix[4]arenes in 1,3-*alternate* conformation (whose cylindrical shape features a molecular channel) are known, and they all belong to the head-to-head[5] or to the tail-to-tail[6] series. We report herein the synthesis of a 1,3-distal bridged double calix[4]arene in 1,3-*alternate* conformation, the first X-ray crystal structure of such a dimer, and a preliminary NMR study of its complexation with silver(I) ions.

The 1,3-distal O-alkylated derivative **2** was obtained from the parent *p*-H-calix[4]arene **1** (2.2 equiv potassium carbonate, 2.2 equiv 2-ethoxyethyl tosylate, acetonitrile, 2 atm, 130 °C, 74% yield). Reaction of **2** with *N*-bromosuccinimide in 2-butanone gave the dibromo compound **3** as the major component (76% yield after chromatography) and small amounts of the monobromo derivative **4** (1–4% yield). The ^1H[7] and ^{13}C NMR spectra[8] of these compounds indicate that they are in *cone* conformations.

Dibromo compound **3** was then fully O-alkylated under Reinhoudt's conditions (15 equiv cesium carbonate, 12 equiv 2-ethoxyethyl tosylate, DMF, 80 °C)[9] to give **5** as a 92:8 mixture of 1,3-*alternate* and *partial-cone* conformers from which the major 1,3-*alternate* conformer was isolated in 82% yield.

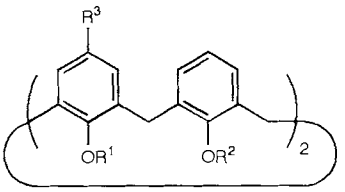

1 $R^1 = R^2 = R^3 = H$
2 $R^1 = R^3 = H$; $R^2 = CH_2CH_2OCH_2CH_3$
3 $R^1 = H$; $R^2 = CH_2CH_2OCH_2CH_3$; $R^3 = Br$
5 $R^1 = R^2 = CH_2CH_2OCH_2CH_3$; $R^3 = Br$
6 $R^1 = R^2 = CH_2CH_2OCH_2CH_3$; $R^3 = N_3$

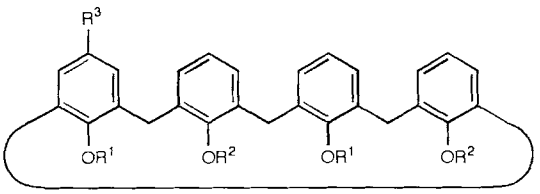

4 $R^1 = H$; $R^2 = CH_2CH_2OCH_2CH_3$; $R^3 = Br$
7 $R^1 = R^2 = CH_2CH_2OCH_2CH_3$; $R^3 = N_3$

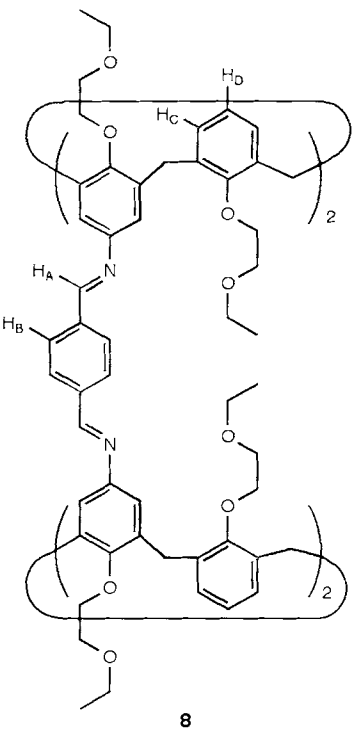

8

Bromine/lithium exchange (2.2 equiv *tert*-butyllithium, THF, −78 °C) followed by addition of tosyl azide and heating to reflux gave diazide **6** (56% yield) and small amounts of monoazide **7** (4% yield). Finally, aza-Wittig condensation of diazide **6** with terephthaldialdehyde afforded double calix[4]arene **8** in 30% yield.

In ^1H NMR spectra of compounds **5** and **8** isochronous signals at $\delta \approx 3.6$ were observed for the methylene bridge protons, even though AB systems, like those in the spectra of compounds **6** and **7**, were expected based on the substitution pattern of the aromatic rings. In the ^{13}C NMR spectra the signals of the

[*] Prof. Dr. P. Prados, Prof. Dr. J. de Mendoza, J.-A. Pérez-Adelmar, Dr. H. Abraham, Dr. C. Sánchez
Departamento de Química Orgánica
Universidad Autónoma de Madrid
Cantoblanco, E-28049 Madrid (Spain)
Fax: Int. code +(1)397-3966
Prof. Dr. K. Rissanen
Department of Chemistry, University of Jyväskylä, Jyväskylä (Finland)

[**] This work was supported by Dirección General de Investigación Científica y Técnica (DGICYT PB93 0283) and by the Finnish Academy (project no. 8588).

methylene groups in compounds **5**–**8** ranged between $\delta = 33.4$ and 35.4, deviating slightly from the typical value of $\delta = 37$ for calixarenes with 1,3-*alternate* conformations.[8] Reinhoudt et al. found similar deviations ($\delta \approx 35$) for calix[4]arenes whose X-ray structures showed distorted 1,3-*alternate* conformations.[9, 10]

The 1,3-*alternate* conformation of compound **8** was established unambiguously by a single-crystal X-ray structure determination (Fig. 1).[11] The double calix[4]arene **8** has a tubular shape with a cross section of 12 Å and a length of 28 Å (Fig. 1a). The inner diameter of the 1,3-*alternate* calix[4]arene termini varies from 4.1 to 4.5 Å, whereas the separation between nitrogen atoms at the bridges is 4.3 Å. Furthermore, the benzene rings of the terephthaloyl spacers are parallel to each other and separated by 3.3–3.9 Å. Due to the symmetry of **8** the ethoxyethyl arms at the end of the cylinder are twisted by 90° relative to each other in a suitable orientation to "shake hands" with the ethoxyethyl arms of an adjacent molecule. This creates an infinite channel-type structure in the crystal lattice (Fig. 1b). These infinite channels are tightly packed along the *a*-axis; the packing is enhanced by the close contacts of the central ethoxyethyl arms (Fig. 1c). The X-ray structure of **8** is the first reported of a double calix[4]arene in 1,3-*alternate* conformation[14] and shows how these compounds can self-assemble in the solid state as organic zeolite-type structures.

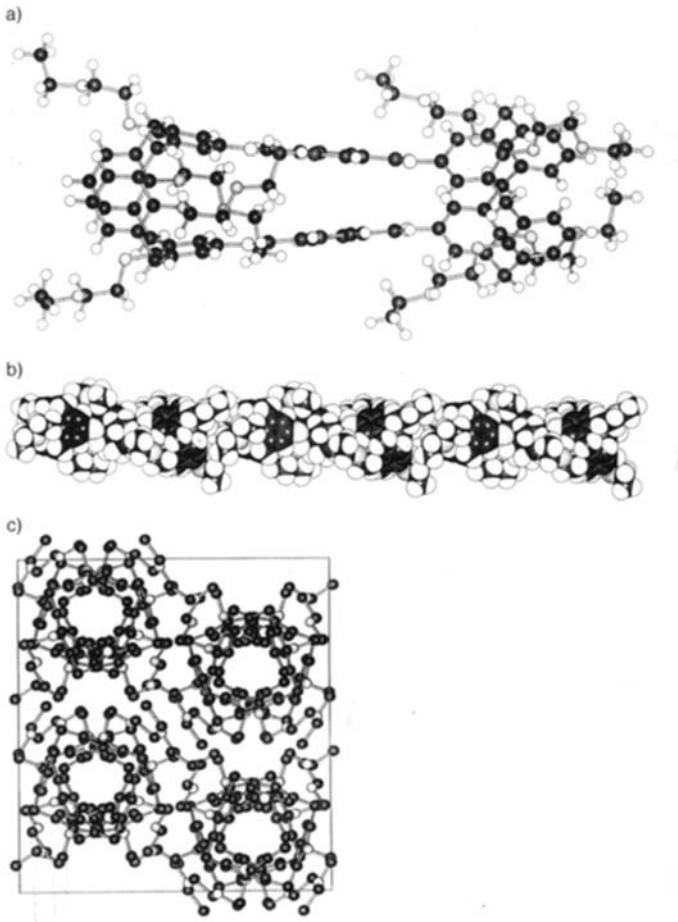

Fig. 1. Crystal structure of **8**. a) Side view. b) Side view of a CPK model of three aligned molecules, showing the tubular structure. c) Top view along the *a*-axis, showing the internal diameter of **8**.

Preliminary ^{1}H NMR experiments revealed that compound **8** shows affinity for silver(I) ions. Addition of increasing amounts of silver(I) triflate caused significant changes in the spectrum (Fig. 2). At room temperature the signals of the imine protons H_A and the protons H_B of the aromatic spacer are shifted significantly downfield, although no new signals appeared. When more than two equivalents of silver(I) had been added, the signals of the calixarene aromatic protons (such as H_C and H_D) shifted as well. Thus, it is likely that two metal ions are complexed initially by the imine nitrogen atoms and then two further cations are complexed at the calixarenes ends by the oxygen-containing chains. At $-80\,^\circ$C new signals appeared upon addition of up to two equivalents of silver(I), corresponding to mixtures of "frozen" species (free ligand, one and two metal atoms). Addition of an excess of the silver salt resulted in a single compound corresponding to the tetranuclear complex. In agreement with the NMR observations, the FAB-MS spectrum of **8** (*meta*-nitrobenzyl alcohol (*m*NBA) matrix) in the presence of an excess of silver(I) triflate shows peaks at *m/z* (%) 2561.1 (0.4) $[(M \cdot Ag \cdot 3AgOTf)^+]$, 2304.2 (3) $[(M \cdot Ag \cdot 2AgOTf)^+]$, 2046.2 (100) $[(M \cdot Ag \cdot AgOTf)^+]$, and 1790.0 (62.4) $[(M \cdot Ag)^+]$.

Addition of small amounts of potassium picrate induced downfield shifts of the signals of the calixarene H_C and H_D aromatic protons. Experiments aimed to study complexation

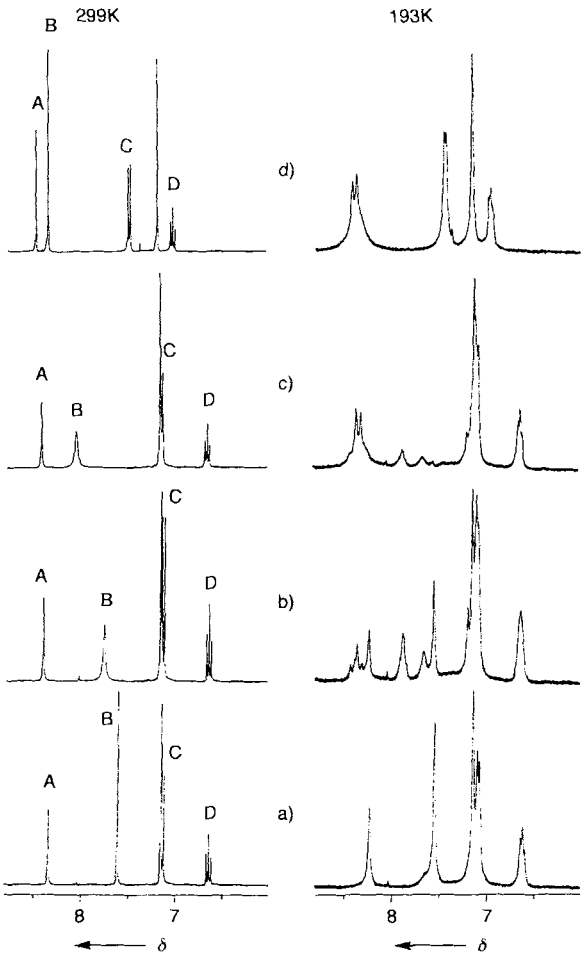

Fig. 2. ^{1}H NMR spectrum of **8** (300 MHz, $CDCl_3/CD_3OD$ 4/1 (v/v)] between $\delta = 6.0$ and 8.8 at 299 K (left) and 193 K (right): a) pure **8**, b) **8** with 1.0, c) 2.0, and d) 10.0 equiv silver(I) triflate.

 © VCH Verlagsgesellschaft mbH, D-69451 Weinheim, 1996 0570-0833/96/3509-1010 $ 15.00+.25/0

and/or scrambling of potassium cations at the ends of the dimeric structure in the presence of one or two silver(I) ions, which could block the channel at the central imine binding sites, are currently underway.

Experimental Procedure

8: To a solution of **6** (310 mg, 0.39 mmol) and Ph_3P (246 mg, 2.4 equiv, 0.94 mmol) in dry toluene (150 mL) was added a solution of terephthaldialdehyde (52 mg, 1 equiv, 0.39 mmol) in toluene (10 mL) under Ar. The mixture was stirred at room temperature for 7 d, the solvent was removed in vacuo, and the residue was triturated with diethyl ether and filtered. The filtrate was concentrated to dryness and the resulting solid was triturated with acetonitrile and filtered. Column chromatography (ethyl acetate/hexane, 1:1) afforded **8** (110 mg, 30%). M.p. > 300 °C; ^{1}H NMR (300 MHz, $CDCl_3$): δ = 8.31 (s, 4H, CH=N), 7.58 (s, 8H, ArH), 7.15 (d, J = 7.5 Hz, 8H, ArH), 7.13 (s, 8H, ArH), 6.65 (t, J = 7.5 Hz, 4H, ArH), 4.10–3.93 (m, 24H, OCH_2CH_2O), 3.83–3.80 (m, 8H, OCH_2CH_2O), 3.69 (q, J = 7.0 Hz, 8H, OCH_2CH_3), 3.68 (q, J = 7.0 Hz, 8H, OCH_2CH_3), 3.60 (s, 16H, $ArCH_2Ar$), 1.35 (t, J = 7.0 Hz, 12H, OCH_2CH_3), 1.27 (t, J = 7.0 Hz, 12H, OCH_2CH_3); ^{13}C NMR (75 MHz, $CDCl_3$, Heteronuclear Multiple Bond Correlation (HMBC), Heteronuclear Multiple Quantum Correlation (HMQC)): δ = 157.8 (CH=N), 155.7, 154.2, 145.3, 135.2, 133.9 (ArC), 130.3, 128.3, 122.5, 121.5 (ArCH), 72.3, 72.2, 70.2, 69.9 (OCH_2CH_2O), 66.6 (OCH_2CH_3), 34.5 ($ArCH_2Ar$), 15.2 (OCH_2CH_3); FAB-HRMS (*m*NBA matrix): *m/z*: 1681.8746 [$M^+ + 1$]; calcd. for $C_{104}H_{121}N_4O_{16}$, 1681.8777.

Received: November 27, 1995 [Z85951E]
German version: *Angew. Chem.* **1996**, *108*, 1088–1090

Keywords: calixarenes · silver compounds

[1] C. D. Gutsche in *Calixarenes: Monographs in Supramolecular Chemistry, Vol. 1* (Ed.: J. F. Stoddart), Royal Society of Chemistry, Cambridge, **1989**; J. Vicens, V. Böhmer, *Calixarenes, a Versatile Class of Macrocyclic Compounds*, Kluwer, Dordrecht, **1990**; V. Böhmer, *Angew. Chem.* **1995**, *107*, 785; *Angew. Chem. Int. Ed. Engl.* **1995**, *34*, 713.

[2] a) J.-D. van Loon, D. Kraft, M. J. J. Ankoné, W. Verboom, S. Harkema, W. Vogt, V. Böhmer, D. N. Reinhoudt, *J. Org. Chem.* **1990**, *55*, 5176; b) D. Kraft, J.-D. van Loon, M. Owens, W. Verboom, W. Vogt, M. A. McKervey, V. Böhmer, D. N. Reinhoudt, *Tetrahedron Lett.* **1990**, *31*, 4941; c) G. Ulrich, R. Ziessel, *ibid.* **1994**, *35*, 6299; d) Z.-L. Zhong, Y.-Y. Chen, X.-R. Lu, *ibid.* **1995**, *36*, 6735; e) R. Milbradt, J. Weiss, *ibid.* **1995**, *36*, 2999; f) F. Ohseto, S. Shinkai, *J. Chem. Soc. Perkin Trans. 2* **1995**, 1103.

[3] a) V. Böhmer, H. Goldman, W. Vogt, J. Vicens, Z. Asfari, *Tetrahedron Lett.* **1989**, *30*, 1391; b) A. Arduini, G. Manfredi, A. Pochini, A. R. Sicuri, R. Ungaro, *J. Chem. Soc. Chem. Commun.* **1991**, 936; c) K. Araki, K. Sisido, K. Hisaichi, S. Shinkai, *Tetrahedron Lett.* **1993**, *34*, 8297; d) A. Arduini, S. Fanni, G. Manfredi, A. Pochini, R. Ungaro, A. R. Sicuri, F. Ugozzoli, *J. Org. Chem.* **1995**, *60*, 1448.

[4] a) W. Wasikiewicz, G. Rokichi, J. Kielkiewicz, V. Böhmer, *Angew. Chem.* **1994**, *106*, 230; *Angew. Chem. Int. Ed. Engl.* **1994**, *33*, 214; b) P. D. Beer, P. A. Gale, D. Hesek, *Tetrahedron Lett.* **1995**, *36*, 767.

[5] a) Z. Asfari, R. Abidi, F. Arnaud, J. Vicens, *J. Inclusion Phenom. Mol. Recognit. Chem.* **1992**, *13*, 163; b) Z. Asfari, J. Weiss, S. Pappalardo, J. Vicens, *Pure Appl. Chem.* **1993**, *65*, 585; c) Z. Asfari, S. Wenger, J. Vicens, *ibid.* **1995**, *67*, 1037.

[6] A. Ikeda, S. Shinkai, *J. Chem. Soc. Chem. Commun.* **1994**, 2375.

[7] C. D. Gutsche, B. Dhawan, J. A. Levine, K. Hylen, L. J. Bauer, *Tetrahedron* **1983**, *39*, 409.

[8] C. Jaime, J. de Mendoza, P. Prados, P. M. Nieto, C. Sánchez, *J. Org. Chem.* **1991**, *56*, 3372.

[9] W. Verboom, S. Datta, Z. Asfari, S. Harkema, D. N. Reinhoudt, *J. Org. Chem.* **1992**, *57*, 5394.

[10] In agreement with this, the spectrum of the isomer of **5** having a *partial cone* conformation shows an AX system (δ = 4.21 and 3.00) for methylene bridges in *syn* orientation and an AB system (δ = 3.62 and 3.72) for those *anti* oriented (HMQC). The corresponding ^{13}C signals appear at δ = 30.4 and 34.2, respectively.

[11] Crystal structure analysis of **8**: $C_{104}H_{120}N_4O_{16}$, M_r = 1682.1, monoclinic, space group $C2/c$ (no. 15), a = 27.029(6), b = 19.612(3), c = 19.540(4) Å, β = 110.63(2)°, V = 9693(4) Å^3, Z = 4, ρ_{calcd} = 1.153 g cm^{-3}, $F(000)$ = 3658, T = 296 ± 1 K. The data were collected from a colorless crystal with dimensions 0.30 × 0.30 × 0.45 mm. Of 6956 collected reflections, 5586 were unique (R_{int} = 0.040), recorded with a SYNTEX $P2_1$ diffractometer using graphite-monochromated $Cu_{K\alpha}$ radiation [λ = 1.5418 Å] and a ω-scan mode to 2θ = 113° (h: −29 → 27, k: 0 → 21, and l: 0 → 21), 3167 reflections with $I > 2\sigma(I)$ were used for refinement. Lp correction, but no absorption correction was applied, $\mu(Cu_{K\alpha})$ = 0.613 mm^{-1}. The structure was solved by direct methods (SHELXS) [12] and subjected to full-matrix refinement [13]. The ratio F_o/(number of parameters) was 5.46, R = 0.121, and R_w = 0.143 for 580 parameters; $w = w'[1.0 - (\Delta F/6\sigma F)^2]^2$, where w' = Chebychev polynomial for F_c with three coefficients (2.79, 3.34, 1.54), S = 1.18, convergence, max. shift/error < 0.08. A final difference map displayed no electron density higher than 0.73 e Å^{-3}. Crystallographic data (excluding structure factors) for the structure reported in this paper have been deposited with the Cambridge Crystallographic Data Centre as supplementary publication no. CCDC-179-20. Copies of the data can be obtained free of charge on application to The Director, CCDC, 12 Union Road, Cambridge CB21EZ, UK (fax: Int. code +(1223) 336-033; e-mail: teched@chemcrys.cam.ac.uk).

[12] G. M. Sheldrick in *Crystallographic Computing 3* (Eds.: G. M. Sheldrick, C. Krüger, R. Goddard), Oxford University Press, Oxford, **1985**, p. 175.

[13] D. Watkin, J. R. Carruthers, P. W. Betteridge, *CRYSTALS*, Chemical Crystallography Laboratory, Oxford, **1990**.

[14] For an X-ray crystal structure of a double calix[4]arene in *cone* conformation, see ref. [3d]. No crystal structures have been reported for the double calixarenes in 1,3-*alternate* conformation [5, 6].

A Stable Tetraazafulvalene**

T. Andrew Taton and Peter Chen*

We report the synthesis, X-ray crystal structure, and chemical behavior of the electron-rich olefinic dimer of an *N,N'*-dialkylimidazol-2-ylidene (an Arduengo carbene). The carbenes were recently found,[1] much to everyone's surprise, to be isolable compounds, raising the question as to the C=C bond dissociation enthalpy of the tetraazafulvalene-type dimer of the carbenes. Qualitative theoretical considerations had predicted the bond enthalpy of tetraazafulvalenes to be close to zero, or possibly even negative. In the first thermochemical study of the dimerization of an *N,N'*-dialkylimidazol-2-ylidene, we find the bond dissociation enthalpy of *N,N',N'',N'''*-tetraalkyltetraazafulvalenes to be only slightly greater than zero.

The tetraazafulvalene **1** (n,m = 3) was prepared by two separate routes (Scheme 1). Double deprotonation of the

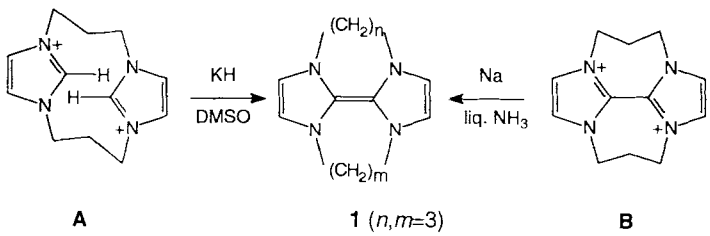

Scheme 1. Synthesis of **1** (n,m = 3).

doubly bridged bis(imidazolium) dication **A** by treatment with KH in dimethyl sulfoxide (DMSO) or alternatively with $NaNH_2$ in NH_3 afforded **1** rather than the biscarbene **1'** (n,m = 3). Reduction of a doubly bridged biimidazolium dication **B**[2] with sodium in liquid ammonia, evaporation of the ammonia, extraction of the residue with hexane, and finally

[*] Prof. Dr. P. Chen, T. A. Taton
Laboratorium für Organische Chemie
der Eidgenössischen Technischen Hochschule
Universitätstrasse 16, CH-8092 Zürich (Switzerland)
Fax: Int. code +(1)632-1280
e-mail: peter@chen2.ethz.ch

[**] The research was supported by the Schweizerische Nationalfonds zur Förderung der wissenschaftlichen Forschung. The authors acknowledge the generous assistance of Prof. Dr. Bernhard Jaun (ETH Zürich) and Paul Seiler (ETH Zürich, X-ray structure analysis).

recrystallization of the crude product by slow evaporation yielded pale yellow prisms whose spectroscopic properties[3] are identical to those of **1** ($n,m = 3$) produced by the other route.

The presence of a genuine double bond between the two imidazol-2-ylidene moieties is evident from the ^{13}C NMR chemical shift of central olefinic carbon in **1**. For the carbenes this signal occurs at $\delta = 210-220$, whereas for the tetraazafulvalene **1** ($n,m = 3$) it is found at $\delta = 127.5$. Furthermore, in the X-ray crystal structure[4] of **1** ($n,m = 3$) (Fig. 1) the C–C distance is

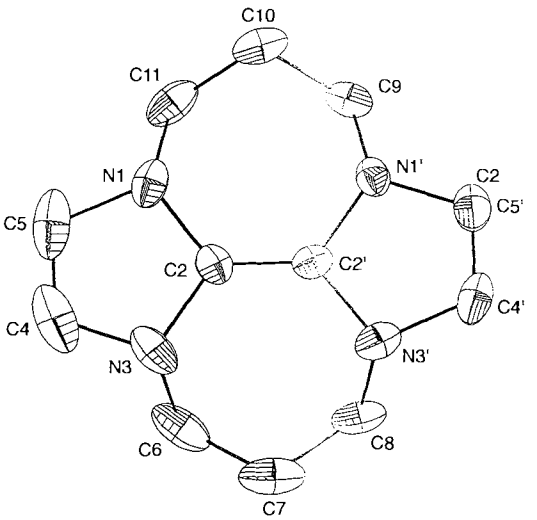

Fig. 1. X-ray crystal structure of **1** ($n,m = 3$). The H atoms are omitted for clarity. Selected distances [Å] and angles [°]: C2–C2' 1.337(5), C2/2'–N1/3/1'/3' 1.429(4) (av), N1/3/1'/3'–C4/5/4'/5' 1.410(6) (av), C4/4'–C5/5' 1.294(9) (av); N1/1'-C2/2'-N3/3' 107.9(3) (av).

1.337(5) Å, and the central olefinic portion of the molecule close to planar, which is completely consistent with the presence of a bona fide double bond. Although further details of the structure will be discussed in a separate report, one should mention here that the two trimethylene bridges are strongly puckered, permitting considerable flexibility in the molecule. It is noteworthy that in the X-ray structures of the related doubly bridged (also with two trimethylene bridges) bis(benzimidazolone)[5] the two heterocyclic rings are placed face-to-face to minimize steric repulsions, in sharp contrast to **1** ($n,m = 3$). We find **1** ($n,m = 3$) to be stable at room temperature both in solution and in the solid state for days under anhydrous, anaerobic conditions. Furthermore, no change in the ^1H NMR spectrum of **1** ($n,m = 3$) was observed even upon heating to 100 °C in [D_6]DMSO for 15 minutes or more.

Preparation of **1** ($n,m = 4$) by reduction of the corresponding biimidazolium salt in liquid ammonia, extraction, and recrystallization also produced yellow crystals, which, upon warming to room temperature, rapidly changed into a white powder. The powder was identified as the doubly bridged biscarbene **1'** ($n,m = 4$) by its characteristic ^1H NMR spectrum.[6] All attempts to prepare the monobridged tetraazafulvalenes **2** and the unbridged species **3** yielded only the corresponding carbenes **2'** and **3'**

The theoretical prediction of a near-zero or negative bond enthalpy for tetraazafulvalenes is based on a valence-bond promotion energy picture,[7] most recently expounded by Carter and Goddard with ab initio calculations in support.[8] The overall scheme is closely related to valence state arguments from spin-valence theory,[9] the DSSE (= divalent state stabilization

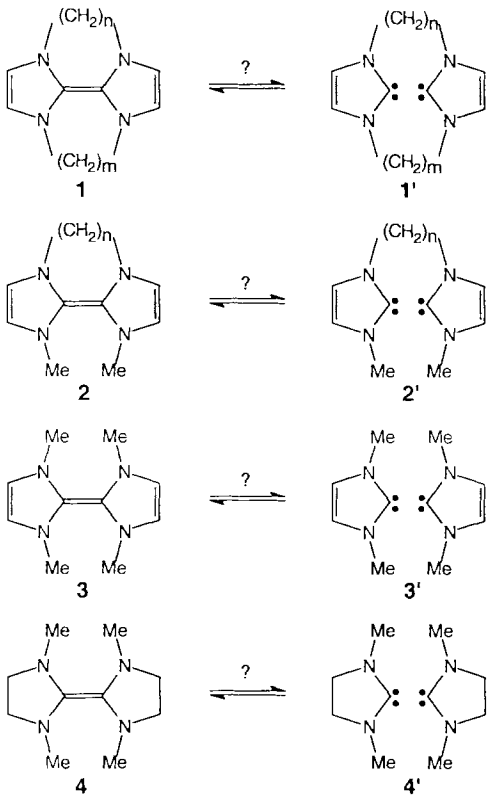

energy) model by Walsh[10] and the valence-bond curve-crossing model by Pross and Shaik.[11] In the Carter and Goddard formulation, the strength of the C=C bond in the formal dimer of a pair of singlet carbenes should correspond to that of a canonical C=C bond (usually that of ethene) minus the sum of the singlet–triplet energy difference for the two carbenes. The singlet–triplet splitting in imidazol-2-ylidenes has been predicted by ab initio calculations[12] to be approximately 85 kcal mol^{-1}, which is the largest value known for any divalent carbon compound other than CO or isocyanides. Accordingly, one expects the bond strength in a tetraazafulvalene to be approximately $[172 - (2 \times 85)] \approx 2$ kcal mol^{-1}. The failure of previous attempts to isolate tetraazafulvalenes has been attributed to the nearly nonexistent bond between the two halves of the molecule. One notes that the tetraaminoethene **4**, which is a formal dimer of imidazolidin-2-ylidene **4'**, has been known for over 30 years,[13] and the dibenzo analogs of **1** ($n,m = 3$) have been recently reported.[5] In these cases, the singlet–triplet energy gap of the carbene is reduced[12] by saturation of the heterocyclic carbene or benzannelation, which increases the strength of the C=C bond in the dimer. However, it is absolutely essential to acknowledge that isolability of either the carbene or its dimer gives no actual information about the C=C bond strength. The surprising preparation and X-ray crystal structure determination of the *N,N'*-dimesitylimidazolidin-2-ylidene[14] related to carbene **4'**, together with the long-known isolability of **4**, underlines the point that isolability only means that a kinetic barrier exists to either dimerization or dissociation. Because we have prepared a series of tetraazafulvalenes that differ only in the number and length of the methylene bridges, and observed the entire range of possibilities from stable dimers, to interconverting dimers and carbenes, to stable carbenes, we can make the following hypothesis. Based on the ready conversion of **1** ($n,m = 4$) to **1'** ($n,m = 4$), we can surmise that the kinetic barrier to dissociation is low enough so that the conversion **1** ($n,m = 3$) to **1'** ($n,m = 3$) would occur if it were thermochemically favorable.

Detailed equilibrium and kinetic studies will be the subject of a future report, but we can already place relatively narrow bounds on the enthalpy of dissociation of the central C=C bond in *N,N',N'',N'''*-tetraalkyltetraazafulvalenes. The problem in determining the enthalpy of C=C bond scission in **1** is similar to that in describing the energetics of intramolecular reactions[15] or of the formation of intramolecular hydrogen bonds in flexible systems.[16] Assuming that the enthalpy of dissociation is approximately constant across the series **1**, **2**, and **3**, the differences in the free energy of dissociation, which is positive for **1** ($n,m = 3$), near-zero or slightly negative for **1** ($n,m = 4$), and more strongly negative for **2** and **3**, should arise principally from differences in the entropy of dissociation. A lower bound of $\Delta H > 0$ is based on the stability of **1** ($n,m = 3$). Given that dissociation is kinetically possible in this case, only a positive ΔH could give a positive ΔG when ΔS for the reaction **1** ($n,m = 3$) → **1'** ($n,m = 3$) is positive. An upper bound on the ΔS value for dissociation of any of the tetraazafulvalenes is $\Delta S < 35\ \mathrm{cal\,mol^{-1}\,K^{-1}}$, which would correspond to the reaction **3** → **3'**. That places, in turn, an upper bound of $\Delta H < 10\ \mathrm{kcal\,mol^{-1}}$ for **1**, **2**, and **3**. Because the ΔH value is actually bracketed by the difference in $T\Delta S$ for the two reactions, **1** ($n,m = 3$) → **1'** ($n,m = 3$) and **1** ($n,m = 4$) → **1'** ($n,m = 4$), and ΔS for **1** ($n,m = 4$) → **1'** ($n,m = 4$) is certainly much less than the upper bound of $35\ \mathrm{cal\,mol^{-1}\,K^{-1}}$, we can estimate with confidence that the bond dissociation enthalpy for an *N,N',N'',N'''*-tetraalkyltetraazafulvalene is $\Delta H = 4 \pm 3\ \mathrm{kcal\,mol^{-1}}$. The exceedingly weak bond is a striking confirmation of the quantitative accuracy of a qualitative theory.

We have prepared and characterized a series of tetraazafulvalenes of varying stability, including one that is isolable at room temperature. Its structure was determined unambiguously by NMR spectroscopy and X-ray crystallography. An estimate of the bond dissociation enthalpy for tetraazafulvalenes agrees very well with expectations from qualitative theory, and confirms the existence of a very weak C=C bond in the formal dimers of singlet carbenes.[17]

Received: February 14, 1996 [Z 8822IE]
German version: *Angew. Chem.* **1996**, *108*, 1098–1100

Keywords: carbenes · imidazol-2-ylidenes

[1] A. J. Arduengo III, R. L. Harlow, M. Kline, *J. Am. Chem. Soc.* **1991**, *113*, 361; A. J. Arduengo III, H. V. R. Dias, R. L. Harlow, M. Kline, *ibid.* **1992**, *114*, 5530; A. J. Arduengo III, H. V. R. Dias, D. A. Dixon, R. L. Harlow, W. T. Klooster, T. F. Koetzle, *ibid.* **1994**, *116*, 6812; M. Regitz, *Angew. Chem.* **1996**, *108*, 791; *Angew. Chem. Int. Ed. Engl.* **1996**, *35*, 725.

[2] Synthesis of the doubly bridged biimidazolium dications followed the general procedure in: R. P. Thummel, V. Goulle, B. Chen, *J. Org. Chem.* **1989**, *54*, 3057.

[3] M.p. 102–103 °C (decomp); ^{1}H NMR ([D$_8$]dioxane): $\delta = 5.62$ (s, 4H), 2.58 (m, 8H), 1.58 (m, 4H); ^{13}C NMR ([D$_8$]dioxane, $T_1 = 10$ s): $\delta = 127.5$, 120.3, 54.3, 31.5; IR (C_6H_6): $\tilde{\nu} = 3107$, 2929, 2820, 1604, 1440, 1374, 1342, 1309, 1236, 1148, 1077, 927, 882, 812, 698, 620, 566 cm^{-1}; EI MS (70 eV): *m/z* (%): 216 [M^+], 188, 174, 159, 146, 134, 119, 106, 94, 81, 68, 53, 41 (100); UV/Vis (hexane): λ_{max} (ε) = 330 nm (8000).

[4] A yellow crystal of **1** ($n, m = 3$) suitable for X-ray diffraction analysis was grown by slow evaporation of a saturated hexane solution and mounted in an ultrathin sealed capillary. Crystal data for **1** ($n,m = 3$) at 213 K: crystal dimensions [mm]: ca. $0.2 \times 0.3 \times 0.3$, monoclinic, space group $P2_1/n$ (no. 14), $a = 8.715(2)$, $b = 9.518(2)$, $c = 14.171(8)$ Å, $\beta = 97.84(0)°$, $V = 1164.5(7)$ Å^3, $Z = 4$, $\rho_{calcd} = 1.23\ \mathrm{g\,cm^{-3}}$, $F(000) = 464$; 2168 reflections with $\theta < 25.0°$. Structure solution and refinement for 1260 independent reflections with $I > 2.0\sigma(I)$ and 163 parameters. $R = 0.057$; $R(w) = 0.067$. Residual electron density max. 0.32, min. $-0.66\ \mathrm{e\,Å^{-3}}$. Nonius CAD4 diffractometer, $Mo_{K\alpha}$ radiation ($\mu = 5.68\ \mathrm{mm^{-1}}$); graphite monochromator. Structure solution and refinement was carried out using SHELXTL PLUS, with hydrogen atoms included in calculated positions. Crystallographic data (excluding structure factors) for the structure reported in this paper have been deposited with the Cambridge Crystallographic Data Centre as supplementary publication no. CCDC-179-27. Copies of the data can be obtained free of charge on application to The Director, CCDC, 12 Union Road, Cambridge CB2 1EZ, UK (fax: int. code +(1223) 336-033; e-mail: teched@chemcrys.cam.ac.uk).

[5] Z. Shi, R. P. Thummel, *Tetrahedron Lett.* **1994**, *35*, 33; *ibid.* **1995**, *36*, 2741.

[6] **1** ($n,m = 4$): ^{1}H NMR ([D$_8$]toluene, −50 °C): $\delta = 5.48$ (s, 4H), 3.20 (br. m, 8H), 1.68 (br. m, 8H); **1'** ($n,m = 4$): ^{1}H NMR ([D$_7$]DMF): $\delta = 6.83$ (s, 4H), 3.75 (br. m, 8H), 1.75 (br. m, 8H). The ^{1}H NMR NMR spectrum of bridged biscarbene **1'** is essentially identical to those for the monomeric carbenes reported in ref. [1] and differs from that of **1** principally in the downfield shifts of the vinylic protons.

[7] J. A. Blush, H. Clauberg, D. W. Kohn, D. W. Minsek, X. Zhang, P. Chen, *Acc. Chem. Res.* **1992**, *25*, 385.

[8] E. A. Carter, W. A. Goddard, *J. Phys. Chem.* **1986**, *90*, 998.

[9] J. N. Murrell, S. F. A. Kettle, J. M. Tedder, *The Chemical Bond*, 2nd ed., Wiley, New York, **1985**, pp. 247–249. See also: J. P. Simons, *Nature* **1965**, *205*, 1308.

[10] R. Walsh, *Acc. Chem. Res.* **1981**, *14*, 246; *Pure Appl. Chem.* **1987**, *59*, 69; R. S. Grev, H. F. Schaefer III, K. Baines, *J. Am. Chem. Soc.* **1990**, *112*, 9458.

[11] A. Pross, S. S. Shaik, *Acc. Chem. Res.* **1983**, *16*, 363.

[12] C. Heinemann, W. Thiel, *Chem. Phys. Lett.* **1994**, *217*, 11; D. A. Dixon, A. J. Arduengo III, *J. Phys. Chem.* **1991**, *95*, 4180.

[13] H. W. Wanzlick, *Angew. Chem.* **1962**, *74*, 129; H. Schönherr, H. W. Wanzlick, *Chem. Ber.* **1970**, *103*, 1037.

[14] A. J. Arduengo III, J. R. Goerlich, W. J. Marshall, *J. Am. Chem. Soc.* **1995**, *117*, 11027.

[15] M. I. Page, W. P. Jencks, *Proc. Nat. Acad. Sci. USA* **1971**, *68*, 1678; L. Mandolini, *Bull. Chim. Soc. Fr.* **1988**, 173.

[16] M. S. Searle, D. H. Williams, *J. Am. Chem. Soc.* **1992**, *114*, 10690.

[17] We have just been informed of an independent preparation of **1** ($n,m = 3$) by bulk electrolysis of a doubly bridged bis(imidazolium) salt (Z. Shi, V. Goulle, R. P. Thummel, *Tetrahedron Lett.*, in press). The ^{1}H and ^{13}C NMR spectra in that work are essentially identical to those in the present report.

Synthesis and Characterization of Bis(chlorin)s from the McMurry Reaction of Formylchlorins**

Laurent Jaquinod, Daniel J. Nurco, Craig J. Medforth, Ravindra K. Pandey, Timothy P. Forsyth, Marilyn M. Olmstead, and Kevin M. Smith*

Arrays of porphyrins linked by rigid spacer groups have become important for the understanding the interchromophore electron-transfer mechanisms responsible for the primary charge separation in photosynthesis[1] and for their potential uses as electronic devices such as conducting polymers (molecular wires),[2] photovoltaic devices,[3] and molecular logic devices;[4] dimers with "face-to-face" or "gable" arrangements are also effective catalysts for the four-electron reduction of dioxygen to water,[5] and the oxidation of organic substrates.[6] Previous work in our laboratories has focused on the synthesis of dimers with ethylene or stilbene linking units through coupling with low-valent titanium (McMurry coupling),[7, 8] as well as through reductive couplings of benzochlorins bearing an acrolein side group.[8] Although these and other porphyrins have proven to be valuable model compounds, we felt that chlorin–chlorin dimers would be a useful step toward the preparation of more biologically relevant model systems. In this paper we describe the reductive coupling of 20-formyl- and 3-formylchlorin derivatives (**1–3**), and some of the unusual

[*] Prof. Dr. K. M. Smith, Dr. L. Jaquinod, D. J. Nurco, Dr. C. J. Medforth, Dr. R. K. Pandey,[+] T. P. Forsyth, Dr. M. M. Olmstead
Department of Chemistry
University of California, Davis, CA 95616 (USA)
Fax: Int. code +(916)752-8995
e-mail: smith@chem.ucdavis.edu

[+] Permanent address: Department of Radiation Biology, Roswell, Park Cancer Institute, Buffalo, NY 14263 (USA)

[**] This work was supported by grant CHE-93-05577 from the National Science Foundation, and a grant from Oncologic Foundation of Buffalo.

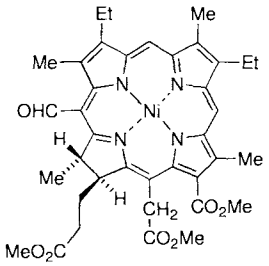

1

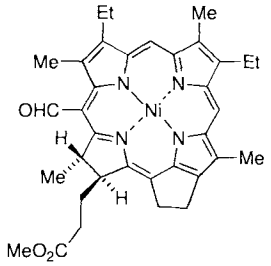

2

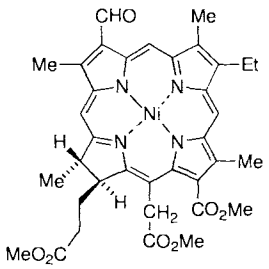

3

structural and spectroscopic properties of the bis-systems obtained from these reactions.

McMurry coupling of nickel(II) 20-formylmesochlorin-e_6 trimethyl ester (**1**) at room temperature or in 1,2-dimethoxymethane (DME) at reflux led to the production of a single bis(chlorin) in 52% yield.[9] X-ray crystallography (Fig. 1)[10]

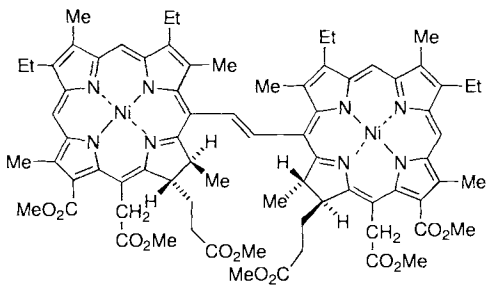

4

showed the molecular structure of the dimer to be **4**, in which two crystallographically independent Ni^{II}-chlorin molecules are covalently linked by an ethylene bridge (C=C 1.330(8) Å). To the best of our knowledge, **4** is the first structurally characterized ethene-linked bis(chlorin), though an ethane-linked bis(octaethylchlorin) has been reported.[12] In **4** the nickel-chlorin units are in a *trans* arrangement about the ethylene bridge, with a mean deviation of the porphyrin core atoms from the least squares plane of 0.35 Å and an average Ni-N distance of 1.915 Å. The latter are consistent with the known tendency of nickel porphyrins to favor nonplanar structures with short Ni-N distances.[13, 14] The ^{1}H NMR spectrum of **4** at room temperature shows apparent C_2 symmetry, but upon cooling to 174 K in CS_2/CD_2Cl_2 (3/1) many of the signals broaden and split into two signals of unequal intensity. For the vinyl protons, the downfield signal ($\delta = 7.56$) is favored over the upfield signal ($\delta = 6.28$) by a ratio of 2.1:1 ($\Delta G^{\circ}_{175\,K} = 1.1$ kJ mol^{-1}). The energy barrier for this process estimated from the coalescence temperature of the vinyl protons is $\Delta G^{*}_{223\,K} = 41.6$ kJ mol^{-1}. At present, the most likely explanation for the dynamic behavior exhibited by **4** is restricted rotation about the $C_{meso}-C_{vinyl}$ bonds, with slow exchange between conformations which have the reduced rings on the same side of the dimer (as in the crystal form shown in Fig. 1) and a structure in which both chlorins are rotated 180° about the $C_{meso}-C_{vinyl}$ bond. Other dynamic processes, such as inversion of the nonplanar macrocycles,[15, 16] were considered but could not be used to rationalize the observed dynamic behavior in **4**. Note that in contrast to bis(porphyrins),[17] heating **4** at reflux in deoxygenated boiling acetic acid did not yield significant *cis-trans* isomerization, perhaps because of the steric repulsions present in a dimer with *cis* chlorin substituents.

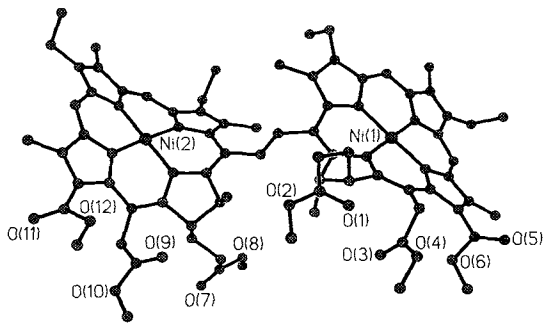

Fig. 1. Molecular structure of *trans*-bis(chlorin) **4**.

Coupling of the related chlorin, nickel(II) methyl-20-formyl-13^1-deoxomesopyropheophorbidea (**2**) gave the corresponding bis(pheophorbide) **5a** in 72% yield. Variable-temperature proton NMR studies also revealed a dynamic process for this dimer ($\Delta G^{*}_{223\,K} = 41.9$ kJ mol^{-1}). The ratio of the intensities of the signals from the two components is reversed relative to **4**: the upfield vinyl signal ($\delta = 6.57$) is favored over the downfield one ($\delta = 7.61$) by a ratio of 6:1 in favor of the structure in which the chlorin units are rotated by 180° ($\Delta G^{\circ}_{174\,K} = 2.6$ kJ mol^{-1}). Coupling of nickel(II) 3-formyl-3-devinylchlorin-e_6 trimethyl ester[18] (**3**) gave a 67% yield of a bis(chlorin) identified as **6a**, in which the macrocycles are linked by an ethylene bridge at a pyrrole position rather than a *meso* position. Variable-temperature proton NMR studies

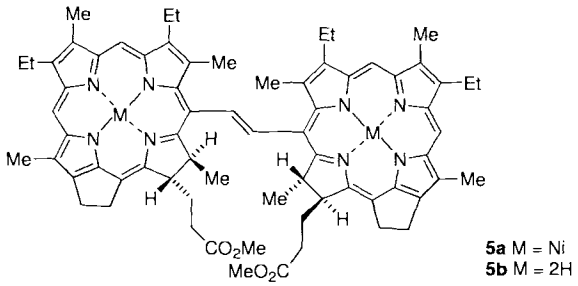

5a M = Ni
5b M = 2H

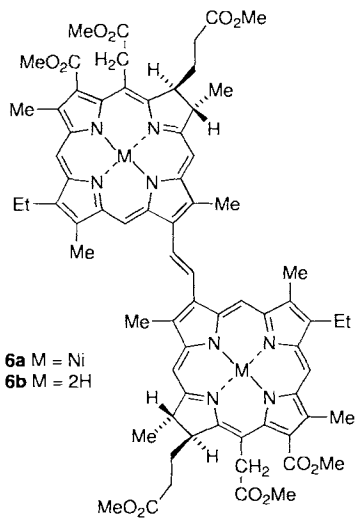

6a M = Ni
6b M = 2H

of **6a** revealed broadening and coalescence of some signals upon cooling, although the nature of the dynamic process was not clear for this bis(chlorin). Interestingly, the behavior of chlorin **3** in the coupling reaction is quite different from that observed for nickel(II) 2-formyl-3,7,8,12,13,17,18-heptaethylporphyrin, which gives a bis(porphyrin carbinol) upon McMurry coupling, rather than an ethylene-linked dimer.[8]

Attempts to demetalate bis(chlorin)s **5a** and **6a** with concentrated H_2SO_4 led to decomposition, so metal-free bis-systems **5b** and **6b** were accessed by performing the coupling reaction in which Zn^{II} is the coordinated metal ion, followed by demetalation of the McMurry product with trifluoroacetic acid (TFA). Previous attempts to couple Zn^{II} porphyrins have led to substantial decomposition.[19] In the present work, the coupling was performed in THF at room temperature in the presence of 3.5 equivalents of pyridine (to prevent any HCl formed during the reduction of $TiCl_3$ from demetalating the acid-labile Zn^{II}-chlorins prior to the coupling). The molecular structure was determined crystallographically (Fig. 2)[10] for the free base **5b** of

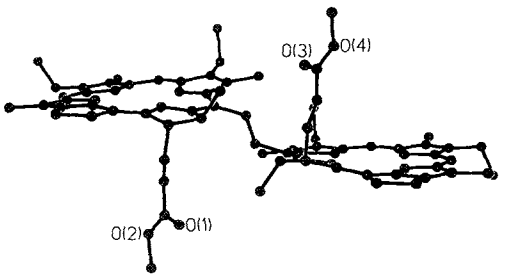

Fig. 2. Molecular structure of metal-free *trans*-bis(chlorin) **5b**.

dimer **5a**, and also shows a *trans* arrangement of the chlorin rings about an ethylene linkage [C=C 1.295(4) Å]. A noticeable difference between the structures of **5b** and the Ni^{II} complex **4** is evident in the increased planarity of the former, where the mean deviation of the macrocyclic core atoms from the least squares plane is only 0.13 Å. Variable-temperature proton NMR studies of **5b** also revealed broadening of some signals upon cooling, although again the nature of the dynamic process is not clear for this system. Treatment of **5b** and **6b** with $[Ni(acac)_2]$ in refluxing chloroform gave nickel complexes **5a** and **6a**.

A striking difference was observed between the bis(chlorin)s linked at a pyrrole position (**6**) and those linked at a *meso* position (**4** and **5**) upon oxidation in refluxing toluene/acetic acid (3/1) in the presence of air. The pyrrole-linked dimer **6a** could not be properly oxidized under these conditions, whereas the *meso*-linked dimer **4** provided the porphyrin–chlorin system **7** in 50% yield, and the *trans*-bis(porphyrin) **8** in 30% yield. Most interestingly, oxidation of **5a** under the same conditions yielded the *cis*-bis(porphyrin) **9** in 80% yield. The molecular structure of **9** (Fig. 3)[10] shows two nonplanar Ni^{II} porphyrins (mean deviation of the porphyrin core atoms from the least squares plane 0.21 Å,

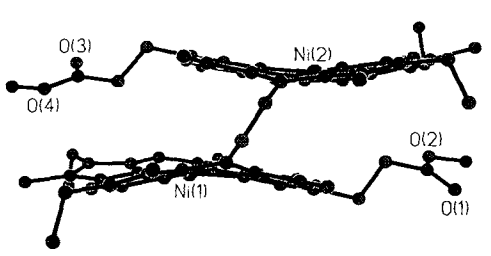

Fig. 3. Molecular structure of *cis*-bis-porphyrin **9**.

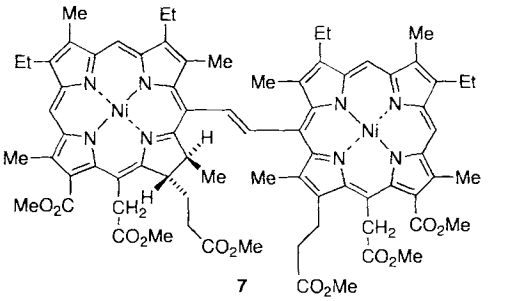

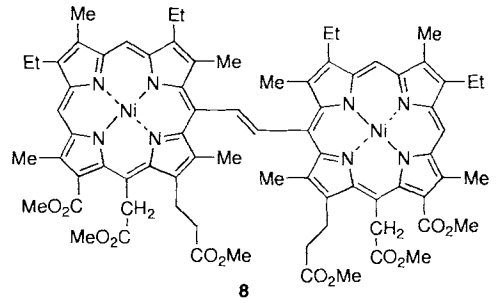

average Ni–N distance 1.925 Å) joined by an ethylene bridge (C=C 1.327(16) Å). No dynamic process was seen for **9** in variable-temperature proton NMR spectroscopy, presumably because the macrocycles cannot rotate about the $C_{meso}-C_{vinyl}$ bond when they are in a *cis* configuration. However, consistent with the molecular structure of **9**, large upfield shifts are seen for the exocyclic ring protons. Finally, the formation of **9** is stereoselective, in contrast to *cis*-octaethyl-1,2-bis-(coproporphyrinyl)ethene ester, which is isolated as a mixture of two atropisomers.[20]

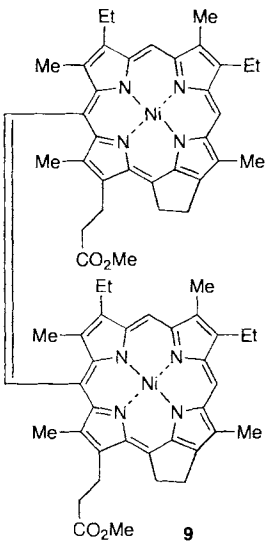

Experimental Procedure

In a typical McMurry coupling reaction, $[TiCl_3(dme)_{1.5}]$ (365 mg, 1.26 mmol) and Zn–Cu couple (335 mg, 4.65 mmol) were added to a dry flask in a dry box. Anhydrous DME (15 mL) was added to the reaction flask, and the resulting mixture was heated at reflux for 2 h under an inert atmosphere. Ni^{II} formylchlorin (0.10 mmol) was added, and the mixture heated at reflux for 3 h. After being cooled to room temperature, the reaction mixture was passed through a short Brockmann Grade III alumina plug with dichloromethane/methanol (10/1) as eluent. The solvents were removed, and the resulting residue was further purified by chromatography on a silica gel column eluted with 5% acetone in dichloromethane. The major green band was then collected and recrystallized from dichloromethane/methanol.

McMurry couplings of Zn^{II}-chlorins were performed in a similar manner except that pyridine (3.5 equiv) was added to the reaction mixture before addition of the Zn^{II} formylchlorin.

UV/Vis data of selected compounds: **4**: λ_{max} (CH_2Cl_2) = 416 (ε = 170000), 458 sh (53600), 648 (51000), 732 sh nm (14000). **5a**: λ_{max} (CH_2Cl_2) = 408 (ε = 119000), 454 sh (57000), 622 (40800), 710 nm sh (11000). **5b**: λ_{max} (CH_2Cl_2) = 416 (ε = 192000), 504 (31400), 550 (15800), 594 (16400), 648 nm (57100). **6a**: λ_{max} (CH_2Cl_2) = 409 (ε = 135600), 500 (10000), 556 (7700), 672 nm (63000). **7**: λ_{max} (CH_2Cl_2) = 420 (ε = 54000), 485 (64300), 588 (19900), 681 nm (30500)). **9**: λ_{max} (CH_2Cl_2) = 397 (ε = 185000), 548 (16000), 588 nm (13700).

Received: November 27, 1995 [Z8597IE]
German version: *Angew. Chem.* **1996**, *108*, 1085–1087

Keywords: low-valent compounds · McMurry reactions · porphyrinoids · titanium compounds

[1] M. R. Wasielewski, *Chem. Rev.* **1992**, *92*, 435–461.
[2] M. J. Crossley, P. L. Burn, *J. Chem. Soc. Chem. Commun.* **1991**, 1569–1571.
[3] A. Lamrabte, M. Momenteau, P. Malliard, P. Seta, *J. Mol. Elec.* **1990**, *6*, 145–153.
[4] E. E. Bonfantini, D. L. Officer, *J. Chem. Soc. Chem. Commun.* **1994**, 1445–1446.
[5] J. P. Collman, F. C. Anson, C. E. Barnes, C. S. Bencosme, T. Geiger, E. R. Evitt, R. P. Kreh, K. Meier, R. B. Pettman, *J. Am. Chem. Soc.* **1983**, *105*, 2694–2699.
[6] Y. Naruta, M. Sasayama, K. Maruyama, *Chem. Lett.* **1992**, 1267–1270.
[7] M. O. Senge, K. R. Gerzevske, M. G. H. Vicente, T. P. Forsyth, K. M. Smith, *Angew. Chem.* **1993**, *105*, 745–747; *Angew. Chem. Int. Ed. Engl.* **1993**, *32*, 750–754.
[8] M. G. H. Vicente, K. M. Smith, *J. Org. Chem.* **1991**, *56*, 4407–4418.
[9] All compounds were characterized by UV/Vis and ^{1}H NMR spectroscopy and gave satisfactory mass spectra and elemental microanalyses.
[10] Data collection and structure refinement information (**4**, **5b**, and **9**): Syntex $P2_1$ diffractometer, $\lambda(CuK_\alpha) = 1.54178$ Å, 130(2) K in $\theta/2\theta$ scan mode, $2\theta_{max} = 114°$ (**4**, **9**); for **5b**: Siemens P4 diffractometer with rotating anode, $\lambda(Cu_{K\alpha}) = 1.54178$ Å, 130(2) K in $\theta/2\theta$ scan mode, $2\theta_{max} = 112°$. The structures were solved by direct methods and refined (based on F^2 with all independent data) by full matrix least squares methods (Siemens SHELXTL V. 5.02). Number of parameters: 904 (**4**), 800 (**5b**), 813 (**9**). The NH protons of **5b** were located on a difference map and found to be on rings A and C; all hydrogens were treated as riding. The absolute stereochemistry of **4** and **5b** was correlated with the known absolute stereochemistry of chlorophyll a from which these compounds were derived. The handedness of **9** could not be reliably determined. Reported R values are $R1$ (based on F and observed data) and $wR2$ (based on F^2 and all data). Absorption corrections were performed with XABS2 [11]. T_{min}/T_{max} values: 0.71/0.85 (**4**), 0.84 and 0.94 (**5b**), 0.87 and 0.92 (**9**); m values: 1.27 mm^{-1} (**4**), 0.62 mm^{-1} (**5b**), 1.19 mm^{-1} (**9**). Single crystals of **4** suitable for X-ray diffraction were obtained by slow diffusion of methanol into a solution of **4** in chloroform. A block-shaped green crystal of **4**·0.35 H_2O was selected, dimensions 0.40 × 0.24 × 0.10 mm ($\rho_{calcd} = 1.392$ g cm^{-3}), triclinic, space group $P\bar{1}$, $a = 12.190(2)$, $b = 12.219(3)$, $c = 14.181(3)$ Å, $\alpha = 89.96(2)$, $\beta = 70.300(14)$, $\gamma = 60.780(15)°$, $V = 1700.7(6)$ Å^3, $Z = 1$. Of 4612 reflections measured ($+h, \pm k, \pm l$) 4607 were independent, and 4450 had $I > 2\sigma$, $R_{int} = 0.0145$. Final R factors: $R1 = 0.0425$, $wR2 = 0.1127$, max. residual electron density 0.63 e Å^{-3}. Single crystals of **5b** suitable for X-ray diffraction were obtained by slow diffusion of MeOH into a solution of **5b** in CH_2Cl_2. A needle of **5b**·1.24 H_2O was chosen, dimensions 0.56 × 0.20 × 0.12 mm ($\rho_{calcd} = 1.199$ g cm^{-3}), orthorhombic, space group $P2_12_12$, $a = 25.596(2)$, $b = 13.663(2)$, $c = 17.190(2)$ Å, $V = 6011.5(10)$ Å^3, $Z = 4$. Of 8590 reflections measured ($+h, +k, +l$ and $-h, -k, -l$) 4389 were independent, and 4214 had $I > 2\sigma$, $R_{int} = 0.0294$. Final R factors: $R1 = 0.0439$, $wR2 = 0.1161$, max. residual electron density 0.38 e Å^{-3}. Disorder was encountered in the propyl methyl ester groups. Single crystals of **9** suitable for X-ray diffraction were obtained by slow diffusion of MeOH into a solution of **9** in DMSO. A prismatic crystal of **9**·2 CH_3OH was selected, dimensions 0.42 × 0.14 × 0.06 mm ($\rho_{calcd} = 1.303$ g cm^{-3}), monoclinic space group $P2_1$, $a = 8.789(1)$, $b = 21.406(4)$, $c = 17.295(3)$ Å, $\beta = 96.530(10)°$, $V = 3232.7(9)$ Å^3, $Z = 2$. Of 4841 reflections measured ($+h, +k, \pm l$) 4509 were independent, and 3027 had $I > 2\sigma$, $R_{int} = 0.032$. Final R factors: $R1 = 0.0743$, $wR2 = 0.2097$, max. residual electron density was 0.64 e Å^{-3}. Crystallographic data (excluding structure factors) for the structure(s) reported in this paper have been deposited with the Cambridge Crystallographic Data Centre as supplementary publication no. CCDC-179-19. Copies of the data can be obtained free of charge on application to The Director, CCDC, 12 Union Road, Cambridge CB2 1EZ, UK (fax: int. code +(1223) 336-033; e-mail: teched@chemcrys.cam.ac.uk).
[11] S. R. Parkin, B. Moezzi, H. Hope, *J. Appl. Crystallogr.* **1995**, *28*, 53–56.
[12] M. O. Senge, H. Hope, K. M. Smith, *J. Chem. Soc. Perkin Trans. 2* **1993**, 11–16.
[13] C. Kratky, R. Waditschatka, C. Angst, J. E. Johansen, J. C. Plaquevent, J. Schreiber, A. Eschenmoser, *Helv. Chim. Acta* **1985**, *68*, 1312–1337.
[14] L. D. Sparks, C. J. Medforth, M.-S. Park, J. R. Chamberlain, M. R. Ondrias, M. O. Senge, K. M. Smith, J. A. Shelnutt, *J. Am. Chem. Soc.* **1993**, *115*, 581–592.
[15] K. M. Barkigia, M. D. Berber, J. Fajer, C. J. Medforth, M. W. Renner, K. M. Smith, *J. Am. Chem. Soc.* **1990**, *112*, 8851–8857.
[16] C. J. Medforth, M. O. Senge, K. M. Smith, L. D. Sparks, J. A. Shelnutt, *J. Am. Chem. Soc.* **1992**, *114*, 9859–9869.
[17] G. V. Ponomarev, V. V. Borokov, K. Sugiura, Y. Sakata, A. M. Shul'ga, *Tetrahedron Lett.* **1993**, *34*, 2153–2156.
[18] R. K. Pandey, F.-Y. Shiau, M. Isaac, S. Ramaprasad, T. J. Dougherty, K. M. Smith, *Tetrahedron Lett.* **1992**, *33*, 7815–7818.
[19] M. O. Senge, M. G. H. Vicente, K. R. Gerzevske, T. P. Forsyth, K. M. Smith, *Inorg. Chem.* **1994**, *33*, 5625–5638.
[20] G. V. Ponomarev, V. V. Borovkov, A. M. Shul'ga, Y. Sakata, *J. Chem. Soc. Chem Commun.* **1994**, 1927–1928.

Oxindigo: Color Deepening, Strong Fluorescence, and Large Stokes Shift by Donor-Substitution

Heinz Langhals* and Barbara Wagner

Oxindigo (**1**)[1, 2] has never attained any technical importance as a chromophore and has been the subject of only few publications in contrast to indigo (**2**), its N-analogue, or to thioindigo,

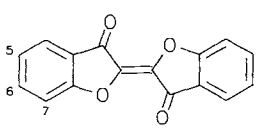

1

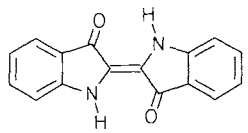

2

its S-analogue. This discrepancy is due to its hypsochromic absorption (413 nm in cyclohexane[3]), low coefficient of extinction (13800[3]), lack of fluorescence,[3] and difficult synthesis. We have now discovered that the influence of substituents in the conjugating positions 6 and 6′ is particularly interesting in this respect.

The starting material for oxindigo is coumaranone (benzofuran-2(3H)-one, **7**), which is prepared from **3** and then oxidatively coupled. We sought a new coupling procedure for **7** (Scheme 1), because the synthesis by Fries et al.[1] and Stoermer[2] requires several steps, and the method of Chovin[4] gives other products.[5]

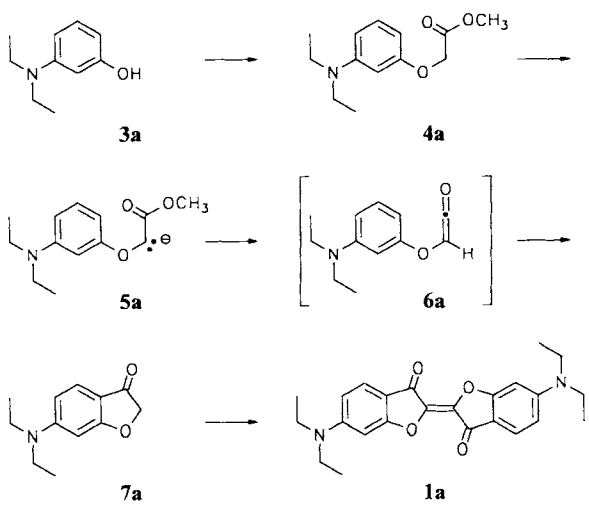

Scheme 1.

The thermal coupling of **7** results in low yields (< 1%) of **1**, whereas the reaction of **3** with atmospheric oxygen under basic conditions produces up to 10% of **1a** with appreciable formation of resin (ethyl chloroacetate and LDA (lithium diisopropylamide), or **3a** to **4a** with KOH in DMSO[6–8] and **4a** to **1a** with

[*] Prof. Dr. H. Langhals, Dr. B. Wagner
Institut für Organische Chemie der Universität
Karlstrasse 23, D-80333 München (Germany)
Fax: Int. code +(89) 5902-483
e-mail: ui26101@sunmail.lrz-muenchen.de

[**] This work was supported by the Deutsche Forschungsgemeinschaft and the Fonds der Chemischen Industrie.

LDA). The formation of resin is less pronounced under acidic reaction conditions: for example, the reaction of **3a** with chloroacetic acid chloride and silica gel[9] yields 12% of **1a** under very simple reaction conditions, whilst the reaction of **3a** with bromoacetic acid chloride, $POCl_3$, PCl_3, and $FeCl_3$ yields 20% of **1a**,[10] which is the highest yield of oxindigo and its derivatives yet attained. This latter reaction is a more general synthetic procedure, especially for compounds containing longer alkyl substituent groups at the nitrogen atoms of **3**.

Only the *trans* isomer of indigo (**2**) is obtained by the oxidative dimerization of indoxyl, and special structural requirements[11] are necessary for the preparation of *cis* isomers. In contrast, the analogous preparation of oxindigo compounds also yields *cis* isomers. Traces of *cis*-**1a** are formed in equilibrium with *trans*-**1a** at high reaction temperatures (at reflux in toluene or in DMF at 110 °C), and this yield can be increased to about 50% by lowering the reaction temperature (20–50 °C, kinetic control of the reaction). Another way to prepare *cis*-**1a** is to reduce the more easily prepared *trans*-**1a** to the leuko form (**8a**), which is reoxidized at low temperature to a 1:1 *cis*–*trans* mixture (Scheme 2). The *cis*-**1** isomer may be completely separated

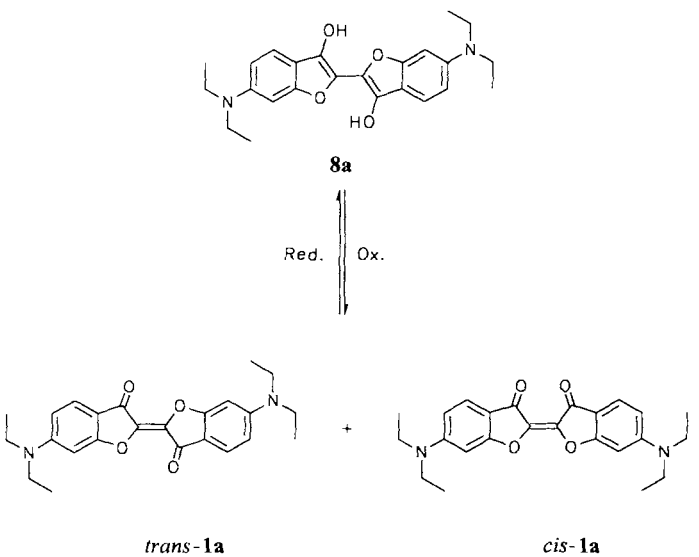

Scheme 2.

from *trans*-**1** by column chromatography. One can reliably distinguish between *cis*-**1** and *trans*-**1** by the carbonyl absorptions in their IR spectra. The *trans* compounds show, as expected, an absorption at 1725 cm^{-1}, whereas a shift to higher wavenumbers (1765 cm^{-1}) is observed for the *cis* compounds because of the interaction of the carbonyl groups, whose dipoles are nearly parallel. (Compare also the corresponding bands of unsubstituted oxindigo[3] and thioindigo.[12])

The UV/Vis spectroscopic properties of **1** are completely changed by the introduction of donor groups into positions 6 and 6'. The unusually large 111 nm bathochromic shift of the absorption to 523.8 nm is striking (see Fig. 1).

The annelation of further rings increases the donor function of the nitrogen atoms by "rigid planarization"; for example the julolidine derivative **1l** exhibits a further bathochromic shift of 34 nm in absorption and fluorescence compared to the value for **1a** (see Fig. 2 and Table 1). The bathochromic shift is less pronounced if the donor function is diminished by phenyl substituents as in **1i**. The spectroscopic data of the methoxy derivative **1k**, which is known,[14] are also in accord with these results.

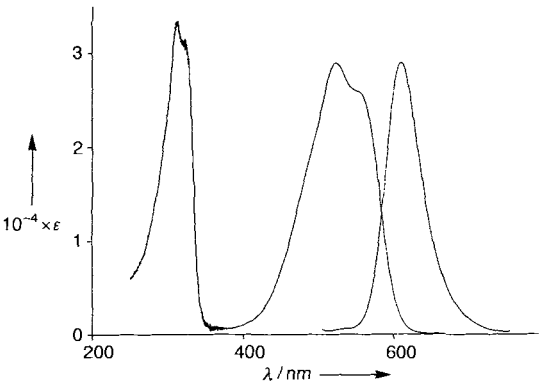

Fig. 1. UV/Vis absorption and fluorescence spectra of *trans*-oxindigo **1a** in $CHCl_3$ (color coordinates [13]: $x = 0.3791$, $y = 0.2169$, $z = 0.4040$ at $T_{max} = 0.1$).

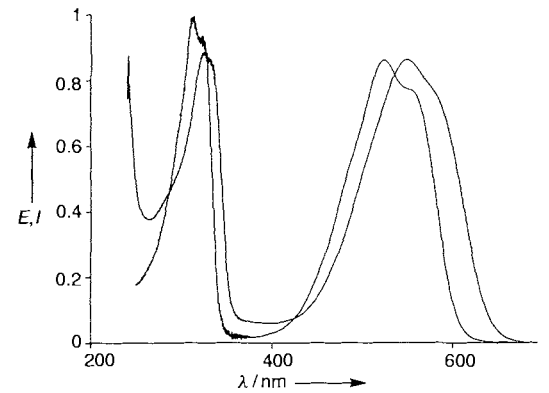

Fig. 2. UV/Vis spectrum of the *trans*-julolidine derivative **1l** (right; color coordinates [13]: $x = 0.2889$, $y = 0.1646$, $z = 0.5472$ at $T_{max} = 0.1$) compared to oxindigo **1a** (left) in $CHCl_3$.

Table 1. Spectroscopic properties of oxindigo derivatives **1** with donor groups in positions 6 and 6'.

No.	R [a]	*cis*/*trans*	λ_{max} (Abs.) [nm] [b]	λ_{max} (Em.) [nm] [c]
1a	$(C_2H_5)_2N$	*trans*	523.8	610.0
		cis	646.9	
1b	$(CH_3)_2N$	*trans*	511.7	602.0
		cis	629.1	
1c	$(n\text{-}C_3H_7)_2N$	*trans*	527.3	620.8
		cis	651.3	
1d	$(n\text{-}C_4H_9)_2N$	*trans*	527.4	619.0
		cis	652.1	
1e	$(n\text{-}C_5H_{11})_2N$	*trans*	524.2	608.1
		cis	653.1	
1f	$(n\text{-}C_6H_{13})_2N$	*trans*	528.1	617.9
		cis	652.0	
1g	$(n\text{-}C_8H_{17})_2N$	*trans*	528.8	615.5
		cis	652.9	
1h	$(n\text{-}C_{12}H_{25})_2N$	*trans*	627.5	614.9
		cis	653.4	
1i	$2\text{-}CH_3C_6H_4$, CH_3N	*trans*	505.1	591.0
1j	$2\text{-}CH_3C_6H_4$, HN	*trans*	488.8	582.0
		cis	602.0	
1k	CH_3O	*trans*	421.4	475.3

[a] Substituent in positions 6 and 6' of **1**. [b] Absorption maximum in chloroform. [c] Fluorescence maximum in chloroform. Fluorimeter: Perkin Elmer 3000.

The parent compound, oxindigo, does not fluoresce. However, a strong red fluorescence is induced by the donor groups in **1a** (Fig. 1), which is of interest for fluorescence applications, because of this dye's high color fastness.[15] Dye **1k** also exhibits a strong fluorescence. The effect of the donor groups on

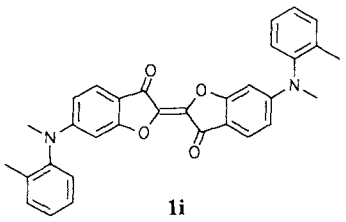

1i

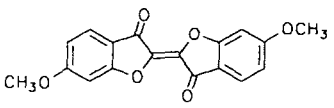

1k

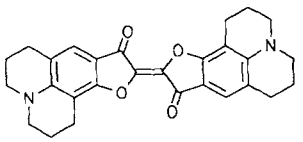

1l

the fluorescence of **1** is exactly opposite to their effect in thioindigo—unsubstituted thioindigo fluoresces strongly, whereas donor groups in positions 6 and 6′ result in a fluorescence quenching.[16] This has been ascribed to an "out-of-phase-conjugation",[16] but the experimental data for oxindigo would seem to contradict this. The remarkably large Stokes shift of 86 nm for **1a** in solution can be taken as an indication of a dynamic process after the electronic excitation. Both the good spectral separation between absorption and fluorescence and the sufficient solubility of the dye are of interest for laser applications.

Although *trans*-**1a** absorbs at remarkably long wavelengths, the absorption of *cis*-**1a**, which forms blue solutions, is at even longer wavelengths (Fig. 3). This behavior is contrary to that of

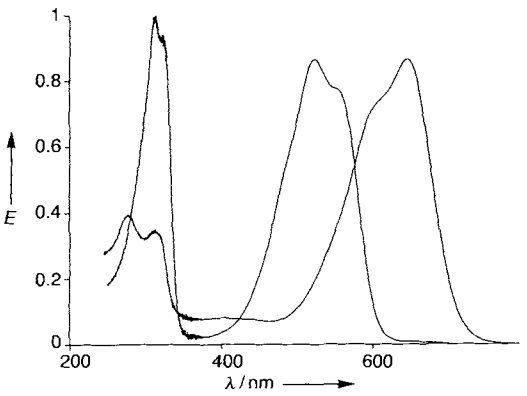

Fig. 3. UV/Vis spectrum of *cis*-**1a** (right; color coordinates [13]: $x = 0.1970$, $y = 0.2300$, $z = 0.5730$ at $T_{max} = 0.1$) compared to *trans*-**1a** (left) in $CHCl_3$.

oxindigo or indigo itself. Whilst *cis*-**1a** does not fluoresce in solution, it exhibits a strong fluorescence in the solid state (see below).

Compound *cis*-**1a** is completely stable as a solid; however, in solution ($CHCl_3$) a photochemical (HPK 125W lamp with yellow filter GG 400, 18 h, see ref. [15]) or thermal[17] transformation into the *trans* isomer takes place. The latter reaction is in contrast to the behavior of unsubstituted oxindigo, which undergoes a thermal decomposition rather than such a transformation,[3] which occurs only photochemically. On the other hand, a photochemical transformation of *trans*-**1a** into *cis*-**1a** is difficult[15]—the strong fluorescence of *trans*-**1a** probably inhibits the reaction through inactivation of the absorbed light.

If the ethyl groups of **1a** are replaced by methyl groups (**1b**), the spectroscopic properties change only slightly. The persistency of the dye, however, is lowered. In contrast, longer alkyl groups at the nitrogen atoms increase the solubility of the dyes without affecting their persistency (for further details see Table 1).

The strong bathochromic shift of **1** by donor groups is satisfactorily supported neither by simple HMO calculations, nor by PPP or by AM1 calculations. This may be attributed to strong intermolecular electrostatic interactions; torsion about the central C=C double bond is less probable as cause both because unsubstituted oxindigo is planar,[18] and because the coefficient of extinction of **1a** is rather high.

The unusually high Stokes shift of **1a** and the differently structured absorption and fluorescence spectra suggest that a relaxation process occurs after the electronic excitation. To gain more insight into this process, quantum mechanical calculations were performed on dye **1b** at the AM1 level (MOPAC). The more stable isomer is *trans*-**1b** with a central C–C bond length of 1.33 Å and a dipole moment of 0.84 D. Isomer *cis*-**1b**, which is also planar, is 1.4 kcal mol^{-1} less stable and has a central C–C bond of 1.34 Å. In the first electronically excited state (**1b**-S_1) the molecule is twisted by 81° (C3, C2, C2′, C3′ angle of torsion) about the central bond which has a length of about 1.37 Å. In this state the molecule has a dipole moment of 12 D. Furthermore, one of the dimethylamino groups is slightly bent out of the π plane (20°).

The relaxation of the planar structure of *trans*-**1b** into the twisted structure of **1b**-S_1 after the electronic excitation can be taken as an explanation both for the large Stokes shift and for the different fine structure of the absorption and the fluorescence spectrum. It may also be the cause for the lack of fluorescence of *cis*-**1b** in solution, because the metastable state **1b**-S_1 might not be reached after the optical excitation. In accord with this concept both the *trans* and the *cis* form exhibit a strong fluorescence in the solid state (*trans*-**1a** 516.5 and 615.8 nm; *trans*-**1l** 666 nm; *cis*-**1e** 722.4, 769.6 and 800 (sh) nm). The *cis* isomers are also of interest for technical applications, because the dyes are very photostable in the solid state and their fluorescence extends far into the NIR region.

Experimental Procedure

trans-**1a**: **3a** (10.0 g, 60.5 mmol) and bromoacetic acid (12.5 g, 90.1 mmol) were allowed to react with $POCl_3$ (7.0 g, 46 mmol), PCl_3 (6.3 g, 46 mmol), and iron(III) chloride (24.6 g, 152 mmol; 24 h, 60 °C). The mixture was worked up with ice, sodium citrate solution, and chloroform, and purified by column separation ($CHCl_3$, silica gel). Yield: 4.0 g of red brown black crystals (19%), m.p. 292 °C. R_f ($CHCl_3$) = 0.70. IR (KBr): $\tilde{\nu}$ [cm^{-1}] = 2970 (m), 2929 (m), 1727 (s, C=O), 1616 (s, C=C), 1521 (m), 1404 (m), 1354 (m), 1347 (m), 1319 (m), 1277 (m), 1147 (m). UV ($CDCl_3$): λ_{max} (ε) [nm] = 311.4 (34200), 321.8 (31900), 523.8 (29000), 555.2 sh (25800). Fluorescence ($CDCl_3$): λ_{max} = 610 nm. ^1H NMR ($CDCl_3$): δ = 1.23 (t, J = 7 Hz, 12H), 3.44 (q, J = 7 Hz, 8H), 6.55 (d, J = 3 Hz, 2H), 6.69 (dd, J = 3, 9 Hz, 2H), 8.93 (d, J = 9 Hz, 2H). ^{13}C NMR ($CDCl_3$): δ = 12.3, 44.7, 97.3, 105.3, 109.7, 121.3, 128.4, 149.6, 154.2, 159.3. MS (70 eV): m/z (%) = 406 (100) [M^+], 391 (81), 362 (10), 347 (35), 188 (16).

cis-**1a**: **3a** (2.3 g, 14 mmol) in toluene (75 mL) was added in small portions to a LDA solution in cyclohexane/toluene/THF (8 mL, 2 M, −78 °C), and this was then added dropwise to a solution of methyl chloroacetate (1.7 g, 15.5 mmol, −78 °C) in toluene (70 mL). A further portion of the LDA solution (8 mL, 2 M) was added, and the mixture then warmed up (60 °C, 12 h), treated with water (300 mL) and 2 N HCl (pH = 6), extracted (chloroform), washed to neutral (H_2O), and purified by column separation ($CHCl_3$, silica gel). First fraction: 510 mg (10%) *trans*-**1a**; second (blue) fraction: 50 mg blue black crystals (1%; yield of *cis*-**1e** 3%); m.p. 285 °C. R_f ($CHCl_3$) = 0.73. IR (KBr): $\tilde{\nu}$ [cm^{-1}] = 2960 (s), 2925 (s), 2854 (s), 1763 (m, C=O), 1625 (s, C=C), 1516 (s), 1467 (s), 1455 (m), 1400 (s), 1377 (m), 1352 (m), 1337 (s), 1279 (s), 1070 (s), 795 (m), 717 (m). UV ($CDCl_3$): λ_{max} [nm] = 277.6, 312.5, 609.8 sh, 646.9. ^1H NMR ($CDCl_3$): δ = 1.15 (t, J = 7 Hz, 12H), 3.38 (q, J = 7 Hz,

8H), 6.29 (d, J = 2.5 Hz, 2H), 6.39 (dd, J = 9, 2.5 Hz, 2H), 8.73 (d, J = 9 Hz, 2H). ^{13}C NMR ($CDCl_3$): δ = 22.69, 45.01, 92.84, 105.14, 112.34, 120.75, 129.63, 150.78, 157.40, 169.45. MS (70 eV): m/z (%) = 406 (100) [M^+], 392 (10), 391 (39), 362 (13), 347 (21), 204 (16), 188 (15). $C_{24}H_{26}N_2O_4$: calcd 406.1887, found 406.1956 (MS).

Received: September 11, 1995
Revised version: January 18, 1996 [Z83901E]
German version: *Angew. Chem.* **1996**, *108*, 1090–1093

Keywords: dyes · fluorescence · indigo · oxindigo

[1] K. Fries, A. Hasselbach, *Ber. Dtsch. Chem. Ges.* **1911**, *44*, 124–128.
[2] R. Stoermer, *Ber. Dtsch. Chem. Ges.* **1909**, *42*, 199–202; R. Stoermer, K. Brachmann, *ibid.* **1911**, *44*, 315–319.
[3] H. Güsten, *J. Chem. Soc. D* **1969**, 133.
[4] P. Chovin, *Bull. Soc. Chim. Fr.* **1944**, *11*, 82–89.
[5] H. Langhals, B. Wagner, *Tetrahedron* **1996**, *52*, 1961–1964.
[6] H. Langhals, M. Julia, D. Mansuy, *Tetrahedron Lett.* **1976**, 3519–3522.
[7] H. Langhals, M. Julia, D. Uguen, *Liebigs Ann. Chem.* **1982**, 2216–2222.
[8] C. Finkentey, E. Langhals, H. Langhals, *Chem. Ber.* **1983**, *116*, 2394–2397.
[9] L. B. Conte, F. N. Apel (Union Carbide), US-A 3098099; *Chem. Abstr.* **1968**, *69*, 27031.
[10] $C_{24}H_{26}N_2O_4$ (406.2): calcd C 70.92, H 6.45, N 6.89; found C 70.85, H 6.54, N 6.66; calcd 406.1887, found: 406.1892 (MS).
[11] See for example M. Klessinger, W. Lüttke, *Chem. Ber.* **1966**, *99*, 2136.
[12] G. M. Wyman, A. Zenhäusern, *J. Org. Chem.* **1965**, *30*, 2348.
[13] H. Zollinger, *Color Chemistry*, 2nd ed., VCH, Weinheim, **1991**.
[14] K. Fries, K. Saftien, *Liebigs Ann. Chem.* **1925**, *442*, 284.
[15] Solutions of **1a** in chloroform or toluene showed no noticeable decomposition after three months exposure to direct sunlight, six hours irradiation with the concentrated light of an HQI-T 2000 W/N lamp (A. Rademacher, S. Märkle, H. Langhals, *Chem. Ber.* **1982**, *115*, 2927–2934) or a mercury vapor lamp (Philips HPK 125) with yellow filter (CG 400 from Schott).
[16] G. M. Wymann, B. M. Zarneger, *J. Phys. Chem.* **1973**, *77*, 831.
[17] In $CHCl_3$ slowly; in ethanol, $k_1 = 4.00 \times 10^{-3}\ s^{-1}$ at 28 °C (r = 0.998, n = 34, 637.5 nm).
[18] H. Pandraud, *Acta Cryst.* **1962**, *15*, 1131–1139.

Synthesis of Novel Difluoroprostacyclin Derivatives: Unprecedented Stabilizing Effect of Fluorine Substituents**

Takashi Nakano, Mayumi Makino, Yoshitomi Morizawa, and Yasushi Matsumura*

Fluorine has unique physical properties mainly derived from its small atomic size and high electron negativity.[1] Introduction of fluorine into biologically active substances such as steroids,[2] nucleic acids,[3] amino acids, and peptides,[4] as well as prostaglandins and thromboxanes,[5] is regarded as an important strategy in drug design. Prostacyclin (**1**) is a particularly attractive target because of its powerful effects as an inhibitor of platelet aggregation and as a vasodilator in maintaining homeostatic circulation.[6] Despite the pharmacological importance, the inherent instability of **1** limits its therapeutical applicability. Research on new prostacyclin mimetics with reasonable stability and beneficial therapeutic profiles has been a major field of interest for over a decade.[7] Nonetheless, the subject is still far from fully developed. Recent advances in molecular biology including the structural elucidation of prostacyclin receptors[8] require the discovery of more selective agonists to give a better understanding of the precise mechanism of action.

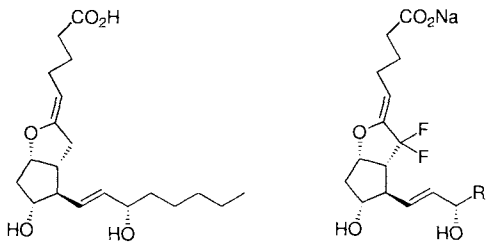

1 **2**

Fluoroprostacyclin derivatives have been targeted by several research groups[9] as potential stable drugs. We are interested in the synthesis of novel prostacyclin mimetics **2**, which have two fluorine atoms at the 7-position. The strong electron-withdrawing effect of the fluorine substituents adjacent to the acid-labile vinyl ether should prevent its hydrolysis. We herein disclose a direct and efficient synthesis of the novel 7,7-difluoroprostacyclin derivative **14** (see Scheme 3), which shows unprecedented stability and potent inhibition of platelet aggregation.[10]

In designing a synthetic plan, we searched for a strategy to construct a characteristic difluorine-substituted vinyl ether employing fluorine-containing building blocks. The conventional route by cyclization of a prostaglandin $F_{2\alpha}$ derivative **3** did not appear promising due to the low reactivity of the electron-deficient double bond bearing two fluorine atoms (Scheme 1). We

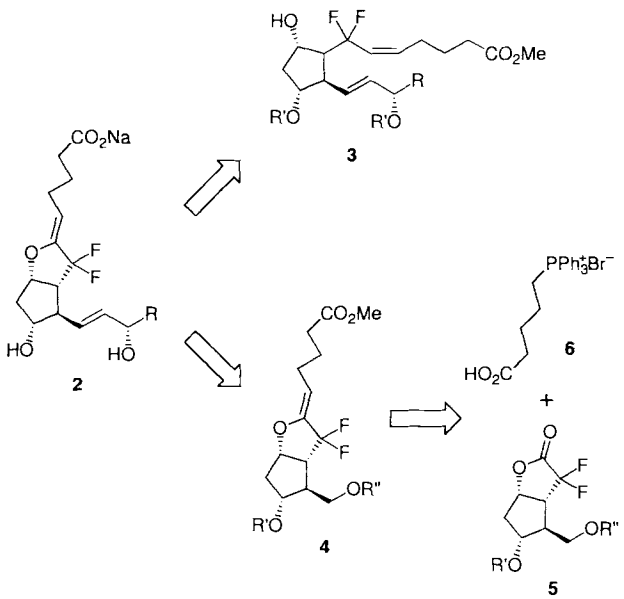

Scheme 1. Retrosynthetic analysis of **2**.

approached the challenge by choosing the vinyl ether **4** as a key intermediate. Advantages of this strategy are: intermediate **4** could serve as a useful starting point for the synthesis of a variety of analogs with modified ω-side chains; the α-side chain could be directly assembled by a stereoselective Wittig reaction of difluorolactone **5** and phosphonium salt **6**; and a novel fluorination reaction with the readily available Corey lactone could provide compound **5**.

Electrophilic fluorination is an attractive method to construct fluorinated building blocks simply from rather complicated molecules. Several new electrophilic fluorinating agents have been developed;[11] however, selective difluorination of carbonyl compounds has not received much attention and remains

[*] Y. Matsumura, T. Nakano, M. Makino, Dr. Y. Morizawa
Research Center, Asahi Glass Co., Ltd.
1150 Hazawa, Kanagawa-ku, Yokohama 221 (Japan)
Fax: Int. code +(45)334-6079
e-mail: yasushi@agc.co.jp

[**] We thank Dr. Arata Yasuda for helpful discussions.

troublesome because of the lack of reactivity of the intermediary α-fluoro enolate.[12] We examined various fluorinating agents and found *N*-fluorobenzenesulfonimide **8**[11h] to be suitable for the reaction. The Corey lactone **7** was treated with lithium *N*,*N*-bis(trimethylsilyl)amide in THF and fluorinated with the sulfonimide **8** at −78 °C to afford monofluorolactone **9** in 61% yield (Scheme 2). The desired difluorolactone **10** could

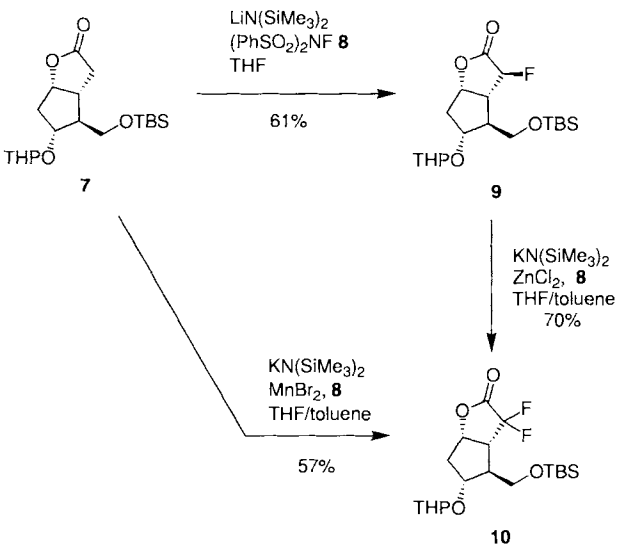

Scheme 2. Synthesis of intermediate **10**. THP = tetrahydropyran, TBS = *tert*-butyldimethylsilyl.

not be obtained in the reaction even when an excess of the base and the sulfonimide **8** were used. On the other hand, fluorination of **9** with reagent **8** after metal exchange with zinc chloride at −78 °C effectively provided the desired difluoride **10** in 70% yield. After many unsuccessful attempts, we found that the fluorination of lactone **7** with **8** in the presence of manganese dibromide gave the desired difluoride **10** directly in 57% yield.

Wittig reaction[13] of the difluorolactone **10** with the phosphonium salt **6** with sodium *N*,*N*-bis(trimethylsilyl)amide in THF at room temperature proceeded smoothly to furnish the vinyl ether **11**, which was obtained as an 87:13 mixture of *Z* and *E* isomers in 63% yield after esterification (Scheme 3). After removal of *tert*-butyldimethylsilyl group with Bu_4NF (94%), Moffatt oxidation to the aldehyde and subsequent Horner–Emmons reaction with the known phosphonate **12**[7c] afforded enone **13** in 90% yield (over two steps). Enone **13** was reduced with $NaBH_4$ in the presence of $CeCl_3$ and the THP group was removed afforded a 1:1 mixture of the (15*S*) and (15*R*) alcohol.[14] The desired more polar (15*S*) isomer was hydrolyzed to provide the carboxylic acid sodium salt **14** as a white solid in 30% yield (over three steps). The (15*R*) isomer could be recovered and converted to **14** by oxidation with manganese dioxide and reduction to the mixture of diastereomeric alcohols.

The stability of **14** in aqueous solution was determined by HPLC. No decomposition was observed in pH 6.5 buffer at 25 °C after 30 days.[15] This is in sharp contrast with natural prostacyclin (**1**), which has very short half-life (76.2 s) under analogous conditions.[16] The high stability of **14** is consistent with the results of a previous study of acid-catalyzed hydration of α-trifluoromethyl vinyl ether in aqueous solution.[17] Protonation of the vinyl ether double bond of **14**, the rate-limiting step in the hydrolysis, should be strongly retarded by the adjacent difluoromethylene group.[18]

The inhibitory activity of **14** on ADP-induced human platelet aggregation in vitro (IC_{50} = 0.07 ng mL^{-1}) is the strongest of all the reported prostacyclin derivatives. In addition, compound **14** was found to be a highly selective prostacyclin agonist with little affinity for various subtypes of the prostaglandin E receptor.[19]

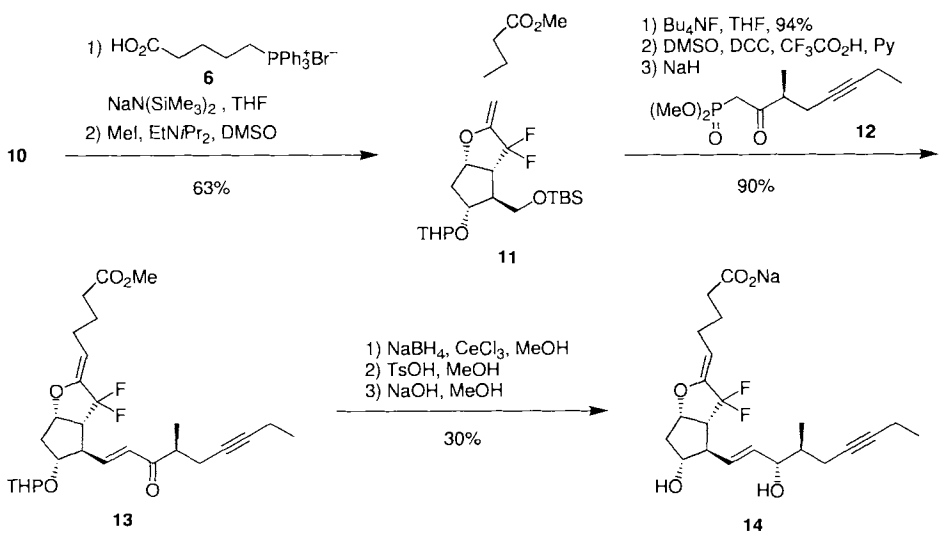

Scheme 3. Synthesis of 7,7-difluoroprostacyclin (**14**). DMSO = dimethyl sulfoxide, DCC = *N*,*N*′-dicyclohexylcarbodiimide, Py = pyridine, Ts = tosyl.

Experimental Procedure

9: To a solution of 1,1,1,3,3,3-hexamethyldisilazane (7.14 mL, 33.8 mmol) in THF (60 mL) was added *n*BuLi (1.66 M hexane solution, 18.7 mL) at −78 °C. The mixture was stirred at −78 °C for 40 min and a solution of **7** (10.0 g, 27.0 mmol) in THF (40 mL) was added. The reaction mixture was stirred at −78 °C for 50 min, and then a solution of **8** (10.7 g, 33.9 mmol) in THF (100 mL) was added. The mixture was stirred at −78 °C for 1 h, poured into saturated $NaHCO_3$, and extracted with EtOAc. The extract was dried, concentrated, and chromatographed on silica gel (hexane/EtOAc 10/1 to 5/1) to give **9** (6.40 g, 61%). ^{1}H NMR ($CDCl_3$): δ = 0.05 (s, 6H), 0.89 (s, 9H), 1.45–2.51 (m, 8H), 2.94 (m, 1H), 3.47–3.87 (m, 4H), 4.63 (m, 1H), 4.92–5.19 (m, 2H); ^{19}F NMR ($CDCl_3$): δ = −178.9 (m).

10: Fluorination of **9**: To a suspension of zinc chloride (25.9 g, 190 mmol) in THF (240 mL) was added a solution of **9** (33.4 g, 86.1 mmol) in THF (240 mL). The mixture was cooled to −78 °C, then potassium *N*,*N*-bis(trimethylsilyl)-amide (0.5 M in toluene, 269 mL) and a solution of **8** (33.9 g, 108 mmol) were added. The mixture was stirred at −78 °C for 1 h and allowed to warm to room temperature. The reaction mixture was poured into saturated $NaHCO_3$ and extracted with EtOAc. The extract was dried, concentrated, and chromatographed on silica gel (hexane/EtOAc 10/1 to 5/1) to furnish difluorolactone **10** (24.3 g, 70%). ^{1}H NMR ($CDCl_3$): δ = 0.06 (s, 6H), 0.88 (s, 9H), 1.25–2.29 (m, 8H), 2.63 (m, 1H), 3.06 (m, 1H), 3.48–3.84 (m, 4H), 4.22 (m, 1H), 4.64 (m, 1H), 5.11 (m, 1H); ^{19}F NMR ($CDCl_3$): δ = −94.3 (m), −115.5 (m); HRMS *m*/*z* calcd for $C_{19}H_{33}O_5F_2Si$ (*M* + 1) 407.2065, found 407.1957.

10: Difluorination of **7**: To a suspension of manganese dibromide (68.7 g, 320 mmol) in THF (500 mL) was added a solution of **8** (101 g, 320 mmol) in THF (500 mL) and the mixture was cooled to −78 °C. To the suspension at −78 °C were added dropwise a solution of **7** (29.6 g, 80 mmol) in THF (200 mL) and a solution of 0.5 M potassium *N*,*N*-bis(trimethylsilyl)amide (800 mL, 400 mmol) in toluene. The mixture was stirred at −60 °C for 2 h then allowed to warm to 0 °C. Saturated $NaHCO_3$ (1000 mL) was added and the mixture was extracted with EtOAc. The extract was dried, concentrated, and chromatographed on silica gel (hexane/EtOAc 10/1) to afford **10** (18.4 g, 57%).

11: To a suspension of **6** (5.45 g, 12.3 mmol) in THF (12 mL) was added sodium *N*,*N*-bis(trimethylsilyl)amide (1 M THF solution, 24.6 mL) at room temperature. The mixture was heated at 70 °C for 1 h, then cooled to room temperature. To the mixture was added a solution of **10** (1.0 g, 2.46 mmol) in THF (8 mL) at room temperature. After stirring for 3 h, the reaction mixture was concentrated, the pH was adjusted to 4, and the mixture was extracted with 50% EtOAc in hexane. The extract was dried and concentrated to give the crude acid, which was dissolved in DMSO (9 mL). To the solution were added *N*,*N*-diisopropylethylamine (1.29 mL) and iodomethane (0.77 mL) at room temperature. The mixture was stirred at room temperature for 18 h, poured into water, and extracted with 50% EtOAc in hexane. The extract was dried, concentrated, and chromatographed on silica gel (hexane/EtOAc 10:1) to afford **11** (757 mg, 63%) as an 87:13 mixture of *Z* and *E* isomers. ^{1}H NMR ($CDCl_3$): δ = 0.05 (s, 6H), 0.88 (s, 9H), 1.25–2.42 (m, 15H), 2.81 (m, 1H), 3.65 (s, 3H), 3.46–3.90 (m, 4H), 4.14 (m, 1H), 4.60–4.78 (m, 3H); ^{19}F NMR ($CDCl_3$): *Z* isomer: δ = −84.1 (m), −116.1 (m); *E* isomer δ = −85.4 (m), −109.7 (d, *J* = 259 Hz); HRMS *m*/*z* calcd for $C_{21}H_{33}O_6F_2Si$ (*M* − *t*Bu) 447.2014, found 447.2001.

13: To a solution of **11** (21.9 g, 43.5 mmol) in THF (300 mL) was added Bu_4NF (1 M THF solution, 66.8 mL) at 0 °C. The mixture was stirred at room temperature for 16 h. After removal of the solvent, the residue was chromatographed on silica gel (hexane/EtOAc 1:1) to give the alcohol (15.9 g, 94%). To the alcohol (9.0 g, 23.1 mmol) in benzene (160 mL) were added DMSO (36 mL), pyridine (2.12 mL), trifluoroacetic acid (0.28 mL), and DCC (14.8 g, 71.7 mmol) at 0 °C. The mixture was stirred at room temperature for 3 h and filtered to remove the precipitate. The filtrate was poured into water and extracted with 15% EtOAc in hexane. The extract was dried and concentrated in vacuo to afford the crude aldehyde. To a suspension of NaH (60% oil dispersion, 1.06 g, 26.5 mmol) in DME (500 mL) was added a solution of **12** (6.57 g, 26.7 mmol) in DME (75 mL) at 0 °C. The mixture was stirred for 1 h, then a solution of the aldehyde in DME (300 mL) was added at 0 °C. The mixture was stirred at room temperature for 30 min, poured into brine, extracted with EtOAc. The extract was concentrated to dryness and chromatographed on silica gel (hexane/EtOAc 4/1) to furnish **13** (10.9 g, 90%). ^{1}H NMR ($CDCl_3$): δ = 1.10 (t, *J* = 7.2 Hz, 3H), 1.19–1.21 (m, 3H), 1.48–2.96 (m, 21H), 3.67 (s, 3H), 3.42–4.15 (m, 3H), 4.60–4.87 (m, 3H), 6.36 (m, 1H), 6.82 (m, 1H); ^{19}F NMR ($CDCl_3$): δ = −84.4 (m), −115.4 (m); HRMS *m*/*z* calcd for $C_{28}H_{38}O_6F_2$ (M) 508.2636, found 508.2573.

14: To a solution of **13** (10.0 g, 19.7 mmol) in MeOH (350 mL) were added $CeCl_3 \cdot 7H_2O$ (11.2 g, 30.1 mmol) and $NaBH_4$ (1.14 g, 30.1 mmol) at −78 °C. The mixture was stirred at −78 °C for 30 min then allowed to warm to room temperature. The mixture was poured into saturated $NaHCO_3$ and extracted with EtOAc. The extract was dried and concentrated to give the crude alcohol (11.0 g). The alcohol was dissolved in MeOH (330 mL), and *p*TsOH·H_2O (0.38 g) was added at room temperature. The reaction mixture was stirred for 1 h, then $NaHCO_3$ (4.4 g) was added. The mixture was concentrated to dryness and chromatographed on silica gel (hexane/EtOAc 1/1 to 1/2) to give the less polar (15*R*) alcohol (3.1 g, 37%), the more polar (15*S*) alcohol (3.3 g, 39%), and a mixture of the isomers (0.4 g). To a solution of the (15*S*) alcohol (0.64 g, 1.5 mmol) in MeOH (22.5 mL) was added 0.1 N NaOH (22.5 mL). The mixture was stirred at room temperature for 13 h, acidified with 0.1 N HCl, and chromatographed on Merck LiChroprep RP-2 (MeOH/H_2O 1/1) to give the acid (507 mg, 82%). The acid was treated with 1 N NaOH to afford the sodium salt **14** as a white powder. IR (KBr): $\tilde{\nu}$ = 3406, 2975, 2938, 1562, 1408, 1300, 1243, 1043, 1017, 971 cm^{-1}; ^{1}H NMR (CD_3OD): δ = 0.97 (d, *J* = 6.8 Hz, 3H), 1.14 (t, *J* = 7.2 Hz, 3H), 1.70–2.78 (m, 15H), 2.63 (m, 1H), 3.89–3.99 (m, 2H), 4.76 (m, 1H), 5.58–5.68 (m, 2H); ^{19}F NMR (CD_3OD): δ = −85.7 (m), −118.7 (d, *J* = 248 Hz); ^{13}C NMR (CD_3OD): δ = 13.1, 14.9, 15.5, 23.0, 25.5, 27.4, 38.7, 40.1, 41.8, 51.3, 52.8, 76.6, 77.8, 78.6, 82.0, 83.5, 102.1, 125.6 (t, *J*(C,F) = 247 Hz), 132.5, 134.9, 150.0, 182.7; HR MS *m*/*z* calcd for $C_{22}H_{29}O_5F_2$ (*M* − Na) 411.1983, found 411.1998.

Received: November 20, 1995 [Z 8570 IE]
German version: *Angew. Chem.* **1996**, *108*, 1082–1084

Keywords: fluorinations · prostacyclins

[1] *Organofluorine Compounds in Medicinal Chemistry and Biomedical Applications* (Eds.: R. Filler, Y. Kobayashi, L. M. Yagupolskii), Elsevier, Amsterdam, **1993**.

[2] J. Fried, E. F. Sabo, *J. Am. Chem. Soc.* **1954**, *76*, 1455.

[3] D. E. Bergstrom, D. J. Swartling in *Fluorine-Containing Molecules, Structure, Synthesis and Applications* (Eds.: J. F. Liebman, A. Greenberg, W. R. Dolbier, Jr.), VCH, New York, **1988**, p. 259.

[4] *Fluorine-containing Amino Acids: Synthesis and Properties* (Eds.: V. P. Kukhar, V. A. Soloshonok), Wiley, Chichester, **1995**.

[5] A. Yasuda in ref. [1], p. 275.

[6] *Therapeutic Applications of Prostaglandins* (Eds.: J. Vane, J. O'Grady), Edward Arnold, London, **1993**.

[7] a) W. Skuballa, H. Vorbrüggen, *Angew. Chem.* **1981**, *93*, 1080; *Angew. Chem. Int. Ed. Engl.* **1981**, *20*, 1046; b) M. Shibasaki, Y. Torisawa, S. Ikegami, *Tetrahedron Lett.* **1983**, *24*, 3493; c) W. Skuballa, E. Schillinger, C. S. Stuerzebecher, H. Vorbrüggen, *J. Med. Chem.* **1986**, *29*, 313; d) K. Ohno, H. Nishiyama, H. Nagase, K. Matsumoto, M. Ishikawa, *Tetrahedron Lett.* **1990**, *31*, 4489; e) W. Bartmann, G. Beck, *Angew. Chem.* **1982**, *94*, 767; *Angew. Chem. Int. Ed. Engl.* **1982**, *21*, 751.

[8] a) T. Namba, H. Oida, Y. Sugimoto, A. Kakizuka, M. Negishi, A. Ichikawa, S. Narumiya, *J. Biol. Chem.* **1994**, *269*, 9986; b) Y. Boie, T. H. Rushmore, A. Darmon-Goodwin, R. Grygorczyk, D. M. Slipetz, K. M. Metters, M. Abramovitz, *ibid.* **1994**, *269*, 12173.

[9] a) J. Fried, D. K. Mitra, M. Nagarajan, M. M. Mehrotra, *J. Med. Chem.* **1980**, *23*, 234; b) K. Bannai, T. Toru, T. Oba, T. Tanaka, N. Okamura, K. Watanabe, A. Hazato, S. Kurozumi, *Tetrahedron* **1983**, *39*, 3807; c) Y. Matsumura, T. Shimada, T. Nakayama, M. Urushihara, T. Asai, Y. Morizawa, A. Yasuda, *ibid.* **1995**, *51*, 8771; d) T. Asai, Y. Morizawa, T. Shimada, T. Nakayama, M. Urushihara, Y. Matsumura, A. Yasuda, *Tetrahedron Lett.* **1995**, *36*, 273.

[10] Y. Matsumura, T. Nakano, M. Makino, Y. Morizawa, preliminary report presented at the AFMC International Medicinal Chemistry Symposium 95, Tokyo, **1995**.

[11] a) W. E. Barnette, *J. Am. Chem. Soc.* **1984**, *106*, 452; b) S. H. Lee, J. Schwartz, *ibid.* **1986**, *108*, 2445; c) S. Singh, D. D. DesMarteau, S. S. Zuberi, M. Witz, H.-N. Huang, *ibid.* **1987**, *109*, 7194; d) E. Differding, R. W. Lang, *Helv. Chim. Acta* **1989**, *72*, 1248; e) T. Umemoto, S. Fukami, G. Tomizawa, K. Harasawa, K. Kawada, K. Tomita, *J. Am. Chem. Soc.* **1990**, *112*, 8563; f) E. Differding, G. M. Ruegg, R. W. Lang, *Tetrahedron Lett.* **1991**, *32*, 1779; g) F. A. Davis, W. Han, *ibid.* **1991**, *32*, 1631; h) E. Differding, H. Ofner, *Synlett* **1991**, 187; i) G. S. Lal, *J. Org. Chem.* **1993**, *58*, 2791.

[12] a) H. Molines, M. H. Massoudi, D. Cantacuzene, C. Wakselman, *Synthesis*, **1983**, 322; b) J. T. Welch, J. S. Plummer, T.-S. Chou, *J. Org. Chem.* **1991**, *56*, 353.

[13] Wittig reaction of perfluorinated esters and amides: a) H. J. Bestmann, H. Dornauer, K. Rostock, *Chem. Ber.* **1970**, *103*, 2011; b) J. P. Begue, D. Bonnet-Delpon, D. Mesureur, G. Nee, S. W. Wu, *J. Org. Chem.* **1992**, *57*, 3807.

[14] The assignment of the configuration was based on the known chromatographic behavior of prostaglandin intermediates.

[15] Compound **14** was approximately 1000 times more stable than 7-fluoro-2,4-methylene-17,20-dimethylprostacyclin [9c,d] under these conditions.

[16] M. J. Cho, M. A. Allen, *Prostaglandins* **1978**, *15*, 943.

[17] A. D. Allen, F. Shahidi, T. T. Tidwell, *J. Am. Chem. Soc.* **1982**, *104*, 2516.

[18] W. Kirmse, A. Wonner, A. D. Allen, T. T. Tidwell, *J. Am. Chem. Soc.* **1992**, 114, 8828.

[19] C.-S. Chang, M. Negishi, T. Nakano, Y. Morizawa, Y. Matsumura, I. Ichikawa, *Prostaglandins*, in press.

Charge Transfer Interactions in Dyed Crystals of Aromatic Carboxylic Acids and Their Relevance to MALDI Mass Spectrometry**

Christine A. Mitchell, Scott Lovell, Keith Thomas, Phil Savickas, and Bart Kahr*

Efforts to understand how and why organic molecules enter crystals of aromatic carboxylic acids have suddenly taken on a new urgency in light of matrix-assisted laser desorption/ionization (MALDI) mass spectrometry,[1] a revolutionary process in which analyte molecules, when precipitated with a crystalline acid matrix, are served-up to the gas phase upon irradiation. The success of the MALDI experiment depends critically upon the host–guest interactions, which at this time are poorly understood.[2] We have been systematically studying a large, neglected literature describing crystals, including aromatic carboxylic

[*] Dr. B. Kahr, C. A. Mitchell, S. Lovell, K. Thomas
Department of Chemistry, Purdue University
West Lafayette, IN 47907-1393 (USA)
Fax: Int. code +(317)494-0239

Dr. P. Savickas
Analytical Sciences Laboratory, The Dow Chemical Company
Midland, MI 48667 (USA)

[**] This work was supported by the National Science Foundation and the Dow Chemical Company. We thank Kim Schrum and Phil Fanwick for their assistance.

acids, grown from solution in the presence of dyes.[3] Such crystals sometimes display regiospecific patterns of color due to the selectivity of the dye molecules for different crystalline surfaces. In this report we describe the essential role of complex formation in the growth of these mixed crystals, and show how it relates to the contemporary development of MALDI mass spectrometry.

Lehmann first described pleochroic crystals of organic acids grown in the presence of both natural and synthetic dyes,[4] but his experiments are difficult to interpret because he paid little attention to crystallographic directions. Sometime later, Gaubert placed this work on a stronger crystallographic foundation[5] by reporting that Crystal Violet (**1**) and Malachite Green (**2**) color the {021} growth sectors of phthalic acid (**3**) crystals.[6] We grew crystals of **3** from saturated aqueous solutions containing **1** or **2** (0.02 M), as well as dyes **5**–**8**. These

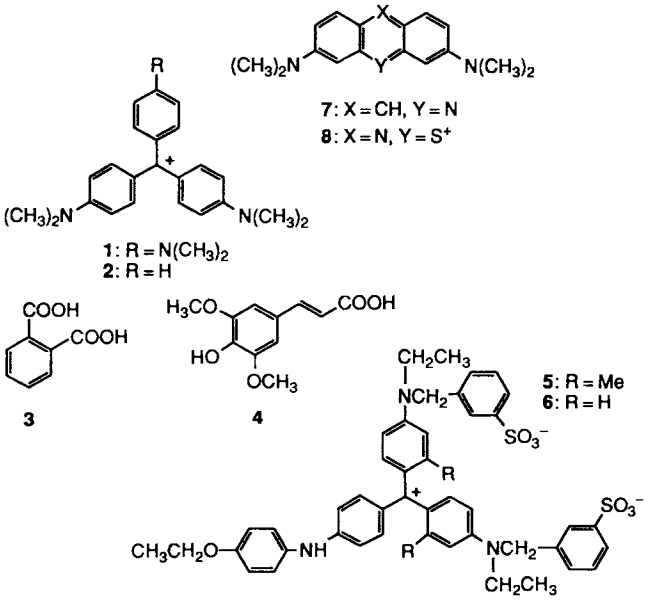

crystals showed characteristic hourglass patterns of coloration resulting from dye inclusion in the {021} growth sectors, in agreement with the previous observations of Gaubert (Fig. 1). We determined, by quantifying the absorption of dissolved mixed crystals, that one dye molecule is included in a colored sector for every $5-15 \times 10^3$ molecules of **3**. The crystals are strongly dichroic for light incident upon the (010) face (Table 1); a maximum absorption was observed when the electric vector made an angle of 45° to [100], the slow vibration direction (Fig. 2).[7, 8]

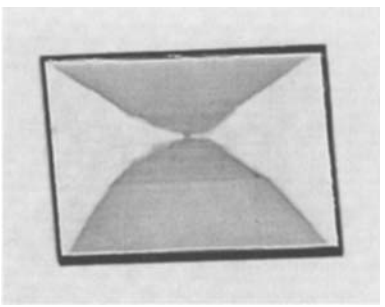

Fig. 1. A mixed crystal (0.7 × 0.5 mm) of **3** and **8** showing its dyed {021} growth sectors and the largest flat faces {010}, viewed in the $-b$ direction.

We determined the X-ray structure[9] of a stoichiometric (1:1) cocrystal of Malachite Green (**2**)·hydrogen phthalate and phthalic acid,[10] which helps to explain the observed dichroism

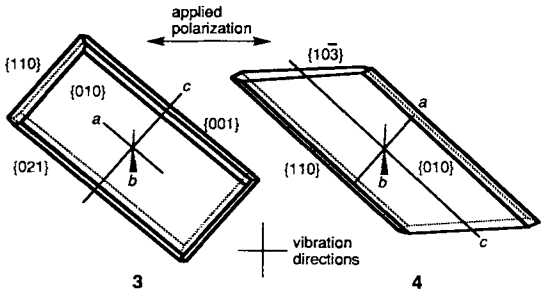

Fig. 2. Morphologies of **3** and **4**. Crystals are oriented with respect to a common set of vibration directions. View is at an angle of 10° from the b axis to emphasize minor facets.

Table 1 Absorption for dyes in phthalic acid crystals and in solution.

Dye	Color index no.[a]	λ_{max} [nm] aq. soln.	λ_{max} [nm] satd. soln. **3**	λ_{max} [nm] crystals **3**	Dichroic ratio, light incident on (010)
1	42555	616	619	630	7.5
2	42000	664	668	669	3.2
5	42655	590	593	601	2.6
6	42660	588	618	625	2.6
7	46005	490	493	505	15.6
8	52015	554	556	575	11.6

[a] *Colour Index*, 3rd ed., Society of Dyers and Colourists, London, **1982**.

in the solid solutions. In this structure the phthalic acid and hydrogen phthalate molecules form a hydrogen-bonded network that may be succinctly described by the graph set $\mathbf{C_2^2(11)S(7)}$.[11] As shown in Figure 3, ion **2** is grossly distorted

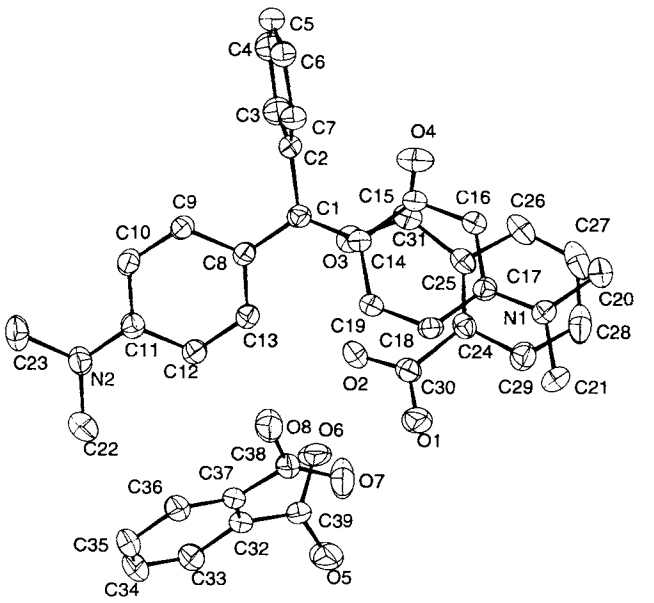

Fig. 3. ORTEP representation (50% ellipsoids) of the crystal structure of **2**·hydrogen phthalate·**3**. Selected bond lengths [Å] and angles [°]: C1–C14 1.41(1), C1–C2 1.49(1), C1–C8 1.44(1), C11–N2 1.35(1), C17–N1 1.33(1), O8–O2 2.59(1), O1–O6 2.57(1), O2–O3 2.45(1); C2-C1-C8 117.0(2), C2-C1-C14 117.8(2), C14-C1-C8 125.2(2), C24-C25-C31-O3 −16.86(2), C25-C24-C30-O2 22.23(2), C37-C32-C39-O6 − 53.88(2), C32-C37-C38-O7 − 29.99(2). Angles [°] between mean planes of aryl rings and the mean plane through C1-C8-C14-C2: C2–C7 67.4(2) C8–C13 17.8(2) C14–C19 21.1(2); Angle between planes C14–C19 and C24–C29 5.3(2)°.

from the expected propeller-like ground state geometry,[12] extending its π system in order to accommodate the interaction with hydrogen phthalate. Such charge transfer interactions were previously identified in solution as red shifts in the absorption maxima.[13] Table 1 lists similar red shifts that we observed in solution and in the mixed crystals.

We calculated the electric transition dipole moment (ETDM) in the **2**·hydrogen phthalate complex by applying the INDO/S[14] method to the coordinates from the X-ray structure analysis. Next, we placed the structure of this complex determined by X-ray crystallography, with its attendant ETDM, within a model of the phthalic acid lattice[15] such that the aromatic ring of the hydrogen phthalate in the complex was least squares fit to a phthalic acid ring in the lattice (Fig. 4). We also considered the superposition of a structure in which the COOH functionality at C24 was moved to C26, assuming that it was only necessary to preserve the interaction between **2** and the carboxylate group at C25. The average projection of the ETDMs for the two possible superpositions gave a predicted dichroic ratio of 5.7 with a maximum absorption in the slow vibration direction. Thus, π-complexation of hydrogen phthalate ions with the cationic dyes would serve to orient the chromophore π systems parallel with the (102) planes, yielding absorption anisotropies in reasonable agreement with experiment. Sensibly, the dichroic ratios are greater for the "flat" cations (**7**, **8**) than for the propellers (**1**, **2**, **5**, **6**) because the ETDM is now constrained to lie in the mean molecular plane of the dye, which will adopt a parallel orientation with respect to hydrogen phthalate in the lattice.

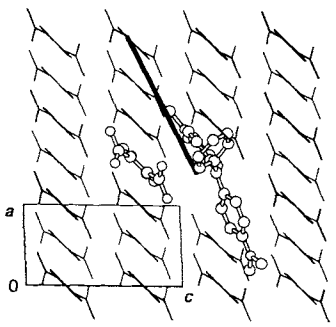

Fig. 4. X-ray structure of Malachite Green incorporated into the phthalic acid lattice, viewed down *b*, such that the complexing hydrogen phthalate ion is superimposed on a phthalic acid molecule in the lattice. The calculated ETDM is indicated as a thick black line.

Recently, researchers attempted to image proteins[16] and oligonucleotides[17] in MALDI host crystals such as sinapic acid (**4**) by first staining the biological molecules with the noncovalent dyes Brilliant Blue G (**5**) and Acridine Orange (**7**), respectively. Since dichroic, facially specific patterns of color were observed only in the presence of the biological molecules, it was reasoned that the proteins and the oligonucleotides carried the dyes into the crystals of **4**. It seemed to us that if crystals of **3** can orient cationic dyes, **4** might produce similar inclusions even in the absence of a biological analyte. We grew crystals of **4** in the presence of **1**, **2**, **5**, **6**, **7**, and **8** under the conditions employed previously by the MALDI researchers (2/1 H_2O/CH_3CN containing 0.1% trifluoroacetic acid at 4 °C).[15] Each dye produced colored crystals of **4** that were dichroic, with the maximum absorptions polarized in the $(10\bar{3})$ planes. No biological cofactors were necessary. Crystals of **4** have a lamellar structure with hydrogen-bonded layers parallel to $(10\bar{3})$, which is the sharpest cleavage plane.[15] It is not surprising, considering our studies with **3**, that dye adsorption occurs on these layers.

The historical literature describes hundreds of other acid/dye solid solutions.[4] We hope that this article will serve to remind researchers of these chemical systems and caution others as to their ubiquity. At the same time, such solid solutions may serve as useful models for the noncovalent interactions that are requisite in forming mixed crystals suited to MALDI mass spectrometry.

Received: December 13, 1995 [Z86561E]
German version: *Angew. Chem.* **1996**, *108*, 1076–1078

Keywords: dichroism · dyes · mass spectrometry · polarization spectroscopy

[1] F. Hillenkamp, M. Karas, R. C. Beavis, B. T. Chait, *Anal. Chem.* **1991**, *63*, 1193A–1203A; S. Borman, *Chem. Eng. News.* **1995**, *73*, (*25*) 23–35.
[2] K. Strupat, M. Karas, F. Hillenkamp, *Int. J. Mass. Spectrom. Ion Processes* **1991**, *111*, 89–102.
[3] B. Kahr, J. Chow, M. J. Peterson, *J. Chem. Educ.* **1994**, *71*, 584–586; M. P. Kelley, B. Janssens, B. Kahr, W. J. Vetter, *J. Am. Chem. Soc.* **1994**, *116*, 5519–5520; M. Rifani, Y.-Y. Yin, D. S. Elliott, M. J. Jay, S.-H. Jang, M. P. Kelley, L. Bastin, B. Kahr, *ibid.* **1995**, *117*, 7572–7573.
[4] O. Lehmann, *Z. Phys. Chem.* **1891**, *8*, 543–553; *Ann. Phys. Chem.* **1894**, *51*, 47–76.
[5] P. Gaubert, *Z. Kristallogr.* **1906**, *43*, 501 (originally in *Bull. Soc. Fr. Mineral.* **1905**, *28*, 286–304); b) P. Gaubert, *C. R. Hebd. Seances Acad. Sci.* **1906**, *142*, 219–221.
[6] Gaubert used Groth's indices obtained from classical goniometry (*Chemische Krystallographie*, *Bd. 4*, Wilhelm Engelmann, Leipzig, **1909**). The *k* values should be doubled in order to conform with modern conventions (see ref. 10).
[7] A. Neuhaus, *Z. Kristallogr.* **1943**, *105*, 161–219; A. N. Winchell, *The Optical Properties of Organic Compounds*, McCrone Research Institute, Chicago, IL, **1987**, p. 122.
[8] The intensity was quantified by using a microabsorption spectrophotometer constructed from an Olympus polarizing microscope.
[9] Metallic green needles of **2**·hydrogen phthalate:**3** were grown by slow evaporation of a 50/50 EtOH/H_2O solution containing 0.4 g (0.024 mol) of **3** and 0.56 g (0.006 mol) **2**·oxalate; m.p. 167–170 °C. Crystal data: $C_{39}H_{36}N_2O_8$, M = 660.72 g mol^{-1}, crystal dimensions 0.29 × 0.20 × 0.16 mm, triclinic, space group $P\bar{1}$ (No. 2), a = 7.251(1), b = 13.655(1), c = 18.345(1) Å, α = 110.87(1), β = 91.76(1), γ = 101.42(1)°, V = 1644.0(1) Å^3, ρ_{calcd} = 1.335 g cm^{-3}, $\mu(Cu_{K_\alpha})$ = 7.275 cm^{-1}, λ = 1.5418 Å, Z = 2, 7270 reflections collected, 4062 observed ($I < 3.0\sigma(I)$) with 5° < 2θ < 149°. Intensity data were recorded at room temperature with an Enraf-Nonius Kappa Axis CAD4 rotating anode diffractometer with ω-2θ scans, and corrected for Lorentz and polarization effects. Heavy atoms were refined anisotropically and hydrogen atoms were placed in idealized positions, except for H1 and H2, which were located in the difference map and refined with a riding model (d(C–H) = 0.96 Å) using the programs contained in CRYSTALS (D. Watkin, Chemical Crystallography Laboratory, Oxford, UK, **1994**). R = 0.058, R_w = 0.073 for 445 parameters, maximum/minimum residual electron density: 0.33/ − 0.40 e Å^{-3}. Crystallographic data (excluding structure factors) for the structure reported in this paper have been deposited with the Cambridge Crystallographic Data Centre as supplementary publication no. CCDC-179-18. Copies of the data can be obtained free of charge on application to The Director, CCDC, 12 Union Road, Cambridge CB2 1EZ, UK (fax: int. code +(1223) 336-033; e-mail: teched(*a* chemcrys.cam.ac.uk).
[10] The compound $C_{39}H_{36}N_2O_8$ was first reported by W. Lindenberg, *Z. Naturforsch. B* **1956**, *11*, 151–157.
[11] J. Bernstein, R. E. Davis, L. Shimoni, N.-L. Chang, *Angew. Chem.* **1995**, *107*, 1687–1706; *Angew. Chem. Int. Ed. Engl.* **1995**, *34*, 1555–1573; M. C. Etter, *Acc. Chem. Res.* **1990**, *23*, 120–126.
[12] For a review on the structures of triarylmethyl cations see: B. Kahr, M. P. Kelly in *Proceedings of the NATO Advanced Research Workshop on Supramolecular Stereochemistry*, (Ed.: J. S. Siegel), Kluwer, Dortrecht, **1995**, pp. 203–222; B. Kahr, J. E. Jackson, D. L. Ward, S.-H. Jang, J. F. Blount, *Acta Crystallogr. Sect. B* **1992**, *48*, 324–329.
[13] S. Hamai, *Bull. Chem. Soc. Jpn.* **1985**, *58*, 2099–2106.
[14] J. Ridley, M. C. Zerner, *Theor. Chim. Acta* **1973**, *32*, 111–134; *ibid.* **1976**, *42*, 223–236.
[15] O. Ermer, *Helv. Chim. Acta* **1981**, *64*, 1902–1909.
[16] R. C. Beavis, J. N. Bridson, *J. Phys. D. Appl. Phys.* **1993**, *26*, 442–447.
[17] K. Schneider, B. T. Chait, *Org. Mass Spectr.* **1993**, *28*, 1353–1361.

 © *VCH Verlagsgesellschaft mbH, D-69451 Weinheim, 1996* *0570-0833/96/3509-1023 $ 15.00+.25/0*

Reflections of a True PhD

The Same and Not the Same. By *R. Hoffmann*. Columbia University Press, New York, 1995. 294 pp., hardcover $ 34.95.—ISBN 0-231-10138-4

A popular oratorical strategy especially common in high-brow rhetoric exploits the "tension field" created by one polar extreme acting against another, usually with the speaker clambering up and down like a preacher (in this case) on a Jacob's ladder of subtly linked dichotomies and contradictions in an attempt to make the obvious more memorable. If the orator is gifted at formulating matters with insight, sensitivity, and circumspection, with wisdom and charm, this approach can also provide a source of reflective pleasure. And when has it been otherwise with Roald Hoffmann? His broad background, his dazzling style, his enviably engaged combinatorial memory—these are characteristics that make him a highly regarded and avidly sought spokesperson for all sorts of occasions related to chemistry, or which he himself shows to be chemistry-related. Drawing upon a great many such occasions, and enhancing the effect with a cleverly tailored set of images, Hoffmann has here assembled a skein of information that affords interesting, stimulating, and affirmative reading from beginning to end. The resulting collage is somewhat reminiscent of a series of essays from another chemist: Primo Levi's *The Periodic Table*, which Hoffmann frequently cites in his extensive bibliography. But Levi's work amounts to a veiled autobiography, whereas this is instead a wide-ranging and fervent plea for reflection with respect to chemistry as a discipline. Understanding comes only through enlightened participation. Hoffmann therefore elucidates, in a marvelously uncomplicated way fully accessible to the layman, the actual problems chemists confront amidst the contradictory technical, emotional, moral, and political tensions surrounding their work.

Roald Hoffmann always knows where to find memorable and apt analogies, illustrations, and examples, and many people have contributed enthusiastically to this particular endeavor. Not least among these is the publisher, incidentally, who has produced a deluxe edition the like of which is seldom seen these days on such an occasion: glossy paper and sharp printing, clear diagrams, and faithful color reproductions, presented in a genuine cloth binding! But this handsome piece certainly should not disappear into the bibliophile's bookcase; it should instead be "consumed", and then shared with other chemists. The effort will be richly rewarded!

The content of the book is easily summarized, but characterizing it is more difficult: call it chemistry transformed by a tincture of wisdom into philosophy. Hoffmann's goal is to convey his thoughts directly to an engaged circle of readers, thoughts as they have occurred to him in the course of his life as a theoretical chemist pursuing research, as a graduate adviser, and as a conscientious citizen. Laymen should have no trouble following him, because the reader will quickly become captivated, and there is no let-up. Insightful chemists will affirm the validity of the way Hoffmann analyzes chemistry's methodology, and they will be uplifted by the discovery that their intellectually guided skills are grounded not only in the dissection and unfolding of the multifaceted, but above all in the art of synthesis: joining together, mediating, creating, and recreating. The self-critical scientific reader will also become more acutely conscious of how arrogant it is in a dispute involving concerned environmentalists to demand that a cost/benefit analysis always be undertaken, believing that the world must be run on the basis of a specialist's insights—not unlike Plato's proposed dictatorship over a society made up of minors.

This is one observation among many that are transmuted here by a chemist, drawing upon both chemical experience and political reflection, into a general principle: that only a combination of knowledge and engagement will create an environment in which chemists, too, can introduce their artistry in a harmonious way. Chemistry must therefore direct its educational skills toward those who will themselves never be chemists; indeed, chemical illiteracy is a threat not because it limits our ability to exploit nature, but rather because it prevents us from understanding the principles according to which nature operates. It isolates us from nature, which in compensation acquires a mystical character. That is in turn damaging, because the public becomes incapable of making decisions based on fact with respect to scientific issues. And it is precisely the public and only the public that must make such decisions: not the scientists, who are themselves simply people, neither priests nor politicians. The one chemist among a thousand citizens will continue to learn the necessary skills anyway, but he or she will not be permitted to practice them if the 999 non-chemists fail to understand his/her intentions. This is one of many instances in which awareness of a critical dichotomy leads to increased insight.

Every chemist is familiar with the polarities of analysis and synthesis, left and right, effective and ineffective, equivalent and nonequivalent, natural and unnatural (as well as a host of others), but here these have been refined into productive philosophy. Roald Hoffmann shares this gift with the adepts of old, whose dreams, deeply embedded within us, are still so very alive: the ability of some agent, some catalyst to participate through a keyhole, to ascend immaculately out of a mêlée with the power to turn raw materials into treasure. Are these not still the essential driving forces? Hoffmann makes us acutely conscious of the role of catalysis in the context of the three-way catalyst and of enzymes, but in

This section contains book reviews and a list of new books received by the editor. Book reviews are written by invitation from the editor. Suggestions for books to be reviewed and for book reviewers are welcome. Publishers should send brochures or (better) books to Dr. Illenora Beckmann, Redaktion Angewandte Chemie, Postfach 101161, D-69451 Weinheim, Federal Republic of Germany. The editor reserves the right of selecting which books will be reviewed. Uninvited books not chosen for review will not be returned.

such a way that we are not deprived of the magic of it all. The magic persists, even if each step along the way can be reconstructed conceptually.

The tragic dichotomy in the deeds and character of the chemist himself is illustrated by a moving sketch of the towering personality of Fritz Haber: rationalist and Don Quixote, world citizen and patriot in both the narrower and the wider sense, career man and visionary, nourisher and destroyer. Haber's fruitful and beneficial ammonia synthesis serves as an elegant starting point for exploring a chemist's activities and thoughts, as well as the leap of genius from paradigmatic routine into the unimagined. Many windows are opened onto the mental universe of the scientist, onto the forces of the mind that guide his or her visions and tools, with a particular chemist serving as an example, but leading to insights that are quite generally valid. We sense the polarities that keep the chemist's world in motion: substances and reactions, discovering and protecting, things and personalities, understanding and feeling, curiosity and power, creative ability and fear, self-control and arrogance, responsibility and exploitation. The crossing-points of various emotions—perceived and unperceived—define the state of the chemist's soul, as they do with all humans, in the contest over the possible, which the chemist seeks in that which holds nature together.

The Janus-faced character of chemistry—its double-barreled quality, its blind spots—is not a new theme, but also not an overly familiar one. Here it becomes a theme for the confessional, at the same time witty and amusing, partly out of personal experience, but with no trace of hubris or hysteria. The chemist as the dull mean—or as the sharp focal point—between a physics obsessed with mathematization and a chaotic biology. Well thought out are the insights so modestly presented on the method of reductionism; beautiful as well are the humility and sense of indebtedness with respect to the humanities which indicate how multidimensional the nexuses are. And the observation that we are tied to linearizing patterns of speech, but at the same time in a desperate search for a "method" of simplification, of enumeration, measurement, and standardization. How easy it all is for chemists, with their conditioned symbolism and the strict conventions of their notation!

Roald Hoffmann's book contains an unimagined treasure trove of thoughts, knowledge, and refinement—from Aeschylus to Zeus, from alchemy to the zodiac, from acetylcholine to xenon tetrafluoride, most of it related to Hoffmann's own scientific efforts or engagements. In effect, it represents the journey of a man out of oppression into freedom, and at the same time his committed gratitude to fate. If the book were to be the subject of an excellent translation it could exert its effect well beyond the bounds of chemistry, and it warrants that opportunity—though the effort might also prove a disappointment, since so much is a function of the marvelous language in which the work is cast, a language the author himself was forced to learn, albeit at an early age.

Lothar Jaenicke
Institut für Biochemie
der Universität Köln (Germany)

Resorcinol. Its Uses and Derivatives. (Series: Topics in Applied Chemistry.) By *H. Dressler*. Plenum, New York, 1994. 500 pp., hardcover $ 115.00.—ISBN 0-306-44850-5

The author of this book is obviously a (former) industrial chemist. This becomes apparent in each chapter, on each page, almost even in each sentence, both in its positive and negative aspects.

The introductory chapter is essentially a list of the book's contents, then in only the first seven pages of the second chapter (three of which are filled by full-page reproductions of the IR, ^{1}H NMR—at 60 MHz!—and ^{13}C NMR spectra of resorcinol) we already find four clear references to the author's firm, including the statement that "this plant has had a good record as to the safety and health of its employees for many years". However, as regards the subject of this chapter, entitled "The Properties and Chemistry of Resorcinol", the reader is given insufficient information. For example, Section 2.6 on "Methods of Analysis" consists of just five sentences.

The following ten chapters deal with industrial and commercial aspects of resorcinol in all conceivable variants. The best way to do justice to the book is to list their titles as follows: 3. "Processes for Making Resorcinol", 4. "The Use of Resorcinol in Rubber Compositions", 5. "Resorcinol/Formaldehyde Resins—Adhesives for Wood and Other Nonrubber Applications", 6. "*m*-Aminophenol", 7. "Agricultural Chemicals, Including Veterinary Products", 8. "Pharmaceuticals, Over-the-Counter Medications, and Diagnostic Aids", 9. "The Uses of Resorcinol/Derivatives in Polymers", 10. "Dyes, Fluorescent Chemicals, Optical Bleaches, Laser Dyes, and Imaging/Recording Technologies", 11. "Additives of Many Types", and 12. "Other Uses for Resorcinol".

In each chapter the author strings together innumerable bits of information, mostly at a rather superficial level (examples of the style: "A large number of... were prepared, and shown to be..."; "A preparation of... was patented..."; "A similar patent covered the use of..."). The few cross-references given, although welcome in principle, seem to have been chosen more or less at random. There is hardly any evidence of the mass of information having been critically evaluated or processed in any way, except perhaps in the flow diagrams describing the large-scale manufacture of the basic chemicals resorcinol and *m*-aminophenol (Chapters 3 and 7). In Chapters 3–12 about 90% of the literature references given are patents. Despite the fact that data on tonnages produced and their value are scattered throughout the text, the author evidently felt it necessary to include a separate chapter on these (13. "Selected Business Aspects").

This is followed by a further two chapters (14. "Occurrence in Nature—A Domain of Academic Researchers", 15. "Other Examples of Mostly Academic Work with Resorcinol") which contain about 400 literature references (not patents), compared with the book's total of slightly over 1800. With regard to these two rather unbalanced chapters, the author comments in the introduction: "The placement... near the end of the book is not intended as an indication of the lesser importance of these topics, but rather as an intent to finish with a note of enthusiasm, to show the burst of ideas and the connection to the whole fabric." Here, as in the book as a whole, one would like to believe in the author's good intentions.

At first glance the book appears nicely produced. It contains many structural formulas which aid the reader's understanding, although the choice of these sometimes seems strange. Whereas Chapter 5 contains no chemical formulas at all, those of *m*-fluorophenol and equally simple compounds included elsewhere could surely have been omitted. Most of the formulas are printed in a clear and uniform style, although sometimes they are badly reproduced (e.g., 15-4 and 15-5) and others have been copied without much thought (e.g., 11-44, a [1.1]metacyclophane!). Similar criticisms apply to the black-and-white photographs (some of which are of poor quality, e.g. those showing a lichen-covered rock and a

 © VCH Verlagsgesellschaft mbH, D-69451 Weinheim, 1996 0570-0833/96/3509-1026 $ 15.00+.25/0

minesweeper). Also, surely it should have been possible to find a better ^{1}H NMR spectrum of resorcinol than the badly reproduced version from the Sadtler Catalog!

The book presents, from the standpoint of a chemist engaged in his own special field, of the mainly technical and commercial uses of resorcinol. The question that one must ask is whether it is useful to have a book devoted arbitrarily to a single chemical compound. The reader who feels that it is and decides to buy the book will find that it gives a very comprehensive survey of the relevant patent literature. This is undoubtedly of some value. However, anyone expecting more will be disappointed.

Volker Böhmer
Fachbereich Chemie
der Universität Mainz (Germany)

Forschung mit Röntgenstrahlen. Bilanz eines Jahrhunderts (1895–1995). Edited by *F. H. W. Heuck* and *E. Macherauch*. Springer, Berlin, 1995. 682 pp., hardcover DM 98.00.—ISBN 540-57718-1

The idea of publishing a book to mark the centenary of the discovery of X-radiation seems at first sight to be a fairly straightforward undertaking. However, questions arise when one comes to consider what should be included in such a book, and what the reader will expect from the title "Research Using X-Rays"—where should one begin?—and how are the boundaries to be defined? X-radiation is used in such diverse fields as medicine (for both diagnosis and therapy), the natural sciences, engineering and technology, art, and archeology. All these are in fact treated in this book. Obviously such a range could not be covered by a single author, and for that reason this substantial 682-page volume contains 44 articles by different authors.

The book opens with a brief historical outline of the discovery of X-radiation and of the life of Röntgen (which, interestingly, is only taken up to the time when he made the discovery). The first half of the book describes radiological diagnostics as applied to the parts of the body with supporting and movement functions and to internal organs, followed by articles on the applications of X-rays in medico-legal practice, radiotherapy, dosimetry, radiobiology, and veterinary science. It can be seen from this list that F. H. W. Heuck, the editor responsible for the medical part of the book, has been especially concerned to present a balanced and comprehensive picture of the research applications of X-rays in this area. From the standpoint of a layman so far as this field is concerned, I found these articles very interesting. The text, written in a way understandable by the nonspecialist, and the excellent illustrations make this part compelling reading. The articles stimulate one's interest in the medical applications of X-radiation and offer the nonspecialist reader an excellent overview of the subject.

The second half of the book is devoted to the natural sciences and technology. It begins with a historical account of the development of methods for generating X-rays, and of the fundamental knowledge that was gained up to about the mid-1920s. The various methods for detecting X-rays are then described, leading up to the modern CCD (charge-coupled device) camera. Separate chapters deal with applications of X-rays in crystallography, chemistry, and biochemistry, with appropriate examples. These are followed by articles on X-ray diffraction in mixed crystals, noncrystalline metals, and alloys. Additional chapters deal with the technologically important topics of texture determination, elastic stress measurements, and studies of macroscopic structure. These chapters, which are mainly concerned with investigating the structures of materials, are followed by others on X-ray spectroscopy, X-ray microscopy, and measurements on X-radiation from outer space. The book concludes with descriptions of the applications of X-radiation in the fields of art, anthropology, and paleontology.

All the articles are readily understandable, and the text is illustrated by many diagrams and instructive photographs. With only a few exceptions, mathematical formulas have been avoided. It is clear that all the authors have aimed to present their subjects in a way that can be understood by readers who are unfamiliar with the field. Each article also contains a list of material for more advanced reading.

The layout and standard of production of the book are excellent. The editors are to be congratulated on having put together a book which, despite the large number of authors involved, achieves a consistent style and quality. Almost every area of research using X-radiation is covered, and the book provides a very good survey of the subject. It can be recommended for everyone with an interest in the field, and should be available in every university library.

Helmut Bertagnolli
Institut für Physikalische Chemie
der Universität Stuttgart (Germany)

 © *VCH Verlagsgesellschaft mbH, D-69451 Weinheim, 1996* *0570-0833/96/3509-1027 $ 15.00+.25/0*

Conceivable orbital interactions
that could stabilize side-on
coordinated alkanes like
side-on coordinated
silanes and
H_2 .

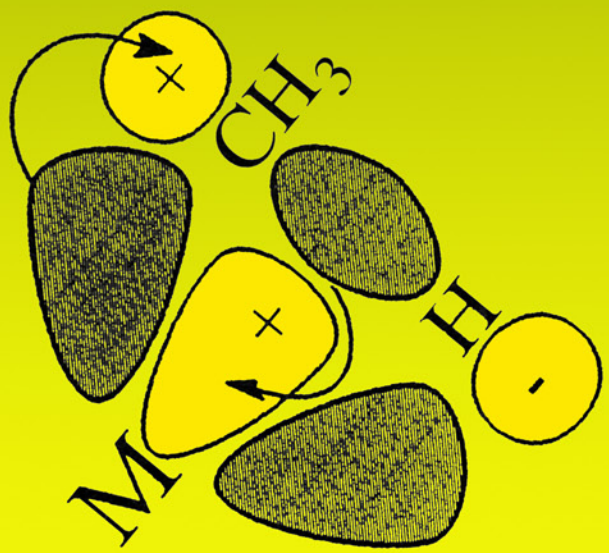

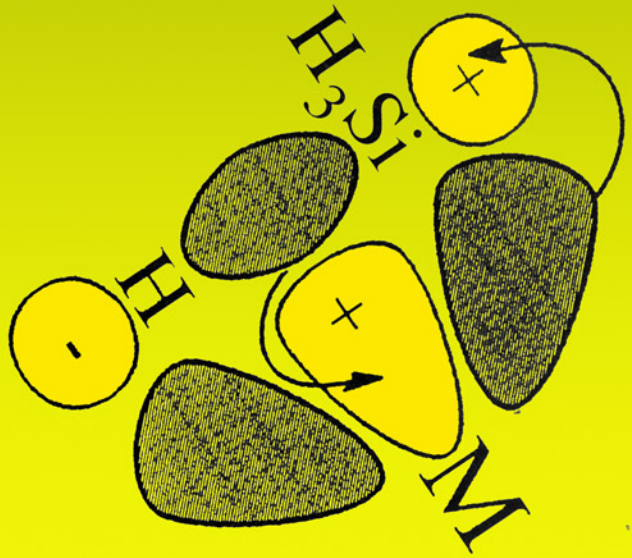

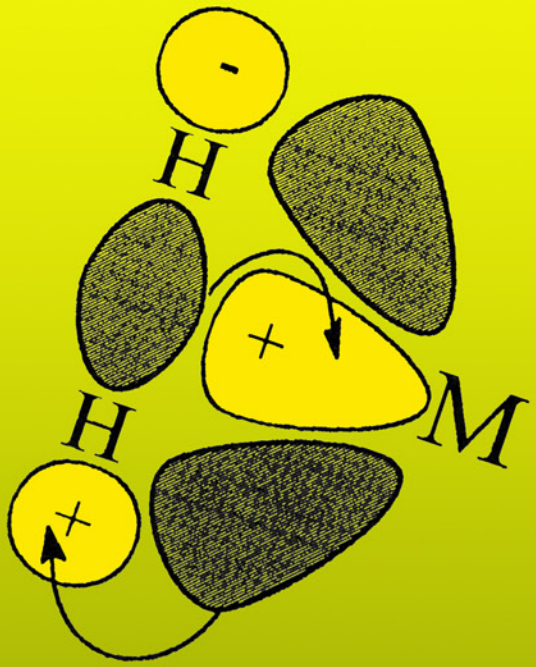

Free-Radical Carbonylations: Then and Now

Ilhyong Ryu* and Noboru Sonoda

Although known since the 1950s, free-radical carbonylation has not received much attention until only recently. In the last few years the application of modern free-radical techniques has revealed the high synthetic potential of this reaction as a tool for introducing CO into organic molecules. Clearly now is the time for a renaissance of this chemistry. Under standard conditions (tributyltin hydride/CO) primary, secondary, as well as tertiary alkyl bromides and iodides can be efficiently converted into the corresponding aldehydes. Aromatic and α,β-unsaturated aldehydes can also be prepared from the parent aromatic and vinylic iodides. If the reaction is carried out in the presence of alkenes containing an electron-withdrawing substituent, the initially formed acyl radical subsequently adds to the alkene, leading to a general method for the synthesis of unsymmetrical ketones. This three-component coupling reaction can be extended successfully to allyltin-mediated reactions. Thus, β,γ-enones can be prepared from organic halides, CO, and allyltributylstannanes. In a remarkable one-pot procedure alkyl halides can be treated with a mixture of alkene, allyltributylstannane, and carbon monoxide in a four-component coupling reaction that provides β-functionalized δ,ε-unsaturated ketones by the formation of three new C–C bonds. The reaction of 4-pentenyl radicals with CO leads to acyl radical cyclization, which provides a useful method for the synthesis of cyclopentanones. Certain useful one-electron oxidations can be combined efficiently with free-radical carbonylations. These findings and others discussed in this article clearly demonstrate that free-radical carbonylation can now be considered a practical alternative to transition metal mediated carbonylation.

Keywords: carbon–carbon coupling · carbon monoxide · carbonylation · radicals · synthetic methods

1. Introduction

As the introduction of carbon monoxide into organic molecules is important in synthesis, many chemists have worked on developing useful and reliable carbonylation reactions. Much of this effort has been centered around the use of transition metals. During the long history of carbonylation chemistry, many industrially important processes have been developed such as the Reppe reaction, the Roelen reaction, and Monsanto's acetic acid synthesis, to name just a few. A wide variety of transition metal complexes can be used to catalyze carbonylation reactions.[1] However, to meet the challenges set by the modern chemical industry, further investigations are needed to obtain new, selective, mild, cheap, and safe carbonylation catalysts.

Transition metal catalysis is not the only means capable of introducing CO into organic compounds. For example, both cationic and anionic species can react with CO to provide carbonyl compounds (Scheme 1).[2, 3] What about the role of free radicals in carbonylation chemistry? Has the potential of free-radical carbonylation been fairly judged? These simple questions initiated our own research into this undeveloped area which began in the late 1980s. Free-radical carbonylation was first investigated in the early 1950s, triggered by the work of Coffman and co-workers, who first documented the peroxide-initiated copolymerization of ethylene and CO.[4] Unfortunately, this type of reaction did not receive much further attention, possibly because some of the initial work employed extremely high CO presssures (> 1000 atm) and kinetic studies were not pursued vigorously. In 1990, however, we reported a highly efficient carbonylation reaction, which takes place in a tin hy-

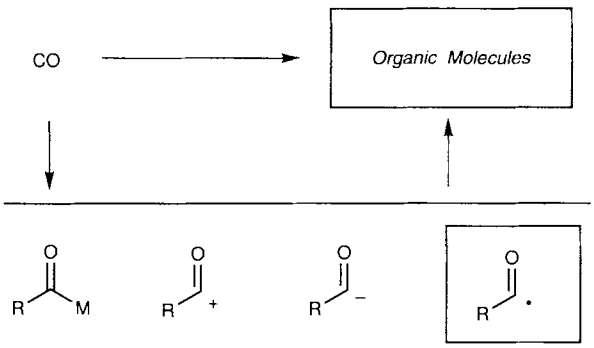

Scheme 1. Possible intermediates in carbonylations with CO.

[*] Prof. I. Ryu, Prof. N. Sonoda
Department of Applied Chemistry, Faculty of Engineering, Osaka University
Suita, Osaka 565 (Japan)
Fax: Int. code +(6)879-7402
e-mail: ryu@chem.eng.osaka-u.ac.jp

dride mediated radical chain reaction system, to give aldehydes from alkyl halides.[5] This work provided the starting point for us and others to reinvestigate free-radical carbonylation reactions as a synthetic tool. Free-radical carbonylations have long been overshadowed by the successful metal-catalyzed or metal-mediated carbonylations, but now the chemistry appears to be experiencing a renaissance. In this review, we will present the first full coverage of free-radical carbonylation in organic synthesis to date. Extensions of the free radical initiated copolymerization of ethylene and CO, which have also received attention recently in view of the need for degradable polymers, will not be covered here.

2. Early Work

The trapping of carbon monoxide by methyl radical was first reported in 1939 by Faltings.[6] He observed that the reaction of ethane with CO under UV irradiation resulted in the production of acetone. The synthetic applications of free-radical carbonylation truly evolved in the 1950s. In 1952 Coffman, Brubaker, and Hoehn, at DuPont, described the peroxide-initiated copolymerization of ethylene and CO to yield polyketones (Scheme 2).[4]

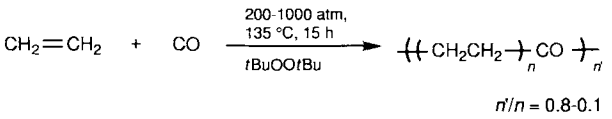

Scheme 2. Free radical mediated copolymerization of ethylene and CO (1952).

The proportion of CO in the copolymers depended on the ratio of CO/C_2H_4 employed, but the incorporation of CO did not exceed 50% even when CO was used in large excess.[7, 8] The work of Coffman et al. was the first example of efficient addition of radicals to CO, and even more importantly it served as the springboard for the development of radical carbonylation reactions for the preparation of carbonyl-containing compounds other than polyketones.[9]

Subsequent work at DuPont aimed at synthesizing aldehydes from an alkanethiol, CO, and ethylene (Scheme 3)[10] or

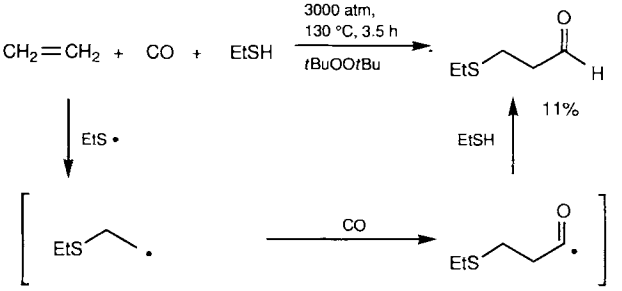

Scheme 3. Thioformylation of ethylene (1956).

acetylene.[11] Unfortunately, the results were not very promising on account of low yields ($\leq 11\%$) even in reactions conducted under extremely high pressures (up to 3000 atm).

In 1957 Cramer reported that pyrolysis of tetraethyllead at 200 °C under 1000 atm of CO gave diethyl ketone as one of the products (Scheme 4).[12] This reaction was proposed to proceed by the coupling of acyl and alkyl radicals, which was first suggested by Faltings. It was also observed that under similar reaction conditions, α-phenylethyl radicals did not give carbonylated products, presumably due to the stability of the radical.

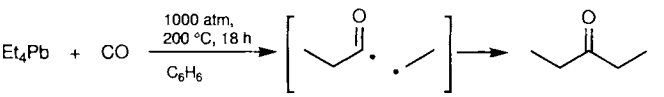

Scheme 4. Formation of diethyl ketone from tetraethyllead and CO (1957). The yield was not given.

Ilhyong Ryu was born near Nagoya (Japan) in 1951, received his BS in 1973 from Nagoya University, and earned his PhD in 1978 at Osaka University, where he worked under the direction of Noboru Sonoda. After spending a couple of years as a JSPS postdoctoral fellow and a research associate at Osaka University, he became Assistant Professor there in 1987 and was promoted to Associate Professor in 1995. He was a visiting scientist at the University of Ottawa with Professor Howard Alper (1991–1992). He received the Progress Award of Synthetic Organic Chemistry, Japan, in 1990. His current research interests include the development of new synthetic methods by means of reactive intermediates such as either free radicals or organometallic species.

I. Ryu

N. Sonoda

Noboru Sonoda was born in Osaka (Japan) in 1933, graduated from Osaka University in 1956, and obtained his doctorate there in 1961. He became Assistant Professor at Osaka University in 1961 and was promoted to Associate Professor in 1967 and then to Professor in 1973. He served as Dean of the Faculty of Engineering during 1993–1995. He has received many awards for research: the Chemical Society of Japan Award for Young Chemists (1965), the Synthetic Chemistry Award, Japan (1987), the Chemical Society of Japan Award (1990), and the Japan Petroleum Institute Award (1995). His research interests include the development of new synthetic methods based on elements such as sulfur, selenium, tellurium, silicon, and tin, and new carbonylation chemistry.

In 1958 Coffman's group and Chiusoli and Minisci independently recorded their efforts to extend the CO trapping reaction to a free-radical carboxylation system. For example, the reaction of *tert*-butyl cyanide with Fenton's reagent ($FeSO_4$, H_2O_2) in the presence of CO yielded β-cyanoisovaleric acid together with the dimer of the starting material (Scheme 5).[13] They

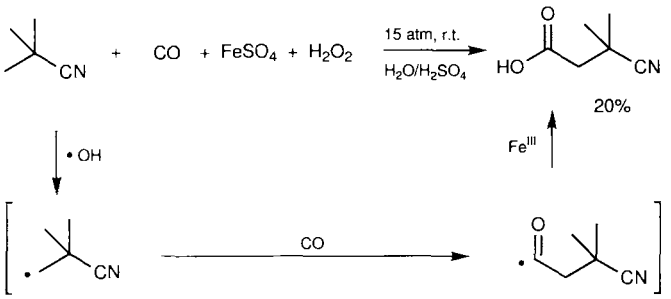

Scheme 5. Free-radical carboxylation with CO at room temperature (r.t.) (1958).

proposed that iron(II) reduces hydrogen peroxide to generate the hydroxyl radical, which abstracts a hydrogen atom from *tert*-butyl cyanide. The resulting radical adds to CO and the acyl radical formed is oxidized by Fe^{III} to give acyl cation, thus regenerating Fe^{II}. The yields of carboxylated products are generally low. Since hydrogen abstraction by the hydroxyl radical from alkanes is not selective, the range of substrates is severely limited. Nevertheless, this work served as a benchmark since it described the incorporation of CO into an "unactivated" C–H bond under remarkably low CO pressures (1–50 atm). Pimeric acid was synthesized from cyclohexanone and CO under similar reaction conditions by β-scission of a cyclohexyloxy radical.[13, 14]

Walling and co-workers also contributed to free-radical carbonylation during the early stages. The decomposition of dibenzoyl peroxide in CCl_4 at 70 °C under 53 atm of CO pressure gave benzoyl chloride in 40% yield (Scheme 6).[15] This product is

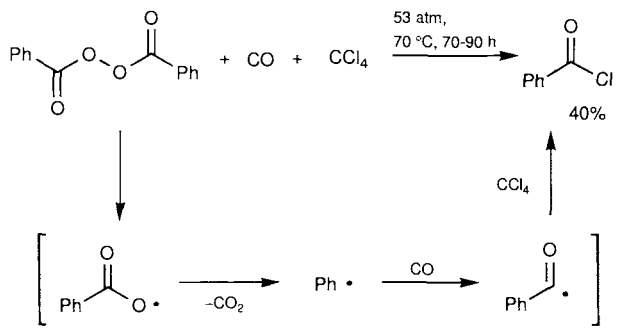

Scheme 6. Carbonylation of Ph' (1960).

thought to result from the addition of phenyl radical, which is generated by the decarboxylation of the initially formed benzoyloxy radical, to CO with subsequent abstraction of chlorine from CCl_4. Interestingly, Walling et al. found that treatment of dibutyl disulfide with CO in the presence of triethyl phosphite afforded *S*-butyl thiovalerate (Scheme 7).[16] Dibutyl sulfide is a by-product of this reaction, but at 325 atm of CO the selectivity for the thioester is very high. Under photolytic conditions the reaction proceeds to some extent even under 1 atm CO. The authors propose the radical chain mechanism shown in Scheme 7, in which disulfide serves not only as a source of butyl radicals but also as a scavenger of acyl radicals.

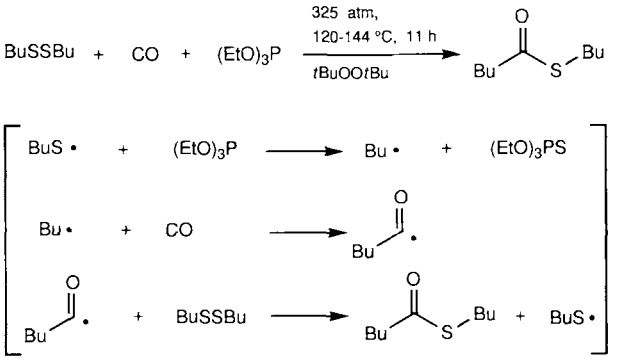

Scheme 7. Formation of a thioester from a disulfide, triethyl phosphite, and CO (1960).

Thaler achieved the conversion of cyclohexane to cyclohexanecarbonyl chloride by subjecting a 2:1 mixture of cyclohexane and CCl_4 to CO under forcing conditions (Scheme 8).[17, 18]

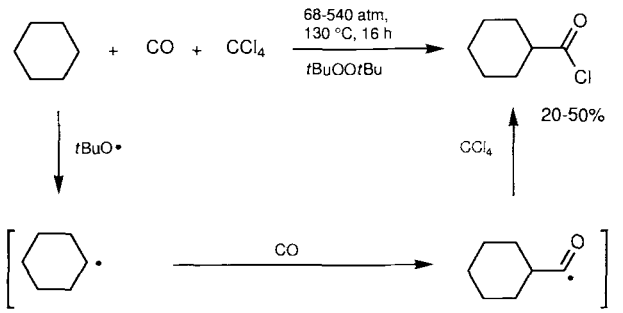

Scheme 8. Preparation of an acid chloride from cyclohexane, CO, and CCl_4 (1966).

The reaction begins by abstraction of hydrogen from cyclohexane by a *tert*-butoxy radical (generated from di-*tert*-butyl peroxide at 130 °C), and the trichloromethyl radical formed in the last step is thought to be the chain carrier. CO pressures of more than 200 atm are required to suppress formation of cyclohexyl chloride.

In 1970 Tsuji and Susuki reported that the reaction of alkenes with CO and CCl_4 in the presence of metal carbonyl catalysts such as $[Co_2(CO)_8]$, $[\{CpFe(CO)_2\}_2]$, and $[\{CpMo(CO)_3\}_2]$ yielded β-trichloromethyl-substituted alkanoyl chlorides (Scheme 9).[19] Carbon tetrachloride served as the solvent and high CO pressures (160–200 atm) were necessary. Although a free-radical mechanism has yet to be verified for the carbonylation step, this reaction is a significant improvement on the original transformation described by

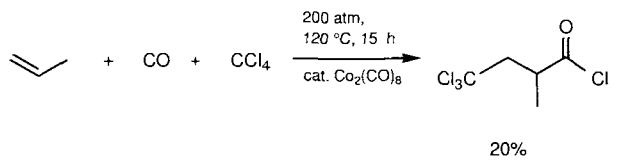

Scheme 9. Carbonylation of propylene with CO and CCl_4 (1970).

Foster et al., which required added peroxide as an initiator and gave poor results.[10]

With the exception of a few studies that were not directed towards preparative applications (see Section 7), the synthetic potential of free-radical carbonylation was mostly neglected until 1990, when our first report appeared.[5] During this period, however, the chemical and physical properties of acyl radicals were largely elucidated.[20] In recent years numerous methods for the formation of acyl radicals, which involve the use of acyl selenides,[21] have modernized and generalized their synthetic applications.[22]

3. Kinetic Studies

Kinetic information provides the basis for designing and understanding free-radical processes. When we started this research program in the late 1980s, only kinetic data for the gas-phase reaction of methyl and ethyl radicals with CO was available.[23, 24] The lack of useful kinetic data for reactions in solution may be one of the main reasons why free-radical carbonylation long failed to come into its own. However, this all changed with the results of kinetic studies by Bakac et al., by Boese and Goldman, and by us (Scheme 10). The addition of

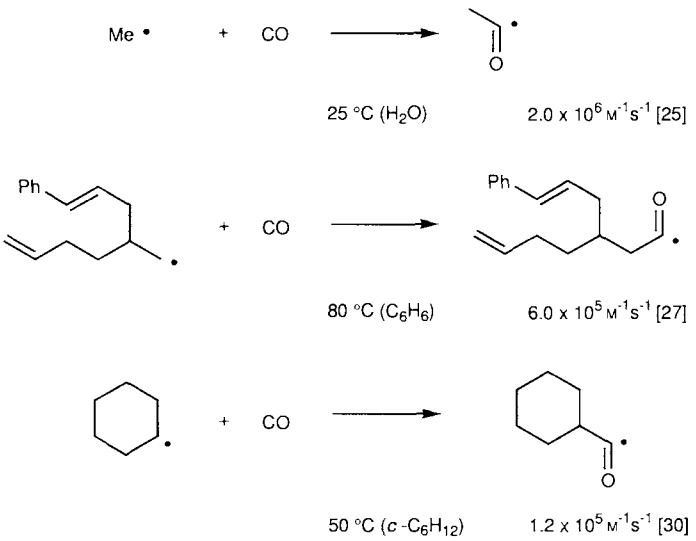

Scheme 10. Rate constants for carbonylation of alkyl radicals in solution.

alkyl radicals to CO in solution was found to be much faster than expected based on the gas-phase data. For the reaction of methyl radical in water the rate constant k_1 was estimated to be $2.0 \times 10^6\ M^{-1}s^{-1}$ at 25 °C.[25, 26] This value is roughly 300 times greater than the reported gas-phase value.[23c] A primary alkyl radical was recently shown by us to add to CO at 80 °C in benzene with a rate constant of $6.0 \times 10^5\ M^{-1}s^{-1}$ and an activation barrier of 6.0 kcal mol^{-1}.[27, 28] The observed rate constant is somewhat smaller than the rate constant for the addition of a primary radical to acrylonitrile ($1.1 \times 10^6\ M^{-1}s^{-1}$, 69 °C) but comparable to that to styrene ($1.5 \times 10^5\ M^{-1}s^{-1}$, 69 °C).[29] The rate constant for the addition of cyclohexyl radical to CO in cyclohexane was reported by Goldman and Boese ($1.2 \times 10^5\ M^{-1}s^{-1}$, 50 °C).[30] When the different temperatures are taken into consideration, this value is similar to our value for the addition of a primary radical extrapolated to 50 °C ($2.7 \times 10^5\ M^{-1}s^{-1}$).

The addition of alkyl radicals to CO is reversible (Scheme 11) and therefore the rate constants for the decarbonylation of acyl radicals (k_{-1}) are useful for the design of free-radical carbonylations. The kinetic parameters for the decarbonylation of pivaloyl and phenylacetyl radicals in solution are well established. For example, at 23 °C the decarbonylation rate constants k_{-1} of pivaloyl and phenylacetyl radicals in hexane are $6.7 \times 10^5\ s^{-1}$[24] ($8.3 \times 10^5\ s^{-1}$[31a]) and $5.3 \times 10^6\ s^{-1}$,[31a] respectively (Scheme 12). The k_{-1} values for the decarbonylation of acyl

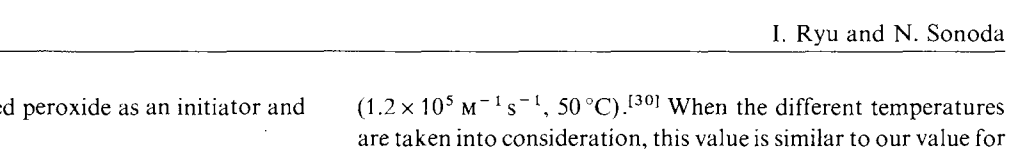

Scheme 11. Carbonylation–decarbonylation equilibrium.

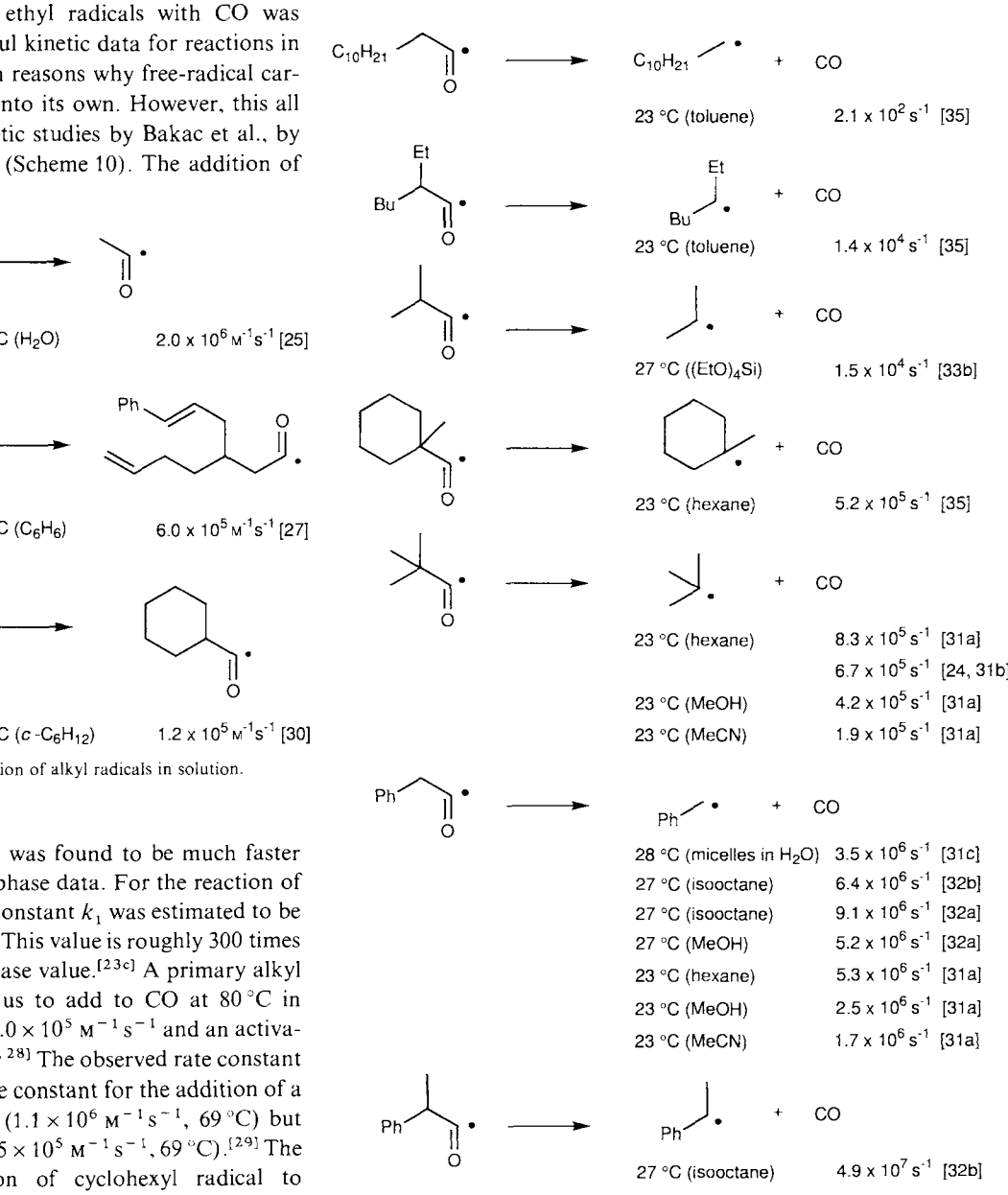

Scheme 12. Rate constants for decarbonylation of acyl radicals in solution.

radicals are solvent dependent,[31a, 32] and the polar nature of acyl radicals is thought to be the origin of the slower rates in polar solvents.

In contrast, the decarbonylation data on secondary and primary acyl radicals are scarce. Some rate constants are known for secondary acyl radicals in solution,[33] but until recently the only available kinetic data for the decarbonylation of primary acyl radicals were measured in the gas phase.[34] In 1995 Chatgilialoglu and Lucarini estimated the approximate rate constants for the decarbonylation of primary, secondary, and tertiary acyl radicals in toluene at 80 °C to be $1.3 \times 10^4\ s^{-1}$, $3.9 \times 10^5\ s^{-1}$, and $1.0 \times 10^7\ s^{-1}$, respectively.[35] Thus the ease of decarbonylation of acyl radicals follows in the order phenylacetyl > pivaloyl > secondary acyl > primary acyl.[36]

4. Free-Radical Formylation: Synthesis of Aldehydes

The transformation of organic halides into aldehydes is one of the most useful carbonylation reactions. A versatile transition metal mediated process is the palladium-catalyzed formylation of allyl, benzyl, and aryl halides with CO and a hydrogen donor such as molecular hydrogen, hydrosilanes, formate ions, and tin hydrides.[1, 37] However, the oxidative addition of simple alkyl halides to metal centers is much slower than that of allyl, benzyl, and aryl halides, and the metal-catalyzed processes are useless with the more common halides.[38, 39] Another serious drawback is that the organometallic product of the oxidative addition reaction is often susceptible to β-hydride elimination and subsequent isomerization.[40] Because formylation by free-radical carbonylation proceeds via completely different intermediates (Scheme 13), β-elimination and the accompanying isomerization cannot arise.

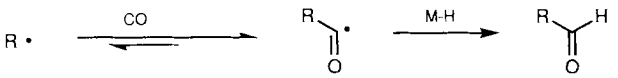

Scheme 13. Concept for free-radical formylation.

In the first attempts at synthesizing aldehydes by free-radical carbonylation (Scheme 3) the marked inefficiency was most likely due to problems with generation of the key alkyl radical, which may hamper the smooth flow of the total free-radical chain system. We believed that this problem could be avoided by employing much more reliable free-radical generation systems like the well-established tin hydride mediated reduction of organohalides.[41] This approach led to a breakthrough. We showed that CO pressures of less than 90 atm can be used for the formylation of alkyl bromides and iodides, when tributyltin hydride and a catalytic amount of 2,2'-azobis(isobutyronitrile) (AIBN) are used.[5] This landmark work marked the first synthetically useful aldehyde synthesis by free-radical carbonylation. Thus, octyl bromide can be formylated to give nonanal in good yield (Scheme 14). Higher dilution conditions have been found to result in better selectivity (formylation vs. reduction).

Scheme 15 illustrates some other examples of free-radical formylation. Secondary alkyl bromides can be formylated successfully, but the efficiency of the reaction of tertiary alkyl bromides varies from substrate to substrate. Thus, 1-bromoadamantane can be formylated smoothly, whereas *tert*-butyl bromide gives pivalaldehyde in relatively low yield. This process is not limited to alkyl halides: aromatic aldehydes can be prepared from the parent iodides.[42] 2-Phenylcyclopropanecarbaldehyde can be prepared from the parent bromide, CO, and tributyltin hydride with high *trans* selectivity. The attack of CO at the least hindered site may account for the selectivity.[43] Selenides can also be used as radical precursors.

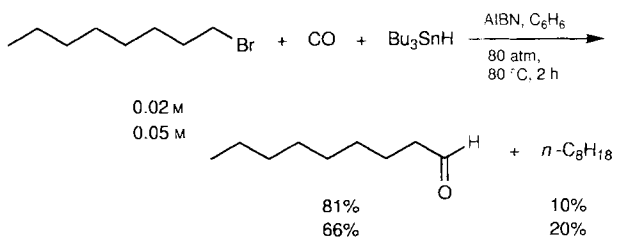

Scheme 14. Free-radical formylation of octyl bromide.

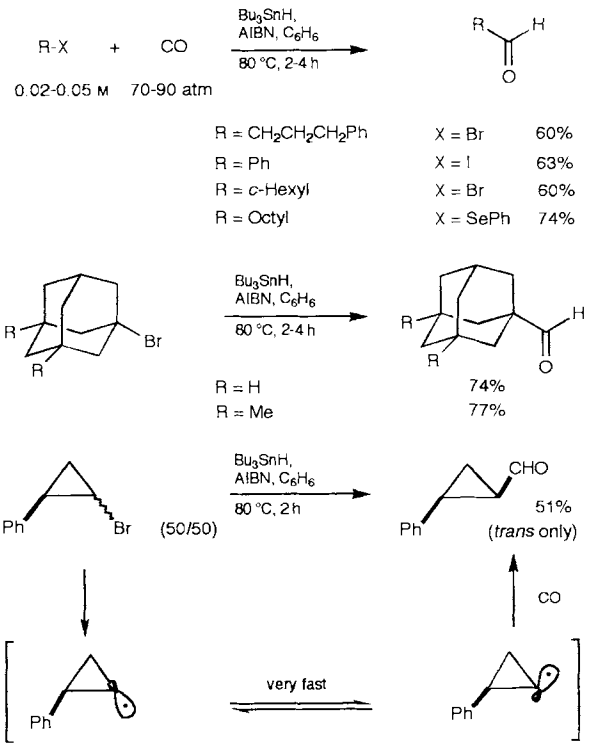

Scheme 15. Free-radical formylation of alkyl halides.

This formylation process can be explained by the free-radical chain propagation mechanism illustrated in Scheme 16. In the initiation step the cyanoisopropyl radical (generated from the decomposition of AIBN) abstracts a hydrogen atom from tributyltin hydride. The resulting stannyl radical abstracts a halogen atom from an alkyl halide furnishing the requisite alkyl radical, which then adds to CO. The resulting acyl radical abstracts a hydrogen atom from tributyltin hydride to give the aldehyde with regeneration of the stannyl radical.

Although alkyl, aryl, and vinyl halides are suitable substrates for free-radical formylations, compounds that yield very stable radicals (i.e. benzyl radical) are not. This is reasonable if one assumes the reverse reaction, decarbonylation of the resulting radicals (see Section 3). Allyl radicals and simple radicals stabi-

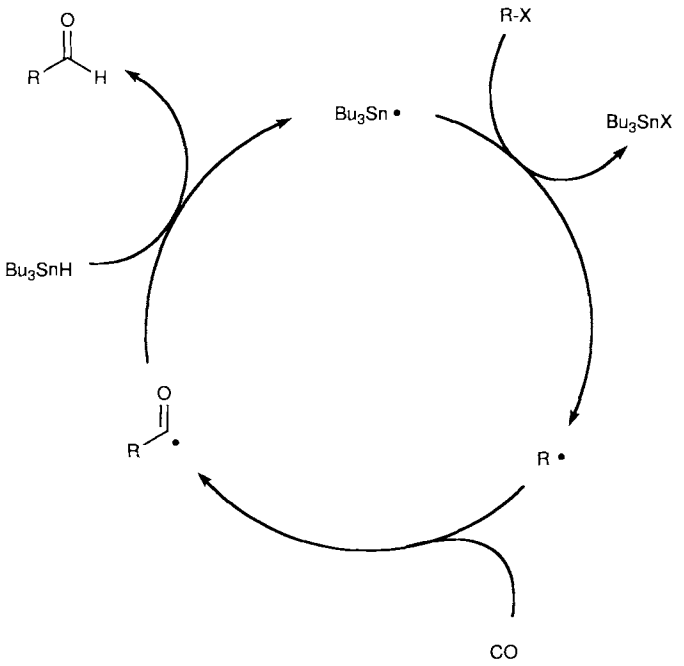

Scheme 16. Mechanism for free-radical formylation of RX (R = alkyl, aryl, vinyl).

lized by adjacent electron-withdrawing groups like cyano and carbonyl groups or electron-donating substituents like an alkoxy group cannot be formylated under the aforementioned conditions.

In these free-radical formylations, high dilutions of 0.02–0.05 M (for organic halides) and high CO pressures of 70–90 atm are required to force the alkyl radicals to add to CO rather than abstract a hydrogen atom from tributyltin hydride. Other ways to obtain high selectivities for carbonylation over reduction include employing free-radical mediators with reduced hydrogen transfer ability. When we used tris(trimethylsilyl)silane (TTMSS),[44] which reacts with primary alkyl radicals six times slower than tributyltin hydride does, we could reduce CO pressures to below 50 atm (Scheme 17).[45]

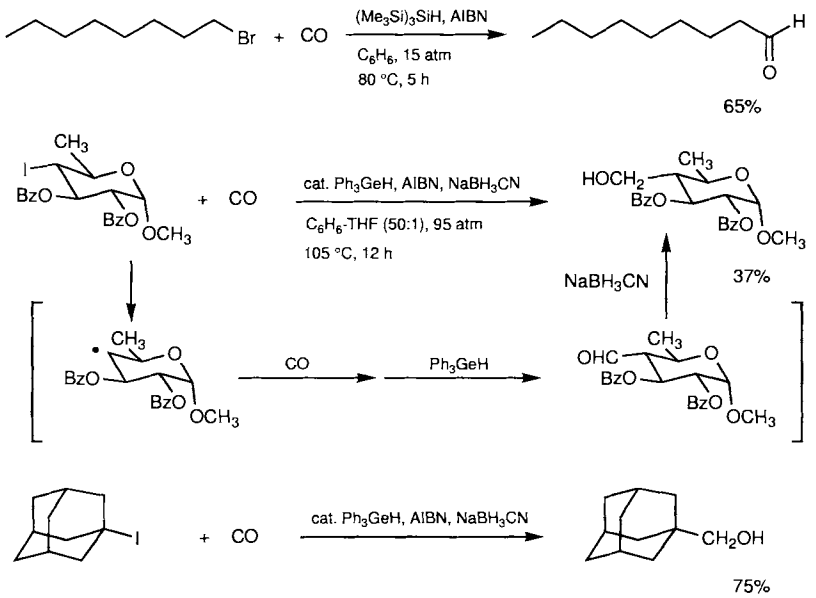

Scheme 17. Free-radical formylations mediated by TTMSS and by Ph_3GeH ([RX] = 0.03–0.05 M).

Gupta and Kahne reported that alkyl iodides are converted to the corresponding hydroxymethyl compounds in good yields with catalytic triphenylgermane and sodium cyanoborohydride/AIBN under CO pressure (Scheme 17).[46] Hydroxymethyl compounds are obtained since the free-radical formylation is followed by in situ reduction. Formylation of alkyl iodides can also be conducted with zinc/copper couple in aqueous media (Luche's system) as the reducing agent.[47] Cyclohexyl iodide and 1-iodoadamantane are formylated in moderate yield with this Zn(Cu)/CO system (Scheme 18).[48] Since the one-electron

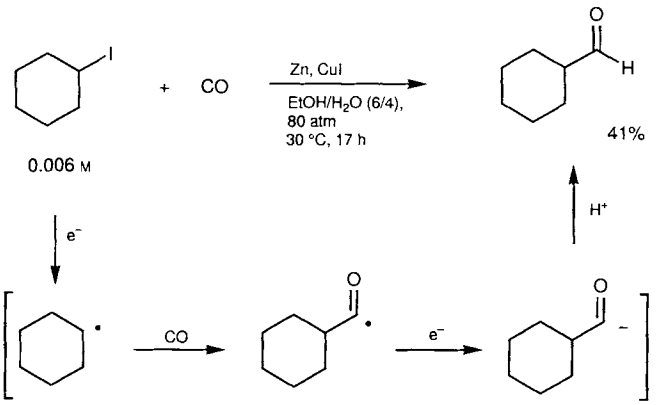

Scheme 18. Free-radical formylation of cyclohexyl iodide mediated by Zn(Cu) couple.

reduction of secondary and tertiary alkyl radicals by zinc is particularly slow, the intermediates add to CO quite smoothly. In contrast, as primary radicals undergo rapid one-electron reduction to the carbanions, the free-radical formylation of a primary alkyl iodide frequently results in a low yield of the aldehyde.

It is interesting to note that a similar formylation catalyzed by palladium(0) complexes also uses tributyltin hydride as a hydrogen source.[37d] Stille and Baillargeon reported that aryl, allyl, and alkenyl halides can be conveniently formylated by tin hydride and CO in the presence of a catalytic amount of $[Pd(PPh_3)_4]$ to yield the corresponding aldehydes. In the proposed mechanism (Scheme 19) the organic halide adds oxidatively to the palladium center to form an organopalladium species. Subsequent CO insertion and reductive elimination then furnish the desired aldehydes. This method is complementary to free-radical formylation, since the latter is not suited to the carbonylation of allylic and benzylic substrates. Conversely, the palladium method is not suited to alkyl halides.

Free-radical formylations are possible not only with organic halides but also with alkynes, 1,6-dienes, and vinylcyclopropanes. The following three examples demonstrate the synthetic potential of these reactions, which are initiated by the addition of heteroatom-centered radicals to unsaturated C–C bonds and therefore inherently lead to heteroatom-substituted aldehydes.

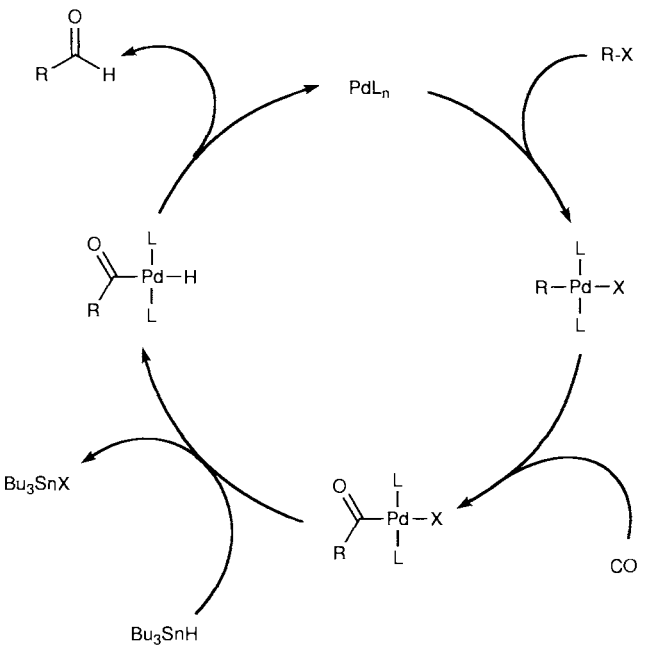

Scheme 19. Mechanism for Stille's Pd-catalyzed formylation of RX (R = aryl, vinyl, allyl).

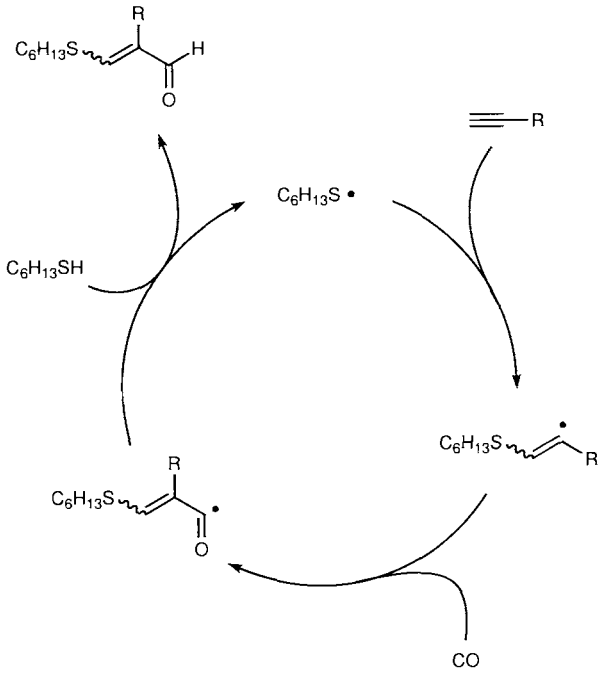

Scheme 21. Mechanism for Yoshida's thioformylation of alkynes.

Yoshida and co-workers reported that treatment of terminal alkynes with aromatic or aliphatic thiols and AIBN under CO afforded α,β-unsaturated β-thioaldehydes in moderate to good yields (Scheme 20).[49] The formation of exclusively *trans* isomers is due presumably to thermodynamic equilibration. The

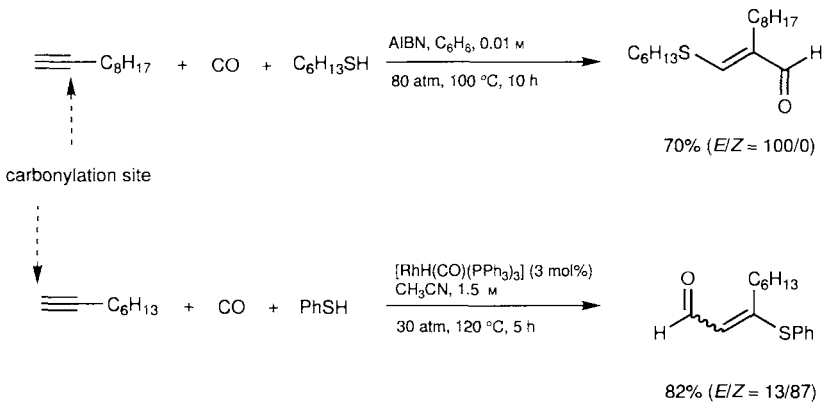

Scheme 20. Two types of thioformylations of alkynes.

reaction follows the mechanism given in Scheme 21. The reactions with alkanethiols gave consistently better results than those with thiophenol. Since alkanethiols have a lower tendency for hydrogen transfer,[50] premature quenching of the vinylic radical prior to reaction with CO is less likely. Thioformylation of alkynes catalyzed by rhodium complexes has been reported recently by Ogawa, Sonoda, and co-workers (Scheme 20).[51] Interestingly, the regioselectivity of the addition to monosubstituted alkynes is the opposite of that in the radical addition.

One of the recent topics in transition metal catalyzed carbonylations is the silylformylation of organic molecules with hydrosilanes and CO;[52] the related stannylformylation has yet to be explored. Free radical based stannylformylation of 1,6-dienes was reported in 1994.[53] In this reaction a 5-*exo*-trig ring closure gives carbocycles having stannylmethyl and formylmethyl groups at adjacent carbons (Scheme 22). The major byproduct of this reaction is the reduced cyclized product.[54] The addition of stannyl radicals to C=C bonds is reversible. Accordingly, in cases where 5-*exo*-trig cyclization of the key radical is relatively slow, as with 1,6-heptadiene, the yields are low as a result of the radical reverting to stannyl radical and the diene. Analogous silylformylation of 1,6-dienes with TTMSS was unsuccessful because the preferred pathway is an intramolecular S_H2-type reaction at silicon.[55] Likewise, stannylformylation of vinylcyclopropanes is accompanied by the ring opening of the cyclopropylmethyl radicals to give γ,δ-unsaturated aldehydes having an allyltin moiety (Scheme 22).[56]

Recently Chatgilialoglu and Lucarini reported some kinetic data for hydrogen abstraction by acyl radicals from tributyltin hydride and TTMSS in nonpolar solvents.[35] At 23 °C a primary acyl radical abstracts hydrogen from tributyltin hydride and TTMSS with rate constants of $4.1 \times 10^5\ M^{-1}s^{-1}$ and $1.6 \times 10^4\ M^{-1}s^{-1}$, respectively. The rates are somewhat slower than those for the analogous hydrogen transfer to alkyl radicals. (For example the rate constant of the reaction of hexyl radical with tributyltin hydride is $1.1 \times 10^6\ M^{-1}s^{-1}$ at 23 °C.[57]) Lusztyk, Ingold, and co-workers also estimated the rate constant for the abstraction of deuterium by propanoyl radical from tributyltin deuteride to be $3.0 \times 10^5\ M^{-1}s^{-1}$ at 23 °C in hexane.[24] The rate constant for the H-abstraction from thiophenol by isopropanoyl radical was

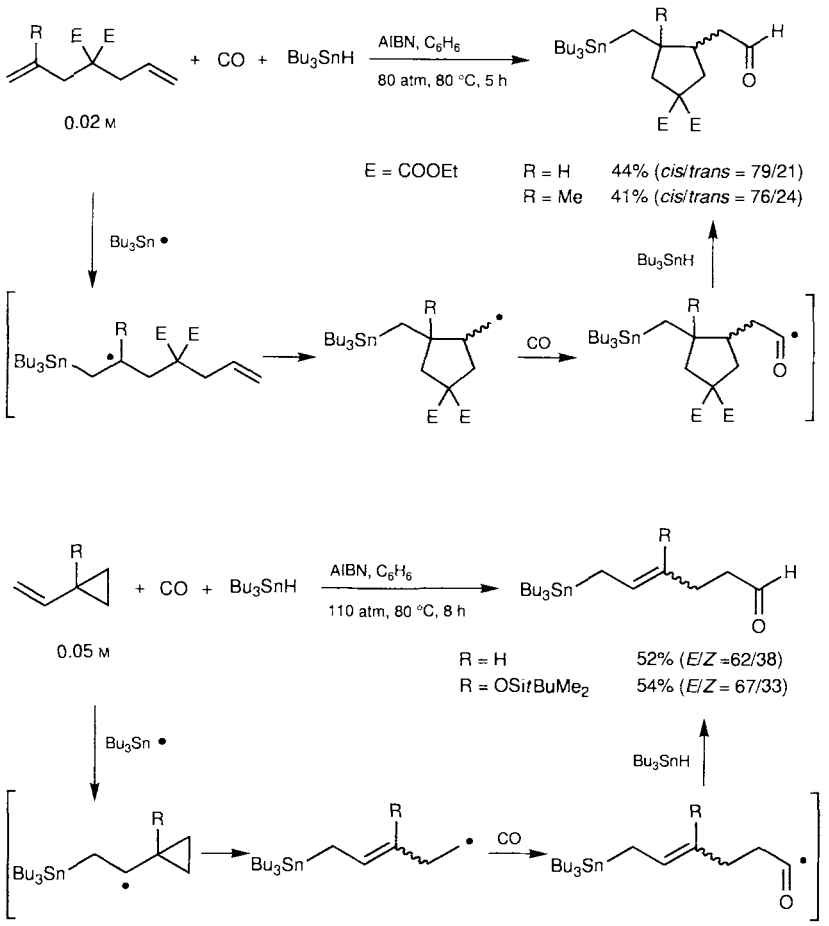

Scheme 22. Stannylformylation of 1,6-dienes and vinylcyclopropanes.

also measured to be 4.4×10^7 $M^{-1}s^{-1}$ at 23 °C in hexane, which is roughly one order of magnitude faster than the corresponding tin hydride reaction.

5. Synthesis of Ketones

As mentioned in the introduction, aside from polyketone synthesis, until recently there were no efficient systems for synthesizing unsymmetrical ketones by free-radical carbonylation. Yet the addition of acyl radicals to alkenes has long been recognized as a useful synthetic method for the preparation of unsymmetrical ketones. In 1949 Kharasch and co-workers reported that the peroxide-initiated chain addition of aldehydes to alkenes yields ketones.[58, 59] A survey of recent examples illustrates the synthetical potential of this ketone synthesis, in which acyl radicals are generated from diverse reagents[60] such as acyl selenides/tin hydride,[60a] acyl tellurides/$h\nu$,[22e] chromium carbene complexes/copper(II),[60b] acylcobalt,[60c, 60e, 22f] and aldehydes/$NO_3^{\cdot}$ radical.[60d] As acyl radicals are nucleophilic, the use of alkenes having an electron-withdrawing substituent facilitates the addition reaction. Kinetic data for reactions in solution indicate that acyl radicals react very rapidly with electron-poor alkenes. Fischer and co-workers have shown that the rate of the addition of pivaloyl radical to acrylonitrile ($k = 5.0 \times 10^5$ $M^{-1}s^{-1}$ at 27 °C) is comparable to that of the analogous reaction of the *tert*-butyl radical ($k = 1.0 \times 10^6$ or 2.4×10^6 $M^{-1}s^{-1}$ at 27 °C).[61] Encouraged by the success of free-radical formylation with tributyltin hydride,[5] we anticipated that the three-component system consisting of RX, CO, and an alkene would lead to unsymmetrical ketones (Scheme 23). The method represents a formal double alkylation of CO, and the transformation is somewhat analogous to Cooke's organotetracarbonylferrate chemistry.[62]

We found that the addition of an alkyl radical to CO could indeed be coupled to the subsequent addition of the resulting acyl radical to an electron-poor alkene to give an unsymmetrical ketone.[63] Competing reactions such as abstraction of hydrogen from tin hydride by acyl radicals to give aldehydes and direct addition of the alkyl radical to the alkene[64] must be supressed. By adjusting the amounts of the alkene and the concentrations ([RI] < 0.02 M) optimal conditions were obtained. Under such high-dilution conditions the ratio of [acyl radical]/[alkyl radical] would be expected to become higher, because the concentration of dissolved CO remains unchanged.

This three-component coupling method has proven to be a general route to a variety of unsymmetrical ketones having diverse functionality. Thus, β-cyano, β-acyl, and β-alkoxycarbonyl ketones can be easily prepared from readily available alkyl halides, functionalized alkenes, and CO (Scheme 24). Styrene can also be used as the alkene component, but the yield of the resulting ketone is rather modest. Reactions conducted with tributyltin hydride require relatively high CO pressures

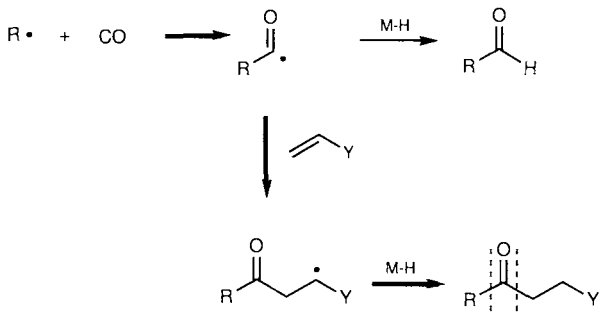

Scheme 23. Concept for the synthesis of unsymmetrical ketones.

of 70–90 atm to encourage the alkyl radicals to capture CO instead of abstracting a hydrogen atom from tin hydride or adding to alkene; however, lower CO pressures should be sufficient when a radical mediator having poorer hydrogen donating ability is used. With TTMSS as a radical mediator, the three-component coupling reaction of primary alkyl halides can be conducted at CO pressures as low as 20 atm.[45] Nevertheless, even with TTMSS higher CO pressures are required to transform secondary and tertiary alkyl radicals into ketones in good yield. One additional advantage of using TTMSS for the three-

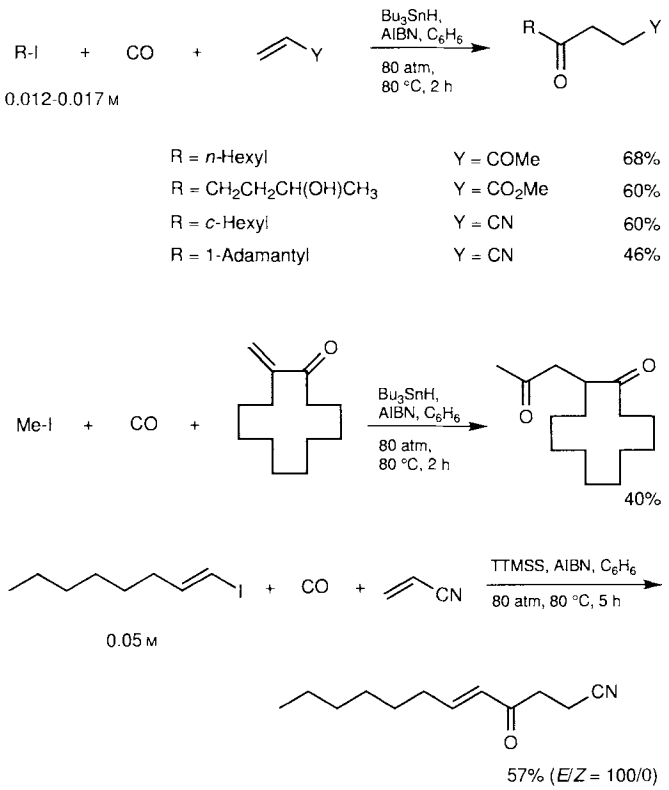

Scheme 24. Representative examples of ketone syntheses.

component coupling is that the reaction can be carried out with only a slight excess of the alkene (generally 1.2 equiv) without a decrease in the yield. This may be because of the slower rate of hydrogen atom abstraction from TTMSS by the acyl radical.[35]

The superiority of TTMSS is further demonstrated by the carbonylation of vinyl radicals (Scheme 24). Vinyl radicals abstract hydrogen from tributyltin hydride considerably faster than alkyl radicals do because of the formation of a strong C–H bond.[65] This often prevents vinyl halides from participating in free-radical carbonylations mediated by tributyltin hydride. For example, the attempted three-component coupling of (*E*)-1-iodooct-1-ene (0.025 M) with CO (80 atm) and acrylonitrile (1.5 equiv) gave 1-octene (45%) as the major product rather than cyanoethyl octenyl ketone (15%). When the same reaction was carried out with TTMSS as the radical mediator, the desired α,β-unsaturated ketone was obtained in 57% yield (Scheme 24).

The chain propagation mechanism of this synthesis of unsymmetrical ketones is illustrated in Scheme 25. This new, efficient synthetic method offers easy access to a variety of structually diverse unsymmetrical ketones, and the use of TTMSS for radical generation increases the versatility of the free-radical carbonylation.

At this point it seems fitting to discuss the efficiency of alkyl radicals in free-radical carbonylations. As discussed in Section 3, the rate constants for the addition of primary and secondary alkyl radicals to CO are large enough for free-radical reactions even at atmospheric pressure, since the values are comparable to the corresponding rate constants for addition of primary alkyl radicals to some reactive alkenes. Nevertheless, high CO pressures are often required for successful free-radical carbonylation. Why? This is mainly because of competing reactions.[66] For example, in the above case of the TTMSS-mediated three-component coupling, competing reactions include direct hydrogen abstraction from TTMSS, addition of the alkyl radicals to alkenes, and even decarbonylation of the resulting acyl radicals. Importantly, free-radical carbonylation in the presence of TTMSS has demonstrated that the reaction with *primary* alkyl radicals is far the more favorable than that of secondary or tertiary alkyl radicals. We consider that this reflects the decarbonylation rates of the corresponding acyl radicals (see Scheme 12).

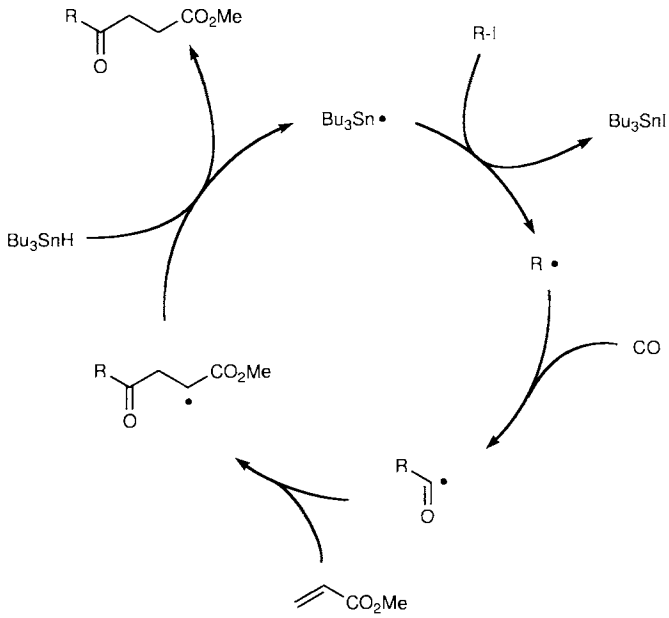

Scheme 25. Radical chain mechanism for the synthesis of unsymmetrical ketones.

Thus, lower CO pressures can be used in the carbonylations of primary alkyl radicals conducted with a slow radical chain mediator. Curran, Giese, and co-workers estimated the rate constant for the addition of primary alkyl radicals to allyltributyltin to be roughly $4 \times 10^4\ M^{-1}s^{-1}$ at 80 C,[67] which is significantly less than the rate of the corresponding H-abstraction from tributyltin hydride (Scheme 26).[57, 65] Thus the direct addition of alkyl radicals to alkenes should not compete with addition to CO. The slow chain propagation of allyltin-mediated process[68, 69] offers valuable insights into the mechanism as well as interesting prospects for synthesis.

The coupling reaction of alkyl iodides, CO, and allyltin yielded β,γ-unsaturated ketones in good yield (Scheme 27).[70, 71] As

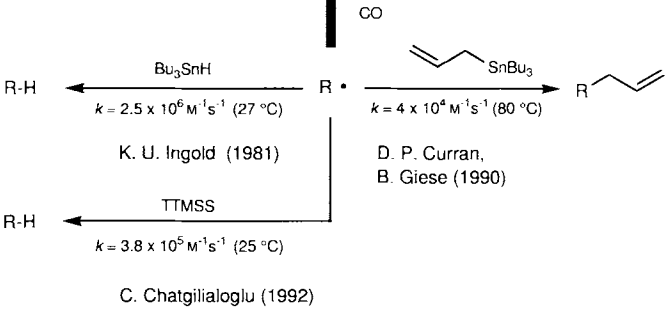

Scheme 26. Rate constants *k* for competing reactions of primary alkyl radicals.

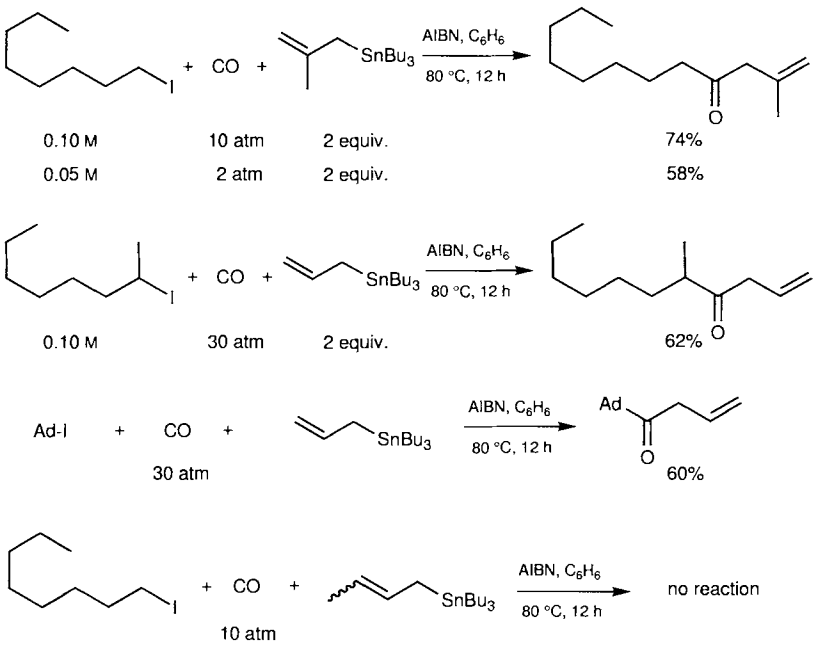

Scheme 27. Allyltin-mediated synthesis of β,γ-unsaturated ketones. Ad = 1-adamantyl.

expected, for the coupling of octyl radical CO pressures of less than 10 atm suffice. In fact, the reaction proceeds efficiently even at 2 atm of CO. For secondary (octyl) and tertiary (adamantyl) radicals, higher CO pressures (30 atm) result in better selectivity for carbonylated products, since the direct S_H2' addition of the alkyl radicals to allyltin is suppressed. Methallyltin can also serve as the alkene component, whereas addition to crotyltin is not possible, presumably due to steric effects.[68]

With electron-deficient alkenes, the four-component coupling reaction of alkyl halides, CO, alkenes, and allyltin takes place efficiently. A variety of β-functionalized (cyano, formyl, acyl, and alkoxycarbonyl), δ,ε-unsaturated ketones can be synthesized conveniently in a single operation.[72] Two examples are given in Scheme 28. In free-radical reactions, the efficiency of

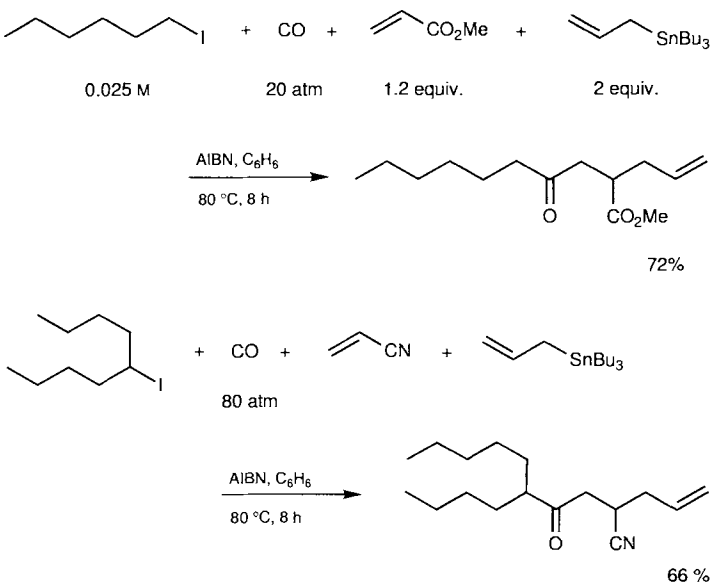

Scheme 28. Allyltin-mediated synthesis of functionalized ketones.

chain propagation does not necessarily reflect the number of the steps. This is also true for allyltin-mediated free-radical carbonylations. Even at low concentrations ([RX] = 0.025 M) the four-component reaction gives better yields than the three-component coupling reaction. The undesirable three-component coupling between an alkyl radical, a reactive alkene, and allyltin[73] without incorporation of CO was suppressed by the strict use of nearly stoichiometric amounts of the electron-poor alkene. The four-component coupling reaction can also be applied to vinyl and aryl iodides. Because these substrates have stronger C_{sp^2}–I bonds, higher concentrations ([RX] = 0.1 M) are required.

Scheme 29 illustrates the mechanism of this reaction. The stannyl radical abstracts an iodine atom from alkyl iodide. The resulting alkyl radical adds to CO to form an acyl radical, which then adds to an alkene. An S_H2' reaction with allyltin yields the desired ketone with regeneration of tributyltin radical.

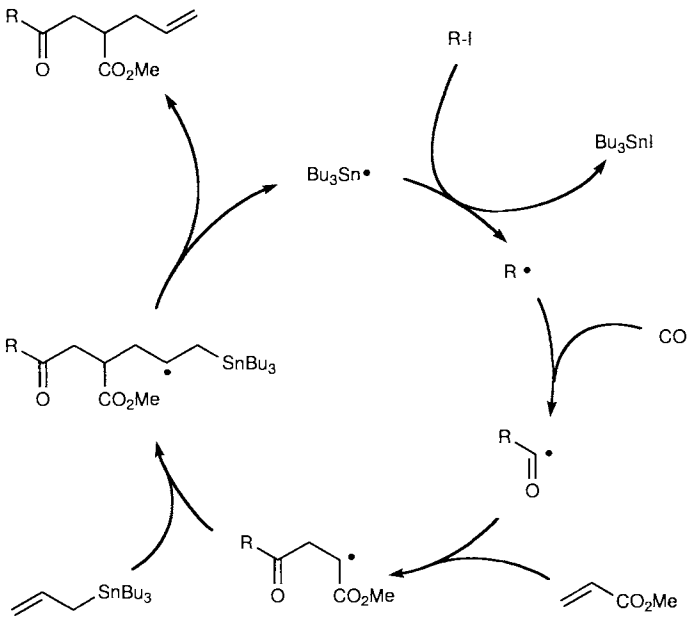

Scheme 29. Radical chain mechanism for the synthesis of functionalized ketones.

6. Synthesis of Cyclic Carbonyl Compounds

It should be possible to combine the concept of free-radical carbonylation with that of radical cyclization to provide access to cyclic ketones. Thus we investigated the (4 + 1) annulation of 4-pentenyl radicals and carbon monoxide with the aim of developing a free-radical carbonylation method for the synthesis of cyclopentanones (Scheme 30).

The reaction of 4-hexenyl bromide, CO, and tributyltin hydride as the free-radical mediator yielded a mixture of 2-ethylcyclopentanone and 2-methylcyclohexanone (Scheme 31).[74] The cyclopentanone results from the addition of the initial rad-

Scheme 30. Concept for carbonylation and cyclization of 4-pentenyl radical.

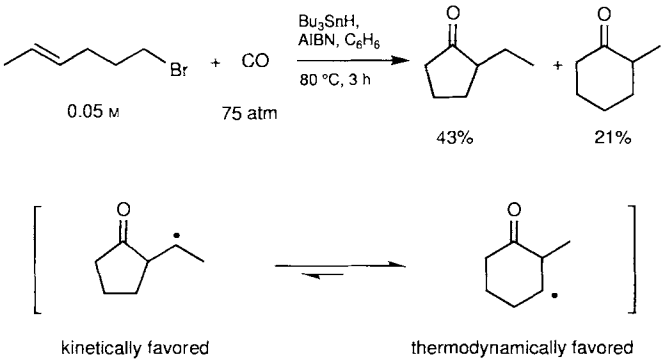

Scheme 31. Carbonylation and cyclization of 4-hexenyl radical.

ical to CO to give the 5-heptenoyl radical, subsequent 5-*exo*-trig cyclization, and abstraction of a hydrogen atom.[75] 2-Methylcyclohexanone may be formed by isomerization of the 1-(2-oxocyclopentyl)ethyl radical to the thermodynamically more stable 2-methyl-3-oxocyclohexyl radical. The propensity of the kinetically favored radical to isomerize is somewhat similar to that in the corresponding cyclization of vinyl radicals.[76] However, the two σ radicals undergo 5-*exo* cyclization at different rates. The rate constant for the cyclization of the 5-hexenoyl radical was estimated by Chatgilialoglu and co-workers to be $6.5 \times 10^5\ s^{-1}$ at 80 °C;[77] Beckwith and co-worker showed that the corresponding cyclization of the vinyl radical is much more rapid, roughly $1.2 \times 10^8\ s^{-1}$ at 80 °C.[76a]

With the judicious choice of substituents one can suppress the undesired isomerization. Introduction of dialkyl and phenyl substituents to pent-4-enyl bromide at C-5 led to the selective formation of 5-*exo* cyclization products (Scheme 32). Similarly,

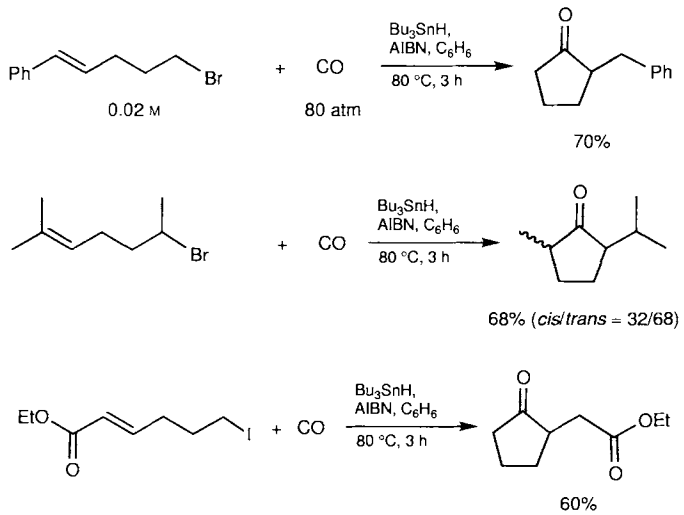

Scheme 32. Synthesis of cyclopentanones.

the reaction of a substrate with terminal carboethoxy moiety resulted in the desired substituted cyclopentanone. The radical carbonylation/cyclization reaction sequence provides a unique and general method for the preparation of cyclopentanones from alkenyl halides and CO.[78] The free-radical chain mechanism is summarized in Scheme 33 with the example of 2-benzylcyclopentanone.

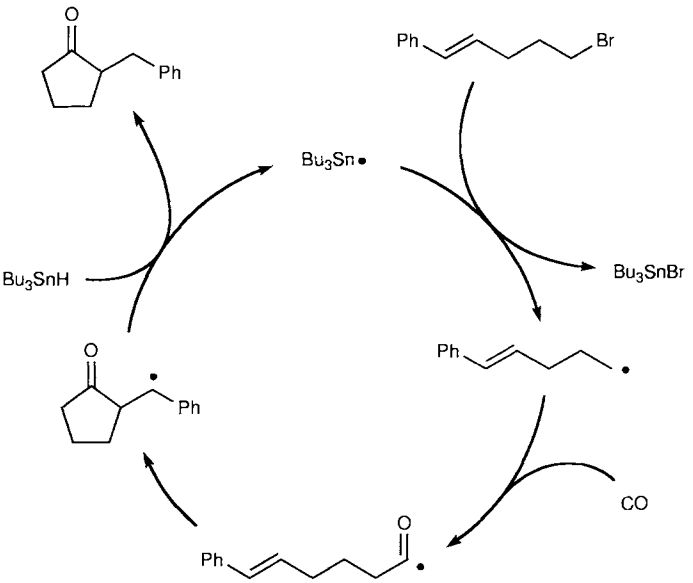

Scheme 33. Radical chain mechanism for the synthesis of a cyclopentanone.

Radical carbonylations can be combined with tandem cyclizations. For example dienyl bromides can be transformed into 1,4-diketones in the presence of a radical initiator, tin hydride, and CO (Scheme 34).[74, 79] In another tandem reaction

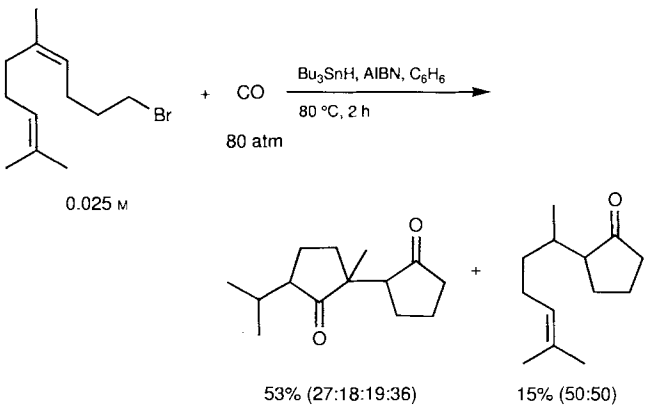

Scheme 34. A cascade reaction consisting of carbonylation and tandem cyclization.

the initially formed cyclic radical is added to allyltributyltin. The reaction of 4-hexenyl iodide with CO (10 atm) in the presence of methallyltin and a catalytic amount of AIBN gave a mixture of five- and six-membered cyclic ketones in the ratio of 6:94 (Scheme 35).[70] This regioselectivity is in stark contrast to that of the carbonylation/cyclization mediated by tributyltin hydride, which gives five-membered ring compounds as the major

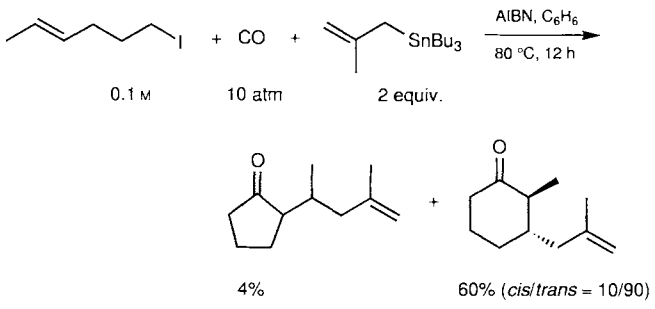

Scheme 35. Carbonylation and cyclization with methallyltin.

products (cf. Scheme 31). The preferential formation of the six-membered ring products suggests that the allyltin-mediated reaction is thermodynamically controlled.

Unlike the (4 + 1) annulation, (5 + 1) annulation in *exo* mode was not successful, since the addition of the 5-hexenyl radical to CO cannot compete well with rapid cyclization leading to the cyclopentylmethyl radical.[70] Thus in this case cyclization precedes carbonylation and cyclopentylmethyl methallyl ketone is formed as the major product (Scheme 36).

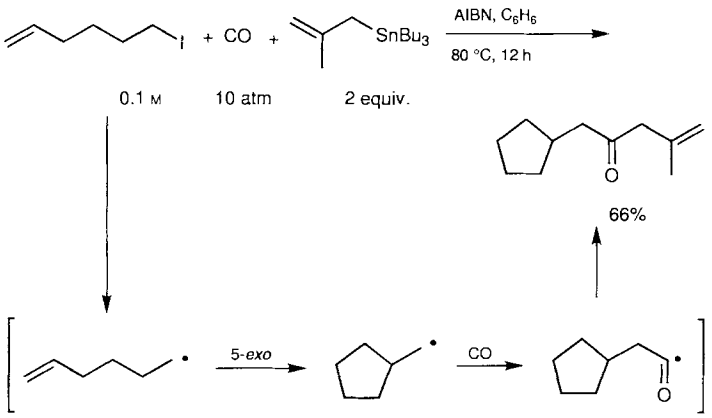

Scheme 36. Cyclization and carbonylation of 5-hexenyl radical.

The (*n* + 1) annulation strategy was, however, extended successfully to macrocyclization reactions, where the intramolecular addition takes place with *endo* selectivity.[80] Thus, macrocyclic 4-oxolactones can be conveniently synthesized from alkyl iodides having a terminal acryloxy moiety and CO in the presence of TTMSS (Scheme 37).[81] This (*n* + 1)-type macrocyclization is possible for the formation of ten-membered rings or for larger rings.[82] To our knowledge, there has been no significant work on (*n* + 1)-type macrocyclization by transition metal catalyzed carbonylation.[83]

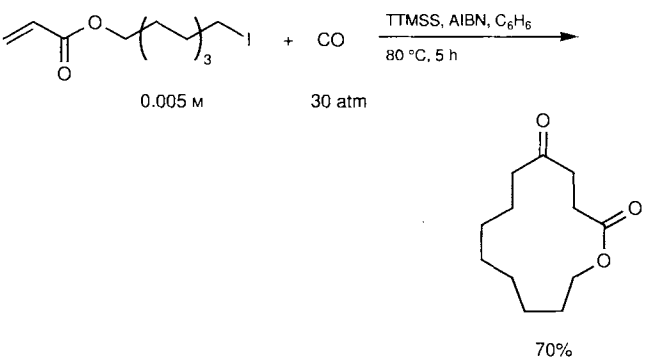

Scheme 37. Synthesis of a macrocyclic oxolactone by (*n* + 1) annulation.

7. Free-Radical Carbonylation Induced by Cleavage of C–M, C–H, and C–C Bonds

In the 1950s it was already suggested that reaction of methyl radical with CO should be exceptionally efficient.[84] The process should have little activation energy due to the inherent instability of the methyl radical. Some examples of the trapping of CO by methyl radical were reported in the 1980s, and more recent kinetic data also indicated that the reaction should be facile.[25] In 1984 Kräutler reported that the irradiation of methylcobalamin with visible light under a CO atmosphere gave acetylcobalamin, and the addition of methyl radical to CO was suggested (Scheme 38).[85] Shortly after this, Bergman and

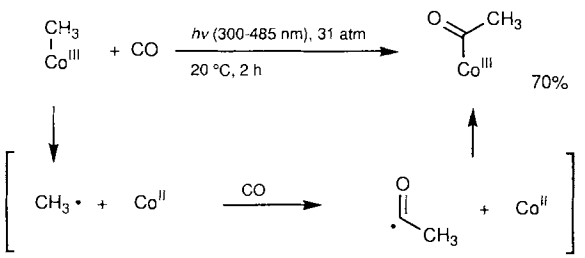

Scheme 38. Carbonylation of methylcobalamin (abbreviated CH_3–Co^{III}) by UV irradiation.

Goldberg reported that UV irradiation of dicarbonyl(cyclopentadienyl)dimethylrhenium under 20 atm of CO pressure yielded 2,4-butanedione.[86] A nonchain radical mechanism is proposed to account for this product. UV irradiation apparently leads to cleavage of the metal–carbon bond, giving the methyl radical. The methyl radical is carbonylated by CO to give acetyl radical, which dimerizes to give 2,3-butanedione (Scheme 39). This work is noteworthy since it emphasizes that free-radical car-

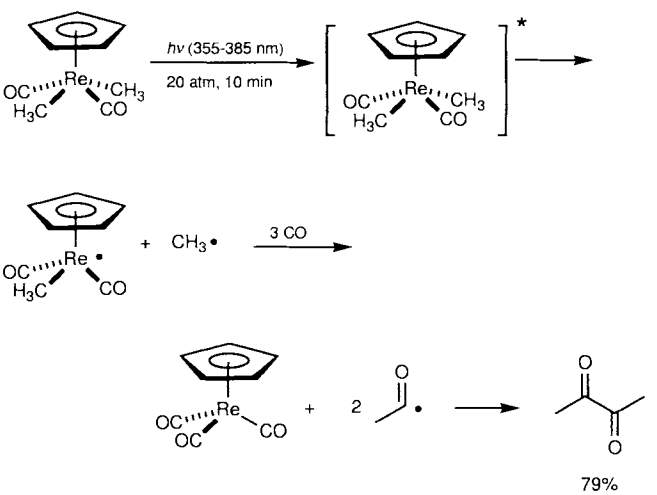

Scheme 39. Photocarbonylation of Bergman's rhenium complex.

bonylation pathways must always be considered when transition metal mediated carbonylations are performed under photolytic conditions.

The functionalization of alkanes is a topic of intense interest, and the introduction of CO into unactivated C–H bonds is an important challenge in this very active field.[87] As mentioned in Section 2, the potential of the free-radical carbonylation of alkanes was first demonstrated in the 1950s, but this chemistry attracted renewed attention only recently. In 1992 Sen and Lin reported the carboxylation of methane by CO and peroxydisulfate.[88] Peroxydisulfate, a powerful oxidizing agent[89] which upon mild thermolysis yields $SO_4^{\bullet -}$, is used to generate methyl radical by abstraction of hydrogen from methane (Scheme 40).

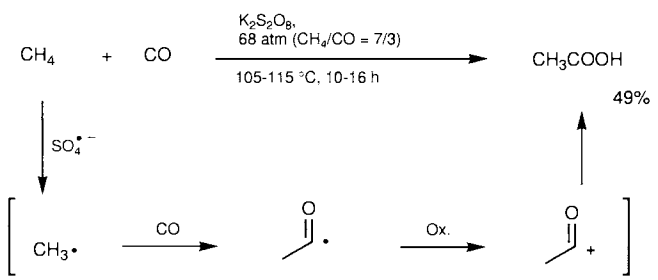

Scheme 40. Synthesis of acetic acid by oxidative carbonylation of methane.

In the next step the methyl radical adds to CO to yield acetyl radical, which is oxidized in situ to give acetic acid. With molecular oxygen as the oxidant, similar carbonylative transformation of short-chain hydrocarbons is effected by catalytic $RhCl_3$[90] and Pd/Cu.[91]

Although the photochemical conversion of alkanes into aldehydes was first achieved in 1987 by Tanaka and co-workers, who used $[RhCl(CO)(PMe_3)_2]$ as the catalyst,[92] the photochemically induced free-radical carbonylation of alkanes was investigated later. In 1991 Crabtree and Ferguson reported the mercury-photosensitized reaction of cyclohexane under CO flow, which gave significant amounts of cyclohexanecarbaldehyde and dicyclohexyl ketone together with uncarbonylated dicyclohexyl (Scheme 41).[93] In 1992 Goldman and Boese reported that aromatic ketones such as benzophenone and 2-trifluoromethylphenyl phenyl ketone photocatalyze the carbonylation of cyclohexane to give cyclohexanecarbaldehyde (Scheme 42).[30]

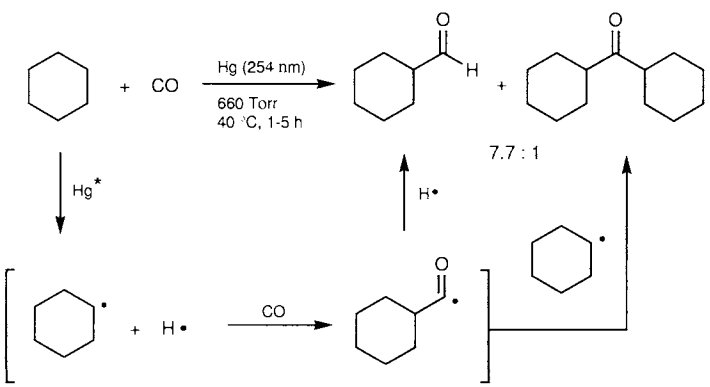

Scheme 41. Hg-photosensitized carbonylation of cyclohexane.

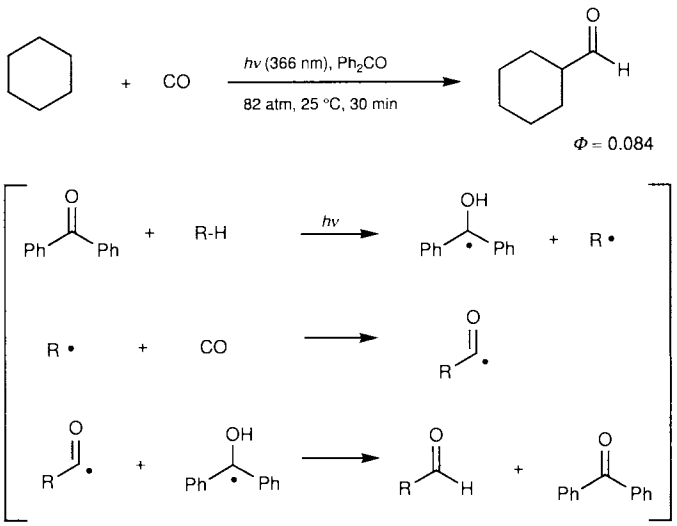

Scheme 42. Photocatalyzed carbonylation of cyclohexane by benzophenone. Φ = quantium yield.

Very recently, Hill and Jaynes found that tetrabutylammonium polytungstate is a good catalyst for the free-radical carbonylation of alkanes under irradiation.[94] For example, the carbonylation of cyclohexane catalyzed by $(Bu_4N)_4[W_{10}O_{32}]$ produced cyclohexanecarbaldehyde with 54 turnovers in 16 h with good selectivity in 8% yield (Scheme 43). The reaction was conducted

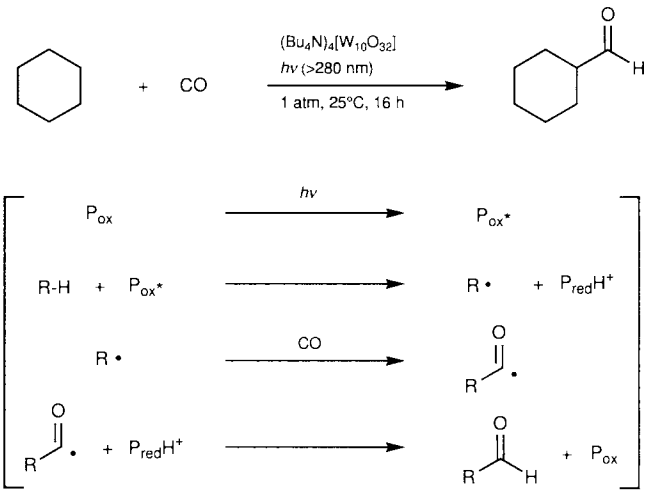

Scheme 43. Photocatalyzed carbonylation of cyclohexane by polyoxotungstate. P = catalyst.

under 1 atm of CO with irradiation from a medium-pressure mercury lamp with a Pyrex filter. Both the turnover levels and the selectivities exceed those of previously reported systems.

These C–H carbonylations are generally not selective for different types of C–H bonds, and only reactions of cyclic alkanes are certain to give uniform products. For this reason we have become interested in the targeted δ-carbonylation of saturated alcohols based on a well-known free-radical reaction, the 1,5-H shift from an alkoxy radical in δ-position.[95] We employed the lead tetraacetate induced oxidation of alcohols[96] to achieve a novel synthesis of δ-lactones from saturated alcohols and CO (Scheme 44).[97] This reaction is quite general for car-

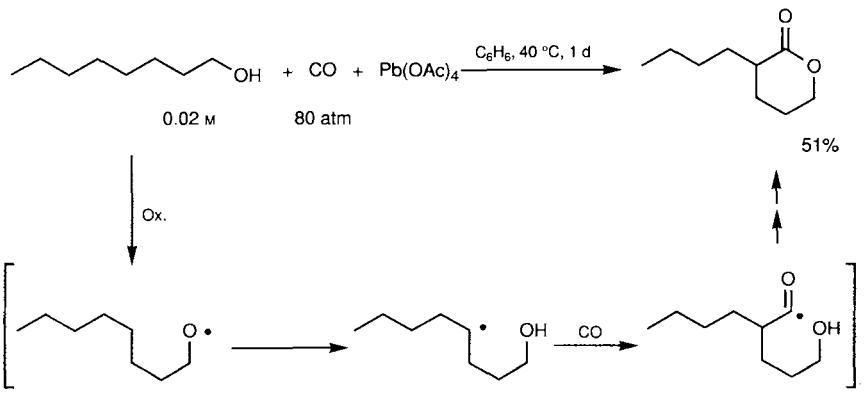

Scheme 44. Carbonylation of 1-octanol induced by lead tetraacetate.

bonylation of primary alcohols and secondary alcohols having primary and/or secondary carbons in δ-position. If an alcohol has both primary and secondary δ-carbons, CO is incorporated preferentially at the secondary position in a 24:1 ratio (Scheme 45). The strategy has been applied to a one-step synthesis of a carpenter bee pheromone starting from commercially available, optically pure (*R*)-(−)-2-hexanol.

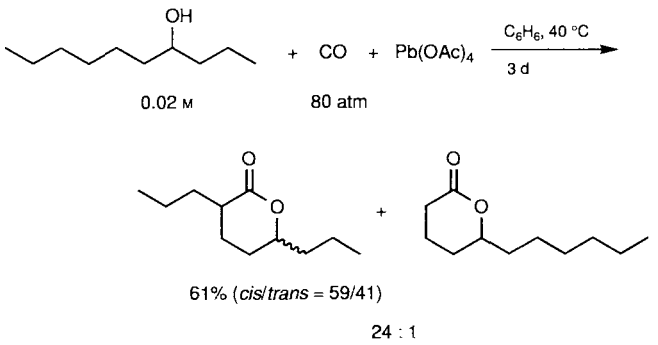

Scheme 45. Carbonylation of 4-decanol induced by lead tetraacetate.

Another approach to generating radicals is the oxidative cleavage of 1-substituted cyclobutanols with lead tetraacetate to give δ-oxoalkyl radicals. Subsequent addition to CO yields acyl radicals, which can be oxidized to afford 5-oxo carboxylic acids.[98] Lead tetraacetate is known to promote decarboxylation of carboxylic acids,[99] but careful examination of the crude reaction mixture by NMR spectroscopy has shown that the primary products are acid anhydrides. In contrast, reaction of 1-unsubstituted cyclobutanols with lead tetraacetate in the presence of CO afforded acetoxy-δ-lactones in moderate yield (Scheme 46).

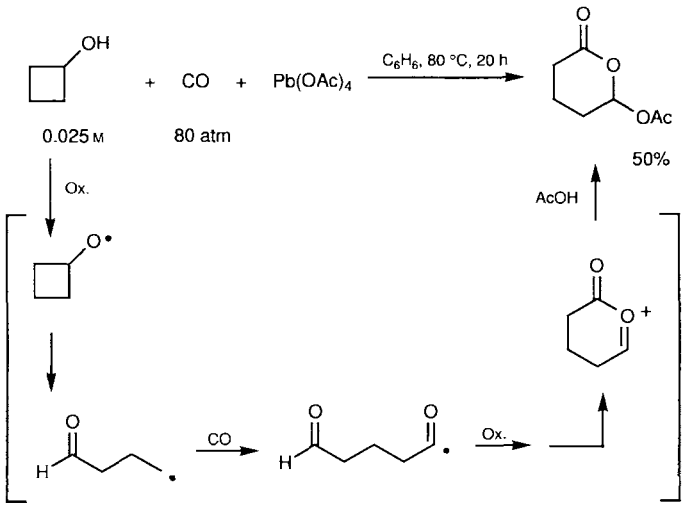

Scheme 46. Carbonylation of cyclobutanol.

The synthetic potential of a carbonylation reaction with a Mn^{III} oxidizing agent has also been demonstrated by Ryu and Alper.[100] For example, dimethyl (4-pentenyl)malonate, when treated with 2.5 equivalents of manganese(III) acetate dihydrate at 41 atm of CO, yields the desired cyclic carboxylic acid in 50% yield (Scheme 47).

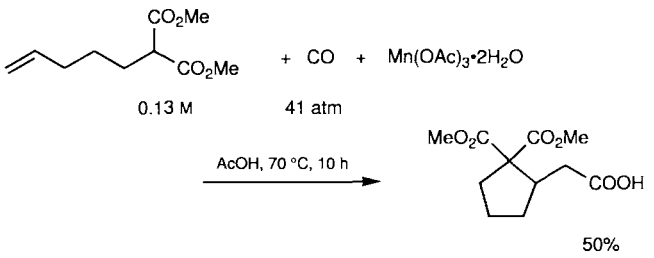

Scheme 47. Oxidative carbonylation with manganese(III) acetate.

8. Summary and Outlook

The rapid development of free-radical methods in the past decade has made a large impact on organic chemistry[101] and motivated us to reexamine the synthetic potential of free-radical carbonylation. As evident in this review, free-radical carbonylations can now be considered to be versatile and promising methods for the introduction of CO into organic molecules. Free-radical carbonylations in combination with tin and silyl radical mediated chain reaction systems offer novel routes to a wide variety of carbonyl-containing compounds.

Free-radical carbonylations have several notable features. An important advantage of free-radical reactions in general is their tolerance of a high level of functionality in the substrates, which makes free-radical carbonylation uniquely suited for the carbonylation of highly functionalized substrates without tedious protection/deprotection sequences. Unlike transition metal mediated methods, which often suffer undesirable side reactions as a result of unstable metal–carbon bonds, a wide range of *alkyl* halides can participate in free-radical carbonylations. A variety of multicomponent coupling reactions with incorporation of CO can be designed based on the abundant kinetic data for free-radical reactions. The combination of free-radical cyclization and carbonylation is a particularly attractive approach for the preparation of cyclic compounds containing a carbonyl moiety. Both reductive and oxidative metal-induced radical reactions can also be utilized in carbonylations. All of the carbonylations described are essentially one-pot reactions performed in an autoclave.

For many years free-radical carbonylation received little attention and thus its full synthetic potential was not probed. Now the opportunity for the facile introduction of CO without the use of transition metals exists and awaits many interesting applications.

The work in Osaka was conducted by an enthusiastic group of graduate students and research staff including Kazuya Kusano, Norio Masumi, Hiroshi Yamazaki, Mitsuharu Hasegawa, Akio Kurihara, Yukihiro Tamura, Kiyoto Nagahara, Hiroshi Fukushima, Hideo Muraoka, Tohru Okuda, Sumiaki Yamasaki, Shinji Tsunoi, Dr. Nobuaki Kambe, and Dr. Akiya Ogawa. We are most thankful to them for their experimental and intellectual contributions. We also thank Professor Mitsuo Komatsu, Dr. Cathleen M. Crudden, and Dr. David C. Falbes for helpful comments. We are grateful to the Ministry of Education, Science and Culture, Japan, for financial support. I. R. thanks the Daicel Chemical Award in Synthetic Organic Chemistry, Japan for partial financial support.

Received: August 11, 1995 [A128IE]
German version: *Angew. Chem.* **1996**, *108*, 1140–1157

[1] a) *Organic Synthesis via Metal Carbonyls, Vol. 2* (Eds: I. Wender, P. Pino), Wiley, New York, **1977**; b) *New Synthesis with Carbon Monoxide* (Ed.: J. Falbe), Springer, Berlin, **1980**; c) H. M. Colquhoun, D. J. Thompson, M. V. Twigg, *Carbonylation: Direct Synthesis of Carbonyl Compounds*, Plenum, New York, **1991**; d) G. P. Chiusoli, *Transition Met. Chem.* **1991**, *16*, 553.

[2] C. Narayana, M. Periasamy, *Synthesis* **1985**, 253.

[3] a) Selenium-catalyzed carbonylations: N. Sonoda, *Pure Appl. Chem.* **1993**, *65*, 699; b) carbonylations of organoboranes: A. Pelter, K. Smith, H. C. Brown, *Borane Reagents*, Academic Press, London, **1988**, p. 274.

[4] M. M. Brubaker, D. D. Coffman, H. H. Hoehn, *J. Am. Chem. Soc.* **1952**, *74*, 1509.

[5] I. Ryu, K. Kusano, A. Ogawa, N. Kambe, N. Sonoda, *J. Am. Chem. Soc.* **1990**, *112*, 1295.

[6] K. Faltings, *Ber.* **1939**, *72B*, 1207.

[7] D. D. Coffman, P. S. Pinkney, F. T. Wall, W. H. Wood, H. S. Young, *J. Am. Chem. Soc.* **1952**, *74*, 3391.

[8] Related work: C. Walling, *J. Polym. Sci.* **1955**, *16*, 315; Y. Chatani, T. Takizawa, S. Murahashi, Y. Sakata, Y. Nishimura, *ibid.* **1961**, *55*, 811; P. Colombo, M. Steinberg, J. Fontana, *J. Polym. Sci. B Polym. Lett.* **1963**, *1*, 447; P. Colombo, M. Steinberg, D. Macchia, *J. Polym. Sci. A Gen. Pap.* **1963**, *1*, 483. A. Sommazzi, N. Cardi, F. Garbassi, C. Chatgilialoglu, U.S. Patent 5 369 187, **1994**.

[9] Reviews on earlier work: a) C. Walling, *Free Radicals in Solution*, Wiley, New York, **1957**, p. 273; b) H. Wilms, *Methoden Org. Chem. (Houben-Weyl) 4th ed. 1952*, Bd. 14/1, **1961**, p. 1154.

[10] R. E. Foster, A. W. Larchar, R. D. Lipscomb, B. C. McKusick, *J. Am. Chem. Soc.* **1956**, *78*, 5606.

[11] J. C. Sauer, *J. Am. Chem. Soc.* **1957**, *79*, 5314; see also ref. [49] and Section 4.

[12] R. Cramer, *J. Am. Chem. Soc.* **1957**, *79*, 6215.

[13] D. D. Coffman, R. Cramer, W. E. Mochel, *J. Am. Chem. Soc.* **1958**, *80*, 2882.

[14] G. P. Chiusoli, F. Minisci, *Gazz. Chim. Ital.* **1958**, *88*, 43.

[15] C. Walling, E. S. Savas, *J. Am. Chem. Soc.* **1960**, *82*, 1738.

[16] C. Walling, O. H. Basedow, E. S. Savas, *J. Am. Chem. Soc.* **1960**, *82*, 2181.

[17] W. A. Thaler, *J. Am. Chem. Soc.* **1966**, *88*, 4278.

[18] W. A. Thaler, *J. Am. Chem. Soc.* **1967**, *89*, 1902.

[19] T. Susuki, J. Tsuji, *J. Org. Chem.* **1970**, 35, 2982.

[20] Pertinent reviews from the 1970s on synthetic applications of acyl radicals: a) M. G. Vinogradov, G. I. Nikishin, *Usp. Khim.* **1971**, *40*, 1960; *Russ. Chem. Rev.* **1971**, *40*, 916; b) T. Caronna, F. Minisci, *Rev. React. Species Chem. React.* **1976**, *1*, 263; c) P. I. Abell in *Free Radicals, Vol. 2* (Ed.: J. K. Kochi), Wiley, New York, **1973**, Chapter 13.

[21] J. Pfenninger, W. Graf, *Helv. Chim. Acta* **1980**, *63*, 1562.

[22] Recent studies with a variety of acyl radical precursors: acyl selenides: a) D. L. Boger, R. J. Mathvink, *J. Am. Chem. Soc.* **1990**, *112*, 4003; b) C. E. Schwartz, D. P. Curran, *ibid.* **1990**, *112*, 9272. c) D. L. Boger, R. J. Mathvink, *J. Org. Chem.* **1992**, *57*, 1429; acyl sulfides: d) J. H. Penn, F. Liu, *ibid.* **1994**, *59*, 2608; acyl tellurides: e) D. Crich, C. Chen, J.-T. Hwang, H. Yuan, A. Papadatos, R. I. Walter, *J. Am. Chem. Soc.* **1994**, *116*, 8937; acyl cobalt compounds: f) D. J. Coveney, V. F. Patel, G. Pattenden, D. M. Thompson, *J. Chem. Soc. Perkin Trans. 1* **1990**, 2721.

[23] a) J. A. Kerr, J. G. Calvert, *J. Phys. Chem.* **1965**, *69*, 1022; b) K. W. Watkins, W. W. Thompson, *Int. J. Chem. Kinet.* **1973**, *5*, 791; c) K. W. Watkins, W. W. Word, *ibid.* **1974**, *6*, 855; d) C. Anastasi, P. R. Maw, *J. Chem. Soc. Faraday Trans. 1* **1982**, *78*, 2423.

[24] For a survey of acyl radical chemistry with particular emphasis on kinetic and spectroscopic studies, see: C. E. Brown, A. G. Neville, D. M. Rayner, K. U. Ingold, J. Lusztyk, *Aust. J. Chem.* **1995**, *48*, 363. We thank Dr. J. Lusztyk informing us of this article prior to publication.

[25] A. Bakac, J. H. Espenson, V. G. Young, Jr., *Inorg. Chem.* **1992**, *31*, 4959.

[26] [CO](1 atm) = 0.00096 M (water): *Solubility Data Series. Carbon Monoxide* (Ed.: R. W. Cargill), Pergamon, New York, **1990**, p. 2.

[27] K. Nagahara, I. Ryu, N. Kambe, M. Komatsu, N. Sonoda, *J. Org. Chem.* **1995**, *60*, 7384.

[28] [CO](1 atm) = 0.0084 M (benzene): *Solubility of Gases in Liquids* (Eds.: P. G. T. Fogg, W. Gerrard), Wiley, New York, **1991**, p. 274.

[29] A. Citterio, A. Arnoldi, F. Minisci, *J. Org. Chem.* **1979**, *44*, 2674.

[30] W. T. Boese, A. S. Goldman, *Tetrahedron Lett.* **1992**, *33*, 2119.

[31] a) Y. P. Tsentalovich, H. Fischer, *J. Chem. Soc. Perkin Trans. 2* **1994**, 729; b) A. G. Neville, C. E. Brown, D. M. Rayner, J. Lusztyk, K. U. Ingold, *J. Am. Chem. Soc.* **1991**, *113*, 1869; c) F. L. Cozens, J. C. Scaiano, *ibid.* **1993**, *115*, 5204.

[32] a) L. Lunazzi, K. U. Ingold, J. C. Scaiano, *J. Phys. Chem.* **1983**, *87*, 529; b) N. J. Turro, I. R. Gould, B. H. Baretz, *ibid.* **1983**, *87*, 531.

[33] a) M. J. Perkins, B. P. Roberts, *J. Chem. Soc. Perkin Trans. 2* **1974**, 297; b) J. Lipscher, H. Fischer, *J. Phys. Chem.* **1984**, *88*, 2555.

[34] Review: H. Fischer, H. Paul, *Acc. Chem. Res.* **1987**, *20*, 200.

[35] a) C. Chatgilialoglu, M. Lucarini, *Tetrahedron Lett.* **1995**, *36*, 1299; b) C. Chatgilialoglu, C. Ferreri, M. Lucarini, P. Pedrielli, G. F. Pedulli, *Organometallics* **1995**, *14*, 2672. We thank Dr. C. Chatgilialoglu for informing us of this article prior to publication.

[36] For relative decarbonylation rates of acyl radicals, see: a) D. E. Applequist, L. Kaplan, *J. Am. Chem. Soc.* **1965**, *87*, 2194; b) D. E. Applequist, J. H. Klug, *J. Org. Chem.* **1978**, *43*, 1729.

[37] a) R. W. Bates, C. J. Gabel, J. Ji, *Tetrahedron Lett.* **1994**, *35*, 6993; b) Y. Misumi, Y. Ishii, M. Hidai, *J. Mol. Cat.* **1993**, *78*, 1; c) R. Takeuchi, Y. Tsuji, M. Fujita, T. Kondo, Y. Watanabe, *J. Org. Chem.* **1989**, *54*, 1831; d) V. P. Baillargeon, J. K. Stille, *J. Am. Chem. Soc.* **1986**, *108*, 452.

[38] a) J. P. Collman, L. S. Hegedus, J. R. Norton, R. G. Finke, *Principles and Applications of Organotransition Metal Chemistry*, University Science Books, Mill Valley, CA, **1987**; b) A. Yamamoto, *Organotransition Metal Chemistry*, Wiley, New York, **1986**; c) J. K. Stille, *Angew. Chem.* **1986**, *98*, 504; *Angew. Chem. Int. Ed. Engl.* **1986**, *25*, 508.

[39] One exception is the synthesis of aldehydes from stoichiometric amounts of acylcarbonylferrates: a) M. Ryang, I. Rhee, S. Tsutsumi, *Bull. Chem. Soc. Jpn.* **1964**, *37*, 341; b) M. Ryang, S. Tsutsumi, *Synthesis*, **1971**, 55; c) Y. Takegami, Y. Watanabe, H. Masada, I. Kanaya, *Bull. Chem. Soc. Jpn.* **1967**, *40*, 1456; d) M. P. Cooke, Jr., *J. Am. Chem. Soc.* **1970**, *92*, 6080.

[40] For work on metal-catalyzed carbonylation of alkyl halides, see: a) H. Urata, H. Maekawa, S. Takahashi, T. Fuchikami, *J. Org. Chem.* **1991**, *56*, 4320; b) T. Ishiyama, N. Miyaura, A. Suzuki, *Tetrahedron Lett.* **1991**, *32*, 6923; c) ref. [37c].

[41] J. G. Noltes, G. J. M. Van der Kerk, *Chem. Ind.* **1959**, 294.

[42] I. Ryu, K. Kusano, N. Masumi, H. Yamazaki, A. Ogawa, N. Sonoda, *Tetrahedron Lett.* **1990**, *31*, 6887.

[43] Related tin hydride reductions: H. Schumann, B. Pachaly, B. C. Schütze, *J. Organomet. Chem.* **1984**, *265*, 145.

[44] a) C. Chatgilialoglu, *Acc. Chem. Res.* **1992**, *25*, 188; b) *Chem. Rev.* **1995**, *95*, 1229.

[45] I. Ryu, M. Hasegawa, A. Kurihara, A. Ogawa, S. Tsunoi, N. Sonoda, *Synlett* **1993**, 143.

[46] V. Gupta, D. Kahne, *Tetrahedron Lett.* **1993**, *34*, 591. The importance of low concentrations for efficient formylation with tin hydride is overlooked in this paper.

[47] C. Dupuy, C. Petrier, L. A. Sarandeses, J. L. Luche, *Synth. Commun.* **1991**, *21*, 643.

[48] S. Tsunoi, I. Ryu, H. Fukushima, M. Tanaka, M. Komatsu, N. Sonoda, *Synlett* **1995**, 1249.

[49] S. Nakatani, J.-i. Yoshida, S. Isoe, *J. Chem. Soc. Chem. Commun.* **1992**, 880.

[50] a) M. V. Encinas, P. J. Wagner, J. C. Scaiano, *J. Am. Chem. Soc.* **1980**, *102*, 1357; b) J. A. Franz, B. A. Bushaw, M. S. Alnajjar, *ibid.* **1989**, *111*, 268.

[51] A. Ogawa, M. Takeba, J.-i. Kawakami, I. Ryu, N. Kambe, N. Sonoda, *J. Am. Chem. Soc.* **1995**, *117*, 7564.

[52] a) F. Monteil, I. Matsuda, H. Alper, *J. Am. Chem. Soc.* **1995**, *117*, 4419; b) I. Ojima, E. Vidal, M. Tzamarioudaki, I. Matsuda, *ibid.* **1995**, *117*, 6797; c) Y. Fukumoto, N. Chatani, S. Murai, *J. Org. Chem.* **1993**, *58*, 4187. d) M. E. Wright, B. B. Cochran, *J. Am. Chem. Soc.* **1993**, *115*, 2059.

[53] I. Ryu, A. Kurihara, H. Muraoka, S. Tsunoi, N. Kambe, N. Sonoda, *J. Org. Chem.* **1994**, *59*, 7570.

[54] S. Hanessian, R. Léger, *J. Am. Chem. Soc.* **1992**, *114*, 3115.

[55] a) K. J. Kulicke, C. Chatgilialoglu, B. Kopping, B. Giese, *Helv. Chim. Acta* **1992**, *75*, 935; b) B. Kopping, C. Chatgilialoglu, M. Zehnder, B. Giese, *J. Org. Chem.* **1992**, *57*, 3994; c) K. Miura, K. Oshima, K. Utimoto, *Chem. Lett.* **1992**, 2477.

[56] I. Ryu, H. Muraoka, S. Tsunoi, N. Kambe, N. Sonoda, unpublished results.

[57] C. Chatgilialoglu, K. U. Ingold, J. C. Scaiano, *J. Am. Chem. Soc.* **1981**, *103*, 7739.

[58] M. S. Kharasch, W. H. Urry, B. M. Kuderna, *J. Org. Chem.* **1949**, *14*, 248.

[59] a) W. H. Urry, E. S. Huyser, *J. Am. Chem. Soc.* **1953**, *75*, 4876; b) T. M. Partrick, Jr. *J. Org. Chem.* **1952**, *17*, 1009, 1269; c) W. H. Urry, D. J. Trecker, H. D, Hartzler, *ibid.* **1964**, *29*, 1663; d) review: C. Walling, E. S. Huyser, *Org. React.* **1963**, *13*, 91.

[60] a) D. L. Boger, R. J. Mathvink, *J. Org. Chem.* **1989**, *54*, 1777; b) H. Sakurai, K. Narasaka, *Chem. Lett.* **1994**, 2017; c) R. Scheffold, R. Orlinski, *J. Am. Chem. Soc.* **1983**, *105*, 7200; d) T. Shono, T. Soejima, K. Takigawa, Y. Yamaguchi, H. Maekawa, S. Kashimura, *Tetrahedron Lett.* **1994**, *35*, 4161; e) T. Punniyamurthy, B. Bhatia, J. Iqbal, *J. Org. Chem.* **1994**, *59*, 850; f) P. Gottschalk, D. C. Neckers, *ibid.* **1985**, *50*, 3498; g) R. Stringat, G. Fabre, R. Fellous, P. Paquet, *Tetrahedron Lett.* **1992**, *33*, 4303

[61] F. Jent, H. Paul, E. Roduner, M. Heming, H. Fischer, *Int. J. Chem. Kinet.* **1986**, *18*, 1113.

[62] M. P. Cooke, Jr., R. M. Parlman, *J. Am. Chem. Soc.* **1977**, *99*, 5222.

[63] I. Ryu, K. Kusano, H. Yamazaki, N. Sonoda, *J. Org. Chem.* **1991**, *56*, 5003.

[64] For reviews on C–C bond formation by addition of free radicals to alkenes, see: B. Giese, *Angew. Chem.* **1983**, *95*, 771; *Angew. Chem. Int. Ed. Engl.* **1983**, *22*, 753; *ibid.* **1985**, *97*, 555 and **1985**, *24*, 553; *ibid.* **1989**, *101*, 993 and **1989**, *28*, 969.

[65] M. Newcomb, *Tetrahedron* **1993**, *49*, 1151.

[66] This is also partly because of the limited solubility of CO [26·28].

[67] D. P. Curran, P. A. van Elburg, B. Giese, S. Gilges, *Tetrahedron Lett.* **1990**, *31*, 2861.

[68] G. E. Keck, E. J. Enholm, J. B. Yates, M. R. Wiley, *Tetrahedron* **1985**, *41*, 4079.

[69] a) M. Kosugi, K. Kurino, K. Takayama, T. Migita, *J. Organomet. Chem.* **1973**, *56*, C11; b) J. Grignon, M. Pereyre, *ibid.* **1973**, *61*, C33.

[70] I. Ryu, H. Yamazaki, K. Kusano, A. Ogawa, N. Sonoda, *J. Am. Chem. Soc.* **1991**, *113*, 8558.

[71] For a method with palladium, see: K. Yasui, K. Fugami, S. Tanaka, Y. Tamaru, *J. Org. Chem.* **1995**, *60*, 1365.

[72] I. Ryu, H. Yamazaki, A. Ogawa, N. Kambe, N. Sonoda, *J. Am. Chem. Soc.* **1993**, *115*, 1187.

[73] K. Mizuno, M. Ikeda, S. Toda, Y. Otsuji, *J. Am. Chem. Soc.* **1988**, *110*, 1288.

[74] I. Ryu, K. Kusano, M. Hasegawa, N. Kambe, N. Sonoda, *J. Chem. Soc. Chem. Commun.* **1991**, 1018; D. P. Curran, H. Liu, *J. Am. Chem. Soc.* **1991**, *113*, 2127.

[75] For examples of cyclizations of 5-hexenoyl radicals, see: a) E. J. Walsh, Jr., J. M. Messinger II, D. A. Grudoski, C. A. Allchin, *Tetrahedron Lett.* **1980**, *21*, 4409; b) J. Lusztyk, E. Lusztyk, B. Maillard, K. U. Ingold, *J. Am. Chem. Soc.* **1984**, *106*, 2923; c) L. Chen, G. B. Gill, G. Pattenden, *Tetrahedron Lett.* **1994**, *35*, 2593; d) M. D. Bachi, E. Bosch, *J. Org. Chem.* **1989**, *54*, 1234; e) D. Batty, D. Crich, S. M. Fortt, *J. Chem. Soc. Chem. Commun.* **1989**, 1366; f) D. L. Boger, R. J. Mathvink, *J. Am. Chem. Soc.* **1990**, *112*, 4003; g) *J. Org. Chem.* **1990**, *55*, 5442; h) D. L. J. Clive, H. W. Manning, T. L. B. Boivin, *J. Chem. Soc. Chem. Commun.* **1990**, 972; i) C. E. Schwartz, D. P. Curran, *J. Am. Chem. Soc.* **1990**, *112*, 9272; j) S. P. Green, D. A. Whiting, *J. Chem. Soc. Chem. Commun.* **1992**, 1753; k) P. A. Evans, J. D. Roseman, *Tetrahedron Lett.* **1995**, *36*, 31.

[76] a) A. L. J. Beckwith, D. M. O'Shea, *Tetrahedron Lett.* **1986**, *27*, 4525; b) G. Stork, R. Mook, Jr., *ibid.* **1986**, *27*, 4529.

[77] M. Ballestri, C. Chatgilialoglu, N. Cardi, A. Sommazzi, *Tetrahedron Lett.* **1992**, *33*, 1787.

[78] For recent examples of transition metal mediate reactions, see: a) T. Sugihara, C. Copéret, Z. Owczarczyk, L. S. Harring, E.. Negishi, *J. Am. Chem. Soc.* **1994**, *116*, 7923; b) Y. Ishii, C. Gao, W.-X. Xu, M. Iwasaki, M. Hidai, *J. Org. Chem.* **1993**, *58*, 6818.

[79] For tandem reactions of geminal radical acceptor/donor synthons, see: I. Ryu, N. Sonoda, D. P. Curran, *Chem. Rev.* **1996**, *96*, 177.

[80] Pioneering studies on free-radical macrocyclizations: a) N. A. Porter, V. H.-T. Chang, D. R. Magnin, B. T. Wright, *J. Am. Chem. Soc.* **1988**, *110*, 3554; b) N. A. Porter, B. Lacher, V. H.-T. Chang, D. R. Magnin, *ibid.* **1989**, *111*, 8309; c) D. M. Scott, A. T. McPhail, N. A. Porter, *J. Org. Chem.* **1993**, *58*, 1178.

[81] I. Ryu, K. Nagahara, H. Yamazaki, S. Tsunoi, N. Sonoda, *Synlett* **1994**, 643.

[82] For macrocyclizations of acyl radicals, see: a) D. L. Boger, R. J. Mathvink, *J. Am. Chem. Soc.* **1990**, *112*, 4008; b) M. P. Astley, G. Pattenden, *Synthesis* **1992**, 101.

[83] a) R. Baker, R. C. Cookson, J. R. Vinson, *J. Chem. Soc. Chem. Commun.* **1974**, 515; b) B. M. Trost, J. R. Granja, *J. Am. Chem. Soc.* **1991**, *113*, 1044.

[84] a) M. Szwarc, *Chem. Rev.* **1950**, *47*, 75; b) D. H. Volman, W. M. Graven, *J. Chem. Phys.* **1952**, *20*, 919; c) G. B. Porter, S. W. Benson, *J. Am. Chem. Soc.* **1953**, *75*, 2773; d) J. G. Calvert, J. T. Gruver, *ibid.* **1958**, *80*, 1313.

[85] B. Kräutler, *Helv. Chim. Acta* **1984**, *67*, 1053.

[86] K. I. Goldberg, R. G. Bergman, *J. Am. Chem. Soc.* **1989**, *111*, 1285.

[87] Reviews: a) C. L. Hill, *Synlett* **1995**, 127; b) B. A. Arndtsen, R. G. Bergman, T. A. Mobley, T. H. Peterson, *Acc. Chem. Res.* **1995**, *28*, 154; c) D. H. R. Barton, D. Doller, *ibid.* **1992**, *25*, 504; d) R. H. Crabtree, *Chem. Rev.* **1985**, *85*, 245.

[88] M. Lin, A. Sen, *J. Chem. Soc. Chem. Commun.* **1992**, 892.

[89] F. Minisci, A. Citterio, C. Giordano, *Acc. Chem. Res.* **1983**, *16*, 27.

[90] M. Lin, A. Sen, *Nature* **1994**, *368*, 613.

[91] M. Kurioka, K. Nakata, T. Jintoku, Y. Taniguchi, K. Takaki, Y. Fujiwara, *Chem. Lett.* **1995**, 244.

[92] a) T. Sakakura, M. Tanaka, *J. Chem. Soc. Chem. Commun.* **1987**, 758; b) T. Sakakura, T. Sodeyama, K. Sasaki, K. Wada, M. Tanaka, *J. Am. Chem. Soc.* **1990**, *112*, 7221.

[93] R. R. Ferguson, R. H. Crabtree, *J. Org. Chem.* **1991**, *56*, 5503.

[94] B. S. Jaynes, C. L. Hill, *J. Am. Chem. Soc.* **1995**, *117*, 4704.

[95] a) D. H. R. Barton, *Pure Appl. Chem.* **1968**, *16*, 1; b) D. P. Curran, W. Shen, *J. Am. Chem. Soc.* **1993**, *115*, 6051.

[96] M. L. Mihailovic, Z. Cekovic, L. Lorenc in *Organic Syntheses by Oxidation with Metal Compounds* (Eds.: W. J. Mijs, C. R. H. I. de Jonge), Plenum, New York, **1986**; p. 758.

[97] S. Tsunoi, I. Ryu, N. Sonoda, *J. Am. Chem. Soc.* **1994**, *116*, 5473.

[98] S. Tsunoi, I. Ryu, Y. Tamura, S. Yamasaki, N. Sonoda, *Synlett* **1994**, 1009.

[99] R. A. Sheldon, J. K. Kochi, *Org. React.* **1972**, *19*, 279.

[100] I. Ryu, H. Alper, *J. Am. Chem. Soc.* **1993**, *115*, 7543.

[101] Review: a) B. Giese, *Radicals in Organic Synthesis: Formation of Carbon–Carbon Bonds*, Pergamon, Oxford, **1986**; b) D. J. Hart, *Science* **1984**, *223*, 883; c) D. P. Curran, *Synthesis* **1988**, 417 and 489; d) in *Comprehensive Organic Synthesis* (Eds.: B. M. Trost, I. Fleming), Pergamon, Oxford, **1991**, *Vol. 4*, Chapters 4.1 and 4.2; e) C. P. Jasperse, D. P. Curran, T. L. Fevig, *Chem. Rev.* **1991**, *91*, 1237; f) W. B. Motherwell, D. Crich, *Best Synthetic Methods, Free Radical Chain Reactions in Organic Synthesis*, Academic Press, London, **1991**; g) D. H. R. Barton, *Aldrichimica Acta* **1990**, *23*, 3; h) A. L. J. Beckwith, *Chem. Soc. Rev.* **1993**, 143; i) A. Ghosez, B. Giese, W. Mehl, J. O. Metzger, H. Zipse, *Methoden Org. Chem. (Houben-Weyl) 4th ed. 1952–*, Bd. E19a, **1989**, Parts 1 and 2; j) P. Dowd, W. Zhang, *Chem. Rev.* **1993**, *93*, 2091.

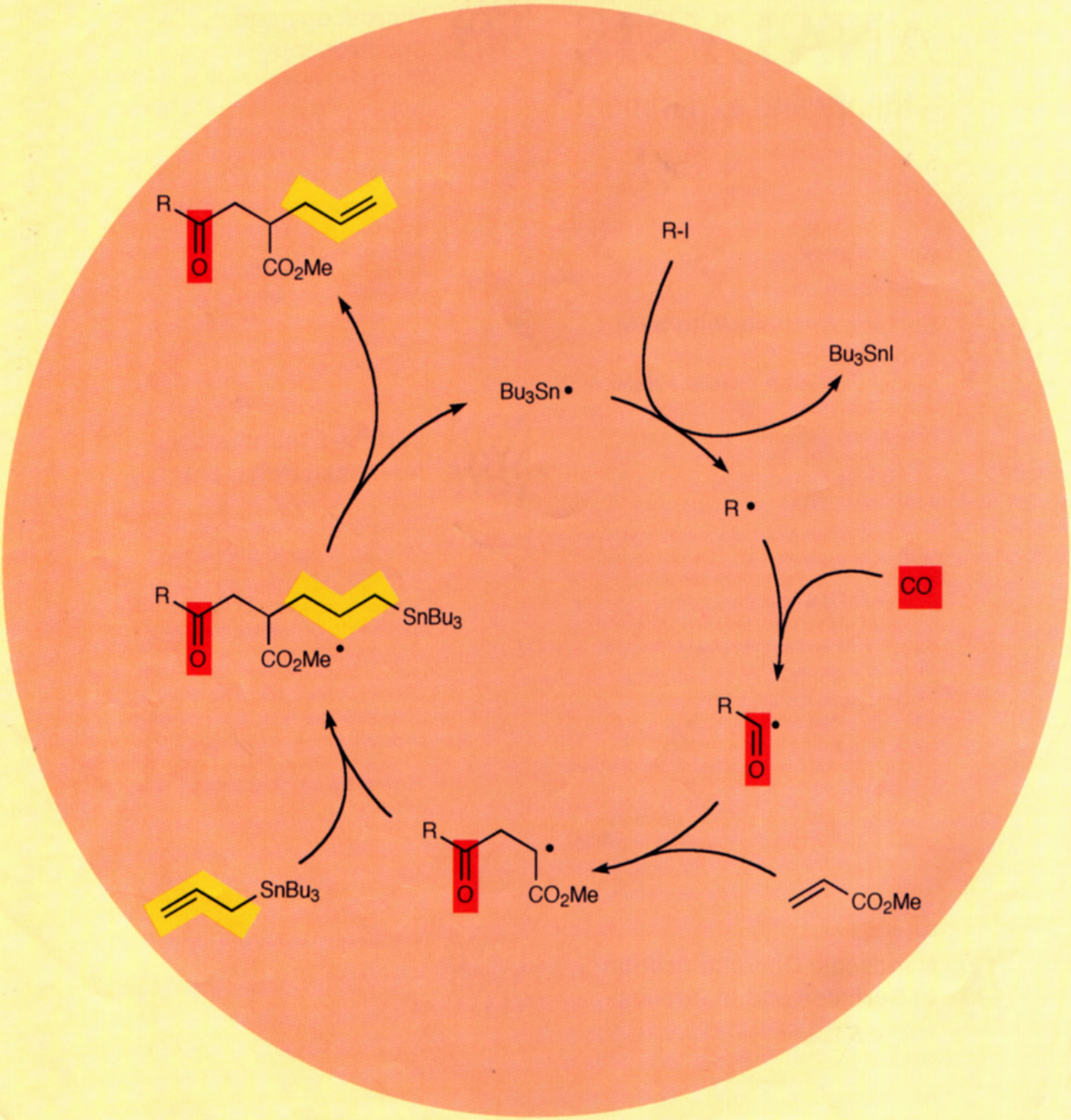

A particularly impressive radical chain reaction: a four-component coupling reaction in which free-radical carbonylation is the first step.

Si–H and C–H Activation by Transition Metal Complexes: A Step Towards Isolable Alkane Complexes?**

Jörg J. Schneider*

The recognition of the fundamental contributions by G. A. Olah on the elucidation of the structure of nonclassical carbocations, in the form of the award of the Nobel prize for chemistry, has recently emphasized the importance of electron-deficient bonds in the understanding of chemical bonding in organic chemistry. In the field of coordination chemistry, the formulation of electron-deficient bonds has been used for some time to describe nonclassical interactions between atoms. Traditional ligands in coordination chemistry such as amines and phosphanes bond to metal centers through their lone pair of electrons. Synergistic bonding effects dominate in the coordination of π-bonded ligands such as alkenes. In the mid-1980s the discovery of dihydrogen complexes having side-on coordination of H_2 gave fresh impetus to transition metal chemistry as well as to the understanding of the interaction of σ-coordinating ligands with transition metals. In the meantime, transiton metal complexes can be obtained with a variety of σ-coordinated X–H fragments, and their mode of bonding can be understood by a common and quite general model. The chemistry of σ-bound silane ligands is particularly varied and well-investigated. These silane ligands enable the investigation of a large range of σ-coordinated metal complex fragments up to complete oxidative addition with cleavage of the Si–H bond and formation of silyl(hydrido) complexes, which has thus also widened our general understanding of the bonding of other σ-bound ligands. Whilst there is a large range of isolable and stable H_2 and SiR_4 complexes available, there are no such alkane analogues known at present. Only when the C–H bond is part of a ligand that is already directly bonded to the transition metal center will the resulting chelate effect stabilize this agostic C-H-M interaction. The complexation of SiH_4, the simplest heavier homologue of CH_4, was achieved recently. This is a further step towards the understanding of the factors which govern σ-complexation of ligands at transition metal centers.

Keywords: C–H activation · complexes with silicon ligands · coordination · methane activation · Si–H activation

1. Introduction

The activation of molecules with σ bonds in the coordination sphere of transition metal is of fundamental interest, particularly with regard to the complexation of hydrocarbons such as methane.[1] As a result of this challenge, the incorporation of molecules with a σ-bonded framework in complexes has developed from what was originally a novel field in the early 1980s to become an important area of research within organometallic chemistry. Nowadays a variety of well-characterized complexes are known that contain σ-coordinated ligands such as (H_2),[2] $(HSiR_3)$,[3] and $(HSnR_3)$.[3] However, comparable stable σ-transition metal complexes of alkanes have not been reported to date.

What is the current level of understanding of the activation and complexation of σ bonds, in particular in H_2, alkanes, and their heavier homologues, the silanes, by oxidative addition at transition metal centers?[4] To what extent can stable SiH_4–transition metal complexes be regarded as having model character for the corresponding CH_4–transition metal complexes? The synthesis, isolation, and structural characterization of the first $M(SiH_4)$ complex **2**[5] [Eq. (a)] was a recent highlight in this area of research. In the following account some of the stages in the development of the transition metal chemistry of σ-bonded ligands will be presented and commented upon.

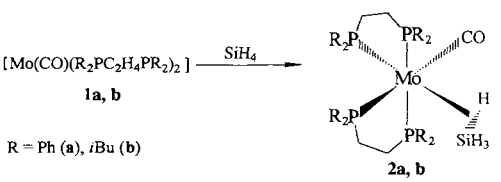

(a)

[*] Priv.-Doz. Dr. J. J. Schneider
Institut für Anorganische Chemie der Universität
Universitätsstrasse 5–7, D-45117 Essen (Germany)
Fax: Int. code +(201)183-2402.
e-mail: joerg.schneider@uni-essen.de.

[**] Abbreviations used: M = transition metal center; (H_2), (CH_4), and $(SiH_4) = (\eta^2\text{-}H_2)$, $(\eta^2\text{-}CH_4)$, and $(\eta^2\text{-}SiH_4)$ respectively, $Cp^* = \eta^5\text{-}C_5Me_5$, INS = inelastic neutron scattering; L = ligand; RHF = restricted Hartree Fock; MP = Moeller–Plesset.

2. σ-Coordinated Dihydrogen and σ-Coordinated Silanes

The simplest ligand that forms exclusively σ complexes with transition metals is the hydrogen molecule H_2. The H–H bond of H_2 always coordinates to a transition metal in a side-on mode.[6] This gives rise to a three-center–two-electron bond, which is comparable to that found in boranes with B-H-B bridges. In analogy to the σ/π bonding formulism for ethene bonding to a transition metal, in H_2 bonding to a transition metal electron density is transferred from an occupied σ_g orbital of the H_2 molecule into an unoccupied metal d_π orbital. By a synergistic interaction, electron density also transfers from an occupied metal d_π orbital into the σ_u^* orbital of the H_2 molecule (Fig. 1). Theoretical investigations,[7] as well as IR,[8a–c] INS,[8d] and Mössbauer[8e] spectroscopic studies confirmed this model of H_2-σ donation and metal(M)-π backbonding. A continual increase of the experimentally obtained intramolecular H–H distances in $M(H_2)$ complexes produce "snapshots" of the oxidative addition of H_2 to a transition metal center.

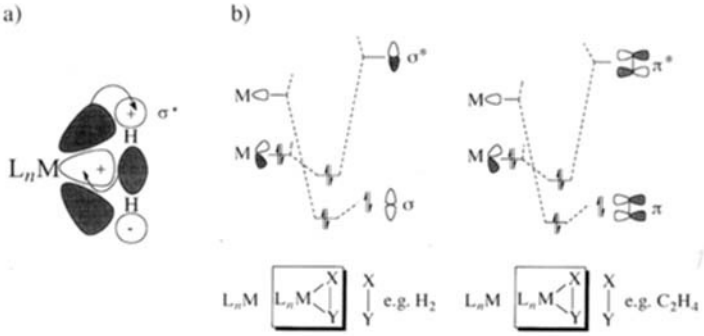

Fig. 1. a) Bonding model for the σ-η^2 side-on coordination of H_2 to a transition metal center; b) comparative representation of the MO interactions in transition metal complexes with σ-coordinating ligands (left) and π-coordinating ligands (right).

At this point the new and surprising results on transition metal free H_2 activation in biosystems should also be mentioned. A hydrogenase found in thermophilic methanogenic archaebacteria is evidently capable of activating H_2 in a catalyzed reaction *without* a redox-active transition metal center.[9] This means that in addition to enzymatic H_2 activation by metal-containing hydrogenases, whose H_2-activating centers contain sulfur and iron or nickel, possibly other modes of H_2 activation occur in nature.

The oxidative addition of a Si–H σ bond is one of the key steps in the mechanism of transition metal catalyzed hydrosilylation.[10] There are numerous examples of the activation of Si–H σ bonds by $M(L_n)$ centers and of complex formation.[3] These reveal that the bonding in silane complexes corresponds to a late step in the oxidative addition to the transition metal center. The ^1H NMR coupling constants and the elongation of the Si–H interatomic distances (from X-ray and neutron scattering investigations) provide a measure of the extent of the oxidative addition in σ-coordinated M-H-SiR_3 complexes (Fig. 2).

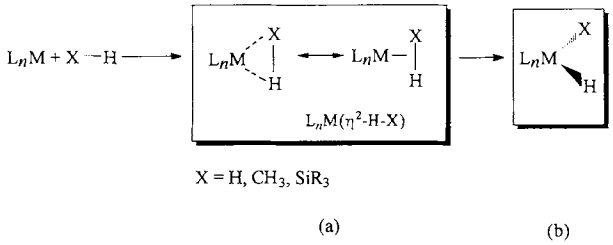

Fig. 2. General scheme for the reaction of a σ-coordinating ligand and a transition metal complex with formation of a side-on σ-η^2 complex (a) and complete oxidative addition of a σ-coordinating ligand to the transition metal complex (b).

3. The C–H Activation of Alkanes

3.1. The C–H Activation of Alkanes by Free Metal Atoms, Metal Oxide Cations, and Metal Clusters

In the case of σ coordination of alkanes to transition metal centers, the weaker basicity, that is the higher electronegativity, of the C–H bond compared to that of the H–H bond has thwarted the successful synthesis and structural characterization of a transition metal stabilized CH_4 complex with methane until now, although both σ bonds have almost equal bond

Jörg J. Schneider was born in 1960 and studied chemistry at the Philipps University in Marburg where he gained his doctorate in inorganic chemistry under C. Elschenbroich in 1986. In 1987/1988, supported by a Fulbright scholarship, he worked as a postdoctoral researcher with K. J. Klabunde at Kansas State University Manhattan/Kansas, USA (two further sojourns there followed in 1991 and 1995). In 1988 he moved to the Max-Planck-Institut für Kohlenforschung at Mülheim an der Ruhr to do further postdoctoral work with G. Wilke, and then remained in Mülheim to start the experimental work for his habilitation in 1989. In 1994 he completed his habilitation in inorganic chemistry at the Universität/Gesamthochschule Essen. In the same year he moved to the Anorganisch-chemisches Institut der Universität/Gesamthochschule Essen as a Heisenberg awardee of the Deutsche Forschungsgemeinschaft. He is currently a lecturer of inorganic chemistry at the University of Essen. His current research focusses on synthesis, structure, and reactivity in organometallic chemistry and on general aspects of high temperature species (atoms and molecules) in synthesis. He is also interested in interdisciplinary research in chemistry, physics, and materials science on which he has recently co-organized two national workshops for graduate students and postdoctoral researchers.

strengths (Me–H: 104.3, H–H: 104.2 ±1 kcal mol^{-1}[11]) and the C–H fragment and the H_2 molecule are isolobal. However, systematic matrix isolation studies of the C–H activation of alkanes by ligand-free transition metal atoms show that even though there is a marked decrease within the group, the reactivity of the transition metal atoms is high (Ru, Os, Rh ≫ Nb, Ta, Mo, Re, Cu, Ag).[12] The crucial factors for the reactivity of all free atoms towards CH_4 were shown to be high M–H dissociation energies and enthalpies of vaporization ΔH_{vap} of the metals. The latter underlines the influence of the kinetic energy of the metal atom in the reactions with CH_4. Ab initio calculations[13] and preparative work on C–H activation with free transition metal atoms[14] confirmed the results from the matrix isolation studies and revealed a particularly high reactivity for the elements Rh and Ru.[15] In the gas phase, the reactivity and selectivity of free transition metal atoms M^0 and ions M^+ towards CH_4 and other alkanes[16] is quite variable and is closely coupled to their electronic configurations and orbital symmetries, as well as to the criteria for spin conservation in these species. Generally, neutral transition metal atoms are less reactive than metal cations in C–H activation. The reason for this is assumed to lie in the $3d^{x-2}4s^2$ ground state electron configuration (x = group number) of neutral atoms which approaches the inert gas character of helium. This means that the charge-induced dipole–dipole interaction with easily polarizable alkanes is distinctly smaller than that for naked metal cations. Precisely this interaction seems to be of crucial importance in the C–H activation of alkanes at transition metal centers in the gas phase, as well as for the differences observed in the reactivity.[16a, 17a] On the basis of ab initio calculations of the gas phase reaction of Pd atoms with CH_4, a complex of type A (Fig. 3) is

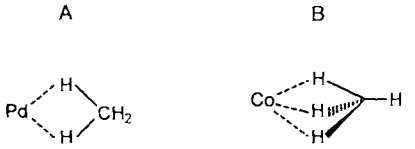

Fig. 3. Intermediates in the C–H activation of methane with Pd atoms in the gas phase (A) [16a,17b] and with Co atoms in solid argon (B) [19].

assumed to be an intermediate[16a, 17a] (A is 4 kcal mol^{-1} more stable by than the reactants Pd_{atoms}/CH_4[18]). Using data from IR matrix-isolation studies, a σ-complex B with C_{3v} symmetry (Fig. 3) is proposed as an intermediate in the oxidative addition of Co atoms with CH_4.[19] The structures A and B are not consistent with the conventional bonding model for σ-H_2 coordination (see above and Fig. 1a). However, interestingly, they are consistent with the results of theoretical calculations of C–H activation of CH_4 with organorhodium complexes (see below and Fig. 6).

In the case of reactions of naked transition metal and transition metal oxide cations with alkanes, there are parallels as well as evident differences in reactivity in the C–H activation of these substrates. Generally, early transition metal oxide cations such as ScO^+, TiO^+, and VO^+ do not react with methane at all. On the other hand, oxide cations of the late transition metals MnO^+ to NiO^+ react very efficiently with methane.[20] The reason for this reduced reactivity of the early metal oxide cations lies in the varying strengths of the M–O bond of these molecules. This bond is particularly strong in the very oxophilic early transition metals and manifests itself in the low reaction efficiency of these transition metal oxide cations with alkanes. The reaction of late transition metal oxide cations with larger alkanes is usually more efficient than that observed with methane; however, this increased reactivity reduces the chemo- and regioselectivity. Additional reaction pathways that may appear, such as the known β-H elimination or even C–C bond activation of the carbon framework of these higher alkanes, may be the cause.[16d, 21] A comprehensive review on the present level of understanding of C–H and C–C activation of alkanes with naked transition metal oxide cations has recently been published by Schröder and Schwarz.[22]

The reactivity of naked metal atom clusters towards CH_4 in the gas phase is size-selective. This was detected for the first time for Pt_2–Pt_{24}; the maximum reactivity occurring for cluster sizes Pt_2–Pt_5.[23a, b] An explanation for the surprisingly high reactivity of such small metal atom clusters is assumed to lie in the low-coordination environment; in contrast larger metal clusters (Pt_6–Pt_{24}) are more highly coordinated and have almost close-packed ordering. In comparative studies of the C–H activation of alkanes in inert gas matrices by free metal atom clusters M_x, the early transition metals were found to be more reactive than the late transition metals.[12] This is consistent with theoretical observations that predict that the activation energy for the dissociative adsorption of alkanes onto metal surfaces increases as the number of d electrons increases.[24]

3.2. Agostic C–H Interactions of Alkanes and Si–H Interactions of Silanes in Transition Metal Complexes

σ-Transition metal alkane complexes of the type $[M(CO)_5(\eta^2\text{-}CH_4)]$ (M = Cr, Mo, W) were detected and characterized spectroscopically as reactive intermediates in alkane/inert gas matrices in the 1970s.[25] Stable, structurally characterized complexes with $(\eta^2\text{-CH})$–M structural elements have only been found to exist so far with agostic bonding;[26] a chelate bridge is responsible for the crucial stabilization of the C-H-M three-center interaction (Fig. 4a). Here the C–H bridge remains close

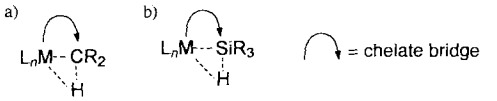

Fig. 4. Agostic interactions in alkane (a) and silane complexes (b).

to the metal center, and the C–H bond is not greatly elongated[2i] (C–H bound: 1.13–1.19 Å, unbound: 1.1 Å), thus preventing complete dissociation and formation of an alkyl(hydrido) complex. In analogy to studies of transition metal complexes with σ-bound silane ligands,[27] an examination of the structural data of transition metal complexes with agostic C-H-M interactions using structural correlation methods[28] has produced a model that describes the approach of the C–H bond towards the metal atom and the stereochemistry during the course of formation of the C-H-M interaction.[2i, 29] Apart from a preliminary stage in which the C–H fragment is more or

less in an end-on orientation ($\sphericalangle$ M-H-C $\approx 150°$), the C–H bond of the alkane approaches the transition metal side-on. Such organometallic complexes with C-H-M interactions have been "arrested" in the early stages of oxidative addition. This is in contrast to compounds with M-Si-H bonds, which, for the most part, do not contain any intramolecular chelate bridges. As a result of the C-H-M interaction, the acidity of the agostically complexed C–H bond increases drastically. In principle, such an intramolecular chelate stabilization should also be possible for Si-H-M interactions (Fig. 4b), and would, of course, lead to the corresponding σ complexes in their early stages of oxidative addition. However, examples of such structures are scarce up to now.[30] If it were possible in future to close this gap with further preparative examples, similar behavior in the coordination of both C–H and Si–H at transition metal centers could certainly be expected.

3.3. C–H Activation of Alkanes in Homogeneous Solution

At the beginning of the 1980s, Bergman, Graham, and Jones and their co-workers in independent work, detected C–H activation reactions of CH_4 and other alkanes in homogeneous solution[31] [Eq. (b)]. Shortly before, Crabtree and Felkin and

$$[(C_5R_5)MLL'] + R'H \xrightarrow{h\nu} [(C_5R_5)ML(R')(H)] + L \qquad (b)$$

R = H, CH_3, R' = CH_3, C_6H_{11}, tBuCH$_2$, Ph
L = CO, $P(CH_3)_3$, L' = CO, H_2, M = Rh, Ir

co-workers had observed the first indications of cycloalkane activation in solution.[32, 33] In the following years Bergman et al. succeeded in detecting conclusively intermediate stages of C–H activation of different alkanes with Ir and Rh complexes.[34] It was frequently the experiments carried out under unconventional, nonclassical conditions, for example in supercritical solvents or in the gas phase, which were of crucial importance for gaining new information on C–H activation. In 1994 it was demonstrated[35] that the photolysis of $[Cp^*Rh(CO)_2]$ in the presence of 2,2-dimethylpropane (neopentane) in liquid krypton produces [Cp*Rh(CO)(Kr)] as an intermediate, which is in equilibrium with the σ-alkane complex $[Cp^*Rh(CO)\{C(CH_3)_4\}]$. These intermediates can be detected *side by side* by IR spectroscopy. The actual end product $[Cp^*Rh(CO)(H)(C_5H_{11})]$ of the oxidative addition reaction of neopentane with the 16 valence electron fragment [Cp*Rh(CO)],[36] arises from an unimolecular reaction [Eq. (c)]. These

$$[Cp^*Rh(CO)_2] \xrightarrow[-CO]{h\nu} [Cp^*Rh(CO)(Kr)] \underset{+Kr,\ k_2}{\overset{+RH,\ k_1}{\rightleftharpoons}} [Cp^*Rh(CO)(RH)] \xrightarrow{k'_2} [Cp^*Rh(CO)(H)(R)] \qquad (c)$$

R = tBuCH$_2$

investigations delivered the first *direct* evidence of an σ-alkane complex as an intermediate in the C–H activation of alkanes. It is worth mentioning at this point that the latest technical developments in apparatus for synthesis in supercritical fluids,[2k] when applied to C–H activations of alkanes, may allow further important advances in this field.

3.4. Heterogeneous C–H Activation of Alkanes

C–H Activation of methane is also known from investigations in heterogeneous phases.[37a–e] For example, the organometallic fragment $[Rh^I(CO)_2]$ exists as an isolated species on oxide surfaces such as Al_2O_3.[37d] On photoactivation there is loss of CO and formation of $[Rh^I(CO)]$. This species can activate CH_4 at temperatures as low as $-40\,°C$,[37e] and cyclohexane at $27\,°C$[37f–h]. The end product of the heterogeneous photochemical C–H activation of CH_4 is the acyl complex $[RhH(CO)(COCH_3)]$, which is formed by migration and insertion reactions of CH_3 into the Rh–CO bond of $[RhH(CO)(CH_3)]$[37e] (Fig. 5). The free coordination site at the Rh center is then filled by a further CO molecule. Such CO insertion reactions have been well documented and represent important key steps in industrial processes, for example the Fischer–Tropsch process,[38a, b] Roelen's hydroformylation,[38c, d, e] or organometallic reactions like the photolytic activation of alkanes with $[RhCl(CO)(PMe_3)_2]$[39] in homogeneous solution.

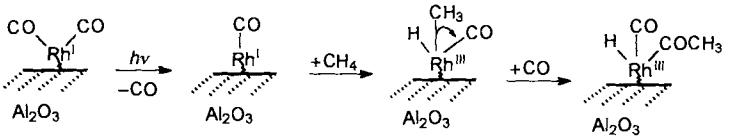

Fig. 5. Reaction scheme for the heterogeneous C–H activation of methane on $[Rh^I(CO)]$ fragments complexed to a surface [37e].

Hitherto, all the known C–H activations at transition metal centers in both homogeneous and heterogeneous phases occur preferentially at primary C–H bonds of alkanes. This gradation in reactivity is contrary to that found for conventional metal-free C–H activations of alkanes with radicals or strong acids[1d, 40] (gradation in reactivity here: *tert*-C-H > *s*-C-H > *primary*-C-H > CH_4), and shows that the environment of the central transition metal center, that is steric effects, have a crucial influence on the reactivity of the C–H activations of alkanes.

3.5. Theoretical Investigations on C–H and Si–H Activation of Alkanes and Silanes

Theoretical studies have accompanied the experimental work on CH_4 and SiH_4 activation on transition metal centers right from the beginning.[41] For intermediates $[L_nRh\cdots(CH_4)]$ of the oxidative addition of CH_4 onto organorhodium complexes, the calculated binding energies, reaction enthalpies ΔH of the total reaction, and the C–H activation energies for the attack of methane by the $[L_nRh]$ fragment, may display strong variations in their absolute values depending on the ab initio procedure used.[41, j, k, 42] However, all the calculations carried out to date gave consistent energy profiles for the C–H activation of CH_4, that is low activation barriers and relatively high reaction enthalpies ΔH, which is consistent with the reactivity of such unsaturated organometallic systems found experimentally. Experimental gas phase investigations of the reaction pathway of the activation of H_2, CH_4 and other alkanes have been carried out using [Cp*Rh(CO)].[34g] In this oxidative addition reaction, the intermediate $[Cp^*(CO)Rh\cdots(CH_4)]$ is formed, which passes through a transition state before transforming into the end

product, a stable methyl(hydrido) complex. Calculations by Morokuma et al. (RHF-MP method) on the H_2, SiH_4, and CH_4 activation at organometallic fragments [Cp*Rh(CO)] and $[RhCl(PH_3)_2]$[39] essentially confirm this reaction pathway.[42b,c] Here, the intermediate of the C–H activation was calculated to have a bidentate structure in which two C–H bonds coordinate simultaneously to the Rh center (Fig. 6). In

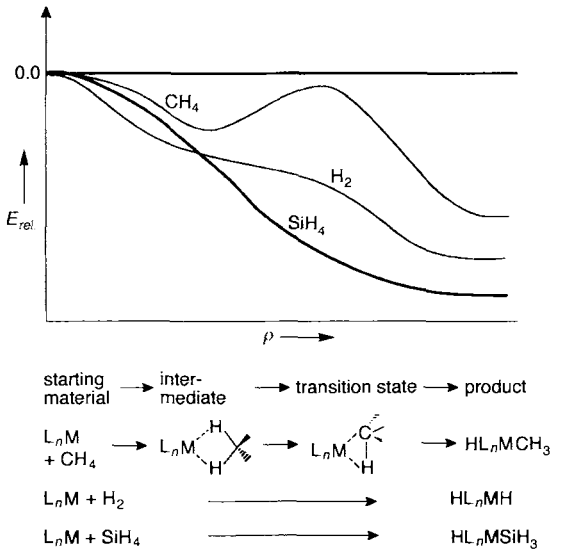

Fig. 6. Reaction profiles for C–H, H–H, and Si–H activation by [Cp*Rh(CO)] and $[RhCl(PH_3)_3]$ according to theoretical investigations [42]. For the structural parameters of the intermediates and the transition states see ref.[42b,c]. ρ = reaction coordinate.

the transition state there is σ-η^2 coordination. Interestingly, calculations on the activation of SiH_4 with both of the above Rh^I complexes gave reaction profiles that did not exhibit a comparable intermediate. The calculated differences in the stabilities of the end products ($HL_nRhSiH_3 > HL_nRhH > HL_nRhCH_3$) of the oxidative additions of H_2, SiH_4 and CH_4 to [Cp*Rh(CO)] and $[RhCl(PH_3)_2]$ correlate well with the $E_{H,Si,C-H}$ ($SiH_4 < CH_2 < CH_4$) and the $E_{H,Si,C-Rh}$ ($SiH_4 > H_2 > CH_4$) bond strengths.[43] This gradation results in a reaction profile for the H–H and the Si–H activation which, in contrast to the C–H activation, only has a downhill gradient without a stable intermediate.

4. Side-On Coordination of SiH_4 as a Model for σ Coordination of CH_4?

Recently, Kubas et al. succeeded in the synthesis, isolation, and structural characterization of a SiH_4 complex [5] by reaction of SiH_4 with the electronically and coordinatively unsaturated 16 valence electron Mo^0 complexes **1**.[44] In the reaction of **1a** ($R = C_6H_5$) or **1b** ($R = i$Bu) with SiH_4, only side-on η^2 coordination is observed both in solution and in the solid state [see Eq. (a)]. Here, the contributions of the ^1H NMR coupling constants of the σ-bound transition metal silane complexes **2** J(Si,bridging-H) and J(Si,H), as well as their differences ΔJ, provide a valuable indication of the extent of the oxidative addition of the SiH_4 ligand at the central Mo atom in **2** in solution (Table 1). Compared to some Mn–silane complexes **5a–c**,[3b]

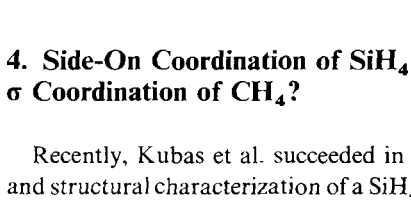

1 R = Ph (**1a**), *i*Bu(**1b**), Et (**1c**)

4 R = z.B. Et, Ph; *R = e.g. Ph, n-C_6H_{13}, H*

Table 1. Selected coupling constants J(Si,H) and J(Si,bridging-H) as well as the differences ΔJ [in Hz] of the $Mo(SiH_4)$ and $Mo(H_2SiR_2)$ complexes **2** and **4**, respectively, in comparison with the silylmolybdenum complex **3** and the manganese silane complexes **5a–c**.

Complex	J(Si,H)	J(Si,bridging-H)	ΔJ [a]
$[Mo(SiH_4)CO(Ph_2PC_2H_4PPh_2)_2]$ **2a**	181	50	131
$[Mo(SiH_4)CO(iBu_2PC_2H_4PiBu_2)_2]$ **2b**	163	31	132
$[Mo(SiH_4)CO(Et_2PC_2H_4PEt_2)_2]$ **2c**	164	35	129
$[MoH(SiH_3)CO(Et_2PC_2H_4PEt_2)_2]$ **3**	143	–	–
$[Mo(SiH_3Ph)CO(Et_2PC_2H_4PEt_2)_2]$ **4a**	164, 170	39	131, 1255
$[Mo(SiH_2Ph_2)CO(Et_2PC_2H_4PEt_2)_2]$ **4b**	172	50	122
$[Mo(SiH_3Ph)CO(Ph_2PC_2H_4PPh_2)_2]$ **4c**	187, 194	57	130, 137
$[Cp'Mn(CO)PMe_3(SiH_2Ph_2)]$ **5a** [b]	188	38	150
$[Cp'Mn(CO)PPh_3(SiH_2Ph_2)]$ **5b** [b]	191	43	148
$[Cp'Mn(CO)\{P(OPh)_3\}(SiH_2Ph_2)]$ **5c** [b]	199	45	154

[a] $\Delta J = J(Si,H) - J(Si,bridging\text{-}H)$. [b] $Cp' = \eta^5$-C_5H_4Me.

the value of ΔJ of about 130 Hz for **2a–c** and for **4a–c**[45] is clearly lower. This indicates the presence of η^2-side-on coordinated silane ligands in **2** and **4** in the "early stage" of the oxidative addition. However, for **1c** there is already an equilibrium between the two tautomeric forms **2c** and **3** in solution; thus, both forms are present at room temperature [Eq. (d)]. This ex-

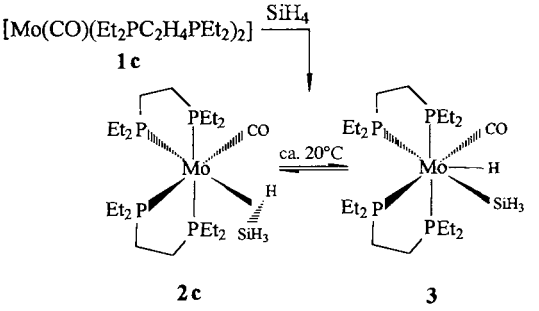

(d)

perimental result indicates a flat energy profile for the activation of SiH_4 by **1**, and is contrary to the theoretical results on Si–H activation obtained by Morokuma et al.; however, it should be kept in mind that his results were obtained with the Rh^I complexes [Cp*Rh(CO)] and $[RhCl(PH_3)]$.[42]

Interestingly, inspection of the electronic situation for the coordination of SiH_4 to the Mo starting complexes **1**, reveals that these complexes exactly fulfil the requirements that Schubert et al. found to be necessary at the beginning of the 1990s for the isolation of stable silane and stannane complexes of Group 6 elements.[46] These results showed that a stepwise increase of the electron density on the metal center due to donor ligands allows the stabilization of σ complexes with silane and stannane ligands. Additionally, the extent of the oxidative addition of

these ligands is directed by factors such as the basicity of the metal center (Cr < Mo < W), the number of phosphane ligands present (Cr, Mo > W), and the electronic situation at the σ-coordinated silane or stannane. In the case of substituted silanes H_xSiR_{4-x}, electron-withdrawing substituents R on the silicon enhance the tendency of σ-Si-H coordination, and increase the activation enthalpy of the reductive elimination of the silane ligand.

Bearing all this in mind, the recent successful σ coordination of SiH_4[5] by means of consequent fine tuning of the electronic situation on both the Mo center and in the ligand sphere of **1** is not quite unexpected; it proves conclusively that such an "optimized" electronic situation at the transition metal center allows the coordination of SiH_4 and thus makes an additional electronic tuning by other ligands on the incoming silicon superfluous. Whether this clearly important step on the way to the coordination of methane can act as a model for the coordination of CH_4 at transition metal centers, as was proposed by Kubas et al.,[4-7] remains to be seen, particularly in view of the electronic differences in the two substrates, CH_4 and SiH_4, and the resulting theoretical and experimental differences for the C–H and Si–H activation at transition metal centers.

5. Final Comments

This account should allow the reader an insight into the comparative C–H and Si–H activation of alkanes and silanes, respectively, at transition metal centers as far as oxidative additions are concerned. Particular consideration has been paid to recent preparative and theoretical results. With respect to the field two recently published review articles by Crabtree[1d, 2j] deserve special attention and will be particularly helpful to the reader.

Completed reactions, that is those that have proceeded to the final oxidative addition of alkanes with transition metals, have already been observed for numerous transition metal atoms and transition metal complex fragments. The σ-transition metal complexes that are formed therein are often only intermediates or transition states on the way to the thermodynamically stable end product, an alkyl(hydrido) complex. In organometallic chemistry it is not rare to find that the high reactivity of a transition metal atom or transition metal complex fragment is associated with a low selectivity or stability of such an intermediate in the corresponding chemical reaction, for example a σ-transition metal complex. This is due in most part to the fact that for highly reactive species there are usually a number of competing reaction channels available. For C–H activation processes this applies in particular to atoms M, complex fragments ML, and highly reactive (unsaturated) complexes ML_n. Therefore, it is necessary to have an accurately tuned electronic and steric situation at the transition metal center to isolate stable σ-alkane complexes as precursors of oxidative additions. For future developments in this field a wide range of ligands with differing electron-directing capabilities and variable spatial requirements will be necessary. They will have to be capable of a) electronic fine tuning of a range of different transition metal centers for σ coordination to the alkane, and b) creating the necessary steric situation at the transition metal center. However, these ligands are probably already largely available. The task facing the organometallic chemist is to find the correct combination of single components—ML fragments and any additional sterically and electron-directing ligands—necessary to obtain complex fragments or complexes that will allow the successful isolation of the first transition metal alkane complexes. Possibly, the use of unconventional preparative methods of synthesis[8c, 25d] will give fresh impetus to the continuation of experimental developments in this area. Moreover, theoretical investigations will continue to be a constant and important partner to the experiments and will aid in understanding the role of the electronic states involved at the transition metal during the C–H activation process.

In summary, inspite of all the successful results obtained so far in the field of C–H activation of alkanes, the understanding of the factors that control the activation of alkanes—and here in particular methane—by transition metals remain a preparative and theoretical challenge.

Received: May 9, 1995
Revised version: November 29, 1995 [A 1431E]
German version: *Angew. Chem.* **1996**, *108*, 1132–1139
Translated by Gillian Scheibelein, Offenburg (Germany)

[1] *Activation and Functionalization of Alkanes* (Ed.: C. L. Hill), Wiley, New York, **1989**; b) G. W. Parshall, *Homogeneous Catalysis*, Wiley Interscience, New York, **1980**; c) A. E. Shilov, *Pure Appl. Chem.* **1978**, *50*, 725; d) R. H. Crabtree, *Chem. Rev.* **1995**, *95*, 987; e) J. H. Lunsford, *Angew. Chem.* **1995**, *107*, 1059; *Angew. Chem. Int. Ed. Engl.* **1995**, *34*, 970; f) M. Lin, A. Sen, *Nature* **1994**, *368*, 613; g) *Perspectives in the Selective Activation of C-H and C-C Bonds in Saturated Hydrocarbons* (Eds.: B. Meunier, B. Chaudret), Scientific Affairs Division, NATO, Brüssel, **1988**; h) N. D. Parkyns, *Chem. Br.* **1990**, *9*, 841.

[2] a) G. J. Kubas, *Comments Inorg. Chem.* **1988**, *7*, 17; b) *Acc. Chem. Res.* **1988**, *21*, 120; c) R. A. Henderson, *Transition Met. Chem.* **1988**, *13*, 474; d) R. H. Crabtree, D. G. Hamilton, *Adv. Organomet. Chem.* **1988**, *28*, 299; e) R. H. Crabtree, *Acc. Chem. Res.* **1990**, *23*, 95; f) R. H. Crabtree, X. Luo, D. Michos, *Chemtracts Inorg. Chem.* **1991**, *3*, 245; g) G. J. Kubas, *Less Common Met.* **1991**, *172–174*, 475; h) D. M. Heinekey, W. A. Oldham, Jr., *Chem. Rev.* **1993**, *93*, 913; i) J. H. Morris, P. G. Jessop, *Coord. Chem. Rev.* **1992**, *121*, 155; j) R. H. Crabtree, *Angew. Chem.* **1993**, *105*, 828; *Angew. Chem. Int. Ed. Engl.* **1993**, *32*, 789; k) J. A. Banister, P. D. Lee, M. Poliakoff, *Organometallics* **1995**, *14*, 3876.

[3] a) W. A. G. Graham, *J. Organomet. Chem.* **1986**, *300*, 81; b) U. Schubert, *Adv. Organomet. Chem.* **1990**, *30*, 151; c) theoretical treatment: H. Raaba, J.-Y. Saillard, U. Schubert, *J. Organomet. Chem.* **1987**, *330*, 397.

[4] a) E. L. Muetterties, *Chem. Soc. Rev.* **1982**, *11*, 283; b) R. H. Crabtree, *Chem. Rev.* **1984**, *85*, 245; c) M. Ephritikhine, *Nouv. J. Chim.* **1986**, *10*, 9; d) for an up to date overview of further reaction pathways on the C–H activation of CH_4 see also [1d] and for a recent compilation of theoretical and experimental results see a special volume on aspects of C–H activation, *J. Organomet. Chem.* **1995**, *504*, 1–155.

[5] X. L. Luo, G. J. Kubas, C.-J. Burns, J. C. Bryan, C. J. Unkefer, *J. Am. Chem. Soc.* **1995**, *117*, 1159.

[6] It is assumed that $[(\sigma\text{-}H_2)Pd]$ is present along with $[(\eta^2\text{-}H_2)Pd]$ in H_2/Kr matrices at 10–12 K: G. A. Ozin, J. Garda-Prieto, *J. Am. Chem. Soc.* **1986**, *108*, 3099.

[7] a) J.-Y. Saillard, R. Hoffmann, *J. Am. Chem. Soc.* **1984**, *106*, 2007; b) H. Raaba, J.-H. Saillard, R. Hoffmann, *ibid.* **1986**, *108*, 4327; c) C. S. Van Der Sluys, J. Eckert, O. Eisenstein, J. H. Hall, J. C. Huffman, S. A. Jackson, T. F. Koetzle, G. J. Kubas, P. J. Vergamini, K. G. Caulton, *ibid.* **1990**, *112*, 4831; d) *Transition Metal Hydrides* (Ed.: A. Dedieu), VCH, Weinheim, **1991**; e) S. Dapprich, G. Frenking, *Angew. Chem.* **1995**, *107*, 383; *Angew. Chem. Int. Ed. Engl.* **1995**, *34*, 354.

[8] a) R. H. Morris, K. A. Earl, R. L. Luck, N. J. Lazarowych, A. Sella, *Inorg. Chem.* **1987**, *26*, 2674; b) S. M. Howdle, M. A. Healy, M. Poliakoff, *J. Am. Chem. Soc.* **1990**, *112*, 4804; c) M. Poliakoff, S. M. Howdle, S. G. Kazarin, *Angew. Chem.* **1995**, *107*, 1409; *Angew. Chem. Int. Ed. Engl.* **1995**, *34*, 1275; d) G. J. Kubas, C. J. Burns, J. Eckert, S. W. Johnson, A. C. Larson, P. J. Vergamini, C. J. Unkefer, G. R. K. Khaba, S. A. Jackson, O. Eisenstein, *J. Am. Chem. Soc.* **1993**, *115*, 569; e) R. H. Morris, M. Schlaf, *Inorg. Chem.* **1994**, *33*, 1725.

[9] a) A. Berkessel, R. K. Thauer, *Angew. Chem.* **1995**, *107*, 2418; *Angew. Chem. Int. Ed. Engl.* **1995**, *34*, 2247; b) L. Jaenicke, *Chem. Uns. Zeit* **1995**, *29*, 276.

[10] a) A. J. Chalk, J. F. Harrod, *J. Am. Chem. Soc.* **1965**, *87*, 1133; b) *ibid.* **1967**, *89*, 1640; c) J. L. Speier, *Adv. Organomet. Chem.* **1979**, *17*, 407.

[11] D. Griller, J. M. Kanobus-Kaminska, A. Maccoll, *J. Mol. Struct. (Theochem)* **1988**, *163*, 125.

[12] a) K. J. Klabunde, G. H. Jeong, A. W. Olsen in ref. [48], Chap. 13, p. 433; b) A. W. Olsen, Dissertation, Kansas State University, USA, **1989**.

[13] a) M. Svennson, M. R. A. Blomberg, P. E. M. Siegbahn, *J. Am. Chem. Soc.* **1991**, *113*, 7076; b) P. E. M. Siegbahn, M. R. A. Blomberg, M. Svennson, *ibid.* **1993**, *115*, 4191; c) P. E. M. Siegbahn, M. Svennson, *ibid.* **1994**, *116*, 10124.

[14] a) J. A. Bandy, M. L. H. Green, D. O'Hare, K. Prout, *J. Chem. Soc. Chem. Commun.* **1984**, 1402; b) J. A. Bandy, M. L. H. Green, D. O'Hare, *J. Chem. Soc. Dalton Trans.* **1987**, 2823; c) M. L. H. Green, D. S. Joyner, J. M. Wallis, *ibid.* **1987**, 2823; d) M. L. H. Green, D. O'Hare, *ibid.* **1986**, 2469; e) in ref. [49], Chap. 16, p. 260.

[15] For the detection of a $[H_2Rh(CH_4)]$ complex see R. J. Van See, S. Li, W. Weltner, Jr., *J. Am. Chem. Soc.* **1993**, *115*, 2976.

[16] a) J. C. Weisshaar, *Acc. Chem. Res.* **1993**, *26*, 213; b) P. B. Armentrout, *Annu. Rev. Phys. Chem.* **1990**, *41*, 313; c) J. A. Martinho-Simoes, J. L. Beauchamp, *Chem. Rev.* **1990**, *90*, 629; d) K. Eller, H. Schwarz, *ibid.* **1991**, *91*, 1121; e) H. Schwarz, *Chem. Uns. Zeit* **1991**, *25*, 268; f) P. B. Armentrout in ref. [48], Chap. 14, p. 467; g) J. L. Beauchamp in ref. [49], Chap. 2, p. 11.

[17] a) D. Ritter, J. C. Weisshaar, *J. Am. Chem. Soc.* **1990**, *112*, 6426; b) J. Caroll, J. C. Weisshaar, *ibid.* **1993**, *115*, 800.

[18] M. R. A. Blomberg, P. E. M. Siegbahn, M. Svennson, *J. Am. Chem. Soc.* **1992**, *114*, 6095.

[19] a) W. E. Billups, S. C. Chang, R. H. Hauge, J. L. Margrave, *J. Am. Chem. Soc.* **1993**, *115*, 2039; b) *ibid.* **1995**, *117*, 1387.

[20] T. C. Jackson, D. B. Jacobson, B. S. Freiser, *J. Am. Chem. Soc.* **1984**, *106*, 1252.

[21] a) S. W. Buckner, B. S. Freiser, *Polyhedron* **1988**, *7*, 1583; b) B. S. Freiser, *Acc. Chem. Res.* **1994**, *27*, 353.

[22] D. Schröder, H. Schwarz, *Angew. Chem.* **1995**, *107*, 2126; *Angew. Chem. Int. Ed. Engl.* **1995**, *34*, 1973.

[23] a) D. J. Trevor, D. M. Cox, A. Kaldor, *J. Am. Chem. Soc.* **1990**, *112*, 3742; b) R. L. Wheeten, D. M. Cox, D. J. Trevor, A. Kaldor, *J. Phys. Chem.* **1985**, *89*, 566; c) Pd clusters: P. Fayet, A. Kaldor, D. M. Cox, *J. Chem. Phys.* **1990**, *92*, 254; d) Rh clusters: M. R. Zakin, D. M. Cox, A. Kaldor, *ibid.* **1988**, *89*, 1201; e) summary of overviews on the reaction of naked metal clusters with alkanes: K. H. Kafafi in ref. [48], Chap. 12, p. 411; D. J. Trevor, A. Kaldor in ref. [49], Chap. 3, p. 43.

[24] a) R. C. Baetzold, *Solid State Commun.* **1982**, *44*, 781; b) E. Shustorovich, R. C. Baetzold, E. L. Muetterties, *J. Phys. Chem.* **1983**, *87*, 1100.

[25] a) M. A. Graham, R. N. Perutz, M. Poliakoff, J. J. Turner, *J. Organomet. Chem.* **1972**, *34*, C34; b) M. Poliakoff, J. J. Turner, *J. Chem. Soc. Dalton Trans.* **1974**, 2276; c) R. N. Perutz, J. J. Turner, *J. Am. Chem. Soc.* **1975**, *97*, 4791; d) R. J. Mawby, R. N. Perutz, M. K. Whittlesley, *Organometallics* **1995**, *14*, 3268; e) C. E. Brown, Y. Ishikawa, P. A. Hackett, D. M. Rayner, *J. Am. Chem. Soc.* **1990**, *112*, 2530; f) T. J. Burkey in *Energetics of Organometallic Species* (Ed.: J. A. M. Simoes), Kluwer, Dordrecht, **1992**.

[26] M. Brookhart, M. L. H. Green, *J. Organomet. Chem.* **1983**, *250*, 395.

[27] a) U. Schubert, K. Ackermann, G. Kraft, B. Woerle, *Z. Naturforsch. B* **1983**, *38*, 1488; b) U. Schubert, G. Scholz, J. Müller, K. Ackermann, B. Woerle, *J. Organomet. Chem.* **1986**, *306*, 303.

[28] H.-B. Bürgi, *Angew. Chem.* **1975**, *87*, 461; *Angew. Chem. Int. Ed. Engl.* **1975**, *14*, 460.

[29] R. H. Crabtree, E. M. Holt, M. Lavin, S. M. Morehouse, *Inorg. Chem.* **1985**, *24*, 1986.

[30] See for example U. Schubert, U. Bader, J. Müller, *J. Organomet. Chem.* **1987**, *327*, 357.

[31] a) A. H. Janowicz, R. G. Bergman, *J. Am. Chem. Soc.* **1982**, *104*, 352; b) *ibid.* **1983**, *105*, 3929; c) J. K. Hoyano, W. A. G. Graham, *ibid.* **1982**, *104*, 3723; d) J. K. Hoyano, A. D. McMaster, W. A. G. Graham, *ibid.* **1983**, *105*, 7190; e) W. D. Jones, F. J. Feher, *ibid.* **1982**, *104*, 4240.

[32] R. H. Crabtree, J. M. Mihelcic, J. M. Quirck, *J. Am. Chem. Soc.* **1979**, *101*, 7738.

[33] D. Baudry, M. Ephritikine, H. Felkin, *J. Chem. Soc. Chem. Commun.* **1980**, 1243.

[34] a) R. A. Periana, R. G. Bergman, *J. Am. Chem. Soc.* **1986**, *108*, 7332; b) J. M. Buchanan, J. M. Stryker, R. G. Bergman, *ibid.* **1986**, *108*, 1537; c) E. P. Wasserman, R. G. Bergman, C. B. Moore, *ibid.* **1988**, *110*, 6076; d) M. B. Sponsler, B. H. Weiller, P. O. Stoutland, R. G. Bergman, *ibid.* **1989**, *111*, 6841; e) B. H. Weiller, E. P. Wasserman, R. G. Bergman, C. B. Moore, G. C. Pimentel, *ibid.* **1989**, *111*, 8288; f) M. J. Hostettler, R. G. Bergman, *ibid.* **1992**, *114*, 7629; g) E. P. Wasserman, C. B. Moore, R. G. Bergman, *Science* **1992**, *255*, 315; h) R. H. Schultz, R. G. Bergman, *J. Am. Chem. Soc.* **1994**, *116*, 7369; i) T. A. Mobley, C. Schade, R. G. Bergman, *ibid.* **1995**, *117*, 7822; j) B. A. Arndtsen, T. A. Mobley, R. G. Bergmann, T. H. Peterson, *Chem. Rev.* **1995**, *28*, 154. Other work: k) Y. Ishikawa, C. E. Brown, P. A. Hackett, D. M. Rayner, *Chem. Phys. Lett.* **1988**, *150*, 506; l) X. Xie, J. D. Simon, *J. Phys. Chem.* **1989**, *93*, 291; m) C. E. C. A. Hop, T. B. McMahon, *J. Am. Chem. Soc.* **1991**, *113*, 355; n) G. R. Dobson, K. J. Asali, C. D. Cate, C. W. Cate, *Inorg. Chem.* **1991**, *30*, 4471; o) J. Belli, C. M. Jensen, *Organometallics* **1996**, *15*, 1532.

[35] A. A. Bengali, R. H. Schultz, C. B. Moore, R. G. Bergman, *J. Am. Chem. Soc.* **1994**, *116*, 9585.

[36] Investigations on the mechanism of photolytic formation of [Cp*Rh(CO)] in C–H activation processes see D. P. Drolet, A. L. Rees, *J. Am. Chem. Soc.* **1992**, *114*, 4186.

[37] a) S. C. Kaliaguine, B. N. Shelimov, V. B. Kazansky, *J. Catal.* **1978**, *55*, 384; b) M. D. Ward, J. F. Bradzil, S. P. Mehandru, A. B. Anderson, *J. Phys. Chem.* **1987**, *91*, 6515; c) K. Wada, K. Yoshida, T. Takatani, Y. Watanabe, *Appl. Catal. A* **1993**, *99*, 21; d) J. T. Yates, Jr., T. M. Duncan, S. D. Worley, R. W. Vaughn, *J. Chem. Phys.* **1979**, *70*, 1219; e) J. C. S. Wong, J. T. Yates, Jr., *J. Phys. Chem.* **1995**, *99*, 12640; f) T. H. Ballinger, J. T. Yates, Jr., *J. Am. Chem. Soc.* **1992**, *114*, 10074; g) *J. Phys. Chem.* **1992**, *96*, 9979; h) J. C. S. Wong, J. T. Yates, Jr., *J. Am. Chem. Soc.* **1994**, *116*, 1610; i) E. A. Wouchoko, J. T. Yates Jr., *ibid.* **1995**, *117*, 12557.

[38] a) F. Calderazzo, *Angew. Chem.* **1977**, *89*, 305; *Angew. Chem. Int. Ed. Engl.* **1977**, *16*, 299; b) D. Foster, *Adv. Organomet. Chem.* **1979**, *17*, 255; c) M. Orchin, G. Rupillius, *Catal. Rev.* **1972**, *6*, 85; d) M. Orchin, *Acc. Chem. Res.* **1981**, *14*, 259; e) B. Cornils, W. A. Herrmann, M. Rasch, *Angew. Chem.* **1994**, *106*, 2239; *Angew. Chem. Int. Ed. Engl.* **1994**, *33*, 2144.

[39] T. Sakakura, T. Sodeyama, K. Sasaki, K. Wada, M. Tanaka, *J. Am. Chem. Soc.* **1990**, *112*, 7221.

[40] a) C–H activation with superacids see L. D. Field in ref. [48], Chap. 8, p. 241; H. Pines, *The Chemistry of Catalytic Hydrocarbon Conversion*, Academic Press, New York, **1981**; G. A. Olah, *Angew. Chem.* **1995**, *107*, 1519; *Angew. Chem. Int. Ed. Engl.* **1995**, *34*, 1393; b) activation with free radicals see W. A. Pryer, *Free Radicals*, McGraw-Hill, New York, **1966**.

[41] a) J. J. Low, W. A. Goddard III, *J. Am. Chem. Soc.* **1984**, *106*, 6928; b) *ibid.* **1984**, *106*, 8321; c) *ibid.* **1986**, *108*, 6115; d) *Organometallics* **1986**, *5*, 609; e) J.-Y. Saillard, R. Hoffmann, *J. Am. Chem. Soc.* **1984**, *106*, 7482; f) E. N. Rodriguez-Arias, L. Rincon, F. Ruette, *Organometallics* **1992**, *11*, 3677; g) M. R. A. Blomberg, P. E. M. Siegbahn, M. Svennson, *J. Am. Chem. Soc.* **1992**, *114*, 6095; h) P. E. M. Siegbahn, M. R. A. Siegbahn, M. Svennson, *New J. Chem.* **1991**, *15*, 727; i) *J. Phys. Chem.* **1991**, *95*, 4313; j) T. Ziegler, V. Tschinke, L. Fan, A. D. Becke, *J. Am. Chem. Soc.* **1989**, *111*, 9177; k) J. Song, M. B. Hall, *Organometallics* **1993**, *12*, 3118; l) J.-Y. Saillard in ref. [48], Chap. 7, p. 207; m) T. R. Cundari, *J. Am. Chem. Soc.* **1994**, *116*, 340; n) *Organometallics* **1993**, *12*, 1998; o) P. Margl, T. Ziegler, P. E. Blöchil, *J. Am. Chem. Soc.* **1996**, *117*, 1262; P. E. M. Siegbahn, *ibid.* **1996**, *118*, 1487.

[42] a) N. Koga, K. Morokuma, *J. Phys. Chem.* **1990**, *94*, 5454; b) *J. Am. Chem. Soc.* **1993**, *115*, 6883; c) D. Musaev, K. Morokuma, *ibid.* **1995**, *117*, 799.

[43] a) Ab initio calculations on C–H and Si–H activation processes on the $[PtR_2]$ fragment gave similar results: S. Sasaki, M. Teki, *J. Am. Chem. Soc.* **1991**, *113*, 5063; *ibid.* **1993**, *115*, 2373; b) for a review of M–L bond strengths from gas phase investigations see P. B. Armentrout in *Bonding Energetics in Organometallic Compounds* (*ACS Symp. Ser.* **1990**, *336*), Chap. 2, p. 18.

[44] M. Sato, T. Tatszumi, T. Kodama, M. Hidai, T. Uchida, Y. Uchida, *J. Am. Chem. Soc.* **1978**, *100*, 4447.

[45] X. L. Luo, G. J. Kubas, J. C. Bryan, C. J. Burns, C. J. Unkefer, *J. Am. Chem. Soc.* **1994**, *116*, 10312.

[46] a) H. Piana, U. Schubert, *J. Organomet. Chem.* **1991**, *411*, 303; b) H. Piana, U. Kirchgässner, U. Schubert, *Chem. Ber.* **1991**, *124*, 743.

[47] G. Kubas, as cited in *Chem. Eng. News* **1995**, *73*(5), 24.

[48] *Selective Hydrocarbon Activation, Principles and Progress* (Eds.: J. A. Davies, P. L. Watson, A. Greenberg, J. F. Liebman), VCH, New York, **1987**.

[49] *High Temperature Processes in Organometallic Chemistry* (*ACS Symp. Ser.* **1987**, *333*).

Nucleophilic Aromatic Substitution—A Possible Key Step in Total Syntheses of Vancomycin**

Kevin Burgess,* Dongyeol Lim, and Carlos I. Martinez

Vancomycin is a natural product with a complicated molecular architecture and clinical significance as an antibiotic for treatment of infections caused by gram positive bacteria. These two attributes have seduced several groups of organic chemists into attempting to prepare this molecule, but no successful synthesis has been reported to date.

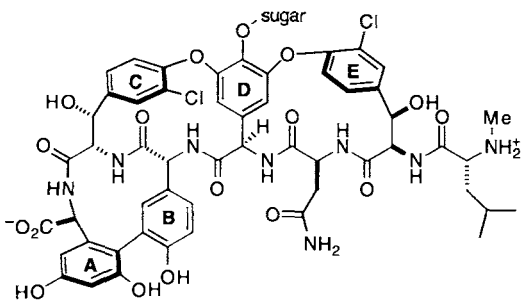

vancomycin

In 1993 there were two reasons to suppose that a total synthesis of vancomycin might be achieved soon.[1] First, the cyclic compound **1** had been prepared;[2] this closely resembles the "southwestern fragment" of vancomycin, which includes the biaryl linkage of rings **A** and **B**. Second, the bicyclic compound **2** had been made;[3] this is closely related to the central region of vancomycin, which incorporates the **C**, **D**, and **E** rings.

Despite this optimism, it apparently has not been convenient to exploit the syntheses of fragments **1** and **2** in a total synthesis, presumably for the following reasons. Vancomycin has only one chlorine atom on rings **C** and **E**, whereas both *ortho* positions on the corresponding aryl rings of **2** are chlorinated. These extra chlorine atoms were critical for the synthesis of **2**, in which two thallium trinitrate-mediated couplings require both *ortho* phenolic positions to be blocked. Furthermore, the formation of **1**, an oxidative coupling of the carbons marked a and b in structure

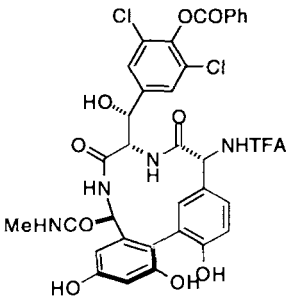

1

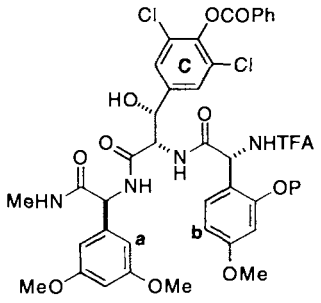

3
(P = 3,4-dichlorobenzyl)

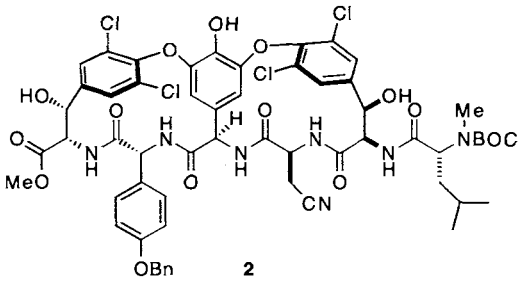

2

3, required harsh conditions (VOF_3, $BF_3 \cdot OEt_2$, TFA, TFAA, CH_2Cl_2, 0 °C, then Zn) that may not be suitable in the absence of chlorine blocking groups at both *ortho* positions of ring **C** in **3**.

Reduction of a single C–Cl bond to a C–H on a dichlorinated aromatic ring is a challenging transformation. When two such monosubstitutions must be made in a molecule containing two dichlorinated aryl rings in a complex molecular skeleton it is more difficult, and if the chlorine atoms on each ring are inequivalent due to atropisomerism,[4] the task is formidable. No further manipulations of **1** and **2** have been reported, implying that a synthetic stalemate has been reached. Strategies involving dichlorinated **C** and **E** rings may be stymied by the selective dehalogenation problem, and in that case a fresh approach is necessary.

Since 1993, relatively new competitors in the vancomycin synthesis arena have provided an impetus that may have sufficient momentum to bring about its total synthesis. Notably, a series of papers from Zhu and co-workers have focused on intramolecular nucleophilic aromatic substitution (S_NAr) reactions as a means to cyclize peptide-based compounds containing biaryl

[*] Prof. K. Burgess, D. Lim, C. I. Martinez
Department of Chemistry, Texas A & M University
College Station, TX 77843-3255 (USA)
Fax: Int. code +(409)845-8839
e-mail: burgess@chemvx.tamu.edu

[**] K. B. thanks The National Institutes of Health for an NIH Research Career Development Award, and The Alfred P. Sloan Foundation for a Fellowship. C. M. thanks The National Institutes of Health for a predoctoral fellowship. Abbreviations: TFA = trifluoroacetic acid, TFAA = trifluoroacetic anhydride, BOC = *tert*-butyloxycarbonyl.

 © VCH Verlagsgesellschaft mbH, D-69451 Weinheim, 1996 0570-0833/96/3510-1077 $ 15.00+.25/0

ether linkages. This approach is a notable improvement on Ullmann coupling procedures using aromatic compounds that are not activated to nucleophilic attack. The latter approach had been explored by Boger and co-workers,[5] but the extreme temperatures and prolonged reaction times preclude application of such classical Ullmann couplings in vancomycin syntheses.

The first efforts in this area by Zhu et al. included a synthesis of the 17-membered ring compound K-13 by biaryl ether formation as the ring closure step.[6] Since then, his group has used related reactions to prepare compound **4**, which has a 14-membered ring, then the 14,16 ring fused system **5** similar to that in teicoplanin (a natural product structurally related to vancomycin).[7–9] Model studies in the vancomycin series showed

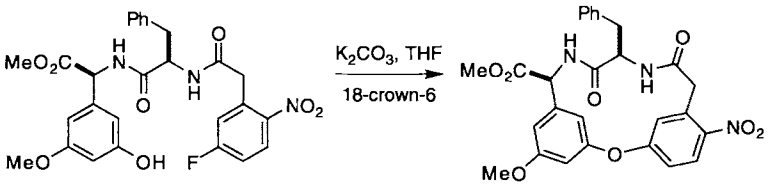

4 71 %

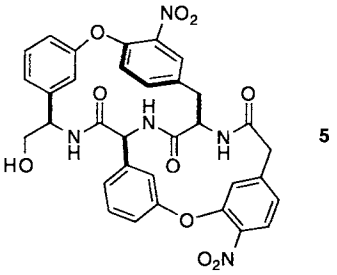

5

that 16-membered peptidic biaryl ethers also could be prepared,[4, 9] an observation that Rao et al. confirmed shortly thereafter.[10] These important studies proved that the ring closure would work even for 16-membered rings of the type found in vancomycin, which had been shown to be difficult to form by other conditions. Moreover, the research by Zhu et al. demonstrated that the cyclization could be performed with minimal racemization at an arylglycine residue within the incipient ring. Indeed, the conditions are sufficiently mild (e.g. K_2CO_3, DMF, 25 °C) that they should be suitable for more complicated substrates. The most recent publication from this group proved that this methodology could be applied to prepare a close analog of the vancomycin **C**-O-**D** ring.[11] Shortly after these studies were published, Boger et al. reported the same type of cyclization method to prepare building blocks for the **C**-O-**D** and **D**-O-**E** rings of vancomycin, compounds **6** and **7**, respectively.[12] The

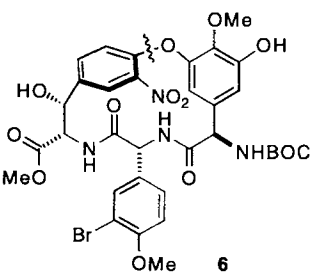

6

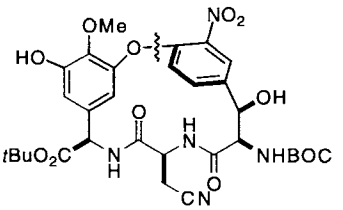

7

intermediate **6** discussed by Boger et al. is notable insofar as it has functionality appropriate for attempted formation of the vancomycin **AB** biaryl fragment.

A total synthesis of vancomycin has not yet been reported. Hurdles that remain include synthesis of the **AB** ring system in such a way that it could be incorporated into the extended product, and coupling of the carbohydrate residues to one of the phenolic oxygen atoms.[13] However, it does seem that the **C**-O-**D**-O-**E** rings of vancomycin, with appropriate chlorine substituents, soon could be synthesized by couplings based on nucleophilic aromatic substitution.

German version: *Angew. Chem.* **1996**, *108*, 1162–1163

Keywords: biaryl ethers · peptides · synthetic methods · total syntheses · vancomycin

[1] A. V. R. Rao, M. K. Gurjar, K. L. Reddy, A. S. Rao, *Chem. Rev.* **1995**, *95*, 2135–2167.
[2] D. A. Evans, C. J. Dinsmore, D. A. Evrard, K. M. DeVries, *J. Am. Chem. Soc.* **1993**, *115*, 6426–6427.
[3] D. A. Evans, J. A. Ellman, K. M. DeVries, *J. Am. Chem. Soc.* **1989**, *111*, 8912–8914.
[4] R. Beugelmans, G. P. Singh, M. Bois-Choussy, J. Chastanet, J. Zhu, *J. Org. Chem.* **1994**, *59*, 5535–5542.
[5] D. L. Boger, Y. Nomoto, B. R. Teegarden, *J. Org. Chem.* **1993**, *58*, 1425–1433.
[6] R. Beugelmans, A. Bigot, J. Zhu, *Tetrahedron Lett.* **1994**, *35*, 7391–7394.
[7] R. Beugelmans, S. Bourdet, J. Zhu, *Tetrahedron Lett.* **1995**, *36*, 1279–1282.
[8] J. Zhu, R. Beugelmans, S. Bourdet, J. Chastanet, G. Roussi, *J. Org. Chem.* **1995**, *60*, 6389–6396.
[9] R. Beugelmans, L. Neuville, M. Bois-Choussy, J. Zhu, *Tetrahedron Lett.* **1995**, *36*, 8787–8790.
[10] A. V. R. Rao, K. L. Reddy, A. S. Rao, *Tetrahedron Lett.* **1994**, *35*, 8465–8468.
[11] J. Zhu, J.-P. Bouillon, G. P. Singh, J. Chastanet, R. Beugelmans, *Tetrahedron Lett.* **1995**, *36*, 7081–7084.
[12] D. L. Boger, R. M. Borzilleri, S. Nukui, *Biorg. Med. Chem. Lett.* **1995**, *5*, 3091–3096.
[13] R. G. Dushin, S. J. Danishefsky, *J. Am. Chem. Soc.* **1992**, *114*, 3471–3475.

 © VCH Verlagsgesellschaft mbH, D-69451 Weinheim, 1996 0570-0833/96/3510-1078 $ 15.00+.25/0

Self-Organized Superlattices of Nanoparticles

Horst Weller*

During the last 50 years, scarcely any field of research in physical chemistry has developed as rapidly as that on nanostructured systems during the last decade. The reason for such avid research arises directly from the dimensions of the ultrasmall solids. With decreasing particle size the ratio of surface to volume increases to such an extent that finally the material properties are much more determined by the surface atoms than by the "classic" lattice atoms. Apart from such surface effects, semiconductors and metals show a drastic change of the electronic structure in the nanometer range, the so-called size-quantization effect, which results from the three-dimensional confinement of electrons and holes within the particles. From the point of view of solid-state physics, the nanoparticles, which are also called Q particles, nanoclusters, nanocrystallites, quantum dots, or artificial atoms, give an impressive example for the quantum mechanical model of a "particle in a three-dimensional box". The chemist may prefer the picture that the overlap of the numerous atomic orbitals in the particles already results in a great number of new states, whereas the energy bands of the macroscopic solid have not yet evolved. It is evident that the optical, catalytic, optoelectronic, magnetic, and electric properties of the particles differ considerably from those of the compact solids. The transition region from molecules to solids is today even described as a new state of matter.

Whereas the first ten years of research were characterized by the investigation of the size-dependent properties of the particles and—as a qualification and precondition for more and more precise measurements—by the development of better and better preparation and characterization methods for monodisperse samples, a new trend of research has recently been established with the aim of arranging individual particles in two- and three-dimensional superlattices and investigating the collective properties resulting from the interaction of the particles. Spectacular results similar to those achieved for the size variation of the isolated particles may be expected.

Ordered superlattices composed of micrometer-sized particles have been known in colloid chemistry for quite a long time; their formation is attributed to the so-called secondary minimum in the potential curves of the colloids. For nanoparticles, this secondary minimum is too small to determine the structure and therefore superlattices can only be formed when the particles are in direct contact through their ligand or stabilizer shells. Opals provide an impressive example for this: the silicon dioxide particles with diameters of about 100–500 nm of which they are composed, form a well-ordered superlattice which is, in fact, the reason for the fascinating interference colors of these precious stones. Up to now, there are only few examples for the crystallization of metal and semiconductor particles. First results have been achieved with iron oxide particles approximately 7 nm in size,[1] followed by investigations of two-dimensional precipitations of gold colloids on carrier foils for electron microscopy.[2–4] Ordered precipitations have also been found in ligand-stabilized Au_{55} and similar clusters.[5, 6] Even more remarkable are the results of a paper recently published by Bawendi et al.[7] who prepared a series of CdSe nanoparticles with diameters between 2 and 6 nm in ordered thin layers as well as in colloid crystals. In both cases crystallization was achieved by slowly removing one component of a solvent mixture, here octane/octanol, thus reducing the solubility of the particles. The alignment of the nanoparticles in a face centered cubic (fcc) superlattice is very clearly shown in high-resolution transmission electron microscope (TEM) images and is supported by X-ray powder diffraction patterns in the narrow- and wide-angle range. These reveal in an impressive way how, as expected, with decreasing particle diameters the superlattice reflections are shifted to higher 2θ values.

Furthermore the authors observed that the fluorescence bands of the crystallized CdSe particles exhibit a long wave length shift in comparison to those in diluted solutions in which the particles are widely separated from each other. In contrast the absorption spectra are identical in both samples. These results are considered to clearly indicate the particle–particle interaction in the superlattice. Similar spectroscopic results have been reported previously for CdS nanoclusters in superlattices.[8] It is certainly incontestable that the fluorescence shift is something to do with the surrounding particles; it remains, however, questionable whether this signifies the formation of collective electronic states, because the change of the ambient dielectric constant or reabsorption might also explain this phenomenon. Therefore further results are eagerly awaited.

The distance between the nanoparticles can be adjusted elegantly by choosing the ligands. This has already been shown for gold particles,[3] and Bawendi et al. have also demonstrated this with the powder diffraction patterns of 4.8 nm crystallites with tributylphosphane oxide, trioctyl phosphane oxide, and hexadecylphosphate as ligands. The distances between the particles change from 0.7 to 1.7 nm.

Unfortunately, Bawendi's nanocluster crystallites measure only few micrometers, so it has not yet been possible to exactly determine the atomic coordinates by single-crystal X-ray diffraction. Such single-crystal data have, however, recently been ascertained for CdS and Cu_2Te nanoclusters and similar compounds with sizes of approximately 1–4 nm. The crystallization and characterization of $[Cu_{146}Se_{73}(PPh)_{30}]$, one of the biggest clusters crystallized up to now, by Fenske et al.[9] is particularly worthy of mention. For semiconductor materials there have recently been remarkable publications on CdS nanoclusters. Following the pioneering work by Dance et al.[10] that led to the crystallization of $[N(CH_3)_4]_2[Cd_{17}S_4(SPh)_{28}]$, Herron et al.[11] succeeded in elucidating the structure of crystallized, electrically neutral $[Cd_{32}S_{14}(SPh)_{36}]\cdot 4DMF$ (DMF = dimethylformamide) nanoclusters, and Vossmeyer et al.[8, 12] reported the corresponding results with $[Cd_{17}S_4(SCH_2CH_2OH)_{26}]$ and $[Cd_{32}S_{14}(SCH_2CH(OH)CH_3)_{36}]\cdot 4H_2O$. All these clusters have a pyra-

[*] Prof. Dr. H. Weller
Institut für Physikalische Chemie der Universität
Bundesstrasse 45, D-20146 Hamburg (Germany)
Fax: Int code +(40)4123-3452

 © VCH Verlagsgesellschaft mbH, D-69451 Weinheim, 1996 0570-0833/96/3510-1079 $ 15.00+.25/0

midal structure, which is best described as a section of the macroscopic zinc blende lattice (Fig. 1). The superlattice structures, however, vary rather strongly. The corners of the neutral $[Cd_{17}S_4(SR)_{26}]$ clusters are covalently linked through sulfur bridges to give the superlattice, the structure of which is an

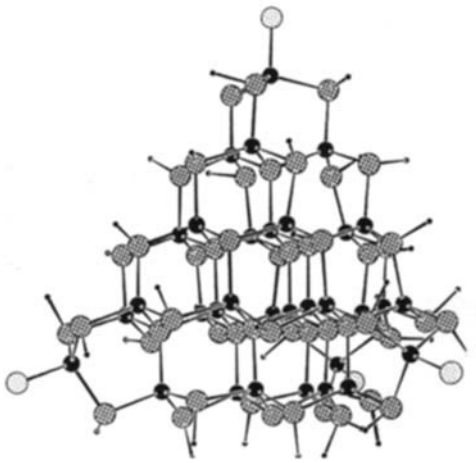

Fig. 1. Structure of the $Cd_{32}S_{14}(SR')_{36}$ nanocluster (● = Cd, ⊛ = S, ○ = H_2O or DMF) [12]. For the sake of clarity the ligands are only indicated. The $[Cd_{17}S_4(SR)_{26}]$ cluster has a very similar structure, the pyramid lacks only the lowest layer of Cd and S, and instead of solvent molecules there are bridging SR groups at the cluster corners. R′ = $CH_2CH(OH)CH_3$ or C_6H_5, R = CH_2CH_2OH.

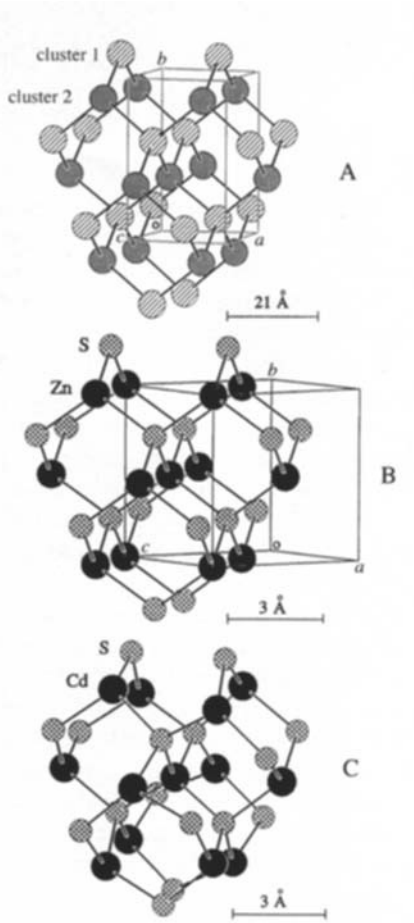

Fig. 2. Section of the $[Cd_{17}S_4(SR)_{26}]$ superlattice (A, each cluster is shown only as a point) and inner structure of the cluster (C); for comparison: zinc blende lattice (B) [8]. The similarity of cluster and superlattice is clearly recognizable. Cluster 1 and cluster 2 in part A of the figure are chemically equivalent, but X-ray crystallographically distinguishable.

enlargement of the inner crystal structure of the individual clusters (Fig. 2). The bigger $[Cd_{32}S_{14}(SR')_{36}]$ clusters form van der Waals type crystals; despite the identical cluster core the superlattices of the latter clusters are totally different. Whereas the thiophenol-stabilized cluster forms a densely packed primitive lattice, the thiopropanol-stabilized cluster forms a rhombohedral lattice in which the clusters build up a double layer structure interspersed with approximately 4 nm cavities filled with water. In addition the absorption bands of both clusters are shifted towards each other by approximately 30 nm in the optical spectra. Evidently, in this range of size the chemistry of the ligands is of importance for the electronic structure of the clusters as well as for their three-dimensional arrangement in the superlattice. Interestingly, the pyramidal structure of the $[Cd_{32}S_{14}(SX)_{36}]$ cluster also occurs in other compounds such as $[Hg_{32}Se_{14}(SePh_3)_{36}]$.[13]

There have been recent reports on a promising attempt at self-organized nanostructuring for gold particles by polymeric and colloidochemical processes. The crux of this method is to prepare the superlattices from colloid phases, here from block copolymer micelles, and to use the micelles as reaction vessel for the preparation of monodispere particles.[14–16] This attempt, that is the control of the synthesis of the particles by host–guest interaction, is not a novel approach, but compared with the present, mostly not very successful attempts, the block copolymer systems offer certain advantages: the polymer structures are sufficiently soft not to be destroyed when the particles are formed—a problem that occurs very often in crystalline inorganic host systems (e.g. zeolites). Furthermore, the block copolymer micelles are exchanged slowly enough to preserve the micelle structure while the particles are precipitated, which is a prerequisite for host–guest systems, but is unfortunately not the case in conventional soap micelles. Block lengths and functionalization of the blocks can be varied rather easily, which is extremely useful for optimizing the materials properties. Figure 3 shows a TEM image of precipitated micelles in the cores of which gold particles have subsequently been generated by reduction. The dense hexagonal packing of the micelles that preforms the resulting superlattice of the gold particles is clearly recognizable.

The examples given illustrate the wide range of variations to be expected when preparing ordered nanocluster materials. In-

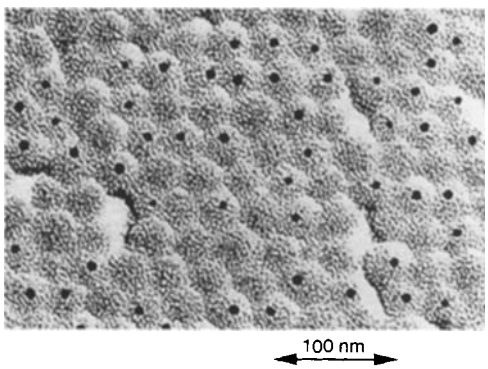

Fig. 3. TEM image of gold particles in polystyrene/poly-4-vinyl pyridine block copolymer micelles. The micelles were loaded with gold salts and precipitated on a carrier net. The reduction of the gold particles was achieved by electron beam; however, other reduction methods are possible [16] (reproduction by kind permission of M. Antonietti and E. Wenz).

cluding the possibility of combining nanoclusters of different size or composition in one superlattice (as can be seen in nature in the case of some opals), it becomes evident how large and varied this field will be in future materials research. It is fascinating to see that it is the self-ordering power of nature that permits the formation of such complex structures and thus at least some of the extremely costly equipment for nanostructuring used today could in future be replaced by the round flask and the beaker. The chemist may even dream of a new structural inorganic chemistry with nanocrystallites serving as building blocks like the atoms in molecular chemistry.[17]

German version: *Angew. Chem.* **1996**, *108*, 1159–1161

Keywords: clusters · colloids · nanoparticles · self-organization · superlattices

[1] M. D. Bentzon, J. van Wonterghem, S. Morup, A. Tholen, C. J. W. Koch, *Philos. Mag. B* **1989**, *60*, 169.
[2] U. Kreibig, K. Fauth, C.-G. Granqvist, G. Schid, *Z. Phys. Chem. (Neue Folge)* **1990**, *169*, 11.
[3] M. Giersig, P. Mulvaney, *J. Phys. Chem.* **1993**, *97*, 6334.
[4] M. Brust, D. Bethell, D. J. Schiffrin, C. J. Kiely, *Adv. Mater.* **1995**, *7*, 795.
[5] G. Schön, U. Simon, *Coll. Polym. Sci.* **1995**, *273*, 101.
[6] R. L. Whetten, J. T. Khoury, M. M. Alvarez, S. Murthy, I. Vezmar, Z. L. Wang, C. Cleveland, W. D. Luedtke, U. Lanzman, *Adv. Mater.* **1996**, *8*, in press.
[7] C. B. Murray, C. R. Kagan, M. G. Bawendi, *Science* **1995**, *270*, 1335.
[8] T. Vossmeyer, G. Reck, L. Katsikas, E. T. K. Haupt, B. Schulz, H. Weller, *Science* **1995**, *267*, 1476.
[9] H. Krautscheid, D. Fenske, G. Baum, M. Semmelmann, *Angew. Chem.* **1993**, *105*, 1363; *Angew. Chem. Int. Ed. Engl.* **1993**, *32*, 1303.
[10] G. S. H. Lee, D. C. Craig, I. Ma, M. L. Scudder, T. D. Bailey, I. G. Dance, *J. Am. Chem. Soc.* **1988**, *110*, 4863.
[11] N. Herron, J. C. Calabrese, W. E. Farneth, Y. Wang, *Science* **1993**, *259*, 1426.
[12] T. Vossmeyer, G. Reck, B. Schulz, L. Katsikas, H. Weller, *J. Am. Chem. Soc.* **1995**, *117*, 12881.
[13] D. Fenske, Karlsruhe, personal communication.
[14] M. Antonietti, E. Wenz, L. Bronstein, M. Seregina, *Adv. Mater.* **1995**, *7*, 1000.
[15] J. P. Spatz, A. Roescher, M. Möller, *Adv. Mater.* **1996**, *8*, 337.
[16] M. Antonietti, E. Wenz, personal communication.
[17] A. Müller, H. Reuter, S. Dillinger, *Angew. Chem.* **1995**, *107*, 2505; *Angew. Chem. Int. Ed. Engl.* **1995**, *34*, 2311.

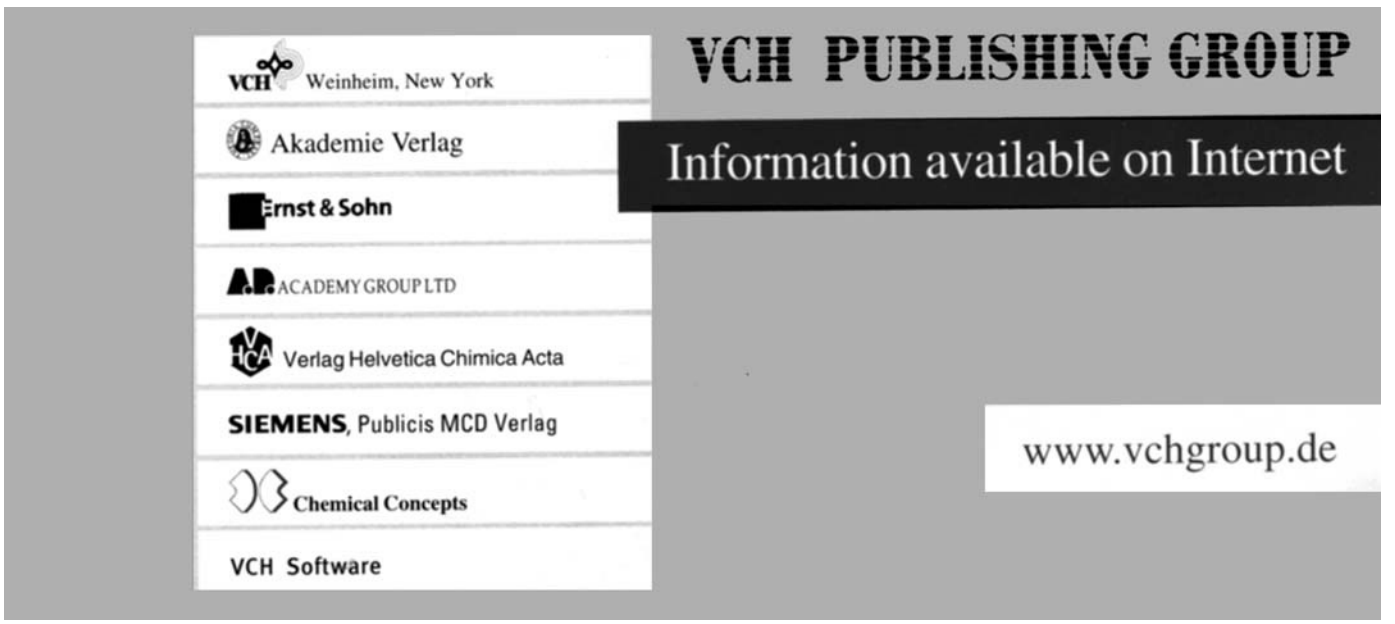

Symmetry-Based Metal Complex Cluster Formation**

Thomas Beissel, Ryan E. Powers, and
Kenneth N. Raymond*

There are examples of non-covalently linked molecular clusters in nature of stunning symmetry and beauty. Two are shown in Figure 1. The 24 individual protein subunits of apoferritin[1, 2] (the elipsoid-shaped subunits on the left of Fig. 1) cluster

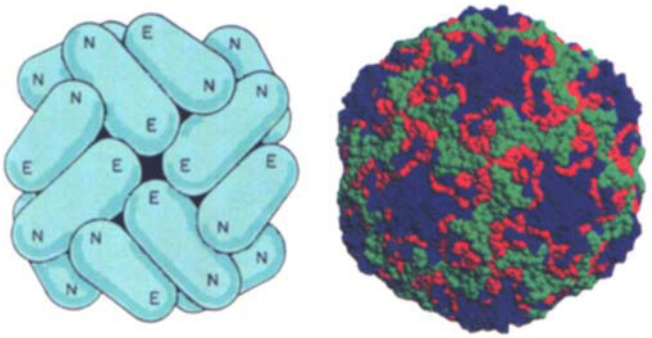

Fig. 1. Models of the apoferritin 24-mer (left) and human rhinovirus 60-mer (right). The view of ferritin is down one of the C_4 axes, the other two C_4 axes of the octahedral cluster are horizontal and vertical, respectively. Along the body diagonal (between three of the elipsoid ends marked N) lies the C_3 axis of the octahedral cluster. The view of the virus is down the C_3 axis, and the regions related by symmetry through the C_2 axis and the C_5 axis are shown in green and blue, respectively.

together to form only this polymeric assemblage (symmetry group O). The approximately spherical cavity can hold over 4000 iron atoms in the form of FeO(OH).[2] When the apoprotein is dissociated into the individual protein subunits and then allowed to reassemble only the highly symmetrical 24-mer of apoferritin forms. Something similar happens with many viruses, in which non-covalently linked protein clusters of virus coats are used to protect the viral nucleic acid. The protein cluster coat of the human rhinovirus (Fig. 1 right)[3] contains 60 protein subunits, which spontaneously assemble to give an icosahedron (symmetry group I). Once again, it is generally true that dissociation and reassembly of the protein coat does not give a random polymer assembly but instead only the highly symmetrical 60-mer.

What is it that leads to the high symmetry of such clusters? What is the relationship of this symmetry to the specificity seen in the formation of a single cluster type with unique cavity size and properties? In each case the individual molecular fragments (the protein subunits) are asymmetric units—the order of the pure rotation groups O and I are 24 and 60, respectively. Can this process be mimicked by using metal–ligand interactions as the driving force? This paper addresses these questions and shows that highly symmetrical clusters can be systematically designed by using the principles of symmetry-driven reactions deduced from natural structures.

In considering the interaction of molecular subunits to make supramolecular assemblages[4] a useful, if extreme, simplification is to consider each intermolecular interaction around the symmetry axis as a molecular lock and key interaction.[5, 6] Such interactions that require different symmetries are incommensurate—they require different stoichiometries at the site of interaction. A useful analogy can be made here with the interaction of incommensurate lattices (Fig. 2). As occurs with some natural

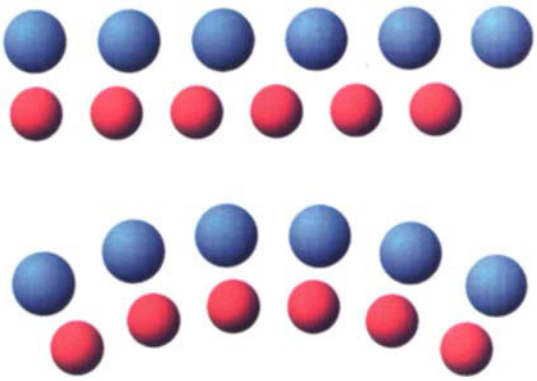

Fig. 2. Lattice 1 (blue) and 2 (red) shown shematically have incommensurate repeat distances (top). If stacked together the lattices must curl in order to remain in register (bottom).

silicates, the superposition of one layer upon another which has a slightly different lattice spacing soon results in a mismatch of the unit cells due to the incommensurate lattice spacings.[7] The two spacings can be kept in register only by curling them, as shown in Figure 2. Similarly, two incommensurate coordination numbers can coexist only by a curvature of the surface lattice of the molecular array.

Consider again the ferritin cluster and its octahedral symmetry. Interaction of the protein subunits at the fourfold axis can be considered as a lock and key interaction in which the lock and key are 90° apart (Fig. 3a). As shown in Figure 3a, this interaction is both a symmetry and stoichiometry requirement: the fourfold symmetry requires formation of tetramers from the monomeric subunit. Similarly the interaction of the protein subunits at the threefold axis can be regarded as a lock and key

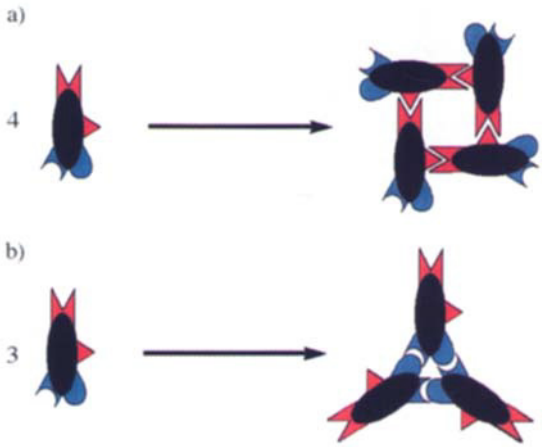

Fig. 3. a) Lock and key interactions that lead to a C_4 symmetric arrangement. b) The same repeating subunit as in a) can lead to a C_3 symmetric arrangement by using a different set of interactions.

[*] Prof. K. N. Raymond, Dr. T. Beissel, R. E. Powers
Department of Chemistry, University of California
Berkeley, CA 94720-1460 (USA)
Fax: Int. code + (510) 486-5283
e-mail: Raymond@garnet.berkeley.edu

[**] Coordination Number Incommensurate Cluster Formation, Part 1. This research was supported in part by the National Institutes of Health, Grant DK32999. T. B. thanks the Alexander von Humboldt-Stiftung for a Postdoctoral Fellowship. We thank Dr. Fred Hollander for his assistance with the structure determination.

interaction in which the lock and key are 60° apart (Fig. 3b). In this case the stoichiometry requirement is to form trimers. The simultaneous satisfaction of these two incommensurate symmetry requirements can only be satisfied by formation of a cluster with octahedral symmetry. In a similar fashion the icosahedral cluster is formed through the combination of incommensurate symmetry number lock and key interactions with fivefold and threefold symmetry, respectively.

The protein–protein interactions described above are formed from many weak interactions. Metal–ligand interactions, which are also highly directional, are much stronger and can be used, instead of many weaker interactions, to direct cluster formation driven by the metal–ligand coordinate bond. Helicates, dimers with molecular D_3 symmetry formed by two pseudo-octahedral metal centers and two bidentate ligands,[8–10] are recent examples of small supramolecular assemblages. The iron complex of the siderophore rhodotorulic acid, and a synthetic hydroxypyridonate analog, are early examples.[11–13] Other examples of spontaneous assembly of metal complex clusters in metal complexes are known,[14–16] however, they seem not to have been designed a priori. It is the goal of this research to *design* such systems, and we present here the most completely characterized of the three types of clusters that have now been prepared.

For simplicity, we begin with the simplest high symmetry polyhedron, the tetrahedron. The pure rotation group T is characterized by incommensurate threefold and twofold symmetry axes. Here the threefold symmetry is induced by using bidentate ligand groups to coordinate to an octahedral metal center. The ligand units are designed to have twofold symmetry, with two bidentate ligand groups, and must be as rigid as possible in order to predispose the coordinating groups to the desired geometry and to prevent geometries which allow a lower stoichiometry.

Hydroxamate ligands were chosen for their high stability and lability with trivalent metals,[17] which provides a strong driving force but also allows formation of the thermodynamically favored cluster over the large number of other intermediate polymers. Molecular modeling[18] was used to design the ligand isophthal-di-*N*-(4-methylphenyl)hydroxamic acid **1** (Scheme 1), which was synthesized by reaction of isophthaloyl dichloride (**A**) with *N*-(4-methylphenyl)hydroxylamine (**B**) (see Experimental Procedure). The reaction of **1** with $[Ga(acac)_3]$ in acetone led to a white microcrystalline precipitate of $[Ga_4L_6]$ (**3**). The dark red compound $[Fe_4L_6]$ **2** was formed in a similar reaction with $[Fe(acac)_3]$. FAB mass spectra and elemental analysis were consistent with the formulation as tetrahedral clustersin both cases.

The 300 MHz ^{1}H NMR spectrum of **3** in CD_2Cl_2 at room temperature shows only six signals, corresponding to the six inequivalent protons of the ligand. This establishes that all six ligands in the cluster are indistinguishable on the NMR time scale. Repeating the synthesis of **3** with excess **1** demonstrates the cooperativity of the cluster formation. The ^{1}H NMR spectrum shows two distinct sets of peaks at room temperature. One set corresponds to the six ligands in the tetrahedron, the other is from the unbound ligand—thus demonstrating no exchange on the NMR time scale.

The solid-state structure[19] of **3** contains two clusters, each of which lies on a special position with $\bar{4}$ symmetry (S_4 an alternative subgroup of the parent T_d group), in which the four metals are separated by an average of 9.0 Å. A space-filling representation of the structure is shown in Figure 4. Figure 5 gives stereo-

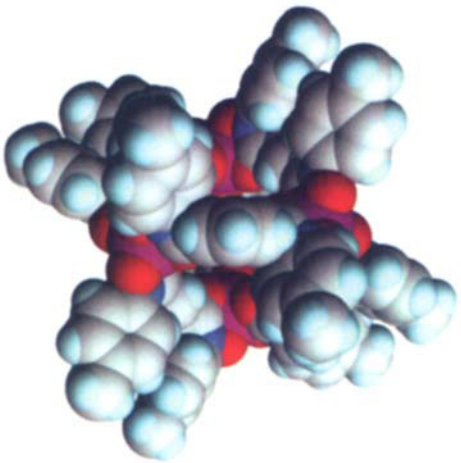

Fig. 4. A space-filling model of **3**, calculated from data from the X-ray structure analysis. View is down the S_4 axis.

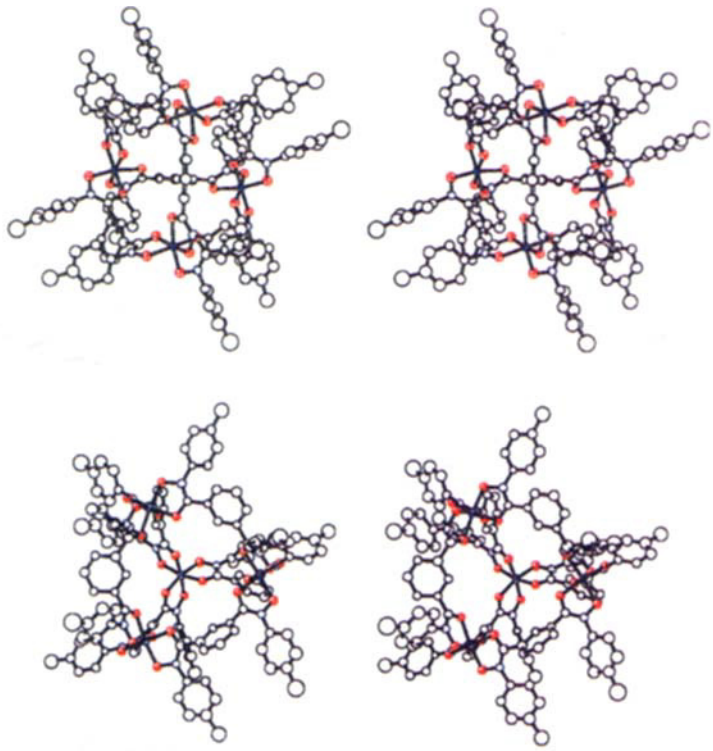

Fig. 5. Stereoviews of **3** looking down the S_4 axis (top) and the pseudo-C_3 axis (bottom).

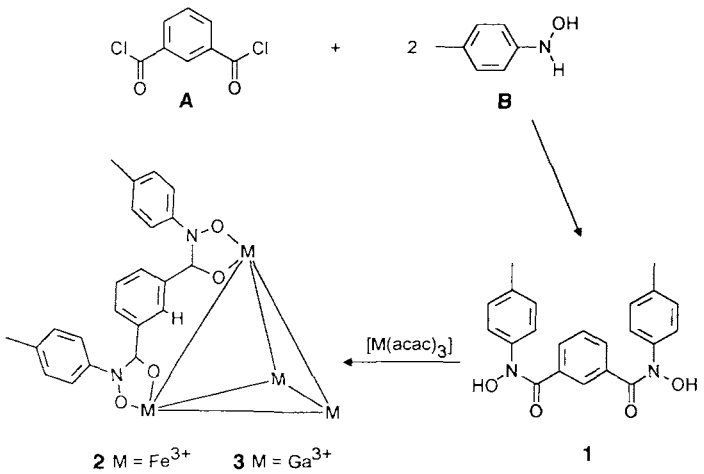

views of the cluster looking down the S_4 axis (top) and the pseudo-C_3 axis (bottom). Each cluster has four crystallographically identical DMF molecules which partially fill the rigid cavity (Fig. 6). The average carbon–carbon distance between the DMF methyl groups within the cluster cavity is 4.0 Å.

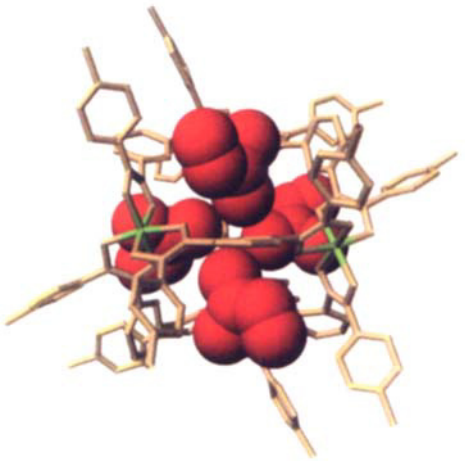

Fig. 6. Stick figure of **3** including a space-filling representation of the absorbed DMF molecules (red).

In summary, the spontaneous assembly of non-covalently linked subunits as seen in the protein clusters of ferritin or viral protein coats has been analyzed in terms of symmetry-driven interactions. The incommensurate coordination numbers for the different lock and key interactions explain the high symmetry (the pure rotation groups *O* and *I*, respectively) seen in these clusters. The unique formation of only one polymer and hence a unique cavity dimension is inextricably linked to the high symmetry. This analysis has been carried forward to the design of supramolecular assemblies based on coordination chemistry interactions. In the first demonstrated design, threefold symmetry at a pseudo-octahedral metal center with bidentate ligands is combined with a rigid ligand system of twofold symmetry to drive formation of a tetrahedral cluster. Both structure and solution experiments indicate that this cluster is the unique product. The success of this *predesigned, symmetry-driven system* supports the explanation of the formation of the highly symmetrical clusters seen in nature. This approach is readily extendible to higher symmetry and larger clusters, studies of which are currently in progress.

Experimental Procedure

1 = LH_2: Pyridine (4 mL, 50 mmol) was added to a solution of **B** (6.1 g, 50 mmol) in dioxane (40 mL). To the resulting mixture, a solution of **A** (5.0 g, 25 mmol) was added dropwise while the temperature of the reaction mixture was maintained below 15 °C. The mixture was then stirred for three hours. The solvents were removed by rotary evaporation and the solid residue was treated with concentrated NH_3/H_2O (100 mL). After the mixture had been stirred for one hour, the white precipitate that had formed was filtered off and then stirred with 0.1 M HCl, filtered, washed with H_2O, and dried. Yield 4.2 g (11 mmol).

B: 4-nitrotoluene (12.00 g, 87.5 mmol) was dissolved in a mixture of NH_4Cl (5.0 g, 93.5 mmol), H_2O (150 mL), and ethanol (150 mL). Zinc (17 g, 260 mmol) was added to the mixture in small portions while the temperature was kept below 10 °C by cooling with an ice/water bath. After the addition of zinc was complete the mixture was stirred for additional three hours and filtered. The precipitate was washed with ethanol, and the combined solvents were reduced by rotary evaporation. The resulting yellow solid was dissolved in diethyl ether, dried with $MgSO_4$, and the ether was removed by rotary evaporation. The yellow residue was washed with hexanes to yield a white, flaky product. Yield 7.3 g (59 mmol).

$[M_4L_6]$ (**2**, M = Fe^{III}, **3**, M = Ga^{III}): A solution of $[M(acac)_3]$ (125 mg, 0.35 mmol) in acetone was added to a solution of **1** (200 mg, 0.53 mmol) and two drops of triethylamine in acetone. The combined solutions were heated to reflux overnight during which time a red microcrystalline precipitate formed. The solid was collected by filtration, washed with a small amount of cold acetone and diethyl ether, and dried. Larger crystals were obtained when DMF was used as the solvent and instead of heating to reflux, the solutions were allowed to stand at ambient temperature for three to five days. Yield: 130 mg (0.05 mmol).

Received: February 19, 1996 [Z.8841IE]
German version: *Angew. Chem.* **1996**, *108*, 1166–1168

Keywords: clusters · lock and key principle · self-assembly

[1] S. H. Banyard, D. K. Stammers, P. M. Harrison, *Nature (London)* **1978**, *271*, 282.
[2] J. Trikha, E. Theil, N. M. Allewell, *J. Mol. Biol.* 1995, *248*, 949.
[3] E. Arnold, M. G. Rossmann, *Acta. Crystallogr. Sect. A.* **1988**, *44*, 270.
[4] J. M. Lehn in *Frontiers in Supramolecular Chemistry and Photochemistry* (Eds.: H. J. Schneider, H. Dürr) VCH, Weinheim, **1991**, pp 1-28.
[5] E. Fischer, *Ber. Dtsch. Chem. Ges.* **1894**, *27*, 2985; see also F. W. Lichtenthaler, *Angew. Chem.* **1994**, *106*, 2456; *Angew. Chem. Int. Ed. Engl.* **1994**, *33*, 2364.
[6] W. L. Jørgensen, *Science* **1991**, *254*, 954.
[7] E. J. W. Whittaker, *Acta Crystallogr.* **1956**, *9*, 855, 862, 865.
[8] M. Albrecht, S. Kotila, *Angew. Chem.* **1995**, *107*, 2285; *Angew. Chem. Int. Ed. Engl.* **1995**, *34*, 2134.
[9] E. C. Constable, *Tetrahedron* **1992**, *48*, 10013.
[10] E. J. Enemark, T. D. P. Stack, *Angew. Chem.* **1995**, *107*, 1082; *Angew. Chem. Int. Ed. Engl.* **1995**, *34*, 996.
[11] C. J. Carrano, S. R. Cooper, K. N. Raymond, *J. Am. Chem. Soc.* **1979**, *101*, 599.
[12] C. J. Carrano, K. Raymond, *J. Am. Chem. Soc.* **1978**, *100*, 5371.
[13] R. C. Scarrow, D. L. White, K. R. Raymond, *J. Am. Chem. Soc.* **1985**, *107*, 6540.
[14] A. J. Amoroso, J. C. Jeffery, P. L. Jones, J. A. McCleverty, P. Thornton, M. D. Ward, *Angew. Chem.* **1995**, *107*, 1577; *Angew. Chem. Int. Ed. Engl.* **1995**, *34*, 1443.
[15] P. Baxter, J.-M. Lehn, A. DeCian, J. Fischer, *Angew. Chem.* **1993**, *105*, 92; *Angew. Chem. Int. Ed. Engl.* **1993**, *32*, 68.
[16] R. W. Saalfrank, R. Burak, A. Breit, D. Stalke, R. Herbst-Irmer, J. Daub, M. Porsch, E. Bill, M. Müther, A. X. Trautwein, *Angew. Chem.* **1994**, *106*, 1697; *Angew. Chem. Int. Ed. Engl.* **1994**, *33*, 1621.
[17] G. Schwarzenbach, K. Schwarzenbach, *Helv. Chim. Acta* **1963**, *46*, 1390.
[18] CAChe version 3. 6.
[19] Compound **3** crystallizes in the tetragonal system, space group $I4_1/a$ (no. 88), with $a = b = 24.059(9)$, $c = 68.547(26)$ Å; $V = 39677$ Å^3, $Z = 8$, $\rho_{calcd} = 1.29\ g\,cm^{-3}$, $\lambda(Mo_{K\alpha}) = 0.710690$ Å. The structure was solved by direct methods and successive Fourier difference syntheses. The initial solution suggested twinning, which could be modeled most satisfactorily as a 76:24 orthogonal twin. The refinements by full-matrix least-squares gave an *R* factor of 0.115 and a weighted *R* factor (R_w) of 0.122 from 4186 reflections with intensity $I \geq 3\sigma(I)$ for 563 variables; linear absorption coefficient $\mu = 6.18$. The gallium atoms were refined anisotropically, all other non-hydrogen atoms were refined isotropically. Four solvent molecules were found in the asymmetric unit, two others were badly disordered. Crystallographic data (excluding structure factors) for the structure(s) reported in this paper have been deposited with the Cambridge Crystallographic Data Centre as supplementary publication no. CCDC-179-32. Copies of the data can be obtained free of charge on application to The Director, CCDC, 12 Union Road, Cambridge CB2 1EZ, UK (fax: Int. code +(1223) 336-033; e-mail: teched@chemcrys.cam.ac.uk).

Allylruthenium(IV) Complexes as Highly Efficient ROMP Catalysts**

Wolfgang A. Herrmann,* Wolfgang C. Schattenmann, Oskar Nuyken, and Stephan C. Glander

Quite early on, Dolgoplosk et al.[1, 2] recognized the suitability of diazoalkanes as initiators for the catalytic metathesis of olefins. Alkylidene metal complexes prepared from diazoalkanes follow the structural concept developed for olefin metathesis catalysts and have been employed successfully as "tailored" molybdenum and tungsten catalysts.[2-4] Nevertheless, there is continued demand for inexpensive, easy-to-handle catalyst systems. Recently, ruthenium(II) complexes have been preferred for the ring-opening metathesis polymerization.[5] Herein we report for the first time a series of easily prepared and exceptionally active ROMP catalysts of tetravalent ruthenium.

The allylruthenium(IV) precursor complex **1** is obtained from isoprene and commercially available ruthenium(III) chloride.[6] Addition of silver tetrafluoroborate to **1** results in the formation of the cationic complexes **2** and **3**.[7] All of these complexes are

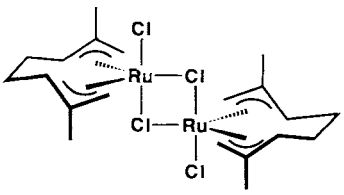

1

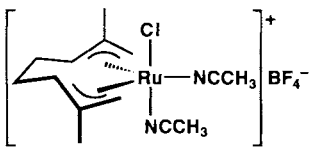

2

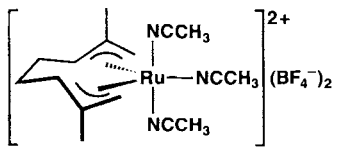

3

stable in air and in solution for several hours; however, due to their ionic character and the resulting solubility in polar solvents, complexes **2** and **3** are suitable for the precipitation polymerization of norbornene.

Complexes **1**–**3** alone are almost completely ROMP-inactive. However, in the presence of aliphatic diazo compounds, for example commercially available ethyl diazoacetate, these complexes show unusual catalytic activity, with the very short reaction times being particularly noteworthy (Table 1). Polymerization experiments performed at a higher monomer-to-catalyst ratio showed that the activity remains high even over extended reaction times.

With catalyst **3** in the presence of ethyl diazoacetate, turnover frequencies (TOF) above $10^5\ h^{-1}$ have been achieved (Table 2). This unoptimized system exhibits activities not previously attained in the ring-opening metathesis polymerization employing ruthenium catalysts.[5] An important advantage of these novel

[*] Prof. Dr. W. A. Herrmann, W. C. Schattenmann
Anorganisch-chemisches Institut der Technischen Universität München
Lichtenbergstrasse 4, D-85747 Garching (Germany)
Fax: Int. code +(89)32093473
Prof. Dr. O. Nuyken, S. C. Glander
Lehrstuhl für Makromolekulare Stoffe der Technischen Universität München
Lichtenbergstrasse 4, D-85747 Garching (Germany)

[**] This work was supported by the Bayerische Forschungsverbund Katalyse (FORKAT).

Table 1. ROMP of norbornene in the presence and absence of ethyl diazoacetate (norbornene/ruthenium = 1000/1; ethyl diazoacetate/ruthenium = 2/1 in 5 mL of MeOH and 15 mL of CH_2Cl_2).

Complex	Diazo cmpd.	Yield [%] [a]	t	TOF [b]	σ_c [%] [c]
1	$N_2{=}CHCO_2Et$	19	5 min	2280	34
1	–	<1	5 min	–	–
1	–	13	21 h	11	33
2	$N_2{=}CHCO_2Et$	8	2.5 min	1920	24
2	–	4	10 h	4	24
3	$N_2{=}CHCO_2Et$	50	30 s	60000	31
3	$N_2{=}CHCO_2Et$	99	2.5 min	24000	31
3 [d]	$N_2{=}CHCO_2Et$	30	2 min	90000	31
3 [d]	$N_2{=}CHCO_2Et$	70	8 min	52500	32
3	–	69	4 h	173	33

[a] Yield relative to isolated polymer. [b] TOF = turnover frequency: mol(polynorbornene)/[mol(catalyst) × h]. [c] σ_c: Percentage of *cis* double bonds in the polymer (as determined from the ^1H NMR signal intensities of the olefinic protons). [d] Norbornene/ruthenium = 10000/1.

Table 2. Influence of solvent composition on the ring-opening metathesis polymerization of norbornene in the presence of ethyl diazoacetate (norbornene/ruthenium = 1000/1; ethyl diazoacetate/ruthenium = 2/1).

Complex	MeOH/ CH_2Cl_2	Yield [%] [a]	t	TOF [b]	$\bar{M}_n$ [c]	PDI [d]	σ_c [%] [e]
3	1/3	50	30 s	0.6×10^5	910×10^3	1.5	31
3	1/1	91	30 s	1.0×10^5	610×10^3	1.7	34
3	6/1	99	30 s	1.2×10^5	380×10^3	1.8	31

[a] Yield relative to isolated polymer. [b] TOF = turnover frequency: mol(polynorbornene)/[mol(catalyst) × h]. [c] $\bar{M}_n$: (number average molecular weight) [g mol^{-1}]. [d] PDI: polydispersity index $\bar{M}_w/\bar{M}_n$. [e] Percentage of *cis* double bonds in the polymer (as determined from the ^1H NMR signal intensities of the olefinic protons).

systems is that the degree of polymerization can be controlled by the choice of solvent. Furthermore, the experimental requirements are easily met: the polymerization can be carried out in air and with ordinary, not strictly anhydrous solvents—unacceptable conditions for most tungsten, molybdenum, and rhenium catalysts.

Similarly, the precise structure of the diazoalkane can also be utilized to control the polymerization. Thus, trimethylsilyldiazomethane develops its full activating power only at molar ratios >1/1 (diazoalkane/ruthenium), whereas the use of ethyl diazoacetate leads to an activity maximum at molar ratios <1/1 (Fig. 1). Possibly a metal carbene intermediate is formed which is stabilized through chelating by the carbonyl groups.[8]

The most active catalyst system to date comprises **3** and ethyl diazoacetate. The ring-opening metathesis polymerization of *endo*-dicyclopentadiene (TOF = 1000 h^{-1}) was accomplished

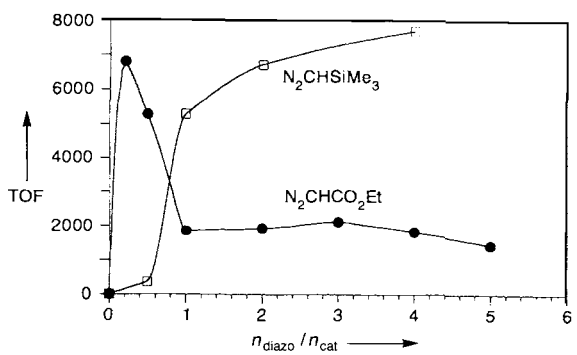

Fig. 1. Dependency of catalyst activity on the ratio diazoalkane/catalyst. TOF = mol(polynorbornene)/[mol(catalyst) × h].

 © VCH Verlagsgesellschaft mbH, D-69451 Weinheim, 1996 0570-0833/96/3510-1087 $ 15.00+.25/0

for the first time.[9] The polymerization of cyclooctene with this system resulted in the formation polymers of low molecular weight, whose ethyl ester end-groups could be identified by NMR spectroscopy. The agreement of the molecular weights determined from ^{1}H NMR spectra and GPC data ($\bar{M}_n$ = 30000; PDI = 1.4) proves the presence of a polyoctenamer with defined end-groups, in other words, a telechelic polymer. This supports the notion that the ruthenium complex and diazoalkane initially form a carbene complex that then initiates the polymerization.

Experimental Procedure

In a typical polymerization experiment norbornene (1.50 g, 16 mmol) was dissolved in solvent (12 mL; CH_2Cl_2 or CH_2Cl_2/MeOH). Next, a 10^{-2} M solution (3.2 mL) of diazo compound in CH_2Cl_2 was added. To this mixture was rapidly added a solution of 1.6×10^{-2} mmol of ruthenium complex **2** or **3** in methanol (5 mL) (or 0.8×10^{-2} mmol **1** in 5 mL of CH_2Cl_2). The precipitating polymer was separated from the solution and washed with methanol. At this stage the polymer is usually sufficiently pure. Further purification can be accomplished by dissolving the product in toluene followed by reprecipitation in methanol. The polymer was dried at room temperature under high vacuum (oil pump) until no further change in weight was observed. The yield was determined gravimetrically. The molecular weight distribution was determined by GPC ($CHCl_3$) with polystyrene as standard.

Received: December 8, 1995 [Z 8622 IE]
German version: *Angew. Chem.* **1996**, *108*, 1169–1170

Keywords: diazoalkanes · catalysis · metathesis · polymerizations · ruthenium compounds

[1] a) B. A. Dolgoplosk, K. L. Makovetskii, E. I. Tyniakova, *Dokl. Akad. Nauk. SSSR Ser. Fiz. Khim.* **1972**, *202*, 95; *Dokl. Phys. Chem.* **1972**, *202*, 95; b) B. A. Dolgoplosk, K. L. Makovetskii, T. G. Golenko, *Eur. Polym. J.* **1974**, *10*, 901.
[2] D. S. Breslow, *Prog. Polym. Sci.* **1993**, *18*, 1141.
[3] W. A. Herrmann, *Angew. Chem.* **1978**, *90*, 855; *Angew. Chem. Int. Ed. Engl.* **1978**, *17*, 800.
[4] *Applied Homogeneous Catalysis with Organometallic Compounds* (Eds.: B. Cornils, W. A. Herrmann), VCH, Weinheim, **1996**, in press.
[5] a) A. Stumpf, E. Saive, A. Demonceau, A. Noels, *J. Chem. Soc. Chem. Commun.* **1995**, 1127; b) P. Schwab, M. B. France, J. W. Ziller, R. H. Grubbs, *Angew. Chem.* **1995**, *107*, 2179; *Angew. Chem. Int. Ed. Engl.* **1995**, *34*, 2039.
[6] a) L. Porri, M. C. Gallazzi, A. Colombo, G. Allegra, *Tetrahedron Lett.* **1965**, *47*, 4187; b) D. N. Cox, R. Roulet, *Inorg. Chem.* **1990**, *29*, 1360.
[7] a) D. N. Cox, R. W. H. Small, R. Roulet, *J. Chem. Soc. Dalton Trans.* **1991**, 2013; b) D. N. Cox, R. Roulet, *J. Chem. Soc. Chem. Commun.* **1988**, 951.
[8] a) M. L. Ziegler, K. Weidenhammer, W. A. Herrmann, *Angew. Chem.* **1977**, *89*, 557; *Angew. Chem. Int. Ed. Engl.* **1977**, *16*, 555; b) W. A. Herrmann, I. Steffl, M. L. Ziegler, K. Weidenhammer, *Chem. Ber.* **1979**, *122*, 1731.
[9] Online literature search in database KKF (Kunstoffe, Kautschuk, Fasern), 1955 through November 1, 1995.

Polymeric Networks of Silver(I) and Copper(I) Ions Linked by an Anionic Acetonyl Derivative of Tetracyanoethylene

Lucia Carlucci, Gianfranco Ciani,*
Davide M. Proserpio, and Angelo Sironi

Many reactions of tetracyanoethylene (TCNE) with metal compounds have been studied in the last few decades,[1] principally because of its ability to form charge-transfer derivatives[2] that are potential conductors and show interesting magnetic properties. The different bonding modes and variable hapticity of TCNE are also of significance for the formation of polymeric networks. Some one-dimensional (1D) coordination polymers with neutral TCNE,[3] and one remarkable two-dimensional (2D) frame, have been described.[4]

We are currently studying the self-assembly of Ag^I cations and polydentate neutral N-donor ligands, and have already reported on interesting 2D and 3D networks, including frames topologically related to the prototypal structures of diamond,[5] α-$ThSi_2$,[6] α-polonium,[7] and $SrSi_2$.[8] The reaction of the potentially tetradentate TCNE with $Ag(CF_3SO_3)$ in H_2O/Me_2CO led to coordination polymer **2**, which unexpectedly contains the anionic acetonyl derivative of TCNE 1,1,2,2-tetracyanopentan-4-one-1-ide, ($AcTCNE^-$; **1**) as ligand. Also in analogous reactions with different silver salts of noncoordinating anions and different solvent systems, no TCNE-containing products were obtained. We report here on **2**, which contains a twofold interpenetrated 2D extended network and on the related Cu^I species **3**, which was

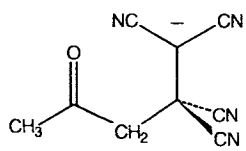

1

[Ag(AcTCNE)] **2**

[Cu(AcTCNE)]·Me_2CO **3**

obtained by reacting $[Cu(MeCN)_4](PF_6)$ with the preformed conjugated acid of **1** (**1**H). Compound **3** exhibits a 3D open zeolite-like framework that belongs to a novel topological type in coordination polymer chemistry.

A complex reaction occurs when a solution of TCNE in acetone is layered over a solution of $Ag(CF_3SO_3)$ in water (molar ratio 1:1). Initially a white powdered material, essentially consisting of AgCN, is precipited (formation of cyanides was reported for other reactions involving TCNE and transition metals[11]). If the reaction solution was left in the dark for a few days, the supernatant solution turned deep orange and elongated pale yellow crystals of **2** formed above the white precipitate.[9] These crystals, which showed IR bands due to the CN and CO stretches of **1**, were suitable for a single-crystal X-ray analysis (see Fig. 1).[11] The synthesis repeatedly gave the same product. However, a fundamental role seems to be played both by the solvent system and by the triflate counterion; attempts to obtain **2** by using other silver salts of noncoordinating anions were unsuccessful.

The structure of **2** consists of 2D infinite undulated nets of hexagonal meshes. These are formed by alternate three-coordinate silver ions and tridentate **1**. Two independent nets of this type interpenetrate to give a layer structure (Fig. 1). The anions

[*] Prof. G. Ciani, Dr. L. Carlucci, Dr. D. M. Proserpio, Prof. A. Sironi
Dipartimento di Chimica Strutturale e Stereochimica Inorganica
and Centro CNR
Via G. Venezian 21, I-20133 Milano (Italy)
Fax: Int. code +(2)70635288

 © VCH Verlagsgesellschaft mbH, D-69451 Weinheim, 1996 0570-0833/96/3510-1088 $ 15.00+.25/0

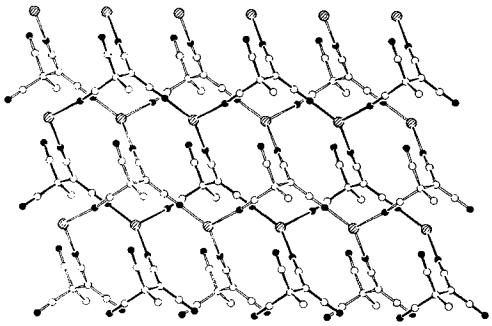

Fig. 1. The twofold interpenetrated layer of **2** (SCHAKAL representation). Only the first carbon atom of the acetonyl groups is shown for clarity. Large hatched circles: Ag; black circles: N; open circles: C.

1 employ the two CN groups bound to the sp^2 hybridized C atom and one CN bound to the sp^3 hybridized C atom for bridging. The Ag^I ions display a distorted trigonal coordination, and show two short Ag–N bonds to the N atoms of the two $C(sp^2)$ nitrile groups (2.114(4) and 2.117(4) Å) and a long one to the N atom of the $C(sp^3)$ nitrile group (2.422(4) Å). The N-Ag-N angles are 146.2(2), 108.1(2), and 105.7(2)°.

The structural type of **2** is rather rare in coordination chemistry. Four classes of interpenetrating 2D networks are presently known, the differences depending on the type of meshes [hexagonal (*h*) or square (*s*)] and on whether the interpenetration occurs in a common plane (type I) or in a mutually perpendicular direction (type II), which results in a 3D array. Complex **2** belongs to class I-*h*, the only previously known compounds of this class are $[AgC(CN)_3]$ (twofold interpenetrated)[12] and a Cd^{II} polymer exhibiting threefold interpenetration described very recently.[13] Very few examples for each of the other classes (I-*s*,[14] II-*h*,[15] and II-*s*[16]) have been reported.

With the aim of accomplishing a more direct and clean synthesis of **2**, we prepared the conjugated acid of **1**, **1**-H, by literature methods.[10] Unfortunately only mixtures that proved difficult to analyze were obtained on reacting **1**-H with a number of silver salts of noncoordinating anions.[17] In contrast, the reaction of $[Cu(MeCN)_4](PF_6)$ with **1**-H in acetone afforded colorless, octahedral crystals of a novel copper(I) 3D polymer **3** that contains **1** as bridging ligand.[18]

The structure of **3** (Fig. 2) consists of a 3D neutral network of four-coordinate copper(I) ions linked by anions **1**. Unlike in **2**, these anions act as tetradentate ligands. The framework resembles a honeycomb with large channels (hexagonal cross-section) extending in the *c* direction. These contain guest acetone molecules. The copper centers reside in distorted tetrahedral environments; the Cu–N bonds and N-Cu-N angles lie in the range 1.938(5)–2.034(5) Å and 103.6(2)–114.3(2)°, respectively. The ability of **1** to coordinate to four metal centers, each attaining an almost tetrahedral geometry, is related to the possibility of free rotation about the $C(sp^2)-C(sp^3)$ bond and to the intrinsic geometry of $C(sp^3)$. Thus, the two planes $C(CN)_2$ are arranged almost perpendicular (dihedral angle of 89.8(2)° in **3** and 82.7(2)° in **2**), and the four CN groups can be considered to be distorted-tetrahedrally oriented (see below).[19]

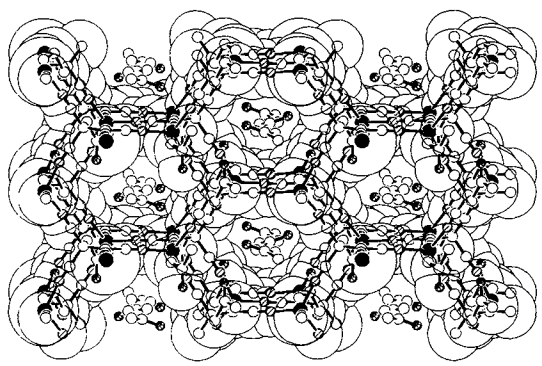

Fig. 2. The structure of **3** (SCHAKAL representation) approximately down the *c* axis. The channels contain acetone molecules. Large black circles: Cu; hatched circles: N; open circles: C; cross-hatched circles: O.

The novel 3D network consists of four-connected (copper atoms) and three-connected (carbon atoms) nodes in the ratio 1:2. However, a more useful topological interpretation can be achieved by replacing the tetradentate anions with their centers (the midpoint of the $C(sp^2)-C(sp^3)$ vector) and connecting them with the copper ions. The resulting fascinating four-connected frame (Fig. 3) belongs to a rare topological type; the shortest circuits starting and ending at each center form squares, hexagons, and octagons in the ratio 2:3:1, hence $4^2 6^3 8$ (specifically net $4^2 6^3 8$-a, according to Wells).[20] Smith, in classifying the framework silicates,[21] cites $(NH_4)LiSO_4$,[22] $RbAlSiO_4$,[23] and the synthetic zeolite Li–A(BW)[24] as examples belonging to this topological type. The prototypal zeolite-like network of **3** may be of interest because of its large channels with an average radius of approximately 4.7 Å, and further studies are in progress to ascertain the possibility of removing or replacing the solvated acetone molecules.

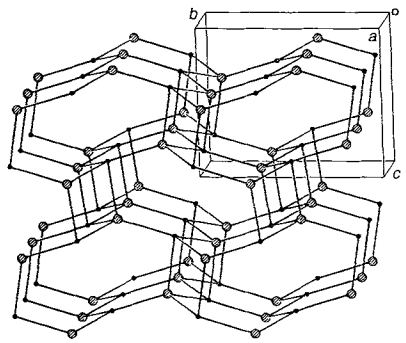

Fig. 3. Schematic view (SCHAKAL representation) of the $4^2 6^3 8$-a network of **3** (large hatched circles: Cu; small black circles: midpoints (C_A) of the $C(sp^2)-C(sp^3)$ bonds of the $AcTCNE^-$ ligands). $\bar{d}(Cu-C_A)$ 4.90(4) Å; C_A-Cu-C_A angle 97–125°; Cu-C_A-Cu angle 80–136°.

The large difference between the structures of the frames in **2** and **3**, in spite of the same stoichiometry, can be related to the higher tendency of Cu^I ions over Ag^I ions to achieve a tetrahedral coordination.

In conclusion, the attempts to obtain novel extended frameworks bridged by the neutral TCNE ligand were unsuccessful. The high reactivity of TCNE, however, led to the unexpected formation of **1**, which exhibits a pronounced tendency to form networks with metal ions. The targeted synthesis of **1** has enabled the preparation of **3**. It is anticipated that this methodology can be extended to other systems with different metal ions and/or with similar polycyano anions.

Experimental Procedure

2: A solution of TCNE (0.130 g, 1.01 mmol) in acetone (3 mL) was layered over a solution of $Ag(CF_3SO_3)$ (0.252 g, 0.98 mmol) in H_2O (3 mL). A white precipitate of AgCN formed immediately. If the solution was left in the dark for 4–5 days, pale yellow elongated crystals of **2** formed above the white precipitate. The mixture was filtered, dried in air, and crystals of **2** were manually separated under a microscope

(yield ca. 15%). The product is air and light stable. A few colorless crystals of **4** were separated successfully from the deep orange mother liquor [9]. Elemental analysis: $C_9H_5AgN_4O$, calcd: C 36.88, H 1.72, N 19.12; found: C 36.10, H 1.83, N 18.84. IR (Nujol): $\tilde{\nu}$(CN) 2251 (w), 2220 (m), 2153 (s), 2127 (s), $\tilde{\nu}$(CO) 1707 (m) cm^{-1}.

3: A solution of TCNE in acetone, acidified with dilute aqueous HCl, was stirred for 24 h. The product (**1**-H), isolated after evaporation of the solution to dryness, was used without further purification. A solution of **1**-H (0.0332 g, 0.178 mmol) in acetone (2 mL) was layered over a solution of $[Cu(MeCN)_4](PF_6)$ (0.0664 g, 0.178 mmol) in acetone (3 mL) under a nitrogen atmosphere in a Schlenk tube. If the reaction mixture was left to stand for a few days, small multifaced colorless crystals of **3** formed. They were filtered off and dried (yield ca. 80%). The product is air stable for days. Elemental analysis: $C_{12}H_{11}CuN_4O_2$, calcd. 46.98, H 3.61, N 18.27; found C 45.95, H 3.40, N 17.95. IR (Nujol): $\tilde{\nu}$(CN) 2258 (vw), 2213 (m), 2162 (s), $\tilde{\nu}$(CO) 1724 (m), 1701 (s) cm^{-1}.

Received: December 8, 1995 [Z8624 IE]
German version: *Angew. Chem.* **1996**, *108*, 1170–1172

Keywords: complexes with nitrogen ligands · coordination polymers · copper compounds · silver compounds · tetracyanoethylene

[1] M. M. Olmstead, G. Speier, L. Szabo, *J. Chem. Soc. Chem. Commun.* **1994**, 541, and references therein.

[2] a) J. S. Miller, J. C. Calabrese, R. W. McLean, A. J. Epstein, *Adv. Mater.* **1992**, *4*, 498; b) V. J. Murphy, D. O'Hare, *Inorg. Chem.* **1994**, *33*, 1833, and references therein.

[3] a) A. G. Bunn, P. J. Carroll, B. B. Wayland, *Inorg. Chem.* **1992**, *31*, 1297, and references therein; b) F. A. Cotton, Y. Kim, J. Lu, *Inorg. Chim. Acta.* **1994**, *221*, 1.

[4] F. A. Cotton, Y. Kim, *J. Am. Chem. Soc.* **1993**, *115*, 8511.

[5] L. Carlucci, G. Ciani, D. M. Proserpio, A. Sironi, *J. Chem. Soc. Chem. Commun.* **1994**, 2755.

[6] L. Carlucci, G. Ciani, D. M. Proserpio, A. Sironi, *J. Am. Chem. Soc.* **1995**, *117*, 4562.

[7] L. Carlucci, G. Ciani, D. M. Proserpio, A. Sironi, *Angew. Chem.* **1995**, *107*, 2045; *Angew. Chem. Int. Ed. Engl.*, **1995**, *34*, 1895.

[8] L. Carlucci, G. Ciani, D. M. Proserpio, A. Sironi, *J. Am. Chem. Soc.* **1995**, *117*, 12861.

[9] The formation of **1** is somewhat surprising since the addition of acetone (or other ketones) to TCNE, to give the conjugated acid **1**H, is slow and was previously accomplished in the presence of catalysts like HCl, BF_3, or "molecular silver" [10]. The complexity of the overall process is, moreover, confirmed by the further reactions of **1**: we have observed the formation of some small platelike colorless crystals of the novel heterocyclic compound, 6-methyl-2(1H)-pyridone-3,4-dicarboxamide monohydrate (**4**) from the mother liquor. We have characterized **4** by a single-crystal X-ray analysis (see [25]). The formation of **4** from **1** presumably occurs by elimination of one equivalent of CN^- as AgCN and partial hydrolysis of the three remaining nitrile groups to amide groups, followed by ring closure by an internal oxime bond and migration of hydrogen.

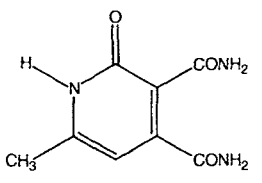

4

[10] W. J. Middleton, R. E. Heckert, E. L. Little, C. G. Krespan, *J. Am. Chem. Soc.* **1958**, *80*, 2783.

[11] A single crystal of **2** was mounted under a coating of cyanoacrylic glue on an Enraf-Nonius CAD-4 diffractometer. Crystal data: monoclinic, *Cc* (no. 9), $a = 6.270(1)$, $b = 19.664(2)$, $c = 8.476(2)$ Å, $\beta = 98.91(1)^\circ$, $V = 1032.4(3)$ Å^3, $Z = 4$, $\rho_{calcd} = 1.885$ Mg m^{-3}, $Mo_{K\alpha}$ radiation ($\lambda = 0.71069$ Å). The data collection was performed at 293 K on an Enraf-Nonius CAD4 diffractometer by the ω scan method, within the limits $3 < \theta < 27^\circ$. The structure was solved by direct methods (SIR92) and refined by full-matrix least-squares against F_o^2 (SHELX93). The final agreement index R was 0.0212 for the correct structure enantiomorph, based on 1034 independent significant $[F_o > 2\sigma(F_o)]$ absorption corrected data. Anisotropic thermal factors were assigned to all the non-hydrogen atoms [25].

[12] J. Konnert, D. Britton, *Inorg. Chem.* **1966**, *5*, 1193.

[13] M. Fujita, Y. J. Kwon, O. Sasaki, K. Yamaguchi, K. Ogura, *J. Am. Chem. Soc.* **1995**, *117*, 7287.

[14] a) T. Soma, T. Iwamoto, *Chem. Lett.* **1994**, 821; b) D. M. L. Goodgame, S. Menzer, A. M. Smith, D. J. Williams, *Angew. Chem.* **1995**, *107*, 605; *Angew. Chem. Int. Ed. Engl.* **1995**, *34*, 574.

[15] a) L. R. McGillivray, S. Subramanian, M. J. Zaworotko, *J. Chem. Soc. Chem. Commun.* **1994**, 1325; b) O. M. Yaghi, G. Li, *Angew. Chem.* **1995**, *107*, 232; *Angew. Chem. Int. Ed. Engl.* **1995**, *34*, 207 c) a similar structural motif is also present in a Mn^{II}/Cu^{II} polymer, but with cross-linking of the perpendicular 2D layers: H. O. Stumpf, L. Quahab, Y. Pei, D. Grandjean, O. Kahn, *Science* **1993**, *261*, 447.

[16] a) R. W. Gable, B. F. Hoskins, R. Robson, *J. Chem. Soc. Chem. Commun.* **1990**, 1677; b) T. Soma, T. Iwamoto, *Chem. Lett.* **1995**, 271.

[17] The reaction of **1**H with $Ag(CF_3SO_3)$ in H_2O/Me_2CO afforded a dark-brown microcrystalline mixture containing some crystals of **4** [9].

[18] Crystal data for **3**. The crystals are monoclinic, space group $P2_1/c$ (no. 14), $a = 7.314(2)$, $b = 15.332(4)$, $c = 12.758(3)$ Å, $\beta = 94.50(2)^\circ$, $V = 1426.2(6)$ Å^3, $Z = 4$, $\rho_{calcd} = 1.429$ Mg m^{-3}. The data collection was performed within the limits $3 < \theta < 25^\circ$. The other experimental details are as for **2**. The final agreement index R was 0.0481 for 1523 independent significant $[F_o > 2\sigma(F_o)]$ absorption corrected data. Anisotropic thermal factors were assigned to all the non-hydrogen atoms [25].

[19] The bond parameters for the anion **1**, in both compounds **2** and **3**, are as expected, with mean bond lengths for $C(sp^2)-C(sp^3)$, $C(sp^2)-C(CN)$, and $C(sp^3)-C(CN)$ of 1.525, 1.384, and 1.489 Å, respectively. Note that as a consequence of the incomplete coordination the $C(sp^3)$ atom in **2** is chiral.

[20] A. F. Wells, *Further studies of Three-dimensional Nets*, ACA Monograph No.8, **1979**; this array is Net 8 in: A. F. Wells, *Three-dimensional Nets and Polyhedra*, Wiley, New York, **1977**.

[21] J. V. Smith, *Am. Mineral.* **1977**, *62*, 703.

[22] W. A. Dollase, *Z. Kristallogr.* **1965**, *121*, 369.

[23] K. H. Klaska, O. Jarchow, *Z. Kristallogr.* **1975**, *142*, 225.

[24] J. S. Kerr, *Z. Kristallogr.* **1974**, *139*, 186.

[25] Crystallographic data (excluding structure factors) for the structure(s) reported in this paper have been deposited with the Cambridge Crystallographic Data Centre as supplementary publication no. CCDC-179-24. Copies of the data can be obtained free of charge on application to The Director, CCDC, 12 Union Road, Cambridge CB2 1EZ, UK (fax: int. code +(1223) 336-033; e-mail: teched(*a*) chemcrys.cam.ac.uk).

Solubilization of NaX Salts in Chloroform by Bifunctional Receptors**

Jurgen Scheerder, John P. M. van Duynhoven, Johan F. J. Engbersen, and David N. Reinhoudt*

Recently, we described bifunctional receptors that are capable of binding and transporting simple salts like KH_2PO_4,[1] CsCl,[2] and NaH_2PO_4.[3] In these bifunctional receptors the (isolated) receptor sites for the anion and cation are covalently linked.[4] Cation complexation did not enhance the anion complexation or vice versa. Now, we report a class of simple, bifunctional receptors that can solubilize NaX salts (X = Cl, Br) in chloroform.[5] In these bifunctional receptors Na^+ complexation is essential for complexation of the anion (positive heterotropic allostery).

Previously we have shown that proper positioning of urea moieties on calix[*n*]arenes ($n = 4$, 6) yields receptors that are capable of binding halide anions exclusively through hydrogen bonding.[6] It has also been established that functionalization of calix[4]arenes with four ethyl ester groups at the lower rim yields ionophores with a high selectivity for Na^+ ions.[7] The combination of these two binding sites on the calix[4]arene skeleton yields molecules that are potential receptors for NaX salts (X = halide). The synthesis of the bifunctional receptors having four ester groups at the lower rim and two or four urea groups at the upper rim is depicted in Scheme 1.

[*] Prof. dr. ir. D. N. Reinhoudt, Dr. ir. J. Scheerder, Dr. J. F. J. Engbersen
Laboratory of Organic Chemistry, University of Twente
P. O. Box 217, NL-7500 AE Enschede (The Netherlands)
Fax: Int. code +(53)489-4645
e-mail: orgchem(*a*) ct.utwente.nl

Dr. J. P. M. van Duynhoven
Laboratory of Chemical Analysis, University of Twente (The Netherlands)

[**] This work was supported by the Netherlands Foundation for Chemical Research (SON) with financial aid from the Netherlands Organization for Scientific Research (NWO). We thank D. M. Rudkevich for helpful discussions.

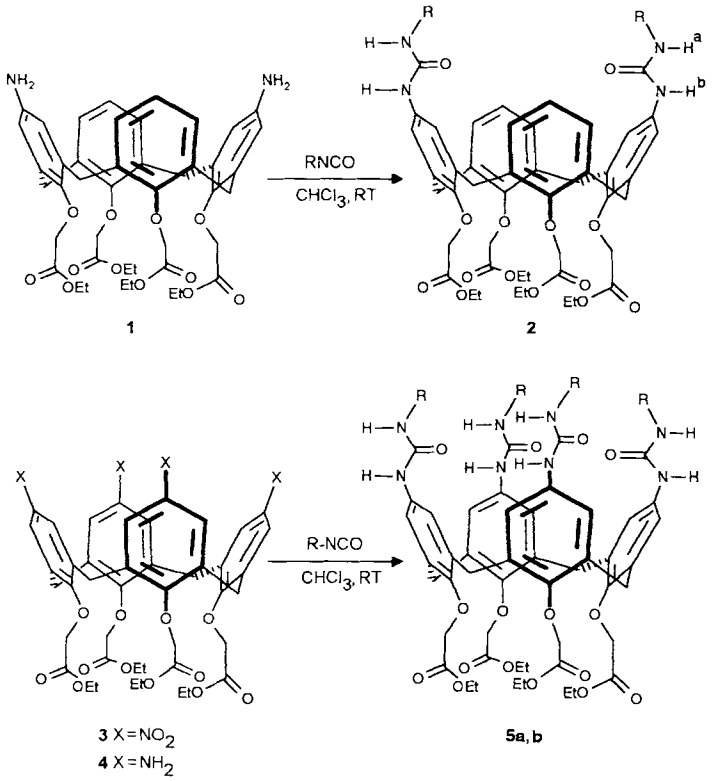

1 2

3 X = NO_2
4 X = NH_2

5a, b

Scheme 1. Synthesis of **2** (R = *n*-octyl), **5a** (R = *n*-octyl), and **5b** (R = *tert*-butyl). The labels on the amide protons are used for the assignment of the NMR spectra in Figure 1. RT = room temperature.

Addition of *n*-octylisocyanate to a solution of 5,17-diaminocalix[4]arene tetra(ethyl ester) **1**[3] in $CHCl_3$ gave the di-(*n*-octylureido)calix[4]arene **2** in 44% yield.[8] Reduction of tetranitrocalix[4]arene **3**[9] (Scheme 1) with $NaBH_4/CoCl_2$ in MeOH at room temperature[10] gave the tetraaminocalix[4]arene **4** in 60% yield. Subsequent addition of the appropriate isocyanates to a solution of **4** in $CHCl_3$ at room temperature gave the tetra(ureido)calix[4]arenes **5a,b** in yields of 60 and 36%, respectively.[8] Calix[4]arene **6**, with only an anion binding site, and calix[4]arene **7**,[7] with only a cation binding site, were included as reference compounds (vide infra). Calix[4]arene **6** was synthesized in analogy to **5a,b**, starting from tetrakis-[(ethoxy(ethoxy)]tetranitrocalix[4]arene.[11]

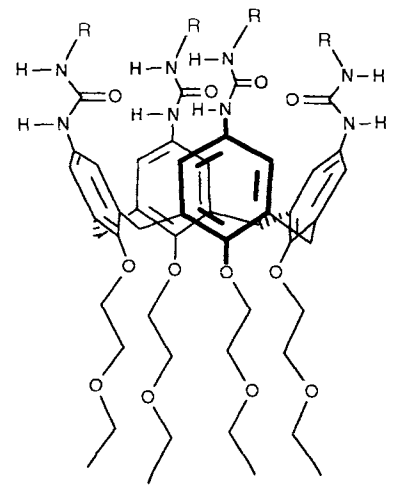

6

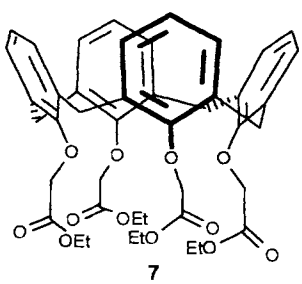

7

Calix[4]arene **2** adopts a pinched *cone* conformation in $CDCl_3$ solution at room temperature due to intramolecular hydrogen bonding between the opposite urea moieties.[12] Recently, Rebek and Shimizu[13] reported that tetrakis(benzyloxy)tetra-(*N*-phenylureido)calix[4]arenes form hydrogen-bonded dimers in $CHCl_3$ solution at room temperature.

Upon addition of Bu_4NCl or Bu_4NBr to a 5 mM solution of **2** in $CDCl_3$, no complexation of halide anions was observed. Due to the pinched *cone* conformation of **2**, the anion binding site is blocked (Scheme 2, left). However, complexation of Na^+

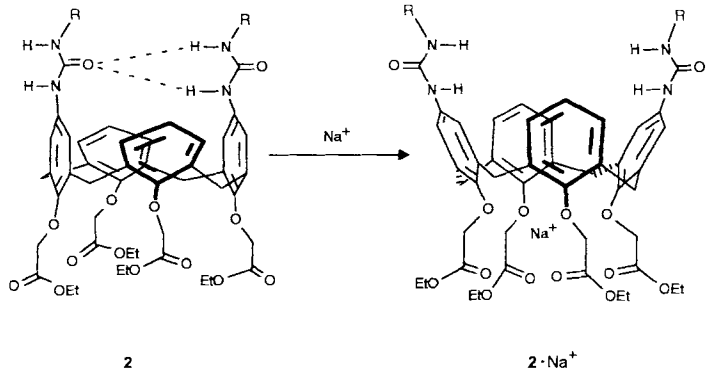

2 2·Na^+

Scheme 2. Complexation of Na^+ ions by **2** (R = *n*-octyl).

ions at the lower rim of **2** converts the pinched *cone* conformation into a symmetrical *cone* conformation. Intramolecular hydrogen bonding at the upper rim is not possible in this conformation due to the rigidification of the calix[4]arene skeleton (Scheme 2, right). This is evident from the large downfield shift of the ^1H NMR signal for the aromatic hydrogens of the substituted aromatic rings (ArH) from $\delta = 6.02$ (Fig. 1a) to $\delta = 7.34$ (Fig. 1b).

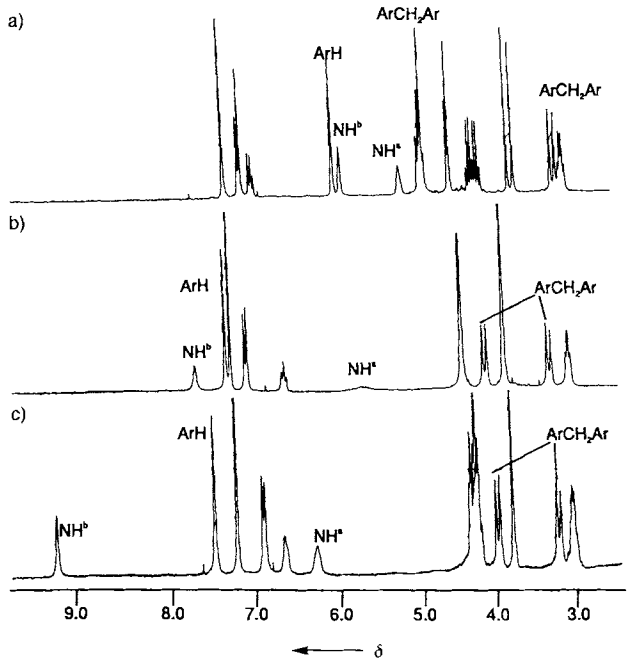

Fig. 1. ^1H NMR spectra of **2** ($CDCl_3$, 5 mM). a) Uncomplexed, b) [**2**·Na]ClO_4, c) [**2**·NaCl]. For NH^a and NH^b see Scheme 1; for ArH and $ArCH_2Ar$ see the text or ref. [14].

The addition of Bu_4NCl and Bu_4NBr to a 5 mM solution of the **2**·Na^+ complex results in a clear downfield shift of the ^1H NMR signals of the urea hydrogens, indicating complexation of the anionic guests through hydrogen bonding.[6] In contrast, the urea hydrogens of **5a,b** are not available for anion complexation due to the formation of a hydrogen-bonded dimer in solution.[14] The addition of Bu_4NBr or Bu_4NCl to a 5 mM solution of **5a,b** in $CDCl_3$ does not result in anion complexation. When **5a,b** is treated with $NaClO_4$, the hydrogen bonding in the dimer is broken, as is evident from the disappearance of the two NMR signals for the aromatic hydrogens and the presence of one signal for these hydrogens.[15] Now the addition of Bu_4NBr or Bu_4NCl to a 5 mM solution of [**5a**·Na]ClO_4 in $CDCl_3$ results in a downfield shift of the signals of the urea hydrogens, indicating hydrogen bonding with the anions. A Job plot[16] indicates a 1:1 stoichiometry for the complex with **5a**, with $K_{ass} \geq 1.0 \times 10^4\ M^{-1}$ for Cl^- and $K_{ass} = 1.3 \times 10^3\ M^{-1}$ for Br^-. The preference for Cl^- ions can be explained by the preference of the "hard" urea hydrogen bond donor for the "harder" hydrogen bond acceptor Cl^-.

The results show that **2** and **5a,b** can simultaneously complex Na^+ and Cl^- or Br^- ions and that cation complexation induces a structural change that is prerequisite for anion complexation. This process resembles a heterotropic allosteric effect.[17] The Na^+ complexation by **5a,b** results in a dissociation of the dimer after which anion complexation can occur.

The bifunctional calix[4]arenes **2** and **5a,b** are capable of solubilizing simple alkali salts in chloroform. The results of the liquid–solid (L–S) extractions[18] of MX (M = Na, K, Cs; X = Cl, Br, I) by **2** and **5a,b** in chloroform are summarized in Table 1. A representative ^1H NMR spectrum of the NaCl com-

Table 1. Percentage of MX complex formed with **2** and **5a,b** after L–S extraction [a].

	2			**5a**			**5b**		
	Na^+	K^+	Cs^+	Na^+	K^+	Cs^+	Na^+	K^+	Cs^+
Cl^-	100	–	–	100	29	–	100	30	–
Br^-	100	16	–	100	62	–	100	75	–
I^-	100	100	–	100	100	–	100	100	–

[a] The concentration of **2** and **5a,b** is 5 mM in $CDCl_3$. See also ref. [18].

plex of **2** is depicted in Figure 1c. Comparison of this ^1H NMR spectrum with that of the free ligand **2** (Fig. 1a) and of [**2**·Na]ClO_4 reveals large downfield shifts of both urea hydrogens and the aromatic hydrogens of the substituted aromatic rings (ArH).

The strong complexation of the NaX salts indicates the strong preference of the receptors for Na^+ ions. Only partial complexation of KX salts is observed, in agreement with the weaker binding of K^+ ions by calix[4]arene tetra(ethyl esters).[7] No complexation of Cs^+ salts is observed, apparently because the Cs^+ ion is too large to fit in the cavity. Although the solubility of the free salts in chloroform is very low and decreases in the order MI > MBr > MCl, the preferential extraction of chloride salts indicates the higher affinity of the urea binding sites for Cl^- ions over Br^- and I^- ions.

Addition of an excess of **2** or **5a,b** to a solution of the salt complexes gives two sets of distinctly separate signals for the complex and the free receptor in the ^1H NMR spectrum. This means that the cation and anion are always complexed to the same molecule and that calix[4]arenes with only a cation or an anion are not present.

The complexation of the salts has also been confirmed by FAB mass spectrometry. When the chloroform solution obtained after L–S extraction of NaCl and NaBr by **5a** is concentrated and the FAB mass spectrum recorded, $[M + Na]^+$ (100%) signals are observed in the positive mode and $[M + Cl]^-$ (100%) or $[M + Br]^-$ (40%) signals in the negative mode. In addition also $[M + Na + Cl]$ (20%) and $[M + Na + Br]$ (20%) signals are present, which clearly proves the salt complexation.

Addition of NaCl or NaBr to a chloroform solution of calix[4]arene **7**, which lacks an anion binding site, did not result in any complexation of Na^+ ions. Addition of NaCl and NaBr to a chloroform solution of calix[4]arene **6**, which lacks the cation binding site, did not result in complexation of Cl^- or Br^- ions. The addition of NaCl or NaBr to a 1:1 mixture of **6** and **7** in $CDCl_3$ did not result in the complexation of Na^+ and Cl^- or Br^- ions. This shows clearly that both the cation binding site and the anion binding site are necessary for the complexation of NaCl or NaBr and that these must be within the same calix[4]arene skeleton.

In conclusion, bifunctional receptors are capable of binding hydrophilic salts MX (M = Na, K; X = Cl, Br, I) in apolar solvents, and the complexation of the cation is essential for anion complexation. Our receptors show a preference for sodium salts with hard anions.[1, 2]

Received: December 7, 1995 [Z86191E]
German version: *Angew. Chem.* **1996**, *108*, 1172–1175

Keywords: allosteric effects · calix[4]arenes · complexes with alkali metal halides · receptors · supramolecular chemistry

[1] a) D. M. Rudkevich, Z. Brzozka, M. Palys, H. C. Visser, W. Verboom, D. N. Reinhoudt, *Angew. Chem.* **1994**, *106*, 480; *Angew. Chem. Int. Ed. Engl.* **1994**, *33*, 467–468; b) H. C. Visser, D. M. Rudkevich, F. de Jong, D. N. Reinhoudt, *J. Am. Chem. Soc.* **1994**, *116*, 11554–11555.

[2] D. M. Rudkevich, J. D. Mercer-Chalmers, W. Verboom, R. Ungaro, F. de Jong, D. N. Reinhoudt, *J. Am. Chem. Soc.* **1995**, *117*, 6124–6125.

[3] D. M. Rudkevich, W. Verboom, D. N. Reinhoudt, *J. Org. Chem.* **1994**, *59*, 3683–3686.

[4] Recently we reported on a bifunctional receptor for NaSCN formed by self-assembly of a cation and an anion receptor. See D. M. Rudkevich, A. N. Shivanyuk, Z. Brzozka, W. Verboom, D. N. Reinhoudt, *Angew. Chem.* **1995**, *107*, 2300–2302; *Angew. Chem. Int. Ed. Engl.* **1995**, *34*, 2124–2126.

[5] Crown ethers having an arylboronic ester center have shown mono- or ditopic binding of potassium salts in organic solvents, depending on the anion. See M. T. Reetz, C. M. Niemeyer, K. Harms, *Angew. Chem.* **1991**, *103*, 1515; *Angew. Chem. Int. Ed. Engl.* **1991**, *30*, 1472–1474.

[6] a) J. Scheerder, M. Fochi, J. F. J. Engbersen, D. N. Reinhoudt, *J. Org. Chem.* **1994**, *59*, 7815–7820; b) J. Scheerder, J. F. J. Engbersen, A. Casnati, R. Ungaro, D. N. Reinhoudt, *J. Org. Chem.* **1995**, *60*, 6448–6454.

[7] F. Arnaud-Neu, E. M. Collins, M. Deasy, G. Ferguson, S. J. Harris, B. Kaitner, A. J. Lough, M. A. McKervey, E. Marques, B. L. Ruhl, M. J. Schwing-Weill, E. M. Seward, *J. Am. Chem. Soc.* **1989**, *111*, 8681–8691.

[8] All new compounds gave correct elemental analyses and had spectral data in full accordance with their structures.

[9] W. Verboom, A. Durie, R. J. M. Egberink, Z. Asfari, D. N. Reinhoudt, *J. Org. Chem.* **1992**, *57*, 1313–1316.

[10] T. Satoh, S. Suzuki, Y. Suzuki, Y. Miyaji, Z. Imai, *Tetrahedron Lett.* **1969**, 4555–4558.

[11] J.-D. van Loon, J. F. Heida, W. Verboom, D. N. Reinhoudt, *Recl. Trav. Chim. Pays-Bas* **1992**, *111*, 353–359.

[12] J. Scheerder, R. Vreekamp, J. F. J. Engbersen, W. Verboom, J. P. M. van Duynhoven, D. N. Reinhoudt, *J. Org. Chem.* **1996**, in press.

[13] K. D. Shimizu, J. Rebek, Jr., *Proc. Natl. Acad. Sci. USA* **1995**, *92*, 12403–12407. We thank Prof. Rebek for providing us with his results on the behavior of the tetra(ureido)calix[4]arenes prior to publication.

[14] NOESY experiments with **5a,b** reveal through-space connectivities between the aromatic hydrogens of the calix[4]arene skeleton and the $NH^aCH_2CH_2$ and $NH^aCH_2CH_2$ hydrogens of **5a** and the *tert*-butyl hydrogens of **5b**. These connectivities cannot result from through-space interactions within a single molecule since in the same molecule these hydrogens are not close enough [14a]. Consequently, these NOE connectivities must result from intermolecular interactions. Furthermore, the sign of the NOE connectivities is positive, suggesting that slow-tumbling entities with increased molecular mass (≥2000) are present

[14a]. Using the initial rate approximation [14b] and the distance between the equatorial and axial calix[4]arene bridging methylene hydrogens as a reference (1.79 Å) the cross relaxation constants (σ_{12}) for a two-spin system involving two atoms (1 and 2) were determined [14c]. The σ_{12} values are an indication of the degree of aggregation of the two atoms involved [14a]. The σ_{12} values for **5a** and **5b** are -0.7 and -0.2, respectively. The negative σ_{12} values suggest the presence of species with a higher molecular mass. These results support the dimeric structure for **5a,b** proposed by Rebek [13]. a) D. Neuhaus, W. P. Williamson, *The Nuclear Overhauser Effect in Structural and Conformational Analysis*, VCH, Weinheim, **1989**; b) R. R. Ernst, G. Bodenhausen, A. Wokaun, *Principles of Nuclear Magnetization Resonance in One and Two Dimensions*, Clarendon, Oxford, **1987**, pp. 490–538; c) Isotropic tumbling and pure dipole–dipole relaxation is assumed. See K. Wüttrich, *NMR of Proteins and Nucleic Acids*, Wiley, New York, **1986**, Chapter 6.

[15] According to Shimizu and Rebek, Jr. the presence of two signals for the aromatic hydrogens of tetra(ureido)calix[4]arenes **5a,b** results from hindered rotation of the urea moieties around the aryl–urea bond due to hydrogen bonding in the dimer [13]. The fact that upon the complexation of Na^+ by **5a,b** one signal for these hydrogens is present in the ^1H NMR spectra indicates that this hindered rotation is absent and that the dimer is no longer present.

[16] K. A. Conners, *Binding Constants*, 1st ed., Wiley, New York, **1987**, p. 24.

[17] J. Rebek, Jr., *Acc. Chem. Res.* **1984**, *17*, 258–264.

[18] A 5 mM solution (0.5 mL) of **2** or **5a,b** in $CDCl_3$ was stirred with an excess of MX for 24 h. The organic layer was separated and the relative amount of complex formed was determined on basis of the intensities of the ^1H NMR signals for the bridging calix[4]arene methylene hydrogens of the complex and the free ligand.

The First Model of the Neocarzinostatin Chromophore with an Epoxide Ring and a Carbonate Moiety**

Matthias Eckhardt* and Reinhard Brückner*

Dedicated to Professor Siegfried Hünig on the occasion of his 75th birthday

Neocarzinostatin is a chromoprotein with exceptionally high antitumor activity.[1] Its chromophore **1** ("NCS") has been established to be its pharmacophore. However, as soon as this compound is separated from the apoprotein, it becomes extremely sensitive towards heat (it is unstable even at room temperature), acid, base, and light. Accordingly, numerous attempts have been made to synthesize dienediyne analogs of **1** that have an in vitro DNA damaging activity comparable to that of the natural product but are hopefully much more stable.[1] In parallel studies analogs of the enediyne anticancer antibiotics esperamycin, calicheamicin, and dynemicin have been sought.[2] In spite of the structural complexity of calicheamicin[3] and dynemicin,[4] their total syntheses either as aglycons or as the fully equipped glycosides found in nature have been achieved. NCS, however, remains an elusive synthetic goal.

In our most recent efforts directed towards the synthesis of NCS analogs we have used bis(enol trifluoromethanesulfonate) **2**[5] ("bistriflate") as a starting material. We found that **2** can be converted into the iodinated dienediyne aldehydes **3a** and **3b** (Scheme 1), and that these compounds cyclize under modified Nozaki–Hiyama conditions to give the dienediyne model compounds **4a** (six-/ten-membered ring system) and **4b** (six-/eleven-membered ring system) of NCS (five-/nine-membered ring system).[6] The cyclized compounds were isolated in quite

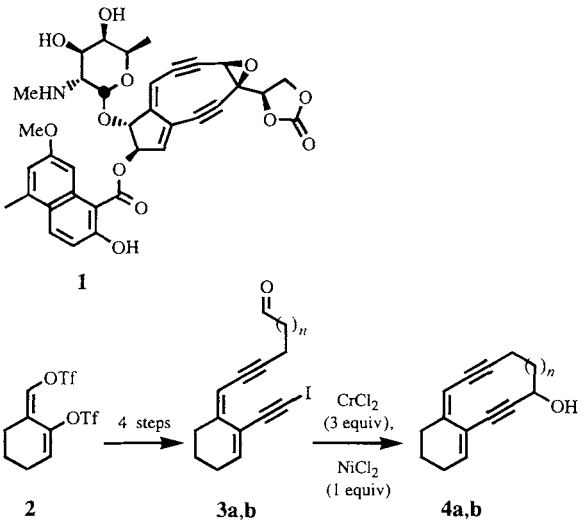

Scheme 1. Tf = CF_3SO_2; **a**, $n = 1$; **b**, $n = 2$.

respectable yields of 51% (**4a**) and 54% (**4b**), indicating that the products are fairly stable. This encouraged us to attempt the synthesis of dienediyne models more closely resembling NCS. To limit ring strain we designed a target compound having the tested[6] unnatural six-/eleven-membered rings in the carbon skeleton, but we also incorporated both the epoxide and the carbonate substructure of the natural product in the correct configurations.

Bistriflate **2**[5] and a 1:1 diastereomeric mixture of the enantiomerically pure alcohols **5**[7] were coupled in the presence of catalytic amounts of $[PdCl_2(PPh_3)_2]$ and CuI to provide the monocoupling product **6** and nearly none of its regioisomer (Scheme 2). The technique and selectivity in this reaction parallel those of similar couplings which we described earlier.[5, 6] Although the monocoupling product **6** was isolable, it was usually used in situ in the next step. When the coupling reaction yielding **6** had gone to completion, we added pentynol to the reaction mixture, which still contained the catalytically active Cu and Pd species. A second coupling reaction occurred with cleavage of the remaining triflate moiety. Standard aqueous work-up and purification by flash chromatography on silica gel[8] furnished the biscoupling product **7** in 73% yield.[9] Product **7** is a 1:1 mixture of diastereomers since the precursor alcohol **5** was used as a 1:1 mixture of diastereomers.

Oxidation of diol **7** with the Dess/Martin periodinane[10] afforded ketoaldehyde **8** in 69% yield (Scheme 2).[9] The 300 MHz ^1H NMR spectrum of compound **8** revealed a minor broadened singlet at $\delta = 5.52$ (impurity) besides a dominant broadened singlet at $\delta = 5.45$ (main product). Such signals are typical for the exocyclic olefinic methine protons of monocyclic *Z*-configurated dienediynes like compound **8**.[5b, 6b] The minor signal indicates the presence of 4 mol% of the regioisomeric biscoupling product, a dienediyne ketoaldehyde in which the positions of the two alkyne arms are interchanged. Product **8** was used without further purification; after the next two steps the contaminating regioisomer could no longer be detected by NMR spectroscopy.

The next transformation, a McMurry coupling,[11] is the key step of our synthesis. In this reaction the monocyclic ketoaldehyde **8** was added by syringe pump to a suspension of low-valent titanium freshly prepared from $TiCl_3 \cdot 1.5\,MeOCH_2CH_2OMe$ (DME) and Zn/Cu couple (Scheme 2). This coupling leads chemoselectively to the bicyclic trienediyne **9**,[9] provided the

[*] Prof. Dr. R. Brückner, Dipl.-Chem. M. Eckhardt
Institut für Organische Chemie der Universität
Tammannstrasse 2, D-37077 Göttingen (Germany)
Fax: Int. code +(551)392944

[**] This work was supported by the Volkswagen-Stiftung (Schwerpunktprogramm "Metallorganische Reaktionen für die Organische Synthese").

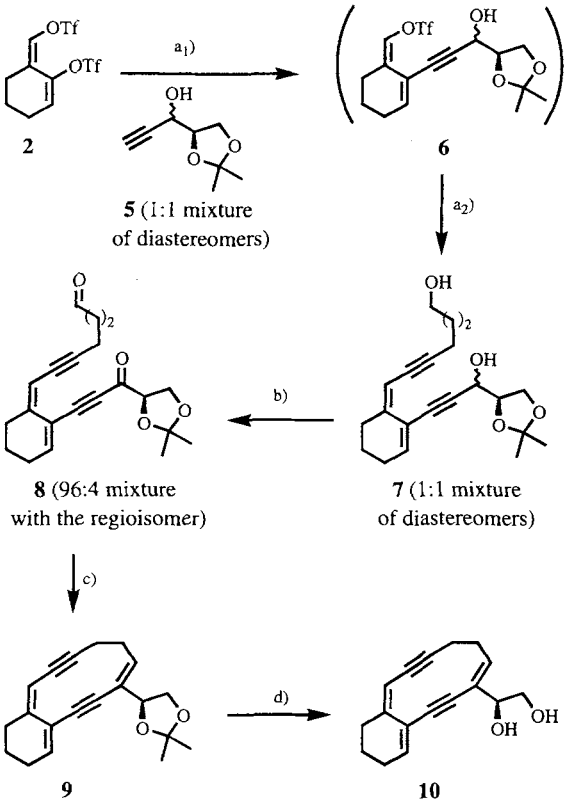

Scheme 2. a_1) Solution of **2** in Et_2O/iPr_2NH (50/17), at room temperature; successive additions of $[PdCl_2(PPh_3)_2]$ (7 mol%), CuI (17 mol%), **5** (1.15 equiv), 4 h; a_2) addition of 4-pentyn-1-ol (1.0 equiv), 18 h; 73% **7**; b) Dess/Martin periodinane (2.6 equiv), a few drops of H_2O, CH_2Cl_2, room temperature, 30 min; 69%; c) DME complex of $TiCl_3$ prereduced with Zn/Cu couple; dropwise addition of **8** ($\approx$0.03 M in DME) at 30–35 °C over 3 h; aqueous workup after another 1 h and purification by flash chromatography on silica gel without complete removal of the eluent; d) conc. HCl in MeOH, room temperature, 4.5 h; 45% yield starting from **8**.

reaction is performed between 30 and 35 °C. The same freshly prepared low-valent titanium reagent effects an intramolecular pinacol coupling of ketoaldehyde **8** if the reaction is conducted at −45 °C. Product **9** was purified by chromatography; however, removal of the eluent initiated its decomposition. Therefore, **9** was used directly in the subsequent reaction, acid-catalyzed removal of the acetonide group through methanolysis (Scheme 2). The trienediynediol **10**[9] was thus obtained in 45% yield based on the ketoaldehyde **8**.

Carbonyl compounds in which the C=O bond is conjugated with a C≡C bond, as in ketoaldehyde **8**, have to our knowledge not been used previously in McMurry reactions.[11] The closest analogy to our coupling **8** → **9** was an intramolecular pinacol coupling of a bisaldehyde of the type H-(O=C)-C≡C-R-C≡C-C(=O)-H;[12] however, an analogous McMurry coupling failed.[12b]

An additional structural feature of ketoaldehyde **8** had to our knowledge[11] never been present hitherto in a McMurry reaction, whether olefination or pinacol coupling: a C–O bond in α-position to the carbonyl group. We had been afraid that substructure O=C-C-OR might be reduced under McMurry conditions to give an enolate rather than the required α-oxygenated ketyl intermediate. Fortunately, this concern was essentially[13] unwarranted.

Our next objective was to epoxidize *one* of the three C=C bonds of the trienediynediol **10** *with stereocontrol* (Scheme 3). The targeted C=C bond is part of both an allylic and a homoallylic alcohol. These circumstances seemed favorable since double bonds of allylic alcohols[14] and of homoallylic alcohols[15] are epoxidized by *t*BuOOH with catalytic $VO(acac)_2$ in preference to other C=C bonds. This is because after the in situ oxidation $V^{IV} \rightarrow V^{V}$ the metal becomes a link between the hydroxyl group and the oxidant and thus directs epoxidation of exclusively the proximal C=C bond. The cyclic transition state also ensures often a high degree of stereocontrol during this attack. The cooperative effect of the OH groups in **10** on treatment with *t*BuOOH/$[VO(acac)_2]$ led to regioselective epoxidation (Scheme 3). However, the stereodirecting effects of the two

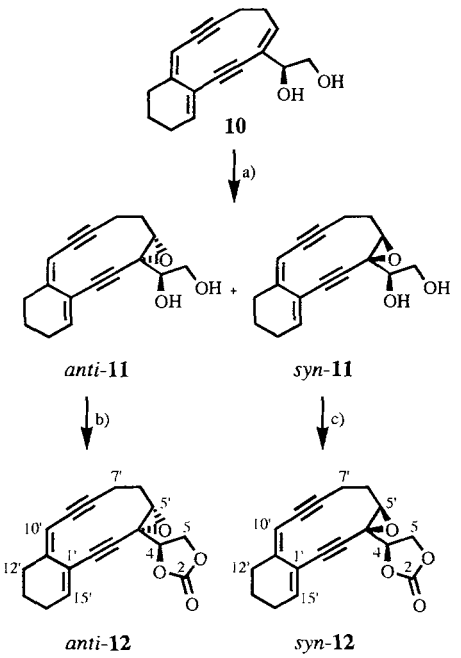

Scheme 3. a) *t*BuOOH (>1.5 equiv), $VO(acac)_2$ (>0.6 mol%/30 min), CH_2Cl_2, room temperature, 3 h; 7% *anti*-**11** and 8% *syn*-**11** after separation by repeated flash chromatography; b) $ClC(=O)OCCl_3$ (>2 equiv), pyridine (>10 equiv), CH_2Cl_2, 0 °C, 15 min; 78%; c) same as b); 78%.

OH groups were either very weak or more likely cancelled each other so that we obtained the epoxy diol **11** as a 1:1 *syn*:*anti* mixture.[9] The configurations of these diols were established after they had been separated and converted into the corresponding carbonates *anti*-**12**[9] and *syn*-**12**.[9] The spectra of these compounds (Table 1) were compared with the spectrum of a sample of *syn*-**12**, which had been obtained by a stereochemically unequivocal route (cf. Scheme 4). Only the spectrum of the carbonate derived from diol *syn*-**11** was identical with the reference spectrum.

We tried to epoxidize trienediynediol **10** with greater stereocontrol by using the double stereodifferentiation of the Sharpless asymmetric epoxidation (Scheme 4).[16] The chiral auxiliary was a stoichiometric quantity of D-(−)-diethyl tartrate (DET) so that the complexed oxidant and the allyl alcohol moiety of the substrate formed a matched pair.[16a] However, stoichiometric amounts of the auxiliary, *t*BuOOH, $Ti(OiPr)_4$, and substrate **10** did not react at −23 °C and decomposed slowly at 0 °C.[17] To sidestep this problem diol **10** was silylated at the primary OH group. With only one remaining OH group in *tert*-butyldimethylsilyl ether **13**, reaction under Sharpless conditions resulted in the desired epoxidation with *complete regio- and stereocontrol* giving the silylated epoxide **14**. In the next, one-pot operation the $tBuMe_2Si$ group was removed with

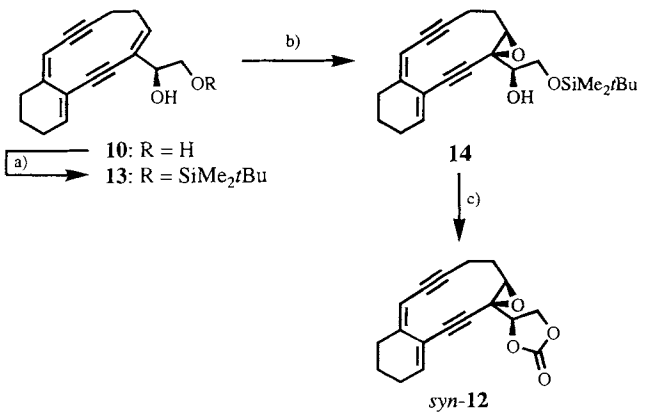

syn-**12**

Scheme 4. a) $ClSiMe_2tBu$ (>1 equiv), imidazole (>1.1 equiv), CH_2Cl_2, 0 °C, 4 h; product purified by flash chromatography but not freed of eluent; b) *t*BuOOH (>2 equiv), $Ti(OiPr)_4$ (>1 equiv), D-(−)-DET (>1.05 equiv), CH_2Cl_2, −23 °C, 2 h; 53% yield starting from **10**; c) Bu_4NF (1.0 M in THF; 1.2 equiv), pyridine (10 equiv), THF, −10 °C, 10 min; $ClC(=O)OCCl_3$ (2 equiv), 30 min; 41%.

Table 1. Analytical data for *anti*-**12** and *syn*-**12**; IR spectra in C_6D_6; ^1H NMR and ^{13}C NMR spectra in C_6D_6 (500 and 126 MHz, respectively; C_6HD_5 as internal standard referenced to $\delta_H = 7.16$ and C_6D_6 as internal standard referenced to $\delta_C = 128.00$, respectively; for numbering see Scheme 3).

anti-**12**: IR: ν = 2930, 2270, 2225, 1825, 1440, 1385, 1320, 1155, 1085, 975, 915, 810, 765 cm^{-1}; ^1H NMR: δ = 1.09–1.26 (m, 13′-H_2), 1.61 (m_c, 6′-H_2), 1.69–1.86 (m, 7′-H^1, 12′-H_2, 14′-H_2), 2.03–2.11 (m, 7′-H^2), 2.74 (dd, $J_{5',6'\ H(1)}$ = 9.5, $J_{5',6'\ H(2)}$ = 4.0, 5′-H), 3.52 (t, $J_{gem} = J_{5\ H(1),4}$ = 8.5, 5-H^1), 3.96 (dd, $J_{4,5\ H(1)}$ = 8.6, $J_{4,5\ H(2)}$ = 5.0, 4-H), 4.20 (dd, J_{gem} = 8.5, $J_{5\ H(2),4}$ = 5.1, 5-H^2), 5.23 (br. s, 10′-H), 6.04 (td, $J_{15',14'}$ = 4.5, $^5J_{15',10'}$ = 1.1, 15′-H); ^{13}C NMR: δ = 15.17 (C-6′), 22.05 (C-13′*), 26.35 (C-14′*), 29.90 (C-7′), 32.61 (C-12′*), 56.58 (C-4′), 60.89 (C-5′), 66.26 (C-5), 75.34 (C-4), 80.02, 84.46, 87.03, and 97.73 (4 sp-C), 106.73 (C-10′), 119.94 (C-1′), 142.60 (C-11′), 143.34 (C-15′), 154.09 (C-2) (*assignments based on the similarity to the chemical shifts of 5,6-benzobicyclo[8.4.0]tetradeca-1(14),5,9-triene-2,7-diyne-4-ylacetate [6b]); $[\alpha]_D^{20} = -27$ (c = 1.01 in C_6D_6); correct high-resolution mass spectrum.

syn-**12**: IR: ν = 2930, 2380, 2270, 1825, 1620, 1450, 1385, 1325, 1155, 1085, 810 cm^{-1}; ^1H NMR: δ = 1.11–1.26 (m, 13′-H_2), 1.60–1.65 (m, 6′-H_2), 1.71–1.88 (m, 7′-H^1, 12′-H_2, 14′-H_2), 2.05–2.13 (m, 7′-H^2), 2.66 (m_c, 5′-H), 3.56 (dd, $J_{gem} = J_{5\ H(1),4}$ = 8.6, 5-H^1), 3.83 (dd, $J_{4,5\ H(1)}$ = 8.3, $J_{4,5\ H(2)}$ = 5.3, 4-H), 4.22 (dd, J_{gem} = 8.7, $J_{5\ H(2),4}$ = 5.3, 5-H^2), 5.21 (br. s, 10′-H), 6.10 (td, $J_{15',14'}$ = 4.4, $^5J_{15',10'}$ = 1.2, 15′-H); ^{13}C NMR: δ = 15.11 (C-6′), 22.03 (C-13′*), 26.35 (C-14′*), 29.76 (C-7′), 32.54 (C-12′*), 56.09 (C-4′), 61.96 (C-5′), 66.34 (C-5), 75.95 (C-4), 80.03, 84.12, 87.85, and 97.59 (4 sp-C), 106.90 (C-10′), 119.99 (C-1′), 142.43 (C-11′), 143.06 (C-15′), 154.14 (C-2) (*assignments based on the similarity to the chemical shifts of 5,6-benzobicyclo[8.4.0]tetradeca-1(14),5,9-triene-2,7-diyne-4-ylacetate [6b]); $[\alpha]_D^{20}$ = 197 (c = 1.14 in C_6D_6); correct high-resolution mass spectrum.

Bu_4NF and the resulting ammonium alcoholate converted into the desired carbonate with diphosgene.[18] The pure carbonate *syn*-**12**[9] (Table 1) was thus available from the McMurry product **9** in 10% overall yield. The configuration of *syn*-**12** is considered established beyond reasonable doubt because the stereoselectivity of the Sharpless oxidation step **13** → **14** cannot possibly deviate from that known from innumerable other applications of this reaction.[16]

Compound *syn*-**12** is a dienediyne analog of NCS (**1**), which is structurally much more closely related to the natural product than many of the earlier analogs. Analog *syn*-**12** has an annulated epoxide ring *and* a cyclic carbonate *both* with the same configuration as the natural product; however, the rings (six-/eleven-membered) in its bicyclic core are larger. The synthesis of analog *syn*-**12** requires only seven steps starting from bistriflate **2** or nine steps starting from formylcyclohexanone.[5, 6]

The known dienediyne analogs closest to NCS are compound **15** from A. G. Myers's lab[19] (five-/nine-membered bicyclic

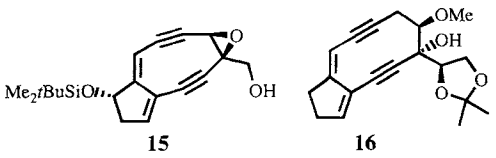

15 **16**

core structure with an annulated epoxide ring[20]) and compound **18** from the group of Terashima[21] (five-/ten-membered bicyclic core structure with incorrectly functionalized oxygen substituents).

Received: December 19, 1995 [Z 8665 IE]
German version: *Angew. Chem.* **1996**, *108*, 1185–1188

Keywords: carbon–carbon coupling · dienediynes · enol triflates · McMurry reactions · neocarzinostatin

[1] Reviews: a) H. Goldberg, *Acc. Chem. Res.* **1991**, *24*, 191–198; b) M. Hirama, *J. Synth. Org. Chem. Jpn.* **1994**, *52*, 980–991.

[2] Reviews: a) K. C. Nicolaou, W.-M. Dai, *Angew. Chem.* **1991**, *103*, 1453–1481; *Angew. Chem. Int. Ed. Engl.* **1991**, *30*, 1387–1416; b) M. E. Maier, *Kontakte (Merck)* **1994** (2), 3–17; c) *Synlett* **1995**, 13–26.

[3] a) K. C. Nicolaou, C. W. Hummel, E. N. Pitsinos, M. Nakada, A. L. Smith, K. Shibayama, H. Saimoto, *J. Am. Chem. Soc.* **1992**, *114*, 10082–10084; b) K. C. Nicolaou, *Angew. Chem.* **1993**, *105*, 1462–1471; *Angew. Chem. Int. Ed. Engl.* **1993**, *32*, 1377; c) R. D. Groneberg, T. Miyazaki, N. A. Stylianides, T. J. Schulze, W. Stahl, E. P. Schreiner, T. Suzuki, Y. Iwabuchi, A. L. Smith, K. C. Nicolaou, *J. Am. Chem. Soc.* **1993**, *115*, 7593–7611; d) A. L. Smith, E. N. Pitsinos, C.-K. Hwang, Y. Mizuno, H. Saimoto, G. R. Scarlato, T. Suzuki, K. C. Nicolaou, *ibid.* **1993**, *115*, 7612–7624; e) K. C. Nicolaou, C. W. Hummel, M. Nakada, K. Shibayama, E. N. Pitsinos, H. Saimoto, Y. Mizuno, K.-U. Baldenius, A. L. Smith, *ibid.* **1993**, *115*, 7625–7635; f) S. A. Hitchcock, M. Y. C. Mayer, S. H. Boyer, S. H. Olson, S. J. Danishefsky, *ibid.* **1995**, *117*, 5750–5756.

[4] a) J. Taunton, J. L. Wood, S. L. Schreiber, *J. Am. Chem. Soc.* **1993**, *115*, 10378–10379; b) A. G. Myers, M. E. Frawley, N. J. Tom, S. B. Cohen, B. Scott, D. J. Madar, *Chem. Biol.* **1995**, *2*, 33–43 (*Chem. Abstr.* **1995**, *123*, 83002); c) M. D. Shair, T.-y. Yoon, S. J. Danishefsky, *Angew. Chem.* **1995**, *107*, 1883–1885; *Angew. Chem. Int. Ed. Engl.* **1995**, *34*, 1720–1723.

[5] a) M. Moniatte, M. Eckhardt, K. Brickmann, R. Brückner, J. Suffert, *Tetrahedron Lett.* **1994**, *35*, 1965–1968; b) experimental details: K. Brickmann, F. Hambloch, J. Suffert, R. Brückner, *Liebigs Ann.* **1996**, 457–471.

[6] a) M. Eckhardt, R. Brückner, J. Suffert, *Tetrahedron Lett.* **1995**, *36*, 5167–5170; b) M. Eckhardt, R. Brückner, *Liebigs Ann.* **1996**, 473–488.

[7] Alcohol **5** was prepared from the acetonide of D-glyceraldehyde and ethynyl magnesium bromide following a procedure given for the addition of the same reagent to an analogous aldehyde (J. Marco-Contelles, M. Bernabé, D. Ayala, B. Sánchez, *J. Org. Chem.* **1994**, *59*, 1234–1235). D-Glyceraldehyde was prepared by oxidative cleavage (procedures: a) D. H. R. Barton, J.-P. Finet, W. B. Motherwell, C. Pichon, *Tetrahedron* **1986**, *42*, 5627–5636; b) C. R. Schmid, J. D. Bryant, M. Dowlatzedah, J. L. Phillips, D. E. Prather, R. D. Schantz, N. L. Sear, C. S. Vianco, *J. Org. Chem.* **1991**, *56*, 4056–4058) of D-1,2:5,6-di-*O*-isopropylidenemannitol (preparation: R. S. Tipson, A. Cohen, *Carbohydr. Res.* **1968**, *7*, 232–243).

[8] W. C. Still, M. Kahn, A. Mitra, *J. Org. Chem* **1978**, *43*, 2923–2925.

[9] All new compounds gave satisfactory ^1H NMR spectra (300 or 500 MHz, $CDCl_3$ or C_6D_6), ^{13}C NMR spectra (75 or 126 MHz, $CDCl_3$ or C_6D_6; except tetraenediyne **17**), IR spectra ($CDCl_3$ or C_6D_6 solution), and high-resolution EI (70 eV) mass spectra.

[10] a) D. B. Dess, J. C. Martin, *J. Org. Chem.* **1983**, *48*, 4155–4156; b) the beneficial effect of added H_2O was reported by S. D. Meyer, S. L. Schreiber, *ibid.* **1994**, *59*, 7549–7552.

[11] Reviews: a) P. Finocchiaro, E. Libertini, A. Recca, *Chim. Ind.* **1982**, *64*, 644–654; b) J. E. McMurry, *Chem. Rev.* **1989**, *89*, 1513–1524; c) B. König, *J. Prakt. Chem.* **1995**, *337*, 250–252.

[12] a) Y. Kuwatani, I. Ueda, *Angew. Chem.* **1995**, *107*, 2017–2019; *Angew. Chem. Int. Ed. Engl.* **1995**, *34*, 1892–1894; b) footnote [11] in ref. [12a].

[13] The early fractions of the chromatographic purification of McMurry product **9** delivered up to 10% of the fully deoxygenated bicycle **17**. Its structure was deduced from the appearance of the following olefin signals in the 300 MHz ^1H NMR spectrum ($CDCl_3$): δ = 5.17 (dd, $J(cis)$ = 10.2 Hz, $J(gem)$ = 1.1 Hz, *E*-2′-H), 5.30 (br. s, 10-H), 5.37 (dd, $J(trans)$ = 17.0 Hz, $J(gem)$ = 1.2 Hz, *Z*-2′-H), 6.07 (t, $J(5,6)$ = 8.3 Hz, 5-H), 6.30 (dd, $J(trans)$ = 17.0 Hz, $J(cis)$ = 10.2 Hz,

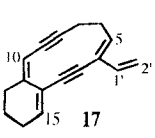

17

1'-H), 6.33 (td, $J(15,14) = 4.4$ Hz, $^5J(15,10) = 1.1$ Hz, 15-H). Compound **17** could arise from reduction of ketoaldehyde **8** to give the mentioned enolate, subsequent fragmentation into acetone and an enolate containing a negatively charged oxygen atom at the sp^3-hybridized β-carbon, coordination of this oxygen atom to titanium, and elimination of both elements together. This would lead to a ketoaldehyde in which a vinyl ketone would have replaced the originally present dioxolanyl ketone moiety. The last step in the conversion of ketoaldehyde **8** into the oxygen-free cyclized compound **19** would correspond to a McMurry ring closure.

[14] S. Tanaka, H. Yamamoto, H. Nozaki, K. B. Sharpless, R. C. Michaelson, J. D. Cutting, *J. Am. Chem. Soc.* **1974**, *96*, 5254–5255.

[15] E. D. Mihelich, K. Daniels, D. J. Eickhoff, *J. Am. Chem. Soc.* **1981**, *103*, 7690–7692.

[16] a) Review: K. B. Sharpless *in Catalytic Asymmetric Synthesis* (Ed.: I. Ojima), VCH, Weinheim, **1993**, pp. 227–272; b) experimental procedure: A. Pfenniger, *Synthesis* **1986**, 89–116.

[17] A similar inertness of an unsaturated 1,2-diol towards Sharpless epoxidation conditions was reported: a) W. Adam, B. Nestler, *Angew. Chem.* **1993**, *105*, 767–769; *Angew. Chem. Int. Ed. Engl.* **1993**, *32*, 733–735; b) W. Adam, B. Nestler, *J. Am. Chem. Soc.* **1993**, *115*, 7226–7231.

[18] Method: W. Nekrassow, N. Melnikow, *J. Prakt. Chem.* **1930**, *126*, 81–96.

[19] A. G. Myers, P. M. Harrington, B.-M. Kwon, *J. Am. Chem. Soc.* **1992**, *114*, 1086–1087.

[20] A carbonate-free five-/ten-membered dienediyne analog of neocarzinostin chromophore containing a spiro-fused epoxide ring rather than an annulated epoxide ring like **1**, **12**, and **15** was prepared by A. G. Myers, P. S. Dragovich, *J. Am. Chem. Soc.* **1993**, *115*, 7021–7022.

[21] a) K. Nakatani, K. Arai, S. Terashima, *J. Chem. Soc. Chem. Commun.* **1992**, 289–291; b) *Tetrahedron* **1993**, *49*, 1901–1912.

Synthesis, Structure, and Thermolysis of N-Apical 1,2λ^5-Azaphosphetidines with a Pentacoordinate P Center and the First Observation of Their N-Equatorial Pseudorotamers**

Takayuki Kawashima,* Tomokazu Soda, and Renji Okazaki*

In the course of our studies on oxetanes in which a high-coordinate main group element is adjacent to oxygen we achieved the syntheses and isolation of 1,2-oxaphosphetanes,[1] 1,2-oxasiletanides,[2] 1,2-oxagermetanides,[3] and 1,2-oxastannetanides,[4] with pentacoordinate P, Si, Ge, and Sn centers, respectively, as well as 1,2-oxaboretanides with a tetracoordinate B center.[5] These compounds correspond to intermediates of the Wittig,[6] Peterson-type,[7] and boron-Wittig reactions,[8] respectively.

Over 30 years ago Bestmann et al. reported that phosphorus ylides undergo a Wittig-type reaction with Schiff bases in place of carbonyl compounds to give the corresponding olefins,[9] possibly via a 1,2λ^5-azaphosphetidine. We now report the synthesis, crystal structure, and thermolysis of N-apical 1,2λ^5-azaphosphetidines with pentacoordinate P centers as well as the first observation of their N-equatorial pseudorotamers.

[*] Prof. Dr. T. Kawashima, Prof. Dr. R. Okazaki, T. Soda
Department of Chemistry, Graduate School of Science
The University of Tokyo
7-3-1 Hongo, Bunkyo-ku, Tokyo 113 (Japan)
Fax: Int. code + (3) 5800-6899
e-mail: takayuki@chem.s.u-tokyo.ac.jp

[**] This work was supported in part by a Kurata Research Grant (T. K.) and by a Grant-in-Aid for General Scientific Research (B) (No. 07454160, T. K.) from the Ministry of Education, Science and Culture. We thank Prof. N. Tokitoh of the University of Tokyo for determining the X-ray crystal structure of **4**, as well as Central Glass and Tosoh Akzo Co. Ltd. for gifts of hexafluorocumyl alcohol and alkyllithium compounds, respectively.

Phosphane oxide **3** was obtained in 44% yield by sequential treatment of methylphenylphosphane oxide **1**, having the Martin ligand,[10] with *n*BuLi, hexamethylphosphoric triamide (HMPA), and *N*-(diphenylmethylene)aniline (**2**) in THF at 0 °C (Scheme 1). Intramolecular cyclization and dehydration of **3**

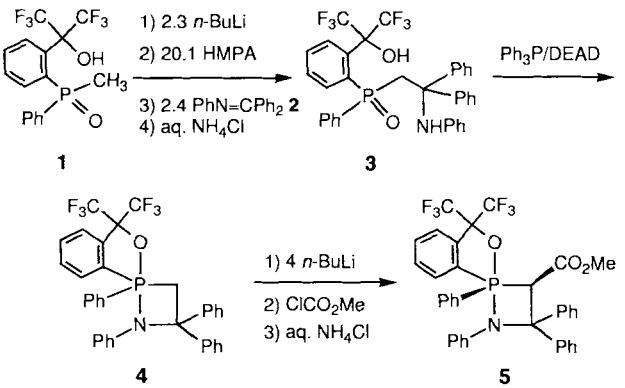

Scheme 1. Synthesis of compounds **3**–**5**. DEAD = diethyl azodicarboxylate.

with the Mitsunobu reagent[11a] provided 1,2λ^5-azaphosphetidine **4** (colorless crystals from ethanol, 93% yield), which was hydrolyzed on silica gel to give the starting compound **3**. This is the first application of the Mitsunobu reagent to the present type of reaction, although phosphorylation of nucleosides by this method has been reported.[11b] The 3-methoxycarbonyl derivative **5** (11% yield)[12] was prepared from **4** by the same method as that reported for the corresponding 1,2λ^5-oxaphosphetane (Scheme 1).[1b]

In the ^{1}H NMR spectrum of **4**, a downfield shift for the *ortho* proton of the Martin ligand was observed at $\delta = 8.27$, which is a typical feature of compounds with a trigonal-bipyramidal (TBP) structure bearing a polar apical bond.[1a, b, 2, 3, 13] Some other selected NMR data are listed in Scheme 2.

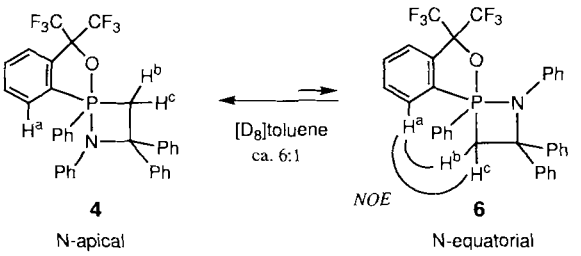

$\delta_P = -29.9$	$\delta_P = -50.9$
H^a: $\delta = 8.27$, $^3J_{HH} = 7.9$ Hz, $^3J_{HP} = 12.1$ Hz	$\delta = 7.64$, $^3J_{HH} = 7.9$ Hz, $^3J_{HP} = 11.6$ Hz
H^b: $\delta = 4.55$, $^2J_{HP} = 21.6$ Hz, $^2J_{HH} = 17.0$ Hz	$\delta = 3.73$, $^2J_{HP} = 7.9$ Hz, $^2J_{HH} = 13.9$ Hz
H^c: $\delta = 4.22$, $^2J_{HP} = 19.6$ Hz, $^2J_{HH} = 17.0$ Hz	$\delta = 3.67$, $^2J_{HP} = 5.6$ Hz, $^2J_{HH} = 13.9$ Hz
$\delta_F = -73.6, -75.5$, $^4J_{FF} = 9.9$ Hz	$\delta_F = -74.2, -75.8$, $^4J_{FF} = 9.3$ Hz

Scheme 2. Selected NMR data of **4** and **6**.

The X-ray crystallographic analysis of **4**[14] (Fig. 1) reveals a distorted trigonal-bipyramidal coordination at phosphorus with apical nitrogen and oxygen atoms, very similar to those of the aforementioned oxa analogues.[1–3] Compound **4** is thus the first example of a pentacoordinate 1,2λ^5-azaphosphetidine.[15] The four-membered ring is similar to that reported for a tetraco-

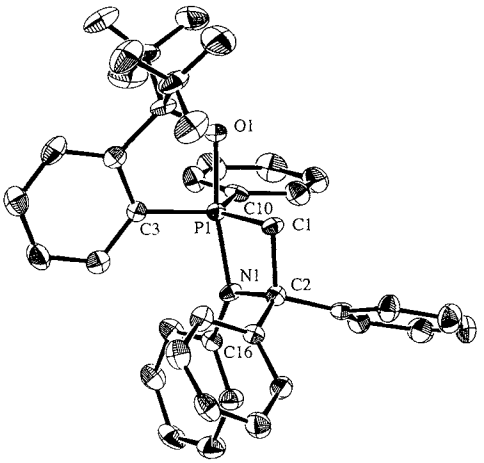

Fig. 1. Crystal structure of **4** (ORTEP, thermal ellipsoids at 30% probability). Selected bond lengths [Å], bond angles [°], and torsion angles [°]: P1-N1 1.798(5), P1-O1 1.796(5), P1-C1 1.818(6), P1-C3 1.816(7), P1-C10 1.822(7), C1-C2 1.542(9), C2-N1 1.486(8); N1-P1-O1 166.9(3), N1-P1-C1 75.1(3), P1-C1-C2 94.3(1), C1-C2-N1 93.1(5), C2-N1-P1 97.5(4), C2-N1-C16 125.4(5), P1-N1-C16 137.1(5), C1-P1-C3 119.9(3), C1-P1-C10 122.5(3), C3-P1-C10 117.5(3); P1-C1-C2-N1 −0.1(5), P1-N1-C2-C1 0.1(5).

ordinate 1,2-azaphosphetidine,[15c] while the length of the apical P1–N1 bond (1.789(5) Å) is close to those in pentacoordinate 1,3,2-diazaphosphetidines (1.799(2) Å[15e] and 1.782(3) Å[15g]). The bond angle between two apical bonds deviates from 180° by 13.1(3)°. The phosphorus atom is placed in the equatorial plane and the torsion angle P1-C1-C2-N1 is −0.1°, indicating that the four-membered ring is almost planar. Interestingly, the nitrogen atom has trigonal-planar coordination and the plane of the benzene ring on the nitrogen lies in the plane of the four-membered ring. When **4** ($\delta(^{31}P) = -29.9$) was dissolved in [D$_8$]toluene, a further signal was observed at $\delta(^{31}P) = -50.9$, probably due to pseudorotamer **6**, in which the nitrogen atom is equatorial (Scheme 2). In the ^{1}H NMR spectrum the signals of the methylene protons of **6** appeared at a slightly higher field than those of **4** and the coupling constants ($^2J_{H,P}$) are smaller. In the NOE difference spectrum correlations between H^a and H^{b,c} were observed in **6** but not in **4**. The signal of the *ortho* proton in **6** (H^a) is not shifted downfield, indicating that the apical P–C bond is less polar than the P–N bond of **4**. These results can be reasonably interpreted as follows: a) Because the apical P–C bond in **6** is more polar and longer than the equatorial P–C bond in **4**, the shielding effect of the increased negative charge results in upfield chemical shifts and in smaller coupling constants. b) The shorter distances between the protons H^a and H^{b,c} in **6** lead to the observed NOE effects, which are not seen for **4**. This is the first observation of such a pseudorotamer; these compounds are not known for the oxygen analogs, 1,2-oxaphosphetanes.[16] This difference may be related to the difference in electronegativity between nitrogen and oxygen. A similar pseudorotamer ($\delta(^{31}P) = -51.0$) was observed also in the case of **5**.

Heating **4** (200 °C, 5 d) or **5** (100 °C, 18 h) in a sealed tube (Scheme 3) gave quantitatively the corresponding olefin **7a** or **7b**

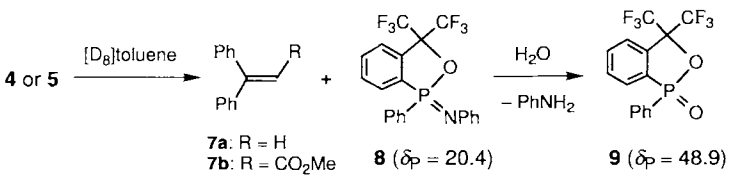

Scheme 3. Reactions of **4** and **5**.

and iminophosphorane **8**, which was hydrolyzed to the corresponding cyclic phosphinate **9** and aniline. Thus **4** and **5** show Wittig reactivity; in other words, a pentacoordinate 1,2-azaphosphetidine can be regarded as an intermediate of the reaction of phosphorus ylides with Schiff bases. The coexistence of both pseudorotamers experimentally supports the argument that the olefin formation occurs via a C-apical pseudorotamer, which has been proposed in the Wittig reaction.[17]

Experimental Procedure

3: To a solution of **1** (1.002 g, 2.62 mmol) in THF (31 mL) were added at 0 °C *n*BuLi (1.62 M solution of hexane, 3.7 mL, 2.3 equiv) and then after 1 h HMPA (9.2 mL, 20.1 equiv) under argon, and the solution was stirred at 0 °C for 2 h. To the solution was added a solution of **2** (1.632 g, 6.34 mmol, 2.4 equiv) in THF (11 mL) at 0 °C, and the reaction mixture was stirred at 0 °C for 3 h and at −10 °C for 18 h. After usual workup the crude mixture was chromatographed on silica gel to give β-aminophosphane oxide **3** (44% yield) (m.p. 177–179 °C (decomp)); **1** was recovered in 23% yield.

4: To a solution of **3** (301 mg, 0.470 mmol) and Ph_3P (380 mg, 1.45 mmol) in dry benzene (20 mL) was added DEAD (0.24 mL, 1.52 mmol) at room temperature (25 °C) under argon. The reaction mixture was stirred for 45 min. The ^{31}P NMR spectrum of the mixture mainly showed signals at $\delta = -29.4$ and 29.8 due to **4** and Ph_3PO, respectively. After removal of the solvent under reduced pressure, the residue was crystallized from absolute EtOH to give almost pure **4** (272 mg, 93% yield). An analytically pure sample was obtained by recrystallization from CH_2Cl_2/EtOH. Single crystals suitable for X-ray analysis were grown from acetone. **4**: M.p. 258–259 °C (decomp); Anal. calcd for $C_{35}H_{26}F_6NOP \cdot H_2O$: C 65.73, H 4.41, N 2.19; found: C 65.45, H 4.20, N 2.27; HRMS (70 eV): *m/z* (M^+) calcd for $C_{35}H_{26}F_6NOP$: 621.1656, found: 621.1656; ^{1}H NMR (500.1 MHz, $CDCl_3$, 27 °C, TMS): $\delta = 4.22$ (dd, $^2J(H,P) = 19.6$, $^2J(H,H) = 17.0$ Hz, 1H, PCHH'), 4.55 (dd, $^2J(H,P) = 21.6$, $^2J(H,H) = 17.0$ Hz, 1H, PCHH'), 6.41 (d, $^3J(H,H) = 8.1$ Hz, 2H), 6.56 (t, $^3J(H,H) = 7.4$ Hz, 1H), 6.78 (dd, $^3J(H,H) = 7.4$, 8.1 Hz, 2H), 7.15–7.17 (m, 3H), 7.26–7.28 (m, 2H), 7.32–7.40 (m, 10H), 7.52–7.56 (m, 1H), 7.78–7.81 (m, 1H), 7.89–7.90 (m, 1H), 8.27 (dd, $^3J(H,P) = 12.1$, $^3J(H,H) = 7.9$ Hz, 1H); ^{31}P NMR (109 MHz, $CDCl_3$, 27 °C, 85% H_3PO_4): $\delta = -29.4$. Satisfactory ^{13}C and ^{19}F NMR spectra were obtained.

Received: November 14, 1995 [Z8548IE]
German version: *Angew. Chem.* **1996**, *108*, 1206–1208

Keywords: 1,2λ^5-azaphosphetidines · heterocycles · olefin formation · pseudorotamers

[1] a) T. Kawashima, K. Kato, R. Okazaki, *J. Am. Chem. Soc.* **1992**, *114*, 4008–4009; b) *Angew. Chem.* **1993**, *105*, 941–942; *Angew. Chem. Int. Ed. Engl.* **1993**, *32*, 869–870.

[2] T. Kawashima, N. Iwama, R. Okazaki, *J. Am. Chem. Soc.* **1992**, *114*, 7598–7599.

[3] T. Kawashima, Y. Nishiwaki, R. Okazaki, *J. Organomet. Chem.* **1995**, *499*, 453–455.

[4] T. Kawashima, N. Iwama, R. Okazaki, *J. Am. Chem. Soc.* **1993**, *115*, 2507–2508.

[5] T. Kawashima, N. Yamashita, R. Okazaki, *J. Am. Chem. Soc.* **1995**, *117*, 6142–6143.

[6] Reviews: I. Gosney, A. G. Rowley in *Organophosphorus Reagents in Organic Synthesis* (Ed.: J. I. G. Cadogan), Academic Press, New York, **1979**, pp. 17–153; B. E. Maryanoff, A. B. Reitz, *Chem. Rev.* **1989**, *89*, 863–927.

[7] Reviews on the Peterson olefination: a) W. P. Weber, *Silicon Reagents for Organic Synthesis*: Springer, New York, **1983**, pp. 58–73; b) E. W. Colvin, *Silicon in Organic Synthesis*, Butterworths, London, **1981**, pp. 141–152; c) D. J. Ager, *Org. React. (N.Y.)* **1990**, *38*, 1–223; d) reviews on Peterson-type reactions: T. Kauffmann, *Top. Curr. Chem.* **1980**, *92*, 109–147; *Angew. Chem.* **1982**, *94*, 401; *Angew. Chem. Int. Ed. Engl.* **1982**, *21*, 410–429; M. Pereyre, J.-P. Quintard, A. Rahm, *Tin in Organic Synthesis*, Butterworths, London, **1987**, pp. 176–177.

[8] Reviews: A. Pelter, K. Smith, H. C. Brown, *Borane Reagents*, Academic Press, London, **1988**, pp. 338–339; A. Pelter, K. Smith in *Comprehensive Organic Synthesis, Vol. 1* (Eds.: B. M. Trost, I. Fleming, S. L. Schreiber), Pergamon, Oxford, **1991**, Chapter 2.2, pp. 487–503; A. Pelter, *Pure Appl. Chem.* **1994**, *66*, 223–233.

[9] H. J. Bestmann, F. Seng, *Angew. Chem.* **1963**, *75*, 475; *Angew. Chem. Int. Ed. Engl.* **1963**, *2*, 393.

[10] The Martin ligand was introduced by using a dilithithio derivative of hexafluorocumyl alcohol: E. F. Perozzi, R. S. Michalak, G. D. Figuly, W. H. Stevenson III, D. B. Dess, M. R. Ross, J. C. Martin, *J. Org. Chem.* **1981**, *46*, 1049–1053.

[11] a) O. Mitsunobu, *Synthesis* **1981**, 1–28 (review); b) O. Mitsunobu, K. Kato, J. Kimura, *J. Am. Chem. Soc.* **1969**, *91*, 6510–6511; J. Kimura, Y. Fujisawa, T. Yoshizawa, K. Fukuda, O. Mitsunobu, *Bull. Chem. Soc. Jpn.* **1979**, *52*, 1191–1196.

[12] Yield of isolated product based on **4**. The yields by NMR analysis were 37, 19, and 35% for **3**, **4**, and **5**, respectively. Only one of two possible diastereomers was obtained, which was determined to have the same configuration as that of the 1,2λ^5-oxaphosphetane [1b] by NOE difference experiments. **5**: M.p. 58–61 °C (decomp); ^{1}H NMR (500.1 MHz, $CDCl_3$, 27 °C, TMS): δ = 3.41 (s, 3H), 5.54 (d, ^2J(H,P) = 18.9 Hz, 1H), 6.30 (d, ^3J(H,H) = 8.1 Hz, 2H), 6.54 (t, ^3J(H,H) = 7.2 Hz, 1H), 6.71–6.74 (m, 2H), 7.13–7.18 (m, 4H), 7.29–7.37 (m, 4H), 7.54–7.58 (m, 1H), 7.75–7.85 (m, 3H), 7.94 (d, ^3J(H,H) = 8.3 Hz, 1H), 8.19 (dd, ^3J(H,P) = 11.7, ^3J(H,H) = 8.0 Hz, 1H); ^{31}P NMR (109 MHz, $CDCl_3$, 27 °C, 85% H_3PO_4): δ = −33.0.

[13] The downfield shift was first reported by J. C. Martin et al.: I. Granoth, J. C. Martin, *J. Am. Chem. Soc.* **1979**, *101*, 4618–4622.

[14] $C_{35}H_{26}F_6NOP$, M_r = 621.56, crystal size 0.25 × 0.25 × 0.05 mm, monoclinic, space group $C2/c$, a = 31.969(6), b = 8.857(7), c = 22.270(4) Å, β = 111.41(2)°, V = 5870(4) Å^3, Z = 8, ρ_{calcd} = 1.406 g cm^{-3}, R = 0.056 (R_w = 0.060). Crystallographic data (excluding structure factors) for the structure reported in this paper have been deposited with the Cambridge Crystallographic Data Centre as supplementary publication no. CCDC-179-22. Copies of the data can be obtained free of charge on application to The Director, CCDC, 12 Union Road, Cambridge CB2 1EZ, UK (fax: int. code + (1223) 336-033; e-mail: teched@chemcrys.cam.ac.uk).

[15] For tetracoordinate 1,2-azaphosphetidienes, see: a) E. S. Gubnitskaya, Z. T. Semashko, A. V. Kirsanov, *Zh. Obshch. Khim.* **1978**, *48*, 2624; b) E. S. Gubnitskaya, V. S. Parkhomenko, Z. T. Semashko, L. I. Samaray, *Phosphorus Sulfur* **1983**, *15*, 257–258; c) M.-J. Menu, Y. Dartiguenave, M. Dartiguenave, A. Baceiredo, G. Bertrand, *Phosphorus Sulfur Silicon* **1990**, *47*, 327–334; d) K. Afarinkia, J. I. G. Cadogan, C. W. Rees, *J. Chem. Soc. Chem. Commun.* **1992**, 285-287. For pentacoordinate 1,2,3-diazaphosphetidines, see: e) A. Schmidpeter, J. Luber, D. Schomburg, W. S. Sheldrick, *Chem. Ber.* **1976**, *109*, 3581–3587; f) H. W. Roesky, K. Ambrosius, W. S. Sheldrick, *ibid.* **1979**, *112*, 1365–1371; g) H. W. Roesky, K. Ambrosius, M. Banek, W. S. Sheldrick, *ibid.* **1980**, *113*, 1847–1854; h) I. M. Abd-ellah, E. H. M. Ibrahim, A. N. El-khazandar, *Phosphorus Sulfur* **1987**, *29*, 239–247.

[16] E. Vedejs, C. F. Marth, *J. Am. Chem. Soc.* **1989**, *111*, 1519–1520.

[17] R. Holler, H. Lischka, *J. Am. Chem. Soc.* **1980**, *102*, 4632–4635; F. Volatron, O. Eisenstein, *ibid.* **1987**, *109*, 1–14; T. Naito, S. Nagase, H. Yamatka, *ibid.* **1994**, *116*, 10080–10088. Whether this reaction follows a C–P heterolysis mechanism or not is open to further investigation. For this mechanism, see: H. J. Bestmann, *Pure Appl. Chem.* **1980**, *52*, 771–788; H. J. Bestmann, O. Vostrowsky, *Top. Curr. Chem.* **1983**, *109*, 85.

Towards the Definition of the Maximum Allowable Tightness of an Electron Transfer Transition State in the Reactions of Radical Anions and Alkyl Halides**

G. Narahari Sastry, David Danovich, and Sason Shaik*

How tightly bonded can the transition state (TS) of an electron transfer (ET) reaction be before it collapses to a classical TS for a bond-forming reaction? In other words: is it possible to define the minimum allowed separation or the maximum allowed bonding between the reactants of an ET process? These fundamental questions are related to the long-standing interest in the mechanistic dichotomy between ET and nucleophilic substitution (SUB) processes,[1] and to renewed interest in the problem through the recent demonstrations of ET/SUB competitions and mechanistic crossovers in the reactions between radical anions and alkyl halides.[2, 3] The present communication addresses the fundamental questions by using the ET and SUB reactions for combinations of formyl radical anions and methyl halides. We have found that within a distinct range of intermolecular distances the TS is transformed from an ET-TS into a SUB-TS.

Following our recent studies described in ref. [4], we investigated a group of reactions between the substituted formyl radical anions and the methyl halides (systems **1** in Scheme 1). These

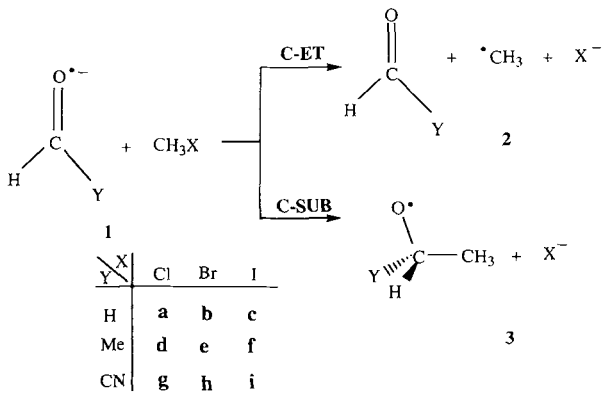

Scheme 1. Reactions studied.

systems undergo three types of reactions: O-alkylation, C-oriented electron transfer (C-ET)[4a] to give **2**, and C-alkylation (C-SUB) to give **3**. While the O-alkylation has generally a distinct TS, which has been discussed before,[4] the C-ET and C-SUB reactions are mutually exclusive and exhibit a mechanistic crossover, C-ET → C-SUB, when the substituents on the formyl radical anion and also the halides are varied. This communication focuses on the latter two processes and addresses precisely the fundamental question posed at the outset.

All the calculations were performed with the Gaussian 92 program package.[5] Geometries were gradient optimized and characterized by frequency analysis. Mechanisms were ascertained by following the reaction path, by using the intrinsic reaction coordinate (IRC) technique with internal (non-mass-weighted) coordinates, IRC(internal).[6, 7] Since spin contamination becomes at times significant along the UHF and UMP2 paths,[6b] the study was carried out with ROHF theory,[6a] which is free of spin contamination and gives geometric and energetic results compatible with those of previous studies.[4a] The 6-31G* basis set was used for C, O, H, and N atoms, while for the halides we used the Hay and Wadt effective core potential (ECP)[9] with the LANL1DZ valence basis set augmented with two sets of uncontracted d-type polarization functions (Cl: α_d = 0.150 and 0.375; Br: α_d = 0.232 and 0.600; I: α_d = 0.270 and 0.730). A comparative all-electron study, which was carried out for X = Cl, using the 6-31G* basis set gave virtually identical results with those of the ECP basis set.

An ion–dipole cluster C_R **4**, precedes the transition state **5**, which proceeds either to the ET products **2** or to the C-SUB products **3**. For each pair of reactants in Scheme 1 the C-attack gave only one TS structure (**5**) either of the C-ET or C-SUB variety, but never both. The critical distances for the various C_R and transition state structures are given in Table 1. In the transition from C_R to TS the R_{CO} distance decreases while R_{CX} increases. For case **f** the TS is early and its C–I bond is shorter than that in the cluster but clearly longer than that in the free

[*] Prof. Dr. S. Shaik, Dr. G. N. Sastry, Dr. D. Danovich
Department of Organic Chemistry
and
The Fritz Haber Centre of Molecular Dynamics
The Hebrew Univerisity, Jerusalem 91904 (Israel)
Fax: Int. code + (2) 658-5345

[**] This research was sponsored by the Volkswagen-Stiftung.

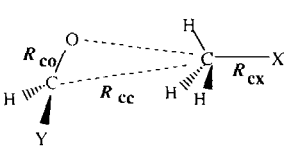

4, C_R

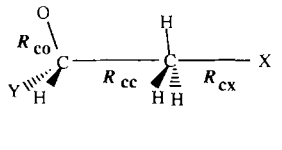

5, TS

Table 1. Important structural parameters [Å] of TS **5** and C_R **4** for the reactions in Scheme 1.

System	Y	X	R_{CO}		R_{CX}		R_{CC}	
			C_R	TS	C_R	TS	C_R	TS
a	H	Cl [a]	1.287	1.262	1.818	2.101	3.289	2.529
			(1.287)	(1.265)	(1.849)	(2.072)	(3.316)	(2.572)
b	H	Br	1.288	1.269	2.031	2.169	3.291	2.679
c	H	I	1.290	1.277	2.200	2.285	3.336	2.846
d	Me	Cl [a]	1.289	1.262	1.815	2.108	3.343	2.524
			(1.290)	(1.265)	(1.822)	(2.081)	(3.360)	(2.565)
e	Me	Br	1.290	1.268	2.028	2.179	3.333	2.667
f	Me	I	1.292	1.276	2.311	2.296	3.236	2.820
					[2.151] [b]			
g	CN	Cl [a]	1.269	1.261	1.816	2.326	3.693	2.250
			(1.269)	(1.259)	(1.824)	(2.297)	(3.680)	(2.314)
h	CN	Br	1.269	1.256	1.992	2.424	3.664	2.370
i	CN	I	1.270	1.252	2.204	2.567	3.630	2.481

[a] Values in the parentheses were obtained with the all-electron 6-31G* basis set. [b] The value in square brackets corresponds to the length of the C–I bond in CH_3I.

reactant, CH_3I. The decrease in R_{CO} promotes the C-ET process (acting to eject the electron from the formyl radical anion), while the increase in R_{CX} is common to both C-ET and C-SUB processes. The IRC(internal) analysis for the C-ET process shows initially a C–C approach followed by C–C recoil. In turn, the C–C recoil is synchronized with C–X bond cleavage; hence this is a dissociative and bonded C-ET process. In contrast, the IRC(internal) analysis for the C-SUB process shows a continuous C–C bond formation synchronized with C–X bond cleavage; hence this is a substitution mechanism. Both types of TSs are connected to cluster C_R in the reverse direction of IRC. Thus, the IRC results for the two processes are distinct and characteristic.

As specified in Table 2, the TS structures for systems **a**–**f** correspond to ET-TS structures. In contrast, systems **g** and **h**, which involve the poorest electron donor, cyanoformaldehyde radical anion, were found to have transition states that correspond to the C-SUB variety, resulting in C-alkylation. Further increase of the acceptor ability of the alkyl halide to X = I in system **i** led to an ET-TS structure even with Y = CN.[6c] Apparently, a mutually exclusive competition exists between the ET and SUB mechanisms along the same C–C–X trajectory of attack, and the entire group of reactions define therefore a mechanistic spectrum with an ET/SUB changeover.

Table 2. Thermochemical quantities [a], entropies of activation [b, c], and α-C^{12}/C^{13} kinetic isotope effects [c, d].

System	Y	X	Process	$\Delta E^{\neq}$	ΔE_{ET} [e]	ΔE_{SUB} [e]	G_{ET} [f, h]	$\Delta S^{\neq}$	α-C^{12}/C^{13}
a	H	Cl [g]	C-ET	6.4	−39.1	−61.3	80.0	−24.9	1.056
				(5.5)	(−48.0)	(−70.2)	(72.4)	(−25.1)	(1.059)
b	H	Br	C-ET	2.8	−50.8	−73.0	45.7	−24.8	1.052
c	H	I	C-ET	0.6	−66.7	−88.9	21.5	−24.9	1.028
d	Me	Cl [g]	C-ET	7.9	−42.4	−57.8	78.1	−25.7	1.057
				(5.8)	(−51.3)	(−66.7)	(70.5)	(−25.8)	(1.058)
e	Me	Br	C-ET	3.4	−54.1	−69.6	43.9	−25.5	1.054
f	Me	I	C-ET	1.4	−70.0	−85.5	19.6	−25.6	1.036
g	CN	Cl [g]	C-SUB	21.7	7.5	−15.8	112.6	−27.7	1.057
				(18.7)	(−1.4)	(−24.7)	(105.0)	(−26.9)	(1.060)
h	CN	Br	C-SUB	14.3	−4.3	−27.5	78.3	−26.1	1.056
i	CN	I	C-ET	9.4	−20.2	−43.4	54.1	−24.6	1.052

[a] In kcal mol^{-1}. [b] The standard state is 1 M at 298.15 K. [c] The parameters correspond to the process **1** → **5**. [d] Frequencies are scaled by the recommended factor 0.8929 to obtain the thermochemical values. [e] ΔE quantities refer to the process from separated reactants **1** to separated products **2** or **3**. [f] G_{ET} corresponds to the energy difference between the ground state $YHC{=}O^{\cdot -}/CH_3X$ and the charge transfer state $YHC{=}O/CH_3X^{\cdot -}$ at the reactants geometry. [g] Values in parentheses were obtained with the all-electron 6-31G* basis set. [h] $G_{SUB} = G_{ET} + \Delta E_{3\pi\pi^*}(YHC{=}O)$. Note that $\Delta E_{3\pi\pi^*}(YHC{=}O)$ is much smaller for Y = CN than for Y = H, CH_3.

Table 2 also gives the computed energies, entropies of activation, and the α-C^{12}/C^{13} kinetic isotope effects. The activation barriers $\Delta E^{\neq}$ depend on X and Y with the following orders: Cl > Br > I for X, and H < Me ≪ CN for Y. All the TS structures contain C–C bonding, as reflected in large values for the entropy of activation for all the reactions and in normal α-C^{12}/C^{13} isotope effects.[10] Even in the "loosest" TS structure in the group, **5c**, exhibits significant bonding, as implied by the normal α-C^{12}/C^{13} isotope effect.

The mechanistic selection follows from a recent valence bond configuration mixing (VBCM) treatment[11] of the problem in terms of three principal VB configurations, which for brevity may be described by the occupancy of the π_{CO} and π^*_{CO} fragment orbitals of the formyl group, and σ_{CX} and σ^*_{CX} orbitals of the alkyl halide moiety. These are: the reactant configuration ($\pi^2_{CO}\ \pi^{*1}_{CO}\ \sigma^2_{CX}$) the charge transfer configuration ($\pi^2_{CO}\ \sigma^2_{CX}\ \sigma^{*1}_{CX}$) and the substitution configuration ($\pi^1_{CO}\ \pi^{*1}_{CO}\ \sigma^2_{CX}\ \sigma^{*1}_{CX}$). The substitution configuration involves triplet excitation of the formyl moiety from π_{CO} to π^*_{CO} in addition to an electron transfer to the σ^*_{CX} orbital. It is the pairing of the two π electrons of the triplet formyl moiety with the electron in the σ^*_{CX} orbital that is eventually responsible for formation of the new C–C bond in the substitution product. At the geometry of the reactants, the energy of the CT state lies above that of the reactant state by the vertical electron transfer energy gap G_{ET}. The vertical energy gap of the substitution state, G_{SUB}, is obtained by adding the triplet $^3\pi\pi^*$ excitation energy of the formyl moiety to G_{ET}. This triplet $^3\pi\pi^*$ excitation energy for formaldehyde and methyl formaldehyde is much larger than that for cyanoformaldehyde, and therefore the $CN(H)C{=}O^{\cdot -}/CH_3X$ reactant pairs are typified both by a higher lying charge transfer configuration and a more closely lying substitution configuration than the configurations of the corresponding pairs, $H_2C{=}O^{\cdot -}/CH_3X$ and $CH_3(H)C{=}O^{\cdot -}/CH_3X$.

These three configurations cross and mix with each other along the C–C–X trajectory.[11b] Consider first the crossing of the reactant and CT configurations in terms of two key quantities shown in Table 2, the reaction exothermicity ΔE_{ET} and the vertical electron transfer energy gap G_{ET}. A large G_{ET} and weakly exothermic ΔE_{ET} will lead to a tighter crossing point with a small intermolecular distance R_{CC}. In turn, the smaller the C–C distance at the crossing point is, the greater the contribution of the substitution configuration will be, until the point at which its mixing with the reactant configuration prevails and the corresponding structure collapses accordingly to a SUB-TS. This effect of the substitution configuration will become significant for the $CN(H)C{=}O^{\cdot -}/CH_3Cl$ and $CN(H)C{=}O^{\cdot -}/CH_3Br$ pairs; the mixing of the substitution configuration will be enhanced by both the large G_{ET} gaps and the low triplet $^3\pi\pi^*$ excitation energy of cyanoformaldehyde.

Since G_{SUB} depends on G_{ET}, a combination of G_{ET} and ΔE_{ET} variations can serve as the minimum necessary predictor of both the C–C distance at the TS as well as in the mechanistic changeover C-ET → C-SUB . The factor $\alpha = 0.5 G_{ET}/(G_{ET} - \Delta E_{ET})$, derived from the Marcus expression,[12] gives effectively the appropriate combination of G_{ET} and ΔE_{ET} that can gauge the earliness of the TS in terms of its R_{CC} distance. Figure 1 is a plot

 © VCH Verlagsgesellschaft mbH, D-69451 Weinheim, 1996 0570-0833/96/3510-1099 $ 15.00+.25/0

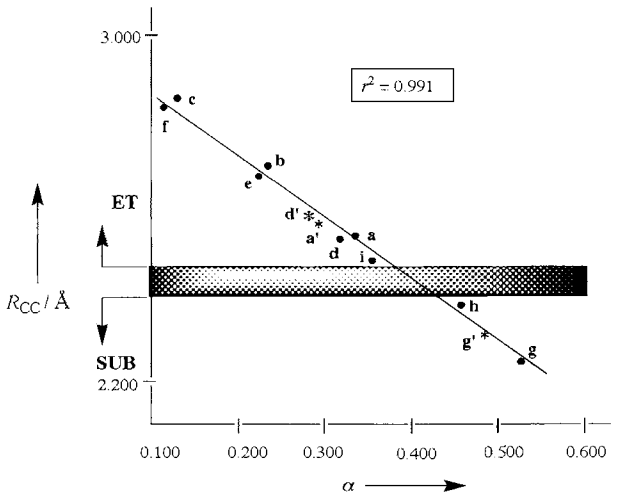

Fig. 1. The variation of C–C distances at the TS as a function of α. Filled circles: results of calculations with the ECP basis set; asterisks: results of calculations with the 6-31G* basis set (systems **a'**, **d'**, and **g'**); gray band: area of mechanistic changeover.

of the R_{CC} distances, calculated for the transition states of the reactions of systems **1**, against the index α. It is seen that the C–C distances in the transition states decrease linearly as α increases; in the ET-TS structures, $R_{CC} \geq 2.481$ Å, while in the SUB-TS structures, $R_{CC} \leq = 2.370$ Å. These two critical values, 2.370 and 2.481 Å, define the mechanistic changeover zone from the C-ET to C-SUB, over a narrow range of approximately 0.1 Å. It follows therefore that the ET/SUB dichotomy characterized by Figure 1 corresponds to two mutually exclusive mechanisms that exhibit a continuous mechanistic spectrum with a narrow changeover zone from C-ET to C-SUB. Thus, while TS earliness is gauged by the Marcus parameter of the ET process, the C-ET → C-SUB mechanistic changeover itself originates in the multiconfigurational nature of the problem, which is characterized by the VB mixing of at least three VB configurations.[11]

We have described here the first structural foundations for the long-sought[1a, b, 3] ET/SUB dichotomy in a set of reactions of radical anions ($A^{\cdot -}$) and alkyl halides (RX). There seems to be a continuous spectrum of distances between the reactants in the ET-TS, and at a certain minimum distance there is a mechanistic changeover to the SUB-TS. Thus, the ET series up to the changeover zone exhibits an ET-TS with variable C–C bonding ranging from weak bonding in cases **c** and **f**, to significant bonding in cases **a**, **d**, and **i**. Of course the choice of the computational method may shift the changeover zone, but nevertheless, the sharpness of the zone indicates that ET-TS structures can indeed be strongly bonded and structurally adjacent to their SUB analogs. The critical zone may of course depend on the nature of the $A^{\cdot -}$/RX family; each family may exhibit its own characteristic changeover zone, and its own point of maximum bonding for the ET-TS.

Received: November 17, 1995 [Z 8564 IE]
German version: *Angew. Chem.* **1996**, *108*, 1208–1211

Keywords: ab initio calculations · electron transfer · radical anions · reaction mechanisms

[1] a) L. Eberson, *Electron Transfer Reactions in Organic Chemistry*, Springer, Heidelberg, **1987**; b) A. Pross, *Acc. Chem. Res.* **1985**, *18*, 212; c) M. Chanon, *Bull. Soc. Chim. Fr.* **1982**, Part II, p. 197.

[2] a) N. Kimura, S. Takamuku, *Bull. Chem. Soc. Jpn.* **1992**, *65*, 1668; b) *ibid.* **1993**, *66*, 3613; c) *J. Am. Chem. Soc.* **1994**, *116*, 4087.

[3] a) K. Daasberg, T. B. Christensen, *Acta Chem. Scand.* **1995**, *49*, 128; b) K. Daasberg, S. U. Pedersen, H. Lund, *ibid.* **1991**, *45*, 424; c) H. Lund, K. Daasberg, T. Lund, S. U. Pedersen, *Acc. Chem. Res.* **1995**, *28*, 313, and references therein; d) J.-M. Savéant, *Adv. Phys. Org. Chem.* **1990**, *26*, 1.

[4] a) G. N. Sastry, S. Shaik, *J. Am. Chem. Soc.* **1995**, *117*, 3290; b) G. N. Sastry, A. C. Reddy, S. Shaik, *Angew. Chem.* **1995**, *107*, 1619; *Angew. Chem. Int. Ed. Engl.* **1995**, *34*, 1495.

[5] M. J. Frisch, G. W. Trucks, M. Head-Gordon, P. M. W. Gill, M. W. Wong, J. B. Foresman, B. G. Johnson, H. B. Schlegel, M. A. Robb, E. S. Replogle, R. Gomperts, J. L. Andres, K. Raghavachari, J. S. Binkley, C. Gonzalez, R. L. Martin, D. J. Fox, D. J. Defrees, J. Baker, J. J. P. Stewart, J. A. Pople, Gaussian 92, Revision C3, Gaussian, Inc., Pittsburgh, PA, **1992**.

[6] The term IRC(internal) is used as in ref. [5]. The reaction pathways were examined also by means of IRC with mass-weighted (MW) coordinates [8], IRC(MW). It was found that the energy along the IRC(internal) path is consistently lower than that along the IRC(MW) path in all the cases. Hence the IRC(internal) path qualifies as the path of steepest descent and was therefore used throughout to designate the mechanisms of the reactions. a) At the ROHF level both IRC(internal) and IRC(MW) gave identical mechanistic conclusions for the combinations **a**–**e**, **g**, and **h** with both the 6-31G* and the ECP basis sets (reaction **a** was tested with many other basis sets—6-31 + G*, 6-31G**, 6-311G*, and 6-311G**—all of which led to the same conclusion, an ET mechanism). b) In UHF (for **a**, **c**, **g**) and UMP2/6-31G* (for **a**, **g**), the IRC(internal) path has a rather small spin contamination throughout and leads to the same mechanistic conclusions as the ROHF path. In contrast, the IRC(MW) path passes through highly spin-contaminated regions (for example $\langle S^2 \rangle = 0.875$ for reaction **a**) and produces nonsmooth energy profiles terminating at C-SUB products. For this reason the ROHF level was preferred over the UHF and UMP2 level in the present study. c) For the reaction in system **i** (Y = CN, X = I) the IRC(MW) at the ROHF level gave a nonsmooth profile resulting in C-SUB, while IRC(internal) produced a consistently steeper path and a smooth energy profile leading to ET. As the path of steepest descent starting from **5i** leads to ET products, **5i** was designated as an ET-TS.

[7] C. Gonzalez, H. B. Schlegel, *J. Chem. Phys.* **1989**, *90*, 2154.

[8] C. Gonzalez, H. B. Schlegel, *J. Phys. Chem.* **1990**, *94*, 5523.

[9] a) P. J. Hay, W. R. Wadt, *J. Chem. Phys.* **1985**, *82*, 270; b) W. R. Wadt, P. J. Hay, *ibid.* **1985**, *82*, 284; c) P. J. Hay, W. R. Wadt, *ibid.* **1985**, *82*, 299.

[10] B. S. Axelsson, B. Långström, O. Matsson, *J. Am. Chem. Soc.* **1987**, *109*, 7233.

[11] a) L. Eberson, S. S. Shaik, *J. Am. Chem. Soc.* **1990**, *112*, 4484. b) Based on Figure 4 in ref. [11a]. The CT state and reactant configurations mix by optimization of the $\pi^*_{CO} - \sigma^*_{CX}$ overlap, while the substitution and reactant configurations mix by optimization of the $\pi_{CO} - \sigma^*_{CX}$ overlap. Hence all three configurations mix along the C···C···X trajectory.

[12] The Marcus expression is given by $\alpha = 0.5(1 + \Delta E_{ET}/\lambda)$, where $\lambda = G_{ET} - \Delta E_{ET}$. Substituting for λ and rearranging leads to $\alpha = 0.5 G_{ET}/(G_{ET} - \Delta E_{ET})$.

Synthesis, Structure, Photophysics, and Excited-State Redox Properties of the Novel Luminescent Tetranuclear Acetylidocopper(I) Complex $[Cu_4(\mu\text{-dppm})_4(\mu_4\text{-}\eta^1,\eta^2\text{-}C{\equiv}C\text{-})](BF_4)_2$**

Vivian Wing-Wah Yam,* Wendy Kit-Mai Fung, and Kung-Kai Cheung

There has been a growing interest in the synthesis of alkynyl metal complexes because of their potential applications as nonlinear optical materials and molecular wires.[1] Moreover, the ability of acetylido ligands to bond to transition metals in a number of different bonding modes to form a variety of mono-

[*] Dr. V. W.-W. Yam, W. K.-M. Fung, Dr. K.-K. Cheung
Department of Chemistry
The University of Hong Kong
Pokfulam Road, Hong Kong (Hong Kong)
Fax: Int. code + (2)857-1586
e-mail: wwyam@hkucc.hku.hk

[**] V. W.-W. Y. acknowledges financial support from the Research Grants Council, the Croucher Foundation, and The University of Hong Kong. W. K.-M. F. acknowledges the receipt of a postgraduate studentship, administered by The University of Hong Kong. dppm = bis(diphenylphosphano)methane.

and polynuclear complexes[2, 3] has also aroused much attention. This together with our recent efforts on the study of the photophysical and photochemical behavior exhibited by polynuclear d^{10} metal complexes[4, 5] have stimulated the present work. Herein we report on the synthesis and luminescent behavior of a highly novel tetranuclear acetylidocopper(I) complex **1**,

$[Cu_4(\mu\text{-dppm})_4(\mu_4\text{-}\eta^1,\eta^2\text{-}C{\equiv}C)](BF_4)_2$ **1**

which contains an acetylido ligand in both η^1 and η^2 bonding modes. Furthermore, the redox properties in the excited state and the crystal structure have also been determined. Complex **1** is the first structure of a tetranuclear d^{10} metal complex with a μ_4-η^1,η^2-acetylido bridge characterized by X-ray crystallography.

Addition of $[Cu_2(\mu\text{-dppm})_2(MeCN)_2](BF_4)_2$ to a solution of *n*-butyllithium and trimethylsilylacetylene in THF under nitrogen at room temperature results in the formation of **1**, which was isolated as air-stable pale yellow crystals. Complex **1** gave satisfactory C, H analyses, and has been characterized by positive FAB-mass spectrometry, IR and ^{1}H NMR spectroscopy, and by crystal structure analysis.[6]

Figure 1 shows the perspective drawing of the cation in **1**. Complex **1** has crystallographic C_2 symmetry. The four copper atoms are arranged in a distorted rectangular array with the four μ-dppm ligands arranged in a saddlelike configuration. A

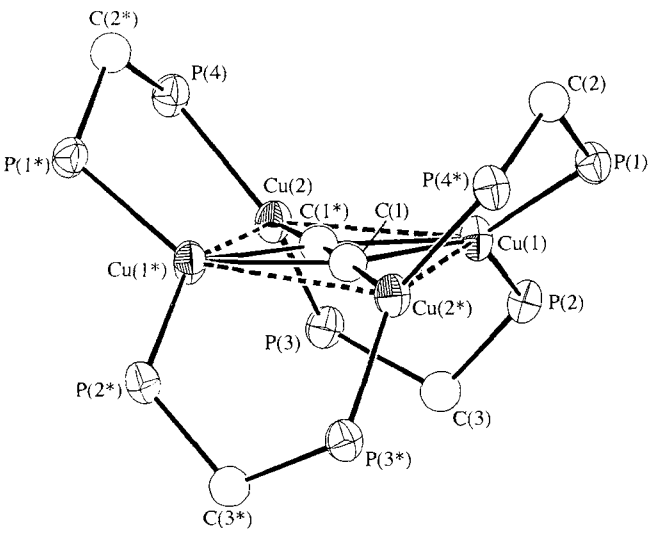

Fig. 1. Perspective drawing of the crystal structure of the cation in **1** with the atomic numbering scheme. Hydrogen atoms and benzene rings have been omitted for clarity. Thermal ellipsoids are shown at the 20% probability levels. Selected bond lengths [Å] and angles [°]: Cu(1)–C(1) 2.13(1), Cu(1)–C(1*) 2.12(1), Cu(2)–C(1*) 1.91(1), Cu(1)–Cu(2) 3.264(2), Cu(1)–Cu(2*) 3.245(2), C(1)–C(1*) 1.26(2), Cu(1)–P(1) 2.273(4), Cu(2)–P(4) 2.236(4), Cu(1)–P(2) 2.270(4), Cu(2)–P(3) 2.230(4); Cu(2)-C(1*)-C(1) 178.2(4), Cu(1)-Cu(2)-Cu(1*) 77.26(6), Cu(2)-Cu(1*)-Cu(2*) 102.60(6), dihedral angle between planes Cu(1)-C(1)-C(1*) and Cu(1*)-C(1*)-C(1) 177.41.

similar configuration has been observed in $[Cu_4(\mu\text{-dppm})_4(\mu_4\text{-S})](PF_6)_2$.[5] The C≡C unit is situated in the middle of the four copper atoms, bridging the four copper atoms in both η^1 and η^2 bonding modes. This represents the first example of a μ_4-η^1,η^2-acetylido-bridged tetranuclear d^{10} copper(I) system. Coordination of this type is also rare in other metal cluster systems.[7] Normal electron counting requires that the C≡C unit acts as a six-electron donor according to the covalent model. While the interaction of the C≡C ligand with each of the Cu_2 units resembles that found in other μ-η^1,η^2-acetylido complexes, best overlap of the two π orbitals of the acetylido ligand with the four copper atoms would require the two Cu_2 units to be orthogonal to each other. However, the π-type bonds from the C≡C unit to Cu(1) and Cu(1*) are close to coplanarity [dihedral angle between Cu(1)-C(1)-C(1*) and Cu(1*)-C(1*)-C(1) is 177.41°]. This may arise as a result of the steric hindrance of the phosphane ligands, which prevents orthogonal geometry for maximum orbital overlap from occurring. A similar type of bonding has also been reported in $[Ru_4(\mu_4\text{-}\eta^1,\eta^2\text{-}C_2)(\mu\text{-}PPh_2)_2(CO)_{12}]$ (**2**).[7a] Unlike in a tetranuclear phenylacetylidocopper(I) complex,[7b] in which true π bonding exists between the C≡CPh unit and the two Cu_2 units arranged in an orthogonal array (dihedral plane 82(1)°), the C≡C bond in **1** (1.26(2) Å) is much shorter than that observed in the phenylacetylide complex (1.38(5) Å),[7b] but comparable to the value of 1.275(11) Å in **2**.[7a] Slightly longer Cu(1)–C(1), Cu(1)–C(1*), Cu(1*)–C(1), and Cu(1*)–C(1*) distances (2.12(1)–2.13(1) Å) have also been observed than the majority of those found in the phenylacetylide complex (1.93(3)–2.18(3) Å).[7b] A Cu(2)-C(1*)-C(1) bond angle of 178.2(4)°, which is close to linearity, is observed. Two of the edges of the Cu_4 unit are shorter than the other two; the copper–copper distances are 3.264(2) and 3.245(2) Å for Cu(1)···Cu(2) and Cu(1)···Cu(2*), respectively. These distances are significantly longer than the sum of van der Waals radii for copper (2.8 Å),[8] which suggests insignificant metal–metal interaction between the four copper atoms. Interestingly, a related tetranuclear M_4 architecture is shown by the $[Pd_4(\mu\text{-}Cl)_2(\mu\text{-dppm})_4]^{2+}$ complex ion.[9]

The electronic absorption spectrum of **1** shows a band at about 262 nm in MeCN, attributable to the intraligand transition of dppm, since free dppm also absorbs strongly in this region. The low-energy absorption at about 374 nm is likely to arise from a $[(C{\equiv}C)^{2-} \rightarrow Cu_4]$ ligand-to-metal charge transfer (LMCT) transition, given the good σ-donating ability of the $(C{\equiv}C)^{2-}$ unit. Upon excitation of complex **1** at $\lambda > 350$ nm at room temperature, intense green and greenish yellow emissions are observed, in the solid state and in solution ($\varphi_{lum} = 0.22$ in acetone), respectively. The photophysical data are summarized in Table 1. The long lifetime of the excited state observed at room temperature in both the solid state and in solution, together with the large Stokes shift suggest that the emission is most likely associated with a spin-forbidden transition from a triplet state. The luminescence of **1** is quenched by pyridinium ion acceptors in an oxidative electron transfer process. The bimolecular rate constants of this quenching are given in Table 2. The reduction potential of the excited state $E^{\circ}(\mathbf{1}^{3+}/\mathbf{1}^{2+*})$ of −1.77 V versus the saturated sodium chloride calomel electrode (SSCE) ($\lambda = 1.39$ eV, and $RT\ln K_{\kappa v} = 0.584$ V vs. SSCE) has been estimated by oxidative quenching studies with a series of structurally related pyridinium ion acceptors, and is indicative of its strong reducing power in the excited state.

Table 1. Photophysical data for complex **1**.

1 (*T*/K)	Absorption λ_{max}/nm (ε_{max}/L mol^{-1} cm^{-1})	Emission λ_{em}/nm (τ_0/μs)	ϕ_{lum}
in acetone (298)	374 (7420)	562 (16.0)	0.22
in acetonitrile (298)	374 sh (6900) 262 (62580)	560 (2.9)	–
as solid (298)		509 (9.8)	
as solid (77)		551	–

 © VCH Verlagsgesellschaft mbH, D-69451 Weinheim, 1996 0570-0833/96/3510-1101 $ 15.00+.25/0

Table 2. Rate constants for the quenching of **1** by pyridinium ion acceptors Q^+ in degassed acetone (0.1 M NBu_4PF_6) at 25 °C.

Quencher [a]	$E(Q^+/Q^0)$/V [b]	k_q'/L mol^{-1} s^{-1} [c]
3,4-dicyano-*N*-methylpyridinium	−0.11	4.05×10^9
2-chloro-*N*-methyl-3-nitropyridinium	−0.37	7.78×10^9
4-cyano-*N*-methylpyridinium	−0.67	5.23×10^9
4-methoxycarbonyl-*N*-methylpyridinium	−0.78	2.59×10^9
4-aminoformyl-*N*-ethylpyridinium	−0.93	9.17×10^8
3-aminoformyl-*N*-methylpyridinium	−1.14	9.56×10^7
N-ethylpyridinium	−1.36	1.13×10^7
4-methyl-*N*-methylpyridinium	−1.49	1.47×10^6

[a] All the cations have hexafluorophosphate counterions except for 3,4-dicyano-*N*-methylpyridinium and 2-chloro-*N*-methyl-3-nitropyridinium which have tetrafluoroborate counterions. [b] Measured against the saturated sodium chloride calomel electrode. [c] k_q' is the rate constant corrected for diffusional effects.

Experimental Procedure

1: To a solution of trimethylsilylacetylene (0.04 mL, 0.30 mmol) in pre-dried, degassed THF (40 mL) under an inert atmosphere of nitrogen, *n*-butyllithium (1.6 M, 0.18 mL, 0.30 mmol) was added at room temperature. A solid sample of $[Cu_2(\mu\text{-dppm})_2(MeCN)_2](BF_4)_2$ (500 mg, 0.43 mmol) was added and stirred at room temperature for 24 h. After evaporation to dryness, the resulting solid was extracted with acetone (3 × 8mL), and the solution was filtered and reduced in volume. Subsequent layering of *n*-hexane into the concentrated solution gave **1** as air-stable pale yellow crystals (yield 200 mg, 46%). ^{1}H NMR (270 MHz, [D$_6$]acetone, 25 °C, relative to TMS): δ = 3.74 (m, 8H; CH_2), 7.00–7.43 (m, 80H; Ph); IR (nujol/KBr): ν[cm^{-1}]: 1057 s, (ν (B–F)); UV/Vis (acetone): λ[nm] (ε_{max}/L mol^{-1}cm^{-1}) = 374 (7420); positive ion FAB-MS: ion cluster at *m/z* 1901 [M^+]. Anal. calcd for $C_{102}H_{88}P_8B_2F_8Cu_4 \cdot H_2O$: C 61.03, H 4.42; found: C 61.13, H 4.45.

Received: December 22, 1995 [Z8678IE]
German version: *Angew. Chem.* **1996**, *108*, 1213–1215

Keywords: bridging ligands · complexes with carbon ligands · coordination · copper compounds · luminescence

[1] T. B. Marder, G. Lesley, Z. Yuan, H. B. Fyfe, P. Chow, G. Stringer, I. R. Jobe, N. J. Taylor, I. D. Williams, S. K. Kurtz, *ACS Symp. Ser.* **1991**, *455*, 605; see also N. J. Long, *Angew. Chem.* **1995**, *107*, 37–56; *Angew. Chem. Int. Ed. Engl.* **1995**, *34*, 21–38.

[2] E. Sappa, A. Tiripicchio, P. Braunstein, *Coord. Chem. Rev.* **1985**, *65*, 219.

[3] R. Nast, *Coord. Chem. Rev.* **1982**, *47*, 89.

[4] V. W. W. Yam, W. K. Lee, T. F. Lai, *Organometallics* **1993**, *12*, 2383; V. W. W. Yam, W. K. Lee, P. K. Y. Yeung, *J. Phys. Chem.* **1994**, *98*, 7545; V. W. W. Yam, W. K. Lee, *J. Chem. Soc. Dalton Trans.* **1993**, 2097; V. W. W. Yam, S. W. K. Choi, *ibid.* **1994**, 2057.

[5] V. W. W. Yam, W. K. Lee, T. F. Lai, *J. Chem. Soc. Chem. Commun.* **1993**, 1571.

[6] a) Crystal Data of **1**: $[(Cu_4P_8C_{102}H_{88})^{2+} \cdot 2BF_4^- \cdot 4(CH_3)_2CO]$, formula weight = 2221.72, orthorhombic, space group *Pccn* (no. 56), a = 21.290(1), b = 23.019(1), c = 22.882(2) Å, V = 11213.7(10) Å^3, Z = 4, ρ_{calcd} = 1.316 g cm^{-3}, $\mu(Mo_{K\alpha})$ = 9.25 cm^{-1}, $F(000)$ = 4576, T = 298 K. A pale yellow crystal of dimensions 0.20 × 0.15 × 0.30 mm mounted inside a capillary glass tube in the presence of some solvent was used for data collection at 25 °C on a Rigaku AFC7R diffractometer with graphite monochromatized $Mo_{K\alpha}$ radiation (λ = 0.71073 Å). ω-2θ scans were used with ω scan angle (0.63 + 0.35 tanθ) at a scan speed of 16.0° min^{-1} (up to four scans for reflections with $I < 15\sigma(I)$). Intensity data (in the range of $2\theta_{max}$ = 45°; h: 0 to 24; k: 0 to 25; l: 0 to 23 and three standard reflections measured after every 300 reflections showed no decay) were corrected for Lorentz and polarization effects, and empirical absorption corrections based on the ψ scan of four strong reflections (minimum and maximum transmission factors 0.925 and 1.000). 8022 reflections were measured, 3357 reflections with $I > 3\sigma(I)$ were considered observed and used in the structural analysis. The space group was determined from systematic absences and the structure was solved by Patterson methods and expanded by Fourier methods (PATTY [6b]) and refinement by full-matrix least squares by using the software package TeXsan [6c] on a Silicon Graphics Indy computer. Only the six heavy atoms (copper and phosphorus) were refined anisotropically. The other 65 non-hydrogen atoms were refined isotropically. 56 hydrogen atoms at calculated positions with thermal parameters equal to 1.3 times that of the attached C atoms were not refined. Convergence for 311 variable parameters by least squares refinement on F with $w = 4F_o^2/\sigma^2(F_o^2)$, where $\sigma^2(F_o^2) = [\sigma^2(I) + (0.012F_o^2)^2]$ for 3357 reflections with $I > 3\sigma(I)$ was reached at R = 0.074 and wR = 0.085 with a goodness-of-fit of 3.00. $(\Delta/\sigma)_{max}$ = 0.04 for the complex cation. Crystallographic data (excluding structure factors) for the structure(s) reported in this paper have been deposited with the Cambridge Crystallographic Data Centre as supplementary publication no. CCDC-179-23. Copies of the data can be obtained free of charge on application to The Director, CCDC, 12 Union Road, Cambridge CB2 1EZ, UK (fax: Int. code + (1223) 336-033; e-mail teched@chemcrys.cam.ac.uk). b) PATTY: P. T. Beurskens, G. Admiraal, G. Beurskens, W. P. Bosman, S. Garcia-Granda, R. O. Gould, J. M. M. Smits, C. Smykalla, **1992**. The DIRDIF program system, Technical Report of the Crystallography Laboratory, University of Nijmegen, The Netherlands; c) TeXsan: Crystal Structure Analysis Package, Molecular Structure Corporation, **1985** and **1992**.

[7] a) M. I. Bruce, M. R. Snow, E. R. T. Tiekink, M. L. Williams, *J. Chem. Soc. Chem. Commun.* **1986**, 701; b) M. G. B. Drew, F. S. Esho, S. M. Nelson, *J. Chem. Soc. Chem. Commun.* **1982**, 1347.

[8] J. C. Slater, *J. Chem. Phys.* **1964**, *41*, 3199.

[9] P. Braunstein, M. A. Luke, A. Tiripicchio, M. T. Camellini, *Angew. Chem.* **1987**, *99*, 802–803; *Angew. Chem. Int. Ed. Engl.* **1987**, *26*, 768–770.

Mesoporous Alumina Molecular Sieves**

Stephen A. Bagshaw and Thomas J. Pinnavaia*

The original synthesis of Mobil M41S mesoporous molecular sieves[1, 2] utilized electrostatic interactions between a positively charged surfactant (S^+) and a negatively charged inorganic precursor (I^-) to assemble the mesostructure. The electrostatic assembly process has been verified[3, 4] and extended to include charge-reversed (S^-I^+) and counterion-mediated ($S^-M^+I^-$ and $S^+X^-I^+$; M^+ = metal cation, X^-) pathways.[5–7] We recently demonstrated that mesostructure assembly, at least in the case of silica, can also be achieved through hydrogen bonding interactions between neutral inorganic precursors (I^0) and neutral alkylamine (S^0) or nonionic polyethylene oxide (N^0) surfactants.[8, 9] More recently, Attard et al.[10] have shown that N^0 surfactants in liquid crystalline form function as authentic templates for the synthesis of M41S silicas with hexagonal, cubic, and lamellar structure. Neutral S^0I^0 and N^0I^0 pathways have important advantages over the electrostatic pathways, in part, because most metals form alkoxides or other neutral complexes suitable for hydrolysis and assembly as I^0 precursors. The diversity of compositions of I^0 precursors allows for the synthesis of mesostructured oxides that are difficult or impossible to achieve by electrostatic assembly mechanisms. We describe here the application of the concept of neutral surfactant templating to the synthesis of the first examples of alumina molecular sieves.

High surface area aluminas are especially important industrial catalysts and catalyst supports.[11, 12] Yet, the performance properties of these widely used phases undoubtedly is limited, because they possess only textural porosity and lack the selective framework/confined pore structure characteristic of a molecular sieve. There have been previous attempts to prepare mesostructured forms of alumina by electrostatic assembly pathways,[5–7] but all afforded products that collapsed upon surfactant removal. However, as shown by the present work, N^0I^0 assembly processes provide highly effective pathways to mesoporous alumina molecular sieves.

[*] Prof. T. J. Pinnavaia, Dr. S. A. Bagshaw
Department of Chemistry and Center for Fundamental Materials Research
Michigan State University
East Lansing, MI 48824 (USA)
Fax: Int. code + (517)432-1225
e-mail: Pinnavaia@cemvax.cem.msu.edu

[**] The support of this research by the National Science Foundation through Chemistry Group Grant CHE-9224102 is gratefully acknowledged.

Table 1. Properties of MSU-X mesoporous alumina molecular sieves calcined at 773 K.

Material designation	Template	Surfactant formulae	Amount of template [a] [mmol]	Surface area [$m^2 g^{-1}$]	d_{100} [nm]	HK pore size [nm]	BJH pore size [nm]	Mesopore volume [b] [mL g^{-1}]
MSU-1	Tergitol 15-S-9 [c]	$C_{11-15}[EO]_9$	10.7	490	8.0	5.5	3.3	0.40
	Tergitol 15-S-12	$C_{11-15}[EO]_{12}$	8.5	425	8.5	6.5	3.5	0.44
	Tergitol 15-S-20	$C_{11-15}[EO]_{20}$	5.8	535	9.0	7.0	4.6	0.68
MSU-2	Igepal RC-760 [d]	$C_{12}Ph[EO]_{18}$	5.9	420	9.6	8.0	4.7	0.64
	Triton X-114 [e]	$C_8Ph[EO]_8$	9.0	460	>9.0	8.0	3.3	0.35
	Triton X-100	$C_8Ph[EO]_{10}$	11.2	445	>9.0	8.0	3.6	0.37
MSU-3	Pluronic 64 L [f]	$[PEO]_{13}[PPO]_{30}[PEO]_{13}$	2.1	430	6.8	4.0	2.4	0.21

[a] All syntheses were performed at a surfactant concentration of 25 wt%. [b] Mesopore volume for pores between 2.0 and 8.0 nm diameter according to the BJH analyses. [c] Tergitol 15-S-x surfactants kindly supplied by Union Carbide. [d] Igepal RC-760 kindly supplied by Rhone-Poulenc. [e] Triton-X surfactants supplied by Aldrich. [f] Pluronic 64 L kindly supplied by BASF.

Three forms of mesoporous aluminas, denoted MSU-1, MSU-2, and MSU-3, were prepared by the hydrolysis of tri-*sec*-butoxyaluminum at ambient temperature in the presence of the nonionic polyethylene oxide surfactants given in Table 1. Typical powder X-ray diffraction (XRD) patterns are shown in Figure 1 for the as-synthesized and calcined forms of MSU-3 alumina prepared from a copolymer surfactant of the type $(PEO)_{13}(PPO)_{30}(PEO)_{13}$ based on polyethylene oxide (PEO) and polypropylene oxide (PPO). Analogous single peak patterns corresponding to large d spacings have been observed for disordered MCM-41,[3, 5] HMS,[8] and MSU-X[9] silicas. However, the reflections for MSU-X aluminas are broader, signifying an even greater degree of structural disorder. Also, the intensities of the XRD lines are substantially larger for the calcined forms of MSU aluminas than for the as-synthesized materials. Analogous changes in XRD intensities have been observed for MCM-41 and HMS silicas.[9] Recent modeling studies by S. D. Mahanti[13] have shown that the removal of the occluded organic template from hexagonal mesostructures enhances the Bragg scattering cross-section. Similar differences in scattering intensities are anticipated for as-synthesized and calcined forms of disordered mesostructures.

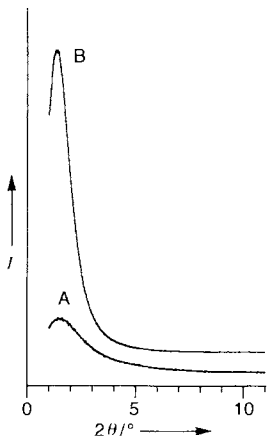

Fig. 1. Powder X-ray diffraction patterns of MSU-3 alumina prepared with Pluronic 64L surfactant: A) As-synthesized sample after air drying at room temperature for 16 h; B) after calcination at 773 K in air for 6 h. The intensity I is in arbitrary units.

PEO-based surfactants are known to adopt spherical to long "wormlike" micellar structures in aqueous solution.[14–16] The pore structures of MSU-X aluminas prepared with these N^0 surfactants reflect the wormlike motif of the micellar structure, as evidenced by the representative transmission electron microscopic (TEM) image (Fig. 2) for a MSU-1 alumina prepared from Tergitol 15-S-9. However, the wormlike channels, though more or less regular in diameter, have no discernible long-range order. That is, the packing of channel system appears to be random, despite the presence of an XRD reflection. In this latter case the regular separation between single channel walls may be giving rise to the XRD reflection. Clearly, the disordered channel system of MSU-X aluminas is in marked contrast to the long-range hexagonal arrangement of channels found for MCM-41[2] and HMS mesostructures.[8]

Fig. 2. TEM image of a calcined (773 K) MSU-1 alumina molecular sieve showing the regular wormlike channel motif, but no discernable long-range channel packing order. The material was prepared by using Tergitol 15-S-9 as the surfactant. The length of the bar corresponds to 60 nm.

Figure 3 provides representative N_2 adsorption/desorption isotherms for a MSU-3 alumina calcined at 773 K. All MSU-X aluminas prepared by using PEO surfactants as templates display a similar broad but well-defined step in the adsorption isotherm at $p/p_0 \approx 0.45-0.8$ and a hysteresis in the desorption isotherm over the same relative pressure range. These features result from the condensation of the adsorbate within the framework-confined mesopores,[17] not from interparticle pores.[18] The lack of textural mesoporosity is indicated further by the absence of a hysteresis loop above $p/p_0 = 0.8$.[8] Some necking of the pore structure is suggested by the sharp curvature in the desorption leg of the hysteresis loop.

Most previously reported studies of mesoporous molecular sieves[1–9] have made use of the Horvath–Kawazoe (HK) model[19] for the determination of pore size distributions from N_2 adsorption isotherms. This model, developed for microporous lamellar carbon materials, assumes the presence of slitlike micropores. Therefore, its applicability to materials with larger,

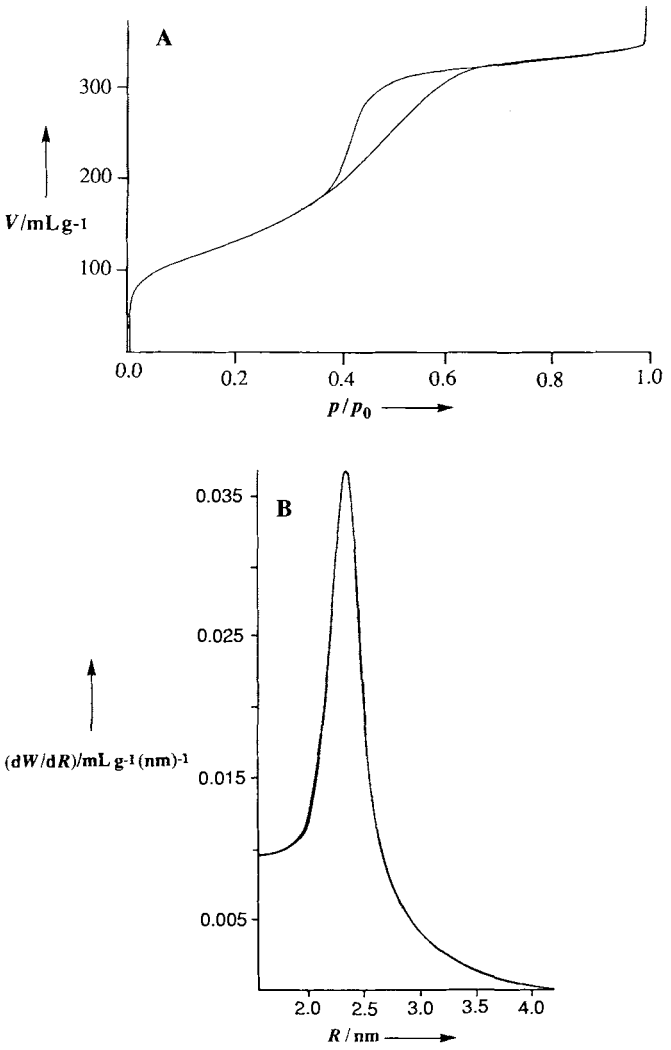

Fig. 3. A) Nitrogen adsorption and desorption isotherms for MSU-3 alumina prepared with the Pluronic 64L surfactant and calcined at 773 K in air for 4 h. The volume of N_2 sorbed is expressed at standard temperature and pressure; p/p_o is the partial pressure of nitrogen in equilibrium with the sample at 77 K. B) Corresponding Barrett–Joiner–Halender pore size distribution determined from the N_2 adsorption isotherm. dW/dR is the derivative of the normalized N_2 volume adsorbed with respect to the diameter of the pores of the adsorbent. Prior to measurement the sample was evacuated at 423 K and 10^{-6} Torr for 16 h.

cylindrical mesopores is likely to be limited. In this report, we have applied in addition to the HK model both the Cranston–Inkley (CI)[20] and the Barrett–Joyner–Halender (BJH)[21] models to the determination of framework pore size. Comparable pore size values were obtained when the CI and BJH models were applied to the N_2 adsorption and desorption branches, respectively. However, HK gave significantly larger pore diameters. For instance, as shown in Figure 3B, the pore distribution determined by the BJH method for MSU-3 alumina is centered at 2.4 nm, whereas the HK model affords a value of 4.8 nm. Measurement of the pores in the TEM image in Figure 2 gave diameters of about 2.6 nm, a value in favorable agreement with the BJH value of 3.3 nm.

Table 1 gives the basal spacings d_{100}, surface areas, pore volumes, and the HK and BJH pore sizes for MSU-X aluminas prepared from different families of PEO-based surfactants. A mesostructure assembly effect is indicated by an increase in both the d spacing and the pore diameters with increasing surfactant size. Since the MSU-X aluminas exhibit similar pore sizes but larger d spacings than MSU-X silicas,[9] we conclude that the channel wall thicknesses is larger for the aluminas than the silicas. This is consistent with the observation that the Brunauer–Emmett–Teller (BET)[18] surface areas of the aluminas calcined in air at 773 K range from 420 to 535 $m^2 g^{-1}$, whereas MSU-X silicas give values twice as large. Nevertheless, the surface areas and pore volumes are substantially larger than those of amorphous and crystalline aluminas[22] prepared by traditional sol–gel or flash-calcination techniques.[23]

The coordination environment of aluminum in MSU-X aluminas was examined by ^{27}Al MAS NMR spectroscopy (MAS = magic angle spinning). Spectra of as-synthesized and calcined MSU-3 alumina (Fig. 4) display three resonance signals, uncorrected for quadrupolar shift, at $\delta = 0$, 35, and 75. These lines are indicative of six-, five-, and four-coordinate metal centers, respectively.[24, 25] In the as-synthesized material the six-coordinate species is dominant, but after dehydration and dehydroxylation at 773 K the four- and five-coordinate centers both increase at the expense of the six-coordinate centers. The presence of five-coordinate aluminum centers is especially noteworthy as they may prove to be of catalytic significance as Lewis acid centers.

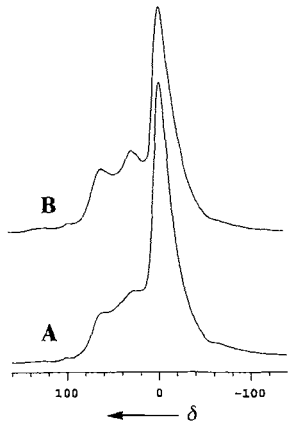

Fig. 4. ^{27}Al MAS NMR spectra of MSU-3 alumina prepared with the Pluronic 64L surfactant: A) As-synthesized sample after air drying at room temperature for 16 h; B) after calcination at 773 K in air for 4 h. The chemical shifts are referenced to external $[Al(H_2O)_6]^{3+}$.

Finally, we note that porous aluminas[26, 27] and aluminates[28] have been prepared previously from alkoxide precursors in the presence of organic pore regulating agents such as methyl cellulose or short-chain quaternary ammonium cations. Although these organic modifiers exhibited structure-directing properties for zeolite syntheses,[29] they afforded aluminas that were X-ray amorphous. Consequently, these earlier alumina synthesis reactions involved modifier encapsulation, but not assembly processes. Alumina aerogels with surface areas near 500 $m^2 g^{-1}$ also have been reported,[30] but the pore structures of these low bulk density materials were purely textural. Because of their thermal stability, high surface area, and multiple aluminum coordination environments, MSU-X alumina molecular sieves offer promising opportunities for new materials applications, particularly as catalysts and catalyst supports.

Experimental Procedure

The synthesis of a representative product, MSU-3 alumina, prepared by using a polyethylene oxide/polypropylene oxide copolymer surfactant illustrates the general procedure for the preparation of a mesoporous alumina molecular sieve. The specific template employed was Pluronic 64L (BASF), a tri-block copolymer with specific stoichiometry $(PEO)_{13}(PPO)_{30}(PEO)_{13}$. A solution containing deionized water (42 mmol) in anhydrous *sec*-butyl alcohol (10 mL) was added very slowly ($\approx$1 mL min^{-1}) to a stirred homogeneous solution containing surfactant (2.1 mmol) and tri-*sec*-butoxyaluminum (21 mmol) in anhydrous *sec*-butyl alcohol (25 mL). The overall reaction stoichiometry, therefore, was 0.1:1.0:2.0 surfactant:Al:water. The resulting gel that formed after stirring for 3 h was diluted with *sec*-butyl alcohol and allowed to react for an additional 16 h. The product was washed with absolute ethanol and dried sequentially at room temperature for 16 h and at 373 K for 6 h. The calcination was carried out by heating to 773 K for 4 h.

XRD patterns were obtained with a Rigaku Rotaflex diffractometer equipped with a rotating anode and $Cu_{K\alpha}$ radiation ($\lambda = 0.15418$ nm). The TEM image was obtained with a JEOL 100CX microscope using an accelerating voltage of 120 kV and a 20 mm objective lens aperture. N_2 isotherms were obtained on a Coulter Om-

 © VCH Verlagsgesellschaft mbH, D-69451 Weinheim, 1996 0570-0833/96/3510-1104 $ 15.00+.25/0

nisorp 360CX Sorptometer operated under continuous adsorption conditions. ^{27}Al MAS NMR spectra were obtained with a Varian VXR-400 NMR spectrometer equipped with a Varian MAS probe and SiN rotor. The spectrometer frequency was 104.22 MHz, pulse width 2 ms, and sample spinning rate 6550 Hz.

Received: November 17, 1995
Revised version: February 14, 1996 [Z8563IE]
German version: *Angew. Chem.* **1996**, *108*, 1180–1183

Keywords: aluminum compounds · mesoporous materials · molecular sieves · surfactants

[1] J. S. Beck, *US-A* 5057296, **1991**.
[2] C. T. Kresge, M. E. Leonowicz, W. J. Roth, J. C. Vartuli, J. S. Beck, *Nature* **1992**, *359*, 710.
[3] C.-Y. Chen, H.-Y. Li, M. E. Davis, *Microporous Mater.* **1993**, *2*, 17.
[4] C.-Y. Chen, H.-Y. Li, S. L. Burkett, M. E. Davis, *Microporous Mater.* **1993**, *2*, 27.
[5] Q. Huo, D. I. Margolese, U. Ciesla, D. G. Demuth, P. Feng, T. E. Gier, P. Sieger, A. Firouzi, B. F. Chmelka, F. Schüth, G. Stucky, *Chem. Mater.* **1994**, *6*, 1176.
[6] Q. Huo, D. I. Margolese, U. Ciesla, P. Feng, T. E. Gier, P. Sieger, R. Leon, P. M. Petroff, F. Schüth, G. Stucky, *Nature* **1994**, *368*, 317.
[7] U. Ciesla, D. Demuth, R. Leon, P. Petroff, G. Stucky, K. Unger, F. Schüth, *J. Chem. Soc. Chem. Commun.* **1994**, 1387.
[8] P. T. Tanev, T. J. Pinnavaia, *Science* **1995**, *267*, 865.
[9] S. A. Bagshaw, E. Prouzet, T. J. Pinnavaia, *Science* **1995**, *269*, 1242.
[10] G. S. Attard, J. C. Glyde, C. G. Göltner, *Nature* **1995**, *378*, 366.
[11] C. Misra, *Industrial Alumina Catalysts*, ACS Monograph Series **1986**, *184*, 133.
[12] G. Tournier, M. Lecroix-Repellin, G. M. Pajonk, *Stud. Surf. Sci. Catal.* **1987**, *31*, 333.
[13] S. D. Mahanti, personal communication.
[14] M. R. Porter, *Handbook of Surfactants*, 2nd ed., Blackie, London, **1994**.
[15] B. Chu, *Langmuir* **1995**, *11*, 414.
[16] Z. Lin, L. E. Scriven, H. T. Davis, *Langmuir* **1992**, *8*, 2200.
[17] P. J. Branton, P. G. Hall, K. S. W. Sing, H. Reichert, F. Schüth, K. K. Unger, *J. Chem. Soc. Faraday Trans.* **1994**, *90*, 2965.
[18] S. J. Gregg, K. S. W. Sing, *Adsorption, Surface Area and Porosity*, 2nd ed., Academic Press, London, **1982**.
[19] G. Horvath, J. Kawazoe, *J. Chem. Eng. Jpn.* **1983**, *16*, 470.
[20] R. W. Cranston, F. A. Inkley, *Adv. Catal.* **1970**, *9*, 143.
[21] E. P. Barrett, L. G. Joyner, P. P. Halender, *J. Am. Chem. Soc.* **1951**, *73*, 373.
[22] R. Poisson, J.-P. Brunelle, P. Nortier in *Catalyst Supports and Supported Catalysts*, (Ed.: A. B. Stiles), Butterworths, Boston, **1987**, p. 11.
[23] B. C. Gates in *Materials Chemistry: An Emerging Discipline*, American Chemical Society, Washington, D. C., **1995**, p. 301.
[24] J. W. Akitt, *Prog. Nucl. Magn. Reson. Spectrosc.* **1989**, *21*, 127.
[25] M. C. Cruickshank, L. S. Dent Glasser, S. A. I. Barri, I. J. Proplett, *J. Chem. Soc. Chem. Commun.* **1986**, 23.
[26] H. Adkins, S. H. Watkins, *J. Am. Chem. Soc.* **1951**, *73*, 2184.
[27] D. Basmadjian, G. Fulford, B. I. Parsons, D. S. Montgomery, *J. Catal.* **1962**, *1*, 547.
[28] R. Sned, *Appl. Catal.* **1984**, *12*, 347.
[29] *Introduction to Zeolite Science and Practice*, (Eds.: H. van Bekkum, E. M. Flanigen, J. C. Jansen) Elsevier, Amsterdam, **1991**.
[30] C.-M. Chen, S.-Y. Chen, S.-Y. Peng, *Studi. Surf. Sci. Catal.* **1995**, *91*, 427.

Design, Synthesis, and Ion-Transport Properties of a Novel Family of Cyclic, Adamantane-Containing Cystine Peptides**

Darshan Ranganathan,* V. Haridas, K. P. Madhusudanan, Raja Roy, R. Nagaraj, G. B. John, and M. B. Sukhaswami

Cyclic peptides have attracted considerable attention in recent years. Apart from acting as templates in the de novo design[1] of artificial proteins, they serve as useful models[2] for the study of preferences in protein secondary structure and also play a pivotal role in ion transport across biological membranes.[3] Recently, a new aspect has developed: the formation of nanotubes from cyclic peptides.[4]

The problem of delineating conformation in cyclic peptides can be overcome by incorporating rigid units in their framework. The potential of this strategy has recently been shown in the design of conformationally constrained, high-affinity ligands for GPIIb/IIIb receptor proteins[5] and in the development of minimal glucocorticoid receptors models.[6] Thus, it was envisaged that when rigid and simultaneously lipophilic units are incorporated into the cyclic peptide framework, not only would the peptide have the desired conformational constraint but it would also interact with lipid bilayers. These cyclic peptides would thereby effectively and preferentially transport ions across biological membranes.

In this communication we provide the first illustration of this strategy and report on the design and synthesis of a unique family of adamantane-containing[7] cystine cyclic peptides with the general structure cyclo(Adm-Cyst)$_n$ (Adm = 1,3-adamantanedicarbonyl; Cyst = L-cystine dimethyl ester; $n = 2-5$), which were constructed in a single step by the reaction of L-cystine dimethyl ester with 1,3-adamantanedicarbonyl dichloride. Further, members of this class of cyclic peptides have been demonstrated to selectively transport sodium and potassium ions in model membranes.

Treatment of 1,3-adamantane dicarbonyl dichloride with L-cystine dimethyl ester in the presence of triethylamine under high-dilution conditions afforded a mixture of four products with similar TLC behavior, which were separated by chromatography on silica gel with ethyl acetate/benzene (80/20) as eluent. The products were isolated in yields of 55 (**1**), 15 (**2**), 12 (**3**), and 2% (**4**), and were fully characterized by spectroscopic and analytical data (Scheme 1, Table 1)).

The highly symmetrical nature of **1**–**4** was evident from the appearance of only single set of resonances for the cystine and adamantane units in their ^{1}H and ^{13}C NMR spectra.[15] The chemical shifts of the adamantane and cystine protons in **2**–**4** were essentially identical to those of **1**, suggesting that these units adopt similar conformations. The ROESY NMR spectra of **1**–**3** and the very enhanced ROE effect[15] between the NH and the adamantane methylene protons suggests that

[*] Dr. D. Ranganathan, V. Haridas
Biomolecular Research Unit, Regional Research Laboratory (CSIR)
Trivandrum, 695019 (India)
Fax: Int. code +(471)490186
Dr. K. P. Madhusudanan, Dr. R. Roy
Medicinal Chemistry Division, Central Drug Research Institute
Lucknow, 226001 (India)
Dr. R. Nagaraj, G. B. John, Dr. M. B. Sukhaswami
Centre for Cellular and Molecular Biology, Hyderabad (India)

[**] This work was supported financially by the Department of Science and Technology, New Delhi (India). We are most grateful to Prof. S. Ranganathan (RRL, Trivandrum) and Prof. D. Balasubramanian (CCMB, Hyderabad) for helpful advice and comments.

 © VCH Verlagsgesellschaft mbH, D-69451 Weinheim, 1996 0570-0833/96/3510-1105 $ 15.00+.25/0

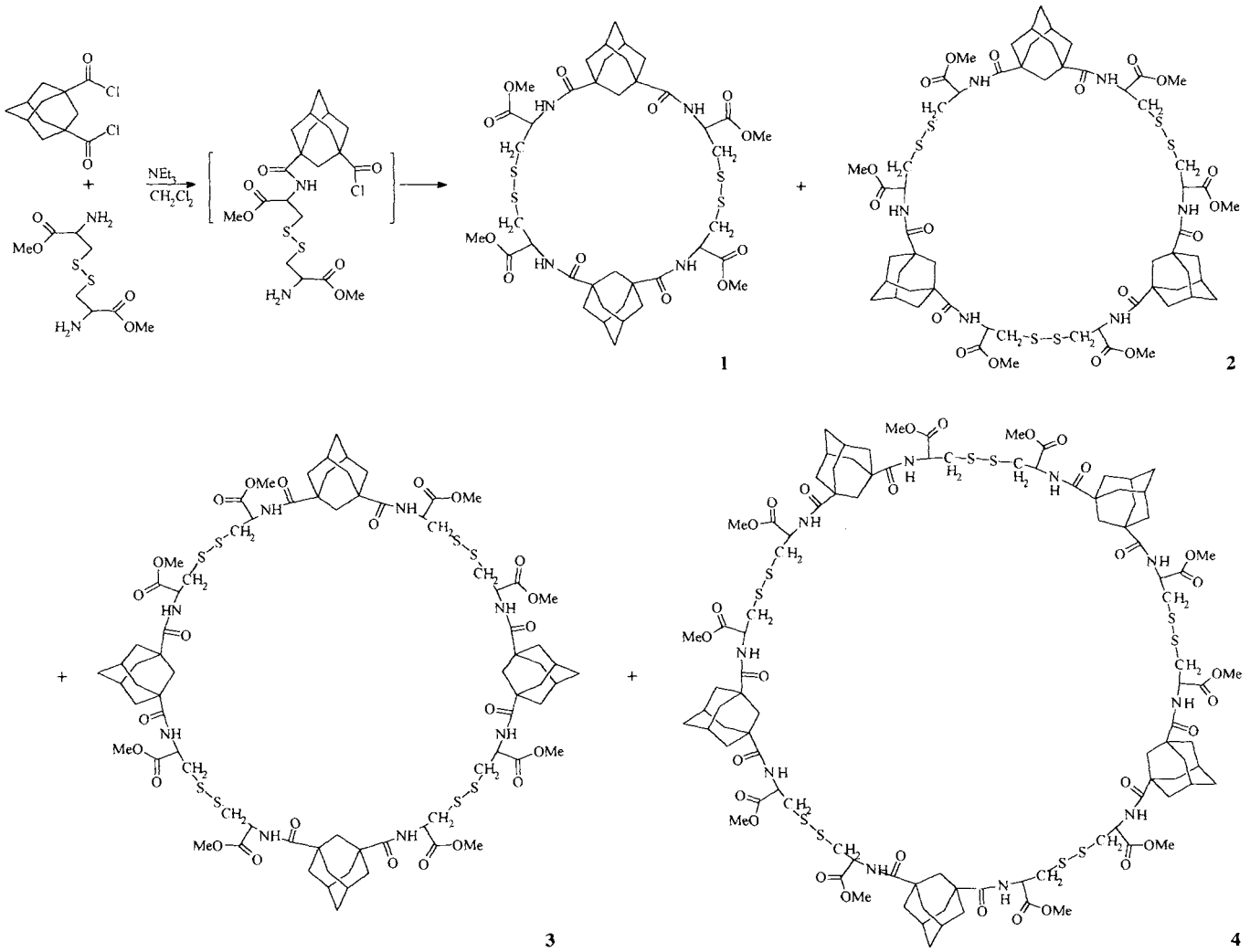

Scheme 1. One-step condensation of 1,3-adamantane dicarbonyl dichloride and cystine dimethyl ester to give macrocycles **1**–**4**.

Table 1. Selected data for compounds **1**–**4**.

1: M.p 110–112 °C; $[\alpha]_D^{25} = -5.99$ ($c = 2.1$ in $CHCl_3$); ^{1}H NMR (300 MHz, $CDCl_3$): $\delta = 1.59$–2.08 (m, 24 H), 2.23 (br. s, 4 H), 3.13 (dd, $J = 9.0$, 4.5 Hz, 4 H), 3.30 (dd, $J = 9.0$, 4.5 Hz, 4 H), 3.78 (s, 12 H), 4.81 (m, 4 H), 6.59 (d, $J = 7.0$ Hz, 4 H); IR (KBr): $\tilde{\nu} = 3365$, 2920, 2862, 1748, 1650, 1522 cm^{-1}; FAB-MS: *m/z* (%): 913 (95) $[M + H]^+$

2: M.p 166–168 °C; $[\alpha]_D^{25} = -1.92$ ($c = 2.35$ in $CHCl_3$); ^{1}H NMR (300 MHz, $CDCl_3$): $\delta = 1.61$–2.11 (m, 36 H), 2.23 (br. s, 6 H), 3.15 (m, 12 H), 3.76 (s, 18 H), 4.80 (m, 6 H), 6.72 (d, $J = 7.0$ Hz, 6 H); IR (KBr): $\tilde{\nu} = 3417$, 2930, 2861, 1748, 1651, 1565, 1536 cm^{-1}; FAB-MS: *m/z* (%): 1369 (100) $[M + H]^+$, 913 (44) $[M^+ -$ Adm-Cyst + H]

3: M.p 190–192 °C; $[\alpha]_D^{25} = +6.04$ ($c = 2.50$ in $CHCl_3$); ^{1}H NMR (300 MHz, $CDCl_3$): $\delta = 1.59$–2.13 (m, 48 H), 2.22 (br. s, 8 H), 3.17 (m, 16 H), 3.76 (s, 24 H), 4.82 (m, 8 H), 6.73 (d, $J = 7.0$ Hz, 8 H); IR (KBr): $\tilde{\nu} = 3368$, 2919, 2861, 1750, 1653, 1522 cm^{-1}; FAB-MS: *m/z* (%): 1825 (86) $[M + H]^+$, 1369 (43) $[M^+ -$ Adm-Cyst + H], 913 (40) $[M^+ - 2 \times$ Adm-Cyst + H]

4: M.p 138–140 °C; ^{1}H NMR (300 MHz, $CDCl_3$): $\delta = 1.50$–2.16 (m, 60 H), 2.21 (br. s, 10 H), 3.18 (m, 20 H), 3.75 (s, 30 H), 4.80 (m, 10 H), 6.71 (br. d, 10 H); IR (KBr): $\tilde{\nu} = 3331$, 2920, 2861, 1748, 1658, 1521 cm^{-1}; FAB-MS: *m/z* (%): 2282 (100) $[M + H]^+$, 1825 (35) $[M^+ -$ Adm-Cyst + H], 1369 (40) $[M^+ - 2 \times$ Adm-Cyst + H], 913 (47) $[M^+ - 3 \times$ Adm-Cyst + H]

Polymer: soluble in DMSO and DMF, insoluble in $CHCl_3$, EtOAc, MeOH; m.p 172–173 °C; thermogravimetric analysis: $T = 250$ °C; ^{1}H-NMR (90 MHz, [D$_6$]DMSO): $\delta = 1.32$–2.37 (m, 14 H), 3.10 (m, 4 H), 3.65 (s, 6 H), 4.60 (m, 2 H), 7.75 (d, $J = 7.0$ Hz, 2 H); IR (KBr): $\tilde{\nu} = 3349$, 2914, 2860, 1750, 1666, 1647, 1562, 1536, 1514, 1441 cm^{-1}

two carbonyl functions are in a *syn-anti* arrangement. The FAB-MS results[15] confirmed that **1**–**4** correspond to the cyclic dimer, trimer, tetramer, and pentamer, respectively, of Adm-Cyst units.[8]

The formation of **1**–**4** containing two, three, four, and five cyclic repeats, respectively, of Adm-Cyst units was rationalized on the basis of further cyclooligomerizations of the initially formed linear Adm-Cyst intermediate (Scheme 1). This notion was supported by the isolation of small amounts (ca. 5%) of linear polymer of the Adm-Cyst unit.

Molecular modeling and energy minimization[9] support the cavitand-like conformation of the 26-, 39-, 52-, and 65-membered macrocycles. The representations of the optimized structures[15] show that while the cavity is hydrophilic, the periphery consisting of repeating adamantane units is largely hydrophobic. This suggests that macrocycles **1**–**4** may harbor metal ions and transport them across membranes. This notion has been demonstrated experimentally.

The capability of compounds **1**–**3** to transport ions across model membranes (small unilamellar vesicles) was evaluated by monitoring the decay of a valinomycin-mediated K^+ diffusion potential[10, 11] and with a chlorotetracycline (CTC)/Ca^{+2} assay.[12, 15] The results show that dimer **1** transports Na^+ in preference to K^+, trimer **2** is more selective towards K^+, and

 © VCH Verlagsgesellschaft mbH, D-69451 Weinheim, 1996 0570-0833/96/3510-1106 $ 15.00+.25/0

tetramer **3** shows negligible transport properties for both ions. None of the compounds were able to transport Ca^{+2} ions across the lipid bilayers, as judged by the CTC assay. The macrocycles did not cause the release of entrapped carboxyfluorescein, indicating that the movement of ions across the lipid bilayer was not due to the formation of large pores or detergentlike action.[13] The ion flux may thus be ascribed to a carrier-type of ion-transport mechanism like that of valinomycin.[14]

The cystine cyclic peptides **1**–**4** described here represent a new family of adamantane-containing cyclic peptides, which are capable of transporting Na^+ and K^+ ions across model membranes. This action and their very simple, short synthesis should be incentive for the design of related compounds in this novel class of cyclic peptides.

Experimental Procedure

A solution of freshly prepared 1,3-adamantane dicarbonyl dichloride (2 mmol) in dry CH_2Cl_2 (100 mL) was added dropwise over 0.5 h to a well-stirred solution of L-cystine dimethyl ester hydrochloride (2 mmol) and triethylamine (9 mmol) in dry CH_2Cl_2 (150 mL) at 0 °C. The reaction mixture was stirred at room temperature for 4–6 h and monitored by TLC. The reaction mixture was washed sequentially with ice-cold 2 N H_2SO_4, H_2O, and 5% $NaHCO_3$ (ca. 20 mL each). The organic layer was dried over $MgSO_4$ and concentrated in vacuo. The residue was chromatographed on silica gel with ethyl acetate/benzene (80/20) as eluent to afford macrocycles **1** (55%), **2** (15%) **3** (12%), and **4**(2%), and a small amount (ca. 5%) of a linear Adm-Cyst polymer.

Received: November 2, 1995
Revised version: February 12, 1996 [Z85221E]
German version: *Angew. Chem.* **1996**, *108*, 1193–1195

Keywords: adamantanes · cyclopeptides · ion transport

[1] A. Grove, M. Mutter, J. E. Rivier, M. Montal, *J. Am. Chem. Soc.* **1993**, *115*, 5919–5924.
[2] J. Rizo, L. M. Gierasch, *Annu. Rev. Biochem.* **1992**, *61*, 387–418, and references therein.
[3] Y. A. Ovchinnikov, V. Yivanov, A. M. Shkrob, *Membrane Active Complexones*, Elsevier, Amsterdam, **1974**; B. C. Pressman, *Annu. Rev. Biochem.* **1976**, *45*, 501; T. J. Marrone, K. M. Merz, Jr., *J. Am. Chem. Soc.* **1992**, *114*, 7542–7549.
[4] M. R. Ghadiri, J. R. Granja, R. A. Milligan, D. E. McRee, N. Khazanovich, *Nature* **1993**, *366*, 324–327; M. R. Ghadiri, J. R. Granja, L. K. Buehler, *ibid.* **1994**, *369*, 301–304; N. Khazanovich, J. R. Granja, D. E. McRee, R. A. Milligan, M. R. Ghadiri, *J. Am. Chem. Soc.* **1994**, *116*, 6011–6012; M. R. Ghadiri, K. Kobayashi, R. K. Chadha, D. E. McRee, *Angew. Chem.* **1995**, *107*, 76–78; *Angew. Chem. Int. Ed. Engl.* **1995**, *34*, 93–95; K. Kobayashi, J. R. Granja, M. R. Ghadiri, *ibid.* **1995**, *107*, 79–81 and **1995**, *34*, 97–98.
[5] A. C. Bach, II, C. J. Eyermann, J. D. Gross, M. J. Bower, R. L. Harlow, P. C. Weber, W. F. DeGrado, *J. Am. Chem. Soc.* **1994**, *116*, 3207–3219; S. Jackson, W. F. DeGrado, A. Dwivedi, A. Parthasarathy, A. Hig, J. Krywko, A. Rockwell, J. Markwalder, G. Wells, R. Wexler, S. Mousa, R. Harlow, *ibid.* **1994**, *116*, 3220–3230.
[6] S. Ranganathan, N. Jayaraman, R. Roy, K. P. Madhusudanan, *Tetrahedron Lett.* **1993**, *34*, 7801–7804.
[7] The 1,3-adamantanediyl unit appeared particularly attractive as a low molecular weight, rigid, lipophilic component for fixing the macrocycle in membranes.
[8] Interestingly, metal ion doping experiments with cyclic peptides **1**–**3** indicated a strong tendency for the uptake of alkali metal ions (FAB-MS). The signal intensity for $(1+M)^+$ and of $(2+M)^+$ appeared in the order of $Li^+ > Rb^+ > Cs^+ > K^+ > Na^+$ and for $(3+M)^+$ in the order of $Rb^+ > Cs^+ > K^+ > Na^+ > Li^+$.
[9] The models for macrocycles **1**–**3** were generated with the Biosym program package, version 2.3.5, a Silicon Graphics IRIS Crimson Elan Work Station. The energy minimization was done with INSIGHT and DISCOVER program packages (Biosym Technologies, San Diego, CA), using a consistent valence force field.
[10] P. J. Sims, A. S. Waggoner, C. H. Wang, J. F. Hoffman, *Biochemistry* **1974**, *13*, 3315–3330.
[11] L. M. Loew, I. Rosenberg, M. Bridge, C. Gitter, *Biochemistry* **1983**, *22*, 837–844; L. M. Loew, L. Benson, P. Lazarovici, I. Rosenberg, *ibid.* **1985**, *24*, 2101–2104; Y. Shai, D. Bach, A. Yanovsky, *J. Biol. Chem.* **1990**, *265*, 20202–20209; S. M. Glaser, M. G. Cumsky, *ibid.* **1990**, *265*, 8808–8816; D. Roise, *Proc. Natl. Acad. Sci. USA* **1992**, *89*, 608–612; R. M. Epand, Y. Shai, J. P. Segrest, G. M. Anantharamaiah, *Biopolymers* **1995**, *37*, 319–338.
[12] R. Nagaraj, M. K. Mathew, P. Balaram, *FEBS Lett.* **1980**, *121*, 365–368.
[13] Ion transport across membranes can take place either by carriers or by channel formers. The two mechanisms can be easily distinguished by monitoring the release of carboxyfluorescein (CF) trapped in lipid vesicles by fluorescence spectroscopy. Since a channel former leads to the formation of large pores in membranes, the trapped CF leaks out of the vesicles into the bulk medium, which causes a sudden enhancement of its fluorescence intensity due to dilution. Carrier molecules, on the other hand, diffuse through the hydrocarbon region of the membrane and do not cause the escape of CF into the medium, and hence no change in fluorescence is seen. In the present case, the absence of any fluorescence enhancement in the presence of macrocycles **1**–**3** implies that trapped CF is not released, and that ion transport occurs by a carrier-type mechanism, like that of valinomycin.
[14] L. A. R. Pioda, V. Stankova, W. Simon, *Anal. Lett.* **1969**, *2*, 665; H. B. Jenny, C. Riess, D. Ammann, B. Mayyar, R. Asper, W. Simon, *Mikrochim. Acta* **1980** (*2*), 309.
[15] Further details may be obtained from the author on request.

Directed Synthesis of Stable Hydrogen Polyphosphides: Preparation and Structural Characterization of HP_{11}^{2-} in $(NBnMe_3)_2HP_{11}$ and $(PBnPh_3)_2HP_{11}$ as Well as Its Comparison with the First "Naked" P_{11}^{3-} Ion in $(NEtMe_3)_3P_{11}$**

Nikolaus Korber,* Jörg Daniels, and Hans Georg von Schnering*

Dedicated to Professor Marianne Baudler on the occasion of her 75th birthday

Recently, the surprisingly stable tetraphenylphosphonium salt of the dihydrogen heptaphosphide $H_2P_7^-$ was isolated and characterized by single-crystal X-ray structure analysis.[1] Even today, very little is known about hydrogen polyphosphides, which are situated between polyphosphanes[2, 3] and polyphosphides.[4] Phosphides and phosphanes with identical phosphorus frameworks (for example, P_7^{3-} [4] and heptaphosphane(3) P_7H_3,[5] both with the nortricyclane cage) are formally related by the Brønsted acid–base concept;[6] however, this formal relationship is difficult to prove experimentally, because the deprotonation of polyphosphanes as well as the protonation of the corresponding polyphosphides both lead to rapid decomposition. Therefore, partially protonated polyphosphides (or partially deprotonated polyphosphanes) are highly reactive species that have rarely been observed in practice. An exception has been a detailed study of the reaction between diphosphane(4) and *n*-butyllithium by Baudler et al., during which several partially lithiated polyphosphanes were detected as highly reactive intermediates by ^{31}P NMR spectroscopy.[7]

In solution, $(PPh_4)H_2P_7$ decomposes as well, yielding undefined higher polyphosphanes; as a crystalline solid, however, it is stable at room temperature and even in air, probably because of the spatial separation of the $H_2P_7^-$ ions by the large cations. $(PPh_4)H_2P_7$ forms in small yields during the reaction of K_3P_{11} with $(PPh_4)Cl$ in liquid NH_3.[1]

[*] Dr. N. Korber, Dipl.-Chem. J. Daniels
Institut für Anorganische Chemie der Universität
Gerhard-Domagk-Strasse 1, D-53121 Bonn (Germany)
Fax: Int. code +(228)735660
e-mail: korber@plumbum.chemie.uni-bonn.de
Prof. Dr. H. G. von Schnering
Max-Planck-Institut für Festkörperforschung
Heisenbergstrasse 1, D-70506 Stuttgart (Germany)
Fax: Int. code +(711)689-1562

[**] The authors are grateful to Dr. W. Hoffbauer for the recording of the solid-state NMR spectra. Bn = benzyl.

Inspired by this serendipitous result, we have investigated possible directed synthetic routes to hydrogen polyphosphides that start from alkali metal polyphosphides. Essential features of such a synthesis are a "soft" protonation of the polyphosphide anions under mild conditions, for example in a solution of liquid NH_3 at low temperatures, and the trapping of the newly formed hydrogen polyphosphide ions with voluminous, noncoordinating cations like quaternary ammonium ions by precipitation as a weakly soluble salt.

We have found that the precise conditions of the protonation reaction were crucial: the simple addition of stoichiometric amounts of the universal acid in the ammonia system (NH_4^+ in the form of halide salts) was unsuccessful. Similarly, the use of urea, which is the ammonia system analogue to carbonic acid, did not produce the desired effect. Only when we employed a reaction that produced the acid in situ were quantitative and reproducible yields achieved. To this end, we used the oxidation of the solvent NH_3 by bromine, which proceeds even at low temperatures (e.g. $-33°C$) according to Equation (a).[8]

$$3Br_2 + 8NH_3 \longrightarrow 6NH_4Br + N_2 \uparrow \qquad (a)$$

Instead of adding bromine directly, it is much more advantageous to use the tribromides Br_3^- of the respective quaternary ammonium cations. Consequently, the halogen generating the acid as well as the quaternary cation that is needed to trap the hydrogen polyphosphide may be added in a simple manner combined in a single reagent.

According to this concept, Cs_3P_{11} and benzyltrimethylammonium tribromide react in liquid NH_3 to yield bis(benzyltrimethylammonium) hydrogen undecaphosphide (**1**), which is surprisingly stable and may even be handled in air for some

$$[N(CH_2C_6H_5)Me_3]_2HP_{11} \quad \mathbf{1}$$

time. HP_{11}^{2-} is the first hydrogen phosphide derived from the pentacyclic cage anion P_{11}^{3-} ("ufosane"),[9] which is built exclusively from fused five-membered rings. The crystal structure[10] confirms the expected cation-to-anion ratio of 2 to 1. The HP_{11}^{2-} anion is located on a twofold crystallographic axis (Fig. 1 top). Although this site symmetry is matched by the symmetry of the phosphorus cage (point group 23-D_3), it is not in agreement with the overall point group symmetry of HP_{11}^{2-}, since the hydrogen atom has to be bound to one of the two symmetry-inequivalent two-bonded phosphorus atoms (P2 and P3). Thus, HP_{11}^{2-} is orientationally disordered with respect to the hydrogen atom, which is difficult to locate by X-ray methods anyway. However, significant distortions of the P_{11} framework permit an unequivocal identification of the phosphorus atom at which the hydrogen atom is located. By the protonation, the atom in question has become a three-bonded phosphorus atom. This should result in longer bond lengths and a larger bond angle with respect to the neighboring atoms.[4] Precisely this is the case for the atom P3, which is situated on the twofold axis (P3–P5 2.196(2) Å compared to P2–P4 2.156(2) Å and P2–P6 2.163(2) Å; P5-P3-P5′ 99.11(8)° compared to P4-P2-P6 96.72(5)°).

Independent evidence for the presence of a hydrogen polyphosphide is provided by the FTIR spectrum, which shows a strong, sharp band at 2245 cm^{-1} assigned to a P–H stretching frequency.

The comparison of **1** with solid $(NEtMe_3)_3P_{11}$ (**2**), which is the first polyphosphide having only quaternary ammonium ions as counter cations, offered further opportunities to confirm our

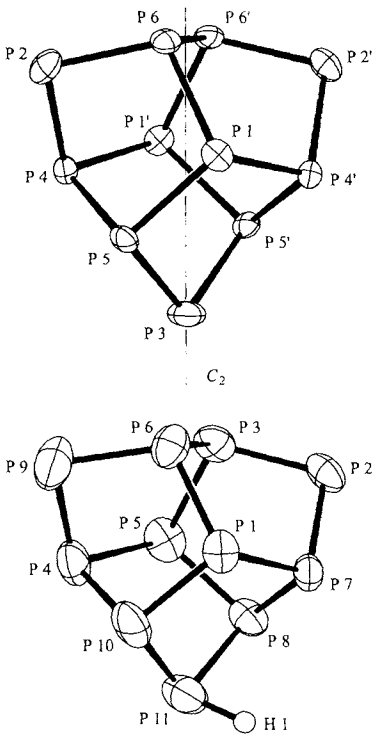

Fig. 1. Top: HP_{11}^{2-} in the crystal structure of **1** (ORTEP, 50% probability). Selected bond lengths [Å] and angles [°]: P1–P5 2.223(1), P1–P4 2.238(1), P1–P6 2.244(1), P2–P4 2.156(2), P2–P6 2.163(2), P3–P5 2.196(2), P4–P5 2.194(2), P4–P1′ 2.239(1), P6–P6′ 2.196(2); P5-P1-P4′ 103.91(5), P5-P1-P6 100.95(5), P4′-P1-P6 103.25(5), P4-P2-P6 96.72(5), P5-P3-P5′ 99.11(8), P2-P4-P5 97.57(6), P2-P4-P1′ 104.66(6), P5-P4-P1′ 102.52(6), P4-P5-P3 96.64(6), P4-P5-P1 102.36(5), P3-P5-P1 102.33(6), P2-P6-P6′ 101.00(8), P2-P6-P1 104.95(6), P6′-P6-P1 100.55(5). Bottom: HP_{11}^{2-} in the crystal structure of **3** (ORTEP, 50% probability). Arbitrarily chosen radius for the hydrogen atom. Selected bond lengths [Å] and angles [°]: P1–P10 2.214(4), P1–P6 2.218(4), P1–P7 2.240(4), P2–P3 2.150(4), P2–P7 2.158(4), P3–P6 2.188(4), P3–P5 2.284(4), P4–P9 2.159(5), P4–P10 2.177(5), P4–P5 2.267(5), P5–P8 2.208(4), P6–P9 2.150(4), P7–P8 2.184(4), P8–P11 2.212(5), P10–P11 2.186(5), P11–H1 1.37(8); P3-P2-P7 96.15(1), P6-P9-P4 95.5(2), P10-P11-P8 98.7(2), P4-P10-P11 94.0(2), H1-P11-P10 105(3), H1-P11-P8 93(3).

results. Recently, some doubts concerning the stability of a compound of this type were caused by a publication by Eichhorn et al., who described the alkylation of P_7^{3-} by tetraalkylammonium ions under very mild conditions.[11] The two-bonded, formally negatively charged phosphorus atoms are evidently very strongly nucleophilic, and cause almost quantitative transfers of alkyl groups from the quaternary ammonium cations, which are known to be rather weak alkylating reagents. In fact, $(PPh_4)_2P_{16}$ was the only example of a polyphosphide with quaternary cations for a long time.[12] Compound **2** can be prepared by simple metathesis in liquid ammonia. It should be mentioned, however, that most of the analogous metathesis reactions with other quaternary ammonium ions are hampered by strong ion-pairing in the solutions, which leads to compounds retaining one or two alkali metal cations per formula unit.[13] The formation of **2** appears to be favored by an especially low solubility. The crystal structure analysis of **2**[14] reveals a further favorable fact: it is the first solid-state structure in which the threefold axis of the ufosane cage corresponds to a crystallographic axis. Therefore, the whole anion is generated by only five symmetry-inequivalent phosphorus atom sites (Fig. 2). A comparison of the bond lengths and angles at the two-bonded phosphorus atom P5 of **2** (P5–P3 2.164(2) Å, P5–P4 2.191(2) Å, P3-P5-P4 95.9(1)°) with the corresponding phosphorus atoms of **1** confirms that the

 © VCH Verlagsgesellschaft mbH, D-69451 Weinheim, 1996 0570-0833/96/3510-1108 $ 15.00+.25/0

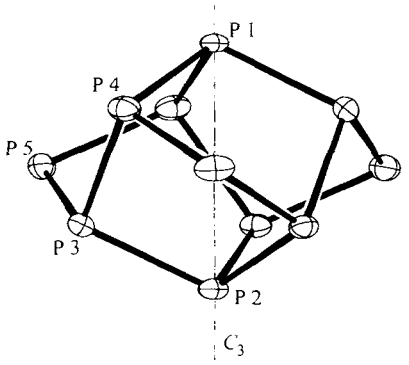

Fig. 2. P_{11}^{3-} in the crystal structure of **2** (ORTEP, 50% probability). Only the enantiomer with the occupancy factor of 87% is shown. Selected bond lengths [Å] and angles [°]: P1-P4 2.239(2), P2-P3 2.243(2), P3-P5 2.164(2), P3-P4 2.190(2), P4-P5 2.191(2); P4-P1-P4 102.0(1), P3-P2-P3 102.8(1), P5-P3-P4 99.7(1), P4-P3-P2 100.8(1), P3-P5-P4 95.9(1).

bonding situation of P3 in **1** (which we believe to be the phosphorus atom where the hydrogen atom is situated) is indeed more similar to that of a three-bonded phosphorus atom; the widening of the P-P-P angle on protonation is particularly significant.

Far more important was the use of **2** as a reference compound in the ^{31}P NMR study of **1**. Since solutions of this hydrogen polyphosphide were again unstable (in analogy to $(PPh_4)H_2P_7$), we had to recur to MAS solid-state NMR spectroscopy (MAS = magic angle spinning). The interpretation of the solid-state NMR spectrum of **1**, which was hampered by rather broad signals and extended overlap of side bands, was greatly facilitated by the comparatively simple NMR spectrum of **2**. Four isotropic signals were observed in the NMR spectrum of **2**, two of which are very close together ($\delta = 174.5$ and 167.9), the remaining signals are at $\delta = -102.3$ and -209.4. The integration of the corresponding signal groups results in a ratio of 6:2:3, which indicates that the two adjoining signals may be assigned to the atoms P3 and P4, which are chemically very similar but crystallographically inequivalent. The signal at $\delta = -102.3$ corresponds to the two atoms on the threefold axis, the signal at $\delta = -209.4$ to the two-bonded atom P5. These assignments helped us to identify the signal of the two-bonded P2 ($\delta = -220$) in the solid-state spectrum of **1**, which displays all the six isotropic signals expected for six crystallographically inequivalent phosphorus atoms. The integration results in a ratio of 2:9 for the signal associated to P2 relative to the remaining signals in the region of three-bonded phosphorus ($\delta = -82, -59, 121, 140, 155$). The latter cannot be separated reliably by integration because of the extended overlap of the side bands. Only the signal at $\delta = 140$ exhibits significant line narrowing following P–H decoupling. It is very probable that this signal can be assigned to the phosphorus atom P3 where the hydrogen atom is situated.

A second synthetic route to hydrogen polyphosphides makes use of large, noncoordinating cations, which are very weak proton donors themselves. A simple example is the benzyltriphenylphosphonium cation, which forms stable benzylidenetriphenylphosphorane upon deprotonation. Accordingly, a second example of a salt of the anion HP_{11}^{2-} was synthesized starting from Cs_3P_{11} and benzyltriphenylphosphonium bromide [Eq. (b)]. Again, a single reagent performs both of the tasks

$$3\,(C_6H_5)_3P^+\text{-}CH_2C_6H_5 + P_{11}^{3-} \longrightarrow \underset{\mathbf{3}}{((C_6H_5)_3PCH_2C_6H_5)_2HP_{11}}\downarrow + (C_6H_5)_3P{=}CHC_6H_5 \qquad \text{(b)}$$

mentioned above: it serves as a proton donor as well as a supply of voluminous cations for the crystallization of the newly formed hydrogen polyphosphide. As was the case with **1**, the distortion of the cage demonstrated by the X-ray data[15] permits the unequivocal identification of the protonated phosphorus atom in **3** (Fig. 1 bottom). Even the position of the hydrogen atom itself was localized and refined (with due caution, because the crystal was of low quality).

Both the synthetic routes described above allow the directed synthesis of hydrogen polyphosphides for the first time. The anions are isolated by the use of quaternary cations as stable solids, offering a convenient access to the chemistry of these species that are highly reactive in solution.

Experimental Procedure

Cs_3P_{11} was synthesized from the elements according to the procedure given in the literature [16] and recrystallized from dry liquid NH_3. All manipulations were carried out under strictly inert conditions. **1**: Cs_3P_{11} (ca. 0.5 mmol) and benzyltrimethylammonium tribromide (Aldrich) were placed into opposite sides of an U-shaped reaction vessel fitted with a glass frit (porosity 3) separating the two sides (molar ratio 1:2). NH_3 (ca. 50 mL) dried over potassium was frozen into the vessel at 77 K. The vessel was allowed to warm slowly to 233 K. After 12 h, **1** formed as red needles of ca. 1 cm length. After the removal of the solvent, CsBr and excess NH_4Br were removed by washing with liquid NH_3 (3 × 20 mL). Yield with respect to Cs_3P_{11}: 94%.

2: Analogous procedure to that for **1**, except that ratio Cs_3P_{11} to ethyltrimethylammonium iodide (Fluka) 1:3. Preparation of single crystals by a longer diffusion path (25 cm). Yield with respect to Cs_3P_{11}: 90%.

3: Analogous procedure to that for **1**, except that ratio Cs_3P_{11} to benzyltriphenylphosphonium bromide (Lancaster) 1:3. Compound **3** formed red ductile crystals, which were mixed with yellow crystals of the benzylidene-phosphorane (identification by X-ray crystal structure analysis). Separation by washing with diethyl ether. Yield: 80%.

Solid-state NMR: Varian Unity 400, ^{31}P frequency 161.419 MHz, spinning frequencies 7–11 kHz, pulse angle 3 ms, 40 (**1**) 240 (**2**) transients, respectively, pause between pulses 120 s, decoupling at 60 kHz, reference 85% H_3PO_4.

Received: June 7, 1995
Revised version: December 21, 1995 [Z8065IE]
German version: *Angew. Chem.* **1996**, *108*, 1186–1188

Keywords: phosphorus compounds · polyphosphides

[1] N. Korber, H. G. von Schnering, *J. Chem. Soc. Chem. Commun.* **1995**, *1713*.
[2] M. Baudler, K. Glinka, *Chem. Rev.* **1993**, 1623.
[3] M. Baudler, K. Glinka, *Chem. Rev.* **1994**,1273.
[4] H. G. von Schnering, W. Hönle, *Chem. Rev.* **1988**, 243.
[5] M. Baudler, R. Riekehof-Böhmer, *Z. Naturforsch. B* **1985**, *40*, 1424.
[6] J. N. Brønsted, *Recl. Trav. Chim. Pays-Bas* **1923**, *42*, 718.
[7] M. Baudler, R. Heumüller, *Z. Naturforsch. B* **1984**, *39*, 1306; M. Baudler, R. Heumüller, J. Germershausen, J. Hahn, *Z. Anorg. Allg. Chem.* **1985**, *526*, 7. M. Baudler, R. Heumüller, *ibid.* **1988**, *559*, 49; M. Baudler, R. Heumüller, D. Düster, *ibid.* **1993**, *619*, 1007.
[8] J. Jander, E. Kurzbach, *Z. Anorg. Allg. Chem.* **1958**, *296*, 117.
[9] W. Wichelhaus, H. G. von Schnering, *Naturwissenschaften* **1973**, *60*, 104.
[10] Crystal structure analysis of **1**: $C_{20}H_{33}N_2P_{11}$, monoclinic, space group $C2/c$, $a = 26.243(7)$, $b = 12.015(2)$, $c = 9.938(3)$ Å, $\beta = 110.12(1)°$, $V = 2943(1)$ Å^3, $\rho_{calcd} = 1.447$ g cm^{-3}, $\mu(Mo_{K\alpha}) = 0.65$ cm^{-1}, $Z = 8$. Enraf-Nonius-CAD4 diffractometer with graphite-monochromated $Mo_{K\alpha}$ radiation, $\lambda = 0.71073$ Å, $T = 193(1)$ K, $\omega/2\theta$ scans, 4620 reflections measured ($1.6 < \theta < 24.0°$), 2316 independent reflections, 1935 observed with $I_o > 2\sigma(I_o)$. Structure solution by direct methods (SHELXS86), Refinement on F^2 (SHELXL93), hydrogen atoms isotropic and in a riding model, 170 parameters, $wR_2 = 0.115$ (all independent reflections), corresponds to conventional $R = 0.042$ using only reflections with $I_o > 2\sigma(I_o)$. Largest peak in the final difference Fourier map 0.59 e Å^{-3}. Further details of the crystal structure investigations are available on request from the Director of the Cambridge Crystallographic Data Centre, 12 Union Road, GB-Cambridge CB2 1EZ (UK), on quoting the full journal citation.
[11] S. Charles, J. C. Fettinger, B. W. Eichhorn, *J. Am. Chem. Soc.* **1995**, *117*, 5303.
[12] H. G. von Schnering, V. Manriquez, W. Hönle, *Angew. Chem.* **1981**, *93*, 606; *Angew. Chem. Int. Ed. Engl.* **1981**, *20*, 594.
[13] N. Korber, H. G. von Schnering, *Chem. Ber.* **1996**, *129*, 155.

[14] Crystal structure analysis of **2**: $C_{15}H_{42}N_3P_{11}$, trigonal, space group $R3c$, $a = 16.984(5)$ Å, $c = 17.446(8)$ Å, $V = 4358(3)$ Å^3, $\rho_{calcd} = 1.38$ g cm^{-3}, $\mu(Mo_{K\alpha}) = 0.66$ cm^{-1}, $Z = 6$. Enraf-Nonius-CAD4-diffractometer with graphite-monochromated $Mo_{K\alpha}$ radiation, $\lambda = 0.71073$ Å, $T = 123(1)$ K, $\omega/2\theta$ scans, 3377 reflections measured ($2.4 > \theta > 22.0$), 1178 independent reflections, 1122 observed with $I_o > 2\sigma(I_o)$. Structure solution by direct methods (SHELXS86), refinement on F^2 (SHELXL93), hydrogen atoms isotropic and in a riding model, 100 parameters, $wR_2 = 0.116$ (all independent reflections), corresponds to conventional $R = 0.045$ using only reflections with $I_o > 2\sigma(I_o)$. The position of P_{11}^{3-} holds both enantiomers of the chiral "ufosane" cage; P1, P2, and P5 belong to both enatiomers, P3 and P4 (occupancy factor 0.87) are matched by two further phosphorus atoms in the second enantiomer (occupancy factor 0.13). Largest peak in the final difference Fourier map 0.44 e Å^{-3} [10].

[15] Crystal structure analysis of **3**: $C_{50}H_{45}P_{13}$, triclinic, space group $P\bar{1}$, $a = 11.226(8)$, $b = 13.550(9)$, $c = 20.20(1)$ Å, $\alpha = 72.46(3)$, $\beta = 88.97(4)$, $\gamma = 65.63(5)$, $V = 2649(3)$ Å^3, $\rho_{calcd} = 1.315$ g cm^{-3}, $\mu(Mo_{K\alpha}) = 0.45$ cm^{-1}, $Z = 2$. Stoe-STADI4 diffractometer with graphite-monochromated $Mo_{K\alpha}$ radiation, $\lambda = 0.71073$ Å, $T = 203(1)$ K, ω scans (width of reflections ca. 2°), 6461 reflections measured ($1.7 < \theta < 22.0$), 6461 independent reflections, 4460 observed with $I_o > 2\sigma(I_o)$. Structure solution by direct methods (SHELXS86), refinement on F^2 (SHELXL93), hydrogen atoms isotropic and in a riding model (except H1), 476 parameters, $wR_2 = 0.284$ (all independent reflections), corresponds to conventional $R = 0.087$ using only reflections with $I_o > 2\sigma(I_o)$. Largest peak in the final difference Fourier map 1.25 e Å^{-3}. The hydrogen atom H1 which is bonded to phosphorus was located by Fourier methods and refined isotropically [10].

[16] T. M. Meyer, Thesis, Universität Stuttgart, **1985**.

Enediyne Generation by a Retro-Diels–Alder Reaction**

Mark E. Bunnage and K. C. Nicolaou*

The enediyne anticancer antibiotics are potent DNA-cleaving agents with highly unusual molecular architecture and fascinating modes of action.[1] The biological activity of these complex molecules derives from the ability of their 1,5-diyn-3-ene ("enediyne") motif to undergo Bergman cycloaromatization[2] (Scheme 1), thereby generating a highly reactive 1,4-diradical that can abstract hydrogen atoms from the backbone of DNA and thus effect DNA scission.[1] Much recent interest in the enediyne field has focused upon the design and synthesis of simple molecules that utilize the enediyne unit as a "warhead" for damaging DNA.[3]

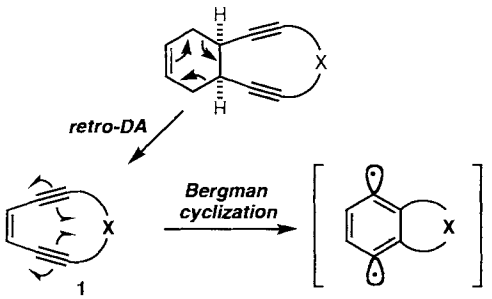

Scheme 1. General concept for the generation of enediynes by the retro-Diels–Alder reaction and Bergman cyclization of the enediynes.

The propensity of a cyclic enediyne to undergo cycloaromatization and form the reactive 1,4-diradical species depends on the nature of the tether (X) between the two alkyne units (Scheme 1). For example, we have shown that while the simple cyclodecenediyne (**1**) (X = $(CH_2)_4$) spontaneously cyclizes at ambient temperature ($t_{1/2} = 18$ h at 37 °C), the corresponding 11-membered ring congener (X = $(CH_2)_5$) is quite stable.[4] Although ring size has a direct bearing on the stability of a cyclic enediyne, many other factors are known to play an important role.[4] This is exemplified by the naturally occurring enediyne antibiotics such as calicheamicin γ_1^I and dynemicin A, in which the enediyne unit is part of a ten-membered ring but rendered stable by conformational restraints.[5] It is believed that the bioactivation of these molecules leads to a change in conformation of the ten-membered ring such that the triple bonds are brought into closer proximity and the Bergman cyclization is initiated.[1]

In light of the above considerations, the incorporation of an intact enediyne unit into a synthetic sequence could prove problematic, and it would be particularly advantageous to develop a convenient and stable masked form from which the enediyne could be readily liberated when desired. Not only could such a precursor prove useful in the preparation of naturally occurring enediynes but, perhaps more importantly, it should also facilitate the synthesis of enediynes containing alternative tethering groups (X). The generation of reactive enediynes in this manner would constitute a triggering mechanism for the formation of 1,4-diradicals and could thus be of potential application in the development of new prodrugs.

A particularly attractive progenitor for an enediyne is the corresponding 1,5-diyne, which lacks the internal double bond and is thus unable to aromatize. A number of groups have investigated procedures for developing enediynes from stable 1,5-diyne precursors,[6] and strategies for olefin generation based on the reductive activation of anthraquinone,[7] benzylic oxidation,[8] base-induced elimination,[9] photochemical elimination,[10] and the Corey–Winter reaction[11] have all been developed. Nevertheless, a variety of other strategies for introduction of the enediyne olefin component can be envisaged, and we were interested in the application of the retro-Diels–Alder reaction (retro-DA) in this context (Scheme 1).

The utility of the retro-Diels–Alder reaction as a method for alkene synthesis has generally been hampered by the high temperatures required to effect cycloreversion (≫150 °C).[12] Since such temperatures would not be compatible with enediyne generation, we sought to identify a system that could be activated under much less forcing conditions. In 1983 Knapp and coworkers[13] demonstrated that Diels–Alder adducts derived from 9-benzyloxymethoxyanthracene (**2**) undergo facile cycloreversion at 25 °C after removal of the benzyloxymethoxy (BOM) protecting group and deprotonation of the resultant alcohol. This important observation has its origins in the remarkable ability of the oxide anion to accelerate pericyclic reactions (often by factors approaching 10^{17}), as first demonstrated by Evans and Golob[14] in the highly exploited anionic oxy-Cope reaction.[15] Although the oxide anion accelerated retro-Diels–Alder reaction has received only scant attention from synthetic organic chemists,[16] it nevertheless appeared ideally suited for our purposes and we decided to investigate the use of **2** as a platform for the generation of enediynes.

We consequently targeted the 1,5-diyne **3** (Scheme 2) as a key intermediate from which a variety of cyclic enediynes could in

[*] Prof. Dr. K. C. Nicolaou, Dr. M. E. Bunnage
Department of Chemistry and The Skaggs Institute of Chemical Biology
The Scripps Research Institute
10550 North Torrey Pines Road, La Jolla, CA 92037 (USA)
and
Department of Chemistry and Biochemistry
University of California, San Diego
9500 Gilman Drive, La Jolla, CA 92093 (USA)
Fax: Int. code +(619) 554-6738

[**] This work was supported financially by CaP CURE, the National Institutes of Health (USA), and The Scripps Research Institute. M. E. B. would like to thank the EPSRC (UK) for a NATO postdoctoral fellowship.

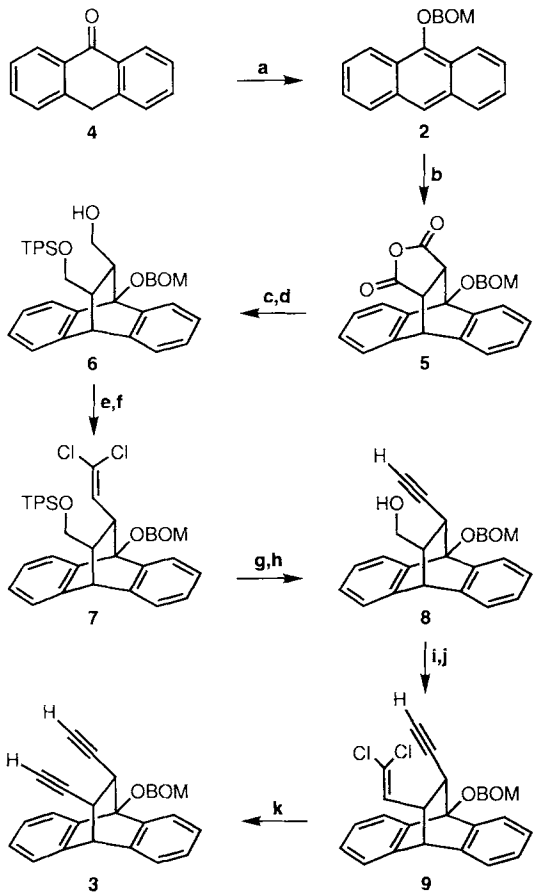

Scheme 2. Synthesis of diyne **3**. Reagents and conditions: a) 1.2 equiv of NaH, THF, 0 °C, 45 min; 1.2 equiv of BOMCl, 1.5 h, 85%; b) 1.0 equiv of maleic anhydride, PhH, reflux, 8 h, 100%; c) 4.25 equiv of $LiAlH_4$, THF, reflux, 12 h, 95%; d) 1.0 equiv of TPSCl, 2.0 equiv of imidazole, 0 → 25 °C, 2.0 h, 63% (+ 25% regioisomer); e) 1.5 equiv of NMO, 0.025 equiv of TPAP, MeCN, 25 °C, 0.5 h, 95%; f) 6 equiv of CCl_4, 3 equiv of $P(NMe_2)_3$, THF, −30 → 0 °C, 1.5 h, 83%; g) 2.1 equiv of *n*BuLi, THF, −78 → 0 °C, 0.5 h, 100%; h) 10 equiv of TBAF, THF, 25 °C, 2 h, 94%; i) 1.5 equiv of NMO, 0.05 equiv of TPAP, CH_2Cl_2/MeCN (9:1), 25 °C, 15 min, 80%; j) 6 equiv of CCl_4, 3 equiv of $P(NMe_2)_3$, THF, −30 °C, 15 min, 84%; k) 3.2 equiv of *n*BuLi, THF, −78 °C, 0.5 h, 45%. BOM = CH_2OCH_2Ph; TPS = *t*$BuPh_2Si$; NMO = 4-methylmorpholine *N*-oxide; TPAP = tetra-*n*-propylammonium perruthenate(VII); TBAF = tetra-*n*-butylammonium fluoride.

tion using the standard Corey–Fuchs procedure[18] was investigated, we obtained superior results by converting the aldehyde to the dichloroolefin **7** with hexamethylphosphorus triamide (HMPA) and CCl_4 in THF at −30 °C (83% yield).[19] Gratifyingly, the transformation of **7** to the desired alkyne occurred in quantitative yield by treatment with *n*-butyllithium, and subsequent desilylation using TBAF cleanly furnished the alcohol **8** (94% yield).

The second alkyne unit was introduced analogously. Thus, oxidation of **8** using TPAP–NMO[17] afforded the corresponding aldehyde in 80% yield. Although rather sensitive, this intermediate aldehyde could be converted, without epimerization, to the dichloroalkene **9** with HMPA/CCl_4 (84% yield). Finally, treatment of **9** with *n*-butyllithium gave the targeted 1,5-diyne **3**[20] in moderate yield (45%).

We were now in a position to investigate whether **3** could function as a platform for the generation of cyclic enediynes. In view of the difficulty in preparing cyclodecenediyne (**1**),[21] and its recognized potential as a DNA-cleaving agent,[4] this enediyne was selected to test the retro-Diels–Alder strategy and, therefore, **10** (Scheme 3) became our next synthetic target. We

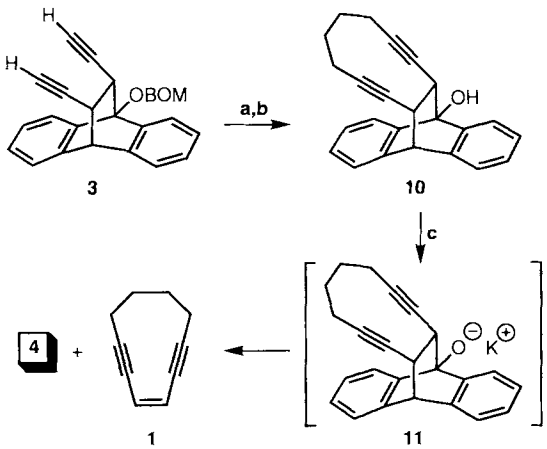

Scheme 3. Synthesis of precursor **10** and base-induced retro-Diels–Alder reaction to form enediyne **1**. Reagents and conditions: a) 2.3 equiv of *n*BuLi, 4 equiv of HMPA, THF, −78 °C, 0.5 h; 1.2 equiv of $I(CH_2)_4I$, −78 → 25 °C, 12 h, 52%; b) 10% TFA in MeOH, reflux, 1 h, 94%; c) KH, THF, 25 °C, 30 min, 90%.

principle be generated. The synthesis of **3** commenced with the preparation of **2** through treatment of the sodium salt of anthrone (**4**) with benzyloxymethyl chloride (BOMCl) (85% yield). The Diels–Alder reaction of **2** with maleic anhydride proceeded without difficulty to afford the adduct **5** in quantitative yield, and this was converted to the corresponding 1,4-diol by reduction with $LiAlH_4$ (95% yield). Initial attempts to oxidize this diol to the dialdehyde proved disappointing, and a stepwise strategy for the introduction of the acetylenic groups was pursued. Thus, protection of the diol with *tert*-butyldiphenylsilyl chloride (TPSCl) provided **6** in 63% yield together with 25% yield of the readily separable regioisomeric alcohol. The selectivity in this reaction (ca. 2:1) is presumably a consequence of the BOM protecting group shielding the proximate hydroxyl moiety from attack, possibly by engaging in intramolecular hydrogen bonding. Importantly, the minor alcohol could be recycled easily through desilylation using tetrabutylammonium fluoride (TBAF) (95% yield).

To prepare for the generation of the first alkyne unit, the alcohol **6** was oxidized to the corresponding aldehyde by the TPAP–NMO protocol[17] (95% yield). Although homologa-

first designed **3** with the supposition that the two alkyne moieties would be locked into a *syn* orientation and intramolecular bisalkylation of the dialkynyl dianion with dihaloalkanes would thus be facilitated.[22] This hypothesis was realized, since treatment of **3** with *n*-butyllithium in THF at −78 °C in the presence of HMPA, followed by addition of 1,4-diiodobutane, led smoothly to the desired cyclic 1,5-diyne in 52% yield. Finally, the target alcohol **10** was revealed (94% yield) by removal of the BOM protecting group using trifluoroacetic acid (TFA) in methanol.[23]

Although alcohol **10** proved highly stable under neutral or acidic conditions, deprotonation to form the oxide anion **11** led, as anticipated, to the desired retro-Diels–Alder cycloreversion. Thus, when **10** was treated with potassium hydride in THF at 25 °C, the reaction mixture developed a deep orange color, consistent with the generation of the potassium salt of anthrone, and **1** was generated cleanly (TLC analysis; $R_f = 0.31$ (silica gel, petroleum ether)[4]). Although **1** does undergo Bergman cycloaromatization at ambient temperature, it is stable enough to isolate,[4] and we were able to secure **1** in 90% yield from **10** by preparative TLC on silica gel.

In conclusion, we have demonstrated that the oxide anion accelerated retro-Diels–Alder reaction can be employed for the facile generation of cyclic enediynes from 1,5-diyne precursors. The use of 9-BOM-anthracene (**2**) to mask the double bond of the enediyne offers the advantages of excellent stability towards a variety of synthetic transformations and convenient removal when desired. Although the enediyne precursor is highly stable under acidic or neutral conditions, treatment with base leads to rapid cycloreversion and development of the enediyne. This methodology offers significant scope for the generation of new cyclic enediynes. Precursors such as **11** have potential as novel prodrugs when conjugated to appropriate delivery systems.

Received: January 4, 1996 [Z8699IE]
German version: *Angew. Chem.* **1996**, *108*, 1178–1180

Keywords: drug design · enediynes · retro-Diels–Alder reactions · synthetic methods

[1] For a review, see: K. C. Nicolaou, W.-M. Dai, *Angew. Chem.* **1991**, *103*, 1453; *Angew. Chem. Int. Ed. Engl.* **1991**, *30*, 1387.
[2] R. G. Bergman, *Acc. Chem. Res.* **1973**, *6*, 25.
[3] For reviews, see: a) K. C. Nicolaou, W.-M. Dai, S.-C. Tsay, V. A. Estevez, W. Wrasidlo, *Science* **1992**, *256*, 1172; b) K. C. Nicolaou, A. L. Smith, *Acc. Chem. Res.* **1992**, *25*, 497; c) K. C. Nicolaou, A. L. Smith, E. W. Yue, *Proc. Natl. Acad. Sci. USA* **1993**, *90*, 5881; d) M. E. Maier, *Synlett* **1995**, 13; e) K. C. Nicolaou, A. L. Smith in *Modern Acetylene Chemistry* (Eds.: P. J. Stang, F. Diederich), VCH, Weinheim, **1995**, pp. 203–283.
[4] K. C. Nicolaou, G. Zuccarello, C. Riemer, V. A. Estevez, W.-M. Dai, *J. Am. Chem. Soc.* **1992**, *114*, 7360; K. C. Nicolaou, G. Zuccarello, Y. Ogawa, E. J. Schweiger, T. Kumazawa, *ibid.* **1988**, *110*, 4866.
[5] For an elegant example of an enediyne, for which the conformation of the tether serves as a triggering device for the Bergman cyclization, see: L. Banfi, G. Guanti, *Angew. Chem.* **1995**, *107*, 2613; *Angew. Chem. Int. Ed. Engl.* **1995**, *34*, 2393.
[6] For a review describing various strategies for enediyne generation, including a section on 1,5-diynes as precursors, see ref. [3d]. See also, H. Hopf, M. Theurig, *Angew. Chem.* **1994**, *106*, 1173; *Angew. Chem. Int. Ed. Engl.* **1994**, *33*, 1099.
[7] A. G. Myers, P. S. Dragovich, *J. Am. Chem. Soc.* **1992**, *114*, 5859.
[8] M. E. Maier, B. Greiner, *Liebigs Ann. Chem.* **1992**, 855; M. E. Maier, T. Brandstetter, *Tetrahedron Lett.* **1991**, *32*, 3679.
[9] H. Audrain, T. Skrydstrup, G. Ulibarri, D. S. Grierson, *Synlett* **1993**, 20; H. Audrain, T. Skrydstrup, G. Ulibarri, C. Riche, A. Chiaroni, D. S. Grierson, *Tetrahedron* **1994**, *50*, 1469.
[10] J. M. Nuss, M. M. Murphy, *Tetrahedron Lett.* **1994**, *35*, 37.
[11] M. F. Semmelhack, J. Gallagher, *Tetrahedron Lett.* **1993**, *34*, 4121.
[12] For a review, see: A. Ichihara, *Synthesis* **1987**, 207.
[13] S. Knapp, R. M. Ornaf, K. E. Rodriques, *J. Am. Chem. Soc.* **1983**, *105*, 5494.
[14] D. A. Evans, A. M. Golob, *J. Am. Chem. Soc.* **1975**, *97*, 4765.
[15] For a review, see: L. A. Paquette, *Angew. Chem.* **1990**, *102*, 642; *Angew. Chem. Int. Ed. Engl.* **1990**, *29*, 609.
[16] See, for example: a) O. Papies, W. Grimme, *Tetrahedron Lett.* **1980**, *21*, 2799; b) T. V. RajanBabu, D. F. Eaton, T. Fukunaga, *J. Org. Chem.* **1983**, *48*, 652; c) J. V. N. Vara Prasad, P. Iyer, C. N. Pillai, *ibid.* **1982**, 47, 1380; d) T. Miyashi, A. Ahmed, T. Mukai, *J. Chem. Soc. Chem. Commun.* **1984**, 179.
[17] W. P. Griffith, S. V. Ley, *Aldrichimica Acta* **1990**, *23*, 13.
[18] E. J. Corey, P. L. Fuchs, *Tetrahedron Lett.* **1972**, 3769.
[19] This combination of reagents has been used for the dichloromethylenation of lactones, see: A. Bandzouzi, M. Lakhrissi, Y. Chapleur, *J. Chem. Soc. Perkin Trans. 1* **1992**, 1471; Y. Chapleur, *J. Chem. Soc. Chem. Commun.* **1984**, 449.
[20] Selected physical data for **3**: $R_f = 0.44$ (silica gel, 20% ether in petroleum ether); IR (film): $\nu_{max} = 3288$, 3066, 3029, 2955, 2919, 1457, 1046, 754 cm^{-1}; ^1H NMR (500 MHz, $CDCl_3$): $\delta = 7.74$ (d, $J = 7.5$ Hz, 1H, Ar), 7.54 (d, $J = 7.5$ Hz, 1H, Ar), 7.50 (d, $J = 7.0$ Hz, 2H, Ar), 7.41–7.14 (m, 9H, Ar), 5.56 (d, $J = 6.0$ Hz, 1H, OCH_2O), 5.51 (d, $J = 6.0$ Hz, 1H, OCH_2O), 5.06 (d, $J = 12.0$ Hz, 1H, OCH_2Ph), 5.02 (d, $J = 12.0$ Hz, 1H, OCH_2Ph), 4.35 (d, $J = 1.5$ Hz, 1H, $ArCHAr$), 3.45 (dd, $J = 10.0$, 2.5 Hz, 1H, $OCCHC{\equiv}C$), 3.26 (m, 1H, $Ar_2CHCHC{\equiv}C$), 2.16 (d, $J = 2.5$ Hz, 1H, $C{\equiv}CH$), 2.07 (d, $J = 2.5$ Hz, 1H, $C{\equiv}CH$); ^{13}C NMR (125 MHz, $CDCl_3$): $\delta = 141.5$, 140.8, 140.7, 137.8, 137.7, 128.4, 128.1, 127.7, 126.7, 126.4, 126.3, 126.2, 125.1, 123.6, 122.4, 121.9, 91.1, 83.4, 83.1, 81.4, 73.5, 72.3, 70.6, 48.8, 38.8, 36.8; HRMS calcd for $C_{28}H_{22}O_2Na$ ($M + Na^+$): 413.1518, found: 413.1538.
[21] We originally prepared **1** in 12% by a Ramberg–Bäcklund reaction, see: ref. [4]. For a novel preparation of **1** based on an intramolecular carbenoid coupling, see: G. B. Jones, R. S. Huber, J. E. Mathews, *J. Chem. Soc. Chem. Commun.* **1995**, 1791. See also the recent Highlight: B. König, *Angew. Chem.* **1996**, *108*, 177; *Angew. Chem. Int. Ed. Engl.* **1995**, *35*, 165.
[22] The intramolecular bisalkylation of dialkynyl dianions has precedent in the work of Semmelhack, see: ref. [11] and M. F. Semmelhack, T. Neu, F. Foubelo, *J. Org. Chem.* **1994**, *59*, 5038; *Tetrahedron Lett.* **1992**, *33*, 3277.
[23] Selected physical data for **10**: $R_f = 0.30$ (silica gel, 20% ether in petroleum ether); IR (film): $\nu_{max} = 3421$ (broad, OH), 2921, 1457, 1069, 754 cm^{-1}; ^1H NMR (500 MHz, $CDCl_3$): $\delta = 7.58$ (m, 1H, Ar), 7.48 (m, 1H, Ar), 7.32–7.13 (m, 6H, Ar), 4.29 (d, $J = 2.5$ Hz, 1H, $ArCHAr$), 3.16 (br s, 1H, OH), 3.10 (m, 1H, $Ar_2CHCHC{\equiv}C$), 3.03 (ddd, $J = 9.5$, 3.5, 1.5 Hz, 1H, $OCCHC{\equiv}C$), 2.06–1.91 (m, 4H, $C{\equiv}CCH_2$), 1.49 (m, 2H, $C{\equiv}CCH_2CH_2$), 1.26 (m, 2H, $C{\equiv}CCH_2CH_2$); ^{13}C NMR (125 MHz, $CDCl_3$): $\delta = 142.3$ 141.5, 140.0, 138.9, 126.4, 126.3, 125.8, 125.6, 125.0, 123.5, 120.8, 120.1, 89.1, 88.1, 81.8, 79.5, 77.4, 48.4, 45.3, 38.1, 28.0, 28.0, 20.6, 20.5; HRMS calcd for $C_{24}H_{20}OCs$ ($M + Cs^+$): 457.0568, found: 457.0554.

Nickel(0) Complexes of Five-Membered Titana- and Zirconacyclocumulenes as Intermediates in the Cleavage of C–C Bonds of Disubstituted Butadiynes**

Siegmar Pulst, Perdita Arndt, Barbara Heller, Wolfgang Baumann, Rhett Kempe, and Uwe Rosenthal*

Dedicated to Professor Paul Binger on the occasion of his 65th birthday

Oxidative addition to transition metal complexes is known for many compounds with a large variety of bonding types, but C–C single bonds react only very rarely in this manner.[1] Due to the high synthetic potential of the functionalization of hydrocarbons, and because of the significance of catalytic conversions, reactions of this kind are currently enjoying a great deal of attention.[2] Among these reactions, the activation and cleavage of the central C–C single bond in certain 1,4-disubstituted 1,3-butadiynes ($R^1C{\equiv}C{-}C{\equiv}CR^2$) by Os,[3a] Ti,[3b] Zr,[3c] and Ni [3d] complexes has been investigated intensely over the last few years. It is already known that when using "Cp_2Ti" and "Cp_2Zr" the success of the cleavage reaction [Eq. (a)] depends on the influence of the metal[3c] and of the substituents,[4] as well as on the stoichiometry.[5]

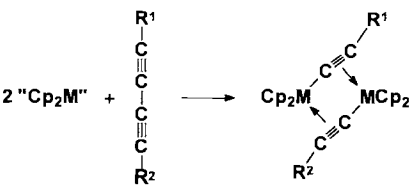

(a)

Moreover, in some cases, the cleavage is only successful if suitable heterobimetallic complexes are used instead of homobimetallic complexes. When the substituents R^1 and R^2 are *tert*-butyl groups, only the combination of Ti and Zr leads to the σ-π-acetylide-bridged complex $[Cp_2Ti(\mu\text{-}\eta^1,\eta^2\text{-}C{\equiv}CR)_2Zr\text{-}Cp_2]$,[5] whereas the reaction with solely "Cp_2Ti" or "Cp_2Zr"

[*] Prof. Dr. U. Rosenthal, Dr. S. Pulst, Dr. P. Arndt, Dr. W. Baumann, Dr. R. Kempe
Max-Planck-Gesellschaft
Arbeitsgruppe "Komplexkatalyse" an der Universität Rostock
Buchbinderstrasse 5-6, D-18055 Rostock (Germany)
Fax: Int. code +(381)4669386
e-mail: urosen@chemie1.Uni-Rostock.DE
Dr. B. Heller
Institut für Organische Katalyseforschung an der Universität Rostock e. V. (Germany)

[**] This work was supported by the Max-Planck-Gesellschaft and the Fonds der Chemischen Industrie.

leads to the formation of the five-membered metallacyclocumulenes $[Cp_2M{-}CR^1{=}C{=}C{=}CR^2]$ (M = Ti,[5] M = Zr[6]). The reaction of butadiyne Ni^0 complexes $[(Ph_3P)_2Ni(\eta^2\text{-}R^1C{\equiv}C{-}C{\equiv}CR^2)]$ with metallocenes has also been employed to cleave diynes. This resulted in substituent-dependent "tweezer-like" ($R^1 = SiMe_3$, $R^2 = Ph$) or unsymmetrical σ-π-acetylide-bridged heterobimetallic complexes ($R^1 = R^2 = SiMe_3$); the mechanism of formation remains the subject of speculation as yet.[7]

We report now that in the reaction of the complex $[(Ph_3P)_2Ni(\eta^2\text{-}PhC{\equiv}C{-}C{\equiv}CPh)]$ with "Cp_2Ti" and "Cp_2Zr" without cleavage of the diyne a new type of complex is formed (**1** and **2** respectively), which can be considered as an intermediate in the heterobimetallic cleavage reactions. This is also of theoretical interest from a bonding point of view as a metallacyclocumulene bonded to a Ni(0) complex fragment [Eq. (b)].

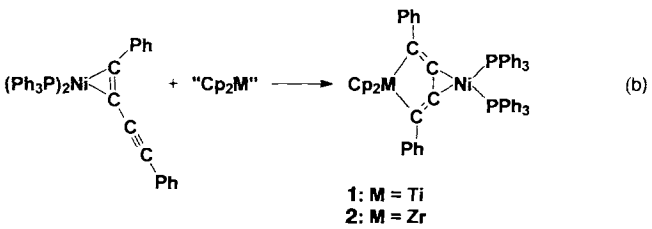

(b)

The titanium compound **1**[8] is readily soluble in benzene and THF, but only slightly soluble in *n*-hexane. In the IR spectrum there are no characteristic peaks for complexed C≡C triple bonds in the region of 1900–1600 cm^{-1}. The ^1H NMR [δ_{Cp} = 5.04 (s, 10H)] and ^{31}P NMR [δ = 21.2 (s)] spectra confirm a symmetrical coordination of the butadiyne.

The crystal structure analysis[9] of **1** (Fig. 1) shows that the central double bond of the titanacyclocumulene complex is formally coordinated to the $Ni(Ph_3P)_2$ fragment. This indicates that the compound $[Cp_2Ti{-}C(tBu){=}C{=}C{=}C(tBu)]$[5] really does exist in the form of a cyclocumulene and not in the form of a complex with η^4-bonded butadiyne.[10] Both the metal centers and the C_4 unit between them lie in a single plane and the P1-Ni-P2 plane is twisted at an angle of 35.0° to this (cf. the twist of the P-Ni-P plane in $[(Ph_3P)_2Ni(H_2C{=}CH_2)]$: 3–7°[11]).

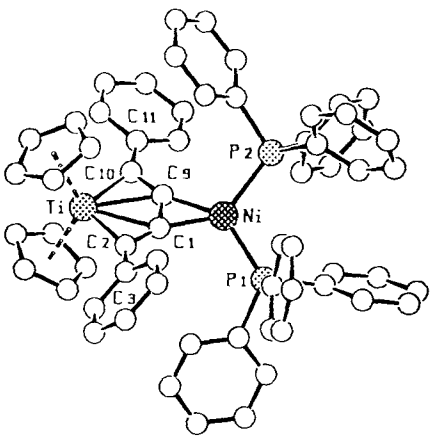

Fig. 1. Selected bond lengths [Å] and angles [°] in **1**: C2-C1 1.316(7), C1-C9 1.419(6), C9-C10 1.334(6), Ni-C1 1.916(5), Ni-C9 1.906(4), Ni-P1 2.227(1), Ni-P2 2.233(1), Ti-C2 2.124(4), Ti-C1 2.325(4), Ti-C9 2.340(5), Ti-C10 2.118(5), Ti-Z1 2.110, Ti-Z2 2.114; C2-C1-C9 137.2(4), C1-C9-C10 135.4(4), C1-C2-C3 134.0(4), C9-C10-C11 132.3(4), C2-Ti-C10 103.7(2), P1-Ni-P2 111.48(5), C9-C1-Ni 67.8(3), C1-C9-Ni 68.6(3), Z1-Ti-Z2 129.36.

Table 1. Selected bond lengths [Å] in **1**, **3**, and **4**.

Bond	1	3	4
Ti-C_α	2.118(5), 2.124(4)	2.252(9), 2.298(10)	2.141(5), 2.172(5)
Ti-C_β	2.325(4), 2.340(5)	2.209(9), 2.213(9)	-
C_α-C_β	1.316(7), 1.334(6)	1.243(13), 1.276(11)	1.369(6), 1.370(6)
C_β-$C_{\beta'}$	1.419(6)	1.339(13)	1.495(6)

Comparison of the data in Table 1 confirms the description of **1** as a titanacyclocumulene coordinated to a Ni^0 compound. The interatomic distances and angles in the TiC_4 unit in **1** are similar to those in the noncoordinated titanacyclocumulene **3**[5] and in the titanacyclopentadiene **4**.[12]

$[Cp_2Ti{-}C(tBu){=}C{=}C{=}C(tBu)]$ **3**

$[Cp_2Ti{-}CPh{=}CPh{-}CPh{=}C(Ph)]$ **4**

The central $C_\beta{-}C_{\beta'}$ bond in **1** (1.419(6) Å) is 0.08 Å longer than that in **3** and thus lies in the range for double bonds in coordinated olefins (cf. $d_{C=C}$ in $[(Ph_3P)_2Ni(H_2C{=}CH_2)]$ 1.43(2) Å[12]). The $C_\alpha{-}C_\beta$ bonds in **1** (1.316(7), 1.334(6) Å) are almost as long as those in **4** (1.369(6), 1.370(6) Å) and the Ti–C_α distances in **1** (2.118(5), 2.124(4) Å) only differ slightly from those in **4** (2.141(5), 2.172(5) Å). Whereas in **3** the Ti–C_β distances (2.209(9), 2.213(9) Å) are shorter than the Ti–C_α distances (2.252(9), 2.298(10) Å), in **1** the situation is the other way around and the Ti–C_β distances (2.325(4), 2.340(5) Å) are about 0.2 Å longer than the Ti–C_α distances.

The zirconocene compound **2** was also synthesized analogously and it displays similar spectroscopic and structural properties.[9, 13] The compounds **1** and **2** can be regarded as coordinated metallacyclocumulenes in which the interaction of the central C=C bond with the Ti atom and the Zr atom[5, 6] is weakened in favor of the interaction with the Ni atom. The isolation of **1** and **2** seems to become possible through the presence of the phenyl substituents on the diyne, because in the case of Me_3Si-substituted butadiynes there is an increased tendency towards activation of the C–C single bond.[3b, 3c, 4]

The significance of the compounds **1** and **2** for the activation of the heterobimetallic C–C single bond lies in that their existence makes the occurrence of metallacyclocumulene intermediates appear probable in the cleavage of butadiynes. Recent investigations also show that in the reverse reaction of the classical combination of acetylide groups with metallocenes to give butadiynes,[10, 14] cyclocumulenes can be identified under photochemical conditions [Eq. (c)].

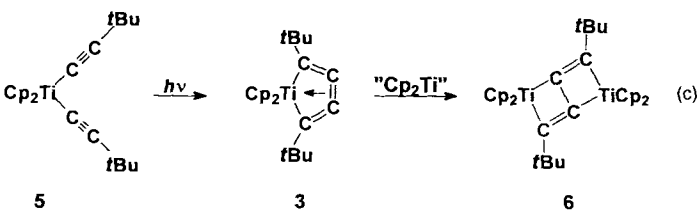

(c)

Under photochemical conditions complexes of the type $[Cp_2TiR_2]$[15] ($R = CH_3$) and $[Cp_2TiAr_2]$[16] ($Ar = C_6H_5$, $CH_3C_6H_4$) can undergo a typical C–C combination which was also suspected for acetylides in earlier works.[17] On irradiating the complex $[Cp_2Ti(C{\equiv}CtBu)_2]$ **5** with light of the wavelength range 390–450 nm, the course of the reaction as shown in Equation (c) could be unequivocally confirmed qualitatively for the

first time by monitoring concentration profiles characteristic of a consecutive reaction by time-dependent NMR spectroscopic techniques (Fig. 2).

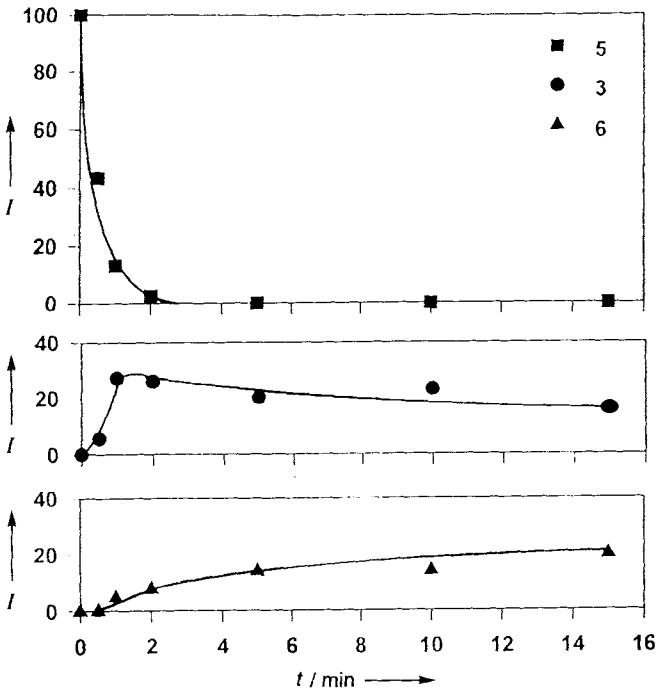

Fig. 2. NMR spectroscopic monitoring of the reaction of **5** to give **6** [see also Eq. (c) and (d)]. Intensities I [%] of the Cp protons of **5** (top), **3** (middle), and **6** (bottom) as a function of time. 0 min: 100% **5**, 0% **3**, 0% **6**; 0.5 min: 43% **5**, 6% **3**, 0% **6**; 1 min: 13% **5**, 27% **3**, 5% **6**; 2 min: 3% **5**, 26% **3**, 8% **6**; 5 min: 0% **5**, 20% **3**, 14% **6**; 10 min: 0% **5**, 23% **3**, 14% **6**; 15 min: 0% **5**, 16% **3**, 20% **6** (total yield 36% with respect to titanium).

According to this, the σ-bis-acetylide **5** decays very rapidly; the amount of the intermediate **3** formed passes through a maximum. This reacts with "Cp_2Ti" as described[5] to give the binuclear complex **6**.[4] In addition, significant amounts of paramagnetic side products are formed. Both the oxidative addition to metallocene systems and the reductive elimination of butadiynes from metallocene systems can thus be explained by the formation of metallacyclocumulenes and their interaction with a second complex (Scheme 1).

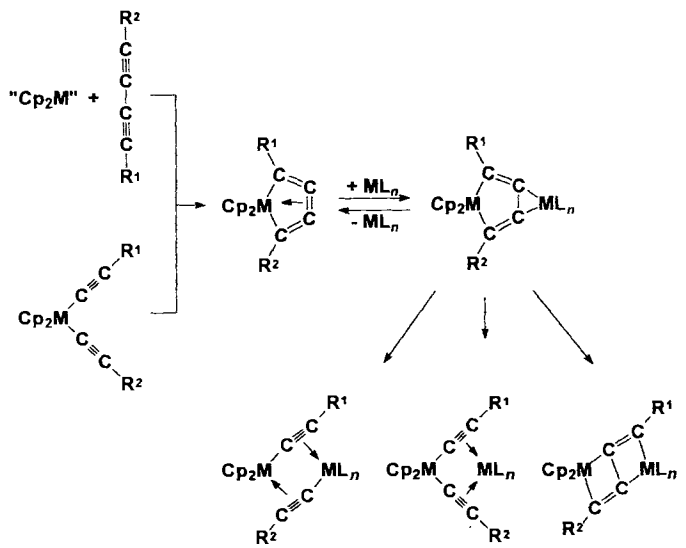

Scheme 1. Formation and reactions of metallacyclocumulenes.

The binuclear complexes formed can then react further in a variety of different ways; the metals, the butadiyne substituents, and the stoichiometry are decisive for the course of the reaction.

Experimental Procedure

All manipulations were carried out under the exclusion of oxygen and moisture.

1: [$(Ph_3P)_2Ni(\eta^2$-PhC≡C–C≡CPh)] (560 mg, 0.71 mmol) in toluene (20 mL) and [$Cp_2Ti(Me_3SiC{\equiv}CSiMe_3)$] (250 mg, 0.71 mmol) in toluene (15 mL) were allowed to react at 40 °C for 4 h. All volatile components were then removed under vacuum and the residue recrystallized from toluene at 50 °C to give dark brown needles of **1**. Yield: 250 mg (36%), m.p. 163–165 °C (decomp.), correct elemental analysis.

2: Dark brown crystals of **2** were obtained analogously to **1** from [$(Ph_3P)_2Ni(\eta^2$-PhC≡C–C≡CPh)] (715 mg, 0.91 mmol) and [$Cp_2Zr(thf)(Me_3SiC{\equiv}CSiMe_3)$] (430 mg, 0.91 mmol) in THF. Yield: 235 mg (25%), correct elemental analysis.

Photolysis of **5**: Six samples of a [D_8]THF solution of **5** (0.04 M) were sealed in NMR tubes and without further cooling irradiated with light of the wavelength range 390–450 nm (HPM-12-Philips 460 W, 1 cm distance) for different periods of time (0.5, 1, 2, 5, 10 and 15 min). NMR spectra were subsequently recorded. The resonances of the protons of the Cp rings in **5**, **3**, and **6** [δ = 6.23 (**5**), 5.05 (**3**), 5.45 (**6**)] in the ^{1}H NMR spectrum ([D_8]THF, quantitative standard C_6H_6) can easily be distinguished from one another.

Received: December 15, 1995 [Z8652IE]
German version: *Angew. Chem.* **1996**, *108*, 1175–1178

Keywords: butadiynes · C–C bond cleavage · nickel compounds · titanium compounds · zirconium compounds

[1] R. H. Crabtree, *Chem. Rev.* **1985**, *85*, 245.
[2] S.-Y. Liou, M. Gozin, D. Milstein, *J. Am. Chem. Soc.*, **1995**, *117*, 9774–9775; and references therein.
[3] a) A. J. Deeming, M. S. B. Felix, P. A. Bates, M. B. Hursthouse, *J. Chem. Soc. Chem. Commun.* **1987**, 461–463; b) U. Rosenthal, H. Görls, *J. Organomet. Chem.* **1992**, *439*, C36–C41; c) U. Rosenthal, A. Ohff, W. Baumann, R. Kempe, A. Tillack, V. V. Burlakov, *Organometallics*, **1994**, *13*, 2903–2906; d) M. Maekawa, M. Munakata, T. Kuroda-Sowa, K. Hachiya, *Inorg. Chem. Acta*, **1995**, *233*, 1–4.
[4] U. Rosenthal, A. Ohff, A. Tillack, W. Baumann, H. Görls, *J. Organomet. Chem.* **1994**, *468*, C4–C8.
[5] V. V. Burlakov, A. Ohff, C. Lefeber, A. Tillack, W. Baumann, R. Kempe, U. Rosenthal, *Chem. Ber.* **1995**, *128*, 967–971.
[6] U. Rosenthal, A. Ohff, W. Baumann, R. Kempe, A. Tillack, V. V. Burlakov, *Angew. Chem.* **1994**, *106*, 1678–1680; *Angew. Chem. Int. Ed. Engl.* **1994**, *33*, 1605–1607.
[7] U. Rosenthal, S. Pulst, P. Arndt, A. Ohff, A. Tillack, W. Baumann, R. Kempe, V. V. Burlakov, *Organometallics* **1995**, *14*, 2961–2968.
[8] **1**: NMR (Bruker ARX 300, [D_8] THF, TMS, 303 K) ^{1}H: δ = 5.04 (10, s, Cp), 6.98–7.05(m), 7.14–7.19(m), 7.70–7.72(m); ^{31}P: δ = 21.2; ^{13}C {^{1}H}: δ = 173.4 (s, C≡C), a quaternary C atom could not be detected. 105.0 (s, Cp), 125.3, 128.2, 128.6, 129.7, 130.5 (each s, Ph), 134.7 (dd, ^2J(C, P) = 10 Hz, ^4J(C, P) = 10 Hz, Ph), 136.4 (dd, ^{1}J(C, P) = 30 Hz, ^3J(C, P) = 20 Hz, Ph), 144.0 (s, Ph).
[9] STOE IPDS Diffractometer, graphite monochromated $Mo_{K\alpha}$ radiation, structure solution using direct methods SHELXS-86 (G. M. Sheldrick, *Acta Crystallogr. Sect. A* **1990**, *46*, 467–473), refinement with full matrix using least-squares methods wrt. F^2 with SHELXL-93 (G. M. Sheldrick, as yet unpublished), structure depiction using SCHAKAL 92 (E. Keller, Universität Freiburg, **1992**). Crystal data from **1**: $C_{62}H_{50}P_2NiTi$, M_r = 963.6 g mol^{-1}, space group $P2_1$, a = 13.199(1), b = 13.443(1), c = 13.967(1) Å, β = 100.848(8)°, V = 2433.9(3) Å^3, Z = 2, ρ_{calcd} = 1.315 g cm^{-3}, 15671 reflections measured, 7232 symmetry-independent reflections of which 6549 observed ($I > 2\sigma(I)$), 595 refined parameters, $R1$ = 0.044, $wR2$ = 0.121, residual electron density 0.22 e Å^{-3}. Crystal data from **2**: $C_{62}H_{50}P_2NiZr$, M_r = 1006.94 g mol^{-1}, space group $P2_1/n$, a = 12.391(2), b = 18.394(3), c = 22.684(3) Å, β = 102.53(1)°, V = 5047.0(13) Å^3, Z = 4, ρ_{calcd} = 1.325 g cm^{-3}, 14821 reflections measured, 8070 symmetry-independent reflections of which 5509 observed ($I > 2\sigma(I)$), 595 refined parameters, $R1$ = 0.043, $wR2$ = 0.113, residual electron density 0.27 e Å^{-3}. Crystallographic data (excluding structure factors) for the structure(s) reported in this paper have been deposited with the Cambridge Crystallographic Data Centre as supplementary publication no. CCDC-179-21. Copies of the data can be obtained free of charge on application to The Director, CCDC, 12 Union Road, Cambridge CB2 1EZ, UK (fax: int. code + (1223) 336-033; e-mail: teched@chemcrys.cam.ac.uk).
[10] B. Temme, G. Erker, R. Fröhlich, M. Grehl, *Angew. Chem.* **1994**, *106*, 1570.
[11] W. Dreissig, H. Dietrich, *Acta Crystallogr. Sect. B.* **1968**, *24*, 108.
[12] J. L. Atwood, W. E. Hunter, H. Alt, M. D. Rausch, *J. Am. Chem. Soc.* **1976**, *98*, 2454–2459.

[13] **2**: NMR (Bruker ARX 400, C_6D_6, TMS, 303 K): ^{1}H: δ = 5.30 (10, s, Cp), 6.60–6.80 (m, 18H), 6.90–7.10 (m, 12H), 7.10–7.20 (m, 6H), 7.85–7.95 (m, 4H); ^{31}P: δ = 18.2 ^{13}C{^{1}H}: δ = 170.4 (s, C≡C), a quaternary C atom could not be detected, 105.0 (s, Cp), 125.3 (s, Ph), 128.4 (d, ^3J(C, P) = 4 Hz, Ph), 128.5, 129.3, 131.0 (each, s, Ph), 134.2 (dd, ^2J(C, P) = 7 Hz, ^4J(C, P) = 7 Hz, Ph), 135.9 (dd, ^1JC, P) = 17 Hz, ^3J(C, P) = 17 Hz, Ph), 144.2 (s, Ph). The crystal structure of **2** is analogous to that of **1**. The dihedral angle between the C1-Ni-C9 and the P1-Ni-P2 planes is 70.0°. Selected bond lengths [Å] and angles [°] in **2**: C2-C1 1.322(5), C1-C9 1.410(5), C9-C10 1.331(5), Ni-C1 1.928(4), Ni-C9 1.911(3), Ni-P1 2.215(1), Ni-P2 2.223(1), Zr-C2 2.238(4), Zr-C1 2.390(3), Zr-C9 2.379(3), Zr-C10 2.223(4), C2-C1-C9 139.4(3), C1-C9-C10 139.8(4), C1-C2-C3 132.2(4), C9-C10-C11 131.4(3), C2-Zr-C10 100.71(13), P1-Ni-P2 123.22(4), C9-C1-Ni 67.8(2), C1-C9-Ni 69.1(2).
[14] J. H. Teuben, H. J. De Liefde Meijer, *J. Organomet. Chem.* **1969**, *17*, 87–93.
[15] H. Alt, M. D. Rausch, *J. Am. Chem. Soc.* **1974**, *96*, 5936.
[16] M. D. Rausch, W. H. Boon, E. A. Mintz, *J. Organomet. Chem.* **1978**, *160*, 81–92.
[17] W. Frömberg, Dissertation, Universität Bochum, **1986**.

Formation of Fe^{IV} and Ni^{IV} by Electrochemical and Chemical Oxidation of an Iron-Substituted Nickel(II) Hydroxide: The Direct Two-Electron Step $Ni^{II} \rightarrow Ni^{IV} + 2e^-$**

Peter Axmann, Christina Freire Erdbrügger, Dieter H. Buss and Oskar Glemser*

Dedicated to Professor Herbert W. Roesky on the occasion of his 60th birthday

Nickel(II) hydroxide crystallizes in the layered structure of brucite. Allmann[1] reported that partial substitution of nickel(II) ions with suitable metal(III) ions results in pyroaurite-type double layered structures of the general formula **1** ($0.2 \leq x \leq 0.4$,

$$\underset{K^{x+}}{[Ni^{II}_{1-x}M^{III}_x(OH)_2]^{x+}}\underset{A^{x-}}{[(X^{n-})_{x/n}(H_2O)_z]^{x-}} \quad \mathbf{1}$$

phase width of the pyroaurite type). The random anionic layers A^{x-} (X = anions of the applied metal salts) are found between the brucite-like cationic layers K^{x+}; the cations in K^{x+} are statistically distributed.[2]

By substitution with Al^{III},[3–5] Co^{III},[4] Mn^{III},[5] and in particular Fe^{III} ions,[6] along with variation of the anion of the metal salt, for example NO_3^-, CO_3^{2-}, SO_4^{2-}, and $SO_4^{2-} + PO_4^{3-}$,[4, 6c, 7] we have been able to improve the electrochemical characteristics of nickel hydroxide with respect to applications as a positive electrode for secondary cells in alkaline electrolytes.[3–7] The molar ratio of Ni^{II}:M^{III} = 4:1 (x = 0.2) was shown to be the best.[3, 8] The substitution with various different M^{III} ions was also successful.[5b]

The remarkable electrochemical characteristics of the Ni/Fe electrode, which we first described,[4, 6] have been confirmed by Delmas et al.[9] During the electrochemical redox process,[10] which is a proton–electron exchange reaction between the pyroaurite-type and γ-NiOOH layers,[11] Faraday yields were found which are larger than the theoretical value for the one-electron step $Ni^{II} \rightarrow Ni^{III} + 1e^-$.[12] This signifies the formation of Ni^{IV} ions.[13] The question of whether the Fe^{III} ions also take part in this electrochemical redox process could be clarified for the first time by studying the Mössbauer spectra[14] of Fe^{III}-substituted pyroaurite-type nickel hydroxides with carbonate as well as sulfate–phosphate ions.[4]

In the following we will present and discuss the results of Mössbauer spectroscopic investigations of the charged and discharged states of an electrode made up of the iron-substituted, carbonate-containing pyroaurite-type nickel hydroxide **2**.[15]

$$[Ni_{4.06}Fe_{0.94}(OH)_{10}]^{+0.94}[(CO_3^{2-})_{0.21}(HCO_3^-)_{0.59}(K^+)_{0.0}\text{-}(H_2O)_{4.66}]^{-0.94} \quad \mathbf{2}$$

The Mössbauer spectrum of the discharged electrode (Fig. 1a) shows two absorption bands. This corresponds to two doublets with isomer shifts δ of +0.34 and +0.44 mm s^{-1},[16]

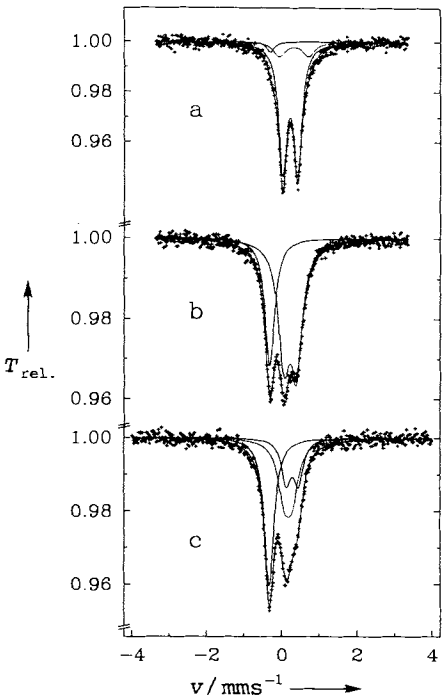

Fig. 1. Mössbauer spectra of an Fe^{III}-substituted pyroaurite-type electrode, v = relative speed between the source and the absorber, T_{rel} = relative transmission. a) Ni/Fe/CO_3 (discharged), b) Ni/Fe/CO_3 (charged), c) NiFe245 (charged); all fits according to model 3 (see text).

which are characteristic for Fe^{III} ions in the high-spin state, as well as to a less intense singlet at $\delta = -0.18$ mm s^{-1}, to whose meaning we will later return. Since both quadrupole doublets show no Lorentz profile, a distribution of quadrupole splittings for the respective isomer shifts must be assumed in order to fit the spectra. This is indicative of different sorts of Fe^{III} ions in slightly varying positions. Similar results were observed with a charged electrode. The quadrupole splittings ΔE_Q presented in Table 1 represent the values at the maxima of the quadrupole distributions.

The typical Mössbauer spectrum of a charged electrode (Fig. 1b) shows signals at $\delta = -0.19, +0.18$, and +0.52 mm s^{-1}. Several interpretation models must be considered.

Model 1: The signals correspond to a doublet and a singlet, both with $\delta = +0.17$ mm s^{-1}; this can be interpreted as low-

[*] Prof. Dr. Ing. O. Glemser, Dr. P. Axmann, Dr. D. H. Buss
Institut für Anorganische Chemie der Universität
Tammannstrasse 4, D-37077 Göttingen (Germany)
Fax: Int. code +(551)39-3373
Dr. C. Freire Erdbrügger
Ammoniak-Labor, BASF, Ludwigshafen (Germany)

[**] Iron-Substituted Nickel Hydroxide Electrodes, Part 4. We thank Prof. Dr. P. Gütlich and Dr. J. Ensling, Institut für Anorganische Chemie und Analytische Chemie der Johannes-Gutenberg-Universität, Mainz, for measuring and interpreting the Mössbauer spectra. We thank the Deutsche Forschungsgemeinschaft, the Fonds der Chemischen Industrie, and the Fa. H. C. Stark, Goslar for their support. Parts 1–3: ref. [6a–c].

Table 1. Mössbauer data for charged and discharged Ni/Fe/CO_3 as well as NiFe245.

Sample	Modell	δ [mm s^{-1}]	ΔE_Q [mm s^{-1}]	Proportion [%]	χ^2
Ni/Fe/CO_3, charged	1	+0.17	0.73	40	1.38
		+0.17	-	60	
	2	+0.52	-	40	1.26
		−0.01	0.37	60	
	3	+0.34	0.34	70	1.13
		−0.19	-	30	
NiFe245	3	+0.40	0.32	23	1.05
		+0.29	≤0.20	37	
		−0.20	-	40	
Ni/Fe/CO_3, discharged	3	+0.34	0.40	82	1.01
		+0.44	0.70	14	
		−0.18	-	4	

spin Fe^{III}. However, with $\chi^2 = 1.38$, this model shows the worst fit of all the alternatives discussed below. This model can be discounted by comparing with the spectrum of another charged electrode with a similar average degree of oxidation but significantly stronger distinction of the signal at $\delta = -0.19$ mm s^{-1} (sample of NiFe245: $\delta = -0.20$ mm s^{-1}, Fig. 1c). The described interpretation can only be applied unter the condition of a strong deviation of the line intensity in the quadrupole doublet. This is highly improbable even with a very large textural contribution.

Model 2: The signals correspond to a doublet at $\delta = -0.01$ mm s^{-1} and a singlet at $\delta = +0.52$ mm s^{-1}. With $\chi^2 = 1.26$ the quality of the fit is better than that for model 1. The isomer shift $\delta = -0.01$ mm s^{-1} is typical for low-spin Fe^{IV}.[17] From a chemical point of view the presence of this state is more probable than the high-spin configuration due to the expected high covalent contribution of the Fe^{IV}–O bond. However, no meaningful explanation can be provided for the singlet. Its isomer shift lies between the typical values for Fe^{III} and Fe^{II} ($\delta = 0.33-0.40$ and 1 mm s^{-1}, respectively), which indicates an increase in electron density on the Fe ion. Such a partial reduction of the Fe^{III} ions is extremely unlikely in the strongly oxidizing γ-NiOOH matrix. Fe^{II} itself is a strong reducing agent in a hydroxide environment. Therefore, this model can also be eliminated.

Model 3: The signals correspond to a singlet at $\delta = -0.19$ and a doublet at $\delta = +0.34$ mm s^{-1}. With $\chi^2 = 1.13$ this model shows the best fit and can be very well applied to the spectrum of the comparison electrode NiFe245 (Fig. 1c): the assignment of two doublets at $\delta = +0.40$ and $+0.29$ mm s^{-1} as well as a singlet at $\delta = -0.20$ mm s^{-1} gives a good fit with $\chi^2 = 1.05$. The signals at $+0.40$ and $+0.29$ mm s^{-1} can be interpreted as high-spin Fe^{III} ions. As described below the singlet at -0.20 mm s^{-1} is from Fe^{IV}. While models 1 and 2 basically require alterations of all the iron ions, in model 3 only a part of the Fe ions are affected. As a result, models 1 and 2 were eliminated and model 3 has been chosen for the basis of the interpretation of the charged electrode.

The measured isomer shift $\delta = -0.19$ mm s^{-1} (Fig. 1b) can, according to literature data, be assigned to high-spin Fe^{IV} ions,[13, 18] which are found in generally about 30% content in the charged Ni/Fe/CO_3 electrodes. The absence of quadrupole splitting indicates approximately undistorted octahedral symmetry of the environment (O_h symmetry of the $Fe^{IV}O_6$ octahedron). The remaining 70% are Fe^{III} ions whose Mössbauer parameters differ only slightly from those of the discharged electrode. In the discharged state small amounts of Fe^{IV} (singlet at $\delta = -0.18$ mm s^{-1}, Fig. 1a) were observed in several different samples. This is probably due to minor amounts of γ-NiOOH which were not accessible during the discharging process because electrical contact was lost to the conducting framework.[19] Noteworthy is the stability of the Fe^{IV} ion in the charged electrode. With $Ni_4Fe/SO_4/PO_4$ samples, no loss of Fe^{IV} was observed even after three months ($T = 290$ K, singlet at $\delta = -0.18$ mm s^{-1}, Fe^{IV} content 23%).[4]

According to the measurements presented, the behavior of the charged electrode is unusual in two ways: 1) The low-spin configuration with two unpaired spins is expected for Fe^{IV}.[20] Unter special condiditions the rarer high-spin configuration can be induced,[20] as in the material investigated here. 2) The high symmetry of the $Fe^{IV}O_6$ octahedron is unusual[21] since d^4 high-spin ions tend to distort their ligand sphere (Jahn–Teller stabilization). This in turn leads to quadrupole splitting of the corresponding signal in the Mössbauer spectrum.[22, 23] In our case a singlet is present. Therefore, the coordination sphere of Fe^{IV} here is not determined by its electron configuration but rather by the γ-NiOOH matrix. This is possible when the distortion of the ligand sphere requires more energy than would be gained by Jahn–Teller stabilization.

The Mössbauer spectra allow for further conclusions. First of all, we can exclude a statistical distribution of the Fe^{IV} ions in the lattice. In this case the Fe^{III} and Fe^{IV} ions would be in similar environments and the Fe^{IV} signal should also show significant quadrupole splitting. Charge delocalization between the nickel ions in varying oxidation states over the total γ-NiOOH lattice would also result in similar environments for the Fe^{III} and Fe^{IV} ions and thereby give rise to signals with comparable quadrupole splitting. This is also not in agreement with the measured Mössbauer spectra.

From this we conclude that domains with local ordering must exist in γ-NiOOH, which force a certain amount of the Fe ions into a regular octahedral corset and simultaneously allow for the transition to the +IV state. How can one imagine this environment to be? In order for the Fe^{IV} ions to have a regular octahedral ligand sphere, the directly adjacent lattice positions must also have O_h symmetry. Within the layer the Fe^{IV} ion can have a maximum of six closest cationic neighbors. In the chosen Ni/Fe molar ratio, these lattice positions are statistically occupied by nickel ions. If we assume that the nickel ions have defined oxidation states, γ-NiOOH with an average degree of oxidation at Ni from +3.0 to +3.3[12] can contain Ni^{III} as well as Ni^{IV} and, as shown here, Ni^{II} in its lattice.

A direct environment of six Ni^{II} ions can be excluded since a fast electron exchange between Fe^{IV} and Ni^{II} would take place. An approximation by which the Fe^{IV} ions are surrounded by six Ni^{III} ions is also not probable. Due to its d^7 configuration, the Ni^{III} ion should be subject to a Jahn–Teller distortion, a situation opposing the formation of a regular environment. In addition, with the given average degree of oxidation the remaining Fe^{III} ions would have environments similar to that of Fe^{IV}. This contradicts the findings from the Mössbauer spectra.

From our point of view the Fe^{IV} ions within the layer must be completely surrounded by Ni^{IV} ions since their d^6 low-spin configuration does not lead to distortion of the ligand sphere (Fig. 2). Use of this domain model also explains the presence of the high-spin state. The high contrapolarizing effect of the Ni^{IV} ions decreases the donor character of the oxygen ions with respect to the Fe ions so that the Fe–O bond has relative ionic character. Simultaneously, the Ni^{IV}–O bonds are sufficiently stabilized, due to their high covalent contribution, to successfully resist distortion of the $Fe^{IV}O_6$ octahedron.

Another possible explanation for the lack of Jahn–Teller distortion in the $Fe^{IV}O_6$ octahedron is presented by the theorem of Höck and Thomas.[24] According to this theorem, a vibronic

 © VCH Verlagsgesellschaft mbH, D-69451 Weinheim, 1996 0570-0833/96/3510-1116 $ 15.00+.25/0

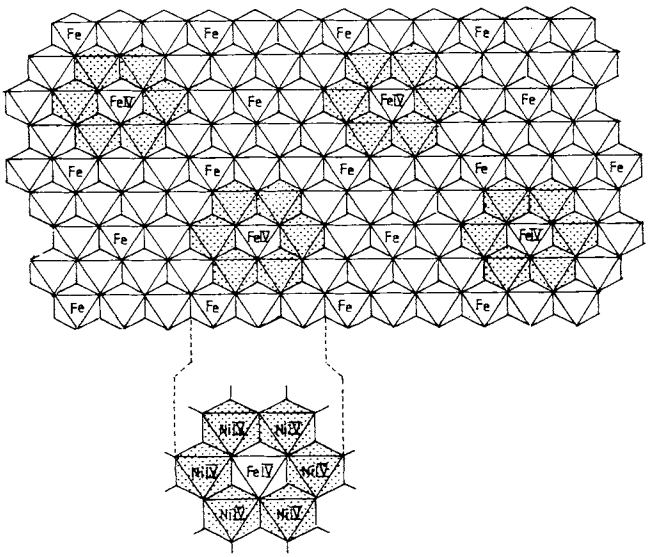

Fig. 2. Domain model for the Fe^{IV} ions in the γ-NiOOH layer.

Jahn–Teller coupling can be suppressed in a strongly electronically delocalized system when the width of the electronic state is larger than the expected ground state splitting. This has been shown for Mn^{III}/Mn^{IV} mixed-oxide crystals[25] and is surely relevant for the domains postulated here.[26]

Such a charge accumulation with seven directly neighboring +IV ions in a layer structure is unusual. However, similar features have been found with ions with significantly higher oxidation states. In the $[TeMo_6O_{24}]^{6-}$ ion,[27] in which the structural unit is derived from CdI_2 and is very similar to the assumed domain structure in γ-NiOOH, the Te^{VI} ion is surrounded by six MoO_6 octahedra. $K_5[I(Mo_6O_{24})]\cdot 5H_2O$ also has a similar structure.[28]

Known data support our ideas for the symmetry of the participating ions. On the basis of Mössbauer and Raman spectroscopic investigations of up to 10 mol% ($x = 0.1$) iron-substituted nickel hydroxide in a charged state, Corrigan et al.[29] assumed that nickel as well as iron ions are present in a highly symmetrical environment. This was confirmed by Kim et al.[30] with X-ray absorption (XAFS) investigations. In contrast to our findings, both groups observed no formation of Fe^{IV}.[31]

Under the assumption of defined charge states, the following is true according to the proposed domain model for the total matrix. In order for all the Fe^{IV} ions to be completely surrounded by Ni^{IV}, the absolute ratio of $Ni^{IV}:Fe^{IV}$ may not be less than 6:1 (limiting case for isolated, intact Ni_6Fe units) (cf. Fig. 2). The Ni^{IV}/Fe^{IV} ratio in the oxidized state of **2** was determined from the Mössbauer spectroscopic, electrochemical, and elemental analytical[15] data.[32–35]

When it is generally assumed that the nickel ions in γ-NiOOH are present in the +III and +IV oxidation states ("$x\,Ni^{IV}O_2\cdot y\,Ni^{III}OOH$"), the Ni^{IV}/Fe^{IV} ratio required for sixfold coordination can not be applied. Almost all of the values obtained from many experiments lie in the range of 2:1 to 4:1. They are therefore not in agreement with the domain model.

The direct two-electron step $Ni^{II} \rightarrow Ni^{IV} + 2e^-$ was postulated relatively early on for the redox reaction in nickel hydroxide.[36] The average degree of oxidation is distributed among the Ni^{II} and Ni^{IV} ions ("$x\,Ni^{IV}O_2\cdot y\,Ni^{II}(OH)_2$"); $Ni^{IV}:Fe^{IV}$ now lies significantly higher than the required 6:1 ratio. Smaller ratios are first expected when the Fe^{IV} content exceeds 40%. However, this high degree of oxidation at nickel could not be achieved electrochemically.

Our experimental results can best be explained by the domain model with the assumption that only Ni^{IV} and Ni^{II} ions are present in the γ-NiOOH phase. This means that the redox process occurs by the direct two-electron step. This is in agreement with the finding that the Mössbauer parameters of the nonoxidized iron ions in γ-NiOOH are barely altered in comparison to the pyroaurite-type starting material. Therefore, there are still mainly Ni^{II} ions in the neighboring positions.

Our arguments are in agreement with investigations by Mansour et al.[37, 38] According to their X-ray absorption measurements (XAFS) of various nickel hydroxides, only two different Ni–O bond lengths, characteristic for Ni^{IV} and Ni^{II}, can be detected. The exclusive presence of Ni in these two oxidation states was also assumed by Greaves et al.,[39] who determined the crystallographic and magnetic structure of Ni_2O_3H from powder neutron diffraction data. Using X-ray data, Wohlfahrt-Mehrens et al.[40] were first to prove that this compound can be formed during electrochemical oxidation in the nickel hydroxide electrode. Thermodynamic considerations of the two-electron step can be found in the paper by Balej and Divisek.[41]

As shown by Mössbauer spectroscopy, the chemical oxidation of a $Ni_4Al_{0.9}Fe_{0.1}$ pyroaurite with peroxodisulfate in 9 M KOH leads to the formation of highly symmetric high-spin Fe^{IV} ions in up to 31% content. An Fe^{IV} content of 35% was achieved in another sample that was electrochemically oxidized.[5b] Therefore oxidized **2** is the first oxidehydroxide produced at room temperature in an aqueous medium showing the γ-NiOOH structure in which both Fe^{IV} and Ni^{IV} are present.

Using Mössbauer spectroscopy and magnetic measurements of iron-substituted γ-NiOOH, Delmas et al.[9] observed the presence of Fe^{IV} in both high- and low-spin states. The samples were prepared by oxidative hydrolysis of the nickelates $NaNi_{1-x}Fe_xO_2$. Noteworthy quadrupole splittings were observed for the respective signals. The given Mössbauer parameters differ significantly from ours. An attempt to fit the spectra of our sample according to the model from Delmas et al.[9] was not successful.

Received: August 3, 1995
Revised version: February 20, 1996 [Z8279IE]
German version: *Angew. Chem.* **1996**, *108*, 1200–1204

Keywords: electrochemistry · Mössbauer spectroscopy · nickel compounds

[1] R. Allmann, *Chimia* **1970**, *24*, 99; H. F. W. Taylor, *Mineral. Mag.* **1973**, *39*, 377.
[2] The general structural principle of double-layered compounds with the layered ions $[M^{II}_{1-x}M^{III}_x(OH)_2]^{x+}$ was observed by Allmann [1] to be the structure type of the mineral pyroaurite $[Mg_6Fe_2(OH)_{16}]^{2+}[CO_3^{2-}\cdot 4H_2O]$ with $M^{II}:M^{III} = 3:1$ ($x = 0.25$). This ratio is also shown by other minerals which Allmann assigned to the type pyroaurite. According to C. F. Frondel (*Am. Mineral.* **1951**, *26*, 295) and W. Hofmeister, H. von Platen (*Cryst. Rev.* **1992**, *3*, 3), the double-layer structure of these minerals displays a regular stacking of the layers with ordered cation distribution within the layers in a ratio of $M^{II}:M^{III} = 3:1$ and 2:1, respectively. They have been named "brucitites" by the authors. In precipitated products, neither we or others have observed this superstructure in the X-ray patterns. This may be due to the precipitation methods used, which may be too fast to allow for a definite ordering of the cations (A. Mendiboure, R. Schöllhorn, *Rev. Chim. Mineral.* **1986**, *23*, 819).
[3] D. H. Buss, J. Bauer, W. Diembeck, O. Glemser, *J. Chem. Soc. Chem. Commun.* **1985**, 81.
[4] C. Freire Erdbrügger, Dissertation, Universität Göttingen, **1991**.
[5] a) O. Glemser, P. Axmann (H. C. Starck GmbH & Co. KG), DE-B 4323997, **1993** [*Chem. Abstr.* **1995**, *122*, 137531]; b) P. Axmann, Dissertation, Universität Göttingen, **1994**.
[6] a) O. Glemser, D. H. Buss, J. Bauer (Varta Batterie AG), DE-A 3520108A1, **1985–1986**, US-A 4696875, **1987** [*Chem. Abstr.* **1987**, *106*, 141186]; b) O. Glemser, D. H. Buss, J. Bauer, H. Löw (Varta Batterie AG), DE-A 3811717A1, **1988–1989**, further patents in USA, Japan, France, and Great

Britain. [*Chem. Abstr.* **1990**, *112*, 59733a]; c) O. Glemser, J. Bauer, D. H. Buss, H. J. Harms, H. Löw, *Power Sources*, **1989**, *12*, 165.

[7] Synthesis of the products by computer-controlled precipitation at constant temperature (32 °C) and constant pH (12.5), characterization by elemental analysis, differential thermal analysis, thermal graviometry, differential thermal graviometry, scanning tunnel microscopy, and IR, Debye–Scherrer, and Mössbauer spectroscopy have been thoroughly described. Electrochemical characterization by measuring the specific charge Q [mAh g^{-1}] in a Cd/$Cd(OH)_2$ test cell with 30% KOH electrolyte has also been described [4, 6c].

[8] J. Bauer, D. H. Buss, H.-J. Harms, O. Glemser, *J. Electrochem. Soc.* **1990**, *137*, 173.

[9] C. Delmas, *Mater. Res. Soc. Symp. Proc.* **1993**, *293*, 15; L. Demourgues-Guerlou, L. Fournès, C. Delmas, *Solid State Ionics Proc. Symp. A2 Int. Conf. Adv. Mater. 1991* **1992**, 109; *J. Solid State Chem.* **1995**, *114*, 6, and references therein.

[10] Electrochemical investigations were carried out in 9 M KOH with a Cd/$Cd(OH)_2$ counter electrode. The sample was charged for 11 h at 50 mA and discharged at 25 mA to a potential of 0 V vs Hg/HgO. The electrode pellet contained 1.00 g of redox-active material, 0.25 g of graphite, and 0.025 g of Teflon and was pressed in a nickel net.

[11] O. Glemser, J. Einerhand, *Z. Anorg. Chem.* **1950**, *261*, 26, 43; R. S. McEwen, *J. Phys. Chem.* **1971**, *75*, 1782.

[12] Examples of Faraday yields [4]: Ni/Fe/CO_3 electrode: $N_{Fe,max} = 131\%$. Ni/Fe/SO_4/PO_4 electrode: $N_{Fe,max} = 130\%$. $N_{Fe,max} = 100\%$ for the theoretical one-electron step $Ni^{II} \rightarrow Ni^{III} + 1e^-$. Participation of Fe in the redox process has not been taken into account here. An average degree of oxidation at nickel of 3.31 was determined from the N_e values [32, 34, 35].

[13] In this article formal charge values such as those describing a bond in its ionic limiting case (complete charge separation) were given for the ions. The actual charge at the metal ions can deviate considerably as a result of covalent bonding contributions (compare also ref. [18]).

[14] The ^{57}Fe Mössbauer spectra were measured ex situ at room temperature in transmission geometry with a ^{57}Co/Rh source with an activity of 25 mCi and an absorber concentration of 3–6 mg cm^{-2}. The speed was calibrated by measuring an α-Fe foil.

[15] Elemental analysis: Ni: 40%, Fe: 8.8%, CO_3: 8%, K: 0.47%. The OH content in the main layer was determined from the number of nickel and iron ions: $n_{OH^-} = 2(n_{Ni} + n_{Fe})$. The IR spectra show a carbonate band ($\tilde{\nu}_{as} = 1480$ cm^{-1}) and a strong hydrogen carbonate band ($\tilde{\nu}_s = 1370$ cm^{-1}), indicating the presence of both anions. Taking into account the potassium ions, the ratio of carbonate to hydrogen carbonate in the interlayer balances the charge of the cationic brucite layer. The water content was found by eliminating all other components. The X-ray structure analysis (hexagonal indexing) provided $a = 3.1$, $c = 23.3$ Å; A. Mendiboure and R. Schöllhorn (*Rev. Chim. Miner.* **1986**, *23*, 819) reported $a = 3.08$, $c = 23.34$ Å for the brucitite with Ni:Fe = 3:1.

[16] The isomer shift δ is given relative to α-iron.

[17] a) G. Demazeau, M. Pouchard, N. Chevreau, J. F. Colombet, M. Thomas, F. Menil, P. Hagenmuller, *J. Less Common Met.* **1980**, *76*, 279: high-spin Fe^{IV} in $Sr_{0.5}La_{1.5}Li_{0.5}Fe_{0.5}O_4(K_2NiF_4)$ at $\delta = -0.19$ mm s^{-1}; b) G. Demazeau, Z. Li-Ming, L. Fournes, M. Pouchard, P. Hagenmuller, *J. Solid State Chem.* **1988**, *72*, 31: for Fe the authors found $\delta = -0.14$ mm s^{-1} in $A^{II}_{0.5}La_{1.5}Li_{0.5}Fe_{0.5}O_4$ (K_4NiF_4-type), which they assigned to the d^4 high-spin state (A = alkaline-earth metals); this result was supported by structural and magnetic data. Further Mössbauer data for low-spin Fe^{IV} ions: c) P. Adler, *J. Solid State Chem.* **1994**, *108*, 275: Sr_2FeO_4: $\delta = -0.017$ mm s^{-1}; d) P. K. Gallagher, J. B. Mac Chesney, D. N. E. Buchanan, *J. Chem. Phys.* **1964**, *41*, 2429: $SrFeO_3$: $\delta = +0.054$ mm s^{-1}; e) M. Takano, N. Nakanishi, Y. Takeda, S. Naka, T. Takada, *Mater. Res. Bull.* **1977**, *12*, 923: $CaFeO_3$: $\delta = +0.073$ mm s^{-1}.

[18] In $SrFeO_3$ the iron is formally in the oxidation state +IV. According to investigations by A. E Bocquet, A. Fujimori, T. Mizokawa, T. Saitoh, H. Namatame, S. Suga, N. Kimizuka, Y. Takeda, M. Takano, *Phys. Rev. B* **1992**, *45*, 1561, the bonding situation in the Fe–O bonds is, as a result of charge transfer, better described by $Fe^{3+}-O^-$ than by $Fe^{4+}-O^{2-}$. According to Demazeau [17a, b], the low-spin state must be assumed for Fe in this compound. The Mössbauer parameters ($\delta = +0.054$ mm s^{-1}) suggest that the extent of back-bonding in $SrFeO_3$ has a greater influence than in the material we describe ($\delta = -0.19$ mm s^{-1}). X-ray photoelectron spectroscopy for chemical analysis (ESCA) would give a more exact description of the bonding situation, but this method is unsuitable for the strongly water-containing hydroxid compounds that we investigated since they decompose in ultrahigh vacuum.

[19] R. Barnard, C. F. Randell, F. L. Tye, *J. Appl. Electrochem.* **1980**, *10*, 109.

[20] G. Demazeau, N. Chevreau, L. Fournès, J.-L. Soubeyroux, Y. Takeda, M. Thomas, M. Pouchard, *Rev. Chim. Miner.* **1983**, *20*, 155.

[21] Cf. P. Gütlich, *Top. Appl. Phys.* **1975**, 53. In an O_h-symmetrical ligand field, the fourth electron in the e_g orbital set is delocalized, and like the ligand field it does not contribute to the electronic field gradients at the nucleus.

[22] The Fe^{III} signal for the discharged electrode and the pure starting material (pyroaurite-type) shows quadrupole splitting. The d^5 high-spin configuration should not contribute to quadrupole splitting due to its symmetrically filled sublevels. Therefore, we attribute this splitting to a minor distortion of the octahedron along the C_3 axis, which can occur in the layered structure.

[23] Quadrupole splitting for high-spin Fe^{IV}, see for example [17a]: $\Delta E_Q = 1.10$ mm s^{-1}.

[24] K.-H. Höck, N. Nickisch, H. Thomas, *Helv. Phys. Acta* **1983**, *56*, 237.

[25] D. Reinen, U. Kesper, D. Belder, *J. Solid State Chem.* **1995**, *116*, 355.

[26] Even under the assumption of low-spin configuration for the ions involved in the cluster, small octahedral distortions of the electronic d states were not registered. This is because strong delocalization would result in the width of this state becoming larger than the relatively small symmetry splittings. An almost regular octahedral symmetry should also here be confirmed by Mössbauer spectroscopy.

[27] H. T. Evans, Jr., *J. Am. Chem. Soc.* **1968**, *90*, 3275.

[28] H. Kondo, A. Kobayashi, Y. Sasaki, *Acta Crystallogr. Sect. B* **1980**, *36*, 661.

[29] D. A. Corrigan, R. S. Conell, C. A. Fierro, D. Scherson, *J. Phys. Chem.* **1987**, *91*, 5009.

[30] S. Kim, D. A. Tryk, M. R. Antonio, R. Carr, D. Scherson, *J. Phys. Chem.* **1994**, *98*, 10269.

[31] Corrigan et al. [29] determined $\delta = +0.22$ mm s^{-1} for Fe^{III}. The values of $\delta = -0.18$ to -0.20 mm s^{-1} that we report correspond unambiguously to Fe^{IV}.

[32] The relative Fe^{IV} content was obtained from the Mössbauer spectra. Based on the iron content in the electrode, as determined by elemental analysis, the portion of iron ions involved in the discharging process $Fe^{IV} + 1e^- \rightarrow Fe^{III}$ (Q_{Fe}) can be determined as follows: 1.00 g of redox-active material contains 0.088 g (8.8%, $n = 1.576 \times 10^{-3}$ mol) of Fe ions. This corresponds to a partial charge of $Q_{100\%,Fe} = nzF = 42.2$ mAh g^{-1} ($z = 1$ and $F = 26803$ mAh mol^{-1}) for complete reaction of $Fe^{IV} + 1e^- \rightarrow Fe^{III}$. If, for example, 30% of the Fe ions, as determined from Mössbauer spectroscopy, participate in the redox process, this corresponds to a value of 12.7 mAh g^{-1} for the electrochemically determined total amount of charge.

[33] The direct galvanostatic determination of the amount of charge for a completely charged electrode is not possible from the charge process. An unmeasureable portion of the charge is lost due to simultaneous electrolyte decomposition with formation of oxygen. For this reason a good approximation of the amount of charge can be obtained from the discharging capacity of the preceeding cycle. In the investigated cycle regions 5–7, consecutive capacity values were nearly the same (deviations < 1%).

[34] To ascertain the portion of nickel ions involved in the discharging process (Q_{Ni}), the value for the Fe^{IV} ions [32] was subtracted from the electrochemically measured total amount of charge ($Q_{Ni+Fe} = 247.0$ mAh g^{-1}) (cf. [33]). In this way a value of $Q_{Ni} = Q_{Ni+Fe} - Q_{Fe} = (247.0 - 12.7)$ mAh g^{-1} = 234.3 mAh g^{-1} was obtained.

[35] Comparing Q_{Ni} to the theoretical capacity value obtained for 100% utilization of the one-electron step $Ni^{III} + 1e^- \rightarrow Ni^{II}$ ($Q_{100\%,Ni}$) provides the average exchanged charge amount per nickel ion as follows: 1.00 g of active material contains 0.40 g (40%, $n = 6.81 \times 10^{-3}$) nickel ions, which corresponds to a charge amount of $Q_{100\%,Ni} = 182.6$ mAh g^{-1} for the theoretical one-electron step. The exchanged charge per nickel ion is then $Q_{Ni}/Q_{100\%,Ni} = 234.3/182.6 = 1.28$, from which an average degree of oxidation for Ni of +3.28 can be determined. The relative content of Ni^{IV} and, under consideration of the analytical Ni/Fe ratio, the absolute Ni/Fe ratio can be calculated from the distribution of the average degree of oxidation on ions in defined charge states.

[36] F. Foerster, *Z. Elektrochem. Angew. Phys. Chem.* **1907**, *28*, 414; O. Glemser, J. Einerhand, *ibid.* **1950**, *54*, 302.

[37] A. N. Mansour, C. A. Melendres, *Extended Abstr. Pap. 186th Meeting Electrochem. Soc.* (Miami Beach, FL) **1994**, *94-2*.

[38] A. N. Mansour, C. A. Melendres, *Physica B (Amsterdam)* **1995**, *208–209*, 583.

[39] C. Greaves, A. M. Malsbury, M. A. Thomas, *Solid State Ionics* **1986**, *18–19*, 763.

[40] M. Wohlfahrt-Mehrens, R. Oesten, R. A. Huggins, *J. Electrochem. Soc.*, submitted.

[41] J. Balej, J. Divisek, *Ber. Bunsen Ges. Phys. Chem.* **1993**, *97*, 929, 933.

Knotted Heterodinuclear Complexes

Christiane O. Dietrich-Buchecker,
Jean-Pierre Sauvage,* Nicola Armaroli, Paola Ceroni,
and Vincenzo Balzani*

Chemical objects whose molecular graphs display topologically nontrivial properties are of special interest, in relation with mathematics, graphical arts, biology, and molecular sciences in general.[1] Molecular knots exist in nature, either based on DNA or on proteins,[2, 3] but they have also been made recently by chemical synthesis.[4] In particular, the use of the 1,3-phenylene group as a spacer between two 1,10-phenanthroline (phen) units in the copper(I)-templated synthesis allows molecular knots to be prepared on a preparative scale.[5]

We report here that the dicopper(I) knot compound $[1CuCu]^{2+}$ is a surprisingly stable species that can be demetalated in a stepwise manner, first to a monocopper(I) complex $[1Cu]^{+}$ and subsequently to the free knotted ligand **1**. In addition, since the singly demetalated species contains a free coordination site, another metal cation can be introduced to afford the disymmetrical complexes $[1CuZn]^{3+}$ and $[1CuAg]^{2+}$. These

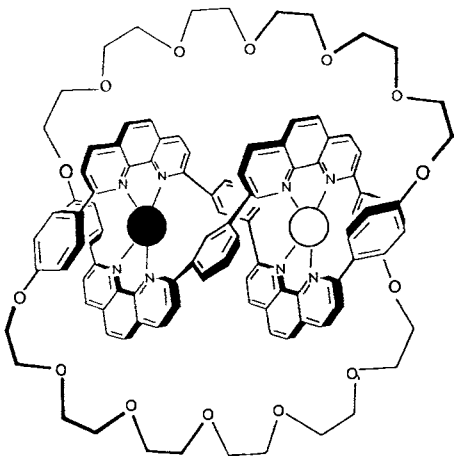

$[1CuCu]^{2+}$, ● = ○ = Cu^{+}
$[1Cu]^{+}$, ● = Cu^{+}, ○ = –
$[1CuZn]^{3+}$, ● = Cu^{+}, ○ = Zn^{2+}
$[1CuAg]^{2+}$, ● = Cu^{+}, ○ = Ag^{+},
1, ● = ○ = –

heterodinuclear species show interesting electro- and photochemical properties, which will also be described herein.

The complex $[1Cu]^{+}BF_4^{-}$ was obtained in quantitative yield by treating $[1CuCu]^{2+}(BF_4^{-})_2$ with a large excess of KCN in CH_2Cl_2/H_2O at room temperature.[6] This complex can be either used as a starting compound for preparing the disymmetrical species, or fully demetalated in refluxing wet CH_3CN to yield the free ligand **1**, which in the presence of protons or metal cations rapidly protonates or remetalates, respectively. The heterodinuclear complexes $[1CuZn]^{3+}$ and $[1CuAg]^{2+}$ were obtained quantitatively after addition of the appropriate metal salt to $[1Cu]^{+}$ at room temperature.[6] ^1H NMR spectroscopy indicates that $[1CuZn]^{3+}$ and $[1CuAg]^{2+}$ contain a helical core analogous to $[1CuCu]^{2+}$. Dinuclear helical complexes of this type containing two different metals have been recently reported.[7, 8] Remarkably, $[1Cu]^{+}$ also displays a helical conformation in spite of its free coordination site. Furthermore, the copper(I) complex subunit of $[1Cu]^{+}$ is even more compact than that in $[1CuCu]^{2+}$ since the release of the first metal ion reduces the conformational strain, allowing better interaction between the remaining copper(I) center and the phenanthroline groups coordinating this center. This is shown by ^1H NMR spectroscopic data which indicate a more pronounced entwining of the ligands, and by the great difficulties associated with trying to remove the second copper(I) ion with CN^{-}.

The decomplexation–recomplexation reactions can be monitored very conveniently by ^1H NMR spectroscopy, as exemplified by the spectra of $[1CuCu]^{2+}$ and $[1CuAg]^{2+}$ in Figure 1, which show the evident loss of symmetry when one of the copper(I) centers is replaced by Ag^{+}.

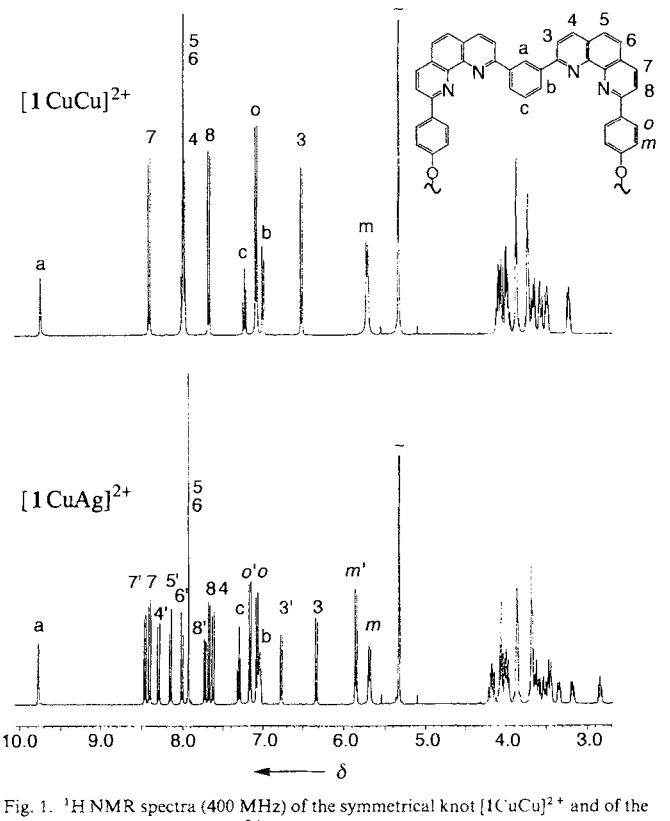

Fig. 1. ^1H NMR spectra (400 MHz) of the symmetrical knot $[1CuCu]^{2+}$ and of the disymmetrical species $[1CuAg]^{2+}$.

The electrochemical data of the complexes have been recorded in CH_3CN. The redox potentials of the Cu^{II}/Cu^{I} couples have been measured against the saturated calomel electrode (SCE), and are all reversible ($\Delta E_p \approx 60$ mV). $[1CuCu]^{2+}$ undergoes two oxidation processes ($[1CuCu]^{3+/2+}$, $E^{\circ} = +0.68$ V; $[1CuCu]^{4+/3+}$, $E^{\circ} = +0.92$ V), whereas $[1CuAg]^{2+}$ and $[1CuZn]^{3+}$ undergo only one oxidation process ($[1CuAg]^{3+/2+}$, $E^{\circ} =$

[*] Dr. J.-P. Sauvage, Dr. C. Dietrich-Buchecker
Laboratoire de Chimie Organo-Minérale URA 422 au CNRS
Faculté de Chimie, Université Louis Pasteur
4, rue Blaise Pascal F-67070 Strasbourg Cedex (France)
Fax: Int. code +88607312
Prof. V. Balzani, N. Armaroli, P. Ceroni
Dipartimento di Chimica "G. Ciamician", Università di Bologna
via Selmi 2, I-40126 Bologna, (Italy)
Fax: Int. code +51259456

[**] We thank Annik Dupont-Gervais, Dr. Emmanuelle Leize, and Dr. Alain van Dorsselaer for ESMS measurements, as well as Jean-Daniel Sauer and Michelle Martigneaux for recording the NMR spectra. This work was supported by CNRS, CNR (Progetto Strategico Tecnologie Chimiche Innovative), MURST, and Galileo Project.

+ 0.69 V; $[1CuZn]^{4+/3+}$, $E^\circ = +0.90$ V). The $[1CuCu]^{3+/2+}$ and $[1CuAg]^{3+/2+}$ reduction potentials are very similar to those found for other copper complexes containing entwined or interlocked ligands.[9] By contrast, the $[1CuCu]^{4+/3+}$ reduction potential is very high and comparable to the value found for the $[1CuZn]^{4+/3+}$ complex. This reflects the strong electron-withdrawing influence of a divalent metal atom located close to the copper center undergoing the redox reaction. As expected, the presence of a positively charged species substantially destabilizes the divalent state of the copper center and thus shifts the Cu^{II}/Cu^{I} redox potential towards anodic values.

The UV absorption spectra of the novel dinuclear knots $[1CuCu]^{2+}$, $[1CuAg]^{2+}$, and $[1CuZn]^{3+}$ (ligand-centered bands) show very similar features, clearly different from those exhibited by the dicopper knot $[2CuCu]^{2+}$ in which the spacer between the phenanthroline moieties is a $(CH_2)_6$ chain instead of a 1,3-phenylene group.[4c] The mononuclear knot $[1Cu]^{+}$ shows distinct spectral features compared with the dinuclear knots of the same family. Such differences are attributed to the presence of uncoordinated phenanthroline ligands in $[1Cu]^{+}$.

In the visible spectral region all the examined compounds show broad bands due to $Cu^{I} \rightarrow$ phen charge-transfer transitions (Fig. 2). A detailed interpretation of the metal-to-ligand

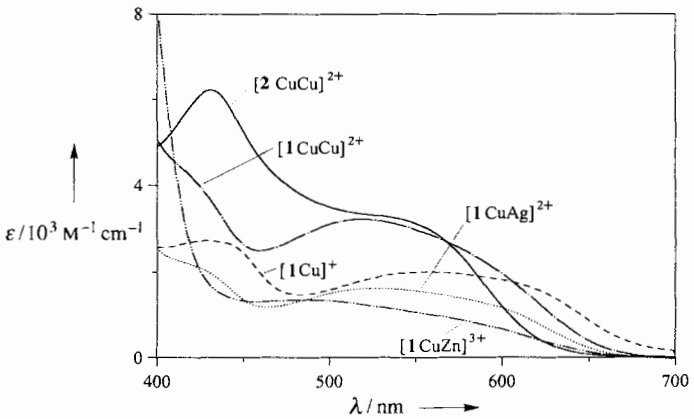

Fig. 2. Electronic absorption spectra in the visible region for the examined compounds in CH_2Cl_2 solution.

charge-transfer (MLCT) bands in Cu^{I} complexes with phenanthroline-type ligands is difficult for several reasons.[10] Nevertheless, some interesting features are apparent from the spectra in Figure 2: a) The intensity of the bands of the compounds containing two Cu^{I} ions is about twice that of the compounds containing only one Cu^{I} ion. b) The spectral features of the complexes of knot **1** are noticeably different from those exhibited by complex $[2CuCu]^{2+}$. c) The spectrum of $[1CuCu]^{2+}$ has exactly the same profile and twice the intensity of the spectrum of $[1CuAg]^{2+}$, which indicates that the coordination environment in the two compounds has substantially the same symmetry. d) The mononuclear complex $[1Cu]^{+}$ has a different spectral profile than the dinuclear $[1CuCu]^{2+}$ and $[1CuAg]^{2+}$ knots; this confirms that the properties of a coordination site are somewhat affected by the presence of a metal in the second coordination site, as inferred from ^1H NMR data (see above).

As is usual for Cu^{I} complexes with phenanthroline-type ligands,[10] the knots investigated herein exhibit a MLCT luminescence in CH_2Cl_2 at room temperature (Table 1).[4c] Noteworthy features are as follows: a) Only one emission band, assigned to the lowest MLCT excited state, is observed; this behavior, and

Table 1. Emission maxima and luminescence properties [a].

Complex cation	λ_{max} [nm] [b]	τ [ns] [c]	Φ_{em} [10^4] [d]	$k_q[O_2]$ [10^{-6} s^{-1}] [e]
$[1Cu]^{+}$	740	120	6	2.6
$[1CuCu]^{2+}$	730	200	9	1.2
$[1CuAg]^{2+}$	725	240	13	1.1
$[1CuZn]^{3+}$	950	11	ca. 0.5	–
$[2CuCu]^{2+}$ [f]	742	210	7	2.5

[a] Deaerated CH_2Cl_2 solution, room temperature. [b] Corrected values of the maximum of the emission band, ± 5 nm. [c] Excited state lifetime, ± 5%. [d] Luminescence quantum yield, ± 20% (uncertainty on relative intensities, ± 5%). [e] Stern–Volmer constant for excited state quenching by dioxygen. [f] From ref. [4c].

the agreement between absorption and excitation spectra all across the UV/vis region, indicate complete conversion of all the upper lying excited states to the lowest emitting MLCT level; this also means that in the compounds containing two distinct chromophoric groups (i.e. $[1Cu]^{+}$, $[1CuAg]^{2+}$, and $[1CuZn]^{3+}$) energy transfer is practically 100% efficient. b) The behavior of $[1CuCu]^{2+}$ and $[1CuAg]^{2+}$ is very similar, which again indicates that the Cu^{I} coordination environment is very similar in the two compounds. c) $[1Cu]^{+}$ shows a shorter excited state lifetime and a smaller luminescence quantum yield than $[1CuCu]^{2+}$, which is consistent with a more rigid structure for the dinuclear complex; this can also explain the difference in the rate constant for the quenching of the excited state by dioxygen in the two compounds. d) The emission band of the $[1CuZn]^{3+}$ complex is strongly red-shifted relative to those of the other complexes; as a consequence (energy gap rule),[11] the radiationless decay of the excited state is faster, which accounts for the shorter lifetime and smaller luminescence quantum yield.

At first sight the decrease in the energy of the lowest $Cu \rightarrow$ phen CT excited state in $[1CuZn]^{3+}$ compared, for example, with that in $[1CuCu]^{2+}$ appear to be contradictory with the Cu^{II}/Cu^{I} reduction potential in $[1CuZn]^{3+}$ (vide supra). In fact, the electrochemical and spectroscopic effects are consistent and can both be explained on the basis of the "conducting" properties of the phenylene spacer. In the ground state, the Cu^{+} ion is more positive in $[1CuZn]^{3+}$, which contains the Cu^{+}-phen-Ph-phen-Zn^{2+} moiety, than in $[1CuCu]^{2+}$, which contains the Cu^{+}-phen-Ph-phen-Cu^{+} moiety, and, as a consequence, oxidation of $[1CuZn]^{3+}$ is more difficult. A more positive Cu^{+} ion should imply a blue shift of the MLCT level; however, it should also be considered that the phen ligand coordinated to Cu^{+} is *much* more positive in $[1CuZn]^{3+}$ than in $[1CuCu]^{2+}$ (i.e. the electron-withdrawing effect of Zn^{2+} is larger on the phen unit coordinated to Cu^{+} than on the Cu^{+} ion). Combination of these two effects leads to a red shift of the MLCT band.

In conclusion, we have synthesized novel knotted heterodinuclear complexes in which the two metal-based components are linked by a 1,3-phenylene spacer. Preparation of these disymmetrical species was made possible by the surprisingly large kinetic inertness of the monocopper(I) complex $[1Cu]^{+}$, which prevents the system from undergoing metal scrambling during the introduction of the second metal center. The presence of a "conducting" spacer leads to electrochemical and spectroscopic properties noticeably different from those of knotted complexes in which the two metal-based components are linked by nonconducting $(CH_2)_n$ spacers.[4c]

Experimental Procedure

Partial demetalation of $[1CuCu]^{2+}$: $[1CuCu]^{2+}2(BF_4^-)$ (132 mg, 0.065 mmol) was dissolved in CH_2Cl_2 (60 mL) and treated with aqueous KCN (400 mg, 6.15 mmol) for 15 h at room temperature. This reaction, monitored by TLC, afforded $[1Cu]^{+}$ (123 mg, 0.065 mmol) after classical work-up and chromatography over alumina

 © VCH Verlagsgesellschaft mbH, D-69451 Weinheim, 1996 0570-0833/96/3510-1120 $ 15.00+.25/0

(quantitative yield, eluent: CH_2Cl_2/EtOH 100/1 to 100/5 v/v). $[1Cu]^+BF_4^-$ ($C_{108}H_{96}N_8O_{14}CuBF_4$): dark brown-red solid. FAB-MS: *m/z*: 1793.5 (calc. for $[1Cu]^+$: 1793.54), 897.3 (calc. for $[1Cu]^+H^+$: 897,2); ^{1}H NMR (CD_2Cl_2, 400 MHz): δ = 9.97 (s, $2H_a$), 8.26 (d, $2H_f$, $J \approx 8.3$ Hz), 8.19 (d, $2H'_d$, $J \approx 8.4$ Hz), 8.06 (d, $2H'_c$, $J \approx 8.3$ Hz), 8.01 (d, $2H_g$, $J \approx 8.7$ Hz), 7.90 (d, $4H'_o$, $J \approx 8.8$ Hz), 7.82 (d, $2H_b$, $J \approx 8.7$ Hz), 7.74 (d, $2H'_3$, $J \approx 8.4$ Hz), 7.72 (AB, $4H'_{5,6}$, $J \approx 8.8$ Hz), 7.56 (d, $2H_g$, $J \approx 8.2$ Hz), 7.13 (d, $2H_4$, $J \approx 8.3$ Hz), 6.96 (d, $4H_o$, $J \approx 8.7$ Hz), 6.91 (t, $2H_e$, $J \approx 7.6$ Hz), 6.77 (d, $2H_b$, $J \approx 7.7$ Hz), 6.71 (d, $2H'_b$, $J \approx 7.7$ Hz), 6.69 (d, $2H'_g$, $J \approx 8.4$ Hz), 6.11 (d, $2H_3$, $J \approx 8.3$ Hz), 5.77 (d, $4H'_m$, $J \approx 8.8$ Hz), 5.52 (d, $4H_m$, $J \approx 8.5$ Hz), 4.15–2.41 (m, 48H, OCH_2CH_2O).

Complete demetalation of $[1Cu]^+$: $[1Cu]^+BF_4^-$ (37 mg, 0.02 mmol) dissolved in CH_3CN (30 mL) was treated with aqueous KCN (1.00 g, 15.3 mmol in 20 mL H_2O) at 80 °C for 24 h. The dark brown coloration of the initial solution faded progressively to be pale yellow at the end. After evaporation of the solvents, the crude product was taken up in CH_2Cl_2/H_2O and decanted. After elimination of excess KCN (washing of the organic layer three times with H_2O), a filtration through silica (eluent CH_2Cl_2/MeOH 100:5) afforded $[1HH]^{2+}(BF_4^-)_2$ (33 mg, ca. 0.02 mmol, quantitative yield), which can be converted to **1** by treatment with aqueous K_2CO_3. **1**: $C_{108}H_{96}N_8O_{14}$. Pale yellow glass. ES-MS: *m/z*: 1731.14, 1731.94, 865.85 (calc. for $[1H]^+$ and $[1HH]^+$, respectively: 1731.00, 1732.01, and 866.00, respectively); ^{1}H NMR (CD_2Cl_2, 200 MHz): δ = 8.77 (dd, $4H_b$, $J \approx 7.7$, 1.4 Hz), 8.71 (s, $2H_a$), 8.37 (d, $4H_1$, $J \approx 8.4$ Hz), 8.28 (d, $4H_d$, $J \approx 8.4$ Hz), 8.13 (d, $8H_o$, $J \approx 8.6$ Hz), 8.09 (d, $4H_f$, $J \approx 8.3$ Hz), 7.90 (d, $4H_g$, $J \approx 8.5$ Hz), 7.68 (t, $2Hc$, $J \approx 7.7$ Hz), 7.55 (AB, $8H_{5,6}$, $J \approx 8.8$ Hz), 6.98 (d, $8H_m$, $J \approx 8.8$ Hz), 4.25 (t, $8H_a$, $J \approx 5.5$ Hz), 3.82–3.60 (m, 40H, OCH_2CH_2O).

$[1CuAg]^{2+}(BF_4^-)_2$: To a solution of $[1Cu]^+BF_4^-$ (46 mg, 0.024 mmol, in 10 mL CH_2Cl_2) was added a large excess of $AgBF_4$ dissolved in C_6H_6 (10 mL, 30 mg, 0.153 mmol) at room temperature. After the mixture had been stirred at room temperature overnight a dark green precipitate was formed (oxidation of Cu^I to Cu^{II} by excess silver salt). Upon addition of water (10 mL) the latter copper(II) complex was easily reduced and $[1CuAg]^{2+}(BF_4^-)_2$ was isolated pure after decantation, washing the organic layer with H_2O, drying over $MgSO_4$, and recrystallization from C_6H_6/CH_2Cl_2 (quantitative yield, 50 mg 0.024 mmol). $[1CuAg]^{2+}(BF_4^-)_2$: $C_{108}H_{96}N_8O_{14}CuAg \cdot 2BF_4$): dark red needles. FAB-MS: *m/z*: 1986.4 (calc. for $[1CuAg]^{2+}BF_4^-$: 1985.8), 1791.5 (calc. for $[1Cu]^+$: 1791.9) and 949.7 (calc. for $[1CuAg]^{2+}$: 950.0); ^{1}H NMR (CD_2Cl_2, 400 MHz): δ = 9.77 (s, $2H_a$), 8.45 (d, $2H'_f$, $J \approx 8.3$ Hz), 8.40 (d, $2H_f$, $J \approx 8.3$ Hz), 8.29 (d, $2H'_d$, $J \approx 8.3$ Hz), 8.15 (d, $2H'_g$, $J \approx 8.8$ Hz), 7.99 (d, $2H_g$, $J \approx 8.8$ Hz), 7.93 (s, $4H_{5,6}$), 7.72 (d, $2H'_g$, $J \approx 8.2$ Hz), 7.67 (d, $2H_g$, $J \approx 8.3$ Hz), 7.62 (d, $2H_4$, $J \approx 8.3$ Hz), 7.30 (t, $2H_c$, $J \approx 7.7$ Hz), 7.16 (d, $4H'_o$, $J \approx 8.6$ Hz), 7.07 (d, $4H_o$, $J \approx 8.8$ Hz), 7.02–7.05 (m, $2H_b + 2H'_b$), 6.76 (d, $2H'_3$, $J \approx 8.3$ Hz), 6.32 (d, $2H_3$, $J \approx 8.4$ Hz), 5.84 (d, $4H'_m$, $J \approx 8.6$ Hz), 5.68 (d, $4H_m$, $J \approx 8.5$ Hz), 4.20–2.80 (m, 48H, OCH_2CH_2O).

$[1CuZn]^{3+}(BF_4^-)_3$: $Zn(NO_3)_2 \cdot 6H_2O$ (20 mg, 0.067 mmol) and $[1Cu]^+BF_4^-$ (16 mg, 0.008 mmol) were mixed and dissolved in CH_2Cl_2 (10 mL) at room temperature: $[1CuZn]^{3+}$, which was poorly soluble in CH_2Cl_2 as NO_3^- salt, precipitated readily as a brown solid. After subsequent anion exchange by addition of a large excess of $NaBF_4$ to the suspension, the complex $[1CuZn]^{3+}(BF_4^-)_3$ was obtained in CH_2Cl_2. A pure sample was obtained by recrystallization from C_6H_6/CH_2Cl_2 (quantitative yield, 18 mg; 0.008 mmol).

$[1CuZn]^{3+}(BF_4^-)_3$: $C_{108}H_{96}N_8O_{14}CuZn.3BF_4$, brown-orange needles. FAB-MS: *m/z*: 2030.4 (calc.for $[1CuZn]^{3+}(BF_4^-)_2$: 2029.8), 971.2 (calc. for $[1CuZn]^{3+}(BF_4^-)$: 971.5) and 1791.4 (calc. for $[1Cu]^+$: 1791.9); ^{1}H NMR (CD_2Cl_2, 400 MHz): δ = 9.06 (s, $2H_a$), 8.84 (d, $2H'_f$, $J \approx 8.4$ Hz), 8.48 (d, $2H_f$, $J \approx 8.4$ Hz), 8.35 (d, $2H'_d$, $J \approx 8.4$ Hz), 8.30 (s, $4H_{5,6}$), 8.25 (d, $2H_d$, $J \approx 8.4$ Hz), 8.10 (AB, $4H_{5,6}$, $J \approx 8.8$ Hz), 7.94 (d, $2H'_g$, $J \approx 8.4$ Hz), 7.69 (d, $2H_g$, $J \approx 8.3$ Hz), 7.55 (t, $2H_c$, $J \approx 7.7$ Hz), 7.34–7.31 (m, $2H_b + 2H'_b$), 6.75 (d, $2H_3$, $J \approx 8.4$ Hz), 6.74 (d, $2H'_3$, $J \approx 8.4$ Hz), ≈6.0 (br $4H'_m$), 5.74 (br d, $4H_m$), 4.08–3.26 (m, 48H, OCH_2CH_2O).

Received: November 24, 1995 [Z8589IE]
German version: *Angew. Chem.* **1996**, *108*, 1190–1193

Keywords: complexes with nitrogen ligands · molecular knots · photophysics

[1] "Topology in Molecular Chemistry", *New. J. Chem.* **1995**, *17*, 617 (special issue).
[2] S. A. Wasserman, N. R. Cozzarelli, *Science* **1986**, *232*, 951 and references therein.
[3] C. Liang, K. Mislow, *J. Am. Chem. Soc.* **1994**, *116*, 11189; *ibid.* **1995**, *117*, 4201.
[4] a) C. O. Dietrich-Buchecker, J.-P. Sauvage, *Angew. Chem.* **1989**, *101*, 192; *Angew. Chem. Int. Ed. Engl.* **1989**, *28*, 189; b) C. O. Dietrich-Buchecker, J. Guilhem, C. Pascard, J.-P. Sauvage, *ibid.* **1990**, *102*, 1202 and **1990**, *29*, 1154; c) C. O. Dietrich-Buchecker, J.-F. Nierengarten, J.-P. Sauvage, N. Armaroli, V. Balzani, L. De Cola, *J. Am. Chem. Soc.* **1993**, *115*, 11237.
[5] C. O. Dietrich-Buchecker, J.-P. Sauvage, A. De Cian, J. Fischer, *J. Chem. Soc., Chem. Comm.* **1994**, 2231.
[6] Characterization of the compounds: see Experimental Procedure.
[7] E. C. Constable, J. Walker, *J. Chem. Soc. Chem. Comm.* **1992**, 884; E. C. Constable, A. J. Edwards, P. R. Raithby, J. Walker, *Angew. Chem.* **1993**, *105*, 1486; *Angew. Chem. Int. Ed. Engl.* **1993**, *32*, 1465.
[8] C. Piguet, G. Hopfgartner, B. Bocquet, O. Schaad, A. Williams, *J. Am. Chem. Soc.* **1994**, *116*, 9092.
[9] C. O. Dietrich-Buchecker, J.-P. Sauvage, J.-M. Kern, *J. Am. Chem. Soc.* **1989**, *111*, 7791.
[10] A. K. I. Gushurst, D. R. McMillin, C. O. Dietrich-Buchecker, J.-P. Sauvage, *Inorg. Chem.* **1989**, *28*, 4070; R. M. Everly, D. R. McMillin, *J. Phys. Chem.* **1991**, *95*, 9071, and references therein.
[11] E. M. Kober, J. V. Caspar, R. S. Lumpkin, T. J. Meyer, *J. Phys. Chem.* **1986**, *90*, 3722.

Bis(diisopropylamino)carbene

Roger W. Alder,* Paul R. Allen, Martin Murray, and A. Guy Orpen

The isolation of stable crystalline imidazol-2-ylidenes by Arduengo and co-workers[1] has aroused great interest. They have shown that derivatives as simple as 1,3,4,5-tetramethylimidazol-2-ylidene (**1**) are stable crystalline solids that show no tendency to dimerize.[2] We are interested in developing these derivatives of diaminocarbene as bases and nucleophilic catalysts, and have recently shown that 1,3-diisopropyl-4,5-dimethylimidazol-2-ylidene (**2**) has a pK_a value of 24 in [D$_6$]DMSO, making it one of the strongest known neutral bases.[3] As an extension of these studies, we started to explore as wide a range of stable diaminocarbene structures as possible. Both imidazol-2-ylidenes and their precursors, imidazolium ions, are aromatic, so aromaticity should not have a first-order effect on the deprotonation. Indeed calculation of the proton affinity (PA) of a range of imidazol-2-ylidenes, dihydroimidazol-2-ylidenes, and acyclic bis(dialkylamino)carbenes, by using the AM1 semiempirical method,[4] showed that PA varied by less than 10 kJ mol^{-1} among similarly substituted examples of these systems (the calculated PAs for **2**, **3**, and **4** are 1066, 1055, and 1063 kJ mol^{-1}, respectively).

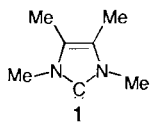

1

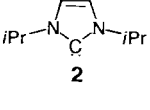

2

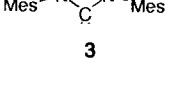

3

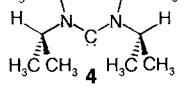

4

This encouraged us to try to generate a diaminocarbene by deprotonation of a suitable amidinium ion, even though it was reported many years ago that *N*,*N*,*N*′,*N*′-tetramethylformamidinium salts are difficult to C-deprotonate.[5] Extensive earlier work by Wanzlick and others[6] showed that 4,5-dihydroimidazol-2-ylidenes were readily generated by a variety of reactions, but apparently always dimerized to give tetraaminoethene derivatives.[7] While our work was in progress however, Arduengo et al.[8] reported the isolation and X-ray crystal structure analysis of the first stable 4,5-dihydroimidazol-2-ylidene **3** by deprotonation of an *N*,*N*′-dimesityl-4,5-dihydroimidazolium ion.

[*] Dr. R. W. Alder, Dr. P. R. Allen, Dr. M. Murray, Prof. A. G. Orpen
School of Chemistry, University of Bristol
Cantock's Close, Bristol, BS8 1TS (UK)
Fax: Int. code +(117)929-8611
e-mail: Rog. Alder@bristol.ac.uk

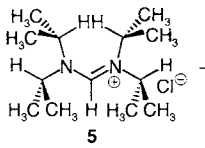

We now report on the isolation of bis(diisopropylamino)-carbene (*N*,*N*,*N*′,*N*′-tetraisopropylformamidinylidene) **4** as a stable solid by deprotonation of *N*,*N*,*N*′,*N*′-tetraisopropylformamidinium chloride **5** with lithium diisopropylamide (LDA) in THF.[9] The formamidinium salt **5** was prepared by reaction of *N*,*N*-diisopropylformamide with phosphorus oxychloride in ether, followed by treatment with diisopropylamine.[10] Reaction of **5** with LDA in THF led to the formation of **4** in 55% yield. Diaminocarbene **4** sublimes readily and is stable under rigorously dry nitrogen, but appears to be significantly more sensitive to oxygen and moisture than other species of this type that we have handled. The X-ray crystal structure of **4** was determined from a crystal grown by sublimation.[11] The structure (Fig. 1) shows that the molecule has approximate C_2

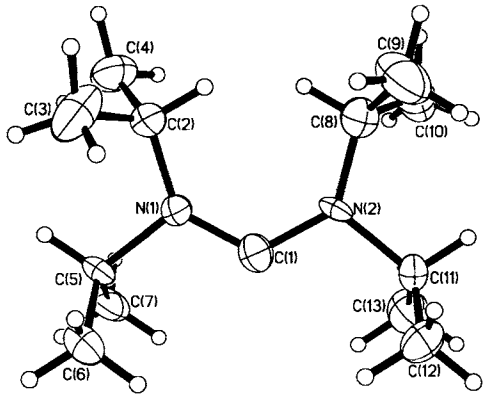

Fig. 1. Molecular structure of **4**. Important bond lengths [Å] bond angles [°] and torsion angles [°]: C(1)-N(1) 1.363(6), C(1)-N(2) 1.381(6), N-CHMe$_2$ (av) 1.492; N(1)-C(1)-N(2) 121.0(5), C(1)-N(1)-C(2) 135.1(4), C(1)-N(1)-C(5) 111.2(4) C(2)-N(1)-C(5) 113.4(4) C(1)-N(2)-C(8) 133.5(4), C(1)-N(2)-C(11) 110.7(4), C(8)-N(2)-C(11) 115.5(4); C(2)-N(1)-C(1)-N(2) −13.7(9), N(1)-C(1)-N(2)-C(8) −10.6(9).

symmetry; the N-C-N angle (121.0°) is much larger than that in any previously studied diaminocarbene derivative (this angle is 104.7° for **3**). The nitrogen atoms are planar, but the C-N-C angles are strongly distorted by the repulsive interactions between the isopropyl groups. The ^{13}C NMR chemical shift of the carbene center at $\delta = 255.5$ is 30–40 ppm downfield of the carbene carbon chemical shifts for imidazol-2-ylidenes, and 10 ppm downfield of that reported for **3**.[8] The further downfield shift for **4** may be related to the increased N-C-N angle.

The ^1H and ^{13}C NMR signals of the *i*Pr groups of **4** are broad at room temperature, and split to reveal two types of *i*Pr groups at −30 °C. The C*H* signals coalesce at −10 °C, leading to a calculated $\Delta G^{\neq}$ of 53 kJ mol^{-1}. Similar behavior was observed for the formamidinium ion precursor **5**, where the coalescence of the C*H* absorptions occurred at +8 °C, $\Delta G^{\neq}$ 55 kJ mol^{-1}. A barrier of 64 kJ mol^{-1} has been reported for the tetramethylformamidinium ion.[12] The fact that the barrier is lower for **5** is understandable in terms of steric destabilization of the ground state relative to the transition state for rotation about a C–N bond. Coalescence of the signals for the *i*Pr groups in **5** must involve rotation about a C–N*i*Pr$_2$ bond, accompanied by rotations about N–*i*Pr$_2$ bonds. In the diaminocarbene **4** interconversion might occur by an inversion mechanism with a linear N-C-N transition state, although AM1 calculations suggest a rotation process will be preferred. However, even if inversion is the observed process, the rotational process must have a higher barrier, and it is therefore clear that there is as much double bond character to the C–N bonds in **4** as those in amidinium ion **5**. Thus, while it is convenient to call **4** a diaminocarbene rather than a formamidinylidene, it would be just as realistic to describe an amidinium ion as a diaminocarbenium ion!

In solutions containing both **4** and **5**, separate NMR signals are seen for these two species, although there is some indication of exchange broadening at higher temperatures. This indicates that proton transfer between **4** and **5** is slow on the NMR time scale. We previously found that proton transfer between **2** and the corresponding imidazolium ion was close to the fast exchange limit at ambient temperature.[3] The slower exchange for **4** is in keeping with the greater steric hindrance in this species. The co-existence in solution of **4** and **5** is interesting from another point of view, since attack of the carbene on the electrophilic carbon atom of the amidimium ion is proposed to be the major route to tetraaminoethenes.[7]

In summary, we have isolated the first acyclic diaminocarbene, and shown that its C–N bonds have substantial double bond character. It will be interesting to discover what minimal steric hindrance is required in these species before dimerization of the carbene sets in, but the preparation of **4** suggests that a wide range of these interesting species can be isolated.

Experimental Procedure

5: Solvents were stored over 3 Å molecular sieves prior to use, and all manipulations were performed under dry nitrogen. Diisopropylformamide (5 mL, 34.5 mmol) in Et_2O (10 mL) was added at 0 °C to a stirred solution of $POCl_3$ (3.2 mL, 34.5 mmol) in Et_2O (25 mL). After the mixture had been stirred for 0.5 h at room temperature, the white precipitate was allowed to settle and the supernatant was removed. The solid was washed with Et_2O (2 × 30 mL), dissolved in dichloromethane (30 mL), and diisopropylamine (4.5 mL, 34.5 mmol) in dichloromethane (10 mL) added dropwise at 0 °C. The solution was stirred at room temperature for 0.5 h, Et_2O (30 mL) added, and the precipitate collected by filtration. The solid, a mixture of the required formamidinium salt and diisopropylammonium chloride (4.4 g), was treated with acetone (30 mL) in which only the formamidinium salt is soluble. After removal of the diisopropylammonium chloride by filtration, Et_2O (30 mL) was added to precipitate the product as a white crystalline solid (2.14 g) which was dried in vacuo over P_2O_5 before use, m. p. 214–220 °C with decomposition. ^1H NMR: (300 MHz, $CDCl_3$): $\delta = 1.49$ (d, 24H), 4.25 (br. s, 4H), 7.60 (s, 1H); ^{13}C NMR (75.45 MHz, $CDCl_3$): $\delta = 22.72$ (br.), 52.0 (br.), 151.05

4: *N*,*N*,*N*′,*N*′-tetraisopropylformamidinium chloride (0.3 g, 1.21 mmol) was added to a solution of LDA (formed by the addition of *n*-butyllithium (0.5 mL, 2.4 M in hexanes) to diisopropylamine (0.21 mL, 1.5 mmol) in tetrahydrofuran at −78 °C). The reaction mixture was allowed to stir at room temperature for 0.5 h by which time complete dissolution had occurred. The solvent was removed under vacuum to give an off-white solid, which was treated with hexane. The supernatant was removed and evaporated under vacuum to give a white solid, which was sublimed at 40 °C/0.2 mm Hg to yield white crystals (0.142 g, 55%), m. p. 51–55 °C. Elemental analysis calculated for $C_{13}H_{28}N_2$: C 73.5, H 13.3, N 13.2%; found: C 73.8, H 13.5, N 13.2; ^1H NMR (500 MHz, [D$_6$]benzene): $\delta = 1.28$ (br., 24H); 3.70 (br., 4H); ^{13}C NMR (125.7 MHz, [D$_6$]benzene): $\delta = 24.2$ (br.), 49.6 (br.), 255.5.

Received: December 8, 1995
Revised version: February 10, 1996 [Z 8626 IE]
German version: *Angew. Chem.* **1996**, *108*, 1211–1213

Keywords: amidinium ions · carbenes · structure elucidation

[1] A. J Arduengo III, R. L. Harlow, M. Kline, M. *J. Am. Chem. Soc.* **1991**, *113*, 361

[2] A. J Arduengo III, H. V. R. Dias, R. L. Harlow, M. Kline, *J. Am. Chem. Soc.* **1992**, *114*, 5530; A. J Arduengo III, H. V. R. Dias, D. A. Dixon, R. L. Harlow, W. T. Klooster, T. F. Koetzle, *ibid.* **1994**, *116*, 6812, report calculations that suggest that dimerization of **1** is endothermic.

[3] R. W. Alder, P. R. Allen, S. J. Williams, *J. Chem. Soc. Chem. Commun.* **1995**, 1267.

[4] Calculation of the proton affinities of a wide range of compounds by this method has been reported: M. J. S. Dewar, K. M. Dieter, *J. Am. Chem. Soc.* **1986**, *108*, 8075.

[5] N. Wiberg, J. W. Buchler, *Z. Naturforsch. B* **1964**, *19*, 953–955.

[6] H.-W. Wanzlick, E. Schikora, *Angew. Chem.*, **1960**, *72*, 494; H.-W. Wanzlick, *Angew. Chem.* **1962**, *74*, 129; *Angew. Chem. Int. Ed. Engl.* **1962**, *1*, 75; H.-J. Schönherr, H.-W. Wanzlick, *Chem. Ber.* **1970**, *103*, 1037–1046, and references therein.

[7] For discussion of this dimerization see: D. M. Lemal, R. A. Lovald, K. I. Kawano, *J. Am. Chem. Soc.* **1964**, *86*, 2518; H. E. Winberg, J. E. Carnahan, D. D. Coffman, M. Brown, *ibid.* **1965**, *87*, 2055; N. Wiberg, J. W. Buchler, *Chem. Ber.* **1963**, *96*, 3000.

[8] A. J. Arduengo III, J. R. Goerlich, W. J. Marshall, *J. Am. Chem. Soc.* **1995**, *117*, 11027.

[9] The ability of *i*Pr groups to stabilize unusual structures at nitrogen is well-known: H. Bock, H. Göbel, Z. Havlas, S. Liedle, H. Oberhammer, *Angew. Chem.* **1991**, *103*, 193; *Angew. Chem. Int. Ed. Engl.* **1991**, *30*, 187.

[10] H. Bredereck, R. Gompper, K. Klemm, H. Rempfer, *Chem. Ber.* **1959**, *92*, 837.

[11] Crystal data for **4**: $C_{13}H_{28}N_2$, $M_r = 212.4$, triclinic, space group $P\bar{1}$ (no. 2), $a = 7.5346(11)$, $b = 8.844(2)$, $c = 12.113(3)$ Å, $\alpha = 110.718(12)$, $\beta = 104.868(12)$, $\gamma = 92.700(9)$°, $V = 721.2(2)$ Å^3, $Z = 2$, $\rho_{calcd} = 0.978$ g cm^{-3}, $\lambda = 0.71073$ Å, $\mu(Mo_{K\alpha}) = 0.57$ cm^{-1}, $F(000) = 240$, $T = 173$ K, crystal size $0.2 \times 0.2 \times 0.2$ mm. All diffraction measurements were made on a Siemens SMART area detector diffractometer, using graphite monochromated $Mo_{K\alpha}$ *X*-radiation. Unit cell dimensions were determined from 89 reflections. Diffracted intensities were measured in a hemisphere of reciprocal space for $3.0 < 2\theta < 45.0$° by 0.3° ω scans, frames observed for 30 s. Crystal decay of about 40% was observed over a period of 13 h. Data collected after about 6 h were discarded because of poor agreement with earlier data. A total of 1259 data were integrated of which 977 had $I > 2\sigma(I)$. No absorption correction was applied. Lorentz and polariation corrections were applied. The structure was solved by direct methods. All non-hydrogen atoms were assigned anisotropic displacement parameters. All hydrogen atoms were located in difference maps and constrained to idealized geometries. Full-matrix least-squares refinement on F^2 of this model using the SHELXL-93 program (SHELXTL version 5.03. Siemens Analytical Xray, Madison WI, 1994) (144 parameters) converged to final residual indices $R1 = 0.084$, $wR2 = 0.198$, $S = 1.15$. Final difference electron density maps showed no features outside the range $+0.26$ to -0.22 e Å^{-3} (cf. methine hydrogen atom peaks 0.39–0.49 e Å^{-3}). Crystallographic data (excluding structure factors) for the structure(s) reported in this paper have been deposited with the Cambridge Crystallographic Data Centre as supplementary publication no. CCDC-179-26. Copies of the data can be obtained free of charge on application to The Director, CCDC, 12 Union Road, Cambridge CB2 1EZ, UK (fax: int. code +(1223) 336-033; e-mail: teched@chemcrys.cam.ac.uk).

[12] J. Schmetzer, J. Daub, P. Fischer, *Angew. Chem.* **1975**, *87*, 489; *Angew. Chem. Int. Ed. Engl.* **1975**, *14*, 487; for barriers for other amidinium ions see: R. C. Neumann and V. Jonas, *J. Phys. Chem.* **1971**, *75*, 3532.

Structures of XeF_7^- and $Xe_2F_{13}^-$**

Arkady Ellern, Ali-Reza Mahjoub, and Konrad Seppelt*

XeF_6 is an amphoteric solvent; however, it has not been investigated very much, mainly because of its extreme fluorinating power, the difficulties associated with its purification, and because of the extraordinary explosive power of its final hydrolysis product, XeO_3. The conductivity of XeF_6 is found to be $1.45 \times 10^{-6}\ \Omega^{-1}$, which suggests a dissociation into fluoroxenon cations and fluoroxenon anions.[1] Nevertheless, the first preparation of Au^V as $Xe_2F_{11}^+AuF_6^-$ was achieved in liquid XeF_6.[2] The chemistry of the fluoroxenon cations of XeF_6 has been established with the ions XeF_5^+ and $Xe_2F_{11}^+$. In solution and in the melt XeF_6 exists as monomer and tetramer in equilibrium,[3] at low temperatures in solution only the tetramer is observed.[4] Tetrameric and (less often) hexameric units are characteristic for the solid state.[5] Because of the amphoteric character of XeF_6 fluoroxenon anions are expected to exist, and XeF_7^- and XeF_8^{2-} have been described.[6] However, only the structure of XeF_8^{2-} has been confirmed; it is square antisprismatic with no detectable steric activity of the nonbonding pair of electrons.[7]

Little is known about the structure of XeF_7^-. It is formed from CsF and XeF_6 as a yellow solid; however, it readily loses XeF_6, resulting in colorless Cs_2XeF_8. Likewise with NOF the final product is XeF_8^{2-}.[6] By using an excess of the weaker fluoride donor NO_2F crystalline, sublimable $NO_2^+XeF_7^-$ is formed; however, this is always multiply twinned therefore not allowing a single-crystal X-ray structure analysis. XeF_7^- presents an interesting structure, since it contains seven identical ligands and a nonbonding electron pair. This is the only example of such a combination known to date in main group chemistry.

$CsXeF_7$ freshly prepared from CsF and XeF_6 dissolves in BrF_5 to give a lemon yellow colored solution, and crystallizes at 4 °C to give yellow crystals. According to the results of a single-crystal X-ray structure determination the anion has a capped octahedral structure, which is strictly obeyed because of the symmetry constraints of the cubic lattice system (Fig. 1).

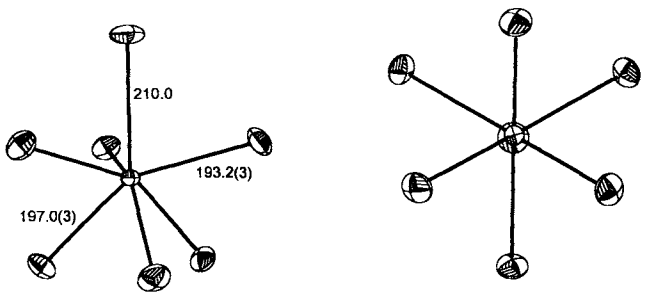

Fig. 1. Structure of the XeF_7^- ion in the crystal of $Cs^+XeF_7^-$ (ORTEP plot, 50% probability). Distances [pm]: Xe–F1 193.2(3), Xe–F2 210.0(6), Xe–F3 197.0(3), Cs···321.7(3), 344.2(4), Cs···F2 3 × 326.5(2), Cs···F3 310.3(3), 341.5(4); angles [°]: F2-Xe-F1 132.2(1), F2-Xe-F3 75.91(1).

In the last few years it has been shown that main group compounds with the coordination number 7 in absence of nonbonding electron pairs always adopt a pentagonal bipyramidal structure (IF_7, TeF_7^-, IOF_6^-, $ROTeF_6^-$, $(RO)_2TeF_5^-$), possibly because this structure has one linear ligand–central atom–ligand arrangement (e.g. I-F-I)—in contrast to all other structural alternatives—to satisfy the high p character of the bonding.[8] Among the comparable transition metal compounds (MoF_7^-, WF_7^-) the capped octahedron is observed;[9] however, not always (ReF_7^-, TeF_7^{2-}).[10–12] The comparison of the capped octahedra of XeF_7^- in $Cs^+XeF_7^-$ with those of MoF_7^- and WF_7^- reveals an important difference. The Xe–F bond to the capping fluorine atom in XeF_7^- is remarkably long (210 pm). Thus, one can assume that this direction in space might also contain the remaining weak influence of the nonbonding electron pair. Whereas the fluorine atoms of the distorted octahedron interact with two cesium ions, the capping fluorine atom interacts with three. This may also explain the length of the bond between xenon and the capping fluorine atom.

[*] Prof. Dr. K. Seppelt
Institut für Anorganische und Analytische Chemie der Freien Universität
Fabeckstrasse 34–36, D-14195 Berlin (Germany)
Telefax: Int. code +(30)838-2424
e-mail: seppelt@blume.chemie.fu-berlin.de

Dr. A. Ellern
Chemistry Department, Ben-Gurion University of the Negev, Beer-Sheva (Israel)

Dr. A.-R. Mahjoub
Department of Chemistry, Tarbiat Modarres University, Teheran (Iran)

[**] We thank the Alexander von Humboldt Stiftung for a stipend for A. E., and the Deutsche Forschungsgemeinschaft and the Fonds der Chemischen Industrie for financial support.

Evidently, this C_{3v} structure is not the only geometry the XeF_7^- ion can adopt. The reaction of NO_2F with excess XeF_6 affords $NO_2^+Xe_2F_{13}^-$ as a colorless, sublimable crystallizate. (Once, but so far not reproducibly, $NO^+Xe_2F_{13}^-$ has also been obtained; which has a very similar structure of the anion.[13]) The dinuclear anion $Xe_2F_{13}^-$ (Fig. 2), following XeF_7^-, is evidently a member of a series which would proceed with $Xe_3F_{19}^-$ and $Xe_4F_{25}^-$. However, experimental difficulties have thus far prevented the isolation of these polynuclear anions.

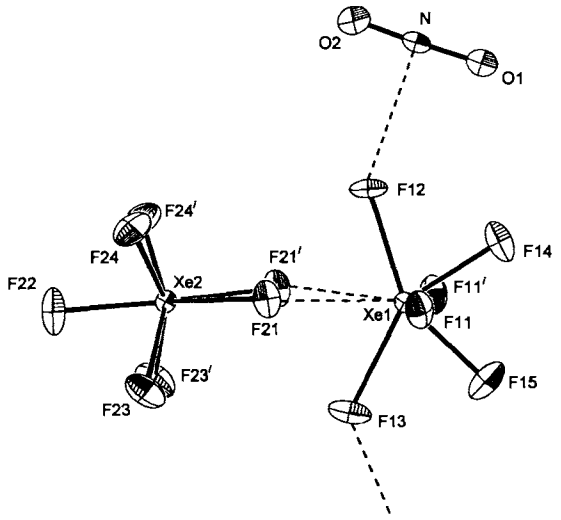

Fig. 2. Structure of a unit $NO_2^+Xe_2F_{13}^-$ in the crystal (ORTEP plot, 50% probability). The crystallographic mirror plane is slightly tilted against the plane of the paper to make symmetry equivalent fluorine atoms visible. Distances [pm]: N···F12 252.2(3), N···F13 247.6(3), Xe1···F21 255.8(3).

The structure of $Xe_2F_{13}^-$ can be separated into a XeF_7^- and a XeF_6 part, if contacts of approximately 255 pm in length are disregarded between F(21) and Xe(1). This view in connection with the long Xe–F bond (210 pm) discussed above is certainly a gross simplification. The XeF_7^- part has a C_{2v} structure as a consequence of lattice symmetry, and the anion has the shape of an ideal capped trigonal prism (Fig. 3). In this case the bond between the capping fluorine atom and the xenon atom is the shortest. The length of the two Xe–F bonds that are opposite to the capping fluorine atom gives the impression that the nonbonding electron pair is located between these long bonds. The structure can also be described as a square pyramidal XeF_5 part with two additional long Xe–F bonds that are pushed away by the nonbonding electron pair. Thus, we conclude that the structure of XeF_7^- is chiefly determined by the lattice symmetry, evidently because energy differences between the different possible geometries of the free anion are marginal.

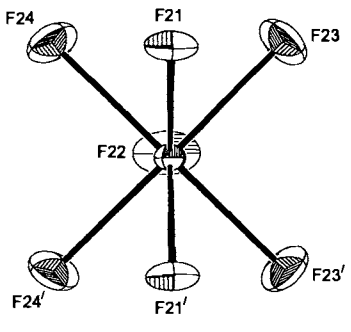

Fig. 3. Capped trigonal prismatic structural unit XeF_7^- in $Xe_2F_{13}^-$. Distances [pm]: Xe2–F21 218.9(2), Xe2–F22 184.2(4), Xe2–F23 190.1(3), Xe2–F24 187.8(3).

The $Xe_2F_{13}^-$ ion holds another surprise—again if the Xe(1)–F(21) contact is not considered—that is, a XeF_6 molecule in a crystalline phase. In agreement with all physical data it is assumed that in the gaseous state XeF_6 has the C_{3v} structure of an octahedron distorted by a nonbonding electron pair. This structure can be interchanged by very small variations of angles into an energetically hardly less optimal C_{2v} structure; the energy barrier between these two structures is very small.[14] In the crystal XeF_6 has a C_{2v} structure with two shorter, two intermediate, and two longer bonds (Fig. 4a). Viewed from a slightly different direction the molecule appears as a distorted C_{3v} structure (Fig. 4b). If one defines the averaged bond angles between opposite fluorine atoms as a measure for the deviation from ideal octahedral symmetry, the angle of 153° for the structures of XeF_6 reveals that it is very distorted (for comparison: IF_6^- 164°, SeF_6^{2-} 172°, and BrF_6^- 180°[15–17]).

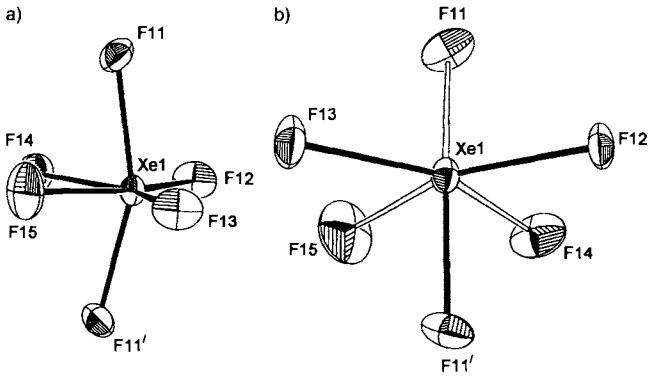

Fig. 4. a) The C_{2v} symmetric XeF_6 molecular unit in $Xe_2F_{13}^-$. b) The same unit as viewed from a slightly different direction to show the approximated C_{3v} structure. Distances [pm] Xe1–F11 188.5(3), Xe–F12 197.2, Xe1–F13 202.1, Xe1–F14 185.5, Xe1–F15 185.6; angles [°]: F11-Xe1-F11′ 157.9(2), F12-Xe-F13 135.2(2), F14-Xe-F15 76.3(2).

Experimental Procedure

$Cs^+XeF_7^-$: An excess of pure XeF_6 [18] was condensed in vacuum (stainless steel system) into a polyperfluoroethene-propene (Teflon FEP) tube on to previously (under exclusion of humidity) powdered CsF. After heating the tube to 40 °C, the excess XeF_6 was pumped off, the crystalline solid was powdered, and again excess XeF_6 was condensed and the procedure repeated. Rapid pumping off of excess XeF_6 afforded a yellow powder of $CsXeF_7$; elemental analysis: found: Xe 34.49, F 34.0%, calcd. Xe 33.46, F 33.4. Raman (solid): $\tilde{\nu}$ = 627.5(10), 555.5(100), 504.5(10), 485(3), 459.5(15), 342(3), 275(3), 207(3) cm^{-1}.

$CsXeF_7$ (ca. 50 mg) was added to a FEP tube, and colorless (Br_2 and BrF_3 free) BrF_5 (3 mL) was condensed onto it. After the tube had been sealed, it was shaken briefly at room temperature to give a clear yellow solution. Discoloration indicated the formation of Cs_2XeF_8. Cooling to 4 °C overnight afforded large yellow crystals.

Crystal structure: A suitable crystal (0.2 × 0.2 × 0.2 mm) was mounted under cooling and in an inert gas atmosphere on an Enraf Nonius CAD-4 cycle diffractometer and measured at −143 °C, a = 896.0(7) pm, $V = 605.7(1) \times 10^6$ pm^3, space group $P2_13$ (No. 198), Z = 8, $2\theta_{max}$ = 70°, $Mo_{K\alpha}$, λ = 71.069 pm, ω scan, 522 measured, 522 independent, 518 used reflections, Lorentz polarization correction, Ψ scan absorption correction, μ = 11.68 mm^{-1}, min/max correction 0.85/1.12. Structure solution was carried out with the program SHELXS 86 [19], refinement with SHELXS 93 [20], 29 parameters, R_1 = 0.035, wR_2 = 0.111, extinction coefficient 0.007(2) [23].

$NO_2^+Xe_2F_{13}^-$: Pure NO_2F [21] and XeF_6 in the molar ratio 1:2 were condensed into a Teflon FEP tube. After the sample had been sealed in vacuum, it was stored at room temperature. Spontaneous sublimation afforded colorless crystals that could be distinguished under the polarization microscope. XeF_6 was optically isotropic, $NO_2^+XeF_7^-$ appeared in the form of square, thin platelets that consist of many, strongly iridescent single crystals, whereas $NO_2^+XeF_{13}^-$ single crystals turn the plane of the polarized light. A single crystal of 0.3 × 0.3 × 0.2 mm dimensions was mounted and measured, as described for $CsXeF_7$, a = 1592.5(3), b = 7543.5(2), c = 864.9(1) pm, β = 94.77(1)°, $V = 1075.8(4) \times 10^6$ pm^3, space group C_2/m (No. 12), Z = 8, $2\theta_{max}$ = 61°, 1732 measured, 1671 independent, 1474 used reflections, DIFABS absorption correction [22], μ = 6.73, min/max correction 6.92/1.12, 97 parameter, R = 0.025, R_2 = 0.068 [23].

Received: December 21, 1995 [Z 8672 IE]
German version: *Angew. Chem.* **1996**, *108*, 1198–1200

Keywords: fluorine compounds · structure elucidation · xenon compounds

[1] H. Selig, A. Mootz, *Inorg. Nucl. Chem. Lett.* **1967**, *3*, 147–148.
[2] N. Bartlett, K. M. Leary, *Rev. Chim. Miner.* **1976**, *13*, 82–97; K. Leary, A. Zalkin, N. Bartlett, *Inorg. Chem.* **1974**, *13*, 775–779.
[3] C. J. Adams, N. Bartlett, *Isr. J. Chem.* **1978**, *17*, 114–125; F. Schreiner, D. W. Osborne, J. G. Malm, G. N. McDonald, *J. Chem. Phys.* **1969**, *51*, 4834–4851.
[4] H. H. Rupp, K. Seppelt, *Angew. Chem.* **1974**, *86*, 669–670; *Angew. Chem. Int. Ed. Engl.* **1974**, *13*, 612–613; K. Seppelt, H. H. Rupp, *Z. Anorg. Allg. Chem.* **1974**, *409*, 331–337; K. Seppelt, N. Bartlett, *ibid.* **1977**, *436*, 122–126.; G. J. Schrobilgen, J. H. Holloway, P. Granger, C. Brevard, *Inorg. Chem.* **1978**, *17*, 980–987.
[5] P. A. Agron, C. H. Johnson, H. A. Levi, *Inorg. Nucl. Chem. Lett.* **1965**, *1*, 145–148; R. D. Burbank, G. R. Jones, *Science* **1971**, *171*, 485–487; *J. Am. Chem. Soc.* **1974**, *96*, 43–48.
[6] R. D. Peacock, H. Selig, I. Shelft, *J. Inorg. Nucl. Chem.* **1966**, *28*, 2561–2567; J. H. Holloway, H. Selig, U. El-Gad, *ibid.* **1973**, *35*, 3624–3625; G. J. Moody, H. Selig, *Inorg. Nucl. Chem. Lett.* **1966**, *2*, 319–321; K. O. Christe, W. W. Wilson, *Inorg. Chem.* **1982**, *21*, 4111–4118.
[7] S. W. Peterson, J. H. Holloway, B. A. Coyle, J. M. Williams, *Science* **1971**, *173*, 1238–1239; A. Ellern, S. Adam, K. Seppelt, *Chem. Eur. J.* **1996**, *4*, 398–402.
[8] K. O. Christe, E. C. Curtis, D. A. Dixon, *J. Am. Chem. Soc.* **1993**, *115*, 1520–1562; T. Vogt, A. N. Fitch, J. K. Cockcroft, *J. Solid State Chem.* **1993**, *103*, 275–279; R. Marx, A.-R. Mahjoub, K. Seppelt, R. M. Ibbeson, *J. Chem. Phys.* **1994**, *101*, 585–593; A. R. Mahjoub, T. Drews, K. Seppelt, *Angew. Chem.* **1992**, *104*, 1047–1050; *Angew. Chem. Int. Ed. Engl.* **1992**, *31*, 1036–1039; K. O. Christe, J. C. P. Sanders, G. J. Schrobilgen, W. W. Wilson, *J. Chem. Soc. Chem. Commun.* **1991**, 837–840; A. R. Mahjoub, K. Seppelt, *ibid.* **1991**, 840–841; K. O. Christe, D. A. Dixon, A. R. Mahjoub, H. P. A. Mercier, J. C. P. Sanders, K. Seppelt, G. J. Schrobilgen, W. W. Wilson, *J. Am. Chem. Soc.* **1993**, *115*, 2696–2706.
[9] S. Giese, K. Seppelt, *Angew. Chem.* **1994**, *106*, 473–475; *Angew. Chem. Int. Ed. Engl.* **1994**, *33*, 461–463.
[10] T. Vogt, A. N. Fitch, J. K. Cockcroft, *Science* **1994**, *263*, 1265–1267.
[11] J. L. Hoard, *J. Am. Chem. Soc.* **1939**, *61*, 1252–1259.
[12] G. Brown, L. A. Walker, *Acta Crystallogr.* **1966**, *20*, 220–229.
[13] $NO^+Xe_2F_{13}^-$: colorless crystals, prepared from NOF and XeF_6; $a = 766.6(1)$, $b = 773.3(1)$, $c = 1600.8(2)$ pm, $\beta = 91.81(3)°$, $Z = 4$, space group $P2_1/n$.
[14] A short review on the structure of XeF_6 in the gaseous state: K. Seppelt, D. Lentz, *Progr. Inorg. Chem.* **1982**, *29*, 167–202.
[15] A. R. Mahjoub, K. Seppelt, *Angew. Chem.* **1991**, *103*, 309–311; *Angew. Chem. Int. Ed. Engl.* **1991**, *30*, 323–324.
[16] A. R. Mahjoub, X. Zhang, K. Seppelt, *Chem. Eur. J.* **1995**, *1*, 261–265.
[17] A. R. Mahjoub, A. Hoser, J. Fuchs, K. Seppelt, *Angew. Chem.* **1989**, *102*, 1528–1529; *Angew. Chem. Int. Ed. Engl.* **1989**, *28*, 1526–1527.
[18] C. L. Chernick, J. G. Malm, S. M. Williamson, *Inorg. Synth.* **1966**, *8*, 258–260; N. Bartlett, F. O. Sladky in *Comprehensive Inorganic Chemistry, The Chemistry of Krypton, Xenon, and Radon, Vol. 1* (Eds.: J. C. Bailor, H. J. Emeleus, R. Nyholm, A. F. Trotman-Dickenson), Pergamon, Oxford, **1973**, p. 294.
[19] G. M. Sheldrick, Program for Crystal Structure Solution, Universität Göttingen, **1986**.
[20] G. M. Sheldrick, SHELX 93, Universität Göttingen, **1993**.
[21] P. J. Bruna, J. E. Sicre, H. J. Shumasher, *J. Chem. Soc. Chem. Commun.* **1970**, 1542–1544.
[22] N. Walker, D. Stuart, *Acta Crystallogr. Sect. A* **1983**, *39*, 158–166.
[23] Further details of the crystal structure investigations may be obtained from the Fachinformationszentrum Karlsruhe, D-76344 Eggenstein-Leopoldshafen (Germany), on quoting the depository numbers CSD-404986 ($CsXeF_7$) and 404987 ($NO_2Xe_2F_{13}$).

Structural Diversity in Alkali Metal Phospholides: A Kalocene-Type Structure

Frédéric Paul, Duncan Carmichael, Louis Ricard, and François Mathey*

The alkali metal derivatives of the cyclopentadienide anions can display four structural forms.[1] Generally, they have bridging η^5-Cp rings incorporated into a polymeric chain, which usually confers low solubility. This structure can be broken down by a donor solvent (Solv) to give monomeric half-sandwich compounds $[CpM(Solv)_n]$. The most interesting structural form, the anionic sandwich complex $[Cp_2M]^-$, has very recently been characterized crystallographically as the lithium compound.[2] A priori, the alkali metal derivatives of phospholide (phosphacyclopentadienide) anions can display the same morphological diversity. However, to date, only lithium tetramethylphospholide, which adopts a half-sandwich structure when crystallized in the presence of tetramethylethylenediamine, has been crystallographically characterized.[3] Some time ago, during a study of a series of flexible tetraphosphole macrocycles,[4] we generated the phospholide anions **2** and **3** in situ by cleavage of one or two P–P bonds of the phosphole tetramer ("P_4") **1** (Scheme 1). As we were interested in the coordination chemistry of these phospholides, we needed precise information on their structures.

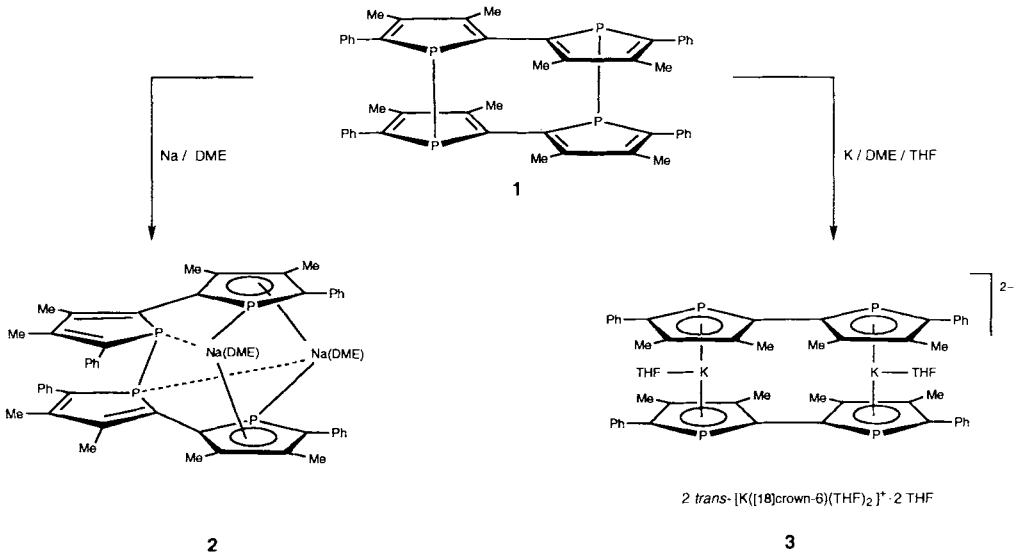

1

2

3

2 *trans*-$[K([18]crown\text{-}6)(THF)_2]^+ \cdot 2\ THF$

Scheme 1.

Compound **2** was prepared as previously described[4] and obtained free from traces of the "P_2"Na_2 derivative by recrystallization from 1,2-dimethoxyethane. The structure of its DME adduct $[\mathbf{2}\cdot(DME)_2]$ is shown in Figure 1. As in the tetrameric precursor **1**,[5] the overall structure of $[\mathbf{2}\cdot(DME)_2]$ is highly skewed. The sodium ion (Na1) is η^5-bound to the first phospholyl ring (P1), σ-bound to the second phospholyl (P20), and chelated by one molecule of DME. The 3.172(2) Å separation between Na1 and P11 (cf. 3.001(1) for Na1–P1 and 3.083(2) Å for Na1–P20) suggests a fifth, weak coordination to the neutral

[*] Prof. Dr. F. Mathey, Dr. F. Paul, Dr. D. Carmichael, Dr. L. Ricard
Laboratoire "Hétéroéléments et Coordination"
URA 1499 CNRS, DCPH
Ecole Polytechnique, F-91128 Palaiseau Cedex (France)
Fax: Int. code +(1) 69 33 39 90

 © VCH Verlagsgesellschaft mbH, D-69451 Weinheim, 1996 0570-0833/96/3510-1125 $ 15.00+.25/0

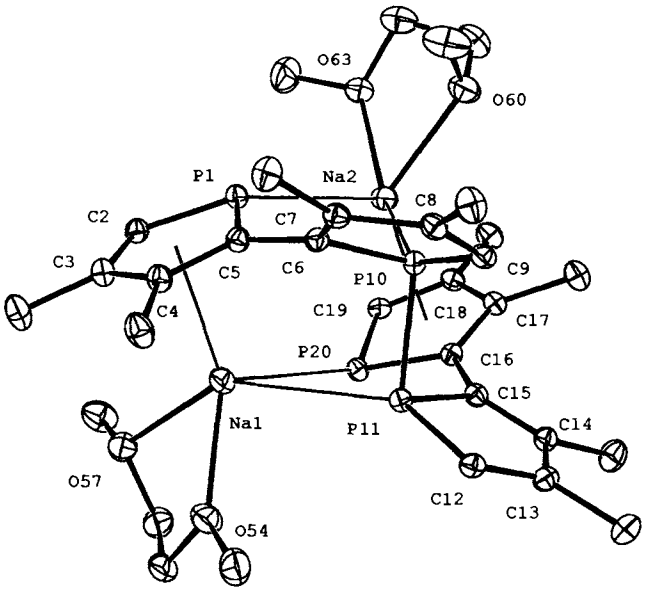

Fig. 1. X-ray crystal structure of **2** (DME adduct); phenyl groups were omitted for clarity. Significant distances [Å] and angles [°]: Na1–P1 3.001(1), Na1–P11 3.172(2), Na1–P20 3.083(2), Na2–P1 2.909(1), Na2–P10 3.250(2), Na2–P20 3.033(2), P10–P11 2.214(3), Na1–O54 2.335(2), Na1–O57 2.433(2), Na2–O60 2.366(2), Na2–O63 2.418(2), P1–C2 1.765(2), P1–C5 1.766(2), P10–C6 1.796(3), P10–C9 1.801(3), C2–C3 1.413(2), C3–C4 1.423(1), C4–C5 1.406(2), C5–C6 1.467(3), C6–C7 1.366(3), C7–C8 1.470(3), C8–C9 1.371(3), Na1–C2 2.807(2), Na1–C5 2.937(2), Na1–C3 2.820(1), Na1–C4 2.891(1). Nonbonding: Na1–Na2 4.264(1). P1-Na1-P11 88.10(4), P1-Na1-P20 87.42(4), P11-Na1-P20 64.85(5), O54-Na1-O57 70.29(7), C2-P1-C5 91.0(1), C6-P10-C9 92.2(1).

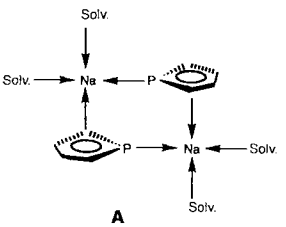

A

phosphorus atom. The simplified representation **A** clearly shows the head-to-tail arrangement of the two phospholyl rings and their η^1-P,η^5-PC_4 bonding mode. Similar coordination modes have been found in some phospholyl–uranium complexes.[6]

The rather short Na1–P20 contact probably reflects a high charge localization of the phospholide anion at phosphorus, as has been predicted by theory.[7] Evidence of high σ-donation from P20 to Na1 is provided by the Na1–phospholyl (P1) distance of 2.569 Å, which is at the high end of the recorded Na–Cp bond lengths (2.40–2.65 Å[11]). $[Cp^*Na(Py)_3]$ ($Cp^* = C_5Me_5$; Py = pyridine), which has three Py donors in the coordination sphere of sodium, has a comparable Na–Cp*(centroid) distance of only 2.40 Å.[8] The influence of the substitution scheme on the structural parameters of the phospholide ring also appears to be significant. For **2**, the relatively small difference in bond lengths ($C_\alpha C_\beta$–$C_\beta C_{\beta'}$) clearly indicates an extensive electronic delocalization throughout the carbon-centered portion of the phospholyl anion. Nonetheless, the P–C separations (1.762(3) and 1.770(3) Å), which are substantially longer than in $[C_4Me_4P][Li(tmeda)]$ (tmeda = *N*,*N*,*N*′,*N*′-tetramethylethylenediamine) (1.750–1.752(2) Å),[3] suggest that phosphorus participates less in cyclic delocalization in **2** than in the tetraalkylphospholide. Thus, it seems possible that extended conjugation between the substituents and the dienic portion of the phospholide may diminish the interaction of the phosphorus with the carbon skeleton of **2**. Such an influence of the substitution pattern on the structural parameters of the phospholide ion is a little unexpected, because calculations suggest that the aromaticity of the parent phospholide anion is only 10% lower than that of Cp^-.[7] However, it has been shown recently that conjugating substituents such as alkynyl groups reduce the degree of aromaticity in the phosphole nucleus.[9] It seems probable that a full understanding of this phenomenon will only be possible from computational analysis.

Compound **3** was prepared in crude form as a yellow precipitate after cleavage of **1** by four equivalents of potassium in DME. Crystals of **3**·2THF suitable for a structural study were obtained by recrystallization from a mixture of THF and [18]crown-6. The X-ray analysis (Fig. 2) shows a double anionic

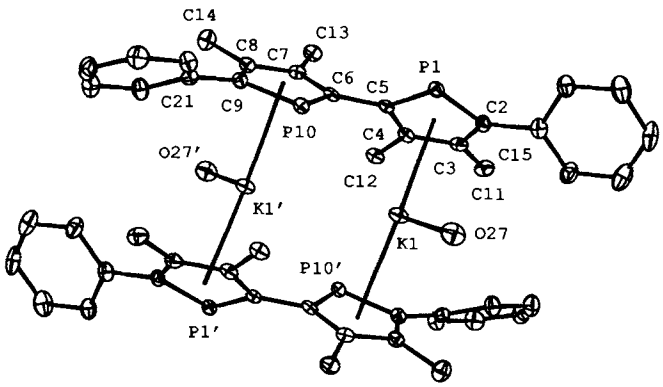

Fig. 2. X-ray crystal structure of the anionic component of **3** (THF adduct). The structure of the cation has been described previously [10] and is not shown. Carbon atoms of the coordinated THF ligand are omitted for clarity. Significant distances [Å] and angles [°]: K1–P1 3.264(1), K1–P10 3.256(1), K1–O27 2.722(3), P1–C2 1.779(4), P1–C5 1.759(3), P10–C6 1.761(4), P10–C9 1.779(4), C2–C3 1.399(5), C3–C4 1.415(5), C4–C5 1.411(5), C5–C6 1.474(5), C6–C7 1.402(5), C7–C8 1.408(5), C8–C9 1.411(5), K–C(α) mean 3.155, K–C(β) mean 3.162, C2-P1-C5 90.8(2), C6-P10-C9 90.8(2).

sandwich related to the previously unknown kalocene anion,[11] which is bent by coordination to THF. Since the structure has a center of symmetry, it is only necessary to discuss the parameters of one P1-K1-P10′ subunit. The two phospholides (P1 and P10′) have a head-to-tail disposition. Their mean planes form an angle of 47°, and the THF molecule is coordinated to the potassium ion on the open side of the tilted sandwich: (P1)centroid-K1-(P10′)centroid = 137.9°, (P1)centroid-K1-O27 = 110.8°, O27-K1-(P10′)centroid = 106.2°. The displacements of the potassium atoms from the phospholyl mean plane (2.855–2.883 Å) are rather large when compared with those in other CpK structures (ca. 2.79 Å).[11] This probably results simply from a relaxation of the K–C distances to accommodate the inherently longer P–K1 separation, which appears to be normal at 3.264(1) Å.[12] Finally, the two 2,2′-biphospholide units unexpectedly adopt a cisoid configuration, and the interaction between the two potassium ions K1 and K1′ is negligible, as shown by their separation of 4.266(2) Å.

From this series of results, it appears that the structural chemistry of alkali metal phospholides is even richer than that of alkali metal cyclopentadienides.

Experimental Procedure

2: Naphthalene (50 mg) was added to sodium metal (1.00 g, 43 mmol) in freshly distilled THF (15 mL) under argon. After five minutes, tetramer **1** (1.00 g, 1.34 mmol) was added. After 2 h the black-green solution was filtered free of sodium with a cannula and treated further with tetramer **1** (0.95 g, 1.28 mmol). The red suspension was then stirred for several hours at room temperature until dissolution of the added tetramer was complete. The solvent was evaporated under vacuum. The red-orange precipitate was washed several times with 20 mL of *n*-pentane and

 © VCH Verlagsgesellschaft mbH, D-69451 Weinheim, 1996 0570-0833/96/3510-1126 $ 15.00+.25/0

dried. Yield: 2.75 g, 97% yield of crude air-sensitive red-orange **2**·4THF. Pure **2**·2DME was obtained by slow diffusion of *n*-hexane into a solution of **2** dissolved in DME. $C_{56}H_{64}Na_2O_4P_4$ (red-orange crystals), $M_r = 971.01$, crystal dimensions $0.32 \times 0.32 \times 0.32$ mm, triclinic, $P\bar{1}$ (No. 2), $a = 11.909(1)$, $b = 14.819(2)$, $c = 16.901(2)$ Å, $\alpha = 95.29(1)$, $\beta = 101.23(1)$, $\gamma = 112.58(1)°$, $V = 2654.0$ (1) Å^3, $Z = 2$, $\rho_{calcd} = 1.215$ g cm^{-3}, $\lambda(Mo_{K\alpha}) = 0.71073$ Å, $\mu = 2.0$ cm^{-1}, $F(000) = 1028$, $T = 123 \pm 0.5$ K. Final $R = 0.044$, $R_w = 0.065$ for 9550 observed unique reflections with $2\theta_{max} = 60°$ having $F_o^2 > 3.0\sigma(F_o^2)$. Solution by direct methods; 595 variables refined using $\omega(|F_o| - |F_c|)^2$ by full matrix least squares, GOF = 1.19. $(\Delta\rho)_{max,min} = 1.05$ Å^3 in the final difference map [13].

3: Potassium metal (0.91 g, 23.3 mmol) and tetramer **1** (4.00 g, 5.38 mmol) were heated to 70 °C in freshly distilled DME (100 mL) for 12 h. The crude precipitate of air-sensitive pale yellow needles was collected, washed with DME, and dried. Yield of **3**·4DME: 6.30 g, 93%. Crystals suitable for X-ray diffraction were grown by diffusion of hexane into a THF solution containing equimolar amounts of **3** and [18]crown-6. $C_{104}H_{156}K_4O_{20}P_4$ (pale yellow crystals), $M_r = 2006.69$, crystal dimensions $0.20 \times 0.30 \times 0.34$ mm, monoclinic, $P21/n$ (No. 14), $a = 17.445(2)$, $b = 15.783(1)$, $c = 20.382(2)$ Å, $\beta = 102.27(1)°$, $V = 5483.5(2)$ Å^3, $Z = 2$, $\rho_{calcd} = 1.215$ g cm^{-3}, $\lambda(Mo_{K\alpha}) = 0.71073$ Å, $\mu = 2.8$ cm^{-1}, $F(000) = 2152$, $T = 123 \pm 0.5$ K. Final $R = 0.056$, $R_w = 0.072$ for 5664 observed unique reflections with $2\theta_{max} = 60°$ having $F_o^2 > 3.0\sigma(F_o^2)$. Solution by direct methods; 595 variables refined using $w(|F_o| - |F_c|)^2$ by full matrix least squares,. GOF = 1.22. $(\Delta\rho)_{max,min} = 0.57$ Å^3 in the final difference map [13].

Received: December 11, 1995 [Z8640IE]
German version: *Angew. Chem.* **1996**, *108*, 1204–1206

Keywords: alkali metal compounds · metallocenes · phospholides · phosphorus compounds

[1] For a recent highlight, see: D. Stalke, *Angew. Chem.* **1994**, *106*, 2256; *Angew. Chem. Int. Ed. Engl.* **1994**, *33*, 2168.
[2] S. Harder, M. H. Prosenc, *Angew. Chem.* **1994**, *106*, 1830; *Angew. Chem. Int. Ed. Engl.* **1994**, *33*, 1744.
[3] T. Douglas, K. H. Theopold, *Angew. Chem.* **1989**, *101*, 1394; *Angew. Chem. Int. Ed. Engl.* **1989**, *28*, 1367.
[4] F. Laporte, F. Mercier, L. Ricard, F. Mathey, *J. Am. Chem. Soc.* **1994**, *116*, 3306.
[5] J. Fischer, A. Mitschler, F. Mathey, F. Mercier, *J. Chem. Soc. Dalton Trans.* **1983**, 841.
[6] D. Baudry, M. Ephritikhine, F. Nief, L. Ricard, F. Mathey, *Angew. Chem.* **1990**, *102*, 1501; *Angew. Chem. Int. Ed. Engl.* **1990**, *29*, 1485.
[7] E. J. Padma Malar, *J. Org. Chem.* **1992**, *57*, 3694 and references therein.
[8] G. Rabe, H. W. Roesky, D. Stalke, F. Pauer, G. M. Sheldrick, *J. Organomet. Chem.* **1991**, *403*, 11.
[9] S. Holand, F. Gandolfo, L. Ricard, F. Mathey, *Bull. Soc. Chim. France*, **1996**, *133*, 33. For a discussion of the validity of the ($C_\alpha C_\beta - C_\beta C_{\beta'}$) criterion see also: P. von R. Schleyer, P. K. Freeman, H. Jiao, B. Goldfuss, *Angew. Chem.* **1995**, *107*, 332; *Angew. Chem. Int. Ed. Engl.* **1995**, *34*, 337.
[10] F. G. N. Cloke, P. B. Hitchcock, A. McCamley, *J. Chem. Soc. Chem. Commun.* **1993**, 248.
[11] In very recent work, in which the existence of the natrocene anion was demonstrated crystallographically, a kalocene anion was also reported. However, no structural data were given. See: J. Wessel, E. Lork, R. Mews, *Angew. Chem.* **1995**, *107*, 2565; *Angew. Chem. Int. Ed. Engl.* **1995**, *34*, 2376. The crystal structure of a triple-decker cesocene complex has also been reported since submission of the present paper: S. Harder, M. H. Prosenc, *Angew. Chem.* **1996**, *108*, 101; *Angew. Chem. Int. Ed. Engl.* **1996**, *35*, 97.
[12] M. Andrianarison, D. Stalke, U. Klingebiel, *Chem. Ber.* **1990**, *123*, 71.
[13] Crystallographic data (excluding structure factors) for the structures reported in this paper have been deposited with the Cambridge Crystallographic Data Centre as supplementary publication no. CCDC-179-25. Copies of the data can be obtained free of charge on application to The Director, CCDC, 12 Union Road, Cambridge CB2 1EZ, UK (fax: int. code +(1223) 336-033; e-mail: teched@chemcrys.cam.ac.uk).

Lithium 2,2′-Biphenyldiyltrimethylsilicate; First Observation of Pentaorganosilicates

Adrianus H. J. F. de Keijzer, Franciscus J. J. de Kanter, Marius Schakel, Robert F. Schmitz, and Gerhard W. Klumpp*

In studies of nucleophilic substitution on silicon and nucleophilic activation of organosilicon compounds,[1] organosilicates with pentavalent silicon bonded to one or several atoms more electronegative than carbon have become very important. By contrast, the addition product of 1,1-dimethylsilacyclobutane and allyl anion, observed in a flowing afterglow experiment, is the only case in which the structure of a pentaorganosilicate (**1**) has been proposed.[2] Otherwise, pentaorganosilicates figure, as yet, only as unproven intermediates in the intramolecular and intermolecular transfer of triorganosilyl groups from neutral to anionic carbon centers. Thus, according to Kumada and co-workers,[3a] the transmetalation of 9,9-diorgano-9*H*,9-silafluorenes such as **2** with organolithiums proceeds via lithium pentaorganosilicates. We now report that we have observed these species at low temperatures by NMR spectroscopy. At higher temperatures they decompose into tetraorganosilane and organolithium. This can result in carbanion exchange between the starting compounds.

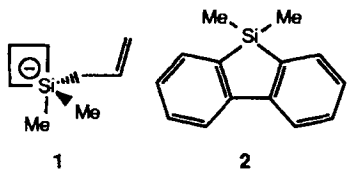

1 **2**

Treatment of bromide **3**[4] with *tert*-butyllithium at −80 °C in THF generated a species whose exceptionally high-field ^{29}Si NMR signal ($\delta = -116.9$) was indicative of pentavalent silicon.[5] Apparently, the lithium compound **4** rearranges instantaneously to the title compound **5**,[6] whose composition was deduced from the 8:9 ratio of the intensities of the biphenylene and methyl proton signals.[7] Raising the temperature converts **5** reversibly into methyllithium and 9,9-dimethyl-9*H*,9-silafluorene (**2**), which was identified in situ by comparison of its ^{29}Si ($\delta = 0.6$), ^{1}H, and ^{13}C NMR spectra with those of authentic material. Conversely, cooling THF solutions of methyllithium plus **2** generates **5**, which is the only species present at approximately −100 °C. Cryoscopy indicated that under these conditions **5** is undissociated: After addition of **2** (0.53 mmol) to a solution in THF of Me_4Li_4 (0.14 mmol), the number of particles contained in the solution (0.52 ± 0.01 mmol **5**) corresponded to the amount of **2** that had been added. In the presence of ten equivalents of hexamethylphosphoric triamide (HMPA), which strongly complexes lithium, the splitting of the ^{7}Li NMR signal by ^{7}Li–^{31}P coupling (−120 °C, $\delta(^7Li) = -2.1$,[8] quintet,

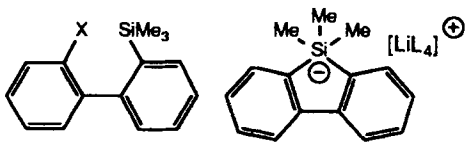

3: X = Br
4: X = Li
5-L_4

[*] Prof. Dr. G. W. Klumpp, Drs. Ing. A. H. J. F. de Keijzer, Dr. F. J. J. de Kanter, Dr. M. Schakel, R. F. Schmitz
Scheikundig Laboratorium Vrije Universiteit
De Boelelaan 1083, NL-1081 HV Amsterdam (The Netherlands)
Fax: Int. code +(20)444-7488

$\delta(^{31}P) = 24.1$, 1:1:1:1 quartet, $^2J(^7Li,^{31}P) = 7.5$ Hz[9]) clearly indicated coordination of four HMPA molecules to the lithium ion of **5**. Since a single ^{29}Si NMR signal at -116.2 persisted from -120 to 20 °C, **5**-L_4 (L = HMPA) must be more stable than **2** plus methyllithium throughout the temperature range studied. A single methyl signal and a single set of six phenylene carbon signals in the ^{13}C NMR spectra indicate that stereoisomers of **5**-L_4 (L = HMPA) interconvert rapidly on the ^{13}C NMR time scale, even at -120 °C.

The reaction of butyllithium (1 equiv) with **2** in THF is analogous to that of methyllithium. At -80 °C the ^{29}Si NMR signal of the *Si*-butyldimethyl analogue of **5** is found at $\delta = -113.6$.[10] By contrast, in ether at -80 °C as well as at higher temperatures, neither the methyllithium/**2** system nor the butyllithium/**2** system exhibits a ^{29}Si NMR signal of pentacoordinated silicon. Above -14 °C formation of 9-butyl-9-methyl-9*H*,9-silafluorene[3a] is evident, strongly suggesting, as Kumada and co-workers[3a] had already proposed for the present reaction and for related ones, that **5** and analogues are accessible kinetically also in ether.[11] However, in this solvent, the thermodynamic stability of **5** and its analogues relative to that of **2** plus methyllithium or butyllithium is so low that they cannot be detected. It appears that the stabilities of ate complexes of Group 4 elements depend to a large degree on the strength of complexation of their countercations by the solvent or other Lewis bases. Thus, organofluorosilicates are most stable as the [18]crown-6 potassium salts.[12] The present order of propensity for complexation of the lithium ions and, thereby, stabilization of **5** and analogues, HMPA > THF > ether, applies also to lithium pentaorganostannates.[13] The fact that **5** is present in THF in substantial concentrations suggests to us optimum complexation of the lithium ion, that is the existence of **5**-L_4 (L = THF). This is in accord with known structures of THF-complexed lithium salts[14] and is supported by the value of the reaction entropy in THF. The ratios of the integrals of the NMR signals of the methyl protons of methyllithium, **5**, and **2**, in THF at eleven temperatures (-54 to -9 °C) were used to determine the equilibrium constant K for the reaction $1/4\,Me_4Li_4 + \mathbf{2} \rightleftharpoons \mathbf{5}$, whence $\Delta H = -55 \pm 2$ kJ mol^{-1}, $\Delta S = -225 \pm 6$ J K^{-1} mol^{-1} were obtained. The value of ΔS indicates a strong decrease of the number of particles, as one would expect for the formation of a tetrasolvate,[15] suggesting that actually reaction (a) is occurring.

$$1/4\,Me_4Li_4 \cdot 4THF + 3THF + \mathbf{2} \rightleftharpoons \mathbf{5}\text{-}L_4\ (L = THF) \qquad (a)$$

Any interpretation of the value of ΔH in terms of silicate formation from tetraorganosilanes and carbanions[16] is precluded by the unknown energy contributions associated with the deaggregation of $Me_4Li_4 \cdot 4THF$ as well as with the separation of ions and the complexation of the lithium ion by THF in **5**-L_4 (L = THF).

Chemical shifts of the ^{29}Si NMR signals arising upon treatment of **2** with phenyllithium and *tert*-butyllithium let us conclude that lithium silicates are also formed in these systems, presumably $Li[SiC_{12}H_8Me_2Ph] \cdot 4THF$, $\delta(^{29}Si, -80\,°C) = -112.7$, and $Li[SiC_{12}H_8Me_2tBu] \cdot 4THF$, $\delta(^{29}Si, -80\,°C) = -102.5$, respectively. A similar high-field resonance ($\delta(^{29}Si, -80\,°C) = -102.3$) in the system tetraphenylsilane/phenyllithium/THF–HMPA proves that lithium pentaorganosilicates (here $Li[SiPh_5] \cdot 4HMPA$) are also formed from tetraphenylsilane.

In summary: In THF equilibria are established between various σ-organolithiums and either 9,9-dimethyl-9*H*,9-silafluorene (**2**) or tetraphenylsilane, and the corresponding lithium silicates. The latter can be monitored by NMR spectroscopy at low temperatures and their stability is increased by coordination of HMPA to lithium. To our knowledge these are the first pentaorganosilicates described. Present studies aim at the preparation of lithium pentaorganosilicates from other tetraorganosilanes.

Received: December 13, 1995
Revised version: February 8, 1996 [Z 8641 IE]
German version: *Angew. Chem.* **1996**, *108*, 1183–1184

Keywords: lithium compounds · NMR spectroscopy · silicon compounds · substitutions

[1] Overview: C. Chuit, R. J. P. Corriu, C. Reye, J. C. Young, *Chem. Rev.* **1993**, *93*, 1371.
[2] S. A. Sullivan, C. H. DePuy, R. Damrauer, *J. Am. Chem. Soc.* **1981**, *103*, 480.
[3] a) M. Ishikawa, T. Tabohashi, H. Sugisawa, K. Nishimura, M. Kumada, *J. Organomet. Chem.* **1983**, *250*, 109; b) N. Tokitoh, T. Matsumoto, H. Suzuki, R. Okazaki, *Tetrahedron Lett.* **1991**, *32*, 2049; c) V. Gevorgyan, L. Borisova, E. Lukevics, *J. Organomet. Chem.* **1992**, *441*, 381.
[4] Prepared by monolithiation of 2,2′-dibromobiphenyl and subsequent reaction with chlorotrimethylsilane. We thank Drs. G. P. M. van Klink for a sample of this compound.
[5] B. J. Helmer, R. West, R. J. P. Corriu, M. Poirier, G. Royo, A. De Saxce, *J. Organomet. Chem.* **1983**, *251*, 295.
[6] ^{13}C NMR (100.63 MHz, [D$_8$]THF, -80 °C): $\delta = 166.92$ (C-2, satellites: $^1J(^{29}Si,^{13}C) = 46.8$ Hz), 145.80 (C-1), 136.05, 125.14, 124.90, 118.40 (C-3 to C-6), 12.37 (CH_3, satellites: $^1J(^{29}Si,^{13}C) = 46.9$ Hz).
[7] ^1H NMR (400.13 MHz, [D$_8$]THF, -80 °C): $\delta = 7.58$ (dd, $^3J(H,H) = 7.5$, $^4J(H,H) = 1.0$ Hz, 2H, Ar), 7.56 (dd, $^3J(H,H) = 7.0$, $^4J(H,H) = 1.4$ Hz, 2H, Ar), 6.93 (ddd, $^3J(H,H) = 7.5$, $^3J(H,H) = 7.1$, $^4J(H,H) = 1.4$ Hz, 2H, Ar), 6.88 (ddd, $^3J(H,H) = 7.0$, $^3J(H,H) = 7.1$, $^4J(H,H) = 1.0$ Hz, 2H, Ar), 0.03 (s, 9H, Me).
[8] External standard: 0.3 M LiCl in methanol.
[9] H. J. Reich, J. P. Borst, R. R. Dykstra, D. P. Green, *J. Am. Chem. Soc.* **1993**, *115*, 8728.
[10] After warming to room temperature, 9-butyl-9-methyl-9*H*,9-silafluorene was isolated [3a].
[11] Calculations indicate that one-step substitution on silicon is always less favorable than reaction via pentacoordinated intermediates (Y. Apeloig, *The Chemistry of Organic Silicon Compounds* (Eds.: S. Patai, Z. Rappoport), **1989**, Wiley, New York, p. 57).
[12] R. Damrauer, S. E. Danahey, *Organometallics* **1986**, *5*, 1490.
[13] H. J. Reich, N. H. Phillips, *J. Am. Chem. Soc.* **1986**, *108*, 2102.
[14] See W. N. Setzer, P. von Ragué Schleyer, *Adv. Organomet. Chem.* **1985**, *24*, 353.
[15] Strikingly, $\Delta S = -110 \pm 29$ J K^{-1} mol^{-1} was found for the reaction $Bu_4Li_4 \cdot 4THF + 4THF \rightleftharpoons 2\,Bu_2Li_2 \cdot 4THF$, in which the tetra(THF) solvate of butyllithium tetramer reacts with four molecules of THF to give two molecules of a new tetra(THF) solvate (J. Heinzer, J. F. M. Oth, D. Seebach, *Helv. Chim. Acta* **1985**, *68*, 1848). This is practically half of the decrease in entropy found in the present study where we postulate formation of a single molecule of tetra(THF) solvate from (formally) 0.25 molecules of the tetra(THF) solvate of methyllithium tetramer, three molecules of THF, and one molecule of **2**.
[16] According to calculations, formation of organosilicates from silanes and carbanions is strongly exothermic: M. S. Gordon, L. P. Davis, L. W. Burggraf, R. Damrauer, *J. Am. Chem. Soc.* **1986**, *108*, 7889.

 © VCH Verlagsgesellschaft mbH, D-69451 Weinheim, 1996 0570-0833/96/3510-1128 $ 15.00+.25/0

Metallopinacolate Intermediates in the Reductive Coupling of Acetone Promoted by Uranium Reagents

Olivier Maury, Claude Villiers, and Michel Ephritikhine*

Reductive coupling of carbonyl compounds by means of low-valent metal species is an extremely useful reaction in organic synthesis, and many efforts have been made to improve the efficiency and to understand the mechanisms of these processes.[1] A number of titanium systems, prepared from $TiCl_4$ or $TiCl_3$ and various reducing agents under different conditions, have been used for coupling ketones. The nature of the products, diols or alkenes, was found to depend markedly upon the structure of the active titanium species and the experimental conditions.[2] A complete rationale for these results is still lacking.[3] In this context, we thought it of interest to consider the potential of uranium compounds in such transformations. Complexes of uranium and Group 4 elements exhibit strong analogies in structure and reactivity, and highly reactive uranium metal powder was effective in the reductive coupling of aromatic ketones.[4] Moreover, the paramagnetic uranium complexes can be easily identified by their NMR spectra. They often crystallize readily and are therefore valuable auxiliaries in synthetic organic chemistry.[5, 6] We reported that benzophenone could be coupled in the presence of uranium tetrachloride and sodium amalgam. For the first time, the pinacolate intermediate previously postulated was isolated, characterized, and transformed into the corresponding alkene, tetraphenylethylene.[6] Subsequently, we found that aliphatic ketones could also be treated with UCl_4 and Na/Hg or Li/Hg to give pinacols or alkenes in good yields. The reaction of the simplest ketone, acetone, was studied in more detail, and the results reported here provide new insights into the intermediates and elementary steps of the coupling and deoxygenation processes. The influence of the reducing agent in these McMurry-type reactions is also defined.

A solution of acetone in tetrahydrofuran (THF) reacted with UCl_4 and Li/Hg in a molar ratio of 1:1:1 to give the bimetallic pinacolate complex **1** (Scheme 1). The mixture was stirred for 3 h at 20 °C and, after filtration and crystallization, **1** was isolated as a greenish powder in 90% yield. An analogous reaction with the components in a 2:1:2 molar ratio led to the formation of the green mononuclear compound **2**, which was also obtained in almost quantitative yield from **1** and two equivalents of Me_2CO and Li/Hg. Comproportionation of **2** and UCl_4 gave **1**. Unequivocal synthesis of **1** and **2** could be achieved in THF by alcoholysis of the amido(chloro)uranium derivatives $[U(NEt_2)Cl_3(THF)]$ and $[U(NEt_2)_2Cl_2]$[7] with pinacol in the presence of LiCl. Compounds **1** and **2** were characterized by their elemental analyses (C, H, Cl) and their ^1H NMR spectra, which exhibit very shifted paramagnetic signals corresponding to the methyl groups, at $\delta = +108$ and $+26$, respectively.[8]

Other products resulted when sodium amalgam was used in place of Li/Hg. The reaction of acetone with UCl_4 and Na/Hg in the molar ratio of 1:1:1 afforded the neutral metallopinacol **3** as the major product (>60% yield), and NaCl precipitated. When a molar ratio of 2:1:2 was employed, the main product was the neutral metallopinacol **4** in similar yields. Other compounds resulting from aldolization of the ketone were also

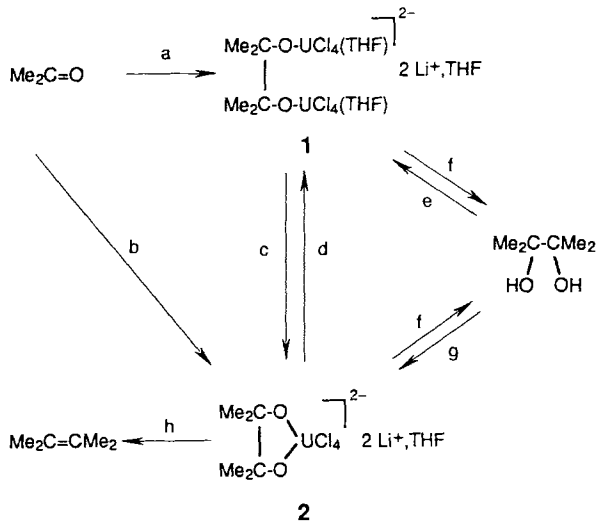

Scheme 1. Synthesis, interconversion, and deoxygenation of the metallopinacols **1** and **2**. Reagents (molar ratios) and reaction times. a) Me_2CO, UCl_4, Li/Hg (1:1:1), 3 h; b) Me_2CO, UCl_4, Li/Hg (2:1:2), 8 h; c) **1**, Me_2CO, Li/Hg (1:2:2), 4 h; d) UCl_4, 1 h; e) $[U(NEt_2)Cl_3(THF)]$, $Me_2C(OH)C(OH)Me_2$, LiCl (2:1:2), 2 h; f) H_2O, 10 min; g) $[U(NEt_2)_2Cl_2]$, $Me_2C(OH)C(OH)Me_2$, LiCl (1:1:2), 2 h; h) 2 Li/Hg, 24 h. All reactions in THF at 20 °C except reaction (h) at 65 °C. The coordination of THF molecules in **1** and **2** is not known; in the formulas here written, uranium is hexacoordinate, as most frequently encountered.

$[\{UCl_3(THF)_2\}_2(\mu\text{-}OCMe_2CMe_2O)]$ **3**

$[UCl_2(OCMe_2CMe_2O)(THF)_x]$ **4**

formed and are currently under investigation. These reactions with Na/Hg, which required three days for completion, were much slower than those with Li/Hg. As expected, complexes **3** and **4**, which were synthesized independently by treating $[U(NEt_2)Cl_3(THF)]$ and $[U(NEt_2)_2Cl_2]$ with pinacol, were converted into **1** and **2** by addition of LiCl. The bimetallic compound **3** was characterized by its ^1H NMR spectrum, which showed a broad resonance at $\delta = +126$. The derivative $[\{UCl_3(HMPA)_2\}_2(\mu\text{-}OCMe_2CMe_2O)]$, prepared by replacement of the THF ligands with hexamethylphosphoric triamide (HMPA), gave satisfactory elemental analyses (C, H, N) and its structure was confirmed by X-ray crystallography.[9] Complex **4**, which presumably has a polymeric structure with Cl bridges, is insoluble in organic solvents and could not be purified by extraction or crystallization.

Complexes **1**–**4** are the first metallopinacolate intermediates to be isolated in the reductive coupling of an aliphatic ketone. A bimetallic species similar to **1** and **3** could not be identified in the reactions of benzophenone with the systems UCl_4 and M/Hg (M = Li or Na). However, metallopinacols have been synthesized recently by reaction of dialdehydes and ketoaldehydes with tin hydrides [10] and by treatment of fluorenone with a samarium(II) alkoxide;[11] these complexes are not intermediates in McMurry-type reactions. Not surprisingly, hydrolysis of **1**–**4** led to the immediate and quantitative liberation of pinacol. More interesting is the formation of the alkene product, which, as previously demonstrated,[6] required further treatment of the pinacolato complexes with the reducing agent. In fact, reaction of **1** with one equivalent of lithium amalgam at 20 °C in THF did not afford the alkene but gave after 4.5 h the metallacycle **2** in 85% yield. Since the violet uranium(III) chloride concomitantly formed, $LiUCl_4$ (or $UCl_3 + LiCl$), is precisely that obtained from UCl_4 and Li/Hg, it was not surprising to observe its total conversion into **1** after further addition of one equivalent of acetone (NMR experiments). These results (Scheme 2) confirmed that **1** is an intermediate in the synthesis of **2** and revealed

[*] Dr. M. Ephritikhine, O. Maury, Dr. C. Villiers
Service de Chimie Moléculaire, DSM, DRECAM, CNRS URA 331
CEA Saclay, F-91191 Gif sur Yvette (France)
Fax: Int. code +(1)69 08 66 40
e-mail: ephri@nanga.saclay.cea.fr

 © VCH Verlagsgesellschaft mbH, D-69451 Weinheim, 1996 0570-0833/96/3510-1129 $ 15.00+.25/0

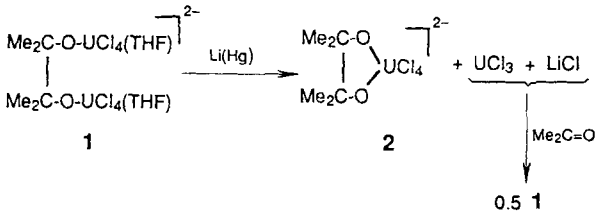

Scheme 2. The role of **1** as an intermediate in the formation of **2**.

two unsuspected points of the reaction mechanism. Firstly, acetone is not involved in the transformation **1** → **2**, which is induced by Li/Hg reduction and generates UCl_3 and LiCl. Secondly, **2** is the true precursor of the alkene, tetramethylethylene. Indeed, **2** was smoothly reduced at 20 °C by Li/Hg to give a not yet identified uranium(III) alkoxide, and complete formation of the alkene could be achieved after the mixture was heated at reflux for 24 h. In agreement with these observations, the reductive coupling of acetone to give pinacol or tetramethylethylene was performed in a one-pot reaction by using the proper quantities of UCl_4 and Li/Hg; the diol was formed by hydrolysis after 8 h at room temperature, whereas the alkene was obtained by heating for 24 h under reflux (quantitative yields by NMR). When the UCl_4 and Na/Hg system was used, the yield of tetramethylethylene did not exceed 10% after 48 h at 65 °C. This difficulty in forming the alkene could be clearly related to the sluggish reduction of the pinacolato intermediate **4**, which was quite inert towards Na/Hg at 20 °C; even after 30 h at 65 °C only about 20% was converted into tetramethylethylene. In contrast, **4** was readily reduced by Li/Hg and transformed completely into the expected alkene after 10 h in refluxing tetrahydrofuran.

We have found that in the reductive coupling of acetone, quite distinct conditions are necessary for both the coupling process leading to the pinacolate intermediates and for the subsequent deoxygenation step giving tetramethylethylene. These differences can be used to achieve remarkable selectivity like that observed with some titanium systems.[1,2] The results also underline the major role of the reducing agent, which determines the structure of the intermediates and is of particular importance in the deoxygenation step. If the first intermediate, a bimetallic species with a bridging $OCMe_2CMe_2O$ ligand, readily reacts with the reducing agent to give a cyclic mononuclear metallopinacol, only this intermediate is transformed under more forcing conditions into the corresponding alkene.

Experimental Procedure

^{1}H NMR (TMS int.): Bruker WP60 (60 MHz). All experiments were carried out under argon (< 5 ppm oxygen and water) using standard Schlenk-vessel and vacuum-line techniques or in a glove box. Solvents were thoroughly dried and deoxygenated by standard methods and distilled immediately before use.

1: A mixture of UCl_4 (354 mg, 0.93 mmol), 1% Li/Hg (640 mg, 0.93 mmol of Li), and acetone (68 μL, 0.93 mmol) in THF (15 mL) was stirred for 3 h at 20 °C. The green solution was filtered and its volume reduced to 5 mL. The green microcrystals of **1** that precipitated upon addition of pentane (10 mL) were filtered off, washed with pentane, and dried under vacuum (464 mg, 90%).

2: By using the same procedure as for **1**, green microcrystals of **2** were isolated in 76% yield from the reaction of UCl_4 (337 mg, 0.88 mmol), 1% Li/Hg (1215 mg, 1.76 mmol of Li) and acetone (102 mg, 1.76 mmol).

3: A mixture of $[U(NEt_2)Cl_3(THF)]$ (253 mg, 0.51 mmol) and pinacol (30.2 mg, 0.25 mmol) in THF (15 mL) was stirred for 2 h at 20 °C. The green solution was filtered and concentrated to dryness, leaving a green powder, which was washed with pentane and dried under vacuum (256 mg, 92%).

4: A mixture of $[U(NEt_2)_2Cl_2]$ (310 mg, 0.68 mmol) and pinacol (81 mg, 0.68 mmol) in THF (15 mL) was stirred for 2 h at 20 °C. The gray precipitate was filtered off, washed with pentane, and dried under vacuum (328 mg).

Received: January 15, 1996 [Z 8718 IE]
German version: *Angew. Chem.* **1996**, *108*, 1215–1216

Keywords: McMurry reactions · pinacol derivatives · reductive couplings · uranium compounds

[1] K. G. Pierce, M. A. Barteau, *J. Org. Chem.* **1995**, *60*, 2405; A. Fürstner, A. Hupperts, *J. Am. Chem. Soc.* **1995**, *117*, 4468; B. Bogdanovic, A. Bolte, *J. Organomet. Chem.* **1995**, *502*, 109; T. Wirth, *Angew. Chem.* **1996**, *108*, 65; *Angew. Chem. Int. Ed. Engl.* **1996**, *35*, 61, and references therein.
[2] Y. Dang, H. J. Geise, *Janssen Chim. Acta* **1988**, *6*, 3; J. E. McMurry, *Chem. Rev.* **1989**, *89*, 1513; A. Fürstner, *Angew. Chem.* **1993**, *105*, 171; *Angew. Chem. Int. Ed. Engl.* **1993**, *32*, 164.
[3] D. Lenoir, *Synthesis* **1989**, 883.
[4] B. E. Kahn, R. D. Rieke, *Chem. Rev.* **1988**, *88*, 733; *Organometallics* **1988**, *7*, 463.
[5] R. Adam, C. Villiers, M. Lance, M. Nierlich, J. Vigner, M. Ephritikhine, *New J. Chem.* **1993**, *17*, 455; R. Adam, C. Villiers, M. Ephritikhine, *Tetrahedron Lett.* **1994**, *35*, 573; C. Villiers, M. Ephritikhine, *J. Chem. Soc. Dalton Trans.* **1994**, 3397.
[6] C. Villiers, R. Adam, M. Lance, M. Nierlich, J. Vigner, M. Ephritikhine, *J. Chem. Soc. Chem. Commun.* **1991**, 1144.
[7] J. C. Berthet, C. Boisson, M. Lance, J. Vigner, M. Nierlich, M. Ephritikhine, *J. Chem. Soc. Dalton Trans.* **1995**, 3019.
[8] ^{1}H NMR (60 MHz, [D$_8$]THF, 30 °C). **1**: $\delta = 108$ (Me, $W_{1/2} = 75$ Hz); **2**: $\delta = 26$ (Me, $W_{1/2} = 50$ Hz); **3**: $\delta = 126$ (Me, $W_{1/2} = 310$ Hz).
[9] O. Maury, C. Villiers, M. Lance, M. Nierlich, M. Ephritikhine, unpublished results.
[10] D. S. Hays, G. C. Fu, *J. Am. Chem. Soc.* **1995**, *117*, 7283.
[11] Z. Hou, T. Miyano, H. Yamazaki, Y. Wakatsuki, *J. Am. Chem. Soc.* **1995**, *117*, 4421.
[12] T. Mukaiyama, T. Sato, J. Hanna, *Chem. Lett.* **1973**, 1041.

Molecular Tweezers as Synthetic Receptors in Host–Guest Chemistry: Inclusion of Cyclohexane and Self-Assembly of Aliphatic Side Chains**

Frank-Gerrit Klärner,* Johannes Benkhoff, Roland Boese, Ulrich Burkert, Markus Kamieth, and Ulf Naatz

Simple synthetic receptors with molecular pockets or cavities can act as models for far more complicated biological systems,[1] for example they are important for protein folding or molecular recognition of substrates in enzymatic processes. The study of such receptors should provide information about the stability and structure of receptor–substrate complexes and the noncovalent interactions responsible for their formation. Besides the relatively strong and therefore often dominant hydrogen bonding[1c–h] and the hydrophobic effects[1d,2g] in aqueous solutions, the arene–arene interaction[2] seems to be of some importance. Here we report on syntheses and some supramolecular properties (complex formation and self-assembly) of the novel molecular tweezers[3] **1a–c**, **2**, and **3**, which because of their rigid ribbon-type structure should be execellently preorganized for the formation of complexes with aromatic guest molecules

[*] Prof. Dr. F.-G. Klärner, Dr. J. Benkhoff, Dipl.-Chem. U. Burkert, Dipl.-Chem. M. Kamieth, Dipl.-Chem. U. Naatz
Institut für Organische Chemie der Universität Gesamthochschule Essen, D-45117 Essen (Germany)
Fax: Int. code +(201)1833082
e-mail: klaerner@oc1.orgchem.uni-essen.de
Prof. Dr. R. Boese
Institut für Anorganische Chemie der Universität Gesamthochschule Essen (Germany)

[**] This work was supported by the Deutsche Forschungsgemeinschaft and the Fonds der Chemischen Industrie. We thank H. Bandmann for conducting the NMR experiments and D. Bläser for performing the crystal structure analyses.

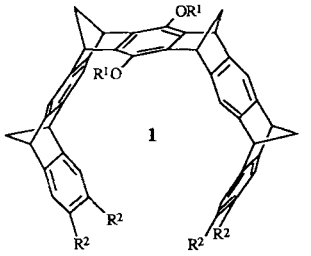

	a	b	c
R^1	CH_3	CH_3	$CH_2CO_2CH_2CH_3$
R^2	CO_2CH_3	H	H

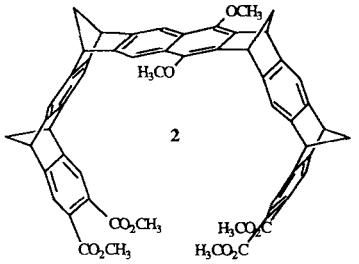

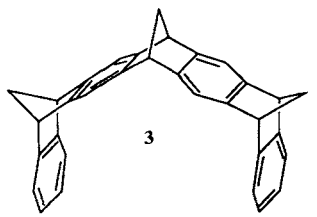

through multiple arene–arene interactions. Furthermore, bond angle distortions, which require little energy, should induce a certain flexibility to these systems allowing the tweezer "arms" to be expanded or compressed in a way comparable to the working principle of mechanical tweezers. Therefore, in their function as receptor they should be able, to a certain extent, to provide a geometrical fit to the structure of the potential substrate.

The key steps in the syntheses of **1a–c**, **2**, and **3** (Scheme 1) are repetitive Diels–Alder reactions[4] which here without exception proceed stereospecifically[5] on the *exo*-face of the bisdienophiles **4a**,[4b] **4c**, **5**,[4b] and **12** and on the *endo*-face of bisdiene **6**[6] or diene **10**.[7] Furthermore Diels–Alder reactions of the resulting bisdienes **7** and **8** with dimethyl acetylenedicarboxylate (DMAD) and subsequent DDQ dehydrogenation (DDQ = 2,3-dichloro-5,6-dicyano-1,4-benzoquinone) yield the desired tetraesters **1a** and **2**, respectively, which can be transformed by ester hydrolysis to the water-soluble sodium salts of the corresponding carboxylic acid.[8] Starting with the bisdienophiles **4a**, **4c**, and **12** and the diene **10**, compounds **1b**, **1c**, and **3**, respectively, could be synthesized in only two steps. The high stereoselectivity of the Diels–Alder reaction of diene **10** with norbornadiene **12** was surprising, because **12** does not show complete *exo*-selectivity[9] and, for example, gives a (60:40) mixture of the *syn*- and the *anti*-adduct[10] in the Diels–Alder reaction with 5,6-bismethylenenorbornene as a diene at 140 °C. The bowl-shaped geometry of **1a**, **1c**, and **2** can be seen from the crystal structure analyses (see below).

Preliminary ^{1}H NMR experiments (300 MHz $CDCl_3$, 25 °C) showed that the potential host molecules **1a** and **2** form complexes with 1,4-dicyanobenzene or 1,4-benzoquinone as guest molecules. Addition of **1a** or **2** (c = 0.09 and 0.08 M, respectively) caused an upfield shift of the ^{1}H NMR signals of 1,4-dicyanobenzene (c = 0.02 M, δ = 7.78 → 7.38 or 7.34, $\Delta\delta$ = 0.40 and 0.44, respectively) and 1,4-benzoquinone (c = 0.02 M, δ = 6.79 → 6.64, $\Delta\delta$ = 0.15 with **2**) which indicates that the hydrogen atoms of the guest molecules are located in the magnetic anisotropy regions of the host–arene units.[11] Contrary to these findings the addition of the host fragments **4a** or **5a** did not result in a change of the chemical shifts in the ^{1}H NMR spectra of 1,4-dicyanobenzene or 1,4-benzoquinone. Surprisingly, the structure analysis of **1a** (Fig. 1), crystallized from a (2:1) mixture of cyclohexane and ethyl acetate as colorless rhombic crystals, shows a (1:1) complex of disordered cyclohexane included in the cavity of **1a**. The orientation of the cyclohexane molecule seems to depend on the positioning of the likewise disordered methoxy groups that are pointed towards the cavity. A similar result is apparent from the structure analysis of crystals of compound **2** prepared in the same way. Here also a disordered cyclohexane molecule is included in the cavity of **2**.

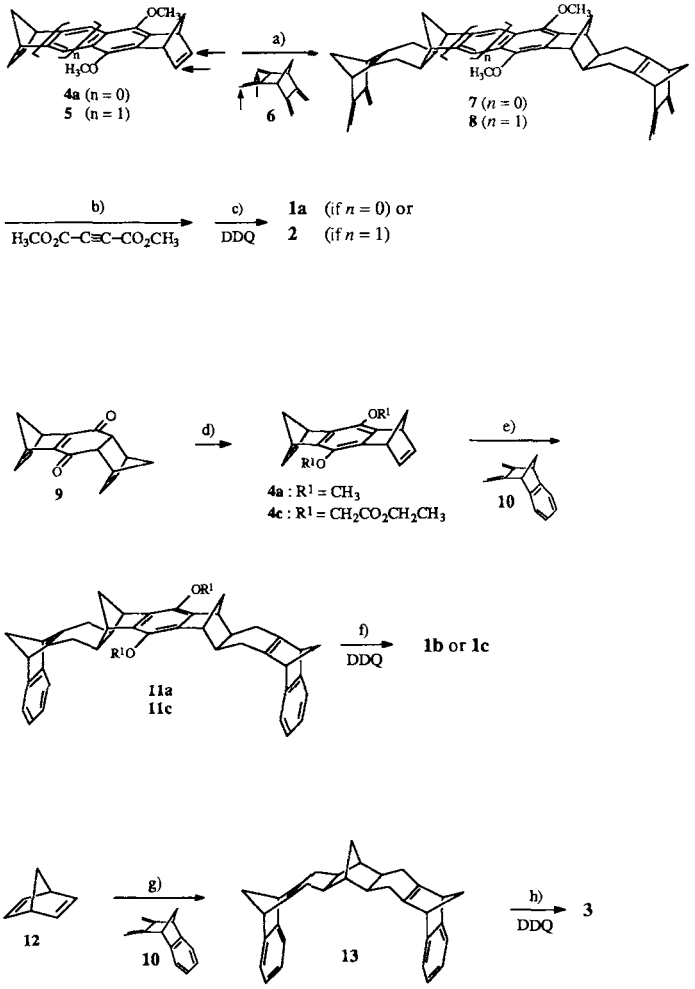

Scheme 1. Synthesis of the molecular tweezers **1a–c** and **2**. Reaction conditions and yields. (The thermolyses were performed in pyrex glass ampoules deactivated by $(C_2H_5)_3N$ and sealed under Ar). a) **6** (fivefold molar excess in each case), $(C_2H_5)_3N$ (catalytic amount), toluene, 125 °C, 3.5 d, 66% **7** (m.p. 210 °C decomp.) and 84% **8** (m.p. >300 °C), respectively. b) Dimethyl acetylenedicarboxylate (DMAD) (fivefold molar excess in each case), toluene, 65–70 °C, 21 h, 46% or 51% (1:2) Diels–Alder adduct (n = 0 or 1). c) DDQ (tenfold molar excess in each case), toluene, 115–120 °C, 5 h, 54% **1a** (m.p. >320 °C) or 61% **2** (m.p. >320 °C). d) $(CH_3O)_2SO_2$, NaOH, H_2O, Ar, 25 °C, 2 d, 94% **4a** (m.p. 148 °C); $BrCH_2CO_2CH_2CH_3$, 1,8-diazabicyclo[5.4.0]undec-7-ene (DBU), KI (catalytic amount), CH_3CN, 70 °C, 24 h, 56% **4c** (m.p. 84 °C). e) **10** (threefold molar excess), toluene, 170 °C, 3 d, 68% **11a**; **10** (fivefold molar excess), $(C_2H_5)_3N$ (catalytic amount), 160–170 °C, 6 d, 65% **11c** (m.p. 124 °C). f) DDQ (1.5-fold molar excess), toluene, 80 °C, 5 h, 44% **1b**; DDQ (twofold molar excess), toluene, 115 °C, 17 h, 43% **1c** (m.p. 246 °C). g) **10** (fourfold molar excess), toluene, 170 °C, 3 d, 60% **13**. h) DDQ (1.5-fold molar excess), toluene, 80 °C, 5 h, 63% **3**.

The geometry of the complex between **1a** and cyclohexane calculated with molecular mechanics (MacroModel: AMBER*)[12] is in good agreement with that derived from the structure analysis. The calculated distance (6.6 Å) between the opposing terminal arene C atoms, that is the tweezer's tips, for example, is well in accord with the experimental result. In the empty tweezer **1a** this distance is calculated to be only 5.6 Å. The

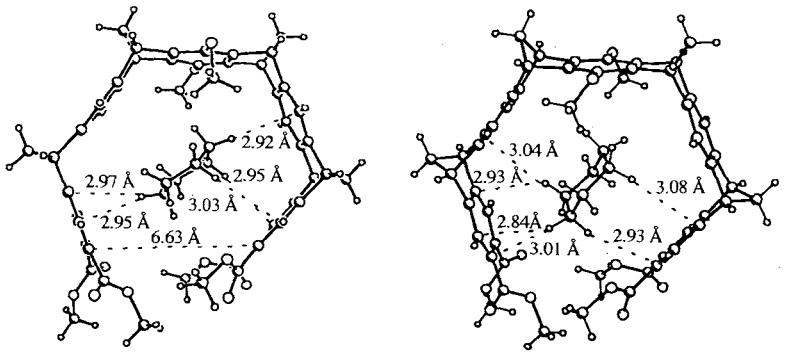

Fig. 1. Crystal structure of the superimposed (1:1) inclusion complex between **1a** and cyclohexane. In both structures the methoxy groups are pointed towards the cavity. The angle of projection between the C atoms of the two OCH_3 groups with the view of O–O axis is 35° in the first case and −55° in the second case. The two cyclohexane rings are twisted by 30° to each other with respect to the C_3 axis.

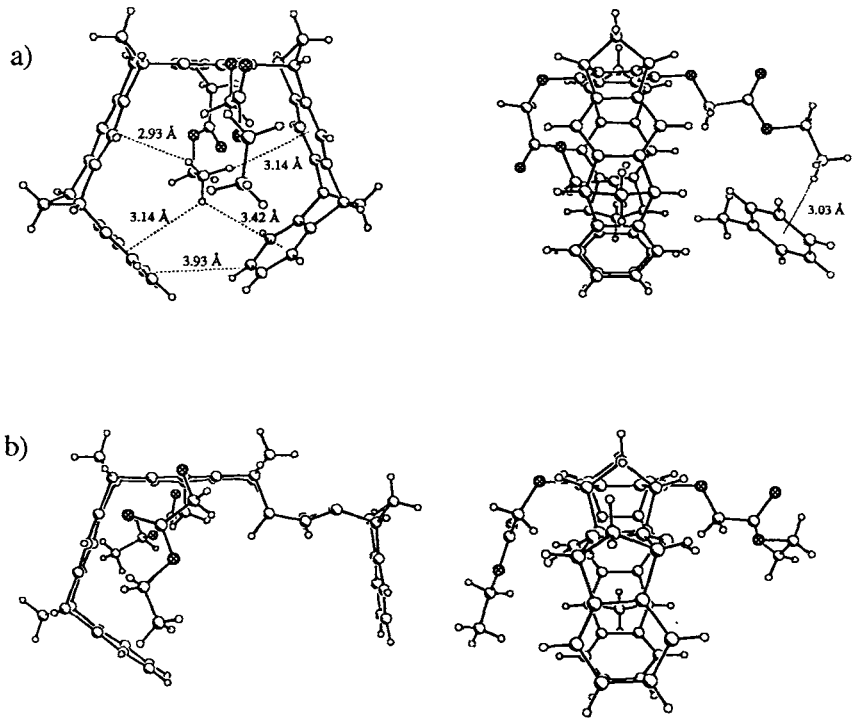

Fig. 2. a) Crystal structure of **1c**. In the side view (top, right) the distance between one methyl hydrogen atom of the extended side chain and the solvent molecule (toluene) is shown. b) Crystal structure of **14c**, the intermediate of the DDQ dehydrogenation **11c** → **1c**.

extra strain energy required for the extension by 1 Å (3 kcal mol^{-1}) is relatively small and can be easily compensated by the attractive noncovalent interactions in the formed complex.[12] For the extension of the corresponding distance in **1b** from 3.8 Å (in the empty tweezer **1b**) to 6.1 Å (in the calculated structure of the complex **1b**/cyclohexane) the extra strain energy is calculated to be 4 kcal mol^{-1}. Corresponding calculations with the tweezer **2** (having a naphthalene spacer unit) show that no change of this distance is necessary for formation of the complex between **2** and cyclohexane.

In the molecular tweezer **1c** a self-assembly of the aliphatic side chains was observed. The first evidence for such a process comes from the unexpected chemical shifts of the OCH_2CH_3 signals in the ^{1}H NMR spectrum of **1c** (Table 1). The upfield shifts indicate that the relevant hydrogen atoms are strongly influenced by the anisotropy of the arene units. The equivalence of the side chains in the NMR spectrum shows that either both side chains are complexed by the arene units in a symmetrical

Table 1. Solvent dependence of the chemical shifts of the OCH_2CH_3 groups in the ^{1}H NMR spectrum of **1c** (300 MHz, 21 °C). The compounds **4c** and **11c** used as references, only show the usual solvent dependence of chemical shifts: $\delta(CH_3) = 1.29$ or 1.23, $\delta(CH_2) = 4.24$ or 4.18 ($CDCl_3$); $\delta(CH_3) = 0.88$ or 0.43, $\delta(CH_2) = 3.85$ or 3.91 ([D_8]toluene).

Solvent	$\delta(CH_3)$	$\delta(CH_3)\delta(CH_2)$
CD_2Cl_2	1.15	4.15
$CDCl_3$	−0.27	3.37
CCl_4	−0.53	3.24
CD_3CN	1.09	4.09
[D_6]acetone	−0.28	3.33
[D_6]benzene	−0.70	3.15
[D_8]toluene	−0.84	3.05

arrangement or that only one side chain is complexed while the other one is free and that there is a rapid exchange between the complexed and the noncomplexed side chain. The results hitherto obtained from low-temperature ^{1}H NMR experiments have not allowed us to make a clear decision[13] between these two possibilities.

The structure analysis of **1c**, however, provides a clear result for the crystalline state (Fig. 2a). Here one side chain is folded and its terminal methyl group is centered in the cavity, whereas the other side chain has an extended conformation. The terminal methyl group of the extended side chain is complexed by a toluene molecule also present in the crystal. A comparison between the structures of **1c** and **14c** (Fig. 2b), an intermediate in the DDQ dehydrogenation **11c** → **1c**, is particularly instructive. Accordingly, the complexation of the side chain with both tweezer arms in **1c** is essential for its folding, whereas the interaction of the side chain with only one tweezer "arm" in **14c** is not sufficient.

The downfield shifts of the OCH_2CH_3 signals observed in the ^{1}H NMR spectra of **1c** in dichloromethane and acetonitrile (Table 1) provide evidence that these small solvent molecules can successfully compete with the one side chain to be included in the cavity of **1c**.[14] Therefore, the chemical shift of the ^{1}H NMR signal of the methyl group seems to be a sensitive probe for the ability of the molecular tweezers to form intermolecular host–guest complexes. The experiments presented here show that even the relatively weak but evidently directed alkane–arene interactions[15] are sufficient for the formation of host–guest complexes and self-assembly, so that they also have to be considered in the explanation of biological systems.

Received: November 23, 1995
Revised version: February 2, 1996 [Z 8582 IE]
German version: *Angew. Chem.* **1996**, *108*, 1195–1198

Keywords: Diels–Alder reactions · molecular tweezers · norbornenes · supramolecular chemistry

[1] a) Monographs: F. Vögtle, *Supramolekulare Chemie*, Teubner, Stuttgart, **1989**; F. Diederich, *Cyclophanes*, The Royal Society of Chemistry, Cambridge, **1994**; J.-M. Lehn, *Supramolecular Chemistry*, VCH, Weinheim, **1995**; examples: b) B. R. Peterson, P. Wallimann, D. R. Carcanages, F. Diederich, *Tetrahedron* **1995**, *51*, 401–421; B. R. Peterson, F. Diederich, *Angew. Chem.* **1994**, *106*, 1688–1690; *Angew. Chem. Int. Ed. Engl.* **1994**, *33*, 1625–1628; c) G. Das, A. D. Hamilton, *J. Am. Chem. Soc.* **1994**, *116*, 11139–11140; d) J. Rebek, Jr., *Acc. Chem. Res.* **1990**, *23*, 399–404; M. M. Conn, G. Deslongchamps, J.

deMendoza, J. Rebek, Jr., *J. Am. Chem. Soc.* **1993**, *115*, 3548–3557; e) S. S. Yoon, W. C. Still, *ibid.* **1993**, *115*, 823–834; f) D. M. Perreault, X. H. Chen, E. V. Anslyn, *Tetrahedron* **1995**, *51*, 353–362; C. Y. Huang, L. A. Cabell, E. V. Anslyn, *J. Am. Chem. Soc.* **1994**, *116*, 2778–2792; g) R. P. Bonarlaw, J. K. M. Sanders, *ibid.* **1995**, *117*, 259–271; h) G. A. Jeffrey, W. Saenger, *Hydrogen Bonding in Biological Structures*, 2nd ed. Springer, Berlin, **1994**; i) T. H. Webb, C. S. Wilcox, *Chem. Soc. Rev.* **1993**, *22*, 383–395.

[2] a) E. G. Cox, D. W. J. Cruikshank, J. A. C. Smith, *Proc. R. Soc. London A* **1958**, *247*, 1–21; K. C. Janda, J. C. Hemminger, J. S. Winn, S. Novick, S. J. Harris, W. Klemperer, *J. Chem. Phys.* **1975**, *63*, 1419; C. Krieger, F. Diederich, *Chem. Ber.* **1985**, *118*, 3620–3631; b) S. K. Burley, G. A. Petsko, *Science* **1985**, *229*, 23–28; *J. Am. Chem. Soc.* **1986**, *108*, 7995–8001; c) J. Singh, J. M. Thornton, *FEBS Lett.* **1985**, *191*, 1–6; *J. Mol. Biol.* **1990**, *211*, 595–614; d) I. Peterson, T. Liljefors, *J. Comput. Chem.* **1987**, *8*, 1139–1145; N. L. Allinger, J.-H. Lii, *ibid.* **1987**, *8*, 1146–1153; C. A. Hunter, J. K. M. Sanders, *J. Am. Chem. Soc.* **1990**, *112*, 5525–5534; C. A. Hunter, *Chem. Soc. Rev.* **1994**, 101–109; e) W. L. Jorgensen, D. L. J. Serverance, *J. Am. Chem. Soc.* **1990**, *112*, 4768–4774; f) G. Karlström, P. Linse, A. Wallquist, B. Jönsson, *ibid.* **1983**, *105*, 3777–3782; P. Hobza, H. L. Selzle, E. W. Schlag, *ibid.* **1994**, *116*, 3500–3506; g) L. F. Newcomb, T. S. Haque, S. H. Gellmann, *ibid.* **1995**, *117*, 6509–6519; h) S. Paliwal, S. Geib, C. S. Wilcox, *ibid.* **1994**, *116*, 4497–4498.

[3] The term "molecular tweezers" was introduced by C. W. Chen, H. Whitlock, *J. Am. Chem. Soc.* **1978**, *100*, 4921–4922. Further examples: S. H. Zimmerman, *Proc. Natl. Acad. Sci. USA* **1993**, *90*, 1190–1193 (review). M. Harmata, C. L. Barnes, S. R. Karra, S. Elahmad, *J. Am. Chem. Soc.* **1994**, *116*, 8392–8393. C. Valdés, U. P. Spitz, L. M. Toledo, S. W. Kubik, J. Rebek, Jr., *ibid.* **1995**, *117*, 12733–12745.

[4] Comparable repetitive Diels–Alder reactions were used in the syntheses of oxa- and methylene-bridged macrocycles and ribbon-type structures: a) F. H. Kohnke, A. M. Z. Slawin, J. F. Stoddart, D. J. Williams, *Angew. Chem.*, **1987**, *99*, 941–943; *Angew. Chem. Int. Ed. Engl.* **1987**, *26*, 892–894; P. R. Ashton, G. R. Brown, N. S. Isaacs, D. Guiffrida, F. H. Kohnke, J. P. Mathias, A. M. Z. Slawin, D. R. Smith, J. F. Stoddart, D. J. Williams, *J. Am. Chem. Soc.*, **1992**, *114*, 6330–6353; J. P. Mathias, J. F. Stoddart, *Chem. Soc. Rev.* **1992**, *21*, 215–225; P. R. Ashton, U. Girreser, D. Giuffrida, F. H. Kohnke, J. P. Mathias, F. M. Raymo, A. M. Z. Slawin, J. F. Stodart, D. J. Williams, *J. Am. Chem. Soc.*, **1993**, *115*, 5422–5429. P. R. Ashton, J. P. Mathias, J. F. Stoddart, *Synthesis* **1993**, 221–224; b) J. Benkhoff, R. Boese, F.-G. Klärner, A. E. Wigger, *Tetrahedron Lett.* **1994**, *35*, 73–76.

[5] *exo*- and *endo*-addition of norbornene and norbornadiene derivatives are surveyed and discussed in a) R. Gleiter, M. C. Böhm, *Pure Appl. Chem.* **1983**, *55*, 237–244; b) F. K. Brown, K. N. Houk, *J. Am. Chem. Soc.* **1985**, *107*, 1971–1978; c) C. G. Wipff, K. Morokuma, *Tetrahedron Lett.* **1980**, *21*, 4445–4449; d) K. N. Houk, M. N. Paddon-Row, P. Caramella, N. G. J. Rondau, *J. Am. Chem. Soc.* **1981**, *103*, 2436–2440.

[6] O. Pilet, P. Vogel, *Helv. Chim. Acta* **1981**, *64*, 2563–2570.

[7] Compound **10** was prepared in four steps starting from indene according to a procedure reported by D. N. Butler, R. A. Snow, *Can. J. Chem.* **1975**, *53*, 256–262 and simplified by M. Kamieth, Diplomarbeit, Universität Gesamthochschule Essen, **1995**.

[8] A. E. Wigger, U. Burkert, F.-G. Klärner, unpublished results.

[9] D. Hochstrate, F.-G. Klärner, *Liebigs Ann. Chem.* **1995**, 745–754.

[10] J. Benkhoff, Dissertation, Universität Gesamthochschule Essen, **1994**. The ratio of the adducts was determined after DDQ dehydrogenation of the central cyclohexene ring to a corresponding benzene ring.

[11] A considerably larger effect on the chemical shift of 1,4-dicyanobenzene ($c = 0.003$ M) is observed during complexation with the tetrasodium tertracarboxylate of **2** ($c = 0.01$ M) in water ($\delta = 7.93 \rightarrow 6.20$, $\Delta\delta = 1.73$). Presently, the association constants (K_a) are determined by the use of ^{1}H NMR titrations in which the host concentrations are varied.

[12] MacroModel V5.0: F. Mohamadi, N. G. I. Richards, W. C. Guida, R. Liskamp, M. Lipton, G. Chang, T. Hendrikson, W. C. Still, *J. Comput. Chem.* **1990**, *11*, 440–467. The complex formed between **1a** and cyclohexane is calculated in vacuum to be more stable by about 10 kcal mol^{-1} than the separated compounds with optimized geometries.

[13] At the minimum temperature of -85 °C obtained with [D_8]toluene as a solvent only specific broadening but neither coalescence nor separation of the CH_3 or CH_2 signals in the ^{1}H NMR spectrum have been observed.

[14] Examples of complex formation with small aliphatic guest molecules like methane, halogenated hydrocarbons or dichloromethane have been reported by L. Garel, J.-P. Dutasta, A. Collet, *Angew. Chem.* **1993**, *105*, 1249–1251; *Angew. Chem. Int. Ed. Engl.* **1993**, *32*, 1169–1171.

[15] M. Nishio, Y. Umezawa, M. Hirota, Y. Takeuchi, *Tetrahedron* **1995**, *51*, 8665–8699.

Systematic Separation

Principles and Practice of Modern Chromatographic Methods. By *K. Robards, P. R. Haddad*, and *P. E. Jackson*. Academic Press, London, 1994. 495 pp., hardcover £ 35.00.—ISBN 0-12-589570-4

Chromatographic methods of separation are among the most versatile and powerful tools available to the analyst, especially when combined with detectors of high sensitivity and selectivity. This is reflected in the fact that international book publishers have supplied the market with a wealth of material in this field, including both general treatments and specialist texts. So why do we need yet another book? The authors of this work aim to reach "as wide an audience as possible" ranging, for example, from analytical chemists whose knowledge does not include all the most recent developments in chromatography to scientists who work in fields other than chemistry but need analytical data from chromatography. It is also recommended that the book should be used by undergraduate students; however, this is likely to be no more than wishful thinking in view of the meager treatment of analytical chemistry in many university courses, at least in Germany. The authors have set out to provide a survey of the whole field of chromatography, including modern developments. They have succeeded in this, even though they have not been able to jettison all the unnecessary historical ballast. Inches and psi appear as units in a few places, and the retention factor k is still referred to as the capacity factor k'. On the other hand, topics such as supercritical fluid chromatography have been fully integrated into the text. (However, the less common name ethoxyethane instead of diethyl ether strikes one as curious rather than modern.)

The chapters have the following titles: 1. Introduction and Overview; 2. Theory of Chromatography; 3. Gas Chromatography; 4. Planar Chromatography; 5. High-Performance Liquid Chromatography--Instrumentation and Techniques; 6. HPLC Separations; 7. Supercritical Fluid Chromatography; 8. Sample Handling in Chromatography. HPLC occupies 150 pages, and is thus given considerably more attention than gas chromatography with only 100 pages. Electrophoretic methods are not covered at all.

The practical orientation and experience of the authors is evident in all the chapters, and the whole text is full of valuable advice. In the theoretical chapter, for example, it is pointed out that the quality of a chromatographic system is not determined solely by the resolution and the number of theoretical plates but also depends on factors such as column bleed and the activity of the column. The authors must also be commended for their clear warnings against misplaced faith in the integrity of instruments: "There is a tendency to uncritically accept the output from a computer system." The need for the analyst to use his or her experience in manually checking the data from instrumental measurements is emphasized repeatedly.

How successful have the authors been in their ambition to write an up-to-date survey? Let us take the chapter on gas chromatography as a test example. The first section discusses the carrier gas, including a reference to the pressure programming facility that is provided in some modern instruments. The section on sample introduction describes the currently used techniques, including the main possible sources of error. In accordance with modern practice, the use of a retention gap is recommended. Fourteen pages are devoted to columns, including a mention of high-temperature developments. The practical orientation of the treatment is illustrated by the fact that this section includes detailed descriptions of how to fit a column into the gas chromatograph, and of how to choose a column of the correct dimensions. The treatment of stationary phases which follows provides a good survey of the most commonly used phases. However, the section on "Special Phases" fails to mention liquid-crystalline phases. Chiral phases are included. A short section on the choice of temperature is then followed by a discussion of detectors; those covered here are TCD, FID, ECD, NPD, and FPD detectors. The reader will at first be disappointed to find no mention of other types such as mass-selective detectors, but these appear 20 pages later under "Ancillary Techniques". This section includes a miscellany of topics: derivatization techniques, pyrolysis-GC, head-space techniques, multidimensional GC, high-speed GC, GC-MS, and GC-IR. The atomic emission detector is not mentioned. The description of mass-selective detectors is limited to the detection characteristics; there is no explanation of the functioning of a quadrupole mass spectrometer or of an ion trap. Lastly, however, the authors have not forgotten to include a practically-orientated section on "Performance Tests".

The 50-page chapter on "Sample Handling" contains information that is rarely found in this form in texts on chromatography; it serves as a valuable supplement to the preceding chapters. With the exception of the microwave techniques on which there is currently much research, all the commonly used methods of sample collection and preparation are described in a clear and understandable way. The final chapter then presents eight examples of analytical applications with quantitative calculations, which are discussed in detail.

The reader who works carefully through the 500 pages of this book will gain a wealth of up-to-date knowledge about the use of chromatographic methods. This can then be followed up in greater depth through further reading in more detailed publications, guided by the comprehensive lists of references given in the book.

Jan Andersson
Anorganisch-chemisches Institut
der Universität Münster (Germany)

This section contains book reviews and a list of new books received by the editor. Book reviews are written by invitation from the editor. Suggestions for books to be reviewed and for book reviewers are welcome. Publishers should send brochures or (better) books to Dr. Illenora Beckmann, Redaktion Angewandte Chemie, Postfach 101161, D-69451 Weinheim, Federal Republic of Germany. The editor reserves the right of selecting which books will be reviewed. Uninvited books not chosen for review will not be returned.

How the understanding of self-assembly in natural systems (e.g. DNA) can be harnessed in the design of self-assembling nanostructures.

Self-Assembly in Natural and Unnatural Systems

Douglas Philp and J. Fraser Stoddart*

Although there are no fundamental factors hindering the development of nanoscale structures, there is a growing realization that "engineering down" approaches, in other words a reduction in the size of structures generated by lithographic techniques below the present lower limit of roughly 1 μm, may become impractical. It has, therefore, become increasingly clear that only by the development of a fundamental understanding of the self-assembly of large-scale biological structures, which exist and function at and beyond the nanoscale, *downwards*, and the extension of our knowledge regarding the chemical syntheses of small-scale structures *upwards*, can the gap between the promise and the reality of nanosystems be closed. This kind of construction of nanoscale structures and nanosystems represents the so-called "bottom up" or "engineering up" approach to device fabrication. Significant progress can be made in the development of nanoscience by transferring concepts found in the biological world into the chemical arena. Central to this mission is the development of simple chemical systems capable of instructing their own organization into large aggregates of molecules through their mutual recognition properties. The precise programming of these recognition events, and hence the correct assembly of the growing superstructure, relies on a fundamental understanding and the practical exploitation of non-covalent bonding interactions between and within molecules. The science of supramolecular chemistry—chemistry beyond the molecule in its very broadest sense—has started to bridge the yawning gap between molecular and macromolecular structures. By utilizing interactions as diverse as aromatic π–π stacking and metal–ligand coordination for the information source for assembly processes, chemists have, in the last decade, begun to use biological concepts such as self-assembly to construct nanoscale structures and superstructures with a variety of forms and functions. Here, we provide a flavor of how self-assembly operates in natural systems and can be harnessed in unnatural ones.

Keywords: molecular recognition · nanochemistry · nanostructures · non-covalent interactions · supramolecular chemistry

1. The Need for Nanochemistry

The creation of nanometer-scale (nanoscale) devices[1–4] has fascinated and inspired the scientific community for more than a quarter of a century. There are no fundamental thermodynamic[5] or quantum mechanical[6] impediments lying in the way of the development of very large scale integrated (VLSI), i.e. nanoscale, electronic architectures. Consequently, the electronics industry is keen to exploit the increased signal processing speeds and lower power consumption VLSI systems offer. The development of a three-dimensional array[7] of switching elements, permitting higher levels of integration, is another primary aim of the industry. These goals, however, conflict with the realization[8] that "engineering down" approaches, in other words a reduction in the size of silicon components below the present 1 μm lower limit, are impractical. For semiconductor devices, difficulties arise as a result of the failure of insulating barriers in the materials used. More specifically, the problems associated with typical insulating barriers in the 0.2 to 1 μm size range include 1) electronic cross-talk between devices as a direct consequence of electron tunneling, 2) quantum mechanical confinement of charge carriers resulting in each device having an energy spectrum dependent on its size, 3) heat dissipation, and 4) the difficulty[9] and cost of fabrication.

Hence, the possibility of "engineering up" from a molecule to functioning electronic devices has become an increasingly attractive prospect.[10–15] The activities associated with this kind of molecular engineering have become synonymous with the quest for molecular electronics. The requirements of molecular electronics demand that we not only provide molecular scale bistable devices (switches), but also the communication infrastructure (input/output) necessary to exchange information with the outside world. Moreover, the switches must be completely controllable, reversible, and readable at the molecular level.[13] It follows that the challenge to the chemist is not only to develop bistable systems (switches), but also to construct the necessary molecular architectures and machineries capable of servicing such systems. To be able to meet these challenges, the chemist must understand and apply[16] the rules of molecular self-organization, self-assembly, and self-synthesis. Fortunately, the chemist is not alone in requiring nanoscale devices. Biological systems display a diverse array of functional nanoscale

[*] Prof. J. F. Stoddart, Dr. D. Philp
School of Chemistry, University of Birmingham
Edgbaston, Birmingham B15 2TT (UK)
Fax: Int. code +(121)414-3531

structures and devices in the size range 1 to 10000 nm. These structures and arrays are constructed by the self-organization and self-assembly of molecular components, which interact chemically and physically in certain well-defined ways. Indeed, the phenomenon of self-organization may have been responsible[17, 18] for the emergence of life itself. The specificity and precision displayed by biological systems is derived from the highly directed mutual recognition displayed by the components of a structure. Clearly, the ultimate goal for the chemist seeking to match and even emulate the achievements of biological systems in creating and maintaining nanoscale structures is to control the assembly and function of synthetic structures from components with the same precision as that displayed by Nature. This objective can only be achieved by firstly understanding the principles behind the self-organization, self-assembly, and self-synthesis processes exhibited by biological systems.[19, 20]

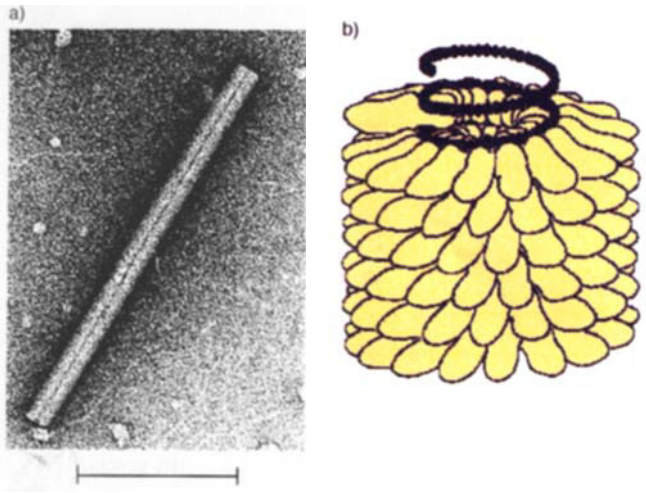

Fig. 1. The tobacco mosaic virus (TMV). a) Electron micrograph, b) schematic representation. The protein subunits are colored yellow (taken from ref. [25]).

2. Self-Assembly in Biological Systems

The tobacco mosaic virus[21] (TMV) is a helical virus particle (Fig. 1), 300 nm in length and 18 nm in diameter, whose self-assembly serves to illustrate many of the features present in self-assembling biological systems.[22–24] The viral particle is composed of 2130 identical subunits, each comprising 158 amino acids, which form a helical sheath around a single strand of RNA, 6390 base pairs (bp) in length. This information illustrates the first point about self-assembling systems—the amount of genetic information required by such structures is remarkably small. If the protein coat of TMV were coded by a single, contiguous gene, then the structure would require a section of RNA approximately 1×10^6 bp long. As 2130 identical subunits capable of self-assembling are utilized to form the protein coat, the complete structure may be coded for in a gene of around 500 bp in length—less than 8% of the total genome.

A further example of the economy in the use of genetic information may be found in the much more complex bacteriophage T4 (Fig. 2).[25] Only 53 out of a total of 135 genes contain information directly related to the construction of this apparently highly complex structure. TMV particles may be dissociated readily into their component parts and then subsequently reassembled accurately in vitro to give totally functional viral particles. In this way, the mechanism of TMV self-assembly has been investigated extensively.[24, 26–28] Under physiological

Douglas Philp was born and educated in and around Glasgow in the West of Scotland. He gained his BSc degree in 1989 from the University of Aberdeen before moving to the laboratories of J. F. Stoddart, first at the University of Sheffield and then at the University of Birmingham. He completed studies toward his PhD in 1992 with a thesis entitled "Self-Assembly in Chemical Systems". He was a Royal Society European Science Exchange Programme Postdoctoral Fellow in the laboratories of Professor François Diederich (ETH, Zürich) before returning to the University of Birmingham in 1994 to take up his current post as a Lecturer in Physical Organic Chemistry. His current research interests focus on the development of self-assembling and self-replicating structures and the application of computational methods in chemistry.

D. Philp

J. F. Stoddart

J. Fraser Stoddart was born and educated in and around Edinburgh in the East of Scotland. He has been Professor of Organic Chemistry at the University of Birmingham since 1990. He was appointed Head of the School of Chemistry there in 1993. Previously, he was a Reader in Chemistry at the University of Sheffield for eight years, where he was also Lecturer from 1970 to 1982. From 1978 to 1981 he was seconded from the University of Sheffield to the ICI Corporate Laboratory in Runcorn. He gained his BSc in 1964, his PhD in 1966, and his DSc in 1980, all from the University of Edinburgh. He was elected to the Fellowship of the Royal Society of London in 1994. He has received many awards, including the International Izatt-Christensen Award in Macrocyclic Chemistry in 1993, and has been a distinguished lecturer in many universities worldwide. Professor Stoddart has published more than 400 communications, papers, reviews, and monographs and has wide-ranging interests in supramolecular science. He is at present developing the transfer of concepts such as self-assembly between the life sciences and materials science.

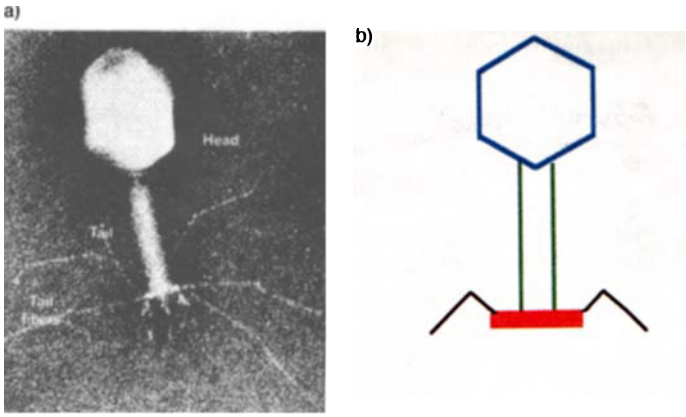

Fig. 2. The bacteriophage T4. a) Electron micrograph (taken from ref. [25]), b) schematic representation. The head is colored blue, the tail green, the base plate red, and the tail fibers black.

conditions[24, 26] the protein subunits form a disk-shaped subassembly (Fig. 3a), which is transformed into a helical form (Fig. 3b) by insertion of a loop of RNA into the central hole of the protein disk. Additional protein disks, each corresponding to two turns of the final helix, associate with the growing viral particle (Fig. 3c and d) until assembly is complete. The association of individual subunits into the disk subassembly through noncovalent interactions permits the overall construction process to be dynamic, that is, at or close to equilibrium. As a result, assembly and disassembly of protein subunits is a facile event and the overall self-assembly process is intrinsically error-checking and self-correcting.

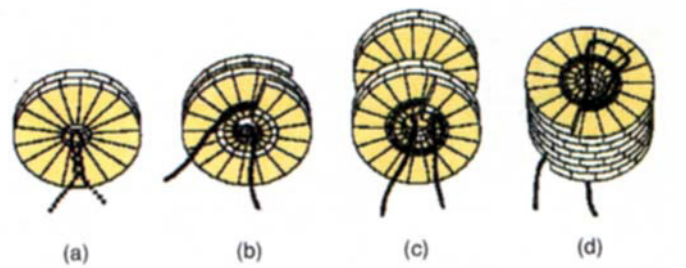

Fig. 3. The self-assembly of the tobacco mosaic virus (taken from ref. [25]).

The assembly of TMV demonstrates the ability of biological systems to construct large, ordered molecular and supramolecular arrays from small, relatively simple subunits by a mechanism of self-assembly. Such processes are responsible for the wide diversity of structure and function observed at both the cellular and subcellular levels in Nature. The evolution of self-assembly pathways in natural systems can be rationalized in terms of the selective advantages conferred upon organisms that utilize such synthetic routes. The common feature of all biological self-assembly processes is the ability to take advantage of many, weak noncovalent interactions between preformed subunits or well-defined subassemblies to guide the formation of a structure. These noncovalent interactions are also responsible for the stability of the final structure. Since self-assembly involves the intermediacy of many weak and reversible interactions, the final structure formed represents a thermodynamic minimum for the system. In addition, owing to the dynamic nature of the assembly process, defective or incorrectly attached subunits are eliminated from the growing structure, ensuring high overall fidelity in the assembly of the final structure. The modular nature of self-assembly processes (Fig. 4), involving the construction of

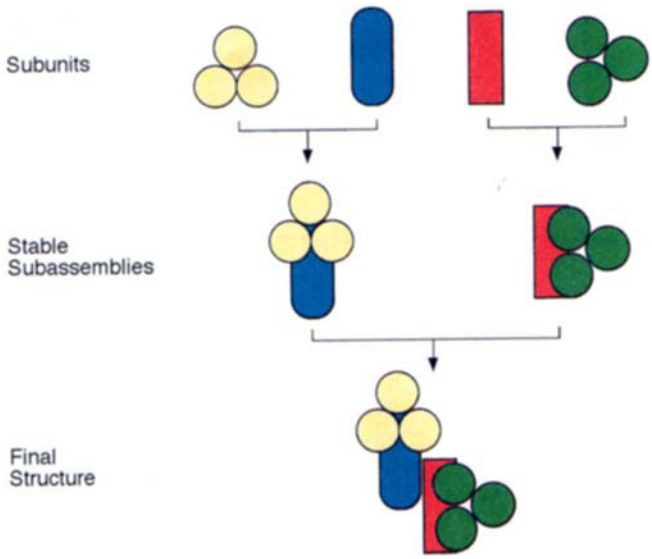

Fig. 4. The modular and convergent nature of biological self-assembly. Subunits aggregate to form stable subassemblies, which in turn form the final structure.

stable subassemblies, which are then carried forward into the final structure, permits great synthetic efficiency; in chemical terms, the synthesis of the final structure is *highly convergent*.[29, 30] The use of several identical subunits within a structure also requires that only a limited set of binding interactions is necessary to form the structure correctly, minimizing the amount of information needed to describe the structure fully. In summary, biological self-assembly processes require assembling subunits to display complementarity in geometric shape and surface electronic properties. The result of this complementarity is a structure stabilized by many, relatively weak, noncovalent bonding interactions, which may be shape-dependent (van der Waals/hydrophobic), or directed (hydrogen bonds/electrostatic interactions), distributed over the whole molecular volume, rather than limited to a few strong, localized covalent bonds. In biological systems, self-assembly pathways utilize both self-assembly in isolation and in harness with the formation of covalent bonds. For these reasons, self-assembly processes fall into two distinct categories, namely strict self-assembly and self-assembly with covalent modification.

2.1. Strict Self-Assembly

The term "strict self-assembly" applies to pathways that produce a final product directly and spontaneously when the correct components are mixed under appropriate conditions. The pathway must be completely reversible and the product should be stable at thermodynamic equilibrium. In addition, the constituent components of the final structure must contain all of the information necessary for correct assembly to occur.

The self-assembly of the DNA double helix from two complementary oligonucleotides is perhaps the most well-known and intensively studied biological paradigm of strict self-assembly. As such, it illustrates many of the salient features of biological self-assembly and, in addition, highlights some of the difficulties associated with the study of self-assembly. An idealized picture of DNA assembly is the contact and recognition of one oligonucleotide strand by another, followed by the propagation of the growing helix by the matching of complementary base pairs. Dynamic assembly and disassembly allow the recovery of the structure from errors in base matching, ultimately leading to correct registration between the two strands, and hence the most stable structure, at thermodynamic equilibrium. In practice, the situation is complicated somewhat by the formation of loops and hairpins, by hydrodynamic effects, and by interstrand penetration.[31] Studies of the nucleic acids $(A)_{17}$ and $(U)_{17}$ have shown that the self-assembly of the double helix is essentially an all-or-nothing process (Fig. 5):[32-34] a certain number

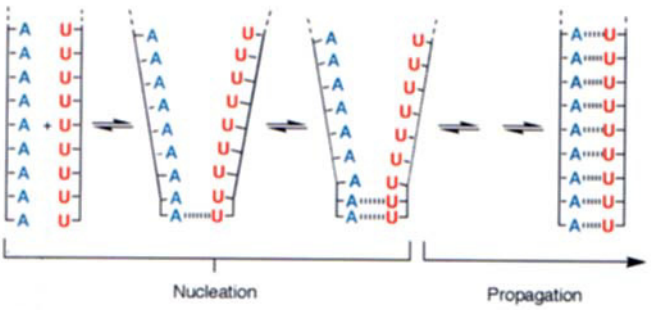

Fig. 5. Nucleation and propagation in nucleic acid self-assembly.

of base pairs are required to form before double helix assembly will occur, but once this particular point is reached, only the fully formed double helix will result. The double helix nucleation structure is believed to consist of three to four base pairs.[32, 34] In terms of its free energy,[35] the formation of a nucleus is unfavorable (Fig. 6). However, additional base pairs formed after nucleation make a large and negative contribution to the overall free energy of double helix formation. Thus, double helix growth proceeds *cooperatively*; base pairing occurs repeatedly, promoting further base pairing until double helix

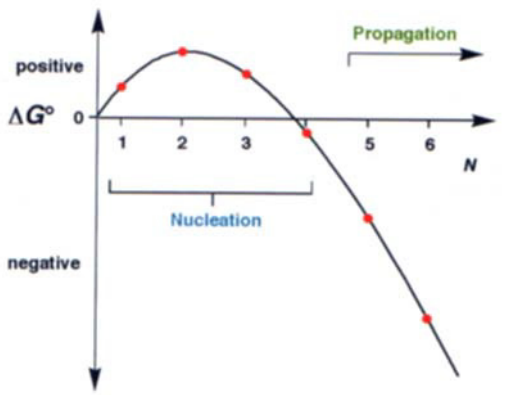

Fig. 6. Free energy profile for the self-assembly of the DNA double helix (adapted from ref. [19]). N = number of base pairs formed.

formation is complete. This pattern of events illustrates a key concept in self-assembly processes: the numerous favorable interactions that occur during the growth of a superstructure can easily overcome the initial unfavorable equilibrium. The favorable noncovalent interactions make up for the entropic price paid to associate the two strands of DNA in solution. Hence, the assembly of a large structure incorporating many noncovalent bonds will be relatively easier than the formation of a small structure incorporating only a few noncovalent bonds.

The study of the folding of ribonuclease, a 124 residue protein containing eight cysteine residues, provides another example of the self-assembly of a thermodynamically stable structure. Native ribonuclease can be reductively denatured[37] to give a random structure carrying eight cysteine SH groups (Fig. 7). When

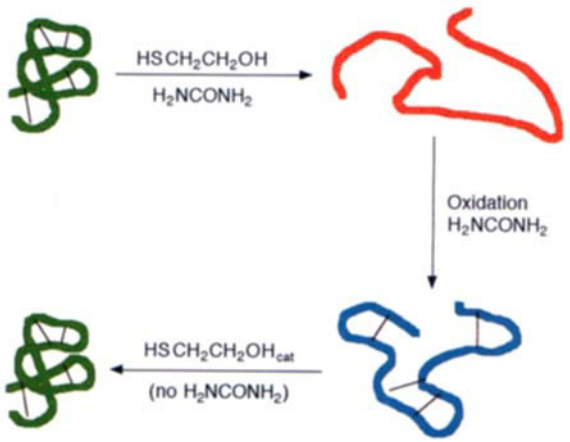

Fig. 7. The folding of ribonuclease. The native structure is colored green, the completely unfolded structure red, and one of the many isomeric, incorrectly folded structures blue.

the protein is reoxidized in the presence of urea (a denaturant), a large number of isomeric disulfide-bonded protein structures are formed. This mixture is essentially enzymatically inactive. Removal of the urea and addition of a catalytic amount of 2-sulfanylethanol, which facilitates disulfide exchange, rapidly regenerates the native structure. These observations demonstrate that, at least in the case of ribonuclease, the native protein structure, under physiological conditions, occupies an energy minimum,[37, 38] and that all of the information necessary for the correct folding of the protein lies in its primary amino acid sequence.

2.2. Self-Assembly with Covalent Modification

Although the folding of ribonuclease could be regarded as an example of self-assembly followed by covalent modification, this category of self-assembly is normally reserved for processes in which the formation of covalent linkages within an assembly is irrevocable and irreversible. Biological self-assembly processes displaying these characteristics fall into three classes:

1. *Precursor Processing*. The preparation of subunits for self-assembly by the covalent processing (Fig. 8) of precursor molecules, or formative processing,[39] is widespread in biological

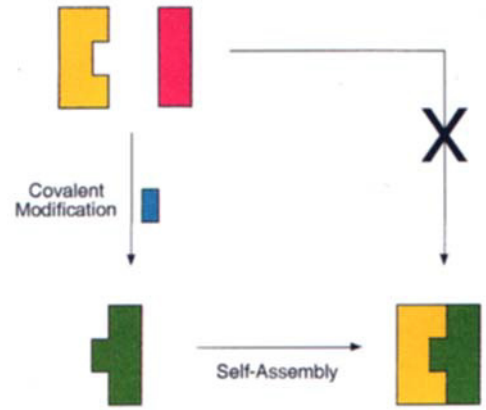

Fig. 8. Structure generation by covalent modification followed by self-assembly. The two subunits (yellow and purple) cannot associate until a covalent modification is performed on one of these subunits (purple to green).

systems. The activation of microtubule assembly by the covalent attachment of GTP to tubulin[40] is an example of such a system (Fig. 9). Microtubules are filamentous assemblies responsible

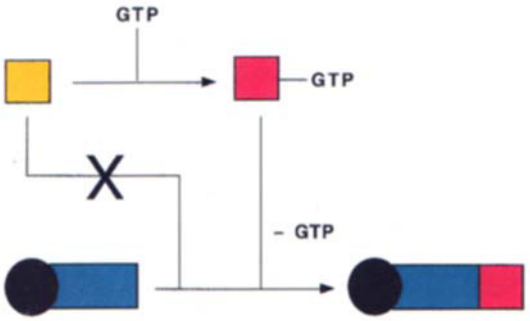

Fig. 9. Microtubule self-assembly. The tubulin subunit (yellow) must be activated by GTP to give an active complex (purple) before it can add to the growing microtubule (blue).

for the movement of vesicles, cellular organelles, and chromosomes (during cell division) through the cytoplasm of the cell. Microtubules are composed of a helical array of alternating protein subunits known as α and β tubulin. They are approximately 250 Å in diameter and of highly variable length. Most microtubules undergo rapid assembly and disassembly from structures known as centrosomes. It transpires that α and β tubulin will only add to the end of the growing chain of the microtubule if they are covalently bound to GTP. The native proteins are completely inactive in promoting the self-assembly process.

2. *Post-Assembly Processing*. Insulin is a mammalian peptide hormone consisting of two covalently linked polypeptide chains—the A chain composed of 21 amino acid residues and the B chain composed of 30 residues. These two chains are linked by two disulfide bridges. Reductive cleavage of these bridges, followed by reoxidation of the tetrathiol does *not* give rise to the native protein; in other words, the two short polypeptide chains do not by themselves contain enough information to assemble correctly the native protein structure. Insulin is, in fact, synthesized by two posttranslational processing steps carried out on a much larger polypeptide, preproinsulin (Fig. 10).[36, 38]

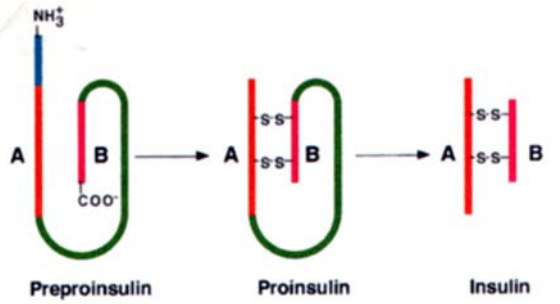

Fig. 10. The posttranslational processing of preproinsulin to form the active hormone, insulin. The signal section is colored blue, the connecting peptide, green.

After cleavage of the signal section, which is used to guide the nascent polypeptide to the correct location within the endoplasmic reticulum, proinsulin is cleaved at two sites in the Golgi complex to give the active hormone in which the A and B chains are linked appropriately by the two disulfide bridges. The generation of insulin from proinsulin serves two functions: firstly, it ensures the correct folding of the protein to form the active tertiary structure, a feat the A and B chains cannot accomplish on their own, and secondly, it permits the storage of insulin as a physiologically inactive precursor.

Self-splicing and self-cleaving RNA structures[41-46] are perhaps the most remarkable examples of post-assembly processing in the biological world. Short stretches of RNA found in a wide range of organisms are capable of performing catalytic processing of themselves after the initial assembly of their structure. The Lucerne Transient Streak Virusoid (LTSV) is a covalently closed loop of RNA, 324 base pairs in length, which infects plant cells. The virus replicates by a "rolling circle mechanism" (Fig. 11). This mechanism requires that the monomeric RNA

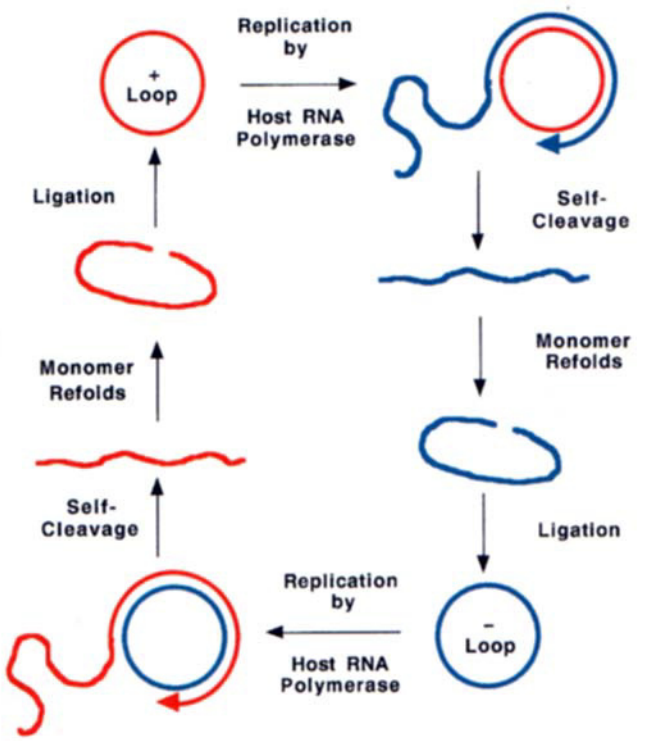

Fig. 11. LTSV replication by a rolling circle mechanism demonstrating catalytic self-excision of RNA strands. The blue loop is capable of cleaving the red polymeric genome into appropriately sized fragments and vice versa.

strand is excised from the growing polymeric RNA molecule produced by this mechanism. Since no cellular enzyme exists to perform this task, and the viral genome is too small to code for such an enzyme, the RNA molecule itself must perform it. In fact, very short strands of LTSV RNA, around 50 base pairs in length, are capable of excising accurately the required monomeric RNA in vitro. Although this remarkable feat of self-assembly followed by self-modification is poorly understood, it is thought to rely upon the catalytic properties of the three-dimensional surface structure of RNA. In essence, RNA is acting as an enzyme. The short stretches of RNA capable of performing this feat have highly conserved sequences, indicating that a sequence-specific three-dimensional structure is involved.

3. *Self-Assembly with Intermittent Processing.* The alternation of self-assembly with pre-assembly or post-assembly covalent processing of subunits or stable subassemblies permits very precise control of the order of events within a biosynthetic pathway. This class of self-assembly is really a fusion of the previous two classes, but offers such fine control over the structure of the final product that it must be considered separately. The best understood examples of this class of self-assembly process are bacteriophage morphogenesis[47] and ribosome assembly.[48] The assembly of ribosomes has been studied extensively in vitro (Fig. 12). It was shown by Nomura in 1968 that a fully functional 30S subunit could be reconstituted in vitro from its constituents, 16S RNA and 21 proteins. The 50S subunit can also be reconstituted in vitro from its constituents, 5S RNA, 23S RNA, and 34 proteins. The significance of these observations is that the assembly of the ribosome must be a self-assembly process; in other words, the components of the ribosome contain all of the information necessary to construct a functional ribosome. In addition, studies on the 30S subunit have shown conclusively that the process occurs in a specific order. A stable intermediate containing the 16S RNA and 15 proteins is isolable when the reconstitution is carried out at 0 °C. It can be converted to a functional 30S subunit by adding the missing proteins and heating to 40 °C. A similar intermediate, containing the two RNAs and 20 of the 34 proteins, is also found in the aggregation of the 50S subunit. This highly programmed assembly route allows the complex ribosomal structure to be assembled with great precision and efficiency.

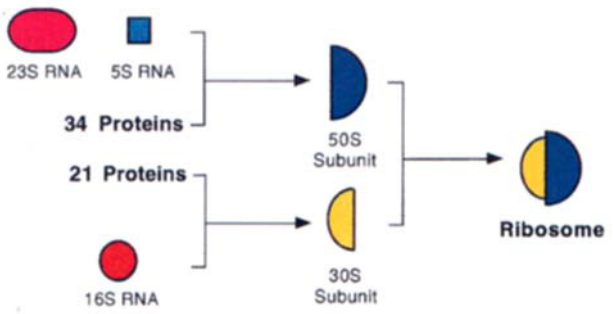

Fig. 12. The self-assembly pathway followed in the construction of a ribosome.

2.3. Lessons to be Learned from Biological Systems

Biological systems point the way forward to chemical systems capable of employing the advantages offered by synthetic routes incorporating self-assembly. The stunning diversity of structure and function found in biological systems, which rely on self-assembly for their genesis, display four common themes for synthetic chemists to exploit:

- Self-assembly processes are economical by virtue of their high convergence.
- Stable, structurally diverse assemblies can be rapidly, accurately, and efficiently synthesized from relatively simple subunits.
- The use of identical subunits within an assembly enables the lexicon of interactions employed to be kept to a minimum, economizing on the amount of information required to describe a structure.
- Molecular recognition by means of many, weak noncovalent bonding interactions leads to a dynamic, reversible, and "intelligent" synthetic pathway, which is self-checking and self-correcting and affords a product representing a thermodynamic minimum.

3. A New Approach to Chemical Synthesis

The science of organic synthesis[29, 30] has, until the present time, been concerned with the construction of assemblies of atoms by the controlled, selective, and sequential formation of covalent bonds. This approach to the generation of large structures has led to syntheses of relatively large molecules such as vitamin B_{12}[49, 50] and palytoxin.[51] The advantages of sequential covalent bond forming techniques lie in their ability to produce arrays of covalently linked atoms in a well-defined and controlled manner. The relative energies of the products may be located far from the global thermodynamic minimum for a particular collection of atoms in a molecule. It follows that the investment of time and manpower necessary to construct assemblies on a nanometer-scale using such an approach must be viewed as prohibitive.[52] Therefore, to construct nanoscale structures, the synthetic chemist must look to novel concepts and new approaches in the search for efficient methods of generating compounds with the desired order and dimensions.[53–58] We can envisage several such approaches:[20]

1. *Covalent Polymerization.* The repetitive reaction of a simple, chemical entity (monomer) with itself under appropriate conditions can give rise to a very large single molecule (polymer). Although this process affords structures that are large in chemical terms ($M_r > 10^5$ Da), the primary molecular constitution is simple and repetitive, and hence this process has limited potential for the controlled generation[59] of three-dimensional structures. Although polymers can produce nanoscale structures as a result of their physical properties, for example phase separation,[60, 61] the approach is limited by the lack of understanding, except in a few cases,[62] of the rules that govern the noncovalent bonding interactions within such polymer systems.

2. *Noncovalent Polymerization or Self-Organization.* Highly organized structures may be formed when many identical mole-

cules aggregate as a direct result of noncovalent bonding interactions. Noncovalent polymerization or self-organization gives rise to a wide variety of supramolecular architectures. Liquid crystals,[63] micelles,[64] monolayers at air–water[65, 66] or air–solid interfaces,[67–69] bilayers,[70] and Langmuir–Blodgett films[71–73] may all be constructed in this manner. However, since the molecules organize themselves, the final structure represents a thermodynamic minimum over which the chemist has only indirect control. Therefore, although self-organization can produce structures of nanometer scale, its application,[74] in isolation from other techniques,[75] is limited by the lack of any precise control.

3. *Self-Assembly*. Biological systems construct and modify functioning nanoscale structures with startling efficiency. It seems logical, therefore, that self-assembly should be the strategy of choice for synthetic chemists wishing to construct nanoscale assemblies. This realization means that the chemist must develop a synthetic regime incorporating the lessons learned from Nature (Fig. 13). In the first instance, sequential

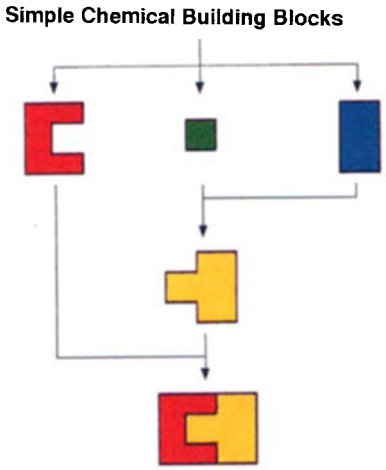

Fig. 13. Synthetic strategy based on self-assembly: conversion of simple building blocks, which can assemble, into complex chemical entities.

covalent synthesis (conventional organic synthesis) has to be used to create subunits which, by relying upon noncovalent bonds, can aggregate with themselves or other synthetic subunits to afford stable, structurally defined supramolecular assemblies. Of paramount importance to this approach is an understanding of the nature of the noncovalent bonding interactions responsible for stabilizing the final assembly. In energy terms, noncovalent bonding interactions are generally several orders of magnitude weaker than covalent bonds. This fundamental feature of bonding means that large areas of complementary surface must be present in the final assemblies in order for them to form stable entities. In addition, the favorable interactions within the superstructure must be sufficient to overcome the entropic penalty that has to be paid for the organization of the assembly's components into an ordered state. Understanding the interactions between noncovalently bonded molecules is crucial to the successful design and synthesis of self-assembling, wholly synthetic structures. Thus, the science of supramolecular[76] or host–guest[77] chemistry is ideally placed to contribute to achieving this goal.

4. Self-Assembly in Chemical Systems

The development of supramolecular or host–guest chemistry in the 29 years since Pederson's discovery[78] of the crown ethers resulted in a diverse array of supramolecular structures. It is not intended in this review to undertake a comprehensive treatment of this field; for this, the reader is directed to numerous reviews[79] and monographs.[80] The number of papers published on self-assembly and self-organization in chemical systems has grown from around 170 in the period 1985 to 1989 to well over 1000 in the period 1990 to 1995. Therefore, in this review, the discussion is limited to an overview of the various types of interactions used by the chemist to create large molecular arrays and how they may be applied to the self-assembly of nanostructures. The reader is directed to the references for a more complete, but still not comprehensive, record of the achievements of chemists in the field of self-assembly.

4.1. Cyclodextrins

The cyclodextrins (CDs) are a series of cyclic oligosaccharides consisting of six or more α-1,4-linked D-glucopyranose rings (Fig. 14).[81, 82] The cyclodextrins are named according to the

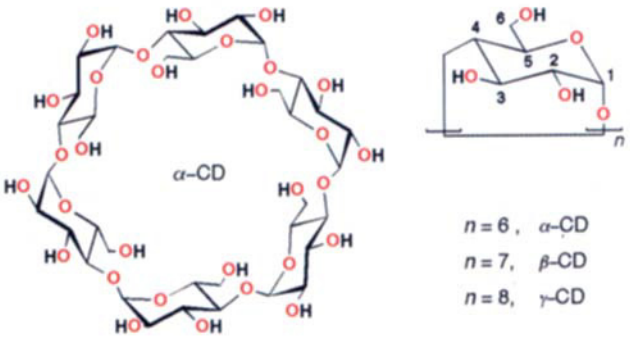

Fig. 14. The chemical structure of the cyclodextrins.

number of glucopyranose rings present: α-CD has six, β-CD has seven, and γ-CD has eight. The most immediately apparent structural feature of the smaller cyclodextrins is the rigid, well-defined cavity resulting from the overall bucket-shape of the molecules (Fig. 15). The open top of the bucket is encircled by the secondary hydroxyl groups at the C2 and C3 positions of the

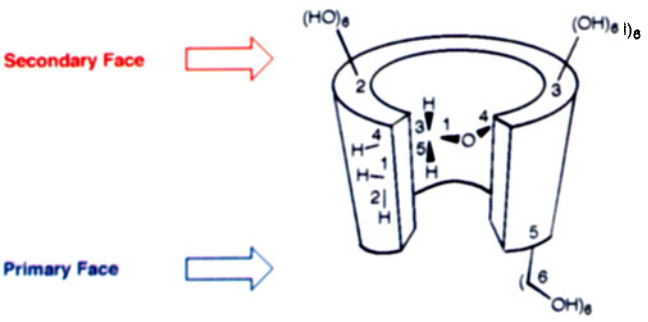

Fig. 15. The gross structure of α-CD.

glucopyranose residues, and the bottom of the bucket is encircled by the primary hydroxyl groups at C6. The interior of the bucket is lined with the oxygen atoms associated with the glycosidic linkages and the hydrogen atoms located at the C3 and C5 positions on the glucose residues. The rigid, relatively hydrophobic cavity of the cyclodextrins gives rise to their voracious appetite for molecular guests of all types. In all cases some part of the guest is bound within the cavity of the cyclodextrin. The precise nature of the binding interactions involved has been the subject of much debate.[81, 83–85] The principal binding interaction in a cyclodextrin–guest complex is most likely a summation of several relatively weak effects, for example van der Waals interactions, hydrophobic binding,[86] and the release of "high-energy water"[81] from the cavity. The contribution from each effect depends on the cyclodextrin, the solvent, and the guest.

Cyclodextrins have been known since 1891, and the first detailed description of their isolation was published in 1903 by Schardinger.[87] Since then, these naturally occurring molecular receptors have been exploited in many ways. Cramer[88] demonstrated that cyclodextrins can form inclusion complexes with a wide variety of substrates. This property was exploited by Bender in his seminal work on enzyme mimics.[89] Their role as catalysts has been further extended and utilized by both Tabushi[90] and Breslow.[91] Cyclodextrins have also been employed as second-sphere ligands in transition metal complexes.[92] Recently, however, the focus of cyclodextrin research has shifted towards their use as ready-made components for the construction of nanoscale structures through self-assembly.[93] The propensity of cyclodextrins to form strong complexes in aqueous solutions with many different types of guests has led to their development as building blocks in the construction of nanoscale devices.

Rotaxanes[94] are a class of molecules in which a dumbbell-shaped component is encircled by a macrocycle; the two components are linked mechanically rather than by a covalent bond. A generally accepted method for the synthesis of rotaxanes is *threading* (Fig. 16).[57] This approach takes advantage of the

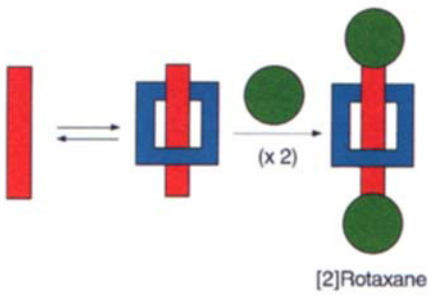

Fig. 16. Schematic representation of the synthesis of a [2]rotaxane by threading.

noncovalent bonding interactions between the rodlike portion of the dumbbell component and a macrocycle. The complex formed between these two species can then be modified with blocking groups to produce the [2]rotaxane. (The prefix [2] indicates the number of mechanically linked components within the molecule.) Clearly, it should be possible to construct rotaxanes by taking advantage of the promiscuous binding properties of cyclodextrins toward guest species of many types. The successful synthesis of a [2]rotaxane, which exploited the binding of α,ω-diaminoalkanes by either α-CD or β-CD, was first reported back in 1981 by Ogino and co-workers.[95] Treatment of such a diaminoalkane with a cyclodextrin yields an inclusion complex, which, after reaction with the cobalt complex $[CoCl_2(en)_2]$ (en = ethylenediamine), yields the [2]rotaxane (Fig. 17). The

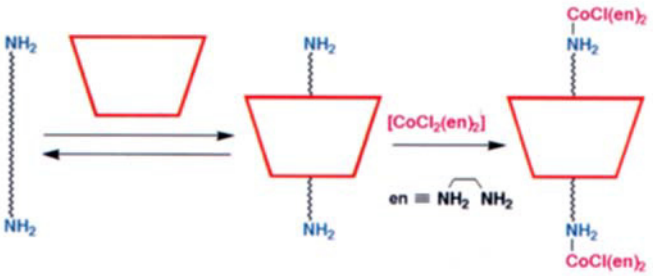

Fig. 17. Cyclodextrin rotaxanes constructed from α,ω-diaminoalkanes and cobalt-based blocking groups synthesized by Ogino and co-workers [95].

terminal metal complexes are apparently too large to permit decomplexation of the diaminoalkane from the cyclodextrin. The concept of utilizing cyclodextrins and metal complexes in the self-assembly of [2]rotaxanes has been described more recently by Wylie and Macartney.[96] In this instance, however, the order of addition of the components—α-CD, 1,1″-(α,ω-alkanediyl)bis(4,4′-pyridylpyridinium) dibromide **1**, and the pentacyanoferrate(II) salt—is unimportant (Fig. 18). Addition of solid $Na_3[Fe(CN)_5NH_3]\cdot 3H_2O$ to an aqueous solution of the [**1**·α-CD] complex results in rapid formation of the [2]rotaxane **2**. This reaction is demonstrated by the appearance of a metal-to-ligand charge transfer transition in the visible spectrum and the appearance of two sets of ligand proton resonances in the ^{1}H NMR spectrum—a direct result of the end-to-end asymme-

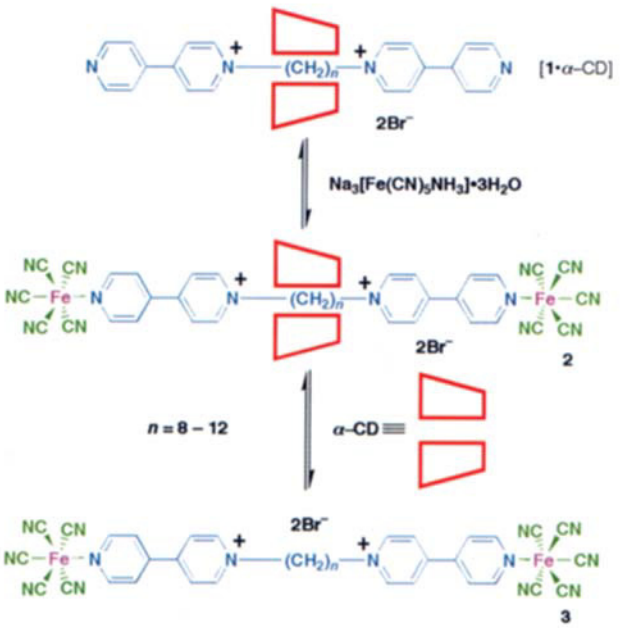

Fig. 18. The cyclodextrin-based [2]rotaxane synthesized by Macartney and co-workers.

try imposed on **1** by the trapped α-CD ring. The [2]rotaxane is also formed by the addition of α-CD to a solution of the bridged dimeric iron complex **3**. This result infers a slow dissociation of the terminal pentacyanoferrate(II) complex, followed by formation of an intermediate semirotaxane, and capping of the free pyridine ligand by reassociation of the pentacyanoferrate(II) complex. The inclusion of the dication within the cavity of α-CD enhances the stability of the coordinate bond between the terminal pyridine ring and the pentacyanoferrate(II) end group. This dissociation precludes the description of this system as a true rotaxane, since the degree of mechanical blocking of dissociation by the terminal groups of the complex is uncertain. It is more appropriate to describe such systems as pseudorotaxanes.[97]

Rao and Lawrence have constructed a "threaded molecular loop" from the bisammonium salt **4** and per-2,6-dimethyl-β-cyclodextrin (DMβ-CD) **5** (Fig. 19).[98] Addition of sodium tetraphenylborate to a solution of the [**4**·**5**] complex results in the precipitation of the [2]rotaxane **6** in 71% yield. ^{1}H and ^{13}C NMR spectroscopic studies confirm the composition of the product. Although FABMS, unsurprisingly, shows only fragment ions, the product **6** can be chromatographed unchanged on cellulose. It is unclear, however, whether the tetraphenylborate anions act as true blocking groups in the [2]rotaxane or simply as counterions. Since ammonium tetraphenylborate salts exist principally as solvent-separated ion pairs in polar solvents,[99] it seems likely that the primary stabilization in the [2]rotaxane **6** is derived from the interaction of **4** and **5**, with little or no contribution from the mechanical capping of the chain termini.

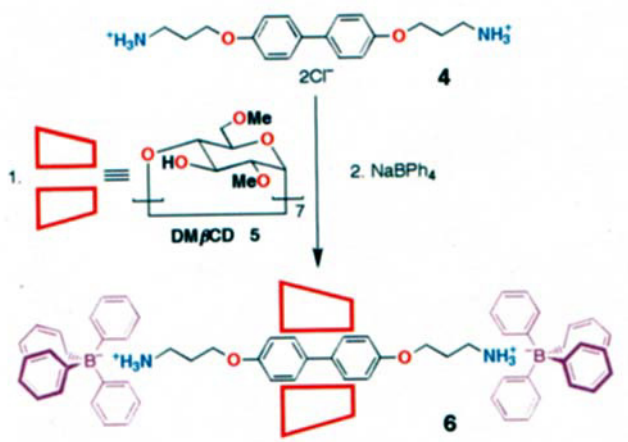

Fig. 19. The threaded molecular loop based on DMβ-CD described by Lawrence and co-workers.

The self-assembly of [2]rotaxanes containing cyclodextrins and covalently attached blocking groups has been reported recently by two research groups. Isnin and Kaifer have demonstrated the self-assembly of asymmetric zwitterionic [2]-rotaxanes incorporating α-CD.[100] Alkyl(ferrocenylethyl)dimethylammonium salts can interact with both α-CD and β-CD (Fig. 20). Termination of the alkyl chain with a carboxylate group provides an attachment point for a blocking group. Although the binding of **7** and **8** by α-CD is pH dependent (K_a(**7**) = 425 M^{-1} (pH 2.6), 71 M^{-1} (pH 8.0)), both are bound in water, and treatment of the complexes [**7**·α-CD] and [**8**·α-CD] with potassium 5-amino-2-naphthalenesulfonate and one equivalent of the coupling reagent 1-ethyl-3-[3-(dimethylamino)-propyl]carbodiimide hydrochloride (EDC) afforded the isomeric zwitterionic [2]rotaxanes **9a** and **10a**, and **9b** and **10b**, respectively. The isomers were separated[101] and the relative orientation of the α-CD component on the asymmetric dumbbell-shaped component of each isomer ascertained. Surprisingly, **9a** and **10a** are stable, whereas their isomers, **9b** and **10b**, unthread slowly.

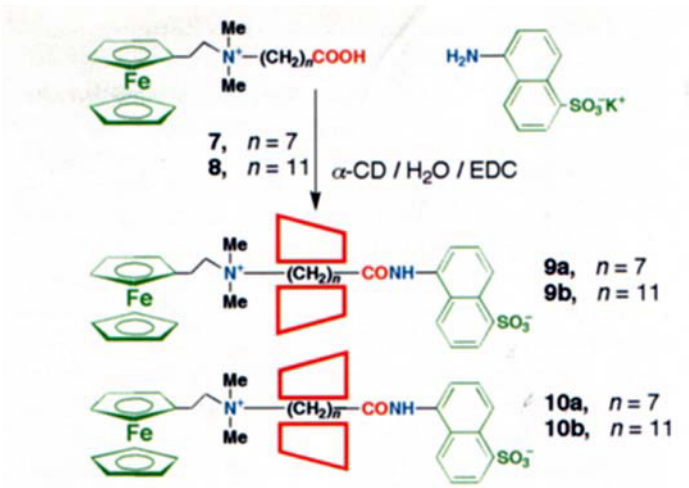

Fig. 20. Isomeric zwitterionic [2]rotaxanes based on α-CD synthesized by Kaifer and Isnin.

Wenz and co-workers[102] have utilized inverse recognition logic to self-assemble a lipophilic [2]rotaxane. Instead of using a hydrophilic cyclodextrin to bind a hydrophobic guest, they designed a lipophilic cyclodextrin that can bind cationic guests in inert organic solvents.[102] Thus, heptakis(3-*O*-acetyl-2,6-di-*O*-butyl)-β-cyclodextrin **11** (Fig. 21) was ob-

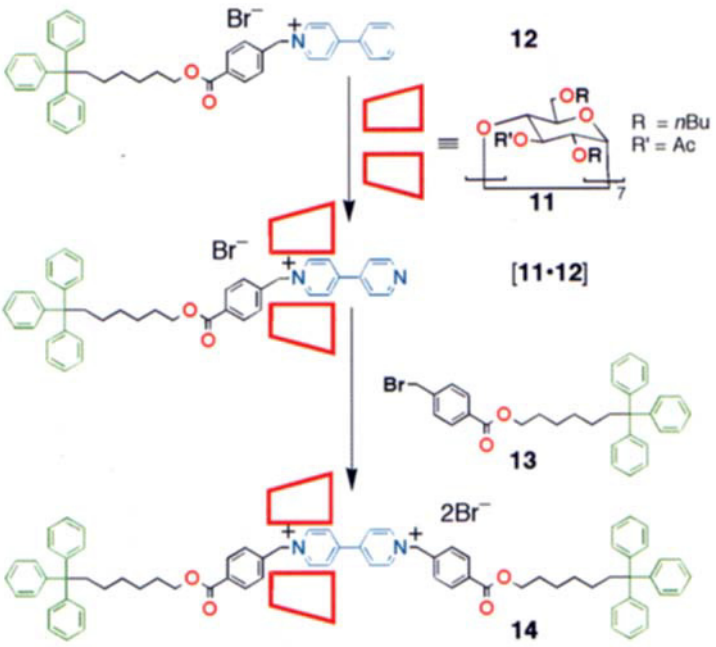

Fig. 21. A lipophilic [2]rotaxane incorporating a chemically modified CD constructed by Wenz and co-workers.

tained by chemical modification of β-CD. The pyridylpyridinium salt **12** was synthesized in nine steps from triphenylmethane. The binding of **12** within the cavity of **11** was demonstrated by ^{1}H NMR spectroscopy, and the association constant was found to be 450 M^{-1} in CD_3CN. The benzylic bromide **13** could then be used to cap the end of complex [**11**·**12**] (Fig. 21). This process affords the [2]rotaxane **14** in 20% yield. The ^{252}Cf plasma desorption mass spectrum of **14** shows a clear molecular ion at m/z 3293 for the intact [2]rotaxane. The ^{1}H NMR spectrum demonstrates that the C_7 symmetry of the cyclic host is maintained in **14**. However, the resonances corresponding to the two CH_2N^+ groups display different signal patterns, one appearing as an AB system and the other as a singlet, illustrating end-to-end asymmetry within the [2]rotaxane.

Polyrotaxanes containing CDs have also been described.[103] Harada and co-workers have reported a polyrotaxane based on poly(ethylene glycol) diamine (PEG-DA) **15**.[104] Polyethylene glycol is known to form an inclusion complex with α-CD.[104] Hence, reaction of 2,4-dinitrofluorobenzene **16** with **15** in DMF solution saturated with α-CD yielded, after extensive purification, the polyrotaxane **17** in 60% yield (Fig. 22). The molecular

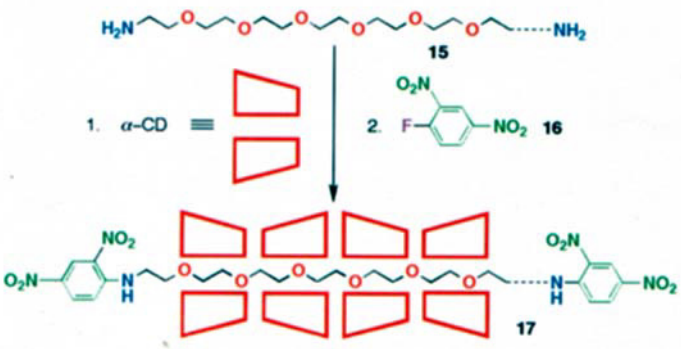

Fig. 22. An α-CD-based polyrotaxane synthesized by Harada and co-workers.

mass of **17** is in the region of 25000 Da, commensurate with the trapping of approximately 22 α-CD beads on the dumbbells. In more recent work Harada et al. have demonstrated the use of a polyrotaxane as a template for the synthesis of a tubular polymer.[105] When the hydroxyl groups of α-cyclodextrin, threaded on to a poly(ethylene glycol) backbone of mass 1450 Da, were allowed to react with epichlorohydrin, the cyclodextrin tori became linked together. Cleavage of the blocking groups with strong base resulted in long tubelike structures with an average molecular mass of 20000 Da.

Wenz and Keller have threaded α-CD with the poly(iminomethylene) chains **18a** and **18b** (Fig. 23).[106] Treatment of **18a** with α-CD gave a product whose ^{1}H NMR spectrum did not change after two hours, whereas the analogous reaction with **18b** required 170 hours to reach equilibrium. The long reaction times are consistent with a stepwise incorporation of the α-CD units: each CD ring must find a chain terminus, and the existing threaded α-CD molecules must shuffle toward the center of the polymer chain to make room for the new rings. Nonspecific reaction of the threaded polymer chain with nicotinyl chloride is expected to trap the CD rings located between the two nicotinamide units on the polymer backbone. This modification should produce a heterogeneous polymer with varying numbers

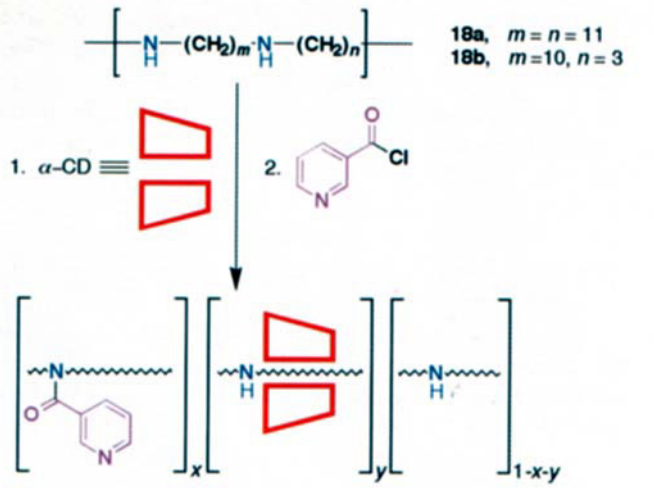

Fig. 23. The α-CD polyrotaxane of Wenz and Keller.

of nicotinyl groups (x), threaded CDs (y), and free polyiminomethylene regions ($1-x-y$) (Fig. 23). Analysis of the product from reaction of [**18b**·(α-CD)$_n$] with nicotinyl chloride revealed a polyrotaxane with a weight-averaged molecular weight of 55000 ± 5000 Da obtained by laser light scattering. The polyrotaxane isolated was shown to possess a degree of polymerization of 55 ± 5 and 37 α-CD rings permanently threaded on to the polymer chain.

The use of CDs as building blocks for the self-assembly of complex molecular architectures has not been restricted to the synthesis of rotaxanes. Lawrence and co-workers have prepared a heme-dependent protein mimic from a tetraarylporphyrin and DMβ-CD by self-assembly (Fig. 24).[107] The protonated te-

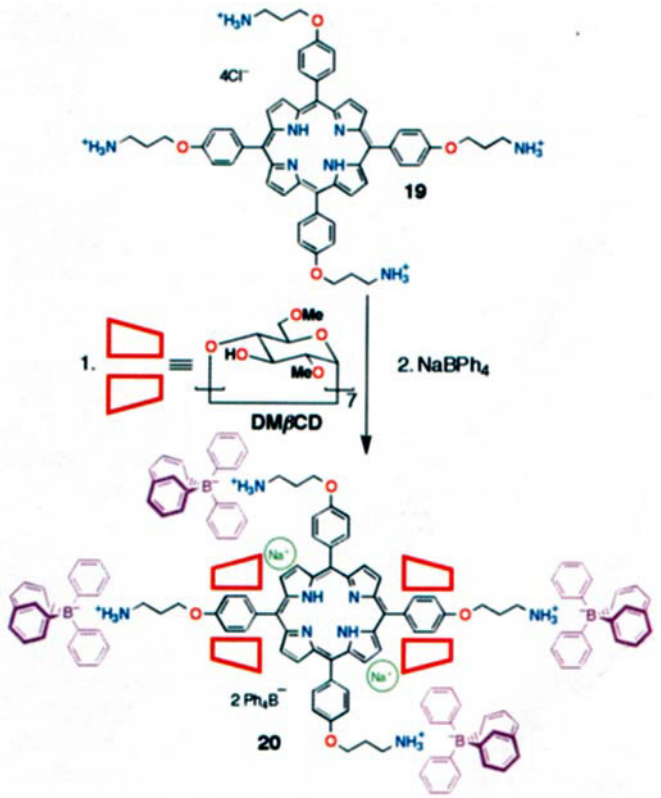

Fig. 24. A self-assembled heme-dependent protein mimic from the group of Lawrence.

traaminoporphyrin **19** forms an inclusion complex on exposure to a tenfold excess of DMβ-CD in aqueous solution at pH 6. The formation of this complex is supported by both a shift in the Soret absorption band of the tetraammonium porphyrin from 444 to 418 nm, and by upfield shifts of the signals for the H3 and H5 protons of DMβ-CD in the ^{1}H NMR spectrum of the complex. The complex is precipitated from aqueous solution by the addition of sodium tetraphenylborate. The precipitation procedure also leads to the incorporation of two Na^+ ions into the structure, which can be removed by complexation with [18]crown-6. Overall, the complete assembly contains eleven components—six tetraphenylborate ions, two Na^+ ions, two DMβ-CDs, and a tetraarylporphyrin—and has a molecular mass of >5000 Da. However, the kinetic stability of this assembly is unlikely to be high since the ammonium tetraphenylborate ion-pairs used as blocking groups are solvent separated[99] in polar solvents.

The synthesis of interlocked or catenated molecules, the catenanes,[108] has fascinated and inspired many scientists for more than 75 years.[109–111] The efficient synthesis of such systems, which has eluded chemists until recently, requires that one ring be threaded by the precursor of the second ring, and that this assembly be held together as the second ring is formed. In other words, one macrocycle must act as a template for the formation of the second macrocycle (Fig. 25). This requirement can be

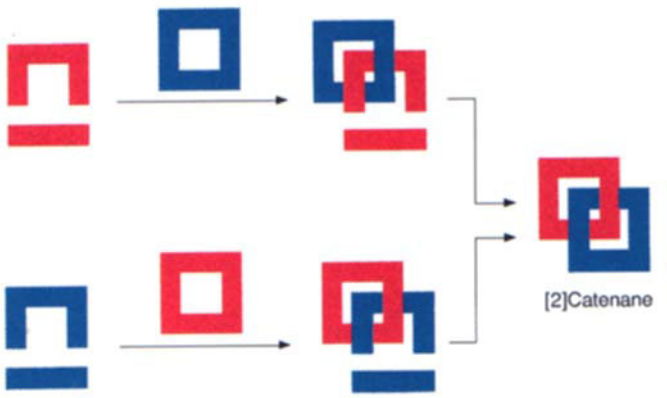

Fig. 25. The assembly of [2]catenanes by different routes. The red ring may be constructed by using the blue ring as the template (top) or vice versa.

fulfilled most easily by exploiting noncovalent bonding between the assembling molecular components. In the first published account of an attempt to synthesize a catenane in 1958, Lüttringhaus, Cramer, Prinzbach, and Henglein[112] endeavored to make use of the weak, noncovalent bonding interaction between α-CD and a series of aromatic guests bearing thiol-terminated alkyloxy substituents. After macrocyclization by oxidative coupling of the thiol groups, they hoped to obtain a catenated α-CD. Although this early attempt was unsuccessful, a number of CD catenanes have now finally been synthesized.[113] DMβ-CD in D_2O binds strongly the diamine **21** incorporating a bitolyl group (Fig. 26). The reaction of **21** with terephthaloyl chloride at 5 °C in 0.01 N NaOH solution in the presence of DMβ-CD affords a mixture of [2]- and [3]catenanes. The [2]catenanes **22** and **23** are produced yields of 3 and 0.8%, respectively, whilst the isomeric [3]catenanes **24a** and **24b** are

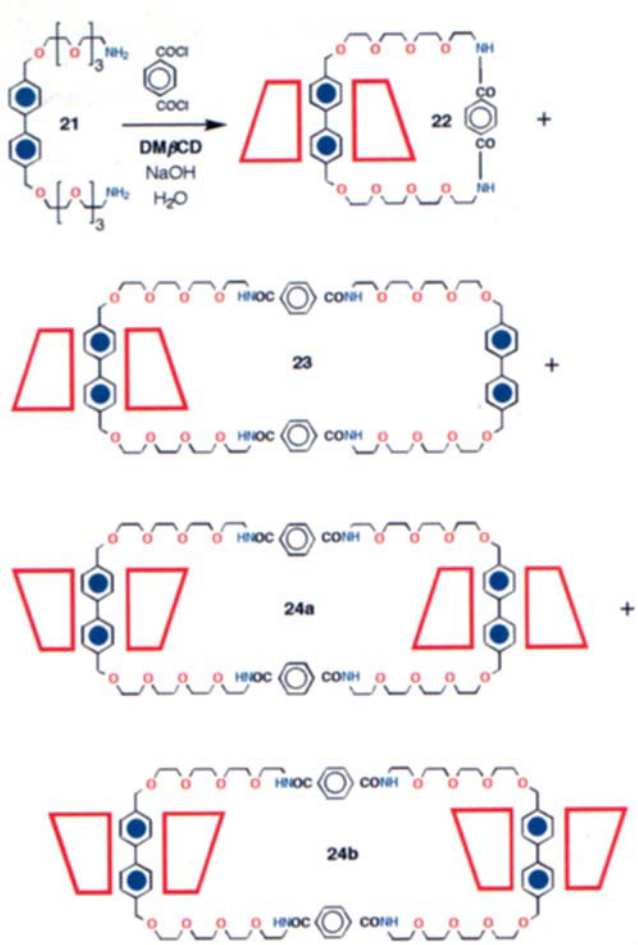

Fig. 26. The first successful synthesis of a series of CD-containing catenanes (facing red quadrilaterals: DMβ-CD).

obtained as an equimolar mixture in 1.1% yield.[114] ^{13}C NMR spectroscopy was used to assign head-to-head or head-to-tail structures to these isomers. The low yields of the catenanes, when compared with the somewhat higher yields for the uncatenated, macrocyclic oligoamides (12% for the bisamide macrocycle and 3% for the tetraamide macrocycle), suggest that the DMβ-CD may be inhibiting the macrocyclizations leading to the catenated species. The single-crystal X-ray structure of **22** reveals that the bitolyl unit is included within the cavity of the CD. Surprisingly, no hydrogen bonding interactions are apparent between the macrocyclic bisamide and the CD torus.

The range of self-assembled structures that can be constructed by utilizing the binding affinities of CDs for very different guests is wide. However, the interaction of CDs with their substrates, although strong, is not directional in other than a general sense. In the next two sections we will highlight the use of noncovalent bonding interactions that are much more directional.

4.2. The Hydrogen Bond

The highly selective and directional nature of the hydrogen bond makes it ideal for use in the construction and stabilization of large noncovalently linked molecular and supramolecular

architectures. Indeed, the biological world is replete with examples of such systems: DNA and protein tertiary structures are amongst the most obvious examples. Hydrogen bonds are formed when a donor (D) with an available acidic hydrogen atom is brought into intimate contact (i.e. a separation less than the sum of the appropriate van der Waals radii) with an acceptor (A) carrying available nonbonding lone pairs of electrons (Fig. 27). Many theoretical approaches to understanding the

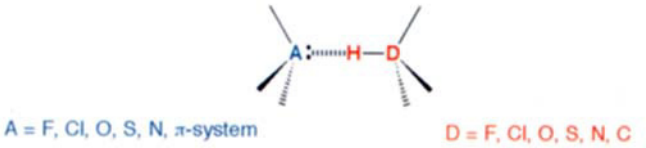

Fig. 27. A hydrogen bond formed between an acidic hydrogen atom (hydrogen bond donor **D** in red) and an appropriate acceptor (**A** in blue).

nature of the hydrogen bond have been advanced,[115] but none are wholly satisfactory in explaining all of the properties of the hydrogen bond. Most likely it involves the summation of several contributions, whereby the importance of each contribution depends on the precise nature of the system involved (Fig. 28). The strength of hydrogen bonds[116] can vary between 1 kcal mol^{-1} for D–H$\cdots\pi$ interactions to 13 kcal mol^{-1} for the Cl–H$\cdots$Cl$^-$ interaction. The geometry of the hydrogen bonds has been studied extensively both by statistical[117] and by X-ray diffraction methods.[118–120] The reader is referred to the literature[121] for a comprehensive survey. Based on X-ray diffraction analyses, certain rules have been proposed for the assembly of superstructures arising from the formation of hydrogen bonds within a system,[122] although many factors influence the nature of the final superstructure.

The use of hydrogen bonding networks to control molecular architectures in the solid state has been exploited by a number of research groups.[92, 123] Etter illustrated the utility of the hydrogen bond as a design element in solid-state organic chemistry.[124] The hydrogen bond directed cocrystallization of diarylureas[125] and acyclic imides[126] with a wide variety of compounds allows the formulation of general rules about the hydrogen bond driven molecular recognition within these molecules. In addition, cocrystallization can be utilized in the investigation of the hydrogen bond preferences of a single compound.[127] 2-Aminopyrimidine **25** (Fig. 29) has two equivalent hydrogen bond donors and two equivalent acceptors. The crystal structure[128] of **25** shows that all donors and acceptors are used in forming continuous chains of hydrogen bonds. However, the addition of either carboxylic acids or dicarboxylic acids can produce four distinct heteromeric structural motifs, depending on the nature of the added carboxylic acid. From the crystal stoichiometries and the patterns shown in Figure 29, rules for hydrogen bond donor and acceptor preferences in this system have been derived.[127]

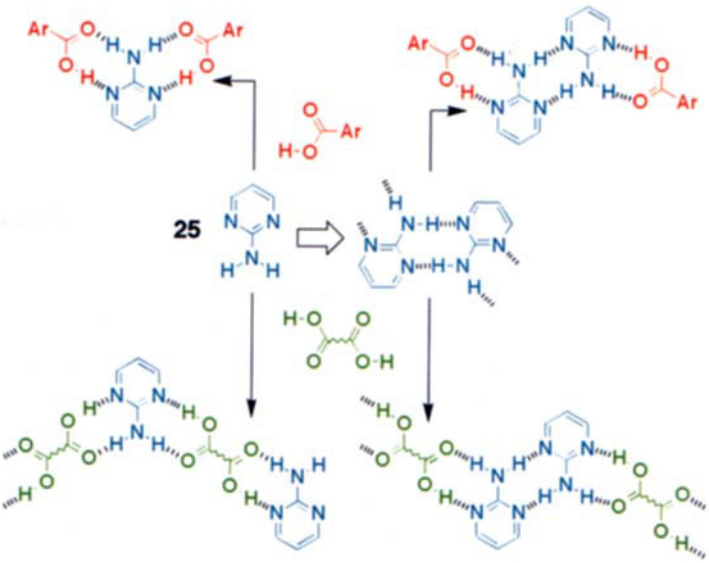

Fig. 29. Cocrystals formed between 2-aminopyrimidine (blue) and carboxylic acids (red) and diacids (green).

The assembly of long-range solid-state superstructures from simple building blocks directed by hydrogen bond formation has been exploited by Wuest et al.[129–131] The observation[129, 130] that the pyridone dimer can be used to control molecular aggregation led to the design and synthesis of the "tecton" **26** (Fig. 30), which contains a rigid tetraarylmethane core with pyridone units held rigidly at a fixed distance from the core.[131] Crystallization of **26** from a mixture of butyric acid, methanol, and hexane yielded crystals of approximate composition **26**·2C_3H_7COOH. X-ray structural analysis of this crystalline material revealed that the tecton had undergone hydrogen bond directed assembly to form an interpenetrating diamondoid network (Fig. 30), in which the voids are filled by the butyric acid molecules and the interpenetrating networks.[132] Crystallization with different carboxylic acids, for example propionic acid, has given similar results.

Hamilton and co-workers[133] have also demonstrated the controlled assembly of solid-state superstructures, resembling molecular sheets, that rely upon hydrogen bonds. Interestingly, they have

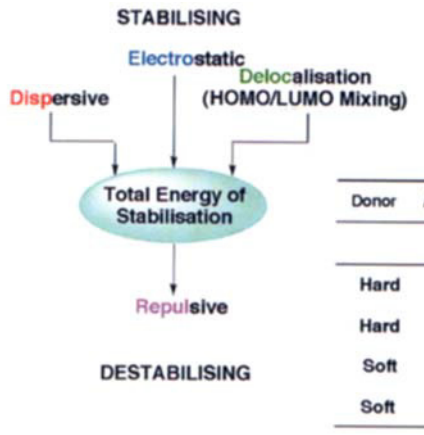

Donor	Acceptor	Interaction Type			
		Electro	Deloc	Disp	Repul
Hard	Hard	++	+/–	–	Similar for all types
Hard	Soft	–	+	+	
Soft	Hard	+	–	–	
Soft	Soft	–	+	+	

Fig. 28. The relative contributions of various types of interactions to the overall strength of a hydrogen bond (table adapted from ref. [261]).

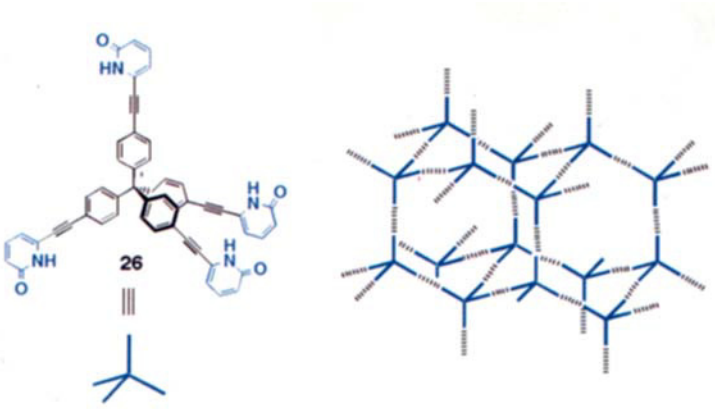

Fig. 30. An interpenetrating diamondoid network arising from hydrogen-bonded tectons (blue) based on the molecular recognition between pyridones.

shown that a conformational change produced by protonation can lead to the self-assembly of solid-state superstructures.[134] 2,6-Diamidopyridine **27** has a parallel arrangement of hydrogen bond donors and acceptors in its free base form (Fig. 31). Protonation at the pyridine nitrogen atom pro-

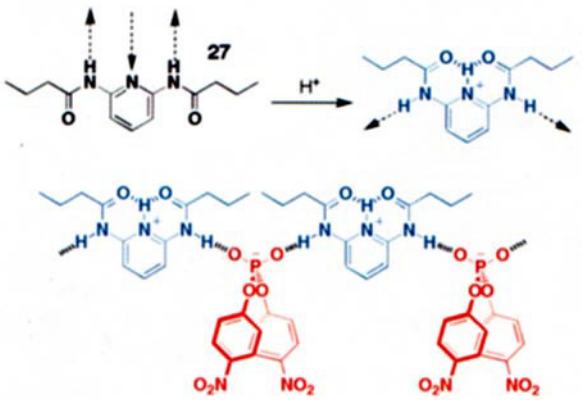

Fig. 31. A conformational change brought about by protonation permits hydrogen bond directed self-assembly to occur.

duces a conformational change: the amide carbonyl oxygen atoms form intramolecular hydrogen bonds and the amide protons are directed outwards. In this conformation, the pyridinium ion can form continuous hydrogen bonded chains with its diaryl phosphate counterions in the solid state (Fig. 31). Hamilton and co-workers have also transferred their design into solution, where (2 + 2) aggregates stablized by a network of hydrogen bonds have been self-assembled successfully.[135] Moreover, they have demonstrated that the aggregation of simple dicarboxylic acids in the solid state is controlled by hydrogen bonding.[136] Six molecules of an appropriately functionalized isophthalic acid form a hexameric aggregate which is stabilized by twelve hydrogen bonds. Hydrogen bonding can also be used to create rodlike structures in the solid state. Crystallization of triamide **28** (Fig. 32) from CH_2Cl_2 and MeOH results in the growth of large rod-shaped crystals up to 1 cm in length![137] X-ray diffraction analysis demonstrates that the triamide molecules form stacks which are stabilized by hydrogen bonds between the three amide NH groups of one molecule and the amide CO groups of the next molecule in the stack.

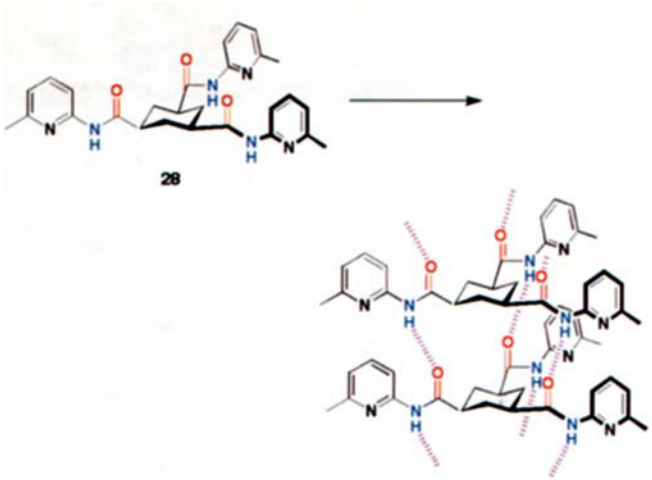

Fig. 32. The hydrogen bond directed self-assembly of molecular rods through hydrogen bonding between amide groups.

Lehn et al.[138] have employed complementary components for the self-assembly of highly ordered strands in the solid state. Cocrystallization of the barbituric acid derivative **29** with the 2,4,6-triaminopyrimidine **30** gives rise to continuous hydrogen-bonded strands (Fig. 33),[138] in which the **A** groups attached to

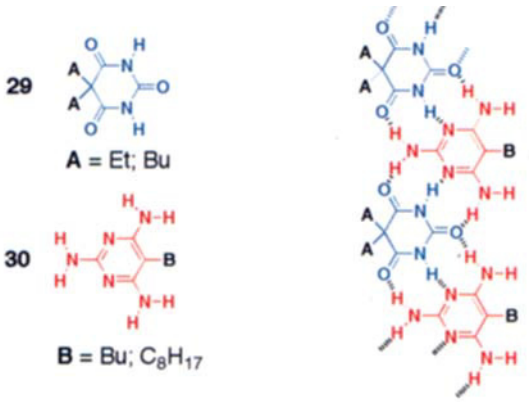

Fig. 33. Cocrystallization of barbituric acid derivatives with triaminopyrimidines forms segregated strands in the solid state through hydrogen bonding.

the barbituric acid nuclei and the **B** groups attached to the triaminopyrimidine nuclei are on opposite sides of the major axis of the hydrogen-bonded strands. The arrangment of side chains could confer specific properties on the cocrystal at the macroscopic level. Such systems open the way for the construction of designed crystal structures for specific applications.

Whitesides and co-workers[139–143] have exploited the strong, multiply hydrogen-bonded lattice formed between cyanuric acid **31** and melamine **32** to construct large, nanometer-scale structures in solution[139, 140] and to direct the assembly of structures in the solid state.[141, 142] Reaction of **31** with **32** gives the insoluble 1:1 complex [**31**·**32**] shown in Figure 34. The linking of three melamine units to a central hub ***H*** (Fig. 35) affords molecule **33**, which is conformationally compatible with the cyanuric acid/melamine lattice. Thus, mixing **33** with three molar equivalents of the alkyl cyanuric acid **34** gives the extremely stable 3:1 complex **35** in $CDCl_3$ solution, which contains one layer of the basic structure of the cyanuric acid/melamine lattice

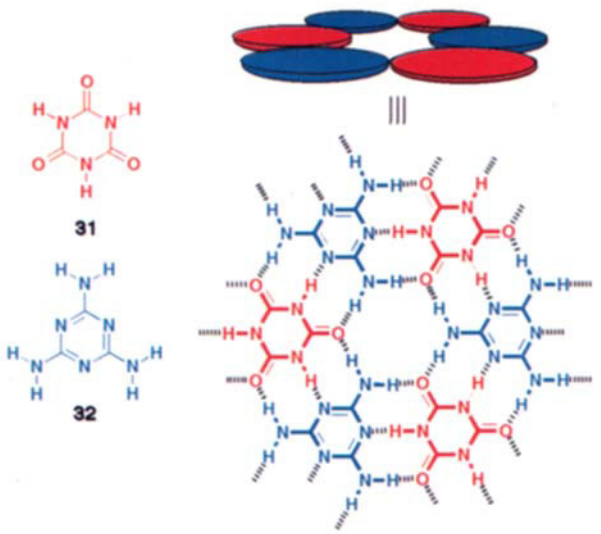

Fig. 34. The stable hexagonal lattice formed between cyanuric acid and melamine.

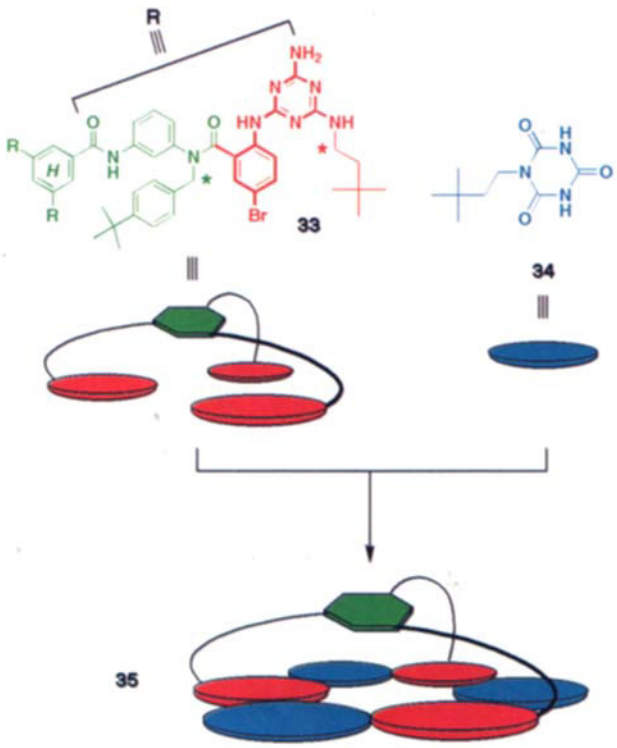

Fig. 35. The hexagonal cyanuric acid/melamine lattice can be transferred into solution. The 3:1 complex between the cyanuric acid derivative (blue) and the hub, which tethers three melamine units, is stabilized by 18 hydrogen bonds.

capped by the trisubstituted benzene hub ***H***. ^{1}H NMR spectroscopy confirms the proposed structure of the 3:1 complex. The two imide NH protons of **33** are in different hydrogen bonding environments and so give rise to separate signals in **35**. In addition, two of the methylene groups of **33** (marked by * in Fig. 35) become diastereotopic in the 3:1 complex, and hence each methylene group gives rise to two separate signals in the ^{1}H NMR spectrum of **35**. NOESY experiments provide further support for the proposed structure. Vapor pressure osmometry (VPO) gives a molecular mass for the species in solution of 2720 Da (c = 2–16 mM), in close agreement with the calculated value of 2733 Da for **35**. The high stability of the complex is a result of two factors: the conformational compatibility of the melamine trimer with the cyanuric acid/melamine lattice, and the preorganization of **33**, namely the connection of the three melamine units to a central aromatic hub ***H***. In subsequent research, Whitesides and co-workers have shown that a bis(cyanuric acid) derivative can aggregate with **33** to form a 3:2 complex of molecular mass > 5500 Da, which incorporates two layers of the cyanuric acid/melamine lattice.[142] Interestingly, cyanuric acid also forms a 1:1 cocrystal with biuret (cyanuric acid is the decomposition product of biuret), which is stabilized by chains of hydrogen bonds running in two directions throughout the crystal lattice.[144] The construction of even larger aggregates is possible using this approach.[145] Mixing the core **36**, containing nine melamine subunits, with an appropriate quantity of the substituted cyanuric acid **37** results in the formation of a single conformation of the decamolecular aggregate **38** (Fig. 36). However, it has not proved possible to deduce by

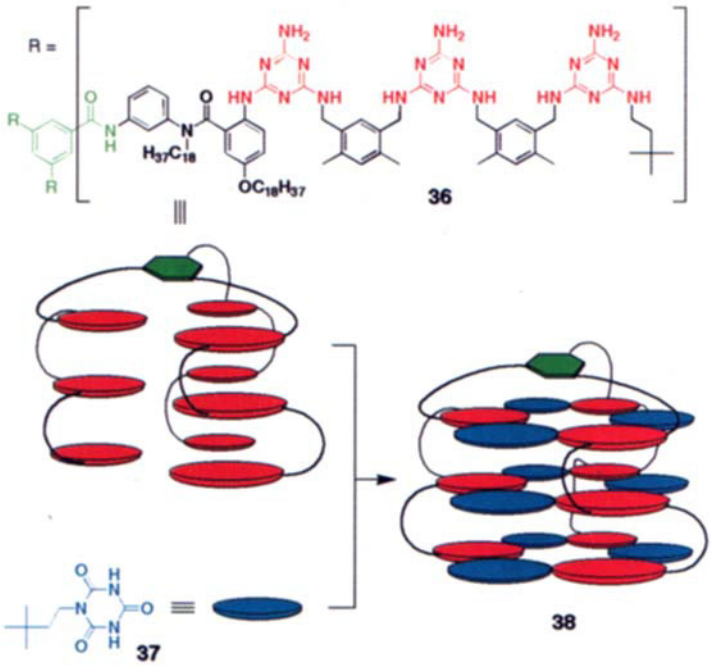

Fig. 36. A triple-decker version of the hexagonal cyanuric acid/melamine lattice can be transferred into solution. The 9:1 complex between cyanuric acid derivative (blue) and the hub, which tethers the melamine units, is stabilized by 54 hydrogen bonds.

NMR spectroscopy which of the many possible conformations is thermodynamically favored and observed. The aggregate **38** contains three layers of the cyanuric acid/melamine lattice, is stabilized by 54 hydrogen bonds, and has a molecular mass in excess of 6000 Da. The successful self-assembly of ten molecules into a single well-defined aggregate, which is stable in solution, demonstrates clearly the power of approaches based on self-assembly for the construction of nanoscale architectures.

Wyler, de Mendoza, and Rebek[146] have extended the range of architectures that have been constructed by hydrogen bond directed self-assembly with the construction of a molecular tennis ball. Molecule **39**, based on diphenylglycouril, is self-complementary and self-associates in solution through the formation of eight hydrogen bonds to form a dimer having an internal cavity (Fig. 37). This dimeric structure is remarkably stable,

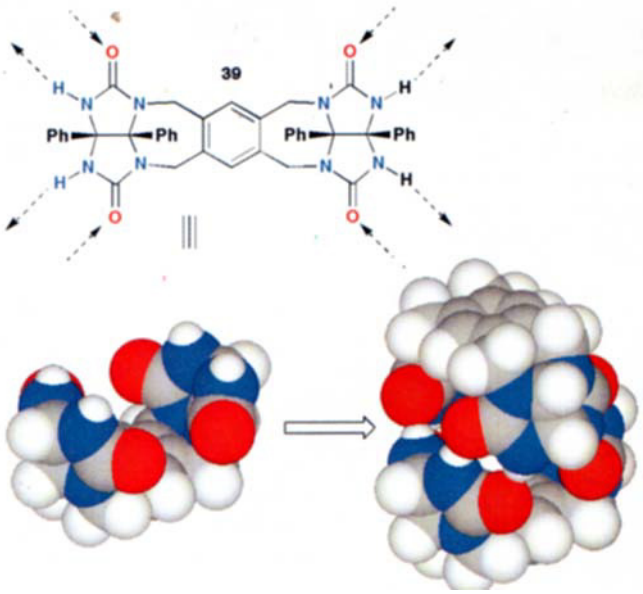

Fig. 37. Self-association of the cyclic bis(urea) derivative through eight hydrogen bonds gives a structure that resembles a tennis ball. The phenyl rings have been omitted from the space-filling representations for clarity.

persisting in $CDCl_3$ containing up to 20% CD_3SOCD_3. The encapsulation of small molecules within these self-assembled cavities has been demonstrated in this system and in others.[147]

Molecular recognition driven by hydrogen bonding can also be used to effect a phase change within a system. Lehn and co-workers have demonstrated the formation of a liquid-crystalline polymer, which is derived from the association of two complementary ditopic components through hydrogen bonds.[148] Mixing equimolar amounts of the complementary, nonmesogenic components **40** and **41** results in the formation of the hydrogen-bonded polymer **42** (Fig. 38), which displays liquid-crystalline behavior from $<25\,^{\circ}C$ up to $200\,^{\circ}C$. The formation of the liquid-crystalline polymer is largely unaffected by the stereochemistry of the components (both the DL and *meso* forms of **40** and **41** give thermotropic mesophases), but the internal

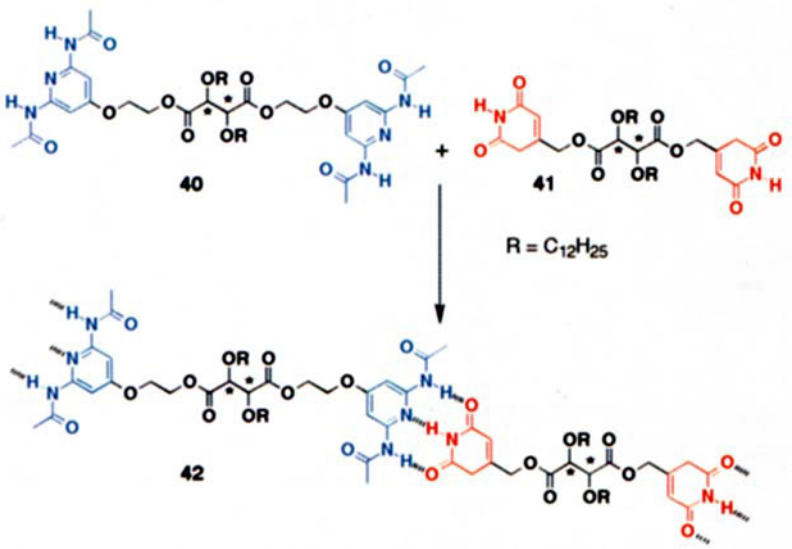

Fig. 38. The formation of a thermotropic liquid crystal by hydrogen bond directed molecular recognition. Compounds **40** and **41** have either DL or *meso* configurations.

structures of the mesophases formed by the stereoisomeric pairs are vastly different. Thus, this system illustrates how the process of self-assembly, through molecular recognition directed by hydrogen bonding, can lead to drastic changes in the physical properties of the system. The formation of a macroscopic mesophase is an expression of microscopic molecular recognition at a macroscopic level. Other systems in which molecular recognition at the microscopic level is manifest in macroscopic physical properties have been reported.[149]

Ghadiri and co-workers have reported the self-assembly of a remarkable series of nanoscale tubules based on cyclic peptides.[150] The basic design utilizes a cyclic peptide whose primary sequence consists of alternating D- and L-amino acids (Fig. 39). Such peptides possess flat "donutlike" conformations in solution. This conformation promotes the face-to-face association of the cyclic peptides into nanoscale tubules, which are stabilized along their length by hydrogen bonding interactions between the amide groups in the peptide backbone. Depending on the conditions, such peptides can be assembled into highly ordered aggregates of nanotubes in the solid state or into transmembrane pores.

Receptors that can catalyze bond-making reactions by forming a superstructure, which converts an intermolecular reaction into an intramolecular one, that is, an artificial enzyme, have been the focus of research by many groups. Kelly et al.[151] have reported the design and synthesis of a "bisubstrate reaction template" **43**, which is capable of a sixfold acceleration in the reaction between the benzylic bromide **44** and the amine **45** (Fig. 40). This rate acceleration is a result of the ability of **43** to bind the two reaction substrates through a network of hydrogen bonds and hold them in place while reaction occurs. The two binding sites in **43** are identical and thus many unproductive ternary complexes may form. Severe product inhibition could also be anticipated in this system since the product will be bound to **43** by no less than six hydrogen bonds. Fortuitously, however, the product precipitates as its HBr salt and is thus removed from the reaction mixture, ensuring at least a modest turnover in the catalytic cycle. The efficacy of this system can be improved by modification of the receptor **43** to reduce the number of nonproductive complexes formed. This goal has been achieved by modification of the right-hand binding site in **43**, resulting in a 12-fold rate enhancement in the second-generation system.[152]

The bisubstrate reaction template described by Kelly et al. is a general case of a catalytic system based on a ternary complex. In such systems two reaction channels exist: an uncatalyzed bimolecular reaction and a catalyzed ternary reaction. When the reaction product can serve as a template for its own formation and, in addition, is capable of conserving and expressing its structure, then the reaction is termed a *self-replication process*. Examples of self-replication have been observed in the nonenzymatic ligation of nucleotides,[153] as demonstrated by the research groups led by von Kiedrowski[154–156] and Orgel.[157, 158]

Minimal models of self-replication in wholly synthetic systems, based on the model shown schematically in Figure 41, have also appeared recently.

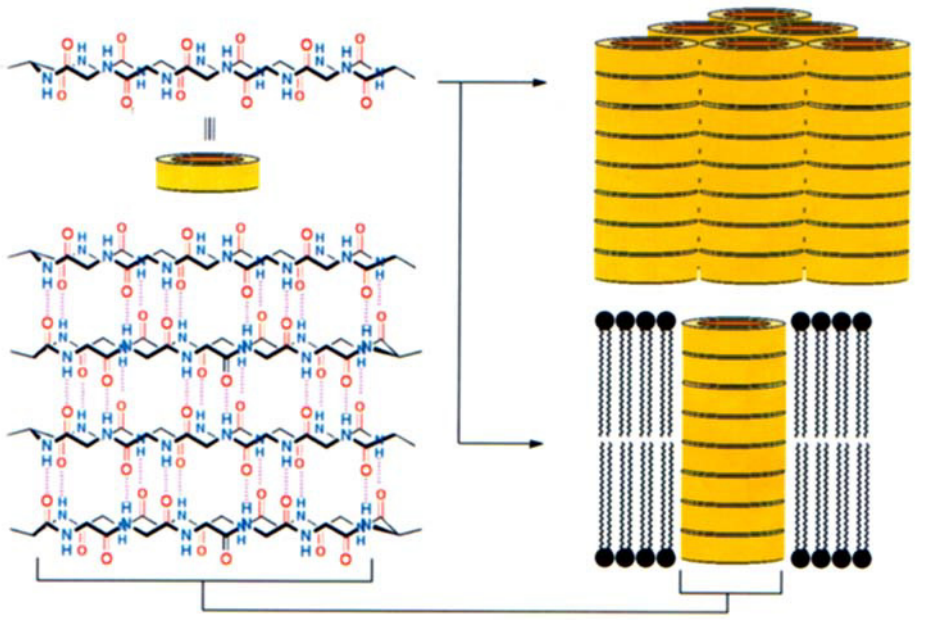

Fig. 39. The self-assembly of cyclic peptides, in which the amino acids have alternating D and L configurations, into tubular superstructures through hydrogen bonding between the amide groups.

Rebek and co-workers[159–161] have built on their experience with molecular receptors based on Kemp's triacid and have developed a self-replicating system.[162] The Kemp's triacid derivative **46** can recognize and bind the adenine derivative **47** to give the complex **48** (Fig. 42).[163, 164] This complex is stabilized, not only by the hydrogen bonding between the imide unit of **46** and the adenine residue of **47**, but also by the $\pi-\pi$ stacking interaction between the adenine base of **47** and the naphthalene moiety of **46**. This assembly is arranged perfectly for the formation of a *cis* amide bond between **46** and **47** by attack of the amino function of **47** on the activated ester of **46**. The *cis* amide linkage in **49** is, however, thermodynamically less stable than the *trans* isomer **50** and isomerization occurs. It opens up two new

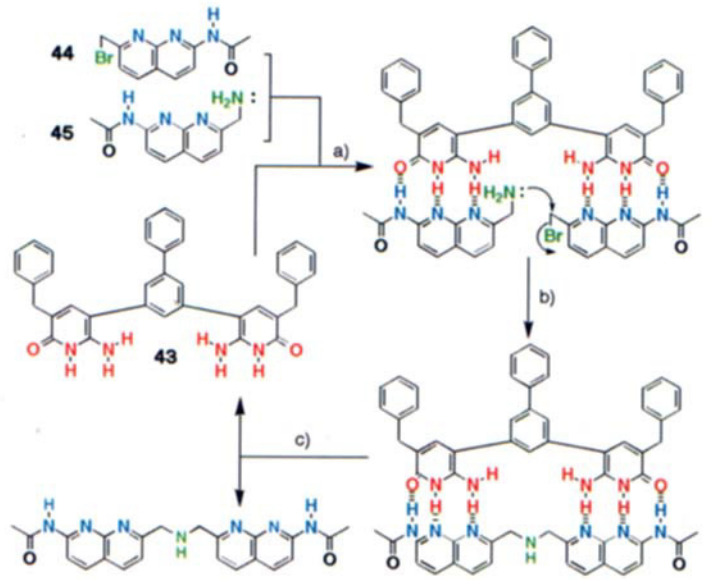

Fig. 40. Rate acceleration through hydrogen bond directed binding of reactants in a bisubstrate reaction template. a) Association, b) reaction, c) dissociation.

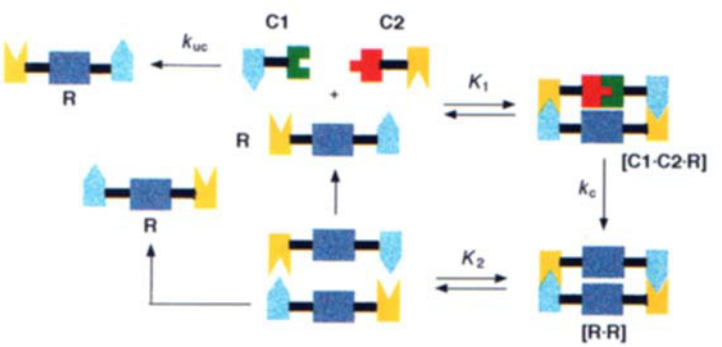

Fig. 41. A minimal model of self-replication. The synthesis of the replicator **R** is accelerated by its binding of components C1 and C2 to form the catalytic ternary complex [C1·C2·**R**]. This autocatalytic cycle is in competition with the uncatalyzed bimolecular reaction.

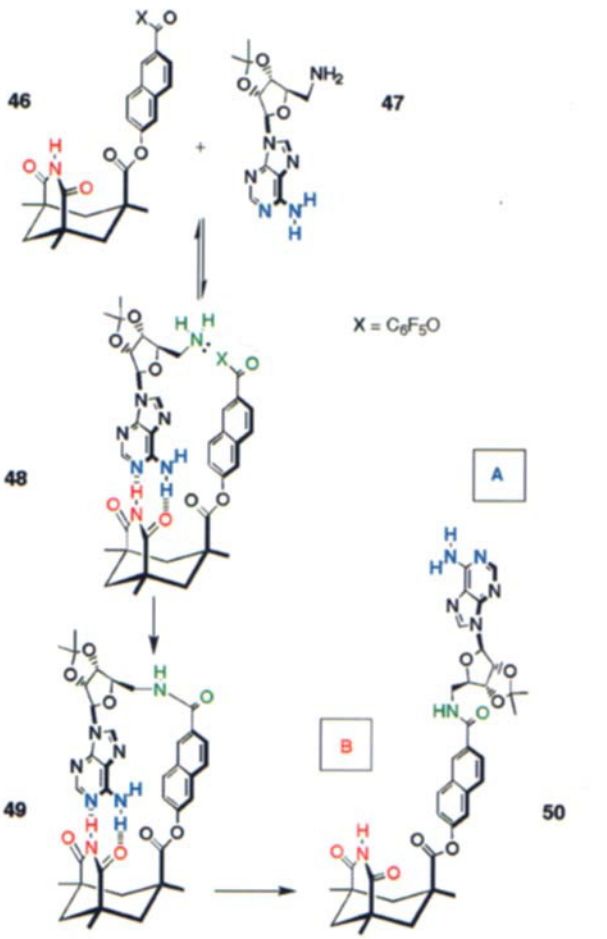

Fig. 42. The construction of a self-replicating system based on adenine recognition, through hydrogen bonding and amide bond formation. Binding sites A and B are available after *cis–trans* isomerization of the amide linkage (**49** → **50**).

binding sites A and B, which are capable of binding **46** and **47**, respectively. The binding of **46** and **47** by **50** is analogous to the formation of the ternary complex containing the bisubstrate reaction template **43**. However, since the product of the reaction between **46** and **47** is ultimately **50**, the formation of **50** must be autocatalytic along this reaction channel. In other words, **50** is self-replicating, when provided with the appropriate components. Since **50** is self-complementary[165] (dimerization constant, $K_D = 630\ M^{-1}$) some product inhibition must occur. Rebek et al. have subsequently identified a sigmoidal rate profile in a related system, demonstrating that the autocatalytic reaction channel is dominant.[166] Competition, reciprocal template effects, and mutation have also been demonstrated in these and other systems,[166, 167] as well as self-replication in systems not based on the Kemp's triacid core.[168]

The condensation of 3-aminobenzamidines and 2-formylphenoxyacetic acids has been exploited[169] by Terfort and von Kiedrowski in the design of a self-replicating system (Fig. 43).

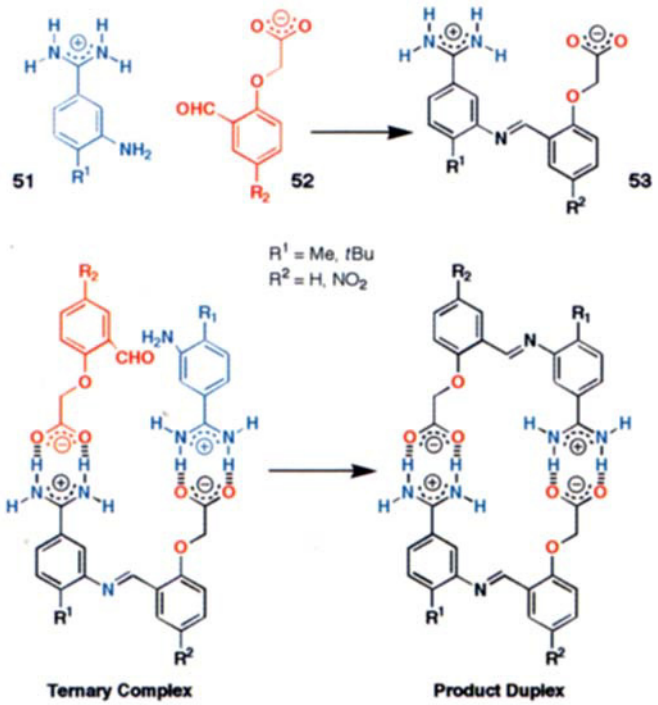

Fig. 43. The construction of a self-replicating system based on carboxylate recognition, through hydrogen bonding and ion pairing, and subsequent imine formation.

By utilizing the same minimal model of self-replication, the amidinium–carboxylate salt bridges formed between **53** and its precursor components, aminobenzamidine **51** and formylphenoxyacetic acid **52**, promote the formation of the central C=N bond of **53** by holding the reactants in close proximity in a ternary complex. Interestingly, kinetic data suggests that in certain cases the ternary complex [**51**·**52**·**53**] is more stable than the [**53**·**53**] duplex. This research indicates that self-replication with exponential autocatalysis can be achieved if the structure of the product can be modified to destabilize the product duplex further with respect to the catalytic ternary complex.[170]

Hunter[171] has designed and synthesized the macrocycle **54** (Fig. 44), which binds *p*-benzoquinone through a combination

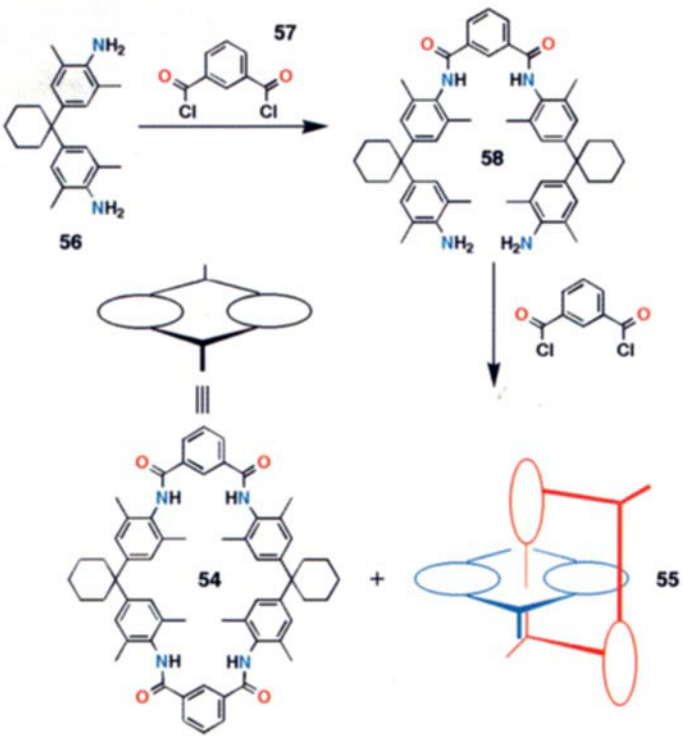

Fig. 44. The synthesis of an amide-based [2]catenane. (The cyclic dimer of **54** is formed as a side-product.)

of hydrogen bonds to the polar amide bridges and CH–π interactions[172] between the acidic hydrogen atoms of the quinone and the arene rings of **54**. In the original synthesis,[171] **54** was prepared in 10% yield by the single-step, high-dilution macrocyclization of the diamine **56** with isophthaloyl chloride **57**. In a modified synthesis,[173] reaction of isophthaloyl chloride **57** with the diamine **58** resulted in three major products: the receptor **54** in 51% yield, a cyclic dimer of **54** in 5% yield, and a product, which was identified as the [2]catenane **55** containing two interlocked units of **54**, in 34% yield. Although the exact mechanism of the self-assembly of **55** is still unclear, the remarkable efficiency of the process dictates that it must involve the complexation of a reaction intermediate with **54** through the hydrogen bonding and π–π interactions that are so effective in the binding of *p*-benzoquinone by **54**. The production of catenated products in such systems is not limited to the use of isophthaloyl chloride.[174] Clearly, a full mechanistic explanation for catenane formation must await complete elucidation[175] of all of the interactions within the system.

In the 29 years since Pedersen's discovery of crown ethers, the binding of ammonium (NH_4^+) and primary ammonium ions (RNH_3^+) by [18]crown-6 and its derivatives through hydrogen bonding interactions has been reported widely.[79] In contrast, studies on the binding of secondary ammonium ions ($R_2NH_2^+$) have been limited to smaller macrocycles such as diaza-[12]crown-4.[176] In principle, enlargement of the complexing macrocycle should provide an environment suitable for the pseudorotaxane-like insertion of the cation through the center of the macrocyclic polyether (Fig. 45). This pseudorotaxane superstructure should be stabilized by hydrogen bonding between the acidic hydrogen atoms of the ammonium group and the oxygen atoms of the crown ether. The realization of this concept

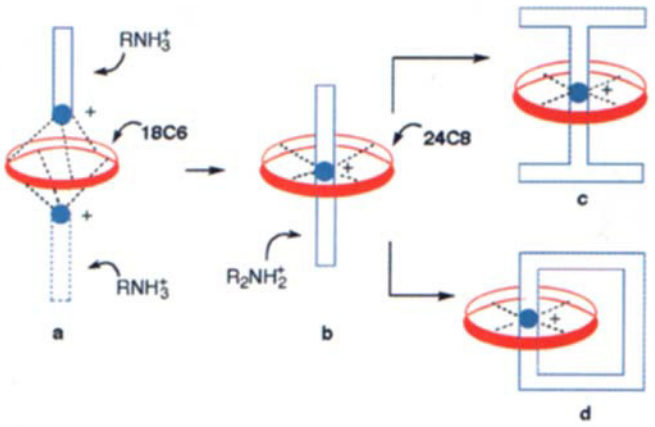

Fig. 45. The progression from a) a complex between a primary ammonium cation and [18]crown-6(18C6) with a "perched" geometry through b) a complex between a secondary ammonium cation and [24]crown-8(24C8) with a pseudorotaxane-like geometry to c) rotaxanes and d) catenanes.

has been described simultaneously by two research groups. We have exploited the recognition between large crown ethers and various dialkylammonium ions to demonstrate that this hypothesis is, in fact, correct.[177] Dibenzo-[24]crown-8 (**DB24C8**) can bind both dibenzylammonium and bis(*n*-butyl)ammonium ions in a pseudorotaxane-like manner (Fig. 46). Interestingly,

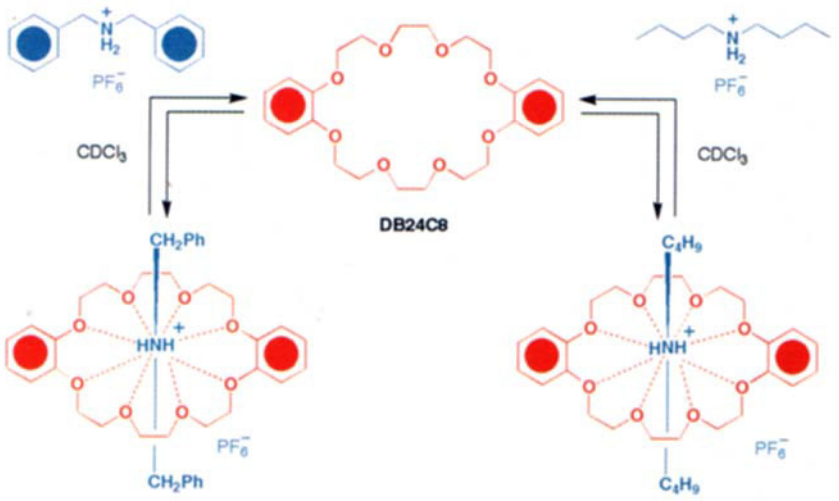

Fig. 46. Dibenzo-[24]crown-8 forms pseudorotaxane-like complexes with both dibenzylammonium hexafluorophosphate and di-*n*-butylammonium hexafluorophosphate.

the exchange of free and bound dibenzylammonium ions is slow on the ^{1}H NMR timescale. This kinetic effect is a result of the large steric barrier encountered by the phenyl rings of the cation when attempting to pass through the **DB24C8** torus, rather than a particularly high binding constant (27000 M^{-1} in $CDCl_3$). This new recognition motif has been extended to the self-assembly of doubly encircled and doubly stranded pseudorotaxanes[177] (Fig. 47). Busch and co-workers have described the synthesis and characterization of a [2]rotaxane based on the recognition of the salts of either 4-(anthracen-9-yl)butylamine or *N*-1-(anthracen-9-yl)methylethan-1,2-diamine by **DB24C8**.[178] The synthesis of the [2]rotaxane proceeded in modest yield

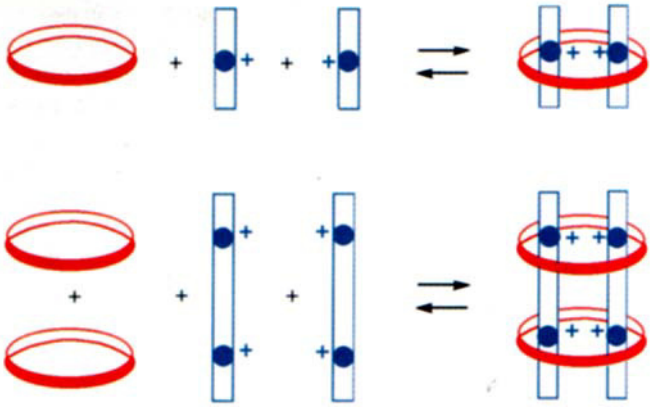

Fig. 47. Secondary ammonium ions can direct the assembly of doubly stranded (top) and doubly encircled (bottom) pseudorotaxanes.

(20%) and the insertion of the ammonium ion through the torus of the **DB24C8** macrocycle has been demonstrated by X-ray crystallography.

4.3. Metal–Ligand Interactions

Metal–ligand interactions have been known and studied since the turn of the century.[179] Werner, building on earlier ideas[180] that metal centers could bind neutral molcules or ligands,[181] introduced the idea of specific metal–ligand geometries in first decade of this century. The stereochemical ideas of Werner were consolidated and expanded on by Lewis and Sidgwick, who introduced the concept of a metal–ligand interaction being the sharing of an electron pair. Later, the idea of chelating and macrocyclic ligands for metal centers emerged.[182, 183] Metal coordination chemistry has many useful features that can be applied to the field of self-assembly. Metal–ligand bonds can be strong, lending stability to a structure, yet kinetically labile, allowing reorganization to occur. Additionally, metal–ligand interactions provide the chemist with a lexicon of well-defined geometries for the design of a wide range of structural forms. One of the earliest examples of molecular self-assembly was provided by the field of metal coordination chemistry.[184–186] In 1960 Curtis reported the one-pot synthesis of a yellow crystalline product from the reaction of $[Ni(en)_3]^{2+}$ (en = ethylenediamine) in dry acetone (Fig. 48). At first this product was assigned incorrectly to a complex of the bisimine species **59**. However, the extreme stability of the complex—it survives boiling acid and alkali—did not support this structural assignment. It was shown subsequently that the yellow product was, in fact, a mixture of the isomeric macrocyclic Ni^{II} complexes **60** and **61**. Although the precise mechanism of this self-assembly process is not clear, it may involve repetitive imine formation with subsequent attack of an acetonyl carbanion on the Ni-coordinated imine; in other words, the Ni^{2+} cation acts as the template[187] around which the macrocycle is assembled.

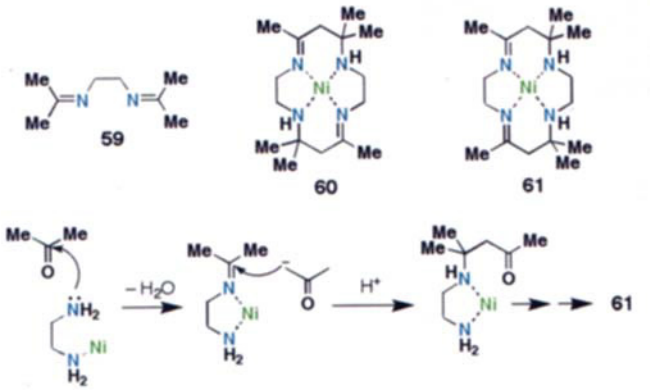

Fig. 48. The self-assembly of a macrocycle around a Ni^{II} ion (Curtis et al. [184–186]).

Sanders and co-workers have extended their earlier investigations of flexible bisporphyrin receptors[188, 189] to utilize the axial ligand site[190] of zinc porphyrins for the directed self-assembly of a diverse array of novel porphyrin-containing macrocycles. Although the macrocyclic porphyrin trimer **63a** can be synthesized by untemplated oxidative coupling of the diacetylenic porphyrin monomer **62a** (Fig. 49),[191] the yield is relatively low (47%) and the crude product contains many other cyclic and acyclic oligomers. If, however, the monomer **62b** is oxidatively coupled in the presence of s-2,4,6-tri-4-pyridyltriazine (**64**), then the amount of cyclic trimer **63b** formed is dramatically enhanced.[192] Surprisingly, bifunctional pyridine ligands such as di-4-pyridylpropane are almost as efficient at

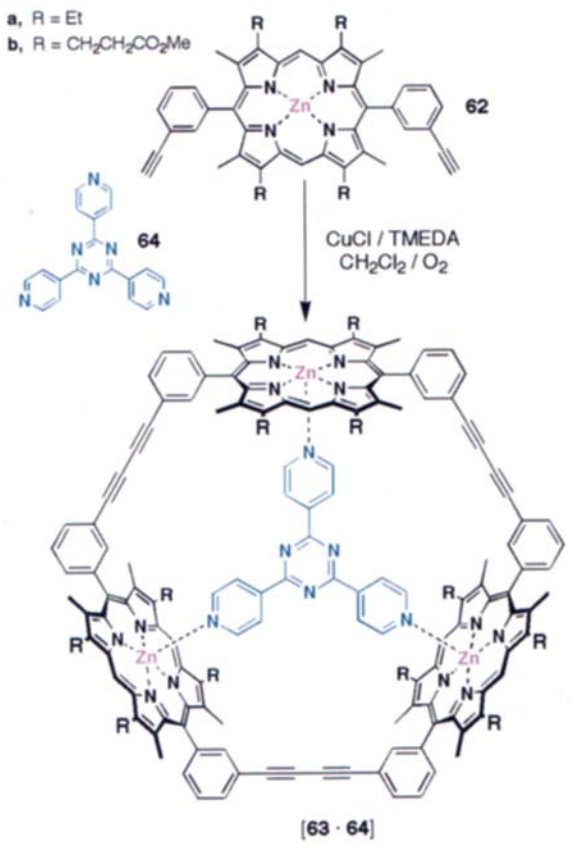

Fig. 49. s-Tripyridyl triazine can act as an efficient template for the formation of a trimeric macrocyclic porphyrin array.

templating the synthesis of **63b**. This observation indicates that **64** acts as a "negative template": it promotes trimer formation passively by inhibiting dimer formation actively. The cyclic dimer can also be synthesized in high yield by employing 4,4′-bipyridine as a "positive template". The attempted template-directed synthesis of an enlarged, platinum-linked cyclic trimer of **62a**, using a chiral aluminium-based ligand designed for the purpose, has also been reported.[193] The multifarious roles of the amine templates within these systems has been further extended by the introduction of the "scavenger template".[194, 195] A scavenger template allows efficient dimerization of singly reactive species in statistical mixtures of unreactive, singly, and doubly reactive species by forcing doubly reactive species to cyclize, thus allowing the singly reactive species to react with themselves. The supermacrocyles formed in these remarkable template-directed syntheses have large internal cavities in which several molecules can be brought together and bound in close proximity. Sanders and co-workers have described the acceleration of an *exo*-selective intermolecular Diels–Alder cycloaddition reaction between a maleimide and a furan derivative, which occurs within the cavity of a cyclic porphyrin trimer.[196] The diene **65** and dienophile **66** can bind in a favorable orientation within the cavity of the trimeric macrocycle **63a** (Fig. 50). The

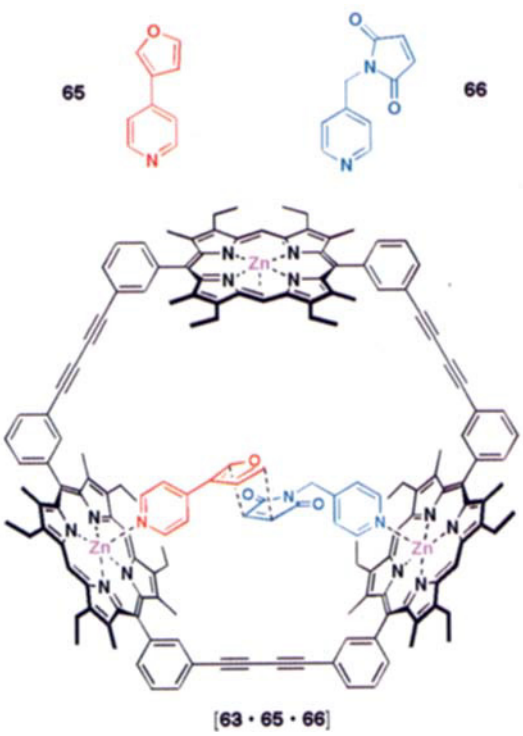

Fig. 50. A trimeric porphyrin array can act as an efficient catalyst for the Diels–Alder reaction between and a furan derivative (red) and a maleimide (blue).

porphyrin trimer acts as a very effective linear template[195] both kinetically, by accelerating the reaction, and thermodynamically, by stabilizing the *exo* product. Trimer **63a** is regarded as a significant step[196] towards the development of artificial enzyme systems as it decouples recognition and orientation of the reactants from the reaction itself. Therefore, it should be possible to bring together a range of substrates within its cavity by rational design changes.

Fujita, Yazaki, and Ogura[197, 198] have exploited metal coordination in the formation of macrocycles of a different kind. When $[M(en)(NO_3)_2]$ (M = Pt, Pd) is treated with bipyridine, a cyclic tetrameric macrocycle **67**—a molecular box—is formed as the thermodynamic product (Fig. 51). The mechanism pre-

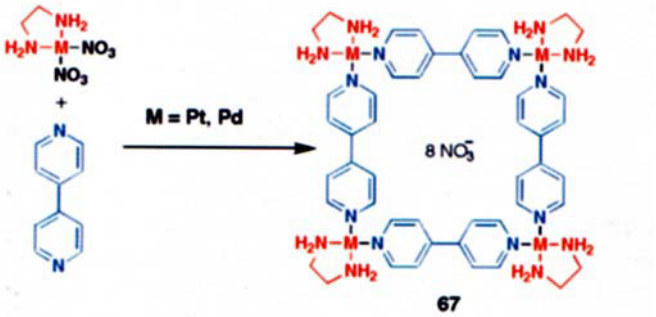

Fig. 51. Tetrameric bipyridine macrocycles are formed readily through metal directed self-assembly.

sumably involves stepwise displacement of the nitrate ligands by bipyridine. Interestingly, in the reaction of the platinum complex, the kinetic product is an oligomeric species which is converted slowly into the thermodynamic, tetrameric product when the reaction mixture is heated at 100 °C. This observation suggests slow exchange within the ligand set around the metal center. In the palladium complex, ligand exchange must be rapid since no oligomeric products are observed by ^{1}H NMR spectroscopy and the thermodynamic product is formed immediately. The macrocycle **67** is capable of binding π-electron rich aromatic guests such as 1,3,5-trimethoxybenzene within its cavity.[199] Other groups have also reported self-assembling molecular boxes based on metal coordination chemistry.[200]

Fujita et al. have extended the concepts used to construct the molecular boxes to the assembly of a wide array of structures[201] such as molecular networks, ladders, and bricks. A spectacular example of the power of these self-assembly processes is the quantitative self-assembly of a [2]catenane from a pair of preformed molecular rings.[202] This synthesis of a [2]catenane exploits the relatively lability of the Pd^{II}–N coordinate bond. When the Pd^{II} complex $[Pd(en)(NO_3)_2]$ **68** is treated with one molar equivalent of 1,4-bis(4-pyridylmethyl)benzene (**69**) in D_2O, the macrocycle **70** is formed initially (Fig. 52). However, as the concentration of the solution is increased, another compound is formed which was shown to have the catenated structure **71** (>90% yield for c(**68**), c(**69**) > 50 mM). Initially, a "double-differential complexation" mechanism was proposed for the assembly of the [2]catenane, in which two molecules of **70** bind each other in their cavities. A control experiment in which the Pd^{II} is replaced by Pt^{II} established that the breaking and reforming of the Pd–N bond is crucial in the efficient formation of the [2]catenane. In the case of Pt^{II}, a kinetic mixture of the [2]catenane together with other products is observed. Dilution of this mixture does not affect the product ratio—the Pt–N coordinate bond cannot be broken under these conditions. However, recent work has shown that a novel "Möbius strip" mechanism, in fact, operates.[202] The different behavior of the Pt^{II} system has been exploited in the assembly of a "molecular lock" based on the [2]catenane struc-

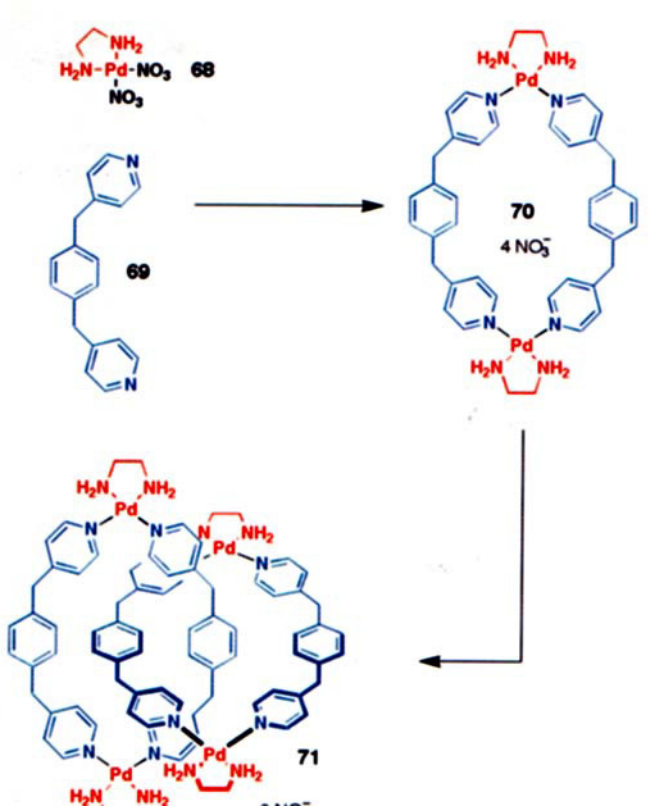

Fig. 52. Metal-directed self-assembly produces first macrocycle **70**. When the concentrations of the appropriate species are increased, [2]catenane **71** forms almost spontaneously and almost quantitatively.

ture **71**.[203] The Pt–N bond in the [2]catenane can only be "unlocked" under certain conditions, and hence the stepwise assembly of the [2]catenane structure can be controlled precisely.

A wide variety of macromolecular biological structures display molecular helicity,[204] for example, the protein α-helix. Lehn and co-workers[205, 206] have described a series of oligobipyridine ligands, which spontaneously order themselves around an appropriate number of Cu^I metal centers to give helical complexes (Fig. 53). These helical species display many of the features normally associated with self-organizing biological systems. The assembly of the helicates shows positive cooperativity;[207] in other words, the binding of the first Cu^I ion facilitates the binding of the second and so on. Hence, their assembly is highly nonlinear, as evidenced by the fact that at all Cu^I concentrations examined only free ligand and fully formed helicate exist in solution. In addition, the binding of the ligands by Cu^I displays self–self selection;[208] that is, given a mixture of ligands, a forming helical species will bind selectively a second ligand of the same size, and thus no overlapping polymeric structures are formed in solution. This phenomenon has been termed the "instructed system paradigm". The assembly of bipyridine ligands carrying pendant nucleoside units around Cu^I centers has also been demonstrated by Lehn et al.[209] In this case, the final structure, a so-called deoxyribonucleohelicate, recalls Pauling's (incorrect) structure for DNA proposed in 1953[210] in that the pyrimidine bases are divergent from the helix core. These systems may have applications as complementary ligands for the selective binding of regions of the DNA

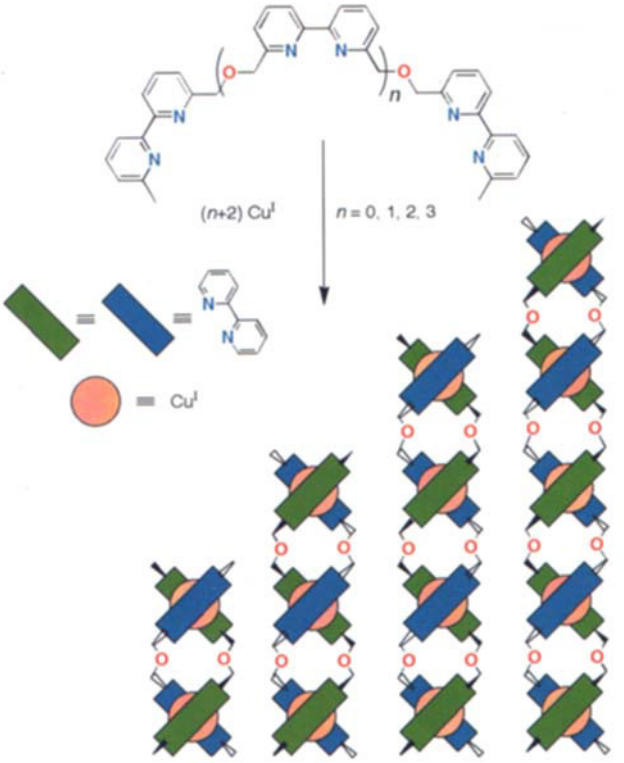

Fig. 53. Cu^{I} ion directed self-assembly of oligobipyridine-based double helices.

double helix, but at the very least they are beautiful examples of the power of self-assembly to create large, unnatural structures in a highly selective and ordered manner. More recently, Lehn and co-workers have reported the self-assembly of triple helices from Ni^{II} ions and oligobipyridine ligands,[211] as well as the spontaneous formation of a cylindrical complex from five ligands and six Cu^{I} ions.[212]

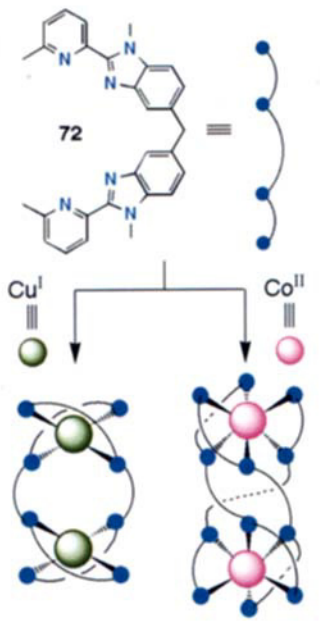

Fig. 54. Different metals instruct the self-assembly of different structures. Ligand **72** can form a double or a triple helical complex depending on the metal ion employed in the self-assembly process.

Constable and co-workers[213–217] have utilized oligopyridine ligands in the self-assembly of both single and double helical metal–ligand complexes with a wide variety of metal centers. The requirements for helix formation in the case of single helices have been elucidated. Helical superstructures arise when the oligopyridine ligands interact with a small, charged center that can impose a clear stereochemical preference on the system.[218] The formation of stereochemically well-defined complexes has been applied by Constable et al. to the efficient template-directed synthesis of the ligands themselves.[219]

By combining pyridine and benzimidazole subunits within the same ligand, Piguet, Bernardinelli, and Williams have been able to self-assemble a wide range of double and triple helices containing both transition metal and lanthanide centers.[220] A degree of control can be exercised over the outcome of these self-assembly processes. When ligand **72** is mixed in a 3:2 ratio with an appropriate source of Co^{II} ions, a dinuclear triple helicate forms spontaneously (Fig. 54).[221] However, the analogous reaction with Cu^{I} ions results in spontaneous formation of a dinuclear double helicate. In this case, the outcome of the self-assembly process is governed by the coordination geometries of the metal centers.

Lehn and co-workers have explored the use of metal coordination for the construction of molecular racks, ladders, and grids (Fig. 55).[222] When ligand **73** is mixed with 1.5 equivalents of $AgSO_3CF_3$, a three-by-three molecular grid self-assembles spontaneously from nine Ag^{I} ions and six ligands (Fig. 56). Analysis of the product by ^{109}Ag NMR spectroscopy indicates that, as expected, there are three types of Ag^{I} ions in the structure in the ratio 4:4:1, corresponding to the metal ions at the vertices, those on the edges, and the single Ag^{I} ion at the center of the grid, respectively.

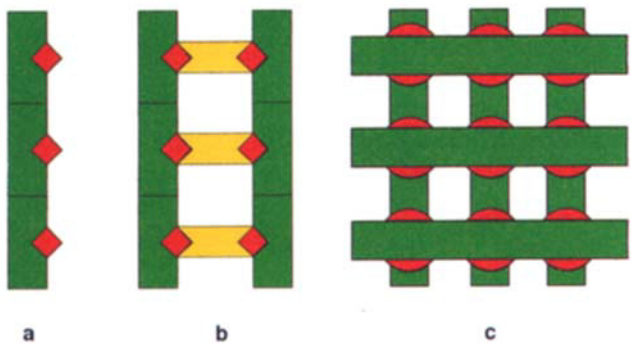

Fig. 55. Rack (a), ladder (b), and grid structures (c).

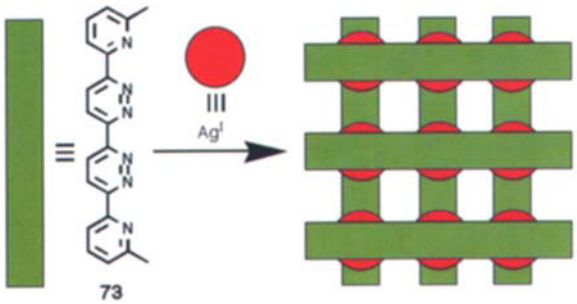

Fig. 56. Nine Ag^{I} cations and six ligands form a molecular grid by self-assembly.

Balzani, Campagna, Denti, and co-workers have described the synthesis and photophysical properties of a series of decanuclear homo- and heterometallic polypyridine complexes incorporating Ru^{II} and Os^{II} metal centers (Fig. 57).[223] These com-

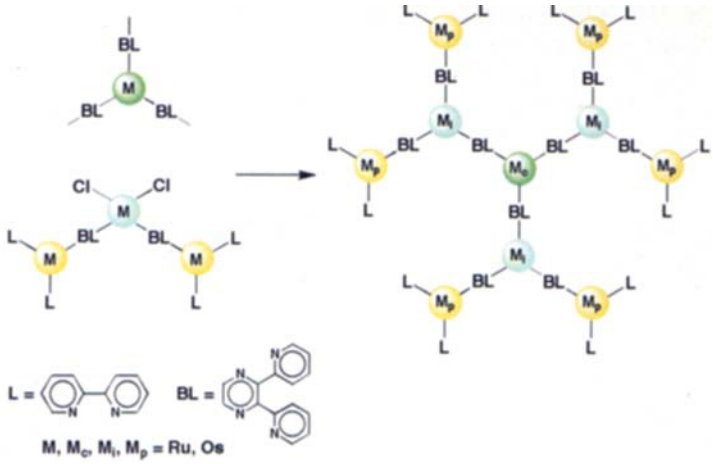

Fig. 57. Energy transfer within the multinuclear dendritic metal complexes is controlled by the identity of the metals and ligands at the various sites within the complex.

pounds have remarkable photophysical properties: when they are irradiated, energy is transferred through the system in a manner predetermined by the nature of the metal in each of the ligand sites. For example, upon irradiation of the complex with $M_c = Os^{II}$, M_i, $M_p = Ru^{II}$, and L = bipyridine, the energy is transferred from the central metal toward the periphery of the assembly.

Sauvage et al. have exploited the coordination geometry of 2,9-disubstituted 1,10-phenanthroline ligands around a Cu^I center to provide the first example of a practical, efficient synthesis of a catenated species (Fig. 58).[224] Sauvage has termed the

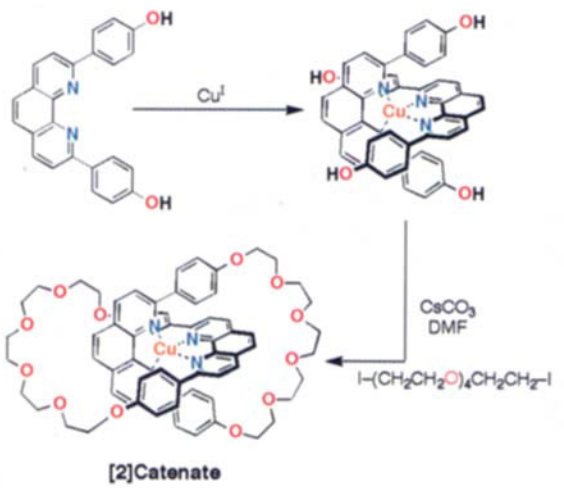

Fig. 58. The interaction between a Cu^I ion and a 9,10-phenanthroline ligand can be used to direct the formation of a [2]catenate.

metalated structures catenates and the corresponding demetalated species catenands (*caten*ane + lig*and*). This research has been extended to encompass both further [2]catenanes containing a variety of metal centers,[225, 226] [3]catenanes,[227, 228] the investigation of higher catenanes by electrospray mass spectrometry,[229] and more recently, [2]rotaxanes containing a Cu^I–phenanthroline core with differentially metalated porphyrin stoppers or with fullerene-based stoppers,[230] and pseudorotaxanes containing several Cu^I centers.[231] Perhaps the most exquisite example of the application of metal–ligand interactions in self-assembly is the synthesis by Sauvage et al. of a molecular trefoil knot.[232] The trefoil knot may be synthesized from a tetrafunctionalized helicoidal complex (Fig. 59), which

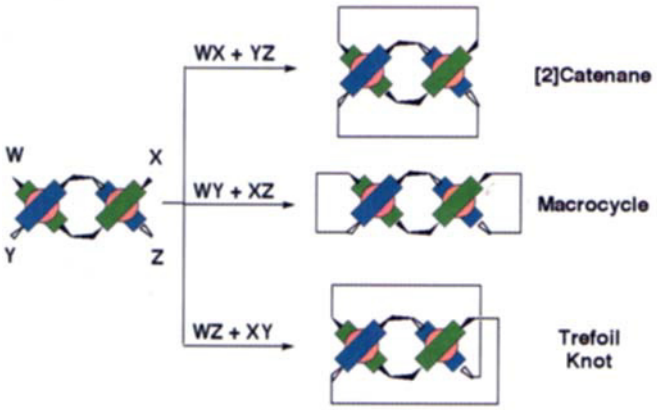

Fig. 59. The possible products of a reaction in which the termini of a double helical complex are linked.

has a number of possible cyclization pathways. In particular, if point W is linked to point Z, and point X to point Y, a trefoil knot results. Other connections produce either macrocyclic or catenated species. Using an extension of their copper–phenanthroline methodology, Sauvage et al. were able to synthesize

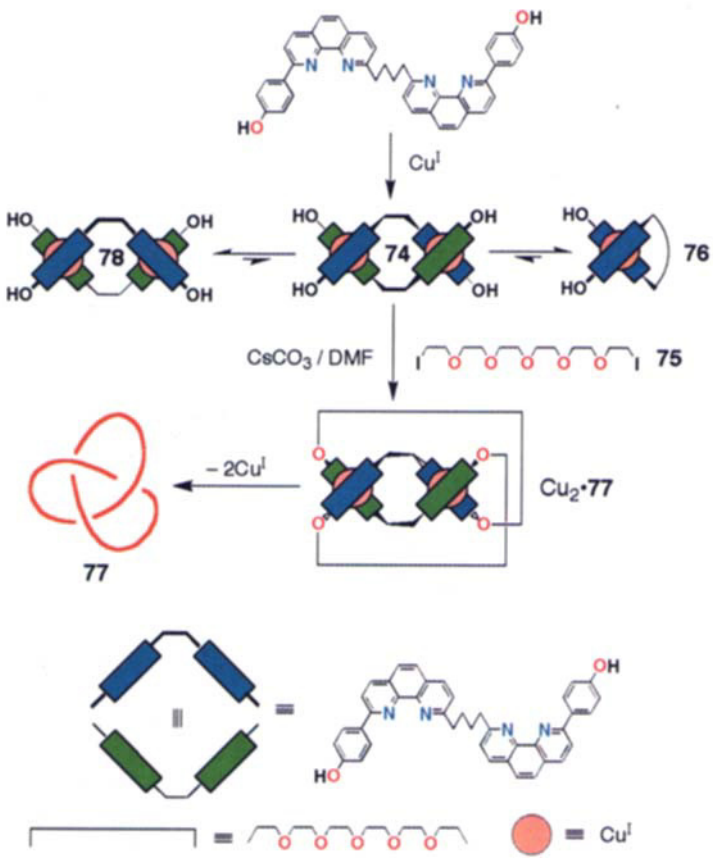

Fig. 60. The double helix formed by two Cu^I cations and a bis(9,10-phenanthroline) ligand can be used to direct the synthesis of a trefoil knot.

trefoil knot **77** in 3% yield from the helical dinuclear Cu^{I} complex **74** and hexaethyleneglycol diiodide **75** (Fig. 60). Although the yield of the trefoil knot appears to be low, it should be noted that the helical dinuclear complex **74** is in equilibrium with the mononuclear Cu^{I} complex **76**, and that the equilibrium lies far to the side of mononuclear complex. In addition, the equilibrium of the helical complex **74** with its face-to-face isomer **78** is also unfavorable (**74**:**78** = 1:10). The effects of these deleterious equilibria can be overcome by the use of a rigid 1,3-substituted phenylene spacer in place of the flexible oligo(methylene)spacer in the original bis(phenanthroline) ligand.[233] The redesigned ligand permits the synthesis of a trefoil knot in a remarkable 30% yield, marking a high point in the synthetic applications of self-assembly.[234]

4.4. Self-Assembling Systems Based on π-Donors and π-Acceptors

The donor–acceptor interactions between π-systems have been known[235] and studied[236] for over 40 years. Although the exact nature of these interactions is still a matter for some debate,[237] they are an important class of noncovalent bonding interactions. The 1,1′-dimethyl-4,4′-bipyridinium dication 79^{2+}, better known as the bipyridinium herbicide paraquat,[238–240] is an extensively studied electron acceptor. It offers a planar π-system in which two positive charges are delocalized[241] as well as a rich and reversible electrochemistry.[242] Unsurprisingly, the dication 79^{2+} forms a wide range of electron donor–acceptor complexes with a variety of electron donors.[243–244] Of most interest in the context of the present research activity are those involving π-donors. Among the species that form relatively weak ($\Delta G^{\circ} < -1$ kcal mol^{-1}) π-donor/π-acceptor complexes with the paraquat dication[245] are aniline, *o*-phenylenediamine, catechol, and hydroquinone. In the crystal structure of the complex formed between hydroquinone **80** and 1,1′-dimethyl-4,4′-bipyridinium diiodide (Fig. 61)[246] the dication and the π-donor have a face-to-face arrangment with a mean separation[247] between the two π-planes of 3.38 Å.

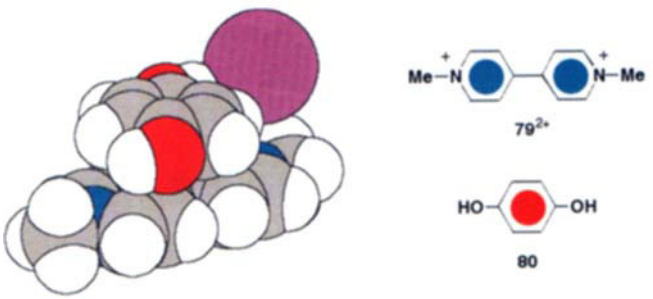

Fig. 61. The X-ray crystal structure of the paraquat diiodide/hydroquinone complex. Note that the second iodide counterion has been removed for clarity.

The bipyridinium herbicides are also capable of forming complexes with macrocyclic π-donors. The dicationic platinum complex 81^{2+} forms a strong complex (K_a = 191000 M^{-1}) with the crown ether dibenzo-[30]crown-10 (**DB30C10**) (Fig. 62).[248] This prompted us to exploit the constitutional similarities between 81^{2+} and the diquat dication 82^{2+} and show that the latter also forms a strong 1:1 complex (K_a = 4100 M^{-1}) with **DB30C10** (Fig. 62).[249] The principal stabilizing interactions in

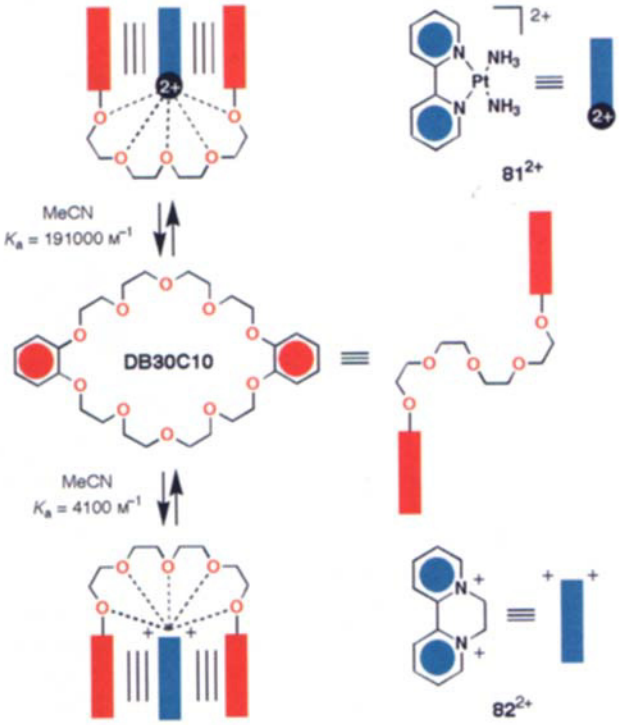

Fig. 62. The binding of $[Pt(bpy)(NH_3)_2]^{2+}$ and the bipyridinium herbicide diquat by **DB30C10**. The counterions have been omitted for clarity. In addition, in the cartoon representation of **DB30C10**, only one of the tetraethylene glycol chains is shown.

the complexes are: 1) the solvation of the positive charge by the oxygen atoms of the polyether chains within **DB30C10** through electrostatic interactions including hydrogen bonding and 2) the π-donor/π-acceptor and charge transfer (CT) interactions between the electron-rich catechol units of **DB30C10** and the electron-deficient π-system in both dications. The CT interaction gives rise to the characteristic orange color of these complexes. Subsequently, we demonstrated that the paraquat dication 79^{2+} can also be bound strongly by bisparaphenylene-[34]crown-10 (**BPP34C10**), a constitutional isomer of the dibenzo crown **DB30C10**.[250–252] **BPP34C10** binds **79**·2PF_6 in acetone solution with a stability constant of 730 M^{-1} for the 1:1 complex (Fig. 63). Furthermore, the X-ray crystal structure of this complex revealed a highly ordered superstructure in which the rod-like 79^{2+} dication is inserted into the cavity of **BPP34C10** centrosymmetrically, such that the methyl groups are positioned on opposite faces of the crown ether in a pseudorotaxane-like manner.[97] The complex is stabilized both by electrostatic interactions, including [C–H···O] hydrogen bonding between the acidic hydrogen atoms of 79^{2+} and the polyether oxygen atoms, and by dispersive forces including CT between the complementary π-systems of **BPP34C10** and 79^{2+}. Like [**82**·**DB30C10**]$^{2+}$, the [**79**·**BPP34C10**]$^{2+}$ complex has a deep orange color as a result of the CT interactions.

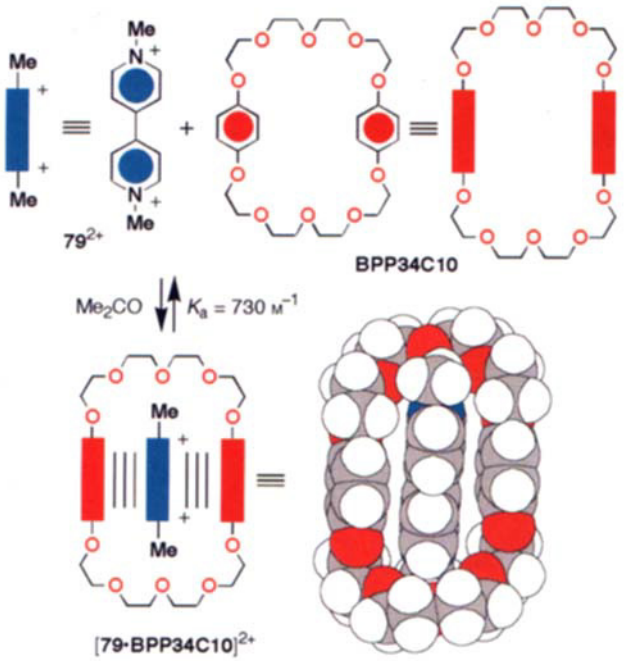

Fig. 63. The complexation of the bipyridinium herbicide paraquat by ***BPP34C10***. The counterions have been omitted for clarity.

Both of these examples illustrate how π-donor/π-acceptor interactions can be used to bind a π-electron deficient *guest* inside a π-electron rich *host*. There is no conceptual or practical reason why the roles of the π-donor and the π-acceptor cannot be reversed to produce a π-electron deficient *host* capable of binding a π-electron rich *guest*. Indeed, this objective has been achieved with the synthesis of the tetracationic cyclophane **83**$^{4+}$ (Fig. 64) as its tetrakis(hexafluorophosphate) salt.[253] This cyclophane, incorporating two π-electron deficient 4,4′-bipyridinium dications, is capable of binding a wide variety of π-electron rich guests within its rigid rectangular cavity. Guests that can be bound include catechol and hydroquinone dimethyl ethers,[254] substituted 1,5-dioxynaphthalene derivatives,[255] aromatic amino acids,[256] tetrathiafulvalene,[257] and derivatives of indole.[258] The X-ray crystal structure of the complex formed between **83**·4PF_6 and 1,4-dimethoxybenzene **84** reveals that the π-electron rich **84** is inserted centrosymmetrically inside the cavity of **83**$^{4+}$ in a pseudorotaxane-like manner (Fig. 64). The principal stabilizing feature in this 1:1 complex is the π-donor/π-acceptor interaction, with no additional stabilization from hard electrostatic interactions such as hydrogen bonding. The absence of efficient electrostatic stabilizing forces is reflected in the low value of the stability constant, namely 17 M^{-1}. Interestingly, there are also weakly stabilizing (<0.3 kcal mol^{-1}) edge-to-face interactions between the electropositive hydrogen atoms on the phenylene ring of **84** and the π-system of the rigid *p*-xylyl unit of **83**$^{4+}$. This type of interaction has been found in widely diverse structures such as in the solid-state structure of benzene and in the crystal structures of proteins rich in aromatic amino acids.[259–261]

The observation that it is possible to bind a π-electron deficient guest within a π-electron rich cavity (e.g. [**79**·**BP34C10**]$^{2+}$) and a π-electron rich guest within a π-electron deficient cavity (e.g. [**83**·**84**]$^{4+}$) strongly suggests the possibility of combining these two supramolecular design features within the same

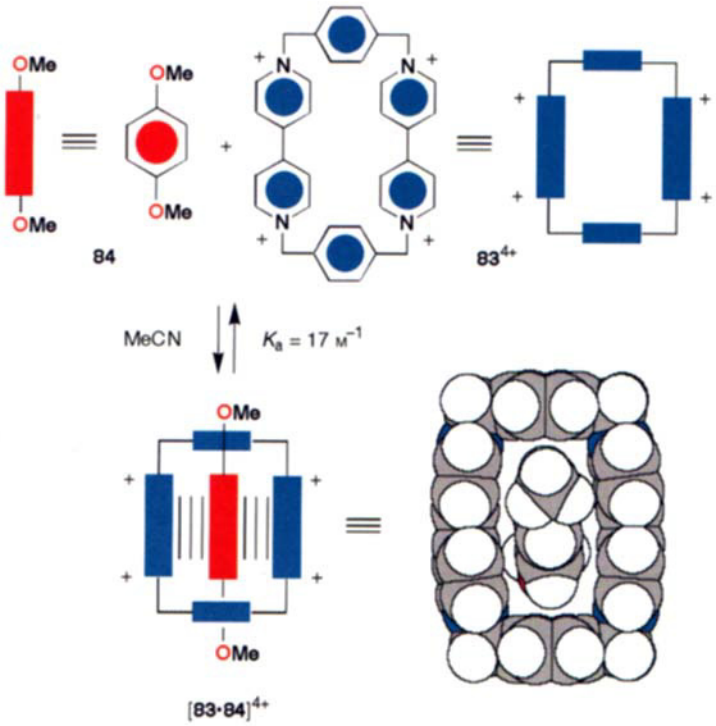

Fig. 64. The complexation of 1,4-dimethoxybenzene by the rigid tetracationic receptor cyclobis(paraquat-*p*-phenylene). The counterions have been omitted for clarity.

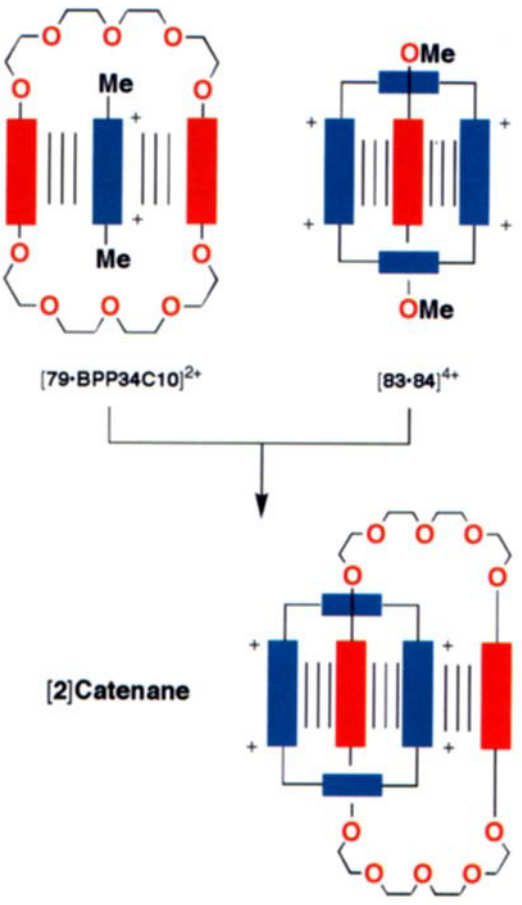

Fig. 65. The emergence of the design of a [2]catenane based on the simple receptor chemistry shown in Figs. 63 and 64.

molecular assembly. This proposition was reinforced by the observation that a continuous π-donor/π-acceptor stack is formed in the solid state when 1,5-dinaphtho-[44]crown-12 crystallizes with two molar equivalents of $\mathbf{79}^{2+}$; one dication is included within the crown ether host and the second is clathrated between adjacent complexes in the crystal.[262] Thus, the design of a [2]catenane emerged quite logically from the supramolecular chemistry of complementary π-donors and π-acceptors (Fig. 65). When the reaction between the bis(pyridylpyridinium) salt $\mathbf{85}^{2+}$ and 1,4-bis(bromomethyl)benzene **86** is performed in acetonitrile at room temperature in the presence of three molar equivalents of the crown ether **BPP34C10**, the [2]catenane **88**·4 PF_6 is formed in 70% yield, following purification and counterion exchange (Fig. 66).[263] This extremely high

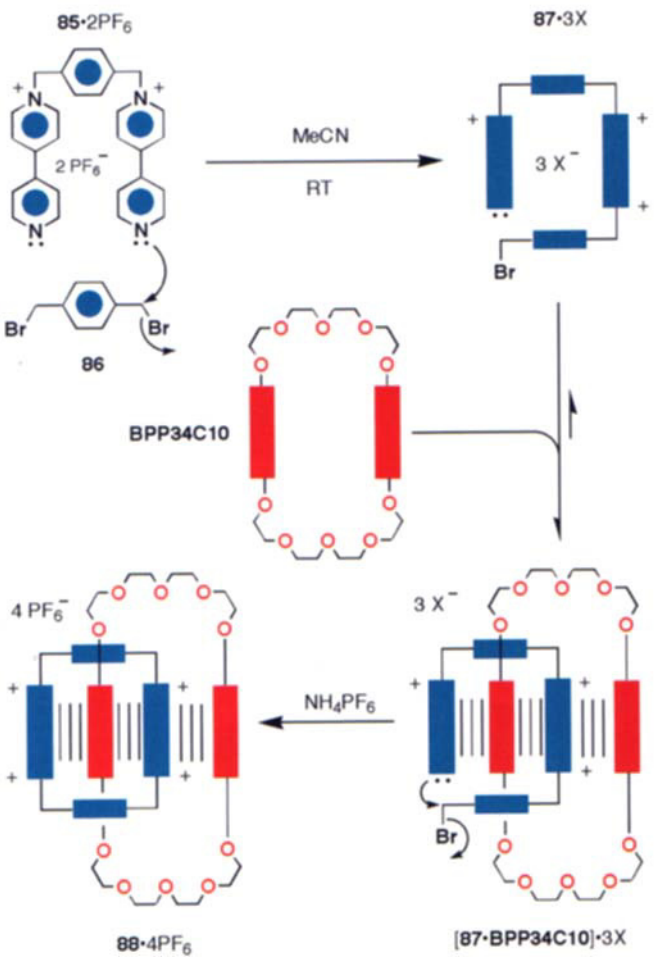

Fig. 66. The self-assembly of a [2]catenane directed by the mutual recognition between appropriately located π-donors (red) and π-acceptors (blue). The critical phase of this reaction scheme is the binding of the paraquat-like tricationic intermediate **87**·3X by **BPP34C10**. RT = room temperature.

yield contrasts starkly with the harsh conditions required and low yields obtained in the synthesis of both the **BPP34C10** and $\mathbf{83}^{4+}$ macrocycles as separate compounds. The mechanism involves initial alkylation of the dication $\mathbf{85}^{2+}$ by 1,4-bisbromomethylbenzene **86** to produce the tricationic intermediate $\mathbf{87}^{3+}$.[264] The 4,4′-bipyridinium component of this trication is then rapidly and strongly complexed by **BPP34C10**. This 1:1 complex will be stabilized by the electrostatic, CT, and π–π stacking interactions between the π-electron rich hydroquinone rings of the crown ether and the π-electron deficient 4,4′-bipyridinium residue of $\mathbf{87}^{3+}$. This intermediate complex $[\mathbf{87}\cdot\mathbf{BPP34C10}]^{3+}$ is ideally disposed to undergo a second ring-closing nucleophilic displacement of bromide ion to form the [2]catenane. The X-ray crystal structure of **88**·4 PF_6·5 MeCN reveals continuous stacks of the [2]catenanes along one of the crystallographic directions such that π-donors and π-acceptors alternate both intra- and intermolecularly[266] with a spacing of 3.5 Å (Fig. 67).[263, 265] Dynamic ^{1}H NMR spectroscopy reveals that the [2]catenane is also highly ordered in solution.[263, 265] Three dynamic processes are observable (Fig. 68). The first is the circumrotation of the neutral **BPP34C10** through the cavity of the $\mathbf{83}^{4+}$ cyclophane (Process I, Fig. 68). This process is relatively high in energy as it involves the disruption of all noncovalent π–π interactions within the [2]catenane, and consequently, at 25 °C this process occurs only 22 times per second. The second process is the pirouetting of the **BPP34C10** around the periphery of the $\mathbf{83}^{4+}$ cyclophane (Process II, Fig. 68). Since this process involves the disruption of only one of the π–π interactions within the [2]catenane, it has a much lower energy barrier than the first dynamic process. As a result, the pirouetting motion occurs 7000 times per second at 25 °C. The third dynamic process observed (Process III, Fig. 68) is the rocking motion of the hydroquinone ring within the cavity of the tetracationic cyclophane. At low temperatures the exchange of the hydroquinone ring protons between the two magnetic enviroments becomes slow on the ^{1}H NMR timescale and two signals arise. At 25 °C, however, this process is extremely fast, occurring 1.6×10^6 times per second. The self-assembly process that forms

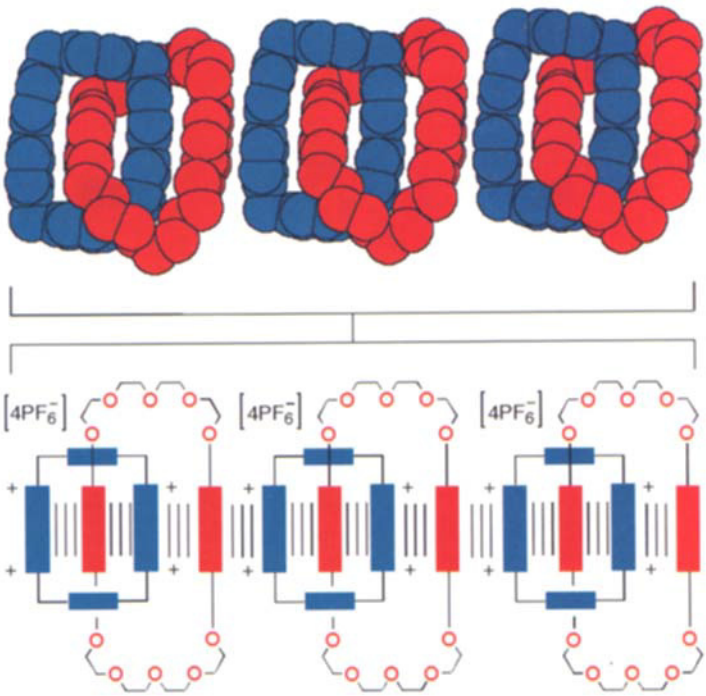

Fig. 67. The mutual recognition between the appropriately located π-donors (red) and π-acceptors (blue), which directs the formation of the [2]catenane, is in action both within the molecule and beyond the molecule in the solid state, where the [2]catenanes form continuous π-donor/π-acceptor stacks.

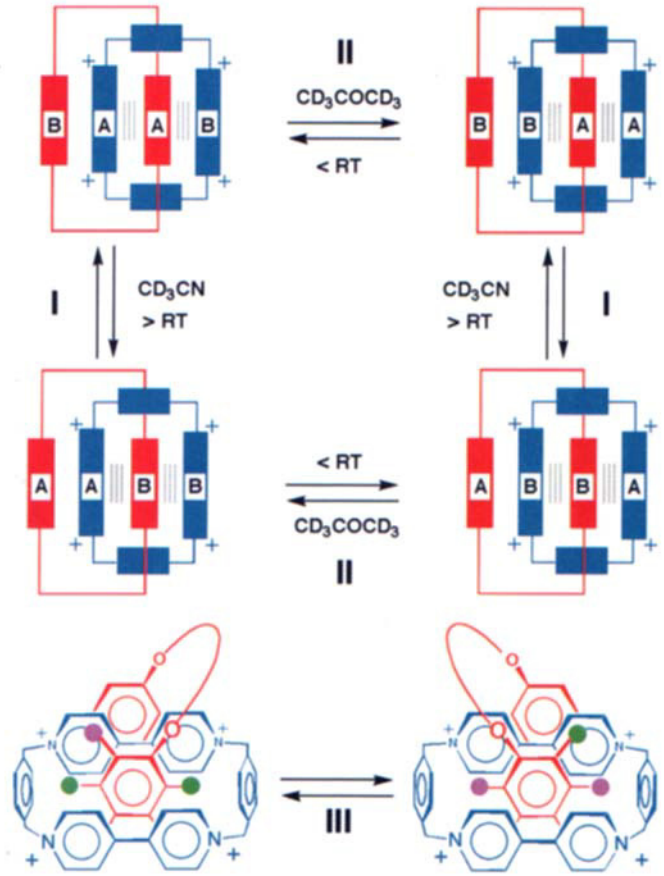

Fig. 68. The three dynamic processes that can occur within the [2]catenane. A detailed commentary is provided in the text.

the [2]catenane **88**·4PF_6 is remarkably robust and can tolerate the incorporation of both other crown ethers[265, 267] and the alteration of the bridging *p*-xylyl unit in the 83^{4+} ring.[265, 268]

To proceed from simple [2]catenane to higher [*n*]catenanes, one or other of the macrocyclic components must be enlarged. Reaction of the expanded crown ether **TPP68C20** with **85**·2PF_6 and **86** in dimethylformamide at room temperature and pressure affords, after appropriate workup, the [2]catenane **89**·4PF_6 in 12% yield (Fig. 69).[269] The dynamic processes characterizing the smaller [2]catenane **88**·4PF_6 also occur in **89**·4PF_6. However, the low-energy process, the pirouetting of the **TPP68C20** around the periphery of the 83^{4+} cyclophane, has a much lower energy barrier as a result of the larger cavity in **TPP68C20** and hence it occurs 28000 times per second at room temperature. The motion of the **TPP68C20** ring through the cavity of the 83^{4+} cyclophane can be observed by variable-temperature ^{1}H NMR spectroscopy. The 83^{4+} cyclophane visits each of the hydroquinone rings in turn as it moves round the perimeter of the **TPP68C20** macrocycle 300 times per second at room temperature—leading us to christen **89**·4PF_6 the "molecular train".[269] When the same catenane-forming reaction is repeated at 10 kbar pressure, the [3]catenane **90**·8PF_6, in which two 83^{4+} cyclophanes have been catenated with the **TPP68C20** macrocycle, is produced in 11% yield (Fig. 70).[269] As in **89**·8PF_6 the 83^{4+} cyclophanes in **90**·8PF_6 move between each of the hydroquinone units in the **TPP68C20** macrocycle. However, dynamic ^{1}H NMR spectroscopy shows that the symmetry

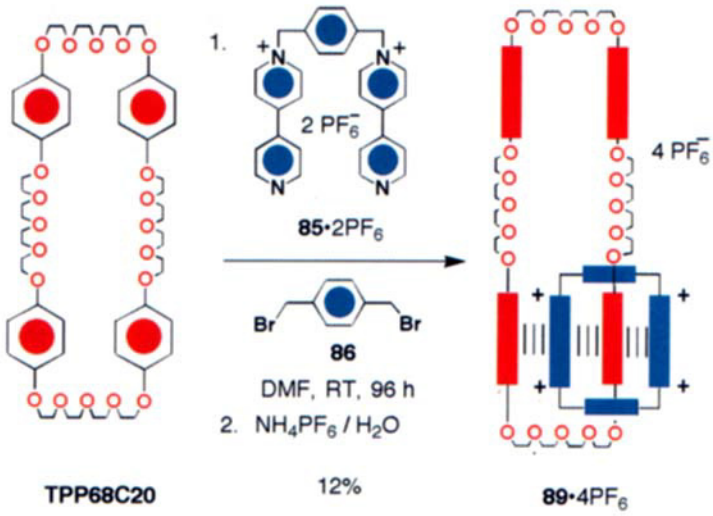

Fig. 69. The synthesis of a [2]catenane that behaves like a molecular train.

of the molecule is maintained. Hence, only the translational isomer[270] in which the 83^{4+} rings are separated by an uncomplexed hydroquinone ring is present in solution: on this "molecular merry-go-round" crashes do not happen.

Molecular modeling indicated that if the *p*-xylyl spacer in 83^{4+} is replaced by a *p*-bitolyl unit, it should be possible to accommodate two hydroquinone rings side-by-side simultaneously within the enlarged cyclophane cavity. The synthesis of this enlarged cyclophane has proven problematic.[271] However, when the dicationic precursor **91**·2PF_6 of the enlarged cyclophane was treated with bis(bromomethyl)biphenyl **92** in the presence of **BPP34C10** or alternatively **1/5DN38C10**, then the [3]catenanes **93**·4PF_6 and **94**·4PF_6 were produced in yields of 20 and 31%, respectively (Fig. 71).[272] Single-crystal X-ray structural analysis confirmed that two hydroquinone rings do indeed sit side-by-side in the 11 × 11 Å cavity of the charged macrocycle, and dynamic ^{1}H NMR spectroscopy showed that the dynamic processes observed in the other catenanes also oc-

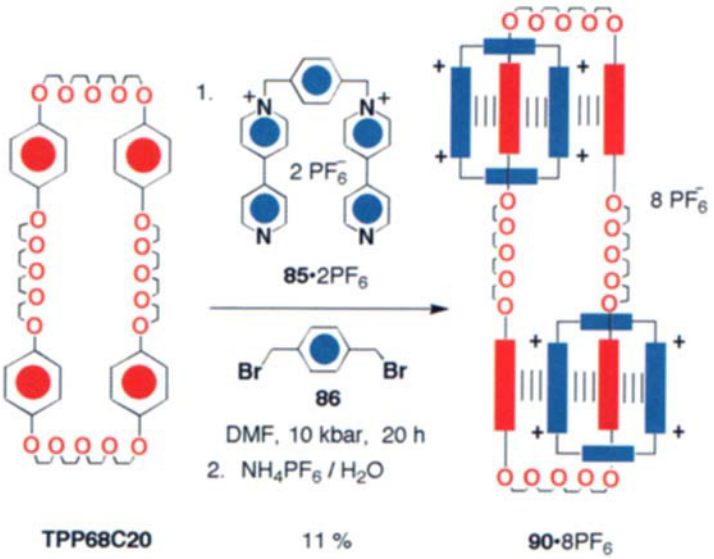

Fig. 70. The synthesis of a [2]catenane that behaves like a molecular merry-go-round.

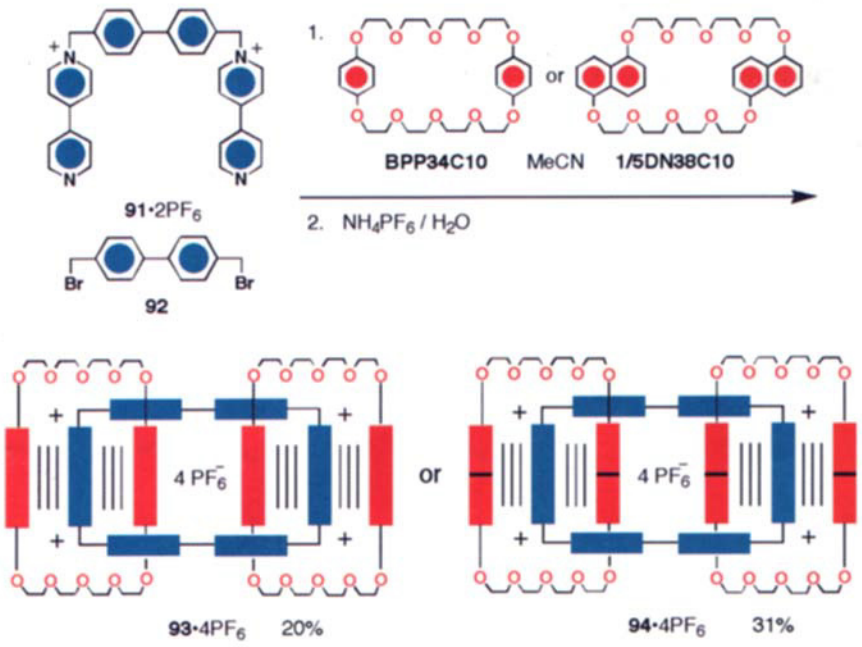

Fig. 71. The syntheses of [3]catenanes containing an enlarged tetracationic cyclophane.

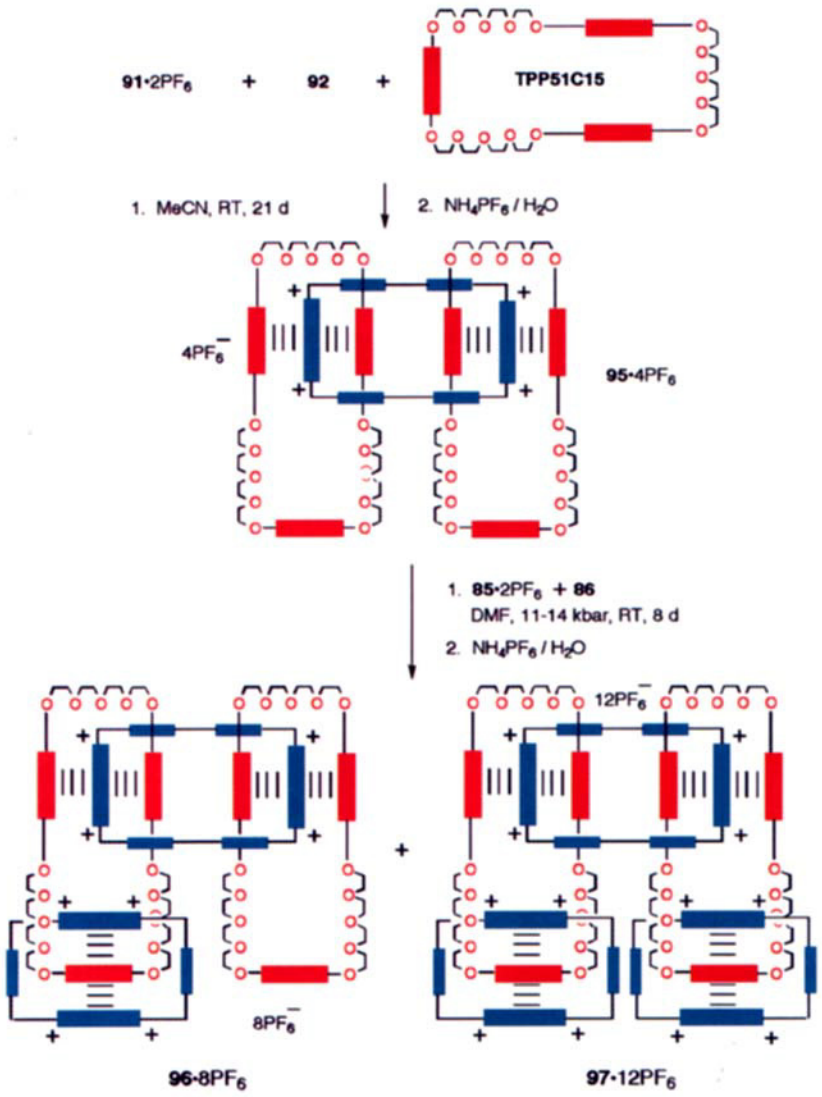

Fig. 72. The syntheses of a [4]- and a [5]catenane.

cur in these new [3]catenanes – the neutral rings circumrotate through the charged ring some 8000 times per second at room temperature.

The successful synthesis by self-assembly of the [2]catenane **89**·4PF_6 and the [3]catenanes **93**·4PF_6 and **94**·4PF_6 suggested to us that it may in fact be possible to construct a [5]catenane by combining these two syntheses. Hence, we anticipated that synthesis of **89**·4PF_6, followed by catenation with **91**·2PF_6 and **92**, could lead to a [5]catenane. Alternatively, we reasoned that it might be possible to synthesize a [3]catenane incorporating **TPP68C20** and the enlarged macrocycle derived from **91**·2PF_6, and subsequently catenate two **83**$^{4+}$ rings in a reaction analogous to that which produces **90**·8PF_6. Unfortunately, all of these expectations were unfulfilled. A reappraisal of the system suggested that the **TPP68C20** macrocycle might be too flexible to allow efficient molecular recognition to occur between it and the forming charged macrocycles. Hence, we decided to explore the use of a crown ether of intermediate size, namely **TPP51C15**, whose ring size is exactly halfway between that of the successful **BPP34C10** and the unsuccessful **TPP68C20**. Thus, reaction of **91**·2PF_6 and **92** in the presence of **TPP51C15** afforded the [3]catenane **95**·4PF_6 in 3.5% yield (Fig. 72).[273] Reaction of **95**·4PF_6 with **85**·2PF_6 and **86** under ultrahigh-pressure conditions afforded both the [4]catenane **96**·8PF_6 in 22% yield and a trace of the [5]catenane **97**·12PF_6. The reluctance of the [4]catenane **96**·8PF_6 to react with further **85**·2PF_6 and **86** was perplexing. This problem was eventually overcome by replacing the hydroquinone units in the crown ether by 1,5-dioxynaphthalene rings. Substitution of **1/5TN57C15** for the **TPP51C15** in the reaction scheme shown in Figure 72 led to the successful synthesis of macroscopic quantities of a [5]catenane, which was dubbed "Olympiadane" (Fig. 73a).[273] Dynamic ^{1}H NMR spectroscopy (Fig. 73b) attests to the high symmetry of this molecule. At 60 °C the ^{1}H NMR spectrum is remarkably simple showing that the motion of all of the catenated rings with respect to each other is fast on the NMR timescale.

The self-assembly of chiral catenated systems is also possible.[274, 275] Reaction of **85**·2PF_6, **98**, and **BPP34C10** in acetonitrile at room temperature for ten days afforded the bis([2]catenane) **99**·8PF_6 in 13% yield (Fig. 74).[274] This system shows remarkable selectivity during self-assembly for the reaction of *para*-related bromomethyl groups within **98**—the only catenated product isolated

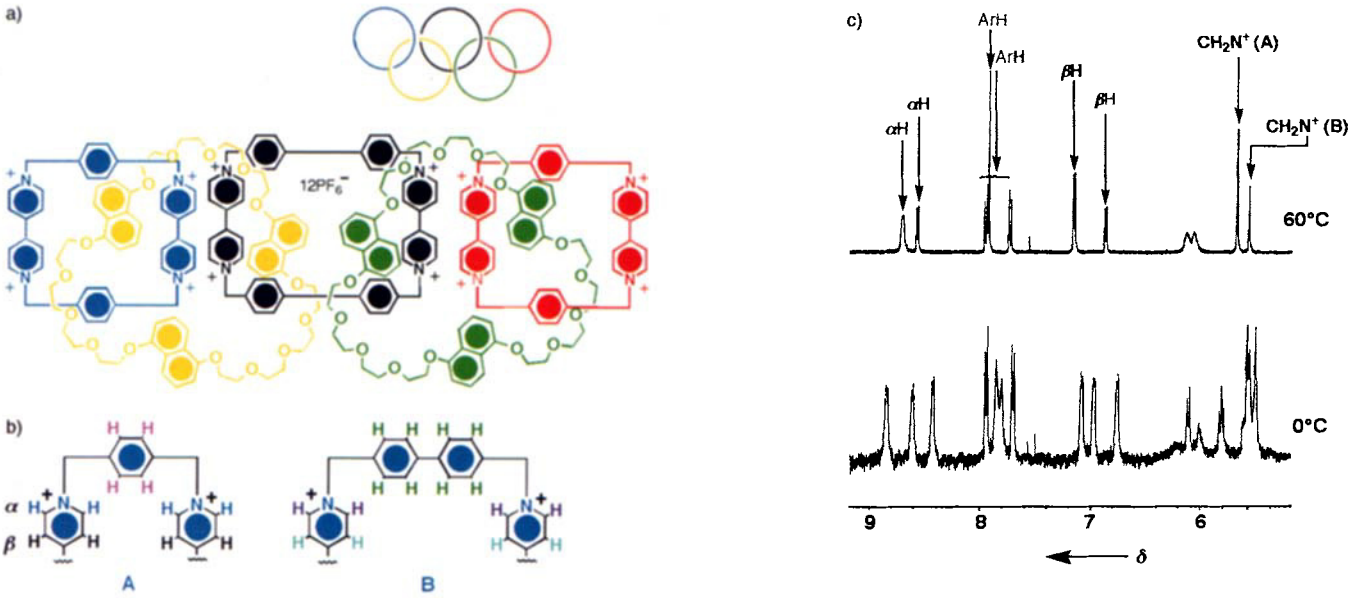

Fig. 73. Olympiadane: a) chemical structure, b) subunits for the assignment, and c) section of the 400 MHz ^{1}H NMR spectra at 0 and 60 °C. The small macrocycles colored blue, black, and red are labeled **A**; the large macrocycles colored yellow and green are labeled **B**.

is **99**·8 PF_6. This molecule has planar chirality, as evidenced by the observation of a highly diagnostic AB system for the four homotopic groups of diastereotopic benzylic methylene protons attached to the central tetrasubstituted benzene core. Interestingly, it is not possible to synthesize **99**·8 PF_6 from the tetracation **100**·4 PF_6 and **86** in the presence of **BPP34C10** (Fig. 74). This highly selective, one-step construction of a chiral bis([2]catenane) from five molecular components demonstrates clearly the power of our synthetic strategy based on self-assembly driven by molecular recognition between complementary π-donors and π-acceptors.

The control of the dynamic processes occurring within the catenated structures has also been investigated. Highly selective translational isomerism can be observed by altering the nature of the π-electron deficient or the π-electron rich component.[276]

Progress has also been made toward the construction of polymeric catenanes with the synthesis and characterization of two bis([2]catenanes) (Fig. 75).[277] In principle a polymeric structure can be achieved by linking π-electron rich components that have been catenated with a dimeric π-electron deficient component (Fig. 75a), or by linking π-electron deficient components that have been catenated with a dimeric π-electron rich component (Fig. 75b). The bis([2]catenanes) **101**·8 PF_6 and **102**·8 PF_6 are protoypes for these two approaches.

The utility of complementary π-donors and π-acceptors is not limited to the construction of catenated structures. [2]Rotaxanes can also be synthesized by self-assembly.[265] In the threading approach (Fig. 76a), the complexed diol is trapped by the addition of silyl ether blocking groups; in the clipping procedure (Fig. 76b), the tetracationic cyclophane is assembled around the dumbbell-shaped template. The successful synthesis of [2]-rotaxanes is not limited to these simple examples containing only one π-donor. Reaction of **85**·2 PF_6 and **86** in the presence of the bis(silyl ether) **103** affords the [2]rotaxane **104**·4 PF_6 in 32% yield (Fig. 77).[278] Since this [2]rotaxane contains two equivalent hydroquinone sites in the threadlike component, the charged ring darts back and forth between the two sites 1800 times per second at room temperature. If the solution is cooled to −50 °C, this shuttling motion ceases and the hydroquinone sites become nonequivalent, as indicated by the ^{1}H NMR spectrum. This type of system has been referred to as a "molecular shuttle". Such molecular shuttles could form the basis for molecular scale devices. Replace-

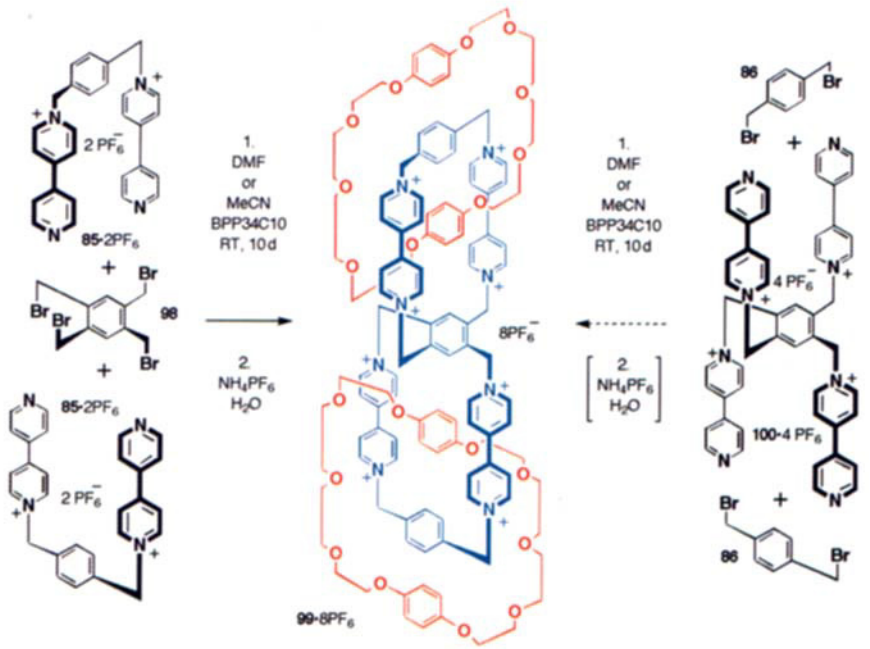

Fig. 74. The synthesis of a chiral bis([2]catenane). Note that the bis([2]catenane) can be formed from its components by only one of the two possible methods.

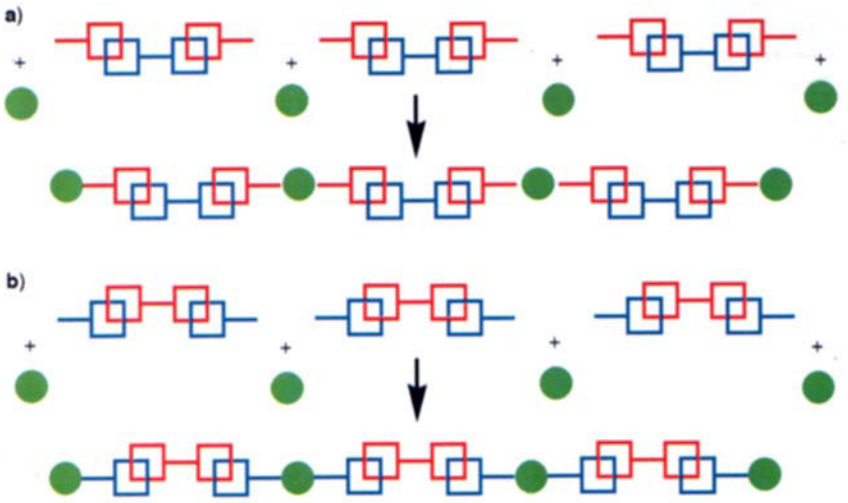

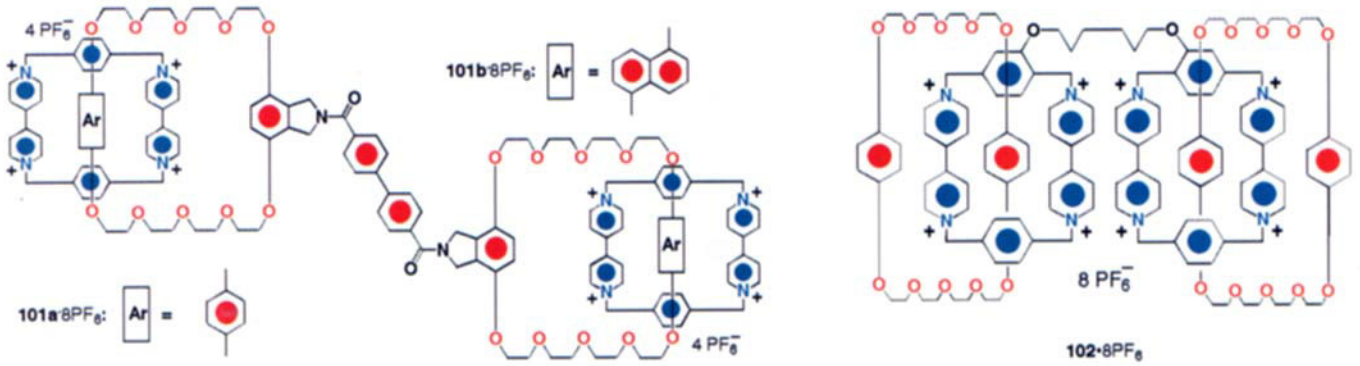

Fig. 75. Conception (a, b) for the synthesis of two series of polymeric catenanes and prototypes of the corresponding starting compounds, **101** and **102**.

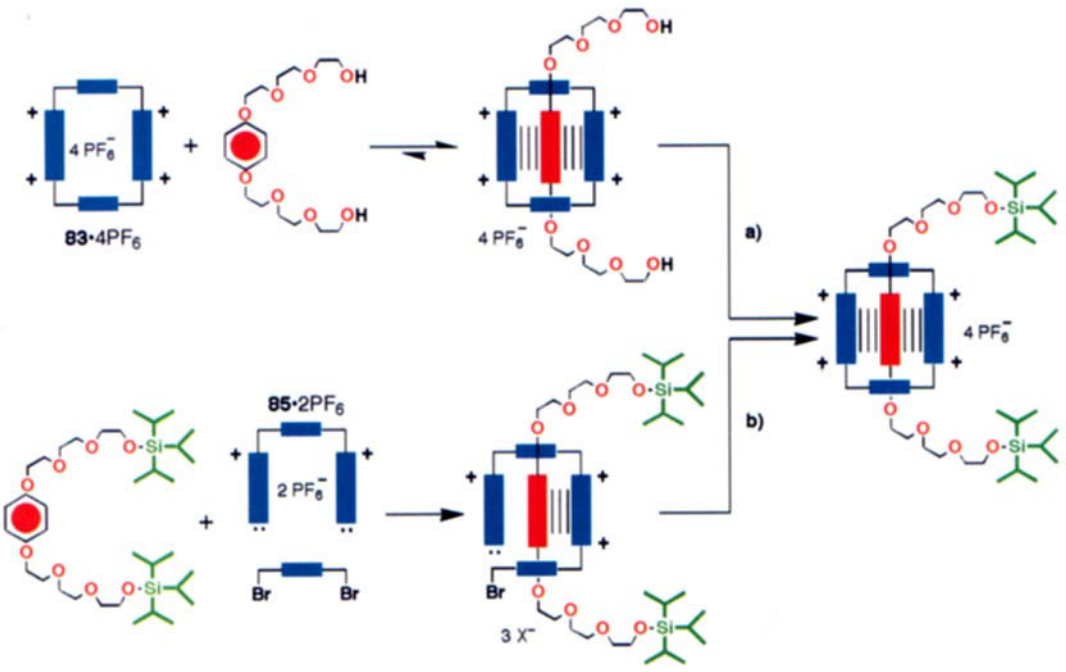

Fig. 76. The self-assembly of [2]rotaxanes directed by complementary π-donors and π-acceptors through a) threading and b) clipping.

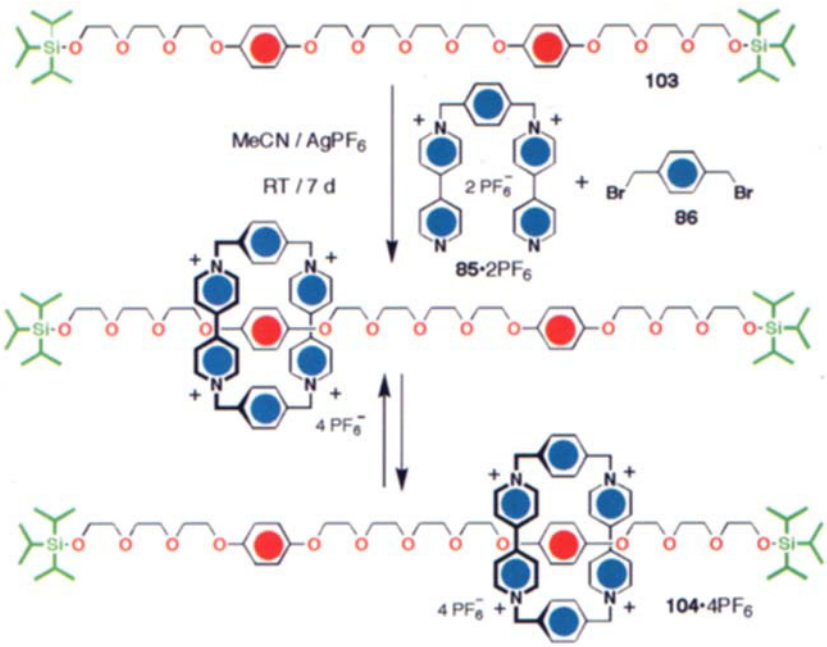

Fig. 77. The self-assembly of a [2]rotaxane, which behaves as a molecular shuttle, by a clipping procedure directed by complementary π-donors and π-acceptors.

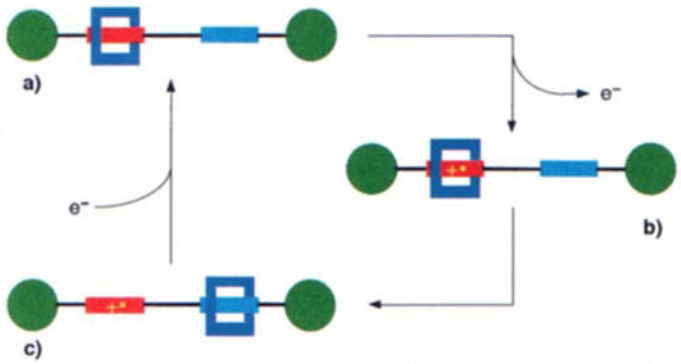

Fig. 78. Electrochemical control of the position of the tetracationic cyclophane in a molecular shuttle (see text for details).

ment of one of the twohydroquinone rings with another unit of either lesser or greater π-donating ability (colored red and light blue, respectively, in Fig. 78), should, in principle, cause the charged macrocycle to be localized in the ground state. In general, the tetracationic cyclophane will be localized at the site of greatest π-donating ability (a). One can then envisage oxidation of the occupied π-donor to form a radical cation (b), drastically reducing the donating ability of this site to a level below that of the second, poorer π-donor site. Hence, the charged ring would then be expected to move along the thread to the second π-donor site (c). Reversal of the electrochemical cycle should return the system to the starting position, thus effecting an off–on–off switching cycle. Three such systems have been designed and studied.[258, 279, 280] The first system incorporated a hydroquinone ring as the better π-donor and a *p*-xylyl unit as the poorer π-donor (Fig. 79a).[279] Unfortunately, the tetracationic macrocycle partitions itself between the two π-donor sites, with 70% occupation of the hydroquinone site and 30% occupation of the *p*-xylyl site at −30 °C. Such partitioning leads to severe complications for the electrochemical control of the cyclophane position. The second system incorporated within its dumbbell component an indole unit as the better π-donor and a hydroquinone as the poorer π-donor (Fig. 79b).[258] In this case, contrary to our expectations, the tetracationic cyclophane occupied the hydroquinone site preferentially, rendering this molecular shuttle functionally incompetent. In the third-generation system,[280] a tetrathiafulvalene (TTF) unit[281] served as the better π-donor and two equivalent hydroquinone rings as the poorer π-donors within the dumbbell component (Fig. 79c). The position of the tetracationic cyclophane within this system shows an interesting solvent dependency. In CD_3COCD_3 at room temperature the cyclophane is located exclusively on one of the hydroquinone rings. However, in CD_3SOCD_3 the cyclophane partitions itself between the TTF residue and the hydroquinone rings (3:1). The addition of small amounts of D_2O to a CD_3SOCD_3 solution of the [2]rotaxane shifts the equilibrium further in favor of occupation of the

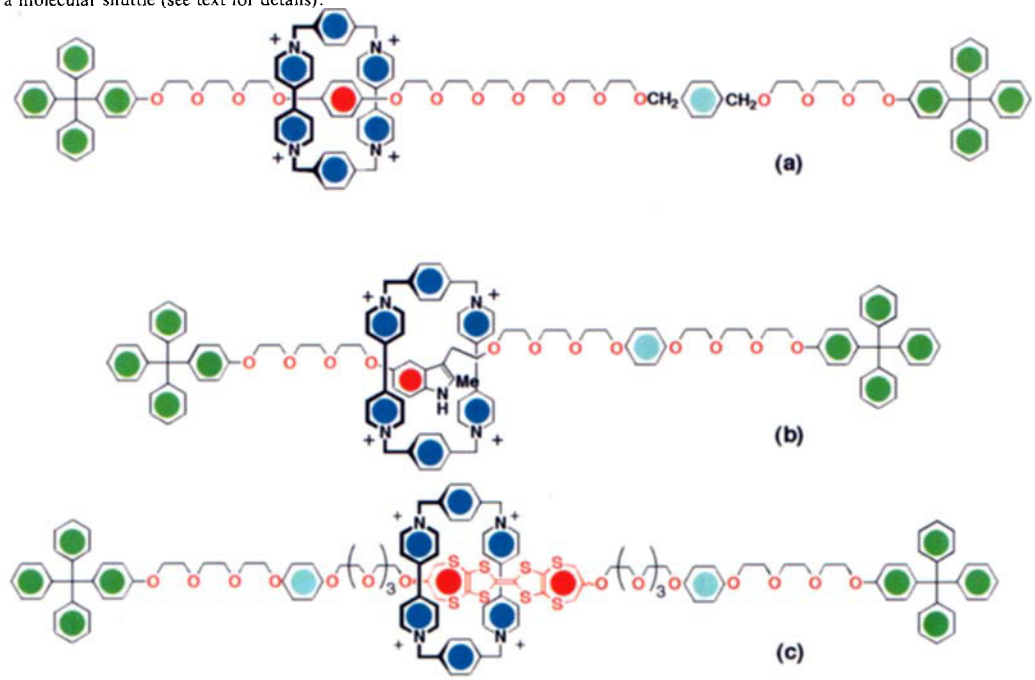

Fig. 79. Three prototypes of controllable molecular shuttles.

TTF residue, thus rendering electrochemical control of this system experimentally feasible.

The synthesis of a chemically and electrochemically switchable molecular shuttle has now been achieved utilizing the same basic design principles.[282] By designating a biphenol residue as the poor π-donor and a benzidine moiety as the good π-donor, control of the position of the tetracationic cyclophane within the molecular shuttle **105**·4PF_6 can be achieved by either chemical or electrochemical means (Fig. 80). In the ground state, the benzidine:biphenol site occupancy is 84:16 in CD_3CN at 229 K. Upon addition of trifluoroacetic acid, the benzidine nitrogen atoms are protonated, and tetracation occupies the biphenol site exclusively. The original site occupancy can be restored by the addition of pyridine to the solution. Electrochemical oxidation of the benzidine moiety, generating the corresponding radical cation, also results in a similar change in site occupancy.

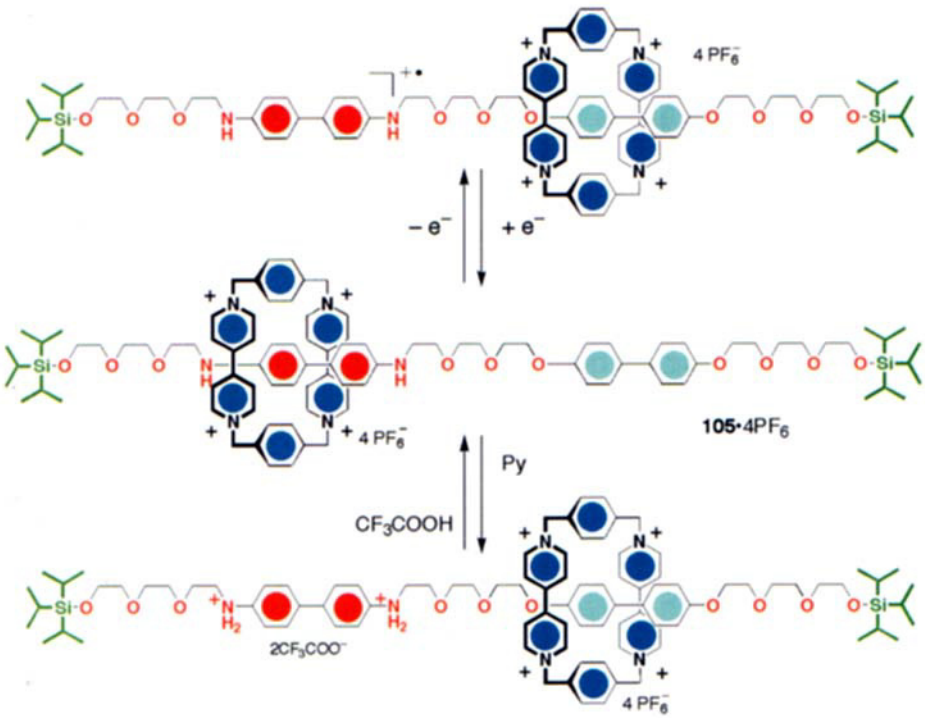

Fig. 80. Electrochemical and chemical control of the translational isomerism in a molecular shuttle based on complementary π-donors and π-acceptors. Py = pyridine.

The redox processes required to drive a molecular shuttle need not be driven electrochemically; photochemical control is also possible. We have demonstrated a simple photochemically driven molecular machine (Fig. 81).[283] When the cyclophane **83**·4Cl and the diol **106** are mixed in deaerated 0.1 M sodium acetate solution, a strong, pseudorotaxane-like complex [**83**·**106**]·4Cl forms, which has a characteristic purple color due to a CT absorption centered on 520 nm. In addition, the fluorescence of the naphthalene ring in **106** is quenched. 9-Anthracenecarboxylic acid, a photosensitizer (**PS**) whose excited state is a powerful reductant, is added and the system is irradiated. Electrons are transferred from **PS** to the [**83**·**106**]·4Cl complex, reducing the $\mathbf{83}^{4+}$ cyclophane to the $\mathbf{83}^{3+}$ radical cation (Fig. 81). To prevent the fast back electron-transfer reaction from $\mathbf{83}^{3+}$ to **PS**, a sacrificial reductant, triethanolamine, is added to reduce **PS** back to its ground state. The interaction between the reduced cyclophane $\mathbf{83}^{3+}$ and **106** is no longer strong enough to hold the complex together, and so dissociation occurs and the fluorescence of the naphthalene ring in **106** reappears. Under the experimental conditions 35% of the pseudorotaxane was unthreaded after 25 minutes of irradiation. The pseudorotaxane can be rethreaded by allowing oxygen to enter the system, whereupon $\mathbf{83}^{3+}$ is promptly reoxidized to $\mathbf{83}^{4+}$ and the [**83**·**106**]·4Cl complex reforms. The ideas demonstrated by this system can be incorporated into molecular shuttles in which the photosensitizer is located in one of the stoppers. A prelude to this type of system is the successful synthesis[284] of a porphyrin-stoppered molecular shuttle.[285]

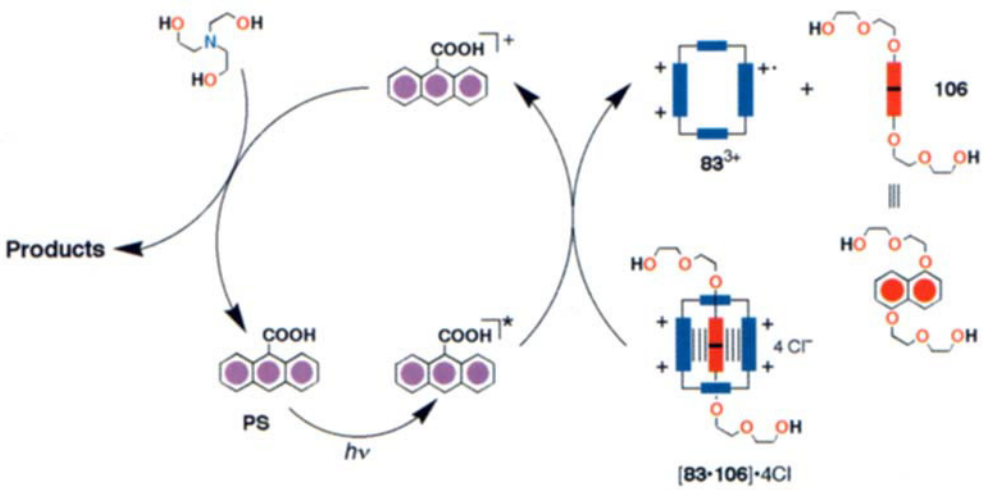

Fig. 81. A simple photochemically driven molecular machine.

The successful control of these supramolecular processes leaves us with three major challenges: firstly, to achieve the control processes in a more facile and selective manner, secondly, to improve the material properties of the compounds we synthesize, and thirdly, to connect our controllable systems to the outside world.

Up to this point we have been concerned with molecular shuttles in which the π-donors have been located in the dumbbell-shaped component and the π-acceptors have been located in the macro-

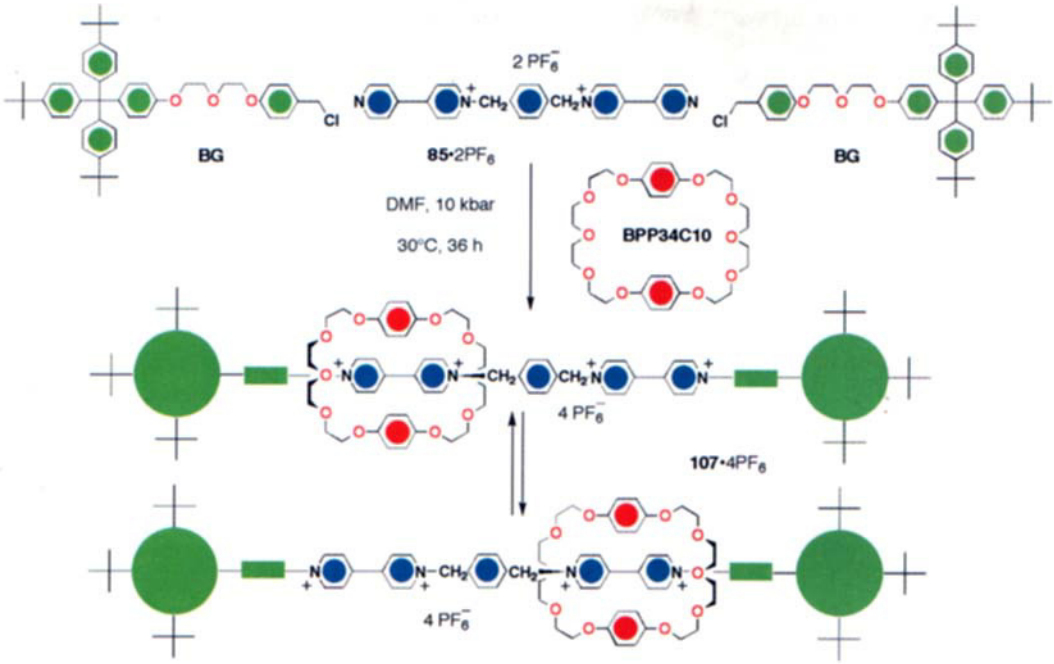

Fig. 82. The self-assembly of a [2]rotaxane, which behaves as a molecular shuttle, directed by complementary π-donors and π-acceptors.

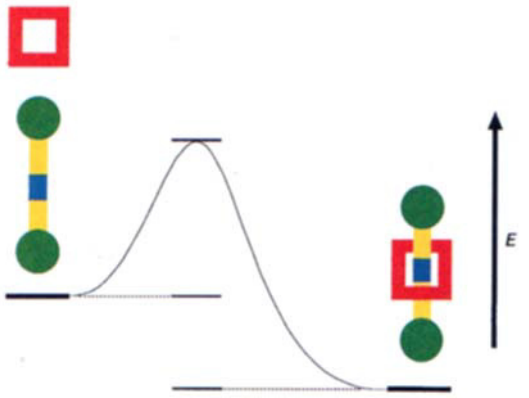

Fig. 83. The energy diagram for rotaxane synthesis by slippage. The molecular recognition between dumbbell and macrocycle provides a thermodynamic trap.

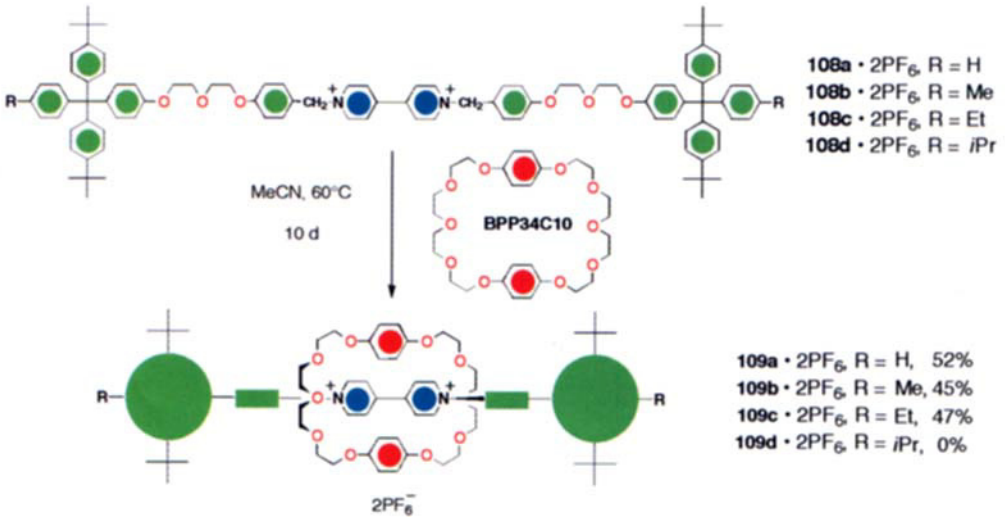

Fig. 84. The syntheses of simple [2]rotaxanes by a slippage route.

cyclic component. There is, of course, no fundamental reason for choosing this design logic; it should be possible to invert the design logic and place the π-donors within the macrocyclic component and the π-acceptors within the dumbbell-shaped component. Thus, reaction of **85**·2PF$_6$ with an appropriately designed blocking reagent **BG** together with **BPP34C10** in stoichiometric amounts affords the molecular shuttle **107**·4PF$_6$ in 23% yield (Fig. 82).[286] Dynamic ^{1}H NMR spectroscopy reveals that the **BPP34C10** macrocycle moves between the two equivalent paraquat sites 340000 times per second at room temperature. The reaction forming **107**·4PF$_6$ seems to show some selectivity since the major product of the reaction is the [2]rotaxane and not the [3]rotaxane in which two **BPP34C10** rings have been incorporated. The observed selectivity depends on the reaction conditions, but is in the region of 10:1 in favor of the [2]rotaxane. Thus, if we wish to obtain a [3]rotaxane incorporating two **BPP34C10** rings, an alternative strategy must be sought. We reasoned that if the large stoppers at the ends of the dumbbell-shaped component were the right size, **BPP34C10** could slip over the stoppers (Fig. 83) at elevated temperatures. The mutual interaction of the π-donors within the crown ether and the π-acceptors within the dumbbell-shaped component then provides a "thermodynamic trap" for the **BPP34C10** macrocycle, raising the activation energy for extrusion of the **BPP34C10**, and so rendering the [2]rotaxanes thus formed stable at room temperature. Hence, heating the dumbbell-shaped compounds **108a**·2PF$_6$–**108d**·2PF$_6$ with an excess of **BPP34C10** in acetonitrile at 60 °C for ten days permitted the isolation of the [2]rotaxanes **109a**·2PF$_6$–**109c**·2PF$_6$ in 45 to 52% yield (Fig. 84).[287] The [2]rotaxane **109d**·2PF$_6$ could not be formed in isolable quantities under these reaction conditions. Examination of the relative rates of slippage revealed that for **108d**·2PF$_6$, slippage was ten times slower than for **109a**·2PF$_6$–**109c**·2PF$_6$. The concept of slippage can be extended to the synthesis of the [3]rotaxanes mentioned above, which are inaccessible by other means. Thus, reac-

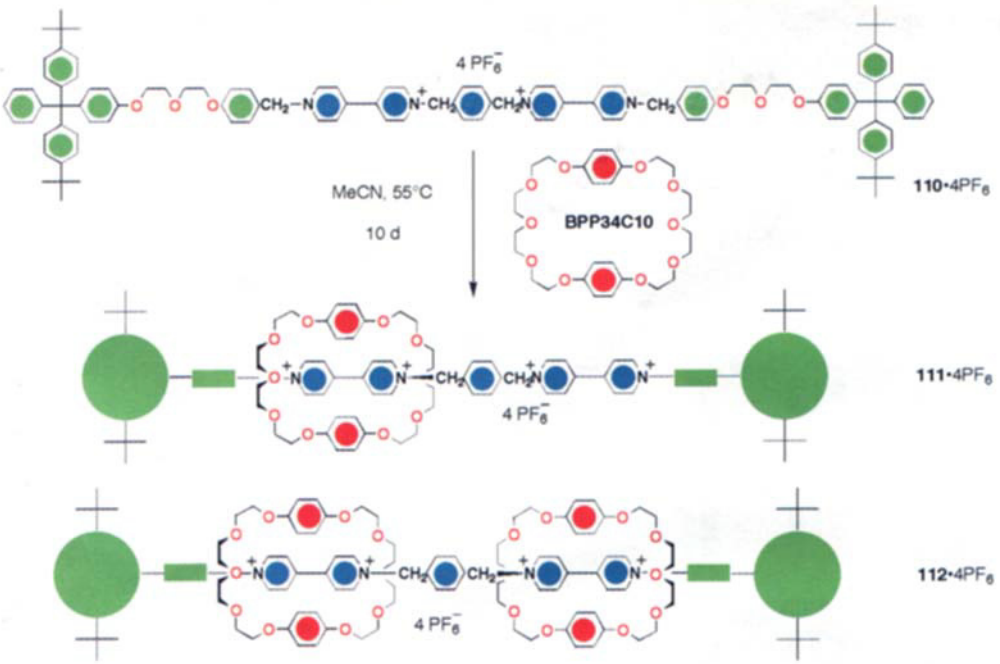

Fig. 85. The syntheses by slippage of [2]- and [3]rotaxanes.

tion of **110**·4PF$_6$ with an threefold excess of **BPP34C10** in acetonitrile at 55 °C for ten days affords both the [2]rotaxane **111**·4PF$_6$ in 31% yield and the [3]rotaxane **112**·4PF$_6$ in 8% yield (Fig. 85).[287] The yields of **111**·4PF$_6$ and **112**·4PF$_6$ could be increased to 20 and 55%, respectively, when a tenfold excess of **BPP34C10** was employed under the same conditions. The ^{1}H NMR spectra of **111**·4PF$_6$ display a temperature dependence commensurate with its properties as a molecular shuttle. In contrast, the ^{1}H NMR spectrum of **112**·4PF$_6$ shows the **BPP34C10** rings to be static and localized on the two paraquat residues as expected. Thus, it can be seen that slippage is an important third method of rotaxane synthesis, which exploits two features fundamental to supramolecular chemistry—size-complementarity (between macrocycle and stoppers) and mutual, noncovalent interactions (as a thermodynamic trap). The slippage approach may be extended to the construction of branched [*n*]rotaxanes (Fig. 86).[288, 289] These systems may be regarded as the first step on the road toward dendritic rotaxanes as well as polyrotaxanes.[289]

For error-checking to be possible in self-assembly processes, the pathways must operate under equilibrium control; in other words, the final assembly is the thermodynamic product for the system. Other methods of selection can operate in systems that utilize intermittent processing. The demonstration of kinetic selection in [2]catenane assembly illustrates this point.[290] In a system in which competing reactions can occur (Fig. 87), the product ratios reflect, not the relative binding efficiencies (*K* or *K'*), for example between the crown ethers and 4,4'-bipyri-

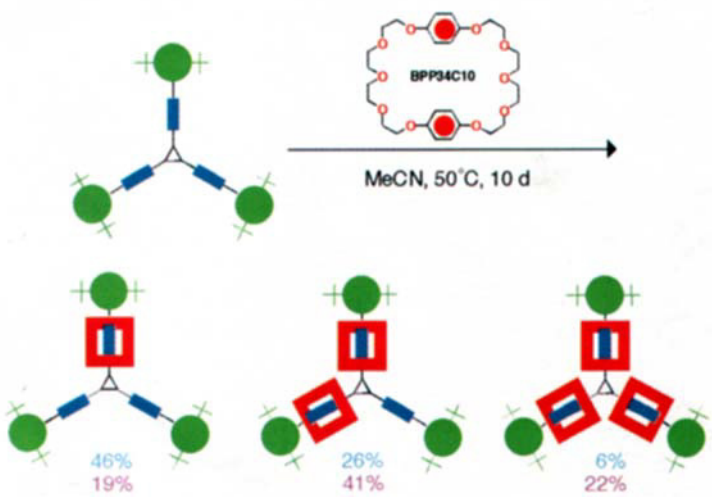

Fig. 86. Towards dendritic polyrotaxanes. The syntheses of branched [2]-, [3]-, and [4]rotaxanes by slippage. The yields in light blue refer to reactions with 2 molar equivalents of **BPP34C10**, those in pink with 15 molar equivalents. In the cartoon representation the formal charges have been omitted for clarity from the blue blocks representing the 4,4'-bipyridinium dications.

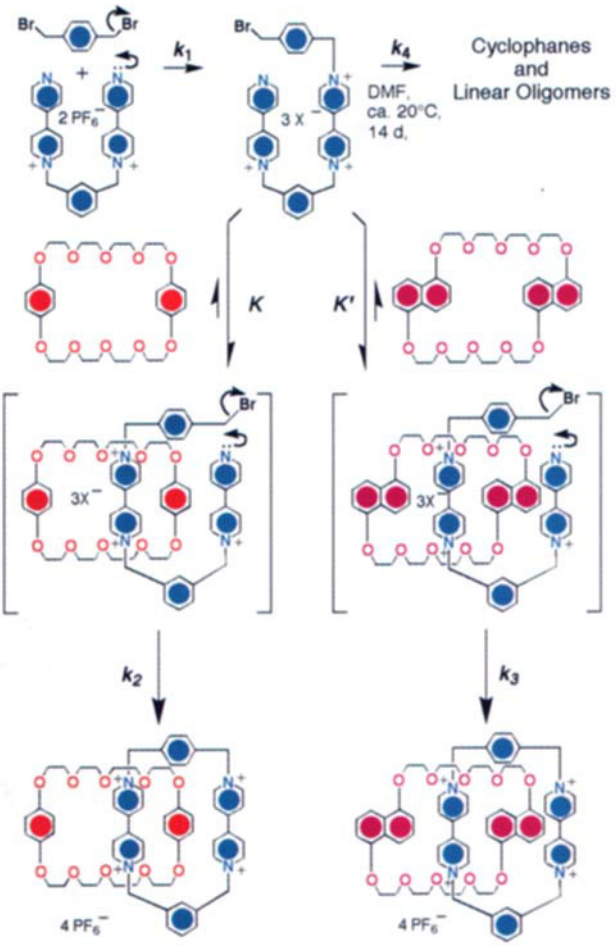

Fig. 87. Kinetic selection in the self-assembly of [2]catenanes. (The products are obained as PF$_6$ salts after ion exchange with NH_4PF_5/H_2O.)

dinium dications, but rather the rate at which the final bond-forming step occurs (k_2 or k_3). In other words, the structure that predominates is selected kinetically, not thermodynamically, during the self-assembly process; Curtin–Hammett type kinetics[291] are operating.

Recently, it has proven possible to combine π-electron deficient and π-electron rich recognition sites within the same molecule to create the self-complementary cyclophane **113**·4PF$_6$ (Fig. 88).[292] The X-ray crystal structure of **113**·4PF$_6$ reveals a

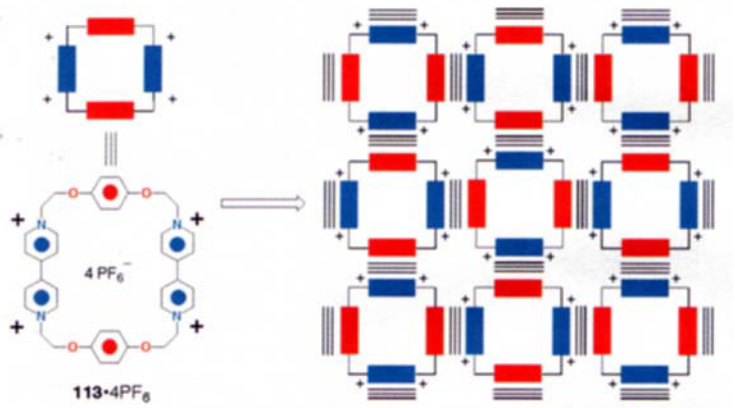

Fig. 88. Schematic representation of the X-ray crystal structure of the molecular mosaic formed by the self-complementary cyclophane **113**·4PF$_6$.

remarkable degree of ordering. The cyclophane itself is almost square and packs in layers in which each cyclophane is rotated 90° with respect to its neighbors. This packing arrangement results in a two-dimensional π-acceptor/π-donor mosaic in the solid state (Fig. 88). Even though adjacent sheets of cyclophanes are separated by counterions and solvent, the cyclophanes are in register and form continuous channels about 1 nm square in the third dimension of the structure. The cyclophane is capable of binding ferrocene,[293] and the crystal structure of this adduct retains the structural features of the free macrocycle. The information present in the self-complementary cyclophane facilitates the efficient self-assembly of a regular three-dimensional supramolecular array in the solid state.

Self-assembling systems based on neutral π-donors and positively charged π-acceptors are particularly easy to design and construct.[294] They give rise to molecular and supramolecular systems with the kinds of physical and chemical properties that make them attractive to work with from the point of view of their forms (for example, depending on the counterion, they are soluble in a wide range of solvents) and their functions (for example, mechanical behavior can be controlled by altering redox properties).

5. The Messages from Self-Assembly

There is no doubt that self-assembly can be utilized to construct a wide diversity of structural types with apparent ease. This situation is a result of the inherent synthetic advantages offered by self-assembly processes.

- Self-assembly can utilize both covalent and *noncovalent* bonding. Hence, noncovalently driven self-assembly can be used to create a primary structure which may be captured and consolidated upon by the subsequent formation of covalent bonds.
- Self-assembly often operates under *equilibrium control*. Thus, a growing structure can reorganize during assembly to maximize complementary surface contacts. The final structure thus represents the thermodynamic minimum for a particular collection of atoms with a given connectivity.
- Self-assembly is, more often than not, a *cooperative* process.
- Self-assembly is *efficient*. A large structure requires a small number of subunit types. Its assembly is *error-checking* and defective recognition features in a subunit are rejected.
- Synthesis is *convergent*. Thus, the synthetic load is significantly lighter.

It follows that, as a synthetic tool, self-assembly has much to offer the chemist.[295] In this review we have met examples in chemical systems of self-assembly that utilize three basic types of interactions. The first type is nonspecific and it operates in the case of the cyclodextrins. This approach has the advantage of being an essentially off-the-shelf model. However, the information content of the system, depending as it does on the hydrophobic effect, is largely nonspecific. The second type is specific and depends upon highly directional interactions such as hydrogen bonding and metal–ligand interactions. These two systems have high information contents as a consequence of the very specific interaction geometries involved. However, the use of such interactions for the construction of large-scale structures requires a high degree of design of the complementary components for the precise matching of hydrogen bonding or the existence of a satisfactory metal–ligand geometry. Self-assembling systems based on interactions between π-donors and π-acceptors fall into an intermediate class. Although they are reasonably specific and hence have a moderate information content and are somewhat directional, they do not require highly regulated design features to function successfully in a self-assembling system.

The establishment of efficient synthetic routes for the construction of nanometer-scale architectures is of paramount importance if the goals of molecular electronics are to be realized. To achieve this aim, the art of chemical synthesis must undergo a profound revolution. Conventional chemical synthesis relies heavily on the use of protecting groups and sophisticated reagents and catalysts to introduce relatively small groups, in terms of molecular mass, in a controlled and stepwise manner. It is difficult to see how this approach can be applied successfully to the construction of mesomolecular systems. Biological systems demonstrate clearly the advantages to be gained by employing what is tantamount to a conceptual leap in synthetic strategy, away from the methods used traditionally in the preparation of small molecular systems, toward construction by self-assembly and self-synthesis. In Nature, processes such as light harvesting, which are apparently very difficult for the scientist to mimic, are accomplished by use of complex systems that are constructed with apparent ease by the processes of self-organization and self-assembly. The research described in this review demonstrates that the chemist, by appropriate choice of noncovalently interacting species, can begin to mimic some of the synthetic strategies so prevalent in Nature. The use of "intelligent substrates", preprogrammed with all of the stereoelec-

tronic information necessary to define molecular recognition within a superstructure, for the assembly of large mesomolecular superstructures such as pseudorotaxanes and double helices or organized molecular assemblies such as catenanes and rotaxanes, demonstrates that self-assembly is a viable synthetic paradigm for the construction of nanometer-scale structures and that there are inherently simple and efficient methods for constructing complex unnatural products without the need for external reagent control or catalysis. At present, the function of the wholly synthetic mesomolecular structures constructed by self-assembly processes is largely unimportant. The development of self-assembly as a viable synthetic paradigm for the efficient construction of nanometer-scale structures and the establishment of the principles governing its use are more important. In any case, the "engineering up" approach to molecular electronic devices requires the construction of not only the devices themselves, but also the infrastructure to serve them—scaffolds to support the devices and a means to connect them to the outside world. Self-assembly offers a synthetic method capable of providing many of these things. It is somewhat ironic that synthetic chemists have developed *wholly unnatural methods* for the synthesis of *natural products*, yet the *wholly unnatural products* required in the quest for molecular electronic devices will be constructed using principles such as self-organization, self-assembly, self-synthesis, and self-replication, which are *natural in origin*.

6. Reflections and Rewards

What has self-assembly to offer to chemists and chemistry in particular, and scientists and science in general? Hopefully, the short commentary[296] that follows will encourage the reader to reflect for a few minutes and then decide that it is actually quite a lot—particularly if the reader is a chemist!

Chemistry can be likened to "language". The atoms are the "letters". The molecules are the "words". Assemblies of molecules make up the "sentences". The sets of assembled molecules or supermolecules are the "paragraphs". The ways in which the molecular assemblies and supramolecular arrays contain and express information are the "chapters". The manner in which this information is conveyed at both a molecular level is the "book". Ultimately, chemistry has to tell a "story". The life sciences are composed of really wonderful chemical "stories". They have been written by nature using "ancient languages".

Chemists are just starting to write their own "stories". They know how to produce the "words". Now, they are learning how to write the "sentences". The "grammar" they will use will be dictated by the nature of the noncovalent bond. The "modern languages" are about to evolve. Materials science and the life sciences will be a beneficiaries. As a discipline, chemistry will be enriched.

There are always many people and organizations it is a pleasure to thank. In particular, we would like to express our gratitude to the University of Birmingham for providing us with contemporary surroundings and a stimulating environment in which to do science. We are indebted to the many funding bodies including the Research Councils in the United Kingdom, European government agencies, the European Community, charities and industrial companies, who have provided the financial support necessary to push our science forward during recent years. None of the research described in Section 4.4 would have been achieved without the contributions of the many talented postgraduate and postdoctoral co-workers whose names appear in the references. Collaboration is right at the heart of scientific discovery. We have been fortunate to have enjoyed many collaborations over the years, but those with Professors Vincenzo Balzani (Bologna), Angel Kaifer (Miami), Helmut Ringsdorf (Mainz), and David Williams (London) have been particularly rewarding. Finally, we would like to thank Professor François Diederich for his critique of an earlier incarnation of the text of this review.

Received: August 30, 1995 [A134IE]
German version: *Angew. Chem.* **1996**, *108*, 1242–1286

[1] R. P. Feynman, *Eng. Sci.* **1960**, *23(2)*, 22; *Sat. Rev.* **1960**, *43* (April 2), 45.
[2] A. S. Moffat, *MOSAIC* **1990**, *21*, 30.
[3] K. E. Drexler, *Engines of Creation*, Fourth Estate, London, **1990**; *Nanosystems: Molecular Machinery Manufacturing and Computation*, Wiley, New York, **1992**; *Annu. Rev. Biophys. Biomol. Struct.* **1994**, *23*, 377.
[4] *Equinox–Little by Little*, Channel 4 Television Publications, London, **1989**; E. Regis, *Nano! Remaking the World Atom by Atom*, Brown/Bantam, **1995**.
[5] C. H. Bennett, *Int. J. Theor. Phys.* **1982**, *21*, 905.
[6] R. P. Feynman, *Found. Phys.* **1986**, *16*, 507.
[7] M. J. Little, J. Grinberg, *Byte* **1988**, *13(12)*, 311.
[8] A. L. Robinson, *Science* **1984**, *223*, 267.
[9] M. A. Clarkson, *Byte* **1989**, *14(5)*, 268.
[10] F. L. Carter, *NRL Memo. Rep.* **1979**, *3960*, 121.
[11] J. R. Barker, *Hybrid Circuits* **1987**, *14(9)*, 19.
[12] D. Haarer, *Angew. Chem. Adv. Mater.* **1989**, *101*, 1576; *Angew. Chem. Int. Ed. Engl. Adv. Mater.* **1989**, *28*, 1544; *Adv. Mater.* **1989**, *1*, 362.
[13] R. C. Haddon, A. A. Lamola, *Proc. Natl. Acad. Sci. USA* **1985**, *82*, 1874.
[14] J. S. Miller, *Adv. Mater.* **1990**, *2*, 378, 495, 601.
[15] H. Kuhn in *Molecular Electronics* (Ed.: F. T. Hong), Plenum, New York, **1989**, p. 5.
[16] F. L. Carter, *Physica D (Amsterdam)* **1984**, *10*, 175.
[17] H. Kuhn, J. Waser, *Angew. Chem.* **1981**, *93*, 495; *Angew. Chem. Int. Ed. Engl.* **1981**, *20*, 500.
[18] M. Eigen, P. Schuster, *The Hypercycle*, Springer, Berlin, **1979**.
[19] J. S. Lindsey, *New J. Chem.* **1991**, *15*, 153; "Host–Guest Interactions: From Chemistry to Biology": J. F. Stoddart, *Ciba Found. Symp.* **1991**, *158*, 5; D. S. Lawrence, T. Jiang, M. Levett, *Chem. Rev.* **1995**, *95*, 2229.
[20] G. M. Whitesides, J. P. Mathias, C. T. Seto, *Science* **1991**, *254*, 1312.
[21] A. Klug, *Angew. Chem.* **1983**, *95*, 579; *Angew. Chem. Int. Ed. Engl.* **1983**, *22*, 565.
[22] A collection of papers under on the topic "Assembly Mechanisms": *J. Supramol. Struct.* **1974**, *2*, 81.
[23] A collection of papers on the topic "Macromolecular Assembly Analysed by Converging Structural Techniques": *Biophys. J.* **1986**, *49(1)*, 1.
[24] *Self-Assembling Architecture* (Ed.: J. E. Varner), Alan R. Liss, New York, **1988**.
[25] L. Stryer, *Biochemistry*, 3rd ed., W. H. Freeman, New York, **1988**, p. 852.
[26] H. Fraenkel-Conrat, R. C. Williams, *Proc. Natl. Acad. Sci. USA* **1955**, *41*, 690.
[27] M. A. Lauffer, *Entropy-Driven Processes*, Springer, New York, **1975**.
[28] G. Lebeurier, A. Nicholaieff, K. E. Richards, *Proc. Natl. Acad. Sci. USA* **1977**, *75*, 150.
[29] E. J. Corey, X. M. Cheng, *The Logic of Chemical Synthesis* Wiley, New York, **1989**; E. J. Corey, *Angew. Chem.* **1991**, *103*, 469; *Angew. Chem. Int. Ed. Engl.* **1991**, *30*, 455.
[30] K. C. Nicolaou, E. J. Sorensen, *Classics in Total Synthesis*, VCH, Weinheim, **1996**.
[31] C. R Cantor, P. R. Schimmel, *Biophysical Chemistry, Part III*, W. H. Freeman, San Francisco, **1980**, p. 1215.
[32] D. Pörschke, M. Eigen, *J. Mol. Biol.* **1971**, *62*, 361.
[33] D. Pörschke, in *Chemical Relaxation in Molecular Biology* (Eds.: I. Pecht, R. Rigler), Springer, Berlin, **1977**, p. 191.
[34] M. E. Craig, D. M. Crothers, P. Doty, *J. Mol. Biol.* **1971**, *62*, 383.
[35] W. Saenger, *Principles of Nucleic Acid Structure*, Springer, New York, **1984**, p. 116.
[36] C. B. Anfinsen, *Science* **1973**, *181*, 223.
[37] C. J. Epstein, R. F. Goldberger, C. B. Anfinsen, *Cold Spring Harbor Symp. Quant. Biol.* **1963**, *28*, 439.
[38] C. B. Anfinsen, *Harvey Lect.* **1967**, *61*, 95.
[39] A. Hershko, M. Fry, *Annu. Rev. Biochem.* **1975**, *44*, 775.
[40] M. Kirschner, T. Mitchison, *Cell* **1986**, *45*, 329.

[41] S. Altman, *Angew. Chem.* **1990**, *102*, 735; *Angew. Chem. Int. Ed. Engl.* **1990**, *29*, 749.

[42] T. R. Cech, *Sci. Am.* **1986**, *255(5)*, 76; *Angew. Chem.* **1990**, *102*, 745; *Angew. Chem. Int. Ed. Engl.* **1990**, *29*, 759.

[43] T. R. Cech, B. L. Bass, *Annu. Rev. Biochem.* **1986**, *55*, 599; T. R. Cech, *Science* **1987**, *236*, 1532.

[44] J. M. Buzayan, W. L. Gerlach, G. Bruening, *Nature* **1986**, *323*, 349.

[45] L. M. Epstein, J. G. Gall, *Cell* **1987**, *48*, 535.

[46] J. D. Watson, N. H. Hopkins, J. W. Roberts, J. A. Streitz, A. L. Weiner, *Molecular Biology of the Gene*, 4th ed., Benjamin-Cummings, **1987**, p. 1107.

[47] R. L. Thompson, N. S. Goel, *BioSystems* **1985**, *18*, 23.

[48] M. Nomura, *Science* **1973**, *179*, 864.

[49] R. B. Woodward, *Pure Appl. Chem.* **1973**, *33*, 145. See also ref. [30], p. 99.

[50] A. E. Eschenmoser, C. E. Wintner, *Science* **1977**, *196*, 1410. See also ref. [30], p. 99.

[51] R. W. Armstrong, J.-M. Beau, S. H. Cheon, W. J. Christ, H. Fujioka, W. H. Ham, L. D. Hawkins, H. Jin, S. H. Kang, Y. Kishi, M. J. Martinelli, W. W. McWhorter, M. Mizuno, M. Nakata, A. E. Stutz, F. X. Talamas, M. Taniguchi, J. A. Tino, K. Ueda, J. Uenishi, J. B. White, M. Yonaga, *J. Am. Chem. Soc.* **1989**, *111*, 7525. See also ref. [30], p. 711.

[52] The total synthesis of palytoxin spanned almost 10 years and involved more than 100 researchers. This level of effort was required to produce a compound with a molecular mass of 2680 Da and dimensions an order of magnitude smaller than the 10–100 nm dimensions usually regarded as nanoscale. Clearly, extrapolation of this type of synthetic strategy to a structure with a molecular mass of ca. 10000 Da would be prohibitive both in terms of time and manpower.

[53] H. Ringsdorf, B. Schlarb, J. Venzmer, *Angew. Chem.* **1988**, *100*, 117; *Angew. Chem. Int. Ed. Engl.* **1988**, *27*, 113; T. Kunitake, *ibid.* **1992**, *104*, 692 and **1992**, *31*, 709; J. H. Fuhrhop, *Membranes and Molecular Assemblies: The Synkinetic Approach*, Royal Society of Chemistry, Cambridge, **1994**.

[54] G. M. Whitesides, *Angew. Chem.* **1990**, *102*, 1247; *Angew. Chem. Int. Ed. Engl.* **1990**, *29*, 1209.

[55] J. M. Lehn, *Angew. Chem.* **1990**, *102*, 1347; *Angew. Chem. Int. Ed. Engl.* **1990**, *29*, 1304; *Science* **1993**, *260*, 1762; *Supramolecular Chemistry*, VCH, Weinheim, **1995**.

[56] D. Seebach, *Angew. Chem.* **1990**, *102*, 1363; *Angew. Chem. Int. Ed. Engl.* **1990**, *29*, 1320.

[57] D. Philp, J. F. Stoddart, *Synlett* **1991**, 445; R. Hoss, F. Vögtle, *Angew. Chem.* **1994**, *106*, 389; *Angew. Chem. Int. Ed. Engl.* **1994**, *33*, 375.

[58] G. W. Gokel, J. C. Medina, C. Li, *Synlett* **1991**, 677.

[59] Starburst dendrimers are a novel class of highly branched monodisperse polymers with diverse three-dimensional structures, which can be synthesized, divergently or convergently, from multifunctional building blocks by repetitive, near-quantitative reactions. For general reviews of this topic, see: D. A. Tomalia, A. M. Naylor, W. A. Goddard III, *Angew. Chem.* **1990**, *102*, 119; *Angew. Chem. Int. Ed. Engl.* **1990**, *29*, 138; H.-B. Mekelburger, W. Jaworek, F. Vögtle, *ibid.* **1992**, *104*, 1609 and **1992**, *31*, 1571; G. R. Newkome, C. N. Moorefield, G. R. Barker, *Aldrichimica Acta* **1992**, *25*, 31; D. A. Tomalia, H. D. Hurst, *Top. Curr. Chem.* **1993**, *165*, 193; D. A. Tomalia, *Aldrichimica Acta* **1993**, *26*, 91; J. M. J. Fréchet, *Science* **1994**, *263*, 1710; J. Issberner, R. Moors, F. Vögtle, *Angew. Chem.* **1994**, *106*, 2507; *Angew. Chem. Int. Ed. Engl.* **1994**, *33*, 2413. For examples of the convergent approach to dendritic macromolecules, see: C. J. Hawker, J. M. J. Fréchet, *J. Am. Chem. Soc.* **1990**, *112*, 7638; K. L. Wooley, C. J. Hawker, J. M. J. Fréchet, F. Wudl, G. Srdanov, S. Shi, C. Li, M. Kao, *ibid.* **1993**, *115*, 9836; K. L. Wooley, C. J. Hawker, J. M. J. Fréchet, *Angew. Chem.* **1994**, *104*, 123; *Angew. Chem. Int. Ed. Engl.* **1994**, *33*, 82. The growing importance of multiplex and combinatorial methods of synthesis for the rapid generation of libraries of structurally diverse organic compounds should be noted. For some examples, overviews, and commentaries, see: A. Plückthun, G. Liming, *Angew. Chem.* **1991**, *103*, 301; *Angew. Chem. Int. Ed. Engl.* **1991**, *30*, 296; C. Y. Cho, E. J. Moran, S. Cherry, J. Stephans, S. P. A. Fodor, C. Adams, A. Sundaram, J. W. Jacobs, P. G. Schultz, *Science* **1993**, *261*, 1303; B. A. Bunin, J. A. Ellman, *J. Am. Chem. Soc.* **1992**, *114*, 10997; B. A. Bunin, M. J. Plunkett, J. A. Ellman, *Proc. Natl. Acad. Sci. USA* **1994**, *91*, 4708; C. X. Chen, L. A. Randall, R. B. Miller, A. D. Jones, M. J. Kurth, *J. Am. Chem. Soc.* **1994**, *116*, 2661; J. Neilsen, *Chem. Ind.* **1994**, 902; A. Borchardt, W. C. Still, *J. Am. Chem. Soc.* **1994**, *116*, 373; J. A. Ellman, *Chemtracts* **1995**, *8*, 1; M. C. Pirrung, *ibid.* **1995**, *8*, 5; A. W. Czarnik, *ibid.* **1995**, *8*, 13; L. A. Mitscher, *ibid.* **1995**, *8*, 18; J. Rohr, *Angew. Chem.* **1995**, *107*, 963; *Angew. Chem. Int. Ed. Engl.* **1995**, *34*, 881; J. J. Baldwin, J. J. Burbaum, I. Henderson, M. H. J. Ohlmeyer, *J. Am. Chem. Soc.* **1995**, *117*, 5588; T. Carell, E. A. Wintner, A. J. Sutherland, J. Rebek, Jr., Y. M. Dunayevsky, *Chem. Biol.* **1995**, *2*, 171.

[60] D. A. Frankel, H. Lamparski, U. Liman, D. F. O'Brien, *J. Am. Chem. Soc.* **1989**, *111*, 9262.

[61] K. R. Shull, K. I. Winey, E. L. Thomas, E. J. Kramer, *Macromolecules* **1991**, *24*, 2748.

[62] D. Tanner, J. A. Fitzgerald, B. R. Phillips, *Angew. Chem. Adv. Mater.* **1989**, *101*, 665; *Angew. Chem. Int. Ed. Engl. Adv. Mater.* **1989**, *28*, 649; *Adv. Mater.* **1989**, *1*, 151.

[63] P. S. Pershan, *Structure of Liquid Crystal Phases*, World Scientific, Singapore, **1988**; P. J. Collings, *Liquid Crystals–Nature's Delicate Phase of Matter*, Hilger, Bristol, **1990**.

[64] A. R. Kortan, R. Hull, R. L. Opila, M. G. Bawendi, M. L. Steigerwald, P. J. Carroll, L. E. Brus, *J. Am. Chem. Soc.* **1990**, *112*, 1327.

[65] G. L. Gaines, *Insoluble Monolayers at Liquid-Gas Interfaces*, Wiley, New York, **1966**.

[66] D. Möbius, H. Möhwald, *Adv. Mater.* **1991**, *3*, 19.

[67] A. Ullman, *Adv. Mater.* **1990**, *2*, 573; A. Kumar, N. L. Abbott, E. Kim, H. A. Biebuyck, G. M. Whitesides, *Acc. Chem. Res.* **1995**, *28*, 219.

[68] C. D. Bain, E. B. Troughton, Y. T. Tao, J. Evall, G. M. Whitesides, R. G. Nuzzo, *J. Am. Chem. Soc.* **1989**, *111*, 321; G. M. Whitesides, P. E. Laibinis, *Langmuir* **1990**, *6*, 87; L. H. Dubois, R. G. Nuzzo, *Annu. Rev. Phys. Chem.* **1992**, *43*, 437; G. P. Lopaz, M. W. Albers, S. L. Schreiber, R. Caroll, E. Peralta, G. M. Whitesides, *J. Am. Chem. Soc.* **1993**, *115*, 5877; N. L. Abbott, D. R. Rolison, G. M. Whitesides, *Langmuir* **1994**, *10*, 2672; C. B. Gorman, H. A. Biebuyck, G. M. Whitesides, *Chem. Mater.* **1995**, *7*, 526; P. E. Laibinis, C. D. Bain, R. G. Nuzzo, G. M. Whitesides, *J. Phys. Chem.* **1995**, 99, 7663.

[69] For examples of the types of structures that can be formed at air–solid interfaces, see: A. K. Kakkar, S. Yitzchaik, S. B. Roscoe, F. Kubota, D. S. Allan, T. J. Marks, W. Lin, G. K. Wong, *Langmuir* **1993**, *9*, 388; J. Li, A. E. Kaifer, *ibid.* **1993**, *9*, 591; O. Chailapakul, R. M. Crooks, *ibid.* **1993**, *9*, 884; A. R. Bernardo, T. B. Lu, E. Córdova, L. T. Zhang, G. W. Gokel, A. E. Kaifer, *J. Chem. Soc. Chem. Commun.* **1994**, 529; M. T. Rojas, R. Königer, J. F. Stoddart, A. E. Kaifer, *J. Am. Chem. Soc.* **1995**, *117*, 336; B. H. Huisman, E. U. T. Vanvelzen, F. C. J. M. Vanveggel, J. F. J. Engberson, D. N. Reinhoudt, *Tetrahedron Lett.* **1995**, *36*, 3273; E. U. T. Vanvelzen, J. F. J. Engberson, P. J. Delange, J. W. G. Mahy, D. N. Reinhoudt, *J. Am. Chem. Soc.* **1995**, *117*, 6853; B.-H. Huisman, D. M. Rudekevich, F. C. M. van Veggel, D. N. Reinhoudt, *ibid.* **1996**, *118*, 3523.

[70] H. T. Tien, *Adv. Mater.* **1990**, *2*, 316.

[71] M. Sugi, *Thin Solid Films* **1987**, *152*, 305.

[72] "Langmuir-Blodgett Films 3": D. Möbius, *Thin Solid Films* **1988**, *159* and *160*.

[73] *Adv. Mater.* **1991**, *3(1)* (Special issue).

[74] F. M. Menger, *Angew. Chem.* **1991**, *103*, 1104; *Angew. Chem. Int. Ed. Engl.* **1991**, *30*, 1086.

[75] M. Ahlers, W. Müller, A. Reichert, H. Ringsdorf, J. Venzmer, *Angew. Chem.* **1990**, *102*, 1310; *Angew. Chem. Int. Ed. Engl.* **1990**, *29*, 1269.

[76] J. M. Lehn, *Angew. Chem.* **1988**, *100*, 91; *Angew. Chem. Int. Ed. Engl.* **1988**, *27*, 89.

[77] D. J. Cram, *Angew. Chem.* **1988**, *100*, 1041; *Angew. Chem. Int. Ed. Engl.* **1988**, *27*, 1009.

[78] C. J. Pedersen, *J. Am. Chem. Soc.* **1967**, *89*, 2495; 7017; *Aldrichimica Acta* **1971**, *4*, 1; *Angew. Chem.* **1988**, *100*, 1053; *Angew. Chem. Int. Ed. Engl.* **1988**, *27*, 1021.

[79] J. F. Stoddart, *Chem. Soc. Rev.* **1979**, *8*, 85; D. N. Reinhoudt, *Adv. Phys. Org. Chem.* **1980**, *17*, 279; J. F. Stoddart, *Annu. Rep. Prog. Chem. Sect. B* **1984**, 353; I. O. Sutherland, *Chem. Soc. Rev.* **1986**, *15*, 63; D. N. Reinhoudt, *J. Coord. Chem.* **1988**, *18*, 21; F. N. Diederich, *Angew. Chem.* **1988**, *100*, 372; *Angew. Chem. Int. Ed. Engl.* **1988**, *27*, 362; J. F. Stoddart, *Annu. Rep. Prog. Chem. Sect. B* **1989**, 353; I. O. Sutherland, *J. Inclusion Phenom. Mol. Recognit. Chem.* **1989**, *7*, 213; *Pure Appl. Chem.* **1989**, *61*, 1547; H.-J. Schneider, *Angew Chem.* **1991**, *103*, 1419; *Angew Chem. Int. Ed. Engl.* **1991**, *30*, 1417; D. J. Cram, *Nature* **1992**, *356*, 29.

[80] J. F. Stoddart, *Nature* **1988**, *334*, 10; C. D. Gutsche, *Calixarenes*, Royal Society of Chemistry, Cambridge, **1989**; F. N. Diederich, *Cyclophanes*, Royal Society of Chemistry, Cambridge, **1991**; G. W. Gokel, *Crown Ethers and Cryptands*, Royal Society of Chemistry, Cambridge, **1991**; F. Vögtle, *Supramolecular Chemistry*, Wiley, Chichester, **1991**; B. Dietrich, P. Viout, J. M. Lehn, *Macrocyclic Chemistry*, VCH, New York, **1993**; D. J. Cram, *Container Molecules and their Guests*, Royal Society of Chemistry, Cambridge, **1994**.

[81] W. Saenger, *Angew. Chem.* **1980**, *82*, 343; *Angew. Chem. Int. Ed. Engl.* **1980**, *19*, 344.

[82] J. F. Stoddart, *Carbohydrate Res.* **1989**, *192*, xii.

[83] R. J. Bergeron, *Inclusion Comp.* **1984**, *3*, 391.

[84] M. L. Bender, M. Komiyama, *Cyclodextrin Chemistry*, Springer, New York, **1978**.

[85] J. Szejtli, *Inclusion Comp.* **1984**, *3*, 331.

[86] N. Muller, *Acc. Chem. Res.* **1990**, *23*, 23; W. Blokzjil, J. B. F. N. Engberts, *Angew. Chem.* **1993**, *105*, 1610; *Angew. Chem. Int. Ed. Engl.* **1993**, *32*, 1545.

[87] F. Schardinger, *Z. Unters. Nahr. Genussm. Gebrauchsgegenstaende* **1903**, *6*, 865.

[88] F. Cramer, *Chem. Ber.* **1951**, *84*, 851; *Angew. Chem.* **1952**, *64*, 136; *Chem. Ber.* **1953**, *86*, 1576; *Einschlussverbindungen*, Springer, Berlin, **1954**; in *Cyclodextrins and their Industrial Uses* (Ed.: D. Duchêne), Editions de Santé, Paris, **1987**, p. 11.

[89] D. W. Griffiths, M. L. Bender, *Adv. Catal.* **1973**, *23*, 209.

[90] I. Tabushi, *Acc. Chem. Res.* **1982**, *15*, 66.

[91] R. Breslow, *Acc. Chem. Res.* **1980**, *13*, 170; *Science* **1982**, *218*, 532; *Chem. Br.* **1983**, *19*, 126; *Inclusion Comp.* **1984**, *3*, 473; *Acc. Chem. Res.* **1995**, *28*, 146.

[92] H. M. Colquhoun, J. F. Stoddart, D. J. Williams, *Angew. Chem.* **1986**, *98*, 483; *Angew. Chem. Int. Ed. Engl.* **1986**, *25*, 487; J. F. Stoddart, R. Zarzycki, *Recl. Trav. Chim. Pays-Bas* **1988**, *107*, 515; in *Cation Binding by Macrocycles: Complexation of Cationic Species by Crown Ethers* (Eds.: Y. Inoue, G. W. Gokel), Marcel Decker, New York, **1990**, p. 631.

[93] J. F. Stoddart, *Angew. Chem.* **1992**, *104*, 860; *Angew. Chem. Int. Ed. Engl.* **1992**, *31*, 846; G. Wenz, *ibid.* **1994**, *106*, 851 and **1994**, *33*, 803.

[94] G. Schill, *Catenanes, Rotaxanes and Knots*, Academic Press, New York, **1971**. See also: "Topology in Molecular Chemistry" (Ed.: J. P. Sauvage): *New J. Chem.* **1993**, *17*, Nos. 10–11.

[95] H. Ogino, *J. Am. Chem. Soc.* **1981**, *103*, 1303; *Inorg. Chem.* **1984**, *23*, 3312; *New J. Chem.* **1993**, *17*, 683. For similar [2]rotaxanes, see also: K. Yamanari, Y. Shimura, *Bull. Chem. Soc. Jpn.* **1983**, *56*, 2283; *ibid.* **1984**, *57*, 1596.

[96] R. S. Wylie, D. H. Macartney, *J. Am. Chem. Soc.* **1992**, *114*, 3136; *Supramol. Chem.* **1993**, *3*, 29; D. H. Macartney, C. A. Waddling, *Inorg. Chem.* **1994**, *33*, 5912.

[97] The name "rotaxane" is derived from the Latin "rota" meaning wheel and "axis" meaning axle [94]. The addition of the prefix "pseudo" indicates that the wheels are free to dissociate from the axle as in a more conventional type of complex. In chemical terms, this means that the components of the pseudorotaxane are held together only be their mutual noncovalent interaction and not (also) by a mechanical feature.

[98] T. V. S. Rao, D. S. Lawrence, *J. Am. Chem. Soc.* **1990**, *112*, 3614.

[99] T. L. Buxton, J. A. Caruso, *J. Am. Chem. Soc.* **1974**, *96*, 6033.

[100] R. Isnin, A. E. Kaifer, *J. Am. Chem. Soc.* **1991**, *113*, 8188; *Pure Appl. Chem.* **1993**, *65*, 495.

[101] See comments by R. Dagani in *Chem. Eng. News* **1992**, *70(15)*, 39.

[102] G. Wenz, E. von der Bay, L. Schmidt, *Angew. Chem.* **1992**, *104*, 758; *Angew. Chem. Int. Ed. Engl.* **1992**, *31*, 783; G. Wenz, F. Wolf, M. Wagner, S. Kubik, *New J. Chem.* **1993**, *17*, 729.

[103] Y. S. Lipatov, T. E. Lipatova, L. F. Kosyanchuk, *Adv. Polym. Sci.* **1989**, *88*, 49; H. W. Gibson, H. Marand, *Adv. Mater.* **1993**, *5*, 11; H. W. Gibson, P. T. Engen, *New J. Chem.* **1993**, *17*, 723; H. W. Gibson, M. C. Bheda, P. T. Engen, *Prog. Polym. Sci.* **1994**, *19*, 843.

[104] A. Harada, M. Kamachi, *J. Chem. Soc. Chem. Commun.* **1990**, 1322; A. Harada, J. Li, M. Kamachi, *Nature* **1992**, *356*, 325; A. Harada, J. Li, T. Nakamitsu, M. Kamachi, *J. Org. Chem.* **1993**, *58*, 7524; A. Harada, J. Li, M. Kamachi, *J. Am. Chem. Soc.* **1994**, *116*, 3192.

[105] A. Harada, J. Li, M. Kamachi, *Nature* **1993**, *364*, 516; *ibid.* **1994**, *370*, 126. The formation of molecular nanotube aggregates of β- and γ-cyclodextrins linked by diphenylhexatrienes has also been reported: G. Li, L. B. McGown, *Science* **1994**, *264*, 249.

[106] G. Wenz, B. Keller, *Angew. Chem.* **1992**, *104*, 201; *Angew. Chem. Int. Ed. Engl.* **1992**, *31*, 197. For side-chain polyrotaxanes with a tandem structure based on cyclodextrins and a polymethacrylate main chain, see: M. Born, H. Ritter, *ibid.* **1995**, *107*, 342 and **1995**, *34*, 309. For an example of a polyrotaxane, incorporating cyclodextrins, with a blocking group in every structural unit of the polymer chain, see I. Yamaguchi, K. Osakada, T. Yamamoto, *J. Am. Chem. Soc.* **1996**, *118*, 1811.

[107] J. S. Manka, D. S. Lawrence, *J. Am. Chem. Soc.* **1990**, *112*, 2440; D. L. Dick, T. V. S. Rao, D. Sukumaran, D. S. Lawrence, *ibid.* **1992**, *114*, 2664. Other groups have prepared similar pseudorotaxane-type structures: J. T. Rademacher, A. W. Czarnik, *J. Am. Chem. Soc.* **1993**, *115*, 3018; S. Matile, T. Hansen, A. Stocker, W.-D. Waggon, *Helv. Chim. Acta* **1994**, *77*, 1087.

[108] The name "catenane" is derived from the Latin word "catena" meaning chain [94]. In chemical terms, such molecules can be viewed as being composed of two or more macrocycles that are connected mechanically but not by any covalent chemical bond. The prefix indicates the number of interlocked components. Thus, a [2]catenane contains two interlocked rings.

[109] For early work on the synthesis of catenanes, see: H. L. Frisch, E. Wasserman, *J. Am. Chem. Soc.* **1961**, *83*, 3789, and references therein. For early work on the configuration and topology of catenanes, see: S. J. Tauber, *J. Res. Natl. Bur. Stand. Sect. A* **1963**, *67*, 591. For an interesting historical footnote, see: D. M. Walba, *New J. Chem.* **1993**, *17*, 618; N. van Gulick, *ibid.* **1993**, *17*, 619.

[110] For reviews and discussions concerning topologically interesting molecules, see: D. M. Walba, *Tetrahedron* **1985**, *41*, 3161; C. O. Dietrich-Buchecker, J.-P. Sauvage, *Bioorg. Chem. Front.* **1991**, *2*, 195; C. Weber, *New J. Chem.* **1993**, *17*, 627; D. M. Walba, T. C. Homan, R. M. Richards, R. C. Haltiwanger, *ibid.* **1993**, *17*, 661; D. B. Amabilino, I. W. Parsons, J. F. Stoddart, *Trends Polym. Sci.* **1994**, *2*, 146; D. B. Amabilino, J. F. Stoddart, *Chem. Rev.* **1995**, *95*, 2725.

[111] Interestingly, catenated structures are relatively common in DNA: B. Hudson, J. Vinograd, *Nature* **1967**, *216*, 647; M. I. Baldi, P. Benedetti, E. Mattoccia, G. P. Tocchini-Valentini, *Cell* **1980**, *20*, 461; S. A. Wasserman, N. R. Cozzarelli, *Proc. Natl. Acad. Sci. USA* **1985**, *82*, 1079. E. Shekhtman, S. A. Wasserman, N. R. Cozarelli, M. J. Solomon, *New J. Chem.* **1993**, *17*, 757.

[112] A. Lüttringhaus, F. Cramer, H. Prinzbach, F. M. Henglein, *Chem. Ber.* **1958**, *613*, 185.

[113] D. Armspach, P. R. Ashton, C. P. Moore, N. Spencer, J. F. Stoddart, T. J. Wear, D. J. Williams, *Angew. Chem.* **1993**, *105*, 944; *Angew. Chem. Int. Ed. Engl.* **1993**, *32*, 854.

[114] The two isomeric [3]catenanes **24a** and **24b** can be separated readily by HPLC: D. Armspach, P. R. Ashton, R. Ballardini, V. Balzani, A. Godi, C. P. Moore, L. Prodi, N. Spencer, J. F. Stoddart, M. S. Tolley, T. J. Wear, D. J. Williams, *Chem. Eur. J.* **1995**, *1*, 27.

[115] A general introduction can be found in S. Bratoz, *Adv. Quantum Chem.* **1967**, *3*, 209.

[116] M. D. Joeston, *J. Chem. Educ.* **1982**, *79*, 362.

[117] R. Taylor, O. Kennard, *Acc. Chem. Res.* **1984**, *17*, 320.

[118] The poor scattering of X-rays by the hydrogen atom gives rise to large errors (0.05–0.1 Å) for N–H and O–H distances determined by this method. Although, in principle, neutron diffraction can give distances with an accuracy one order of magnitude better, its expense is prohibitive. Instead, X-ray diffraction methods employ a normalization procedure, which fixes the D–H distance at a standard value.

[119] R. Taylor, O. Kennard, *Acta Crystallogr. Sect. B* **1983**, *39*, 133.

[120] G. A. Jeffrey, L. Lewis, *Carbohydr. Res.* **1978**, *60*, 179.

[121] B. Pedersen, *Acta Crystallogr. Sect. B* **1974**, *30*, 289; R. Taylor, O. Kennard, W. Verischel, *J. Am. Chem. Soc.* **1984**, *106*, 244; G. A. Jeffrey, W. Saenger, *Hydrogen Bonding in Biological Structures*, Springer, Berlin, **1991**; J. Bernstein, R. E. Davis, L. Shimoni, N.-L. Chang, *Angew. Chem.* **1995**, *107*, 1689; *Angew. Chem. Int. Ed. Engl.* **1995**, *34*, 1555.

[122] M. C. Etter, *Acc. Chem. Res.* **1990**, *23*, 120. For a general overview of crystal engineering, see: G. R. Desiraju, *Crystal Engineering – The Design of Organic Solids*, Elsevier, Amsterdam, **1989**; C. B. Aakeröy, K. R. Seddon, *Chem. Soc. Rev.* **1993**, *23*, 397; M. Mascal, *Contemp. Org. Synth.* **1994**, *1*, 31; D. B. Amabilino, J. F. Stoddart, D. J. Williams, *Chem. Mater.* **1994**, *6*, 1159; M. J. Zaworotko, *Chem. Soc. Rev.* **1994**, *24*, 283; J. Bernstein, R. E. Davis, L. Shimoni, N. L. Chang, *Angew. Chem.* **1995**, *107*, 1689; *Angew. Chem. Int. Ed. Engl.* **1995**, *34*, 1555; G. A. Desiraju, *ibid.* **1995**, *107*, 2541 and **1995**, *34*, 2311; A. D. Burrows, C. W. Chan, M. M. Chowdhry, J. E. McGrady, D. M. Mingos, *Chem. Soc. Rev.* **1995**, *25*, 329; S. Valiyaveettil, V. Enkelmann, G. Mössner, K. Mullen, *Macromolecular Symposia* **1996**, *102*, 165; V. R. Thalladi, R. S. Goud, V. J. Hoy, F. H. Allen, J. A. K. Howard, G. R. Desiraju, *Chem. Commun.* **1996**, 401.

[123] The earliest examples of crystal engineering employing two building blocks that recognize each other, both in a ditopic manner, by complementary hydrogen bonding were found in research carried out in the 1970s and 1980s on the second-sphere coordination of transition metal ammine and aqua complexes by [18]crown-6 and its derivatives. For a discussion of the X-ray crystal structures of $([Cu(NH_3)_4(H_2O)([18]crown\text{-}6)]^{2+})_n(PF_6^-)_{2n}$ and $([Pt(H_2NCH_2CH_2NH_2)(H_2O)([18]crown\text{-}6)]^{2+})_n(PF_6^-)_{2n}$, which form hydrogen bonded chain copolymers in which the transition metal complex and the crown ether alternate to form tubular arrays, see: H. M. Colquhoun, J. F. Stoddart, D. J. Williams, *J. Chem. Soc. Chem. Commun.* **1981**, 847, 849; H. M. Colquhoun, D. F. Lewis, J. F. Stoddart, D. J. Williams, *J. Chem. Soc. Dalton Trans.* **1983**, 607. The X-ray crystal structure of $([PhCOCH_2SMe_2([18]crown\text{-}6)]^+)_n(PF_6^-)_n$ provides a rare example of a hydrogen-bonded tubular array in which an *organic cation* replaces the transition metal in a 1:1 polymeric adduct: B. L. Allwood, J. Crosby, D. A. Pears, J. F. Stoddart, D. J. Williams, *Angew. Chem.* **1984**, *96*, 987; *Angew. Chem. Int. Ed. Engl.* **1984**, *23*, 977. For references to other examples, particularly the hydrogen bondined copolymers formed between aqua complexes and [18]crown-6, see ref. [92].

[124] M. C. Etter, *J. Phys. Chem.* **1991**, *95*, 4601.

[125] M. C. Etter, Z. Urbanczyk-Lipkowska, M. Zia-Ebrahimi, T. W. Panunto, *J. Am. Chem. Soc.* **1990**, *112*, 8415.

[126] M. C. Etter, S. M. Reutzel, *J. Am. Chem. Soc.* **1991**, *113*, 2586.

[127] M. C. Etter, D. A. Adsmond, *J. Chem. Soc. Chem. Commun.* **1990**, 589.

[128] J. Scheinbein, E. Schempp, *Acta Crystallogr. Sect. B* **1976**, *32*, 607.

[129] M. Gallant, M. T. P. Viet, J. D. Wuest, *J. Am. Chem. Soc.* **1991**, *113*, 721.

[130] M. Gallant, M. T. P. Viet, J. D. Wuest, *J. Org. Chem.* **1991**, *56*, 2284.

[131] M. Simard, D. Su, J. D. Wuest, *J. Am. Chem. Soc.* **1991**, *113*, 4696. For an earlier example of diamondoid lattices, see: O. Ermer, A. Eling *Angew. Chem.* **1988**, *100*, 856; *Angew. Chem. Int. Ed. Engl.* **1988**, *27*, 829; O. Ermer, *J. Am. Chem. Soc.* **1988**, *110*, 3747; X. Wang, M. Simard, J. D. Wuest, *ibid.* **1994**, *116*, 12119; for an alternative type of molecular tectonics, see F. Hajek, E. Graf, M. W. Hosseini, X. Delaigue, A. Decian, J. Fischer, *Tetrahedron Lett.* **1996**, *37*, 1401; M. W. Hosseini, G. Brand, P. Schaeffer, R. Ruppert, A. Decian, J. Fischer, *Tetrahedron Lett.* **1996**, *37*, 1405.

[132] For an example of a diamondoid lattice constructed using hydrogen bonds between 1,2-diaminoethane and a organomanganese species, see: S. B. Copp, S. Subramanian, M. J. Zaworotko, *J. Am. Chem. Soc.* **1992**, *114*, 8719; *J. Chem. Soc. Chem. Commun.* **1993**, 1078.

[133] F. Garcia-Tellado, S. J. Geib, S. Goswami, A. D. Hamilton, *J. Am. Chem. Soc.* **1991**, *113*, 9265; S. J. Geib, C. Vicent, E. Fan, A. D. Hamilton, *Angew. Chem.* **1993**, *105*, 83; *Angew. Chem. Int. Ed. Engl.* **1993**, *32*, 119.

[134] S. J. Geib, S. C. Hirst, C. Vicent, A. D. Hamilton, *J. Chem. Soc. Chem. Commun.* **1991**, 1283.

[135] J. Yang, E. Fan, S. J. Geib, A. D. Hamilton, *J. Am. Chem. Soc.* **1993**, *115*, 5314.

[136] J. Yang, J. L. Marendaz, S. J. Geib, A. D. Hamilton, *Tetrahedron Lett.* **1994**, *35*, 3665; E. Fan, C. Vicent, S. J. Geib, A. D. Hamilton, *Chem. Mater.* **1994**, *6*, 1113.

[137] E. Fan, J. Yang, S. J. Geib, T. C. Stoner, M. D. Hopkins, A. D. Hamilton, *J. Chem. Soc. Chem. Commun.* **1995**, 1251. For an alternative class of molecular rods, see: M. Kotera, J. M. Lehn, J. P. Vigneron, *Tetrahedron* **1995**, *51*, 1953.

[138] J.-M. Lehn, M. Mascal, A. De Cian, J. Fischer, *J. Chem. Soc. Chem. Commun.* **1990**, 479; *J. Chem. Soc. Perkin Trans 2* **1992**, 461. Barbituric acid derivatives have also been used to construct hydrogen bonded networks at air–water interfaces: R. Ahuja, P.-L. Caruso, D. Möbius, W. Paulus, H. Ringsdorf, G. Wildburg, *Angew. Chem.* **1993**, *105*, 1082; *Angew. Chem. Int. Ed. Engl.* **1993**, *32*, 1033. Bilayer membranes can also be self-organized using a complementary hydrogen bonding network: N. Kimizuka, T. Kawasaki, T. Kunitake, *J. Am. Chem. Soc.* **1993**, *115*, 4387; N. Kimizuka, T. Kawasaki, K. Hirata, T. Kunitake, *ibid.* **1995**, *117*, 6360. For an example of an ion pair reinforced molecular ribbon, see:: M. Mascal, P. S. Fallon, A. S. Batsanov, B. R. Heywood, S. Champ, M. Colclough, *J. Chem. Soc. Chem. Commun.* **1995**, 805. See also T. Kawamoto, B. S. Hammes, B. Haggerty, G. P. A. Yap, A. L. Rheingold, A. S. Borovik, *J. Am. Chem. Soc.* **1996**, *118*, 285. For the use of hydrogen bonding to organise metal chelates, see C. W. Chan, D. M. P. Mingos, A. J. P. White, D. J. Williams, *Chem. Commun.* **1996**, 81; A. D. Burrows, D. M. P. Mingos, A. J. P. White, D. J. Williams, *ibid.* **1996**, 97.

[139] C. T. Seto, G. M. Whitesides, *J. Am. Chem. Soc.* **1990**, *112*, 6409.

[140] C. T. Seto, G. M. Whitesides, *J. Am. Chem. Soc.* **1991**, *113*, 712.

[141] J. A. Zerkowski, C. T. Seto, D. A. Wierda, G. M. Whitesides, *J. Am. Chem. Soc.* **1990**, *112*, 9025; J. A. Zerkowski, C. T. Seto, G. M. Whitesides, *ibid.* **1992**, *114*, 5473.

[142] J. A. Zerkowski, J. C. Macdonald, C. T. Seto, D. A. Wierda, G. M. Whitesides, *J. Am. Chem. Soc.* **1994**, *116*, 2382; J. A. Zerkowski, G. M. Whitesides, *ibid.* **1994**, *116*, 4298; J. A. Zerkowski, J. C. Macdonald, G. M. Whitesides, *Chem. Mater.* **1994**, *6*, 1250; J. C. Macdonald, G. M. Whitesides, *Chem. Rev.* **1994**, *94*, 2383.

[143] For full accounts of these and other systems, see: C. T. Seto, G. M. Whitesides, *J. Am. Chem. Soc.* **1993**, *115*, 905; C. T. Seto, J. P. Mathias, G. M. Whitesides, *ibid.* **1993**, *115*, 1321; C. T. Seto, G. M. Whitesides, *ibid.* **1993**, *115*, 1330; J. P. Mathias, C. T. Seto, E. E. Simanek, G. M. Whitesides, *ibid.* **1994**, *116*, 1725; J. P. Mathias, E. E. Simanek, G. M. Whitesides, *ibid.* **1994**, *116*, 4326; E. E. Simanek, M. Mammen, D. M. Gordon, D. Chin, J. P. Mathias, C. T. Seto, G. M. Whitesides, *Tetrahedron* **1995**, *51*, 607; D. N. Chin, D. M. Gordon, G. M. Whitesides, *J. Am. Chem. Soc.* **1994**, *116*, 12033; G. M. Whitesides, E. E. Simanek, J. P. Mathias, C. T. Seto, D. Chin, M. Mammen, D. M. Gordon, *Acc. Chem. Res.* **1995**, *28*, 37; X. Li, D. N. Chin, G. M. Whitesides, *J. Org. Chem.* **1996**, *61*, 1779; X. Cheng, Q. Gao, R. D. Smith, E. E. Simanek, M. Mammen, G. M. Whitesides, *ibid.* **1996**, *61*, 2204.

[144] N. M. Stainton, K. D. M. Harris, R. A. Howie, *J. Chem. Soc. Chem. Commun.* **1991**, 1781. For other solid-state structures supported by networks of hydrogen bonds, see: S. B. Copp, S. Subramanian, M. J. Zaworotko, *Angew. Chem.* **1993**, *105*, 755; *Angew Chem. Int. Ed. Engl.* **1993**, *32*, 706; *J. Chem. Soc. Chem. Commun.* **1993**, 952; S. Subramanian, M. J. Zaworotko, *Can. J. Chem.* **1993**, *71*, 433; S. D. Christie, S. Subramanian, L. K. Thompson, M. J. Zaworotko, *J. Chem. Soc. Chem. Commun.* **1994**, 2563; M. Munakata, L. P. Wu, M. Yamamoto, T. Kuroda-Sowa, M. Maekawa, *J. Am. Chem. Soc.* **1996**, *118*, 3117.

[145] J. P. Mathias, E. E. Simanek, C. T. Seto, G. M. Whitesides, *Angew. Chem.* **1993**, *105*, 1848; *Angew. Chem. Int. Ed. Engl.* **1993**, *32*, 1766.

[146] R. Wyler, J. de Mendoza, J. Rebek, Jr., *Angew. Chem.* **1993**, *105*, 1820; *Angew. Chem. Int. Ed. Engl.* **1993**, *32*, 1699.

[147] N. Branda, R. Wyler, J. Rebek, Jr., *Science* **1994**, *263*, 1267; N. Branda, R. M. Grotzfeld, C. Valdes, J. Rebek, Jr., *J. Am. Chem. Soc.* **1995**, *117*, 85; R. S. Meissner, J. Rebek, Jr., J. de Mendoza, *Science* **1995**, *270*, 1485; C. Valdes, U. P. Spitz, S. W. Kubik, J. Rebek, Jr., *Angew. Chem.* **1995**, *107*, 2031; *Angew. Chem. Int. Ed. Engl.* **1995**, *34*, 1885; C. Valdes, U. P. Spitz, L. M. Toledo, S. W. Kubik, J. Rebek Jr., *J. Am. Chem. Soc.* **1995**, *117*, 12733; K. D. Shimizu, J. Rebek, Jr., *Proc. Natl. Acad. Sci. USA* **1995**, *92*, 12403.

[148] C. Fouquey, J.-M. Lehn, A.-M. Levelut, *Adv. Mater.* **1990**, *2*, 254; T. Gulik-Krzywicki, C. Fouquey, J.-M. Lehn, *Proc. Natl. Acad. Sci. USA* **1993**, *90*, 163; W. S. Yang, S. G. Chen, X. D. Chai, Y. W. Cao, R. Lu, W. P. Chai, Y. S. Jiang, T. J. Li, J. M. Lehn, *Synth. Metals* **1995**, *71*, 2107.

[149] For other examples of self-assembled liquid crystals, see : S. Bonazzi, M. M. De Morais, G. Gottarelli, P. Mariani, G. P. Spada, *Angew. Chem.* **1993**, *105*, 251; *Angew. Chem. Int. Ed. Engl.* **1993**, *32*, 248; A. Garbesi, G. Gottarelli, P. Mariani, G. P. Spada, *Pure Appl. Chem.* **1993**, *65*, 641; C. C. Ling, R. Darcy, W. Risse, *J. Chem. Soc. Chem. Commun.* **1993**, 438; G. Johansson, V. Percec, G. Ungar, D. Abramic, *J. Chem. Soc. Perkin Trans. 1* **1994**, 447; F. Ciuchi, G. Di Nicola, H. Franz, G. Gottarelli, P. Mariani, M. G. P. Bossi, G. P. Spada, *J. Am. Chem. Soc.* **1994**, *116*, 7064; R. Kleppinger, C. P. Lillya, C. Yang, *Angew. Chem.* **1995**, *107*, 1762; *Angew. Chem. Int. Ed. Engl.* **1995**, *34*, 1637. V. Percec, D. Schlüter, J. C. Ronda, G. Johansson, G. Ungar, J. P. Zhou, *Macromolecules* **1996**, *29*, 1464. For other examples of interesting structures constructed using hydrogen bonding interactions, see: P. Tecilla, R. P. Dixon, G. Slobodkin, D. S. Alavi, D. H. Waldbeck, A. D. Hamilton, *J. Am. Chem. Soc.* **1990**, *112*, 8408; A. Harriman, Y. Kubo, J. L. Sessler, *ibid.* **1992**, *114*, 388; S. Hanessian, A. Gomtysan, M. Simard, S. Roelens, *ibid.* **1994**, *116*, 4495; S. Hanessian, M. Simard, S. Roelens, *ibid.* **1995**, *117*, 7630; O. F. Schall, G. W. Gokel, *ibid.* **1994**, *116*, 6089; F. M. Menger, Y. Yamasaki, K. K. Catlin, T. Nishimi, *Angew. Chem.* **1995**, *107*, 616; *Angew. Chem. Int. Ed. Engl.* **1995**, *34*, 585. For an excellent review of the photochemistry of self-assembled supramolecular systems, see: V. Balzani, *Tetrahedron* **1992**, *48*, 10443.

[150] N. Khazanovich, J. R. Granja, D. E. McRee, R. A. Milligan, M. R. Ghadiri, *J. Am. Chem. Soc.* **1994**, *116*, 6011; M. R. Ghadiri, K. Kobayashi, J. R. Granja, R. K. Chadha, D. E. McRee, *Angew. Chem.* **1995**, *107*, 76; *Angew. Chem. Int. Ed. Engl.* **1995**, *34*, 93; M. R. Ghadiri, *Adv. Mater.* **1995**, 7, 675. For examples of self-assembling ion channels, see: G. G. Cross, T. M. Fyles, T. D. James, M. Zojaji, *Synlett* **1993**, 449; T. M. Fyles, T. D. James, A. Pryhatka, M. Zojaji, *J. Org. Chem.* **1993**, *58*, 7456; T. M. Fyles, T. D. James, K. C. Kaye, *J. Am. Chem. Soc.* **1993**, *115*, 12315.

[151] T. R. Kelly, C. Zhao, G. J. Bridger, *J. Am. Chem. Soc.* **1989**, *111*, 3744.

[152] T. R. Kelly, G. J. Bridger, C. Zhao, *J. Am. Chem. Soc.* **1990**, *112*, 8024.

[153] For a review of replication and mutation in DNA, see: P. Strazewski, C. Tamm, *Angew. Chem.* **1990**, *102*, 37; *Angew. Chem. Int. Ed. Engl.* **1990**, *29*, 36.

[154] G. von Kiedrowski, *Angew. Chem.* **1986**, *98*, 932; *Angew. Chem. Int. Ed. Engl.* **1986**, *25*, 932.

[155] G. von Kiedrowski, B. Wlotzka, J. Helbing, *Angew. Chem.* **1989**, *101*, 1259; *Angew. Chem. Int. Ed. Engl.* **1989**, *28*, 1235; G. von Kiedrowski, B. Wlotzka, J. Helbing, M. Matzen, S. Jordan, *ibid.* **1991**, *103*, 456 and **1991**, *30*, 423.

[156] G. von Kiedrowski, *Bioorg. Chem. Front.* **1993**, *3*, 113; T. Achilles, G. von Kiedrowski, *Angew. Chem.* **1993**, *105*, 1225; *Angew. Chem. Int. Ed. Engl.* **1993**, *32*, 1198; D. Sievers, G. von Kiedrowski, *Nature* **1994**, *369*, 221.

[157] W. S. Zielinski, L. E. Orgel, *Nature* **1987**, *327*, 346.

[158] T. Wu, L. E. Orgel, *J. Am. Chem. Soc.* **1992**, *114*, 317.

[159] J. Rebek, Jr., *Angew. Chem.* **1990**, *102*, 261; *Angew. Chem. Int. Ed. Engl.* **1990**, *29*, 245.

[160] J. Rebek, Jr. in *Inclusion Phenomena and Molecular Recognition* (Ed.: J. Atwood), Plenum, New York, **1990**, p. 1.

[161] J. Rebek, Jr., *Acc. Chem. Res.* **1990**, *23*, 399.

[162] M. Famulok, J. S. Nowick, J. Rebek, Jr., *Acta Chem. Scand.* **1992**, *46*, 315.

[163] T. Tjivikua, P. Ballester, J. Rebek, Jr., *J. Am. Chem. Soc.* **1990**, *112*, 1249.

[164] J. S. Nowick, Q. Feng, T. Tjivikua, P. Ballester, J. Rebek, Jr., *J. Am. Chem. Soc.* **1991**, *113*, 8831.

[165] For a description of a self-complementary system designed to self-replicate, which is unsuccessful: F. Persico, J. D. Wuest, *J. Org. Chem.* **1993**, *58*, 95. For another use of this building block, see: E. Boucher, M. Simard, J. D. Wuest, *ibid.* **1995**, *60*, 1408.

[166] V. Rotello, J.-I. Hong, J. Rebek, Jr., *J. Am. Chem. Soc.* **1991**, *113*, 9422; J.-I. Hong, Q. Feng, V. Rotello, J. Rebek, Jr., *Science* **1992**, *255*, 848. See also I. Amato, *Science* **1992**, *255*, 800; E. A. Wintner, M. M. Conn, J. Rebek, Jr., *Acc. Chem. Res.* **1994**, *27*, 198; M. M. Conn, E. A. Wintner, J. Rebek, Jr., *Angew. Chem.* **1994**, *106*, 1665; *Angew. Chem. Int. Ed. Engl.* **1994**, *33*, 1577; R. J. Pieters, I. Huc, J. Rebek, Jr., *ibid.* **1994**, *106*, 1667 and **1994**, *33*, 1579; E. A. Wintner, M. M. Conn, J. Rebek, Jr., *J. Am. Chem. Soc.* **1994**, *116*, 8877; R. J. Pieters, I. Huc, J. Rebek, Jr., *Tetrahedron* **1995**, *51*, 485.

[167] The difficulties associated with the demonstration of self-replicating behavior in complex systems are highlighted by the fact that the claim that the production of **50** proceeds by the mechanism described in the text has been challenged, defended, and rechallenged since its initial publication five years ago. Lead references for the argument and counterargument on this controversial subject: F. M. Menger, A. V. Eliseev, N. A. Khanjin, *J. Am. Chem. Soc.* **1994**, *116*, 3613; M. M. Conn, E. A. Wintner, J. Rebek, Jr., *ibid.* **1994**, *116*, 1577; F. M. Menger, A. V. Eliseev, N. A. Khanjin, M. J. Sherrod, *J. Org. Chem.* **1995**, *60*, 2870; E. A. Wintner, B. Tsao, J. Rebek, Jr., *ibid.* **1995**, *60*, 7997.

[168] T. K. Park, Q. Feng, J. Rebek, Jr., *J. Am. Chem. Soc.* **1992**, *114*, 4529.

[169] A. Terfort, G. von Kiedrowski, *Angew. Chem.* **1992**, *104*, 626; *Angew. Chem. Int. Ed. Engl.* **1992**, *31*, 654.

[170] The destabilization of the **[53·53]** duplex must be a result of the reduced strength of the salt bridges. Normally, the duplex should be more stable than the ternary complex for entropic reasons.

[171] C. A. Hunter, *J. Chem. Soc. Chem. Commun.* **1991**, 749.

[172] W. L. Jorgensen, D. L. Severance, *J. Am. Chem. Soc.* **1990**, *112*, 4768; C. A. Hunter, J. K. M. Sanders, *ibid.* **1990**, *112*, 5525; C. A. Hunter, *J. Mol. Biol.* **1993**, *250*, 1025; *Angew. Chem.* **1993**, *105*, 1653; *Angew. Chem. Int. Ed. Engl.*, **1993**, *32*, 1584; *Chem. Soc. Rev.* **1994**, *23*, 101; M. Nishio, Y. Umezawa, M. Hirota, Y. Takeuchi, *Tetrahedron* **1995**, *51*, 8665.

[173] C. A. Hunter, *J. Am. Chem. Soc.* **1992**, *114*, 5303. A combination of hydrogen bonding to the polar amide bridges and $\pi-\pi$ interactions has also been used to construct a "molecular zipper": A. P. Bisson, F. J. Carver, C. A. Hunter, J. P. Waltho, *ibid.* **1994**, *116*, 10292.

[174] The templating of catenations by the interaction between bisamides and 1,5-dicarbonyl compounds appears to be a relatively general phenomenon: C. A. Hunter, D. H. Purvis, *Angew. Chem.* **1992**, *104*, 779; *Angew. Chem. Int. Ed. Engl.* **1992**, *31*, 792; F. Vögtle, S. Meier, R. Hoss, *ibid.* **1992**, *104*, 1628 and

1992, *31*, 1619; S. Ottens-Hildebrandt, S. Meier, W. Schmidt, F. Vögtle, *ibid.* **1994**, *106*, 1818 and **1994**, *33*, 1767; F. J. Carver, C. A. Hunter, R. J. Shannon, *J. Chem. Soc. Chem. Commun.* **1994**, 1277; S. Ottens-Hildebrandt, M. Nieger, K. Rissanen, J. Rouvinen, S. Meier, G. Harder, F. Vögtle, *ibid.* **1995**, 777; H. Adams, F. J. Carver, C. A. Hunter, *ibid.* **1995**, 809; A. G. Johnston, D. A. Leigh, R. J. Pritchard, M. D. Deegan, *Angew. Chem.* **1995**, *107*, 1324; *Angew. Chem. Int. Ed. Engl.* **1995**, *34*, 1209; A. G. Johnston, D. A. Leigh, L. Nezhat, J. P. Smart, M. D. Deegan, *ibid.* **1995**, *107*, 1327 and **1995**, *34*, 1212; D. A. Leigh, K. Moody, J. P. Smart, K. J. Watson, A. M. Z. Slawin, *ibid.* **1996**, *108*, 326 and **1996**, *35*, 306. Catenanes containing sulfonamide units have also been synthesized: S. Ottens-Hildebrandt, T. Schmidt, J. Harren, F. Vögtle, *Liebigs Ann.* **1995**, 1855. For the template-directed synthesis of amide-based rotaxanes, see: F. Vögtle, M. Handel, S. Meier S. Ottenshildebrandt, F. Ott, T. Schmidt, *ibid.* **1995**, 739.

[175] L. R. Hanton, C. A. Hunter, D. H. Purvis, *J. Chem. Soc. Chem. Commun.* **1992**, 1134.

[176] J. C. Metcalfe, J. F. Stoddart, G. Jones, *J. Am. Chem. Soc.* **1977**, *99*, 8317; J. C. Metcalfe, J. F. Stoddart, G. Jones, W. E. Hull, A. Atkinson, I. S. Kerr, D. J. Williams, *J. Chem. Soc. Chem. Commun.* **1980**, 540.

[177] P. R. Ashton, P. J. Campbell, E. J. T. Chrystal, P. T. Glink, S. Menzer, D. Philp, N. Spencer, J. F. Stoddart, P. A. Tasker, D. J. Williams, *Angew. Chem.* **1995**, *107*, 1997; *Angew. Chem. Int. Ed. Engl.* **1995**, *34*, 1865; P. R. Ashton, E. J. T. Chrystal, P. T. Glink, S. Menzer, C. Schiavo, J. F. Stoddart, P. A. Tasker, D. J. Williams *ibid.* **1995**, *107*, 2001 and **1995**, *34*, 1869; P. R. Ashton, P. T. Glink, J. F. Stoddart, P. A. Tasker, A. J. P. White, D. J. Williams, *Chem. Eur. J.* **1996**, *2*, 193; P. R. Ashton, E. J. T. Chrystal, P. T. Glink, S. Menzer, C. Schiavo, N. Spencer, J. F. Stoddart, P. A. Tasker, A. J. P. White, D. J. Williams, *ibid.* **1996**, *2*, 213; P. T. Glink, C. Schiavo, J. F. Stoddart, D. J. Williams, *Chem. Commun.*, in press.

[178] A. G. Kolchinski, D. H. Busch, N. W. Alcock, *J. Chem. Soc. Chem. Commun.* **1995**, 1289.

[179] For a basic introduction to metal–ligand complexes, see: F. A. Cotton, G. A. Wilkinson, *Comprehensive Inorganic Chemistry*, 5th ed., Wiley, **1988**, Chapter 2.

[180] A. Werner, *Neuere Anschauungen auf dem Gebiete der anorganischen Chemie*, Braunschweig, **1905**; translation of the 2nd edition: A. Werner, *New Ideas in Chemistry*, E. P. Hedley, London, **1911**.

[181] W. H. Brock, K. A. Jensen, C. Jørgensen, G. B. Kaufman, *Polyhedron* **1983**, *2*, 1.

[182] G. A. Melson, *Coordination Chemistry of Macrocyclic Compounds*, Plenum, New York, **1979**.

[183] L. F. Lindoy, *The Chemistry of Macrocyclic Ligand Complexes*, Cambridge University Press, Cambridge, **1989**.

[184] N. F. Curtis, *J. Chem. Soc.* **1960**, 4409.

[185] N. F. Curtis, D. A. House, *Chem. Ind.* **1961**, 1708.

[186] N. F. Curtis, Y. M. Curtis, H. K. Powell, *J. Chem. Soc. A* **1966**, 1015.

[187] Interestingly, the metal-free macrocycle can be synthesized by utilizing a network of hydrogen bonds as the template: R. W. Hay, G. A. Lawrance, N. F. Curtis, *J. Chem. Soc. Dalton Trans.* **1975**, 591.

[188] C. A. Hunter, M. N. Meah, J. K. M. Sanders, *J. Am. Chem. Soc.* **1990**, *112*, 5773.

[189] H. L. Anderson, C. A. Hunter, M. N. Meah, J. K. M. Sanders, *J. Am. Chem. Soc.* **1990**, *112*, 5780.

[190] The zinc metal center can become five-coordinate, which permits the zinc porphyrin to accept an additional fifth axial ligand in addition to the four nitrogen ligands porvided by the pyrrole residues of the porphyrin.

[191] H. L. Anderson, J. K. M. Sanders, *J. Chem. Soc. Chem. Commun.* **1989**, 1714.

[192] H. L. Anderson, J. K. M. Sanders, *Angew. Chem.* **1990**, *102*, 1478; *Angew. Chem. Int. Ed. Engl.* **1990**, *29*, 1400.

[193] L. G. Mackay, H. L. Anderson, J. K. M. Sanders, *J. Chem. Soc. Chem. Commun.* **1992**, 43; J. K. M. Sanders, H. L. Anderson, L. G. Mackay, *J. Chem. Soc. Perkin Trans. 1* **1995**, 2269.

[194] S. Anderson, H. L. Anderson, J. K. M. Sanders, *Angew. Chem.* **1992**, *104*, 921; *Angew. Chem. Int. Ed. Engl.* **1992**, *31*, 907; H. L. Anderson, A. Bashall, K. Henrick, M. McPartlin, J. K. M. Sanders, *ibid.* **1994**, *106*, 445 and **1994**, *33*, 429; S. Anderson, H. L. Anderson, A. Bashall, M. McPartlin, J. K. M. Sanders, *ibid.* **1995**, *107*, 1196 and **1995**, *34*, 1096.

[195] "Supramolecular Chemistry": H. L. Anderson, R. P. Bonar-Law, L. G. Mackay, S. Nicholson, J. K. M. Sanders, *NATO ASI Ser. Ser. C* **1992**, *371*, 359; S. Anderson, H. L. Anderson, J. K. M. Sanders, *Acc. Chem. Res.* **1993**, *26*, 455; J. K. M. Sanders, H. L. Anderson, S. Anderson, *J. Chem. Soc. Perkin Trans. 1* **1995**, 2255, 2247.

[196] C. J. Walter, H. L. Anderson, J. K. M. Sanders, *J. Chem. Soc. Chem. Commun.* **1993**, 458; C. J. Walter, J. K. M. Sanders, *Angew. Chem.* **1995**, *107*, 223; *Angew. Chem. Int. Ed. Engl.* **1995**, *34*, 217. For an acyl transfer reaction performed inside the cavity of a porphyrin trimer, see: L. G. Mackay, R. S. Wylie, J. K. M. Sanders, *J. Am. Chem. Soc.* **1994**, *116*, 3141; *Tetrahedron* **1995**, *51*, 513; J. K. M. Sanders, H. L. Anderson, *J. Chem. Soc. Perkin Trans. 1* **1995**, 2223.

[197] M. Fujita, J. Yazaki, K. Ogura, *J. Am. Chem. Soc.* **1990**, *112*, 5645.

[198] M. Fujita, J. Yazaki, K. Ogura, *Chem. Lett.* **1991**, 1031.

[199] M. Fujita, J. Yazaki, K. Ogura, *Tetrahedron Lett.* **1991**, *32*, 5592; M. Fujita, S. Nagao, M. Iida, K. Ogata, K. Ogura, *J. Am. Chem. Soc.* **1993**, *115*, 1574. For the self-assembly of ten molecules into nanometer-sized organic host frameworks, see: M. Fujita, D. Oguro, M. Miyazawa, H. Oka, K. Yamaguchi, K. Ogura, *Nature* **1995**, *378*, 469.

[200] P. J. Stang, D. H. Cao, *J. Am. Chem. Soc.* **1994**, *116*, 4981; P. J. Stang, D. H. Cao, S. Saito, *ibid.* **1995**, *117*, 6273; P. J. Stang, B. Olenyuk, J. Fan, A. M. Arif, *ibid.* **1996**, *118*, 904; J. Lee, A. W. Schwabacher, *ibid.* **1994**, *116*, 8382; C. A. Hunter, L. D. Sarson, *Angew. Chem.* **1994**, *106*, 2424; *Angew. Chem. Int. Ed. Engl.* **1994**, *33*, 2313; R. W. Saalfrank, R. Burak, S. Reihs, N. Löw, F. Hampel, H. D. Stachel, J. Lentmaier, K. Peters, E. M. Peters, H. G. von Schnering, *ibid.* **1995**, *107*, 1085 and **1995**, *34*, 993; C. A. Hunter, *ibid.* **1995**, *107*, 1181 and **1995**, *34*, 1079. X. L. Chi, A. J. Guerin, R. A. Haycock, C. A. Hunter, L. D. Sarson, *J. Chem. Soc. Chem. Commun.* **1995**, 2563, 2567. For an octahedral coordination polymer with large square channels, see: S. Subramanian, M. J. Zaworotko, *ibid.* **1995**, *107*, 2295 and **1995**, *34*, 2127. For another example of a microporous metal–organic framework, see: O. M. Yaghi, G. Li, H. Li, *Nature* **1995**, *378*, 703.

[201] M. Fujita, Y. J. Kwon, S. Washizu, K. Ogura, *J. Am. Chem. Soc.* **1994**, *116*, 1151; M. Fujita, S. Nagao, K. Ogura, *ibid.* **1995**, *117*, 1649; M. Fujita, Y. J. Kwon, O Sasaki, K. Yamaguchi, K. Ogura, *ibid.* **1995**, *117*, 7287.

[202] M. Fujita, F. Ibukuro, H. Hagihara, K. Ogura, *Nature* **1994**, *367*, 720. For a discussion of the unusual Möbius strip mechanism of [2]catenane formation, see: M. Fujita, F. Ibukuro, H. Seki, O. Kamo, M. Imanari, K. Ogura, *J. Am. Chem. Soc.* **1996**, *118*, 899.

[203] M. Fujita, F. Ibukuro, K. Yamaguchi, K. Ogura, *J. Am. Chem. Soc.* **1995**, *117*, 4175.

[204] For brief overviews of molecular helicity in chemical systems see: E. C. Constable, *Nature* **1990**, *346*, 314; *Angew. Chem.* **1991**, *103*, 1482; *Angew. Chem. Int. Ed. Engl.* **1991**, *30*, 1450. A comprehensive survey of the use of oligopyridine ligands for the construction of molecular helices can be found in: E. C. Constable, *Tetrahedron* **1992**, *48*, 10013. Molecular helices can also be constructed with hydrogen bonds as the stabilizing noncovalent interactions: S. J. Geib, C. Vicent, E. Fan, A. D. Hamilton, *Angew. Chem.* **1993**, *105*, 83; *Angew. Chem. Int. Ed. Engl.* **1993**, *32*, 119. For the self-assembly of a double helical complex with sodium ions, see: T. W. Bell, H. Jousselin, *Nature* **1994**, *367*, 441.

[205] J.-M. Lehn, A. Rigault, J. Siegel, J. Harrowfield, B. Chevrier, D. Moras, *Proc. Natl. Acad. Sci. USA* **1987**, *84*, 2565.

[206] J.-M. Lehn, A. Rigault, *Angew. Chem.* **1988**, *100*, 1121; *Angew. Chem. Int. Ed. Engl.* **1988**, *27*, 1095.

[207] A. Pfeil, J.-M. Lehn, *J. Chem. Soc. Chem. Commun.* **1992**, 838.

[208] R. Kramer, J.-M. Lehn, A. Marquis-Rigault, *Proc. Natl. Acad. Sci. USA* **1993**, *90*, 5394.

[209] U. Koert, M. M. Harding, J.-M. Lehn, *Nature* **1990**, *346*, 339; M. M. Harding, U. Koert, J. M. Lehn, A. Marquis-Rigault, C. Piguet, J. Siegel, *Helv. Chim. Acta* **1991**, *74*, 594. For the interaction of helicates with DNA, see: B. Schoentjies, J. M. Lehn, *ibid.* **1995**, *78*, 1.

[210] L. Pauling, R. B. Corey, *Nature* **1953**, *171*, 346.

[211] R. Kramer, J.-M. Lehn, A. De Cian, J. Fischer, *Angew. Chem.* **1993**, *105*, 764; *Angew. Chem. Int. Ed. Engl.* **1993**, *32*, 703. For the applications of double helicates in macromolecular chemistry, see: C. D. Eisenbach, U. S. Schubert, G. R. Baker, G. R. Newkome, *J. Chem. Soc. Chem. Commun.* **1995**, 69. For another example of the use of bipyridine ligands in metal-based self-assembly, see: K. T. Potts, K. A. Gehysen Raiford, M. Keshavarz, *J. Am. Chem. Soc.* **1993**, *115*, 2793. For another example of Ni^{II} ions in self-assembly, see: O. F. Schall, K. Robinson, J. L. Atwood, G. W. Gokel, *ibid.* **1991**, *113*, 7434. Cram et al. also described a helical ligand system: J. K. Judice, S. J. Keipert, D. J. Cram, *J. Chem. Soc. Chem. Commun.* **1993**, 1323. See also M. Mascal, C. J. Moody, A. I. Morrell, A. M. Z. Slawin, D. J. Williams, *J. Am. Chem. Soc.* **1993**, *115*, 813.

[212] P. Baxter, J.-M. Lehn, A. De Cian, J. Fischer, *Angew. Chem.* **1993**, *105*, 92; *Angew. Chem. Int. Ed. Engl.* **1993**, *32*, 69. For an example of self-assembly induced by Cu^{II} ions, see: R. W. Saalfrank, O. Struck, K. Peters, H. G. von Schnering, *Chem. Ber.* **1993**, *126*, 837.

[213] E. C. Constable, M. G. B. Drew, M. D. Ward, *J. Chem. Soc. Chem. Commun.* **1987**, 1600.

[214] M. Barley, E. C. Constable, S. A. Corr, R. C. S. McQueen, J. C. Nutkins, M. D. Ward, M. G. B. Drew, *J. Chem. Soc. Dalton Trans.* **1988**, 2655.

[215] E. C. Constable, M. G. B. Drew, D. A. Tocher, *J. Am. Chem. Soc.* **1990**, *112*, 1256.

[216] E. C. Constable, R. Chotalia, D. A. Tocher, *J. Chem. Soc. Chem. Commun.* **1992**, 771.

[217] a) E. C. Constable, S. M. Elder, P. R. Raithby, M. D. Ward, *Polyhedron* **1991**, *10*, 1395; b) E. C. Constable, J. V. Walker, D. A. Tocher, *J. Chem. Soc. Chem. Commun.* **1992**, 768; c) E. C. Constable, A. J. Edwards, P. R. Raithby, J. V. Walker, *Angew. Chem.* **1993**, *105*, 1486; *Angew. Chem. Int. Ed. Engl.* **1993**, *32*, 1465.

[218] E. C. Constable, M. G. B. Drew, G. A. Forsyth, M. D. Ward, *J. Chem. Soc. Chem. Commun.* **1988**, 1450; E. C. Constable, S. M. Elder, J. V. Walker, P. D. Wood, D. A. Tocher, *ibid.* **1992**, 229; E. C. Constable, J. V. Walker, *ibid.* **1992**, 884; ref. [217c]. See also G. S. Hanan, J. M. Lehn, N. Kyritsakas, J. Fischer, *J. Chem. Soc. Chem. Commun.* **1995**, 765.

[219] E. C. Constable, R. Chotalia, *J. Chem. Soc. Chem. Commun.* **1992**, 64.

[220] A. F. Williams, C. Piguet, R. F. Carina in *Transition Metals in Supramolecular Chemistry* (Eds.: L. Fabbrizzi, A. Poggi), Kluwer, **1994**, p. 409. See also G. Bernardinelli, C. Piguet, A. F. Williams, *Angew. Chem.* **1992**, *104*, 1626; *Angew. Chem. Int. Ed. Engl.* **1992**, *31*, 1622; C. Piguet, J.-C. G. Bünzli, G. Bernardinelli, G. Hopfgartner, A. F. Williams, *J. Am. Chem. Soc.* **1993**, *115*, 8197; R. F. Carina, G. Bernardinelli, A. F. Williams, *Angew. Chem.* **1993**, *105*, 1483; *Angew. Chem. Int. Ed. Engl.* **1993**, *32*, 1463; C. Piguet, B. Bocquet, G. Hopfgartner, *Helv. Chim. Acta* **1994**, *77*, 931; C. Piguet, G. Hopfgartner, A. F. Williams, J.-C. G. Bünzli, *J. Chem. Soc. Chem. Commun.* **1995**, 491; L. J. Charbonniere, M. F. Gilet, K. Bernauer, A. F. Williams, *Chem. Commun.* **1996**, 39.

[221] A. F. Williams, C. Piguet, G. Bernardinelli, *Angew. Chem.* **1991**, *103*, 1530; *Angew. Chem. Int. Ed. Engl.* **1991**, *30*, 1490; C. Piguet, G. Bernardinelli, B. Bocquet, A. Quattropani, A. F. Williams, *J. Am. Chem. Soc.* **1992**, *114*, 7440.

[222] P. N. W. Baxter, J. M. Lehn, J. Fischer, M. T. Youinou, *Angew. Chem.* **1994**, *106*, 2432; *Angew. Chem. Int. Ed. Engl.* **1994**, *33*, 2284. Molecular racks: H. Sleiman, P. N. W. Baxter, J. M. Lehn, K. Rissanen, *J. Chem. Soc. Chem. Commun.* **1995**, 715; G. S. Hanan, C. R. Arana, J. M. Lehn, D. Fenske, *Angew. Chem.* **1995**, *107*, 1191; *Angew. Chem. Int. Ed. Engl.* **1995**, *34*, 1122. For a different class of porphyrin-based molecular grids, see: C. M. Drain, J. M. Lehn, *J. Chem Soc. Chem. Commun.* **1994**, 2313; **1995**, 503.

[223] G. Denti, S. Campagna, S. Serroni, M. Ciano, V. Balzani, *J. Am. Chem. Soc.* **1992**, *114*, 2944; S. Campagna, G. Denti, S. Serroni, A. Juris, M. Venturi, V. Ricevuto, V. Balzani, *Chem. Eur. J.* **1995**, *1*, 211. For a discussion of large self-assembled organopalladium spheres, see: W. T. S. Huck, F. C. J. M. van Veggel, B. L. Kropman, D. H. A. Blank, E. G. Keim, M. M. A. Smithers, D. N. Reinhoudt, *J. Am. Chem. Soc.* **1995**, *117*, 8293.

[224] C. O. Dietrich-Buchecker, J. P. Sauvage, J. P. Kintzinger, *Tetrahedron Lett.* **1983**, *24*, 5095; C. O. Dietrich-Buchecker, J. P. Sauvage, J. M. Kern, *J. Am. Chem. Soc.* **1984**, *106*, 3043.

[225] C. O. Dietrich-Buchecker, J. P. Sauvage, *Bioorg. Chem. Front.* **1991**, *2*, 197; *Chem. Rev.* **1987**, *87*, 795, and references therein.

[226] J. P. Sauvage, *Acc. Chem. Res.* **1990**, *23*, 319; J.-C. Chambron, C. O. Dietrich-Buchecker, J. P. Sauvage, *Top. Curr. Chem.* **1993**, *165*, 131. For the synthesis of a doubly interlocked [2]catenane, see: J. F. Nierengarten, C. O. Dietrich-Buchecker, J. P. Sauvage, *J. Am. Chem. Soc.* **1994**, *116*, 375.

[227] J. P. Sauvage, J. Weiss, *J. Am. Chem. Soc.* **1985**, *107*, 6108.

[228] C. O. Dietrich-Buchecker, A.-K. Khémiss, J. P. Sauvage, *J. Chem. Soc. Chem. Commun.* **1986**, 1376; N. Amaroli, V. Balzani, F. Barigelletti, L. De Cola, L. Flamigni, J. P. Sauvage, C. Hemmert, *J. Am. Chem. Soc.* **1994**, *116*, 5211. For multiring catenanes with a macrobicyclic core, see: C. O. Dietrich-Buchecker, B. Fromberger, I. Lüer, J. P. Sauvage, F. Vögtle, *Angew. Chem.* **1993**, *105*, 1526; *Angew. Chem. Int. Ed. Engl.* **1993**, *32*, 1434. For a [2]catenate containing a TTF unit, see: T. Jørgensen, J. Becher, J. C. Chambron, J. P. Sauvage, *Tetrahedron Lett.* **1994**, *25*, 4339. For other catenated structures based on metal coordination, see: H. O. Stumpf, L. Ouahab, Y. Pei, D. Grandjean, O. Kahn, *Science* **1993**, *261*, 447; H. O. Stumpf, L. Ouahab, Y. Pei, D. Grandjean, P. Bergerat, O. Kahn, *J. Am. Chem. Soc.* **1994**, *116*, 3866; D. M. L. Goodgame, S. Menzer, A. M. Smith, D. J. Williams, *Angew. Chem.* **1995**, *107*, 605; *Angew. Chem. Int. Ed. Engl.* **1995**, *34*, 574; *J. Chem. Soc. Chem. Commun.* **1995**, 1975; C. Piguet, G. Bernardinelli, A. F. Williams, B. Bocquet, *Angew. Chem.* **1995**, *107*, 618; *Angew. Chem. Int. Ed. Engl.* **1995**, *34*, 582.

[229] F. Bitsch, C. O. Dietrich-Buchecker, A.-K. Khémiss, J. P. Sauvage, A. van Dorsselaer, *J. Am. Chem. Soc.* **1991**, *113*, 4023; F. Bitsch, G. Hegy, C. O. Dietrich-Buchecker, E. Leize, J. P. Sauvage, *New J. Chem.* **1994**, *18*, 801.

[230] J.-C. Chambron, V. Heitz, J. P. Sauvage, *J. Chem. Soc. Chem. Commun.* **1992**, 1131; *J. Am. Chem. Soc.* **1993**, *115*, 12378; F. Diederich, C. O. Dietrich-Buchecker, J.-F. Nierengarten, J. P. Sauvage, *J. Chem. Soc. Chem. Commun.* **1995**, 781; J. C. Chambron, V. Heitz, J. P. Sauvage, *Bull. Soc. Chim. Fr.* **1995**, 340; C. Wu, P. R. Lecavalier, Y. X. Shen, H. W. Gibson, *Chem. Mater.* **1991**, *3*, 569.

[231] J.-C. Chambron, C. O. Dietrich-Buchecker, J.-F. Nierengarten, J. P. Sauvage, *J. Chem. Soc. Chem. Commun.* **1993**, 801; J.-C. Chambron, C. O. Dietrich-Buchecker, J.-F. Nierengarten, J. P. Sauvage, N. Solladie, A. M. Albrecht-Gary, M. Meyer, *New J. Chem.* **1995**, *19*, 409.

[232] C. O. Dietrich-Buchecker, J. P. Sauvage, *Angew. Chem.* **1989**, *101*, 192; *Angew. Chem. Int. Ed. Engl.* **1989**, *28*, 189; C. O. Dietrich-Buchecker, J.-F. Nierengarten, J. P. Sauvage, N. Amaroli, V. Balzani, L. De Cola, *J. Am. Chem. Soc.* **1993**, *115*, 11237; J.-C. Chambron, C. O. Dietrich-Buchecker, J.-F. Nierengarten, J. P. Sauvage, *Pure Appl. Chem.* **1994**, *66*, 1543; J.-C. Chambron, C. O. Dietrich-Buchecker, V. Heitz, J.-F. Nierengarten, J. P. Sauvage, C. Pascard, J. Guilhem, *ibid.* **1995**, *67*, 233; D. B. Amabilino, C. O. Dietrich-Buchecker, J. P. Sauvage, *J. Am. Chem. Soc.* **1996**, *118*, 3285.

[233] C. O. Dietrich-Buchecker, J. P. Sauvage, A. De Cian, J. Fischer, *J. Chem. Soc. Chem. Commun.* **1994**, 2231.

[234] The synthesis of molecular with a rubber glove toplogy has been reported recently, which relied on a combination of Cu^{I}–phenanthroline chemistry and the hook-and-ladder approach: D. M. Walba, Q. Y. Zheng, K. Schilling, *J. Am. Chem. Soc.* **1992**, *114*, 6259. Knotted DNA has also been reported: S. T. Mullins, N. K. Annan, P. R. Cook, G. Lowe, *Biochemistry* **1992**, *31*, 842; N. C. Seeman, J. Chen, S. M. Du, J. E. Mueller, Y. Zhang, T. J. Fu, Y. Wang, H. Wang, S. Zhang, *New J. Chem.* **1993**, *17*, 739.

[235] Molecular donor–acceptor complexes were first noted in 1949 by Benesi and Hildebrand (H. A. Benesi, J. H. Hildebrand, *J. Am. Chem. Soc.* **1949**, *71*, 2703), when they observed an additional band in the electronic spectrum of a mixture of iodine and benzene which could not be attributed to either of the separate components of the system. Subsequently, such complexes were much studied by Mulliken, who proposed a resonance theory description of such complexes (R. S. Mulliken, *ibid.* **1952**, *74*, 811). In Mulliken's model, the complex is viewed as being a resonance between a no-bond structure $\Psi(D\cdots A)$ and a charge transfer state $\Psi(D^{+}\cdots A^{-})$. Later, Dewar proposed a molecular orbital treatment of such complexes in which the mixing of the HOMO of the donor and the LUMO of the acceptor can be treated by perturbation theory (M. J. S. Dewar, A. R. Lepley, *ibid.* **1961**, *83*, 4560).

[236] For reviews, see: R. S. Mulliken, W. B. Person, *Annu. Rev. Phys. Chem.* **1962**, *8*, 107; R. Foster, *Organic Charge-Transfer Complexes*, Academic Press, New York, **1969**; *J. Phys. Chem.* **1980**, *84*, 2135.

[237] See for example: F. Cozzi, M. Cinquini, R. Annuziata, J. S. Siegel, *J. Am. Chem. Soc.* **1993**, *115*, 5330.

[238] A. J. Bard, A. Ledwith, J. Shine, *Adv. Phys. Org. Chem.* **1976**, *13*, 155.

[239] L. A. Summers, *The Bipyridinium Herbicides*, Academic Press, London, **1980**.

[240] L. A. Summers, *Adv. Heterocycl. Chem.* **1984**, *35*, 282.

[241] An SCF-MO calculation of the charge distribution in the Paraquat dication using the AM1 method reveals that significant positive charge is located at the positions α and γ to the nitrogen atoms, and especially on the hydrogen atoms at the α position. Significant positive charge is also located on the hydrogen atoms of the methyl groups: M. J. S. Dewar, E. G. Zoebisch, E. F. Healy, J. J. P. Stewart, *J. Am. Chem. Soc.* **1985**, *107*, 3902.

[242] M. Heyrovsky, *J. Chem. Soc. Chem. Commun.* **1987**, 1856.

[243] A. Nakahara, J. C. Wang, *J. Phys. Chem.* **1963**, *67*, 496.

[244] R. Haque, W. R. Coshow, L. F. Jonson, *J. Am. Chem. Soc.* **1969**, *91*, 3822.

[245] B. G. White, *Trans. Faraday Soc.* **1969**, 2000.

[246] M. M. Mahmoud, S. C. Wallwork, *Acta Crystallogr. Sect. B* **1976**, *32*, 440.

[247] The situation in this complex is somewhat complicated by the fact that the iodide counterion also forms a donor–acceptor complex with the Paraquat dication and a continuous hydrogen bonded chain with the phenolic OH groups of the hydroquinone. The fact that the hydroquinone molecule does not position itself to achieve maximum overlap with the Paraquat π-system probably reflects this fact.

[248] H. M. Colquhoun, J. F. Stoddart, J. B. Wolstenholme, D. J. Williams, R. Zarzycki, *Angew. Chem.* **1981**, *93*, 1093; *Angew. Chem. Int. Ed. Engl.* **1981**, *20*, 1051; H. M. Colquhoun, S. M. Doughty, J. M. Maud, J. F. Stoddart, D. J. Williams, J. B. Wolstenholme, *Isr. J. Chem.* **1985**, *25*, 16.

[249] H. M. Colquhoun, E. P. Goodings, J. M. Maud, J. F. Stoddart, J. B. Wolstenholme, D. J. Williams, *J. Chem. Soc. Perkin Trans. 2* **1985**, 607.

[250] B. L. Allwood, N. Spencer, H. Shahriari-Zavareh, J. F. Stoddart, D. J. Williams, *J. Chem. Soc. Chem. Commun.* **1987**, 1064.

[251] P. R. Ashton, A. M. Z. Slawin, N. Spencer, J. F. Stoddart, D. J. Williams, *J. Chem. Soc. Chem. Commun.* **1987**, 1066.

[252] A. M. Z. Slawin, N. Spencer, J. F. Stoddart, D. J. Williams, *J. Chem. Soc. Chem. Commun.* **1987**, 1070.

[253] B. Odell, M. V. Reddington, A. M. Z. Slawin, N. Spencer, J. F. Stoddart, D. J. Williams, *Angew. Chem.* **1988**, *101*, 1605; *Angew. Chem. Int. Ed. Engl.* **1988**, *27*, 1547.

[254] P. R. Ashton, B. Odell, M. V. Reddington, A. M. Z. Slawin, J. F. Stoddart, D. J. Williams, *Angew. Chem.* **1988**, *100*, 1608; *Angew. Chem. Int. Ed. Engl.* **1988**, *27*, 1550.

[255] M. V. Reddington, A. M. Z. Slawin, N. Spencer, J. F. Stoddart, C. Vicent, D. J. Williams, *J. Chem. Soc. Chem. Commun.* **1991**, 630.

[256] T. T. Goodnow, M. V. Reddington, J. F. Stoddart, A. E. Kaifer, *J. Am. Chem. Soc.* **1991**, *113*, 4335; A. R. Bernado, J. F. Stoddart, A. E. Kaifer, *ibid.* **1992**, *114*, 10624.

[257] D. Philp, A. M. Z. Slawin, N. Spencer, J. F. Stoddart, D. J. Williams, *J. Chem. Soc. Chem. Commun.* **1991**, 1584.

[258] P. R. Ashton, R. A. Bissell, R. Górski, D. Philp, N. Spencer, J. F. Stoddart, M. S. Tolley, *Synlett* **1992**, 919.

[259] R. O. Gould, A. M. Gray, P. Taylor, D. Walkinshaw, *J. Am. Chem. Soc.* **1985**, *107*, 5921.

[260] S. K. Burley, G. A. Petsko, *J. Am. Chem. Soc.* **1986**, *108*, 7995.

[261] M. Nishio, M. Hirota, *Tetrahedron* **1989**, *45*, 7201.

[262] J.-Y. Ortholand, A. M. Z. Slawin, N. Spencer, J. F. Stoddart, D. J. Williams, *Angew. Chem.* **1989**, *101*, 1402; *Angew. Chem. Int. Ed. Engl.* **1989**, *28*, 1394.

[263] P. R. Ashton, T. T. Goodnow, A. E. Kaifer, M. V. Reddington, A. M. Z. Slawin, N. Spencer, J. F. Stoddart, C. Vicent, D. J. Williams, *Angew. Chem.* **1989**, *101*, 1404; *Angew. Chem. Int. Ed. Engl.* **1989**, *28*, 1396; C. L. Brown, D. Philp, J. F. Stoddart, *Synlett* **1991**, 459, 462.

[264] C. L. Brown, D. Philp, N. Spencer, J. F. Stoddart, *Isr. J. Chem.* **1992**, *32*, 61.
[265] P. L. Anelli, P. R. Ashton, R. Ballardini, V. Balzani, M. Delgado, M. T. Gandolfi, T. T. Goodnow, A. E. Kaifer, D. Philp, M. Pietraszkiewicz, L. Prodi, M. V. Reddington, A. M. Z. Slawin, N. Spencer, J. F. Stoddart, C. Vicent, D. J. Williams, *J. Am. Chem. Soc.* **1992**, *114*, 193; D. B. Amabilino, P. R. Ashton, C. L. Brown, E. Córdova, L. A. Godínez, T. T. Goodnow, A. E. Kaifer, S. P. Newton, M. Pietraszkiewicz, D. Philp, F. M. Raymo, A. S. Reder, M. T. Rutland, A. M. Z. Slawin, N. Spencer, J. F. Stoddart, D. J. Williams, *ibid.* **1995**, *117*, 1271.
[266] The alternation of donors and acceptors within this stack can be used as a conceptual basis for the self-assembly of other structures: P.-L. Anelli, P. R. Ashton, N. Spencer, A. M. Z. Slawin, J. F. Stoddart, D. J. Williams, *Angew. Chem.* **1991**, *103*, 1052; *Angew. Chem. Int. Ed. Engl.* **1991**, *30*, 1036; P. R. Ashton, D. Philp, N. Spencer, J. F. Stoddart, *J. Chem. Soc. Chem. Commun.* **1991**, 1677; P. R. Ashton, D. Philp, M. V. Reddington, A. M. Z. Slawin, N. Spencer, J. F. Stoddart, D. J. Williams, *ibid.* **1991**, 1680; P. R. Ashton, D. Philp, N. Spencer, J. F. Stoddart, *Makromol. Chem. Macromol. Symp.* **1992**, *54/55*, 441; P. R. Ashton, R. A. Bissell, D. Philp, N. Spencer, J. F. Stoddart, *NATO ASI Ser. Ser. C* **1992**, *371*, 1; P. R. Ashton, D. Philp, N. Spencer, J. F. Stoddart, D. J. Williams, *J. Chem. Soc. Chem. Commun.* **1994**, 181; D. B. Amabilino, P. R. Ashton, S. Menzer, J. F. Stoddart, D. J. Williams, *ibid.* **1994**, 2479; R. S. Lokey, B. L. Iverson, *Nature* **1995**, *375*, 303.
[267] P. R. Ashton, C. L. Brown, E. J. T. Chrystal, T. T. Goodnow, A. E. Kaifer, K. P. Parry, D. Philp, A. M. Z. Slawin, N. Spencer, J. F. Stoddart, D. J. Williams, *J. Chem. Soc. Chem. Commun.* **1991**, 634; P. R. Ashton, M. Blower, D. Philp, N. Spencer, J. F. Stoddart, M. S. Tolley, R. Ballardini, M. Ciano, V. Balzani, M. T. Gandolfi, L. Prodi, *New J. Chem.* **1993**, *17*, 689.
[268] D. B. Amabilino, P. R. Ashton, M. S. Tolley, J. F. Stoddart, D. J. Williams, *Angew. Chem.* **1993**, *105*, 1358; *Angew. Chem. Int. Ed. Engl.* **1993**, *32*, 1297; F. Vögtle, W. M. Müller, U. Müller, M. Bauer, K. Rissanen, *ibid.* **1993**, *105*, 1356 and **1993**, *32*, 1295.
[269] P. R. Ashton, C. L. Brown, E. J. T. Chrystal, K. P. Parry, M. Pietraszkiewicz, N. Spencer, J. F. Stoddart, *Angew. Chem.* **1991**, *103*, 1058; *Angew. Chem. Int. Ed. Engl.* **1991**, *30*, 1042.
[270] The term "translational isomerism" is attributed to Schill and co-workers: G. Schill, K. Rissler, W. Vetter, *Angew. Chem.* **1981**, *93*, 197; *Angew. Chem. Int. Ed. Engl.* **1981**, *20*, 187; K. Rissler, G. Schill, H. Fritz, W. Vetter, *Chem. Ber.* **1986**, *119*, 1374.
[271] F. M. Raymo, J. F. Stoddart, *Pure Appl. Chem.* **1996**, *68*, 313.
[272] P. R. Ashton, C. L. Brown, E. J. T. Chrystal, T. T. Goodnow, A. E. Kaifer, K. P. Parry, M. Pietraszkiewicz, A. M. Z. Slawin, N. Spencer, J. F. Stoddart, D. J. Williams, *Angew. Chem.* **1991**, *103*, 1055; *Angew. Chem. Int. Ed. Engl.* **1991**, *30*, 1039.
[273] D. B. Amabilino, P. R. Ashton, A. S. Reder, N. Spencer, J. F. Stoddart, *Angew. Chem.* **1994**, *106*, 450; *Angew. Chem. Int. Ed. Engl.* **1994**, *33*, 433; *ibid.* **1994**, *106*, 1316 and **1994**, *33*, 1286. For the original suggestion that the first, fully characterized pentacatenane be named "Olympiadane", see: N. van Gulick, *New J. Chem.* **1993**, *17*, 619.
[274] P. R. Ashton, A. S. Reder, N. Spencer, J. F. Stoddart, *J. Am. Chem. Soc.* **1993**, *115*, 5286.
[275] Chirality has also been incorporated into a [2]catenane by more traditional means: See P. R. Ashton, I. Iriepa, A. M. Z. Slawin, N. Spencer, J. F. Stoddart, D. J. Williams, *Tetrahedron Lett.* **1994**, *35*, 4835.
[276] For a description of [2]catenanes in which resorcinol rings replace sequentially hydroquinone rings in the macrocyclic polyether component and *meta*-xylyl replace sequentially the *para*-xylyl spacers in the tetracationic cyclophane component, see: D. B. Amabilino, P. R. Ashton, G. R. Brown, W. Hayes, J. F. Stoddart, *J. Chem. Soc. Chem. Commun.* **1994**, 2475; D. B. Amabilino, P. R. Ashton, J. F. Stoddart, *Supramol. Chem.* **1995**, *5*, 5; D. B. Amabilino, P. L. Anelli, P. R. Ashton, G. R. Brown, E. Córdova, L. A. Godinez, W. Hayes, A. E. Kaifer, D. Philp, A. M. Z. Slawin, N. Spencer, J. F. Stoddart, M. S. Tolley, D. J. Williams, *J. Am. Chem. Soc.* **1995**, *117*, 11142. For description of [2]catenanes in which 1,5-dioxynaphthalene rings replace sequentially hydroquinone rings in the macrocyclic polyether component and *trans*-bis(pyridinium)ethylene units replace sequentially bipyridinium units in the tetracationic cyclophane component, see: P. R. Ashton, R. Ballardini, V. Balzani, M. T. Gandolfi, D. J. F. Marquis, L. Pérez-García, L. Prodi, J. F. Stoddart, M. Venturi, *J. Chem. Soc. Chem. Commun.* **1994**, 177; R. Ballardini, V. Balzani, A. Credo, M. T. Gandolfi, L. Prodi, M. Venturi, L. Pérez-García, J. F. Stoddart, *Gazz. Chim. Ital.* **1995**, *125*, 1; P. R. Ashton, L. Pérez-García, J. F. Stoddart, A. J. P. White, D. J. Williams, *Angew. Chem.* **1995**, *107*, 607; *Angew. Chem. Int. Ed. Engl.* **1995**, *34*, 571; P. R. Ashton, R. Ballardini, V. Balzani, M. T. Gandolfi, S. Menzer, L. Pérez-García, L. Prodi, J. F. Stoddart, M. Venturi, A. J. P. White, D. J. Williams, *J. Am. Chem. Soc.* **1995**, *117*, 11171. For a description of [2]catenanes in which the polyether chains of the **BPP34C10** ((bisparaphenylene-[34]crown-10)) are intercepted by a) catechol residues, b) furan, and c) pyridine residues, see: a) D. B. Amabilino, J. F. Stoddart, *Rec. Trav. Chim. Pays Bas* **1993**, *112*, 429; b) P. R. Ashton, M. A. Blower, S. Iqbal, C. H. McLean, J. F. Stoddart, M. S. Tolley, D. J. Williams, *Synlett* **1994**, 1059; c) P. R. Ashton, M. A. Blower, C. H. McLean, J. F. Stoddart, *ibid.* **1994**, 1063. For a description of [2]catenanes in which thiophene residues replace sequentially the paraphenylene units in the tetracationic cyclophane component, see: P. R. Ashton, J. A. Preece, J. F. Stoddart, M. S. Tolley, A. J. P. White, D. J. Williams, *Synthesis* **1994**, 1344.
[277] P. R. Ashton, J. A. Preece, J. F. Stoddart, M. S. Tolley, *Synlett* **1994**, 789; *Polym. Prepr. Am. Chem. Soc. Div. Polym. Chem.* **1995**, *36*, 587; P. R. Ashton, J. Huff, S. Menzer, I. W. Parsons, J. A. Preece, J. F. Stoddart, M. S. Tolley, A. J. P. White, D. J. Williams, *Chem. Eur. J.* **1996**, *2*, 123; J. Huff, J. A. Preece, J. F. Stoddart, *Macromol. Symp.* **1996**, *102*, 1.
[278] P.-L. Anelli, N. Spencer, J. F. Stoddart, *J. Am. Chem. Soc.* **1991**, *113*, 5131; P. R. Ashton, M. Grognuz, A. M. Z. Slawin, J. F. Stoddart D. J. Williams, *Tetrahedron Lett.* **1991**, *33*, 6235; E. Córdova, R. A. Bissell, N. Spencer, P. R. Ashton, J. F. Stoddart, A. E. Kaifer, *J. Org. Chem.* **1993**, *58*, 6550.
[279] P. R. Ashton, R. A. Bissell, N. Spencer, J. F. Stoddart, M. S. Tolley, *Synlett* **1992**, 914.
[280] P. R. Ashton, R. A. Bissell, N. Spencer, J. F. Stoddart, M. S. Tolley, *Synlett* **1992**, 923; R. A. Bissell, J. F. Stoddart in *Computational for the Nanoscale* (Eds.: P. E. Blöchl, A. J. Fisher, C. Joachim), Kluwer, Dordrecht, **1993**, p. 141; Z. T. Li, P. C. Stein, N. Svenstrup, K. H. Lund, J. Becher, *Angew. Chem.* **1995**, *107*, 2719; *Angew. Chem. Int. Ed. Engl.* **1995**, *34*, 2524; Z. T. Li, J. Becher, *Chem. Commun.* **1996**, 639.
[281] For a reviews of TTF chemistry, see: A. Krief, *Tetrahedron* **1986**,*42*, 1209; T. Jørgensen, T. K. Hansen, J. Becher, *Chem. Soc. Rev.* **1994**, *24*, 41.
[282] R. A. Bissell, E. Córdova, A. E. Kaifer, J. F. Stoddart, *Nature* **1994**, *369*, 133; E. Córdova, R. A. Bissell, A. E. Kaifer, *J. Org. Chem.* **1995**, *60*, 1033; R. A. Bissell, E. Córdova, J. F. Stoddart, A. E. Kaifer in *Molecular Engineering for Advanced Materials* (Eds.: J. Becher, K. Schaumberg), Kluwer, Dordrecht, **1995**, p. 29.
[283] R. Ballardini, V. Balzani, M. T. Gandolfi, L. Prodi, M. Venturi, D. Philp, H. G. Ricketts, J. F. Stoddart, *Angew. Chem.* **1993**, *105*, 1362; *Angew. Chem. Int. Ed. Engl.* **1993**, *32*, 1301. For examples of chemically driven molecular machines, see: R. Ballardini, V. Balzani, A. Credi, M. T. Gandolfi, S. J. Langford, S. Menzer, L. Prodi, J. F. Stoddart, M. Venturi, D. J. Williams, *Angew. Chem.* **1996**, *108*, 1054; *Angew. Chem. Int. Ed. Engl.* **1996**, *35*, 976; P. R. Ashton, S. Iqbal, J. F. Stoddart, N. D. Tinker, *Chem. Commun.* **1996**, 479; M. Asakawa, S. Iqbal, J. F. Stoddart, N. D. Tinker, *Angew. Chem.* **1996**, *108*, 1056; *Angew. Chem. Int. Ed. Engl.* **1996**, *35*, 978.
[284] P. R. Ashton, M. R. Johnston, J. F. Stoddart, M. S. Tolley, J. W. Wheeler, *J. Chem. Soc. Chem. Commun.* **1992**, 1128.
[285] Porphyrin-containing [2]catenanes have also been prepared by self-assembly, and their dynamic properties have been investigated in solution by ^{1}H NMR spectroscopy: M. J. Gunter, M. R. Johnston, *J. Chem. Soc. Chem. Commun.* **1992**, 1163; *ibid.* **1994**, 829; M. J. Gunter, D. C. R. Hockless, M. R. Johnston, B. W. Skelton, A. H. White, *J. Am. Chem. Soc.* **1994**, *116*, 4810. Phenyl glycosides can also be bound by cyclobis(paraquat-*p*-phenylene), see: S. A. Stanley, B. D. Smith, *Tetrahedron Lett.* **1996**, *37*, 283; M. A. Lipton, *ibid.* **1996**, *37*, 287. Photochemically active azobenzene units have been incorporated into [2]catenanes: M. Bauer, W. M. Müller, U. Müller, K. Rissanen, F. Vögtle, *Liebigs Ann.* **1995**, 649. For a description of photoactive anthracene- and ferrocene-stoppered [2]rotaxanes, see: A. C. Benniston, A. Harriman, *Angew. Chem.* **1993**, *105*, 1553; *Angew. Chem. Int. Ed. Engl.* **1993**, *32*, 1459; A. C. Benniston, A. Harriman, V. M. Lynch, *Tetrahedron Lett.* **1994**, *35*, 1473; *J. Am. Chem. Soc.* **1995**, *117*, 5275. For a discussion of photoactive supramolecular assemblies, see: A. C. Benniston, A. Harriman, D. Philp, J. F. Stoddart, *ibid.* **1993**, *115*, 5298; M. Seiler, H. Dürr, I. Wilner, E. Joselevich, A. Doron, J. F. Stoddart, *ibid.* **1994**, *116*, 3399. In the quest for functioning supramolecular materials, the first steps toward introducing pseudorotaxanes and [2]catenanes incorporating cyclobis(paraquat-*p*-phenylene) into Langmuir films and Langmuir–Blodgett multilayers have been taken: R. C. Ahuja, P.-L. Caruso, D. Möbius, G. Wildburg, H. Ringsdorf, D. Philp, J. A. Preece, J. F. Stoddart, *Langmuir* **1993**, *9*, 1534. Finally, for a discussion of the self-assembly of a gold surface attached [2]catenane, see: T. B. Lu, L. T. Zhang, G. W. Gokel, A. E. Kaifer, *J. Am. Chem. Soc.* **1993**, *115*, 2542. For photoinduced electron transfer in supramolecular assemblies based on cyclobis(paraquat-*p*-phenylene), see M. Kropf, E. Joselevich, H. Dürr, I. Willner, *J. Am. Chem. Soc.* **1996**, *118*, 655.
[286] P. R. Ashton, D. Philp, N. Spencer, J. F. Stoddart, *J. Chem. Soc. Chem. Commun.* **1992**, 1124; *Spec. Publ. R. Soc. Chem.* **1992**, *111*, 53.
[287] P. R. Ashton, M. Bělohradsky, D. Philp, J. F. Stoddart, *J. Chem. Soc. Chem. Commun.* **1993**, 1269.
[288] D. B. Amabilino, P. R. Ashton, M. Bělohradsky, F. M. Raymo, J. F. Stoddart, *J. Chem. Soc. Chem. Commun.* **1995**, 751; P. R. Ashton, M. Bělohradsky, D. Philp, N. Spencer, J. F. Stoddart, *ibid.* **1993**, 1274; M. Asakawa, P. R. Ashton, S. Iqbal, J. F. Stoddart, N. D. Tinker, A. J. P. White, D. J. Williams, *ibid.* **1996**, 483.
[289] Slippage can also be used to create [*n*]rotaxanes containing several constitutionally different components: D. B. Amabilino, P. R. Ashton, M. Bělohradsky, F. M. Raymo, J. F. Stoddart, *J. Chem. Soc. Chem. Commun.* **1995**, 747. Polyrotaxanes have been prepared by the reaction of bis(2-hydroxyethyl)-4,4'-bipyridinium bis(hexafluorophosphate) with bis(*p*-isocyanatophenyl)-methane in the presence of bisparaphenylene-[34]crown-10: H. W. Gibson, P. T. Engen, Y. X. Shen, J. Sze, C. Lim, M. C. Bheda, *Makromol. Chem.*

Macromol. Symp. **1992**, *54/55*, 519. The inverse design logic has been employed in the synthesis of a pseudopolyrotaxane incorporating cyclobis(-paraquat-*p*-phenylene) around a polymer prepared by reacting a three-hydroquinone ring-containing thread with bis(*p*-isocyanatophenyl)methane: X. Sun, D. B. Amabilino, P. R. Ashton, I. W. Parsons, J. F. Stoddart, M. S. Tolley, *Makromol. Chem. Macromol. Symp.* **1994**, *77*, 191. Hydrogen-bonded pseudopolyrotaxanes have also been assembled: M. Asakawa, P. R. Ashton, G. R. Brown, W. Hayes, S. Menzer, J. F. Stoddart, A. J. P. White, D. J. Williams, *Adv. Mater.* **1996**, *8*, 37. Function is also being built into polymers by designing them to bind paraquat. For a discussion of the properties of conducting pseudopolyroatxanes containing paraquat receptor sites, see: M. J. Marsella, P. J. Carroll, T. M. Swager, *J. Am. Chem. Soc.* **1994**, *116*, 9347. For an example of energy migration in conjugated polymers carrying paraquat receptor sites, see: Q. Zhou, T. M. Swager, *ibid.* **1995**, *117*, 7017. For the strong binding of paraquat and polymeric paraquat derivatives by basket-shaped hosts, see: A. P. H. J. Schenning, B. Debruin, A. E. Rowan, H. Kooijman, A. L. Spek, R. J. M. Nolte, *Angew. Chem.* **1995**, *107*, 2288; *Angew. Chem. Int. Ed. Engl.* **1995**, *34*, 2132.

[290] D. B. Amabilino, P. R. Ashton, L. Pérez-García, J. F. Stoddart, *Angew. Chem.* **1995**, *107*, 2569; *Angew. Chem. Int. Ed. Engl.* **1995**, *34*, 2378.

[291] J. I. Seeman, *Chem. Rev.* **1983**, *83*, 83; *J. Chem. Educ.* **1986**, *63*, 42.

[292] P. R. Ashton, C. G. Claessens, W. Hayes, S. Menzer, J. F. Stoddart, A. J. P. White, D. J. Williams, *Angew. Chem.* **1995**, *107*, 1994; *Angew. Chem. Int. Ed. Engl.* **1995**, *34*, 1862.

[293] The template-directed synthesis of cyclobis(paraquat-4,4′-biphenylene) has been accomplished recently using a 1,1′-disubstituted ferrocene derivative as the template: P. R. Ashton, S. Menzer, F. M. Raymo, G. Shimizu, J. F. Stoddart, D. J. Williams, *Chem. Commun.* **1996**, 487; M. Asakawa, P. R. Ashton, S. Menzer, F. M. Raymo, J. F. Stoddart, A. J. P. White, D. J. Williams, *Chem. Eur. J.* **1996**, *2*, no. 7.

[294] For a number of shorter and more specific reviews covering different parts of the research conducted in our own laboratories during the last decade, see: J. F. Stoddart, *Chem. Br.* **1991**, *27*, 714; *Chem. Aust.* **1992**, *59*, 576; *An. Quim.* **1993**, *89*, 51; D. B. Amabilino, J. F. Stoddart, *Pure Appl. Chem.* **1993**, *65*, 2351; H. G. Ricketts, J. F. Stoddart, M. M. Hann, *NATO ASI Ser. Ser. C* **1994**, *426*, 377; J. A. Preece, J. F. Stoddart, *Nanobiology* **1994**, *3*, 149; in *Molecular Engineering for Advanced Materials* (Eds: J. Becher, K. Schaumberg), Kluwer, Dordrecht, **1995**, p. 1; in *Ultimate Limits of Fabrication and Measurement* (Eds.: M. E. Welland, J. K. Gimzewski), Kluwer, Dordrecht, **1995**, pp. 1, 255; S. J. Langford, L. Pérez-García, J. F. Stoddart, *Supramol. Chem.* **1995**, *6*, 11, D. Pasini, F. M. Raymo, J. F. Stoddart, *Gazz. Chim. Ital.* **1995**, *125*, 431; M. Belohradsky, F. M. Raymo, J. F. Stoddart, *Coll. Czech Chem. Comm.* **1996**, *61*, 1.

[295] Self-assembly is a highly interdisciplinary and fast-moving research area. Between 1985 and 1989 around 170 articles were published on this topic. Between 1990 and 1995 well over 1000 articles concerning self-assembly. In 1996 the following highlights have already appeared. Chiral double helical structures: N. Ohata, H. Masuda, O. Yamauchi, *Angew. Chem.* **1996**, *108*, 570; *Angew. Chem. Int. Ed. Engl.* **1996**, *35*, 531; heteroduplex helicates: B. Hasenkopf, J. M. Lehn, G. Baum, D. Fenske, *Proc. Natl. Acad. Sci. USA* **1996**, *93*, 1397; self-assembling dendrimers: S. C. Zimmerman, F. W. Zeng, D. E. C. Reichert, S. V. Kolotuchin, *Science* **1996**, *271*, 1095; self-assembling host system: R. M. Grotzfeld, N. Branda, J. Rebek, Jr., *Science* **1996**, *271*, 487; anionic helicates: J. Sanchezquesada, C. Seel, P. Prados, J. de Mendoza, I. Dalcol, E. Giralt, *J. Am. Chem. Soc.* **1996**, *118*, 277; Peptide nanotubes: J. D. Hartgerink, J. R. Granja, R. A. Milligan, M. R. Ghadiri, *ibid.* **1996**, *118*, 43; multi-heme self-assembly: J. Lahiri, G. D. Fate, S. B. Ungashe, J. T. Groves, *ibid.* **1996**, *118*, 2347; multi-porphyrin supramolecular macrocycle: C. M. Drain, K. C. Russell, J. M. Lehn, *Chem. Commun.* **1996**, 337; novel water-soluble molecular clips : J. N. H. Reek, A. Kros, R. J. M. Nolte, *ibid.* **1996**, 337.

[296] J. P. Mathias, J. F. Stoddart in *The Encyclopedia of Advanced Materials* (Eds.: D. Bloor, R. J. Brook, M. C. Flemings, S. Mahajan), Pergamon, Oxford, **1994**, p. 2729.

Application of π-Arene–Ruthenium Complexes in Peptide Labeling and Peptide Synthesis

Roland Krämer*

Organotransition metal complexes with biologically relevant ligands have attracted considerable attention in recent years. The term "bioorganometallic chemistry" has been coined to describe the research in this area.[1, 2] The combination of naturally occurring ligands (bioligands) with organometallic compounds with characteristic physical and chemical properties opens interesting perspectives for biochemical and synthetic applications. Examples include the developement of a carbonyl-metalloimmunoassay,[1, 3] the investigation of receptor and enzyme active sites using organometallic-labeled substrates,[1] and the application of organotransition metal complexes with amino acid ligands as enantioselective catalysts.[4] This highlight focuses on some "bioorganometallic curiosities" from the field of [Ru(π-arene)] peptide complexes. In the examples considered herein two characteristics of the π-arene–Ru^{II} interaction play a fundamental role: the remarkable thermal stability of π-arene–Ru bond and the Ru-induced activation of arenes that carry good leaving groups for nucleophilic substitution (S_NAr) reactions.

The facile preparation of [CpRu] sandwich complexes (Cp = η^5-C_5H_5) with aromatic amino acids by reaction of N/O-protected phenylalanine (Phe), tryptophane (Trp), and tyrosine (Tyr) with $[CpRu(MeCN)_3](PF_6)$ was first reported by Moriarty and co-workers.[5] Recently Sheldrick et al. have discovered that this methodology is also applicable to unprotected amino acids[6] and peptides.[7] The [Cp*Ru^{II}] dipeptide complex **1** (Cp* = η^5-C_5Me_5) is obtained readily by reaction of Phe–Phe with two equivalents of $[Cp^*Ru(MeCN)_3](CF_3SO_3)$. The analogous reaction with Trp–Trp affords bis(sandwich) complexes with regioselective η^6-coordination of the six-membered indole ring.

An alternative N/O chelate coordination, which is observed in the reaction of [Cp*Ru] with phenylalanine at room temperature,[6] can be suppressed by applying elevated reaction temperatures. The investigations have been extended to the use of [(η^6-arene)Ru^{II}] fragments as organometallic markers.[8] Sheldrick et al. have also shown that [Cp*Ru]-labeled aromatic amino acids can be incorporated into peptides by using the classic carbodiimide coupling reaction.[7] Thus, reaction of

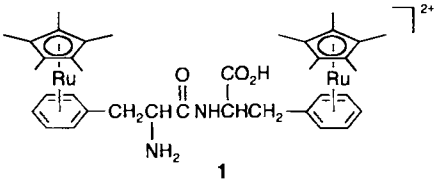

1

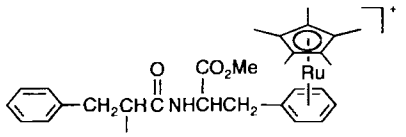

2

[Cp*Ru]-labeled phenylalanine methyl ester with N-protected phenylalanine affords the dipeptide derivative **2** (92%) with specific [Cp*Ru] labeling of the C-terminal Phe residue. The remarkable stability of the η^6-arene–Ru bond is clearly demonstrated by isolation of the intact sandwich complex after removal of the N-terminal protecting group with glacial acetic acid.

The above-mentioned straightforward methods for organometallic labeling of peptides—either by direct attachment of [Cp*Ru] to aromatic side chains or by incorporation of a [Cp*Ru]-substituted amino acid by peptide synthesis—are relevant to biochemical applications. Ruthenocene derivatives that display selective enrichment behavior in tissues are of considerable interest as radiopharmaceuticals (^{97}Ru, ^{103}Ru, ^{106}Ru). For example, radiolabeled ruthenocenylalanine has been applied as a pancreatic imaging agent.[9] In addition, [Cp*Ru] derivatives of bioactive peptides could open new analytical perspectives for the investigation of the substrate binding sites of receptors. [Cp*Ru]-labeled estradiol has already been employed succesfully to gain insights into hormone receptor–substrate interactions.[1]

The next example refers to the utilization of π-arene–Ru^{II} chemistry to the synthesis of important peptide-derived antibiotics. Cyclic biphenyl ethers are structural components of many biologically active peptide derivatives such as the vancomycins and the protease inhibitor K-13. A challenging problem in the synthesis of these compounds is the sensitivity of the amino acid functionality, which is unable to with-

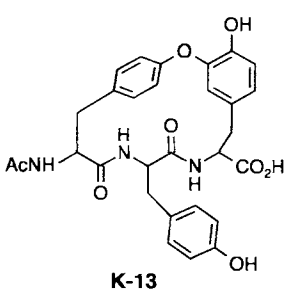

K-13

[*] Dr. R. Krämer
Anorganisch-chemisches Institut der Universität
Wilhelm-Klemm-Strasse 8, D-48149 Münster (Germany)
Fax: Int. code +(251)838366
e-mail: kramerr@vnwz01.uni-muenster.de

 © VCH Verlagsgesellschaft mbH, D-69451 Weinheim, 1996 0570-0833/96/3511-1197 $ 15.00+.25/0

stand the harsh reaction conditions usually required for construction of the diaryl ether linkage. Pearson et al. have reported a formal total synthesis of K-13 in which the diaryl ether coupling is effected under very mild conditions with participation of a ruthenium-activated chloroarene.[10] Nucleophilic substitution (S_NAr)[11] of the chloro substituents in the [CpRu^{II}] derivative of protected *p*-chlorophenylalanine (**3**) by the phenolate function of an isotyrosine dipeptide affords **4** without racemization at the α-C atoms of the amino acid building blocks (Scheme 1).

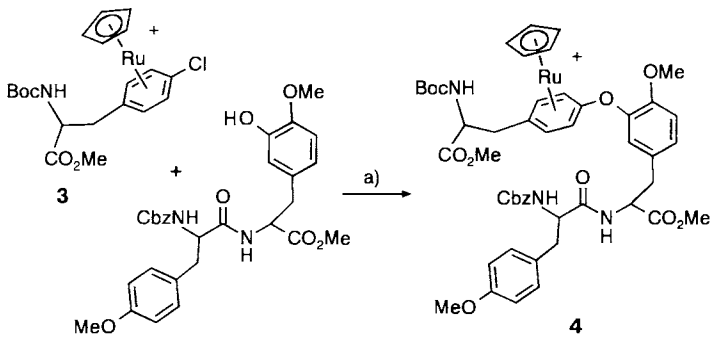

Scheme 1. Boc = *tert*-butoxycarbonyl. Cbz = carbobenzoxy. a) Sodium 2,6-di-*tert*-butylphenoxide.

The [CpRu] group can be readily photochemically removed; $[CpRu(CH_3CN)_3]PF_6$, which was used for the preparation of **3**, is recovered in 85% yield. Synthesis of the K-13 analogue is completed by deprotection and cyclization of the linear tripeptide **4** by intramolecular coupling of a peptide bond. The low yields in the final cyclization step are a weak point of the reaction sequence.

Recently Rich et al. have overcome this problem by an elegant variation of the synthetic route.[12] By coupling of [CpRu(*N*-Boc-*p*-Cl-Phe)]$^+$ with an isotyrosine dipeptide, the tripeptide backbone was constructed *prior* to formation of the aryl ether bond. The linear tripeptide complex **5** is converted to the macrocyclic product **6** by *intramolecular* nucleophilic substitution (Scheme 2). After photolytic removal of the [CpRu] fragment, the 17-membered macrocyclic ring system was isolated in 60% yield!

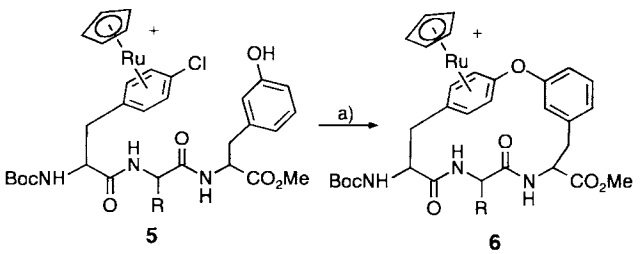

Scheme 2. R = *sec*-butyl, benzyl, 4-(*tert*-butoxy)benzyl. a) Sodium 2,6-di-*tert*-butylphenoxide.

A possible explanation for the surprisingly high yield in the cyclization reaction is an intramolecular preorganization of the electron-poor π-complexed ring and of the electron-rich phenol ring by π-π interactions, which favors formation of the macrocycle over polymerization. The versatility of the approach developed by Rich et al. should facilitate the creation of libraries of cyclic biphenyl ether peptides. Numerous analogues of K-13 and of related antibiotics should be available by varying the N-terminal substituent, the central amino acid, and the C-terminal substituent in a combinatorial fashion during the synthesis.

The final example considered here is a remarkable peptide synthesis in which a π-arene-coordinated ruthenium(II) center directly promotes amide bond formation. The chloro-bridged complex $[\{(\eta^6\text{-hexamethylbenzene})Ru(\mu\text{-Cl})(Cl)\}_2]$ reacts smoothly with peptide esters by formation of *N,N*-chelate complexes.[13] With aromatic amino acids no competitive formation of sandwich complexes is observed. In the glycylglycine methyl ester compound $[(\eta^6\text{-hexamethylbenzene})Ru(GlyGlyOMe)Cl]$ **7**, the dipeptide is coordinated by NH_2 and a deprotonated amide nitrogen atom. On addition of amino acid esters in the presence of base, **7** undergoes a remarkable peptide bond formation reaction that was discovered earlier with related [Cp*M] complexes (M = Rh^{III}, Ir^{III}).[14] The new amino acid is incorporated at the amino terminus of the coordinated peptide chain, and the tripeptide ester complexes **8** are obtained in 80–90% yield.[15] A plausible mechanism involves nucleophilic attack of a metal-bound aminoanion at the carbonyl group of the N-coordinated amino acid ester. The pseudooctahedral $[(C_6Me_6)Ru]$ fragment with three available, facially orientated coordination sites functions as a template.

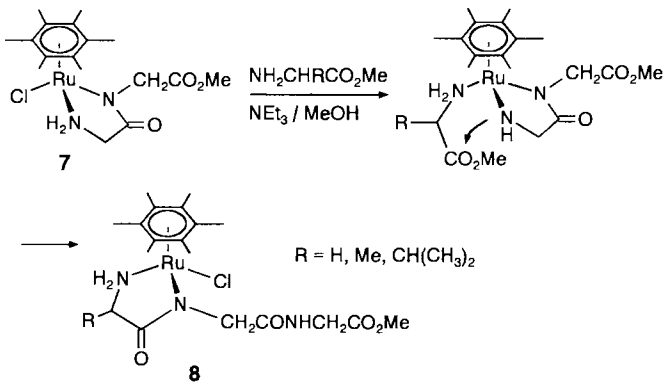

It has been demonstrated that even longer peptides can be constructed in this fashion (Scheme 3). The tetrapeptide Ser-GlyGlyGly was prepared sequence specifically in a one-pot reaction by successive addition of GlyOMe and SerOMe to a diglycine complex.[14] In some respects this reaction is reminiscent of the action of a ribosome in biological systems, in which peptide bonds are formed by nucleophilic attack of NH_2 at the carboxy group which is esterified with the ribose moiety of a tRNA molecule. Whereas biological peptide synthesis proceeds

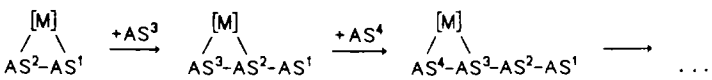

Scheme 3. AS: amino acid building block. AS^1: C-terminal amino acid. [M]: organometallic complex fragment.

by incorporation of the new amino acid at the C-terminus of the peptide chain, the peptide synthesis by the metal-based "artificial ribosome" occurs in the reverse direction.

German version: *Angew. Chem.* **1996**, *108*, 1287–1289

Keywords: bioorganometallic chemistry · complexes with carbon ligands · peptides · ruthenium compounds · sandwich complexes

[1] G. Jaouen, A. Vessières, I. S. Butler, *Acc. Chem. Res.* **1993**, *26*, 361; see also: A. D. Ryabov, *Angew. Chem.* **1991**, *103*, 945–955; *Angew. Chem. Int. Ed. Engl.* **1991**, *30*, 931–941.
[2] D. P. Smith, E. Baralt, B. Morales, M. M. Olmstead, M. F. Maestre, R. H. Fish, *J. Am. Chem. Soc.* **1992**, *114*, 10647–10649.
[3] A. Vessières, M. Salmain, V. Philomin, G. Jaouen, *Immunoanal. Biol. Spec.* **1992**, *31*, 9; M. Salmain, A. Vessières, P. Brossier, I. S. Butler, G. Jaouen, *J. Immunol. Methods* **1992**, *148*, 65.
[4] K. Drauz, A. Kleemann, J. Martens *Angew. Chem.* **1982**, *94*, 590–613; *Angew. Chem. Int. Ed. Engl.* **1982**, *21*, 584–608; H. Brunner, *ibid.* **1983**, *95*, 921–931 and **1983**, *22*, 879–907; H. Brunner, B. Reiter, G. Riepl, *Chem. Ber.* **1984**, *117*, 1330–1354; P. Kvintovics, B. R. James, B. Heil, *J. Chem. Soc. Chem. Commun.* **1986**, 1810–1811; G. Süss-Fink, T. Jenke, H. Heitz, M. A. Pellinghelli, A. Trippicchio, *J. Organomet. Chem.* **1989**, *379*, 311–323.
[5] R. M. Moriarty, Y.-Y. Ku, U. S. Gill, *J. Chem. Soc. Chem. Commun.* **1987**, 1837–1838.
[6] W. S. Sheldrick, A. Gleichmann, *J. Organomet. Chem.* **1994**, *470*, 183–187.
[7] A. J. Gleichmann, J. M. Wolff, W. S. Sheldrick, *J. Chem. Soc., Dalton Trans.* **1995**, 1549–1554.
[8] J. M. Wolff, A. J. Gleichmann, C. Schmidt, W. S. Sheldrick, *J. Inorg. Biochem.* **1995**, *59*, 219.
[9] W. H. Soine, C. E. Guyer, F. F. Knapp, Jr., *J. Med. Chem.* **1984**, *27*, 803.
[10] A. J. Pearson, K. Lee, *J. Org. Chem.* **1994**, *59*, 2304–2313.
[11] Review: M. F. Semmelhack in *Comprehensive Organic Synthesis, Vol. 4*, (Eds.: B. M. Trost, I. Fleming), Pergamon, Oxford, **1991**, pp. 517–549.
[12] J. W. Janetka, D. H. Rich, *J. Am. Chem. Soc.* **1995**, *117*, 10585–10586.
[13] R. Krämer, M. Maurus, R. Bergs, K. Polborn, K. Sünkel, B. Wagner, W. Beck, *Chem. Ber.* **1993**, *126*, 1969–1980.
[14] W. Beck, R. Krämer, *Angew. Chem.* **1991**, *103*, 1492–1493; *Angew. Chem. Int. Ed. Engl.* **1991**, *30*, 1467–1468.
[15] M. Maurus, Dissertation, Universität München, **1994**.

From Oxides to Nitrides: Recent Developments in the Structural Chemistry of Alkali/Alkaline Earth Metal Sub-Compounds

Caroline Röhr*

Almost a hundred years after the discovery of the structurally remarkable rubidium and cesium suboxides and over twenty years since the elucidation of their structures and their thermoanalytical characterization by Simon,[1] this structural chemistry has been extended to the corresponding ternary sodium–barium nitrides in the last few years. The compound $Na_{14}Ba_{14}CaN_6$[2] recently described by Simon and Steinbrenner forms a link between the new subnitrides and the classic suboxides. With a degree of face-sharing of coordination octahedra about O/N never achieved before, the quaternary phase is more than just a new final member in the series of "inverse clusters" of the sub-compounds; it is an important extension of the structural chemistry of this class of compounds, since in this case cations are also present in the saltlike interior of a cluster.

The chemical bonding and the characteristic building units of the structures are similar in the Rb/Cs suboxides and the Na–Ba subnitrides. A remarkable and at the same time special feature of these compounds are clusters comprising face-shared, X-centered octahedra (X = O,N) of the electropositive partners (A) rubidium and cesium, and barium, respectively. The bonds within the octahedra are ionic, whereas between the clusters coordination numbers and interatomic distances occur such as those in metals. Rubidium and cesium as well as barium form the "cluster skin" and act as a link between the ionic and the metallic region. The metallic matrix and thus the composition of the phases can be varied over a wide range in all systems. That compounds with this kind of remarkable bonding also show unusual physical properties (color, low electronic work function, etc.) is as unsurprising as the fact that many of the clusters were detected, for example, also in molten metals.

A special position among the subnitrides is held by the alkaline earth metal nitrides A_2N (A = Ca, Sr, Ba), which crystallize in the anti-$CdCl_2$ type, and thus are the only sub-compounds to exhibit N-centered alkaline earth metal octahedra that are connected not through faces but through six of the twelve edges of the octahedron. All the other suboxides and subnitrides can be arranged according to the increasing linkage of the A octahedra (A = Rb, Cs, Ba, Ca) in the inverse cluster around the anions X ($X = O^{2-}, N^{3-}$) and to the corresponding decreasing ratio A/X (A = number of corners of the octahedra, X = number of centers of octahedra; Table 1, Fig. 1). The series begins at the maximum ratio $A/X = 6$ for discrete $[NBa_6]$ octahedra in $Na_{16}Ba_6N$,[3] which are arranged body-centered cubic and are

Table 1. Summary of the structural elements in suboxides and nitrides (A = Ba, Rb, Cs; A′ = Ca; X = O, N; *: additional Na, Rb, or Cs atoms in the metallic matrix).

Structural element	Fig. 1	Nitride	Oxide	A/X
discrete octahedra $[XA_6]$	a	$Na_{16}Ba_6N^*$		6
$^0_7[X_2A_9]$ cluster	b		Rb_9O_2 Rb_6O^*	4.5
$^0_\infty[X_3A_{11}]$ cluster	c		Cs_7O^* $Cs_{11}O_3$ Cs_4O^*	3.67
strand of octahedra $^1_\infty[XA_{6/2}]$	d	$NaBa_3N^*$ $Na_5Ba_3N^*$	Cs_3O	3
$^0_\infty[X_6A'A_{14}]$ cluster from six octahedra $[XA'A_5]$	e	$Na_{14}Ba_{14}CaN_6$		2.5

[*] Dr. Ing. C. Röhr
Eduard-Zintl-Institut der Technische Hochschule, Anorganische Chemie II
Hochschulstrasse 10, D-64289 Darmstadt (Germany)
Fax: Int. code +(6151)166029
e-mail: caroline@iisirius.ac.chemie.th-darmstadt.de

 © *VCH Verlagsgesellschaft mbH, D-69451 Weinheim, 1996* *0570-0833/96/3511-1199 $ 15.00+.25 0*

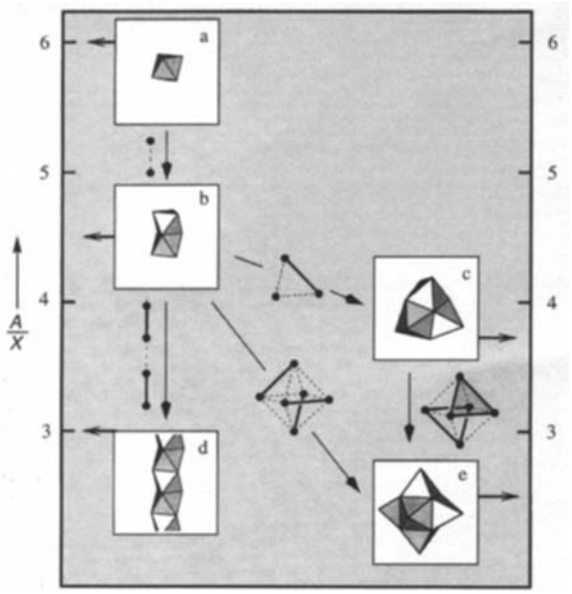

Fig. 1. The clusters in the crystal structures of the suboxides and subnitrides $Na_{16}Ba_6N$ (a), Rb_9O_2 (b), $Cs_{11}O_3$ (c), Cs_3O, $NaBa_3N$, and Na_5Ba_3N (d) as well as $Na_{14}Ba_{14}CaN_6$ (e). *A*: number of corners of octahedra, *X*: number of centers of octahedra.

separated from one another by a large number of sodium atoms. All Rb suboxides show clusters $[X_2A_9]$ comprising two face-sharing octahedra, which in Rb_9O_2[4] are discrete and in Rb_6O[5] are present together with "metallic" rubidium. Units comprising three octahedra condensed through three common faces with a common edge are prevalent in the Cs oxides. These clusters $[X_3A_{11}]$ form the saltlike part in the crystals of $Cs_{11}O_3$,[7] Cs_4O,[8] Cs_7O,[6] (in the latter two again together with additional Cs that does not participate in the construction of the octahedra). The linkage of octahedra each through two opposite faces to give infinite strands occurs both in Cs_3O[10] (which has not been fully characterized by X-ray crystallography) and in $NaBa_3N$[9] and Na_5Ba_3N.[11] The Na atoms in these two compounds are located between the strands of octahedra. With the synthesis of the quaternary nitride $Na_{14}Ba_{14}CaN_6$ Simon and Steinbrenner have achieved the preparation of a "heterocluster" containing both barium (at the cluster periphery) and calcium (in the center of the cluster) for the first time:[2] six octahedrally arranged octahedra $[NBaBa_{4/3}Ca_{1/6}]$ are face-shared in such a way that the calcium ion forms the common corner of all six octahedra and thus in total eight common edges between three octahedra as well as 24 common faces are present per cluster—a cubic close packing with (distorted) octahedra! Alternatively and directly related to the Rb/Cs suboxides, the $[Ba_{14}CaN_6]$ cluster can also be derived from three $[X_2A_9]$ or from two $[X_3A_{11}]$ building units, which clearly shows that this cluster is a new, (provisionally) final member in the series of sub-clusters. As in the other Na–Ba subnitrides, in $Na_{14}Ba_{14}CaN_6$ the clusters, which are arranged face-centered cubic in the crystal, are separated from one another by Na atoms (Fig. 2). If one considers the large variability of the contents A and the crystal structures, for example, of Cs suboxides containing the same cluster, and the possibility of incorporating different amounts of Na between the rigid one-dimensional infinite strands of octahedra in $NaBa_3N$ and Na_5Ba_3N, it appears

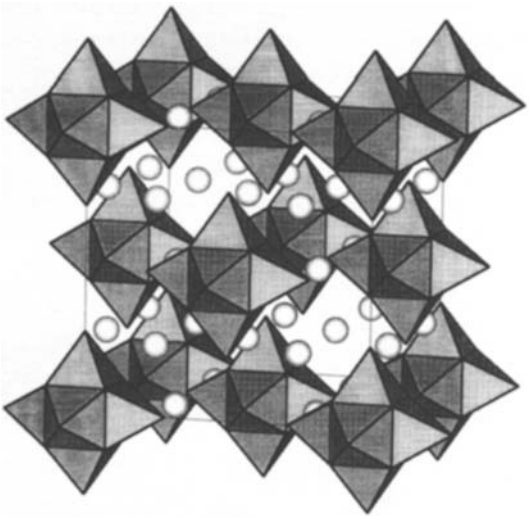

Fig. 2. Section of the crystal structure of the subnitride $Na_{14}Ba_{14}CaN_6$ (octahedra: $[NCaBa_5]$, spheres: Na), which shows the cubic face-centered arrangement of the clusters $[Ba_{14}CaN_6]$.

correct to assume the existence of further stoichiometric phases of the composition $Na_nBa_{14}CaN_6$ ($n = 17, 21, 22$).

A common feature of the suboxides and subnitrides are regions with ionic partial structures in a metal matrix, in which the atoms of the "cluster skin" (for the nitrides to date only Ba and for the oxides only Cs and Rb) play a "mediating role", corresponding approximately to oxidation states between Ba^0 and Ba^{2+}. The bonding becomes clear based on the A–A distances: The edges of the octahedra within the cluster are short and the A–A distances resemble those in electrovalent[*] binary oxides and nitrides; the A–A distances between the clusters are large (interatomic distances as in the metals), and the lengths of the edges of the $[XA_6]$ octahedra on the cluster skin vary with the number of octahedra in which the respective edge participates.

That despite the severe face-sharing of octahedra the N–N distances in $Na_{14}Ba_{14}CaN_6$ are even a little longer than those in the ternary Na–Ba subnitrides is attributed to the displacement of the X atoms from the centers of the A octahedra (away from the common faces of the octahedra towards the cluster periphery) known for suboxide clusters. Consequently, the N–Ca distances are large and the N–Ba distances are small in comparison to the typical distances observed for ionic bonds.

The distribution of the electropositive bonding partners in the crystal structure is interesting, particularly with regard to the quaternary compound. All the results obtained so far indicate that only the large "soft" Ba can form the cluster skin. Although Na and Ca have similar ionic and metallic radii as well as ionization energies, the distribution of elements determined follows the formation of compounds in the binary phases: Ca nitrides are known, Na_3N is unknown. However, binary intermetallic phases are known in the Na–Ba system, but not for Ca–Ba. In the $[Ba_{14}CaN_6]$ cluster Ca occupies the position (the common corner of six coordination octahedra) with the highest positive charge. A similar situation occurs in the mixed Rb–Cs suboxide $Rb_6Cs_5O_3$,[12] in whose structure the lighter homologue prefer-

[*] Compounds are referred to as electrovalent when the valence electrons, in accord with common assumptions, can be attributed unequivocally to specific atoms.

 © VCH Verlagsgesellschaft mbH, D-69451 Weinheim, 1996 0570-0833/96/3511-1200 $ 15.00+.25/0

ably substitutes the Cs atoms of the common edge of all three $[OCs_6]$ octahedra of the $[Os_3Cs_{11}]$ cluster.

The nature of the structural units formed in each of the subcompounds is evidently primarily determined by types of atoms that make up the cluster: $[O_3Cs_{11}]$ predominates in the Cs oxides, dimeric $[X_2A_9]$ units are known only in the Rb–O system, and infinite chains of octahedra $^1_\infty[NBa_{6/2}]$ are the characteristic building unit in the Na–Ba nitrides. $Na_{14}Ba_{14}CaN_6$ represents a remarkable subnitride of the Na-Ca-Ba-N system: It contains a new cluster, in which the calcium ion plays an important dual role with respect to the stability both for geometrical reasons (distortion of the octahedra for the extreme face-sharing) and for electronic reasons (first example of a "real" cation (Ca^{2+}) in the saltlike interior of a sub-cluster).

German version: *Angew. Chem.* **1996**, *108*, 1289–1291

Keywords: clusters · subnitrides · suboxides

[1] A. Simon, *Struct. Bonding (Berlin)* **1979**, *36*, 81.
[2] U. Steinbrenner, A. Simon, *Angew. Chem.* **1996**, *108*, 595–597; *Angew. Chem. Int. Ed. Engl.* **1996**, *35*, 552–554.
[3] G. J. Snyder, A. Simon, *Angew. Chem.* **1994**, *106*, 713–715; *Angew. Chem. Int. Ed. Engl.* **1994**, *33*, 689–691.
[4] A. Simon, *Naturwissenschaften* **1971**, *58*, 623.
[5] A. Simon, *Naturwissenschaften* **1971**, *58*, 623.
[6] A. Simon, *Naturwissenschaften* **1971**, *58*, 622–623.
[7] A. Simon, E. Westerbeck, *Angew. Chem.* **1972**, *84*, 1190–1191; *Angew. Chem. Int. Ed. Engl.* **1972**, *11*, 1105–1106.
[8] H. Deiseroth, E. Westerbeck, B. Hillenkoetter, *Z. Anorg. Allg. Chem.* **1976**, *423*, 203–211.
[9] P. E. Rauch, A. Simon, *Angew. Chem.* **1992**, *104*, 1505–1506; *Angew. Chem. Int. Ed. Engl.* **1992**, *31*, 1519–1521.
[10] K. R. Tsai, P. M. Harris, E. N. Lassettre, *J. Phys. Chem.* **1956**, *60*, 345–347.
[11] G. J. Snyder, A. Simon, *J. Am. Chem. Soc.* **1995**, *117*, 1996–1999.
[12] H. J. Deiseroth, A. Simon, *Rev. Chim. Miner.* **1983**, *20*, 475–487.

Time is money...

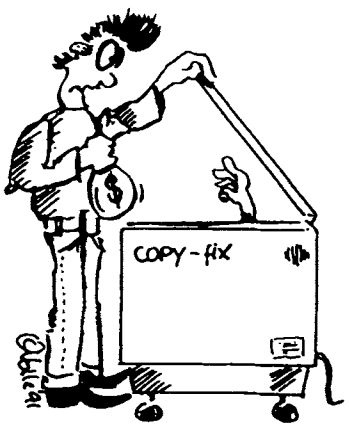

Save both by starting a personal subscription to *Angewandte Chemie* (now with *Chemistry - A European Journal*). At 9¢ per page you can't go wrong. With your own private copy you can read the "hot" articles before they cool, and waste less time in front of the copier.

Order now!
An order form can be found on the last page of this issue.

A Topochemically Controlled, Regiospecific Fullerene Bisfunctionalization**

Bernhard Kräutler,* Thomas Müller, Joseph Maynollo, Karl Gruber, Christoph Kratky, Philippe Ochsenbein, Dieter Schwarzenbach, and Hans-Beat Bürgi

Fullerenes, molecular allotropes of carbon,[1, 2] have opened new areas of research at the interface of molecular and solid-state sciences.[3] Exohedral derivatization in solution[5, 6] has recently led to some highly functionalized fullerenes[7–9] in impressively regioselective addition reactions. Crystal engineering[10] and solid-state chemistry could provide an alternative, novel synthetic entry to specific organo-substituted fullerenes. Here we report a highly uniform and topochemically[11, 12] controlled fullerene refunctionalization, which is based on a thermal, intermolecular anthracene-transfer reaction, unprecedented in the solid state. In addition we describe the X-ray structure analysis of the crystalline cycloadduct **2** of C_{60} (**1**) and 1,3-cyclohexadiene.[13] The observed molecular packing in single crystals of **2** stimulated this investigation, as it shows a linear stacking of fullerene and cyclohexene moieties. The approach presented here promises to open new routes in solid-state chemistry.[10]

The crystalline 6,6-monoadduct **3** prepared from **1** and anthracene[14–16] undergoes a regiospecific thermal transformation into a solid 1:1 mixture of **1** and the antipodal 6,6-bisanthracene adduct **4**.[15, 16] Heating a deoxygenated sample of

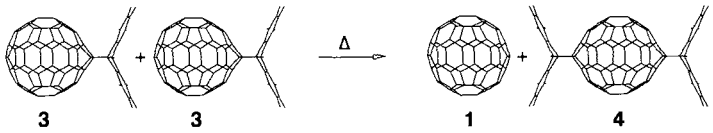

3 **3** **1** **4**

crystalline **3** at 180° C for 10 min afforded 48% each of the fullerene **1** and the antipodal bisadduct **4** (96% conversion; no other components detected). The bisadduct **4**, first described in ref. [15], was isolated and its structure confirmed by NMR spectroscopy and (FAB) mass spectrometry, as well as by single-crystal structure analysis.[17] The relative amounts of **3** and **4** in the reaction mixture were established by ^{1}H NMR spectroscopy (at 500 MHz), and after chromatographic separation the absolute amounts of **1**, **3**, and **4** were determined. The result of the solid-state thermolysis contrasts with that in solution, in which **3** has been noted to decompose to **1** and anthracene.[15] As a control, the monoadduct **3** (76 mM) and anthracene (160 mM) were allowed to react in a carbon disulfide solution at room temperature for 28 days. This led to 52% conversion with 45% yield of a mixture of five bisadducts, about 3% yield of **1**, and the antipodal bisadduct **4** as only a minor product (1.6%).

Crystals of the Diels–Alder adduct **2** formed from **1** and 1,3-cyclohexadiene[13] were obtained from a solution of **2** in *o*-

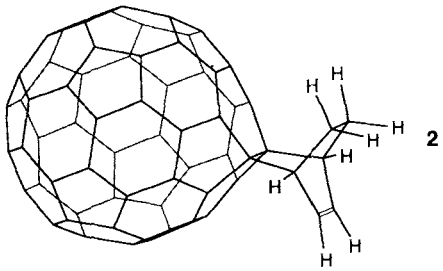

2

dichlorobenzene and analyzed by X-ray diffraction.[18] The crystal lattice with composition $\{\mathbf{2}\cdot 2C_6H_4Cl_2\}$ shows a columnar stacking of molecules of **2** mediated by intermolecular contacts between the convex fullerene surface and the concave cyclohexene moiety (Fig. 1, top). The molecules are arranged such that the part of the fullerene surface recognized by a neighboring cyclohexene moiety is antipodal to its own cyclohexene unit. Note that the fullerene 6,6-bond (C(55)–C(60)) involved in the contact is parallel to the vector between the bridgehead atoms (C(1a) and (C4a)) in the neighboring cyclohexene moiety (Fig. 1, bottom). Similar contacts, two per molecule, have been

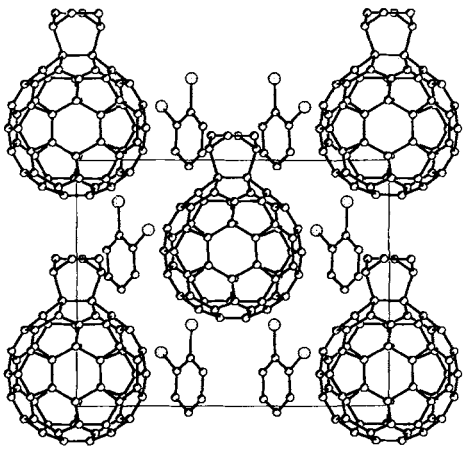

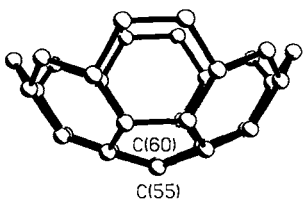

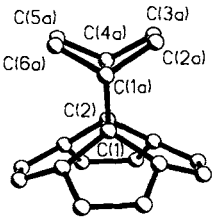

Fig. 1. Top: Crystal packing of $\{\mathbf{2}\cdot 2C_6H_4Cl_2\}$ in the crystallographic *a,b* plane; molecular stacks are parallel to the *b* axis. Bottom: Intermolecular contacts between the convex [60]fullerene (**1**) and the concave cyclohexene receptor moiety, shortest intermolecular distances [Å]: C(55)···C(2a) and C(60)···C(5a) 3.51, C(55)···C(6a) and C(60)···C(3a) 3.53 Å. Due to crystal symmetry the HC=CH and H_2C-CH_2 bonds of the cyclohexene fragment of **2** are disordered.

[*] Prof. Dr. B. Kräutler, Mag. T. Müller, Mag. J. Maynollo
Institut für Organische Chemie der Universität
Innrain 52a, A-6020 Innsbruck (Austria)
Fax: Int. code +(512)507-2892
e-mail: Bernhard.Kraeutler@uibk.ac.at
Dr. K. Gruber, Prof. Dr. C. Kratky
Institut für Physikalische Chemie der Universität Graz (Austria)
Dr. P. Ochsenbein, Prof. Dr. H.-B. Bürgi[+]
Laboratorium für Kristallographie der Universität Bern (Switzerland)
Prof. Dr. D. Schwarzenbach
Laboratoire de Crystallographie, Université de Lausanne (Switzerland)
[+] Address for correspondence concerning the X-ray analysis.

[**] We would like to thank Dr. R. Konrat and M. Tollinger for NMR spectra, Univ.-Doz. Dr. K.-H. Ongania and Mag. A. Rieder for mass spectra, and Dr. G. Färber for some of the graphics.

 © VCH Verlagsgesellschaft mbH, D-69451 Weinheim, 1996 0570-0833/96/3511-1204 $ 15.00+.25/0

observed in the bisadduct **4**.[17] Single crystals of **3** were too small for a complete structure analysis; however, it was possible to determine the unit cell constants ($a = 12.8(1)$, $b = 16.9(1)$, $c = 16.6(1)$ Å, $\beta = 94.2(1)^\circ$) and the space group ($P2_1/m$ or $P2_1$). Together, these two observations lead to the conclusion that the molecules of **3** form layers of stacks analogous to those in crystalline **2** (cf. Fig. 1).[19]

The selective thermal transformation of the monoadduct **3** into the fullerene **1** and its antipodal bisadduct **4** is thus suggested to proceed by intermolecular anthracene transfer, in which one molecule of the starting compound acts as an intimate anthracene donor for the neighboring fullerene, which acts as acceptor. The occurrence of this reaction can be rationalized by the specific packing of molecules of **3** in the crystal. There, the crucial 6,6-bonds are properly aligned for anthracene transfer. Such an alignment not only renders the reaction geometrically feasible, but also makes it thermally allowed in terms of orbital symmetry, as a combination of (potentially synchronized) [4 + 2]cycloreversion and [4 + 2]cycloaddition steps.

A second aspect of the transformation of **3** into **1** and **4** in the solid state is the high overall conservation of atomic positions between the starting material and products. Due to their spherical architecture, the fullerene cores undergo only minimal overall deformation in the cycloaddition/cycloreversion reactions. Furthermore, the mode of coaxial alignment, inferred for the crystalline starting material, appears to be carried over to the product state (Fig. 2). Cocrystals of the product components **1** and **4** can be reconstituted from concentrated solutions containing a 1:1 molar ratio of fullerene **1** and the bisadduct **4**. All of the points discussed are in agreement with topochemical control of the anthracene-transfer reaction.

The solid-state reaction reported here not only produces the antipodal bisadduct **4** with high regioselectivity, but it also proceeds with high conversion. Apparently, this reaction is favored both kinetically and thermodynamically in the ordered solid state. Calculated dehydrogenation energies of 1,2-dihydro[60]-fullerenes and of the corresponding antipodal tetrahydro-[60]fullerenes[6] hint at a small enthalpic contribution to the thermodynamic driving force for this reaction. The structural information available shows that the coaxial alignment of the convex fullerene spheres and the concave receptor sites of the diene addends is rigid and restricted in its motion, whereas unsubstituted spherical fullerene molecules often show orientational disorder[20] or reorientational motion.[21, 22] Thus, the increased rotational mobility of the product molecule **1** (but not **4**) in the solid state may stabilize the product state; that is, the highly selective transformation of **3** into **1** and **4** seems to be driven largely by an increase in entropy.

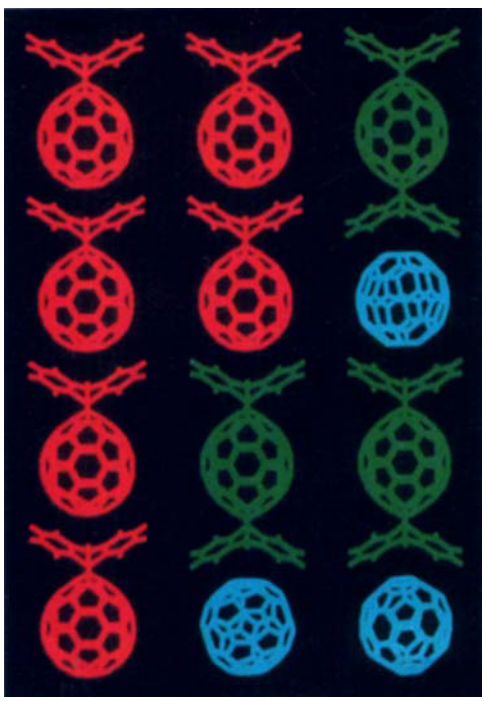

Fig. 2. Schematic description of the anthracene-transfer reaction. A stack of molecules of **3** in the solid state (left) transform into a stack of alternating molecules of **1** and **4** (right).

The results presented here indicate that crystal engineering[10] in combination with topochemical reactions[11] can lead to novel approaches for the preparation of specific fullerene derivatives. Fullerenes, in turn, may serve as versatile scaffolds for the design and for the synthesis of programmed molecular components,[23] which may assemble into useful, ordered solid materials. The exceptional, spherical buildup of fullerenes provides the field of supramolecular chemistry[23] with new structural motifs, which may add a dimension to crystal design[10] and, in this way, contribute fruitfully to new developments in materials science.

Received: December 21, 1995 [Z8675IE]
German version: *Angew. Chem.* **1996**, *108*, 1294–1296

Keywords: crystal engineering · fullerenes · solid-state chemistry · topochemistry

[1] H. W. Kroto, J. R. Heath, S. C. O'Brien, R. F. Curl, R. E. Smalley, *Nature* **1985**, *318*, 162–163.
[2] W. Krätschmer, L. D. Lamb, K. Fostiropoulos, D. R. Huffmann, *Nature* **1990**, *347*, 354–356.
[3] F. Diederich, Y. Rubin, *Angew. Chem.* **1992**, *104*, 1123–1292; *Angew. Chem. Int. Ed. Engl.* **1992**, *31*, 1101–1124.
[4] *The Fullerenes* (Eds: H. W. Kroto, D. R. M. Walton), Cambridge University Press, Cambridge, **1993**.
[5] F. Wudl, *Acc. Chem. Res.* **1992**, *25*, 157–161.
[6] A. Hirsch, *The Chemistry of the Fullerenes*, Thieme, Stuttgart, **1994**.
[7] A. Hirsch, I. Lamparth, T. Grösser, H. R. Karfunkel, *J. Am. Chem. Soc.* **1994**, *116*, 9385–9386.
[8] L. Isaacs, R. F. Haldimann, F. Diederich, *Angew. Chem.* **1994**, *106*, 2434–2437; *Angew. Chem. Int. Ed. Engl.* **1994**, *33*, 2339–2342.
[9] B. Kräutler, J. Maynollo, *Angew. Chem.* **1995**, *107*, 69–71; *Angew. Chem. Int. Ed. Engl.* **1995**, *34*, 87–89.
[10] G. R. Desiraju, *Crystal Engineering -- The Design of Organic Solids*, Elsevier, Amsterdam, **1989**; *Angew. Chem.* **1995**, *107*, 2541–2558; *Angew. Chem. Int. Ed. Engl.* **1995**, *34*, 2311–2327.
[11] *Organic Solid State Chemistry* (Ed.: G. R. Desiraju), Elsevier, Amsterdam, **1987**.
[12] H.-B. Bürgi, J. D. Dunitz, *Helv. Chim. Acta* **1993**, *76*, 1115–1166.
[13] B. Kräutler, J. Maynollo, *Tetrahedron* **1996**, *52*, 5038–5042.
[14] J. A. Schlueter, J. M. Seaman, S. Taha, H. Cohen, K. R. Lykke, H. H. Wang, J. M. Williams, *J. Chem. Soc. Chem. Commun.* **1993**, 972.
[15] M. Tsuda, T. Ishida, T. Nogami, S. Kurono, M. Ohashi, *J. Chem. Soc. Chem. Commun.* **1993**, 1296.
[16] T. Ishida, M. Tsuda, T. Nogami, S. Kurono, M. Ohashi, *Fullerene Sci. Technol.* **1994**, *2*, 155–164.
[17] B. Kräutler, T. Müller, P. Ochsenbein, H.-B. Bürgi, unpublished.
[18] Crystal structure determination of **2**: crystal dimensions $0.38 \times 0.17 \times 0.14$ mm^3, monoclinic, space group $C2_1$, $a = 16.418(3)$, $b = 12.720(3)$, $c = 10.466(2)$ Å, $\beta = 105.00(3)^\circ$, $\rho_{calcd} = 1.722$ g cm^{-3}, $2\theta_{max} = 75.9^\circ$, $\lambda(Cu_{K\alpha}) = 1.54178$ Å, $\omega/2\theta$-scan, $T = 178(2)$ K, 4216 reflections collected. 2232 independent ($R_{int} = 0.0644$), Lp-correction, $\mu = 3.030$ mm^{-1}, structure determination by direct methods, full matrix least-squares on all independent F^2, C and Cl atoms anisotropic, H atoms isotropic, 374 parameters, 20 restraints. The solvent molecules were restrained to be planar ($\sigma = 0.02$ Å) and to have six equal C–C distances ($\sigma = 0.02$ Å) and two equal C–Cl distances ($\sigma = 0.02$ Å). The direction of the C–H vectors were fixed and the C–H distances were allowed to vary. *R*1 ($|F|$, all data) = 0.056, $\omega R2(F^2$, all data) = 0.107, GOOF (F^2) = 3.55, max. and min. residual electron densities 0.6 and -0.66 e Å^{-3}, respectively. Calculations performed with SHELXL92. (G. M. Sheldrick, Program for the Refinement of Crystal Structures, University of Göttingen, Ger-

 © VCH Verlagsgesellschaft mbH, D-69451 Weinheim, 1996 0570-0833/96/3511-1205 $ 15.00+ .25/0

many, **1992**). Crystallographic data (excluding structure factors) for the structure reported in this paper have been deposited with the Cambridge Crystallographic Data Centre as supplementary publication no. CCDC-179-29. Copies of the data can be obtained free of charge on application to The Director, CCDC, 12 Union Road, Cambridge CB21EZ, UK (fax: Int. code +(1223)336-033; e-mail: teched(@chemcrys.cam.ac.uk).

[19] From the unit cell volume of **3** (ca. 3595 Å^3) and the space group symmetry, it is probable that the unit cell contains four molecules of **3** and no solvent. With this assumption the calculated density is ca. 1.67 g cm^{-3}, intermediate to those of **2** (1.722 g cm^{-3}) and **4** (1.561 g cm^{-3}). The space group symmetry requires two layers of molecules, one at y and the other at $y+\frac{1}{2}$. The distribution of 1171 intensity measurements with $I(hkl)/\sigma(I) \geq 3$ shows that intensities for $(h+l)$ even are twice as frequent and on average twice as intense as those for $(h+l)$ odd. This indicates a pseudotranslation period of $(a+c)/2$. Within one layer, molecules of **3** must be related by translation along a. This implies that each C_{60} unit of **3** has six nearest neighbors, two at 10.1 Å ($\pm a/2 \pm c/2$), two at 10.8 Å ($\pm a/2 \pm c/2$), and two at 12.8 Å ($\pm a$). These distances are similar to those found in **2**, where they are 10.38 Å between stacks and 12.8 Å within stacks. The former value in **2** is close to the average of 10.45 = (10.1 + 10.8)/2 Å in **3**; the latter value in **2** is almost the same as the value of 12.8 Å in **3**. From these similarities we conclude that layers of **3** show a packing of stacks analogous to that in **2** (see Fig. 1). This conclusion is corroborated by the crystal structure of **4**, which shows linear C_{60}-anthracene$\cdots C_{60}$ motifs and a distance of 12.77 Å between C_{60} centers [17] (vs. 12.8 Å in the postulated linear C_{60}-anthracene$\cdots C_{60}$ motifs of **3**). We thank Dr. F. Pichierri and S. Capelli for help with measurements at the Swiss-Norwegian Beam Line (European Synchrotron Radiation Facility, Grenoble).

[20] O. Ermer, *Helv. Chim. Acta* **1991**, *74*, 1339–1351.

[21] H.-B. Bürgi, E. Blanc, D. Schwarzenbach, S. Lu, Y. Lu, M. M. Kappes, J. A. Ibers, *Angew. Chem.* **1992**, *104*, 667–670; *Angew. Chem. Int. Ed. Engl.* **1992**, *31*, 640–643.

[22] H.-B. Bürgi, R. Restori, D. Schwarzenbach, *Acta Crystallogr. Sect. B* **1993**, *49*, 832–838.

[23] J.-M. Lehn, *Supramolecular Chemistry*, VCH, Weinheim, **1995**.

Molybdenum Blue: A 200 Year Old Mystery Unveiled

Achim Müller,* Jochen Meyer, Erich Krickemeyer, and Ekkehard Diemann

"This is a substance or group of substances about which there has been much discussion" is a statement we read in an older standard textbook of inorganic chemistry.[1] It refers to an (usually) amorphous blue material that was first mentioned by C. W. Scheele in 1778 and today is known as "molybdenum blue".[2] The first source of information about its composition dates back to J. J. Berzelius in 1826.[3] Since then this material has been the topic of numerous publications,[4, 5] and generations of students and chemists have applied the "molybdenum blue test" as a simple, fast, and sensitive method for a qualitative analysis of molybdenum.[6] However, the constitution of the compound (or compounds) has remained mysterious[7–10] and therefore it is not surprising that most of its remarkable properties could not be explained. We can now show that the anion of the crystalline, blackish-blue compound **1** ($n \approx 350$), prepared recently by us according to a useful strategy[11] for obtaining ever larger clusters,[12] is archetypical for the compounds referred to in the literature as "amorphous molybdenum blue".[13]

$$(NH_4)_{25\pm5}[Mo_{154}(NO)_{14}O_{420}(OH)_{28}(H_2O)_{70}]\cdot nH_2O \quad \mathbf{1}$$

After repeating some general preparation methods as well as analytical test procedures leading to "molybdenum blue", and comparing the properties of the products with those of **1**, significant similarities immediately became apparent (see Fig. 1).[17] In particular, we have studied the reduction of acidified aqueous solutions of molybdates a) with $(N_2H_6)SO_4$, b) with $SnCl_2$, c) with elemental Fe, and d) with elemental Zn[4] as well as e) the photochemically induced reduction with formic acid.[15] Whereas for c) and d) only "amorphous" precipitates with a correspondingly low degree of crystallinity were obtained, we isolated small amounts of a blackish-blue homogeneous material with a higher degree of crystallinity for a) and b). Hence, for the latter it was now possible to obtain spectroscopic data of a homogeneous well-defined compound and compare them with those of the amorphous blue precipitates (of possibly varying compositions). The IR spectra of these compounds are very similar to those of the earlier reported compound **1**,[12] except for a pronounced band at 728 cm^{-1} associated with one of the two stretching vibrations of the {MoNO} group (Fig. 1A). The same

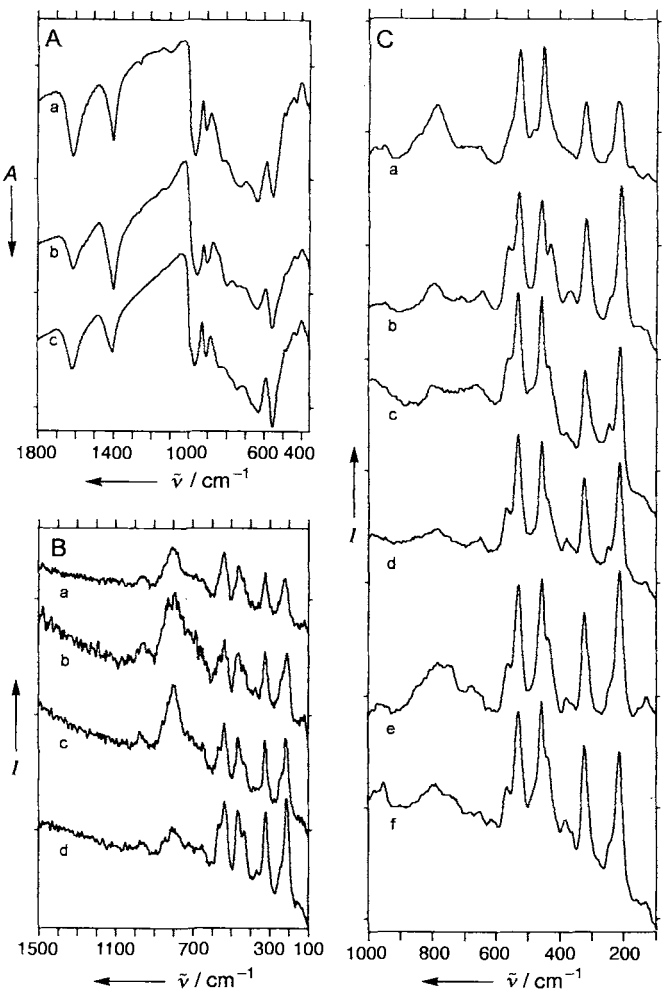

Fig. 1. A) IR spectra (KBr pellet) of **1** (a), of "molybdenum blue" obtained by reduction of molybdate with $(N_2H_6)SO_4$ (b), and $SnCl_2$ (c). B) Solid-state Raman spectra (λ_e = 1064 nm) corresponding to the samples given in A) and of a soluble blue "amorphous" precipitate obtained by reduction with Fe (d). C) Solution Raman spectra (λ_e = 1064 nm) of the products of B), of a molybdate solution (pH 1.4) reduced with Zn (e), and of a molybdate solution (pH 1.4) irradiated with an UV lamp in the presence of formic acid (f).

[*] Prof. Dr. A. Müller, Dipl.-Chem. J. Meyer, E. Krickemeyer, Dr. E. Diemann
Fakultät für Chemie der Universität
Lehrstuhl für Anorganische Chemie I
Postfach 100131, D-33501 Bielefeld (Germany)
Fax: Int. code +(521)106-6003
e-mail: amueller@cheops.chemie.uni-bielefeld.de

[**] We thank Dr. H. Bögge, F. Hellweg, Dipl.-Chem. B. Hollmann, Dipl.-Chem. C. Menke, Dipl.-Chem. F. Nonnenbruch, Dipl.-Ing. M. Ohm, Dipl.-Chem. F. Peters, Dipl.-Chem. M. Randerath and Dipl.-Chem. C. Serain for their contributions.

holds for the corresponding resonance Raman spectra (Nd:YAG laser: $\lambda_e = 1064$ nm; inter-valence-charge-transfer (IVCT) band ≈ 1070 nm), which show a series of five characteristic bands in the region between 900 and 200 cm^{-1} (Fig. 1B). According to a simplified normal coordinate analysis, these bands are assigned to vibrations of $\{(Mo^{V/VI})_mO\}$ fragments ($m = 2,3,4$).[23] Furthermore, the resonance Raman spectra of solutions of "molybdenum blue" obtained by the different given synthetic pathways resemble the corresponding solution spectrum of **1** (Fig. 1C). The differences in the intensity and the shape of one particular band at about 800 cm^{-1} are most probably due to variations in the electron populations of the cluster anions. This band becomes gradually more intense and its half-width decreases upon increasing the degree of reduction (ratio Mo^V/Mo^{VI}) of an acidified (pH 1.4) molybdate solution from 10% to 20%. Above a degree of reduction of 20% this band dominates the spectrum (according to a model calculation it can be assigned to a particular $\{(Mo^{V/VI})_3\mu_3\text{-}O\}$ fragment, in which the IVCT transitions responsible for the resonance effect mainly occur).[23] In addition, the electronic absorption spectra of the reduced molybdate solutions resemble that of **1**; however, the absorbance and to a lesser extent the positions of the absorption maxima vary significantly with the degree of reduction.

Futhermore, Raman spectroscopic investigations[24] show that the dominant species in non-reduced molybdate solutions (pH 1–2) is the large isopolymolybdate $[Mo_{36}O_{112}(H_2O)_{16}]^{8-}$ ($\equiv[(MoO_2)_2H_{24}\{Mo_{17}\}_2]^{8-}$),[24, 25] which itself, or the intrinsic $\{Mo_{17}\}$ ($\equiv\{Mo_{17}O_{60}(H_2O)_2\}$) fragment, is considered to act as a template (cf. also ref. [12a]) for the formation of the ring-shaped anions like that of **1**.[12] The greenish by-product of the synthesis of **1**[12a] was identified as the water-insoluble polymeric compound $\{(NH_4)HMo_5O_{16}(H_2O)\cdot H_2O\}_n$, which was also reported to be formed from solutions containing the $[Mo_{36}O_{112}(H_2O)_{16}]^{8-}$ ion.[24]

The X-ray powder diffractograms of the "molybdenum blue" precipitates obtained from different synthetic pathways have almost identical patterns. They show (with the exception of the characteristic sharp reflections of the parts (corresponding to **1**) with the higher degree of crystallinity) only diffuse scattering maxima ($2\theta \approx 26$, 29.5, and 51°; $Cu_{K\alpha} = 154.18$ pm), as usually observed for noncrystalline compounds. However, the intensity pattern corresponds quite well to the envelope of the powder pattern of **1**. This implies that a species at least structurally very similar to the anion of **1** should be present in all these materials.

The results available so far imply that a highly abundant species of "amorphous molybdenum blue" corresponds to a "*molecular* molybdenum trioxide" with a varying degree of protonation and reduction and a (probable) formula of $[(MoO_3)_{154}(H_2O)_{70}H_x]^{y-}$.[23] This formula is derived by replacing the 14 $\{MoNO\}^{3+}$ groups of the anion of **1** by the corresponding number of $\{MoO\}^{4+}$ groups[11] (see also the existence of the comparable cluster pairs $[Mo_{36}(NO)_4O_{108}(H_2O)_{16}]^{12-}$/$[Mo_{36}O_{112}(H_2O)_{16}]^{8-}$[11] as well as $[Mo_6(NO)O_{18}]^{3-}$/$[Mo_6O_{19}]^{2-}$[26]). Interesting in this context is that $MoO_3\cdot 2H_2O$ as well as the homologous oxides CrO_3 and $WO_3\cdot 2H_2O$ are end products of condensation processes caused by acidification. In the present case the formation of neutral polymeric compounds with solid-state structures is prevented by reduction (anion formation).

The knowledge of the basic structure of "molybdenum blue" enables us now to understand for the first time some of its unusual properties:

a) The amorphous character of the predominant part of the obtained samples of molybdenum blue has to be attributed to the difficulties of positioning extremely large anions into a highly ordered crystal lattice. The understanding of the stochastic nature of fluctuations during the nucleation phase of the crystallization process with the help of the Langevin equation[27] presents a fascinating challenge. There are virtually no related investigations in the context of ionic crystals with extremely large ions.

b) The large hydrophilic inner and outer surface built up by the exceptionally large number of H_2O molecules and OH groups as ligands (70 and 28, respectively, in the case of **1**, Fig. 2) explains the high solubility in water,[4] and even (to a lesser extent) in methanol, 95% ethanol, or aqueous acetone.

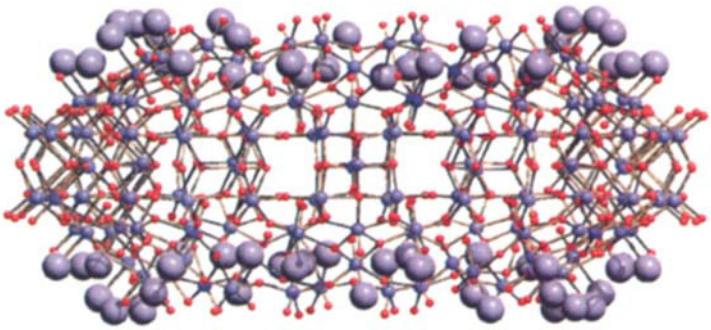

Fig. 2. Ball-and-stick representation of $[(MoO_3)_{154}(H_2O)_{\sim 6}H_x]^{y-}$, derived from **1** by replacing the $\{MoNO\}^{3+}$ by $\{MoO\}^{4+}$ groups (view along the approximated C_2 axis); the 70 H_2O ligands are represented as large gray spheres, the Mo and O atoms as smaller blue and red spheres, respectively.

c) The large surface area is responsible for the high affinity to adsorbents (charcoal, cotton, silk etc.)[28] and models that of solids, for example of mixed-valence transition metal oxides with catalytic activities.[29]

d) The solutions have been described as colloidal (showing a Tyndall effect) with a tendency towards the formation of micelles, but with properties very close to those of "real" solutions.[4, 30] This can be attributed to the size of the anions, and the ability of the species to aggregate, which was recently confirmed by us by dynamic light scattering experiments.[31]

e) The migration of "molybdenum blue" to the anode in an electric field[32] is due to the true anionic nature of the cluster ions and not—as normally in the case of colloids—to nonstoichiometric surface charges.

Other interesting properties are: the nanometer-sized cavity and the corresponding host properties, the high density of states in the HOMO/LUMO region that gives rise to a pseudo-band structure with a narrow band gap resulting in a small-sized semiconductor, the electron-storage properties and the thus related potential suitability as a redox catalyst as well as the remarkable intense color, which, according to resonance Raman investigations, can be attributed to IVCT transitions.

According to the experimental results presented here there is significant evidence that the (anionic) structure of **1** represents the basic structural type of the investigated "molybdenum blue compounds".[13] The high complexity of the molecular system together with its manifold properties may explain the confusion about the nature of this material in literature. With the determination of the structure of **1** and the consistency of its main properties with those reported for "amorphous molybdenum blue", a more than 200 year old mystery has been partly unveiled.

Experimental Procedure

Precipitates of "amorphous molybdenum blue" were obtained from reduced, acidified aqueous solutions of molybdates according to general preparation methods [4,5]. With $(N_2H_6)SO_4$ and with $SnCl_2$ a homogeneous blackish-blue material with a high degree of crystallinity was formed in small amounts that had to be separated mechanically from by-products. All products were stored under inert atmosphere.

Reduction with hydrazinium sulfate: A solution of $(N_2H_6)SO_4$ (0.16 g, 1.2 mmol) in water (8 mL) was added to a solution of $(NH_4)_6[Mo_7O_{24}]\cdot 4H_2O$ (1.12 g, 0.9 mmol) and 50% acetic acid (0.24 mL) in water (12 mL) at 20 °C. 2 mL of the resulting green solution was allowed to stand for about two months (without shaking) in a closed 20 mL test tube for crystallization.

Reduction with tin(II) chloride: A solution of $SnCl_2$ (6.66 mL, 0.025 M; pH 1.4, adjusted with hydrochloric acid) was added to a solution of $(NH_4)_6[Mo_7O_{24}]\cdot 4H_2O$ (10 mL, 0.014 M; pH 1.4) under inert atmosphere. The resulting blue solution was kept under inert atmosphere and allowed to stand for two months (without shaking) for crystallization.

Reduction with elemental iron: Iron powder (5 g, 89 mmol; 150 μm, Merck) was added to a solution of $(NH_4)_6[Mo_7O_{24}]\cdot 4H_2O$ (20 g, 16 mmol) in water (250 mL) in a 300 mL Erlenmeyer flask (wide-necked). Under stirring the pH value was adjusted to 1.0 with 25% hydrochloric acid (colorless precipitate). The mixture was kept at 20° C for 18 h without stirring (Erlenmeyer flask covered with a watch glass). After filtration the solution was kept at 20 °C in a closed test tube for 3 d. The blue precipitate that formed slowly from the deep blue solution was filtered off under an argon atmosphere and dried.

Received: December 20, 1995 [Z 8676 IE]
German version: *Angew. Chem.* **1996**, *108*, 1296–1299

Keywords: clusters · colloids · molybdenum compounds · polyoxometalates

[1] N. V. Sidgwick, *The Chemical Elements And Their Compounds, Vol. II*, Clarendon, London, **1962**, p. 1046.
[2] C. W. Scheele, *Sämtliche Physische und Chemische Werke, Vol. II* (Ed.: D. S. F. Hermbstädt), **1793**, reprint: Martin Sändig oHG, Niederwalluf/Wiesbaden, **1971**, pp. 185–200.
[3] J. J. Berzelius, *Poggendorff's Ann. Phys. Chem.* **1826**, *6*, 385.
[4] *Gmelins Handbuch der Anorganischen Chemie, Mo*, Verlag Chemie, Berlin, **1935**, pp. 134–147.
[5] *Gmelin Handbook of Inorganic Chemistry, Mo. Suppl., Vol. B3a*, Springer, Berlin, **1987**, pp. 61–68.
[6] G. Jander, E. Blasius, *Einführung in das anorganisch-chemische Praktikum*, Hirzel, Stuttgart, **1977**, p. 143.
[7] P. Souchay, *Polyanions et polycations*, Gauthier-Villars, Paris, **1963**, pp. 143–147.
[8] F. B. Schirmer Jr., L. F. Audrieth, S. T. Gross, D. S. McClellan, L. J. Seppi, *J. Am. Chem. Soc.* **1942**, *64*, 2543.
[9] W. D. Treadwell, Y. Schaeppi, *Helv. Chim. Acta* **1946**, *29*, 771.
[10] O. Glemser, G. Lutz, *Z. Anorg. Allg. Chem.* **1951**, *264*, 17.
[11] a) A. Müller, E. Krickemeyer, S. Dillinger, H. Bögge, W. Plass, A. Proust, L. Dloczik, C. Menke, J. Meyer, R. Rohlfing, *Z. Anorg. Allg. Chem.* **1994**, *620*, 599; b) A. Müller, W. Plass, E. Krickemeyer, S. Dillinger, H. Bögge, A. Armatage, A. Proust, C. Beugholt, U. Bergmann, *Angew. Chem.* **1994**, *106*, 897; *Angew. Chem. Int. Ed. Engl.* **1994**, *33*, 849.
[12] a) A. Müller, E. Krickemeyer, J. Meyer, H. Bögge, F. Peters, W. Plass, E. Diemann, S. Dillinger, F. Nonnenbruch, M. Randerath, C. Menke, *Angew. Chem.* **1995**, *107*, 2293; *Angew. Chem. Int. Ed. Engl.* **1995**, *34*, 2122. Compound **1** contains an extremely large cluster anion (stoichiometry $(MoO_3)_{154}N_{14}(H_2O)_{70}H_{28}$) with a large cavity (diameter >2 nm). It is the largest, anthropogenic, discrete ion characterized by X-ray structure analysis to date and consists of 140 MoO_6 octahedra and 14 pentagonal bipyramidal $\{MoO_6(NO)\}$ subunits; b) A. Müller, H. Reuter, S. Dillinger, *Angew. Chem.* **1995**, *107*, 2505; *Angew. Chem. Int. Ed. Engl.* **1995**, *34*, 2328. c) By changing the reaction parameters the formation of the by-product $\{(NH_4)HMo_5O_{16}(H_2O)\cdot H_2O\}_n$ [12a] could be prevented and **1** could be obtained in 80% yield with a higher degree of crystallinity.
[13] The subject of this article are the blue solutions that can be obtained by (partial) reduction of acidified molybdate(VI) solutions with a large number of different reducing agents (but also by electrolytical [14] or photochemically induced reduction [15]) and that are usually used for a qualitative test for the presence of molybdenum. Solids precipitated from these solutions are known as "amorphous molybdenum blue(s)"—in contrast to blue crystalline oxide–hydrates (prepared from MoO_3 suspensions) and anhydrous blue oxides with typical framework structures [10]. They have also to be distinguished from the "heteropoly blues" with an additional element [16].
[14] G. Marchetti, *Z. Anorg. Chem.* **1899**, *19*, 391.
[15] J. Duclaux, R. Titéica, *Rev. Gen. Coll.* **1929**, *7*, 289.
[16] a) M. T. Pope, *Heteropoly and Isopoly Oxometalates*, Springer, Berlin, **1983**, pp. 101–117; b) M. T. Pope, A. Müller, *Angew. Chem.* **1991**, *103*, 56; *Angew. Chem. Int. Ed. Engl.* **1991**, *30*, 34; c) N. Casañ-Pastor, L. C. W. Baker in *Polyoxometalates: From Platonic Solids to Anti-Retroviral Activity*, (Eds.: M. T. Pope, A. Müller), Kluwer, Dordrecht, **1994**, p. 203
[17] In the early publications the stoichiometric composition of the mixed-valence compounds (Mo^V/Mo^{VI}, type III [18]) was normally given as $MoO_{3-x}\cdot nH_2O$ (see Table in ref.[4]). Surprisingly, the real anionic nature of "molybdenum blue" was overlooked in most of the earlier investigations even in those cases where molybdates were used as starting materials and even though the problem of obtaining "electrolyte" or cation-free samples of "molybdenum blue" was sometimes mentioned [3,19] (exceptions [15, 20–22]).
[18] M. B. Robin, P. Day, *Adv. Inorg. Chem. Radiochem.* **1967**, *10*, 247.
[19] A. Dumanski, *Z. Chem. Ind. Kolloide* **1910**, *7*, 20.
[20] P. Klason, *Ber. Dtsch. Chem. Ges.* **1901**, *34*, 158.
[21] W. F. Jakób, W. Trzebiatowski, *Roczn. Chem.* **1929**, *9*, 676.
[22] S. Ostrowetsky, *Bull. Soc. Chim. Fr.* **1964**, *5*, 1003.
[23] Principally, also the presence of different and larger ring-shaped species (and fragments) with a general composition of $\{(MoO_3)_m(H_2O)_nH_p\}$ cannot be ruled out completely either by powder diffractometry or by IR and Raman spectra *alone*. This corresponds to the general problem of structure determination of amorphous substances (see for instance A. Müller, V. Fedin, K. Hegetschweiler, W. Amrein, *J. Chem. Soc. Chem. Commun.* **1992**, 1795, in the case of a molybdenum sulfide). Both methods together, however, give a strong hint that *mainly* only one kind of those species is abundant. The IR spectra of the very large polyoxomolybdates (type $\{Mo_{36}\}$, $\{Mo_{57}\}$ [11], $\{Mo_{154}\}$ [12]) can be modeled very nicely by superposition of the subspectra resulting from weakly coupled (!) characteristic vibrations of different $\{Mo_mO\}$ fragments ($m = 2, 3, 4$; with the heavy Mo centers preventing (diminishing) coupling. This facilitates the proof of functional groups but complicates, for example, the differentiation of species with different numbers of these base fragments (A. Müller, M. Ohm, H. Bögge, unpublished results).
[24] K. H. Tytko, B. Schönfeld, *Z. Naturforsch. B* **1975**, *30*, 471; K. H. Tytko, B. Schönfeld, B. Buss, O. Glemser, *Angew. Chem.* **1973**, *85*, 305; *Angew. Chem. Int. Ed. Engl.* **1973**, *12*, 330.
[25] B. Krebs, I. Paulat-Böschen, *Acta Crystallogr. B* **1976**, *32*, 1697; B. Krebs, S. Stiller, K. H. Tytko, J. Mehmke, *Eur. J. Solid State Inorg. Chem.* **1991**, *28*, 883.
[26] P. Gouzerh, Y. Jeannin, A. Proust, F. Robert, *Angew. Chem.* **1989**, *101*, 1377; *Angew. Chem. Int. Ed. Engl.* **1989**, *28*, 1363.
[27] See for example I. Oppenheimer, K. E. Schuler, G. H. Weiss in *Encyclopedia of Physics*, 2nd ed., (Eds.: R. G. Lerner, G. L. Trigg), VCH, New York, **1991**, p. 1177.
[28] W. Biltz, *Ber. Dtsch. Chem. Ges.* **1905**, *38*, 2963.
[29] *The Surface Science of Metal Oxides*, (Eds.: V. E. Henrich, P. A. Cox), Cambridge Univ. Press, Cambridge, **1995**.
[30] W. Biltz, W. Geibel, *Nachr. Ges. Wiss. Göttingen Math. Phys. Kl.* **1906**, 141.
[31] A. Müller, C. Serain, A. Herrmann, W. Eimer, T. Hellweg, unpublished results.
[32] W. Biltz, *Ber. Dtsch. Chem. Ges.* **1904**, *37*, 1095.

Stabilization of an Unusual Coordination Geometry at Li^+ in the Interior of a Cryptand-Type Helicate**

Markus Albrecht* and Sirpa Kotila

The metal-directed self-assembly of linear ligands to form triple-stranded helicates proceeds with high stereoselectivity.[1–3] Recently we reported the first example of an achiral *meso*-helicate, which is obtained by self-assembly of three bis(catecholate) ligands with two titanium(IV) ions.[4] We proposed that the stereochemistry of helicate versus *meso*-helicate

[*] Dr. M. Albrecht
Institut für Organische Chemie der Universität
Richard-Willstätter-Allee, D-76131 Karlsruhe (Germany)
Fax: Int. code +(721)698529
Dr. S. Kotila
Organisch-chemisches Institut der Universität Münster (Germany)

[**] This work was supported by the Fonds der Chemischen Industrie (Liebig Stipendium), the Deutsche Forschungsgemeinschaft, and the Academy of Finland. We thank Dr. H. Röttele (NMR), Mrs. B. Wibbeling (X-ray), Dr. R. Fröhlich (X-ray), and Dr. D. Röttger (CSD search) for their help.

formation depends on the zigzag conformation of the alkyl spacer connecting the ligand moieties. An even number of methylene units should favor the helicate, an odd number the *meso*-helicate structure. To test this assumption we have synthesized a binuclear triple $(CH_2)_2$-bridged titanium(IV) complex.

$Li_4[(\mathbf{1})_3Ti_2]$ is formed quantitatively by self-assembly of three equivalents of 3,3′-ethane-1,2-diylbis(1,2-benzenediol) [1,2-bis(2,3-dihydroxyphenyl)ethane] ($\mathbf{1\text{-}H_4}$)[5] with two equivalents of $[(acac)_2TiO]$ (acac = acetyl acetonate) in the presence of two equivalents of lithium carbonate as base.

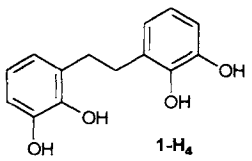

1-H$_4$

Only one diastereoisomer can be detected by ^1H NMR and ^{13}C NMR spectroscopy ([D$_4$]methanol), but the spectra do not allow an assignment to the helicate or *meso*-helicate structure.[6] The ^1H NMR spectrum (400 MHz) at room temperature shows the signals of the aromatic moiety at $\delta = 6.46-6.39$ (m, 12H) and 6.29 (dd, $J = 1.4$, 7.4 Hz, 6H) as well as a broad signal at $\delta = 2.80$ (12H) for the protons of the ethylene spacer. When the sample is cooled to 194 K, the signal for the ethylene spacer is split into two multiplets at $\delta = 3.25$ (6H) and 2.31 (6H). Coalescence is observed at 233 K, indicating an energy barrier of $\Delta G^{\neq} = 10.3$ kcal mol^{-1} for the racemization of the two octahedrally coordinated chiral titanium centers.

Figure 1a shows the structure of the tetraanion $[(\mathbf{1})_3Ti_2]^{4-}$ in the crystal.[7] As proposed, the binuclear $[(\mathbf{1})_3Ti_2]^{4-}$ ion possesses the chiral helicate form. Two of the ligands **1** induce a helical turn leading to transfer of chiral information from one titanium(IV) center to the other. The third ligand adopts a more linear orientation (vide infra). This helicate structure indicates the possibility of controlling the stereochemistry in the self-assembly process of achiral components.[8] Simple conformational changes influence the diastereoselectivity in such a way that exclusively one diastereoisomer is formed.

In contrast to the analogous oligonuclear coordination compounds formed from linear nitrogen donors (for example, oligo(2,2′-bipyridine) ligands),[2] the catecholate complexes possess additional lone pairs of electrons at the donor atoms. In the solid state as well as in solution these are capable of binding alkali cations in a cryptand-type fashion.[9,10] Thus, $[(\mathbf{1})_3Ti_2]^{4-}$ encapsulates one of the lithium counterions in its cavity, thereby forcing an extraordinary coordination geometry at this alkali ion (Fig. 1b). The lithium ion bridges the two internal oxygen atoms of the linearly coordinated bis(catecholate) ligand **1**, leading to an O2-Li1-O2* angle of 164.2(5)°. Vacant coordination sites at this Li^+ ion are saturated by two water molecules, which are each fixed in the cavity by hydrogen bonding interactions with the internal oxygen atoms of the two helically orientated ligand strands. The $O10_{water}$-Li1-$O10^*_{water}$ angle is 148.7(6)°. Thus, the tetracoordinate Li1 atom does not adopt the expected tetrahedral geometry. The coordination geometry can be described best as distorted square planar or as trigonal prismatic with one equatorial ligand missing. The free equatorial position is blocked by the ethylene spacer of the linear ligand **1** (Li1···C7(spacer) 2.78(1) Å).

A few rare examples of compounds containing lithium coordinated in a square-planar fashion have been described. Li^+ shows a planar tetracoordinate coordination geometry in porphyrins[11] or phthalocyanines[12] and bis(acetyl acetonate) complexes.[13] In the case of $[\{Li(H_2O)_2\} \subset \{(\mathbf{1})_3Ti_2\}]^{3-}$ the unusual geometry seems to result from constraints of the cavity. The internal oxygen atoms of the Li-binding ligand are 4.01 Å apart. Effective coordination to lithium can only take place if the O2-Li1-O2* angle widens. Steric effects force the water molecules to move outwards. Further stabilization is obtained by the hydrogen bonding interactions of the water. The combination of steric effects with hydrogen bonding stabilization allows the distorted square-planar geometry. Attempts to detect the inclusion of the lithium cation in solution were unsuccessful. ^6Li NMR ([D$_4$]methanol/methanol 1:1, 58.9 MHz) of a sample of $^6Li_4[(\mathbf{1})_3Ti_2]$ at various temperatures (193–300 K) showed only one resonance at $\delta = 0.92$. This indicates that the exchange of encapsulated and solvated lithium ions is fast with respect to the NMR time scale.

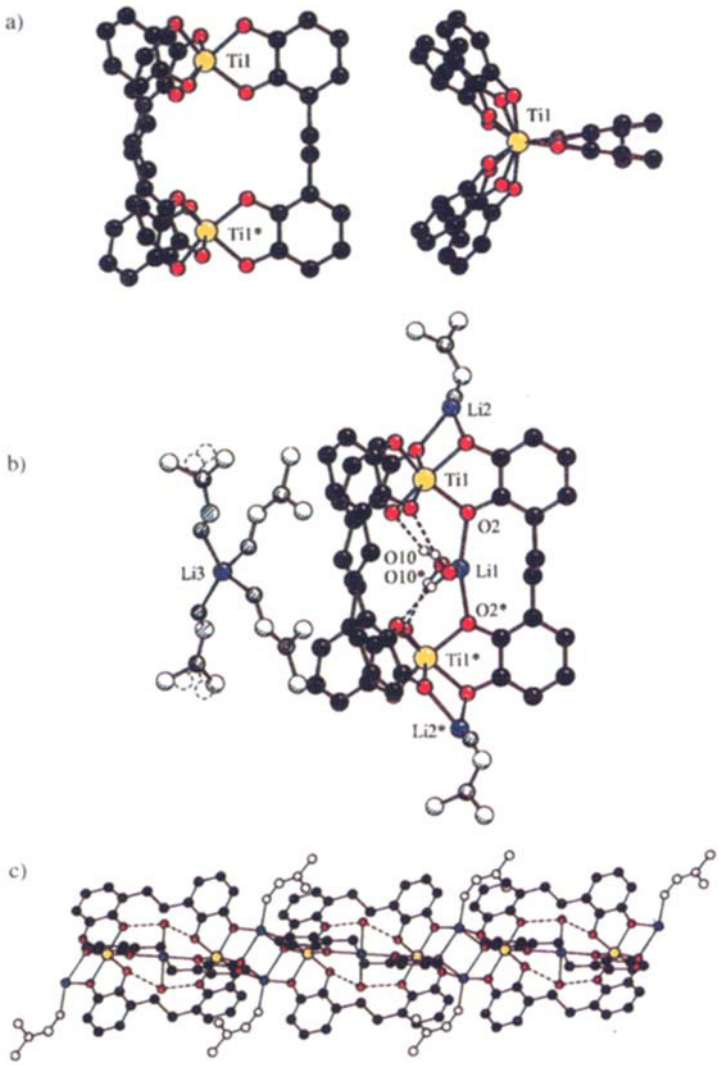

Fig. 1. Molecular structure of $Li_4[(\mathbf{1})_3Ti_2]\cdot 6DMF\cdot 2H_2O$. a) The tetraanion $[(\mathbf{1})_3Ti_2]^{4-}$; side view (left) and view along the Ti–Ti axis (right); b) monomeric unit; c) polymeric structure. Black: carbon, red: oxygen, yellow: titanium, blue: lithium; for clarity only the H atoms forming hydrogen bonds are shown; solvent molecules are not colored; disorder is indicated by dotted lines.

In the crystal, in addition to Li1 two further Li^+ cations are exohedrally bound to external catecholate oxygen atoms at the "ends" of the helicate anion. These two ions form a bridge by interaction with two DMF molecules, resulting in an infinite chain in the solid state (Fig. 1c).[14] Coordination geometries at these two lithium ions are trigonal bipyramidal. The remaining fourth lithium ion is tetrahedrally surrounded by four DMF molecules.

In summary, we have shown that the stereochemistry of the self-assembly processes of achiral components is influenced by small conformational changes of the participating substrates.

Furthermore, the aggregates formed can act as receptors and bind small molecules (water) or ions (Li^+), stabilizing unusual geometries in its cavity. This shows some relevance to the function of enzymes and antibodies that can stabilize the geometry of reaction intermediates by a combination of stereoelectronic effects and hydrogen bonding networks.[15]

Received: January 11, 1996 [Z8711IE]
German version: *Angew. Chem.* **1996**, *108*, 1299–1300

Keywords: catechol · complexes with oxygen ligands · self-assembly · supramolecular chemistry · titanium compounds

[1] Reviews: D. S. Lawrence, T. Jiang, M. Levett, *Chem. Rev.* **1995**, *95*, 2229; E. C. Constable, *Tetrahedron* **1992**, *48*, 10013, and references therein.

[2] A. F. Williams, C. Piguet, G. Bernardinelli, *Angew. Chem.* **1991**, *103*, 1530; *Angew. Chem. Int. Ed. Engl.* **1991**, *30*, 1490; G. Bernardinelli, C. Piguet, A. F. Williams, *ibid.* **1992**, *104*, 1626 and **1992**, *31*, 1622; R. Krämer, J.-M. Lehn, A. De Cian, J. Fischer, *ibid.* **1993**, *105*, 764 and **1993**, *32*, 703; K. T. Potts, C. P. Horwitz, A. Fessak, M. Keshavarz-K, E. Nash, P. J. Toscano, *J. Am. Chem. Soc.* **1993**, *115*, 10444; D. Zurita, P. Baret, J.-L. Pierre, *New. J. Chem.* **1994**, *18*, 1143; C. Piguet, G. Hopfgartner, A. F. Williams, J.-C. G. Bünzli, *J. Chem. Soc. Chem. Commun.* **1995**, *491*.

[3] D. L. White, K. N. Raymond, *J. Am. Chem. Soc.* **1985**, *107*, 6540; E. J. Corey, C. L. Cywin, M. C. Noe, *Tetrahedron Lett.* **1994**, *35*, 69; E. J. Enemark, T. D. P. Stack, *Angew. Chem.* **1995**, *107*, 1082, *Angew. Chem. Int. Ed. Engl.* **1995**, *34*, 996.

[4] M. Albrecht, S. Kotila, *Angew. Chem.* **1995**, *107*, 2285; *Angew. Chem. Int. Ed. Engl.* **1995**, *34*, 2134.

[5] M. Albrecht, *Synthesis* **1996**, 230.

[6] $Li_4[(\mathbf{1})_3Ti_2]$: ^{13}C NMR (100 MHz, BB/DEPT, [D$_4$]methanol): δ = 158.9 (C), 157.5 (C), 128.0 (C), 120.4 (CH), 118.4 (CH), 110.7 (CH), 32.6 (CH_2); UV/Vis (methanol): λ = 209, 274, 363 nm; positive ion FAB-MS (glycerine): m/z = 839 $[H_3Li_2[(\mathbf{1})_3Ti_2]^+]$, 845 $[H_2Li_3[(\mathbf{1})_3Ti_2]^+]$, 851 $[HLi_4[(\mathbf{1})_3Ti_2]^+]$; $C_{42}H_{30}Li_4O_{12}Ti_2 \cdot 6H_2O \cdot 5MeOH$ (1118.6): calcd.: C 50.47, H 5.59; found C 50.16, H 5.54.

[7] Crystals of $Li_4[(\mathbf{1})_3Ti_2] \cdot 2H_2O \cdot 6DMF$ were obtained by slow diffusion of ether in a solution of the compound in DMF/water (10:1). Crystal data for $Li_4[(\mathbf{1})_3Ti_2] \cdot 2H_2O \cdot 6DMF$: Formula $C_{60}H_{76}Li_4N_6O_{20}Ti_2$, formula weight 1324.83, brownish yellow plates (0.4 × 0.3 × 0.2 mm^3), monoclinic, space group $C2/c$ (No. 15), a = 1208.7(2), b = 2280.0(3), c = 2337.2(2) pm, β = 100.26(1)°, $V = 6338 \times 10^6$ pm^3, Z = 4, $F(000)$ = 2776, T = −100 °C, $\rho_{calcd.}$ = 1.388 g cm^{-3}, μ = 3.3 cm^{-1}, empirical absorption correction from Ψ scans ($C_{min/max}$ = 0.940/0.999), Enraf-Nonius MACH3 diffractometer, λ = 71.073 pm, ω-2θ scans, 5504 reflections measured ($\pm h$, $-k$, $+l$, $2\theta_{max}$ = 49°) of which 5363 were independent and 3066 observed [$I \geq 2\sigma(I)$], 449 refined parameters, R = 0.050, wR^2 = 0.122, residual electron density max./min. 0.50/−0.36 e Å^{-3}. The structure was solved by direct methods (SHELXS-86) and refined against F^2 (SHELXL-93), hydrogen atoms were introduced to their calculated positions and refined isotropically as riding atoms, the hydrogen atoms of the crystalline water molecules were located from the difference Fourier map. Asymmetric unit was one half of the monomer and the other half was generated by symmetry operation $-x, y, 0.5-z$. One DMF molecule was disordered (59:41) and it was refined using geometrical and and thermal restraints. The figures were drawn with the schakal program. Further details of the X-ray crystal structure analysis are available upon request from the Fachinformationszentrum Karlsruhe, D-76344 Eggenstein-Leopoldshafen, on quoting the depository number CSD-404667.

[8] For a further example of diastereoselectivity in the self-assembly of achiral components, see for example: R. W. Saalfrank, B. Hörner, D. Stalke, J. Salbeck, *Angew. Chem.* **1993**, *105*, 1223; *Angew. Chem. Int. Ed. Engl.* **1993**, *32*, 1179.

[9] J.-M. Lehn, *Angew. Chem.* **1988**, *100*, 92; *Angew. Chem. Int. Ed. Engl.* **1988**, *27*, 90.

[10] M. Albrecht, H. Röttele, P. Burger, unpublished results.

[11] J. Arnold, D. Y. Dawson, C. G. Hoffman, *J. Am. Chem. Soc.* **1993**, *115*, 2707.

[12] H. Sugimoto, M. Mori, M. Masuda, T. Taga, *J. Chem. Soc. Chem. Commun.* **1986**, 962.

[13] F. A. Schröder, H. P. Weber, *Acta Cryst. B* **1975**, *31*, 1745; R. J. Morris, G. S. Girolami, *Polyhedron* **1988**, *7*, 2001.

[14] F. E. Hahn, M. Keck, K. N. Raymond, *Inorg. Chem.* **1995**, *34*, 1402.

[15] See, for example: P. G. Schulz, R. A. Lerner, *Science* **1995**, *269*, 1835.

Crystal Growth in Zeolite Y Revealed by Atomic Force Microscopy**

Michael W. Anderson,* Jonathan R. Agger, John T. Thornton, and Nicola Forsyth

Zeolites form one of the most important classes of heterogeneous catalyst. Their microporous nature and consequent high surface area impart both high selectivity and high activity. Although well over one hundred zeolite-like compounds can now be synthesized with a wide range of pore geometries their synthesis remains very much a "black art". Generally, zeolites are synthesized from an alkaline aluminosilicate gel that sometimes contains organic cations. At least two main routes to crystallization have been identified: first, gel globules crystallize without transport of material resulting in globular, highly twinned crystals; second, single zeolite crystals grow by transport of nutrient from the gel phase to a growing zeolite crystal. It is the second route that is dealt with in this study.

Novel frameworks are often produced by incorporating large organic cations into the synthesis mixture, but whether these cations act as structure templates or as structure blockers is not well understood. There are a number of examples of syntheses in which the organic molecule fits very snugly into the resulting tunnel structure, for example the tetrapropylammonium ion in ZSM-5, and it is tempting in these cases to think of the molecules as templates. However, often the same structure can be made with other organic molecules or with no organic molecules at all—again ZSM-5 is a good example of a zeolite that can be made with a wide variety of organic molecules or simply in the presence of Na^+ ions.

Zeolite Y (structure designation FAU) is probably the single most important zeolite from a catalytic standpoint, since it is used for the catalytic cracking of petroleum. An interesting recent example of structure-directing through the use of organic molecules is the synthesis of the hexagonal polymorph of zeolite Y (structure designation EMT) in the presence of [18]crown-6 and Na^+ ions.[1] Both FAU and EMT can be constructed by linking sodalite cages (truncated octahedra) through double six-membered rings. The relationship of the sodalite cages is as for zinc blend in FAU and as for wurtzite in EMT. It has been shown[2] that a $[Na([18]crown-6)]^+$ macrocation is located within the oblate cages of EMT into which it sits very snugly. The structure of EMT was originally proposed by Breck[3] and was known as Breck structure six (BSS) but proved elusive to synthesize. The cubic polymorph of zeolite Y on the other hand is extremely easy to synthesize and can be prepared from an aluminosilicate gel containing only Na^+ ions. As EMT and FAU are constructed from the same building units they easily form random intergrowths, and this has been observed in many preparations containing a variety of organic molecules.[4] Like EMT the FAU structure can also be prepared by using a crown ether

[*] Dr. M. W. Anderson, Dr. J. R. Agger
Department of Chemistry, UMIST
PO Box 88, Manchester, M60 1QD (UK)
Fax: Int. code +(161)236 7677
e-mail: M. Anderson@umist.ac.uk
J. T. Thornton
Digital Instruments,
520 E. Montecito St., Santa Barbara, CA (USA)
Dr. N. Forsyth
L. O. T. Oriel,
1 Mole Business Park, Leatherhead, KT22 7AU (UK)

[**] We thank the European Commission through ESPRIT and EPSRC for funding J. R. A., Osamu Terasaki for useful discussions and Ian Brough for the scanning electron micrographs.

([15]crown-5), and it has been shown that by mixing [18]crown-6 with [15]crown-5 controlled intergrowths of the two materials can be prepared.[5-9] A mechanism has been postulated[6,7] in which [18]crown-6 acts to stabilize the EMT structure during crystallization. This mechanism views the crystallization in terms of a layer growth (supported by high-resolution electron microscopy (HREM) of surface growth steps) in which [18]crown-6 decorates a growth layer. This decoration occurs at pocket sites on the growing surface and forces the next growing surface to grow with a mirror symmetry rather than an inversion symmetry to the decorated layer. Such mirror related growth gives EMT rather than FAU structure. The postulation of layer growth was based primarily on electron microscopy which only provides a projected image through the crystal, therefore, although the presence of growth steps was identified, the true morphology of the related terraces circumscribed by these steps was unclear.

Atomic force microscopy (AFM) has recently been used to monitor the surface features in zeolite minerals[10] and also the details of crystal growth of a number of organic[11] and inorganic[12] materials. In this present study we have utilized AFM to scan the surface of crystals of FAU and EMT synthesized by using crown ether templates to reveal the growth face morphology. The crown ether preparations result in relatively large (> 1 mm), defect-free crystals compared with conventional routes for the synthesis of zeolite Y making study by AFM feasible.

Scanning electron micrographs of FAU and EMT samples (Fig. 1) reveal characteristic octahedral and hexagonal crystal

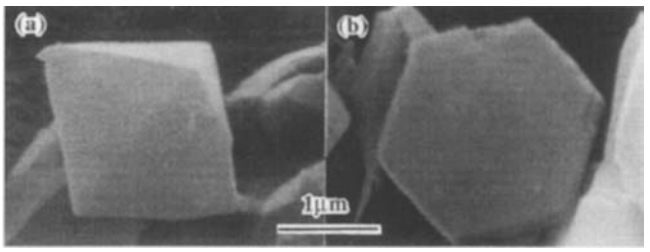

Fig. 1. Scanning electron micrographs of a) a FAU crystal showing octahedral habit with a crystal edge length of about 1 μm and b) an EMT crystal showing hexagonal prism habit with edge length about 1 μm.

morphology, respectively. In FAU the faces of the crystal are all $\{111\}_c$, in EMT the top and bottom faces are $\{001\}_h$ and the side faces are $\{100\}_h$, where c and h depict cubic and hexagonal phases, respectively. Figure 2a shows the AFM image of one of the $\{111\}_c$ faces of FAU. The triangular nature of the face with edge length about 1 μm is immediately apparent. On the crystal surface a host of triangular terraces are observed with the triangles rotated by 60° to the crystal edges. A section analysis (Fig. 2b) reveals that the triangular terraces have a highly uniform thickness of approximately 1.5 nm. This thickness is in very good agreement with the thickness of one faujasite layer of 1.43 nm, calculated crystallographically, (see [110] projection in Scheme 1) and in very good agreement with the step heights observed previously by HREM.[7]

A number of important features are observed in the AFM image of FAU structure: 1) the triangular edges of the terraces are rotated by 60° about $[111]_c$ from the crystal edges; 2) the orientation of all triangular terraces is the same; 3) the spacing between the terrace edges decreases towards the edges of the crystal.

The first feature is at first surprising. One might expect the orientation to be the same; however, the rotated sense of the terraces will result in layer growth which circumvents the whole crystal as illustrated in Scheme 1 in which eight growing terraces

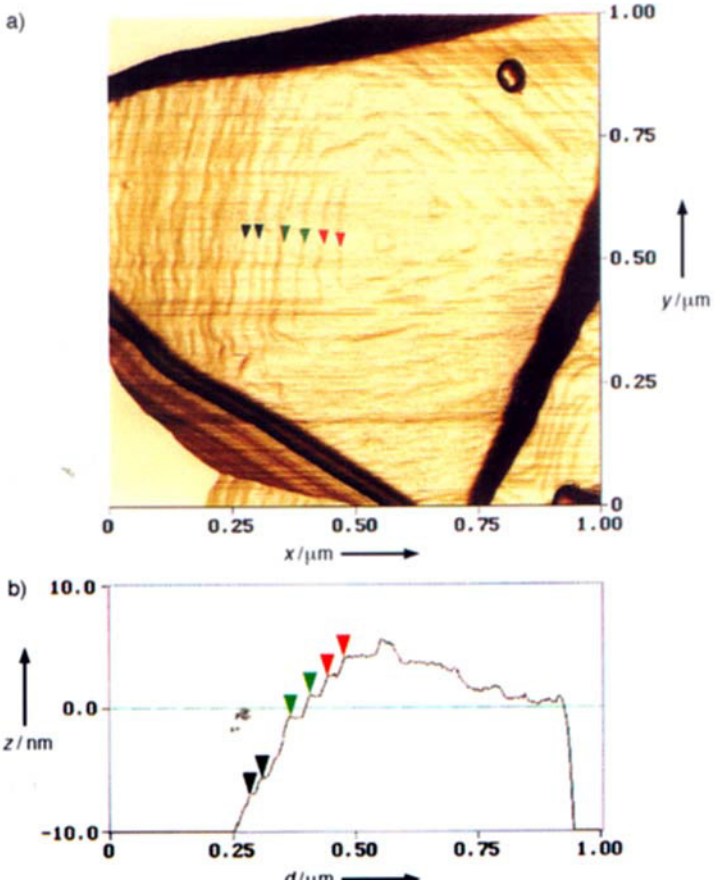

Fig. 2. a) AFM image (TappingMode) of FAU structure showing the $(111)_c$ face. The triangular terraces are growth steps each about 1.5 nm in height. This value was derived from section analysis (b), which shows height and separation of crystal steps (d: lateral shift in the xy plane). The colored arrows correspond to the following step heights and (in parentheses) lateral step separations, respectively: red: 1.5 nm (33 nm); green: 1.7 nm (39 nm); black: 1.4 nm (25 nm).

are shown with one highlighted in black. The growing terraces nucleate on the $\{111\}_c$ face and have a triangular appearance, as the [111] projection shows. In these projections vertices represent silicon or aluminum atoms linked by oxygen bridges. The oxygen atoms are not shown for clarity but lie approximately half way along each line. The trigonal symmetry of one faujasite sheet can be seen in the [111] projection where U and D represent up and down, respectively, and indicate displacement of sodalite cage building units. This trigonal symmetry is reflected in the triangular appearance of the growing terraces. As the triangular terraces enlarge they will merge with other growing terraces on other $\{111\}_c$ faces to form the six-sided faces of a truncated octahedron. Such a growth front ensures that the crystal will grow in a uniform manner on all $\{111\}_c$ faces. If the triangular terraces were to grow in the same sense as the crystal faces, each face would in effect grow independently of neighboring faces which might result in more irregular crystals.

The second feature, that is the fact that on any given crystal face, all triangular terraces grow in the same sense is due both to the threefold symmetry of the faujasite layer (Scheme 1) and to the relationship between interconnected layers. A pure cubic faujasite crystal is composed of an ABCABC stacking of faujasite layers. The different layers are shifted laterally to one another but are not rotated. A rotation of one layer by 60° would result in an unfavorable planar fault and the creation of a small amount of EMT structure. For example a layer stacking

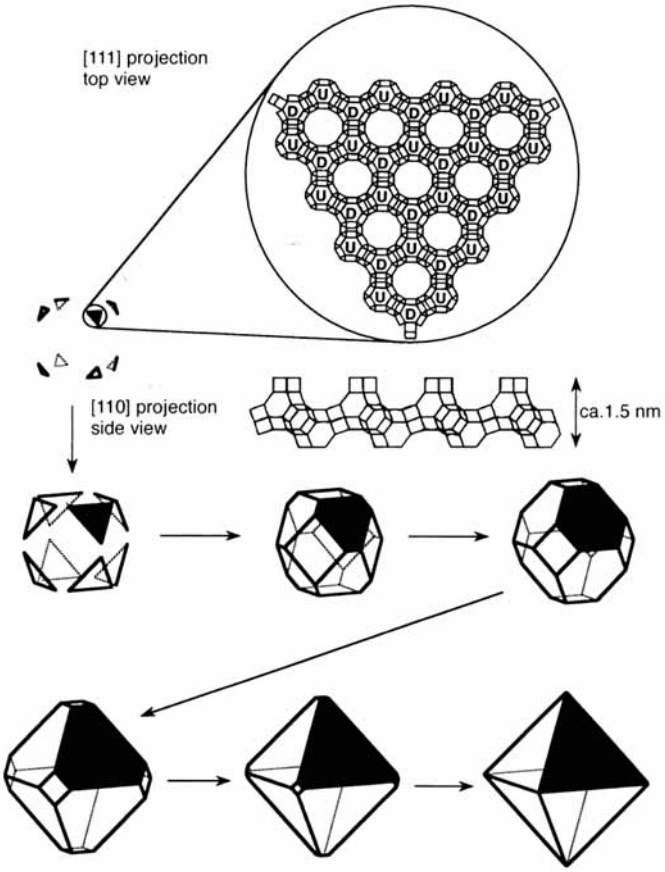

Scheme 1. Schematic representation of terrace growth on a $\{111\}_c$ face of a FAU crystal.

ABCAB*ABCABC which is shown with the EMT section in bold and the one rotated B layer highlighted with an asterisk. In order to force this unfavorable rotation between interconnected layers [18]crown-6 must be used as a structure-directing agent.

The last feature, that is the decreasing spacing between terrace edges has been observed previously in HREM images[7] and can be explained in terms of the growth mechanism. If the terraces grow by a terrace-ledge-kink (TLK) mechanism (see Fig. 3 inset), growth rate perpendicular to a growing face is governed by the nucleation time of a new terrace. If it is assumed that this terrace nucleation time is a constant, the terrace number provides a unit measurement of time (the smallest triangular terrace is numbered as one). The size of each terrace will depend upon the time for which it has been growing (that is those with a low terrace number have been growing for the shortest period and will therefore be smallest). If the terraces grow by deposition of nutrient from solution at a kink site (a site with constant area), the area of a terrace will increase at a constant rate. Consequently, a plot of growing time (or terrace number) versus terrace area (or area coefficient, which is the square of any linear parameter of the triangle—we have used the square of the triangle height, h^2) should be linear. Terrace steps will consequently get closer and closer together as the step separation is related to the square root of the terrace area. Figure 3 shows a linear relationship between the terrace growth time (terrace number n) and terrace area coefficient h^2 which is consistent with such a growth mechanism.

It should be remembered that analysis by AFM, as with analysis by HREM, is essentially a "post-mortem" on a crystal following growth. It is not possible to determine whether the surface structure has altered following removal of the crystals from the supernatant solution. Further, it is well known that as

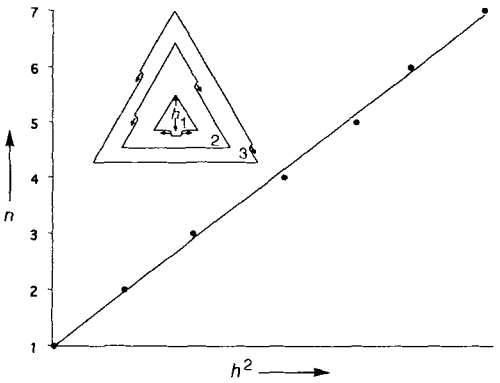

Fig. 3. Linear plot of terrace number n versus area coefficient h^2 (arbitrary units) for growing terraces. The inset shows a schematic representation of kink growth.

the supersaturation of a synthesis medium drops, the first faces to stop growing are the low index faces[13] such as $\{111\}_c$. In FAU, however, the only faces exposed are $\{111\}_c$ and therefore these will all behave in an equivalent manner. The regular nature of the surface terraces coupled with the excellent linear relationship between terrace area and growth time is compelling evidence that these terraces are indeed fundamental units in the growth process and that zeolite Y grows by a layer mechanism. The definitive, yet challenging, experiment will be an in situ AFM study to monitor crystal growth.

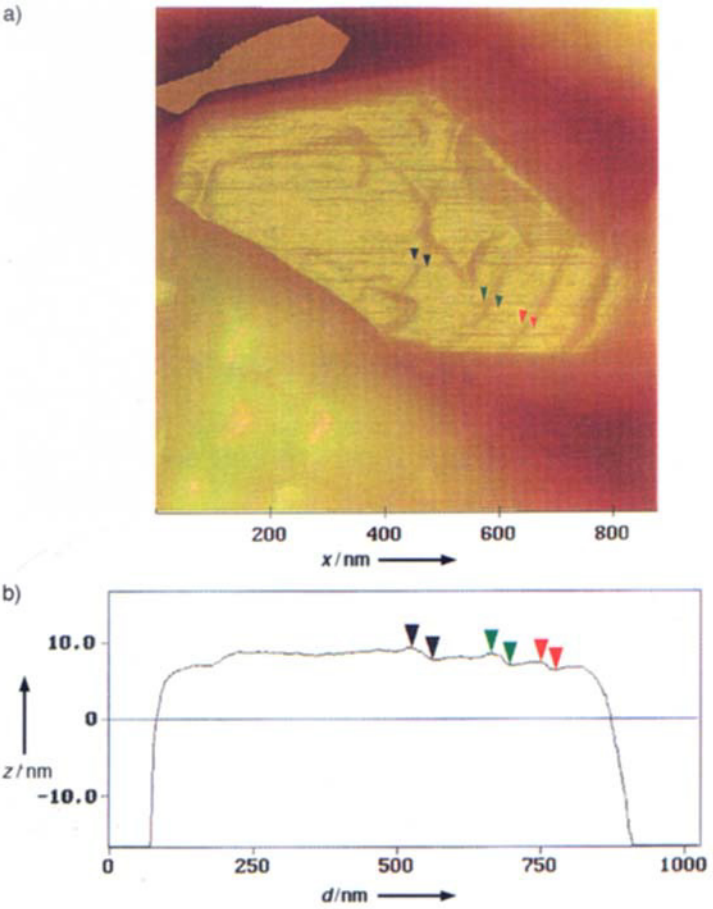

Fig. 4. a) AFM image (TappingMode) of EMT structure showing a partially obscured $(001)_h$ face. These terraces are about 1.5 nm in height, as revealed by the section analysis (b), corresponding to one faujasite sheet (d: lateral shift in xy plane). The colored arrows correspond to the following step heights: red: 1.0 nm; green: 1.5 nm; black: 1.5 nm.

 © VCH Verlagsgesellschaft mbH, D-69451 Weinheim, 1996 0570-0833/96/3511-1212 $ 15.00+.25/0

Figure 4a shows the AFM image of one partially obscured $\{001\}_h$ face of EMT. The hexagonal nature of the face with edge length about 0.6 μm is immediately apparent. Though the overall terrace topology on the crystal surface is not as well defined as for FAU, both a hexagonal nature and a diminishing terrace width towards the edge of the crystal are evident. This hexagonal terrace morphology is a consequence of the symmetry generated along the $[001]_h$ direction by the ABAB stacking of faujasite layers. Although individually the A and B layers have threefold symmetry (see Scheme 1) they are rotated with respect to one another by 60° thereby generating a pseudo sixfold axis. Section analysis again reveals that the terraces are approximately 1.5 nm thick and this thickness is highly uniform. The growth terraces of the EMT structure are less well defined than those of the FAU structure which is a reflection of the larger number of defects in EMT than FAU.[7]

Experimental Procedure

The zeolites were synthesized in the system $10SiO_2:1.0Al_2O_3:2.4Na_2O:140H_2O:1.0$ crown ether. The sources of material were 40 wt% colloidal silica (HS-40 Ludox); 40 wt% sodium aluminate solution; [15]crown-5 and [18]crown-6 (Aldrich). Gels were aged for two days at room temperature followed by crystallization in Teflon bottles for eight days at 95 °C.

AFM images were recorded on a Nanoscope Multimode Microscope from Digital Instruments operating in TappingMode. Samples were secured on an adhesive surface to prevent lateral movement. A first order planefit was conducted on the images in the x and y directions to level the crystal terraces, and simulated illumination is used to emphasize the crystal steps. Dark areas around crystal edges are due to the surface topography possessing a greater slope than the side of the tip. Thus, these areas contain information on the tip shape only and do not contain topographical information.

Received: October 30, 1995 [Z 8513 IE]
German version: *Angew. Chem.* **1996**, *108*, 1301–1304

Keywords: atomic force microscopy · crystallization · zeolites

[1] E. Delprato, L. Delmotte, J. L. Guth, L. Huve, *Zeolites* **1990**, *10*, 546–552.
[2] C. Baerlocher, L. B. McCusker, R. Chiapetta, *Microporous Mater.* **1994**, *2*, 269–280.
[3] D. W. Breck, *Zeolite Molecular Sieves*, Wiley, New York, **1974**, p.56.
[4] J. M. Thomas, M. Audier, J. Klinowski, *J. Chem. Soc. Chem. Commun.* **1981**, 1221–1222; M. M. J. Treacy, J. M. Newsam, R. A. Beyerlein, M. E. Leonowicz, D. E. W. Vaughan, *ibid.* **1986**, 1211–1213; J. M. Newsam, M. M. J. Treacy, D. E. W. Vaughan, K. G. Stohmaier, W. J. Mortier, *ibid.* **1989**, 493–495; J. A. Martens, P. A. Jacobs, S. Cartlidge, *Zeolites* **1989**, *9*, 423–427; S. Ernst, G. T. Kokotailo, J. Weitkamp, *ibid.* **1987**, *7*, 180–182; M. M. J. Treacy, J. M. Newsam, D. E. W. Vaughan, R. A. Beyerlein, S. B. Rice, C. B. deGruyter, *Mater. Res. Soc. Symp. Proc.* **1988**, *111*, 177–190; D. E. W. Vaughan (Exxon), *Eur. Pat. Appl.* 315461, **1988** (*Chem. Abstr. 108*, 115126m); D. E. W. Vaughan, M. G. Barret (Exxon), US-A 4333859, **1982** (*Chem. Abstr. 98*, 75170n); J. Jiric (Mobil Oil), *ibid.* 3972983, **1976** (*Chem. Abstr. 86*, 92954r), *ibid.* 4021331, **1977** (*Chem. Abstr. 86*, 195783p); V. Fülöp, G. Borbély, H. K. Beyer, S. Ernst, J. Weitkamp, *J. Chem. Soc. Faraday Trans. 1* **1989**, *85*, 2127–2139.
[5] M. W. Anderson, K. S. Pachis, F. Prébin, S. W. Carr, O. Terasaki, T. Ohsuna, V. Alfredsson, *J. Chem Soc. Chem Commun.* **1991**, 1660–1664.
[6] O. Terasaki, T. Ohsuna, V. Alfredsson, J.-O. Bovin, D. Watanabe, S. W. Carr, M. W. Anderson, *Chem. Mater.* **1993**, *5*, 452–458.
[7] T. Ohsuna, O. Terasaki, V. Alfredsson, J.-O. Bovin, D. Watanabe, S. W. Carr, M. W. Anderson, *Proc. R. Soc. London A*, in press.
[8] J. P. Arhancet, M. E. Davis, *Chem. Mater.* **1991**, *3*, 567–569.
[9] S. L. Burkett, M. E. Davis, *Microporous Mater.* **1993**, *1*, 265–282.
[10] A. L. Weisenhorn, J. E. MacDougall, S. A. C. Gould, S. D. Cox, W. S. Wise, J. Massie, P. Maivald, V. B. Elings, G. D. Stucky, P. K. Hansma, *Science* **1990**, *247*, 1330–1333; J. E. MacDougall, S. D. Cox, G. D. Stucky, A. L. Weisenhorn, P. K. Hansma, W. S. Wise, *Zeolites* **1991**, *11*, 429–433; M. Komiyama, T. Yashima, *Jpn J. Appl. Phys. Part 1* **1994**, *33*, 3761–3763.
[11] S. Manne, J. P Cleveland, G. D. Stucky, P. K. Hansma, *J. Cryst. Growth* **1993**, *130*, 333–340; S. D. Durbin, W. E. Carlson, *ibid.* **1992**, *122*, 71–79.
[12] P. E. Hillner, A. J. Gratz, S. Manne, P. K. Hansma, *Geology* **1992**, *20*, 359–362; P. E. Hillner, S. Manne, A. J. Gratz, P. K. Hansma, *Ultramicroscopy* **1992**, *42*, 1387–1393; A. J. Gratz, S. Manne, P. K. Hansma, *Science* **1991**, *251*, 1343–1346.
[13] W. K. Burton, N. Cabrera, F. C. Frank, *Phil. Trans. R. Soc. A* **1951**, *243*, 299–358.

Controlled Assembly of Nanosized Metallodendrimers**

Wilhelm T. S. Huck, Frank C. J. M. van Veggel,* and David N. Reinhoudt*

There is considerable interest in the synthesis of well-defined structures of nanometer dimensions.[1] These structures can be constructed by formation of covalent bonds, but this requires multistep synthesis.[2] Therefore, various other strategies have been developed that rely on self-assembly through noncovalent interactions, for example hydrogen bonds. Whitesides et al.[3] obtained stable rosettelike structures constructed of melamine and barbituric acid units held together by strong hydrogen bonds. The nanotubular assemblies prepared by Ghadiri et al.[4] are another beautiful example of hydrogen-bonded assemblies. Dative bonds to transition metals can also be employed in self-assembly. Lehn et al. have applied the coordination of oligopyridines to transition metals to form triple helices, ladder polymers, and molecular grids.[5] Previously, we have described the self-assembly of small aggregates and ribbonlike polymers using the uranyl cation.[6] In this paper we describe the synthesis of metallodendrimers by controlled assembly.

Dendrimers are attractive, nanosize compounds with very specific architectures.[7, 8]] Dendrimers can be synthesized by following either a convergent or a divergent route,[9] in which an increasing number of new covalent bonds are formed in each generation. A few dendrimers containing transition metals have been reported.[10] Van Koten et al.[11] have used metalated dendrimers as homogeneous catalysts. Balzani and co-workers reported the synthesis of metallodendrimers containing transition metals in every generation, which relied on sequential reactions on the metal centers and protection/deprotection of ligands.[12] In contrast, Achar and Puddephat built dendrimers by oxidative additions to Pt^{II} complexes.[13]

We have recently described the synthesis of large organopalladium spheres by "genuine" self-assembly.[14] Now we report here that we can control this process and use this method for the synthesis of first-, second-, and third-generation metallodendrimers. Our approach is based on controlled assembly of building blocks that contain all the necessary information. We make use of the coordination chemistry of Pd^{II} and have combined in building block **BB-Cl** two kinetically inert tridentate "pincer-type" ligands and one labile coordinating cyano group (Scheme 1). The nucleus $\mathbf{G_0}$ has in this case C_3 symmetry with three Pd centers.

The temporary protection of the metal center by a strongly coordinating Cl^- ion prevents coordination by cyano groups. Further growth of Pd complex $\mathbf{G_0}$ is achieved by replacing the Cl^- ion for a noncoordinating BF_4^- ion, by reaction with $AgBF_4$. Subsequent addition of three equivalents of the protected building block **BB-Cl** yields the next generation dendrimer $\mathbf{G_1}$. By repeating this sequence twice it is possible to build the third-generation metallodendrimer $\mathbf{G_3}$.

The synthesis of **BB-Cl** and $\mathbf{G_0}$ is outlined in Scheme 2. The S-C-S pincer ligand was prepared in seven steps from dihydroxy-

[*] Dr. Ir. F. C. J. M. van Veggel, Prof. Dr. Ir. D. N. Reinhoudt, Drs. W. T. S. Huck
Laboratory of Organic Chemistry and MESA Research Institute
University of Twente
P. O. Box 217, NL-7500 AE Enschede (Netherlands)
Fax: Int. code +(53)4894645
e-mail: orgchem@ct.utwente.nl

[**] We thank the Dutch Foundation for Chemical Research (SON) for financial support. We are grateful to Prof. N. Nibberink and R. Fokkens (Institute of Mass Spectrometry, University of Amsterdam) for ES-MS measurements.

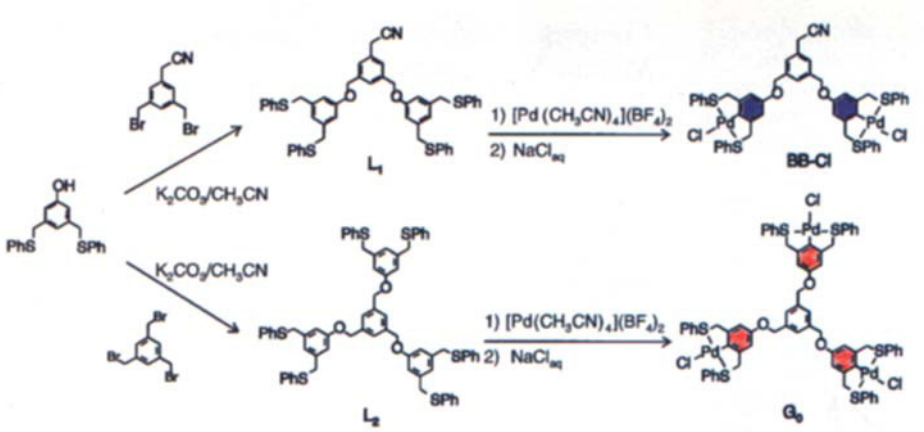

Scheme 1. Graphical representation of the controlled assembly process.

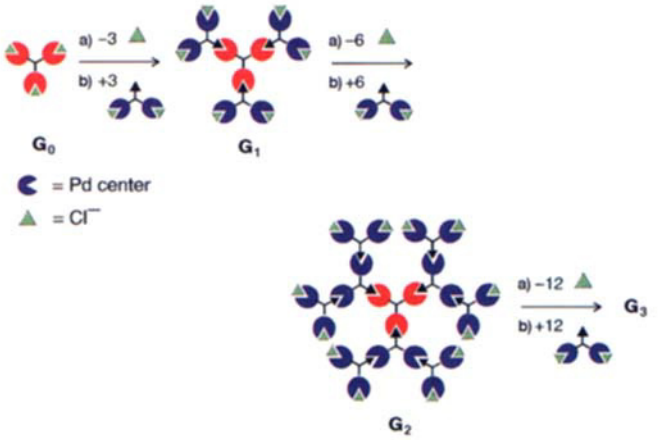

Scheme 2. Synthesis of dendrimer building blocks.

isophthalic acid.[14] The pincer ligands were coupled to a tribromomesitylene spacer to afford the nucleus $\mathbf{L_2}$, or to dibromomonocyanomesitylene to yield the dendrimer building block $\mathbf{L_1}$. Simple cyclopalladation of $\mathbf{L_1}$ and $\mathbf{L_2}$ with $[Pd(CH_3CN)_4(BF_4)_2]$[15] gave in quantitative yield the bis- and trispalladium complexes, which were directly converted into the chloride complexes **BB-Cl** and $\mathbf{G_0}$, respectively, by stirring with aqueous NaCl. The palladation is quantitative and occurs exclusively at the position activated by both S donor atoms, as can be deduced from ^{1}H NMR spectroscopy. A broad singlet at $\delta = 4.4$ for the CH_2S protons reflects the slow conformational interconversion of the five-membered Pd cycle, and the absence of a singlet at $\delta = 6.85$ indicates complete cyclopalladation. After purification by column chromatography (silica gel, eluting with CH_2Cl_2/MeOH 97/3) **BB-Cl** and $\mathbf{G_0}$ were obtained in yields of 70 and 40%, respectively.

Nucleus $\mathbf{G_0}$ was activated by stirring with three equivalents of $AgBF_4$ in CH_2Cl_2/nitromethane (1/1), and three equivalents of **BB-Cl** were added to form the assembly $\mathbf{G_1}$. Repeating the same procedure yielded in a very simple way metallodendrimers $\mathbf{G_2}$ and $\mathbf{G_3}$. These complexes were purified by filtration over hyflo and column chromatography (silica gel reversed phase, eluting with nitromethane) to remove the precipitated silver chloride. The yellow-colored metallodendrimers were obtained as a single fraction in quantitative yield after chromatography. The synthesis of an nth generation metallodendrimer is a one-pot procedure, because intermediate generations need not be isolated. The assembly process is controlled by the repetitive addition of $AgBF_4$ and **BB-Cl**. Dendrimers $\mathbf{G_1}$–$\mathbf{G_3}$ were fully characterized by ^{1}H and ^{13}C NMR and FT-IR spectroscopy,[16] electrospray mass spectrometry (ES-MS), and elemental analysis (Table 1).

The ^{1}H NMR spectra of $\mathbf{G_1}$–$\mathbf{G_3}$ are remarkably simple because of the high symmetry of the nucleus and the similarity of the building blocks. The formation of the desired compounds can be deduced from the ratios of the intensities of the signals of the CH_2CN and CH_2O protons, which is 1:3 for $\mathbf{G_1}$, 3:7 for $\mathbf{G_2}$, and 1:2 for $\mathbf{G_3}$. The signals in the ^{1}H NMR spectrum of $\mathbf{G_3}$ show some broadening, indicating the restricted motion of the inner generations. The ^{13}C NMR spectra show no shifts on going from $\mathbf{G_0}$ to $\mathbf{G_3}$.[17]

Molecular masses were determined by ES-MS. The transformed ES mass spectra (Fig. 1)[18] show signals at m/z 1516.2

Table 1. Selected physical data for $\mathbf{G_0}$–$\mathbf{G_3}$.

$\mathbf{G_0}$: M.p. 164–166 °C; ^{1}H NMR ($CDCl_3$): δ = 7.81 (m, 12H; Ar_5H), 7.39 (s, 3H; ArH), 7.35 (m, 18H; Ar_5H), 6.63 (s, 6H; $Ar_{Pd}H$), 4.93 (s, 6H; CH_2O), 4.53 (br. s, 12H; CH_2S); ^{13}C NMR ($CDCl_3$): δ = 156.5, 150.2, 137.7, 132.3, 131.4, 129.8, 129.7, 109.2, 69.8, 51.7; ES-MS: m/z: 1516.2 $[M-Cl]^+$. Analysis: calcd for $C_{69}H_{57}O_3S_6Pd_3Cl_3 \cdot H_2O$: C 52.78, H 3.79; found: C 52.51, H 3.70.

$\mathbf{G_1}$: M.p. 154–157 °C; ^{1}H NMR (CD_3NO_2): δ = 7.63 (m, 36H; Ar_5H), 7.45 (s, 3H; ArH), 7.40 (s, 9H; ArH), 7.29 (m, 54H; Ar_5H), 6.62 (s, 18H; $Ar_{Pd}H$), 4.93 (s, 18H; CH_2O), 4.49 (br. s, 36H; CH_2S), 3.78 (s, 6H; CH_2CN); ^{13}C NMR (CD_3NO_2, 80 °C): δ = 153.1, 147.0, 145.8, 134.9, 128.3, 127.9, 126.4, 125.8, 106.1, 46.2, 19.8; ES-MS: m/z: 4759.5 $[M-2Cl-2BF_4]^+$. Analysis calcd for $C_{219}H_{177}B_3N_3O_9F_{12}S_{18}Cl_6Pd_9 \cdot CH_3NO_2$: C 51.47, H 3.58, N 1.11, Cl 4.20; found: C 51.99, H 3.74, N 1.33, Cl 4.09.

$\mathbf{G_2}$: M.p. 148–152 °C; ^{1}H NMR (CD_3NO_2): δ = 7.75 (m, 84H; Ar_5H), 7.4 (m, 156H; ArH), 6.75 (s, 42H; $Ar_{Pd}H$), 5.00 (s, 42H; CH_2O), 4.54 (br. s, 84H; CH_2S), 3.89 (s, 18H; CH_2CN); ^{13}C NMR (CD_3NO_2, 80 °C): δ = 153.1, 147.0, 145.8, 134.9, 128.2, 127.9, 126.5, 125.8, 122.8, 106.1, 66.2, 46.2, 19.8; ES-MS: m/z: 11907.0 $[M]^+$. Analysis calcd for $C_{519}H_{426}B_9N_9O_{21}F_{36}S_{42}Cl_{12}Pd_{21} \cdot 2CH_3NO_2$: C 51.99, H 3.62, N 1.29, Cl 3.53; found: C 51.74, H 3.75, N 1.86, Cl 3.16.

$\mathbf{G_3}$: M.p. 139–142 °C; ^{1}H NMR (CD_3NO_2): δ = 7.7 (m, 180H; Ar_5H), 7.5 (m, 336H; ArH), 6.8 (s, 90H; $Ar_{Pd}H$), 5.0 (s, 90H; CH_2O), 4.5 (br. s, 180H; CH_2S), 3.9 (s, 42H; CH_2CN); ^{13}C NMR (CD_3NO_2, 80 °C): δ = 153.1, 147.0, 145.8, 134.9, 128.2, 127.9, 126.5, 125.8, 122.8, 106.1, 66.2, 46.2, 19.8; ES-MS: m/z: 24032 $[M-19BF_4]^+$. Analysis calcd for $C_{1119}H_{918}B_{21}N_{21}O_{45}F_{84}S_{90}Cl_{24}Pd_{45} \cdot 10CH_3NO_2$: C 51.16, H 3.60, N 1.74, Cl 3.22; found: C 51.16, H 3.61, N 2.22, Cl 3.21.

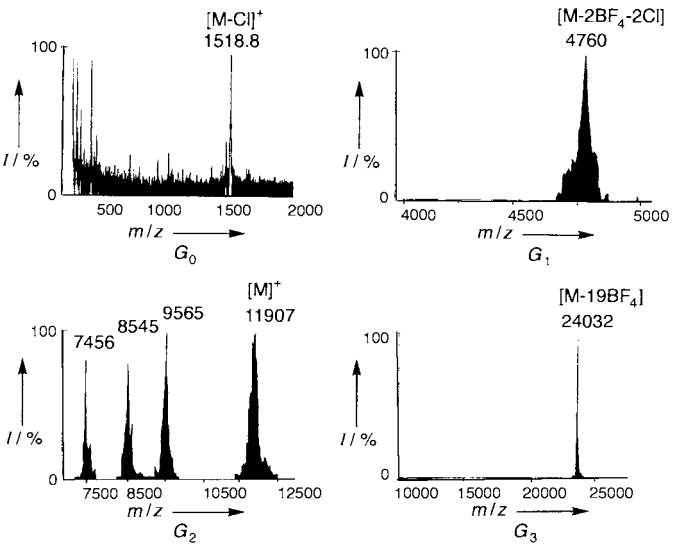

Fig. 1. ES mass spectra for $\mathbf{G_1}$–$\mathbf{G_3}$.

($[\mathbf{G_0} - \mathrm{Cl}]^+$), 4783.5, ($[\mathbf{G_1} - \mathrm{Cl} - 2\,\mathrm{BF_4}]^+$), 11907.0 ($[\mathbf{G_2}]^+$) and 24030.2 ($[\mathbf{G_3} - 19\,\mathrm{BF_4}]^+$). The loss of anions takes place inside the mass spectrometer, generating the multiply charged ions needed for detection and calculation of the molecular weight.[19]

Molecular mechanics calculations[20] were performed on $\mathbf{G_0}$–$\mathbf{G_3}$. The square-planar coordination environment of the Pd centers is well preserved. It is clear that after the second generation the structure of the dendrimer becomes quite entangled (Fig. 2).

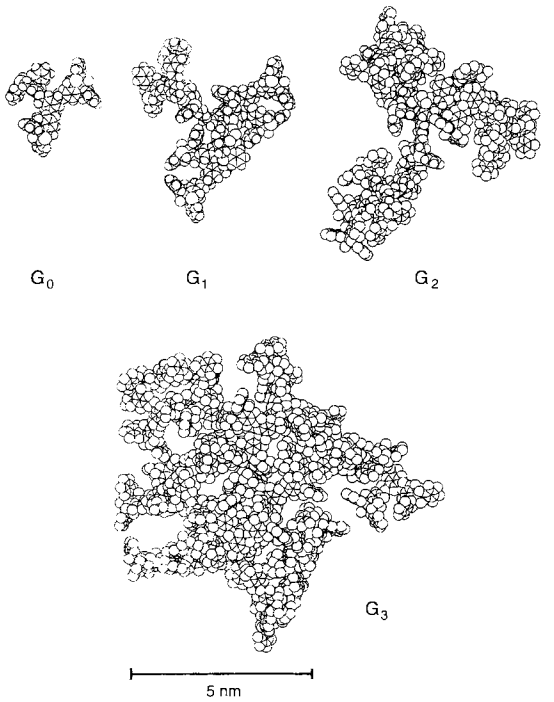

Fig. 2. Optimized structures of $\mathbf{G_0}$–$\mathbf{G_3}$.

We have shown that organometallic structures of nanometer dimensions can now be constructed in a very simple and controlled way. This method of controlled assembly provides a new and versatile tool for dendrimer synthesis. The method allows large variation in the metal in each generation, the coordinating ligands, and the structure of the nucleus.

Received: December 29, 1995 [Z 8690 IE]
German version: *Angew. Chem.* **1996**, *108*, 1304–1306

Keywords: dendrimers · palladium complexes · supramolecular chemistry

[1] Review: G. Ozin, *Adv. Mater.* **1992**, *15*, 612–648.
[2] For the synthesis of a receptor molecule with a nanosize cavity see: P. Timmerman, W. Verboom, F. C. J. M. van Veggel, W. P. van Hoorn, D. N. Reinhoudt, *Angew. Chem.* **1994**, *106*, 1313–1316; *Angew. Chem. Int. Ed. Engl.* **1994**, *33*, 1292–1295.
[3] J. P. Mathias, E. E. Simanek, G. M. Whitesides, *J. Am. Chem. Soc.* **1994**, *116*, 4326–4340.
[4] N. Khazanovich, J. R. Granja, D. E. McRee, R. A. Milligan, M. R. Ghadiri, *J. Am. Chem. Soc.* **1994**, *116*, 6011–6012.
[5] J.-M. Lehn, *Supramolecular Chemistry*, VCH, Weinheim, **1995**, pp. 139–197, and references therein.
[6] D. M. Rudkevich, W. Verboom, Z. Brzøzka, M. J. Palys, W. P. R. V. Stauthamer, G. J. van Hummel, S. M. Franken, S. Harkema, J. F. J. Engbersen, D. N. Reinhoudt, *J. Am. Chem. Soc.* **1994**, *116*, 4341–4351.
[7] D. A. Tomalia, A. M. Naylor, W. A. Goddard III, *Angew. Chem.* **1990**, *102*, 119–156; *Angew. Chem. Int. Ed. Eng.* **1990**, *29*, 138–175.
[8] J. F. G. A. Jansen, E. M. M. de Brabander-van den Berg, E. W. Meijer, *Science* **1994**, *266*, 1226–1229.
[9] C. J. Hawker, J. M. J. Fréchet, *J. Am. Chem. Soc.* **1990**, *112*, 7638–7642.
[10] Y. H. Liao, J. R. Moss, *J. Chem. Soc. Chem. Commun.* **1993**, 1774–1777; G. R. Newkome, F. Cardullo, E. C. Constable, C. N. Moorefield, A. M. W. Cargill Thompson, *ibid.* **1993**, 925–927; M. F. Ottaviani, S. Bossmann, N. J. Turro, D. A. Tomalia, *J. Am. Chem. Soc.* **1994**, *116*, 661–671; A. Miedaner, C. J. Curits, R. M. Barkley, D. L. Dubois, *Inorg. Chem.* **1994**, *33*, 5483–5498; G. R. Newkome, R. Guther, C. N. Moorefield, F. Cardullo, L. Echegoyen, E. Perèz-Cordero, H. Luftmann, *Angew. Chem.* **1995**, *107*, 2159–2162; *Angew. Chem. Int. Ed. Engl.* **1995**, *34*, 2023–2026.
[11] J. W. J. Knapen, A. W. van der Made, J. C. de Wilde, P. W. N. M. van Leeuwen, P. Wijkens, D. M. Grove, G. van Koten, *Nature* **1994**, *372*, 659–662.
[12] S. Campagna, G. Denti, S. Serroni, A. Juris, M. Venturi, V. Ricevuto, V. Balzani, *Chem. Eur. J.* **1995**, *1*, 211–221.
[13] S. Achar, R. J. Puddephat, *Angew. Chem.* **1994**, *106*, 895–897; *Angew. Chem. Int. Ed. Engl.* **1994**, *33*, 847–849.
[14] W. T. S. Huck, F. C. J. M. van Veggel, B. L. Kropman, D. H. A. Blank, E. G. Keim, M. M. A. Smithers, D. N. Reinhoudt, *J. Am. Chem. Soc.* **1995**, *117*, 8293–8294.
[15] S. J. Loeb, G. K. H. Shimizu, *J. Chem. Soc. Chem. Commun.* **1993**, 1395–1397.
[16] Coordination of the cyano group is deduced from the characteristic shift from 2252 cm^{-1} (free C≡N) to 2290 cm^{-1} upon coordination. B. N. Storhoff, H. C. Lewis, *Coord. Chem. Rev.* **1977**, *23*, 1–23.
[17] M. H. P. van Genderen, M. W. P. L. Baars, J. C. M. van Hest, E. M. M. de Brabander-van den Berg, E. W. Meijer, *Recl. Trav. Chim. Pays-Bas* **1994**, *113*, 573–574.
[18] The signals at lower *m/z* values in the spectrum of $\mathbf{G_2}$ correspond to species after the respective loss of one, two, and three dendrimer building blocks and corresponding anions.
[19] Examples of loss of counterions are known from literature: E. Leize, A. van Dorsselaer, R. Krämer, J.-M. Lehn, *J. Chem. Soc. Chem. Commun.* **1993**, 990–993; G. Hopfgarter, C. Piguet, J. D. Henion, A. F. Williams, *Helv. Chim. Acta* **1993**, *76*, 1759–1766.
[20] Universal Force Field in the Cerius² program package: A. K. Rappé, C. J. Casewit, K. S. Colwell, W. A. Goddard, III, W. M. Skiff, *J. Am. Chem. Soc.* **1992**, *114*, 10024–10035.

Molecular Boxes Based on Calix[4]arene Double Rosettes**

Remko H. Vreekamp, John P. M. van Duynhoven, Martin Hubert, Willem Verboom, and David N. Reinhoudt*

The construction of noncovalently bonded, well-defined aggregates has received increasing attention over the last few years. The study of molecular self-assembly is expected to provide information on how interactions between molecular functionalities lead to entities with new shapes and functions. The shapes of recently described ensembles range from boxes[1, 2] and channels[3] to more complex three-dimensional networks and other discrete aggregates.[4–6] Reported molecular boxes based on noncovalent interactions all have rather small cavities, since they result from the dimerization of two molecules with concave structures.[2] Recently we prepared receptors with large hydrophobic cavities by the covalent combination of calix[4]arenes and resorcin[4]arenes.[7] The successful synthesis

[*] Prof. Dr. ir. D. N. Reinhoudt, Dr. ir. R. H. Vreekamp, M. Hubert, Dr. W. Verboom
Laboratory of Organic Chemistry and MESA Research Institute
University of Twente
P. O. Box 217, NL-7500 AE Enschede (The Netherlands)
Fax: Int. code +(53)4894645
e-mail: orgchem@ct.utwente.nl
Dr. J. P. M. van Duynhoven
Laboratory of Chemical Analysis, University of Twente

[**] We gratefully acknowledge financial support from Akzo Nobel Central Research b.v.

of these molecules indicates that calix[4]arene[8] is a suitable molecular building block for the construction of molecular boxes because it offers a rigid concave surface.

In this communication we describe the formation of large self-assembled boxes, which have a "double-rosette structure". The calix[4]arene skeleton[9] serves as a spacer between the two rosettes and as molecular platform that preorganizes the hydrogen bonding groups. This spacer ensures that the centers of the two rosettes are separated by as much as 8.5 Å (based on CPK molecular models).[10] The formation of the hydrogen-bonded rosette is the result of hydrogen bonding between melamine moieties and barbituric or cyanuric acid derivatives. This motif is being studied intensively by Whitesides et al.,[11] and recently Lehn et al. have also used this motif for self-assembly.[12]

We have used three different calix[4]arenes as components for the double rosettes: the dimelamine derivative **1**, upper-rim substituted isocyanuric acid derivative **2**, and the lower-rim substituted isocyanuric acid derivative **3**.[13]

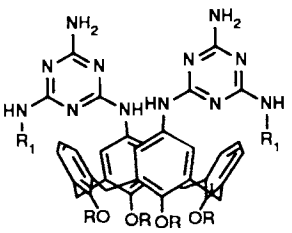

1

R = $C_{12}H_{25}$, R_1 = C_4H_9

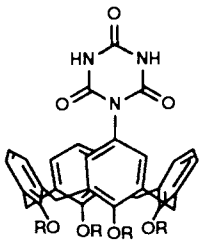

2

R = $C_{12}H_{25}$

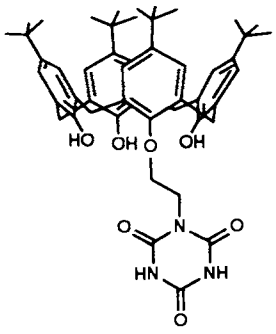

3

^{1}H NMR titration of **1** with diethylbarbituric acid (BA) in $CDCl_3$ showed several characteristic features (Fig. 1). Very interestingly, already at low concentrations of BA two signals (a, b) were evident at very low field.These resonances, which remain at δ = 14.10 and 13.32 regardless of the **1**:BA ratio, are assigned to the hydrogen-bonded NH protons of BA in the **1**·BA complex. When the amount of barbituric acid is increased, the signal corresponding to the NH_2 protons of free **1** decreases in intensity but remains at the same position. At the same time, signals at δ = 8.37 (c) and 7.43 (d) appear, which correspond to the two secondary amine protons of **1** in the hydrogen-bonded complex. At a ratio of **1**:BA of 1:2 the spectrum is sharp, which indicates the absence of free **1**. The 1:2 ratio is consistent with the double-rosette structure schematically represented in Figure 2. Dilution of this solution did not give rise to changes in the ^{1}H NMR spectrum, indicating that the

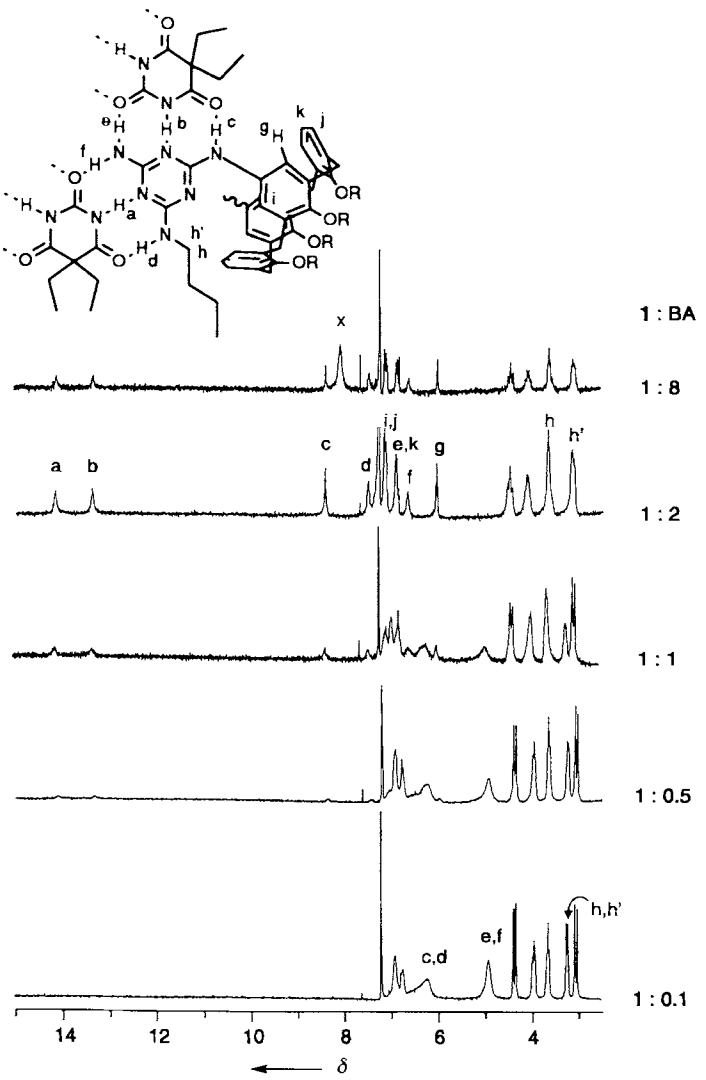

Fig. 1. ^{1}H NMR titration of **1** with BA measured at 400 MHz at ambient temperature. Separate 10 mM solutions of **1** and BA in $CDCl_3$ were mixed in various ratios. x = signal for the free acid.

presence of high-order aggregates is less probable. When more than two equivalents of barbituric acid are present, the signal for the NH protons in free BA is observed alongside the two for the hydrogen-bonded BA. This indicates that exchange between hydrogen-bonded and free BA is slow on the NMR time scale.[15] In the rosette the two NH protons are observed at different chemical shifts as a result of the unsymmetrical substitution of the melamine units. Two signals are observed for both the two NH_2 protons (e, f) and for the two protons of the *n*-butyl chain next to the nitrogen (h, h'), indicating diastereotopicity.[16]

The aromatic protons of the melamine-substituted aromatic ring of calix[4]arene **1** give rise to signals at δ = 7.15 (i) and 6.03 (g). In free **1** these protons display broad signals at δ = 7.05–6.70 and 6.65–6.05, respectively. The resonance at δ = 6.03 is in accordance with a pinched *cone* structure[17] in which the two melamines approach each other.[18]

Titration of **1** with **2** gave similar results. Large downfield shifts are observed for the NH protons (δ = 15.43 and 14.15), free and hydrogen-bonded species do not exchange on the NMR time scale, and a 1:2 ratio is indicated. At ratios beyond 1:2 (i.e. excess **1**) only signals corresponding to the saturated double

 © VCH Verlagsgesellschaft mbH, D-69451 Weinheim, 1996 0570-0833/96/3511-1216 $ 15.00+.25/0

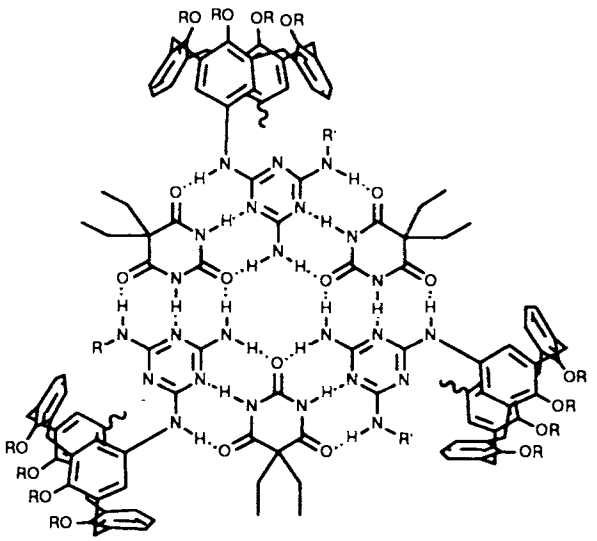

1•BA

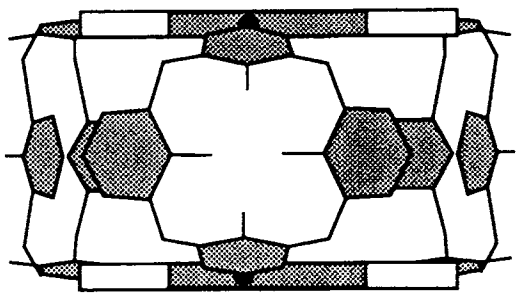

1•BA

Fig. 2. Schematic representation of the proposed structure of a double rosette consisting of 1 and BA. Top: top view (for clarity only the upper rosette is shown). Bottom: side view.

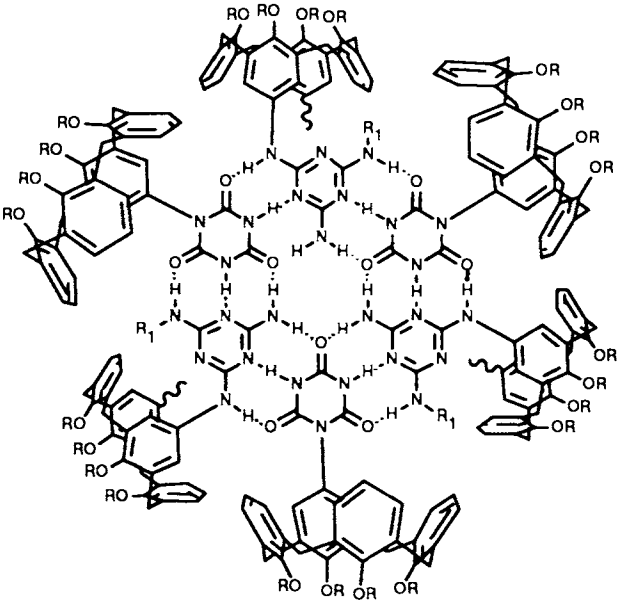

1•2

Fig. 3. Schematic representation of the proposed structure of a double rosette consisting of 1 and 2 (for clarity only the upper rosette is shown).

Table 1. Distances [Å] between the H atoms in 1·BA, 1·2, and 1·3 [a].

H Atoms	1·BA	1·2	1·3
a–d	2.8	2.5	2.7
a–f	3.4	3.1	3.0
b–e	3.2	3.0	2.9
b–c	3.5	2.9	2.9
c–g	3.2	2.9	

[a] Deviation ±0.1 Å.

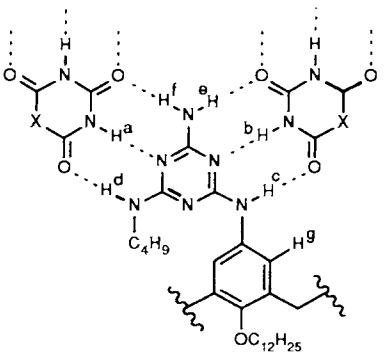

rosette and free 1 are observed. No other signals are present at low field, in particular, which means that no intermediate structures such as partly filled double rosettes or linear aggregates exist. This suggests that rosette formation as depicted in Figure 3 is a cooperative process, in which the formation of one rosette preorganizes the remaining units, favoring the formation of the second rosette.

The ^{1}H NMR titration of **1** with **3** was, to a certain extent, similar to that of **1** with BA. The hydrogen-bonded NH protons were observed at slightly higher field ($\delta = 15.17$ and 14.47). At a **1**:**3** ratio of 1:2 the signals of free **1** disappear, indicating the formation of a double rosette.[19]

The distances between the relevant protons in the three double-rosette structures were determined by 2D NOESY experiments (400 MHz) using the initial rate approximation (Table 1).[20, 21] The distances are slightly larger than those obtained from CPK molecular models and molecular modeling of similar hydrogen-bonding motifs,[22, 23] but provide sufficient evidence for the proposed rosette structure.

The above results strongly indicate the formation of rosettes.[24] Further evidence for the formation of the rosettes was derived from build-up curves measured for the NOE interactions between the methylene bridge protons. From these data cross relaxation rates can be derived, the magnitude and sign of which relate to the rotation correlation time τ_c. If the random isotropic tumbling of a spherical molecule/aggregate and the absence of internal motion are assumed, τ_c can be related to the hydrodynamic volume.[23, 25, 26] By using the initial rate approximation, the cross relaxation rates for the methylene bridge protons of the three aggregates together with those for the free **3** and **1** were determined, and from these values the corresponding τ_c values were calculated. Generally, the τ_c values increase as the expected molecular masses of the aggregates increase. Qualitatively a good correlation is present with the curve of the calculated τ_c values (Fig. 4).[27]

The absolute deviations between the calculated and experimental values are most likely caused by the uncertain assumptions regarding density and shape. Assumptions regarding shape are not likely to hold for the somewhat flattened double rosettes. It is known that a greater ellipticity of a molecule leads to a larger effective correlation time, which correlates to a larger apparent molecular weight.[28]

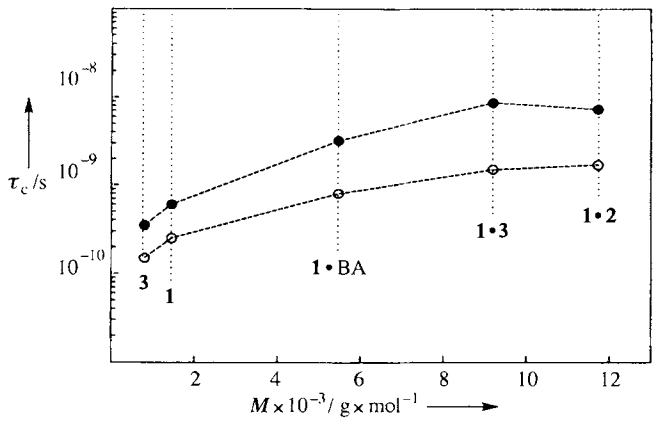

Fig. 4. Rotation correlation times τ_c determined from cross relaxation constants as a function of the molecular weights of the species in question. ● = experimental (400 MHz, 25 mM in $CDCl_3$); ○ = theoretical.

In conclusion, strong indications for the formation of the calix[4]arene-based double-rosette structure from three different combinations of bis(melamine)calix[4]arene and isocyanuric acid derivatives were obtained from ^{1}H NMR titrations and from the distances determined by NOE spectroscopy between the protons involved in hydrogen bonds. The results are in accordance with the expected 1:2 stoichiometry and suggest that the formation of the double rosettes is a highly cooperative process. In addition measurements of cross relaxation rates give further support for the formation of the large entities; the formation of aggregates is reflected by an increase in rotation correlation times. We feel that the determination of cross relaxation rates provides a valuable tool for the characterization of supramolecular structures in general. Future work will focus on complexation of guests, control of the cavity size and openings, and the introduction of chemical functionalities.

Received: December 12, 1995 [Z 8638 IE]
German version: *Angew. Chem.* **1996**, *108*, 1306 – 1309

Keywords: calixarenes · hydrogen bonds · self-assembly · supramolecular chemistry

[1] O. F. Schall, G. W. Gokel, *J. Am. Chem. Soc.* **1994**, *116*, 6089 – 6100.
[2] N. Branda, R. M. Grotzfeld, C. Valdés, J. Rebek, Jr., *J. Am. Chem. Soc.* **1995**, *117*, 85 – 88.
[3] M. R. Ghadiri, J. R. Granja, L. K. Buehler, *Nature* **1994**, *369*, 301 – 304.
[4] S. J. Geib, C. Vicent, E. Fan, A. D. Hamilton, *Angew. Chem.* **1993**, *105*, 83 – 85; *Angew. Chem. Int. Ed. Engl.* **1993**, *32*, 119 – 121.
[5] S. C. Zimmerman, B. F. Duerr, *J. Org. Chem.* **1992**, *57*, 2215 – 2217.
[6] J. L. Sessler, B. Wang, A. Harriman, *J. Am. Chem. Soc.* **1995**, *117*, 704 – 714.
[7] a) P. Timmerman, W. Verboom, F. C. J. M. van Veggel, J. P. M. van Duynhoven, D. N. Reinhoudt, *Angew. Chem.* **1994**, *106*, 1313 – 1315; *Angew. Chem. Int. Ed. Engl.* **1994**, *33*, 1292 – 1295. b) P. Timmerman, K. G. A. Nierop, E. A. Brinks, W. Verboom, F. C. J. M. van Veggel, W. P. van Hoorn, D. N. Reinhoudt, *Chem. Eur. J.* **1995**, *1*, 124 – 131.
[8] For a recent review on calixarenes see: V. Böhmer, *Angew. Chem.* **1995**, *107*, 785 – 818; *Angew. Chem. Int. Ed. Engl.* **1995**, *34*, 713 – 745.
[9] A few calix[4]arene-based hydrogen-bonded aggregates have been reported: a) J.-D. van Loon, R. G. Janssen, W. Verboom, D. N. Reinhoudt, *Tetrahedron Lett.* **1992**, *35*, 5125 – 5128. b) K. Koh, K. Araki, S. Shinkai, *ibid.* **1994**, *35*, 8255 – 8258. c) A. Arduini, M. Fabbi, M. Mantovani, L. Mirone, A. Pochini, A. Secchi, R. Ungaro, *J. Org. Chem.* **1995**, *69*, 1454 – 1457.
[10] This is substantially more than when a simple *meta*-xylene spacer is used (1 – 2 Å): J. P. Mathias, E. E. Simanek, G. M. Whitesides, *J. Am. Chem. Soc.* **1994**, *116*, 4326 – 4340.
[11] For a review see: G. M. Whitesides, E. E. Simanek, J. P. Mathias, C. T. Seto, D. N. Chin, M. Mammen, D. M. Gordon, *Acc. Chem. Res.* **1995**, *28*, 37 – 44.
[12] K. C. Russell, E. Leize, A. van Dorsselaer, J.-M. Lehn, *Angew. Chem.* **1995**, *107*, 244 – 248; *Angew. Chem. Int. Ed. Engl.* **1995**, *34*, 209 – 213.
[13] Calix[4]arene **1** was synthesized in five steps starting from de-*tert*-butylated calix[4]arene in an overall yield of 19%. The reactions include alkylation of the lower rim, selective nitration of the upper rim [14] followed by reduction to the diamine, and reaction with cyanuric chloride, ammonia, and finally *n*-butylamine. The first four steps of the synthesis of **2** are very similar to those of the synthesis of **1**. Mononitrated de-*tert*-butylated calix[4]arene was reduced to the monoamine. Subsequent reaction with nitrobiuret gave the biuret derivative, which was converted to the isocyanuric acid by treatment with diethylcarbonate to give pure **2** in an overall yield of 22%. The synthesis of **3** started with monoalkylation of *p*-*tert*-butylcalix[4]arene with 2-bromoethylphthalimide. The resulting phthalimido derivative was quantitatively reduced to the monoamine, which was then reacted with nitrobiuret. Subsequent reaction with diethylcarbonate gave the pure monoisocyanuric acid **3**. All new compounds were fully characterized by ^{1}H NMR and ^{13}C NMR spectroscopy, FAB mass spectrometry, and elemental analysis.
[14] J.-D. van Loon, J. F. Heida, W. Verboom, D. N. Reinhoudt, *Recl. Trav. Chim. Pays-Bas* **1992**, *111*, 353 – 359.
[15] From the large difference in chemical shifts for free and complexed BA (Fig. 1) an upper limit for the dissociation rate constant of about 2000 s^{-1} can be estimated. Assuming that the formation rate constant is diffusion limited, an overall binding constant of $\geq 10^5$ M^{-1} can be estimated.
[16] For the assignment of the signals of **1**·BA and the other assemblies discussed in this paper NOE, ROE, and J-correlation spectroscopy were used.
[17] "Pinched" means that two opposite aromatic rings become almost parallel while the other two twist outward and "flatten" the calix.
[18] The rosette is also stable in acetonitrile and toluene; however, addition of > 10% DMSO or MeOH to a $CDCl_3$ solution resulted in slow decomposition.
[19] In this case probably higher aggregates are formed as a result of hydrogen bonding between free **3** and the hydroxyl groups of **3** in the aggregate when more than two equivalents of **3** are present. This was concluded from the appearance of new signals in the ^{1}H NMR spectrum.
[20] R. R. Ernst, G. Bodenhausen, A. Wokaun in *Principles of Nuclear Magnetic Resonance in One and Two Dimensions*, International Series of Monographs on Chemistry, Vol. 14 (Eds.: R. Breslow, J. B. Goodenough, J. Halpern, D. Rowlinson), Clarendon, Oxford, **1987**, pp. 490 – 538.
[21] A value of 1.79 Å for the distance between the axial and the equatorial protons of the methylene bridges was used as calibration.
[22] J. Pranata, S. G. Wierschke, W. L. Jorgensen, *J. Am. Chem. Soc.* **1991**, *113*, 2810 – 2819.
[23] K. Wüttrich, *NMR of Proteins and Nucleic Acids*, Wiley, New York, **1986**.
[24] Rosette formation for the complexes **1**·BA and **1**·**2** was also confirmed by electrospray MS: *m*/*z* values of 5770 (calcd for M + 7MeCN 5768) and 11727 (calcd for M + 3H 11727), respectively, were obtained. In the case of **1**·**2** complex VPO measurements in $CHCl_3$ at 29 °C gave a molecular weight of $10.0 \pm 1.8 \times 10^3$ g mol^{-1} (calcd 9199).
[25] D. C. Fry, S. A. Kuby, A. S. Mildvan, *Biochemistry* **1985**, *24*, 4680 – 4693.
[26] The hydrodynamic volume is related to the molecular mass via the density ρ. Equation (a) is used to determine τ_c. This equation expresses the relationship

$$\sigma_{12} = \frac{1}{10}\left(\frac{\mu_0}{4\pi}\right)^2 \frac{\gamma^4\hbar^2}{r^6}\left\{\frac{6\tau_c}{1+4\omega^2\tau_c^2} - \tau_c\right\} \qquad \text{(a)}$$

between τ_c and the cross relaxation constant, σ_{12}, for a two-spin system involving atoms 1 and 2. Isotropic tumbling and pure dipole–dipole relaxation are assumed. μ_0 = dielectric constant, γ = gyromagnetic constant, r = distance between atoms 1 and 2, ω = Larmor frequency.
[27] For these calculations the following values were substituted in the Stokes equation: T = 303 K; η_0 = 0.514 cP.
[28] a) T. L. James, G. B. Matson, I. D. Kuntz, *J. Am. Chem. Soc.* **1978**, *100*, 3590 – 3594. b) C. F. Morgan, T. Schleich, G. H. Caines, D. Michael, *Biopolymers* **1990**, *29*, 469 – 480.

Binuclear Lanthanide Complexes as Catalysts for the Hydrolysis of Bis(*p*-nitrophenyl)-phosphate and Double-Stranded DNA**

Kaliappa G. Ragunathan and Hans-Jörg Schneider*

The catalysis of phosphate ester hydrolysis is of particular interest from two diametric points of view. The formation and cleavage of these ester linkages in nucleic acids are among the most important molecular functions in living systems. At the same time, as chemical warfare agents phosphate esters are the most disastrous inventions of synthetic chemistry; however, it is often forgotten that as insecticides the related aryl phosphates have saved the lives of millions of people. The present communication addresses the hydrolysis of both kinds of esters catalyzed by binuclear metal complexes.

Recent work in particular by Breslow,[1] Komiyama,[2] Morrow,[3] Chin,[4] and their collaborators has shown that highly charged cations, in particular of lanthanides, can greatly accelerate phosphate hydrolysis.[5] Our own efforts are directed primarily towards the development of ligands that form sufficiently stable complexes and enhance the catalytic activity of these lanthanide complexes.[6] The presence of several metal ions, both in enzymes as well as in synthetic analogs, is known to enhance rates of hydrolysis substantially.[7] In very recent studies with carefully designed binuclear zinc complexes Chapman and Breslow[8] have demonstrated how the catalytic efficiency depends critically on the distance between the metal centers and the conformation of the spacer. However, the rate of hydrolysis[9] for UpU as a DNA model was enhanced only by a factor of 2, and for bis(*p*-nitrophenyl)phosphate (BNPP) the rate enhancement factor was around 12.[8] In other recent reports the application of binuclear complexes having peroxo ligands,[10] zinc complexes for the hydrolysis of dinucleotides,[11] and intramolecular metal complexes[12] for the hydrolysis of phosphonates have been described. With binuclear complexes based on imidazoles, Trogler et al.[13] found a ligand rate factor[9] of only 2 for BNPP hydrolysis; in studies with double-stranded DNA binding but no cleavage was observed. We describe here binuclear lanthanide systems that lead to ligand rate factors[9] of up to 72 for the hydrolysis of BNPP and to dramatic enhancements for the cleavage of plasmid DNA.

Ligands **1**–**4** were synthesized according to literature procedures[14] and treated with two equivalents of Eu^{3+} or Pr^{3+} salts in anhydrous methanol. The complexes with nitrate ions were insoluble in methanol and precipitated immediately from the reaction mixture; the complexes with chloride ions were soluble in methanol and were precipitated by slow addition of acetonitrile. The washed precipitates were generally analytically pure. The elemental analyses and titrations of the complexes with EDTA (the complexes were dissolved in water at pH 2; the pH was then increased to 5.2) indicate that all of the solid complexes contain two metal ions. Unfortunately, the complexes with ligands **1** and **2**, containing the more lipophilic benzene rings, were water-soluble only as nitrate salts, which makes comparison to the more reactive chloride salts with **4** difficult. Nitrates are known to form particularly stable complexes with lanthanides.[15] This might be one explanation for the lower, yet still remarkable rate enhancements for BNPP hydrolysis obtained with Pr^{3+} complexes (Table 1, Scheme 1). The rate enhancement factor of 72 observed with Pr_2^{3+}·**4** indicates that the metal centers should have a certain separation; complexes with ligands **1**–**3** have a smaller distance between the metal binding sites and lead to only moderate rate enhancements at best. In line with the report of Chapman and Breslow[8] such a separation seems to be necessary for simultaneous electrostatic stabilization of the bound phosphate group at one end of the complex and activation of water at the other.[16]

The analysis of the reaction kinetics (van't Hoff method, second-order kinetics) indicates that the catalysis arises from the action of *two* metal ions in the transition state. A plot (Fig. 1) of lg v versus lg [M] at constant ligand concentration, where v is the initial rate (measured at $<10\%$ conversion) and [M] is the metal

Table 1. Summary of the results of phosphate ester and DNA hydrolysis catalyzed by lanthanide complexes.

Macrocycle	F for BNPP [a]		DNA cleavage [% RF II] [b]	
1	$Eu(NO_3)_3$	$Pr(NO_3)_3$	$Eu(NO_3)_3$	$Pr(NO_3)_3$
	1.5	4.5	17	5
2	$Eu(NO_3)_3$	$Pr(NO_3)_3$	$Eu(NO_3)_3$	$Pr(NO_3)_3$
	3	14.6	23	7
3	$Eu(NO_3)_3$	$Pr(NO_3)_3$		
	1.5	6		
4	$EuCl_3$	$PrCl_3$	$EuCl_3$	$PrCl_3$
	14	72	77	80
– [c]	$EuCl_3$	$PrCl_3$	$EuCl_3$	$PrCl_3$
	1 [d]	1 [d]	46	42

[a] Efficiency of binuclear complexes for the hydrolysis of BNPP is given as $F = k_{M_2L}/k_M$ from rates at 1 mM [M_2L] and 2 mM [M]; [BNPP] = 3.35×10^{-5} M; $T = 50$ °C; *N*-(2-hydroxyethyl)piperazine-*N'*-propane sulfonic acid (EPPS) buffer (0.01 M), pH 7.0. The hydrolysis was followed by UV-Vis spectroscopy by measuring the increase in absorbance at 400 nm due to the release of *p*-nitrophenol during hydrolysis. [b] Cleavage of double-stranded DNA is given as the percent of the open circular form RF II after correction for the amount of this form in the starting sample of DNA; incubation for 2 h at 37 °C with plasmid DNA (pBR322; concentration 1.95×10^{-5} per base pair), [M_2L] = 1×10^{-3} M or [M] = 2×10^{-3} M; EPPS buffer (0.01 M), pH 7.0. The solutions of the metal complexes were prepared by dissolving the freshly prepared complexes in dimethyl sulfoxide (5% DMSO in the final solution), adding buffer, and adjusting the pH. The macrocyclic polyamines inhibit the migration of DNA in the gel electrophoresis; this was overcome by using ion exchange resins as previously reported [6b]. Densitometry after electrophoresis showed, in double determinations, average deviations of $\pm 2.5\%$. [c] Without ligands. [d] Relative rate = 1; absolute rate k with $EuCl_3$ is 6.0×10^{-3}, with $PrCl_3$ 7×10^{-4} min^{-1}.

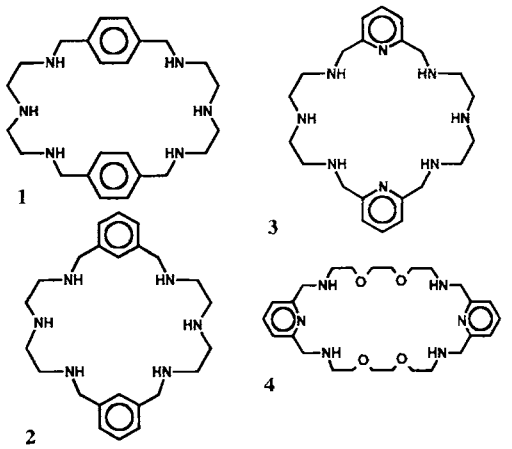

Scheme 1. Structures of ligands **1**–**4**.

[*] Prof. Dr. H.-J. Schneider, Dr. K. G. Ragunathan
FB Organische Chemie der Universität des Saarlandes
D-66041 Saarbrücken (Germany)
Fax: Int. code +(681)302 4105
e-mail: CH12hsvr@SBUSOL. RZ. UNI-SB. DE

[**] Supramolecular Chemistry, Part 58. This work was supported by the Deutsche Forschungsgemeinschaft and the Fonds der Chemischen Industrie. K. R. thanks the Alexander von Humboldt Foundation for a fellowship. Part 57: H.-J. Schneider, F. Eblingen, J. Sartorius, J. Rammo, *J. Mol. Recogn.*, in press.

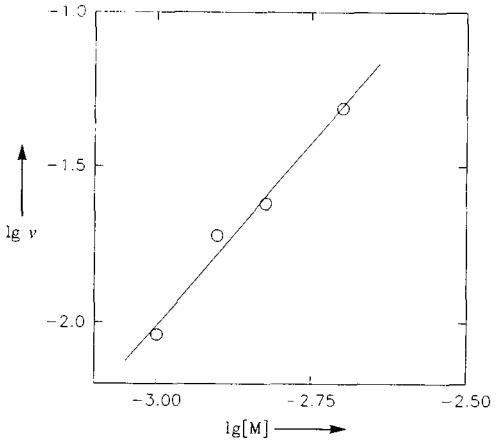

Fig. 1. Plot of lg v (from initial rate v of BNPP hydrolysis at $<10\%$ conversion, [BNPP] $=7\times10^{-5}$ M) versus lg[M], where [M] = [Pr^{3+}] at constant concentration of ligand **4** (1 mM). The concentration of the metal was varied between 1 and 2 mM. Observed slope $=2.3\pm0.2$. For details on the preparation of the metal complexes see text, footnotes in Table 1, and ref. [17].

concentration (between 1 and 2 mM), gives a line with a slope of 2 within experimental error. This treatment neglects the (small) contributions of free metal ions and mononuclear complexes. The van't Hoff plot (Fig. 1) proves that *two* metal ions are involved in the rate-determining step. Spectroscopic or other methods that indicate a 2:1 complex in the solid state or in solution are not conclusive, as the catalytically active complex could be thermodynamically less favorable. Alternative explanations for the observed van't Hoff slope of 2 could be the participation either of two free cations or—even more unlikely—of a single ion complex ML and a free M cation. The first alternative is excluded by the clean first-order reaction observed with uncomplexed lanthanide ions[6a] and by the 72-times slower reaction with the metal cation alone. The second alternative is excluded by the fact that the reaction catalyzed by a 1:1 complex in the presence of an equimolar amount of free Ln^{3+} ions is five times slower than that catalyzed by the 2:1 complex. The 1:1 complex was prepared from equimolar amounts of Ln^{3+} and the ligand in water instead of methanol. The complexes with varying metal content were prepared by mixing L and M in methanol (dried over magnesium methanolate), which was then was removed at 40 °C, and then dissolving the residue in water. The slow rates of complex formation require special conditions in all cases.[17] When EDTA is added (1 mM in the final solution) the reaction rate decreases by about 70% within minutes; with 2 mM EDTA no reaction is observed. This indicates that the complexes are not stable to exchange with EDTA, in line with similar findings by Morrow et al.[18]

Surprisingly, the activity of the complexes of **1**–**4** with plasmid DNA follows the same sequence as that with BNPP, although the nitrophenolate leaving group could lead to a change of mechanism.[19] After the reaction of plasmid DNA with $Pr_2^{3+}\cdot$**4**, electrophoresis and densitometry indicates that single cleavage of form RF I yields 80% of the open circular form RF II (after correction for the RF II form present in the starting material). Visual inspection of the gels shows only form RF II as the cleavage product (Fig. 2). This is to our knowledge the highest proportion of hydrolytic cleavage yet reported for plasmid DNA. In contrast to radical cleavage processes no further cleavage products such as the linear form RF III are apparent in the agarose gels (Fig. 2).[20] That the cleavage occurs by hydrolysis like that with enzymes is furthermore in line with the recent observations of Chin et al.[10] and Komiyama et al.[2b] Even

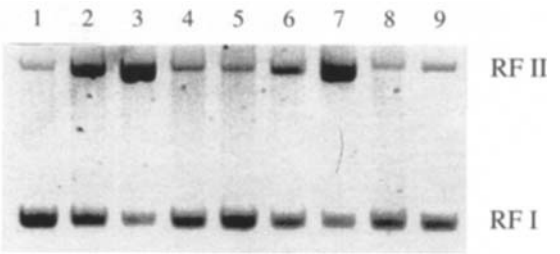

Fig. 2. Electrophoresis gel demonstrating cleavage of double-stranded DNA after 2 h. For conditions see the footnote [b] in Table 1. Lane 1: DNA alone; lane 2: DNA and Eu^{3+}; lane 3: DNA and $Eu_2^{3+}\cdot$**4**; lane 4: DNA and $Eu_2^{3+}\cdot$**2**; lane 5: DNA and $Eu_2^{3+}\cdot$**1**; lane 6: DNA and Pr^{3+}; lane 7: DNA and $Pr_2^{3+}\cdot$**4**; lane 8: DNA and $Pr_2^{3+}\cdot$**2**; and lane 9: DNA and $Pr_2^{3+}\cdot$**1**.

redox-active Ce^{4+} ions act as hydrolytic catalysts. The fact that the rate of DNA cleavage is not accelerated when hydrogen peroxide is added[6b] also speaks against oxidative radical-based mechanisms.

We have shown[6b] that the cleavage of plasmid DNA by lanthanide ions after electrophoretic separation and densitometry is characterized by clean pseudo-first-order rate constants, which then may be used to derive Michaelis–Menten-*type* equilibrium and rate constants K_M and k_{cat}, respectively, from saturation kinetics. We applied the same procedures to study the cleavage of double-stranded DNA with the binuclear complexes prepared from ligand **4**. The observed rates with $Eu_2^{3+}\cdot$**4** and $Pr_2^{3+}\cdot$**4** showed the expected increase with catalyst concentration, but was limited by solubility problems at higher concentrations. The corresponding saturation curve for $Pr_2^{3+}\cdot$**4** (Fig. 3)

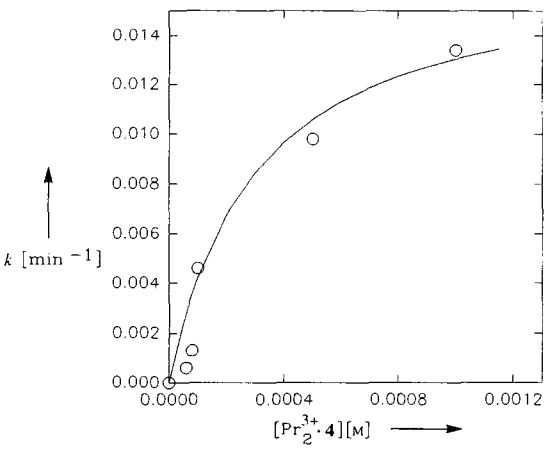

Fig. 3. Saturation kinetics of the cleavage of plasmid DNA by $Pr_2^{3+}\cdot$**4**. The theoretical curve corresponds to $K_M=3.3\times10^{-4}$ M and $k_{cat}=1.7\times10^{-2}$ min^{-1}.

with K_M around 3×10^{-4} M and k_{cat} around 1.5×10^{-2} min^{-1} agree with values found with other lanthanide systems.[6b] The rate constant with $Pr_2^{3+}\cdot$**4** at 37 °C is approximately 2×10^6 times greater than that of the uncatalyzed hydrolysis of double-stranded DNA at 25° and pH 7.0, which was previously determined only very approximately.[21]

In conclusion, binuclear lanthanide complexes can accelerate the cleavage of double-stranded DNA by almost two orders of magnitude over that with metal ions alone. The structure of the ligands, in particular the distance between the metal centers, plays an important role. Unexpectedly, the trends observed with the different ligands are similar for hydrolysis of both activated nitrophenyl phosphates and plasmid DNA. The half-life of

 © VCH Verlagsgesellschaft mbH, D-69451 Weinheim, 1996 0570-0833/96/3511-1220 $ 15.00+.25/0

BNPP is reduced from approximately 75 years[22] to as little as 8 min (with $Eu_2^{3+}\cdot$**4** at 50 °C and pH 7.0); that of double-stranded DNA from approximately 2000 years[21] to 50 min (with $Pr_2^{3+}\cdot$**4** at 37 °C and pH 7.0).

Received: September 25, 1995
Revised version: December 29, 1995 [Z 8424 IE]
German version: *Angew. Chem.* **1996**, *108*, 1314–1316

Keywords: DNA cleavage · hydrolyses · phosphorus compounds supramolecular chemistry · lanthanide compounds

[1] R. Breslow, D.-L. Huang, *Proc. Natl. Acad. Sci. USA* **1991**, *88*, 4080.
[2] a) M. Komiyama, K. Matsamura, Y. Matsumoto, *J. Chem. Soc. Chem. Commun.* **1992**, 640; b) M. Komiyama, N. Takeda, Y. Takahashi, H. Uchida, T. Shiiba, T. Kodama, M. Yashiro, *J. Chem. Soc. Perkin Trans. 2* **1995**, 269, and references therein.
[3] J. L. Morrow, L. A. Buttrey, V. M. Shelton, K. A. Berback, *J. Am. Chem. Soc.* **1992**, *114*, 1903.
[4] D. Wahnon, R. C. Hynes, J. Chin, *J. Chem. Soc. Chem. Commun.* **1994**, 1441.
[5] Lanthanides were used to catalyze the hydrolysis of phosphate esters decades ago without recognition of their full potential. For a review see E. Bamann, H. Trapman, *Adv. Enzymol. Relat. Subj. Biochem.* **1959**, *21*, 169.
[6] a) H.-J. Schneider, J. Rammo, R. Hettich, *Angew. Chem.* **1993**, *105*, 1773; *Angew. Chem. Int. Ed. Engl.* **1993**, *32*, 1716; b) J. Rammo, R. Hettich, A. Roigk, H.-J. Schneider, *J. Chem. Soc. Chem. Commun.* **1996**, 105–107.
[7] For a review on the use of binuclear metal complexes as catalysts for different hydrolysis reactions see: M. W. Göbel, *Angew. Chem.* **1994**, *106*, 1201; *Angew. Chem. Int. Ed. Engl.* **1994**, *33*, 1141.
[8] W. H. Chapman, Jr., R. Breslow, *J. Am. Chem. Soc.* **1995**, *117*, 5851.
[9] As the factor F characterizing the efficiency of a ligand we use the ratio k_{M_2L}/k_M for the reaction with the complex $[M_2L]$ and with the corresponding metal M alone at the same concentration as with the ligand L.
[10] B. K. Takasaki, J. Chin, *J. Am. Chem. Soc.* **1995**, *117*, 8582.
[11] M. Yashiro, A. Ishikubo, M. Komiyama, *J. Chem. Soc. Chem. Commun.* **1995**, 1793.
[12] A. Tsubouchi, T. C. Bruice, *J. Am. Chem. Soc.* **1995**, *117*, 7399.
[13] E. A. Kesicki, M. A. DeRosch, L. H. Freeman, C. L. Walton, D. F. Harvey, W. C. Trogler, *Inorg. Chem.* **1993**, *32*, 5851.
[14] a) D. Chen, A. E. Martell, *Tetrahedron* **1991**, *47*, 6895 for **1** and **3**; b) R. Menif, A. E. Martell, P. J. Squattrito, A. Clearfield, *Inorg. Chem.* **1990**, *29*, 4723 for **2**; c) R. Menif, D. Chen, A. E. Martell, *ibid.* **1989**, *26*, 4633 for **4**.
[15] R. B. King, R. Heckley, *J. Am. Chem. Soc.* **1974**, *96*, 3118.
[16] J. Chin, *Acc. Chem. Res.* **1991**, *24*, 145.
[17] The rate constant observed for the 1:1 complex of ligand **4** and Pr^{3+} prepared in buffer solution by equilibriating 1 mM **4** and 1 mM Pr^{3+} for 8 h at 25 °C and 30 min at 50 °C was only 4.1×10^{-3} min^{-1}, and that for the complex prepared in methanol (dried over $Mg(OMe)_2$) by mixing the ligand and the metal in 1:1 ratio and warming the solution to 40 °C to remove methanol was 9.1×10^{-3} min^{-1}. The van't Hoff plot for the hydrolysis of BNPP by the complexes of ligand **4** and various amounts of Pr^{3+}, prepared directly in the buffer solution, gave a slope of only 1.2. When the ligand **4** and Pr^{3+} in the ratio 2:1 were warmed in anhydrous methanol, catalysis with the resulting complex was even slower than with free Pr^{3+} alone. This could be due to formation of the 2:1 sandwich complex, in which the metal is shielded against reaction with the ester and/or water.
[18] J. R. Morrow, L. A. Buttrey, V. M. Shelton, K. A. Berback, *J. Am. Chem. Soc.* **1992**, *114*, 1903.
[19] A. J. Kirby, M. Younas, *J. Chem. Soc. B* **1970**, 510.
[20] J.-L. Sagripanti, K. H. Kraemer, *J. Mol. Biol.* **1989**, *264*, 1729.
[21] J. Eigner, H. Boedtker, G. Michaels, *Biochim. Biophys. Acta.* **1961**, *51*, 165.
[22] J. Chin, M. Banaszczyk, V. Jubian, X. Zou, *J. Am. Chem. Soc.* **1989**, *111*, 186.

Efficient Synthesis of New 2-Cycloalk(en)ylpropanoic Acid Derivatives—Medium and Large Rings as Bioisosteres of Alkylphenyl Moieties?**

Björn Greve, Peter Imming,* and Stefan Laufer

Dedicated to Professor Gunther Seitz on the occasion of his 60th birthday

Ring systems with 9–12 (or 7–14) members are classed as medium-sized rings. They occur less frequently and are more difficult to prepare than five- and six-membered and large rings, and their applicability is restricted.[1] In an evaluation of two standard encyclopedias of chemistry and pharmacy[2] we found only 132 compounds with an eight-, 23 with a nine-, 26 with a ten-, 12 with an eleven-, 28 with a twelve-, and 6 with a thirteen-membered ring. Of these, 81% are natural products and 73% are heterocycles. In medicinal chemistry particular 9–12-membered lactams are of current interest as mimics of β-turns.[3] In this paper we introduce a new approach to the use of medium and large ring systems.

Medium-sized carbocycles can be seen as lipophilic "clusters" and should be bioisosteric to alkylphenyl moieties. In comparison to these they will bind more weakly to electrophilic protein side chains, but because of their conformative flexibility they should display better adaptation to binding domains of proteins.[4] Medium-sized carbocycles also provide a far more versatile framework than phenyl and "normal" rings (five- and six-membered rings) for the regio- and stereodefined attachment of substituents.

To test our concept we prepared compounds that are structurally derived from both arachidonic acid (**1**) (the physiological substrate of cyclo- (COX) and lipoxygenases (LOX)) and inhibitors of these enzymes[5] like 2-(alkylphenyl)propanoic acids (for example ibuprofen (**2**)). In the active site of the enzyme[6] and in solution[7] arachidonic acid adopts a bent conformation as shown. A substrate with a medium-sized ring should at least partly mimic the conformation of **1**.

We have developed a synthetic route to 2-cycloalk(en)ylpropanoic acids of the general formula **3** (MR = medio-/macro-

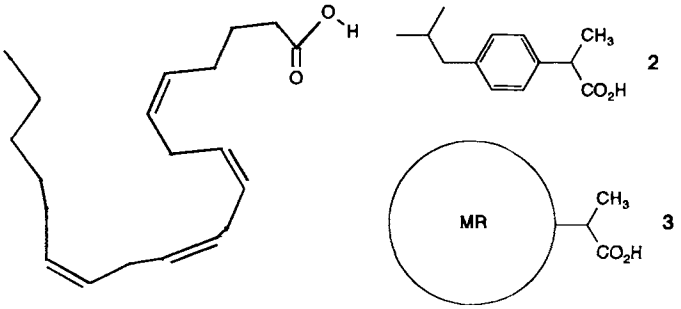

1

[*] Priv.-Doz. Dr. P. Imming, Dipl.-Chem. B. Greve
Institut für Pharmazeutische Chemie der Universität
D-35032 Marburg (Germany)
Fax: Int. code +(6421) 287052
e-mail: imming@pharmazie.uni-marburg.de
Dr. S. Laufer
Merckle GmbH
Postfach 1161, D-89135 Blaubeuren (Germany)

[**] This work was supported by the Fonds der Chemischen Industrie and the Bundesministerium für Forschung und Technologie. We thank Hüls AG (Marl) and Firmenich S. A. (Genf) for financial and material support.

cycle), which leads to the desired compounds in excellent overall yield (Scheme 1). In the first step we treated cycloalkanones **4** with a modified Reformatsky reagent prepared from **5**. (This new type of reagent was developed several years ago.[8])

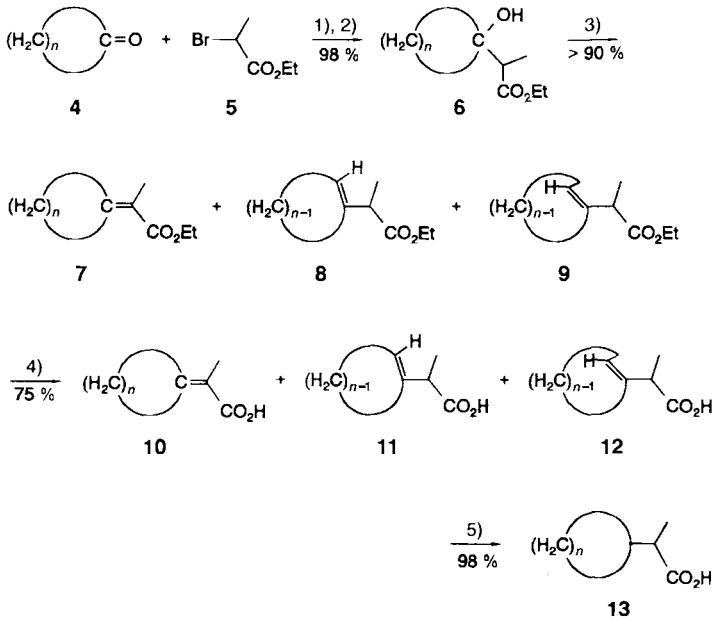

Scheme 1. Synthetic route to 2-cycloalk(en)ylpropanoic acid derivatives with $n = 4-12, 14$. 1) Zn, THF; CuCN, LiCl; 0/ − 50/0 °C. 2) THF; −78 °C to room temperature, 12 h. 3) *p*-TsOH, toluene; reflux; 48 h. 4) KOH/MeOH; room temperature; 24 h. 5) H_2 (3 bar), 10% Pd/C; 55 °C; 6 h.

Organozinc compounds, which had not been treated with medium-sized and larger cycloalkanones previously, were found to have excellent reactivity towards these ketones. Analogous reactions with other organometallic reagents, including organocerium compounds (where one has to use the more expensive alkyl iodides)[9] were not as satisfactory.

The subsequent water elimination proceeded almost regioselectively in the case of the medium-sized rings, yielding the endocyclic, nonconjugated olefins **8**. The introduction of two sp^2 centers in the ring is energetically more favorable than conjugation with the ester group. Through this, our study proves the applicability of H. C. Brown's I-strain (internal strain) concept,[10] which had been supported theoretically by a force-field analysis.[10b] After hydrolysis we isolated the pure (*E*) esters **11**, and after the final hydrogenation the carboxylic acids **13**.

Pharmacological tests[11] showed interesting differences in activities depending on ring size. Table 1 summarizes the test results. We did not measure significant activities up to a ring size of ten. The derivatives of cycloundecane, cyclododecene, and cyclopentadecene (**13a**, **11b**, and **11c**, respectively) inhibit COX-1 with about twice the activity of aspirin. In contrast to the cyclododecene derivative **11b**, the cycloundecene and cyclododecatriene derivatives, **11a** and **15**, respectively, inhibit 5-LOX more effectively than COX-1. (In the synthesis of **15** from **14**[12] we obtained

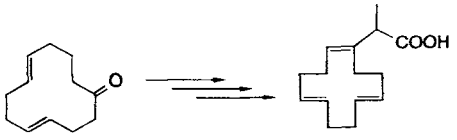

14 **15**

Table 1. Pharmacological activities of some compounds with medium-sized rings in comparison to known drugs [a].

		5-LOX	COX-1	COX-2
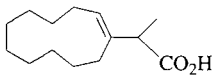	**11a**	2.9	35% inhibition at 10 μM	
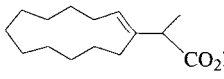	**11b**	<10% at 10 μM	3.15	
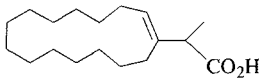	**11c**	3.1	3.2	29
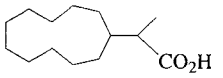	**13a**	4.0	3.2	
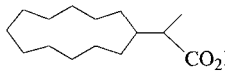	**13b**	<10% at 10 μM	not determined	
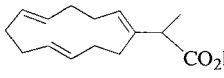	**15**	1.9	40	
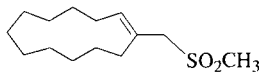	**16**	45% inhibition at 10 μM	<10% at 10 μM	
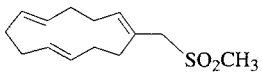	**17**	48% inhibition at 10 μM	<10% at 10 μM	
acetylsalicylic acid			6	
ketoprofen			0.01	
nordihydroguaiaric acid		0.6		
indomethacin				200

[a] In vitro tests. IC_{50} in μM.

the (*E*,*E*,*E*) isomer with 100% *de*.) The almost equal inhibition of both enzymes by the saturated 11-membered and olefinic 15-membered rings **13a** and **11c** makes them promising candidates for the development of "dual action" antirheumatics, a very recent research strategy for the reduction of the gastrointestinal side effects of these drugs.[13] According to present knowledge, a further simultaneous inhibition of COX-2 would be advantageous though not sufficient for the suppression of the symptoms.[14] We thus regard our cyclopentadecene derivative **11c** to be a promising lead for the development of a mimic of arachidonic acid with a (medium) large ring that will have the desired activity profile.

We also prepared the derivatives **16** and **17**, which have a methylsulfonyl instead of a carboxyl function, in a similar fashion. The starting materials were dimethyl sulfone and cyclododeca(die)none. The methylsulfonyl group typical of COX-2 inhibitors[14a] led in our case to a strong decrease in activity towards 5-LOX and COX-1.

In summary, our work has shown for the first time that a differentiated inhibition of enzymes is possible with medium rings of various sizes and degrees of saturation. We propose that unsaturated medium-sized and larger carbocycles are bioisos-

 © VCH Verlagsgesellschaft mbH, D-69451 Weinheim, 1996 0570-0833/96/3511-1222 $ 15.00+.25/0

teric to alkylphenyl moieties. This opens up extensive synthetic possibilities and offers a new approach to the rational application of medium-sized and larger carbocycles beyond medicinal chemistry.

Experimental Procedure

All new compounds gave correct analyses or high-resolutaion mass spectra.

6 ($n = 11$): To a suspension of 6.5 g (100 mmol) of zinc (activated with $SiMe_3Cl$ and dibromoethane) in 30 mL of anhydrous THF was added dropwise 9.1 g (50 mmol) of **5** at 0 °C. The ice bath was removed. After excess zinc had settled, the supernatant was transferred dropwise into a solution of CuCN·2 LiCl (50 mmol) in 100 mL of THF at −50 °C. The mixture was warmed to 0 °C, stirred for 30 min, and cooled to −78 °C. Then 8.2 g (45 mmol) of **4** ($n = 11$) was added. The mixture was allowed to warm to room temperature overnight and was worked up as described [8] to yield 12.6 g (98%) of a white solid, which was of sufficient purity for further transformations. ^{1}H NMR (400 MHz, $CDCl_3$): δ = 4.10–4.04 (m, 2H), 3.18 (s, 1H), 2.37–2.32 (m, 2H), 1.62–1.53 (m, 2H), 1.34–1.10 (m, 24H); $^{13}C\{^1H\}$ NMR (125 MHz, $CDCl_3$): δ = 178.3, 75.3, 61.0, 45.9, 35.0, 30.9, 27.0, 26.9, 26.6, 23.1, 23.0, 22.62, 22.56, 20.0, 19.6, 14.7, 12.3.

7/**8**/**9** ($n = 11$): A solution of **6** ($n = 11$) in toluene was heated to reflux with a catalytic amount of 4-toluenesulfonic acid for 48 h. After vacuum distillation (104–106 °C/1.8×10^{-2} Torr) we obtained the isomeric olefins in 93% yield. They were purified by chromatography on silica gel eluting with pentane/diethyl ether (8/2). **8**: ^{1}H NMR (400 MHz, $CDCl_3$): δ = 5.21 (t, J = 8 Hz, 1H), 4.08–3.96 (m, 2H), 2.98 (q, J = 7 Hz, 1H), 2.13–1.91 (m, 4H), 1.48–1.10 (m, 22H); $^{13}C\{^1H\}$ NMR (125 MHz, $CDCl_3$): δ = 175.1, 138.0, 127.3, 59.9, 43.8, 26.8, 26.3, 25.1, 24.7, 24.6, 24.5, 24.2, 23.8, 22.5, 22.1, 16.6, 13.9.

11b ($n = 11$): We obtained the compound in 74% yield after vacuum distillation (100 °C/1.8×10^{-2} Torr), by stirring 18 mmol of **8** in 18 mL of methanol with 30 mL of a 3 M methanolic KOH solution for 24 h; m.p. 69–70 °C (pentane). ^{1}H NMR (400 MHz, $CDCl_3$): δ = 11.58 (s, 1H), 5.30 (t, J = 8 Hz, 1H), 3.04 (q, J = 7 Hz, 1H), 2.12–1.91 (m, 5H), 1.50–1.12 (m, 18H); $^{13}C\{^1H\}$ NMR (125 MHz, $CDCl_3$): δ = 181.8, 137.8, 128.1, 43.9, 27.0, 26.7, 25.4, 24.93, 24.88, 24.87, 24.5, 24.1, 22.7, 16.7.

13b ($n = 11$): A 1 M solution of **11b** in ethyl acetate was hydrogenated for 6 h at 3 bar and 55 °C with 10% Pd/C catalyst. We isolated a 94% yield of a white solid, m.p. 46–48 °C. ^{1}H NMR (400 MHz, $CDCl_3$): δ = 11.04 (s, 1H), 2.45–2.28 (m, 1H), 1.79–1.77 (m, 1H), 1.39–1.18 (m, 22H), 1.03 (d, J = 7 Hz, 3H); $^{13}C\{^1H\}$ NMR (125 MHz, $CDCl_3$): δ = 183.4, 42.3, 36.6, 27.1, 25.8, 24.5, 23.9, 23.7, 23.6, 23.2, 23.1, 22.3, 21.3, 13.4.

Received: September 7, 1995
Revised version: March 1, 1996 [Z8374IE]
German version: *Angew. Chem.* **1996**, *108*, 1312–1314

Keywords: cycloalkanones · cyclooxygenase inhibitors · medium-sized rings · zinc compounds

[1] See for example M. Braun, *Nachr. Chem. Tech. Lab.* **1985**, *33*, 1066; B. Dietrich, P. Viout, J.-M. Lehn, *Macrocyclic Compounds Chemistry*, VCH, Weinheim, **1993**; E. L. Eliel, S. H. Wilen, *Stereochemistry of Organic Compounds*, Wiley, New York, **1994**, p. 762ff.

[2] a) S. Budavari, *The Merck Index*, Merck & Co., Rahway, NJ, USA, **1989**; b) J. Falbe, M. Regitz, *Römpp Chemie Lexikon*, Thieme, Stuttgart, **1989–1992**.

[3] See for example a) G. Hölzemann, *Kontakte (Merck)* **1991** (1), 3–12; *ibid.* **1991** (2), 55–63; b) A. Giannis, T. Kolter, *Angew. Chem.* **1993**, *105*, 1303; *Angew. Chem. Int. Ed. Engl.* **1993**, *32*, 1244; c) J. Gante, *ibid.* **1994**, *106*, 1780 and **1994**, *33*, 1699.

[4] a) *Tetrahedron* **1993**, *49*, 3433ff. (Symposia-in-print No. 50); b) G. J. Moore, *Trends Pharmacol. Sci.* **1994**, *15*, 124.

[5] For COX and LOX inhibitors see J. Vane, *Nature* **1994**, *367*, 215.

[6] D. Picot, P. J. Loll, R. M. Garavito, *Nature* **1994**, *367*, 243.

[7] a) P. Gund, T. Y. Shen, *J. Med. Chem.* **1977**, *20*, 1146; b) S. R. Wilson, W. Cui, J. W. Moskowitz, K. E. Schmidt, *Tetrahedron Lett.* **1988**, *29*, 4373; c) A. R. Leach, K. Prout, *J. Comput. Chem.* **1990**, *11*, 1193.

[8] P. Knochel, R. D. Singer, *Chem. Rev.* **1993**, *93*, 2117, and references therein.

[9] Ce: T. Imamoto, K. Kusumoto, Y. Tawarayama, Y. Sugiura, T. Mita, Y. Hatanaka, M. Yokoyama, *J. Org. Chem.* **1984**, *49*, 3904; Li/Mg (including a discussion of contradictory reports): L. I. Zakharkin, I. M. Churilova, P. V. Petrovskii, *Russ.* Chem. Bull. **1993**, *42*, 863; see also P. Ballester, A. Costa, A. Garcia-Raso, R. Mestres, *J. Chem. Soc. Perkin Trans. 1* **1989**, 21.

[10] a) H. C. Brown, M. Gerstein, *J. Am. Chem. Soc.* **1950**, *72*, 2926; b) H.-J. Schneider, G. Schmidt, F. Thomas, *ibid.* **1980**, *105*, 3556; c) E. L. Eliel, S. H. Wilen, *Stereochemistry of Organic Compounds*, Wiley, New York, **1994**, p. 769ff.

[11] COX-1 tests were performed with thrombocytes from fresh human blood, 5-LOX tests with polymorphnuclear leukocytes from fresh human blood (K. Stolingwa, S. Baur, Diploma Theses, Fachhochschule Isny, **1995**), COX-2 tests with isolated recombinant enzyme (J. A. Mitchell, P. Akarasereenont, C. Thiemermann, R. J. Flower, J. R. Vane, *Proc. Natl. Acad. Sci. USA* **1993**, *90*, 11693).

[12] G. Wilke (Studiengesellschaft Kohle mbH), DBP 1058987, **1959** [*Chem. Abstr.* **1961**, *55*, 11435]; G. Wilke, P. W. Borner (Studiengesellschaft Kohle mbH), DBP 1075601, **1960** [*Chem. Abstr.* **1961**, *55*, 13340].

[13] S. Laufer, J. Augustin, G. Dannhardt, W. Kiefer, *J. Med. Chem.* **1994**, *37*, 1894, and references therein.

[14] a) D. J. Pinto, W. J. Pitts, R. A. Copeland, M. B. Covington, J. Trzaskos, R. Magolda, *Med. Chem. Res.* **1995**, *5*, 394, and references therein; b) J. L. Masferrer, B. S. Zweifel, P. T. Manning, S. D. Hauser, K. M. Leahy, W. G. Smith, P. C. Isakson, K. Seibert, *Proc. Natl. Acad. Sci. USA* **1994**, *91*, 3228, and references therein.

A Zirconium Bis(porphyrinate) Sandwich Complex with an Appended Quinone**

Gregory S. Girolami,* Christopher L. Hein, and Kenneth S. Suslick*

The development of our understanding of the chemical and physical properties of the photosynthetic reaction center (RC) has been greatly assisted by studies of synthetic analogs. For example, remarkably long-lived charge-separated states have been observed in synthetic porphyrin–quinone tetrads and pentads, and the physiological significance of chromophore orientation and donor–acceptor energetics in reaction centers has been addressed through studies of gable porphyrin dimers and porphyrin–quinone complexes, respectively.[1] The distinctive structural feature of the RC, however, is the closely stacked "special pair" of bacteriochlorophylls that act as the primary photoelectron donor; unfortunately, no model compounds to date feature such a closely spaced cofacial porphyrin dimer as the primary electron donor. Stacked porphyrin macrocycles constrained by rigid organic tethers do not closely resemble the special pair because their mean porphyrin–porphyrin separation is relatively large, typically 5 Å.[1, 2] Much better building blocks for synthetic analogues of the RC are bis(porphyrin) metal sandwich complexes in which the porphyrin–porphyrin separations are about 3 Å.[3] We now describe the first compounds that combine two key structural features present in the reaction center of photosynthetic organisms: a donor consisting of a cofacial arrangement of two porphyrinic macrocycles held about 3 Å apart, and a quinone electron acceptor.

We have previously developed a method to convert the sandwich complex $[Zr(TTP)_2]$ **1** (TTP = 5,10,15,20-tetra(*p*-tolyl)-porphyrinato dianion) to the amine-substituted bis(porphyrin) zirconium species $[Zr(TTP)(TTP\text{-}NH_2)]$ **2**, in which the amine group is attached to a β-pyrrole site on one of the porphyrin rings.[4, 5] In such bis(porphyrin) zirconium species, the two porphyrin rings are cofacial with an N_4 mean plane separation of

[*] Prof. Dr. G. S. Girolami, Prof. Dr. K. S. Suslick, C. L. Hein
School of Chemical Sciences
The University of Illinois at Urbana-Champaign
Urbana, IL 61801 (USA)
Fax: Int. code +(217)333-2685
e-mail: girolami@aries.scs.uiuc.edu
ksuslick@uiuc.edu

[**] This work was supported by the U. S. National Institutes of Health (PHS 5R01-HL25934). We thank Dr. Alex I. Smirnov, Illinois, for the EPR spectrum.

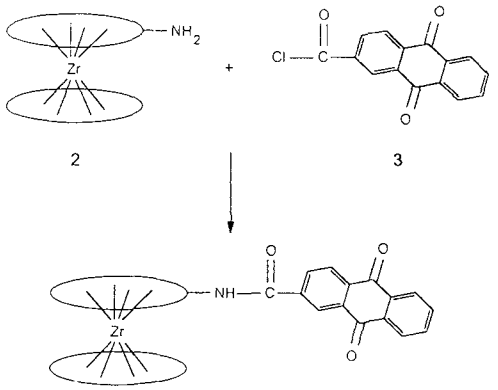

Scheme 1.

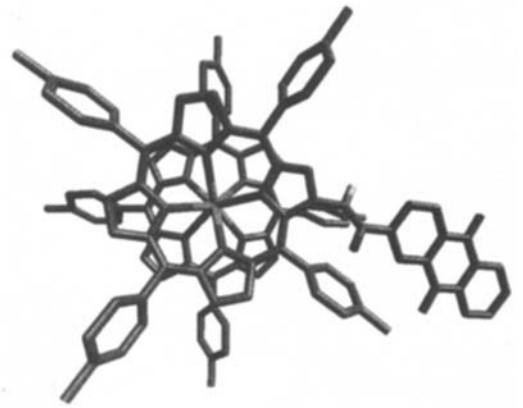

Fig. 1. Schematic representation of **4** (minimum energy configuration) illustrating the proximity of the anthraquinone substituent to two of the *p*-tolyl groups. The structure was calculated by using the programs Quanta and Charm.

2.56 Å; the mean plane separation for all 24 atoms of the porphyrin is 3.28 Å. These strongly interacting porphyrin subunits closely resemble the "special-pair" of chlorophylls in the photosynthetic reaction center, both in their cofacial architecture and spacing and in their electronic properties.[3] Condensation of **2** with 2-(chlorocarbonyl)anthraquinone (**3**) (Scheme 1) in excess pyridine yields the quinone-derivatized bis(porphyrin) complex [Zr(TTP)(TTP-NHCOAQ)] **4** (Fig. 1).[6]

The UV/Vis spectrum of **4** contains a Soret band at 400 nm and several Q bands at 511, 557, and 696 nm; these values are essentially unchanged from those obtained for the parent complex **1** (Fig. 2). Holten et al.[7] have assigned the Q″ band at 511 nm to a charge-resonance state having a wavefunction described as $(A^+B^- + A^-B^+)/\sqrt{2}$, where A and B represent the two porphyrin rings. The absorption at 557 nm is ascribed to a "normal" metalloporphyrin Q band. The lowest energy absorption at 696 nm, called Q′, involves a π-π^* transition that is characteristic of all porphyrin dimers in which the macrocycles are separated by about 3 Å.[7] The anthraquinone unit absorbs strongly at 258 nm, and the features seen are again only slightly altered relative to those of 2-(phenylamidocarbonyl)-anthraquinone (**5**).

The cyclic voltammogram of the quinone-derivatized porphyrin complex **4** contains two oxidation and four reduction waves. The first two reduction waves involve the anthraquinone unit, while the third and fourth involve the bis(porphyrin) π-electron system, as judged from comparisons with the redox potentials of related species (Table 1). The oxidation potential of the porphyrin π-electron system in **4** is approximately 100 mV

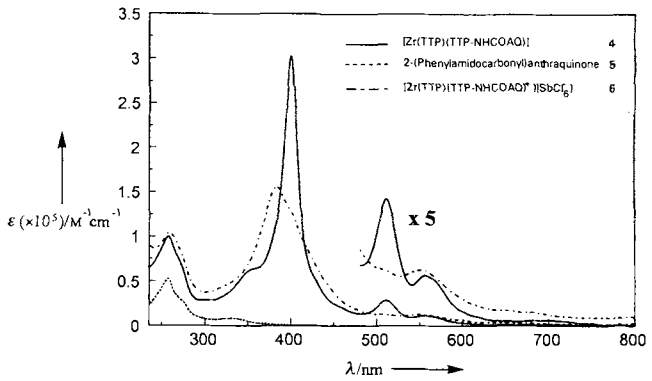

Fig. 2. UV/Vis spectra of complexes **4** and **6** and of quinone **5** in CH_2Cl_2.

Table 1. Electrochemical potentials of the zirconium bis(porphyrinate) sandwich complexes and of the quinone **5** [a].

Porphyrin compound	Porphyrin $Oxid_2$	Porphyrin $Oxid_1$	Quinone $Redn_1$	Quinone $Redn_2$	Porphyrin $Redn_1$	Porphyrin $Redn_2$
1	940	515			−1322	−1674
2	836	432			−1357	−1710
4	947	523	−819	−1265	−1363	−1678
5			−782	−1285		

[a] All potentials measured [mV] in CH_2Cl_2 vs Ag/AgCl. [nBu$_4$NPF$_6$] = 0.1 M. Scan speed = 100 mVs^{-1}. [$FeCp_2$] oxidation occurs at 493 mV under these conditions.

higher than that of the amine-substituted sandwich complex **2**. Furthermore, the reduction potentials for the anthraquinone substituent in **4** are shifted cathodically by about 40 mV relative to those seen for quinone **5**. These changes in the redox potentials suggest that the quinone substituent is electron-withdrawing. The reduction potentials of the porphyrin π-electron system in **4** remain nearly unchanged.

Oxidized dimeric porphyrins exhibit characteristic near-IR absorptions due to electronic transitions between bonding and antibonding molecular orbitals.[8] Treatment of **4** with phenoxathiinylium hexachloroantimonate[9] yields the $SbCl_6^-$ salt **6**

[Zr(TTP)(TTP-NHCOAQ)][SbCl$_6$] **6**

of the double-decker quinone monocation. Both chemical and electrochemical oxidation takes place from the porphyrin HOMO. The near-IR absorption band for **6** occurs at 1096 nm compared to that for $[Zr(TPP)_2]^+$ at 1075 nm.[8] Such electronic transitions are of particular interest since a broad transition (1300 nm) is also found for the special pair of bacteriochlorophyll-b, $[(BChl)_2]^+$.[10] Oxidation of the bis(porphyrin) π-electron system increases the extent of π-π overlap between the two porphyrin rings; consequently, the Soret band of **6** is shifted to higher energy (Fig. 2).[11]

We have also prepared the pyromellitimide-substituted bis(porphyrin) sandwich complex **7** by treatment of **2** with hexylamine and pyromellitic dianhydride (Scheme 2).[12] The mass spectrum confirms the presence of an *N*-hexyl-pyromellitimide group bound to the bis(porphyrin)ziconium core (m/z 1725). The UV spectrum of **7** shows absorptions due to the pyromellitimide substituent at 310 and 320 nm. Porphyrin–pyromellitimide complexes are ideal systems with which to study light-induced charge separation processes because reduced pyromellitimide absorbs strongly at 715 nm, a wavelength at which the bis(porphyrin) subunit is optically transparent.[12]

Until now, models of the photosynthetic reaction center have all relied on monomeric porphyrins as the electron donor. The

 © VCH Verlagsgesellschaft mbH, D-69451 Weinheim, 1996 0570-0833/96/3511-1224 $ 15.00+.25/0

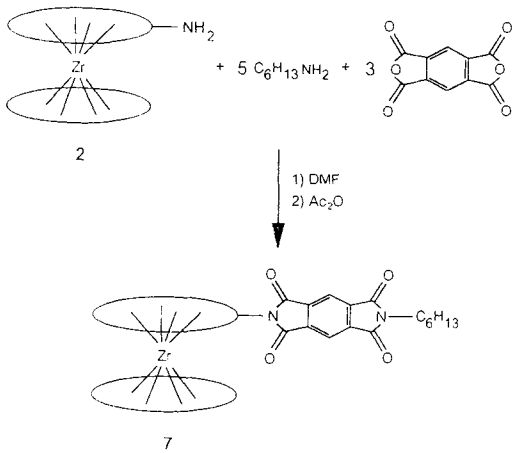

Scheme 2.

two new structural analogs of the reaction center presented here are the first in which an electron acceptor is attached to a porphyrin pair in which the porphyrin planes are held within 3 Å of each other. Comparisons of the electron transfer kinetics and the excited-state lifetimes of **4** and **7** with those of the reaction center are currently under investigation.[13, 14]

Experimental Procedure

4: A solution of **3** (64 mg, 0.24 mmol) in toluene was added dropwise to a suspension of **2** (140 mg, 0.097 mmol) in toluene and pyridine (2 mL), and the resulting mixture was stirred at room temperature for 2 d under Ar. The solvent was removed and the residue was extracted with CH_2Cl_2. The extract was purified by thin layer chromatography on silica plates with toluene as the eluting solvent ($R_f = 0.18$). Product **4** was then recrystallized by slow diffusion of hexane into a toluene solution at 25 °C. Yield : 104 mg (66%). Calcd. for [Zr(TTP)(TTP-NHCOAQ)]: C 79.4, H 4.75, N 7.51, Zr 5.44; found: C 79.2, H 4.66, N 7.59, Zr 5.31. IR (Nujol): $\tilde{\nu} = 1678\ cm^{-1}$ (C=O). UV Vis (CH_2Cl_2): λ_{max} (ε) = 258 (98000), 400 (295000), 511 (28000), 557 (11000), 696 nm (1300). ^1H NMR (CD_2Cl_2, 500 MHz, −80 °C): $\delta = 9.63-9.3$ (8 d, *o*-H), 9.30 (s, pyrr-H adjacent to AQ), 9.0 (br. s amido N-H), 8.74 (s, AQ H1), 8.49 - 8.45 (m, AQ H4-H8), 8.43--8.02 (14 d, pyrr-H), 8.01–7.62 (8 d, *m*-H), 7.88–7.82 (m, AQ H3), 7.09 -6.81 (8 d, *m'*-H), 6.34–5.88 (8 d, *o'*-H), 2.69–2.57 (8 s, *p*-CH_3). FAB MS (8 kV, 3-nitrobenzyl alcohol): *m/z* (%): 1676 (100) [M^+ + H].

6: Phenoxathiinylium hexachloroantimonate (34 mg, 0.064 mmol) was added to **4** (100 mg, 0.060 mmol) in CH_2Cl_2 (75 mL), and the resulting mixture was stirred for 1 h under Ar. The solution was concentrated to about 1 mL and crystals of the salt **6** were obtained by slow diffusion of toluene into the CH_2Cl_2 solution at −78 °C. Yield: 72 mg (60%). Calcd. for [Zr(TTP)(TTP-NHCOAQ)][$SbCl_6$]·0.5 CH_2Cl_2: C 65.2, H 3.92, N 6.13, Zr 4.44, Sb 5.92, Cl 12.1; found: C 64.6, H 4.01, N 6.08, Zr 4.35, Sb 6.01, Cl 11.8. IR (Nujol): $\tilde{\nu} = 1678$ (C=O), 1302 (cation marker band), 1292 cm^{-1} (cation marker band). UV/Vis NIR (CH_2Cl_2): λ_{max} (ε) = 259 (104000), 383 (156000), 554 (12000), 1096 nm (fwhm = 1300 cm^{-1}). EPR (95 K, 1:1 CH_2Cl_2:C-H_n): g = 2.0037, linewidth = 6.41 G. Electrospray ionization MS: 1675 [M^+], 2005, [$M$$SbCl_6^-$].

7: Pyromellitic dianhydride (11 mg, 0.05 mmol) was added to a mixture of **2** (15 mg, 0.01 mmol) and hexylamine (3 mg, 0.03 mmol) in *N,N*-dimethylformamide (DMF) (2 mL). The resulting mixture was heated to reflux for 12 h. The solvent was removed, acetic anhydride (2 mL) was added, and the mixture was allowed to reflux for 1 d. The solvent was removed and the resulting product **7** was purified by thin layer chromatography on silica plates ($R_f = 0.16$). Yield: 1 mg (6%). UV Vis (CH_2Cl_2): λ_{max} (ε) = 310 (117000), 319 (129000), 400 (295000), 511 (27000), 555 (13000), 689 nm (5000). FAB MS (8 kV, 3-nitrobenzyl alcohol): *m/z* (%): 1725 (30) [M^+ + H].

Received: September 7, 1995
Revised version: February 6, 1996 [Z83721E]
German version: *Angew. Chem.* **1996**, *108*, 1310–1312

Keywords: photosynthesis · porphyrinoids · quinones · sandwich complexes · zirconium compounds

[1] M. R. Wasielewski, *Chem. Rev.* **1992**, *92*, 435–461; D. Gust, T. A. Moore in *The Photosynthetic Reaction Center, Vol. 2* (Eds.: J. Deisenhofer, J. R. Norris), Academic Press, San Diego, **1993**, pp 419–464; J. L. Sessler, *Isr. J. Chem.* **1993**, *32*, 449–467; H. Kurreck, M. Huber, *Angew. Chem.* **1995**, *107*, 929–947; *Angew. Chem. Int. Ed. Engl.* **1995**, *34*, 849–866.

[2] H. A. Staab, M. Tercel, R. Fischer, C. Krieger, *Angew. Chem.* **1994**, *106*, 1531–1534; *Angew. Chem. Int. Ed. Engl.* **1994**, *33*, 1463–1466; H. A. Staab, T. Carell, *ibid.* **1994**, *106*, 1534–1536 and **1994**, *33*, 1466–1468.

[3] J. W. Buchler, A. De Cian, J. Fischer, M. Kihn-Botulinski, H. Paulus, R. Weiss, *J. Am. Chem. Soc.* **1986**, *108*, 3652–3659; G. S. Girolami, S. N. Milam, K. S. Suslick, *Inorg. Chem.* **1987**, *26*, 343–344; G. S. Girolami, S. N. Milam, K. S. Suslick, *J. Am. Chem. Soc.* **1988**, *110*, 2011–2012; K. Kim, W. S. Lee, H.-J. Kim, S.-H. Cho, G. S. Girolami, P. A. Gorlin, K. S. Suslick, *Inorg. Chem.* **1991**, *30*, 2652–2656; J. W. Buchler, A. De Cian, J. Fischer, P. Hammerschmitt, R. Weiss, *Chem. Ber.* **1991**, *124*, 1051–1058; J. W. Buchler, A. De Cian, F. Elschner, J. Fischer, P. Hammerschmitt, R. Weiss, *ibid.* **1992**, *125*, 107–115.

[4] G. S. Girolami, P. A. Gorlin, K. S. Suslick, *Inorg. Chem.* **1994**, 33, 626–627.

[5] TTP is represented schematically as an ellipse in Scheme 1 and 2.

[6] Compound **4** crystallizes in space group *Fddd*, with a = 34.898, b = 37.551, c = 30.537 Å. We thank Prof. Andrew Wang and Dr. Yi-Gui Gao for collecting the data set. The refinement is still in progress.

[7] X. Yan, D. Holten, *J. Phys. Chem.* **1988**, *92*, 409–414; O. Bilsel, J. Rodriguez, D. Holten, *ibid.* **1990**, *94*, 3508–3512; O. Bilsel, J. Rodriguez, D. Holten, G. S. Girolami, S. N. Milam, K. S. Suslick, *J. Am. Chem. Soc.* **1990**, *112*, 4075–4077; O. Bilsel, J. W. Buchler, P. Hammerschmitt, J. Rodriguez, D. Holten, *Phys. Chem. Lett.* **1991**, *182*, 415–421; O. Bilsel, J. Rodriguez, S. N. Milam, P. A. Gorlin, G. S. Girolami, K. S. Suslick, D. Holten, *J. Am. Chem. Soc.* **1992**, *114*, 6528–6538.

[8] R. J. Donohoe, J. K. Duchowski, D. F. Bocian, *J. Am. Chem. Soc.* **1988**, *110*, 6119–6124; J. K. Duchowski, D. F. Bocian, *Inorg. Chem.* **1990**, *29*, 4158–4160; J.-H. Perng, J. K. Duchowski, D. F. Bocian, *J. Phys. Chem.* **1990**, *94*, 6684–6691; P. C. Martin, J. Arnold, D. F. Bocian, *J. Phys. Chem.* **1993**, *97*, 1332–1338.

[9] P. Gans, J.-C. Marchon, C. A. Reed, J.-R. Regnard, *Nouv. J. Chim.* **1981**, *5*, 203–204; E. T. Shimomura, M. A. Phillippi, H. M. Goff, W. F. Scholz, C. A. Reed, *J. Am. Chem. Soc.* **1981**, *103*, 6778–6780.

[10] M. S. Davis, A. Forman, L. K. Hanson, J. P. Thornber, J. Fajer, *J. Phys. Chem.* **1979**, *83*, 3325–3332.

[11] G. S. Girolami, P. A. Gorlin, S. N. Milam, K. S. Suslick, *J. Coord. Chem.* **1994**, *32*, 173–212.

[12] T. Nagata, *Bull. Chem. Soc. Jpn.* **1991**, *64*, 3005–3016; A. Osuka, H. Yamada, K. Maruyama, N. Mataga, T. Asahi, M. Ohkouchi, T. Okada, I. Yamazaki, Y. Nishimura, *J. Am. Chem. Soc.* **1993**, *115*, 9439–9452; A. Osuka, S. Nakajima, K. Maruyama, N. Mataga, T. Asahi, I. Yamazaki, Y. Nishimura, T. Ohno, K. Nozaki, *ibid.* **1993**, *115*, 4577–4589; D. W. Dixon, V. Kumar, *New J. Chem.* **1992**, *16*, 555–558.

[13] Whereas the fluorescence intensity of [$Zr(TPP)_2$] (**1**) remains relatively unchanged in a range of solvent polarities, excitation of [Zr(TTP)(TTP-NHCOAQ)] (**4**) gives a considerably weaker fluorescence signal with increasing solvent polarity. This suggests that the singlet excited state of **4** undergoes electron transfer to form a charge-separated state (porphyrin$^+$-quinone$^-$). Dewey Holten and Steve Gentemann (Washington University, St. Louis, Mo), personal communication.

[14] A quinone-bridged cerium bis(porphyrin) complex has also been recently synthesized. J. W. Buchler (Technische Hochschule Darmstadt), personal communication.

Synthesis and Encapsulation Behavior of New Redox-Active Dimeric Assemblies**

Xavier Garcías and Julius Rebek, Jr.*

Molecular assemblies are suitable systems for the study of recognition phenomena, and self-complementary molecules are advantageous in this regard. These compounds can dimerize through hydrogen bonding,[1] and the dimers present closed-shell capsules capable of surrounding of smaller, complemen-

[*] Prof. Dr. J. Rebek,[+] Jr., Dr. X. Garcías
Department of Chemistry, Massachusetts Institute of Technology
Cambridge, MA 02139 (USA)
Fax: Int. code + (617) 253-7929
e-mail: jrebek@mit.edu

[+] After July 1, 1996: Institute for Chemical Biology, The Scripps Research Institute, 10550 N. Torrey Pines Rd, La Jolla, CA 92037 (USA).

[**] This work was supported by the National Institutes of Health. X. G. is grateful to the Ministerio de Educación y Ciencia of Spain for a postdoctoral MEC/Fulbright fellowship.

tary guest species.[2] Here we describe systems that feature varied interior linings, and the consequences for the binding of guests are reported.

The new systems are structurally related to the original **1**, but present either electron-rich or electron-deficient surfaces to encapsulated species. Their enhanced solubility in organic media is a consequence of the peripheral ester groups, for example, in **2**.[3] The syntheses follow the methods described earlier: the new hydroquinone **3** was prepared by the condensation of 1,4-bis(acetoxy)-2,3,5,6-tetrakis(bromomethyl)benzene[4] with an excess of the appropriate glycoluril. The corresponding quinone **4** was obtained, without apparent side reactions, through NO_2 oxidation of **3** in CH_2Cl_2.

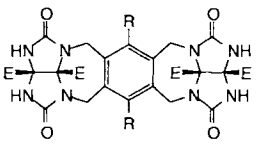

1: R = H; E = C_6H_5
2: R = H; E = $CO_2(C_2H_5)$
3: R = OH; E = $CO_2(n\text{-}C_4H_9)$

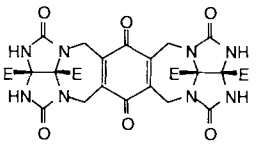

4: E = $CO_2(n\text{-}C_4H_9)$

In organic solvents such as chloroform, both **3** and **4** show the spectroscopic earmarks of well-defined assemblies.[5] Downfield NH resonances ($\delta \approx 9$) and generally sharp NMR signals spectra indicate that the dimeric capsule is the dominant species in solution. Moreover, the dimer **2**, a species closely related in structure, exists as a dimeric capsule in the crystalline state.[6]

In addition to self-assembly into homodimers, disproportionations into heterodimers[7] were observed in mixtures of the hydroquinone **3** and the quinone **4**, or either of these with the capsule **2** (Fig. 1). This behavior is in accord with observations

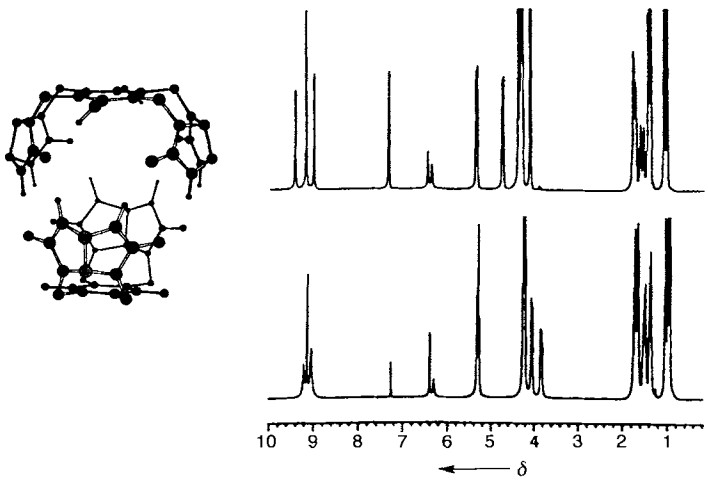

Fig. 1. Left: Energy-minimized [8] structure of the heterodimer **3-4** (glycoluril esters are omitted for clarity). Right: 500 MHz ^{1}H NMR spectra of equimolar mixtures of **2** and **3** (top), and **3** and **4** (bottom).

in our laboratories and elsewhere. The heterodimers present cavities of nearly identical volume to those of the original **1-1** or **2-2** featuring the benzene spacer, but offer a π surfaces with different electron densities to their encapsulated guests.

The encapsulation of small, complementary molecular guests could be observed directly by NMR spectroscopic techniques, and the association constants for the formation of the encapsulation complexes were calculated as described previously.[2] The data are given in Table 1, and the NMR chemical shifts for the signals of encapsulated guests are listed in Table 2. In addition

Table 1. Association constants K_a (M^{-1}, 298 K) for the encapsulation of guests in the dimers **N-N** (**N** = **2**, **3**, **4**). ($K_{a,298}$ = [N-guest.N]/[N-N] × [free guest]).

Guest	Host 2-2	3-3	4-4
CH_4	33	70	10
C_2H_6	51	51	13
CH_3F	10	17	<0.3
CF_4	0.7	0.6	<0.2

Table 2. $\delta(^1H)$ and $\delta(^{19}F)$ values for guests encapsulated in the hosts **N-N** and for the free guests.

Guest	Host 2-2	3-3	4-4	Free guest
CH_4	−1.51/–	−1.33/–	−0.57/–	0.22/–
C_2H_6	−0.99/–	−0.81/–	0.02/–	0.85/–
CH_3F	2.50/−176.35	2.68/−175.76	–/–	4.27/−175.06
CF_4	–/ −61.11	–/ −60.24	–/–	–/ −62.48

to methane[9] and ethane, methyl fluoride (CH_3F) and tetrafluoromethane (CF_4) were examined as guests. The studies of the fluorinated methanes were inspired by recent calculations[10] that predict CF_4 to be as well suited as CH_4 as a guest for these capsules. We had, however, been unable to observe the encapsulation of CF_4 by **1** at 298 K by either ^{1}H or ^{19}F NMR methods.[2]

The association constants for the encapsulation of methane and ethane by all of the capsules were similar in magnitude, although the hydroquinone was generally a better host than the quinone. In addition, the upfield shifts observed for guests inside the quinone ($\Delta\delta \approx 0.8$ ppm) were considerably smaller than those for the hydroquinone ($\Delta\delta \approx 1.7$ ppm). This likely reflects the lower anisotropy experienced by guests in the electron-deficient quinone. The fluorinated methanes presented some experimental problems, but CH_3F encapsulated in **2-2** or **3-3** could be directly observed. Figure 2 shows both ^{19}F and ^{1}H NMR spec-

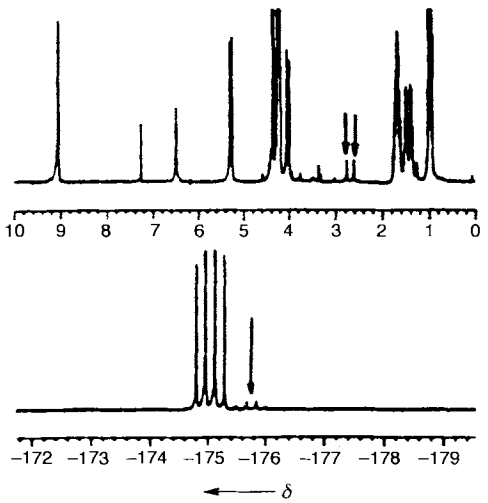

Fig. 2. Top: ^{1}H NMR spectrum (300 MHz) of **3** (28.5 mM) in $CDCl_3$ containing CH_3F (155 mM). Bottom: ^{19}F NMR spectrum (282 MHz) of the same sample. Signals for included CH_3F are marked with arrows.

 © VCH Verlagsgesellschaft mbH, D-69451 Weinheim, 1996 0570-0833/96/3511-1226 $ 15.00+.25/0

tra of encapsulated CH_3F in **3**. The encapsulation results in an upfield shift, as expected for a molecule held between two π surfaces. Dimer **4-4** failed to encapsulate CH_3F under similar conditions and an upper limit of $K_{a,298} = 0.3\ M^{-1}$ can be calculated, assuming that no more than 5% of the capsule was occupied.

The ^{19}F NMR spectrum of CF_4 was recorded at high amplitude and 298 K with or without added **1** (Fig. 3a). No new upfield signals for encapsulated CF_4 were observed at this temperature. The low solubility of both **1** and CF_4 may be the cause (the solubility of **1-1** in $CDCl_3$ is only 3 mM). However, a very small peak (0.8% of the signal for free CF_4) could be observed when the temperature was lowered to 273 K (Fig. 3b), but it

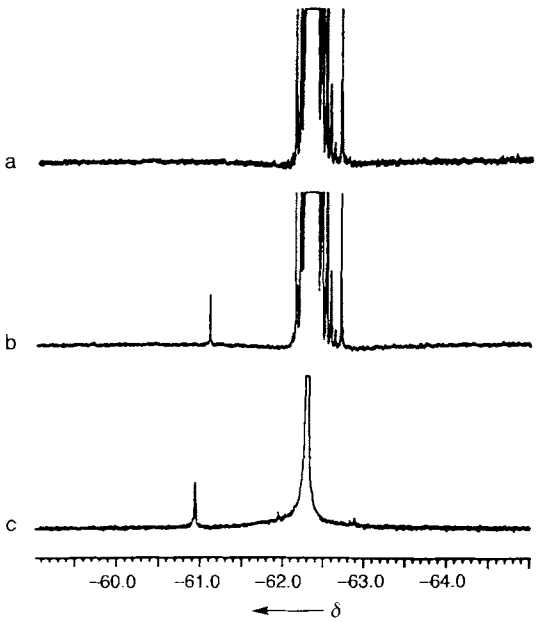

Fig. 3. ^{19}F NMR spectra of **1** in $CDCl_3$ saturated with CF_4 at 298 K (a, 470 MHz) and at 273 K (b, 470 MHz), and of **2** in $CDCl_3$ saturated with CF_4 at 298 K (c, 282 MHz).

appeared downfield of the signal for free CF_4. If this signal represents encapsulated CF_4,[11] the $K_{a,273}$ can be calculated as $2.8\ M^{-1}$. To test the reproducibility of this signal, the more soluble **2-2** was used in $CDCl_3$ saturated with CF_4, with C_6F_6 added as an internal ^{19}F integration standard. Again, the downfield signal was observed only when the capsule was present (Fig. 3c). Integration permits an association constant of $0.7\ M^{-1}$ to be calculated for the encapsulation of this species, presumably CF_4, by **2-2** at 298 K. Similar results were obtained with **3-3**. The association constants for CH_4 are three to four times smaller than those observed for the cryptophanes by Collet et al., who also noted a diminution of affinity when F is substituted for H in chloromethanes.[9]

Why the ^{19}F NMR signal of the encapsulated CF_4 appears downfield of that of free CF_4 ($\delta = -62.48$, referenced to CCl_3F) remains a mystery. It has not been possible to observe this downfield signal for CF_4 in **4-4**, and an upper limit for $K_{a,298} = 0.2\ M^{-1}$ can be calculated if no more than 1% of the CF_4 is encapsulated. Fox et al. have calculated the free energies and suggested that the order of binding affinity to **1-1** should be $CHCl_3 < CF_4 < CH_4$, an order that is confirmed by the experiments described here.[10] The calculations were less successful quantitatively, in that the strength of binding (relative to CH_4) was overestimated for CF_4 and underestimated for $CHCl_3$.

Finally, qualitative evidence for the encapsulation of nitric oxides in **4-4** was obtained. Earlier attempts to bind NO in **1-1** led to decomposition,[2] but the successful oxidation of **3** to **4** with NO_2 suggested the following experiment. Treatment of **3-3** with excess NO_2 in CH_2Cl_2 followed by evaporation of the volatiles gave a solid residue, which was taken up in $CDCl_3$. This solution showed the characteristic NMR spectrum of pure **4-4**. When an equivalent amount of **3-3** was added to this material, only **4-4** was observed by NMR in the solution. Apparently, the $CDCl_3$ solution contained an oxidizing agent—most likely an encapsulated oxide of nitrogen—capable of converting **3** into **4**. The assignment of structure for the encapsulated oxidant awaits further research.[12] In the meantime, we note that many unusual properties of encapsulated guests have been observed in covalent hosts.[13]

Experimental Procedure

NMR experiments: All experiments reported were conducted in spectroscopic grade $CDCl_3$. Methane, ethane, or methyl fluoride were bubbled into a solution of a known weight of the appropiate host at room temperature. The the total volume of the solution was measured and the concentrations of the species (empty/full host and free/included guest) were calculated by integration (^1H and/or ^{19}F NMR). Tetrafluoromethane was bubbled for 15 min into a solution cooled at −40 °C of a known weight of **2**, **3**, or **4**. Hexafluorobenzene (2 μL) was added as internal standard for integration and the tube was sealed while cold. The concentrations of free and encapsulated CF_4 were determined by integration with respect to the C_nF_n. For example, in the case of **2**, the data found were: [**2**] = 42 mg in 0.5 mL = 120 mM; [**2-2**] = 60 mM; $[CF_4]_{total} = 21$ mM; $[CF_4]_{free} = 20.2$ mM; $[CF_4]_{included} = 0.8$ mM; $K_{a,298} = 0.8 \times 10^3/59.2 \times 20.2 = 0.7\ M^{-1}$.

Preparation of **3**: Potassium *tert*-butoxide (1.68 g, 15 mmol) was added all at once to a solution of 5.13 g (15 mmol) of 1,5-bis(carboxybutyl)glycoluril (prepared as described for the corresponding ethyl derivative [3]) in 50 mL of dry DMSO at room temperature. The mixture was stirred until dissolution was complete (about 45 min), then solid 1,4-bis(acetoxy)-2,3,5,6-tetrakis(bromomethyl)benzene [4] (562 mg, 1 mmol) was added, and stirring was continued at room temperature for an additional 2 h. The yellowish mixture was poured into a vigorously stirred solution of 500 mL of 0.1 N HCl. The resulting suspension was filtered by suction, and the solid was washed with water (5 × 100 mL). The white solid was dried and then triturated with hot CH_2Cl_2 (3 × 100 mL) and filtered. The combined filtrates were evaporated yielding 250 mg of crude **3**. After column chromatography (CH_2Cl_2/CH_3OH 98/2), 168 mg (20% yield) of pure material was obtained. ^1H NMR (300 MHz, $CDCl_3$): $\delta = 9.13$ (s, 4H, NH), 6.39 (s, 2H, OH), 5.30 (d, $J = 16.0$ Hz, 4H, benzylic CH), 4.23 (m, 8H, CH_2O), 4.03 (d, $J = 16.0$ Hz, 4H, benzylic CH), 1.75–1.33 (m, 16H, CH_2CH_2), 0.98 (t, $J = 7.3$ Hz, 3H, CH_3), 0.94 (t, $J = 7.3$ Hz, 3H, CH_3); ^{13}C NMR (75 MHz, $CDCl_3$): $\delta = 165.93$, 165.30, 160.13, 146.20, 128.15, 82.3, 67.12, 37.59, 30.47, 19.20, 19.04, 13.77; HRMS: calcd for $[M+H]^+$ $C_{38}H_{51}N_8O_{14}$ 843.3525, found 843.3519.

Preparation of **4**: Bisglycoluril **3** (42 mg, 0.05 mmol) was treated for 1 h at room temperature with 0.5 mL of a solution of CH_2Cl_2 saturated with NO_2. The solvent was evaporated to obtain a quantitative yield of **4**. ^1H NMR (300 MHz, $CDCl_3$): $\delta = 9.01$ (s, 4H, NH), 5.31 (d, $J = 16.3$ Hz, 4H, benzylic CH), 4.20 (m, 8H, CH_2O), 3.83 (d, $J = 16.3$ Hz, 4H, benzylic CH), 1.76–1.31 (m, 16H, CH_2CH_2), 1.03 (t, $J = 7.3$ Hz, 3H, CH_3), 0.93 (t, $J = 7.3$ Hz, 3H, CH_3); ^{13}C NMR (75 MHz, $CDCl_3$): $\delta = 183.50$, 165.56, 162.21, 158.45, 140.96, 81.94, 75.29, 67.02, 35.28, 30.24, 19.00, 18.85, 13.55; HRMS: calcd for $[M+2H]^+$ $C_{38}H_{50}N_8O_{14}$ 842.3447, found 843.3439.

Received: January 8, 1996 [Z8703IE]
German version: *Angew. Chem.* **1996**, *108*, 1328–1330

Keywords: host–guest chemistry

[1] R. Wyler, J. de Mendoza, J. Rebek, Jr., *Angew. Chem.* **1993**, *105*, 1820; *Angew. Chem. Int. Ed. Engl.* **1993**, *32*, 1699.
[2] N. Branda, R. Wyler, J. Rebek, Jr., *Science* **1994**, *263*, 1267; R. M. Grotzfeld, N. Branda, J. Rebek, Jr., *ibid.* **1996**, *271*, 487.
[3] N. Branda, R. M. Grotzfeld, C. Valdés, J. Rebek, Jr., *J. Am. Chem. Soc.* **1995**, *117*, 85.
[4] A. D. Thomas, L. L. Miller, *J. Org. Chem.* **1986**, *51*, 4160.
[5] A variety of these characteristics in molecular assemblies, are described in other reports: a) C. Seto, G. M. Whitesides, *J. Am. Chem. Soc.* **1991**, *113*, 712; b) P. Baxter, J.-M. Lehn, A. DeCian, J. Fischer, *Angew. Chem.* **1993**, *105*, 92; *Angew. Chem. Int. Ed. Engl.* **1993**, *32*, 69; c) J. Yang, E. Fan, S. Geib, A. D. Hamilton, *J. Am. Chem. Soc.* **1993**, *115*, 5314; d) M. R. Ghadiri, J. R. Granja, L. K. Buehler, *Nature* **1994**, *369*, 133; e) M. R. Ghadiri, K. Kobayashi, J. R. Granja, R. K. Chadha, D. E. McRee, *Angew. Chem.* **1995**, *107*, 76; *Angew. Chem. Int. Ed. Engl.* **1995**, *34*, 93.

[6] C. Valdés, U. P. Spitz, L. M. Toledo, S. W. Kubik, J. Rebek, Jr., *J. Am. Chem. Soc.* **1995**, *117*, 12733.
[7] C. Valdés, U. P. Spitz, S. W. Kubik, J. Rebek, Jr., *Angew. Chem.* **1995**, *107*, 2031; *Angew. Chem. Int. Ed. Engl.* **1995**, *34*, 1885; R. G. Chapman, J. C. Sherman, *J. Am. Chem. Soc.* **1995**, *117*, 9081.
[8] Molecular modeling was performed using MacroModel 3.5X (MM2* force field): F. Mohamadi, N. G. Richards, W. C. Guida, R. Liskamp, M. Lipton, C. Caufield, G. Chang, T. Hendrickson, W. C. Still, *J. Comput. Chem.* **1990**, 11, 440.
[9] For methane encapsulation inside a cryptophane see: L. Garel, J.-P. Dutasta, A. Collet, *Angew. Chem.* **1993**, *105*, *32*, 1169; *Angew. Chem. Int. Ed. Engl.* **1993**, *32*, 1169.
[10] T. Fox, B. E. Thomas, M. McCarrick, P. A. Kollman, *J. Phys. Chem.*, submitted. We thank these authors for helpful correspondence and a preprint of their manuscript.
[11] The other possibilities are encapsulated C_2F_6, C_2F_4, or C_2F_2 as contaminants in the commercial CF_4.
[12] Oxidation by O_2 catalyzed by residual nitrogen oxides has not been ruled out: R. Rathore, E. Bosch, J. K. Kochi, *Tetrahedron Lett.* **1994**, *35*, 1335.
[13] For examples, see: a) D. J. Cram, *Nature* **1992**, *356*, 29; b) D. J. Cram, R. Jaeger, K. Deshayes, *J. Am. Chem. Soc.* **1993**, *115*, 10111; c) C. N. Eid, Jr., C. B. Knobler, D. A. Gronbeck, D. J. Cram, *ibid.* **1994**, *116*, 8506; d) A. Collet, *Tetrahedron* **1987**, *13*, 5725; e) R. M. Hatt, J. S. Bradshaw, K. Pawlak, R. L. Bruening, B. J. Tarbet, *Chem. Rev.* **1992**, *92*, 1261; f) P. Timmermann, W. Verboom, F. C. J. M. van Veggel, J. P. M. van Duynhoven, D. N. Reinhoudt, *Angew. Chem.* **1994**, *106*, 2437; *Angew. Chem. Int. Ed. Engl.* **1994**, *33*, 2345.

Self-Complementarity of 7,9-Dimethylguanine: A Base Pair Containing Three Hydrogen Bonds**

Susanne Metzger and Bernhard Lippert*

Molecular recognition of *complementary* molecules through hydrogen bonding is a common feature in biochemistry[1] as well as in supramolecular chemistry.[2, 3] Base pairing according to the Watson–Crick and Hoogsteen scheme[1] and also substrate–receptor recognition[2–4] may serve as examples. Molecular recognition between *identical* molecules is a much less common phenomenon usually restricted to molecules containing "complementary ends".[5] Although many cases of pairwise hydrogen bond formation between identical molecules, including nucleobases,[1] are known, this kind of association should not be referred to as "molecular recognition" since the association constants in solution are low.

With the assumption that at least three hydrogen bonds are required for self-recognition between naturally occurring nucleobases, homo base pairing can be realized between cytosines (partially protonated) and guanines (partially deprotonated) only (Fig. 1). Adeninium base pairs, although known, are difficult to prove in solution. It is well known that cytosines form base pairs at a pH corresponding to their pK_a values (4–5), leading to helical structures in the case of poly(dC), which are sufficiently stable to exist at physiological pH.[6] In the case of guanine, half of the protons at the N1 position must be removed to achieve self pairing (Fig. 1). Considering the high pK_a value of guanine derivatives (9–10) it is not surprising that triple H bonding between guanine nucleobases has not yet been described.

[*] Prof. Dr. B. Lippert, Dipl.-Chem. S. Metzger
Fachbereich Chemie der Universität
Otto-Hahn-Strasse 6, D-44227 Dortmund (Germany)
Fax: Int. code +(231)755-3797

[**] Our work was supported by the Deutsche Forschungsgemeinschaft and the Fonds der Chemischen Industrie (grant for S. M.). We thank Dr. M. Linscheid and C. Siethoff (Institut für Spektrochemie, Dortmund) for recording the ESI mass spectra.

However, in the course of our studies on N7-platinated guanines, we were able to prove the formation of guanine–guanine base pairs by spectroscopic methods and X-ray analysis in two cases (Fig. 2).[7, 8] The acidification of the N1 position ($pK_a = 8–9$) as a consequence of Pt coordination at N7 facilitates base pairing at a pH significantly lower than that required for pairing of the free base.

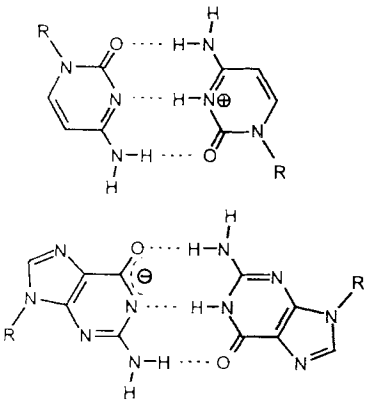

Fig. 1. Partially protonated cytosine ($HC^+\equiv C$) and partially deprotonated guanine ($HG\equiv G^-$).

Using 7,9-dimethylguanine (7,9-DimeG) we have now found a guanine derivative capable of base pairing at pH 7, that is, at physiological pH. 7,9-DimeG can be regarded a model for the naturally occurring 7-methylguanosine, which is known to display a number of biologically interesting functions. Its role as a rare RNA base[9] and as the main product of DNA methylation by carcinogenic and mutagenic agents,[10] its mutagenicity as a consequence of mispairing,[11] and its occurrence in the 5′-cap of mRNA[12] are some of these. 7,9-DimeG is zwitterionic in its neutral form (2-amino-7,9-dimethyl-6-oxodihydropurinium betaine, herbipoline).[13] With a pK_a of 7.19,[13] 7,9-DimeG exists as a 1:1 mixture of its neutral and its cationic form at physiological pH (Fig. 3). Upon titration of an aqueous solution of 7,9-DimeG with an acid HX, a poorly water-soluble precipitate of composition [7,9-DimeGH·7,9-DimeG]X·n H_2O forms in the pH range of 7 ± 1.[14] Attempts to obtain single crystals suitable for X-ray analysis were unsuccessful. IR spectra[15] of the various hydrogen-bonded complexes are almost identical except for anion bands. The electrospray ionization mass spectrum for the complex with $X = ClO_4^-$[16] clearly indicates the existence of a hydrogen-bonded dimer (m/z 359). The poor solubility of [7,9-DimeGH·7,9-DimeG]X in all common solvents does not permit comprehensive characterization of the adduct by NMR spectroscopy.[17] In solutions of the dimer ($X = ClO_4^-$) in DMSO, for example, the maximum concentration is 0.0067 mol L^{-1} (per dimer). Even the choice of a more hydrophobic anion (tetraphenylborate) does not improve solubility because the poor solubility of the neutral 7,9-DimeG is the limiting factor. Attempts to estimate the association constant by a dilution experiment[18] failed, as the $\Delta\delta$ values of the NH_2 signals in the ^1H NMR spectrum ([D_6]DMSO) could be deter-

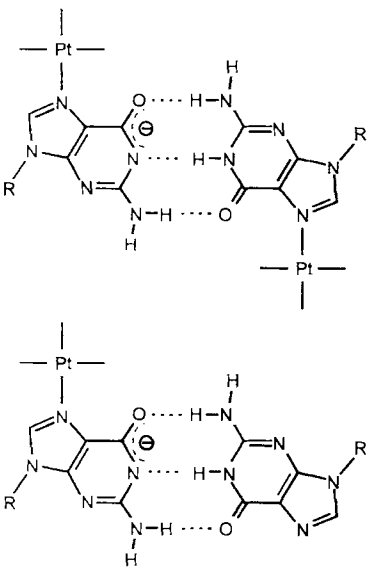

Fig. 2. Guanine–guanine base pairing between two cations of N7-platinated 9-R-guanines and between a cation of N7-platinated 9-R-guanine and neutral, nonplatinated guanine.

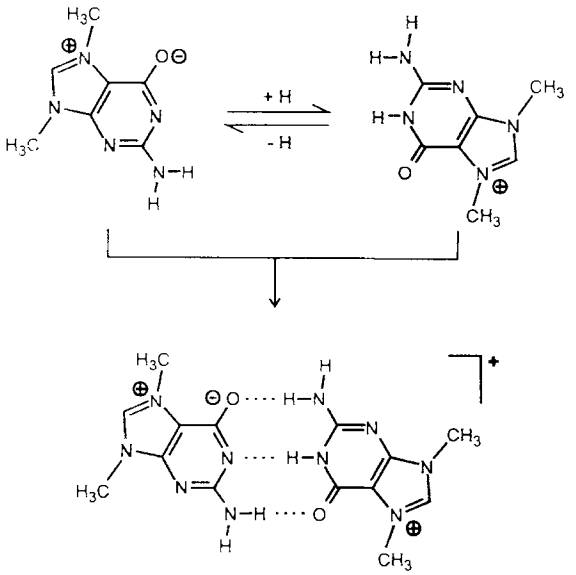

Fig. 3. Acid - base equilibrium of 7,9-dimethylguanine and adduct formation between the two species.

mined for the nonlinear part of the dilution curve only. Nevertheless, the following qualitative conclusions can be drawn from the ^{1}H NMR experiments: First, the upfield shift of the NH_2 signals of the dimer upon dilution significantly exceeds that of the NH_2 signals of 9-ethylguanine (9-EtGH) and 1-methylcytosine (1-MeC) in the same solvent and concentration range.[19] Second, 1-MeC is not capable of replacing 7,9-DimeG from its adduct with 7,9-DimeGH$^+$.[20] Third, for the betaine 7,9-DimeG, no hydrogen bond formation with 1-MeC can be detected in [D$_6$]DMSO, whereas H bonding to 9-EtGH is readily deduced from ^{1}H NMR spectra.[21]

It remains to be clarified if the ability of the rare nucleobase 7,9-dimethylguanine to act as a proton acceptor as well as a proton donor is of relevance to its biological function. In any case, the strong association between 7,9-dimethylguanine and its conjugate acid is exceptional. The positive charge of this base pair is not expected to restrict its occurrence in physiological systems.[22] The high affinity of 7,9-DimeG to guanine may also offer a new strategy for the design of guanine receptors different from conventional ones.[23] Furthermore, it seems feasible that the pK_a value of the N1 proton of guanines may be tuned by substituents at the 7 and 8 positions such that guanine receptors suitable for different pH ranges could be designed.

Received: December 22, 1995 [Z8680IE]
German version: *Angew. Chem.* **1996**, *108*, 1321–1323

Keywords: base pairing · hydrogen bonds · nucleobases · supramolecular chemistry

[1] W. Saenger, *Principles of Nucleic Acid Structure*, 1st ed., Springer, New York, **1984**, p. 117.

[2] *Frontiers in Supramolecular Chemistry and Photochemistry*, (Eds.: H.-J. Schneider, H. Dürr), VCH, Weinheim, **1991**.

[3] J.-M. Lehn, *Supramolecular Chemistry: Concepts and Perspectives*, 1st ed., VCH, Weinheim, **1995**; J. S. Lindsey, *New. J. Chem.* **1991**, *15*, 153–180; G. M. Whitesides, E. E. Simanek, J. P. Mathias, C. T. Seto, D. N. Chin, M. Mammen, D. M. Gordon, *Acc. Chem. Res.* **1995**, *28*, 37–44, and references therein.

[4] V. M. Rotello, E. A. Viani, G. Deslongchamps, B. A. Murray, J. Rebek, Jr., *J. Am. Chem. Soc.* **1993**, *115*, 797–798; T. J. Murray, S. C. Zimmerman, *ibid.* **1992**, *114*, 4010–4011; M. Kotera, J.-M. Lehn, J.-P. Vigneron, *J. Chem. Soc. Chem. Commun.* **1994**, 197–199; M. Inouye, T. Konishi, K. Isagawa, *J. Am. Chem. Soc.* **1993**, *115*, 8091–8095; A. Harriman, Y. Kubo, J. L. Sessler, *ibid.* **1992**, *114*, 388–390; S. J. Geib, C. Vicent, E. Fan, A. D. Hamilton, *Angew. Chem.* **1993**, *105*, 83–85; *Angew. Chem. Int. Ed. Engl.* **1993**, *32*, 119–121.

[5] E. A. Winter, M. M. Conn, J. Rebek, Jr., *Acc. Chem. Res.* **1994**, *27*, 198–203.

[6] K. Gehring, J.-L. Leroy, M. Guéron, *Nature* **1993**, *363*, 561–565, and references therein; J.-L. Mergny, L. Lacroix, X. Han, J.-L. Leroy, C. Hélène, *J. Am. Chem. Soc.* **1995**, *117*, 8887–8898.

[7] R. Faggiani, C. J. L. Lock, B. Lippert, *J. Am. Chem. Soc.* **1980**, *102*, 5418–5419; R. Faggiani, B. Lippert, C. J. L. Lock, R. A. Speranzini, *Inorg. Chem.* **1982**, *21*, 3216–3225; B. Lippert, *J. Am. Chem. Soc.* **1981**, *103*, 5691–5697.

[8] G. Schröder, B. Lippert, M. Sabat, C. J. L. Lock, R. Faggiani, B. Song, H. Sigel, *J. Chem. Soc. Dalton Trans.* **1995**, 3767–3775.

[9] J. A. McCloskey, S. Nishimura, *Acc. Chem. Res.* **1977**, *10*, 403–410.

[10] R. F. Newbold, W. Warren, A. S. C. Medcalf, J. Amos, *Nature* **1980**, *283*, 596–599.

[11] P. D. Lawley, P. Brookes, *Nature* **1961**, *192*, 1081–1082.

[12] H. F. Lodish, *Ann. Rev. Biochem.* **1976**, *45*, 39; M. Kozak, *Microbiol. Rev.* **1983**, *47*, 1.

[13] W. Pfleiderer, *Liebigs Ann. Chem.* **1961**, *647*, 167–173.

[14] Preparation: Concentrated aqueous solutions of 7,9-dimethylguanine (ca. 50 mmol L^{-1}) were adjusted to a pH of 7.2 by addition of either $HClO_4$, HNO_3, or HCl, and precipitation was completed by cooling to 4 °C. The colorless solids were filtered off, washed with H_2O, and dried in high vacuum. Yields were between 70 and 85%. C, H, N analyses are in agreement with the proposed compositions (monohydrates for $X = NO_3^-$ and Cl^-; hemihydrate for $X = ClO_4^-$).

[15] The most intensive bands in the C=C stretching region and in the fingerprint region are: 1709.6 (vs), 1684.4, 1617.4, 1592.2, 1576.5, 1560.0 and 786.5, 767.6, 747.5 cm^{-1}, respectively. Spectra were recorded on a FT-IR spectrometer Bruker IFS 28 (32 scans between 200 to 4000 cm^{-1}, KBr). The program Opus, version 2.0 by Bruker, was used for data processing.

[16] MS: *m/z* 359: [7,9-DimeGH·7,9-DimeG]$^+$; *m/z* 180: DimeGH$^+$. Mass spectra were recorded on a Finnigan MAT90 spectrometer using an electrospray source of our own construction at an acceleration potential of +5000 V. 89 scans were recorded in the range of *m/z* 50–800 (scan speed 8.27 s per scan). The solution (H_2O/ methanol) was infused by means of a E540101 pump (TSE) through a 50 µm fused silica capillary (flow rate = 0.5 ML min^{-1}). A sheet flow of methanol (1 µL min^{-1}) was applied for stabilization.

[17] ^{1}H NMR spectra were recorded on a Bruker DRX-400 spectrometer at a frequency of 400.13 MHz in [D$_6$]DMSO without presaturation of the solvent and H_2O signals. The resonance of nondeuterated DMSO was used as internal reference ($\delta = 2.50$).

[18] C. S. Wilcox in ref. [2], pp. 123–143.

[19] Upon dilution of a solution of [7,9-DimeGH·7,9-DimeG]ClO_4 in [D$_6$]DMSO from $c = 6.7$ mmol L^{-1} to $c = 0.42$ mmol L^{-1}, the NH_2 resonance of 7,9-dimethylguanine is shifted upfield by 0.30. The upfield shift of the NH_2 resonance of 9-ethylguanine (9-EtGH) upon addition of an equimolar amount of 1-methylcytosine (1-MeC) in the same concentration range is 0.05 at $c = 6.7$ mmol L^{-1} and 0.0 at $c = 0.42$ mmol L^{-1}. The shift of the NH resonance is $\Delta\delta = 0.1$, as expected. This shift value is twice that of the NH_2 resonance since the NH_2 signal is an average of two protons, one of which is H bonded while the other is not. In the case of [7,9-DimeGH·7,9-DimeG]X this resonance is not observed as a consequence of chemical exchange.

[20] Addition of 1-MeC to a solution of [7,9-DimeGH·7,9-DimeG]ClO_4 in [D$_6$]DMSO does not cause changes in the chemical shifts of any of the two components but leads to clean superpositions only.

[21] Addition of a tenfold excess of 9-ethylguanine to a saturated solution of 7,9-dimethylguanine in [D$_6$]DMSO (c(7,9-DimeG) = 0.36 mmol L^{-1} at 18 °C) results in a downfield shift of the NH_2 resonance of 7,9-DimeG by roughly 0.39 ppm. (7,9-DimeG is expected to exist exclusively in its H bonded form under these conditions.)

[22] M. F. Goodman, *Nature* **1995**, *378*, 237–238; A. Douhal, S. K. Kim, A. H. Zewail, *ibid.* **1995**, *378*, 260–263.

[23] H. Furuta, D. Magda, J. L. Sessler, *J. Am. Chem. Soc.* **1991**, *113*, 978–985; C. Seel, F. Vögtle, *Angew. Chem.* **1991**, *103*, 433–436; *Angew. Chem. Int. Ed. Engl.* **1991**, *30*, 442–445.

[24] Note added in proof (May 2, 1996): After completion of this manuscript we became aware that the results of an X-ray crystal structure determination of a nucleoside analogue, of hemiprotonated 7-methylguanosine (as the iodide salt), have been reported: K. Tomita, *Yakugaku Zasshi* **1989**, *109*, 439–459. The results confirm the existence of the proposed G,G base pair. Neither the title nor the English abstract of this review article provide any indication of this compound. We feel that this is the reason why this work escaped our attention.

Synthesis of Glycopeptides and Lipopeptides by Chemoselective Ligation**

Stefano E. Cervigni, Pascal Dumy, and Manfred Mutter*

An important feature of natural glycoproteins is their structural diversity. Posttranslational glycosylation in eukaryotic cells plays a key role in various phenomena such as protein stabilization against denaturation, intercellular communication processes, and regulation of cell growth.[1] For a better understanding of the contribution of the carbohydrate moieties of glycoproteins in biological processes much effort has been devoted recently to improving the chemical synthesis of glycopeptides as models for glycosylated proteins. Moreover, the glycosylation of peptides is an important tool in drug design for modulating the biological activity and improving the bioavailability and solubility of natural peptides.[2]

The regiospecific chemical synthesis of glycopeptides remains a difficult task due to the weakness of the glycosidic linkage and the need for selective protection of several functional groups.[3] Recent developments in the ligation of unprotected peptide fragments by chemoselective methods[4] have opened new routes to multifunctional peptides and proteins of high complexity. Consequently, numerous applications of this elegant concept have emerged in protein de novo design,[5] for example peptide dendrimers[6] and protein conjugates.[7]

Here we report on a general strategy based on chemoselective formation of oxime bonds[8] for the attachment of unprotected multifunctional peptides to aldehyde-containing compounds such as carbohydrates and lipids. In sharp contrast with other methods applied for the synthesis of glycopeptides,[9] this procedure permits preservation of the cyclic nature of the saccharide unit.[10]

As shown in Scheme 1, amino acids containing selectively addressable amino-oxy functions can be incorporated into the peptide sequence. After the sequential deprotection of the amino-oxy function and subsequent reaction with the aldehyde group of any of a variety of compounds, an oxime bond is formed regioselectively under mild aqueous conditions in a one-pot reaction. This simple method enables the direct linkage of unprotected peptides with free carbohydrates, lipids, and other substrates.

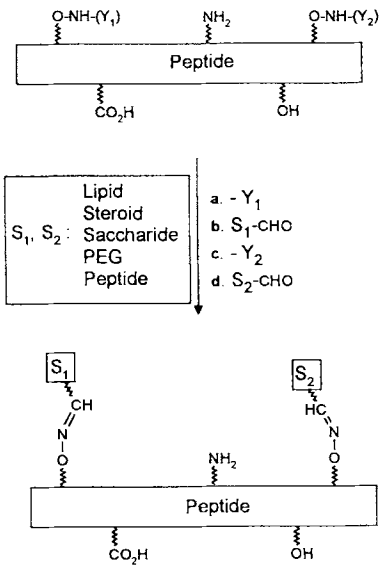

Scheme 1. Strategy for regioselective oxime bond formation. a) and c) Selective deprotection of the amino-oxy functions (Y_1, Y_2: orthogonal protecting groups such as *tert*-butyloxycarbonyl (Boc) and allyloxycarbonyl (Alloc); b) and d) Oxime formation in acetate buffer (S_1, S_2: aldehyde-containing compounds). PEG = polyethyleneglycol.

For example, orthogonally protected peptides were assembled by using standard Fmoc solid-phase chemistry on a Rink amide resin. Subsequently, the N-terminal amino group of the peptide and/or the ε-amino group of lysine were selectively derivatized with differently protected amino-oxyacetyl groups as previously described.[11] After acid treatment the amino-oxyacetyl peptide was reacted with aldehyde groups either on a sugar or lipid to form the corresponding oxime. The reaction was found to occur smoothly, selectively, and independently of the peptide primary sequence.[12] As demonstrated by the preparation of a series of derivatives (**8**–**13**) of the amino-oxyacetylated somatostatin analogue RC-160[13] **1** (Table 1 and

NH_2OCH_2CO-(D)Phe-Cys-Tyr-(D)Trp-Lys-Val-Cys-Trp-NH_2 **1**

Scheme 2), the procedure offers a variety of possibilities for modulating the physical, chemical, and biological properties of peptides.

Table 1. Yields and reaction times of the oxime derivatives of **1**.

Aldehyde	Derivative	*T* [h][a]	Yield [%] [b]
2 glycosone [14]	**8**	5	65
3 glucose	**9**	25	60
4 gentobiose	**10**	75	70
5 maltose	**11**	100	75
6 maltotriose	**12**	120	70
7 decanal	**13**	1	70

[a] As determined by analytical HPLC. [b] Yield of isolated product.

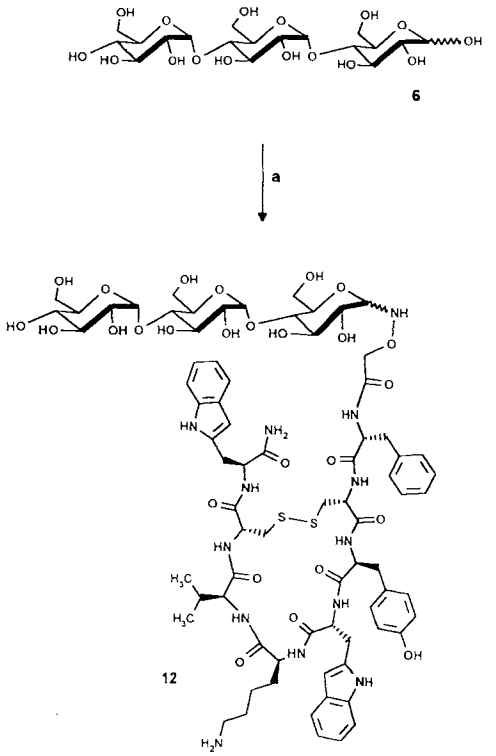

Scheme 2. Linkage of maltotriose **6** and **1** through formation of an oxime bond (for the sake of clarity only the cyclic form of **12** is represented) [10]. a) Acetate buffer/acetonitrile, pH 3, **1**, 120 h; preparative HPLC, **12**: 70%, ESI-MS: 1689.8.

[*] Prof. Dr. M. Mutter, Dipl.-Chem. S. E. Cervigni, Dr. P. Dumy
Institute of Organic Chemistry, University of Lausanne
BCH-Dorigny, CH-1015 Lausanne (Switzerland)
Fax: Int. code +(21)6924015
e-mail: mmutter@ulys.unil.ch

[**] This work was supported by the Swiss National Science Foundation. The authors thank M. Mathieu for synthesizing peptide **14**.

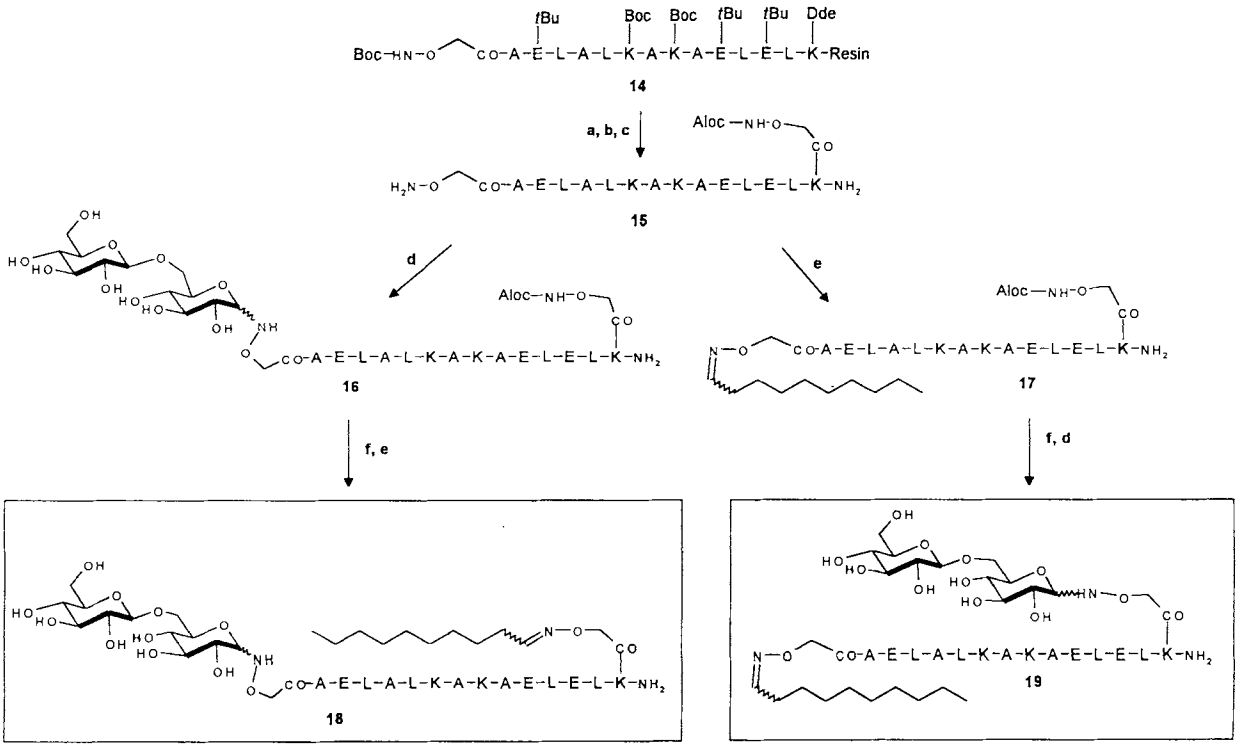

Scheme 3. Chemical pathway for the synthesis of isomeric bis-oxime-containing peptides **18** and **19** (for the sake of clarity only the cyclic form is represented) [10]. a) 3% NH_2NH_2 in DMF; b) Alloc-NHOCH$_2$CO$_2$Su (Su = succinimidyl) in DMF; c) 50% TFA in CH_2Cl_2 (1:1); d) gentobiose **4**, acetate buffer pH 3; e) decanal **7**, acetate buffer pH 3; f) [$(Ph_3P)_2PdCl_2$], nBu$_3$SnH in CH_2Cl_2/AcOH (96:4).

For comparison, the Lys^5(Dde)-protected RC-160 analogue **1a** (Dde = 1-(4,4-dimethyl-2,6-dioxocyclohexylidene)ethyl) was

[H-(D)Phe-Cys-Tyr-(D)Trp-Lys(Dde)-Val-Cys-Trp-NH_2] **1a**

prepared and conjugated to glucosone **2**, gentobiose **4**, and maltotriose **6** by reductive amination[9] with $NaBH_3CN$. Oxime formation leading to the oxime compounds **8**, **10**, and **12** was much faster than the reductive alkylation yielding the corresponding reduced compounds **8a**, **10a**, and **12a**, especially for longer saccharides. With lipid components the chemoselective ligation was even faster and proceeded with remarkably high yields (Table 1). The decreased reactivity of carbohydrates can be explained by the low concentration of the reactive aldehyde form of the reducing sugar in solution. This finding is confirmed by the difference in the reaction times with glucosone **2** and glucose **3**.

To demonstrate the flexibility of the method, two isomeric oxime-ligated glycolipo- (**18**) and lipoglycopeptides (**19**) were prepared (Scheme 3). To this end, we chose an amphiphilic "switch-peptide" designed to undergo solvent-induced conformational changes,[15] and the multifunctional peptide was derivatized with selectively addressable amino-oxyacetyl sites. Removal of Boc/*t*Bu protecting groups of **14** allowed the regioselective attachment of gentobiose (or decanal) to **15** through an oxime bond giving **16** (or **17**). After Pd^{II}-catalyzed cleavage of the Alloc group, **16** was treated with decanal and **17** with gentobiose to provide the oxime-containing lipoglycopeptides **18** and **19** in overall yields of 60 and 65%,[16] respectively.

We have shown that chemoselective oxime bond formation in association with orthogonal protection techniques can be used to attach a variety of compounds such as glycosides and lipids regioselectively to completely unprotected peptides under mild aqueous conditions. In analogy to the posttranslational glycosylation process, the method described above can be considered as a "postsynthetic" modification of unprotected peptides by chemoselective oxime ligation. The approach may be easily extended to any aldehyde-containing compound such as ligands, nucleic acids, and proteins. Its flexibility can greatly facilitate access to more complex targets of pharmaceutical interest. Furthermore, this ligation technique may be applied in combinatorial chemistry and thus extend the potential for creating new chimeric peptide libraries.

Experimental Procedure

Typical procedure for solid-phase peptide synthesis: The linear protected peptide was assembled using *N*α-Fmoc amino acids (3.0 equiv) on Rink amide resin (preactivated with hydroxybenzotriazole (3.0 equiv) and *N*,*N*-diisopropylcarbodiimide (3.0 equiv) in DMF for 15 min) and coupled in the presence of diisopropylethylamine (3.0 equiv) in DMF for 45 min. The Fmoc protecting groups were removed by treatment with piperidine (20% v/v in DMF, 20 min). The amino-oxyacetyl moiety was coupled at the N-terminus of the peptide and/or the ε-amino group of the lysine residue by coupling *N*α-Boc- or *N*α-Alloc- protected amino-oxyacetic acid derivatives. Subsequently, the protected peptide was cleaved from the resin with 50% trifluoroacetic acid in CH_2Cl_2 and the solvent removed under reduced pressure.

Typical conditions for chemoselective ligation: A solution of the amino-oxyacetylated peptide (10 μmol) was dissolved in 2 mL of a 1:1 mixture of 0.1 M (pH 4.0) acetate buffer and CH_3CN and added dropwise to a solution of the carbohydrate or the lipid (100 μmol) in the same buffer. The mixture was acidified to pH 3 with 100 μL of glacial acetic acid, and the coupling reaction was monitored by analytical HPLC. Purification by semipreparative HPLC followed by lyophylization gave the desired glyco- or lipopeptide as a white powder, which was characterized by ESI-MS.

Typical procedure for Aloc cleavage: A solution of the peptide **16** or **17** (15 mg, 0.008 mmol) and [$(Ph_3P)_2PdCl_2$] (2–3 mg) in CH_2Cl_2/4% AcOH (2.5 mL) was treated with nBu$_3$SnH (10 μL, 0.035 mmol) and the reaction was monitored by HPLC. The orange solution was filtered and concentrated in vacuo, and diethyl ether was added. The resulting precipitate was isolated by centrifugation and the

ether phase decanted. The precipitate was washed several times with ether and finally dried to give the deprotected product as a white powder (13 mg, 91%).

The reductive amination was carried out using a modification of a published procedure [13]. In a typical experiment, the protected peptide **1a** (10 μmol) was dissolved in 2 mL of a 10:1 mixture of 0.1 M phosphate buffer (pH 6.0) and CH_3CN. To this peptide solution were added the carbohydrate (200 μmol) dissolved in 2 mL of the same buffer and sodium cyanoborohydride (200 μmol) as a solid. The mixture was stirred at room temperature and progress of the coupling reaction monitored by analytical HPLC. The glycopeptides were purified by semipreparative HPLC and characterized by ESI-MS.

Received: December 22, 1995 [Z8684IE]
German version: *Angew. Chem.* **1996**, *108*, 1325–1328

Keywords: glycopeptides · lipopeptides · oximes · solid-phase syntheses

[1] I. J. Goldstein, R. C. Hugues, M. Monsigny, T. Osawa, N. Sharon, *Nature* **1980**, *285*, 66; N. Sharon, H. Lis, *The Proteins, Vol. 5*, Academic Press, New York, **1982**, pp. 1–123.
[2] J. F. Fisher, A. W. Harrison, G. L. Bundy, K. F. Wilkinson, B. D. Rush, M. J. Ruwart, *J. Med. Chem.* **1991**, *34*, 3140–3143.
[3] H. Kunz, *Angew. Chem.* **1987**, *99*, 297; *Angew. Chem. Int. Ed. Engl.* **1987**, *26*, 294–308; U. Sprengard, G. Kretzschmar, E. Bartnick, C. Hüls, H. Kunz, *ibid.* **1995**, *107*, 1104 and **1995**, *34*, 990–993; O. Frey, M. Hoffmann, H. Kessler, *ibid.* **1995**, *107*, 2194–2195 and **1995**, *34*, 2026–2028.
[4] M. Schnölzer, S. B. H. Kent, *Science* **1992**, *256*, 221–225; P. E. Dawson, T. W. Muir, I. Clark-Lewis, S. B. H. Kent, *ibid.* **1994**, *266*, 776–779; G. Tuchscherer, *Tetrahedron Lett.* **1993**, *34*, 8419–8422.
[5] P. E. Dawson, S. B. H. Kent, *J. Am. Chem. Soc.* **1993**, *115*, 7263–7266.
[6] J. Shao, J. P. Tam, *J. Am. Chem. Soc.* **1995**, *117*, 3893–3899.
[7] I. Fisch, G. Künzi, K. Rose, R. E. Offord, *Bioconjugate Chem.* **1992**, *3*, 147–153.
[8] K. Rose, *J. Am. Chem. Soc.* **1994**, *116*, 30–33.
[9] B. A. Schwartz, G. R. Gray, *Arch. Biochem. Biophys.* **1977**, *181*, 542–549.
[10] P. Finch, Z. Merchant, *J. Chem. Soc. Perkin Trans. 1*, **1975**, 1682–1686. Preliminary ^1H and ^{13}C NMR investigations on amino-oxy acetic acid D-glucose oxime demonstrate the presence in solution of a mixture of three interconvertible isomers: the β-cyclic form and the acyclic *syn* (*E*) and *anti* (*Z*) forms.
[11] P. Dumy, I. M. Eggleston, S. Cervigni, U. Sila, X. Sun, M. Mutter, *Tetrahedron Lett.* **1995**, *36*, 1255–1258.
[12] The use of different peptides did not particularly affect the course of the reaction.
[13] R. Albert, P. Marbach, W. Bauer, U. Briner, G. Fricker, C. Bruns, J. Pless, *Life Sci.* **1993**, *53*, 517–525.
[14] Glucosone **2** (D-*arabino*-hexos-2-ulose) was prepared following the procedure of D. J. Walton, T. Hvidt, W. A. Szarek, *Carbohydrate Res.* **1987**, *167*, 123.
[15] M. Mutter, R. Hersperger, *Angew. Chem.* **1990**, *102*, 115; *Angew. Chem. Int. Ed. Engl.* **1990**, *29*, 185–187.
[16] The pure products **18** and **19** were characterized by electrospray ionization mass spectroscopy (ESI-MS). Found: 2135.6 (calcd: 2135.2).

Charge and Potential: Arenes as Oxidants**

Robert Weiss,* Robert May, and Bernd Pomrehn

We have shown that the transition from neutral to cationic sets of substituents achieved for both inorganic and organic systems by using the trimethylsilyltriflate-assisted poly(onio) substitution method developed by us leads to a marked increase in their electrophilicities and electron affinities.[1–5] This is attributed primarily to the electrostatic field effects of the cationic substituents. Recently we reported on the first per(onio) substitution of hexafluorobenzene with 4-dimethylaminopyridine (DMAP) as a preliminary highlight of this development.[6] We considered whether the electrostatic activation of the electron affinity of aromatic systems could be raised to such an extent that their "antiaromatic" (LUMO-filled) reduction products would be capable of existing as thermodynamically stable compounds such that their chemical properties could be investigated. This would open up new perspectives in the chemistry even of conventional aromatic compounds.

The protocol for transforming arenes into powerful oxidants by electrostatic activation is based on the fundamental conditions of Coulomb's Law:

1) introduction of the maximum number of onio substituents structurally possible at the organic π-electron system (per(onio) substitution);
2) the use of onium centers of the highest possible electropositivity so as to generate high pole strengths;
3) choice of the shortest possible distances of the positive poles from the organic system.

For a given structural type there is no freedom of choice with criterion 1). However, for criteria 2) and 3) it must be considered carefully whether the use of an element from the first period as an onium center produces a more efficient electrostatic effect than an isoelectronic element from a higher period, because the development of the positive charge of the onium center and its distance from the central system in this comparison are inversely related. Semiempirical calculations show that phosphonio substitutents are far more efficient for our purpose than triorganoammonio substituents.[7] This is consistent with the comparatively higher stability of phosphonium relative to ammonium ylides.

The attempt to achieve per(onio) substitution on hexafluorobenzene (**1**) by the reaction with PR_3/Me_3SiOTf (Tf = trifluoromethanesulfonyl) under a variety of conditions led only to the formation of the 1,4-bis-phosphonio-substituted system **4a,b** (Scheme 1).[8]

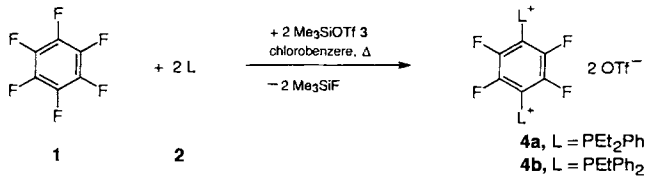

Scheme 1. Synthesis of 1,4-bis-phosphonio-substituted benzene derivatives.

Cyclic voltammetric investigations of the salts **4a,b** reveal two quasi-reversible redox steps at remarkably positive potentials (Table 1).[9] In spite of the relatively high electron affinity of **4a,b** these salts are not activated towards further nucleophilic substitution. This in sharp contrast to the analogous substitution of hexafluorobenzene with DMAP, which under autoactivation leads to per(onio)-substituted products.[6] In this case, in

Table 1. Half-wave potentials of the poly(onio)-substituted arenes [a].

Compound [9]	1st Reduction [V]	2nd Reduction [V]
4a	− 0.83 (q)	− 1.46 (q)
4b	− 0.76 (q)	− 1.36 (q)
6	0.04 (q)	− 0.09 (i)
7a	0.03 (r)	− 0.19 (r)
7b	0.14 (r)	− 0.06 (r)
9a	0.60 (r)	− 0.04 (r)
10	0.80 (r)	0.14 (r)

[a] r = reversible, q = quasi-reversible, i = irreversible.

[*] Prof. Dr. R. Weiss, Dr. R. May, Dr. B. Pomrehn
Institut für Organische Chemie der Universität Erlangen-Nürnberg
Henkestrasse 42, D-91054 Erlangen (Germany)
Fax: Int. code +(9131)859132

[**] This work was supported by the Deutsche Forschungsgemeinschaft and the Fonds der Chemischen Industrie.

ether phase decanted. The precipitate was washed several times with ether and finally dried to give the deprotected product as a white powder (13 mg, 91%).

The reductive amination was carried out using a modification of a published procedure [13]. In a typical experiment, the protected peptide **1a** (10 μmol) was dissolved in 2 mL of a 10:1 mixture of 0.1 M phosphate buffer (pH 6.0) and CH_3CN. To this peptide solution were added the carbohydrate (200 μmol) dissolved in 2 mL of the same buffer and sodium cyanoborohydride (200 μmol) as a solid. The mixture was stirred at room temperature and progress of the coupling reaction monitored by analytical HPLC. The glycopeptides were purified by semipreparative HPLC and characterized by ESI-MS.

Received: December 22, 1995 [Z8684IE]
German version: *Angew. Chem.* **1996**, *108*, 1325–1328

Keywords: glycopeptides · lipopeptides · oximes · solid-phase syntheses

[1] I. J. Goldstein, R. C. Hugues, M. Monsigny, T. Osawa, N. Sharon, *Nature* **1980**, *285*, 66; N. Sharon, H. Lis, *The Proteins, Vol. 5*, Academic Press, New York, **1982**, pp. 1–123.
[2] J. F. Fisher, A. W. Harrison, G. L. Bundy, K. F. Wilkinson, B. D. Rush, M. J. Ruwart, *J. Med. Chem.* **1991**, *34*, 3140–3143.
[3] H. Kunz, *Angew. Chem.* **1987**, *99*, 297; *Angew. Chem. Int. Ed. Engl.* **1987**, *26*, 294–308; U. Sprengard, G. Kretzschmar, E. Bartnick, C. Hüls, H. Kunz, *ibid.* **1995**, *107*, 1104 and **1995**, *34*, 990–993; O. Frey, M. Hoffmann, H. Kessler, *ibid.* **1995**, *107*, 2194–2195 and **1995**, *34*, 2026–2028.
[4] M. Schnölzer, S. B. H. Kent, *Science* **1992**, *256*, 221–225; P. E. Dawson, T. W. Muir, I. Clark-Lewis, S. B. H. Kent, *ibid.* **1994**, *266*, 776–779; G. Tuchscherer, *Tetrahedron Lett.* **1993**, *34*, 8419–8422.
[5] P. E. Dawson, S. B. H. Kent, *J. Am. Chem. Soc.* **1993**, *115*, 7263–7266.
[6] J. Shao, J. P. Tam, *J. Am. Chem. Soc.* **1995**, *117*, 3893–3899.
[7] I. Fisch, G. Künzi, K. Rose, R. E. Offord, *Bioconjugate Chem.* **1992**, *3*, 147–153.
[8] K. Rose, *J. Am. Chem. Soc.* **1994**, *116*, 30–33.
[9] B. A. Schwartz, G. R. Gray, *Arch. Biochem. Biophys.* **1977**, *181*, 542–549.
[10] P. Finch, Z. Merchant, *J. Chem. Soc. Perkin Trans. 1*, **1975**, 1682–1686. Preliminary ^1H and ^{13}C NMR investigations on amino-oxy acetic acid D-glucose oxime demonstrate the presence in solution of a mixture of three interconvertible isomers: the β-cyclic form and the acyclic *syn* (*E*) and *anti* (*Z*) forms.
[11] P. Dumy, I. M. Eggleston, S. Cervigni, U. Sila, X. Sun, M. Mutter, *Tetrahedron Lett.* **1995**, *36*, 1255–1258.
[12] The use of different peptides did not particularly affect the course of the reaction.
[13] R. Albert, P. Marbach, W. Bauer, U. Briner, G. Fricker, C. Bruns, J. Pless, *Life Sci.* **1993**, *53*, 517–525.
[14] Glucosone **2** (D-*arabino*-hexos-2-ulose) was prepared following the procedure of D. J. Walton, T. Hvidt, W. A. Szarek, *Carbohydrate Res.* **1987**, *167*, 123.
[15] M. Mutter, R. Hersperger, *Angew. Chem.* **1990**, *102*, 115; *Angew. Chem. Int. Ed. Engl.* **1990**, *29*, 185–187.
[16] The pure products **18** and **19** were characterized by electrospray ionization mass spectroscopy (ESI-MS). Found: 2135.6 (calcd: 2135.2).

Charge and Potential: Arenes as Oxidants**

Robert Weiss,* Robert May, and Bernd Pomrehn

We have shown that the transition from neutral to cationic sets of substituents achieved for both inorganic and organic systems by using the trimethylsilyltriflate-assisted poly(onio) substitution method developed by us leads to a marked increase in their electrophilicities and electron affinities.[1–5] This is attributed primarily to the electrostatic field effects of the cationic substituents. Recently we reported on the first per(onio) substitution of hexafluorobenzene with 4-dimethylaminopyridine (DMAP) as a preliminary highlight of this development.[6] We considered whether the electrostatic activation of the electron affinity of aromatic systems could be raised to such an extent that their "antiaromatic" (LUMO-filled) reduction products would be capable of existing as thermodynamically stable compounds such that their chemical properties could be investigated. This would open up new perspectives in the chemistry even of conventional aromatic compounds.

The protocol for transforming arenes into powerful oxidants by electrostatic activation is based on the fundamental conditions of Coulomb's Law:

1) introduction of the maximum number of onio substituents structurally possible at the organic π-electron system (per(onio) substitution);
2) the use of onium centers of the highest possible electropositivity so as to generate high pole strengths;
3) choice of the shortest possible distances of the positive poles from the organic system.

For a given structural type there is no freedom of choice with criterion 1). However, for criteria 2) and 3) it must be considered carefully whether the use of an element from the first period as an onium center produces a more efficient electrostatic effect than an isoelectronic element from a higher period, because the development of the positive charge of the onium center and its distance from the central system in this comparison are inversely related. Semiempirical calculations show that phosphonio substitutents are far more efficient for our purpose than triorganoammonio substituents.[7] This is consistent with the comparatively higher stability of phosphonium relative to ammonium ylides.

The attempt to achieve per(onio) substitution on hexafluorobenzene (**1**) by the reaction with PR_3/Me_3SiOTf (Tf = trifluoromethanesulfonyl) under a variety of conditions led only to the formation of the 1,4-bis-phosphonio-substituted system **4a,b** (Scheme 1).[8]

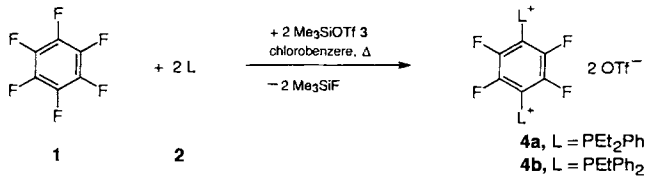

Scheme 1. Synthesis of 1,4-bis-phosphonio-substituted benzene derivatives.

Cyclic voltammetric investigations of the salts **4a,b** reveal two quasi-reversible redox steps at remarkably positive potentials (Table 1).[9] In spite of the relatively high electron affinity of **4a,b** these salts are not activated towards further nucleophilic substitution. This in sharp contrast to the analogous substitution of hexafluorobenzene with DMAP, which under autoactivation leads to per(onio)-substituted products.[6] In this case, in

Table 1. Half-wave potentials of the poly(onio)-substituted arenes [a].

Compound [9]	1st Reduction [V]	2nd Reduction [V]
4a	− 0.83 (q)	− 1.46 (q)
4b	− 0.76 (q)	− 1.36 (q)
6	0.04 (q)	− 0.09 (i)
7a	0.03 (r)	− 0.19 (r)
7b	0.14 (r)	− 0.06 (r)
9a	0.60 (r)	− 0.04 (r)
10	0.80 (r)	0.14 (r)

[a] r = reversible, q = quasi-reversible, i = irreversible.

[*] Prof. Dr. R. Weiss, Dr. R. May, Dr. B. Pomrehn
Institut für Organische Chemie der Universität Erlangen-Nürnberg
Henkestrasse 42, D-91054 Erlangen (Germany)
Fax: Int. code +(9131)859132

[**] This work was supported by the Deutsche Forschungsgemeinschaft and the Fonds der Chemischen Industrie.

addition to steric effects, electronic effects are probably responsible for the resulting products. According to PM3 calculations the LUMO of **4a,b** is predominantly localized on C atoms positioned α to the phosphonio substitutents, so that the electronic prerequisites for further onio substitution are unfavorable.

The hitherto unknown per(onio) substitution on naphthalene should, because of the larger number of cationic substituents and the inherently higher electron affinity of naphthalene, lead to a further increase of the electron affinity relative to that of the analogous benzene derivatives. By using DMAP/Me_3SiOTf and octafluoronaphthalene (**5**) we achieved per(onio) substitution in the naphthalene system for the first time. The octacationic salt **6** could be isolated as a stable, water-soluble, pale yellow compound in almost quantitative yield (Scheme 2). The replacement

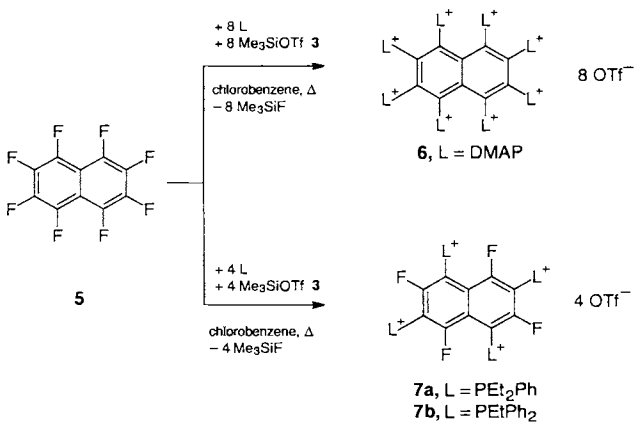

Scheme 2. Octakis- and tetrakis(onio) substitution of octafluoronaphthalene.

of DMAP with tertiary phosphanes led under otherwise identical conditions exclusively to the formation of good yields of the tetrasubstituted products **7a,b**, in which the fluoro and triorganophosphonio substituents alternated along the periphery of the naphthalene core. Investigations into the regiochemistry of the S_NAr reaction at octafluoronaphthalene indicate that substitutions at C-2/C-6 precede those at C-4/C-8.[10] The interplay of steric and electronic factors evidently hinders per(onio) substitution by phosphonio substituents as for the benzene system.

Electrochemical measurements on salts **6** and **7a,b** confirm an unprecedented high electron affinity for benzenoid aromatic compounds (cf Table 1). Remarkably, four triorganophosphonio substituents are as effective in raising the redox potentials as eight pyridinio substituents—an expected trend (see above) in view of the higher capability of phosphonio substituents to stabilize carbanions. The tetraphosphonio-substituted salts **7a,b** represent the ox-forms of a new, completely reversible two-step redox system whose oxidizing power is similar to that of chloranil.[11]

According to PM3 model calculations, replacement of the CF groups by N in salts of the type **7a,b** should lead to an even larger increase in the electron affinity.[7] This could be confirmed experimentally. The reaction of tetrachloropyrimido-[5,5-*d*]pyrimidine[12] (**8**) with four molar equivalents of PEt_3/Me_3SiOTf led smoothly to the formation of the corresponding tetrakis(onio)-substituted salt **9a** (Scheme 3).[13]

The "aromatic" compound **9a** is the ox-form of a completely reversible two-step redox system (Table 1) and, with a half-wave potential of 0.60 V (vs. Ag/AgCl) for the transition ox/sem, has at least the oxidizing power of 2,3-dichloro-5,6-dicyanobenzoquinone (DDQ) one of the most powerful organic oxidizing

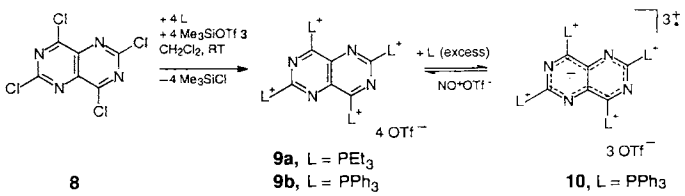

Scheme 3 Onio substitution of tetrachloropyrimido[5,4-*d*]pyrimidine. RT = room temperature.

agents used in organic synthesis.[11] As a consequence of the increasing positive charge on the phosphorus center when alkyl is replaced by aryl[8b] the intially formed salt **9b**, obtained when PPh_3 is used analogously as a nucleophile, already has such a high electron affinity that it is quantitatively reduced by excess phosphane to the new tricationic radical salt **10**. The latter is a deep green isolable salt that has been fully characterized, including by a high-resolution ESR spectrum. With a strong oxidizing agent such as NO^+ **10** may be reconverted to **9b**. The measured half-wave potential for this conversion of 0.80 V (vs. Ag/AgCl) establishes this compound as the most powerful "aromatic oxidant" known to date. Calculations show that the charge distributions in the antiaromatic red-forms of the polyphosphonio salts **4, 7, 9** are characterized by a maximum charge pairing in terms of the bis-ylidic mesomeric structures **A** and **B/C** (Fig. 1).

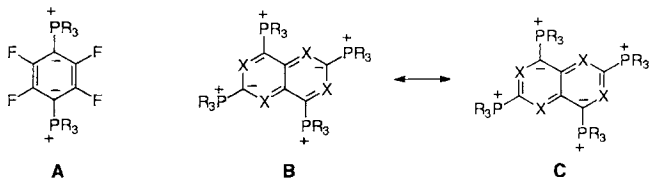

Fig. 1. Bis-ylidic mesomeric structures of the red-forms. X = CF, N.

The position of the pertinent redox potentials and the reversibility of the corresponding reduction steps (cf Table 1) opens up the prospect of generating such systems in a straightforward manner by chemical methods. With the synthesis of the sem-form **10** the first step in this direction has already been taken. Owing to the clear structural analogy with the corresponding quinones we designate the red-forms **A**–**C** as "quinobis-ylides".[14] The controlled reductive generation of suitable representatives of this class of substances is the subject of current investigations.

Experimental Procedure

All reactions were carried out under N_2 and in dried solvents. Correct C, H, N analyses were obtained for all compounds prepared.

4a,b: Compound **3** (2 mmol) and PEt_2Ph or $PEtPh_2$ (2 mmol) were added to a solution of **1** (1 mmol) in chlorobenzene (20 mL) and the solution was stirred under reflux. After 24 h (**4a**; or 72 h for **4b**) the white precipitate was filtered off, washed with Et_2O (5 × 5 mL) and dried for 12 h under high vacuum.

4a: Yield: 99%; ^1H NMR (400.05 MHz, CD_3NO_2/CF_3COOD, 21 °C, TMS): δ = 7.95 (m, 6H; H-2/H-4/H-6, phenyl), 7.80 (m, 4H; H-3/H-5, phenyl), 3.20 (m, 8H; CH_2), 1.38 (dt, $^3J(H,P)$ = 22.21 Hz, $^3J(H,H)$ = 7.56 Hz, 12H; CH_3); ^{13}C NMR (100.5 MHz, CD_3NO_2/CF_3COOD, 21 °C, TMS): δ = 150.27 (dm, $^1J(C,F)$ = – 255.5 Hz; C2/C3/C5/C6, benzene), 137.54 (s; C4, phenyl), 133.61 (d, $^2J(C,P)$ = 9.2 Hz; C2/C6, phenyl), 132.03 (d, $^3J(C,P)$ = 12.8 Hz; C3/C5, phenyl), 121.67 (q, $^1J(C,F)$ = – 319.8 Hz; CF_3), 116.40 (d, $^1J(C,P)$ = 84.5 Hz; C1, phenyl), 109.43 (dm, $^1J(C,P)$ = 84.5 Hz; C1/C4, benzene), 15.65 (d, $^1J(C,P)$ = 49.7 Hz; CH_2), 6.09 (d, $^2J(C,P)$ = 3.7 Hz; CH_3); ^{31}P NMR (161.7 MHz, CD_3NO_2/CF_3COOD, 21 °C, ext. H_3PO_4): δ = 35.53 (s).

4b: Yield: 50%; ^1H NMR (400.05 MHz, CD_3NO_2/CF_3COOD, 23 °C, TMS): δ = 7.99 (m, 12H; H-2/H-4/H-6, phenyl), 7.85 (m, 8H; H-3/H-5, phenyl), 3.54 (m,

4H; CH_2), 1.41 (dt, $^3J(H,P) = 22.70$ Hz; $^3J(H,H) = 7.33$ Hz; 6H; CH_3); ^{13}C NMR (100.5 MHz, CD_3NO_2, CF_3COOD, 23 °C, TMS): $\delta = 150.14$ (dm, $^1J(C,F) = -265.7$ Hz; C2/C3/C5/C6, benzene), 137.83 (d, $^4J(C,P) = 3.6$ Hz; C4, phenyl), 134.82 (d, $^2J(C,P) = 11.1$ Hz; C2/C6, phenyl), 132.14 (d, $^3J(C,P) = 12.9$ Hz; C3/C5, phenyl), 121.71 (q, $^1J(C,F) = -318.0$ Hz; CF_3), 115.80 (d, $^1J(C,P) = 88.3$ Hz; C1, phenyl), 110.65 (dm, $^1J(C,P) = 88.3$ Hz; C1/C4, benzene), 19.36 (d, $^1J(C,P) = 49.7$ Hz; CH_2), 6.94 (d, $^2J(C,P) = 5.5$ Hz; CH_3); ^{31}P NMR (161.7 MHz, CD_3NO_2, CF_3COOD, 23 °C, ext. H_3PO_4): $\delta = 26.71$ (s).

6: Compound **3** (0.80 mL, 4.43 mmol) and **6** (0.605 g, 4.95 mmol) were added to a solution of **5** (0.149 g, 0.55 mmol) in chlorobenzene (20 mL) and the solution was stirred under reflux. After 12 h the yellow precipitate was filtered off, washed with CH_2Cl_2 (4 × 5 mL) and dried for 12 h under high vacuum. Yield: 1.24 g (98%); ^1H NMR (400.05 MHz, CD_3CN, 24 °C, TMS): $\delta = 8.05$ (d, $^3J(H,H) = 7.57$ Hz, 8H; H-2/H-6), 7.83 (d, $^3J(H,H) = 7.57$ Hz, 8H; H-2/H-6), 6.87 (d, $^3J(H,H) = 7.57$ Hz, 8H; H-3/H-5), 6.86 (d, $^3J(H,H) = 7.57$ Hz, 8H; H-3/H-5), 3.24 (s, 24H; CH_3), 3.20 (s, 24H; CH_3); ^{13}C NMR (100.5 MHz, CD_3CN, 24 °C, TMS): $\delta = 157.30$ (s; C4, DMAP), 156.81 (s; C4, DMAP), 142.29 (s; C2/C6, DMAP), 140.42 (s; C2/C6, DMAP), 140.37 (s; C1/C4/C5/C8, naphthalene), 138.49 (s; C2/C3/C6/C7, naphthalene), 131.34 (s; C9/C10, naphthalene), 121.88 (q, $^1J(C,F) = -319.9$ Hz; CF_3), 110.86 (s; C3/C5, DMAP), 110.70 (s; C3/C5, DMAP), 41.80 (s; CH_3), 41.60 (s; CH_3); ^{19}F NMR (470.4 MHz, CD_3CN, 20 °C, C_6F_6): $\delta = -77.9$ (s; CF_3).

7a,b: Compound **3** (2 mmol) and PEt_2Ph or $PEtPh_2$ (2 mmol) were added to a solution of **5** (0.5 mmol) in chlorobenzene (20 mL) and the solution was stirred under reflux. After 48 h the suspension was cooled to −20 °C, the precipitation was completed by the addition of Et_2O (20 mL), and the precipitate was filtered off, washed with Et_2O (5 × 5 mL), and dried for 12 h under high vacuum.

7a: pale yellow powder; yield: 95%; ^1H NMR (400.05 MHz, CD_3CN, 24 °C, TMS): $\delta = 7.85$ (m, 8H; H-2/H-6, phenyl), 7.73 (m, 4H; H-4, phenyl), 7.67 (m, 8H; H-3/H-5, phenyl), 2.85 (m, 16H; CH_2), 1.06 (dt, $^3J(H,P) = 21.73$ Hz, $^3J(H,H) = 7.57$ Hz, 12H; CH_3), 1.01 (dt, $^3J(H,P) = 22.22$ Hz, $^3J(H,H) = 7.32$ Hz, 12H; CH_3); ^{13}C NMR (100.5 MHz, CD_3CN, 24 °C, TMS): $\delta = 167.65$ (dd, $^1J(C,F) = -262.9$ Hz, $^2J(C,F) = 10.1$ Hz; C4/C8, naphthalene), 166.26 (dm, $^1J(C,F) = -270.3$ Hz; C2/C6, naphthalene), 136.82 (d, $^4J(C,P) = 3.7$ Hz; C4, phenyl), 135.99 (s; C4, phenyl), 133.39 (d, $^2J(C,P) = 11.0$ Hz; C2/C6, phenyl), 132.27 (d, $^2J(C,P) = 9.2$ Hz; C2/C6, phenyl), 131.63 (d, $^3J(C,P) = 12.8$ Hz; C3/C5, phenyl), 131.46 (d, $^3J(C,P) = 12.9$ Hz; C3/C5, phenyl), 129.88 (m; C9/C10, naphthalene), 121.92 (q, $^1J(C,F) = -319.9$ Hz; CF_3), 120.01 (d, $^1J(C,P) = 86.4$ Hz; C1, phenyl), 116.31 (d, $^1J(C,P) = 84.6$ Hz; C1, phenyl), 106.46 (m; C3/C7, naphthalene), 102.26 (dd, $^1J(C,P) = 75.3$ Hz, $^2J(C,F) = 19.4$ Hz; C1/C5, naphthalene), 17.78 (d, $^1J(C,P) = 44.1$ Hz; CH_2), 15.40 (d, $^1J(C,P) = 47.8$ Hz; CH_2), 6.64 (d, $^2J(C,P) = 3.7$ Hz; CH_3), 6.11 (d, $^2J(C,P) = 5.5$ Hz; CH_3); ^{19}F NMR (470.4 MHz, CD_3CN, 20 °C, C_6F_6): $\delta = -78.0$ (s, 12F; CF_3), −74.8 (m, 2F; F-4/F-8), −67.9 (m, 2F; F-2/F-6); ^{31}P NMR (161.7 MHz, CD_3CN, 20 °C, ext. H_3PO_4): $\delta = 42.98$ (dd, $^3J(P,F) = 18.4$ Hz; $^3J(P,F) = 8.2$ Hz; P-3/P-7), 35.71 (d, $^3J(P,F) = 6.2$ Hz; P-1/P-5).

7b: pale orange powder; yield: 88%; ^1H NMR (400.05 MHz, CD_3CN, 21 °C, TMS): $\delta = 7.85$–7.62 (m, 40H; phenyl), 3.33 (m, 8H; CH_2), 1.11 (m, 12H; CH_3); ^{13}C NMR (100.5 MHz, CD_3CN, 21 °C, TMS): $\delta = 137.19$ (s; C4, phenyl), 136.69 (s; C4, phenyl), 133.34 (d, $^2J(C,P) = 11.0$ Hz; C2/C6, phenyl), 132.55 (d, $^2J(C,P) = 11.1$ Hz; C2/C6, phenyl), 131.66 (d, $^3J(C,P) = 14.7$ Hz; C3/C5, phenyl), 130.70 (d, $^3J(C,P) = 12.9$ Hz; C3/C5, phenyl), 129.66 (m; C9/C10, naphthalene), 121.92 (q, $^1J(C,F) = -319.9$ Hz; CF_3), 119.10 (d, $^1J(C,P) = 86.4$ Hz; C1, phenyl), 115.57 (d, $^1J(C,P) = 84.6$ Hz; C1, phenyl), 103.72 (m; C3/C7, naphthalene), 101.18 (m; C1/C5, naphthalene), 18.53 (d, $^1J(C,P) = 51.5$ Hz; CH_2), 17.44 (d, $^1J(C,P) = 53.3$ Hz; CH_2), 8.21 (d, $^2J(C,P) = 5.5$ Hz; CH_3), 7.09 (d, $^2J(C,P) = 3.7$ Hz; CH_3); ^{19}F NMR (470.4 MHz, CD_3CN, 20 °C, C_6F_6): $\delta = -78.0$ (s, 12F; CF_3), −69.0 (m, 2F; F-4/F-8), −66.6 (m, 2F; F-2/F-6); ^{31}P NMR (161.7 MHz, CD_3CN, 20 °C, ext. H_3PO_4): $\delta = 32.63$ (d, $^3J(P,F) = 18.2$ Hz; P-3/P-7), 26.07 (d, $^3J(P,F) = 4.1$ Hz; P-1/P-5).

9a: Compound **9** (1 mmol) was suspended in CH_2Cl_2 (30 mL) and **3** (4 mmol) was added. Subsequently, PEt_3 (4 mmol) dissolved in CH_2Cl_2 (10 mL) was added to the mixture. After the mixture had been stirred for 12 h at room temperature, the pale green precipitate was filtered off, washed with CH_2Cl_2 (3 × 5 mL) and dried for 12 h under high vacuum. Yield: 62%; ^1H NMR (399.65 MHz, CD_3CN, 20 °C, TMS): 2.85 (m, 24H; CH_2) 1.29 (m, 36H; CH_3).

10: Compound **9** (1 mmol) was suspended in CH_2Cl_2 (20 mL) and **3** (4 mmol) was added. Subsequently PPh_3 (6 mmol) dissolved in CH_2Cl_2 (20 mL) was added to the mixture. After the mixture had been stirred for 12 h at room temperature Et_2O (100 mL) was added to precipitate a green solid. The solid was filtered off, washed with Et_2O (3 × 5 mL) and dried for 12 h under vacuum. Yield: 69%; UV/Vis (CH_3CN): λ_{max} (ε) = 668 (4870), 614 (5355), %72 (2920), 439 (6330), 382 (8520), 270 (37085), 214 (91945).

Received: December 15, 1995 [Z 8655 IE]
German version: *Angew. Chem.* **1996**, *108*, 1319–1321

Keywords: arenes · heterocycles · nucleophilic aromatic substitutions · phosphonium salts · polycations

[1] R. Weiss, N. J. Salomon, G. E. Miess, R. Roth, *Angew. Chem.* **1986**, *98*, 925; *Angew. Chem. Int. Ed. Engl.* **1986**, *25*, 917.
[2] R. Weiss, R. Roth, *J. Chem. Soc. Chem. Commun.* **1987**, 317.
[3] R. Weiss, R. Roth, *Synthesis* **1987**, 870.
[4] R. Weiss, J. Seubert, *Angew. Chem.* **1994**, *106*, 900; *Angew. Chem. Int. Ed. Engl.* **1994**, *33*, 891.
[5] R. Weiss, J. Seubert, F. Hampel, *Angew. Chem.* **1994**, *106*, 2038; *Angew. Chem. Int. Ed. Engl.* **1994**, *33*, 1952.
[6] R. Weiss, B. Pomrehn, F. Hampel, W. Bauer, *Angew. Chem.* **1995**, *107*, 1446; *Angew. Chem. Int. Ed. Engl.* **1995**, *34*, 1319.
[7] B. Pomrehn, Dissertation, Universität Erlangen-Nürnberg, **1996**.
[8] The corresponding salts of the benzene parent structure have already been reported: a) L. Horner, G. Mummenthey, H. Moser, P. Beck, *Chem. Ber.* **1966**, *99*, 2782; b) H. Bock, U. L. Knoblauch, P. Hamel, *ibid.* **1986**, *119*, 3749.
[9] The electrochemical investigations were carried out at room temperature under N_2 with ferrocene as the internal standard in a 0.1 N NEt_4BF_4/CH_3CN electrolyte solution against a saturated Ag/AgCl electrode immersed in a 0.1 N NEt_4Cl/CH_3CN solution. Auxiliary and working electrodes were made of platinum.
[10] C. L. Cheong, B. J. Wakefield, *J. Chem. Soc. Perkin Trans. 1* **1988**, 3301.
[11] M. E. Peover, *J. Chem. Soc.* **1962**, 4540.
[12] F. G. Fischer, J. Roch, W. P. Neumann, *Liebigs Ann. Chem.* **1960**, *631*, 147.
[13] R. May, Dissertation, Universität Erlangen-Nürnberg, **1993**.
[14] Because of the inverse polarity of the functional groups the red-forms may also be designated as "antiquinones".

A New Mode of Reaction of *tert*-Butylphosphaethyne: Trinuclear Cyclopentadienylcobalt Clusters with P, PS, and PO as μ_3 Complex Ligands**

Jan Foerstner, Falk Olbrich, and Holger Butenschön*

Dedicated to Professor Erwin Weiss on the occasion of his 70th birthday

"Phosphaalkynes correspond to alkynes in all aspects, to nitriles in nothing." This remark by Regitz[1] is substantiated by the results of our investigations of the chemistry of [ω-phosphanyl(ethylcyclopentadienyl)]cobalt complexes. Herein we report on reactions of such complexes with *tert*-butylphosphaethyne that in addition to diphosphete complexes result in the formation of μ_3-phosphido clusters in good yields. The "naked" phosphorus ligand in these clusters can be oxidized with elemental sulfur or with oxygen in the air to give PS and PO ligands, respectively.

The chemistry of phosphaethynes has been investigated intensely in the past few years.[2] In a few cases mononuclear transition metal complexes with a monomeric phosphaethyne ligand have been prepared.[3–5] Because we were able to coordinate alkynes with the [(ω-di-*tert*-butylphosphanyl)ethylcyclopentadienyl]cobalt (Cp'Co) fragment without di- or trimerization,[6, 7] we investigated reactions of Cp'Co complexes with *tert*-butylphosphaethyne. The paramagnetic chloride **1** and the

[*] Prof. Dr. H. Butenschön, Dipl.-Chem. J. Foerstner
Institut für Organische Chemie der Universität
Schneiderberg 1B, D-30167 Hannover (Germany)
Fax: Int. code +(511)762-4616
e-mail: holger.butenschoen@mbox.oci.uni-hannover.de
Dr. F. Olbrich
Chemisches Institut der Universität Magdeburg (Germany)

[**] We thank the Deutsche Forschungsgemeinschaft and the Fonds der Chemischen Industrie for their financial support and BASF AG, Bayer AG, Chemetall GmbH, and Hüls AG for donations of chemicals. We are indebted to ENRAF-NONIUS for their kind support in performing the X-ray crystal structure analysis. We thank Dr. G. Remberg, Göttingen, and Dr. A. Kornick, Hannover, for mass spectra and helpful discussions.

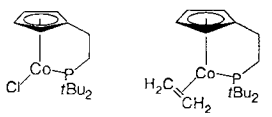

1 2

ethene complex **2** generated from **1** proved to be good starting materials for Cp'Co complexes: they were applied either in the presence of sodium/amalgam (**1**) or directly (**2**) with a new ligand. The reaction starting with **1** avoids the detour via the ethene complex **2** and usually results in higher yields. Compound **2** should be used as starting material in reactions with ligands (for example arenes) that can undergo side reactions with sodium amalgam.[7]

Treatment of **1** in the presence of sodium amalgam at $-50\,^{\circ}C$ with a threefold molar excess of *tert*-butylphosphaethyne, followed by allowing the mixture to warm up to $-30\,^{\circ}C$ gives the diphosphete complex **3**, in which the "phosphane arm" has been decomplexed, in 71% yield (Scheme 1). A compound analagous

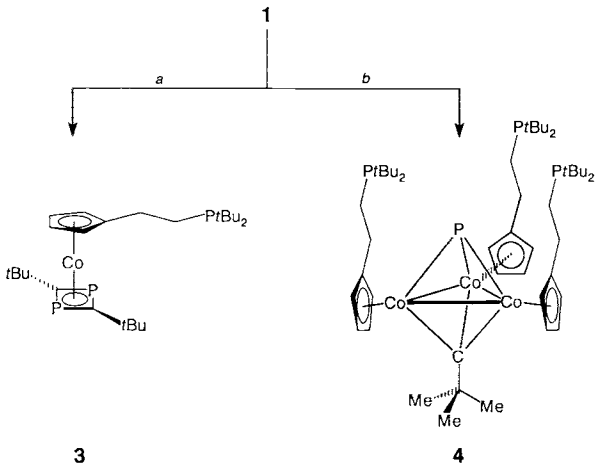

3 4

Scheme 1. a) 3 equiv PC*t*Bu, Na/Hg, THF, $-50 \rightarrow -30\,^{\circ}C$, 4 h, 71%; b) 0.33 equiv PC*t*Bu, Na/Hg, THF, $-50 \rightarrow 20\,^{\circ}C$, 90 min, 85%.

to **3** is obtained by the reaction of cyclopentadienyldi(ethene)cobalt(I) with *tert*-butylphosphaethyne.[8, 9] However, treatment of *tert*-butylphosphaethyne with a threefold excess of **1** at 20 °C leads unexpectedly to the μ_3-carbyne-μ_3-phosphidotricobalt cluster **4** as the sole product in 85% yield. Treatment of **2** with an equimolar amount of *tert*-butylphosphaethyne results in the diphosphete complex **3** (50% yield) together with cluster **4** (5% yield). Such a mode of reaction of *tert*-butylphosphaethyne, which is characterized by a complete breakage of the phosphorus–carbon triple bond and coordination of the phosphorus atom and the carbyne fragment on opposite faces of the tricobalt plane, was hitherto unkown. The quotation of Regitz mentioned at the beginning is confirmed impressively, however, because such reactions of alkynes have been observed at high temperatures (195 °C) and lead to biscarbyne clusters.[10–12] Zenneck et al.[13] and Stone et al.[14] have described compounds that result from cleavage of the P–C bond of *tert*-butylphosphaethyne and subsequent reformation of new P–C bonds.

The question of how important is it to start from cyclopentadienylcobalt complexes like **1** or **2** with a phosphanylalkyl substituent for the formation of clusters like **4** was studied by treating common cyclopentadienyl- and pentamethylcyclopentadienylcobalt compounds with *tert*-butylphosphaethyne. The reaction of cyclopentadienyldi(ethene)cobalt with *tert*-butylphosphaethyne for 3 h at 20 °C, followed by evaporation of the solvent, and heating up to 180 °C for 5 min gave no evidence for the formation of a cluster corresponding to **4**.

Treatment of a 1.5 molar excess of $[\{Cp^*CoCl\}_2]$,[15] the dimer corresponding to **1** with pentamethylcyclopentadienyl (Cp*) ligands instead of the Cp' ligand, under the conditions chosen for **1** resulted in a mixture of the diphosphete complex[16] and traces of cluster **5** corresponding to **4** in an overall yield of 57%. When the reaction mixture was heated to 180 °C, **5** was obtained as the only isolated product in 1-2% yield. Thus, the "phosphane arm" promotes the formation of **4** extraordinarily. Possibly in the reaction sequence leading to **4**, initially the originally desired complex with *tert*-butylphosphaethyne is formed, which then reacts further with excess **1** leading to the formation of the tricobalt cluster. Compound **3** does not react with **1** to give **4**, and therefore it is not regarded as an intermediate in the formation of **4**. To date there are only a few μ_3-phosphido clusters known; these have been generated by treatment of phosphorus(III) halides or even P_4 with low-valent transition metal complexes.[17–21]

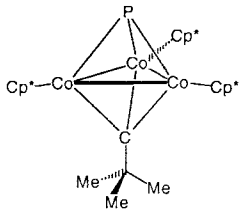

5 $Cp^* = C_5Me_5$

Preliminary studies on the reactivity were performed by treating the cluster **4** with elemental sulfur. Within 20 min **4** reacts with S_8 in diethyl ether at 20 °C to give the air-stable sulfuration product **6** in 77% yield, in which all four phosphorus atoms have been oxidized (Scheme 2). Compound **6** is one of the very rare complexes with PS as a ligand.[22, 23] In addition to the main product **6**, the phosphorus monoxide complex **7** was separated by column chromatography in low but reproducible yield (1–2%). It is probably generated from incompletely sulfurated product on the chromatography phase silica gel and adsorbed oxygen. This suggests that **4** is initially sulfurated at the phosphorus atoms of the phosphane fragments and then at the phosphido ligand. Oxidation of **4** with oxygen in air leads to the cluster **8**, which is oxidized at all four phosphorus atoms, in good yield (68%). This was characterized by mass spectrometry but decomposes very fast. Compounds **7** and **8** are examples of a rare class of complexes with PO as ligand, first discovered by Scherer et al., which otherwise were only found in interstellar space or as short-lived extremely reactive species.[24–26] The new compounds were characterized by spectroscopy and mass spectrometry (Table 1), and the structure of the PO complex **7** was determined by X-ray structure analysis (Fig. 1).[33]

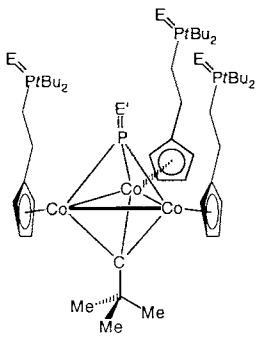

6: E = E' = S
7: E = S, E' = O
8: E = E' = O

6 + **7** $\xleftarrow{a}$ **4** $\xrightarrow{b}$ **8**

Scheme 2. a) 1. S_8, Et_2O, 20 °C, 20 min; 2. column chromatography on silica gel (petroleum ether/diethyl ether 6:1, red fraction), **6** (77%), elution with diethyl ether (orange fraction) **7** (1–2%). b) 1. Air oxygen, diethyl ether; 2. column chromatography on silica gel, ethyl acetate/ethanol 1:1, red fraction) **8** (68%).

The structure of **7** in the crystal shows a distorted, nearly C_3 symmetrical trigonal bipyramid in which three cobalt atoms Co1, Co2, and Co3 form the base. The phosphorus atom P4 of the PO ligand is located nearly perpendicular above the center of this plane, below which the carbon atom C16 of the *tert*-butylcarbyne ligand is located. The axis comprising the atoms O, P4, C16, and C17 is almost linear (angle O-P4-C16 179.3°,

Table 1. Selected spectroscopic data of new compounds (+ and − denote the positive (C, CH_3) and negative phase (CH, CH_3), respectively, in APT ^{13}C NMR spectra). All compounds gave satisfactory elemental analyses or high-resolution mass spectra.

3: ^1H NMR (200 MHz, C_6D_6): $\delta = 1.04$ (s, 18H), 1.27 (d, 18H, $^3J(P,H) = 11$ Hz), 2.08 (dt, 2H, $^3J(P,H) = 11$ Hz, $^3J(H,H) = 6$ Hz), 3.08 (m, 2H, $^2J(P,H) = 13$ Hz, $^3J(H,H) = 6$ Hz), 4.8 (m, 2H, $SJ = 4$ Hz), 5.23 (m, 2H). ^{13}C NMR (50 MHz, C_6D_6): $\delta = 23.7$ (+, d, PCH_2CH_2, $^2J(P,C) = 22$ Hz), 30.3 (−, $PCCH_3$, $^2J(P,C) = 13.8$ Hz), 31.5 (−, t, P_2CCCH_3, $^3J(P,C) = 4.6$ Hz), 31.6 (+, d, $PCCH_3$, $^1J(P,C) = 23$ Hz), 34.5 (+, t, P_2CCCH_3, $^2J(P,C) = 6.9$ Hz), 40.6 (+, d, PCH_2CH_2, $^1J(P,C) = 17.6$ Hz), 79.5 (−, cyclopentadienyl-*C*H), 81.1 (−, cyclopentadienyl-*C*H), 105.6 (+, d, cyclopentadienyl-*C*CH$_2$, $J(C,P) = 14$ Hz), 108.5 (+, t, $^1J(P,C) = 54.3$ Hz). ^{31}P NMR (81 MHz, C_6D_6, ext. standard H_3PO_4): $\delta = 37.8$ (P_2CCCH_3), 28.9 ($PCCH_3$). MS (70 eV): *m/z*: 496 (M^+, 3%).

4: ^1H NMR (400 MHz, C_6D_6): $\delta = 1.20$ (d, 54H, $PCCH_3$, $^3J(P,H) = 10.7$ Hz), 1.70 (m, 2H, PCH_2CH_2), 2.39 (m, 2H, PCH_2, $^2J(P,H) = 8.3$ Hz), 2.45 (s, 9H, Co_3CCCH_3), 4.42 (AA'BB', 2H, cyclopentadienyl-H, $\Sigma J = 4$ Hz), 4.96 (AA'BB', 2H, cyclopentadienyl-H). ^{13}C NMR (100 MHz, C_6D_6): $\delta = 24.2$ (+, d, CH_2), 24.3 (+, d, CH_2), 29.9 (−, d, $PCCH_3$, $^2J(P,C) = 13.5$ Hz), 31.4 (+, d, $PCCH_3$, $^1J(P,C) = 24.5$ Hz), 37.3 (−, Co_3CCCH_3), 59.9 (+, Co_3CCCH_3), 67.9 (+, d, Co_3CCCH_3, $^2J(P,C) = 10.1$ Hz), 81.0 (−, cyclopentadienyl-*C*H), 81.9 (−, d, cyclopentadienyl-*C*H, $J(P,C) = 1.9$ Hz), 103.8 (+, d, cyclopentadienyl-*C*CH$_2$, $J(P,C) = 15.2$ Hz). ^{31}P NMR (162 MHz, C_6D_6, ext. standard H_3PO_4): $\delta = 27.0$ (s), 189.9 (br. s). MS (CI - methane): *m/z*: 989.9 (M^+, 10%).

5: ^1H NMR (200 MHz, CD_2Cl_2): $\delta = 1.63$ (s, 45H), 2.29 (s, 9H). MS (70 eV): *m/z*: 682 (M^+, 100%).

6: IR (KBr): $\tilde{\nu}$[cm^{-1}] = 2963, 1262, 1099, 1025, 804, 735 (PS), 650 (CCo_3). ^1H NMR (200 MHz, $CDCl_3$): $\delta = 1.33$ (d, 54H, $PCCH_3$, $^3J(P,H) = 15$ Hz), 2.06 (m, 6H, PCH_2CH_2), 2.28 (m, 6H, PCH_2), 2.33 (s, 9H, Co_3CCCH_3), 4.5 (m, 6H, cyclopentadienyl-H), 4.72 (m, 6H, cyclopentadienyl-H). ^{13}C NMR (50 MHz, $CDCl_3$): $\delta = 23.8$ (+, d, PCH_2CH_2, $^2J(P,C) = 13.6$ Hz), 24.2 (+, d, PCH_2, $^1J(P,C) = 26.2$ Hz), 27.6 (−, $PCCH_3$), 37.8 (+, d, $PCCH_3$, $^1J(P,C) = 41.6$ Hz), 62.2 (+, Co_3CCCH_3), 65.8 (+, Co_3CCCH_3), 82.5 (−, cyclopentadienyl-*C*H), 86.3 (−, cyclopentadienyl-*C*H), 102.4 (+, d, cyclopentadienyl-*C*CH$_2$, $J(P,C) = 15.4$ Hz). ^{31}P NMR (81 MHz, $CDCl_3$, ext. standard H_3PO_4): $\delta = 78.5$ [$C(tBu_3)_2P{=}S$], 578 ($Co_3P{=}S$). MS [FAB (*ortho*-nitrobenzyl)alcohol]: $m/z = 1117$ ($M^+ + 1$, 15%).

7: IR ($CHCl_3$): $\tilde{\nu}$[cm^{-1}] = 2964, 2928, 1604, 1260, 1228, 1132. ^1H NMR (200 MHz, $CDCl_3$): $\delta = 1.35$ (d, 54H, $PCCH_3$, $^3J(P,H) = 15$ Hz), 2.07 (m, 6H, PCH_2CH_2), 2.22 (m, 6H, PCH_2), 2.31 (s, 9H, Co_3CCCH_3), 4.53 (m, 6H, cyclopentadienyl-C*H*), 4.98 (m, 6H, cyclopentadienyl-C*H*). ^{13}C NMR (50 MHz, $CDCl_3$): $\delta = 25.1$ (+, d, PCH_2CH_2 or PCH_2CH_2, $J(P,C) = 20$ Hz), 27.6 (−, $PCCH_3$), 37.6 (−, Co_3CCCH_3), 37.9 (+, d, $PCCH_3$), 62.5 (+, Co_3CC), 81.8 (−, cyclopentadienyl-*C*H), 84.4 (−, cyclopentadienyl-*C*H), 102.5 (+, d, cyclopentadienyl-*C*CH$_2$, $J(P,C) = 16.3$); signal for Co_3CC was not observed due to low sample concentration. MS (70 eV): *m/z*: 1100 (M^+, 100%).

8: MS (70 eV, 300 °C): $m/z = 1052$ (M^+, 18%), 1036 (21), 963 (37), 891 (17), 782 (18), 565 (21), 312 ($CoCp^*O$, 71).

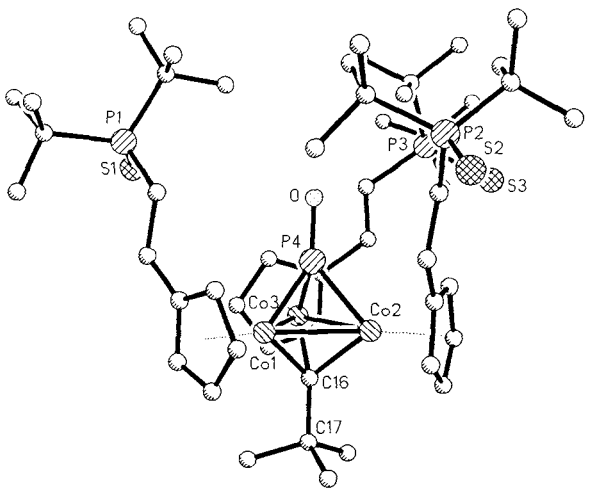

Fig. 1. Molecular structure of **7** in the crystal. Selected bond lengths [Å] and angles [°]: Co1–Co2 2.4751(8), Co2–Co3 2.4691(9), Co1–Co3 2.4592(8), Co1–P4 2.0959(13), Co2–P4 2.0964(13), Co3–P4 2.0941(13), P4–O 1.489(3), Co1–C16 1.885(4), Co2–C16 1.885(4), Co3–C16 1.890(5), Co–C(Cp) 2.070(5)–2.106(4), P–S 1.965(2); Co1-Co2-Co3 59.66(2), Co2-Co3-Co1 60.29(2), Co3-Co1-Co2 60.05(3), Co1-P4-Co2 72.37(4), Co2-P4-Co3 72.20(4), Co3-P4-Co1 71.88(4), Co1-C16-Co2 82.1(2), Co2-C16-Co3 81.7(2), Co3-C16-Co1 81.3(2), Co1-P4-O 137.4(2), Co2-P4-O 136.55(15), Co3-P4-O 137.5(2), Co1-C16-C17 130.4(3), Co2-C16-C17 130.6(3), Co3-C16-C17 131.8(3). Distance P4–C16 2.773(4) Å.

P4-C16-C17 179.2°). In the Co_3 plane the Co–Co distances range between 2.459–2.475 Å. The bond lengths Co–P4 are 2.095 Å, the bond lengths Co–C16 1.887 Å. The P4–O distance of 1.489 Å is nearly the same as that found by Scherer in the first P–O complex (1.46, 1.48 Å).[27] A substituted cyclopentadienyl ligand is attached to each Co atom at the periphery of the cluster with the coordinated carbon atoms at about the same distance from the cobalt atom (av Co–C(Cp) 2.084 Å). Remarkably, all three "phosphane arms" point in the direction of the face of the Co_3 plane to which the PO ligand is coordinated. The reason for this might be the steric hindrance of the *tert*-butylcarbyne ligand at the opposite face. An attractive interaction from the O atom to the atoms P1, P2, or P3 was not observed (the shortest distance is 4.643 Å for O–P1).

We have discovered a hitherto unkown mode of reactivity of *tert*-butylphosphaethyne, which in analogy to the reaction of alkynes with cyclopentadienylcobalt complexes leads to μ_3-carbyne-μ_3-phosphidotricobalt clusters with the [ω-phosphanyl-(ethylcyclopentadienyl)]cobalt complexes **1** and **2**, whose phosphido ligand can be oxidized to PS and PO ligands, respectively. The "phosphane arm" in **1** and **2** is evidently needed for the formation of the cluster, since comparable cyclopentadienyl or pentamethylcyclopentadienyl metal complexes form analogous clusters at best in traces. We are currently investigating the role of the "phosphane arm" in the formation of **4**.

Received: December 22, 1995 [Z8679IE]
German version: *Angew. Chem.* **1996**, *108*, 1323–1325

Keywords: clusters · cobalt compounds · phosphaalkynes · phosphorus compounds

[1] M. Regitz, Lecture, GDCh-Ortsverband Hannover, June 1, 1995.
[2] *Multiple Bonds and Low Coordination in Phosphorous Chemistry* (Eds.: M. Regitz, O. J. Scherer), Thieme, Stuttgart, **1990**, pp. 478.
[3] S. I. Al-Resayes, S. I. Klein, H. W. Kroto, M. F. Meidine, J. F. Nixon, *J. Chem. Soc. Chem. Commun.* **1983**, 930–932.
[4] J. C. T. R. Burckett-St. Laurent, P. B. Hitchcock, H. W. Kroto, J. F. Nixon, *J. Chem. Soc. Chem. Commun.* **1981**, 1141–1143.
[5] P. B. Hitchcock, M. J. Maah, J. F. Nixon, J. A. Zora, G. J. Leigh, M. A. Bakar, *Angew. Chem.* **1987**, *99*, 497–498; *Angew. Chem. Int. Ed. Engl.* **1987**, *26*, 474–475.
[6] R. T. Kettenbach, W. Bonrath, H. Butenschön, *Chem. Ber.* **1993**, *126*, 1657–1669.
[7] J. Foerstner, R. Kettenbach, R. Goddard, H. Butenschön, *Chem. Ber.* **1996**, *126*, 319–325.
[8] P. Binger, R. Milczarek, R. Mynott, M. Regitz, W. Rösch, *Angew. Chem.* **1986**, *98*, 645–646; *Angew. Chem. Int. Ed. Engl.* **1986**, *25*, 644–645.
[9] P. Binger, R. Milczarek, R. Mynott, C. Krüger, Y.-H. Tsay, E. Raabe, M. Regitz, *Chem. Ber.* **1988**, *121*, 637–645.
[10] J. R. Fritch, K. P. C. Vollhardt, M. R. Thompson, V. W. Day, *J. Am. Chem. Soc.* **1979**, *101*, 2768–2770.
[11] H. Yamazaki, Y. Wakatsuki, K. Aoki, *Chem. Lett.* **1979**, 1041–1044.
[12] J. R. Fritch, K. P. C. Vollhardt, *Angew. Chem.* **1980**, *92*, 570–572; *Angew. Chem. Int. Ed. Engl.* **1980**, *19*, 559-561.
[13] M. Driess, D. Hu, H. Pritzkow, H. Schäufele, U. Zenneck, M. Regitz, W. Rösch, *J. Organomet. Chem.* **1987**, *334*, C35–C38.
[14] A. F. Hill, J. A. K. Howard, T. P. Spaniol, F. G. A. Stone, J. Szameitat, *Angew. Chem.* **1989**, *101*, 213–214; *Angew. Chem. Int. Ed. Engl.* **1989**, *28*, 210–211.
[15] U. Kölle, F. Khouzami, B. Fuss, *Angew. Chem.* **1982**, *94*, 132; *Angew. Chem. Int. Ed. Engl.* **1982**, *21*, 131; U. Kölle, F. Khouzami, B. Fuss, *Angew. Chem. Suppl.* **1982**, 250–256.
[16] P. B. Hitchcock, M. J. Maah, J. F. Nixon, *J. Chem. Soc., Chem. Commun.* **1986**, 737–738.
[17] O. J. Scherer, *Angew. Chem.* **1990**, *102*, 1137–1155; *Angew. Chem. Int. Ed. Engl.* **1990**, *29*, 1104–1122.
[18] G. Ciani, A. Sironi, *J. Organomet. Chem.* **1983**, *241*, 385–393.
[19] A. Gourdon, Y. Jeannin, *J. Organomet. Chem.* **1986**, *304*, C1–C3.
[20] H. Lang, G. Huttner, B. Sigwarth, I. Jibril, L. Zsolnai, O. Orama, *J. Organomet. Chem.* **1986**, *304*, 137–155.
[21] H. Lang, G. Huttner, L. Zsolnai, G. Mohr, B. Sigwarth, U. Weber, O. Orama, I. Jibril, *J. Organomet. Chem.* **1986**, *304*, 157–179.
[22] A. Vizi-Orosz, G. Pályi, L. Markó, *J. Organomet. Chem.* **1973**, *60*, C25–C26.
[23] C. E. Laplaza, W. M. Davis, C. C. Cummings, *Angew. Chem.* **1995**, *107*, 2181–2183; *Angew. Chem. Int. Ed. Engl.* **1995**, *34*, 2042–2044.

[24] O. J. Scherer, J. Braun, P. Walther, G. Heckmann, G. Wolmershäuser, *Angew. Chem.* **1991**, *103*, 861–863; *Angew. Chem. Int. Ed. Engl.* **1991**, *30*, 852–854.
[25] W. A. Herrmann, *Angew. Chem.* **1991**, *103*, 835–836; *Angew. Chem. Int. Ed. Engl.* **1991**, *30*, 818–819.
[26] J. F. Corrigan, S. Doherty, N. J. Taylor, A. J. Carty, *J. Am. Chem. Soc.* **1994**, *116*, 9799–9800.
[27] X-ray crystal structure analysis of **7**: DIP2020 Image Plate from Enraf-Nonius, $Mo_{K\alpha}$ radiation, graphite monochromator. Structure resolution was performed with direct methods (SHELXS-86), refinement with full-matrix least-squares refinement at F^2 (SHELXL-93). $C_{50}H_{87}Co_3OP_4S_3$, $M_r = 1101.05$, orthorhombic, space group $Pna2_1$, $Z = 4$, $a = 23.446(3)$ $b = 22.794(2)$ $c = 10.531(2)$ Å, $V = 5628.1(14)$ Å^3, $\rho_{calcd} = 1.30$ g cm^{-3}, $\mu = 1.13$ mm^{-1}, 34477 measured reflections, 8159 independent, and 7446 observed reflections for $I > 2\sigma(I)$, temperature 20 °C. All non-hydrogen atoms were refined anisotropically, H atoms calculated for idealized positions. $R_1 = 0.0375$, $wR_2 = 0.0859$ (all data) for 569 parameters and 1 restraint. Further details of the crystal structure investigation may be obtained from the Fachinformationszentrum Karlsruhe, D-76344 Eggenstein-Leopoldshafen (Germany), on quoting the depository number CSD-404656.

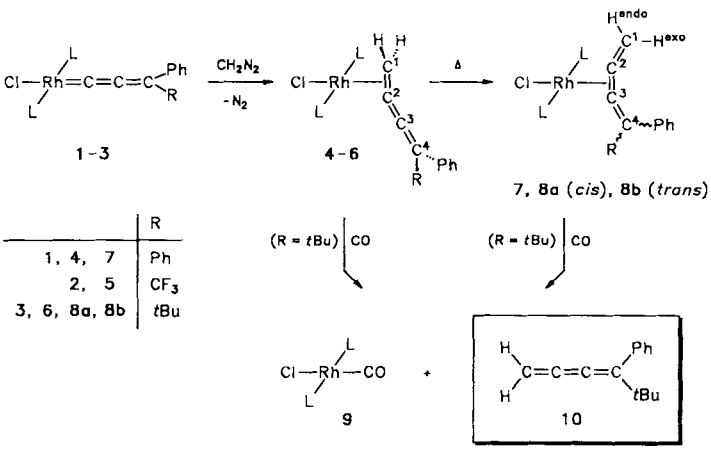

Scheme 1. L = P*i*Pr$_3$.

Methyl Iodide as a Source of CH_2: Two Routes for Generating 1,1-Disubstituted Butatrienes in the Coordination Sphere of a Transition Metal**

Helmut Werner,* Matthias Laubender, Ralf Wiedemann, and Bettina Windmüller

Dedicated to Professor Max Herberhold on the occasion of his 60th birthday

Following the reports on the synthesis of vinylidene complexes of the general type *trans*-[RhCl(=C=CHR)(P*i*Pr$_3$)$_2$],[1] we recently also described an efficient preparative route to the corresponding allenylidene compounds *trans*-[RhCl(=C=C=CRR′)(P*i*Pr$_3$)$_2$].[2] In the course of investigations into the reactivity of these compounds, we have now discovered that the allenylidene unit can be converted by two different pathways into 1,1-disubstituted butatrienes $H_2C{=}C{=}C{=}CRR'$, which because of their lability are otherwise hardly accessible. We note that up to now there is no precedent for the coupling of a CH_2 fragment, generated from CH_2N_2 or CH_3I, with an allenylidene moiety to yield a butatriene. Moreover, allenes can likewise be obtained from allenylidenerhodium complexes.

In contrast to compounds *trans*-[RhCl(=C=CHR)(P*i*Pr$_3$)$_2$] (R = Ph, *t*Bu, CO_2Me), which are inert in the presence of CH_2N_2,[3] complexes **1**–**3**[4] react with excess diazomethane at room temperature within a few minutes.[5] The red or orange butatriene complexes **4**–**6** (Scheme 1), which are only moderately sensitive to air and water, were isolated in nearly quantitative yield. The compositions of **4**–**6** have been confirmed by elemental analysis. The proposed structure shown in Scheme 1 is particularly supported by the ^{13}C NMR spectra (Table 1), which display four signals between $\delta = 180$ and 12 for the carbon atoms of the butatriene ligand. Two of these signals show a relatively large Rh–C coupling and are thus assigned to the C atoms of the butatriene ligand bonded to the metal. The chemical shift of the C^1 resonance as well as the ^1J(CH) coupling constant (161.4 Hz) of **4** indicate a predominant sp^3 character of this carbon atom which implies that the bonding between Rh, C^1, and C^2 is related to that of a metallacyclopropane.

The X-ray crystal structure analysis of **4** (Fig. 1)[6] reveals a distorted square-planar coordination around the central atom;

Table 1. Selected spectroscopic data of complexes **4**–**8** and **12**–**14**, and of the cumulenes **10** and **16** (without data for phosphane ligands, phenyl and *tert*-butyl groups); for assignment C^1–C^4 and H^{exo}, H^{endo} see Scheme 1.

4: ^{1}H NMR (400 MHz, C_6D_6): $\delta = 2.61$ [dvt, $N = 10.8$, J(H,H) = 1.6 Hz, CH_2]; ^{13}C NMR (100.6 MHz, C_6D_6): $\delta = 181.50$ (s, *C*=CPh$_2$), 111.39 (s, *C*Ph$_2$), 108.51 [dt, J(Rh,C) = 22.1, J(P,C) = 8.0 Hz, *C*=CH$_2$], 13.03 [d, J(Rh,C) = 13.6 Hz, CH$_2$]

5: ^{1}H NMR (400 MHz, $CDCl_3$): $\delta = 2.87$ and 2.78 [each dddd, J(Rh,H) = 6.0, J(P^1,H) = 5.6, J(P^2,H) = 5.6, J(H,H) = 1.6 Hz, 1H each of CH$_2$]; ^{13}C NMR (100.6 MHz, $CDCl_3$): $\delta = 183.83$ [s, *C*=C(Ph)CF$_3$], 125.02 [q, J(F,C) = 272.2 Hz, CF$_3$], 109.86 [dt, J(Rh,C) = 22.1, J(P,C) = 4.0 Hz, *C*=CH$_2$], 99.34 [q, J(F,C) = 34.0 Hz, *C*(Ph)CF$_3$], 16.12 [d, J(Rh,C) = 14.7 Hz, CH$_2$]; ^{19}F NMR (376.5 MHz, $CDCl_3$): $\delta = -58.60$ (s)

6: ^{13}C NMR (100.6 MHz, C_6D_6): $\delta = 179.30$ [s, *C*=C(Ph)*t*Bu], 100.17 [s, *C*(Ph)*t*Bu], 109.40 [dt, J(Rh,C) = 23.1, J(P,C) = 5.0 Hz, *C*=CH$_2$], 12.52 [d, J(Rh,C) = 13.4 Hz, CH$_2$]

7: ^{1}H NMR (400 MHz, $CDCl_3$): $\delta = 5.46$ and 5.00 (each s, br, 1H each of CH$_2$); ^{13}C NMR (100.6 MHz, $CDCl_3$): $\delta = 142.69$ [dt, J(Rh,C) = 17.1, J(P,C) = 4.0 Hz, C^2/C^3], 137.96 [dt, J(Rh,C) = 20.1, J(P,C) = 5.0 Hz, C^2/C^3], 127.59 (s, br, *C*Ph$_2$), 98.36 (s, br, CH$_2$)

8a: ^{1}H NMR (400 MHz, $CDCl_3$): $\delta = 5.62$ [t, J(P,H) = 2.4 Hz, 1H of CH$_2$], 5.21 (s, br, 1H of CH$_2$); ^{13}C NMR (100.6 MHz, $CDCl_3$): $\delta = 143.57$ [dt, J(Rh,C) = 16.1, J(P,C) = 4.0 Hz, C^2/C^3], 134.27 [s, *C*(Ph)*t*Bu], 132.59 [dt, J(Rh,C) = 18.1, J(P,C) = 4.0 Hz, C^2/C^3], 100.20 (s, CH$_2$); ^{31}P NMR (162.0 MHz, $CDCl_3$): $\delta = 28.05$ [d, J(Rh,P) = 119.2 Hz]

8b: ^{1}H NMR (400 MHz, $CDCl_3$): $\delta = 4.65$ and 4.19 (each s, br, 1H each of CH$_2$); ^{31}P NMR (162.0 MHz, $CDCl_3$): $\delta = 28.99$ [d, J(Rh,P) = 119.5 Hz]

10: IR (C_6H_6): $\tilde{\nu}$ [cm^{-1}] = 2050 (C=C=C); ^{1}H NMR (400 MHz, $CDCl_3$): $\delta = 5.13$ and 5.05 [each d, J(H,H) = 7.6 Hz, 1H each of CH$_2$]; ^{13}C NMR (100.6 MHz, $CDCl_3$): $\delta = 168.64$ and 158.69 (each s, =C=), 135.27 (s, *C*Ph$_2$), 89.31 (s, CH$_2$)

12: ^{1}H NMR (400 MHz, $CDCl_3$): $\delta = 5.13$ and 4.78 (each s, 1H each of CH$_2$); ^{13}C NMR (100.6 MHz, $CDCl_3$): $\delta = 142.43$ [dt, J(Rh,C) = 18.1, J(P,C) = 3.0 Hz, C^2/C^3], 135.87 [dt, J(Rh,C) = 20.1, J(P,C) = 5.0 Hz, C^2/C^3], 127.49 (s, br, *C*Ph$_2$), 98.31 (s, CH$_2$)

13: ^{1}H NMR (400 MHz, $CDCl_3$): $\delta = 2.41$ [dt, J(Rh,H) = 2.1, J(P,H) = 5.1 Hz, CH$_2$]; ^{13}C NMR (100.6 MHz, $CDCl_3$): $\delta = 173.34$ [dt, J(Rh,C) = 23.1, J(P,C) = 6.0 Hz, =C=], 123.10 (s, *C*Ph$_2$), 16.40 [d, J(Rh,C) = 13.1 Hz, CH$_2$]

14: ^{1}H NMR (400 MHz, $CDCl_3$): $\delta = 2.62$ (m, CH$_2$); ^{13}C NMR (100.6 MHz, $CDCl_3$): $\delta = 179.00$ (m, =C=), 122.47 [q, J(F,C) = 277.4 Hz, CF$_3$], 112.85 [q, J(F,C) = 27.3 Hz, *C*(Ph)CF$_3$], 18.86 [d, br, J(Rh,C) = 13.9 Hz, CH$_2$]; ^{19}F NMR (188.3 MHz, $CDCl_3$): $\delta = -59.44$ (s)

16: MS (70 eV): *m*/*z* 184 (M^+); IR (C_6H_6): $\tilde{\nu}$ [cm^{-1}] = 1955 (C=C=C); ^{1}H NMR (400 MHz, C_6D_6): $\delta = 4.75$ [q, J(F,H) = 3.2 Hz, CH$_2$]; ^{13}C NMR (100.6 MHz, C_6D_6): $\delta = 210.20$ [q, J(F,C) = 5.0 Hz, =C=], 124.19 [q, J(F,C) = 273.7 Hz, CF$_3$], 102.02 [q, J(F,C) = 32.2 Hz, *C*(Ph)CF$_3$], 83.12 (s, CH$_2$); ^{19}F NMR (188.3 MHz, C_6D_6): $\delta = -60.70$ (s)

[*] Prof. Dr. H. Werner, Dipl.-Chem. M. Laubender, Dipl.-Chem. R. Wiedemann, Dipl.-Chem. B. Windmüller
Institut für Anorganische Chemie der Universität
Am Hubland, D-97074 Würzburg (Germany)
Fax: Int. code +(931)888-4605

[**] This work was supported by the Volkswagen Foundation, the Deutsche Forschungsgemeinschaft (SFB 347), and Degussa AG.

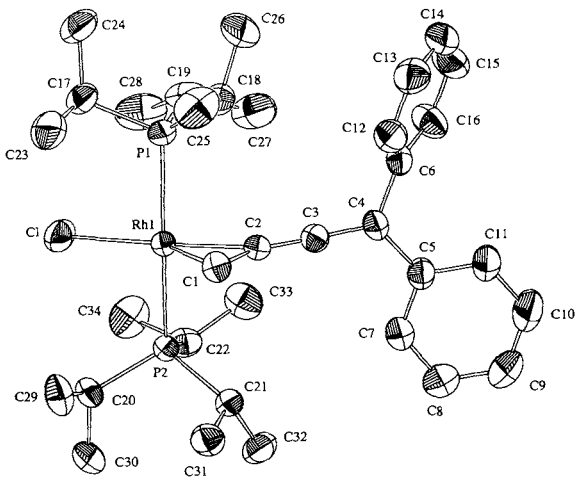

Fig. 1. Molecular structure of **4** (ORTEP plot) in the crystal. Selected bond lengths [Å] and angles [°]: Rh–P1 2.365(1), Rh–P2 2.355(1), Rh–Cl 2.349(1), Rh–C1 2.060(2), Rh–C2 2.063(2), C1–C2 1.408(3), C2–C3 1.272(3), C3–C4 1.335(3); P1-Rh-P2 166.45(2), P1-Rh-Cl 88.16(3), P1-Rh-C1 96.70(7), P1-Rh-C2 90.56(6), P2-Rh-Cl 87.42(2), P2-Rh-C1 94.35(7), P2-Rh-C2 92.89(6), Cl-Rh-C1 144.36(7), Cl-Rh-C2 175.65(6), C1-Rh-C2 40.0(1), Rh-C1-C2 70.1(1), Rh-C2-C1 69.9(1), C1-C2-C3 144.7(2), C2-C3-C4 174.8(2).

the Cl, Rh, and C1–C4 atoms lie in one plane. The Cl-Rh-C2 axis is almost linear (175.65(6)°), while the P1-Rh-P2 axis (166.45(2)°) deviates somewhat more from linearity. Despite the unsymmetrical coordination of the $C{=}CH_2$ unit to the metal, the Rh–C1 and Rh–C2 bond lengths are nearly identical. This is in contrast to the structurally similar compound *trans*-$[RhCl\{(1,2\text{-}\eta)\text{-}C^1H_2{=}C^2{=}C^3HC^4O_2Et\}(P\mathit{i}Pr_3)_2]$, in which the Rh–C1 and Rh–C2 bond lengths are 2.120(5) and 1.991(5) Å, respectively.[7]

Upon heating in toluene to 80–90 °C for several hours, compounds **4** and **6** rearrange to the thermodynamically more stable complexes **7** and **8**, respectively. The isomerization can easily be monitored by a change of color from red to yellow. In the case of **8**, a mixture of isomers **8a**/**8b** is formed that differ in the relative position of the phenyl and *tert*-butyl groups to the metal center. If the rearrangement of **6** is monitored by ^{31}P NMR spectroscopy, a **8a**:**8b** ratio of about 2:1 is observed initially that after 10 h in toluene at 90 °C changes to 10:1. Under these conditions, a complete conversion of **8b** to **8a** does not occur. Complex **8a** has been isolated analytically pure upon fractional crystallization from acetone (−78 °C) and, by comparison of the ^1H NMR data with those of **8b**, identified as the isomer in which the phenyl group at C^4 is directed towards the metal. The assignment of the signals for the H^{endo} and H^{exo} protons at C^1 follows from the work of Gladysz at al.[8] who assigned the resonances of the CH_2 protons of the allene complex $[C_5H_5Re(\eta^2\text{-}CH_2{=}C{=}CH_2)(NO)(PPh_3)]BF_4$ based on NOE measurements. We note that in all of the previously described 1,1,4,4-tetrasubstituted butatrienerhodium(I) compounds *trans*-$[RhCl\{(2,3\text{-}\eta)\text{-}R_2C^1{=}C^2{=}C^3{=}C^4R'_2\}(PPh_3)_2]$, which were prepared from $[RhCl(PPh_3)_3]$ and corresponding butatrienes,[9] the central C=C bond is coordinated to the metal; the linkage of a terminal $R_2C{=}C$ bond not to rhodium(I) but to platinum(0) was recently reported by Stang.[10]

Similarly to the butenyne complex *trans*-$[RhCl\{(1,2\text{-}\eta)\text{-}PhC^1{\equiv}C^2C^3H{=}C^4HPh\}(P\mathit{i}Pr_3)_2]$,[11] compounds **4**–**8** also react rapidly with CO in benzene at room temperature yielding the carbonyl complex **9**[12] by ligand exchange. Of the butatrienes formed in these conversions, those with CPh_2 and $C(Ph)CF_3$ as the terminal unit are quite labile and undergo secondary reactions. The hitherto unknown compound **10** was characterized by GC/MS and by comparison of the spectroscopic data with those of other butatrienes.[13, 14]

Surprisingly, there is also a second route to convert a metal-bonded allenylidene moiety into a butatriene ligand (Scheme 2).

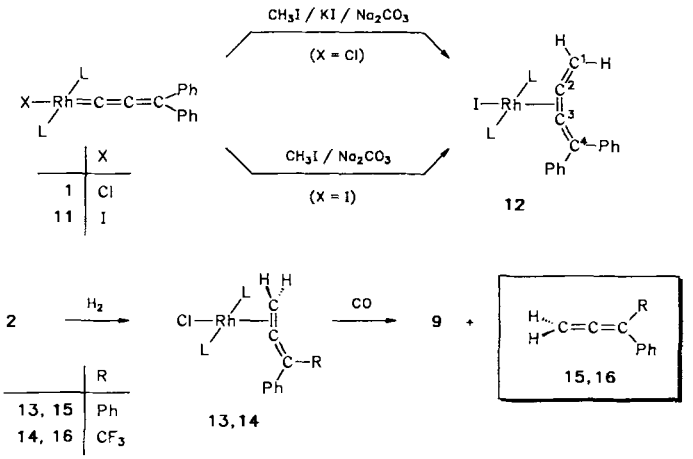

Scheme 2. L = $P\mathit{i}Pr_3$.

Complex **1** does not react, as we expected, with CH_3I to give a methylrhodium(III) compound. Instead, in the presence of excess Na_2CO_3, a mixture of products is formed, which besides **7** also contains the corresponding iodo derivative **12**.[15] A subsequent reaction of the mixture of products with KI yields **12** almost quantitatively. If compound **11**[2a] is treated with CH_3I and Na_2CO_3 in acetone/THF at room temperature, the butatriene complex **12** can be isolated in 76% yield. As far as the mechanism of formation of **12** is concerned, we assume that in the initial step an oxidative addition of CH_3I at the rhodium center takes place that is followed by an insertion of the allenylidene unit into the $Rh{-}CH_3$ bond. The intermediate $Rh{-}C(CH_3){=}C{=}CPh_2$ then reacts by a β-H shift to give a butatriene(hydrido)diiodorhodium(III) complex, which upon reductive elimination of HI generates the product **12**. Analogous to the first two steps is the formation of $[IrCl(I)\{C(CH_3){=}CH_2\}(P\mathit{i}Pr_3)_2]$ and $[IrI\{C(CH_3){=}CH_2\}\{N(SiMe_2CH_2PPh_2)_2\}]$ from the corresponding vinylidene complexes and methyl iodide;[16] in these cases, however, a subsequent β-H shift does not occur. Preliminary studies indicate that under the same conditions the dideuterated compound *trans*-$[RhCl\{(2,3\text{-}\eta)\text{-}C^1D_2{=}C^2{=}C^3{=}C^4Ph\}(P\mathit{i}Pr_3)_2]$ is formed from **11** and CD_3I. Kinetic studies, now in progress, should provide a more detailed insight into the mechanism of this unexpected reaction.

Compounds **1** and **2** are hydrogenated by H_2 at a different rate. While the reaction of **1** with H_2 in benzene at room temperature is rather slow and completed after 40 h, the corresponding reaction of **2** takes only 30 min. In both cases, the allene complexes **13** and **14** are quantitatively formed by cleavage of the Rh=C double bond.[17] Remarkably, under the chosen conditions no hydrogenation of the allene ligand occurs. Only after increasing the reaction time to 10 days and raising the temperature of the reaction to 60 °C, is the formation of a new rhodium-containing product observed, which according to the NMR data is $[RhH_2Cl(P\mathit{i}Pr_3)_2]$.[18] With regard to the structure of **13** and **14** it is important to note that the ^1H NMR spectra display only one signal for the CH_2 protons, thus confirming the coordination of the *unsubstituted* double bond of the allene to the metal center. A slippage of the $[RhCl(P\mathit{i}Pr_3)_2]$

 © VCH Verlagsgesellschaft mbH, D-69451 Weinheim, 1996 0570-0833/96/3511-1238 $ 15.00+.25/0

fragment along the axis of the cumulene, as has been observed for $[Fe(\eta^2\text{-}Me_2C{=}C{=}CMe_2)(CO)_4]$[19] and $[PtCl_2(\eta^2\text{-}Me_2C{=}C{=}CMe_2)]$,[20] could not be detected.

In the same way as for **6** and **8**, on treatment of **13** and **14** with CO (benzene, 10 °C, 1 min) the olefinic ligand can be displaced leading to the 1,1-diphenylallene **15**, which is already known,[21] and the allene derivative **16**, which has been characterized by ^1H, ^{13}C, and ^{19}F NMR spectroscopy (see Table 1).

Received: December 18, 1995 [Z8659IE]
German version: *Angew. Chem.* **1996**, *108*, 1330–1332

Keywords: allenylidene complexes · butatrienes · isomerizations · rhodium compounds

[1] a) F. J. Garcia Alonso, A. Höhn, J. Wolf, H. Otto, H. Werner, *Angew. Chem.* **1985**, *97*, 401–402; *Angew. Chem. Int. Ed. Engl.* **1985**, *24*, 406–407; b) H. Werner, F. J. Garcia Alonso, H. Otto, J. Wolf, *Z. Naturforsch. B* **1988**, *43*, 722–726; c) H. Werner, U. Brekau, *ibid.* **1989**, *44*, 1438–1446.

[2] a) H. Werner, T. Rappert, *Chem. Ber.* **1993**, *126*, 669–678; b) H. Werner, N. Mahr, T. Rappert, R. Wiedemann, J. Wolf, *Organometallics* **1994**, *13*, 2721–2727.

[3] F. J. Garcia Alonso, U. Brekau, unpublished results.

[4] The synthesis of **1** has been reported [2a]; compounds **2** and **3** are analogously accessible from $[\{RhCl(PiPr_3)_2\}_2]$ and HC≡CCPh(R)OH (R = CF_3, *t*Bu) in 90–95% yield.

[5] General procedure for **4**–**6**: A solution of **1**, **2**, or **3** (0.15 mmol) in benzene (3 mL) was treated dropwise with a 0.28 M solution of CH_2N_2 (1.5 mL) in ether at room temperature. After the solution had been stirred for 5 min, the solvent was removed, and the residue was recrystallized from pentane (−78 °C). Bright red (**4**), red (**5**), or orange crystals (**6**); yield 95%.

[6] Data for X-ray structure analysis: crystals from pentane (−10 °C), $C_{34}H_{54}ClP_2Rh$ (663.1); crystal dimensions 0.3 × 0.3 × 0.4 mm; monoclinic; space group $P2_1/c$ (No. 14); $a = 18.52(1)$, $b = 11.193(3)$, $c = 16.523(9)$ Å, $\beta = 93.35(3)°$, $Z = 4$, $V = 3420(3)$ Å^3; $\rho_{calcd.} = 1.288$ g cm^{-3}; $T = 293(2)$ K; max. $2\theta = 48°$; 5567 reflections measured; 5351 unique, 4654 observed [$I > 2\sigma(I)$]; Enraf-Nonius CAD4 diffractometer, Mo_{K_α} radiation (λ = 0.70930 Å), graphite monochromated, zirkon filter (factor 16.4); Lorentz polarization and empirical absorption correction (Ψ scan method, min. transmission 97.49%); Patterson method, refinement with full-matrix, least-squares method; $R1 = 0.0214$, $wR2 = 0.0568$ [for 4654 reflections with $I > 2\sigma(I)$], $R1 = 0.0305$, $wR2 = 0.0610$ (for all 5351 data); data-to-parameter ratio 8.33; residual electron density +0.296/−0.170 e Å^{-3}. Crystallographic data (excluding structure factors) for the structure reported in this paper have been deposited with the Cambridge Crystallographic Data Centre as supplementary publication no. CCDC-179-30. Copies of the data can be obtained free of charge on application to The Director, CCDC, 12 Union Road, Cambridge CB2 1EZ, UK (fax: int. code +(1223) 336-033; e-mail: teched@chemcrys.cam.ac.uk).

[7] H. Werner, D. Schneider, M. Schulz, *J. Organomet. Chem.* **1993**, *451*, 175–182.

[8] J. Pu, T.-S. Peng, A. M. Arif, J. A. Gladysz, *Organometallics* **1992**, *11*, 3232–3241.

[9] a) L. Hagelee, R. West, J. Calabrese, J. Norman, *J. Am. Chem. Soc.* **1979**, *101*, 4888–4892; b) P. J. Stang, M. R. White, G. Maas, *Organometallics* **1983**, *2*, 720–725.

[10] M. R. White, P. J. Stang, *Organometallics* **1983**, *2*, 1654–1658.

[11] M. Schäfer, N. Mahr, J. Wolf, H. Werner, *Angew. Chem.* **1993**, *105*, 1377–1379; *Angew. Chem. Int. Ed. Engl.* **1993**, *32*, 1315–1318.

[12] a) C. Busetto, A. D'Alfonso, F. Maspero, G. Perego, A. Zazzetta, *J. Chem. Soc. Dalton Trans.* **1977**, 1828–1834; b) K. Wang, G. P. Rosini, S. P. Nolan, A. S. Goldman, *J. Am. Chem. Soc.* **1995**, *117*, 5082–5088.

[13] W. Runge, W. T. Brady, *The Chemistry of Ketenes, Allenes and Related Compounds Vol. 1* (Ed.: S. Patai), Wiley, New York, **1980**.

[14] H. Westmijze, J. Nap, J. Meijer, H. Kleijn, P. Vermeer, *Recl. Trav. Chim. Pays-Bas* **1983**, *102*, 154–157, and references therein.

[15] Preparative procedure for **12**: A solution of **1** (88 mg, 0.14 mmol) and Na_2CO_3 (500 mg, 4.72 mmol) in acetone/THF (1:1) (4 mL) was treated dropwise with CH_3I (60 μL, 135 mg, 0.95 mmol) at room temperature. After the solution had been stirred for 6 h, the solvent was removed, and the residue was extracted with CH_2Cl_2 (3 mL). The extract was concentrated to dryness in vacuo, the residue was dissolved in THF (4 mL), and KI (300 mg, 1.81 mmol) was added to the solution. After the mixture had been stirred at room temperature for 3 h, the solvent was removed, the residue was extracted with benzene (5 mL), the extract was concentrated, and the yellow precipitate was washed with acetone (3 × 2 mL) (0 °C); yield 83 mg (82%); m.p. 146 °C decomp.

[16] a) A. Höhn, H. Werner, *J. Organomet. Chem.* **1990**, *382*, 255–272; b) M. D. Fryzuk, L. Huang, N. T. McManus, P. Paglia, S. J. Rettig, G. S. White, *Organometallics* **1992**, *11*, 2979–2990.

[17] General procedure for **13** and **14**: A solution of **1** or **2** (0.20 mmol) in benzene (5 mL) was stirred under a H_2 atmosphere for 40 h (**1**) or 30 min (**2**). After the solvent had been removed, the yellow residue was washed with pentane (0 °C) (2 × 1 mL) and dried in vacuo; yield 95%.

[18] H. Werner, J. Wolf, A. Höhn, *J. Organomet. Chem.* **1985**, *287*, 395–407.

[19] R. Ben-Shoshan, R. Pettit, *J. Am. Chem. Soc.* **1967**, *89*, 2231–2232.

[20] K. Vrieze, H. C. Volger, A. P. Praat, *J. Organomet. Chem.* **1970**, *21*, 467–475.

[21] P. Beltrame, D. Pitea, A. Marzo, M. Simonetta, *J. Chem. Soc. B* **1967**, 71–75.

Imine Substituent Effects on [2+2]Cycloadditions with Ketenes**

Claudio Palomo,* Jesus M. Aizpurua,* Marta Legido, Regina Galarza, Pere M. Deya, Jacques Dunoguès, Jean Paul Picard, Alfredo Ricci, and Giancarlo Seconi

The cycloaddition of imines with ketenes, generated from acid chlorides and tertiary amines, is recognized as one of the most convenient approaches to β-lactams.[1] However, virtually all of the investigations have dealt with the use of non-enolizable imines derived from aldehydes and, therefore, subsequent steps are often required to obtain the desired target product. In fact, ketene-enolizable aldimine cycloadditions, which would generate a wider range of substitution patterns at the C_4 position of the β-lactam ring, have not been viable, because of the instability of the starting imines and the presence of competitive deprotonations. We report herein on our initial findings on the development of this approach to a general asymmetric synthesis of 3-amino-4-alkyl β-lactams. The significance of these compounds as valuable precursors of β-lactam antibiotics, more complex organic compounds, large and medium heterocycles, and amino acid derivatives is apparent.[2] We thought that α-(trimethylsilyl)methyl imines[3] might provide a solution to the above-mentioned problems for two reasons: first, because of the ability of silyl groups to stabilize electron-deficient carbon centers in the β- and/or γ-position[4] and, second, because of the zwitterionic character of the reaction intermediate proposed for this kind of cycloaddition.[5]

[*] Prof. Dr. C. Palomo, Dr. J. M. Aizpurua, M. Legido, R. Galarza
Departamento de Química Orgánica
Universidad del País Vasco, Facultad de Química
Apdo 1072, E-20080 San Sebastián (Spain)
Fax: Int. code +(43)212236
e-mail: qppaiipj@sc.ehu.es

Dr. P. M. Deya
Departament de Química
Universitat de les Illes Balears, E-07071 Palma de Mallorca (Spain)

Prof. Dr. J. Dunoguès, Dr. J. P. Picard
Laboratoire de Chimie Organique et Organometallique Université de Bordeaux, F-33405 Talence (France)

Prof. Dr. A. Ricci
Dipartimento di Chimica Organica, Università di Bologna
I-40136 Bologna (Italy)

Dr. G. Seconi
C. N. R.-Istituto dei Composti del Carbonio contenenti Eteroatomi e loro Applicazioni
I-40064 Bologna (Italy)

[**] This work was supported by the E. U. (Project: SC1 CT 91/0646) and, in part, by Basque Government (Project: PI9386). Grants to M. L. from Spanish Education Ministry and to R. G. from Gobierno Navarro are acknowledged.

The reaction of **1**[6] with **2**[7] resulted exclusively in the formation of β-lactams *cis*-**3** and *trans*-**3** with good to excellent diastereomeric selectivities and, most notably, with complete asymmetric induction at the C_3 position. The results summarized in Table 1 illustrate the efficiency of this method for the

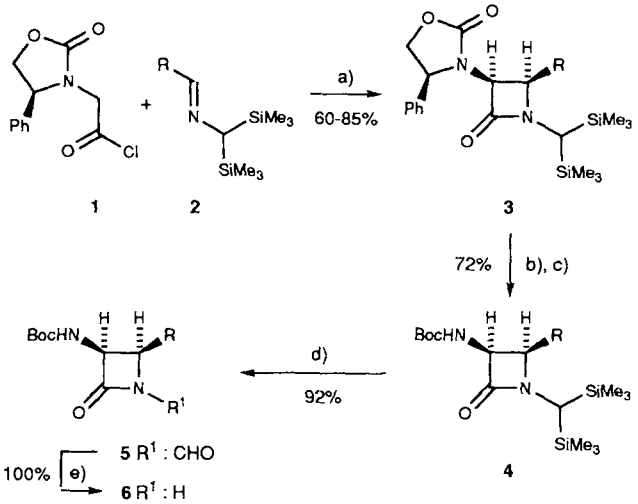

Scheme 1. a) NEt_3, $CHCl_3$, reflux 20 h; b) Li (6 equiv), NH_3, THF, *t*BuOH (33, 10, 1 equiv), −78 °C, 10 min; c) $(Boc)_2O$, CH_2Cl_2, room temperature, 3 h; d) $(NH_4)_2Ce(NO_3)_6$, MeCN, H_2O, 0 °C, 6 h; e) $NaHCO_3$, $NaHSO_3$, Na_2CO_3, H_2O, Me_2CO, room temperature, 5 h.

Table 1. Cycloadditions of **1** with the imines **2** [a].

Cmpd. [b]	R	Solvent	Yield [%] [c]	*cis*-**3**: *trans*-**3** [d]	*cis*-**3**-Isomer [e] m.p. [°C]	$[\alpha]_D^{25}$
3a	CH_3	CH_2Cl_2 [f]	48	80:20	142–144	+91.9
		C_6H_6	70	70:30		
		$CHCl_3$	65 (70) [g]	81:19		
3b	CH_3CH_2	$CHCl_3$	60 (75) [g]	>98:2	152–154	+74.1
3c	$CH_3CH_2CH_2$	$CHCl_3$	70 (75) [g]	90:10	138–139	+67.1
3d	$PhCH_2CH_2$	C_6H_6	72 [g]	83:17	syrup	+30.2
		$CHCl_3$	82 [g]	92:2		
3e	$PhCH_2$	$CHCl_3$	55 [g]	>98:2	syrup	+80.0
3f	$(CH_3)_2CH$	C_6H_6	60	90:10	160–162	+91.1
		$CHCl_3$	78 [g]	>98:2		
3g	$PhCH_2OCH_2$	$CHCl_3$	70	>98:2	syrup	+73.8
3h	$tBuO_2CCH_2CH_2$	$CHCl_3$	65	88:12	110–112	+44.9

[a] Reactions were conducted on a 10 mmol scale in refluxing benzene or $CHCl_3$; ratio of acid chloride:imine:triethylamine 1.2:1:1.4. [b] The crude imines were used directly. For imine **2a** the *E*:*Z* isomer ratio was 90:10. All other imines showed *E*:*Z* ratios >98:2 as determined by ^1H NMR spectroscopy (300 MHz). [c] Yield of the corresponding mixture of *cis* and *trans* β-lactams. [d] Determined by integration of the doublets at $\delta \approx 4.51$ and ≈ 4.40, which correspond to the *cis*- and *trans*-positioned protons at C3, respectively. [e] Pure compounds crystallized from hexanes/CH_2Cl_2 (10/1). All data recorded in CH_2Cl_2 ($c = 1.0$). [f] Reaction carried out at −78 °C to room temperature overnight. [g] Reaction carried out using a twofold excess of acid chloride and triethylamine.

direct construction of homochiral β-lactams with linear as well as branched chains at the C_4 position. In each case tested, yields were uniformly good when the reactions were carried out in boiling benzene or chloroform, and the use of a twofold excess of acid chloride **1** resulted in a noticeable increase in the yield, particularly when chloroform was used as solvent. Lowering the reaction temperatures led to a decrease in yield with no significant improvement in the ratio of *cis* to *trans* diastereomers. Noteworthy, even the imine **2e** derived from the easily enolizable phenylacetaldehyde, afforded the expected β-lactam, whereas the corresponding *N*-benzyl or *N*-(4-methoxy)phenyl imines gave only enamides and hydrolysis products.[8]

The absolute stereochemistry of the cycloaddition products was established by the conversion of the azetidinone *cis*-**3a** into the known compound **6a** (Scheme 1),[9] and a uniform reaction mechanism was assumed for the other derivatives. Thus, cleavage of the oxazolidinone moiety and subsequent *N*-Boc protection (Boc = *tert*-butoxycarbonyl) of the resulting free amino derivative gave **4a** [syrup, $[\alpha]_D^{25} = +32.8$ ($c = 1.0$ in CH_2Cl_2)] in 72% yield. Subsequent removal of the bis(trimethylsilyl)-methyl moiety by treatment with ammonium cerium(IV) nitrate in acetonitrile/water afforded the corresponding *N*-formyl-β-lactam **5a** in 92% yield. Remarkably, this novel method of deprotection of *N*-[bis(trimethylsilyl)methyl] amides expands considerably their usefulness in synthesis, complementing, as a cationic umpolung, the known fluoride-mediated reactivity of α-amido carbanions.[10] The cleavage of the formyl group from the ring N atom[11] in compound **5a**, which was carried out in a slightly basic medium, afforded **6a** in almost quantitative yield.[12] In addition to this two-step method to remove the *N*-[bis(trimethylsilyl)methyl] substituent from cycloaddition products **4**, we also found that prolonged exposure of β-lactams **3** to ammonium cerium(IV) nitrate in methanol instead of in acetonitrile/water led directly to the corresponding *N*-unsubstituted β-lactams in almost quantitative yields. This is illustrated (Scheme 2) by the synthesis of the loracarbef precursor **7** from **3h**.[13]

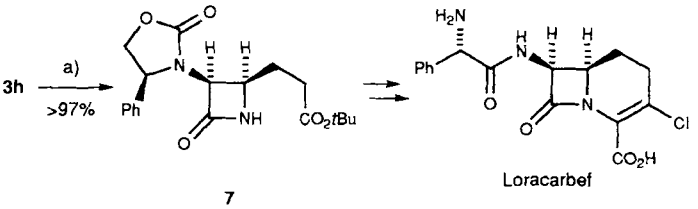

Scheme 2. a) $(NH_4)_2Ce(NO_3)_6$, MeOH, 0 °C, 6 h.

In summary, our results help to fill the gap with regard to the unexplained behavior of enolizable aldimines in [2+2]cycloadditions with ketenes[14] and offer for the first time a general asymmetric convergent synthesis to 3-amino-4-alkyl-β-lactams. It is expected that this new methodology for preventing enolization could be extended to further reactions involving zwitterionic species.

Experimental Procedure

Preparation of β-lactams **3**: *C*,*C*-bis(trimethylsilyl)methylamine (1.75 g, 10 mmol) was added to a solution of the corresponding enolizable aldehyde (10 mmol) in dry dichloromethane (10 mL) containing 4 Å molecular sieves. The mixture was stirred at 20 °C and monitored by GC-MS until completion (typically, 30 min). The molecular sieves were filtered off, the solvent was evaporated, and replaced by new dried molecular sieves (3 g) and freshly distilled dry chloroform (30 mL). To this solution, kept under nitrogen, triethylamine (5.6 mL, 40 mmol) and a solution of **1** (4.78 g, 20mmol) in chloroform (10 mL) were added dropwise at 0 °C, and the resulting mixture was heated to reflux for approximately 20 h. After work-up [10b] the corresponding β-lactams **3a–h** were obtained.

Deprotection of the β-lactams **3**: To a solution of the appropriate β-lactam **3** (5 mmol) in dry methanol (40 mL), ammonium cerium (IV) nitrate (10.96 g, 20 mmol) was added at 25 °C, and the suspension was stirred at the same temperature and monitored by TLC. After 6 h, the reaction mixture was taken up in water (50 mL) and extracted with ethyl acetate (3 × 80 mL). The organic layer was washed successively with aqueous $NaHCO_3$ (100 mL, saturated solution), aqueous

aqueous $NaHSO_3$ (3 × 50 mL, 40%), aqueous $NaHCO_3$ (100 mL, saturated solution), and aqueous NaCl (100 mL, saturated solution). Drying and evaporation of solvents yielded quantitatively fairly pure **6**.

Received: November 14, 1995
Revised version: February 23, 1996 [Z8528IE]
German version: *Angew. Chem.* **1996**, *108*, 1317–1318

Keywords: asymmetric syntheses · cycloadditions · imines · β-lactams

[1] For comprehensive reviews, see: a) J. Backes in *Methoden Org. Chem. (Houben-Weyl)*, 4th ed. *Band E16B*, **1991**, p. 31; b) L. Ghosez, J. Marchand-Brynaert in *Comprehensive Organic Synthesis*, *Vol. 5* (Eds.: B. Trost, I. Fleming), Pergamon, Oxford, **1991**, p. 85; c) R. C. Thomas in *Recent Progress in the Chemical Synthesis of Antibiotics* (Eds.: G. Lukacs, M. Ohno), Springer, Berlin, **1988**, p. 533; d) F. H. Van der Steen, G. Van Koten, *Tetrahedron* **1991**, *47*, 7503; f) G. I. Georg, V. T. Ravikumar in *The Organic Chemistry of β-Lactams*, (Ed.: G. I. Georg), VCH, New York, **1992**, p. 295.

[2] For some reviews on β-lactam antibiotics, see: a) W. Dürkheimer, J. Blumbach, R. Lattrell, K. H. Scheunemann *Angew. Chem.* **1985**, *97*, 183; *Angew. Chem. Int. Ed. Engl.* **1985**, *24*, 180; b) *Chemistry and Biology of β-Lactam Antibiotics*, *Vol. 1–3* (Eds.: R. B. Morin, M. Gorman), Academic Press, New York, **1982**. For reviews on amino acids and heterocycles derived from β-lactams, see: c) M. S. Manhas, D. R. Wagle, J. Chiang, A. K. Bose, *Heterocycles* **1988**, *27*, 1755; d) M. Hesse in *Ring Enlargement in Organic Chemistry*, VCH, Weinheim, **1991**; e) I. Ojima in *The Organic Chemistry of β-Lactams*, (Ed.: G. I. Georg), VCH, New York, **1992**, p.197.

[3] a) A. Capperucci, A. Ricci, G. Seconi, J. Dunoguès, S. Grelier, J. P. Picard, C. Palomo, J. M. Aizpurua, *J. Organomet. Chem.* **1993**, *458*, C1; b) M. Dal Colle, G. Distefano, D. Jones, A. Guerrini, G. Seconi, A. Modelli, *J. Chem. Soc. Perkin Trans. 2* **1994**, 789.

[4] a) L. A. Paquette, *Science* **1982**, *217*, 793; b) J. B. Lambert, *Tetrahedron* **1990**, *46*, 2677.; c) J. M. White, *Aust. J. Chem.*, **1995**, *48*, 1227. The β-silyl effect was suggested by Colvin to govern the regiochemistry of the cycloaddition between allylsilanes and chlorosulfonyl isocyanate to give racemic β-lactams. see: d) E. W. Colvin, M. A. Loreto, M. Monteith, I. Tommasini in *Frontiers of Organosilicon Chemistry*, (Eds.: A. R. Bassindale, P. P. Gaspar), The Royal Society of Chemistry, London, **1991**, p. 356.

[5] a) J. A. Sordo, J. González, T. Sordo, *J. Am. Chem. Soc.* **1992**, *114*, 6249; b) F. P. Cossio, J. M. Ugalde, X. Lopez, B. Lecea, C. Palomo, *ibid.* **1993**, *115*, 995.

[6] a) D. A. Evans, E. B. Sjögren, *Tetrahedron Lett.* **1985**, *26*, 3783; b) *idem.*, *ibid.* **1985**, *26*, 3787.

[7] These ketimines were prepared from the corresponding aldehydes and *C,C*-bis(trimethylsilyl)methylamine. For the preparation of the latter compound in multigram quantities from the commercially available *N,N*-dimethylcyanamide, see: S. Grelier, T. Constantieux, D. Deffieux, M. Bordeau, J. Dunoguès, J. P. Picard, C. Palomo, J. M. Aizpurua, *Organometallics* **1994**, *13*, 3711.

[8] The same enolization trend was observed for *N*-(4-methoxy)phenyl imines derived from acetaldehyde, propionaldehyde, and phenylacetaldehyde. See also: D. Dugat, G. Just, S. Sahoo, *Can. J. Chem.* **1987**, *65*, 88.

[9] L. S. Hegedus, J. Montgomery, Y. Narukawa, D. C. Snustad, *J. Am. Chem. Soc.* **1991**, *113*, 5784.

[10] a) C. Palomo, J. M. Aizpurua, J. M. García, I. Ganboa, F. P. Cossío, B. Lecea, M. C. López, *J. Org. Chem.* **1990**, *55*, 2498; b) C. Palomo, J. M. Aizpurua, J. M. García, J. P. Picard, J. Dunoguès, *Tetrahedron Lett.* **1990**, *31*, 1921; c) C. Palomo, J. M. Aizpurua, M. Legido, J. P. Picard, J. Dunoguès, T. Constantieux, *ibid.* **1992**, *33*, 3903.

[11] G. I. Georg, P. He, J. Kant, Z. J. Wu, *J. Org. Chem.* **1993**, *58*, 5771.

[12] A similar transformation sequence was achieved starting from *trans*-**3a** that confirmed the (*S*)-configuration at C3 in all diastereomers obtained. Selected data: **5**: M.p. 156–157 °C, $[\alpha]_D^{25} = -43.4$ ($c = 1.0$ in CH_2Cl_2); **6**: M.p. 182–183 °C, $[\alpha]_D^{25} = +55.0$ ($c = 1.0$ in MeOH).

[13] For a comprehensive review, see: R. D. G. Cooper in *The Chemistry of β-Lactams* (Ed.: M. I. Page), Chapman and Hall, London, **1992**, p. 272.

[14] A semiempirical SCF-MO AM1 theoretical study carried out in our laboratories to establish the dependence of the enamide or β-lactam pathway upon imine nitrogen substituents (CH_3 or $CH(SiMe_3)_2$) was consistent with experimental results, and suggests that the "β-effect" exerted by the two σ HC-$SiMe_3$ bonds is the responible for the chemoselectivity observed. These results will be published in due course.

Lateral Thinking on Organic Textbooks

Aspekte der Organischen Chemie. Band 1: Struktur. Edited by *G. Quinkert, E. Egert* and *C. Griesinger*. Verlag Helvetica Chimica Acta, Basel, 1995. 503 pp., hardcover DM 148.00.—ISBN 3-906390-11-X The English version is planned for later this year (ISBN 3-906390-15-2).

It can be said straight away that this first volume, on structure, in the series *Aspekte der Organischen Chemie* forms an excellent addition to the existing range of textbooks, and it can be recommended both for students and for all involved in the teaching and practice of chemistry. In its approximately 500 pages it offers the reader a view of organic chemistry from a mainly structural standpoint, which cannot be found elsewhere. Many of the topics included, such as the analysis of the crystal structure of diamond and the Prelog catalog of regular tetrahedral structures, are treated didactically for the first time in a structural context. The presentation of the subject matter is esthetically pleasing with a carefully written text, thus helping the reader to understand the more difficult concepts. Nevertheless, the book is not easy reading, and the novice will probably need to use it in conjunction with a more conventional textbook. The intention of the editors and authors is to develop the student's ability for independent learning, for which the excellent bibliographies at the ends of the chapters are a valuable aid. Many of the chapters begin with an interesting historical introduction which provides some light relief. At the beginning of Chapter 8 there is even a short introduction to the ideas of Karl Popper concerning the philosophy of science.

The volume is divided into two parts, with a gray stripe throughout the margin of Part 2 to emphasize the distinction. Part 1 consists of eight chapters which introduce the structural aspects of organic chemistry [constitution, configuration, and conformation (Chapter 2), chirality and symmetry (Chapter 3), molecular topology (Chapter 4)] and discuss examples of their application to specific topics in classical and modern chemistry. Other chapters explain the fundamentals needed for understanding this part of the book. In a very thorough didactic style the book introduces some highly topical areas of research in biological chemistry, thereby bridging the gap between organic chemistry and biology, with special emphasis on the structural analysis of supermolecules and their constituent units. Thus, structural considerations are applied not only to compounds such as carbohydrates and steroids (Chapters 5 and 6) but also to supramolecular structures such as the diamond lattice (Chapter 7). The latter chapter in Part 1 also contains an excellent discussion of the stereostructural aspects of DNA, homo-DNA, and pyranosyl-RNA. Other topics covered include base-pairing, the various conformations of DNA, and antigen and antisense strategies. There is a particularly good description of the conformational analysis of peptides and their secondary structural features, which is probably not treated better in any other book. The setting-up and "tagging" of peptide libraries is also described. Here the authors have taken the bold step of including detailed results from very recent studies. However, they caution that their experimental results, theories, and hypotheses need to undergo a period of expert criticism before being accepted (see Chapter 1: the outline of the book's aims and the overall conclusion). The last chapter of Part 1 discusses the qualitative MO model. The authors then use this model to interpret some conformational observations that cannot be explained on the basis of the classical structure model developed in Chapters 2–6.

Part 2 highlights some important aspects of modern organic chemistry and examines them in detail, and treats some of the topics already mentioned in Part 1 in greater depth. These include the use of information from data banks (Chapter 9), symmetry, point groups, and space groups (Chapter 11), the determination of absolute configuration (Chapter 12), an introduction to NMR spectroscopy (Chapter 13), and aromaticity (Chapter 14). Chapter 15 discusses hydrogen-bonding, which plays an essential role in the formation of supramolecular structures in chemistry and biology. However, the treatment of this topic is not really complete, as it does not include aspects such as secondary electrostatic interactions. Based on the foregoing discussions, the final chapter then deals with base-pairing in biology and chemistry, explaining the basic principles underlying classical and modern molecular biology. The Periodic System is shown inside the front cover of the book and the genetic code inside the back cover. The work provides an excellent demonstration of the interdisciplinary nature of the field and the wide-ranging relevance of organic chemistry. This volume on structure represents a notable advance for the teaching of organic chemistry, and will be of great benefit to students, not least because of the excellent quality of the writing. It is not a textbook in the conventional sense; instead it aims to stimulate thought, and presents organic chemistry in a slightly different and sometimes unusual way. After this first volume of the series we await with interest Volume 2 (reactivity), Volume 3 (synthesis), and Volume 4 (structure determination).

Thomas Carell
Institut für Organische Chemie
Eidgenössische Technische Hochschule
Zürich
(Switzerland)

This section contains book reviews and a list of new books received by the editor. Book reviews are written by invitation from the editor. Suggestions for books to be reviewed and for book reviewers are welcome. Publishers should send brochures or (better) books to Dr. Illenora Beckmann, Redaktion Angewandte Chemie, Postfach 101161, D-69451 Weinheim, Federal Republic of Germany. The editor reserves the right of selecting which books will be reviewed. Uninvited books not chosen for review will not be returned.

 © *VCH Verlagsgesellschaft mbH, D-69451 Weinheim, 1996* *0570-0833/96/3511-1243 $ 15.00+.25/0*

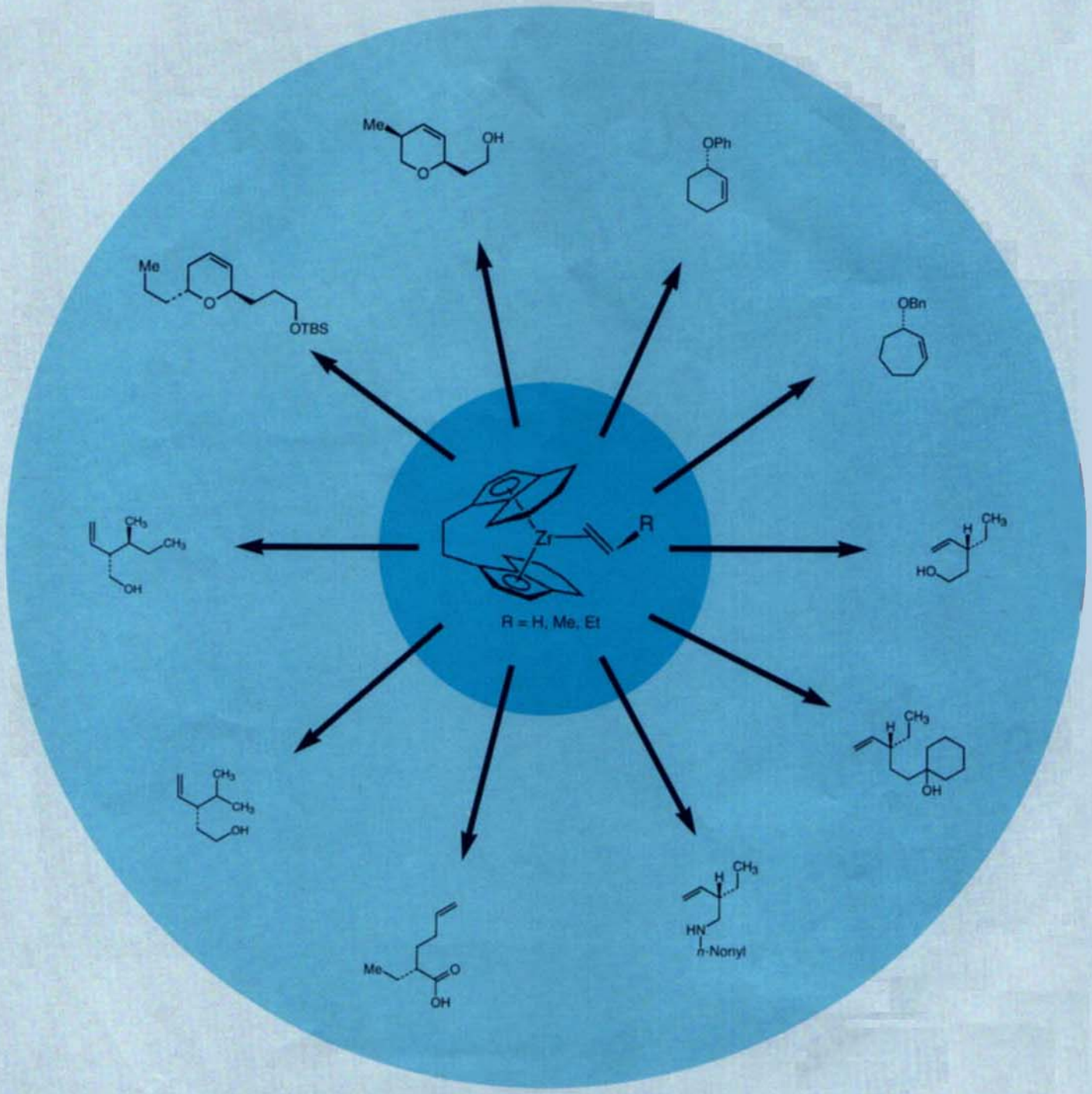

Chiral zirconocenes are good catalysts for a variety of enantioselective reactions. More on the subject can be found in the review by A. H. Hoveyda and J. P. Morken.

Enantioselective C–C and C–H Bond Formation Mediated or Catalyzed by Chiral ebthi Complexes of Titanium and Zirconium**

Amir H. Hoveyda* and James P. Morken

Dedicated to our mentor Professor Stuart L. Schreiber

The development of catalytic processes that effect enantioselective bond formation under mild conditions is an important and challenging task in modern chemical synthesis. In this connection, chiral C_2-symmetric *ansa*-metallocenes (bridged metallocenes) have found notable applications as catalysts. This article discusses the chemistry of this class of chiral metallocene complexes with regard to their utility in catalytic and enantioselective C–C and C–H bond formation reactions. In addition, where applicable, a brief comparison with other related catalytic enantioselective processes is offered. Many of the reactions effected with high levels of enantioselectivity by catalytic amounts of these complexes are of great significance to the preparation of new materials and in the synthesis of therapeutic agents. For example, zirconocene complexes readily catalyze the enantioselective addition of alkylmagnesium halides to alkenes, and cationic zirconocene complexes may promote the highly stereoregulated copolymerization of terminal alkenes. Furthermore, the related chiral titanocenes are involved in an impressive range of useful asymmetric catalytic reactions, including the enantioselective hydrogenation of olefins and reduction of imines or ketones. This review attempts to bring together the practical aspects of the use of [(ebthi)M] complexes of Group 4 transition metals (catalyst synthesis and resolution), outline the manner in which the C_2-symmetric chiral ligands are believed to initiate stereoselective bond formation, and highlight the aspects of this chemistry that are less well understood and require further research.

Keywords: asymmetric syntheses · asymmetric catalysis · enantiomeric resolution · metallocenes · sandwich complexes

1. Introduction

The design and development of catalytic processes that effect bond formation under mild conditions in a highly enantioselective fashion (>90% enantiomeric excess) stands as one of the most important and challenging tasks in modern chemical synthesis.[1] Organometallic systems that possess well-defined three-dimensional structures—metal complexes whose structural integrity in solution can be reliably predicted—offer a particularly attractive option in the design of enantioselective reactions, since the intricacies of substrate–catalyst association can be studied in appreciable detail. Within this context, chiral C_2-symmetric *ansa*-metallocenes, also referred to as bridged metallocenes, have found extensive use as catalysts for enantioselective bond formation.[2] In general, bridged ebti-metallocene dichlorides such as **1**–**3** put forth attractive options for the development of asymmetric reactions because their structures are conformationally constrained and they are relatively easy to prepare. The purpose of this article is to provide a review of the chemistry of these and related chiral metallocene complexes, particularly in relation to their utility in catalytic and enantioselective C–C and C–H bond formation.

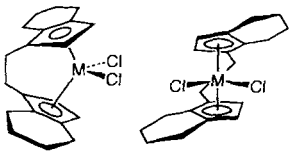

1 M = Ti
2 M = Zr
3 M = Hf

2. Chiral, Nonracemic ebthi Complexes of Group 4 Transition Metals: Synthesis and Resolution

2.1. A Historical Perspective

The chiral titanocene derivative **1** was first prepared by Brintzinger and co-workers, as part of their pioneering work in the design and synthesis of configurationally stable Group IV complexes.[3] Their 1982 account describes the preparation of the racemic chiral titanocene, a procedure for separating the chiral complex from the corresponding *meso* isomer, and a method for resolving the racemate as the binaphtholate derivative. In addition, Brintzinger's landmark paper offered the first X-ray crystal structure of a member of this class of C_2-symmet-

[*] Prof. Dr. A. H. Hoveyda, Dr. J. P. Morken
Department of Chemistry, Merkert Chemistry Center
Boston College
Chestnut Hill, MA 02167 (USA)
Fax: Int. code +(617)552-2705
e-mail: hoveyda@hermes.bc.edu

[**] ebthi = ethylenebis(tetrahydroindenyl).

ric metallocenes. A report detailing studies on the zirconocene complex **2** was published by the Brintzinger laboratory in 1985. The synthesis and X-ray crystal structure of the hafnium complex **3** was reported in 1987 by Ewen and Atwood.[4]

Collins and co-workers in 1988 reported a refinement of the original crystal structures of **1** and **2**.[5] In 1995 Piemontesi and Sironi published crystal structures of *rac*- and *meso*-[(ebi)$ZrCl_2$] (ebi = ethylenebis(indenyl);[6] these researchers also disclosed a detailed spectroscopic study of the organometallic complexes, unveiling many of their subtle conformational preferences.

Collins et al.[5] described experimental modifications in the synthesis of zirconocene complexes; the new protocol allowed for improved yields, rendering these organometallic complexes more accessible. Additional modifications of the synthesis route by Buchwald et al. enhanced the efficiency of the catalyst preparation; this included use of KH to deprotonate bis(indene) (Scheme 1) and utilization of a double-dilution technique to complex the bis(indenyl) ligand with [$ZrCl_4(thf)_2$].[7] Interestingly, Buchwald's procedural adjustments also led to the formation of roughly 30% of the corresponding *meso* isomer (2:1 *rac*:*meso*).

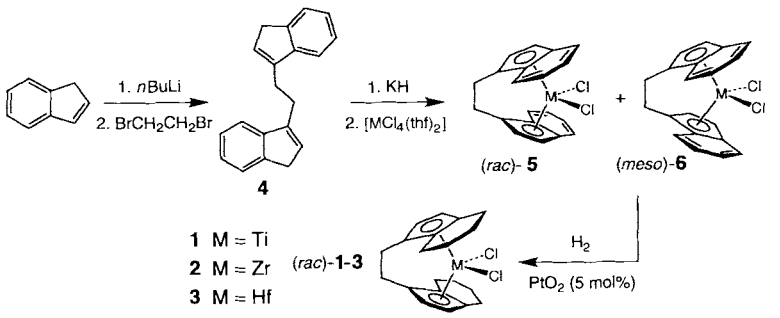

Scheme 1. General synthesis scheme for the preparation of chiral metallocenes **1**–**3**.

2.2. General Procedure for Catalyst Preparation

2.2.1. Synthesis of Racemic [(ebthi)M] Complexes

As illustrated in Scheme 1, **4** is produced through alkylation of dibromoethane with the lithium salt derived from indene (*n*BuLi, −78 °C, THF). When the bis(indenyl) dianion is complexed to the solvated metal tetrachloride,[8] *rac*-[(ebi)MCl_2] **5** and *meso*-[(ebi)$ZrCl_2$] **6** form. In principle, **5** (after appropriate enantiomeric resolution) can be used in asymmetric transformations; however, chiral metallocenes **5** are not as readily soluble as the ebthi complexes **1**–**3** and tend to be somewhat less stable than complexes that are formed by hydrogenation of the pendant cyclohexadiene groups. Accordingly, Pt-catalyzed hydrogenation of a mixture of **5** and **6** is typically carried out to afford metallocenes **1**–**3**.[9]

Most recently, Jordan et al. have described a convenient method for the synthesis of *rac*-[(ebi)$ZrCl_2$], in which the *meso* and racemic [(ebi)$Zr(NMe_2)_2$] complexes (prepared by reaction of reaction of **4** with [$Zr(NMe_2)_4$]) undergo rapid equilibration under appropriate reaction conditions.[10] Whereas the initial ratio after two hours is 2:1 (*rac*:*meso*), after 17 hours at 100 °C it is increased to 13:1; subsequent recrystallization of the amido complex affords the desired chiral metallocene in 95% yield. Subsequent treatment with $Me_2NH \cdot HCl$ affords **6** in 69% yield. (The entire operation can be carried out in a single vessel as well.) Most likely, *rac*-[(ebi)-$Zr(NMe_2)_2$] can itself be used for a large number of reactions in which the dichloride is typically employed.

2.2.2. Resolution of Racemic ebthi Complexes

2.2.2.1. Resolution through Mandalate Complexes

Resolution procedures have so far been developed only for the titanium and zirconium metallocenes **1**

Amir H. Hoveyda was born in Tehran in 1959. He received his BA degree from Columbia University in 1981. He then moved to New Haven, where he was a graduate student at Yale University with Professor Stuart L. Schreiber. After receiving his PhD in 1986, he joined Professor David Evans at Harvard as an American Cancer Society postdoctoral fellow. In June 1990 he joined the faculty at Boston College, where he is now professor of chemistry. His research interests are the design and development of new stereoselective reaction methods, organometallic chemistry, the study of reaction mechanisms, asymmetric catalysis, and the synthesis of natural products. His honors include the Young Investigator award of the National Science Foundation, the Pfizer Award in Synthetic Organic Chemistry, a Sloan Fellowship, a Camille Dreyfus Teacher–Scholar Award, and a Johnson & Johnson Focused Award.

A. H. Hoveyda

J. P. Morken

James P. Morken was born in Concord, California, in 1967. He received his BS at the University of California, Santa Barbara, in 1989, after which he joined Professor Hoveyda's research group at Boston College. His graduate work focused on the development of zirconium-catalyzed asymmetric carbomagnesation reactions, for which in 1993 he was awarded a graduate fellowship by the American Chemical Society, sponsored by Glaxo, Inc. Dr. Morken received his PhD in 1995. He is currently an NSF postdoctoral fellow at Harvard University in the laboratories of Professor Stuart L. Schreiber.

and **2**. Two methods for the effective separation of the metallocene enantiomers involve the displacement of the bound chloro ligands with appropriate chiral, nonracemic ligands. Separation of the resulting diastereomers, followed by reinstallation of the chloro ligands, affords the optically pure metallocene dichlorides. The successful procedure illustrated in Scheme 2 calls for the use of *O*-acetylmandelic acid. Diastereomeric mandelate salts **7** and **8** may thus be separated by recrystallization.[11] Treatment of the derived nonracemic mandalates with hydrochloric acid, or formation of the dimethyl metallocene (after treatment with MeLi), followed by the addition of HCl, readily converts **7** and **8** to chiral nonracemic metallocenes **1** and **2**.

2.2.2.2. Resolution through Binaphtholate Complexes

Although the mandelic acid used in the previously mentioned resolution procedure is relatively inexpensive (roughly \$5 per gram), the fractional recrystallization required to separate the diastereomeric derivatives **7** and **8** is somewhat tedious. A more popular procedure for metallocene resolution[3a, 11] relies on the fact that nonracemic binaphtholates (Na[3a] or Li salts[11]) efficiently react with only one enantiomer in the racemic mixture of chiral metallocenes (Scheme 3). Hence, treatment of racemic **1** or **2** with 0.5 equivalents of nonracemic lithium binaphtholate results in the formation of (*R*)-[(ebthi)M(binol)] **9** together with 0.5 equivalents of the unreacted nonracemic metallocene dichloride. The latter may be separated by treatment with silica gel or alumina, since in contrast to the binaphthol derivatives, dichlorides are adsorbed onto these chromatographic supports. Air-stable binaphtholate salts such as **9** are often used directly as precatalysts for various asymmetric processes. Alternatively, these chiral nonracemic metallocene complexes can be converted into the corresponding dichlorides by treatment with HCl. (For the zirconocene **1**, pretreatment with MeLi to form [(ebthi)$ZrMe_2$] is required to separate the free binaphtholate from the metal complex).

3. Stereoselective Reactions with *ansa*-Metallocenes as Reagents

3.1. Enantioselective, Zirconocene-Mediated Synthesis of Allylic Amines

Buchwald and co-workers have reported a procedure that employs metallocene complex **2** for the highly enantioselective preparation of chiral nonracemic allylic amines.[12] Although this protocol requires stoichiometric amounts of the chiral metallocene complex, it offers a reliable and highly enantioselective route towards these important chiral materials. As shown in Equation (a), the net transformation is an asymmetric reductive coupling of an alkyne to the α-carbon of a secondary amine.

As illustrated in Scheme 4, the zirconocene-mediated synthesis of allylic amines begins with (*S*)-[(ebthi)$ZrMe_2$] **10**, prepared by treatment of binaphtholate **9** (Scheme 3) with two equivalents of methyllithium. Reaction of dimethylzirconocene **10** with one equivalent of trifluoromethanesulfonic acid at −78 °C affords the zirconium methyltriflate **11**, which upon treatment with the appropriate lithium amide is readily converted to **12**. At this point, warming of the reaction mixture to 80 °C results in the formation of the zirconocene–imine complexes **13** and **14**. It is not clear whether β-H abstraction furnishes **13** selectively, or if equilibrium between **13** and **14** is rapidly established at elevated temperatures.[13] In the latter case, the equilibrium should lie on the side of **14**, due to the minimization of steric interactions between the alkyl substituent (R) and the cyclohexyl moiety of the chiral ligand (these steric repulsions likely exist in **13**). Regardless, addition of the alkyne substrate leads to a highly regioselective insertion to provide the five-membered zirconacycle **17**. Subsequent hydrolysis of the metallacyclopentane furnishes the desired allylic amine in excellent enantiopurity (Table 1).

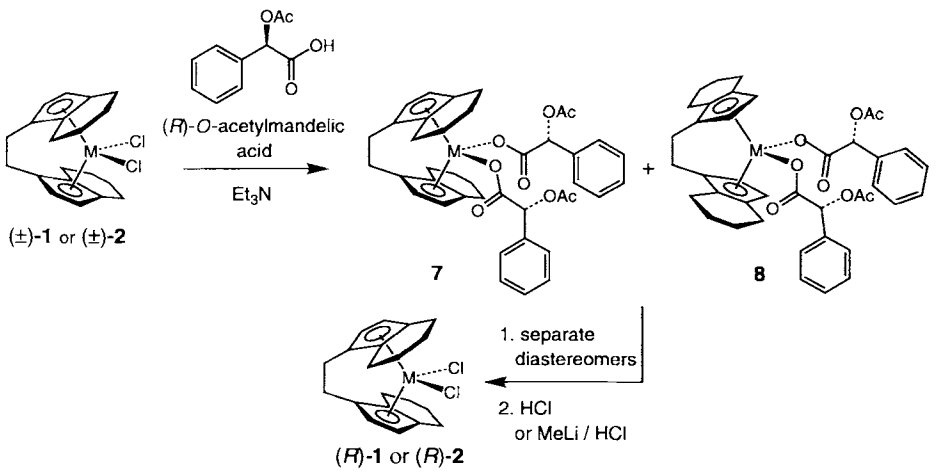

Scheme 2. Resolution of metallocene enantiomers through separation of their diastereomeric mandalate salts.

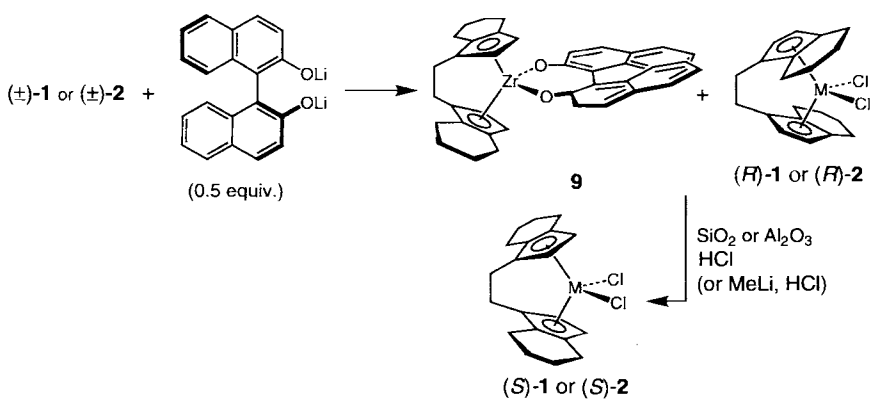

Scheme 3. Resolution of metallocene enantiomers through separation of their diastereomeric binaphtholate derivatives.

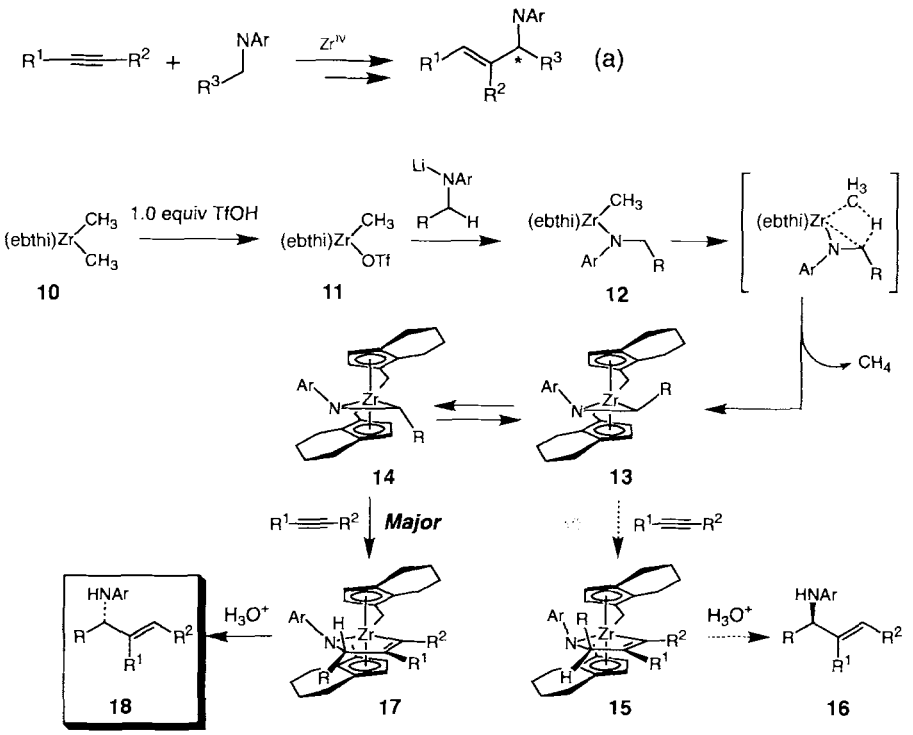

Scheme 4. Buchwald's protocol for [(ebthi)Zr]-mediated enantioselective coupling of alkynes and imines. For R, R^1, and R^2 see Table 1.

Table 1. Zirconocene-mediated enantioselective synthesis of secondary allylic amines.

Entry	Alkyne	Lithium amide	Product	Yield [%]	*ee* [%]
1	Me—≡—Me	PhNLi, Me	HNPh, Me, Me, Me	72	> 95
2	Ph—≡—Me	PhNLi, Me	HNPh, Me, Ph, Me	50	> 90
3	Me_3Si—≡—OTBS	PhNLi, Me	HNPh, Me, $SiMe_3$, OTBS	59	> 95
4	Me	PhNLi, Ph	HNPh, Ph, Me, Me	54 [a]	> 90
5	Me, O, H	PhNLi, Ph	HNPh, Ph, Me, OH	43 [b]	94

[a] 8:1 mixture of diastereomers. [b] 7:1 mixture of diastereomers.

As the examples in Table 1 illustrate, the zirconocene-mediated synthesis of allylic amines tolerates a variety of functional groups in both the alkyne and amine starting materials. Simple alkyl-substituted alkynes, as well as silylacetylenes, terminal alkenes, and aldehydes, may be employed as substrates. Unsymmetrical alkynes can be used; in cases where the steric bulk of the two alkyne substituents is significantly different, high levels of regiocontrol are observed (entries 2 and 3, Table 1). It is worthy of note that reactions with terminal alkenes (entry 4, Table 1) and an aldehyde substrate (entry 5) occur with useful levels of diastereoselectivity.

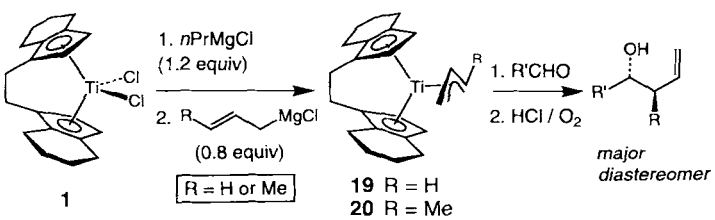

Scheme 5.

3.2. Diastereoselective Titanocene-Mediated Addition of Allylmetal Complexes to Aldehydes

Stereoselective addition of chiral allyl- and crotyltitanocenes to aldehydes, as shown in Scheme 5, has been reported by Collins.[14] Treatment of titanocene dichloride **1** with propylmagnesium chloride, followed by the addition of either allyl- or crotylmagnesium chloride, affords the titanium(III)-π-allyl complex **19** or **20**. Upon subsequent addition of an aldehyde substrate, C–C bond formation takes place, affording the corresponding homoallylic alkoxides (Scheme 5). Workup with anhydrous gaseous HCl, followed by exposure to O_2 results in alkoxide protonation and reoxidation of the titanocene reagent (to **1**). Therefore, chiral titanocene **1**, although required in stoichiometric quantities, can be recovered from the reaction and reused for subsequent transformations.

Whereas excellent diastereoselectivity (40:1 *anti*:*syn*) is achieved in the above addition of allylmetal compounds, with chiral nonracemic metallocenes, C–C bond formation is effected with only moderate levels of enantioselectivity; reaction of pivaldehyde with the crotyltitanocene **20** proceeds with a diastereoselectivity of 36:1 but in 55% *ee* (83% yield). As shown in Scheme 6, other experiments with the crotyl reagent **20** indicate that decreasing the size of the aldehyde substituent results in diminished diastereo- and enantiocontrol in the alkylation.

Transition structures **I** and **II** in Scheme 7 have been suggested by Collins to rationalize the observed

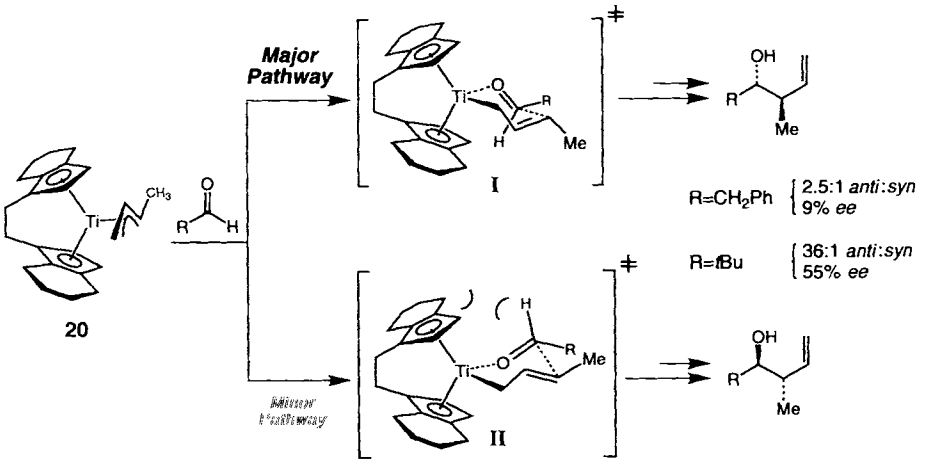

Scheme 6. Addition of [(ebthi)Ti(crotyl)] to aldehydes and the related transition state structures proposed by Collins.

trends in stereoselectivity in the Ti-catalyzed additions of allylmetal compounds to aldehydes. It has been proposed that transformations with **20** proceed through a six-membered chairlike transition state structure,[15] in which both the R group of the aldehyde and methyl group adopt the energetically more favorable pseudoequatorial position. The *anti* diastereomer therefore emerges the major product (Schemes 5 and 6). This mechanistic hypothesis offers a rationale for the higher levels of diastereoselectivity that are observed when aldehyde substrates with bulky alkyl substituents are used. Steric repulsion between the aldehyde substrate and cyclohexyl group of the catalyst disfavor transition structure **II** (Scheme 6). It is therefore tenable that allylmetalation of aldehydes with crotyltitanocene **20** proceeds selectively through transition structure **I**.

It is noteworthy that reactions of allyl- and crotyltitanocene reagents with aldehydes have dissimilar stereochemical consequences. The reaction of aldehyde substrates having larger alkyl substituents proceeds with higher levels of relative and absolute stereoselectivity when crotylmetallocene **20** is employed (Scheme 6). However, when allylmetallocene **19** is used (Scheme 7), the more sterically demanding aldehydes provide

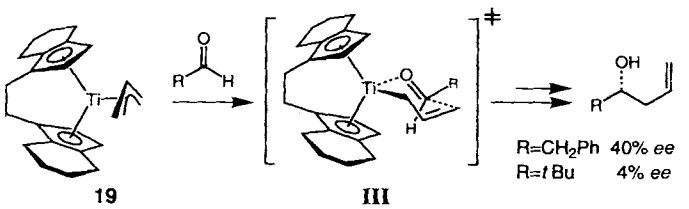

Scheme 7. Addition of [(ebthi)Ti(allyl)] to aldehydes and the related transition state structures proposed by Collins.

inferior levels of stereochemical control. Furthermore, alkylations with **20** generally proceed with higher enantioselectivity than those of **19** (cf. Schemes 6 and 7).

The chairlike transition state structures presented in Schemes 6 and 7 have been invoked by Collins to explain the observed trends in diastereo- and enantioselectivity in reactions of crotyltitanocene **19** and **20** to aldehydes. However, they do not rationalize the stereochemical outcomes observed in alkylations with allyltitanocene **19**. It is plausible that the carbonyl oxygen binds to the metal in such a way that the alkyl group (R) is oriented pseudoequatorially, allowing the reaction to proceed through transition structure **III** (Scheme 7) to furnish the (*R*)-configurated product predominantly. Nevertheless, it is not entirely clear why increasing the steric bulk of the aldehyde should decrease stereoselectivity.

The chiral titanocene-promoted allylation reactions described above are important since, although modest degrees of enantioselectivity are obtained, high levels of diastereoselectivity in the C–C bond forming reactions are detected. In addition, these studies shed light on a variety of subtle interactions between the allylmetal compound and various aldehyde substrates; such principles should prove critical in future developments involving these chiral metallocene complexes. However, as far as stereochemical control in this general class of transformations is concerned, a number of other stoichiometric reactions have been reported that provide outstanding levels of enantioselectivity. Reactions reported by Brown,[16] Mukaiyama,[17] Riediker,[18] Corey,[19] Hafner and Duthaler,[20] Roush,[21] and Hoffman[22] are some notable examples.[23]

More recently, impressive advances in the area of catalytic asymmetric additions of allylmetal compounds to carbonyls have reported. Procedures put forth by Yamamoto [Eq. (b)][24] and Keck and Tagliavini [Eq. (c)][25] indicate that both

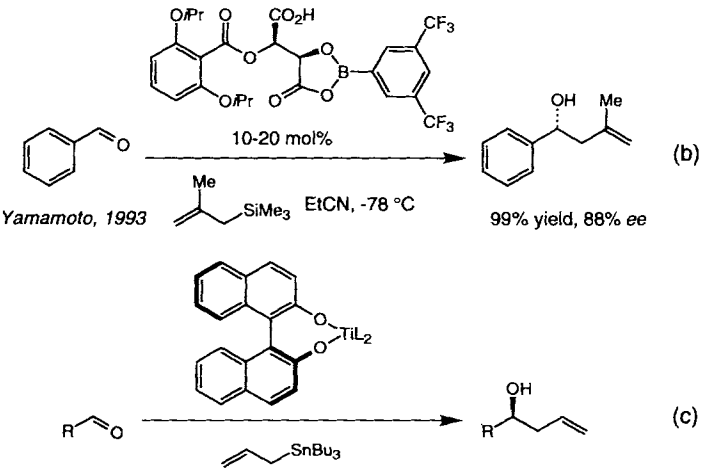

Ti- and B-based chiral Lewis acids can effect C–C bond forming reactions efficiently and with excellent enantioselectivity.

3.3. Stereoselective Alkene Insertion Reactions with Cationic Zirconocene Complexes

Inspired by the ability of cationic *ansa*-zirconocene complexes to catalyze stereocontrolled olefin polymerization reactions (see Section 4.1.1), Jordan has recently reported the stereoselective insertion of simple alkenes to both [(ebi)Zr(η^2-pyrid-2-yl)] **22** and [(ebthi)Zr(η^2-pyrid-2-yl)] **23**.[26] As shown in Equations (d)

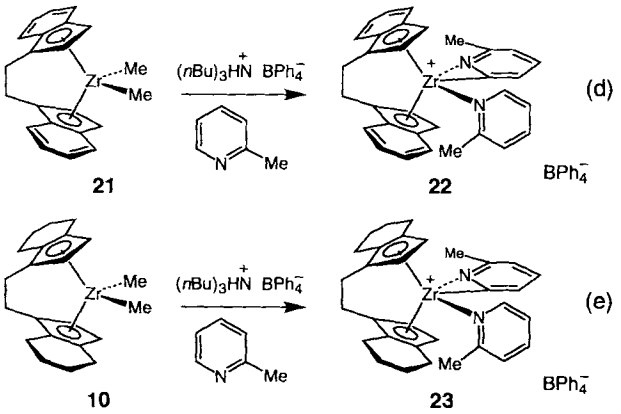

and (e), treatment of *rac*-[(ebi)$ZrMe_2$] **21** and *rac*-[(ebthi)$ZrMe_2$] **10** with $[(n\text{Bu})_3\text{HN}]^+(\text{BPh}_4)^-$ in the presence of 2-picoline affords complexes **22** and **23**, respectively. (The $B(C_6F_5)$ derivatives may also be prepared and are in fact reported to be more convenient to use.) These metallocenes exist as mixtures of isomers which rapidly exchange at 23 °C and are differentiated structurally by the orientation of the η^2-pyridyl ligand ("N-inside" and "N-outside").

When **22** and **23** are treated with a variety of alkene substrates, facile insertion into the azazirconacycle takes place. The resulting azazirconacyclopentanes are formed with various, but generally high, levels of diastereoselectivity, depending on the substituents on the alkene. The cases shown in Scheme 8 are illustrative. Whereas reactions with olefins that bear relatively small substituents (Me or *n*Bu) afford metallacyclopentane isomers **24**, **25**, and **27** selectively, terminal olefins such as styrene or trimethylsilyl vinylsilane with sterically more demanding substituents yield **26** and **28** with high selectivity.

The observed trends in regio- and stereoselectivity have been rationalized by Jordan as resulting from the minimization of steric interactions between alkene substituents and the pyridyl ligand. Scheme 9 illustrates three modes of alkene insertion into **25**. In all the pyridyl complexes the aromatic ring is tilted so as to avoid unfavorable steric interactions with the chiral ebthi group. The coordination mode of structure **IV** is preferred with smaller alkyl substituents: (ebthi)Zr–alkene association occurs such that the less substituted C atom is involved in the C–Zr bond, and pyridyl–olefin interaction leads to the approach of the olefin with the stereochemistry shown (R group towards cyclohexyl group of chiral ligand). In structure **V** steric repulsion between the R group and the pyridyl ligand is proposed to be energetically prohibitive. Accordingly, with groups larger then methyl at the *ortho* position of the pyridyl ligand, structure **IV** is even more preferred, since the resulting larger tilt of the heterocyclic ligand (to avoid the ebthi moiety) increases the severe steric interactions between the pyridyl *ortho* H and the alkene R group in **V**. It thus follows that with smaller *ortho* substituents, selectivity decreases. Additionally, when the R group is large such as *tert*-butyl, steric interactions with the chiral ligand

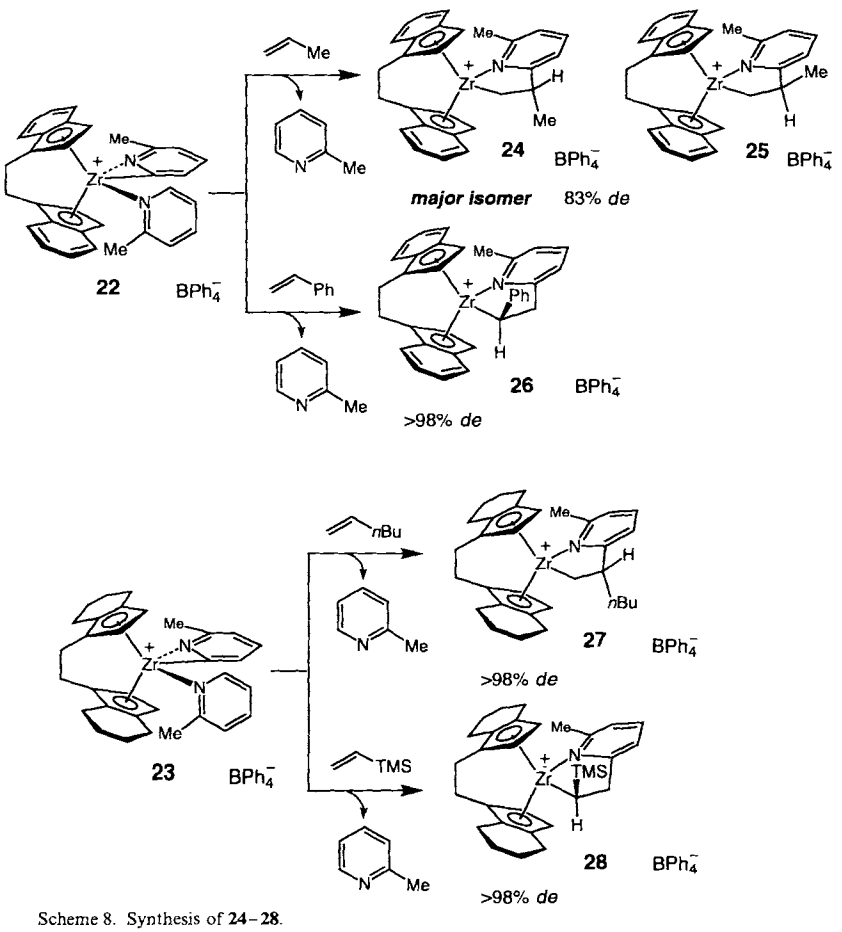

Scheme 8. Synthesis of **24**–**28**.

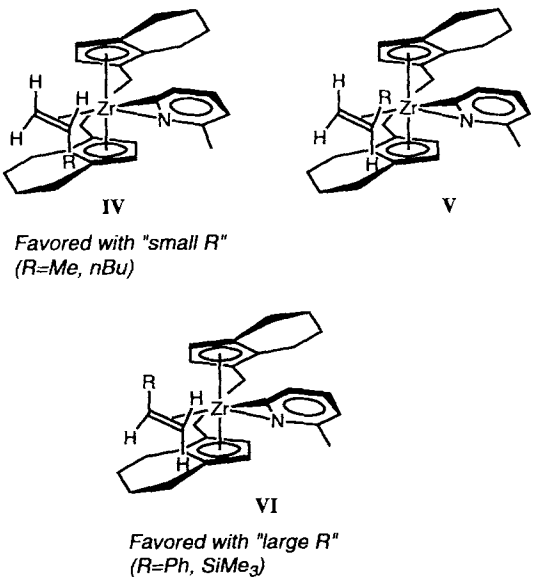

Scheme 9. Various modes of alkene–metallocene complexation proposed by Jordan for the stereoselective insertion of terminal alkenes into chiral zirconocene–pyridyl systems.

in **IV** lead to reduced stereoselectivity. With alkene substituents such as phenyl or trimethylsilyl, which can stabilize an adjacent partial negative charge on a carbon (developed in the formation of the C–Zr bond),[27] the coordination mode in structure **VI** is favored. However, whereas electronic effects can explain the turnover in the regioselectivity of olefin–metal binding, steric effects between these large alkene substituents and the cyclohexyl unit of the ebthi group provide a plausible rationale for the stereochemical preference of this metal–olefin coordination mode.

As illustrated in Equation (f), the nonracemic complex **23** has been shown to catalyze an asymmetric C–C bond forming reaction. This observation augurs well for future applications of cationic metallocene complexes in the design of catalytic enantioselective reactions.

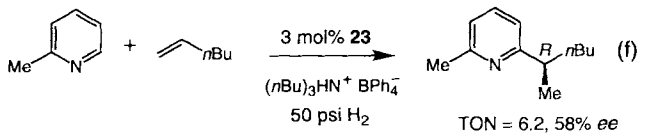

(f)

4. Catalytic Reactions Effected by *ansa*-Metallocenes

4.1. Catalytic Asymmetric C–C Bond Forming Reactions

4.1.1. Asymmetric Polymerization of Propylene

ansa-Metallocenes were initially used by Ewen and co-workers to control tacticity in the polymerization of propylene and butylene. These studies demonstrate that with titanium complexes **5** and **6** (see Scheme 1) product mixtures of isotactic and atactic polymers can be obtained.[28] Kaminsky and Brintzinger reported in 1985 that $[Cp_2ZrMe_2]$ induces the formation of predominantly atactic polymer structures when methylalumoxane (MAO) is used for catalyst activation (Scheme 10).[3c] In contrast, with catalytic $[(ebthi)ZrCl_2]$, polymers of 91% isotacticity and an average of 60 monomers in each isotactic sequence are produced. The activity of the bridged metallocene catalyst was thus demonstrated to be remarkably high: 7700 kg of polypropylene per hour may be produced for every mole of zirconocene; such values correspond to approximately 180000 propene insertions per catalyst molecule per hour.

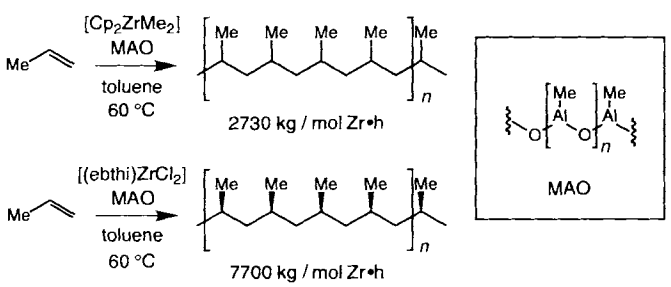

Scheme 10. Propene is polymerized more efficiently by $[(ebthi)ZrCl_2]$/MAO than by the original catalyst system $[Cp_2ZrMe_2]$/MAO. The top polymer is atactic, the bottom polymer is 91% isotactic.

Because isotactic polymers do not have inherent chirality associated with the main chain, efforts have been extended to control the absolute stereochemistry in oligomerization reactions. Oligomers are produced when chain termination steps are facilitated in relation to propagation events;[29] these principles were recently discussed in an excellent review article.[29b] One method of promoting termination steps is to conduct the polymerization in the presence of H_2 gas. It has been proposed that hydrogenation of the intermediate alkyl–metal species effectively inhibits chain growth at the oligomer stage, thus affording a fully saturated product, as well as the corresponding metal hydride.[30] Alternatively, it is possible that addition of hydrogen enhances the relative rate of hydrogenation versus chain growth. If the reaction is conducted at lower alkene concentration, β-hydride elimination may compete with chain propagation and thus lead to the desired short polymers.[31] Indeed, both approaches have been employed in attempts to produce optically pure organic molecules by *ansa*-zirconocene catalysis.

Pino and co-workers demonstrated that when H_2 is introduced into a polymerization reaction with $[(ebthi)ZrCl_2]$/MAO as catalyst, propene oligomers such as **29** are formed with moderate enantioselectivity (Scheme 11).[32] In this process, **29** constitutes only 0.5% (by weight) of the total reaction product, a significant amount, as the system allows for 64000 propene insertions per molecule of catalyst. It is noteworthy that, although the majority (roughly 80%) of the reaction products are high molecular weight polymers, other oligomers obtained (e.g. **30**) exhibit appreciable optical activity as well.

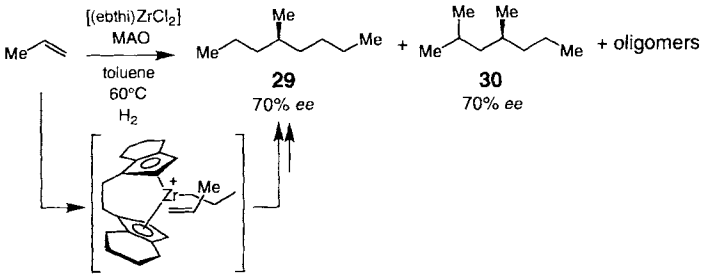

Scheme 11. Synthesis of **29** and **30**.

As was previously mentioned, an alternate method for producing oligomers is to reduce alkene concentration in a polymerization reaction, thereby slowing chain propagation relative to β-H elimination. Kaminsky and co-workers have found that polymerization of butene at low substrate concentration results in the desired low molecular weight polymers (e.g. **31**),[31] albeit with low levels of asymmetric induction [Eq. (g)]. Nevertheless, small oligomers do constitute a large percentage of the reaction product (roughly 18% by weight), and low catalyst loadings (0.01 mol% compared to butene) are sufficient for the reaction to proceed efficiently.

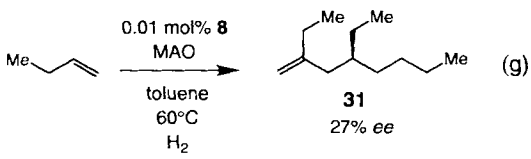

(g)

4.1.2. *Asymmetric Cyclopolymerization of Dienes*

In contrast to the polymerization of terminal alkenes, the cyclopolymerization reaction recently developed by Waymouth and Coates affords isotactic polymers with main-chain chirality.[33] The cyclopolymerization of 1,5-hexadiene depicted in Scheme 12 begins with the insertion of one of the double bonds

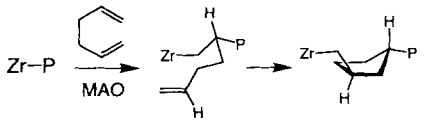

Scheme 12. P = polymer.

of the diene into the metal–carbon bond of the growing polymer. Insertion of the remaining double bond results in cyclization of the monomer to afford the polymer elongated by one five-membered carbocycle; subsequent insertion steps account for the continued chain growth.

It is worthy of note that of the four types of polymers that can in principle be obtained from a cyclopolymerization reaction, only the (*rac*)-diisotactic product is chiral by virtue of its main-chain stereochemistry (Scheme 13). The other products contain mirror planes within the repeating subunits that make up the polymer.

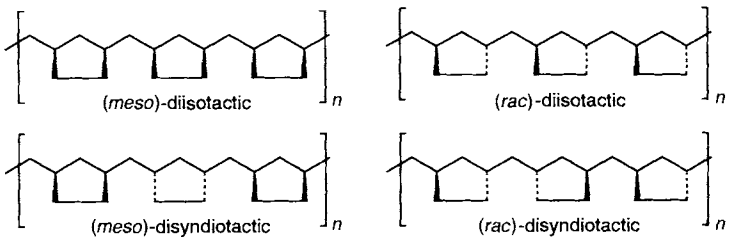

Scheme 13. Possible stereoisomeric products that may be obtained from cyclopolymerization of 1,5-hexadienes.

Initial studies with the racemic *ansa*-metallocene **9** demonstrated that the predominant product from the cyclopolymerization of 1,5-hexadiene is the chiral (*rac*)-diisotactic polymer;[34a] 68% of the rings in the product have *trans* configuration. Furthermore, optically enriched metallocene catalysts lead to optically active polymers; for the polymer formed with catalyst **9** [Eq. (h)] the molar optical rotation (per monomer unit), $[\alpha]_{405}^{28}$, is +50.1 ($c = 7.8$, $CHCl_3$). Waymouth and Coates therefore concluded that isotactic polymers are the major products in the cyclopolymerization. It is interesting that, although *cis*-configurated rings are present in the polymer structure, the corresponding molar optical rotations (per monomer unit) are considerably higher than that of the model system, *trans*-(1*R*,3*R*)-1,3-dimethylcyclopentane. In this connection, the Stanford researchers suggest that the polymer may adopt conformations in solution that contribute to the observed optical rotation.

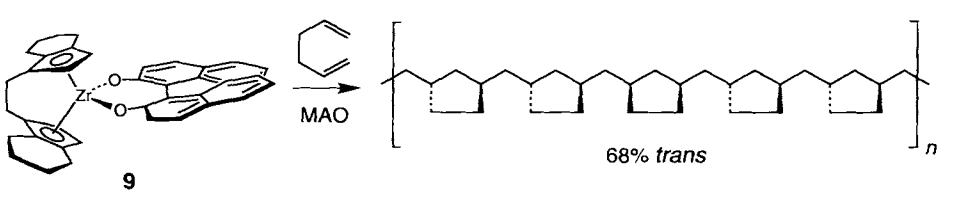

(h)

Comparison with Related Catalytic Enantioselective Processes

Stereospecific olefin polymerization reactions catalyzed by chiral metallocene catalysts are particularly important and were recently reviewed by Brintzinger, Fischer, Mulhaupt, Rieger, and Waymouth.[29b] These homogeneous catalysts, alongside enantioselective methods reported by Natta and Farina for polymerization of pentadienes[34] and benzofurans,[35] may be used in highly enantioselective polymerization and cyclopolymerization processes.[36] More importantly, these homogeneous catalytic systems offer unique opportunities in reaction design and engineering, as the polymerization reactions discussed above are effected by a single, well-defined metal complex with a reasonably well understood coordination sphere. In brief, chiral metallocenes have greatly expanded the scope and versatility of the readily accessible types of polymers. Nonetheless, the studies summarized in this section are likely to be the harbinger of other great contributions to the metal-catalyzed enantioselective polymerization reactions.

4.1.3. *Asymmetric Diels–Alder Reactions*

Collins and co-workers have examined catalytic enantioselective Diels–Alder reactions in which *ansa*-metallocene **32** is utilized as a chiral catalyst.[37] The cycloadditions are typically efficient (ca. 90% yield), but proceed with modest stereoselectivity (26–52% *ee*). Collins's studies provide important mechanistic insights that may ultimately be utilized in the design and development of more selective metallocene-based chiral catalysts.

The catalyst used in the asymmetric Diels–Alder reaction is the cationic complex $[(ebthi)Zr(O\text{-}t\text{Bu})(thf)]^+$ **32** [Eq. (i)].

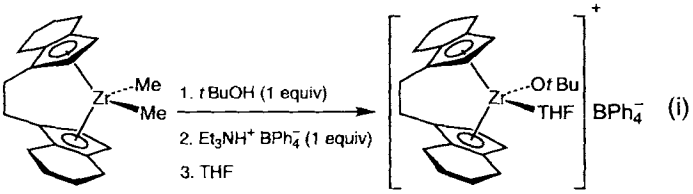

10 32 (i)

Treatment of the dimethylzirconocene **10**[38] with one equivalent of *tert*-butyl alcohol, followed by protonation with one equivalent of $(Et_3NH)(BPh_4)$ results in the formation of the requisite chiral cationic complex **32**, which is used to catalyze the [4 + 2] cycloaddition of acrylate and acrolein derivatives with cyclopentadiene.

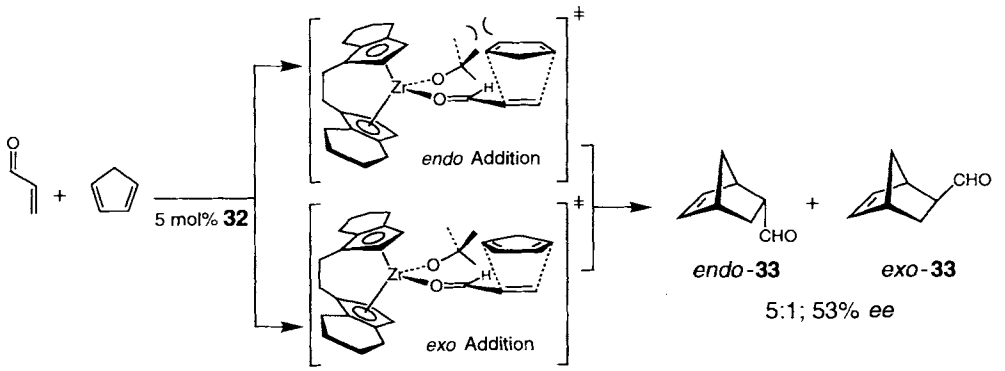

Scheme 14. Stereoselective [(ebthi)Zr]-catalyzed [4 + 2] cycloaddition and the corresponding transition state structures proposed by Collins.

In the presence of 5 mol% **32**, the [4 + 2] cycloaddition reaction of acrolein and cyclopentadiene proceeds efficiently to afford **33** in 93% yield and 53% *ee*, as a 5:1 mixture of *endo*:*exo* isomers (Scheme 14). ^{1}H NMR experiments indicate that the preferred orientation for binding between acrolein and the chiral metallocene is as shown in Scheme 14. Accordingly, Collins proposed that acrolein is coordinated to the chiral zirconocene complex so that the vinyl group is oriented away from the bulky alkoxide unit. It is plausible that approach of cyclopentadiene in the *endo* mode (Scheme 14) leads to unfavorable interactions between the diene and the *tert*-butoxy ligand, thus resulting in modest levels of diastereoselectivity (5:1 *endo*:*exo*). Molecular models indicate that any significant steric influence by the chiral ligand on the stereochemical outcome (both absolute and relative) of the cycloaddition is unlikely; the observed low enantioselectivity (53% *ee*) may thus be the result of inefficient asymmetric induction by the chiral ebthi moiety.[39]

In reactions in which methylacrylate is used as the dienophile (Scheme 15), cycloadditions occur with low enantioselectivity (23% *ee* compared to 53% *ee* with acrolein; the absolute configuration of the major product **34** is opposite to that of **33**), but with significantly higher diastereoselectivity (17:1, *endo*:*exo*). As before, formation of the *endo* isomer may be preferred, since the transition structure that leads to the *exo* isomer should include energetically unfavorable interactions between the diene and the metal-bound *tert*-butoxy group. Higher levels of *endo* selectivity are detected in the reaction of the methyl ester (Scheme 15); this is perhaps because, at least in part, the dienophile π-system is oriented towards the *tert*-butoxy ligand where the steric influence of the bulky substituent is expected to be more pronounced. Collins and co-workers put forth the transition state structures shown in Scheme 15 based on previous reports regarding the preferred stereochemistry of Lewis acid association with carboxylic esters.[40]

Most recently, Collins and co-workers reported on a highly enantioselective catalytic Diels–Alder cycloaddition, in which zirconocene and titanocene bis(triflate) complexes are used as catalysts.[41] Most noteworthy is the influence of the solvent polarity on enantioselectivity. For example, as shown in Scheme 16, with CH_2Cl_2 as solvent and 1 mol% **35** the *endo* product, **36**, is formed in 30% *ee* (30:1 *endo*:*exo*, 88% yield), whereas with CH_3NO_2 as solvent and 5 mol% **35** the enantioselectivity is raised to 89% (7:1 *endo*:*exo*, 85% yield). Extensive ^{1}H and ^{19}F NMR studies further indicate that a mixture of metallocene–dienophile complexes exist in both solutions (ca. 6:1 in CH_2Cl_2 and ca. 2:1 in CH_3NO_2, Scheme 16), and that most likely it is the minor complex isomer that is more reactive and leads to the observed major enantiomer. For example, in NOE experiments when the resonance frequency of H_b in the minor complex is irradiated, 5% enhancement of the signals of the adjacent Cp ring is observed. In contrast, no enhancements are observed when the resonance frequency of H_a in the major complex is irradiated.

These recent results illustrate, for the first time, that metallocene-based chiral Lewis acids can effectively catalyze [4 + 2] cycloadditions with excellent levels of enantiofacial selectivity. Perhaps more importantly, the reported NMR studies and the observed dramatic solvent effect should pave the way for future endeavors in the rational design of better chiral metallocenes.

Comparison with Related Catalytic Enantioselective Processes

The cycloaddition reactions catalyzed by titanocene and zirconocene complexes described in this section provide additional useful methods in enantioselective C–C bond forming reactions and offer deeper insights into the inner workings of the [(ebthi)M] class of chiral catalysts. Nonetheless, other catalytic systems can generally be used to carry out these and other similar reactions with better selectivity.[42] Related asymmetric cy-

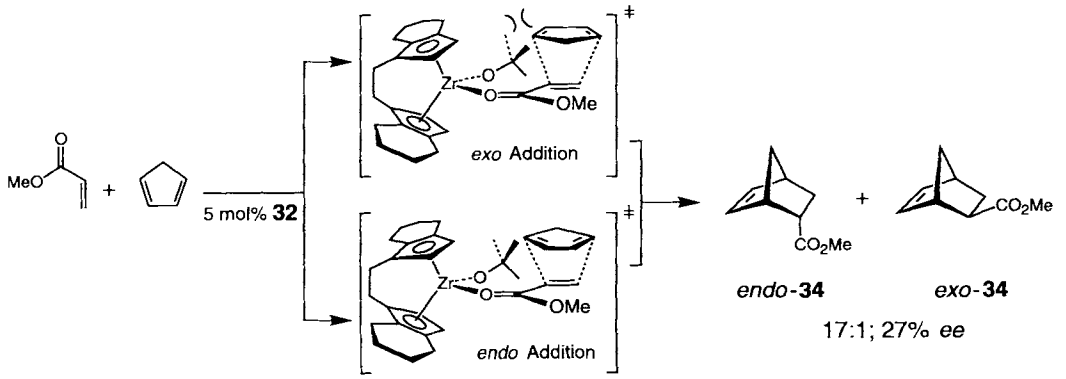

Scheme 15. Stereoselective [(ebthi)Zr]-catalyzed [4 + 2] cycloaddition and the corresponding transition structures proposed by Collins.

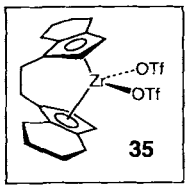

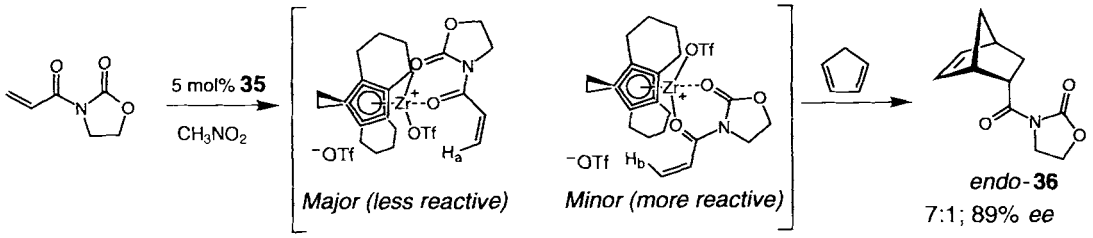

Scheme 16. Stereoselective [(ebthi)Zr(OTf)$_2$]-catalyzed [4 + 2] cycloaddition and the corresponding transition structures proposed by Collins.

cloadditions have been reported in which oxazolidinones similar to those in Collins's work serve as dienophiles. For example, Narasaka [Eq. (j)],[43] Corey [Eq. (k)],[44] Evans [Eq. (l)],[45] and Kobayashi [Eq. (m)][46] have described systems that offer similar or frequently even higher levels of relative and absolute stereoselectivity. As further indicated by papers cited in reference [42], asymmetric catalytic [4 + 2] cycloadditions continue to be the subject of extensive investigations in a number of research groups, a fact that reflects the significance of this class of C–C bond forming transformations. However, it should be noted that the enantioselective Diels–Alder cycloaddition is far from being a "generally solved problem". The high enantioselectivities reported in the literature, although extremely important, only concern a specific, relatively small and highly reactive class of dienes and dienophiles.[47] In brief, considering the importance of the [4 + 2] cycloadditions in organic chemistry, future research in this area should continue to provide notable contributions to the field of asymmetric synthesis.

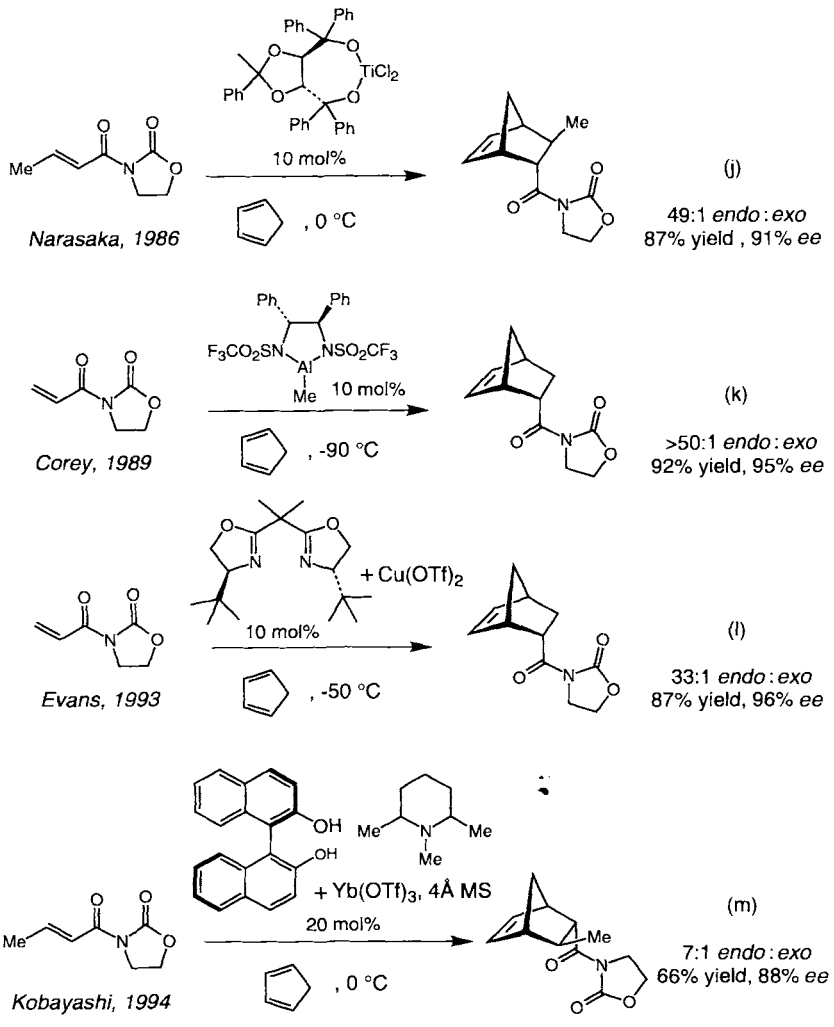

4.1.4. *Asymmetric Carbomagnesation Reactions*

4.1.4.1. *Asymmetric Synthesis through Catalytic Carbomagnesation*

Work in our laboratories in connection to the zirconocene-catalyzed carbomagnesation as a convenient method for selective C–C bond formation has resulted in the development of catalytic processes that are carried out at ambient temperature to afford synthetically useful products with excellent enantiomeric purity. As illustrated in Table 2, in the

Table 2. [(ebthi)Zr]-catalyzed enantioselective ethylmagnesation of unsaturated heterocycles [a].

Entry	Substrate	Product	*ee* [%]	Yield [%]
1		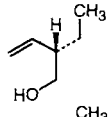	> 99	65
2	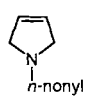	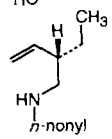	> 95	75
3		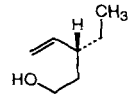	95	73
4	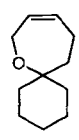	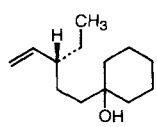	92	75

[a] Reaction conditions: 10 mol% (*R*)-**2**, 5.0 equiv EtMgCl, THF, 22 °C for 6–12 h. Entry 1 with 2.5 mol% (*R*)-**2**.

presence of 2.5–10 mol% nonracemic [(ebthi)$ZrCl_2$] (or [(ebthi)Zr(binol)] and with EtMgCl as the alkylating agent, five-, six-, and seven-membered unsaturated heterocycles undergo facile asymmetric ethylmagnesation.[48]

The rate of ethylmagnesation of the terminal double bonds of the reaction products is sufficiently slower, so that unsaturated alcohols and amines can be isolated in high yield (the second alkylation is not generally stereoselective). Catalytic asymmetric carbomagnesation thus affords nonracemic reaction products that bear a C=C bond and a hydroxyl or amino group, functional groups that are readily amenable to a wide range of subsequent derivatizations.

Within this context, we have recently utilized the stereoselective ethylmagnesation shown in entry 1 of Table 2 as a key step in the synthesis of the aglycon macrolactam of the antifungal agent Sch 38516.[49] As illustrated in Scheme 17, further functionalization of the product of the Zr-catalyzed ethylmagnesation through three subsequent catalytic procedures yields the requisite carboxylic acid unit in >99% *ee*. This synthesis route underlines the utility of the Zr-catalyzed carbomagnesation protocol: the reaction product, since it carries a C=C bond and a hydroxyl group, can be readily functionalized to provide a variety of other nonracemic intermediates.

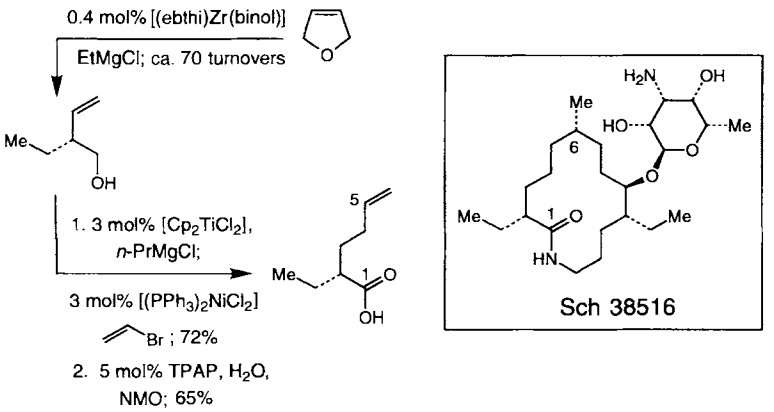

Scheme 17. Demonstration of the utility of [(ebthi)Zr]-catalyzed ethylmagnesation in the enantioselective synthesis of the aglycon of the macrolactam Sch 38516.

The catalytic cycle that we have proposed to account for the enantioselective ethylmagnesation is shown in Scheme 18. The reaction is initiated by the chiral zirconocene–ethylene complex (*R*)-**37**, formed upon reaction of dichloride (*R*)-**2** with EtMgCl.[50] Coupling of the alkene substrate with (*R*)-**37** leads to the formation of the zirconacyclopentane intermediate **VII**. Reaction of **VII** with EtMgCl affords zirconate **VIII**, which undergoes Zr–Mg ligand exchange to yield **IX**. Subsequent β-hydride abstraction, accompanied by intramolecular magnesium–alkoxide elimination leads to the release of the carbomagnesation product and regeneration of (*R*)-**37**.

An important aspect in the carbomagnesation of six-membered and larger heterocycles is that the intermediate metallacyclopentanes formed preferentially lead to reaction products in which the C–Zr bond is formed at the carbon α to the heterocycle C–X bond. Whether the regioselectivity in the formation of the zirconacycle is kinetically nonselective and rapidly reversible, as is the case when only one regioisomer is active in the catalytic cycle, or whether formation of the metallacycle is kinetically selective (stabilization of electron density upon formation of C–Zr bond by the adjacent C–X bond),[27] has not been rigorously determined. However, as will be discussed below, the regioselectivity with which the intermediate zirconacyclopentane is formed is critical in the [(ebthi)Zr]-catalyzed kinetic resolution of heterocyclic alkenes.

It is plausible that the observed enantioselectivity arises from minimization of unfavorable steric and torsional interactions in the complex formed between (*R*)-**37** and the unsaturated heterocycle (Scheme 18). The alternative mode of addition, illustrated in Figure 1, would lead to costly steric repulsions between the heterocycle and the cyclohexyl group of the chiral ligand.[51] Thus, reactions of

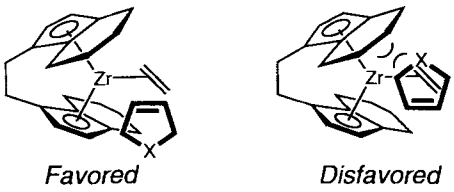

Fig. 1. Substrate–catalyst interactions favor a specific mode of alkene insertion into the zirconocene–alkene complex in carbomagnesation.

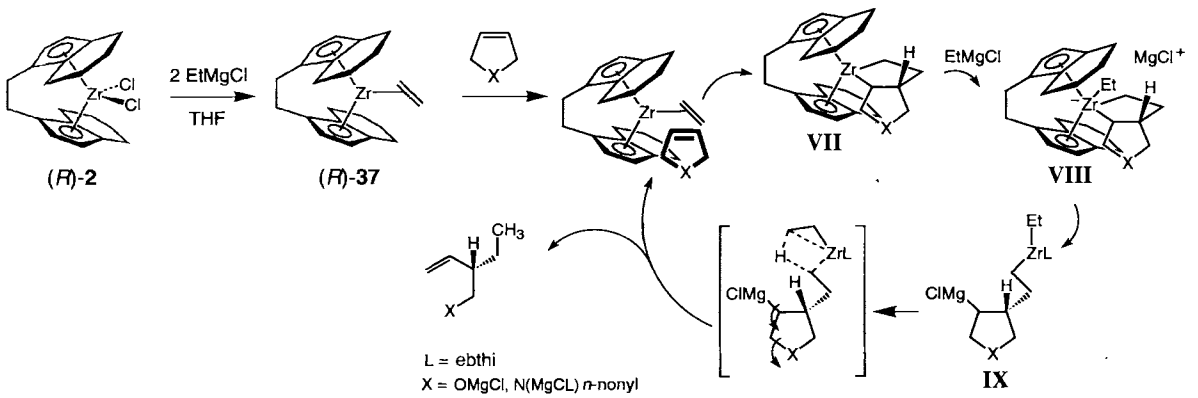

Scheme 18. Catalytic cycle proposed by Hoveyda for the [(ebthi)Zr]-catalyzed ethylmagnesation of unsaturated heterocycles.

Table 3. [(ebthi)Zr]-catalyzed enantioselective carbomagnesation of unsaturated heterocycles with longer chain alkylmagnesium chlorides [a].

Entry	Substrate	Major product(s)	T [°C]	RMgCl	Regioselectivity	*ee* [%]	Diastereoselectivity
1		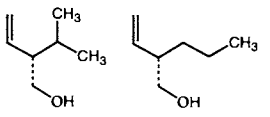 **38** **39**	22	*n*PrMgCl	2:1	99 (**38**), 99 (**39**)	–
2			70	*n*PrMgCl	20:1	94 (**38**)	–
3		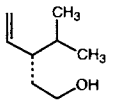	22	*n*PrMgCl	> 25:1	98	–
4		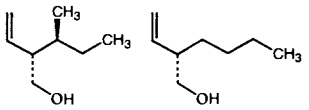 **40** **41**	22	*n*BuMgCl	2:1	> 99 (**40**), > 99 (**41**)	15:1
5			70	*n*BuMgCl	15:1	90 (**40**)	13:1
6		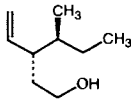	22	*n*BuMgCl	> 25:1	> 95	> 25:1

[a] Reaction conditions: 5 equiv RMgCl, 10 mol% (*R*)-**2**, 16 h. All yields: 35–40% after silica gel chromatography.

simple terminal olefins under identical conditions result in little or no enantioselectivity. This is presumably because when the alkene carbon that bonds to the zirconium center in **VII** has no substituent, the aforementioned steric interactions are ameliorated and the olefin substrate reacts indiscriminately through both modes of substrate–catalyst binding represented in Figure 1.

As shown in Table 3, reactions in which higher magnesium alkyls are used, namely *n*PrMgCl and *n*BuMgCl, proceed less efficiently (35–40% yield) but with similarly high enantioselectivity (>90% *ee*). Two issues in connection to the data illustrated in Table 3 merit comment. 1) With 2,5-dihydrofuran as substrate, at 22 °C a mixture of branched (**38** and **40**) and *n*-alkyl products (**39** and **41**) are obtained. When the reaction mixture is heated to 70 °C, the branched adducts **38** and **40** become the major product isomers. In contrast, with the six-membered heterocycle, reactions at 22 °C are highly selective (entries 3 and 6, Table 3). 2) With *n*BuMgCl as the alkylating agent, excellent diastereoselectivity is observed as well (entry 6).

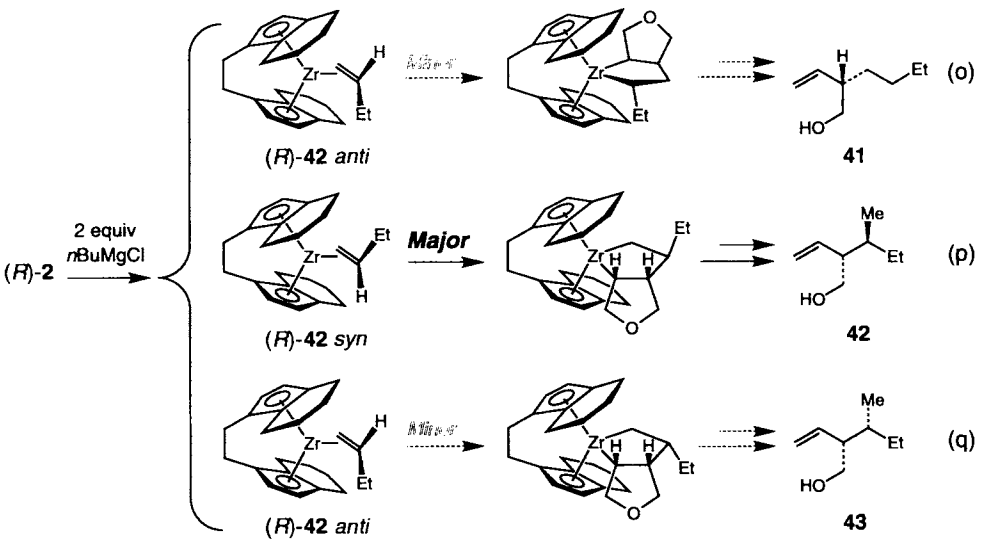

These observations carry significant mechanistic implications. As illustrated in Equations (o) through (q), the zirconocene–alkene complexes derived from the longer chain alkylmagnesium halides present several additional selectivity issues: 1) The transition metal–alkene complex can exist in two diastereomeric forms, (*R*)-**42** *anti* and *syn*, which can lead to the formation of different product diastereomers [cf. Eqs. (o) and (p), and Eqs. (p) and (q)]. The data in Table 3 indicate that the alkylation product arises from the mode of addition shown in Equation (p). 2) As illustrated in Equations (o) and (q), the carbomagnesation process can afford either the branched or the *n*-alkyl product. Insertion of the alkene substrate from the more substituted front of the zirconocene–alkene system affords the branched isomer [Eq. (q)], whereas reaction from the less substituted end leads to the formation of the straight-chain product [Eq. (o)]. The results shown in Table 3 indicate that, depending on the reaction conditions, products derived from the two isomeric metallacyclopentane formation can be competitive.

Detailed studies from our laboratories shed light on the mechanistic intricacies of asymmetric catalytic carbomagnesations and lead to a better understanding of the above trends in regio- and stereoselectivity.[52] Importantly, our mechanistic studies clearly indicate that there is no preference for the formation of either the *anti* or the *syn* [(ebthi)Zr]–alkene isomers (e.g. **42** *anti* vs **42** *syn*); it is only that one metallocene–alkene diastereomer

(*syn*) is more reactive. Our mechanistic studies also indicate that zirconacyclopentane intermediates (**VII** in Scheme 18) do not spontaneously eliminate to give the derived zirconocene–alkoxide; Zr–Mg ligand exchange is likely a prerequisite for the alkoxide elimination and formation of the terminal alkene.

4.1.4.2. Kinetic Resolution through Catalytic Carbomagnesation

The high levels of enantioselectivity obtained in the asymmetric catalytic carbomagnesation reactions (Tables 2 and 3) imply highly organized interactions between the [(ebthi)Zr]–alkene complex and the heterocyclic alkene substrates. It therefore follows that if a racemic mixture of chiral unsaturated pyrans or furans are employed, the resident center of asymmetry may induce different rates of reaction, such that after roughly 50% conversion one enantiomer of the chiral product can be recovered in high enantiomeric purity. Molecular models indicate that with a 2-substituted dihydropyran, as shown in Figure 2, the mode of addition labeled **X** should be significantly favored over **XI** and **XII**, in which the catalyst–substrate complex is destabilized by unfavorable steric interactions.

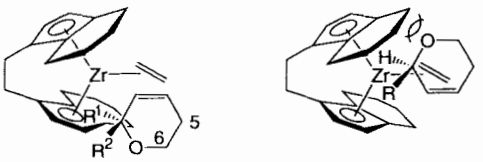

X **XII**
XI

Fig. 2. Possible modes of association for pyran enantiomers with the [(ebthi)Zr(C_2H_2)] complex. **X**: R^1 = H, R^2 = alkyl. **XI**: R^1 = alkyl, R^2 = H. **XII**: R = alkyl.

As the data in Table 4 indicate, in the presence of catalytic amounts of nonracemic [(ebthi)$ZrCl_2$], a variety of unsaturated pyrans can be resolved effectively to deliver these synthetically useful heterocycles in excellent enantiomeric purity.[53] A number of important issues in connection to the catalytic kinetic resolution of dihydropyrans are noteworthy: 1) Reactions performed at elevated temperatures (70 °C) afford recovered starting material with significantly higher levels of enantiomeric purity than that isolated from processes carried out at 22 °C. For example, the 2-substituted dihydropyran shown in entry 1 of Table 4, when subjected to the same reaction conditions but at room temperature, is recovered after 60% conversion in only 88% *ee* (vs 96% *ee* at 70 °C). Experiments that help establish the mechanistic basis of the above temperature effects are in progress. 2) Consistent with the models illustrated in Figure 2, 6-substituted dihydropyrans (Table 1, entry 2) are not resolved effectively (C5 substituent should not strongly interact with the catalyst structure; see Fig. 2); however, when a substituent at C2 is also present, resolution proceeds with excellent efficiency (entry 3). 3) Dihydropyrans substituted at C5 are resolved with high selectivity as well (entry 4). In this class of substrates, one enantiomer reacts more slowly, presumably because its association with the zirconocene–alkene complex leads to unfavorable steric interactions between the C5 alkyl unit and the coordinated ethylene ligand.

Table 4. [(ebthi)Zr]-catalyzed kinetic resolution of unsaturated pyrans [a].

Entry	Substrate		Conv. [%]	Cat. [mol%]	Config. *ee* [%] [b]
1	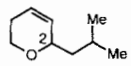		60	10	*R*, 96
2	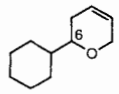		60	10	*S*, 41
3	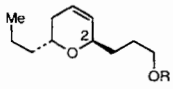	R = MgCl R = TBS	56 60	10 10	*R*, > 99 *R*, > 99
4	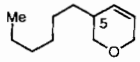		58	20	*R*, 99
5	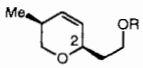	R = MgCl R = TBS	63 61	10 10	*R*, > 99 *R*, 94

[a] Reaction conditions: indicated mol% (*R*)-**2**, 5.0 equiv EtMgCl, 70 °C, THF. Mass recovery in all reactions > 85%. [b] Configuration and *ee* value of recovered alkene.

Zirconocene-catalyzed kinetic resolution of dihydrofurans is also possible (Scheme 20).[54] Unlike their six-membered ring counterparts, both of the heterocyclic enantiomers react readily, but through distinctly different reaction pathways, to afford readily separable constitutional isomers in high diastereomeric and enantiomeric purity. A plausible explanation for the difference in the reactivity of dihydropyrans and -furans is that in the latter both olefinic carbons are adjacent to a C–O bond: formation of the C–Zr bond can take place at either end of the π-system. Thus, the dihydrofuran substrate and the [(ebthi)Zr]–alkene complex (*R*)-**37** approach one another so that unfavorable steric interactions are avoided, leading to the formation of readily separable nonracemic products (see Scheme 19).

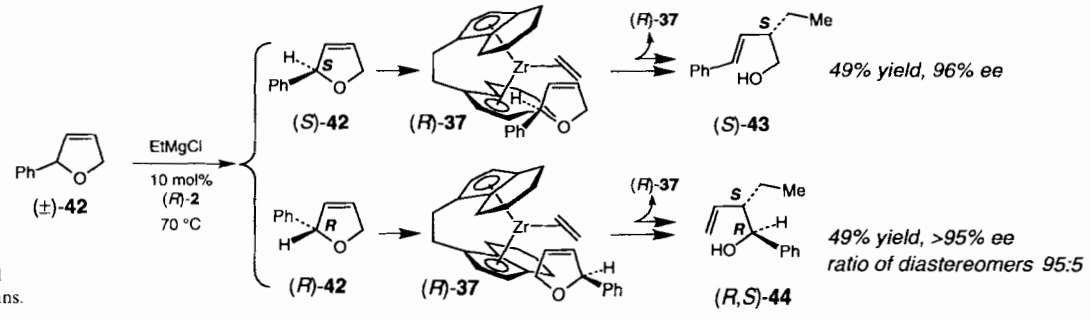

Scheme 19. [(ebthi)Zr]-catalyzed kinetic resolution of dihydrofurans.

Comparison with Related Catalytic Enantioselective Processes

The zirconocene-catalyzed enantioselective carbomagnesation accomplishes an important and unique task: addition of an alkylmagnesium halide to an alkene to provide a carbometalation product suitable for a variety of additional functionalization reactions (see Scheme 17). Excellent enantioselectivity is obtained in reactions with ethyl-, propyl, and butylmagnesium chloride, and the catalytic resolution processes allow for preparation of a variety of nonracemic heterocycles. Nonetheless, the development of reaction processes for the efficient and enantioselective addition of a larger range of alkyl groups (e.g. methyl, vinyl, phenyl, etc.) to unfunctionalized alkenes remains an important and challenging goal. The reaction described recently by Negishi [Eq. (r)], in which a nonbridged chiral zirconocene[55] is used as catalyst, is an example of research towards this end.[56]

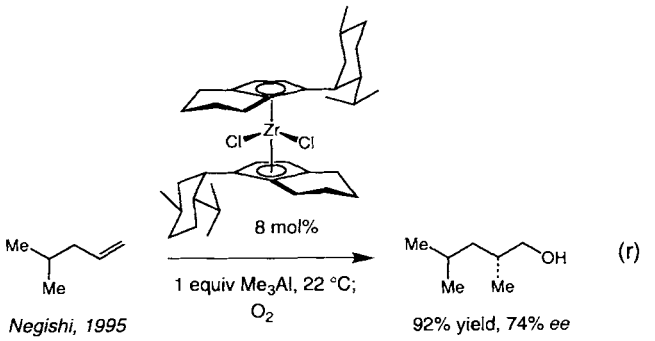

4.2. Catalytic Asymmetric Formation of C–H Bonds

4.2.1. Asymmetric Hydrogenation of Terminal and 1,1-Disubstituted Alkenes

In the last five years much progress has been made in the *ansa*-metallocene-catalyzed hydrogenation of alkenes. Both Zr- and Ti-based catalytic systems have been used for this purpose; terminal and 1,1-disubstituted olefins, as well as trisubstituted alkenes have been used as substrates. By far the most successful hydrogenations involve trisubstituted alkenes, for which enantioselectivities from 83 to 99% *ee* have been reported. In initial studies in this area, carried out by Waymouth and Pino, the polymerization catalyst [(ebthi)ZrX_2]/MAO was used in the presence of H_2 to effect alkene hydrogenation.[29] Pino and Waymouth had recognized that in certain instances olefin polymerization proceeds sluggishly because hydrogenation of the metal–alkyl intermediate is significantly faster than alkene insertion, leading to the formation of hydrogenated monomers in large excess.

Table 5 illustrates the marked difference in reaction efficiency that arises when different metallocene sources are employed in the [(ebthi)Zr]-catalyzed hydrogenation. The mechanism by which MAO converts the zirconium(IV) salts into active zirconium–hydride species remains unclear.[57] However, it has been proposed that when the catalytically inactive zirconium dichloride salt is used, a chlorine atom may form an η^2-bridge between aluminum and zirconium, thus preventing formation of the active cationic metal center.[29]

As was mentioned before, and as illustrated in Table 6, an important prerequisite for efficient cationic [(ebthi)Zr]-catalyzed hydrogenation is that the alkene should not be able to polymerize readily. Whereas with 1-decene as substrate the hydrogenation product is obtained in only 28% yield (Table 6, entry 1; the main product is the polymer), 2-methyl-1-pentene affords 97% of the hydrogenation product (Table 6, entry 3). Interestingly, in a competition experiment, *trans*-2-hexene is hydrogenated much faster than the *cis* isomer (Table 6, entry 4).

Table 5. Hydrogenation of styrene as a function of the zirconium catalyst precursor.

Catalyst precursor	Gas	P_o [kPa; atm]	Yield [%]
[(ebthi)$ZrMe_2$]	H_2	2.0×10^3; 20	93
[(ebthi)Zr(binol)]	D_2	1.7×10^3; 17.5	89
[(ebthi)$ZrCl_2$]	H_2	2.0×10^3; 20	0

Table 6. Hydrogenation of alkenes with [(ebthi)$ZrMe_2$]/MAO as precatalyst.

Entry	Substrate	P_o [kPa; atm]	Conv. [%]	Yield [%]
1	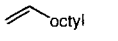	10^3; 10	95	28
2	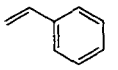	2×10^3; 20	94	93
3	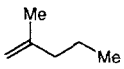	2×10^3; 20	100	97
4	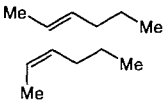	10^2; 1	96 4	50 [a]
5	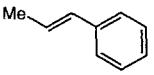	2×10^3; 20	20	20

[a] Combined yield.

Data in Table 7 illustrate that when the nonracemic [(ebthi)Zr] system is used to catalyze the hydrogenation of prochiral alkenes, moderate levels of enantiofacial differentiation are observed (23–65% *ee*). Enantioselective deuteration of pentene occurs in low yield but shows noticeable enantioselectivity (23% *ee*). The same reaction with styrene proceeds in 61% yield and with moderate enantioselectivity (65% *ee*). Hydrogenation of 2-phenyl-1-pentene proceeds in excellent yield (95%) but with poor control of stereochemistry (36% *ee*).

An interesting aspect of these hydrogenations and deuterations of alkenes is that the induced stereochemistry is opposite to that of similar oligomerization reactions. Thus, as the example in Scheme 20 illustrates, the prochiral π-face that is hy-

Table 7. Enantioselective hydrogenation and deuteration of alkenes catalyzed by (*R*)-[(ebthi)Zr(binol)] and MAO at 25 °C.

Substrate	Gas	Cat. [mol%]	Yield [%]	*ee* [%]	Prod. config.
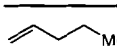	D_2	–	10	23	*R*
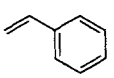	D_2	6.0×10^{-4}	61	65	*R*
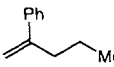	H_2	2.2×10^{-4}	95	36	*R*

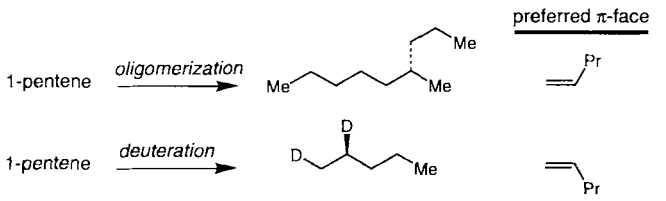

Scheme 20. Variations in enantiofacial selectivity in reactions catalyzed by [(ebthi)Zr(binol)] MAO.

drogenated is opposite to that on which carbon–carbon bond formation takes place in the related polymerization process.

As an explanation Waymouth has suggested that a sterically demanding polymer chain would prefer to associate with the zirconocene catalyst in the manner shown in Scheme 21. That is,

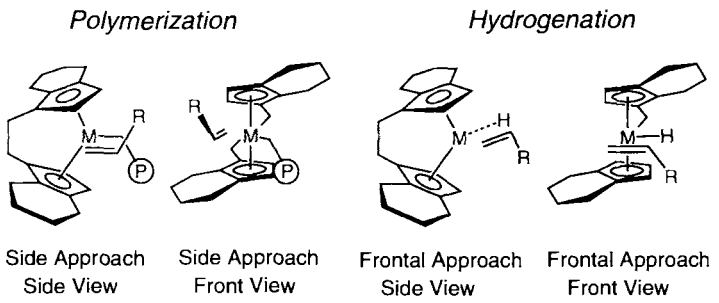

Scheme 21. Transition state structures proposed by Waymouth for the polymerization and hydrogenation of alkenes by [(ebthi)ZrX]/MAO. Ⓟ = polymer chain.

the pendant groups on the alkene substrate may be oriented such that most steric interactions with the ebthi ligand are avoided. This mode of catalyst–substrate interaction necessitates that the reacting alkene approach the [(ebthi)Zr] system side-on in the oligomerization or polymerization processes. In contrast, in the hydrogenation of alkenes the small hydrogen atom may readily adopt the side position below the tetrahydroindenyl ligand, allowing the larger alkene to approach the metal hydride from the sterically more accessible front face (Scheme 21).

4.2.2. *Asymmetric Hydrogenation of Trisubstituted Alkenes*

Hydrogenation of unfunctionalized trisubstituted olefins with bridged titanocene complexes as catalyst precursors has been reported recently by Buchwald and co-workers.[58] Unfunctionalized alkenes are appropriate substrates and excellent levels of enantioselectivity are observed. The active catalyst in these systems is postulated to be chiral titanocene (*S*)-**45**, which is produced by treatment of nonracemic [(ebthi)Ti(binol)] with two equivalents of butyllithium under H_2 atmosphere, followed by the addition of 2.5 equivalents of phenylsilane [Eq. (s)].

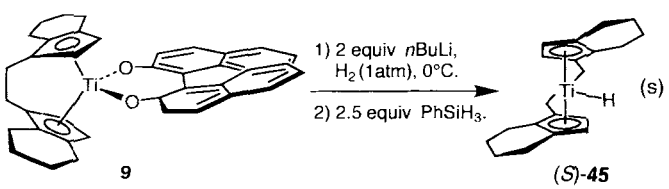

As evident in Table 8, hydrogenation of trisubstituted olefins catalyzed by 5 mol% (*S*)-**45** occurs in high yields and >90% *ee*. Aromatic olefins as well as allylic amines and ethers are suitable substrates (entries 4 and 5). Although it is not a stated prerequisite, all substrates reported are alkenes attached to an aromatic ring. Interestingly, *E* and *Z* alkenes react with much different efficiencies under the reported conditions. (*E*)-α,β-Dimethyl-*p*-methoxystyrene is hydrogenated in 48 h to give a 79% yield of the (*R*) enantiomer of the product in 95% *ee* (entry 2, Table 8). However, when a 2:1 mixture of *E*:*Z* alkenes is used as starting material, the reaction requires 146 h to give an 80% yield of the (*R*) isomer in only 31% *ee*.[59]

Table 8. Enantioselective hydrogenation of trisubstituted alkenes with [(ebthi)TiH] [a].

Entry	Alkene	Product [b]	Yield [%]	*ee* [%]
1	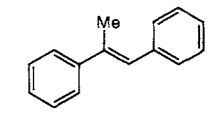	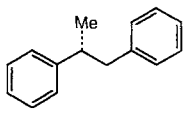	91	>99
2	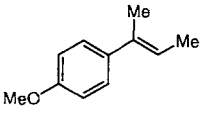	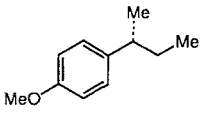	79	95
3	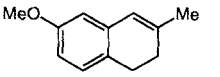	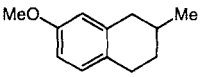	77	92
4	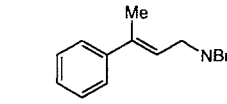	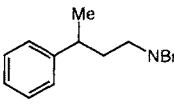	75	95
5	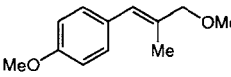	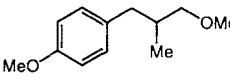	86	94

[a] Reaction conditions: 5 mol% (*S*)-[(ebthi)TiH], 1.38×10^4 kPa (2000 psi H_2), 65 °C, THF. [b] Absolute configuration was determined only for entries 1 and 2.

Transition state structures have been put forth by Buchwald to rationalize the absolute stereochemistry afforded by the [(ebthi)Ti]-catalyzed hydrogenation.[58] In the proposed mechanism the substituent attached to the monosubstituted terminus of the C=C bond appears to control which face of the prochiral alkene reacts preferably. If we assume that the hydride attached to titanium takes the side position beneath the cyclohexyl ring of the ebthi ligand, then the alkene should approach the metal center from the front face of the complex (Ti prefers to bond to the less substituted carbon of the alkene; Scheme 22). Hence, there are two modes of attack for each type of alkene substrate (*E* or *Z*) that could lead to the hydrogenation product; in both instances, one mode of reaction involves interaction of two of the alkene substituents with the large cyclohexyl ring of the catalyst (**XIV** and **XVI**). Because the lower energy path involves an alkene–cyclohexyl interaction (**XIII** and **XV**), there is a reactivity difference between *E* and *Z* alkenes in the hydrogenation reaction.

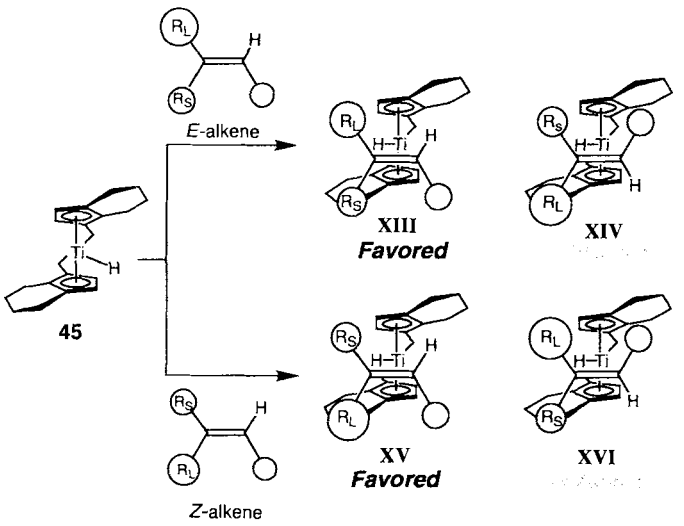

Scheme 22. Transition structure models proposed by Buchwald for [(ebthi)Ti]-catalyzed hydrogenation of alkenes. R_s = small group, R_L = large group.

Table 9. Enantioselective hydrogenation of imines with [(ebthi)Ti(binol)] as precatalyst [a].

Entry	Substrate	Product	Yield [%]	*ee* [%]
1	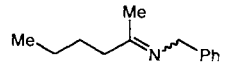	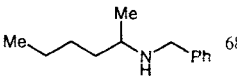	68	58
2	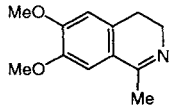	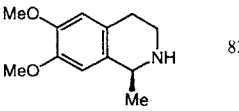	82	98
3	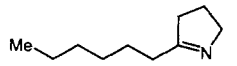	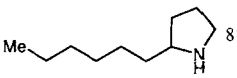	81	98
4	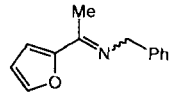	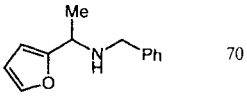	70	53

[a] Reaction conditions: 5 mol% (*S*)-**45**, 1.38×10^4 kPa (2000 psi) H_2, 65 °C, THF. [b] Absolute configuration was determined only for entry 2.

Comparison with Related Catalytic Enantioselective Processes

Significant advances have been made in the area of enantioselective hydrogenation with various rhodium, ruthenium, and cobalt complexes as catalysts.[60] However, similar processes with trisubstituted alkenes as substrates are often nonstereoselective.[61] Therefore, the titanocene-catalyzed hydrogenation of trisubstituted alkenes reported by Buchwald represents the first catalytic transformation that accomplishes this important task with excellent efficiency and enantioselectivity. The development of other new catalytic methods for the hydrogenation of a wider range of olefinic substrates will undoubtedly remain a preoccupation of researchers active in this area. In this context, the highly enantioselective hydrogenation of α,β-unsaturated carbonyl compounds by Pfaltz [Eqs. (t) and (u)] represents a major advance in the field.[62]

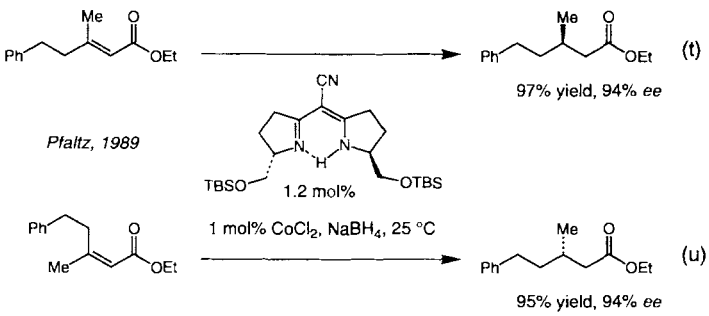

4.2.3. Asymmetric Hydrogenation of Imines

4.2.3.1. Asymmetric [(ebthi)Ti]-Catalyzed Reduction of Imines

Buchwald and co-workers have reported that titanocene **45** is an effective catalyst for enantioselective hydrogenation of imines (Table 9).[63] With 5 mol% of the chiral Ti complex and under 1.38×10^4 kPa (2000 psi) H_2 at 65 °C, imines are reduced to amines in good yield and with 58–98% *ee*.[64a] In the reduction of acyclic imines the selectivity is lower than that obtained with cyclic substrates. This could arise because acyclic imines are often composed of a mixture of *cis* and *trans* isomers; similar to the hydrogenation of alkenes, the two imine isomers might be expected to react through opposite enantiofaces.[64]

In more recent work, Buchwald has demonstrated that the [(ebthi)Ti]-catalyzed reduction of cyclic imines proceeds notably faster than that of related acyclic substrates.[64b] Kinetic studies indicate that the catalytic cycle shown in Scheme 23

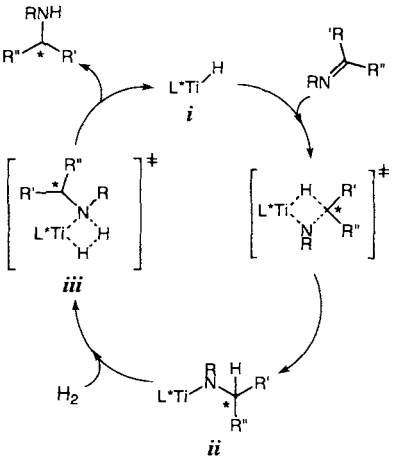

Scheme 23. Proposed mechanism for the [(ebthi)Ti]-catalyzed reduction of imines.

represents a plausible mechanism for the Ti-catalyzed reduction. Specifically, experimental evidence indicates that hydrogenolysis of the Ti–N bond (*ii* → *iii* → *i*) may be the rate-determining step in the titanium-catalyzed reduction of imines.[64c] Buchwald has suggested that when the substrate is a cyclic amine in which the two nitrogen substituents are tethered, the Ti–N bond is generally more accessible to the incoming H_2 molecule and therefore undergoes hydrogenation (*iii* → *i*, Scheme 24) faster than an analogous acyclic system in which the Ti–N bond is effectively more hindered.[65]

Buchwald and co-workers subsequently established that with cyclic imines, 551 kPa (80 psi) H_2 pressure is sufficient for the Ti-catalyzed reduction to proceed smoothly.[64b] Thus, **46**–**53** (Scheme 24) are reduced with 5 mol% **45** [see Eq. (s)] under

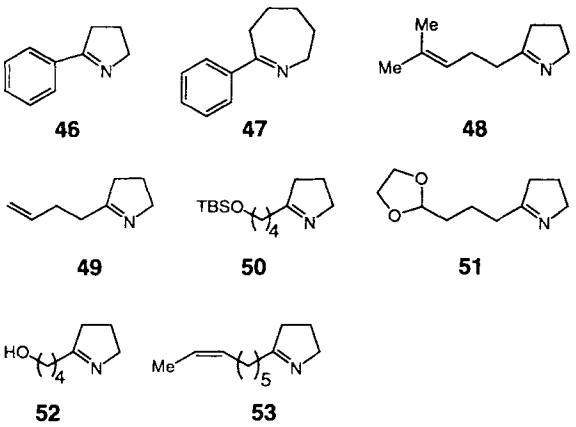

Scheme 24. Substrates suitable for [(ebthi)TiH]-catalyzed reduction of imines.

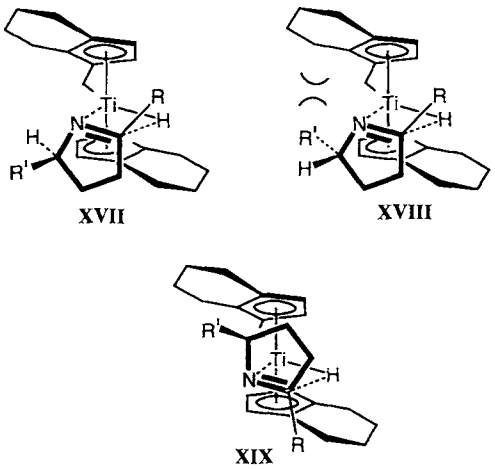

Scheme 25. Transition state models proposed by Buchwald for the [(ebthi)TiH]-catalyzed reduction of cyclic imines. **XVII**: no steric hindrance. **XVIII**: with steric hindrance. **XIX** is not possible.

551 kPa (80 psi) H_2 to yield the desired amines in >70% yield and >98% *ee*. In addition, these workers reported that the more reactive cyclic imines exemplified by **46** are reduced with as little as 1 mol% catalyst. Whereas terminal C=C bonds in the substrate may be hydrogenated along with the imine, di- and trisubstituted C=C bonds are relatively inert under these reaction conditions (ca. 16% of **53** contained the (*E*) alkene and ca. 17% of the substrate was the saturated analog). In the case of hydroxyl-substituted imines, phenylsilane is used for the in situ protection of hydroxyl group; hence hydroxyl imines may be subjected to the catalytic reduction conditions as well (e.g. **52** with excess phenylsilane). Five-, six-, and seven-membered cyclic imines, as well as substrates bearing silylethers, acetals, and protected pyrroles can be utilized in these transformations.

4.2.3.2. Kinetic Resolution through [(Ebthi)Ti]-Catalyzed Reduction of Imines

The catalytic kinetic resolution of chiral imines through the titanium-catalyzed enantioselective hydrogenation reaction has been investigated by Buchwald.[66] As shown in Table 10, when (±)-5-methyl-2-phenyl-1-pyrroline is subjected to the hydrogenation conditions, after about 50% conversion both the recovered starting material and the product in 99% *ee* are obtained (entry 1, Table 10). Whereas pyrrolines substituted at C5 are readily resolved, those carrying substituents at C3 and C4 undergo catalytic resolution less efficiently (cf. entries 1 and 2 to entries 3 and 4).

The proposed transition state structures depicted in Scheme 25, accounting for the reactivity and selectivity patterns observed in [(ebthi)Ti]-catalyzed reduction of imines, are similar to those offered for the catalytic hydrogenation of alkenes (cf. Scheme 22). It has been suggested that in the intermediate in which C–H bond formation occurs, the Ti–H bond is positioned such that it can overlap with the π^* orbital of the imine.[67] That is, bond formation proceeds through a four-centered transition state structure, in which the pyrroline ring is positioned such that steric interactions between the R group attached to the imine carbon and the tetrahydroindenyl ligand are avoided (**XVII** and **XVIII** in Scheme 25). A complex of type **XIX** would be destabilized by interactions between R and the cyclohexyl group of the chiral ligand. Furthermore, it should be preferable that the heterocycle is situated such that the R′ substituent on the stereogenic carbon is oriented away from the catalyst, as in **XVII**. In the transition state structure for the mismatched substrate enantiomer **XVIII**, the R′ group is positioned directly under the cyclohexyl group of the ligand and suffers from unfavorable steric interaction with the cyclopentadienyl ring of the chiral catalyst.[68]

According to the models proposed for the [(ebthi)Ti]-catalyzed reduction of imines, it may be predicted that the C3- and C4-substituted imines should be efficiently resolved under these conditions with equal efficiency. How-

Table 10. [(ebthi)Ti]-catalyzed kinetic resolution of cyclic imines [a].

Entry	Substrate	Product	Yield [%] *ee* [%]	Recovered substrate	Yield *ee* [%]
1	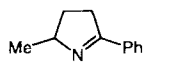	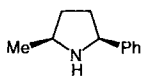	34 [99]	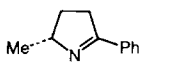	37 [99]
2	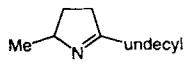	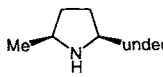	41 [> 95]	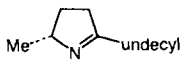	41 [> 95]
3	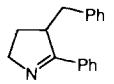	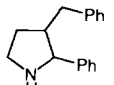 *syn:anti 6:1*	42 [> 95]	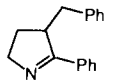	- [75]
4	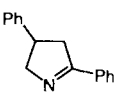	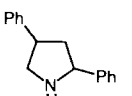 *syn:anti 3:1*	44 [99]	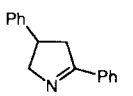	33 [49]

[a] Reaction conditions: 5 mol% (*S*)-[(ebthi)TiH], 551 kPa (80 psi) H_2, 65 °C, THF.

ever, as shown in Table 10 (entry 4), the steric bulk of a phenyl group at C4 is not sufficient to allow effective kinetic resolution, and reduction of a substrate having a benzyl substituent at the C3 site (entry 3) is significantly less selective than that with the corresponding C5-substituted isomers (entries 1 and 2). Thus, it is likely that there are other conformations of the pyrroline ring that allow the alkyl groups at C4 to escape interaction with the ligands of the metal catalyst.

Comparison with Related Catalytic Enantioselective Processes

The synthesis of nonracemic amines through reduction of their unsaturated precursors has been the target of a number of important investigations. Procedures described by Brunner and Wiegrebe [Eq. (v)],[69] Fryzuk and James [Eq. (w)],[70] Osborn [Eq. (x)],[71] Spindler [Eq. (y)],[72] and Burk [Eq. (z)][73] offer alternative enantioselective methods. Comparison of this previous work to that described in this section clearly indicates that the [(ebthi)Ti]-catalyzed reduction of imines developed by Buchwald is an important, valuable, and useful addition to the variety of available methods for the reduction of imines.

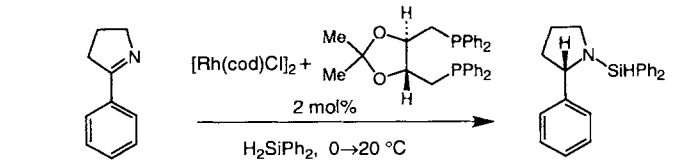

Brunner & Wiegrebe, 1985 — 85% yield, 59% *ee* (v)

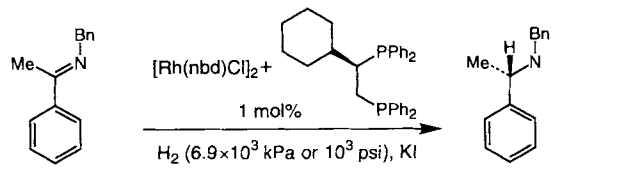

Fryzuk & James, 1988 — >99% yield, 84% *ee* (w)

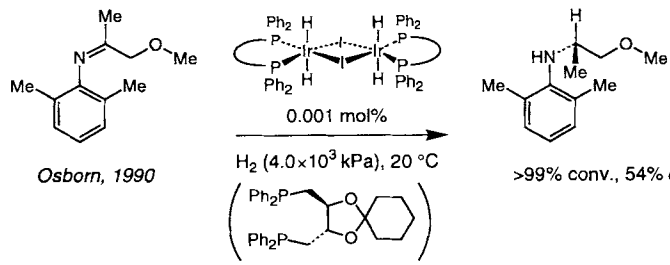

Osborn, 1990 — >99% conv., 54% *ee* (x)

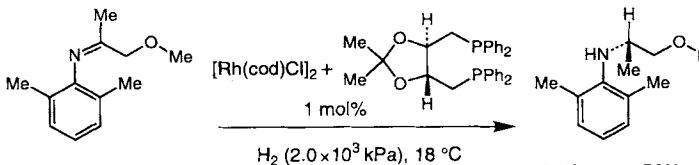

Spindler, 1990 — 77% conv., 56% *ee* (y)

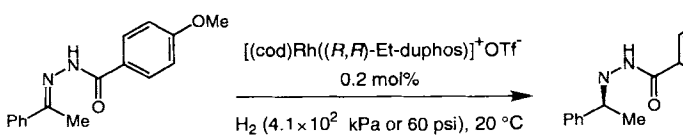

Burk, 1992 — 95% yield, 91% *ee* (z)

In the context of related catalytic kinetic resolution procedures, Lensink reported in 1993 an effective method for the catalytic kinetic resolution of chiral acyclic imines;[74] an example of this process is illustrated below [Eq. (aa)]. Thus, the

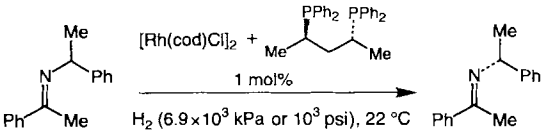

Lensink, 1993 — 83% *ee*, 67% conv. (aa)

Rh-catalyzed and the [(ebthi)Ti]-catalyzed resolution methods complement each other in offering convenient routes for the efficient enantioselective syntheses of a variety of chiral imines in nonracemic form.

4.2.4. *Asymmetric Hydrogenation of Enamines*

Buchwald and Lee have reported the [(ebthi)TiH]-catalyzed asymmetric hydrogenation of enamines.[75] The reaction conditions are sufficiently mild that aromatic chlorides, ethers, and trisubstituted alkenes can be considered as compatible functional groups. However, when an aryl bromide is used as a substrate, the the C–Br bond is reduced, presumably by a titanium(III) hydride complex. As shown in Table 11, α-aryl tertiary amines are produced in good yield and with exceptional enantioselectivity. Cyclic tertiary amines are most often employed as substrates; however, acyclic methyl benzyl enamines are suitable starting materials as well (entry 2, Table 11). It is worthy of note that the C=C bond in the cyclohexenyl enamine substrate in entry 3 of Table 11 is not hydrogenated under the reaction conditions.

Transition state models that account for the selectivity observed in the [(ebthi)Ti]-catalyzed asymmetric hydrogenation of enamines have been proposed by Buchwald and are depicted in Scheme 26. It has been suggested that one transition state structure would be significantly favored if the phenyl group rotates out of conjugation with the enamine

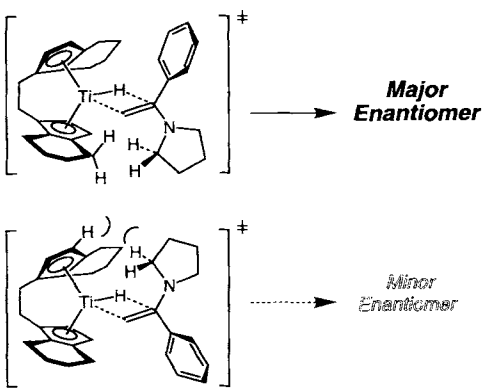

Scheme 26. Transition state structures proposed by Buchwald for the [(ebthi)TiH]-catalyzed reduction of enamines.

Table 11. Catalytic and enantioselective hydrogenation of selected enamines with [(ebthi)TiH] [a].

Entry	Substrate	Product	Yield [%]	*ee* [%] [b]
1	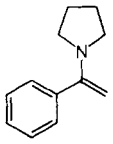	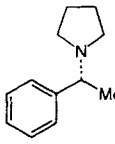	75	92
2	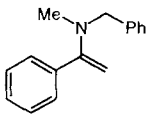	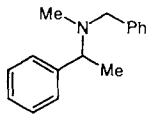	83	96
3	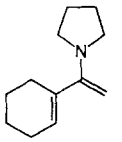	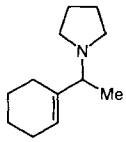	72	95
4	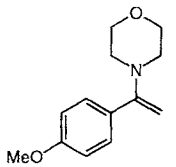	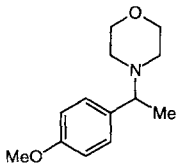	88	91

[a] Reaction conditions: 5 mol% (*S*)-[(ebthi)Ti(binol)], 103–551 kPa (15–80 psi) H_2, 65 °C, THF. [b] Absolute configuration was determined only for entry 1.

Table 12. Catalytic and enantioselective reduction of selected ketones with (*R*)-[(ebthi)TiH] [a].

Entry	Substrate	Product	Yield [%]	*ee* [%]
1	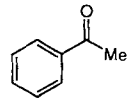	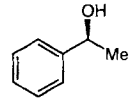	73	97
2	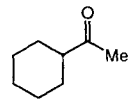	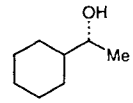	67	24
3	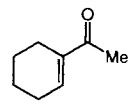	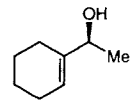	72	90 [b]
4	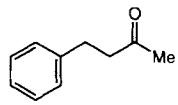	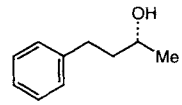	88	12
5	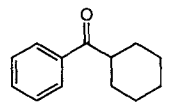	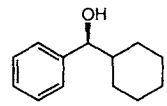	88	82 [c]

[a] Product shown is that obtained after treatment of the hydrosilation products with TBAF or HCl. [b] 9 mol% catalyst used. [c] $PhSiH_3$ used.

C=C bond; as a result the nonbonding pair of electrons on nitrogen could retain their overlap with the olefin π-cloud. Severe A(1,2) allylic strain would exist if both the phenyl π-system and the nonbonding electrons on nitrogen were to remain coplanar with the C=C bond. These conformational considerations lead to the preference for the top transition structure in Scheme 26. Although there is no experimental evidence in support of such conformational tendencies, the above mechanistic paradigm readily accounts for the observed enantioselectivities.

Comparison with Related Catalytic Enantioselective Processes

Catalytic enantioselective methods for the hydrogenation of enamides has been the subject of a number of reports.[76] However, the Buchwald study describes the first examples of asymmetric and catalytic reductions of enamines. Therefore, the [(ebthi)TiH] system has provided the synthetic chemist with a unique tool for the efficient preparation of a variety of nonracemic amines in high enantiopurity.

4.2.5. Asymmetric Hydrosilation of Ketones

The development of methods for the enantioselective reduction of ketones has been the subject of intense study in recent years. In general, the reported methods are most effective when the two groups attached to the carbonyl group differ significantly in size. In an effort to extend the scope of this transformation, Buchwald and co-workers have employed the [(ebthi)TiH] complex in the asymmetric catalytic reduction of ketones.[77] Thus, in the presence of polymethylhydrosilane, (*R*)-[(ebthi)TiH] complex (generated from (*R*)-[(ebthi)Ti(binol)] and two equivalents of butyllithium) catalyzes the reduction of various ketones in high yield and with excellent enantioselectivity.

Aryl, methyl, and vinyl ketones are selectively reduced to the corresponding nonracemic secondary alcohols (Table 12). Selectivity is markedly reduced, however, when both of the ketone substituents are aliphatic (entry 4). The selective reduction of cyclohexyl phenyl ketone (entry 5), in which the ketone substituents are of similar size, indicates that electronic effects can play a notable role in controlling stereoselectivity. In connection to the last case, Buchwald suggests that the two substituents may have different effective sizes. The phenyl and carbonyl π-systems may remain coplanar and hence conformationally constrained, whereas the cyclohexyl ring might rotate to avoid costly steric interactions with the chiral ligand. Structures that account for the enantiofacial selectivity in the hydrosilation of ketones are similar to those discussed previously for the hydrogenation of alkenes, imines, and enamines (cf. Schemes 22, 25, and 26).

Comparison with Related Catalytic Enantioselective Processes

Shown below are examples of other highly enantioselective reductions of carbonyl compounds reported by Corey [Eq. (bb)],[78] Evans [Eq. (cc)],[79] Bolm [Eq. (dd)],[80] Ito [Eq. (ee)],[81] Noyori [Eq. (ff)],[82] and Mukaiyama [Eq. (gg)].[83] The Corey method has been utilized in the synthesis of a variety of important target molecules: the prostaglandin precursor **54**,[84] and trichloromethyl alcohol **55**,[85] which is used in the preparation of unnatural amino acids in the nonracemic form, are illustrative.[86] Buchwald's [(ebthi)TiH]-catalyzed method presents a useful complement to other available catalytic methods for the enantioselective reduction of ketones. For example, the hydrosilation procedure reported by Ito [Eq. (ee)] affords the allylic alcohol with enantioselectivity similar to that reported by the MIT group (entry 3, Table 12); however, a subsequent desilylation is required in the Ito method. On the other

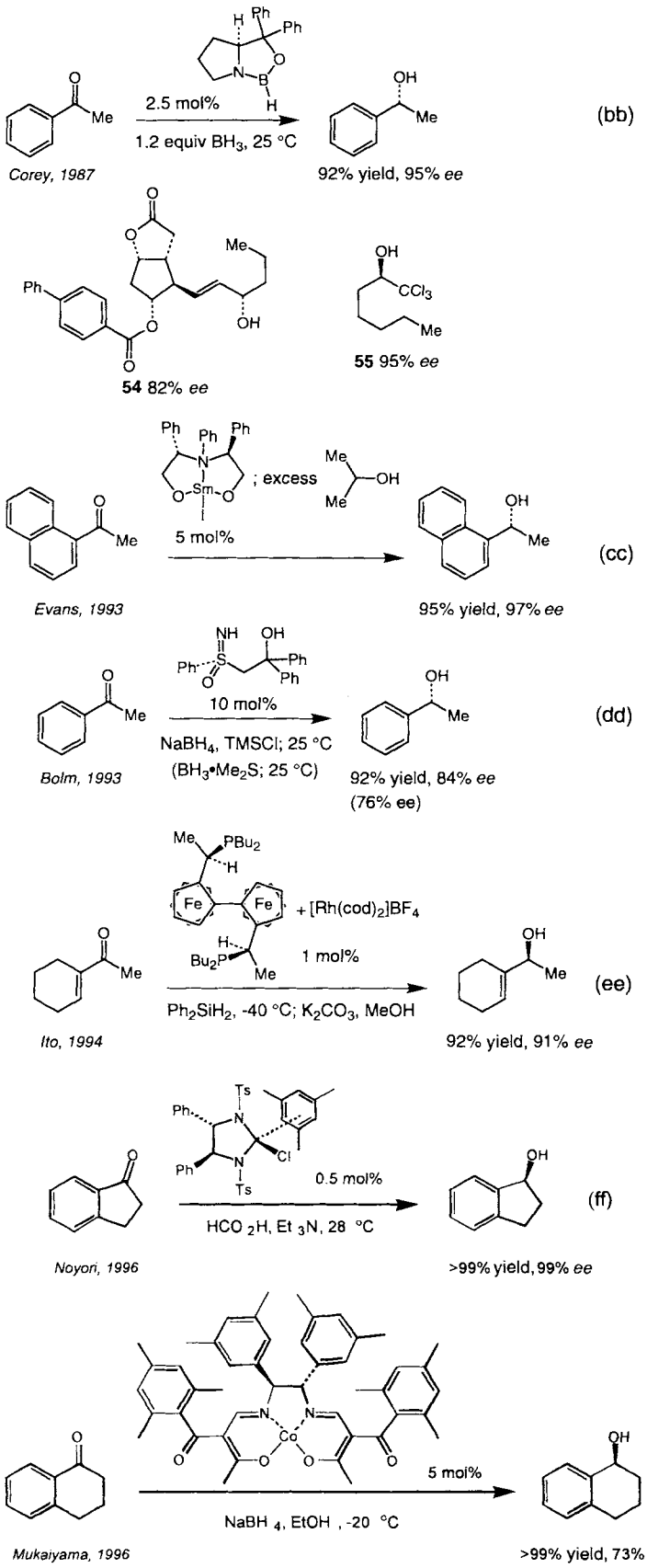

hand the cyclohexyl methyl ketone shown in entry 2 of Table 12 is reduced in 80% *ee* by the Ito approach (vs. 24% *ee* by the Ti-catalyzed protocol). The most recent advance reported by Noyori affords outstanding enantioselectivities in a reaction in which the hydride source (formic acid) efficiently reduces the ketone substrate. This is in contrast to the reaction with the more conventional hydride source 2-propanol, which suffers from the reverse process and thus less than ideal conversions.

5. Summary and Outlook

The chemistry described in this article demonstrates that chiral *ansa*-metallocene complexes can be used to effect a number of useful and important catalytic asymmetric transformations in excellent yield and with high levels of enantioselectivity. Because of the direct involvement of the metal center in the bond-forming process, reactions that involve the insertion of a functional group (for example an alkene, imine, enamine, or ketone) into a metal–hydride or metal–carbon bond most often proceed with outstanding regio- and stereoselectivity. However, when bond formation takes place at a site more remote from the transition metal center (as in allylmetalation or Lewis acid catalyzed Diels–Alder reaction), less efficient chirality transfer is observed. Future studies may nonetheless show that in the latter class of transformations alteration of the chiral ligand allows for a higher degree of chirality transfer in metallocene-mediated or -catalyzed reactions.

Although ebthi metallocenes have proven to be effective at promoting a variety of transformations, the equipment required to prepare such catalysts (glovebox and high-pressure hydrogenation apparatus), as well as costs associated with the required metallocene resolution (nonracemic binaphthol costs $45 per gram), may preclude everyday use of these chiral controlling agents in large-scale organic synthesis. In this context, promising advances toward practical syntheses of inexpensive and chiral [(ebthi)MX_2] equivalents may eventually provide more practical alternatives to this powerful class of transition metal catalysts. These organometallic complexes should not only allow for widespread application of the enantioselective and catalytic transformations discussed in this review, they may also be able to effect selective transformations not readily achieved with nonracemic [(ebthi)M] ensembles. Regardless, there is little doubt that the chemistry discussed in this article adumbrates future exciting discoveries in the design and development of useful asymmetric catalytic transformations.

We are grateful to the National Institutes of Health (GM-47480) and the National Science Foundation (CHE-9257580) for generous support of our research in connection to the development of the Zr-catalyzed carbomagnesation reaction. Additional support from Pfizer, Eli Lilly, Zeneca, Glaxo, and Monsanto is also gratefully acknowledged. We are grateful to our co-workers and colleagues Z.-M. Xu, Ahmad F. Houri, Mary T. Didiuk, Michael S. Visser, Charles W. Johannes, Nina R. Horan, and Derek A. Cogan for their important contributions to aspects of the carbomagnesation project described here. We thank Professors Robert Waymouth and Richard Jordan for many useful suggestions and a critical reading of this manuscript, and Professor Steve Buchwald for a helpful discussion.

Received: August 11, 1995 [A 129IE]
German version: *Angew. Chem.* **1996**, *108*, 1378–1401

[1] For a general overview of recent advances in this area, see: *Catalytic Asymmetric Synthesis* (Ed.: I. Ojima), VCH, New York, Weinheim, **1993**.

[2] For a recent review on chiral metallocene complexes, see: a) R. L. Halterman, *Chem. Rev.* **1992**, *92*, 969–994; b) J. Okuda, *Angew. Chem.* **1992**, *104*, 49; *Angew. Chem. Int. Ed. Engl.* **1992**, *31*, 47–48.

[3] a) F. R. W. P. Wild, L. Zsolnai, G. Huttner, H. H. Brintzinger, *J. Organomet. Chem.* **1982**, *232*, 233–247; b) F. W. R. P. Wild, M. Wasiucionek, G. Huttner, H. H. Brintzinger, *J. Organomet. Chem.* **1985**, *288*, 63–67; c) W. Kaminsky, K. Kulper, H. H. Brintzinger, F. W. R. P. Wild, *Angew. Chem.* **1985**, *97*, 507; *Angew. Chem. Int. Ed. Engl.* **1985**, *24*, 507–508.

[4] J. A. Ewen, L. Haspeslagh, J. L. Atwood, H. Zhang, *J. Am. Chem. Soc.* **1987**, *109*, 6544–6545.

[5] S. Collins, B. A. Kuntz, N. J. Taylor, D. G. Ward, *J. Organomet. Chem.* **1988**, *342*, 21–29.

[6] F. Piemontesi, I. Camurati, L. Resconi, D. Balboni, A. Sironi, M. Moret, R. Zeigler, N. Piccolrovazzi, *Organometallics* **1995**, *14*, 1256–1266.

[7] R. B. Grossman, R. A. Doyle, S. L. Buchwald, *Organometallics* **1991**, *10*, 1501–1505.

[8] For preparation of solvated Group IV metal tetrachlorides from the anhydrous metal salts, see: L. E. Manzer, *Inorg. Synth.* **1982**, 135–140.

[9] For studies on the stereochemistry of hydrogenation of [(ebi)$ZrCl_2$] (**5**), see: R. M. Waymouth, F. Bangerter, P. Pino, *Inorg. Chem.* **1988**, *27*, 758–759.

[10] G. M. Diamond, S. Rodewald, R. F. Jordan, *Organometallics* **1995**, *15*, 5–7.

[11] A. Schafer, E. Karl, L. Zsolnai, G. Huttner, H. H. Brintzinger, *J. Organomet. Chem.* **1987**, *328*, 87–89.

[12] R. B. Grossman, W. M. Davis, S. L. Buchwald, *J. Am. Chem. Soc.* **1991**, *113*, 2321–2322.

[13] A similar equilibration has recently been proposed for the zirconium-catalyzed isomerization of *cis* and *trans* alkenes that do not bear β-hydrides, see: E. I. Negishi, D. Choueiry, T. B. Nguyen, D. R. Swanson, D. R. Suzuki, T. Takahashi, *J. Am. Chem. Soc.* **1994**, *116*, 9751–9752.

[14] S. Collins, B. A. Kuntz, Y. Hong, *J. Org. Chem.* **1989**, *54*, 4154–4158.

[15] A similar transition state structure has been proposed to explain the stereochemistry of addition of achiral allyl titanocenes to aldehydes. See: F. Sato, K. Iida, S. Iijima, H. Moriya, M. Sato, *J. Chem. Soc. Chem. Commun.* **1981**, 1140–1141.

[16] H. C. Brown, P. K. Jadhav, *J. Am. Chem. Soc.* **1983**, *105*, 2092–2093.

[17] N. Minowa, T. Mukaiyama, *Bull. Chem. Soc. Jpn.* **1987**, *60*, 3697–3704.

[18] M. Riediker, R. O. Duthaler, *Angew. Chem.* **1989**, *101*, 488; *Angew. Chem. Int. Ed. Engl.* **1989**, *28*, 494–495.

[19] E. J. Corey, C.-M. Yu, S. S. Kim, *J. Am. Chem. Soc.* **1989**, *111*, 5495–5496.

[20] A. Hafner, R. O. Duthaler, R. Marti, G. Rihs, P. Rothe-Streit, F. Schwarzenbach, *J. Am. Chem. Soc.* **1992**, *114*, 2321–2336.

[21] a) W. R. Roush, L. K. Hoong, M. A. J. Palmer, J. C. Park, *J. Org. Chem.* **1990**, *55*, 4109–4117; b) W. R. Roush, P. T. Grover, X. Lin, *Tetrahedron Lett.* **1990**, *31*, 7563–7566; c) W. R. Roush, P. T. Grover, *ibid.* **1990**, *31*, 7567–7570; d) W. R. Roush, J. C. Park, *ibid.* **1991**, *32*, 6285–6288.

[22] R. Sturmer, R. W. Hoffmann, *SynLett.* **1990**, 759–760.

[23] For similar enantioselective addition of allenic and acetylenic units, see: a) E. J. Corey, G. B. Jones, *Tetrahedron Lett.* **1991**, *32*, 5713–5716; b) E. J. Corey, K. A. Cimprich, *J. Am. Chem. Soc.* **1994**, *116*, 3151–3152; c) G. E. Keck, D. Krishnamurthy, X. Chen, *Tetrahedron Lett.* **1994**, *35*, 8323–8324.

[24] K. Ishihara, M. Mouri, Q. Gao, T. Maruyama, K. Furuta, H. Yamamoto, *J. Am. Chem. Soc.* **1993**, *115*, 11490–11495.

[25] a) G. H. Keck, K. H. Tarbet, L. S. Geraci, *J. Am. Chem. Soc.* **1993**, *115*, 8467–8468; b) A. L. Costa, M. G. Piazza, E. Tagliavini, C. Trombini, A. Umani-Ronchi, *ibid.* **1993**, *115*, 7001–7002; c) P. Bedeschi, S. Casolari, A. L. Costa, E. Tagliavini, A. Umani-Ronchi, *Tetrahedron Lett.* **1995**, *36*, 7897–7900.

[26] S. Rodewald, R. F. Jordan, *J. Am. Chem. Soc.* **1994**, *116*, 4491–4492.

[27] a) A. S. Guram, R. F. Jordan, *Organometallics* **1990**, *9*, 2190–2192; b) *ibid.* **1991**, *10*, 3470–3479.

[28] J. A. Ewen, *J. Am. Chem. Soc.* **1984**, *106*, 6355–6364.

[29] For a brief introduction to the oligomerization process, see: a) J. P. Collman, L. S. Hegedus, J. R. Norton, R. G. Finke, in *Principles and Applications of Organotransition Metal Chemistry*, University Science Books, Mill Valley, CA, **1987**, 593–600; b) For a recent review, see: H. H. Brintzinger, D. Fischer, R. Mulhaupt, B. Reiger, R. M. Waymouth, *Angew. Chem.* **1995**, *107*, 1255–1283; *Angew. Chem. Int. Ed. Engl.* **1995**, *34*, 1143–1170.

[30] R. M. Waymouth, P. Pino, *J. Am. Chem. Soc.* **1990**, *112*, 4911–4914.

[31] W. Kaminsky, A. Ahlers, N. Moller-Lindenhof, *Angew. Chem.* **1989**, *101*, 1304; *Angew. Chem. Int. Ed. Engl.* **1989**, *28*, 1216–1218.

[32] P. Pino, P. Cioni, J. Wei, *J. Am. Chem. Soc.* **1987**, *109*, 6189–6191.

[33] a) G. W. Coates, R. M. Waymouth, *J. Am. Chem. Soc.* **1991**, *113*, 6270–6271; b) *ibid.* **1993**, *115*, 91–98. For an additional example of an optically active synthetic polymer with main-chain chirality, see: M. Brookhart, M. J. Wagner, G. G. A. Balavoine, H. A. Haddou, *J. Am. Chem. Soc.* **1994**, *116*, 3641–3642.

[34] a) G. Natta, L. Porri, S. Valenti, *Makromol. Chem.* **1963**, *67*, 225–228; b) T. Tsunetsugu, T. Fueno, J. Furukawa, *ibid.* **1968**, *112*, 220–224; c) M. Farina, G. Audisio, G. Natta, *J. Am. Chem. Soc.* **1967**, *89*, 5071; d) G. Costa, P. Locatelli, A. Zambelli, *Makromolecules* **1973**, *6*, 653–654.

[35] G. Natta, M. Farina, M. Peraldo, G. Bressan, *Makromol. Chem.* **1961**, *43*, 68–75.

[36] For stereoselective polymerization of racemic 4-methyl-1-hexene through heterogeneous metal catalysis, see: P. Pino, R. Mulhaupt, *Angew. Chem.* **1980**, *92*, 921; *Angew. Chem. Int. Ed. Engl.* **1980**, *19*, 857–875, and references therein.

[37] Y. Hong, B. A. Kuntz, S. Collins, *Organometallics* **1993**, *12*, 964–969.

[38] [(ebthi)$ZrMe_2$] is prepared by treatment of [(ebthi)Zr(binol)] with two equivalents of methyllithium, see ref. [12].

[39] With [Cp_2Zr(O*t*Bu)(thf)] as catalyst selectivities are generally around 20:1 *endo*:*exo*. See: S. Collins, B. E. Koene, R. Ramachandran, N. J. Taylor, *Organometallics* **1991**, *10*, 2092–2094.

[40] J. M. Hawkins, S. Loren, *J. Am. Chem. Soc.* **1991**, *113*, 7794–7795, and references therein.

[41] J. B. Jaquith, J. Guan, S. Wang, S. Collins, *Organometallics* **1995**, *14*, 1079–1081.

[42] For a review of catalytic asymmetric Diels–Alder reactions, see: H. B. Kagan, O. Riant, *Chem. Rev.* **1992**, *92*, 1007–1019. For representative reports on catalytic asymmetric [4 + 2] cycloadditions that have appeared subsequent to this review, see: a) Q. Gao, T. Maruyama, M. Mouri, H. Yamamoto, *J. Org. Chem.* **1992**, *57*, 1951–1952; b) K. Hattori, H. Yamamoto, *ibid.* **1992**, *57*, 3264–3265; c) E. J. Corey, T.-P. Loh, *Tetrahedron Lett.* **1993**, *34*, 3979–3982; d) J. Bao, W. D. Wulff, A. L. Rheingold, *J. Am. Chem. Soc.* **1993**, *115*, 3814–3815; e) I. E. Marko, G. R. Evans, *Tetrahedron Lett.* **1993**, *35*, 2771–2774; f) E. P. Kündig, B. Bourdin, G. Bernardinelli, *Angew. Chem.* **1994**, *106*, 1931–1934; *Angew. Chem. Int. Ed Engl.* **1994**, *33*, 1856–1858; g) J. Bao, W. D. Wulff, *ibid.* **1994**, *36*, 3321–3324; h) K. Ishihara, H. Yamamoto, *J. Am. Chem. Soc.* **1994**, *116*, 1561–1562; i) K. Mikami, Y. Motoyama, M. Terada, *ibid.* **1994**, *116*, 2812–2820; j) K. Ishihara, M. Miyata, M., K. Hattori, T. Tada, H. Yamamoto, *ibid.* **1994** *116*, 10520–10524; k) E. J. Corey, A. Guzman-Perez, T.-P. Loh, *ibid.* **1994**, *116*, 3611–3612; l) W. Odenkirk, B. Bosnich, *J. Chem. Soc. Chem. Commun.* **1995**, 1181–1182; m) K. Fuji, T. Kawabata, A. Kuroda, T. Taga, *J. Org. Chem.* **1995**, *60*, 1914–1915; n) E. J. Corey, M. A. Letavic, *J. Am. Chem. Soc.* **1995**, *117*, 9616–9617; o) G. E. Keck, X.-Y. Li, D. Krishnamurthy, *J. Org. Chem.* **1995**, *60*, 5998–5999; p) K. Ishihara, H. Kurihara, H. Yamamoto, *J. Am. Chem. Soc.* **1996**, *118*, 3049–3050.

[43] K. Narasaka, N. Iwasawa, M. Inoue, T. Yamada, M. Nakashima, J. Sugimori, *J. Am. Chem. Soc.* **1989**, *111*, 5340–5345, and references therein.

[44] a) E. J. Corey, R. Imwinkelried, S. Pikul, Y.-B. Xiang, *J. Am. Chem. Soc.* **1989**, *111*, 5493–5495; b) E. J. Corey, N. Imai, H.-Y. Zhang, *ibid.* **1991**, *113*, 728–729; this paper reports cycloaddition reactions catalyzed by complexes with bis(oxazoline) chiral ligands (also utilized by Evans in ref. [45]).

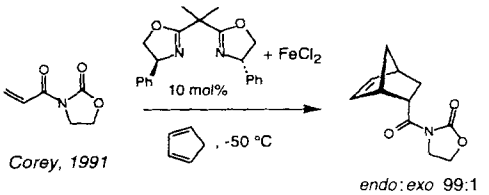

[45] a) D. A. Evans, S. J. Miller, T. Lectka, *J. Am. Chem. Soc.* **1993**, *115*, 6460–6461; b) D. A. Evans, J. A. Murry, P. Von Matt, R. D. Norcros, S. J. Miller, *Angew. Chem.* **1993**, *107*, 864; *Angew. Chem. Int. Ed. Engl.* **1995**, *34*, 798–800.

[46] S. Kobayashi, H. Ishitani, *J. Am. Chem. Soc.* **1994**, *116*, 4083–4084, and references therein. For a recent review, in which Sc-catalyzed enantioselective cycloadditions are discussed, see: S. Kobayashi, *SynLett.* **1994**, 689–701.

[47] For reports that address the reactivity issue (reactions with less reactive dienes) in the asymmetric Diels-Alder reactions, see: a) E. J. Corey, S. Sarshar, D.-H. Lee, *J. Am. Chem. Soc.* **1994**, *116*, 12089–12090; b) ref. [45b].

[48] J. P. Morken, M. T. Didiuk, A. H. Hoveyda, *J. Am. Chem. Soc.* **1993**, *115*, 6997–6998; see also: H.-G. Schmalz, *Nachr. Chem. Tech. Lab.* **1994**, *42*, 724–729.

[49] A. F. Houri, Z.-M. Xu, D. A. Cogan, A. H. Hoveyda, *J. Am. Chem. Soc.* **1995**, *117*, 2943–2944; see also: H.-G. Schmalz, *Angew. Chem.* **1995**, *107*, 1981–1984; *Angew. Chem. Int. Ed. Engl.* **1995**, *34*, 1833–1836.

[50] A. H. Hoveyda, J. P. Morken, *J. Org. Chem.* **1993**, *58*, 4237–4244.

[51] Kinetic measurements performed in our laboratories [52] indicate that the Zr–Mg ligand exchange (e.g., *i* → *iii* in Scheme 19) is likely the turnover-limiting step. However, formation of the zirconacyclopentane may well be the stereochemistry-determining event in the catalytic cycle. That is, either both metallacycle isomers undergo ligand exchange at the same rate and, therefore, the more predominant metallacycle leads to the final major isomer, or Zr–Mg ligand exchange may be somewhat faster in the minor zirconacycle, but the higher concentration of one intermediate metallacycle may more than compensate for the aforementioned rate difference.

[52] M. T. Didiuk, C. W. Johannes, J. P. Morken, A. H. Hoveyda, *J. Am. Chem. Soc.* **1995**, *117*, 7097–7104.

[53] J. P. Morken, M. T. Didiuk, M. S. Visser, A. H. Hoveyda, *J. Am. Chem. Soc.* **1994**, *116*, 3123–3124. For a recent report on Zr-catalyzed kinetic resolution of related medium-ring systems, see: M. S. Visser, N. M. Heron, M. T. Didiuk, J. F. Segal, A. H. Hoveyda, *J. Am. Chem. Soc.* **1996**, *118*, 4291–4298. For a recent report on the Zr-catalyzed kinetic resolution of exocyclic ethers, see: M. S. Visser, J. P. A. Harrity, A. H. Hoveyda, *J. Am. Chem. Soc.* **1996**, *118*, 3779–3780.

[54] M. S. Visser, A. H. Hoveyda, *Tetrahedron* **1995**, 4383–4394.

[55] G. Erker, M. Aulbach, M. Knickmeier, D. Wingbermuhle, C. Kruger, M. Nolte, S. Werner, *J. Am. Chem. Soc.* **1993**, *115*, 4590–4601.

[56] a) D. Y. Kondakov, E. Negishi, *J. Am. Chem. Soc.* **1995**, *117*, 10771–10772; b) D. Y. Kondakov, E. Negishi, *J. Am. Chem. Soc.* **1996**, *118*, 1577–1578.

[57] For studies related to the characterization of Ziegler–Natta polymerization intermediates with $[Cp_2ZrCl_2]$ as catalyst, see: P. Gassman, M. R. Callstrom, *J. Am. Chem. Soc.* **1987**, *109*, 7875–7876.

[58] R. D. Broene, S. L. Buchwald, *J. Am. Chem. Soc.* **1993**, *115*, 12569–12570.

[59] With a 64:36 mixture of *E*:*Z* alkene isomers and 100% conversion, a value of 83% *ee* can be calculated for the hydrogenation product of the (*Z*) alkene: 64% (95% *ee R*) + 36% (83% *ee S*) = 100% (31% *ee R*).

[60] a) A. Pfaltz, *Acc. Chem. Res.* **1993**, *26*, 339–345; b) R. Noyori, *Science* **1990**, *248*, 1194–1199; c) H. Takaya, T. Ohta, R. Noyori, in *Catalytic Asymmetric Synthesis* (Ed.: I. Ojima), VCH, New York, Weinheim, **1993**, pp. 1–39, and references therein; d) I. Ojima, N. Clos, C. Bastos, *Tetrahedron* **1989**, *45*, 6901–6939, and references therein.

[61] M. Tanaka, I. Ogata, *J. Chem. Soc. Chem. Commun.* **1975**, 735.

[62] U. Leutenegger, A. Madin, A. Pfaltz, *Angew. Chem.* **1989**, *101*, 61; *Angew. Chem. Int. Ed. Engl.* **1989**, *28*, 60–61.

[63] For other examples of metal-catalyzed asymmetric hydrogenation of imines, see: a) Rhodium catalysis: J. Bakos, I. Toth, B. Heil, G. Szalontai, L. Parkanyi, V. Fulop, *J. Organomet. Chem.* **1989**, *370*, 263 b) Iridium catalysis: Y. N. C. Chan, J. A. Osborn, *J. Am. Chem. Soc.* **1990**, *112*, 9400–9401.

[64] a) C. A. Willoughby, S. L. Buchwald, *J. Am. Chem. Soc.* **1992**, *114*, 7562–7564; b) *ibid.* **1994**, *116*, 8952–8965; c) *ibid.* **1994**, *116*, 11703–11714.

[65] C. A. Willoughby, S. L. Buchwald, *J. Org. Chem.* **1993**, *58*, 7627–7629.

[66] A. Viso, N. E. Lee, S. L. Buchwald, *J. Am. Chem. Soc.* **1994**, *116*, 9373–9374.

[67] Alkene insertion reactions generally involve a transition state in which the alkene and metal–hydride bond are coplanar. See: R. H. Crabtree in *The Organometallic Chemistry of the Transition Metals*, Wiley, New York **1988**, pp. 148–153.

[68] Buchwald has shown that in the [(ebthi)TiH]-catalyzed reduction of achiral imines, the rate-determining step is hydrogenolysis of the Ti–N bond (Scheme 23). Therefore, insertion of an imine into the Ti–H bond is not necessarily a kinetically significant process. However, the proposed mechanistic arguments, in which the major product stereoisomer is predicted based on the minimization of steric interactions within the [(ebthi)TiH] π-complex, provide a convenient tool for the reliable prediction of stereochemical outcome of the reaction. It is possible that, in fact, enamine or alkene association with the chiral Ti–H complex is the stereochemistry-determining step. In other words, although the Ti–N hydrogenation may be rate-determining, there is little energy difference between the slow steps of the various pathways that lead to enantiomeric products: the predominant product isomer arises from the most abundant transition metal–substrate complex.

[69] R. Becker, H. Brunner, S. Mahboobi, W. Wiegrebe, *Angew. Chem.* **1985**, *97*, 993; *Angew. Chem. Int. Ed. Engl.* **1985**, *24*, 995–996.

[70] G.-J. Kang, W. R. Cullen, M. D. Fryzuk, B. R. James, J. P. Kutney, *J. Chem. Soc. Chem. Commun.* **1988**, 1466–1467; see also: a) ref. [63a]; b) J. Bakos, A. Orosz, B. Heil, M. Laghmari, P. Lhoste, D. Sinou, *J. Chem. Soc. Chem. Commun.* **1991**, 1684–1685; c) A. G. Becalski, W. R. Cullen, M. D. Fryzuk, B. R. James, G.-J. Kang, S. J. Rettig, *Inorg. Chem.* **1991**, *30*, 5002–5008.

[71] Y. N. C. Chan, J. A. Osborn, *J. Am. Chem. Soc.* **1990**, *112*, 9400–9401.

[72] F. Spindler, B. Pugin, H.-U. Blaser, *Angew. Chem.* **1990**, *102*, 561; *Angew. Chem. Int. Ed. Engl.* **1990**, *29*, 558–559.

[73] M. J. Burk, J. E. Feaster, *J. Am. Chem. Soc.* **1992**, *114*, 6266–6267. The structure of Et-duphos is shown below. For details of the synthesis of this class of ligands, see: M. J. Burk, J. E. Feaster, W. A. Nugent, R. L. Harlow, *J. Am. Chem. Soc.* **1993**, *115*, 10125–10138.

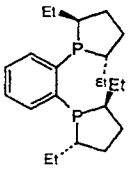

[74] C. Lensink, J. G. de Vries, *Tetrahedron Asymmetry* **1993**, *4*, 215–222.

[75] N. E. Lee, S. L. Buchwald, *J. Am. Chem. Soc.* **1994**, *116*, 5985–5986.

[76] For recent review of enantioselective hydrogenation of enamides, see: a) R. Noyori, *Asymmetric Catalysis in Organic Synthesis*, Wiley, New York, **1994**, pp. 33–38; b) ref. [60b], pp. 9–10 and ref. [60c].

[77] M. B. Carter, B. Schiott, A. Gutierrez, S. L. Buchwald, *J. Am. Chem. Soc.* **1994**, *116*, 11667–11670.

[78] E. J. Corey, R. K. Bakshi, S. Shibata, *J. Am. Chem. Soc.* **1987**, *109*, 5551–5553.

[79] D. A. Evans, S. G. Nelson, M. R. Gagne, A. R. Muci, *J. Am. Chem. Soc.* **1993**, *115*, 9800–9801.

[80] a) C. Bolm, A. Seger, M. Felder, *Tetrahedron Lett.* **1993**, *34*, 8079–8080; b) C. Bolm, M. Felder, *ibid.* **1993**, *34*, 6041–6044.

[81] M. Sawamura, R. Kuwano, Y. Ito, *J. Am. Chem. Soc.* **1994**, *33*, 111–113.

[82] A. Fujii, S. Hashiguchi, N. Uematsu, T. Ikariya, R. Noyori, *J. Am. Chem. Soc.* **1996**, *118*, 2521–2522.

[83] T. Nagata, K. Yorozu, T. Yamada, T. Mukaiyama, *Angew. Chem.* **1995**, *107*, 2309–2311; *Angew. Chem. Int. Ed. Engl.* **1995**, *34*, 2145–2147.

[84] E. J. Corey, R. K. Bakshi, S. Shibata, C.-P. Chen, V. K. Singh, *J. Am. Chem. Soc.* **1987**, *109*, 7925–7926.

[85] E. J. Corey, J. O. Link, *J. Am. Chem. Soc.* **1992**, *114*, 1906–1908.

[86] For other less enantioselective catalytic reductions of ketones, see: a) K. Yamamoto, T. Hayashi, M. Kumada, *J. Organomet. Chem.* **1972**, *46*, C65–C67; b) K. Tamao, H. Yamamoto, H. Matsumoto, N. Miyake, T. Hayashi, M. Kumada, *Tetrahedron Lett.* **1977**, 1389–1392; c) R. L. Halterman, T. M. Ramsay, Z. Chen, *J. Org. Chem.* **1994**, *59*, 2642–2644.

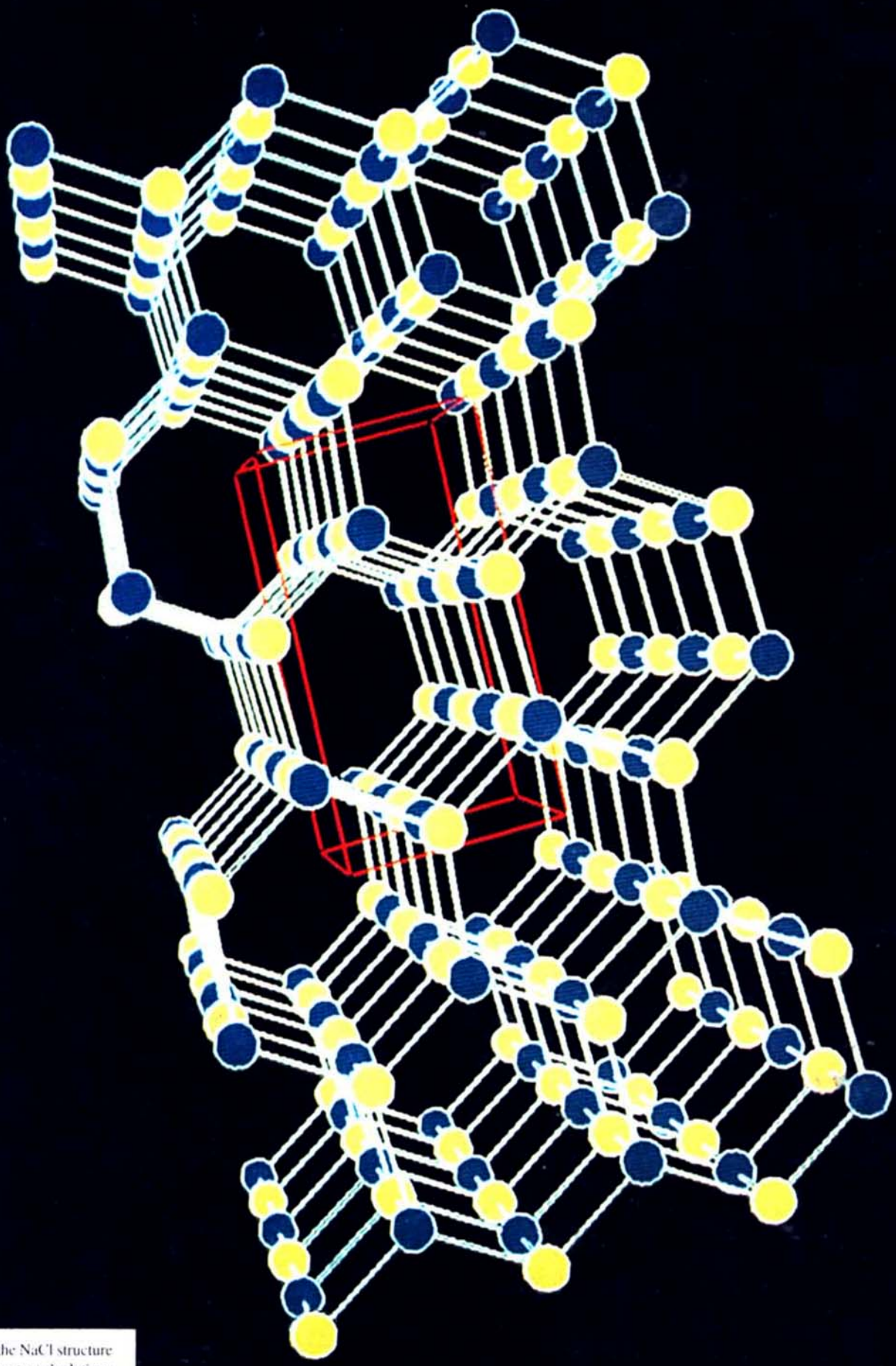

A variant of the NaCl structure that according to calculations should be stable at low temperatures or in the presence of included particles

First Step Towards Planning of Syntheses in Solid-State Chemistry: Determination of Promising Structure Candidates by Global Optimization

J. Christian Schön and Martin Jansen*

A method is presented here that allows, in principle, the prediction of the existence and structure of (meta)stable solid compounds. It is based on a set of adjustable modules that are applied to the study of the energy function of the chemical system of interest. The main elements are a set of routines for global optimization and local minimization, as well as algorithms for the investigation of the phase space structure near local minima of the potential energy, and the analysis and characterization of the structure candidates. The current implementation focuses on ionic compounds, for which empirical potentials are used for the evaluation of the energy function in the first stage, and a Hartree–Fock algorithm for refinements. The global optimization is performed with a stochastic simulated annealing algorithm, and the local minimization employs stochastic quenches and gradient methods. The neighborhoods of the local minima are studied with the threshold algorithm. The results of this approach are illustrated with a number of examples: compounds of binary noble gases, and binary and ternary ionic compounds. These include several substances that have not been synthesized yet, but should stand a fair chance of being kinetically stable, for example further alkali metal nitrides besides Li_3N, as well as Ca_3SiBr_2 or $SrTi_2O_5$.

Keywords: computer chemistry · solid-state structures · structure prediction · synthesis planning

1. Introduction and Philosophy

A touchstone for judging the stage of the development of a scientific field is the degree to which it is possible to predict experimental results from basic principles. Considering the main goals of chemistry, namely synthesis and analysis of new compounds, one must ask whether it is feasible to predict the existence of hypothetical compounds under given thermodynamic boundary conditions, and also to develop realistic routes for their synthesis.

Already with respect to the predictability of (meta)stable compounds, dramatic differences exist among the different branches of preparative chemistry. In the molecular chemistry of carbon and some of the other nonmetals, an impressive ability in the design, that is, the prediction of such molecules, has been reached. In addition, a large repertoire of techniques has been developed that allow the systematic planning of specific synthetic routes. As just one of many examples, we mention the "retro-synthesis" technique[1] systematized and developed in the work of Corey;[2, 3] another remarkable approach is the systematic classification of possible reaction sites and paths by Ugi et al.[4]

Prof. Dr. M. Jansen, Dr. J. C. Schön
Institut für Anorganische Chemie der Universität
Gerhard-Domagk-Strasse 1, D-53121 Bonn (Germany)
Fax: Int. code + (228)735660
e-mail: unc419@ibm.rhrz.uni-bonn.de

In preparative solid-state chemistry, however, it is neither possible to predict whether some hypothetical compound can exist at all nor what structure(s) it would exhibit. In most cases, the research is experimental in the classical sense of the word. Of course, the success of such an exploration can be improved through clever choices of starting materials, and appropriate temperature and pressure settings during the synthesis. But a control of the reactions involved that would be sufficient for an a-priori design of a specific synthetic route is not available at this time. The obvious great differences with respect to both the methods and the general approach have caused, for example, Harald Schäfer to remark[5] that a separation of preparative chemistry into the subfields "solid-state chemistry" and "molecular chemistry" were more appropriate than the historically founded one into "organic" and "inorganic" chemistry, and similar sentiments have been expressed by others since.[6]

In Table 1 we have tried to illustrate the complementary, even nearly antagonistic, character of these two subfields through a comparison of the crucial laws and processes pertaining to each. Homogeneous equilibria between molecular starting materials and products dispersed within a solution are compared with the phase equilibria among macroscopically distributed reaction partners in solid-state reactions. From this follows the well-known fact that in homogeneous equilibria all participants in the reaction are present in finite concentrations, while in solid-state reactions the solid starting materials can be used up completely. Thus, with appropriate control of the reaction, only the

Table 1. Comparison of molecular and solid-state chemistry with respect to selected features of reactions within these fields.

Molecular Chemistry	Solid-State Chemistry
homogeneous equilibrium	heterogeneous equilibrium
in equilibrium all reactants are present in finite amounts	reactions may proceed until one of the condensed phases has disappeared, or even until only one remains
low reaction temperatures	high reaction temperatures
kinetic reaction control	thermodynamic reaction control
conservation of molecular framework, reaction at functional groups	destruction of the structure of the starting materials
transport distance: about 5–10 Å	transport distance: about 10^4–10^6 Å
diffusion coefficients: about 10^{-5} $cm^2 sec^{-1}$	diffusion coefficients: about 10^{-10}–10^{-14} $cm^2 sec^{-1}$

pure product can remain in equilibrium as a single condensed phase, in agreement with Gibbs' phase rule.[7]

Already from this observation follows another, usually very clear, difference: since the reactions of molecules dispersed in homogeneous media can be made to proceed with little thermal activation and to involve the opening and closing of only a single or at most very few bonds at a time, these reactions are kinetically controlled to a large degree. In contrast, due to the rather drastic temperature and pressure conditions employed during solid-state reactions, these are usually controlled thermodynamically, and result in a complete reorganization of the structures of the initial compounds. Finally, the actual synthesis techniques strongly reflect the fundamental differences in the conditions for the transport of the atoms involved during the different types of reactions, that is, the distances separating the reactants, the available transport paths, and the diffusion coefficients of the atoms/molecules in the solid or the solution (cf. Table 1).

From this simplified phenomenological comparison, one can draw the conclusion that the regiospecificity of reactions in molecules together with the mainly kinetic control of the reactions constitute an efficient toolbox for planning molecular syntheses, while similar tools are usually not available for solid-state syntheses. One must ask, however, how the molecular chemist can predict whether the final, and also the intermediate, molecules are capable of existing in the first place, and, furthermore, how he can recognize the validity of the proposed reaction steps.

The basis for the understanding of the details of molecular chemistry lies in the hierarchical structure of the participating quantities and the relatively small number of participating atoms. The local environment of an atom within a suggested molecule is dominated by the bonds to the neighboring atoms and to a lesser extent by spatial packing requirements. Since "allowed" local configurations are well-known from experience, both with respect to their geometry and their stability, any presumably stable molecule can be easily constructed by using these local configurations as a system of stable structural increments. On the next level, one can investigate the secondary (topological) structure consisting of rings, chains, or clusters, etc., which again must follow certain simple rules based on size and bonding angle requirements. Finally, in larger molecules or emsembles, the arrangement of secondary structure elements into a higher tertiary or quaternary structure must be considered. This hierarchical approach reflects the fact that the energy function for the kinetically stable molecules usually encountered by the molecular chemist can be described by a sum of local (short-range) interactions. Even up to rather large distortions, this local description appears to remain a valid approximation, and the effects of distortions on the energy of the system are often known and have been accounted for in the models. In the past two decades, such potentials[8, 9] have been implemented successfully in molecular modeling packages that may be seen as a way to "quantify" the intuitive understanding of the molecular chemist.

In contrast, it appears nearly impossible to predict even the existence of stable solid phases with a given fixed composition, not to mention *all* the metastable phases that might exist.[10] Why should Li_3N exist, but not Na_3N or Cs_3N? Why is TiO_2 found in a large number of stable modifications such as rutile,

Martin Jansen, born in 1944 on Pellworm, studied chemistry at the Justus-Liebig-Universität Giessen, where he gained his doctorate in 1973 under the supervision of R. Hoppe. After his habilitation in 1978, he was offered and accepted a professorial chair for Inorganic Chemistry at the Universität Hannover. In 1987 he moved to the Rheinische Friedrich Wilhelms Universität in Bonn. His main research lie in the field of preparative solid-state chemistry, crystal chemistry, materials research, and the structure–property relationship of solids. Among others, he was awarded the Gottfried Wilhelm Leibniz prize and the Otto Bayer prize.

M. Jansen

J. C. Schön

J. Christian Schön was born in Bonn in 1957. He studied physics at the Universität Bonn and at the Massachusetts Institute of Technology, where he received his MS im mathematical physics in 1982, and his PhD in theoretical solid state physics in 1988. Afterwards he undertook postdoctoral studies in applied mathematics at San Diego State University until the end of 1991, where he worked on mathematical models in the areas of materials science and thermodynamics. After being a visitor at the University of Odense (Denmark), he carried out further postdoctoral research in the physics department of Copenhagen University. Since 1993 he has been at the Institut für Anorganische Chemie der Universität Bonn, where he is investigating the energy landscapes of solids, with a particular emphasis on modeling and predicting structures.

anatas, and brookite, while for MgF_2 only one structure has been reliably reported? Indubitably, it is also often possible in solid-state chemistry to estimate whether a suggested structure of a previously unknown compound is reasonable or strange; and a number of empirical rules exist, for example the radius ratio rule,[11-13] the valence electron concentration rule,[14, 15] Pauling's bond valence rules,[13, 16] and the analysis of partial Madelung constants,[17] that help us to pronounce judgement, after the fact. But even with the help of these rules and some empirical information about (formal) ionic charges and ionic radii, or some guidelines about the typical number of bonds a certain atom usually tries to establish, it is very difficult even to derive three-dimensional structures for a hypothetical compound of a given composition. And we are not even addressing the question, which structure might be the thermodynamically stable one (if any exists at all), or whether any of the competing ones might be kinetically stable. Of course, planning a synthesis route is inconceivable without a realistic synthetic target.

That one cannot predict the existence of a solid compound and its structure based on common sense can be seen in the difficulty to write down a simple energy function that—as is the case for an organic molecule—is dominated by a restricted set of local interactions. Of course, for a given existing structure, one can always construct a-posteriori some purely short-range potential containing empirical parameters derived from, for example, certain elastic constants and cell parameters. Because of the way it was constructed, such a potential can be used to justify, but not to predict, the local coordination polyhedra observed.

However, since such a very specific potential cannot be easily transferred even to another polymorphic modification of a given compound, it usually lacks the versatility inherent in the successful potentials used to describe the interactions within molecules. Most "general" forms of effective energy functions need to contain terms that describe long-range interactions, if they are to be of any use in comparing many hypothetical different structures of an unknown compound. However, once such terms are introduced, the simple building blocks one needs to construct consistent structures, in analogy to the visualization of a molecule, become increasingly fuzzy. In addition, we are dealing with practically infinite three-dimensional solids (extended solids), and thus, the number of possible arrangements of simple building blocks such as coordination polyhedra into periodic structures appears to be limitless, not to mention the possibility of amorphous structures and quasi-crystals. Apart from "social" arguments like "each atom of a given type should have the same environment" or "the structure with the higher symmetry should be more prevalent", there appears to be no obvious way to quickly choose among configurations that exhibit the same local structure but are otherwise different.

Nevertheless, the preceding considerations point towards a possible solution of the problems one faces when searching for new solids to synthesize. While it is still impossible to safely predict new and interesting solids by intuition or simple rules alone, with the advent of powerful computers other approaches have become feasible. From a physical point of view,[7] a kinetically stable compound is equivalent to a local minimum on the hypersurface of the potential energy[18] or Gibbs enthalpy of the chemical system, when this minimum is surrounded by energy and/or entropy barriers that are high enough to prevent a decomposition or a transformation into another structure within some (temperature-dependent) "survival time" $\tau_{life}(T)$.[18] Thus, in principle, it is possible to find all the (meta)stable compounds of a given system by studying the corresponding energy hypersurface. At this point, molecular and solid-state chemistry meet again in the sense that the complete range of possible molecules and solid compounds is already present on the energy hypersurface of a given chemical system.[19] Although the main goal of such a detailed study of the energy hypersurface is the recognition of promising synthetic targets and the evaluation of their kinetic stability, the neighborhood structure of the set of local minima may even yield hints for possible synthetic routes.

Since the direct quantum mechanical approach, that is solving the Schrödinger equation for an unknown realistic chemical system, is not yet feasible,[20] we feel that it is necessary to follow a stepwise procedure: first, possible candidate structures are determined with relatively fast but not very accurate methods, and then analyzed with respect to their properties, especially their kinetic and thermodynamic stability. The most promising ones can subsequently be refined by using more advanced and more precise, but also more time-consuming, algorithms. Attempts to implement such a procedure lead directly to the modular approach described in the next two sections.

In Section 4 we present the details of the current implementation, that is, the type of algorithms used, and the type of chemical systems that have been studied so far. Thereafter, we give an overview of the results obtained up to now, followed by a critical discussion of the current procedure. Our method constitutes a new approach to the planning of syntheses in solid-state chemistry; in the final section, we show the links between the method presented and the application of energy minimizations in the field of structure determination and structure refinement in solids, and studies of the energy hypersurface of molecules or clusters.

2. The Elements of the Modular Approach

We have chosen to implement the stepwise procedure described above by splitting it into five modules: input and database, preselector, optimizer, property analyzer, stability analyzer. Each element is devoted to a certain set of tasks, and it may employ algorithms of different degrees of refinement, depending on the stage of the procedure. During the analysis of a chemical system of interest, these modules will be called upon many times, until the most promising candidate structures have been determined.

2.1. Input and Database

The first module consists of two parts. First, there is the database containing as much of the a priori knowledge about the system as can be gleaned from theoretical and/or experimental studies of similar and/or related systems. This can include general properties like ionization energies and electron affinities, effective radii of the participating atoms or ions, and the number of valence electrons. But the database also contains

ranges of allowed parameters in effective potentials, basis sets for ab initio calculations, that is, the quantities necessary to evaluate the energy function within the most useful approximation.

The second part of the module is the traditional input one has to choose for any numerical calculation. Besides fixing the "physical" boundary conditions such as external tensions (e.g. pressure) or electromagnetic fields, we have to decide what the "chemical" boundary conditions should be. Since we can only represent a system of limited size in the computer, it is usually necessary to employ periodic boundary conditions, that is, a simulation cell of arbitrary variable shape containing a possibly fluctuating but nevertheless finite number of atoms is repeated periodically.[21] Evidently, this excludes quasi-crystals and amorphous systems, although one would expect that for very large simulation cells corresponding systems could occur.[22] If the system under investigation is completely unexplored, it might be most useful to impose no further restrictions and to let the subsequent optimization procedures determine which compositions, ionic charges, crystallographic unit cells, etc. characterize the most promising structures. On the other hand, one often has some a-priori interest, for example, in a certain composition, and thus one might want to prescribe fixed ratios of the numbers of different atoms within the simulation cell.

2.2. Preselector

This module represents the "controller" of the structure determination procedure. Like an "expert system", it analyzes the information provided by the other four modules and then decides upon the next step in the procedure. Of course, the general sequence of global and local optimizations, and the analyses of the best local minima is basically fixed. But the choice of initial configurations for the next optimization run(s) and the choice of the parameters of the various algorithms, in particular, is strongly influenced by the outcomes of the previous run(s). Depending on the problem at hand, one may want to program the preselector to follow a fixed schedule, or one may prefer a more dynamic approach. In the latter case, one would also decide (or have the preselector decide on its own), what method to use to evaluate the energy of the system, and how to vary the parameters of the empirical potentials and ab initio algorithms, in order to judge the robustness of the candidate structures.

2.3. Optimizer

The task of this module is rather straightforward. Based on the boundary conditions, initial configurations, and optimization parameters provided by the preselector and input modules, global and/or local optimization algorithms are employed to determine and/or refine local minima of the hypersurface of the potential energy of the system. The lowest local minima are often called sub-optima, since for most difficult optimization problems there is no guarantee that the global minimum can be found during a finite global optimization run.[23–25]

2.4. Property Analyzer

Since the hypersurface of the potential energy contains a very large number of local minima, one can expect that each optimization run will result in a different result. It is thus necessary, to analyze these structures, and to place them into certain structural categories. Furthermore, one might want to identify useful substructures that could serve as the initial configuration of a later optimization run. Finally, we are, of course, interested in the properties of the best structure candidates.[26] The determination and classification of the properties of the candidate structures is the task of the property analyzer module. It must contain algorithms to analyze the geometry of a given structure, and it may include additional algorithms for other properties of interest such as elastic constants.

2.5. Stability Analyzer

This module could have been discussed as part of the previous one, but since it deals with the analysis of the local environment and the kinetic stability of a minimum on the energy hypersurface, it is somewhat different from the usual algorithms that are used to evaluate the properties of a given fixed structure. As was pointed out in Section 2.4, the number of local minima on the energy hypersurface is very large, and this remains true, even after configurations with "similar" structure have been reduced to just one typical structure representative. At a temperature of $T = 0$ K, all these minima could in principle exist. But in most chemical systems, only a small number of (meta)stable periodic structures will actually be accessible synthetically. One criterion that presumably would eliminate many weak candidates, is the kinetic stability of the structure. If the energy barriers around a metastable minimum are too low, even very low temperatures will be enough to provide the activation energy necessary for a phase transformation to a different structure. Therefore, the stability analyzer module consists of algorithms that determine the heights of the energy barriers and the phase space volume near a local minimum.

3. General Aspects of the Search Procedure

Before turning to the specific algorithms we have used for the study of example systems, we would like to outline, how the stepwise procedure might work for an unknown chemical system containing the elements A, B, and C. After all the relevant information about the participating atoms A, B, and C has been placed in the database, the physically reasonable range of parameters for empirical potentials that appear appropriate for the system A/B/C must be estimated, either from general theoretical considerations or empirical data, if, for example, information about binary compounds in the systems A/B, B/C, and A/C is available. Such a range of parameters has to be considered, since even in systems in which a compound is known and potentials have already been parametrized successfully it is far from clear whether the perhaps very specialized shape of the potential is appropriate for the modeling of alternative modifications.

After the external pressure, the initial number of atoms N etc. have been set to some fixed values, the preselector module will create an initial configuration consisting of N atoms with a randomly selected composition $A_nB_mC_l$ ($n+m+l=N$). The atoms are placed at random positions within a simulation cell that is characterized by three cell vectors of random length and orientation. By choosing the empirical potential that allows the fastest evaluation of the energy function, a global optimization is now performed with module 3; the system may be changed, in principle, in all of its aspects as far as the number, identity, state,[27] and location of the atoms, and the size and shape of the simulation cell are concerned. The final results of the global optimization, perhaps including some intermediate configurations, are usually close to but not identical with a local minimum. Thus, a local optimization is performed on each interesting configuration, and the outcomes of module 3 are analyzed in module 4 and classified into structure types. The results are stored, and the global optimization is repeated for different initial configurations until a statistically relevant set of optimized structure candidates has been collected. If the quality of the empirical potentials was not very high, the parameters of the energy function would also be varied to judge the robustness of the structure types observed so far.

Next, the preselector analyzes the observed distribution of local minima with respect to, for example, common compositions, ionic charges, or coordination polyhedra. Based on the results of this analysis, perhaps together with a-priori information about, for example, "characteristic" ionic charges etc., more restricted optimization runs with certain fixed compositions and/or fixed ionic charges, and fixed numbers of atoms can be performed. For each fixed composition etc., global optimizations are performed. Usually at this stage, most runs will result in chemically and physically reasonable structures. If the system is very complex, even now the minimum configurations found may frequently consist of a mixture of only locally (within the simulation cell) optimized structure elements. In this case, it is a good strategy to use these building blocks to construct structure candidates on purely geometric grounds that then could again serve as initial configurations for another set of optimization runs.

While simple empirical potentials can produce many promising structures, the precise values of, for example, their cell parameters or the exact locations of the atoms in the cell are not to be expected. Such details would require performing another optimization round for fixed composition, etc., using a more realistic potential. Preferably, one would want to employ either highly refined (semi)empirical potentials[28–32] or some ab initio method.[33–35] However, it would be very time-consuming to perform a *global* optimization, especially in the latter case. But, since in most cases many promising structure candidates have already been accumulated at this point, one would restrict oneself to essentially *local* minimizations for each structure type, each time using the best representative as initial configuration.

After completion of the optimization stage, the candidate structures with the lowest ground state energy are analyzed with respect to their stability using module 5. The final result of the whole procedure would now consist of an overview of a large number of preferred compositions, and possible structure types and structure elements that would be expected to occur under certain conditions in the system A/B/C, together with estimates of the relative ground state energies and kinetic stability of the most promising ones. The latter information allows the tentative identification of thermodynamically stable and metastable structures.

4. Specific Algorithms

4.1. Construction of Potentials and Choice of Initial Configurations

We have already applied the modular approach to two classes of systems, noble gases[36] and their mixtures,[37,38] and binary[39–42] and ternary[43,44] ionic compounds. The reason for this choice lies in the possibility of employing relatively simple two-body potentials capable of capturing many qualitative and also some semi-quantitative aspects of the energy hypersurface of the compound in the construction of effective energy functions for such test systems. Since one single run of a global optimization procedure typically involves hundreds of thousands or millions of energy evaluations, and it is, in general, necessary to perform hundreds of such runs to acquire sufficient statistics on the distribution of deep-lying minima, any reduction in the number of function evaluations involved in the calculation of the energy is of great importance.

For noble gases, we employ Lennard-Jones potentials [Eq. (a)], for which the parameters ε_{ij} and σ_{ij} are available from experimental and theoretical investigations.[45]

$$V_{ij}(r_{ij}) = \varepsilon_{ij}\left[\left(\frac{\sigma_{ij}}{r_{ij}}\right)^{12} - \left(\frac{\sigma_{ij}}{r_{ij}}\right)^{6}\right] \qquad \text{(a)}$$

The approximate potentials for the description of ionic systems [Eq. (b)] consist of three terms, a damped Coulomb term, $r^{-1}\exp(-\alpha r)$, a repulsive term, r^{-n}, usually $n=12$, and an attractive dispersion term r^{-6}. If the damping factor in the Coulomb term is not present, that is, $\alpha = 0$, the energy function is evaluated by using the summation method suggested by deLeeuw et al.[46]

$$V_{ij}(r_{ij}) = \frac{q_i q_j \exp(-\alpha r_{ij})}{4\pi\varepsilon_0 r_{ij}} + \varepsilon_{ij}^1\left(\frac{\sigma_{ij}}{r_{ij}}\right)^n - \varepsilon_{ij}^2\left(\frac{\sigma_{ij}}{r_{ij}}\right)^6 \qquad \text{(b)}$$

In addition to these two-body terms, the energy function contains one-body terms $E_0(i)$ (the ionization energy or the electron affinity) and $\mu(i)$ (the chemical potential), and the latter is relevant if the number of atoms is allowed to change during the optimization. Thus, the energy function per atom takes the form given in Equation (c).

$$E = \frac{E_{\text{pot}}}{N} = \frac{1}{2N}\sum_{i\neq j} V_{ij}(r_{ij}) + \frac{1}{N}\sum_i E_0(i) + \mu(i) \qquad \text{(c)}$$

This choice has influenced the type of algorithms we employ in the first two modules. The main task in module 1 is the determination of the free parameters in the potential. Three major routes are available, depending on the amount of preknowledge about the system. If the participating atoms have already been studied extensively in the context of molecular studies using ab initio methods, it is sometimes possible to

derive effective two- and three-body potentials based on these theoretical results.[20, 47, 48] Experience shows, however, that so far this path does involve considerable effort, taking months of investigation.[49] Furthermore, the potentials cannot always be transferred with the required (and hoped-for) accuracy from the molecular environment to the one in the solid state.[49] Thus, one is usually forced to fit the parameters to some experimental observations. Here, two options are available: either one may adjust the parameters according to the properties of some known compound(s) of the binary system, for example, bond lengths and elastic behavior, or one may concentrate on the average properties of the participating atoms, for example ionic radii and deformabilities of the ions. The former option is especially useful for the study of ternary systems when the corresponding binary compounds are already known. For the case of binary systems, however, there are two problems. First, if no compound of the system is known beforehand, obviously no fit can be performed. Second, if a compound is already available experimentally, the model can very easily be prejudiced by using only this substance for fitting, and thus suppressing alternative minima of the (true) energy hypersurface. In contrast, the use of "atomic" properties averaged over many different compounds and local atomic environments should result in somewhat more unbiased effective potentials (recently, the use of parameters averaged over many binary compounds has been proposed by Bush et al.[50]). A disadvantage, of course, lies in the lack of specificity of the potential. Because of this possible trade-off between accuracy and generality, the fit procedure is chosen according to the specific circumstances of the calculation. In both cases, but especially when using average atomic parameters, the optimization runs should be repeated by varying the potential about the "best" values chosen originally. Averaged properties of the ions necessary to construct the effective potential have been placed into a databank, while the allowed variation of the parameters mentioned above is performed by the preselector. The fitting to properties of binary compounds has so far not been automated, and is carried out separately for each case. In a number of instances, it is also possible to refer to tabulated values.[29]

For the final analysis of "good" structure candidates, we use the Hartree–Fock type ab initio program CRYSTAL92.[34] Here, too, a certain freedom in the choice of basis sets and pseudo-potential parameters exists, and it is usually necessary to adjust these parameters for each chemical system or even structure candidate.

The current implementation of the preselector creates random initial configurations with as much built-in order and/or restrictions on the type of atoms (enforced composition and/or ionic charges) as desired. Usually, the atoms are placed at positions chosen at random and the volume of the cell is about ten times as large as that expected for a dense packing of all the atoms initially placed into the simulation cell.

4.2. Global and Local Optimization Methods

The availability of a global optimization procedure is of key significance to our procedure. While it is well-known that more and more refined optimization algorithms can be devised based on more and more detailed knowledge of the energy surface of the system, we have so far used only one family of algorithms, which are based on the stochastic simulated annealing algorithm[51] introduced by Kirkpatrick et al.[52] and Cerny.[53] The great advantage of this method lies in the relative ease of implementation and the very general applicability, regardless of the specific optimization problem.

Simulated annealing is based on the Metropolis (Monte–Carlo) algorithm,[54] which implements a weighted random walk through configuration space. Starting from a current configuration i, a neighboring configuration $i+1$ is chosen at random according to a set of rules (the "moveclass"). If the energy E_{i+1} is below or equal to E_i, the move is always accepted, that is, $i+1$ becomes the new current configuration. Otherwise, the move is only accepted with the probability $\exp(-(E_{i+1}-E_i)/C)$, where C is a control parameter of the random walk. Thus during a sequence of such MC steps, the system can climb over barriers of the energy surface. It can be shown that in the long-time limit ($t \rightarrow \infty$) for an ergodic system the probability $p(i)$ of visiting state (= the configuration) i is given by the Boltzmann distribution for the system at a temperature given by $T = C/k_B$.[55] Furthermore, in analogy to the annealing procedure of a real material, we can reduce the control parameter C down to zero, and expect that the system will end up, with a high probability, in some deep-lying minimum. It can be shown that during such a simulated annealing run, an ergodic system will reach the global minimum,[25, 51, 56] at least for $t \rightarrow \infty$.

Clearly, the most important parameters of this optimization procedure are the temperature program, that is, the rule according to which C is decreased to zero, and the moveclass, that is, the selection of the next trial configuration $i+1$ from the current one i. While a considerable effort has been devoted to the development of efficient general temperature programs,[56–64] the choice of a good moveclass still remains an open question, since it is highly dependent on the problem at hand.

For our explorations of the energy landscapes of solids, the best results seem to be gained from a moveclass in which 60–80% of the moves are devoted to movements of single atoms, about 10% each to the change of ionic charges and the addition/removal/exchange of atoms, while the remaining ones should be used to adjust the size and shape of the simulation cell. However, the selection of the moveclass should also take the size of the system, the goals of the current optimization, and the design of the temperature program into account. Often it might even be useful to vary the moveclass as a function of temperature.

As far as the temperature program is concerned, reasonable results have been achieved by using $T_n = T_0 f^n$ ($n = 0 \ldots n_{max}$), with m MC steps between temperature updates. Here, T_0, f, n_{max}, and m should be chosen according to the size of the system, the moveclass, and the objective of the current optimization run. The latter refers to the fact that different strategies have to be chosen, if one wants to find as deep a minimum as possible for a given amount of computer time or whether one tries to gain a general overview of the statistical distribution of local minima and their accessibility.

An extreme option consists of essentially replacing the global optimization with many local optimizations. In this method it is hoped that the initial configurations are chosen such that all

relevant regions of the configuration space are covered. This requires that either the barrier structure is simple enough that quench runs are not always stranded in high-lying minima even when starting from random initial configurations, or that the starting configurations are already so close to the best sub-optima that only some final adjustments are necessary to reach the desired minimum configurations. The latter case applies if realistic initial states are constructed by some special algorithm, or if the initial configurations are based on the results of earlier optimization runs.

We have employed two algorithms for the purpose of local optimization: a stochastic quench, which corresponds to a simulated annealing algorithm with $C = 0$, and a steepest descent algorithm with a line search option.[23] While the stochastic quench can be used with the full moveclass including charge transfer and atom exchange, the gradient descent is only useful when only the cell parameters and the atom positions need to be adjusted.

4.3. Findcell Algorithm

For the purpose of structure element recognition and structure classification, we have constructed the "findcell" algorithm.[65, 66] By using this one can determine whether the simulation cell contains primitive unit cells that can be used to describe either the full structure or substantial regions of the optimal configuration(s). The latter option is of special interest for large simulation cells, since it will often happen that the configurations reached during the optimization contain several distinct regions each showing a distinct but individually viable structure. Each such substructure should then be investigated in detail by using it as the initial configuration of another global or local optimization run. Note that if these substructures exhibit different compositions, their joint appearance may indicate a possible tendency of the system towards phase separation.

If the primitive cell can reproduce the full configuration, the system can then be further classified crystallographically using combinations of already available algorithms.[67–69]

4.4. Threshold Algorithm

The final algorithm we employ is the threshold or lid algorithm.[70] It is an adaptation of the "lid-method"[71] that has been used to classify the local energy landscape of discrete multiminima systems in the neighborhood of a local minimum.[72, 73] Starting from a given local minimum, a sequence of energy lids slightly above the energy of the local minimum is chosen. For each lid value a random walk is performed with the only restriction that no moves above the energy lid are allowed. Periodically, the system is quenched into the nearest local minimum. There will be some value of the lid above which not all of these quenches will return the system to its starting minimum but end up in a different configuration. This lid value gives an upper limit on the height of the energy barrier that separates the starting minimum from other local minima belonging to the newly accessible region of configuration space. Furthermore, the distribution of energies seen during the random walk(s) provides information on the local density of states of the system. Combining the information about energy barriers and local densities of states, we can construct a model of the energy hypersurface that consists of a tree-graph with weighted nodes. This model can then be used to estimate the stability of structure candidates and find their most likely transformation paths into competing structures.

5. Examples

The modular approach has been tested for two types of chemical systems so far: noble gases and ionic compounds. In this section, we will give a short summary of the results and discuss some characteristic examples. Unless explicitly stated otherwise, the initial configurations of the global optimization run were constructed by placing neutral atoms at random positions inside a large simulation cell with cell volume about ten times the volume of all the participating atoms.

5.1. Noble Gases

5.1.1. Lennard-Jones Gas Consisting of Only One Kind of Particles[36]

Since the Lennard-Jones potential has proved to be a very successful approximation for the potential energy of noble gases, we have used a system of atoms interacting through this potential to test the applicability of the simulated annealing algorithm to the problem of finding sub-optima of the energy hypersurface. Up to 36 atoms within the simulation cell were used. The results showed that the best sub-optimal configurations were hexagonal and cubic close-packed arrangements of the atoms. The next best ones were close-packed arrangements with one atom missing in the arrangement, that is, the optimal ones containing one point defect per simulation cell. The remaining runs resulted in strongly distorted or amorphous structures.

To gain a better understanding of this result, we have performed threshold runs for two-dimensional structures (sixteen atoms in the simulation cell) of a Lennard-Jones gas exhibiting one or more point defects.[38, 70] The barrier structure, and the analysis thereof, showed quite clearly that the structure missing one atom per simulation cell from the sites of a close packing constitutes both the deepest side minimum and the most stable one. It is thus no surprise that this structure candidate was the most likely to appear besides the two sub-optima during relatively short or medium length optimization runs in the three-dimensional case.

5.1.2. Binary Noble Gases[37, 38]

While the details of the energy and length scales were irrelevant for the study of a Lennard-Jones gas consisting of a single component, it was necessary to use appropriate values of the parameters ε_{ij} and σ_{ij} for the case of binary noble gases within the Lennard-Jones potential approximation. These values were

taken from experiment as far as available, and corrected or interpolated from theoretical models, depending on whether the values were slightly contradictory or missing, respectively.[45] The number of atoms in the simulation cell was kept fixed at values ranging from 8 to 64. The optimal structures found were refined by using stochastic quench and steepest descent algorithms.

For most of the runs the composition was kept fixed at 1:1.[74] Very long optimization runs were performed, and for the combinations Ne/Ar, Ne/Kr, Ne/Xe, and Ar/Xe the best sub-optimal structures (in 90% of the cases) were found to consist of two regions in the simulation cell, each containing a dense packing of only one component. In contrast, the best configurations (in 90% of the cases) found for the Ar/Kr system showed a close-packed solid solution of Ar and Kr atoms. Finally, Kr/Xe resulted in phase separation in about 50% of the runs, while the remaining 50% resulted in a joint dense packing. These results indicate that Ar and Kr could form a solid solution at low temperatures, in agreement with experiment,[75] while, with the possible exception of Kr/Xe, the other combinations with composition 1:1 would tend to show phase separation instead.

Table 2. Best results of simulated annealing runs for ionic compounds, including a comparison with the observed structures. During the optimization, many additional structures, corresponding to local minima of the energy hypersurface, have been found in these systems.

Input	Structure (calculated)	Structure (observed)
Na/Cl	NaCl structure	NaCl structure
Cs/Cl	CsCl structure	CsCl structure
Li/F	NaCl structure	NaCl structure
Na/F	NaCl structure	NaCl structure
K/F	NaCl/CsCl structure	NaCl structure
Rb/F	NaCl/CsCl structure	NaCl structure
Cs/F	NaCl/CsCl structure	NaCl structure
Ba/O	NaCl structure	NaCl structure
Li/I	NaCl structure	NaCl structure
Sr/O	NaCl structure	NaCl structure
Ni/O	NaCl structure	NaCl structure
Ca/O	NaCl structure	NaCl structure
Mg/O	NaCl structure	NaCl structure
Ca/F	fluorite structure	fluorite structure
Mg/F	rutile structure	rutile structure
Li/O	antifluorite structure	antifluorite structure
K/O	antifluorite strucutre	antifluorite strucutre
Sr/Cl	fluorite structure	fluorite structure
Ca/Cl	$CaCl_3$ structure	$CaCl_2$ structure
Sn/O	rutile structure	rutile structure
Ti/O	rutile structure	rutile structure
Na/O	antifluorite structure	antifluorite structure
Si/O	cristobalite structure, tridymite structure	e.g. tridymite strucutre, cristobalite structure

5.2. Ionic Compounds

The second class of materials chosen as test systems were the (inorganic) ionic compounds. Both binary and ternary compounds have been investigated; the latter including mostly unknown or at least not-yet-synthesized compounds. The general form of the potential was as given in Section 4.1 (see [Eq. (b)]). The effective potential has been constructed by using both $\alpha = 0$, which requires an Ewald summation, and $\alpha > 0$ (= damped Coulomb potential). Average ionic radii and information about the polarizability or "hardness" of the ions were used to establish starting values of the free parameters in the potential, n, ε_{ij}, and σ_{ij}.

In order to test the applicability of the optimization procedure to ionic systems, we have investigated[39] a large number of binary systems using long simulated annealing runs that are expected to reach a very good sub-optimum of the energy hypersurface ($> 10^6$ MC steps). For most of these runs, the composition of the system and the number of atoms in the simulation cell was kept fixed. Initially, electron transfer between randomly chosen pairs of atoms/ions was allowed. Of course, once the preferred ionic charges had been established as part of the global optimization procedure, additional studies of the system using ions with fixed charges were admissible. The results are listed in Table 2. We note that in nearly all instances the best sub-optimum found during the simulated annealing run turned out to be either the structure seen experimentally to be the preferred one or the structure that agreed with the radius ratio rule.

5.2.1. *Binary Systems*

While the above results clearly show that it is possible to determine very good sub-optima of the energy hypersurface of binary ionic compounds using effective potentials based on characteristic atomic quantities, it was felt necessary to investigate in more detail the energy hypersurface of some particular systems. We have chosen NaCl as a representative AB system,[39] and MgF_2, $MgCl_2$, CaF_2, and $CaCl_2$ as AB_2 systems.[41, 42] The parameters in the effective potential were varied slowly from each set of optimization runs to the next to study the robustness of the candidate structures. Each such set of runs consisted of 14 or 20 global optimizations of 10^5 to 3×10^5 simulated annealing steps, the only difference being the initial value of the random number generator. Thus, for each system, several hundred global optimization runs were performed. Since it had already been established during several sets of optimization runs in which charge transfer was allowed that the best sub-optima occurred when the "fully" ionized ions were present (Na^+, Mg^{2+}, Ca^{2+}, F^-, Cl^-), the ionic charges were fixed at these values, and the moveclass consisted of movement/exchange of the ions, and variation of the size and shape of the simulation cell.

Na/Cl

A large number of structure candidates corresponding to local minima of the energy hypersurface were found in the Na/Cl system. They have been listed in Table 3. Two of these structures were judged to be of special interest, the 5-5 variant (Fig. 1) consisting of trigonal bipyramids of Cl^- ions around the Na^+ ions, and a NiAs-type variant. Recently, Martin and Corbett have succeeded in synthesizing an unprecedented monohalide, LaI, exhibiting the NiAs structure type.[76] For each of these variants, the energy barriers separating them from other local minima were determined by using the threshold algorithm. While NaCl in the NiAs-type structure exhibited a barrier in excess of 0.13 eV per atom ($T \approx 1300$ K), the lowest energy barrier for the 5-5 structure was found to be approximately 0.02 eV per atom ($T \approx 200$ K). Thus, the latter structure would not be expected to survive at high temperatures unless it were stabilized

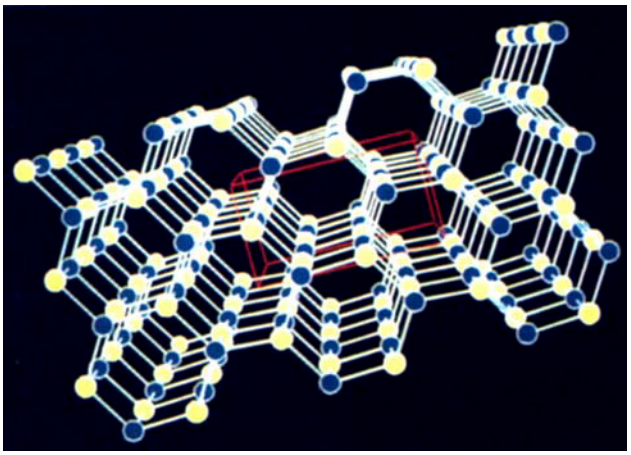

Fig. 1. 5-5 structure of NaCl, consisting of trigonal bipyramids of Cl (blue) about Na (yellow). Ions are not drawn to scale. Average Na–Cl distance is 2.7 Å.

Table 3. Overview of the minima found for the system Na/Cl with composition 1:1. The terms "dense open structures" refer to arrangements of different coordination polyhedra without and with large channels or cavities in the structure, respectively.

Coordination number of Na by Cl	Structure types structure elements	occurrence [%]
4	anti-PtS-structure sphalerite edge-shared tetrahedra	5.5
5	edge-shared trigonal bipyramids	6.8
5	edge-shared square pyramids	3.0
6	NaCl structure	37.2
6	NiAs structure	20.0
6	anti-NiAs structure	4.3
6	other structures	1.8
7	monocapped prisms (Fig. 2)	0.3
8	CsCl structure	0.1
mixed	"dense" structures	12.0
mixed	"open" structures	9.0

in some fashion. In this context, it should be noted that for a set of optimization runs in which large amounts of excess chlorine atoms were present, the 5-5 structure with the excess chlorine located within the channels occurred as the major stable alternative to the phase separation into one region filled with neutral chlorine and a second one containing the standard NaCl structure. Thus, one might expect that in the presence of some third component that could fill the channels in the 5-5 structure, this structure might be stabilized.

Another point to note is the robustness of the deepest local minima with respect to quite large variations of the parameters in the potential. In this context, it was tested, whether there were differences between using a damping factor or an Ewald summation for the electrostatic terms. It was found that the distribution of local minima encountered during the optimizations did not change significantly when using a damping factor ($\alpha > 0$).

To gain some insight with respect to general aspects of the global optimization for large pressures, we have considered pressures of 1, 10, 100, and 10^3 GPa by adding a term pv' to the energy function, where p is the pressure, and v' the volume per atom: $H = E + pv'$. By minimizing the enthalpy H, we have found that for pressures up to 10 GPa, the NaCl structure was the deepest minimum, while above 100 GPa the sevenfold (Fig. 2) and eightfold (CsCl structure) coordinations of Na by

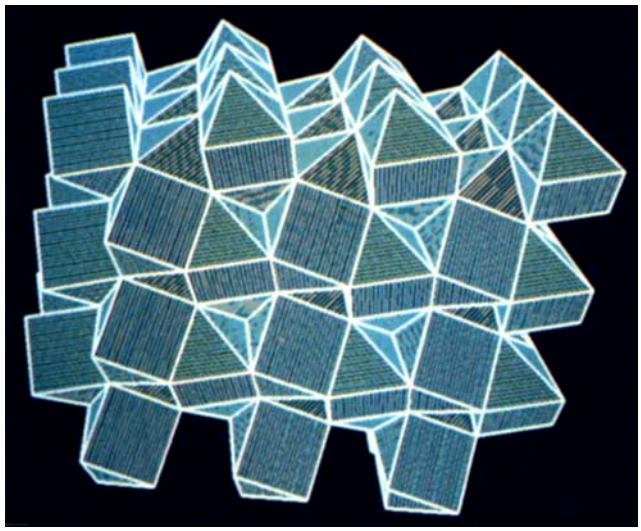

Fig. 2. Structure candidate for NaCl, consisting of face-shared monocapped Cl^- prisms about the Na^+ ions (polyhedral representation).

Cl are preferred compared to the sixfold ones. This agrees qualitatively with the experimental observation that the high-pressure modification of NaCl probably shows a CsCl structure above 29 GPa.[77]

AB_2 Systems

Since layered structures are important variants in AB_2 systems (for example, the CdI_2 and $CdCl_2$ families of structures), it was deemed necessary to always use a Coulomb potential without a damping term. The method chosen to perform the full Coulomb sum was the one suggested by de Leeuw et al.[46] Again, the resulting structure candidates, in general, did not depend on the exact values of the effective potential.

The most common structure types found are summarized in Table 4. We note that these include many commonly found structures like anatas and fluorite, but also layer structures like CdI_2. Although the energies of the latter structure candidates usually are higher than the best sub-optima, it is a pleasant surprise that these layer structures were competitive even in a purely ionic model. One very interesting class of candidate

Table 4. Overview of the most important structure types/elements seen in the systems MgF_2, CaF_2, $MgCl_2$, and $CaCl_2$. The polyhedra listed always refer to the coordination of the cation by the anions. The frequency of occurrence during optimization runs is given in percent.

Structure elements, structure types	MgF_2	$MgCl_2$	CaF_2	$CaCl_2$
(e.g., HgI_2 structure, ZnO_2 substructure of $SrZnO_2$)	0	31	3	4
edge-/corner-shared trigonal bipyramids	6	1	0	0
$CdCl_2$/CdI_2 structure	20	7	5	16
rutile	37	45	9	0
anatas	2	0	0	0
$CaCl_2$ structure	0	0	0	44
other structures based on octahedra	7	10	0	10
edge-/corner-shared prisms	3	0	0	2
edge-/corner-shared monocapped prisms	21	0	15	22
fluorite	0	0	66	0
other structures	4	6	2	2

structures is that in which the cations are surrounded by seven anions forming monocapped prisms. By using the threshold algorithm, it was found that these structures constituted very shallow minima located on a broad saddle of the energy hypersurface between the sixfold and eightfold coordinated structures of the rutile and fluorite type. Also, certain trends among the orientations of, for example, the octahedra in the rutile-type structures could be seen, indicating that $CaCl_2$ should really be more likely to be found in a $CaCl_2$-type structure than MgF_2, whose structure tended to be very close to that of the ideal rutile struture.

Encouraged by these results, we have also applied the effective (ionic) potential to the partly covalent Si/O system. Here, the best sub-optimal structures encountered were the tridymite and cristobalite structures.

AB_3 Systems

Finally several sets of optimization runs were performed for AB_3 systems.[40] We used as examples the alkali metal nitrides Li_3N, Na_3N, K_3N, Rb_3N, and Cs_3N. During the initial (long) runs in which charge transfer was allowed, it was found that in the first two cases the full oxidation states (Li^+, Na^+, N^{3-}) were reached easily, while the latter three did not succeed in completely crossing the barriers on the energy hypersurface separating the configurations with fully ionized from those with the partly ionized building blocks. Both Li_3N and Na_3N exhibited several interesting candidate structures as good sub-optima: the Li_3N structure known to occur in nature and a sheared SrO_3 substructure of the $SrTiO_3$ perovskite structure (both in the cubic and hexagonal variant; see Fig. 3). Based on these results, it appears reasonable to suggest that Na_3N, if it can be synthesized, will crystallize in one of these three structure types.

For the nitrides of the heavier alkali metals, additional optimizations were performed with K^+, Rb^+, Cs^+, and N^{3-} ions for the initial configuration. The observed structures ranged from the ReO_3 structure for Cs_3N and a cubelike variant of the Li_3N structure for Rb_3N and Cs_3N to 11-fold (tetragonal close packing) and 12-fold (like Na_3N) coordinations of the N^{3-} ions by the cations in K_3N. This decrease in the coordination number with increasing size of the cation is reminiscent of the radius ratio rule.

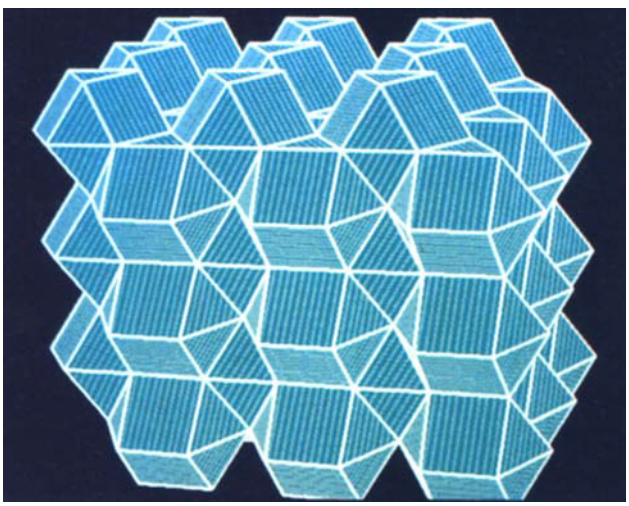

Fig. 3. Sheared SrO_3 substructure of the perovskite structure as a model for the hypothetical compound Na_3N. N^{3-} ions are contained within the fcc arrangement of cuboctahedra formed by the Na^+ ions (polyhedral representaion). Average Na–Na and Na–N distance is about 2.6 Å.

5.2.2. *Ternary Ionic Systems*

When moving from binary to ternary systems, an alternative for the construction of the effective potentials is possible, since in many instances binary compounds of the components are known, and can serve to fit the parameters of the energy function. Even if this option is available, one should still use the less biased approach based on purely atomic parameters for comparison. Since the energy hypersurface of these systems is often rather complex, the optimization runs tend to be quite lengthy.

Ca/Ti/O

To test whether it is possible to find good structure candidates in ternary ionic compounds, we have performed[43] several sets of optimization runs for the system Ca/Ti/O. Of course, there exists a large range of compositions that allow for "full" ionization (Ca^{2+}, Ti^{4+}, O^{2-}) of the system: $Ca_nTi_mO_p$ with $p = n + 2m$. While in binary compounds the composition corresponding to the "fully" ionized case is established nearly automatically during a general global optimization run, a number of equally valid options now exist that correspond to deep local minima separated by rather high energy barriers.

For our test runs, we have chosen besides the simplest one, $n = 1$ and $m = 1$, that is $CaTiO_3$, the three cases $n = 2$, $m = 1$; $n = 1$, $m = 2$; and $n = 3$, $m = 1$. The potential was constructed by using only the average ionic radii, under the assumption that the ions were of medium hardness and the Coulomb potential contained a damping factor.

In half of the relatively short (2×10^5 steps) runs for the case ($n = 1$, $m = 1$), the best sub-optima found were perovskite-type structures, while in only 20% of the runs, the system ended in a configuration without complete ionization ($Ca^{2+}Ti^{3+}O^-(O^{2-})_2$). This agrees well with the experimentally observed[12] structure of $CaTiO_3$, which is considered to be a distorted perovskite-structure. In addition, we estimated the heat of formation from CaO and TiO_2 at $T = 0$ K to be about 130 kJ mol^{-1}. Considering the highly simplified model for the potential energy, this compares reasonably well[78] with the value[79] of 90 kJ mol^{-1} found experimentally under standard conditions. For the other three compositions we have investigated, the best sub-optimal structures also contained fully ionized building blocks. However, so far only some layered structures of Ca_2TiO_4, related to the structure of Ca_2SnO_4,[80] were found to be thermodynamically stable (about 40 kJ mol^{-1}) with respect to dissociation into CaO and TiO_2.

As no calculations using a more refined (for example, Hartree–Fock level) model for the energy were performed for this system, no statement with regard to ferroelectric instabilities can be made, since this would require a more detailed analysis of the covalent aspects of the system.[81]

Sr/Ti/O

The optimizations described for the Ca/Ti/O system were repeated[43] analogously for the Sr/Ti/O system. It was again observed that $SrTiO_3$ should form a pervoskite structure with an enthalpy of formation of about 220 kJ mol^{-1} with respect to the binary compounds (experimental value:[79] 140 kJ mol^{-1} under standard conditions). Possibly stable structure candidates of the composition Sr_2TiO_4 were found, which exhibited strands of edge-sharing TiO_6 octahedra similar to those present in the already known structure.[82] A beautiful structure was found for the composition $SrTi_2O_5$, consisting of layers of SrO_{12} anticuboctahedra interlaced with hexagonal arrangements of TiO_5 trigonal bipyramids (Fig. 4).

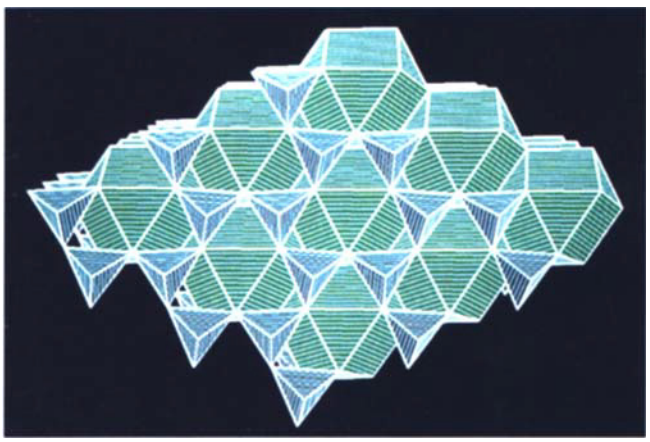

Fig. 4. Structure candidate for $SrTi_2O_5$. The Ti–O substructure consists of corner-sharing trigonal bipyramids (blue) of oxygen about the titanium atoms. The Sr^{2+} ions are located inside the O^{2-} anticuboctahedra (green) between the layers of trigonal bipyramids.

Ca/Si/Br

Apart from the alkali metal nitrides, we have so far only described systems that contain at least one experimentally known compound. Since the goal of our approach is the prediction of unknown solids that might be capable of existence, we need to test the method by applying it to an unexplored system, and subsequently synthesizing the predicted structure candidates. The Ca/Si/Br system appears to be well-suited for this purpose. From the participating components, one would conclude that a hypothetical ternary compound of, for example, the composition Ca_3SiBr_2 should have sufficient ionic character (Ca^{2+}, Si^{4-}, Br^-) to justify the use of the simple potential function for ionic crystals we have been testing so far. Furthermore, the binary components (Ca_2Si, $CaBr_2$) are known, and it is therefore possible to fit the parameters in the two-body potentials to their properties. Last but not least, intensive attempts to synthesize such a ternary compound from this system appear not to have been caried out to date.

During the test runs needed for fitting the parameters, the binary (ionic) compounds proved to be stable local minima. Therefore, we did not precede the long global optimization runs by optimizations involving charge transfer. Instead, the ionic charges were fixed from the outset, and these ions were then, as usual, placed at random positions in a large simulation cell. We have concentrated[44] on the composition Ca_3SiBr_2; each simulated annealing run involved several million optimization steps, in which up to four formula units (24 ions) per simulation cell were used.

The structure candidates belonging to the two best sub-optima found are shown in Figures 5 and 6. The structure in Figure 5 can be derived from a NaCl-type structure, in which the Na sublattice is occupied by the Ca^{2+} ions, while the Cl sublattice contains the Si^{4-} and Br^- ions in such a way that the Si^{4-} ions are as far away as possible from each other while still allowing for a relaxation of the inevitable distortions due to the somewhat different sizes and hardnesses of the Si^{4-} and Br^- ions. In Figure 6, an alternative structure is shown, derived from the CsCl type. Again, the anions occupy the Cl sublattice, while the cations are located on the sites of the Cs sublattice.

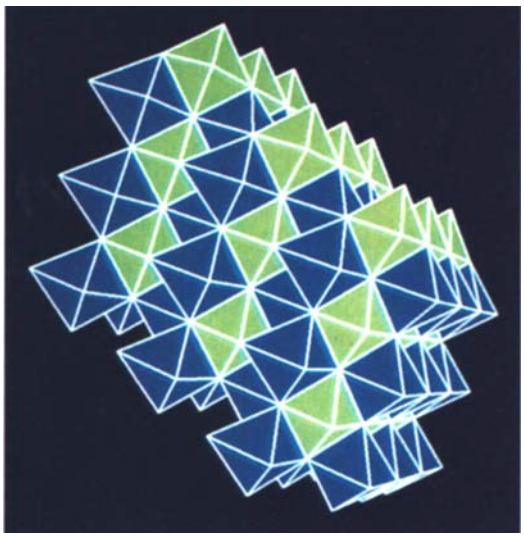

Fig. 5. Structure candidate for Ca_3SiBr_2 based on the NaCl structure. Si^{4+} ions are located within the green octahedra of Ca^{2+} ions, Br^- ions within the blue ones (polyhedral representation). Note the distortions of the octahedra due to the different anion species.

Fig. 6. Structure candidate for Ca_3SiBr_2 based on the CsCl structure. Si^{4-} ions are located within the green cubes of Ca^{2+} ions, Br^- ions within the blue ones (polyhedral representation) Note the distortions of the cubes due to the different anion species

Since no obvious way exists to judge the quality of these structure candidates (at least until the compound has been synthesized!), the ground state energies of these sub-optimal structures were also calculated by using the Hartree–Fock program CRYSTAL92[34] (no global optimization runs). It turned out these ground state energies lie so close together that it was not possible to decide which structure candidate should actually be preferred: E_{HF}(NaCl type) = − 5.15 eV per atom, E_{HF}(CsCl type) = − 5.11 eV per atom compared to E(NaCl type) = − 5.53 eV per atom and E(CsCl type) = − 5.49 eV per atom for the simple potentials.

$Si_3B_3N_7$

The compound $Si_3B_3N_7$ may serve as a final example of a ternary system. So far, it exists only as a kinetically very stable amorphous solid;[83] it is questionable whether it will be possible to ever synthesize a ternary crystalline variant. Although the bonding within this compound is expected to be well-represented by a covalent network, we have applied our usual effective (ionic) potential to the system. After several long global optimization runs, a plausible crystalline structure (Fig. 7) has been found that exhibits the expected coordination of Si^{4+} and B^{3+} by N^{3-} (tetrahedral and trigonal planar environment, respectively). Even each of the N^{3-} ions was surrounded by three cations in an approximately trigonal planar arrangement. It seems that in the case of $Si_3B_3N_7$ already the purely ionic part of the potential is sufficient to generate a structure that is reasonable even in a covalent model.

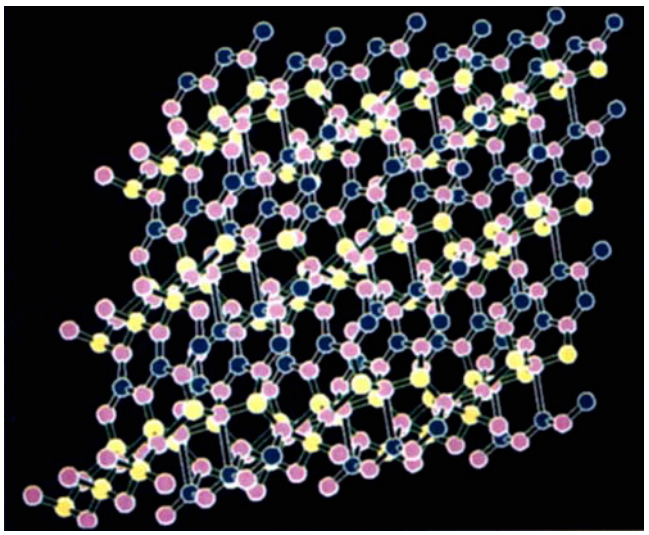

Fig. 7. Structure candidate for crystalline $Si_3B_3N_7$. Si^{4+} ions are represented by yellow spheres, B^{3+} ions by blue spheres, and N^{3-} ions by pink spheres. Nearest neighbors are connected, exhibiting the tetrahedral environment of Si and the trigonal planar one of B. Ions are not drawn to scale.

6. Critical Discussion

The results in the preceding section have shown that the modular approach and our current implementation as described in Sections 2–4 is suitable in general, and already successful in ionic systems, for the determination of reasonable structure candidates of hypothetical compounds, where nothing is known besides the identity of the components and, perhaps, their composition. To gain a better insight into the basic concept of the approach presented, particularly with regard to understanding its strengths and limitations, it is necessary to analyze both the general approach and the implementation chosen.

6.1. Construction of the Energy Hypersurface

The fundamental ingredient to our approach for the prediction of metastable compounds is the assumption that a detailed study of the (potential) energy hypersurface of a chemical system, as a function of atomic/ionic configurations, will yield sufficient information to achieve our goal. This definitely agrees with the basic understanding of classical physical systems for $T = 0$ K, since all configurations that can exist as (meta)stable compounds at $T = 0$ K correspond to local minima of the potential energy of the system.

However, in equilibrium quantum statistical mechanics,[7] only the ground state will be populated at $T = 0$ K, the other local minima are irrelevant. Nevertheless, in most instances of chemical interest, parts of the classical picture still hold in quantum mechanics, as long as one can show that the wave functions corresponding to the classical local minimum configurations have a long lifetime. This is often true, since the energy barriers separating potential energy minima usually are large enough to prevent the decay of a metastable configuration by tunneling. This presupposes, of course, that it is possible to construct such a potential energy surface in the first place.

In general, the eigenfunctions of a solid are complicated functions of both the ionic and the electronic degrees of freedom. Every classical ionic configuration, and its excited states will be a linear combination of many such eigenfunctions. To construct an energy hypersurface (for the electronic ground state) as a parametric function of classical ionic configurations alone, it is necessary that a) the electronic and ionic degrees of freedom can approximately be separated (Born–Oppenheimer approximation[84]), and b) the ionic part of the wave function, in addition, can be separated approximately into well-defined, nearly classical localized particles plus a (negligible) set of zero-point vibrations. Clearly there are some obvious problems: there are many systems in which electron–phonon interactions play an important role in stabilizing or destabilizing an otherwise unstable/stable structure. Thus, both the Born–Oppenheimer approximation and the assumption of negligible zero-point vibrations can lead to errors.[85–87]

Nevertheless, these issues are somewhat beside the point: while structural details (distortions away from a high symmetry, precise dimensions of the unit cell), electronic properties (metal, insulator), and the degree of stability of the compounds may change upon analyzing a given structure in greater detail, we are primarily concerned with the existence and the general structure type of a hypothetical compound. Unless there are reasons to believe that the neglected quantum mechanical effects will destroy or create important local minimum configurations outright, for example superfluidity in liquid helium, the construction of the (potential) energy hypersurface is a good first step.

A much more dubious step is the use of effective potentials instead of using ab initio methods for every energy evaluation. Of course, if a system is studied in great detail using ab inito methods, it is possible to design effective potentials that will provide very good fits to the real potential energy. However, this is very time-consuming, and the additional effort might not be justified by the improvement of the results. Especially, if no a-priori information about the hypothetical compounds is available, it is easy to miss important structure elements that should enter the design of the potential. Furthermore, in many systems the potentials have to involve long-range terms, in order to be sufficiently realistic for global (in contrast to local) optimizations. This requires the use of rather large clusters for ab initio calculations, increasing the time necessary. Because of this problem, we have decided to employ ab initio methods only in later steps of the modular approach, that is, after a first round of optimizations have been performed, and interesting structure candidates have been found. Since then the most important (sub)structures are known, the selective use of first-principle techniques appears to be more efficient as far as computer resources are concerned.[88]

This leaves us with the problem of designing useful effective potentials. We have been guided by the application of basic principles both as far as the expected physics and chemistry of the compound are concerned and with respect to the requirements of efficient global optimization algorithms. First, the potentials have to reflect correctly both the local and the long-range interactions between the atoms/ions: the atoms must not be allowed to overlap too much, and, except through electrostatic forces, they must not interact directly at long distances. Additional terms will enter that reflect the local bonding situation of the atoms, and here usually a selection takes place, depending on whether we want to stress, for example, the covalent, ionic, or metallic character of the hypothetical compound. This first selection is in our opinion the most regrettable approximation in the construction of effective potentials, because it tends to exclude a large variety of possible structures by changing the weight of certain configurations, possibly resulting even in both the elimination of actual minima and the creation of spurious local minima. Nevertheless, we currently see no way of avoiding such a preselection, that is, constructing simple potentials that can describe equally well ionic, covalent, and metallic compounds. Somewhat less critical is the subsequent choice of fit parameters for a given potential, although it can often be a contentious issue[89]—should it be based on (averaged) atomic quantities, (averaged) binary compounds, elastic constants of already-known modifications, etc.?

The advantages and disadvantages of the highly simplified form of our effective ionic potential are quite evident: ease of computation, simple physical and chemical origin of the terms within the potential, simple dependence on atomic quantities based on averaged properties of the atoms within many ionic compounds on the one hand, and lack of quantitative accuracy, use of averaged parameters, restriction to spherically symmetric ions, exclusion of three-body-effects, on the other. Clearly, for a completely unknown (ionic) system full quantitative agreement of a semi-phenomenological with the actual energy hypersurface cannot be achieved purely from knowledge about other systems involving these ions, but requires ab initio calculations instead. Nevertheless, we feel that the simple potential we employ does exhibit the correct qualitative features of the true energy hypersurface and delivers the necessary information for the second round of calculations, which can then be made more precise with the use of more accurate methods. Similarly, since we are registering many good sub-optima, usually exhibiting many different ion coordinations, during the global optimizations, and expect to have included among these the structures actually accessible to the chemist, the use of averaged parameters is not a critical problem. Nevertheless, we feel it is important to vary these parameters slightly to judge which of the local minima found are the most robust ones. In most of the test systems for which the structures of already existing compounds are known, our results indicate that the most robust candidate structures correspond to those that are observed in reality.

The surprising success of the ionic model in reproducing the proper local environment of the atoms within the solid even in some strongly covalently bonded materials is based on the fact that in many instances the optimal or sub-optimal local arrangements within the ionic and the covalent model are identical. This appears to be an expression of a basic rule of crystal chemistry that realistic crystal structures capable of existence tend to be optimized in all relevant aspects, including the contribution of the electrostatic energy in the case of a predominantly covalent solid. The greatest difficulties occur, and the ionic model usually fails, when the covalent bonds result in a poor use of the available space in the structure, for example in the formation of twofold linear coordinations[90] of Cu^+ or Ag^+, or of a square-planar environment with "room" above the plane (e.g. for Ag^{3+}),[91] which in the ionic model would tend to distort into a tetrahedron. Nevertheless, even such coordinations can appear as very good sub-optima under suitable circumstances.[92]

Clearly, it would be interesting to include nonspherical ions or components that can be modeled in such a fashion, for example ions with lone pairs of electrons (Sn^{2+}, transition metal ions) or complex ions ($(O_2^{2-}$, SO_4^{2-}, $O_3^-)$, into the purview of our model potential. Apart from the additional computational effort, there are, in principle, no problems. However, the evaluation of the repulsion between such neighboring ions and also the calculation of the corresponding polarization term could become rather cumbersome. Similarly, the three-body terms usually required for a proper description of covalent bonds add considerably to the time needed for each energy evaluation; and it appears reasonable to eschew their use in the first stages of the optimization, as long as their exclusion does not topple the whole edifice.

6.2. Technical Details of the Algorithms

Once the parameters of the potential have been chosen, the energy of each possible configuration of ions and atoms is determined within the framework of the model. Nevertheless, there are still several open issues and choices left. The most important of these are the boundary conditions (open = cluster, or periodic = crystal), number of atoms in the simulation cell, and the choice of moveclass for the simulated annealing algorithm.

For our purposes, the choice of crystal-like boundary conditions is reasonable, since we are for the most part interested in

(meta)stable crystalline structures. Since we start initially from systems at gaseous densities and allow free variation of the cell, the requirement of periodicity is not very restrictive. A greater problem is the use of fixed numbers of formula units during the optimization. Clearly, if the number of atoms is not allowed to change during a run, only those structures can be found that can be constructed on the basis of some unit cell that contains exactly those atoms. In principle, this problem can be solved by varying the number of atoms arbitrarily during a given run. However, it has often proven to be more efficient to keep the composition fixed during a given run and, instead, to repeat the optimization with all the other promising compositions afterwards. Since this restriction makes the addition and removal of atoms rather awkward, fixing the composition usually implies fixing the number of atoms, too. Therefore, we also need to repeat the runs for a given composition with different numbers of formula units in the simulation cell.[93] Our observations have shown that if, for example, the number of formula units is doubled, the same minima are still present, but that, of course, many additional sub-minima appear. As pointed out in the introduction, the number of possible metastable periodic structures appears to be limitless.

Finally, we have to be aware that the choice of moveclass can, in principle, change the features of the energy landscape. As long as the allowed moves are physical (movements of the atoms, variation of the cell = collective movement of all atoms, charge transfer, etc.) and reasonably complete (no exclusion of physically possible microscopic changes of the configuration), each local minimum found during the optimization will also be a kinetically stable one. Usually this condition is not violated. But if the only goal is to reach the global minimum as fast as possible, it is, of course, useful to try to improve the optimization algorithm by including nonphysical moves, avoiding or eliminating metastable minima in the process. Obviously, for our purposes such a high-efficiency moveclass is a double-edged sword. Thus, we have allowed only those nonphysical moves that remove or exchange whole ions in the simulation cell, since these operations will only lead to the elimination of realistic sub-optima in very special cases.[94]

6.3. Feasibility of the Modular Approach for General Thermodynamic Boundary Conditions

As we pointed out in the introduction, our current investigations are concerned with the prediction of possible (meta)stable structures of a compound at $T = 0$ K and $p \approx 0$ Pa that are characterized by the requirement that they are local minima of the energy hypersurface of the system. Thus, our optimizations are performed with respect to an energy function that is defined in the configuration space, *not* in the thermodynamic space. To address the issue of high-pressure or high-temperature modifications, we have to carefully distinguish between the space of all hypothetical configurations of the chemical system; each configuration is characterized by the number and type of participating atoms, their position vectors, ionic charges, etc., and the usual space of thermodynamic variables, p, T, N_i, etc..

In principle, there is no problem in studying the system under external constraints like pressure p and stationary external electric fields $\boldsymbol{E}$ at $T = 0$ K. Instead of minimizing the potential energy, one now minimizes the enthalpy $H = E + pv'$, or similar extensions of the energy function.[7] A greater practical problem lies in the usually unknown dependence of the parameters of the effective potential on pressure or other external fields. This also holds true for potentials fitted to binary systems, but it can be alleviated somewhat by choosing the parameters to, for example, reproduce measured elastic constants.

The determination of "high-temperature structures" is a much more subtle enterprise. For $T = 0$ K, it is very clear what constitutes a (meta)stable structure: it is the one, and only one, configuration that is associated with a local minimum of the energy hypersurface. In contrast, for $T > 0$ K, equilibrium statistical mechanics tells us that each configuration has a nonzero probability of being present at a given time. This implies that the concept of a single unique configuration that represents the system at $T > 0$ K at all times no longer applies. However, it is often possible to group many of the configurations together according to certain common characteristic properties (e.g. time-averaged structure). If this common quantity is denoted R,[95] it is possible to calculate the probability that the system will be found in some configuration exhibiting property R according to Equation (d).

$$p(R) = \sum_{i \in R} p(i) = \frac{Z(R)}{Z} = \frac{\exp(-F(R)/kT)}{\exp(-F/kT)} \qquad \text{(d)}$$

Here, $Z(R)$ is the partition sum for that region of phase space that is associated with R, and $F(R)$ is defined as the free energy for structure R. Clearly, finding the most likely structure representing the system at temperature T corresponds to finding the minimum of the restricted free energy $F(R)$ with respect to R. While in special cases it is possible to a certain degree to write down analytical expressions for $F(R)$, finding $F(R)$, in general, is very difficult, and we have not yet attempted to adapt our approach to this question.

7. Links with Earlier Studies of the Energy Hypersurface of Complex Systems

As far as we know, the basic concept of our approach, that is the planning of solid-state syntheses through a (as general as possible) determination of possible (meta)stable solid compounds in a chemical system using global and subsequent local optimizations, has not been proposed before. Nevertheless, there are many links to past and present work dealing with, for example, the calculation of the energy of solids or the use of optimization methods to assist in structure determination problems.

In the field of solid-state theory, there is a long tradition of attempts[96] to understand the structure of solids, be they crystalline or amorphous, of macroscopic size or microscopic like clusters. It has always been clear that (meta)stable structures of solids at low temperatures can be identified by determining the minima of the energy hypersurface of the chemical system, apart from certain systems that are dominated by quantum effects. Especially in the early days of solid-state physics,[97, 98] much effort was devoted to the calculation of cohesive energies (ground state energies) of already known compounds,[85] and the derivation of elastic constants by varying the lattice parameters.

With the development of computers and fast algorithms, new tools became available to solid-state theory. A clear path of steady improvement runs from the molecular dynamics studies of Alder and Wainwright,[99] who modeled liquids with hard spheres as building blocks, to ab initio molecular dynamic simulations with the Car–Parrinello algorithm,[35] which are capable of performing local optimizations of the structure of simple solids.[100] This work has been paralleled by developments in the theory of molecules and their structure.[101] It is now standard procedure to employ some local optimization routine during ab initio studies of molecules.

A combination of these two strands of research has come about in the investigation of clusters,[102–128] which can often be viewed either as large molecules or as nanoscopic solids. An early example is the work by Welch et al.[129] in which, in the context of the shell model,[130] local energy minimizations were performed with gradient methods for alkali metal halide clusters containing up to 44 dimers. More recently, for instance, Phillips et al.[131] studied the geometry of NaCl clusters and cluster ions again using a shell model. The global optimization was replaced by a large number of local optimizations with gradient methods; each reasonable initial configuration was generated by adding positive and negative ions in alternating positions of the cluster. Similarly, Rose and Berry[120] have used Born–Mayer potentials and multiple gradient minimizations during molecular dynamics simulations runs to study phase transitions in $(KCl)_{32}$ clusters. Both $(KCl)_n$ and $(LiF)_n$ clusters ($n \leq 15$) have been investigated by Ochsenfeld and Ahlrichs[102] at the SCF (MP2) level by using SCF force field calculations in order to determine local minima. Other work using ab initio density functional calculations together with (relatively short) molecular dynamics simulated annealing runs has been performed by Jones and Seifert[116] for phosphorus clusters ($n \leq 11$). To generate useful starting configurations, they employed simulated annealing with a simple effective potential on the LCAO-trial function level. Of course, this is only a very small sample of the efforts being undertaken in the study of ionic and covalent systems, not to mention the large amount of comparable work on noble gas and metal clusters.

While the clusters studied so far are often too small to really justify being viewed as extended solids, the work on such mesoscopic systems has had a profound effect on the way one approaches the analogous problem of structure optimization in solids. Two difficulties common to these systems have become apparent:[128, 132–134] the number of possible structures of a cluster/solid characterized as local minima of the energy hypersurface is very large, and it is not clear at all how to decide on the best or typical one without studying the energy landscape in great detail. This involves both the calculation of the depth of the local minima, the study of the density of states associated with these minima, and finally the determination of the barrier heights of the saddle points connecting the different structures.

While the importance of the lowest saddle points between two local minima has always been appreciated in the study of molecular reactions,[135–139] this has been perhaps less so when dealing with solids, in which usually only one structure has been considered at a time. The justification for this traditional procedure lies in the kinetic stability of solids, which is related to the idea of broken ergodicity by Palmer,[140] that is, in realistic large systems, it can often happen that at low temperatures thermodynamic equilibrium is not obtained globally. Only for a certain subset of the phase space of the system does the time-average, which is accessible to observation, equal the ensemble average. Thus, the thermodynamic behavior of a solid may depend only on the small region of the energy landscape around some (meta)stable structure.

It has therefore been perfectly reasonable to concentrate on the local environment of some already known or expected interesting structure, and to perform local optimizations of some energy function. Such local optimizations[35, 100, 141, 142] have been performed with varying degrees of restrictions on the number of atoms, symmetry of the structure, and size of the cell parameters. For example, Wentzcovitch and Martins[100] have modeled liquid Li using molecular dynamics techniques; at each step the Kohn–Sham equations were solved. This procedure is thus somewhat more suited to deal with volume changes during the (still rather local) optimization than the original Car–Parrinello algorithm, for which a fictitious electron dynamics has to complement the movement of the ion cores. In this context, one should also mention the modeling of proteins,[143] water,[144] and amorphous structures.[47, 145] In the latter case, one aims for a disordered arrangement of the atoms: thus, instead of finding a good sub-optimum by using some global optimization method, a local minimization is performed, resulting in an amorphous structure.

An interesting application of the use of global optimization methods in the determination of the structures of solids from powder diffraction data has been introduced in recent years by Pannetier, Newsam, Freeman, Catlow, and others.[31, 146–150] In their work, it is generally assumed that some experimental information about the compound is already available, for example, as a X-ray powder diffractogram. Thus, the size and shape of the unit cell, the composition of the compound, the ionic charges, and the number of formula units present in the cell are assumed to be known. It "only" remains to determine the exact positions of the atoms within this cell, a task that often tends to be quite involved, especially if only data from X-ray or neutron powder diffraction experiments are available. Imposing the above constraints, the authors perform global or local minimizations of special cost functions that combine some energy terms based on effective potentials with penalty terms reflecting, for example, Pauling's bond-valence rule[148] or the requirement of an even distribution of ions within the unit cell.[147] If the penalty terms and the effective potential are chosen appropriately,[151] the minimization produces a number of reasonable structure candidates, which then can serve as input either of a structure solving program or a refinement optimization using a more realistic energy function. In the extreme case, the cost function is solely constructed from penalty terms and equals a "figure of merit" that reflects a-priori knowledge of the typical bonding arrangements in the solid.[152, 153]

For example, Pannetier et al.[148] have used a combination of bond-valence and Coulomb terms as cost function to perform simulated annealing optimizations of the positions of the ions within a fixed unit cell of known ion content, for example, for NbF_4 or K_2NiF_4. Similarly, Freeman et al.[147] also used a unit cell for which size, shape, and ion content were known from experiment for their detemination of the structure of TiO_2 poly-

morphs. Using purely repulsive interactions as cost function, initial configurations were created by simulated annealing followed by conjugate gradient. Starting from these configurations, local minimizations were performed by using an empirical potential. Recently, Bush et al.[154] have demonstrated that genetic algorithms as global optimization method can also be used to assist in the determination of the structures of compounds for which only powder diffraction data and the composition of the unit cell are available. Again, an effective cost function similar to the one used by Pannetier et al.[148] was employed during the global optimization.

Alternative approaches[155-159] to understanding or for the determination of structures employ a-priori knowledge about bonding preferences and/or spacial constraints, often assuming a known unit cell, together with bond-valence rules to suggest possible structures. An interesting derivation of covalent structure elements of phosphorus (P_n, $n \leq 70$) using local ab initio optimizations on heuristically constructed network structures has recently been presented by Böcker and Häser.[160]

Our approach parallels the above-mentioned cluster studies in the sense that the basic concept of an in-depth study of the energy landscape is applied to the case of solids on a global scale instead of only very close to a given structure. While one usually considers the difference between cluster and solid to be the number of atoms, we would like to stress the use of periodic boundary conditions versus open boundary conditions in distinguishing between the two views. In this sense, one might consider our simulation cell plus its first shell(s) of neighbor cells as being equivalent to a cluster, that is, the effort required to deal with a cluster of about N atoms should in some way correspond to a calculation of a simulation cell with about $N/27$ atoms. Of course, there are a number of important differences deriving from the periodicity: long-range (e.g. Coulombic) forces have to be treated more carefully, and the free variation of the size and shape of the simulation cell plays a highly important role in the optimization. Together with the variation of composition and ionic charges, this last point is also a crucial step beyond the work on structure determination based on a-priori information about the unit cell of the already synthesized compound, described at the beginning of this section. In our opinion, this freedom during the global optimization is absolutely necessary to reach the goal of being able to plan syntheses in solid-state chemistry.

8. Conclusions

We have presented a method for the prediction of reasonable structure candidates for solid compounds. Thus, the state of planned solid-state syntheses has, in principle, become comparable to the one in the molecular chemistry of carbon and other nonmetals with respect to the formulation of concrete synthetic *targets* for those systems. It is expected that in both fields the further development of effective potentials appropriate for global optimizations will be a major area of future research. However, an important difference still remains: in solid-state chemistry, there is as yet no set of theoretical tools for the detailed design of the synthetic *route* to reach the predicted substance comparable to the aids available in molecular chemistry.

We would like to thank the participants of the structure seminar at the Institut für Anorganische Chemie der Universität Bonn for interesting discussions, and especially Dipl.-Chem. H. Putz and M. Wevers for their contributions. One of us, C. S., would also like to thank the participants of the Telluride Summer Research Center 1993 for useful comments. Funding by the Leibniz program of the Deutsche Forschungsgemeinschaft and by the Pinguin-Stiftung are gratefully acknowledged.

Received: July 3, 1995 [A 121 IE]
German version: *Angew. Chem.* **1996**, *108*, 1358–1377

[1] E. Hjelt, *Geschichte der Organischen Chemie*, Vieweg, Braunschweig, **1916**
[2] E. J. Corey, *Angew. Chem.* **1991**, *103*, 469–479; *Angew. Chem. Int. Ed. Engl.* **1991**, *30*, 455–465.
[3] E. J. Corey, *Pure Appl. Chem.* **1967**, *14*, 19–37.
[4] I. Ugi, J. Bauer, K. Bley, A. Dengler, A. Dietz, E. Fontain, B. Gruber, R. Herges, M. Knauer, K. Reitsam, N. Stein, *Angew. Chem.* **1993**, *105*, 210–239; *Angew. Chem. Int. Ed. Engl.* **1993**, *32*, 201–227.
[5] H. Schäfer, *Angew. Chem.* **1971**, *83*, 35–42; *Angew. Chem. Int. Ed. Engl.* **1971**, *10*, 43–50.
[6] R. Dronskowski, R. Hoffmann, *Adv. Mater.* **1992**, *4*, 514–520.
[7] L. D. Landau, E. M. Lifshitz, *Statistical Physics, Part 1*, 3rd ed., Pergamon, New York, **1985**.
[8] O. Ermer, *Aspekte von Kraftfeldrechnungen*, Wolfgang Baur Verlag, München, **1981**
[9] S. R. Niketic, K. Rasmussen, *The Consistent Force Field*, Springer, New York, **1977**.
[10] M. Jansen, *Abh. Rheinisch. Westfael. Akad. Wiss.* **1996**, *N 342*, in press.
[11] V. M. Goldschmidt, *Skrift. Nor. Vidensk. Akad. Kl. 1: Mat. Naturvidensk. Kl.* **1926**, *I*.
[12] A. R. West, *Solid State Chemistry and Its Applications*, Wiley, New York, **1984**.
[13] L. Pauling, *The Nature of the Chemical Bond*, Cornell University Press, Ithaca, **1960**.
[14] W. Hume-Rothery, *J. Inst. Met.* **1926**, *35*, 295–303.
[15] U. Müller, *Anorganische Strukturchemie*, Teubner, Stuttgart, **1992**.
[16] I. D. Brown, R. D. Shannon, *Acta Crystallogr. Sect A* **1973**, *29*, 266–282.
[17] R. Hoppe, *Adv. Fluorine Chem.* **1970**, *6*, 387–438.
[18] Strictly speaking most of the subsequent discussion deals with those structures that can be stabilized by energy barriers alone, that is, phases that could in principle exist at $T = 0$ K. For those phases that can only exist at high temperatures (e. g. the liquid state), we refer to the discussion in Section 6.3.
[19] The design and synthesis of a new compound correspond to the theoretical and experimental exploration of this energy landscape; thus, a chemist plays a role closer to that of an intrepid discoverer of strange and foreign lands and less to that of a creator of new worlds.
[20] J.-R. Hill, J. Sauer, *J. Phys. Chem.* **1994**, *98*, 1238–1244.
[21] Note that the use of periodic boundary conditions does not imply anything about the final symmetry of the candidate structures.
[22] An alternative is the use of open boundary conditions, that is, the simulation of a cluster. To deal with surface effects, this cluster should be embedded possibly in an effective medium, which reflects the average interaction with the remainder of the solid, .
[23] D. A. Pierre, *Optimization Theory with Applications*, Dover Publications, New York, **1986**.
[24] L. Davis, *Genetic Algorithms and Simulated Annealing*, Pitman, London, **1987**.
[25] P. J. M. van Laarhoven, Ph.D. Thesis, De Erasmus Universiteit Rotterdam, **1988**.
[26] Depending on the objectives of the simulation, one might want to exclude the ones with uninteresting properties. For example, if one searches for insulators, one would not want to spend time refining structures that exhibit metallic behavior.
[27] The term "state" refers to the electronic configuration of the atoms entering the approximate description of the solid, such as ionic charge or "type" and occupation of orbitals.
[28] S. M. Foiles, M. I. Baskes, M. S. Daw, *Phys. Rev. B* **1986**, *33*, 7983–7991.
[29] A. M. Stoneham, *Handbook of Interatomic Potentials. I. Ionic Crystals* (preprint, **1981**)
[30] M. P. Tosi, F. G. Fumi, *J. Phys. Chem. Solids* **1964**, *25*, 45–52.
[31] C. R. A. Catlow, R. G. Bell, J. D. Gale, *J. Mater. Chem.* **1994**, *4*, 781–792.
[32] M. Finnis, *Acta Metall. Mater.* **1992**, *40*, S25–S37.
[33] N. Chetty, K. Stokbro, K. W. Jacobsen, J. K. Nørskov, *Phys. Rev. B* **1992**, *46*, 3798–3809.
[34] C. Pisani, R. Dovesi, C. Roetti, *Hartree–Fock ab initio Treatment of Crystalline Systems*, Springer, Heidelberg, **1988**.
[35] R. Car, M. Parrinello, *Phys. Rev. Lett.* **1985**, *55*, 2471–2474.

[36] J. C. Schön, M. Jansen, *Ber. Bunsen Ges. Phys. Chem.* **1994**, *12*, 1541–1544.
[37] H. Putz, J. C. Schön, M. Jansen, *Ber. Bunsen Ges. Phys. Chem.* **1995**, *99*, 1148–1153.
[38] H. Putz, Diplom Thesis, Universität Bonn, **1994**.
[39] J. C. Schön, M. Jansen, *Comput. Mater. Sci.* **1995**, *4*, 43–58.
[40] J. C. Schön, M. Jansen, unpublished results.
[41] M. Wevers, J. C. Schön, M. Jansen, unpublished results.
[42] M. Wevers, Diplom Thesis, Universität Bonn, **1995**.
[43] J. C. Schön, M. Jansen, unpublished results.
[44] H. Putz, J. C. Schön, M. Jansen, unpublished results.
[45] M. Waldman, A. T. Hagler, *J. Comput. Chem.* **1993**, *14*, 1077–1084.
[46] S. W. de Leeuw, J. W. Perram, E. R. Smith, *Proc. R. Soc. London, A* **1980**, *373*, 27–56.
[47] F. H. Stillinger, T. A. Weber, *J. Phys. Chem.* **1987**, *91*, 4899–4907.
[48] C. Oligschleger, H. R. Schober, *Physica A* **1993**, *201*, 391–394.
[49] C. Oligschleger, Aachen, personal communication, **1995**.
[50] T. S. Bush, J. D. Gale, C. R. A. Catlow, P. D. Battle, *J. Mater. Chem.* **1994**, *4*, 831–837.
[51] P. J. M. van Laarhoven, E. H. L. Aarts, *Simulated Annealing*, Reidel, Dordrecht, Holland, **1987**.
[52] S. Kirkpatrick, C. D. Gelatt, Jr., M. P. Vecchi, *Science* **1983**, *220*, 671–680.
[53] V. Cerny, *J. Optim. Theory Appl.* **1985**, *45*, 41–51.
[54] N. Metropolis, A. Rosenbluth, M. Rosenbluth, A. Teller, E. Teller, *J. Chem. Phys* **1953**, *21*, 1087–1092.
[55] From this we can conclude that, in certain circumstances, we may interpret T as an actual temperature.
[56] S. Geman, D. Geman, *IEEE, PAMI* **1984**, *6*, 721–741.
[57] B. Andresen, K. H. Hoffmann, K. Mosegaard, J. Nulton, J. M. Pedersen, P. Salamon, *J. Phys. (Paris)* **1988**, *49*, 1485–1492.
[58] L. Goldstein, *Mean Square Rates of Convergence in the Continuous Time Simulated Annealing Algorithm on Rd* (preprint, **1985**).
[59] B. Hajek, *Math. Oper. Res.* **1988**, *13*, 311–329.
[60] J. Lam, J.-M. Delosme, *An Adaptive Annealing Schedule* (preprint, **1987**).
[61] J. M. Pedersen, K. Mosegaard, M. O. Jakobsen, *Optimized Optimization*, (preprint, **1989**).
[62] J. M. Pedersen, K. Mosegaard, M. O. Jakobsen, P. Salamon, (preprint, **1990**).
[63] G. Ruppeiner, J. M. Pedersen, P. Salamon, *J. Phys. I* **1991**, *1*, 455–470.
[64] P. Salamon, J. Nulton, J. Robinson, J. Pedersen, G. Ruppeiner, L. Liao, *Comput. Phys. Commun.* **1988**, *49*, 423–428.
[65] J. C. Schön et al., unpublished results.
[66] A. Hannemann, J. C. Schön, M. Jansen in *Tagungsband der Arbeitstagung des Arbeitskreises Nichtkristalline und Partiellkristalline Strukturen der DKG* (Eds.: B. Müller), Schmiedefeld, **1995**.
[67] H. Zimmermann, H. Burzlaff, *Z. Kristallogr.* **1985**, *170*, 241–246.
[68] L. C. Andrews, H. J. Bernstein, *Acta Crystallogr. Sect A* **1988**, *44*, 1009–1018.
[69] Y. LePage, *J. Appl. Crystallogr.* **1987**, *20*, 264–269.
[70] J. C. Schön, H. Putz, M. Jansen, *J. Phys. Condens. Matter*, **1996**, *8*, 143–156.
[71] P. Sibani, J. C. Schön, P. Salamon, J.-O. Andersson, *Europhys. Lett.* **1993**, *22*, 479–485.
[72] P. Sibani, J.-O. Andersson, *Physica A* **1994**, *206*, 1–12.
[73] P. Sibani, P. Schriver, *Phys. Rev. B* **1994**, *49*, 6667–6671.
[74] For several optimization runs, the composition was allowed to vary freely, too. In these cases, the candidate structures were dominated by a close packing of the heavier atoms, while the lighter noble gases tended to be removed from the simulation cell, indicating that phase separation was a very important option for all of these systems.
[75] R. Heastie, *Nature* **1955**, *176*, 747–748
[76] J. D. Martin, J. D. Corbett, *Angew. Chem.* **1995**, *107*, 234–236; *Angew. Chem. Int. Ed. Engl.* **1995**, *34*, 233–235..
[77] W. F. Sherman, A. A. Stadtmuller, *Experimental Techniques in High-Pressure Research*, Wiley, New York, **1987**.
[78] Note that our energy of formation with respect to the binary compounds is calculated at $T = 0$ K and $p = 0$ Pa, while the experimental value is valid at standard conditions. Since the resulting difference in enthalpy is basically given by the integral over the specific heat, and the contribution from the binary compounds will to a large degree cancel the contribution from the ternary compound, the rough comparison we perform appears to be reasonable.
[79] I. Barin, *Thermochemical Data of Pure Substances*, VCH, New York, **1989**.
[80] M. Troemel, *Z. Anorg. Allg. Chem.* **1969**, *371*, 237–247.
[81] R. E. Cohen, H. Krakauer, *Phys. Rev. B* **1990**, *42*, 6416–6423.
[82] K. Lukaszewicz, *Rocz. Chem.* **1959**, *33*, 239–242.
[83] H.-P. Baldus, O. Wagner, M. Jansen in *Materials Research Society Fall Meeting* (Eds.: W. G. Klemperer, C. J. Brinker), Materials Research Society, Boston, **1992**, 821–826
[84] J. Callaway, *Quantum Theory of the Solid State*, Academic Press, New York, **1974**.
[85] N. W. Ashcroft, N. D. Mermin, *Solid State Physics*, Harcourt Brace College, New York, **1976**.
[86] J. K. Burdett, S. Lee, *J. Am. Chem. Soc.* **1983**, *105*, 1079–1083.
[87] E. Canadell, M.-H. Whangbo, *Chem. Rev.* **1991**, *91*, 965–1034.
[88] It is curious to note that the energy differences of the local minima in Ca_3SiBr_2 computed by using the effective potential were actually quite similar to those computed with the Hartree–Fock method (c.f. Section 5.2). This coincidence should not be over-interpreted, of course, nevertheless, their agreement shows that one might expect the optimizations using the simple effective potential to yield at least reasonable qualitative results.
[89] M. Kunz, T. Armbruster, *Acta Crystallogr. B* **1992**, *48*, 609–622.
[90] A. F. Wells, *Structural Inorganic Chemistry*, Clarendon, Oxford, **1975**, 107.
[91] M. Jansen, B. Standke, *Z. Anorg. Allg. Chem.* **1986**, *535*, 39–46.
[92] For example, for the quaternary system $Sr_2NiO_2Cl_2$, the best configuration we have found so far shows an A-B-A-layer structure reminiscent of the K_2NiF_4 structure, in which each layer is based on a square O^{2-} lattice with Ni^{2+} filling every other square. Above and below each Ni^{2+} ion, a Cl^- ion is placed, resulting in an elongated octahedron around Ni. The Sr^{2+} ions lie above and below those O^{2-} squares that do not contain a Ni^{2+} ion. Finally, the Cl^- ions "coat" the Sr-Ni-O layer, leading to the NiO_4Cl_2 octahedra, and a O_4Cl_4 coordination of Sr.
[93] One other observation of note is the fact that for the systems with many atoms in the simulation cell the sub-optimal solutions tend to exhibit point defects (cf. Section 5.1). It is possible to "remove" the defects by performing considerably longer optimization runs. However, the effective use of the computer resources becomes quickly an issue, especially, if the optimal candidate structures can already easily be perceived from the sub-optimal structures containing these defects.
[94] Such an instance might be systems that show tendencies to form solid solutions of nearly equal size atoms.
[95] Note that R (sometimes called an order parameter) is usually not a thermodynamic variable like T, p, or V. Its definition is arbitrary and only represents one possible (but very useful if chosen cleverly!) way to partition the configuration space.
[96] M. L. Cohen, *Phys. Scr. T* **1982**, *1*, 5–10.
[97] M. P. Tosi in *Solid State Physics Vol 16*, (Eds.: F. Seitz, D. Turnbull), Academic Press, New York, **1964**, 1–120.
[98] J. E. Jones, A. E. Ingham, *Proc. R. Soc. A* **1925**, *107*, 636–653.
[99] B. J. Alder, T. E. Wainwright, *J. Chem. Phys.* **1957**, *27*, 1208–1209.
[100] R. M. Wentzcovitch, J. L. Martins, *Solid State Commun.* **1991**, *78*, 831–834.
[101] *Modern Techniques in Computational chemistry: MOTECC-90*, (Ed.: E. Clementi), ESCOM, Leiden, **1992**.
[102] C. Ochsenfeld, R. Ahlrichs, *Ber. Bunsen Ges. Phys. Chem.* **1994**, *98*, 34–47.
[103] V. Bonačić-Koutecký, P. Fantucci, J. Koutecky, *Chem. Rev.* **1991**, *91*, 1035–1108.
[104] W. Andreoni in *The Chemical Physics of Atomic and Molecular Clusters* (Eds.: G. Scoles), North-Holland, Amsterdam, **1990**, pp. 159–175.
[105] R. S. Berry, *Z. Phys. D* **1989**, *12*, 161–165.
[106] S. Björnholm, *Contemp. Phys.* **1990**, *31*, 309–324.
[107] E. Blaisten-Barojas, D. Levesque, *Phys. Rev. B* **1986**, *34*, 3910–3916.
[108] L. A. Bloomfield, C. W. S. Conover, Y. A. Yang, Y. J. Twu, N. G. Phillips, *Z. Phys. D* **1991**, *20*, 93–96.
[109] J. Buttet, *Z. Phys. D* **1986**, *3*, 155–157.
[110] A. W. Castleman, Jr., R. G. Keesee, *Chem. Rev.* **1986**, *86*, 589–618.
[111] W. Damgaard Kristensen, E. J. Jensen, R. M. J. Cotterill, *J. Chem Phys.* **1974**, *60*, 4161–4169.
[112] R. D. Etters, R. Danilowicz, J. Kaelberer, *J. Chem. Phys.* **1977**, *67*, 4145–4148.
[113] U. Even, N. Ben-Horin, J. Jortner, *Phys. Rev. Lett.* **1989**, *62*, 140–143.
[114] R. M. Graves, G. E. Scuseria, *J. Chem. Phys.* **1991**, *95*, 6602–6606.
[115] M. R. Hoare, *Adv. Chem. Phys.* **1979**, *40*, 49–135.
[116] R. O. Jones, G. Seifert, *J. Chem. Phys.* **1992**, *96*, 7564–7572.
[117] A. Maiti, L. M. Falicov, *Phys. Rev. A* **1991**, *44*, 4442–4449.
[118] C. D. Maranas, C. A. Floudas, *J. Chem. Phys.* **1992**, *97*, 7667–7678.
[119] C. Ochsenfeld, R. Ahlrichs, *J. Chem. Phys.* **1992**, *97*, 3487–3497.
[120] J. P. Rose, R. S. Berry, *J. Chem. Phys.* **1993**, *98*, 3246–3260.
[121] J. Uppenbrink, D. J. Wales, *J. Chem. Phys.* **1992**, *96*, 8520–8534.
[122] D. G. Vlachos, L. D. Schmidt, R. Aris, *J. Chem. Phys.* **1992**, *96*, 6891–6901.
[123] D. G. Vlachos, L. D. Schmidt, R. Aris, *J. Chem. Phys.* **1992**, *96*, 6880–6890.
[124] D. J. Wales, *J. Chem. Phys.* **1989**, *91*, 7002–7010.
[125] D. J. Wales, *Mol. Phys.* **1993**, *78*, 151–171.
[126] R. S. Berry, P. A. Braier, R. J. Hinde, H.-P. Cheng, *Israel J. Chem.* **1990**, *30*, 39–44.
[127] R. S. Berry in *The Chemical Physics of Atomic and Molecular Clusters* (Eds.: G. Scoles), North-Holland, Amsterdam, **1990**, pp. 3–22.
[128] R. S. Berry, *Chem. Rev.* **1993**, *93*, 2379–2394.
[129] D. O. Welch, O. W. Lazareth, G. J. Dienes, R. D. Hatcher, *J. Chem. Phys.* **1978**, *68*, 2159–2171.
[130] B. G. Dick, Jr., A. W. Overhauser, *Phys. Rev.* **1958**, *112*, 90–103.
[131] N. G. Phillips, C. W. S. Conover, L. A. Bloomfield, *J. Chem. Phys.* **1991**, *94*, 4980–4987.
[132] R. S. Berry, *J. Phys. Chem.* **1994**, *98*, 6910–6918.
[133] R. E. Kunz, R. S. Berry, *Phys. Rev. Lett.* **1993**, *71*, 3987–3990.
[134] R. E. Kunz, R. S. Berry, *Phys. Rev. E* **1994**, *49*, 1895–1908.
[135] B. Jeziorski, R. Moszynski, K. Szalewicz, *Chem Rev.* **1994**, *94*, 1887–1930.

[136] M. D. Newton, *Chem. Rev.* **1991**, *91*, 767–792.
[137] J. E. Eksterowicz, K. N. Houk, *Chem. Rev.* **1993**, *93*, 2439–2461.
[138] M. Page, J. W. McIver, Jr., *J. Chem. Phys.* **1988**, *88*, 922–935.
[139] J. Pancik, *Coll. Czech. Chem. Commun.* **1975**, *40*, 1112–1118.
[140] R. G. Palmer, *Adv. Phys.* **1982**, *31*, 669–735.
[141] C. R. A. Catlow, A. N. Cormack, *Int. Rev. Phys. Chem.* **1987**, *6*, 227–250.
[142] M. P. Teter, *Int. J. Quantum Chem. Quantum Chem Symp.* **1993**, *27*, 155–162.
[143] M. Wagener, J. Gasteiger, *Angew. Chem.* **1994**, *106*, 1245–1248; *Angew. Chem. Int. Ed. Engl.* **1994**, *33*, 1189–1192.
[144] I. Ohmine, H. Tanaka, *Chem. Rev.* **1993**, *93*, 2545–2566.
[145] C. Oligschleger, PhD Thesis, RWTH Aachen, **1994**.
[146] C. M. Freeman, C. R. A. Catlow, *J. Chem. Soc. Chem. Commun.* **1992**, 89–91.
[147] C. M. Freeman, J. M. Newsam, S. M. Levine, C. R. A. Catlow, *J. Mater. Chem.* **1993**, *3*, 531–535.
[148] J. Pannetier, J. Bassas-Alsina, J. Rodriguez-Carvajal, V. Caignaert, *Nature* **1990**, *346*, 343–345.
[149] P. A. Wright, S. Natarajan, J. M. Thomas, R. G. Bell, P. L. Gai-Boyes, R. H. Jones, J. Chen, *Angew. Chem.* **1992**, *104*, 1526–1529; *Angew. Chem. Int. Ed. Engl.* **1992**, *31*, 1472–1475.
[150] D. K. Belashenko, *Inorg. Mater. (Engl. Trans.)* **1994**, *30*, 966–976.
[151] Since these penalty terms do not correspond to a physical energy term, but only reflect some intuitive chemical or physical knowledge about the system, they have to be treated very carefully when being assigned a quantitative meaning compared to terms from an effective potential.
[152] M. W. Deem, J. M. Newsam, *J. Am. Chem. Soc.* **1992**, *114*, 7189–7198.
[153] M. W. Deem, J. M. Newsam, *Nature* **1989**, *342*, 260–262.
[154] T. S. Bush, C. R. A. Catlow, P. D. Battle, *J. Mater. Chem.* **1995**, *5*, 1269–1272.
[155] N. Engel, *Acta Crystallogr. Sect. B* **1991**, *47*, 849–858.
[156] I. D. Brown, R. Duhlev, *J. Solid State Chem.* **1991**, *95*, 51–63.
[157] R. Duhlev, I. D. Brown, C. Balarew, *J. Solid State Chem.* **1991**, *95*, 39–50.
[158] I. D. Brown, *Z. Kristallogr.* **1988**, *185*, 503.
[159] I. D. Brown, *Acta Crystallogr. Sect. B* **1992**, *48*, 553–572.
[160] S. Böcker, M. Häser, *Z. Anorg. Allg. Chem.* **1995**, *621*, 258–286.

Time is money...

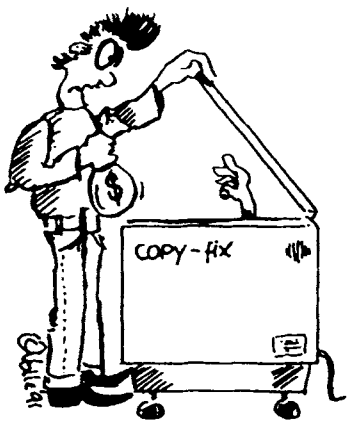

Save both by starting a personal subscription to *Angewandte Chemie* (now with *Chemistry - A European Journal*). At 9¢ per page you can't go wrong. With your own private copy you can read the "hot" articles before they cool, and waste less time in front of the copier.

Order now!
An order form can be found on the last page of this issue.

Cationic Iridium(III) Complexes: A Step Towards Synthetic Applicability of C–H Activation

John C. W. Lohrenz* and Heiko Jacobsen*

A problem in modern chemistry that still remains only partially solved is the functionalization of unreactive compounds. Here, the activation of C–H bonds in hydrocarbons by transition metals is of central interest.[1] The significance attributed to this question is apparent from the fact that the selective C–H activation was described as a "holy grail of chemistry",[1, 2] and recently an entire issue of the *Journal of Organometallic Chemistry*[3] was dedicated to this topic.

Despite their low reactivitiy C–H bonds are not completely inert, and reactions with selected transition metal complexes have been known for some time in which alkanes can be cleaved successfully. It would be beneficial to be able to use this route to catalytically transform the compounds that occur in large quantities in oil and gas into "valuable" products.

A recent paper by Arndtsen and Bergman,[4] which describes an unusually mild and selective cleavage of C–H bonds in alkanes and arenes by the iridium complex **1a** ([BArf]$^-$ = [B(3,5-

$[Cp^*Ir(PMe_3)(CH_3)(ClCH_2Cl)][BAr_f]$ **1a**

$C_6H_3(CF_3)_2)_4]^-$), is certainly a milestone on the route to efficient C–H activation. Based on this work, herein we wish to take the opportunity to summarize most recent developments in C–H activation by late transition metal complexes.[5]

Since the early work in the research groups of Graham,[6] Jones,[7] and Bergman,[8] significant advances in the design of metal complexes have been made. All three research groups employ electronically unsaturated complexes of the late transition metals with vacant coordination sites. The first positive results had been achieved in 1982 by Janowicz and Bergman who utilized the iridium complex **2a**,[8] a compound that mainly activates aromatic C–H bonds. The analogous rhodium complex **2b** was employed by Jones and Feher in 1984 for the oxidative addition to C–H bonds.[7] Activation of methane was achieved for the first time by Graham and co-workers in 1983, who used the iridium complex **3**.[6] As promising as these results

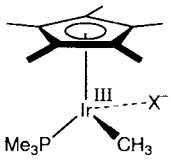

1a $X^- = Cl\text{-}CH_2Cl\ [BAr_f]^-$
1b $X^- = [OSO_2CF_3]^-$
1c $X^- = Cl^-$

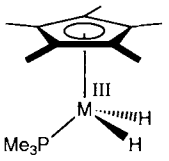

2a M = Ir
2b M = Rh

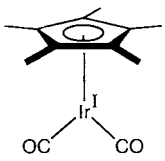

3

were, several significant disadvantages were apparent for all of the systems. First, the catalysts had to be either photochemically or thermally activated, second the presented complexes are quite unselective with respect to the C–H bond to be activated. Finally, so far these complexes can be used in stoichiometric quantities only, and cannot be included satisfactorily in a catalytic cycle.

In the photolysis of compounds **2a,b** and **3**, H_2 or one equivalent of CO are lost, leading to the 16-electron complexes $[Cp^*M(PMe_3)]$ and $[Cp^*Ir(CO)]$, respectively. These, however, could not be observed directly (Scheme 1). In the next step the hydrocarbon oxidatively adds to the metal center. In the initial stage of this process the C–H bond probably coordinates through an agostic interaction to the metal.[9] The product of the addition can be worked up with bromoform, leading to the corresponding bromoalkane.

Indeed, ab initio MP2 calculations[10] on the interaction of the 16-electron model system [CpRh(CO)] with methane revealed a stabilization of the agostic intermediate by $-14.8\ kcal\,mol^{-1}$, which agrees well with the experimental results of Wasserman et al.[9] Furthermore, a moderate activation barrier of $4.1\ kcal\,mol^{-1}$ was obtained for the oxidative addition. Finally, the reaction enthalpy was calculated to be $-30.6\ kcal\,mol^{-1}$. This nicely shows how an activation of hydrocarbons can be achieved by the previously assumed 16-electron intermediates.

Going to the electron-deficient Ir^{III} complex **1b** results in a new class of extremely reactive compounds[11] that are capable of cleaving C–H bonds without prior photochemical activation. The key role of the counterion in the complexes **1** becomes clear when one considers that **1c** with the strongly coordinating chloride ion does not react with benzene below 100 °C, whereas the latter adds quantitatively to the triflate complex **1b** already at

[*] Dr. J. C. W. Lohrenz
Organisch-chemisches Institut der Universität Zürich
Winterthurerstrasse 190, CH-8057 Zürich (Switzerland)
Fax: Int. code +(1)361-9895
e-mail: lohrenz@oci.unizh.ch

Dr. H. Jacobsen
Anorganisch-chemisches Institut der Universität Zürich
Winterthurerstrasse 190, CH-8057 Zürich (Switzerland)
e-mail: jacobsen@aci.unizh.ch

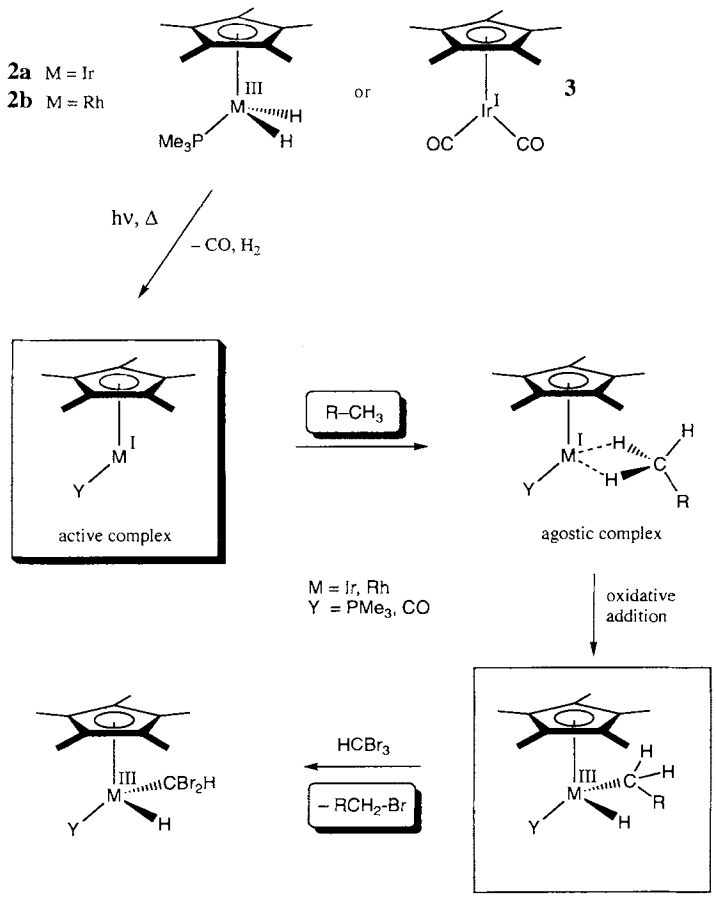

Scheme 1. Mechanism of the C–H activation by complexes **2** and **3**.

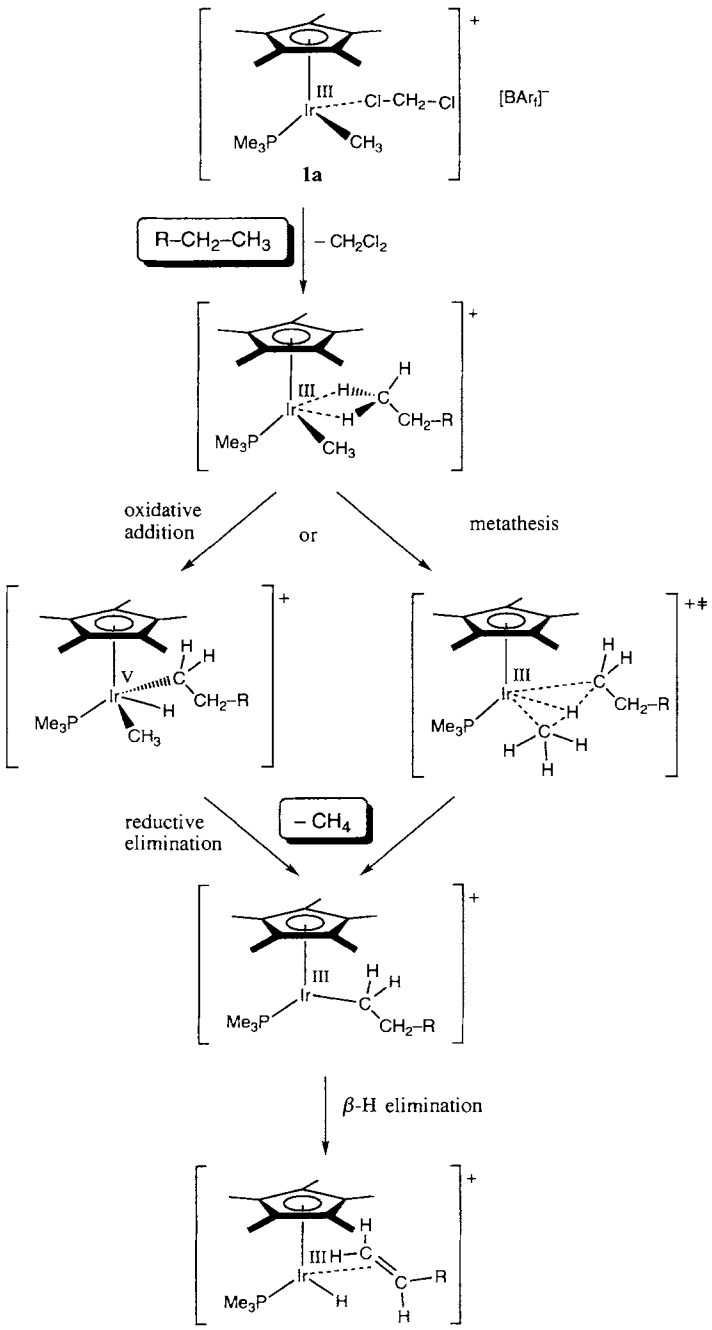

Scheme 2. Postulated mechanism of the C–H activation by complex **1a**.

25 °C. These observations suggest that the active species is the free cation formed after dissociation of the counterion.

The reaction of **1a,b** with hydrocarbons leads to the elimination of methane. This indicates the possibility of a reaction by a σ-bond metathesis mechanism, as is also known for complexes of early transition metals (Scheme 2, right branch). Such an interpretation is supported by the fact that the larger electrophilicity of **1a,b** (or to be more precise that of the corresponding cation) makes its chemistry comparable to that of early transition metals.[11] Oxidative addition with subsequent reductive elimination (Scheme 2, left branch), however, cannot be ruled out completely.

The efforts to trap the cationic intermediate led to the very active complex **1a**, in which the triflate ion was replaced by the noncoordinating $[BAr_f]^-$ ion.[4] An X-ray structure analysis revealed that the vacant coordination site of the 16-electron intermediate in **1a** is occupied by a weakly coordinating dichloromethane molecule (Fig. 1). The counterion $[BAr_f]^-$ and a second molecule of dichloromethane have no contacts to the cation. Thus, the dissociated ion pair exists in the crystal.

Compound **1a** reacts with benzene already at −30 °C and activates methane at 10 °C. As assumed by Arndtsen and Bergman, the extremely high reactivity is based on the weak bond between the dichlomethane molecule and the metal center. This could be shown by ^{1}H NMR spectroscopy by a rapid exchange with CD_2Cl_2 at −90 °C.

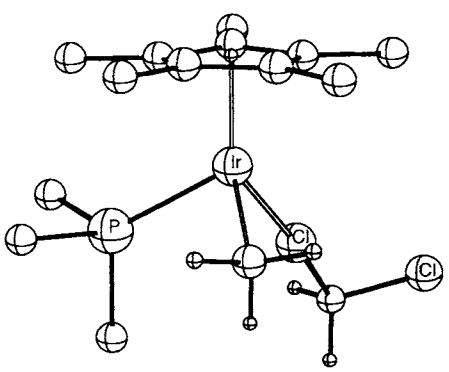

Fig. 1. Structure of **1a**·CH_2Cl_2 in the crystal [4]. The borate counterion and the second dichloromethane molecule do not form contacts to the cation and are therefore omitted.

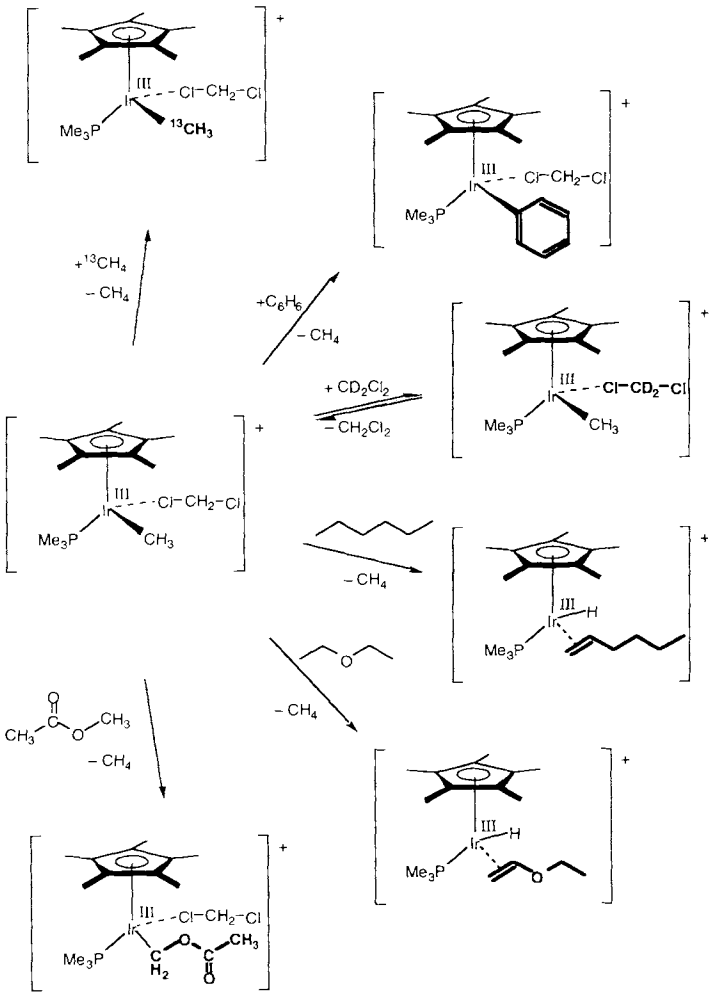

Scheme 3. Reactions of the cation in **1a**.

Selected reactions of the cation in **1a** are given in Scheme 3. Compound **1a** reacts better with primary than with secondary C–H bonds, and in the presence of β hydrogen atoms ultimately leads to olefin complexes. Here, the initial C–H activation step probably is followed by a β-H elimination (Scheme 2). Furthermore, the selectivity of **1a** is shown by the reaction with methyl acetate, in which only the *O*-methyl group reacts. This is remarkable since here a methyl group is activated in the presence of the considerably more acidic protons of an acetyl group. The complex **1a** even tolerates functional groups and thus also enables the targeted cleavage of C–H bonds in "complex" molecules. Diethyl ether, for example, which is still inert toward **1b**, reacts smoothly with **1a** to give the corresponding vinyl ether complex.

The observations outlined in the last section show that the initially described problems of activity and selectivity can be well controlled with complex **1a**. The method developed by Arndtsen and Bergman, however, still requires the complex in stoichiometric quantities. The development of a catalytic process demands in addition the simultaneous activation of an oxidizing agent such as oxygen. For the future, it will be interesting to see whether and how the as yet unresolved problem of *catalytic* C–H activation is mastered.

German version: *Angew. Chem.* **1996**, *108*, 1403–1405

Keywords: C–H activation · iridium compounds · rhodium compounds

[1] B. A. Arndtsen, R. G. Bergman, T. A. Mobley, T. H. Peterson, *Acc. Chem. Res.* **1995**, *28*, 154–162.
[2] A. J. Bard, G. M. Whitesides, R. N. Zare, F. W. McLafferty, *Acc. Chem. Res.* **1995**, *28*, 92.
[3] All publications in *J. Organomet. Chem.* **1995**, *504*, 1–155.
[4] B. A. Arndtsen, R. G. Bergman, *Science* **1995**, *270*, 1970–1973.
[5] C–H Activations are also known with complexes of the early transition metals [J. P. Rothwell in *Selective Hydrocarbon Activation. Principles and Progress* (Eds.: J. A. Davies, P. L. Watson, J. F. Liebman, A. Greenberg), VCH, Weinheim, **1990**, pp. 43–78] as well as with those of rare earth metals [P. L. Watson, *ibid.*, pp.79–112].
[6] J. K. Hoyano, A. D. McMaster, W. A. G. Graham, *J. Am. Chem. Soc.* **1983**, *105*, 7190–7191.
[7] W. D. Jones, F. J. Feher, *J. Am. Chem. Soc.* **1984**, *106*, 1650.
[8] A. H. Janowicz, R. G. Bergman, *J. Am. Chem. Soc.* **1982**, *104*, 352–354.
[9] E. P. Wasserman, C. B. Moore, R. G. Bergman, *Science* **1993**, *255*, 315–318.
[10] J. Song, M. B. Hall, *Organometallics* **1993**, *12*, 3118–3126.
[11] P. Burger, R. G. Bergman, *J. Am. Chem. Soc.* **1993**, *115*, 10462–10463.

 © VCH Verlagsgesellschaft mbH, D-69451 Weinheim, 1996 0570-0833/96/3512-1307 $ 15.00+.25/0

The Sharpless Asymmetric Aminohydroxylation of Olefins

Oliver Reiser*

"The time has come for me to discover something new, but there is so much chemistry out there!" With these words Barry Sharpless closed the Merck–Schuchardt lecture 1995 in Göttingen, Germany.[1] After about 10 years of continuous optimization, the asymmetric dihydroxylation (AD) of olefins had developed into one of the most versatile catalytic asymmetric reactions to date.[2]

An "obvious" extension of the AD process would be the asymmetric transfer of heteroatoms other than oxygen to a C–C double bond. Indeed, the osmium-catalyzed[3] or palladium-mediated[4] aminohydroxylation of alkenes has been known for 20 years. The resulting β-amino alcohols are an important structural element in biologically active compounds as well as the starting point in the design of many chiral ligands. However, to develop this reaction into a catalytic, asymmetric process several problems had to be overcome.

According to the original protocol[3] alkenes can be converted to racemic, N-tosyl-protected β-amino alcohols in the presence of catalytic amounts of osmium tetroxide using Chloramine-T as the nitrenoid source and water as the hydroxyl source [Eq. (a)]. However, unlike the AD process, the aminohydroxylation of unsymmetrical alkenes can lead to two regioisomeric products, which was a drawback in the early stages of its development. Moreover, the direct reaction of osmium tetroxide with the alkene could not be completely surpressed, and diols were sometimes observed as side products.

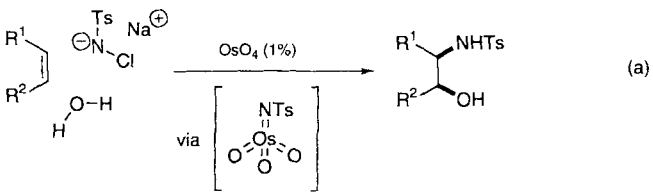

(a)

Although the first, albeit stoichiometric, example of this asymmetric aminohydroxylation reaction had already been observed in 1980,[5] the discovery of the titanium-catalyzed asymmetric epoxidation (AE)[6] at about the same time probably also "interfered" with an earlier development of today's catalytic asymmetric aminohydroxylation (AA) process.

Since the discovery of the catalytic AD in 1987, there have been numerous attempts in the Sharpless group to render the old catalytic aminohydroxylation process asymmetric.[7] Until recently, the obvious approach of adding the chiral ligands of the AD reaction, but otherwise staying close to the original protocol[3] led to extremly slow catalyst turnover. The present breakthrough[8] was not due to a sudden conceptual insight but rather to the luck of making a number of small changes, all of which had been tried before but never in concert. Suddenly the turnover was decent, diol side products were greatly reduced, and good regioselectivity was seen for the first time.[7] Most exciting of all, the products were obtained with moderate to high enantioselectivities, and with complimentary discrimination of the enantiotopic faces of the alkene by the two ligands, $(DHQ)_2PHAL$ and $(DHQD)_2PHAL$.[9] The same sense of asymmetric induction as in the AD is observed, indicating that the transfer of chirality occurs by a similar pathway. Moreover, due to the highly crystalline nature of the products they can often be raised to enantiopurity by simple recrystallization.

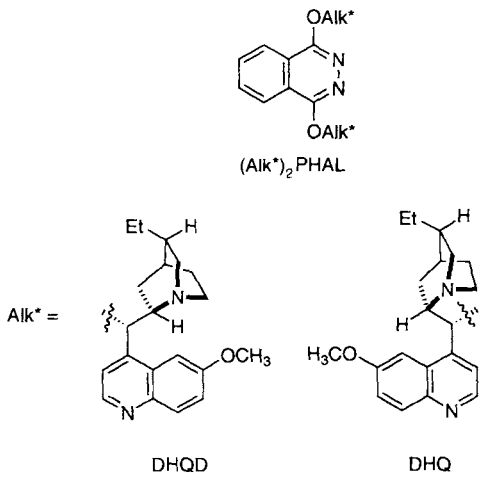

What types of alkenes undergo this reaction (Scheme 1)? In contrast to the AD reaction also strongly electron-poor alkenes are suitable substrates probably due to the greater polarization of the Os=NTs group compared to that of the Os=O group. Thus, acrylates in general give good results in the AA (**5** → **6**), but even dimethyl fumarate (**1**) reacts rapidly—**1** is a very poor AD substrate—to give the 2-hydroxy aspartic acid derivative **2**. Cinnamates **3** can be converted to α-hydroxy-β-amino acids **4**, giving, for example, a most effective entry to the side chain amino acid of taxol.[10] One of the most remarkable effects of the chiral ligand is on the regioselectivity. In the absence of the ligand the cinnamates **3** give roughly equal amounts of the regioiosmers (that is **4** plus its 2-NHTs, 3-OH isomer).[3] *Para*-substitution of the aryl group in **3** by electron-donating or -withdrawing groups is well tolerated, however, *meta*- and, in particular, *ortho*-substitution results in some loss of enantio- and regioselectivity. While most of the reactions to date were carried out with 4 mol%Os/5 mol% ligand, in large scale runs the amount of catalyst required has been successfully reduced by half.

Less electron-poor alkenes like stilbenes (**7** and **9**) are also viable substrates, but the enantioselectivities are generally low-

[*] Priv.-Doz. Dr. O. Reiser
Institut für Organische Chemie der Universität
Tammannstrasse 2, D-37077 Göttingen (Germany)
Fax: Int. code +(551)39-9475
e-mail: oreiser@gwdg.de

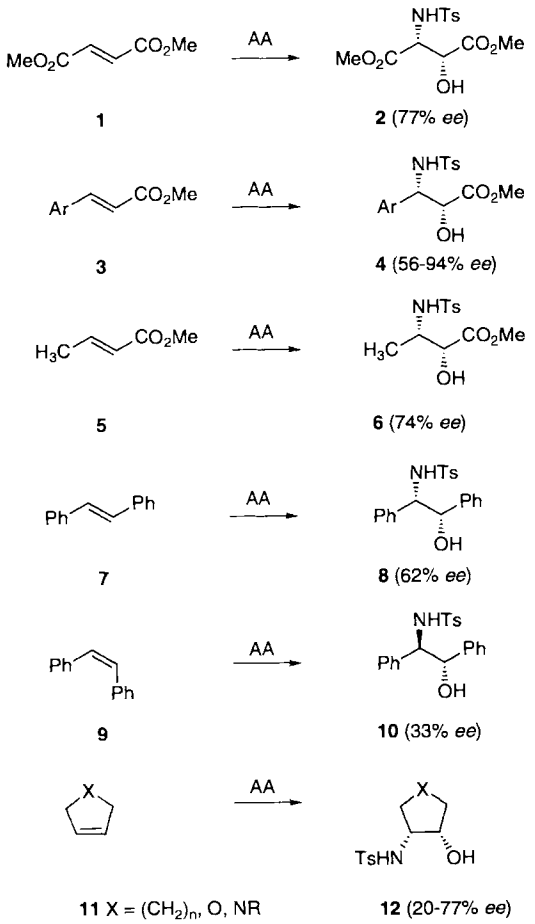

Scheme 1. AA: TsNClNa (3.5 equiv), *t*BuOH/H_2O 1/1 or CH_3CN/H_2O 1/1, room temperature $K_2[OsO_2(OH)_4]$ (4.0 mol%), $(DHQ)_2$-PHAL (5 mol%); $(DHQD)_2$-PHAL leads to the enantiomeric products.

er. Direct comparison of **8** and **10** also indicates, that (*E*)-alkenes are—in analogy to the AD process—better substrates than (*Z*)-alkenes. Nevertheless, it is already clear at this stage that (*Z*)-alkenes, and, in particular, symmetrical (*Z*)-alkenes, are useful substrates in the AA. A *syn*-dihydroxylation of the latter class of olefins leads to *meso* diols and is therefore not suitable in relation of the concept of asymmetric dihydroxylation. Cyclic (*Z*)-alkenes (**11**) ($n = 1, 2$) also have given promising results, and heteroatoms can be present as long as they are not directly attached to the double bond.[7]

1,3-, 1,4-, and 1,5-dienes as well as certain 1-alkenes also have given encouraging results in the AA, but additional regioselectivity and reactivity problems arise with these substrates. Alkenes that seem to be problematic so far are allylic halides, allylic alcohols, and allylic amines, no matter if protected or not. Several allylic acetals have also given poor results.[7]

The products obtained by the AA process can be easily transformed into aziridines or into precursors for α,β-diamino acids (Scheme 2).[7] Moreover, some derivatives like **4** can be deprotected without loss of stereochemical integrity[10] even under the quite harsh conditions (HBr/HOAc/phenol 75 °C) required to remove the N-tosyl group. The recent and exciting introduction of the nitrobenzenesulfonyl group for amine protection,[11] a group combining the virtues of the tosyl group with that of being easily removable, should dramatically advance the chemistry of these and other reactions wherein the purpose is creating new C–N bonds under mild conditions.

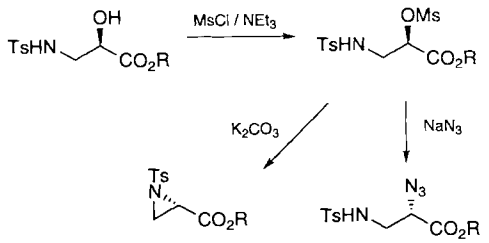

Scheme 2. Possible reactions with the product of an AA.

Is it too early to write a "highlight" on this new reaction? Most certainly not! At the present stage of development there are many desirable improvements concerning the range of substrates and the selectivities, as well as optimized reaction conditions. The influence of numerous parameters for the AA process like temperature, solvent, and additives are currently being investigated intensively in the Sharpless group. Also, the openness with which Sharpless et al. is presenting this discovery to the synthetic community is most impressive in that not only short communications but simultaneously full papers with detailed experimental procedures are currently in press. Looking back at the great and successful effort undertaken for the catalytic AD process, one would not be surprised to witness a similar rapid development of this catalytic asymmetric aminohydroxylation process. Moreover, there are already two other oxidative amination processes on the horizon, namely allylic amination of olefins [Eq. (b)] and 1,2-diamination of 1,3-dienes [Eq. (c)].[12] Could these useful, but stochiometric transformations be rendered catalytic and perhaps also asymmetric some day?

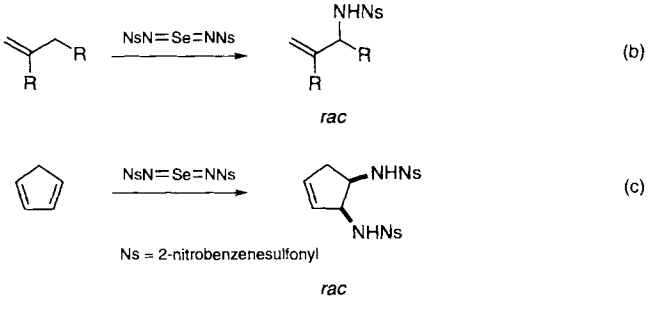

German version: *Angew. Chem.* **1996**, *108*, 1406–1408

Keywords: aminations · β-amino alcohols · asymmetric aminohydroxylation · Chloramine-T · osmium compounds

[1] Universität Göttingen, April 28, 1995. The day of the AA discovery was June 14, 1995.
[2] H. C. Kolb, M. S. VanNieuwenhze, K. B. Sharpless, *Chem. Rev.* **1994**, *94*, 2483.
[3] a) K. B. Sharpless, A. O. Chong, K. Oshima, *J. Org. Chem.* **1976**, *41*, 177; b) E. Herranz, K. B. Sharpless, *ibid.* **1978**, *43*, 2544.
[4] J. E. Bäckvall, *Tetrahedron Lett.* **1975**, 2225.
[5] S. Hentges, K. B. Sharpless, *J. Am. Chem. Soc.* **1980**, *102*, 4263.
[6] T. Katsuki, B. Sharpless, *J. Am. Chem. Soc.* **1980**, *102*, 5447.
[7] K. B. Sharpless, personal communication.
[8] G. Li, H.-T. Chang, K. B. Sharpless, *Angew. Chem.* **1996**, *108*, 451; *Angew. Chem. Int. Ed. Engl.* **1996**, *35*, 451.
[9] H. Becker, K. B. Sharpless, *Angew. Chem.* **1996**, *108*, 447; *Angew. Chem. Int. Ed. Engl.* **1996**, *35*, 448.
[10] G. Li, K. B. Sharpless, *Acta Chem. Scand.* **1996**, *50*, in press.
[11] T. Fukuyama, C.-K. Jow, M. Cheung, *Tetrahedron Lett.* **1995**, *36*, 6373.
[12] M. Bruncko, T.-A. V. Khuong, K. B. Sharpless, *Angew. Chem.* **1996**, *108*, 453; *Angew. Chem Int. Ed. Engl.* **1996**, *35*, 454.

A Steroid-Based Cryptand for Halide Anions**

Anthony P. Davis,* John F. Gilmer, and Justin J. Perry

Supramolecular chemistry is founded largely on the early discoveries of the crown ethers and cryptands, *neutral organic molecules* capable of surrounding inorganic cations, binding them through the cooperative action of several preorganized centers, and providing lipophilic exteriors, which promote solubility in nonpolar organic media.[1] The study of anion recognition was a natural extension of this work and has resulted in a variety of elegant and effective systems.[2] However, there are still rather few molecules that may be described in the fullest sense as "anion-equivalents" of crown ethers or cryptands in that they bind inorganic anions using convergent, preorganized functionality mounted on a macrocyclic framework and are a) electrically neutral, b) essentially organic in nature, and c) soluble in nonpolar organic solvents. In order to meet these criteria, a receptor must act either through ion–dipole attraction[2a, b] or through hydrogen-bond donation.[2d–k] While the latter is probably the more potent force, there are few (if any) molecules with good neutral H-bond donor groups that do not also contain H-bond acceptors. The design of multivalent hosts is therefore complicated by a tendency towards intramolecular H-bond formation (which can close the binding cleft or cavity) and intermolecular association (which lowers solubility).

We now report a neutral, macrocyclic organic receptor for halide anions in which these problems are minimized by a lipophilic exterior featuring flexible alkyl chains to maintain solubility in nonpolar organic media and a rigid framework to maintain a binding cavity and limit the possibilities for intramolecular H-bond formation. The new host **1** is conceptually related to the "cholaphanes" reported previously from this laboratory,[3] being a macrodilactam derived from two molecules of the inexpensive steroid cholic acid **2**.[4] However, whereas the cholaphanes surround medium-sized organic molecules, **1** was designed to possess a compact and rigid structure encompassing a much smaller cavity, bordered by a high density of convergent, polar functional groups. In particular, the hydroxyl groups were intended to create an environment mimicking the aqueous solvation of a spherical anion, but preorganized for binding and surrounded by a lipophilic envelope. As a crown ether or cryptand may be thought to provide "preorganized aquation" for a spherical cation, receptor **1** would perform a complementary function for an anion.

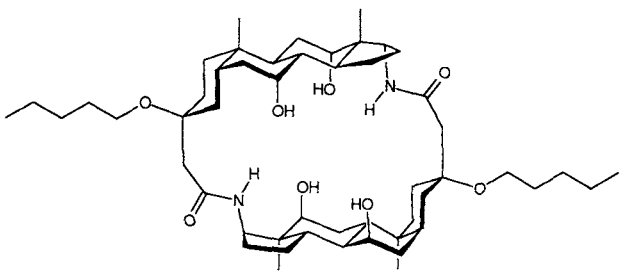

1

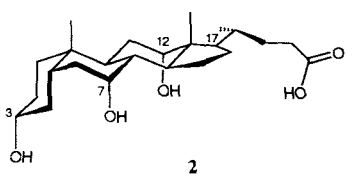

2

The synthesis of **1** from **2** hinged on replacement of the side chain at C17 with an α-NH_2 group and installation of CH_2CO_2R as a short spacer in the 3α position in addition to the solubilizing β-alkoxy substituent. The early intermediate **3** was prepared by Baeyer–Villiger oxidation[5] of the corresponding 17β-acetyl-5β-androstane, which was obtained from **2** by a degradation sequence developed by Barton and co-workers.[6] The remaining steps are shown in Scheme 1. An apparent cu-

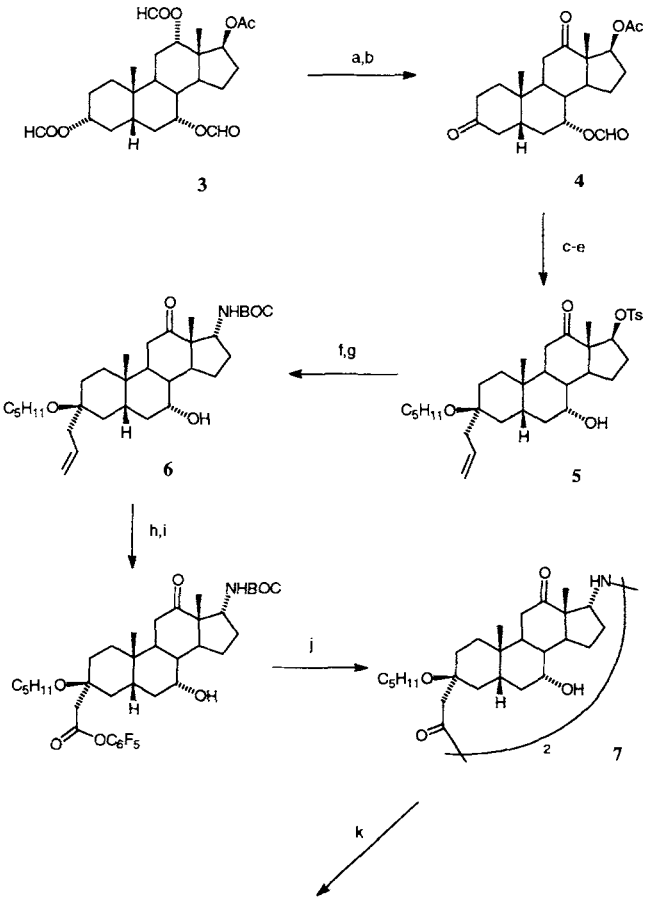

Scheme 1. a) K_2CO_3, THF, H_2O, MeOH; b) pyridinium chlorochromate, CH_2Cl_2; c) $Me_3SiCH_2CH{=}CH_2$, $Me_3SiOC_5H_{11}$, Me_3SiOTf (cat.), CH_2Cl_2, $-40\,^{\circ}C$; d) NaOMe, MeOH; e) TsCl, pyridine; f) NaN_3, DMPU (*N,N'*-dimethyl-*N,N'*-propylene urea), 130 °C, 48 h; g) Zn, AcOH, then $(BOC)_2O$ (BOC = *tert*-butoxycarbonyl), CH_2Cl_2, Et_3N; h) O_3, CH_2Cl_2, then H_2O_2; i) C_6F_5OH, DCC (dicyclohexylcarbodiimide); j) TFA (trifluoroacetic acid), CH_2Cl_2, then DMAP (4-dimethylaminopyridine), Et_3N, CH_2Cl_2 (2 mL per mg of substrate); k) H_2, PtO_2, EtOAc, AcOH.

riosity is the oxidation of the C12-OH at the start of the sequence, and its regeneration through a stereoselective reduction on macrocycle **7**. This (somewhat desperate) measure was adopted after we discovered that a 12α-O substituent had a strongly deleterious effect on the azide displacement at C17 (as required for **5** → **6**). Also of note is the regio- and stereoselective application of the "silyl-modified Sakurai" reaction, incorpo-

[*] Prof. A. P. Davis, J. F. Gilmer, J. J. Perry
Department of Chemistry, Trinity College
Dublin 2 (Ireland)
Fax: Int. code +(1)6712826
e-mail: adavis@mail.tcd.ie

[**] Financial support for this work was provided by Materials Ireland. We are grateful to Peter Ashton (University of Birmingham) for mass spectra, and to Freedom Chemical Diamalt GmbH for generous gifts of cholic acid.

rating both a spacer in α position and a solubilizing group in β position at C3 during the conversion of **4** to **5**.[7] All the steps in Scheme 1 gave satisfactory yields, the lowest (about 70%) being that of the macrocyclization to form **7**. Despite its congregation of polar groups, the tetraol **1**[8] was found to be highly soluble in chloroform and most other organic solvents.

The prospects for anion recognition by **1** were assessed by molecular modeling. A Monte Carlo search[9] on the receptor revealed a single dominant framework conformation, common to all the structures saved up to 39 kJ mol^{-1} above baseline. The macrocycle possesses an ovoid cavity about 3.3 Å long by 2.2 Å broad, sufficient to accommodate a fluoride and possibly chloride or bromide ion,[10] but too small for significant penetration by chloroform solvent molecules. The cavity is bounded by inward-directed NH groups at the ends of its long axis and CH and OH groups across its breadth, and is closed on one face by a transannular hydrogen bond between the two 7α-OH groups. Although this means that one 7α-OH group may be unavailable for H-bond donation to an enclosed anion, the second may be directed into the cavity as exemplified by the conformation shown in Figure 1 (which is just 2.1 kJ mol^{-1} above baseline).

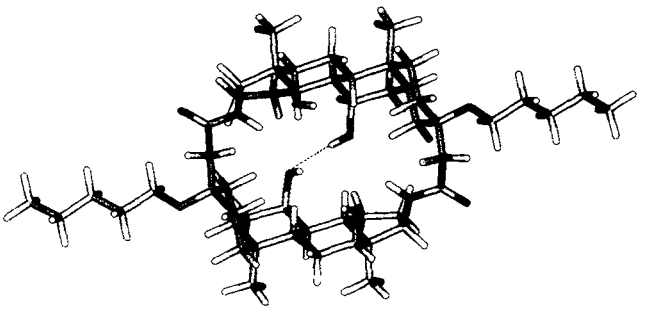

Fig. 1. One of the lower energy conformations of **1** found by computer-based molecular modeling. The macrocycle is viewed from the "C12 face", with the C7–OH···O C7 hydrogen bond (shown as a dotted line) at the base of the cavity. All the conformers located up to 39 kJ mol^{-1} above baseline possessed essentially the same framework conformation, and differed only in torsion angles about the three free OH groups ($1 \times 7\alpha$ and $2 \times 12\alpha$) and the bonds in the pentyloxy groups. The structure shown, which was found at 2.1 kJ mol^{-1} above baseline, is selected to illustrate the possibility of an inward-directed C7–OH (in the bottom left section of the cavity).

The two 12α-OH groups may also rotate inwards to form hydrogen bonds with a guest. The distance between the amide hydrogen atoms (5.6 Å) is probably too great to allow simultaneous formation of two NH···X$^-$ hydrogen bonds. However, as shown in Figure 2, an anion situated towards one end of the cavity can adopt a position about 2 Å from each of four donor hydrogen atoms (one NH, three OH) without significant adjustment of the framework conformation.[11] It should be stressed that Figure 2 is intended to illustrate the general suitability of **1** for halide binding, and does not represent a proposed structure for an actual complex (vide infra).

The recognition properties of **1** towards fluoride, chloride, and bromide anions were studied through NMR titrations employing the tetrabutylammonium salts of the anions in $CDCl_3$. Addition of all three halides resulted in substantial downfield shifts of the signal due to the NH protons on the receptor, consistent with NH···X$^-$ hydrogen bond formation. The shifts could be analyzed in terms of 1:1 binding, giving the association constants (K_a) recorded in Table 1. The macrocycle discriminates quite well between the anions, favoring, not unexpectedly, the smaller and more basic guests, which also gave the larger complexation-induced shifts. The receptor is clearly less potent

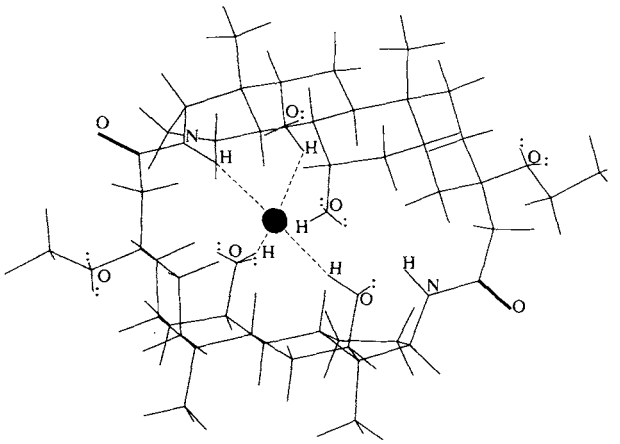

Fig. 2. Modeling H-bond formation to a hypothetical spherical anion within the cavity of **1**. Starting from the conformation in Figure 1, this configuration resulted from manual adjustment of the three OH torsions and anion position, followed by minimization of the receptor with the OH torsions held in place, and return of the anion. The hydrogen bonds (broken lines) range between 1.99 and 2.18 Å.

than those employing positively charged binding centers, for which association constants larger than 10^3 are commonly observed even in aqueous media.[12] However the binding constant for fluoride, and the selectivities, compare well with those of earlier neutral organic receptors.[2e, 2j] The H-bond donor groups in **1** are not especially potent by themselves.[13] When the secondary amide **8**, chosen to model the NH groups in **1**,[14] was titrated with tetrabutylammonium fluoride in $CDCl_3$, the observed change in NH chemical shift was small ($\Delta\delta = 0.05$) and essentially linear with concentration. The preorganized arrangement of groups in **1** must therefore be crucial for its effectiveness.

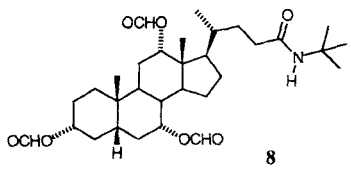

8

It would have been interesting to compare **1** with a "monomeric analogue" of the form **9**. Unfortunately, we were

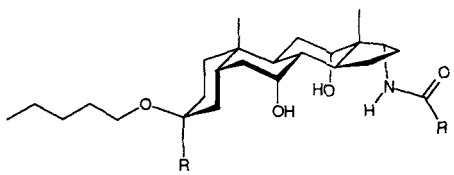

9

prevented from doing so by our inability to reduce the 12-keto group with the necessary stereoselectivity in acyclic intermediates.[15] However, molecular modeling on the more accessible[16] amido diol **10** suggested that, although its H-bond donor groups are more widely separated than those in **9**, they should be able to act in concert to bind the larger halides.[17] NMR titrations of **10** against tetrabutylammonium chloride and bromide under the conditions used for **1** did indeed provide evidence for 1:1 complex formation. Interesting-

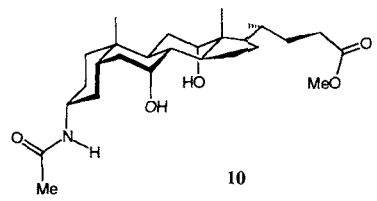

10

 © VCH Verlagsgesellschaft mbH, D-69451 Weinheim, 1996 0570-0833/96/3512-1313 $ 15.00+.25/0

Table 1. Results from ^{1}H NMR titrations of **1** with tetrabutylammonium halides in $CDCl_3$ [a].

Halide	K_a [M^{-1}]	$-\Delta G^0$ [KJ mol^{-1}]	$\Delta\delta$ [b] NH	7β-H	12β-H	17β-H
F^-	3220 ± 350	20.01	1.569	−0.134	−0.27	−0.21
Cl^-	990 ± 80	17.09	0.611	−0.101	−0.168	−0.06
Br^-	250 ± 20	13.68	0.393	−0.13	−0.11	~0

[a] Halides were added to **1** (2–4 mM) in $CDCl_3$ that had been partially dried and deacidified over K_2CO_3. The experiments were performed at 298 K. Binding constants K_a were calculated with an iterative, nonlinear, least-squares curve-fitting programme. Saturation levels of greater than 70% were achieved in all cases. [b] Signal shifts induced by complexation, extrapolated to 100% saturation. Negative values imply upfield movements on addition of the guest.

ly, the limits of the downfield shifts of the NH signal in **10** ($\Delta\delta = 1.15$ and 0.8 for Cl^- and Br^- ions, respectively) were approximately twice those obtained for macrocycle **1**, consistent with our supposition that the amide groups in **1** cannot both participate in binding. However, as expected, the acyclic receptor proved less effective than the macrocycle, binding Cl^- and Br^- with $K_a = 53 \pm 2\ M^{-1}$ and $36 \pm 1\ M^{-1}$, respectively.

A distinctive feature of receptors derived from **2** is the profusion of distinguishable ^{1}H NMR resonances resulting from the low symmetry of the steroidal nucleus.[18] In favorable cases these NMR signals may be used to report on recognition behavior from a variety of positions in the structure. As shown in Table 1, there were several protons apart from the NH which could be followed during the course of the titrations (see also Fig. 3). The signals due to the 7β and 12β *H*COH moved upfield

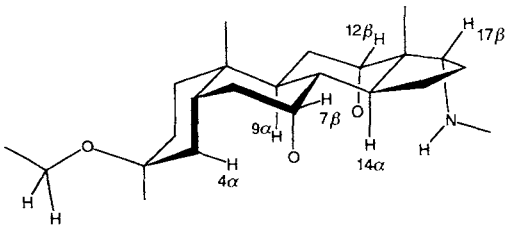

Fig. 3. Section of the structure of **1**, indicating the protons serving, or thought to serve, as NMR probes for complex formation.

in each case, consistent with H-bond donation by OH,[19] which therefore implies that hydroxyl groups in both environments take part in binding.[20] Analysis of this data, where feasible, provided support for the results obtained from the NH signal. The 17β *H*CNH moved upfield on binding to fluoride and chloride, but was unaffected by bromide. In addition to the signals in Table 1, a broad resonance corresponding to three protons from the steroid nucleus moved downfield by about $\Delta\delta = 0.3$ on binding to fluoride. We suspect that these are protons on the interior surface of the host, which are coming into contact with the anionic guest.[21] Our experience with other systems suggests that they may be the 4α-, 9α-, and 14α-H atoms (Fig. 3). A similar but smaller effect was observed on addition of chloride ($\Delta\delta \approx 0.15$). The externally positioned OCH_2 protons were also informative. These nuclei are remote from the expected binding site, but modeling suggests that steric effects should couple their orientations to changes in the conformation of the macrocycle. In **1** they appeared as a complex multiplet, but after binding to fluoride they gave individual signals separated by $\Delta\delta = 0.18$. Similar changes were observed on formation of the chloride complex, but not on addition of bromide. We infer that binding to fluoride and chloride does cause **1** to alter its conformation, whereas its mode of interaction with bromide may be qualitatively different.

Finally, the anion-binding capability of **1** was confirmed by negative-ion LSI-MS. Equal quantities of tetrabutylammonium fluoride and bromide were added to the sample, which was then dissolved in a *p*-nitrobenzyl alcohol matrix. Unexpectedly, it was the bromide complex ($M + Br^-$) that was detected, at 75% the level of the base peak ($M - H^+$). No evidence was found for $M + F^-$. This result is probably due to the nature of the matrix, emphasizing the difficulty of binding fluoride in competition with a protic solvent.

In conclusion, we have designed and synthesized a neutral, lipophilic macrocyclic host molecule with a well-defined cavity, which excludes solvent but is preorganized to bind spherical anions by multiple H-bond donation. NMR studies confirm that it does indeed act as a receptor for halide ions, showing interesting potency and selectivity. Macrocycle **1** joins a select band of neutral molecules that can fairly be termed "anion-equivalents" of crown ethers or cryptands.

Received: August 21, 1995
Revised: February 22, 1996 [Z8326IE]
German version: *Angew. Chem.* **1996**, *108*, 1410–1413

Keywords: host–guest chemistry · molecular recognition · steroids · supramolecular chemistry

[1] J.-M. Lehn, *Angew. Chem.* **1988**, *100*, 91; *Angew. Chem. Int. Ed. Engl.* **1988**, *27*, 89; F. Vögtle, *Supramolecular Chemistry*, Wiley, Chichester, **1991**.

[2] Review: a) B. Dietrich, *Pure Appl. Chem.* **1993**, *65*, 1457. Examples: b) K. Worm, F. P. Schmidtchen, A. Schier, A. Schäfer, M. Hesse, *Angew. Chem.* **1994**, *106*, 360; *Angew. Chem. Int. Ed. Engl.* **1994**, *33*, 327; c) P. B. Savage, S. K. Holmgren, S. H. Gellman, *J. Am. Chem. Soc.* **1994**, 116, 4069; d) K. Worm, F. P. Schmidtchen, *Angew. Chem.* **1995**, *107*, 71; *Angew. Chem. Int. Ed. Engl.* **1995**, *34*, 65; e) P. D. Beer, P. A. Gale, D. Husek, *Tetrahedron Lett.* **1995**, *36*, 767; f) W. B. Farnham, D. C. Roe, D. A. Dixon, J. C. Calabrese, R. L. Harlow, *J. Am. Chem. Soc.* **1990**, *112*, 7707; g) R. A. Pascal, J. Spergel, D. Van Engen, *Tetrahedron Lett.* **1986**, *27*, 4099; h) S. Valiyaveettil, J. F. J. Engbersen, W. Verboom, D. N. Reinhoudt, *Angew. Chem.* **1993**, *105*, 942; *Angew. Chem. Int. Ed. Engl.* **1993**, *32*, 900; i) Y. Morzherin, D. M. Rudkevich, W. Verboom, D. N. Reinhoudt, *J. Org. Chem.* **1993**, *58*, 7602 j) J. Scheerder, M. Fochi, J. Engbersen, D. N. Reinhoudt, *ibid.* **1994**, *59*, 7815; k) C. Raposo, N. Pérez, M. Almaraz, M. L. Mussons, M. C. Caballero, J. R. Morán, *Tetrahedron Lett.* **1995**, *36*, 3255; l) P. J. Smith, M. V. Reddington, C. S. Wilcox, *ibid.* **1992**, *33*, 6085; m) X. Yang, C. B. Knobler, Z. Zheng, M. F. Hawthorne, *J. Am. Chem. Soc.* **1994**, *116*, 7142; n) D. M. Rudkevich, W. Stauthamer, W. Verboom, J. Engbersen, S. Harkema, D. N. Reinhoudt, *ibid.* **1992**, *114*, 9671; o) P. D. Beer, Z. Chen, A. J. Goulden, A. Graydon, S. E. Stokes, T. Wear, *J. Chem. Soc. Chem. Commun.* **1993**, 1834; p) J. L. Sessler, M. Cyr, H. Furuta, V. Král, T. Mody, T. Morishima, M. Shionoya, S. Weghorn, *Pure Appl. Chem.* **1993**, *65*, 393; q) C. L. Hannon, E. V. Anslyn, *Bioorg. Chem. Front.* **1993**, *3*, 193; r) C. Andreu, A. Galán, K. Kobiro, J. de Mendoza, T. K. Park, J. Rebek, Jr., A Salmerón, N. Usman, *J. Am. Chem. Soc.* **1994**, *116*, 5501; s) E. Fan, S. Van Arman, S. Kincaid, A. D. Hamilton, *ibid.* **1993**, *115*, 369.

[3] See, for example, R. P. Bonar-Law, A. P. Davis, B. A. Murray, *Angew. Chem.* **1990**, *102*, 1497; *Angew. Chem. Int. Ed. Engl.* **1990**, *29*, 1407; K. M. Bhattarai, R. P. Bonar-Law, A. P. Davis, B. A. Murray, *J. Chem. Soc. Chem. Commun.* **1992**, 752.

[4] Survey on the use of cholic acid in molecular recognition chemistry: A. P. Davis, *Chem. Soc. Rev.* **1993**, *22*, 243. Recent developments: D. Albert, M. Feigl, *Tetrahedron Lett.* **1994**, *35*, 565; R. Boyce, G. Li, H. P. Nestler, T. Suenaga, W. C. Still, *J. Am. Chem. Soc.* **1994**, *116*, 7955; D. Roy, D. M. Birney, *Synlett* **1994**, 798; U. Maitra, L. J. D'Souza, *J. Chem. Soc. Chem. Commun.* **1994**, 2793; H.-P. Hsieh, J. G. Muller, C. J. Burrows, *J. Am. Chem. Soc.* **1994**, *116*, 12077; R. P. Bonar-Law, J. K. M. Sanders, *ibid.* **1995**, *117*, 259.

[5] J. R. Diaz, R. Ramachandra, *Org. Prep. Proced. Int.* **1977**, *9*, 109.

[6] D. H. R. Barton, J. Wozniak, S. Z. Zard, *Tetrahedron* **1989**, *45*, 3741.

[7] A. Mekhalfia, I. E. Markó, *Tetrahedron Lett.* **1991**, *32*, 4779; T. Mukaiyama, M. Ohshima, N. Miyoshi, *Chem. Lett.* **1987**, 1121.

[8] **1**: ^{1}H NMR (300 MHz, $CDCl_3$): $\delta = 0.76$ (s, 3H, 18-Me), 0.89 (m, 6H, 19-Me and 3β-O(CH$_2$)$_4$C*H*$_3$), 2.20 (d, $J = 14$ Hz, 1H, 3α-C(H)*H*′C=O), 2.46 (d, $J = 14$ Hz, 1H, 3α-C(H)H′*H*C=O), 3.47 (m, 2H, OCH_2), 3.86 (t, $J = 5$ Hz, 1H, 17β-H), 3.92 (m, 1H, 7β-H), 4.13 (m, 1H, 12β-H), 7.94 (d, 1H, $J = 12$ Hz, N-H); ^{13}C NMR (75.5 MHz, $CDCl_3$) 14.1 (3β-O(CH$_2$)$_4$*C*H$_3$), 19.1 (18-Me),

22.4 (19-Me), 22.6, 24.1, 26.1, 28.7, 29.5, 29.7, 30.1, 30.6, 31.6, 31.8, 34.4 (C-10), 34.5, 37.5, 38.2, 40.0, 46.2, (C-13), 49.2 (3α-CH_2), 59.6 (C-17), 61.4 (3β-OCH_3), 69.1 (C-7), 74.1 (C-12), 74.5 (C-3), 170.4 (C=O); LSI-MS *m/z* 889 (MNa^+).

[9] Performed within MacroModel V4.0 (Silicon Graphics 4D25TG workstation). See F. Mohamadi, N. G. J. Richards, W. C. Guida, R. Liskamp, C. Caufield, G. Chang, T. Hendrickson, W. C. Still, *J. Comput. Chem.* **1990**, *11*, 440. The search employed 1000 MC steps, the MM2* force field, and GB SA (chloroform) solvation.

[10] At first sight this may seem to be in doubt, given the conventional ionic radii of 1.33, 1.81, and 1.96 Å (diameters of 2.66, 3.62, and 3.92 Å) of fluoride, chloride, and bromide, respectively (Y. Marcus, *J. Chem. Soc. Faraday Trans.* **1991**, *87*, 2995). However, it is questionable whether these figures are relevant to the present circumstances. For example, Farnham et al. (ref. [2f]) record CH···F$^-$ distances of between 1.94 and 2.12 Å. As the standard van der Waals radius for hydrogen (used in our modeling) is 1.2 Å, one might conclude that a radius of about 0.8 Å might be more appropriate for fluoride in a hydrocarbon environment. The figures for chloride and bromide presumably need similar adjustment.

[11] An examination of halide hydrate structures present in the Cambridge Structural Database suggested that "ideal" OH···X$^-$ distances are in the region of 1.75 Å for X = F, 2.3 Å for X = Cl, and 2.4 Å for X = Br.

[12] See, for example, refs. [2a] and [2d]. Very high binding constants (10^6–10^8 M^{-1}) can be obtained with charged receptors operating in nonpolar solvents; see, for example, M. Shionoya, H. Furuta, V. Lynch, A. Harriman, J. L. Sessler, *J. Am. Chem. Soc.* **1992**, *114*, 5714.

[13] M. H. Abraham, *Chem. Soc. Rev.* **1993**, *22*, 73.

[14] The examination of CPK models suggests that the steric environment of the NH in **8** should be roughly similar to that in **1**. It should be noted that the steroidal moiety in **8** serves merely as a convenient appendage, without contributing in any specific way to the value of **8** as a control.

[15] Attempts to separate mixtures of 12α and 12β alcohols were also ineffectual. Our success in reducing **7** to **1** presumably results from steric protection of the steroidal α-face in the macrocyclic structure.

[16] The 3α-amido group was introduced by a double inversion (Mitsunobu reaction followed by azide displacement); cf. A. P. Davis, J. J. Walsh, *J. Chem. Soc. Chem. Commun.* **1996**, 449.

[17] Modeling indicated that the NH and two OH groups in **10** should be able to form H-bonds of 2.5–2.6 Å to a centrally located anion. These figures are not greatly in excess of the "ideal" OH···X$^-$ distances inferred from X-ray crystallography for X = Cl and Br [11]. See also Ref. [20] below.

[18] R. P. Bonar-Law, A. P. Davis, *Tetrahedron* **1993**, *49*, 9845.

[19] C.-Y. Huang, L. A. Cabell, E. V. Anslyn, *J. Am. Chem. Soc.* **1994**, *116*, 2778.

[20] The binding experiments on **10** revealed similar upfield shifts of the *H*COH signals (Δδ between 0.124 and 0.153), supporting our hypothesis that all three H-bond donor groups are involved in halide recognition by this "acyclic analogue" of **1**.

[21] See ref. [2f] for a downfield shift resulting from formation of a CH···F$^-$ hydrogen bond.

Reactions of Silyllithium with C_{60}: Isolation and X-ray Crystallographic Characterization of an Unusual Bissilylated-C_{60} Adduct**

Takahiro Kusukawa and Wataru Ando*

The unique structure of C_{60} and its derivatives have sparked much research activity bridging the disciplines of chemistry, physics, and materials science.[1–5] Recently closed 1,2-, opened 1,6- (5,6-annulenes), and 1,4-adducts have been isolated. Nucleophilic addition to C_{60} is among the most common reaction types in fullerene chemistry.[6] We have reported a few examples of the photochemical formation of silylfullerene derivatives to date.[7] Yet in spite of those developments, the methods available for silylfullerene derivatives is limited, allowing access to only specific patterns of silicon substituents and ring arrangements. However, the use of silyllithium compounds has not previously been reported. Herein we report the isolation of an unusual bissilylated-C_{60} adduct by reactions of bulky substituted silyllithium with C_{60}, whose adduct was characterized by single X-ray crystal analysis.

In earlier work with C_{60} and Ph_3SiLi the formation of a brown precipitate was observed at −78 °C, and when the suspension was quenched with EtOH, only C_{60} was recovered. The analogous reaction with other silyllithium compounds ($Me_2PhSiLi$, $MePh_2SiLi$, $Et_2PhSiLi$, $EtPh_2SiLi$) leads to similar results. On the other hand, diisopropylphenylsilyllithium **1a** reacted with C_{60} under these conditions to produce **2a** (78% yield, based on unchanged C_{60}, for spectroscopic data see Table 1) upon quenching with EtOH (Scheme 1).

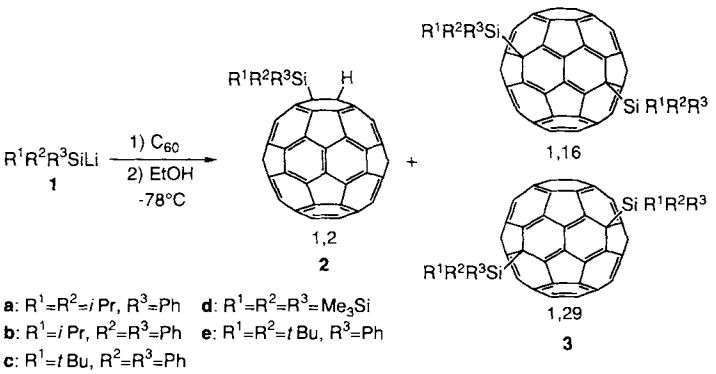

a: $R^1=R^2=i$Pr, R^3=Ph **d**: $R^1=R^2=R^3=Me_3Si$
b: $R^1=i$Pr, $R^2=R^3$=Ph **e**: $R^1=R^2=t$Bu, R^3=Ph
c: $R^1=t$Bu, $R^2=R^3$=Ph

Scheme 1. Synthesis of the mono- and disilyl C_{60} adducts **2** or **3**. For spectroscopic data of the products see Table 1. 1,2 etc. represents the type of addition.

The FAB mass spectrum of **2a** exhibits one peak at *m/z* 912–915 for the molecular ion and one for C_{60} at *m/z* 720–723. The ^{13}C NMR spectrum of **2a** displays 30 signals for C_{60} carbon, supporting C_s symmetry for the molecule. One signal has a relative intensity of 4, one a relative intensity of 3, 25 signals have a relative intensity of 2, and three a relative intensity of 1; thus, the number of carbon atoms sums up to 60. Of the 30, two fullerene carbon atoms resonate at δ = 58.87 and 60.94. The signals of all other carbons appear in the region between δ = 130–160.

The partial structure of the fragment bound to the C_{60} moiety derives from the NMR spectroscopic properties for **2a**: The presence of one hydrogen connected to C_{60} is deduced from one doublet at δ = 58.87 and one singlet at δ = 6.93 in the ^{13}C NMR and ^1H NMR spectrum, respectively. The ^{29}Si NMR spectrum of **2a** shows one peak at δ = 5.42, which is assigned to the silicon atoms of **2a**.

The most probable addition pattern for the fullerene moiety is a 1,2-addition.[6c] In the case of a 1,6-addition 60 signals for C_{60} carbon would be expected. The possibility of 1,4-addition can be eliminated by the ^{13}C–^1H COLOC (Correlation Spectroscopy via Long-Range Coupling) spectroscopic method. It was shown that the proton resonance at δ = 6.93 correlates with quaternary carbon (δ = 60.94) on the C_{60}. Under similar conditions, diphenylisopropyl- and diphenyl-*tert*-butylsilyllithium, **1b** and **1c** react with C_{60} to give monoadducts **2b** (80% yield, based on unchanged C_{60}) and **2c** (50% yield, based on unchanged C_{60}), respectively. On the other hand, the reaction of tris(trimethylsilyl)silyllithium **1d** with equivalent amounts of C_{60} at −78 °C give bisadduct **3d** in 69% yield (based on unchanged C_{60}), and monoadduct **2d** could not be detected.

[*] Prof. Dr. W. Ando, Dr. T. Kusukawa
Department of Chemistry, University of Tsukuba
Tsukuba, Ibaraki 305 (Japan)
Fax: Int. code +(298)53-6503

[**] This work was supported by a Grant-in-Aid for Scientific Research for Ministry of Education, Science and Culture of Japan.

Table 1. Selected spectroscopic data of compounds **2a–c**, **3d**, and **3e** [a].

2a: Brown solid; ^{1}H NMR δ = 1.58 (d, J = 7.5, 6H), 1.73 (d, J = 7.5, 6H), 2.33 (sept, J = 7.5, 2H), 6.93 (s, 1H), 7.5–7.6 (m, 3H), 8.1–8.2 (m, 2H); ^{13}C NMR δ = 12.79 (d), 19.53 (q), 19.99 (q), 58.87 (d, 1C), 60.94 (s, 1C), 128.20 (d), 130.22 (d), 131.22 (s), 134.01 (s, 2C), 135.69 (s, 2C), 136.08 (d), 140.03 (s, 2C), 140.11 (s, 2C), 141.19 (s, 2C), 141.28 (s, 2C), 141.41 (s, 2C), 141.58 (s, 2C), 141.69 (s, 2C), 142.10 (s, 2C), 142.33 (s, 2C), 142.38 (s, 2C), 143.35 (s, 2C), 144.29 (s, 2C), 144.40 (s, 2C), 144.52 (s, 2C), 145.18 (s, 2C), 145.32 (s, 2C), 145.35 (s, 2C), 145.95 (s, 3C), 146.10 (s, 2C), 146.18 (s, 2C), 146.21 (s, 2C), 146.48 (s, 1C), 147.08 (s, 4C), 147.42 (s, 2C), 153.87 (s, 2C), 157.36 (s, 2C); ^{29}Si NMR δ = 5.42; FAB-MS: m/z: 912–915 (M^+)

2b: brown solid; ^{1}H NMR δ = 1.43 (d, J = 7.3, 6H), 2.35 (sept, J = 7.3, 1H), 7.03 (s, 1H), 7.5–7.6 (m, 6H), 8.2–8.3 (m, 4H); ^{13}C NMR δ = 11.88 (d), 19.19 (q), 59.29 (d, 1C), 60.68 (s, 1C), 128.33 (d), 130.39 (s, 2C), 130.62 (d), 134.53 (s, 2C), 135.70 (s, 2C), 136.98 (d), 140.10 (s, 2C), 140.22 (s, 2C), 141.38 (s, 4C), 141.52 (s, 2C), 141.69 (s, 2C), 141.81 (s, 2C), 142.20 (s, 2C), 142.44 (s, 2C), 142.47 (s, 2C), 143.40 (s, 2C), 144.47 (s, 2C), 144.53 (s, 2C), 144.61 (s, 2C), 145.31 (s, 2C), 145.37 (s, 2C), 145.46 (s, 2C), 146.02 (s, 2C), 146.08 (s, 2C), 146.21 (s, 2C), 146.30 (s, 2C), 146.32 (s, 2C), 146.63 (s, 1C), 147.20 (s, 1C), 147.32 (s, 2C), 147.47 (s, 2C), 153.95 (s, 2C), 157.03 (s, 2C); ^{29}Si NMR δ = 0.88; FAB-MS: m/z: 946–949 (M^+)

2c: brown solid; ^{1}H NMR δ = 1.59 (s, 9H), 7.14 (s, 1H), 7.5–7.6 (m, 6H), 8.3–8.4 (m, 4H); ^{13}C NMR δ = 22.03 (s), 29.60 (q), 60.11 (d, 1C), 60.99 (s, 1C), 128.03 (d), 130.35 (d), 131.30 (s, 2C), 134.81 (s, 2C), 135.76 (s, 2C), 137.69 (d), 139.79 (s, 2C), 140.10 (s, 2C), 141.25 (s, 2C), 141.30 (s, 2C), 141.47 (s, 2C), 141.73 (s, 2C), 141.79 (s, 2C), 142.16 (s, 2C), 142.44 (s, 2C), 142.47 (s, 2C), 143.38 (s, 2C), 144.49 (s, 2C), 144.55 (s, 2C), 144.56 (s, 2C), 145.27 (s, 2C), 145.29 (s, 2C), 145.41 (s, 2C), 146.04 (s, 2C), 146.08 (s, 2C), 146.29 (s, 4C), 146.61 (s, 1C), 147.10 (s, 1C), 147.39 (s, 2C), 147.60 (s, 2C), 153.95 (s, 2C), 156.96 (s, 2C); ^{29}Si NMR δ = −0.46; FAB-MS: m/z: 960–963 [(M^+ + 1)cluster]

3d: dark red solid; ^{1}H NMR δ = 0.38 (s, 54H); ^{13}C NMR δ = 2.63 (q), 60.88 (s, 2C), 135.02 (s, 2C), 135.76 (s, 2C), 139.36 (s, 2C), 140.06 (s, 2C), 140.62 (s, 2C), 140.82 (s, 2C), 141.83 (s, 2C), 142.49 (s, 2C), 142.71 (s, 2C), 143.30 (s, 2C), 143.66 (s, 2C), 143.81 (s, 2C), 144.37 (s, 2C), 145.20 (s, 2C), 145.66 (s, 2C), 146.00 (s, 2C), 146.14 (s, 2C), 146.22 (s, 2C), 146.25 (s, 2C), 146.38 (s, 4C), 147.09 (s, 2C), 147.43 (s, 2C), 147.90 (s, 2C), 148.75 (s, 2C), 151.55 (s, 2C), 151.67 (s, 2C), 164.76 (s, 2C), 165.71 (s, 2C); ^{29}Si NMR δ = −52.72, −9.95; FAB-MS: m/z: 1215–1218 (M^+)

3e: dark red solid; ^{1}H NMR δ = 1.56 (s, 9H), 1.57 (s, 9H), 7.2–7.4 (m, 3H), 8.0–8.1 (m, 2H); ^{13}C NMR δ = 25.22 (s, 2C), 31.85 (q), 31.89 (q), 65.74 (s, 2C), 127.30 (d), 129.55 (d), 131.66 (s, 1C), 136.40 (s, 2C), 137.11 (d), 138.65 (s, 2C), 139.48 (s, 2C), 140.57 (s, 2C), 141.13 (s, 2C), 141.54 (s, 2C), 141.89 (s, 2C), 141.98 (s, 2C), 142.20 (s, 2C), 143.51 (s, 2C), 143.98 (s, 2C), 144.19 (s, 2C), 145.31 (s, 2C), 145.33 (s, 2C), 145.99 (s, 2C), 146.02 (s, 2C), 146.11 (s, 2C), 146.14 (s, 2C), 146.36 (s, 2C), 146.59 (s, 2C), 146.94 (s, 2C), 147.39 (s, 2C), 147.72 (s, 2C), 148.57 (s, 2C), 150.31 (s, 2C), 152.74 (s, 2C), 162.66 (s, 2C), 165.19 (s, 2C); ^{29}Si NMR δ = 5.22; FAB-MS: m/z: 1159–1162 (M^+).

[a] 500 MHz ^{1}H, 126 MHz ^{13}C, and 60 MHz ^{29}Si NMR spectra in a 1/2 mixture (for all ^{1}H spectra, as well as the ^{13}C and ^{29}Si NMR spectra of **2a**) or 1/1 mixture (all other spectra) of $CDCl_3/CS_2$; J values in Hz.

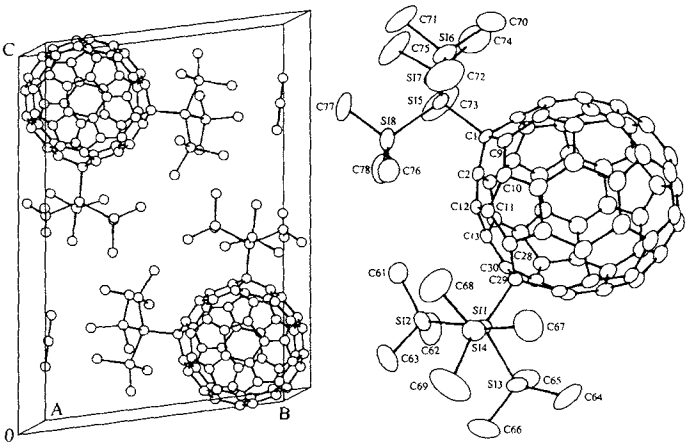

Fig. 1. X-ray crystallographic characterization of **3d**·CS_2. Left: arrangement in the unit cell. Right: Crystal structure of one of the two enantiomorphic molecules in the unit cell. The ellipsoids represent 50% probability.

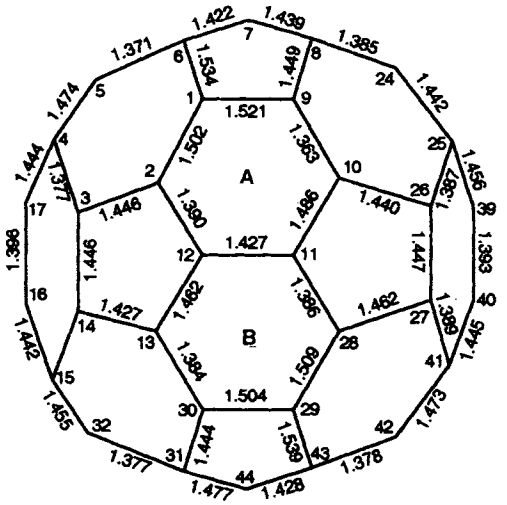

Fig. 2. Bond lengths [Å] in **3d** and selected bond angles [°]: C2-C1-C6 121.9, C2-C1-C10 109.1, C6-C1-C10 117.3, C1-C2-C3 123.2, C2-C3-C4 110.2, C3-C4-C5 124.0, C4-C5-C6 120.6, C1-C6-C5 117.2, C1-C6-C7 122.0, C5-C6-C7 108.9, C6-C7-C8 123.3, C7-C8-C9 109.7, C8-C9-C10 124.3, C1-C10-C9 120.4. The standard deviation in the last digit is 7–8 Å.

The FAB mass spectrum of **3d** exhibits one peak at m/z 1215–1218 for the molecular ion), as well as one for C_{60} at m/z 720–723. The ^{13}C NMR spectrum of **3d** displays 29 signals for all quaternary carbon atoms, of which one fullerene carbon atom resonates at δ = 60.88. All other signals appear in the region between δ = 135–165. Symmetry arguments support the 1,6-addition or 1,4-addition to C_{60}; however addition of the bulky substituent [$(Me_3Si)_3Si$] is unfavorable for 1,6-addition. In order to obtain information of the structure for **3d**, we carried out the X-ray crystallographic analysis.[8]

Compound **3d** crystallized in the triclinic space group $P\bar{1}$, with two enantiomorphic molecules of **3d** and two CS_2 molecules in the unit cell (Fig. 1, left). The crystal structure of **3d** is shown in Figure 1 (right), and selected bond lengths and angles are given in Figure 2.

The C–C bond lengths C12–C2, C9–C10, C11–C28, and C30–C13 are within 1.363(7)–1.390(7) Å, which are close to the C–C double bond length. The bond angles at the fullerene C atoms excluding the bonds in rings A and B, are 107.3(4)–109.2(4)° in the pentagons and 118.3(4)–121.5(5)° in the hexagons, values which are within the normal range. The length of the C_{60} skeleton, excluding the bonds in rings A and B, range from 1.371(7) to 1.474(8) Å (Fig. 2). The structure of **3d** is a new type of addition mode to the C_{60}.

Relative stabilities of the dihydrofullerenes (given as the energy of formation from C_{60} and H_2) were reported by Dixon et al., who determined them with semiempirical calculations:[9] 1,2 (776.1 kcal mol^{-1}) > 1,4 (780.0 kcal mol^{-1}) > 1,16 or 1,29 (791.6 kcal mol^{-1}) > 1,6 (794.5 kcal mol^{-1}). Accordingly, our new bissilylated-C_{60} (**3d**, 1,16 or 1,29 addition) is about 15.5 kcal mol^{-1} more unstable than the 1,2 form, but 2.9 kcal mol^{-1} more stable than the 1,6 adduct. Additions of two $(Me_3Si)_3Si$ groups at the 1,2 (6,6 addition) and 1,4 positions are unfavorable because of the steric hindrance, so the two $(Me_3Si)_3Si$ groups might be bound to the 1,16 (or 1,29) positions.

Di-*tert*-butylphenylsilyllithium **1e** also reacts with C_{60} to give bisadduct **3e** in 72% yield (based on unchanged C_{60}). The structure of the adduct **3e** was determined in a similar manner by use of NMR techniques.

The UV/Vis absorption spectrum of **2a–2c** shows absorption at 416–417 nm and 444–445 nm in toluene. On the other hand, bisadducts **3d** and **3e** show broad absorption at 520 nm–600 nm.

The formation of **3** poses a question on the mechanism of the addition of silyllithium to C_{60}. The structure of **3** resulted from the introduction of two organosilyl groups at the 1,16 or 1,29 positions of the two six-membered rings. Considering the bisadduct formation by Grignard reagents,[6e] we initially proposed that the formation of **3** involved radical processes. To clarify the mechanistic pathway of the formation of **3**, we examined the photochemical reaction (254 nm) of $[(Me_3Si)_3Si]_2$ with C_{60}, which did not give the bisadduct **3d**. From these findings, the $(Me_3Si)_3Si$ radical is probably not be involved in the formation of **3**. Further studies are in progress in order to establish the mechanism of this interesting addition reaction.

Experimental Procedure

A solution of the silyllithium compound (**1a**-**1e**, 138.9 μmol) in THF (1.7 mL) was added by syringe to a solution of C_{60} (138.9 μmol) in dry toluene (120 mL) at −78 °C over 30 min. After the addition, the solution was quenched with EtOH and warmed to room temperature. The solvent was evaporated, and the residue purified by gel-permeation chromatography (Jaigel 1H and 2H columns, Japan Analytical Industry Co. Ltd.; eluent toluene), to afford the adducts **2a**-**2c**, **3d**, and **3e**.

Received: November 23, 1995
Revised: February 13, 1996 [Z8581IE]
German version: *Angew. Chem.* **1996**, *108*, 1416–1418

Keywords: fullerenes · lithium compounds · silicon compounds

[1] a) H. W. Kroto, A. W. Allaf, S. P. Balm, *Chem. Rev.* **1991**, *91*, 1213; b) H. W. Kroto, J. R. Heath, S. C. O'Brien, R. F. Curl, R. E. Smalley, *Nature* **1985**, *318*, 162; c) W. Krätschmer, L. Lamb, K. Fostiropoulos, D. R. Huffman, *ibid* **1990**, *347*, 354; d) W. Krätschmer, K. Fostiropoulos, D. R. Huffman, *Chem. Phys. Lett.* **1990**, *170*, 167.

[2] *Acc. Chem. Res.* **1992**, *25*, 98–175, special issue.

[3] F. Diederich, L. Isaacs, D. Philip, *Chem. Soc. Rev.* **1994**, 243.

[4] A. Hirsch, *Angew. Chem.* **1993**, *105*, 1189; *Angew. Chem. Int. Ed. Engl.* **1993**, *32*, 1138.

[5] *Fullerenes: Synthesis, Properties, and Chemistry of Large Carbon Clusters* (Eds.: G. Hammond, V. J. Kuck), (*ACS Symp. Ser.* **1992**, 481).

[6] a) F. Wudl, A. Hirsch, K. C. Khemani, T. Suzuki, P.-M. Allemand, A. Koch, H. Eckert, G. Srdanov, H. Webb, in Ref [5], pp. 161–175; b) P. J. Fagan, P. J. Krusic, D. H. Evans, S. A. Leake, E. Johnston, *J. Am. Chem. Soc.* **1992**, *114*, 9697; c) A. Hirsch, A. Soi, H. R. Karfunckel, *Angew. Chem.* **1992**, *104*, 808; *Angew. Chem. Int. Ed. Engl.* **1992**, *31*, 766; d) A. Hirsch, T. Grösser, A. Skiebe, A. Soi, *Chem. Ber.* **1993**, *126*, 1061; e) H. Nagashima, H. Terasaki, E. Kimura, K. Nakajima, K. Itoh, *J. Org. Chem.* **1994**, *59*, 1246; f) H. L. Anderson, R. Faust, Y. Rubin, F. Diederich, *Angew. Chem.* **1994**, *106*, 1427; *Angew. Chem. Int. Ed. Engl.* **1994**, *33*, 1366.

[7] a) T. Akasaka, W. Ando, K. Kobayashi, S. Nagase, *J. Am. Chem. Soc.*, **1993** *115*, 10366; *ibid* **1993**, *115*, 1605; b) T. Akasaka, E. Mitsuhida, W. Ando, K. Kobayashi, S. Nagase, *ibid* **1994**, *116*, 2627; c) T. Kusukawa, Y. Kabe, T. Erata, B. Nestler, W. Ando, *Organometallics*, **1994**, *13*, 4186; d) T. Kusukawa, Y. Kabe, W. Ando, *ibid* **1995**, *14*, 2142; e) T. Kusukawa, A. Shike, W. Ando, *Tetrahedron*, in press.

[8] X-ray structure analysis of **3d**: needles of single crystals $(C_{78}H_{54}Si_8)\cdot(CS_2)$ grown from CS_2. $T = 296$ K, $M_r = 1292.1$, triclinic, space group $P\bar{1}$ (no. 2), $\rho_{calcd} = 1.35$ g cm^{-3}, $Z = 2$, $a = 9.921(2)$, $b = 15.198(2)$, $c = 21.523(2)$ Å, $\alpha = 82.79(1)$, $\beta = 85.36(1)$, $\gamma = 80.80(2)$, $V = 3171.9$ Å^3. Enraf-Nonius CAD4 diffractometer, $Cu_{K\alpha}$ radiation, $\lambda = 1.5418$ Å. The structure was solved by direct methods and refined by full-matrix least-squares analysis. Final $R(F) = 0.062$, $wR(F) = 0.068$ for 802 variables and 7027 observed reflections with $F > 3\sigma(F)$ and $\theta < 60$°. Hydrogen atoms were located and added to the structure factor calculations but their positions were not refined. Crystallographic data (excluding structure factors) for the structure(s) reported in this paper have been deposited with the Cambridge Crystallographic Data Centre as supplementary publication no. CCDC-179-31. Copies of the data can be obtained free of charge on application to The Director, CCDC, 12 Union Road, Cambridge CB2 1EZ, UK (fax: Int. code +(1223) 336-033; e-mail: teched@chemcrys.cam.ac.uk).

[9] N. Matsuzawa, D. A. Dixon, T. Fukunaga, *J. Phys. Chem.* **1992**, *96*, 7594.

The Long Elusive Acepentalene—Experimental and Theoretical Evidence for its Existence**

Rainer Haag, Detlef Schröder, Tosja Zywietz, Haijun Jiao, Helmut Schwarz,* Paul von Ragué Schleyer,* and Armin de Meijere*

In 1964, Woodward et al. proposed triquinacene (**2**) as a logical precursor to the still elusive acepentalene (**1**, Scheme 1).[1] The nowadays easily accessible $C_{10}H_{10}$ hydrocarbon **2**[2, 3] has the same carbon skeleton as **1**, but contains only three isolated double bonds, and therefore is far less strained. Introduction of two additional double bonds into triquinacene **2** would result in the highly strained acepentalene **1**, which, like cyclobutadiene and pentalene, is an antiaromatic species.[4, 5] The Hückel molecular orbital (HMO) theory predicts that, on the assumption of a D_{3h} symmetric geometry, the $C_{10}H_6$ hydrocarbon **1** has a triplet diradical ground state.[4a] However, Jahn–Teller distortion to a lower symmetry singlet is possible. In addition, the angle strain of the three widened C,C,C angles on the three outer bridgeheads disfavors a planar geometry of **1**. After all, the aromatic acepentalene dianion $\mathbf{1}^{2-}$, which is formed by treatment of **2** with a superbasic mixture,[6] has a curved molecular surface.[7, 8]

Several disubstituted dehydrotriquinancenes with four double bonds have been synthesized, but none of them has been transformed successfully into **1**.[3, 5] The bis(trimethylstannyl)-dihydroacepentalene **3**, which was obtained by trapping the dianion $\mathbf{1}^{2-}$ with trimethyltin chloride (Scheme 1),[8] is a stable species (under inert atmosphere), despite the strain due to the central bridgehead–bridgehead double bond.

The slight elongation of the carbon–tin bond (X-ray analysis)[8b, 9] suggests that compound **3** might serve as a particularly good precursor for the fully unsaturated acepentalene **1**. How-

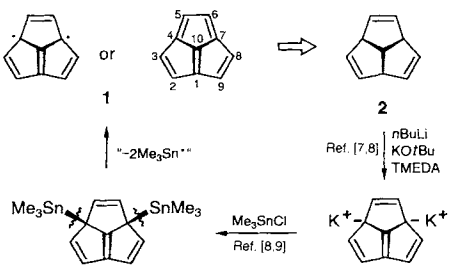

Scheme 1. Pathway for the generation of acepentalene **1**.

[*] Prof. Dr. A. de Meijere, Dr. R. Haag, T. Zywietz
Institut für Organische Chemie der Universität
Tammanstrasse 2, D-37077 Göttingen (Germany)
Fax: Int. code +(551)399475
e-mail: ameijer1@gwdg.de
Prof. Dr. H. Schwarz, Dr. D. Schröder
Institut für Organische Chemie der Technischen Universität
Strasse des 17. Juni 135, D-10623 Berlin (Germany)
Fax: Int. code +(30)314-21102
email: schw0531@zrzsp5.chem.tu-berlin.de
Prof. Dr. P. von R. Schleyer, Dr. H. Jiao
Institut für Organische Chemie der Universität
Henkestrasse 42, D-91054 Erlangen (Germany)
Fax: Int. code +(9131)859132
e-mail: pvrs@organik.uni-erlangen.de

[**] This work was supported by the Deutsche Forschungsgemeinschaft, the Fonds der Chemischen Industrie, the Volkswagen-Stiftung and the Convex Computer Corporation. R. H. is indebted to the Fonds der Chemischen Industrie for a graduate fellowship. We are grateful to the companies BASF, Bayer, Hoechst, Degussa, and Hüls AG for generous gifts of chemicals.

ever, attempts to cleave off both trimethyltin substituents from **3** homolytically (either thermally or photolytically) to generate acepentalene **1** have not been successful.[8b, 10a]

Neutralization–reionization mass spectrometry (NRMS) is a potential approach to the neutral acepentalene **1**.[11] In such experiments, appropriate precursors are ionized in the ion source of a mass spectrometer and subjected to double collision: The fast moving ions are neutralized in the first collision, the remaining ions are deflected, and the beam of neutrals is reionized in the second collision event.

Electron or chemical ionization of bis(trimethylstannyl)-dihydroacepentalene **3** in the positive ion mode does not lead to an intense $[C_{10}H_6]^{\bullet+}$ signal, and tin-containing cations prevail in the mass spectrum. Further, the integrity of the acepentalene skeleton is not guaranteed in the radical cation, because cationized hydrocarbons are known to undergo extensive structural rearrangements.[12] In contrast, negative-ion chemical ionization (NICI)[13] of **3**, with N_2O as the reagent gas, affords large amounts of the acepentalene anion radical, $[C_{10}H_6]^{\bullet-}$. The high yield of $[C_{10}H_6]^{\bullet-}$ points to a relatively high electron affinity[14] of neutral **1** (see below). A significant electron affinity of the acepentalene skeleton was already indicated by a previous study of the tribenzo derivative.[15]

The $[C_{10}H_6]^{\bullet+}$ ion radical formed by reionization of the intermediate neutral molecule **1** is observed in the NR mass spectrum of $\mathbf{1}^{\bullet-}$ (Fig. 1). This process is quite efficient and reionized neutral **1** is the base peak in the NR spectrum. In addition, the observation of $[C_{10}H_6]^{\bullet+}$ demonstrates that neutral **1** is stable for at least 1 μs, which is the time scale of the NR experiment. The intrinsic stability of **1** is further demonstrated by elongating the flight time of the neutral in the NR experiment by a factor 8: This hardly changes the features of the NR mass spectrum and reionized **1** is the predominant base peak.[10b]

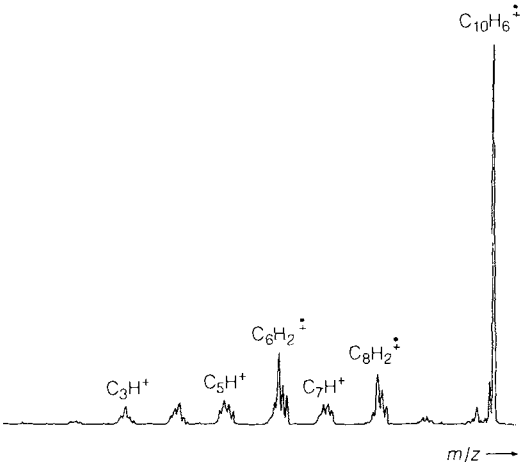

Fig. 1. Neutralization–reionization mass spectrum of $[C_{10}H_6]^{\bullet-}$ generated by chemical ionization of **3** with oxygen (each 80% transmission) in both collision cells.

The generation of the neutral hydrocarbon by collisional electron detachment from the corresponding anion radical is also advantageous in that structural rearrangements are much less likely to occur in this process[16, 17] than in the neutralization of cationic species. The absence of rearrangements is further supported by the finding that $[C_{10}H_6]^{\bullet-}$ undergoes neither unimolecular nor collision-induced fragmentation (except for electron detachment), even though potential fragments exhibit positive electron affinities (for example, acetylide anions).[14] Although mass spectrometry cannot prove structures directly, the fragmentation pattern in the NR spectrum is consistent with the connectivity of the acepentalene skeleton, for example, predominant losses of ethyne and oligoyne fragments (C_2H_2, C_4H_2, C_6H_2 etc.).

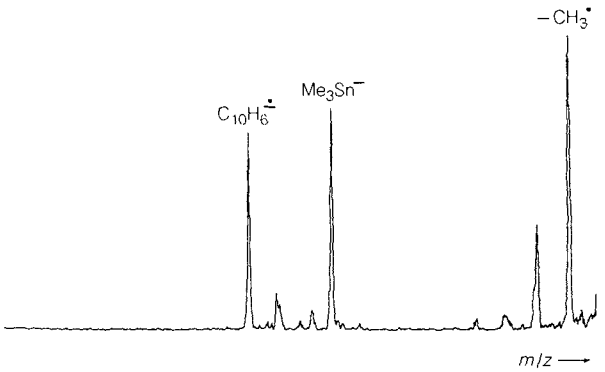

Fig. 2. Collisional activation mass spectrum of $[\mathbf{1}/SnMe_3]^-$ (He, 80% transmission).

Collisional activation (CA) of $[\mathbf{1}/SnMe_3]^-$ is another approach to generate neutral **1**. $[\mathbf{1}/SnMe_3]^-$ is also generated by NICI of **3** with N_2O in a simple substitution process of **3** with $O^{\bullet-}$ [reaction (a)] in which rearrangements are unlikely to occur. In the CA mass spectrum of $[\mathbf{1}/SnMe_3]^-$ (Fig. 2) two competing processes [reactions (b) and (b')], which only differ in the placement of the negative charge in the products, become apparent.

$$\mathbf{3} + O^{\bullet-} \longrightarrow [\mathbf{1}/SnMe_3]^- + MeSn^{\bullet} \quad (a)$$

$$[\mathbf{1}/SnMe_3]^- \longrightarrow Me_3Sn^- + C_{10}H_6 \quad (b)$$

$$[\mathbf{1}/SnMe_3]^- \longrightarrow [C_{10}H_6]^{\bullet-} + Me_3Sn^{\bullet} \quad (b')$$

According to Cooks's kinetic method,[18] the near unit ratio of the Me_3Sn^- and $[C_{10}H_6]^{\bullet-}$ ions implies that the electron affinities (EAs) of both fragments are comparable. While $EA(Me_3Sn^{\bullet})$ has not been determined yet,[19] $EA(Me_3Sn^{\bullet}) \approx 1.5$ eV can be estimated from the available literature data for silicon, germanium, and tin compounds.[14] This value agrees well with the calculated value for **1** (1.8 eV, see Table 1). Also note that the competition of reactions (b) and (b') implies that fragmentation of $[\mathbf{1}/SnMe_3]^-$ leads to neutral **1** in its electronic ground state (see below).

These experimental data can be compared with the results of density functional theory computations on acepentalene.[20] The Becke3LYP/6-31G* optimized structural parameters for singlet $\mathbf{1}(S_0)$ and triplet acepentalene $\mathbf{1}(T_0)$ are given in Figure 3. At Becke3LYP/6-31G*, $\mathbf{1}(T_0)$ and $\mathbf{1}(S_0)$ are energy minima (NIMAG = 0). The C_s symmetric $\mathbf{1}(S_0)$ shows the localized single and double bond lengths expected for a singlet antiaromatic species. In contrast, $\mathbf{1}(T_0)$ is C_{3v} symmetric and has a

Table 1. Calculated total [Hartree] and relative [kcal mol^{-1}] energies as well as ZPVE (kcal mol^{-1}) for **1** (C_s, singlet), **1** (C_{2v}, singlet), **1** (C_{3v}, triplet), and $\mathbf{1}^{\bullet-}$ (C_s).

Species (point group)	Becke3LYP/ 6-311 + G* [a]	ZPVE [b, c]	E_{rel}
1 S_0 (C_s)	−384.57448	74.14 (0)	0.0
1 S_0 (C_{2v})	−384.56280	73.90 (1)	7.5
1 T_0 (C_{3v})	−384.56943	73.45 (0)	3.9
$\mathbf{1}^{\bullet-}$ (C_s)	−384.63873	73.59 (0)	−40.8 [d]

[a] Single-point energies using Becke3LYP/6-31G* geometries. [b] Becke3LYP/6-31G* values, scaled by 0.97. [c] Number of imaginary frequencies, in parentheses. [d] This corresponds to EA $\mathbf{1}(S_0) = 1.8$ eV.

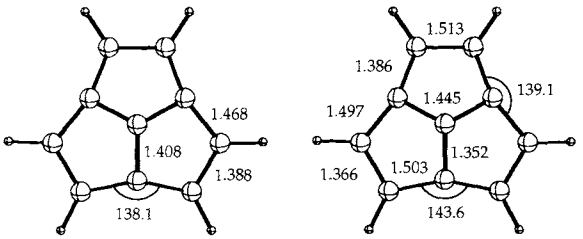

Fig. 3. Bond lengths [Å] and bridgehead C,C,C angles [ ] for **1** (C_{3v}, triplet, left) and **1** (C_s, singlet, right).

delocalized π system. The bond lengths, compared to the **1**(S_0) state, show partial equalization of formal single and double bonds. This is supported by the computed natural atomic charges and Wiberg bond indices.[21]

Table 1 summarizes the total and relative energies for **1**(T_0, C_{3v}), **1**(S_0, C_s), **1**(S_0, C_{2v}) and $\mathbf{1}^{\bullet-}(C_s)$. In contrast to the HMO results,[1a] the C_s singlet acepentalene **1**(S_0) is 3.9 kcal mol^{-1} lower in energy than the triplet state at the Becke3LYP/6-311 + G*//Becke3LYP/6-31G* + ZPVE (Becke3LYP/6-31G*) level. The singlet state is stabilized by Jahn–Teller distortion, which is typical for almost all antiaromatic compounds.[22] The inversion of the S_0 state proceeds via a C_{2v} transition structure with an associated barrier of 7.5 kcal mol^{-1} (Table 1).

Experimental Procedure

The experiments were performed with a modified VG ZAB HF AMD 604 four-sector mass spectrometer of BEBE configuration (B stands for magnetic and E for electric sectors), as described previously [23]. The anion radical of acepentalene, $[C_{10}H_6]^{\bullet-}$, was generated by chemical ionization (CI) of **3** with N_2O as electron-moderating and reagent gas [24]. For the CA spectra, $[C_{10}H_6]^{\bullet-}$ was mass-selected with B(1)E(1) at a mass resolution of $m/\Delta m = 3000$, collided with helium [80% transmission], and the products were analyzed with B(2). In the NR experiments [11], mass-selected $[C_{10}H_6]^{\bullet-}$ collided with oxygen (80% transmission) in the first of two collision cells in the field-free region preceding B(2). Subsequently, all remaining ions were deflected by charging an electrode to a potential of 1000 V. The beam of fast neutrals proceeded to the second collision cell in which oxygen (80% transmission) was present as reionizing gas. The cations formed were analyzed by scanning B(2) in the positive ion mode. The occurrence of a "recovery signal" for the reionized neutral $C_{10}H_6$ demonstrates that the neutral must be stable for at least 1 μs, since it survived the flight between the two collision cells (distance 10 cm). Longer flight times for the neutrals were achieved by using a collision cell for neutralization located after the end of E(1) such that the distance between the neutralization and reionization chambers was about 80 cm [25]. All spectra were accumulated and processed on-line with the AMD/Intectra data system; 5 to 15 scans were averaged to improve the signal-to-noise ratio.

Received: November 22, 1995
Revised version: March 11, 1996 [Z8576IE]
German version: *Angew. Chem.* **1996**, *108*, 1413–1416

Keywords: acepentalene · density functional theory · hydrocarbons · mass spectrometry · strained rings

[1] R. B. Woodward, T. Fukunaga, R. C. Kelly, *J. Am. Chem. Soc.* **1964**, *86*, 3162.
[2] a) I. T. Jacobsen, *Acta Chem. Scand.* **1967**, *21*, 2235; b) M. J. Wyvratt, L. A. Paquette, *Tetrahedron Lett.* **1974**, 2433; c) P. Deslongchamps, U. O. Cheriyan, Y. Lambert, J. C. Mercier, L. Ruest, R. Russo, P. Soucy, *Can. J. Chem.* **1978**, *56*, 1687; d) A. K. Gupta, G. S. Lannoye, G. Kubiak, J. Schkeryantz, S. Wehrli, J. M. Cook, *J. Am. Chem. Soc.* **1989**, *111*, 2169.
[3] a) H. Butenschön, A. de Meijere, *Tetrahedron Lett.* **1983**, 4563; b) *ibid.* **1984**, 1693; c) *Chem. Ber.* **1985**, *118*, 2557; d) *Helv. Chim. Acta* **1985**, *68*, 1658.
[4] a) A. Streitwieser Jr., *Molecular Orbital Theory for Organic Chemists*, Wiley, New York, **1961**; b) R. Zahradnik, J. Michl, J. Koutecky', *Coll. Czech. Chem. Commun.* **1964**, *29*, 1932; c) R. Zahradnik, J. Michl, *ibid.* **1965**, *30*, 3529; d) B. A. Hess Jr., L. J. Schaad, *J. Org. Chem.* **1971**, *36*, 3418; e) I. Gutman, N. Trinajstic, *Croat. Chem. Acta* **1975**, *47*, 35; f) F. Thomas, J. I. Fernandez-Alonso, *An. Quim.* **1976**, 122; g) I. Gutman, M. Milun, N. Trinajstic, *J. Am. Chem. Soc.* **1977**, *99*, 1692; h) V. Bonacic-Koutecky', J. Koutecky', J. Michl, *Angew. Chem.* **1987**, *99*, 216; *Angew. Chem. Int. Ed. Engl.* **1987**, *26*, 170; i) C. Glidewell, D. Lloyd, *Chem. Scr.* **1988**, *28*, 385.
[5] H. Butenschön, A. de Meijere, *Tetrahedron* **1986**, *42*, 1721.
[6] a) L. Lochmann, J. Pospisil, D. Lim, *Tetrahedron Lett.* **1966**, 257; b) M. Schlosser, S. Strunk, *ibid.* **1984**, 741; c) L. Brandsma, H. D. Verkruijsse, C. Schade, P. von R. Schleyer, *J. Chem. Soc. Chem. Commun.* **1986**, 260; d) M. Schlosser, *Pure Appl. Chem.* **1988**, *60*, 1627.
[7] T. Lendvai, T. Friedel, H. Butenschön, T. Clark, A. de Meijere, *Angew. Chem.* **1986**, *98*, 734; *Angew. Chem. Int. Ed. Engl.* **1986**, *25*, 719.
[8] a) R. Haag, R. Fleischer, D. Stalke, A. de Meijere, *Angew. Chem.* **1995**, *107*, 1642; *Angew. Chem. Int. Ed. Engl.* **1995**, *34*, 1492; b) R. Haag, *Dissertation*, Universität Göttingen, **1995**.
[9] The length of the C4(7)-Sn bond in **3** is 221 pm (average) and thereby 6 pm longer than usual C–Sn bonds: R. Haag, M. Schüngel, T. Haumann, R. Boese, A. de Meijere, unpublished results.
[10] a) Matrix isolation experiments have been performed in an argon matrix at 10 K with flash pyrolysis (600 and 750 °C) and photolysis (254 and 313 nm) techniques. In all cases decomposition of the starting material **3** was observed, but no sound evidence for the formation of acepentalene **1** collected: R. Haag, H. P. Reisenauer, G. Maier, A. de Meijere, unpublished results. b) Although this proves a half life of **1** on the order of at least 10 μs, it is unlikely that it will ever be prepared at room temperature. Most probably though, it will one day be generated and characterized by spectroscopic methods in a low temperature matrix from an appropriate precursor.
[11] Recent review: N. Goldberg, H. Schwarz, *Acc. Chem. Res.* **1994**, *27*, 347.
[12] M. Saunders, H. A. Jiménez-Vázquez, *Chem. Rev.* **1991**, *91*, 375 and references therein.
[13] a) A. G. Harrison, *Chemical Ionization Mass Spectrometry*, CRC Press, Boca Raton, **1983**; b) H. Budzikiewicz, *Mass Spectrom. Rev.* **1986**, *5*, 345.
[14] S. G. Lias, J. E. Bartmess, J. F. Liebman, J. L. Holmes, R. D. Levin, W. G. Mallard, *Gas Phase Ion and Neutral Thermochemistry*, *J. Phys. Chem. Ref. Data, Suppl. 1* **1988**, *17*.
[15] a) D. Kuck, A. Schuster, B. Ohlhorst, V. Sinnwell, A. de Meijere, *Angew. Chem.* **1989**, *101*, 626; *Angew. Chem. Int. Ed. Engl.* **1989**, *28*, 595; b) R. Haag, B. Ohlhorst, M. Noltemeyer, R. Fleischer, D. Stalke, A. Schuster, D. Kuck, A. de Meijere, *J. Am. Chem. Soc.* **1995**, *117*, 10474.
[16] P. C. H. Eichinger, S. Dua, J. H. Bowie, *Int. J. Mass Spectrom. Ion Processes* **1994**, *133*, 1.
[17] For a related study to generate the elusive neutral vinylidene, see: a) D. Sülzle, H. Schwarz, *Chem. Phys. Lett.* **1989**, *156*, 397; see also: b) G. Vacek, J. R. Thomas, B. J. DeLeeuw, Y. Yamaguchi, H. F. Schaefer III, *J. Chem. Phys.* **1993**, *98*, 4766.
[18] a) S. A. McLuckey, D. Cameron, R. G. Cooks, *J. Am. Chem. Soc.* **1981**, *103*, 1313; b) for a review, see R. G. Cooks, J. S. Pattrick, T. Kotiaho, S. A. McLuckey, *Mass Spectrom. Rev.* **1994**, *13*, 287; for an application to bracket EAs, c) see D. J. Burinsky, E. K. Fukada, J. E. Campana, *J. Am. Chem. Soc.* **1984**, *106*, 2770.
[19] R. G. Kostyanovsky, *Tetrahedron Lett.* **1968**, 2721.
[20] Geometry optimizations and frequency calculations were carried out at the Becke3LYP/6-31G* level by using the Gaussian 94 [25] program package. Stationary points were characterized to be energy minima with no imaginary frequencies (NIMAG = 0) or to be transition structures having only one imaginary frequency (NIMAG = 1). Natural atomic charges (NAC) and bond orders (Wiberg bond index, WBI [27]) were derived from the natural bond orbital analysis (NBO) of Reed et al. [28]. Single-point energies were obtained at the Becke3LYP level with the 6-311 + G* basis set with the Becke3LYP/6-31G* geometries.
[21] Wiberg bond indices (Becke3LYP/6-31G*) for **1** (C_{3v}, triplet) and **1** (C_s, singlet, values in parentheses): C(1)–C(2): 1.143 (1.054); C(2)–C(3): 1.638 (1.694); C(3)–C(4): 1.143 (1.061); C(4)–C(5): 1.143 (1.579); C(5)–C(6): 1.638 (1.048); C(1)–C(10): 1.223 (1.815); C(4)–C(10): 1.223 (1.096). Natural atomic charges for **1** (C_{3v}, triplet) and **1** (C_s, singlet, in parentheses): C(1): 0.020 (0.036); C(2): −0.222 (−0.218); C(3): −0.222 (−0.164); C(4): 0.020 (0.080); C(5): −0.222 (−0.145); C(10): −0.161 (−0.072).
[22] H. Jiao, P. von R. Schleyer, *AIP Conference Proceedings 330*, E. C:C:C.1, *Computational Chemistry* (Eds.: F. Bernadi, J. L. Rivail), American Institute of Physics, Woodbury, New York, **1995**.
[23] a) R. Srinivas, D. Sülzle, T. Weiske, H. Schwarz, *Int. J. Mass Spectrom. Ion Processes* **1991**, *107*, 368; b) R. Srinivas, D. Sülzle, W. Koch, C. H. DePuy, H. Schwarz, *J. Am. Chem. Soc.* **1991**, *113*, 5970.
[24] K. J. van den Berg, S. Ingeman, N. M. M. Nibbering, *Org. Mass Spectrom.* **1993**, *28*, 527.
[25] For the details of the increase in the flight length, see C. A. Schalley, D. Schröder, H. Schwarz, *Int. J. Mass Spectrom. Ion Processes*, in press.
[26] *Gaussian 94, Revision B.2*, M. J. Frisch, G. W. Trucks, H. B. Schlegel, P. M. W. Gill, B. G. Johnson, M. A. Robb, J. R. Cheeseman, T. Keith, G. A. Petersson, J. A. Montgomery, K. Raghavachari, M. A. Al-Laham, V. G. Zakrzewski, J. V. Ortiz, J. B. Foresman, J. Cioslowski, B. B. Stefanov, A. Nanayakkara, M. Challacombe, C. Y. Peng, P. Y. Ayala, W. Chen, M. W. Wong, J. L. Andres, E. S. Replogle, R. Gomperts, R. L. Martin, D. J. Fox, J. S. Binkley, D. J. Defrees, J. Baker, J. P. Stewart, M. Head-Gordon, C. Gonzalez, and J. A. Pople, Gaussian, Inc., Pittsburgh PA, **1995**.
[27] K. B. Wiberg, *Tetrahedron* **1968**, *24*, 1083.
[28] A. E. Reed, L. A. Curtiss, F. Weinhold, *Chem. Rev.* **1988**, *88*, 899.